PERGAMON

www.elsevier.nl/locate/poly

Polyhedron 19 (2000) 1–5

POLYHEDRON

Synthesis and X-ray structural study of magnesium (1,3-propanediaminetetraacetato)cuprate(II) octahydrate, $Mg[Cu(1,3\text{-}pdta)]\cdot 8H_2O$. Stereochemistry of hexadentate copper(II)–edta-type complexes in relation to the structure of the ligand

Urszula Rychlewska [a], Dušanka D. Radanović [b], Violeta S. Jevtović [b], Dušan J. Radanović [b,*]

[a] *Faculty of Chemistry, A. Mickiewicz University, 60-780 Poznan, Poland*

[b] *Department of Chemistry, Faculty of Science, University of Kragujevac, 34000 Kragujevac, Serbia, Yugoslavia*

Received 16 April 1999; accepted 13 October 1999

Abstract

The hexadentate complex $Mg[Cu(1,3\text{-pdta})]\cdot 8H_2O$ (**1**) (where 1,3-pdta represents the 1,3-propanediaminetetraacetate ion) has been prepared and isolated and its structure established by X-ray crystallography. The structure converged to $R = 0.030$ for 1537 observed reflections. The Cu(II) ion is surrounded by two nitrogen atoms and four oxygen atoms of the ligand, making a tetragonally elongated octahedron ($T = 0.868$). The Mg cation is bonded octahedrally to six water molecules. Both complex ions utilize a two-fold symmetry axis that is present in the crystal. The conformations of the chelate rings were found to be *envelope* for the glycinates and *skew-boat* for the six-membered diamine (T) ring. Comparison of the structures of the hexadentate copper(II)–edta-type complexes shows an expected variation in their stereochemistry, depending on the structure of the ligand. Infrared (carboxylate region) and electronic absorption spectra are also given. ©2000 Elsevier Science Ltd All rights reserved.

Keywords: Copper(II)–edta-type complexes; Crystal structures; Stereochemistry

1. Introduction

Many transition metal ions take a coordination number of six when complexed with the ethylenediaminetetraacetate ion (edta), and such hexadentate $[M(edta)]^{n-}$ complexes are well known: M = Co(III) [1,2], Cr(III) [3], Fe(III) [4,5], Mn(III) [6,7], Zn(II) [8], Cu(II) [8–11], Co(II) [12,13] and Ni(II) [14]. The format for describing the various chelate rings formed in these types of chelates was credited to Weakliem and Hoard [1]. The ethylenediamine ring is referred to as the E ring, the axially coordinated glycinate ring as the R ring, and the equatorially coordinated glycinate ring as the G ring. The G rings in these types of complexes are more strained than the R rings because the sum of the ring angles of the latter is closer to the expected value for a five-membered chelate ring with glycinate. Another ligand displaces a G ring more easily than an R ring [15], and such a complex of $[Cu(H_2edta)(H_2O)]$ (the edta acting as a pentadentate) has been well established [16].

The ethylenediaminetetra-3-propionate ion (edtp), forming four β-alaninate rings, is likely to function as a hexadentate with larger metal ions: M = Co(III) [17], Cr(III) [17], Ni(II) [18] or Rh(III) [19]. Contrary to this, the edtp ligand acts as a pentadentate in the square-pyramidal $[Cu(edtp)]^{2-}$ complex, and this dominant geometry has been verified crystallographically [20]. However, the tetragonal octahedral Cu(II) complexes of some other edta-type ligands that form six-membered rings, such as the favoured *trans*(O_6)-Cu(II) isomers of 1,3-propanediamine-*N*,*N*′-diacetate-*N*,*N*′-di-3-propionate ion (1,3-pddadp) and the Λ-*trans*(O_5)-Cu(II) isomer of the 2*S*,2*S*′-ethylenediamine-*N*,*N*′-disuccinate ion (*SS*-edds), have also been established [21–23].

With respect to $[M(edta)]^{n-}$ [1–14], the in-plane strain is eased for the $[M(1,3\text{-pdta})]^{n-}$ complexes containing an in-plane six-membered diamine (T) ring, as evidenced by their crystal structures [24–27].

* Corresponding author. Tel.: +381-34-336230; fax: +381-34-335040; e-mail: rivan@eunet.yu

0277-5387/100/$ - see front matter ©2000 Elsevier Science Ltd All rights reserved.
PII S0277-5387(99)00316-2

This study deals with the preparation of an octahedral hexadentate complex, $Mg[Cu(1,3\text{-pdta})]\cdot 8H_2O$ (**1**), for which X-ray data are reported. Structural parameters of this complex and the other tetragonal octahedral Cu(II)–edta-type complexes are compared and discussed in relation to their stereochemistry, the structure of the ligand and the size of its chelate rings. Infrared (IR) and electronic absorption spectral data of the studied complex are also reported.

2. Experimental

All commercially obtained reagent-grade chemicals were used without further purification.

2.1. Preparation of barium(1,3-propanediaminetetraacetate) dihydrate, $Ba_2(1,3\text{-pdta})\cdot 2H_2O$

The barium salt of 1,3-propanediaminetetraacetic acid was prepared according to the procedure of Wayh and Hamm [28], with a minor modification. The condensation mixture of 1,3-propanediamine (15 g, 0.20 mol) and chloroacetic acid (96 g, 0.91 mol) in aqueous KOH solution was prepared; deposited KCl was removed by filtration. A hot solution of $BaCl_2\cdot 2H_2O$ (98 g, 0.40 mol in 200 cm^3 of H_2O) was then added to the mixture, which was stirred (90°C) for 2 h. The white precipitate of $Ba_2(1,3\text{-pdta})\cdot 2H_2O$, which was practically insoluble in water, was filtered, washed with warm water and air-dried ($\approx$100 g).

Found: C, 21.04; H, 2.63; N, 4.53; Ba, 44.74; H_2O, 5.90%. Calc. for $Ba_2(1,3\text{-pdta})\cdot 2H_2O$, $Ba_2C_{11}H_{18}N_2O_{10}$ (FW = 612.93): C, 21.55; H, 2.96; N, 4.57; Ba, 44.81; H_2O, 5.88%.

The barium salt of the ligand was used directly for the preparation of the corresponding hexadentate Cu(II) complex.

2.2. Preparation of magnesium(1,3-propanediaminetetraacetato)cuprate(II) octahydrate, $Mg[Cu(1,3\text{-pdta})]\cdot 8H_2O$ (1)

$Cu(SO_4)\cdot 5H_2O$, 7.50 g (0.0300 mol) in 100 cm^3 of H_2O, was stirred at 80°C for 10 min. To this solution, solid $Ba_2(1,3\text{-pdta})\cdot 2H_2O$ (18.39 g, 0.0300 mol) was added and the blue solution (pH $\sim$7) was then stirred at 80°C for 3 h. The deposited $BaSO_4$ was removed by filtration. The obtained filtrate was then poured into a 5×60 cm column containing Dowex 1X8 (200–400 mesh) anion-exchange resin in the Cl^- form. The column was then washed with H_2O and eluted with 0.05 M $MgCl_2$ ($\sim$0.5 cm^3/min). The obtained eluate was reduced to a volume of 150 cm^3 and allowed to stand at room temperature for several days. The crystals of $Mg[Cu(1,3\text{-pdta})]\cdot 8H_2O$ were collected, washed with ethanol, then ether, and air-dried; the yield was 10 g (66%). Found: C, 24.84; H, 4.84; N, 5.04%. Calc. for $Mg[Cu(1,3\text{-pdta})]\cdot 8H_2O$ (**1**), $MgCuC_{11}H_{30}N_2O_{16}$ (FW = 534.21): C, 24.73; H, 5.66; N, 5.24%.

2.3. Physical measurements

$Mg[Cu(1,3\text{-pdta})]\cdot 8H_2O$ (**1**): a pale-blue crystal having approximate dimensions of $0.35\times 0.40\times 0.45$ mm, obtained from an aqueous solution, was used for data collection. Intensity measurements were made on a four-circle KM-4 (KUMA Diffraction) diffractometer using graphite monochromated Mo Kα radiation (293°K).

Crystal data: $MgCuC_{11}H_{30}N_2O_{16}$ (F_w = 534.21), orthorhombic, space group *Pnna*, a = 13.264(3), b = 11.711(4), c = 13.684(4) Å, V = 2125.6 Å^3, Z = 4, D_c = 1.669 g cm^{-3}, $F(000)$ = 1116, μ(Mo Kα) = 11.38 cm^{-1}. The cell constants and the orientation matrix were obtained from a least-squares fit of 48 centred reflections with θ in the range 7.7–12.5°. The structure was solved by direct methods using SHELXS-86 [29] and refined by least-squares techniques with SHELXL-93 [30], to $R1 = 0.030$ ($wR2 = 0.079$) for 1537 reflections ($I > 2\sigma(I)$) of 2114 reflections collected in the range $2.14 < \theta < 26.05°$. The intensity data were corrected for Lorentz and polarization effects as well as for absorption. The non-hydrogen atoms were refined anisotropically, and all hydrogen atoms were refined using a riding model with isotropic temperature factors 30% higher than the isotropic equivalent for the atom to which the hydrogen atom was bonded. The function minimized was $\Sigma[w(F_o^2 - F_c^2)^2]$ with $w = 1/[\sigma^2(F_o)^2 + (aP)^2 + bP]$, where $P = (F_o^2 + 2F_c^2)/3$, a = 0.0453 and b = 0.46. The final difference map showed minima and maxima ranging from -0.57 to 0.29 e Å^{-3}. A Siemens Stereochemical Workstation was used to prepare drawings [31].

IR spectra were recorded on a JASCO FT/IR-5300 spectrophotometer using KBr pellets. Electronic absorption spectra were recorded on a Varian Cary 17D spectrophotometer. For these measurements 1×10^{-2} M aqueous solutions were used. Electronic reflectance spectra were run on a Varian Cary 2300 spectrophotometer. Elemental microanalyses for carbon, hydrogen, nitrogen and barium were performed by the Microanalytical Laboratory, Faculty of Chemistry, University of Belgrade.

3. Results and discussion

3.1. Description of the crystal structure of $Mg[Cu(1,3\text{-pdta})]\cdot 8H_2O$ (1)

An ORTEP drawing of the complex anion, $[Cu(1,3\text{-pdta})]^{2-}$, is shown in Fig. 1; the numbering scheme adopted for the respective atoms is also given. Bond lengths and valency angles are listed in Table 1.

The structural unit consists of $[Cu(1,3\text{-pdta})]^{2-}$ and $[Mg(H_2O)_6]^{2+}$ octahedra and two water solvent molecules, all of which lie on a special position in the unit cell. The

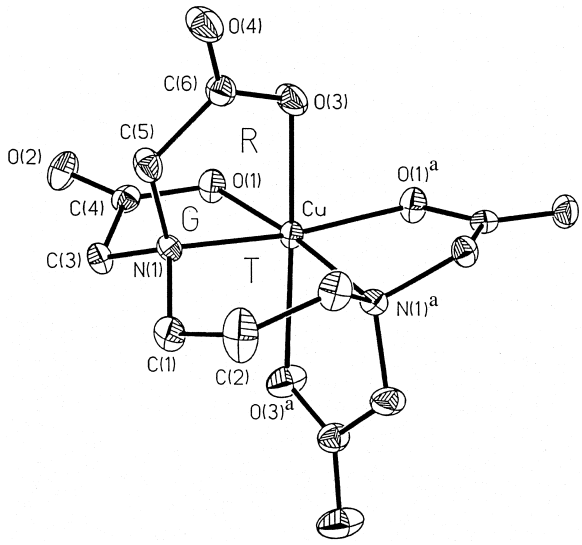


Fig. 1. View of the $[Cu(1,3\text{-pdta})]^{2-}$ octahedron with labelling scheme. Thermal ellipsoids were drawn with 40% probability.

Table 1
Bond lengths (Å) and valency angles (°) for $Mg[Cu(1,3\text{-pdta})]\cdot 8H_2O$

Cu–O(1)	1.974(2)	O(3)–C(6)	1.254(3)
Cu–N(1)	2.047(2)	O(4)–C(6)	1.244(3)
Cu–O(3)	2.272(2)	N(1)–C(3)	1.478(3)
Mg–O(1W)	2.034(2)	N(1)–C(5)	1.479(3)
Mg–O(2W)	2.072(2)	N(1)–C(1)	1.487(3)
Mg–O(3W)	2.066(2)	C(1)–C(2)	1.517(3)
O(1)–C(4)	1.268(3)	C(3)–C(4)	1.517(3)
O(2)–C(4)	1.236(3)	C(5)–C(6)	1.515(3)
$O(1)^a$–Cu–O(1)	96.2(1)	C(4)–O(1)–Cu	114.4(1)
O(1)–Cu–N(1)	84.0(1)	C(6)–O(3)–Cu	112.4(1)
O(1)–Cu–$N(1)^a$	172.4(1)	C(3)–N(1)–C(5)	110.0(2)
N(1)–Cu–$N(1)^a$	96.8(1)	C(3)–N(1)–C(1)	109.3(2)
O(1)–Cu–$O(3)^a$	92.2(1)	C(5)–N(1)–C(1)	111.3(2)
N(1)–Cu–$O(3)^a$	94.0(1)	C(3)–N(1)–Cu	102.9(1)
O(1)–Cu–O(3)	93.6(1)	C(5)–N(1)–Cu	112.2(1)
N(1)–Cu–O(3)	80.2(1)	C(1)–N(1)–Cu	110.7(1)
$O(3)^a$–Cu–O(3)	171.3(1)	N(1)–C(1)–C(2)	115.2(2)
$O(1W)^b$–Mg–O(1W)	174.3(1)	$C(1)^a$–C(2)–C(1)	119.4(3)
O(1W)–Mg–$O(3W)^b$	92.3(1)	O(2)–C(4)–O(1)	124.9(2)
O(1W)–Mg–O(3W)	91.8(1)	O(2)–C(4)–C(3)	119.4(2)
$O(3W)^b$–Mg–O(3W)	87.7(1)	O(1)–C(4)–C(3)	115.7(2)
O(1W)–Mg–O(2W)	87.0(1)	N(1)–C(3)–C(4)	111.1(2)
O(3W)–Mg–O(2W)	176.8(1)	N(1)–C(5)–C(6)	116.6(2)
O(1W)–Mg–$O(2W)^b$	89.1(1)	O(4)–C(6)–O(3)	126.0(2)
O(3W)–Mg–$O(2W)^b$	89.4(1)	O(3)–C(6)–C(5)	118.5(2)
O(2W)–Mg–$O(2W)^b$	93.6(1)	O(4)–C(6)–C(5)	115.5(2)

[a] Symmetry codes: $x, -y+0.5, -z+0.5$.
[b] Symmetry codes: $x, -y-0.5, -z+0.5$.

highest symmetry (C_2) axis of the complex passes through the Cu, Mg and C(2) atoms and bisects the N(1)–Cu–N1(1)[a] bond angle, making the two glycinate (R) rings (as well as the G rings) identical. The Cu–O bond distances differ considerably, the equatorial and axial distances being 1.974(2) and 2.272(2) Å, respectively (Table 1). The four basal atoms N(1), N(1)[a], O(1) and O(1)[a] are nearly coplanar and the Cu(II) ion lies in this plane. The *cis* angles at the Cu(II) ion (Table 1) range from 80.2(6) to 96.8(1)° and the *trans* angles are 171.3(1) and 172.4(1)°. The six-membered diamine (T) ring (Fig. 1) adopts a *skew-boat* conformation (λ for the enantiomorph presented in Fig. 1 having Δ configuration). The R rings are nearly planar and are in an *envelope* conformation. The G rings are much more puckered and are halfway between an *envelope* and a *twist* conformation.

An increase of the backbone ring in the complex **1** causes significant changes in equatorial valency angles. We observed widening of N–Cu–N valency angle (96.8(1)°; Table 1) compared with those of hexadentate $[Cu(edta)]^{2-}$ [8–11] (av. 88.5(0.9)°), whereas the equatorial N–Cu–O valency angles in these structures were nearly the same. However, the O–Cu–O angle of complex **1**, 96.2(1)°, was larger than the 90° expected for a regular octahedron, but much less with respect to those of hexadentate Cu(II)–edta complexes (av. 106.7(2.7)°).

$[Cu(1,3\text{-pdta})]^{2-}$ octahedra form discrete units, a phenomenon that is not common either in $[Cu(edta)]^{2-}$ [8–11] or in $[M(1,3\text{-pdta})]^{-}$ complexes [24–27]. The discrete Cu(II) and Mg(II) complex ions are arranged in the unit cell in a very much the same way as in the sodium chloride structure. This packing is determined by an extended network of hydrogen bonds predominantly involving the water molecules coordinated to Mg(II) (acting as donors) and carboxylate oxygens (acting as acceptors).

3.2. Structural parameters correlating stereochemistry of tetragonal octahedral Cu(II)–edta-type complexes

Tetragonal octahedral Cu(II)–edta-type complexes of known structure are listed in Table 2 (complexes **1**–**8**); copper–ligand bond-length data are also given. Within these complexes (oxygen ligands) the variation in R_S is less ($\sim$0.04 Å) than that in R_L ($\sim$0.2 Å) and, as expected [32–35], there is an increase in the value of R_S (not exactly for **1**, **5** and **6**) as T increases. The extent of distortion of these complexes is restricted by the chelation of the multidentate edta-type ligand and depends on its structure. The parameter (T) for listed complexes increases in the order: $\mathbf{2} \le \mathbf{3} < \mathbf{4} < \mathbf{5} < \mathbf{6} < \mathbf{1} < \mathbf{7} < \mathbf{8}$. The tetragonality ($T$) of these complexes increases with the decreasing number of six-membered rings incorporated in the complex (complexes **2**, **3**, **4** and **1**; Table 2). Complexes **2** [21] and **3** [22], containing the 1,3-pddadp ligand and forming three six-membered rings (*trans*(O_6) coordination), are much more elongated and have a tetragonality ($T \sim 0.80$) the same as that obtained for tetragonal octahedral complexes [34,35]. Other complexes listed in Table 2 (complexes **1** and **4**–**8**, *trans*(O_5) coordination) have higher T values of 0.818–0.884 (for oxygen ligands) and 0.902 for **8** (for nitrogen ligands), as was observed for elongated rhombic octahedral complexes [34]. We observed that the variation in tetragonalities of edta complexes (complexes **5**–**7**; Table 2) depends on the packing in their crystal structures and interaction of the axially coordinated carboxylate group involved in the covalent bond with

Table 2
Copper–ligand bond length data for elongated tetragonal and rhombic octahedral Cu(II)–edta-type complexes involving mixed (nitrogen–oxygen) donor atoms

Complex	R_S	R_L	T	Asymmetry in tetragonal bonds (Δ, Å)	Ref.
trans(O_6)-[Cu($H_2$1,3-pddadp)]·1.5H_2O (**2**)	1.954	2.448	0.798	0.014	[21]
trans(O_6)-Na_2[Cu(1,3-pddadp)]·$NaNO_3$·2H_2O (**3**)	1.953	2.445	0.799	0.000	[22]
trans(O_5)-Mg[Cu(*SS*-edds)]·7H_2O (**4**)	1.984	2.425	0.818	0.242	[23]
[Cu(en)$_2$(H_2O)$_2$][Cu$_2$(edta)$_2$Cu(en)$_2$]·10H_2O (**5**)	1.959	2.337	0.838	0.028	[10]
K_2[Cu(edta)]·3H_2O (**6**)	1.978	2.302	0.859	0.157	[9]
Mg[Cu(1,3-pdta)]·8H_2O (**1**)	1.974	2.272	0.868	0.000	This work
[Mn(H_2O)$_4$][Cu(edta)]·2H_2O (**7**)	1.991	2.252	0.884	0.074	[8]
[Cu(H_2edta)(H_2O)] [a] (**8**)	2.066	2.291	0.902	0.176	[16]

[a] Ligand acting as pentadentate (the tetragonality is taken as the comparison of the Cu–N lengths). Other complexes listed are hexadentates, for which the tetragonality given is taken as the comparison of the Cu–O lengths.

the counter ion. Generally, the stereochemistry of the copper(II) ion present varies from elongated tetragonal octahedral (complexes **1** and **3**), through elongated rhombic octahedral (complex **2**) to (in approximation) the square-based pyramidal configuration (complexes **4**–**8**) (Table 2).

3.3. Spectral characteristics of the complex

The complex studied (**1**) exhibits one very strong band in an expected IR carboxylate region (at 1601 cm^{-1}) corresponding to the asymmetric stretching vibrations of the five-membered (glycinate) rings. This band shows evidence of separation (the small band at 1693 cm^{-1}) and should be expected to be overlapped by the $\delta(H_2O)$ mode. One strong band of $\nu_s(COO^-)$ at 1404 cm^{-1} was also recorded.

The ligand field absorption spectra are considered only for complexes forming six-membered (T) rings and having the same 5–6–5 combination of the ring members in the G plane (studied complex (**1**) and complexes **2** and **3** of known structures and spectral characteristics [21,22]; Table 3). All blue complexes having C_2 molecular symmetry (in approximately C_2 for **2**) exhibit single unsymmetrical absorption bands. These bands can be assigned to the d_{z^2}, d_{xy}, d_{xz}, $d_{yx} \rightarrow d_{x^2-y^2}$ transitions with a $d_{x^2-y^2}$ ground state. The reflectance spectra of complexes **1**, **2** and **3**, with respect to data taken from solution (Table 3), are only slightly changed and retain almost the same shape and position of the band maxima, suggesting that the geometry of these complexes is the same in both, solution and solid state. In the case of [Cu(1,3-pdta)]$^{2-}$ (**1**), with respect to **2** and **3** (*trans*(O_6) coordination), the stronger axial interaction increases the energy of the d_{z^2} orbital and the energy of the $d_{x^2-y^2}$ orbital would therefore be lowered. The lowering of the energy of the d–d transitions for **1** would be expected and is found (Table 3).

Table 3
Absorption data (solution or solid state) for hexadentate Cu(II)–edta-type complexes forming six-membered diamine rings

Complex	ν ($10^3 \times cm^{-1}$) [a]	ε	Ref.
[Cu(1,3-pdta)]$^{2-}$ (**1**)	14.16 (~14.17)	86	This work
trans(O_6)-[Cu(1,3-pddadp)]$^{2-}$ (**3**)	14.97 (~14.97)	80	[22]
trans(O_6)-[Cu($H_2$1,3-pddadp)] (**2**)	15.97 (~15.97)	54	[21,22]

[a] Data for reflectance spectra are given in parentheses.

Supplementary data

Crystallographic data have been deposited with the CCDC (12 Union Road, Cambridge, CB2 1EZ, UK) and are available on request, quoting deposition number 116779.

Acknowledgements

The authors are grateful to the Serbian Ministry for Science and Technology for financial support.

References

[1] H.A. Weakliem, J.L. Hoard, J. Am. Chem. Soc. 81 (1959) 549.
[2] K. Okamoto, T. Tsukihara, J. Hidaka, Y. Shimura, Bull. Chem. Soc. Jpn. 51 (1978) 3534.
[3] Y. Kushi, K. Morimasa, H. Yoneda, Presented at the 49th Annual Meeting of the Chemical Society of Japan, Tokyo, April 1984, abstract 1N31.
[4] N.V. Novozhilova, T.N. Polynova, M.A. Porai-Koshits, N.I. Pechurova, L.I. Martynenko, A. Khadi, Zh. Strukt. Khim. 14 (1973) 745.
[5] Y. Kushi, K. Morimasa, K. Yoshitsugu, H. Yoneda, 35th Symposium Coordination Chemistry, Hiroshima, Japan, 1985, abstract 2B01.
[6] T. Lis, Acta Crystallogr., Sect. B 34 (1978) 1342.
[7] J. Stein, J.P. Fackler Jr., G.J. McClune, J.A. Fee, L.T. Chan, Inorg. Chem. 18 (1979) 3511.
[8] X. Solans, M. Font-Altaba, J. Oliva, J. Herrera, Acta Crystallogr., Sect. C 39 (1983) 435.
[9] M.A. Porai-Koshits, N.V. Novozhilova, T.N. Polynova, T.V. Filippova, L.I. Martynenko, Kristallografiya 17 (1973) 89.
[10] T.F. Sysoeva, V.M. Agre, V.K. Trunov, N.M. Dyatlova, N.N. Barkhanova, Zh. Strukt. Khim. 25 (1984) 107.
[11] M.V. Leont'eva, A. Ya. Fridman, N.M. Dyatlova, V.M. Agre, T.F. Sysoeva, Zh. Neorg. Khim. 32 (1987) 2494.
[12] E.F.K. McCandlish, T.K. Michael, J.A. Neal, E.C. Lingafelter, N.J. Rose, Inorg. Chem. 17 (1978) 1384.
[13] A.I. Pozhidaev, N.N. Neronova, T.N. Polynova, M.A. Porai-Koshits, V.A. Logvinenko, Zh. Strukt. Khim. 13 (1972) 344.
[14] E. Coronado, M. Drillon, A. Fuertes, D. Beltran, A. Mosset, J. Galy, J. Am. Chem. Soc. 108 (1986) 900.
[15] H. Ogino, M. Shimura, Adv. Inorg. Bioinorg. Mech. 4 (1986) 107.

[16] F.S. Stephens, J. Chem. Soc. A (1969) 1723.
[17] M. Parvez, C. Maricondi, D.J. Radanović, M.I. Djuran, B.E. Douglas, Inorg. Chim. Acta 182 (1991) 177.
[18] D.J. Radanović, S. Ianelli, G. Pelosi, Z.D. Matović, S. Tasić-Stojanović, B.E. Douglas, Inorg. Chim. Acta 278 (1998) 66.
[19] D.J. Radanović, M.I. Djuran, B.E. Douglas, Inorg. Chem. 24 (1985) 4239.
[20] U. Rychlewska, D.D. Radanović, M. Dj. Dimitrijević, D.J. Radanović, unpublished results.
[21] B.V. Prelesnik, D.D. Radanović, Z.D. Tomić, P.T. Djurdjević, D.J. Radanović, D.S. Veselinović, Polyhedron 15 (1996) 3761.
[22] D.J. Radanović, B.V. Prelesnik, D.D. Radanović, Z.D. Matović, B.E. Douglas, Inorg. Chim. Acta 262 (1997) 203.
[23] J. Soldánová, F. Pavelčik, J. Majer, Acta Crystallogr., Sect. B 37 (1981) 921.
[24] T. Yamamoto, K. Mikata, K. Miyoshi, H. Yoneda, Inorg. Chim. Acta 150 (1988) 237.
[25] R. Nagao, F. Marumo, Y. Saito, Acta Crystallogr., Sect. B 28 (1972) 1852.
[26] R. Herak, G. Srdanov, M.I. Djuran, D.J. Radanović, M. Bruvo, Inorg. Chim. Acta 83 (1984) 55.
[27] J.C. Robles, Y. Matsuzaka, S. Inomata, M. Shimoi, W. Mori, H. Ogino, Inorg. Chem. 32 (1993) 13.
[28] J.A. Weyh, R.E. Hamm, Inorg. Chem. 7 (1968) 2431.
[29] G.M. Sheldrick, SHELXS86, Program for the Solution of Crystal Structures, University of Göttingen, Germany, 1986.
[30] G.M. Sheldrick, SHELXL93, Program for the Refinement of Crystal Structures, University of Göttingen, Germany, 1993.
[31] Stereochemical Workstation Operation Manual, Release 3.4, Siemens Analytical X-Ray Instruments, Inc., Madison, WI, 1989.
[32] A.A.G. Tomlinson, B.J. Hathaway, D.E. Billing, P. Nichols, J. Chem. Soc. A (1969) 65.
[33] I.M. Procter, B.J. Hathaway, P. Nichols, J. Chem. Soc. A (1968) 1678.
[34] B.J. Hathaway, in: G. Wilkinson, R.D. Gillard, J.A. McCleverty (Eds.), Comprehensive Coordination Chemistry, vol. 5, Pergamon, Oxford, 1987, Ch. 53.
[35] B.J. Hathaway, P.G. Hodgson, J. Inorg. Nucl. Chem. 35 (1973) 4071.

PERGAMON

www.elsevier.nl/locate/poly

Polyhedron 19 (2000) 7–21

POLYHEDRON

Synthesis, characterization and crystal structure of a series of ruthenium nitrosonaphthol complexes

Xiao-Xia Liu, Wing-Tak Wong *

Department of Chemistry, The University of Hong Kong, Pokfulam Road, Hong Kong, PR China

Received 6 July 1999; accepted 13 October 1999

Abstract

A monosubstituted decarbonylation reaction was performed on *cis*-,*cis*-[Ru{η^2-N(O)$C_{10}H_6$O}$_2$(CO)$_2$] (*cis*-NO, *cis*-O) (**A**), *trans*-,*cis*-[Ru{η^2-N(O)$C_{10}H_6$O}$_2$(CO)$_2$] (*trans*-NO, *cis*-O) (**B**), *cis*-,*cis*-[Ru{η^2-O$C_{10}H_6$N(O)}$_2$(CO)$_2$] (**C**), *trans*-,*cis*-[Ru{η^2-O$C_{10}H_6$N(O)}$_2$(CO)$_2$] (**D**) and *cis*-,*trans*-[Ru{η^2-O$C_{10}H_6$N(O)}$_2$(CO)$_2$] (*cis*-NO, *trans*-O) (**E**) with donor ligand (L) 4-phenylpyridine (ppy), 4-{2-(9-anthryl)vinyl}pyridine (avpy) or triphenylphosphine (PPh_3) to give substituted complex *cis*-,*cis*-[Ru{η^2-N(O)$C_{10}H_6$O}$_2$(CO)L] (**1a**, L = ppy; **2a**, L = avpy; **3a**, L = PPh_3), *trans*-,*cis*-[Ru{η^2-N(O)$C_{10}H_6$O}$_2$(CO)L] (**1b**, L = ppy), *cis*-,*cis*-[Ru{η^2-O$C_{10}H_6$N(O)}$_2$(CO)L] (**1c**, L = ppy; **2c**, L = avpy), *trans*-,*cis*-[Ru{η^2-O$C_{10}H_6$N(O)}$_2$(CO)L] (**1d**, L = ppy; **2d** L = avpy) or *cis*-,*trans*-[Ru{η^2-O$C_{10}H_6$N(O)}$_2$(CO)L] (**1e**, L = ppy). Progressive substitution of the carbonyl ligands of **A** by tributylphosphine (PBu_3) or functionalized pyridine 4-formylpyridine (fpy), 4-ethylpyridine (epy) or 4-dimethylaminopyridine (mapy) gave a centrosymmetric bisubstituted complex *trans*-,*trans*-[Ru{η^2-N(O)$C_{10}H_6$O}$_2$L$_2$] (**8a**, L = PBu_3; **9a**, L = fpy; **10a**, L = epy; **11a**, L = mapy) together with the corresponding mono-CO-substituted complex *cis*-,*cis*-[Ru{η^2-N(O)$C_{10}H_6$O}$_2$(CO)L] (**4a**, L = PBu_3; **5a**, L = fpy; **6a**, L = epy; **7a**, L = mapy). The electronic absorption spectra and metal-localized oxidation formal potentials changed significantly for the bisubstituted complexes compared with the monosubstituted ones. ©2000 Elsevier Science Ltd All rights reserved.

Keywords: Crystal structures; Nitrosonaphthol; Ruthenium nitrosonaphthol complexes

1. Introduction

1-Nitroso-2-naphthol (referred to as 1,2-naphthoquinone-1-oxime, abbreviated as 1-nqoH) was the first organic substance that was found to form precipitates with metal ions [1]. This reagent and its isomer 2-nitroso-1-naphthol (1,2-naphthoquinone-2-oxime, 2-nqoH) have been used extensively for analytical purposes [2,3]. Metal complexes containing these ligands have attracted much attention; however, most of the studies have been concerned with first-row transition metals. It is well documented that direct coordination of first-row transition metal salts with these ligands or their sodium salts gives complexes of M(nqo)$_2$ [4–6] or M(nqo)$_3$ [7,8] type, which normally exist in oligomeric form. Charalambous and coworkers demonstrated that the internal redox reactions of Cu(nqo)$_2$ upon treatment with amine [9] or triphenylphosphine [10] led to the deoxygenation of the 1,2-naphthoquinone-mono-oximato ligands. Cu(nqo)$_2$ can also form adducts with acetone [11] or H_2O [12]. The structural analyses by X-ray crystallography that are available on these adducts reveal an interesting coordination mode in which the 1,2-naphthoquinone-mono-oximato moiety acts as a bidentate ligand and chelates to the central metal atom through the nitroso nitrogen atom and the naphtholic oxygen atom.

Charalambous and his group also demonstrated rhodium, iridium and ruthenium complexes derived from 1,2-naphthoquinone-mono-oxime that were produced through direct coordination of the metal salt with the ligand or its sodium salt [13,14]. Structural analyses of the complexes containing pyridine in their coordination sphere, such as [pyH][Ir(1-nqo)(py)Cl$_3$] [13] and [Ru(1-nqo)$_2$(py)$_2$]·1.5py [14], were available. However, the chemistry of second-row transition metals with these ligands has not been well established. Recently, we demonstrated that the reaction between triruthenium dodecacarbonyl and 1-nqoH or 2-nqoH lead to the mononuclear complexes *cis*-,*cis*- and *trans*-,*cis*-[Ru{η^2-N(O)$C_{10}H_6$O}$_2$(CO)$_2$] [15] or *cis*-,*cis*- and *trans*-,*cis*-[Ru{η^2-O$C_{10}H_6$N(O)}$_2$(CO)$_2$] [16], respectively. As a continuation of our studies on this type of complex, we document here the progressive carbonyl substitution reaction by

* Corresponding author. Tel.: +86-852-2547 2933; fax: +86-852-2857-1586; e-mail: wtwong@hkucc.hku.hk

0277-5387/100/$ - see front matter ©2000 Elsevier Science Ltd All rights reserved.
PII S0277-5387(99)00317-4

pyridine- and phosphine-type donor ligands in which an unusual structural rearrangement occurs in the bicarbonyl substitution reactions. The properties of some substituted complexes are also investigated by electronic absorption spectroscopy and electrochemical techniques.

2. Results and discussion

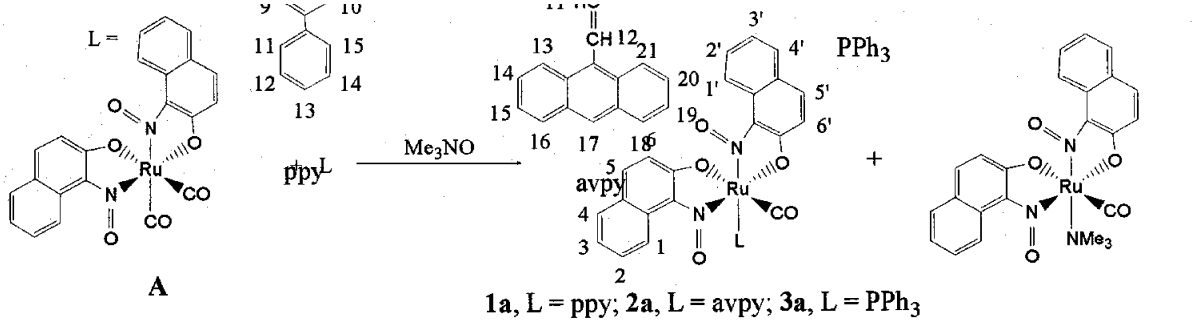
2.1. Monocarbonyl substitution reaction

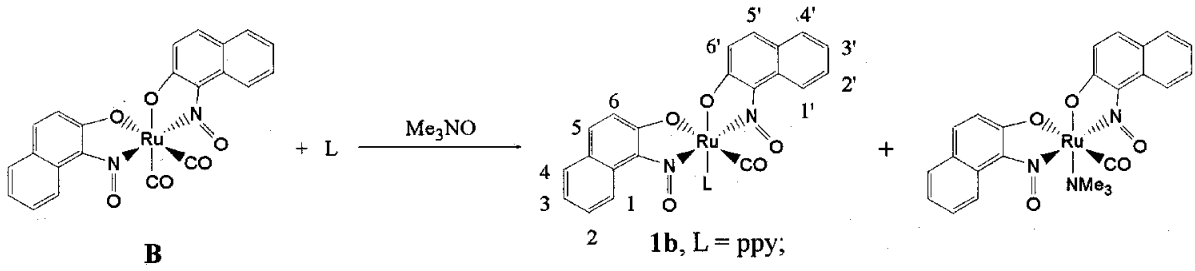
A monocarbonyl substitution reaction of the ruthenium carbonyl complexes derived from 1,2-naphthoquinone-1-oxime, *cis*-,*cis*-[Ru{η^2-N(O)$C_{10}H_6$O}$(CO)_2$] (**A**) and *trans*-,*cis*-[Ru{η^2-N(O)$C_{10}H_6$O}$_2(CO)_2$] (**B**) [15], or the complexes derived from 1,2-naphthoquinone-2-oxime, *cis*-,*cis*-[Ru{η^2-$OC_{10}H_6$N(O)}$_2(CO)_2$] (**C**) and *trans*-,*cis*-[Ru{η^2-$OC_{10}H_6$N(O)}$_2(CO)_2$] (**D**) [16], with donor ligand (L) 4-phenylpyridine (ppy) or 4-{2-(9-anthryl)vinyl}pyridine (avpy), respectively, was performed by the addition of trimethylamine *N*-oxide to the reaction mixture at room temperature. The desired complex with one carbonyl substituted by pyridine donor ligand, *cis*-,*cis*-[Ru{η^2-N(O)$C_{10}H_6$O}$_2$(CO)L] (**1a**, L = ppy; **2a**, L = avpy), *trans*-,*cis*-[Ru{η^2-N(O)$C_{10}H_6$O}$_2$(CO)L] (**1b**, L = ppy), *cis*-,*cis*-[Ru{η^2-$OC_{10}H_6$N(O)}$_2$(CO)L] (**1c**, L = ppy; **2c**, L = avpy) or *trans*-,*cis*-[Ru{η^2-$OC_{10}H_6$N(O)}$_2$(CO)L] (**1d**, L = ppy; **2d**, L = avpy), is obtained as the major product with a small amount of NMe_3-substituted complex *cis*-,*cis*- or *trans*-,*cis*-[Ru{η^2-N(O)$C_{10}H_6$O}$_2$(CO)(NMe_3)] [17]; *cis*-,*cis*- or *trans*-,*cis*-[Ru{η^2-$OC_{10}H_6$N(O)}$_2$(CO)(NMe_3)] [16] is obtained upon thin-layer chromatographic (TLC) separation using CH_2Cl_2–n-hexane as eluent (Scheme 1). Complexes **2a**, **2c** and **2d** are too light sensitive to allow study of their conducting properties, and the CO-substituted complex of **B** by avpy cannot be isolated and characterized because of its instability. When *cis*-,*cis* complexes (**A** or **C**) are used as the starting material, the reaction proceeds through the substitution of a carbonyl *trans* to the oximato group, which demonstrates the strong *trans* influence of this group. Substitution by triphenylphosphine (PPh_3) was also performed on **A** and again the carbonyl *trans* to the oximato group was replaced by donor ligand to give *cis*-,*cis*-[Ru{η^2-N(O)$C_{10}H_6$O}$_2$(CO)(PPh_3)] (**3a**) as the major product together with a small amount of *cis*-,*cis*-[Ru{η^2-N(O)$C_{10}H_6$O}$_2$(CO)(NMe_3)] (**12a**).

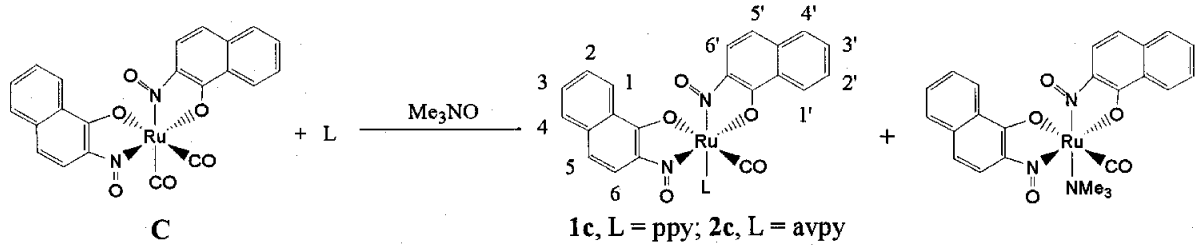
Reaction of **C** with avpy leads to a new orange compound (**E**) in addition to the carbonyl-substituted products. The chromatographic behaviour of **E** is very similar to that of **C**. Only after repeated TLC separation could we isolate **E** in sufficient purity for characterization. The ^{1}H NMR spectrum of **E** shows no pyridine ring signal but one set of proton signals for the 2-nqo ligands. Its infrared (IR) spectrum shows two strong bands in the region of carbonyl absorption, which is consistent with a *cis*-dicarbonyl arrangement [16]. Single crystal X-ray analysis (see Fig. 6) revealed that **E** is the isomer of **C** and **D** with the formula *cis*-,*trans*-[Ru{η^2-$OC_{10}H_6$N(O)}$_2(CO)_2$]. This isomer could not initially be detected in the reaction of $Ru_3(CO)_{12}$ with 2-nitroso-1-naphthol [16]. The naphtholic groups in **E** are *trans* to each other and both CO groups are also *trans* to oximato groups. We believe that isomer **E** was formed in very small quantity during the reaction of $Ru_3(CO)_{12}$ and 2-nitroso-1-naphthol. However, in the presence of isomer **C**, it is very difficult to separate and purify **E**, but, upon careful substitution of **C** by the pyridine type of nucleophile, the existence of **E** becomes apparent. **E** can also undergo carbonyl substitution by ppy under similar reaction conditions to give *cis*-,*trans*-[Ru{η^2-$OC_{10}H_6$N(O)}$_2$(CO)(ppy)] (**1e**) in which a CO group *trans* to oximato is replaced by ppy (see Fig. 7).

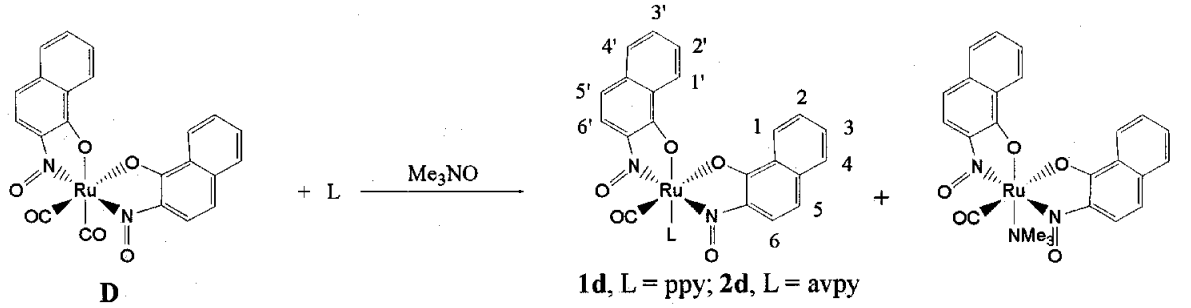
2.2. Bicarbonyl substitution reaction

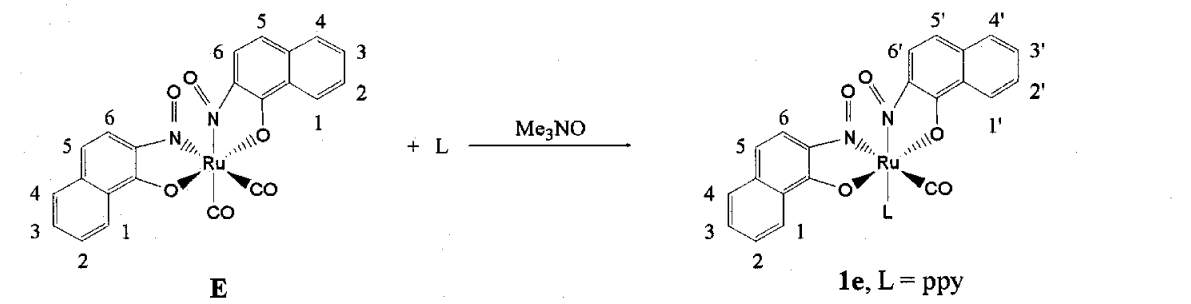
Higher ligand and Me_3NO to metal ratios and extended reaction time are required to substitute two carbonyl groups by donor ligand (L) tributylphosphine (PBu_3) or *para*-functionalized pyridine 4-formylpyridine (fpy), 4-ethylpyridine (epy) or 4-dimethylaminopyridine (mapy) when using **A** as the starting material. Upon TLC separation, a light purple (when using PBu_3 as donor ligand) or a purple-blue (when using fpy, epy or mapy as donor ligands) complex is obtained together with the reddish-brown monocarbonyl-substituted product *cis*-,*cis*-[Ru{η^2-N(O)$C_{10}H_6$O}$_2$(CO)L] (**4a–7a**) (**4a**, L = PBu_3; **5a**, L = fpy; **6a**, L = epy; **7a**, L = mapy) and *cis*-,*cis*-[Ru{η^2-N(O)$C_{10}H_6$O}$_2$(CO)(NMe_3)] (**12a**) (Scheme 2), in which the donor ligand replaces the carbonyl *trans* to the oximato nitrogen atom as in **1a–3a**. In ^{1}H NMR spectra, the new complex shows one set of donor ligand signals and one set of 1-nqo ligand signals in an integral ratio of 1:1. There is no significant feature in the IR spectra in the region of carbonyl absorption, and the mass-spectrometric (MS) data show that the molecular formula is consistent with the bisubstitution complex *trans*-,*trans*-[Ru{η^2-N(O)$C_{10}H_6$O}$_2L_2$] (**8a**, L = PBu_3; **9a**, L = fpy; **10a**, L = epy; **11a**, L = mapy). X-ray analysis of **8a** (see Fig. 8) confirms that both of the carbonyls in **A** are substituted by phosphine ligands that are *trans* to each other, with the two 1-nqo ligands located in an equatorial coordination plane containing the ruthenium metal centre. Due to the steric effect, both the oximato and naphtholic groups also adopt the *trans* configuration, as in [Cu{η^2-N(O)$C_{10}H_6$O}$_2$]·2$(CH_3)_2$CO [11]. The structure of the molecule is consistent with its ^{1}H NMR and ^{31}P NMR spectroscopic data. The *para*-functionalized pyridine substitution products (**9a–11a**) should have the same ligand spatial orientation since they have very similar ^{1}H NMR spectra for 1-nqo ligands to that of **8a**. For the reaction of **A** with the donor ligand, only mono-CO-substituted complex is detected in the first 24 h of reaction; the bi-CO-substituted complex is detected after 48 h, which indicates that the substitution evolves progressively. We suspect that the ligand rearrange-


L =
ppyL
Me3NO
avpy
PPh3
A
1a, L = ppy; 2a, L = avpy; 3a, L = PPh3

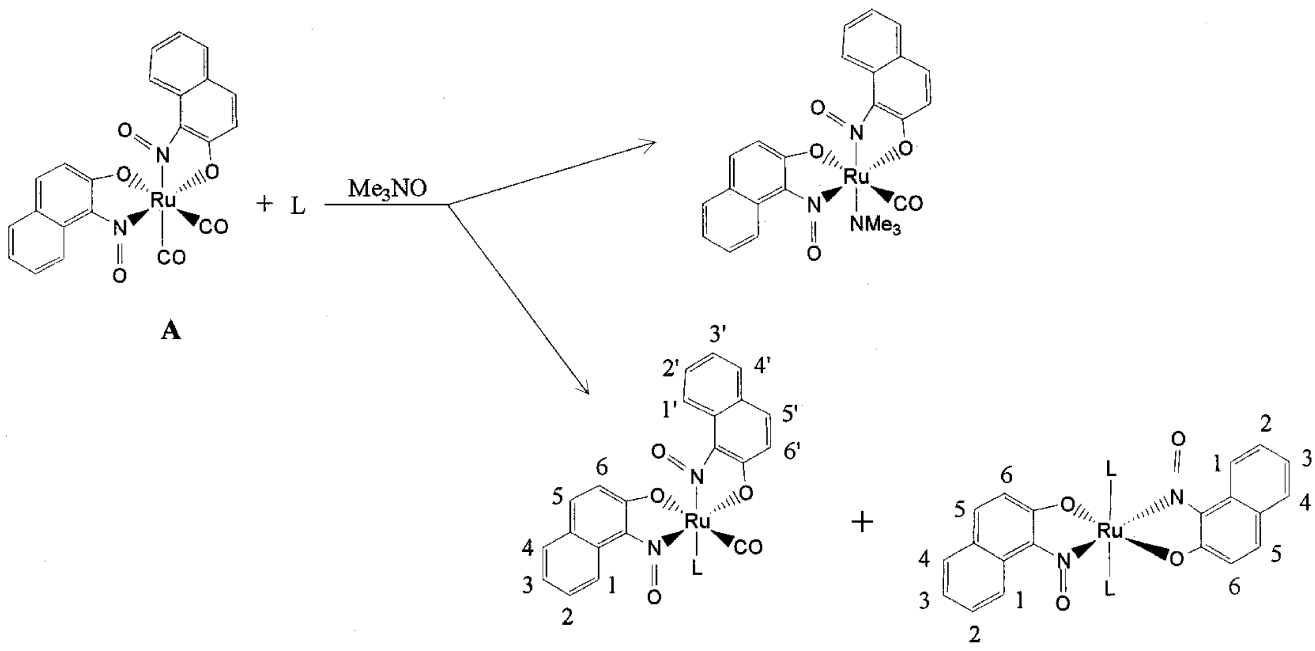

+ L
Me3NO
B
1b, L = ppy;


+ L
Me3NO
C
1c, L = ppy; 2c, L = avpy


+ L
Me3NO
D
1d, L = ppy; 2d, L = avpy


+ L
Me3NO
E
1e, L = ppy

Scheme 1.



L =			
$P\{(CH_2)_3CH_3\}_3$ (7 8)	**4a**	**8a**
7 8 9 10 CHO (11)	**5a**	**9a**
7 8 9 10 CH_2CH_3 (11 12)	**6a**	**10a**
7 8 9 10 $N(CH_3)_2$ (11)	**7a**	**11a**

Scheme 2.

ment takes place in the second CO substitution, rather than first the formation of the *cis*-,*cis*-bisubstituted complex followed by ligand rearrangement.

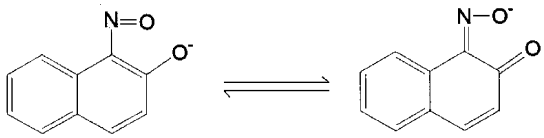
2.3. Characterization

The IR spectra of monosubstituted complexes show one strong carbonyl band ranging from 1976 to 1989 cm^{-1}, which is lower than that of the starting dicarbonyl complexes. This is because, when one CO group is substituted by a weaker π acid ligand (phosphine or pyridine), there will be a greater donation of dπ electrons from the metal to the vacant π* orbital of CO than when two CO groups are present at *cis* positions [18]. ^1H NMR spectra show definite signals for 1,2-naphthoquinone-mono-oximato and donor ligand, respectively. The assignment of the signals proceeds on the basis of ^1H–^1H correlation spectroscopy (COSY) for most of the complexes, or in a similar manner (Table 1) [17,19].

The electronic absorption spectral data for the series of carbonyl-substituted complexes (**1a**, **3a–12a**) together with those of the starting material (**A**) and 1-nqoH ligand are summarized in Table 2. The spectra of **6a** and **10a** in CH_2Cl_2 in the visible region are shown in Fig. 1.

The electronic spectra of mono-CO-substituted complexes are dominated in the visible region by two absorption bands, with the high energy band appearing at nearly the same absorption maximum (about 420 nm) as that of the starting material (**A**). Early work by Chatterjee [20] showed that a similar band appeared for the copper complex of 1-nitroso-2-naphthol [$Cu(NOC_{10}H_6O)_2$] (420 nm) and the corre-

sponding ligand in an alkaline medium (425 nm). The band was assigned as charge resonance between structures (I) and (II).



(I) (II)

The low-energy intense band (10^3 dm^3 mol^{-1} cm^{-1} < ε < 10^4 dm^3 mol^{-1} cm^{-1}) which appears at 480 nm for **A** and red-shifts as one CO is substituted by a donor ligand should be assigned as ruthenium to 1-nqo charge transfer. Pyridine or phosphine is a good σ donor and a poor π acceptor compared with carbonyl; thus, the substitution of CO by these two ligands will result in destabilization of the ground state and stabilization of the excited state for metal-to-ligand charge transfer (MLCT) to 1-nqo and the band will shift to lower energy as a result [21]. The MLCT band of phosphine substitution complexes (**3a** and **4a**) appears to be at higher energy than that of pyridine substitution complexes (**1a**, **5a**−**7a**); this is because phosphine is a better π acceptor and a poorer σ donor than pyridine.

In the spectra of bicarbonyl-substituted complexes, the MLCT to 1-nqo band red-shifts further with a higher extinction coefficient ($\varepsilon > 10^4$ dm^3 mol^{-1} cm^{-1}). The functional group at the *para* position of the pyridine ring has some influence on the energy of this band. As the functional group changes from electron-withdrawing to electron-donating (from formyl to dimethylamino), the band shifts to a lower energy (from 568 to 592 nm). This trend further supports the band as charge transfer to 1-nqo rather than to pyridine since the donating group in the pyridine ring further destabilized the ground state and stabilized the excited state for MLCT to 1-nqo. Compared with its *cis*-,*cis* analogue, the *trans*-,*trans* spatial orientation of ligands shows a more intense ($\varepsilon > 10^4$ dm^3 mol^{-1} cm^{-1}) lower energy MLCT band than *trans*-[Ru(NH$_3$)$_4$L$_2$] (L = pyridyl ligand) [22,23]. The high energy band is very sensitive to the *para* functional group on the pyridine ring. As the *para* functional group on the pyridine ring changes from withdrawing (formyl) to donating (dimethylamino), this band blue-shifts from 515 to 476 nm, indicating that the withdrawing group contributes to lowering the energy of the accepting π* orbital and the donating group contributes to raising it; thus this band should be assigned as MLCT to the pyridine ligand [24].

2.4. Crystallographic studies

X-ray analyses have been carried out on prisms of **3a**, **7a**, **8a**, **1b**, **1c**, **E** and **1e**, which were obtained by slow evaporation of the corresponding solvent mixture at −20°C. The molecular structure and selected bond parameters of complex **3a** are shown in Fig. 2 and Table 3, respectively. A distorted octahedral coordination of the ruthenium metal centre is revealed and the molecule consists of two 1-nqo ligands, a triphenylphosphine and a carbonyl group. The two 1-nqo ligands chelate to the ruthenium centre with the naphtholic oxygen [Ru–O(2) 2.088(2) Å; Ru–O(4) 2.071(2) Å] and oximato nitrogen [Ru–N(1) 2.072(3) Å; Ru–N(2) 2.000(3) Å] atoms to form a five-membered ring [O(2)–Ru–N(1) 77.8(1)°; O(4)–Ru–N(2) 79.5(1)°] as in the par-

Table 1
Spectroscopic data for compounds **1a–11a**, **1b**, **1c–2c**, **1d–2d**, **E** and **1e**

Complex	IR spectra [a]: ν(CO) (cm^{-1})	Mass spectra [b] (*m*/*z*)	^{1}H NMR spectra: δ, *J* (Hz)	^{31}P NMR spectra [c,e,f]: δ
1a	1985s	629 (629)	9.32 (d, 1H, *J* = 8.4, H^1), 9.09 (d, 1H, *J* = 8.3, H$^{1'}$), 8.74 (dd, 2H, *J* = 5.3, 1.4, H^{7,8}), 7.79 (d, 1H, *J* = 9.4, H$^{5'}$), 7.66 (d, 1H, *J* = 9.3, H^5), 7.64 (m, 1H, H^2), 7.59–7.56 (m, 6H, H$^{4,4',9,10,11,15}$), 7.53–7.47 (m, 4H, H$^{2',12,13,14}$), 7.39 (m, 1H, H$^{3'}$), 7.37 (m, 1H, H^3), 7.23 (d, 1H, *J* = 9.4, H$^{6'}$), 6.97 (d, 1H, *J* = 9.3, H^6) [e,g]	–
2a	1985s	755 (755)	9.26 (d, 1H, *J* = 8.4, H^1), 9.04 (d, 1H, H = 8.2, H$^{1'}$), 8.72 (br.d, 2H, *J* = 6.6, H^{7,8}), 8.47 (s, 1H, H^{17}), 8.24 (d, 1H, *J* = 16.7, H^{11}), 8.20 (m, 2H, H^{13,21}), 8.04 (m, 2H, H^{16,18}), 7.83 (d, 1H, *J* = 9.4, H$^{5'}$), 7.71 (d, 1H, *J* = 9.4, H^5), 7.71–7.60 (m, 3H, H$^{2,4,4'}$), 7.62 (br.d, 2H, *J* = 6.6, H^{9,10}), 7.55 (m, 1H, H$^{2'}$), 7.55–7.47 (m, 4H, H^{14,15,19,20}), 7.42(m, 2H, H$^{3,3'}$), 7.25 (d, 1H, *J* = 9.4, H$^{6'}$), 6.97 (d, 1H, *J* = 9.4, H^6), 6.93 (m, 1H, H^{12}) [d,g]	–
3a	1985s	736 (736)	8.99 (d, 1H, *J* = 8.2, H^1), 8.72 (d, 1H, *J* = 8.4, H$^{1'}$), 7.71 (d, 1H, *J* = 9.5, H$^{5'}$ or H^5), 7.55 (br.d, 1H, *J* = 7.5, H^4), 7.48–7.36 (m, 10H, H$^{2,2',4',5 \text{ or } 5'}$, 6H of phenyl), 7.34 (m, 1H, H^3), 7.31–7.19 (m, 10H, H$^{3'}$, 9H of phenyl), 7.02 (d, 1H, *J* = 9.5, H$^{6'}$or H^6), 6.61 (d, 1H, *J* = 9.3, H^6 or H$^{6'}$) [d,g,h]	38 (s)
4a	1976s	676 (676)	9.06 (d, 1H, *J* = 8.3, H^1), 8.99 (d, 1H, *J* = 8.2, H$^{1'}$), 7.67 (d, 1H, *J* = 9.4, H$^{5'}$ or H^5), 7.66 (d, 1H, *J* = 9.3, H^5 or H$^{5'}$), 7.55 (m, 3H, H$^{2,4,4'}$), 7.44 (m, 1H, H$^{2'}$), 7.32 (m, 2H, H$^{3,3'}$), 6.99 (d, 1H, *J* = 9.4, H$^{6'}$ or H^6), 6.89 (d, 1H, *J* = 9.3, H^6 or H$^{6'}$), 1.18 (m, 18H, H^7), 0.78 (t, 9H, *J* = 7.0, H^8) [d,g,h]	25 (s)

Table 1 (*continued*)

Complex	IR spectra [a]: ν(CO) (cm^{-1})	Mass spectra [b] (m/z)	^{1}H NMR spectra: δ, J (Hz)	^{31}P NMR spectra [c,e,f]: δ
5a	1987s	581 (581)	9.98 (s, 1H, H^{11}), 9.13 (d, 1H, J=8.4, H^1), 8.93 (m, 1H, $H^{1\prime}$), 8.92 (m, 2H, $H^{7,8}$), 7.76 (d, 1H, J=9.4, $H^{5\prime}$), 7.72 (dd, 2H, J=5.0, 1.5, $H^{9,10}$), 7.61 (d, 1H, J=9.3, H^5), 7.57 (m, 2H, $H^{2,4\prime}$), 7.52 (br.d, 1H, J=7.9, H^4), 7.47 (m, 1H, $H^{2\prime}$), 7.34 (m, 1H, $H^{3\prime}$), 7.32 (m, 1H, H^3), 7.14 (d, 1H, J=9.4, $H^{6\prime}$), 6.84 (d, 1H, J=9.3, H^6) [d,g]	–
6a	1983s	581 (581)	9.13 (d, 1H, J=8.4, H^1), 8.93 (d, 1H, J=8.3, $H^{1\prime}$), 8.45 (dd, 2H, J=5.1, 1.5, $H^{7,8}$), 7.73 (d, 1H, J=9.4, $H^{5\prime}$), 7.59 (d, 1H, J=9.3, H^5), 7.55 (m, 2H, $H^{2,4\prime}$), 7.51 (br.d, 1H, J=7.9, H^4), 7.45 (ddd, 1H, J=8.3, 7.2, 1.3, $H^{2\prime}$), 7.32 (m, 1H, $H^{3\prime}$), 7.30 (m, 1H, H^3), 7.16 (m, 2H, $H^{9,10}$), 7.12 (d, 1H, J=9.4, $H^{6\prime}$), 6.84 (d, 1H, J=9.3, H^6), 2.58 (q, 2H, J=7.6, H^{11}), 1.12 (t, 3H, J=7.6, H^{12}) [d,g,h]	–
7a	1979s	596 (596)	9.13 (d, 1H, J=8.3, H^1), 8.94 (d, 1H, J=8.2, $H^{1\prime}$), 8.02 (dd, 2H, J=5.8, 1.4, $H^{7,8}$), 7.72 (d, 1H, J=9.4, $H^{5\prime}$), 7.59 (d, 1H, J=9.3, H^5), 7.57–7.50 (m, 3H, $H^{2,4,4\prime}$), 7.44 (m, 1H, $H^{2\prime}$), 7.32 (m, 1H, $H^{3\prime}$), 7.30 (m, 1H, H^3), 7.13 (d, 1H, J=9.4, $H^{6\prime}$), 6.85 (d, 1H, J=9.3, H^6), 6.41 (dd, 2H, J=5.8, 1.4, $H^{9,10}$), 2.90 (s, 6H, H^{11}) [d,g]	–
1b	1981s	629 (629)	9.36 (d, 1H J=8.7, H^1), 9.24 (d, 1H, J=8.4, $H^{1\prime}$), 8.55 (dd, 2H, J=5.3, 1.5, $H^{7,8}$), 7.73 (m, 1H, H^5), 7.71 (m, 1H, $H^{5\prime}$), 7.67 (m, 1H, H^4), 7.66 (m, 1H, H^2), 7.64–7.61 (m, 3H, $H^{2\prime,11,15}$), 7.60 (br.d, 1H, J=7.8, $H^{4\prime}$), 7.56 (dd, 2H, J=5.3, 1.5, $H^{9,10}$), 7.50–7.46 (m, 4H, $H^{3,12,13,14}$), 7.39 (m, 1H, $H^{3\prime}$), 7.05 (d, 1H, J=9.4, H^6), 7.01 (d, 1H, J=9.3, $H^{6\prime}$) [d,f,h]	–

ent complex **A** [15]. The nitroso oxygen atoms are non-coordinating and a similar arrangement is found in those complexes with quinone-oxime ligands [10–16]. The aver-

Table 1 (*continued*)

Complex	IR spectra [a]: ν(CO) (cm^{-1})	Mass spectra [b] (m/z)	^{1}H NMR spectra: δ, J (Hz)	^{31}P NMR spectra [c,e,f]: δ
1c	1989s	629 (629)	8.77 (m, 2H, $H^{7,8}$), 8.76 (m, 1H, H^1), 8.39 (d, 1H, J=8.0, $H^{1\prime}$), 7.73 (m, 1H, H^3), 7.69 (m, 1H, H^4), 7.65–7.59 (m, 5H, $H^{2,9,10,11,15}$), 7.56 (m, 1H, $H^{4\prime}$), 7.54 (m, 1H, $H^{3\prime}$), 7.51–7.47 (m, 3H, $H^{12,13,14}$), 7.34 (m, 1H, $H^{2\prime}$), 7.32 (d, 1H, J=9.4, $H^{6\prime}$), 7.17 (d, 1H, J=9.5, H^6), 6.88 (d, 1H, J=9.5, H^5), 6.84 (d, 1H, J=9.4, $H^{5\prime}$) [d,g]	–
2c	1989s	755 (755)	8.81 (br.d, 2H, J=6.6, $H^{7,8}$), 8.78 (m, 1H, H^1), 8.46 (s, 1H, H^{17}), 8.45 (d, 1H, J=7.8, $H^{1\prime}$), 8.23 (d, 1H, J=16.6, H^{11}), 8.17 (m, 2H, $H^{13,21}$), 8.02 (m, 2H, $H^{16,18}$), 7.71 (m, 1H, H^3), 7.68 (m, 1H, H^4) 7.61 (br.d, 2H, J=6.6, $H^{9,10}$), 7.60 (m, 1H, H^2), 7.56 (m, 2H, $H^{3\prime,4\prime}$), 7.51–7.44 (m, 4H, $H^{14,15,19,20}$), 7.38 (d, 1H, J=9.4, $H^{6\prime}$), 7.34 (m, 1H, $H^{2\prime}$), 7.22 (d, 1H, J=9.5, H^6), 6.91 (d, 1H, J=16.6, H^{12}), 6.86. (d, 1H, J=9.5, H^5), 6.82 (d, 1H, J=9.4, $H^{5\prime}$) [e,g]	–
1d	1985s	629 (629)	8.42 (dd, 2H, J=5.4, 1.5, $H^{7,8}$), 8.34 (d, 1H, J=8.2, H^1), 8.28 (d, 1H, J=8.0, $H^{1\prime}$), 7.55 (m, 3H, $H^{3\prime,4\prime}$, 1H of phenyl), 7.51 (m, 3H, $H^{3,4}$, 1H of phenyl), 7.44 (dd, 2H, J=5.4, 1.5, $H^{9,10}$), 7.40–7.37 (m, 3H, $H^{12,13,14}$), 7.36 (d, 1H, J=9.4, $H^{6\prime}$), 7.34 (m, 1H, $H^{2\prime}$), 7.30 (m, 1H, H^2), 7.23 (d, 1H, J=9.4, H^6), 6.89 (d, 1H, J=9.4, $H^{5\prime}$), 6.76 (d, 1H, J=9.4, H^5) [d,g,h]	–
2d	1985s	755 (755)	8.57 (br.d, 2H, J=6.0, $H^{7,8}$), 8.46 (m, 1H, H^1), 8.44 (s, 1H, H^{17}), 8.41 (d, 1H, J=7.9, $H^{1\prime}$), 8.18 (d, 1H, J=16.7, H^{11}), 8.16 (d, 2H, J=9.4, $H^{13,21}$), 8.02 (m, 2H, $H^{16,18}$), 7.60–7.54 (m, 4H, $H^{3,3\prime,4,4\prime}$), 7.50–7.43 (m, 6H, $H^{9,10,14,15,19,20}$), 7.40–7.36 (m, 3H, $H^{2,2\prime,6\prime}$), 7.25 (m, 1H, H^6), 6.94 (d, 1H, J=9.5, $H^{5\prime}$), 6.87 (m, 1H, H^{12}), 6.83 (m, 1H, H^5) [e,g]	–

Table 1 (*continued*)

Complex	IR spectra [a]: ν(CO) (cm^{-1})	Mass spectra [b] (m/z)	^{1}H NMR spectra: δ, J (Hz)	^{31}P NMR spectra [c,e,f]: δ
1e	1989s	629 (629)	8.76 (m, 2H, $H^{1,1'}$), 8.75 (dd, 2H, J=5.3, 1.5, $H^{7,8}$), 7.74–7.70 (m, 2H, 2-nqo), 7.69–7.65 (m, 2H, 2-nqo), 7.64–7.60 (m, 4H, 2H of 2-nqo, 2H of phenyl), 7.60 (dd, 2H, J=5.3, 1.5, $H^{9,10}$), 7.51–7.47 (m, 3H, phenyl), 7.16 (d, 1H, J=9.3, H^5 or $H^{5'}$), 7.10 (d, 1H, J=9.4, $H^{5'}$ or H^5), 6.88 (d, 1H, J=9.3, H^6 or $H^{6'}$), 6.82 (d, 1H, J=9.4, $H^{6'}$ or H^6) [d,f,h]	–
E	2026s, 2076s	501 (501)	8.57 (d, 2H, J=8.0, H^1), 7.74 (m, 2H, H^3), 7.64 (br.d, 2H, J=7.8, H^4), 7.62 (m, 2H, H^2), 7.10 (d, 2H, J=9.5, H^6), 6.93 (d, 2H, J=9.5, H^5) [d,f,h]	–
8a		850 (850)	9.45 (d, 2H, J=8.2, H^1), 7.55 (m, 2H, H^2), 7.54 (d, 2H, J=7.7, H^4), 7.50 (d, 2H, J=9.2, H^5), 7.29 (m, 2H, H^3), 7.08 (d, 2H, J=9.2, H^6), 0.95 (m, 36H, H^7), 0.59 (t, 18H, J=6.9, H^8) [d,g,h]	8 (s)
9a		660 (660)	9.90 (s, 2H, H^{11}), 8.97 (d, 2H, J=8.3, H^1), 8.91 (dd, 4H, J=5.0, 1.4, $H^{7,8}$), 7.59 (d, 2H, J=9.3, H^5), 7.57 (m, 4H, $H^{9,10}$), 7.52 (br.d, 2H, J=6.7, H^4), 7.37 (d, 2H, J=9.3, H^6), 7.33 (m, 2H, H^2), 7.18 (m, 2H, H^3) [d,g]	–
10a		660 (660)	9.01 (d, 2H, J=8.3, H^1), 8.47 (dd, 4H, J=5.1, 1.5, $H^{7,8}$), 7.57 (d, 2H, J=9.4, H^5), 7.52 (br.d, 2H, J=7.8, H^4), 7.36 (d, 2H, J=9.4, H^6), 7.32 (m, 2H, H^2), 7.16 (m, 2H, H^3), 7.03 (br.d, 4H, J=6.4, $H^{9,10}$), 2.51 (q, 4H, J=7.6, H^{11}), 1.07 (t, 6H, J=7.6, H^{12}) [d,g]	–
11a		690 (690)	9.03 (d, 2H, J=8.4, H^1), 8.09 (br.d, 4H, J=7.0, $H^{7,8}$), 7.56 (d, 2H, J=9.4, H^5), 7.53 (m, 2H, H^4), 7.34 (d, 2H, J=9.4, H^6), 7.32 (m, 2H, H^2), 7.13 (m, 2H, H^3), 6.31 (br.d, 4H, J=7.0, $H^{9,10}$), 2.85 (s, 12H, H^{11}) [d,g]	–

[a] In CH_2Cl_2.
[b] Calculated values in parentheses.
[c] With ^{1}H decoupled.

Table 1 (*continued*)

Complex	IR spectra [a]: ν(CO) (cm^{-1})	Mass spectra [b] (m/z)	^{1}H NMR spectra: δ, J (Hz)	^{31}P NMR spectra [c,e,f]: δ

[d] In CD_2Cl_2.
[e] In $CDCl_3$.
[f] DPX-500 ^{1}H NMR spectrometer.
[g] DPX-300 ^{1}H NMR spectrometer.
[h] ^{1}H–^{1}H COSY NMR.

age N–O bond distance of the nitroso group is 1.260(4) Å, which is within the range of most metal complexes with N-bonded nitroso groups such as [Cu{η^2-N(O)$C_{10}H_6$O}$(PPh_3)_2$] [1.287(13) Å] [10], [Hpy][Ir{η^2-N(O)$C_{10}H_6$O}(py)Cl_3] (py = pyridine) [1.274(8) Å] [13] and the parent complex *cis*-,*cis*-[Ru{η^2-N(O)$C_{10}H_6$O}$_2$$(CO)_2$] [1.258(5) and 1.256(5) Å] [15]. The two naphtholic oxygen atoms as well as the two nitroso nitrogen atoms of the two 1-nqo ligands are located *cis* to each other. The carbonyl group is *trans* to the naphtholic oxygen [O(4)–Ru–C(1) 173.3(1)°] in one 1-nqo ligand and the phosphine *trans* to the oximato group [N(1)–Ru–P 170.31(9)°] in another 1-nqo ligand, with the carbonyl and the phosphine *cis* to each other [P–Ru–C(1) 90.7(1)°]. The

Table 2
Summary of electronic absorption data [a]

Compound	λ (nm) (log ε, $dm^3\ mol^{-1}\ cm^{-1}$)
1-nqoH	274 (4.43), 379 (4.05)
A	295 (4.20), 420 (4.13), 480 (3.71)
3a	302 (4.22), 422 (4.04), 496 (3.79)
4a	300 (4.29), 380(sh), 422 (4.16), 511 (3.92)
5a	300 (4.21), 382(sh), 425 (4.15), 528 (3.86)
1a	303(sh), 380(sh), 423 (4.01), 531 (3.78)
6a	302 (4.24), 389 (4.02), 423 (4.09), 530 (3.88)
12a	302 (4.20), 389(sh), 425 (4.09), 536 (3.87)
7a	294 (4.39), 387 (4.05), 419 (4.08), 540 (3.89)
8a	279 (4.12), 345 (4.08), 400(sh) 541 (4.25)
9a	334 (4.00), 393 (3.97), 515(sh), 568 (4.25)
10a	336 (4.01), 370(sh), 474 (3.64), 578 (4.22)
11a	340(sh), 380(sh), 476 (3.73), 592 (4.18)

[a] In CH_2Cl_2. ε is the molar extinction coefficient.

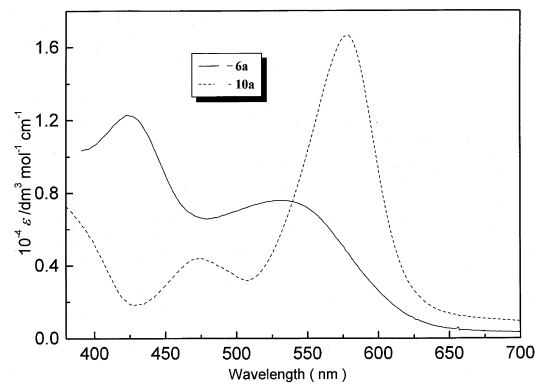


Fig. 1. Comparison of electronic absorption spectra of **6a** and **10a** in CH_2Cl_2.

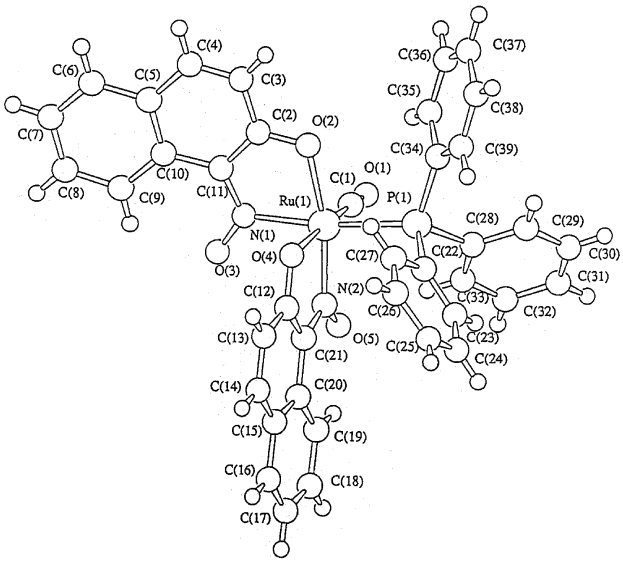


Fig. 2. The molecular structure of *cis*-,*cis*-[Ru{η^2-N(O)$C_{10}H_6$)}$_2$(CO)(PPh_3)] (**3a**), showing the atom numbering scheme.

Ru–P distance of 2.372(1) Å is comparable to other ruthenium phosphine complexes such as [Ru(pyca)$_2$(PPh_3)$_2$]·2MeOH [2.397(1) Å] (Hpyca = pyridine-2-carboxylic acid) [25].

Fig. 3 shows the molecular structure of **7a** and the selected bond parameters are listed in Table 3. The molecule of **7a** also adopts an approximately octahedral coordination around the ruthenium centre as in **3a**, but the position *trans* to the oximato group in one 1-nqo ligand is occupied by 4-dimethylaminopyridine. The pyridine ligand is coordinated to the ruthenium centre via its nitrogen atom with a Ru–N(3) bond length of 2.129(5) Å, which is comparable with the distance between the ruthenium centre and the nitrogen atom of pyridine *trans* to the oximato group [2.120(4) Å] in [Ru{η^2-N(O)$C_{10}H_6$O}$_2$(py)$_2$] [14]. The bond distance between the ruthenium centre and the oximato nitrogen atom *trans* to the pyridine ring [Ru–N(1) 2.029(5) Å] is shorter than when it is *trans* to phosphine in **3a** [2.072(3) Å] and when it is *trans* to carbonyl in the parent complex **A** [2.062(4) Å] [15], indicating the *trans* influence of the pyridine ring. The same ligand spatial orientation of complexes **3a** and **7a** results in very similar ^{1}H NMR signals for 1-nqo ligands. The other complexes derived from **A** (**1a–2a**, **4a–6a**) did not yield single crystals of X-ray quality; however, they all have very similar ^{1}H NMR signals for the 1-nqo ligands to that of **3a** and **7a**. Hence, their structures can be proposed to have the same ligand orientation as **3a** and **7a**.

The molecular structure of **1b** and the selected bond parameters are given in Fig. 4 and Table 3, respectively. The structure is similar to that of **7a**, with the two 1-nqo ligands, 4-phenylpyridine and a carbonyl group around the ruthenium centre in a distorted octahedral geometry. In contrast, the oximato nitrogen atoms are *trans* to each other [N(1)–Ru–N(2) 169.2(5)°] whereas the naphtholic oxygen atoms of the two 1-nqo ligands are also in a *cis* configuration [O(2)–Ru–O(4) 86.0(3)°].

The molecular structure of **1c** is depicted in Fig. 5 and the relevant structural parameters are listed in Table 3. The ruthenium centre adopts an approximately octahedral geometry as in **1b** but with two 2-nqo ligands chelating to the ruthenium centre instead of 1-nqo ligand. Both the naphtholic oxygen atoms as well as the oximato nitrogen atoms of the two 2-nqo ligands are in a *cis* configuration. The nitrogen atom of the pyridine ring coordinates to the ruthenium centre *trans* to an oximato group [N(1)–Ru–N(3) 170.7(8)°] of the 2-nqo ligand. From ^{1}H NMR data, the molecular structure of **2c** can be presumed to have the same ligand spatial orientation as in **1c**.

Fig. 6 shows the molecular structure of **E** and selected bond parameters are given in Table 4. The structure of **E** is very similar to *trans*-,*cis*-[Ru{η^2-$OC_{10}H_6N(O)$}$_2$(CO)$_2$] (**D**) [16] but with the naphtholic oxygen atoms *trans* to each other [O(2)–Ru–O(2*) 170.2(1)°] instead of the *trans* arrangement of oximato nitrogen atoms in **D** [16]. In contrast, there is a crystallographically imposed 2-fold rotational axis through the central ruthenium atom, resulting in exactly the same coordination configuration for the two 2-nqo ligands with the same bond length as Ru–N [2.076(3) Å] and Ru–O [2.061(2) Å], which is comparable to the isomer **D**. This configuration is consistent with the ^{1}H NMR spectrum in which only one set of signals for 2-nqo ligands appears. Both of the carbonyl groups are located *trans* to the oximato nitrogen atom in the 2-nqo ligand [N(1)–Ru–C(1) 174.5(1)°] with the same Ru–C bond length of 1.919(4) Å, which is longer than that in **D** [1.87(2) and 1.90(2) Å] [16].

Fig. 7 shows the molecular structure of complex **1e**; the selected structure parameters are listed in Table 3. The configuration of the molecule is a distorted octahedron around the ruthenium centre similar to the parent complex **E**, with a 4-phenylpyridine ligand occupying the position of one carbonyl in **E**. The bond length between the ruthenium centre and the coordinated pyridine nitrogen atom is 2.11(2) Å, which is comparable to that in **7a** [2.129(5) Å] in which the pyridine ligand is also located *trans* to the nitroso group. The bond distance between this nitoso nitrogen atom and the ruthenium centre is also shortened [Ru–N(1) 2.01(2) Å] compared with the parent complex **E** [Ru–N 2.076(3) Å]. The structures of **3a**, **7a**, **1b**, **1c** and **1e** confirm that no rearrangement of the two coordinated naphtholic oximato ligands occurred during substitution; thus it can be assumed that, in the molecular structures of **1d** and **2d**, one carbonyl *trans* to a naphtholic oxygen atom was substituted by the pyridine ligand (Scheme 1).

The molecular structure and selected bond parameters of complex **8a** are shown in Fig. 8 and Table 5, respectively. The structure is centrosymmetric and the geometry of the central ruthenium atom is a slightly distorted octahedron. The 1-nqo ligands coordinate to the central ruthenium atom through the naphtholic oxygen and the oximato nitrogen atoms to give a five-membered chelate ring. The two chelate rings locate in an equatorial plane containing the ruthenium metal centre as in [Cu(1-nqo)$_2$]·2$(CH_3)_2$CO [11] and

Table 3
Selected bond lengths (Å) and bond angles (°) for compounds **3a**, **7a**, **1b, 1c** and **1e**

	3a	**7a**	**1b**	**1c**	**1e**
Ru–O(2)	2.088(2)	2.078(4)	2.067(8)	2.11(1)	2.07(1)
Ru–N(1)	2.072(3)	2.029(5)	2.06(1)	2.04(2)	2.01(2)
Ru–O(4)	2.071(2)	2.085(4)	2.061(8)	2.11(1)	2.05(2)
Ru–N(2)	2.000(3)	1.990(5)	2.042(9)	2.00(2)	2.06(2)
Ru–P	2.372(1)	–	–	–	–
Ru–N(3)	–	2.129(5)	2.077(9)	2.09(2)	2.11(2)
Ru–C(1)	1.852(4)	1.877(8)	1.88(2)	1.87(3)	1.85(3)
O(1)–C(1)	1.144(4)	1.120(8)	1.11(1)	1.11(3)	1.15(3)
O(3)–N(1)	1.252(4)	1.253(6)	1.22(1)	1.24(2)	1.19(2)
O(5)–N(2)	1.268(4)	1.251(6)	1.27(1)	1.26(2)	1.22(2)
O(2)–C(2)	1.285(4)	1.288(7)	1.29(2)	1.29(2)	1.32(3)
O(4)–C(12)	1.295(4)	1.295(7)	1.28(1)	1.26(2)	1.27(3)
N(1)–C(11)	1.368(4)	1.372(8)	1.37(1)	1.37(2)	1.35(3)
N(2)–C(21)	1.375(4)	1.383(8)	1.38(1)	1.35(2)	1.34(3)
C(2)–C(11)	1.416(5)	1.438(9)	1.42(2)	1.44(3)	1.39(3)
C(12)–C(21)	1.415(5)	1.420(9)	1.47(2)	1.41(3)	1.42(3)
P–C(22)	1.824(4)	–	–	–	–
P–C(28)	1.822(4)	–	–	–	–
P–C(34)	1.821(4)	–	–	–	–
N(3)–C(22)	–	1.353(8)	1.35(1)	1.29(2)	1.34(3)
N(3)–C(26)	–	1.355(8)	1.35(1)	1.40(2)	1.29(3)
O(2)–Ru–O(4)	90.09(9)	88.8(2)	86.0(3)	90.0(5)	175.2(7)
O(2)–Ru–N(1)	77.8(1)	79.2(2)	79.7(4)	80.0(7)	80.5(9)
O(2)–Ru–N(2)	167.3(1)	168.3(2)	96.0(4)	170.0(7)	95.0(8)
O(2)–Ru–N(3)	–	92.6(2)	172.7(4)	91.4(6)	92.7(8)
O(2)–Ru–P	93.33(7)	–	–	–	–
O(2)–Ru–C(1)	95.5(1)	98.3(2)	94.7(4)	95.9(9)	93.5(10)
O(4)–Ru–N(1)	83.5(1)	87.2(2)	90.5(4)	88.3(6)	98.1(9)
O(4)–Ru–N(2)	79.5(1)	79.8(2)	79.3(4)	80.7(7)	80.4(8)
O(4)–Ru–N(3)	–	91.0(2)	88.4(3)	88.2(6)	88.4(7)
O(4)–Ru–P	92.69(7)	–	–	–	–
O(4)–Ru–C(1)	173.3(1)	172.1(2)	176.6(5)	174.0(9)	91.1(10)
N(1)–Ru–N(2)	93.6(1)	97.5(2)	169.2(5)	96.0(7)	90.5(8)
N(1)–Ru–N(3)	–	171.7(2)	95.7(4)	170.7(8)	172.4(10)
N(1)–Ru–P	170.31(9)	–	–	–	–
N(1)–Ru–C(1)	94.0(1)	90.9(3)	92.9(5)	91.8(9)	90(1)
N(2)–Ru–N(3)	–	90.1(2)	87.5(4)	92.0(7)	86.8(7)
N(2)–Ru–P	94.44(8)	–	–	–	–
N(2)–Ru–C(1)	94.5(1)	92.9(3)	97.3(5)	93(1)	171(1)
N(3)–Ru–C(1)	–	92.0(2)	91.1(5)	92.6(8)	93.2(10)
P–Ru–C(1)	90.7(1)	–	–	–	–

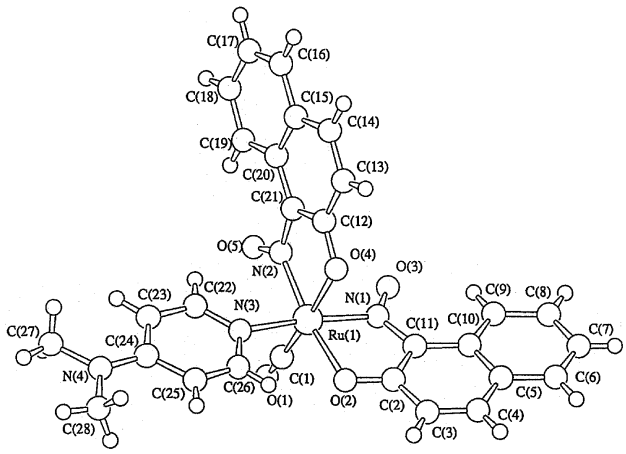


Fig. 3. The molecular structure of *cis*-,*cis*-[Ru{η^2-N(O)$C_{10}H_6$)}$_2$(CO)(mapy)] (**7a**), showing the atom numbering scheme.

[Cu(2-nqo)$_2$]·H_2O [12], and the PBu_3 ligands lie nearly perpendicular to the plane with a deviation of 3.3(6)°. As far as we are aware, this configuration is the first structurally characterized example of ruthenium nitrosonaphthol complexes. The Ru–O distance of the naphtholic group is 2.076(5) Å and the Ru–N distance is 2.011(7) Å, which is comparable with the bond length between the ruthenium centre and the oximato nitrogen atom [2.029(5) Å] *trans* to the nitrogen atom of pyridine in **7a**. The N–O bond distance is found to be 1.266(8) Å, which is in reasonable agreement with previously mentioned complexes [10,11,13–15]. The structure of other bisubstituted complexes (**9a**–**11a)** can be deduced to have the same ligand spatial orientation as that of **8a** from the very similar ^{1}H NMR signals for 1-nqo ligands and the one set of signals for the two pyridine ligands.

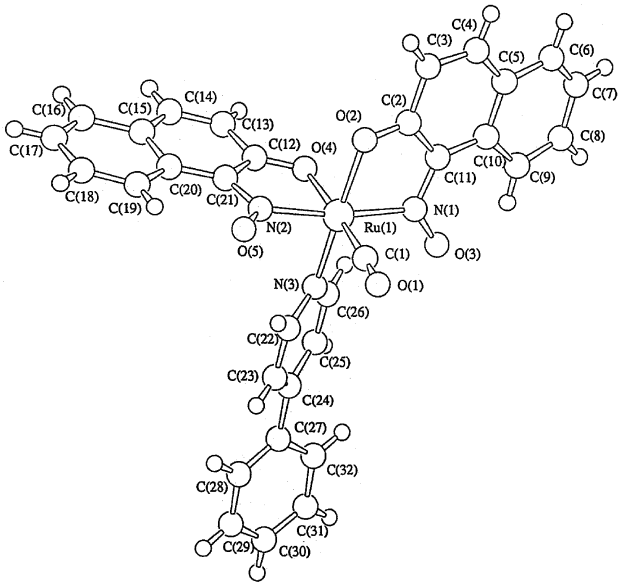


Fig. 4. The molecular structure of *trans*-,*cis*-[Ru{η^2-$N(O)C_{10}H_6$}$_2$(CO)(ppy)] (**1b**), showing the atom numbering scheme.

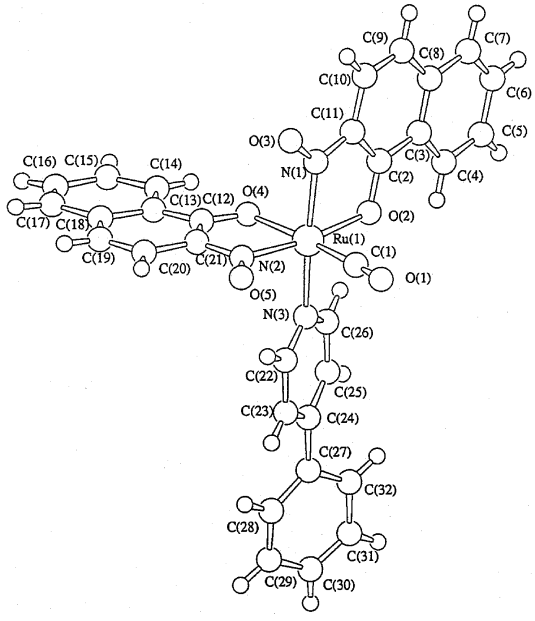


Fig. 5. The molecular structure of *cis*-,*cis*-[Ru{η^2-$OC_{10}H_6N(O)$}$_2$(CO)(ppy)] (**1c**), showing the atom numbering scheme.

2.5. Electrochemical studies

The redox potentials of the pyridyl complexes and the parent compound **A** were obtained by cyclic voltammetry in acetonitrile and are listed in Table 6. Representative cyclic voltammograms of **10a** and **6a** are shown in Fig. 9.

The cyclic voltammograms of bisubstituted complexes **9a**–**11a** are characteristic of a reversible one-electron process on the positive side. The peak presents an anodic-to-cathodic peak separation of 69–78 mV, which is close to the theoretical separation (59 mV at 25°C). The effect of variation of the pyridyl ligand on the formal potential of the peak is very similar to that of the Ni(II)/Ni(III) couple in nickel quinone-mono-oxime complexes [Ni(MeQ)$_2$(py)$_2$] (MeQ = 4-methyl-1,2-benzoquinone-2-oximato; py = pyridine, 4-methylpyridine and 4-aminopyridine, respectively) [26]. The peak can be similarly assigned to the Ru(II)/Ru(III) couple as that for Ni(II)/Ni(III) in [Ni(cbqo)$_2$] (cbqo = 4-chloro-1,2-benzoquinone-2-oximato) which appeared at 0.64 V (vs. ferrocene/ferrocenium) as a quasi-reversible one-electron oxidation process [27]. Some tris-1,2-quinone-2-oxime complexes also show a similar metal-based redox process [26,28–30]. Other Ru(II) complexes have an oxidation potential near to that of the Ru(II)/Ru(III) couple; for example, [Ru(NH$_3$)$_5$(isn)](PF$_6$) (isn = isonicotinamide) and [Ru(NH$_3$)$_5$(pz)](PF$_6$)

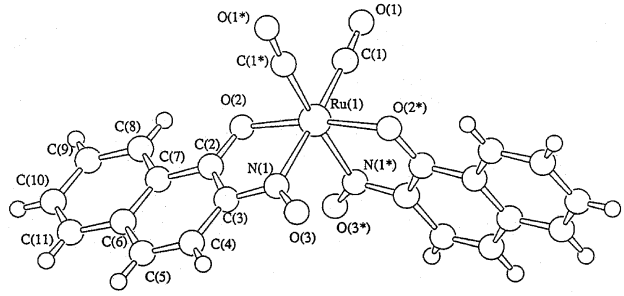


Fig. 6. The molecular structure of *cis*-,*trans*-[Ru{η^2-$OC_{10}H_6N(O)$}$_2$(CO)$_2$] (**E**), showing the atom numbering scheme.

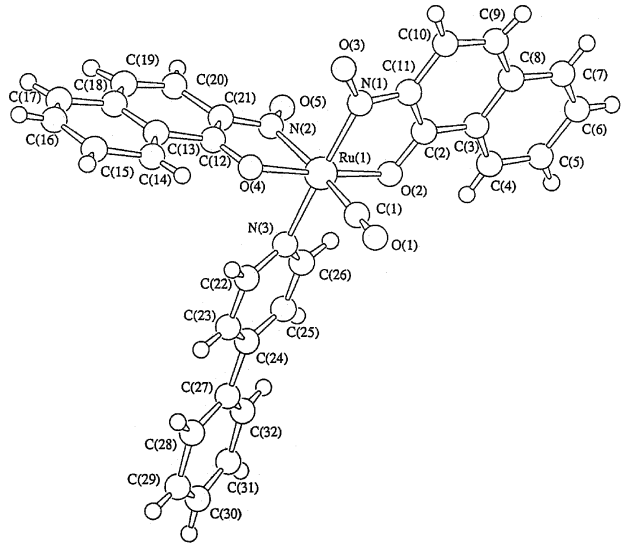


Fig. 7. The molecular structure of *cis*-,*trans*-[Ru{η^2-$OC_{10}H_6N(O)$}$_2$(CO)(ppy)] (**1e**), showing the atom numbering scheme.

Table 4
Selected bond lengths (Å) and bond angles (°) for compound **E** [a]

Ru–O(2)	2.061(2)	Ru–N(1)	2.076(3)
Ru–C(1)	1.919(4)	O(1)–C(1)	1.125(4)
O(3)–N(1)	1.252(3)	O(2)–C(2)	1.279(4)
N(1)–C(3)	1.358(4)	C(2)–C(3)	1.427(4)
O(2)–Ru–O(2*)	170.2(1)	O(2)–Ru–N(1*)	93.61(10)
O(2)–Ru–N(1)	79.14(10)	O(2)–Ru–C(1*)	91.7(1)
O(2)–Ru–C(1)	95.4(1)	N(1)–Ru–N(1*)	85.0(2)
N(1)–Ru–C(1*)	94.5(1)	N(1)–Ru–C(1)	174.5(1)
C(1)–Ru–C(1*)	86.5(2)	Ru–N(1)–O(3)	125.4(2)

[a] Symmetry code: *2 − *x*, *y*, (3/*z*) − *z*.

Table 5
Selected bond lengths (Å) and bond angles (°) for compound **8a** [a]

Ru–P(1)	2.370(2)	Ru–O(1)	2.076(5)
Ru–N(1)	2.011(7)	O(2)–N(1)	1.266(8)
O(1)–C(1)	1.279(10)	N(1)–C(10)	1.40(1)
P(1)–C(11)	1.819(10)	P(1)–C(15)	1.838(9)
P(1)–C(19)	1.830(9)		
P(1)–Ru–P(1*)	180.0	P(1)–Ru–O(1)	89.5(2)
P(1)–Ru–O(1*)	90.5(2)	P(1)–Ru–N(1)	90.6(2)
P(1)–Ru–N(1*)	89.4(2)	O(1)–Ru–O(1*)	180.0
O(1)–Ru–N(1)	78.6(3)	O(1)–Ru–N(1*)	101.4(3)
N(1)–Ru–N(1*)	180.0	Ru–P(1)–C(11)	115.4(3)
Ru–P(1)–C(15)	114.4(3)	Ru–P(1)–C(19)	113.6(3)
Ru–N(1)–O(2)	124.4(5)		

[a] Symmetry code: *$2-x, -y, 2-z$.

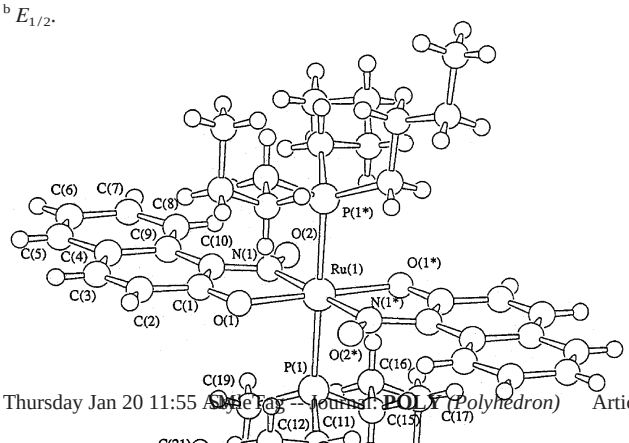
(pz = pyrazine) have $E_{1/2}$ values of 0.115 and 0.225 V (vs. Ag/Ag^+), respectively [31]. The monosubstituted complexes **1a**, **5a–7a** and **12a** exhibit an irreversible oxidation peak, which is a significantly positive shift to the potential common for the Ru(II)/Ru(III) couple [21,24] from that for the bisubstituted complexes. This may be due partly to the change in the surrounding ligands, which stabilizes Ru(III) less than Ru(II), and partly to the change of spatial orientation of the ligands. The parent complex (**A**) exhibits a more positive oxidation potential, which is due to the appearance of two carbonyl groups with slightly better π acceptor and poor σ donor properties, thus favoring the destabilization of Ru(III) relative to Ru(II) [22]. A similar effect was observed for poly$[Ru(II)(vbpy)_2(py)_2]^{2+}$ (vbpy = 4-vinyl-4′-methyl-2,2′-bipyridine; py = pyridine), where the oxidation potential shifted from 0.89 V to 0.39 V and further to −0.03 V (vs. Ag/Ag^+) as one and two py were progressively replaced by Cl^- [32]. However, the possibility of ligand-centred oxidation could not be eliminated because a similar compound, 2-propanone oxime, showed an irreversible oxidation peak at 1.47 V (vs. NHE) [33].

The change of the donor ligand results in a change of electronic absorption spectra and electrochemical properties in the same direction. As the donor ligand becomes more electron-donating, the oxidation potential becomes more cathodic and the band of MLCT to 1-nqo decreases in energy, both of them showing stabilization of Ru(III) compared to Ru(II) by the more electron-donating ligand.

Table 6
Formal potentials for complexes **1a**, **5a − 7a**, **9a − 12a** and **A** [a]

Complex	$[E^{\circ\prime}(ox)]$	$[E^{\circ\prime}(red)]_1$	$[E^{\circ\prime}(red)]_2$	$[E^{\circ\prime}(red)]_3$	$[E^{\circ\prime}(red)]_4$
9a	0.38 [b]	−1.25	−1.45	−1.61	–
10a	0.28 [b]	−1.38	−1.54	−1.89	–
11a	0.14 [b]	−1.48	−1.61	−2.00	–
5a	1.19	−1.11	−1.22	−1.59	−1.76
1a	1.17	−1.15	−1.25	−1.59	−1.88
6a	1.15	−1.13	−1.26	−1.52	−1.70
12a	1.14	−1.22	−1.27	−1.52	−1.67
7a	1.05	−1.17	−1.28	−1.57	−1.92
A	1.44	−0.98	−1.07	−1.40	−1.65

[a] All potentials are in volts vs. Ag (0.1 mol dm^{-3} Ag^+). In MeCN, containing 0.1 mol dm^{-3} TBAH.
[b] $E_{1/2}$.



3. Experimental

All manipulations were carried out under nitrogen using standard Schlenk techniques. Chemicals were purchased from commercial sources (Aldrich, Strem) and used as received unless stated otherwise. The compounds *cis*-,*cis*- and *trans*-,*cis*-$[Ru\{\eta^2\text{-}N(O)C_{10}H_6O\}_2(CO)_2]$, *cis*-,*cis*- and *trans*-,*cis*-$[Ru\{\eta^2\text{-}OC_{10}H_6N(O)\}_2(CO)_2]$ were prepared according to our previously described procedure [15,16]. Trimethylamine *N*-oxide (Aldrich) was dried by azeotropic distillation in benzene and sublimed prior to use. Dichloromethane and acetonitrile were distilled from CaH_2. Preparative thin-layer chromatographic (TLC) plates were prepared

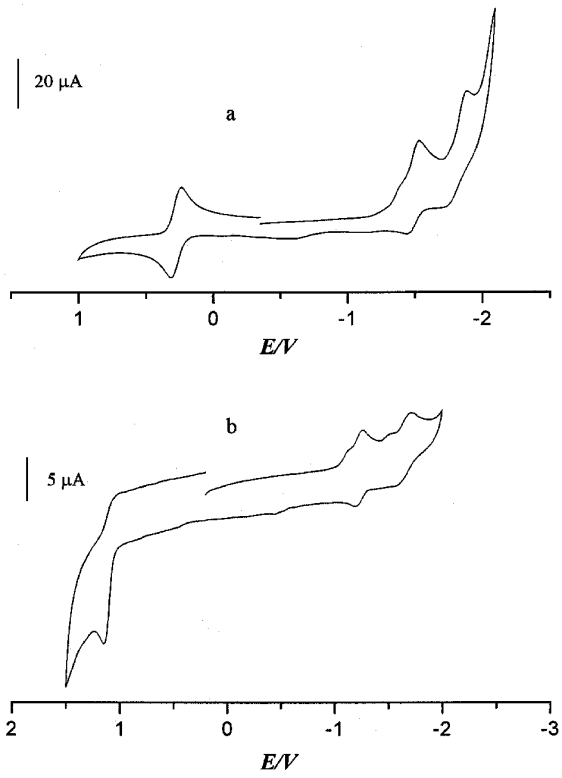


Fig. 9. Cyclic voltammograms of **10a** (a) and **6a** (b) in MeCN containing 0.1 mol dm^{-3} Bu_4NPF_6; glassy carbon working electrode; $AgNO_3$ reference electrode (Ag 0.1 mol dm^{-3}); scan rate, 50 mV s^{-1}.

were recorded on a Finnigan MAT 95 mass spectrometer. Electronic absorption spectra were obtained on a Hewlett-Packard 8453 spectrophotometer at room temperature. Cyclic voltammetric experiments were carried out using a Princeton Applied Research Model 273A potentiostat/galvanostat. All electrochemical data were obtained using acetonitrile containing 0.1 mol dm^{-3} n-tetrabutylammonium hexafluorophosphate (TBAH) as a supporting electrolyte at room temperature, with a gas-sealed (argon) two-compartment cell, equipped with a glassy carbon working electrode, a $AgNO_3$ reference electrode (Ag 0.1 mol dm^{-3}) and a platinum wire as the auxiliary electrode.

3.1. Preparation of cis-,cis- (1a) and trans-,cis- (1b) [Ru{η²-N(O)C₁₀H₆O}₂(CO)(ppy)]

Solid samples of *cis-,cis*-[Ru{η^2-N(O)$C_{10}H_6O$}$_2$(CO)$_2$] (**A**) or *trans-,cis*-[Ru{η^2-N(O)$C_{10}H_6O$}$_2$(CO)$_2$] (**B**) (50 mg, 0.1 mmol) and the donor ligand 4-phenylpyridine (ppy) (17 mg, 0.11 mmol) were dissolved in 40 cm^3 of CH_2Cl_2 at room temperature. A CH_2Cl_2 solution (10 cm^3) of Me_3NO (7.5 mg, 0.1 mmol) was added dropwise to this and an instantaneous colour change from orange to reddish-brown was observed. After stirring for 1 h, the solvent was removed in vacuo and the residue was chromatographed by TLC using a solvent mixture of n-hexane–CH_2Cl_2 (1:1, v/v) as eluent to afford three bands. The first, orange, band was unreacted **A** or **B**. The second, reddish-brown, band was *cis-,cis*-[Ru{η^2-N(O)$C_{10}H_6O$}$_2$(CO)(NMe$_3$)] or *trans-,cis*-[Ru{η^2-N(O)$C_{10}H_6O$}$_2$(CO)(NMe$_3$)] and the third fraction of reddish-brown colour was **1a** or **1b**. Reddish-brown crystals of **1b** were obtained by slow evaporation of cyclohexane–$CHCl_3$ solution at −20°C. (Found for **1a**: C, 61.2; H, 3.5; N, 6.5%. Found for **1b**: C, 61.2; H, 3.6; N, 6.6%. Calc. for $C_{32}H_{21}N_3O_5Ru_1$: C, 61.1; H, 3.4; N, 6.7%).

3.2. Preparation of cis-,cis- (1c) and trans-,cis- (1d) [Ru{η²-OC₁₀H₆N(O)}₂(CO)(ppy)]

A procedure analogous to that of the preparation of **1a** and **1b** was followed, using *cis-,cis-* or *trans-,cis*-[Ru{η^2-$OC_{10}H_6N(O)$}$_2$(CO)$_2$] (**C** or **D**) as starting material; a colour change from red to dark purple indicated completion of the reaction. TLC separation using a solvent mixture of n-hexane–CH_2Cl_2 (1:1, v/v) as eluent gave three bands. The first red band for the reaction of **D** was the unreacted starting material (**D**). The second band was dark purple *cis-,cis*-[Ru{η^2-$OC_{10}H_6N(O)$}$_2$(CO)(NMe$_3$)] or *trans-,cis*-[Ru{η^2-$OC_{10}H_6N(O)$}$_2$(CO)(NMe$_3$)] and the third fraction, also dark purple, was **1c** or **1d**. Dark purple crystals of **1c** were obtained by slow evaporation of cyclohexane–$CHCl_3$ solution at −20°C. (Found for **1c**: C, 61.1; H, 3.3; N, 6.7%. Found for **1d**: C, 61.3; H, 3.4; N, 6.7%. Calc. for $C_{32}H_{21}N_3O_5Ru_1$: C, 61.1; H, 3.4; N, 6.7%).

3.3. Preparation of cis-,cis-[Ru{η²-N(O)C₁₀H₆O}₂(CO)(PPh₃)] (3a)

A procedure analogous to that for the preparation for **1a** and **1b** was followed, using triphenylphosphine (PPh_3) (29 mg, 0.11 mmol) as donor ligand and observing the colour change from orange to brown to ensure completion of the reaction. TLC separation using a solvent mixture of n-hexane–CH_2Cl_2 (2:3, v/v) as eluent gave three bands. The first orange band was unreacted starting material (**A**). The second band was reddish-brown **12a** and the third fraction, orange-red in colour, was **3a**. Orange-red crystals of **3a** were obtained by slow evaporation of n-hexane–CH_2Cl_2 solution at −20°C. (Found: C, 63.6; H, 3.5; N, 3.7; P, 4.1%. Calc. for $C_{39}H_{27}N_2O_5P_1Ru_1$: C, 63.7; H, 3.7; N, 3.8; P, 4.2%).

3.4. Preparation of cis-,cis-[Ru{η²-N(O)C₁₀H₆O}₂(CO)(avpy)] (2a)

A solid sample of complex **A** (50 mg, 0.1 mmol) and the donor ligand 4-{2-(9-anthryl)vinyl}pyridine (avpy) (31 mg, 0.11 mmol) were dissolved in 40 cm^3 of CH_2Cl_2 at room temperature. A CH_2Cl_2 solution (10 cm^3) of Me_3NO (7.5 mg, 0.1 mmol) was added dropwise to this solution mixture in the dark. After stirring for 1 h, the solvent was removed in vacuo and the residue was separated by TLC using the solvent mixture of n-hexane–CH_2Cl_2 (1:5, v/v) as eluent to afford three bands. The entire procedure until the separation was protected from light by aluminium foil. The first orange band was unreacted **A**. The second, reddish-brown, band was **12a**;

the third fraction, reddish-brown in colour, was **2a**, which should be protected from the light. (Found: C, 66.7;H, 3.7;N, 5.6%. Calc. for $C_{42}H_{27}N_3O_5Ru_1$: C, 66.8; H, 3.6; N, 5.6%).

3.5. Preparation of cis-,cis- (2c) and trans-,cis- (2d) [Ru{η²-OC₁₀H₆N(O)}₂(CO)(avpy)]

A procedure analogous to that for the preparation of **2a** was followed by using **C** or **D** as starting material. After completion of reaction and upon TLC separation, protected from light, using the solvent mixture n-hexane–CH_2Cl_2 (1:5, v/v) as eluent, the first red band for reaction of **D** was found to be the unreacted starting material. In the reaction using **C** as starting material, the first band was *cis-,trans-*[Ru{η²-$OC_{10}H_6N(O)$}$_2$(CO)$_2$] (**E**) which was orange in colour and at the exact position on the TLC plate as **C**. The second band was the dark purple *cis-,cis-* or *trans-,cis-*[Ru{η²-$OC_{10}H_6N(O)$}$_2$(CO)(NMe$_3$)]; the third fraction, also dark purple, was **2c** or **2d**, and should be also kept from light. Orange crystals of **E** were obtained by slow evaporation of n-hexane–CH_2Cl_2 solution at −20°C. (Found for **2c**: C, 66.6; H, 3.5; N, 5.7%. Found for **2d**: C,66.8; H, 3.7; N, 5.7%. Calc. for $C_{42}H_{27}N_3O_5Ru_1$: C, 66.8; H, 3.6; N, 5.6%. Found for **E**: C, 52.6; H, 2.3; N, 5.6%. Calc. for $C_{22}H_{12}N_2O_6Ru_1$: C, 52.7;H, 2.4; N, 5.6%).

*3.6. Separation of **E** from **C***

A solid sample of **E** (50 mg, 0.1 mmol) dissolved in a minimum amount of CH_2Cl_2 was re-chromatographed by TLC using a solvent mixture of n-hexane–diethyl ether (10:1, v/v) as eluent. Two bands appeared: the first, red, band was **C** (47 mg, 94%; $R_f = 0.30$); the second, orange, band was **E** (2 mg, 4%; $R_f = 0.25$).

3.7. Preparation of cis-,trans-[Ru{η²-OC₁₀H₆N(O)}₂(CO)(ppy)] (1e)

A procedure analogous to that for the preparation of **1a** and **1b** was followed using **E** as the starting material. TLC separation was conducted using the same eluent to afford two bands. The first, orange, band was the unreacted starting material (**E**); the second, dark-brown, band was *cis-,trans-*[Ru{η²-$OC_{10}H_6N(O)$}$_2$(CO)(ppy)] (**1e**). Dark-brown crystals of **1e** were obtained by slow evaporation of n-hexane–$CHCl_3$ solution at −20°C. (Found: C, 61.2; H, 3.4; N, 6.8%. Calc. for $C_{32}H_{21}N_3O_5Ru_1$: C, 61.1; H, 3.4; N, 6.7%).

3.8. Preparation of cis-,cis-[Ru{η²-N(O)C₁₀H₆O}₂(CO)(PBu₃)] (4a) and trans-,trans-[Ru{η²-N(O)C₁₀H₆O}₂(PBu₃)₂] (8a)

A procedure analogous to that for the preparation of **1a** and **1b** was followed, using tributylphosphine (PBu_3) as donor ligand, with ligand:metal and Me_3NO:metal ratios of 5:1 and 2:1, respectively. The reaction period of 2 days ensured completion of the reaction. TLC separation of the dark-brown residue using a solvent mixture of n-hexane–CH_2Cl_2 (1:2, v/v) as eluent gave three bands. The first, bright purple, band was *trans-,trans-*[Ru{η²-$N(O)C_{10}H_6O$}$_2$(PBu_3)$_2$] (**8a**), the second, reddish-brown, band was *cis-,cis-*[Ru{η²-$N(O)C_{10}H_6O$}$_2$(CO)(PBu_3)] (**4a**), the third fraction being **12a**. Bright purple crystals of **8a** were obtained by slow evaporation of n-hexane solution at −20°C. (Found for **4a**: C, 58.5; H, 5.7; N, 4.2; P, 4.4%. Calc. for $C_{33}H_{39}N_2O_5P_1Ru_1$: C, 58.7; H, 5.8; N, 4.2; P, 4.6%. Found for **8a**: C, 62.2; H, 7.7; N, 3.2; P, 7.1%. Calc. for $C_{44}H_{66}N_2O_4P_2Ru_1$: C, 62.2; H, 7.8; N, 3.3; P, 7.3%).

3.9. Preparation of cis-,cis-[Ru{η²-N(O)C₁₀H₆O}₂(CO)L] (5a, L = fpy; 6a, L = epy; 7a, L = mapy) and trans-,trans-[Ru{η²-N(O)C₁₀H₆O}₂L₂] (9a, L = fpy; 10a, L = epy; 11a, L = mapy)

A procedure analogous to that for the preparation of **4a** and **8a** was followed, using *para*-functionalized pyridine as donor ligand; the colour change was from orange to dark blue. After completion of the reaction, the dark blue residue was separated by TLC using a solvent mixture of n-hexane–CH_2Cl_2 (1:5 to 1:6, v/v) as eluent to give three bands. The first band was reddish-brown **12a**. The second, reddish-brown, band was *cis-,cis-*[Ru{η²-$N(O)C_{10}H_6O$}$_2$(CO)(py)] (**5a–7a**) and the third, purple-blue, fraction was *trans-,trans-*[Ru{η²-$N(O)C_{10}H_6O$}$_2$(py)$_2$] (**9a**–**11a**). Reddish brown crystals of **7a** were obtained by slow evaporation of n-hexane − CH_2Cl_2 solution at −20°C. (Found for **5a**: C, 55.7; H, 3.0; N, 7.3%. Calc. for $C_{27}H_{17}N_3O_6Ru_1$: C, 55.9; H, 3.0; N, 7.2%. Found for **9a**: C, 58.1; H, 3.2; N, 8.6%. Calc. for $C_{32}H_{22}N_4O_6Ru_1$: C, 58.3; H, 3.4; N, 8.5%. Found for **6a**: C, 58.2; H, 3.5; N, 7.3%. Calc. for $C_{28}H_{21}N_3O_5Ru_1$: C, 58.0; H, 3.6; N, 7.2%. Found for **10a**: C, 62.0; H, 4.5; N, 8.3%. Calc. for $C_{34}H_{30}N_4O_4Ru_1$: C, 61.9; H, 4.6; N, 8.5%. Found for **7a**: C, 56.6; H, 3.9; N, 9.3%. Calc. for $C_{28}H_{22}N_4O_5Ru_1$: C, 56.5; H, 3.7; N, 9.4%. Found for **11a**: C, 59.2; H, 4.6; N, 12.3%. Calc. for $C_{34}H_{32}N_6O_4Ru_1$: C, 59.2; H, 4.7; N, 12.2%).

4. Crystallography

Single crystals of **3a**, **7a**, **8a**, **1b**, **1c**, **E** and **1e** for X-ray analysis were obtained as described above. A crystal of **3a** was mounted on top of a glass fibre using epoxy resin, whereas crystals of **7a**, **8a**, **1b**, **1c**, **E** and **1e** were sealed in Lindemann glass capillaries. Crystal intensity data were collected on a MAR research image-plate scanner using graphite-monochromated Mo Kα radiation ($\lambda = 0.71073$ Å) for unit-cell determination and data collection. The intensity data were corrected for Lorentz and polarization effects. An approximation to absorption correction by inter-image scaling was also applied. Summaries of the crystallographic data, structure solution and refinement are given in Table 7. Scat-

Table 7
Crystal data and data collection parameters for compound **3a**, **7a**, **1b**, **1c**, **E**, **1e** and **8a**

	3a	**7a**	**1b**	**1c**	**E**	**1e**	**8a**
Empirical formula	$RuPO_5N_2C_{39}H_{27}$	$RuO_5N_4C_{29}H_{24}Cl_2$	$RuO_5N_3C_{34}H_{23}Cl_6$	$RuO_5N_3C_{34}H_{23}Cl_6$	$RuO_6N_2C_{22}H_{12}$	$RuO_5N_3C_{34}H_{23}Cl_6$	$RuP_2O_4N_2C_{44}H_{66}$
M	735.70	680.51	867.36	867.36	501.42	867.36	850.03
Crystal colour, habit	orange-red, needle	reddish-brown, block	reddish-brown, block	dark purple, block	orange, block	brown, prism	purple, needle
Crystal dimensions (mm)	0.07×0.10×0.33	0.12×0.23×0.24	0.21×0.21×0.23	0.18×0.33×0.38	0.15×0.22×0.24	0.22×0.23×0.24	0.10 × 0.21 × 0.34
Crystal system	Monoclinic	triclinic	triclinic	monoclinic	monoclinic	triclinic	triclinic
Space group	$P2_1/n$ (no. 14)	$P\bar{1}$ (no. 2)	$P\bar{1}$ (no. 2)	$P2_1/n$ (no. 14)	$C2/c$ (no. 15)	$P\bar{1}$ (no. 2)	$P\bar{1}$ (no. 2)
a (Å)	18.558(2)	10.032(1)	11.528(1)	13.046(1)	20.8560	11.734(1)	8.8540
b (Å)	10.118(1)	11.985(1)	12.613(2)	19.026(3)	8.3930	12.700(1)	10.8600
c (Å)	18.811(2)	12.715(1)	13.177(2)	16.253(2)	12.1640	12.987(1)	11.9930
α (°)	–	109.26(1)	95.85(2)	–	–	101.36(2)	92.4100
β (°)	107.26(2)	92.09(2)	97.08(2)	114.13(2)	115.3010	93.71(2)	93.3000
γ (°)	–	98.28(1)	107.19(2)	–	–	106.12(2)	90.6100
U (Å^3)	3373.1(7)	1422.4(3)	1797.0(6)	3681.7(9)	1924.9919	1808.1(4)	1150.1509
Z	4	2	2	4	4	2	1
D_c (g cm^{-3})	1.449	1.589	1.603	1.565	1.730	1.593	1.227
μ (Mo Kα) (cm^{-1})	5.59	7.85	9.27	9.05	8.59	9.21	4.50
Reflections collected	31457	13909	16867	38392	8253	18226	12049
Unique reflections	6480	3413	4100	3558	1788	2189	2369
Observed reflections [$I > 1.5\sigma(I)$]	4486	2511	2593	1848	1458	1314	1743
R	0.042	0.049	0.082	0.112	0.032	0.095	0.069
R'	0.041	0.047	0.086	0.110	0.036	0.106	0.068
Goodness of fit, S	1.33	1.26	1.67	2.13	1.36	1.67	1.46

tering factors were taken from Cromer and Waber [34] and anomalous dispersion effects were included in *Fc* [35]. The position of ruthenium atom were determined by direct methods (SIR92) [36]. The remaining non-hydrogen atoms were determined by subsequent Fourier and Fourier-difference techniques. The structures were refined by full-matrix least-squares analysis on F with all non-hydrogen atoms refined anisotropically until convergence was reached. The hydrogen atoms of the organic moieties were generated in their ideal positions (C–H, 0.95 Å). They were included in the structure factor calculations on a Silicon-Graphics computer using the program package TEXSAN [37]. The R values for most of the complexes are reasonally good, except for **1b**, **1c** and **1e**. This is probably due to the positional disorder associated with the solvent molecules present in the crystal.

Supplementary data

Supplementary data are available from the CCDC, 12 Union Road, Cambridge CB2 1EZ, UK, on request, quoting deposition number 129645.

Acknowledgements

We gratefully acknowledge financial support from the Hong Kong Research Grants Council and the University of Hong Kong. Xiao-Xia Liu acknowledges the receipt of a demonstratorship administered by the Department of Chemistry, University of Hong Kong.

References

[1] F. Feigl, Chemistry of Specific, Selective and Sensitive Reactions, Academic Press, New York, 1949, pp. 251–280.
[2] O.K. Borggaard, H.E.M. Christensen, S.P. Lund, Analyst 109 (1984) 1179.
[3] O.K. Borggaard, H.E.M. Christensen, T.K. Nielsen, M. Willems, Analyst 107 (1982) 1479.
[4] D.K. Allen, J. Charalambous, M.H. Johri, R. Sims, Inorg. Chim. Acta 29 (1978) L235.
[5] J. Charalambous, P. Maple, N.A. Nassef, F.B. Taylor, Inorg. Chim. Acta 26 (1978) 107.
[6] J. Charalambous, M.J. Frazer, F.B. Taylor, J. Chem. Soc. A (1969) 2787.
[7] J. Charalambous, G. Soobramanien, A. Betts, J. Bailey, Inorg. Chim. Acta 60 (1982) 151.
[8] J. Charalambous, M.J. Frazer, R. Sims, Inorg. Chim. Acta 18 (1976) 247.
[9] R.G. Buckley, J. Charalambous, E.G. Brain, J. Chem. Soc., Perkin Trans. 1 (1982) 1075.
[10] R.G. Buckley, J. Charalambous, M.J. Kensett, M. McPartlin, D. Mukerjee, E.G. Brain, J.M. Jenkins, J. Chem. Soc., Perkin Trans. 1 (1983) 693.
[11] H. Saarinen, J. Korvenranta, Acta Chem. Scand., Ser. A 29 (1975) 409.

[12] J. Korvenranta, H. Saarinen, Acta Chem. Scand., Ser. A 29 (1975) 861.
[13] J. Charalambous, K. Henrick, Y. Musa, R.G. Rees, R.N. Whiteley, Polyhedron 6 (1987) 1509.
[14] J. Charalambous, W.C. Stoten, K. Henrick, Polyhedron 8 (1989) 103.
[15] K.K.-H. Lee, W.-T. Wong, J. Chem. Soc., Dalton Trans. (1997) 2987.
[16] K.K.-H. Lee, W.-T. Wong, J. Organomet. Chem. 547 (1997) 329.
[17] X.-X. Liu, W.-T. Wong, Inorg. Chim. Acta 198 (2000).
[18] K. Goswami, M.M. Singh, J. Inorg. Nucl. Chem. 39 (1977) 1718.
[19] W.-Y. Wong, W.-T. Wong, J. Chem. Soc., Dalton Trans. (1996) 1853.
[20] K.K. Chatterjee, Anal. Chim., Acta 20 (1959) 423.
[21] B. Hong, S.R. Woodcock, S.K. Saito, J.V. Ortega, J. Chem. Soc., Dalton Trans. (1998) 2615.
[22] M.L. Bento, E. Tfouni, Inorg. Chem. 27 (1988) 3410.
[23] L.A. Pavanin, Z.N. da Rocha, E. Giesbrecht, E. Tfouni, Inorg. Chem. 30 (1991) 2185.
[24] J.M. Calvert, D.L. Peebles, R.J. Nowak, Inorg. Chem. 24 (1985) 3111.
[25] M.C. Barral, R. Jimenez-Aparicio, E.C. Royer, M.J. Saucedo, F.A. Urbanos, E. Gutierrez-Puebla, C. Ruiz-Valero, J. Chem. Soc., Dalton Trans. (1991) 1609.
[26] D. Ray, A. Chakravorty, Inorg. Chem. 27 (1988) 3292.
[27] C.B. Castellani, A. Buttafava, O. Carugo, A. Poggi, J. Chem. Soc., Dalton Trans. (1988) 1497.
[28] P. Basu, A. Chakravorty, J. Chem. Soc., Chem. Commun. (1992) 809.
[29] P. Basu, S. Pal, A. Chakravorty, J. Chem. Soc., Chem. Commun. (1989) 977.
[30] P. Basu, S.B. Choudhury, S. Pal, A. Chakravorty, Inorg. Chem. 28 (1989) 2680.
[31] I. Ando, H. Fujimoto, K. Nakayama, K. Ujimoto, H. Kurihara, Polyhedron 10 (1991) 1139.
[32] R.M. Leasure, W. Ou, J.A. Moss, R.W. Linton, T.J. Meyer, Chem. Mater. 8 (1996) 264.
[33] M.F.C. Guedes da Silva, Y.A. Izotova, A.J.L. Pombeiro, V.Y. Kukushkin, Inorg. Chim. Acta 277 (1998) 83.
[34] D.T. Cromer, J.T. Waber, International Tables for X-Ray Crystallography, vol. 4, Kynoch Press, Birmingham, 1974, Table 2.2.B.
[35] D.T. Cromer, J.T. Waber, International Tables for X-Ray Crystallography, vol. 4, Kynoch Press, Birminghma, 1974, Table 2.3.1.
[36] M.C. Burla, M. Camalli, G. Cascarano, C. Giacovazzo, G. Polidori, R. Spagana, D. Viterbo, J. Appl. Crystallogr. 22 (1989) 389.
[37] TEXSAN, Crystal Structure Analysis Package, Molecular Structure Corporation, Houston, TX, 1985 and 1992.

PERGAMON

www.elsevier.nl/locate/poly

Polyhedron 19 (2000) 23–34

POLYHEDRON

Synthesis and coordination chemistry of 4′,4″-disubstituted 2,2′:6′,2″:6″,2‴-quaterpyridines and crystal and molecular structures of nickel(II) and cobalt(II) complexes

Edwin C. Constable *, Michael J. Hannon, Peter Harverson, Markus Neuburger, Diane R. Smith, Verena F. Wanner, Louise A. Whall, Margareta Zehnder

Institut für Anorganische Chemie der Universität Basel, Spitalstrasse 51, CH 4056 Basel, Switzerland

Received 16 July 1999; accepted 30 September 1999

Abstract

A range of symmetrical 4′,4″-disubstituted 2,2′:6′,2″:6″,2‴-quaterpyridines has been prepared and their coordination behaviour with metal ions having a preference for tetrahedral and octahedral geometries has been studied. The new ligands reacted with copper(I) and silver(I) salts to form dinuclear double-helical complexes; reaction with nickel(II) or cobalt(II) salts gave mononuclear species. The crystal structures of three mononuclear complexes are reported and demonstrate that the ligand binds in a tetradentate mode to the equatorial plane of the octahedral metal centre. ©2000 Elsevier Science Ltd All rights reserved.

Keywords: Helical structures; Supramolecular chemistry; Transition metals; X-ray crystal structures

1. Introduction

Oligopyridines are versatile ligands that form coordination complexes with almost all metal ions [1–6]. We and others have investigated the coordination behaviour of 2,2′:6′,2″:6″,2‴-quaterpyridine (**1**) [2,7–35] and have shown that coordination to octahedral six-coordinate metal centres results in the formation of mononuclear complexes, whereas bonding to four-coordinate tetrahedral metal ions gives dinuclear double-helical complexes [4,5]. As part of our ongoing interest in the use of supramolecular interactions in the synthesis of extended dendritic or starburst systems [36,37], we intended to incorporate a dinuclear double helicate at the centre of a metallodendrimer using 2,2′:6′,2″:6″2‴-quaterpyridines bearing substituents on the two central rings. However, we have recently shown that the introduction of substituents onto the terminal rings of 2,2′:6′,2″:6″,2‴-quaterpyridines results in significant changes in the coordination behaviour and has a major effect on the pitch of helicates. Accordingly, we decided to make preliminary investigations of the coordination behaviour of symmetrical 4′,4″-disubstituted 2,2″:6′,2″:6″,2‴-quaterpyridines.

* Corresponding author. Tel.: +41-61-267-1001; fax: +41-61-267-1015; e-mail: constable@ubaclu.unibas.ch

2. Experimental

2.1. General procedures

Infrared spectra were recorded on a Mattson Genesis Fourier-transform spectrophotometer with samples in compressed KBr discs. Proton nuclear magnetic resonance (^{1}H NMR) spectra were recorded on Varian Gemini 300, Bruker AM 400 or WM 250 spectrometers. Electron impact (EI) and fast atom bombardment (FAB) mass spectra were recorded using Kratos MS-50, Kratos MS-890, VG 70-250 or Kratos MS-902 instruments; for FAB spectra the sample was loaded using acetonitrile as a solvent and 3-nitrobenzyl alcohol as supporting matrix. Matrix-assisted laser desorption ionization time-of-flight (MALDI-TOF) mass spectra were measured using a PerSeptive Biosystems Voyager-RP Biospectrometry Workstation. Electrochemical measurements were performed with an Eco Chemie Autolab PGSTAT 20 system using platinum bead working and auxiliary electrodes with an Ag/AgCl electrode as reference, purified acetonitrile as solvent and 0.1 M $[Bu^n_4N][BF_4]$ as supporting electrolyte. Ferrocene was added at the end of each experiment as an internal reference. *N*-[2-(2-Pyridyl)-2-oxethyl]pyridinium iodide was prepared according to the procedure in the literature [38]. All other compounds were used as supplied.

0277-5387/100/$ - see front matter ©2000 Elsevier Science Ltd All rights reserved.
PII S0277-5387(99)00318-6

2.2. 1,6-Diarylhexa-1,5-diene-3,4-diones (9–14)

Piperidine (0.2 ml, 0.17 g, 20 mmol) and glacial acetic acid (0.12 ml, 20 mmol) were added to a stirred solution of diacetyl (0.88 ml, 0.86 g, 10 mmol) and the substituted benzaldehyde (40 mmol) in methanol (5 ml). The mixture was heated under reflux for 2 h and then the methanol and unreacted diacetyl were removed in vacuo. The solution was placed in a freezer overnight and the orange crystals that had formed were isolated by filtration.

9, **10**: properties as previously reported [39,40].

11 (0.210 g, 7%): m.p. 172–173°C. Found: C, 74.32; H, 5.61. Calc. for $C_{20}H_{18}O_4$: C, 74.52; H, 5.63%. IR: 2959 w, 2836 w, 1679 m, 1597 s, 1251 s, 1176 m, 1029 m, 995 m, 830 w, 816 w, 789 w, 686 w, 552 w cm^{-1}. Mass spectrum (EI): *m/z* 322 {M}. ^{1}H NMR ($CDCl_3$): δ 3.87 (6H, s, OMe), 6.95 (4H, d, J = 8.7 Hz, H^m), 7.34 (2H, d, J = 16 Hz, H^1), 7.62 (4H, d, J = 8.7 Hz, H^o), 7.83 (2H, d, J = 16 Hz, H^2).

12 (0.330 g, 11%): m.p. 185–186°C. Found: C, 82.49; H, 6.32. Calc. for $C_{20}H_{18}O_2$: C, 82.73; H, 6.25%. IR: 1669 s, 1596 vs, 1509 w, 1328 w, 1305 w, 1294 w, 1181 m, 994 s, 805 s, 682 s, 518 w cm^{-1}. Mass spectrum (EI): *m/z* 290 {M}. ^{1}H NMR ($CDCl_3$): δ 2.40 (6H, s, Me), 7.23 (4H, d, J = 7.8 Hz, H^m), 7.41 (2H, d, J = 16 Hz, H^1), 7.55 (4H, d, J = 7.8 Hz, H^o), 7.85 (2H, d, J = 16 Hz, H^2).

13 (0.16 g 4%): m.p. 190°C. Found: C, 59.67; H, 3.13. Calc. for $C_{20}H_{12}F_6O_2$: C, 60.31; H, 3.04%. IR: 1673 s, 1605 vs, 1574 s, 1415 m, 1319 vs, 1278 m, 1206 w, 1171 s, 1137 s, 1113 m, 1067 s, 1015 m, 992 w, 825 m, 714 m cm^{-1}. Mass spectrum (EI): *m/z* 398 {M}. ^{1}H NMR ($CDCl_3$): δ 7.66 (2H, d, J = 16.2 Hz, H^1), 7.68 (4H, d, J = 8.2 Hz, H^m), 7.76 (4H, d, J = 8.2 Hz, H^o), 7.89 (2H, d, J = 16.2 Hz, H^2).

14 (0.88 g, 3%): m.p. 219–220°C. Found: C, 64.90; H, 3.73. Calc. for $C_{18}H_{12}Cl_2O_2$: C, 65.28; H, 3.65%. IR: 1670 s, 1607 vs, 1588 s, 1562 m, 1489 m, 1326 m, 1295 m, 1096 m, 998 s, 809 s, 748 s cm^{-1}. Mass spectrum (EI): *m/z* 332/330 {M}. ^{1}H NMR ($CDCl_3$): δ 7.42 (4H, d, J = 8.0 Hz, H^m), 7.48 (2H, d, J = 16 Hz, H^1), 7.60 (4H, d, J = 8.0 Hz, H^o), 7.83 (2H, d, J = 16 Hz, H^2).

2.3. 4′,4″-Diaryl-2,2′:6′,2″:6″,2‴-quaterpyridines (3–8)

The appropriate 1,6-diarylhexa-1,5-diene-3,4-dione (0.5 mmol) was added to a solution of *N*-[2-(2-pyridyl)-2-oxethyl]pyridinium iodide (0.4 g, 1 mmol) and anhydrous ammonium acetate (4 g, excess) in ethanol (40 ml) and the mixture heated under reflux for 4 h. After cooling, the off-white precipitate was filtered off and recrystallized from ethanol to give the desired ligand.

3, **4**: properties as previously reported [39,40].

5 (0.100 g, 38%): m.p. > 250°C. Found: C, 75.79; H, 5.25; N, 10.34. Calc. for $C_{34}H_{26}N_4O_2 \cdot H_2O$: C, 75.54; H, 5.21; N, 10.36%. IR: 1583 s, 1567 m, 1547 m, 1515 s, 1472 m, 1383 m, 1255 m, 1185 m, 831 m, 794 m, 575 m cm^{-1}. Mass spectrum (MALDI-TOF): *m/z* 522 {M}. ^{1}H NMR ($CDCl_3$): δ 3.87 (6H, s, OCH_3), 7.10 (4H, d, J = 8.7 Hz, H^m), 7.38 (2H, ddd, J = 7.5, 4.8, 1 Hz, H^5), 7.92 (6H, m, $H^{o,4}$), 8.72 (2H, m, H^6), 8.76 (2H, m, H^3), 8.74 (H, d, J = 1.7 Hz, $H^{3'/5'}$), 8.92 (2H, d, J = 1.7 Hz, $H^{3'/5'}$).

6 (0.157 g, 32%): m.p. > 250°C. Found: C, 80.29; H, 5.46; N, 10.89. Calc. for $C_{34}H_{26}N_4 \cdot H_2O$: C, 80.29; H, 5.55; N, 11.02%. IR: 1595 m, 1582 s, 1568 m, 1546 m, 1514 m, 1469 m, 1379 m, 822 m, 795 m, 733 w, 718 w, 661 w cm^{-1}. Mass spectrum (MALDI-TOF): *m/z* 490 {M}. ^{1}H NMR ($CDCl_3$): δ 1.57 (6H, s, CH_3), 7.38 (6H, m, $H^{m,5}$), 7.86 (4H, d, J = 8.1 Hz, H^o), 7.91 (2H, td, J = 7.8, 1.5 Hz, H^4), 8.72 (2H, d, J = 7.8 Hz, H^6), 8.74 (2H, m, H^3), 8.77 (2H, d, J = 1.7 Hz, $H^{3'/5'}$), 8.94 (2H, d, J = 1.7 Hz, $H^{3'/5'}$).

7 (122 mg, 41%): m.p. > 250°C. Found: C, 67.6; H, 3.4; N, 9.2. Calc. for $C_{34}H_{20}F_6N_4 \cdot 0.5H_2O$: C, 67.2; H, 3.5; N, 9.2%. IR: 1619 vw, 1597 w, 1584 m, 1567 w, 1549 m, 1475 w, 1380 m, 1331 vs, 1164 m, 1119 s, 1109 s, 1074 s, 1037 vw, 1016 w, 840 m, 795 m, 723 w cm^{-1}. Mass spectrum (MALDI-TOF): *m/z* 598 {M}. ^{1}H NMR ($CDCl_3$): δ 7.38 (2H, ddd, J = 6.0, 4.8, 1.1 Hz, H^5), 7.82 (4H, d, J = 8.0 Hz, H^m), 7.91 (2H, td, J = 7.7, 1.7 Hz, H^4), 8.01 (4H, d, J = 8.2 Hz, H^o), 8.68 (2H, d, J = 8.0 Hz, H^3), 8.74 (2H, dd, J = 4.3, 0.9 Hz, H^6), 8.77 (2H, d, J = 1.7 Hz, $H^{5'/3'}$, 8.92 (2H, d, J = 1.7 Hz, $H^{3'/5'}$).

8 (0.055 g, 52%): m.p. > 250°C. Found: C, 68.88; H, 3.87; N, 10.07. Calc. for $C_{32}H_{20}Cl_2N_4 \cdot 1.5H_2O$: C, 68.82; H, 4.16; N, 10.03%. IR: 1602 m, 1585 s, 1566 m, 1547 m, 1494 m, 1472 w, 1379 m, 1090 m, 1012 w, 821 m, 790 m, 752 w, 739 w cm^{-1}. Mass spectrum (EI): *m/z* 530 {M}. ^{1}H NMR ($CDCl_3$): δ 7.39 (2H, ddd, J = 7.7, 4.8, 1.4 Hz, H^5), 7.55 (4H, d, J = 8.7 Hz, H^m), 7.88 (4H, d, J = 8.7 Hz, H^o), 7.93 (2H, td, J = 7.7, 1.4 Hz, H^4), 8.70 (2H, d, J = 7.8 Hz, H^6), 8.75 (2H, d, J = 1.5 Hz, $H^{3'/5'}$), 8.76 (2H, m, H^3), 8.90 (2H, d, J = 1.5 Hz, $H^{3'/5'}$).

2.4. Copper complexes $[Cu_2L_2][PF_6]_2$ (L = 3–8)

The appropriate ligand (20 mg) and an equimolar amount of $[Cu(MeCN)_4][PF_6]$ were heated under dinitrogen in degassed methanol (10 ml) for 3 h. After cooling, the red–brown precipitate was collected by filtration and washed with diethyl ether.

$[Cu_2(\mathbf{3})_2][PF_6]_2$ (0.020 g, 77%): m.p. > 250°C. IR: 1608 s, 1542 w, 1459 w, 1403 m, 841 vs, 766 m, 558 s cm^{-1}. Mass spectrum (MALDI-TOF): *m/z* 1197 $\{Cu_2(\mathbf{3})_2(PF_6)\}^+$, 1052 $\{Cu_2(\mathbf{3})_2\}$, 525 $\{Cu(\mathbf{3})\}$. ^{1}H NMR (CD_3COCD_3): δ 7.21 (2H, dd, J = 6,8, 5.9 Hz, H^5), 7.60 (6H, m, $H^{m,p}$), 7.80 (6H, m, $H^{o,4}$), 8.14 (2H, d, J = 4.4 Hz, H^6], 8.19 (6H, m, $H^{3,3',5'}$). UV–Vis (MeCN): λ_{max} (log ε) 553 (3.78), 443 (4.03), 274 (4.99), 240 (sh), 198 nm (5.14).

$[Cu_2(\mathbf{4})_2][PF_6]_2$ (0.014 g, 51%): m.p. > 250°C. IR: 2923 m, 1601 m, 1368 m, 1115 w, 1016 w, 842 s, 739 w, 557 m cm^{-1}. Mass spectrum (MALDI-TOF): *m/z* 1419 $\{Cu_2(\mathbf{4})_2(PF_6)\}$, 1281 $\{Cu_2(\mathbf{4})_2\}$. ^{1}H NMR (CD_3COCD_3): δ 1.39 (18H, s, $C(CH_3)_3$), 6.72 (2H, m, H^5), 6.93 (4H, d, J = 7.6 Hz, H^m), 7.14 (4H, d, J = 7.6 Hz, H^o), 7.30 (2H, m, H^4), 7.76 (2H, dm, J = 7.6 Hz, H^6), 7.84 (6H, m, $H^{3,3'5'}$).

UV–Vis (MeCN): λ_{max} (log ε) 550 (3.58), 444 (3.80), 298 (4.66), 207 (4.69).

$[Cu_2(\mathbf{5})_2][PF_6]_2$ (0.029 g, 94%): m.p. > 250°C. Found: C, 55.94; H, 3.67; N, 7.41. Calc. for $C_{68}H_{52}Cu_2F_{12}N_8O_4P_2$: C, 55.86; H, 3.58; N, 7.66%. Mass spectrum (MALDI-TOF): *m/z* 1316 $\{Cu_2(\mathbf{5})_2(PF_6)\}$, 1171 $\{Cu_2(\mathbf{5})_2\}$. ^{1}H NMR (CD_3COCD_3): δ 2.17 (6H, s, OCH_3), 6.48 (4H, d, J = 8.5 Hz, H^m), 6.72 (2H, td, J = 6.6, 1 Hz, H^5), 7.24 (4H, d, J = 8.5 Hz, H^o), 7.30 (2H, td, J = 3.2, 1.6 Hz, H^4), 7.72 (2H, d, J = 1 Hz, $H^{3'/5'}$), 7.76 (2H, dm, J = 4.9 Hz, H^6), 7.78 (2H, d, J = 1 Hz, $H^{3'/5'}$), 7.86 (2H, d, J = 8.2 Hz, H^3). UV–Vis (MeCN): λ_{max} (log ε) 554 (3.64), 438 (3.90), 315 (4.76), 199 nm (4.87).

$[Cu_2(\mathbf{6})_2][PF_6]_2$ (0.027 g, 93%): m.p. > 250°C. Found: C, 57.42; H, 3.71; N, 7.99. Calc. for $C_{68}H_{52}Cu_2F_{12}N_8P_2 \cdot H_2O$: C, 57.67; H, 3.84; N, 7.91%. IR: 1601 m, 843 s, 787 w, 557 m cm^{-1}. Mass spectrum (MALDI-TOF): *m/z* 1252 $\{Cu_2(\mathbf{6})_2(PF_6)\}$, 1107 $\{Cu_2(\mathbf{6})_2\}$, 699 $\{Cu(\mathbf{6})\}$. ^{1}H NMR (CD_3COCD_3): δ 1.57 (6H, s, CH_3), 6.72 (2H, ddd, J = 7.1, 6.3, 1 Hz, H^5), 6.78 (4H, d, J = 8.1 Hz, H^m), 7.18 (4H, d, J = 8.1 Hz, H^o), 7.32 (2H, td, J = 7.2, 1.2 Hz, H^4), 7.74, (2H, dm, J = 4.5 Hz, H^6), 7.80 (2H, s, $H^{3'/5'}$), 7.82 (2H, s, $H^{3'/5'}$), 7.88 (2H, d, J = 8.1 Hz, H^3). UV–Vis (MeCN): λ_{max} (log ε) 551 (3.50), 440 (3.73), 281 nm (4.71).

$[Cu_2(\mathbf{7})_2][PF_6]_2$ (0.019 g, 80%): m.p. > 250°C. Found: C, 50.22; H, 2.57; N, 6.87. Calc. for $C_{68}H_{40}Cu_2F_{24}N_8P_2 \cdot H_2O$: C, 50.60; H, 2.50; N, 6.94%. IR: 1609 m, 1543 w, 1395 w, 1322 s, 1170 m, 1114 m, 1061 m, 1016 w, 852 s, 834 vs, 789 m, 557 m cm^{-1}. Mass spectrum (MALDI-TOF): *m/z* 1469 $\{Cu_2(\mathbf{7})_2(PF_6)\}$, 1343 $\{Cu_2(\mathbf{7})_2\}$, 662 $\{Cu(\mathbf{7})\}$. ^{1}H NMR (CD_3COCD_3): δ 7.44 (2H, ddd, J = 7.0, 6.7, 1 Hz, H^5), 7.94 (4H, d, J = 8.0 Hz, H^m), 8.03 (2H, td, J = 7.3, 1.3 Hz, H^4), 8.18 (4H, d, J = 8.0 Hz, H^o), 8.46, (2H, d, J = 4.3 Hz, H^6), 8.58 (2H, d, J = 8.1 Hz, H^3), 8.62 (2H, s, $H^{3'/5'}$), 8.66 (2H, s, $H^{3'/5'}$). UV–Vis (MeCN): λ_{max} (log ε) 563 (3.52), 4.42 (3.71), 283 nm (4.85).

$[Cu_2(\mathbf{8})_2][PF_6]_2$ (0.025 g, 88%): m.p. > 250°C. IR: 1608 m, 844 s, 789 m, 558 m cm^{-1}. Mass spectrum (MALDI-TOF): *m/z* 1334 $\{Cu_2(\mathbf{8})_2(PF_6)\}$, 1189 $\{Cu_2(\mathbf{8})_2\}$, 740 $\{Cu(\mathbf{8})\}$. ^{1}H NMR (CD_3COCD_3): δ 6.78 (2H, ddd, J = 7.2, 5, 1 Hz, H^5), 6.98 (4H, d, J = 8.7 Hz, H^m), 7.32 (4H, d, J = 8.7 Hz, H^o), 7.36 (2H, m, H^4), 7.76 (2H, d, J = 4.9, H^6), 7.88 (2H, d, J = 1.2 Hz, $H^{3'/5'}$), 7.89 (2H, d, J = 8.1 Hz, H^3), 7.90 (2H, d, J = 1.2 Hz, $H^{3'/5'}$). UV–Vis (MeCN): λ_{max} (log ε) 555 (3.48), 445 (3.70), 286 (4.90), 226 nm (4.94).

2.5. Silver complexes $[Ag_2L_2][PF_6]_2$ (L = **3**–7)

The appropriate ligand (20 mg) and an equimolar amount of silver acetate were heated under dinitrogen in degassed methanol (10 ml) for 3 h. After cooling to room temperature, a methanolic solution of $[NH_4][PF_6]$ was added. The off-white precipitate that formed was isolated by filtration and washed with diethyl ether.

$[Ag_2(\mathbf{3})_2][PF_6]_2$ (0.018 g, 58%): m.p. > 250°C. IR: 1597 s, 1552 m, 1480 w, 1449 w, 1396 w, 844 vs, 763 s, 558 s cm^{-1}. Mass spectrum (MALDI-TOF): *m/z* 1285 $\{Ag_2(\mathbf{3})_2(PF_6)\}$, 1139 $\{Ag_2(\mathbf{3})_2\}$, 1032 $\{Ag(\mathbf{3})_2\}$, 677 $\{Ag_2(\mathbf{3})\}$. ^{1}H NMR (CD_3CN): δ 7.15 (2H, dd, J = 6.8, 5.1 Hz, H^5), 7.65 (6H, m, $H^{m,p}$), 7.95 (8H, m, $H^{o,4,6}$), 8.13 (2H, d, J = 8.1 Hz, H^3), 8.22 (2H, s, $H^{3'/5'}$), 8.43 (2H, s, $H^{3'5'}$).

$[Ag_2(\mathbf{4})_2][PF_6]_2$ (0.019 g, 67%): m.p. > 250°C. IR: 2962 w, 1597 m, 1479 w, 1390 w, 844 s, 791 w, 558 m cm^{-1}. Mass spectrum (MALDI-TOF): *m/z* 1364 $\{Ag_2(\mathbf{4})_2\}$, 1256 $\{Ag(\mathbf{4})_2\}$, 790 $\{Ag_2(\mathbf{4})\}$. ^{1}H NMR (CD_3COCD_3): δ 1.43 (18H, s, $C(CH_3)_3$), 6.66 (2H, ddd, J = 7.7, 5.0, 1 Hz, H^5), 7.02 (4H, d, J = 8.5 Hz, H^m), 7.32 (4H, d, J = 5 Hz, H^o), 7.44 (2H, td, J = 7.7, 1.5 Hz, H^4), 7.70 (2H, dm, J = 5 Hz, H^6), 7.82 (2H, d, J = 7.7 Hz, H^3), 7.86 (2H, d, J = 1Hz, $H^{3'/5'}$), 8.06 (2H, d, J = 1 Hz, $H^{3'/5'}$). UV–Vis (MeCN): λ_{max} (log ε) 281 (4.98), 255 (sh), 221 (sh), 198 nm (5.19).

$[Ag_2(\mathbf{5})_2][PF_6]_2$: (0.027 g, 92%): m.p. > 250°C. IR: 2924 w, 1599 s, 1518 m, 1257 w, 1184 w, 843 m, 789 w cm^{-1}. Mass spectrum (MALDI-TOF): *m/z* 1260 $\{Ag_2(\mathbf{5})_2\}$, 1152 $\{Ag(\mathbf{5})_2\}$, 738 $\{Ag_2(\mathbf{5})\}$. ^{1}H NMR (CD_3COCD_3): δ 3.93 (6H, s, OCH_3), 7.16 (6H, m, $H^{5,m}$), 7.90 (6H, m, $H^{o,4}$), 8.04 (2H, dm, J = 4.5 Hz, H^6), 8.10 (2H, d, J = 8.2 Hz, H^3), 8.15 (2H, d, J = 1 Hz, $H^{3'/5'}$), 8.33 (2H, d, J = 1 Hz, $H^{3'/5'}$). UV–Vis (MeCN): λ_{max} (log ε) 307 (sh), 294 (4.95), 247 (4.81), 221 (sh), 197 nm (5.20).

$[Ag_2(\mathbf{6})_2][PF_6]_2$ (0.027 g, 88%): m.p. > 250°C. Found: C, 53.9; H, 3.6; N, 8.0. Calc. for $C_{68}H_{52}N_8Ag_2P_2F_{12} \cdot H_2O$: C, 54.3; H, 3.6; N, 7.5%. IR: 1598 m, 1546 w, 1392 m, 842 s, 788 m, 557 m cm^{-1}. Mass spectrum (MALDI-TOF): *m/z* 1196 $\{Ag_2(\mathbf{6})_2\}$, 1088 $\{Ag(\mathbf{6})_2\}$, 598 $\{Ag(\mathbf{6})\}$. ^{1}H NMR (CD_3COCD_3) δ 1.57 (6H, s, CH_3), 6.66 (2H, ddd, J = 7.0, 6.7, 1 Hz, H^5), 6.82 (4H, d, J = 8.0 Hz, H^m), 7.32 (4H, d, J = 8.0 Hz, H^o), 7.42 (2H, td, J = 7.3, 1.3 Hz, H^4), 7.64, (2H, dm, J = 4.3 Hz, H^6), 7.84 (2H, d, J = 8.1 Hz, H^3), 7.86 (2H, s, $H^{3'/5'}$), 8.04 (2H, s, $H^{3'/5'}$). UV–Vis (MeCN): λ_{max} (log ε) 279 (4.93), 257 (4.86), 220 (sh), 196 nm (5.2).

$[Ag_2(\mathbf{7})_2][PF_6]_2$ (0.038 g, 76%): m.p. > 250°C. Found: C, 47.1; H, 2.5; N, 6.4. Calc. for $C_{68}H_{40}N_8P_2F_{24}Ag_2 \cdot 2H_2O$: C, 47.0; H, 2.6; N, 6.4%. IR: 1597 m, 1548 m, 1481 w, 1450 w, 1388 m, 1327 vs, 1173 m, 1120 s, 1075 m, 1065 m, 1016 m, 840 vs, 792 m, 730 w, 558 m cm^{-1}. Mass spectrum (MALDI-TOF): *m/z* 1412 $\{Ag_2(\mathbf{7})_2\}$, 1304 $\{Ag(\mathbf{7})_2\}$, 814 $\{Ag_2(\mathbf{7})\}$, 706 $\{Ag(\mathbf{7})\}$. ^{1}H NMR (CD_3COCD_3): δ 7.21 (2H, ddd, J = 7.0, 6.7, 1 Hz, H^5), 7.89 (6H, m, $H^{4,m}$), 8.01 (4H, d, J = 8.0 Hz, H^o), 8.17, (4H, m, $H^{3,6}$), 8.26 (2H, s, $H^{3'/5'}$), 8.49 (2H, s, $H^{3'/5'}$).

2.6. Nickel(II) complexes (L = **3**–7)

The ligand (20 mg) and an equimolar amount of nickel(II) acetate were heated under dinitrogen in methanol or ethanol (10 ml) for 3 h. After cooling to room temperature, a methanolic solution of $[NH_4][PF_6]$ was added and the yellow precipitate that formed was collected by filtration and washed with diethyl ether.

[Ni(**3**)(OAc)(H_2O)][PF_6] (0.016 g, 63%): m.p. > 250°C. Found: C, 55.0; H, 3.5; N, 7.6. Calc. for $C_{34}H_{29}N_4O_3NiPF_6$: C, 54.9; H, 3.7; N, 7.5%. IR: 1606 s, 1533 vs, 1460 m, 1406 s, 1243 w, 1017 w, 843 vs, 792 w, 766 s, 734 w, 691 w, 642 w, 632 w, 557 s cm^{-1}. Mass spectrum (MALDI-TOF): *m/z* 744 {Ni(**3**)(OAc)(PF_6)(F)}, 725 {Ni(**3**)(OAc)(PF_6)}, 580 {Ni(**3**)(OAc)}, 521 {Ni(**3**)}. ^{1}H NMR (CD_3CN): δ 10, 11, 34, 39, 46, 50, 60.

[Ni(**4**)(MeCN)(H_2O)][PF_6]$_2$ (0.014 g, 51%): m.p. > 250°C. Recrystallized from MeCN–diethyl ether. Found: C, 51.3; H, 4.4; N, 6.8. Calc. for $C_{42}H_{43}N_5NiOP_2F_{12}$: C, 51.3; H, 4.4; N, 7.1%. IR: 2964 w, 1605 m, 1550 w, 1460 w, 1400 w, 1016 w, 842 s, 798 w, 559 m cm^{-1}. Mass spectrum (MALDI-TOF): *m/z* 651 {Ni(**4**)(H_2O)}, 633 {Ni(**4**)}. ^{1}H NMR (CD_3COCD_3): δ 3, 8 (×2), 12, 13, 34, 63, 67, 91. UV–Vis (MeCN): λ_{max} (log ε) 349 (4.2), 292 (4.66), 238 (4.56), 202 nm (4.88).

[Ni(**5**)(MeCN)$_2$][PF_6]$_2$ (22 mg, 80%): m.p. > 250°C. Recrystallized from MeCN–diethyl ether. Found: C, 47.7; H, 3.5; N, 8.9. Calc. for $C_{38}H_{32}N_6O_2NiP_2F_{12}$: C, 47.9; H, 3.4; N, 8.8%. IR: 1559 s, 1552 w, 1520 m, 1460 m, 1404 m, 1246 m, 1191 m, 1024 m, 845 s, 794 m, 558 m cm^{-1}. Mass spectrum (MALDI-TOF): *m/z* 726 {Ni(**5**)(PF_6)}, 581 {Ni(**5**)}. ^{1}H NMR (CD_3COCD_3): δ 4, 7, 11, 12, 33, 62, 65, 89. UV–Vis (MeCN): λ_{max} (log ε) 334 (4.68), 298 (4.64), 245 (4.70), 200 nm (4.73).

[Ni(**6**)(OAc)(H_2O)][PF_6] (25 mg, 85%): m.p. > 250°C. Found: C, 54.8; H, 3.8; N, 7.2. Calc. for $C_{36}H_{31}N_4O_3NiPF_6 \cdot H_2O$: C, 54.8; H, 4.2; N, 7.1%. IR: 1604 m, 1552 w, 1459 w, 1400 w, 1020 w, 840 s, 794 m, 558 m cm^{-1} Mass spectrum (MALDI-TOF): *m/z* 585 {Ni(**6**)(H_2O)$_2$}, 549 {Ni(**6**)}. ^{1}H NMR (CD_3COCD_3): δ 10 (×2), 11 (×2), 12, 33, 62, 66, 90. UV–Vis (MeCN): λ_{max} (log ε) 348 (4.20), 293 (4.68), 238 (4.56), 202 nm (4.91).

[Ni(**7**)(OAc)(MeCN)][PF_6]$_2$ (0.017 g, 72%): m.p. > 250°C. Recrystallized from MeCN–diethyl ether. Found: C, 49.7; H, 3.0; N, 7.6. Calc. for $C_{38}H_{26}N_5NiO_2PF_{12} \cdot H_2O$: C, 49.6; H, 3.1; N, 7.6%. IR: 1612 s, 1566 m, 1460 m, 1397 m, 1328 vs, 1172 m, 1121 s, 1070 m, 1015 m, 843 vs, 794 m, 735 w, 558 m cm^{-1}. Mass spectrum (MALDI-TOF): *m/z* 744 {[Ni(**7**)(OAc)(PF_6)(F)}, 725 {Ni(**7**)(OAc)(PF_6)}, 580 {Ni(**7**)(OAc)}, 521 {Ni(**7**)}. ^{1}H NMR (CD_3COCD_3): δ 10, 11, 32, 39, 46, 50, 60. UV–Vis (MeCN): λ_{max} (log ε) 349 (4.22), 292 (4.65), 240 (4.62), 204 nm (4.93).

*2.7. Cobalt(II) complexes (L = **3**–**7**)*

Preparation was the same as for the nickel complexes but using cobalt(II) acetate; orange–yellow solids were formed.

[Co(**3**)(OAc)(H_2O)][PF_6] (0.025 g, 78%): m.p. > 250°C. Found: C, 54.9; H, 3.6; N, 7.6. Calc. for $C_{34}H_{27}N_4O_3CoPF_6$: C, 54.9; H, 3.7; N, 7.5%. IR: 1614 s, 1576 m, 1557 s, 1488 w, 1463 m, 1407 m, 848 vs, 768 m, 559m cm^{-1}. Mass spectrum (FAB): *m/z* 537 {Co(**3**)(H_2O)}, 521 {Co(**3**)}. ^{1}H NMR (CD_3CN): δ 6, 9, 12, 22, 32, 40, 50, 71, 72, 159. UV–Vis (MeCN): λ_{max} (log ε) 296 (4.70), 225 (4.66), 202 nm (4.91).

[Co(**4**)(MeCN)(H_2O)][PF_6]$_2$ (0.013 g, 67%): m.p. > 250°C. Recrystallized from MeCN–diethyl ether. Found: C, 51.4; H, 4.6; N, 6.8. Calc. for $C_{42}H_{43}N_5OCoP_2F_{12}$: C, 51.3; H, 4.4; N, 7.1%. IR: 2966 w, 1608 m, 1547 w, 1448 w, 1400 s, 1050 m, 848 s, 793 w, 557 m cm^{-1}. Mass spectrum (MALDI-TOF): *m/z* 923 {Co(**4**)(PF_6)$_2$}, 692 {Co(**4**)(H_2O)(MeCN}, 669 {Co(**4**)(H_2O)$_2$}, 651 {Co(**4**)(H_2O)}, 633 {Co(**4**)}. ^{1}H NMR (CD_3COCD_3): δ 4, 6, 9, 21, 30, 48, 69, 73, 164. UV–Vis (MeCN): λ_{max} (log ε) 297 (4.74), 223 (4.72), 202 nm (4.93).

[Co(**5**)(H_2O)$_2$][PF_6]$_2$ (0.026 g, 94%): m.p. > 250°C. Found: C, 47.2; H, 3.3; N, 6.6. Calc. for $C_{34}H_{30}N_4O_2CoP_2F_{12}$: C, 46.6; H, 3.45; N, 6.4%. IR: 1603 s, 1554 m, 1523 m, 1460 m, 1404 m, 1302 w, 1244 m, 1194 m, 1018 w, 849 s, 793 w, 559 m cm^{-1}. Mass spectrum (MALDI-TOF): *m/z* 871 {Co(**5**)(PF_6)$_2$}, 640 {Co(**5**)(H_2O)(MeCN)}, 617 {Co(**5**)(H_2O)$_2$}, 599 {Co(**5**)(H_2O)}, 581 {Co(**5**)}. ^{1}H NMR (CD_3COCD_3): δ 6, 9, 48, 63, 73, 169. UV–Vis (MeCN): λ_{max} (log ε) 356 (sh), 332 (4.57), 292 (4.65), 226 (sh), 202 nm (4.90).

[Co(**6**)(OAc)(MeCN)][PF_6] (0.024 g, 83%): m.p. > 250°C. Recrystallized from MeCN–diethyl ether. Found: C, 56.8; H, 4.0; N, 9.1. Calc. for $C_{38}H_{32}N_5O_2CoPF_6$: C, 57.5; H, 4.1; N, 8.8%. IR: 1610 m, 1553 m, 1460 w, 1400 w, 1246 w, 1014 w, 846 s, 791 m, 558 m cm^{-1}. Mass spectrum (MALDI-TOF): *m/z* 839 {Co(**6**)(PF_6)$_2$}, 694 {Co(**6**)(PF_6)}, 608 {Co(**6**)(H_2O)(MeCN)}, 585 {Co(**6**)(H_2O)$_2$}, 567 {Co(**6**)(H_2O)}, 549 {Co(**6**)}. ^{1}H NMR (CD_3COCD_3): δ 4 (×2), 9 (×2), 21, 28, 47, 68, 72, 162. UV–Vis (MeCN): λ_{max} 297 (4.71), 224 (4.72), 204 nm (4.92).

[Co(**7**)(OAc)(MeCN)][PF_6] (0.020 g, 75%): m.p. > 250° C. Found: C, 50.4; H, 3.1; N, 7.7. Calc. for $C_{38}H_{26}N_5OPF_{12}Co$: C, 50.6; H, 2.9; N, 7.8%. IR: 1613 m, 1577 m, 1555 m, 1460 m, 1397 m, 1327 vs, 1169 w, 1132 m, 1120 m, 1016 m, 844 vs, 795 w, 557 m cm^{-1}. Mass spectrum (MALDI-TOF): *m/z* 807 {Co(**7**)(PF_6)}, 657 {Co(**7**)}. ^{1}H NMR (CD_3COCD_3): δ 6, 10, 22, 35, 49, 71, 159.

*2.8. Crystal structure determinations of [Ni(**4**)(MeCN)$_2$][PF_6]$_2$ (**15**), [Ni(**3**)(OAc)(MeOH)][PF_6]·2MeOH·H_2O (**16**) and [Co(**3**)(OAc)(MeCN)][PF_6]·1.64MeCN·0.36·H_2O (**17**)*

In each case, crystals were grown by the diffusion of diethyl ether vapour into a solution of the crude complex in acetonitrile. Measurements were made, as previously described, using an Enraf-Nonius CAD4 diffractometer [41]. The conditions used for crystallographic data collection and structure refinement are summarized in Table 1; selected geometric data are given in Table 2. Structures were elucidated by direct methods using SIR92 [42]. Anisotropic least-

Table 1
Crystal data and structure refinement for **15**–**17**

	15	**16**	**17**
Formula	$C_{44}H_{44}N_6Ni \cdot 2F_6P$	$C_{35}H_{18}NiN_4O_3 \cdot F_6P \cdot 2CH_4O \cdot H_2O$	$C_{36}H_{28}CoN_5O_2 \cdot F_6P \cdot 1.64C_2H_3N \cdot 0.36H_2O$
Crystal system	orthorhombic	triclinic	triclinic
Space group	*Pbn*21	$P\bar{1}$	$P\bar{1}$
Crystal colour, habit	pale green plate	yellow–green needle	yellow–orange cube
Crystal dimensions (mm)	0.05×0.16×0.18	0.12×0.14×0.28	0.20×0.26×0.42
a (Å)	9.8573(7)	10.709(1)	11.959(1)
b (Å)	20.1490(17)	13.089(1)	12.738(2)
c (Å)	23.2486(38)	14.809(1)	13.124(2)
α (°)	90	65.369(5)	89.75(1)
β (°)	90	88.515(6)	71.53(1)
γ (°)	90	87.626(8)	87.07(1)
Z	4	2	2
D_c (g cm^{-3})	1.45	1.46	1.47
Temperature (K)	293	223	223
Radiation, Cu Kα (λ, Å)	1.54180	1.54180	1.54180
Scan type	ω-2θ	ω-2θ	ω-2θ
Maximum 2θ	133.48	155.0	155.0
No. data collected	3239	6997	6699
No. unique data	3124	6638	6457
No. observed data	3124	4635, $I > 3.00\sigma(I)$	4354, $I > 3.00\sigma(I)$
No. variables	586	497	549
Absorption correction	psi-scans	DIFABS [45]	DIFABS [45]
Weighting scheme	Chebychev [44]	Chebychev [44]	Chebychev [44]
R	0.1160 (all data)	0.0827	0.0757
R_W	0.2370 (all data)	0.0795	0.0865
$\Delta\rho_{max}$, $\Delta\rho_{max}$ (e, Å^{-3})	0.72, −0.92	0.954, −0.906	0.71, −0.92

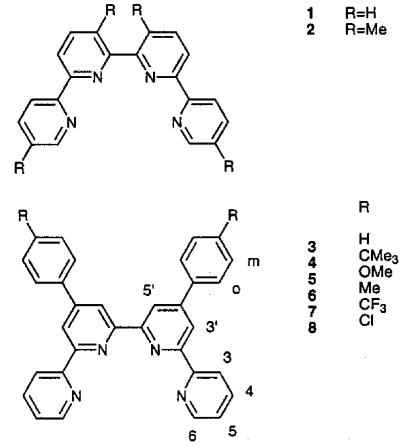
squares full-matrix refinement was carried out on all non-hydrogen atoms using the program CRYSTALS [43] and a Chebychev weighting scheme [44]. The positions of the hydrogen atoms were determined geometrically.

For compound **15**, a poor dataset was obtained and the structure was refined against F^2 using all the data. For **17**, problems were encountered refining disordered solvent molecules. The space around the special position 0.5, 0, 0.5 is occupied by MeCN and H_2O molecules. The frequency was not constrained during refinement, but the total site occupancy was fixed to 1. The ratio of 0.64–0.36 suggests that the two solvent molecules can have two alternative orientations created by the centre of symmetry, or that two MeCN molecules are present in the cavity without H_2O. Another disordered MeCN molecule has been localized in the difference map. The two alternating positions have been refined using appropriate restraints. Because of difficulties in centering the sample on the diffractometer using the oil-drop method at low temperature, psi-scans did not give a good estimate of the absorption; refinement was therefore made using DIFABS [45].

3. Results and discussion

3.1. Ligand synthesis

2,2′:6′,2″:6″,2‴-Quaterpyridine (**1**) was first synthesized in 1938 by the high-temperature coupling of 6-halo-2,2′-bipyridines in the presence of copper powder [28]; this method has also been utilized in the preparation of **2** [23]. More recently, nickel reagents have been utilized for the synthesis of **1** [7]. The preparation of 4′,4″-disubstituted ligands by the coupling reactions of halo-2,2′-bipyridines is not easy, but they can be obtained using the methodology described by Sorenson [40]. We have shown that diacetyl is an excellent precursor for the formation of oligopyridines and that the 4′,4″-diaryl-substituted compounds **3** and **4** can be prepared from this starting material [39].



We have now extended this methodology to the preparation of a range of 4′,4″-disubstituted-2,2′:6′,2″:6″,2″-quaterpyridines (**3**–**8**), which were synthesized according to Scheme 1. The reaction of diacetyl with the appropriate substituted

Table 2
Selected bond lengths (Å) and angles (°) for **15**–**17**

15		**16**		**17**	
Ni(1)–N(1)	2.11(1)	Ni(1)–N(1	2.140(4)	Co(1)–N(1)	2.211(5)
Ni(1)–N(2)	1.982(9)	Ni(1)–N(2)	2.020(4)	Co(1)–N(2)	2.156(4)
Ni(1)–N(3)	2.06(1)	Ni(1)–N(3)	2.009(4)	Co(1)–N(3)	2.158(4)
Ni(1)–N(4)	2.091(9)	Ni(1)–N(4)	2.174(4)	Co(1)–N(4)	2.196(4)
Ni(1)–N(5)	2.09(1)	Ni(1)–O(1	2.133(3)	Co(1)–O(1)	2.171(4)
Ni(1)–N(6)	2.09(1)	Ni(1)–O(2)	2.052(3)	Co(1)–O(2)	2.293(3)
				Co(1)–N(51)	2.156(5)
N(1)–Ni(1)–N(2)	76.4(4)	N(1)–Ni(1)–N(2)	76.7(2)	N(1)–Co(1)–N(3)	145.0(1)
N(1)–Ni(1)–N(3)	156.1(4)	N(1)–Ni(1)–N(3)	154.1(2)	N(2)–Co(1)–N(3)	72.4(1)
N(2)–Ni(1)–N(3)	79.7(4)	N(2)–Ni(1)–N(3)	77.6(2)	N(1)–Co(1)–N(4)	140.6(2)
N(1)–Ni(1)–N(4)	127.7(4)	N(1)–Ni(1)–N(4)	128.9(2)	N(2)–Co(1)–N(4)	144.0(1)
N(2)–Ni(1)–N(4)	155.9(4)	N(2)–Ni(1)–N(4)	153.6(2)	N(3)–Co(1)–N(4)	72.5(1)
N(3)–Ni(1)–N(4)	76.3(4)	N(3)–Ni(1)–N(4)	76.4(2)	N(1)–Co(1)–O(1)	97.4(1)
N(1)–Ni(1)–N(5)	88.6(4)	N(1)–Ni(1)–O(1)	88.1(2)	N(2)–Co(1)–O(1)	91.0(1)
N(2)–Ni(1)–N(5)	93.3(4)	N(2)–Ni(1)–O(1)	91.1(2)	N(3)–Co(1)–O(1)	87.7(1)
N(3)–Ni(1)–N(5)	93.9(4)	N(3)–Ni(1)–O(1)	89.6(2)	N(4)–Co(1)–O(1)	95.4(1)
N(4)–Ni(1)–N(5)	86.3(4)	N(4)–Ni(1)–O(1)	84.5(2)	N(1)–Co(1)–O(2)	78.1(1)
N(1)–Ni(1)–N(6)	90.2(4)	N(1)–Ni(1)–O(2)	90.3(1)	N(2)–Co(1)–O(2)	134.4(1)
N(2)–Ni(1)–N(6)	91.6(4)	N(2)–Ni(1)–O(2)	91.7(2)	N(3)–Co(1)–O(2)	131.8(1)
N(3)–Ni(1)–N(6)	89.4(4)	N(3)–Ni(1)–O(2)	93.2(2)	N(4)–Co(1)–O(2)	77.2(1)
N(4)–Ni(1)–N(6)	90.2(4)	N(4)–Ni(1)–O(2)	94.0(2)	O(1)–Co(1)–O(2)	58.7(1)
N(5)–Ni(1)–N(6)	174.5(4)	O(1)–Ni(1)–O(2)	176.4(2)	N(1)–Co(1)–N(51)	80.8(2)
				N(1)–Co(1)–N(2)	72.9(1)
				N(2)–Co(1)–N(51)	93.0(2)
				N(3)–Co(1)–N(51)	96.4(2)
				N(4)–Co(1)–N(51)	83.2(2)
				O(1)–Co(1)–N(51)	175.0(1)
				O(2)–Co(1)–N(51)	116.3(1)

benzaldehyde in MeOH with piperidinium acetate as catalyst resulted in the formation of 1,6-diarylhexa-1,5-diene-3,4-diones **9**–**14** as bright orange crystals. Although the yields were poor, unreacted material can be recovered; moreover, the convenience of this synthesis and the low cost of the starting materials make these attractive intermediates for oligopyridine synthesis. The compounds were all isolated with the *E,E* configuration, as confirmed by the observation of a single AB system with a coupling constant J_{AB} of $\approx$16 Hz in each of the ^{1}H NMR spectra. The carbonyl group of the enone gives rise to a characteristic absorption in the IR spectrum, with $\bar{\nu}$ = 1669–1679 cm^{-1}. Characterization data for these compounds are collated in Section 2.

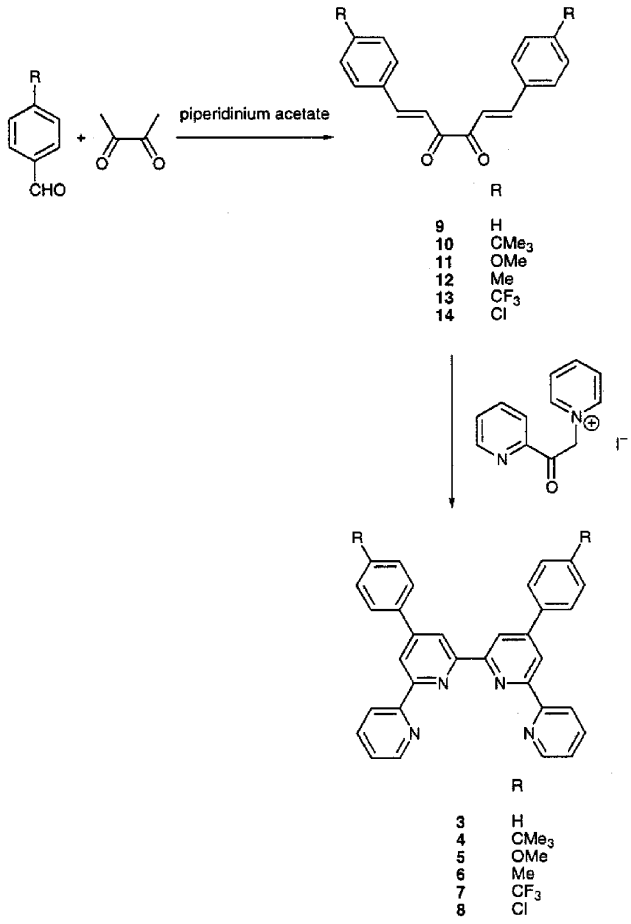
The quaterpyridines **3**–**8** were isolated as off-white solids in yields of 30–60% from the reaction of **9**–**14** with the Kröhnke reagent, *N*-[2-(2-pyridyl)-2-oxethyl]pyridinium iodide [38], in the presence of ammonium acetate. The ^{1}H NMR spectra of these compounds are characteristic, with ligands **3**–**6** giving nine resonances and **7** and **8** giving only eight resonances. All of the chemical shifts and coupling constants were within the normal ranges and the spectra were fully assigned (see Section 2) by inspection, comparison with known compounds and by correlation spectroscopy (COSY).

3.2. Complexes with metals favouring tetrahedral coordination

The four nitrogen donor atoms of quaterpyridine ligands can be partitioned into two didentate bipyridine domains upon interaction with metal ions favouring tetrahedral coordination, because it is not possible for all four donors to occupy the vertices of a tetrahedron [1–5].

3.2.1. Copper(I) complexes

Copper(I) forms dinuclear double-helical complexes with 2,2′:6′,2″:6″,2‴-quaterpyridines [1–5] in which the precise geometrical properties are dependent upon the nature and position of any ligand substituents. The reaction of **3**–**8** with an equimolar amount of [Cu(MeCN)$_4$][PF$_6$] in methanol under nitrogen gave deep red–brown solutions from which the salts [Cu$_2$L$_2$][PF$_6$]$_2$ (L = **3**–**8**) were isolated as solids varying in colour from red–brown through purple to black in 50–90% yield. Microanalysis confirmed the 1:1 metal:ligand stoichiometry, and evidence for the dinuclear structures came from mass spectrometry, which revealed ions corresponding to {[Cu$_2$L$_2$][PF$_6$]}$^+$ and {[Cu$_2$L$_2$]}$^+$ in each case (where L represents quaterpyridine (qtpy) or substituted quaterpyridine). Molecular modelling combined with structural data for a number of [Cu$_2$L$_2$]$^{2+}$ complexes confirms that a dinuclear formulation requires a double-helical structure; no



Scheme 1.

Table 3
Cyclic voltammetric data for copper complexes in MeCN (vs. internal Fc/Fc$^+$)

Complex	$[Cu(I)_2L_2]^{2+}$/ $[Cu(I)Cu(II)L_2]^{3+}$ (V)	$[Cu(II)L]^{2+}$/ $[Cu(I)L]^+$ (V)	$E_a - E_c$ (V)
$[Cu_2(qtpy)_2]^{2+}$	0.005	−0.420	0.470
$[Cu_2(\mathbf{3})_2]^{2+}$	−0.030	−0.360	0.330
$[Cu_2(\mathbf{4})_2]^{2+}$	0.044	−0.294	0.338
$[Cu_2(\mathbf{5})_2]^{2+}$	0.028	−0.331	0.359
$[Cu_2(\mathbf{6})_2]^{2+}$	0.133	−0.370	0.503
$[Cu_2(\mathbf{7})_2]^{2+}$	0.270	−0.371	0.641
$[Cu_2(\mathbf{8})_2]^{2+}$	0.071	−0.289	0.360

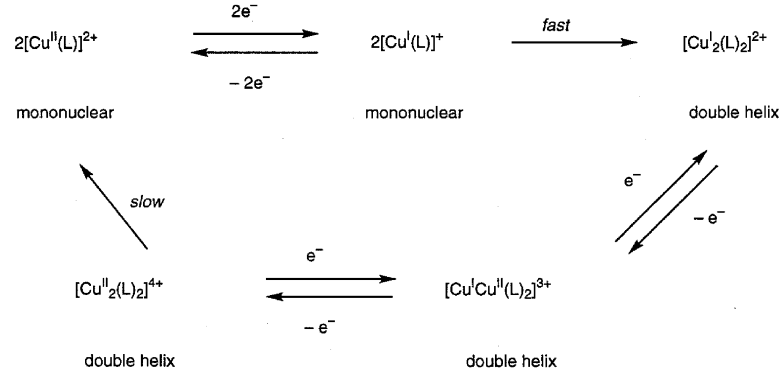
achiral structure is possible. The ^{1}H NMR spectra of CD_3COCD_3 or CD_3CN solutions of the complexes were simple and assigned with the aid of ^{1}H NMR COSY experiments. Only nine (**3**–**6**) or eight (**7**, **8**) different proton environments were observed, indicating a single symmetrical solution species. Comparison with the ^{1}H NMR spectra of solutions of $[Cu_2(qtpy)_2][PF_6]_2$, for which X-ray data have established a double-helical solid-state species, indicates that the solution species are similar. Although the ^{1}H NMR data cannot distinguish between dinuclear and mononuclear solution species, we have used chiral ligands to unambiguously establish that the solution species are dinuclear [17]. Taken in conjunction with the electrochemical data, we can now confidently state that the 4′,4″-disubstituted quaterpyridine ligands give dicopper(I) double-helical complexes in both the solid state and solution. The complexes are indefinitely stable in air in the solid state or in MeCN, although they are slowly oxidized in MeOH solution.

The electronic spectra of the dicopper(I) complexes in MeCN solution show absorption maxima at very similar wavelengths (550–555 and 438–445 nm), with the exception of the complex with **7**, which is significantly red-shifted (563 and 448 nm). Compared with $[Cu_2(qtpy)_2][PF_6]_2$ (λ_{max} 543, 432 nm) [11], the metal-to-ligand charge transfer (MLCT) bands of the complexes with **3**–**8** have been red-shifted, consistent with the lowering of the energy of the ligand π^* acceptor orbital upon the introduction of the conjugated aromatic substituents.

The dicopper(I) complexes are all electrochemically active and show irreversible metal-centred oxidation and reduction processes (Table 3) together with ligand-based reductions at ≈ -1.50 and ≈ -1.75 V. The separation between the metal-centred processes is variable and the data are in accord with earlier studies of simple quaterpyridine derivatives and are compatible with the electrochemical processes outlined in Scheme 2 [22–25].

3.2.2. Silver(I) complexes

The reaction of **3**–**7** with an equimolar amount of AgOAc in methanol gave pale yellow solutions from which the salts $[Ag_2L_2][PF_6]_2$ (L = **3**–**7**) were isolated as white solids in 58–92% yield. Microanalysis confirmed the 1:1 metal:ligand formulations and mass spectrometry confirmed a dinuclear



Scheme 2.

formulation. Arguments similar to those presented above lead to unambiguous assignment of dinuclear double-helical structures to both solid-state and solution species. The ^{1}H NMR spectra of CD_3COCD_3 or CD_3CN solutions of the complexes were simple and only nine (**3**–**6**) or eight (**7**) proton environments were observed, indicating a single symmetrical solution species. The complexes are air-stable both in the solid state and in solution.

All of the complexes exhibit an irreversible process in the range -0.30 and -0.4 V (versus Fc/Fc^+), leading to complex decomposition and plating of silver on the electrode.

All of these data are in accord with the formation of dinuclear double-helical complexes (Scheme 3) with copper(I) and silver(I) in which the 4′,4″-substituents will, at most, control the pitch of the double helix. Despite numerous attempts, we have been unable to obtain X-ray-quality crystals of copper or silver complexes with any of these ligands. As the original aim was to ascertain that the introduction of the 4′,4″-substituents did not affect the formation of dinuclear double helicates, the non-structural evidence was strong enough for us to develop more highly functionalized quaterpyridine ligands for use as dendritic cores [46]. Fig. 1 shows an MM2 minimized structure representing the dicopper(I) complex with **3**. The crystallographic coordinates for the $[Cu_2(qtpy)_2]^{2+}$ cation were taken [9,11] and the 4′- and 4″-H atoms replaced by phenyl groups. The core structure was constrained and the phenyl groups were minimized. There are no short contacts between the substituents and the dinuclear core, and the phenyl substituents are arrayed in a quasi-tetrahedral fashion.

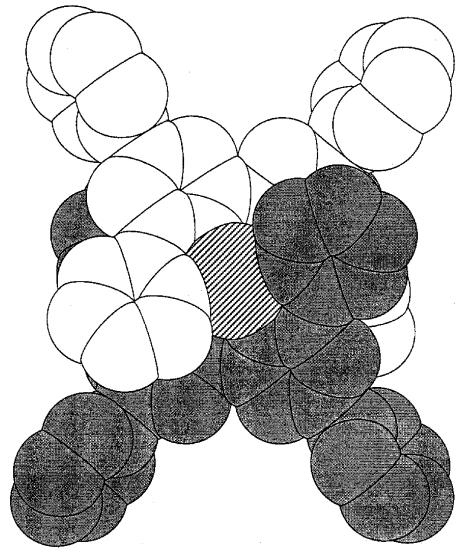


Fig. 1. Modelled structure of the dicopper(I) double helicate obtained with **3**, showing the distribution of the aryl substituents. For clarity, hydrogen atoms have been omitted and one of the ligand strands has been shaded.

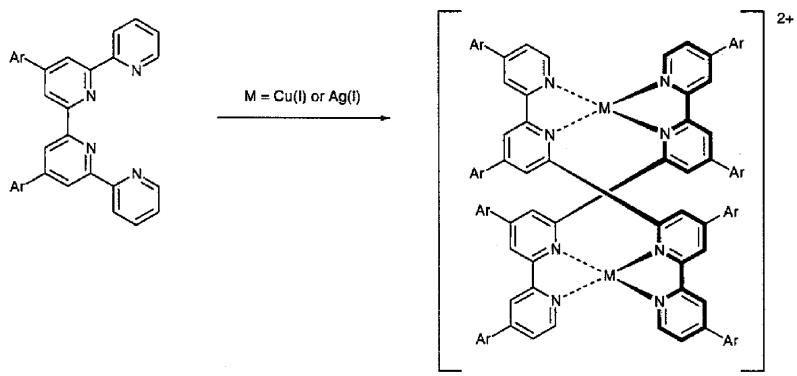
3.3. Complexes with metals favouring octahedral coordination

Octahedral metal centres could form two types of complexes with quaterpyridine ligands: (a) the four nitrogen donors of the ligand could occupy the equatorial sites of a mononuclear octahedral complex, or the ligand could be partitioned into two bipyridine domains to give (b) a dinuclear double helix with two additional ligands per metal centre or (c) a dinuclear triple helix. Modelling suggests that the triple helix (c) is too strained with quaterpyridine ligands, but both (a) and (b) should be possible. Although known structures of cobalt(II) [29,30] and nickel(II) [7,11] complexes are all of type (a), the desired $\{M''(bpy'')_2X_2\}$ coordination subunit is present in the dinuclear double-helical complexes $[M_2(qpy)_2(OAc)]^{3+}$ (M = Ni, Co; qpy = 2,2′:6′,2″:6″,2‴:6‴,2⁗-quinquepyridine; X_2 = OAc). We hoped that the introduction of substituents onto the quaterpyridine might force the adoption of structure (b).

3.3.1. Nickel(II) complexes

The reaction of **3**–**7** with an equimolar amount of nickel(II) acetate in MeOH or EtOH gave yellow solutions from which yellow-green salts were obtained upon the addition of $[NH_4][PF_6]$. In all cases, microanalysis indicated complexes with a 1:1 M:L stoichiometry. It was also apparent that a number of additional ligands or anions were present in each case. In particular, microanalysis indicated that acetate was present in many of the isolated complexes. Because we had previously characterized the acetate-free mononuclear cations $[Ni(qtpy)(S)_2]^{2+}$ (S = MeCN or H_2O), we hoped that the inclusion of acetate was evidence for the formation of the dinuclear double helices.

The precise species formed depended upon the ligand, but isolated complexes included $\{[NiL(OAc)(S)][PF_6]\}_n$



Scheme 3.

(L = **3**, **6**, **7**, S = MeCN, H_2O) and $\{[NiL(S)_2][PF_6]_2\}_n$ (L = **4**, **5**, S = MeCN, H_2O). Mass spectrometry only provided evidence for the formation of mononuclear complexes in each case (see Section 2), although the complexes containing acetate gave ions $\{NiL(OAc)(PF_6)\}^+$ and $\{[NiL(OAc)\}^+$, thereby providing evidence for coordination of the carboxylate. The ^1H NMR spectra of acetone solutions of the complex were very broad, with paramagnetically shifted resonances observed between δ 10 and 100. It has not been possible to assign these spectra fully, but they are consistent with the formation of a single, symmetrical, solution species. Cyclic voltammetry of MeCN solutions of the complexes revealed no nickel(II/III) redox processes, but in each case two-ligand-centred reduction was observed at ≈ -1.60 and -1.85 V. IR spectroscopy did not provide unambiguous data regarding the coordination mode of the carboxylate in the complexes containing acetate. The mass-spectrometric data suggest that the substituted quaterpyridine ligands form mononuclear complexes similar to those formed with quaterpyridine itself. In order to confirm this and to establish the nature of the acetate in these complexes, we determined the solid-state structures of $[Ni(\mathbf{4})(MeCN)_2][PF_6]_2$ and $[Ni(\mathbf{3})(OAc)(MeOH)][PF_6]\cdot 2MeOH\cdot H_2O$.

3.3.2. Crystal structures of $[Ni(\mathbf{4})(MeCN)_2][PF_6]_2$ and $[Ni(\mathbf{3})(OAc)(MeOH)][PF_6]\cdot 2MeOH\cdot H_2O$

The crystal structures of $[Ni(\mathbf{4})(MeCN)_2][PF_6]_2$ and $[Ni(\mathbf{3})(OAc)(MeOH)][PF_6]\cdot 2MeOH\cdot H_2O$ were determined; the relevant data are presented in Tables 1 and 2. The crystal structure of $[Ni(\mathbf{4})(MeCN)_2][PF_6]_2$ (**15**) revealed a mononuclear complex with a pseudo-octahedral cation containing an equatorial **4** ligand and two axial acetonitrile ligands (Fig. 2), closely resembling that in $[Ni(qtpy)(MeCN)_2]^{2+}$ [7,11]. The quaterpyridine is near planar with interplanar angles of 1.9°, 4.7° and 2.6° between the pyridine rings. The aryl substituents are twisted out of the plane of the ligand, one by 21.7° and the other by 35.1°. Nickel(II) is slightly too small to fit in the ligand cavity and the pyridine rings flex inwards towards the metal ion, resulting in small distortions quantified by the bite angles: ∠N(1)–Ni(1)–N(2), 76.4(4)°; N(2)–Ni(1)–N(3), 79.7(4)°; ∠N(3)–Ni(1)–N(4), 76.3(4)°. As expected, the metal–ligand bond lengths to the central pyridyl rings are longer than those to the terminal rings: $Ni–N_{terminal}$, 2.11(1), 2.091(9) Å; $Ni–N_{central}$, 1.982(9), 2.06(1) Å. The axial ligands are close to ideally located: ∠N(5)–Ni(1)–N(6), 174.5(4)°. There are no short contacts between the cations and anions in the lattice.

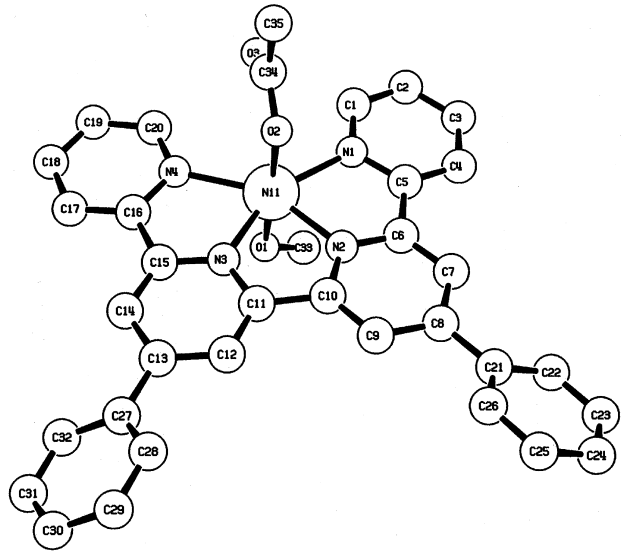


Fig. 3. Molecular structure of the cation present in $[Ni(\mathbf{3})(OAc)(MeOH)][PF_6]\cdot 2MeOH\cdot H_2O$; hydrogen atoms have been omitted for clarity.

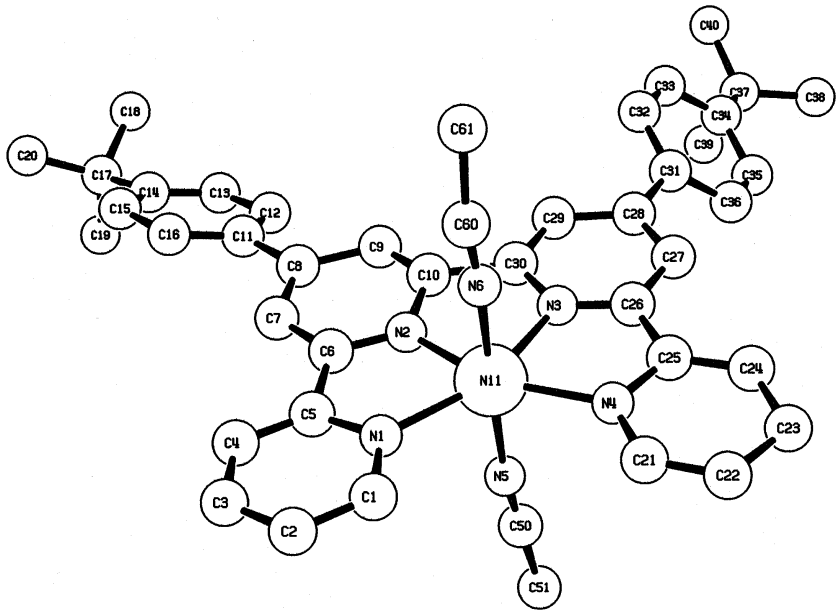


Fig. 2. Molecular structure of the cation present in $[Ni(\mathbf{4})(MeCN)_2][PF_6]_2$; hydrogen atoms have been omitted for clarity.

Analysis of the crystal structure also revealed [Ni(**3**)(OAc)(MeOH)][PF_6] (**16**) contains a mononuclear cation, with an equatorial **3** ligand and axial MeOH and monodentate acetate ligands (Fig. 3). The quaterpyridine is near planar (interplanar angles between pyridine rings of 5.3°, 1.2° and 3.6°), but the phenyl substituents are twisted out of this plane, one by 23.7° and the other by 27.2°. Bond lengths and angles involving the nickel and the quaterpyridine ligand resemble those for **15** (Table 2). The axial ligands are again near-ideally located: ∠O(1)–Ni(1)–O(2), 176.4(2)°. The acetate is monodentate (Ni(1)···O(3), 3.004 Å), with the non-coordinated oxygen lying in the void between the two terminals rings of the quaterpyridine ligand. Consequently, there are two short (2.642, 2.606 Å) contacts between the carboxylate O(3) and the H^6 protons of the terminal rings (Fig. 4). There are no other short contacts between the cations and anions in the lattice. To conclude, in the two structures discussed, the quaterpyridines behave as tetradentate ligands occupying the equatorial sites in near-octahedral cations.

3.3.3. Cobalt(II) complexes

The reaction of **3**–**7** with an equimolar amount of cobalt(II) acetate in MeOH or EtOH gave orange solutions from which orange salts were obtained upon the addition of [NH_4][PF_6]. In general, the isolated complexes closely resembled those with nickel(II), and microanalysis indicated complexes with a 1:1 M:L stoichiometry with additional ligands or anions present. Once again, acetate was present in many of the isolated complexes. On standing in air, some of the complexes decomposed to give green powders.

Mass spectrometry indicated only the formation of mononuclear complexes (see Section 2). We have shown that ^{1}H NMR spectroscopy is a powerful technique for the study of paramagnetic cobalt(II) complexes [47] and, in each case, shifted resonances were observed in the range −20 to 170 ppm. A typical example is seen for the complex [Co(**3**)(OAc)(H_2O)][PF_6], which in CD_3CN solution exhibits ten resonances at δ 6, 9, 12, 22, 32, 40, 50, 71, 72, 159. The resonance at δ 6 is tentatively assigned to the acetate group on the basis of signal intensity. Cyclic voltammetry of MeCN solutions of the complexes showed no cobalt(II/III) redox processes, but ligand-centred reduction was observed at ≈ −1.60 and −1.85 V. The data suggest that the substituted ligands form mononuclear cobalt(II) complexes similar to those formed with nickel(II). In order to confirm this we have determined the solid-state structure of [Co(**3**)(OAc)(MeCN)][PF_6]·1.64MeCN·0.36H_2O.

*3.3.4. Crystal structure of [Co(**3**)(OAc)(MeCN)][PF_6]·1.64MeCN·0.36H_2O (**17**)*

Recrystallization of [Co(**3**)(OAc)(H_2O)][PF_6] from MeCN gave orange crystals of [Co(**3**)(OAc)(MeCN)][PF_6]·1.64MeCN·0.36H_2O. Severe problems were encountered in the refinement of this structure as a result of extensive disorder of the lattice solvent molecules; data are presented in Tables 1 and 2. Discussion centres upon the mononuclear [Co(**3**)(OAc)(MeCN)]$^+$ cation, the structure of which is presented in Fig. 5. The cation is best described as seven-coordinate and contains an equatorial **3** ligand, an axial MeCN and an axial chelating but asymmetric didentate acetate ligand. The quaterpyridine is essentially planar (interplanar angles 2.5°, 0.2°, 0.4°) with the phenyl substituents twisted out of the plane by 10.1° and 26.9°. The metal–ligand bond lengths to the central pyridyl rings are longer than those to the terminal rings. The major difference from the cation in **16** arises in the bonding mode of the acetate. In the the nickel(II) complex, the acetate is essentially monodentate, with the non-bonded contact Ni(1)…O(3) greater than 3 Å; in complex **17**, the two Co…= distances are similar (2.171(4) and 2.293(3) Å), with the shorter contact being to the 'axial' position and the longer to the oxygen bent into the void between the terminal pyridine rings. Once again, ≈2.5 Å contacts between O(2) and the pyridine H^6 protons are observed.

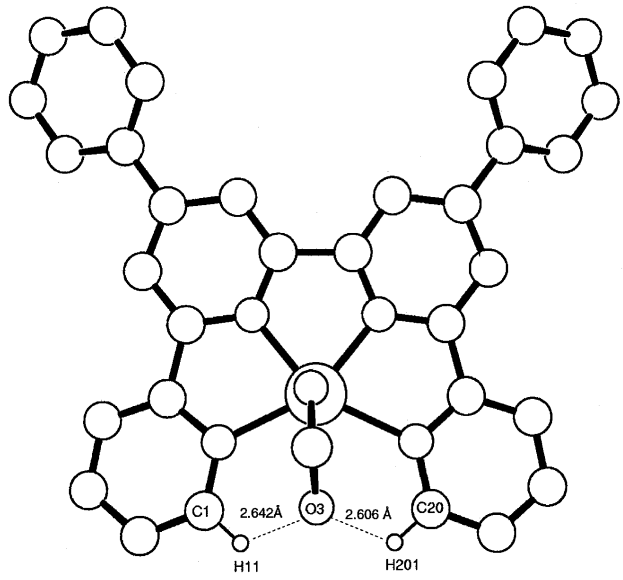


Fig. 4. A view of the cation present in [Ni(**3**)(OAc)(MeOH)][PF_6]·2MeOH·H_2O, showing the contacts between the acetate and pyridine H^6; all hydrogen atoms except H(11) and H(201) have been omitted for clarity, as have the methanol ligand and the acetate methyl group.

4. Conclusions

A series of 2,2′:6′,2″:6″,2‴-quaterpyridine ligands bearing substituents in the 4′- and 4″-positions have been prepared and their coordination chemistry has been investigated. Incorporation of the substituents does not change the basic patterns of reactivity: with silver(I) and copper(I), dinuclear double helicates are formed, whereas, with cobalt(II) and nickel(II), a variety of mononuclear structures are formed.

Supplementary data

Supplementary data are available, upon request, from the CCDC, 12 Union Road, Cambridge CB2 1EZ, UK, quoting the deposition numbers 124959, 124960 and 124961.

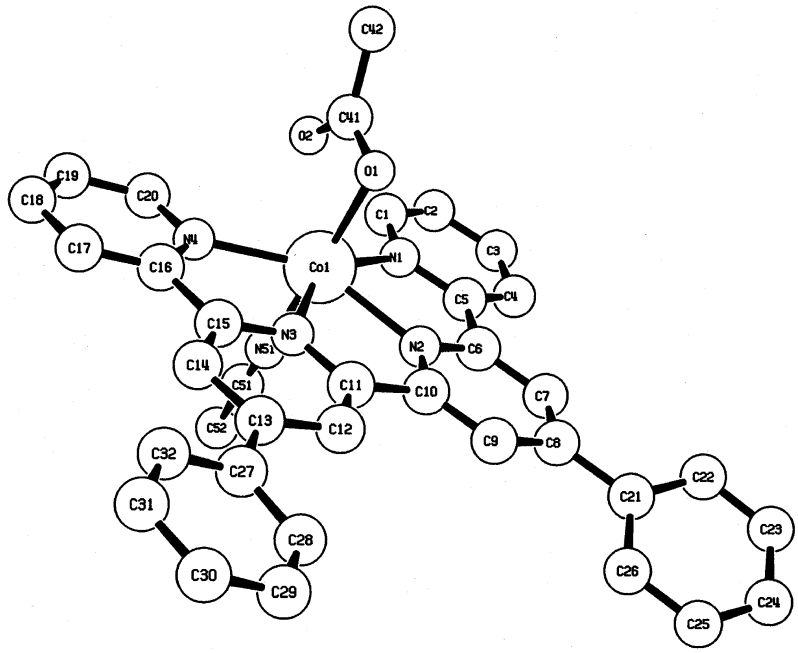


Fig. 5. Molecular structure of the cation present in $[Co(\mathbf{3})(OAc)(MeCN)][PF_6]\cdot 1.64MeCN\cdot 0.36H_2O$; hydrogen atoms have been omitted for clarity.

Acknowledgements

We gratefully acknowledge the Schweizerischer Nationalfonds zur Förderung der wissenenschaftlichen Forschung, the European Community (associated contract CEC ERBCHRXCT 940492/A2) and the University of Basel for financial support.

References

[1] E.C. Constable, Tetrahedron 48 (1992) 10013.
[2] E.C. Constable, Adv. Inorg. Chem. Radiochem. 30 (1987) 69.
[3] E.C. Constable, Progr. Inorg. Chem. 34 (1989) 1.
[4] E.C. Constable, in: J.L. Atwood, J.E.D. Davies, D.D. MacNicol, F. Vögtle (Eds.), Comprehensive Supramolecular Chemistry, vol. 9, Pergamon Press, Oxford, 1996, p. 213 and references therein.
[5] C. Piguet, G. Bernardinelli, G. Hopfgartner, Chem. Rev. 97 (1997) 2005.
[6] E.C. Constable, D.R. Smith, The Polymeric Materials Encyclopedia, CRC Press, Boca Raton, 1996, p. 4237.
[7] E.C. Constable, S.M. Elder, J.A. Healy, D.A. Tocher, J. Chem. Soc., Dalton Trans. (1990) 1669.
[8] E.C. Constable, S.M. Elder, D.A. Tocher, Polyhedron 11 (1992) 1337.
[9] E.C. Constable, M.J. Hannon, A. Martin, P.R. Raithby, D.A. Tocher, Polyhedron 11 (1992) 2967.
[10] E.C. Constable, S.M. Elder, D.A. Tocher, Polyhedron 11 (1992) 2599.
[11] E.C. Constable, S.M. Elder, M.J. Hannon, A. Martin, P.R. Raithby, D.A. Tocher, J. Chem. Soc., Dalton Trans. (1996) 2423.
[12] E.C. Constable, F.R. Heirtzler, M. Neuburger, M. Zehnder, J. Am. Chem. Soc. 119 (1997) 5606.
[13] G. Baum, E.C. Constable, D. Fenske, T. Kulke, Chem. Commun. (1997) 2043.
[14] E.C. Constable, S.M. Elder, J.A. Healy, M.D. Ward, D.A. Tocher, J. Am. Chem. Soc. 112 (1990) 4590.
[15] E.C. Constable, F.R. Heirtzler, M. Neuburger, M. Zehnder, Supramol. Chem. 5 (1995) 197.
[16] G. Baum, E.C. Constable, D. Fenske, C.E. Housecroft, T. Kulke, Chem. Commun. (1999) 195.
[17] G. Baum, E.C. Constable, D. Fenske, C.E. Housecroft, T. Kulke, Chem. Eur. J. 5 (1999) 1862.
[18] C.-M. Che, C.-W. Chan, S.-M. Yang, C.-X. Guo, C.-Y. Lee, S.-M. Peng, J. Chem. Soc., Dalton Trans. (1995) 2961.
[19] C.W. Chan, T.F. Lai, C.M. Che, J. Chem. Soc., Dalton Trans. (1994) 895.
[20] S.M. Yang, K.K. Cheung, C.M. Che, J. Chem. Soc., Dalton Trans. (1993) 3515.
[21] C.-W. Chan, C.-M. Che, M.-C. Cheng, Y. Wang, Inorg. Chem. 31 (1992) 4874.
[22] K.T. Potts, M. Keshavarz-K, F.S. Tham, H.D. Abruna, C.R. Arana, Inorg. Chem. 32 (1993) 4422.
[23] J.-M. Lehn, J.-P. Sauvage, J. Simon, R. Ziessel, C. Piccinni-Leopardi, G. Germain, J.-P. Declercq, M. Van Meerssche, Nouv. J. Chim. 7 (1983) 413.
[24] J.-P. Gisselbrecht, M. Gross, J.-M. Lehn, J.-P. Sauvage, R. Ziessel, C. Piccinni-Leopardi, J.M. Arrieta, G. Germain, M. Van Meerssche, Nouv. J. Chim. 8 (1984) 661.
[25] F. Arnaud-Neu, M. Sanchez, M.-J. Schwing-Weill, New J. Chem. 10 (1986) 165.
[26] K.N. Lam, K.Y. Wong, S.M. Yang, C.M. Che, J. Chem. Soc., Dalton Trans. (1995) 1103.
[27] A. Juris, R. Ziessel, Inorg. Chim. Acta 225 (1994) 251.
[28] F.H. Burstall, J. Chem. Soc. (1928) 1662.
[29] E.N. Maslen, C.L. Raston, A.H. White, J. Chem. Soc., Dalton Trans. (1975) 323.
[30] W. Von Henke, S. Kremer, D. Reinen, Z. Anorg. Allg. Chem. 491 (1982) 124.
[31] C.-W. Chan, C.-M. Che, S.-M. Peng, Polyhedron 12 (1993) 2169.
[32] C.-M. Che, Y.-P. Wang, K.-S. Yeung, K.-Y. Wong, S.-M. Peng, J. Chem. Soc., Dalton Trans. (1992) 2675.
[33] F. Calderazzo, L. Labella, F. Marchetti, J. Chem. Soc., Dalton Trans. (1998) 1485.
[34] E.C. Constable, T. Kulke, G. Baum, D. Fenske, Inorg. Chem. Commun. 1 (1998) 80.
[35] S.-M. Yang, K.-K. Cheung, C.-M. Che, J. Chem. Soc., Dalton Trans. (1993) 3515.
[36] E.C. Constable, Chem. Commun. (1997) 1073 and references therein.
[37] E.C. Constable, P. Harverson, Polyhedron (in press).

[38] F. Kröhnke, Synthesis (1976) 1.
[39] E.C. Constable, M.J. Hannon, D.R. Smith, Tetrahedron Lett. 35 (1994) 6657.
[40] N.A. Sorenson, E. Samuelsen, F.R. Oxaal, Acta Chem. Scand. 1 (1947) 458.
[41] E.C. Constable, T. Kulke, M. Neuburger, M. Zehnder, New J. Chem. 21 (1997) 633.
[42] A. Altomare, G. Cascarano, G. Giacovazzo, A. Guagliardi, M.C. Burla, G. Polidori, M. Camalli, J. Appl. Crystallogr. 27 (1994) 435.
[43] D.J. Watkin, J.R. Carruthers, P. Betteridge, CRYSTALS, Chemical Crystallography Laboratory, Oxford, 1985.
[44] J.R. Carruthers, D.J. Watkin, Acta Crystallogr., Sect. A 35 (1979) 698.
[45] N. Walker, D. Stuart, Acta Crystallogr., Sect. A 39 (1983) 158.
[46] E.C. Constable, P. Harverson, unpublished results.
[47] E.C. Constable, T. Kulke, M. Neuburger, M. Zehnder, New J. Chem. 21 (1997) 1091.

PERGAMON

www.elsevier.nl/locate/poly

Polyhedron 19 (2000) 35–42

POLYHEDRON

Group 4 and 5 metal derivatives of 2,2′-methylene-bis(6-phenylphenoxide)

Douglas R. Mulford, Phillip E. Fanwick, Ian P. Rothwell *

Department of Chemistry, 1393 Brown Building, Purdue University, West Lafayette, IN 47907, USA

Received 21 June 1999; accepted 29 September 1999

Abstract

Addition of the phenol 2,2′-methylene-bis(6-phenylphenol) [$(HOC_6H_3Ph)_2CH_2$] (**1**) (1 equiv. per Ti) to hydrocarbon solutions of [$TiCl_4$] or [$Ti(OPr^i)_4$] leads to dimeric products [$Ti\{(OC_6H_3Ph)_2CH_2\}Cl_2]_2$ (**2**) and [$Ti\{(OC_6H_3Ph)_2CH_2\}(\mu\text{-}OPr^i)(OPr^i)]_2$ (**3**). Structural studies show **2** ($CHCl_3$ solvate) to consist in the solid state of two tetrahedral titanium centers linked by one end of two di-aryloxide ligands. In contrast, **3** contains five-coordinate titanium atoms linked directly by two bridging isopropoxide ligands. Treatment of [MCl_5] (M = Nb, Ta) with 1 equiv. of **1** leads to sparingly soluble trichlorides **4** and **5** which react with pyridine to form soluble adducts [$M\{(OC_6H_3Ph)_2CH_2\}Cl_3(py)$] (M = Nb, **6**; M = Ta, **7**). Compounds **6** and **7** are isostructural in the solid state (benzene solvates) with a *mer* arrangement of chloride groups and the pyridine *trans* to one of the di-aryloxide oxygen atoms. Treatment of **7** with PMe_2Ph leads to the products [$Ta\{(OC_6H_3Ph)_2CH_2\}Cl_3(PMe_2Ph)$] (**8**) and [$HPMe_2Ph$][$Ta\{(OC_6H_3Ph)_2CH_2\}Cl_4$] (**9**). Structurally characterized **9** (benzene solvate) presumably arises via the presence of trace amounts of water during workup. Reaction of **1** with [$Ta(NMe_2)_5$] allows isolation of derivatives [$Ta\{(OC_6H_3Ph)_2CH_2\}_2(NMe_2)(HNMe_2)$] (**10**) (*cis*-nitrogen atoms by NMR) and [H_2NMe_2][$Ta\{(OC_6H_3Ph)_2CH_2\}_3$] (**11**) depending on the stoichiometry. The anion in **11** was shown by crystallography to contain an octahedral arrangement of oxygen atoms about the tantalum metal center. The crystallographic study of **11** is complicated by a disorder of the cation and partial occupancies for the three types of benzene solvate molecule. The niobium trichloride **4** acts as a catalyst precursor for benzene hydrogenation although with lower activity than reported for monodentate aryloxide precursors. During the catalysis the *ortho*-phenyl rings of the di-aryloxide ligand are not hydrogenated. ©2000 Elsevier Science Ltd All rights reserved.

Keywords: Titanium; Tantalum; Nobium; Aryloxide; Bisphenol; Hydrogenation

1. Introduction

There has recently been increased interest in the chemistry of 2,6-di-aryl-phenoxide ligation attached to early d-block metal centers [1–8]. Part of this work has been stimulated by the demonstrated ability of niobium and tantalum hydride compounds containing aryloxide ligation to catalyze the hydrogenation of a variety of arene substrates [9]. In the case of 2,6-diphenylphenoxide ligands, both partial and total intramolecular hydrogenation of *ortho*-phenyl rings has been observed [10,11]. As an extension of this research we have examined the early d-block metal chemistry of the chelating ligand 2,2′-methylene-bis(6-phenylphenol) [$(HOC_6H_3Ph)_2CH_2$] (**1**) [12]. This paper reports the synthesis and characterization of Group 4 and 5 metal derivatives of this ligand as well as an evaluation of the hydrogenation activity of niobium and tantalum catalyst precursors.

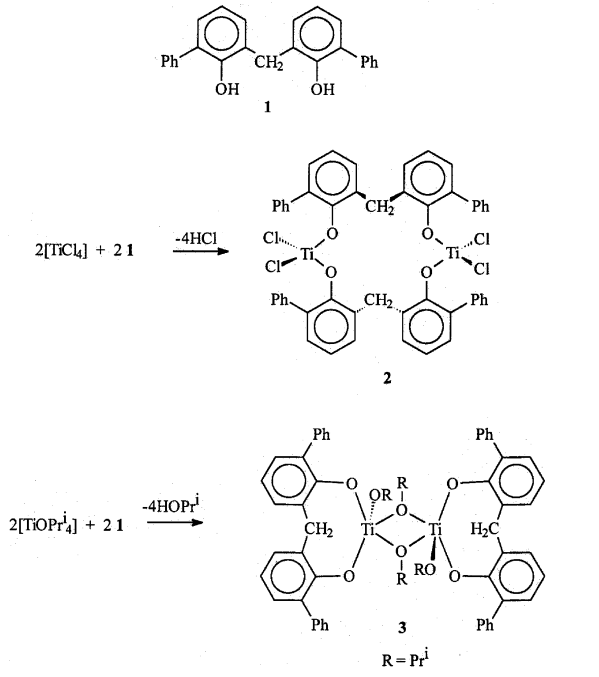
* Corresponding author. Tel.: +1-765-494-7012; fax: +1-765-494-0239; e-mail: rothwell@chem.purdue.edu

2. Results and discussion

2.1. Synthesis and spectroscopy of compounds

The addition of the parent phenol 2,2′-methylene-bis(6-phenylphenol) ($(HOC_6H_3Ph)_2CH_2$ **1**) (1 equiv. per Ti) to hydrocarbon solutions of [$TiCl_4$] or [$Ti(OPr^i)_4$] leads to formation of the corresponding mono(di-aryloxide) compounds **2** and **3** respectively (Scheme 1). The di-chloride **2** is only sparingly soluble and hence purification was difficult. The ^1H NMR spectrum of **2** in C_6D_6 is not very informative, showing, in addition to the aromatic resonances, a single pair of doublets for the methylene protons CH_2 of the ligand. Previous work on 2,2′-methylene-bisphenoxides [13–17] has shown that the puckered eight-membered ring formed by chelation to metal centers undergoes slow flipping on the NMR timescale. Hence the methylene protons in the chelate backbone are typically diastereotopic at ambient temperatures. The ^1H NMR spectral data for **3** are equally uniform-

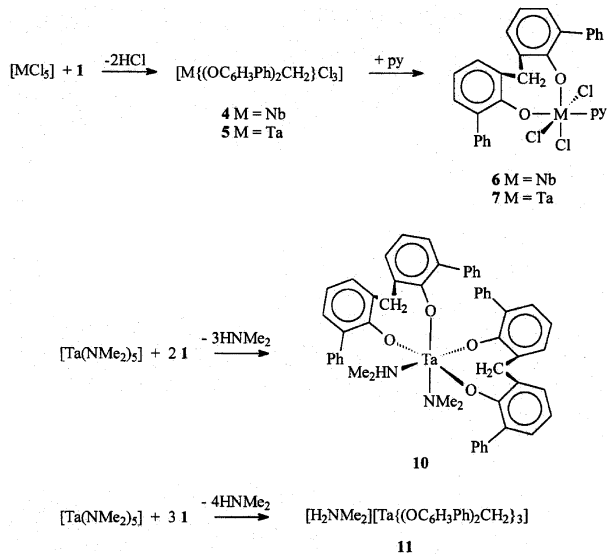
0277-5387/00/$ - see front matter ©2000 Elsevier Science Ltd All rights reserved.
PII S0277-5387(99)00319-8



Scheme 1.

ative, simply showing broad resonances for the di-aryloxide ligands and OPr^i groups.

The reaction of **1** with the chlorides $[M_2Cl_{10}]$ (M = Nb, Ta) produces sparingly soluble trichlorides $[M_2\{(OC_6H_3Ph)_2CH_2\}Cl_3]$ (M = Nb, **4**; M = Ta, **5**) (Scheme 2). Previous work with monodentate aryloxides has shown that for bulky ligands square pyramidal structures are formed for trichlorides $[M(OAr)_2Cl_3]$ (M = Nb, Ta; OAr = $OC_6H_3Bu^t_2$-2,6, various 2,6-diphenylphenoxides) with an axial aryloxide [18,19]. With a slightly smaller aryloxide a dimeric structure $[(ArO)_2Cl_2Ta(\mu\text{-}Cl)]_2$ is formed, where the 2,6-di-isopropylphenoxide ligands are *trans* to the bridging chloride groups [20]. Previously the compound $[Nb\{(OC_6H_2Bu^t_2\text{-}4,6)_2CH_2\}_2Cl]$ has been reported and shown to adopt a tbp structure with an equatorial cloride [17].



Scheme 2.

In the case of **4** and **5**, the bidentate aryloxide is probably not sufficiently bulky to generate a monomeric environment. A dimeric structure in hydrocarbon solvents is consistent with the low solubility, but whether there are chloride or aryloxide bridges is unknown. The addition of the donor ligand pyridine leads to much more soluble adducts $[M\{(OC_6H_3Ph)_2CH_2\}Cl_3(py)]$ (M = Nb, **6**; M = Ta, **7**, Scheme 2). In the ^1H NMR spectra of **6** and **7** (Fig. 1), well resolved sharp multiplets are observed. The diastereotopic methylene protons in the chelate ring are separated by over 2 ppm. The solid state structure (vide infra) would lead to a virtual plane of symmetry in the molecule if the eight-membered chelate were undergoing rapid flipping. The sharp AX pattern observed for the methylene group of **6** and **7** shows that inversion is much slower than the NMR timescale. A similar phosphine adduct of **7** is generated by addition of PMe_2Ph. In this case the resulting product **8** shows broad ligand resonances consistent with partial ligand dissociation in solution. During the workup of **8**, a few well-formed crystals of a salt identified as $[HPMe_2Ph][Ta\{(OC_6H_3Ph)_2CH_2\}Cl_4]$ (**9**) were obtained. It is believed that adventitious amounts of water led to the formation of **9** which has the elements of HCl added to **8**.

The addition of **1** to $[Ta(NMe_2)_5]$ is found to lead to a mixture of substitution products (serious safety concerns have been raised with respect to the original procedure [21], for the synthesis of $[Ta(NMe_2)_5]$, see [22]). With 2 equiv. of **1**, a six-coordinate dimethylamine adduct is produced of formula $[Ta\{(OC_6H_3Ph)_2CH_2\}_2(NMe_2)(HNMe_2)]$ (**10**) (Scheme 2). In the ^1H NMR spectrum of **10** two diastereotopic methylene groups CH_2 indicate non-equivalence of the two di-aryloxide ligands. The spectrum also shows a pair of broad doublets at δ 1.73 and 0.87 ppm. These we assign to the diastereotopic HN*Me*$_2$ methyl groups shifted upfield of their normal position by the anisotropy of adjacent phenyl groups of the aryloxides. Two geometries are possible for six-coordinate **10** (Scheme 2). In one the amine is located *trans* to the amido nitrogen while in the second these groups are mutually *cis*. The assigned *cis*-geometry (Scheme 2) automatically gives rise to non-equivalent di-aryloxide groups as well as diastereotopic HN*Me*$_2$ methyl groups. Even if the di-aryloxide rings in the *trans* geometry fold so as to become non-equivalent, they will still maintain a plane of symmetry through the Ta-HNMe$_2$ group. The reaction of $[Ta(NMe_2)_5]$ with the bulkier ligand 2,2′-methylene-bis(6-tert-butyl-4-methylphenoxide) has been shown to produe $[Ta\{(OC_6H_2Bu^t\text{-}6\text{-}Me\text{-}4)_2CH_2\}(NMe_2)_3]$ with one amide and di-aryloxide oxygen atom *trans* within a tbp structure [16]. When more than 2 equiv. of **1** are reacted with $[Ta(NMe_2)_5]$, a mixture (NMR) is produced from which a sparingly soluble product **11** precipitates. This compound was identified by crystallographic methods as a salt, $[H_2NMe_2][Ta\{(OC_6H_3Ph)_2CH_2\}_3]$ (**11**). Disorder of the cation and the presence of three benzene molecules of solvate complicated solution of the crystal structure of **11**. Two of the benzene molecules had partial occupancies of 0.59 and

0.72, respectively, possibly due to loss of solvent from the unit cell. However, the anion clearly contains a tantalum metal center chelated by three di-aryloxide ligands (vide infra).

2.2. Structural studies

The solid-state structures of **2**, **6**, **7**, **9** and **11** were determined (Tables 1–5, Figs. 2–6). All five compounds formed crystals containing solvent molecules within the unit cell. In the case of **2**, two molecules of chloroform per di-titanium unit were present while the other four compounds contained varying amounts of benzene of solvation. Previous work on the bulky ligand 2,2′-methylene-bis(6-tert-butyl-4-methylphenol) ($(HOC_6H_2Bu^t\text{-}6\text{-}Me\text{-}4)_2CH_2$) has led to the isolation of a series of monomeric species $[Ti\{(OC_6H_2Bu^t\text{-}6\text{-}Me\text{-}4)_2CH_2\}X_2]$ (X = Cl, OR, R) [13].

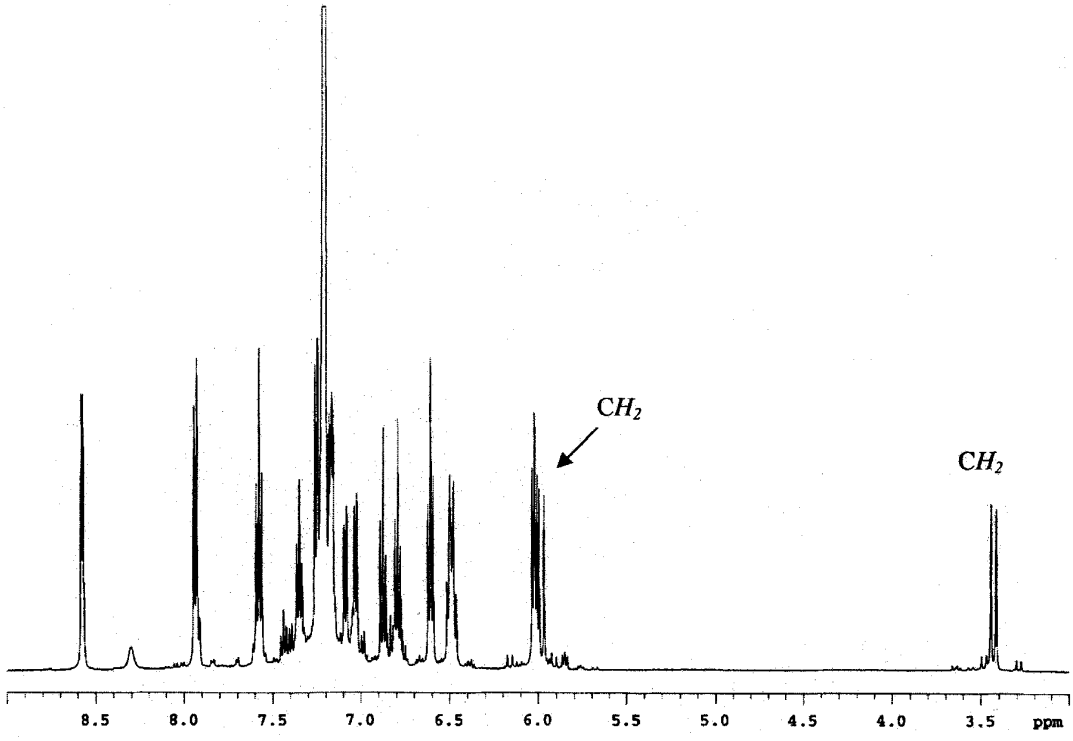


Fig. 1. ^1H NMR (C_6D_6, 500 MHz) of $[Nb\{(OC_6H_3Ph)_2CH_2\}Cl_3(py)]$ (**6**).

Structural studies show a pseudo-tetrahedral geometry about Ti with O–Ti–O angles of 106.5(2)° (X = Cl) and 112.7(2)° (X = Me). In the case of the dichloride a five-coordinate thf adduct was also isolated and structurally characterized as

Table 1
Selected bond distances (Å) and angles (°) for $[Ti\{(OC_6H_3Ph)_2CH_2\}Cl_2]_2\cdot 2CHCl_3$ (**2**)

Ti–O(10)	1.746(5)	Ti–Cl(1)	2.216(3)
Ti–O(20)	1.754(5)	Ti–Cl(2)	2.219(3)
O(10)–Ti–O(20)	111.7(2)	Cl(1)–Ti–Cl(2)	105.9(1)
O(10)–Ti–Cl(1)	110.0(2)	C(11)–O(10)–Ti	161.9(5)
O(10)–Ti–Cl(2)	111.1(2)	C(21)–O(20)–Ti	168.2(5)
O(20)–Ti–Cl(1)	109.4(2)	O(20)–Ti–Cl(2)	108.6(2)

Table 2
Selected bond distances (Å) and angles (°) for $[Nb\{(OC_6H_3Ph)_2CH_2\}Cl_3(py)]\cdot 1/2C_6H_6$ (**6**)

Nb–O(2)	1.867(2)	Nb–Cl(1)	2.371(1)
Nb–O(1)	1.863(2)	Nb–Cl(2)	2.377(1)
Nb–N	2.329(3)	Nb–Cl(3)	2.383(1)
O(1)–Nb–O(2)	93.0(1)	O(2)–Nb–Cl(3)	93.14(9)
O(1)–Nb–N	174.2(1)	N–Nb–Cl(1)	86.62(9)
O(1)–Nb–Cl(1)	99.06(9)	N–Nb–Cl(2)	85.39(8)
O(1)–Nb–Cl(2)	93.80(8)	N–Nb–Cl(3)	82.84(9)
O(1)–Nb–Cl(3)	91.45(8)	Cl(1)–Nb–Cl(2)	87.26(5)
O(2)–Nb–N	88.1(1)	Cl(1)–Nb–Cl(3)	91.45(3)
O(2)–Nb–Cl(1)	88.69(8)	Cl(2)–Nb–Cl(3)	89.81(4)
O(2)–Nb–Cl(2)	172.53(9)	Nb–O(1)–C(1)	141.5(2)
Nb–O(2)–C(13)	161.6(2)		

Table 3
Selected bond distances (Å) and angles (°) for $[Ta\{(OC_6H_3Ph)_2CH_2\}Cl_3(py)]\cdot 1/2C_6H_6$ (**7**)

Ta–O(2)	1.865(2)	Ta–Cl(1)	2.360(1)
Ta–O(1)	1.871(2)	Ta–Cl(2)	2.376(1)
Ta–N	2.311(3)	Ta–Cl(3)	2.368(1)
O(1)–Ta–O(2)	93.8(1)	O(2)–Ta–Cl(3)	91.57(9)
O(1)–Ta–N	88.1(1)	N–Ta–Cl(1)	86.40(9)
O(1)–Ta–Cl(1)	89.21(9)	N–Ta–Cl(2)	85.15(9)
O(1)–Ta–Cl(2)	172.60(8)	N–Ta–Cl(3)	83.4(1)
O(1)–Ta–Cl(3)	92.48(8)	Cl(1)–Ta–Cl(2)	87.38(5)
O(2)–Ta–N	174.7(1)	Cl(1)–Ta–Cl(3)	169.63(3)
O(2)–Ta–Cl(1)	98.53(9)	Cl(2)–Ta–Cl(3)	89.73(5)
O(2)–Ta–Cl(2)	93.20(9)	Ta–O(1)–C(1)	161.5(2)
Ta–O(2)–C(13)	139.9(2)		

Table 4
Selected bond distances (Å) and angles (°) for $[HPMe_2Ph][Ta\{(OC_6H_3Ph)_2CH_2\}Cl_4]\cdot C_6H_6$ (**9**)

Ta–Cl(1)	2.384(1)	Ta–Cl(4)	2.422(1)
Ta–Cl(2)	2.416(1)	Ta–O(1)	1.851(3)
Ta–Cl(3)	2.400(1)	Ta–O(9)	1.892(3)
O(1)–Ta–O(9)	91.5(1)	O(9)–Ta–Cl(4)	174.5(1)
O(1)–Ta–Cl(1)	92.0(1)	Cl(1)–Ta–Cl(2)	90.8(5)
O(1)–Ta–Cl(2)	177.1(1)	Cl(1)–Ta–Cl(3)	176.5(1)
O(1)–Ta–Cl(3)	89.7(1)	Cl(1)–Ta–Cl(4)	92.7(1)
O(1)–Ta–Cl(4)	92.8(1)	Cl(2)–Ta–Cl(3)	87.5(1)
O(9)–Ta–Cl(1)	88.7(1)	Cl(2)–Ta–Cl(4)	87.8(1)
O(9)–Ta–Cl(2)	88.1(1)	Cl(3)–Ta–Cl(4)	89.3(1)
O(9)–Ta–Cl(3)	94.2(1)		

Table 5
Selected bond distances (Å) and angles (°) for $[H_2NMe_2][Ta\{(OC_6H_3Ph)_2CH_2\}_3]\cdot 2.31C_6H_6$ (**11**)

Ta–O(11)	1.939(5)	Ta–O(22)	1.973(9)
Ta–O(12)	1.941(5)	Ta–O(31)	2.014(9)
Ta–O(21)	1.938(5)	Ta–O(32)	1.96(1)
O(11)–Ta–O(12)	92.7(2)	O(12)–Ta–O(32)	90.8(2)
O(21)–Ta–O(22)	93.8(2)	O(22)–Ta–O(31)	90.7(2)
O(31)–Ta–O(32)	89.8(2)	O(11)–Ta–O(21)	176.1(2)
O(12)–Ta–O(22)	88.8(2)	O(12)–Ta–O(31)	178.8(2)
O(21)–Ta–O(31)	87.9(2)	O(22)–Ta–O(32)	176.0(2)
O(11)–Ta–O(32)	88.7(2)		

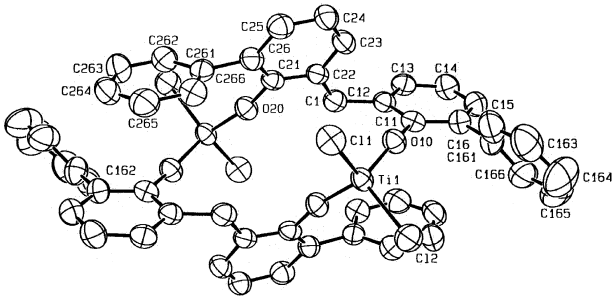


Fig. 2. Molecular structure of $[Ti\{(OC_6H_3Ph)_2CH_2\}Cl_2]_2\cdot 2CHCl_3$ (**2**).

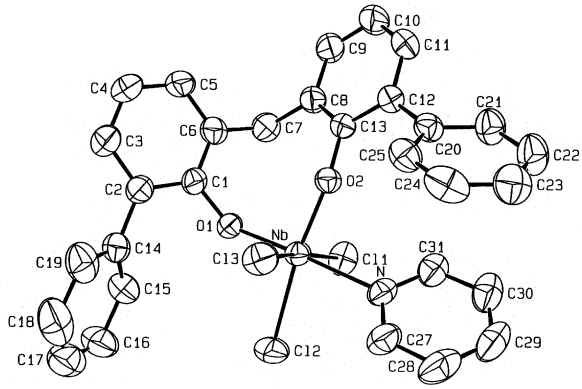


Fig. 3. Molecular structure of $[Nb\{(OC_6H_3Ph)_2CH_2\}Cl_3(py)]\cdot 1/2C_6H_6$ (**6**).

pseudo-trigonal bipyramidal about Ti with the thf axial and *trans* to one end of the chelating di-aryloxide [15]. The O–Ti–O angle of 96.2(1)° for the chelate shows the flexibility of the eight-membered ring in occupying coordination sites about the metal center. In contrast the dichloride **2** can be seen to adopt a dinuclear structure in the solid state (Fig. 2). Each Ti metal center is pseudo-tetrahedral and bound to one end of two di-aryloxides. The O–Ti–O angle is 111.7(2)°, only slightly larger than that found for $[Ti\{(OC_6H_2Bu^t\text{-}6\text{-}Me\text{-}4)_2CH_2\}Cl_2]$. The question arises as to what factors are important in determining whether a monomeric structure is formed or a dimeric unit as in **2**. The dimeric structure does

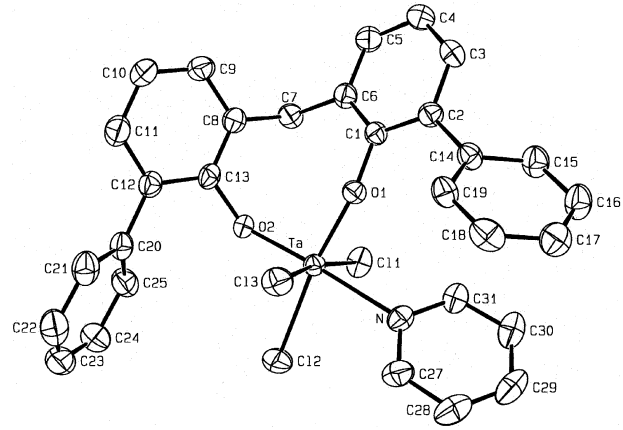


Fig. 4. Molecular structure of $[Ta\{(OC_6H_3Ph)_2CH_2\}Cl_3(py)]\cdot 1/2C_6H_6$ (**7**).

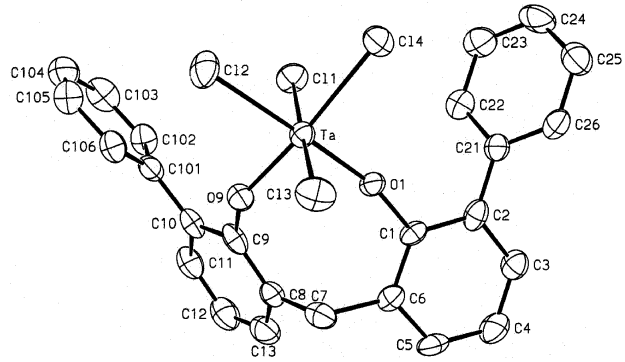


Fig. 5. Molecular structure of $[HPMe_2Ph][Ta\{(OC_6H_3Ph)_2CH_2\}Cl_4]\cdot C_6H_6$ (**9**).

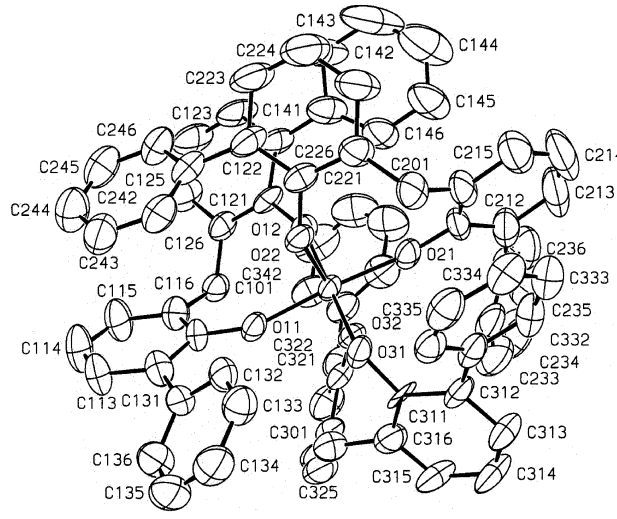


Fig. 6. Molecular structure of $[H_2NMe_2][Ta\{(OC_6H_3Ph)_2CH_2\}_3]\cdot C_6H_6$ (**11**).

not contain either chloro or oxygen bridges which might alleviate the electron deficiency of the metal center. It may very well be that the bulkier *ortho*-tert-butyl substituents preclude formation of a dimer. However, an electronic rationale for the dimeric structure is that it allows for larger Ti–O–Ar angles. In monomeric $[Ti\{(OC_6H_2Bu^t\text{-}6\text{-}Me\text{-}4)_2CH_2\}Cl_2]$ these angles are 143.6(4) and 155.8(4)° while in **2** they open up to 161.9(5) and 168.2(5)°. This could imply greater oxygen-p to metal-d π-bonding. However, the Ti–O distances in $[Ti\{(OC_6H_2Bu^t\text{-}6\text{-}Me\text{-}4)_2CH_2\}Cl_2]$, 1.760(4) and 1.742(4) Å, are essentially identical to values of 1.746(5) and 1.754(5) Å found for **2**. It is now well established that the degree of π-donation does not correlate with M–O–Ar angles for early d-block metal aryloxides [23,24]. It appears that a larger database of related compounds is needed to reach any conclusions concerning the relative stabilities of these two structural motifs. The formation of dimeric units has been enforced by use of fluorenediol ligation where the di-aryloxide structure precludes chelation [25].

A data set collected on the isopropoxide **3** indicates a dimeric structure in the solid state with terminal chelated di-aryloxide and bridging isopropoxides as shown in Scheme 1. Unfortunately the refinement could not be completed owing to disorder among the methyl units of the Pr^i groups [26]. It would appear in this case that the electron deficiency of the titanium atoms is relieved by the formation of alkoxide bridges leading to a pseudo square pyramidal geometry about each metal center.

Both of the pyridine adducts **6** and **7** have been structurally characterized (Figs. 3 and 4). A large number of adducts $[M(OAr)_x(Cl)_{5-x}(L)]$ (M = Nb, Ta; OAr = various monodentate aryloxides; L = O, N or P donor ligands) have been reported [20]. Structural studies of the tri-chlorides ($x = 3$) show a *cis-mer* geometry with the donor ligand *trans* to one of the aryloxides. These molecules consistently show a distortion from octahedral geometry in which four of the anionic ligands are bent towards the *cis*-donor ligand. This distortion has been studied theoretically [20,27]. It can be seen that compounds **6** and **7** are related to the previously isolated monodentate aryloxide complexes. The chloride ligands are arranged in a *mer* fashion with the pyridine *trans* to one of the chelating aryloxide oxygen atoms. The O–M–O angles are 93–94°, again showing the flexibility of this ligand. The metal–ligand distances (Tables 2 and 3) are very similar to those reported for *cis-mer*-$[M(OC_6H_3Pr^i_2\text{-}2,6)_2Cl_3(py)]$ (M = Nb, Ta). In order to quantify the distortion from octahedral geometry in adducts of this type, the parameter $\Sigma\alpha$ defined as follows, $\Sigma\alpha = \Sigma[(cis\text{-L-M-X}) - 90]$, was introduced [20]. The value of $\Sigma\alpha$ is −17.6 and −17.0 for **6** and **7**, respectively. These values are slightly smaller than values of −23.5 and −22.6 found in *cis-mer*-$[M(OC_6H_3Pr^i_2\text{-}2,6)_2Cl_3(py)]$ (M = Nb, Ta) but still indicate a significant distortion from octahedral geometry.

The molecular structures of the anions in **9** and **11** (Figs. 5 and 6) are unexceptional. In both cases the geometry about the metal center is very close to octahedral. The O–Ta–O angle in **9** of 91.5(1)° accommodates the octahedral geometry very well. The bite of the three chelates in the anion of **11** scans the range 89.8(2)–93.8(2)°. Also in tris(chelate) **11** the folding of the chelate rings is such that there are two types of di-aryloxide. Unfortunately the lack of solubility of this compound precluded confirmation of this by NMR. The closest analog of **9** is the salt $[HPMe_2Ph][Nb(OC_6H_3Pr^i_2\text{-}2,6)_3Cl_3]$ formed as a minor product by addition of PMe_2Ph to $[Nb(OC_6H_3Pr^i_2\text{-}2,6)_2Cl_3]$ [20]. The anion in tris(chelate) **11** can be related to the hexa(aryloxide) anion $[Nb(OC_6H_3Me_2\text{-}3,5)_6]$ [28].

2.3. Reactivity studies

The potential of the trichloride compounds **4** and **5** as catalyst precursors for the hydrogenation of arene rings was evaluated. A sample of the trichloride (0.5 mmol) was placed in benzene and activated with a standardized solution of n-BuLi (3 equiv.). The resulting mixture (20 ml total volume) was pressurized with H_2 (1200 psi) and heated at 120°C for 24 h. The tantalum compound showed no detectable activity for benzene hydrogenation. However, the niobium precursor **4** did produce cyclohexane (80 equiv. per Nb). This compares with 240 equiv. previously reported to be produced by the precursor $[Nb(OC_6HPh_4\text{-}2,3,5,6)_2Cl_3]$ under the same conditions [9]. Under these conditions in the presence of 20 equiv. of PPh_3, compound **4** showed some conversion to $PCyPh_2$ and PCy_2Ph, but the activity was much lower than when the monodenate precursor $[Nb(OC_6HPh_4\text{-}2,3,5,6)_2Cl_3]$ was used. Analysis of these reaction mixtures after hydrolysis showed (NMR and GC) the presence of **1** with only very minor signals that may be attributable to cyclohexyl phenols. It therefore appears that the chelation of the di-aryloxide at niobium metal centers inhibits the intramolecular hydrogenation of the *ortho*-phenyl rings, a reaction that is facile for monodentate *ortho*-phenylphenoxides [10,11].

3. Experimental

3.1. General

All operations were carried out under a dry nitrogen atmosphere or in vacuo either in a Vacuum Atmosphere Dri-Lab or by standard Schlenk techniques. Hydrocarbon solvents were dried by distillation from sodium/benzophenone and stored under dry nitrogen. Reagents were purchased from Aldrich Chemical Co. and were dried over 3 Å molecular sieves prior to use. The ^1H NMR spectra were recorded on a Varian Associates Gemini 200 and a General Electric QE-300 spectrometer and were referenced using protio impurities of commercial benzene-d_6 as an internal standard. Microanalytical data were obtained in-house at Purdue. All high-pressure reactions were performed in a Parr model 4561, 300

ml internal volume minireactor. The X-ray diffraction studies were completed in-house at Purdue University.

3.2. Synthesis of compounds

3.2.1. [Ti{$(OC_6H_3Ph)_2CH_2$}Cl_2]$_2$ (2)

To a suspension of 2,2′-methylene-bis(6-phenylphenol) (4.23 g, 12.0 mmol) in benzene (100 ml) was added [$TiCl_4$] (2.0 g, 10.5 mmol) by standard Schlenk techniques under a dry N_2 atmosphere. The resulting red solution was stirred for 3 h before being dried in vacuo to produce a red solid which was washed twice with pentane to yield compound **2**. Yield 4.10 g (83.2%). *Anal.* Calc. for $TiCl_2O_2C_{25}H_{18}$: C, 63.99; H, 3.86; Cl, 15.11. Found: C, 62.41; H, 4.03; Cl, 15.31%. ^{1}H NMR ($CDCl_3$, 30°C): δ 7.16–7.56 (m, 16H, aromatics); 4.32 (d, 1H, CH_2); 3.92 (d, 1H, CH_2). Crystals suitable for X-ray diffraction were obtained from $CHCl_3$–pentane mixtures.

3.2.2. [Ti{$(OC_6H_3Ph)_2CH_2$}(μ-OPr^i)(OPr^i)]$_2$ (3)

A mixture of 2,2′-methylene-bis(6-phenylphenol) (24.6 g, 69.8 mmol) and [$Ti(OPr^i)_4$] (20.0 g, 70.4 mmol) in benzene (100 ml) was stirred for 1 h then dried in vacuo. The resulting red/orange solid was washed three times with hexane and recrystallized from toluene. The resulting orange plate-like crystals of **3** were dried in vacuo. Yield 13.85 g (38.1%). *Anal.* Calc. for $TiO_4C_{31}H_{32}$: C, 72.01; H, 6.24. Found: C, 72.17; H, 6.25%. ^{1}H NMR (C_6D_6, 30°C): δ 7.45 (d, 2H, aromatic); 7.09 (m, 12H, aromatic); 6.73 (t, 2H, aromatic); 4.35 (broad, 2H, C*H*Me_2); 4.19 (broad, 1H, CH_2); 3.45 (broad, 1H, CH_2); 0.85 (broad, 12H, CH*Me*$_2$).

3.2.3. [Nb{$(OC_6H_3Ph)_2CH_2$}Cl_3] (4)

A sample of 2,2′-methylene-bis(6-phenylphenol) (13.3 g, 37.76 mmol) was added to a solution of [$NbCl_5$] (10.2 g, 37.7 mmol) in benzene (100 ml) to give a red solution which was stirred for 5 h under a dry N_2 atmosphere. The resulting red/brown precipitate of **5** was dried in vacuo. Yield 17.5 g (84%). *Anal.* Calc. for $NbCl_3O_2C_{25}H_{18}$: C, 54.63; H, 3.30; Cl, 19.35. Found: C, 53.89; H, 3.40; Cl, 17.33%. ^{1}H NMR (C_6D_6, 30°C): δ 6.65–7.24 (m, 16H, aromatics); 3.10 (s, 2H, CH_2).

3.2.4. [Ta{$(OC_6H_3Ph)_2CH_2$}Cl_3] (5)

A sample of 2,2′-methylene-bis(6-phenylphenol) (1.02 g, 2.89 mmol) was added to a solution of [$TaCl_5$] (1.02 g, 2.87 mmol) in benzene (25 ml) to give a brown/red solution which was stirred for 1.5 h under a dry N_2 atmosphere. The resulting yellow/orange precipitate of **4** was dried in vacuo. Yield 1.47g (75%). *Anal.* Calc. for $TaCl_3O_2C_{25}H_{18}$: C, 47.10; H, 2.84; Cl, 16.68. Found: C, 47.10; H, 2.84; Cl, 14.59%. ^{1}H NMR (C_6D_6, 30°C): δ 6.65–7.44 (m, 16H, aromatics); 3.24 (s, 2H, CH_2).

3.2.5. [Nb{$(OC_6H_3Ph)_2CH_2$}Cl_3(py)] (6)

To a suspension of **4** (0.50 g, 0.91 mmol) in benzene was added pyridine (0.13 g 1.64 mmol, 1.80 equiv.) and the resulting solution was stirred for 1 day during which time the solution changed from brown to red. The solution was layered with pentane and the resulting solid **6** was washed once with pentane and dried in vacuo. Yield 0.48 g (83.0%). *Anal.* Calc. for $NbNO_2Cl_3C_{30}H_{23}\cdot 0.5C_6H_6$: C, 59.35; H, 3.92; N, 2.10; Cl, 15.92. Found: C, 58.82; H, 4.06; N, 2.14; Cl, 16.04%. ^{1}H NMR (C_6D_6, 30°C): δ 8.48 (d, aromatic); 7.83 (d, aromatic); 7.48 (t, aromatic); 7.16 (d, aromatic); 6.78 (t, aromatic); 6.70 (t, aromatic); 6.51 (t, aromatic); 6.39 (d, aromatic); 5.93 (t, aromatic); 5.88 (d, 1H, CH_2); 3.33 (d, 1H, CH_2).

3.2.6. [Ta{$(OC_6H_3Ph)_2CH_2$}Cl_3(py)] (7)

To a suspension of **5** (0.50 g, 0.78 mmol) in benzene was added pyridine (0.09 g 1.14 mmol, 1.5 equiv.) resulting in the formation of a yellow solution. The solution was layered with pentane causing yellow crystals of **7** to form, which were dried in vacuo. Yield 0.30 g (52.8%). *Anal.* Calc. for $TaNO_2Cl_3C_{30}H_{23}\cdot 0.5C_6H_6$: C, 52.44; H, 3.47; N, 1.85; Cl, 14.07. Found: C, 51.77; H, 3.81; N, 1.50; Cl, 13.94%. ^{1}H NMR (C_6D_6, 30°C): δ 8.52 (d, aromatic); 7.84 (d, aromatic); 7.47 (t, aromatic); 7.14 (d, aromatic); 6.77 (t, aromatic); 6.70 (t, aromatic); 6.50 (t, aromatic); 6.43 (d, aromatic); 5.93 (t, aromatic); 5.81 (d, 1H, CH_2); 3.42 (d, 1H, CH_2).

3.2.7. [Ta{$(OC_6H_3Ph)_2CH_2$}Cl_3(PMe_2Ph)] (8) and [$HPMe_2Ph$][Ta{$(OC_6H_3Ph)_2CH_2$}Cl_4] (9)

To a suspension of **5** (0.32 g, 0.50 mmol) in benzene was added PMe_2Ph (0.155 g, 1.12 mmol) and the solution was stirred for 20 min. Yellow powder of **8** formed overnight and was washed twice with pentane and dried in vacuo. Yield 0.35 g (70%). *Anal.* Calc. for $TaO_2Cl_3PC_{33}H_{29}$: C, 51.08; H, 3.79; P, 3.99; Cl, 13.71. Found: C, 50.82; H, 3.83; P, 3.61; Cl, 13.57%. ^{1}H NMR (C_6D_6, 30°C): δ 6.89–7.17 (m, 21H, aromatic); 5.95 (broad, 1H, CH_2); 3.25 (broad, 1H, CH_2); 1.026 (s, 6H, P*Me*$_2$Ph). ^{31}P NMR (C_6D_6, 30°C): δ −10.536 (s, 1P, *P*Me_2Ph). Layering of the supernatant with pentane resulted in the formation of a few well formed crystals of **9** (benzene solvate) presumably due to adventitious amounts of moisture. ^{1}H NMR (C_6D_6, 30°C): δ 6.89–7.17 (m, 21H, aromatic); 5.95 (broad, 1H, CH_2); 3.25 (broad, 1H, CH_2); 0.489 (d, 6H, P*Me*$_2$Ph). ^{31}P NMR (C_6D_6, 30°C): δ −10.505 (d, 1P, H*P*Me_2Ph, $^2J_{P\text{-}H}$ = 461.43 Hz).

3.2.8. [Ta{$(OC_6H_3Ph)_2CH_2$}$_2$(NMe_2)($HNMe_2$)] (10)

To a suspension of [$Ta(NMe_2)_5$] (0.25 g, 0.62 mmol) in benzene was added 2,2′-methylene-bis(6-phenylphenol) (0.44 g, 1.24 mmol) by standard Schlenk techniques under an N_2 atmosphere. The solution was stirred for 2 h and allowed to stand overnight before being dried in vacuo to produce a yellow powder. The resulting powder was suspended in a minimum amount of benzene and layered with pentane, resulting in the formation of a yellow crystalline material. Yield 0.486 g (78.4%). *Anal.* Calc. for $TaN_2O_4C_{54}H_{49}\cdot C_6H_6$: C, 68.70; H, 5.28; N, 2.67. Found: C,

68.84; H, 5.33; N, 2.44%. ^{1}H NMR (C_6D_6, 30°C): δ 6.73–7.86 (m, 32H, aromatics); 6.41 (d, 1H, CH_2); 5.56 (d, 1H, CH_2); 3.59 (d, 1H, CH_2); 3.46 (d, 1H, CH_2); 2.51 (s, 16H, NCH_3); 1.73 (d, 3H, HNCH_3); 0.87 (d, 3H, HNCH_3).

*3.2.9. [H_2NMe_2][Ta{($OC_6H_3Ph)_2CH_2$}$_3$] (**11**)*

To a suspension of [Ta(NMe_2)$_5$] (0.25 g, 0.62 mmol) in benzene was added 2,2′-methylene-bis(6-phenylphenol) (0.66 g, 1.86 mmol) by standard Schlenk techniques under an N_2 atmosphere. Upon stirring for 1 h a small amount of **11** was formed as a white precipitate which was isolated. Upon standing, the supernatant produced a few crystals of **11** (benzene solvate) suitable for X-ray analysis. *Anal*. Calc. for $TaNO_6C_{77}H_{62}\cdot 2C_6H_6$: C, 74.52; H, 5.20; N, 1.00. Calc. for $TaNO_6C_{77}H_{62}\cdot 3C_6H_6$: C, 75.43; H, 5.33; N, 0.93. Found: C, 74.22; H, 5.40; N, 1.65%. The crystals analyzed by crystallography contained 2.31 equiv. of benzene per Ta within the unit cell.

3.2.10. Hydrogenation experiment

A sample of [Nb{($OC_6H_3Ph)_2CH_2$}Cl_3] (**4**) (0.28 g, 0.51 mmol) was suspended in benzene (17 ml, 400 equiv.) in a 50 nl round bottomed flask. To this was added n-BuLi (3 equiv. in hexane). The flask containing the mixture was placed in a Parr model 4561, 300 ml high pressure minireactor and pressurized to 1200 psi hydrogen and heated to 80°C for 24 h. After cooling, a small amount of the resulting solution was diluted with C_6D_6 and the degree of hydrogenation (20%, 80 equiv.) of cyclohexane determined by ^{1}H.

4. Supplementary data

Crystal data and data collection parameters are contained in Tables 6 and 7. Crystallographic data for the structural analyses have been deposited with the Cambridge Crystallographic Data Center, CCDC numbers 133328 (**2**), 133329 (**6**), 133330 (**7**), 133331 (**9**) and 133332 (**11**). Copies of this information may be obtained free of charge from The Director, CCDC, 12 Union Road, Cambridge, CB2 1EZ, UK (fax: +44-1223-336-033) or e-mail deposit@ccdc.cam.ac.uk or http://www.ccdc.cam.ac.uk.

Table 7
Crystal data and data collection parameters

	9	**11**
Formula	$TaCl_4O_2C_{33}H_{30}P\cdot C_6H_6$	$TaO_6NC_{77}H_{62}\cdot 2.31C_6H_6$
Formula weight	890.45	1458.75
Space group	$P2_1/c$ (no. 14)	$P\bar{1}$ (no. 2)
a (Å)	15.1411(2)	14.1691(5)
b (Å)	12.2725(3)	15.2004(5)
c (Å)	21.3744(3)	18.5104(6)
α (°)	90	96.427(2)
β (°)	110.5051(12)	94.398(2)
γ (°)	90	105.3996(19)
V (Å^3)	3720.1(2)	3795.8(5)
Z	4	2
ρ_{calc} (g cm^{-3})	1.590	1.276
Temperature (K)	203.	193.
Radiation (wavelength, Å)	Mo Kα (0.71073)	Mo Kα (0.71073)
R	0.025	0.065
R_W	0.055	0.148

Acknowledgements

We thank the Department of Energy, Basic Energy Sciences, for financial support of this research.

References

[1] M.G. Thorn, Z.C. Etheridge, P.E. Fanwick, I.P. Rothwell, Organometallics 17 (1998) 3636.

Table 6
Crystal data and data collection parameters

	2	**6**	**7**
Formula	$Ti_2Cl_4O_4C_{50}H_{36}\cdot 2CHCl_3$	$NbCl_3O_2NC_{30}H_{23}\cdot 1/2C_6H_6$	$TaCl_3O_2NC_{30}H_{23}\cdot 1/2C_6H_6$
Formula weight	1177.21	667.85	755.89
Space group	$P\bar{1}$ (no. 2)	$P\bar{1}$ (no. 2)	$P\bar{1}$ (no. 2)
a (Å)	8.5013(14)	10.8086(4)	10.683(4)
b (Å)	10.2239(16)	11.0418(4)	11.023(3)
c (Å)	15.117(2)	13.6563(5)	13.579(3)
α (°)	85.736(12)	67.0451(17)	67.15(2)
β (°)	84.716(9)	84.929(2)	84.59(2)
γ (°)	78.217(11)	87.293(2)	86.90(2)
V (Å^3)	1278.7(5)	1494.75(14)	1466.7(9)
Z	1	2	2
ρ_{calc} (g cm^{-3})	1.529	1.484	1.711
Temperature (K)	203.	296.	203.
Radiation (wavelength, Å)	Mo Kα (0.71073)	Mo Kα (0.71073)	Mo Kα (0.71073)
R	0.087	0.049	0.026
R_W	0.244	0.130	0.071

[2] M.G. Thorn, J.E. Hill, S.A. Waratuke, E.S. Johnson, P.E. Fanwick, I.P. Rothwell, J. Am. Chem. Soc. 119 (1997) 8630.
[3] E.S. Johnson, G.J. Balaich, I.P. Rothwell, J. Am. Chem. Soc. 119 (1997) 7685.
[4] S.A. Waratuke, E.S. Johnson, M.G. Thorn, P.E. Fanwick, I.P. Rothwell, Chem. Commun. (1996) 2617.
[5] G.J. Balaich, I.P. Rothwell, Tetrahedron 51 (1995) 4463.
[6] G.J. Balaich, J.E. Hill, S.A. Waratuke, P.E. Fanwick, I.P. Rothwell, Organometallics 14 (1995) 656.
[7] J.E. Hill, G.J. Balaich, P.E. Fanwick, I.P. Rothwell, Organometallics 12 (1993) 2911.
[8] I.P. Rothwell, Acc. Chem. Res. 21 (1988) 153.
[9] I.P. Rothwell, Chem. Commun. (1997) 1331.
[10] M.A. Lockwood, M.C. Potyen, B.D. Steffey, P.E. Fanwick, I.P. Rothwell, Polyhedron 14 (1995) 3293.
[11] M.A. Lockwood, P.E. Fanwick, I.P. Rothwell, Polyhedron 14 (1995) 3363.
[12] G. Casiraghi, G. Casnati, A. Pochini, G. Puglia, R. Ungaro, G. Sartori, Synthesis (1981) 143.
[13] C. Floriani, F. Corazza, W. Lesueur, A. Chiesi-Villa, C. Guastini, Angew. Chem., Int. Ed. Engl. 28 (1989) 66.
[14] F. Corazza, C. Floriani, A. Chiesi-Villa, C. Guastini, Inorg. Chem. 30 (1991) 145.
[15] J. Okuda, S. Fokken, H.-C. Kang, W. Massa, Chem. Ber. 128 (1995) 221.
[16] M.H. Chisholm, J.-H. Huang, J.C. Huffman, W.E. Streib, D. Tiedtke, Polyhedron 16 (1997) 2941.
[17] L. Higham, M. Thornton-Pett, M. Bochmann, Polyhedron 17 (1998) 3047.
[18] L.R. Chamberlain, I.P. Rothwell, J.C. Huffman, Inorg. Chem. 23 (1984) 2575.
[19] M.A. Lockwood, M.C. Potyen, B.D. Steffey, P.E. Fanwick, I.P. Rothwell, Polyhedron 14 (1995) 3293.
[20] J.R. Clark, A.L. Pulverenti, P.E. Fanwick, M. Sigalas, O. Eisenstein, I.P. Rothwell, Inorg. Chem. 36 (1997) 3623.
[21] D.C. Bradley, M. Thomas, Can. J. Chem. 40 (1962) 1355.
[22] R.W. Chesnut, I.P. Rothwell, M. Banasak Holl, P.T. Wolczanski, Chem. Eng. News 68 (1990) 2.
[23] B.D. Steffey, P.E. Fanwick, I.P. Rothwell, Polyhedron 9 (1990) 963.
[24] G.D. Smith, P.E. Fanwick, I.P. Rothwell, Inorg. Chem. 29 (1990) 3221.
[25] O. Saied, M. Simard, J.D. Wuest, Inorg. Chem. 37 (1998) 2620.
[26] P.E. Fanwick, personal communication.
[27] C.A. Bayse, M.B. Hall, Organometallics 17 (1998) 4861.
[28] T.W. Coffindaffer, B.D. Steffey, I.P. Rothwell, K. Folting, J.C. Huffman, W.E. Streib, J. Am. Chem. Soc. 111 (1989) 4742.

PERGAMON

www.elsevier.nl/locate/poly

Polyhedron 19 (2000) 43–45

POLYHEDRON

Synthesis and structure of a novel dimeric molybdenum oxyhalide anion

T. Ozeki* [1, a], M. Sakaguchi [b], A. Yagasaki* [2,b]

[a] *Department of Chemistry and Materials Science, Tokyo Institute of Technology, O-okayama, Meguro-ku, Tokyo 152-8551, Japan*
[b] *Department of Chemistry, Kwansei Gakuin University, Uegahara, Nishinomiya 662-8501, Japan*

Received 2 August 1999; accepted 21 October 1999

Abstract

Reaction of $[(n\text{-}C_4H_9)_4N]_2[Mo_2O_7]$ with concentrated hydrochloric acid in an aprotic solvent yields a molecular molybdenum oxychloride anion $[Mo_2O_5Cl_4]^{2-}$ as a tetra-*n*-butylammonium salt. X-ray structural analysis of $[(n\text{-}C_4H_9)_4N]_2[Mo_2O_5Cl_4]\cdot 1/3(C_2H_5)_2O$ revealed that the dimeric anion consists of two MoO_3Cl_3 octahedra sharing a common face with a relatively long Mo–Mo distance (3.279 Å). The compound has the highest acidity as a polynuclear molybdate isolated so far. ©2000 Elsevier Science Ltd All rights reserved.

Keywords: Polyoxometalate; Oxyhalide; Molybdenum; X-ray structure; High acidity

1. Introduction

Since the discovery of molybdophosphate by Berzelius, many isopoly- and heteropoly-molybdates have been isolated and structurally characterized [1,2]. Their structures vary from relatively simple $[Mo_2O_7]^{2-}$ [3] to highly complex $[Mo_{36}O_{112}(H_2O)_{18}]^{8-}$ [4]. On the other hand, their acidity values *Z* [5–7] are confined in a narrow range of 1.0–2.0. The existence of a dimeric cation that has a *Z* value of 3 was repeatedly postulated in different solution studies [8–13], but such a species has never been isolated. Recently, we have isolated a novel molybdenum oxychloride anion that has the same *Z* value as this proposed dimer. Here we report its synthesis and structural characterization.

2. Experimental

2.1. Reagents, solvents, and general procedures

The following were purchased from commercial sources and used without further purification: concentrated hydrochloric acid, B_2O_3, and $Na_2MoO_4\cdot 2H_2O$ (Kishida), and P_2O_5 (Wako). Acetonitrile, diethyl ether, and acetone (Kishida or Wako) were distilled under N_2 atmosphere before use over P_2O_5, sodium benzophenone ketyl, and B_2O_3, respectively. Procedures described in the literature [14] were followed for the preparation of $[(n\text{-}C_4H_9)_4N]_2[Mo_2O_7]$. Elemental analysis was performed by Toray Research Center, Shiga, Japan. Infrared spectra were recorded from mineral oil (Nujol) mulls between KBr plates on a Hitachi I-3000 spectrometer. Absorptions are described as follows: strong (s), medium (m), weak (w), and shoulder (sh).

2.2. Preparation of $[(n\text{-}C_4H_9)_4N]_2[Mo_2O_5Cl_4]$

Concentrated hydrochloric acid (0.085 ml, 1.0 mmol) was added to a solution of $[(n\text{-}C_4H_9)_4N]_2[Mo_2O_7]$ (0.20 g, 0.25 mmol) in 2 ml of acetonitrile. The resulting pale yellow solution was refluxed under N_2 atmosphere for 1 h. A small amount of yellow crystals that formed on cooling the solution to ambient temperature was filtered off, and the filtrate was evaporated under vacuum to yield a crude product as a colorless tacky solid. The crude product was crystallized by dissolving it into 4 ml of acetone, adding 10 ml of diethyl ether to the solution, heating the mixture to boiling, filtering off a small amount of solid that formed, and allowing the filtrate to stand at ambient temperature for several hours. The colorless plate-shaped crystals thus obtained weighed 0.037 g (0.041 mmol, 16%) after drying under vacuum. *Anal*. Calc. for $C_{32}H_{72}N_2Mo_2Cl_4O_5$: C, 42.77; H, 8.08; N, 3.12; Cl, 15.78; Mo, 21.4. Found: C, 42.56; H, 7.94; N, 3.15; Cl, 15.62; Mo, 21.3%. IR (Nujol, 1000–400 cm^{-1}): 942 (s), 912 (s), 878 (m), 798 (w), 736 (m), 722 (m), 690 (s), 670 (sh), 546 (m).

[1] *Corresponding author. Tel.: +81-798-54-6405; fax: +81-798-51-0914; e-mail: yagasaki@kwansei.ac.jp
[2] *Corresponding author.

0277-5387/00/$ - see front matter ©2000 Elsevier Science Ltd All rights reserved.
PII S0277-5387(99)00320-4

2.3. Crystal structure determination

Diffraction data from a colorless plate shaped crystal were collected on a Siemens SMART CCD diffractometer [15] at 115 K. The structure was solved by the direct method using the SHELXS-97 [16] program and was refined by the full-matrix least-squares method on F^2 with the SHELXL-97 [17] program for 822 parameters and 16564 independent reflections. Mo, Cl and O atoms were refined with anisotropic displacement parameters. Hydrogen atoms were refined with the riding model. Crystallographic data for $3[(n\text{-}C_4H_9)_4N]_2[Mo_2O_5Cl_4]\cdot(C_2H_5)_2O$: empirical formula $Mo_6Cl_{12}O_{16}N_6C_{100}H_{226}$, space group $P2_1/c$, $a=28.723(6)$, $b=16.357(3)$, $c=29.692(6)$ Å, $\beta=104.25(3)°$, $Z=4$, crystal size $0.30\times0.15\times0.04$ mm, $\lambda=0.7107$ Å, $T=115$ K, $R[F_o^2>2\sigma(F_o^2)]=0.065$, $R_w[F_o^2>2\sigma(F_o^2)]=0.166$ ($R=\sum||F_o|-|F_c||/\sum|F_o|$, $R_w=[\sum w(F_o^2-F_c^2)^2/\sum w(F_o^2)^2]^{1/2}$, $w=1/[\sigma^2(F_o^2)+(0.070P)^2+103.0P]$, where $P=(F_o^2+2F_c^2)/3$). The anions A and B are roughly related by a center of symmetry at (0.25 0.25 0.25), with which the space group would be $I2/a$. Lattice centering with respect to these anions leads to much smaller intensities for the reflections with $h+k+l=2n+1$ than those with $h+k+l=2n$. However, the refinement with the space group $P2_1/c$ using both reflection classes is essential for the successful refinement of the anions C and D and the tetra-*n*-butylammonium cations. An asymmetric unit contains four independent $[Mo_2O_5Cl_4]^{2-}$ anions, six tetra-*n*-butylammonium cations and one diethyl ether molecule of crystallization. Two of the four independent $[Mo_2O_5Cl_4]^{2-}$, anions C and D, are disordered and their occupancies were refined with the constraint that the sum of them is 1.0. Selected geometric parameters are listed in Table 1.

Table 1
Interatomic distances (Å) and angles (°) for $[Mo_2O_5Cl_4]^{2-}$ anions

	Anion			
	A	B	C	D
Mo1···Mo2	3.278(1)	3.279(1)	3.272(2)	3.248(3)
Mo1–O1	1.687(5)	1.694(5)	1.697(10)	1.686(16)
Mo1–O2	1.699(5)	1.690(5)	1.708(10)	1.689(21)
Mo1–O5	1.921(5)	1.906(5)	1.910(9)	1.803(18)
Mo1–Cl1	2.370(2)	2.375(2)	2.367(4)	2.388(7)
Mo1–Cl3	2.708(2)	2.688(2)	2.689(4)	2.683(7)
Mo1–Cl4	2.696(2)	2.698(2)	2.648(3) [a]	2.796(3) [a]
Mo2–O3	1.690(5)	1.694(5)	1.678(8)	1.670(18)
Mo2–O4	1.691(5)	1.694(5)	1.683(10)	1.671(20)
Mo2–O5	1.899(5)	1.914(4)	1.917(9)	1.911(19)
Mo2–Cl2	2.380(2)	2.379(2)	2.379(6)	2.418(7)
Mo2–Cl3	2.701(2)	2.695(2)	2.680(4)	2.651(7)
Mo2–Cl4	2.691(2)	2.698(2)	2.629(3) [a]	2.802(3) [a]
Mo1–O5–Mo2	118.3(2)	118.2(2)	117.5(5)	122.0(10)
Mo1–Cl3–Mo2	74.62(5)	75.04(5)	75.09(10)	75.03(19)
Mo1–Cl4–Mo2	74.98(5)	74.83(5)	76.63(8) [a]	70.93(8) [a]

[a] $Cl4_C$ and $Cl4_D$ are located very close to each other, expected to be 0.26 Å apart. Thus, a Cl atom representing superimposed image of these two Cl was introduced and was refined with the occupancy factor of 1.0. Distances and angles involving this Cl atom are therefore less reliable.

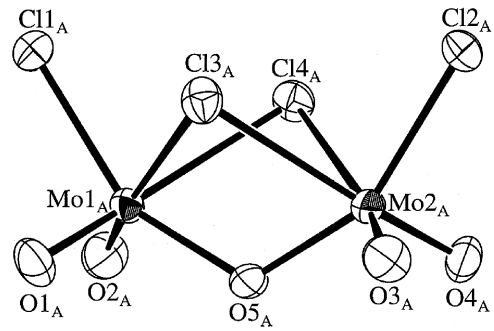


Fig. 1. Perspective view of the anion A. Displacement ellipsoids are scaled to enclose 50% probability levels.

3. Results and discussion

Reaction of $[(n\text{-}C_4H_9)_4N]_2[Mo_2O_7]$ [14] with concentrated hydrochloric acid in acetonitrile yields a novel molybdenum oxychloride anion as a tetra-*n*-butylammonium salt.

$$[(n\text{-}C_4H_9)_4N]_2[Mo_2O_7]+4HCl\rightarrow$$
$$[(n\text{-}C_4H_9)_4N]_2[Mo_2O_5Cl_4]+2H_2O$$

X-ray structural analysis revealed that single crystals of $[(n\text{-}C_4H_9)_4N]_2[Mo_2O_5Cl_4]\cdot1/3(C_2H_5)_2O$ are composed of $[(n\text{-}C_4H_9)_4N]^+$ cations, diethyl ether molecules of crystallization, and discrete $[Mo_2O_5Cl_4]^{2-}$ (**1**) anions having the structure shown in Fig. 1. The dimeric oxychloride anion consists of two octahedral MoO_3Cl_3 units sharing a common face, where all the Cl atoms are positioned *trans* to the O atoms. The Mo–O bond lengths in **1** are comparable to those found in the face-sharing dioctahedral units of $[(CH_3)_2AsMo_4O_{15}H]^{2-}$ [18–20], $[AsMo_8O_{30}H_2]^{5-}$ [21], $[AsMo_8O_{30}]^{7-}$ [21], $[Mo_4O_{10}(O_3PCH_2PO_3)_2]^{4-}$ [22], $[(Bu^tP)_2Mo_6O_{24}]^{4-}$ [22], $[Mo_4O_{12}F_3]^{3-}$ [23], $[Mo_2O_6F_3]^{3-}$ [24], $[(C_{14}H_8)Mo_4O_{15}(OH)]^{2-}$ [25], $[CeMo_{12}O_{42}]^{8-}$ [26], and many molybdate–polyalcohol complexes [23,27–31]. The Mo···Mo distance in **1**, however, is 3.279 Å and unusually long for a face-sharing octahedral molybdenum(VI) compound. The corresponding distances are 3.163 Å in $[(CH_3)_2AsMo_4O_{15}H]^{2-}$, 3.193 and 3.188 Å in $[AsMo_8O_{30}H_2]^{5-}$, 3.113 Å in $[AsMo_8O_{30}]^{7-}$, 3.129 and 3.122 Å in $[Mo_4O_{10}(O_3PCH_2PO_3)_2]^{4-}$, 3.106 and 3.245 Å in $[(Bu^tP)_2Mo_6O_{24}]^{4-}$, 3.152 Å in $[Mo_4O_{12}F_3]^{3-}$, 3.205 Å in $[Mo_2O_6F_3]^{3-}$, 3.143 Å in $[(C_{14}H_8)Mo_4O_{15}(OH)]^{3-}$, 3.13 Å in $[CeMo_{12}O_{42}]^{8-}$, and 3.14 Å [32] in different dimeric molybdate–polyalcohol compounds. More interestingly, the molybdenum–oxygen bond lengths and angles (and hence the Mo···Mo distance) in **1** are extremely similar to those of the $(MoO_3)_6$ rings found in Anderson type [33–40] and $X_2Mo_6O_{18}$ type ($X=CH_3AsO_3$, $H_2NC_6H_4AsO_3$, AsO_4, MoO_4, VO_4, TeO_3) [31,41–46] structures. It might be better to describe the structure of **1** as

a Mo_2O_5 unit cut out from a $(MoO_3)_6$ ring and coordinated by four chloride ligands rather than to depict it as two MoO_3Cl_3 octahedra sharing a common face. In fact, the IR spectrum of $[(n\text{-}C_4H_9)_4N]_2[Mo_2O_5Cl_4]$ exhibits a feature characteristic for the compounds that have a $(MoO_3)_6$ ring (see Section 2) and it is impossible to distinguish the current compound from an Anderson type polymolybdate by IR spectra alone.

As mentioned earlier, **1** has a very high acidity ($Z=3$). Just like $[Mo_2O_7]^{2-}$ ($Z=1$) opened up a new synthetic route and aspect in polymolybdate chemistry that had been traditionally constrained by the chemical nature of MoO_4^{2-} ($Z=0$), the current compound is expected to serve as an entree to the chemistry of polymolybdates of higher acidity.

Supplementary data

Supplementary data are available from the CCDC, 12 Union Road, Cambridge, CB2 1EZ, UK on request, quoting the deposition number CCDC 132906.

Acknowledgements

A.Y. thanks Ms Y. Sakai, Ms A. Nishitani, and Mr M. Okada for technical help.

References

[1] For reviews, see for example, Polyoxometalate Chemistry, Kikan Kagaku Sosetsu, 20 (1993).
[2] See for example Polyoxymetalates, Chem. Rev. 98 (1998).
[3] V.W. Day, M.F. Fredrich, W.G. Klemperer, W. Shum, J. Am. Chem. Soc. 99 (1977) 6146.
[4] B. Krebs, I. Paulat-Boeschen, Acta Crystallogr., Sect. B 38 (1982) 1710.
[5] The acidity value of a polymolybdate is defined as the amount of H^+ consumed per Mo atom assuming the species is formed from MoO_4^{2-} [6,7]. Thus $Z=8/7=1.17$ for $[Mo_7O_{24}]^{6-}$ ($8H^+ + 7MoO_4^{2-} \rightarrow [Mo_7O_{24}]^{6-} + 4H_2O$).
[6] Y. Sasaki, L.G. Sillén, Arkiv Kemi 29 (1968) 253.
[7] M.T. Pope, Heteropoly and Isopoly Oxometalates, Springer, Berlin, 1983, pp. 33–34, 42.
[8] Y. Sasaki, L.G. Sillén, Acta Chem. Scand. 18 (1964) 1014.
[9] J.F. Ojo, R.S. Taylor, A.G. Sykes, J. Chem. Soc., Dalton Trans. (1975) 500.
[10] J.J. Cruywagen, J.B.B. Heyns, E.F.C.H. Rohwer, J. Inorg. Nucl. Chem. 40 (1978) 53.
[11] S. Himeno, M. Hasegawa, Inorg. Chim. Acta 83 (1984) L5.
[12] K. Yokoi, N. Matsubayashi, T. Miyanaga, I. Watanabe, K. Murata, S. Ikeda, Chem. Lett. (1987) 1453.
[13] J.M. Coddington, M. Taylor, J. Chem. Soc., Dalton Trans. (1990) 41.
[14] N.H. Hur, W.G. Klemperer, R.-C. Wang, Inorg. Synth. 27 (1990) 79.
[15] SMART and SAINT: Area Detector Control and Integration Software, Siemens Analytical X-ray Systems, Inc., Madison, WI, 1996.
[16] G.M. Sheldrick, SHELXS-97, Program for the Solution of Crystal Structures, University of Göttingen, Germany, 1997.
[17] G.M. Sheldrick, SHELXL-97, Program for the Refinement of Crystal Structures, University of Göttingen, Germany, 1997.
[18] K. Barkigia, L.M. Rajkovic, M.T. Pope, C.O. Quicksall, J. Am. Chem. Soc. 97 (1975) 146.
[19] K.M. Barkigia, L.M. Rajkovic-Blazer, M.T. Pope, E. Prince, C.O. Quicksall, Inorg. Chem. 19 (1980) 2531.
[20] K.Y. Matsumoto, Bull. Chem. Soc. Jpn. 52 (1979) 5284.
[21] K.-F. Hsu, S.-L. Wang, Inorg. Chem. 36 (1997) 3049.
[22] Y.-D. Chang, J. Zubieta, Inorg. Chim. Acta 245 (1996) 177.
[23] N. Buchholz, R. Mattes, Angew. Chem., Int. Ed. Engl. 25 (1986) 1104.
[24] R. Mattes, K. Mennemann, N. Jäckel, H. Rieskang, H.-J. Brockmeyer, J. Less-Common Met. 76 (1980) 199.
[25] Q. Chen, S. Liu, H. Zhu, J. Zubieta, Polyhedron 8 (1989) 2915.
[26] D.D. Dexter, J.V. Silverton, J. Am. Chem. Soc. 90 (1968) 3589.
[27] L.O. Atovmyan, V.V. Tkachev, T.G. Shiskova, Dokl. Akad. Nauk SSSR 205 (1970) 609.
[28] C.G. Pierpont, R.M. Buchanan, J. Am. Chem. Soc. 97 (1975) 6450.
[29] C.G. Pierpont, R.M. Buchanan, Inorg. Chem. 21 (1982) 652.
[30] A.M. El-Hendawy, W.P. Griffith, C.A. O'Mahoney, D.J. Williams, Polyhedron 8 (1989) 519.
[31] L. Ma, S. Liu, J. Zubieta, Polyhedron 8 (1989) 1571.
[32] An average for six different compounds. The standard deviation is 0.04 Å.
[33] A. Perloff, Inorg. Chem. 9 (1970) 2228; H.T. Evans Jr., Acta Crystallogr., Sect. B 30 (1974) 2095.
[34] H. Kondo, A. Kobayashi, Y. Sasaki, Acta Crystallogr., Sect. B 36 (1980) 661.
[35] U. Lee, Y. Sasaki, Chem. Lett. (1984) 1294.
[36] F. Ito, T. Ozeki, H. Ichida, H. Miyamae, Y. Sasaki, Acta Crystallogr., Sect. C 45 (1989) 946.
[37] Y. Ozawa, Y. Hayashi, K. Isobe, Acta Crystallogr., Sect. C 47 (1991) 637.
[38] H.Y. Lee, K.M. Park, U. Lee, H. Ichida, Acta Crystallogr., Sect. C 47 (1991) 1959.
[39] U. Lee, Acta Crystallogr., Sect. C 50 (1994) 1657.
[40] C.C. Allen, R.C. Burns, G.A. Lawrance, P. Turner, T.W. Hambley, Acta Crystallogr., Sect. C 53 (1997) 7.
[41] W. Kwak, L.M. Rajkovic, J.K. Stalick, M.T. Pope, C.O. Quicksall, Inorg. Chem. 15 (1976) 2778.
[42] B. Hedman, Acta Crystallogr., Sect. B 36 (1980) 2241.
[43] J. Fuchs, H. Hartl, Angew. Chem., Int. Ed. Engl. 15 (1976) 375.
[44] V.W. Day, M.F. Fredrich, W.G. Klemperer, W. Shum, J. Am. Chem. Soc. 99 (1977) 952.
[45] A. Björnberg, Acta Crystallogr., Sect. B 35 (1979) 1995.
[46] V. Balraj, K. Vidyasagar, Inorg. Chem. 37 (1998) 4764.

PERGAMON

www.elsevier.nl/locate/poly

Polyhedron 19 (2000) 47–54

POLYHEDRON

Synthesis and structural characterisation of new manganese(II) and (III) complexes. Study of their photolytic and catalase activity and X-ray crystal structure of [Mn(3-OMe, 5-Br-*salpn*)(EtOH)(H_2O)]ClO_4

M. Maneiro [a], M.R. Bermejo [a,*], A. Sousa [a], M. Fondo [a], A.M. González [a], A. Sousa-Pedrares [a], Charles A. McAuliffe [b]

[a] *Departamento de Química Inorgánica, Facultade de Química, Universidade de Santiago de Compostela, 15706 Santiago de Compostela, Galicia, Spain*
[b] *Department of Chemistry, University of Manchester, Institute of Science and Technology, PO Box 88, Manchester M60 1QD, UK*

Received 30 June 1999; accepted 13 October 1999

Abstract

New [$Mn^{II}L(H_2O)_2$] and [$Mn^{III}L(H_2O)_2$]ClO_4 complexes, where L are substituted *N*,*N*′-bis(salicylidene)propane-1,3-diamine (H_2*salpn*) ligands have been prepared and thoroughly characterised by elemental analysis, IR and mass spectroscopy, conductivity and magnetic measurements at room temperature (and, in the case of **1**, at variable temperature). Cyclic and normal pulse voltammetry measurements were also performed. All these studies support an octahedral geometry around the metal with the Schiff base in the equatorial plane acting as tetradentate and solvent molecules in the axial positions. Crystallographic characterisation of **6** confirms this geometry and shows a supramolecular structure involving π–π stacking and hydrogen bonding interactions. The ability to split water by these complexes and their catalase activity has also been studied. ©2000 Elsevier Science Ltd All rights reserved.

Keywords: Manganese complexes; Schiff bases; Manganoenzymes; Photolysis; Catalase; Dioxygen

1. Introduction

The existence of natural catalysts with a manganese centre raises the question of whether other synthetic complexes can mimic the reactivity of these biological sites. This has prompted the vast interest developed by bioinorganic chemists in manganese complexes as models for water photoinduced oxidation or catalysts with catalase-like activity, for example.

Photosynthetic organisms have a high ability for conversion of light energy to chemical energy under favourable conditions [1]. The oxygen-evolving complex (OEC), which induces the oxidation of water to dioxygen, is thought to contain a cluster of four manganese atoms [2,3].

The binding domain for the manganese cluster remains an issue of uncertainty; nevertheless, data on the physical structure of the metal centre have been recently summarised and provide a model for the catalytic site [4]. The most popular model, according to EXAFS experiments by Klein and coworkers [5], implies a natural site composed by two di-μ-oxo $Mn_2(\mu\text{-}O)_2$ units linked by a μ-oxo-bis-μ-carboxylate bridge. Hoganson and Babcock [6] proposed that a tyrosine radical is involved in the water oxidation process by abstraction of hydrogen atoms from substrate water molecules bound as terminal ligands to two of the four manganese ions.

The advances in the knowledge of the natural OEC structure have been accompanied by the synthesis of artificial models [7,8]. However, those tetramanganese synthetic models, designed in an attempt to reproduce the structure of the natural centre [9–11], have not had much success in mimicking the natural OEC properties. We focused our efforts on the study of some types of monomers and dimers [12–14], in order to find artificial catalysts for the decomposition of water. We have reported some μ-aquo dimeric manganese-Schiff base complexes [12,15] containing coordinated water molecules with a Mn–Mn distance of about 5 Å which possesses this ability. These complexes have shown a polymeric array in their solid state supramolecular structure [16] due to π stacking and hydrogen bonding, involving the phenyl rings of the Schiff base, the coordinated water molecules and even the perchlorate counterions.

On the other hand, catalases protect organisms from oxidative damage by removing the appreciable levels of hydro-

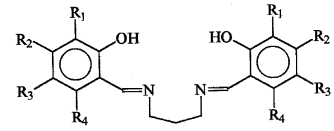
* Corresponding author. Tel.: +34-981-591-076; fax: +34-981-597-525; e-mail: qimb45@uscmail.usc.es

0277-5387/00/$ - see front matter ©2000 Elsevier Science Ltd All rights reserved.
PII S0277-5387(99)00321-6

gen peroxide produced during O_2 metabolism in cells. The hydroxyl radicals, derived from the peroxide, are potent oxidants which are capable of oxidising all cellular components they come in contact with [17].

L-edge X-ray absorption spectroscopy measurements indicate that the octahedral component of the ligand field, which splits the valence 3d orbitals of the reduced *Lactobacillus plantarum* Mn catalase, is about 1.1 eV. This is a typical value for a manganese centre surrounded by O or N ligands, with a coordination number of six [18]. Furthermore, some manganese complexes with derivative *salpn* ligands have shown excellent ability for the disproportionation of hydrogen peroxide [19].

As a result of these previous findings, it seems that manganese Schiff base complexes could be functional models for the reactivity of the manganese OEC active site or manganese catalases. Thus, we extended our investigations on this type of compound to new complexes containing substituted Schiff base ligands, in order to find a correlation Schiff base/structure/activity (Scheme 1).



	R_1	R_2	R_3	R_4
H_2L^1	H	H	Cl	H
H_2L^2	H	H	NO_2	H
H_2L^3	OEt	H	H	H
H_2L^4	Br	H	Cl	H
H_2L^5	Br	H	NO_2	H
H_2L^6	OMe	H	Br	H
H_2L^7	H	OMe	H	OMe

Scheme 1.

2. Experimental

2.1. Chemicals

Salicylaldehydes (Maybridge), 1,3-diaminopropane (Aldrich), manganese(II) perchlorate hexahydrate (Fluka) and *p*-benzoquinone (Aldrich) were used as received without further purification.

2.2. Physical measurements

Elemental analyses were performed on a Carlo Erba model 1108 CHNS-O elemental analyser. The IR spectra were recorded as KBr discs on a Nicolet PC5 FT-IR spectrophotometer and UV–Vis spectra on a Hewlett-Packard 8452A instrument. ^{1}H NMR spectra were recorded on a Bruker WH 300 MHz spectrometer using $CDCl_3$ as solvent and $SiMe_4$ as an internal reference. FAB mass spectra were recorded on a Kratos MS50 TC spectrometer connected to a DS90 data system, using metanitrobenzyl alcohol as a matrix. Λ_M was measured by using a WTW type LF 3 conductivimeter. Room temperature magnetic susceptibilities were measured using a Digital Measurement system 1660 vibrating magnetometer operating at 5000 G. $HgCo(NCS)_4$ was employed as a susceptibility standard. Magnetic susceptibility measurements in the 5–300 K temperature range were obtained using a SQUID magnetometer operating at 5000 G.

2.3. Electrochemical measurements

All measurements were performed using an EG&G PAR model 273 potentiostat, controlled by EG&G PAR model 270 software. A Metrohm model 6.1204.000 graphite disc coupled to a Metrohm model 628-10 rotating electrolyte device was used as a working electrode. A saturated calomel electrode was used as a reference and a platinum wire as an auxiliary electrode.

All measurements were made with ca. 10^{-3} mol dm^{-3} solutions of the complexes in dimethylformamide using 0.2 mol dm^{-3} NBu_4PF_6 as a supporting electrode. Cyclic voltammetry measurements were performed with a static graphite electrode, whilst direct current and pulse voltammograms were recorded with the graphite disc rotating at 2000 rev min^{-1}.

2.4. Preparation of the ligands

The symmetrical Schiff bases (R-*salpn*) were prepared in an analogous manner by the reaction of the corresponding substituted salicylaldehyde with diamine. This can be typified by the following preparation.

To an ethanol solution (100 ml) of 1,3-diaminopropane (0.84 ml, 9.82 mmol) was added 3Br,5Cl-salicylaldehyde (4.63 g, 19.64 mmol). This mixture was refluxed in a round bottom flask fitted with a Dean Stark trap to remove the water produced during the reaction. After refluxing for 3 h, the solution was concentrated to yield a yellow solid. The product was collected by filtration, washed with diethyl ether and dried in air.

Yields were almost quantitative.

H_2L^1 (Found: C, 58.0; H, 4.8; N, 8.4. Calc. for $C_{17}H_{16}Cl_2N_2O_2$: C, 58.1; H, 4.6; N, 8.0%); ^{1}H NMR δ 2.13 (q, 2H), 3.75 (t, 4H), 6.8–7.3 (m, 6H), 8.30 (s, 2H), 13.33 (s, 2H); IR ν(C=N) 1634, ν(C–O) 1281 cm^{-1}; m.p. 84°C.

H_2L^2 (Found: C, 54.7; H, 4.3; N, 14.6. Calc. for $C_{17}H_{16}N_4O_6$: C, 54.8; H, 4.3; N, 15.0%); ^{1}H NMR δ 2.10 (q, 2H), 3.90 (t, 4H), 7.0–8.0 (m, 6H), 8.40 (s, 2H); IR ν(C=N) 1660, ν(C–O) 1309 cm^{-1}; m.p. 234°C.

H_2L^3 (Found: C, 67.5; H, 6.9; N, 7.3. Calc. for $C_{21}H_{19}N_2O_4$: C, 68.1; H, 7.0; N, 7.6%); ^{1}H NMR δ 1.50 (t, 6H), 2.09 (q, 2H), 3.75 (t, 4H), 4.20 (q, 4H), 6.8–7.0 (m, 6H), 8.38 (s, 2H), 13.98 (s, 2H); IR ν(C=N) 1625, ν(C–O) 1271 cm^{-1}; m.p. 74°C.

H_2L^4 (Found: C, 39.5; H, 3.0; N, 5.3. Calc. for $C_{17}H_{14}Br_2Cl_2N_2O_2$: C, 40.1; H, 2.8; N, 5.5%); ^{1}H NMR δ 2.07 (q, 2H), 3.71 (t, 4H), 7.1–7.5 (m, 6H), 8.20 (s, 2H), 14.42 (s, 2H); IR ν(C=N) 1625, ν(C–O) 1286 cm^{-1}; m.p. 147°C.

H_2L^5 (Found: C, 38.8; H, 3.0; N, 10.9. Calc. for $C_{17}H_{14}Br_2N_4O_6$: C, 38.5, H, 2.7; N, 10.6%); ^{1}H NMR δ 2.17 (q, 2H), 3.78 (t, 4H), 8.2–8.4 (m, 6H), 8.83 (s, 2H), 13.22

(s, 2H); IR ν(C=N) 1655, ν(C–O) 1318 cm^{-1}; m.p. 264°C.

H_2L^6 (Found: C, 46.0; H, 4.3; N, 5.9. Calc. for $C_{19}H_{20}Br_2N_2O_4$: C, 45.6; H, 4.0; N, 5.6%); ^1H NMR δ 2.10 (q, 2H), 3.73 (t, 4H), 3.89 (s, 6H), 7.0–7.3 (m, 6H), 8.27 (s, 2H), 14.24 (s, 2H); IR ν(C=N) 1632, ν(C–O) 1275 cm^{-1}; m.p. 141°C.

H_2L^7 (Found: C, 62.2; H, 6.6; N, 7.1. Calc. for $C_{21}H_{26}N_2O_6$: C, 62.6; H, 6.5; N, 7.0%); ^1H NMR δ 2.11 (q, 2H), 3.64 (t, 4H), 3.84 (s, 6H), 3.91 (s, 6H), 5.6–6.0 (m, 6H), 8.40 (s, 2H), 14.28 (s, 2H); IR ν(C=N) 1642, ν(C–O) 1282 cm^{-1}; m.p. 99°C.

2.5. Complex preparation

All the complexes were synthesised by air oxidation of the solution made up from $Mn(ClO_4)_2 \cdot 6H_2O$ and the Schiff base [20]. A typical preparation is outlined below.

$[MnL^1(H_2O)_2]ClO_4$ (**1**), 2.85 mmol (1.0 g) of H_2L^1 were dissolved in 100 ml of a 1:1 methanol–ethanol mixture and 2.85 mmol (1.03 g) of $Mn(ClO_4)_2 \cdot 6H_2O$ were added to the initial yellow solution which changed to green. (**Caution**: Although no problems have been encountered in this work, perchlorates are potentially explosive and should be handled in only small quantities and with care!) After stirring for 10 min, 5.70 mmol (0.23 g) of NaOH, dissolved in a small quantity of water, were added and the mixture turned dark. The progress of the reaction was followed by TLC for three days and the mixture was then filtered. The complex was obtained from the filtrate as a brown solid after crystallisation. It was isolated by filtration and washed with diethyl ether and dried in air, yield: 0.80 g, 52% (Found: C, 37.7; H, 3.5; N, 5.3. Calc. for $MnC_{17}H_{18}Cl_3N_2O_8$: C, 37.8; H, 3.3; N, 5.2%).

$[MnL^2(H_2O)_2]$ (**2**), 2.69 mmol (1.0 g) of H_2L^2; 2.69 mmol (0.97 g) of $Mn(ClO_4)_2 \cdot 6H_2O$; 5.38 mmol (0.22 g) of NaOH; yield: 1.12 g, 86% (Found: C, 44.5; H, 3.9; N, 12.2. Calc. for $MnC_{17}H_{18}N_4O_8$: C, 44.3; H, 3.9; N, 12.2%).

$[MnL^3(H_2O)_2]ClO_4$ (**3**), 1.62 mmol (0.6 g) of H_2L^3; 1.62 mmol (0.59 g) of $Mn(ClO_4)_2 \cdot 6H_2O$; 3.24 mmol (0.13 g) of NaOH; yield: 0.71 g, 82% (Found: C, 45.4; H, 4.8; N, 5.1. Calc. for $MnC_{21}H_{28}ClN_2O_{10}$: C, 45.1; H, 5.0; N, 5.0%).

$[MnL^4(H_2O)_2]ClO_4$ (**4**), 1.96 mmol (1.0 g) of H_2L^4; 1.96 mmol (0.71 g) of $Mn(ClO_4)_2 \cdot 6H_2O$; 4.0 mmol (0.16 g) of NaOH; yield: 0.62 g, 47% (Found: C, 29.9; H, 2.2; N, 4.1. Calc. for $MnC_{17}H_{16}Br_2Cl_3N_2O_8$: C, 29.5; H, 2.3; N, 4.0%).

$[MnL^5(H_2O)]$ (**5**), 1.87 mmol (1.0 g) of H_2L^5; 1.87 mmol (0.68 g) of $Mn(ClO_4)_2 \cdot 6H_2O$; 3.77 mmol (0.15 g) of NaOH; yield: 1.05 g, 91% (Found: C, 33.0; H, 2.4; N, 8.6. Calc. for $MnC_{17}H_{14}Br_2N_4O_7$: C, 33.0; H, 2.6; N, 9.0%).

$[MnL^6(H_2O)_2]ClO_4$ (**6**), 2.0 mmol (1.0 g) of H_2L^6; 2.0 mmol (0.72 g) of $Mn(ClO_4)_2 \cdot 6H_2O$; 4.0 mmol (0.16 g) of NaOH; yield: 0.82 g, 61% (Found: C, 33.5; H, 3.2; N, 4.1. Calc. for $MnC_{19}H_{22}Br_2ClN_2O_{10}$: C, 33.2; H, 3.2; N, 4.1%).

$[MnL^7(H_2O)_2]ClO_4$ (**7**), 2.49 mmol (1.0 g) of H_2L^7; 2.49 mmol (0.90 g) of $Mn(ClO_4)_2 \cdot 6H_2O$; 4.98 mmol (0.20 g) of NaOH; yield: 1.20 g, 85% (Found: C, 42.2; H, 4.5; N, 4.6. Calc. for $MnC_{21}H_{28}ClN_2O_{12}$: C, 42.7; H, 4.7; N, 4.7%).

2.6. Irradiation experiments

The irradiation of aqueous solutions of the manganese complexes was carried out in a colourless two-neck glass flask (1 l) placed in a metacrilate thermostatted water-bath. In a typical experiment a magnetically stirred solution of **1** (10^{-5} mol; 4.9 mg) and *p*-benzoquinone (2×10^{-4} mol; 21.6 mg) in deoxygenated, deionised water was irradiated with light from a 200 W tungsten lamp for 24 h. The solution was connected to a UV spectrophotometer through a peristaltic pump and a flow cell. One neck of the flask was closed by a septum whilst an oxygen meter Oxi 92 entered into the solution through the other neck of the flask, to measure the amount of oxygen evolved during the irradiation. Oxygen readings were recorded as percentage dissolved oxygen where 100% corresponds to a fully saturated aqueous solution at 25°C (6 $cm^3\ O_2\ dm^{-3}$) and 0% corresponds to no dissolved oxygen.

Reproducible results were obtained with this method provided that the temperature of the bath remained constant (25.0 ± 0.1°C) and a constant stirring rate was also maintained.

2.7. Catalase probes

Oxidation of 2,2′-azinobis(3-ethylbenzothiazoline)-sulfonic (ABTS) acid with H_2O_2 was tested in the presence of the complexes at ca. pH 7. An aqueous solution of ABTS (50 μl; 0.009 M; 4.5×10^{-7} mol) and a methanol solution of the complex (10 μl; 10^{-3} M; 10^{-8} mol) were added to water (3 ml). The oxidation of ABTS starts immediately after addition of an aqueous solution of H_2O_2 (50 μl; 10 M; 5×10^{-4} mol).

2.8. X-ray diffraction studies

Crystals of **6** suitable for X-ray studies were obtained by slow evaporation of an ethanol solution of the complex. Crystal data for **6**: $C_{42}H_{52}Br_4Cl_2Mn_2N_4O_{20}$, triclinic, space group $P\bar{1}$, $a = 14.224(10)$, $b = 19.509(7)$, $c = 10.337(7)$ Å, $\alpha = 89.98(5)$, $\beta = 112.14(5)$, $\gamma = 89.83(5)°$, $Z = 2$, Mo Kα radiation, $\lambda = 0.71073$ Å, $T = 293(2)$ K, dark brown colour, crystal size $0.40 \times 0.35 \times 0.20$ nm. Measurements were made on a Rigaku AFC6S diffractometer (transmission 0.3222–0.5280). 9759 reflections were collected (theta range for data collection from 1.04 to 25.00°) giving 9335 unique data with $R_{int} = 0.1111$; the completeness to $2\theta = 25.00$ is 99.7%. All data were corrected for Lorentz polarisation effects. The structure was solved by direct methods [21] and refined using full-matrix least-squares [22] on F^2. An absorption correction (psi scan technique) was applied. Non-hydrogen atoms were

Table 1
Magnetic moments, IR and mass spectrometric data of the complexes

Compound	ν(C=N)	ν(C–O)	$\nu_3(ClO_4^-)$	$\nu_4(ClO_4^-)$	FAB [b]	μ_{eff} [c]
1	1630vs (1634) [a]	1292m (1281)	1122vs	622s	404	4.7
2	1641vs (1660)	1339s (1309)			426	5.9
3	1612s (1625)	1307m (1271)	1122vs	625s		5.0
4	1610vs (1625)	1300m (1286)	1121vs	630s	563	4.9
5	1637vs (1655)	1335s (1318)			584	5.6
6	1624s (1632)	1294m (1275)	1119vs	625s	554	4.6
7	1611vs (1642)	1327m (1282)	1122vs	625s	456	4.5

[a] Bands corresponding to the free ligands in parentheses; vs very strong, s strong, m medium.
[b] Peaks corresponding to $[MnL]^+$.
[c] Values in Bohr magnetons (BM).

refined anisotropically. Hydrogen atoms were included in idealised positions. At convergence, $wR = \{\sum[w(F_o^2 - F_c^2)^2]/\sum[wF_o^2)_2]\}^{1/2} = 0.1830$ for all data, conventional $R = 0.0656$ on F values of 9335 reflections with $I > 2\sigma(I)$, goodness of fit 0.977 for all F^2 values and 692 refined parameters. A final difference synthesis contained no features outside the range 0.604 to -0.589 e Å^{-3}.

3. Results and discussion

3.1. IR spectroscopic studies

All the complexes show similar IR spectral features (Table 1), exhibiting a strong band between 1641–1611 cm^{-1} attributable to ν(CN), which is shifted 4–31 cm^{-1} lower than in the free Schiff base ligand.

Complexes **1**, **3**, **4**, **6** and **7** show broad unsplit bands at ca. 1100 cm^{-1}, together with bands at 630 cm^{-1}, that are indicative of the presence of a non-coordinated perchlorate counterion. These stretching frequencies were not observed for complexes **2** and **5**.

3.2. Mass spectra

FAB mass spectra show peaks relating to fragments $[MnL]^+$ for all the complexes, indicating the coordination of the ligand to the metal centre (Table 1). No traces of dimeric peaks were found and the presence of the $[MnL(OH_2)_2]^+$ fragment can be deduced from some minor peaks.

3.3. Magnetic studies

The magnetic moments in BM are listed in Table 1. Those complexes formulated as $[MnL(H_2O)]ClO_4$ exhibit room temperature magnetic moments close to the spin-only value of 4.9 BM, as expected for a high-spin magnetically diluted d^4 manganese(III) ion. Complexes containing the 5-NO_2-substituted ligands show magnetic moments close to the spin-only value of 5.9 BM, which agree with the presence of a high-spin d^5 magnetically diluted manganese(II) ion in **2** and **5**.

Magnetic studies at variable temperature have been done for **1** (between 300 and 40 K) and the magnetic behaviour is illustrated in Fig. 1. This study shows little or no antiferromagnetic interaction between neighbouring metal centres. This behaviour is typical of magnetically diluted manganese atoms and is in accordance with the quite long Mn···Mn distance (5.17(1) Å) [23].

3.4. Crystallographic studies

Slow evaporation of an ethanol solution of **6** gives crystals, suitable for X-ray diffraction studies, of $[MnL^6(EtOH)(H_2O)]ClO_4$. The crystal structure is shown in Fig. 2 and main bond distances and angles in Table 2.

The monomer is composed of an approximately octahedral $[MnL^6(EtOH)(H_2O)]^+$ cation with a crystallographically independent ClO_4^- anion. The planar tetradentate Schiff-base ligand is tightly bound to the manganese(III) ion via the N_{imine} and O_{phenol} atoms (Mn–N_{imine} bond lengths of 2.017(17) and 2.029(17) Å and Mn–O_{phenol} bond lengths of 1.863(13) and 1.868(14) Å). A capping water molecule (Mn–O_{water} 2.203(15) Å) and a coordinated ethanol molecule (Mn–$O_{ethanol}$ 2.275(14) Å) from the crystallisation solvent, complete the coordination sphere of the distorted octahedral manganese centre. The ability of the ethanol sol-

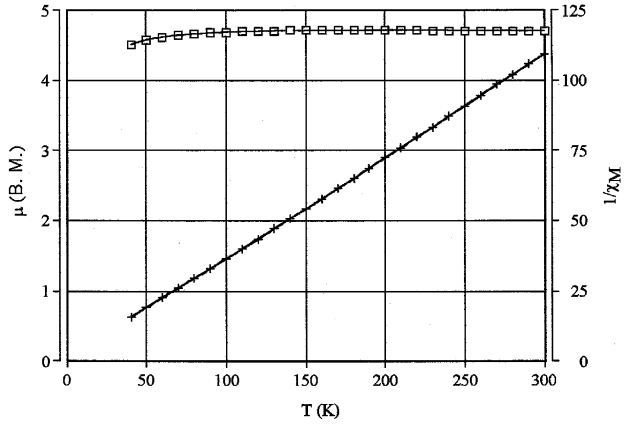


Fig. 1. Plots of μ_{eff} (□) and $1/\chi_M$ (+) vs. temperature for **1**.

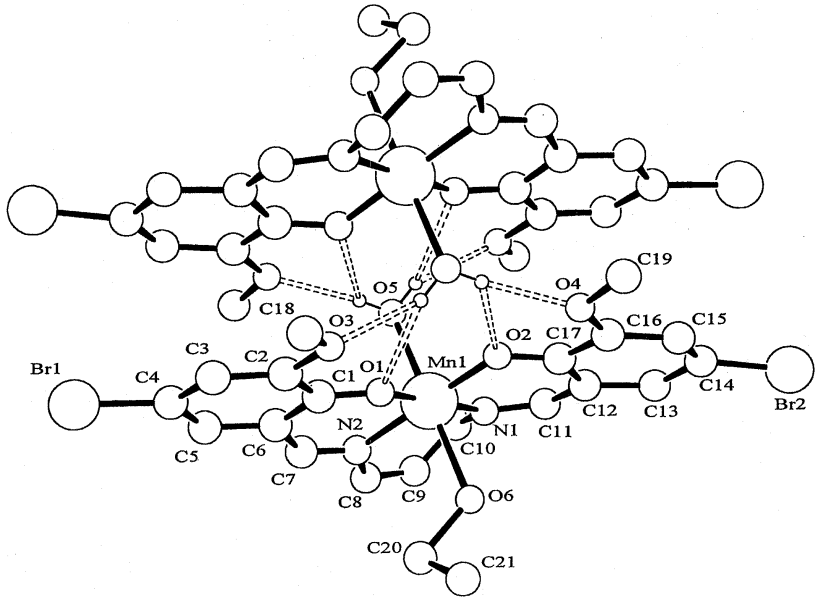


Fig. 2. Crystal structure for **6**; broken lines represent the hydrogen bonds between axially coordinated water molecules and phenoxy and methoxy oxygens.

Table 2
Selected bonds lengths (Å) and angles (°) for complex **6**

Mn1–O1	1.863(13)	Mn1–N1	2.029(17)
Mn1–O2	1.868(14)	Mn1–N2	2.017(17)
Mn1–O5	2.203(15)	Mn1–O6	2.275(14)
O1–Mn1–O2	86.5(6)	N2–Mn1–O5	90.5(7)
O1–Mn1–N2	90.6(7)	N1–Mn1–O5	89.3(6)
O2–Mn1–N2	177.0(6)	O1–Mn1–O6	89.8(6)
O1–Mn1–N1	176.5(7)	O2–Mn1–O6	91.2(6)
O2–Mn1–N1	91.1(6)	N2–Mn1–O6	87.8(7)
N2–Mn1–N1	91.8(7)	N1–Mn1–O6	87.7(6)
O1–Mn1–O5	93.3(6)	O5–Mn1–O6	176.5(6)
O2–Mn1–O5	90.5(5)		

vent to displace a water molecule during crystallisation, shows the bond lability of such coordinated molecules, which can be substituted by other substrates in catalytic processes.

The superstructure of the complex involves associations via a combination of π–aryl interactions and hydrogen bonds between capping water and phenoxy and methoxy oxygen atoms of the neighbouring Schiff base ligand (see Fig. 2). An extended spiral is formed as consequence of these interactions. This results in Mn–Mn distances of 5.08 Å, which are quite short for monomeric compounds; these types of systems have been reported in the literature [24] as μ-aquo dimers. We have previously proposed this type of structure as the active species in the photolytic splitting of water following a mechanism originally reported by us [15].

Recrystallisation of **1** gave crystals suitable for single-crystal X-ray diffraction studies. However, **1** shows the same crystal structure as a compound previously reported by us [23]. The related complex was obtained by a different method, by reorganisation of a MnL_2 complex (where L represents the asymmetrical Schiff base obtained by condensation of 8-amino-4-methyl-5-azaoct-3en-2-one and 5-chlorosalicyladehyde) in solution.

We have proposed a mechanism [25] for this rearrangement process which we have found a few times for unsymmetrical ligands; this reorganisation in solution indicates the higher stability of the symmetrical versus the unsymmetrical compound in this medium.

The crystal structure of **1** has essentially the same highlights as **6**. This fact, together with the comparison of other physical properties for all the complexes presented in this work, suggests a similar structure for all of them. Subsequently reported structures of comparable compounds support this idea [16,26].

3.5. Conductivity measurements

The conductivity data suggest a non-ionogenous nature for **2** and **5**, considering that their Λ_M values in DMF are 11.7 and 22.1 μS, respectively. In contrast, Λ_M values in acetone range from 115 to 140 μS for complexes **1**, **3**, **4**, **6** and **7**, indicating a behaviour attributable to 1:1 electrolytes [27].

3.6. Electrochemical studies

Cyclic voltammograms of the complexes were measured in dimethylformamide (DMF) over a potential range from +1.00 to −1.00 V. In DMF solution, all the complexes exhibit a quasi-reversible one-electron reduction–oxidation wave, which at slow scan rates of about 0.02 V s^{-1} is reversible (Fig. 3, Table 3). The reduction waves of **1**, **3**, **6** and **7** (−0.06, −0.13, −0.04, −0.35 V versus saturated calomel electrode, SCE) are observed at slightly negative potentials; meanwhile **2**, **4** and **5** have reduction waves (0.108, 0.04 and 0.168 V) at positive potentials.

Normal pulse voltammetry confirms the reversible nature of these systems. Thus cathodic or anodic currents were observed by this technique with reference to the current observed without electroactive compounds.

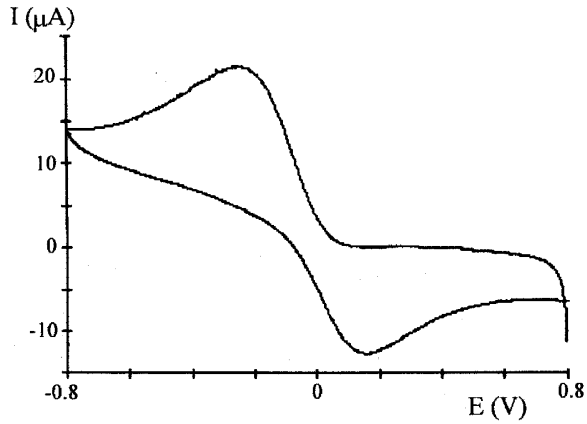


Fig. 3. Cyclic voltammogram for **6** at a scan rate of 0.02 V s^{-1}.

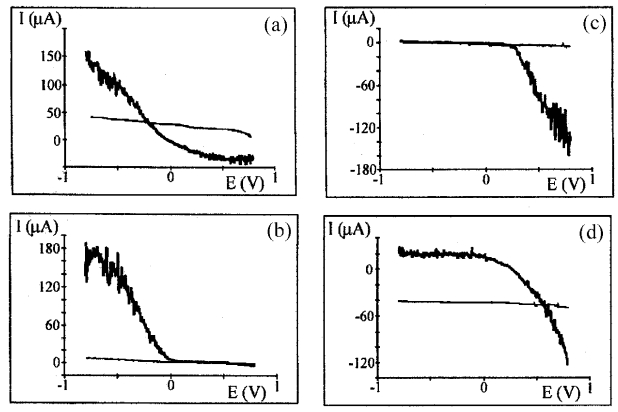


Fig. 4. Normal pulse voltamograms for **5** and **6**: (a) and (b) are, respectively, anodic and cathodic scans of **6**, a Mn(III) complex; (c) and (d) are, respectively, anodic and cathodic scans of **5**, a Mn(II) compound.

The study of these species by pulse voltammetry allows us to distinguish between Mn^{II} and Mn^{III} complexes as we have already reported [28].

Mn^{III} complexes (**1**, **3**, **4**, **6** and **7**) showed anodic and cathodic currents when an anodic potential scan was performed, but when a cathodic potential scan was used, only cathodic currents were observed (Fig. 4). This behaviour implies that only the oxidised forms of the implied redox systems Mn^{II}–Mn^{III} are present in solution.

However, **2** and **5** (Mn^{II} complexes) present the opposite behaviour: when the initial potentials were more positive than the wave range, both anodic and cathodic currents were observed, meanwhile only an anodic current was recorded when the initial potentials were more negative than the wave voltage range (Fig. 4). The presence of the redox systems Mn^{II}–Mn^{III} in reduced forms is in accordance with these voltammograms.

Magnetic measurements of the complexes have confirmed these oxidation states proposed by electrochemical studies.

The stabilisation of the manganese oxidation states (II), (III) or (IV) in complexes obtained by the Boucher method, is attributed to the electron donor or electron withdrawing character of the substituents about the phenyl ring of the Schiff base [28,29]. Thus, strong electron-withdrawing groups (e.g. nitro) stabilise Mn^{II} complexes and strong donor substituents lead to Mn^{IV} complexes [30–32].

3.7. Water photolysis experiments

The experiments were carried out in the presence of *p*-benzoquinone, a water-soluble hydrogen-atom acceptor. Photoactivated *p*-benzoquinone is able to abstract hydrogen atoms from H_2O [33]. Consequently, the role of this molecule in our system is similar to that of tyrosine in the natural PSII, as recent studies have pointed out [6].

Irradiation of Mn(III) complexes and *p*-benzoquinone solutions results in an increased dioxygen concentration in solution, as monitored by using an O_2 electrode (Table 4, Fig. 5) and conversion of the quinone to a hydroquinone, as determined by spectrophotometric monitoring of the reaction.

Awad and Anderson [34] have carried out a mechanistic quantum study of the photogeneration of O_2 from H_2O coordinated to active Mn^{III} complexes in the presence of *p*-benzoquinone. They suggest the possibility of dimerization by this type of $[LMn^{III}(H_2O)_2]$ monomers via μ-aquo bridges. They also propose that the H_2O molecules bonded to Mn^{III} in the monomer or as bridges in the Mn^{III} dimer starts off the reaction sequence by transferring a hydrogen atom to an O^- created by a $\pi^* \leftarrow n$ optical excitation in *p*-benzoquinone. As a result of this process, Mn^{III} is oxidised to Mn^{IV} and OH^- groups are tightly bound (Mn–O bond distance of 1.64 Å). The deprotonation of the OH^- groups is feasible because they are sufficiently polarised. The di-μ-oxo Mn^{IV} complex,

Table 3
Cyclic and normal pulse voltammetry data for the complexes at scan rate of 0.02 V s^{-1}; potential vs. SCE

Compound	E_{ox} (V)	E_{red} (V)	$E_{1/2}$ (V)	ΔE_{ox-red}	NPV [a]
1	−0.002	−0.064	−0.033	0.062	Mn^{III}
2	0.350	0.108	0.229	0.242	Mn^{II}
3	−0.028	−0.132	−0.080	0.104	Mn^{III}
4	0.102	0.040	0.071	0.062	Mn^{III}
5	0.492	0.168	0.330	0.324	Mn^{II}
6	0.068	−0.040	0.014	0.108	Mn^{III}
7	−0.204	−0.352	−0.278	0.148	Mn^{III}

[a] Normal pulse voltammetry indicates which is the oxidation state in solution (Mn^{II}/Mn^{III}).

Table 4
Variation of the percentages of saturation of O_2 during the photolysis experiments ($T = 25$°C; final measurements after 24 h) and values of the intensity of the wavelengths of the UV spectra corresponding to the $ABTS^+$ formed in the catalase experiments

Compound	% sat O_2		Absorbance of $ABTS^+$ UV signals			
	Initial	Final	λ = 415	λ = 650	λ = 735	λ = 815
1	3.0	11.0	0.061	0.036	0.038	0.045
2	2.8	9.0	0.080	0.026	0.030	0.027
3	3.0	5.0	0.122	0.035	0.057	0.051
4	2.5	14.2	0.200	0.067	0.076	0.075
5	3.0	7.0	0.082	0.041	0.041	0.050
6	2.4	5.1	0.206	0.068	0.097	0.092
7	3.0	8.2	0.103	0.042	0.040	0.058

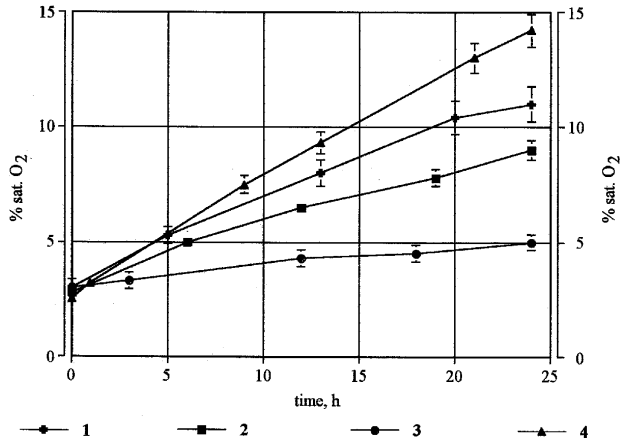


Fig. 5. Graph of percentage O_2 dissolved in solution vs. time for complexes **1**, **2**, **3** and **4**.

which forms either by oxidation of the H_2O-bridged Mn^{III} dimer or by dimerisation of oxidised monomers, cannot release O_2 because it is too stable. However, the disproportionation of two dimers together through a four-manganese intermediate can evolve O_2. This tetramanganese intermediate is reminiscent of the proposed structure of the natural OEC in the PSII.

In the case of the present complexes, it can be seen from Table 4 that most of them show slight catalytic activity. Complexes **1** and **4** show the highest rate of oxygen evolution. Thus, they have the greatest ability to split water. A comparison of these complexes shows one point in common: both of them contain a chlorine substituted Schiff base. These results confirm previous assumptions [15,32] and although it is not possible to establish a general pattern, it seems clear that halide substitution over the aromatic rings of the Schiff bases favours the photolytic activity.

3.8. Catalase probes

ABTS is a colourless water-soluble compound used for clinical peroxidase assays because of its excellent characteristics [35,36]. ABTS on oxidation forms a stable green cation radical ($ABTS^+$) with several strong absorptions in the visible and near-IR [37]. The formation of $ABTS^+$ is monitored conveniently at its wavelengths of 415, 650, 735 and 815 nm [38] and measured quantitatively at $\lambda = 650$ nm, since $\varepsilon = 12\,000\ M^{-1}\ cm^{-1}$ has been determined. The oxidation potentials of ABTS and the fully reduced species to provide $ABTS^+$ are invariable over a wide range of pH. In the absence of the complex, a solution of ABTS and H_2O_2 is stable for several hours without showing any formation of $ABTS^+$. The reaction of ABTS with H_2O_2 in the presence of **1**–**7** generates $ABTS^+$ and the characteristic absorption bands of this species could be established (Table 4, Fig. 6). Further oxidation to the corresponding dication [39] was not observed.

Nevertheless, the rate of formation of $ABTS^+$ of about 2% or even less indicates a poor capacity of disproportionation of H_2O_2 by the complexes. The present compounds do not seem to be efficient functional models for the reactivity of the manganese catalases, in contrast with other Mn–Schiff base systems. These results suggest the need for dimanganese sites involved in the catalase activity, since the monomeric complexes are insufficient models for this aim.

Probably, compounds of this type are able to bind directly the substrate, H_2O_2, by displacement of a water ligand molecule, but a subsequent oxidation of the hydroperoxide to

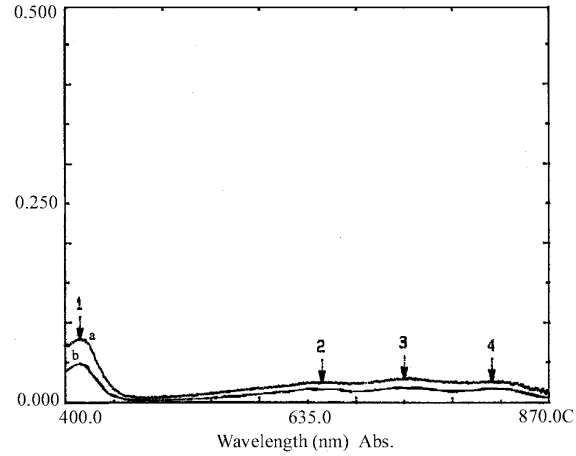


Fig. 6. UV–Vis absorption spectra of (a) $ABTS + H_2O_2 +$ **3**, (b) $ABTS + H_2O_2$, each recorded 10 min after mixing the solutions. (1) λ = 415; (2) λ = 650; (3) λ = 735; (4) λ = 815.

generate O_2 is forbidden, as this would involve an intramolecular two-electron transfer reaction that would reduce the manganese atom(s). The electrochemical studies of the present complexes showed their facility for one-electron oxidation–reduction between Mn^{II}–Mn^{III}, by reversible processes at potentials near to 0 V. Thus, we suppose that two manganese atoms are necessary for the implied two-electron transfer reaction. Thus, this binuclear system could suffer a two-electron reduction from {III,III} to {II,II}. Although crystallographic studies indicate an interaction between monomers by π stacking and H bonding, this feature is not enough to involve neighbouring manganese atoms in the electron transfer reaction once the substract is bound to the metal centre. The moderate extension of the catalase reaction for our complexes suggests a monomer/aquo-bridged dimer equilibrium in aqueous solution as reported for similar compounds [40].

The test of the catalase activity for new characterised manganese monomeric/dimeric complexes might confirm or reject their role in this catalysis because alternative mechanisms have been proposed [41] and monomers should not be set aside yet. In this sense, further studies are necessary in order to find better synthetic models of manganese catalases and to determinate their mechanism of action.

Supplementary data

Supplementary data are available from the CCDC, 12 Union road, Cambridge CB2 1EZ, UK on request, quoting the deposition number 127776.

Acknowledgements

The authors would like to thank Xunta de Galicia (Spain) for financial support (PGIDT99PXI20903B). One of us (M.M.) thanks Universidad de Santiago de Compostela (USC) for a postdoctoral fellowship.

References

[1] C. Tommos, G.T. Babcock, Acc. Chem. Res. 31 (1998) 18.
[2] K. Wieghardt, Angew. Chem., Int. Ed. Engl. 28 (1989) 1153.
[3] V.K. Yachandra, K. Sauer, M.P. Klein, Chem. Rev. 96 (1996) 2927.
[4] R.D. Britt, in: D.R. Ort, C.F. Yocum (Eds.), Oxygenic Photosynthesis: The Light Reactions, Kluwer, Dordrecht, 1996, p. 137.
[5] V.K. Yachandra, V.J. DeRose, M.J. Latimer, I. Mukerji, K. Sauer, M.P. Klein, Science 260 (1993) 675.
[6] C.W. Hoganson, G.T. Babcock, Science 277 (1997) 1953.
[7] V.L. Pecoraro, M.J. Baldwin, A. Gelasco, Chem. Rev. 94 (1994) 807.
[8] W. Rüttinger, G.C. Dismukes, Chem. Rev. 97 (1997) 5.
[9] See, for example: W. Rüttinger, C. Campana, G.C. Dismukes, J. Am. Chem. Soc. 1196 (1997) 670.
[10] M.N.C. Dunand-Sauthier, A. Deronzier, A. Piron, X. Pradon, S. Mènage, J. Am. Chem. Soc. 120 (1998) 5373.
[11] L. Stelzig, A. Steiner, B. Chansou, J.P. Tuchages, Chem. Commun. (1998) 771.
[12] F.M. Ashmawy, C.A. McAuliffe, R.V. Parish, J. Tames, J. Chem. Soc., Dalton Trans. (1985) 1391.
[13] R. Ramaraj, A. Kira, M. Kaneko, Angew. Chem., Int. Ed. Engl. 25 (1986) 825.
[14] J. Limburg, J.S. Vrettos, L.M. Liable-Sands, A.L. Rheingold, R.H. Crabtree, G.W. Brudvig, Science 283 (1999) 1524.
[15] N. Aurangzeb, C.E. Hulme, C.A. McAuliffe, R.G. Pritchard, M. Watkinson, M.R. Bermejo, A. García-Deibe, M. Rey, J. Sanmartín, A. Sousa, J. Chem. Soc., Chem. Commun. (1994) 1153.
[16] M.R. Bermejo, M. Fondo, A. García-Deibe, M. Rey, J. Sanmartín, A. Sousa, M. Watkinson, C.A. McAuliffe, R.G. Pritchard, Polyhedron 15 (1996) 4185.
[17] G.C. Dismukes, Chem. Rev. 96 (1996) 2909.
[18] M.M. Grush, J. Chen, T.L. Stemmler, S.J. George, C.Y. Ralston, R.T. Stibrany, A. Gelasco, S.M. Gorun, J.E. Penner-Hahn, S.P. Cramer, J. Am. Chem. Soc. 118 (1996) 65.
[19] A. Gelasco, S. Bensiek, V.L. Pecoraro, Inorg. Chem. 37 (1998) 3301.
[20] L.J. Boucher, C.G. Coe, Inorg. Chem. 14 (1975) 1289.
[21] G.M. Sheldrick, Acta Crystallogr., Sect. A 46 (1990) 467.
[22] G.M. Sheldrick, SHELX-97, Program for Crystal Structure Refinement, University of Göttingen, Germany, 1997.
[23] C.A. McAuliffe, R.G. Pritchard, A. García-Deibe, A. Sousa, M.R. Bermejo, Acta Crystallogr., Sect. C 48 (1992) 364.
[24] F.M. Ashmawy, B. Beagley, C.A. McAuliffe, R.V. Parish, R.G. Pritchard, J. Chem. Soc., Chem. Commun. (1990) 936.
[25] M.R. Bermejo, A. García-Deibe, M. Rey, J. Sanmartín, A. Sousa, N. Aurangzeb, C.E. Hulme, C.A. McAuliffe, R.G. Pritchard, M. Watkinson, M. Helliwell, J. Chem. Soc., Dalton Trans. (1994) 1265.
[26] A. García-Deibe, M.R. Bermejo, A. Sousa, C.A. McAuliffe, P. McGlynn, P.T. Ndifon, R.G. Pritchard, J. Chem. Soc., Dalton Trans. (1993) 1605.
[27] W.I. Geary, Coord. Chem. Rev. 7 (1971) 81.
[28] M.R. Bermejo, A. Castiñeiras, J.C. García-Monteagudo, M. Rey, A. Sousa, M. Watkinson, C.A. McAuliffe, R.G. Pritchard, R.L. Beddoes, J. Chem. Soc., Dalton Trans. (1996) 2935.
[29] J.A. Bonadies, M.J. Maroney, V.L. Pecoraro, Inorg. Chem. 28 (1989) 2044.
[30] M.J. Baldwin, T.L. Stemmler, P.J. Riggs-Gelasco, M.L. Kirk, J.E. Penner-Hahn, V.L. Pecoraro, J. Am. Chem. Soc. 116 (1994) 11349.
[31] M. Watkinson, M. Fondo, M.R. Bermejo, A. Sousa, C.A. McAuliffe, R.G. Pritchard, N. Jaiboon, N. Aurangzeb, M. Naeem, J. Chem. Soc., Dalton Trans. (1999) 31.
[32] M. Maneiro, M.R. Bermejo, A. Sousa, M. Fondo, J. Sanmartín, J.C. García-Monteagudo, C.A. McAuliffe, R.G. Pritchard, V.V. Lukov, J. Chem. Soc., Dalton Trans. (submitted for publication).
[33] A.I. Ononye, A.R. McIntosh, J.R. Bolton, J. Phys. Chem. 90 (1986) 6266.
[34] M.K. Awad, A.B. Anderson, J. Am. Chem. Soc. 111 (1989) 802.
[35] H. Gallati, J. Clin. Biochem. 17 (1979) 1.
[36] J. Puetter, R. Becker, in: H.U. Bergmeyer (Ed.), Methods of Enzymatic Analysis, vol. 3, Verlag Chemie, Weinheim, 3rd edn., 1983, p. 286.
[37] M.F. Zipplies, W.A. Lee, T.C. Bruice, J. Am. Chem. Soc. 108 (1986) 4433.
[38] B. Eulering, M. Schmidt, V. Pinkernell, U. Karst, B. Krebs, Angew. Chem., Int. Ed. Engl. 35 (1996) 1973.
[39] S. Hüning, H. Balli, H. Conrad, A. Schott, Justus Liebigs Ann. Chem. 676 (1964) 36.
[40] F.M. Ashmawy, C.A. McAuliffe, R.V. Parish, J. Tames, J. Chem. Soc., Chem. Commun. (1984) 14.
[41] A.E. Meier, M.M. Whitaker, J.W. Whitaker, Biochemistry 35 (1996) 348.

PERGAMON

www.elsevier.nl/locate/poly

Polyhedron 19 (2000) 55–61

POLYHEDRON

Solution speciation and spectral studies on oxovanadium(IV) complexes of pyridinecarboxylic acids

E. Kiss [a], K. Petrohán [a], D. Sanna [b], E. Garribba [b], G. Micera [b], T. Kiss [c,*]

[a] *Department of Inorganic and Analytical Chemistry, Lajos Kossuth University, PO Box 21, H-4010 Debrecen, Hungary*
[b] *Dipartimento di Chimica, Università di Sassari, Via Vienna 2, I-07100 Sassari, Italy*
[c] *Department of Inorganic and Analytical Chemistry, Attila József University, PO Box 440, H-6701 Szeged, Hungary*

Received 8 June 1999; accepted 20 October 1999

Abstract

Complex formation between oxovanadium(IV) and several pyridinecarboxylic acids (picolinic acid, 3-hydroxypicolinic acid and 2-hydroxynicotinic acid) was studied in aqueous solution by pH-potentiometric and spectroscopic (electron paramagnetic resonance and electronic absorption) techniques. The results demonstrated that picolinic acid forms mono and bis complexes with the VO(IV) ion, coordinated through the pyridine nitrogen and the carboxylate group. The pyridine nitrogen is also involved in the complexation of VO(IV) by 3-hydroxypicolinic acid and 2-hydroxynicotinic acid in the acidic pH range, but as the pH is increased deprotonation of the phenolic hydroxy group occurs and complexes with salicylate-type (COO^-,O^-)-coordination are formed. In the VO(IV)–3-hydroxypicolinic acid system, the ligand coordinates to the metal ion in a tridentate fashion via the (N,COO^-,O^-) donor set, forming a tetrameric complex $(VOA)_4$ in the pH range 6–8. ©2000 Elsevier Science Ltd All rights reserved.

Keywords: Oxovanadium(IV) complexes; Pyridinecarboxylic acids; pH-metry; Spectral studies; Speciation

1. Introduction

Vanadium is an important trace element for different organisms. Oxovanadium(IV) and vanadate(V) are the main species present in solution under physiological conditions. The physiological effects are in many cases a consequence of the good complexation behaviour of the VO^{2+} ion, and the chemical similarity between phosphate and vanadate. A few vanadium compounds seem to have therapeutic effects [1]. One of the results of the intensive investigation of vanadium over the past two decades has been the discovery that vanadium compounds have insulin-mimetic properties [2]. Among others, bis(picolinato)oxovanadium(IV) [$VO(pic)_2$] has proved to be an orally active and long-acting insulin-mimetic compound with which insulin-dependent diabetes mellitus (IDDM) may be treated in rats [3].

Vanadium in its oxidation states +4 and +5 is able to interact with metal ion binders of biological systems containing negatively charged oxygen donors such as carboxylate, phenolate, phosphate, phosphonate, catecholate and hydroxamate [4–10]. Its interactions with small biomolecules containing nitrogen and sulfur atoms are weaker than those with oxygen donors. Picolinic acid (pyridine-2-carboxylic acid) contains a carboxylic group, which has significant affinity for the VO(IV) ion, and a pyridine nitrogen in a sterically favourable position to this group. Hence, the formation of (N,COO^-) chelates can be expected.

Pyridinecarboxylic acids and their derivatives are present in many natural products. They are also of special interest to medicinal chemists because of the wide variety of physiological properties displayed by the natural and also many synthetic derivatives [11]. Metal complexes of pyridinecarboxylic acids are particularly interesting model systems because of their physiological properties.

Complex formation in the VO(IV)–picolinic acid system was studied earlier [12–16], but to our knowledge, no data on the formation of VO(IV) complexes with 3-hydroxypicolinic acid or 2-hydroxynicotinic acid have been reported so far.

The interactions of VO(IV) with picolinic acid in the absence and presence of some dicarboxylic acids (oxalic, phthalic and maleic acids) has been studied by potentiometry. The formation of (N,COO^-)-coordinated 1:1 and 1:2 VO(IV)–picolinate chelates and the hydrolysis of VOA were indicated. In the ternary systems, 1:1:1 mixed ligand com-

* Corresponding author. Fax: +36 62 420505; e-mail: tkiss@chem.u-szeged.hu

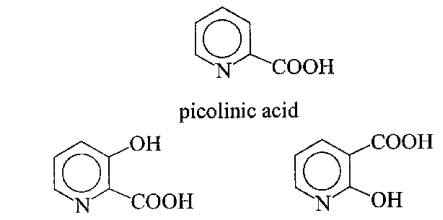
0277-5387/00/$ - see front matter ©2000 Elsevier Science Ltd All rights reserved.
PII S0277-5387(99)00323-X

plexes were also observed [12]. The results were recently confirmed by Duma and Hancock, who also detected the formation of complexes of the same type, VOA and VOA_2 [13]. The tendency of the VO(IV)–picolinate chelates to undergo hydrolysis was studied by Kaden and Fallab, who provided spectrophotometric evidence that OH^- is in a *trans* position to the VO group in the mixed hydroxo complex $VOA_2(OH)$ [14]. The bis(picolinato)oxovanadium(IV) complex has been isolated in the solid form and characterised by elemental analysis, visible and IR absorption, electron spin resonance spectra, magnetic susceptibility and partition coefficient. The relationship between its structure and insulin-mimetic activity has also been examined [15].

Vanadium in oxidation states other than +4 also forms stable complexes with picolinic acid. The synthesis, structural characterisation and reactivity of a highly stable vanadium(III) complex of picolinic acid, $V(pic)_3 \cdot H_2O$, have been reported. An X-ray diffraction study revealed that the pyridine nitrogen and the carboxylate oxygen are coordinated to the metal ion and the vanadium is in a highly distorted octahedral environment [17].

The interactions of vanadate(V) with picolinic acid, 3-hydroxypicolinic acid and 2-hydroxynicotinic acid in aqueous solution have been studied by using ^{51}V NMR spectroscopy [18]. Picolinic acid proved to form mono and bis chelates, although interaction between the pyridine-N and vanadate(V) is not favoured. 3-Hydroxypicolinic acid forms a mixture of complexes, through condensation of vanadate with the nitrogen and carboxylate and possibly with the carboxylate and the hydroxy groups. 2-Hydroxynicotinic acid reacts as a weak chelating ligand to give a complex in which the carboxylate and the adjacent OH group are coordinated to the vanadate [18].

In the present work we have studied the complexation of VO(IV) with picolinic acid, 3-hydroxypicolinic acid or 2-hydroxynicotinic acid (Scheme 1) in order to establish how the position of a further strong VO(IV)-binder, a phenolate, affects the binding properties of the ligand. We report here the coordination properties of the above-mentioned three pyridinecarboxylic acids with the VO(IV) ion. Their solution speciation was studied by pH-potentiometric and spectral (EPR and electronic absorption) methods.



Scheme 1.

2. Experimental

2.1. Chemicals

The ligands (Sigma or Fluka products of the highest available quality) were used without further purification. Their purities were checked and the exact concentrations of solutions were determined by the Gran method [19]. The oxovanadium(IV) stock solution was prepared as described in Ref. [20] and standardised for metal ion concentration by permanganate titration and for hydrogen ion concentration by potentiometry, using the appropriate Gran function. The ionic strength was adjusted to 0.20 mol dm^{-3} KCl in each solution studied. In all cases, the temperature was 25.0 ± 0.1°C.

2.2. Potentiometric measurements

The stability constants of the proton and VO(IV) complexes of the ligands were determined by pH-potentiometric titration of 25.0 cm^3 samples. The ligand concentration was 0.004 mol dm^{-3} or 0.006 mol dm^{-3} and the metal ion to ligand molar ratio was 0:1, 1:1, 1:2 or 1:4 (plus 1:6 and 1:8 for the VO(IV)–2-hydroxynicotinic acid system).

pH was measured with a Radiometer pHM 84 instrument equipped with a Metrohm combined glass electrode, calibrated for hydrogen ion concentration according to Irving et al. [21]. pK_w calculated from strong acid–strong base titrations was 13.76 ± 0.01. The titrations of the systems were performed in the pH range 2–11, or until precipitation occurred, with a carbonate-free KOH solution of known concentration ($\sim$0.2 mol dm^{-3}) under an argon atmosphere, in order to avoid the oxidation of the metal ion.

Equilibria corresponding to the formation of the hydroxo complexes of VO(IV) were taken into account in the calculation of the stability constants of the complexes. The following species were assumed: $[VO(OH)]^+$ ($\log \beta_{1-1} = -5.94$), $[(VO)_2(OH)_2]^{2+}$ ($\log \beta_{2-2} = -6.95$, calculated from the data published by Henry et al. [22], the Davies equation being used to take into account the different ionic strengths), $[VO(OH)_3]^-$ ($\log \beta_{1-3} = -18.0$) and $[(VO)_2(OH)_5]^-$ ($\log \beta_{2-5} = -22.0$, taken from Ref. [23]).

The concentration stability constants $\beta_{pqr} = [M_pA_qH_r]/[M]^p[A]^q[H]^r$ were calculated with the PSEQUAD computer program [24].

2.3. Spectroscopic measurements

In order to confirm the speciation results and establish the binding modes of the ligands in the complexes, spectral measurements were performed. Anisotropic X-band EPR spectra (9.15 GHz) were recorded at 140 K in aqueous solutions, with a Varian E-9 spectrometer using quartz tubes. As usual, the samples for low-temperature measurements contained a few drops of DMSO to ensure good glass formation in frozen solutions. Absorption spectra were recorded with a Hewlett

Packard HP 8453 spectrophotometer. All manipulations and titrations were carried out under an atmosphere of argon.

3. Results and discussion

The protonation constants of picolinic acid (HA), 3-hydroxypicolinic acid (H_2A) and 2-hydroxynicotinic acid (H_2A) are listed in Table 1. The significant decreases in acidity of the carboxylic group in the 3-hydroxypicolinic acid and 2-hydroxynicotinic acid ligands ($\log K(COO^-) \sim 1$) can be attributed to the formation of intramolecular hydrogen-bonding between the COO^- and the phenolic-OH, and in the case of picolinic acid between the COO^- and NH^+ groups, which makes the liberation of the first proton more favoured. The protonation constant of the pyridine nitrogen is about 10^5, as in pyridine itself ($\log K = 5.24$ [25]) and its derivatives 3-hydroxypyridine ($\log K = 4.89$ [26]) and nicotinic acid ($\log K = 4.66$ [26]). The basicity of the phenolic group is increased significantly as compared with phenol ($\log K = 9.82$ [27]), 2-hydroxypyridine ($\log K = 9.5$ [26]) and 3-hydroxypyridine ($\log K = 8.50$ [26]). The phenolic pK of the ligands is high, as in the case of salicylic acid ($\log K = 13.4$ [28]). This is again a result of stabilisation of the monoprotonated, hydrogen-bonded forms of the ligands. The protonation constants presented here for these ligands are in good agreement with those reported in previous papers, when the difference in ionic strength is taken into account [13–16,29,30].

3.1. Complexes of picolinic acid

Picolinic acid forms mono and bis complexes with the VO(IV) ion (Table 2). The concentration distribution curves for the complexes formed as a function of pH are depicted in Fig. 1. The complexation starts with formation of complexes VOA and VOA_2 at pH < 2 [16]. In VOA, the pyridine nitrogen and the carboxylate group of the ligand coordinate to the metal ion and form a five-membered chelate. The EPR spectra confirm this binding mode, as the mono-chelated species VOA has the following parameters: $g_\parallel = 1.939$, $A_\parallel = 175 \times 10^{-4}$ cm^{-1}. The bis complex is the predominant species in the pH range 3–6.5. The spectral parameters remain unchanged in this pH range, which suggests the exclusive formation of a single species ($g_\parallel = 1.945$, $A_\parallel = 165 \times 10^{-4}$ cm^{-1}, λ_{max} (ε (mol^{-1} cm^{-1} dm^3)) 735 nm (35), 547 nm (16) (shoulder)). On the basis of the additivity rules for the coupling constant of VO(IV) complexes [31], the EPR parameters could be supportive of two N donors in the equatorial plane of the metal ion. The behaviour of the system suggests a *cis* geometrical isomeric form, in which one of the ligands occupies two equatorial sites, while the other adopts an equatorial–axial coordination mode, presumably with the carboxylate group as the apical donor, and a water molecule in *cis* position to the oxo group of VO(IV) completes the donor set in the equatorial plane [15]. In fact, in the presence of an excess of ligand, deprotonation of the complex VOA_2 occurs, with p$K = 6.98$. This value is lower than expected for the ionisation of a weakly bound axial water molecule, and suggests the deprotonation of an equatorial water molecule. Therefore, both the observation of an EPR-active species VOA_2H_{-1} and the concomitant spectral change ($g_\parallel = 1.947$, $A_\parallel = 160 \times 10^{-4}$ cm^{-1}) support the *cis* arrangement of the coordinating ligands in VOA_2. At pH > 8, stepwise displacement of the ligands by hydroxide ion takes place and through a dihydroxo bridged mixed hydroxo complex $(VOAH_{-1})_2$, and results in the formation of oligonuclear binary hydroxo complexes, which is supported by the disappearance of the EPR signal.

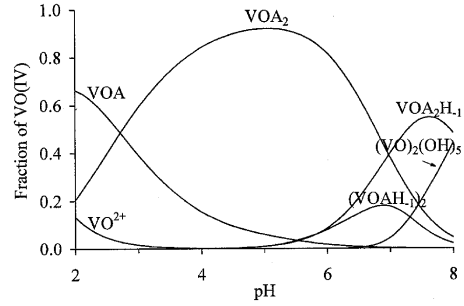


Fig. 1. Speciation curves for complexes formed in the VO(IV)–picolinic acid system, $c_{VO(IV)} = 0.002$ mol dm^{-3} and $c_{ligand} = 0.004$ mol dm^{-3}.

Table 1
Protonation constants of picolinic acid, 3-hydroxypicolinic acid and 2-hydroxynicotinic acid at 25.0 ± 0.1°C and $I = 0.20$ mol dm^{-3} (KCl)

log K	Picolinic acid	3-Hydroxypicolinic acid	2-Hydroxynicotinic acid
HA	5.19(2)	10.9(1)	11.9(2)
H_2A	~1	5.08(2)	4.98(2)
H_3A		~1	<1

Table 2
VO(IV) ($\log \beta_{pqr}$) stability constants for the complexes of picolinic acid at 25.0 ± 0.1°C and $I = 0.20$ mol dm^{-3} (KCl)

Complex	$\log \beta_{pqr}$
VOA	6.66(2)
$(VOAH_{-1})_2$	6.15(3)
VOA_2	12.11(2)
VOA_2H_{-1}	5.13(3)
Fitting [a]	1.38×10^{-2}
No. points	202

[a] The average difference between the calculated and experimental titration curves expressed in cm^3 of titrant.

3.2. Complexes of 3-hydroxypicolinic acid

Because of the spatial arrangement of the donor groups, the molecule can form complexes with metal ions through the pyridine nitrogen and carboxylate group (picolinate-like coordination) or carboxylate and phenolate groups (salicylate-like coordination). For steric reasons, the three donor groups cannot coordinate to the same metal ion simultaneously. Stability constants for the VO(IV) complexes of 3-

hydroxypicolinic acid, and the derived equilibrium constants calculated for different complex formation steps, are listed in Tables 3 and 4. For comparison, some derived equilibrium constants for the VO(IV) complexation of picolinic acid and salicylic acid are also listed in Table 4.

Analysis of the pH-potentiometric titration curves indicates the liberation of two protons per ligand molecule, by pH ~ 5, i.e. the formation of a species with the stoichiometry VOA or $(VOA)_n$. All dissociable protons can be liberated from the ligand molecule by pH ~ 5 only through its tridentate coordination: in the case of bidentate picolinate-type or salicylate-type coordination, the non-coordinated third donor (phenolate-O or pyridine-N, respectively) remains protonated. Molecular modelling indicates that tridentate coordination cannot occur in monomeric, dimeric or trimeric forms; the tetrameric complex is the lowest oligomer where the steric conditions allow this type of coordination. Accordingly, titration curves were evaluated with a tetrameric species $(VOA)_4$ in addition to the relevant mononuclear complexes.

A comparison of the derived equilibrium data calculated for the VO(IV)–3-hydroxypicolinato complexes involving the different binding modes with those of the VO(IV)–picolinic acid and VO(IV)–salicylic acid model systems suggests the dominant binding modes in the complexes (see Table 4). In the equations for the calculation of these derived constants, 3-hydroxypicolinic acid is denoted as (H)A(H) (more precisely $^{+}$HNAOH, in which $^{+}$HN means the imino group, while OH means the phenolic-OH group).

The speciation curves calculated with the stability constants listed in Table 3 are depicted in Fig. 2. The EPR spectra of the 1:2 VO(IV)–ligand system at different pH values are shown in Fig. 3. It is seen from the speciation diagram that complexation starts with the formation of VOAH in the acidic pH range. The ligand coordinates through the pyridine nitrogen and the carboxylate group, as in the VO(IV)–picolinic acid complex. This binding mode is confirmed by comparison of the EPR parameters of the complex VOAH ($g_{\parallel} = 1.938$, $A_{\parallel} = 174 \times 10^{-4}$ cm^{-1}) with those of VOA formed with picolinic acid (vide extra) and by the good agreement between the derived constants (see first row in Table 4).

In the pH range 3–5, the complex VOA_2H_2 is also formed in considerable amounts at a ligand excess. In this complex, a $2\times$(N,COO$^-$) coordination mode and a *cis* arrangement are again consistent with the derived data of the two bis

Table 3
VO(IV) (log β_{pqr}) stability constants for the complexes of 3-hydroxypicolinic acid at 25.0 ± 0.1°C and $I = 0.20$ mol dm^{-3} (KCl)

Complex	Log β_{pqr}
VOAH	17.27(3)
VOA_2H_2	33.93(2)
VOA_2H	28.31(4)
VOA_2	20.50(3)
VOA_2H_{-1}	10.03(4)
$(VOA)_4$	66.70(8)
Fitting [a]	1.54×10^{-2}
No. points	290

[a] The average difference between the calculated and experimental titration curves expressed in cm^3 of titrant.

Table 4
Some derived constants for the VO(IV) complexes of picolinic acid, 3-hydroxypicolinic acid and salicylic acid at 25.0 ± 0.1°C and $I = 0.20$ mol dm^{-3} (KCl)

Reaction	Picolinic acid	3-Hydroxy-picolinic acid	Salicylic acid [27]
VO + A(H) = VOA(H)	6.66	6.37	
VO + (H)A = VO(H)A		12.19	12.97
VOA(H) + A(H) = VO[A(H)]$_2$	5.45	5.76	
VO(H)A + (H)A = VO[(H)A]$_2$		11.58	9.84
log(K_1/K_2)	1.21	0.61	3.13

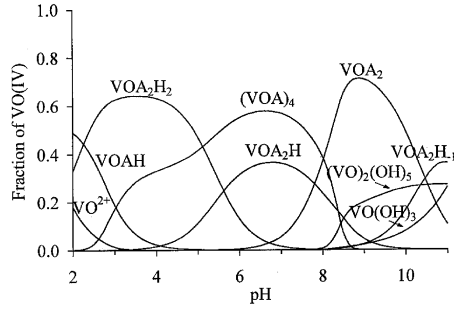


Fig. 2. Speciation curves for complexes formed in the VO(IV)–3-hydroxypicolinic acid system, $c_{VO(IV)} = 0.002$ mol dm^{-3} and $c_{ligand} = 0.004$ mol dm^{-3}.

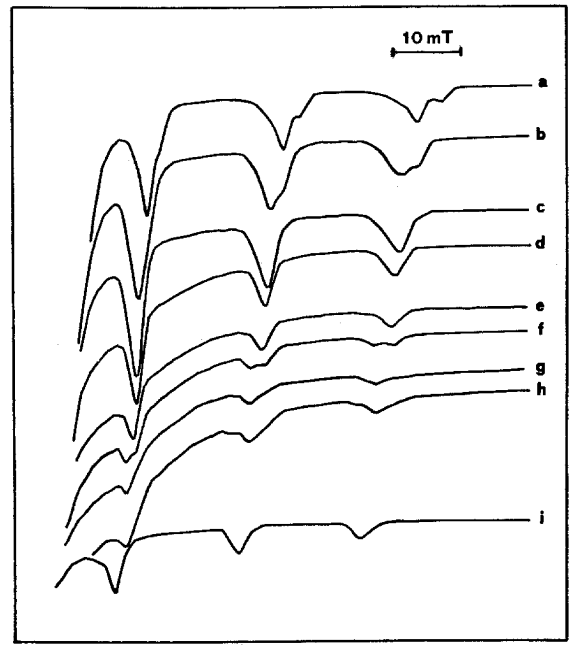
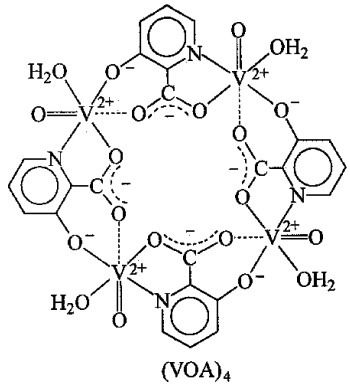


Fig. 3. High field parallel region of frozen solution EPR spectra (X-band) recorded at 140 K on the VO(IV)–3-hydroxypicolinic acid 1:2 system at various pH values: (a) 1.95, (b) 2.30, (c) 3.00, (d) 6.30, (e) 7.35, (f) 8.35, (g) 9.13, (h) 10.20, (i) 10.95. $c_{VO(IV)} = 0.004$ mol dm^{-3}.

complexes (cf. log $K = 5.76$ for VOA_2H_2 and log $K = 5.45$ for $VO(pic)_2$). The low values of $\log(K_1/K_2)$, indicating the favoured coordination of the second ligand, confirm picolinate-like binding. However, on the basis of the EPR parameters (cf. $g_\parallel = 1.940$, $A_\parallel = 170 \times 10^{-4}$ cm^{-1} for VOA_2H_2 and $g_\parallel = 1.945$, $A_\parallel = 165 \times 10^{-4}$ cm^{-1} for VOA_2 formed with picolinic acid), a *cis* arrangement involving one of the N atoms in the apical position is more likely. The salicylate-like (COO^-,O^-)-coordination mode in these species VOAH and VOA_2H_2 (with the protonated pyridine nitrogen) is less likely, as substantiated by a comparison of the derived constants and the EPR parameters (see the data in rows 2, 4 and 5 of Table 4).

As discussed above, an oligomeric complex, presumably $(VOA)_4$, is assumed in the pH range 6–8. Molecular modelling demonstrates that, while dimeric or trimeric species involve considerable steric hindrance, a cyclic tetramer can be formed without any strain provided that one of the carboxylate oxygens coordinates to vanadium in the apical position and there is a water molecule in the equatorial plane of the metal ion (see Scheme 2). The EPR results also suggest the oligonuclear model: in the pH range 6–8, a broad, featureless band is observed at $g = 2$, indicating a significant interaction between the paramagnetic centres (Fig. 4). This broad band is superimposed by signals due to mononuclear complexes formed at low concentration. The visible spectral parameters for this complex (λ_{max} (ε (mol^{-1} cm^{-1} dm^3)) 775 nm (43), 550 nm (20) (shoulder)) are similar for those of 1:2 VO(IV)–salicylate (775 nm (42), 562 nm (27)) [27].



Scheme 2.

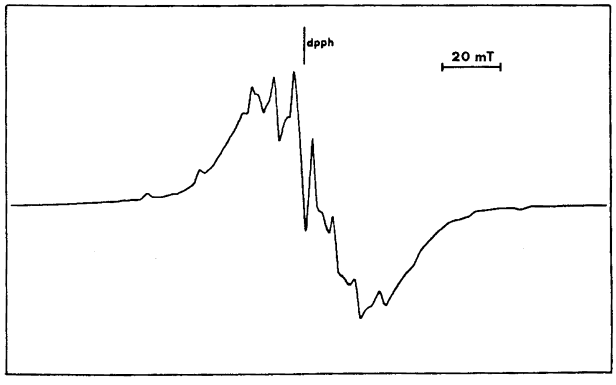


Fig. 4. Frozen solution EPR spectrum recorded at 140 K on the VO(IV)–3-hydroxypicolinic acid 1:1 system at pH 7.65. $c_{VO(IV)} = 0.004$ mol dm^{-3}.

At an excess of ligand, in addition to formation of the tetrameric species, stepwise deprotonation of the complex VOA_2H_2 occurs. These processes are accompanied by a continuous rearrangement from the picolinate-like coordination to the salicylate-type coordination via a mixed binding mode. The EPR parameters of the complex VOA_2H ($g_\parallel = 1.943$, $A_\parallel = 167 \times 10^{-4}$ cm^{-1}) indicate a (N,COO^-)(COO^-,O^-) donor set, with the stronger N and O donors in the equatorial plane. The parameters for VOA_2 ($g_\parallel = 1.946$, $A_\parallel = 165 \times 10^{-4}$ cm^{-1}) are similar to those of some salicylate derivatives (e.g. $g_\parallel = 1.947$, $A_\parallel = 166 \times 10^{-4}$ cm^{-1} for the complex VOA_2 of 2,4-dihydroxybenzoic acid [28]) and again indicate $2 \times (COO^-,O^-)$ coordination with the stronger donors in the equatorial plane of the metal ion. The complex VOA_2 loses a proton from the coordinated water molecule with p$K = 10.47$ and a mixed hydroxo complex is formed ($VOA_2H_{-1} = VOA_2(OH)$) with EPR parameters $g_\parallel = 1.950$ and $A_\parallel = 161 \times 10^{-4}$ cm^{-1}. The EPR detection of this species indicates that in VOA_2 the two ligands adopt a *cis* arrangement, with a carboxylate group in the axial position. The deprotonation of the water molecule, i.e. replacement of the water molecule by a hydroxo ligand, is consistent with the spectral change. The p*K* value is significantly higher than the corresponding one measured with picolinic acid (see Table 2), probably as a consequence of the negative charge of VOA_2.

3.3. Complexes of 2-hydroxynicotinic acid

2-Hydroxynicotinic acid is a constitutional isomer of 3-hydroxypicolinic acid (Scheme 1). The stability constants and speciation curves for the VO(IV) complexes of 2-hydroxynicotinic acid (Table 5, Fig. 5) reveal that the complex-forming properties of 2-hydroxynicotinic acid are rather different from those of 3-hydroxypicolinic acid. Depending on the metal ion to ligand ratio, a precipitate starts to form in the pH range pH 4–5.5 in samples with 1:1, 1:2 or 1:4 metal ion to ligand ratios; this dissolves by pH > 9, where only binary hydroxo complexes of VO(IV) can be detected. However, titrations could be carried out without precipitation

Table 5
VO(IV) (log β_{pqr}) stability constants for the complexes of 2-hydroxynicotinic acid at 25.0 ± 0.1°C and $I = 0.20$ mol dm^{-3} (KCl)

Complex	Log β_{pqr}
VOAH	17.30(3)
VOA_2H_2	33.71(3)
VOA_2H	26.69(8)
VOA_2	19.09(9)
VOA_2H_{-1}	10.71(11)
Fitting [a]	1.61×10^{-2}
No. points	291

[a] The average difference between the calculated and experimental titration curves expressed in cm^3 of titrant.

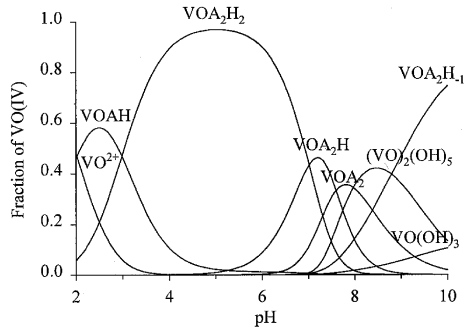


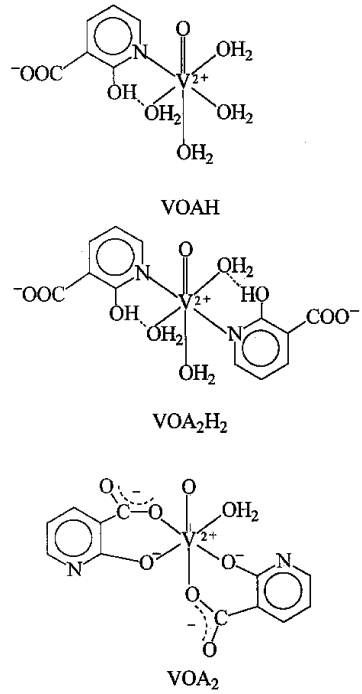
Fig. 5. Speciation curves for complexes formed in the VO(IV)–2-hydroxynicotinic acid system, $c_{VO(IV)} = 0.0006$ mol dm^{-3} and $c_{ligand} = 0.0036$ mol dm^{-3}.

throughout the whole pH range at metal ion to ligand ratios of 1:6 and 1:8. It is seen in Fig. 5 that at low pH, complexation starts with the monoprotonated 1:1 complex VOAH (λ_{max} (ε (mol^{-1} cm^{-1} dm^3)) 780 nm (30), 600 nm (12)), while the species VOA_2H_2 (λ_{max} (ε (mol^{-1} cm^{-1} dm^3)) 803 nm (49), 595 nm (24)) is predominant in the pH range 3.5–6.5. This latter neutral complex has rather low solubility in water and is precipitated at lower excesses of ligand. For example, at a metal ion concentration of 4×10^{-3} mol dm^{-3} precipitation of the complex is almost complete by pH ~ 5.5 and samples display hardly any EPR activity. However, in more dilute solutions at a metal ion concentration of 5×10^{-4} mol dm^{-3} and at high excesses of ligand (higher than 1:6), oversaturated solutions are probably formed, this being the reason why this complex could be studied by both potentiometry and spectroscopy. The derived equilibrium constant calculated for the VO(IV) complexes of 2-hydroxynicotinic acid and for comparison for those of salicylic acid may help us to suggest the most likely binding modes of the ligands in the complexes formed. For instance, the equilibrium constant obtained for the 1:1 complex VOAH of 2-hydroxynicotinic acid assuming salicylate-type (COO^-,O^-) coordination mode is in fairly good agreement with that for the analogous complex of salicylic acid (see rows 1 and 4 in Table 6). There is, however, a large difference in the ratio of the stepwise formation constants of the 1:1 and 1:2 complexes ($\log(K_1/K_2)$) of 2-hydroxynicotinic acid and salicylic acid (see rows 3 and 6 in Table 6), that cannot be explained. Accordingly, salicylate-type coordination of the ligand in the protonated complexes VOAH and VOA_2H_2 is very unlikely.

Table 6
Some derived constants for the VO(IV) complexes of 2-hydroxynicotinic acid and salicylic acid at 25.0 ± 0.1°C and $I = 0.20$ mol dm^{-3} (KCl)

Ligand	Reaction	log K
2-Hydroxynicotinic acid	VO + (H)A = VO(H)A	12.32
	VO(H)A + (H)A = VO(H)$_2$A$_2$	11.43
	$\log(K_{VOAH}/K_{VOA_2H_2})$	0.89
Salicylic acid [27]	VO + A = VOA	12.97
	VOA + A = VOA_2	9.84
	$\log(K_{VOA}/K_{VOA_2})$	3.13

In fact, the EPR data ($g_\parallel = 1.938$, $A_\parallel = 175\times10^{-4}$ cm^{-1} for VOAH; $g_\parallel = 1.942$, $A_\parallel = 168\times10^{-4}$ cm^{-1} for VOA_2H_2) are more consistent with the coordination of nitrogen donors. Similar parameters have been observed for the monodentate coordination of imidazole and pyrazole ligands to VO(IV) (imidazole: $g_\parallel = 1.938$, $A_\parallel = 177\times10^{-4}$ cm^{-1} for VOA, $g_\parallel = 1.943$, $A_\parallel = 171\times10^{-4}$ cm^{-1} for VOA_2; pyrazole: $g_\parallel = 1.937$, $A_\parallel = 176\times10^{-4}$ cm^{-1} for VOA, $g_\parallel = 1.941$, $A_\parallel = 172\times10^{-4}$ cm^{-1} for VOA_2) [32]. The stability constant derived for the complex with monodentate coordination of pyridine nitrogen ($\log K_{VO(H)A} = \log K_{VOAH} - \log K_{HA} = 5.40$), however, is significantly higher than expected and only about one order of magnitude lower than that for the VO(IV)–picolinate chelate ($\log K_{VOA} = 6.66$). Therefore, it can be supposed that in the protonated complexes VOAH and VOA_2H_2, in addition to the pyridine nitrogen, the protonated phenolic-OH also coordinates, presumably in an indirect way through hydrogen bonding between this phenolic-OH group and an equatorial water molecule in the VO(IV) coordination sphere (see Scheme 3). Support for the above conclusion is provided by the spectral changes accompanying the stepwise deprotonation of the complex VOA_2H_2. Two species, VOA_2H and VOA_2, are formed, with pK = 7.02 and 7.60, respectively. A comparison of the EPR spectral parameters ($g_\parallel = 1.945$, $A_\parallel = 166\times10^{-4}$ cm^{-1}) for VOA_2 with those for 3-hydroxypicolinic acid and other salicylate derivatives (vide extra) clearly indicates a structural rearrangement of the complex to the salicylate-type (COO^-,O^-) binding mode (Scheme 3). On the other hand, the parameters for VOA_2H ($g_\parallel = 1.941$, $A_\parallel = 173\times10^{-4}$ cm^{-1}) point to a mixed coordination (COO^-,O^-)(N, H_2O) with a *cis* arrangement, i.e. the N donor is in the apical position.



Scheme 3.

At pH > 8 and at high ligand excess, A:M > 6, a species VOA_2H_{-1} is formed by deprotonation of the complex VOA_2 ($pK = 8.38$). The EPR parameters ($g_{\parallel} = 1.947$, $A_{\parallel} = 162 \times 10^{-4}\ cm^{-1}$) are consistent with a *cis* arrangement of the ligands, which brings two strong O^- donors, a COO^- and an OH^- ion, into the equatorial coordination sites, while the second carboxylate group occupies the axial position. This may suggest that VOA_2 also adopts a *cis* arrangement (or that there is an equilibrium between the *cis* and *trans* isomeric forms). Above pH 8 hydroxide ions displace the ligands from the coordination sphere and oligonuclear binary hydroxo complexes of VO(IV) are formed.

4. Conclusions

The interactions between VO(IV) and several ligands containing pyridine nitrogen, such as picolinic acid and its hydroxy derivatives 3-hydroxypicolinic and 2-hydroxynicotinic acids, were investigated in order to clarify the effects of the positions of the donor groups in the ligands on their complex-forming properties. In the acidic pH range, 3-hydroxypicolinic acid behaves like picolinic acid, forming chelated complexes through the pyridine nitrogen and the carboxylate oxygen. In the pH range 6–8, a very stable tetramer $(VOA)_4$, containing tridentately coordinated ligands is detected, while at higher pH values bis complexes involving salicylate-type (COO^-,O^-) coordination are formed. The VO(IV) complexes of 2-hydroxynicotinic acid involve pyridine nitrogen-phenolic hydroxyl (N, OH) binding mode in the acidic pH range and salicylate-type (COO^-,O^-) coordination in the weakly basic pH range. Both 3-hydroxypicolinic acid and 2-hydroxynicotinic acid contain a salicylate (COO^-,O^-) donor set in addition to a pyridine nitrogen. The stability data and spectral behaviour of the complexes suggest that a pyridine nitrogen in a position adjacent to a carboxylate group is a more effective binding site for VO(IV) than that adjacent to a phenolic hydroxyl group.

Acknowledgements

The work was carried out in the frame of COST D8 collaboration and was supported by the Hungarian Scientific Research Fund (OTKA 23776/97) and the Hungarian Ministry of Education (FKFP 0013/97).

References

[1] D. Rehder, Met. Ions Biol. Syst. 31 (1995) 1.
[2] C. Orvig, K.H. Thompson, M. Battell, J.H. McNeill, Met. Ions Biol. Syst. 31 (1995) 575.
[3] H. Sakurai, K. Fujii, H. Watanabe, H. Tamura, Biochem. Biophys. Res. Commun. 214 (1995) 1095.
[4] T. Kiss, P. Buglyó, G. Micera, A. Dessì, D. Sanna, J. Chem. Soc., Dalton Trans. (1993) 1849.
[5] T. Kiss, P. Buglyó, D. Sanna, G. Micera, P. Decock, D. Dewaele, Inorg. Chim. Acta 239 (1995) 145.
[6] J. Costa Pessoa, S.M. Luz, R.D. Gillard, Polyhedron 14 (1995) 1495.
[7] P. Buglyó, N. Culeddu, T. Kiss, G. Micera, D. Sanna, J. Inorg. Biochem. 60 (1995) 45.
[8] D. Sanna, G. Micera, P. Buglyó, T. Kiss, J. Chem. Soc., Dalton Trans. (1996) 87.
[9] P. Buglyó, A. Dessi, T. Kiss, G. Micera, D. Sanna, J. Chem. Soc., Dalton Trans. (1993) 2057.
[10] A. Messerschmidt, R. Weaver, Proc. Natl. Acad. Sci. USA 93 (1996) 392.
[11] K.A. Idriss, M.S. Saleh, H. Sedaira, M.M. Seleim, E.Y. Hashem, Monatsch. Chem. 122 (1991) 507.
[12] S.P. Singh, J.P. Tandon, Acta Chim. Acad. Sci. Hung. 84 (1975) 419.
[13] T.W. Duma, R.D. Hancock, J. Coord. Chem. 31 (1994) 135.
[14] T.H. Kaden, S. Fallab, Chimica 20 (1966) 51.
[15] S. Fujimoto, K. Fujii, H. Yasui, R. Matsushita, J. Takada, H. Sakurai, J. Clin. Biochem. Nutr. 23 (1997) 113.
[16] A. Napoli, A.L. Magri, Ann. Chim. (Rome) 77 (1987) 783.
[17] M Chatterjee, S. Ghosh, A.K. Nandi, Polyhedron 16 (1997) 2917.
[18] B. Galeffi, A.S. Tracey, Inorg. Chem. 28 (1989) 1727.
[19] G. Gran, Acta Chem. Scand. 4 (1950) 559.
[20] I. Nagypál, I. Fábián, Inorg. Chim. Acta 61 (1982) 109.
[21] H.M. Irving, M.G. Miles, L.D. Pettit, Anal. Chim. Acta 38 (1967) 475.
[22] R.P. Henry, P.C.H. Mitchell, J.E. Prue, J. Chem. Soc., Dalton Trans. (1973) 1156.
[23] A. Komura, M. Hayashi, H. Imanaga, Bull. Chem. Soc. Jpn. 50 (1977) 2927.
[24] L. Zèkany, I. Nagypál, in: D. Leggett (Ed.), Computational Methods for the Determination of Stability Constants, Plenum, New York, 1985.
[25] A.E. Martell, R.M. Smith, Critical Stability Constants, vol. 2, Plenum, New York, 1975.
[26] A.E. Martell, R.M. Smith, Critical Stability Constants, vol. 6, Plenum, New York, 1989.
[27] A.E. Martell, R.M. Smith, Critical Stability Constants, vol. 3, Plenum, New York, 1977.
[28] M. Jezowska-Bojczuk, H. Kozlowski, A. Zubor, T. Kiss, M. Branca, G. Micera, A. Dessì, J. Chem. Soc., Dalton Trans. (1990) 2903.
[29] L.D. Pettit, H.K.J. Powell, The IUPAC Stability Constants Database, Academic Software and IUPAC, Royal Society of Chemistry, London, 1992–1997.
[30] A.K.W. Stephens, C. Orvig, Inorg. Chim. Acta 273 (1998) 47.
[31] N.D. Chasteen, Vanadyl(IV) EPR spin probes, inorganic and biochemical aspects. In: L.J. Berliner, J. Reuben (Eds.), Biological Magnetic Resonance, vol. 3, Plenum, New York, 1981.
[32] D. Sanna, G. Micera, L. Strinna Erre, M.G. Molinu, E. Garribba, J. Chem. Res. (1996) 40.

PERGAMON

www.elsevier.nl/locate/poly

Polyhedron 19 (2000) 63–68

POLYHEDRON

New phosphoranes with five- and seven-membered rings: influence of the nature of the substituents on hydrogen bonding

C. Muthiah [a], Musa A. Said [a], M. Pülm [b], R. Herbst-Irmer* [1,b], K.C. Kumara Swamy* [2,a]

[a] *School of Chemistry, University of Hyderabad, Hyderabad 500046, India*

[b] *Institut für Anorganische Chemie der Universität Göttingen, Tammannstrasse 4, D-37077 Göttingen, Germany*

Received 30 June 1999; accepted 15 October 1999

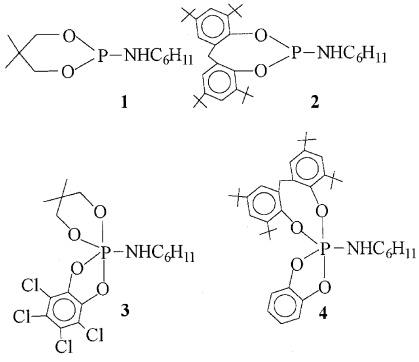
Abstract

Several pentacoordinated phosphoranes with a primary amino substituent have been synthesized by oxidative addition reactions on a cyclic phosphite. X-ray structures of three of these, i.e. $(C_6H_{11}NH)P(2,2'\text{-}O\text{-}C_6H_4\text{-}C_6H_4\text{-}O)(1,2\text{-}O_2C_6Cl_4)$ (**6**), $(C_6H_{11}NH)P(9,10\text{-}O_2C_{14}H_8)(1,2\text{-}O_2C_6H_4)$ (**7**) and $(MeNH)P(2,2'\text{-}O\text{-}C_6H_4\text{-}C_6H_4\text{-}O)(1,2\text{-}O_2C_6H_4)$ (**8**) have been determined. While **6** does not show hydrogen bonding interactions involving the NH proton, compound **7** is a weak dimer with hydrogen bonding interactions between the NH proton and the apical oxygen of the catecholate ring. By contrast in **3**, although hydrogen bonding again involves the NH proton and apical oxygen of the five-membered catecholate ring, a polymeric chain structure is formed. ©2000 Elsevier Science Ltd All rights reserved.

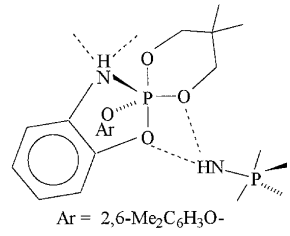
Keywords: Phosphoranes; Pentacoordination; X-ray structure; Hydrogen bonding

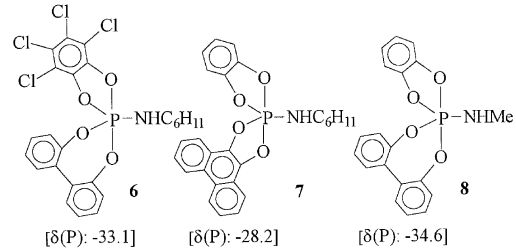
1. Introduction

We have been interested in looking at hydrogen bonding interactions and their influence on the structures of cyclic phosphorus compounds. We feel that studies such as these could be important in understanding the nature of the pentacoordinated transition state in the reactions of phosphates conducted in protic media (see Ref. [1] and references cited therein). In this direction we have recently reported the synthesis and X-ray structures of compounds **1**–**4**, all of which possess a cyclohexylamino group [2].



Although hydrogen bonding involving the NH proton and one of the ring oxygens was observed in the tricoordinated compounds **1** and **2**, a similar feature was not observed in the corresponding pentacoordinated structures **3** and **4**. In contrast to this, studies on the phosphorane **5** revealed hydrogen bonding involving an NH proton and a ring oxygen [3]. This



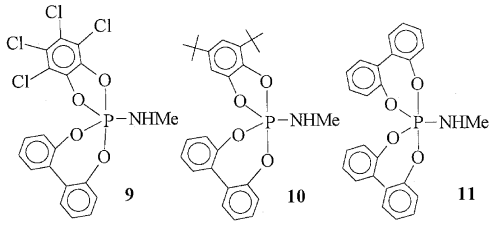


prompted us to examine the primary amino substituted phosphoranes further. Herein we report the synthesis and structures of three such phosphoranes **6**–**8**. We also report the synthesis of **9**–**11** bearing a primary amino group.

[1] *Corresponding author.

[2] *Corresponding author. Fax: +91-40-301-0120; e-mail: kckssc@uohyd.ernet.in

0277-5387/00/$ - see front matter ©2000 Elsevier Science Ltd All rights reserved.
PII S0277-5387(99)00324-1



2. Experimental

Chemicals were procured from Aldrich or from local manufacturers; they were purified when required. Solvents were purified according to standard procedures [4]. NMR spectra were recorded on a Bruker 200 MHz spectrometer. Chemical shifts ($CDCl_3$, ppm) were measured against tetramethylsilane (^1H, ^{13}C) or ext. 85% H_3PO_4. IR spectra were recorded on a Perkin-Elmer 1310 spectrophotometer. Elemental analysis was performed on a Perkin-Elmer 240C CHN analyzer.

The precursors ($C_6H_{11}NH$)P(1,2-$O_2C_6H_4$) (**12**; δ(P) 139.8) and ($C_6H_{11}NH$)P(2,2′-O-C_6H_4-C_6H_4-O) (**13**; δ(P) 151.0) were prepared by following a reported procedure [5].

*2.1. Preparation of (MeNH)P(2,2′-O-C_6H_4-C_6H_4-O) (**14**)*

Into a stirred solution of ClP(2,2′-O-C_6H_4-C_6H_4-O) [5] (3.00 g, 11.97 mmol) in diethyl ether at −60°C was condensed an excess of methylamine gas for 0.5 h at −60°C. The residue, obtained after filtration and removal of solvent, was subjected to vacuum distillation to afford **14** as a viscous liquid (b.p. 180°C/3 mm Hg). Yield 2.7 g (93%). ^1H NMR: δ 2.63 (dd, 3H, P–NHCH_3, ^3J(HH) = 5.8 Hz, ^3J(P–H) = 9.2 Hz), 2.95–3.15 (m, 1H, N*H*), 7.25–7.46 (m, 8H, Ar–*H*). ^{31}P NMR: δ 150.8. IR: 3399 cm^{-1} (ν(NH)). *Anal*. Calc. for $C_{13}H_{12}NO_2P$: C, 63.67; H, 4.90; N, 5.71. Found: C, 63.50; H, 4.85; N, 5.62%.

*2.2. Preparation of ($C_6H_{11}NH$)P(2,2′-O-C_6H_4-C_6H_4-O)-(1,2-$O_2C_6Cl_4$) (**6**), ($C_6H_{11}NH$)P(9,10-$O_2C_{14}H_8$)-(1,2-$O_2C_6H_4$) (**7**), (MeNH)P(2,2′-O-C_6H_4-C_6H_4-O)-(1,2-$O_2C_6Cl_4$) (**9**) and (MeNH)P(2,2′-O-C_6H_4-C_6H_4-O)-(3,5-(Bu^t)$_2$-1,2-$O_2C_6H_2$) (**10**)*

These compounds were prepared by the reaction of the respective aminophosphite with the corresponding quinone in yields of >85%. A typical procedure for the synthesis of **9** is given below.

To a solution of **14** (0.99 g, 4 mmol) in toluene (5 ml) was added *o*-chloranil (1.00 g, 4 mmol) slowly (5 min) under nitrogen. The mixture was stirred for 10 min more and allowed to stand. Compound **9** was obtained as a crystalline solid over a period of ca. 2 days in a yield of 94%.

A similar procedure was adopted to prepare **6** and **10**. In the case of **7**, the two reactants were heated in neat condition at 150°C for 1/2 h; the solid obtained after cooling was recrystallized from CH_2Cl_2–hexane (1:1) mixture.

6: M.p. 170°C. ^1H NMR: δ 0.81–1.85 (m, 10H, cyclohexyl–CH_2), 3.20–3.40 (m, 2H, N*H* + NC*H*), 7.15–7.48 (m, 8H, Ar–*H*). ^{31}P NMR: δ −34.7. *Anal*. Calc. for $C_{24}H_{20}Cl_4NO_4P$: C, 51.54; H, 3.58; N, 2.51. Found: C, 51.46; H, 3.51; N, 2.60%.

7: M.p. 88–90°C. ^1H NMR: δ 0.86–3.40 (m, 12H, cyclohexyl–*H* + N*H*), 6.93–8.68 (m, 12H, Ar–*H*). ^{31}P NMR: δ −28.2. IR: 3310 cm^{-1} (ν(NH)). *Anal*. Calc. for $C_{26}H_{24}NO_4P$: C, 70.09; H, 5.44; N, 3.14. Found: C, 69.95; H, 5.32; N, 3.08%.

9: M.p. 214–216°C. ^1H NMR: δ 2.72 (dd, 3H, ^3J(HH) = 5.0 Hz, ^3J(HH) = 13.4 Hz, PNHCH_3), 3.30–3.40 (m, 1H, N*H*), 7.03–7.59 (m, 8H, Ar–*H*). ^{31}P NMR: δ −33.0. IR: 3402 cm^{-1} (ν(NH)). *Anal*. Calc. for $C_{19}H_{12}Cl_4NO_4P$: C, 46.46; H, 2.46; N, 2.85. Found: C, 46.41; H, 2.41; N, 2.91%.

10: M.p. 142–144°C. ^1H NMR: δ 1.32 (s, 9H, C(CH_3)$_3$), 1.35 (s, 9H, C(CH_3)$_3$), 2.76 (dd, 3H, ^3J(HH) = 5.1 Hz, ^3J(PH) = 12.8 Hz, NHCH_3), 3.19–3.30 (m, 1H, N*H*), 6.82–7.61 (m, 10H, Ar–*H*). ^{31}P NMR: δ −34.7. IR: 3403 cm^{-1} (ν(NH)). *Anal*. Calc. for $C_{27}H_{32}NO_4P$: C, 69.65; H, 6.94; N, 3.00. Found: C, 69.58; H, 6.85; N, 2.94%.

*2.3. Preparation of (MeNH)P(2,2′-O-C_6H_4-C_6H_4-O)-(1,2-$O_2C_6H_4$) (**8**) and (MeNH)P(2,2′-OC_6H_4-C_6H_4O)$_2$ (**11**): typical procedure for **8***

To a stirred solution of the phosphite **14** (0.3 g, 1.22 mmol) in toluene (10 ml) maintained at −60°C was added first *N*-chlorodiisopropylamine (0.16 g, 1.22 mmol) in toluene (3 ml) and then catechol (0.13 g, 1.22 mmol) in toluene (3 ml) over a period of (total) 15 min with continuous stirring. The reaction mixture was brought to 30°C, stirred overnight and filtered. Solvent was removed and the residue crystallized from toluene (5 ml) to give **8**. Yield 0.4 g (93%). M.p. 146–148°C. ^1H NMR: δ 2.70 (dd, 3H, ^3J(HH) = 5.0 Hz, ^3J(PH) = 13.0 Hz, NHCH_3), 3.10–3.25 (m, N*H*), 6.78–7.57 (m, 12H, Ar–*H*). ^{31}P NMR: δ −34.6. IR: 3435 cm^{-1} (ν(NH)). *Anal*. Calc. for $C_{19}H_{16}NO_4P$: C, 64.58; H, 4.57; N, 3.96. Found: C, 64.54; H, 4.50; N, 3.85%.

In the above reaction, if catechol is added first, followed by *N*-chlorodiisopropylamine, the reaction mixture shows other products (~50%) in addition to **8** (see Fig. 1).

Compound **11** was prepared similarly, but in this case the order of addition did not matter and compound **11** was obtained in >85% yield. **11**: M.p. 136–138°C. ^1H NMR: δ 2.77 (dd, 3H, ^3J(HH) = 4.9 Hz, ^3J(PH) = 12.7 Hz, NHCH_3), 3.34–3.46 (m, 1H, N*H*), 7.21–7.55 (m, 16H, Ar–*H*). ^{31}P NMR: δ −38.2. IR: 3443 cm^{-1} (ν(NH)). *Anal*. Calc. for $C_{25}H_{20}NO_4P$: C, 69.91; H, 4.70; N, 3.26. Found: C, 70.21; H, 4.75; N, 3.35%.

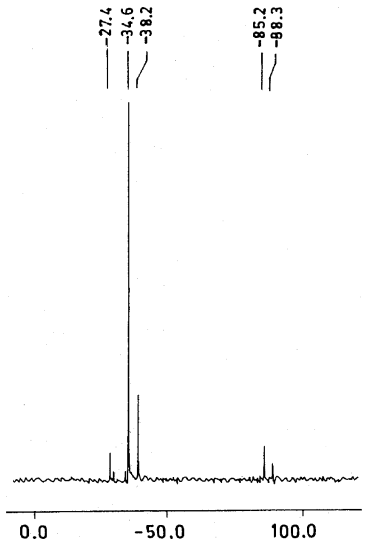


Fig. 1. The ^{31}P NMR spectrum (0 to −100 ppm) of the product mixture from reaction of the cyclic phosphite **14** with catechol and $ClN(Pr^i)_2$; catechol was added first to the phosphite.

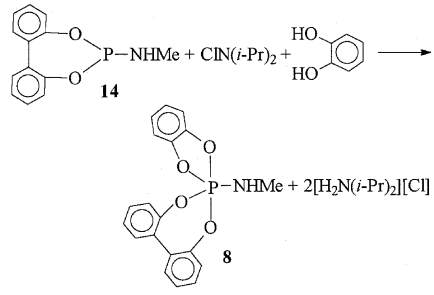
2.4. X-ray crystallography

X-ray data were collected on a Stoe-Siemens-Huber diffractometer (compound **6** at 153 K) or an Enraf-Nonius MACH3 diffractometer (compounds **7** and **8** at 293 K) using monochromated Mo Kα ($\lambda = 0.71073$ Å) radiation. The structures were solved by direct methods; all non-hydrogen atoms were refined anisotropically [6–8]. For the hydrogen atoms bonded to carbon, the riding model was used. The hydrogens bonded to nitrogens were located in a difference map. They were refined with distance restraints. Crystal data are summarized in Table 1.

3. Results and discussion

3.1. Synthesis and spectroscopy

Synthesis of compounds **6**, **7**, **9** and **10** is achieved by oxidative addition of the corresponding quinone to the cyclic phosphites $(C_6H_{11}NH)P(1,2\text{-}O_2C_6H_4)$ (**12**), $(C_6H_{11}NH)$-$P(2,2'\text{-}O\text{-}C_6H_4\text{-}C_6H_4\text{-}O)$ (**13**) and $(MeNH)P(2,2'\text{-}O\text{-}C_6H_4\text{-}C_6H_4\text{-}O)$ (**14**) as the case may be. Compounds **8** and **11** were obtained by the *N*-chlorodiisopropylamine route [10,11] which is represented in Eq. (1) for **8**.



(1)

In this reaction involving the aminophosphites, the order of addition of the reagents is important. Instead of adding $ClN(Pr^i)_2$ first followed by diol, if the diol is added first and

Table 1
Crystal data for **6–8**

	6	**7**	**8**
Empirical formula	$C_{24}H_{20}Cl_4NO_4P$	$C_{26}H_{24}NO_4P$	$C_{19}H_{16}NO_4P$
Formula weight	559.18	445.43	353.30
Crystal system	monoclinic	monoclinic	monoclinic
Space group	$P2_1/n$	$C2/c$	$P2_1$
a (Å)	14.256(2)	17.820(4)	10.333(5)
b (Å)	12.053(2)	10.415(2)	9.449(3)
c (Å)	15.193(2)	25.895(5)	17.543(16)
β (°)	114.28(1)	108.89(3)	96.77(5)
V (Å^3)	2379.7(6)	4547(2)	1700.9(18)
Z	4	8	4
D_{calc} (g cm^{-3})	1.561	1.301	1.380
μ (mm^{-1})	0.598	0.154	0.185
$F(000)$	1144	1872	736
Crystal size (mm)	0.4×0.2×0.2	0.3×0.2×0.2	0.4×0.3×0.3
2θ max	50	45	52
Total reflections	7974	5777	3726
Observed reflections ($I > 2\sigma(I)$)	3311	1202	3151
Data/restraints/parameters	4222/1/310	2990/1/293	3546/2/461
$R1$ [a] ($I > 2\sigma(I)$)	0.0373	0.0438	0.0395
$wR2$ [b] (all data)	0.0877	0.1329	0.1227
S (all data)	1.024	1.096	1.052
Max./min. peak in difference map (e Å^{-3})	0.302/−0.360	0.188/−0.191	0.355/−0.390
Absolute structure parameter [9]			0.1(1)

[a] $R1 = (\Sigma||F_o| - |F_c||)/\Sigma|F_o|$.
[b] $wR2 = \{\Sigma[w(F_o^2 - F_c^2)^2]/\Sigma[w(F_o^2)^2]\}^{1/2}$.

then $ClN(Pr^i)_2$, other side reactions also take place; thus if the former order is maintained in Eq. (1), compound **8** is formed exclusively whereas if the latter order is followed, other pentacoordinated and hexacoordinated phosphorus species are formed as shown by ^{31}P NMR in Fig. 1 [12]. What is interesting is the observation of two signals in the hexacoordinated phosphorus region at −85.2 and −88.2 ppm. On the basis of available literature, these signals may be ascribable to compounds of the type $[MeNH_3]^+[P(2,2'\text{-}OC_6H_4\text{-}C_6H_4O)(1,2\text{-}O_2C_6H_4)_2]^-$ or $[MeNH_3]^+[P(1,2\text{-}O_2C_6H_4)_3]^-$ [13,14]. Thus here, in addition to exchange of the amino group by the catecholic –OH, ring exchange also appears to be taking place and the signal in the ^{31}P NMR in Fig. 1 at −38.2 ppm is assignable to compound **11**. Such an exchange reaction, however, is not observed in an analogous reaction of **14** with 2,2′-biphenol.

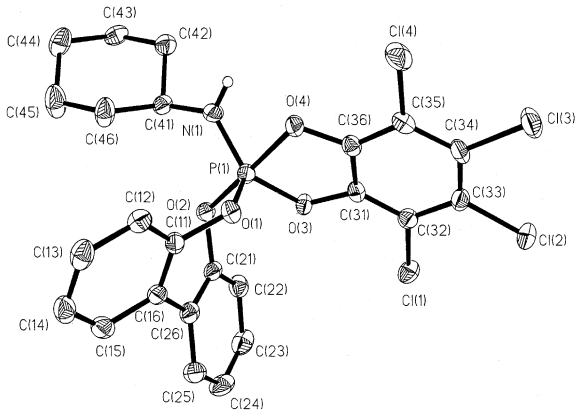


Fig. 2. Molecular structure of **6** (probability level of displacement ellipsoids 50%).

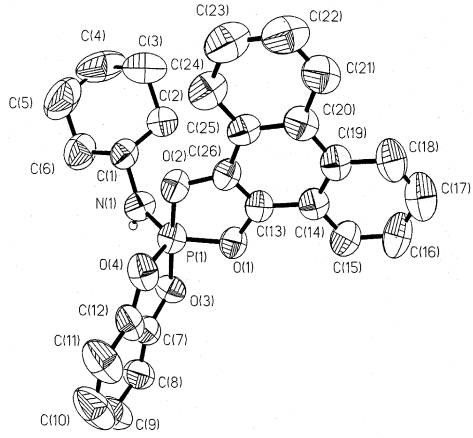


Fig. 3. Molecular structure structure of **7** (probability level of displacement ellipsoids 50%).

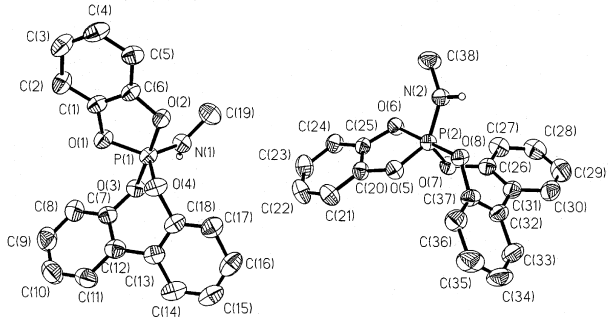


Fig. 4. Molecular structure of **8**; both the molecules in the asymmetric unit are shown (probability level of displacement ellipsoids 50%).

The ^{31}P NMR spectra of **6**–**11** in solution are consistent with a pentacoordinated structure. The peak for the (7 + 7) ring compound **11** appears upfield to (7 + 5) ring compounds **8**–**10** and the (5 + 5) ring compound **7** has the most downfield chemical shift in this series. In the ^1H NMR spectra, the methyls of the methylamino group show up as a doublet of a doublet in the P(III) precursor **14** (δ 2.63, $^3J(HH) = 5.8$ Hz; $^3J(PH) = 9.2$ Hz) as well as as in the phosphoranes ($^3J(HH) = 5.0$ Hz, $^3J(HH) = 13.0$ Hz for **11**), but the $^3J(PH)$ value is greater for the pentacoordinated systems. At least in **8**, dilution broadens the N*H*CH_3 signal, although no discernible change in the δ value is noticed.

Table 2
Selected bond distances (Å) and angles (°) for **6** with e.s.d.s in parentheses

P(1)–N(1)	1.618(2)	P(1)–O(3)	1.654(2)
P(1)–O(1)	1.604(2)	P(1)–O(4)	1.759(2)
P(1)–O(2)	1.635(2)		
N(1)–P(1)–O(1)	123.2(1)	O(1)–P(1)–O(3)	107.3(1)
N(1)–P(1)–O(2)	90.9(1)	O(1)–P(1)–O(4)	87.7(1)
N(1)–P(1)–O(3)	129.0(1)	O(2)–P(1)–O(3)	89.5(1)
N(1)–P(1)–O(4)	86.3(1)	O(2)–P(1)–O(4)	174.8(2)
O(1)–P(1)–O(2)	97.6(1)	O(3)–P(1)–O(4)	88.8(1)

Table 3
Selected bond distances (Å) and angles (°) for **7** with e.s.d.s in parentheses

P(1)–N(1)	1.620(4)	P(1)–O(3)	1.718(3)
P(1)–O(1)	1.637(3)	P(1)–O(4)	1.634(3)
P(1)–O(2)	1.688(3)		
N(1)–P(1)–O(1)	124.3(2)	O(1)–P(1)–O(3)	86.8(2)
N(1)–P(1)–O(2)	92.4(2)	O(1)–P(1)–O(4)	115.9(2)
N(1)–P(1)–O(3)	90.1(2)	O(2)–P(1)–O(3)	177.5(2)
N(1)–P(1)–O(4)	119.7(2)	O(2)–P(1)–O(4)	87.9(2)
O(1)–P(1)–O(2)	91.5(2)	O(3)–P(1)–O(4)	91.1(2)

Table 4
Selected bond distances (Å) and angles (°) for **8** with e.s.d.s in parentheses

P(1)–N(1)	1.608(4)	P(2)–N(2)	1.611(3)
P(1)–O(1)	1.634(3)	P(2)–O(5)	1.635(3)
P(1)–O(2)	1.725(3)	P(2)–O(6)	1.718(3)
P(1)–O(3)	1.660(3)	P(2)–O(7)	1.609(3)
P(1)–O(4)	1.606(3)	P(2)–O(8)	1.662(3)
N(1)–P(1)–O(1)	126.4(2)	N(2)–P(2)–O(5)	128.6(2)
N(1)–P(1)–O(2)	90.6(2)	N(2)–P(2)–O(6)	91.0(2)
N(1)–P(1)–O(3)	88.9(2)	N(2)–P(2)–O(7)	121.4(2)
N(1)–P(1)–O(4)	121.6(2)	N(2)–P(2)–O(8)	87.6(2)
O(1)–P(1)–O(2)	89.7(2)	O(5)–P(2)–O(6)	89.3(2)
O(1)–P(1)–O(3)	89.0(2)	O(5)–P(2)–O(7)	110.1(2)
O(1)–P(1)–O(4)	111.9(2)	O(5)–P(2)–O(8)	88.8(2)
O(2)–P(1)–O(3)	177.8(2)	O(6)–P(2)–O(7)	88.4(2)
O(2)–P(1)–O(4)	87.2(2)	O(6)–P(2)–O(8)	176.3(2)
O(3)–P(1)–O(4)	94.9(2)	O(7)–P(2)–O(8)	95.3(2)

Table 5
P–N bond lengths in selected tri-, tetra- and penta-coordinated compounds

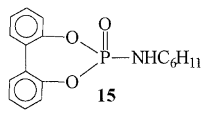
Sample	Compound	P–N (Å)	Coordination number	Reference
1	$(C_6H_{11}NH)P(OCH_2CMe_2CH_2O)$	1.656 (mean)	3	[2]
2	$(C_6H_{11}NH)P\{[O\text{-}4,6\text{-}(Bu^t)_2C_6H_2]_2CH_2\}$	1.635	3	[2]
3	$(C_6H_{11}NH)P(O)[2,2'\text{-}OC_6H_4\text{-}C_6H_4O]$	1.609	4	[15]
4	$N_3P_3Cl_4[(Pr^i)NCH_2CH_2CH_2N(Pr^i)]$	1.623 (mean) [a] 1.623 (mean) [b]	4	[18]
5	$N_4P_4Cl_6[(Pr^i)NCH_2CH_2CH_2N(Pr^i)]$	1.574 (mean) [a] 1.626 (mean) [b]	4	[18]
6	$(C_6H_{11}NH)P(OCH_2CMe_2CH_2O)(1,2\text{-}O_2C_6Cl_4)$	1.619	5	[2]
7	$(C_6H_{11}NH)P\{[O\text{-}4,6\text{-}(Bu^t)_2C_6H_2]_2CH_2\}[1,2\text{-}O_2C_6H_4]\cdot 1/2Et_2O$	1.629	5	[2]
8	**6**	1.618	5	this work
9	**7**	1.620	5	this work
10	**8**	1.608 (molecule 1) 1.611 (molecule 2)	5	this work
11	$H_2NP[OC(CF_3)_2C(CF_3)_2O]_2$	1.590	5	[19]

[a] *P*(spiro)-phosphazene ring.
[b] *P*(spiro)-saturated ring.

3.2. X-ray structural analysis

The molecular structures of **6**–**8** are shown in Figs. 2–4 respectively. Selected bond parameters are given in Tables 2–4.

All the three compounds have a trigonal bipyramidal geometry around phosphorus with the cyclic substituents spanning apical-equatorial dispositions. As expected, the P–O(apical) bonds are longer than the P–O(equatorial) bonds; the P–O bonds in the five-membered rings are comparatively longer than those found in the seven-membered ring. The P–O distances in the seven-membered ring in **6** or **8**, however, are slightly longer than those observed in the phosphate ester **15** [15].



15

The P–N bonds in the three compounds are in the range 1.607–1.620 Å and thus are significantly shorter than the accepted P–N single bond length [16,17]. It is thus intriguing to note that in a large number of cases, whether phosphorus is tri-, tetra- or penta-coordinated (like that reported here), the formal P–N single bond is very short and close (or equal) in length to those in cyclophosphazenes where unsaturated P–N bonds are expected [18]. These distances for selected compounds are given in Table 5. At the moment this is only an observation and a detailed analysis encompassing all these classes of compounds would be more revealing as regards the the nature of the P–N bond.

The five-membered rings are nearly planar in all three structures. The seven-membered rings in **6** and **8** show a conformation between a twist boat and a boat [20]; this is analogous to that in the hexacoordinated structures reported previously [12].

In contrast to **15** where hydrogen bonding is present, in **6** such a feature is absent. Even in the the (5+5) spirophosphorane **7**, the closest intermolecular N–O distance is 3.312 Å [21]. The molecules organize themselves as weakly hydrogen bonded dimers (Fig. 5) with only the apical oxygen O(3) of the catecholate residue involved in hydrogen bonding. A stronger interaction is observed in **8**. Here primarily the atoms N(1) and O(2) of molecule 1 as well as N(2) and O(6) of molecule 2 are involved in hydrogen bonding interactions; the relevant intermolecular N–O contact distances are 2.981 and 3.126 Å respectively. In contrast to the dimer formation in **7**, hydrogen bonding in **8** results in a chain structure (Fig. 6). Again only the apical oxygens of the catecholate residue are involved in significant hydrogen bonding.

To summarize, in the reaction of aminophosphites with diols/$ClN(Pr^i)_2$ the order of addition of the diol and $ClN(Pr^i)_2$ to the phosphite is important. Where there is no significant steric inhibition, hydrogen bonding in primary amino substituted tetraoxyphosphoranes is observed; this interaction involves the *apical* oxygens (and not the *equatorial* ones) of the trigonal bipyramidal structure. This observation is perhaps useful in arriving at probable transition state

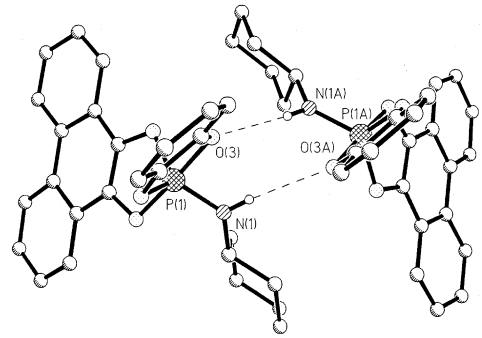


Fig. 5. A diagram showing the dimeric structure via hydrogen bonding in **7**.

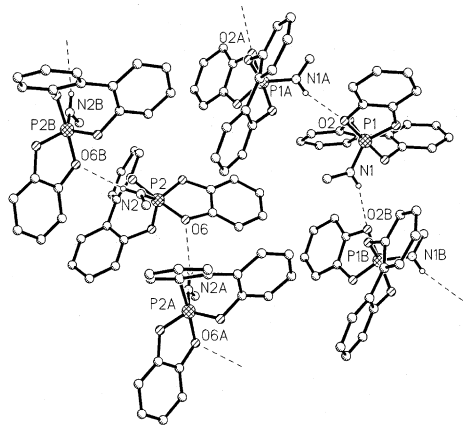


Fig. 6. A diagram showing the chain structure via hydrogen bonding in **8**.

pentacoordinated species in the nucleophilic substitution reactions of phosphate esters.

Supplementary data

Supplementary data are available from the CCDC, 12 Union Road, Cambridge CB2 1EZ, UK on request, quoting the deposition numbers 124695–124697.

Acknowledgements

We thank the Department of Science and Technology (New Delhi) for funding and for setting up a National Single Crystal Diffractometer Facility at the University of Hyderabad. Thanks are also due to UGC, India (COSIST and Special Assistance Programme), as well as the AvH Foundation (Germany) for instrumental facilities. We are thankful to Professor Dr G.M. Sheldrick for his interest in a part of this work.

References

[1] R.R. Holmes, J.A. Deiters, Inorg. Chem. 33 (1994) 3235.
[2] M.A. Said, M. Pülm, R. Herbst-Irmer, K.C. Kumara Swamy, Inorg. Chem. 36 (1997) 2044.
[3] R.O. Day, K.C. Kumara Swamy, J.M. Holmes, R.R. Holmes, J. Am. Chem. Soc. 113 (1991) 1627.
[4] D.D. Perrin, W.L.F. Armarego, D.R. Perrin, Purification of Laboratory Chemicals, Pergamon, Oxford, 1986.
[5] M.A. Said, K.C. Kumara Swamy, M. Veith, V. Huch, J. Chem. Soc., Perkin Trans. 1 (1995) 2945.
[6] G.M. Sheldrick, SHELXS-90, Acta Crystallogr., Sect. A 46 (1990) 467.
[7] G.M. Sheldrick, SHELX-93, University of Göttingen, Germany, 1993.
[8] G.M. Sheldrick, SHELX-97, University of Göttingen, Germany, 1997.
[9] H.D. Flack, Acta Crystallogr., Sect. A 39 (1983) 876.
[10] S. Antczak, S.A. Bone, J. Brierly, S. Trippett, J. Chem. Soc., Perkin Trans. 1 (1977) 278.
[11] K.C. Kumara Swamy, R.O. Day, J.M. Holmes, R.R. Holmes, J. Am. Chem. Soc. 112 (1990) 6095.
[12] In the reaction of $Me_2NP(OCH_2CMe_2CH_2O)$ with 2,2′-biphenol + $ClN(Pr^i)_2$ we have also observed a similar situation. The addition of $ClN(Pr^i)_2$ first leads to the phosphorane $(Me_2N)P(OCH_2CMe_2CH_2O)(2,2'\text{-}O\text{-}C_6H_4\text{-}C_6H_4O)$ (δ(P) −45.9) exclusively whereas addition of 2,2′-biphenol first leads to several products (δ(P) −66.5, −66.4, −58.1, −56.6, −56.3, −45.9) in the pentacoordinated region.
[13] M.A. Said, M. Pülm, R. Herbst-Irmer, K.C. Kumara Swamy, J. Am. Chem. Soc. 118 (1996) 9841.
[14] M. Koenig, A. Klaebe, A. Munoz, R. Wolf, J. Chem. Soc., Perkin Trans. 2 (1979) 40.
[15] C. Muthiah, K.C. Kumara Swamy, Acta Crystallogr., Sect. C 55 (1999) 110.
[16] E. Hobbs, D.E.C. Corbridge, B. Raistrick, Acta Crystallogr. 6 (1953) 621.
[17] T.S. Cameron, R.E. Cordes, B.R. Vincent, Acta Crystallogr., Sect. C 42 (1986) 1242.
[18] S. Kumaraswamy, M. Vijjulatha, C. Muthiah, K.C. Kumara Swamy, U. Engelhardt, J. Chem. Soc., Dalton Trans. (1999) 891.
[19] W. Storzer, D. Schomburg, G.V. Röschenthaler, Z. Naturforsch., Teil B 36 (1981) 1071.
[20] I.K. Boessenhool, J.C.A. Boeyens, J. Cryst. Mol. Struct. 10 (1980) 11.
[21] Although the N(1)–O(3) (intramolecular) distance is 2.364 Å, it is more likely because of geometrical restriction rather than true hydrogen bonding.

PERGAMON

www.elsevier.nl/locate/poly

Polyhedron 19 (2000) 69–76

POLYHEDRON

Vanadium complexes as models for vanadium species of marine organisms. Synthesis, X-ray structure of oxo(*O*,*O*-sulfate)(2,2′:6′,2″-terpyridine)vanadium(IV) hydrate, and density functional geometry optimization analysis of vanadyl complexes

Claudia Pifferi, Maria Pia Picchi, Renzo Cini *

Dipartimento di Scienze e Tecnologie Chimiche e dei Biosistemi, Università di Siena, Pian dei Mantellini 44, 53100 Siena, Italy

Received 30 June 1999; accepted 15 October 1999

Abstract

The addition of an alcoholic solution of 2,2′:6′,2″-terpyridine (terpy) to a vanadyl sulfate ($VOSO_4 \cdot 3H_2O$) aqueous solution (molar ratio 1:1) produced a dark green solution from which brown single crystals suitable for X-ray diffraction studies grew within 12 h. The crystals contain neutral complex molecules [VO(terpy)(*O*,*O*-SO_4)] and water molecules (at a ratio 1:0.5). The complex molecules have a hexa-coordinate vanadium(IV) center linked to the three nitrogen atoms from terpy, to the apical *oxo* ligand and to two oxygen atoms from sulfate. The analysis of the geometrical parameters relevant to the VSO_4 group shows some significant distortion of the SO_4^{2-} ligand upon chelation to the V(IV)O core. The two S–O(d, donor) bonds (lengths: 1.495(3) *trans* to *oxo*; 1.546(3) Å *cis* to *oxo*) are stretched differently when compared to the S–O(t, terminal) bonds (1.447(3) Å). The effect is not due to packing forces but comes from electronic effects. This is shown by a DFT geometry optimization analysis carried out at the density functional B3LYP/LANL2DZ level on model complexes of the type $[VO(H_2O)]^{2+}$, $[VOL]^{2+}$ (L, *N*H=CH–CH=*N*–C(=CH_2)–CH=*N*H), $[VO(H_2O)_2L]^{2+}$ and [VOL(*O*,*O*-SO_4)]. This analysis shows also that the $[VOL]^{2+}$ moiety has a very large affinity for the sulfate anion; the formation energy at the gas phase for [VOL(*O*,*O*-SO_4)] from $[VOL]^{2+}$ and SO_4^{2-} is -448.11 kcal mol^{-1}, much higher than the corresponding value for $[VO(H_2O)_2L]^{2+}$ (-91.47). This can be a rationale for the role vanadyl–sulfate interactions play in blood cells of Ascidians. ©2000 Elsevier Science Ltd All rights reserved.

Keywords: Vanadium; Vanadyl; Terpyridine; Density functional theory

1. Introduction

The discovery by Henze that Ascidian blood cells contain high concentrations of vanadium and that the blood cell lysis produces sulfuric acid [1] raised interest and much research work has been done since then on the matter [2–5]. It is generally accepted that vanadium is stored mainly in the unstable state V(III) [2]. However 5–10% of vanadium is estimated as *oxo* vanadium(IV) (vanadyl, VO^{2+}) and it can occur as an intermediate of a reductive process after vanadate has been absorbed from sea water, or by O_2-oxidation of V(III). At least for Ascidian *ceratodes*, V(III)-sulfate and vanadyl sulfate species are invoked for interpreting NMR, EXAFS and EPR data from blood cells [2].

Some vanadium complexes are insulin mimics and have been tested in humans for the treatment of diabetes [6–8]. The molecular mechanism through which such vanadium complexes act is not known.

Research efforts on coordination chemistry of vanadium have increased significantly after the discovery of vanadium enzymes [9] such as vanadium haloperoxidase which is widely present in marine algae. The catalyst is involved in the production of halogenated species and contains vanadium(V). The coordination environment of vanadium is not fully understood. EXAFS analysis of the reduced vanadium(IV) enzyme is indicative of a pseudo-octahedral coordination sphere consisting of a strongly bound *oxo* donor and five weakly bound light atoms (O or N) [10].

It is evident that all research efforts devoted to detailed analysis of the molecular and electronic structures of V(V), vanadyl and V(III) complexes contribute to throwing light on the field. On the basis of this reasoning and as a continuation of projects from this laboratory to investigate vanadium complexes related to biological systems [11], we wish to

* Corresponding author. Tel.: +39-577-232-041; fax: +39-577-232-004; e-mail: cini@unisi.it

0277-5387/00/$ - see front matter ©2000 Elsevier Science Ltd All rights reserved.
PII S0277-5387(99)00325-3

report here on the synthesis and the crystal and molecular structure of the title compound at 173 K and on a DFT geometry optimization analysis of model vanadyl complexes performed at the density functional B3LYP/LANL2DZ level.

2. Experimental

2.1. Starting materials

Commercial reagent-grade chemicals $VOSO_4 \cdot 3H_2O$ (Aldrich) and 2,2′:6′,2″-terpyridine (terpy, Fluka) were used without further purification.

2.2. Preparation of $[VO(O,O\text{-}SO_4)(C_{15}H_{11}N_3)] \cdot 0.5H_2O$, $\mathbf{1} \cdot 0.5H_2O$

A clear aqueous solution of $VOSO_4 \cdot 3H_2O$ (8 mg, 0.037 mmol; 2 ml H_2O) was mixed with a clear alcoholic solution of terpy (9 mg, 0.039 mmol; 1 ml EtOH). The dark green solution, stored at room temperature, produced brown crystals within 12 h. The crystals were collected through suction filtration, washed with a few drops of cold water, then with 1 ml of EtOH, stored in air at room temperature for 4 h and finally stored in a closed vessel at 5°C. Yield: 10 mg, 67%. *Anal*. Calc. for $C_{15}H_{12}N_3O_{5.5}SV$ ($\mathbf{1} \cdot 0.5H_2O$; 405.3): C, 44.45; H, 2.98; N, 10.37. Found: C, 44.02; H, 2.70; N, 10.03%.

2.3. X-ray crystallographic study

A brown crystal was chosen at the polarizing microscope and mounted on a glass fiber for the X-ray data collection which was performed at 173 K through a Siemens P4 diffractometer. The unit cell dimensions were refined by a least-squares algorithm using 27 randomly selected high intensity reflections in the range $10 \leq 2\theta \leq 30°$. Selected crystallographic data are reported in Table 1. A total of 2770 reflections (2301 considered observed) were collected in the range $4 \leq 2\theta \leq 47°$ and corrected for Lorentz polarization and absorption (ψ-scan method) effects. Three reflections monitored during the collection (every 97) did not show any appreciable decay.

The structure was solved using the Patterson and Fourier techniques of SHELX 97 [12]. All the hydrogen atoms were located from the Fourier-difference map and their positions were refined freely. The model was refined by full-matrix least-squares methods. The non-hydrogen atoms were refined anisotropically, whereas all the hydrogen atoms were treated isotropically and their thermal parameters were restrained to 1.2 times the U_{eq} of the atoms to which they are bound. The oxygen atom of the free water molecule sits on a crystallographic two-fold axis so that the occupancy for O(1W) was assigned the value of 0.5.

All the calculations were carried out using Pentium 200 MHz machines with SHELX 97 [12] and PARST 97 [13] packages, as well as the molecular graphics XPMA-ZORTEP 98 [14] and ORTEP 32 [15] software.

Table 1
Selected crystal data and structure refinement for $[V(O)(terpy)(O,O\text{-}SO_4)] \cdot 0.5H_2O$, $\mathbf{1} \cdot 0.5H_2O$

Parameter	Value
Empirical formula	$C_{15}H_{12}N_3O_{5.5}SV$
Formula weight	405.28
Temperature (K)	173(2)
Wavelength (Å)	0.71073
Crystal system, space group	monoclinic, $C2/c$ (no. 15)
Unit cell dimensions	
a (Å)	17.146(2)
b (Å)	16.5380(10)
c (Å)	13.131(2)
β (°)	123.770(10)
Volume (Å^3)	3095.2(6)
Z, Calculated density (Mg m^{-3})	8, 1.739
Absorption coefficient (mm^{-1})	0.814
Reflections collected/unique	2770/2301 ($R_{int} = 0.0206$)
Refinement method	Full-matrix least-squares on F^2
Data/restraints/parameters	2301/0/269
Final R indices ($I > 2\sigma(I)$)	$R1 = 0.0403$, $wR2 = 0.0907$
R indices (all data)	$R1 = 0.0639$, $wR2 = 0.1013$

2.4. Computational procedure

All the density functional calculations were performed using the GAUSSIAN94/DFT [16] package implemented on a CRAY C90 and an Origin 2000 SG machine located at CINECA (Interuniversity Computing Center), Bologna, Italy. Geometry optimizations, energy calculations and population analysis were obtained by using the B3LYP method [17,18] and the LANL2DZ [16] basis set. This consists of 6-31G like functions for non-transition metal atoms and a valence double-zeta basis set for 3s, 3p, 3d and 4s electrons and orbitals along with an effective core potential (Hay and Wadt [19]) for the metal. All the geometrical parameters were fully optimized without symmetry constraints. Other details are as those reported in Ref. [20]. The molecules optimized were $[VO(H_2O)]^{2+}$, $[VO(NH{=}CH{-}CH{=}N{-}C(=CH_2){-}CH{=}NH)]^{2+}$, $[VO(H_2O)_2(NH{=}CH{-}CH{=}N{-}C(=CH_2){-}CH{=}NH)]^{2+}$ and $[VO(NH{=}CH{-}CH{=}N{-}C(=CH_2){-}CH{=}NH)(O,O\text{-}SO_4)]$. The starting structure of the coordination sphere for the optimization of the complex molecules was very close to that found at the solid state for $[VO(terpy)(O,O\text{-}SO_4)]$ (**1**), except that terpy was substituted by $NH{=}CH{-}CH{=}N{-}C(=CH_2){-}CH{=}NH$ in the model complexes. For better reproduction of S-containing molecules, polarization functions should be taken into account. In fact the computation of SO_4^{2-} at the B3LYP/LANL2DZ level (6-31G basis set for all the atoms) does not reproduce well the S–O bond distance (computed, 1.678 Å; experimental solid state, 1.49 [21]). Results are much better at the B3LYP/6-3G** level (computed S–O, 1.537 Å) and at RHF/6-31G** (1.497). Attempts to optimize the

[VO(*N*H=CH–CH=*N*–C(=CH_2)–CH=*N*H)(*O*,*O*-SO_4)] model molecule at the 6-31G** level for the S atom did not succeed. Therefore, it was decided to use the B3LYP/LANL2DZ level also for the sulfur-containing [VO(*N*H=CH–CH=*N*–C(=CH_2)–CH=*N*H)(*O*,*O*-SO_4)] molecule. All the molecules were fully optimized excluding the [VO(*N*H=CH–CH=*N*–C(=CH_2)–CH=*N*H)(*O*,*O*-SO_4] model molecule which was optimized by the following procedure: (1) the structure of the V(*N*H=CH–CH=*N*–C(=CH_2)–CH=*N*H) moiety was that of the fully optimized [VO(H_2O)$_2$(*N*H=CH–CH=*N*–C(=CH_2)–CH=*N*H)]$^{2+}$ molecule and it was fixed; (2) all the geometrical parameters for the $VOSO_4$ group were freely refined; (3) the starting geometry of the $N_3V(O)SO_4$ group was roughly C_s; (4) the optimization produced first a saddle point structure for maximum force and rms force shifts of 0.000359, 0.000079 (Gaussian 94 criteria, 0.000450, 0.000300, respectively), and for maximum displacement and rms displacement 0.037317, 0.007613 (Gaussian 94 criteria, 0.001800, 0.001200, respectively), the symmetry remained C_s. These conditions were reached after 18 cycles of refinement or ca. 50 h cpu time of a SG Origin 2000 machine. The optimization was then continued up to convergence on the basis of the Gaussian 94 criteria (ca. 100 h cpu time), the symmetry was C_1.

Molecular drawings were obtained through XPMA-ZORTEP [14] and ORTEP 32 [15] packages implemented on a Pentium machine.

3. Results and discussion

3.1. X-ray structure analysis

A drawing of the complex molecule and of the proximal water molecule of **1**·0.5H_2O is reported in Fig. 1(a). Selected bond distances and angles are listed in Tables 2 and 3.

The vanadium(IV) center has a pseudo-octahedral coordination sphere consisting of the three nitrogen atoms (N(1), N(2), N(3)) from the terpy ligand and one oxygen atom (O(2)) from the chelating SO_4^{2-} anion in the equatorial positions; the *oxo* (O(1X)) donor and a second oxygen atom (O(1)) from SO_4^{2-} are in the apical positions. The metal atom is displaced 0.3842(8) Å from the plane defined by the equatorial N(1)/N(2)/N(3)/O(2) set, towards O(1X) and the bond angles between the V–O(1X) vector, and the V–N and VO(2) vectors range between 96.3(1) (N(3)) and 107.6(1)° (N(2)), so that the coordination sphere assumes the typical umbrella shape of V(IV)OL_5 groups.

The V–O(1X) distance is 1.593(3) Å, in nice agreement with previously reported data for vanadyl sulfate, 1.59 (rombohedral) and 1.63 (tetragonal) [21], [VO(H_2O)(ada)] (H_2ada, *N*-(carbamoylmethyl)iminodiacetic acid; V–O(*oxo*), 1.601(2) Å) [10] and analogous complexes; with [VO(H_2O)(Hhida)] (H_3hida, *N*-(2-hydroxyethyl)-iminodiacetic acid; V–O(*oxo*), 1.596(5) Å) [6] and with [VO(mp)$_2$]$^{2-}$ (H_2mp, 2-mercaptophenol; V–O, 1.611(5) Å) [22].

The V–N bond distances are 2.124(3), 2.037(3) and 2.131(3) Å for N(1), N(2) and N(3), respectively, showing the common feature of a strongest coordination linkage of

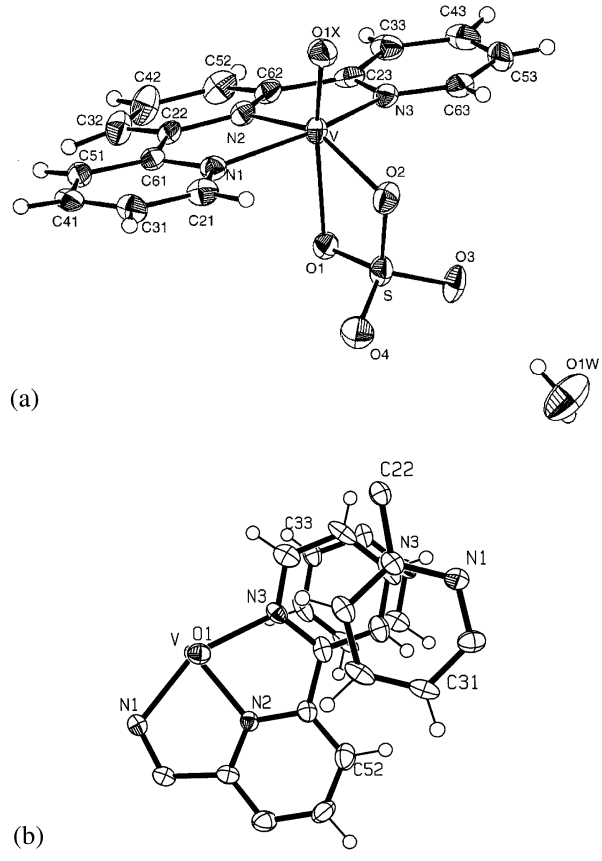


Fig. 1. (a) Drawing of the complex molecule and the proximal water molecule for **1**·0.5H_2O. The ellipsoids enclose 30% probability. (b) The diagram shows a selected stacking interaction between terpy moieties in the structure of **1**·0.5H_2O.

Table 2
Selected bond lengths (Å) for [V(O)(terpy)(*O*,*O*-SO_4)]·0.5H_2O, **1**·0.5H_2O

Vector	Length
V–O(1X)	1.593(3)
V–O(1)	2.239(3)
V–O(2)	1.996(3)
V–N(1)	2.124(3)
V–N(2)	2.037(3)
V–N(3)	2.131(3)
N(1)–C(21)	1.338(5)
N(1)–C(61)	1.357(5)
N(2)–C(62)	1.354(5)
N(2)–C(22)	1.357(5)
N(3)–C(63)	1.340(5)
N(3)–C(23)	1.359(5)
S–O(1)	1.495(3)
S–O(2)	1.546(3)
S–O(3)	1.455(3)
S–O(4)	1.439(3)

Table 3
Selected bond angles (°) for [V(O)(terpy)(*O*,*O*-SO_4)]·0.5H_2O, **1**·0.5H_2O

Vector	Angle
O(1X)–V–O(1)	169.17(13)
O(1X)–V–O(2)	102.39(13)
O(1X)–V–N(1)	96.94(13)
O(1X)–V–N(2)	107.61(13)
O(1X)–V–N(3)	96.29(13)
O(2)–V–O(1)	66.79(10)
N(1)–V–O(1)	85.54(10)
N(2)–V–O(1)	83.22(11)
N(3)–V–O(1)	85.84(11)
O(2)–V–N(1)	99.53(12)
O(2)–V–N(2)	150.01(12)
O(2)–V–N(3)	100.35(12)
N(2)–V–N(1)	77.02(12)
N(1)–V–N(3)	153.10(13)
N(2)–V–N(3)	76.69(12)
C(21)–N(1)–V	126.0(3)
C(61)–N(1)–V	114.9(2)
C(62)–N(2)–V	119.6(2)
C(22)–N(2)–V	119.3(2)
C(63)–N(3)–V	125.8(3)
C(23)–N(3)–V	115.4(2)
S–O(1)–V	92.13(13)
S–O(2)–V	100.49(14)
C(21)–N(1)–C(61)	118.7(3)
C(62)–N(2)–C(22)	120.6(3)
C(63)–N(3)–C(23)	118.6(3)
O(1)–S–O(2)	100.56(15)
O(3)–S–O(1)	110.91(16)
O(4)–S–O(1)	113.55(17)
O(3)–S–O(2)	108.87(16)
O(4)–S–O(2)	109.46(17)
O(4)–S–O(3)	112.73(18)
N(1)–C(21)–C(31)	122.4(4)
N(1)–C(61)–C(51)	121.6(4)
N(1)–C(61)–C(22)	115.4(3)
N(2)–C(22)–C(32)	120.9(4)
N(2)–C(22)–C(61)	113.0(3)
N(2)–C(62)–C(52)	120.1(4)
N(2)–C(62)–C(23)	113.4(3)
N(3)–C(23)–C(33)	121.5(4)
N(3)–C(23)–C(62)	114.6(3)
N(3)–C(63)–C(53)	122.2(4)

the middle nitrogen of the terpy ligand. The only structure containing the terpy ligand bound to a vanadium(IV) center which could be found through the Cambridge Structural Database on requesting the combination of the words *vanadium* and *terpyridine* is [$V(S_2)_2$(terpy)] [23]. In this case the three V–N bond distances are 2.112(2), 2.083(2) and 2.118(2) Å and have a similar trend to that of the present structure. Complexes of terpy with other metals show the same trend, too; see for example [(terpy)Cu(oxalate)-VO(oxalate)(H_2O)] [24].

The two V–O(sulfate) bond distances have very different values: 1.996(3) and 2.239(3) Å for O(2) and O(1), respectively, the O(1) donor experiencing a high *trans influence* from the *oxo* donor, as expected. The O(1)–V–O(1X), O(2)–V–O(1X) and O(1)–V–O(2) bond angles are 169.2(1), 102.4(1) and 66.8(1)° in agreement with a steric strain imposed by a coordination four-member ring. The V–O(sulfate) bond distances are 2.03 and 2.04 Å for the two forms of vanadyl sulfate in both of which the SO_4^{2-} ions bridge four octahedrally coordinate vanadium centers [21].

The structure of the sulfate molecule undergoes significant distortions from pure T_d symmetry upon complexation. The S–O(d, donor) bond distances (1.495(3), O(1); 1.546(3) Å, O(2)) are significantly larger than the S–O(t, terminal) bond lengths (1.455(3), O(3); 1.439(3) Å, O(4)). The O(3) atom interacts with the water molecule via a H-bond. The S–O bond distance for sulfate anions not significantly covalently liked to *block d* metal ions is reported to be 1.49 in Ref. [21], and is in the range 1.452(4)–1.491(4) Å (average, 1.468(4)) for the compound [$Cu(oaoH_2)_2(H_2O)]SO_4$ ($oaoH_2$, oxamide oxime) [25]. For this latter structure the longest S–O distance (1.491(4)) has to be related to a strong H-bond between the sulfate oxygen and the H_2O ligand.

The sulfate ligand which bridges two copper atoms in [$Cu(oaoH_2)(H_2O)(\mu$-$SO_4)]_2$ and [$Cu(oaoH_2)(H_2O)(\mu$-$SO_4)]_n$ has S–O(b, bridging) distances of 1.481(3) (average) and 1.489(3) Å, respectively [25].

The vanadium(II) complex [$V(bpy)_2$(*O*,*O*-SO_4)] has S–O(d) and S–O(t) bond lengths of 1.500(3) and 1.446(3) Å [26], respectively.

It is evident from these data that, at least at the solid state, the S–O(d) bond lengths enlarge upon coordination to the metal or upon H-bonding formation, whereas the S–O(t) bond lengths shorten upon the formation of metal–O(d) bonds. This work proves that the lengthening effect caused on a S–O(d) bond (namely, S–O(2)) is significant and much larger than that found for the other S–O(d) bond (namely, S–O(1)). In fact the S–O(2) length is close to the S–OH bond distance (up to 1.541 Å) found for the hydrogen sulfate anion of monoclinic $N(CH_3)HSO_4$ at 175 K [27] and to the S–OH bond distance (1.537(3)) found for the salt [$(C_6H_5)_2SONH_2$]HSO_4 [28].

The bond angles with respect to sulfur are in the range 100.6(1)–113.6(2)° in the structure of **1**, the smallest values belong to O(1)–S–O(2) as expected because it is part of the flat four-member ring. This value is even smaller than the corresponding value reported previously for [$V(bpy)_2$(*O*,*O*-SO_4)] (102.0(1)°) [26].

Therefore, the (terpy)V=O unit has a high affinity for the sulfate anion (as appears from the short V–O(2) bond distance) and it is particularly suited to induce a sort of activation on SO_4^{2-} because of the highly different electronic and steric effects induced by the *oxo* ligand and the donor atoms from terpy.

The terpy ligand deviates significantly from planarity. The dihedral angles between the three rings are as high as 7.7(2)° (rings 1/2) 3.7(1)° (rings 1/3) and 7.9(2)° (rings 2/3); the vanadium atom deviates from the least squares planes of 0.1938(8), −0.1994(8) and 0.1755(8) Å when compared

to the position of O(1X). The bond distances and angles for the terpy moiety have normal values.

The analysis of the crystal packing shows several interesting intermolecular interactions. First, the terpy ligand is involved in strong stacking interactions mostly through the two peripheral pyridine rings, as depicted in Fig. 1(b). The shortest stacking interatomic distance is 3.274(8) Å, between two C(51) atoms of molecules located at x, y, z and $-x+1, y, -z+2.5$. Second, a complicated web of hydrogen bonds links all the molecules in the crystal. The water molecule (O(1W)) bridges two complex molecules through the O(3) atoms: O(1W)···O(3), 2.891(5) Å; O(1W)–H···O(3), 178(6)°. The water molecule also has two C–H(53)··· O(1W) hydrogen bonds. The *oxo* ligand is surrounded by at least four H atoms from terpy moieties, the shortest contact distance being C(43)H···O(1X), 2.71(5) Å. All the oxygen atoms of sulfate interact also with hydrogen atoms from terpy moieties.

3.2. Density functional analysis

The geometry optimized molecules are pictured in Figs. 2–5. The total energy for the optimized molecules is reported in Table 4. The formation energy for selected formal reactions is reported in Table 5. Selected bond distances and bond angles are listed in Tables 6 and 7, respectively. Atomic coordinates can be retrieved from Supporting Material.

Structures of molecules: The optimized structure of L, *N*H=CH–CH=*N*–C(=CH_2)–CH=*N*H, has C–N bond distances of 1.300 Å and the backbone C–C bond lengths in the range 1.419–1.491 in agreement with values found in the solid state for the terpy ligand of **1**·0.5H_2O. The angles around the N atoms are also in acceptable agreement with those for terpy. The overall conformation of the optimized L

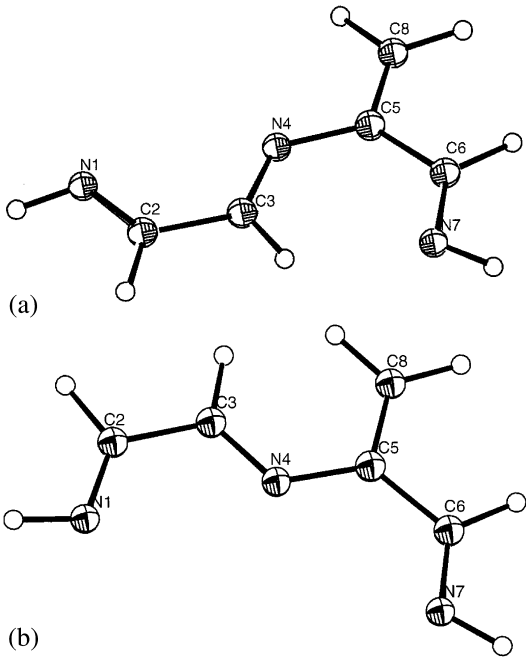


Fig. 2. (a) Drawing of the optimized structure for L, *N*H=CH–CH=*N*–C(=CH_2)–CH=*N*H, EZEE conformation, as computed at the B3LYP/6-31G level. (b) Representation of *N*H=CH–CH=*N*–C(=CH_2)–CH=*N*H, EZZE conformation.

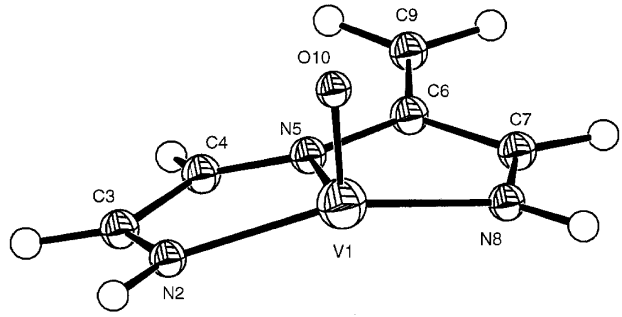


Fig. 3. Drawing of the [VO(*N*H=CH–CH=*N*–C(=CH_2)–CH=*N*H)]$^{2+}$ molecule computed at the B3LYP/LANL2DZ level (full optimization).

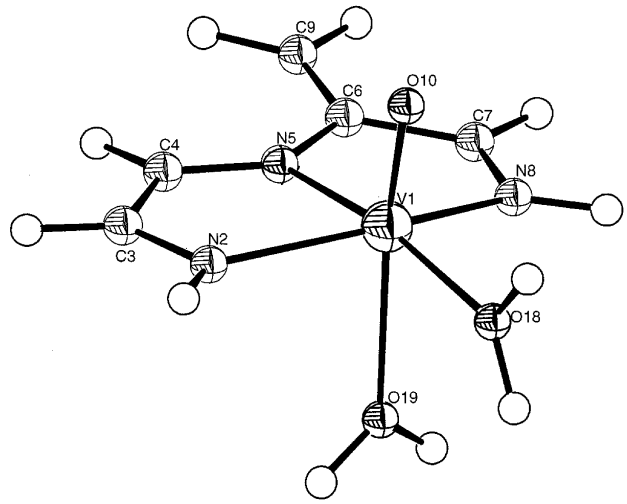


Fig. 4. Drawing of the *cis*-[VO(H_2O)$_2$(*N*H=CH–CH=*N*–C(=CH_2)–CH=*N*H)]$^{2+}$ molecule computed at the B3LYP/LANL2DZ level (full optimization).

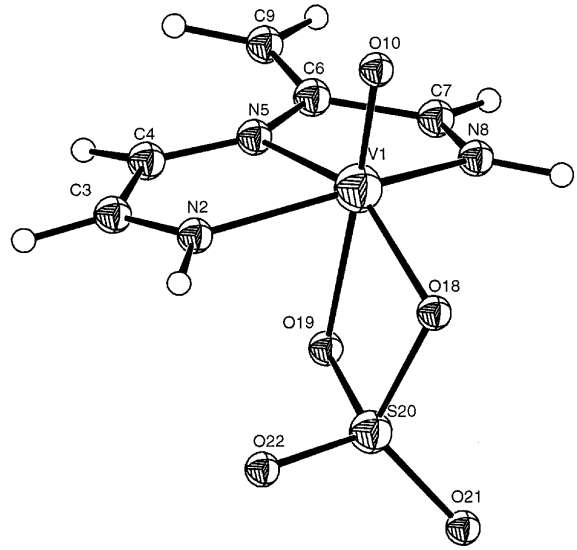


Fig. 5. Drawing of the [VO(*N*H=CH–CH=*N*–C(=CH_2)–CH=*N*H)(*O*,*O*-SO_4)] molecule computed at the B3LYP/LANL2DZ level (full optimization, see Section 2.4). The symmetry of the $VOSO_4$ group is C_1.

Table 4
Total energy (hartrees) for the geometry optimized molecules at the B3LYP/LANL2DZ level (Gaussian 94) unless otherwise specified. L, *N*H=CH–CH=*N*–C(=CH_2)–CH=*N*H (for the meaning of the symbols EZEE and EZZE, see Fig. 2)

Molecule	Energy
O^{2-}	−74.66876
H_2O	−76.41432
SO_4^{2-}	−310.71954
SO_4^{2-} (B3LYP/6-31G**) [a]	−310.94493
SO_4^{2-} (RHF/6-31G**) [a]	−309.23020
L, EZEE	−358.83496
L, EZZE	−358.80802
V^{4+}	−67.45070
VO^{2+}	−145.60945
$[VO(H_2O)]^{2+}$	−222.16805
$[VOL]^{2+}$	−504.92920
$[VO(H_2O)_2L]^{2+}$	−657.90360
$[VOL(O,O\text{-}SO_4)]$ (C_s for the $VOSO_4$ group)	−816.36188
$[VOL(O,O\text{-}SO_4)]$ (C_1 for the $VOSO_4$ group)	−816.36285
$[TiOL]^{2+}$	−491.71709
$[TiOL(O,O\text{-}SO_4)]$ (C_1 for the $VOSO_4$ group)	−803.16652

[a] Oxygen atoms were applied the 6-31G basis set.

Table 5
Formation energy (kcal mol^{-1}) for selected formal reactions as computed at the DFT B3LYP/LANL2DZ level, unless otherwise specified. L, *N*H=CH–CH=*N*–C(=CH_2)–CH=*N*H (for the meaning of the symbols EZEE and EZZE, see Fig. 2)

Reaction	ΔE
$VO^{2+} + H_2O \rightarrow [VO(H_2O)]^{2+}$	−90.54
$VO^{2+} + L(EZEE) \rightarrow [VOL]^{2+}$	−304.21
$VO^{2+} + L(EZZE) \rightarrow [VOL]^{2+}$	−321.12
$[VOL]^{2+} + 2H_2O \rightarrow [VO(H_2O)_2L]^{2+}$	−91.47
$[VOL]^{2+} + SO_4^{2-} \rightarrow [VOL(O,O\text{-}SO_4)]$ (C_1)	−448.11
$[TiOL]^{2+} + SO_4^{2-} \rightarrow [TiOL(O,O\text{-}SO_4)]$ (C_1)	−458.01

ligand can be described as EZEE (Fig. 2(a)), different from the EZZE conformation (Fig. 2(b)) of the starting structure and from that of the N–C–C–N–C–C–N backbone of terpy in the structure of **1**. The energy gap between the EZEE and EZZE conformations as computed at the B3LYP/6-31G level is 16.91 kcal mol^{-1}. The instability of the EZZE structure comes from the steric hindrance between a hydrogen atom from the =CH_2 arm and a second hydrogen atom from the backbone. Short intramolecular H···H contacts are also present within the chelating terdentate terpy ligand. These steric repulsions are probably one of the reasons for deviations from coplanarity of the three aromatic rings of terpy in the solid state structure of **1**.

The V–O(*oxo*) bond distance increases significantly from 1.537 Å, VO^{2+}, to 1.557 Å, $[VO(H_2O)]^{2+}$, showing that even the addition of a weak field ligand such as H_2O in the *trans* position weakens appreciably the V–O(*oxo*) bond. The hexacoordinate $[VO(H_2O)_2L]^{2+}$ and $[VOL(O,O\text{–}SO_4)]$ complexes have V–O(*oxo*) bond lengths of 1.581 and 1.608 Å respectively, in excellent agreement with the value found for **1** in the solid state.

The V–O(H_2O, *trans*) bond distances are 2.023 and 2.254 Å for the $[VO(H_2O)]^{2+}$ and $[VO(H_2O)_2L]^{2+}$ species,

Table 6
Selected bond distances (Å) for the molecules optimized at the DFT-B3LYP/LANL2DZ level, unless otherwise specified. t, terminal; d, donor; *trans* and *cis* are referred to the *oxo* ligand

Molecule	S–O(t)	S–O(d)	V=O	V–O(*trans*)	V–O(*cis*)	V–N(2) [a]	V–N(5) [a]	V–N(8) [a]
SO_4^{2-}	1.678							
SO_4^{2-} (B3LYP/6-31G**) [b]	1.537							
SO_4^{2-} (RHF/6-31G**) [b]	1.497							
VO^{2+}			1.537					
$[VO(H_2O)]^{2+}$			1.557	2.023				
$[VOL]^{2+}$			1.561			2.084	2.061	2.039
$[VO(H_2O)_2L]^{2+}$			1.581	2.254	2.078	2.126	2.109	2.083
$[VOL(O,O\text{-}SO_4)]$	1.614	1.721	1.609	2.226	1.921	2.106	2.104	2.099
($VOSO_4$, C_s)		1.773						
$[VOL(O,O\text{-}SO_4)]$	1.606	1.719	1.608	2.247	1.932	2.108	2.100	2.099
($VOSO_4$, C_1)	1.633	1.766						

[a] The numbering of the atoms is that reported in Figs. 2–5.
[b] Oxygen atoms were applied the 6-31G basis set.

Table 7
Selected bond angles (°) for the molecules optimized at the DFT B3LYP/LANL2DZ level

Molecule	O(t)–S–O(t)	O(d)–S–O(d)	O=V–O(*trans*)	O=V–O(*cis*)	O(S/H)–V–O(S/H)	O=V–N(5)
$[VOL]^{2+}$						107.8
$[VO(H_2O)_2L]^{2+}$			168.3	89.9	78.6	101.4
$[VOL(O,O\text{-}SO_4)]$ (C_1)	118.9	91.8	176.7	110.1	73.1	102.5

showing that the *cis*-L ligand has a large effect. It is worth noting that the computed V–O(*trans*) distance of [VOL(*O*,*O*-SO_4)] is 2.226–2.247 Å, close to the value computed for the diaqua-derivative and in excellent agreement with the experimental value for **1** (2.239(3) Å).

The computed V–O(*cis*) bond distance is 2.078 Å for $[VO(H_2O)_2L]^{2+}$ and 1.932 Å for [VOL(*O*,*O*-SO_4)], showing that the V–sulfate bond is much stronger than the V–water linkage at that coordination site (the strength of the vanadyl sulfate interaction is reflected in the value of the bond formation energy, see below).

The computed V–N bond lengths reproduce well the experimental solid state values; the largest difference between experiment (for **1**) and theory (for [VOL(*O*,*O*-SO_4)]) is 0.063 Å.

As mentioned above (Section 2.4) the S–O bond distances are overestimated (up to 0.18 Å), compared to experimental values, when the basis set is 6-31G for all the first, second and third raw elements. A certain overestimation (ca. 0.05 Å) persists on using 6-31G set for first and second raw elements, and 6-31G** type orbitals for sulfur. However the relative changes caused by chelation of sulfate to the VOL^{2+} group on the S–O bond distances are well estimated at the B3LYP/LANL2DZ level. The S–O(t) vectors undergo a shortening effect upon complexation of 0.04 Å (found for **1**, based on the S–O distance of 1.49 [21]), whereas the computed effect is 0.06 Å. Similarly, the found and computed lengthening of S–O(d, *cis* to *oxo*) is 0.06 and 0.08 Å, respectively.

The structures of $[TiOL]^{2+}$ and [TiOL(*O*,*O*-SO_4)] (C_1) were also optimized for comparison purposes. The computed Ti–O(*cis*) bond distance is 1.877 Å whereas the Ti–O(*trans*) bond length is 2.302 Å. The equatorial oxygen of sulfate is more strongly linked to the metal than the axial oxygen, when compared to the vanadyl complex.

Metal–ligand binding energies: The computed formation energy for $[VO(H_2O)]^{2+}$ is −90.54 kcal mol^{-1}, lower than that of $[Zn(H_2O)]^{2+}$ (−108.40) [20] and higher than that of $[Zn(H_2O)(Imz)]^{2+}$ (Imz, imidazole) (−81.80) [20] from $[Zn(Imz)]^{2+}$ and H_2O. The formation of $[VOL]^{2+}$ from L-EZZE is exothermic for −321.12 kcal and it compares well with the value for $[Zn(H_2O)(Imz)_3]^{2+}$ from $[Zn(H_2O)]^{2+}$ and 3Imz (−298.22 kcal) [29].

The addition of two water molecules to $[VOL]^{2+}$ has a small enthalpic effect (−91.47 kcal) but, interestingly, the addition of the sulfate anion produces a high amount of energy: −448.11 kcal. The latter enthalpic effect is even higher than the formation energy of the tetra-coordinate $[Zn(H_2O)(Imz)_3]^{2+}$ molecule from Zn^{2+}, H_2O and 3Imz (−406.6 kcal) [20]. Even though these values are computed at the gas phase and solvation effects can play a very important role, it is evident that sulfate and N_3VO^{2+} groups have a large affinity. It has to be noted that the high enthalpic effect of the addition of sulfate is not peculiar to the $[VOL]^{2+}$ species. In fact the formal reaction of the sulfate anion with $[TiOL]^{2+}$ to give [TiOL(*O*,*O*-SO_4)] (C_1) produces an even larger amount of energy, −458.01 kcal.

Atomic charges: The atomic charges calculated from the Mulliken population analysis are listed in Table 8. The charge on the V atom decreases down to 1.839*e* from 4, upon V–O(*oxo*) bond formation. The effect of donation from H_2O trans to *oxo* is small: charge on V for $[VO(H_2O)]^{2+}$, 1.632*e*. On the contrary, the addition of L to VO^{2+} has a large effect: charge on V for $[VOL]^{2+}$, 1.185*e*. As expected, chelating sulfate causes a larger effect than two water molecules on the charge of V: 0.927*e* for [VOL(*O*,*O*-SO_4)], 1.057*e* for $[VO(H_2O)_2L]^{2+}$.

The atomic charge of the *oxo* donor is highly influenced by the coordination environment on vanadium: it is 0.161*e* for vanadyl, 0.087*e* for $[VO(H_2O)]^{2+}$ and −0.239*e* for $[VO(H_2O)_2L]^{2+}$. The large negative charge on the *oxo* donor of [VOL(*O*,*O*-SO_4)], −0.368*e*, is in agreement with the presence of several short (C)H···O(*oxo*) contacts found in the crystal structure of **1**·0.5H_2O. The atomic charges on the hydrogen atoms of the L ligand of the [VOL(*O*,*O*-SO_4)] molecule are in the range 0.240–0.357*e*. The charges on the oxygen atoms of the sulfate ligand are highly negative and this explains why several (S)O···H(H_2O) and (S)O···H(C) interactions exists at the solid state for **1**·0.5H_2O.

Computed vibrational frequencies: The IR ν(V–O(*oxo*)) stretching frequency for $[VO(H_2O)]^{2+}$ is 999.1 cm^{-1}, the intensity of the absorption being weak–medium (52.0 km mol^{-1}). The IR ν(V–O(H_2O)) stretching frequency for the same molecule is 489.1 cm^{-1}, weak–medium (38.2), whereas the ν(O–H) stretching frequencies are 3489.0 and 3558.6 cm^{-1} and intense (558.3 and 388.7).

Table 8
Selected atomic charges (*e*) from the Mulliken population analysis at the B3LYP/LANL2DZ level (terms *cis* and *trans* are relevant to the position of the *oxo* ligand; t, terminal)

Molecule	O(*oxo*)	O(*trans*)	O(*cis*)	O(t)	N(2)	N(5)	N(8)	S	V
SO_4^{2-}				−0.811				1.243	
L(EZZE)					−0.218	0.022	−0.246		
VO^{2+}	0.161								1.839
$[VO(H_2O)]^{2+}$	0.087	−0.805							1.632
$[VOL]^{2+}$	−0.157				−0.493	−0.376	−0.545		1.185
$[VO(H_2O)_2L]^{2+}$	−0.239	−0.753	−0.740		−0.453	−0.285	−0.503		1.057
[VOL(*O*,*O*-SO_4)] (C_1)	−0.368	−0.593	−0.618	−0.576	−0.385	−0.267	−0.403	1.252	0.927

4. Conclusion

This work produced the structural characterization of the first complex ever reported of vanadyl with chelating sulfate and a terdentate polypyridine. The X-ray analysis gave accurate geometrical parameters for the complex molecule and in particular for the vanadyl–sulfate grouping. From this, it is evident that the sulfate anion has a strong interaction with the vanadyl group mostly through the oxygen atom which occupies the equatorial position. The chelation causes a large distortion of the sulfate tetrahedron with a significant elongation of a S–O bond and a shortening of two S–O bonds. The angles around sulfur are also significantly altered. The result is a type of activation of SO_4^{2-} towards SO_3. Similar effects happen for the *oxo*-titanium(IV) derivative.

The molecular orbital analysis carried out on several isolated molecules confirms that: (1) the $(terpy)VO^{2+}$ and SO_4^{2-} molecules have a large affinity as estimated by an enthalpic contribution for the formal reaction of -448.11 kcal; (2) the distortion of the sulfate ligand found in the crystal of $\mathbf{1}\cdot 0.5H_2O$ has electronic intramolecular origin and it does not depend significantly on the packing forces inside the crystal; (3) bond distances and bond angles for a $N_3V(O)O_2$ grouping can be excellently reproduced at the B3LYP/LANL2DZ level of computation.

Supplementary data

Supplementary data are available from the CCDC, 12 Union Road, Cambridge CB2 1EZ, UK, deposition number 114535.

Acknowledgements

Professor Francesco Pietra, University of Trento, Italy, is gratefully acknowledged for providing a useful reference list about vanadium in Ascidia and other marine organisms. The University of Siena (Fondo 60%), Italian Ministry for University and Scientific and Technological Research, MURST, Rome (grant COFIN.MURST 97 CIFSIB) and Italian National Counsel for Research, CNR, Rome, are acknowledged for funding. Thanks are due to Mr Francesco Berrettini, Interdepartmental Center for Analysis and Structural Determinations, CIADS, University of Siena, for the X-ray data collection.

References

[1] M. Henze, Hoppe-Seyler's Z. Physiol. Chem. 79 (1912) 215; 72 (1911) 494.
[2] S.W. Taylor, C.J. Hawkins, D.L. Parry, J.H. Swinchart, J.R. Hanson, J. Inorg. Biochem. 56 (1994) 97.
[3] D.H. Anderson, J.H. Swinehart, Comp. Biochem. Physiol. 99A (1991) 585.
[4] E.M. Holtz, S. Pollack, T. Delohery, M.J. Smith, M. Ojika, S. Lee, K. Kustin, K. Nakanishi, Experientia 45 (1989) 186.
[5] S.G. Brand, C.J. Hawkins, A.T. Marshall, G.W. Nette, D.L. Parry, Comp. Biochem. Physiol. 93B (1989) 425.
[6] M. Mahroof-Tahir, A.D. Keramidas, R.B. Goldfarb, O.P. Anderson, M.M. Miller, D.C. Crans, Inorg. Chem. 36 (1997) 1657.
[7] N. Cohen, M. Halberstam, P. Shlimovich, C.J. Chang, H. Shamoon, L. Rossetti, J. Clin. Invest. 95 (1995) 2501.
[8] A.B. Goldfine, D.C. Simonson, F. Folli, M.-E. Patti, C.R. Kahn, J. Clin. Endocrinol. Metab. 80 (1995) 3311.
[9] M.J. Clague, A. Butler, in: G.L. Eichhorn, L.G. Marzilli (Eds.), Advances in Inorganic Biochemistry, Models in Inorganic Chemistry, vol. 9, ch. 6, PTR Prentice Hall, Englewood Cliffs, NJ, 1994.
[10] B.J. Hamstra, A.L.P. Houseman, G.J. Colpas, J.F. Kampf, R. LoBrutto, W.D. Frasch, V.L. Pecoraro, Inorg. Chem. 36 (1997) 4866.
[11] R. Cini, G. Giorgi, F. Laschi, M. Sabat, A. Sabatini, A. Vacca, J. Chem. Soc., Dalton Trans. (1989) 575.
[12] G.M. Sheldrick, SHELX 97, Program for the Refinement of Crystal Structures, University of Göttingen, 1997.
[13] M. Nardelli, PARST 97, A System of Computer Routines for Calculating Molecular Parameters from Results of Crystal Structure Analyses, University of Parma, 1997.
[14] L. Zsolnai, XPMA-ZORTEP 98, University of Heidelberg, 1998.
[15] C.K. Johnson, M.N. Burnett, ORTEP-3 for Windows, Oak Ridge National Laboratory, 1998. 32-bit Implementation by L.J. Farrugia, University of Glasgow.
[16] M.J. Frisch, G.W. Trucks, H.B. Schlegel, P.M.W. Gill, B.G. Johnson, M.A. Robb, J.R. Cheeseman, T. Keith, G.A. Petersson, J.A. Montgomery, K. Raghavachari, M.A. Al-Laham, V.G. Zakrzewski, J.V. Ortiz, J.B. Foresman, J. Cioslowski, B.B. Stefanov, A. Nanayakkara, M. Challacombe, C.Y. Peng, P.Y. Ayala, W. Chen, M.W. Wong, J.L. Andres, E.S. Replogle, R. Gomperts, R.L. Martin, D.J. Fox, J.S. Binkley, D.J. Defrees, J. Baker, J.P. Stewart, M. Head-Gordon, C. Gonzalez, J.A. Pople, Gaussian, Inc., Pittsburgh, PA, 1995.
[17] A.D. Becke, J. Chem. Phys. 88 (1988) 1053.
[18] C. Lee, W. Yang, R.G. Parr, Phys. Rev. B 37 (1988) 785.
[19] P.J. Hay, W.R. Wadt, J. Chem. Phys. 82 (1985) 299.
[20] R. Cini, D.G. Musaev, L.G. Marzilli, K. Morokuma, J. Mol. Struct. (Theochem) 392 (1997) 55.
[21] A.F. Wells, Structural Inorganic Chemistry, Oxford University Press, 1984, and references cited therein.
[22] P.R. Klich, A.T. Daniher, P.R. Challen, D.B. McConville, W.J. Youngs, Inorg. Chem. 35 (1996) 347.
[23] F.T. Al-Ani, D.L. Hughes, C.J.Pickett, J. Chem. Soc., Dalton Trans. (1988) 1705.
[24] R. Cortés, M.K. Urtiaga, L. Lezama, M.I. Arriortua, T. Rojo, Inorg. Chem. 33 (1994) 829.
[25] H. Endres, D. Nöthe, E. Rossato, W.E. Hatfield, Inorg. Chem. 23 (1984) 3467.
[26] L.M. Daniels, C.A. Murillo, K.C. Rodríguez, Inorg. Chim. Acta 229 (1995) 27.
[27] N.L. Speziali, G. Chapuis, Acta Crystallogr., Sect. B 47 (1991) 757.
[28] J.J. Longridge, J.M. Rawson, N. Feeder, P.R. Raithby, Acta Crystallogr., Sect. C 54 (1998) 398.
[29] R. Cini, D.G. Musaev, L.G. Marzilli, K. Morokuma, unpublished data.

PERGAMON

www.elsevier.nl/locate/poly

Polyhedron 19 (2000) 77–83

POLYHEDRON

Synthesis and characterization of homo- and heterobimetallic diethanolaminates of alkaline earth metals

M. Sharma, A. Singh* [1], R.C. Mehrotra* [2]

Department of Chemistry, University of Rajasthan, Jaipur-302 004, India

Received 4 August 1999; accepted 20 October 1999

Abstract

Heteroleptic heterobimetallic isopropoxide diethanolaminate derivatives of the type $\{Al(OPr^i)_2\}_2\{M[(OC_2H_4)_2NH]_2\}$ (M = Mg, Ca, Sr, Ba) have been prepared by the reactions of homometallic precursor derivatives $H_2M\{(OC_2H_4)_2NH\}_2$ (**1a**–**1d**) with $Al(OPr^i)_3$ in 1:2 molar ratio in benzene. The insoluble homometallic precursor derivatives (**1a**–**1d**) have been synthesized by two alternative routes: (1) reactions of $M(OPr^i)_2$ with diethanolamine in 1:2 molar ratio; and (2) reactions of the metals Mg, Ca, Sr and Ba with diethanolamine in 1:2 molar ratio in refluxing toluene. The new homo- and heterobimetallic diethanolaminate derivatives have been characterized by elemental analysis, molecular weight measurements and spectroscopic [IR, NMR (^1H, ^{13}C, ^{27}Al)] studies. ©2000 Elsevier Science Ltd All rights reserved.

Keywords: Alkaline earth metals; Heterobimetallic diethanolaminates; Homobimetallic diethanolaminates

1. Introduction

Although homo- and heterobimetallic triethanolaminate derivatives of a number of metals have been reported [1–3], the corresponding diethanolaminates are still rare, except the reported [1] synthesis of homometallic diethanolaminates of B, Al, Ge, Sn and Nb as well as those of organosilicon [4] and organogermanium [5].

During the last few decades, we have been interested in the development of coordination chemistry of non-classical chelating ligands [3,6,7] (i.e. alkoxometallates such as $Al(OPr^i)_4^-$, $Zr_2(OPr^i)_9^-$, $Nb(OPr^i)_6^-$, etc.), which led to the emergence of diverse structural patterns and recognition of the potentiality of such derivatives as important precursors in the sol–gel process for the synthesis of advanced mixed-metal oxide systems. The organic chelating ligands such as β-diketones [8], carboxylic acids [9], amino alcohols and other polyhydroxy alcohols [10–13] have been found to play an important role in modulating the reactivity of the highly reactive metal alkoxides to such an extent that formation of gel during the hydrolysis process can be accomplished instead of precipitation.

In view of the above, we report herein for the first time the synthesis and characterization of heterobimetallic diethanolaminates of alkaline earth metals, which assume special significance due to the importance of barium as a constituent of superconducting mixed-metal oxide systems [14,15]. Further, the diethanolaminate group as a chelating ligand possesses potential advantages, such as ability to (1) control the reactivity of metal alkoxides; (2) reduce the nuclearity of the oligomeric metal alkoxides; and (3) enhance the volatility and solubility (in common organic solvents) of the resulting derivatives.

2. Experimental

All the preparative reactions were performed under strictly anhydrous conditions. Benzene (BDH), isopropyl alcohol (BDH), n-hexane and toluene (BDH) were dried and purified [16,17] by the usual methods. Diethanolamine was purified by distillation at 213°C, 760 mm.

$Al(OPr^i)_3$ was prepared by the literature method [1]. Freshly cut and dried pieces of alkaline earth metals (Ca, Sr, Ba) were used. Magnesium was used as a foil.

Strontium, barium and aluminium were estimated [18] gravimetrically as strontium sulphate, barium sulphate and aluminium oxinate, respectively. Magnesium and calcium were estimated volumetrically by complexometric titrations using eriochrome black-T as indicator. Nitrogen was estimated [18] by the Kjeldahl method.

Infrared spectra (4000–200 cm^{-1}) were recorded on a Nicolet Magna-550 spectrophotometer in Nujol mulls. NMR

[1] *Corresponding author.

[2] *Corresponding author. Tel.: +91-141-650 800; fax: +91-141-511 557.

0277-5387/00/$ - see front matter ©2000 Elsevier Science Ltd All rights reserved.
PII S0277-5387(99)00327-7

spectra for ^{1}H (in $CDCl_3$ or dimethylsulphoxide, DMSO-d_6), ^{13}C (in CCl_4 or DMSO) and ^{27}Al (in CCl_4 or C_6H_6) were recorded on a JEOL FX 90 Q spectrometer. Molecular weights of soluble derivatives were measured ebullioscopically in benzene using a Gallenkamp ebulliometer with thermistor sensing device.

2.1. Syntheses

Homometallic diethanolaminate derivatives of alkaline earth metals have been prepared either by the reactions of metals or of metal isopropoxides with diethanolamine. Reactions of these insoluble bisdiethanolaminates of alkaline earth metals, $H_2M\{(OC_2H_4)_2NH\}_2$ with $Al(OPr^i)_3$ in 1:2 molar ratio yielded soluble products with the composition $\{Al(OPr^i)_2\}_2\{M[(OC_2H_4)_2NH]_2\}$.

Alternatively, the heterobimetallic isopropoxide-diethanolaminate derivatives have also been prepared by the (1:2) reactions of $M\{Al(OPr^i)_4\}_2$ with diethanolamine.

Due to similarity in the methods of preparation of the new derivatives, the preparation of only one typical compound of each type is described below, while preparative and analytical details for other compounds are listed in Tables 1–4.

2.1.1. Synthesis of homometallic derivative $H_2Ba\{(OC_2H_4)_2NH\}_2$

Surface-cleaned Ba metal (0.75 g, 5.46 mmol) and diethanolamine (1.15 g, 10.92 mmol) were taken in toluene (~50 ml), and refluxed for ~10 h. Removal of the volatiles

Table 1
Reactions of metals with diethanolamine in 1:2 molar ratio

Derivative	Reactants (g, mmol)		Time of refluxing (h)	Empirical formula of the product/ Colour and nature/Yield (g, %)	*Anal.* found (calc.)	
	Metal	Diethanolamine			M = Mg/Ca/ Sr/Ba	N
1a	Mg (0.22, 9.05)	(1.90, 18.17)	30	$H_2Mg\{(OC_2H_4)_2NH\}_2$ Colourless solid [a] (2.01, 98)	10.31 (10.45)	11.81 (12.04)
1b	Ca (0.33, 8.23)	(1.74, 15.56)	20	$H_2Ca\{(OC_2H_4)_2HN\}_2$ Colourless solid [a] (2.01, 98)	16.01 (16.14)	11.47 (11.28)
1c	Sr (0.32, 3.65)	(0.76, 7.23)	10	$H_2Sr\{(OC_2H_4)_2NH\}_2$ Colourless solid [a] (1.08, 91)	29.52 (29.61)	9.23 (9.47)
1d	Ba (0.75, 5.46)	(1.15, 10.92)	10	$H_2Ba\{(OC_2H_4)_2NH\}_2$ Colourless solid [a] (1.88, 98)	39.64 (39.74)	8.01 (8.10)

[a] Insoluble in common organic solvents.

Table 2
Reactions of $M(OPr^i)_2$ with diethanolamine in 1:2 molar ratio

Derivative number	Reactants (g, mmol)		Time of refluxing (h)	Liberated Pr^iOH found (calc.)	Empirical formula of the product/ Colour and nature/Yield (g, %)	*Anal.* found (calc.)	
	$M(OPr^i)_2$	Diethanolamine				M = Mg/Ca/ Sr/Ba	N
1a	M = Mg (0.94, 6.59)	(1.38, 13.12)	10	0.78 (0.79)	$H_2Mg\{(OC_2H_4)_2NH\}_2$ Colourless solid [a] (1.53, 93)	10.16 (10.45)	12.00 (12.04)
1b	M = Ca (1.05, 6.64)	(1.39, 13.22)	9	0.79 (0.80)	$H_2Ca\{(OC_2H_4)_2HN\}_2$ Colourless solid [a] (1.64, 93)	16.03 (16.14)	11.09 (11.28)
1c	M = Sr (3.73, 18.13)	(3.80, 36.33)	8	2.18 (2.18)	$H_2Sr\{(OC_2H_4)_2NH\}_2$ Colourless solid [a] (5.29, 92)	29.33 (29.61)	9.31 (9.47)
1d	M = Ba (1.17, 4.58)	(0.96, 9.14)	6	0.54 (0.55)	$H_2Ba\{(OC_2H_4)_2NH\}_2$ Colourless solid [a] (1.56, 97)	39.56 (39.74)	8.11 (8.10)

[a] Insoluble in common organic solvents.

under reduced pressure yielded a colourless powdery solid (1.88 g, 98%). Analytical details are listed in Table 1.

Freshly prepared $Ba(OPr^i)_2$ (1.17 g, 4.58 mmol) was taken in a solution containing diethanolamine (0.96 g, 9.14 mmol), in benzene (~70 ml). The mixture was refluxed for ~6 h, and the isopropyl alcohol in the azeotrope was estimated periodically until the distillate showed negligible presence of isopropyl alcohol. After removal of the volatiles from this suspension, a colourless solid powder was obtained (1.56 g, 97%). Analytical details are listed in Table 2.

2.1.2. Synthesis of heterobimetallic diethanolaminate derivative $\{Al(OPr^i)_2\}_2\{Ba[(OC_2H_4)_2NH]_2\}$

$H_2Ba\{(OC_2H_4)_2NH\}_2$ (0.73 g, 2.11 mmol) and $Al(OPr^i)_3$ (0.86 g, 4.20 mmol) were taken in benzene solution (~70 ml), which was refluxed for ~6 h under a fractionating column with continuous removal and oxidimetric estimation of the liberated isopropyl alcohol. After completion of the reaction, the solvent was removed under reduced pressure from this yellow coloured solution, yielding a yellow coloured powder (1.26 g, 98%), which on recrystallization from n-hexane and toluene mixture at −20°C yielded the title derivative (1.07 g, 85%). Analytical details are listed in Table 3.

2.1.3. Synthesis of $Ba\{Al(OPr^i)_2[(OC_2H_4)_2NH]\}_2$

The reaction mixture containing freshly prepared $Ba\{Al(OPr^i)_4\}_2$ (2.45 g, 3.69 mmol) in benzene solution (~50 ml) and diethanolamine (0.78 g, 7.38 mmol) was refluxed under a fractionating column for ~6 h with contin-

Table 3
Preparation of heterobimetallic diethanolaminates of alkaline earth metals

Derivative number	Reactants (g, mmol)		Time of refluxing (h)	Liberated Pr^iOH found (calc.)	Empirical formula of the product/ Colour and nature/Yield (g, %)	*Anal.* found (calc.)			Molecular weight found (calc.)
	$H_2M\{(OC_2H_4)_2NH\}_2$	$Al(OPr^i)_3$				M = Mg/ Ca/Sr/Ba	Al	N	
2	M = Mg (1.22, 5.25)	(2.13, 10.41)	6	0.63 (0.63)	$\{Al(OPr^i)_2\}_2\{Mg[(OC_2H_4)_2NH]_2\}$ Colourless solid [a] (2.70, 65)	4.44 (4.67)	10.01 (10.36)	5.13 (5.38)	510 (521)
3	M = Ca (1.43, 5.76)	(2.33, 11.40)	6	0.69 (0.69)	$\{Al(OPr^i)_2\}_2\{Ca[(OC_2H_4)_2NH]_2\}$ Colourless solid [a] (3.04, 69)	7.22 (7.47)	9.81 (10.06)	5.10 (5.22)	529 (537)
4	M = Sr (3.06, 10.34)	(4.11, 20.12)	6	1.24 (1.24)	$\{Al(OPr^i)_2\}_2\{Sr[(OC_2H_4)_2NH]_2\}$ Colourless solid [a] (5.88, 92)	14.45 (14.99)	8.96 (9.24)	4.31 (4.80)	590 (584)
5	M = Ba (0.73, 2.11)	(0.83, 4.06)	6	0.24 (0.25)	$\{Al(OPr^i)_2\}_2\{Ba[(OC_2H_4)_2NH]_2\}$ Colourless solid [a] (1.26, 85)	21.15 (21.66)	8.08 (8.51)	4.18 (4.42)	618 (634)

[a] Soluble in common organic solvents.

Table 4
Reactions of $M\{Al(OPr^i)_4\}_2$ with diethanolamine in 1:2 molar ratio

Derivative number	Reactants (g, mmol)		Time of refluxing (h)	Liberated Pr^iOH found (calc.)	Empirical formula of the product/ Colour and nature/Yield (g, %)	*Anal.* found (calc.)			Molecular weight found (calc.)
	$M\{Al(OPr^i)_4\}_2$	Diethanolamine				M = Mg/ Ca/Sr/ Ba	Al	N	
6	M = Mg (3.35, 6.08)	(1.28, 12.17)	6	1.45 (1.46)	$Mg\{Al(OPr^i)_2[(OC_2H_4)_2NH]\}_2$ Colourless solid [a] (3.15, 84)	4.28 (4.67)	9.97 (10.36)	5.33 (5.38)	531 (521)
7	M = Ca (3.15, 5.56)	(1.17, 11.13)	6	1.34 (1.34)	$Ca\{Al(Opr^i)_2[(OC_2H_4)_2NH]\}_2$ Colourless solid [a] (2.97, 77)	7.21 (7.47)	9.96 (10.06)	5.43 (5.22)	545 (537)
8	M = Sr (2.21, 3.60)	(0.76, 7.23)	6	0.86 (0.87)	$Sr\{Al(OPr^i)_2[(OC_2H_4)_2NH]\}_2$ Colourless solid [a] (2.10, 66)	14.60 (14.99)	9.02 (9.24)	4.27 (4.80)	575 (584)
9	M = Ba (2.45, 3.69)	(0.78, 7.38)	6	0.88 (0.89)	$Ba\{Al(OPr^i)_2[(OC_2H_4)_2NH]\}_2$ Colourless solid [a] (2.39, 76)	21.29 (21.66)	8.28 (8.51)	4.17 (4.42)	645 (634)

[a] Soluble in common organic solvents.

uous collection of the liberated isopropyl alcohol, which was periodically estimated. On completion of the reaction (as indicated by negligible reduction of $K_2Cr_2O_7$), the resulting solution was dried under reduced pressure to afford a light yellow solid (2.39 g, 97%), which was recrystallized in 76% yield from n-hexane and toluene mixture at −20°C. Analytical details are listed in Table 4.

3. Results and discussion

Reactions of alkaline earth metals with diethanolamine in 1:2 molar ratio in refluxing toluene yield insoluble derivatives according to the following reaction:

$$M + 2HN(C_2H_4OH)_2 \xrightarrow[\sim 18\ h]{C_6H_5CH_3} H_2M\{(OC_2H_4)_2NH\}_2\downarrow + H_2\uparrow \quad (1)$$

(1a) : M = Mg
(1b) : M = Ca
(1c) : M = Sr
(1d) : M = Ba

The synthesis of Mg and Ca derivatives by the above route requires a small amount (∼1 ml) of isopropyl alcohol and $HgCl_2$ as a catalyst.

As the preparation of the derivatives **1a**–**1d** by reaction (1) requires ∼18 h of refluxing, these derivatives have been precipitated out slowly at room temperature by mixing diethanolamine in benzene solution of $M(OPr^i)_2$ in 1:2 molar ratio. This mixture is refluxed under a fractionating column with continuous removal of liberated isopropyl alcohol:

$$M(OPr^i)_2 + 2HN(C_2H_4OH)_2 \xrightarrow[\sim 8\ h]{C_6H_6} H_2M\{(OC_2H_4)_2NH\}_2\downarrow + 2Pr^iOH\uparrow \quad (2)$$

(1a) : M = Mg
(1b) : M = Ca
(1c) : M = Sr
(1d) : M = Ba

Interestingly, the reactions of the above insoluble derivatives (**1a**–**1d**) with $Al(OPr^i)_3$ in 1:2 molar ratio in refluxing benzene afford soluble heterobimetallic isopropoxide-diethanolaminate derivatives (**2**–**5**) and 2 mol of isopropyl alcohol, which is quantitatively fractionated out with benzene in the form of an azeotrope:

$$H_2M\{(OC_2H_4)_2NH\}\downarrow + 2Al(OPr^i)_3 \xrightarrow[\sim 6\ h]{C_6H_6}$$

$$\{Al(OPr^i)_2\}_2\{M[(OC_2H_4)_2NH]_2\}_2 + 2Pr^iOH\uparrow \quad (3)$$

where M = Mg (**2**), M = Ca (**3**), M = Sr (**4**) and M = Ba (**5**).

The reactions of $M\{Al(OPr^i)_4\}_2$ derivatives with diethanolamine in 1:2 molar ratio can be represented by Eq. (4). These products could be expected to have a composition of the type $M\{Al(OPr^i)_2[(OC_2H_4)_2NH]\}_2$:

$$M\{Al(OPr^i)_4\}_2 + 2(HOC_2H_4)_2NH \xrightarrow[\sim 6\ h]{C_6H_6}$$

$$M\{Al(OPr^i)_2[(OC_2H_4)_2NH]\}_2 + 4Pr^iOH\uparrow \quad (4)$$

where M = Mg (**6**), M = Ca (**7**), M = Sr (**8**) and M = Ba (**9**).

It would be interesting to investigate the tendencies (if any) of the interconversion of the structural form of products **6**–**9** with those represented by **2**–**5**.

All these colourless homo- and heterobimetallic diethanolaminate derivatives (**1**–**9**) are moisture-sensitive. On heating, compounds **1a**–**1d** tend to decompose around 280°C; compounds **2**–**9** appear to be more stable, but decompose around 350°C without melting. The insoluble nature of the homometallic derivatives (**1a**–**1d**) in benzene precluded molecular weight measurements. These derivatives (**1a**–**1d**) are insoluble in common organic solvents, but freely soluble in DMSO, whereas the heterobimetallic derivatives (**2**–**9**) are soluble in common organic solvents and display a monomeric nature in benzene.

3.1. IR spectra

The diethanolamine ligand shows infrared absorptions [19] (in cm^{-1}) at: 3475 (br) νO–H, 3274 (br) νNH, 2950 (br) νC–H, 1447 $\delta_s(CH_2)$, 905 (br) νC–C and 1060 νC–H.

The homometallic derivatives (**1a**–**1d**) show broad absorptions (Table 5) in the regions 3298–3281 νOH, 3188–3175 νNH, 900–830 νC–C, 1063–1008 νC–O and 576–547 νM–O [6,7] (M = Mg, Ca, Sr, Ba). A comparison of νNH data for the above metal derivatives with that of the free ligand shows lowering of 85–100 cm^{-1}, indicating the possibility of coordination through nitrogen to the central metal atom. Furthermore, the shifting of νOH in homometallic derivatives to lower wave numbers tends to indicate the possibility of extensive hydrogen bonding, making them insoluble due to polymerization, as observed [2] in the case of $H_3La\{(OCH_2CH_2)_3N\}_2$.

The heteroleptic heterobimetallic derivatives (**2**–**9**) show absorptions (Table 5) characteristic of both the isopropoxy (1175–1140, 1127–1096, νOPr^i, 1079–1032 νC–O) and the diethanolaminate groups (3189–3161 νNH, 2939–2905 νC–H) as well as absorption bands at 675–611 νAl– and 577–436 νM–O. The lowering (58–146 cm^{-1}) of νNH compared with that of uncomplexed diethanolamine ligand indicates the possibility of involvement of nitrogen in bonding.

3.2. NMR spectra

The ^1H NMR spectrum of diethanolamine shows signals at δ 2.80 (t (J = 6.1 Hz), CH_2N), 3.80 (t (J = 6.1 Hz), CH_2O) and 4.37 (broad, N*H* and O*H*).

The ^1H NMR spectra (Table 6) of homometallic derivatives $H_2M\{(OC_2H_4)_2NH\}_2$ (**1a**–**1d**) show triplet (J = 6.1 Hz) at δ 2.60–2.68 (CH_2N), broad peaks at 3.37–3.70

Table 5
IR spectral data (cm^{-1}) for homo- and heterobimetallic diethanolaminates of Mg, Ca, Sr and Ba

Derivative number	Compound	νOH	νNH	νOPr^i	νC–O	νM–O (Mg, Ca, Sr, Ba)	νAl–O
	$NH(C_2H_4OH)_2$	3475	3274		1060		
1a	$H_2Mg\{(OC_2H_4)_2NH\}_2$	3281	3175		1008	547	
1b	$H_2Ca\{(OC_2H_4)_2NH\}_2$	3297	3188		1063	555	
1c	$H_2Sr\{(OC_2H_4)_2NH\}_2$	3298	3185		1063	548	
1d	$H_2Ba\{(OC_2H_4)_2NH\}_2$	3281	3188		1032	576	
2	$\{Al(OPr^i)_2\}_2\{Mg[(OC_2H_4)_2NH]_2\}$		3187	1166, 1120	1063, 1047	577	675
3	$\{Al(OPr^i)_2\}_2\{Ca[(OC_2H_4)_2NH]_2\}$		3189	1125, 1101	1079, 1048	532	659
4	$\{Al(OPr^i)_2\}_2\{Sr[(OC_2H_4)_2NH]_2\}$		3170	1165, 1111	1079, 1063	595	659, 643
5	$\{Al(OPr^i)_2\}_2\{Ba[(OC_2H_4)_4NH]_2\}$		3166	1175, 1127	1079, 1032	476, 436	658, 611
6	$Mg\{Al(OPr^i)_2[(OC_2H_4)_2NH]\}_2$		3101	1127, 1096	1095, 1040	595	675
7	$Ca\{Al(OPr^i)_2[(OC_2H_4)_2NH]\}_3$		3172	1159, 1111	1063, 1016	492	675
8	$Sr\{Al(OPr^i)_2[(OC_2H_4)_2NH]\}_2$		3167	1173, 1119	1079, 1032	595	675, 659
9	$Ba\{Al(OPr^i)_2[(OC_2H_4)_2NH]\}_2$		3161	1143, 1111	1063, 1016	523	659, 632

Table 6
^{1}H NMR spectral data (δ, ppm) for homometallic diethanolaminates of Mg, Ca, Sr and Ba

Derivative number	Compound	
	$NH(C_2H_4OH)_2$	2.80(t (J=6.1 Hz), 4H, CH_2N); 3.80(t (J=6.1 Hz), 4H, CH_2O); 4.42(br, 2H, (OH+NH))
1a	$H_2Mg\{(OC_2H_4)_2NH\}_2$	2.60(t (J=6.1 Hz), 8H, CH_2N); 3.57 (br, 8H, CH_2O); 4.74 (br, 4H, (OH+NH))
1b	$H_2Ca\{(OC_2H_4)_2NH\}_2$	2.68(t (J=6.0 Hz), 8H, CH_2N); 3.57(br, 8H, CH_2O); 4.63 (br, 4H, (OH+NH))
1c	$H_2Sr\{(OC_2H_4)_2NH\}_2$	2.48(t (J=6.0 Hz), 8H, CH_2N); 3.37(br, 8H, CH_2O); 4.52 (br, 4H, (OH+NH))
1d	$H_2Br\{(OC_2H_4)_2NH\}_2$	2.55(t (J=6.0 Hz), 8H, CH_2N); 3.70(br, 8H, CH_2O); 4.41(br, 4H, (OH+NH))

Table 7
NMR (^{1}H, ^{27}Al) spectral data (δ, p.p.m.) for heterobimetallic diethanolaminates of Mg, Ca, Sr and Ba

Derivative number	Compound	^{1}H	^{27}Al
2	$\{Al(OPr^i)_2\}_2\{Mg[(OC_2H_4)_2NH]_2\}$	1.21(d (J=6.0 Hz), 24H, CHMe_2); 2.46(br, 8H, CH_2N); 2.95(br, 8H, CH_2O); 3.62(br, 2H, NH); 4.36(sept (J=6.0 Hz), 4H, CHMe$_2$)	63.20
3	$\{Al(OPr^i)_2\}_2\{Ca[(OC_2H_4)_2NH]_2\}$	1.24(d (J=6.0 Hz), 24H, CHMe_2); 2.42(br, 8H, CH_2N); 2.95(br, 8H, CH_2O); 3.74(br, 2H, NH); 4.17(sept (J=6.0 Hz), 4H, CHMe$_2$)	66.41
4	$\{Al(OPr^i)_2\}_2\{Sr[(OC_2H_4)_2NH]_2\}$	1.26(d (J=6.0 Hz), 24H, CHMe_2); 2.59(br, 8H, CH_2N); 2.86(br, 8H, CH_2O); 3.66(br, 2H, NH); 4.13(sept (J=6.0 Hz), 4H, CHMe$_2$)	59.10
5	$\{Al(OPr^i)_2\}_2\{Ba[(OC_2H_4)_2NH]_2\}$	1.26(d (J=6.0 Hz), 24H, CHMe_2); 2.59(br, 8H, CH_2N); 2.95(br, 8H, CH_2O); 3.68(br, 2H, NH); 4.16(sept (J=6.0 Hz), 4H, CHMe$_2$)	60.29
6	$Mg\{Al(OPr^i)_2[(OC_2H_4)_2NH]\}_2$	1.24(d (J=6.0 Hz), 24H, CHMe_2); 2.64(br, 8H, CH_2N); 2.99(br, 8H, CH_2O); 3.84(br, 2H, NH); 4.22(sept (J=6.0 Hz), 4H, CHMe$_2$)	63.16
7	$Ca\{Al(OPr^i)_2[(OC_2H_4)_2NH]\}_2$	1.26(d (J=6.0 Hz), 24H, CHMe_2); 2.64(br, 8H, CH_2N); 2.95(br, 8H, CH_2O); 3.80(br, 2H, NH); 4.16(sept (J=6.0 Hz), 4H, CHMe$_2$)	57.20
8	$Sr\{Al(OPr^i)_2[(OC_2H_4)_2NH]\}_2$	1.25(d (J=6.0 Hz), 24H, CHMe_2); 2.55(br, 8H, CH_2N); 3.06(br, 8H, CH_2O); 3.73(br, 2H, NH); 4.18(sept (J=6.0 Hz), 4H, CHMe$_2$)	59.20
9	$Ba\{Al(OPr^i)_2[(OC_2H_4)_2NH]\}_2$	1.26(d (J=6.0 Hz), 24H, CHMe_2); 2.60(br, 8H, CH_2N); 3.00(br, 8H, CH_2O); 3.71(br, 2H, NH); 4.23(sept (J=6.0 Hz), 4H, CHMe$_2$)	61.55

(CH_2O) and 4.41–4.74 (OH+NH). The low field shifting ($\sim$0.04–0.32 ppm) of OH and NH protons indicates involvement of these groups in bonding. Further, the appearance of only a single set of resonances indicates rapid hydrogen isomerism.

The heteroleptic heterobimetallic derivatives $\{Al(OPr^i)_2\}_2\{M[(OC_2H_4)_2NH]_2\}$ (**2–5**) and $M\{Al(OPr^i)_2[(OC_2H_4)_2NH]\}_2$ (**6–9**) show peaks (Table 7) at δ 2.42–2.64 (br, CH_2N), 2.86–3.00 (br, CH_2O), 3.61–3.84 (br, NH), 1.21–1.26 (d (J=6.0 Hz), CHMe_2) and 4.13–4.36 (sept (J=6.0 Hz), CHMe$_2$).

The ^{13}C NMR spectrum of diethanolamine shows signals at δ 50.54 (CH$_2$N) and 59.70 (CH$_2$O), whereas these signals in the derivatives (**1a–1d**) are observed at δ 49.13–50.69

(CH_2N) and 58.02–59.48 (CH_2O). The mixed-ligand derivatives (**2**–**9**) show peaks due to isopropoxo groups at δ 25.62–28.44 ($CHMe_2$) and 62.75–66.73 ($CHMe_2$) as well as due to the diethanolamino groups at δ 49.13–50.69 (CH_2N) and 58.02–59.13 (CH_2O).

The heterobimetallic derivatives (**2**–**9**) exhibit ^{27}Al NMR chemical shifts in the range δ 58–66, characteristic of tetrahedral [20–22] aluminium compounds.

4. Suggested structures

The insolubility of the products **1a**–**1d** in non-polar organic solvents (e.g. C_6H_6) indicated their polymeric nature, which may be due either to association through diethanolaminate bridges or to the core structure (Fig. 1) with the chelated diethanolaminate ligand becoming associated through hydrogen bonding. The latter possibility appears to be more feasible as these insoluble homometallic diethanolaminates readily yield monomeric bimetallic derivatives (**2**–**5**) in which hydrogen bonding is not possible.

The plausible structure for **1a**–**1d** shown in Fig. 1 is in conformity with spectroscopic (IR, ^{1}H, ^{13}C) data. Similarly, the spectroscopic data (including ^{27}Al NMR) for the heterometallic derivatives (**2**–**5**) are consistent with the plausible structure depicted in Fig. 2.

The broad ^{27}Al NMR signals at δ 57–63 and insignificant change in the position of νNH with that of the diethanolamine ligand for the derivatives **6**–**9** (prepared by the interaction of $M\{(\mu\text{-}OPr^i)_2Al(OPr^i)_2\}_2$ with diethanolamine in 1:2 molar ratio) tend to favour the structure shown in Fig. 3.

It may, however, be pointed out that, due to the significant size and electronegativity differences between alkaline earth metals and aluminium, shifting of diethanolaminate moieties from aluminium to the alkaline earth metal centres may be possible to render coordinatively saturated structures similar to that shown in Fig. 2.

Such type of shifting of a chelating ligand (e.g. $Zr_2(OPr^i)_9^-$) from the smaller less electropositive Cd to the larger more electropositive Ba atom has been recently established X-ray crystallographically by Veith et al. [23] for the product obtained by the reaction shown below:

$$[Zr_2(OPr^i)_9]CdI + KBa(OPr^i)_3 \longrightarrow \{Zr_2(OPr^i)_9\}Cd\{Ba(OPr^i)_3 + KI\downarrow$$

$$\downarrow$$

$$\{Zr_2(OPr^i)_9\}Ba\{Cd(OPr^i)_3\}$$

Although repeated efforts to obtain crystals suitable for X-ray crystallography have not been yet successful, the solubility of the heterometallic derivatives $\{Al(OPr^i)_2\}_2\{M[(OC_2H_4)_2NH]_2\}$ (**2**–**5**) and in contrast to the insolubility of homometallic precursors $H_2\{M[(OC_2H_4)_2NH]_2\}$ (**1a**–**1d**) in hydrocarbon solvents along with no tendency of the derivatives (**2**–**9**) to eliminate $Al(OPr^i)_3$ even on heating up to 200°C, 0.1 mm, confirm their individuality beyond any reasonable doubt, and the structures suggested to be acceptable on the basis of the spectroscopic data discussed in the text are in conformity with suggested plausible structures.

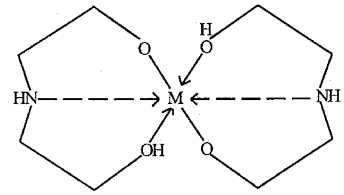


Fig. 1. Proposed structure for the derivatives $H_2M\{(OC_2H_4)_2NH\}_2$; M = Mg (**1a**), Ca (**1b**), Sr (**1c**), Ba (**1d**). Dashed lines represent the tentative involvement of coordination through nitrogen depending upon the size of the metal atom.

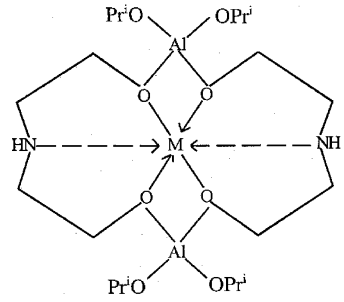


Fig. 2. Proposed structure for the derivatives $\{Al(OPr^i)_2\}_2\{M[(OC_2H_4)_2NH]_2\}$ (**2**–**5**).

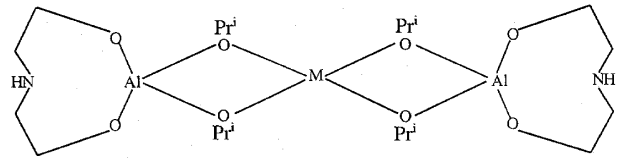


Fig. 3. Proposed logical structure for the derivatives $M\{Al(OPr^i)_2[(OC_2H_4)_2NH]\}_2$ (**6**–**9**).

Acknowledgements

We are grateful to the CSIR and the DST (Government of India) for financial support.

References

[1] D.C. Bradley, R.C. Mehrotra, D.P. Gaur, Metal Alkoxides, Academic Press, London, 1978.
[2] V.G. Kessler, L.G. Hubert-Pfalzgraf, S. Halut, J.C. Daran, J. Chem. Soc., Chem. Commun. (1994) 705.
[3] R.C. Mehrotra, A. Singh, Prog. Inorg. Chem. 46 (1997) 239.
[4] J.J. Daly, F. Sanz, J. Chem. Soc., Dalton Trans. (1974) 2051.
[5] V.F. Mironov, Main Group Metal Chem. 12 (1989) 355.
[6] R.C. Mehrotra, A. Singh, S. Sogani, Chem. Soc. Rev. 23 (1994) 215.
[7] R.C. Mehrotra, A. Singh, S. Sogani, Chem. Rev. 94 (1994) 1643.
[8] R.C. Mehrotra, R. Bohra, D.P. Gaur, Metal β-Diketones and Allied Derivatives, Academic Press, London, 1978.
[9] R.C. Mehrotra, R. Bohra, Metal Carboxylates, Academic Press, London, 1983.
[10] Q. Chen, J. Zubieta, Coord. Chem. Rev. 107 (1992) 114.
[11] Q. Chen, J. Zubieta, Inorg. Chim. Acta 95 (1992) 198.
[12] T.J. Boyle, R.W. Schwartz, R.J. Doedens, J.W. Ziller, Inorg. Chem. 34 (1995) 1110.

[13] M.I. Khan, J. Zubieta, Prog. Inorg. Chem. 43 (1995) 1.
[14] J.G. Bednorz, A. Müller, Z. Phys. B. Condens. Matter 64 (1986) 189.
[15] A. Müller, J.G. Bednorz, Science 217 (1987) 1133.
[16] S. Sogani, A. Singh, R.C. Mehrotra, Polyhedron 14 (1995) 621.
[17] M. Bhagat, Ph.D. Thesis, University of Rajasthan, Jaipur, 1998.
[18] A.I. Vogel, A Text Book of Quantitative Analysis, 5th ed., Longman, London, 1978.
[19] R.M. Silverstein, G. Bassler, T.C. Morrill, Spectroscopic Identification of Organic Compounds, 4th ed., Wiley, New York, 1981.
[20] J.W. Akitt, A. Farthing, J. Chem. Soc., Dalton Trans. (1980) 1615.
[21] J.W. Akitt, A. Farthing, J. Chem. Soc., Dalton Trans. (1981) 1624.
[22] J.W. Akitt, G. Gessner, J. Chem. Soc., Dalton Trans. (1984) 147.
[23] M. Veith, S. Mathur, V. Huch, J. Am. Chem. Soc. 118 (1996) 903.

PERGAMON

www.elsevier.nl/locate/poly

Polyhedron 19 (2000) 85–91

POLYHEDRON

Formation and crystal structures of novel seven-coordinate 15-crown-5 complexes of manganese(II), iron(II) and cobalt(II)

Jerry L. Atwood [a], Peter C. Junk [b,*]

[a] *Department of Chemistry, University of Missouri, Columbia, MO 65211, USA*
[b] *Department of Chemistry, James Cook University, Townsville, Qld 4811, Australia*

Received 2 August 1999; accepted 13 October 1999

This paper is dedicated to Dr Jonathan Steed on the occasion of his 30th birthday

Abstract

The reactions of $Mn(CO)_5Br$, $Fe(CO)_5$ and $Co_2(CO)_8$ with $HCl_{(g)}$ in the presence of 15-crown-5 and H_2O in toluene have been explored. These reactions were promoted with the use of UV radiation and formed liquid clathrates almost immediately upon reaction. For each metal species, oxidation of the metal center from either [+1] (for Mn) or [0] (for Fe, Co) to [+2] occurred. For manganese, the Mn^{II} species $[Mn^{II}(H_2O)_2 \cdot 15\text{-crown-5}][Br^-Cl^-]$ (**1**) was obtained from the liquid clathrate layer in the reaction mixture. For iron the Fe^{II} species $[Fe^{II}Cl(H_2O) \cdot 15\text{-crown-5}][H_5O_2^+][Fe^{II}Cl_4^{2-}]$ (**2**) rapidly formed, and for cobalt the Co^{II} species $[Co^{II}(H_2O) \cdot 15\text{-crown-5}]$-$[H_9O_4^+][Co^{II} \cdot 15\text{-crown-5}][H_9O_4^+][Co^{II}(H_2O) \cdot 15\text{-crown-5}][Co^{II}Cl_4^{2-}]_4$ (**3**) was deposited from the liquid clathrate layer. It was established by X-ray crystallography that each species contains a seven-coordinate metal center with pentagonal bipyramidal stereochemistry. Complex **1** is a hydrogen-bonded single-stranded polymer through bridging halide atoms. Complex **2** has a $H_5O_2^+$ oxonium ion hydrogen-bonded to the cations and complex **3** has a remarkable H_2O–Co^{2+}–$H_9O_4^+$–Co_2^+–$H_9O_4^+$–Co_2^+–H_2O cationic chain. ©2000 Elsevier Science Ltd All rights reserved.

Keywords: 15-Crown-5 complexes; Liquid clathrates; X-ray crystallography; Oxonium ion

1. Introduction

We have isolated a number of complexes from liquid clathrate systems in which we are able to stabilize H_3O^+ in aromatic media [1–9]. For this, we use the coordinating power and the lipophilic nature of 18-crown-6. Further, we are able to use these cations to prepare liquid clathrates in which simple transition metal species act as counterions [6–9]. In moving to the smaller crown ethers which are not suitable for the isolation of H_3O^+ because of the limited diameter of the macrocycle, we find interesting results, with 12-crown-4, where a range of oxonium ions $[H^+ \cdot (H_2O)_n]$, $n = 1$, 2 and 3 were isolated, and with 15-crown-5, $H_5O_2^+$ spanned successive crown ethers [10,11]. In these complexes, the oxonium ions, while hydrogen bonded to the crown ethers, were bound to the faces of the crowns and participated with other molecules in the crystal to form a network of hydrogen-bonded ions.

We now present a study of similar systems with 15-crown-5 and the first row transition metals manganese, iron and cobalt. In moving to first row transition metal ions, the metal center can compete with oxonium ions for coordination sites within the crown ether. It has been established that metal complexation by a crown ether can readily occur if the ratio of the metal ion diameter to the crown cavity diameter (R) falls within the range 0.75–0.90 [12]. For first row transition metals, this is readily achieved for 15-crown-5 (diameter 1.7–2.2 Å [13]); however, for 12-crown-4 (diameter 1.2–1.5 Å [13]) and 18-crown-6 (diameter 2.6–3.2 Å [14]), complexation by the crown does not typically occur. X-ray studies have indicated that transition metal ions have a weaker affinity for crown ethers than non-transition metals. Typically the crowns are hydrogen-bonded to metal-coordinated water molecules, rather than being bound directly to the metal ion [15]. Therefore, an investigation for the propensity of the

* Corresponding author. Tel.: +61-7-47-814-523; fax: +61-7-47-251-394; e-mail: peter.junk@jcu.edu.au

0277-5387/00/$ - see front matter ©2000 Elsevier Science Ltd All rights reserved.
PII S0277-5387(99)00328-9

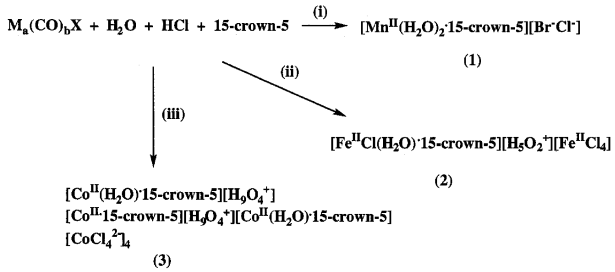
crown ether to coordinate either the transition metal ions (where the size of the ion is perfectly suited for complexation) or an oxonium species appeared to be warranted.

As part of our study of liquid clathrate systems [16–18], particularly of the $[H_3O^+ \cdot 18\text{-crown-6}]$ ion, we have now investigated the formation of anionic manganese, iron and cobalt complexes of the $[(H_2O)_nH^+ \cdot 15\text{-crown-5}]$ system. Our studies of transition metal complexes existing within liquid clathrate media displays the potential for catalytically active species being formed within these systems.

Herein we report the synthesis and crystal structures of $[Mn^{II}(H_2O)_2 \cdot 15\text{-crown-5}][Br^-Cl^-]$ (**1**), $[Fe^{II}Cl(H_2O) \cdot 15\text{-crown-5}][H_5O_2^+][Fe^{II}Cl_4^{2-}]$ (**2**) and $[Co^{II}(H_2O) \cdot 15\text{-crown-5}][H_9O_4^+][Co^{II} \cdot 15\text{-crown-5}][H_9O_4^+][Co^{II}(H_2O) \cdot 15\text{-crown-5}][Co^{II}Cl_4^{2-}]_4$ (**3**), which were all isolated from aromatic media. All three species display seven-coordinate metal centers with pentagonal bipyramidal geometry. In complex **1**, the hybrid chloride/bromide species was isolated. In complexes **2** and **3**, oxonium ions were evident and were involved in hydrogen-bonding frameworks. Complex **3** contained an $[H_9O_4^+]$ oxonium ion which bridged successive Co^{2+} centers, representing an unusual case where a cation is involved as a ligand on a cationic metal center.

2. Preparation of complexes

Complexes studied in this investigation were synthesized according to the novel reaction conditions presented in Scheme 1. In all reactions the reaction mixture quickly separated into two phases yielding liquid clathrate species. The upper layer in these reactions was neat toluene, while the metal complexes formed were completely dissolved within the clathrate layer. Reactions were performed in contact with air, followed by sealing the reaction vessel from aerial contact. Promotion of CO removal was aided by irradiating the reaction mixtures with UV light. In all reactions oxidation of the metal center occurred, from [+1] to [+2] for **1** and from [0] to [+2] for **2** and **3**. In other reactions where we have performed the experiment in the total exclusion of oxygen, no oxidation of the metal center takes place. Instead, for chromium and tungsten we have formed complexes of the type $[M(CO)_5Cl^-]$ [9].



Scheme 1. Reagents and conditions: (i) M = Mn, $a = 0$, $b = 5$, X = Br, toluene, UV; (ii) M = Fe, $a = 0$, $b = 5$, X = O, toluene, UV; (iii) M = Co, $a = 2$, $b = 8$, X = O, toluene, UV.

In the reactions reported herein we obtained seven-coordinate metal species, where complexation of the metal center by the 15-crown-5 macrocycle took place. In complexes **2** and **3**, the oxonium ions $[H_5O_2^+]$ and $[H_9O_4^+]$ were isolated. In complex **1** where $Mn(CO)_5Br$ was used as the source of metal, the chloride/bromide hybrid was produced. These reactions are similar to those that we have established in forming other oxonium ion-crown ether complexes of transition metals [6–9].

Reaction conditions throughout were optimized to yield liquid clathrates and X-ray-quality crystals. To identify the species present in the liquid clathrate layers, all the compounds investigated were structurally authenticated using X-ray crystallography. The complexes were obtained in moderate yields, and no attempts were made to maximize the yields.

3. Structural results

Details for the diffraction experiments are given in Section 5 and Table 1. Selected bond distances and angles for complexes **1**–**3** are shown in Tables 2–4.

3.1. $[Mn^{II}(H_2O)_2 \cdot 15\text{-crown-5}][Br^-Cl^-]$ (1)

This complex does not crystallize as discrete anions and cations, but rather as one-dimensional polymeric strands held together by hydrogen bonding where the $[Mn^{II}(H_2O)_2 \cdot 15\text{-crown-5}]$ cations hydrogen-bond through the terminal water molecules to Br^- and Cl^- (Fig. 1).

The cation resides on a two-fold axis (through Mn and O(1)) and exists as a distorted pentagonal bipyramidal structure. The Mn center is bound to five equatorial crown oxygen atoms and two axial water molecules. The Mn–Wat length is

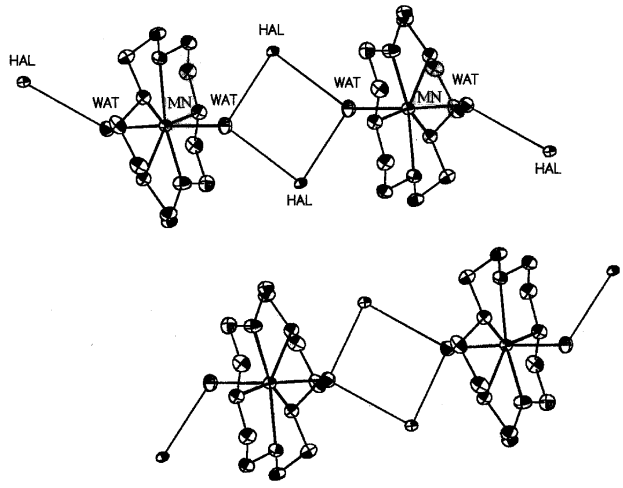


Fig. 1. Structure of $[Mn^{II}(H_2O) \cdot 15\text{-crown-5}][Br^-][Cl^-]$ (**1**), showing the hydrogen bonding between the axial water molecule and the halogen ions. Structural parameters: Mn–Wat, 2.162(6); average Mn–O(crown), 2.23(5); Wat···Hal, 3.16 Å; Hal–Wat–Hal, 99.4°.

Table 1
Crystal data and summary of data collection for complexes **1**–**3**

Compound	$[Mn^{II}(H_2O)_2 \cdot 15\text{-crown-5}][Br^-Cl^-]$ (**1**)	$[Fe^{II}Cl(H_2O) \cdot 15\text{-crown-5}][H_5O_2^+][Fe^{II}Cl_4^{2-}]$ (**2**)	$[Co^{II}(H_2O) \cdot 15\text{-crown-5}][H_9O_4^+][Co^{II} \cdot 15\text{-crown-5}][H_9O_4^+][Co^{II}(H_2O) \cdot 15\text{-crown-5}][Co^{II}Cl_4^{2-}]_4$ (**3**)
Molecular formula	$C_{10}H_{24}BrClMnO_7$	$C_{10}H_{27}Cl_5Fe_2O_8$	$C_{30}H_{82}Cl_{16}Co_7O_{25}$
Molecular weight	426.6	564.3	1822.6
Space group	$C2/c$	$P\bar{1}$	$C2/c$
a (Å)	13.672(2)	7.720(1)	24.031(3)
b (Å)	15.626(3)	12.358(5)	15.869(2)
c (Å)	7.694(1)	12.594(4)	18.789(2)
α (°)	90	94.74(7)	90
β (°)	97.64(1)	103.82(6)	114.63(1)
γ (°)	90	100.02(5)	90
V (Å^3)	1629(2)	1139	6513
Molecules/unit cell	4	2	4
D_c (g cm^{-3})	1.746	1.651	1.866
μ (cm^{-1})	34.1	19.02	24.8
Radiation	Mo Kα	Mo Kα	Mo Kα
Scan width (°)	$0.80 + 0.20 \tan\theta$	$0.80 + 0.20 \tan\theta$	$0.80 + 0.20 \tan\theta$
2θ range (°)	2–50	2–36	2–50
No. reflections collected	1541	2787	4827
No. observed reflections	922	1733	2629
No. parameters varied	92	238	405
Sigma cut-off	3σ	3σ	3σ
Weighting scheme	unit weights	unit weights	unit weights
Temperature of data collection (°)	23	23	23
R	0.054	0.083	0.072
R_w	0.062	0.093	0.076

Table 2
Selected bond distances (Å) and angles (°) for $[Mn^{II}(H_2O)_2 \cdot 15\text{-crown-5}][Br^-Cl^-]$ (**1**)

Atoms	Distance	Atoms	Distance
Mn(1)–Wat	2.162(6)	Mn(1)–O(1)	2.163(9)
Mn(1)–O(4)	2.285(6)	Mn(1)–O(7)	2.237(6)
Atoms	**Angle**	**Atoms**	**Angle**
O(1)–Mn(1)–Wat	88.4(2)	O(4)–Mn(1)–Wat	88.2(2)
O(7)–Mn(1)–Wat	98.7(2)	O(1)–Mn(1)–O(4)	71.0(2)
O(1)–Mn(1)–O(7)	143.5(1)	O(4)–Mn(1)–O(7)	73.4(2)

Table 3
Selected bond distances (Å) and angles (°) for $[Fe^{II}Cl(H_2O) \cdot 15\text{-crown-5}][H_5O_2^+][FeCl_4^{2-}]$ (**2**)

Atoms	Distance	Atoms	Distance
Fe(1)–Cl(1)	2.325(6)	Fe(1)–Cl(2)	2.302(6)
Fe(1)–Cl(3)	2.262(6)	Fe(1)–Cl(4)	2.327(6)
Fe(2)–Wat	2.15(1)	Fe(2)–O(1)	2.20(1)
Fe(2)–O(4)	2.23(1)	Fe(2)–Cl(5)	2.472(5)
Fe(2)–O(7)	2.17(1)	Fe(2)–O(10)	2.21(1)
Fe(2)–O(13)	2.25(1)		
Atoms	**Angle**	**Atoms**	**Angle**
Cl(1)–Fe(1)–Cl(2)	105.9(2)	Cl(1)–Fe(1)–Cl(3)	108.5(2)
Cl(2)–Fe(1)–Cl(3)	115.0(3)	Cl(1)–Fe(1)–Cl(4)	111.1(2)
Cl(2)–Fe(1)–Cl(4)	107.8(3)	Cl(3)–Fe(1)–Cl(4)	108.6(2)
O(1)–Fe(2)–Wat	89.9(5)	O(4)–Fe(2)–Wat	81.5(5)
O(7)–Fe(2)–Wat	91.6(6)	O(10)–Fe(2)–Wat	93.7(6)
O(13)–Fe(2)–Wat	83.3(5)	O(1)–Fe(2)–O(4)	72.3(5)
Wat–Fe(2)–Cl(5)	175.2(4)	O(1)–Fe(2)–Cl(5)	86.1(4)
O(4)–Fe(2)–Cl(5)	94.8(3)	O(7)–Fe(2)–Cl(5)	90.2(4)
O(10)–Fe(2)–Cl(5)	91.1(4)	O(13)–Fe(2)–Cl(5)	98.0(3)
O(1)–Fe(2)–O(7)	144.8(5)	O(4)–Fe(2)–O(7)	73.1(5)
O(1)–Fe(2)–O(10)	143.4(5)	O(4)–Fe(2)–O(10)	144.2(5)
O(7)–Fe(2)–O(10)	71.6(5)	O(1)–Fe(2)–O(13)	72.8(4)
O(4)–Fe(2)–O(13)	141.8(5)	O(7)–Fe(2)–O(13)	142.2(5)
O(10)–Fe(2)–O(13)	71.4(5)		

2.162(6) Å, while the average Mn–O(crown) distances are slightly longer at 2.23(5) Å. The O(crown)–Mn–Wat angles of 88.4(2), 88.2(2) and 98.7(2)° reflect the distorted pentagonal bipyramidal stereochemistry. The O(crown)–Mn–O(crown) angles of 71.0(2) to 73.4(2)° are close to that expected for this stereochemistry. The Mn center resides 0.13 Å out of the plane generated by the crown oxygen atoms.

The anions in this complex are the chloride/bromide hybrid. These anions, which hydrogen bond to the metal-bound water molecule at 3.16 Å, are equally disordered over the two sites, and form hydrogen-bonded bridges to the next cation, generating polymeric strands. The Hal–Wat–Hal angle is 99.4°.

Table 4
Selected bond distances (Å) and angles (°) for $[Co^{II}(H_2O)\cdot 15\text{-crown-}5][H_9O_4^+][Co^{II}\cdot 15\text{-crown-}5][H_9O_4^+][Co^{II}(H_2O)\cdot 15\text{-crown-}5][Co^{II}Cl_4^{2-}]_4$ (**3**)

Atoms	Distance	Atoms	Distance
Co(1)–Cl(1)	2.296(4)	Co(1)–Cl(2)	2.257(4)
Co(1)–Cl(3)	2.252(4)	Co(1)–Cl(4)	2.268(4)
Co(2)–Ox(1)	2.06(1)	Co(2)–Wat(1)	2.07(1)
Co(2)–O(1)	2.16(1)	Co(2)–O(4)	2.168(8)
Co(2)–O(7)	2.254(9)	Co(2)–O(10)	2.176(9)
Co(2)–O(13)	2.25(1)	Co(3)–Ox(4)	2.06(1)
Co(3)–O(1)	2.11(3)	Co(3)–O(22)	2.28(2)
Co(3)–O(1)	2.14(2)	Co(3)–O(42)	2.21(3)
Co(3)–O(1)	2.22(3)		
Atoms	Angle	Atoms	Angle
Cl(1)–Co(1)–Cl(2)	108.1(2)	Cl(1)–Co(1)–Cl(3)	108.1(2)
Cl(2)–Co(1)–Cl(3)	111.3(2)	Cl(1)–Co(1)–Cl(4)	109.5(2)
Cl(2)–Co(1)–Cl(4)	109.2(2)	Cl(3)–Co(1)–Cl(4)	110.6(2)
Wat(1)–Co(2)–Ox(1)	179.6(3)	O(1)–Co(2)–Ox(1)	85.2(4)
O(1)–Co(2)–Wat(1)	95.2(4)	O(4)–Co(2)–Ox(1)	95.8(4)
O(4)–Co(2)–Wat(1)	84.5(4)	O(7)–Co(2)–Ox(1)	84.6(4)
O(7)–Co(2)–Wat(1)	95.2(4)	O(10)–Co(2)–Ox(1)	91.8(4)
O(10)–Co(2)–Wat(1)	87.7(4)	O(13)–Co(2)–Ox(1)	91.3(5)
O(13)–Co(2)–Wat(1)	88.7(5)	O(1)–Co(2)–O(4)	74.0(4)
O(1)–Co(2)–O(7)	144.5(3)	O(4)–Co(2)–O(7)	73.4(3)
O(1)–Co(2)–O(10)	143.1(4)	O(4)–Co(2)–O(10)	142.8(4)
O(7)–Co(2)–O(10)	71.2(4)	O(1)–Co(2)–O(13)	71.6(4)
O(4)–Co(2)–O(13)	144.1(4)	O(7)–Co(2)–O(13)	142.5(3)
O(10)–Co(2)–O(13)	71.7(4)	O(12)–Co(3)–Ox(4)	93(1)
O(22)–Co(3)–Ox(4)	87.9(8)	O(32)–Co(3)–Ox(4)	93.1(8)
O(42)–Co(3)–Ox(4)	84.3(8)	O(52)–Co(3)–Ox(4)	98.4(8)
O(12)–Co(3)–O(22)	146(1)	O(12)–Co(3)–O(32)	105(1)
O(22)–Co(3)–O(32)	41(1)	O(12)–Co(3)–O(42)	106(1)
O(22)–Co(3)–O(42)	108(1)	O(32)–Co(3)–O(42)	149(1)
O(12)–Co(3)–O(52)	144(1)	O(22)–Co(3)–O(52)	69(1)
O(32)–Co(3)–O(52)	108(1)	O(42)–Co(3)–O(52)	42(1)

3.2. $[Fe^{II}Cl(H_2O)\cdot 15\text{-crown-}5][H_5O_2^+][Fe^{II}Cl_4^{2-}]$ (**2**)

In this complex the $[Fe^{II}Cl(H_2O)\cdot 15\text{-crown-}5]$ cations and the $[Fe^{II}Cl_4^{2-}]$ anions are held together in a hydrogen-bonded network through the $[H_5O_2^+]$ ions (see Fig. 2).

In the $[Fe^{II}Cl(H_2O)\cdot 15\text{-crown-}5^+]$ cation, the geometry around the Fe center is a distorted pentagonal bipyramid, bound to five equatorial crown oxygen atoms and a water and chloride ligand in the axial positions. The bonding parameters around the Fe(2) center are (Å): Fe(2)–Cl(5), 2.472(5) Å; Fe(2)–Wat, 2.15(1) Å; and Fe(2)–O(crown), average = 2.21(3). The Cl(5)–Fe(2)–Wat angle is 175.2(4)°, while the Wat–Fe(2)–O(crown) and Cl(5)–Fe(2)–O(crown) angles are in the range 81.5(5)–93.7(6)° and 86.1(4)–98.0(3)° respectively, and reflect the distortion from a regular pentagonal bipyramid. The O(crown)–Fe(2)–O(crown) angles of 71.4(5)–73.1(5)° and 141.8(5)–144.8(5)° are typical of this stereochemistry. The Fe^{II} center resides 0.08 Å out of the plane generated by the crown oxygen atoms.

The $[H_5O_2^+]$ oxonium ions form a hydrogen-bonded array with the $[Fe^{II}Cl(H_2O)\cdot 15\text{-crown-}5^+]$ cations and $[FeCl_4^{2-}]$ anions, where the oxonium ions bridge the Cl(5) ligands of the cation with the Cl(1) and Cl(4) ligands of the anion. These distances of Oa···Cl(1) 3.130, Oa···Cl(4) 3.152 and Ob···Cl(5) 3.023 and 3.024 Å are within the accepted limits for this type of hydrogen bonding [19]. The Oa···Ob distance of 2.337 Å is relatively short for this type of ion, and indicates a strong hydrogen bond [20]. Typical O···O distances of 2.41–2.45 Å are found in $[H_5O_2^+]$ oxonium ions [21].

The $[FeCl_4^{2-}]$ anions exhibit a typical tetrahedral array.

3.3. $[Co^{II}(H_2O)\cdot 15\text{-crown-}5][H_9O_4^+][Co^{II}\cdot 15\text{-crown-}5][H_9O_4^+][Co^{II}(H_2O)\cdot 15\text{-crown-}5][Co^{II}Cl_4^{2-}]_4$ (**3**)

In this complex two $[Co^{II}(H_2O)\cdot 15\text{-crown-}5]$ cations are bridged through $[H_9O_4^+]$ ions to a central $[Co^{II}\cdot 15\text{-crown-}5]$ ion. The bridging $[H_9O_4^+]$ ions coordinate the terminal $[Co^{II}(H_2O)\cdot 15\text{-crown-}5]$ ions through the Co centers (see Fig. 3). $[Co^{II}Cl_4^{2-}]$ counterions, which exhibit the typical tetrahedral array, balance the charge of the compound.

In the structure of the cations, the central $[Co^{2+}\cdot 15\text{-crown-}5]$ ion resides on a center of inversion. The crown is 50:50 disordered, which is a requirement for the molecule to reside on a center of inversion. The three Co^{2+} centers have pentagonal bipyramidal stereochemistry. The remarkable feature of this structure is the Co^{2+} being spanned by cationic $H_9O_4^+$. For the two terminal Co atoms there is a water molecule and an oxygen of the $H_9O_4^+$ in axial positions and five oxygen atoms from the ring in equatorial positions. The central Co atom also has five equatorial oxygen atoms, but has an oxygen of the $H_9O_4^+$ in each axial position. The two

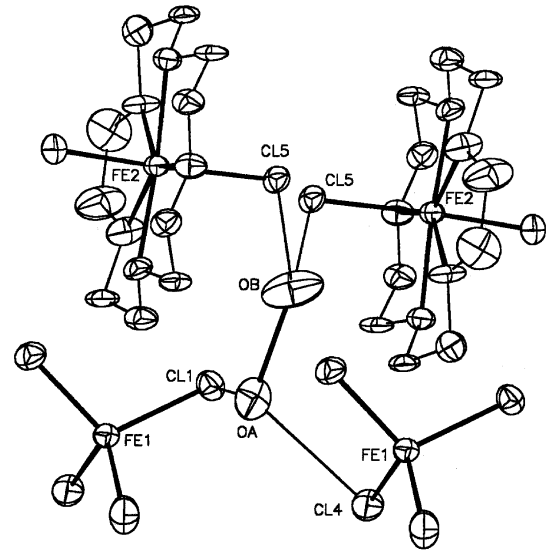


Fig. 2. Arrangement of the anions and cations in $[Fe^{II}Cl(H_2O)\cdot 15\text{-crown-}5][H_5O_2^+][Fe^{II}Cl_4^{2-}]$ (**2**), showing the hydrogen bonding between the $[H_5O_2^+]$ ion and the $[Fe^{II}Cl(H_2O)\cdot 15\text{-crown-}5]$ cations and $[Fe^{II}Cl_4^{2-}]$ anions. Bonding distances (Å): Fe(2)–Cl(5), 2.472(5); Fe(2)–Wat, 2.15(1); average Fe(2)–O(crown), 2.21(3).

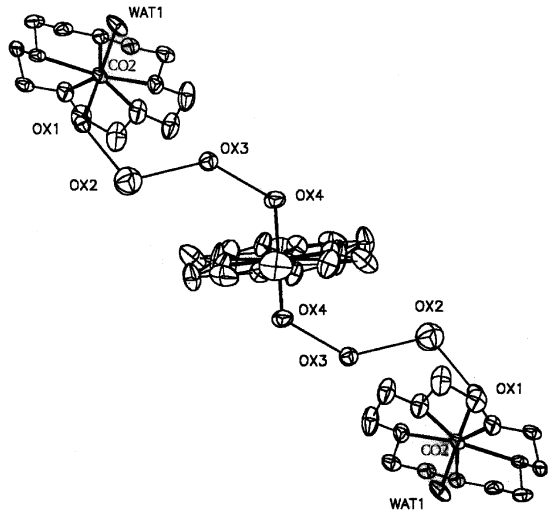


Fig. 3. Structure of the $[Co^{II}(H_2O)\cdot 15\text{-crown-}5][H_9O_4^+][Co^{II}\cdot 15\text{-crown-}5][H_9O_4^+][Co^{II}(H_2O)\cdot 15\text{-crown-}5]$ oligomeric cationic strand in **3**. Bonding distances (Å): Co(2)–Ox(1), 2.06(1); Ox(1)···Ox(2), 2.573; Ox(2)···Ox(3), 3.036; Ox(3)···Ox(4), 2.585; Co(1)–Ox(4), 2.06(1).

$H_9O_4^+$ oxonium ions link together the three cobalt containing 15-crown-5 molecules in a polycationic strand terminated by water molecules. The average Co–O(crown) distances are 2.20(4) Å. The Co–Ox distances are both 2.06(1) Å, the Ox(2)···Ox(3) distance is 3.036 Å and the Ox(1)···Ox(2) and Ox(3)···Ox(4) distances are 2.573 and 2.585 Å. Further intermolecular Cl···H–O hydrogen-bondings between the $[CoCl_4^{2-}]$ anions and the oxonium ions and the terminal H_2O molecule are evident (Cl···O distances 3.067–3.483 Å). These intermolecular hydrogen-bonding contacts terminate the oligomeric cationic strand. The Co^{II} center resides 0.01 Å out of the plane defined by the crown oxygen atoms.

4. Discussion

The preparation of the complexes herein is a novel approach: a metal in its [0] or [+1] oxidation state is treated with HCl gas under UV radiation. The products isolated are of lowest energy which self-assemble from the liquid clathrate medium. We have shown in other publications that this self-assembly is a rather general approach for similar oxonium ion/crown ether complexes of transition metal coordination compounds [6–9].

In all other preparations of transition metal complexes we have utilized metal [0] carbonyls as starting materials. In the case of the manganese complex we used $Mn(CO)_5Br$ to ascertain the generality of this type of reaction. To our surprise, the product obtained was the chloride/bromide hybrid species (**1**). In this reaction, there must be sufficient quantities of HBr produced to remain in solution for further reaction. When we performed the analogous reaction in the presence of 18-crown-6, we isolated the known complex $[H_3O^+\cdot 18\text{-crown-}6]_2[MnCl_4^{2-}]$ [22,23].

For complexes **2** and **3**, oxonium ions were isolated, which formed hydrogen-bonded networks throughout the structure (see below).

In the three complexes discussed, complexation by 15-crown-5 occurred, forming seven-coordinate pentagonal bipyramidal structures. For Mn^{II}, Fe^{II} and Co^{II}, values of *R* (the ratio of the metal ion diameter to the crown cavity diameter) are 0.61–0.78, 0.71–0.92 and 0.68–0.88, respectively. Complexation of the metal by a crown ether can readily occur if *R* falls within the range 0.75–0.90 [9]. In all three cases the metal center resides between 0.01 and 0.13 Å out of the plane of the crown oxygen atoms, and thus snugly fits within the macrocycle. When we perform the analogous reactions in the presence of 18-crown-6 instead of 15-crown-5 the $[H_3O^+\cdot 18\text{-crown-}6]$ complexes of $[MnCl_4^{2-}]$, $[FeCl_4^-]$ and $[CoCl_4^{2-}]$ are isolated [6–8,22]. For 18-crown-6 (diameter 2.6–3.2 Å [14]), *R* values of 0.42–0.51, 0.49–0.60 and 0.47–0.57 are obtained for Mn, Fe and Co, and therefore complexation by the crown does not occur. In contrast to reports that transition metal ions have a weaker affinity for crown ethers than non-transition metals [15], we have shown that, for 15-crown-5, complexation is readily achieved. In all three cases, the crown has a greater tendency to complex the transition metal than to coordinate oxonium ions, as in 18-crown-6 and 12-crown-4 complexes (but also 15-crown-5 where the metal does not 'fit' the crown) [6–11].

There are several reports of seven-coordinate pentagonal bipyramidal stereochemistry for manganese(II) [24,25]. In these, the seven-coordinate Mn^{II} complex $[Mn(HL)(OH_2)_2Cl]Cl\cdot H_2O$ [L = 2,6-diacetylpyridine-mono-(2-aminobenzoylhydrazone)] was characterized by X-ray crystallography [24]. In another, $(MnBr_2)_2$(benzo-15-crown-5)·3/2acetone·H_2O was characterized spectroscopically [25]. The data were consistent with either (1) the Mn^{II} center having eight-coordination comprising five ether oxygens, one oxygen from acetone and two bridging halogens to a second tetrahedrally bound transition metal ion, or (2) the metal having pentagonal bipyramidal geometry in the cation and tetrahedral geometry in the anion. While we obtained neither of these two types of species in **1**, by analogy with complexes **2** and **3** the structure of $(MnBr_2)_2$(benzo-15-crown-5)·3/2acetone·H_2O is most likely that described in (2).

The hydrogen bonding displayed in complex **1**, where the halide ions are bridging successive $[Mn^{II}(H_2O)_2\cdot 15\text{-crown-}5]$ ions and have O···Hal separations of 3.16 Å, this length is slightly longer than typical O–H···Cl separations of 3.10 Å and shorter than expected O–H···Br distances [19]. These distances support the hybrid model found in the X-ray crystallography. Although the protons on the water molecules were not found, the Hal–O–Hal angle of 99.4° suggests that the O–H···Hal linkage is close to linear.

The seven-coordinate pentagonal bipyramidal structure of iron(II) is known in $[Fe(L')(OH_2)_2][BF_4]_2$ (the structure of L′ is shown in Fig. 4) where there are five equatorial

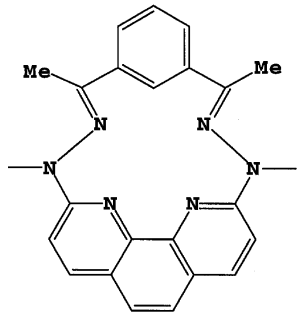


Fig. 4. The structure of L′.

nitrogen atoms and two axial water molecules [26]. The structure we obtained is similar to that postulated using spectroscopic evidence for Mn, Co and Ni complexes of benzo-15-crown-5 [25] except that we isolated a complex with an axial H_2O and Cl^- ligands with a bridging $H_5O_2^+$ molecule between the cations and anions.

The O···Cl distances of 3.01–3.15 Å between the chloride ligands and the $[H_5O_2^+]$ ion in **2** are typical. The O···O separation in the $[H_5O_2^+]$ ion (2.337 Å) is rather short and suggests a strongly hydrogen-bonded oxonium ion [20]. Emsley has stated that a hydrogen bond of >0.3 Å less than the sum of the van der Waals radii of the two elements is classified as a strong hydrogen bond [20]. In this case the O···O separation is some 0.46 Å less than the sum of the van der Waals radii for oxygen [27]. Typical O···O separations in $[H_5O_2^+]$ ions is 2.40–2.45 Å [21].

The seven-coordinate pentagonal bipyramidal stereochemistry for cobalt is not uncommon [14,28]. Compound **3** is closely related to $[Co^{2+}(H_2O)_2\cdot 15\text{-crown-5}][NO_3^-]_2$ [14]. The outstanding difference between the two structures is that, for the NO_3^- species, the nitrate anion is hydrogen-bonded to the axial water molecule, whereas in the present case the axial H_2O molecules are hydrogen-bonded to a positively charged cation, H_3O^+, with further water molecules generating the oligomeric cationic strand of $H_9O_4^+$ and Co^{2+}.

In the linear-chain $[H_9O_4^+]$ ions in compound **3**, the Ox(2)···Ox(3) distance of 3.036 Å precludes the $[H_9O_4^+]$ structure from being considered as an $H_5O_2^+$ ion with terminal H_2O molecules as in the case of $[(H_5O_2^+)(H_9O_4^+)(\text{benzo-15-crown-5})_2][UOCl_4]$ [29]. Typical O···O separations in $H_5O_2^+$ range from 2.40 to 2.45 Å. The Ox(1)···Ox(2) and Ox(3)···Ox(4) distances of 2.573 and 2.585 Å are surprisingly short, being bound to the positive Co^{2+} center. In the uranium complex above the corresponding distances are 2.60 and 2.66 Å [29].

It is interesting to note that, while cationic ligands for metal complexes have been sought for many years, self-assembly of single components in the present system have succeeded where designed systems have often failed [30–33].

5. Experimental

$Mn(CO)_5Br$ and $Fe(CO)_5$ were obtained from Aldrich Chemical Co., $Co_2(CO)_8$ from Alfa and HCl gas was purchased from Atlas Co. Complexes **1**–**3** were prepared exposed to air, prior to the reaction mixture being sealed in an air-tight screw-top tube. In all cases, yields were moderate ($\sim$70–80%), but reactions were conducted to obtain X-ray-quality crystals, so no attempts were made to optimize yields. Attempts at obtaining microanalytical data were thwarted by solvent loss, so are not reported.

*5.1. Preparation of $[Mn^{II}(H_2O)_2\cdot 15\text{-crown-5}][Br^-Cl^-]$ (**1**)*

To a sample of 15-crown-5 (1.00 g, 4.50 mmol) in toluene, was added H_2O (0.08 g, 4.50 mmol) and $Mn(CO)_5Br$ (1.24 g, 4.50 mmol) and stirred rapidly for 15 min. $HCl_{(g)}$ was then rapidly bubbled through the mixture for approx. 1 h while irradiating with UV radiation. A colorless liquid clathrate separated from the solvent during the addition of $HCl_{(g)}$. Colorless crystals of the title complex deposited from the liquid clathrate layer after approx. 24 h.

*5.2. Preparation of $[Fe^{II}Cl(H_2O)\cdot 15\text{-crown-5}][H_5O_2^+]$-$[Fe^{II}Cl_4^{2-}]$ (**2**)*

To a sample of 15-crown-5 (0.80 g, 3.62 mmol) in toluene, was added H_2O (0.065 g, 3.62 mmol) and $Fe(CO)_5$ (0.71 g, 3.62 mmol) and stirred rapidly for 15 min. $HCl_{(g)}$ was then rapidly bubbled through the mixture for approx. 1 h while irradiating with UV radiation. During this time a colorless liquid clathrate separated from the toluene layer. Colorless crystals of the title complex deposited from the liquid clathrate layer after approx. 30 h.

*5.3. Preparation of $[Co^{II}(H_2O)\cdot 15\text{-crown-5}][H_9O_4^+]$-$[Co^{II}\cdot 15\text{-crown-5}][H_9O_4^+][Co^{II}(H_2O)\cdot 15\text{-crown-5}]$-$[Co^{II}Cl_4^{2-}]_4$ (**3**)*

A sample of 15-crown-5 (0.80 g, 3.62 mmol) was moistened with distilled water (0.065 ml, 3.62 mmol) and approx. 100 ml of toluene added. $Co_2(CO)_8$ (1.24 g, 3.62 mmol) was then added and $HCl_{(g)}$ was rapidly bubbled through the mixture for approx. 1 h while irradiating with UV light. After this time, a bright blue liquid clathrate separated from the solvent. Bright blue crystals of the title complex deposited from the clathrate layer after approx. 24 h.

5.4. Collection of X-ray diffraction data, and solution and refinement of the structures

Single crystals of **1**, **2** and **3** were sealed in thin-walled glass capillaries under an atmosphere of toluene. Final lattice parameters as determined from the least-squares refinement of the angular settings of 24 high-angle reflections ($2\theta > 30°$) accurately centered on an Enraf-Nonius CAD4 diffractometer are given in Table 1. A summary of data collection parameters is also given in Table 1. An empirical absorption correction based on psi scan data was performed. Calculations were

carried out using the SHELX system of computer programs [34].

Positions of heavy atoms were determined from a three-dimensional Patterson function. All other non-hydrogen atoms were located from a difference-Fourier synthesis. All non-hydrogen atoms were refined with anisotropic thermal parameters. Hydrogen atoms on the water molecules and oxonium ions in **1**, **2** and **3** were not located on the difference map. All other hydrogen atoms were placed at calculated positions and their parameters were not refined. The halides in compound **1** were disordered over two sites. The structure was successfully refined with each halide site being occupied by 50% Br^- and 50% Cl^-. In compound **2**, there was high thermal motion in C(8), C(9), O(a) and O(b), but the model refined successfully. In compound **3** the 15-crown-5 molecule on the central Co^{2+} was 50:50 disordered over two sites, and Ox(3) and one of the $CoCl_4^{2-}$ were also disordered. They were refined successfully. Refinements converged with $R = 0.062$ for 922 observed reflections for **1**, $R = 0.083$ for 1733 observed reflections for **2**, and $R = 0.072$ for 2629 observed reflections for **3**.

Supplementary data

Crystallographic data for the structures have been deposited with the Cambridge Crystallographic Data Centre (CCDC deposition numbers CCDC 132777, CCDC 132778, CCDC 132779). Copies of the data can be obtained upon request from CCDC, 12 Union Road, Cambridge CB2 1EZ, UK, quoting the deposition numbers.

Acknowledgements

We are grateful to the National Science Foundation for support of this research. We also acknowledge the Department of Chemistry at the University of Alabama for collection of the X-ray data.

References

[1] J.L. Atwood, S.G. Bott, A.W. Coleman, K.D. Robinson, S.B. Whetstone, C.M. Means, J. Am. Chem. Soc. 109 (1987) 8100.
[2] J.L. Atwood, S.G. Bott, C.M. Means, A.W. Coleman, H. Zhang, M.T. May, Inorg. Chem. 29 (1990) 467.
[3] J.L. Atwood, S.G. Bott, K.D. Robinson, E.J. Bishop, M.T. May, J. Cryst. Spec. Res. 21 (1991) 459.
[4] J.L. Atwood, P.C. Junk, M.T. May, K.D. Robinson, J. Chem. Crystallogr. 24 (1994) 243.
[5] P.C. Junk, L.R. MacGillivray, M.T. May, K.D. Robinson, J.L. Atwood, Inorg. Chem. 34 (1995) 5395.
[6] P.C. Junk, J.L. Atwood, J. Chem. Crystallogr. 24 (1994) 247.
[7] J.L. Atwood, S.G. Bott, P.C. Junk, M.T. May, J. Coord. Chem. 37 (1996) 89.
[8] J.L. Atwood, P.C. Junk, M.T. May, K.D. Robinson, J. Coord. Chem. 40 (1996) 247.
[9] J.L. Atwood, S.G. Bott, P.C. Junk, M.T. May, J. Organomet. Chem. 487 (1995) 7.
[10] P.C. Junk, J.L. Atwood, J. Coord. Chem. (submitted for publication).
[11] P.C. Junk, J.L. Atwood, J. Organomet. Chem. 565 (1998) 179.
[12] J.J. Christensen, J.O. Hill, R.M. Izatt, Science 174 (1971) 459.
[13] N.K. Dalley, R.M. Izatt, J.J. Christensen, Synthetic Multidentate Macrocyclic Compounds, Academic Press, New York, 1978, pp. 207–244.
[14] E.M. Holt, N.W. Alcock, R.R. Hendrixson, G.D. Malpass Jr., R.G. Ghirardelli, R.A. Palmer, Acta Crystallogr., Sect. B 37 (1981) 1080.
[15] B. Chiswell, E.D. McKenzie, L.F. Lindsoy, G. Wilkinson, R.D. Gillard, J.A. McCleverty, Comprehensive Coordination Chemistry, vol. 4, Pergamon, New York, 1987, p. 80.
[16] J.L. Atwood, in: J.L. Atwood, J.D. Davies, D.D. MacNicol (Eds.), Inclusion Compounds, vol. 1, Academic Press, London, 1984, pp. 375–405.
[17] J.L. Atwood, in: C.J. King, J.D. Navratil (Eds.), Chemical Separations, Litarvan, Denver, CO, 1986, pp. 335–354.
[18] J.L. Atwood, in: N.N. Li, H. Strathmann (Eds.), Separation Technology, United Engineering Trustees, New York, 1988, pp. 46–56.
[19] W.C. Hamilton, J.A. Ibers, Hydrogen Bonding in Solids, Benjamin Press, New York, 1968, p. 12.
[20] J. Emsley, J. Chem. Soc. Rev. 9 (1980) 91.
[21] N.N. Greenwood, A. Earnshaw, Chemistry of the Elements, Pergamon, New York, 1984, p. 739.
[22] P.C. Junk, J.L. Atwood (unpublished results).
[23] R. Chenevert, D. Chamberland, M. Simard, F. Brisse, Can. J. Chem. 68 (1990) 797.
[24] C. Pelizzi, G. Pelizzi, P. Tarasconi, J. Chem. Soc., Dalton Trans. (1985) 215.
[25] M.E. Farago, Inorg. Chim. Acta 25 (1977) 71.
[26] M.M. Bishop, J. Lewis, T.D. O'Donoghue, P.R. Raithby, J.N. Ramsden, J. Chem. Soc., Dalton Trans. (1979) 1390.
[27] R.D. Shannon, Acta Crystallogr. A32 (1976) 751.
[28] F. Mathieu, R. Weiss, J. Chem. Soc., Chem. Commun. (1973) 816.
[29] R.D. Rogers, A.H. Bond, W.G. Hipple, A.N. Rollins, R.F. Henry, Inorg. Chem. 30 (1991) 2671.
[30] C. Ercolani, J.V. Quagliano, L.M. Vallarino, J. Chem. Soc., Chem. Commun. (1969) 1094.
[31] C. Ercolani, J.V. Quagliano, L.M. Vallarino, Inorg. Chim. Acta 3 (1969) 421.
[32] V.L. Goedkin, L.M. Vallarino, J.V. Quagliano, Inorg. Chem. 10 (1971) 2682.
[33] W.D. Perry, J.V. Quagliano, L.M. Vallarino, Inorg. Chim. Acta 7 (1973) 175.
[34] G.M. Sheldrick, SHELX76: A System of Computer Programs for X-Ray Structure Determination, University of Cambridge, UK, 1976.

PERGAMON

www.elsevier.nl/locate/poly

Polyhedron 19 (2000) 93–98

POLYHEDRON

Synthesis, crystal structure and magnetic properties of novel dinuclear complexes of manganese, cobalt and nickel with 4-acetylbispyrazolone

Luqin Yang *, Wenzheng Jin [1], Jianhua Lin

State Key Laboratory of Rare Earth Materials Chemistry and Applications, College of Chemistry and Molecular Engineering, Peking University, Beijing 100871, PR China

Received 24 June 1999; accepted 28 October 1999

Abstract

Five novel transition metal complexes, $MnL \cdot 2C_2H_5OH \cdot 3H_2O$ (**1**), $MnL \cdot 2.5DMF \cdot 0.5H_2O$ (**2**), $Co(HL)(NO_3) \cdot C_2H_5OH$ (**3**), $CoL \cdot 2.5H_2O$ (**4**), and $NiL \cdot C_2H_5OH \cdot 2H_2O$ (**5**), have been synthesized and characterized. H_2L represents bis(1′-phenyl-3′-methyl-5′-pyrazolone-4′)-1,5-pentanedione (L^{2-} and HL^- are the deprotonated forms of H_2L). Spectroscopic data reveal that the title complexes are dimers. The tetraketone ligand L coordinates to the metal ions through two β-diketonates. The β-diketonate is mainly in the delocalized enol form. The enol-keto form β-diketone (HL^-, one β-diketone remains in keto form and the other is in deprotonated enol form) also exists in the Co complex **3**. The crystal structure of $MnL \cdot 2.5DMF \cdot 0.5H_2O$ (**2**) was determined by X-ray diffraction. The ligand L is in a bridging mode connecting two metal ions. Mn^{2+} is six-coordinated with a distorted octahedral coordination sphere. A variable temperature magnetic susceptibility investigation showed that a weak antiferromagnetic exchange interaction exists between the metal centers in the complexes. The $2J$ values based on $\boldsymbol{H} = -2J/\boldsymbol{S}_1\boldsymbol{S}_2$ are -0.71 cm^{-1} (Mn1), -1.96 cm^{-1} (Co2), -1.74 cm^{-1} (Co3), and -2.02 cm^{-1} (Ni).
©2000 Elsevier Science Ltd All rights reserved.

Keywords: Crystal structures; Magnetic properties; Dinuclear complexes; Manganese; Cobalt ; Nickel

1. Introduction

Molecular based materials are a promising frontier research field in both chemistry and materials science [1–3], and has attracted great interest recently. Metal complexes play an important role in the design and synthesis of molecular materials [4]. Some β-diketonate manganese complexes show extraordinary structures and interesting magnetic properties [5]. Owing to their effective properties with respect to extracting metal ions, β-diketone compounds have attracted most interest in recent decades. They can also be used in laser materials, proton NMR shift reagents, MOCVD, the petroleum industry, and analytical chemistry [6–10]. There are only a few reports on poly-β-diketone complexes [11]. 4-Acetyl-bipyrazolone is a new type of chelating ligand which contains two β-diketones. It is more efficient than 4-acetyl-pyrazolone derivatives in extracting hard Lewis acid metal ions [12] and can form different types of coordination compounds owing to the use of four donor sites in its molecule. The rare earth complexes of bispyrazolone show very strong fluorescence [13–18] and some also have antitumor activity in vitro, and high herbicidal activities. Based on the structure of the tetraketone, it should be efficient in forming multinuclear complexes. In order to investigate the magnetic and fluorescence properties of multinuclear complexes, we synthesized a series of multinuclear transition metal and rare earth complexes. To our knowledge, no crystal structures of bispyrazolone transition metal complexes have been reported in the literature. Recently we obtained the single structure of a manganese complex. This paper reports the crystal structure of the novel manganese complex with 1,5-bis(1′-phenyl-3′-methyl-5′-pyrazolone-4′)-1,5-pentanedione. The magnetic properties of complexes Mn(II), Co(II), Ni(II) were also studied.

2. Experimental

2.1. Materials and measurements

1,5-bis(1′-phenyl-3′-methyl-5′-pyrazolone-4′)-1,5-pentanedione (H_2L) was synthesized according to the method

* Corresponding author; e-mail: lqyang@chemms.chem.pku.edu.cn

[1] Current address: Department of Materials Science and Engineering, University of Utah, Salt Lake City, UT 84112, USA.

0277-5387/00/$ - see front matter ©2000 Elsevier Science Ltd All rights reserved.
PII S0277-5387(99)00329-0

described in the literature [19]. $Ni(ClO_4)_2 \cdot 6H_2O$ was prepared by our laboratory. The other reagents used for synthetic experiments were of analytical grade available commercially without further purification.

Elemental analyses were carried out on a Perkin-Elmer 240 analyzer. FAB-MS was carried out on a HS-ZAB spectrometer. TG and DTA were carried out on a LCT-1 thermoanalyzer. FT-IR spectra were carried out on a magna 750 IR spectrometer. Solid state reflection UV–Vis spectra were recorded on a Shimadzu UV-3100 spectrophotometer. Variable temperature magnetic susceptibilities were measured on an extracting sample magnetometer CF-1. Di-magnetic corrections were made using Pascal's constants. Effective magnetic moments of complexes were calculated with $\mu_{eff} = 2.828(\chi T)^{1/2}$.

2.2. Preparation of complexes

$MnL \cdot 2C_2H_5OH \cdot 3H_2O$ (**1**). An ethanolic solution containing 1 mmol $MnAc_2 \cdot 4H_2O$ was added to the ethanolic solution containing 1 mmol H_2L with magnetic stirring. The resulting solution was refluxed for 20–25 h. Then the fine crystalline precipitate was collected and washed with ethanol, dried in vacuo at room temperature. The yield of complex was above 85%. The product was obtained as a light pink solid. Found: C, 54.52; H, 5.72; N, 8.55. Calc. for $C_{29}H_{40}N_4O_9Mn$: C, 54.12; H, 6.22; N, 8.71%. IR (KBr, cm^{-1}): 1614 (vs, ν(C=O)), 1531 (w, ν(C=C)), 1489 (vs, ν(C=O)). Thermogravity (TG): 82°C, loss weight 16.2% (calc. for $2C_2H_5OH$, 17.1%, endothermic); 82–268°C, loss weight 8.2% (calc. for $3H_2O$, 8.4%, endothermic). Molar conductivity Λ_M(DMF) = 5.8 S cm^2 mol^{-1}. UV–Vis: 336 nm.

$CoHL(NO_3) \cdot C_2H_5OH$ (**3**). This pink crystalline solid product was obtained following a similar procedure as described for compound **1** by replacing $MnAc_2 \cdot 4H_2O$ with $Co(NO_3)_2 \cdot 6H_2O$. Found: C, 53.11; H, 4.90; N, 11.30. Calc. for $C_{27}H_{29}N_5O_8Co$: C, 53.12; H, 4.75; N, 11.48%. IR(KBr, cm^{-1}): 1661, 1642 (s, ν(C=O)), 1621 (vs, ν(C=O)), 1501 (vs, ν(C=O)). TG: 62–149°C, loss weight 7.2% (calc. for C_2H_5OH, 7.5%, endothermic); 255°C, loss weight 9.8% (calc. for HNO_3, 10.0%, exothermal). Λ_M(DMF) = 75 S cm^2 mol^{-1}.

$CoL \cdot 2.5H_2O$ (**4**). 2 mmol NaOH aqueous solution (0.6 mol^{-1}) was added to an ethanolic solution containing 1 mmol H_2L with stirring. A light yellow–orange solution was obtained (pH 5–6). Then an ethanolic solution containing 1 mmol $CoCl_2 \cdot 6H_2O$ was added to the above solution under magnetic stirring. Stirring was continued at room temperature for about 10 h. The precipitate was collected and washed thoroughly with ethanol, water, ethanol, respectively, then dried in vacuo over P_2O_5 at room temperature. The product was obtained as a pink solid. The yield was above 85%. Found: C, 55.39; H, 4.65; N, 10.49. Calc. for $C_{25}H_{27}N_4O_{6.5}Co$: C, 54.94; H, 4.95; N, 10.26%. IR (KBr, cm^{-1}): 1611 (vs, ν(C=O)), 1530 (w, ν(C=C)), 1494 (vs, ν(C=O)). TG: 74°C, loss weight 8.4% (calc. for $2.5H_2O$, 8.2%, endothermic). UV–Vis: 340, 562, 1164, 1374 nm.

$NiL \cdot C_2H_5OH \cdot 2H_2O$ (**5**). The light green solid product was obtained following a similar procedure as described for compound **1** by replacing $MnAc_2 \cdot 4H_2O$ with $Ni(ClO_4)_2 \cdot 6H_2O$. Found: C, 55.34; H, 5.43; N, 9.21. Calc. for $C_{27}H_{32}N_4O_7Ni$: C, 55.60; H, 5.49; N, 9.61%. IR (KBr, cm^{-1}): 1616 (vs, ν(C=O)), 1534 (w, ν(C=C)), 1504, 1494 (vs, ν(C=O)). Λ_M(DMF) = 4.2 S cm^2 mol^{-1}. FAB-MS (M/e): 1002 [Ni_2L_2, M^+], 562 [Ni_2L, M − 2], 502 [NiL, M + 1]. UV–Vis: 327, 661, 723, 1122 nm.

2.3. Preparation, X-ray data collection, structure determination and refinement of a single crystal of $Mn_2L_2 \cdot 5DMF \cdot H_2O$ (2)

The colorless single crystals of $Mn_2L_2 \cdot 5DMF \cdot H_2O$ (**2**) were obtained by slowly evaporating the DMF solution of complex **1** at ambient temperature for over 2 months. They lost the solvent molecules easily in air.

A single crystal of $C_{32.5}H_{40.5}MnN_{6.5}O_7$ with dimensions $0.05 \times 0.15 \times 0.30$ mm was mounted on an Enraf-Nonius CAD-4 X-ray diffractometer. The data were measured using graphite-monochromated Mo Kα radiation ($\lambda = 0.71073$ Å) in the θ range 4.5–23° with an ω–2θ scan mode. Accurate cell parameters were obtained from a least squares fit of the setting angles of 25 reflections with θ range 8.93–12.74° at 299 ± 1 K. The data collection gave 5237 reflections from which 4787 were independent ($R_{int} = 0.058$). 1824 reflections were considered to be observed ($I \geq 2\sigma(I)$) and were used in the following refinement. A correction for Lorentz polarization effects was applied to the data.

Crystals are triclinic, space group $P\bar{1}$, with a = 10.773(5), b = 13.397(5), c = 14.811(3) Å, α = 65.04(3), β = 70.93(3), γ = 80.54(3)°, V = 1831(1) Å^3, M_r = 689.18, Z = 2, D_x = 1.254 g cm^{-3}, μ = 3.946 cm^{-1}.

The structure was solved with direct methods. The positions of two manganese ions were located on an E-map. All the other non-hydrogen atoms were determined from the successive difference Fourier synthesis.

The entire structure was refined by the full-matrix least-squares technique with anisotropic thermal parameters for all of the non-hydrogen atoms, except for the uncoordinated solvent molecules for which the isotropic thermal parameters were used. The agreement factors were $R = \sum||F_o| - |F_c||/\sum|F_o| = 0.067$ and $wR = [\sum w(||F_o|^2 - |F_c|^2|/\sum|F_o|^2)]^{1/2} = 0.072$ (unit weights for all observed reflections).

3. Results and discussion

3.1. Constituent and general properties

The composition of the complexes was determined by elemental analyses, FT-IR and TG analysis. The molar ratio M:L in all the complexes is 1:1. The tetraketone ligand H_2L

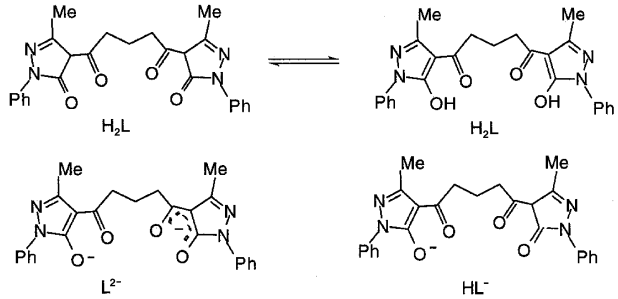


Fig. 1. Structures of of H_2L, HL^- and L^{2-} (one tautomer of each).

is coordinated to the metal ions as HL^- in complex **3** and as L^{2-} in the other complexes (Fig. 1).

All the complexes are insoluble in water or ethanol, but dissolve in DMF or DMSO. The molar conductivity of complexes in DMF shows that complex **3** is a 1:1 electrolyte and the others are non-electrolytes [20].

Thermal analyses (TG and DTA) of the complexes indicate that they lose the solvent molecules below 150°C with an endothermic peak in DTA. When the temperature is above 280°C, the complexes are decomposed into metal oxides with strong exothermic DTA peaks.

The FAB-mass spectrum of the nickel complex was also recorded. In the FAB-mass spectrum of the nickel complex (DMF), the largest mass number 1002 can be assigned to a Ni_2L_2 (M^+) fragment, 562 to Ni_2L $(M-2)^+$, and 502 to NiL $(M+1)^+$. All these fragments indicate that the complex is a dimer. The zinc complex appears also to be a dimer from FAB-MS and this is verified by its crystal structure [21]. TG analysis and IR spectra of the complexes confirmed the existence of some coordinated solvent molecules. The liquid–liquid extraction of copper ion with bipyrazolone has two extracts: 1:2 and 2:2 (metal ion/ligand molar ratio). The 2:2 extract is a dimer [22]. For the 1:2 ratio it is easy to form a coordination polymer, and the solid copper(II) [21] and VO(II) (not published) complexes have this kind of structure. Given their similar solubilities, the structures of Mn(II), Co(II) and Ni(II) complexes may be analogous. The primary molecular structures of Co(II) and Ni(II) are similar to that of $Mn_2L_2 \cdot 5DMF \cdot H_2O$.

The solid state reflection UV–Vis spectra of the complexes were recorded. d–d-Transitions are observed in Co, Ni complexes: 562, 1164, 1374 nm for **4** and 661, 723, 1122 nm for **5** The absorption around 320–360 nm in Mn, Co, Ni can be attributed to the L–L* transition of coordinated ligand.

3.2. Crystal structure

A perspective view of complex **2** is shown in Fig. 2. Selected bond distances and bond angles are listed in Table 1.

In the molecule $Mn_2L_2 \cdot 5DMF \cdot H_2O$, L behaves as a tetradentate ligand, acting as a bis-bidentate ligand. The ligand L is a bridge connecting the two manganese ions with its two β-diketone groups. The complex is binuclear and each manganese ion is six-coordinated. The six-coordination oxygen atoms come from two tetraketone ligands L (O1, O2, O3a, O4a) and two dimethylformamide molecules (O41, O51). The bond distance Mn–O ranges from 2.123 (Mn–O2) to 2.178 Å (Mn–O51) (mean Mn–O 2.143 Å). The coordination polyhedron of the manganese ion is a distorted octahedron (Fig. 3). The dihedral angle between plane 1 (O1, O4, O3, O41) and plane 2 (O1, O2, O3′, O51) is 89.36°; the angle between plane 1 and plane 3 (O2, O4′, O41, O51) is 89.62°; the angle between plane 2 and plane 3 is 86.43°; the angle between plane 4 (O1, O2, O4′) and plane 10 (O3′, O41, O51) is 12.71°; the angle between plane 5 (O1, O2, O41) and plane 11 (O3′, O4′, O51) is 168.34°; the angle between plane 6 (O1, O41, O51) and plane 8 (O2, O3′, O4′) is 15.19°; the angle between plane 7 (O1, O4, O51) and plane 9 (O2, O3′, O41) is 5.56°.

β-Diketones in the ligand H_2L are all in the deprotonated form (L^{2-}). From the bond distances C=O (O1–C17, 1.266; O2–C1, 1.26; O3–C5, 1.21; O4–C27, 1.25 Å) and the connecting C–C distances (C1–C2, 1.56; C1–C18, 1.39; C17–C18, 1.45; C4–C5, 1.53; C5–C28, 1.44; C27–C28, 1.45 Å) it can be deduced that the β-diketones are in delocalized form.

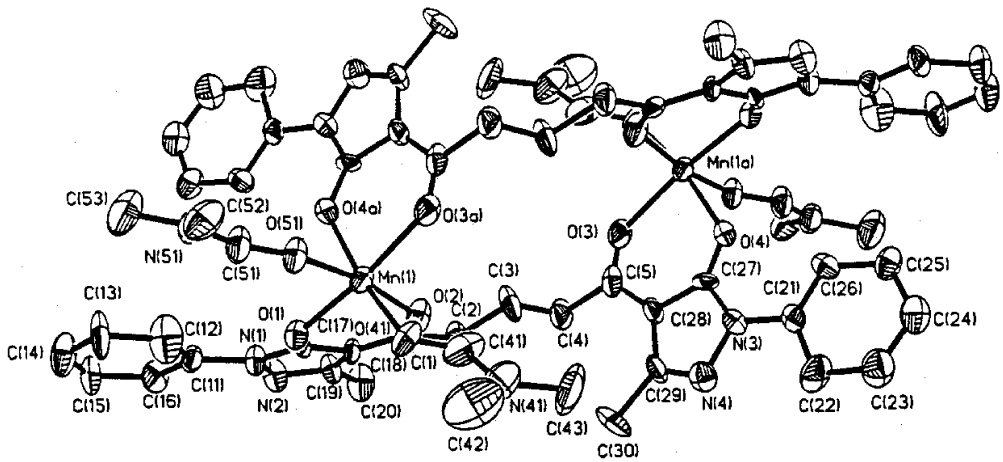


Fig. 2. Molecular structure of $Mn_2L_2 \cdot 5DMF \cdot H_2O$.

Table 1
Selected bond distances (Å) and angles (°) for the complex $Mn_2L_2 \cdot 5DMF \cdot H_2O$

Mn(1)–O(1)	2.124(5)	Mn(1)–O(2)	2.123(6)
Mn(1)–O(3a)	2.157(8)	Mn(1)–O(4a)	2.134(7)
Mn(1)–O(41)	2.131(6)	Mn(1)–O(51)	2.178(6)
O(1)–C(17)	1.266(8)	O(2)–C(1)	1.26(1)
C(17)–C(18)	1.45(2)	C(1)–C(18)	1.39(2)
C(18)–C(19)	1.40(1)	C(1)–C(2)	1.56(1)
C(17)–N(1)	1.358(8)	C(2)–C(3)	1.61(1)
C(19)–N(2)	1.325(9)	C(3)–C(4)	1.52(1)
N(1)–N(2)	1.434(8)	C(4)–C(5)	1.53(1)
O(3)–C(5)	1.21(1)	C(5)–C(28)	1.44(1)
C(28)–C(27)	1.45(1)	C(28)–C(29)	1.43(1)
O(4)–C(27)	1.25(1)	O(41)–C(41)	1.26(1)
C(41)–N(41)	1.29(1)	N(41)–C(43)	1.48(2)
O(51)–C(51)	1.22(1)	C(51)–N(51)	1.31(2)
N(51)–C(53)	1.47(1)	O(61)–C(61)	1.19(3)
C(61)–N(61)	1.37(3)	N(61)–C(63)	1.26(2)
O(1)–Mn(1)–O(2)	83.5(3)	O(1)–Mn(1)–O(3)	165.4(3)
O(1)–Mn(1)–O(4)	84.0(2)	O(1)–Mn(1)–O(41)	105.7(3)
O(1)–Mn(1)–O(51)	89.7(2)	O(2)–Mn(1)–O(3)	91.5(3)
O(2)–Mn(1)–O(4)	95.9(2)	O(2)–Mn(1)–O(41)	87.3(2)
O(2)–Mn(1)–O(51)	169.8(3)	O(3a)–Mn(1)–O(4a)	82.9(3)
O(3a)–Mn(1)–O(41)	87.7(3)	O(3a)–Mn(1)–O(51)	96.9(2)
O(4a)–Mn(1)–O(41)	170.1(3)	O(4a)–Mn(1)–O(51)	91.0(2)
O(41)–Mn(1)–O(51)	87.2(2)	Mn(1)–O(1)–C(17)	119.9(5)
Mn(1)–O(2)–C(1)	129.9(5)	Mn(1a)–O(3)–C(5)	134.2(7)
Mn(1a)–O(3)–C27	127.0(6)	Mn(1)–O(41)–C(41)	120.5(8)
Mn(1)–O(51)–C(51)	120.1(6)	O(1)–C(17)–C(18)	131.8(7)
O(1)–C(17)–N(1)	122.79(8)	O(2)–C(1)–C(18)	123.8(9)
O(2)–C(1)–C(2)	116.5(7)	C(18)–C(1)–C(2)	119.6(8)
C(1)–C(2)–C(3)	106.8(7)	O(51)–C(51)–N(51)	122.4(9)
C(51)–N(51)–C(52)	121.8(8)	C(51)–N(51)–C(53)	119.2(9)
C(52)–N(51)–C(53)	119.0(9)	O(61)–C(61)–N(61)	109(3)
C(61)–N(61)–C(62)	107(2)	C(61)–N(61)–C(63)	111(2)
C(62)–N(61)–C(63)	141(3)		

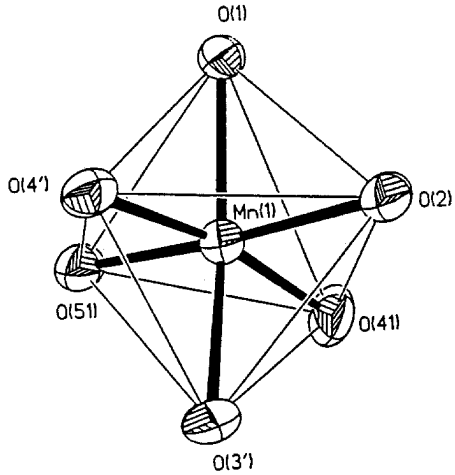


Fig. 3. Coordination geometry of manganese in $Mn_2L_2 \cdot 5DMF \cdot H_2O$.

The resonance structure of the β-diketonate is similar to that in the diterbium complex [23,24] (in forms I or IV, Fig. 4). The benzene ring and the connected pyrazolone ring are approximately coplanar. The dihedral angles between them are 7.23° (plane 12 (C11–C16) and plane 13 (N1–N2, C17–C19)) and 3.27° (plane 14 (C21–C26) and plane 15 (N3–N4, C27–C29)). C20, C1 and O1 are in the connected pyrazolone plane 13 with the maximum deviation −0.12 Å (O1). C30, C5 and O4 are in plane 15 with the maximum deviation −0.074 Å (C5). The dihedral angles between planes 12 and 14, planes 12 and 15, and planes 13 and 15 are 90.56, 91.65 and 98.86°, respectively. The two benzene planes in ligand L^{2-} are almost perpendicular.

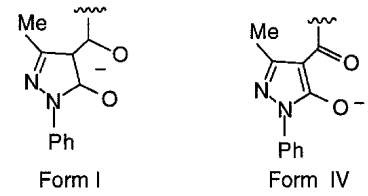


Fig. 4. The resonance structures of the β-diketonates in $Mn_2L_2 \cdot 5DMF \cdot H_2O$.

There are some changes in bond distances and angles when DMF is coordinated to manganese ions (Table 1). The uncoordinated DMF and water are distributed through the crystal lattice. There is a tetragonal hole in the molecule of the manganese complex.

3.3. FT-IR spectra

The complexes have similar IR spectra which differ from that of H_2L. In the FT-IR spectra of the complexes, the absorption assigned to $\nu(Ac^-)$ or $\nu(ClO_4^-)$ does not appear in the spectra of the manganese and nickel complexes. The ligand H_2L must coordinate to metal ions with the deprotonated enol form L^{2-}. The appearance of $\nu(NO_3^-)$ (at 1380 cm^{-1}, typical ionic NO_3^- absorption) in the cobalt complex **3** is indicative of the mono deprotonated HL^-. The molar conductivity and elemental analysis of complex **3** are in accordance with this observation. The IR spectra verify the formation of the complexes [25].

The stretching vibrations of C=O shift to lower frequencies in the complexes (1611–1616 and 1480–1504 cm^{-1}), compared to the free ligand H_2L which shows peaks at 1621, 1562, 1500 cm^{-1}. This indicates the carbonyl groups of ligand L coordinate directly to metal ions. The peaks at 1661, 1642 cm^{-1} in the cobalt complex **3** can be assigned to the keto form $\nu(C{=}O)$ of HL^-. Both enol and keto β-diketones exist in complex **3**. The weak absorption around 1532 cm^{-1} in all complexes is assigned to $\nu(C{\cdots}C)$, which comes from delocalized β-diketonate. This assignment is verified by FT-Raman spectra of a similar zinc complex. This vibration shows a very strong peak in Raman spectra. The result is in accordance with the delocalized diketone form of ligands in the complexes.

The weak sharp peak at 3605–3625 cm^{-1} in Ni and Co (**4**) complexes reveals the existence of crystalline water in these complexes. The broad, strong absorption around 3400 cm^{-1} in all the complexes is assigned to the stretching OH vibration of water and ethanol molecules. There is a weak

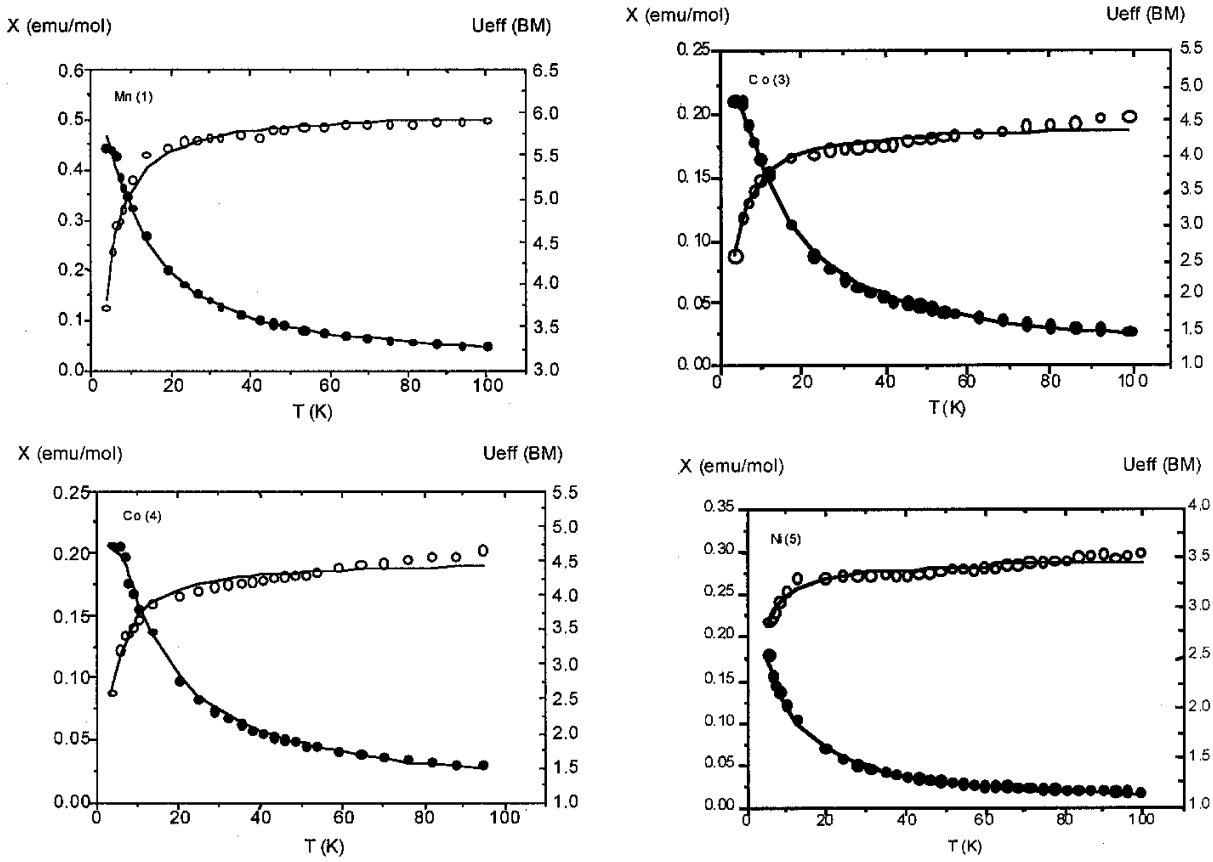


Fig. 5. Temperature dependence of magnetic susceptibility (χ–T) and moment (μ_{eff}–T) per molar metal ion for complexes (the symbols represent experimental values, the curves are fitted lines).

shoulder peak around 1630 cm^{-1} in complexes **1**, **4** and **5**, which can be assigned to the δHOH of water [26].

3.4. Magnetic properties

Variable temperature dependent magnetic susceptibilities of complexes were measured in the range 2–100 K. Fig. 5 shows the temperature dependent magnetic susceptibilities and the effective magnetic moments of the complexes.

The magnetic moments of binuclear complexes decrease smoothly above 20 K on decreasing the temperature. The changes become more rapid at lower temperature. The data of effective magnetic moments indicate some antiferromagnetic interaction exists in the complexes.

The susceptibility data of complexes are fitted with the binuclear magnetic equations [27–29] deduced from the Hamiltonian $\boldsymbol{H} = -2J\boldsymbol{S}_1\boldsymbol{S}_2$.

Table 2
Magnetic parameters

Complex	g	$2J$ (cm^{-1})	$F\times10^3$
Mn(1)	2.03	−0.71	0.48
Co(3)	2.28	−1.86	1.3
Co(4)	2.32	−1.96	7
Ni(5)	2.46	−2.02	8

$$\chi_A = N\beta^2 g^2 (kT)^{-1} AB^{-1}$$

Mn^{2+} (d^5, $S=5/2$): $A = 55+30X^{10}+14X^{18}+5X^{24}+X^{28}$;

$B = 11+9X^{10}+7X^{18}+5X^{24}+3X^{28}+X^{30}$

Co^{2+} (d^7, $S=3/2$): $A = 14+5X^6+X^{10}$;

$B = 7+5X^6+3X^{10}+X^{12}$

Ni^{2+} (d^8, $S=1$): $A = 5+X^4$;

$B = 5+3X^4+X^6$

where $X = \exp[-J/kT]$; N, g, β, k and T have their usual meanings; J is the exchange integral between metal ions in binuclear unit and χ_A the susceptibility per mole metal ion. The agreement factor F, is defined as $\Sigma(\chi_i^{obs}-\chi_i^{calc})^2$-$(\chi_i^{obs})^{-1}$ [30,31].

A good agreement factor is reached in fitting the experimental susceptibility data. The results are given in Table 2. Small negative $2J$ values indicate weak antiferromagnetic interaction exists between metal ions in the binuclear unit for Mn, Co and Ni complexes. The $-2J$ values have the order $J_{Ni^{2+}-Ni^{2+}}(Ni^{2+}, d^8, S=1) > J_{Co^{2+}-Co^{2+}}(Co^{2+}, d^7, S=3/2) > J_{Mn^{2+}-Mn^{2+}}(Mn^{2+}, d^5, S=5/2)$, which is in accordance with the order predicted by Hoffmann for different spin interaction centers [32]. The small $2J$ value is also in agreement with the molecular structure. The saturated chain is not an efficient bridge conducting the magnetic exchange inter-

action between metals. The two cobalt complexes have similar $2J$ and g values, which may indicate the similarity in coordination structures. The g values of complexes are also in accordance with the octahedron coordination structures of transition metal ions.

Supplementary data

Supplementary crystallographic data for the manganese complex are available from the CCDC, 12 Union Road, Cambridge CB2 1EZ, UK on request, quoting the deposition number CCDC 127572.

Acknowledgements

This work was supported by the National Natural Science Foundation of China (No. 29801001), Science Foundation of Peking University and National Key Project for Fundamental Research of China.

References

[1] O. Kahn, C.J. Martinez, Science 279 (1998) 44.
[2] A. Harriman, R. Ziessel, Chem. Commun. (1996) 1707.
[3] O. Sato, T. Iyoda, A. Fujishima, K. Hashimoto, Science 272 (1996) 704.
[4] D.W. Bruce, D. O'Hare, 'Inorganic Materials', Wiley, 2nd edn., 1996.
[5] G.L. Abbati, A. Cornia, A.C. Fabretti, A. Caneschi, D. Gatteschi, Inorg. Chem. 37 (1998) 1430, 3759.
[6] H. Samelson, A. Lempicki, J. Chem. Phys. 39 (1963) 110.
[7] R.G. Charles, E.P. Riedel, J. Inorg. Nucl. Chem. 28 (1966) 3005.
[8] C.C. Hinckley, J. Am. Chem. Soc. 91 (1969) 5160.
[9] W.DeW. Horrocks Jr, J.P. Sipe III, J. Am. Chem. Soc. 93 (1971) 6800.
[10] E.W. Berg, J.J.C. Acosta, Anal. Chim. Acta 40 (1968) 101.
[11] R.L. Lintvedt, N. Ahmad, Inorg. Chem. 21 (1982) 2356.
[12] X. Dong, F. Liu, Y. Zhao, Acta Chim. Sinica 41 (1983) 848.
[13] L. Yang, R. Yang, Polyhedron 14 (1995) 507.
[14] L. Yang, R. Yang, Acta Chim. Sinica 47 (1989) 911.
[15] L. Yang, R. Yang, Chem. J. Chin. Univ. 10 (1989) 225.
[16] L. Yang, J. Wu, Z. Xu, Y. Dong, X. Ju, Optronics Lasers (Suppl.) 6 (1995) 539.
[17] L. Yang, R. Yang, W. Dong, J. Liu, Acta Chim. Sinica 47 (1989) 633.
[18] X. Li, R. Yang, Polyhedron 11 (1992) 1545.
[19] L. Yang, R. Yang, J. Lanzhou Univ.(Nat. Sci.) 24 (1988) 134.
[20] W.J. Geary, Coord. Chem. Rev. 7 (1971) 81.
[21] L. Yang, J. Lin, J. Wu, J. Funct. Mater. 29 (1998) 1182.
[22] S. Miyazaki, H. Mukai, S. Umetani, S. Kihara, M. Matsui, Inorg. Chem. 28 (1989) 3014.
[23] L. Yang, R. Yang, J. Mol. Struc. 380 (1996) 75.
[24] L. Yang, R. Yang, J. Coord. Chem. 33 (1994) 303.
[25] K. Nakamoto, Infrared and Raman Spectroscopy of Inorganic and Coordination Compounds, Wiley, New York, 4th edn., 1986.
[26] J. Wu (Ed.), Morden Fourier Transform Infrared Spectroscopy Technology and Applications, Science and Technology Document Publishing House, Beijing, 1994.
[27] M. Mikuriya, Y. Kawasaki, T. Tokii, S. Yanai, A. Kawamori, Inorg. Chim. Acta 156 (1989) 21.
[28] P.W. Ball, A.B. Blake, J. Chem. Soc., Dalton Trans. (1974) 852.
[29] N. Mahootian, C. Kiknchi, W. Viehmann, J. Chem. Phys. 48 (1968) 1097.
[30] The spin-orbital interaction in Co(II) (d^7, $S=3/2$) complexes was not considered directly. All the effects which make S not a good quantum number were included in the g value (assuming S is a good quantum number when using this simplified model). The zero field splitting of Ni(II) (d^8, $S=1$) was not considered. Given no maximum value in the χ_A–T curve in the range of temperature measured, the zero field splitting of Ni(II) may occur at very low temperature.
[31] R.S. Drago, Physical Methods for Chemists, Surfside Scientific Publishers, 2nd edn., 1992.
[32] P.J. Hay, J.C. Thibeault, R. Hoffmann, J. Am. Chem. Soc. 97 (1975) 4884.

PERGAMON

www.elsevier.nl/locate/poly

Polyhedron 19 (2000) 99–107

POLYHEDRON

Comparative hydrolysis behavior of the rare earths and yttrium: the influence of temperature and ionic strength

Greta D. Klungness, Robert H. Byrne *

University of South Florida, Department of Marine Science, St. Petersburg, FL 33701, USA

Received 24 June 1999; accepted 11 October 1999

Abstract

In this work two techniques are used to determine hydrolysis constants (β_1*(M)) of yttrium and the rare earths (YREEs), where β_1*(M) = [MOH^{2+}][H^+][M^{3+}]$^{-1}$. Potentiometric experiments were conducted on time scales as long as 15 min and spectrophotometric experiments were complete on time scales much shorter than 500 ms. The stability constant patterns produced by both procedures are in excellent agreement. Potentiometric results obtained over a temperature range between 25 and 55°C indicate that enthalpies appropriate to YREE hydrolysis can be reasonably approximated as ΔH^0(M) = 11.3 kcal mol^{-1} for all YREEs. The dependence of YREE hydrolysis constants on temperature (T), ionic strength (I), and YREE identity (M) can be expressed as $\log \beta_1$*(M) = $\log {}^0\beta_1$*(M) − {2.044$I^{1/2}$/(1 + 5.52$I^{1/2}$) + 1.84 × $10^{-3}I$} − 2446K/T + 8.204 where the $\log {}^0\beta_1$*(M) values, appropriate at 25°C and zero ionic strength, are given as follows: $\log {}^0\beta_1$*(Y) = −7.80, $\log {}^0\beta_1$*(La) = −8.81, $\log {}^0\beta_1$*(Ce) = −8.34, $\log {}^0\beta_1$*(Pr) = −8.32, $\log {}^0\beta_1$*(Nd) = −8.18, $\log {}^0\beta_1$*(Sm) = −7.84, $\log {}^0\beta_1$*(Eu) = −7.76, $\log {}^0\beta_1$*(Gd) = −7.83, $\log {}^0\beta_1$*(Tb) = −7.64, $\log {}^0\beta_1$*(Dy) = −7.59, $\log {}^0\beta_1$*(Ho) = −7.56, $\log {}^0\beta_1$*(Er) = −7.52, $\log {}^0\beta_1$*(Tm) = −7.39, $\log {}^0\beta_1$*(Yb) = −7.24, $\log {}^0\beta_1$*(Lu) = −7.27. ©2000 Elsevier Science Ltd All rights reserved.

Keywords: Yttrium; Rare earth elements; Hydrolysis; Enthalpy; Ionic strength; Spectrophotometry

1. Introduction

Solution equilibria strongly influence the environmental behavior of the trivalent rare earths and yttrium (YREE). Important environmental YREE species include carbonate, hydroxide, sulfate, fluoride and chloride complexes. Among all the equilibria currently known to influence YREE solution speciation in natural waters, hydrolysis equilibria are probably the least well understood.

The first hydrolysis step for trivalent YREEs, written as

$$M^{3+} + H_2O \Leftrightarrow MOH^{2+} + H^+ \quad (1)$$

can be quantitatively characterized with hydrolysis constants written in the form

$$\beta_1^*(M) = [MOH^{2+}][H^+][M^{3+}]^{-1} \quad (2)$$

where M^{3+} is a trivalent YREE and brackets denote concentrations of each indicated species. Previous experimental determinations of β_1*(M) do not provide a coherent representation of YREE hydrolysis behavior. The $\log \beta_1$*(M) data shown in Fig. 1 [1–27] at zero ionic strength exhibit an overall range of approximately two orders of magnitude. These data show no discernable pattern in the magnitudes of $\log \beta_1$*(M) across the YREE series other than a general, but poorly defined, increase between the lightest rare earth elements (REEs) and the heaviest REEs. In addition to the very large range in previous $\log \beta_1$*(M) estimates for the YREEs, there are essentially no previous observations of the influence of temperature and ionic strength on YREE hydrolysis constants. In view of the extreme paucity of experimental $\log \beta_1$*(M) data obtained using consistent procedures for all YREEs, and the absence of $\log \beta_1$*(M) data obtained over a range of temperatures and ionic strengths, further experimental observations are required over a range of conditions appropriate to the natural environment.

In this work two procedures have been used to determine the hydrolysis constants of yttrium and all rare earths (except Pm). Both methods involve measurement of pH in solutions buffered by M^{3+}/MOH^{2+} hydrogen ion exchange-couples. In the first procedure, pH is measured spectrophotometrically with *meta*-cresol purple, a pH indicator calibrated previously [28] at ionic strengths appropriate to seawater. Spectrophotometric pH measurements in systems buffered by M^{3+}/

* Corresponding author. Tel.: +1-727-553-1508; fax: +1-727-553-1189; e-mail: Byrne@seas.marine.usf.edu

0277-5387/00/$ - see front matter ©2000 Elsevier Science Ltd All rights reserved.
PII S0277-5387(99)00332-0

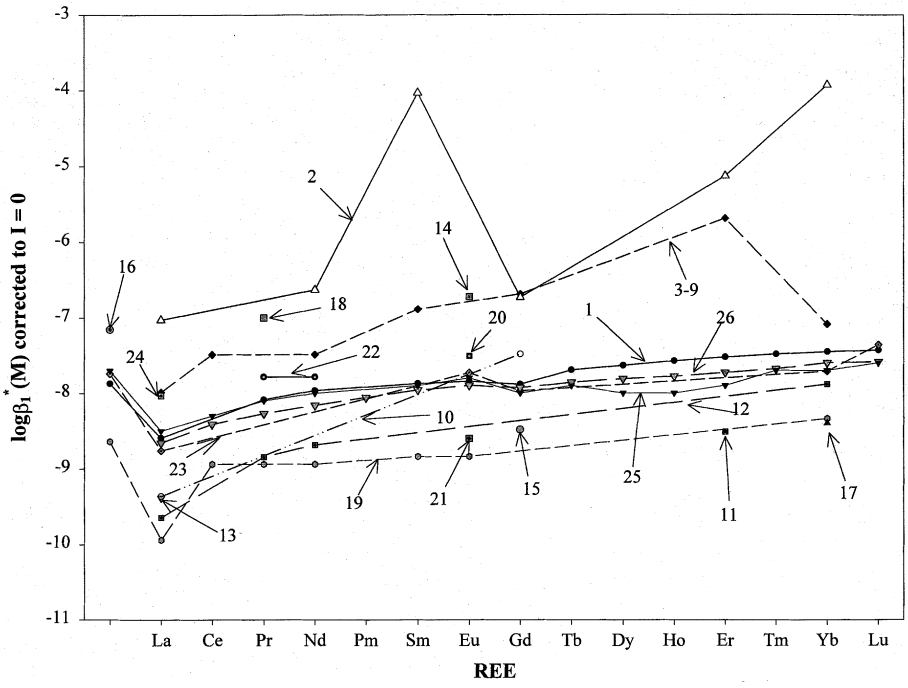


Fig. 1. Hydrolysis constant estimates at 25°C and zero ionic strength. Ionic strength corrections were performed using the hydrolysis behavior of Fe^{III} as an appropriate analog [27].

MOH^{2+} couples involved the use of a stopped flow rapid scan spectroscopy system to observe pH via indicator absorbance ratios on a time scale of zero to 500 ms. This procedure was used as a means of separating the first hydrolysis step (Eq. (1)) from slower hydrolysis steps leading to formation of solid $M(OH)_3(s)$. The second measurement procedure involved the use of electrodes to measure pH in solutions having much higher total metal concentrations but lower pH (higher $[M^{3+}]/[MOH^{2+}]$ ratios) than those in our spectrophotometric experiments. These measurements at low pH substantially lowered the saturation state of our solutions with respect to formation of solid $M(OH)_3(s)$. The overall experimental design in this work acknowledges the importance of obtaining consistent results using independent methodologies. Direct comparisons are obtained between potentiometrically and spectrophotometrically derived log β_1*(M) results at 25°C and ionic strength (I) equal to 0.7 molar. Additional potentiometric results at $I=0.7$ molar are used to determine log β_1*(M) at 40°C and 55°C. Finally, log β_1*(M) is determined at $I=0.1$ molar and 25°C for all YREEs, and the ionic strength dependence of log β_1*(Ho) is observed at 25° for ionic strengths between 0.04 and 5.4 molar.

2. Analytical procedures

2.1. Theory

The potentiometric and spectrophotometric procedures used to determine log β_1*(M) in this work account for all significant acid–base equilibria. The metal ion buffers used in potentiometric experiments were composed by combining acidic solutions, containing $HClO_4$ and either dissolved $M(ClO_4)_3$ or $M(NO_3)_3$, with solutions of NaOH. These acid and base titrants were added to solutions containing $NaClO_4$ as the background electrolyte. The charge balance equation describing the final buffered solution at equilibrium is

$$3[M^{3+}]+2[MOH^{2+}]+[H^+]+[Na^+]-[ClO_4^-]-[OH^-]=0 \quad (3)$$

The concentrations of M^{3+} and MOH^{2+} in this buffer can be expressed as

$$M_T=[M^{3+}](1+\beta_1^*(M)[H^+]^{-1})=[M^{3+}]+[MOH^{2+}] \quad (4)$$

where M_T is the total concentration of a given YREE. The $[Na^+]$ and $[ClO_4^-]$ concentrations in Eq. (3) have four sources: $NaClO_4$, $HClO_4$, $M(ClO_4)_3$ and NaOH. The Na^+ and ClO_4^- added as $NaClO_4$ are balanced ($[Na^+]=[ClO_4^-]$) and need not be considered in Eq. (4). As such, the difference between $[Na^+]$ and $[ClO_4^-]$ in Eq. (4) equals the $[Na^+]$ added as NaOH minus $[ClO_4^-]$ added as $HClO_4$ and $M(ClO_4)_3$. Thus we can write

$$[Na^+]-[ClO_4^-]=[\Delta]-3M_T \quad (5)$$

where $[\Delta]$ can be conceptualized as the concentration of base (NaOH) added in excess of acid ($HClO_4$), and $3M_T$ is the concentration of ClO_4^- in solution from added $M(ClO_4)_3$. Combining Eqs. (3)–(5), Eq. (2) can be written as

$$\log \beta_1^* = -\mathrm{pH} + \log\left\{\frac{[\Delta]+[H^+]-K_w[H^+]^{-1}}{M_T-[\Delta]+K_w[H^+]^{-1}-[H^+]}\right\} \quad (6)$$

Under the conditions of each experiment both $[H^+]$ and $[OH^-]$ (i.e. $K_w[H^+]^{-1}$) are small (≤ 2 μmol dm^{-3}) whereby the final term in Eq. (6) is nearly equal to the term $\log [MOH^{2+}]/[M^{3+}]$. For each experiment, performed at constant temperature and ionic strength, the terms Δ and $M_T-\Delta$ were held very nearly constant. In this case, the pattern of $\log \beta_1^*(M)$ values in each experiment was very nearly identical to the pattern of directly observed equilibrium pH values.

The equations used in our spectrophotometric experiments are identical to those used in our potentiometric experiments with one exception. Spectrophotometric experiments contained two forms of *m*-cresol purple, L^{2-} and HL^-. Consequently, two additional terms must be added to Eq. (3). These terms, $-2[L^{2-}]-[HL^-]$, are added to the left side of Eq. (3). Additionally, since our indicator solutions were composed by dissolving Na_2L in NaOH, the $[Na^+]$ term in Eq. (3) must include the additional Na^+ added to solutions along with *m*-cresol purple. In spectrophotometric experiments, $\log \beta_1^*(M)$ values can also be calculated using Eq. (6). However, in this case $[\Delta]$ includes the following term

$$2[L]_T-2[L^{2-}]-[HL^-]=[HL^-] \quad (7)$$

Consequently, whereas Eq. (6) is used to calculate $\log \beta_1^*(M)$ directly in potentiometric experiments, as used in spectrophotometric experiments one additional term ($[HL^-]$) is added to the term $[\Delta]$ in Eq. (6).

2.2. Methods

Potentiometric $\log \beta_1^*(M)$ determinations were conducted by mixing two solutions and measuring solution pH over a 15 min period. One of these two solutions consisted of a rare earth element, total concentration 0.01 molar, in $NaClO_4$ at $[H^+]=1\times10^{-4}$. The second solution was a 0.1 N volumetric standard NaOH solution. The mixture of these solutions produced a buffering ratio ($[\Delta]/(M_T-[\Delta])$ on the order of 0.11, whereby the measured solution pH was approximately one log unit more positive than the $\log \beta_1^*(M)$ appropriate to a given element.

Two experiments were conducted at 25°C and 0.7 molar ionic strength (I) and two experiments at $I=0.7$ molar were conducted at each of two higher temperatures (40 and 55°C). Two additional experiments were conducted at 25°C and 0.1 molar ionic strength. The procedures described above were conducted using all YREEs except Pm. Experiments at 25°C were also conducted using a single element (Ho) over a range of ionic strengths between 0.04 and 5.4 molar.

The glass electrode used in these experiments was calibrated on the free hydrogen ion concentration scale by titrating unbuffered $NaClO_4$ with a standard $HClO_4$ solution which had been calibrated against a standard NaOH solution (0.1 N NaOH). In all cases, the Orion Ross-type combination electrode used in this work exhibited Nernstian behavior. The acidic solutions used in each experiment were freshly prepared prior to each experiment. Each acidic solution was stored in a plastic beaker under an atmosphere of ultra high purity N_2, and was thermostated at the desired experimental temperature prior to mixing. The basic solution was kept in its original container and placed in the temperature bath to maintain the appropriate temperature prior to mixing. Experiments were initiated by combining a small volume of the standard NaOH solution with a large volume of each solution containing a 0.01 molar YREE. The NaOH addition was made with a variable capacity Eppendorf pipette. All pipettes used in this work were calibrated gravimetrically. Replicate gravimetric/volumetric analyses indicated that volumetric additions were accurate to $\pm 1\%$ or better. In all potentiometric experiments, a Lauda K-4R thermocooler was used to provide constant thermal conditions (25, 40, 55°C). These temperatures were monitored directly in each experimental solution and were constant to ± 0.1°C. Prior to additions of the NaOH titrant, the combination electrode was equilibrated in the acidic YREE-containing solution until the electrode potential was constant within ± 0.1 mV for 5 min. The small $K_w[H^+]^{-1}$ terms in Eq. (6) were calculated using the ionic strength dependence of K_w in $NaClO_4$ summarized by Baes and Mesmer [25], and the temperature dependence of Harned and Owen [29].

The procedures used in spectrophotometric experiments were nearly identical to the procedures used in the potentiometric work. In spectrophotometric experiments the pH term in Eq. (6) is calculated as

$$\mathrm{pH} = \mathrm{p}K_2 + \log\left(\frac{R-e_1}{e_2-e_3R}\right) \quad (8)$$

where pK_2 refers to the HL^- dissociation constant, R is a measured absorbance ratio at the absorbance maxima of L^{2-} and HL^- (578 and 434 nm), and the terms e_1, e_2 and e_3 are molar absorptivity ratios [25,30,31]. The use of *meta*-cresol purple and Eq. (8) to measure the pH of seawater on the total hydrogen ion concentration scale is described in Clayton and Byrne [28]. On the free hydrogen ion concentration scale pH ($-\log[H^+]$) is higher than the total scale pH (expressed as $\mathrm{pH}_T = -\log[H^+]_T$ where $[H^+]_T = [H^+] + [HSO_4^-]$) by 0.14 log units [32]. Consequently, $pK_2 = 8.1456$ at 25°C and $I=0.7$ molar ionic strength. Subsequent to calculating pH in each spectrophotometric experiment using absorbance ratios (R), the term $[HL^-]$ which is included in the $[\Delta]$ term of Eq. (8) is given as

$$[HL^-] = [L]_T\left(1+\frac{K_2}{[H^+]}\right)^{-1} \quad (9)$$

Spectrophotometric experiments involved the use of an OLIS RSM-1000 to measure absorbance ratios at a rate of 1000 scans per second. Using absorbance observations at the

isosbestic point of *m*-cresol purple, the instrument was adjusted to mix two solutions in a one to one ratio. One solution consisted of 4×10^{-5} molar *m*-cresol purple (25°C) and either 1×10^{-3} molar or 6×10^{-4} molar NaOH in 0.7 molar $NaClO_4$ (25°C). The second solution consisted of a 2×10^{-3} molar YREE in 0.7 molar $NaClO_4$ (25°C) at $[H^+]=1\times10^{-4}$. Each of these solutions as well as the mixing and measurement chambers were submerged in a thermostated solution whose temperature (25°C) was constant within ±0.1°C. Nine absorbance scans, recorded against an absorbance baseline obtained using pure 0.7 molar $NaClO_4$, were used to construct an average pH profile for each YREE. Maximum absorbance ratios, generally obtained between 70 and 80 ms, were used to calculate the pH used for log β_1*(M) calculations in Eq. (6).

2.3. Materials

Potentiometric analyses (pH determinations) were conducted using a Corning model 129 pH meter in the absolute millivolt mode. The pH electrode used in this work was an Orion Ross-type combination electrode (Orion no. 8102BN). The volumetric pipettes used in this were Eppendorf variable capacity 100–1000 μl and 1000–5000 μl pipettes.

Yttrium and rare earth element oxides (99.99%) were obtained from Aldrich, Milwaukee, WI. Ce, Pr, and Tb were obtained as $Ce(NO_3)_3$, $Pr(NO_3)_3$, and $Tb(NO_3)_3$ (99.99%). YREE stock solutions were prepared by dissolving salts in perchloric acid to make solutions that were 0.1 molar in each YREE and 0.01 molar in $HClO_4$. Solutions were stored in glass volumetric flasks (250 ml) and the YREE concentration of each flask was determined via ICP-MS analysis using YREE standards obtained from SPEX (Metuchen, NJ). Anhydrous $NaClO_4$ was obtained from Sigma (St. Louis, MO). $NaClO_4$ (4 molar) stock solutions were prepared by (a) dissolving $NaClO_4$ in MilliQ water (Millipore), (b) adding sufficient NaOH to raise the pH to values between 10 and 11, (c) filtering these solutions through clean 0.4 μm polycarbonate membrane filters (Poretics® Products, Livermore, CA) after storage in a sealed volumetric flask overnight. Each solution was subsequently acidified to pH 4.0 to avoid uptake of CO_2 and was likewise stored in a glass volumetric flask.

Perchloric acid was obtained from Aldrich (Milwaukee, WI). The concentrations of concentrated $HClO_4$ standard solutions were determined titrimetrically using volumetric standard NaOH solutions obtained from Fisher Scientific (Pittsburgh, PA). *Meta*-cresol purple salts were obtained from Eastman Kodak (Rochester, NY). Ultra high Purity N_2 was obtained from Air Products and Chemicals Inc. (Allentown, PA).

3. Results

3.1. YREE hydrolysis patterns

Equilibrium pH values for each potentiometric experiment were based on millivolt readings recorded 5 min after mixing. Typical pH profiles through time are shown in Fig. 2. Typical pH profiles for spectrophotometric experiments are shown in Fig. 3. The decrease in solution pH after the observed maxima was anticipated at the high pH of these experiments owing to polymerization/precipitation reactions. Fig. 4 shows the results of two potentiometric log β_1*(M) determinations at 25°C along with the average log β_1*(M) results for five spectrophotometric experiments at 25°C. The standard errors shown in Fig. 4 refer to the spectrophotometric average. The potentiometric results in Fig. 4 were obtained using a buffer ratio ($[MOH^{2+}]/[M^{3+}]$) on the order of 0.11, whereby the measured pH in each experiment was approximately 1 unit above the Fig. 4 calculated log β_1*(M) values. Two buffer ratios were used in the spectrophotometric experiments, $[MOH^{2+}]/[M^{3+}]\cong0.43$ and $[MOH^{2+}]/[M^{3+}]\cong1$. While the absolute magnitudes of spectrophotometrically derived log β_1*(M) values varied significantly in these experiments (as reflected by the standard errors shown in the figure), the pattern of log β_1*(M) values across the series of YREEs was highly consistent in every spectrophotometric and potentiometric experiment. This observation indicates that the log β_1*(M) standard errors shown for each YREE are highly correlated. Notably, the averaged log β_1*(M) results obtained using spectrophotometric procedures are in excellent agreement with the result of each potentiometric experiment. The only exception to this generalization is seen in the hydrolysis behavior of Ce. Spectrophotometric experiments, conducted on very short time scales, provide a sequence of log β_1*(M) values for La, Ce and Pr that are closely consistent with the patterns of hydrolysis constants estimated for these elements using linear free energy relationships [26]. While it is possible to suggest that accessibility to the tetravalent oxidation state, unique to Ce in aqueous solutions, may be responsible for the observed Ce anomaly, Ce oxidation is expected to be extremely slow under these experimental conditions. As such, the origin of the Fig. 4 discrepancies in log β_1*(Ce) values estimated from spectrophotometric and potentiometric procedures is uncertain.

Fig. 5 compares the grand average of all potentiometric and spectrophotometric experiments performed at 25°C and 0.7 molar ionic strength with the results of two potentiometric experiments performed at 25°C and 0.1 molar ionic strength. The standard errors shown on this graph refer to the seven experiments performed at 0.7 molar ionic strength. The potentiometrically derived log β_1*(M) patterns in this figure are in excellent agreement with the spectrophotometrically and potentiometrically derived patterns shown in Fig. 4 and indicate that the log β_1*(M) pattern across the YREE series

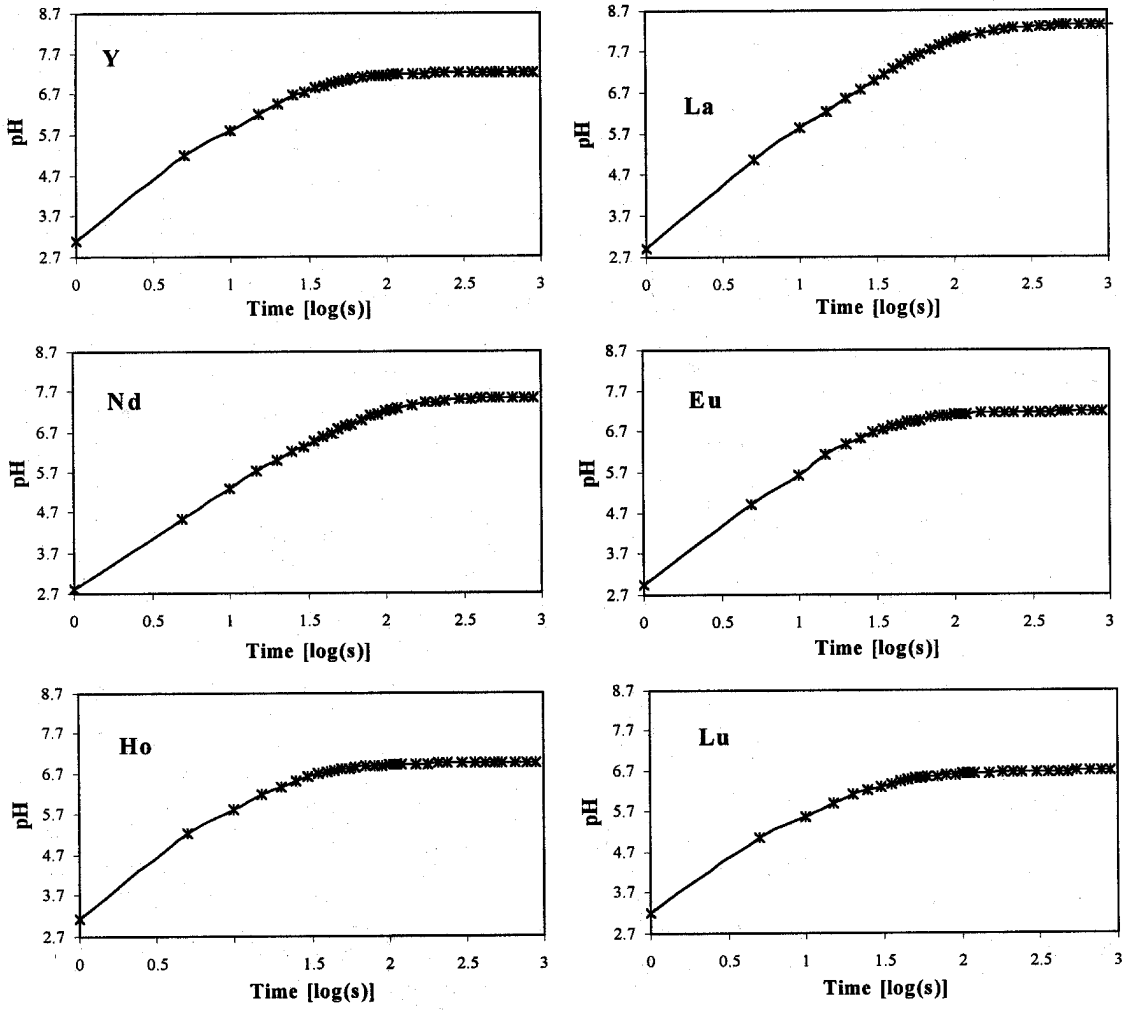


Fig. 2. Representative potentiometric data vs. time.

is insensitive to changes in ionic strength. Constancy in YREE stability constant patterns over a range of ionic strengths has also been observed for YREE complexation by NTA^{3-} [33] and F^- [34].

The log β_1*(M) observations obtained in our work (Fig. 5) are broadly consistent with the observations of Frolova (Fig. 1). However, our work indicates that comparative YREE hydrolysis constants deviate significantly from the generally smooth patterns observed by Frolova [1]. In the present study prominent variations in slope (log β_1*(M) plotted against atomic number) are observed between Gd and Lu. Similar variations have also been observed for CO_3^{2-} complexation constants [35] obtained via solvent exchange analysis and for F^- complexation [34,36] obtained via specific ion electrode and ion exchange analysis.

In spite of the close similarity in the ionic radii of Ho^{3+} and Y^{3+} [37], the hydrolysis behavior of Y^{3+} is intermediate to that observed for Sm^{3+} and Eu^{3+} (Fig. 5). This is consistent with behavior expected for Y^{3+} and REE complexation by a highly covalent ligand [38]. Yttrium is a harder ion than any of the rare earths [39]. It is more weakly complexed than Ho in cases where REE–ligand interactions are significantly covalent [40], and is more strongly complexed than Ho^{3+} for bonding which is strongly electrostatic in character.

3.2. Influence of ionic strength on log β_1*(M)

On the basis of the observed insensitivity of log β_1*(M) patterns to variations in ionic strength, our investigations of the influence of ionic strength on YREE hydrolysis were confined to a single element, Ho. The log β_1*(M) results obtained for Ho between ionic strengths 0.04 molar and 5.7 molar are shown graphically in Fig. 6. As is the case for log β_1*(M) results obtained potentiometrically at ionic strengths 0.7 and 0.1 molar, the results shown in Fig. 6 were obtained with a $[HoOH^{2+}]/[Ho^{3+}]$ ratio on the order of 0.11. Since a relatively high Ho^{3+} concentration ($[Ho^{3+}]$) was used in these experiments, the ionic strength range in these measurements did not include values smaller than 0.04. The ionic strength dependence of the data shown in Fig. 6 was described quantitatively using an equation identical in

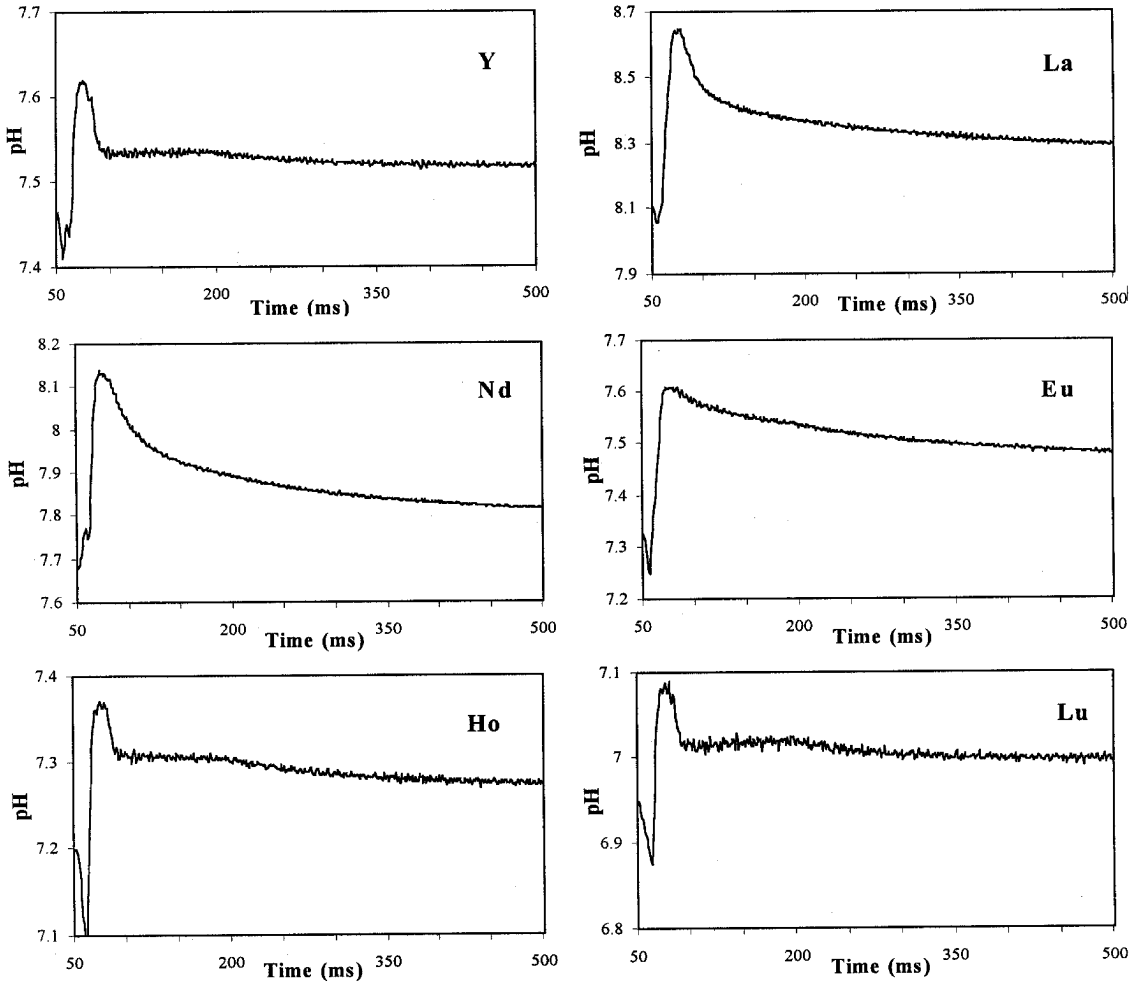


Fig. 3. Representative spectrophotometric data vs. time.

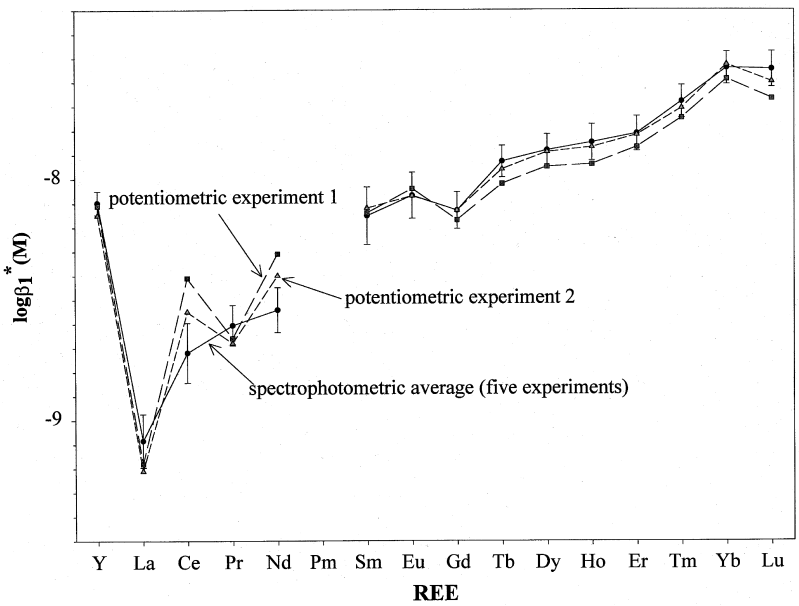


Fig. 4. Log β_1*(M) determinations at $I = 0.7$ molar and 25°C. Average of five spectrophotometric experiments with standard errors plus the results of two potentiometric experiments.

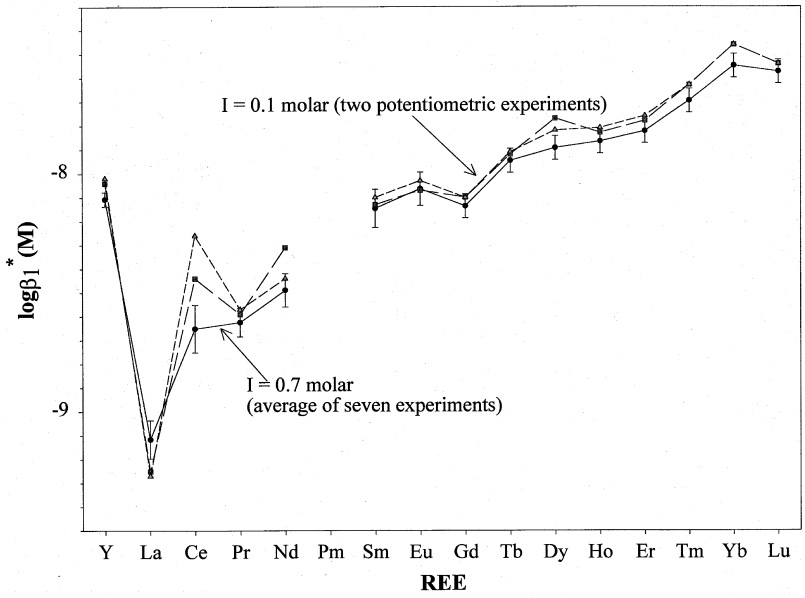


Fig. 5. Average log β_1*(M) determinations for all experiments at $I=0.7$ molar and 25°C plus the results of two potentiometric experiments at 25°C and $I=0.1$ molar. The standard errors shown in this figure refer to the seven experiments performed at 0.7 molar ionic strength.

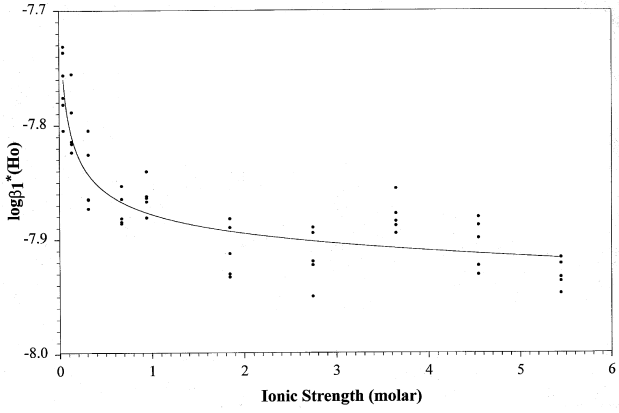


Fig. 6. Ionic strength dependence of log β_1*(Ho) at 25°C. Note that the difference ($\cong 0.05$) between log β_1*(M) for heavy REEs at 0.7 molar and 0.1 molar ionic strengths (Fig. 5) is consistent with the observations shown in this figure.

form to that employed in descriptions of YREE complexation by F^- and NTA^{3-}. The best fit curve in Fig. 6 is given by

$$\log \beta_1^*(\mathrm{Ho}) = \log {}^0\beta_1^*(\mathrm{Ho}) - 2.044 I^{1/2} / (1+5.52 I^{1/2}) - 1.84\times10^{-3} I \quad (10)$$

where $\log {}^0\beta_1^*(\mathrm{Ho}) = -7.56$ is the hydrolysis constant appropriate to 25°C and zero ionic strength.

3.3. Temperature dependence of YREE hydrolysis constants

The temperature dependence of YREE hydrolysis constants was determined by conducting additional potentiometric experiments at 40 and 55°C. The results shown in Fig. 7 are the average of two potentiometric experiments at $I=0.7$ molar for each temperature. Fig. 7 shows that the patterns of log β_1*(M) values obtained at 40 and 55°C closely resemble the patterns obtained potentiometrically at 25°C. The log β_1*(M) data in Fig. 7 were fitted using the van't Hoff equation. The enthalpy values obtained in these fits are given in Table 1. The average ΔH^0(M) value for all YREEs is 11.3 kcal mol^{-1}. In consideration of the standard errors given with each ΔH^0(M) estimate in Table 1, this enthalpy is in good agreement with values obtained for all elements except Ce. Enthalpies ranged from 13.6 kcal mol^{-1} for Ce to 10 kcal mol^{-1} for Yb and Lu. The standard errors given with each ΔH^0(M) value in Table 1 indicate that reaction enthalpies appropriate to Eq. (1) are much better defined for the heavy rare earths than is the case for for the lightest rare earths (La–Nd).

The results obtained in this work allow log β_1*(M) values to be calculated over a wide range of temperatures and ionic strengths. Table 2 provides the grand average YREE hydrolysis constants appropriate at 25°C and the ionic strength of

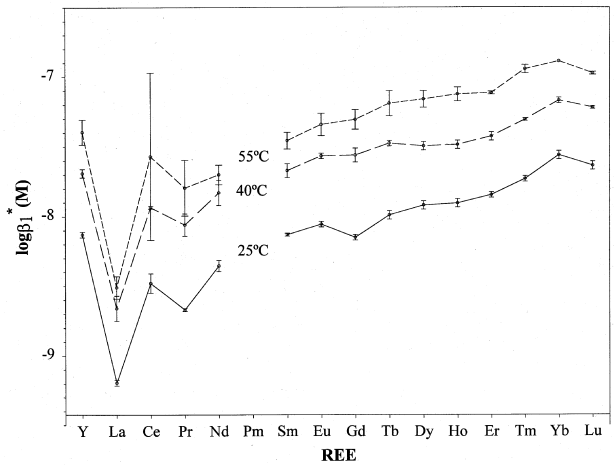


Fig. 7. Potentiometric log β_1*(M) results (0.7 molar) at 25, 40 and 55°C. Error limits shown in this figure indicate the range in log β_1*(M) for two measurements at each temperature.

Table 1
Enthalpy data (kcal mol^{-1}) for YREE hydrolysis

REE	$\Delta H \pm$ S.E.
Y	11.0 ± 1.1
La	10.3 ± 2.0
Ce	13.6 ± 6.4
Pr	13.0 ± 2.7
Nd	9.9 ± 2.0
Pm	
Sm	10.2 ± 1.3
Eu	10.8 ± 1.3
Gd	12.6 ± 1.6
Tb	12.0 ± 1.3
Dy	11.3 ± 0.8
Ho	11.7 ± 0.7
Er	11.0 ± 0.5
Tm	11.7 ± 0.4
Yb	10.0 ± 0.5
Lu	9.9 ± 0.7

Table 2
YREE hydrolysis constants at 25°C are shown for $I = 0.7$ molar ($\log \beta_1^*(M) \pm$ S.E.) and $I = 0.0$ ($\log {}^0\beta_1^*(M)$)

REE	$\log \beta_1^*(M) \pm$ S.E.	$\log {}^0\beta_1^*(M)$
Y	−8.11 ± 0.03	−7.80
La	−9.12 ± 0.08	−8.81
Ce	−8.65 ± 0.10	−8.34
Pr	−8.62 ± 0.06	−8.32
Nd	−8.49 ± 0.07	−8.18
Pm		
Sm	−8.15 ± 0.08	−7.84
Eu	−8.06 ± 0.07	−7.76
Gd	−8.14 ± 0.05	−7.83
Tb	−7.95 ± 0.05	−7.64
Dy	−7.89 ± 0.05	−7.59
Ho	−7.87 ± 0.05	−7.56
Er	−7.82 ± 0.05	−7.52
Tm	−7.70 ± 0.05	−7.39
Yb	−7.55 ± 0.05	−7.24
Lu	−7.57 ± 0.05	−7.27

seawater (0.7 molar). The $\log {}^0\beta_1^*(M)$ values given in Table 2 were calculated using the ionic strength behavior observed for Ho, and the average $\log \beta_1^*(M)$ results obtained for all experiments performed at 25°C and 0.7 molar ionic strength. Using $\Delta H^0(M) = 11.3$ kcal mol^{-1} as a reasonable approximation for all YREEs, hydrolysis constants can be estimated as a function of temperature and ionic strength (I) with the following equation

$$\log \beta_1^*(M) = \log {}^0\beta_1^*(M) - \{2.044 I^{1/2}/(1+5.52 I^{1/2}) + 1.84\times10^{-3} I\} - 2446 K/T + 8.204 \quad (11)$$

where T is the temperature in degrees Kelvin and $\log {}^0\beta_1^*(M)$ values are given in Table 2.

4. Conclusions

The $\log \beta_1^*(M)$ values obtained in this work are in general agreement with the previous measurements of Frolova [1]. However, observations obtained in the present study show much more structure than the Frolova [1] results. The nearest neighbor $\log \beta_1^*(M)$ relationships observed for YREEs in this work are broadly consistent with those observed in LFER characterizations of YREE stability constants with a wide variety of organic ligands [26,39]. The nearest neighbor hydrolysis constants observed in our study also resemble YREE stability constant patterns observed for CO_3^{2-} and F^- complexation [34–36].

Our hydrolysis constant observations indicate that for surface seawater at 25°C (pH ≅ 8.2) the ratio $[MOH^{2+}]/[M^{3+}]$ varies from values smaller than unity for La to values on the order of five for Lu. The enthalpy values obtained for the first YREE hydrolysis step are in good agreement with values predicted [41] using the enthalpy estimation systematics of Baes and Mesmer [42]. For the enthalpies observed in the present work ($\Delta H^0 = 11.3$ kcal mol^{-1}) YREE hydrolysis constants are predicted to decrease by more than a factor of four between 25°C and temperatures characteristic of the deep ocean ($0°C \le t \le 6°C$). Consequently MOH^{2+} is a minor species for the YREEs in ocean waters relative to carbonate complexes, MCO_3^+ and $M(CO_3)_2^-$.

Hydrolysis constants have been advocated as proxies for metal ion adsorption constants appropriate to the surfaces of metal oxides and hydrous oxides and organic particles [43–47]. The application of surface complexation models to YREEs has generally involved the use of $\log \beta_1^*(M)$ values obtained from linear free energy relationships [26] or the hydrolysis data recommended by Baes and Mesmer [25]. The $\log \beta_1^*(M)$ data obtained in the present work provide a basis for refined YREE scavenging models (adsorptive transport) in seawater and freshwater systems.

Acknowledgements

This work was supported by contract OCE-95-22878 from the National Science Foundation. The authors gratefully acknowledge the constructive criticism of two anonymous reviewers.

References

[1] U.K. Frolova, V.N. Kumok, V.V. Serebrennikov, Izv. Vyssh. Uchebn. Zaved. Khim. Khim. Tekhnol. 9 (1966) 176.
[2] R. Guillamont, B. Désiré, M. Galin, Radiochem. Radioanal. Lett. 8 (1971) 189.
[3] J. Kragten, L.G. Decnop-Weever, Talanta 25 (1978) 147.
[4] J. Kragten, L.G. Decnop-Weever, Talanta 26 (1979) 1105.
[5] J. Kragten, L.G. Decnop-Weever, Talanta 27 (1980) 1047.
[6] J. Kragten, L.G. Decnop-Weever, Talanta 29 (1982) 219.
[7] J. Kragten, L.G. Decnop-Weever, Talanta 29 (1983) 131.
[8] J. Kragten, L.G. Decnop-Weever, Talanta 31 (1984) 731.
[9] J. Kragten, L.G. Decnop-Weever, Talanta 34 (1987) 861.
[10] T. Amaya, H. Kakihana, M. Maeda, Bull. Chem. Soc. Jpn. 46 (1973) 1720.
[11] K.A. Burkov, L.S. Lilich, N. Din Ngo, Izv. Vyssh. Uchebn. Zaved. Khim. Khim. Tekhnol. 18 (1975) 181.

[12] K.A. Burkov, E.A. Bus'ko, I.V. Pichugina, Russ. J. Inorg. Chem. 27 (1982) 362.
[13] G. Biedermann, L. Ciavatta, Acta Chem. Scand. 15 (1961) 1347.
[14] M.S. Caceci, G.R. Choppin, Radiochim. Acta 33 (1983) 101.
[15] N. Din Ngo, K.A. Burkov, Russ. J. Inorg. Chem. 19 (1974) 1249.
[16] Yu.P. Davydov, N.I. Voronik, Russ. J. Inorg. Chem. 28 (1983) 1270.
[17] B.N. Ivanov-Emin, A.M. Egorov, V.I. Romanyuk, E.N. Siforova, Russ. J. Inorg. Chem. 15 (1970) 628.
[18] H. López-González, M. Jiménez-Reyes, A. Rojas-Hernández, M. Solache-Rios, Talanta 44 (1997) 1891.
[19] T. Moeller, J. Phys. Chem. 50 (1946) 242.
[20] G.M. Nair, K. Chander, J.K. Joshi, Radiochim. Acta 29 (1982) 37.
[21] K.H. Schmidt, J.C. Sullivan, S. Gordon, R.C. Thompson, Inorg. Nucl. Chem. Lett. 14 (1978) 429.
[22] R.S. Tobias, A.B. Garret, J. Am. Chem. Soc. 80 (1958) 3532.
[23] L.N. Usherenko, N.A. Skorik, Russ. J. Inorg. Chem. 17 (1972) 1533.
[24] E.J. Wheelwright, F.H. Spedding, G. Schwarzenbach, J. Am. Chem. Soc. 75 (1953) 4196.
[25] C.F. Baes Jr, R.E. Mesmer, The Hydrolysis of Cations, Wiley, New York, 1976.
[26] J.H. Lee, R.H. Byrne, Geochim. Cosmochim. Acta 56 (1991) 1127.
[27] R.M. Milburn, W.C. Vosburgh, J. Am. Chem. Soc. 77 (1955) 1352.
[28] T.D. Clayton, R.H. Byrne, Deep-Sea Res. 40 (1993) 2115.
[29] H.S. Harned, B.B. Owen, The Physical Chemistry of Electrolytic Solutions, Reinhold, New York, 1958.
[30] G.L. Robert-Baldo, M.J. Morris, R.H. Byrne, Anal. Chem. 55 (1985) 2564.
[31] R.H. Byrne, Anal. Chem. 59 (1987) 1479.
[32] J.A. Breland, R.H. Byrne, Deep-Sea Res. 40 (1993) 629.
[33] B. Li, R.H. Byrne, Aqua. Geochem. 3 (1997) 99.
[34] Y.-R. Luo, R.H. Byrne, The ionic strength dependence of rare earth and yttrium fluoride complexation at 25°C, submitted 1999.
[35] X. Liu, R.H. Byrne, J. Sol. Chem. 27 (1998) 803.
[36] J. Schijf, R.H. Byrne, Determination of stability constants for the mono- and difluoro complexes of Y and the REE, using a cation-exchange resin and ICP-MS, Polyhedron 18 (1999) 2839.
[37] R.D. Shannon, Acta Crystallogr., Sect. A 32 (1976) 751.
[38] R.D. Hancock, A.E. Martell, Chem. Rev. 89 (1989) 1875.
[39] R.H. Byrne, J.H. Lee, Mar. Chem. 44 (1993) 121.
[40] V.N. Kumok, V.V. Serebrennikov, Russ. J. Inorg. Chem. 10 (1965) 1095.
[41] R.H. Byrne, L.R. Kump, K.J. Cantrell, Mar. Chem 25 (1988) 163.
[42] C.F. Baes, R.E. Mesmer, Am. J. Sci. 281 (1981) 935.
[43] C. Huang, W. Stumm, J. Colloid Interface Sci. 43 (1973) 409.
[44] L. Balistrieri, P.G. Brewer, J.W. Murray, Deep-Sea Res. 28A (1981) 101.
[45] P.W. Schindler, W. Stumm, in: W. Stumm (Ed.), Aquatic Surface Chemistry, Wiley, New York, 1987, p. 83.
[46] D.A. Dzombak, F.M.M. Morel, Surface Complexation Modeling, Wiley, New York, 1990.
[47] K.H. Johannesson, K.J. Stetzenbach, V.F. Hodge, Geochim. Cosmochim. Acta 61 (1997) 3605.

PERGAMON

www.elsevier.nl/locate/poly

Polyhedron 19 (2000) 109–114

POLYHEDRON

Syntheses, structures and electrochemistry of $[Zn(L^1)_2](BF_4)_2 \cdot 2H_2O$ and $[Zn(L^1)(Tp^R)]BF_4$ (L^1 = 1-{pyrid-2-yl}-3-{2′,5′-dimethoxyphenyl}pyrazole; $[Tp^R]^-$ = tris-{3-arylpyrazolyl}borate)

Li Mei Lindy Chia [a], Andrew E.H. Wheatley [a], Neil Feeder [a], John E. Davies [a], Malcolm A. Halcrow [b,*]

[a] *Department of Chemistry, University of Cambridge, Lensfield Road, Cambridge CB2 1EW, UK*
[b] *School of Chemistry, University of Leeds, Woodhouse Lane, Leeds LS2 9JT, UK*

Received 7 September 1999; accepted 9 November 1999

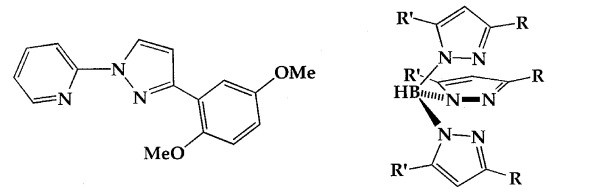
Abstract

Complexation of hydrated $Zn(BF_4)_2$ by 1-{pyrid-2-yl}-3-{2′,5′-dimethoxyphenyl}pyrazole (L^1) in MeCN, followed by layering with Et_2O, affords a white polycrystalline material analysing as $[Zn(L^1)_2](BF_4)_2 \cdot 2H_2O$ (**1**). Reaction of **1** with $K[Tp^{Ph}]$, $K[Tp^{Tol}]$ or $K[Tp^{PhF}]$ ($[Tp^{Ph}]^-$ = tris-{3-phenylpyrazolyl}borate; $[Tp^{Tol}]^-$ = tris-{3-[4-methylphenyl]pyrazolyl}borate; $[Tp^{PhF}]^-$ = tris-{3-[4-fluorophenyl]-pyrazolyl}borate) in 4:1 CH_2Cl_2:MeCN gives $[Zn(L^1)(Tp^{Ph})]BF_4$ (**2**), $[Zn(L^1)(Tp^{Tol})]BF_4$ (**3**) and $[Zn(L^1)(Tp^{PhF})]BF_4$ (**4**) in low-to-moderate yields. The single crystal structure of **2** shows a five-coordinate zinc ion, with a very distorted square-pyramidal geometry. A variable temperature NMR study of **2** in CD_2Cl_2 demonstrates a fluxional process involving libration of the L^1 ligand within one 'wedge' of the $[Tp^R]^-$ tripod. Cyclic voltammograms of **1**–**3** in CH_2Cl_2/0.5 M $NBu^n{}_4PF_6$ or MeCN/0.1 M $NBu^n{}_4PF_6$ each show one irreversible L^1-based oxidation at $E_{pa} = +1.0$–1.1 V versus ferrocene/ferrocenium, and two principle daughter waves at $E_{pc} = 0.0$ V and $E_{1/2} = -0.5$ V. This differs from the cyclic voltammograms of their previously published copper-containing analogues, which do not show oxidative EC reactivity. The reasons for these differences, and the nature of the decomposition products of zinc-coordinated $[L^{1\bullet}]^+$, are discussed. ©2000 Elsevier Science Ltd All rights reserved.

Keywords: Zinc; Tris-pyrazolylborate; Crystal structures; Electrochemistry

1. Introduction

We have recently described the complexes $[Cu(L^1)(Tp^R)]BF_4$ (L^1 = 1-{pyrid-2-yl}-3-{2′,5′-dimethoxyphenyl}pyrazole; $[Tp^R]^-$ = tris-{3-phenylpyrazolyl}borate ($[Tp^{Ph}]^-$), tris-{3-[4-methylphenyl]pyrazolyl}borate ($[Tp^{Tol}]^-$), tris-{3-[4-fluorophenyl]pyrazolyl}borate ($[Tp^{PhF}]^-$); Scheme 1), which exhibit an intramolecular π–π stacking interaction between the pendant dimethoxyphenyl substituent of L^1 and a $[Tp^R]^-$ aryl moiety [1]. The cyclic voltammograms of these complexes in CH_2Cl_2/0.5 M $NBu^n{}_4PF_6$ at room temperature contain a fully reversible one-electron oxidation by cyclic voltammetry, attributable to oxidation of the L^1 dimethoxyphenyl moiety to a radical cation [1]. In contrast, however, $[Cu(L^1)(Tp^{Cy})]BF_4$ (Cy = cyclohexyl) shows an *irreversible* ligand oxidation under the same conditions [2]. We therefore proposed that the π–π stacking interaction in $[Cu(L^1)(Tp^R)]^+$ (R = Ph, Tol, PhF) was kinetically stabilising the $[Cu(L^{1\bullet+})(Tp^R)]^{2+}$ oxidation product [1], a suggestion that appeared to be confirmed by the spectroscopic characterisation of the extremely long-lived species $[Cu(L^{1\bullet+})(Tp^R)]^{2+}$ (R = Ph, PhF; Scheme 1) [2]. This is a result of relevance to the



Scheme 1. Ligands referred to in this study.

* Corresponding author. Tel.: +44-113-233-6506; fax: +44-113-233-6565; e-mail: m.a.halcrow@chem.leeds.ac.uk

0277-5387/00/$ - see front matter ©2000 Elsevier Science Ltd All rights reserved.
PII S0277-5387(99)00343-5

properties of amino acid radicals in proteins, several examples of which are involved in π–π stacking interactions to neighbouring aromatic side-chains [3], as well as to the production of molecule-based conducting or magnetic materials [4].

As a complement to these initial studies, we were eager to prepare analogues of $[M(L^1)(Tp^R)]^+$ (M = Cu) containing a diamagnetic metal ion. In principle, this would allow the characterisation of the intramolecular π–π stacking interaction in solution by ^{1}H NMR spectroscopy, as well as removing Cu-based spectroscopic features that complicate the characterisation of $[M(L^{1\bullet+})(Tp^R)]^{2+}$ by EPR and UV–Vis spectroscopies. We therefore describe here the synthesis, solid state and solution structures and electrochemistry of $[Zn(L^1)(Tp^{Ph})]BF_4$. Throughout this paper, the Trofimenko nomenclature scheme for tris-pyrazolylborate ligands is employed [5].

2. Experimental

All manipulations were carried out in air. $Zn(BF_4)_2\cdot xH_2O$ ($x\approx2$, Aldrich) and all solvents were used as supplied. L^1 [1], K[Tp] [6], K[Tp*] [7], $K[Tp^{Ph}]$ [8], $K[Tp^{Tol}]$ [9] and $K[Tp^{PhF}]$ [1] were prepared by the literature procedures.

2.1. $[Zn(L^1)_2](BF_4)_2\cdot 2H_2O$ (1)

A mixture of L^1 (0.40 g, 1.4×10^{-3} mol) and $Zn(BF_4)_2\cdot xH_2O$ ($x\approx2$; 0.17 g, 7.2×10^{-4} mol) in MeCN (25 cm^3) was stirred at room temperature for 1 h, affording a colourless solution, which was filtered, concentrated and layered with Et_2O. White microcrystals formed over several days (yield 0.54 g, 89%). *Anal*. Found: C, 46.0; H, 4.0; N, 10.0. Calc. for $C_{32}H_{34}B_2F_8N_6O_6Zn$: C, 45.9; H, 4.1; N, 10.0%. IR (cm^{-1}): 1614m, 1532m, 1495s, 1480s, 1444s, 1331m, 1304m, 1290m, 1266m, 1244m, 1221m, 1184m, 1060vs, 1049s, 934m, 787m, 722m, 521m. FAB mass spectrum (fragment, %): 645 ($[^{65}Zn(L^1)_2(OH_2)]^+$, 17), 627 ($[^{65}Zn(L^1)_2]^+$, 3), 364 ($[^{65}Zn(L^1)(OH_2)]^+$, 100) with correct isotopic distributions. ^{1}H NMR (CD_3CN, 298 K): δ 8.52 (d, 2.7 Hz, 1H, Pz H^5), 8.25 (vbr, 1H, Py H^6), 8.14 (t, 7.7 Hz, 1H, Py H^4), 7.82 (d, 7.7 Hz, 1H, Py H^3), 7.39 (br, 1H, Py H^5), 6.82 (br, 1H, Pz H^4), 6.67 (br, 2H, Ph H^3+H^4), 6.44 (br, 1H, Ph H^6), 3.82 (s, 3H, OCH_3), 3.17 (s, 3H, OCH_3).

2.2. $[Zn(L^1)(Tp^{Ph})]BF_4$ (2)

A solution of $K[Tp^{Ph}]$ (0.12 g, 2.4×10^{-4} mol) and $[Zn(L^1)_2](BF_4)_2\cdot2H_2O$ (0.20 g, 2.4×10^{-4} mol) in 4:1 CH_2Cl_2:MeCN (25 cm^3) was stirred at room temperature for 1 h. Filtration and concentration of the colourless solution, followed by layering with Et_2O, afforded pale yellow crystals (yield 0.065 g, 31%). *Anal*. Found: C, 58.6; H, 4.3; N, 14.2. Calc. for $C_{43}H_{37}B_2F_4N_9O_2Zn$: C, 59.0; H, 4.3; N, 14.4%. IR (cm^{-1}): 2496w, 1615m, 1579m, 1530s, 1494s, 1306m, 1264m, 1220m, 1185m, 1060vs, 953m, 766m, 730m, 701m, 521m. FAB mass spectrum (fragment, %): 786 ($[^{65}Zn(L^1)(H^{11}B\{pz^{Ph}\}_3)]^+$, 100), 642 ($[^{65}Zn(L^1)(H^{11}B\{pz^{Ph}\}_2)-H]^+$, 7), 505 ($[^{65}Zn(H^{11}B\{pz^{Ph}\}_3)]^+$, 48), 361 ($[^{65}Zn(H^{11}B\{pz^{Ph}\}_2)-H]^+$, 44), 346 ($[^{65}Zn(L^1)]^+$, 13) with correct isotopic distributions. NMR spectra (CD_2Cl_2, 298 K) ^{1}H: δ 8.28 (d, 2.8 Hz, 1H, L^1 Pz H^5), 7.95 (d, 2.3 Hz, 3H, Tp^{Ph} Pz H^5), 7.91 (pseudo-td, 8.8 and 1.6 Hz, 1H, L^1 Py H^4), 7.69 (d, 8.8 Hz, 1H, L^1 Py H^3), 7.50 (d, 4.9 Hz, 1H, L^1 Py H^6), 7.11 (m, 9H, Tp^{Ph} Ph $H^{2/6}+H^4$), 6.98 (m, 6H, Tp^{Ph} Ph $H^{3/5}$), 6.79 (dd, 9.0 and 3.1 Hz, 1H, L^1 Ph H^4), 6.76 (d, 2.8 Hz, 1H, L^1 Pz H^4), 6.70 (d, 9.0 Hz, 1H, L^1 Ph H^3), 6.61 (dd, 8.8 and 4.9 Hz, L^1 Py H^5), 6.34 (d, 2.3 Hz, 3H, Tp^{Ph} Pz H^4), 5.96 (d, 3.1 Hz, 1H, L^1 Ph H^6), 3.51 (s, 3H, L^1 OCH_3), 3.48 (s, 3H, L^1 OCH_3). ^{13}C: δ 156.1, 154.8, 154.7, 153.1, 148.3 (L^1 Py C^2+Pz C^3+Ph C^2+C^5), 148.4 (L^1 Py C^6), 145.6 (L^1 Py C^4), 140.0 (Tp^{Ph} Pz C^5), 133.4 (Tp^{Ph} Pz C^1), 131.2 (L^1 Pz C^5), 130.7 (Tp^{Ph} Ph C^4), 130.0, 129.0 (Tp^{Ph} Ph $C^{2/6}+C^{3/5}$), 123.8 (Tp^{Ph} Ph C^1), 117.3, 115.7 (2C), 114.2, 113.1, 109.5 (L^1 Py C^3+C^5+Pz C^4+Ph $C^3+C^4+C^6$), 106.5 (Tp^{Ph} Pz C^4), 57.1 (L^1 OCH_3), 56.8 (L^1 OCH_3).

2.3. $[Zn(L^1)(Tp^{Tol})]BF_4$ (3)

Method as for **2**, using $K[Tp^{Tol}]$ (0.13 g, 2.4×10^{-4} mol). The product was a white microcrystalline solid (yield 0.065 g, 22%). *Anal*. Found: C, 59.5; H, 4.7; N, 13.9. Calc. for $C_{46}H_{43}B_2F_4N_9O_2Zn$: C, 60.3; H, 4.7; N, 13.7. IR (cm^{-1}): 2508w, 1616m, 1578w, 1531m, 1492s, 1331m, 1305m, 1292m, 1263m, 1220m, 1182m, 1060vs, 952m, 819m, 776m, 732m, 721m, 521m. FAB mass spectrum (fragment, %): 828 ($[^{65}Zn(L^1)(H^{11}B\{pz^{Tol}\}_3)]^+$, 100), 547 ($[^{65}Zn(H^{11}B\{pz^{Tol}\}_3)]^+$, 46), 389 ($[^{65}Zn(H^{11}B\{pz^{Tol}\}_2)-H]^+$, 59), 281 ($[L^1]^+$, 26) with correct isotopic distributions. NMR spectra (CD_2Cl_2, 298 K) ^{1}H: δ 8.61 (d, 2.8 Hz, 1H, L^1 Pz H^5), 8.06 (d, 8.8 Hz, 1H, L^1 Py H^3), 7.96 (pseudo-t, 8.8 Hz, 1H, L^1 Py H^4), 7.84 (d, 2.3 Hz, 3H, Tp^{Tol} Pz H^5), 7.44 (d, 5.0 Hz, 1H, L^1 Py H^6), 6.93 (d, 8.0 Hz, 6H, Tp^{Tol} Ph $H^{3/5}$), 6.75 (m, 8H, Tp^{Tol} Ph $H^{3/5}+L^1$ Pz H^4+L^1 Ph H^4), 6.63 (d, 8.8 Hz, 1H, L^1 Ph H^3), 6.57 (dd, 8.8 and 5.0 Hz, L^1 Py H^5), 6.27 (d, 2.3 Hz, 3H, Tp^{Tol} Pz H^4), 6.00 (d, 3.1 Hz, 1H, L^1 Ph H^6), 3.51 (s, 3H, L^1 OCH_3), 3.41 (s, 3H, L^1 OCH_3), 2.22 (s, 9H, Tp^{Tol} CH_3). ^{13}C: δ 154.3, 152.7, 152.6, 151.2, 146.5 (L^1 Py C^2+L^1 Pz C^3+L^1 Ph C^2+L^1 Ph C^5), 146.4 (L^1 Py C^6), 143.5 (L^1 Py C^4), 139.1 (Tp^{Tol} Pz C^5), 137.7 (Tp^{Tol} Pz C^1), 130.2 (L^1 Pz C^5), 128.7, 126.8 (Tp^{Tol} Ph $C^{2/6}+C^{3/5}$), 128.4 (Tp^{Tol} Ph C^4), 121.4 (L^1 Ph C^1), 117.9, 115.5, 115.2, 113.9, 113.1, 111.0 (L^1 Py C^3+C^5+Pz C^4+Ph $C^3+C^4+C^6$), 104.3 (Tp^{Tol} Pz C^4), 55.2 (L^1 OCH_3), 54.8 (L^1 OCH_3), 21.0 (Tp^{Tol} CH_3).

2.4. $[Zn(L^1)(Tp^{PhF})]BF_4$ (4)

Method as for **2**, using $K[Tp^{PhF}]$ (0.13 g, 2.4×10^{-4} mol). The white solid thus obtained (0.085 g) was recrystallised

three times from CH_2Cl_2:Et_2O (yield 0.015 g, 7%). *Anal.* Found: C, 55.8; H, 3.9; N, 13.2. Calc. for $C_{43}H_{34}B_2F_7N_9O_2Zn$: C, 55.6; H, 3.7; N, 13.6. IR (cm^{-1}): 2493w, 1610m, 1578w, 1532s, 1494s, 1306w, 1263w, 1221s, 1183m, 1156m, 1060vs, 954m, 841m, 780m, 734m, 722m, 605m, 521m. FAB mass spectrum (fragment, %): 840 ($[^{65}Zn(L^1)(H^{11}B\{pz^{PhF}\}_3)]^+$, 100), 678 ($[^{65}Zn(L^1)(H^{11}B\{pz^{PhF}\}_2)–H]^+$, 5), 559 ($[^{65}Zn(H^{11}B\{pz^{PhF}\}_3)]^+$, 26), 397 ($[^{65}Zn(H^{11}B\{pz^{PhF}\}_2)–H]^+$, 38), 346 ($[^{65}Zn(L^1)]^+$, 8) with correct isotopic distributions. NMR spectrum (CD_2Cl_2, 298 K) ^1H: δ 8.38 (d, 2.7 Hz, 1H, L^1 Pz H^5), 7.95 (pseudo-t, 8.5 Hz, 1H, L^1 Py H^4), 7.93 (d, 2.3 Hz, 3H, Tp^{PhF} Pz H^5), 7.78 (d, 8.5 Hz, 1H, L^1 Py H^3), 7.54 (d, 4.3 Hz, 1H, L^1 Py H^6), 7.07 (dd, 8.2 and 5.4 Hz, 6H, Tp^{PhF} Ph $H^{2/6}$), 6.89 (d, 2.8 Hz, 1H, L^1 Pz H^4), 6.81 (dd, 9.2 and 3.0 Hz, 1H, L^1 Ph H^4), 6.72 (m, 8H, Tp^{PhF} Ph $H^{3/5}$ + L^1 Py H^5 + L^1 Ph H^3), 6.33 (d, 2.3 Hz, 3H, Tp^{PhF} Pz H^4), 6.04 (d, 3.0 Hz, 1H, L^1 Ph H^6), 3.50 (s, 3H, L^1 OCH_3), 3.47 (s, 3H, L^1 OCH_3).

2.5. X-ray structure determination of $[Zn(L^1)(Tp^{Ph})]BF_4$

Diffusion of Et_2O into a solution of the complex in CH_2Cl_2 yielded pale yellow–green plates. Experimental details for the structure determination are given in Table 1. The structure was solved by direct methods (SHELXTL Plus [10]), and developed by least-squares refinement against $|F^2|$ (SHELXL93 [11]). During refinement, the BF_4^- anion was found to be disordered by rotation about the B(2)–F(1) bond. This was modelled using two orientations with a 60:40 occupancy ratio, with all B–F and F···F distances restrained to be equal. All non-H atoms with occupancy >0.5 were refined anisotropically, while H atoms were placed in calculated positions.

2.6. Other measurements

IR spectra were obtained as Nujol mulls pressed between KBr windows between 400–4000 cm^{-1} using a Perkin–Elmer Paragon 1000 spectrophotometer. NMR spectra were run on a Bruker DPX250 spectrometer, operating at 250.1 MHz (^1H) and 62.9 MHz (^{13}C); low temperature ^1H spectra were obtained using a Bruker AM400 instrument operating at 400.1 MHz. Positive ion fast atom bombardment (3-NOBA matrix) mass spectra were performed on a Kratos MS890 spectrometer. Microanalyses were performed by the University of Cambridge Department of Chemistry microanalytical service. All electrochemical measurements were carried out using an Autolab PGSTAT20 voltammetric analyser, in CH_2Cl_2 or MeCN containing 0.5 or 0.1 M $Bu^n_4NPF_6$, respectively, as supporting electrolyte. Cyclic voltammetric experiments involved the use of a double platinum working/counter electrode and a silver wire reference electrode; all potentials quoted in the text are referenced to an internal ferrocene/ferrocenium standard and were obtained at a scan rate of 100 mV s^{-1}.

Table 1
Experimental details for the single crystal structure determination of $[Zn(L^1)(Tp^{Ph})]BF_4$ (**2**)

Formula	$C_{43}H_{37}B_2F_4N_9O_2Zn$
M_r	874.81
Crystal habit	pale yellow plate
Crystal size (mm)	$0.40\times0.30\times0.15$
Crystal system, space group	monoclinic, $P2_1/n$
a (Å)	15.756(16)
b (Å)	10.604(3)
c (Å)	24.329(7)
β (°)	100.52(8)
U (Å^3)	3996(4)
Z	4
μ (mm^{-1})	0.684
T (K)	180(2)
Diffractometer	Rigaku AFC 7-R
Radiation	graphite-monochromated Mo Kα
λ (Å)	0.71073
Scan type	ω–2θ
Measured reflections	7312
Independent reflections	7038
R_{int}	0.071
Absorption correction	semi-empirical (Ψ-scans)
Min. transmission	0.83
Max. transmission	1.00
Observed reflections ($I>2\sigma(I)$)	4216
Range in 2θ (°)	$5\le2\theta\le50$
Range in h	$0\le h\le18$
Range in k	$0\le k\le12$
Range in l	$-28\le l\le28$
No. of parameters	562
No. of restraints	87
$R(F)$ [a], $wR(F^2)$ [b]	0.070, 0.161
GOF	1.017
Weighting scheme [c]	$w=1/[\sigma^2(F_o^2)+(0.01740P)^2+10.0908P]$
Max. shift/e.s.d	0.073
$\Delta\rho_{min}$, $\Delta\rho_{max}$ (e Å^{-3})	−0.40, 0.50

[a] $R=\Sigma[\,|F_o|-|F_c|\,]/\Sigma|F_o|$.
[b] $wR=[\Sigma w(F_o^2-F_c^2)/\Sigma wF_o^4]^{1/2}$.
[c] $P=(F_o^2+2F_c^2)/3$.

3. Results and discussion

Our initial attempts to prepare $[Zn(L^1)(Tp^{Ph})]BF_4$ followed the same method employed for its copper-containing analogues [1]. However, in contrast to the copper system, treatment of hydrated $Zn(BF_4)_2$ with equimolar amounts of L^1 and $K[Tp^{Ph}]$ in a variety of solvents gave only an intractable mixture of products. Reactions of $[ZnCl(Tp^{Ph})]$ [12,13] or $[Zn(O_2CMe)(Tp^{Ph})]$ [12] with L^1 in the presence of $NaBF_4$ or $AgBF_4$ were similarly unsuccessful. We therefore sought an alternative route to our target compounds.

Treatment of hydrated $Zn(BF_4)_2$ with 2 molar equivalents of L^1 in MeCN yields a colourless solution, from which a white polycrystalline material can be isolated upon layering with ether. This material analyses reproducibly as $[Zn(L^1)_2](BF_4)_2\cdot2H_2O$ (**1**), a formulation supported by IR spectroscopy, which shows the presence of L^1 and BF_4^- only, and FAB mass spectrometry, which exhibits a highest molec-

ular ion corresponding to $[^{65}Zn(L^1)_2(OH_2)]^+$, at $m/z=$ 645. The ^1H NMR spectra of this compound in CD_3CN or CD_3NO_2 exhibit the correct number of peaks expected for coordinated L^1, but are rather broadened. This presumably reflects fluxionality or partial solvolysis of the zinc centre upon dissolution. We have been unable to grow X-ray quality crystals of **1**, so its molecular structure remains uncertain. In particular, it is unclear whether **1** contains tetrahedral $[Zn(L^1)_2]^{2+}$ centres analogous to the isoelectronic complex $[Cu(L^1)_2]BF_4$ [14], or whether one or both of the water molecules present in **1** are metal bound to afford a higher coordination number zinc ion.

Reaction of $[Zn(L^1)_2](BF_4)_2\cdot 2H_2O$ with 1 equiv. of $K[Tp^{Ph}]$ or $K[Tp^{Tol}]$ in 4:1 CH_2Cl_2:MeCN at room temperature gives cloudy, very pale yellow solutions; filtration, concentration and addition of a large excess of Et_2O to these solutions affords white microcrystalline products in variable yields ranging from 20–35%. These solids analysed as the desired products $[Zn(L^1)(Tp^{Ph})]BF_4$ (**2**) and $[Zn(L^1)(Tp^{Tol})]BF_4$ (**3**) without further purification. In contrast, however, analogous reactions involving $K[Tp^{PhF}]$ gave white solid products of variable composition by microanalysis. Multiple recrystallisations of these crude solids from $CH_2Cl_2\cdot Et_2O$ did afford small amounts of analytically pure $[Zn(L^1)(Tp^{PhF})]BF_4$ (**4**), however. The reduced efficiency of this synthesis for **4** compared to **2** and **3** may relate to the reduced nucleophilicity of the $[Tp^{PhF}]^-$ ligand, caused by its electron-withdrawing fluoro substituents (the donor capabilities of pyrazolylborates are sensitive to the nature of the pyrazole 3-substituents [15]). Owing to the small amounts of **4** available, and since its solution properties are likely to be identical to those of **2** and **3**, only basic characterisation of this compound was undertaken.

The assignment of **2**–**4** as the desired compounds was supported by IR spectroscopy, which demonstrated the presence of L^1, BF_4^- and the appropriate pyrazolylborate. It was also supported by NMR spectroscopy (see below), and by FAB mass spectrometry which in each case gave a highest molecular ion corresponding to $[^{65}Zn(L^1)(Tp^R)]^+$ (R = Ph, $m/z=787$; R = Tol, $m/z=828$; R = PhF, $m/z=840$). In none of these mass spectra were molecular ions attributable to $[^{65}Zn(L^1)_2]^+$ ($m/z=627$) or $[^{65}Zn(Tp^R)_2]^+$ (R = Ph, $m/z=947$; R = Tol, $m/z=1031$; R = PhF, $m/z=1055$) observed. In addition, the IR spectra of microcrystalline **2**–**4** are almost superimposable on that of single crystals of **2** (see below). Both of these latter observations suggest that **2**–**4** are homogeneous solids, containing the $[Zn(L^1)(Tp^R)]^+$ (R = Ph, Tol, PhF) complex cations only.

Under the conditions used to prepare **2**–**4**, reactions of **1** with K[Tp] or K[Tp*] were unsuccessful, the resultant solutions yielding impure powders when layered with ether or pentane which did not give reproducible microanalyses. In the latter case a small number of crystals of $[Zn(Tp^*)_2]$ [16] also formed, implying that the reduced cone angles of these smaller pyrazolylborates [15] were allowing ligand disproportionation products to form from these reactions. In contrast to **4**, repeated recrystallisations of the products of these reactions did not yield pure material.

X-ray-quality crystals of **2** were grown from CH_2Cl_2/Et_2O. The structure shows one cation and anion per asymmetric unit, lying on a general position (Fig. 1, Table 2). The complex adopts the expected five-coordinate geometry, the closest contact between Zn(1) and the dimethoxyphenyl pendant being Zn(1)···C(66) = 3.557(5) Å. In contrast to the $[Cu(L^1)(Tp^R)]^+$ complexes [1], which adopt a near-regular square-pyramidal coordination sphere with one lengthened apical Cu–N bond, the geometry about Zn(1) is rather distorted. The pattern of three short and two long Zn–N distances (Table 1) is suggestive of a trigonal bipyramidal geometry, which would implicate N(3) and N(5) as the axial donors (Fig. 1). However the 'τ' index of Addison and Reedijk [17], which can vary between 0 and 1 corresponding to the limiting square-pyramidal or regular trigonal-bipyramidal geometries respectively, is only 0.28 for **2**. This is at the low end of the range observed for other known $[Zn(L)(Tp^R)]$ (L = bidentate ligand) species, all of which exhibit a 'three

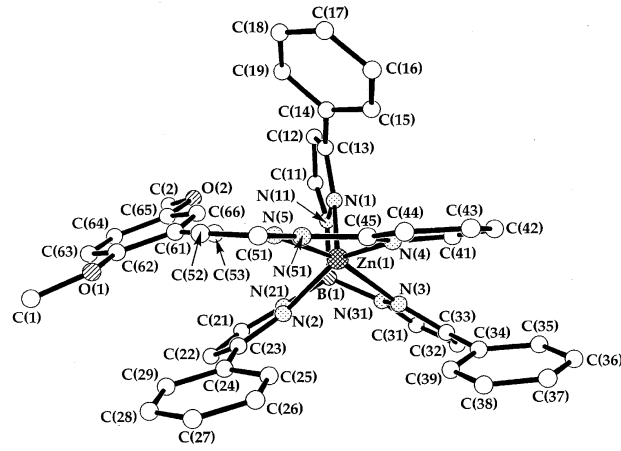


Fig. 1. View of the $[Zn(L^1)(Tp^{Ph})]^+$ cation in the single crystal structure of **2**, showing the atom numbering scheme employed. For clarity, all H atoms have been omitted.

Table 2
Selected bond lengths (Å) and angles (°) in the crystal structure of $[Zn(L^1)(Tp^{Ph})]BF_4$ (**2**)

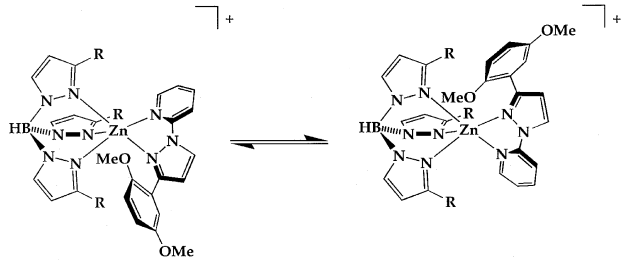
Zn(1)–N(1)	2.028(5)
Zn(1)–N(2)	2.061(4)
Zn(1)–N(3)	2.225(5)
Zn(1)–N(4)	2.054(4)
Zn(1)–N(5)	2.201(5)
N(1)–Zn(1)–N(2)	99.6(2)
N(1)–Zn(1)–N(3)	91.0(2)
N(1)–Zn(1)–N(4)	114.9(2)
N(1)–Zn(1)–N(5)	106.9(2)
N(2)–Zn(1)–N(3)	82.5(2)
N(2)–Zn(1)–N(4)	145.4(2)
N(2)–Zn(1)–N(5)	92.7(2)
N(3)–Zn(1)–N(4)	97.8(2)
N(3)–Zn(1)–N(5)	162.0(2)
N(4)–Zn(1)–N(5)	76.4(2)

short, two long' pattern of bond lengths to zinc and show $\tau = 0.21$–0.64 [18–22]. By comparison, τ for $[Cu(L^1)(Tp^{Ph})]BF_4$ is 0.19 [1].

The change in geometry between **2** and its Cu(II) analogue corresponds to a ca. 15° twist of the L^1 ligand about the central metal ion. This has the effect of weakening the π-stacking interaction in **2** between the Tp^{Ph} Ph ring (C(24)–C(29)) and L^1 dimethoxyphenyl pendant (C(61)–C(66)), since while these two moieties are still nearly coplanar (dihedral angle 9.0(2)°), their centroids are offset by 3.5 Å. By comparison, in $[Cu(L^1)(Tp^R)]BF_4$ the centroids of the two stacked arene rings are offset by 3.0 Å [1], which is an ideal value for an attractive stacking interaction between two monocyclic arenes [23].

The room temperature ^1H NMR spectra of **2**–**4** in CD_2Cl_2 exhibit the expected number of peaks and integral ratios for a 1:1 L^1:$[Tp^{Ph}]^-$ stoichiometry, and display three-fold symmetry of the pyrazolylborate ligand. This is inconsistent with the geometry of **2** in the crystal, for which each $[Tp^{Ph}]^-$ pyrazole ring is chemically distinct, and suggests that these zinc centres are fluxional in this solvent. For **2**, near 220 K, decoalescence of the $[Tp^{Ph}]^-$ Pz H^4 peak (6.34 ppm (d, 3H) at 298 K) into two peaks at δ 6.46 (1H) and 6.23 (2H) ppm is observed; partial decoalescence of the $[Tp^{Ph}]^-$ Pz H^5 and C_6H_5 peaks also takes place at this temperature. Similarly, a ^{13}C spectrum of **2** at 208 K showed splitting of the following resonances from the $[Tp^{Ph}]^-$ ligand: Pz C^3 (156.1 ppm at 298 K) into 154.1 (1C) + 153.3 (2C); Pz C^4 (104.7) into 104.2 (1C) + 104.7 (2C); Pz C^5 (140.0) into 137.9.2 (1C) + 138.3 (2C); Ph C^1 (133.4) into 132.9 (1C) + 130.3 (2C). These results strongly suggest that dissolution of **2** does not result in ligand disproportionation, and shows that the low temperature NMR structure of **2** contains a plane of symmetry through the $[Tp^{Ph}]^-$ ligand. This could either correspond to a static trigonal-bipyramidal geometry at zinc in solution, or to a fluxional process involving libration of coordinated L^1 within one 'wedge' defined by two of the $[Tp^{Ph}]^-$ pyrazole rings (Scheme 2). Given the irregular coordination geometry shown by **2** in the crystal, the latter scenario seems more likely.

The cyclic voltammogram (CV) of **1** in CH_2Cl_2/0.5 M $NBu^n_4PF_6$ at room temperature consists of an oxidation at $E_{pa} = +1.11$ V versus ferrocene/ferrocenium at a scan rate ν of 100 mV s^{-1}. This process is irreversible between $10 \leq \nu \leq 1000$ mV s^{-1} and has two associated daughter peaks: a weak irreversible reduction at $E_{pc} = 0.00$ V and a stronger *quasi*-reversible process at $E_{1/2} = -0.45$ V ($\Delta E_p = 150$ mV at 100 mV s^{-1}). An essentially identical CV was obtained in MeCN/0.1 M $NBu^n_4PF_6$, with no additional processes being observed (Fig. 2(a)). The CVs of **2** and **3** in CH_2Cl_2/0.5 M $NBu^n_4PF_6$ also exhibit an irreversible oxidation, at $E_{pa} = +1.00 \pm 0.01$ V. For both compounds this process becomes slightly *quasi*-reversible at higher scan rates, with I_{pc}:$I_{pa} \approx 0.15$ at $\nu = 1000$ mV s^{-1}. Weak daughter peaks associated with this oxidation were also observed at similar potentials to those exhibited by **1**, at $E_{pc} = -0.05$ V and



Scheme 2. Proposed fluxional process undergone by **2** in solution at low temperatures.

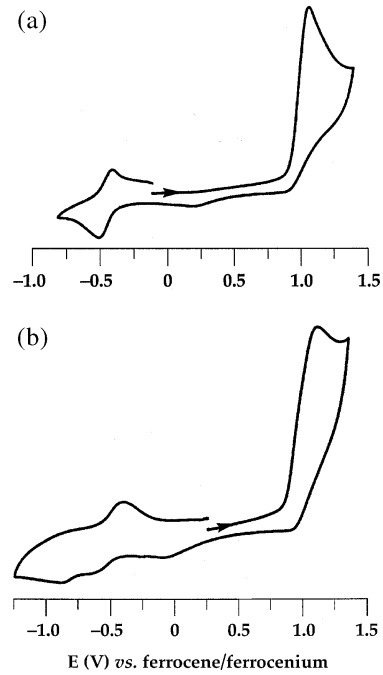


Fig. 2. Cyclic voltammograms in MeCN/0.1 M $NBu^n_4PF_6$ at 298 K with $\nu = 100$ mV s^{-1} of (a) **1** and (b) **2**.

$E_{1/2} = -0.50$ V. This suggests that **1** and **2** undergo the same EC processes at the anode. The CVs of **2** and **3** in MeCN have a similar form to those in CH_2Cl_2 (Fig. 2(b)), but with the following small differences: the initial oxidation occurs at the slightly higher potential of $E_{pa} = 1.10 \pm 0.02$ V; the daughter peaks are significantly more intense; and an additional daughter wave at $E_{pc} = -0.89$ V is also present. As expected, no electrochemical processes attributable to the zinc ion were detected within the solvent window for any of these compounds.

The irreversible oxidation exhibited by **1**–**3** can be assigned to the oxidation of each coordinated L^1 ligand to a $[L^{1\bullet}]^+$ radical cation [1,14,24]. From our previous work, the site of oxidation is the non-coordinated dimethoxyphenyl moiety on each ligand [1,2]. Interestingly, the CVs of free L^1, $[Cu(L^1)_2](BF_4)_2$ and $[Cu(L^1)(Tp^R)]BF_4$ (R = Ph, Tol, PhF) each exhibit no daughter products arising from decomposition of $[L^{1\bullet}]^+$ under these conditions [1], suggesting that the EC processes observed for **1**–**3** must be promoted by the zinc ion. Although precedent exists for 1,4-dialkoxybenzenes to undergo oxidative electropolymerisation under cer-

tain conditions [25], there was no evidence for polymer formation in the CVs of **1**–**3**. However, 1,4-dimethoxybenzyl radical cations are also known to be susceptible to nucleophilic attack at the 1- and 4-positions [26–28] following electrooxidation. In particular, a metal-promoted hydrolysis of electrooxidised 1,4-dimethoxy-2,5-di-*tert*-butylbenzene to 2,5-di-*tert*-butyl-1,4-benzoquinone has been reported [28]; a similar oxidative hydrolysis could conceivably take place for **1** owing to its lattice or ligated water content. However, the *quasi*-reversible daughter wave shown by **1** at -0.45 V is about 0.5 V more positive than that expected for a putative aryl-substituted benzoquinone EC product [29]. Hence, the nature of the EC reaction undergone by **1**–**3** is uncertain.

The irreversibility of the L^1-based oxidation shown by **2** and **3** contrasts with the behaviour of $[Cu(L^1)(Tp^R)]BF_4$ (R = Ph, Tol), which exhibit a chemically reversible ligand oxidation at $E_{1/2} = +0.97$ V [1]. This appears to support our proposition that the species $[Cu(L^{1\bullet+})(Tp^R)]^{2+}$ are kinetically stabilised by the presence of an intramolecular π–π stacking interaction [1,2], since in the crystal structure of **2** this π–π interaction is geometrically less favourable than in its copper-containing congener (see above). Additional investigations of this phenomenon using other metal/ligand systems are in progress, and will be reported in due course.

Supplementary data

The full crystallographic data are available from the CCDC, 12 Union Road, Cambridge CB2 1EZ, UK on request, quoting the deposition number 134090.

Acknowledgements

We thank the Royal Society (London) for a University Research Fellowship to M.A.H., the government of Singapore for a studentship to L.M.L.C., the EPSRC for a studentship to A.E.H.W., the University of Cambridge and the University of Leeds for financial support.

References

[1] M.A. Halcrow, E.J.L. McInnes, F.E. Mabbs, I.J. Scowen, M. McPartlin, H.R. Powell, J.E. Davies, J. Chem. Soc., Dalton Trans. (1997) 4025.
[2] X. Liu, L.M.L. Chia, S. Radojevic, L.J. Yellowlees, M. McPartlin, M.A. Halcrow, to be submitted.
[3] J. Stubbe, W.A. van der Donk, Chem. Rev. 98 (1998) 705.
[4] D.W. Bruce, D. O'Hare (Eds.), Inorganic Materials, Wiley, Chichester, 2nd edn., 1996.
[5] S. Trofimenko, Chem. Rev. 93 (1993) 943.
[6] S. Trofimenko, J. Am. Chem. Soc. 89 (1967) 3170.
[7] S. Trofimenko, J. Am. Chem. Soc. 89 (1967) 6288.
[8] D.M. Eichhorn, W.H. Armstrong, Inorg. Chem. 29 (1990) 3607.
[9] S. Trofimenko, J.C. Calabrese, J.K. Kochi, S. Wolowiec, F.B. Hulsbergen, J. Reedijk, Inorg. Chem. 31 (1992) 3943.
[10] G.M. Sheldrick, SHELXTL PLUS PC version, Siemens Analytical X-ray Instruments Inc., Madison, WI, 1990.
[11] G.M. Sheldrick, SHELXL93, Program for the Refinement of Crystal Structures, University of Göttingen, Germany, 1993.
[12] R. Alsfasser, A.K. Powell, S. Trofimenko, H. Vahrenkamp, Chem. Ber. 126 (1993) 685.
[13] F. Hartmann, W. Kläui, A. Kremer-Aach, D. Mootz, A. Strerath, H. Wunderlich, Z. Anorg. Allg. Chem. 619 (1993) 2071.
[14] M.A. Halcrow, N.L. Cromhout, P.R. Raithby, Polyhedron 16 (1997) 4257.
[15] N. Kitajima, W.B. Tolman, Prog. Inorg. Chem. 43 (1995) 419.
[16] W.R. McWhinnie, Z. Monsef-Mirzai, M.C. Perry, N. Shaikh, T.A. Hamor, Polyhedron 12 (1993) 1193.
[17] A.W. Addison, T.N. Rao, J. Reedijk, J. van Rijn, G.C. Verschoor, J. Chem. Soc., Dalton Trans. (1984) 1349.
[18] N. Kitajima, S. Hikichi, M. Tanaka, Y. Moro-oka, J. Am. Chem. Soc. 115 (1993) 5496.
[19] U. Hartmann, H. Vahrenkamp, Chem. Ber. 127 (1994) 2381.
[20] M. Ruf, R. Burth, K. Weis, H. Vahrenkamp, Chem. Ber. 129 (1996) 1251.
[21] M. Ruf, K. Weis, I. Brasack, H. Vahrenkamp, Inorg. Chim. Acta 250 (1996) 271.
[22] M. Ruf, K. Weis, H. Vahrenkamp, Inorg. Chem. 36 (1997) 2130.
[23] C.A. Hunter, J.K.M. Sanders, J. Am. Chem. Soc. 112 (1990) 5525.
[24] A. Zweig, W.G. Hodgson, W.H. Jura, J. Am. Chem. Soc. 86 (1965) 4124.
[25] B. Fabre, K. Michelet, N. Simonet, J. Simonet, J. Electroanal. Chem. 425 (1997) 67.
[26] S. Andreades, E.W. Zahnow, J. Am. Chem. Soc. 91 (1969) 4181.
[27] A. Nilsson, U. Palmquist, T. Pettersson, A. Ronlán, J. Chem. Soc., Perkin Trans. 1 (1978) 708.
[28] M. Michman, M. Oron, Electrochim. Acta 39 (1994) 2781.
[29] J.Q. Chambers, in: S. Patai (Ed.), The Chemistry of the Quinoid Compounds, Part 2, Wiley Interscience, 1974, ch. 14, pp. 737–791.

PERGAMON

www.elsevier.nl/locate/poly

Polyhedron 19 (2000) 115–121

POLYHEDRON

Synthesis and characterization of novel symmetrical phthalocyanines substituted with mono- or bi-macrocycles

Mehmet Kandaz [a], İsmail Yılmaz [b], Özer Bekaroğlu [b,*]

[a] *Department of Chemistry, Sakarya University, 5400 Adapazarı, Sakarya, Turkey*
[b] *Department of Chemistry, Technical University of Istanbul, 80626 Maslak, Istanbul, Turkey*

Received 11 May 1999; accepted 10 November 1999

Abstract

A new generation of soluble metallophthalocyanine derivatives (**5a**, **5b**, **6a**, **6b**, **7b**, **8b** and **8b**·2KSCN) bearing four 14-membered [1,4,8,11] dioxadiaza macrocycles, 14-membered [1,4,8,11] diazadithia-macrocycles or 14-membered [1,4,8,11] diazadithia-macrocycles fused to a 15-membered crown-ether have been prepared by cyclotetramerization of the newly synthesized dicyano macrocycle (**3a**, **3b** and **4b**) in the presence of appropriate metal salts in non-aqueous solvents. The *N*-tosylated derivatives are extensively soluble in apolar solvents. The interaction of the alkaline metal salts with the crown-ether groups of the complex **8b** resulted in products of less solubility. Elemental analysis results and IR, UV–Vis, ^{1}H NMR, mass spectral data on the newly synthesized intermediates and all phthalocyanines are in accordance with the proposed structures. ©2000 Elsevier Science Ltd All rights reserved.

Keywords: Phthalocyanine complexes; Phthalonitrile derivatives; Crown-ether; Copper; Nickel; Cobalt; Alkaline metal extraction

1. Introduction

Phthalocyanines and metallophthalocyanines, commonly used for many years as dyes and catalysts, have recently undergone an enormous renaissance [1–3]. Over the last 20 years or so, a new generation of phthalocyanine derivatives with purpose-designed substitution patterns has been developed [4–9]. Thanks to the development of the methodology of synthesis during the last two decades, these compounds and many of their derivatives exhibit properties that are interesting for many potential technical applications in a variety of new high technology fields such as semiconductor devices, molecular electronics, electrochromic display devices, photovoltaic and solar cells, gas sensors, synthetic metals, liquid crystals, non-linear optics, optical disks, electrophotography, and photodynamic cancer therapy [1,2,10,11]. The rich coordination chemistry of phthalocyanine complexes has encouraged researchers to 'tailor' specific products with certain properties which are required for high technology applications. The two variables are the central metal ion and peripheral substituents: when the possibility of inserting a great number of different metal ions into the phthalocyanine core is combined with the unlimited number and type of substituents, the variety of novel products is infinite. The introduction of bulky substituents on the peripheral position of the macrocycle increases drastically their solubility in organic solvents. In addition to solubility, the spectral and electrochemical properties of phthalocyanines are also strongly influenced by the peripheral substituents on the macrocycles [12–15].

Our work has been heavily engaged in the synthesis of new phthalocyanines with various functional groups and/or macrocycles. Among these we may cite the N-, O- and S-containing functionalities such as crown ethers [16–20], monoaza [21], tetraaza, tetrathia [22,23], diazatrioxa [24], tetraaza double layer and some homo- and heteropentanuclear complexes [8,20,24–26]. In all these macrocycle-substituted phthalocyanines so far, the starting point is 4,5-bis(bromomethyl)-1,2-dibromobenzene or 4,5-dichlorophthalonitrile which has been substituted with O- and S-nucleophiles through base-catalyzed nucleophilic aromatic displacement [16,27].

In the present work, as a further part of our previous studies on phthalocyanines with multifunctional substituents, starting from 4,5-bis(2′-aminophenoxy)-1,2-dicyanobenzene and 4,5-bis(2′-aminophenolsulfanyl)-1,2-dicyanobenzene (**1a** and **1b**), we report here for the first time a generalizable procedure for the preparation and characterization of a benzo-fused 14-membered dioxadiaza macrocycle, 14-membered

* Corresponding author. Tel.: +90-212-2853436; fax: +90-212-2856386; e-mail: obek@itu.edu.tr

0277-5387/00/$ - see front matter ©2000 Elsevier Science Ltd All rights reserved.
PII S0277-5387(99)00344-7

diazadithia macrocycle or 14-membered diazadithia macrocycle fused to a crown-ether, and metal phthalocyanines (Cu, Ni, Co) derived from these macrocycles. In this way, we introduce new derivatives carrying four N_2S_2 or N_2O_2 macrocycles on the periphery [8,27].

2. Experimental

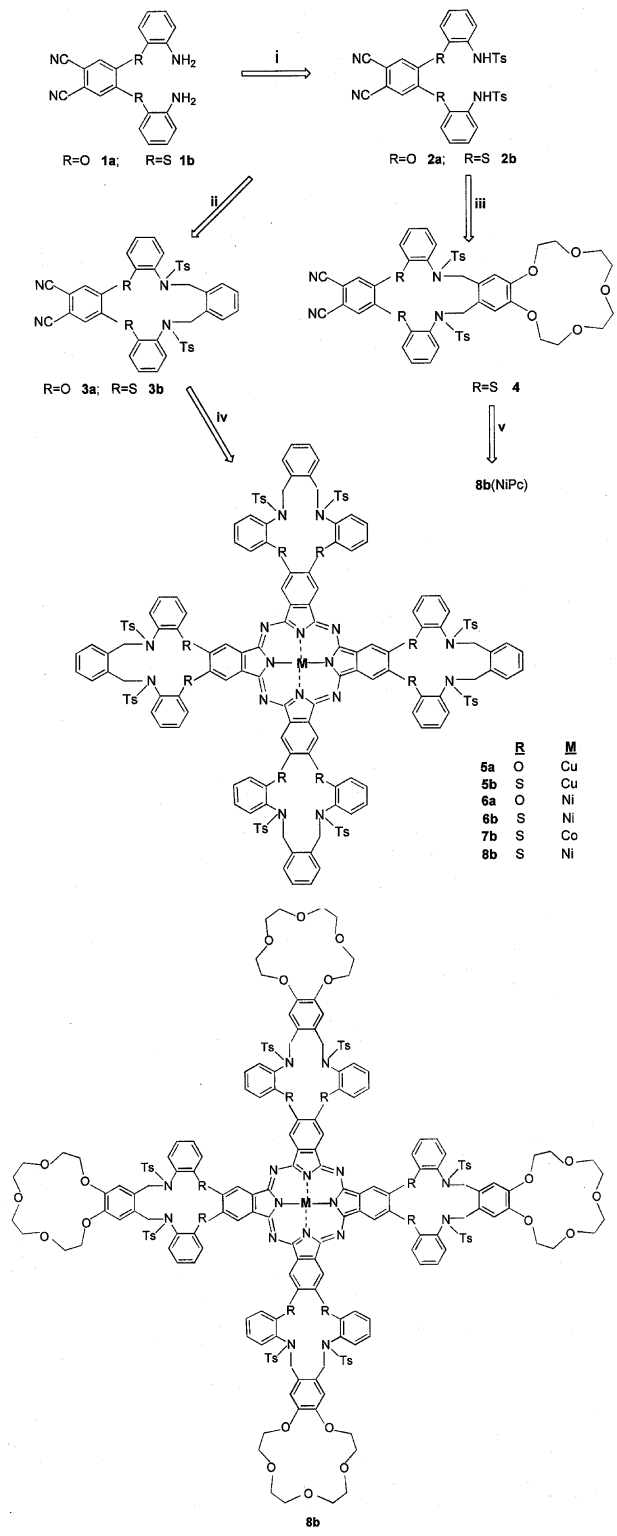
FTIR (KBr) spectra were measured on an ATI-Unicom-Mattson 1000 spectrometer using KBr pellets. Elemental analyses (C, H and N) were carried out at the instrumental analysis laboratory of Tubitak Gebze Research Center. ^{1}H NMR spectra were recorded on a Bruker 200 MHz spectrometer using $CDCl_3$ and DMSO-d_6 (99.9%). Mass spectra (EI and FAB) were measured on a VG-Zubspec GS-MS spectrometer. The metal contents of some complexes were determined with a Hitachi 180-80 atomic absorption spectrometer in solution prepared by decomposition of the compounds in conc. HCl and conc. HNO_3 (3:1) solution followed by dilution in water. The homogeneity of the products was tested at each step by TLC (SiO_2–chloroform, $CHCl_3$:MeOH).

2.1. Materials and synthesis

4,5-Dichloro-1,2-benzendicarboxylic acid was purchased from Aldrich Chemical Co. and used as received. 4,5-Dichloro-1,2-dicyanobenzene was synthesized according to reported procedures [8,27] by a multistep reaction sequence; yield 75%, m.p. 182°C. 4′,5′-bis(chloromethyl)(benzo-15-crown-5) was prepared from benzo-15-crown-5 and *p*-formaldehyde in the presence of conc. HCl by the reported procedure [26]; yield 88%, m.p. 146–148°C. As a multifunctional ligand, 4,5-bis(2′-aminophenoxy)-1,2-dicyanobenzene and 4,5-bis(2′-aminophenolsulfanyl)-1,2-dicyanobenzene (**1a** and **1b**) were synthesized starting from 2-aminophenol, 2-aminothiophenol and 4,5-dichloro-1,2-dicyanobenzene with maximum caution via base-catalyzed nucleophilic aromatic displacement of 4,5-dichloro-1,2-dicyanobenzene with O- and S-nucleophiles, respectively [8,27] (Scheme 1); yield 73%; for **1b** the yield was rather low (20%). Owing to instability of the amines **1a** and **1b**, all the preparations described below require the use of freshly prepared and purified samples of these ligands.

*2.2. 4,5-bis(2′-p-tolylsulfanylaminophenoxy)-1,2-dicyanobenzene (**2a**)*

4,5-bis(2′-aminophenoxy)-1,2-dicyanobenzene (**1a**), (0.1 g, 0.32 mmol) was dissolved in dry pyridine (7 ml) under nitrogen and powdered toluene-*p*-sulfonylchloride (0.14 g, 0.75 mmol) was added portionwise over 0.5 h to the stirred and ice-salt-cooled solution at −10°C. Stirring and cooling of the reaction mixture was continued for 1.5 h at −10°C, then the mixture was stirred at room temperature overnight. The solution was poured slowly on ice (100 g)



Scheme 1. (i) *p*-toluenesulfanylchloride, pyridine, −10°C; (ii) K_2CO_3, DMF, 1,2-bis(bromomethyl)benzene; (iii) K_2CO_3, DMF, 4′,5′-bis(chloromethyl)[benzo-15-crown-5], 35°C; (iv) quinoline, ethylene glycol in the presence of anhydrous $CuCl_2$, $NiCl_2$, $CoCl_2$; (v) quinoline, anhydrous $NiCl_2$.

and diluted with water (100 ml). The precipitated ditosylate was filtered off and washed with water (100 ml) until neutral, then with cold ethanol and diethyl ether. The creamy colored

ditosylate was crystallized from ethanol and chromatographed (silica gel, chloroform). Recrystallization from EtOH (20 ml) gave the pure ditosylate. This compound is soluble in chloroform, dichloromethane, THF, DMSO, DMF and pyridine. Yield of **2a** 0.05 g (22%); m.p. 182°C. *Anal*. Calc. for $C_{34}H_{26}N_4O_6S_2$: C, 62.76; H, 4.00; N, 8.61. Found: C, 62.35; H, 3.99; N, 8.20%. IR (KBr, cm^{-1}): ν 3250 (–NH), 3060 (Ar, C–H), 2950–2840 (aliph, –CH), 2220 (–C=N), 1590 (N–H bending), 1490, 1340–1150 (SO_2), 1280, 1260, 1120, 980, 830, 700, 670, 575, 510. ^{1}H NMR (200 MHz, DMSO-d_6, ppm): δ 10.2 (s, 2H, aromatic N–H), 7.9 (s, 2H, Ar–H), 6.6–7.6 (m, 16H, Ar–H), 2.3 (s, 6H, CH_3). EI MS *m/z* 649.1 $[M^+ - 1]$.

*2.3. 4,5-bis(2′-p-tolylsulfanylaminothiophenoxy)-1,2-dicyanobenzene (**2b**)*

4,5-bis(2′-aminophenolsulfanyl)-1,2-dicyanobenzene (**1b**) (1 g, 2.67 mmol) was dissolved in dry pyridine (10 ml) under nitrogen at −10°C in the presence of cold-salt-ice bath. Powdered toluene-*p*-sulfonylchloride (1.12 g, 5.94 mmol) was added portionwise to the stirred and ice-cold solution over a period of 1.5 h at a rate such that the temperature of salt and reaction mixture never exceeded 0°C. Stirring and cooling was continued for 3 h at −10°C then the mixture was stirred at room temperature overnight. After 16 h at room temperature, the reaction mixture was poured over crushed ice (200 g). The precipitated ditosylate was filtered off and washed with water until neutral (100 ml) or free of any pyridine residue, and with cold ethanol and diethyl ether. Recrystallization from EtOH (30 ml) gave the pure ditosylate. This compound is soluble in chloroform, dichloromethane, THF, DMSO, DMF and pyridine. Yield of **2b** 1.4 g (76.87%); m.p. 267°C. *Anal*. Calc. for $C_{34}H_{26}N_4O_4S_4$: C, 59.82; H, 3.81; N, 8.21. Found: C, 59.55; H, 3.70; N, 7.95%. IR (KBr, cm^{-1}): ν 3250, 3020, 2950–2840, 2200, 1600, 1480, 1370, 1250, 1150, 1100, 970, 810, 790, 610, 500. ^{1}H NMR (200 MHz, DMSO-d_6): δ 10.1 (s, 2H, Ar–NH), 7.6 (s, 2H, Ar–H), 6.7–7.5 (m, 16H, Ar–H), 2.25 (s, 6H, Ar–CH_3). EI MS *m/z* 682 (54) $[M^+]$.

*2.4. Diazadithia macrocycle (**3a**) and dioxadiaza macrocycle (**3b**)*

Compound **2a** (0.15 g, 0.23 mmol) or compound **2b** (0.157 g, 0.23 mmol) was dissolved in dry DMF (10 ml) under nitrogen containing finely ground anhydrous excess K_2CO_3 (0.067 g, 0.048 mmol) for **2a** and (0.070 g, 0.51 mmol) for **2b** and the mixtures were stirred for 1 h at 30°C. A solution of 1,2-bis(bromomethyl)benzene 0.061 g (0.23 mmol) for **2a** and 0.061 g (0.23 mmol) for **2b** in dry DMF (10 ml) was added dropwise over 0.5 h and the mixture was stirred at the same temperature for 48 h. It was then poured on ice-water (100 g) and stirred for 20 min. The precipitate was filtered off, washed successively with water until the filtrate was neutral, then with cold ethanol, diethyl ether and dried in vacuo. Recrystallization from toluene + EtOH gave a creamy colored product. This compound was soluble in chloroform, dichloromethane, DMF, DMSO. Yield of compound **3a** 0.08 g (46.25%); m.p. 167°C. *Anal*. Calc. for $C_{42}H_{32}N_4O_6S_2$: C, 67.02; H, 4.25; N, 7.44. Found: C, 66.87; H, 4.33; N, 7.39%. IR (KBr, cm^{-1}): ν 3040 (–Ar–CH), 2925 (aliph–CH), 2200 (–C=N), 1370–1150 (SO_2), 1260, 1050, 950, 760, 670, 500. ^{1}H NMR (200 MHz, $CDCl_3$): δ 7.70–6.73 (m, 22H, tosyl Ar–H and Ar–H), 4.50 (s, 4H, CH_2–N), 2.40 (s, 6H, Ar–CH_3). EI MS (70 eV) *m/e* (%) 751 (27) $[M^+ - 1]$. Yield of compound **3b** 0.11 g (61.08%); m.p. 180°C. *Anal*. Calc. for $C_{42}H_{32}N_4O_4S_4$: C, 64.29; H, 4.08; N, 7.14. Found: C, 63.87; H, 4.12; N, 6.95%. IR (KBr, cm^{-1}): ν 3060 (Ar, –CH), 2930 (aliph–CH), 2210 (–C=N), 1350–1150 (SO_2), 1210 (R–S–R), 1070, 840, 550, 490. ^{1}H NMR (200 MHz, $CDCl_3$): δ 7.50–6.40 (m, 22H, tosyl Ar–H and Ar–H), 4.32 (s, 4H, Ar–CH_2–N), 2.35 (s, 6H, Ar–CH_3). EI MS (70 eV) *m/z* (%) 784 (28) $[M^+]$.

*2.5. Bicyclic dicyano compound **4***

Compound **2b** (0.1 g, 0.15 mmol) was dissolved in dry DMF (10 ml) containing finely ground anhydrous K_2CO_3 excess (0.044 g, 0.32 mmol) and stirred under nitrogen at 35°C for 1 h. A solution of 4,5-bis(chloromethyl)[benzo-15-crown-5] (0.08 g, 0.29 mmol) in dry DMF (7 ml) was added dropwise over 2 h and the mixture was stirred at the same temperature (35–40°C) for 60 h. The reaction mixture was then poured onto ice-water (100 g) and stirred for 1 h. The precipitate was filtered off, washed successively with water until the filtrate was neutral, then washed with ethanol, diethyl ether and dried in vacuo. Recrystallization from EtOH (10 ml) gave the pure bicyclic dicyano compound. This compound is soluble in chloroform, dichloromethane, DMSO and DMF. Yield of **4** 0.02 g (14.06%); m.p. 197°C. *Anal*. Calc. for $C_{50}H_{46}N_4O_5S_4$: C, 61.60; H, 4.72; N, 5.75. Found: C, 61.10; H, 4.32; N, 5.65%. IR (KBr, cm^{-1}): ν 3020 (Ar–CH), 2920 (aliph, C–H), 2220, 1480, 1370–1150 (SO_2), 1210 (R–S–R), 1100, 950, 840, 700, 660, 550. ^{1}H NMR (200 MHz, $CDCl_3$): δ 7.74–7.62 (s, 8H, tosyl Ar–H), 7.86 (s, 2H, Ar–H), 6.64 (s, 2H, –CH_2), 4.25 (s, 4H, Ar–CH_2–N), 2.40 (s, 6H, Ar–CH_3), EI MS (70 eV) *m/e* (%) 974 (15) $[M^+]$.

*2.6. [Octakis(N-p-tosyl)tetrakis(macrocycle)phthalocyaninato]copper(II) (**5a** and **5b**)*

A mixture of **3a** (0.1 g, 0.13 mmol), **3b** (0.1 g, 0.13 mmol), anhydrous $CuCl_2$ (~0.0033 g, 0.033 mmol) and TMU or quinoline (0.3 ml) was heated and stirred at 100°C in a sealed tube for 5 h under nitrogen. After cooling to room temperature, the dark green mixture was diluted with EtOH (15 ml) and crude product was precipitated. It was filtered off and washed with the solvent to remove the unreacted organic impurities. The procedure was repeated three times. The dark greenish-blue powders (**5a** and **5b**) were then iso-

lated by silica gel column chromatography with chloroform. These compounds are soluble in chloroform, dichloromethane, DMSO, DMF and quinoline. Yield of **5a** 0.010 g (9.57%); m.p. > 200°C. *Anal*. Calc. for $C_{168}H_{128}N_{16}O_{24}S_8Cu$: C, 65.63; H, 4.16; N, 7.29. Found: C, 65.19; H, 3.94; N, 6.86%. IR (KBr, cm^{-1}) ν 3060 (Ar, C–H), 2930 (aliph, C–H), 1600, 1490, 1370–1160 (SO_2), 1250 (R–O–R), 1050, 875, 780, 590, 500. FAB$^+$ MS *m/z* 3074.5 [$(M+H)^+$]. Yield of **5b** 0.016 g (15.60%); m.p. > 200°C. *Anal*. Calc. for $C_{168}H_{128}N_{16}O_{16}S_{16}Cu$: C, 63.00; H, 4.03; N, 6.99. Found: C, 62.70; H, 4.00; N, 6.84%. IR (KBr, cm^{-1}) ν 3070 (Ar–H), 2920 (aliph, C–H), 1600, 1470, 1370–1150 (SO_2), 1230 (R–S–R), 1130, 1100, 1070, 900, 860, 700, 590, 510. FAB$^+$ MS (matrix: trifluoroaceticacid-glycerine) *m/z* 3199.5 [M^+].

*2.7. [Octakis(N-p-tosyl)tetrakis(macrocycle)phthalocyaninato]nickel(II) (**6a** and **6b**)*

A mixture of **3a** (0.1 g, 0.13 mmol), **3b** (0.1 g, 13 mol), anhydrous $NiCl_2$ (0.0050 g, 0.038 mmol) and quinoline (0.5 ml) was heated and stirred at 190°C for 6 h in a sealed glass tube under nitrogen. After cooling to room temperature, the dark blue mixture was diluted with ethanol (5 ml) until the crude product precipitated and the product was filtered off and washed with the same solvent hot. The dark green metallophthalocyanine was isolated on a silica gel column with $CHCl_3$ as the eluent. The products were soluble in chloroform, dichloromethane, DMSO, DMF, quinoline and THF. Yield of **6a** 0.015 g (14.10%); m.p. > 200°C. *Anal*. Calc. for $C_{168}H_{128}N_{16}O_{24}S_8Ni$: C, 65.75; H, 4.17; N, 7.30. Found: C, 65.23; H, 4.34; N, 7.00%. IR (KBr, cm^{-1}): ν 3050–2940 (Ar, C–H, aliph, C–H), 1600, 1470, 1450, 1360 (SO_2), 1240 (R–O–R), 1170 (SO_2), 1070, 990, 790, 600, 510. ^{1}H NMR (200 MHz, DMSO-d_6): δ 7.97–6.95 (m, 88H, tosyl Ar–H and Ar–H), 4.45 (s, 16H, Ar–CH_2–N), 2.43 (s, 24H, Ar–CH_3). FAB$^+$ MS *m/z* 3066 [M^+]. Yield of compound **6b** 0.020 g (18.8%); m.p. > 200°C. *Anal*. Calc. for $C_{168}H_{128}N_{16}O_{16}S_{16}Ni$: C, 63.11; H, 4.00; N, 7.01. Found: C, 62.82; H, 3.91; N, 6.86%. IR (KBr, cm^{-1}): ν 3040 (Ar, C–H), 2930 (aliph, C–H), 1600, 1450, 1370 (SO_2), 1230 (R–S–R), 1150 (SO_2), 1060, 880, 750, 610, 500. ^{1}H NMR (200 MHz, DMSO-d_6): δ 7.78–6.73 (m, 88H, tosyl Ar–H and Ar–H), 4.30 (s, 16H, Ar–CH_2–N), 2.36 (s, 24H, Ar–CH_3). FAB$^+$ MS *m/z* 3194 [$(M^+ + H)^+$].

*2.8. [Octakis(N-p-tosyl)tetrakis(macrocycle)phthalocyaninato]cobalt(II) (**7b**)*

A mixture of dicyano compound **3b** (0.15 g, 19 mmol), anhydrous $CoCl_2$ (0.0069 g, 0.054 mmol), and anhydrous ethylene glycol (4 ml) was heated and stirred at 200°C for 10 h under nitrogen in a round-bottom flask. After cooling to room temperature the reaction mixture was treated with EtOH (10 ml) and water to precipitate the dark green product, and then with EtOH to remove the unreacted organic materials. The blue-greenish powder was dissolved in chloroform (10 ml) and the solution filtered. The product was purified by column chromatography with silica gel (chloroform as the eluent). This product is soluble in chloroform, dichloromethane, THF, DMSO, DMF and quinoline. Yield 0.011 g (7.19%); m.p. > 200°C. *Anal*. Calc. for $C_{168}H_{128}N_{16}O_{16}S_{16}Co$: C, 63.08; H, 4.00; N, 7.01. Found: C, 62.93; H, 3.93; N, 6.86%. IR (KBr, cm^{-1}): ν 3040 (Ar, C–H), 2930 (aliph, C–H), 1600, 1490, 1460, 1400, 1350 (SO_2), 1240 (R–S–R), 1150 (SO_2), 1120, 1100, 860, 750, 690, 600, 510.

*2.9. Two-fold macrocycle substituted nickel(II) phthalocyanine (**8b**)*

A mixture of **4** (0.1 g, 0.10 mmol), anhydrous $NiCl_2$ (0.037 g, 0.030 mmol) and anhydrous quinoline (0.4 ml) in a sealed tube was heated and stirred at 195°C for 5 h under nitrogen. After cooling to room temperature, it was treated with ethanol (5 ml), the product was filtered off and washed with the same solvent hot, then with ethyl acetate, acetone and diethyl ether to remove unreacted organic materials. The product was dissolved in $CHCl_3$ (10 ml) and to the solution was added dropwise successively warm ethanol, ethyl acetate and acetone. The procedure was repeated several times to purify two-fold nickel(II) phthalocyanine. Finally, this product was purified by column chromatography with silica gel (chloroform as eluent); yield 0.010 g (9.87%); m.p. > 200°C. *Anal*. Calc. for $C_{200}H_{184}N_{16}S_{16}O_{36}Ni$: C, 60.69; H, 4.65; N, 5.66. Found: C, 60.01; H, 4.53; N, 5.44%. IR (KBr, cm^{-1}): ν 3020 (Ar, C–H), 2920 (aliph, C–H), 1600, 1590, 1350 (SO_2), 1260 (R–S–R), 1150 (SO_2), 1060, 970, 830, 690. ^{1}H NMR (200 MHz, DMSO-d_6): δ 7.91–6.61 (m, 22H, tosyl Ar–H and Ar–H), 4.62–3.54 (m, 80H, CH_2 of aryl, CH_2–O, CH_2–N), 2.38 (s, 24H, Ar–CH_3).

*2.10. Synthesis of the adduct of alkali metal salt with [ML] (**8b**·KSCN)*

To a stirred solution of the nickel phthalocyanine **8b** (0.07 g, 0.000018 mmol) dissolved in chloroform (20 ml) was added a solution of the desired alkali metal salt KSCN (0.0082 g, 0.000085 mmol, 10% in excess) in ethanol (5 ml) and the mixture was heated at 50°C for 8 h, then cooled to room temperature. The compound was filtered off, then it was washed successively with chloroform, ether and dried under vacuum. Yield 0.042 g (60%); m.p. > 200°C. *Anal*. Calc. for **8b**·2KSCN: C, 58.15; H, 4.41; N, 6.04. Found: C, 58.10; H, 4.17; N, 5.92%. IR (KBr, cm^{-1}): ν 3060, 3030 (Ar–CH), 2970, 2910 (aliph, CH), 2050 (KSCN), 1620, 1580, 1370 (SO_2), 1260 (R–S–R), 1150 (SO_2), 1120–1100 (C–O–C), 1040, 970, 790, 550.

3. Results and discussion

As in the case of most of the other substituted phthalocyanines, a rational method for the synthesis of this type

of compound is to start with the 4,5-dibromo-1,2-bis(bromomethyl)benzene and 4,5-dichloro-1,2-dicyano derivative of the corresponding macrocycle compound. To overcome difficulties such as low yields in the conversion from the dibromo derivatives by a Rosenmund von Broun reaction into dicarbonitrile and in order not to obtain other phthalocyanines except CuPc, new macrocycles were designed directly by the phthalonitrile unit from the beginning [8,25,27].

Recently, 1,2-dichloro-4,5-dicyanobenzene was used to prepare 4,5-disubstituted phthalonitrile derivatives, such as 4,5-bis(2′-aminophenoxy)-1,2-dicyanobenzene and 4,5-bis(2′-aminophenolsulfanyl)-1,2-dicyanobenzene (**1a** and **1b**) through base-catalyzed nucleophilic aromatic displacement [8,27].

The aromatic amine groups of 4,5-disubstituted-1,2-dicyanobenzene were then tosylated in pyridine at −10°C with *p*-toluenesulfonylchloride to protect amino groups and to make use of the high reactivity of tosylamides in further cyclization reactions. Under weak carbonate base conditions, 1,2-bis(bromomethyl)benzene reacts with the 1,2-bis(2′-*p*-tolylsulfanylaminophenoxy)-1,2-dicyanobenzene (**2a**) or 1,2-bis(2′-*p*-tolylsulfanylaminothiophenoxy)-1,2-dicyanobenzene (**2b**) to form the 14-membered dioxadiaza or 14-membered diazadithia macrocycles **3a** and **3b**. On the other hand, 4,5-bis(chloromethyl)benzo-15-crown-5 reacts with the 1,2-bis(2′-*p*-tolylsulfanylaminothiophenoxy)-1,2-dicyanobenzene in DMF at 35°C to form crown-ether fused 14-membered [1,2,8,11] diazadithia macrocycle (bicyclic compounds) (**4**). The yield in ring-closure reaction between two bifunctional reactants is relatively low (14%).

Compounds **3a**, **3b** and **4** were converted into desired metal phthalocyaninates **5a**, **5b**, **6a**, **6b**, **7b**, **8b** by using anhydrous metal salts ($CuCl_2$, $NiCl_2$, $CoCl_2$) in the presence of anhydrous solvents with high boiling points (e.g. quinoline or ethylene glycol) [1,28–30]. The yields of these reactions were rather low depending on the metal ions, as encountered for phthalocyanines with other bulky groups [15,26].

The most characteristic feature of complexes **5a**, **5b**, **6a**, **6b**, **7b** and **8b** is their high solubility in common organic solvents, e.g. chloroform, dichloromethane, dimethylformamide, dimethylsulfoxide. The two-fold substitution in **8b** results in a more bulky group on the periphery, so the solubility is higher than for the other phthalocyanines [15,19,24–26]. The crude dark-green cyclotetramerization products required final column chromatography with silica gel for purification. All attempts at detosylation of phthalocyanines to form pentanuclear phthalocyanine complexes in conc. sulfuric acid at 125°C for 5 h failed owing to decomposition of the phthalocyanines [23–25].

The interaction of the alkali metal salts with crown-ether groups of complex **8b** results in less solubility. The alkali metal binding ability of **8b**, having four crown-ether units, was estimated by solvent extraction of alkali metal picrates. Highest affinity was observed for K^+ amongst alkali metal cations. The stoichiometry of the complex isolated from a mixture of **8b** and KSCN was also found to be 1:2 [15,16,19].

Elemental analysis results and the spectral data (^{1}H NMR, UV–Vis, IR, MS) of all the new products are consistent with the assigned formulations.

In the IR spectra of **1a** and **1b**, the intense absorption bands at 2220 and 3460–3340 cm^{-1} for **1a** and 2200, 3450–3350 cm^{-1} for **1b**, respectively, corresponding to the $–NH_2$ groups, disappear after the conversion to the tosylamino compounds. The rest of the spectra of **1a** and **1b** resembles closely that of **2a** and **2b** including the characteristic vibrations of aromatic –CH, ethers (R–O–R), (R–S–R), –CN and other groups. On formation of 14-membered macrocycle and 14-membered crown-ether fused bicyclic compounds, the peaks related to tosylamino groups in **2a** and **2b** at 3350 and 1150 disappear and aliphatic peaks of macrocycles appear. In the case of crown-ether substituted 14-membered macrocycles, the extra aliphatic peaks coming from crown-ether appear in the finger-trace region. A diagnostic feature of the formation of phthalocyanines from cyano derivatives **3a**, **3b** and **4** is the disappearance of sharp intense –CN vibration bands at 2220 cm^{-1} of the reactants in the IR spectrum. The same similarities in the IR spectrum of the ligands (**3a**, **3b** except **4**) were seen in the IR spectrum of the phthalocyanines attached to the same macrocycle moieties, except **8b** for which were seen additional aliphatic, aromatic and etheric peaks (CH_2–O–). Upon the complexation of **8b** with alkali metal, vibration of the SCN^- counter anion in the case of **8b**·KSCN appears at 2050 cm^{-1}.

^{1}H NMR spectra of **2a**, **2b** and **3a**, **3b** are almost identical, with only small changes in shifts. With the addition of D_2O in **2a** and **2b**, the chemical shifts of tosylamide from about 5 to 10 ppm peaks disappear after deuterium exchange. The difference between the two spectra of tosylated amino and free amino groups **1a**, **1b** and **2a**, **2b** is clear from the presence of sulfonamide bands in **2a**, **2b** and **4** at 10.2, 10.1 ppm, respectively. In addition to aromatic protons in diazadithia, dioxadiaza or crown-ether bicyclic compounds **3a**, **3b**, **4**, $–CH_2N$ in **3a**, **3b** and the etheral protons ($–CH_2O$) of crown-ether in **4** appear at 4.50, 4.32, 4.25 ppm, respectively. ^{1}H NMR spectra of phthalocyanines **6a**, **6b**, **8b** show very small downfield shifts when compared to spectra of dinitrile starting materials **3a**, **3b**, **4**. ^{1}H NMR measurements were precluded owing to the paramagnetic nature of the copper(II) phthalocyanines **5a**, **5b** and cobalt(II) phthalocyanine **7b** [1]. ^{1}H NMR spectra of phthalocyanines **6a**, **6b** and **8b** are rather broad, owing probably to the aggregation of phthalocyanine which is frequently encountered at the concentrations used for NMR [1]. The signals for the tosyl aromatic and aromatic protons of the phthalocyanine core in **6a**, **6b** and **8b** appear as expected at 7.97–6.95, 7.78–6.73, 7.91–6.61 ppm, respectively as multiplets, and those for the tosyl aromatic and aromatic protons of the macrocycle dicyano starting materials **3a**, **3b**, **4** appear at 7.70–6.73, 7.50–6.40, 7.74–7.62 ppm respectively as multiplets. Phthalocyanines containing 14-membered dioxadiaza, diazadithia, crown-ether fused-

diazadithia macrocycles show typical electronic spectra with two absorption regions at 600–700 and 300–350 nm as Q and B bands. The UV–Vis spectra of the phthalocyanines **5a**, **5b**, **6a**, **6b**, **7b**, **8b** in chloroform and **8b**·KSCN in DMSO show Q-band absorption at 683, 694, 673, 684, 690, 674, 677 nm and B-band absorption at 343, 327, 342, 335, 330, 342, 343 nm (Table 1 and Fig. 1). These values are consistent with the results obtained previously for similar phthalocyanines [16,24,25]. An increase in the concentration leads to aggregation which is easily monitored by the position of the Q-band which is shifted to shorter wavelengths, and to a decrease in molar absorption coefficient [15–26]. In order to test the effect of the central metal ion on the changes in the Q-band, the spectra of all phthalocyanines **5**–**8** in apolar solvents have been carefully investigated (Table 1) [12–26]. The obvious effect of alkali metal ions complexed in the crown-ether groups on the Q-band transition of the phthalocyanine unit should be appreciated. Compared with the spectrum of **8b**·KSCN in DMSO, the shoulder around 648 nm is present to a lesser extent but shows no appreciable change with concentration [15–26].

A close investigation of the mass spectra of phthalonitrile derivatives **2a**, **2b**, **3a**, **3b**, **4** and phthalocyanines **5a**, **5b**, **6a**, **6b** confirmed the proposed structures. The mass spectra of **5a**, **5b**, **6a**, **6b** were obtained by the FAB technique using matrix (matrix: trifluoroaceticacid–glycerine) in the region of molecular ion peaks [M^+] *m/z* 3074.5 [$(M+H)^+$], *m/z* 3199.5 [M^+], *m/z* 3066 [M^+], *m/z* 3194 [$(M+H)^+$] with the other various mass fragments (especially [M^+–tosyl], [M^+–2tosyl], [M^+–3tosyl], [M^+–4tosyl] and the others). The mass spectra results obtained from **1a** and **1b** are interpreted in our previous paper [8].

Table 1
Electronic spectral data for the phthalocyanine complexes in chloroform

Compound	λ_{max} (nm) ($10^{-4}\varepsilon$ ($dm^3\ mol^{-1}\ cm^{-1}$))			
5a [a]	683 (14.7)	620 (4.0)	602 (3.2)	343 (14.5)
5b [a]	694 (12.5)	652 (3.2)	626 (3.1)	327 (7.1)
6a [a]	673 (7.2)	628 (3.6)	600 (3.5)	342 (6.4)
6b [a]	684 (12.4)	643 (4.3)	609 (3.8)	335 (11.2)
7b [a]	690 (7.6)	626 (5.4)	612 (2.2)	330 (9.7)
8b [a]	674 (11.3)	635 (5.7)	605 (5.0)	342 (11.0)
8b·2KSCN [b]	677 (7.0)	648 (2.3)	612 (2.5)	343 (6.9)

[a] In chloroform.
[b] In DMSO.

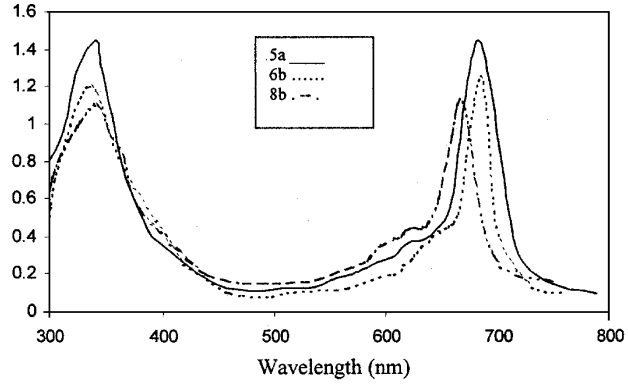


Fig. 1. UV–Vis spectra of phthalocyanine complexes.

4. Conclusions

We have presented new dicyano starting materials (ligands) and their conversion to metallophthalocyanines that are soluble in a number of solvents. We have extended the range of reactions further than in former works. We succeeded in alkali-metal binding to the endocyclic cavity of crown-ethers by alkali metal ions, causing distinct changes in the UV–Vis spectrum compared with those of the diazadithia macrocycle substituted compounds. Among the alkaline metal cations, the highest affinity was observed for K^+ which can be attributed to sandwich-type adduct formation between 15-crown-5 units and the cation. The approach described here allows the preparation of a wide number of novel penta and nona nuclear complexes whose properties will be the subject of future reports.

Acknowledgements

We thank the Research Fund of Technical University of Istanbul for financial Support and one of us Ö. Bekaroğlu thanks Turkish Academy of Science (TUBA).

References

[1] C.C. Leznoff, A.B.P. Lever (Eds.), Phthalocyanines—Properties and Applications, vols. I–V, VCH, Weinheim, 1989, 1993, 1996.
[2] J. Simon, P. Bossoul, in: C.C. Leznoff, A.B.P. Lever (Eds.), Phthalocyanines—Properties and Applications, vol. II, VCH, Weinheim, 1989, 1993, 1996.
[3] H. Schultz, H. Lehman, M. Rein, M. Hanack, Structure Bonding 74 (1991) 41–146.
[4] Z.Z. Öztürk, E. Musluoğlu, V. Ahsen, A. Gül, Ö. Bekaroğlu, J. Mater. Sci. (1992) 6183.
[5] F.T. Baumann, J.W. Sibert, M.M. Olmstead, G.M. Barett, B.M. Hoffman, J. Am. Chem. Soc. 116 (1994) 2639.
[6] J. Li, L.R. Subramanian, M. Hanack, Eur. J. Chem. (1998) 2759.
[7] S. Dabak, A. Gül, Ö. Bekaroglu, Chem. Ber. 127 (1994) 2009.
[8] M. Kandaz, Ö. Bekaroglu, Chem. Ber. 130 (1997) 1833.
[9] N. Kobayashi, M. Togashi, T. Osa, K. Ishii, S. Yamauchi, H. Hino, J. Am. Chem. Soc. 118 (1996) 1073.
[10] N. Kobayashi, in: C.C. Leznoff, A.B.P. Lever (Eds.), Phthalocyanines—Properties and Applications, vol. II, VCH, Weinheim, 1993, chapter 3.
[11] E.A. Lucyanets, Electronic Spectra of Phthalocyanines and Related Compounds, Tcherkassy, Moscow, 1989.
[12] Ö. Bekaroglu, Appl. Organomet. Chem. 10 (1996) 605.
[13] R. Polley, H. Heckmann, M. Hanack, in: Methoden der Organischen Chemie, vol. E9, Thieme, Stuttgart, 4th ed., 1997, p. 718.
[14] I. Rosenthal, E. Ben-Hur, S. Greenberg, A. Conception-Lam, M.D. Drew, C.C. Leznoff, Photochem. Photobiol. 46 (1991) 959.

[15] S.V. Kudrevich, A. Hasrat, J.E. Lier, J. Chem. Soc., Perkin Trans. 1 (1994) 2767.
[16] M. Kandaz, Ö. Bekaroğlu, J. Porphyrin Phthalocyanines 3 (1999) 339.
[17] A.I. Okur, A. Gül, A. Cihan, N. Tan, Ö. Bekaroğlu, Synth. React. Inorg. Met. Org. Chem. 20 (1990) 139.
[18] S. Sarigül, Ö. Bekaroğlu, Chem. Ber. 122 (1989) 291.
[19] M. Koçak, A.I. Okur, Ö. Bekaroğlu, J. Chem. Soc., Dalton Trans. (1994) 323.
[20] E. Musluoglu, A. Gül, Ö. Bekaroğlu, Chem. Ber. 124 (1991) 2531.
[21] A. Gürek, V. Ahsen, A. Gül, Ö. Bekaroğlu, J. Chem. Soc., Dalton Trans. (1991) 3367.
[22] A. Gürek, Ö. Bekaroğlu, Helv. Chim. Acta 77 (1994) 1616.
[23] G. Gümüş, Z. Öztürk, V. Ahsen, A. Gül, Ö. Bekaroğlu, J. Chem. Soc., Dalton Trans. (1992) 2485.
[24] I. Yilmaz, Ö. Bekaroğlu, Chem. Ber. 129 (1996) 967.
[25] M. Kandaz, Ö. Bekaroğlu, 2nd Int. Symp. on Phthalocyanines, Edinburgh, September 1998.
[26] E. Weber, K. Scobridis, M. Ouchi, T. Hakushi, Y. Inoue, Bull. Chem. Soc. Jpn. 63 (1990) 3670.
[27] D. Wöhrle, M. Eskes, K. Shigehera, A. Yamada, Synthesis (1993) 194.
[28] N. Kobayashi, A.B.P. Lever, J. Am. Chem. Soc. 109 (1987) 7433.
[29] M.J. Cook, A.J. Dunn, S.D. Howe, A.J. Thomson, K.J. Harrison, J. Chem. Soc., Perkin Trans. 1 (1998) 2453.
[30] S. Hayashida, N. Hayushi, Chem. Lett. (1990) 2137.

PERGAMON

www.elsevier.nl/locate/poly

Polyhedron 19 (2000) 123–124

POLYHEDRON

Observations concerning the constitution of some 'rhodium(II) dithiocarbamato complexes'

George Exarchos, Stephen D. Robinson *

Department of Chemistry, King's College London, Strand, London WC2R 2LS, UK

Received 13 August 1999; accepted 18 October 1999

Abstract

Mononuclear rhodium(II) dithiocarbamato complexes 'Rh(S_2CNR_2)$_2$(PPh_3)' and 'Rh(S_2CNR_2)$_2$', (R = Me, Et) have been shown to be mixtures of various rhodium(III) dithiocarbamato complexes. ©2000 Elsevier Science Ltd All rights reserved.

Keywords: Rhodium(II); Dithiocarbamates

1. Introduction

The coordination chemistry of rhodium(II) is dominated by the numerous diamagnetic binuclear rhodium(II/II) complexes with the now familiar quadruple bridged 'lantern' structure [1,2]. Examples of mononuclear paramagnetic rhodium(II) complexes are known but remain relatively rare [3,4]. The latter are purported to include two pairs of dithiocarbamato derivatives, 'Rh(S_2CNR_2)$_2$(PPh_3)' and 'Rh(S_2CNR_2)$_2$', (R = Me, Et), obtained from the reactions of $RhCl_2(NO)(PPh_3)_2$ with the appropriate sodium dithiocarbamate salt in cold and refluxing benzene respectively [5]. Although the reactions apparently involved the reduction of rhodium(III), no mention was made of precautions to exclude air. In connection with our current work on bis(dithiocarbamato) complexes of bivalent metals [6], we sought to repeat these syntheses with a view to investigating further the chemistry of the rhodium(II) products and, hopefully, developing a parallel route to analogous iridium complexes Ir(S_2CNR_2)$_2$ containing that metal in the rare bivalent state. Unfortunately, we have been unable to confirm the formation of the reported rhodium(II) dithiocarbamato complexes. Instead only rhodium(III) species, notably the simple tris(chelate) species Rh(S_2CNR_2)$_3$, could be detected.

* Corresponding author. Tel.: +44-181-546-7940; e-mail: stephen.robinson@ukgateway.net

2. Experimental

2.1. Attempted preparation of the complexes 'Rh(S_2CNR_2)$_2$(PPh_3)' (R = Me, Et)

The preparations were conducted as reported in the original paper [5], using the prescribed ratio of rhodium complex to sodium dithiocarbamate salt, and were then repeated using stoichiometric amounts (1:2 ratio). The reactions were also repeated using (a) a reaction time of 72 h in place of 6 h, and (b) acetone as solvent in place of benzene. In each case the prescribed work-up procedure was followed and products identical in appearance to those described in the original paper were obtained.

2.2. Reaction of $RhBr_2(NO)(PPh_3)_2$ with NaS_2CNEt_2

Stoichiometric amounts of $RhBr_2(NO)(PPh_3)_2$ and NaS_2CNEt_2 (1:2 ratio) were stirred together in cold benzene for 72 h, and the mixture then filtered and worked up in the prescribed manner.

2.3. Attempted preparation of the complexes 'Rh(S_2CNR_2)$_2$' (R = Me, Et)

The reactions were conducted as reported in the original paper [5] and gave orange crystalline products identical in appearance to those previously described.

0277-5387/00/$ - see front matter ©2000 Elsevier Science Ltd All rights reserved.
PII S0277-5387(99)00346-0

3. Results and discussion

The original report on the synthesis of adducts $Rh(S_2CNR_2)_2(PPh_3)$ in cold benzene specified, either by error or by design, the use of a stoichiometric deficiency of dithiocarbamate salt. The syntheses were therefore attempted using the prescribed quantities of reagents and repeated using stoichiometric amounts. In each case the reagents failed to react or even dissolve to any appreciable extent within the allotted 6 h period of stirring. The reaction times were therefore extended to 72 h, and the mixtures filtered prior to work-up in the prescribed manner. In an attempt to overcome the solubility problem, the reactions were also repeated using cold acetone as solvent. Yellow products, similar in appearance to those described in the original paper [5], were obtained in each case. However, the $^{31}P\{^1H\}$ NMR spectra of the products showed none of the paramagnetic shifts or line broadening effects expected for mononuclear rhodium(II) species. Instead they displayed an array of sharp doublets ($^1J_{Rh-P}$ ca. 80–120 Hz) characteristic of rhodium(III) triphenylphosphine species [7,8], together with singlets at δ 29.90 and 44.05 attributable to Ph_3PO and Ph_3PS respectively. In addition, proton NMR spectra reveal the presence of significant amounts of the tris(dithiocarbamato) complexes $Rh(S_2CNR_2)_3$, particularly when the higher amounts of dithiocarbamate salt were employed. Thus the characteristic pattern arising from the diastereotopic methylene protons of $Rh(S_2CNEt_2)_3$ is clearly visible in the spectrum of the diethyldithiocarbamate reaction products.

In an attempt to identify the various rhodium(III) triphenylphosphine intermediates present in these reaction mixtures, a parallel series of reactions involving the corresponding bromo complex, $RhBr_2(NO)(PPh_3)_2$, was undertaken. Two doublets (δ 34.23, $^1J_{Rh-P}$ 115 Hz and δ 33.18, $^1J_{Rh-P}$ 119.5 Hz) common to both series are attributed to halide free intermediates. However, we have not been able to make definitive assignments for these resonances or for the further five doublets seen in the spectra recorded for the products of the various $RhCl_2(NO)(PPh_3)_2$ based reactions.

The reaction of $RhCl_2(NO)(PPh_3)_2$ with sodium diethyldithiocarbamate in refluxing benzene gave an orange crystalline material similar in appearance to that originally reported [5]. However, the spectroscopic properties of this product are identical with those displayed by an authentic sample of $Rh(S_2CNEt_2)_3$ prepared from $RhCl_3 \cdot 3H_2O$. In particular the ^1H NMR spectrum displayed the resonance pattern characteristic for ethyl groups containing diastereotopic methylene protons which would be expected for the ethyl groups in octahedral $Rh(S_2CNEt_2)_3$ but not for those in square planar $Rh(S_2CNEt_2)_2$.

Attempts to obtain rhodium(II) dithiocarbamato complexes by excluding air from the syntheses were unsuccessful; in all cases good yields of the corresponding rhodium(III) products were obtained. Finally, attempts to achieve a rational synthesis of $Rh(S_2CNEt_2)_2$ from $Rh_2(O_2CMe)_4$ and NaS_2CNEt_2, similar to that previously employed in the syntheses of $[NBu^n_4]_2[Rh\{S_2C_2(CN)_2\}_2]$ [9], afforded instead good yields of the rhodium(III) species $Rh(S_2CNEt_2)_3$. We therefore conclude that the original report concerning the syntheses and characterisation of mononuclear rhodium(II) dithiocarbamato complexes is in error, and that such complexes, if accessible, are likely to prove highly susceptible to oxidation to the trivalent state.

References

[1] E.B. Boyar, S.D. Robinson, Coord. Chem. Rev. 50 (1983) 109.
[2] T.R. Felthouse, Prog. Inorg. Chem. 29 (1982) 74.
[3] F.P. Pruchnik, Pure Appl. Chem. 61 (1989) 795.
[4] K.K. Pandey, Coord. Chem. Rev. 121 (1992) 1.
[5] K.K. Pandey, D.T. Nehete, R.B. Sharma, Polyhedron 9 (1990) 2013.
[6] G. Exarchos, S.D. Robinson, Polyhedron 17 (1998) 1257.
[7] T.H. Brown, P.J. Green, J. Am. Chem. Soc. 91 (1969) 3378.
[8] T.H. Brown, P.J. Green, J. Am. Chem. Soc. 92 (1970) 2359.
[9] E. Billig, S.I. Shupack, J.H. Waters, R. Williams, H.B. Gray, J. Am. Chem. Soc. 86 (1964) 926.

PERGAMON

www.elsevier.nl/locate/poly

Polyhedron 19 (2000) 125–128

POLYHEDRON

Synthesis and spectroscopic characterization of organophosphoryl polyoxotungstates $[C_6H_{11}P(O)]_2X^{n+}W_{11}O_{39}^{(8-n)-}$ ($X^{n+} = P^{5+}$, Si^{4+}, B^{3+}, Ga^{3+})

Zhen-Gang Sun, Qun Liu, Jing-Fu Liu *

Department of Chemistry, Northeast Normal University, Changchun 130024, PR China

Received 7 July 1999; accepted 14 October 1999

Abstract

In the presence of NBu_4Br acting as a phase-transfer reagent, the monovalent polyoxotungstates α-$X^{n+}W_{11}O_{39}^{(12-n)-}$ (X = P, Si, B, Ga) react with electrophilic cyclohexane phosphonyl chloride to give hybrid organophosphoryl polyoxotungstates $[(C_6H_{11}P(O)]_2$-$XW_{11}O_{39}^{(8-n)-}$, which have been characterized by elemental analysis and IR, ^{31}P and ^{183}W NMR spectroscopy. The six-line ^{183}W spectra indicate that the hybrid anions possess C_s symmetry in solution. According to spectroscopic observations and chemical analyses, the hybrid anion consists of an α-$[XW_{11}O_{39}]$ framework on which are grafted two equivalent $C_6H_5P(O)$ groups through P–O–W bridges. ©2000 Elsevier Science Ltd All rights reserved.

Keywords: Organophosphoryl polyoxotungstate; Polyoxometalate; Synthesis; ^{183}W NMR

1. Introduction

Derivatized polyoxometalates have received increasing attention during the last 20 years owing to their potential use in catalysis, medicine and materials science [1]. It has been recognized for a long time that, by grafting appropriate organic and organometallic groups onto the polyoxometalate surface, the solubility and other physical properties of the complexes may be modified, which would increase their utility and versatility in catalysis and various medical applications, including antiviral and antitumoral chemotherapy [2–4]. The reactivity of lacunary polyoxotungstates with organic and organometallic groups has been summarized [5]. To date, the reaction of lacunary polyoxotungstates with organophosphonic acid has been reported rarely, except for a unique study by Kim et al. [6] on PhPO derivatives of monovalent tungstophosphate and tungstosilicate, and that of Mayer and Thouvenot [7] on RPO derivatives of trivalent tungstophosphate. As a continuation of these studies, we report here the synthesis and spectroscopic characterization of the title compounds $[C_6H_{11}P(O)]_2XW_{11}O_{39}^{(8-n)-}$ (X = P, Si, B, Ga).

* Corresponding author. Tel.: +86-564-9825; e-mail: sdjingfu@public.cc.jl.cn

2. Experimental

2.1. Reagents and apparatus

All reagents were of analytical or guaranteed purity. CH_3CN was distilled over P_2O_5 and used immediately. Sodium and potassium salts of $X^{n+}W_{11}O_{39}^{(12-n)-}$ (X = P, Si, B, Ga) were prepared using procedures describd in the literature [8,9]. Cyclohexanephosphonyl chloride was prepared according to a published method [10]. IR spectra were recorded on an Alpha Centauri FTIR spectrometer (2000–400 cm^{-1} range) with KBr pellets. ^{31}P NMR spectra were recorded with a JNM-FX-100 NMR spectrometer, and chemical shifts were given with respect to external 85% H_3PO_4 for ^{31}P in CD_3CN. ^{183}W NMR spectra were recorded at 16.64 MHz on a Unity-400 spectrometer using a 10-mm diameter NMR tube at 20°C; chemical shifts were referenced to 2 M Na_2WO_4 in D_2O.

2.2. Preparation of the compounds

2.2.1. $[NBu_4]_3[C_6H_{11}P(O)]_2PW_{11}O_{39}$ (1)

α-$Na_7PW_{11}O_{39}\cdot 13H_2O$ (1.42 g, 0.5 mmol) and NBu_4Br (0.97 g, 3 mmol) were suspended in CH_3CN (25 ml), and an acetonitrile solution of $C_6H_{11}POCl_2$ (0.201 g, 1 mmol in 15 ml of acetonitrile) was added dropwise under vigorous

0277-5387/00/$ - see front matter ©2000 Elsevier Science Ltd All rights reserved.
PII S0277-5387(99)00326-5

stirring. The flask was sealed with a septum stopper, and the mixture was stirred for 48 h at room temperature. After separation of a white solid (NaCl, NaBr and traces of $Na_7PW_{11}O_{39}$), the resulting solution was concentrated on a rotary evaporator, and was then diluted with 100 ml of absolute ethanol to produce a white precipitate. The white precipitate was isolated by filtration, and the solid isolated was reprecipitated again from 5 ml of acetonitrile solution by adding 100 ml of ethanol to give 1.1 g (49.12%) of a white powder. Found: C, 19.31; H, 3.58; N, 1.19; P, 2.82; W, 55.82. Calc. for $C_{60}H_{130}N_3O_{41}P_3W_{11}$: C, 19.65; H, 3.50; N, 1.15; P, 2.54; W, 55.23%.

2.2.2. $[NBu_4]_4[C_6H_{11}P(O)]_2SiW_{11}O_{39}$ (2)

This compound was similarly synthesized from α-$K_6Na_2SiW_{11}O_{39}\cdot 13H_2O$ (2.54 g, 0.8 mmol), NBu_4Br (1.29 g, 4 mmol) and $C_6H_{11}POCl_2$ (0.32 g, 1.6 mmol). Yield: 1.4 g (44.87%). Found: C, 23.48; H, 4.30; N, 1.47; Si, 0.74; P, 1.62; W, 51.62. Calc. for $C_{76}H_{166}N_4O_{41}P_2SiW_{11}$: C, 23.36; H, 4.25; N, 1.43; Si, 0.72; P, 1.59; W, 51.84%.

2.2.3. $[NBu_4]_4H[C_6H_{11}P(O)]_2BW_{11}O_{39}$ (3)

This compound was similarly synthesized from α-$K_7NaHBW_{11}O_{39}\cdot 13H_2O$ (2.54 g, 0.8 mmol), NBu_4Br (1.29 g, 4 mmol) and $C_6H_{11}POCl_2$ (0.32 g, 1.6 mmol). Yield: 1.35 g (43.41%). Found: C, 26.72; H, 4.33; N, 1.48; B, 0.26; P, 1.61; W, 52.14. Calc. for $C_{76}H_{167}N_4O_{41}P_2BW_{11}$: C, 26.54; H, 4.29; N, 1.44; B, 0.28; P, 1.59; W, 52.06%.

2.2.4. $[NBu_4]_4K[C_6H_{11}P(O)]_2GaW_{11}O_{39}$ (4)

This compound was similarly synthesized from α-$K_9GaW_{11}O_{39}\cdot 13H_2O$ (2.64 g, 0.8 mmol), NBu_4Br (1.29 g, 4 mmol) and $C_6H_{11}POCl_2$ (0.32 g, 1.6 mmol). Yield: 1.28 g (40.15%). Found: C, 22.62; H, 4.24; N, 1.45; Ga, 1.72; K, 0.96; P, 1.59; W, 50.68. Calc. for $C_{76}H_{166}N_4KO_{41}P_2GaW_{11}$: C, 22.89; H, 4.17; N, 1.41; Ga, 1.76; K, 0.98; P, 1.56; W, 50.79%.

2.3. Chemical analyses

Tungsten, phosphorus, silica, boron and gallium were determined by means of inductively coupled plasma–Auger electron spectroscopy (ICP–AES). K was determined by atomic absorption spectroscopy. C, H, N were determined using a PE-2400 elemental analyzer.

3. Results and discussion

3.1. Synthesis

The monovalent polyoxotungstates α-$X^{n+}W_{11}O_{39}{}^{(12-n)-}$ react with electrophilic cyclohexane phosphonyl chloride in acetonitrile to yield organic/inorganic species $[C_6H_{11}P(O)]_2\,X^{n+}W_{11}O_{39}{}^{(8-n)-}$ ($X^{n+}=P^{5+}$, Si^{4+}, B^{3+}, Ga^{3+}), using NBu_4Br acting as a phase-transfer reagent. The overall reaction is:

$$X^{n+}W_{11}O_{39}^{(12-n)-}+C_6H_{11}P(O)Cl_2 \xrightarrow[NBu_4Br]{MeCN} [C_6H_{11}P(O)]_2X^{n+}W_{11}O_{39}^{(8-n)-}$$

After filtration of a white solid consisting of NaCl, NaBr or KCl, KBr and a small amount of unchanged sodium or potassium polyoxotungstate, the acetonitrile solution contains a single hybrid anionic species, which has been isolated as its tetrabutylammonium salt. Elemental analysis results are consistent with the formulation of the title compounds. In contrast, the reaction between the sodium salt of α-$[PW_{11}O_{39}]^{7-}$ with $C_6H_{11}P(O)Cl_2$ in water did not show any evidence for the attachment of the organic group. This indicates that the anhydrous condition is needed for the reaction of $C_6H_{11}P(O)Cl_2$ with the lacunary polyoxotungstate. In addition, direct reaction of the lacunary precursor with $C_2H_5OP(O)Cl_2$ in acetonitrile does not give any isolable product, showing that a highly electrophilic organophosphonoyl moiety is needed for the above reaction.

3.2. Infrared spectra

The infrared spectra of all the compounds are very similar; all data and IR assignments are given in Table 1. The P–O stretching vibration bands of the organic group and central PO_4 moiety are observed between 1000 and 1060 cm^{-1} and the highest wavenumber (1120–1150 cm^{-1}) is assigned to the stretching vibration of the P–C bond of the $C_6H_{11}P(O)$ unit. The low wavenumber region ($\nu<1000$ cm^{-1}) is characteristic of the W–O stretching and bending vibration in the polyoxotungstate. It is of interest to compare the ν_3 stretching modes of the PO_4 unit (F_2) [11] for compound **1** with the IR spectra of the other structurally related anions. It is well known that a decrease in symmetry from T_d (XW_{12}) to C_s (XW_{11}) leads to splitting of the ν_3 vibration (F_2) of the PO_4 group into two components. The value of the splitting, $\Delta\nu$, is decreased when the triply bridging oxygen of the PO_4 unit interacts with a transition metal ion [11,12].

It can be seen from Table 1 that the value of $\Delta\nu$ is decreased when two organophosphoryl groups are bound in the cavity, and the stretching vibrational bands, ν_{as} ($W=O_{ter}$) and ν_{as} ($W–O_b–W$), are shifted to a higher frequency than those of the starting lacunary polyanions. This effect is attributed to a partial saturation of the polyoxometallic moiety through attachment of RPO units.

3.3. ^{31}P NMR spectra

The attachment of phosphoryl groups onto the polyoxotungstate surface is demonstrated by the resonances in the ^{31}P NMR spectra, which are all distinct from that of $C_6H_{11}P(O)Cl_2$ (Table 2).

Table 1
Comparison of infrared stretching frequencies (cm^{-1})

Q_3PW_{12} [a]	$Q_4H_2NaPW_{11}$ [a]	Compound				Assignment
		1	**2**	**3**	**4**	
		1120	1148	1144	1119	ν (P–C)
		1043	1042	1039	1026	ν_{as} (P–O) [b]
1080	1107	1060				ν_{as} (P–O) [c]
	1051	1027				
977	958	976	974	970	954	ν_{as} (W–O_d)
			916	913	566	ν_{as} (X–O_a) [d]
896	884	880	889	832	881	ν_{as} (W–O_b)
830	828	827	811	788	790	ν_{as} (W–O_c)
808	807	795	738	741	763	
	752	740			701	
513	517	525	534	532	566	δ (W–O–W)

[a] $Q = (n\text{-}C_4H_9)_4N^+$.
[b] $C_6H_{11}PO$.
[c] PO_4.
[d] X = Si, B, Ga.

Table 2
^{31}P NMR data for $[C_6H_{11}P(O)]_2X^{n+}W_{11}O_{39}^{(8-n)-}$

Compound	Chemical shift (δ, ppm)
$C_6H_{11}P(O)Cl_2$	58.5
$[Bu_4N]_3[C_6H_{11}P(O)]_2PW_{11}O_{39}$	34.2, −13.7
$[Bu_4N]_4[C_6H_{11}P(O)]_2SiW_{11}O_{39}$	31.4
$[Bu_4N]_4H[C_6H_{11}P(O)]_2BW_{11}O_{39}$	35.2
$[Bu_4N]_4K[C_6H_{11}P(O)]_2GaW_{11}O_{39}$	29.9

The ^{31}P NMR spectrum of compound **1** exhibits two lines at 34.2 and −13.7 ppm with a relative intensity of 2:1 (see Fig. 1). The high-frequency resonance is attributed to the phosphoryl group, and the low-frequency singlet is assigned to the central PO_4 unit of the polyoxotungstate. This chemical shift, which is intermediate between that of the starting lacunary anion α-$[PW_{11}O_{39}]^{7-}$ ($\delta = -10.4$ ppm) and that of α-$[PW_{12}O_{40}]^{3-}$ ($\delta = -14.9$ ppm), is in accord with a partially saturated tungstophosphate structure. The relative intensity is consistent with the grafting of only two phosphoryl groups. A heteropolyanion with a Keggin structure becomes the C_s lacunary polyanion $X^{n+}M_{11}O_{39}^{(12-n)-}$ after losing one heavy atom and its terminal oxygen, which contains three W_3O_{13} triads and one W_2O_{10} diad. These anions have a hole surrounded by five oxygen atoms, one O_a, two O_b and two O_c (see Fig. 2).

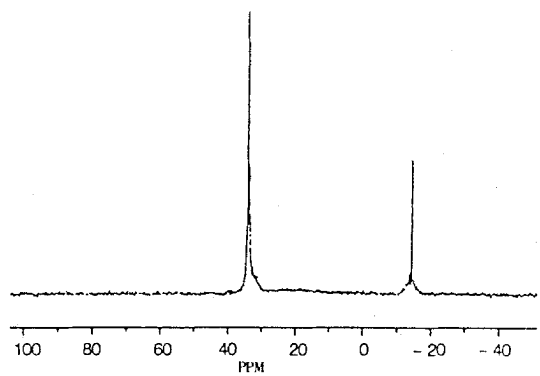


Fig. 1. The ^{31}P NMR spectrum of compound **1** in CD_3CN (0.075 M).

When two double-bonded phosphoryl groups each bridges two of the five oxygen atoms that define the hole in the lacunary polyanion, there are two possibilities, i.e. the groups can bridge the oxygens such that they are either unequivalent or equivalent. The single resonance in the ^{31}P NMR spectra indicates that the mode of attachment of the organic groups to the lacunary anion is equivalent, i.e. each organic group is connected to two W atoms belonging to a triad and a diad, respectively (see Fig. 3).

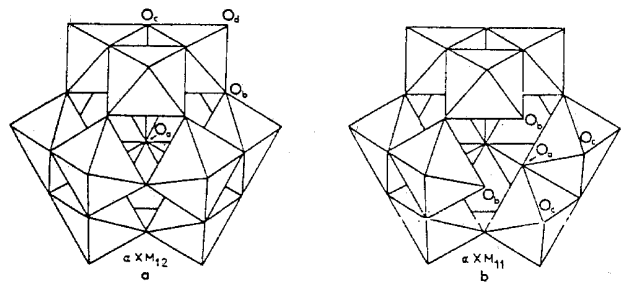


Fig. 2. Idealized structures of α-XM_{12} (Keggin structure) (a) and α-XM_{11} (defective Keggin structure) (b). O_a, oxygen shared by three MO_6 octahedra and the XO_4 tetrahedron; O_b and O_c, oxygen linked to two different M atoms; O_d, terminal unshared oxygen.

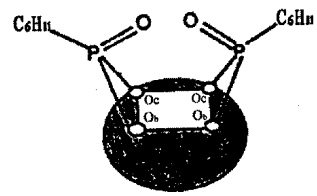


Fig. 3. Schematic representation of α-$[C_6H_{11}P(O)_2]X^{n+}W_{11}O_{39}^{(8-n)-}$.

Table 3
^{183}W NMR data for $[C_6H_{11}P(O)]_2X^{n+}W_{11}O_{39}^{(8-n)-}$

Compound	Chemical shift ($-\delta$, ppm)
$[Bu_4N]_3[C_6H_{11}P(O)]_2PW_{11}O_{39}$	80.9(2), 82.9(2), 96.6(1), 103.1(2), 113.5(2), 121.5(2)
$[Bu_4N]_4[C_6H_{11}P(O)]_2SiW_{11}O_{39}$	82.5(2), 98.3(2), 111.2(1), 123.5(2), 140.1(2), 180.9(2)
$[Bu_4N]_4H[C_6H_{11}P(O)]_2BW_{11}O_{39}$	91.9(2), 110.3(2), 115.7(1), 122.2(2), 190.3(3), 196.8(2)
$[Bu_4N]_4K[C_6H_{11}P(O)]_2GaW_{11}O_{39}$	62.5(2), 70.9(1), 93.1(2), 96.3(2), 126.3(2), 147.9(2)

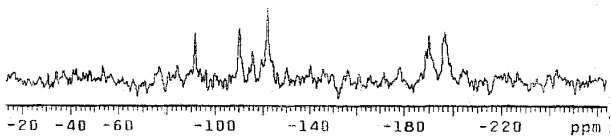


Fig. 4. The ^{183}W NMR spectrum of compound **3** in CD_3CN (0.08 M).

3.4. ^{183}W NMR spectra

The ^{183}W NMR spectrum of compound **3** and chemical shifts of all compounds are shown in Fig. 4 and Table 3, respectively.

The ^{183}W NMR spectra of all species consist of six peaks, establishing that all species have C_s symmetry in solution. This feature was observed for other derivatives of Keggin-type heteropolytungstates that bear organometallic ligands [13].

4. Conclusions

The sodium or potassium of $X^{n+}W_{11}O_{39}^{(12-n)-}$ (X = P, Si, B, Ga) and tetra-n-butylammonium bromide (NBu_4Br) were suspended in acetonitrile, and an acetonitrile solution of $C_6H_{11}POCl_2$ was added dropwise under vigorous stirring. After filtration, the resulting solution was concentrated and was then diluted with absolute ethanol to produce a white precipitate; the solid isolated was reprecipitated again from acetonitrile solution by adding absolute ethanol. Despite all our efforts to grow suitable crystals of the $C_6H_{11}(O)$ derivatives of $X^{n+}W_{11}O_{39}^{(12-n)-}$ (X = P, Si, B, Ga), no X-ray diffraction study was possible. Thus the compounds have to be characterized in solid state by IR spectroscopy and in the CD_3CN solution by ^{31}P and ^{183}W NMR. This hybrid anion consists of an α-$[XW_{11}O_{39}]$ framework on which are grafted two equivalent $C_6H_5P(O)$ groups through P–O–W bridges; each organic group is connected to two W atoms belonging to a triad and diad, respectively.

Acknowledgements

The support of the National Natural Science Foundation of China (No. 29571008) is gratefully acknowledged.

References

[1] M.T. Pope, A. Muller, Angew. Chem., Int. Ed. Engl. 30 (1991) 34.
[2] N. Mizuno, M. Misono, Chem. Rev. 98 (1998) 199.
[3] M. Weeks, C.L. Hill, R.F. Schinazi, J. Med. Chem. 35 (1992) 1216.
[4] Y. Chen, J. Liu, Q. Liu, Y. Xing, Y. Lin, H. Jia, Polyhedron 18 (1998) 481.
[5] P. Gouzerh, A. Proust, Chem. Rev. 98 (1998) 77.
[6] G.S. Kim, K.S. Hagen, C.L. Hill, Inorg. Chem. 31 (1992) 5316.
[7] C.R. Mayer, R. Thouvenot, J. Chem. Soc., Dalton Trans. (1998) 7.
[8] C. Brevard, R. Schimpf, G. Tourne, C.M. Tourne, J. Am. Chem. Soc. 105 (1983) 7059.
[9] N. Haraguchi, Y. Okaue, T. Isobe, Y. Matsuda, Inorg. Chem. 33 (1994) 1015.
[10] J.O. Clayton, W.L. Jensen, J. Am. Chem. Soc. 70 (1948) 3880.
[11] C. Rocchiccioli-Deltcheff, R. Thouvenot, J. Chem. Res. Synop. (1977) 46.
[12] F. Zonnevijlle, C.M. Tourné, G.F. Tourné, Inorg. Chem. 21 (1982) 2742.
[13] O.A. Gansow, R.K.C. Ho, W.G. Klemperer, J. Organomet. Chem. 187 (1980) C27.

PERGAMON

www.elsevier.nl/locate/poly

Polyhedron 19 (2000) 129–135

POLYHEDRON

The structures of bis-maltolato-zinc(II) and of bis-3-hydroxy-1,2-dimethyl-4-pyridinonato–zinc(II) and –lead(II)

Suada I. Ahmed [a,1], John Burgess [a,*], John Fawcett [a], Simon A. Parsons [a,2], David R. Russell [a], Stuart H. Laurie [b]

[a] *Chemistry Department, University of Leicester, Leicester LE1 7RH, UK*
[b] *Chemistry Department, De Montfort University, Leicester LE1 9BH, UK*

Received 10 August 1999; accepted 28 October 1999

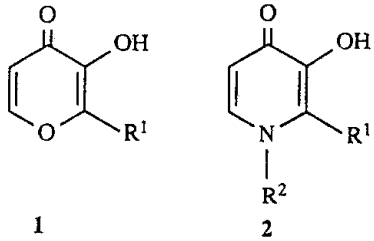
Abstract

The structures of bis-(3-hydroxy-4-pyronato)zinc(II) {bis-maltolato-zinc(II), $Zn(malt)_2 \cdot 1.5H_2O$}, bis-(1,2-dimethyl-3-hydroxy-4-pyridinonato)zinc(II) {$Zn(L1)_2 \cdot 7H_2O$}, and bis-(1,2-dimethyl-3-hydroxy-4-pyridinonato)lead(II) {$Pb(L1)_2 \cdot 7H_2O$}, determined by X-ray diffraction techniques, are reported. The zinc in {$Zn(L1)_2 \cdot 7H_2O$} is five coordinated; in $Zn(malt)_2 \cdot 1.5H_2O$ zinc occurs in both five- and six-coordination. $Pb(L1)_2 \cdot 7H_2O$ is dimeric; each lead has five oxygens, two of them bridging, in its coordination shell. All three compounds contain water molecules coordinated to the metal; both L1 complexes also contain water of crystallisation in the form of extended chains. All three compounds are extensively hydrogen bonded. ©2000 Elsevier Science Ltd All rights reserved.

Keywords: Zinc complexes; Lead(II) complexes; Maltol; 3-Hydroxy-4-pyranone; 3-Hydroxy-4-pyridinone; 1,2-Dimethyl; Crystal structures

1. Introduction

There has in recent years been growing interest in chelating ligands of the 3-hydroxy-4-pyranone (**1**) and 3-hydroxy-4-pyridinone (**2**) type, both for the control of levels of metals in the body and for their oral administration for diagnostic or therapeutic purposes [1].



1 2

Thus they have been proposed both for the introduction of iron to anaemic patients and for the removal of excess of iron from patients suffering from bodily overload as in thallasaemia or haemochromatosis. Their use to reduce aluminium levels in the body and thus perhaps to slow the progress of dementias has been suggested; they may also have a role to play in the administration of, for example, ^{67}Ga or ^{111}In radiopharmaceuticals or of gadolinium for magnetic resonance imaging (MRI) [2].

Zinc is an essential element for man. It plays a central, if still only dimly understood, role in a number of healing processes. Zinc citrate [3], probably acting as a convenient source of bio-active $Zn^{2+}(aq)$ [4], appears to aid dental care by inhibiting plaque formation [5]. Indeed, the beneficial therapeutic effects of compounds of zinc have been recognised for at least a thousand years [6]. More recently the isotopes ^{63}Zn and ^{69m}Zn have found application in radiopharmaceuticals. Absorption of zinc depends strongly on the form in which it is administered. It appears that the simple aqua-ion $Zn^{2+}(aq)$ and its phytate complex [7] are not well absorbed, but that complexes with citrate, histidine [8], prolinate, several EDTA-derivatives [3], and 3-hydroxy-4-pyranones and 3-hydroxy-4-pyridinones [9] are absorbed by the body. The determination of stability constants for zinc(II) complexes of a number of maltol derivatives [10] may point to a new route for the administration of zinc.

In contrast to zinc, lead is, of course, toxic [11,12], though this fact did not prevent the use in former times of lead(II) acetate for the treatment for diarrhoea and currently for the darkening of grey hair, nor of lead(II) acetate, stearate, and

* Corresponding author. Tel.: +44-116-252-2089; fax: +44-116-252-3789; e-mail: jbx@le.ac.uk

[1] On secondment from: Department of Chemistry, De Montfort University, Leicester LE1 9BH, UK.

[2] Present address: School of Water Sciences, Cranfield University, Cranfield, Beds. MK43 0AL, UK.

0277-5387/00/$ - see front matter ©2000 Elsevier Science Ltd All rights reserved.
PII S0277-5387(99)00330-7

oleate for certain skin complaints, nor of lead(II) iodide in ointment for application to arthritic swellings [13]. Again there are lead isotopes of radiopharmaceutical value: ^{203}Pb has proved useful in tomography [14]; ^{212}Pb may prove valuable as a source of the very cytotoxic ^{212}Bi [15].

For both zinc and lead, there is thus a need for ligands and complexes which can be orally administered. Several chelators are available for the treatment of lead poisoning, including EDTA, penicillamine, thiohydroxamates [16] and 2,3-dimercapto-propane-1-sulfonate [17], but a cheap, simple, user-friendly (maltol is a benign natural product, much used in the baking industry) chelator would be a useful addition to the lead detoxification armoury.

A great deal is known about the preparation, structures, and solvation characteristics of tris-hydroxy-pyronato– and tris-hydroxy-pyridinato–metal(III) complexes; much less is known about analogous bis-ligand complexes of metal(II) ions. The crystal structure of bis(1,2-dimethyl-3-hydroxy-4-pyridinonato)zinc(II) has been determined, but does not appear to have been published [18]; crystal structures of two ternary ruthenium(II)–bis-maltolate complexes have been reported [19]. As an essential preliminary to a planned study of solvation of such bis-ligand metal(II) complexes, we have prepared three zinc and lead complexes and determined their crystal structures by X-ray methods. None of the complexes had the hoped for simple anhydrous structure, which meant that they were not suitable for the assessment of solvation through solubility measurements. However, the complexes revealed several interesting features, both in relation to the coordination environment of the metal centres and to the extensive hydrogen-bonding in each structure, which are described below.

2. Experimental

2.1. Preparation of complexes

Bis-maltolato-zinc(II) (**3**) was prepared by dissolving 2.0 g zinc sulfate heptahydrate in the minimum amount of water and adding this solution to a solution containing 2.0 g maltol dissolved in the minimum amount of a 1:1 methanol:water mixture. Aqueous ammonia (S.G. 0.880) was added dropwise to raise the pH to 7. The volume of the solution was reduced to half by gentle heating, and the resultant solution left to stand overnight. 2.25 g (91% yield) of orange-tinged white crystals were obtained. Recrystallisation from 1:1 methanol:water gave colourless needle-shaped crystals; m.p. 199–202°C (dec).

Bis-(3-hydroxy-1,2-dimethyl-4-pyridinonato)zinc(II) (**4**) was prepared by adding 0.4 g of ligand to 0.2 g zinc(II) chloride dissolved in 10 ml methanol, and bringing the pH to 7 by dropwise addition of dilute sodium hydroxide solution. The solution was concentrated to 5 ml on a water bath; clear colourless crystals appeared on cooling. The yield was 0.52 g (90%); the product decomposed above 190°C.

Bis-(3-hydroxy-1,2-dimethyl-4-pyridinonato)lead(II) (**5**) was prepared by dissolving lead dichloride (0.5 g) and ligand (0.5 g) in 10 ml methanol; the pH of the solution was raised to 8 by dropwise addition of dilute sodium hydroxide solution. The solution was concentrated to 5 ml on a water bath, then cooled in ice. Colourless crystals appeared during the course of 24 h. The yield was 0.81 g (72%); the product decomposed above 190°C.

2.2. X-ray crystallography

Block-shaped sections of crystals of **3**, **4**, and **5** suitable for X-ray crystallography were obtained by appropriate cutting of needle-shaped crystals from recrystallised material prepared as described in the preceding paragraphs. Crystal data for **3**, **4**, and **5**, and a summary of data collection and structure refinement parameters are given in Table 1. See also Supplementary data. Data were measured on a Siemens P4 diffractometer at 293 K using graphite-monochromated Mo Kα radiation ($\lambda = 0.7107$ Å) with omega scans. Crystals were glued onto glass fibres. Unit cell dimensions were determined by least-squares refinement of optimised setting angles. The data were corrected for Lorentz and polarisation effects. The structures were solved by Patterson methods (SHELXS86), and refined by full-matrix least-squares on F^2 using SHELXTL/PC. The H atoms bonded to O in **3** and **4** were located from difference Fourier maps; (O)H atoms in **5** were neither located nor included in refinement. All C(H) atoms were included in calculated positions (C–H = 0.96 Å). Located and calculated H atoms were fixed as riding on the bonded atom with isotropic displacement parameters proportional to the U_{iso} value of that atom. All non-H atoms were refined with anisotropic displacement parameters.

3. Results and discussion

We start by dealing with the main features and metal environment for each compound separately. Thereafter we discuss the angles subtended at the metal ions in the three complexes, then some features of the geometry of the coordinated ligands, and finally deal with hydrogen-bonding in our complexes.

3.1. Metal ion coordination: bis-maltolatozinc(II)

The structure of bis-maltolatozinc(II) is shown in Fig. 1, with selected bond distances and angles given in Table 2. The overall structure can be viewed as layers of ABA sandwiches, i.e. …ABA…ABA…, with layers A consisting of five-coordinated zinc complexes, layers B of the six-coordinate complexes. The structure shows two unusual features, the occurrence in the unit cell of two molecules with different coordination numbers, five and six, for the zinc ion, and that the five-coordinate zinc ion is in an approximately square-pyramidal coordination environment. Zn1 is on a centre of

Table 1
Data collection and refinement parameters for **3**, **4** and **5**

	3	**4**	**5**
Formula	$C_{24}H_{30}O_{17}Zn_2$	$C_{14}H_{30}N_2O_{11}Zn$	$C_{14}H_{30}N_2O_{11}Pb$
Molecular weight	721.22	467.77	609.59
Crystal system	orthorhombic	triclinic	monoclinic
Space group	*Pbcn*	$P\bar{1}$	$P2_1/c$
a (Å)	16.162(3)	6.806(1)	10.142(3)
b (Å)	13.125(1)	10.706(2)	12.188(4)
c (Å)	13.404(1)	14.332(3)	18.190(6)
α (°)	90	90.12(1)	90
β (°)	90	94.86(1)	91.88(2)
γ (°)	90	91.50(1)	90
V (Å^3)	2843.2(6)	1040.2(3)	2247.3(12)
Z	4	2	4
$F(000)$	1480	492	1192
D_c (g cm^{-3})	1.685	1.487	1.802
μ (mm^{-1})	1.768	1.237	7.561
Crystal size (mm)	0.67×0.42×0.29	0.38×0.24×0.18	0.71×0.37×0.31
Crystal colour/shape	colourless/block	colourless/block	colourless/needle
Abs. corr. T_{max}/T_{min}	0.711, 0.489	0.866, 0.710	0.251, 0.039
Scan range θ (°)	2.51–27.00	2.37–25.00	2.01–28.17
Scan index limits (h,k,l)	$-\leq h\leq 20,\ 0\leq k\leq 16,\ -1\leq l\leq 17$	$-1\leq h\leq 7,\ -12\leq k\leq 12,\ -17\leq l\leq 17$	$-1\leq h\leq 13,\ -1\leq k\leq 16,\ -24\leq l\leq 24$
Data collected	3563	4518	6745
Unique data	3074	3518	5355
Goodness of fit on F^2 [a]	1.046	1.071	1.120
R_{int}	0.018	0.020	0.033
Observed data ($I>2\sigma(I)$) $R1$	0.0350	0.0409	0.0407
$wR2$ (all data)	0.0963	0.1099	0.1112
Parameters n	197	253	253
ΔF (e Å^{-3})	+0.339, −0.358	+0.477, −0.602	+1.523, −1.329

[a] $R1=\Sigma||F_o|-|F_c||/\Sigma|F_o|$, $wR2=[w(F_o^2-F_c^2)^2/(F_o^2)^2]^{1/2}$, goodness of fit $s=[\Sigma w(F_o^2-F_c^2)^2/(n-p)]^{1/2}$ where n = number of reflections and p = total number of parameters; $w=1/[\sigma^2(F_o^2)+(aP)^2+bP]$ where $P=(F_o^2+2F_c^2)/3$.

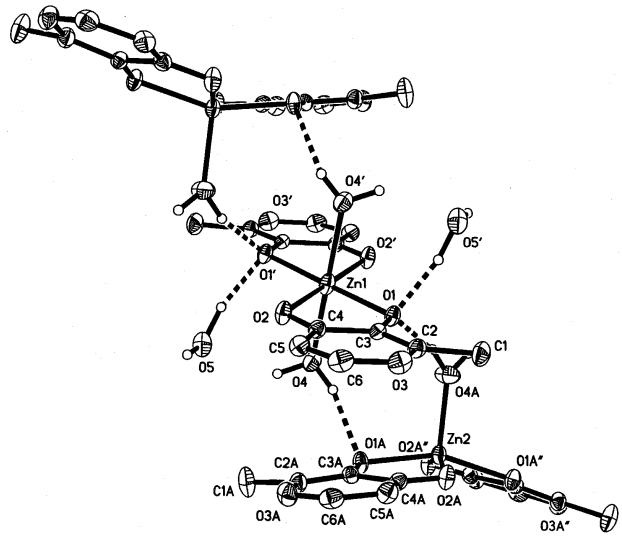


Fig. 1. Molecular structure of **3** showing 30% displacement ellipsoids; (C)H atoms are omitted for clarity. Single prime atoms are generated by a centre of symmetry ($1-x$, $1-y$, $-z$); double prime atoms are generated by a 2-fold axis through Zn2 and O4a ($-x$, $1+y$, $1/2-z$).

symmetry, with a unique half molecule and primed ligand atoms generated by $1-x$, $1-y$, $-z$. Zn2 is on a 2-fold axis, with the half molecule generated by $-x$, $1+y$, $1/2-z$; one water is associated with the asymmetric unit. Another example of a metal occurring in both five- and six-coordination in a compound is provided by the tetranuclear iron compound $Fe_4Cl_8(thf)_6$ [20]. Further examples of five-coordinated zinc include a modelled carbonic anhydrase derivative containing a second, more distant, water molecule [21], and others which appear below.

The zinc to water-oxygen distance in the five-coordinated aqua-ion is 2.01 Å. This may be compared with the value of 2.20 Å in $Zn(acac)_2\cdot H_2O$ (where the zinc is in coordination

Table 2
Selected bond distances (Å) and angles (°) for bis-maltolato-zinc(II) (**3**)

Zn(1)–O(1)	2.033(2)	Zn(2)–O(1A)	2.010(2)
Zn(1)–O(2)	2.075(2)	Zn(2)–O(2A)	2.076(2)
Zn(1)–O(4)	2.259(2)	Zn(2)–O(4A)	2.003(2)
O(1)–Zn(1)–O(1′)	180	O(1A)–Zn(2)–O(1A″)	156.80(12)
O(1)–Zn(1)–O(2)	82.09(7)	O(1A)–Zn(2)–O(2A″)	93.64(7)
O(1)–Zn(1)–O(2′)	97.91(7)	O(1A)–Zn(2)–O(2A)	82.10(7)
O(1′)–Zn(1)–O(4)	87.46(8)	O(1A″)–Zn(2)–O(4A)	101.60(6)
O(1′)–Zn(1)–O(4′)	92.54(8)	O(2A)–Zn(2)–O(2A″)	158.83(13)
O(2)–Zn(1)–O(4)	89.65(8)	O(2A)–Zn(2)–O(4A)	100.58(7)
O(2′)–Zn(1)–O(4)	90.35(8)		
O(2)–Zn(1)–O(2′)	180		

Table 3
Selected bond distances (Å) and angles (°) for bis(3-hydroxy-1,2-dimethyl-4-pyridinonato)zinc(II) (**4**)

Zn(1)–O(1)	2.021(2)	Zn(1)–O(11)	2.034(2)
Zn(1)–O(2)	2.050(2)	Zn(1)–O(12)	2.047(2)
Zn(1)–O(3)	2.043(3)		
O(1)–Zn(1)–O(2)	81.68(8)	O(2)–Zn(1)–O(11)	97.85(9)
O(1)–Zn(1)–O(3)	109.82(10)	O(2)–Zn(1)–O(12)	165.14(10)
O(1)–Zn(1)–O(11)	146.20(10)	O(3)–Zn(1)–O(11)	103.74(10)
O(1)–Zn(1)–O(12)	90.54(9)	O(3)–Zn(1)–O(12)	96.49(11)
O(2)–Zn(1)–O(3)	98.05(11)	O(11)–Zn(1)–O(12)	81.59(9)

geometry intermediate between trigonal-bipyramidal and square-pyramidal, though closer to the latter) [22], with zinc–oxygen distances of between 1.99 and 2.31 Å in the approximately trigonal-bipyramidal $[Zn(H_2O)_5]^{2+}$ entity in crystals of penta-aquazinc(II) bis(3,3′,3′-phosphinetriyltripropionato)dizincate(II,II), [23] and with Zn–OH_2 = 2.00 Å in $[Zn(bipy)(O_2CCCl_3)_2(H_2O)]$, where the water ligand is equatorial [24]. The coordination number of the zinc in the $[Zn(maltolate)_2(H_2O)]$ units is indubitably five, with no evidence for even a weak interaction at the vacant sixth coordination site. One has to go further than 5 Å from the metal in this direction before finding the nearest neighbouring atom. Indeed two oxygen atoms of water ligands (O4, Fig. 1) in octahedral $[Zn(maltolate)_2(H_2O)_2]$ units (see below) in the adjacent layer of the sandwich are, at 3.94 Å, closer than this, but on the same side of the zinc as the coordinated water (O4A).

In the octahedral aqua-ion, the two waters are *trans* to each other, with Zn–O rather long at 2.26 Å; Zn–O is, for example, 2.03 Å in the octahedral $[Zn(H_2O)_4Cl_2]$ entities in zinc chloride hydrate ($ZnCl_2 \cdot 4/3H_2O$) and 2.08 Å in the octahedral aqua-ion $Zn(H_2O)_6^{2+}$ in aqueous solution [25,26]. The complex $[Zn(dimethyl\text{-}3\text{-}oxopentanedioate)_2(H_2O)_2]$ has a structure analogous to that of the present $[Zn(maltol)_2(H_2O)_2]$; the pentanedioate complex has Zn–O = 2.18 Å to the mutually *trans* water ligands, 2.02 and 2.08 Å to the other coordinated oxygens [27]. We are very interested in establishing metal to water distances in an analogous copper(II) bis-aqua bis-pyronato-species, but unfortunately our extensive efforts to grow a suitable single crystal have so far been unsuccessful.

The zinc to maltol-oxygen distances are all within the relatively narrow range of 2.01 to 2.08 Å, normal for zinc to coordinated oxygen bond lengths. The two maltolate ligands are effectively in the *trans* configuration to each other in the planar $Zn(maltolate)_2$ unit in the octahedral species.

3.2. Metal ion coordination: bis(1,2-dimethyl-3-hydroxy-4-pyridinonato)zinc(II)

The zinc ion is five-coordinated in this complex, again with a distorted square-pyramidal geometry around the metal ion. Selected bond distances and angles are listed in Table 3; atom numbering is shown in Fig. 2. The zinc to water-oxygen distance is 2.05 Å, marginally longer than in the five-coordinate zinc-maltol species. The zinc to hydroxypyridinonate-oxygen distances are between 2.02 and 2.05 Å, within the range for zinc-maltol. As is the case for the $[Zn(maltolate)_2(H_2O)]$ units in the maltol complex, the coordination number of the metal is again indubitably five, with no significant interaction along the axis in the opposite direction to the coordinated water. Fig. 2 shows how the water molecules containing O7′, O8′, and O9′ effectively block the sixth coordination site at the zinc without themselves interacting with the metal.

3.3. Metal ion coordination: bis(1,2-dimethyl-3-hydroxy-4-pyridinonato)lead(II)

An atom-numbered view of this complex, with water of crystallisation, is shown in Fig. 3, with selected bond distances and angles listed in Table 4. Here the main structural interest lies in the binuclear nature of the complex, with additional interest in whether the lone pair on the lead has a

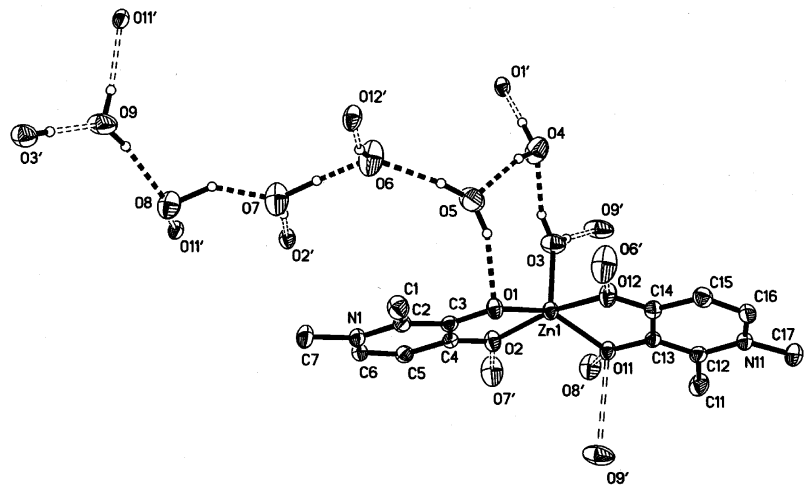


Fig. 2. Molecular structure of **4** showing 30% displacement ellipsoids; (C)H atoms are omitted for clarity. Full dashed lines show O–H···O hydrogen bonds; open dashed lines and primed atoms indicate extended symmetry-related hydrogen bonds.

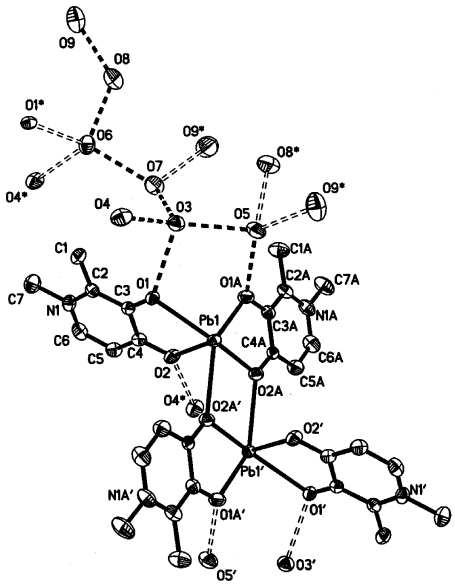


Fig. 3. Molecular structure of **5** showing 30% displacement ellipsoids; (C)H atoms are omitted for clarity. Single prime atoms are generated by a centre of symmetry $(1-x, 1-y, -z)$. Full dashed lines show show probable O–H···O hydrogen bonds (O···O < 2.9 Å); open dashed lines and starred atoms indicate further symmetry-related hydrogen bonds.

Table 4
Selected bond distances (Å) and angles (°) for bis(3-hydroxy-1,2-dimethyl-4-pyridinonato)lead(II) (**5**)

Pb(1)–O(1)	2.544(5)	Pb(1)–O(1A)	2.358(5)
Pb(1)–O(2)	2.300(5)	Pb(1)–O(2A)	2.370(5)
		Pb(1)–O(2A′)	2.684(5)
O(1)–Pb(1)–O(1A)	91.4(2)	O(1A)–Pb(1)–O(2A)	69.5(2)
O(1)–Pb(1)–O(2)	67.6(2)	O(1A)–Pb(1)–O(2A′)	135.8(2)
O(1)–Pb(1)–O(2A)	141.6(2)	O(2)–Pb(1)–O(2A)	79.3(2)
O(1)–Pb(1)–O(2A′)	119.1(2)	O(2)–Pb(1)–O(2A′)	74.8(2)
O(1A)–Pb(1)–O(2)	90.6(2)	O(2A)–Pb(1)–O(2A′)	66.9(2)

significant stereochemical influence. The lead complex has the expected 2:1 ligand:metal stoichiometry, but instead of containing monomeric entities it consists of binuclear molecules each containing two ligands bridging through one of their oxygen atoms. There are several examples of dinuclear copper(II) complexes with bridging 2-pyridinone ligands [28], but we believe this is the first dinuclear complex with 4-pyridinonate bridges. The $Pb_2(\mu\text{-}O)_2$ moiety is a parallelogram with ∠O–Pb–O = 67°; the Pb–O distances are 2.38 and 2.68 Å.

The coordination geometry around lead(II) continues to be a matter of interest [29], especially the extent to which the lone pair is stereochemically active. It has long been realised that a lone pair on lead(II) is in general less stereochemically active than one in an analogous tin(II) compound [30,31]. Nonetheless, at least two recently published structures indicate stereoactive lone pairs in lead(II) complexes [32,33]. In the present complex, each lead atom has only five oxygen atoms in its coordination shell: two bridging oxygens, the second oxygen donor from one of the bridging ligands,

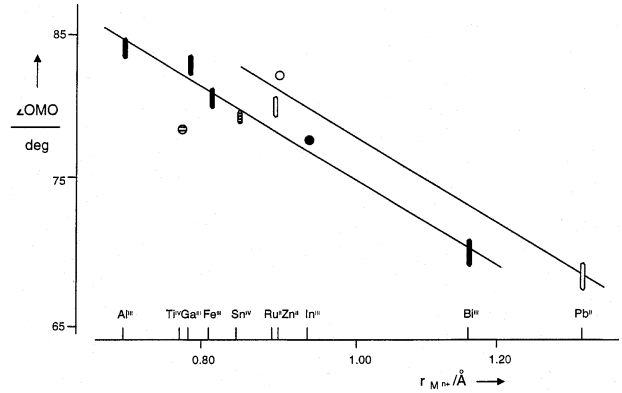


Fig. 4. Relation between ligand chelate bite angles subtended by coordinated 3-hydroxy-4-pyranonate and 3-hydroxy-4-pyridinonate ligands and ionic radii of the respective central metal ions. ○ M^{2+}; ● M^{3+}; ⊜ M^{4+}; elongated symbols cover the range of bite angles for cases where more than one structure has been determined, or where there are two or more different bite angles in a given complex.

and two oxygen atoms from a non-bridging ligand. There is thus space for a stereoactive lone pair, and indeed the arrangement of the oxygens around the lead strongly suggest that the lone pair is playing a significant stereochemical role. There is a stereoactive lone pair in the closely related tris-ethylmaltolato-bismuth(III) complex [34].

3.4. Angles subtended at the metal

The ligand L1 subtends a much smaller angle at lead, 67.6° and 69.5° (the former for the non-bridging ligand), than either L1 or maltol at zinc. It seemed to us likely that this was simply a consequence of the larger size of lead(II) and therefore we assembled data on the angles subtended at metals by coordinated 3-hydroxy-4-pyranones and 3-hydroxy-4-pyridinones. The data are presented graphically in Fig. 4, which suggests a close correlation between bite angle and metal radius [3] for M^{2+} (lower line) and for M^{3+} (upper line). The correlations for the two oxidation states are parallel but separate. The very limited data (two compounds) for M^{4+} do not quite conform to the pattern for the M^{2+} and M^{3+} complexes. This may, however, be a reflection on the published estimate for the ionic radius for Sn^{4+} rather than deviation from the pattern for M^{2+} and M^{3+}.

3.5. Coordinated ligand geometry

The carbon–oxygen and carbon–carbon bond distances in the chelate rings of tris-1,2-dimethyl-3-hydroxypyridinato–metal(III) complexes reveal significantly greater bond delocalisation than in the parent ligand. This is shown in Fig. 5, which also contains bond distances for our zinc(II) and lead(II) bis-ligand analogues. The difference between the two carbon–oxygen bond lengths in the chelate rings of $Zn(L1)_2$ is not significantly different from the analogous

[3] In the absence of a published ionic radius for Ru^{2+} we have used an estimated value of 0.88 Å, derived from published estimates for Ru^{3+} and Ru^{4+}; O–Ru–O angles are from Ref. [19].

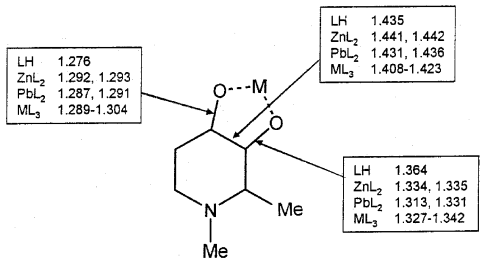


Fig. 5. Comparison of intra-ligand bond distances in the chelate rings of the bis-ligand complexes of zinc and of lead with analogous distances in tris-ligand metal(III) and in the free ligand, for the ligand 3-hydroxy-1,2-dimethyl-4-pyridinonate.

differences for tris-ligand metal(III) complexes, consistent with greater delocalisation in the chelated ligand than in the free ligand. However, the carbon–carbon bond distances in the chelate rings of the zinc(II) complex are, within their respective uncertainties, the same as in the free ligand, in contrast to its shortening in the chelate rings of the metal(III) complexes. Analogous comments can be made about the lead complex, whose binuclear structure seems to have no significant effect on ligand geometry.

The differences in bond length that we are seeking are comparable in magnitude to their uncertainties, but it would not be unreasonable to suggest that the pattern of carbon–oxygen and carbon–carbon bond distances in the chelate rings and in the free ligand is consistent with slightly greater π-delocalisation in the metal(II) complexes than in the free ligand, and again slightly greater in the metal(III) complexes. Unfortunately we have so far been unable to grow crystals of the zirconium(IV) complex $Zr(L1)_4$ of sufficient quality for X-ray diffraction investigation, while our structural data on related tin(IV) and titanium(IV) compounds [35] are not strictly comparable since the ligand in these cases is a 2-ethyl analogue of 1,2-dimethyl-3-hydroxypyridinate, and there are also chloride ligands on the metal in both cases. We are therefore unable to test our suggestion of a dependence of π-delocalisation on metal cation charge by comparison with metal(IV) analogues.

3.6. Hydrogen-bonding

Since the description of the first structure of a complex of this type, i.e. $Al(L1)_3 \cdot 12H_2O$ [36], it has been clear that this class of complex is extensively hydrogen bonded. The hydrogen bonding usually involves water–water, water–donor atom, and inter-ligand interactions. Several tris-ligand–metal(III) complexes of 3-hydroxy-4-pyranones and 3-hydroxy-4-pyridinones exist as dodecahydrates, which contain chains of water molecules which are hydrogen bonded both to each other and to ligand-oxygen-donor atoms. This creates a three-dimensional framework of water molecules with embedded molecules of complex, a type of clathrate structure.

Both our L1 complexes are heavily hydrated, if less so than the dodecahydrates just mentioned, with seven waters per metal ion in both the zinc and the lead complex. The waters of crystallisation in both these L1 complexes form extended chains, which are themselves hydrogen bonded to donor oxygen atoms. This is apparent from Figs. 2 and 3. It is noteworthy that the O–O distances between adjacent water molecules are essentially within the same range as the O–O distances between water and donor oxygen. The ranges are 2.714–2.824 and 2.701–2.815 Å, respectively.

By way of contrast, our zinc-maltol complex is lightly hydrated, with only 1.5 water molecules per zinc. All these water molecules are coordinated to zinc ions. The water in the five-coordinated zinc units is hydrogen bonded to ligand-oxygen in adjacent six-coordinated zinc units; the water in the latter is also coordinated to ligands in the former. As noted above, the layer structure of the zinc-maltol complex (shown in Fig. 1) consists of ABA sandwiches, A consisting of five-coordinated, B of six-coordinated complexes. There is strong A···B···A inter-layer hydrogen-bonding interaction, but there are no hydrogen-bonding interactions between adjacent ABA 'sandwiches'.

Supplementary data

All other crystallographic data may be obtained from the Cambridge Crystallographic Data Centre, where CIF files have been deposited (Deposition Numbers 129249 for **3**, 129250 for **4**, and 129251 for **5**).

Acknowledgements

We are grateful to Paul Hynes for a preliminary X-ray examination of bis-(1,2-dimethyl-3-hydroxy-pyridinato)-zinc(II).

References

[1] R.C. Hider, A.D. Hall, Progr. Med. Chem. 28 (1991) 41.
[2] J. Burgess, Transition Met. Chem. 18 (1993) 439.
[3] J.R. Duffield, D.R. Williams, Chem. Br. (1989) 375.
[4] C.C. Coombes, D.R. Williams, J. Inorg. Biochem. 43 (1991) 685.
[5] R.J. Gilbert, G.S. Ingram, J. Pharm. Pharmacol. 40 (1988) 399.
[6] C.A. Pasternak, G.M. Alder, C.L. Bashford, D. Mahadevan, J. Inorg. Biochem. 43 (1991) 394.
[7] P.J. Sadler, Adv. Inorg. Chem. 36 (1991) 1.
[8] R.J. Davie, J.D. Phillips, N.J. Birch, J. Inorg. Biochem. 43 (1991) 686.
[9] R.C. Hider, G. Kontoghiorghes, J. Silver, M.A. Stockham, GB Patent Application 2 148 896, 1985.
[10] G. Choux, R.L. Benoit, Bull. Soc. Chim. Fr. (1967) 2920.
[11] H.A. Waldron, in: H.A. Waldron (Ed.), Metals in the Environment, Chapter 6, Academic Press, New York, 1980.
[12] R.F. Labbé, Clin. Chem. 36 (1990) 1870.
[13] E.W. Lucas, The Book of Prescriptions (Beasley), 9th edn., Churchill, London, 1907.
[14] L.L. Camin, W.W. Layne, M.P. Liteplo, S.K. Nigam, P.A. Simard, J. Labelled Compd. Radiopharm. 16 (1979) 198.

[15] K. Kumar, M. Magerstädt, O.A. Gansow, J. Chem. Soc., Chem. Commun. (1989) 145.
[16] K. Abu-Dari, F.E. Hahn, K.N. Raymond, J. Am. Chem. Soc. 112 (1990) 1519.
[17] R.M. Maiorino, R.C. Dart, D.E. Carter, H.V. Aposhian, J. Pharmacol. Exp. Ther. 259 (1991) 808.
[18] J. Charalambous, A. Dodd, M. McPartlin, S.O.C. Matondo, N.D. Pathirana, H.R. Powell, Polyhedron 7 (1988) 2235.
[19] M.D. Fryzuk, M.J. Jonker, S.J. Rettig, Chem. Commun. (1997) 377.
[20] F.A. Cotton, R.L. Luck, K.-A. Son, Inorg. Chim. Acta 179 (1991) 11.
[21] A. Vedani, D.W. Huhta, J. Am. Chem. Soc. 112 (1990) 4759.
[22] H. Montgomery, E.C. Lingafelter, Acta Crystallogr. 16 (1963) 748.
[23] J. Podlahová, B. Kratochvil, J. Podhala, J. Hašek, J. Chem. Soc., Dalton Trans. (1985) 2393.
[24] S. Sen, S. Mitra, P. Kundu, M.K. Saha, C. Krüger, J. Bruckman, Polyhedron 16 (1997) 2475.
[25] J. Burgess, Metal Ions in Solution, Ellis Horwood, Chichester, 1978, Section 4.4.1.
[26] J. Burgess, Ions in Solution, Horwood, Chichester, 2nd ed., 1999, Chapter 3, p. 185, and References therein.
[27] J. Fawcett, R.D.W. Kemmitt, D.R. Russell, K. Singh, Acta Crystallogr., Sect. C53 (1997) 1422.
[28] A.J. Blake, R.O. Gould, J.M. Rawso, R.E.P. Winpenny, J. Chem. Soc., Dalton Trans. (1994) 2005, and References therein.
[29] J. Parr, Polyhedron 16 (1997) 551.
[30] A.F. Wells, Structural Inorganic Chemistry, Oxford, 5th ed., 1984, see especially pp. 1182–1189.
[31] D.L. Reger, Syn. Lett. (1992) 469.
[32] P.L. Jones, K.L.V. Mann, J.C. Jeffery, J.A. McCleverty, M.D. Ward, Polyhedron 16 (1997) 2435.
[33] W. Radecka-Paryzek, M. Gdaniec, Polyhedron 16 (1997) 3681.
[34] J. Burgess, J. Fawcett, S.A. Parsons, D.R. Russell, Acta Crystallogr., Sect. C50 (1994) 1911.
[35] S. Alshehri, J. Burgess, J. Fawcett, S.A. Parsons, D.R. Russell, Polyhedron 19 (2000).
[36] W.O. Nelson, S.J. Rettig, C. Orvig, J. Am. Chem. Soc. 109 (1987) 4121.

PERGAMON

www.elsevier.nl/locate/poly

Polyhedron 19 (2000) 137–145

POLYHEDRON

TCNE and TCNQ ligands as efficient bridges in mixed-valence complexes containing iron–cyclopentadienyl and other organometallic systems

Carlos Diaz [a,*], Alejandra Arancibia [b]

[a] *Departamento de Quimica, Facultad de Ciencias, Universidad de Chile, Casilla 653, Santiago, Chile*
[b] *Facultad de Quimica, P. Universidad Catolica de Chile, Casilla 306, Santiago, Chile*

Received 10 May 1999; accepted 4 October 1999

Abstract

Reaction between the π-accepting tetracyanoethene (TCNE) or tetracyano-*p*-quinodimethane (TCNQ) ligands and the π-electron-rich organometallic species $Cp(dppe)Fe^{+}$ results in the formation of the complexes $[\{Cp(dppe)Fe\}_n\{\eta^n\text{-TCNX}\}](PF_6)_n$ ($n=1$, 2 and 4). Infrared spectroscopy, magnetic moment measurements, electron-spin resonance (ESR) and cyclic voltammetry data indicate a net transfer of one π electron to the TCNX acceptor ligand. The polynuclear complexes have an intense intervalence electron transfer absorption band in the near-infrared region. The values for the intervalence parameters $\alpha=0.02$–0.06 and $V_{ab}=200$–$600\ cm^{-1}$ indicate that these complexes can be classified as class II according to Robin-Day. Estimation of the rate of electron transfer affords values in the order of $10^8\ s^{-1}$, which are compared and discussed with values estimated for other polynuclear systems containing TCNE and TCNQ ligands as bridges. The solvent effect on the intervalence transition follows Hush's prediction for highly polar solvents, thereby permitting evaluation of the reorganizational energy. For the related series $[\{Cp(dppe)Fe\}_n\text{–}(\mu\text{-X})](PF_6)_n$, the reorganization energy appears to depend mainly on the inner reorganization energy through changes to vibrational modes of the bridge. Reorganizational energy is not as important in determining the electron transfer rate as the activation energy, E_a. A linear relationship is found between the rate constant $\ln(k_{et})$ and the activation energy. These results can be discussed within the Marcus theory of electron transfer. The fast and efficient electron transfer between the metal fragments is discussed using molecular orbital arguments. ©2000 Elsevier Science Ltd All rights reserved.

Keywords: Hush theory; Iron complexes; Mixed valence; TCNE complexes; TCNQ complexes

1. Introduction

Tetracyanoethene (TCNE) and the related tetracyano-*p*-quinodimethane (TCNQ) are molecules that present interesting acceptor properties, which are associated with their unusual electrical and magnetic behaviour [1–4]. TCNE and TCNQ can act as σ ligands (via the nitrile-N lone pair) as a π-type arrangement (via the C=C olefinic bond in TCNE) or 'free' (ion pair) mode II (Fig. 1) [5].

Many coordination compounds with considerable metal ligand delocalization have been reported [6–10]. Several special features make such compounds interesting for practical purposes: (1) intense charge-transfer absorption bands in the visible and near-infrared regions can make such systems useful as dyes for information storage using optic fibre and diode laser [11,12]; (2) the communication between metal-connected ligands and/or ligand-connected metals has received attention in the area of low-dimensional polymers with electron-propagating capabilities and within the concept of 'molecular electronics' [13]; (3) the existence of several close-lying and easily accessible redox transitions renders

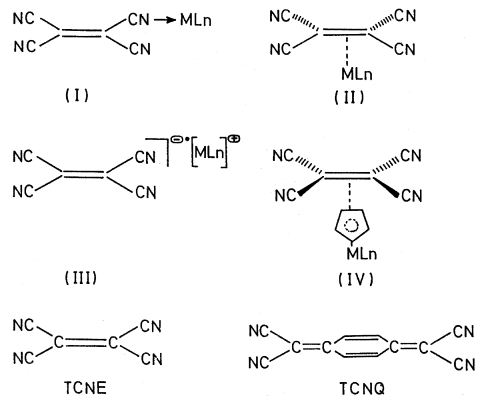


Fig. 1. Coordination modes of TCNE and TCNQ ligands.

* Corresponding author. Tel./fax: +56-2-271-3888

0277-5387/00/$ - see front matter ©2000 Elsevier Science Ltd All rights reserved.
PII S0277-5387(99)00331-9

these compounds suitable as 'electron reservoirs', especially because small structural changes during the redox transitions of extensively delocalized systems favour rapid electron transfer due to the small reorganization barriers [14–16].

Non-reduced TCNE and TCNQ are rather poor ligands for metal centres; however, on electron uptake by back-donation or full reduction with one or two electrons, they can bind metal fragments via modes I–IV.

In connection with points (2) and (3), we report here the preparation of the complexes $[\{Cp(dppe)Fe\}_n\{\eta^n\text{-TCNX}\}](PF_6)_n$ and the study of the intermetallic electron transfer in the following polynuclear systems:

$[Cp(dppe)Fe(TCNE)]PF_6$ (**1**)
$[\{Cp(dppe)Fe\}_2(TCNE](PF_6)_2$ (**2**)
$[Cp(dppe)Fe(TCNQ)]PF_6$ (**3**)
$[\{Cp(dppe)Fe\}_4(TCNQ](PF_6)_4$ (**4**)

While several di- and polynuclear complexes with extensive π delocalization including the metal centre have been reported [6–10], no detailed quantitative studies on the electron transfer via TCNE and TCNQ bridges have been reported.

We have selected the fragment $Cp(dppe)Fe^+$ because its electron richness permits efficient electronic delocalization [11–21], it binds strongly to nitrogen cyanide containing ligands [22–25] and the iron in the fragment is electrochemically active [11–21].

2. Results and discussion

2.1. Mononuclear complexes

$Cp(dppe)FeI$ reacts with an excess of TCNE or TCNQ in the presence of NH_4PF_6 or $TlPF_6$ in CH_3OH or CH_2Cl_2, respectively, to give dark black–green solids whose elemental analysis and spectroscopic properties agree with the mononuclear formulation $[Cp(dppe)Fe(TCNX)]PF_6$. As observed for another d^5 paramagnetic mononuclear complex $[(C_5R_5)Mn(CO)_2(\eta^1\text{-TCNX})]$ and others [8–10], magnetic resonance investigations of complexes **1** and **3** have been hampered by the paramagnetism of the complexes. The dark-black colour is typical of complexes of the type $Cp(dppe)Fe^{III}$ [19–21]. Additional evidence for the reduction of the TCNX ligand is provided by from IR spectra [5] (see Table 1). As for other monodentate TCNX complexes, three ν_{CN} bands were observed [26] as expected for the non-symmetrically bound ligands [5,27–33]. The ν_{CN} IR bands are quite intense and shifted to lower wavenumbers compared to those of the free, non-reduced ligands. This indicates nitrile-N coordination and sizeable back-donation of π electron density from the metal fragments to the TCNX ligand [5,27–33]. The ν_{CN} wavenumber of the complexes lies between those of the free anion radicals and the values found for the dianions.

Thus, the mononuclear complexes are distinguished from polynuclear complexes and from the free ligands as the highest intensity is displayed by the low-energy band for the polynuclear systems [6–10]. In the IR spectra of complexes **1** and **3** the highest intensity corresponds to the high-energy band. IR bands for the $Cp(dppe)Fe^+$ fragment appear normally [34]; the main values are displayed in Table 1.

2.1.1. Magnetic measurements

Magnetic moments for complexes **1** and **3** are typical values for $[Cp(dppe)FeX]^+$ complexes [19,20], corresponding to one unpaired electron in low spin Fe^{III}. The unpaired electron arising from the radical $TCNX^-$ could not be observed due to spin coupling between them in solid state.

Table 1
IR data for complexes **1**–**4** [a]

Complex	$\nu(C_5H_5)$ [b]	ν(dppe) [c]	$\nu(PF_6)$	ν(CN)	
				Solid	Solution
TCNE				2257	2251
				2220	2210
$[Cp(dppe)Fe(TCNE)]PF_6$ (**1**)	1098	696	843	2171	2200
				2059	2136
				1995	2065
					1994
$[\{Cp(dppe)Fe\}_2(TCNE)](PF_6)_2$ (**2**)	1106	706	847	2197(sh)	2197(sh)
				2173	2173
TCNQ				2223	2223
$[Cp(dppe)Fe(TCNQ)]PF_6$ (**3**)	1094	694	847	2173	2185
				2128	2129
				2067	
$[\{Cp(dppe)Fe\}_4(TCNQ)](PF_6)_4$ (**4**)	1096	697	838	2099	2114
				2032	2035

[a] In KBr pellets, unless other indicated; data given in cm^{-1}.
[b] δ(C–H) bending in-plane vibration.
[c] δ(C–H) bending out-of-plane vibration.

Table 2
Long-wavelength absorption maxima λ (nm), magnetic and ESR data for TCNX complexes

Complex	λ_{max} [a] (CH_2Cl_2)	μ (eff) [c]	ESR [c]: g_1, g_2, g_3
1	545 (1187), 619 (1245)	1.8	2.0189; 2.1912; 2400
2	441 [b] (2262), 512 (1769) [b], 1073 (969)	0.7	1.9880; 2.2086; 2.420
3	498 (1189)	1.9	1.9883; 2.0095; 2.2439
4	498 (5741), 1008 (14300)	2.5	1.9940; 2.0393; 2.2417

[a] Molar extinction coefficients (M^{-1}) are given in parentheses.
[b] Shoulder.
[c] In solid state.

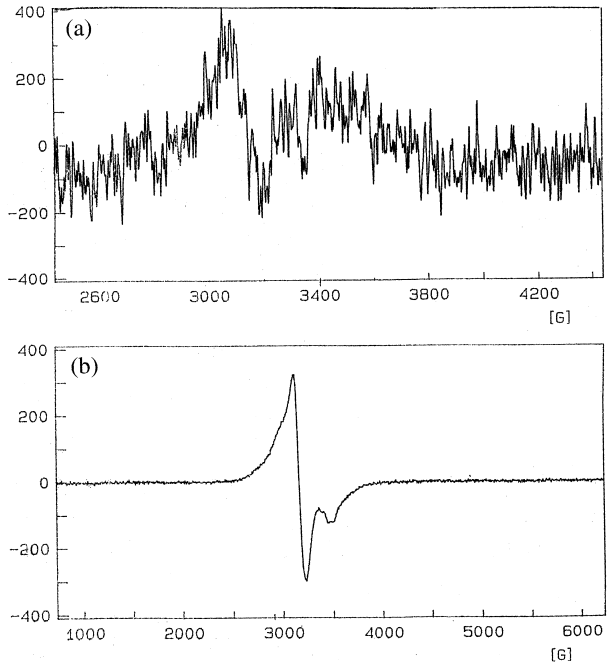


Fig. 2. ESR spectra of complex **1** in CH_2Cl_2 solution (a) and in solid state (b) at room temperature.

The ESR data discussed below are also in agreement with this argument. Values are shown in Table 2.

2.1.2. ESR spectra

The ESR spectra of mononuclear complexes **1** and **3** at room temperature in solid state exhibit one single signal, characteristic of $Cp(dppe)Fe^{III}X$ complexes [35–37]. Three well-separated features corresponding to the three components of the **g** tensor — expected for low symmetry pseudo-octahedral piano–stool complexes — were observed (see Fig. 2). Data are shown in Table 2. This indicates that the signal observed in both cases may correspond to the unpaired electron centred on the metal. The signal corresponding to the $TCNE^-$ and $TCNQ^-$ radical ligands was not observed, probably due to intramolecular spin coupling between the $TCNX^-$ molecules in the solid state. Consistent with this, in CH_2Cl_2 solution the ESR spectra of **1** and **3** exhibit several complex signals with various features (see Fig. 2), which presumably include the signal of $Cp(dppe)Fe^{III}L$ as well as the signals of $TCNX^-$. As found for other $LnM(\eta^1\text{-}TCNX^-)$ complexes [38,39], owing to the lowered symmetry, 16 (four different nitrogen) or 1296 (four different nitrogen and four different ^1H) lines for TCNE and TCNQ, respectively, could be observed.

2.1.3. Cyclic voltammetry

Mononuclear systems are reduced at more negative potentials than TCNX ligands (Table 3). This is a consequence of metal-to-ligand electron transfer in the ground state, which leaves either the single reduced ligand or the oxidized metal fragment available for reduction at relatively negative potentials.

Oxidation of the complexes is almost always irreversible; it may thus be safely assumed that these are metal-based. Thus peak potentials of about 0.7–0.8 V versus SCE

Table 3
Electrochemical data [a] for TCNX ligands and their complexes

Compound	$E^{ox}_{1/2}$ (metal)	E^{red}_1 (0/1−) [d]	E^{red}_2 (−/2−) [d]
TCNE		0.18	−0.85
$[Cp(dppe)Fe(TCNE)]PF_6$ (**1**)	0.83 [b]	−0.61	−0.95
$[\{Cp(dppe)Fe\}_2(TCNE)](PF_6)_2$ (**2**)	0.89, 0.70 [c]	−0.53	−0.88
TCNQ		0.25	−0.31
$[Cp(dppe)Fe(TCNQ)]PF_6$ (**3**)	0.78 [b]	−0.49	−0.70
$[\{Cp(dppe)Fe\}4(TCNQ)](PF_6)_4$ (**4**)	0.93, 0.75 [c]	−0.65	−0.80

[a] In CH_2Cl_2–0.1 M Bu_4NPF_6; potential (in V) vs. SCE.
[b] Anodic peak potential are given for irreversible oxidation processes.
[c] Two very near quasi-reversible waves were observed.
[d] Quasi-reversible waves.

(saturated calomel electrode) for complexes [Cp(dppe)-Fe(nitrile)]PF_6 have been observed [22–25].

2.1.4. Electronic spectroscopy

Complexes **1** and **3** exhibit intense bands at about 545 and 619 nm, which are typical of the absorption behaviour of [Cp(dppe)Fe^{III}L]$(PF_6)_2$ complexes [17–21] (Fig. 3). Table 2 summarizes the data obtained. No absorption was observed above 700 nm. This constitutes strong evidence for the Fe^{III}–($TCNX^-$) state because Fe^{II}–NCR complexes exhibit only one band at about 450 nm [40].

2.2. Polynuclear complexes

TCNE or TCNQs react with an excess of Cp(dppe)FeI in the presence of NH_4PF_6 or $TlPF_6$ in CH_3OH or CH_2Cl_2, respectively, to give black–green solids of composition {[Cp(dppe)Fe]$_2$TCNE}$(PF_6)_2$ and {[Cp(dppe)Fe]$_4$-TCNQ}$(PF_6)_4$. Similarly to complexes **1** and **3**, NMR studies are precluded due to the paramagnetism of the complexes. In agreement with this, the related complex [$Ru(NH_3)$]$_4$–(μ-TCNX)]$^{10+}$ is also paramagnetic [7]. No suitable crystals were obtained for X-ray structural determination of the complexes.

2.2.1. Infrared spectra

As pointed out by Kaim [8] and others [28], for [MLn]$_n$–(TCNX) complexes some information about the structure of the complexes can be obtained from IR spectroscopy. The number and the pattern of bands observed by IR depend on the symmetry of the complexes; for the binuclear systems [MLn]$_2$–(μ-TCNX) three isomers can be expected: 1,2-*trans* (C_{2h}), 1,2-*cis* (C_{2v}) or 1,1′ (C_{2v}). According to their symmetry, two or four bands could be observed for the isomers 1,2-*trans*, 1,1-*cis* or 1,2-*cis*, respectively. This is consistent with IR data for [MLn]$_n$–(μ-TCNX) complexes having a 1,2-*trans* geometry: [$(PPh_3)_2$(CO)Ir]$_2$TCNE [29], (2176(m), 2097 vs); [L′L_2Cu(μ-TCNE)CuL_2]$_n$ [30], (2190, 2147); [$Rh_2(O_2CCF_3)_4$]$_2$TCNE [31], (2230, 2210); [Tl(18-crown-6)TCNQ] [32], (2181, 2154); [$Ru(PPh_3)_2$]$_2$TCNQ [33] (2170, 2140).

In agreement with this, the binuclear complex **2** exhibits two bands (one as a shoulder), suggesting the 1,2-*trans* configuration for this complex. This is the favoured configuration for bulky fragments [5] such as CpFe(dppe). As expected for tetranuclear complexes (with a slightly perturbed D_{2h} symmetry), two bands are observed for complex **4**. Thus complexes [$Ru(NH_3)_5$–(μ_4-TCNX)] and [C_5Me_5–$Mn(CO)_2$]$_4$–(μ_4-TCNX) exhibit bands at: 2163, 2121 cm^{-1} for the Ru–TCNE complex; 2153, 2096 cm^{-1} for the Ru–TCNQ complex; 2160, 2110 cm^{-1} for the Mn–TCNE complex; and 2170, 2105 cm^{-1} for the Mn–TCNQ complex. As observed for similar $(MLn)_2TCNX^{n+}$ and $(MLn)_4$-$TCNX^{n+}$ complexes the highest intensity is displayed by the low-energy band, behaviour that is characteristic of polynuclear systems [6–10].

2.2.2. Magnetic measurements

The low magnetic moment for the binuclear complex **2** could be due to the delocalization of the unpaired electron between the two iron atoms, which couple antiferromagnetically with the unpaired electron of the $TCNE^-$ ligand. On the other hand the tetranuclear complex **4** exhibits the highest magnetic moment, which could be due to the complex interaction of several paramagnetic Fe^{III} centres. Similar magnetic moments have been observed for tetranuclear {[Cp*Mn(CO)$_2$]$_4$–(μ-TCNE)} complexes [6–10].

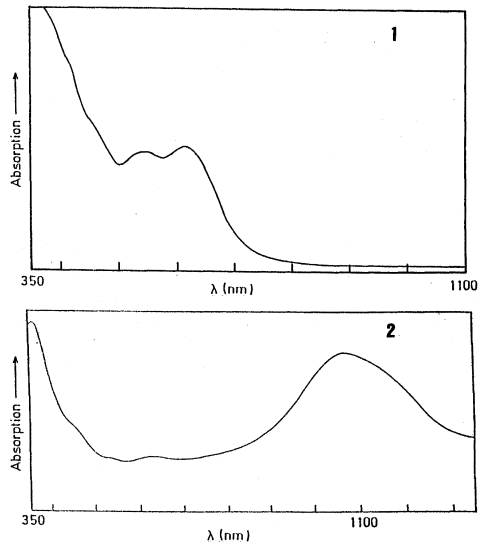


Fig. 3. Electronic absorption spectra of complexes **1** and **2** in CH_2Cl_2 solution.

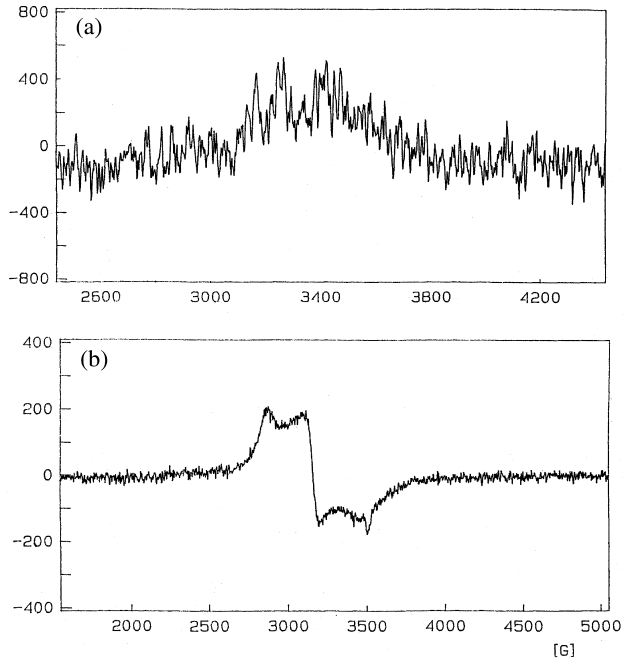


Fig. 4. ESR spectra of compound **2** in CH_2Cl_2 solution (a) and in solid state (b) at room temperature.

Table 4
Intervalence band parameters and derived electronic coupling parameter for the mixed-valence complexes [a]

Complex	ν_{max} (cm^{-1})	ε ($M^{-1}\,cm^{-1}$)	$\Delta\nu_{1/2}$ (cm^{-1})	α	d (Å)	V_{ab} (cm^{-1})	E_a (cm^{-1})	E_m (cm^{-1})	K_{th} (seg^{-1})
2	9320	968	1635	0.027	9.9	253	2330	9320	2.18×10^{8}
4	9978	5960	3159	0.063	14.2	625	2480	9921	1.22×10^{8}

[a] In CH_2Cl_2 solution.

2.2.3. ESR spectra

The ESR spectrum of compound **2** in solid state shows a broad line exhibiting recognizable anisotropic features (Fig. 4), behaviour typical of delocalized mixed-valence systems [35–37]. The spectrum of compound **4** displays a similar pattern with the **g** factors summarized in Table 3. As observed for other multinuclear Ru–TCNX compounds [7], the ESR signal for the radical $TCNX^-$ ligand was not observed. In CH_2Cl_2 solution, similarly to the mononuclear complexes, the signal of the iron centre as well as the complex signal of the organic $TCNX^-$ radical were observed (see Fig. 4).

2.2.4. UV–Vis spectra

The UV–Vis spectra of complexes **2** and **4** revealed, in addition to absorptions typical for $Cp(dppe)Fe^{III}L$ [17–21] and $Cp(dppe)Fe^{II}L$ [40] chromophores, a new absorption band at about 1100 nm. The electronic spectrum of compound **2** in CH_2Cl_2 is shown in Fig. 3.

These observations coupled with data on similar $Cp(dppe)Fe^{III}$–L–$Fe^{II}(dppe)Cp$ systems [11–21] allow us to assign this near-IR band to an intervalence transfer transition. Thus, on reducing the mixed valence complexes **2** and **4** with Red Al, sodium bis(2-methoxyethoxy)aluminium hydride, the intervalence absorption disappears.

2.2.5. Cyclic voltammetry

The reduction potential of the polynuclear complexes with TCNE and TCNQ (Table 3) are more negative than those of the corresponding free ligands; this is consistent with the electron transfer involved in the formation of the complexes, leaving the ligands as $TCNX^-$ or $TCNX^{2-}$.

Table 5
Electronic interaction parameter and electron transfer rate constants for **2**, **4** and other polynuclear mixed-valence complexes containing TCNE and TCNQ bridges

Complexes	V_{ab} (cm^{-1})	k_{et} (seg^{-1})
$[\{Cp^*(CO)_2Mn\}_2(\mu\text{-TCNE})]$ [a]	1302	1.27×10^{10}
$[\{(NH_3)_5Ru\}_4(\mu\text{-TCNE})](PF_6)_8$ [a]	2980	2.7×10^{8}
$[\{(NH_3)_5Ru\}_4(\mu\text{-NCC(t-Bu)CN})]$ [a]	1256	1.26×10^{9}
$[\{(NH_3)_5Ru\}_4(\mu\text{-TCNQ})](PF_6)_8$ [a]	1860	2.1×10^{9}
$[\{Cp(dppe)Fe\}_2(\mu\text{-TCNE})](PF_6)_2$ [b]	253	2.2×10^{8}
$[\{Cp(dppe)Fe\}_4(\mu\text{-TCNQ})](PF_6)_4$ [b]	625	6.2×10^{8}

[a] Determined using Eq. (4) and literature data [11–16,27–33] for the intervalence transition.
[b] This work.

$$(Cp(dppe)Fe^{II})^+ + TCNX \rightarrow (Cp(dppe)Fe^{III}\text{–}[TCNX])^{\bullet -} \quad (1)$$

In the oxidation region of the metal fragment, the cyclic voltammogram exhibits two non-well-defined waves which probably involve the oxidation of the metal centres. The difference in peak potential indicates a considerable coupling between the metal centres. From the wave separation, the comproportionation constant, K_c, relative to the following equilibrium:

$$Fe^{II}\text{–}TCNX\text{–}Fe^{II} + Fe^{III}\text{–}TCNX\text{–}Fe^{III} \leftrightarrow 2Fe^{II}\text{–}TCNX\text{–}Fe^{III} \quad (2)$$

can be computed as $K_c = 1626$ and 1202 for complexes **2** and **4**, respectively. The relatively high K_c values indicate a considerable electronic interaction between the iron atoms.

2.2.6. Electronic interaction in the mixed-valence species

Information about the degree of metal–metal interaction in the mixed-valence complexes can be obtained from the intervalence absorption band using the Hush formalism [11–16,41–45]. According to this, the degree of delocalization parameter is given by the formula:

$$\alpha = \frac{(4.2\times10^{-4})\,\varepsilon_{max}\Delta\nu_{1/2}}{\nu_{max}d^2} \quad (3)$$

where $\Delta\nu_{1/2}$ is the bandwidth at half-maximum (cm^{-1}), ε_{max} is the maximum extinction coefficient, ν_{max} is the band position (cm^{-1}) and d is the metal–metal distance in Å. Because no X-ray determination is available for complexes **2** and **4**, the metal–metal distance was estimated from structural data for similar complexes [46–48]. The α values shown in Table 4 indicate a class II Robin-Day system.

On the other hand the electronic coupling term, V_{ab}, can be determined by the following formula [41–45]:

$$V_{ab} = \alpha^{1/2}\nu_{max} \quad (4)$$

The calculated values, displayed in Table 4, indicate a more or less strong metal–metal coupling, although somewhat less than for the cyanide ligand. From intervalence transfer transition data for other organometallic systems, the interaction parameter V_{ab} was estimated using Eq. (4). Values shown in Table 5 for other complexes indicate that metallic fragments such as $(NH_3)_5Ru$ permit a stronger interaction than the iron fragment, which can be due to steric hindrance of the $Cp(dppe)Fe^+$ arising from the bulky dppe [46]. From data

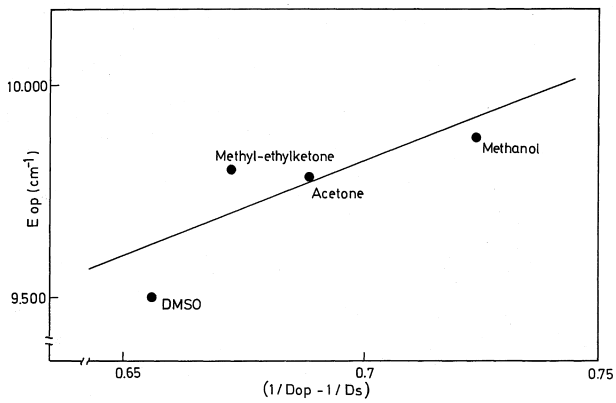


Fig. 5. Plot of intervalence absorption energy for E_{op} vs. $(1/D_{op}-1/D_s)$.

in Table 5, it can also be concluded that the interaction between the metal centres is highly dependent on the nature of the organometallic fragment.

An approximate estimation of the rate of electron transfer between the metal centres in complexes **2** and **4** can be made using the expression [41–45]:

$$k_{th}=\left[\frac{2\pi(V_{ab})^2}{h}\right]\left[\frac{\pi}{KTE_m}\right]^{1/2}\left[e\left(-\frac{E_a}{RT}\right)\right] \quad (5)$$

where $E_m=E_{op}$ and $E_a=[(E_m)^2/4E_m]$. E_m, the total reorganization energy, has two components: the outer-reorganization energy E_o, and the inner-reorganization energy E_i; thus $E_m=E_i+E_o$.

Although these equations differ in absolute values from those measured experimentally, comparison for a related series of compounds is valid [18]. The values about $10^8\ s^{-1}$ calculated for compounds **2** and **4** indicate a fast electron transfer between the iron atoms. Similar rates are obtained using Eq. (5) for other organometallic systems, as can be seen in Table 5. The similar k_{et} values, notwithstanding the different organometallic fragment, mean that the nature of the bridge is most important in determining the electron transfer rate. It is interesting to compare the TCNX ligands as bridges with the cyanide bridging ligand for which electron-transfer rates of $10^4\ s^{-1}$ were estimated in the mixed-valence complexes $[Cp(dppe)Fe–CN–MLn]PF_6$ (MLn = $Cp(dppe)Fe$, $Mn(CO)_2(dppm)P(OPh)_3$) [18].

The solvent effect on the intervalence transition gives information about the reorganization energy arising from rearrangements of the inner and outer coordination spheres [49,50]. With the assumption of a dielectric continuum model, the dependence of E_{op} on solvent polarization is given by:

$$E_{op}=E_i+E_o \quad (6)$$

$$E_{op}=E_i+e^2\left(\frac{1}{2a_1}+\frac{1}{2a_2}-\frac{1}{d}\right)\times\left(\frac{1}{D_{op}}-\frac{1}{D_s}\right)$$

The intercept of a plot of E_{op} versus $(1/D_{op}-1/D_s)$ for several solvents affords the E_i values (Fig. 5 and Table 6). From Eq. (6) the outer-sphere reorganizational parameters E_o can be estimated. Values for complexes **2** and **4** and for other complexes containing the CpFe(dppe) moiety are shown in Table 6. Some comments can be made from this data: comparing the E values for complexes **2** and **4**, mostly larger variations on the outer-reorganizational parameters than for the inner-reorganization values are observed (differences of 21% on E_i and of 43% on E_o are observed). This can be explained by the similar metal–ligand vibration modes involved in the electron-transfer process. Attention must be drawn to the high inner-reorganization energies involved in electron-transfer events in the complex $\{[Cp(dppe)]_2–(\mu\text{-}S–C_5H_5N)\}(PF_6)_2$. This may be due to an enhanced change on vibrational modes of the thiopyridine ligand upon electron transfer.

It is interesting to note that, although the complexes displayed in Table 7 all have the same fragment CpFe(dppe), the reorganization energy is very different. For instance, compare $E_m=12\,697\ cm^{-1}$ for $[CpFe(dppe)]_2–(\mu\text{-}S–C_5H_5N)](PF_6)_2$ [21] with $E_m=6038\ cm^{-1}$ for $\{[CpFe(dppe)]_2–\mu\text{-}CN\}PF_6$ [18].

This means that, for this series, the reorganizational energy is highly dependent on some properties of the bridge ligand. Because the data in Table 7 indicate that the main contribution to the reorganizational energy arises from the inner-reorganization energy, the observed variations E_m might stem from changes in the vibrational mode of the bridging ligand.

Recent studies of electron transfer in the mixed-valence systems $[(NC)_5M^{II}–CN–Ru^{III}(NH_3)_5]^-$ (M = Fe or Ru)

Table 6
Solvent dependence of the intervalence transition in complexes **2** and **4**

Complex	Solvent	E_{op} (cm^{-1})	$(1/D_{op}-1/D_s)$	E_i (cm^{-1})	E_o (cm^{-1})	E_m
2	Dimethylsulfoxide (DMSO)	9128	0.6551	6621	2587	9128
2	Acetone	9238	0.6886			
2	MeOH	9208	0.7234			
2	CH_2Cl_2	9320	0.5899			
4	DMSO	9501	0.6550	8394	1448	9501
4	MeOH	9872	0.7234			
4	Ethyl methyl ketone	9799	0.6722			
4	Acetone	9780	0.6886			
4	CH_2Cl_2	9978	0.5899			

Table 7
Solvent reorganization energies [a] for complexes **2**, **4** and other related complexes containing the moiety CpFe(dppe)$^+$

Complex	E_i (cm^{-1})	E_o (cm^{-1})	E_m (cm^{-1})
[{CpFe(dppe)}$_2$–(μ-TCNE)](PF$_6$)$_2$	8394	1448	9842
[{CpFe(dppe)}$_4$–(μ-TCNQ)](PF$_6$)$_4$	6621	2587	9208
[{CpFe(dppe)}$_2$–(μ-S–C$_5$H$_4$N)](PF$_6$)$_2$	12470	227	12697
[{CpFe(dppe)}$_2$–(μ-CN)]PF$_6$	2096	3942	6038

[a] Values of E_m, E_i and E_o were determined from E_{op} vs. $(1/D_{op}-1/D_s)$ plots. Values for complexes other than complexes **2** and **4** were taken from [11–21].

have shown that a large part of the reorganization energy comes from modes assigned to the bridging ligand [51,52].

Comparing the reorganizational values with electron-transfer rates it can be observed that there does not exist a correlation between them. According to semiclassical electron-transfer theory [41–45], electron-transfer reaction rates (k_{et}) are governed by three parameters (Eq. (5)): (1) the electronic coupling (V_{ab}) between reactants and products, (2) the free-energy change for the reaction (ΔG°) and (3) the total reorganization energy.

From Tables 5 and 7 it can be seen that no correlation exists between k_{et} and the electron coupling or the reorganization energy. However, the electron-transfer rate appears to be related to ΔG° through the relation $E_a=(E_{op})^2/(E_{op}-\Delta G^\circ)$. In fact, a linear correlation between $\ln(k_{th})$ and E_a holds, as shown in Fig. 6. Furthermore, this expression has the shape of the most general and simple relationship between k_{et} and E_a, the classical Marcus equation $k_{et}=Ae(-E_a)$ [41–45]. We believe that this is a remarkable example where the general electron rate theory of Marcus works well in mixed-valence complexes.

*2.3. Nature of the electron transfer in binuclear complexes **2** and **4***

The efficient and fast electron transfer between the metal centres in complexes **2** and **4** can be explained by considering the molecular orbitals involved in the Fe–N interaction. These can be adequately established from an orbital interaction diagram built from the molecular orbital (MO) fragments of CpFe(dppe)$^+$ and nitriles [53–56]. As shown in Fig. 7, the HOMO of complexes involves a π-delocalized molecular orbital throughout the Fe–TNCX–Fe moiety.

3. Experimental

All operations were conducted under a pure dinitrogen or argon atmosphere using standard Schlenk and glovebox techniques. Solvents were dried according to established protocols and degassed prior to use. Unless otherwise specified, reagents were obtained from commercial supplies and used as received. Magnetic measurements were carried out by Gouy's method at room temperature using a Johnson Matthey magnetic susceptibility balance with tetrathiocyanate cobaltate(II) as calibrant balance. ESR spectra were recorded on Bruker ECS 106 spectrometer. FTIR spectra were recorded on an FT–IR Perkin Elmer 2000 spectrophotometer. Electronic absorption spectra were recorded on a Shimadzu UV 160. Cyclic voltammetry was performed on a three-electrode configuration (glassy-carbon working electrode, satured calomel as reference) with 0.1 M solution of NH_4PF_6 as electrolyte support in CH_2Cl_2. Cp(dppe)FeI was prepared as previously reported [22–25].

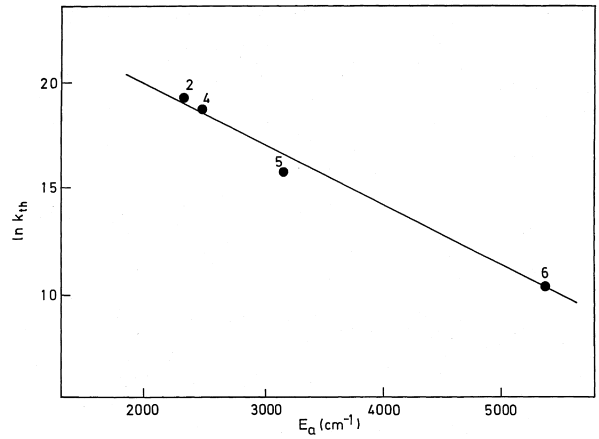


Fig. 6. Estimated electron-transfer rates vs. activation energy E_a for complexes **2**, **4**, {[CpFe(dppe)]$_2$–(μ-S–C$_5$H$_4$N)}(PF$_6$)$_2$ (**5**) and {[CpFe(dppe)]$_2$–(μ-CN)} PF$_6$ (**6**).

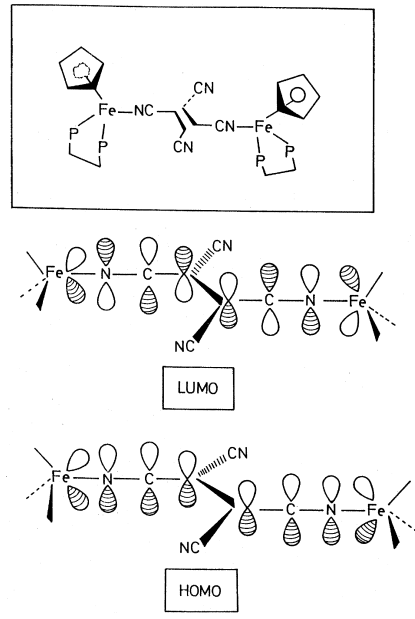


Fig. 7. Proposed HOMO-LUMO of complexes **2** and **4**.

3.1. [Cp(dppe)Fe–(TCNE)]PF_6 (**1**)

A solution of Cp(dppe)FeI (70 mg, 0.10 mmol) in 20 ml of CH_3OH was added dropwise over 0.03 g, 0.23 mmol of $C_2(CN)_4$ and 0.03 g, 0.18 mmol of NH_4PF_6. The mixture was stirred at room temperature for 24 h. The reaction mixture was then evaporated to dryness, and the solid residue redissolved in 30 ml and the solution filtered through Celite and evaporated to about 15 ml. After this a black solid was formed, which was decanted and washed twice with hexane–ether and dried in vacuo. Yield: 28 mg (29%). *Anal*. Calc. for $C_{41}H_{29}F_6N_4P_3Fe \cdot CH_2Cl_2$: C, 52.08; H, 3.54; N, 6.38. Found: C, 51.73; H, 4.02; N, 5.90%.

3.2. [{Cp(dppe)Fe}$_2$–(μ-TCNE)]$(PF_6)_2$ (**2**)

To a solution of Cp(dppe)FeI, 0.15 g, 0.23 mmol in 10 ml of CH_3OH, was added dropwise slowly over 0.015 g, 0.11 mmol of $C_2(CN)_4$ in 20 ml of CH_3OH in the presence of NH_4PF_6 (0.03 g, 0.18 mmol). The mixture was stirred at room temperature for 24 h and then concentrated to dryness under reduced pressure. The solid was dissolved in CH_2Cl_2 (30 ml) and filtered through Celite. The solution was concentrated in vacuum to about 15 ml and the black solid precipitated was washed twice with hexane–ether and dried in vacuo. Yield: 0.045 g (28%). *Anal*. Calc. for $C_{72}H_{58}F_{12}N_8P_2Fe_2$: C, 62.26; H, 4.4; N, 5.0. Found: C, 61.7; H, 5.0; N, 5.0%.

3.3. [Cp(dppe)Fe–(TCNQ)]PF_6 (**3**)

A solution of Cp(dppe)FeI, 0.15 g, 0.23 mmol in 10 ml of CH_3OH, was added dropwise over 0.07 g, 0.34 mmol of TCNQ and in the presence of NH_4PF_6 (0.06 g, 0.36 mmol). Following the procedure outlined for separation and purification of compound **1**, 0.2 g of black solid was obtained. Yield: 68%. *Anal*. Calc. for $C_{43}H_{33}F_6N_4PFe \cdot CH_2Cl_2$: C, 55.43; H, 3.6; N, 5.8. Found: C, 54.3; H, 3.0; N, 4.8%.

3.4. [{Cp(dppe)Fe}$_4$–(μ-TCNQ)]$(PF_6)_4$ (**4**)

To a solution of Cp(dppe)FeI, 0.15 g, 0.23 mmol in 20 ml of CH_3OH, was added dropwise slowly over 0.03 g, 0.14 mmol of TCNQ in 20 ml of CH_3OH in the presence of NH_4PF_6 (0.04 g, 0.25 mmol). The mixture was stirred at room temperature for 24 h. Separation and purification procedures similar to that for compound **3** afforded a black powder. Yield: 0.2 g (48%). *Anal*. Calc. for $C_{136}H_{120}F_{24}N_4P_4Fe_4 \cdot 2CH_2Cl_2$: C, 57.09; H, 4.2; N, 1.96. Found: C, 55.39; H, 4.26; N, 2.6%.

3.5. Preparation of complexes **1–4** using $TlPF_6$ as halide abstractor and CH_2Cl_2 as solvent

Similar compounds were obtained using the following typical procedure.

3.5.1. [Cp(dppe)Fe–(TCNE)]PF_6

A mixture of 0.15 g, 0.25 mmol of Cp(dppe)FeI, 0.04 g, 0.31 mmol of TCNE and 0.16 g, 0.45 mmol of $TlPF_6$ (**caution**: thallous salts are very poisonous and should be handled with care) in 30 ml of CH_2Cl_2 was stirred at room temperature for 3 days. The solution was then filtered through Celite and the filtrate was removed in vacuo to about 15 ml. The black solid precipitated was isolated by decantation and washed twice with n-hexane–ether, and dried in vacuo to give 0.12 g, 60% yield.

Acknowledgements

Financial support of this work from D.I.D., Universidad de Chile (Project 98-018), is gratefully acknowledged.

References

[1] K.R. Dunbar, Angew. Chem., Int. Ed. Engl. 35 (1996) 1659.
[2] J.S. Miller, A.J. Epstein, Angew. Chem. 106 (1994) 399.
[3] J.S. Miller, A.J. Epstein, Angew. Chem., Int. Ed. Engl. 33 (1994) 385.
[4] J.S. Miller, Adv. Mater. 6 (1994) 322.
[5] W. Kaim, M. Moscherosch, Coord. Chem. Rev. 129 (1994) 157.
[6] E. Waldhor, W. Kaim, M. Lawson, J. Jordanov, Inorg. Chem. 36 (1997) 3248.
[7] M. Moscherosch, E. Waldhor, H. Binder, W. Kaim, J. Fiedler, Inorg. Chem. 34 (1995) 4326.
[8] R. Gross-Lannert, W. Kaim, B. Olbrich-Deussner, Inorg. Chem. 29 (1990) 5046.
[9] R. Gross-Lannert, W. Kaim, Angew. Chem., Int. Ed. Engl. 26 (1987) 251.
[10] W. Kaim, T. Roth, B. Olbrich-Deussner, R. Gross-Lannert, J. Jordanov, E.K.H. Roth, J. Am. Chem. Soc. 114 (1992) 5693.
[11] J. Fabian, K. Zahradnik, Angew. Chem. 101 (1989) 693.
[12] J. Fabian, K. Zahradnik, Angew. Chem., Int. Ed. Engl. 28 (1989) 677.
[13] D. Astruc, Acc. Chem. Res. 30 (1997) 383.
[14] D. Astruc, Electron Transfer and Radical Processes in Transition-Metal Chemistry, VCH, New York, 1995.
[15] D. Astruc, Acc. Chem. Res. 12 (1986) 377.
[16] M.H. Desbois, D. Astruc, J. Guillin, F. Varret, A.X. Trautwein, G. Villaneuve, J. Am. Chem. Soc. 111 (1989) 5800.
[17] G. Barrado, G.A. Carriedo, C. Díaz, V. Riera, Inorg. Chem. 30 (1991) 4416.
[18] C. Díaz, A. Arancibia, Inorg. Chim. Acta 269 (1998) 246.
[19] C. Díaz, C. Leal, N. Yutronic, J. Organomet. Chem. 516 (1996) 59.
[20] C. Díaz, Polyhedron 16 (1997) 999.
[21] C. Díaz, A. Arancibia, unpublished results.
[22] C. Díaz, N. Yutronic, Synth. React. Inorg. Met.-Org. Chem. 27 (1997) 119.
[23] C. Díaz, R. Latorre, Bol. Soc. Chil. Quim. 37 (1992) 211.
[24] C. Díaz, A. Arancibia, Bol. Soc. Chil. Quim. 43 (1998) 303.
[25] G.A. Carriedo, A. Arancibia, C. Diaz, N. Yutronic, E.P. Carreño, S.G. Granda, J. Organomet. Chem. 508 (1996) 23.
[26] Strictly four bands must be observed for a C_s local symmetry of the η^1-nitrogen linked ligand. However, three bands are normally observed, the fourth being observed as a shoulder, or masked for the most intense absorption; see [5–10] and references cited in [27].
[27] B. Olbrich-Deubner, R. Gross, W. Kaim, J. Organomet. Chem. 366 (1989) 155.

[28] J.L. Wesemann, M.H. Chisholm, Inorg. Chem. 36 (1997) 3258.
[29] G.T. Yee, J.C. Calabrese, C. Vazquez, J.S. Miller, Inorg. Chem. 32 (1993) 377.
[30] M.M. Olmstead, G. Speier, L. Szabó, J. Chem. Soc., Chem. Commun. (1994) 541.
[31] F.A. Cotton, Y. Kim, J. Am. Chem. Soc. 221 (1993) 1.
[32] M.C. Grossel, S.C. Wester, J. Chem. Soc., Chem. Commun. (1992) 1510.
[33] I. Ito, S. Kitazume, A. Yamamoto, S. Ikeda, J. Am. Chem. Soc. 92 (1970) 3011.
[34] M.M. Campos, C. Díaz, K. Figueroa, L. Padilla, N. Lara, G. Díaz, Vibration Spectrosc. 7 (1994) 61.
[35] P. Hamon, I.R. Hamon, C. Lapinte, J. Chem. Soc., Chem. Commun. (1992) 1602.
[36] P. Hamon, L. Toupet, J.R. Hamon, C. Lapinte, J. Chem. Soc., Chem. Commun. (1994) 931.
[37] V. Mathias, S. Cron, L. Toupet, C. Lapinte, Organometallics 15 (1996) 5393.
[38] T. Roth, W. Kaim, Inorg. Chem. 31 (1992) 1930.
[39] S.E. Bell, J.S. Field, R.J. Haines, M. Moscherosh, W. Matheis, W. Kaim, Inorg. Chem. 31 (1992) 3269.
[40] C. Díaz, B. Weiss, Polyhedron 12 (1993) 1403.
[41] N.S. Hush, Prog. Inorg. Chem. 8 (1967) 391.
[42] N.S. Hush, Electrochim. Acta 13 (1968) 1005.
[43] N.S. Hush, Coord. Chem. Rev. 64 (1985) 135.
[44] R.A. Marcus, N. Sutin, Biochim. Biophys. Acta 811 (1985) 265.
[45] Y. Dong, J.T. Hupp, Inorg. Chem. 31 (1992) 3170.
[46] P.E. Riley, C.E. Capshew, R. Pettit, R.E. Davis, Inorg. Chem. 17 (1978) 408.
[47] L. Ballester, M. Carmen Barral, A. Gutierrez, R. Jimenez-Aparicio, J. Martinez-Muyo, M.F. Perspiñan, M.A. Monge, C. Ruiz-Valero, J. Chem. Soc., Chem. Commun. (1991) 1395.
[48] D. Ewan, A.J. Blake, T.A. Stephenson, M. Schroder, L.J. Tellouless, J. Chem. Soc., Chem. Commun. (1988) 1533.
[49] M.D. Newton, N. Sutin, Annu. Rev. Phys. Chem. 35 (1984) 437.
[50] N. Sutin, B.S. Brunschrirg, C. Creutz, J.R. Winkler, Pure Appl. Chem. 60 (1998) 1817.
[51] P. Forlano, F.D.C. Kiernik, O. Poizat, J. Olabe, J. Chem. Soc., Dalton Trans. (1997) 1595.
[52] K.S. Door, P.O. Stoutland, R.B. Dyer, H.W. Woodruff, Am. Chem. Soc. 114 (1992) 3133.
[53] For frontier OM of fragment $Cp(dppe)Fe^{+}$ see: J.F. McGrady, T. Lowell, R. Stranger, M.G. Humphrey, Organometallics 16 (1997) 4004.
[54] See also our studies in [40].
[55] N.M. Kostic, R.F. Fenske, Organometallics 1 (1992) 1979.
[56] For frontier OM for TCNX, see [6,8].

PERGAMON

www.elsevier.nl/locate/poly

Polyhedron 19 (2000) 147–153

POLYHEDRON

Monodentately coordinated *o*-phenylenediacetonitrile seven-coordinate complexes of molybdenum(II) and tungsten(II): X-ray crystal structure of $[WI_2(CO)_3\{1,2\text{-}C_6H_4(CH_2CN)_2\text{-}N\}_2]$

Paul K. Baker [a,*], Emily Samson [a], Patrick L. Veale [a], Michael G.B. Drew [b]

[a] *Department of Chemistry, University of Wales, Bangor, Gwynedd LL57 2UW, UK*

[b] *Department of Chemistry, University of Reading, Whiteknights, Reading RG6 6AD, UK*

Received 9 August 1999; accepted 1 November 1999

Abstract

Treatment of $[MI_2(CO)_3(NCMe)_2]$ (M = Mo or W) with 2 equiv. of *o*-phenylenediacetonitrile ($1,2\text{-}C_6H_4(CH_2CN)_2$) gives the complexes $[MI_2(CO)_3\{1,2\text{-}C_6H_4(CH_2CN)_2\text{-}N\}_2]$ (**1** and **2**) via displacement of the acetonitrile ligands. The tungsten complex $[WI_2(CO)_3\{1,2\text{-}C_6H_4(CH_2CN)_2\text{-}N\}_2]$ (**2**) has been characterised crystallographically. The geometry surrounding the coordination sphere is capped octahedral with a carbonyl group in the unique capping position, an iodide and two carbonyls in the capped face and an iodide and two nitrogen atoms from nitrile groups in the uncapped face. Reactions of **1** and **2** with equimolar amounts of L (L = PPh_3, $AsPh_3$, $SbPh_3$, $P(OPh)_3$) affords $[MI_2(CO)_3(NCMe)L]$, which followed by an in situ reaction with 1 equiv. of $1,2\text{-}C_6H_4(CH_2CN)_2$ gives the new mixed ligand complexes $[MI_2(CO)_3\{1,2\text{-}C_6H_4(CH_2CN)_2\text{-}N\}L]$ (**3**–**10**) in high yield. Reaction of $[MI_2(CO)_3(NCMe)_2]$ and $[MI_2(CO)_3(NCMe)(PPh_3)]$ with 2 and 1 equiv. of L^1 ($L^1 = [WI_2(CO)_3\{1,2\text{-}C_6H_4(CH_2CN)_2\text{-}N\}_2]$ (**2**)) gives the first trimetallic $[MI_2(CO)_3L^1{}_2]$ (**11** and **12**) and bimetallic $[MI_2(CO)_3L^1(PPh_3)]$ (**13** and **14**) *o*-phenylene diacetonitrile bridged complexes in high yield. ©2000 Elsevier Science Ltd All rights reserved.

Keywords: Molybdenum(II); Tungsten(II); Crystal structures; *o*-Phenylenediacetonitrile; Bimetallic complexes; Trimetallic complexes; Nitrile-bridged complexes; Seven-coordinate complexes; Halocarbonyls

1. Introduction

Since our initial report in 1986 [1], of the synthesis and characterisation of the bis(acetonitrile) complexes $[MX_2(CO)_3(NCMe)_2]$ (M = Mo or W; X = Br or I), we have described the preparation and structural characterisation of a number of seven-coordinate complexes of molybdenum(II) and tungsten(II) containing ligands with one nitrile functional group attached to the metal [2–12]. Hitherto, no examples with ligands containing two nitrile functional groups have been reported of any type of seven-coordinate complexes of molybdenum(II) and tungsten(II).

In this paper we describe the reactions of the seven-coordinate complexes $[MI_2(CO)_3(NCMe)_2]$ (M = Mo or W) and $[MI_2(CO)_3(NCMe)L]$ (L = PPh_3, $AsPh_3$, $SbPh_3$ or $P(OPh)_3$) with the bis(nitrile) functionalised ligand *o*-phenylenediacetonitrile ($1,2\text{-}C_6H_4(CH_2CN)_2$). The molecular structure of $[WI_2(CO)_3\{1,2\text{-}C_6H_4(CH_2CN)_2\text{-}N\}_2]$ is also discussed. The structure of $[WI_2(CO)_3\{1,2\text{-}C_6H_4\text{-}(CH_2CN)_2\text{-}N\}_2]$ shows that only one nitrile group is attached to the tungsten in this complex. In view of this observation, we also describe the synthesis and characterisation of the first trimetallic and bimetallic *o*-phenylenediacetonitrile-bridged complexes $[MI_2(CO)_3L^1{}_2]$ (M = Mo, W; $L^1 = [WI_2(CO)_3\{1,2\text{-}C_6H_4(CH_2CN)_2\text{-}N\}_2]$) and $[MI_2\text{-}(CO)_3L^1(PPh_3)]$.

2. Experimental

The seven-coordinate complexes $[MI_2(CO)_3(NCMe)_2]$ (M = Mo or W) [1] and $[MI_2(CO)_3(NCMe)L]$ (L = PPh_3, $AsPh_3$, $SbPh_3$, $P(OPh)_3$) [4], were prepared by literature methods. All chemicals were purchased from commercial sources, and CH_2Cl_2 was dried over calcium hydride and distilled before use.

Elemental analyses (C, H and N) were determined using a Carlo Erba elemental analyser MOD 1108 (using helium

* Corresponding author. Tel.: +44-1248-351-151; fax: +44-1248-370-528.

0277-5387/00/$ - see front matter ©2000 Elsevier Science Ltd All rights reserved.
PII S0277-5387(99)00335-6

Table 1
Physical and analytical data [a] for the *o*-phenylenediacetonitrile 1,2-$C_6H_4(CH_2CN)_2$ seven-coordinate complexes of molybdenum(II) and tungsten(II)

Complex	Colour	Yield (%)	Analysis		
			C (%)	H (%)	N (%)
$[MoI_2(CO)_3\{1,2\text{-}C_6H_4(CH_2CN)_2\text{-}N\}_2]$ (**1**)	brown	72	37.9 (37.0)	2.4 (2.2)	7.6 (7.5)
$[WI_2(CO)_3\{1,2\text{-}C_6H_4(CH_2CN_2)_2\text{-}N\}_2]$ (**2**)	red–brown	75	33.0 (33.3)	2.0 (1.9)	6.3 (6.7)
$[MoI_2(CO)_3\{1,2\text{-}C_6H_4(CH_2CN)_2\text{-}N\}(PPh_3)]$ (**3**)	dark brown	86	43.8 (43.7)	3.0 (2.7)	3.6 (3.3)
$[WI_2(CO)_3\{1,2\text{-}C_6H_4(CH_2CN)_2\text{-}N\}(PPh_3)]$ (**4**)	yellow	89	40.0 (39.6)	2.6 (2.5)	3.1 (3.0)
$[MoI_2(CO)_3\{1,2\text{-}C_6H_4(CH_2CN)_2\text{-}N\}(AsPh_3)]$ (**5**)	dark brown	80	41.5 (41.6)	2.8 (2.6)	3.3 (3.1)
$[WI_2(CO)_3\{1,2\text{-}C_6H_4(CH_2CN)_2\text{-}N\}(AsPh_3)]$ (**6**)	orange	85	37.8 (37.9)	2.4 (2.4)	2.9 (3.0)
$[MoI_2(CO)_3\{1,2\text{-}C_6H_4(CH_2CN)_2\text{-}N\}(SbPh_3)]$ (**7**)	brown	80	40.0 (39.5)	2.8 (2.5)	3.5 (3.0)
$[WI_2(CO)_3\{1,2\text{-}C_6H_4(CH_2CN)_2\text{-}N\}(SbPh_3)]$ (**8**)	dark orange	45	36.1 (35.7)	2.3 (2.1)	2.8 (3.0)
$[MoI_2(CO)_3\{1,2\text{-}C_6H_4(CH_2CN)_2\text{-}N\}\{P(OPh)_3\}]$ (**9**)	light brown	82	41.3 (41.4)	2.7 (2.6)	2.1 (3.1)
$[WI_2(CO)_3\{1,2\text{-}C_6H_4(CH_2CN)_2\text{-}N\}\{P(OPh)_3\}]$ (**10**)	yellow	73	37.2 (37.7)	2.7 (2.3)	2.4 (2.8)
$[MoI_2(CO)_3(L^1)_2]$ (**11**)	dark brown	63	28.6 (28.0)	1.5 (1.5)	5.0 (5.9)
$[WI_2(CO)_3(L^1)_2]$ (**12**)	brown	67	27.5 (26.9)	1.8 (1.5)	4.9 (5.1)
$[MoI_2(CO)_3(L^1)(PPh_3)]$ (**13**)	light brown	77	33.9 (34.5)	1.5 (2.0)	3.4 (3.7)
$[WI_2(CO)_3(L^1)(PPh_3)]\cdot CH_2Cl_2$ (**14**)	light brown	71	33.8 (33.4)	2.3 (2.0)	3.5 (3.5)

[a] Calculated values in parentheses.

Table 2
IR data [a] for the *o*-phenylenediacetonitrile seven-coordinate complexes of molybdenum(II) and tungsten(II)

Complex	ν(C≡O) (cm^{-1})			ν(N≡C) (cm^{-1}) (coordinated)	ν(N≡C) (cm^{-1}) (uncoordinated)
1	2035(s)	1962(s)	1937(s)	2360	2305
2	2070(s)	2029(s)	1948(s)	2361	2306
3	2038(s)	1978(s)	1937(s)	2359	2305
4	2033(s)	1966(s)	1917(s)	2359	2304
5	2038(s)	1980(s)	1917(s)	2348	2304
6	2034(s)	1966(s)	1914(s)	2360	2306
7	2024(s)	1958(br,s)		2361	2305
8	2033(s)	1945(s)	1917(s)	2359	2308
9	2053(s)	2001(br,s)		2358	2305
10	2047(s)	1989(s)	1925(s)	2360	2305
11	2028(s)	1949(br,s)		2360	2306
12	2028(s)	1947(br,s)		2359	2309
13	2032(s)	1963(br,s)		2348	2305
14	2028(s)	1947(br,s)		2358	2305

[a] Spectra recorded as thin $CHCl_3$ films between NaCl plates.

as a carrier gas). The IR spectra were recorded as thin $CHCl_3$ films between NaCl plates on a Perkin–Elmer 1600 series FTIR spectrophotometer. ^1H (referenced to $SiMe_4$) NMR spectra were recorded using a Bruker AC 250 MHz NMR spectrometer. Molecular weights were determined by Rast's method [13], using camphor as the standard.

2.1. $[WI_2(CO)_3\{1,2\text{-}C_6H_4(CH_2CN)_2\text{-}N\}_2]$ (2)

To a stirred solution of $[WI_2(CO)_3(NCMe)_2]$ (0.50 g, 0.83 mmol) in CH_2Cl_2 (20 cm^3) was added 1,2-$C_6H_4(CH_2CN)_2$-*N* (0.260 g, 1.66 mmol). After stirring the solution at room temperature for 1 h, the mixture was filtered and the solvent removed in vacuo to give a red–brown powder of $[WI_2(CO)_3\{1,2\text{-}C_6H_4(CH_2CN)_2\text{-}N\}_2]$ (**2**). Recrystallisation from CH_2Cl_2–Et_2O (50:50 ratio) and cooling to −17°C gave suitable single crystals for X-ray analysis. Yield of pure product 0.518 g, 75%.

A similar reaction of $[MoI_2(CO)_3(NCMe)_2]$ with 2 equiv. of 1,2-$C_6H_4(CH_2CN)_2$ in CH_2Cl_2 at room temperature gives $[MoI_2(CO)_3\{1,2\text{-}C_6H_4(CH_2CN)_2\text{-}N\}_2]$ (**1**) after recrystallisation from CH_2Cl_2–Et_2O. See Tables 1–3 for physical, analytical and spectroscopic data.

2.2. $[WI_2(CO)_3\{1,2\text{-}C_6H_4(CH_2CN)_2\text{-}N\}(PPh_3)]$ (4)

To a stirred solution of $[WI_2(CO)_3(NCMe)_2]$ (0.500 g, 0.83 mmol) in CH_2Cl_2 (20 cm^3) was added PPh_3 (0.218 g, 0.83 mmol). After 1 min, 1,2-$C_6H_4(CH_2CN)_2$ (0.130 g, 0.83 mmol) was added, and the solution was stirred at room temperature for a further 30 min, after which filtration, followed by removal of the solvent in vacuo, gave the yellow complex $[WI_2(CO)_3\{1,2\text{-}C_6H_4(CH_2CN)_2\text{-}N\}(PPh_3)]$ (**4**), which was recrystallised from CH_2Cl_2–Et_2O (yield 0.694 g, 89%).

Similar reactions of $[MI_2(CO)_3(NCMe)_2]$ with 1 equiv. of L (L = PPh_3 (1 min), $AsPh_3$ (3 min), $SbPh_3$ (5 min), or

Table 3
^{1}H NMR data [a] for the *o*-phenylenediacetontrile seven-coordinate complexes of molybdenum(II) and tungsten(II)

Complex	^{1}H (δ) (ppm)
1	7.3–7.6 (br, m, 8H, 1,2-$C_6H_4(CH_2CN)_2$); 4.0 (s, 4H, [(Mo–$NCCH_2$)] coord.); 3.8 (s, 4H, [–$NCCH_2)_2$] uncoord.)
2	7.3–7.5 (br, m, 8H, 1,2-$C_6H_4(CH_2CN)_2$); 4.0 (s, 4H, [(W–$NCCH_2)_2$] coord.); 3.8 (s, 4H, [–$(NCCH_2)_2$] uncoord.)
3	7.3–7.7 (br, m, 19H, 1,2-$C_6H_4(CH_2CN)_2$ and P*Ph*$_3$); 4.0 (s, 2H, [(Mo–$NCCH_2$)] coord.); 3.75 (s, 2H, [–$(NCCH_2)$] uncoord.)
4	7.3–7.6 (br, m, 19H, 1,2-$C_6H_4(CH_2CN)_2$ and P*Ph*$_3$); 4.0 (s, 2H, [(W–$NCCH_2$)] coord.); 3.7 (s, 2H, ($NCCH_2$) uncoord.)
5	7.3–7.7 (br, m, 19H, 1,2-$C_6H_4(CH_2CN)_2$ and As*Ph*$_3$); 4.0 (2, 2H, [(Mo–$NCCH_2$)] coord.); 3.85 (s, 2H, [–$(NCCH_2)$] uncoord.)
6	7.3–7.6 (br, m, 19H, 1,2-$C_6H_4(CH_2CN)_2$ and As*Ph*$_3$); 4.0 (s, 2H, [(W–$NCCH_2$)] coord.); 3.8 (s, 2H, [–$(NCCH_2)$] uncoord.)
7	7.3–7.7 (br, m, 19H, 1,2-$C_6H_4(CH_2CN)_2$ and Sb*Ph*$_3$); 4.0 (s, 2H, [(Mo–$NCCH_2$)] coord.); 3.85 (s, 2H, [–$(NCCH_2)$] uncoord.)
8	7.4–7.7 (br, m, 19H, 1,2-$C_6H_4(CH_2CN)_2$ and Sb*Ph*$_3$); 4.0 (s, 2H, [(W–$NCCH_2$)] coord.); 3.8 (s, 2H, [–$(NCCH_2)$] uncoord.)
9	7.3–7.6 (br, m, 19H, 1,2-$C_6H_4(CH_2CN)_2$ and P*Ph*$_3$); 4.0 (s, 2H, [(Mo–$NCCH_2$)] coord.); 3.8 (s, 2H, [–$(NCCH_2)$] uncoord.)
10	7.2–7.7 (br, m, 19H, 1,2-$C_6H_4(CH_2CN)_2$ and P(O*Ph*)$_3$); 4.0 (s, 2H, [(W–$NCCH_2$)] coord.); 3.8 (s, 2H, [(–$NCCH_2$)] uncoord.)
11	7.3–7.6 (br, m, 16H, 1,2-$C_6H_4(CH_2CN)_2$); 4.0 (s, 4H, [–(W–$NCCH_2)_2$] coord.); 3.8 (s, 12H, [–$(NCCH_2)_2$] uncoord.)
12	7.3–7.6 (br, m,16H, 1,2-$C_6H_4(CH_2CN)_2$); 4.0 (s, 4H, 2×[–(W–$NCCH_2)_2$] coord.); 3.8 (s, 12H, [–$(NCCH_2)_2$] uncoord.)
13	7.4–7.9 (br, m, 23H, 1,2-$C_6H_4(CH_2CN)_2$ and P*Ph*$_3$); 4.0 (s, 6H, [–(W–$NCCH_2)_2$] coord.); 3.8 (s, 4H, [–$(NCCH_2)_2$] uncoord.)
14	7.3–7.9 (br, m, 23H, 1,2-$C_6H_4(CH_2CN)_2$ and P*Ph*$_3$); 5.3 (s, 2H, C*H*$_2$Cl$_2$); 4.0 (s, 6H, [–(W–$NCCH_2)_2$] coord.); 3.8 (s, 2H, [–$(NCCH_2)_2$] uncoord.)

[a] Spectra recorded in $CDCl_3$ (+25°C, referenced to $SiMe_4$).

P(OPh)$_3$ (5 min)) in CH_2Cl_2 gives [$MI_2(CO)_3$(NCMe)L], followed by an in situ reaction of an equimolar amount of 1,2-$C_6H_4(CH_2CN)_2$ affords [$MI_2(CO)_3${1,2-C_6H_4-$(CH_2CN)_2$-*N*}L] (**3**, **5–10**). The complexes are then recrystallised from CH_2Cl_2–Et_2O to give the pure products. For physical, analytical and spectroscopic data, see Tables 1–3.

2.3. [$MoI_2(CO)_3L^1{}_2$] (**11**)

To a stirred solution of [$MoI_2(CO)_3(NCMe)_2$] (0.093 g, 0.18 mmol) in CH_2Cl_2 (20 cm^3) was added [$WI_2(CO)_3${1,2-$C_6H_4(CH_2CN)_2$-*N*}$_2$] (L^1) (0.30 g, 0.36 mmol). After stirring at room temperature for 15 h, the mixture was filtered and the solvent removed in vacuo to give a dark brown powder of [$MoI_2(CO)_3L^1{}_2$] (**11**). Recrystallisation from CH_2Cl_2–Et_2O (50:50 ratio) and cooling to −17°C gave pure complex **11**. Yield of pure product 0.239 g, 63%. Molecular weight for complex **11** 2102; molecular weight found by Rast's method [13] 1933.

A similar reaction of [$WI_2(CO)_3(NCMe)_2$] with 2 equiv. of L^1 in CH_2Cl_2 gives the trimetallic complex [$WI_2(CO)_3L^1{}_2$] (**12**). See Tables 1–3 for physical, analytical and spectroscopic data. Molecular weight for complex **12** 2190; molecular weight found by Rast's method [13] 2442.

2.4. [$WI_2(CO)_3L^1(PPh_3)]\cdot CH_2Cl_2$ (**14**)

To a stirred solution of [$WI_2(CO)_3(NCMe)_2$] (0.300 g, 0.50 mmol) in CH_2Cl_2 was added PPh_3 (0.13 g, 0.50 mmol). After 1 min, [$WI_2(CO)_3${1,2-$C_6H_4(CH_2CN)_2$-*N*}$_2$] (0.414 g, 0.50 mmol) was added, and the solution was stirred at room temperature for a further 15 h, after which filtration, followed by removal of the solvent in vacuo, gave the light brown complex [$WI_2(CO)_3L^1(PPh_3)]\cdot CH_2Cl_2$ (**14**), which was recrystallised from CH_2Cl_2–Et_2O. Yield of pure product 0.568 g, 71%. Molecular weight for complex **14** 1618; molecular weight found by Rast's method [13] 1717.

A similar reaction of [$MoI_2(CO)_3(NCMe)_2$] with 1 equiv. of PPh_3 for 1 min in CH_2Cl_2 followed by an in situ addition of L′ gave the bimetallic complex [$MoI_2(CO)_3L^1(PPh_3)$] (**13**) which was recrystallised from CH_2Cl_2–Et_2O. Molecular weight for complex **13** 1530; molecular weight found by Rast's method [13] 1333.

2.5. X-ray crystallography

Single crystals for X-ray crystallography of [$WI_2(CO)_3${1,2-$C_6H_4(CH_2CN)_2$-*N*}$_2$] (**2**) were grown as described in Section 2.1.

Selected bond lengths and angles are given in Table 4. $C_{25}H_{22}I_2N_4O_4W$; *M* 880.12; orthorhombic; space group *Pnma*; $a=8.531(9)$, $b=19.69(2)$, $c=17.74(2)$ Å; $U=2980(5)$ Å^3; $Z=4$; $D_{calc}=1.962$ Mg m^{-3}; $\mu=5.983$ mm^{-1}; $F(000)=1648$; reflections collected 9337; independent reflections 2858 ($R_{int}=0.0707$).

Data were collected with Mo Kα radiation using the MAR-research Image Plate System. The crystal was positioned at 70 mm from the Image Plate. 95 frames were measured at 2° intervals with a counting time of 2 min. Data analysis was carried out with the XDS program [14]. The structure was solved using direct methods with the SHELX86 program [15]. The molecule had crystallographic C_s symmetry. The non-hydrogen atoms were refined with anisotropic thermal parameters. The hydrogen atoms were included in geometric positions. A solvent ethanol molecule was located and given 50% occupancy. An empirical absorption correction was carried out [16]. The structure was then refined on F^2 using SHELX [17]. Final *R* indices ($I>2\sigma(I)$) were $R_1=0.0759$, $wR_2=0.1826$ with *R* indices (all data) $R_1=0.0923$, $wR_2=0.1986$. All calculations were carried out on a Silicon Graphics R4000 Workstation at the University of Reading.

Table 4
Bond lengths (Å) and angles (°) in the metal coordination sphere for **1**

W(1)–C(200)	1.98(3)
W(1)–C(100)	1.987(13)
W(1)–C(100)#1	1.987(13)
W(1)–N(4)#1	2.195(10)
W(1)–N(4)	2.195(10)
W(1)–I(2)	2.810(3)
W(1)–I(3)	2.872(3)
C(200)–W(1)–C(100)	74.9(8)
C(200)–W(1)–C(100)#1	74.9(8)
C(100)–W(1)–C(100)#1	103.7(7)
C(200)–W(1)–N(4)#1	124.6(7)
C(100)–W(1)–N(4)#1	81.9(5)
C(100)#1–W(1)–N(4)#1	160.4(5)
C(200)–W(1)–N(4)	124.6(7)
C(100)–W(1)–N(4)	160.4(5)
C(100)#1–W(1)–N(4)	81.9(5)
N(4)#1–W(1)–N(4)	87.0(6)
C(200)–W(1)–I(2)	136.6(12)
C(100)–W(1)–I(2)	78.7(5)
C(100)#1–W(1)–I(2)	78.7(5)
N(4)#1–W(1)–I(2)	84.1(3)
N(4)–W(1)–I(2)	84.1(3)
C(200)–W(1)–I(3)	68.2(12)
C(100)–W(1)–I(3)	115.1(4)
C(100)#1–W(1)–I(3)	115.1(4)
N(4)#1–W(1)–I(3)	78.0(3)
N(4)–W(1)–I(3)	78.0(3)
I(2)–W(1)–I(3)	155.18(6)

3. Results and discussion

The seven-coordinate starting materials $[MI_2(CO)_3(NCMe)_2]$ (M = Mo or W) used in this research have been prepared by reacting *fac*-$[M(CO)_3(NCMe)_3]$ (prepared in situ [18]) with an equimolar amount of I_2 at 0°C. [1]. In an attempt to see whether the ligand *o*-phenylenediacetonitrile can act as a chelate ligand, the reactions of equimolar amounts of $[MI_2(CO)_3(NCMe)_2]$ and 1,2-$C_6H_4(CH_2CN)_2$ in CH_2Cl_2 at room temperature for varying periods of time were carried out, giving only oily products which were difficult to isolate in a pure state. From the results of the next section, whereby the reaction of $[MI_2(CO)_3(NCMe)_2]$ with 2 equiv. of 1,2-$C_6H_4(CH_2CN)_2$ gives the bis-monodentately attached *o*-phenylenediacetonitrile complexes $[MI_2(CO)_3\{1,2\text{-}C_6H_4(CH_2CN)_2\text{-}N\}_2]$ (**1** and **2**), as expected, it is likely that 1,2-$C_6H_4(CH_2CN)_2$ cannot behave as a simple chelate ligand in this system. This was confirmed by the X-ray crystal structure of the tungsten derivative (Fig. 1), which shows the unattached nitrile groups are well away from possible coordination to the tungsten as a chelate ligand. It is likely that reaction of $[WI_2(CO)_3(NCMe)_2]$ with an equimolar amount of 1,2-$C_6H_4(CH_2CN)_2$ initially gives the mixed nitrile complex $[WI_2(CO)_3(NCMe)\{1,2\text{-}C_6H_4(CH_2CN)_2\text{-}N\}]$, which probably dimerises to give $[\{W(\mu\text{-}I)I(CO)_3(1,2\text{-}C_6H_4(CH_2CN)_2\text{-}N)\}_2]$, as we have previously observed with other mixed monodentate nitrogen donor ligand complexes [19].

Reaction of $[MI_2(CO)_3(NCMe)_2]$ (M = Mo or W) with 2 equiv. of 1,2-$C_6H_4(CH_2CN)_2$ in CH_2Cl_2 at room temperature affords the acetonitrile displaced products $[MI_2(CO)_3\{1,2\text{-}C_6H_4(CH_2CN)_2\text{-}N\}_2]$ (**1** and **2**) in 72% (**1**) and 75% (**2**) yield. Complexes **1** and **2** have been characterised by elemental analysis (C, H and N) (Table 1), IR (Table 2) and ^{1}H NMR spectroscopy (Table 3) and for M = W, by X-ray crystallography. The complexes are very soluble in CH_2Cl_2 and $CHCl_3$, but only slightly soluble in diethyl ether. The complexes are air sensitive in the solid state and in solution, however, the complexes can be stored for prolonged periods of time under an inert atmosphere. The IR spectrum of, for example, **2** has, as expected, three carbonyl bands in the solution state spectrum ($CHCl_3$) at 2070, 2029 and 1948 cm^{-1}, similar to other bis(nitrile) complexes previously described [2–7]. The spectrum also shows bands due to coordinated nitrile at 2361 cm^{-1}, and unbound nitrile at 2306 cm^{-1}, which is confirmed by the X-ray crystal structure shown in Fig. 1.

Single crystals suitable for X-ray analysis of $[WI_2(CO)_3\{1,2\text{-}C_6H_4(CH_2CN)_2\text{-}N\}_2]$ (**2**) were grown from a CH_2Cl_2–Et_2O (50:50) concentrated solution of **2** at −17°C. The molecular structure of **2** is shown in Fig. 1, together with the atomic numbering scheme. The molecule has crystallographic C_s symmetry. The metal atom is seven-coordinate, being bonded to three carbonyls, two iodides and two substituted methyl cyanides. The geometry of the structure can be described as a distorted capped octahedron similar to the structures $[WI_2(CO)_3(NCR)_2]$ (R = Me, Et) [9]. A carbonyl group is in the unique capping position (W–C(200) 1.98(3) Å), with the capped face containing one iodide (I(3) (W–I(3) 2.872(3) Å) and two more carbonyl groups at W–C(100) 1.98(3) Å. The uncapped face is occupied by the two nitrogen atoms (2.195(10) Å), and the remaining iodide W–I(2) 2.810(3) Å. The crystallographic mirror plane

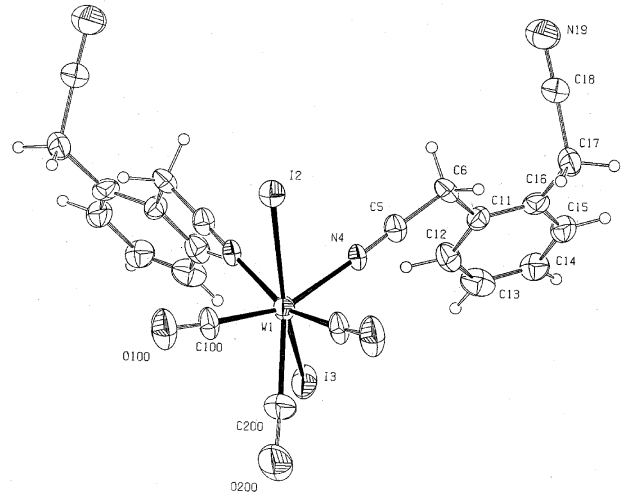


Fig. 1. The structure of $[WI_2(CO)_3\{1,2\text{-}C_6H_4(CH_2CN)_2\text{-}N\}_2]$ (**2**) with the atomic numbering scheme. Ellipsoids are shown at 30% occupancy. Hydrogen atoms are shown as small circles of arbitrary radii.

passes through the metal W, both iodides and the capping carbonyl atom. It is interesting to note that an equivalent crystallographic mirror plane is observed in $[WI_2(CO)_3(NCR)_2]$ [9,10]. As in those structures, the bond to the iodide in the capped face is significantly longer than the bond to the iodide in the uncapped face where there is less steric crowding. The dimensions in the metal coordination sphere are listed in Table 4. The room temperature ^1H NMR spectra (Table 3) of **1** and **2** showed the expected resonances for the monodentate donor *o*-phenylenediacetonitrile ligands. A number of unsuccessful attempts to obtain low temperature ^{13}C NMR spectra of **2** were made, and although resonances for the nitrile groups were obtained, the resonances of coordinated carbon monoxide groups could not be observed.

Treatment of $[MI_2(CO)_3(NCMe)_2]$ (M = Mo or W) with an equimolar amount of L (L = PPh_3, $AsPh_3$, $SbPh_3$ or $P(OPh)_3$) in CH_2Cl_2 at room temperature gives $[MI_2(CO)_3(NCMe)L]$, which when reacted in situ with 1 equiv. of 1,2-$C_6H_4(CH_2CN)_2$, yields the mixed ligand complexes $[WI_2(CO)_3\{1,2\text{-}C_6H_4(CH_2CN)_2\text{-}N\}L]$ (**3–10**) in high yield. Complexes **3–10** have been characterised by elemental analysis (C, H and N), IR and ^1H NMR spectroscopy (Tables 1–3). The complexes are considerably less soluble than complexes **1** and **2** in CH_2Cl_2 and $CHCl_3$, and only very slightly soluble in diethyl ether, except for the $P(OPh)_3$ complexes **9** and **10**, which are more soluble. Complexes **3–10** are more stable in air than complexes **1** and **2**, however, they still decompose in solution when exposed to air. The IR spectra (Table 2) for complexes **3–10** all show three carbonyl bands, in similar positions to other related mixed-ligand complexes of the type $[MI_2(CO)_3(NCR)L]$ (M = Mo or W; R = Me, Et or Ph; L = PPh_3, $AsPh_3$, $SbPh_3$ or $P(OPh)_3$), and since the X-ray crystal structures of $[WI_2(CO)_3(NCR)(AsPh_3)]$ (R = Et, Ph) [3] and $[WI_2(CO)_3(NCMe)(PPh_3)]$ [11] have been described previously, and have either distorted capped trigonal prismatic or distorted capped octahedral geometries [20–24], it is likely that complexes **3–10** will have similar structures. The IR spectra also show two nitrile bands at approximately 2360 and 2300 cm^{-1} for the coordinated and uncoordinated nitrile groups for complexes **3–10**, which confirm the expected monodentate coordination mode of the *o*-phenylenediacetonitrile ligand in these complexes.

The mechanisms of these acetonitrile replacement reactions are likely to proceed via dissociative mechanisms, since the complexes $[MI_2(CO)_3(NCMe)_2]$ and $[MI_2(CO)_3(NCMe)L]$ obey the effective atomic number rule. Also Tripathi et al. [25] have previously prepared and isolated the 16-electron complexes $[MoX_2(CO)_3L]$ (X = Cl, Br or I; L = PPh_3, $AsPh_3$ or $SbPh_3$), which are proposed as intermediates as shown in Scheme 1.

Having prepared and structurally characterised the tungsten complex $[WI_2(CO)_3\{1,2\text{-}C_6H_4(CH_2CN)_2\text{-}N\}_2]$ (**2**) which has the *o*-phenylenediacetonitrile coordinated in a monodentate fashion, this section describes the successful

(i) $[MI_2(CO)_3(NCMe)_2] \rightarrow [MI_2(CO)_3(NCMe)] + NCMe$

(ii) $[MI_2(CO)_3(NCMe)] + L \rightarrow [MI_2(CO)_3(NCMe)L]$

(iii) $[MI_2(CO)_3(NCMe)L] \rightarrow [MI_2(CO)_3L] + NCMe$

(iv) $[MI_2(CO)_3L] + 1,2\text{-}C_6H_4(CH_2CN)_2 \rightarrow [MI_2(CO)_3\{1,2\text{-}C_6H_4(CH_2CN)_2\text{-}N\}L]$

Scheme 1. Proposed mechanism for the formation of $[MI_2(CO)_3\{1,2\text{-}C_6H_4(CH_2CN)_2\text{-}N\}L]$ from $[MI_2(CO)_3(NCMe)_2]$.

attempts to prepare and characterise the first *o*-phenylenediacetonitrile-bridged complexes of tungsten(II). Reaction of $[MI_2(CO)_3(NCMe)_2]$ (M = Mo or W) with 2 equiv. of $[WI_2(CO)_3\{1,2\text{-}C_6H_4(CH_2CN)_2\text{-}N\}_2]$ (L^1) in CH_2Cl_2 at room temperature affords the trimetallic complexes $[MI_2(CO)_3L^1{}_2]$ (**11** and **12**). Complexes **11** and **12** have been characterised in the normal manner (Tables 1–3). The trimetallic nature of complexes **11** and **12** was confirmed by molecular weight measurements using Rast's method [13] (see Section 2.3). Several attempts were made to obtain mass spectrometric data but, as with many of our diiodo-complexes, no parent ion was observed. These complexes represent the first bridging nitrile complexes of this type to be described. The complexes are air sensitive in solution, and must be stored in the solid state under a dinitrogen atmosphere. They are soluble in CH_2Cl_2 and $CHCl_3$, but only slightly soluble in Et_2O and hydrocarbon solvents. The IR spectra for complexes **11** and **12** show bands for the *o*-phenylenediacetonitrile groups at 2360, 2309 cm^{-1} (for **11**) and 2359, 2309 cm^{-1} (for **12**).

The structures of both the acetonitrile complexes $[MI_2(CO)_3(NCMe)_2]$ (M = Mo [12] or W [9]) have been determined crystallographically and are very similar, based on a capped octahedron with a carbonyl ligand capping an octahedral face which has two terminal carbonyl groups and an iodo ligand. Also, the structure of the tungsten nitrile ligand **2** has also been determined (see Fig. 1). If the acetonitrile ligands have been replaced in a stereoselective manner, the geometry of the products would be as shown in Fig. 2. The IR and ^1H NMR data conform with the proposed structure. Many unsuccessful attempts were made to grow suitable single crystals for X-ray analysis of **11** and **12** using a wide range of mixed solvent and temperature conditions.

Reaction of $[MI_2(CO)_3(NCMe)_2]$ (M = Mo or W) with 1 equiv. of PPh_3 gives, after 1 min, $[MI_2(CO)_3(NCMe)(PPh_3)]$, which reacts in situ with an equimolar amount of L^1 ($[WI_2(CO)_3\{1,2\text{-}C_6H_4(CH_2CN)_2\text{-}N\}_2]$) to afford the new bimetallic complexes $[MI_2(CO)_3(L^1)(PPh_3)]$ (**13** and **14**) in good yield. Complexes **13** and **14** have been fully characterised (Tables 1–3), and also the bimetallic nature was confirmed by molecular weight measurements using Rast's method [13] (see Section 2.4). Complex **14** was confirmed as a CH_2Cl_2 solvate by repeated elemental analyses and ^1H NMR spectroscopy. Since the structure of the tungsten complex $[WI_2(CO)_3(NCMe)(PPh_3)]$ has been determined crystallographically and has distorted capped octahedral geometry, the most likely structure for **13** and **14** might be as shown in Fig. 3. Many unsuccessful attempts were made to grow suitable single crystals for X-ray analysis of **13** and **14**

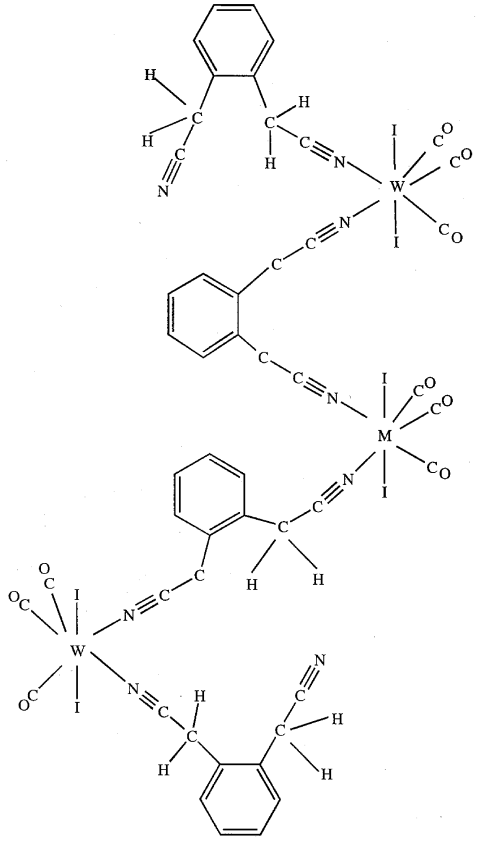


Fig. 2. Proposed structure of the trimetallic complexes $[MI_2(CO)_3(L^1)_2]$ (**11** and **12**) ($L^1 = [WI_2(CO)_3\{1,2\text{-}C_6H_4(CH_2CN)_2\text{-}N\}_2]$ (**2**)).

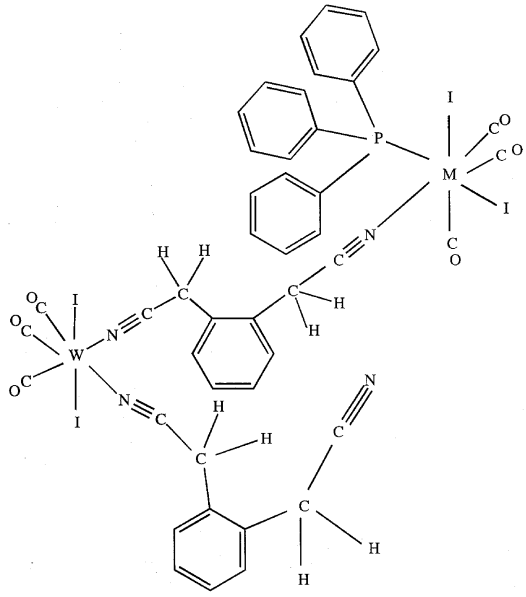


Fig. 3. Proposed structure of the bimetallic complexes $[MI_2(CO)_3L^1(PPh_3)]$ (**13** and **14**).

using a wide range of mixed solvent and temperature conditions. However, it should be noted that we have very recently [26] obtained the X-ray crystal structure of the related succinonitrile-bridged tungsten complex $[\{WI_2(CO)_3(PPh_3)\}_2\{\mu\text{-}NC(CH_2)_2CN\}]$. This also conforms with a more definitive assignment of the bimetallic and trimetallic nature of complexes **11–14.** IR and ^{1}H NMR data (Tables 2 and 3) conform with the structure shown in Fig. 3.

4. Conclusions

In conclusion, the potentially chelating ligand, 1,2-$C_6H_4(CH_2CN)_2$ coordinates in a monodentate manner in the seven-coordinate complexes $[MI_2(CO)_3\{1,2\text{-}C_6H_4(CH_2CN)_2\text{-}N\}_2]$ (M = Mo and W) and $[MI_2(CO)_3\{1,2\text{-}C_6H_4(CH_2CN)_2\text{-}N\}L]$ described in this paper. The molecular structure of $[WI_2(CO)_3\{1,2\text{-}C_6H_4(CH_2CN)_2\text{-}N\}_2]$ (**2**) shows definitively that *o*-phenylenediacetonitrile is coordinated in a monodentate manner in these complexes. In view of these observations, the use of **2** as a novel monodentate nitrile donor ligand has been successfully explored, and two trimetallic ($[MI_2(CO)_3L^1{}_2]$ $L^1 = \mathbf{2}$) and two bimetallic ($[MI_2(CO)_3L^1(PPh_3)]$) complexes have been successfully prepared and characterised during the course of this work.

Acknowledgements

E. Samson thanks the Training for Work Scheme for support. P.L. Veale thanks the ESF for support. We also thank A.W. Johans for help with the crystallographic work, and thank the EPSRC and the University of Reading for funds towards the purchase of the image plate system.

References

[1] P.K. Baker, S.G. Fraser, E.M. Keys, J. Organomet. Chem. 309 (1986) 319.
[2] P.K. Baker, M.B. Hursthouse, A.I. Karaulov, A.J. Lavery, K.M.A. Malik, D.J. Muldoon, A. Shawcross, J. Chem. Soc., Dalton Trans. (1994) 3493.
[3] P.K. Baker, M.E. Harman, M.B. Hursthouse, A.I. Karaulov, A.J. Lavery, K.M.A. Malik, D.J. Muldoon, A. Shawcross, J. Organomet. Chem. 494 (1995) 205.
[4] P.K. Baker, S.G. Fraser, Transition Met. Chem. 12 (1987) 560.
[5] P.K. Baker, A. Bury, J. Organomet. Chem. 359 (1989) 189.
[6] P.K. Baker, D. ap Kendrick, J. Organomet. Chem. 466 (1994) 139.
[7] P.K. Baker, T. Birkbeck, S. Bräse, A. Bury, H.M. Naylor, Transition Met. Chem. 17 (1992) 401.
[8] P.K. Baker, K.R. Flower, H.M. Naylor, K. Voigt, Polyhedron 12 (1993) 357.
[9] M.G.B. Drew, P.K. Baker, E.M. Armstrong, S.G. Fraser, D.J. Muldoon, A.J. Lavery, A. Shawcross, Polyhedron 14 (1995) 617.
[10] P.K. Baker, D.J. Muldoon, M.B. Hursthouse, S.J. Coles, A.J. Lavery, A. Shawcross, Z. Naturforsch., Sect. B. 51 (1996) 263.
[11] P.K. Baker, S.J. Coles, M.C. Durrant, S.D. Harris, D.L. Hughes, M.B. Hursthouse, R.L. Richards, J. Chem. Soc., Dalton Trans. (1996) 4003.
[12] P.K. Baker, M.M. Meehan, M.G.B. Drew, Transition Met. Chem. 24 (1999) 333.
[13] F.G. Mann, B.C. Saunders, Practical Organic Chemistry, Longmans Green, New York, 1954, pp. 342–344.
[14] W. Kabsch, J. Appl. Crystallogr. 21 (1988) 916.

[15] G.M. Sheldrick, SHELX86, Acta Crystallogr., Sect. A 46 (1990) 467.
[16] N. Walker, D. Stuart, Acta Crystallogr., Sect. A 39 (1983) 158.
[17] G.M. Sheldrick, SHELX, Program for Crystal Structure Refinement, University of Göttingen, Germany.
[18] D.P. Tate, W.R. Knipple, J.M. Augl, Inorg. Chem. 1 (1962) 433.
[19] P.K. Baker, S.G. Fraser, J. Organomet. Chem. 329 (1987) 209.
[20] M.G.B. Drew, Prog. Inorg. Chem. 23 (1977) 67.
[21] M. Melník, P. Sharrock, Coord. Chem. Rev. 65 (1985) 49.
[22] C.W. Haigh, P.K. Baker, Polyhedron 13 (1994) 417.
[23] P.K. Baker, Adv. Organomet. Chem. 40 (1996) 45.
[24] P.K. Baker, Chem. Soc. Rev. 27 (1998) 125.
[25] S.C. Tripathi, S.C. Srivastava, D.P. Pandey, Transition Met. Chem. 2 (1977) 52.
[26] P.K. Baker, M.G.B. Drew, J. Gardiner, unpublished results.

PERGAMON

www.elsevier.nl/locate/poly

Polyhedron 19 (2000) 155–163

POLYHEDRON

Dinuclear diimine palladium(II) and platinum(II) hydroxo and amido complexes: synthesis and X-ray crystal structures

S. Kannan, A.J. James, P.R. Sharp *

Department of Chemistry, University of Missouri-Columbia, Columbia, MO 65211, USA

Received 9 August 1999; accepted 5 October 1999

Abstract

Treatment of L_2MCl_2 with $AgBF_4$ in wet tetrahydrofuran (THF)–CH_2Cl_2 or wet CH_2Cl_2–ethanol yields the dinuclear palladium(II) and platinum(II) hydroxo complexes $[L_2M(\mu\text{-}OH)]_2(BF_4)_2$ (L_2 = diimine, M = Pd, Pt). Reaction of the dihydroxo bridged complexes with aromatic amines ($ArNH_2$) yields the corresponding diamido bridged complexes $[L_2M(\mu\text{-}NHAr)]_2(BF_4)_2$. $[L_2M(\mu\text{-}OH)]_2(BF_4)_2$ is unstable in methanol and converts to $[L_2M(\mu\text{-}OMe)]_2(BF_4)_2$. The structures of several of these complexes were determined by single crystal X-ray diffraction and show the expected edge-shared square-planar Pt centers with bridging hydroxo, methoxo, or amido groups. Attempts to deprotonate the hydroxo and amido complexes were not successful. ©2000 Elsevier Science Ltd All rights reserved.

Keywords: Amido; Diimine; Dimer; Hydroxo; Palladium; Platinum

1. Introduction

The synthesis and chemistry of palladium(II) and platinum(II) hydroxo and amido complexes have attracted interest for their relevance to the anti-tumor activity of Pt(II) complexes [1,2] and to the formation of C–O and C–N bonds in synthesis and catalysis [3–15]. The hydroxo complexes are also useful as synthetic precursors taking advantage of the nucleophilic character of the hydroxo ligand [8,15–22].

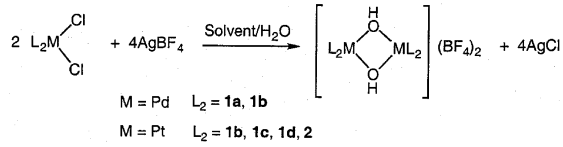
We have been interested in these complexes for their conjugate acid relationship to oxo and imido complexes, which are also relevant to C–O and C–N bond-forming reactions in catalytic processes [23–31]. The majority of our work in this area has been limited to phosphine ligand systems. Our initial attempts to expand to pyridine and bipyridine ligand systems met with limited success due to the poor solubility of the complexes [32]. Reports of soluble Pt(II) and Pd(II) complexes with non-cyclic diimine ligands [33–36] prompted us to explore the hydroxo and amido chemistry of Pt(II) and Pd(II) with these diimine ligands. This work is reported here.

* Corresponding author. Tel.: +1-573-882-7715; fax: +1-573-882-2754; e-mail: sharpp@missouri.edu

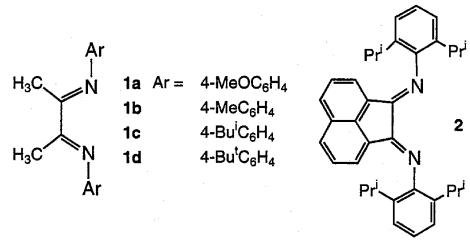
2. Results

2.1. Hydroxo complexes

Treatment of L_2MCl_2 (see Scheme 1 for identification of L_2) with $AgBF_4$ in wet solvents yields the dinuclear hydroxo complexes $[L_2M_2(\mu\text{-}OH)]_2(BF_4)_2$:



The hydroxo group is detected in the IR spectra of the complexes as a broad band at 3526–3550 cm^{-1}. ^1H NMR spectra show the expected diimine peaks. The hydroxo proton peaks are typically broad with shift values that depend on the



Scheme 1.

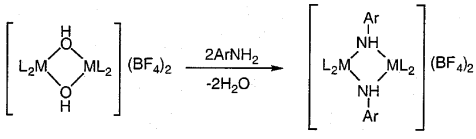
0277-5387/00/$ - see front matter ©2000 Elsevier Science Ltd All rights reserved.
PII S0277-5387(99)00338-1

metal and the solvent. Negative shifts are observed in $CDCl_3$ and in CD_2Cl_2. The Pd complexes typically give the lowest shift values (-2.70 and -3.02 ppm) with the Pt complexes just below 0 ppm (-0.60 to -0.63 ppm). Negative hydroxo group shifts are common for Pt and especially Pd hydroxo complexes in non-hydrogen-bonding solvents [17,21,37–40]. In deuterated acetone, the hydroxo peak shift values for the Pt complexes are positive and are found in the range 3.22–3.80 ppm. The downfield shift in acetone is presumably the result of hydroxo group hydrogen bonding to the acetone.

The dinuclear nature of the complexes is confirmed by X-ray crystal structure determinations on two of the complexes (M = Pd, L_2 = **1a** and M = Pt, L_2 = **1d**). ORTEP (Oak Ridge thermal ellipsoid plot) drawings are given in Figs. 1 and 2. An abbreviated summary of crystal data and data collection and processing is given in Table 1. Selected bond distances and angles are listed in Table 2. The expected μ-hydroxo groups, edge bridging two square planar metal centers, are observed for the cationic portions. The bond distances within the two structures are essentially identical. A difference in the two structures is observed in the M_2O_2 'diamond' core. The Pd core is non-planar with a fold angle at the O–O hinge of 140°. The Pt structure is almost planar with a fold angle of 170°. Other differences, related to the fold angle, are the metal–metal distances and the M–O–M angles. The metal–metal distance and the M–O–M angle are greater for Pt. Although there is doubt in the positions of the hydroxo group hydrogen atoms (located in a difference Fourier but not refined for Pd and ideal hydrogen bonded to THF positions for Pt), the hydrogen atoms are *cis* for Pd and *trans* for Pt. Detailed analysis of such structures reveals small energy differences between planar and non-planar forms [41–44].

2.2. Amido complexes

The dihydroxo complexes react readily with aromatic amines yielding the corresponding amido-bridged dinuclear complexes $[L_2M_2(\mu\text{-NHAr})]_2(BF_4)_2$:



M = Pd L_2 = **1a** Ar = *p*-$NO_2C_6H_4$, *p*-MeC_6H_4

M = Pt L_2 = **1b** Ar = Ph, *p*-MeC_6H_4

IR spectra of the diamido complexes show the presence of the bridging NH groups at 3248–3281 cm^{-1}. ^1H NMR spectra show the diimine ligand and broad peaks for the NH groups. The NH peaks are at positive shift values. Although the data are limited, the shift values in $CDCl_3$ appear to be lower for Pd (0.45 ppm) than for Pt (1.81 and 1.82), as is observed for the dihydroxo complexes.

The structure of two of the diamido complexes (M = Pd, L_2 = **1a**, Ar = *p*-$NO_2C_6H_4$; M = Pt, L_2 = **1b**, Ar = *p*-tol) were determined. ORTEP diagrams are shown in Figs. 3 and 4. An

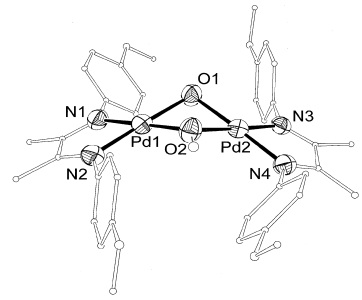


Fig. 1. ORTEP drawing of the cationic portion of $[L_2Pd(\mu\text{-OH})]_2(BF_4)_2$ (L_2 = **1a**).

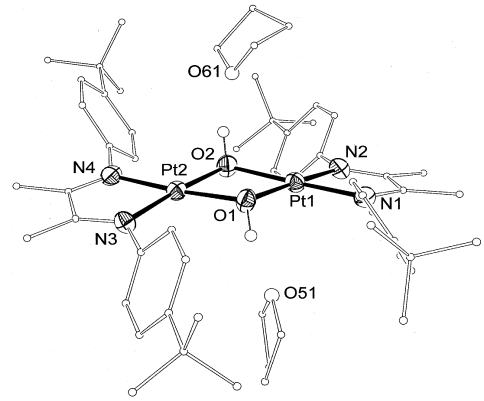


Fig. 2. ORTEP drawing of the cationic portion of $[L_2Pt(\mu\text{-OH})]_2(BF_4)_2$ (L_2 = **1d**) including hydrogen-bonded THF molecules.

abbreviated summary of crystal data and data collection and processing is given in Table 1. Selected bond distances and angles are listed in Table 3. The cationic portions of the structures consist of two edge-shared square-planar Pt centers with bridging NHAr groups. As with the hydroxo complexes above, bond distances within the two structures are essentially identical, but the Pd structure is non-planar while the Pt structure is planar (by symmetry). The fold angle for the Pd complex is 156°. The folding is again reflected in the metal–metal distances and the M–N–M angles, which are greater for the planar Pt structure. The amido group hydrogen atoms are at ideal calculated positions.

2.3. Attempted deprotonations

The reactions of the complexes with $LiN(SiMe_3)_2$ were investigated with the intent of forming oxo and imido complexes by deprotonation of the hydroxo and amido groups. Black precipitates, believed to be Pd metal, are obtained for the reactions of the Pd complexes. The Pt complexes generally gave a series of intense color changes (violet, blue, green, yellow, green and finally red) on addition of base. ^1H NMR spectra of the final red–brown products show broad resonances in the aliphatic and aromatic region. We were unable to purify or crystallize the products.

2.4. Miscellaneous

In at least one case the hydroxo complex reacts with alcohols. Slow evaporation of a solution of $[L_2Pd(\mu\text{-OH})]_2$-

Tuesday Feb 01 09:30 AM

Table 1
Crystallographic and data collection parameters at 173 K [a]

Complex	$[L_2Pd(\mu\text{-}OH)]_2(BF_4)_2$, L_2 = **1a**	$[L_2Pt(\mu\text{-}OH)]_2(BF_4)_2$, L_2 = **1d**	$[L_2Pd(\mu\text{-}NHR)]_2(BF_4)_2$, L_2 = **1a**, R = *p*-$C_6H_4NO_2$	$[L_2Pt(\mu\text{-}NHR)]_2(BF_4)_2$, L_2 = **1b**, R = *p*-tol	$[L_2Pd(\mu\text{-}OMe)]_2(BF_4)_2$, L_2 = **1a**	$[L_2Pt(\mu\text{-}Cl)]_2(BF_4)_2$, L_2 = **1b**
Formula	$C_{36}H_{42}N_4O_6Pd_2(BF_4)_2 \cdot CH_2Cl_2 \cdot 0.5C_4H_{10}O_2$	$C_{62}H_{54}N_2P_4Pt_2 \cdot 2(C_4H_8O) \cdot x$(solvent) [d]	$C_{48}H_{50}N_8O_8Pd_2(BF_4)_2 \cdot 1.5(C_2H_4Cl_2) \cdot H_2O$	$C_{50}H_{56}N_6O_2Pt_2(BF_4)_2 \cdot 5(C_4H_8O)$	$C_{38}H_{46}N_4O_6Pd_2(BF_4)_2$	$C_{36}H_{40}N_4Cl_2Pt_2(BF_4)_2$
Color/habit	orange–yellow/plate	orange/plate	red–orange/flat needle	red–orange/prism	red–brown/prism	red/prism
Crystal size (mm)	0.3×0.3×0.1	0.3×0.3×0.15	0.4×0.2×0.1	0.3×0.3×0.2	0.3×0.2×0.2	0.3×0.3×0.2
Crystal system	triclinic	orthorhombic	triclinic	triclinic	monoclinic	monoclinic
Space group (*Z*)	*P*1(2)	*Pbca*(8)	*P*1(2)	*P*1(1)	$P2_1/c$(2)	$P2_1/c$(2)
a (Å)	13.0847(6)	21.9439(11)	13.6261(7)	9.5790(5)	12.7857(7)	11.358(1)
b (Å)	13.3313(6)	21.3468(11)	14.4140(7)	12.4670(6)	13.3337(8)	13.049(3)
c (Å)	14.0272(7)	31.4621(16)	16.8682(8)	15.2335(8)	13.3354(8)	14.220(2)
α (°)	74.263(1)		95.576(1)	98.697(1)		
β (°)	81.306(1)		107.509(1)	90.653(1)	106.600(1)	108.400(9)
γ (°)	79.943(1)		100.243(1)	94.101(1)		
Total/unique/R_{int}	14305/9847/0.040	80911/16300/0.080	18326/12641/0.020	11042/7628/0.021	12577/4715/0.031	10375/4208/0.021
Observed/cut-off	7250/2σ(*I*)	11501/2σ(*I*)	9797/2σ(*I*)	6942/2σ(*I*)	3418/2σ(*I*)	3738/2σ(*I*)
θ_{max}/% measured	27.23/96	27.21/99	27.17/92	27.15/96	27.11/98	27.18/94
R_1 [b]/wR_2 [c]	0.108/0.257	0.069/0.120	0.052/0.129	0.037/0.086	0.042/0.100	0.020/0.048

[a] Siemens CCD system (omega scans), SADABS absorption correction.
[b] $R_1 = (\Sigma||F_o| - |F_c||)/\Sigma|F_o|$.
[c] $wR_2 = [(\Sigma w(F_o^2 - F_c^2)^2)/\Sigma w(F_c^2)^2]^{1/2}$.
[d] *x*(solvent) refers to a chemically unidentified collection of atoms refined as half-occupancy carbon atoms.

StyleTag -- Journal: **POLY** (*Polyhedron*) Article: **3291**

Table 2
Selected distances (Å) and angles (°) for $[L_2Pd(\mu\text{-}OH)]_2(BF_4)_2$, L_2 = **1a** and $[L_2Pt(\mu\text{-}OH)]_2(BF_4)_2$, L_2 = **1d**

Pd		Pt	
Pd1–Pd2	2.9838(9)	Pt1–Pt2	3.1365(4)
Pd1–O2	2.009(6)	Pt1–O1	2.034(5)
Pd1–O1	2.024(6)	Pt1–O2	2.027(5)
Pd2–O2	2.003(6)	Pt2–O1	2.026(5)
Pd2–O1	2.023(6)	Pt2–O2	2.024(5)
Pd1–N2	1.990(8)	Pt1–N1	1.989(6)
Pd1–N1	1.991(8)	Pt1–N2	1.990(6)
Pd2–N3	1.956(7)	Pt2–N3	1.988(6)
Pd2–N4	1.996(7)	Pt2–N4	1.983(6)
O2–Pd1–O1	76.5(3)	O2–Pt1–O1	78.2(2)
N2–Pd1–N1	78.9(3)	N2–Pt1–N1	79.1(3)
N2–Pd1–O2	101.7(3)	N2–Pt1–O2	101.5(2)
N1–Pd1–O2	178.4(3)	N1–Pt1–O2	178.0(2)
N2–Pd1–O1	177.8(3)	N2–Pt1–O1	177.3(2)
N1–Pd1–O1	102.9(3)	N1–Pt1–O1	101.3(2)
N3–Pd2–N4	79.4(3)	N4–Pt2–N3	79.0(3)
N3–Pd2–O2	177.8(3)	N4–Pt2–O2	101.3(2)
N4–Pd2–O2	102.5(3)	N3–Pt2–O2	174.8(2)
N3–Pd2–O1	101.5(3)	N4–Pt2–O1	174.9(2)
N4–Pd2–O1	178.0(3)	N3–Pt2–O1	101.6(2)
O2–Pd2–O1	76.6(3)	O2–Pt2–O1	78.4(2)
Pd1–O1–Pd2	95.0(3)	Pt1–O1–Pt2	101.2(2)
Pd2–O2–Pd1	96.1(3)	Pt2–O2–Pt1	101.5(2)

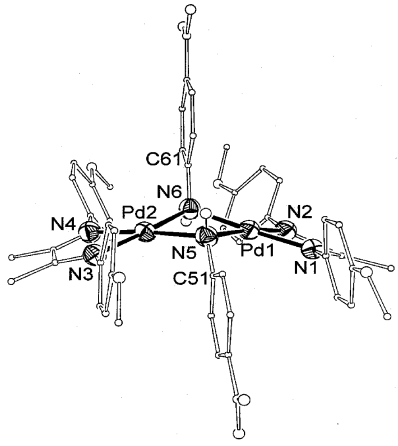


Fig. 3. ORTEP drawing of $[L_2Pd(\mu\text{-}NHAr)]_2(BF_4)_2$ (L_2 = **1a**, Ar = *p*-$NO_2C_6H_4$).

$(BF_4)_2$ (L_2 = **1a**) in MeOH yields red–brown crystals of $[L_2Pd(\mu\text{-}OMe)]_2(BF_4)_2$. An ORTEP diagram is shown in Fig. 5. An abbreviated summary of crystal data and data collection and processing is given in Table 1. Selected bond distances and angles are listed in Table 4. The cationic portion of the structure is similar to the hydroxo and amido complexes and consists of two edge-shared square-planar Pd centers with bridging OMe groups. The complex is planar by symmetry with a *trans* orientation of the methoxo methyl groups.

Poorly soluble $[L_2Pt(\mu\text{-}Cl)]_2(BF_4)_2$ (L_2 = **1b**) is obtained from the reaction of the hydroxo complex with $BF_3 \cdot OEt_2$ in CH_2Cl_2. The solvent is the apparent chloride source. An ORTEP diagram of the cationic portion is shown

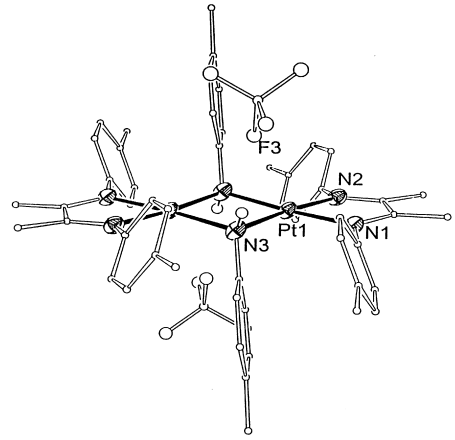


Fig. 4. ORTEP drawing of $[L_2Pt(\mu\text{-}NHAr)]_2(BF_4)_2$ (L_2 = **1b**, Ar = *p*-tol).

Table 3
Selected distances (Å) and angles (°) for $[L_2Pd(\mu\text{-}NHR)]_2(BF_4)_2$, L_2 = **1a**, R = *p*-$C_6H_4NO_2$, and $[L_2Pt(\mu\text{-}NHR)]_2(BF_4)_2$, L_2 = **1b**, R = *p*-tol [a]

Pd		Pt	
Pd1–Pd2	3.0544(4)	Pt1–Pt1	3.1738(4)
Pd1–N1	2.035(4)	Pt1–N1	2.021(4)
Pd1–N2	2.024(4)	Pt1–N2	2.031(4)
Pd2–N3	2.040(4)		
Pd2–N4	2.015(4)		
Pd1–N5	2.068(4)	Pt1–N3	2.060(4)
Pd1–N6	2.037(4)	Pt1–N3′	2.048(4)
Pd2–N5	2.074(4)		
Pd2–N6	2.038(4)		
N5–C51	1.427(6)	N3–C31	1.446(6)
N6–C61	1.416(6)		
N2–Pd1–N1	78.68(15)	N1–Pt1–N2	78.16(17)
N4–Pd2–N3	79.02(15)		
N1–Pd1–N5	102.20(15)	N1–Pt1–N3	100.68(17)
N3–Pd2–N5	102.43(15)		
N2–Pd1–N6	97.72(15)	N2–Pt1–N3′	102.72(17)
N4–Pd2–N6	97.12(15)		
N1–Pd1–N6	175.74(14)	N1–Pt1–N3′	175.34(17)
N3–Pd2–N6	176.07(15)		
N2–Pd1–N5	173.32(15)	N2–Pt1–N3	175.27(17)
N4–Pd2–N5	175.01(16)		
N6–Pd1–N5	81.65(15)	N3–Pt1–N3′	78.81(17)
N6–Pd2–N5	81.48(14)		
C51–N5–Pd1	115.4(3)	C31–N3–Pt1	112.7(3)
C51–N5–Pd2	116.5(3)	C31–N3–Pt1′	114.1(3)
C61–N6–Pd1	115.0(3)		
C61–N6–Pd2	115.9(3)		
Pd1–N5–Pd2	95.04(15)	Pt1–N3–Pt1′	101.19(17)
Pd1–N6–Pd2	97.11(16)		

[a] Atoms with a ‘’ suffix are symmetry-related to those without the suffix.

in Fig. 6. An abbreviated summary of crystal data and data collection and processing is given in Table 1. Selected bond distances and angles are listed in Table 5. The cationic portion of the structures is again similar to the hydroxo, methoxo and amido complexes and consists of two edge-shared square-planar Pt centers with bridging Cl atoms. The structure is planar by symmetry.

Table 4
Selected distances (Å) and angles (°) for $[L_2Pd(\mu\text{-}OMe)]_2(BF_4)_2$, L_2 = **1a** [a]

Pd–Pd	3.0783(5)	Pd–N1	2.000(3)	Pd′–O3	2.024(3)
Pd–N2	1.986(3)	Pd–O3	2.020(3)	O3–C5	1.479(6)
N2–Pd–N1	79.65(13)	N1–Pd′–O3	177.99(12)		
N2–Pd–O3	176.48(12)	C5–O3–Pd	112.0(3)		
N1–Pd–O3	99.96(11)	C5–O3–Pd′	112.3(3)		
O3–Pd–O3′	80.86(11)	Pd–O3–Pd′	99.14(11)		
N2–Pd′–O3	99.65(12)				

[a] Atoms with a ‘′’ suffix are symmetry-related to those without the suffix.

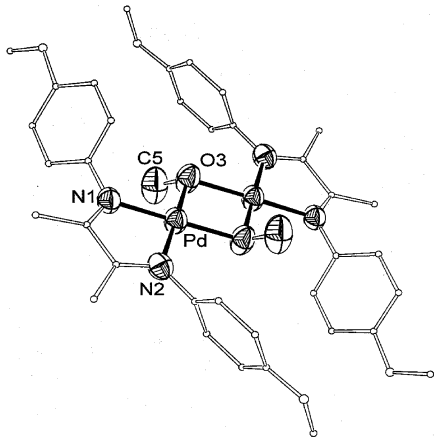


Fig. 5. ORTEP drawing of the cationic portion of $[L_2Pd(\mu\text{-}OMe)]_2(BF_4)_2$ (L_2 = **1a**).

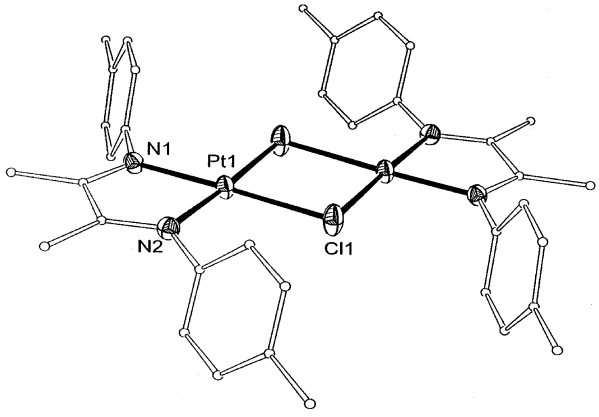


Fig. 6. ORTEP drawing of the cationic portion of $[L_2Pt(\mu\text{-}Cl)]_2(BF_4)_2$ (L_2 = **1b**).

3. Discussion

Diimine ligands have drawn attention recently for their great flexibility in synthesis and their tuneability to give desired electronic and steric properties [33–36]. Here we have shown that these ligands may be used to generate hydroxo and amido Pt and Pd dimers. The reaction that gives the hydroxo complexes has been used extensively in the synthesis of Pt and Pd hydroxo complexes. Chloride removal from L_2PdCl_2 and L_2PtCl_2 with Ag salts of non-coordinating anions has yielded binuclear hydroxo complexes for L = phosphines, arsines, pyridine, bipy, amines and sulfoxides [14,15,22,32,37,45–52]. Monomeric aqua and hydroxo complexes $[L_2M(OH_2)_2]^{2+}$ and $[L_2M(OH)_2]$, trinuclear hydroxo complexes $[L_2M(\mu\text{-}OH)]_3^{3+}$ and tetranuclear hydroxo complexes $[L_2M(\mu\text{-}OH)]_4^{4+}$ have also been isolated for some of these ligand systems [15,22,46,47,53–62]. Equilibria between these various species have been studied and are pH dependent [15,22,46,60,63,64]. We observe only the dimeric hydroxo complexes under the conditions employed.

Table 5
Selected distances (Å) and angles (°) for $[L_2Pt(\mu\text{-}Cl)]_2(BF_4)_2$, L_2 = **1b** [a]

Pt1–N1	1.981(2)	Pt1 Cl1	2.3256(8)
Pt1–N2	1.991(2)	Pt1 Cl1′	2.3196(8)
N1–Pt1–N2	79.26(10)	N2 Pt1′ Cl1	177.13(7)
N1–Pt1–Cl1	177.89(7)	Cl1 Pt1 Cl1′	83.15(3)
N2–Pt1–Cl1	99.72(7)	Pt1 Cl1 Pt1′	96.85(3)
N1–Pt1′–Cl1	97.87(7)		

[a] Atoms with a ‘′’ suffix are symmetry-related to those without the suffix.

Aminolysis of the hydroxo complexes to amido complexes has been less extensively applied and, for Pt and Pd, has been restricted to phosphine and aryl/alkyl ligand systems [17,38,65]. Our synthesis of the diimine amido complexes provides the first examples of Pt and Pd diamido complexes supported by diimine ligands.

4. Experimental

Experiments were routinely performed in air except for the reactions using $LiN(SiMe_3)_2$, which were conducted under a dinitrogen atmosphere in a Vacuum Atmospheres Corporation drybox, or by Schlenk techniques. Solvents and reagents were reagent grade and used as received except in the reactions of $LiN(SiMe_3)_2$, where the solvents were dried by standard methods. Solvent mixtures were prepared on a volume basis. Ethanol was 95%. The diimine ligands were prepared from the corresponding diketones by reported methods [35]. The starting chloro compounds L_2MCl_2 (M = Pd or Pt, L_2 = diimine) were prepared by procedures similar to those previously reported [36]. ^1H and ^{19}F NMR spectra were recorded on a Bruker AMX-250 spectrometer using internal trimethylsilane (TMS) (^1H) and external $CFCl_3$ (^{19}F) as references. Chemical shifts are reported in ppm with negative values upfield of the reference. IR spectra were recorded on a Nicolet 550 Magnum FTIR spectrometer using mineral oil

mulls between NaCl plates. Frequencies are reported in cm^{-1}. Spectra were recorded at ambient temperatures unless otherwise indicated. M-H-W Laboratories (Arizona) or National Chemical Consulting, Inc. (New Jersey) performed the microanalyses (inert atmosphere).

4.1. Preparation of $[L_2M(\mu\text{-}OH)]_2(BF_4)_2$

4.1.1. M = Pd, L_2 = **1a**

A THF (5 ml) solution of $AgBF_4$ (510 mg, 2.63 mmol) was added to a stirred CH_2Cl_2–THF (1:1, 50 ml) suspension of L_2PdCl_2 (600 mg, 1.27 mmol) containing a few drops of water. The mixture immediately precipitated AgCl. Stirring was continued for 3 h and then the mixture was filtered through a bed of diatomaceous earth. The clear red–orange filtrate was evaporated to dryness. The residue was dissolved in 2 ml of CH_2Cl_2 and filtered. The filtrate was layered with 3 ml of THF and cooled at −20°C overnight. The resulting red–orange crystalline product was filtered-off, washed with cold THF and ether, and dried. Recrystallization from CH_2Cl_2–THF afforded red–orange crystals. Yield: 420 mg (66%). *Anal*. Calc. (found) for $C_{36}H_{42}B_2F_8N_4O_6Pd_2 \cdot THF$: C, 44.3 (44.4); H, 4.6 (4.6); N, 5.2 (5.2)%. Crystals for the X-ray analysis were grown from CH_2Cl_2–DME.

^{1}H NMR (CD_2Cl_2): −2.70 (br s, 2H, OH), 2.27 (s, 12H, CH_3), 3.87 (s, 12H, OCH_3), 6.65 and 6.96 (m, 16H, C_6H_4). ^{19}F NMR (CD_2Cl_2): −150.6. IR: 3550 (OH), 1604 (C=N), 1050 (B–F).

4.1.2. M = Pd, L_2 = **1b**

The procedure was similar to that used for M = Pd, L_2 = **1a** and gave the product as a yellow solid. Yield: 97%. *Anal*. Calc. (found) for $C_{36}H_{42}N_4O_2B_2F_8Pd_2$: C, 45.6 (45.2); H, 4.5 (4.1); N, 5.9 (5.8)%.

^{1}H NMR (CD_2Cl_2): −3.02 (s, 2H, OH), 2.24 (s, 12H, CH_3), 2.41 (s, 12H, CH_3), 6.9 (s, 16H, C_6H_4). ^{19}F NMR (CD_2Cl_2): −148.7. IR: 3539 (OH), 1606 (C=N), 1063 (B–F).

4.1.3. M = Pt, L_2 = **1b**

A solution of $AgBF_4$ (355 mg, 1.83 mmol) in ethanol (5 ml) was added to a stirred CH_2Cl_2–ethanol (1:1, 40 ml) suspension of L_2PtCl_2 (485 mg, 0.91 mmol). The solution was stirred for 3 h and then filtered to remove AgCl. The clear red–brown filtrate was evaporated in air and the residue was extracted with 3 ml of CH_2Cl_2 and filtered. The filtrate was layered with 5 ml of ether and stored at −20°C overnight. The resulting red–brown crystals were filtered-off, washed with ether, and dried. Recrystallization from CH_2Cl_2–THF gave red–brown crystals. Yield: 480 mg (93%). *Anal*. Calc. (found) for $C_{36}H_{42}N_4O_2B_2F_8Pt_2 \cdot H_2O$: C, 37.8 (37.9); H, 3.9 (3.7); N, 4.9 (4.8)%.

^{1}H NMR (CD_2Cl_2): −0.60 (s, 2H, OH), 2.08 (s, 12H, CH_3), 2.47 (s, 12H, CH_3), 7.02 (d, J_{HH} = 8.3 Hz, 8H, C_6H_4), 7.11 (d, J_{HH} = 8.3 Hz, 8H, C_6H_4). ^{19}F NMR (CD_2Cl_2): −150.1. IR: 3634 (H_2O), 3534 (OH), 1633 (C=N), 1060 (B–F).

4.1.4. M = Pt, L_2 = **1c**

The procedure was similar to that used for M = Pt, L_2 = **1b** and gave the product as a red–brown solid. Yield: 90%. *Anal*. Calc. (found) for $C_{48}H_{66}N_4O_2B_2F_8Pt_2 \cdot H_2O$: C, 43.9 (44.2); H, 5.2 (5.1); N, 4.3 (4.1)%.

^{1}H NMR ($CDCl_3$, broad poorly resolved peaks): −0.61 (s, 2H, OH), 0.88 and 1.26 (m, 12H and 12H, $CH_3CH_2CHCH_3$), 1.56 (m, 8H, $CH_3CH_2CHCH_3$), 2.04 (s, 12H, CH_3), 2.58 (m, 4H, $CH_3CH_2CHCH_3$), 7.09–7.26 (br, 16H, C_6H_4).

^{1}H NMR (acetone-d_6): 0.90 (t, J_{HH} = 7.3 Hz, 12H, $CH_3CH_2CHCH_3$), 1.31 (dd, J_{HH} = 6.9, 1.0 Hz, 12H, $CH_3CH_2CHCH_3$), 1.68 (quint, J_{HH} = 7.3 Hz, 8H, $CH_3CH_2CHCH_3$), 2.15 (s, 12H, CH_3), 2.74 (sext, J_{HH} = 7.0 Hz, 4H, $CH_3CH_2CHCH_3$), 3.22 (s, 2H, OH), 7.25 (d, J_{HH} = 8.5 Hz, 8H, C_6H_4), 7.34 (d, J_{HH} = 8.5 Hz, 8H, C_6H_4). ^{19}F NMR ($CDCl_3$): −153.5. IR: 3598 (H_2O), 3526 (OH), 1630 (C=N), 1060 (BF).

4.1.5. M = Pt, L_2 = **1d**

The procedure was similar to that used for M = Pt, L_2 = **1b** and gave the product as a red–brown crystalline solid. Recrystallization from CH_2Cl_2–THF gave red–brown crystals. Yield: 85.6%. *Anal*. Calc. for $C_{48}H_{66}N_4O_2B_2F_8Pt_2 \cdot H_2O$: C, 43.9 (43.8); H, 5.2 (5.2); N, 4.2 (4.2)%.

^{1}H NMR (acetone-d_6): 1.36 (s, 36H, Bu^t), 2.06 (s, 12H, CH_3), 3.80 (s, 2H, OH), 7.22 (d, 8.5 Hz, J_{HH} = 8H, C_6H_4), 7.46 (d, J_{HH} = 8.5Hz, 8H, C_6H_4). ^{19}F NMR (acetone-d_6): −150.0. IR: 3600–3542 (br, OH), 1629 (C=N), 1063 (BF).

4.1.6. M = Pt, L_2 = 2

The procedure was similar to that used for M = Pt, L_2 = **1b** and gave the product as a red–brown solid. Yield: 97%. *Anal*. Calc. for $C_{72}H_{82}O_2N_4B_2F_8Pt_2$: C, 54.1 (53.9); H, 5.2 (5.3); N, 3.5 (3.4)%. The hydrogen atom numbering scheme in the ^{1}H NMR spectra is taken from [36].

^{1}H NMR (CD_2Cl_2): −0.63 (s, 2H, OH), 1.00 (d, J_{HH} = 6.8 Hz, 24H, $CH(CH_3)_2$), 1.37 (d, J_{HH} = 6.8 Hz, 24H, $CH(CH_3)_2$), 3.17 (sept, J_{HH} = 6.8 Hz, 8H, $CH(CH_3)_2$), 7.00 (d, J_{HH} = 7.3 Hz, 4H, H_3), 7.38 (d, J_{HH} = 7.8 Hz, 8H, H_{10}), 7.62, 7.66 (overlapping t, J_{HH} = 7.9 Hz, 8H, H_4 and H_{11}), 8.45 (d, J_{HH} = 8.3 Hz, 4H, H_5).

^{1}H NMR (acetone-d_6): 0.99 (d, J_{HH} = 6.8 Hz, 24H, $CH(CH_3)_2$), 1.50 (d, J_{HH} = 6.8 Hz, 24H, $CH(CH_3)_2$), 2.77 (s, 2H, OH), 3.44 (sept, J_{HH} = 6.8 Hz, 8H, $CH(CH_3)_2$), 6.84 (d, J_{HH} = 7.3 Hz, 4H, H_3), 7.52 (d, J_{HH} = 7.8 Hz, 8H, H_{10}), 7.72, 7.75 (overlapping t, J_{HH} = 7.6 Hz, 8H, H_4 and H_{11}), 8.57 (d, J_{HH} = 8.3 Hz, 4H, H_5). ^{19}F NMR (CD_2Cl_2): −152.5. IR: 3535 (br, H_2O, OH), 1642 (OH), 1607 (C=N), 1061 (BF).

4.2. Preparation of $[L_2M(\mu\text{-}NHAr)]_2(BF_4)_2$

4.2.1. M = Pd, L_2 = **1a**, Ar = p-$NO_2C_6H_4$

p-Nitroaniline (15 mg, 0.108 mmol) was slowly added to a stirred 1,2-dichloroethane solution (2 ml) of $[L_2M(\mu\text{-}OH)]_2(BF_4)_2$ (55 mg, 0.054 mmol). The mixture was stirred for 5 min and then filtered. The clear red–orange filtrate was stored in a closed vial at room temperature. Red crystals deposited overnight. These were filtered-off, washed with cold 1,2-dichloroethane, and dried. Yield: 64 mg (94%). *Anal*. Calc. (found) for $C_{48}H_{50}O_8N_8B_2F_8Pd_2$: C, 45.0 (45.1); H, 4.0 (4.1); N, 8.9 (8.9)%.

^{1}H NMR (DMSO-d_6): 1.87 (s, 12H, CH_3), 2.15 (s, 2H, NH), 3.81 (s, 12H, OCH_3), 6.09 (br s, 4H, amido-C_6H_4), 6.59 (br s, 8H, C_6H_4), 7.22–7.42 (br m, 12H, C_6H_4). ^{19}F NMR (CD_2Cl_2): −149.1. IR: 3271 (NH), 1609 (C=N).

4.2.2. M = Pd, L_2 = **1a**, Ar = p-tol

p-Toluidine (28.5 mg, 0.266 mmol) was slowly added to a stirred CH_2Cl_2 (5 ml) solution of $[L_2M(\mu\text{-}OH)]_2(BF_4)_2$ (120 mg, 0.118 mmol). The mixture immediately turned dark red–orange and was stirred for 2 h. The solution was reduced in volume to 2 ml, layered with ether and stored at −20°C overnight. The resulting orange solid was filtered-off, washed with ether, and dried. Yield: 125 mg (88.6%). *Anal*. Calc. (found) for $C_{50}H_{56}N_6B_2F_8O_4Pd_2$: C, 50.4 (49.9); H, 4.7 (4.4); N, 7.1 (7.1)%.

^{1}H NMR ($CDCl_3$): 0.45 (s, 2H, NH), 2.06 (s, 12H, CH_3), 2.17 (s, 6H, amido-CH_3), 3.81 (s, 12H, OCH_3), 5.88 (d, J_{HH} = 8.2 Hz, 4H, amido-C_6H_4), 6.31 (br d, J_{HH} = 8 Hz, 4H, C_6H_4), 6.37 (d, J_{HH} = 8.2 Hz, 4H, amido-C_6H_4), 6.45 (m, 4H, C_6H_4), 6.99 (br d, J_{HH} = 8 Hz, 4H, C_6H_4), 7.44 (br d, J_{HH} = 8 Hz, 4H, C_6H_4). ^{19}F NMR ($CDCl_3$): −149.8. IR: 3281, 3238 (NH), 1604 (C=N).

4.2.3. M = Pt, L_2 = **1b**, Ar = p-tol

The procedure was similar to that used for M = Pd, L_2 = **1a**, Ar = *p*-tol and gave the product as a red–brown solid. Yield: 85%. *Anal*. Calc. (found) for $C_{50}H_{56}N_6B_2F_8Pt_2 \cdot H_2O$: C, 45.4 (45.5); H, 4.4 (4.1); N, 6.4 (6.4)%.

^{1}H NMR (CD_2Cl_2): 1.81 (s, 12H, CH_3), 2.20 (s, 6H, amido-CH_3), 2.43 (s, 12H, CH_3), 3.07 (br s, 2H, NH), 6.01 (br d, J_{HH} = 7 Hz, 4H, C_6H_4), 6.08 (d, 8.1 Hz, 4H, C_6H_4), 6.43 (d, 8.1 Hz, 4H, C_6H_4), 6.83 (br d, J_{HH} = 7 Hz, 4H, C_6H_4), 7.44 (br s, 8H, C_6H_4). ^{19}F NMR (CD_2Cl_2): −151.0. IR: 3256 (br, NH), 1609 (C=N), 1060 (BF).

4.2.4. M = Pt, L_2 = **1b**, Ar = Ph

Aniline (17 mg, 0.18 mmol) in 1,2-dichloroethane (1 ml) was slowly added to a 1,2-dichloroethane (2 ml) solution of $[L_2M(\mu\text{-}OH)]_2(BF_4)_2$ (100 mg, 0.089 mmol). The mixture was stirred for 3 h. Then the solution was reduced in volume to 1 ml, layered with ether (2 ml), and stored at −20°C overnight. The red–brown crystalline product was filtered-off, washed with ether, and dried. Yield: 98 mg (86%). *Anal*. Calc. (found) for $C_{48}H_{52}N_6B_2F_8Pt_2$: C, 45.2 (45.2); H, 4.1 (3.9); N, 6.6 (6.4)%.

^{1}H NMR (CD_2Cl_2): 1.82 (s, 12H, CH_3), 2.43 (s, 12H, CH_3), 3.08 (br, 2H, NH), 5.99 (br m, 4H, C_6H_4), 6.20 (br d, J_{HH} = 8 Hz, 4H, Ph), 6.62 (m, 4H, Ph), 6.79 (m, 6H, Ph and C_6H_4), 7.59 (br d, J_{HH} = 8 Hz, 8H, C_6H_4). ^{19}F NMR (CD_2Cl_2): −151.2. IR: 3256, 3248 (NH), 1628(C=N), 1059 (BF).

4.3. Reactions with $LiN(SiMe_3)_2$

4.3.1. Pd complexes

A 1 ml solution of $LiN(SiMe_3)_2$ (33 mg, 0.198 mmol) was slowly added to a stirred suspension of $[L_2Pd(\mu\text{-}OH)]_2(BF_4)_2$, L_2 = **1a** (100 mg, 0.098 mmol) in THF. The solution immediately turned black and deposited a black solid assumed to be palladium metal. The reaction was repeated at −30°C with similar results. Identical results were obtained with L_2 = **1b** and with $[L_2Pd(\mu\text{-}NHAr)]_2(BF_4)_2$, L_2 = **1a**, Ar = *p*-$NO_2C_6H_4$ and *p*-tol.

4.3.2. Pt complexes

A 1 ml solution of $LiN(SiMe_3)_2$ (21 mg, 0.125 mmol) was slowly added to a stirred suspension of $[L_2Pt(\mu\text{-}OH)]_2(BF_4)_2$, L_2 = **1c** (70 mg, 0.062 mmol) in THF. A flash of violet was observed on the surface at the point of contact but this changed immediately to blue on stirring. Within a few minutes the solution became green followed by green–yellow and finally red. The clear red solution was stirred for 2 h and evaporated to dryness. The resulting red–brown powder was washed with ether and dried. Attempts to crystallize the product were unsuccessful. ^{1}H NMR spectra of the crude product were very broad. Similar results were obtained at −30°C and with L_2 = **1b**, **1c** and **1d** and with $[L_2Pt(\mu\text{-}NHAr)]_2(BF_4)_2$, L_2 = **1b**, Ar = Ph and *p*-tol. However, with $[L_2Pt(\mu\text{-}NHAr)]_2(BF_4)_2$, L_2 = **1b**, Ar = *p*-$NO_2C_6H_4$, a reasonably stable dark-blue solution was obtained but the ^{1}H NMR spectrum, while not broad, contained many peaks.

4.4. Reaction of $[L_2Pd(\mu\text{-}OH)]_2(BF_4)_2$ (L_2 = **1a**) with MeOH

$[L_2Pd(\mu\text{-}OH)]_2(BF_4)_2$ was suspended in methanol and stirred overnight. Slow evaporation of the resulting clear red–brown solution yielded red–brown crystals and yellow solid starting material ($[L_2Pd(\mu\text{-}OH)]_2(BF_4)_2$). One of the red–brown crystals was subjected to X-ray diffraction analysis and shown to be $[L_2Pd(\mu\text{-}OMe)]_2(BF_4)_2$.

4.5. Reaction of $[L_2Pt(\mu\text{-}OH)]_2(BF_4)_2$ (L_2 = **1b**) with $BF_3 \cdot OEt_2$

Two drops of $BF_3 \cdot OEt_2$ were added to a stirred red–brown dichloromethane solution of $[L_2Pt(\mu\text{-}OH)]_2(BF_4)_2$ (100 mg). The mixture became dark-red and was filtered and stored in a closed vial for 12 h. The resulting red crystals

were subjected to X-ray diffraction study and proved to be $[L_2Pt(\mu\text{-}Cl)]_2(BF_4)_2$. Poor solubility prevented characterization by NMR.

4.6. Crystal structure analyses

Crystal data, reflection collection and processing parameters, and solution and refinement data are summarized in Table 1. Full details are available from the CCDC. Crystals were mounted by pipetting crystals and mother liquor into a pool of heavy oil. A suitable crystal was selected and removed from the oil with a glass fiber. With the oil-covered crystal adhering to the end of the glass fiber the sample was transferred to a N_2 cold stream on the diffractometer and data were collected at 173 K.

Supplementary data

Full crystal structure information has been deposited with the Cambridge Crystallographic Data Centre (deposition numbers CCDC 133158-CCDC 133163).

Acknowledgements

The Division of Chemical Sciences, Office of Basic Energy Sciences, Office of Energy Research, US Department of Energy (grant DE-FG02-88ER13880) is gratefully acknowledged for financial support of this work. Grants from the National Science Foundation provided a portion of the funds for the purchase of the X-ray (NSF-CHE-9011804) and NMR (grants 8908304 and 9221835) equipment.

References

[1] S.J. Lippard, Platinum, Gold, and Other Metal Chemotherapeutic Agents: Chemistry and Biochemistry, American Chemical Society, Washington, DC, 1983.
[2] S.E. Sherman, S.J. Lippard, Chem. Rev. 87 (1987) 1153.
[3] B.H. Yang, S.L.J. Buchwald, Organomet. Chem. 576 (1999) 125.
[4] J.P. Wolfe, S. Wagaw, J.F. Marcoux, S.L. Buchwald, Acc. Chem. Res. 31 (1998) 805.
[5] J.F. Hartwig, Angew. Chem., Int. Ed. Engl. 37 (1998) 2047.
[6] J.F. Hartwig, Acc. Chem. Res. 31 (1998) 852.
[7] R. Gavagnin, M. Cataldo, F. Pinna, G. Strukul, Organometallics 17 (1998) 661.
[8] G. Strukul, A. Varagnolo, F. Pinna, J. Mol. Catal. A 117 (1997) 413.
[9] O. Hamed, P.M. Henry, Organometallics 16 (1997) 4903.
[10] J.-E. Backvall, E.E. Bjorkman, L. Pettersson, P. Siegbahn, J. Am. Chem. Soc. 106 (1984) 4369.
[11] J.-E. Backvall, E.E. Bjorkman, L. Pettersson, P. Siegbahn, J. Am. Chem. Soc. 107 (1985) 7265.
[12] M.A. Bennett, H. Jin, S.H. Li, L.M. Rendina, A.C. Willis, J. Am. Chem. Soc. 117 (1995) 8335.
[13] S. Ganguly, D.M. Roundhill, Organometallics 12 (1993) 4825.
[14] S. Ganguly, J.T. Mague, D.M. Roundhill, Inorg. Chem. 31 (1992) 3831.
[15] A. Fujii, E. Hagiwara, M. Sodeoka, J. Am. Chem. Soc. 121 (1999) 5450.
[16] V.F. Kuznetsov, C. Bensimon, G.A. Facey, V.V. Grushin, H. Alper, Organometallics 16 (1997) 97.
[17] J. Ruiz, N. Cutillas, J. Samperdo, G. López, J.A. Hermoso, M. Martínez-Ripoll, J. Organomet. Chem. 526 (1996) 67.
[18] V.V. Grushin, C. Bensimon, H. Alper, Organometallics 14 (1995) 3259.
[19] M. Akita, T. Miyaji, Y.J. Moro-oka, Chem. Commun. (1998) 1005.
[20] S. Park, A.L. Rheingold, D.M. Roundhill, Organometallics 10 (1991) 615.
[21] G. López, J. Ruiz, G. García, C. Vicente, J.M. Marti, J.A. Hermoso, A. Vegas, M. Martinez-Ripoll, J. Chem. Soc., Dalton Trans. (1992) 53.
[22] T.K. Miyamoto, Chem. Lett. (1994) 1971.
[23] M. Shelef, Chem. Rev. 95 (1995) 209.
[24] V. Schmatloch, N. Kruse, Surf. Sci. 269/270 (1992) 488.
[25] S. Lee, Methanol Synthesis and Technology, CRC Press, Boca Raton, FL, 1990.
[26] W.H. Cheng, H.H. Kung, Methanol Production and Use, Marcel Dekker, New York, 1994.
[27] P.M. Jones, J.A. May, J.B. Reitz, E.I. Solomon, J. Am. Chem. Soc. 120 (1998) 1506.
[28] K.D. Karlin, Y. Gultneh, Prog. Inorg. Chem. 35 (1987) 219.
[29] A.E. Martell, D.T. Sawyer, Oxygen Complexes and Oxygen Activation by Transition Metals, Plenum, New York, 1988.
[30] X.-C. Guo, R.J. Madix, J. Am. Chem. Soc. 117 (1995) 5523.
[31] R.J. Madix, J.T. Roberts, in: R.J. Madix (Ed.), Surface Reactions, Springer, New York, 1994, pp. 5–53.
[32] J.J. Li, W. Li, P.R. Sharp, Inorg. Chem. 35 (1996) 604.
[33] L.K. Johnson, S. Mecking, M. Brookhart, J. Am. Chem. Soc. 118 (1996) 267.
[34] L.K. Johnson, C.M. Killian, M. Brookhart, J. Am. Chem. Soc. 117 (1995) 6414.
[35] R. van Asselt, C.J. Elsevier, W.J.J. Smeets, A.L. Spek, R. Benedix, Recl. Trav. Chim. Pay-Bas 113 (1994) 88.
[36] R. van Asselt, C.J. Elsevier, C. Amatore, A. Jutand, Organometallics 16 (1997) 317.
[37] A.L. Bandini, G. Banditelli, F. Demartin, M. Manassero, G. Minghetti, Gazz. Chim. Ital. 123 (1993) 417.
[38] M.S. Driver, J.F. Hartwig, Organometallics 16 (1997) 5706.
[39] V.V. Grushin, H. Alper, Organometallics 12 (1993) 1890.
[40] V.V. Grushin, H. Alper, Organometallics 15 (1996) 5242.
[41] G. Aullon, G. Ujaque, A. Lledós, S. Alvarez, P. Alemany, Inorg. Chem. 37 (1998) 804.
[42] G. Aullon, G. Ujaque, A. Lledós, S. Alvarez, Chem. Eur. J. 5 (1999) 1391.
[43] R.H. Summerville, R. Hoffmann, J. Am. Chem. Soc. 98 (1976) 7240.
[44] M. Capdevila, W. Clegg, P. Gonzàlez-Duarte, A. Lledós, Inorg. Chem. 35 (1996) 490.
[45] G.W. Bushnell, K.R. Dixon, R.G. Hunter, J.J. McFarland, Can. J. Chem. 50 (1972) 3694.
[46] J.R. Marvin, E.H. Abbott, Inorg. Chim. Acta 247 (1996) 267.
[47] S. Fallis, G.K. Anderson, N.P. Rath, Organometallics 10 (1991) 3180.
[48] Z. Burgarcic, K. Lovqvist, A. Oskarsson, Acta Crystallogr., Sect. C 50 (1994) 1028.
[49] F.D. Rochon, R. Melanson, A. Morneau, Magn. Reson. Chem. 30 (1992) 697.
[50] V. Ericson, K. Lovqvist, B. Noren, A. Oskarsson, Acta Chem. Scand. 46 (1992) 854.
[51] G. Trovo, G. Bandoli, U. Casellato, B. Corain, M. Nicolini, B. Longata, Inorg. Chem. 29 (1990) 4616.
[52] F.D. Rochon, F. Guay, Acta Crystallogr., Sect. C 43 (1987) 43.
[53] J.A. Whiteford, C.V. Lu, P.J. Stang, J. Am. Chem. Soc. 119 (1997) 2524.

[54] P.J. Stang, B. Olenyuk, J. Fan, A.M. Arif, Organometallics 15 (1996) 904.
[55] P.J. Stang, D.H. Cao, G.T. Poulter, A.M. Arif, Organometallics 14 (1995) 1110.
[56] F.D. Rochon, A. Morneau, R. Melanson, Inorg. Chem. 27 (1988) 10.
[57] J.-P. Macquet, S. Cros, A.L. Beauchamp, J. Inorg. Biochem. 25 (1985) 197.
[58] R. Faggiani, B. Lippert, C.J.L. Lock, B. Rosenberg, Inorg. Chem. 17 (1978) 1941.
[59] R. Faggiani, B. Lippert, C.J.L. Lock, B. Rosenberg, Inorg. Chem. 16 (1977) 1192.
[60] S. Wimmer, P. Castan, F.L. Wimmer, N.P.J. Johnson, Chem. Soc., Dalton Trans. (1989) 403.
[61] M. Sperrle, V. Gramlich, G. Consiglio, Organometallics 15 (1996) 5196.
[62] F. Benetollo, R. Bertani, G. Bombieri, L. Toniolo, Inorg. Chim. Acta 233 (1995) 5.
[63] S.J. Barton, Inorg. Chim. Acta 273 (1998) 8.
[64] T.G. Appleton, J.R. Hall, S.F. Ralph, C.S.M. Thompson, Inorg. Chem. 28 (1989) 1989.
[65] J.J. Li, W. Li, A.J. James, T. Holbert, T.P. Sharp, P.R. Sharp, Inorg. Chem. 38 (1999) 1563.

PERGAMON

www.elsevier.nl/locate/poly

Polyhedron 19 (2000) 165–176

POLYHEDRON

Chelated fluoroboron cations
II. Synthesis and NMR studies involving aromatic chelating ligands

J. Stephen Hartman *, James A.W. Shoemaker [1]

Department of Chemistry, Brock University, St. Catharines, Ontario L2S 3A1, Canada

Received 2 August 1999; accepted 10 October 1999

Abstract

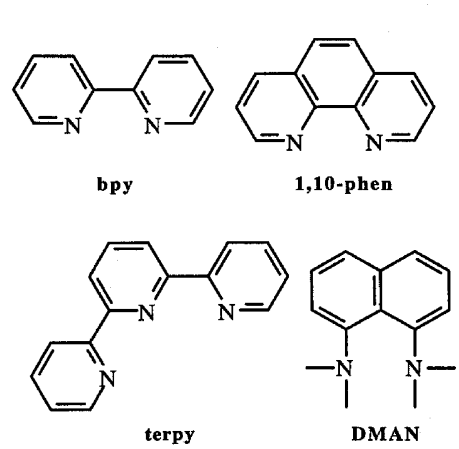
Possible methods of formation of chelated fluoroboron cations $(DD)BF_2^+$ and $(DD)BFX^+$, where DD is 2,2′-bipyridine (bpy), 1,10-phenanthroline (1,10-phen), 2,2′,6′,2″-terpyridine (terpy) and 1,8-bis(dimethylamino)naphthalene (DMAN, 'proton sponge'), have been investigated, primarily by ^{19}F and ^{11}B NMR and fast atom bombardment mass spectrometry. The most successful method involves displacement of weakly basic isoxazole (ISOX) and heavy halide ion from $ISOX \cdot BF_2X$ and $ISOX \cdot BFX_2$ (X = Cl, Br). Displacement of pyridine from $py \cdot BF_2Cl$ and $py \cdot BFCl_2$ is less effective because pyridine, more basic than isoxazole, competes with the chelating donor in forming fluoroboron cations when displaced from its adducts. 1,10-Phen, terpy and DMAN form $(DD)BF_2^+ \cdot BF_4^-$ when reacted with $Et_2O \cdot BF_3$ or with $ISOX \cdot BF_3$ under our conditions, but bpy does not. None of these chelating ligands can displace pyridine from $(py)_2BF_2^+ \cdot PF_6^-$ under conditions that are effective with tertiary-amine chelating donors. $(1,10\text{-Phen})BF_2^+$ but not the other $(DD)BF_2^+$ species is attacked by dimethylsulfoxide (DMSO), to form first $(DMSO)_2BF_2^+$ and finally $DMSO \cdot BF_3$. ©2000 Elsevier Science Ltd All rights reserved.

Keywords: 2,2′-Bipyridine; 1,8-Bis(dimethylamino)naphthalene; Boron-11 NMR; Chelated fluoroboron cations; Fast atom bombardment mass spectrometry; Fluorine-19 NMR; 1,10-Phenanthroline; 2,2′,6′,2″-Terpyridine

1. Introduction

There have been sporadic reports of the formation of chelated BF_2^+ cations with bidentate N-donor ligands over the past 30 years. Typically the ligand has been reacted with $Et_2O \cdot BF_3$ at room temperature or with BF_3 at −196°C, followed by slow warming [1–6]. The resulting species have been identified, but not very convincingly in some cases, by elemental analysis and/or by NMR [5–7]. Our studies [8–12] of the formation of fluoroboron cations by heavy halide ion displacement from mixed boron trihalide adducts [13], initially by monodentate ligands [8–11], have provided new approaches to the formation of chelated fluoroboron cations. Using these approaches we have formed BF_2^+, $BFCl^+$ and $BFBr^+$ cations of tertiary-amine chelating ligands [12], and established the conditions required to form the chelated cation, compared with those that give only the bis-BF_3 adduct $F_3B \cdot DD \cdot BF_3$. We now report our extension of these studies to aromatic N-donor chelating ligands, which behave very differently from the saturated-amine chelating ligands.

2,2′-Bipyridine (bpy), 1,10-phenanthroline (1,10-phen), and 2,2′,6′,2″-terpyridine (terpy) are well-known chelating ligands which coordinate to a wide range of metal ions [14,15], while 1,8-bis(dimethylamino)naphthalene (DMAN; also known as 'proton sponge') is noteworthy for its very high Bronsted basicity ($pK_b^1 = 1.7$) [4,16] but very high steric hindrance about the nitrogens which inhibits its reactivity with Lewis acids. All but terpy have been reported to form difluoroboron cations [5,6], as well as dichloroboron



* Corresponding author. Tel.: +1-905-688-5550, ext. 3849; e-mail: shartman@chemiris.labs.brocku.ca

[1] Present address: Symyx Technologies, Inc., Santa Clara, CA, USA.

0277-5387/00/$ - see front matter ©2000 Elsevier Science Ltd All rights reserved.
PII S0277-5387(99)00339-3

[5,6,17] and (except for DMAN) dibromoboron [17] cations.

Kinetic simulations, based on Janzen's 'coordination model' of reaction mechanisms [18], indicate that reactions of bidentate nitrogen donor molecules with BF_3 should give only the non-chelated bis-BF_3 adduct $F_3B \cdot DD \cdot BF_3$ rather than the chelated $(DD)BF_2^+ \cdot BF_4^-$ [19]. This is borne out in some cases [20,21], whereas in other cases the chelated species do form in high yield [1,2]. Preliminary work in Janzen's laboratory, involving reaction of ethylenediamine (en) and bpy with BF_3 in a variety of solvents, has given only low yields of chelated $(en)BF_2^+$ and $(bpy)BF_2^+$ under only a few of the reaction conditions tried, and even in these cases these products are always accompanied by much larger amounts of the corresponding bis-BF_3 adduct [22]. We here explore the formation of chelated fluoroboron cations of aromatic chelating ligands from the BF_3 sources $Et_2O \cdot BF_3$ and isoxazole $\cdot BF_3$, in addition to their formation by heavy halide ion displacement from mixed boron trihalide adducts.

2. Experimental

2.1. Materials and methods

Materials were handled with standard inert-atmosphere Schlenk line and glove bag techniques. 2,2′-Bipyridine (Aldrich, 99+%), 1,10-phenanthroline (Aldrich, 99+%), 2,2′,6′,2″-terpyridine (Aldrich, 98%), and 1,8-bis(dimethylamino)naphthalene (Aldrich, 99%) were used without further purification. All chelating donors were stored in desiccators over Drierite. Boron trifluoride (Aldrich, 99.5%), boron trifluoride etherate (Aldrich), boron trichloride (Matheson, 99.5%) boron tribromide (Aldrich, 99.9%), isoxazole (Aldrich 99%) (ISOX), ammonium hexafluoro-



ISOX

phosphate (Aldrich, 95+%), and pyridine (Aldrich, 99.5%) were handled as described previously [9,10,12]. Solvents were used without further purification, and were dried as described previously [12].

Most ^{19}F and ^{11}B spectra were obtained on a Bruker AC-200 4.7 Tesla multinuclear Fourier transform NMR spectrometer operating at 188.31 MHz (^{19}F) and 64.20 MHz (^{11}B), using 5 mm NMR tubes. ^{19}F spectra were obtained with 16K FIDs, 16K zero-filling, and spectral windows of up to 35 000 Hz, with between 256 and 4096 30° pulses and a relaxation delay of 1.0 s. The 90° pulse length was 6.6 μs. ^{19}F chemical shifts are accurate to ± 0.1 ppm and were internally referenced to C_6F_6 as a secondary standard (-162.7 ppm from $CFC1_3$), and are reported in ppm from $CFC1_3$. $^1J_{BF}$ coupling constants are accurate to ± 1 Hz. ^{11}B spectra were obtained with 16K FIDs, 16K zero-filling, and spectral windows of up to 6400 Hz, with between 256 and 4096 30° pulses and a relaxation delay of between 0.5 and 10 s. The 90° pulse length was 17.1 μs. ^{11}B chemical shifts are accurate to ± 0.1 ppm and were externally referenced to $Et_2O \cdot BF_3$. The NMR data were manipulated using WIN NMR software, normally with the application of 1.5 Hz of line broadening (^{19}F).

Some ^{19}F, ^{11}B, and $^{11}B\{^{19}F\}$ NMR spectra were obtained at 30°C on a Bruker DRX-500 11.7 Tesla multinuclear Fourier transform NMR spectrometer (McMaster University) operating at 470.53 MHz (^{19}F) and 160.46 MHz (^{11}B) using between 40 and 128 30° pulses with 32K FIDs. The 90° pulse durations were 7.5 μs (^{19}F) and 15.0 μs (^{11}B). Spectral windows of 42 016 Hz (^{19}F) and 40 000 Hz (^{11}B) were used. $^{11}B\{^{19}F\}$ decoupling experiments used selective and broad band decoupling pulse power between 25 and 35 dB.

^1H, ^1H–^1H COSY and ^{13}C spectra were obtained on a Bruker DPX-300 7.4 Tesla multinuclear Fourier transform NMR spectrometer operating at 300.13 and 75.45 MHz, respectively, and referenced to internal tetramethylsilane (TMS).

^{11}B solid state magic angle spinning (MAS) NMR spectra were obtained on a Bruker DPX-300 7.4 Tesla multinuclear Fourier transform NMR spectrometer operating at 96.29 MHz, using a Bruker MAS probe with 4 mm spinners (capacity ~100 mg) and spin rates of 5–12.5 KHz. Between 256 and 2048 scans were obtained, with relaxation delays of 0.5–5.0 s between scans. 32K data points were obtained, and Fourier transformed with 5–15 Hz of line broadening. Trimethyl borate was used as the external standard, with its chemical shift being set to 18.3 ppm from $Et_2O \cdot BF_3$.

Positive and negative ion FAB spectra were obtained on a Concept 1S double beam mass spectrometer with 8 kV accelerating voltage, using Xe collision gas at 7.5 W power. Data were collected on a Kratos DART data system with SUN Spectrostation 10, using XMACH3 software. 3-Nitrobenzyl alcohol (NBA) was used as the liquid matrix. This matrix can protonate bases, so protonated-base FAB peaks, which are often of high intensity, can be generated in the instrument; they do not necessarily indicate a high concentration of protonated base in the original sample.

The $py \cdot BF_nCl_{3-n}$, $ISOX \cdot BF_nCl_{3-n}$ and $ISOX \cdot BF_nBr_{3-n}$ adduct systems were prepared in Schlenk vessels (using methods previously described [9,11]) and transferred either directly to NMR tubes (for the pyridine adduct systems with all products soluble) or to 2 ml septum-capped GC–MS vials (Hewlett Packard) for ease of centrifugation of precipitates and solvent removal (for the ISOX adduct systems which normally give insoluble products). Typical reactions of the $py \cdot BF_nCl_{3-n}$, $ISOX \cdot BF_nCl_{3-n}$ and $ISOX \cdot BF_nBr_{3-n}$ systems with the chelating donors were carried out using 20–25 mg of $py \cdot BF_3$ or $ISOX \cdot BF_3$ in 0.5–1.0 ml of $CHCl_3$ or $CDCl_3$, with the appropriate amount of BCl_3 or BBr_3 added to give the desired F:Cl or F:Br ratio. The chelating ligand (neat if liquid; in concentrated solution in chloroform if

solid) was added by syringe to the mixed boron trihalide adduct solution (followed by stirring if in an NMR tube; very rapid precipitation occurs with many ISOX systems). With the $py \cdot BF_nCl_{3-n}$ system a standard ratio of reagents corresponding to $py \cdot BF_3$:BCl_3:chelating donor = 5:2:3:5 was used. With the $ISOX \cdot BF_nCl_{3-n}$, system, two standard ratios of reagents were used: 'fluorine-rich', with ISOX:BF_3:BCl_3:chelating donor = 2:1:1:2; and 'chlorine-rich', with ISOX:BF_3:BCl_3:chelating donor = 4:1:3:4. With the $ISOX \cdot BF_nBr_{3-n}$ systems, similar ratios were used: 'fluorine-rich', ISOX:BF_3:BBr_3:chelating donor = 5:2:3:5; and 'bromine-rich', ISOX:BF_3:BBr_3:chelating donor = 4:1:3:4.

Reactions of $Et_2O \cdot BF_3$ and $ISOX \cdot BF_3$ with the chelating donors were carried out by adding neat $Et_2O \cdot BF_3$, or $ISOX \cdot BF_3$ dissolved in the reaction solvent, to 1–15 ml of solution containing 20–100 mg of the chelating donor in benzene, chloroform, acetone, or diethyl ether. Mole ratios of $Et_2O \cdot BF_3$ or $ISOX \cdot BF_3$ to chelating donor varied from 3:1 to 1:1.

$(py)_2BF_2^+ \cdot PF_6^-$ was prepared by a modification of the method used previously [9], involving precipitation from a 1:1 chloroform–ethanol solution. Reactions of $(py)_2BF_2^+ \cdot PF_6^-$ with the chelating donors were attempted in acetone solutions containing 20 mg ml^{-1} of $(py)_2BF_2^+ \cdot PF_6^-$, to which a 2- or 10-fold molar excess of chelating donor was added.

2.2. Specific reactions

2.2.1. $Py \cdot BF_nCl_{3-n}$ plus bpy

The clear colourless solution turned pink on standing, with white crystals of $(bpy)BF_2^+ \cdot Cl^-$ and $(py)_2BF_2^+ \cdot Cl^-$ precipitating. Positive ion FAB mass spectra of the solution: $py \cdot H^+$ [80 *m/z* (3.1%)]; $bpy \cdot H^+$ [157 *m/z* (100%)]; $(bpy)BF_2^+$ [205 *m/z* (2.1%)]; $(py)_2BF_2^+$ [207 *m/z* (8.6%)]. Positive ion FAB mass spectra of the white crystals: $bpy \cdot H^+$ [157 *m/z* (100%)]; $(bpy)BF_2^+$ [205 *m/z* (63.2%)]; $(py)_2BF_2^+$ [207 *m/z* (47.8%)]. These crystals were soluble in sulpholane. ^{19}F signals: $(bpy)BF_2^+$, −154.0 ppm [splittings due to $^1J_{BF}$ not visible]; $(py)_2BF_2^+$, −155.7 ppm [$^1J_{BF}$ = 22.8 Hz]; BF_4^-, −152.8 ppm [9]. In the less viscous 3:1 acetone–sulpholane mixed solvent the $(bpy)BF_2^+$ signal is split into a 1:1:1:1 quartet [$^1J_{BF}$ = 23.4 Hz].

2.2.2. $Py \cdot BF_nCl_{3-n}$ plus 1,10-phen

1,10-Phen reacted with $py \cdot BF_2Cl$, to give $(1,10\text{-phen})BF_2^+$ along with $(py)_2BF_2^+$ and some BF_4^-, detected by ^{19}F NMR (Table 1). White crystals precipitated over ten days. Positive ion FAB mass spectra of the crystals and the

Table 1
NMR parameters of haloboron cations

	^{19}F chemical shift (ppm) in:		^{11}B chemical shift (ppm) in:		$^1J_{BF}$ (Hz) in:	
	$CDCl_3$	CH_3NO_2	$CDCl_3$	CH_3NO_2	$CDCl_3$	CH_3NO_2
$(Bpy)BF_2^+$	−154.4	−155.7		5.7		23.5
$(Py)_2BF_2^+$ [a]	−155.6		1.7		22.9	
$(1,10\text{-Phen})BF_2^+$		−149.8		7.0		24.4
$(Terpy)BF_2^+$	−146.0	−145.2	5.0	6.0	[b]	25.2
$(Py)(2\text{-Mepy})BF_2^+$ [a]	−147.5		2.1		25.4	
$(DMAN)BF_2^+$	−164.4		1.9		30.3	
$(Me_3N)_2BF_2^+$ [c]	−165.4		1.9		36.2	
$(Bpy)BFCl^+$	−142.3	−143.6	7.4	8.4	~55	51.7
$(Py)_2BFCl^+$ [a]	−146.9		6.2		47.8	
$(1,10\text{-Phen})BFCl^+$	−139.4	−139.1	8.7	9.8	[b]	52.9
$(Terpy)BFCl^+$	−129.8	−128.0	7.6	8.7	49.9	49.1
$(Bpy)BFBr^+$		−137.5		6.1		61.5
$(Py)_2BFBr^+$ [a]	−142.4		4.9		58.1	
$(1,10\text{-Phen})BFBr^+$		−135.3		7.1		63.2
$(Terpy)BFBr^+$	−126.7	−125.1		5.4	[b]	60.6
$(Py)(2\text{-Mepy})BFBr^+$ [a]	−129.4		5.2		62.1	
$(Bpy)BCl_2^+$			7.8	8.8		
$(Py)_2BCl_2^+$ [a]			8.4			
$(1,10\text{-Phen})BCl_2^+$			9.1	10.2		
$(Terpy)BCl_2^+$			8.0	9.0		
$(Bpy)BBr_2^+$				0.0		
$(Py)_2BBr_2^+$ [a]			2.6			
$(1,10\text{-Phen})BBr_2^+$				0.6		
$(Terpy)BBr_2^+$			−1.4	−0.9		

[a] Values from [9].
[b] Unresolved.
[c] Values from [8].

solution did not give a detectable $(1,10\text{-phen})BF_2^+$ signal, but only $1,10\text{-phen}\cdot H^+$ and $(py)_2BF_2^+$ signals.

2.2.3. $Py\cdot BF_nCl_{3-n}$ plus terpy

Terpy reacted with $py\cdot BF_2Cl$, giving $(terpy)BF_2^+$ along with BF_4^- and $(py)_2BF_2^+$ after 48 h, as detected by ^{19}F NMR. White crystals precipitated, apparently the chloride salts of $(terpy)BF_2^+$ and $(py)_2BF_2^+$. Positive ion FAB mass spectra of the solution: $terpy\cdot H^+$ [234 m/z (100%)]; $(terpy)BF_2^+$ [282 m/z ($\sim$2%)]; $(py)_2BF_2^+$ [207 m/z (5.4%)]. Positive ion FAB mass spectra of the white crystals: $terpy\cdot H^+$ [234 m/z (100%)]; $(terpy)BF_2^+$ [282 m/z (4.3%)]; $(py)_2BF_2^+$ [207 m/z (12.4%)].

2.2.4. $ISOX\cdot BF_nCl_{3-n}$ plus bpy

A pink precipitate formed immediately, and the colourless supernatant liquid gave ^{11}B and ^{19}F NMR spectra consistent with very low concentrations of $(bpy)BF_2^+$, $(bpy)BFCl^+$, $(bpy)BCl_2^+$ and BF_4^- (Table 1). Positive ion FAB mass spectra of the precipitates obtained from the fluorine-rich and chlorine-rich reaction mixtures gave signals as follows (with peak intensities from the fluorine-rich reaction mixture listed first): $(bpy)BF_2^+$ [205 m/z (100%; 100%); $(bpy)BFCl^+$ [221 m/z (29.1%; 69.2%)]; $(bpy)BCl_2^+$ [237 m/z (0.0%; 19.4%)]. ^{11}B and ^{19}F spectra of the precipitate, dissolved in 3:1 acetone–sulpholane or nitromethane, confirm the presence of $(bpy)BF_2^+$, $(bpy)BFCl^+$ and BF_4^- (only a trace in the chlorine-rich sample), plus (in the chlorine-rich sample) $(bpy)BCl_2^+$ and a large amount of BCl_4^- (7.7 ppm).

2.2.5. $ISOX\cdot BF_nCl_{3-n}$ plus 1,10-phen

An orange precipitate formed immediately, and the yellow supernatant liquid gave ^{11}B and ^{19}F NMR spectra indicating very low concentrations of $(1,10\text{-phen})BFCl^+$, $(1,10\text{-phen})BCl_2^+$ (chlorine-rich sample only) and BF_4^-. Positive ion FAB mass spectra of the precipitate (fluorine-rich and chlorine-rich samples, respectively): $1,10\text{-phen}\cdot H^+$ [181 m/z (100%; 100%)]; $(1,10\text{-phen})BF_2^+$ [229 m/z (95.7%; 85.8%)]; $(1,10\text{-phen})BFCl^+$ [245 m/z (25.7%; 54.0%)]; $(1,10\text{-phen})BCl_2^+$ [261 m/z (0.0%; 6.7%)]. ^{11}B and ^{19}F NMR spectra of the precipitate, dissolved in 3:1 acetone–sulpholane or nitromethane, confirm the presence of $(1,10\text{-phen})BF_2^+$, $(1,10\text{-phen})BFCl^+$ and BF_4^-, plus (in the chlorine-rich sample) $(1,10\text{-phen})BCl_2^+$ and a large amount of BCl_4^-. Both ^{11}B NMR spectra and positive ion FAB mass spectra show that the amount of $(1,10\text{-phen})BCl_2^+$ is less than the amount of $(bpy)BCl_2^+$ in the correspconding bpy system.

2.2.6. $ISOX\cdot BF_nCl_{3-n}$ plus terpy

A very small amount of brown precipitate formed immediately, and the yellow supernatant liquid gave ^{11}B and ^{19}F NMR spectra indicating the presence of $(terpy)BF_2^+$, $(terpy)BFCl^+$, BF_4^- and (in the chlorine-rich sample) $(terpy)BCl_2^+$. FAB mass spectra obtained from the chloroform solution (fluorine-rich) gave peaks corresponding to: $terpy\cdot H^+$ [234 m/z (100%)]; $(terpy)BF_2^+$ [282 m/z (90.1%)]; $(terpy)BFCl^+$ [298 m/z (29.1%)]. FAB mass spectra of the precipitate gave peaks corresponding to (fluorine-rich and chlorine-rich samples, respectively): $terpy\cdot H^+$ [234 m/z (85.8%; 99.6%)]; $(terpy)BF_2^+$ [282 m/z (100%; 41.1%)]; $(terpy)BFCl^+$ [298 m/z (29.6%; 100%)]; $(terpy)BCl_2^+$ [314 m/z (0.0%; 14.9%)]. (The proportion of $(terpy)BFCl^+$ in the chlorine-rich sample appeared to be much larger from the FAB spectrum than from the ^{11}B NMR spectrum.) ^{11}B and ^{19}F NMR spectra of the precipitate, dissolved in 3:1 acetone–sulpholane or nitromethane, confirmed the presence of $(terpy)BF_2^+$, $(terpy)BFCl^+$, BF_4^-, plus (in the chlorine-rich sample) $(terpy)BCl_2^+$ and a large amount of BCl_4^-.

2.2.7. $ISOX\cdot BF_nCl_{3-n}$ plus DMAN

Reaction of DMAN with the chlorine-rich $ISOX\cdot BF_nCl_{3-n}$ solution gave a series of colour changes over several hours: successively yellow, orange, brown, red, gold, and brown, before settling on deep purple. Strong ^{11}B NMR signals arose that can be assigned to BCl_4^- (6.9 ppm), $BFCl_3^-$ (7.0 ppm [$^1J_{BF}=81.8$ Hz]), and $BF_2Cl_2^-$ (5.0 ppm [$^1J_{BF}=54.8$Hz]) [10,23]. This was confirmed by ^{19}F NMR showing that $BFCl_3^-$ and $BF_2Cl_2^-$ were indeed the major fluorine-containing species, making up over 50% of the total ^{19}F intensity: -95.4 ppm [$^1J_{BF}=81.6$ Hz]; -105.4 ppm [$^1J_{BF}=54.7$ Hz], respectively [10,23]. Typical ^{11}B signal intensities were: BCl_4^- and $BFCl_3^-$ (overlapping), 53%; BF_2Cl_2, 27%; broad signals in the 4 to 1 ppm region, 20%. Only in the presence of an excess of DMAN to ISOX, and with heating at 50°C, did significant amounts of $(DMAN)BF_2^+$ form: ^{11}B 1:2:1 triplet at 1.9 ppm [$^1J_{BF}=30.3$ Hz] (lit.: 2.3 ppm, $^1J_{BF}=27$ Hz [4]; 1.9 ppm [5]; the chemical shifts were listed as negative values in these papers because the old sign convention was in use, with positive values to low frequency, (high field); ^{19}F 1:1:1:1 quartet at -164.4 ppm [$^1J_{BF}=30.3$ Hz]. NMR signals of unreacted $ISOX\cdot BCl_3$ and $ISOX\cdot BFCl_2$ were still present. The positive ion FAB mass spectrum showed only two major species: $DMAN\cdot H^+$ [215 m/z (100%)]; $(DMAN)BF_2^+$ [263 m/z (5.6%)].

2.2.8. $ISOX\cdot BF_nBr_{3-n}$ plus bpy

A yellow precipitate formed immediately on addition of $ISOX\cdot BF_nBr_{3-n}$ to chloroform solutions containing bpy; BF_4^- in low concentration was the only species detectable in the supernatant liquid by ^{19}F NMR. FAB mass spectra of the precipitate gave peaks corresponding to (fluorine-rich and bromine-rich samples, respectively): $bpy\cdot H^+$ [157 m/z (37.2%, 42.9%)]; $(bpy)BF_2^+$ [205 m/z (29.2%, 18.3%)]; $(bpy)BBr^+$ [246 m/z (21.4%, 17.6%)]; $(bpy)BFBr^+$ [265 m/z (5.7%, 5.7%)]; $(bpy)BBr_2^+$ [327 m/z (100%, 100%)]. Thus $(bpy)BBr_2^+$ predominates in the solids prepared from both fluorine-rich and bromine-rich reaction mixtures. The precipitate, dissolved in nitromethane, gave ^{19}F and ^{11}B NMR signals corresponding to $(bpy)BF_2^+$,

(bpy)$BFBr^+$, (bpy)BBr_2^+ and BF_4^-. The ^{11}B multiplets of the difluoro- and fluorobromoboron cations overlap at 4.7 Tesla, but are readily distinguished at 11.7 Tesla.

2.2.9. ISOX·BF_nBr_{3-n} plus 1,10-phen

A brown oil settled out over several hours, following which only BF_4^- in low concentration could be detected in the supernatant liquid by ^{19}F and ^{11}B NMR. NMR monitoring, carried out before the oil began to separate, on a bromine-rich sample (equimolar 1,10-phen and total ISOX) indicated very rapid reaction of ISOX·BF_2Br and ISOX·$BFBr_2$, only their reaction products (1,10-phen)BF_2^+ and (1,10-phen)-$BFBr^+$ being detectable in the initial spectrum. ISOX·BF_3 and ISOX·BBr_3 reacted slowly, giving further (1,10-phen)BF_2^+ from the BF_3 adduct and (1,10-phen)BBr_2^+ from the BBr_3 adduct, as the oil began to separate. The oil gave FAB mass spectral peaks consistent with (fluorine-rich and chlorine-rich samples, respectively): 1,10-phen·H^+ [181 *m/z* (100%, 100%)]; (1,10-phen)BF_2^+ [229 *m/z* (35.3%, 45.8%)]; (1,10-phen)BBr^+ [270 *m/z* (3.7%, 7.3%)]; (1,10-phen)$BFBr^+$ [289 *m/z* (8.1%, 16.4%)]; (1,10-phen)BBr_2^+ [351 *m/z* (12.3%, 30.8%)]. The oil, dissolved in nitromethane, gave ^{11}B and ^{19}F NMR signals arising from (1,10-phen)BF_2^+, (1,10-phen)$BFBr^+$, (1,10-phen)BBr_2^+ and BF_4^-, with the fluorine-rich system giving more BF_4^- and less (1,10-phen)BBr_2^+.

2.2.10. ISOX·BF_nBr_{3-n} plus terpy

NMR monitoring of a bromine-rich sample (equimolar terpy and total ISOX) showed very rapid reaction of ISOX·BF_2Br and ISOX·$BFBr_2$, giving (terpy)BF_2^+ and (terpy)$BFBr^+$, but slow reaction of ISOX·BF_3 and ISOX·BBr_3. The resulting homogeneous yellow solutions gave ^{11}B and ^{19}F spectra consistent with (terpy)BF_2^+, (terpy)$BFBr^+$, (terpy)BBr_2^+ and BF_4^-, the 4.7 Tesla ^{11}B signals of (terpy)BF_2^+ and (terpy)$BFBr^+$ being poorly resolved. Removal of the chloroform left a brown oil which dissolved in nitromethane to give well-resolved NMR signals. The chloroform solution, and the oil respectively, gave FAB mass spectral peaks that correspond to: terpy·H^+ [234 *m/z* (100%, 73.9%)]; (terpy)BF_2^+ [282 *m/z* (24.2%, 71.1%)]; (terpy)BBr^+ [323 *m/z* (2.5%, 11.2%)]; (terpy)$BFBr^+$ [342 *m/z* (5.4%, 6.0%)]; (terpy)BBr_2^+ [404 *m/z* (15.3%, 100%)].

2.2.11. ISOX·BF_nBr_{3-n} plus DMAN

Multiple colour changes occurred, similar to those observed with DMAN plus ISOX·BF_nCl_{3-n}. ^{19}F NMR monitoring of bromine-rich samples of DMAN and ISOX·BF_nBr_{3-n} showed very rapid reaction of ISOX·BF_2Br (minutes), slower reaction of ISOX·$BFBr_2$ (hours) and very slow reaction of ISOX·BF_3 and ISOX·BBr_3 (days); (DMAN)BF_2^+ was the only identifiable haloboron cation. No mixed tetrahaloborate anion ($BF_nBr_{4-n}^-$) NMR signals [23] were detected. The positive ion FAB mass spectrum of the solution showed the same two species as on reaction with ISOX·BF_nCl_{3-n}: DMAN·H^+ [215 *m/z* (100%)]; (DMAN)BF_2^+ [263 *m/z* (6.7%)].

2.2.12. Bpy plus $Et_2O·BF_3$

Reaction of bpy with $Et_2O·BF_3$ in 1:1 ether–acetone, chloroform, or benzene at mole ratios of $Et_2O·BF_3$ to bpy of 1:1, 2:1 and 3:1 gave either bpy$H^+·BF_4^-$ as principal product in some attempts (^{19}F chemical shift −150.5 ppm), or a precipitate as principal product which, dissolved in nitromethane, gave a broad ^{19}F peak at −150.2 ppm (no splittings visible) and an ^{11}B peak at −0.6 ppm. These NMR parameters are inconsistent with those observed for (bpy)BF_2^+ as obtained by substitution reactions of the mixed boron trihalide adducts (Table 1), and could arise from the mono- or the bis-BF_3 adduct of bpy, by analogy with known chemical shifts of pyridine adducts [9]; bis-BF_3 adducts of chelating tertiary-amine donors have chemical shifts very similar to those of the mono-BF_3 adducts [12]. Elemental analysis of the precipitate from a bpy:$Et_2O·BF_3$ = 1:3 system in benzene solvent: C, 46.84; H, 2.98; N, 10.92%. Calc. for bpy·$(BF_3)_2$: C, 41.16; H, 2.76; N. 9.60%. Calc. for bpy·BF_3: C, 53.62; H, 3.60; N, 12.50%. Calc. for bpy·$H^+·BF_4^-$: C, 49.23; H, 3.71; N, 11.48%. The results are the most consistent with 1.5 BF_3 units per bpy unit, i.e. a mixture of bpy·BF_3 and bpy·$(BF_3)_2$.

2.2.13. Bpy plus ISOX·BF_3

Reaction of bpy with ISOX·BF_3 in chloroform gives the same insoluble species as on reaction with $Et_2O·BF_3$ (similar broad ^{19}F peak at −150.2 ppm in nitromethane). Attempted reaction of bpy with ISOX·BF_3 (and also with $Et_2O·BF_3$) in nitromethane gave a more complex ^{19}F spectrum, with broad peaks at −139.9, −141.4 and −150.5 ppm, in addition to the broad signal at −150.2 ppm arising from the bpy·BF_3 species. (BF_3 alone, bubbled into nitromethane, gives a broad ^{19}F singlet, apparently the BF_3 adduct, at −146.7 ppm.) Positive ion FAB mass spectra gave no evidence of (bpy)BF_2^+ in any of these samples.

2.2.14. 1,10-Phen plus $Et_2O·BF_3$

Addition of $Et_2O·BF_3$ to a benzene solution containing 1,10-phen in a mole ratio of $Et_2O·BF_3$:1,10-phen = 1:1 gave rapid formation of a white precipitate which, when dissolved in nitromethane, gave a ^{19}F signal at −149.8 ppm [$^1J_{BF}$ = 24.4 Hz] arising from (1,10-phen)BF_2^+ (also seen in the mixed boron trihalide displacement studies described above; Table 1) and a BF_4^- signal (−150.5 ppm) with twice the intensity. ^1H NMR and ^1H–^1H COSY NMR spectra (obtained in acetonitrile-d_3) showed that only half of the 1,10-phen had reacted with the $Et_2O·BF_3$, the remainder forming 1,10-phen·H^+. Addition of $Et_2O·BF_3$ to a benzene solution of 1,10-phen in a $Et_2O·BF_3$:bpy mole ratio of 2:1 gave a white precipitate which, dissolved in acetonitrile-d_3, gave ^{19}F signals at −149.2 ppm [$^1J_{BF}$ = 23.4 Hz] [(1,10-phen)BF_2^+] and −150.0 ppm (BF_4^-) in a 1:2 ratio. ^1H and ^{13}C NMR spectra showed that over 95% of the 1,10-phen had

formed (1,10-phen)BF_2^+. ^{1}H chemical shifts in acetonitrile-d_3: δ 9.36 [5.23 Hz (d) (1H)]; 9.22 [8.36 Hz, 0.72 Hz (dd) (1H)]; 8.44 [(s) (1H)]; 8.41 [8.40 Hz, 5.41 Hz (dd) (1H)]. ^{13}C chemical shifts (ppm) in acetonitrile-d_3: 146.2; 145.9; 129.6; 129.2; 128.6; 126.9. Positive ion FAB mass spectra of the precipitate gave peaks at 229 m/z [(1,10-phen)BF_2^+] (100%) and 181 m/z [1,10-phen·H^+] (46.5%). Negative ion FAB mass spectra gave a small peak at 403 m/z [(1,10-phen)$BF_2^+ \cdot (BF_4^-)_2$] in addition to the main peak at 87 m/z [BF_4^-].

2.2.15. 1,10-phen plus ISOX·BF_3

(1,10-Phen)$BF_2^+ \cdot BF_4^-$ also formed readily on reacting a chloroform solution of ISOX·BF_3 with 1,10-phen in a 2:1 mole ratio. Found: C, 45.70; H, 2.83; N, 9.01%. Calc.: C, 45.64; H, 2.55; N, 8.87%.

2.2.16. Terpy plus $Et_2O \cdot BF_3$

Addition of $Et_2O \cdot BF_3$ to terpy solutions in 1:1 ether–acetone or benzene, at $Et_2O \cdot BF_3$ to terpy mole ratios of 1:1, 2:1 and 3:1, gave a pale yellow precipitate over several minutes. The precipitate, dissolved in nitromethane, gave a ^{19}F signal at −145.2 ppm [$^1J_{BF}$ = 25.2 Hz] (also seen in the mixed boron trihalide displacment studies described above), arising from (terpy)BF_2^+, and a much larger BF_4^- signal at −150.5 ppm, the ratio of the two signals varying from 1:6 to 1:20 in different samples. ^{1}H spectra and ^{1}H–^{1}H COSY spectra (obtained in acetonitrile-d_3) showed that only 10–30% of the terpy had reacted with the $Et_2O \cdot BF_3$ in different samples, the remainder having formed terpy·$H^+ \cdot BF_4^-$. Positive ion FAB mass spectra of the precipitate gave peaks at: 282 m/z [(terpy)BF_2^+] (100%); 234 m/z [terpy·H^+] (58.2%). Negative ion FAB mass spectra gave a small peak at 240 m/z [(BF_4^-)(NBA); NBA is the matrix liquid, 3-nitrobenzoic acid] in addition to the base peak at 87 m/z [BF_4^-].

2.2.17. Terpy plus ISOX·BF_3

(Terpy)$BF_2^+ \cdot BF_4^-$ also formed on reacting a chloroform solution of ISOX·BF_3 with terpy in a 2:1 mole ratio. The yields for the yellow precipitate are similar to those reported above with $Et_2O \cdot BF_3$.

2.2.18. DMAN plus $Et_2O \cdot BF_3$

Addition of $Et_2O \cdot BF_3$ to a solution of DMAN in benzene, in a $Et_2O \cdot BF_3$:DMAN ratio of 1:1, gave a red precipitate after 24 h which, dissolved in nitromethane, gave a ^{19}F signal at −162.2 ppm [$^1J_{BF}$ = 29.2 Hz], consistent with (DMAN)BF_2^+, and a BF_4^- signal at −150.5 ppm, of relative intensities 1:1.9. ^{19}F NMR parameters in acetonitrile-d_3 are very similar: (DMAN)BF_2^+, −162.5 ppm [$^1J_{BF}$ = 29.2 Hz]; BF_4^-, −150.0 ppm. ^{1}H NMR indicated that only half of the DMAN had formed (DMAN)BF_2^+. A DMAN:$Et_2O \cdot BF_3$ ratio of 1:2 caused more than 95% of the DMAN to form (DMAN)BF_2^+, as shown by a combination of ^{19}F, ^{1}H, and ^{13}C NMR studies and confirmed by the high intensity of the positive ion FAB signal arising from (DMAN) BF_2^+. ^{1}H chemical shifts in acetonitrile-d_3: δ 8.21 [8.29 Hz (d) (1H)]; 8.15 [7.89 Hz (d) (1H)]; 7.83 [8.13 Hz (t) (1H)]; 3.44 [(s) (3H)]. ^{13}C chemical shifts (ppm) in acetonitrile-d_3: 139.4; 136.2; 131.9; 128.5; 122.7; 52.9. Positive ion FAB mass spectra of the precipitate gave peaks at: 263 m/z [(DMAN)BF_2^+] (100%); 248 m/z [(DMAN-Me)BF_2^+] (9.9%); 215 m/z [DMAN.H^+] (86.8%); 200 m/z [(DMAN-Me)·H^+] (4.7%). Negative ion FAB mass spectra gave a small peak at 437 m/z [(DMAN)-$BF_2^+(BF_4^-)_2]^-$ in addition to the base peak at 87 m/z [BF_4^-].

2.2.19. DMAN plus ISOX·BF_3

(DMAN)$BF_2^+ \cdot BF_4^-$ also formed readily on reacting a chloroform solution of ISOX·BF_3 with DMAN in a 2:1 mole ratio, with similar yield for the red precipitate as when $Et_2O \cdot BF_3$ was used.

3. Results and discussion

3.1. Reactions with py·BF_nCl_{3-n} adducts

Bpy, 1,10-phen and terpy react with py·BF_2Cl, but with none of the other py·BF_nCl_{3-n} (n = 0–3) adducts, in chloroform over a period of several days, to form the chelated (DD)BF_2^+ cations, identified by their ^{19}F and ^{11}B NMR signals (^{19}F 1:1:1:1 quartet, ^{11}B 1:2:1 triplet, Table 1) and by positive ion fast atom bombardment mass spectra. Fig. 1 shows ^{19}F NMR monitoring of the reaction with bpy. The ^{19}F 1:1:1:1 quartet of py·BF_2Cl diminishes and a poorly resolved 1:1:1:1 quartet of (bpy)BF_2^+ appears, along with signals of BF_4^- and (py)$_2BF_2^+$. The latter arises from displacement of Cl^- from py·BF_2Cl by free pyridine (which was itself displaced from py·BF_2Cl by the chelating ligand). In all three

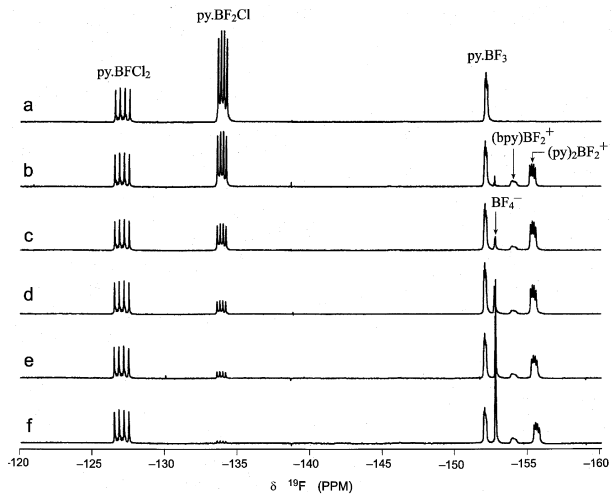


Fig. 1. 188.31 MHz ^{19}F NMR spectra of the py·BF_nCl_{3-n} (n = 0–3) adducts in $CDCl_3$ (mole ratio py:BF_3:BCl_3 = 5:2:3). (a) Initial solution; (b) after addition of bpy (same number of moles as moles of pyridine present) and standing for 2 days at room temperature; (c–f) same as (b) after standing for a total of 4 days (c), 6 days (d), 8 days (e), 10 days (f).

systems white crystals precipitate on standing, while the $(DD)BF_2^+$ and $(py)_2BF_2^+$ ^{19}F signal intensities decrease compared to the $py \cdot BF_3$ and $py \cdot BFCl_2$ ^{19}F signal intensities. The latter two signals stay constant except for a slight diminution of the $py \cdot BF_3$ signal, which seems to be related to the growth of the BF_4^- signal, as illustrated in Fig. 1. Both $(DD)BF_2^+$ and $(py)_2BF_2^+$ precipitate as their chloride salts, $(DD)BF_2^+ \cdot Cl^-$ being less soluble than $(py)_2BF_2^+ \cdot Cl^-$. No intermediate non-chelated $(py)(DD)BF_2^+$ species could be detected by NMR, unlike the situation with tertiary-amine chelating donors [12]. Furthermore, the three aromatic chelating ligands react with $py \cdot BF_2Cl$ much more slowly (days versus hours) than the tertiary-amine chelating ligands [12], and the yields are much poorer. Yields vary in the order $(bpy)BF_2^+ > (terpy)BF_2^+ > (1,10\text{-phen})BF_2^+$, i.e., inversely with ligand steric hindrance and rigidity. The most hindered ligand, DMAN, does not react with any of the $py \cdot BF_nCl_{3-n}$ adducts under the same conditions.

3.2. Reactions with $ISOX \cdot BF_nX_{3-n}$ (X = Cl, Br) adducts

Isoxazole, a much weaker base than pyridine, is much more easily displaced from its adducts than pyridine is from the corresponding pyridine adducts, and also differs from pyridine in being more easily displaced than Cl^- or Br^- [12]. Thus the $ISOX \cdot BF_nCl_{3-n}$ adducts are much more reactive than their pyridine analogues, and the $ISOX \cdot BF_nBr_{3-n}$ adducts are still more reactive due to the greater ease of displacement of Br^- than Cl^-. Because of this the mixed boron trihalide adducts of isoxazole are attractive intermediates for preparing chelated fluoroboron cations. However, they suffer from the disadvantage of an unfavourable halogen redistribution equilibrium, and do not form in large amounts. ^{11}B NMR spectra of the equilibrated $ISOX \cdot BF_nCl_{3-n}$ and $ISOX \cdot BF_nBr_{3-n}$ adduct systems (Fig. 2) illustrate this. Especially in the F,Br system, the mixed-halogen adducts are present in very small proportions.

Halogen redistribution in mixed boron trihalide adducts occurs spontaneously at room temperature when the donor–acceptor bond is sufficiently weak [13], i.e. with isoxazole but not with pyridine. The equilibria among mixed- and unmixed-halogen adducts can be expressed as the equilibrium constants K_1 and K_2, as follows [24]:

$$K_1 = \frac{[D \cdot BF_2X][D \cdot BX_3]}{[D \cdot BFX_2]^2} \quad (1)$$

$$K_2 = \frac{[D \cdot BF_3][D \cdot BFX_2]}{[D \cdot BF_2X]^2} \quad (2)$$

These can be near-statistical ($K_1 = K_2 = 0.33$) or, with soft donors, can strongly favour the unmixed-halogen over the mixed-halogen adducts (see Table 1 of [13]). The latter situation is in accord with Pearson's 'symbiotic principle' [25]: hard ligands tend to cluster together on a central atom, as do soft ligands. In accord with this principle, fluorine-heavy halogen redistribution equilibria increasingly favour

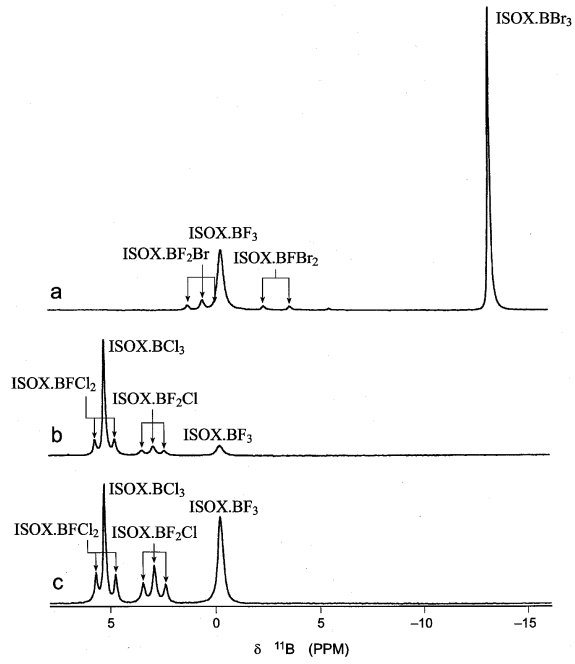


Fig. 2. 64.20 MHz ^{11}B NMR spectra of $CDCl_3$ solutions of $ISOX \cdot BF_nX_{3-n}$, illustrating the much greater concentration of unmixed-halogen than mixed-halogen adducts at equilibrium at ambient temperature (22°C). (a) $ISOX \cdot BF_nBr_{3-n}$ (mole ratio $ISOX:BF_3:BBr_3 = 4:1:3$); (b) $ISOX \cdot BF_nCl_{3-n}$ (mole ratio $ISOX:BF_3:BCl_3 = 4:1:3$); (c) $ISOX \cdot BF_nCl_{3-n}$ (mole ratio $ISOX:BF_3:BCl_3 = 2:1:1$).

the unmixed-halogen adducts over the mixed-halogen adducts as the heavy halogen changes from Cl to Br to I. This trend occurs in the isoxazole adduct system, as illustrated in Fig. 2. The spectra of Fig. 2 correspond to equilibrium constants K_1 and K_2 of 7.8 and 0.58 for the $ISOX \cdot BF_nCl_{3-n}$ system, and 42 and 2.5 for the $ISOX \cdot BF_nBr_{3-n}$ system. [K_1 is always larger than K_2 (Table 1 of [13]), consistent with favouring the only 'all-soft' adduct, $D \cdot BCl_3$, when the donor molecule is soft.] Despite this strong discrimination against the synthetically useful mixed-halogen adducts in the equilibrium mixture, their concentrations are sufficient to give detectable amounts of reaction products, mixed however with products of reaction of the more abundant BCl_3 and BBr_3 adducts. Our routinely used 'fluorine-rich' and 'heavy halogen-rich' proportions of reagents optimize the amounts of the desirable $ISOX \cdot BF_2X$ and $ISOX \cdot BFX_2$ adducts, respectively.

Bpy, 1,10-phen and terpy react with all of the $ISOX \cdot BF_nCl_{3-n}$ and $ISOX \cdot BF_nBr_{3-n}$ adducts, displacing heavy halide and generating mixtures of $(DD)BF_2^+$, $(DD)BFX^+$ and $(DD)BX_2^+$ (X = Cl, Br), along with some BF_4^- and, from chlorine-rich $ISOX \cdot BF_nCl_{3-n}$ samples, a large amount of BCl_4^-. There is insufficient tetrahaloborate ion present to balance the cation charge, consistent with the principal counterion being chloride or bromide ion.

The Cl- and Br-containing systems differ in that Cl^- can displace ISOX from its BCl_3 adduct, giving BCl_4^- (^{11}B chemical shift 6.7 ppm [23]), whereas there is no evidence for BBr_4^- formation in the Br-containing system (expected

^{11}B chemical shift −24.1 ppm [23]; note that the chemical shifts of [23] are converted to ppm to *high* frequency from $Et_2O \cdot BF_3$, from the opposite sign convention used in the original paper). ^{11}B MAS NMR spectra of the solids that precipitate from the chlorine- and bromine-rich reaction mixtures of bpy with $ISOX \cdot BF_nCl_{3-n}$ and $ISOX \cdot BF_nBr_{3-n}$, and ^{11}B NMR spectra of the same materials dissolved in nitromethane, are shown in Figs. 3 and 4, respectively. There are no absorptions within 20 ppm of the BBr_4^- chemical shift position. (F,Br exchange, rapid on the NMR time scale at room temperature [23], would be likely if both BF_4^- and BBr_4^- were present [23], but there is no exchange averaging of the BF_4^- signal.) Although resolution is poor in the ^{11}B MAS NMR spectra (Fig. 3), consistent with strong dipolar coupling to ^{19}F [26], the major peaks are consistent with those in nitromethane solution (Fig. 4) and with the chemical shift ranges of the closely related non-chelated $py_2BF_2^+$, py_2BFX^+ and $py_2BX_2^+$ [9].

Unlike the situation with tertiary-amine chelating donors which readily displace ISOX and form intermediate monodentate (DD)BF_nX_{3-n} adducts before undergoing chelation [12], no non-chelated boron trihalide adducts of bpy, 1,10-phen, terpy or DMAN could be detected by NMR. Such monodentate species are very unlikely on steric grounds for 1,10-phen and DMAN in which the nitrogens are held close together, but are plausible for bpy and terpy. Indeed, the monodentate analogue of bpy, 2-phenylpyridine, reacts readily with the $ISOX \cdot BF_nX_{3-n}$ adducts to give the corresponding 2-Phpy$\cdot BF_nX_{3-n}$ adducts, the ^{19}F resonances of which are shifted from 12–20 ppm to the high frequency of the corresponding py$\cdot BF_nX_{3-n}$ adduct signals (e.g. 2-Phpy$\cdot BF_3$ absorbs at −139.1 ppm), indicative of high steric hindrance at the donor site [27], although some of the effect could arise from the ring current of the phenyl group. Our inability to detect monodentate bpy$\cdot BF_nX_{3-n}$ and terpy$\cdot BF_nX_{3-n}$ species is consistent with the low steric hindrance of two-coordinate pyridine nitrogen giving very efficient ring closure. The increased pre-organization [28] of the more rigid aromatic ligands, with the second donor site being held close to the boron atom once the first site coordinates, would also assist in ring closure.

Bromine-containing systems usually react more rapidly than their chlorine-containing analogues, so it is unusual that bpy, 1,10-phen and terpy all react rapidly with the $ISOX \cdot BF_nCl_{3-n}$ adducts (giving precipitates), while only bpy reacts equally rapidly with the $ISOX \cdot BF_nBr_{3-n}$ adducts. With the slower-reacting 1,10-phen and terpy the reaction could be monitored by NMR, and in both cases the $ISOX \cdot BF_nBr_{3-n}$ adducts react in the order $BF_2Br \geq BFBr_2 > BF_3 > BBr_3$; i.e. the mixed-halogen adducts and especially the BF_2Br adduct are the most reactive, consistent with our previous studies of haloboron cation formation [8–12].

DMAN reacts very differently than the other chelating donors. With the $ISOX \cdot BF_nCl_{3-n}$ adducts the reaction favours formation of BCl_4^- and the mixed tetrahaloborate anions $BFCl_3^-$ and $BF_2Cl_2^-$ over formation of (DMAN)BF_2^+. Only in the presence of an excess of DMAN over ISOX, and with heating to 50°C, are significant amounts of (DMAN)BF_2^+ produced. Neither (DMAN)$BFCl^+$ nor (DMAN)BCl_2^+ are formed under our conditions, despite a

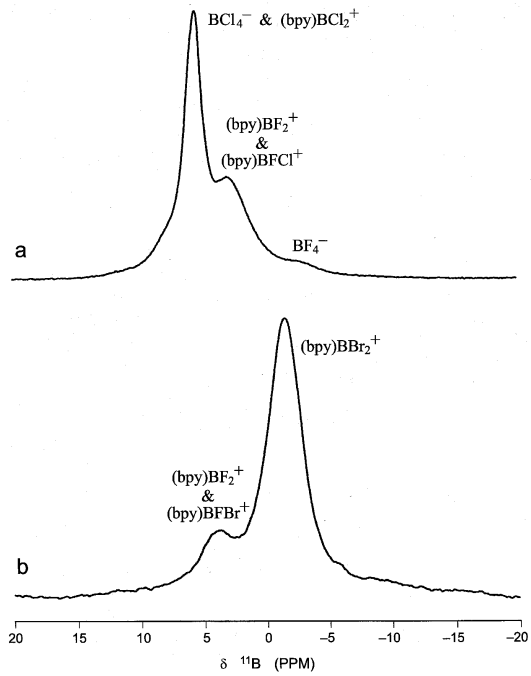


Fig. 3. 96.29 MHz ^{11}B magic-angle spinning NMR spectra of the precipitates formed on reaction of chloroform solutions of $ISOX \cdot BF_nX_{3-n}$ (mole ratio ISOX:BF_3:BX_3 = 4:1:3) with bpy (same number of moles as total moles of ISOX). (a) $ISOX \cdot BF_nCl_{3-n}$ plus bpy; (b) $ISOX \cdot BF_nBr_{3-n}$ plus bpy. No BBr_4^- signal was present at −26 ppm (off scale).

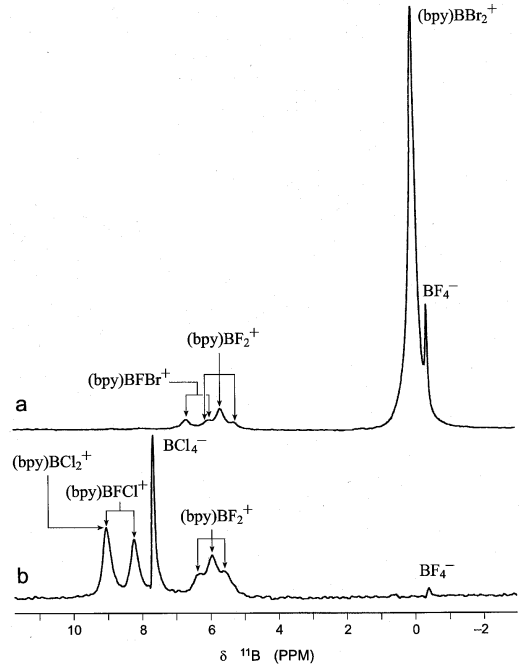


Fig. 4. 64.20 MHz ^{11}B NMR spectra of the precipitates of Fig. 3, dissolved in nitromethane. (a) $ISOX \cdot BF_nBr_{3-n}$ plus bpy; (b) $ISOX \cdot BF_nCl_{3-n}$ plus bpy.

previous report of the existence of $(DMAN)BCl_2^+$ [5]. Also, in some samples we are able to detect short-lived ^{11}B NMR signals in the three-coordinate boron region of the spectrum (at about 35, 24 and 16 ppm), in the early stages of the reaction; these disappear as the tetrahaloborate peaks grow (Fig. 5). These samples also appear to give off a small amount of a volatile material which fumes on contact with air, consistent with the behaviour of such three-coordinate boron compounds as BCl_3. (However, the ^{11}B chemical shift of BCl_3 in chloroform is 46.2 ppm, so BCl_3 does not give rise to one of these signals.)

DMAN reacts with the $ISOX \cdot BF_nBr_{3-n}$ adducts to give multiple colour changes similar to those observed when it reacts with the $ISOX \cdot BF_nCl_{3-n}$ adducts, but there are no corresponding mixed tetrahaloborate ion ($BF_nBr_{4-n}^-$ or $BF_mCl_nBr_{4-(m+n)}^-$) NMR signals [23]. If such species form at all they are too short-lived to detect. These anions undergo chemical exchange that is rapid on the NMR time scale [23], but there is no averaged ^{19}F NMR signal consistent with this. $(DMAN)BF_2^+$ is the only new fluorine-containing species formed, besides a very small amount of an unknown species absorbing near −151 ppm, which may be BF_4^-. Unlike the corresponding reaction with the $ISOX \cdot BF_nCl_{3-n}$ adducts, no transitory ^{11}B NMR signals could be detected in the three-coordinate boron region. DMAN reacts with the $ISOX \cdot BF_nBr_{3-n}$ adducts in the order $ISOX \cdot BF_2Br$ (minutes) ≫ $ISOX \cdot BFBr_2$ (hours) ≫ $ISOX \cdot BF_3 \sim ISOX \cdot BBr_3$ (days) (Fig. 6). Fluorine–bromine exchange must occur among the $ISOX \cdot BF_nBr_{3-n}$ adducts in order to give primarily a BF_2-containing product.

The unusual reaction of DMAN with the $ISOX \cdot BF_nCl_{3-n}$ adducts, giving the mixed chlorofluoroborate ions and BCl_4^- as primary products, is reminiscent of the behaviour of amidine $\cdot BF_nCl_{3-n}$ adduct systems [10]. Similar colour changes occurred, the mixed chlorofluoroborate ions were produced (including BF_3Cl^-, which is formed in only very small amounts in the present case) and protonated amidine was the counterion to the $BF_nCl_{4-n}^-$ anions (or ions). In the amidine systems the $BF_nCl_{4-n}^-$ anions forms only in the presence of excess boron trihalide [10], and we proposed a concerted mechanism involving dichlorocarbene formation from chloroform, assisted by free boron trihalide which would increase the effective basicity of the amidines which are not normally basic enough to drive carbene formation [29]. DMAN is almost as basic as the amidines in our previous study ($pK_b^1 = 1.7$, compared with 1.1 and 0.5 for the amidines [10]), but the DMAN reactions contrast with the amidine reactions in that the $BF_nCl_{4-n}^-$ anions form under excess base conditions as well. The extreme differences in steric hindrance, low in the amidines but very high in DMAN, no doubt contribute to the differences in behaviour. DMAN can only with great difficulty take up a second proton despite its very high affinity for the first proton, which led to the term 'proton sponge' for this and related compounds [30,31]. DMAN is too hindered to form simple covalent Lewis acid–base complexes, and this apparently allows boron to briefly become

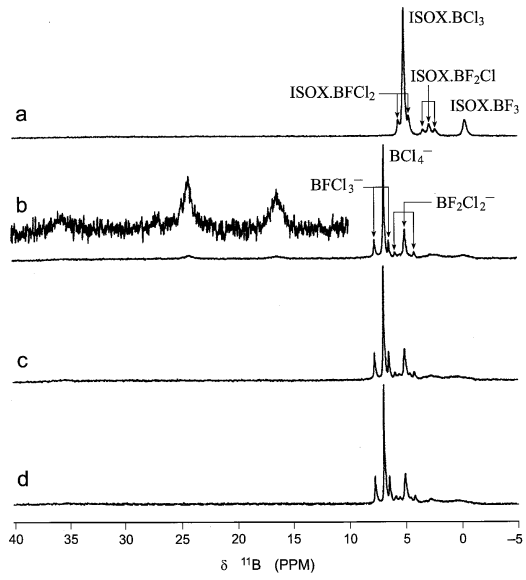


Fig. 5. 64.20 MHz ^{11}B NMR spectra of the $ISOX \cdot BF_nCl_{3-n}$ ($n = 0$–3) adducts in $CDCl_3$ (mole ratio $ISOX:BF_3:BCl_3 = 4:1:3$). (a) Initial solution. (b) After addition of DMAN (same number of moles as moles of ISOX present) and standing for 4 min at room temperature (inset spectrum: 10-fold vertical expansion); the $ISOX \cdot BCl_3$ peak overlaps the central peak of the $BF_2Cl_2^-$ triplet. (c) After standing for 8.4 min. (d) After standing for 17 min.

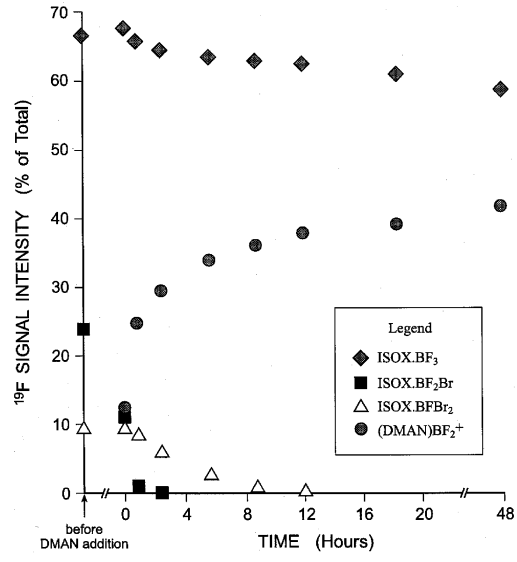


Fig. 6. Plot of relative ^{19}F signal intensity versus time for the reaction of DMAN with $ISOX \cdot BF_nBr_{3-n}$ in $CDCl_3$ (mole ratio $ISOX:BF_3:BBr_3:DMAN = 4:1:3:4$).

three-coordinate during the reaction of DMAN with the $ISOX \cdot BF_nCl_{3-n}$ adducts. The identities of the three-coordinate species are not obvious. Further studies are required to identify these and to determine the mechanism of reaction of DMAN with the $ISOX \cdot BF_nCl_{3-n}$ adducts.

Few $D \cdot BF_nCl_{3-n}$ systems give rise to the $BF_nCl_{4-n}^-$ anions , but it is of interest that they do form in the (tetramethylurea) $\cdot BF_nCl_{3-n}$ adduct system, which unlike the DMAN or amidine systems does not involve an especially

strong base [32]. Much remains to be learned about halogen redistribution in such systems.

3.3. Reactions of chelating ligands with $Et_2O \cdot BF_3$ and $ISOX \cdot BF_3$

$Et_2O \cdot BF_3$ is a well-known laboratory reagent; its very weak donor–acceptor bond readily dissociates, providing a convenient source of BF_3 for many uses including formation of BF_3 adducts of stronger donors and, in some favourable cases, formation of chelated $(DD)BF_2^+ \cdot BF_4^-$ species [1–6]. $ISOX \cdot BF_3$ behaves much like $Et_2O \cdot BF_3$ as a source of $(DD)BF_2^+ \cdot BF_4^-$, being successful with the same chelating donors. 1,10-Phen, terpy and DMAN, but not bpy, readily form the chelated $(DD)BF_2^+ \cdot BF_4^-$ on reaction with either $Et_2O \cdot BF_3$ or $ISOX \cdot BF_3$, along with large amounts of $DD \cdot H^+ \cdot BF_4^-$ unless the BF_3 source is present in excess. None of 1,10-phen, terpy or DMAN give any evidence of BF_3 adduct formation.

In contrast, bpy under the same conditions does not form $(bpy)BF_2^+$, a species which we have prepared by reaction with the mixed boron trihalide adducts and which is readily identifiable by NMR and by FAB MS. Instead our product gives analytical results consistent with 1.5 BF_3 units per bpy unit, i.e. a mixture of $bpy \cdot BF_3$ and $bpy \cdot (BF_3)_2$. The contrast between bpy and the other aromatic donors is striking. Not even trace amounts of $(bpy)BF_2^+$ are formed. Two overlapping ^{19}F 1:1:1:1 quartets of similar chemical shift, each poorly resolved, from $bpy \cdot BF_3$ and $bpy \cdot (BF_3)_2$, might account for the broadness and absence of fine structure of our ^{19}F signal.

$(bpy)BF_2^+ \cdot BF_4^-$ was previously reported to form under very similar conditions [5,6]. However, elemental analysis, which cannot distinguish this species from its coordination isomer the bis-BF_3 adduct, was the only evidence provided for the structure. Our results indicate that the previous workers actually isolated the bis-BF_3 adduct. Our bpy-BF_3 adduct has a similar ^{11}B chemical shift in DMSO (0.0 ppm) to the values reported for $(bpy)BF_2^+ \cdot BF_4^-$ by Axtell et al. (0.6 ppm) [6] and by Koch and Madelung (1.6 ppm) [5], whereas the actual $(bpy)BF_2^+$, synthesized by us from the mixed-halogen adducts, appears at 5.7 ppm in nitromethane. Furthermore, our $(bpy)BF_2^+$ does not react with DMSO, whereas the materials prepared by Axtell et al. and by Koch and Madelung reacted readily. This confirms that neither Axtell et al. nor Koch and Madelung prepared $(bpy)BF_2^+ \cdot BF_4^-$, but instead the bis-BF_3 adduct. Koch and Madelung suggested that $(bpy)BF_2^+$ undergoes rapid solvolysis by DMSO and reacts before it can be detected in solution by NMR, whereas the rigid $(1,10\text{-phen})BF_2^+$ is much more stable towards DMSO [5]. Our results show that the opposite is true.

The rigidity and steric hindrance of 1,10-phen and DMAN, with their two nitrogens held close together, should strongly hinder the formation of the mono-BF_3 adducts and preclude the formation of the bis-BF_3 adducts, and indeed over 95% of these ligands can be incorporated into the $(DD)BF_2^+$ species. Terpy is more flexible and like bpy should be able to form mono- and bis-BF_3 adducts, or even the tris-BF_3 adduct, but these are not observed. We detect $(terpy)BF_2^+$ instead, but only a small proportion (up to 30%) of terpy can be incorporated into $(terpy)BF_2^+$. It is not clear why bpy gives only adduct under the same conditions, but terpy is clearly an intermediate case: it does form the chelated cation but not in the high yields obtained with 1,10-phen and DMAN.

3.4. Reaction of chelated fluoroboron cations with DMSO

Previous attempts to prepare $(bpy)BF_2^+ \cdot BF_4^-$ and $(1,10\text{-phen})BF_2^+ \cdot BF_4^-$ involved the use of DMSO as solvent [5,6]. However, DMSO is a potent Lewis base, and we have shown that it reacts readily with $(py)_2BF_2^+$ to form $(DMSO)_2BF_2^+$ [33]. The more recent of the previous studies showed that DMSO solvolysis of $(1,10\text{-phen})BF_2^+ \cdot BF_4^-$ does indeed occur [5]. However, these authors assigned the ^{11}B NMR signals incorrectly. The $(DMSO)_2BF_2^+$ signal (2.2 ppm, $^1J_{BF} = 12.5$ Hz) was assigned to $(1,10\text{-phen})BF_2^+$, while the true $(1,10\text{-phen})BF_2^+$ signal (9.0 ppm; $^1J_{BF}$ unresolved) was tentatively assigned to $1,10\text{-phen} \cdot BF_3$, a species that we have not been able to prepare and that seems unlikely because of high steric hindrance. We here describe the reactions of DMSO with our chelated fluoroboron cation systems.

^{11}B NMR monitoring of the reaction of $(1,10\text{-phen})BF_2^+ \cdot BF_4^-$ with an excess of DMSO (Fig. 7) shows the transitory appearance of a small $(DMSO)_2BF_2^+$ signal (identified in a separate study [33]) after 6 min of reaction as the $(1,10\text{-phen})BF_2^+$ signal diminishes. The $(DMSO)_2BF_2^+$ signal (with 1:2:1 triplet structure that shows up more

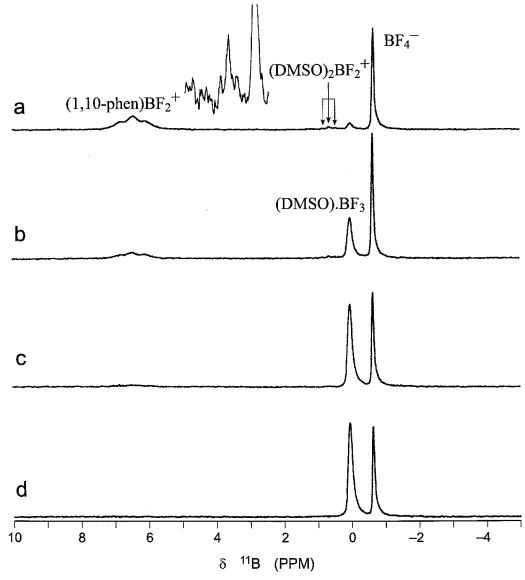


Fig. 7. 64.20 MHz ^{11}B NMR spectra of $(1,10\text{-phen})BF_2^+ \cdot BF_4^-$ in acetonitrile-d_3, following addition of a 4-fold molar excess of DMSO, after standing for: (a) 6 min (inset spectrum: 20-fold vertical expansion); (b) 12 min; (c) 24 min; (d) 72 min.

clearly in the expansion of Fig. 7a) never becomes large. Instead, fluorine redistribution occurs, the ionic $(DMSO)_2BF_2^+ \cdot BF_4^-$ converting to its covalent coordination isomer $DMSO \cdot BF_3$. The (1,10-phen)BF_2^+ signal is no longer detectable after 72 min. The BF_4^- signal intensity decreases but does not disappear as $DMSO \cdot BF_3$ becomes predominant, consistent with the remaining BF_4^- being present as the counterion of protonated 1,10-phen.

In samples prepared from mixed boron trihalide adducts and containing (1,10-phen)$BFCl^+$ and (1,10-phen)BCl_2^+ as well as (1,10-phen)BF_2^+, as chloride salts in nitromethane, only (1,10-phen)BF_2^+ reacts with a large excess of DMSO, to form first $(DMSO)_2BF_2^+$ and eventually $DMSO \cdot BF_3$. Samples containing (1,10-phen)BF_2^+, (1,10-phen)$BFBr^+$ and (1,10-phen)BBr_2^+, as bromide salts in nitromethane, behave similarly, with only (1,10-phen)BF_2^+ reacting. In these systems in which the predominant counterion of (1,10-phen)BF_2^+ is chloride or bromide, the conversion of (1,10-phen)BF_2^+, with two fluorines per boron, into $DMSO \cdot BF_3$, with three fluorines per boron, must involve further halogen redistribution reactions. These remain to be investigated.

None of the bpy-containing haloboron cations, (bpy)BF_2^+, (bpy)$BFCl^+$, (bpy)BCl_2^+, (bpy)$BFBr^+$ or (bpy)BBr_2^+, that are present in samples prepared by various methods as described earlier, react with a large excess of DMSO over 48 h at room temperature. (Terpy)BF_2^+ and (terpy)BBr_2^+ are similarly unreactive, but (terpy)$BFBr^+$, present in the same solution, does react with DMSO with the appearance of a new and not yet explained ^{11}B signal at about 22 ppm, in the three-coordinate boron spectral region.

(DMAN)$BF_2^+ \cdot BF_4^-$ is unreactive with DMSO, not surprisingly in view of its high steric hindrance. $(Quinuclidine)_2BF_2^+$, also highly sterically hindered, is unreactive with various Lewis bases [11]. Surprisingly, the less hindered (ethylenediamine)BF_2^+ does not react with DMSO over a period of several months [34].

3.5. Attempted reactions with $(py)_2BF_2^+ \cdot PF_6^-$

None of bpy, 1,10-phen, terpy or DMAN react with $(py)_2BF_2^+ \cdot PF_6^-$ in acetone solution under conditions that allow pyridine to be displaced by saturated-amine chelating donors to give chelated (DD)BF_2^+ [12], or by quinuclidine to give (py)(quinuclidine)BF_2^+ [11]. This is consistent with the steric hindrance and inflexibility of the aromatic donors. Instead there is decomposition of $(py)_2BF_2^+ \cdot PF_6^-$, requiring weeks at 20°C or hours at 50°C, with $py \cdot H^+$ and BF_4^- being major products. With DMAN, small amounts of BF_3OH^- [35,36] and additional unidentified fluorine-containing species also form. The reactions of $(py)_2BF_2^+ \cdot PF_6^-$, including decomposition in the presence of bases such as these, will be discussed elsewhere [33].

3.6. NMR parameters

The ^{19}F chemical shifts and $^1J_{BF}$ values reported here follow established patterns [37]. The ^{19}F and ^{11}B NMR parameters of the chelated species (Table 1) are fairly typical of haloboron cations except for a chelation shift to high frequency (low field). Table 1 includes NMR parameters for a few analogous non-chelated species for comparison. The chelation shift is less regular than was observed previously with tertiary-amine chelating donors [12], probably because of competing ring current effects which differ in their effectiveness in different species. The ^{19}F chemical shifts of $(py)_2BF_2^+$ and (bpy)BF_2^+ differ by only 1.2 ppm but their ^{11}B chemical shifts differ by about 3 ppm. (Bpy)BCl_2^+ and (bpy)BBr_2^+ also show ^{11}B chelation shifts to higher frequency ($+0.6$ and $+3.6$ ppm, respectively) compared with the analogous bis-pyridine species. There are large ^{19}F chemical shift differences among the (DD)BF_2^+ cations (5.9 ppm between the bpy and 1,10-phen cations, and a further 4.6 ppm between the 1,10-phen and terpy cations), whereas the ^{11}B chemical shifts of these species cover a range of only 1.3 ppm. The $^1J_{BF}$ values of the aromatic (DD)BF_2^+ cations are within a few Hz of each other, as are the $^1J_{BF}$ values of the corresponding (DD)$BFCl^+$ and (DD)$BFBr^+$ cations. (DMAN)BF_2^+ has NMR parameters typical of tertiary-amine ligands, the greatest similarity in chemical shifts being to $(Me_3N)_2BF_2^+$, although the $^1J_{BF}$ value of the chelated system is appreciably smaller. Chemical shift comparisons are limited by the need to use both $CHCl_3$ and CH_3NO_2 as solvents in different systems due to solubility limitations. ^{11}B chemical shifts are usually about 1 ppm to lower frequency in nitromethane and ^{19}F shifts differ by up to 1.5 ppm in either direction between the solvents.

4. Conclusions

Chelated fluoroboron cations of aromatic donors are accessible by displacement reactions from mixed boron trihalide adducts, and in most cases by reaction of the chelating ligand with $Et_2O \cdot BF_3$ or $ISOX \cdot BF_3$, but not by displacement of pyridine from $py_2BF_2^+$. Bipyridyl, unlike 1,10-phenanthroline, terpyridyl, or 1,8-bis(dimethylamino)naphthalene (DMAN), does not form the chelated difluoroboron cation on reaction with $Et_2O \cdot BF_3$ or $ISOX \cdot BF_3$, but this ion is readily formed by displacement of donor and heavy halide ion from $py \cdot BF_2Cl$, $ISOX \cdot BF_2Cl$ and $ISOX \cdot BF_2Br$. Reaction of DMAN with the $ISOX \cdot BF_nCl_{3-n}$ and $ISOX \cdot BF_nBr_{3-n}$ adduct systems has unique features, apparently related to DMAN's combination of high Bronsted basicity and low Lewis basicity, that merit further investigation.

Acknowledgements

We thank Tim Jones for assistance with the instrumentation, W.R. (Rick) Szerminski and Paul Ragogna for synthesis of $(py)_2BF_2^+ \cdot PF_6^-$, Prof. Alex F. Janzen (University of

Manitoba) and Prof. Fred Capretta (Brock University) for helpful discussions, Dr Don Hughes and Brian Sayer (McMaster University) for assistance with the 11.7 Tesla NMR instrument, and the Natural Sciences and Engineering Research Council of Canada for financial support.

References

[1] N. Wiberg, J.W. Buchler, Chem. Ber. 96 (1963) 3000.
[2] N. Wiberg, J.W. Buchler, J. Am. Chem. Soc. 85 (1963) 243.
[3] N.M.D. Brown, P. Bladon, J. Chem. Soc., Sect. A (1969) 526.
[4] T. Onak, H. Rosendo, G. Siwapinyoyos, R. Kubo, L. Liauw, Inorg. Chem. 18 (1979) 2943.
[5] K.R. Koch, S. Madelung, Polyhedron 10 (1991) 2221.
[6] D.D. Axtell, A.V. Campbell, P.C. Keller, J.V. Rund, J. Coord. Chem. 5 (1976) 129.
[7] S. Hünig, I. Wehner, Heterocycles 28 (1989) 359.
[8] M.J. Farquharson, J.S. Hartman, Can. J. Chem. 67 (1989) 1711.
[9] M.J. Farquharson, J.S. Hartman, Can. J. Chem. 74 (1996) 1309.
[10] J.S. Hartman, Z. Yuan, A. Fox, A. Nguyen, Can. J. Chem. 74 (1996) 2131.
[11] J.S. Hartman, E.I. Ilnicki, J.A.W. Shoemaker, R.W. Szerminski, Z. Yuan, Can. J. Chem. 76 (1998) 1317.
[12] J.A.W. Shoemaker, J.S. Hartman, Can. J. Chem. 77 (1999) 1856.
[13] J.S. Hartman, J.M. Miller, Adv. Inorg. Chem. Radiochem. 21 (1978) 147.
[14] E.C. Constable, Metals and Ligand Reactivity, 2nd ed., VCH, New York, 1996.
[15] N.N. Greenwood, A. Earnshaw, Chemistry of the Elements, Pergamon Press, Oxford, 1984, Chapter 19.
[16] P.R. Mallinson, K. Wozniak, C.C. Wilson, K.L. McCormack, D.S. Yufit, J. Am. Chem. Soc. 121 (1999) 4640, and references therein.
[17] R.M.K. Deng, K.B. Dillon, Polyhedron 11 (1992) 397.
[18] A.F. Janzen, Coord. Chem. Rev. 130 (1994) 355.
[19] X. Ou, R. Wallace, A.F. Janzen, Can. J. Chem. 71 (1993) 51.
[20] H.C. Brown, B. Singaram, J.R. Schwier, Inorg. Chem. 18 (1979) 51.
[21] H.C. Brown, B. Singaram, Inorg. Chem. 18 (1979) 53.
[22] J.S. Hartman, A.F. Janzen, X. Ou, 79th Annual Canadian Chemical Conference, St John's Newfoundland, 23–26 June 1996, paper 57.
[23] J.S. Hartman, G.J. Schrobilgen, Inorg. Chem. 11 (1972) 940.
[24] K. Moedritzer, Adv. Organomet. Chem. 6 (1968) 171.
[25] R.G. Pearson, J. Songstad, J. Am. Chem. Soc. 89 (1967) 1827.
[26] C.A. Fyfe, Solid State NMR for Chemists, CFC Press, Guelph, Ontario, 1983, Chapter 1.
[27] A. Fox, J.S. Hartman, R.E. Humphries, J. Chem. Soc., Dalton Trans. (1982) 1275.
[28] A.E. Martell, R.D. Hancock, R.J. Motekaitis, Coord. Chem. Rev. 133 (1994) 39.
[29] F.A. Carey, R.J. Sundberg, Advanced Organic Chemistry. Part B: Reactions and Synthesis, 2nd ed., Plenum, New York, 1983, Section 9.1.
[30] H.A. Staab, T. Saupe, Angew. Chem., Int. Ed. Engl. 27 (1988) 865.
[31] R.W. Alder, Chem. Rev. 89 (1989) 1215.
[32] J.S. Hartman, G.J. Schrobilgen, Inorg. Chem. 13 (1974) 874.
[33] J.S. Hartman, A.F. Janzen, P.J. Ragogna, J.A.W. Shoemaker, W.R. Szerminski (in preparation).
[34] A.F. Janzen (personal communication).
[35] R.E. Mesmer, A.C. Rutenberg, Inorg. Chem. 12 (1973) 699.
[36] K. Kuhlmann, D.M. Grant, J. Phys. Chem. 68 (1964) 3208.
[37] S. Berger, S. Braun, H.-O. Kalinowski, NMR Spectroscopy of the Non-Metallic Elements, Wiley, Chichester, 1997, Chapter 6.

PERGAMON

www.elsevier.nl/locate/poly

Polyhedron 19 (2000) 177–183

POLYHEDRON

Titanium(IV) complexes of the crystallographically characterised fluorene-Schiff base *N*-2-fluorenyl(salicylideneimine) and related bi- and tetradentate ligands

Simon J. Coles [a], Michael B. Hursthouse [a], David G. Kelly [b,*], Andrew J. Toner [b]

[a] *Department of Chemistry, University of Southampton, Highfield, Southampton SO17 1BJ, UK*

[b] *Department of Chemistry and Materials, The Manchester Metropolitan University, Chester Street, Manchester M1 5GD, UK*

Received 23 August 1999; accepted 4 November 1999

Abstract

Schiff base ligands have been prepared by the condensation of 2-aminofluorene with salicylaldehyde (**1**, flusalH) or 3-methoxy-2-hydroxybenzaldehyde (**2**, MeOflusalH). Compound **1** reacts with $TiCl_4$ in a 1:1 stoichiometry to afford [$TiCl_3$(flusal)] (**3**) and in a 2:1 ratio to yield [$TiCl_4$(flusalH)$_2$] (**4**). The reaction of excess $TiBz_4$ with compound **1** results in the isolation of the octahedral Ti(IV) complex [Ti(flusal)$_2$(flusalaBz)$_2$] (**5**). Crystallographic and spectroscopic data for the latter indicate a complex containing two Schiff base ligands present as conventional N,O chelates and a further two ligands in which the C=N function is reduced by the addition of benzyl and hydrogen moieties producing an O-bound species with pendant amine. The single crystal X-ray diffraction structure of compound **1** has been obtained and compared with the published data for compound **5**. Similar ligand alkylation to that observed in compound **5** is also achieved by the reaction of organolithium reagents with compounds **1** and **2**; the reaction of PhLi and compound **2** followed by aqueous hydrolysis affords MeOflusalaPhH (**6**). Although reactivity does occur between $TiCl_4$ and compound **6**, the products could not be fully characterised. Thus tetradentate reduced Schiff base ligands were synthesised by the reaction of salenH_2 with MeLi or PhLi, giving salenaMe_2H_2 (**7**) and salenaPh_2H_2 (**8**), respectively. Reaction of compound **8** and $TiCl_4$ affords the quadruply deprotonated amido complex [Ti(salenamidoPh_2)] (**9**), which hydrolyses in air to the μ-oxo amine complex [Ti(salenaPh_2)O] (**10**). ©2000 Elsevier Science Ltd All rights reserved.

Keywords: Additions; Alkylation; Insertions; Nucleophilic; Schiff bases; Titanium

1. Introduction

The recent interest in group 4 complexes incorporating the fluorenyl ligand stems from the discovery that *ansa*-metallocene zirconium complexes containing linked fluorenyl-cyclopentadienyl ligands are involved in the syndiospecific polymerisation of α-olefins [1–11]. Examples of unsupported fluorenyl coordination to group 4 metals are far less numerous than the corresponding indenyl and cyclopentadienyl moieties [12]; the preparation of [(η^5-$C_{13}H_9$)$_2$-$TiCl_2$], from sodium fluorenyl and titanium(IV) chloride, and of [(η^5-$C_{13}H_9$)(η^5-C_5H_5)$TiCl_2$], from thallium fluorenyl and [$CpTiCl_3$], are the only examples of titanium(IV) metallocene precursors containing the fluorenyl moiety [13,14], although a large number of monodithiocarbamate derivatives have been synthesised from [(η^5-$C_{13}H_9$)$_2TiCl_2$] [15]. Recently bis-fluorenyltitanium(0) has also been formed by metal vapour deposition (MVD) methods [16]. In the present work the relative coordination affinities of Schiff base and fluorenyl moieties contained within potentially chelating ligands are assessed. Part of this work has previously been the subject of a brief communication [17].

2. Results and discussion

2.1. Titanium(IV) complexes of flusalH and derivatives

Schiff base ligands can be readily formed by the condensation of 2-aminofluorene and salicylaldehyde (**1**, flusalH) or 3-methoxy-2-hydroxybenzaldehyde (**2**, MeOflusalH) (Table 1). The synthetic route, outlined in Scheme 1, is conventional and employs published methods [18]. Although compounds **1** and **2** appear visually very different in colour, visible reflectance spectra display similar features, with a shift in absorbance to higher wavelength occurring as

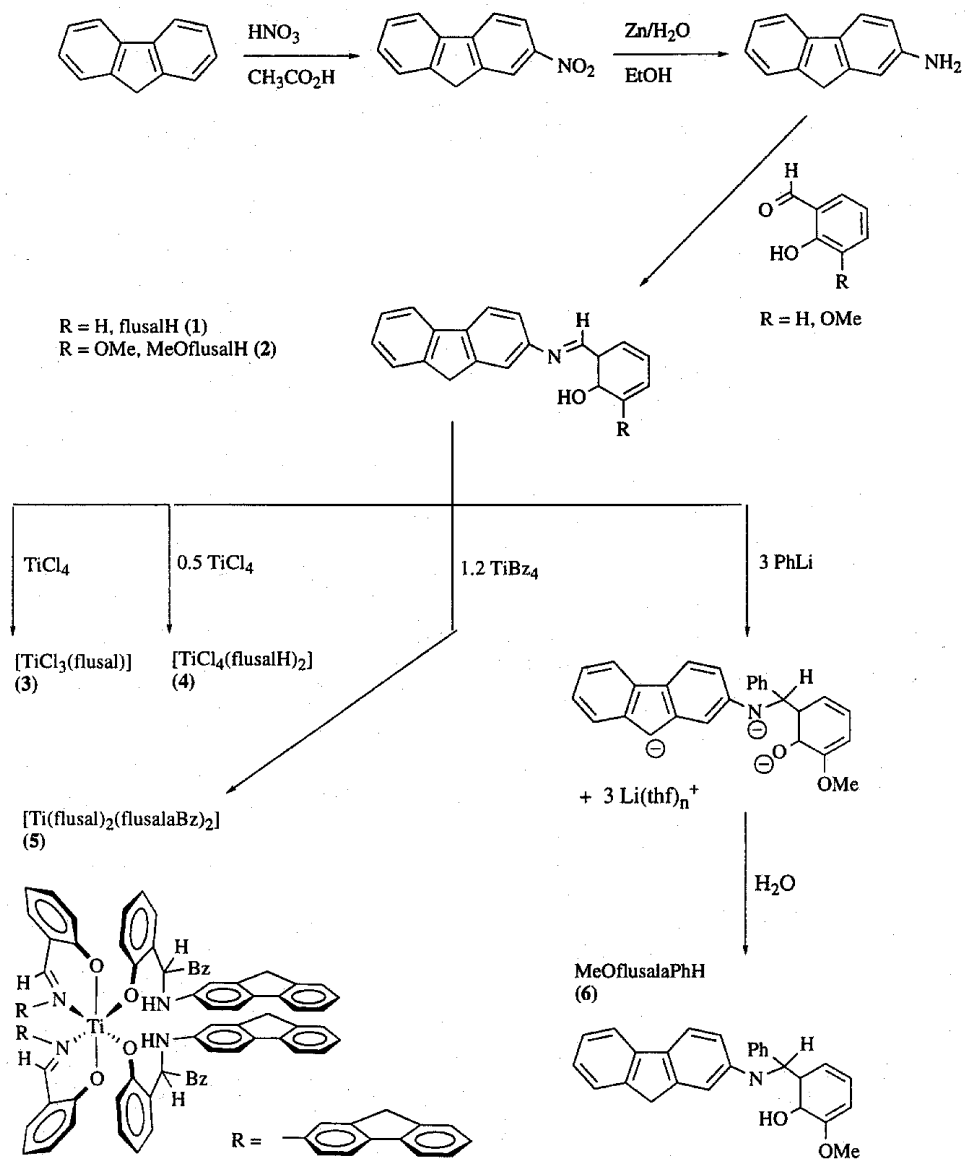
* Corresponding author. Tel: +44-161-247-1425; fax: +44-161-247-6357; e-mail: d.g.kelly@mmu.ac.uk

0277-5387/00/$ - see front matter ©2000 Elsevier Science Ltd All rights reserved.
PII S0277-5387(99)00340-X

Table 1
Analytical and spectroscopic data for compounds **1**–**10**

Compound	Colour	Yield (%)	^{1}H NMR (δ, ppm)		IR [a] (cm^{-1})		Elemental analysis			
			*H*C=N	*H*CR–NH	ν(C=N)	ν(N–H)	C	H	N	Cl
FlusalH (**1**)	yellow	80	8.70		1618		84.6 (84.2)	5.2 (5.3)	4.9 (4.9)	
MeOflusalH (**2**)	orange	75	8.71		1618		80.0 (80.0)	5.8 (5.4)	4.4 (4.4)	
$TiCl_3$(flusal) (**3**)	red	95	insoluble		1612		54.4 (54.7)	3.5 (3.2)	3.1 (3.2)	23.7 (24.3)
$TiCl_4$(flusalH)$_2$ (**4**)	red	99	insoluble		1620 [b]		62.6 (63.0)	4.6 (4.4)	3.7 (3.4)	17.8 (17.4)
[Ti(flusal)$_2$(flusalaBz)$_2$] (**5**)	orange	25	8.75	4.10	1612	3376, 3389	82.2 (82.5)	5.6 (5.3)	3.8 (4.1)	
MeOflusalaPhH (**6**)	cream	96		3.95		3414, 3475	82.7 (82.4)	6.3 (5.9)	3.2 (3.6)	
$SalenaMe_2H_2$ (**7**)	white	45		3.88		3299	72.1 (72.0)	8.2 (8.0)	9.2 (9.3)	
$SalenaPh_2H_2$ (**8**)	white	80		3.88		3303	80.0 (79.2)	6.8 (6.6)	6.2 (6.6)	
[Ti(salenamidoPh_2)] (**9**)	brown	90		not obsvd.	Abs		70.4 (71.8)	5.8 (5.1)	6.0 (6.0)	
[Ti(salenaPh_2)O] (**10**)	yellow	93		insoluble	[c]	3255, 3374	69.2 (69.2)	5.4 (5.4)	5.6 (5.8)	

[a] Nujol mull.
[b] Also C=O 1645 cm^{-1}.
[c] Also Ti–O 756 cm^{-1}.



Scheme 1. Synthesis and reactivity of compounds **1** and **2**.

a consequence of the electron donating methoxy substituent in compound **2** (Fig. 1). Considering the coordination potential of compounds **1** and **2**, it is of note that the pK_a of fluorene is significantly larger than that of indene or cyclopentadiene [19]. Moreover, the extended delocalisation of charge within the deprotonated fluorene results in far lower coordination affinities than either indenyl or cyclopentadienyl moieties. Thus, the stoichiometric reaction of titanium(IV) chloride and compound **1** in dichloromethane yields the deep red complex [$TiCl_3$(flusal)] (**3**), which on the basis of IR evidence displays ligand bonding through the Schiff base moiety by chelation of nitrogen and the deprotonated oxygen centre. The significant change in colour from compound **1** to compound **3** is common in Schiff base systems and does not imply more complex interactions or processes (Fig. 1). Although the formation of compound **3** is entirely normal, it is of note that compound **3** is nominally five coordinate . The fact that this compound strongly retains solvent, and affords an insoluble high melting solid once dried, suggests six coordinate geometry is achieved by the formation of halide bridged dimers. Molecular weight measurements for related 1:1 complexes have been indicative of such behaviour [20]. Reaction of titanium(IV) chloride with two equivalents of compound **1** in tetrahydrofuran (THF) yields a red sticky and intractable solid which retains solvent. After suspension in dry, deaerated acetone, [$TiCl_4$(flusalH)$_2$]·$(Me)_2CO$ (**4**) is isolated as a free-flowing powder from which acetone is not liberated even at elevated temperatures in vacuo. The insolubility of compound **4** limits the extent of its characterisation (Table 1); however, the various forms of Schiff base denticity and deprotonation have been explored in detail for both titanium(IV) and zirconium(IV) [20–24]. By analogy with this work it is possible to suggest that compound **4** exists as a six coordinate complex containing N-bound ligands in which acetone hydrogen bonds to the phenolic protons of the pendant OH functionalities. It is the presence of the latter and their interactions with solvents which are likely to cause the difficulties in handling and drying the complex [25–27].

Complexes **3** and **4** are typical Schiff base complexes in which the fluorenyl moiety is entirely passive. To induce reactivity at this centre, interaction with organometallic reagents was examined. Since considerable problems are associated with the alkylation of group 4 Schiff base complexes using alkyllithium and Grignard reagents [28,29], compound **1** was reacted directly with $TiBz_4$ [17]. Thus, the addition of compound **1** to a hexane solution of $TiBz_4$ (1:1.2) at −20°C affords, after work-up, the complex [Ti(flusal)$_2$(flusalaBz$_2$)$_2$] (**5**) (Scheme 1). ^{1}H NMR data are consistent with the crystallographic characterisation of the complex [17], which indicates the presence of two chelating flusal ligands in the octahedral titanium(IV) coordination sphere. The remaining sites are occupied by reduced Schiff base ligands, reduction having occurred as a consequence of benzyl and hydrogen addition to the C=N moieties to afford pendant amine functions. IR data are also consistent with amine and imine absorbances being observed. Once again there is no

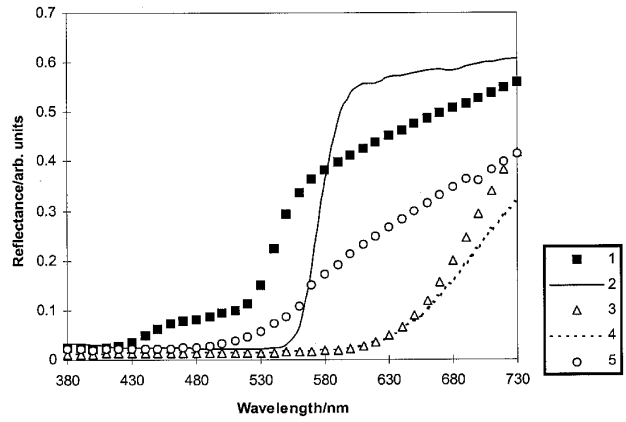


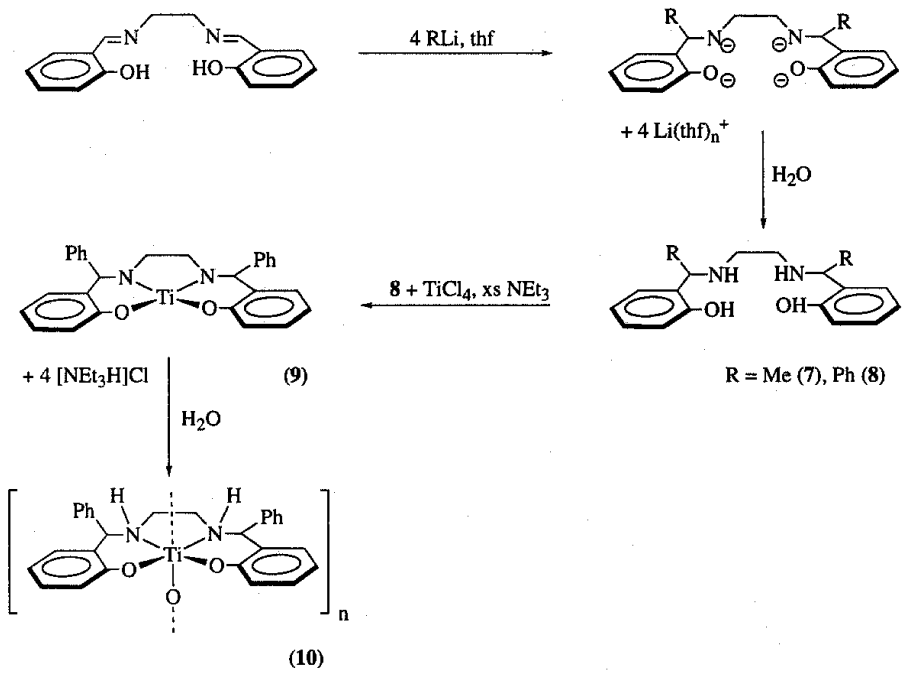
Fig. 1. Diffuse reflectance visible spectra of compounds **1–5**.

evidence for reactivity at the fluorene moiety. However, these extended aromatic systems do appear to influence the overall structure; π–π interaction of the fluorene groups of the two reduced ligands inducing a *cis* orientation of the monodentate donors.

A mechanistic appreciation of the formation of compound **5** is difficult to obtain, although several groups have considered the reactivity of systems containing alkyl functionalities, Schiff base ligands and group(4) metals [28–32]. Although direct interaction of metal and alkyl groups can occur, reactivity is complicated by the potential for metal reduction and/or nucleophilic attack of the alkyl at the Schiff base C=N group resulting in amide formation. The isolation of compound **5** extends the latter reactivity, with imine reduction to amines resulting from the effective addition of benzyl and hydrogen moieties to the C=N group. It has not proved possible to follow this process stepwise, although Bz migration to the coordinate d flusalH ligand followed by intramolecular proton transfer is clearly realistic. Such a mechanism has been explored using the reactivity of compounds **1** and **2** with organolithium reagents.

2.2. Reactivity of organolithium reagents with flusalH and derivatives

Three equivalents of organolithium reagent are consumed in the reaction of compound **1** with PhLi or n-BuLi and of compound **2** with MeLi or t-BuLi. Reaction stoichiometry suggests that highly air-sensitive intermediates are formed as a consequence of the deprotonation at hydroxyl and 9-fluorenyl protons, and nucleophilic alkyl attack at the imine centre (Scheme 1). Aqueous hydrolysis protonates all three basic sites leaving imine reduction by R-addition as the single permanent change. The formation of amines is confirmed in each reaction by the observation of parent ions in the respective mass spectra, with additional characterisation of the product obtained from the reaction of compound **2** and PhLi, i.e. MeOflusalaPhH (**6**) (Table 1). Since reducing the reaction stoichiometry to a 2:1 RLi/ligand ratio results in the complete recovery of compounds **1** and **2**, it can be assumed that the relative pK_a of the three acidic sites is OH < 9-fluorenyl



Scheme 2. Synthesis and reactivity of compounds **7** and **8**.

<HC=N. This view is supported by the reactivity observed between compound **1** or **2** and $Li[N(SiMe_3)_2]$. Addition of excess $Li[N(SiMe_3)_2]$, followed by hydrolysis, results in the quantitative recovery of compounds **1** and **2**. Although steric control cannot be ignored, this behaviour suggests that this less basic reagent is not capable of nucleophilic attack at the imine moiety.

The reactivity of compounds **1** and **2** with organolithium reagents demonstrates the general principle that nucleophilic alkyl attack at the imine function, followed by protonation, can afford amines. However, clear differences in selectivity are apparent. The 1:1.2 **1**/$TiBz_4$ reaction stoichiometry which affords compound **5** provides an excess of alkylating agent, but titanium coordination and stoichiometric availability of phenolic protons moderate reactivity. As a consequence, it can be proposed that the initial N,O coordination of the Schiff base ligand enhances intramolecular nucleophilic attack of the Bz moiety and facilitates intramolecular proton transfer. That imine alkylation remains marginal is demonstrated by the 50:50 ratio of amine and imine moieties in compound **5**. However, it is evident that in the formation of compound **5** imine reactivity is preferred to that of the fluorene function, a clear contrast to the reactivity observed with organolithium reagents.

The reactivity of compound **6** and $TiCl_4$ also provides a useful contrast to the formation of compound **5**. It is apparent that reactivity occurs between compound **6** and $TiCl_4$; however, the insolubility of the products precludes the separation and characterisation of what appears to be several metal-containing complexes. The elimination of HCl from the reaction $TiCl_4$ with ammine and amine ligands is well established, and such reactivity may be the source of multiple products here [33]. To increase the potential to form a single characterisable product, quadradentate reduced Schiff base ligands were prepared by the reaction of $salenH_2$ with organolithium reagents.

2.3. Synthesis and reactivity of reduced salenH_2 ligands

In an analogous manner to the reaction of flusalH and organolithium reagents, the reaction of MeLi or PhLi, followed by aqueous hydrolysis, affords $salenaMe_2H_2$ (**7**) and $salenaPh_2H_2$ (**8**), respectively (Scheme 2). Stoichiometric reaction of compound **8** and $TiCl_4$ in the presence of NEt_3 results in complete deprotonation of the N_2O_2 donor set and the isolation of [Ti(salenamidoPh_2)] (**9**). Similar tetra-anionic species have been synthesised using reduced Schiff base ligands and zirconium(IV) [34]. In the latter, the octahedral geometry is completed by pyridine coordination. Although compound **9** is nominally four coordinate, the classical octahedral geometry may be completed by intermolecular dative bonding by the oxygen centres. Such behaviour is well established in the corresponding titanium Schiff base chemistry [31,32,35,36]. Compound **9** is unstable in moist air, undergoing rapid hydrolysis to the polymeric μ-oxo diamine complex [Ti($salenaPh_2$)O] (**10**). Once again the relative stability of such μ-oxo species has been demonstrated by the formation of a number of dimeric, oligomeric and polymeric complexes in which the μ-oxo group is readily identified by a strong ν(Ti–O) IR vibration [32,37,38].

2.4. Crystallographic characterisation of N-2-fluorenyl-(salicylideneimine) (1)

Crystallographic characterisation of *N*-2-fluorenyl-(salicylideneimine) allows direct structural comparison with

the titanium complex **5**. Structural elucidation of compound **1** indicates similarities with the bond lengths and angles that are observed in single crystal X-ray diffraction studies of the fluorene and simple Schiff base ligands such as salenH_2 [39,40], Fig. 2. Comparison of geometries in the deprotonated flusal and reduced flusala ligands of compound **5** with compound **1** demonstrates the effects of both coordination and reduction (Table 2). The imine flusalH bond, N(1)–C(14), is slightly elongated in the coordinate d Schiff base of compound **5**, although it must be noted that the O(1)···H···N(1) hydrogen bond of flusalH is replaced by metal coordination in compound **5**. Thus, the relatively modest elongation on titanium coordination must be viewed in the context of substituting one Lewis acid interaction at N(1) with another. More significantly, lengthening of the same bond occurs by reduction in the pendant amine of the same complex — clearly a direct consequence of changing bond order. The corresponding nitrogen–fluorene linkages, N(1)–C(12), shorten in both metal-bound forms. Perhaps most notably, little change in the C(12)–N(1)–C(14) bond angle occurs between the hydrogen bonded free Schiff base and the reduced flusala moiety of compound **5**, despite the change from sp^2 to sp^3 hybridisation. In contrast, the coordinated imine moiety displays a shift towards sp character — a feature which may optimise a Ti(dπ)–N(pπ) interaction. Moreover, the significant structural changes which occur on coordination help to rationalise the differing functional group selectivity observed for the reactivity of RLi or $TiBz_4$ with compound **1**.

3. Conclusion

Titanium(IV) complexes containing Schiff base ligands and their reduced analogues may be synthesised by direct reaction of metal salt and ligand. More complex reactivity occurs between Schiff base ligands and the organotitanium reagent $TiBz_4$, involving partial imine alkylation and reduction. Reduced ligands can react with $TiCl_4$ to afford amido functionalities, which may themselves be hydrolysed to regenerate coordinate d amines. Thus by manipulation of reagents and conditions a range of ligand-centred transformations involving imine, amine and amido functionalities may occur within the group 4 metal coordination sphere.

4. Experimental

4.1. Crystallographic characterisation

Recrystallisation of compound **1** from THF–Et_2O using vapour diffusion techniques gave yellow-brown crystals ($0.07\times0.07\times0.11$ mm) suitable for single crystal X-ray analysis. Data collection and structure solution of compound **1** was performed using previously described methods, resulting in the following crystal data [41–44].

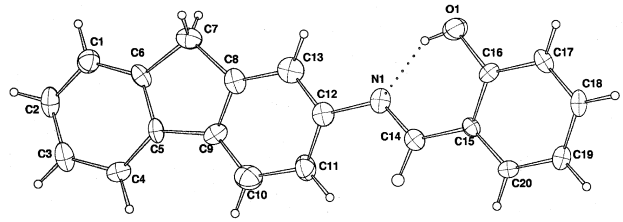


Fig. 2. Single crystal X-ray structure of compound **1**.

Table 2
Bond lengths and angles in **1** and **5**

Molecular dimensions	**1**	**5** [a]	
		Flusal moiety	Flusala moiety
Bond lengths (Å)			
N(1)–C(12)	1.469(5)	1.409(10)	1.379(12)
N(1)–C(14)	1.272(5)	1.317(10)	1.449(10)
C(14)–C(15)	1.449(5)	1.419(11)	1.507(11)
O(1)–C(16)	1.362(4)	1.318(10)	1.370(9)
O(1)–H	0.820(1)		
N(1)–H	1.805(4)		
O(1)–N(1)	2.528(4)		
Bond angles (°)			
C(13)–C(12)–N(1)	113.9(5)	120.9(9)	119.3(11)
C(12)–N(1)–C(14)	119.3(4)	128.7(9)	118.8(8)
C(14)–C(15)–C(16)	120.6(4)	121.7(10)	114.2(8)
C(15)–C(16)–O(1)	122.0(4)	119.7(10)	115.3(9)
O(1)–H–N(1)	146.2(2)		

[a] From [17].

Crystal data for $C_{18}H_{15}NO$ (**1**): $M=285.33$; monoclinic; space group $P2_1a$, $a=11.048(42)$, $b=7.936(15)$, $c=15.899(35)$ Å; $\beta=97.39(8)°$; $U<1478.3(6)$ Å^3; $D_c=1.371$ g cm^{-3}; $Z=4$; $T=145(2)$ K; $\mu=0.084$ mm^{-1}; $F(000)=600$; λ(Mo Kα) = 0.71069 nm; $2.58<\theta<25.07$; total observed reflections = 2124; observed reflections [$I>2\sigma(I)$] 734; $R=0.0489$; $R_w=0.0958$ (observed data).

4.2. Data collection and structure solution

Collection, FAST TV area detector; absorption correction, DIFFABS (min./max. factors 0.748 and 1.324, respectively); solution, direct methods (SHELXS-86); refinement, full matrix least squares on F^2 (SHELX-92), non-hydrogen atoms anisotropic, hydrogen atoms riding.

4.3. Synthetic procedures

Solvents were dried using standard methods. All titanium reactions were performed under nitrogen [32]. RLi reagents [R = Me, Ph, n-Bu, t-Bu, N(SiMe$_3$)$_2$] were purchased from Aldrich. 2-Aminofluorene, lithiumfluorenyl and $TiBz_4$, were prepared using published methods [18,45–47]. ^{1}H NMR spectra were obtained at 270 MHz in $CDCl_3$ unless stated otherwise. Elemental analysis and important characterisation data are given in Table 1.

*4.3.1. N-2-Fluorenyl(salicylideneimine), flusalH (**1**)*

The ligand was prepared by the dropwise addition of one equivalent of 2-aminofluorene in THF to an ethanolic solution of freshly distilled salicylaldehyde. After refluxing for 1 h the solution was cooled to afford crude compound **1**, which was washed in Et_2O and dried in vacuo. Recrystallisation of the crude material from ethanol–chloroform gave compound **1** as a yellow-brown crystalline solid (80%). ^{1}H NMR: δ 3.95 (s, 2H, CH_2), 6.92–7.84 (m, 11H, aromatic), 8.70 (s, 1H, CH), 13.30 (s, 1H, OH). EI^+ MS: *m/z* 285 (100%, $[\mathbf{1}]^+$). IR (Nujol) (cm^{-1}): ν(C=N) 1618, ν(O–H) 3460.

*4.3.2. N-2-Fluorenyl(3-methoxysalicylideneimine) (**2**)*

Compound **2** was prepared by the same method as compound **1** and recrystallised from ethanol (75% yield). ^{1}H NMR ($CDCl_3$): δ 3.94 (s, 3H, MeO) and (s, 2H, CH_2) (methylene protons obscured by the methoxy resonance), 6.84–7.83 (m, 11H, Ph), 8.71 (s, 1H, CH), 13.83 (s, 1H, OH). EI^+ MS: *m/z* 316 (100%, $[2+H]^+$). IR (Nujol) (cm^{-1}): ν(C=N) 1618, ν(O–H) 3460.

*4.3.3. [$TiCl_3$(flusal)] (**3**)*

A toluene solution of titanium(IV) chloride (1.0 M, 3.15 cm^3, 3.15 mmol) was added dropwise to compound **1** (0.9 g, 3.2 mmol) in CH_2Cl_2 (approx. 30 cm^3). A deep red precipitate immediately formed. The solution was refluxed for 1 h, after which the solid was separated by filtration, washed with hexane (5×10 cm^3) and dried in vacuo to afford compound **3** as a maroon free-flowing solid. Yield: 1.3 g (95%). Compound **3** is insufficiently soluble to obtain ^{1}H NMR spectroscopic data. FAB^+ MS: *m/z* 437 (15%, $[\mathbf{3}]^+$). M.p. dec.: 306–310°C.

*4.3.4. [$TiCl_4$(flusalH)$_2$] (**4**)*

Compound **1** (2.0 g 7.0 mmol) in THF (approx. 50 cm^3) was treated with titanium(IV) chloride (1.0 M, 3.5 cm^3, 3.5 mmol). A deep red solid precipitated, after which the solution was refluxed for 1 h. The colourless solvent was then decanted from the solid which was washed with THF (2×30 cm^3), also resulting in colourless extracts. The solid was slurried in acetone and cooled to −20°C. After 1 day, decantation of the solvent and drying in vacuo gave 2.8 g of [$TiCl_4$(flusalH)$_2$]·Me_2CO (**4**) as a deep red, air-stable solid in quantitative yield. Insolubility precluded ^{1}H NMR spectroscopic characterisation. FAB^+ MS: *m/z* 286 (100%, $[1+H^+]$), 348 (40%, [Ti(=O)(flusal)]$^+$). IR (Nujol) (cm^{-1}): ν(C=O) 1645, ν(C=N) 1620, ν(O–H) 3361.

*4.3.5. [Ti(flusal)$_2$(flusalaBz$_2$)$_2$] (**5**)*

Compound **1** (0.50 g, 1.8 mmol) was added in a single portion to a hexane solution (20 cm^3) of $TiBz_4$ (0.87 g, 2.1 mmol) at −20°C. The dark brown precipitate which formed over 0.5 h was filtered, washed with hexane and extracted with toluene. The resultant brown solution becomes progressively pale orange. Addition of hexane and storage at −20°C affords toluene solvated compound **5** over about 3 days. ^{1}H NMR: δ 3.22 (m, 4H, Ph*CH*$_2$CHNH), 3.72 (s, 2H, 9-fluorene CH_2), 3.96 (s, 2H, 9-fluorene CH_2), 4.18 (s, 2H, PhCH$_2$CH*NH*), 4.60 (m, 2H, PhCH$_2$*CH*NH), 6.67–7.86 (m, 54H, aromatic), 8.75 (s, 2H, *CH*). FAB^+ MS: *m/z* 268 (100%, $[\mathbf{1}]^+$), 1368 (10%, $[\mathbf{5}]^+$). IR (Nujol) (cm^{-1}): ν(C=N) 1612(s), ν(N–H) 3376(s), 3389(s).

*4.3.6. N-2-Fluorenyl(α-phenyl-3-methoxysalicylideneamine) (**6**)*

Compound **2** (3.0 g, 9.5 mmol) in THF (approx. 40 cm^3) was cooled to −20°C and PhLi (1.8 M, 15.9 cm^3, 28.6 mmol) was added dropwise. During addition the solution developed a deep red colour. After stirring for 1 h, deaerated distilled water was added. The mixture was diluted with Et_2O and the organic layer was separated. The aqueous layer was shaken with two portions of Et_2O (approx. 2×30 cm^3) and the combined organic fractions were dried over magnesium sulfate. Following filtration the solvent was removed under reduced pressure to yield crude compound **6** (3.7 g, ≈96%) as a gelatinous, off-white solid. Recrystallisation from THF–Et_2O afforded cream, crystalline material. ^{1}H NMR: δ 1.18 (s br, 1H, *NH*), 3.68 (s, 2H, *CH*$_2$), 3.83 (s, 3H, *CH*$_3$O), 4.40 (s br, 1H, *OH*), 5.82 (s, 1H, CH), 6.73–6.83, 7.07–7.35 (m, Ph). FAB^+ MS: *m/z* 393 (55%, $[\mathbf{6}]^+$). IR (Nujol) (cm^{-1}): ν(N–H) 3414, 3475 (vs), ν(O–H) 1375.

Similar reactions carried out using compounds **1** and **2** with other organolithium reagents afforded products analogous to compound **6**. These products did not lend themselves to crystallisation and thus produced ^{1}H NMR spectra containing residual solvent, and tolerable but somewhat variable elemental analysis. However, molecular ions of significant intensity could be recorded in each case. Thus *N*-2-fluorenyl(α-phenyl-salicylideneamine) [EI MS: *m/z* 363, 85%] and *N*-2-fluorenyl(α-n-butyl-salicylideneamine) [FAB^+ MS: *m/z* 344, 100%] were recovered from the reaction of compound **1** with phenyllithium and butyllithium, respectively. The methoxyl derivatives *N*-2-fluorenyl(α-methyl-3-methoxysalicylideneamine) [FAB^+ MS: *m/z* 331, 20%] and *N*-2-fluorenyl(α-t-butyl-3-methoxysalicylideneamine) [FAB^+ MS: *m/z* 374, 100%] were also isolated from the reaction of compound **2** with methyllithium and t-butyllithium.

*4.3.7. N,N′-(1,2-Ethlyenebis(α-methylsalicylaldamine)] (**7**)*

An ET_2O solution of methyllithium (1.4 M, 21.3 cm^3, 29.9 mmol) was added dropwise to a THF solution of salenH_2 (2.0 g, 7.46 mmol) at −20°C. The resultant colourless solution was stirred for 1 h before deaerated, distilled water was added (approx. 20 cm^3). Addition of Et_2O produced two layers. After separation, the aqueous layer was washed with ether (3×30 cm^3). The combined organic phases were concentrated, dried with $MgSO_4$ and further reduced to produce a paste which was recrystallised from THF–Et_2O to afford compound **7** (1.0 g, 45%). ^{1}H NMR (CD_2Cl_2): δ 1.38 (s, 3H, *Me*), 1.41 (s, 3H, *Me*), 1.53 (b s, *NH*), 2.66 (m, 2H,

CH_2), 2.79 (m, 2H, CH_2), 3.88 (q, 2H, *CH*), 6.70–7.13 (m, 8H, *Ph*), 11.03 (bs *OH*). EI MS: m/z 300 (100%, $[\mathbf{7}]^+$).

*4.3.8. N,N′-(1,2-Ethylenebis(α-phenylsalicylaldamine)] (**8**)*

The compound was prepared by the same route as compound **7**, giving a white solid in 80% yield. ^{1}H NMR: δ 1.42 (b s, *NH*), 2.93 (m, 4H, CH_2), 4.88 (s, 2H, *CH*), 6.72–7.31 (m, 18H, *Ph*), 11.50 (bs *OH*). FAB$^+$ MS: m/z 425 (30%, $[\mathbf{8}]^+$).

*4.3.9. [Ti(salenamidoPh$_2$)] (**9**)*

A toluene solution of compound **8** (1.76 g, 4.15 mmol) and triethylamine (3.5 cm^3, 25 mmol) was treated dropwise with $TiCl_4$ (1.0 M toluene, 4.15 cm^3, 4.15 mmol). After stirring for 12 h, an orange solution was filtered from the precipitated $[NEt_3H]Cl$, and after concentration and addition of hexane afforded compound **9** as a brown crystalline solid (1.8 g, 90%). FAB$^+$ MS: m/z 468 (50%, $[\mathbf{9}]^+$).

*4.3.10. [Ti(salenaPh$_2$)O] (**10**)*

An orange toluene solution of compound **9** (1.0 g, 2.14 mmol) was filtered in air and rapidly formed a pale yellow precipitate. After 0.5 h the precipitate was filtered and washed with dry hexane to afford compound **10** (1.8 g, 93%). Compound **10** could be crystallised from CH_2Cl_2–Et_2O as an analytically pure microcrystalline solid. FAB$^+$ MS: m/z 955 (100%, $[\mathbf{10}_2 - O]^+$).

5. Supplementary data

Crystallographic data for the structural analyses have been deposited with the Cambridge Crystallographic Data Centre, CCDC, No. 127639. Copies of this information can be obtained free of charge from The Director, CCDC, 12, Union Road, Cambridge CB2 1EZ (fax: +44-1223-336-033; e-mail: deposit@ccdc.cam.ac.uk or http://www.ccdc.cam.ac.uk).

References

[1] J.A. Ewen, R.L. Jones, A. Razavi, J.D. Ferrara, J. Am. Chem. Soc. 110 (1988) 6255.
[2] J.A. Ewen, M.J. Elder, R.L. Jones, L. Haspeslagh, J.L. Atwood, S.G. Bott, K. Robinson, Makromol. Chem., Makromol. Symp. 48/49 (1991) 235.
[3] J.A. Ewen, M.J. Elder, Makromol. Chem., Makromol. Symp. 66 (1993) 179.
[4] A. Razavi, J.D. Ferrara, J. Organomet. Chem. 435 (1992) 299.
[5] A. Razavi, U. Thewalt, J. Organomet. Chem. 445 (1993) 111.
[6] A. Razavi, J.L. Atwood, J. Organomet. Chem. 459 (1993) 117.
[7] B. Rieger, J. Organomet. Chem. 420 (1991) C17.
[8] B. Rieger, M. Steinmann, R. Fawzi, Chem. Ber. 125 (1993) 2373.
[9] M. Bochmann, S.J. Lancaster, M.B. Hursthouse, M. Mazid, Organometallics 12 (1993) 4718.
[10] G.S. Herrmann, H.G. Alt, M.D. Rausch, J. Organomet. Chem. 401 (1991) C5.
[11] N.G. Alt, W. Milius, S.J. Palackal, J. Organomet. Chem. 472 (1994) 113.
[12] E.W. Abel, F.G.A. Stone, G. Wilkinson (Eds.), Comprehensive Organometallic Chemistry II, vol. 4, Pergamon, Oxford, 1995, Chapter 5.
[13] E. Samuel, R. Seltan, J. Organomet. Chem. 4 (1965) 156.
[14] A.K. Sharma, N.K. Kaushik, Acta Chim. Hung. 116 (1984) 361.
[15] N.K. Kaushik, A.K. Sharma, G.S. Sodhi, Indian J. Chem. 20 (1981) 847.
[16] F.G.N. Cloke, A.R. Dias, A.M. Galvao, J.L.F. daSilva, J. Organomet. Chem. 548 (1997) 177.
[17] S.J. Coles, M.B. Hursthouse, D.G. Kelly, A.J. Toner, N.M. Walker, Can. J. Chem. (in press).
[18] W.E. Kuhn, Org. Synth. 13 (1933) 447.
[19] W.K. McEwen, J. Am. Chem. Soc. 58 (1936) 1124.
[20] J.A. Garcia-Vasquez, M. Lûpez-Becerra, J.R. Masaguer, Transition Metal Chem. 8 (1983) 233.
[21] N.S. Biradar, V.H. Kulkarni, J. Inorg. Nucl. Chem. 33 (1971) 3847.
[22] F.L. Bowden, D. Ferguson, J. Chem. Soc., Dalton Trans. (1974) 460.
[23] S.J. Coles, M.B. Hursthouse, D.G. Kelly, A.J. Toner, N.M. Walker, J. Chem. Soc., Dalton Trans. (1998) 3489.
[24] F. Corazza, E. Solari, C. Floriani, A. Chiesi-Villa, C. Guastini, J. Chem. Soc., Dalton Trans. (1990) 1335.
[25] A.D. Garnovskii, A.L. Nivorozhkin, V.L. Minkin, Coord. Chem. Rev. 126 (1993) 1.
[26] S. Yamada, Coord. Chem. Rev. 1 (1966) 415.
[27] U. Casellata, P.A. Vigato, M. Vidali, Coord. Chem. Rev. 23 (1977) 31.
[28] C. Floriani, E. Solari, F. Corazza, A. Chiesi-Villa, C. Guastini, Angew. Chem., Int. Ed. Engl. 28 (1989) 64.
[29] E. Solari, C. Floriani, A. Chiesi-Villa, C. Rizzoli, J. Chem. Soc., Dalton Trans. (1992) 367.
[30] E.B. Tjaden, D.C. Swenson, R.F. Jordan, J.L. Petersen, Organometallics 14 (1995) 371.
[31] S.J. Coles, M.B. Hursthouse, D.G. Kelly, A.J. Toner, N.M. Walker, Polyhedron 15 (1996) 4307.
[32] S.J. Coles, M.B. Hursthouse, D.G. Kelly, A.J. Toner, N.M. Walker, J. Organomet. Chem. 580 (1999) 304.
[33] A.D. Norman, Inorganic Reactions and Methods, vol. 8, VCH, New York, 1991, p. 80.
[34] P. Woodman, P.B. Hitchcock, P. Scott, J. Chem. Soc., Chem. Commun. (1996) 2735.
[35] M. Mazzanti, S. Gambarotta, C. Floriani, A. Chiesi-Villa, C. Guatini, Inorg. Chem. 25 (1986) 2308.
[36] J.-M. Rosset, C. Floriani, M. Mazzanti, A. Chiesi-Villa, C. Guatini, Inorg. Chem. 29 (1990) 3991.
[37] K. Nakajima, C. Sasaki, M. Kojima, T. Aoyama, S. Ohba, Y. Saito, J. Fujita, Chem. Lett. (1987) 2189.
[38] E. Gallo, E. Solari, F. Franceschi, C. Floriani, A. Chiesi-Villa, C. Rizzoli, Inorg. Chem. 34 (1995) 2495.
[39] G.M. Brown, M.H. Bortner, Acta Crystallogr. 7 (1954) 139.
[40] N. Bresciani-Pahor, M. Calligaris, G. Nardin, L. Randaccio, Acta Crystallogr., Sect. B 34 (1978) 1360.
[41] J.A. Darr, S.R. Drake, M.B. Hursthouse, K.M.A. Malik, Inorg. Chem. 32 (1993) 5704.
[42] G.M. Sheldrick, Acta Crystallogr., Sect. A 46 (1990) 467.
[43] G.M. Sheldrick, SHELX-93, University of Göttingen, Germany, 1993.
[44] N.P.C. Walker, D. Stuart, Acta Crystallogr. Sect. A39 (1983) 158 (adapted for FAST geometry by A. Karaulov, University of Wales, Cardiff, 1991).
[45] G.W.H. Scherf, R.K. Brown, Can. J. Chem. 38 (1960) 2450.
[46] U. Zucchini, E. Albizzati, U. Giannini, J. Organomet. Chem. 26 (1971) 357.
[47] J.J. Felten, W.P. Anderson, J. Organomet. Chem. 36 (1972) 87.

PERGAMON

www.elsevier.nl/locate/poly

Polyhedron 19 (2000) 185–192

POLYHEDRON

Mono- and polynuclear complexes of Fe(II), Co(II), Ni(II), Cu(II), Zn(II) and Cd(II) with *N,N′*-bis(3-hydroxysalicylidene)-1,3-diamino-2-propanol

Jesús Sanmartín [a], Manuel R. Bermejo [a,*], Ana M. García-Deibe [a], Marcelino Maneiro [a], Carmen Lage [a], Antonio J. Costa-Filho [b]

[a] *Departamento de Química Inorgánica, Facultade de Química, Campus Sur, Universidade de Santiago de Compostela, E-15706 Santiago de Compostela, Galicia, Spain*

[b] *Instituto de Física de São Carlos, Universidade de São Paulo, C.P. 369, 13560-970 São Carlos, SP, Brazil*

Received 15 September 1999; accepted 8 November 1999

Abstract

Mono- and polynuclear neutral complexes have been obtained by direct electrochemical reaction of metal anodes with the potentially heptadentate and tetracompartmental ligand *N,N′*-bis(3-hydroxysalicylidene)-1,3-diamino-2-propanol (H_5L). Physicochemical data suggest that the ligand behaves as a di- or tetra-anion in mono- and polynuclear complexes, respectively. Metal ions are held together by μ-phenoxo oxygen bridges in polynuclear complexes. Nickel and copper environments are distorted to tetrahedral and square-planar, respectively. Zinc and cadmium could be hexa-coordinated in the mononuclear complexes. Finally, iron and cobalt ions seem to be in pseudo-octahedral fields. ©2000 Elsevier Science Ltd All rights reserved.

Keywords: Electrochemical synthesis; Mononuclear complexes; Phenoxo bridges; Polyhydroxyl ligands; Polynuclear complexes; Schiff base ligands

1. Introduction

Attempts to obtain homodinuclear nickel and copper(II) complexes from *N,N′*-bis(3-hydroxysalicylidene)-1,3-diamino-2,2-dimethylpropane, following an accepted procedure for this type of ligand, were unsuccessful [1]. Usually, di- and polynuclear complexes are prepared by refluxing the appropriate metal(II) acetate and LiOH in methanol with the previously prepared mononuclear complex. However, a homodinuclear iron(III) complex containing this ligand has been prepared using template synthesis [2].

Recently, we have synthesised and structurally characterised $Cu_3(SB)(H_2SB)\cdot 2H_2O$ [3] and $Zn_8(SB)_4(H_2O)_3\cdot 3CH_3CN$ [4], which contain the symmetrical hexadentate Schiff base *N,N′*-bis(3-hydroxysalicylidene)-1,4-diaminobutane. A notable feature of this ligand, that we found previously, is that it shows a high ability to hold together metal ions by μ-phenoxo oxygen bridges. In fact, it can simultaneously coordinate up to five metal centres in different ways, resulting in complex structures. An additional interest in the study of these systems is that the bis-helical [4+4+4] compound $Cu_3(SB)(H_2SB)\cdot 2H_2O$ presents some intermetallic distances, and a metal centre triangular array, similar to those observed in some copper proteins [3,5,6].

Here we describe the direct electrochemical synthesis and structural characterisation of mono- and polynuclear Fe, Co, Ni, Cu, Zn and Cd(II) complexes with the symmetrical and potentially tetracompartmental Schiff base ligand *N,N′*-bis(3-hydroxysalicylidene)-1,3-diamino-2-propanol (H_5L).

2. Experimental

2.1. Materials

Iron, cobalt, nickel, copper, zinc and cadmium were used as sheets 0.5 mm thick. 2,3-Dihydroxybenzaldehyde and 1,3-diamino-2-propanol were commercial products (Aldrich) and were used without further purification, as were all solvents. The Schiff base ligand was prepared by condensation of the aldehyde and the diamine, in 2:1 molar ratio, and refluxing in chloroform for 3 h.

* Corresponding author. Tel.: +34-981-591076; fax: +34-981-597525; e-mail: qimb45@uscmail.usc.es

0277-5387/00/$ - see front matter ©2000 Elsevier Science Ltd All rights reserved.
PII S0277-5387(99)00341-1

Table 1
Experimental conditions in the synthesis of the complexes

Complexes	Amount H_5L/(g)	Calculated [a] M/mg (g)	Solved M/mg (g)	Electrolysis time/s (h) [a]	Initial voltage [b] (V)	Yield (%)	E_f (mol F^{-1})
$Fe(H_3L)(H_2O)_2$	0.1	17	16	5760	9.2	79	0.5
$[Fe_2(HL)(H_2O)_5]_n$	0.1	34	27	10800	21.4	88	0.4
$Co(H_3L)(H_2O)_3$	0.2	37	36	11520	8.5	73	0.5
$[Co_2(HL)(H_2O)_2]_n$	0.1	37	37	11520	9.3	51	0.5
$Ni(H_3L)(H_2O)$	0.1	18	14	5700	17.2	86	0.4
$[Ni_2(HL)(H_2O)_2]_n$	0.1	36	30	10500	21.7	98	0.5
$[Cu_2(HL)(H_2O)]_n$	0.1	39	30	4680	12.6	44	1.0
$Zn(H_3L)(H_2O)_2$	0.1	20	18	5760	11.4	68	0.5
$[Zn_2(HL)(H_2O)]_n$	0.1	39	34	12000	16.3	75	0.5
$Cd(H_3L)(H_2O)_2$	0.1	34	29	5700	27.7	78	0.4
$[Cd_2(HL)(H_2O)_2]_n$	0.1	68	62	11400	17.6	97	0.5

[a] The amount of metal was calculated in accordance with the quantitative yield with respect to the amount of ligand in the processes: $2M_{(s)} + H_5L_{(MeCN)} \rightarrow [M_2(HL)(H_2O)_x]_n + 2H_{2(g)}$ and $M_{(s)} + H_5L_{(MeCN)} \rightarrow M(H_3L)(H_2O)_x + H_{2(g)}$.
[b] Voltage to produce a current of 10 mA.

2.2. Complexes synthesis

The electrochemical method [7] has been widely employed by us [3,4,8–11] in the synthesis of mono- and polynuclear complexes. The cell was a 100 cm^3 tall form beaker fitted with a rubber bung through which the electrical leads entered. The metal anode, which had been previously weighed, was suspended from a platinum wire; a second platinum wire was the cathode. H_5L, 0.1–0.2 g, was dissolved with heat in about 80 ml of acetonitrile. Then, a small amount of tetramethylammonium perchlorate (about 10 mg) was added as supporting electrolyte. (Caution: although no problem has been encountered in this work, all perchlorate compounds are potentially explosive, and should be handled in small quantities and with great care.) Direct current was obtained from a purpose-built DC power supply. Applied voltages of between 8.5 and 27.7 V allowed sufficient current flow to obtain the solution of the required mass of metal anodes (see Table 1). The electrolysis times were calculated with respect to the amount of ligand and in accordance with the following reactions: $M_{(s)} + H_5L \rightarrow M(H_3L)(H_2O)_x + H_{2(g)}$ and $2M_{(s)} + H_5L \rightarrow [M_2(HL)(H_2O)_x]_n + 2H_{2(g)}$. Metal solved is calculated after re-weighing the anode. The experimental conditions for the synthesis of complexes are set out in Table 1. In all cases, hydrogen was evolved at the cathode. Cells can be summarised as: $M_{(+)}|MeCN + H_5L|Pt_{(-)}$.

Solid products were readily isolated from the electrolysis solution by filtration. The insoluble products obtained were washed with acetonitrile and diethyl ether to remove any excess ligand and vacuum dried.

The amount of metal solved was evaluated in order to postulate an empirical formula for the complexes and the processes involved in their synthesis. The calculated E_f value is useful for the latter. Electrodes were cleaned with a dilute HCl solution.

2.3. Physicochemical measurements

Elemental analyses of C, H, N and O were carried out on a Fisons Instruments EA 1108 CHNS-O. The empirical formulae deduced from these results are listed in Table 2.

A Varian E-109 spectrometer together with an ITC503 Oxford cryogenic system were used to perform electron paramagnetic resonance (EPR) measurements at 9.3 GHz (X band). The spectrometer is equipped with a rectangular resonant cavity and 100 kHz field modulation. A HP5352B frequency counter was used to measure the microwave frequency. A powdery sample of $[Cu_2(HL)(H_2O)]_n$ was measured at 4.0 K. The EPR spectrum was acquired and digitised by a microcomputer equipped with a standard data acquisition card with an analogue to digital converter. Magnetic susceptibilities were measured using a SQUID magnetometer. Diamagnetic corrections were made using Pascal's constants.

^1H NMR spectra were recorded on a Bruker 300 AC spectrometer. The positive ion electrospray mass spectra up to 1000 *m/z* were registered on an LC/MSD HP1100 spectrom-

Table 2
Analytical data for the compounds [a]

Compound	C	H	N	O
H_5L	61.7 (61.8)	5.6 (5.5)	8.3 (8.5)	24.0 (24.2)
$Fe(H_3L)(H_2O)_2$	48.3 (48.5)	4.7 (4.8)	7.0 (6.7)	27.1 (26.7)
$[Fe_2(HL)(H_2O)_5]_n$	38.9 (38.7)	4.2 (4.5)	5.3 (5.3)	30.3 (30.3)
$Co(H_3L)(H_2O)_3$	45.8 (46.3)	4.5 (5.0)	6.9 (6.4)	28.5 (29.0)
$[Co_2(HL)(H_2O)_2]_n$	42.2 (42.5)	4.0 (3.8)	6.1 (5.8)	23.8 (23.3)
$Ni(H_3L)(H_2O)$	50.6 (50.4)	4.8 (4.4)	7.2 (6.9)	23.4 (23.7)
$[Ni_2(HL)(H_2O)_2]_n$	43.0 (42.6)	3.7 (3.8)	5.7 (5.8)	24.0 (23.4)
$[Cu_2(HL)(H_2O)]_n$	41.7 (41.7)	3.9 (3.7)	5.8 (5.7)	22.7 (22.9)
$Zn(H_3L)(H_2O)_2$	47.8 (47.5)	4.4 (4.7)	6.2 (6.5)	25.8 (26.1)
$[Zn_2(HL)(H_2O)]_n$	43.2 (43.3)	3.6 (3.4)	6.0 (5.9)	22.2 (22.7)
$Cd(H_3L)(H_2O)_2$	42.6 (42.8)	4.2 (4.2)	5.9 (5.9)	23.9 (23.5)
$[Cd_2(HL)(H_2O)_2]_n$	34.8 (34.8)	3.2 (3.1)	4.8 (4.8)	18.7 (19.1)

[a] Data are expressed in percentages. Calculated values are in parentheses.

eter at 190 V with acetonitrile as solvent. IR spectra were recorded as KBr pellets on a FT-IR Mattson Instruments 2020 spectrophotometer. Diffuse reflectance spectra were recorded on a Shimadzu UV-3103 PC spectrophotometer. Electronic spectra in solution were registered on a HP 8452 A diode array spectrophotometer. Melting points were measured on a Gallenkamp apparatus.

The water content and decomposition temperature were evaluated using a PL differential scanning calorimeter. Tests were performed in air. Aluminium was used as reference material. The temperature programme used was a gradient from 30 to 600°C for 1 h.

3. Results and discussion

As mentioned in Section 1, a N_2O_2 coordinated mononuclear iron complex and a homodinuclear iron(III) compound with *N*,*N*′-bis(3-hydroxysalicylidene)-1,3-diamino-2,2-dimethylpropane using N_2O_2 and O_4 donor sets have been obtained. However, when the metal ion was nickel(II) or copper(II), homodinuclear complexes could not be prepared [1].

We have found that the anodic oxidation of iron, cobalt, nickel, copper, zinc and cadmium in the presence of H_5L is a simple and efficient route to obtain homopolynuclear complexes. The variation in the amount of metal solved, which is controlled by means of the reaction time and voltage, leads to mono- or polynuclear complexes. Only in the case of copper do these conditions seem not to be critical, at least for the times and voltages tested. Thus, even when mild reaction conditions are used, such as low voltage and short electrolysis time, the electrochemical method yields only the polynuclear copper compound. Complexes have been studied by elemental analysis (Table 2), IR and mass spectrometry and, in appropriate cases, by ^{1}H NMR and UV–Vis spectroscopy, thermal analysis, magnetism or EPR. The data allow identification of the coordination site and the geometry of the molecule.

All the powdery solids isolated are light- and air-stable, but their behaviour in solution appears to be different. Complexes gradually lose Schiff base ligand to yield new compounds in which water (in a higher ratio than for original complexes) and/or hydroxo groups are present. As an example, a mixture of compounds can be obtained from water or ethanol solutions of $Zn(H_3L)(H_2O)_2$. The elemental analyses of successive isolated mixtures show a significant and gradual decrease of the C, H and N percentage values, and IR spectroscopy shows an increase of the ν(OH) intensity at about 3400 cm^{-1}, as well as the presence of two new bands. One band, at about 1060 cm^{-1}, is attributed to the Zn–O–H bending mode, and the other, near 470 cm^{-1}, is probably due to ν(Zn–O).

Finally, we have found that cadmium oxidation (for 3960 s at 17 V and 5 mA) in the presence of a dimethylsulfoxide (DMSO) solution containing $Zn(H_3L)(H_2O)_2$ yields $[Cd_2(HL)(H_2O)_2]_n$, similar to that prepared by direct electrochemical synthesis. [Found: C, 34.0; H, 2.6; N, 4.5. Calc. for $C_{17}H_{20}Cd_2N_2O_7$: C, 34.8; H, 3.1; N, 4.8%. ν_{max} (cm^{-1}): 3415 (OH), 1626 (CN), 1458 and 1261 (CO)]. This behaviour seems to correspond to a transmetalation process [12,13].

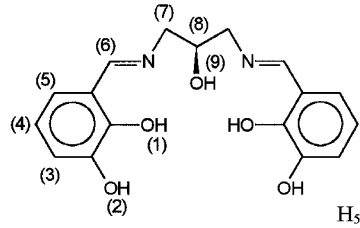
3.1. Efficiency

In keeping with previous practice, we have measured the electrochemical efficiency, which is defined as the quantity of metal dissolved per faraday of charge. E_f values are listed in Table 1. The values close to 0.5 mol F^{-1} are in keeping with a one-step mechanism for the redox reaction at the anode. The E_f value for $[Cu_2(HL)(H_2O)]_n$ (1.0 mol F^{-1}) implies a reaction to form a Cu(I) complex at the anode followed by an oxidative addition reaction to give the Cu(II) complex. Such oxidation steps have been previously observed for other copper complexes [14].

3.2. ^{1}H NMR spectroscopy

^{1}H NMR spectra of H_5L and diamagnetic mononuclear complexes were recorded in DMSO-d_6. Data are listed in

Table 3
^{1}H NMR data (in ppm) for diamagnetic compounds using DMSO-d_6 as solvent



H_5L

Compound	2H(1)	2H(2)	2H(6)	2H(5)	2H(3)	2H(4)	1H(9)	1H(8)	4H(7)
H_5L	13.69 b	8.89 b	8.48 s	6.86 d	6.83 d	6.63 t	5.35 b	4.00 b	3.80 d, 3.60 d
$Zn(H_3L)(H_2O)_2$		7.88 b	8.11 s	6.62 d	6.59 d	6.21 t	4.99 b	3.89	3.89, 3.57
$Cd(H_3L)(H_2O)_2$			8.13 s	6.62 d	6.60 d	6.27 t		3.85	3.85, 3.58

Table 3. The very low solubility of polynuclear compounds prevents their study. Assignment of signals is according to our experience with similar Schiff bases [15] and the literature [2,16]. The symmetry of the ligand makes its spectrum very simple. For the free ligand, all O*H* protons are detectable as three broad signals. The presence of the hydroxyl group in the aliphatic chain causes a split of the signal attributed to H(7) protons. The aromatic proton in the *ortho* position with respect to the iminic group is observed downfield (6.86 ppm), very near to the proton sited in close proximity to the outer phenolic OH. The remaining aromatic proton shows a signal at higher field (6.63 ppm).

For $Zn(H_3L)(H_2O)_2$, hydroxylic and outer phenolic oxygen atoms remain protonated and are apparently not coordinated, as reported for several other compounds [16–19]. The absence of the inner phenolic protons and the strong shift of the outer O*H* signal confirm the complexation of zinc ion in the inner N_2O_2 compartment of the ligand. The low solubility of $Cd(H_3L)(H_2O)_2$ makes its study difficult. Thus, the fact that H(2) and H(9) were not observed is probably due to the low intensity of these broad signals. An upfield shift with respect to the free ligand is observed for all the proton signals of these metal complexes, excluding those assigned as H(7) which are not significant.

In contrast with our observations [20] and those described for similar Schiff base complexes when the metal was nickel [2], the complexation of zinc or cadmium into the inner N_2O_2 compartment produces a marked change in the relative positions of H(2) and H(6) signals. This is caused by the weak upfield shift undergone by H(6), whereas for nickel complexes both H(2) and H(6) signals suffer an equivalent shift. However, the resulting difference between H(2) and H(6) signals after coordination is not very different from that found before. The correct assignment of the H(2) signal was confirmed by the observation of its absence after a small addition of D_2O. The presence of the metal centre also produces a slight and opposite shift of both H(7) and H(8), which results in a unique signal at 3.89 ppm.

The conjugation of C=N bonds with the aromatic rings limits the geometric variety of the mononuclear complexes containing salpn-type ligands. Thus, it is very common to find square-planar or octahedral coordination geometries with the Schiff base donor atoms occupying equatorial positions [15–17]. In analogy with those described for Mn(III) complexes containing 2-OH-salpn [17] and according to the empirical formulae of these complexes, we propose an octahedral geometry for $Zn(H_3L)(H_2O)_2$ and $Cd(H_3L)(H_2O)_2$ with water molecules in axial positions.

3.3. ES mass spectroscopy

Positive ion electrospray (ES) mass spectra for mononuclear complexes show peaks related to fragments of the type $M(H_3L)$ between 384 and 441 *m/z*. This indicates the ligand coordination to the metal centre. Some important mass peaks are given in Table 4. The low solubility of the polynuclear iron and cadmium complexes makes their study difficult.

The observation of peaks related to fragments of the type $M_2(HL)$ at about 450 *m/z* for polynuclear complexes shows that each ligand unit coordinates at least two metal centres. Although this could be indicative of both metal ions occupying the inner N_2O_2 and the outer O_4 compartments, the presence of peaks corresponding to heavier fragments such as $M_3(HL)_2$ at about 840 *m/z* and $M_4(HL)_2$ near to 900 *m/z*, for Co(II), Ni(II), Cu(II) and Zn(II) complexes, indicates that metal ions could be coordinated to two different ligand units, as observed for $Cu_3(SB)(H_2SB)\cdot 2H_2O$ [3] and $Zn_8(SB)_4(H_2O)_3\cdot 3CH_3CN$ [4]. These facts seem to be in agreement with a polymeric behaviour of the complexes rather than with a monomeric one.

The low abundance for the peaks considered is very probably due to the low solubility and high fragmentation of the

Table 4
Some important mass peaks, colour, UV–Vis and magnetic moment (at room temperature) for the studied compounds

Compound	Mass peaks (m/z)	Colour	λ (nm)	μ_B
H_5L	331 (31×10^3)	orange	225 [a], 270 [a], 290 [a], 330 [a], 425 [a]	
$Fe(H_3L)(H_2O)_2$	384 (3×10^3)	purple		5.0
$[Fe_2(HL)(H_2O)_5]_n$		purple		7.5
$Co(H_3L)(H_2O)_3$	387 (23×10^3)	purple	490 [b], 630 [b], 1300 [b], 480 [c], 610 [c]	5.0
$[Co_2(HL)(H_2O)_2]_n$	445 (20×10^3), 830 (10×10^3), 889 (3×10^3)	brown	500 [b], 640 [b], 1300 [b]	6.6
$Ni(H_3L)(H_2O)$	387 (23×10^3)	brown	630 [b], 1250 [b]	3.8
$[Ni_2(HL)(H_2O)_2]_n$	445 (27×10^3), 831 (2.5×10^3), 888 (2.5×10^3)	brown	630 [b], 1250 [b]	3.6
$[Cu_2(HL)(H_2O)]_n$	454 (28×10^3), 844 (5×10^3), 909 (7×10^3)	green	630 [a], 620 [b,c,d], 600 [e]	2.4
$Zn(H_3L)(H_2O)_2$	394.5 (4×10^3)	ochre		
$[Zn_2(HL)(H_2O)]_n$	458 (4.5×10^3), 851 (1.5×10^3), 917 (1×10^3)	ochre		
$Cd(H_3L)(H_2O)_2$	441.0 (1×10^3)	ochre		
$[Cd_2(HL)(H_2O)_2]_n$		brown		

[a] Registered in methanol.
[b] Registered in solid state.
[c] Registered in ethanol.
[d] Registered in DMSO.
[e] Registered in DMF.

complexes. Thus, two weak peaks, one at 331 *m/z* for H_5L, and another attributable to $M(H_3L)$ fragments, are detected in most of the spectra.

3.4. Differential scanning calorimetry (DSC) results

Coordinated and/or lattice water is present in all complexes. Thermal analyses of iron, copper and cadmium compounds show a water loss (endothermic peak) under an air flux in the range 77–85°C. Some of the DSC data are given in Table 5. DSC thermograms exhibit one or two endothermic peaks in the range 230–410°C. These peaks are usually associated with some decompositions, reductions or phase transitions. All compounds decompose without melting between 388 and 434°C.

DSC thermograms for $Cd(H_3L)(H_2O)_2$ and $[Cd_2(HL)(H_2O)_2]_n$ are shown in Fig. 1. Their thermal behaviour is quite different, as expected for two compounds of different nature. Exothermic processes in the 210–350°C range usually correspond to chemical reactions such as polymerisations that seem to occur for $Cd(H_3L)(H_2O)_2$. Decomposition of mono- and polynuclear cadmium complexes occurs at about 434°C; however, for the polynuclear complex, this is followed by a transformation between 450 and 550°C. Endothermic processes seem to be more important in $[Cd_2(HL)(H_2O)_2]_n$ than in $Cd(H_3L)(H_2O)_2$.

$[Cu_2(HL)(H_2O)]_n$ suffers endothermic decomposition at about 388°C, leading to a final compound that is stable up to 600°C. The decomposition product was characterised as CuO, in agreement with X-ray powder diffraction analyses. This decomposition temperature is significantly lower than those reported [21] for $[CuLa(L^1)(NO_3)]\cdot H_2O$ (550°C) and $[CuBa(L^1)]\cdot 2H_2O$ (480°C), leading to $CuLa_2O_4 + CuO$ and $CuBa_2O_4$, respectively [H_4L^1: *N,N′*-bis(3-hydroxysalicylidene)-1,2-diaminoethane].

3.5. Electron spectroscopy, magnetic susceptibility and EPR results

The free ligand spectrum in methanol solution shows two strong bands at about 225 and 270 nm, two shoulders at about 290 and 330 nm and, finally, another band of medium intensity at about 425 nm. All complexes display intense absorption bands in the range 225–425 nm that are clearly charge transfer bands in origin. Therefore, the electronic spectra of all the complexes, in the solid state or in solution, are characterised by low-intensity absorption bands or shoulders that can be associated with d–d transitions. Data are listed in Table 4.

Solid state susceptibility measurement for $[Cu_2(HL)(H_2O)]_n$ showed a magnetic moment (per complex) of 2.41 μ_B at 270 K. The diffuse reflectance spectrum of this complex shows a clear shoulder at about 620 nm (Fig. 2) which was also observed in methanol, ethanol, dimethylformamide (DMF) and DMSO solutions. This suggests that, even in donor solvents, the copper environments are similar in both

Table 5
DSC data for some complexes

Compounds	Water loss (°C)	Endothermic peaks (°C)	Decomposition process (°C)
$Fe(H_3L)(H_2O)_2$	79	402	420
$[Cu_2(HL)(H_2O)]_n$	77	231, 302	388
$Cd(H_3L)(H_2O)_2$	85	390, 410	434
$[Cd_2(HL)(H_2O)_2]_n$	79	385	431

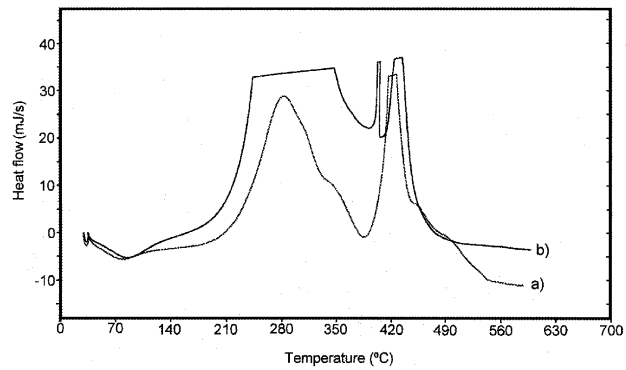


Fig. 1. DSC thermograms for (a) $[Cd_2(HL)(H_2O)_2]_n$ and (b) $Cd(H_3L)(H_2O)_2$.

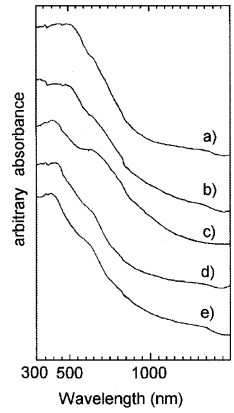


Fig. 2. Diffuse reflectance spectra for (a) $[Co_2(HL)(H_2O)_2]_n$ (b) $Co(H_3L)(H_2O)_3$, (c) $[Cu_2(HL)(H_2O)]_n$ (d) $Ni(H_3L)(H_2O)$ and (e) $[Ni_2(HL)(H_2O)_2]_n$.

phases. Although the observed energy is somewhat lower than those generally quoted for copper(II) in a square-planar field, similar absorption bands have been assigned to this geometry [17,22]. We ascribe this discrepancy to a tetrahedral distortion.

The EPR spectrum of $[Cu_2(HL)(H_2O)]_n$ at 4 K is characteristic of a magnetically non-dilute Cu(II) compound with like metal environments. The usual line around the $\mathbf{g} = 2$ region is observed in Fig. 3. This line shows rhombic or axial symmetry characteristics without hyperfine coupling. This could be explained by an exchange coupling between copper ions. These local symmetries are in good agreement with the postulated molecular structure for $[Cu_2(HL)(H_2O)]_n$.

The diffuse reflectance spectra (Fig. 2) of $Ni(H_3L)(H_2O)$ and $[Ni_2(HL)(H_2O)_2]_n$ show a shoulder and a low-intensity

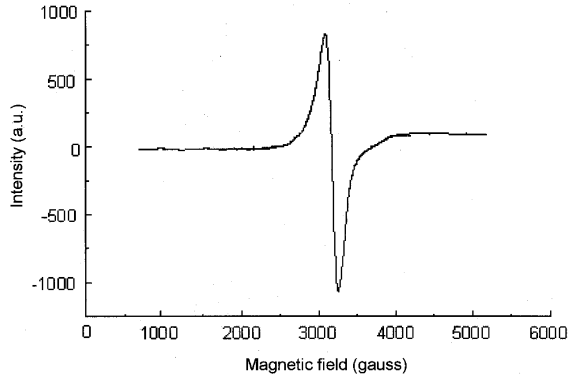


Fig. 3. X-band EPR spectrum of $[Cu_2(HL)(H_2O)]_n$ at 4.0 K.

band at about 630 and 1250 nm, respectively, that are characteristic of nickel(II) ions in tetrahedral coordination environments. The lower energy band can be attributed to the $^3A_2 \leftarrow {}^3T_1(F)$ and the higher one to $^3T_1(P) \leftarrow {}^3T_1(F)$ transitions. The low solubility of these nickel complexes in ethanol solutions prevents the detection of the expected shoulders. The $\mu_{spin\text{-}only}$ calculated value for Ni(II) is 2.8 μ_B and thus octahedral complexes, with not a very significant orbital contribution, lie in the range 2.9–3.3 μ_B. However, magnetic moments of tetrahedral compounds, with a temperature-dependent orbital contribution, are found to lie in the range 3.2–4.1 μ_B. Electron delocalisation on to the ligands and distortions from ideal tetrahedral symmetry reduce the μ value towards $\mu_{spin\text{-}only}$. The room temperature magnetic moments observed for $Ni(H_3L)(H_2O)$ and $[Ni_2(HL)(H_2O)_2]_n$ (3.8 and 3.6 μ_B, respectively) are in keeping with a tetrahedral geometry. This is in contrast with $Ni(H_2L^2)$, which is characterised as square-planar in the literature [1] ($H_4L^2 = N,N'$-bis(3-hydroxysalicylidene)-1,2-diaminomethylpropane).

UV–Vis data for $Co(H_3L)(H_2O)_3$ in solid state and solution suggest a high-spin distorted octahedral Co(II) environment. The spectra show two shoulders at about 490 and 620 nm, and a low-intensity band at about 1300 nm (only in solid state; Fig. 2) which is attributed to $^4T_{1g}(P) \leftarrow {}^4T_{1g}(F)(\nu_3)$, $^4A_{2g} \leftarrow {}^4T_{1g}(F)(\nu_2)$ and $^4T_{2g}(P) \leftarrow {}^4T_{1g}(F)(\nu_1)$ transitions, respectively. The low solubility of $[Co_2(HL)(H_2O)_2]_n$ prevents its study in ethanol and DMF solution. Its solid state spectrum is similar to that obtained for the mononuclear cobalt complex and, consequently, a pseudo-octahedral geometry can also be postulated. However, it must be noted that this study does not exclude other possibilities such as five coordinations and various non-regular structures. The room temperature magnetic moments observed for $Co(H_3L)(H_2O)_3$ and $[Co_2(HL)(H_2O)_2]_n$, with values of 5.0 and 6.6 μ_B (per complex), respectively, are in keeping with the postulated geometry.

The diffuse reflectance studies for $Fe(H_3L)(H_2O)_2$ and $[Fe_2(HL)(H_2O)_5]_n$ are almost identical and suggest that these complexes could have the same geometry. They display a multicomponent band with a maximum absorption between 250 and 525 nm but no bands are detected about 1000 (high spin octahedral field) or 2500 nm (tetrahedral field). Magnetic moments of tetrahedral iron(II) complexes are reported to lie in the range 5.0–5.4 μ_B, but these high values are difficult to explain. High-spin distorted octahedral iron(II) complexes mostly show magnetic moments about 5.2 μ_B in magnetically dilute compounds. Thus, the value of 5.0 μ_B calculated for $Fe(H_3L)(H_2O)_2$ is not far from that. Consequently, the Fe(II) environment could be pseudo-octahedral in this mononuclear complex. This is supported by the described tendency of the ligand to give square-planar or octahedral complexes [15–17].

3.6. Infrared spectroscopy

The most characteristic IR bands of the complexes in which ligands are coordinated via both nitrogen and oxygen atoms are listed in Table 6. They have been assigned following the literature [2]. A comparison of the spectra of free ligand and complexes shows a remarkable similarity in the range 1650–1200 cm^{-1}. ν(C=N), ν(C=O) and ν(C–O) are present as three very strong bands in the ranges 1630–1650, 1450–1460 and 1235–1260 cm^{-1}, respectively.

ν(C–O) is significantly affected by the coordination to the metal ions. Thus, an up-frequency shift between 10 and 20 cm^{-1} was detected. The same tendency was observed for ν(C=O), but, in this case, the shift was between 5 and 10 cm^{-1}. ν(C=N) was also shifted (± 10 cm^{-1}) because of the complexation. The split broad band at about 3250 and 3360 cm^{-1} is due to disappearance of the phenol OH groups of the ligand, and a very broad band at about 3400 cm^{-1} is now present in all complexes. The presence of this broad band is associated with coordinated and/or solvated water molecules, but unfortunately interferes with the observation of uncoordinated hydroxyl groups [16] in mono- and polynuclear complexes. Finally, no significant differences are observed in the spectra of polynuclear complexes compared with those of the corresponding mononuclear compounds.

Table 6
Some significant IR bands (cm^{-1}) for the compounds (as KBr pellets)

Compounds	ν(O–H)	ν(C=N)	ν(C=O)	ν(C–O)
H_5L	3360 s, 3250 s	1640 vs	1460 vs	1235 vs
$Fe(H_3L)(H_2O)_2$	3406 b	1643 vs	1451 vs	1253 vs
$[Fe_2(HL)(H_2O)_5]_n$	3407 b	1650 vs	1453 vs	1253 vs
$Co(H_3L)(H_2O)_3$	3422 b	1634 vs	1458 vs	1258 vs
$[Co_2(HL)(H_2O)_2]_n$	3408 b	1634 vs	1456 vs	1256 vs
$Ni(H_3L)(H_2O)$	3370 b	1630 vs	1465 vs	1253 vs
$[Ni_2(HL)(H_2O)_2]_n$	3400 b	1630 vs	1457 vs	1252 vs
$[Cu_2(HL)(H_2O)]_n$	3353 b	1630 vs	1453 vs	1260 vs
$Zn(H_3L)(H_2O)_2$	3410 b	1635 vs	1455 vs	1253 vs
$[Zn_2(HL)(H_2O)]_n$	3400 b	1637 vs	1457 vs	1252 vs
$Cd(H_3L)(H_2O)_2$	3424 b	1643 vs	1453 vs	1245 vs
$[Cd_2(HL)(H_2O)_2]_n$	3370 b	1637 vs	1450 vs	1249 vs

4. Conclusions

We have demonstrated the versatility of the potentially heptadentate ligand *N,N′*-bis(3-hydroxysalicylidene)-1,3-diamino-2-propanol. The presence of four phenolic groups seems to result in high nuclearity. It could behave simply as a mononucleating N_2O_2 donor or could even be simultaneously coordinated up to four metal centres in $O_2+ONO+ONO+O_2$ compartments. All the oxygen atoms could act as bridges between the metal centres. However, we have not detected any evidence of coordination through the hydroxyl group of the methylene chain, which remains protonated in these neutral complexes.

Therefore, the metal environment in mononuclear complexes can be described as N_2O_2 coordinated in the inner compartment, whereas, for polynuclear complexes, at least two possible coordinating behaviours are in accordance with the $[M_2(L)(H_2O)_x]_n$ formula, the chemical nature of the metal centres and the data from their mass spectra. A schematic representation of these is shown in Fig. 4.

A first alternative (Fig. 4a) could be that each ligand coordinates a metal ion in its inner N_2O_2 compartment, and it also could coordinate two more metal centres through both phenolic oxygen atoms of each aldehyde residue. These would be in O_4 environments, where *cis* sites would be occupied by outer phenolic oxygen atoms and μ-phenoxo bridges for tetra-coordinated metal centres. This tricompartmental behaviour $(O_2+N_2O_2+O_2)$ has been previously observed for both $Cu_3(SB)(H_2SB)\cdot 2H_2O$ [3] and $Zn_8(SB)_4(H_2O)_3\cdot 3CH_3CN$ [4].

A second possibility (Fig. 4b) would consist of each ligand unit acting as tetranucleating by coordination of two metal ions to both inner *NO* donor sets, as we have previously reported [3,11]. Another two metal ions could be coordinated through the outer *O* atoms and μ-phenoxo bridges. Coordination environments would be completed by two neighbouring ligand units, resulting in NO_3 chromophores for tetra-coordinated metal centres. This could occur if a ligand behaved as H_2SB in $Cu_3(SB)(H_2SB)\cdot 2H_2O$, but being totally deprotonated $(O_2+ON+NO+O_2)$.

Physicochemical data of the studied complexes suggest that nickel and copper environments are pseudo-tetrahedral and square-planar, respectively. Additionally, iron and cobalt ions seem to be in pseudo-octahedral fields, due to the presence of coordinated water molecules. Finally, zinc and cadmium could be also hexa-coordinated in mononuclear complexes.

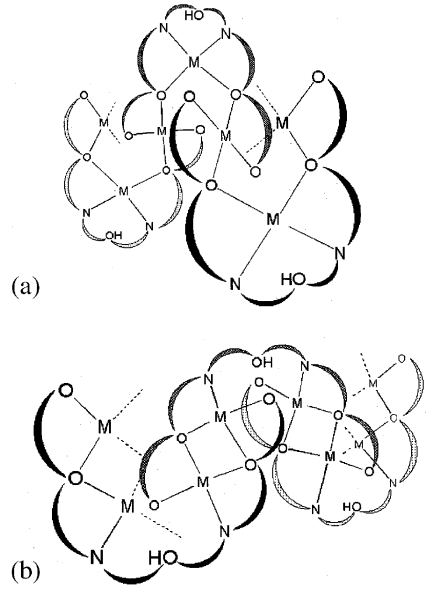


Fig. 4. Schematic representation of two possible polynucleating ligand behaviours using their $O_2+N_2O_2+O_2$ (a) or $O_2+ON+NO+O_2$ (b) donor sets.

Acknowledgements

The authors would like to thank the Xunta de Galicia (Spain) (XUGA20903B99) and the Brazilian agencies FAPESP, CNPq and CAPES for financial support. EPR analysis software was furnished by grant no. RR01811 from the Illinois ESR Research Center, NIH Division of Research Resources.

References

[1] P. Guerriero, S. Tamburini, P.A. Vigato, U. Russo, C. Benelli, Inorg. Chim. Acta 213 (1993) 279.
[2] U. Casellato, P. Guerriero, S. Tamburini, P.A. Vigato, C. Benelli, Inorg. Chim. Acta 207 (1993) 39.
[3] J. Sanmartin, M.R. Bermejo, A.M. Garcia-Deibe, O. Piro, E.E. Castellano, Chem. Commun. (1999) 1953.
[4] M.R. Bermejo (unpublished).
[5] A. Messerschmidt, A. Rossi, R. Ladenstein, R. Huber, M. Bolognesi, G. Gatti, A. Marchesini, R. Petruzelli, A. Finazzo-Agró, J. Mol. Biol. 206 (1989) 513.
[6] K.A. Magnus, H. Ton-That, J.E. Carpenter, Bioinorganic Chemistry of Copper, Chapman & Hall, New York, 1993.
[7] C. Oldham, D.G. Tuck, J. Chem. Educ. 59 (1982) 420.
[8] J. Sanmartín, M.R. Bermejo, J.A. García-Vázquez, J. Romero, A. Sousa, A. Brodbeck, A. Castiñeiras, W. Hiller, J. Strähle, Z. Naturforsch., Teil B 48 (1993) 431.
[9] J. Sanmartín, M.R. Bermejo, J.A. García-Vázquez, J. Romero, A. Sousa, Transition Met. Chem. 18 (1993) 528.
[10] J. Sanmartín, M.R. Bermejo, J.A. García-Vázquez, J. Romero, A. Sousa, Transition Met. Chem. 19 (1994) 209.
[11] M.R. Bermejo, M. Fondo, A.M. González, O.L. Hoyos, A. Sousa, C.A. McAuliffe, W. Hussein, R.G. Pritchard, V.M. Novotorsev, J. Chem. Soc., Dalton Trans. (1999) 2211.
[12] S. Brooker, R.J. Kelly, P.G. Plieger, Chem. Commun. (1998) 1079.
[13] H. Adams, N.A. Bailey, S.R. Collinson, D.E. Fenton, J.C. Kitchen, J.S. Kitchen, J. Organomet. Chem. 550 (1998) 7.
[14] N.M. Atherton, D.E. Fenton, G.J. Heroson, C.H. McLean, R. Bastida, J. Romero, A. Sousa, E.E. Castellano, J. Chem. Soc., Dalton Trans. (1988) 1059.
[15] M.R. Bermejo, M. Fondo, A. García-Deibe, M. Rey, J. Sanmartín, A. Sousa, M. Watkinson, C.A. McAuliffe, R.G. Pritchard, Polyhedron 15 (1996) 4185.

[16] W. Mazurek, A.M. Bond, M.J. O'Connor, A.G. Wedd, Inorg. Chem. 25 (1986) 906.
[17] K. Bertoncello, G.D. Fallon, K.S. Murray, E.R.T. Tiekink, Inorg. Chem. 30 (1991) 3562.
[18] M.S. Okamoto, E.K. Barefield, Inorg. Chem. 13 (1974) 2611.
[19] T.G. Appleton, J.R. Hall, Inorg. Chem. 11 (1972) 117.
[20] I.M. Rivas, Graduation Work, University of Santiago de Compostela, 1997.
[21] U. Casellato, P. Guerriero, S. Tamburini, S. Sitran, P.A. Vigato, J. Chem. Soc., Dalton Trans. (1991) 2145.
[22] W. Maruzek, K.J. Berry, K.S. Murray, M.J. O'Connor, M.R. Snow, A.G. Wedd, Inorg. Chem. 21 (1982) 3071.

PERGAMON

www.elsevier.nl/locate/poly

Polyhedron 19 (2000) 193–197

POLYHEDRON

A multinuclear NMR study of the complexation of W(VI) with *meso*-2,3-dimercaptosuccinic acid (DMSA)

M. Madalena Caldeira, M. Luísa Ramos, Gilberto G. Pereira, Victor M.S. Gil *

Department of Chemistry, University of Coimbra, 3000 Coimbra, Portugal

Received 27 September 1999; accepted 10 November 1999

Abstract

Meso-2,3-dimercaptosuccinic acid (DMSA), which is used as an antidote for heavy metal poisoning and in complexes of ^{99m}Tc for diagnostic purposes, forms several complexes with tungsten(VI) in aqueous solutions, as found by ^{1}H, ^{13}C, ^{17}O and ^{183}W NMR spectroscopy. In the pH range ~4–7, there are four complexes in which the acid acts as a bidentate ligand through one carboxyl group and the adjacent sulfhydryl group (a dominant 2:2 species and three 1:2 metal–ligand isomers are proposed) and 2:1 complexes in which the ligand is twisted in order to use the four binding groups. It is proposed that in both the 2:2 and 2:1 cases the S atoms bridge the two W atoms. At lower pH, the acid is again predominantly a tetradentate ligand in m:n associations with the metal (m > n). ©2000 Elsevier Science Ltd All rights reserved.

Keywords: *meso*-2,3-dimercaptosuccinic acid; Multinuclear NMR; Tunsgsten

1. Introduction

2,3-Dimercaptosuccinic acid (DMSA; HO_2C-CHSH-CHSH-CO_2H), in both the *meso* form and as the racemic mixture, has been used in pharmacology for more than four decades, mainly as an antidote for heavy metal poisoning, particularly lead(II), in humans [1–5]; more recently, DMSA has been used as the complexing agent in the administration of technetium (^{99m}Tc) for diagnostic purposes [6–9]. Several research groups have compared the antidotal actions of *meso*- and *rac*-DMSA and studied the biotransformation of the acid, in addition to more chemically oriented studies [10–12]. In particular, the ionization and the complexation equilibria have been discussed in terms of the conformations of the acids [12]. One of the advantages of the racemic mixture is the greater solubility of the complexes in water. One disadvantage is that it leads to a greater loss of endogenous zinc(II) than the *meso* form, because of differences in the formation constants of the complexes [13].

The complexation of DMSA with metal oxo ions has been reported in two cases: (1) oxovanadium(IV) complexes [14] in relation to the importance of V–S coordination in various biomolecules; and (2) arsenate and arsenite complexes in connection with the biotransformation of arsenic and the transfer of arsenite from glutathione to dithiols [15]. In the presence of As(V), the acid is readily oxidized and the formation of a 2:3 (metal–ligand) complex with As(III) was proposed involving only the SH groups as donors [15]. With V(IV), the carboxyl groups are also involved in chelation [14]. As for As(V), the oxo ions of vanadium(V) and molybdenum(VI) are strong oxidizing agents of DMSA, but the same does not apply to tungstate. Comparison with the complexes of W(VI) with tartaric acid [16,17] and with thiolactic [18] and thiomalic acids [19] leads us to expect the formation of stable complexes of DMSA with tungsten(VI). Tungsten is the active centre of some enzymes. It was only recently found that this metal can have a positive biological role, contrary to the traditional view of W as an antagonist of the biological functions of Mo (for a review, see [20]). In this paper we report the complexation of W(VI) with *meso*-2,3-dimercaptosuccinic acid in aqueous solution, at various pH and concentration conditions. Multinuclear magnetic resonance spectroscopy was used in one and two dimensions.

2. Experimental

Commercially available dihydrate sodium tungstate and *meso*-DMSA were used. Because of the low solubility of the acid, the metal–ligand mixtures were prepared by adding the

* Corresponding author. Fax: +351-39-27703

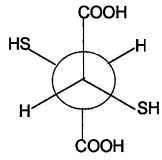
0277-5387/00/$ - see front matter ©2000 Elsevier Science Ltd All rights reserved.
PII S0277-5387(99)00342-3

appropriate amount of the solid acid to the tungstate solutions. D_2O solutions were used throughout. The concentration range for the metal and the ligand was 0.025–2.0 M and 0.10–1.0 M, respectively. The pH was adjusted by adding DCl and NaOD in D_2O. Drastic changes of concentration were avoided in order to reduce local disturbances of equilibria that may be slow to disappear. The pH* values quoted (from 2.5 to 9) are the direct pH-meter readings (room temperature) after standardization with aqueous (H_2O) buffers.

The NMR spectra were obtained on a Varian UNITY-500 spectrometer. The residual water signal was reduced using the Presat sequence.

3. Results and discussion

The ^{1}H NMR spectrum due to the CH groups of the acid in aqueous solution is a singlet, but the doublet corresponding to the ^{13}C–H satellites shows an HH vicinal coupling constant which varies from 10.3 to 11.4 Hz on increasing pH* from 2.1 to 7.5. This proves that, irrespective of ionization of the carboxylic groups, the *meso*-2,3-DMSA exists preferentially in the conformation:



In this conformation, the repulsion between the bulky sulfhydryl groups is minimized. Essentially the same result is found for methanol–water mixtures as a solvent of lower dielectric constant.

In the presence of sodium tungstate, and depending on the molar ratio and on pH, a large number of signals (at higher frequency relative to free ligand) is observed corresponding to bound ligand. Except at low pH and in the presence of excess of metal ion, free ligand is also present, in slow exchange (in the NMR time scale) with the bound ligands. Apart from one set of broad signals close to the residual water (DHO) signal, each bound ligand gives rise to two comparatively sharp doublets of equal intensity (AX spectrum) instead of singlets. The vicinal HH coupling constant is now directly obtained. A set (six AX spectra) dominant at moderate pH ($\sim$4–7) and for metal–ligand molar ratios equal or below to 1 (group A complexes) shows couplings between 7.5 and 9.2 Hz and proton shifts that vary from 0.3 to 0.6 ppm for one of the doublets and from 0.9 to 1.2 ppm for the other, as illustrated in Fig. 1 and tabulated in Table 1. In the same pH range but for metal–ligand molar ratios greater than 1, a set of four to six broad singlets are recorded at 1.2–1.4 ppm to high frequency of free ligand (group B complexes).

At low pH ($\sim$3) and for metal–ligand ratios greater than 1, a set of five well-resolved AX spectra of about the same intensity are recorded, showing splittings that lie between 3.0 and 3.8 Hz and high-frequency shifts relative to free ligand

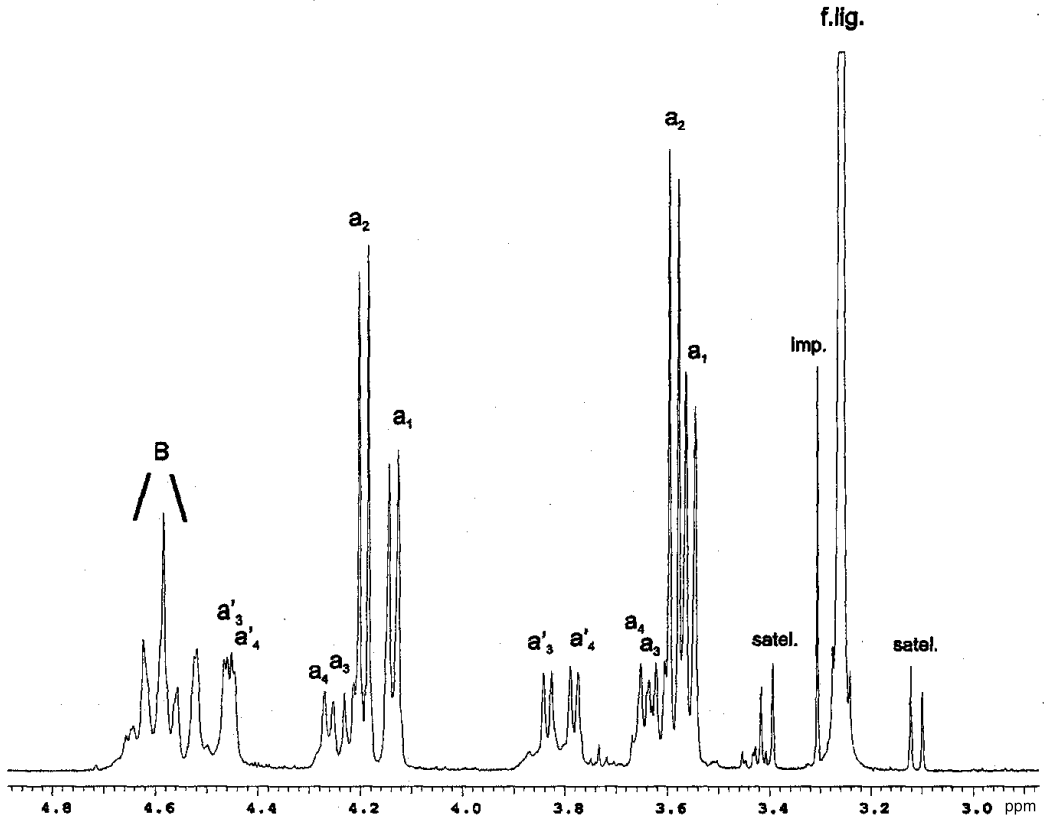


Fig. 1. 500 MHz ^{1}H NMR spectrum of a 0.10 M:0.40 M solution of sodium tungstate and *meso*-DMSA in D_2O, pH* 5.4, 298 K. f. lig. denotes free ligand; imp. denotes ligand impurity; satel. denotes satellite.

Table 1
^{1}H NMR parameters [a] for W(VI) + *meso*-DMSA (at 298 K)

pH 5.4					
Free ligand	$\delta = 3.26$				$^3J_{HH} = 11.2$
B	$\delta = 4.5$–4.7				
	δ_A	$\Delta\delta_A$	δ_x	$\Delta\delta_x$	$^3J_{HH}$
a_1	3.55	0.29	4.13	0.88	9.2
a_2	3.59	0.33	4.19	0.93	8.9
a_3	3.61	0.35	4.22	0.96	8.9
a'_3	3.83	0.57	4.46	1.20	7.5
a_4	3.64	0.38	4.26	1.00	8.2
a'_4	3.78	0.52	4.45	1.19	7.2
pH 2.9					
Free ligand	$\delta = 3.40$				$^3J_{HH} = 10.5$
	δ_A	$\Delta\delta_A$	δ_x	$\Delta\delta_x$	$^3J_{HH}$
C_1	4.4	1.0	4.92	1.51	3.2
C_2	4.4	1.0	4.93	1.52	3.4
C_3	4.42	1.02	4.95	1.55	3.8
C_4	4.39	0.99	4.99	1.58	3.2
C_5	4.37	0.97	5.02	1.61	3.0

[a] δ values are in ppm relative to Me_4Si, using *tert*-butyl alcohol ($\delta_H = 1.2$) as internal reference; *J* values are in Hz.

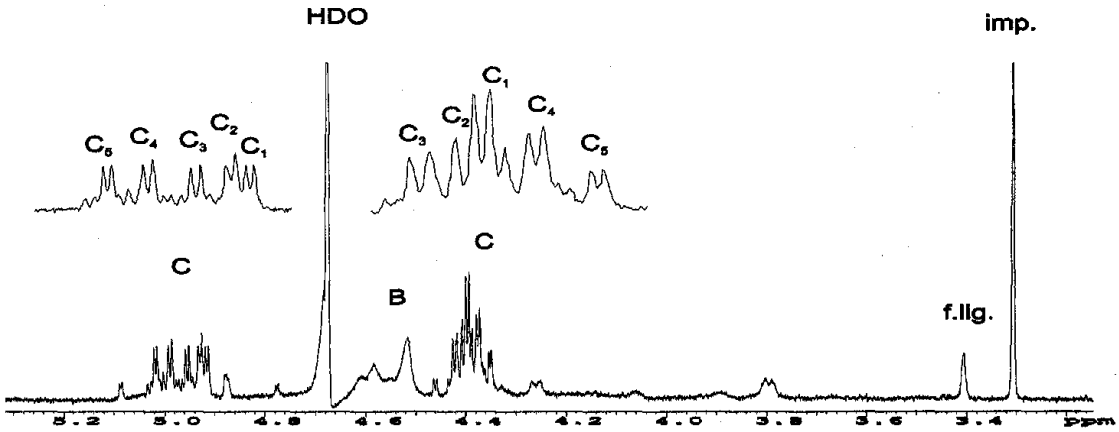


Fig. 2. 500 MHz ^{1}H NMR spectrum of a 0.40 M:0.10 M solution of sodium tungstate and *meso*-DMSA in D_2O, pH* 2.9, 298 K. f. lig. denotes free ligand; imp. denotes ligand impurity.

of about 1.0 and 1.6 ppm (group C complexes) (Fig. 2 and Table 1). Some weaker signals are also detected in the latter case. The assignment of each pair of doublets in each AX spectrum was made on the basis of the coupling constants and, in the case of doubt, by proton decoupling and COSY spectra.

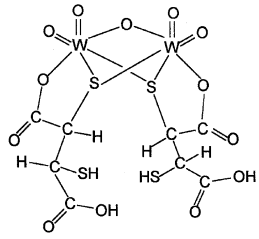
The number of complexes is likely to be smaller than the number of spectra of bound ligand, as magnetic non-equivalence of ligands may occur in complexes having more than one ligand molecule. For example, the AX spectra a_3 and a_3' in Fig. 1 always have the same intensity irrespective of pH and concentration conditions, and the same is found for a_4 and a_4'. This suggests that each of these pairs of AX spectra arise from the same complex, probably having 1:2 (metal–ligand) stoichiometry. Accordingly, there will be four complexes in group A. When a Job's plot is constructed based on the ^{1}H NMR intensities for complexes A, at pH* 5.5, a clear maximum at 1:1 is obtained for the dominant complex, A_1, which points to an n:n stoichiometry. Due to the presence of various competing species, no other firm conclusion can be directly extracted from that plot alone, but 1:2 complexes are likely to be formed by analogy with thiolactic [18] and thiomalic acids [19] and tartaric acid [16,17].

The existence of one small high-frequency proton shift (0.3–0.6 ppm) upon complexation together with a higher one (0.9–1.2 ppm) indicate the involvement of only one sulfhydryl group in complexes A, whereas the observation of high-frequency shifts (1.0–1.6 ppm) for both CH protons in complexes B and C show that both S atoms are bound to the metal. This is corroborated by the corresponding ^{13}C shifts relative to free ligand in the same conditions. In fact, for complex A (at pH* 5.5), high-frequency complexation shifts between 4.0 and 5.0 ppm are observed for the ^{13}C bonded to the more deshielded H atom, and almost no shift for the other. For complexes B and C, the two ^{13}C(SH) complexation shifts (at pH* 2.8) lie in the range 7–8 ppm. Whenever necessary,

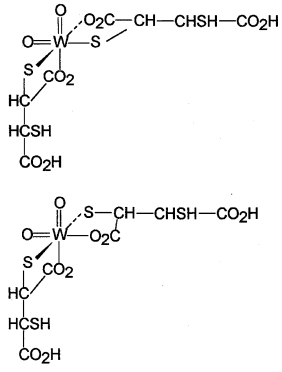
the assignment of the ^{13}C signals was made by running HETCOR 2D spectra.

Complexes A also involve only one of the carboxylate groups in bonding to the metal, as shown by a high-frequency shift on complexation (in the range 5–7 ppm) of one of the CO_2^- groups, together with a low-frequency shift of about −0.8 ppm for the other group. On the other hand, both carboxylate ^{13}C signals of complexes B and C shift between 7 and 8 ppm to high frequency, which shows that both carboxylate groups now participate in complexation.

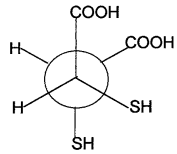
Based on the above data, we can propose that the acid acts as a bidentate ligand in complexes A, involving one carboxylic group and the adjacent SH group, irrespective of the stoichiometry being n:n or 1:2. The conformation of DMSA is slightly changed on complexation, as indicated by HH couplings of 7.5–9.2 Hz in the complexes compared with 10–11 Hz in the free ligand. Since a 1:1 complex, involving two water molecules bound to the metal, is not expected to be particularly stable, we propose a 2:2 species with the following structure, in which the ligand molecules are magnetically equivalent:



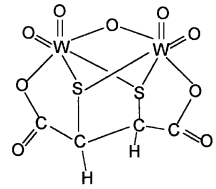
Regarding complexes having 1:2 stoichiometry, we note that several diastereoisomers are possible, for example:



In complexes B and C, the ligand acts as tetradentate and undergoes much alteration of conformation on binding to the metal. In fact, the HH coupling constants recorded for complexes C lie between 3.0 and 3.8 Hz, showing that the conformation of bound DMSA is now close to:



The same conclusion must apply to complexes B, as the line width of each signal is about 3 Hz. In spite of this conformational change, a molecular model suggests that it is highly unlikely that a tetradentate DMSA molecule is bound to just one W atom. The same has been recently advanced in the case of complexes of DMSA with tin [21]. The formation of several polynuclear species must then occur. This is corroborated by the fact that complexes B are dominant for high metal–ligand molar ratios. One of the possible structures is



which is similar to that previously found by X-ray diffraction for a 2:1 complex of Mo(VI) with L-dithiothreitol [22].

Broad ^1H NMR signals are a result of complexes B having close proton resonances (a range of 0.2 ppm) that no longer correspond to first-order spectra.

The proposal of similar metal centres, $W_2O_5^{2+}$, for the most abundant complexes A and B (2:2 and 2:1 species, respectively), which are present in a 1.0:1.0 M W(VI)–*meso*-DMSA solution in D_2O, at pH* 7.0, is corroborated by the occurrence of ^{183}W resonances between +579 and +592 ppm with respect to an external reference of Na_2WO_4 in D_2O (pH* 9.5), besides the three signals due to uncomplexed $W_7O_{24}^{6-}$ (at +269, −92 and −179 ppm) [23,24]. Values close to +600 ppm were also recorded for the systems W(VI)–thiolactic acid and W(VI)–thiomalic acid. The ^{17}O spectra of the same solution shows the signals of $W_7O_{24}^{6-}$ (terminal and bridging O atoms) [23,24] and some new signals: a major peak at +534.5 ppm (relative to D_2O as external reference) which lies in the region of W=O resonances [25] and a smaller one at +270.8 ppm in the region of W–O–W signals [25]. This also points to the presence of a $W_2O_5^{2+}$ moiety in the 2:2 and 2:1 complexes.

For a 2.0:0.5 M solution at pH* 4.3, where complexes B dominate, we have again several ^{183}W signals between +580 and +593 ppm (besides those of $W_7O_{24}^{6-}$). An additional and sharp signal appears at −120 ppm, the resonance of the α-metatungstate ion, α-$H_2W_{12}O_{40}^{6-}$ [23]. A similar signal has been detected in solutions of tungstate and mandelic or isocitric acids and attributed to 2:2 complexes involving two oxygen bridges [17]. We prefer to attribute the above resonance to the isopolyanion expected to be present at low pH, but additional studies are necessary.

Regarding signals C, dominant for high metal–ligand molar ratios and low pH, which are the conditions for polytungstate anions to be present in significant concentrations, we again propose an m:n complexation, with m > n. The fact that there are five AX spectra in this set, all with approximately the same intensity, suggests that a major polynuclear complex C is present involving five ligands in slightly different magnetic conditions. However, further studies are needed to clarify this and other points of such a complicated

system. We therefore plan to go back to our previous work on simpler systems [18,19] and carefully run ^{17}O and ^{183}W NMR spectra.

Acknowledgements

This work has been supported by a grant from the Fundação para a Ciência e Tecnologia (Praxis Qui-63/96) of the Portuguese Ministry of Science and Technology.

References

[1] Y. Liang, C. Chu, Y. Tsen, K. Ting, Acta Physiol. Sin. 21 (1957) 24.
[2] H.V. Aposhian, Annu. Rev. Pharmacol. Toxicol. 23 (1983) 193.
[3] D.C. Jones, G.L. Smith, P.M. May, D.R. Williams, Inorg. Chim. Acta 93 (1984) 93.
[4] M. Rivera, H.V. Aposhian, Q. Fernando, J. Inorg. Biochem. 37 (1989) 283.
[5] H.V. Aposhian, R.M. Maiorino, D. Gonzalez-Ramirez, M. Zumiga-Charles, Z. Xu, K.M. Hurlbut, P. Junko-Munoz, R.C. Dart, M.M. Aposhian, Toxicology 97 (1995) 23.
[6] T.H. Lin, A. Khentigan, H.S. Winchell, J. Nucl. Med. 15 (1974) 34.
[7] I. Ikeda, I. Osamu, K. Kurata, J. Nucl. Med. 18 (1977) 1222.
[8] H. Ohta, K. Yamamoto, K. Endo, T. Mori, D. Hamanaka, A. Shimazu, K. Ikekubo, K. Makimoto, Y. Iida, J. Konishi, R. Morita, N. Hata, K. Horiuchi, A. Yokoyama, K. Torizuka, K. Kuma, J. Nucl. Med. 25 (1984) 323.
[9] K. Horinchi, S. Hiedo, A. Yokoyama, Nucl. Med. Biol. 25 (1998) 689.
[10] X. Fang, Q. Fernando, Chem. Res. Toxicol. 7 (1994) 148.
[11] X. Fang, Q. Fernando, Chem. Res. Toxicol. 7 (1994) 882.
[12] X. Fang, Q. Fernando, Chem. Res. Toxicol. 8 (1995) 525.
[13] X. Fang, Q. Fernando, Chem. Res. Toxicol. 7 (1994) 770.
[14] T. Kiss, P. Buglyó, G. Micera, A. Dessi, D. Sanna, J. Chem. Soc., Dalton Trans. (1993) 1849.
[15] M. Delnomdedieu, M.M. Basti, J.D. Otvos, D.J. Thomas, Chem. Res. Toxicology 6 (1993) 598.
[16] A.M. Cavaleiro, J.D. Pedrosa de Jesus, R.D. Gillard, P.A. Williams, Transition Met. Chem. 9 (1984) 81.
[17] M. Hlaibi, S. Chapelle, M. Benaissa, J.-F. Verchère, Inorg. Chem. 34 (1995) 4434.
[18] M.M. Caldeira, V.M.S. Gil, Polyhedron 5 (1986) 381.
[19] M.M. Caldeira, V.M.S. Gil, Can. J. Chem. 62 (1984) 2094.
[20] M.K. Johnson, D.C. Rees, M.W.W. Adams, Chem. Rev. (1996) 2817.
[21] K. Gajda-Schrantz, L. Nagy, E. Kuzmann, A. Vértes, J. Holecek, A. Lycka, J. Chem. Soc., Dalton Trans. (1997) 2201.
[22] S.J.N. Burgmayer, E.I. Stiefel, Inorg. Chem. 27 (1988) 2518.
[23] J.J. Hastings, O.W. Howarth, J. Chem. Soc., Dalton Trans. (1992) 209.
[24] R.I. Maksimovskaya, K.G. Burtseva, Polyhedron 4 (1985) 1559.
[25] M.L. Ramos, M.M. Caldeira, V.M.S. Gil, Carbohydr. Res. 299 (1997) 209.

PERGAMON

www.elsevier.nl/locate/poly

Polyhedron 19 (2000) 199–204

POLYHEDRON

New complexes of lanthanide chlorides. Reversible isomerization in octahedral $[LaCl_3(HMPA)_3]$ and the crystal structure of *fac*-$[SmCl_3(HMPA)_3]$

S. Petriček *, A. Demšar, L. Golič, J. Košmrlj

University of Ljubljana, Faculty of Chemistry and Chemical Technology, Aškerčeva 5, 1001 Ljubljana, Slovenia

Received 9 August 1999; accepted 10 November 1999

Abstract

Complexes of $[LnCl_3L]$ (Ln = La, Nd, Sm, Eu, and L = diethylene glycol dimethyl ether, diglyme; Ln = La, Pr, and L = dimethoxyethane, DME) were prepared from the lanthanide oxides and hydrogen chloride, which was formed in situ from chlorotrimethylsilane and water. When hexamethylphosphoramide (HMPA) was added to the suspension of the prepared DME and diglyme complexes in toluene, *fac*-$[LnCl_3(HMPA)_3]$ (Ln = La, Pr, Nd, Sm, Eu, Gd) complexes, isomorphous according to the unit cell determination, were formed. The crystal structure of $[SmCl_3(HMPA)_3]$ was determined. Each samarium atom is octahedrally coordinated by three chlorine atoms and three HMPA molecules, which are distributed in a facial mode. The exchange of coordinated and free HMPA, as well as the reversible *fac–mer* isomerization of $[LaCl_3(HMPA)_3]$, was observed by variable temperature ^1H NMR spectroscopy. The associative mechanism of the exchange and isomerization was proposed. ©2000 Elsevier Science Ltd All rights reserved.

Keywords: Crystal structures; *Fac* isomers; Isomerization; Lanthanide chloride complexes; Octahedral complexes

1. Introduction

An important source of information regarding the reactivity of coordination and organometallic compounds are studies of fluxionality, isomerization [1] and ligand exchange [2]. Transition metal six-coordinate complexes are rather rigid [3]. On the other hand, the small crystal-field splitting and larger ionic radii of six-coordinate lanthanide complexes promise enhanced fluxionality and facile coordination sphere extension [4]. The isolation of solid state six-, seven- and eight-coordinate complex ions $[Ln(NCS)_n]^{(n-3)-}$ ($n = 6$, 7, 8) [5], six-coordinate $[LnCl_3(HMPA)_3]$ (HMPA = hexamethylphosphoramide) [6] and seven-coordinate $[LaBr_3(HMPA)_4]$ [7] suggests that little energy is required for transition among six-, seven- and eight-coordinate species. The facile dissociation and binding of ligands are important for the catalytic activity of coordination and organometallic compounds.

The growing interest in the reactivity of lanthanide compounds is stimulated by their use as versatile reagents and catalysts [8–12]. The solution dynamics of eight- and higher coordinate solvated lanthanide ions [4] and the lanthanide magnetic resonance imaging agents [13] have attracted much interest, but six-coordinate lanthanide compounds have been studied less intensively.

We report on the synthesis of new $[LnCl_3(DME)]$ (Ln = La, Pr; DME = dimethoxyethane) and $[LnCl_3$-(diglyme)] (Ln = La, Nd, Sm, Eu; diglyme = diethylene glycol dimethyl ether) complexes directly from the corresponding lanthanide oxides and chlorotrimethylsilane. Two similar synthetic routes for the preparation of lanthanide chloride complexes have been reported, the first starting from lanthanide metals and chlorotrimethylsilane [14] and the second from lanthanide oxides using tionyl chloride [15]. The $[LnCl_3(DME)]$ (Ln = La, Pr) and $[LnCl_3(diglyme)]$ (Ln = La, Nd, Sm, Eu) complexes were used in the preparation of *fac*-$[LnCl_3(HMPA)_3]$ (Ln = La, Pr, Nd, Sm, Eu, Gd) isomers. The solution dynamics of $[LaCl_3(HMPA)_3]$ are also described.

2. Experimental

2.1. Materials

All manipulations were carried out under an atmosphere of purified argon using Schlenk tubes or in a dry box. Lan-

* Corresponding author. Tel.: +386-61-176 0556; fax: +386-61-125 8220; e-mail: sasa.petricek@guest.arnes.si

0277-5387/00/$ - see front matter ©2000 Elsevier Science Ltd All rights reserved.
PII S0277-5387(99)00345-9

thanide oxides (Aldrich), diglyme (Fluka), DME (Fluka), chlorotrimethylsilane (Aldrich) and HMPA (Aldrich) were used as received. Tetrahydrofuran (THF) and toluene were dried with Na–K alloy and distilled before use.

2.2. Physical measurements

The samples were ground in a Nujol mull and IR spectra were recorded on a Perkin-Elmer 1720X instrument between 400 and 4000 cm^{-1}.

The chlorine content was determined by a potentiometric titration of chlorine ions with silver nitrate. The lanthanide content was determined by gravimetric analysis. Elemental analyses were obtained using a Perkin-Elmer 2400 CHN analyser at the University of Ljubljana (Department of Organic Chemistry).

The ^{1}H, ^{31}P and ^{139}La NMR spectra were recorded on a Bruker DPX 300 spectrometer. Variable temperature spectra were recorded using the variable temperature controller of the spectrometer. Deuterated toluene was dried with potassium and distilled under reduced pressure.

2.3. Synthesis

2.3.1. [$LaCl_3$(DME)]

To 0.440 g (1.35 mmol) of La_2O_3 were added 12.91 g (143 mmol) of DME, 13.09 g (121 mmol) of $(CH_3)_3SiCl$ and 0.10 g (5.55 mmol) of water. The suspension was stirred for 4 days and after drying in vacuo 0.904 g (99.8% yield) of the complex [$LaCl_3$(DME)] was gained. Found: La, 42.0; Cl, 31.5. Calc. for [$LaCl_3$(DME)]: La, 41.4; Cl, 31.7%. IR (Nujol) (cm^{-1}): 1082 s, 1041 vs, 1019 s, 1001 s and 858 s.

2.3.2. [$LaCl_3$(diglyme)]

To 0.330 g (1.01 mmol) of La_2O_3 were added 35 ml of THF, 13.71 g (126 mmol) of $(CH_3)_3SiCl$, 0.850 g (6.3 mmol) of diglyme and 0.120 g (6.7 mmol) of water. The suspension was stirred for 4 days and after drying in vacuo 0.769 g (100% yield) of the complex [$LaCl_3$(diglyme)] was gained. Found: La, 36.5; C, 18.96; H, 3.55. Calc. for [$LaCl_3$(diglyme)]: La, 36.6; C, 18.99; H, 3.72%. IR (Nujol) (cm^{-1}): 1289 w, 1261 m, 1213 vw, 1090 vs, 1064 m, 1048 vs, 1005 m, 951 m, 873 s, 832 m, 801 m.

2.3.3. [$LaCl_3$(HMPA)$_3$]

2.3.3.1. Method A. HMPA (0.850 g, 4.74 mmol) was added to a suspension of [$LaCl_3$(DME)] (0.238 g, 0.710 mmol) in toluene (25 ml). A clear solution resulted immediately. Bright, colourless crystals of the complex [$LaCl_3$(HMPA)$_3$] grew out of the solution during slow evaporation of the solvent. The crystals were filtered off and washed with pentane three times. Found: La, 17.4; C, 27.58; H, 7.00; N, 15.83. Calc. for [$LaCl_3$(HMPA)$_3$]: La, 17.7; C, 27.62; H, 6.95; N, 16.10%. IR (Nujol) (cm^{-1}): 1302 s, 1193 m, 1163 m, 1130 vs, 1067 w, 986 vs, 802 w, 752 s, 482 m. ^{1}H NMR (300 MHz, [D_8]toluene): δ 2.50, J(PH) 9Hz. ^{31}P NMR (121 MHz, [D_8]toluene): δ 26.1.

2.3.3.2. Method B. HMPA (0.700 g, 3.91 mmol) was added to a suspension of [$LaCl_3$(diglyme)] (0.338 g, 0.891 mmol) in toluene (20 ml). A clear solution resulted immediately. Bright, colourless crystals of the complex [$LaCl_3$(HMPA)$_3$] grew out of the solution during slow evaporation of the solvent. Found: La, 17.4; C, 27.41; H, 7.00; N, 15.86. Calc. for [$LaCl_3$(HMPA)$_3$]: La, 17.7; C, 27.62; H, 6.95; N, 16.10%. IR (Nujol) (cm^{-1}): 1303 s, 1194 m, 1163 m, 1130 vs, 1067 w, 988 vs, 753 s, 482 m.

2.3.4. [$PrCl_3$(DME)]

To 0.495 g (0.48 mmol) of Pr_6O_{11} were added 13.6 g (151 mmol) of DME, 13.6 g (125 mmol) of $(CH_3)_3SiCl$ and 0.10 g (5.55 mmol) of water. The suspension was stirred for 4 days and after drying in vacuo 0.950 g (96.8% yield) of the dark brown complex [$PrCl_3$(DME)] was gained. Found: Cl, 31.0. Calc. for [$PrCl_3$(DME)]: Cl, 31.5%. IR (Nujol) (cm^{-1}): 1082 s, 1039 vs, 1019 s, 1001 s, 859 s.

2.3.5. [$PrCl_3$(HMPA)$_3$]

HMPA (1.06 g, 5.92 mmol) was added to a suspension of [$PrCl_3$(DME)] (0.289 g, 0.86 mmol) in toluene (25 ml). A clear solution resulted immediately. Bright, colourless crystals of the complex [$PrCl_3$(HMPA)$_3$] grew out of the solution during slow evaporation of the solvent. Found: C, 27.51; H, 6.89; N, 15.68. Calc. for [$PrCl_3$(HMPA)$_3$]: C, 27.55; H, 6.93; N, 16.06%. IR (Nujol) (cm^{-1}): 1302 s, 1261 w, 1195 m, 1165 m, 1131 vs, 1068 w, 986 vs, 802 w, 759 s, 481 m.

2.3.6. [$NdCl_3$(diglyme)]

To 0.340 g (1.01 mmol) of Nd_2O_3 were added 20 ml of THF, 12.86 g (118 mmol) of $(CH_3)_3SiCl$, 0.890 g (6.6 mmol) of diglyme and 0.120 g (6.7 mmol) of water. The suspension was stirred for 4 days and after drying in vacuo 0.777 g (100% yield) of the pale violet complex [$NdCl_3$(diglyme)] was gained. Found: Nd, 37.6; C, 18.90; H, 3.75. Calc. for [$NdCl_3$(diglyme)]: Nd, 37.5; C, 18.73; H, 3.67%. IR (Nujol) (cm^{-1}): 1290 w, 1260 s, 1213 w, 1091vs, 1048 vs, 1006 s, 953 m, 875 s, 834 m, 803 m.

2.3.7. [$NdCl_3$(HMPA)$_3$]

HMPA (0.640 g, 3.75 mmol) was added to a suspension of [$NdCl_3$(diglyme)] (0.338 g, 0.878 mmol) in toluene (15 ml). A clear solution resulted immediately and the colour changed to light blue. Bright, pale blue crystals of the complex [$NdCl_3$(HMPA)$_3$] grew out of the solution during slow evaporation of the solvent. Found: Nd, 18.7; C, 27.12; N, 15.43; H, 6.81. Calc. for [$NdCl_3$(HMPA)$_3$]: Nd, 18.3; C, 27.43; N, 15.99; H, 6.91%. IR (Nujol) (cm^{-1}): 1302 s, 1193 m, 1163 m, 1133 vs, 1064 w, 986 vs, 759 s, 481 m.

2.3.8. [$SmCl_3$(diglyme)]

To 0.490 g (1.41 mmol) of Sm_2O_3 were added 20 ml of THF, 12.96 g (119 mmol) of $(CH_3)_3SiCl$, 0.930 g (6.93 mmol) of diglyme and 0.080 g (4.44 mmol) of water. The suspension was stirred for 4 days and after drying in vacuo 1.099 g (100% yield) of the complex [$SmCl_3$(diglyme)] was gained. Found: Sm, 38.0; C, 18.47; H, 3.55. Calc. for [$SmCl_3$(diglyme)]: Sm, 38.4; C, 18.44; H, 3.61%. IR (Nujol) (cm^{-1}): 1290 w, 1261 w, 1245 w, 1092 vs, 1064 s, 1048 vs, 1006 m, 954 m, 876 vs, 834 m, 824 m, 803 w.

2.3.9. [$SmCl_3(HMPA)_3$]

2.3.9.1. Method A. HMPA (0.710 g, 3.96 mmol) was added to a suspension of [$SmCl_3(DME)_2$] (0.296 g, 0.677 mmol) [16] in toluene (28 ml). A clear solution resulted immediately. Bright, colourless crystals of the complex [$SmCl_3(HMPA)_3$] grew out of the solution during slow evaporation of the solvent. Found: Sm, 19.3; C, 27.39; H, 6.82; N, 15.42. Calc. for [$SmCl_3(HMPA)_3$]: Sm, 18.9; C, 27.22; H, 6.85; N, 15.87%. IR (Nujol) (cm^{-1}): 1303 s, 1196 m, 1169 m, 1135 vs, 1067 w, 986 vs, 759 s, 482 m.

2.3.9.2. Method B. HMPA (0.580 g, 3.24 mmol) was added to a suspension of [$SmCl_3$(diglyme)] (0.265 g, 0.678 mmol) in toluene (25 ml). A clear solution resulted immediately. Bright, colourless crystals of the complex [$SmCl_3(HMPA)_3$] grew out of the solution during slow evaporation of the solvent. Found: Sm, 19.4; C, 27.05; N, 15.64; H, 6.97. Calc. for [$SmCl_3(HMPA)_3$]: Sm, 18.93; C, 27.22; N, 15.87; H, 6.85%. IR (Nujol) (cm^{-1}): 1302 s, 1193 m, 1167 m, 1134 vs, 1068 m, 985 vs, 798 w, 752 s, 481 m.

2.3.10. [$EuCl_3$(diglyme)]

To 0.340 g (0.97 mmol) of Eu_2O_3 were added 20 ml of THF, 10.54 g (97 mmol) of $(CH_3)_3SiCl$, 0.790 g (5.89 mmol) of diglyme and 0.130 g (7.2 mmol) of water. The suspension was stirred for 4 days and after drying in vacuo 0.760 g (99.8% yield) of the white complex [$EuCl_3$(diglyme)] was gained. Found: Eu, 39.0; C, 18.2; H, 3.52. Calc. for [$EuCl_3$(diglyme)]: Eu, 38.72; C, 18.36; H, 3.60%. IR (Nujol) (cm^{-1}): 1290 w, 1261 m, 1245 w, 1213 vw, 1092 vs, 1049 vs, 1006 m, 955 m, 877 s, 835 m, 825 w, 803 vw.

2.3.11. [$EuCl_3(HMPA)_3$]

HMPA (1.10 g, 8.20 mmol) was added to a suspension of [$EuCl_3$(diglyme)] (0.77 g, 1.96 mmol) in toluene (40 ml). A clear solution resulted immediately. Bright, colourless crystals of the complex [$EuCl_3(HMPA)_3$] grew out of the solution during slow evaporation of the solvent. Found: Eu, 19.30; C, 27.23; N, 15.38; H, 6.86. Calc. for [$EuCl_3(HMPA)_3$]: Eu, 19.09; C, 27.16; N, 15.84; H, 6.84%. IR (Nujol) (cm^{-1}): 1301 m, 1195 m, 1170 m, 1137 vs, 1068 w, 986 vs, 759 s, 482 m.

2.3.12. [$GdCl_3(HMPA)_3$]

To 0.410 g (1.13 mmol) of Gd_2O_3 were added 20 ml of THF, 13.18 g (121 mmol) of $(CH_3)_3SiCl$, 0.850 g (6.33 mmol) of diglyme and 0.130 g (7.2 mmol) of water. The suspension was stirred for 5 days and dried in vacuo. The dried residual was suspended in toluene (25 ml) and 1.60 g (10.9 mmol) HMPA was added. The white powder partly dissolved. The insoluble substance was filtered off. Bright, colourless crystals of the complex [$GdCl_3(HMPA)_3$] grew out of the solution during slow evaporation of the solvent. Found: Gd, 19.9; C, 26.90; N, 15.56; H, 6.93. Calc. for [$GdCl_3(HMPA)_3$]: Gd, 19.6; C, 26.98; N, 15.73; H, 6.79%. IR (Nujol) (cm^{-1}): 1303 s, 1193 m, 1170 m, 1138 vs, 1067 w, 985 vs, 798 vw, 753 m, 481 m.

2.4. Crystal structure determination

Hygroscopic crystals of [$LnCl_3(HMPA)_3$] (Ln = La, Pr, Nd, Sm, Eu, Gd) were fixed and covered by nail polish and used for cell determination on an Enraf-Nonius CAD-4 diffractometer with graphite monochromatized Mo Kα radiation, $\lambda = 0.7107$. Accurate unit cell parameters of [$LnCl_3(HMPA)_3$] (Ln = La, Pr, Nd, Sm, Eu, Gd) were obtained from a least-squares refinement of the angular settings of 75 reflections $8 < \theta < 15°$. Crystals of [$LnCl_3(HMPA)_3$] (Ln = La, Pr, Nd, Sm, Eu, Gd) are monoclinic, with space group $P2_1/c$, no. 14, $C_{18}H_{54}N_9Cl_3O_3P_3Ln$, $Z = 4$; unit cell parameters are presented in Table 1.

A colourless block-shaped crystal of [$SmCl_3(HMPA)_3$], with dimensions $0.4 \times 0.5 \times 0.6$ mm, sealed in a capillary purged with argon was used for data collection. Intensities were collected at 293(2) K in the ω scan mode to $2\theta_{max} = 28°$ in the range h 0 to 20, k 0 to 26, l −31 to 31; 19 139 total data were measured; equivalent reflections merged into a set

Table 1
Unit cell parameters of [$LnCl_3(HMPA)_3$] (Ln = La, Pr, Nd, Sm, Eu, Gd)

Ln	a (Å)	b (Å)	c (Å)	β (°)	V (Å^3)
La	15.885(1)	20.326(2)	23.820(2)	90.04(1)	7705(2)
Pr	15.826(4)	20.285(5)	23.679(6)	90.00(2)	7602(6)
Nd	15.794(9)	20.215(7)	23.686(7)	90.14(8)	7562(6)
Sm	15.783(1)	20.179(2)	23.606(2)	90.18(1)	7518(2)
Eu	15.772(3)	20.152(3)	23.571(3)	90.01(1)	7492(3)
Gd	15.774(2)	20.147(3)	23.557(3)	90.03(1)	7486(3)

of 11 007 independent reflections, $R_{int} = 0.029$, 6961 with $I > 2.5\sigma(I)$ were observed. Correction was made for analytical absorption. The structure was solved by direct methods, with full-matrix least-squares refinement; H atoms at calculated positions with isotropic temperature factors were included only in structure factor calculations. In the final least-squares cycle there were 6961 reflections and 667 variables. The final R factors were $R = 0.086$ and $R_w = 0.091$, and goodness-of-fit was 1.103. All calculations were performed with the Xtal3.4 system of crystallographic programs [17].

3. Results and discussion

3.1. Synthesis and characterization

Chlorotrimethylsilane reacts with water, generating hydrogen chloride in situ. The generated hydrogen chloride reacts with lanthanide oxides in dimethoxyethane giving the complexes $[LnCl_3(DME)]$ (Ln = La, Pr), as well as with diglyme in tetrahydrofuran resulting in $[LnCl_3(diglyme)]$ (Ln = La, Nd, Sm, Eu). The method is very simple since the syntheses are carried out at room temperature and the side products, HCl and $(CH_3)_3SiOSi(CH_3)_3$, are volatile and easily removed. All prepared products are anhydrous based on the absence of OH stretching bands in the IR spectra. $[LaCl_3(DME)]$ and $[PrCl_3(DME)]$ were prepared for the first time in the same way as previously described $[SmCl_3(DME)_2]$ [16]. The very low solubilities of $[LnCl_3(DME)]$ in common solvents hamper the preparation of single crystals and also suggest the polymeric structure of the compounds, in contrast to the monomeric $[LnCl_3(DME)_2]$ [18–20]. This indicates a possible structural diversity in $[LnCl_3(DME)_n]$ complexes as previously reported for $[LnCl_3(THF)_n]$ [20–28]. The stoichiometry of the prepared diglyme complexes has been found in the octahedral $[ScCl_3(diglyme)]$ [29]. We tried to prepare more soluble $[LnCl_3L]$ (L = diglyme, DME) derivatives by introducing ligand HMPA. When HMPA was added to a suspension of the prepared $[LnCl_3L]$ (L = DME, diglyme) in toluene, the complexes $[LnCl_3(HMPA)_3]$ were formed in high yield in all cases. The syntheses of $[MCl_3(HMPA)_3]$ (M = all rare earth, Sc) have been already reported [6]. The X-ray structure determination of the previously prepared $LnCl_3(HMPA)_3$ (Ln = Pr, Dy, Yb) revealed the meridional distribution of the ligands in the octahedron [30–32]. The ^1H NMR spectrum of $[LaCl_3(HMPA)_3]$ from our synthesis suggested a facial isomer. The X-ray structure analysis of the prepared $[SmCl_3(HMPA)_3]$ confirmed the proposed facial distribution of the ligands. The prepared $[LnCl_3(HMPA)_3]$ (Ln = La, Pr, Nd, Eu, Gd) complexes are isomorphous to the *fac*-$[SmCl_3(HMPA)_3]$ isomer according to the unit cell determination (Table 1). Decreasing volumes of the unit cells from lanthanum to gadolinium complexes are expected, due to lanthanide contraction.

3.2. Crystal structure of $[SmCl_3(HMPA)_3]$

The molecular structure of $[SmCl_3(HMPA)_3]$ is shown in Fig. 1 and selected bond lengths and angles are listed in Table 2. An asymmetric unit consists of two slightly different molecules. This is in contrast to the *mer* isomers with only one molecule in the asymmetric unit [30–32], resulting in the doubling of the unit cell volume in the *fac* compounds. The coordination polyhedron around samarium in *fac*-$[SmCl_3(HMPA)_3]$ is a slightly distorted octahedron with angles Cl–Sm–O from 168.0(4) to 173.1(4)°. The angles between chlorine atoms are wider, Cl–Sm–Cl, from 93.2(2) to 98.0(3)° and sharper between oxygen atoms, O–Sm–O, from 81.4(5) to 87.6(5)°. The bond lengths are from 2.657(8) to 2.680(7) Å for Sm–Cl and from 2.290(13) to 2.388(18) Å for Sm–O. The values for bond lengths are between those listed for *mer*-$[PrCl_3(HMPA)_3]$ [30] and *mer*-$[DyCl_3(HMPA)_3]$ [31], as expected. Sm–Cl bond lengths are also similar to those in the seven-coordinate com-

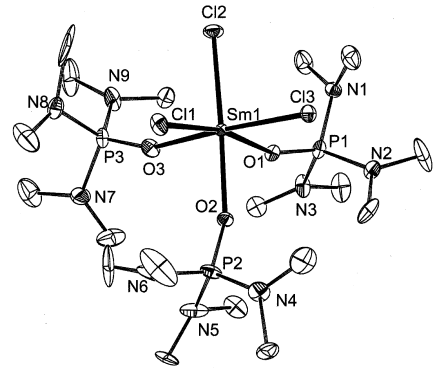
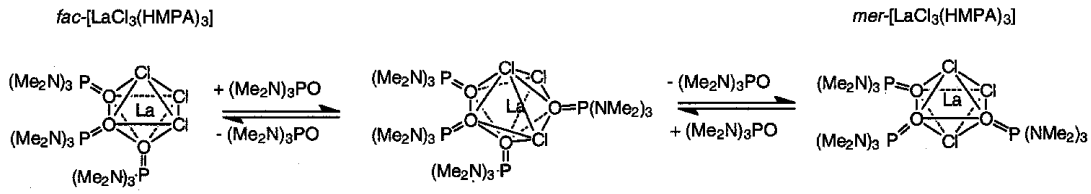


Fig. 1. The molecular structure of $[SmCl_3(HMPA)_3]$. Hydrogen atoms are omitted for clarity.

Table 2
Selected bond lengths (Å) and bond angles (°) in $[SmCl_3(HMPA)_3]$

Sm1–Cl1	2.680(7)	Sm2–Cl4	2.660(6)
Sm1–Cl2	2.668(7)	Sm2–Cl5	2.665(7)
Sm1–Cl3	2.657(8)	Sm2–Cl6	2.662(8)
Sm1–O1	2.388(18)	Sm2–O4	2.349(15)
Sm1–O2	2.338(14)	Sm2–O5	2.305(13)
Sm1–O3	2.290(13)	Sm2–O6	2.331(17)
Cl1–Sm1–Cl2	94.0(2)	Cl4–Sm2–Cl5	94.4(2)
Cl1–Sm1–Cl3	93.2(2)	Cl4–Sm2–Cl6	93.4(2)
Cl1–Sm1–O1	172.9(5)	Cl4–Sm2–O4	173.1(4)
Cl1–Sm1–O2	91.7(4)	Cl4–Sm2–O5	91.3(4)
Cl1–Sm1–O3	89.1(4)	Cl4–Sm2–O6	88.7(4)
Cl2–Sm1–Cl3	98.0(3)	Cl5–Sm2–Cl6	96.4(3)
Cl2–Sm1–O1	87.0(5)	Cl5–Sm2–O4	86.2(4)
Cl2–Sm1–O2	172.4(4)	Cl5–Sm2–O5	172.7(4)
Cl2–Sm1–O3	93.6(4)	Cl5–Sm2–O6	93.7(5)
Cl3–Sm1–O1	93.7(5)	Cl6–Sm2–O4	93.3(4)
Cl3–Sm1–O2	86.8(4)	Cl6–Sm2–O5	87.9(4)
Cl3–Sm1–O3	168.0(4)	Cl6–Sm2–O6	169.5(5)
O1–Sm1–O2	86.8(6)	O4–Sm2–O5	87.6(5)
O1–Sm1–O3	83.8(6)	O4–Sm2–O6	84.4(5)
O2–Sm1–O3	81.4(5)	O5–Sm2–O6	81.8(6)



Scheme 1. The proposed mechanism of *fac–mer* isomerization and HMPA exchange in $[LaCl_3(HMPA)_3]$. The central seven-coordinate species is either an interchange transition state, an intermediate or a stable molecule.

plexes $[SmCl_3(THF)_4]$ (2.635–2.683) [26] and $[SmCl_3(DME)(THF)_2]$ (2.646–2.668) [33].

The six-coordinate complexes of lanthanide chlorides include *mer*-$[LnCl_3(HMPA)_3]$ (Ln = Pr, Dy, Yb) [30–32] and *mer*-$[LnCl_3(THF)_3]$ (Ln = Yb, Lu) [28,34], as well as complexes with bulky ligands in a facial conformation: $[CeCl_3(OAsPh_3)_3]$ [35], $[GdCl_3(C_7H_8O_2)_3]$ [36], $[YbCl_3(C_6H_{10}O_2)(THF)_2]$ [27] and $[PrCl_3(CCl_3C(O)N(H)P(O)(NEt_2)_2)_3]$ [37].

3.3. The NMR solution dynamics study of $[LaCl_3(HMPA)_3]$

The existence of *fac* and *mer* isomers of $[PrCl_3(HMPA)_3]$ prompted us to study *fac–mer* isomerization. The ^{1}H NMR spectrum of $[LaCl_3(HMPA)_3]$ shows a doublet consistent with three equivalent HMPA ligands in the *fac* isomer (Fig. 2a). The doublet in the ^{1}H NMR spectrum of the sample containing only traces of free HMPA[1] is converted (at 362 K in 2.5 h) to two doublets in the approximate ratio of intensities of 2:1, consistent with the formation of the *mer* isomer (Fig. 2b, c). The change is reversible, the slow reappearance of the *fac* isomer being observed at room temperature (Fig. 2d, e). Splitting of the doublet at 362 K was not detected, either with the sample containing pure $[LaCl_3(HMPA)_3]$ or in the solution containing $[LaCl_3(HMPA)_3]$ and HMPA in the molar ratio 1:0.5.

The addition of free HMPA to the $[D_8]$toluene solution of $[LaCl_3(HMPA)_3]$ causes a shift of the HMPA resonance in the ^{1}H NMR spectra to the lower frequency, suggesting the fast exchange of free and coordinated HMPA. The shifts of 0.043 and 0.055 ppm were observed after addition of 3 and 9 moles of HMPA to 1 mole of complex, respectively. The separated resonances of free HMPA at lower frequency and of coordinated HMPA at higher frequency were observed at 182 K in a 0.01 M toluene solution containing equimolar amounts of $[LaCl_3(HMPA)_3]$ and free HMPA (Fig. 3). The resonances coalesced at 196 K.

We propose a reversible *fac–mer* isomerization of $[LaCl_3(HMPA)_3]$ by an associative mechanism (Scheme 1). However, we are not able to distinguish between the associative interchange mechanism and seven-coordinate intermediate. An equilibrium of $[LaCl_3(HMPA)_3]$ and $[LaCl_3(HMPA)_4]$ also can not be excluded, since $[LaBr_3(HMPA)_4]$ was isolated in the solid state [7]. The

[1] Crystals of $[LaCl_3(HMPA)_3]$ were taken in a dry box from the mother liquor containing free HMPA, gently dried with paper and dissolved in deuterated toluene.

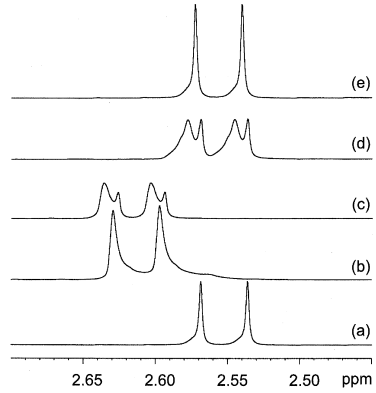


Fig. 2. The ^{1}H NMR spectra of $[LaCl_3(HMPA)_3]$ with traces of free HMPA during thermal treatment ($[D_8]$toluene solution). (a) Starting spectrum at 303 K. The sample was then heated to 362 K, and after 0.5 and 2.5 h at this temperature spectra (b) and (c) were recorded. The sample was cooled down to 303 K and after 1 h the spectrum (d) was recorded. The sample was then left at 298 K for 36 h, and the spectrum (e) resulted.

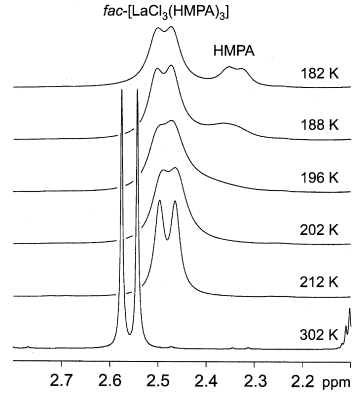


Fig. 3. The variable temperature ^{1}H NMR spectra of $[LaCl_3(HMPA)_3]$ with added free HMPA (molar ratio 1:1, $[D_8]$toluene solution).

fac isomer is dominant at room temperature and the *mer* isomer at 362 K.

According to the proposed mechanism, the exchange and isomerization are second-order reactions, depending on the concentrations of the complex and free HMPA. The exchange of two different environments of HMPA ligand in *mer*-$[LaCl_3(HMPA)_3]$ is slow on the ^{1}H NMR time scale only in the presence of traces of free HMPA (Fig. 2c, d). At a 1:0.5 molar ratio of complex to free HMPA, only one HMPA resonance was observed at 362 K, indicating the fast exchange of all the coordinated HMPA molecules in *mer*-$[LaCl_3(HMPA)_3]$ and free HMPA.

The coalescence of resonances of free and coordinated HMPA at 196 K gave a second-order rate constant k_2(196

K) of $1.0(2)\times10^{4}\ M^{-1}\ s^{-1}$ and $\Delta G^{\neq}(196\ K) = 32\pm1$ kJ/mol.

Only a broad ^{31}P NMR singlet was observed for *fac* and *mer* isomers of $[LaCl_3(HMPA)_3]$. We were not able to detect a ^{139}La NMR resonance.

4. Conclusions

The *fac*-$[LnCl_3(HMPA)_3]$ (Ln = La, Pr, Nd, Sm, Eu, Gd) complexes were prepared by the reaction of $[LnCl_3L]$ (L = diglyme and DME) with excess HMPA at room temperature in toluene solution. The previously reported *mer*-$[PrCl_3(HMPA)_3]$ was obtained by the reaction of $PrCl_3$ in hot ethanol, crystallized at 0°C and then recrystallized from benzene [6,30]. The ^{1}H NMR study of $[LaCl_3(HMPA)_3]$ shows exchange of coordinated and free HMPA. In addition, *fac*-$[LaCl_3(HMPA)_3]$ observed in toluene solution at room temperature is reversibly converted to the *mer* isomer at 362 K in the presence of traces of free HMPA. The conversion was not observed without free HMPA. On this basis, the mechanism was proposed for reversible *fac–mer* isomerization in the presence of free HMPA. However, the polar solvent ethanol, used in the synthesis of *mer*-$[PrCl_3(HMPA)_3]$ [6,30], could alter the relative stabilities of *fac* and *mer* isomers, making the *mer* isomer more stable at 0°C. *mer*-$[PrCl_3(HMPA)_3]$ could not be converted to the *fac* isomer during recrystallization from non-polar benzene since no free HMPA was present.

Supplementary data

Crystallographic data concerning the crystal structure determination of $[SmCl_3(HMPA)_3]$ are available from the Cambridge Crystallographic Data Centre, 12 Union Road, Cambridge CB2 1EZ, UK, on request, quoting deposition number CCDC 132917.

Acknowledgements

This work was supported by the Ministry of Science and Technology, Republic of Slovenia.

References

[1] J.W. Faller, in: R.B. King (Ed.), Encyclopedia of Inorganic Chemistry, vol. 7, Wiley, Chichester, 1994, p. 3914.
[2] M.L. Tobe, J. Burgess, Inorganic Reaction Mechanisms (1999) Longman, Harlow, 1999, Chapter 7.
[3] F.A. Cotton, G. Wilkinson, C.A. Murillo, M. Bochmann, Advanced Inorganic Chemistry, 6th ed., Wiley, Chichester, 1999, p. 13.
[4] L. Helm, A.E. Merbach, Coord. Chem. Rev. 187 (1999) 151.
[5] S.A. Cotton, R.B. King, Encyclopedia of Inorganic Chemistry, Wiley, Chichester, vol. 7, 1994, p. 3595.
[6] J.T. Donoghue, D.A. Peters, J. Inorg. Nucl. Chem. 31 (1969) 467.
[7] D. Barr, A.T. Brooker, M.J. Doyle, S.R. Drake, P.R. Raithby, R. Snaith, D.S. Wright, Angew. Chem., Int. Ed. Engl. 29 (1990) 285.
[8] Y. Li, T.J. Marks, J. Am. Chem. Soc. 120 (1998) 1757.
[9] W.J. Evans, K.J. Forrestal, M.A. Ansari, J.W. Ziller, J. Am. Chem. Soc. 120 (1998) 2180.
[10] W. Xie, Y. Jin, P.G. Wang, Chemtech 29 (1999) 23.
[11] W.J. Evans, K.J. Forrestal, J.W. Ziller, Angew. Chem., Int. Ed. Engl. 36 (1997) 774.
[12] H. Berberich, P.W. Roesky, Angew. Chem., Int. Ed. Engl. 37 (1998) 1569.
[13] E. Toth, L. Helm, A.E. Merbach, R. Hedinger, K. Hegetschweiler, A. Janossy, Inorg. Chem. 37 (1998) 4104 and references therein.
[14] S.H. Wu, Z.D. Ding, X.J. Li, Polyhedron 13 (1994) 2679.
[15] D. Belli Dell'Amico, F. Calderazzo, C. della Porta, A. Merigo, P. Biagini, G. Lugli, T. Wagner, Inorg. Chim. Acta 240 (1995) 1.
[16] S. Petriček, A. Demšar, L. Golič, Polyhedron 18 (1999) 529.
[17] S.R. Hall, G.S.D. King, J.M. Stewart, Xtal3.4 User's Manual, 1995, University of Western Australia, Lamb, Perth.
[18] Crystallographic data obtained through the Cambridge Crystallographic Data Centre, $[GdCl_3(dme)_2]$, refcode: VAKMID, G. Wei, H. Gao, Z. Jin, Q. Shen, J. Struct. Chem. 8 (1989) 61.
[19] S. Anfang, K. Dehnicke, J. Magull, Z. Naturforsch. Teil B51 (1996) 531.
[20] S. Anfang, M. Karl, N. Faza, W. Massa, J. Magull, K. Dehnicke, Z. Anorg. Allg. Chem. 623 (1997) 1425.
[21] G.R. Willey, T.J. Woodman, M.G.B. Drew, Polyhedron 16 (1997) 3385.
[22] G.R. Willey, P.R. Meehan, T.J. Woodman, M.G.B. Drew, Polyhedron 16 (1997) 623.
[23] G.B. Deacon, T. Feng, B.W. Skelton, A.N. Sobolev, A.H. White, Aust. J. Chem. 51 (1998) 75.
[24] S.H. Lin, Z.C. Dong, J.S. Huang, Q.E. Zhang, J.X. Lu, Acta Crystallogr. Sect. C47 (1991) 426.
[25] C. Wenqi, J. Zhongsheng, X. Yan, F. Yugou, Y. Guangdi, Inorg. Chim. Acta 130 (1987) 125.
[26] Crystallographic data obtained through the Cambridge Crystallographic Data Centre, $[SmCl_3(thf)_4]$, refcode: YADWOP, G.Y. Lin, G.C. Wei, Z.S. Jin, W.Q. Chen, J. Struct. Chem. 11 (1992) 200.
[27] J.W. Evans, J.L. Shreeeve, J.W. Ziller, R.J. Doedens, Inorg. Chem. 34 (1995) 576.
[28] G.B. Deacon, T. Feng, S. Nickel, B.W. Skelton, A.H. White, J. Chem. Soc., Chem. Commun. (1993) 1328.
[29] V. Ripert, L.G. Hubert-Pfalzgraf, J. Vaissermann, Polyhedron 18 (1999) 1845.
[30] L.J. Radonovich, M.D. Glick, J. Inorg. Nucl. Chem. 35 (1972) 2745.
[31] X.W. Zhang, X.F. Li, F. Benetollo, G. Bombieri, Inorg. Chim. Acta 139 (1987) 103.
[32] Z. Hou, K. Kobayashi, H. Yamazaki, Chem. Lett. 268 (1991) 265.
[33] Crystallographic data obtained through the Cambridge Crystallographic Data Centre, $[SmCl_3(dme)(thf)_2]$, refcode: SERXIW, Z. Jin, G. Nie, N. Hu, W. Chen, Chin. J. Appl. Chem. 6 (1989) 68.
[34] Crystallographic data obtained through the Cambridge Crystallographic Data Centre, $[LuCl_3(thf)_3]$, refcode: HAFWAM, G.K.I. Magomedov, A.Z. Voskoboinikov, N.I. Kirillova, A.I. Gusev, I.N. Parshina, I.P. Beletskaya, Metalloorg. Khim. 5 (1992) 679.
[35] R.R. Ryan, E.M. Larson, Inorg. Chim. Acta 131 (1987) 267.
[36] C.B. Castellani, V. Tazzoli, Acta Crystallogr., Sect. C40 (1984) 1832.
[37] V.M. Amirhanov, V.A. Ovchinnikov, A.A. Kapshuk, V.V. Skopenko, Zh. Neorg. Khim. 40 (1995) 1869.

PERGAMON

www.elsevier.nl/locate/poly

Polyhedron 19 (2000) 205–210

POLYHEDRON

Host–guest interaction and dynamics of haloferrocenes enclathrated in deoxycholic acid as inferred from ^{57}Fe Mössbauer measurements[1]

Satoru Nakashima [a,b,*], Naoki Ichikawa [c], Hiroaki Komatsu [c], Koji Yamada [c], Tsutomu Okuda [c]

[a] *Radioisotope Center, Hiroshima University, Kagamiyama, Higashi-Hiroshima 739-8526, Japan*

[b] *Department of Mathematical and Life Sciences, Graduate School of Science, Hiroshima University, Higashi-Hiroshima 739-8526, Japan*

[c] *Department of Chemistry, Graduate School of Science, Hiroshima University, Higashi-Hiroshima 739-8526, Japan*

Received 18 May 1999; accepted 16 November 1999

Abstract

^{57}Fe Mössbauer spectroscopy shows that the molecular motion of haloferrocenes enclathrated in deoxycholic acid is similar to that of ferrocene in deoxycholic acid but the onset temperature of the precession and anisotropic vibration of haloferrocenes as a whole in the deoxycholic acid becomes higher as the interaction increases between deoxycholic acid and the halogen atoms in the ferrocene derivatives. It is also shown that increasing the number of halogen atoms has a tendency to increase the interaction with the host lattice. Powder X-ray diffraction patterns show that all the inclusion compounds have similar crystal structures, and the unit cell volume of haloferrocenes enclathrated in deoxycholic acid decreases with increasing van der Waals radius of the halogen atom. ©2000 Elsevier Science Ltd All rights reserved.

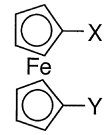
Keywords: Deoxycholic acid; Ferrocene derivatives; Inclusion compounds; Molecular motion; ^{57}Fe Mössbauer spectroscopy; Powder X-ray diffraction patterns

1. Introduction

Crystal engineering has become a major problem in chemistry [1]. Control of the solid state structure of supramolecule substances can provide us with a wide range of new molecular-based materials. One of the strategies to construct crystals is the use of host–guest phenomena. The onset and cessation of the rotational motion of guest molecules having dipole moments in the host lattice result in a change of dielectric constant, giving the possibility of making a molecular-based switch. Therefore, there is considerably current interest in the dynamics of guest molecules in host lattices [2]. It is known that deoxycholic acid forms a channel in the solid state, and that it includes a variety of organic molecules. Miki et al. first reported an X-ray diffraction study of the ferrocene (FcH)–deoxycholic acid (DCA) (1:2) inclusion compound; the FcH was fixed in the DCA channel [3]. Using NMR methods, Imashiro et al. detected a precession of FcH in the DCA inclusion compound [4].

^{57}Fe Mössbauer spectroscopy is a useful technique to investigate molecular motion in inclusion compounds [5]. Recently, the present author applied ^{57}Fe Mössbauer spectroscopy to study the molecular motion of FcH in the DCA channel [6]. The existence of the precession was confirmed and it was first suggested, using ^{57}Fe Mössbauer spectroscopy, that an anisotropic vibration of the FcH molecule as a whole is coupled with the precession.

In the present study, the molecular motion of haloferrocenes having dipole moments such as monochloro- (FcCl), monobromo- (FcBr), monoiodo- (FcI), 1,1′-dichloro- ($FcCl_2$), 1,1′-dibromo- ($FcBr_2$) and 1,1′-diiodoferrocene (FcI_2) (Scheme 1) enclathrated in DCA was investigated by means of ^{57}Fe Mössbauer spectroscopy and was compared with that of the ferrocene molecule enclathrated in DCA. The molecular motion of 1,1′-dimethylferrocene ($FcMe_2$) in DCA was also investigated and compared with those of haloferrocenes in DCA to bring out the interaction of the halogen atoms and the DCA lattice. The crystal data obtained from powder X-ray diffraction patterns were compared with



Scheme 1. Guest molecules: FcH (X = Y = H), FcCl (X = Cl, Y = H), FcBr (X = Br, Y = H), FcI (X = I, Y = H), $FcCl_2$ (X = Y = Cl), $FcBr_2$ (X = Y = Br), FcI_2 (X = Y = I), $FcMe_2$ (X = Y = Me).

* Corresponding author. Tel.: +81-824-24-6291; fax: +81-824-24-0700; e-mail: snaka@ipc.hiroshima-u.ac.jp

[1] A preliminary report of the present study was published in the Proceedings of the International Conference on the Applications of the Mössbauer Effect [Hyperfine Interact. C3 (1998) 121].

0277-5387/00/$ - see front matter ©2000 Elsevier Science Ltd All rights reserved.
PII S0277-5387(99)00351-4

each other, and revealed an interesting contraction of the unit cell volume with an increase in the van der Waals radius of the substituent, which suggests an apparent interaction of the halogen atoms and the host lattice.

2. Experimental

All haloferrocenes were synthesized according to the usual procedure [7] and the purity was confirmed by ^{1}H NMR. The 1,1′-dimethylferrocene used was commercially available (Aldrich). The needle-like crystals of the ferrocene derivative–DCA (1:2) inclusion compounds were obtained from methanol solution except for FcI–DCA, which was obtained from butanol solution. The presence of inclusion compounds was confirmed by powder X-ray diffraction patterns and elemental analyses. Found for FcCl–DCA: C, 69.33; H, 9.07%. Calc. for $C_{24}H_{40}O_4 \cdot 1/2(C_{10}H_9FeCl)$: C, 69.26; H, 8.92%. Found for FcBr–DCA: C, 66.63; H, 8.79%. Calc. for $C_{24}H_{40}O_4 \cdot 1/2(C_{10}H_9FeBr)$: C, 66.34; H, 8.54%. Found for FcI–DCA: C, 63.58; H, 8.71%. Calc. for $C_{24}H_{40}O_4 \cdot 1/2(C_{10}H_9FeI)$: C, 63.49; H, 8.18%. Found for $FcCl_2$–DCA: C, 67.19; H, 8.99%. Calc. for $C_{24}H_{40}O_4 \cdot 1/2(C_{10}H_8FeCl_2)$: C, 66.97; H, 8.53%. Found for $FcBr_2$–DCA: C, 62.27; H, 8.36%. Calc. for $C_{24}H_{40}O_4 \cdot 1/2(C_{10}H_8FeBr_2)$: C, 61.70; H, 7.86%. Found for FcI_2–DCA: C, 57.79; H, 7.55%. Calc. for $C_{24}H_{40}O_4 \cdot 1/2(C_{10}H_8FeI_2)$: C, 57.16; H, 7.25%. Found for $FcMe_2$–DCA: C, 72.10; H, 9.91%. Calc. for $C_{24}H_{40}O_4 \cdot 1/2(C_{12}H_{14}Fe)$: C, 72.10; H, 9.50%.

Powder X-ray diffraction patterns were measured using Cu Kα radiation (RIGAKU) at room temperature.

A ^{57}Co (Rh) source moving in a constant acceleration mode was used for ^{57}Fe Mössbauer spectroscopic measurements. Variable-temperature ^{57}Fe Mössbauer spectra were obtained in the range of 80–363 K using a Toyo Research spectrometer, a proportional counter and a continuous-flow cryostat or home-built high-temperature apparatus. All spectra were measured on powdered samples. The isomer shift values are referred to a metallic iron foil at room temperature. The Mössbauer parameters were obtained by least-squares fitting to Lorentzian peaks. The error limits of isomer shift, quadrupole splitting values, half-width and area ratio are 0.005 mm s^{-1}, 0.010 mm s^{-1}, 0.005 mm s^{-1} and 0.035, respectively.

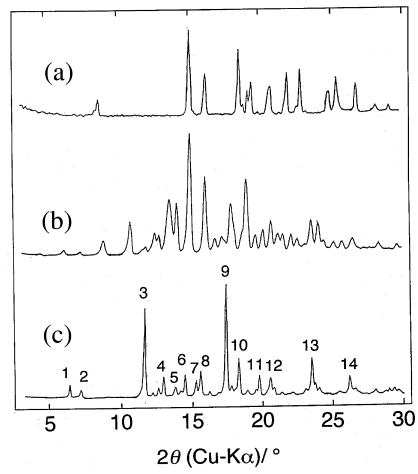


Fig. 1. Powder X-ray diffraction patterns at room temperature of chloroferrocene (a), DCA (b) and the chloroferrocene–DCA inclusion compound (c). The indices obtained using the orthorhombic lattice constants of FcH–DCA are: 1 (010), 2 (110), 3 (310), 4 (001), 5 (020), 6 (220), 7 (211), 8 (301), 9 (510), 10 (420), 11 (130), 12 (321), 13 (430), 14 (530).

3. Results and discussion

The powder X-ray diffraction patterns for chloroferrocene, DCA and the chloroferrocene–DCA inclusion compound are shown in Fig. 1. It can easily be seen from Fig. 1 that the pattern for the chloroferrocene–DCA inclusion compound is not the superposition of those of chloroferrocene and DCA. The patterns from chloroferrocene and DCA are not observed in the inclusion compound. The pattern of FcCl–DCA is similar to that of ferrocene–DCA. It is known that the ferrocene molecule is fixed in the DCA channel in the ratio 1:2 [3]. It can be judged from the similarity of the patterns that chloroferrocene is also included in the DCA lattice in a similar manner, and that the ratio of FcCl–DCA is 1:2. The elemental analysis also supports the ratio. We suppose here that the crystal structure of FcCl–DCA is the same as that of FcH–DCA. In this situation, the reflections of FcCl–DCA can be indexed by using the orthorhombic lattice constants of FcH–DCA. The indices are also shown in Fig. 1. By using these indices we calculated the lattice constants of FcCl–DCA; these are summarized in Table 1. The unit cell volume of FcCl–DCA is larger than that of FcH–DCA. Other inclusion compounds show similar powder X-ray diffraction patterns; the calculated crystal data are also summarized in Table 1.

Variable-temperature ^{57}Fe Mössbauer spectra of the FcCl–DCA inclusion compound are shown in Fig. 2. The Möss-

Table 1
Crystal data of ferrocene derivative–DCA inclusion compounds

Guest	FcH	FcCl	FcBr	FcI	$FcCl_2$	$FcBr_2$	FcI_2	$FcMe_2$
Radius of X (Å) [a]	1.2	1.80	1.95	2.15	1.80	1.95	2.15	2.0
a (Å)	27.29	27.64	28.06	27.63	27.52	26.26	27.22	27.19
b (Å)	13.68	13.82	13.63	13.74	13.8	13.87	13.66	13.63
c (Å)	7.07	7.42	7.27	7.07	7.24	7.35	7.05	7.26
V (Å^3)	2640	2834	2780	2684	2750	2677	2621	2766

[a] van der Waals radii are taken from [13].

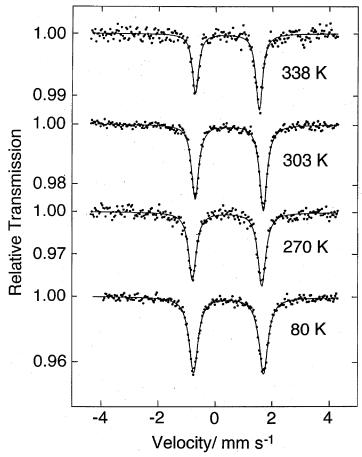


Fig. 2. Variable-temperature ^{57}Fe Mössbauer spectra of chloroferrocene–DCA inclusion compound.

bauer parameters are summarized in Table 2. It can easily be seen that the symmetric doublets are observed at low temperatures, whereas at high temperatures the doublet becomes asymmetric. It can also be seen that the quadrupole splitting (QS) values at high temperatures are smaller than those at low temperatures. Variable-temperature ^{57}Fe Mössbauer spectra of the FcBr–DCA inclusion compound also showed a similar temperature dependence at higher temperatures. The Mössbauer parameters are also summarized in Table 2.

The temperature dependences of the area intensity ratio of the high-energy peak to the low-energy peak and of the QS values in the ^{57}Fe Mössbauer spectra of FcCl–DCA and FcBr–DCA are shown in Figs. 3 and 4, respectively, compared with those of FcH–DCA. It can be seen from Fig. 3 that the doublets are symmetric from 80 to ~300 K for FcCl–DCA and from 80 to ~320 K for FcBr–DCA, whereas at higher temperatures the doublet becomes asymmetric in intensity. The asymmetry in intensity for FcCl–DCA appears above ~300 K, which is higher than that for FcH–DCA (~270 K) and is lower than that for FcBr–DCA (~320 K). The asymmetry in intensity increases with increase in temperature as is the case for FcH–DCA. It is known that the asymmetry of the doublet is caused by a preferred orientation of the molecule and/or an anisotropic recoilless fraction (Gol'danskii–Karyagin effect) [8,9]. The anisotropic recoilless fraction is independent of the orientation of the sample. It is thought that the present asymmetry in intensity is due to the Gol'danskii–Karyagin effect, because the samples in the present study were powdered and the asymmetry showed a temperature dependence. The effect of preferred orientation does not change with a change of temperature. The asymmetric doublet observed at high temperatures reverted to a symmetric doublet upon remeasuring the same sample at low temperatures. It is known that the electric field gradient (V_{zz}) of FcH is positive [10]. It is also known that the introduction of substituents to FcH has little effect upon the electric field gradient at the iron nucleus [11]. Therefore, we assume that the electric field gradients in the present derivatives are positive as is the case of FcH. In this case ($V_{zz} > 0$) the increase in the area ratio of the high-energy peak to the low-energy peak means that the vibration in a direction perpendicular to the molecular axis becomes more intense than that in a direction parallel to the axis at high temperatures ($\langle u_z^2 \rangle < \langle u_{x,y}^2 \rangle$) for the axially symmetric crystal [12]. We suppose here from

Table 2
^{57}Fe Mössbauer parameters for ferrocene derivative–DCA inclusion compounds

Sample	T (K)	δ [a] (mm s^{-1})	ΔE_q (mm s^{-1})	Γ (mm s^{-1})	Area ratio [b]
FcCl–DCA	350	0.43	2.20	0.25	1.33
	340	0.43	2.23	0.28	1.28
	330	0.45	2.31	0.29	1.21
	313	0.44	2.38	0.31	1.15
	303	0.42	2.40	0.31	1.11
	290	0.45	2.41	0.37	1.09
	270	0.46	2.42	0.33	1.09
	200	0.50	2.45	0.37	1.04
	80	0.51	2.44	0.38	1.01
FcBr–DCA	363	0.43	2.32	0.31	1.18
	343	0.46	2.38	0.34	1.09
	323	0.44	2.42	0.30	1.06
	290	0.45	2.43	0.28	1.01
	240	0.47	2.44	0.32	1.02
	160	0.51	2.46	0.38	1.01
	80	0.53	2.46	0.42	0.99
FcI–DCA	363	0.42	2.37	0.37	1.49
	323	0.45	2.38	0.37	1.45
	298	0.45	2.38	0.29	1.26
	200	0.49	2.40	0.31	1.03
	80	0.52	2.42	0.38	1.04
$FcCl_2$–DCA	363	0.44	2.45	0.27	1.16
	333	0.44	2.48	0.28	1.06
	313	0.44	2.48	0.28	1.01
	290	0.43	2.49	0.28	1.01
	200	0.48	2.49	0.34	1.00
	80	0.52	2.50	0.47	0.99
$FcBr_2$–DCA	363	0.45	2.49	0.29	1.01
	353	0.43	2.44	0.28	0.96
	343	0.43	2.43	0.30	0.99
	323	0.44	2.43	0.29	1.01
	303	0.44	2.43	0.30	1.00
	290	0.44	2.43	0.29	1.01
	80	0.52	2.52	0.48	1.01
FcI_2–DCA	358	0.39	2.45	0.27	1.02
	348	0.40	2.47	0.25	1.00
	338	0.40	2.47	0.24	1.00
	328	0.40	2.48	0.23	0.98
	318	0.41	2.48	0.23	0.99
	290	0.42	2.49	0.22	0.95
	220	0.47	2.50	0.26	0.96
	150	0.50	2.51	0.28	0.96
	80	0.52	2.51	0.40	0.97
$FcMe_2$–DCA	356	0.40	2.33	0.22	1.23
	343	0.40	2.36	0.25	1.13
	333	0.40	2.39	0.23	1.08
	323	0.40	2.39	0.25	1.08
	313	0.40	2.41	0.24	1.06
	290	0.41	2.42	0.24	1.04
	270	0.43	2.43	0.38	1.03
	220	0.45	2.44	0.30	0.97
	80	0.50	2.44	0.27	0.98

[a] Isomer shift data are reported with respect to iron foil.
[b] Area intensity ratio of the high-energy peak to the low-energy peak in the doublet.

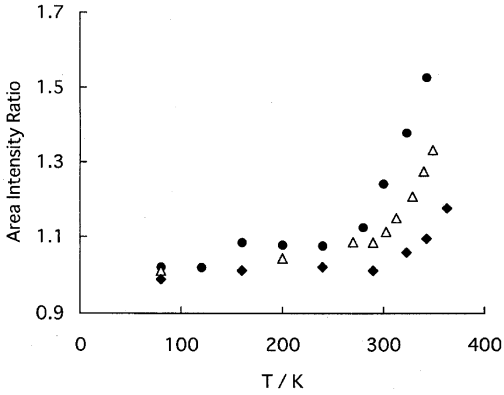


Fig. 3. Temperature dependence of the area intensity ratio of the high-energy peak to the low-energy peak in the ^{57}Fe Mössbauer doublet: ●, FcH–DCA; △, FcCl–DCA; ◆, FcBr–DCA.

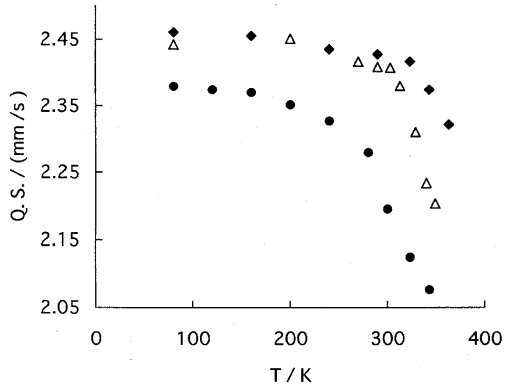


Fig. 4. Temperature dependence of the quadrupole splitting value in the ^{57}Fe Mössbauer spectra: ●, FcH–DCA; △, FcCl–DCA; ◆, FcBr–DCA.

the results of powder X-ray diffraction patterns that the crystal structure of the present inclusion compound is the same as that of FcH–DCA. In the FcH–DCA inclusion compound, DCA makes a channel and the ferrocene molecules are included in this channel in such a way that the molecular axis of ferrocene is perpendicular to the channel. In this case it can be supposed that the direction with the larger mean square amplitude of vibration is the channel direction. It is thought that $\langle u_y^2 \rangle$ is the channel direction. Although the axial symmetry does not hold in the present case, we can easily imagine the relation of $\langle u_x^2 \rangle \approx \langle u_z^2 \rangle$ and $\langle u_y^2 \rangle \gg \langle u_z^2 \rangle$. The temperature dependence of the area ratio in the present ^{57}Fe Mössbauer spectra is not inconsistent with the crystal structure.

The QS values for FcCl–DCA and FcBr–DCA are larger than those of FcH–DCA at the same temperature. It can be seen from Fig. 4 that the QS values of FcCl–DCA are almost constant from 80 to ~300 K and the values decrease suddenly above ~300 K. The QS values of FcBr–DCA are also almost constant from 80 to ~320 K and the values decrease suddenly above ~320 K. The onset temperature (~300 K) for FcCl–DCA is higher than that for FcH–DCA (~280 K) and is lower than that for FcBr–DCA (~320 K). The temperatures are consistent with those at which the doublet starts to become asymmetric in intensity. The changes can be explained by the precession of the FcCl and FcBr molecules in the DCA channel, as is the case of FcH in the DCA lattice [6]. The precession of the FcH molecule in the DCA channel is also suggested from the solid-state NMR [4]. The electric field gradient depends on the precession angle. The electric field gradient decreases in proportion to the cosine of the precession angle. Thus the decrease in the QS value is explained by the precession of guest molecules. It can be thought that the precession angle increases with increasing temperature.

As mentioned in Section 2, the FcI–DCA inclusion compound was not obtained from methanol solution. One possible reason for this may be a stronger interaction of methanol–DCA than of FcI–DCA. The inclusion compound was produced using butanol as solvent. It was not obtained as needle-like crystals but rather as a powder, whereas the other inclusion compounds in the present study, as well as FcH–DCA, were obtained as needle-like crystals. This difference might reflect the poor fit of the FcI molecule into the DCA lattice in the FcI–DCA obtained from butanol solution. The elemental analysis shows that the ratio of DCA to FcI is still 2.

The asymmetry of the FcI–DCA doublet was easily observed even at room temperature, and the asymmetry became larger with increasing temperature, but the abrupt decrease of the QS value was not observed. It is puzzling that, in the FcI–DCA inclusion compound, the changes of asymmetry in the intensity and of the QS values are not consistent with each other. One of the reasons for the discrepancy between the onset temperatures of asymmetry in intensity and of the decrease in the QS value may be the poor fit of FcI into the DCA lattice. This poor fit makes the anisotropic vibration of the FcI molecule in the channel direction easier as a whole and does not make room for the precession.

The 1,1′-diiodoferrocene (FcI_2)–DCA inclusion compound was easily obtained from methanol solution. This difference in the inclusion phenomena between FcI–DCA and FcI_2–DCA remains unexplained. The variable-temperature ^{57}Fe Mössbauer spectra of FcI_2–DCA are shown in Fig. 5.

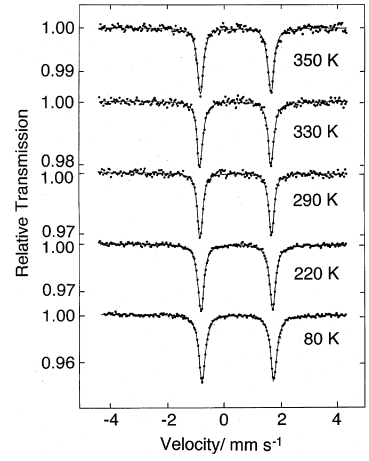


Fig. 5. Variable-temperature ^{57}Fe Mössbauer spectra of 1,1′-diiodoferrocene–DCA inclusion compound.

Symmetric doublets are observed and they do not show the remarkable asymmetry in intensity with increasing temperature, which is contrary to the results for monohaloferrocene–DCA. 1,1′-Dibromoferrocene ($FcBr_2$)–DCA also did not show remarkable temperature dependences, while evidence of molecular motion is observed in 1,1′-dichloroferrocene ($FcCl_2$)–DCA at high temperature. The temperature dependences of the area intensity ratio of the high-energy peak to the low-energy peak and of the QS values in the ^{57}Fe Mössbauer spectra of FcI_2–DCA, $FcBr_2$–DCA and $FcCl_2$–DCA are shown in Figs. 6 and 7, respectively. The large asymmetry in intensity for FcX_2 (X = Cl, Br, I) at high temperatures was not seen in Fig. 6 as compared with Fig. 3. The abrupt decrease of the QS values for FcX_2 (X = Cl, Br, I) at high temperatures was also not seen in Fig. 7 as compared with Fig. 4. The results observed in the halogen-disubstituted ferrocene derivatives in the DCA lattice contrast with those observed in the halogen-monosubstituted derivatives in DCA. It may be supposed that increasing the number of halogen atoms tends to increase the interaction with DCA.

For purposes of comparison we measured the variable-temperature ^{57}Fe Mössbauer spectra of 1,1′-dimethylferrocene ($FcMe_2$)–DCA (Fig. 8). The temperature dependences of the asymmetry in intensity and of the QS values for $FcMe_2$–DCA are also plotted in Figs. 6 and 7, respectively. The doublet becomes asymmetric in intensity and the QS value becomes smaller with increasing temperature abruptly over ~300 K. The temperature is higher than that of ferrocene–DCA because of the steric effect of the methyl substituents. The results in the methyl-disubstituted derivative–DCA show a major contrast with those in halogen-disubstituted derivative–DCA. We attribute this difference between them to an apparent interaction of halogen atoms with deoxycholic acid.

To investigate the difference among DCA inclusion compounds with the series of haloferrocenes we rechecked the results of powder X-ray diffraction patterns, which revealed that the crystal structures in the present study are similar to that of FcH–DCA inclusion compound. As described above, the reflections were indexed by using the orthorhombic lattice constants of FcH–DCA. The crystal data were calculated using the indices obtained from the assumption that the crystal structures in the present inclusion compounds are the same as that of FcH–DCA. Table 1 summarizes the crystal data. Surprisingly it can be seen that, in the monohaloferrocene series, the volume of the unit cell becomes smaller upon increasing the van der Waals radius of the halogen atom. It can also be seen in the dihaloferrocene series that the volume of the unit cell becomes smaller upon increasing the van der Waals radius of the halogen atom. The unit cell volumes of the dihaloferrocenes are smaller than those of the corresponding monohaloferrocenes having the same halogen substituents. In the extreme case, the unit cell volume of FcI_2–DCA is smaller than that of FcH–DCA. The van der Waals radius of the methyl group is 2.0 Å [13], which is slightly larger than that of bromine. An interesting point is that all the unit cell volumes of FcX_2–DCA (X = Cl, Br, I) are smaller than that of $FcMe_2$–DCA in spite of the larger van der Waals radius of iodine. The difference in the temperature dependence of the ^{57}Fe Mössbauer spectra between $FcMe_2$–DCA and FcX_2–

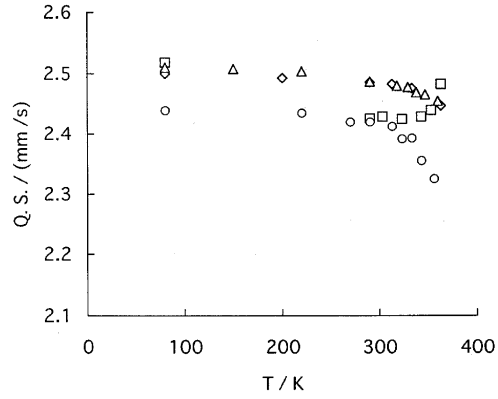


Fig. 7. Temperature dependence of the quadrupole splitting value in the ^{57}Fe Mössbauer spectra: ◇, $FcCl_2$–DCA; □, $FcBr_2$–DCA; △, FcI_2–DCA; ○, $FcMe_2$–DCA.

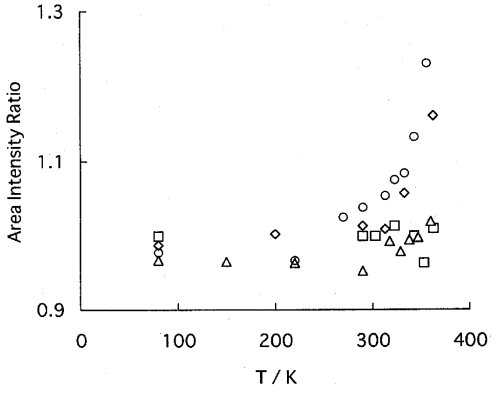


Fig. 6. Temperature dependence of the area intensity ratio of the high-energy peak to the low-energy peak in the ^{57}Fe Mössbauer doublet: ◇, $FcCl_2$–DCA; □, $FcBr_2$–DCA; △, FcI_2–DCA; ○, $FcMe_2$–DCA.

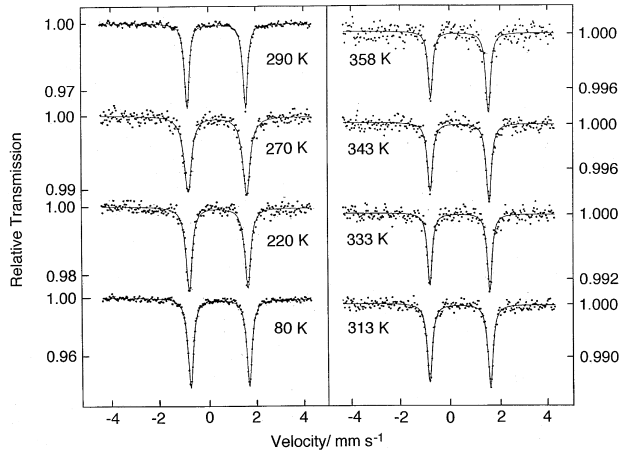


Fig. 8. Variable-temperature ^{57}Fe Mössbauer spectra of 1,1′-dimethylferrocene–DCA inclusion compound.

DCA (X = Cl, Br, I) clearly reveals the existence of the interaction between halogen atoms and the DCA lattice.

Deoxycholic acid has both hydrophobic and hydrophilic planes. It is known that the ferrocene molecule is enclathrated into the hydrophobic plane of deoxycholic acid [3]. The similarity of the present X-ray powder patterns suggests that the halogen-substituted ferrocenes and 1,1′-dimethylferrocene are also enclathrated into the hydrophobic plane of the DCA. FcCl–DCA shows a lower onset temperature than FcBr–DCA, suggesting that the interaction is not an electrostatic one. The enclathrated position and the results of X-ray powder patterns show that the increased van der Waals interaction raises the onset temperature.

It can be concluded that there is an apparent van der Waals interaction between halogen atom in the ferrocene derivatives and the DCA lattice. The interaction suppresses the precession and anisotropic vibration of the ferrocene derivatives as a whole in the DCA lattice. At higher temperatures the precession and anisotropic motion start. In the disubstituted haloferrocenes, these motions are almost unable to begin because of the increased interaction of the halogen atoms in the ferrocene derivatives and the DCA lattice. The precession of the haloferrocenes will result in a change of dielectric constant, which results in a molecular-based switch. Finally, the onset temperature can be controlled by changing the identity and number of the halogen atoms.

Acknowledgements

We thank Professor G. Wulfsberg, Middle Tennessee State University for reading the manuscript.

References

[1] J.-M. Lehn, Supramolecular Chemistry, Concepts and Perspectives, VCH, Weinheim, 1995.
[2] W. Tam, D.F. Eaton, J.C. Calabrese, I.D. Willeams, Y. Wang, A.G. Anderson, Chem. Mater. 1 (1989) 128.
[3] K. Miki, N. Kasai, H. Tsutsumi, M. Miyata, K. Takemoto, J. Chem. Soc., Chem. Commun. (1987) 545.
[4] F. Imashiro, N. Kitazaki, D. Kuwahara, T. Nakai, T. Terao, J. Chem. Soc., Chem. Commun. (1991) 85.
[5] T.C. Gibb, Principles of Mössbauer Spectroscopy, Chapman and Hall, London, 1976.
[6] S. Nakashima, M. Nakashita, H. Sakai, Chem. Lett. (1996) 927.
[7] R.F. Kovar, M.D. Rausch, H. Rosenberg, Organometal. Chem. Syn. 1 (1970) 173.
[8] V.I. Gol'danskii, E.F. Makarov, V.V. Khrapov, Phys. Lett. 3 (1963) 334.
[9] S.V. Karyagin, Dokl. Akad. Nauk SSSR 148 (1963) 1102.
[10] R.L. Collins, J. Chem. Phys. 42 (1965) 1072.
[11] R.M.G. Roberts, J. Silver, J. Organomet. Chem. 263 (1984) 235.
[12] P. Gütlich, R. Link, A. Trautwein, Mössbauer Spectroscopy and Transition Metal Chemistry, Springer, Berlin, 1978.
[13] L. Pauling, The Nature of the Chemical Bond, Cornell University Press, New York, 3rd ed., 1960.

PERGAMON

www.elsevier.nl/locate/poly

Polyhedron 19 (2000) 211–215

POLYHEDRON

Synthesis and X-ray single crystal structures of bis(diisobutyldithiophosphinato)cadmium(II) or zinc(II): Potential single-source precursors for II/VI materials

C. Byrom, M.A. Malik, P. O'Brien *, A.J.P. White, D.J. Williams

Department of Chemistry, Imperial College of Science, Technology and Medicine, South Kensington, London SW7 2AY, UK

Received 20 August 1999; accepted 12 November 1999

Abstract

Bis(diisobutyldithiophosphinato)cadmium(II) (**1**) and bis(diisobutyldithiophosphinato)zinc(II) (**2**) have been synthesised and their X-ray single crystal structures determined. Both compounds have been used as precursors to grow thin films of CdS and ZnS, respectively, by low-pressure metal organic chemical vapour deposition (LP-MOCVD). ©2000 Elsevier Science Ltd All rights reserved.

Keywords: Dithiophosphinates; Low-pressure metal organic chemical vapour deposition; II/VI Semiconductors

1. Introduction

Dithiophosphinates have many important industrial and agricultural applications, including solvent extraction reagents for metals [1], insecticides and pesticides, flotation agents for mineral ores and additives to lubricant oils [2]. Metal complexes of such ligands have the potential to be new precursors for use in low-pressure metal organic chemical vapour deposition (LP-MOCVD). The deposition of II/VI semiconductors had been previously achieved with zinc and cadmium dimethyldithiophosphinates by Takahashi et al. [3]. They grew good-quality ZnS and CdS films on silver-plated glass substrates between 400 and 500°C. Films grown on normal glass substrates were of poor quality in terms of thickness even when grown at higher substrate temperatures.

In the present paper we report the X-ray crystal structures of the new compounds bis(diisobutyldithiophosphinato)-cadmium(II) (**1**) and bis(diisobutyldithiophosphinato)-zinc(II) (**2**), their comparison with those of $[Zn(S_2PEt_2)_2]_2$ [4], $[Zn(S_2PPr^n_2)_2]_2$ [5], $[Cd(S_2PEt_2)_2]_2$ [6–8] and $[Cd(S_2PPh_2)_2]_2$ [9], and the growth of thin films of CdS and ZnS by LP-MOCVD.

* Corresponding author. Present address: Department of Chemistry, and The Manchester Materials Science Centre, Manchester University, Oxford Road, Manchester M13 9PL, UK; e-mail: paul.obrien@man.ac.uk

2. Experimental

2.1. Chemicals

Sodium diisobutyldithiophosphinate (50% solution in water) was obtained from Aldrich Chemical Co. Ltd. Zinc sulfate (99%) and cadmium sulfate (99%) and solvents were obtained from BDH.

2.2. Physical measurements

NMR spectra were recorded using a Bruker AM250 pulsed Fourier transform instrument. Infrared spectra were carried out using a Matteson Polaris FT-IR spectrometer as Nujol mulls; mass spectra were recorded by a micromass Autospec-Q using micromass OPUS software. An electron impact energy of 70 eV at 10^{-7} Torr was used to initiate mass fragmentation. Melting points were measured in sealed tubes with an electrothermal melting point apparatus and are uncorrected. Microanalyses were carried out by the Imperial College London service. X-ray powder diffraction (XRD) analysis was performed using a Siemens D500 automated diffractometer. Samples were mounted flat and scanned from 10 to 60° in steps of 0.04°, with a count time of 2 s. Scanning electron microscopy (SEM) and energy dispersive analytical X-ray analysis (EDAX) was carried out on a JEOL J535CM scanning electron microscope with a LINK QX2000 energy

0277-5387/00/$ - see front matter ©2000 Elsevier Science Ltd All rights reserved.
PII S0277-5387(99)00352-6

dispersive X-ray analysis unit. Thermogravimetric analysis (TGA) was carried out using a Shimadzu TGA-50 at a rate of 10°C min^{-1}.

2.3. Synthesis

2.3.1. $[Cd(S_2P^iBu_2)_2]_2$ (1)

Cadmium diisobutyldithiophosphinate was prepared by the method of Kuchen et al. [10]. In a typical reaction $3CdSO_4 \cdot 8H_2O$ (2.76 g, 11 mmol) in aqueous solution was reacted with sodium diisobutyldithiophosphinate (5 g, 22 mmol) in aqueous solution. The white precipitate formed (5.24 g, 9.9 mmol, 90% yield) was filtered under vacuum, washed with distilled water and recrystallised from acetone to give transparent cubic crystals. Yield 8.24 g (70.7%), m.p. 125°C. (Found: C, 36.3; H, 7.0. Calc.: C, 36.2; H, 6.8%.)

^{1}H NMR ($CDCl_3$, 500 MHz) δ (ppm): 1.13 (d, 24H, $^3J_{H-H}$ = 6.6 Hz, CH_3), 2.17 (dd, 8H, $^3J_{H-H}$ = 6.1 Hz, CH_2), 2.36 (m, 4H, $^3J_{H-H}$ = 6.5 Hz, CH). ^{13}C{^{1}H} NMR ($CDCl_3$, 125 MHz) δ (ppm): 24.72 (d, J_{P-C} = 9.02, CH_3), 25.34 (d, J_{P-C} = 4.31, CH), 48.56 (d, J_{P-C} = 44.65, CH_2). ^{31}P NMR ($CDCl_3$, 202 MHz) δ (ppm): 76.79 (s). IR major bands and tentative assignments: 588 cm^{-1}, ν(Cd–S); 758 cm^{-1}, ν(P=S). Mass spectrum (m/z): M^+ 532 $[Cd(S_2P^iBu_2)_2]_2$, base peak 57 $\{CH_2CH(CH_3)_2\}$, 87 $\{PCH_2CH(CH_3)_2\}$, 177 $\{SP[CH_2CH(CH_3)_2]_2\}$, 209 $\{S_2P[CH_2CH(CH_3)_2]_2\}$, 323 $\{CdS_2P[CH_2CH(CH_3)_2]_2\}$, 419 $\{PS_2CdS_2P[CH_2CH(CH_3)_2]_2\}$.

2.3.2. $[Zn(S_2P^iBu_2)_2]_2$ (2)

This was prepared from sodium diisobutyldithiophosphinate and zinc sulfate by a similar method to that for compound **1**. Solid product crystallised from acetone to give transparent crystals. Yield 7.8 g (73%), m.p. 112°C. (Found: C, 39.6; H, 7.4. Calc.: C, 39.7; H, 7.5%.)

^{1}H NMR ($CDCl_3$, 500 MHz) δ (ppm): 1.13 (d, 24H, $^3J_{H-H}$ = 6.6 Hz, CH_3), 2.08 (dd, 8H, $^3J_{H-H}$ = 6.2 Hz, CH_2), 2.35 (m, 4H, $^3J_{H-H}$ = 6.5 Hz, CH). ^{13}C{^{1}H} NMR ($CDCl_3$, 125 MHz) δ (ppm): 25.04 (d, J_{P-C} = 9.0, CH_3), 25.44 (d, J_{P-C} = 4.5, CH), 48.29 (d, J_{P-C} = 43.0, CH_3). ^{31}P NMR ($CDCl_3$, 202 MHz) δ (ppm): 74.56 (s). IR major bands and tentative assignments: 602 cm^{-1}, ν(Zn–S); 767 cm^{-1}, ν(P=S). Mass spectrum (m/z): M^+ 482 $[Zn(S_2P^iBu_2)_2]_2$, base peak 426 $\{(CH_3)_2CHCH_2PS_2ZnS_2P[CH_2CH(CH_3)_2]_2\}$, 57 $\{CH_2CH(CH_3)_2\}$, 87 $\{PCH_2CH(CH_3)_2\}$, 177 $\{SP[CH_2CH(CH_3)_2]_2\}$, 209 $\{S_2P[CH_2CH(CH_3)_2]_2\}$, 273 $\{ZnS_2P[CH_2CH(CH_3)_2]_2\}$, 368 $\{PS_2ZnS_2P[CH_2CH(CH_3)_2]_2\}$.

2.4. Growth of CdS or ZnS

CdS and ZnS films were deposited from $[Cd(S_2P^iBu_2)_2]_2$ and $[Zn(S_2P^iBu_2)_2]_2$, respectively, using a home-made cold-wall low-pressure reactor (10^{-2} Torr), described in detail elsewhere [11]. Glass substrates were used and these were heated by the action of a quartz halogen lamp on a graphite susceptor. The $[Cd(S_2P^iBu_2)_2]_2$ precursor was held in a tube furnace [12] heated at temperatures between 400 and 450°C.

2.5. X-ray crystallography

2.5.1. Crystal data for compound 1

$C_{32}H_{72}P_4S_8Cd_2$, M = 1062.1, monoclinic, space group $P2_1/c$ (no. 14), a = 11.140(2), b = 12.070(2), c = 18.836(3) Å, β = 92.54(1)°, V = 2530.1(7) Å^3, Z = 2 (the molecule has crystallographic C_i symmetry), D_c = 1.394 g cm^{-3}, μ(Mo Kα) = 13.2 cm^{-1}, $F(000)$ = 1096, T = 293 K; clear prisms, 0.50 × 0.33 × 0.20 mm, Siemens P4/PC diffractometer, ω-scans, 4467 independent reflections. The structure was solved by direct methods; the non-hydrogen atoms were refined anisotropically using full-matrix least-squares based on F^2 to give R_1 = 0.051, wR_2 = 0.113 for 2990 independent observed absorption corrected reflections [$|F_o| > 4\sigma(|F_o|)$, $2\theta \leq 50°$] and 208 parameters [13].

2.5.2. Crystal data for compound 2

$C_{32}H_{72}P_4S_8Zn_2$, M = 968.0, orthorhombic, space group $Fdd2$ (no. 43), a = 48.602(2), b = 11.665(1), c = 18.000(1) Å, V = 10205(1) Å^3, Z = 8 (the molecule has crystallographic C_2 symmetry), D_c = 1.260 g cm^{-3}, μ(Cu Kα) = 55.5 cm^{-1}, $F(000)$ = 4096, T = 293 K; clear platy prisms, 0.37 × 0.33 × 0.13 mm, Siemens P4/PC diffractometer, ω-scans, 2167 independent reflections. The structure was solved by direct methods; the major occupancy non-hydrogen atoms were refined anisotropically using full-matrix least-squares based on F^2 to give R_1 = 0.057, wR_2 = 0.155 for 1718 independent observed reflections [$|F_o| > 4\sigma(|F_o|)$, $2\theta \leq 127°$] and 221 parameters. The polarity of the structure was unambiguously determined by a combination of R-factor tests [R_1^+ = 0.0571, R_1^- = 0.0580] and by use of the Flack parameter [$x^+ = -0.03(19)$, $x^- = +1.03(19)$] [13].

3. Results and discussion

Compounds **1** and **2** were both prepared by the reaction of sodium diisobutyldithiophosphinate with cadmium or zinc sulfate. Both are soluble in most organic solvents and can be recrystallised from acetone at room temperature to give transparent crystals. Compounds **1** and **2** gave satisfactory elemental analysis and were further characterised by NMR (^{1}H, ^{13}C, ^{31}P), IR, TGA and X-ray methods. Both compounds are stable at room temperature for a period of months.

3.1. X-ray structures

The cadmium complex (**1**) has a classic C_i symmetric two-step ladder (or 'chair') structure (Fig. 1) of type 23 for the central eight-membered $Cd_2S_4P_2$ ring [2]. This geometry contrasts with the C_2 symmetric 'boat' conformation observed for the closely related isopropoxide ligand $Cd_2[(i$-

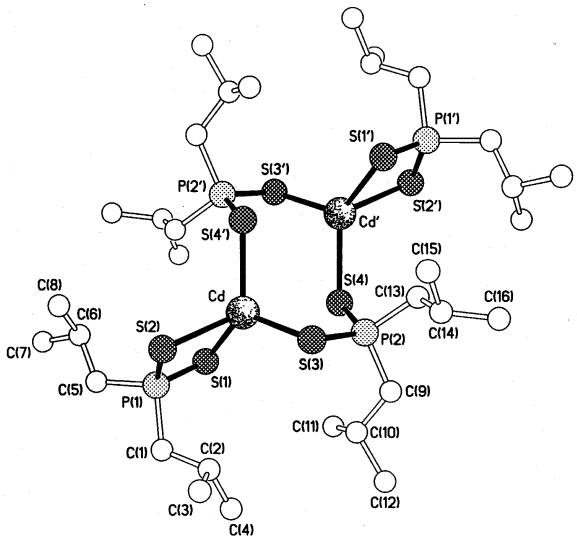


Fig. 1. The molecular structure of the C_i symmetric complex (**1**), showing its 'chair' conformation.

$C_3H_7O)_2PS_2]_4$ (**1***) [14]. The pattern of bonding within the eight-membered ring is similar, however, with both the Cd–S and P–S bonds in compound **1** being, in all but one instance, longer then their counterparts in the isopropoxide analogue **1*** (Table 1). The four-membered chelate ring has a slightly folded geometry (ca. 9° about the S···S vector) with both Cd–S and P–S bonds that are distinctly asymmetric, an asymmetry that was observed for the Cd–S bonds in **1*** but not for the P–S bonds. The geometry at cadmium is severely distorted tetrahedral, with angles ranging between 78.82(6) and 128.63(7)°, the acute angle being associated with the bite of the chelating ligand (Table 2). Indeed, the coordination geometry could almost be considered as distorted trigonal pyramidal, with S(1), S(3) and S(4′) forming the basal plane and S(2) in the apical position. The cadmium atom lies only 0.20 Å out of this basal plane, whereas it lies between 0.95 and 1.08 Å out of the planes of the other three faces. A similar distortion of the coordination geometry is present in compound **1***, where the cadmium lies 0.41 Å out of the basal plane of the trigonal pyramid [14]. Distortions from tetrahedral geometry at the phosphorus centres are relatively small. The packing of the molecules is largely dominated by the hydrophobic isobutyl groups, and there are no short intermolecular S···S contacts.

Table 1
Comparative selected bond lengths (Å) for complexes **1**, $Cd_2[(i\text{-}C_3H_7O)_2PS_2]_4$ (**1***), **2** and $Zn_2[(i\text{-}C_3H_7O)_2PS_2]_4$ (**2***)

	1 [M = Cd]	**1***	**2** [M = Zn]	**2***
M–S(1)	2.544(2)	2.552(7)	2.358(3)	2.351(5)
M–S(2)	2.654(2)	2.590(8)	2.451(4)	2.409(5)
M–S(3)	2.534(2)	2.486(7)	2.309(3)	2.306(5)
M–S(4')	2.545(2)	2.499(7)	2.325(3)	2.302(6)
M···S(4)	3.112(2)	3.194(8)	3.399(4)	3.347(6)
P(1)–S(1)	2.025(3)	1.974(12)	2.002(5)	1.984(7)
P(1)–S(2)	2.002(3)	1.972(12)	2.005(4)	1.968(7)
P(2)–S(3)	2.002(2)	1.957(11)	1.991(5)	1.957(7)
P(2)–S(4)	2.026(3)	1.962(9)	2.020(4)	1.971(7)

X-ray analysis of the zinc complex (**2**) shows that it adopts a geometry for the $Zn_2S_8P_4$ core that is virtually identical to that seen in the cadmium and zinc complexes with *O*,*O*-diisopropylphosphordithioate (compounds **1*** and **2***, respectively) (Fig. 2) [14]. Indeed, a best fit of the 14 heteroatoms of the two zinc structures has a root mean square deviation of only 0.078 Å, with a maximum deviation of 0.096 Å for P(2)/P(2′). The four-membered chelate ring, as in the cadmium structure (**1**), has a slightly folded geometry (ca. 10° about the S···S vector) and also has noticeably asymmetric Zn–S distances; the differences in the P–S bond lengths are not statistically significant (Table 1). A consequence of the change from the 'chair' conformation for the

Table 2
Selected bond angles (°) for complexes **1** and **2**

	1 [M = Cd]	**2** [M = Zn]
S(1)–M–S(2)	78.82(6)	85.76(12)
S(1)–M–S(3)	127.00(8)	118.1(2)
S(1)–M–S(4′)	128.63(7)	112.37(14)
S(2)–M–S(3)	99.90(8)	106.15(14)
S(2)–M–S(4′)	108.31(7)	110.13(14)
S(3)–M–S(4′)	102.44(8)	118.71(12)
S(1)–P(1)–S(2)	110.11(12)	109.6(2)
S(1)–P(1)–C(1)	109.3(4)	111.2(6)
S(2)–P(1)–C(1)	112.1(4)	114.5(6)
S(1)–P(1)–C(5)	111.4(3)	107.1(7)
S(2)–P(1)–C(5)	113.2(3)	113.4(7)
C(1)–P(1)–C(5)	100.2(4)	100.5(9)
S(3)–P(2)–S(4)	113.01(12)	116.7(2)
S(3)–P(2)–C(9)	109.9(3)	108.1(6)
S(3)–P(2)–C(13)	111.3(3)	103.0(6)
S(4)–P(2)–C(9)	109.1(4)	109.4(5)
S(4)–P(2)–C(13)	109.3(3)	106.1(7)
C(9)–P(2)–C(13)	103.8(4)	113.5(9)

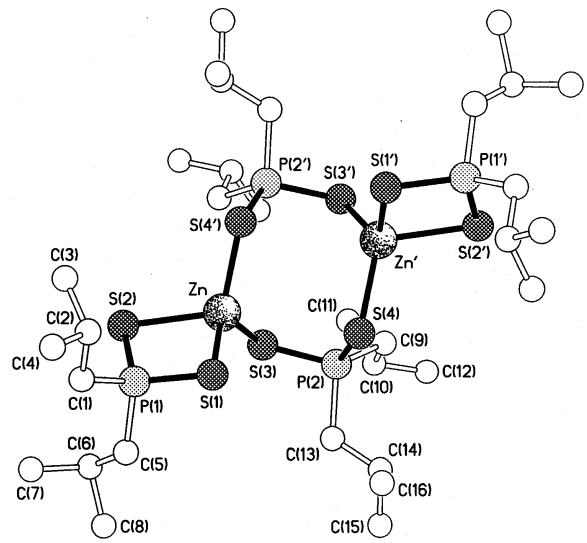


Fig. 2. The molecular structure of the C_2 symmetric complex (**2**), showing its 'boat' conformation.

eight-membered metallocyclic ring in the cadmium complex (**1**) to the 'boat' conformation seen here is a marked difference in the transannular M···S distances which are shorter in the cadmium 'chair' conformer [3.112(2) Å] than in the zinc 'boat' conformer [3.399(4) Å]. There are similar, but not quite so pronounced, distortions in the tetrahedral geometry at the metal centre (Table 2), with the zinc atom lying only 0.45 Å out of the S(1), S(3), S(4′) basal plane. There are no short intermolecular contacts of note.

It has previously been postulated that a probable reason for a change from a C_i symmetric chair to a C_2 symmetric boat conformation for the central eight-membered metallocyclic ring for phosphordithioates/dithiocarbamates is a consequence of the packing requirements of the differently sized R groups. Both the cadmium [15,16] and zinc [17] diethyldithiocarbamate species have a C_i symmetric chair conformation, whereas the corresponding cadmium and zinc diisopropylphosphordithioate complexes (**1*** and **2***, respectively) both have the C_2 symmetric 'boat' conformation (see above). In the present study we see the cadmium (**1**) and zinc (**2**) diisobutylphosphordithioate complexes exhibiting C_i chair and C_2 boat conformations, respectively. We therefore consider that both conformations are likely to occur for both species, and that consequently different polymorphs may be accessible under alternative crystallisation conditions.

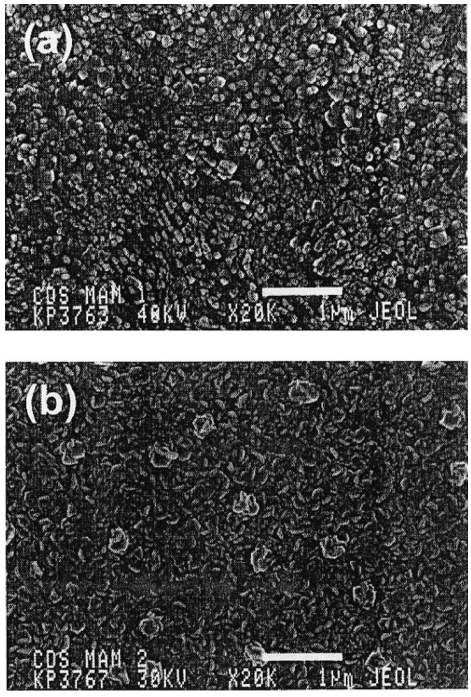


Fig. 3. SEM of CdS thin films grown on glass at substrate temperatures of 400°C (a) and 450°C (b).

Table 3
X-ray powder diffraction data for the CdS (hexagonal) thin film grown on glass at 450°C substrate temperature

hkl	*d*-spacing (Å) (Int: %)	JCPDS [a] (Int: %)
100	3.585(78)	3.58(75)
002	3.365(71)	3.36(59)
101	3.152(100)	3.16(100)
100	2.069(32)	2.06(57)
220	1.759(28)	1.79(17)

[a] JCPDS = joint committee on powder diffraction spectra.

3.2. Growth work

CdS thin films were grown onto glass substrates using bis(diisobutyldithiophosphinato)cadmium(II) under different conditions. Good-quality films were grown at a substrate temperature of 400–450°C (Fig. 3). The films grown at higher temperature gave slightly larger crystallites (Fig. 3b). The EDAX pattern gave peaks for cadmium and sulfur that indicated a slight excess of cadmium (0.97:1.00). SEM showed that the films are crystalline with an average crystallite size of 0.1 μm. The XRD pattern showed the films to be hexagonal (Table 3 and Fig. 4). The films grown at lower temperature during the same period of time were very thin and difficult to characterise by XRD. TGA showed that both complexes start subliming at ca. 273°C and decompose at ca. 375°C (Fig. 5). No growth occurred below 250°C precursor temperature. Bis(diisobutyldithiophosphinato)cadmium(II) appears to be less volatile than the corresponding dithiocarbamates [18–22] and hence the growth rate is lower.

Only very thin films of ZnS were grown using bis(diisobutylthiophosphinato)zinc(II), even at higher growth tem-

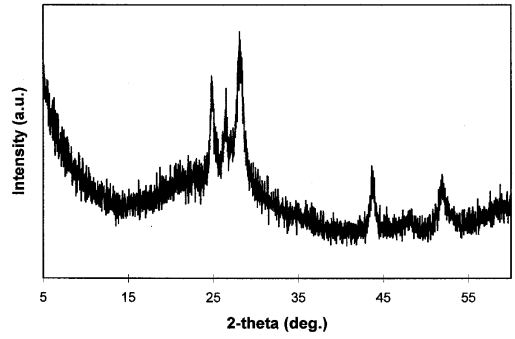


Fig. 4. XRD pattern of CdS grown from $Cd[S_2P^iBu_2]_2$ on glass substrate at 450°C.

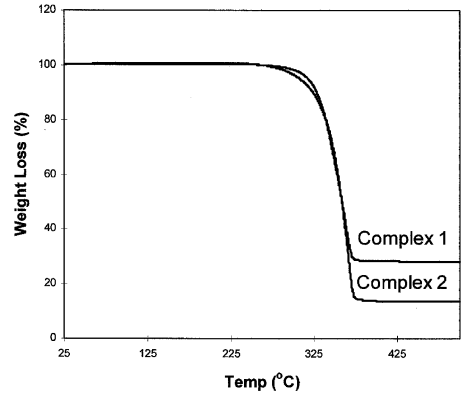


Fig. 5. TGA curves of complexes $Cd[S_2P^iBu_2]_2$ (**1**) and $Zn[S_2P^iBu_2]_2$ (**2**).

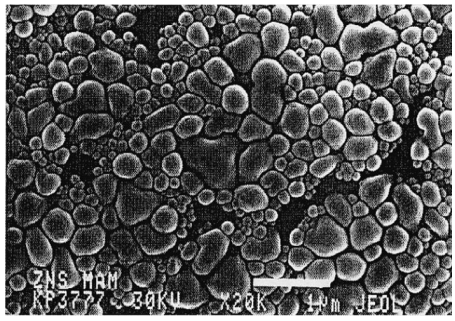


Fig. 6. SEM of ZnS thin films grown on glass at 450°C.

perature. The XRD pattern showed a broad hump, indicating the amorphous nature of the films. SEM (Fig. 6) also confirmed that the films are powdery and the EDAX pattern showed that the Zn:S ratios are close to 1:1. Dithio derivatives of zinc precursors give thin powdery films at ca. 450°C [18]. In general, zinc dithiocarbamato or dithiophosphinato derivatives are not good precursors for the growth of ZnS by LP-MOCVD, but may be useful as precursors for the growth of TOPO (trioctylphosphine oxide)-capped nanoparticles of ZnS [23].

4. Conclusions

Two new compounds, bis(diisobutyldithiophosphinato)-cadmium(II) (**1**) and bis(diisobutyldithiophosphinato)-zinc(II) (**2**), have been synthesised and characterised by NMR (^{1}H, ^{13}C, ^{31}P), IR, TGA and X-ray single crystal methods. The structures of both compounds are based on dimers with eight-membered metallocyclic rings, $M_2S_4P_2$, formed by chelating and bridging of dithiophosphinate ligands. The cadmium complex has a 'chair' conformation whereas the zinc complex has a 'boat' conformation.

The two complexes have been used as precursors to grow thin films of CdS and ZnS, respectively, onto glass substrates by LP-MOCVD. The cadmium complex gave crystalline hexagonal CdS films whereas the zinc complex gave only amorphous films. The films grown were characterised by XRD, EDAX and SEM. Dithiophosphinate of cadmium and zinc proved to be less volatile than the corresponding dithiocarbamates; hence, the growth rate was lower. However, these complexes can be useful precursors for the growth of nanocrystals of ZnS or CdS by thermolysis in tricotylphosphineoxide (TOPO), where volatility of the precursors is not a requirement.

Supplementary data

Supplementary data for the Crystallography are available from the Cambridge Crystallographic Data Centre, 12 Union Road, Cambridge, CB2 1EZ, UK; fax: +44-1223-336033; e-mail: deposit@ccdc.cam.ac.uk or www:http://www.ccdc.cam.ac.uk (deposition numbers CCDC 133287 and 133288).

Acknowledgements

C.B. thanks STS/Sumitomo for a case award and the EPSCRC for a grant. P.O.B. is the Sumitomo/STS Professor of Materials Chemistry. We would like to thank J.H. Park for the XRD measurements and assistance with growth work, K. Pell (Queen Mary and Westfield College) for the EDAX and SEM measurements, S. Boyer (University of North London) for the CHN analyses and Dr M. Odlyha (Birkbeck) for the TGA work.

References

[1] W. Rickelton, R. Boyle, Solvent Extr. Ion Exch. 8 (1990) 783.
[2] I. Haiduc, D. Bryan-Sowerby, Lu Shao-Fang, Polyhedron 14 (1995) 3389.
[3] Y. Takahashi, R. Yuki, M. Sugiura, S. Motojima, K. Sugiyama, J. Cryst. Growth 50 (1980) 491.
[4] M. Calligaris, G. Nardin, A. Ripamonti, J. Chem. Soc., Sect. A (1970) 714.
[5] H. Wunderlich, Acta Crystallogr., Sect. B 38 (1982) 614.
[6] H. Wunderlich, Z. Kristallogr. 159 (1982) 136.
[7] H. Wunderlich, Acta Crystallogr., Sect. C 42 (1986) 631.
[8] G. Svensson, J. Albertsson, Acta Chem. Scand. 45 (1991) 820.
[9] J.S. Casas, M.S. Garcia-Tasende, A. Sanchez, J. Sordo, E.M. Vazquez-Lopez, E.E. Castellano, J. Zukermann-Schepctor, Inorg. Chim. Acta 219 (1994) 115.
[10] W. Kuchen, J. Metten, A. Judat, Chem. Ber. 97 (1964) 2306.
[11] M.A. Malik, P. O'Brien, Adv. Mater. Opt. Electron. 3 (1994) 171.
[12] E.A. Jeffry, T. Mole, Aust. J. Chem. 21 (1968) 1187.
[13] SHELXTL PC version 5.03, Siemens Analytical X-Ray Instruments, Inc., Madison, WI, 1994.
[14] S.L. Lawton, G.T. Kokotailo, Inorg. Chem. 8 (1969) 2410.
[15] E.A. Shugam, V.M. Agre, Kristallografiya 13 (1968) 253.
[16] E.A. Shugam, V.M. Agre, Sov. Phys. Crystallogr. 13 (1968) 197.
[17] M. Bonamico, G. Mazzone, A. Vaciago, L. Zambonelli, Acta Crystallogr. 19 (1965) 898.
[18] D.M. Frigo, O.F.Z. Khan, P. O'Brien, J. Cryst. Growth 96 (1989) 989.
[19] M.A. Malik, M. Motevalli, T. Saeed, P. O'Brien, Adv. Mater. 5 (9) (1993) 653.
[20] M. Chunggaze, J. McAleese, P. O'Brien, D.J. Otway, Chem. Commun. (1998) 833.
[21] P. O'Brien, D.J. Otway, J.R. Walsh, Adv. Mater. 3 (1997) 227.
[22] M. Chunggaze, M.A. Malik, P. O'Brien, J. Mater. Chem. 9 (1999) 2433.
[23] N. Revaprasadu, M.A. Malik, G. Wakefield, P. O'Brien, J. Mater. Res. 14 (1999) 3237.

PERGAMON

www.elsevier.nl/locate/poly

Polyhedron 19 (2000) 217–223

POLYHEDRON

New tetraazamacrocyclic ligand with neutral pendent groups 1,4,7,10-tetrakis(2-cyanoethyl)-1,4,7,10-tetraazacyclododecane (L) and its cobalt(II), nickel(II) and copper(II) complexes: synthesis, structural characterization and antitumor activity

De-Yuan Kong* [1,a], Lin-Hua Meng [b], Jian Ding [b], Yu-Yuan Xie* [2,b], Xiao-Ying Huang [c]

[a] *Department of Chemistry, Texas A&M University, College Station, TX 77842-3012, USA*

[b] *Shanghai Institute of Materia Medica, Chinese Academy of Sciences, Taiyuan Road 294, Shanghai 200031, PR China*

[c] *Fujian Institute of Research on the Structure of Matter, Chinese Academy of Sciences, Fuzhou 350002, PR China*

Received 3 September 1999; accepted 22 November 1999

Abstract

A new tetraazamacrocyclic ligand (L) with four neutral 2-cyanoethyl pendent groups, and its divalent transition-metal complexes $[Co(L)(NO_3)]NO_3 \cdot H_2O$ (**1**), $[Ni(L)(NO_3)]NO_3 \cdot 3H_2O$ (**2**) and $[Cu(L)(H_2O)](NO_3)_2$ (**3**) have been synthesized. The crystal structures of **1** and **3** have been determined by X-ray analysis. In complex **1** the cobalt atom is coordinated by four nitrogen atoms and two oxygen atoms of a nitrate anion, which define a distorted octahedron. The other nitrate ion lies in the lattice as a counter ion. Complex **3** is five-coordinated by four nitrogen atoms and an axial aqua ligand, which form a tetragonal pyramid. In complex **3** the two nitrate anions exist as counter ions. Pharmaceutical tests showed that all three metal complexes exhibit antitumor activity against HL-60 and BEL-7404 tumor cell lines in vitro, even at a concentration of 10^{-8} mol l^{-1}. Complex **1** can partially cleave supercoiled pBR 322 DNA to form nicked DNA in aerobic solution, and complex **3** can convert double strand DNA into nicked DNA completely in the presence of MPA. Complex **3** causes perturbation to K562 tumor cell lines in the G_1 phase. ©2000 Elsevier Science Ltd All rights reserved.

Keywords: Transition metals; Synthesis; Structural characterization; Antitumor activity

1. Introduction

Successful applications of several 1,4,7,10-tetraazacyclododecane (cyclen) stem mainly from their use as models for protein–metal binding sites in biological systems [1–4], and as selective complexants of metallic ions [5–8], i.e. therapeutic reagents for the treatment of metal intoxication [9,10]. Recently, interest has focussed on the synthesis of macrocyclic complexes with potential medicinal applications, as contrast-enhancing agents in magnetic resonance imaging (MRI) [11,12], as NMR shift and relaxation reagents [13,14], and in RNA cleavage catalysis [15,16]. The effective anti-solid tumor drug *cis*-platinum has been found to form a covalent 1,2-intrastrand adduct at N^7 of the guanine base of DNA [17,18]. Screening new metal complexes with antitumor activity is among our research interests. It has been reported that macrocyclic complexes with a tetraazamacrocyclic ligand, such as cyclen, cyclam and bicyclam, exhibit antitumor or anti-HIV virus activity [19–23]. These potential and versatile applications are stimulating researchers to exploit new cyclen-based ligands and complexes with potential chemical, biological and catalytic properties.

In this paper we report the synthesis of a new cyclen-based ligand, with four neutral pendent groups at N sites, and its metal complexes. X-ray diffraction was used to determine the structure of $[Co(L)(NO_3)]NO_3 \cdot H_2O$ (**1**) and $[Cu(L)(H_2O)](NO_3)_2$ (**3**). Complexes **1**, **2** and **3** show antitumor activity against HL-60 and BEL-7404 tumor cell lines in vitro with MTT and SRB assays. Having found that these three complexes exhibited antitumor activity, we wanted to determine possible mechanisms for this behavior. In a study of the cell cycle, complex **3** was found to perturb the G_1 phase. In preliminary tests, complex **3** showed effective direct interaction on double strand DNA in the presence of a reductant. This result provided a rationale for the antitumor activity of these metal complexes in relation to DNA.

[1] *Corresponding author. Tel.: +1-409-845-2232; fax: +1-409-845-4719; e-mail: kong@mail.chem.tamu.edu

[2] *Corresponding author.

0277-5387/00/$ - see front matter ©2000 Elsevier Science Ltd All rights reserved.
PII S0277-5387(99)00369-1

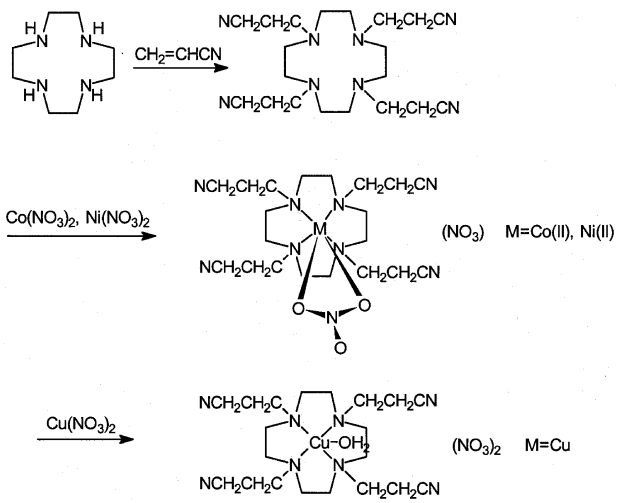
2. Results and discussion

2.1. Synthesis of ligand and complexes

The starting macrocyclic parent cyclen was synthesized according to the method reported by Atkins [24] and Bünzli [25] with improved yield by detosylation in 48% HBr–acetic acid. Although Weisman reported a new and simple synthetic route for cyclen, the initial material is not easily obtainable [26]. The new ligand L was synthesized conveniently via Michael addition according to Scheme 1.

N-alkylation with alkylating reagents, such as alkyl or aryl halide as nucleophile attacking reagents, are common in the synthesis of DOTA and TETA [27–29]. In our synthesis of a similar macrocyclic ligand, 1,4,7,10-tetrakisbenzyl-1,4,7,10-tetraazacyclododecane, benzyl chloride was used as the alkylating reagent. Even in the presence of a transphase catalyst, triethylbenzylammonium chloride, the yield was still not higher than 54% [30]. Accordingly, four neutral pendent cyanoethyl groups were easily introduced into the parent tetraazamacrocycle in high yield (86%) using Michael addition reaction with acrylonitrile as the alkylating reagent, which can make full use of the initial material cyclen. An excessive amount of acrylonitrile was used to produce tetrakisalkylated L to suppress the formation of mono-, di- or tri-substituted products, and L was further purified by recrystallization from $CHCl_3$–EtOH as white needles. This is a versatile route for the synthesis of similar neutral functionalized tetraazamacrocyclic ligands.

The new ligand was treated with 1 equiv. of divalent transitional metal ions in different solvents to produce 1:1 complexes. The results of elemental analysis (C, H, N) indicated stoichiometric formulas $[M(L)(NO_3)]NO_3 \cdot H_2O$ (M = Co, $n = 1$; M = Ni, $n = 3$) and $[M(L)(H_2O)](NO_3)_2$ (M = Cu, $n = 1$). Whether the nitrate ions coordinate with central metal ions can be revealed by the IR spectrum. The IR spectra of the nitrato complexes contain bands of both coordinated and ionic nitrates in complexes **1** and **2**. The bands around 1460 and 1320 cm^{-1} are due to ν(N=O) (ν_1) and $\nu_{asym}(NO_2)$ (ν_5), respectively, of the coordinated nitrate. The $\nu_{sym}(NO_2)$ vibration (ν_2) at 1030 cm^{-1} is characteristic of a bidentate chelating nitrate. The separation ($\Delta\nu$) of the nitrate stretching fundamentals ($\nu_1 - \nu_5$) has been used as a criterion to distinguish between mono- and bidentate chelating nitrates, increasing as the coordination changes from mono- to bidentate or bridging, The magnitude of this separation ($\Delta\nu = 153$ and $\Delta\nu = 132$ for Co and Ni complexes, respectively) is indicative of bidentate coordination of the nitrate ion [31]. The strong and sharp band around 1384 cm^{-1} is characteristic of ionic nitrate [32]. In complex **3**, only the characteristic band of ionic nitrate was observed at 1385 cm^{-1}. In all three complexes the broad and medium intensity band at ca. 3425 cm^{-1} is due to the symmetric and anti symmetric O–H stretching vibrations of lattice water. From the aforementioned IR data it can be concluded that there are two kinds of nitrate ion in complexes **1** and **2**, whereas only ionic nitrate ions exist in complex **3**. The X-ray diffraction results of Co (**1**) and Cu (**3**) substantiate this conclusion.



Scheme 1. Synthetic route for L and complexes **1**, **2** and **3**.

Molar conductance measurements were carried out in freshly prepared DMSO solution at 25°C and 10^{-3} mol l^{-1}. The values for these complexes are 96(1), 84(2) and 57(3) scm^{-1} mol^{-1}, respectively, all suggesting 1:1 electrolytes in the measuring solution [33].

2.2. Structure of complexes *1* and *3*

The crystal structures of complexes **1** and **3** were determined by X-ray diffraction, which supported the existence of ion pairs in these two complexes. An ORTEP drawing of the $[Co(L)(NO_3)]^+$ ion in complex **1** is shown in Fig. 1. The central Co atom coordinates with N(1), N(2), N(3), N(4),

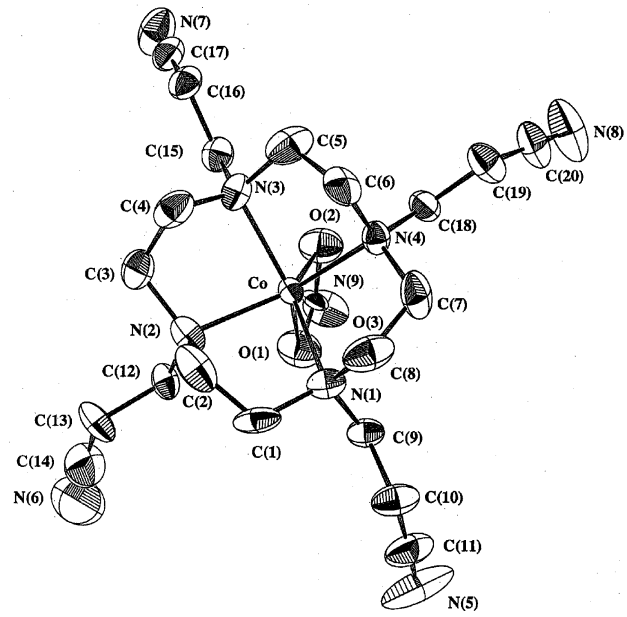


Fig. 1. Perspective view of the $[Co(L)(NO_3)]^+$ cation in **1** showing the atom labeling scheme. Thermal ellipsoids are drawn at 50% probability level. The hydrogen atoms are omitted for clarity.

O(1) and O(2) which define a distorted octahedral geometry. The teraazamacrocyclic ligand serves as a tetradentate ligand and the four pendent groups are not coordinated with the central metal atom. Two oxygen atoms of the nitrate ion coordinate to the cobalt atom bidentately. The equatorial basal nitrogen atoms (N(1), N(2), N(3) and N(4)) lie in one plane with mean deviation 0.0222 Å. The cobalt atom is displaced from this plane by −0.8411 Å. The Co, O(1), O(2), O(3) and N(9) atoms are coplanar with mean deviation 0.0039 Å. The dihedral angle between these two least-squares planes is 90.26°. Selected bond distances and angles are shown in Table 1.

In the cation $[Cu(L)(H_2O)]^{2+}$, complex **3**, the Cu atom coordinates to four nitrogen atoms of L and an aqua ligand, which define a tetragonal pyramid (Fig. 2). The nitrogen atoms are coplanar with mean deviation 0.0053 Å, and Cu deviates from this plane by 0.492 Å. Selected bond lengths and angles are shown in Table 1. Comparing the structure of both complexes, one nitrate ion lies in the coordination sphere of the Co atom in **1** as a bidendate ligand, but neither nitrate ion is bound to the Cu atom in **3**. The reason may be attributed to the fact that the ionic radius of Co is larger than that of Cu, which makes the Co coordination sphere less saturated and more accessible to an additional ligand. Thus Co tends to form a six-coordinated complex, whereas Cu easily forms a four or five-coordinated complex.

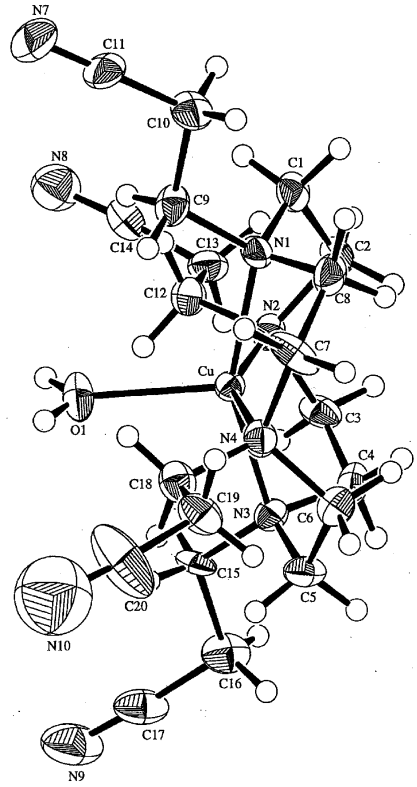


Fig. 2. Perspective view of the $[Cu(L)(H_2O)]^{2+}$ ion in **3** showing the atom labeling scheme. Thermal ellipsoids are drawn at 50% probability level. The hydrogen atoms are omitted for clarity.

3. Pharmaceutical results and discussion

3.1. Antitumor activity in vitro

All three complexes exhibited promising antitumor activity in vitro, especially against the BEL-7404 cell line. Even when the concentration of complexes was diluted to 10^{-8} mol l^{-1}, the antitumor activity could still be observed. Complexes **2** and **3** showed higher than 10% antitumor activity. The percentages of growth inhibition against HL-60 and BEL-7404 tumor cell lines are listed in Table 2. All complexes are effective at a concentration of 10^{-4} mol l^{-1} against HL-60 tumor cell lines. However, the antitumor activity decreased quickly to zero after the concentration of complexes was diluted to 10^{-6} mol l^{-1}.

Table 1
Selected bond lengths (Å) and angles (°) for Co (**1**) and Cu (**3**)

Co–O(1)	2.310(7)	Co–N(2)	2.187(7)
Co–O(2)	2.256(7)	Co–N(3)	2.201(7)
Co–N(1)	2.214(7)	Co–N(4)	2.156(7)
O(1)–Co–N(4)	126.2(3)	O(1)–Co–N(2)	94.8(3)
O(1)–Co–N(3)	132.4(3)	O(1)–Co–N(1)	91.2(3)
O(1)–Co–O(2)	56.5(3)	N(4)–Co–N(2)	135.7(3)
N(4)–Co–N(3)	81.6(3)	N(4)–Co–N(1)	82.4(3)
N(2)–Co–N(3)	81.1(3)	N(4)–Co–O(2)	92.7(2)
N(2)–Co–N(1)	80.9(3)	N(2)–Co–O(2)	127.2(3)
N(3)–Co–N(1)	133.9(3)	N(3)–Co–O(2)	88.5(3)
N(1)–Co–O(2)	135.2(3)		
Cu–O(1)	2.154(8)	Cu–N(1)	2.05(1)
Cu–N(2)	2.05(1)	Cu–N(3)	2.04(1)
Cu–N(4)	2.08(1)		
O(1)–Cu–N(1)	105.1(4)	O(1)–Cu–N(2)	105.3(4)
O(1)–Cu–N(3)	102.4(4)	O(1)–Cu–N(4)	102.6(4)
N(1)–Cu–N(2)	86.6(4)	N(1)–Cu–N(3)	152.4(3)
N(1)–Cu–N(4)	86.9(4)	N(2)–Cu–N(3)	85.9(4)
N(2)–Cu–N(4)	152.1(4)	N(3)–Cu–N(4)	87.4(4)

3.2. Perturbation of K562 tumor cell cycle progression

The changes in cell cycle after exposing K562 tumor cell lines to two concentrations (10 and 50 μmol l^{-1}) for 24 h are shown in Fig. 3.

From Fig. 3, complex **3** caused a significant increase in the proportion of cells in the G_1 phase, from 26.57 to 40.45%. Accompanied by a decrease in the S phase, from 54.38 to 46.91%, a slight change was observed in the G_2–M phase at the same time, from 19.05 to 10.65 to 12.64%.

The results show that complex **3** regulated an important cell cycle-related mechanism: the progression of proliferating cells through the G_1 phase. This indicates that cells continue to undergo mitosis but cannot get past the G_1 phase into the S phase and fail to trigger DNA synthesis. Nevertheless, this possible explanation needs to be verified by further experiments.

Table 2
The percentage of growth inhibition data

Complex	Cell line						
	HL-60		BEL-7404				
	10^{-4}	10^{-5}	10^{-4}	10^{-5}	10^{-6}	10^{-7}	10^{-8}
$[Co(L)(NO_3)]NO_3 \cdot H_2O$	94.7	86.0	100	97.8	31.9	5.5	4.4
$[Ni(L)(NO_3)]NO_3 \cdot 3H_2O$	93.0	57.0	96.7	95.6	19.8	7.7	14.3
$[Cu(L)H_2O](NO_3)_2$	42.1	0	63.3	15.6	78.0	5.6	10.0

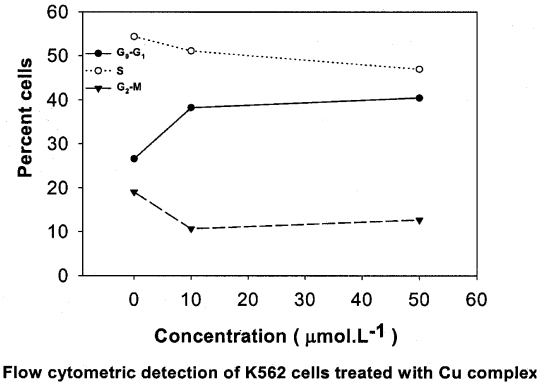


Fig. 3. The perturbation of the cell cycle by complex **3**.

3.3. Measurements of the interaction with pBR 322 DNA

In light of some reports [34–36] that these kinds of complexes can catalyze the hydrolysis of diphosphoresters under physiological conditions, which would effectively cleave DNA, we planned to investigate whether these complexes have direct interactions with DNA, so we treated them with supercoiled DNA. Fig. 4 shows the preliminary electrophoresis result of the interaction of Co complex **1** with pBR 322 DNA. Line 1 is the control group with DNA alone, and lines 2–4 are the measuring groups with concentration varying from 10^{-4} to 10^{-6} mol l^{-1}. From line 2 and line 4 it can be observed that the amount of nicked DNA increased, but supercoiled DNA still existed. The Co complex can only partially cleave double helix DNA to form nicked DNA. At a concentration of 10^{-5} mol l^{-1} the complex has no interaction with DNA.

Interestingly, we found that the Cu complex **3** can cleave supercoiled DNA to nicked and linear DNA at the same time. From Fig. 5 it can be observed that the circular supercoiled DNA is converted to nicked DNA via single-strand cleavage (lanes 2–4). With the increase in complex concentration, the supercoiled DNA decreased and was finally completely converted to nicked and linear DNA. In order to deduce the possible mechanism of this cleavage, we repeated the experiment in the presence of MPA (2-mercaptopropionic acid) as a reducing agent. Under this experimental condition, no linear DNA was formed as no apparent change was observed in lines 3–7 in Fig. 6. However, in line 6 the supercoiled DNA almost completely converted to nicked DNA. This result is similar to that found for the Cu–salen complex as chemical

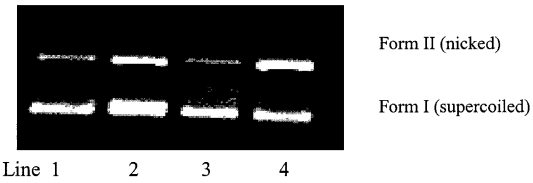


Fig. 4. Effect of Co (**1**) on supercoiled pBR 322 DNA after incubation for 2 h at 37°C. Line 1: control, DNA alone. Line 2: 100 μmol l^{-1} Co (**1**) + DNA. Line 3: 10 μmol l^{-1} Co (**1**) + DNA. Line 4: 1 μmol l^{-1} Co (**1**) + DNA. Forms I and II refer to the supercoiled double helix DNA and nicked DNA, respectively.

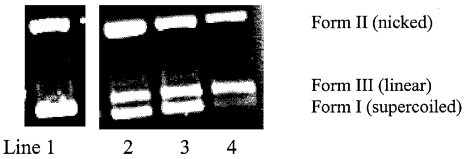


Fig. 5. Cleavage of pBR 322 DNA to nicked and linear DNA with Cu (**3**). Line 1: DNA alone. Line 2: 10 μmol l^{-1} Cu (**3**) + DNA. Line 3: 50 μmol l^{-1} Cu (**3**) + DNA. Line 4: 100 μmol l^{-1} Cu (**3**) + DNA.

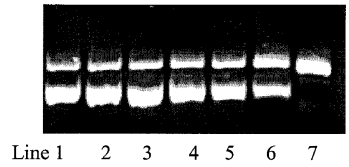


Fig. 6. Effect of Cu (**3**) on supercoiled pBR 322 DNA in the presence of MPA. Line 1: DNA alone. Line 2: MPA + DNA. Line 3: 10 μmol l^{-1} Cu (**3**) + DNA + MPA. Line 4: 20 μmol l^{-1} Cu (**3**) + DNA + MPA. Line 5: 40 μmol l^{-1} Cu (**3**) + DNA + MPA. Line 6: 100 μmol l^{-1} Cu (**3**) + DNA + MPA. Line 7: 500 μmol l^{-1} Cu (**3**) + DNA + MPA.

nuclease reported by Bailly and co-workers [37,38], who suggested that the reactive species in this cleavage were oxygen-based radicals. As pointed out by Sigman et al. [39], the four-coordinated Cu complex were more favorable for cleavage than the six-coordinated Co(II) complex, owing to its facilitative conformation. In many cases Cu(I) was the major active species. In our case, the experimental conditions are different, which means two different cleaving mechanisms may co-exist. Further work is in progress to elucidate the detailed mechanism of antitumor activity of these complexes.

4. Experimental

All reactions were carried out under nitrogen, using solvents which were distilled before use. Cyclen was synthesized

according to the literature. The synthetic route of L is shown in Scheme 1.

NMR spectra were obtained on a Varian GEMINI-300 instrument. IR spectra were recorded in the range 4000–400 cm^{-1} on a Perkin–Elmer 599B spectrometer, as KBr disk. Mass spectra were recorded on a Varian MAT-711 instrument. Microanalyses (C, H, and N) were performed with a Vario EL elemental analyzer.

4.1. Synthesis of ligand

4.1.1. Preparation of 1,4,7,10-tetraazacyclododecane

1,4,7,10-teraazacyclododecane was synthesized according to the scheme reported by Atkins and Bünzli without the isolation of the disodium salt of *N*,*N*′,*N*″-tris(*p*-tolylsulfonyl)diethylenetriamine, m.p. 124–125°C. ^{1}H NMR (300 MHz, $CDCl_3$): δ 2.51 (s, 4H, NH), 2.10 (s,16H, CH_2). *Anal*. Found: C, 55.80; H, 11.72; N, 32.64. Calc. for $C_8H_{20}N_4$: C, 55.78; H, 11.70; N, 32.52%.

4.1.2. Preparation of 1,4,7,10-tetra(2-cycanoethyl)-1,4,7,10-tetraazacyclododecane

Cyclen (172 mg, 10 mmol) in 25 ml acrylonitrile was stirred at room temperature for 2 h then refluxed at 40°C for more than 4 h. The excessive acrylonitrile was removed in vacuo, and the oily residue was crystallized from 20 ml $CHCl_3$–EtOH (1:1) mixed solution. A white precipitate was collected by vacuum suction, and dried in vacuo with P_2O_5. Yield 330 mg, 86%, m.p.110°C. *Anal*. Found: C, 62.15; H, 8.60; N, 29.16. Calc. for $C_{20}H_{32}N_8$: C, 62.47; H, 8.34; N, 29.14%. ^{1}H NMR (300 MHz, $CDCl_3$): δ 2.52 (t, $J_{H-H}=5$, 7, 8H, CH_2CN), 2.68 (s, 16H, NCH_2CH_2N), 2.76 (t, $J_{H-H}=6$, 8, 8H, NCH_2C). EI mass spectrum m/z (assignment, relative intensity): 384 (M^+, 8%), 330 ((M–$CH_2CH_2CN)^+$, 1%), 276 ((M–2$CH_2CH_2CN)^+$, 10%), 222 ((M–3$CH_2CH_2CN)^+$, 18%), 138 (N–$(NCH_2CH_2N)_3^+$, 100%), 53 ($CH_2CH_2CN^+$, 58%). IR spectrum (KBr pellet, cm^{-1}): 2956m, 2806s, 2245s, 1380s, 1097s, 1020s, 737m.

4.2. Synthesis of complexes

4.2.1. [Co(L)(NO_3)]$NO_3\cdot H_2O$ (1)

To the solution of L (96 mg, 0.25 mmol) in 5 ml CH_2Cl_2 was added dropwise $Co(NO_3)_2\cdot 6H_2O$ (73 mg, 0.25 mmol) in 15 ml CH_3OH. The reaction solution was stirred for 12 h at room temperature. Pink solids were filtered and washed with CH_2Cl_2–CH_3OH mixed solution until the filtrate was transparent. The pink solids deposited were dissolved in a minimum amount of water and layered with acetone to precipitate red crystals suitable for X-ray diffraction. Yield 122 mg, 83% (based on L), m.p. 250°C. *Anal*. Found: C, 41.32; H, 5.84; N, 24.16. Calc. for [Co(L)(NO_3)](NO_3)H_2O: C, 41.03; H, 5.85; N, 23.92%. EI mass spectrum m/z: 567 (M^+, Co(L)$(NO_3)_2$). IR (KBr pellet, cm^{-1}): 3438m, 3100m, 2930m, 2252m, 1512s, 1464s, 1385s, 1311s, 1064m, 748w, 594w.

4.2.2. [Ni(L)(NO_3)](NO_3)$\cdot 3H_2O$ (2)

To a solution of L (96 mg, 0.25 mmol) in ethanol was added hydrated $Ni(NO_3)_2\cdot 6H_2O$ (73 mg, 0.25 mmol) in 15 ml methanol. The color of the solution turned rapidly from light green to blue which indicated the occurrence of metal coordination. After filtration in vacuo, the light green solid was washed repeatedly with CH_2Cl_2 and CH_3OH, and then dried under IR light. Yield 133 mg, 86% (based on L), m.p. 232°C. *Anal*. Found: C, 38.32; H, 6.05; N, 22.85. Calc. for [Ni(L)(NO_3)](NO_3)$\cdot 3H_2O$: C, 38.67; H, 6.16; N, 22.54%. FAB mass spectrum m/z: 443 $[L+Ni]^+$, 409 $[L+Na+2H]^+$. IR (KBr pellet, cm^{-1}): 3438(br, m), 3100w, 2950w, 2253m, 1612w, 1512s, 1450m, 1385s, 1318m, 1261s, 1022m, 748w, 594w.

4.2.3. [Cu(L)(H_2O)](NO_3)$_2$ (3)

To a solution of L (192 mg, 0.5 mmol) in 20 ml ethanol was added $Cu(NO_3)_2\cdot H_2O$ (120 mg, 0.5 mmol) and 10 ml ethanol. A blue precipitate formed quickly and the reaction mixture was stirred at room temperature for 12 h. After filtration, the solid complex was washed with CH_2Cl_2 and ether and dried at 50°C for 24 h. Yield 250 mg, 86% (based on L). Crystals suitable for X-ray diffraction were obtained by slow ether diffusion into DMF solution at room temperature, m.p. 240°C. *Anal*. Found: C, 41.21; H, 5.72; N, 24.05. Calc. for [Cu(L)]$(NO_3)_2\cdot H_2O$: C, 41.34; H, 5.72; N, 24.10%. IR (KBr pellet, cm^{-1}): 3345m, 3100w, 2964m, 2253m, 1612w, 1512s, 1465m, 1385s, 1260s, 748w, 596w.

4.3. Crystallography

Crystal data for **1** were measured on an Enraf-Nonius CAD-4 diffractometer equipped with Mo Kα radiation ($\lambda=0.71073$ Å) in the range $3<2\theta<54°$ in $\omega/2\theta$ scanning mode at room temperature (295 K) [40]. The data were corrected for Lorentz and polarization effects, and an absorption correction with empirical scanning technique was applied. Reflections with $I>3\sigma(I)$ were considered to be observed and were used in the following refinements. The structure was solved by direct methods [41–43]. All calculations were performed on a macro VAX 3100 computer with TEXSAN V2.0 package. The non-hydrogen atoms were determined with successive Fourier difference syntheses. The final refinement was done by full-matrix least-squares methods with anisotropic thermal parameters for non-hydrogen atoms ($w=1/[\sigma^2(F)+0.001F^2]$). The coordinates of hydrogen atoms were located according to theoretical models [44,45].

Crystal data for **3** were collected on a Rigaku AFC 7R diffractometer with graphite-monochromated Mo Kα radiation ($\lambda=0.071069$ Å) using the $\omega/2\theta$ mode at 20°C to a maximum 2θ value of 50.0°. An empirical correction, applied using the program DIFABS [46], resulted in correction factors ranging from 0.89 to 1.00. The structure was solved by direct methods [47] and expanded using Fourier techniques [48]. Some non-hydrogen atoms were refined anisotropi-

cally, while the rest were refined isotropically. All hydrogen atoms were introduced in calculated positions. All calculations were performed using the TEXSAN crystallographic software package [49]. Details of data collection and structure refinement are listed in Table 3.

4.4. Cytotoxicity for tumor cells

Three complexes were tested versus two tumor cell lines: HL-60 (human lymphocytic leukemia) and BEL-7404 (human hepatocellular carcinoma). All tumor cells were cultivated in RPMI-1640 medium supplemented with 10% calf serum, 100 units ml^{-1} of penicillin, and 100 μg ml^{-1} of streptomycin. Cells were harvested from exponential-phase maintenance cultures, counted by trypan blue extrusion, and dispensed within 96-well culture plates. Non-adherent cells (HL-60) were added to the complexes after distribution and were measured by MTT assay [50]. Adherent tumor cells (BEL-7404) were allowed to adhere for 24 h before addition of complexes and were measured by SRB assay [51]. The duration of exposure of all tumor cells to complexes was 72 h. Cell inhibition was expressed in terms of the percentage of control absorbance ($\pm$1% SD%) following subtraction of mean blank absorbance in the concentration range 10^{-4}–10^{-8} mol l^{-1}. The percentages of growth inhibition data of three complexes are shown in Table 2.

4.5. Analysis of cell cycle

K562 leukemia cells, 3×10^6, were exposed to complex **3** at concentrations of 0, 10 and 50 μmol l^{-1} for 24 h. Cells were then fixed by 70% ethanol (v/v), washed twice in phosphate-buffered saline solution (PBS) and stained with PBS containing 10 μg ml^{-1} propidium iodide (PI) for 30 min at room temperature in the dark. For each sample, a minimum of 10^4 cells were analyzed by flow cytometry (FACSalibur, Becton Dickinson, USA). Results were analyzed using CELLQUEST and ModFIT for mac V1.01 (Becton Dickinson, USA) and expressed as the percentage of cells found in each phase of the cell cycle.

4.6. DNA electrophoresis

Each reaction mixture contained 4 μl of supercoiled pBR322 DNA, 5 μl of the tested complex at the desired concentration and 2 μl DMSO as solvent. In the case of Cu (**3**), 2 μl MPA (2.5 mmol l^{-1}) was added as reducing reagent. After incubation at 37°C for 2 h, 1 μl of loading buffer (0.25% bromophol blue, 0.25% xylene cyanol, 30% glycerol in H_2O) was added to each tube and the mixed solution was loaded on 1% agarose gel. The electrophoresis was carried out for 2 h at 50 V in TBE buffer (89 mM tris-borate, pH 8.3, 1 mmol l^{-1} EDTA). Gels were stained with ethidium bromide (1 μg ml^{-1}) for 30 min prior to being photographed under UV light. Figs. 5 and 6 give the electrophoresis results of DNA cleavage on agarose gel.

Table 3
Crystallographic data for $[Co(L)(NO_3)](NO_3)_2\cdot H_2O$ (**1**) and $[Cu(L)(H_2O)](NO_3)_2$ (**3**)

	1	**3**
Molecular formula	$C_{20}H_{34}N_{10}O_7Co$	$C_{20}H_{38}N_{10}O_9Cu$
Formula weight	585.48	626.13
Crystal system	monoclinlic	Triclinic
Lattice parameters		
a (Å)	10.569(3)	9.156(4)
b (Å)	21.352(4)	10.128(8)
c (Å)	12.84(4)	8.006(5)
α (°)		96.60(6)
β (°)	113.14(2)	95.79(5)
γ (°)		70.90(5)
V (Å^3)	2665(2)	695.3(8)
Space group	$P2_1/c$	$P1$
Z	4	1
D_{calc} (Mg m^{-3})	1.459	1.495
Crystal size (mm)	0.40×0.25×0.12	0.20×0.20×0.30
Crystal habit	red, plate	blue, prismatic
$F(000)$	1228	329
θ_{max} (°)	27	27
μ (cm^{-1})	6.97	8.52
Index range	$-13\le h\le 13$	$0\le h\le 10$
	$0\le k\le 27$	$-9\le k\le 12$
	$0\le l\le 16$	$-1\le l\le 0$
No. observations ($I>2\sigma(I)$)	2562	1928
No. variables	361	348
Residuals R, R_w	0.076, 0.079	0.063, 0.067
Goodness of fit indicator	1.59	1.70
Maximum shift of final cycle	0.008	0.05
Peak, hole in final difference map (e Å^{-3})	0.66, −0.66	0.89, −0.45

Supplementary data

Atomic coordinates, bond angles, bond distances and thermal parameters for the two complexes **1** and **3** have been deposited at the Cambridge Crystallographic Data Centre, 12 Union Road, Cambridge CB2 1EZ, UK, CIF deposition codes 115874 and 112691, and are available on request.

Acknowledgements

Assistance by the National New Drug Screening Center of Chinese Academy of Sciences, which carried out the antitumor activity measurements, is gratefully acknowledged. We thank Mr Jie Sun of the Shanghai Institute of Organic Chemistry for helping in the structure determination.

References

[1] E. Kimura, Pure Appl. Chem. 65 (1993) 355.
[2] E. Kimura, T. Koike, Chem. Commun. (1998) 1495.
[3] E. Kimura, T. Koike, M. Shionoya, Struct. Bonding 89 (1997) 1.
[4] E. Kimura, T. Koike, Advances in Inorganic Chemistry, vol. 44, Academic Press, 1996, p. 229.

[5] S. Blain, P. Appriou, H. Chaumeil, H. Handel, Anal. Chim. Acta 232 (1990) 331.
[6] E. Kimura, T. Koike, Chem. Soc. Rev. 27 (1998) 179.
[7] H. Tsubuke, T. Yoden, T. Iwachido, M. Zenki, J. Chem. Soc., Chem. Commun. (1991) 1069.
[8] H.F. Handel, R. Muller, R. Guglielmetti, Helv. Chim. Acta 66 (1983) 514.
[9] R.A. Bullman, Struct. Bonding 67 (1987) 41.
[10] D. Bryce-Smith, Chem. Soc. Rev. 15 (1986) 93.
[11] J.L. Bousquet, S. Saini, D.D. Stark, P.F. Hahn, M. Nigam, J. Wittenberg, J. Ferrucci, J. Radiol. 166 (1988) 693.
[12] M.F. Tweedle, G.T. Gaughan, J.H. Hagan, US Patent 4 885 363, 1987.
[13] D.C. Buster, M.M.C.A. Castro, C.F.G.C. Geraldes, C.R. Malloy, A.D. Sherry, T.C. Siemers, Magn. Reson. Med. 15 (1990) 25.
[14] J. Platzek, P. Blaszkiewicz, H. Gries, P. Luger, G. Michl, A. Müller-Fahrnow, B. Radüchel, D. Sülzle, Inorg. Chem. 36 (1997) 686.
[15] S. Aimem, J.R. Morrow, C.R. Lake, M.R. Churchill, Angew. Chem., Int. Ed. Engl. 33 (1994) 773.
[16] B.F. Baker, H. Khalili, N. Wei, J.R. Morrow, J. Am. Chem. Soc. 119 (1998) 8749.
[17] P.M. Takahara, A.H. Rosenzweig, C.A. Friederich, S.J. Lippard, Nature 377 (1995) 649.
[18] S.E. Sherman, D. Gilbson, A.H.-J. Wang, S.J. Lippard, Science 230 (1985) 412.
[19] C. Trabaud, J. Dessolin, P. Vileghe, M. Bouygues, J.C. Chermann, M. Camplo, J.K. Kraus, Bioorg. Med. Chem. Lett. 7 (1997) 1353.
[20] G. Bridger, R. Skerlj, S. Padmanabhan, S. Martellucci, G. Henson, M. Abrams, N. Yamamoto, K. De Vreese, R. Pauwels, E. De Clercq, J. Med. Chem. 38 (1995) 366.
[21] E. DeClerew, N. Yamamoto, R. Pauwels, M. Baba, D. Schols, H. Nakashima, Balzarini, Z.J. Debyser, B.A. Murrer, D. Schwartz, D. Thornton, G. Bridgerm, S. Fricker, G. Henson, M. Abrams, D. Picker, Proc. Natl. Acad. Sci. USA 89 (1992) 5286.
[22] Y. Inoue, E. Kimura, Biol. Pharm. Bull. 19 (1998) 456.
[23] Y. Inoue, E. Kimura, Biol. Pharm. Bull. 17 (1994) 243.
[24] J.E. Richman, T.J. Atkins, J. Am. Chem. Soc. 96 (1974) 2268.
[25] P.A. Pittet, D. Früh, V. Tissières, J.G. Bünzli, J. Chem. Soc., Dalton Trans. (1997) 895.
[26] G.R. Weisman, D.P. Reed, J. Org. Chem. 61 (1996) 5186.
[27] J.F. Desreux, Inorg. Chem. 19 (1980) 1319.
[28] J.F. Desreux, E. Merciny, M.F. Loncin, Inorg. Chem. 20 (1981) 987.
[29] H. Stetter, W. Frank, Angew. Chem., Int. Ed. Engl. 15 (1976) 686.
[30] D.Y. Kong, L.H. Meng, L. Song, Y.Y. Xie, Transition Met. Chem. 24 (1999) 553.
[31] D.S. Kumar, V. Alexander, Inorg. Chim. Acta 238 (1995) 63.
[32] W.T. Carnall, S. Sigel, J.R. Ferraro, B. Tani, E. Gebert, Inorg. Chem. 12 (1973) 560.
[33] W.J. Geary, Coord. Rev. 7 (1971) 113.
[34] R.B. Lauffer, Chem. Rev. 87 (1987) 901.
[35] K.O.A. Chin, J.R. Morrow, Inorg. Chem. 33 (1994) 5036.
[36] S. Amin, J.R. Morrow, C.H. Lake, M.R. Churchill, Angew. Chem., Int. Ed. Engl. 33 (1994) 773.
[37] S. Routier, J.-L. Bernier, M.J. Waring, P. Colson, C. Houssier, C. Bailly, J. Org. Chem. 61 (1996) 2326.
[38] S. Routier, V. Joanny, H. Vezin, J.-P. Catteau, J.-L. Bernier, C. Bailly, J. Chem. Soc., Perkin Trans. 2 (1998) 863.
[39] D.S. Sigman, A. Mazumder, D.M. Perrin, Chem. Rev. 93 (1993) 2295.
[40] Enraf-Nonius, CAD4 Operational Manual Version 5.0, Delft Instruments X-ray Diffraction, PO Box 811, 2600 AV Delft, The Netherlands, 1989.
[41] D.T. Cromer, J.T. Waber, International Tables for X-ray Crystallography, vol. IV, Kynoch Press, Birmingham, 1974, Tables 2.2a, 2.3.1.
[42] G.J. Gilmore, MITHRIL, A Computer Program for the Automatic Solution of the Crystal Structures from the X-ray Data, University of Glasgow, 1983.
[43] C.K. Johnson, ORTEPII, Report ORNI-5138, Oak Ridge National Laboratory, TN, 1976.
[44] Molecular Structure Corporation, TEXSAN, TEXRAY Structure Analysis Package, Revised. MSC, 3200A Research Forest Drive, The Woodlands, TX 77381, USA, 1988.
[45] W.D. Motherwell, W. Clegg, PLUTO, Program for Plotting Molecular and Crystal Structures, University of Cambridge, 1978.
[46] N. Walker, D. Stuart, DIFABS, Acta Crystallogr., Sect. A 39 (1983) 158.
[47] H.-F. Fan, SAPI 91, Structure Analysis Programs with Intelligent Control, Rigaku, Tokyo, 1991.
[48] P.T. Beurskens, G. Admirael, G. Beurskens, W.P. Bosman, S. Garcia-Granda, R.O. Gould, J.M.M. Smits, C. Smykalla, DIRDIF 92, The DIRDIF System, Technical report of the crystallography laboratory, University of Nijmegen, The Netherlands, 1992.
[49] TEXSAN, Crystal Structure of Analysis Package, Molecular Structure Corporation, Houston, TX, 1985–1992.
[50] M.C. Alley, D.A. Scudiero, A. Monks, M.L. Hursey, M.J. Czerwinski, L. Fine, B.J. Abbott, J.G. Mayo, R.H. Shoemaker, M.R. Boyd, Cancer Res. 48 (1988) 589.
[51] P. Skehan, R. Storeny, D. Scudiero, J. Natl. Cancer Inst. 82 (1990) 11.

PERGAMON

www.elsevier.nl/locate/poly

Polyhedron 19 (2000) 225–228

POLYHEDRON

Synthesis and crystal structure of a new mononuclear compound containing alternate nickel(II) and sodium ions in the sheet $[Ni(en)_2(NO_2)_2]NaClO_4 \cdot H_2O$

Inmaculada Resino [a,*], Montserrat Monfort [a], Joan Ribas [a], Mercé Font-Bardia [b], Xavier Solans [b]

[a] *Departament de Química Inorgànica, Universitat de Barcelona, Martí i Franqués 1-11, 08028 Barcelona, Spain*

[b] *Departament de Cristal·lografia i Mineralogia, Universitat de Barcelona, Martí i Franqués s/n, 08028 Barcelona, Spain*

Received 2 August 1999; accepted 18 November 1999

Abstract

The new complex $[Ni(en)_2(NO_2)_2]NaClO_4 \cdot H_2O$ (**1**), where en is ethylenediamine, has been synthesised and characterised crystallographically. Each nickel atom is placed in a pseudo-octahedral environment with two nitrite groups and two diamines. Between these $[Ni(en)_2(NO_2)_2]$ units, there are sodium and perchlorate ions, and one water molecule. Magnetic susceptibility data, measured from 4 to 120 K, show non-interaction between the metals, as is usual in mononuclear compounds following the Curie law. ©2000 Elsevier Science Ltd All rights reserved.

Keywords: Nickel(II); Mononuclear compounds; Crystal structures; Nitrito ligands; Magnetic measurements

1. Introduction

The nitrite ion can coordinate to metal ions in a variety of ways. Monodentate coordination may occur either through nitrogen to give a nitro complex or through oxygen to give a nitrito complex. Bidentate coordination is known to take place either by chelation or by forming a bridge [1]. For this reason, there is a great variety of polynuclear complexes, such as dinuclear [2,3], trinuclear [2,4], pentanuclear [5], heptanuclear [6] and one-dimensional complexes [7–11].

Focusing our attention on ethylenediamine (en), different complexes have been obtained [1,3,5,7,10,12–15] under specific experimental conditions. Our aim is to study the conditions necessary to form dinuclear or polynuclear rather than mononuclear compounds. Unfortunately, this cannot always be achieved.

We present here the synthesis used to obtain a polynuclear complex, but following which only a mononuclear compound was formed. This mononuclear compound is interesting and different from other mononuclear compounds [12–15] because it presents different octahedral units of Ni(II) and Na linked to each other in a sheet. Usually mononuclear compounds have been obtained showing two different formulae: (a) a neutral complex $[Ni(amine)_2(NO_2)_2]$ with two terminal nitrite ligands and (b) a cationic complex $[Ni(amine)_2(NO_2)]X$ with a chelate nitrite ligand. In the present case, the Ni(II) units are neutral, but the complex shows the novelty of cocrystallising with sodium perchlorate. So **1** has been obtained in a fortuitous way.

This new compound $[Ni(en)_2(NO_2)_2]NaClO_4 \cdot H_2O$ (**1**), where (en) is ethylenediamine, has been characterised by its crystal structure and magnetic measurements, as well as IR spectra and elemental analysis.

2. Experimental

Caution! Perchlorate salts of metal complexes with organic ligands are potentially explosive. Only a small amount of material should be prepared and it should be handled with care.

2.1. Synthesis of $[Ni(en)_2(NO_2)_2]NaClO_4 \cdot H_2O$

4 mmol of ethylenediamine (en) dissolved in 10 ml of water were added with stirring to an aqueous solution (20 ml) of 4 mmol of nickel(II) perchlorate hexahydrate. 2 mmol of sodium nitrite in 5 ml of water were added to the green solution formed. Slow evaporation of the resulting solution

* Corresponding author. Fax: +34-93-490-7725; e-mail: iresino@kripto.qui.ub.es

0277-5387/00/$ - see front matter ©2000 Elsevier Science Ltd All rights reserved.
PII S0277-5387(99)00370-8

gave red planar crystals of **1** several days later. *Anal*. Calc. for $C_4H_{18}ClN_6NaNiO_9$: C, 11.7; H, 4.4; Cl, 8.6; N, 20.4. Found: C, 11.4; H, 4.2; Cl, 8.5; N, 20.0%. Yield 62%.

2.2. Spectral and magnetic measurements

The IR spectrum (4000–400 cm^{-1}) was recorded from KBr pellets on a Nicolet 520 FTIR spectrophotometer. Magnetic measurement of a polycrystalline sample was carried out on a MANICS-DSM8 susceptometer equipped with an Oxford Instruments liquid helium cryostat, working in the temperature range 4–120 K, and a Bruker E15 magnet. The magnetic field was approximately 16000 G. Diamagnetic corrections were estimated from the Pascal tables.

2.3. Crystallography

$[Ni(en)_2(NO_2)_2]NaClO_4 \cdot H_2O$ (**1**). A prismatic crystal ($0.1 \times 0.1 \times 0.2$ mm) was selected and mounted on an Enraf-Nonius CAD4 four-circle diffractometer. The crystallographic data, conditions retained for the intensity data collection, and some features of the structure refinement are listed in Table 1. Unit-cell parameters were determined from the automatic centring of 25 reflections ($12 < \theta < 21°$) and refined by the least-squares method. Intensities were collected with graphite monochromatized Mo Kα radiation, using the $\omega/2\theta$ scan-technique. 2778 reflections were measured in the range $2.22 < \theta < 29.96°$. 2022 reflections were assumed as observed, applying the condition $I > 2\sigma(I)$. Three reflections were measured every 2 h as orientation and intensity control; significant intensity decay was not observed. Lorentz polarisation but not absorption corrections were made. The structure was solved by direct methods, using the SHELXS computer program [16] and refined by the full-matrix least-squares method with the SHELX93 computer program [17], using 2563 reflections. The function minimised was $\Sigma w(|F_o|^2 - |F_c|^2)^2$, where $w = [\sigma^2(I) + (0.0397P)^2]^{-1}$, and $P = (|F_o|^2 + 2|F_c|^2)/3$, f, f' and f'' were taken from international tables [18]. The extinction coefficient was 0.0000(11). All H atoms were computed and refined with an overall isotropic temperature factor using a riding model. The final $R(F)$ factor was 0.043, $wR(|F|^2) = 0.089$ and goodness of fit was 1.050 for all observed reflections. The number of refined parameters was 204. The maximum shift/esd was 0.001; the mean shift/esd was 0.07. Maximum and minimum peaks in final difference synthesis were 0.609 and -0.506 e $Å^{-3}$, respectively.

Table 1
Crystal data and structure refinement for $[Ni(en)_2(NO_2)_2]NaClO_4 \cdot H_2O$

Formula	$C_4H_{18}ClN_6NaNiO_9$
FW	411.39
Space group	$P2_1/n$
a (Å) [a]	9.199(2)
b (Å)	13.504(5)
c (Å)	13.191(9)
β (°)	108.63(4)
V (Å^3)	1552.8(13)
Z	4
d_{calc} (g cm^{-3})	1.760
μ(Mo Kα) (cm^{-1})	0.1502
λ(Mo Kα) (Å)	0.71069
T (K)	293(2)
Scan method	$\omega/2\theta$
No. parameters refined	204
R [b]	0.0438
wR [c]	0.0897

[a] The cell parameters were selected according to the IUCr rules for a reduced cell.
[b] $R(F_o) = \Sigma||F_o| - |F_c||/\Sigma|F_o|$.
[c] $R_w(F_o) = \Sigma w||F_o| - |F_c||/\Sigma w|F_o|$.

3. Results and discussion

3.1. IR data

The IR spectrum shows the characteristic bands attributable to the ligands. The nitrite ligand has three vibrational modes: $\nu_{N=O}$ appears at 1273, 1215 cm^{-1} (m), ν_{N-O} at 1326 cm^{-1} (m), and δ at 827 cm^{-1} (w). The bands attributable to (en) appear in the characteristic zone for each vibration: at about 3200 cm^{-1} (N–H); in a wide range between 3000 and 2870 cm^{-1} (C–H); and finally at about 1450 cm^{-1} (C–N). The perchlorate ion shows two main bands centred at 1130 and 625 cm^{-1}.

3.2. Description of the structure

The complex crystallises in the monoclinic system, space group $P2_1/n$ with FW = 411.39, $a = 9.199(2)$, $b = 13.504(5)$, $c = 13.191(9)$ Å, $V = 1552.8(13)$ Å^3, $Z = 4$, $R = 0.0438$, $R_w = 0.0897$. The structure of **1** has three units: two different crystallographic $[Ni(en)_2(NO_2)_2]$ units and another in which there is a sodium ion linked to six oxygens, four from nitrito ligands, one from a perchlorate anion and the other from a water molecule. Each nitrite is coordinated to the Ni(II) by the nitrogen atom, and to the sodium ion by its oxygen. A labelled scheme is shown in Fig. 1. The main bond lengths and angles are gathered in Table 2. We can describe the structure by considering the three units. There are two different pseudo-octahedrally coordinated nickel atoms, with the same environment but different bond parameters. The distance between the nickel atoms is 6.740 Å. The two different nitrito groups are in *trans* arrangement. The Ni–N(diamine) distances are between 2.084 and 2.093 Å. The distances corresponding to Ni–N(nitrite) are 2.133(3) and 2.153(3) Å for Ni(1)–N(3) and Ni(2)–N(6), respectively. The N–Ni–N angles in *trans* arrangement are always 180°, and in *cis* arrangement they are almost 90°; the N(diamine)–Ni–N(diamine) angle is the smallest (82.57°) for the unit with Ni(1), and the largest (97.43°) for the other. The rings formed by diamine with Ni(II) for the unit with Ni(1) form a plane, and with Ni(2) they show a skew-

Table 2
Selected bond lengths (Å) and bond angles (°) for $[Ni(en)_2(NO_2)_2]NaClO_4 \cdot H_2O$

Ni(1)–N(1)	2.084(3)	Ni(1)–N(2)	2.093(3)
Ni(1)–N(3)	2.133(3)	Ni(2)–N(4)	2.088(3)
Ni(2)–N(5)	2.091(3)	Ni(2)–N(6)	2.153(3)
Na–O(1)	2.420(4)	Na–O(1W)	2.396(4)
Na–O(2)#2	2.421(4)	Na–O(3)	2.397(4)
Na–O(4)#3	2.383(4)	Na–O(12)#5	2.515(5)
N(4)–Ni(2)–N(5)	83.51(14)	N(4)–Ni(2)–N(5)#2	96.49(14)
N(4)–Ni(2)–N(6)	91.26(14)	N(4)–Ni(2)–N(6)#2	88.74(14)
N(5)–Ni(2)–N(4)#2	96.49(14)	N(5)–Ni(2)–N(5)#2	180.0
N(5)–Ni(2)–N(6)	89.86(13)	N(5)–Ni(2)–N(6)#2	90.14(13)
N(5)#2–Ni(2)–N(4)#2	83.51(14)	N(5)–Ni(2)–N(6)	89.86(13)
N(6)–Ni(2)–N(4)#2	88.74(14)	N(5)#2–Ni(2)–N(6)	90.14(14)
N(6)#2–Ni(2)–N(4)#2	91.26(14)	N(6)–Ni(2)–N(6)#2	180.0
N(1)–Ni(1)–N(1)#1	180.0	O(4)#3–Na–O(1W)	92.02(14)
N(2)–Ni(1)–N(1)#1	97.43(14)	O(4)#3–Na–O(3)	177.82(13)
N(2)#1–Ni(1)–N(1)#1	82.57(14)	O(4)#3–Na–O(1)	88.56(12)
N(3)–Ni(1)–N(1)#1	90.53(14)	O(4)#3–Na–O(2)#2	90.69(12)
N(3)#1–Ni(1)–N(1)#1	89.47(14)	O(4)#3–Na–O(12)#5	89.64(14)
N(1)–Ni(1)–N(2)	82.57(14)	O(1W)–Na–O(3)	88.41(14)
N(1)–Ni(1)–N(2)#1	97.43(14)	O(1W)–Na–O(1)	93.44(14)
N(1)–Ni(1)–N(3)	89.47(14)	O(1W)–Na–O(2)#2	90.85(14)
N(1)–Ni(1)–N(3)#1	90.53(14)	O(1W)–Na–O(12)#5	170.10(15)
N(2)–Ni(1)–N(2)#1	180.0	O(3)–Na–O(1)	89.28(12)
N(2)–Ni(1)–N(3)	89.07(13)	O(3)–Na–O(2)#2	91.44(12)
N(2)–Ni(1)–N(3)#1	90.93(13)	O(3)–Na–O(12)#5	90.30(12)
N(2)#1–Ni(1)–N(3)	90.93(13)	O(1)–Na–O(2)#2	175.66(14)
N(2)#1–Ni(1)–N(3)#1	89.07(13)	O(1)–Na–O(12)#5	96.35(15)
N(3)–Ni(1)–N(3)#1	180.0	O(2)#2–Na–O(12)#5	79.37(14)
N(4)–Ni(2)–N(4)#2	180.0		

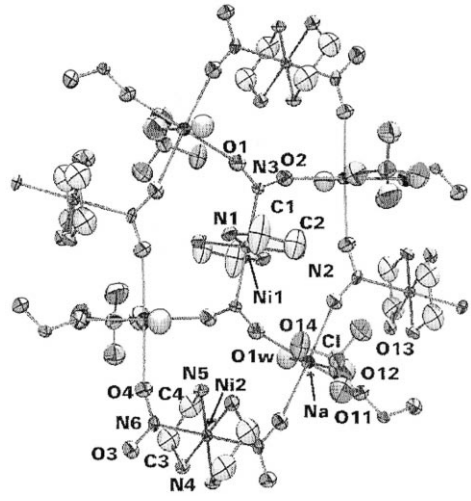


Fig. 1. ORTEP drawing with labelled scheme of $[Ni(en)_2(NO_2)_2]$-$NaClO_4 \cdot H_2O$.

envelope conformation. The chelate ring around Ni(1) is disordered because of the great thermal motion of the C(1) atom. Turning to the unit with the sodium ion, the distances Na–O range from 2.384 to 2.420 Å (oxygen from nitrite and water) whereas the oxygen from the perchlorate ion is at the greatest distance (2.515 Å). The O–Na–O angles in *trans* arrangement are between 170.09 and 177.82°. The same angles in *cis* arrangement are different from 90°, ranging from 79.35 to 96.35°. Each Ni(II) has four nickel atoms in its neighbourhood and four sodium atoms in the next neighbourhood. In the same way, each Na has four different sodium atoms in its neighbourhood and then four nickel atoms. The different entities that form this compound are linked by weak hydrogen bonds, between the nitrogen of (en) and the oxygen of nitrito ligand and perchlorate ion. The orientations of the two $[Ni(en)_2(NO_2)_2]$ units are different: the unit with Ni(1) (Fig. 2) follows the crystallographic [101] axis and the unit

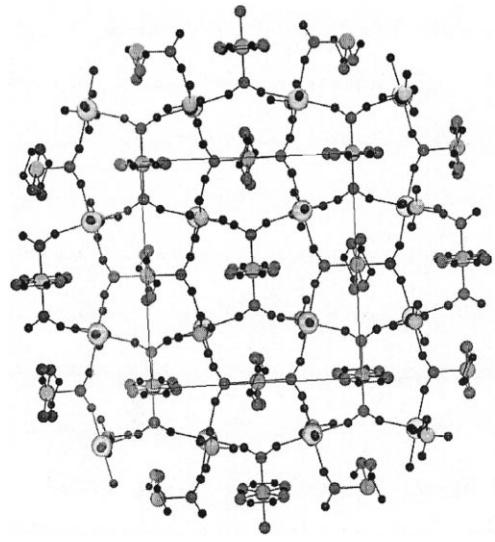


Fig. 2. Ionic sheet with the different units of $[Ni(en)_2(NO_2)_2]$-$NaClO_4 \cdot H_2O$.

with Ni(2) follows the *a* axis. In the (010) plane there are $[Ni(en)_2(NO_2)_2]$ and sodium units alternately.

3.3. Magnetic results

The magnetic susceptibility measurements were carried out in the temperature range 4–120 K. The $\chi_M T$ versus T, χ_M versus T and χ_M^{-1} versus T plots for **1** are shown in Fig. 3. The room temperature $\chi_M T$ value was 1.09 cm^3 K mol^{-1} corresponding to an isolated nickel atom with $g > 2.00$ and was practically constant in the temperature range analysed to 40 K, in which $\chi_M T$ increases to 1.445 cm^3 K mol^{-1} at 5 K. This compound exhibits a quasi-Curie law behaviour with a slight increase after 40 K. This increase in $\chi_M T$ is caused by weak ferromagnetic interactions between the different units of nickel through the sodium cations in the crystal net.

In order to quantify the magnetic behaviour, the experimental data χ_M versus T were fitted to the expression [19] for an isolated nickel ion with ferromagnetic intermolecular interactions:

$$\chi_M = \frac{2Ng^2\mu_\beta^2 S(S+1)}{3kT - zJS(S+1)}$$

where

$$\frac{zJS(S+1)}{3k} = \theta$$

The results of this fit show that the interaction between the different units is very weak. To verify this, we extrapolated the χ_M^{-1} versus T data. As the θ found is positive ($-\theta/C = -2.24$ cm^{-3} mol), we can conclude that the intermolecular interactions are ferromagnetic.

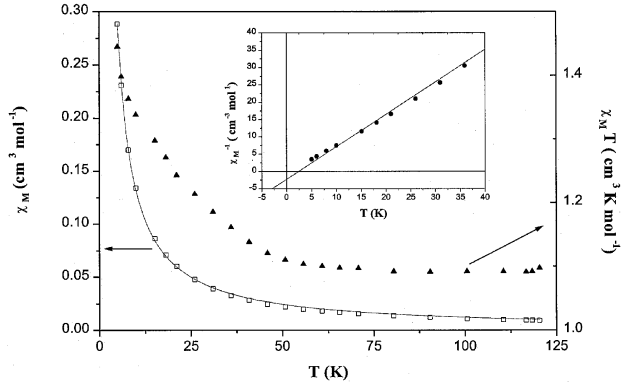


Fig. 3. $\chi_M T$, χ_M and χ_M^{-1} (insert) vs. T plots in the temperature range 4–120 K of a polycrystalline sample of **1**. The solid line corresponds to the best fit.

Supplementary data

Refined atom coordinates, calculated hydrogen coordinates ($\times 10^4$) and anisotropic displacement parameters for non-hydrogen atoms (Å$\times 10^3$) are included in the supplementary material. Observed and calculated structural factors are available on request. Supplementary material has been deposited at the Cambridge Crystallographic Data Centre as publication number CCDC 132682.

Acknowledgements

This work was undertaken with the financial support of CICYT PB96-0163. I.R thanks the Ministerio de Educacion y Cultura for a doctoral FPI fellowship.

References

[1] A.J. Finney, M.A. Hitchman, C.L. Raston, G.L. Rowbottom, A.H. White, Aust. J. Chem. 34 (1981) 2047.
[2] A.J. Finney, M.A. Hitchman, C.L. Raston, G.L. Rowbottom, A.H. White, Aust. J. Chem. 34 (1981) 2125.
[3] A. Gleizes, A. Meyer, M.A. Hitchman, O. Kahn, Inorg. Chem. 21 (1983) 2257.
[4] D.M.L. Goodgame, M.A. Hitchman, D.F. Marsham, P. Phavanantha, D. Rogers, J. Chem. Soc., Dalton Trans. (1969) 1383.
[5] A.J. Finney, M.A. Hitchman, C.L. Raston, G.L. Rowbottom, A.H. White, Aust. J. Chem. 34 (1981) 2139.
[6] M.S. El Fallah, E. Rentschler, A. Caneschi, R. Sessoli, D. Gatteschi, Inorg. Chem. 35 (1996) 3723.
[7] A. Meyer, A. Gleizers, J.J. Girerd, M. Verdaguer, O. Kahn, Inorg. Chem. 21 (1982) 1729.
[8] J.W. Krajewski, P. Gluzinski, B. Korybut-Daszkiewixz, A. Mishnyov, A. Kemme, J. Chem. Soc., Dalton Trans. (1991) 53.
[9] F.J. Llewellyn, J.M. Waters, J. Chem. Soc. (1962) 3845.
[10] A.J. Finney, M.A. Hitchman, C.L. Raston, G.L. Rowbottom, A.H. White, Aust. J. Chem. 34 (1981) 2159.
[11] L.K. Chou, K.A. Abboud, D.R. Talham, W.W. Kim, M.W. Meisel, Chem. Mater. 6 (1994) 2051.
[12] A.E. Shvelashvili, M.A. Porai-Koshits, A.I. Kvitashvili, B.M. Shchedrin, Zh. Strukt. Khim. 15 (1974) 307.
[13] M.G.B. Drew, D.M.L. Goodgame, M.A. Hitchman, D. Rogers, Chem. Commun. (1965) 477.
[14] L.K. Minacheva, A.S. Antsyshkina, M.A. Porai-Koshits, A.E. Shvelashvili, Zh. Strukt. Khim. 11 (1970) 936.
[15] M.A. Porai-Koshits, Acta Crystallogr., Sect. A 31 (1966) 149.
[16] G.M. Sheldrick, Acta Crystallogr., Sect. A 46 (1990) 467.
[17] G.M. Sheldrick, SHELXL93, University of Göttingen, Germany, 1993.
[18] International Tables for X-ray Crystallography, vol. IV, Kynoch Press, Birmingham, 1974, pp. 99–100, 149.
[19] O. Khan, Molecular Magnetism, VCH, 1993, p. 27.

PERGAMON

www.elsevier.nl/locate/poly

Polyhedron 19 (2000) 229–234

POLYHEDRON

Interaction of nitric oxide with cobalt(II) tetrasulfophthalocyanine

Sibulelo Vilakazi, Tebello Nyokong *

Department of Chemistry, Rhodes University, Grahamstown 6140, South Africa

Received 18 August 1999; accepted 30 November 1999

Abstract

The interaction of nitric oxide (NO) with cobalt(II) tetrasulfophthalocyanine [Co(II)TSPc]$^{4-}$ has been studied. Coordination of NO is accompanied by electron transfer from the central metal in [Co(II)TSPc]$^{4-}$, the resulting complex being represented as [(NO$^-$)Co(III)TSPc]$^{4-}$. The rate constant for the formation of this species is $k_f = 142 \pm 7$ dm^3 mol^{-1} s^{-1} and an equilibrium constant of $3.0 \pm 0.5 \times 10^5$ dm^3 mol^{-1} was obtained. When adsorbed to a glassy carbon electrode, [Co(II)TSPc]$^{4-}$ catalyses the oxidation and reduction of NO, with a detection limit of the order of 10^{-9} mol dm^{-3}. Ammonia and hydroxylamine are some of the reduction products obtained for the reduction of NO on [Co(II)TSPc]$^{4-}$-modified glassy carbon electrodes. ©2000 Elsevier Science Ltd All rights reserved.

Keywords: Cobalt; Electrocatalysis; Nitric oxide; Oxidation; Phthalocyanine; Reduction

1. Introduction

Interest in the chemistry of nitric oxide (NO) has intensified in the last few years due to its importance in biological systems including neurotransmission, vascular dilation, cytotoxicity, immune response and regulation of blood pressure [1,2]. Excess concentrations of NO have been implicated as a major factor in a number of conditions, such as septic shock, and Parkinson's and Alzheimer's diseases [3,4]. There has been a surge of interest in the nature of coordination of NO to metalloporphyrins [4–13]. NO interacts with hemoglobin, myoglobin and cytochrome P450 forming NO compounds [14]. NO has a short half-life (depending on the concentration of oxygen) and has high reactivity with oxygen and hydrogen peroxide [1]. Current methods of detecting NO are indirect, relying on the measurement of secondary species such as nitrite and nitrate after removal from biological systems. Measurement of NO using bioassay, chemiluminescence and UV–Vis spectroscopy do not allow for in vivo detection, and require chemical pretreatment of the sample. Thus there is a growing interest in electrochemical sensors for analysis of NO in cells [15–18], based on its electrocatalytic oxidation. Nickel(II) and iron(II) porphyrin complexes and unmetallated porphyrin have been employed in modifying electrodes for the detection of NO [19–27]. The mechanism for the catalytic oxidation of NO by metalloporphyrins is not well understood. For example, the Ni(III)/Ni(II) couple has been implicated in NO determination using electrodes modified with nickel(II) porphyrin complexes [19,20], but other researchers have reported that the Ni(III)/Ni(II) couple plays no role in the electrocatalytic oxidation of NO [25].

Metallophthalocyanine (MPc) complexes have been used successfully as electrocatalysts for many reactions [28–36]. There are only a few reports on the interaction between NO and MPc complexes [37–42]. The use of MPc complexes for the electrocatalytic reduction or oxidation of NO still needs to be explored. It has recently been suggested that [CoTSPc]$^{4-}$ bound to immobilized imidazole-modified silica gel can be used as a water-soluble NO sorbent that does not dimerize, and hence can be used for the removal of NO from flue gas streams [37]. The present study explores the electrocatalytic oxidation and reduction of NO on glassy carbon electrodes modified with cobalt(II) tetrasulfophthalocyanine ([CoTSPc]$^{4-}$; Fig. 1). We also report on the kinetics and equilibria for the interaction between NO and [CoTSPc]$^{4-}$.

2. Experimental

2.1. Materials

Cobalt(II) tetrasulfophthalocyanine (Na_4[Co(II)TSPc]) was synthesized and purified according to the method of

* Corresponding author. Fax: +27-46-6225109; e-mail: t.nyokong@ru.ac.za

0277-5387/00/$ - see front matter ©2000 Elsevier Science Ltd All rights reserved.
PII S0277-5387(99)00373-3

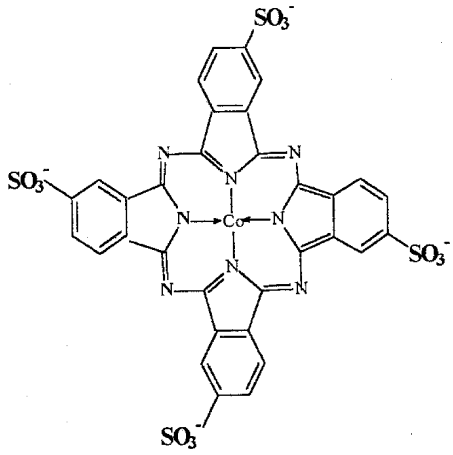


Fig. 1. Molecular structure of cobalt(II) tetrasulfophthalocyanines.

Weber and Busch [43]. NO was prepared by adding saturated sodium nitrite dropwise to a 0.2 mol dm^{-3} solution of H_2SO_4 under nitrogen atmosphere. The NO produced was passed through a column containing solid KOH to remove higher oxides and then bubbled into nitrogen-saturated deionized water. NO solutions in water were prepared freshly before use and kept in glass flasks fitted with a rubber septum. NO concentration in water was determined using the method proposed by Ascenzi et al. [38] or calculated using the reported solubility of 2.2×10^{-3} mol dm^{-3} at 25°C and 1.00 atm [38]. Tetraethylammonium perchlorate (TEAP) was recrystallized from ethanol before use as an electrolyte. Dimethylformamine (DMF) was freshly distilled.

2.2. Electrochemical methods

Electrochemical data were collected with the Bio-Analytical Systems (BAS) model CV-50W voltammetric analyser. For cyclic voltammetry, a glassy carbon electrode (GCE; 3.0 mm diameter) was used as a working electrode and a platinum wire as an auxiliary electrode. The reference electrode was the Ag|AgCl (3 mol dm^{-3} KCl). Concentrations of Na_4[Co(II)TSPc] in water were in the 10^{-4} to 10^{-3} mol dm^{-3} range for cyclic voltammetry. Phosphate buffers pH 4 and 7 were employed for electrochemical experiments. In some experiments sodium sulfate (0.05 mol dm^{-3}) was employed as an electrolyte. For non-aqueous solutions TEAP was employed as an electrolyte.

For electrocatalytic reactions, a glassy carbon electrode modified with Na_4[Co(II)TSPc] (CoTSPc-GCE) was employed as a working electrode. The glassy carbon was modified by anodic electrodeposition from a 10^{-3} mol dm^{-3} solution of $[CoTSPc]^{4-}$ in DMF containing 0.1 mol dm^{-3} TEAP as an electrolyte, as reported before [44]. The deposition was carried out by scanning repetitively at 100 mV s^{-1} between −0.2 and 1.0 V versus Ag|AgCl (non-aqueous). Prior to coating, the GCE was polished with alumina on a Buehler felt pad, followed by soaking in dilute nitric acid and rinsing in water, acetone and the solvent of interest. For bulk electrolysis, a two-compartment cell was employed, with a platinum plate of area 2.2 cm^2 as counter electrode and an Ag|AgCl (3 mol dm^{-3} KCl) reference electrode. The GCE modified by electrodeposition was used as a working electrode for bulk electrolysis. A nitrogen atmosphere was maintained for all electrochemistry experiments. Concentrations of NO were of the order of 10^{-4} to 10^{-3} mol dm^{-3} for electrocatalytic studies. Yields of ammonia were determined by the Nessler method [45] and by monitoring the absorbance at 400 nm. Hydroxylamine was determined spectroscopically using the specific test described in the literature [9].

2.3. Kinetics and equilibria

Kinetic and equilibrium studies were run at 21.0 ± 0.5°C and monitored with a Cary 1E UV–Vis spectrophotometer. We monitored the appearance of the spectra due to the product formed following the addition of NO to solutions of $[CoTSPc]^{4-}$ in water. Typically, a known volume of the aqueous solution of $[CoTSPc]^{4-}$ was added to a cell of 1 cm pathlength and deaerated using nitrogen. Then a known volume of a deaerated aqueous solution of NO was added to the cell and the spectra monitored with time. Bubbling of nitrogen into the cell was continued while adding the NO solution. The cell was fitted with a stopper to avoid oxygen affecting the reaction. Concentrations of $[CoTSPc]^{4-}$ were kept constant at 5.0×10^{-6} mol dm^{-3}, whereas NO concentrations were varied from 1.4×10^{-5} to 5.6×10^{-5} mol dm^{-3}. Concentrations of $[CoTSPc]^{4-}$ in water were determined using the published extinction coefficient of 5.8×10^4 mol^{-1} dm^3 cm^{-1} [46]. Since the concentration of the NO was larger than that of $[CoTSPc]^{4-}$ by a factor of at least 10, pseudo-first-order conditions were assumed for kinetic studies. Solid CoTSPc-NO was prepared by bubbling NO into aqueous solutions of $[CoTSPc]^{4-}$ and allowing the solvent to evaporate.

IR spectra were recorded using a Perkin–Elmer Spectrum 2000 IR spectrophotometer.

3. Results and discussion

3.1. Interactions with NO

The electronic absorption spectral properties of $[CoTSPc]^{4-}$ are well known. Like other tetrasulfonated phthalocyanines, this species forms aggregates in aqueous solution. The electronic absorption spectrum is explained in terms of the monomer/dimer equilibrium. The lower energy band near 670 nm has been attributed to the monomeric species and the higher energy band near 620 to the dimeric species [46]. On coordination of molecules such as nitrite and histidine, the peak due to the monomer increases in intensity and shifts to longer wavelengths, whereas the peak due to the dimeric species decreases in intensity [47,48]. Fig. 2 shows spectral changes that were observed when NO was added to solutions

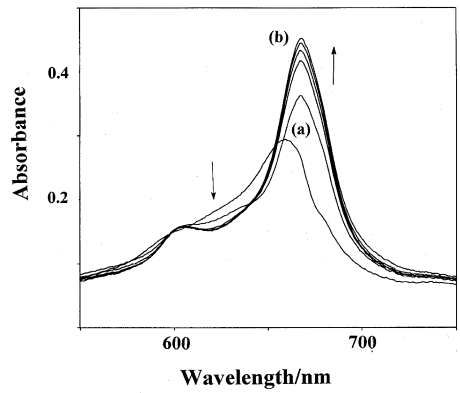


Fig. 2. Electronic absorption spectral changes observed on addition of NO (3.5×10^{-5} mol dm^{-3}) to aqueous solutions of [Co(II)TSPc]$^{4-}$. (a) Spectra immediately after addition of NO; (b) spectra 30 min after addition of NO.

of [Co(II)TSPc]$^{4-}$. The monomeric peak of [CoTSPc]$^{4-}$ was observed at 659 nm before addition of NO (Fig. 2a). The spectrum is typical for [CoTSPc]$^{4-}$ in water, at low electrolyte concentrations; the peak due to the monomer dominates under these conditions [46]. On addition of NO to [Co(II)TSPc]$^{4-}$, a shift in the peak due to the monomer, from 659 to 667 nm, was observed. The intensity of the peak at 667 nm increased isosbestically with time (Fig. 2b). The shift in spectrum is associated with the coordination of NO to the [CoTSPc]$^{4-}$ species. A shift and increase in the monomeric peak of the [CoTSPc]$^{4-}$ species on coordination of histidine and nitrite have been reported [47,48]. An increase and shifting of the monomer peak of [CoTSPc]$^{4-}$ was also observed upon formation of an adduct between this species and oxygen. Oxygen was carefully excluded from the solutions containing NO and [CoTSPc]$^{4-}$ and no spectral changes were observed for [CoTSPc]$^{4-}$ in the absence of NO. Thus the spectral changes shown in Fig. 2 are associated with the formation of an adduct between NO and [CoTSPc]$^{4-}$.

X-ray photoelectron spectroscopy studies have indicated oxidation of the central metal in FePc and CoPc when the complexes are exposed to NO [41]. Electron transfer from Ni(II) to NO has also been implicated during coordination of NO to [Ni(II)TSPc]$^{4-}$, resulting in the formation of the [(NO$^-$)Ni(III)TSPc]$^{4-}$ species [39]. Oxidation of Co(II)Pc to a Co(III)Pc species was also implicated on interaction of NO with CoPc [42]. We suggest that oxidation of the central metal also occurs on coordination of NO to the [CoTSPc]$^{4-}$ species, forming a Co(III)TSPc-NO complex. Oxidation of [CoTSPc]$^{4-}$ using chemical oxidants (e.g. bromine) resulted in the spectrum similar to that shown in Fig. 2b. The lack of an isosbestic point with the spectra of the starting complex in Fig. 2 is most likely a result of the two processes, coordination of NO to [CoTSPc]$^{4-}$ and the subsequent electron transfer between the two molecules, occurring simultaneously.

In nitrosyl complexes, ν(NO) ranges from 1500 to 1900 cm^{-1}. ν(NO) for cobalt tetrakis(*N*-methyl-2-pyridyl)-porphine [Co(2-TMpyP)(NO)] was observed at 1722 cm^{-1} [9] and for CoPc(NO) at 1680 cm^{-1} [42]. IR spectra of the solid formed by reacting [Co(II)TSPc]$^{4-}$ with NO showed a new band at 1730 cm^{-1}, in the range for coordinated NO. This value is higher than those reported for NO coordinated to cobalt porphyrins. Generally oxidized cobalt porphyrin complexes show ν(NO) values at higher frequencies than neutral complexes [12]. Thus the higher ν(NO) values for the (NO)CoTSPc complex could be a consequence of the oxidation of [Co(II)TSPc]$^{4-}$ to [Co(III)TSPc]$^{3-}$ following coordination of NO. As mentioned above, oxidation of [Ni(II)TSPc]$^{4-}$ to [Ni(III)TSPc]$^{3-}$ following coordination of NO has been observed. The IR spectra of the Ni(III)TSPc(NO$^-$) complex showed ν(NO) at 1660 cm^{-1} [39], much lower than the value reported here for the Co(III)TsPc(NO) complex. Vibrational frequencies of NO greater than 1700 cm^{-1} have been associated with linear geometry of M–N=O and those of lower frequency to a bent geometry [39]. The observation of ν(NO) at 1730 cm^{-1} suggests a bent geometry for the Co–NO bond in the CoTSPc(NO) complex. Oxidation of NO to NO_2^- is likely following its coordination to CoTSPc. NO_2^- stretching frequencies were observed at 1401, 1306 and 830 cm^{-1} in Co(III)2-TMpyP(NO). We did not observe new IR bands in this region for the CoTSpc(NO) complex.

The coordination of NO to [Co(II)TSPc]$^{4-}$ can be represented by Eq. (1):

$$[\mathrm{Co(II)TSPc}]^{4-} + \mathrm{NO} \underset{k_r}{\overset{k_f}{\rightleftharpoons}} [(\mathrm{NO}^-)\mathrm{Co(III)TSPc}]^{4-} \quad (1)$$

The number of NO molecules coordinated to the [Co(II)TSPc]$^{4-}$ species was determined using the standard equation [37,42]:

$$\log\left[\frac{A_{eq}-A_0}{A_\infty - A_{eq}}\right] = \log K + n\log[\mathrm{NO}] \quad (2)$$

where A_{eq} is the equilibrium absorbance at 667 nm, A_0 is the absorbance before addition of NO; A_∞, the absorbance after complete formation of the [(NO$^-$)Co(III)TSPc]$^{4-}$ complex, was determined from the final absorbance at 667 nm. Fig. 3a shows a plot of $\log[(A_{eq}-A_0)/(A_\infty - A_{eq})]$ versus log[NO]. A linear plot with a slope $n = 0.97 \pm 0.07$ was obtained, showing that only one molecule of NO is coordinated. The equilibrium constant (K) was determined from the intercept to be $3.0 \pm 0.5 \times 10^5$ dm^3 mol^{-1}.

Plots of the observed rate constant (k_{obs}) versus the concentration of NO were linear (Fig. 3b), showing that the coordination is first-order in NO and obeys the rate law:

$$k_{obs} = k_f[\mathrm{NO}] + k_r \quad (3)$$

where k_f is the rate constant for the formation of the [(NO$^-$)Co(III)TSPc]$^{4-}$ species according to Eq. (1) and k_r is the dissociation of this complex. Least-square analysis of the data presented in Fig. 3b gave $k_f = 142 \pm 7$ dm^3 mol^{-1} s^{-1} from the slope, and $k_r = 5.4 \pm 0.8 \times 10^{-4}$ s^{-1} was

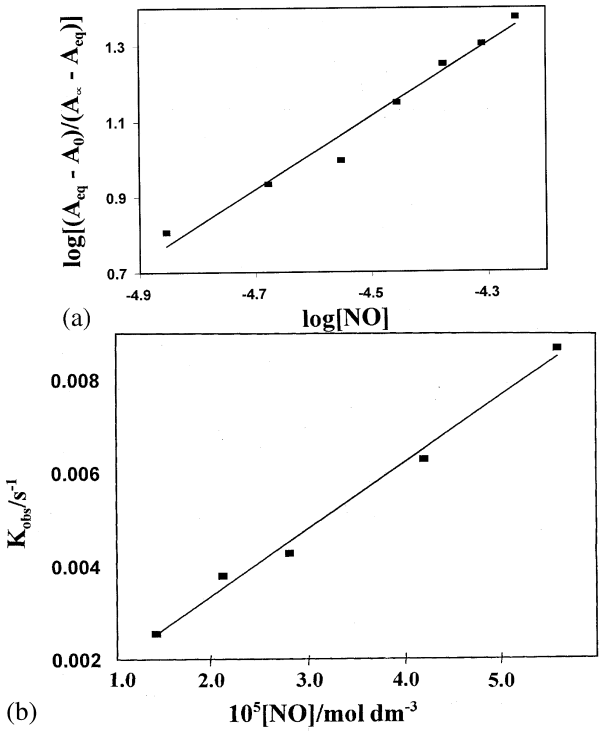


Fig. 3. (a) Plot of $\log[(A_{eq}-A_0)/(A_\infty-A_{eq})]$ vs. log[NO]. (b) Plot of the observed rate constant (k_{obs}) vs. the concentration of NO, for the formation of $[(NO)^-Co(III)TSPc]^{4-}$ species.

obtained from the intercept. Using these values of rate constants, the value of the equilibrium constant for NO coordination to $[Co(II)TSPc]^{4-}$ was estimated to be $K_1 = 2.6\times10^5$ dm^3 mol^{-1} from the relationship $K_1 = k_f/k_r$, which is in excellent agreement, within experimental error, with the value determined above from the equilibrium data.

Table 1 compares the values of the rate constant for the coordination of NO to $[Co(II)TSPc]^{4-}$ with the values for its coordination to iron(II) porphyrin, metmyoglobin and hemoglobin. The values for the coordination of NO to the latter three molecules is much higher than the value for the coordination to $[Co(II)TSPc]^{4-}$. A low rate constant was also reported for the coordination of NO to manganese porphyrin complexes [11]. Axial ligand exchange reactions occur more slowly for CoPc than for FePc complexes [49]. The equilibrium constant for the coordination of NO to $[Co(II)TSPc]^{4-}$ was, however, much larger than for coordination of NO to the Fe(II) porphyrin, metmyoglobin and hemoglobin complexes (Table 1).

3.2. Electrocatalysis

Typical cyclic voltammograms for the reduction of NO on an unmodified GCE and on a GCE modified with $[Co(II)TSPc]^{4-}$ are shown in Fig. 4. On CoTSPc-GCE, a catalytic peak was observed at -0.96 V versus Ag|AgCl for the reduction of NO (Fig. 4b). The voltammogram for the reduction of NO on unmodified GCE is shown in Fig. 4a. The cyclic voltammogram of the adsorbed CoTSPc in buffer alone did not show any peaks. The reduction currents for NO observed on GCE modified with $[Co(II)TSPc]^{4-}$ are much higher than the currents observed for the reduction of the same concentration of NO on an unmodified GCE. The peak currents for the reduction of NO on GCE modified with

Table 1
Equilibrium and rate constants for coordination of NO

Complex	K (dm^3 mol^{-1})	k_f (dm^3 mol^{-1} s^{-1})	Ref.
Fe(III) porphyrin	1.1×10^3	7.2×10^5	[14]
Metmyoglobin	1.4×10^4	1.9×10^5	[14]
Hemoglobin		2.5×10^7	[14]
$[Co(II)TSPc]^{4-}$	3.0×10^5	142	this work

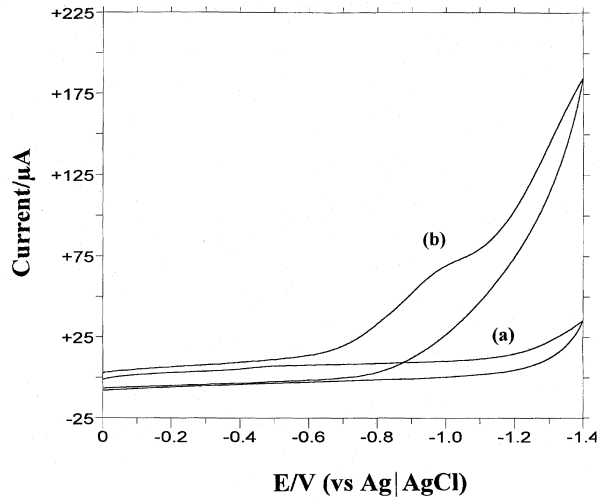


Fig. 4. Cyclic voltammogram for the reduction of 1.0×10^{-5} mol dm^{-3} NO on (a) unmodified GCE and (b) CoTSPc-GCE. Scan rate 100 mV s^{-1}.

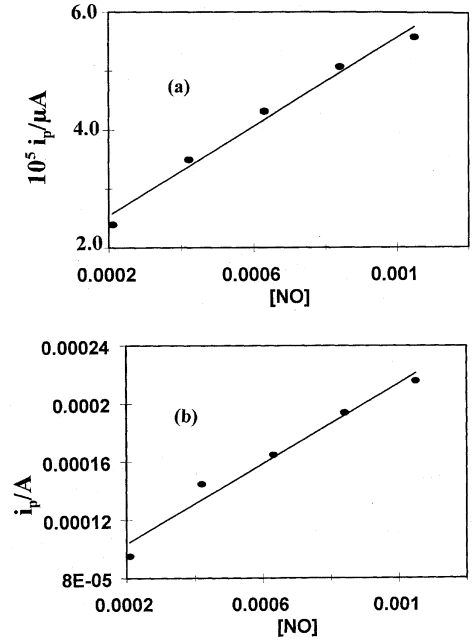


Fig. 5. Plot of the variation of the catalytic currents for (a) reduction and (b) oxidation of NO on CoTSPc-GCE vs. the concentration of NO. Scan rate 100 mV s^{-1}.

$[Co(II)TSPc]^{4-}$ increased with increase in NO concentration as shown in Fig. 5a. The modified electrode showed stability towards the reduction of NO in that the currents did not decrease appreciably with scan number. The peak at -0.96 V versus Ag|AgCl is almost at the same potential as that observed for reduction of NO (-0.93 V) on CoPc-modified GCE [42]. The pH of the media plays an important part in the catalytic reduction or oxidation of NO. The peak for the catalytic reduction of NO in water containing sodium sulfate was observed at -1.2 V versus Ag|AgCl. When the pH 7 buffer was employed the peak was observed at -1.1 V versus Ag|AgCl.

The cyclic voltammograms for the oxidation of NO on an unmodified GCE and on GCE modified with CoTSPc are shown in Fig. 6. There is a considerable enhancement in the oxidation currents of NO when GCE is modified with $[Co(II)TSPc]^{4-}$ compared with unmodified GCE. A weak broad peak is observed for NO on unmodified GCE near 1.1 V. On CoTSPc-GCE, the oxidation peak for NO is well resolved and observed at 1.08 V. The enhancement in oxidation currents when CoTSPc-GCE is employed shows that the $[Co(II)TSPc]^{4-}$ species acts as a catalyst for the oxidation of NO. The currents for the oxidation of NO on CoTSPc-GCE increased with increase in NO concentration, as shown in Fig. 5b. The lowest concentration of NO that could be determined using either the oxidation or reduction of NO on CoTSPc-GCE was of the order of 10^{-9} mol dm^{-3}.

Bulk electrolysis of solutions containing NO at potentials for the catalytic reduction on CoTSPc-GCE gave $n \approx 5$, where n is the number of electrons involved in the reaction. This suggests that ammonia could be one of the reduction products of NO. Analysis of the solution obtained following bulk electrolysis did confirm the presence of ammonia with yields of about 25%. The current efficiency for ammonia production was determined to be 89%. Hydroxylamine was also found to be one of the products.

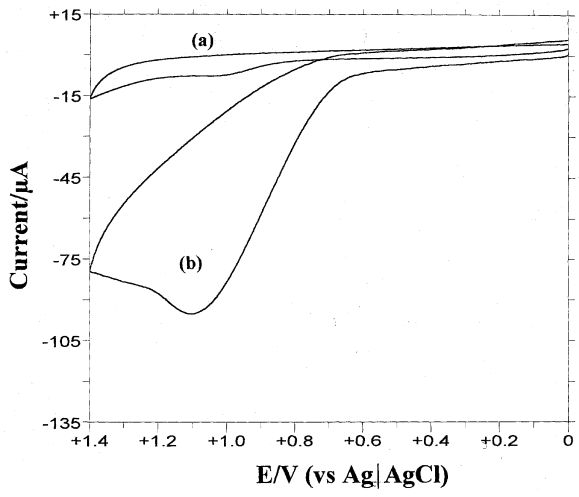


Fig. 6. Cyclic voltammogram for the oxidation of 2.1×10^{-4} mol dm^{-3} NO on (a) unmodified GCE and (b) CoTSPc-GCE. Scan rate 100 mV s^{-1}.

In conclusion, NO has been shown to coordinate to $[Co(II)TSPc]^{4-}$. The coordination is accompanied by electron transfer from the central Co(II) metal and the formation of $[(NO^{-})Co(III)TSPc]^{4-}$ species. The rate constant for the formation of this species is much lower than those reported for the interaction of NO with metmyoglobin, iron(II) porphyrin and hemoglobin. $[Co(II)TSPc]^{4-}$ adsorbed on GCE catalyses both the reduction and oxidation of NO. The lowest concentration of NO that could be detected on GCE modified with $[Co(II)TSPc]^{4-}$ was of the order of 10^{-9} mol dm^{-3}.

Acknowledgements

This work is supported by Rhodes University and by the Foundation of Research Development in South Africa.

References

[1] A.R. Butler, D.L.H. Williams, Chem. Soc. Rev. (1993) 233.
[2] P.L. Feldman, O.W. Griffith, D.J. Stuehr, Chem. Eng. News (1993) 26.
[3] D.D. Rees, S. Celleck, R.M.J. Palmer, S. Moncada, Biochem. Biophys. Res. Commun. 197 (1990) 541.
[4] S. Moncada, R.M.J. Palmer, E.A. Higgs, Biochem. Pharmacol. 38 (1989) 1709.
[5] M.K. Ellison, W.R. Scheidt, Inorg. Chem. 37 (1998) 382.
[6] H. Nasri, M.K. Ellison, S. Chen, B.H. Huynh, W.R. Scheidt, J. Am. Chem. Soc. 119 (1997) 6274.
[7] E.A. Morlino, M.A.J. Rodgers, J. Am. Chem. Soc. 118 (1996) 11798.
[8] L.E. Laverman, M. Hoshino, P.C. Ford, J. Am. Chem. Soc. 119 (1997) 12663.
[9] S.-H. Cheng, Y.O. Su, Inorg. Chem. 33 (1994) 5847.
[10] O.Q. Munro, W.R. Scheidt, Inorg. Chem. 37 (1998) 2308.
[11] C.-H. Yu, Y.O. Su, J. Electroanal. Chem. 368 (1994) 323.
[12] G.B. Richter-Addo, S.J. Hodge, G.-B. Yi, M.A. Khan, T. Ma, E. Van Caemelbecke, N. Guo, K.M. Kadish, Inorg. Chem. 35 (1996) 6530.
[13] M. Frangione, J. Port, M. Baldiwala, A. Judd, J. Galley, M. DeVega, K. Linna, L. Caron, E. Anderson, J.A. Goodwin, Inorg. Chem. 36 (1997) 1904.
[14] M. Hoshino, K. Ozawa, H. Seki, P.C. Ford, J. Am. Chem. Soc. 115 (1993) 9568.
[15] F. Bedioui, S. Trevin, J. Devynck, Electroanalysis 8 (1996) 1085.
[16] B. Fabre, S. Burlet, R. Cespuglio, G. Bidan, J. Electroanal. Chem. 426 (1997) 75.
[17] A.-M. Yu, H.-L. Zhang, H.-Y. Chen, Anal. Lett. 30 (1997) 1013.
[18] S.R. Smith, H.H. Thorp, Inorg. Chim. Acta 273 (1998) 316.
[19] T. Malinski, Z. Taha, S. Grunfeld, A. Burewicz, P. Tomboulian, Anal. Chim. Acta 279 (1993) 135.
[20] T. Malinski, Z. Taha, Nature 358 (1992) 676.
[21] F. Bedioui, S. Trevin, V. Albin, M.G.G. Villegas, J. Devynck, Anal. Chim. Acta 341 (1997) 177.
[22] Š. Mesároš, S. Grunfeld, A. Mesárošová, D. Bustin, T. Malinski, Anal. Chim. Acta 339 (1997) 265.
[23] S. Trévin, F. Bedioui, J. Devynck, Talanta 43 (1996) 303.
[24] J. Hayon, D. Ozer, J. Rishpon, A. Bettelheim, J. Chem. Soc., Chem. Commun. (1994) 619.
[25] A. Ciszewski, E. Kubaszewski, M. Łożyński, Electroanalysis 8 (1996) 293.
[26] S. Trévin, F. Bedioui, J. Devynck, J. Electroanal. Chem. 408 (1996) 261.

[27] F. Lantoine, S. Trévin, F. Bedioui, J. Devynck, J. Electroanal. Chem. 392 (1995) 85.
[28] J.H. Zagal, Coord. Chem. Rev. 119 (1992) 89.
[29] N. Kobayashi, W.A. Nevin, Appl. Organomet. Chem. 10 (1996) 579.
[30] P. Vasudevan, N. Phougat, A.K. Shukla, Appl. Organomet. Chem. 10 (1996) 591.
[31] K. Hanabusa, H. Shirai, C.C. Leznoff, A.B.P. Lever, Phthalocyanines: Properties and Applications, vol. 2, 1993, VCH, New York.
[32] M.K. Halbert, R.P. Baldwin, Anal. Chem. 57 (1985) 591.
[33] Y.H. Tse, P. Janda, A.B.P. Lever, Anal. Chem. 66 (1994) 384.
[34] F. Xu, H. Li, S.J. Cross, T.F. Guarr, J. Electroanal. Chem. 368 (1994) 221.
[35] T. Mafatle, T. Nyokong, J. Electroanal. Chem. 408 (1996) 213.
[36] C. Coutanceau, P. Crouigneau, J.M. Leger, C. Lamy, J. Electroanal. Chem. 379 (1994) 389.
[37] J.W. Owens, M. Perry, D.W. Seybert, Inorg. Chim. Acta 277 (1998) 1.
[38] P. Ascenzi, R. Fruttero, C. Ercolani, F. Monacelli, Analusis 24 (1996) 316.
[39] I. Zilbermann, J. Hayon, T. Katchalski, O. Raveh, J. Rishpon, A.I. Shames, A. Bettelheim, J. Electrochem. Soc. 144 (1997) L228.
[40] P. Ascenzi, M. Brunori, G. Pennesi, G. Ercolani, J. Chem. Soc., Dalton Trans. (1987) 369.
[41] K. Uchida, M. Soma, T. Onishi, K. Tamaru, J. Chem. Soc., Faraday Trans. 1 75 (1979) 2839.
[42] S. Vilakazi, T. Nyokong, Polyhedron 17 (1998) 4415.
[43] J.H. Weber, D.H. Busch, Inorg. Chem. 4 (1965) 469.
[44] J. Limson, T. Nyokong, Electroanalysis 9 (1997) 255.
[45] J. Bassett, R.C. Denney, G.H. Jeffery, J. Mendham, Vogel's Textbook of Quantitative Inorganic Analysis, Longman, New York, 1981.
[46] L.C. Gruen, R.J. Blagrove, Aust. J. Chem. 26 (1973) 319.
[47] N. Chebotareva, T. Nyokong, J. Coord. Chem. 46 (1999) 433.
[48] M. Sekota, T. Nyokong, Polyhedron 16 (1997) 3279.
[49] T. Nyokong, Polyhedron 14 (1995) 2325.

PERGAMON

www.elsevier.nl/locate/poly

Polyhedron 19 (2000) 235–240

POLYHEDRON

Synthesis and properties of ditelluroether complexes of osmium, *trans*-$[OsCl_2(L\text{-}L)_2]$ and *trans*-$[OsCl(PPh_3)(L\text{-}L)_2]PF_6$ (L-L = *o*-$C_6H_4(TeMe)_2$, $RTe(CH_2)_3TeR$ (R = Ph or Me))

Andrew J. Barton, William Levason *, Gillian Reid, Vicki-Anne Tolhurst

Department of Chemistry, University of Southampton, Southampton SO17 1BJ, UK

Received 27 September 1999; accepted 17 November 1999

Abstract

The complexes *trans*-$[OsCl_2(L\text{-}L)_2]$ (L-L = *o*-$C_6H_4(TeMe)_2$, $RTe(CH_2)_3TeR$ (R = Ph or Me)) have been prepared from *trans*-$[OsCl_2(dmso)_4]$ and the ditelluroethers in ethanol. The reaction of $[OsCl_2(PPh_3)_3]$ with the ditelluroethers or $MeSCH_2CH_2SMe$ or $MeSe(CH_2)_3SeMe$ in ethanol in the presence of NH_4PF_6 gave *trans*-$[OsCl(PPh_3)(L\text{-}L)_2]PF_6$. The complexes have been characterised by analysis, IR, UV–Vis and multinuclear NMR spectroscopy. The reaction of OsO_4–HCl–EtOH with $PhTe(CH_2)_3TePh$ results in chlorination of the ligand to $PhTeCl_2(CH_2)_3TePhCl_2$, identified by single-crystal X-ray study. The X-ray structure for *trans*-$[OsCl_2\{PhTe(CH_2)_3TePh\}_2]$ is reported. The reaction of $[OsCl_2(dmso)_4]$ with the distibine $Ph_2Sb(CH_2)_3SbPh_2$ affords *trans*-$[OsCl_2\{Ph_2Sb(CH_2)_3SbPh_2\}_2]$ which has also been characterised crystallographically. ©2000 Elsevier Science Ltd All rights reserved.

Keywords: Osmium; Ditelluroether; X-ray structures

1. Introduction

Osmium forms compounds in formal oxidation states ranging from 8 to −2 and as a consequence has an extremely rich coordination chemistry [1]. However, the absence of labile osmium precursors in the medium oxidation states can make some types of complex difficult to prepare. For example, whilst a wide range of bidentate and polydentate phosphine and arsine complexes of Os(II), Os(III) and Os(IV) are readily made starting from OsO_4–HX–ROH (X = Cl, Br or I) or $[OsX_6]^{2-}$ [1], obtaining complexes with Group 16 donors has proved considerably more difficult. Direct reaction of $[OsX_6]^{2-}$ with dithioethers [2] or diselenoethers [3] generates $[OsX_4(L\text{-}L)]$ type complexes in poor yield, whilst from OsO_4–HX–EtOH and the ligands at low temperatures unstable osmyl complexes $[OsO_2X_2(L\text{-}L)]$ form [4,5]. Further reduction to, for example, $[OsX_2(L\text{-}L)_2]$ does not appear possible by this route. We were interested in extending our previous studies of ditelluroether complexes with platinum group metals, Pt or Pd [6–8], Ir [6,7], Ru or Rh [8], to osmium and report our investigations below.

* Corresponding author. Tel.: +44-1703-543792; fax: +44-1703-593781; e-mail: wxl@soton.ac.uk

2. Results and discussion

The reaction of OsO_4–conc. HCl–EtOH with the three ditelluroether ligands (L-L = *o*-$C_6H_4(TeMe)_2$, or $RTe(CH_2)_3TeR$ (R = Me or Ph)) at 0°C gave brownish-purple solids leaving a dark red solution. These solids lacked the very strong $\nu(OsO_2)$ IR vibration at ca. 850 cm^{-1} typical of *trans*-$[OsO_2Cl_2(L'\text{-}L')]$ (L′-L′ = dithioether or diselenoether) [4,5], ruling out the formation of osmyl species. A similar result was reported with Me_2Te [4,5]. Since telluroethers are both stronger reducing agents and less able to stabilise high oxidation states than their lighter analogues [6–8], their failure to stabilise Os(VI) is not unexpected, but it was hoped that reduction would lead to Os(III) or Os(IV) complexes. The brownish-purple solids have UV–Vis spectra typical of Os(IV), in fact the major features are very similar to those of $[OsCl_6]^{2-}$ [9] and were weakly paramagnetic, which would suggest either Os(IV) and/or Os(III) compounds were present. However, after long accumulations each sample gave a single sharp ^{125}Te NMR resonance at very high frequencies (δ (^{125}Te) ca. 800–900) which would seem to indicate that at least some of the tellurium was present in a diamagnetic material, the shifts being in the range [10] typical of R_2TeCl_2 species. A pale brown crystal was grown (from MeCN) from the $PhTe(CH_2)_3TePh$ reaction and the

0277-5387/00/$ - see front matter ©2000 Elsevier Science Ltd All rights reserved.
PII S0277-5387(99)00376-9

structure solution revealed the diamagnetic tellurium compound to be $PhCl_2Te(CH_2)_3TePhCl_2$.MeCN [1]. The structure is shown in Fig. 1 and selected bond length and angle data are in Table 1. The structure is typical of R_2TeCl_2 type compounds, with $PhCl_2TeCH_2TePhCl_2$ the closest structurally characterised example [11]. The environment about each Te is based upon a distorted trigonal bipyramid with axial $TeCl_2$ groups and with one equatorial position vacant, presumably occupied by the lone pair. The Te–Cl bonds 2.504(2)–2.524(1) Å lie within the usual range [11], and the structure is unexceptional, but serves to identify unequivocally a significant product of the reactions described above.

Similar brownish-purple materials are formed on refluxing $[NH_4]_2[OsCl_6]$ with the ditelluroethers in alcohols. Notably none of the crude materials gave ^{125}Te NMR resonances in the ranges we subsequently observed for the $[OsCl_2(L\text{-}L)_2]$ complexes (below). Although we have been unable to separate any pure osmium species from these reactions, it is clear that the target $[OsCl_2(L\text{-}L)_2]$ are not present in significant amounts.

An alternative route to *trans*-$[OsCl_2(L\text{-}L)_2]$ from Os(II) starting materials was sought, although as indicated in Section 1, most Os(II) materials are kinetically very inert and introducing moderate donor ligands like telluroethers is not easy. We found that the recently characterised [12] *trans*-$[OsCl_2(dmso)_4]$ (dmso = dimethylsulfoxide) reacted with the ditelluroethers under reflux in ethanol to produce poor to moderate yields of *trans*-$[OsCl_2(L\text{-}L)_2]$ as orange or red solids. The isolated complexes are air stable and generally poorly soluble in chlorocarbons or MeCN, which to some extent limited solution spectroscopic studies. Red crystals of $[OsCl_2\{PhTe(CH_2)_3TePh\}_2]$ were obtained by evaporation of a $CHCl_3$ solution of the complex, and the structure solution (Table 2, Fig. 2) revealed a *trans* pseudo-octahedral molecule with the osmium on the inversion centre and with both ditelluroethers in *meso* form. Although the crystals are not isomorphous, the structure is very similar to that previously found in *trans*-$[RuCl_2\{PhTe(CH_2)_3TePh\}_2]$ [8]. The Os–Cl bond length, 2.450(4) Å, is comparable with those found in $[OsCl_2\{Ph_2PCH_2CH_2PPh_2\}_2]$ (2.434(1) Å) [13] and $[OsCl_2\{H_2C{=}C(PPh_2)_2\}_2]$ (2.431(1) Å) [14]. There are no literature data on Os^{II}–TeR_2 bonds, but those in the present complex (2.616(1), 2.6135(9) Å) are, as might be expected, similar to the Ru–Te bonds in the Ru^{II} analogue (2.6247(3), 2.6194(3) Å) [8].

[1] Although $RCl_2Te(CH_2)_nTeRCl_2$ prepared from $RTe(CH_2)_nTeR$ and Cl_2 are white or cream, our crystals were brown, presumably owing to traces of an osmium species.

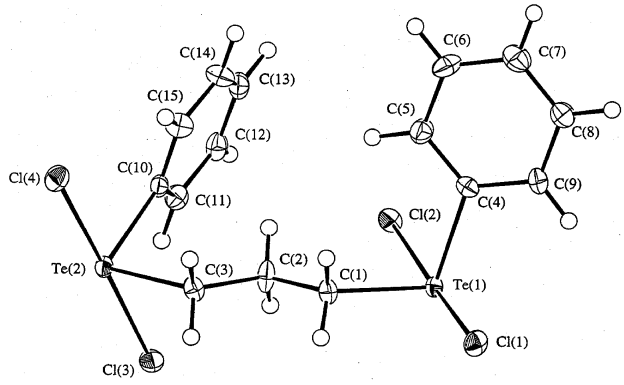


Fig. 1. View of the structure of $PhTeCl_2(CH_2)_3TePhCl_2$ with numbering scheme adopted. Ellipsoids are drawn at 40% probability.

Table 1
Selected bond lengths (Å) and angles (°) for $PhCl_2Te(CH_2)_3TePhCl_2 \cdot MeCN$

Te(1)–Cl(1)	2.507(1)	Te(1)–Cl(2)	2.524(1)
Te(1)–Cl(1)	2.169(5)	Te(1)–C(4)	2.131(6)
Te(2)–Cl(3)	2.520(2)	Te(2)–Cl(4)	2.504(2)
Te(2)–C(3)	2.169(6)	Te(2)–C(10)	2.150(6)
Cl(1)–Te(1)–Cl(2)	175.01(5)	Cl(1)–Te(1)–C(1)	85.3(2)
Cl(1)–Te(1)–C(4)	89.3(2)	Cl(2)–Te(1)–C(1)	93.1(2)
Cl(2)–Te(1)–C(4)	86.2(2)	C(1)–Te(1)–C(4)	99.1(2)
Cl(3)–Te(2)–Cl(4)	176.54(5)	Cl(3)–Te(2)–C(3)	88.1(2)
Cl(3)–Te(2)–C(10)	91.3(2)	Cl(4)–Te(2)–C(3)	89.7(2)
Cl(4)–Te(2)–C(10)	91.5(2)	C(3)–Te(2)–C(10)	94.6(2)
Te(1)–C(1)–C(2)	114.7(4)	C(1)–C(2)–C(3)	110.8(5)
Te(2)–C(3)–C(2)	112.3(4)		

Table 2
Selected bond lengths (Å) and angles (°) for $[OsCl_2\{PhTe(CH_2)_3TePh\}_2]$

Os(1)–Te(1)	2.6135(9)
Os(1)–Te(2)	2.616(1)
Os(1)–Cl(1)	2.450(4)
Te(1)–C(1)	2.18(1)
Te(1)–C(11)	2.13(1)
Te(2)–C(3)	2.18(1)
Te(2)–C(21)	2.14(1)
Te(1)–Os(1)–Te(2)	86.65(3)
Te(1)–Os(1)–Cl(1)	93.15(8)
Te(2)–Os(1)–Cl(1)	93.12(9)

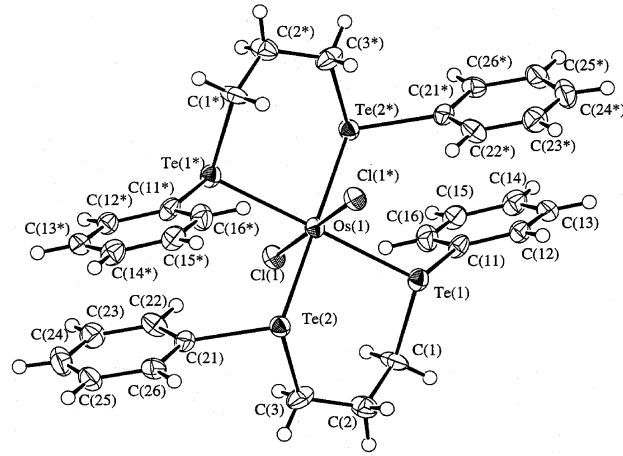


Fig. 2. View of the structure of $[OsCl_2\{PhTe(CH_2)_3TePh_2\}$ with numbering scheme adopted. Ellipsoids are drawn at 40% probability. Atoms marked * are related by a crystallographic inversion centre. H-atoms are omitted for clarity.

The three $[OsCl_2(L\text{-}L)_2]$ complexes have very similar spectroscopic properties (Section 3) including two d–d bands in the range 21000–26000 cm^{-1} as expected for a low spin d^6 complex with local D_{4h} symmetry [9]. The poor solubility made it very difficult to obtain ^{125}Te NMR spectra, but after very long accumulations several resonances were present in each complex, consistent with a mixture of invertomers, showing that pyramidal inversion is slow on the NMR time scale in these systems. As we have discussed elsewhere [8], it is not possible to assign resonances to individual isomers. Notably, for comparable complexes, the $\delta(^{125}Te)$ are found at considerably higher frequency in the ruthenium complexes [8] compared with the present osmium examples, an effect also found for corresponding ruthenium and osmium phosphines [15]. Cyclic voltammetry of the complexes in CH_2Cl_2 revealed a single reversible oxidation for each ($[OsCl_2\{MeTe(CH_2)_3TeMe\}_2]$ +0.35 V versus SCE; $[OsCl_2\{PhTe(CH_2)_3TePh\}_2]$ +0.18 V; $[OsCl_2\{o\text{-}C_6H_4(TeMe)_2\}_2]$ +0.43 V), which contrasts with the quasi-reversible or irreversible oxidations observed in the ruthenium analogues [8], reflecting the expected greater stability of the M(III) state for osmium.

Although $[OsCl_2(dmso)_4]$ provided a satisfactory starting material for the synthesis of the ditelluroether complexes it is still not ideal, and attempts to prepare $[OsCl_2(L'\text{-}L')_2]$ (L′-L′ dithioether or diselenoether) similarly usually result in mixtures containing $[OsCl(dmso)(L'\text{-}L')_2]^+$, $[OsCl_2(dmso)_2(L'\text{-}L')]$ and $[OsCl_2(L'\text{-}L')_2]$, which are not readily separated, and we have not obtained useful amounts of the last complexes.

The reactions of $[OsCl_2(PPh_3)_3]$ with 2 equiv. of the Group 16 ligands in EtOH in the presence of $[PF_6]^-$ gave moderate yields of $[OsCl(PPh_3)(L\text{-}L)_2]PF_6$ (L-L = $RTe(CH_2)_3TeR$, R = Me or Ph), $[OsCl(PPh_3)(MeSCH_2CH_2SMe)_2]PF_6$ and $[OsCl(PPh_3)\{MeSe(CH_2)_3SeMe\}_2]PF_6$ as yellow or brown solids. The complexes are air stable solids which show $[OsCl(PPh_3)(L\text{-}L)_2]^+$ as the highest mass ions in their ES^+ mass spectra. The UV–Vis spectra are uninformative, showing only the $\pi \rightarrow \pi^*$ transitions of the Ph-groups and charge transfer transitions in the near-UV which tail into the visible obscuring the d–d bands, although the absence of significant features below 20000 cm^{-1} confirms the oxidation state as Os(II). The ^1H NMR spectra of the ditelluroether compounds are complex and not very helpful, but the $^{31}P\{^1H\}$ NMR spectra are more useful. For $[OsCl(PPh_3)\{PhTe(CH_2)_3TePh\}_2]PF_6$, in addition to the septet at δ −145 due to $[PF_6]^-$ there are two singlets at −10.5 and −11.8 with approximate intensities 2:1 showing the presence of two major invertomers. The corresponding $^{125}Te\{^1H\}$ NMR spectrum showed five doublets in the range δ 450–565 with $^2J(^{125}Te\text{–}^{31}P)$ of ca. 60–90 Hz. In the case of $[OsCl(PPh_3)\{MeTe(CH_2)_3TeMe\}_2]PF_6$ the $^{31}P\{^1H\}$ NMR spectrum reveals one major invertomer δ −14.5 and there are four doublets in the $^{125}Te\{^1H\}$ NMR spectrum and four δ(Me) resonances in the ^1H NMR spectrum. This is consistent with one invertomer as the major solution form with one *meso* and one *DL* ditelluroether. The pattern of invertomers in these two cases is very similar to that observed in the ruthenium analogues [8]. For the $[OsCl(PPh_3)\{MeSe(CH_2)_3SeMe\}_2]PF_6$ the $^{31}P\{^1H\}$ NMR spectrum shows a singlet at −14.0 and the septet at −145. There are singlets for the Me and CH_2 groups of the diselenoether in the ^1H NMR spectrum. Whilst at first sight this might be taken to indicate one isomer with high symmetry, we were unable to observe a ^{77}Se NMR spectrum from this complex, which suggests that pyramidal inversion is occurring. Finally, for $[OsCl(PPh_3)\{MeS(CH_2)_2SMe\}_2]PF_6$ there is a singlet in the $^{31}P\{^1H\}$ NMR spectrum at δ −15.1, and broad singlets at δ 2.44 and 2.7 (in addition to the Ph multiplet) in the ^1H NMR spectrum, consistent with fast inversion in the dithioether complex. The poor solubility and the number of possible invertomers make these systems poorly suited to VT NMR studies, but comparison of the room temperature spectra shows the usual trends [16,17] in pyramidal inversion barriers Te > Se > S are present.

The reaction of $[OsCl_6]^{2-}$ with Ph_3Sb in alcohols readily yields *mer*-$[OsCl_3(Ph_3Sb)_3]$ which can be reduced by excess ligand and $NaBH_4$ to *trans*-$[OsCl_2(Ph_3Sb)_4]$ [18,19], but attempts to carry out corresponding reactions with ditertiary stibines failed. As a further test of the usefulness of $[OsCl_2(dmso)_4]$ we reacted this with $Ph_2Sb(CH_2)_3SbPh_2$ in ethanol, and readily obtained good yields of yellow *trans*-$[OsCl_2\{Ph_2Sb(CH_2)_3SbPh_2\}_2]$. The spectroscopic data (Section 3) are unexceptional and compare well with the corresponding data on *trans*-$[OsCl_2(Ph_3Sb)_4]$ [18,19] and *trans*-$[OsCl_2(diphosphine)_2]$ [20]. Yellow crystals of *trans*-$[OsCl_2(Ph_2Sb(CH_2)_3SbPh_2)_2]$ were obtained from CH_2Cl_2, and the structure determined. The molecule is shown in Fig. 3 and significant bond lengths and angles are in Table 3. The structure reveals a centrosymmetric molecule, with the d(Os–Cl) 2.477(2) Å typical of an Os(II) centre [13,14]. The d(Os–Sb) 2.5933(8), 2.6030(4) Å are very similar to those in *trans*-$[OsCl_2(Ph_3Sb)_4]$ (2.611(2)–2.630(2) Å) [21].

3. Experimental

Physical measurements were made as described previously [8].

3.1. *[Os{MeTe(CH$_2$)$_3$TeMe}$_2$Cl$_2$]*

$[Os(dmso)_4Cl_2]$ (151 mg, 0.155 mmol), $MeTe(CH_2)_3TeMe$ (100 mg, 0.307 mmol) in MeOH (70 cm^3) were refluxed for 16 h. The solvent was removed in vacuo and CH_2Cl_2 added (2 cm^3). The orange solution was filtered and Et_2O added to precipitate an orange solid. Yield: 0.05 g, 36%. *Anal*. Found: C, 12.9; H, 2.6. Calc. for $C_{10}H_{24}Cl_2OsTe_4$: C, 13.1; H, 2.6%. ^1H NMR ($CDCl_3$, 300 MHz): δ 1.94–3.15 (m, $CH_2 + CH_3$). $^{125}Te\{^1H\}$ NMR ($CDCl_3/CH_2Cl_2$, 113 MHz): δ 236, 267, 274, 286, 293, 329, 339. IR spectrum

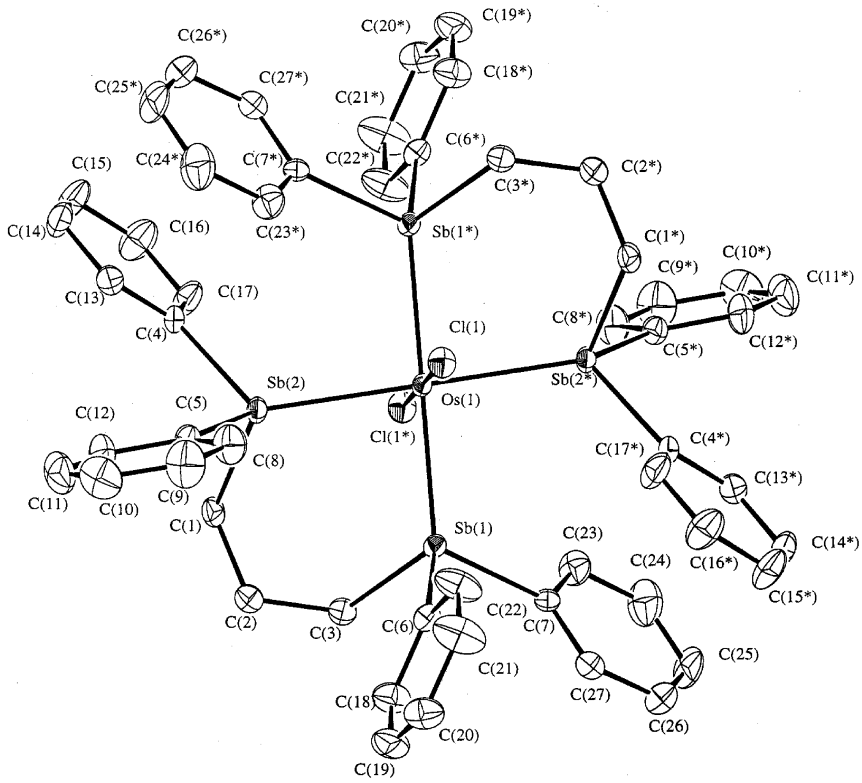


Fig. 3. View of the structure of $[OsCl_2\{Ph_2Sb(CH_2)_3SbPh_2\}_2]$ with number scheme adopted. Ellipsoids are drawn at 40% probability. Atoms marked * are related by a crystallographic inversion centre. H-atoms are omitted for clarity.

Table 3
Selected bond lengths (Å) and angles (°) for $[OsCl_2\{Ph_2Sb(CH_2)_3SbPh_2\}_2]\cdot 2CH_2Cl_2$

Os(1)–Sb(1)	2.5933(8)
Os(1)–Sb(2)	2.6030(4)
Os(1)–Cl(1)	2.477(2)
Sb(1)–C(3)	2.154(7)
Sb(1)–C(6)	2.137(7)
Sb(1)–C(7)	2.149(7)
Sb(2)–C(1)	2.143(7)
Sb(2)–C(4)	2.137(7)
Sb(2)–C(5)	2.144(7)
Sb(1)–Os(1)–Sb(2)	85.73(1)
Sb(1)–Os(1)–Cl(1)	95.53(4)
Sb(2)–Os(1)–Cl(1)	96.76(4)
Os(1)–Sb(1)–C(3)	114.2(2)
Os(1)–Sb(1)–C(6)	124.2(2)
Os(1)–Sb(1)–C(7)	117.1(2)
C(3)–Sb(1)–C(6)	100.1(3)
C(3)–Sb(1)–C(7)	96.9(3)
C(6)–Sb(1)–C(7)	99.7(3)
Os(1)–Sb(2)–C(1)	114.3(2)
Os(1)–Sb(2)–C(4)	118.9(2)
Os(1)–Sb(2)–C(5)	123.6(2)
C(1)–Sb(2)–C(4)	95.7(3)
C(1)–Sb(2)–C(5)	98.5(3)
C(4)–Sb(2)–C(5)	100.8(3)

(CsI disc): 2922 (m), 2855 (w), 1358 (s), 1262 (w), 1091 (s), 1068, 920 (w), 835 (m), 615 (w), 598 (w), 430 (w), 297 (m), 224 (w). UV–Vis spectrum (CH_2Cl_2): $\nu_{max}=22125$ ($\varepsilon_{mol}=330$), 20580 (sh) cm^{-1} (250 $dm^3\,mol^{-1}\,cm^{-1}$).

3.2. *[Os{PhTe(CH$_2$)$_3$TePh}$_2$Cl$_2$]*

The method used was the same as for the previous complex, giving a red powder. Yield: 40 mg, 32%. *Anal*. Calc. for $C_{30}H_{32}Cl_2OsTe_4$: C, 31.0; H, 2.8. Found: C, 30.8; H, 2.9%. ^{1}H NMR ($CDCl_3$, 300 MHz): δ 3.0–3.5 (6H, CH_2), 7.4–7.9 (10H, Ph). ^{125}Te{^{1}H} NMR ($CDCl_3/CH_2Cl_2$ 113 MHz): δ 478, 489, 513, 523, 548. IR spectrum (CsI disc): 3042 (m), 2921 (w), 1571 (m), 1474 (s), 1433 (s), 1415 (m), 1396 (m), 1359 (s), 1200 (m), 1061 (m), 1018 (m), 996 (m), 754 (w), 730 (s), 691 (s), 614 (w), 490 (w), 453 (w), 259 (w), 227 (w). UV–Vis spectrum (MeCN): $\nu_{max}=21000$ ($\varepsilon_{mol}=180$), 24600 (540), 38300 cm^{-1} (18235 $dm^3\,mol^{-1}\,cm^{-1}$).

3.3. *[Os{o-C$_6$H$_4$(TeMe)$_2$}$_2$Cl$_2$]*

The method used was the same as for the previous complex, giving an orange powder. Yield: 29%. *Anal*. Calc. for $C_{16}H_{20}Cl_2OsTe_4$: C, 19.5; H, 2.1. Found: C, 19.4; H, 1.9%. ^{1}H NMR ($CDCl_3$, 300 MHz): δ 2.05–2.3 (6H, CH_3), 7.2–7.8 (4H, C_6H_4). ^{125}Te{^{1}H} NMR ($CDCl_3/CH_2Cl_2$ 113 MHz): δ 656, 663, 671, 672, 673. Electrospray mass spectrum (MeCN) *m/z*: found M^+ 992, 948; calc. for $[^{192}Os\{C_6H_4(^{130}TeMe)\}_2{}^{35}Cl+MeCN]^+$ 1000, $[^{192}Os$-

$\{C_6H_4(^{130}TeMe)\}_2{}^{35}Cl]^+$ 959. IR spectrum (CsI disc): 2923 (w), 2851 (w), 1358 (s) 1260 (w), 1080 (s), 1019 (m), 835 (m), 753 (m), 685 (w), 614 (w), 548 (w), 427 (w), 326 (w), 302 (w). UV–Vis spectrum (MeCN): $\nu_{max}=22600$ cm^{-1} ($\varepsilon_{mol}=590$), 33200 (sh) cm^{-1} (6300 dm^{3}mol^{-1}cm^{-1}).

3.4. $[OsCl(PPh_3)(MeSCH_2CH_2SMe)_2]PF_6$

$[OsCl_2(PPh_3)_3]$ (0.1 g, 0.095 mmol) and $MeSCH_2CH_2SMe$ (0.06 g, 0.29 mmol) were refluxed together in ethanol (10 cm^3) for 2 h, during which time the colour changed from green to orange. After cooling to room temperature, NH_4PF_6 (0.06 g, 0.32 mol) was added and the solution concentrated to 3 cm^3 to give an orange solid, which was filtered off and recrystallised from CH_2Cl_2–Et_2O. Yield: 0.069 g, 70%. *Anal*. Calc. for $C_{26}H_{35}ClF_6OsP_2S_4$: C, 35.5; H, 4.0. Found: C, 35.0; H, 3.3%. Electrospray mass spectrum (MeCN) *m/z*: found M^+ 734; calc. for $[^{192}Os^{35}Cl(PPh_3)(MeSCH_2CH_2SMe)_2]^+$ 733. IR (CsI disc): 2930 (w), 1435 (m), 1357 (m), 1091 (m), 839 (s), 750 (m), 699 (s), 516 (m), 504 (m). ^{1}H NMR (300 MHz $CDCl_3$): δ 2.6 (s), 2.74 (s). $^{31}P\{^1H\}$ (145 MHz, $CH_2Cl_2/CDCl_3$): δ −15.1 (s), −147 (septet).

3.5. $[OsCl(PPh_3)(MeSeCH_2CH_2CH_2SeMe)_2]PF_6$

The method used was similar to that described in Section 3.4, giving a brown solid. Yield: 70%. *Anal*. Calc. for $C_{28}H_{39}ClF_6OsP_2Se_4$: C, 30.9; H, 3.2. Found: C, 30.2; H, 3.0%. Electrospray mass spectrum (MeCN) *m/z*: found M^+ 949; calc. for $[^{192}Os^{35}Cl(PPh_3)(Me^{80}SeCH_2CH_2{}^{80}SeMe)_2]^+$ 753. IR (CsI disc): 2927 (w), 2850 (w), 1434 (w), 1413 (w), 1089 (m), 999 (w), 840 (s), 751 (m), 699 (s), 558 (s), 537 (m), 499 (w), 440 (w). ^{1}H NMR (300 MHz $CDCl_3$): δ 1.72 (q), 2.25 (s), 2.85 (t), 7.4–7.7 (m). $^{31}P\{^1H\}$ (145 MHz, $CH_2Cl_2/CDCl_3$): δ −14.0(s), −147 (septet).

3.6. $[OsCl(PPh_3)\{MeTe(CH_2)_3TeMe\}_2]PF_6$

The method used was the same as described in Section 3.4, giving a yellow solid. Yield: 75%. *Anal*. Calc. for $C_{28}H_{39}ClF_6OsP_2Te_4$: C, 26.1; H, 3.0. Found: C, 26.5; H, 2.1%. Electrospray mass spectrum (MeCN) *m/z*: found M^+ 1143; calc. for $[^{192}Os^{35}Cl(PPh_3)(Me^{130}Te(CH_2)_3Me)_2]^+$ 1153. IR (CsI disc): 2921 (w), 1634 (w), 1417 (w), 1201 (w), 1088 (m), 841 (s), 753 (w), 688 (m), 556 (m), 539 (m), 517 (w), 278 (w). ^{1}H NMR (300 MHz $CDCl_3$): δ 1.57 (m), 1.78 (s), 1.96 (s), 2.02 (s), 2.25 (s), 3.2–3.4 (m), 7.4–7.6 (m). $^{31}P\{^1H\}$ (145 MHz, $CH_2Cl_2/CDCl_3$): δ −13.0 (s), −147 (septet). $^{125}Te\{^1H\}$ NMR (114 MHz, $CH_2Cl_2/CDCl_3$): δ 361, 411, 422, 430.

3.7. $[OsCl(PPh_3)\{PhTe(CH_2)_3TePh\}_2]PF_6$

The method used was the same as described in Section 3.4, giving a yellow solid. Yield: 87%. *Anal*. Calc. for $C_{48}H_{47}ClF_6OsP_2Te_4$: C, 37.5; H, 3.0. Found: C, 37.9; H, 2.4%. Electrospray mass spectrum (MeCN) *m/z*: found M^+ 1391; calc. for $[^{192}Os^{35}Cl(PPh_3)(PhTe(CH_2)_3TePh)_2]^+$ 1401. IR (CsI disc): 3050 (w), 2932 (w), 1477 (w), 1435 (m), 1362 (m), 1088 (m), 1017 (w), 938 (s), 735 (s), 688 (s), 558 (m), 536 (m), 454 (w), 250 (m). ^{1}H NMR (300 MHz $CDCl_3$): δ 2.2 (m), 2.9–3.3 (m), 7.0–7.8 (m). $^{31}P\{^1H\}$ (145 MHz, $CH_2Cl_2/CDCl_3$): δ −10.5(s), −11.8(s), −145 (septet). $^{125}Te\{^1H\}$ NMR (114 MHz, $CH_2Cl_2/CDCl_3$): δ 454, 463, 499, 540, 565.

3.8. $[OsCl_2(Ph_2Sb(CH_2)_3SbPh_2)_2]$

$[OsCl_2(dmso)_4]$ (0.05 g, 0.09 mmol) and $Ph_2Sb(CH_2)_3SbPh_2$ (0.16 g, 0.27 mmol) were refluxed together in ethanol (10 cm^3) for 3 h. The solvent was removed in vacuo, CH_2Cl_2 added to the residue, the solution filtered and the orange product precipitated with Et_2O. Yield: 0.045 g, 35%. *Anal*. Calc. for $C_{54}H_{52}Cl_2OsSb_4\cdot CH_2Cl_2$: C, 43.1; H, 3.4. Found: C, 43.1; H, 2.8%. Electrospray mass spectrum (MeCN) *m/z*: found M^+ 1450. calc. for $[^{192}Os^{35}Cl_2(Ph_2{}^{121}Sb(CH_2)_3{}^{121}SbPh_2)_2]^+$ 1446. IR (CsI disc): 3066 (m), 3049 (m), 1480 (w), 1432 (s), 1360 (m), 1102 (m), 1069 (s), 998 (m), 727 (s), 695 (s), 451 (s), 267 (m). UV–Vis spectrum (CH_2Cl_2): $\nu_{max}=30860$ (sh), ($\varepsilon_{mol}=2200$), 22230 (sh) cm^{-1} (250 dm^3 mol^{-1} cm^{-1}). $^{13}C\{^1H\}$ NMR ($CH_2Cl_2/CDCl_3$): δ 15.8, 24.3, 128–137. CV CH_2Cl_2: reversible +0.3 V versus SCE.

3.9. X-ray structure determination of $PhTeCl_2(CH_2)_3TeCl_2Ph\cdot MeCN$, $[OsCl_2\{PhTe(CH_2)_3TePh\}_2]$ and $[OsCl_2\{Ph_2Sb(CH_2)_3SbPh_2\}_2]\cdot 2CH_2Cl_2$

Details of the crystallographic data collection and refinement parameters are given in Table 4. Data collection used a Rigaku AFC7S four-circle diffractometer operating at 150 K (except for $PhCl_2Te(CH_2)_3TePhCl_2\cdot MeCN$, 295 K), using graphite-monochromated Mo Kα X-ray radiation ($\lambda=0.71073$ Å). For $PhCl_2Te(CH_2)_3TePhCl_2\cdot MeCN$ (295 K) preliminary psi-scans showed no significant absorption. The structure was solved by direct methods [22] and refined by iterative cycles of least-squares refinement [23]. All non-H atoms were refined anisotropically and H atoms were placed in fixed, calculated positions. Selected bond lengths and angles are given in Table 1. For $[OsCl_2\{PhTe(CH_2)_3TePh\}_2]$ preliminary psi scans did not provide a satisfactory absorption correction, hence, with the model at isotropic convergence, the data were corrected for absorption using DIFABS [24]. and for $[OsCl_2\{Ph_2Sb(CH_2)_3SbPh_2\}_2]\cdot 2CH_2Cl_2$ the data were corrected for absorption using psi-scans. Both Os structures were solved by heavy atom methods [25] and developed by iterative cycles of full-matrix least-squares refinement [23] and difference Fourier syntheses. All fully occupied non-H atoms were refined anisotropically and H-atoms were placed in fixed, calculated positions (the H atoms associated with the disordered CH_2Cl_2

Table 4
Crystallographic data

	$PhTeCl_2(CH_2)_3TePhCl_2 \cdot MeCN$	$[OsCl_2\{PhTe(CH_2)_3TePh\}_2]$	$[OsCl_2\{Ph_2Sb(CH_2)_3SbPh_2\}_2] \cdot 2CH_2Cl_2$
Formula	$C_{17}H_{19}Cl_4NTe_2$	$C_{30}H_{32}Cl_2OsTe_4$	$C_{56}H_{56}Cl_6OsSb_4$
FW	639.37	1164.09	1618.98
Crystal system	Monoclinic	monoclinic	triclinic
Space group	$P2_1/n$	$P2_1/n$	P-1
a (Å)	7.931(3)	8.684(5)	12.096(3)
b (Å)	26.889(4)	7.225(6)	12.226(3)
c (Å)	10.695(3)	25.205(2)	11.510(4)
α (°)	90	90	107.43(2)
β (°)	110.20(2)	94.00(2)	114.96(3)
γ (°)	90	90	96.17(2)
U (Å^3)	2140(1)	1577(1)	1417.4(9)
Z	4	2	1
D_{calc} (g cm^{-3})	1.968	2.451	1.897
μ(Mo Kα) (cm^{-1})	32.25	78.54	44.28
Absolute correction (max., min. transmission factors)		1.000, 0.559	1.000, 0.479
Unique observed reflections	3872	3040	4983
Observed reflections with $I_0 > 2\sigma(I_0)$	2785	2254	4308
No. of parameters	217	169	297
R [a]	0.027	0.052	0.036
R_w [b]	0.032	0.058	0.052

[a] $R = \sum(|F_{obs}|_i - |F_{calc}|_i) / \sum |F_{obs}|_i$.
[b] $R_w = \sqrt{[\sum w_i(|F_{obs}|_i - |F_{calc}|_i)^2 / \sum w_i |F_{obs}|_i^2]}$.

solvent molecules were omitted from the final structure factor calculation). In both cases the Os(II) species was found to have crystallographic inversion symmetry, with the Os atom occupying an inversion centre. Two half CH_2Cl_2 solvent molecules, disordered across crystallographic inversion centres, were also identified in the asymmetric unit in the structure of $[OsCl_2\{Ph_2Sb(CH_2)_3SbPh_2\}_2]$. Selected bond lengths and angles are given in Tables 2 and 3.

Supplementary data

Supplementary data have deposited at the Cambridge Crystallographic Data Centre, CCDC reference numbers 135001–135003.

Acknowledgements

We thank the EPSRC for support and Johnson Matthey plc for generous loans of osmium.

References

[1] W.P. Griffith, in: G. Wilkinson, R.R. Gillard, J.A. McCleverty (Eds.), Comprehensive Coordination Chemistry, vol. 4, Pergamon, Oxford, 1987, p. 519.
[2] D.J. Gulliver, W. Levason, K.G. Smith, M.J. Selwood, S.G. Murray, J. Chem. Soc., Dalton Trans. (1980) 1872.
[3] E.G. Hope, W. Levason, M. Webster, S.G. Murray, J. Chem. Soc., Dalton Trans. (1986) 1003.
[4] S.K. Harbron, W. Levason, J. Chem. Soc., Dalton Trans. (1985) 205
[5] S.K. Harbron, W. Levason, J. Chem. Soc., Dalton Trans. (1987) 633.
[6] T. Kemmitt, W. Levason, M. Webster, Inorg. Chem. 28 (1989) 692.
[7] T. Kemmitt, W. Levason, Inorg. Chem. 29 (1990) 731.
[8] W. Levason, S.D. Orchard, G. Reid, V.-A. Tolhurst. J. Chem. Soc., Dalton Trans. (1999) 2071.
[9] A.B.P. Lever, Inorganic Electronic Spectroscopy, Elsevier, New York, 2nd edn., 1984.
[10] N.P. Luthra, J.D. Odom, in: S. Patai, Z. Rappoport (Eds.), The Chemistry of Organic Selenium and Tellurium Compounds, vol. 1, Wiley, New York, 1986, p. 189.
[11] R.J. Batchelor, F.W.B. Einstein, C.H.W. Jones, R.D. Sharma, Organometallics 6 (1987) 2164.
[12] A.M. McDonagh, M.G. Humphrey, D.C.R. Hockless, Aust. J. Chem. 51 (1998) 807.
[13] W. Levason, N.R. Champness, M. Webster, Acta Crystallogr., Sect. C 49 (1993) 1884.
[14] F.A. Cotton, M.P. Diebold, M. Matusz, Polyhedron 6 (1987) 1131.
[15] N.J. Holmes, W. Levason, M. Webster, J. Chem. Soc., Dalton Trans. (1997) 4223.
[16] E.W. Abel, S.K. Bhargava, K.G. Orrell, Prog. Inorg. Chem. 32 (1984) 1.
[17] E.W. Abel, K.G. Orrell, S.P. Scanlan, D. Stephenson, T. Kemmitt, W. Levason. J. Chem. Soc., Dalton Trans. (1991) 591.
[18] N.R. Champness, W. Levason, R.A.S. Mould, D. Pletcher, M. Webster, J. Chem. Soc., Dalton Trans. (1991) 2777.
[19] R.A.S. Mould, Ph.D. Thesis, University of Southampton, 1991.
[20] N.R. Champness, W. Levason, D. Pletcher, M.D. Spicer, M. Webster, J.Chem. Soc., Dalton Trans. (1992) 2201.
[21] N.R. Champness, W. Levason, M. Webster, Inorg. Chim. Acta 208 (1993) 189.
[22] G.M. Sheldrick, SHELXS-86, Acta Crystallogr., Sect. A 46 (1990) 467.
[23] TeXsan: Crystal Structure Analysis Package, Molecular Structure Corporation, TX, 1995.
[24] N. Walker, D. Stuart, Acta Crystallogr., Sect. A 39 (1983) 158.
[25] P.T. Beurskens, G. Admiraal, G. Beurskens, W.P. Bosman, S. Garcia-Granda, R.O. Gould, J.M.M. Smits, C. Smykalla, PATTY, The DIRDIF Program System, Technical Report of the Crystallography Laboratory, University of Nijmegen, The Netherlands, 1992.

PERGAMON

www.elsevier.nl/locate/poly

Polyhedron 19 (2000) 241–245

POLYHEDRON

Copper(II) complexes of deltakephalin and its analogues containing α-hydroxymethylserine

Teresa Kowalik-Jankowska [a,*], Wojciech Leśniak [a], Justyna Brasuń [a], Marcin Stasiak [b], Mirosław T. Leplawy [b]

[a] *Faculty of Chemistry, University of Wrocław, F. Joliot-Curie 14, 50-383 Wrocław, Poland*
[b] *Institute of Organic Chemistry, Technical University of Łódź, 90-924 Łódź, Poland*

Received 13 September 1999; accepted 1 December 1999

Abstract

Potentiometric and spectroscopic data have shown that deltakephalin and its derivatives containing the α-hydroxymethylserine (HmS) residue in the second and in the second and sixth positions form the same series of complexes: CuHL, CuL, $CuH_{-1}L$, $CuH_{-2}L$ and $CuH_{-3}L$ (1N to 4N binding mode). The alcoholic groups in the amino acid side chain are very effective in the stabilization of the complexes formed (the protonation corrected stability constants, log *K**, values of 4N complexes are −22.55 and −21.15 for deltakephalin and its derivative containing the HmS residue in the second and sixth positions, respectively). There is no evidence for the direct involvement of alcoholic groups of HmS in binding of Cu^{2+} ions and there is no indication of binding through the tyrosine-phenolate oxygen atoms, either. ©2000 Elsevier Science Ltd All rights reserved.

Keywords: Copper(II) complexes; Deltakephalins; Stability constants

1. Introduction

α-Hydroxymethylserine (HmS) belongs to the family of α,α-dialkyl amino acids, which are useful replacements for proteinaceous amino acids because of their strong secondary structure-promoting effects and the increased proteolytic stability of the resulting peptides [1,2]. One can expect that in addition to generating specific constraints on the conformational freedom of the peptide chain, HmS would furnish peptides with enhanced hydrophilicity, advantageous for an increase in bioavailability. Preferred conformations of peptides derived from HmS and its *O*,*O*-isopropylidene protected derivative HmS (Ipr) have been reported recently [3,4]. Interest in HmS is stimulated also by its potential to increase the stability of metal complexes. The involvement of the protonated hydroxyl groups of HmS or Ser may stabilize complexes at lower pH [5–11], whereas direct binding of deprotonated hydroxyl oxygen occurring at high pH makes these amino acids efficient chelating agents above pH 8 [5,6,8–11]. The presence of HmS residues in oligopeptides may increase by almost four orders of magnitude the stability constants of copper(II) complexes as compared to homo-oligopeptides such as oligoalanine [11]. This result indicates that there are very effective indirect interactions involving the α-hydroxymethyl side chains, which stabilize the complexes formed.

In the present work the copper(II) complexes of deltakephalin Tyr-(D)-Thr-Gly-Phe-Leu-Thr (**1**) and its analogues Tyr-HmS-Gly-Phe-Leu-Thr (**2**) and Tyr-HmS-Gly-Phe-Leu-HmS (**3**) containing α-hydroxymethylserine were examined.

Deltakephalin (**1**) is an opioid agonist, highly selective toward δ-receptors. In analogues **2** and **3** one or both threonine residues are replaced by α-hydroxymethylserine bearing the additional OH group.

2. Experimental

2.1. Peptide synthesis

Hexapeptide analogues **2** and **3** of deltakephalin **1** were synthesized applying fragment condensation (3 + 3) strategy with the use of TBTU (*O*-benzotriazol-1-yl-*N*,*N*,*N*′,*N*′-tetramethyluronium tetrafluoroborate) [12] as the coupling reagent. The *O*,*O*-isopropylidene (Ipr) protected α-hydroxy-

* Corresponding author. Tel.: +48-71-320431; fax: +48-71-3282348; e-mail: terkow@wchuwr.chem.uni.wroc.pl

0277-5387/00/$ - see front matter ©2000 Elsevier Science Ltd All rights reserved.
PII S0277-5387(99)00377-0

methylserine [13] was incorporated into a peptide chain applying HATU (*O*-7-azabenzotriazol-1-yl-*N*,*N*,*N*′,*N*′-tetramethyluronium hexafluorophosphate) [14] or mixed anhydride [15] method. The benzyl type protective groups were removed from the fully protected hexapeptides by hydrogenation (24–72 h) in the presence of 10% Pd/charcoal catalyst on a Parr apparatus at room temperature and a pressure of 4 kg cm^{-2}. The Boc (t-butoxycarbonyl) and Ipr were then removed by treatment with 90% aq. TFA (trifluoroacetic acid) for 15 min. After evaporation, the products were purified by preparative HPLC. The homogeneity of title hexapeptides was checked by TLC (thin-layer chromatography, butanol:acetic acid:water 3:1:1) and by analytical HPLC (linear gradient over 25 min: 10–40% of acetonitrile in water + 0.1% TFA). FAB-MS spectra were recorded on an APO Electron (MI 12001E) spectrometer. The purity of peptide ligands was checked by potentiometry.

2.2. Potentiometric measurements

Stability constants for proton and Cu^{2+} complexes were calculated from pH-metric titrations carried out in argon atmosphere at 298 K using a total volume of 2.0 cm^3. Alkali was added from a 0.250 cm^3 micrometer syringe which was calibrated by both weight titration and the titration of standard materials.

Experimental details: ligand concentration 2×10^{-3} mol dm^{-3}; metal-to-ligand ratio 1:1.5; ionic strength 0.1 mol dm^{-3} (KNO_3); pH-metric titration on a MOLSPIN pH-meter system using a microcombined glass–calomel electrode, calibrated in concentration using HNO_3 [16]; number of titrations 4; method of calculation SUPERQUAD [17]. The samples were titrated in the pH region 2.5–10.5. Standard deviations (σ values) quoted were computed by SUPERQUAD and refer to random errors only. They are, however, a good indication of the importance of the particular species involved in the equilibria.

2.3. Spectroscopic measurements

EPR spectra were recorded on a Bruker ESP 300E spectrometer at X-band frequency (9.3 GHz) at 120 K. CD spectra were recorded on a Jasco J-600 spectropolarimeter in the range 200–750 nm. The latter results are expressed in $\Delta\varepsilon = \varepsilon_l - \varepsilon_r$, where $\Delta\varepsilon$ is evaluated at the maximum concentration of the particular species as obtained from potentiometric data. Absorption spectra were recorded on a Beckman DU650 spectrophotometer. The metal concentration in all spectroscopic measurements was adjusted to 2×10^{-3} mol dm^{-3} and the metal-to-ligand molar ratio was 1:1.5.

3. Results and discussion

Calculated protonation constants for the studied ligands are given in Table 1. Deltakephalin and its α-hydroxymethylated derivatives (H_3L) have three protonation centres, the phenolate oxygen of the tyrosine residue (log *K* value 9.93–9.67), the terminal amino group (log *K* value 7.24–7.14) and the carboxylate group (log *K* value 3.43–3.25). The acidity of the phenolic proton in the studied ligands is comparable to that measured for N-terminal tyrosine residues in the enkephalin, enkephalin analogues and fragments of the casomorphin series studied previously [18,19]. The insertion of D-threonine or α-hydroxymethylserine into the second position has only a slight effect on the acidity of the amino group of the studied peptides compared to methionine enkephalin (Met-EN, Table 1). The presence of the HmS residue on the C-terminal deltakephalin derivative does not affect the carboxylate p*K* value, similar to results determined for other peptides containing this residue [10,11].

According to potentiometric data calculations, deltakephalin and its α-hydroxymethylated derivatives form with Cu^{2+} ions the series of complexes CuHL, CuL, $CuH_{-1}L$, $CuH_{-2}L$ and $CuH_{-3}L$ (charges omitted for simplicity). The stability constants of copper(II) complexes are collected in Table 2, where $\beta(CuH_jL) = [CuH_jL]/[Cu^{2+}][H]^j[L]$. The species distribution curves are shown in Fig. 1 and the spectroscopic parameters of the complexes formed are given in Table 3.

The coordination pattern for all studied Cu^{2+}–ligand systems was found to be the same with bonding commencing at the N-terminal amino-NH_2 site followed by sequential deprotonation and coordination of neighbouring peptide nitrogens.

Table 1
Protonation constants for deltakephalin, its hydroxymethylated derivatives and comparable peptides at $T = 298$ K and $I = 0.10$ mol dm^{-3} (KNO_3)

Peptide	log β			log *K*		
	HL	H_2L	H_3L	Tyr-O^-	NH_2	COO^-
Tyr-D-Thr-Gly-Phe-Leu-Thr	9.93 ± 0.01	17.17 ± 0.01	20.54 ± 0.01	9.93	7.24	3.37
Tyr-HmS-Gly-Phe-Leu-Thr	9.76 ± 0.01	16.90 ± 0.01	20.33 ± 0.01	9.76	7.14	3.43
Tyr-HmS-Gly-Phe-Leu-HmS	9.67 ± 0.01	16.88 ± 0.01	20.13 ± 0.01	9.67	7.21	3.25
Met-EN [a]	9.82	17.26	20.72	9.82	7.44	3.46
Gly-Gly-Gly-Gly-Gly [a]	7.86	11.25			7.86	3.39
Asn-Ser-Phe-Arg-Tyr-NH_2 [b]	9.62	16.06		9.62	6.44	

[a] Ref. [18].
[b] Ref. [25].

Table 2
Stability constants of Cu(II) complexes of deltakephalin, its hydroxymethylated derivatives and comparable peptides (concentration constants at 298 K and $I = 0.10$ mol dm^{-3} (KNO_3))

	Log β				
	CuHL	CuL	$CuH_{-1}L$	$CuH_{-2}L$	$CuH_{-3}L$
Tyr-D-Thr-Gly-Phe-Leu-Thr	14.34 ± 0.02	9.50 ± 0.01	3.18 ± 0.01	−5.38 ± 0.01	−15.49 ± 0.01
Tyr-HmS-Gly-Phe-Leu-Thr	13.65 ± 0.09	9.65 ± 0.01	3.77 ± 0.01	−4.58 ± 0.01	−14.64 ± 0.01
Tyr-HmS-Gly-Phe-Leu-HmS	14.72 ± 0.02	10.00 ± 0.01	4.31 ± 0.01	−4.27 ± 0.01	−14.07 ± 0.01
Met-EN [a]	14.4	9.25	2.13	−6.36	−16.07
Gly-Gly-Gly-Gly-Gly [a]		5.32	−0.68	−7.58	−15.62
Asn-Ser-Phe-Arg-Tyr-NH_2 [b]	14.13	9.15	2.71	−4.02	−13.50
Values corrected for protonation of Tyr-O^- in deltakephalin and its hydroxymethylated derivatives [c]					
	1N	2N	3N	4N	
Tyr-D-Thr-Gly-Phe-Leu-Thr	4.23	−0.61	−6.93	−15.49	
Tyr-HmS-Gly-Phe-Leu-Thr	3.59	−0.41	−6.29	−14.64	
Tyr-HmS-Gly-Phe-Leu-HmS	4.92	0.20	−5.49	−14.07	
Met-EN [a]	4.69	−0.46	−7.58	−16.07	
Gly-Gly-Gly-Gly-Gly [a]	5.32	−0.68	−7.58	−15.62	
Asn-Ser-Phe-Arg-Tyr-NH_2 [b]	4.65	−0.33	−6.77	−13.50	
	Log K^* values [d]				
	1N	2N	3N	4N	
Tyr-D-Thr-Gly-Phe-Leu-Thr	−2.83	−7.67	−13.99	−22.55	
Tyr-HmS-Gly-Phe-Leu-Thr	−3.25	−7.25	−13.13	−21.48	
Tyr-HmS-Gly-Phe-Leu-HmS	−2.16	−6.88	−12.57	−21.15	
Met-EN [a]	−2.86	−8.01	−15.13	−23.62	
Gly-Gly-Gly-Gly-Gly [a]	−2.54	−8.54	−15.44	−23.48	
Asn-Ser-Phe-Arg-Tyr-NH_2 [b]	−1.93	−6.91	−13.35	−20.08	

[a] Ref. [18].
[b] Ref. [25].
[c] Log K for protonation of Tyr-O^- in deltakephalins calculated from log $\beta(CuH_{-2}L) - \log \beta(CuH_{-3}L)$.
[d] Log $K^* = \log \beta(CuH_jL) - \log \beta(H_2L)$ (or $\beta(HL)$ with Gly-Gly-Gly-Gly-Gly).

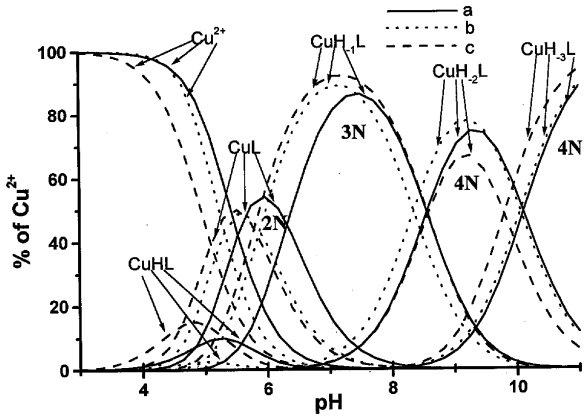


Fig. 1. Comparision of the species distribution curves for 1:1 mixtures of Cu^{2+} with Tyr-D-Thr-Gly-Phe-Leu-Thr (a), Tyr-HmS-Gly-Phe-Leu-Thr (b) and Tyr-HmS-Gly-Phe-Leu-HmS (c) ($C_{Cu(II)} = 0.001$ mol dm^{-3}).

In all these cases the first complex to form, starting at low pH, was the CuHL species, which may be regarded as comparable to the CuL complex of pentaglycine with an additional protonated phenolic residue (on Tyr[1]). The CuHL complex is of low concentration, and it is a minor component of the complex equilibria in Cu^{2+}–linear peptide systems with 1N coordination {NH_2, CO} [20,21]. This species cannot be supported by spectroscopic data because of its low concentration (Fig. 1). With increasing pH, this complex loses the amide proton to give a species of stoichiometry CuL. The EPR parameters $A_\parallel = 170$–180 G and $g_\parallel = 2.251$–2.246, d–d transition energy of 631–622 nm and the presence in the CD spectra of an $N^- \Rightarrow Cu^{2+}$ charge transfer transition at 317–290 nm are consistent with the 2N coordination {NH_2, N^-, CO} of the peptides to copper(II) ions (Table 3) [20].

At pH 6–9, the $CuH_{-1}L$ complex with {NH_2, $2N^-$, CO} coordination mode is formed. This binding mode is easily seen in the EPR, absorption and CD spectra (Table 3). The d–d transition at 561–552 nm, the parameters of the CD spectra as well as $A_\parallel = 191$–198 G and $g_\parallel = 2.213$–2.206 correspond to the three nitrogen bonding mode [20].

Above pH 7, this complex loses the next amide proton to give a $CuH_{-2}L$ species which has four nitrogen donor centres arranged in a square planar geometry around the central copper(II) ion (Fig. 1). The shift of absorption maximum to 526–506 nm, and the EPR parameters $A_\parallel = 213$–201 G,

Table 3
Spectroscopic data for Cu(II) complexes of deltakephalin and its hydroxymethylated derivatives. The values of the molar quantities given in this table are approximate estimates (see text)

Ligand/species	UV–Vis		CD		EPR		Donor set
	λ (nm)	ε	λ (nm)	$\Delta\varepsilon$ (dm^3 mol^{-1} cm^{-1})	$A_\parallel$ (G)	$g_\parallel$	
Tyr-D-Thr-Gly-Phe-Leu-Thr							
CuL	631 [a]	42	569 [a]	+0.243	170	2.251	2N {NH_2, N^-, CO}
			317 [b]	−0.463			
$CuH_{-1}L$	561 [a]	73	538 [a]	+1.071	193	2.213	3N {NH_2, $2N^-$, CO}
			320 [b]	−0.984			
$CuH_{-2}L$	526 [a]	108	515 [a]	+1.583	201	2.195	4N {NH_2, $3N^-$}
			313 [b]	−1.489			
$CuH_{-3}L$	525 [a]	112	513 [a]	+1.757	204	2.184	4N {NH_2, $3N^-$}
			309 [b]	−1.583			
Tyr-HmS-Gly-Phe-Leu-Thr							
CuL	625 [a]	50	658 [a]	+0.175	178	2.246	2N {NH_2, N^-, CO}
			290 [b]	−0.290			
			276 [c]	+0.083			
$CuH_{-1}L$	556 [a]	83	566 [a]	+0.213	191	2.213	3N {NH_2, $2N^-$, CO}
			313 [b]	+0.127			
			281 [c]	+0.077			
$CuH_{-2}L$	511 [a]	105	544 [a]	+0.396	203	2.192	4N {NH_2, $3N^-$}
			319 [b]	+0.044			
$CuH_{-3}L$	505 [a]	121	538 [a]	+0.349	209	2.173	4N {NH_2, $3N^-$}
			321 [b]	−0.161			
			269 [c]	−1.239			
Tyr-HmS-Gly-Phe-Leu-HmS							
CuL	622 [a]	50	675 [a]	+0.076	170	2.251	2N {NH_2, N^-, CO}
			307 [b]	+0.039			
			274 [c]	+0.169			
$CuH_{-1}L$	552 [a]	128	596 [a]	+0.082	198	2.206	3N {NH_2, $2N^-$, CO}
			470 [a]	+0.049			
			300 [b]	+0.203			
			280 [c]	+0.174			
$CuH_{-2}L$	506 [a]	146	536 [a]	+0.082	213	2.172	4N {NH_2, $3N^-$}
			305 [b]	−0.025			
$CuH_{-3}L$	504 [a]	183	537 [a]	+0.160	213	2.170	4N {NH_2, $3N^-$}
			320 [b]	−0.058			
			290 [c]	+0.236			

[a] d–d transition.
[b] $N^- \Rightarrow Cu^{2+}$ charge transfer transition.
[c] $NH_2 \Rightarrow Cu^{2+}$ charge transfer transition.

$g_\parallel = 2.195$–2.172 suggest coordination of the nitrogen donor atom to the copper(II) (Table 3) [20].

Increasing the pH above 8 results in the formation of a species of formula $[CuH_{-3}L]$. This complex has similar bonding mode to that of $[CuH_{-2}L]$ species, with the phenolic oxygen deprotonated. The EPR, CD and absorption parameters of $CuH_{-3}L$ species are similar to those obtained for the $CuH_{-2}L$ complex (Table 3).

The phenolate-O of the Tyr residue does not coordinate to the metal ion which is supported by complete absence of the characteristic charge-transfer band in the CD spectrum at 420 nm (Table 3) [22], and the protonation constant of the $[CuH_{-3}L]$ complex (9.80–10.11) is comparable to that for protonation of the Tyr residue in the free ligand (9.67–9.93) (Tables 1 and 2).

According to the potentiometric data, there is no evidence for the direct involvement of alcoholic groups of HmS in bonding copper(II) ions in the studied pH range (2.50–10.50) because no additional deprotonations are observed in the complexes formed.

Spectroscopic results are in good agreement with potentiometric results indicating the formation of the complexes 1N to 4N.

The stability constants for complexes formed with deltakephalin and its derivatives can be corrected for the phenolate protonation constant of the Tyr residue by subtracting the protonation constant of the $[CuH_{-3}L]$ complex from each to give log values for the stability constants of 1N to 4N complexes (Table 2). These values obtained for deltakephalin are comparable with those for methionine-enkephalin (Met-EN) and pentaglycine. Incorporation of α-hydroxymethylserine into the peptide sequence causes a distinct gain in stability for 3N and 4N complexes. The stability gain of 1.5 log units versus deltakephalin is seen for

the 3N and 4N complexes with the derivative of deltakephalin containing HmS residue in the second and sixth positions.

Stabilization of complexes may be quantified in a number of ways, including by comparing the equilibria:

$$Cu^{2+} + R\text{–}NH_3^+ \Leftrightarrow H^+ + (R\text{–}NH_2)Cu^{2+}$$

Assuming that the phenolic-O^- group of the Tyr residue is protonated, this may be represented by $\log K^* = \log \beta(CuH_jL) - \log \beta(H_2L)$. Values of $\log K^*$ for complexes with 1N to 4N coordination (i.e. j is 1, 0, -1 and -2, respectively) are given in Table 2. These values are the protonation corrected stability constants which are useful for comparing the ability of ligands to bind a metal ion. The data for $\log K^*$ collected in Table 2 for deltakephalin and its derivatives clearly indicate that the incorporation of the second HmS residue in the sixth position causes an increase in stability of a 1N complex by about 1 log unit compared to a derivative containing only one residue of HmS in the second position (Table 2). The amide nitrogen of the HmS residue in the sixth position does not coordinate copper(II) ions but two protonated alcoholic groups of this residue may participate in the stabilization of the 1N complex by the formation of hydrogen bonds with side chains of peptide or with the molecule of water coordinated to the copper(II) ion in the axial position [5–11].

The presence of HmS residues in chelate rings around Cu^{2+} ions in tri-HmS peptide causes an increase in the stability constant of 3N $[CuH_{-2}L]$ species by almost four orders of magnitude when compared to trialanine [11]. The insertion of the HmS residue in the second position of deltakephalin increases the stability ($\log K^*$, Table 2) of the 3N and 4N species by one order of magnitude when compared to deltakephalin. This increase in stability may originate from the partial shielding of the Cu^{2+} binding site from the bulk of the solution both from above and below the coordination plane [23,24]. The HmS residue in the sixth position may also shield the Cu^{2+} binding site. The stabilization of the 1N complex may suggest the presence of this residue above or below the coordination plane.

The stability of copper(II) complexes of deltakephalin derivative containing two HmS residues in the second and sixth positions is comparable to that of the pentapeptide fragment of ANF, Asn-Ser-Phe-Arg-Tyr-NH_2 ($\log K^*$ values in Table 2) [25]. This high stability of the formed complexes may result from the highly organized side chain structures of peptides in copper(II) complexes.

4. Conclusions

α-Hydroxymethylserine residue incorporated into deltakephalin has a distinct influence on the stability of copper(II) complexes. The incorporation of this residue in the second position of this oligopeptide increases the stability of 3N and 4N complexes by about 1 log unit of magnitude compared to deltakephalin. The amide nitrogen of the HmS residue coordinates the copper(II) ions, and two alcoholic groups are situated above and below the coordination plane and may cause shielding of the Cu^{2+} bonding site from the bulk of the solution. The increase in stability of the 1N complex after incorporation of the second HmS residue in the sixth position may suggest further shielding of the Cu^{2+} bonding site (the formation of hydrogen bonds).

Acknowledgements

This work was financially supported by the University of Wrocław, grant 2015/W/WCH/98/2. M.T.L. acknowledges support from the Polish Committee for Scientific Research (grant 3TO9A-11108).

References

[1] C. Toniolo, Janssen Chim. Acta 11 (1993) 10.
[2] C. Toniolo, E. Benedetti, Macromolecules 24 (1991) 4004.
[3] M. Lisowski, M. Stasiak, M.T. Leplawy, Pol. J. Chem. 73 (1999) 313.
[4] W. Wolf, M. Stasiak, M.T. Leplawy, A. Bianco, F. Formaggis, M. Crisma, C. Toniolo, J. Am. Chem. Soc. 120 (1998) 11558.
[5] T. Kowalik-Jankowska, K. Varnagy, C. Bartaln, J. Chem. Res. (S) (1993) 172.
[6] T. Kowalik-Jankowska, H. Kozłowski, K. Kociołek, M.T. Leplawy, G. Micera, Transition Met. Chem. 20 (1995) 23.
[7] L.D. Pettit, J.L.M. Swash, J. Chem. Soc. (1976) 2416.
[8] T. Kiss, C. Simon, Z. Vachter, J. Coord. Chem. 16 (1985) 225.
[9] H. Kozłowski, Z. Siatecki, Chem. Phys. Lett. 54 (1978) 498.
[10] T. Kowalik-Jankowska, H. Kozłowski, M. Stasiak, M.T. Leplawy, J. Coord. Chem. 40 (1996) 113.
[11] T. Kowalik-Jankowska, M. Stasiak, M.T. Leplawy, H. Kozłowski, J. Inorg. Biochem. 66 (1997) 193.
[12] R. Knorr, A. Trzeciak, W. Bannwarth, D. Gillesen, Tetrahedron Lett. 30 (1989) 1927.
[13] M. Stasiak, W.M. Wolf, M.T. Leplawy, J. Peptide Sci. 4 (1998) 46.
[14] L.A. Carpino, J. Am. Chem. Soc. 115 (1993) 4397.
[15] G.W. Andersen, J.E. Zimmerman, F.M. Callahan, J. Am. Chem. Soc. 89 (1967) 5012.
[16] H. Irving, M.G. Miles, L.D. Pettit, Anal. Chim. Acta 38 (1967) 475.
[17] P. Gans, A. Sabatini, A. Vacca, J. Chem. Soc., Dalton Trans. (1985) 1195.
[18] G. Formicka-Kozłowska, L.D. Pettit, I. Steel, C.E. Livera, G. Kupryszewski, K. Rolka, J. Inorg. Biochem. 24 (1985) 299.
[19] E. Chruścińska, J. Olczak, J. Zabrocki, M. Dyba, G. Micera, D. Sanna, H. Kozłowski, J. Inorg. Biochem. 69 (1998) 91.
[20] L.D. Pettit, J.E. Gregor, H. Kozłowski, in: R.W. Hay, J.R. Dilworth, K.B. Nolan (Eds.), Perspectives on Bioinorganic Chemistry, vol. 1, JAI Press, London, 1990, p. 1.
[21] I. Sovago, in: K. Burger (Ed.), Biocoordination Chemistry, Ellis Horwood, New York, 1990, p. 135.
[22] C. Livera, L.D. Pettit, M. Bataille, J. Krembel, W. Bal, H. Kozłowski, J. Chem. Soc., Dalton Trans. (1988) 1357.
[23] W. Bal, G.N. Chmurny, B.D. Hilton, P.J. Sadler, A. Tucker, J. Am. Chem. Soc. 118 (1996) 4727.
[24] P. Młynarz, W. Bal, T. Kowalik-Jankowska, M. Stasiak, M.T. Leplawy, H. Kozłowski, J. Chem. Soc., Dalton Trans. (1999) 109.
[25] W. Bal, H. Kozłowski, G. Kupryszewski, Z. Mackiewicz, L.D. Pettit, R. Robbins, J. Inorg. Biochem. 52 (1993) 79.

PERGAMON

www.elsevier.nl/locate/poly

Polyhedron 19 (2000) 249–257

POLYHEDRON

Structure–property relationships in *ortho*-metallated imine complexes of Re(I)

Marie-Andrée Guillevic, Mark J. Danks, Sarah K. Harries, Simon R. Collinson, Andrew D. Pidwell, Duncan W. Bruce *

School of Chemistry, University of Exeter, Stocker Road, Exeter EX4 4QD, UK

Received 12 May 1999; accepted 16 July 1999

Abstract

Two series of imine liquid crystals, one chiral the other not, have been synthesised and their Re(I) complexes have been prepared. The results have allowed comparisons of the effect of the nature of the terminal group and the position of the imine link on the mesomorphism of both the ligands and the complexes. Broadly speaking, the imines exhibit smectic C and nematic mesophases or, if the terminal chain is chiral, their chiral analogues. Complexation leads to the formation of only a nematic or chiral nematic phase at temperatures which are significantly lower than those for the ligand. ©2000 Elsevier Science Ltd. All rights reserved.

Keywords: Metallomesogens; Rhenium; Nematic phases; Chiral nematic phases

1. Introduction

The study of metal-containing liquid crystals (metallomesogens) has become an active area of interest both to inorganic chemists and to liquid crystal scientists in the last fifteen years or so. In expanding the field, groups have sought to increase the number of metallic elements that may be incorporated into liquid-crystal materials and to understand the relevant structure–property relationships in order to exert control over key parameters, such as melting and clearing points [1]. For many years, the literature of calamitic (rod-like) liquid crystals was dominated by complexes in which the metal was in a planar, four-coordinate environment, therefore necessarily restricting the metals which could be used. As part of our studies in this area, we became interested in the incorporation of metals with higher coordination numbers [2], which led to the synthesis of *ortho*-metallated complexes of Mn(I) [3,4]and Re(I) [5,6], diazabutadiene [7,8] and 2,2′-bipyridine [9,10] complexes of Re(I) and acetylene complexes of Rh(III) [11].

Liquid crystals rely on the presence of anisotropic dispersion forces to stabilise their mesophases, and these arise from a shape anisotropy of the molecules, generally coupled with a significant anisotropy of polarisability. However, while highly anisotropic motifs can be realised with a planar, four-coordinate metal centre, the addition of two extra ligands to generate formally octahedral coordination is likely to reduce significantly the overall anisotropy (see e.g. Ref. [7]). However, we found that this problem could be circumvented if the *liquid-crystalline* ligand were made sufficiently anisotropic so that the perturbation represented by the two 'extra' ligands could be screened out and, therefore, tolerated.

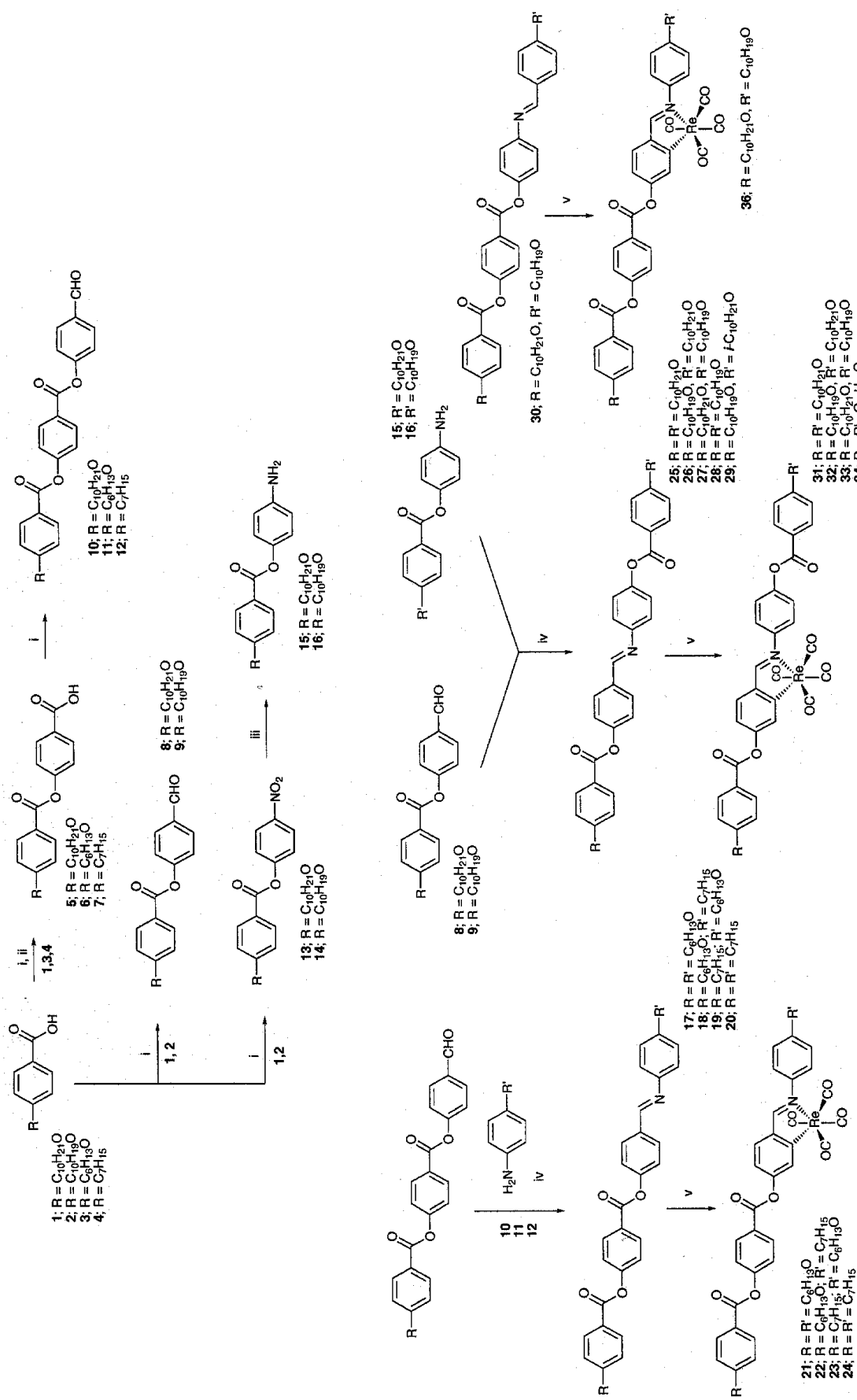
Of all of these systems, the *ortho*-metallated systems (Fig. 1) presented mesophases at the lowest temperatures, with melting points of around 120°C and clearing points as low as about 70°C. We therefore decided that these systems were worthy of greater study in order to minimise further transition temperatures and make them amenable to physical investigation. In this paper, we present the results of investigations which looked at both the introduction of chirality and the removal of the dipolar oxygen in the terminal chains.

2. Synthesis of the ligands and the complexes

The synthetic routes are outlined in Scheme 1. Alkoxybenzoic acids (**1**–**4**) and alkoxybenzaldehydes were obtained via a Williamson ether reaction between the relevant bromoalkane and either ethyl 4-hydroxybenzoate or 4-hydroxybenzaldehyde, followed by hydrolysis of the ethyl 4-alkoxybenzoate in the former case. Alkoxybenzoyloxy-

* Corresponding author. Tel.: +44-1392-263489; Fax: +44-1392-263434; e-mail: d.bruce@exeter.ac.uk

0277-5387/00/$ - see front matter ©2000 Elsevier Science Ltd. All rights reserved.
PII S0277-5387(99)00354-X



Scheme 1. Synthetic route to the ligands and complexes. Reagents and conditions: (i) DCC–DMAP–CH_2Cl_2; (ii) Pd–C, H_2; (iii) $SnCl_2$; (iv) EtOH–THF, room temperature, cat. AcOH; (v) [$ReMe(CO)_5$], toluene, reflux, N_2. *i*-$C_{10}H_{21}O$ refers to the hydrogenated citronellyloxy group (see text).

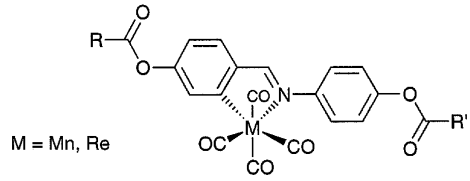


Fig. 1. General structure of the *ortho*-metallated complexes of Mn(I) and Re(I).

benzoic acids (**5**–**7**) were then obtained by esterification of the alkoxybenzoic acid with benzyl 4-hydroxybenzoate, followed by hydrogenolysis of the benzylalkoxybenzoyloxybenzoate; alkoxybenzoyloxybenzoyloxybenzaldehydes (**10**–**12**) were then obtained by subsequent esterification with 4-hydroxybenzaldehyde. Alkoxybenzoyloxynitrobenzenes (**13**, **14**) were obtained by esterification of alkoxybenzoic acids with 4-nitrophenol, and the corresponding amines (**15**, **16**) were obtained by reduction of the nitro group using tin(II) chloride. The target imines (**17**–**20** and **25**–**30**) were synthesised by reaction of a benzaldehyde with an aniline in an ethanol–THF mix with ethanoic acid as catalyst. Two imines are a little different. Thus, **30** was obtained from **5** by esterification with 4-hydroxynitrobenzene, reduction to the amine with $SnCl_2$ and then reaction with 4-citronellyloxybenzaldehyde. For imine **29**, the double bond in the citronellyloxy group is hydrogenated as on one occasion, the reduction of the nitro group in **14** was carried out using hydrogen over palladium on charcoal. The metal complexes (**21**–**24** and **31**–**36**) were finally obtained by reaction of the imine with $[ReMe(CO)_5]$ in toluene at reflux for 20 h. Some of the reactions were carried out only once which accounts for the unoptimised yields in some steps.

3. Mesomorphism of the ligands and their metal complexes

The mesomorphism will be discussed by considering the ligands and complexes in two groups; thus, the chiral and non-chiral materials will be considered separately.

3.1. Non-chiral ligands and complexes

Thermal data are collected in Table 1 and summarised for the ligands in Fig. 2. The ligands (**17**–**20**) differed from those we had synthesised previously in that the imine group used for binding the rhenium was now in a terminal rather than a central bridging position. Although a direct comparison is not possible, consideration of the behaviour of related ligands [3,4,12,13] suggests that the transition temperatures are not greatly affected. The mesomorphism is also similar, showing smectic C and nematic phases and, in some cases, a crystal smectic J phase [14]. However, the interesting comparison is within this series where we have started with an imine with two terminal alkoxy chains, and then gradually replaced them with alkyl chains of the same length. What we see clearly is that the imine with two terminal alkoxy chains (**17**) has the most stable crystal phase and the most stable nematic phase, clearing at 340°C. However, when one alkyl chain is introduced (**18**, **19**), a crystal J phase is observed, the melting point comes down and the nematic phase is reduced in stability. These reductions are greater when the alkoxy chain is found at the end nearest the imine group (**19**). Lowest of all, however, are the transition temperatures found in the imine where both terminal chains are alkyl (**20**). These phenomena can simply be explained by considering the dipolar contri-

Table 1
Thermal data for the non-chiral ligands and complexes

m	Transition	*T* (°C)	Δ*H* (kJ mol^{-1})	Δ*S* (J K^{-1} mol^{-1})
Imines				
17	Crys–S_C	137	35.0	86
	S_C–N	190	0.9	2
	N–I(dec)	340	2.8	5
18	Crys–J	98	4.0	11
	J–S_C	108	16.4	42
	S_C–N	210	0.4	1
	N–I	314	0.2	0
19	Crys–J	105	3.7	9
	J–S_C	114	22.4	59
	S_C–N	207	0.9	2
	N–I	302	0.9	2
20	Crys–J	99	0.6	2
	J–S_C	126	5.5	14
	S_C–N	224	1.0	2
	N–I	299	1.8	3
Rhenium complexes				
21	Crys–N	188	49.4	105
	N–I	204	2.1	4
22	Crys–N	175	40.0	89
	N–I(dec)	190	1.6	3
23	Crys–I	178	47.8	105
	(Crys′–N) [a]	(112)	[b]	
	(N–I)	(170)	[b]	
24	Crys–I	169	48.3	109
	(Crys′–N)	(125)	[b]	
	(N–I)	(160)	(1.7)	(4)

[a] Crys′ is a metastable crystal phase.
[b] Not seen by DSC.

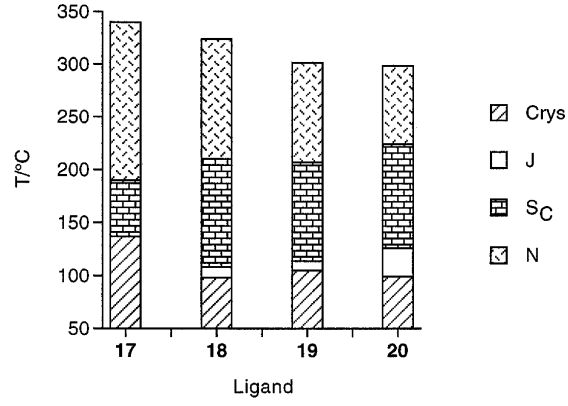


Fig. 2. Graphical illustration of the mesomorphism of the ligands **17**–**20**.

bution made by the oxygen in the alkoxy systems. Thus, intermolecular dipolar interactions will be greater leading to more stable phases.

When the complexes are considered (**21**–**24**), the first point to note is that the mesomorphism changes in as much as the smectic phase(s) seen in the ligands are totally suppressed and only a nematic phase is seen; this is discussed below. Secondly, we find that the clearing points of the complexes are well over 100°C lower than those of the corresponding ligands. Thirdly, we see that exactly the same trend is followed in terms of the stability of the nematic phase, which clears at 204°C in **21**, dropping to 160°C in **24**. The melting points also drop as the number of alkyl chains increases, but an important feature is that these melting points are significantly higher than those observed in complexes we had synthesised previously where the site of metallation was in the centre of the molecule. In these last cases, melting points were in the region of 120–130°C. Indeed, for **23** and **24**, the situation was such that while the nematic phase stability had dropped, the melting point had not and so the phases appeared monotropically. Interestingly, cooling the nematic led to a metastable crystal phase (Table 1, Crys′)which melted back to the nematic at 112 and 125°C for **23** and **24**, respectively.

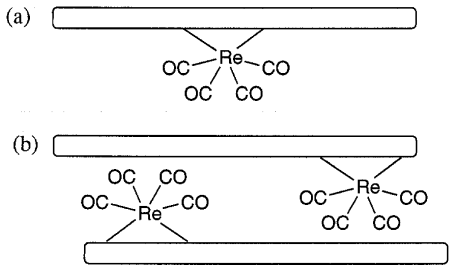


Fig. 3. Schematic diagram to show the poor possibilities for packing when the rhenium is at the centre of the complex (a), which are enhanced when the rhenium is towards the end of the complex (b).

Table 2
Thermal data for the chiral ligands and complexes

M	Transition	*T* (°C)	Δ*H* (kJ mol^{-1})	Δ*S* (J K^{-1} mol^{-1})
Imines				
25	Crys–J	104	17.5	46
	J–S_I	117	23.1	60
	S_I–S_C	129	1.0	2
	S_C–N	232	3.1	6
	N–I	288	1.9	3
26	Crys–Crys′	86	12.5	35
	Crys′–S_C*	93	15.4	42
	S_C*–N*	91	2.9	6
	N*–I	267	1.2	2
27	Crys–S_C*	101	35.5	99
	S_C*–N*	195	1.8	4
	N*–I	256	1.3	2
28	Crys–S_C*	60	13.1	39
	S_C*–N*	158	2.6	6
	N*–I	236	0.5	1
29	Crys–S_C*	71	12.5	36
	S_C*–N*	163	3.6	8
	N*–I	243	1.6	3
30	Crys–S_C*	109	32.7	86
	S_C*–N*	190	1.7	4
	N*–I	259	0.8	2
Rhenium complexes				
31	Crys–N	133	41.7	100
	N–I	160	1.6	4
32	Crys–N*	121	16.4	43
	N*–I	142	0.1	1
33	Crys–I	137	18.1	48
	(N*–I)	(132.5)	[a]	
34	Crys–I	130	39.5	98
35	Crys–I	129	33.0	82
	(Crys–N*)	(107)	(34.0)	(89)
	(N*–I)	(114)	(0.9)	(2)
36	Crys–N*	121	38.9	95
	N*–I	154	0.4	1

[a] Not seen by DSC.

On formation of the complexes, a large, metal tetracarbonyl group is introduced as a lateral substituent. In a very simple way, it is easy to envisage that such a large substituent, particularly near to the centre of a molecule, will disrupt its ability to pack into smectic layers, thus destabilising the smectic C and crystal smectic J phase. However, although the nematic wins out over the smectic phases, the presence of the lateral [$M(CO)_4$] group reduces the molecular anisotropy and thus the attendant anisotropic dispersion forces, which leads to a much lower nematic phase stability in the complexes. Without evidence of the crystal structure (it is not straightforward to grow crystals of such systems), it is a little more difficult to begin to understand the greater stability of the crystal phase of these complexes, but one simple explanation might be as indicated in Fig. 3 where it is possible to envisage a more efficient packing of molecules when the [$Re(CO)_4$] group is situated towards the end of the molecule (Fig. 3(b)) than when it is situated towards the middle (Fig. 3(a)).

3.2. Chiral ligands and complexes

Thermal data are collected in Table 2 and summarised for the ligands in Fig. 4. In this series, for the most part the core was kept the same and the terminal chain was varied. The

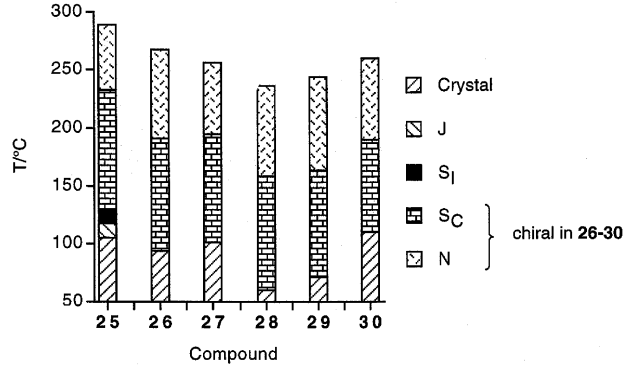


Fig. 4. Graphical illustration of the mesomorphism of the ligands **25**–**30**.

parent compound had two terminal decyloxy chains which were systematically replaced by citronellyloxy chains. Two other compounds are included, namely one (**30**) in which the imine group was moved away from the centre of the molecule as is the case with the series above, and another (**29**) where during preparation, the double bond of one of the citronellyl groups was inadvertently hydrogenated. Rhenium(I) complexes of each ligand were also obtained.

The parent ligand, **25**, melted at 104°C to give a crystal J phase [14] which then gave way to a smectic I phase at 117°C which was characterised on the basis of its optical texture [15]. Then followed a smectic C phase at 129°C and a nematic phase at 232°C which cleared at 288°C. This behaviour is similar to that reported for related ligands which we have described previously [3,4]. When the citronellyl group was introduced at the end of the molecule closest to the *C*-end of the imine link (**26**), the crystal phase was destabilised and melting to a S_C* (chiral smectic C phase) occurred at 93°C; the characteristic [15] petal texture of the S_C* phase is shown in Fig. 5. The S_C* phase was also destabilised with respect to the non-chiral analogue and the phase transition into the N* (chiral nematic or cholesteric) phase was seen at 191°C; the characteristic [15] planar texture of the N* phase is shown in Fig. 6. The N* phase cleared at 267°C. When the citronellyl group was introduced at the end of the molecule closest to the *N*-end of the imine link (**27**), similar destabilisation was observed (Crys 101 S_C* 195 N* 256 I), the transition temperatures of **26** and **27** being broadly similar. However, when both of the terminal groups were citronellyl (**28**), the changes in transition temperature were much more pronounced and the ligand melted at 60°C into a S_C* phase before passing into a N* phase at 158°C and clearing at 236°C. The transition temperatures of **29** in which the citronellyl group at the *C*-end of the molecule was hydrogenated were very similar. Finally, we can see that by moving the imine group within the molecule (**30**), there is little effect on the mesomorphism as the transition temperatures are broadly similar to those of both **26** and **27**.

The overall trend in behaviour in the above ligands can be understood by considering the differences between the decyloxy and citronellyloxy chains (Fig. 7). A decyloxy chain was chosen for this study as it has the same number of carbon atoms as the citronellyl group. Thus, in the former case the chain is not branched in any way and so offers only enhancement of the molecular anisotropy, whereas the latter offers both a double bond (which often appears to lead to a reduction in transition temperatures [16]) and, more significantly, a chain branched in two places. As a branched chain, citronellyl now has the possibility to disrupt the anisotropy of the ligand and so packing in both the crystal state and the mesophases will not be so efficient, leading to a reduction in transition temperatures. Where there are *two* such chains (**28**) then this effect becomes further emphasised and so the transition temperatures drop even further. Of course, the branching also introduces chirality into the system which is responsible for the formation of S_C* and N* phases, rather than their non-

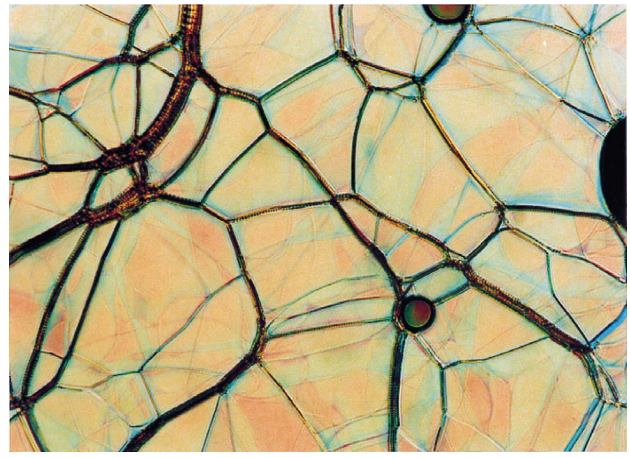


Fig. 5. Petal texture of the S_C* phase of ligand **27** at 109°C, obtained on heating.

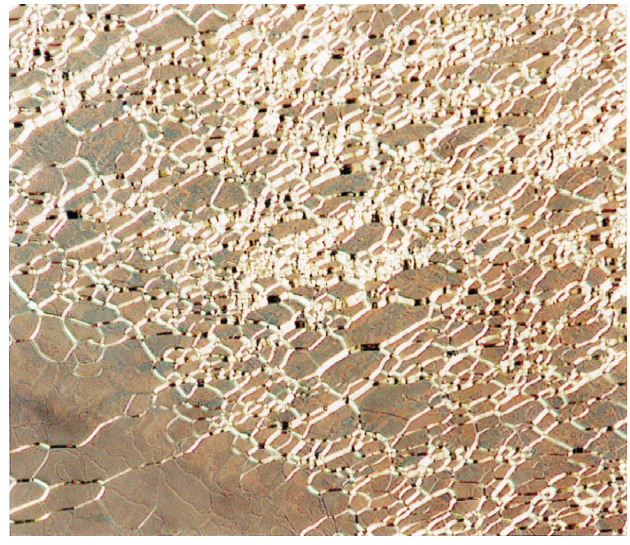


Fig. 6. Planar texture of the chiral nematic (N*) phase of ligand **27** at 262°C, obtained on cooling.

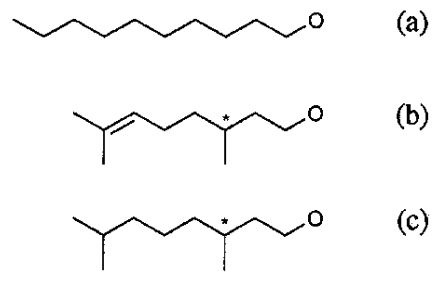


Fig. 7. Structure of the decyloxy chain (a), the citronellyloxy chain (b) and its hydrogenated analogue (c).

chiral counterparts seen in the parent ligand (**25**). Chiral phases [17] are of great technological relevance as the S_C* phase is that used in ferroelectric liquid crystal displays, while the N* phase is responsible for thermochromic effects in liquid crystals (e.g. strip thermometers).

The mesomorphism of the complexes (**31**–**36**) differed from that of the ligands in that now the S_C* phase disappeared and the N* phase was the only one observed. These materials

are therefore interesting from a more general point of view as there are very few metallomesogens known which exhibit a chiral nematic phase which are not derived from dinuclear palladium mesogens [18–21]. In common with the complexes considered above, the melting and clearing points were significantly reduced in comparison with the ligands. The mesomorphism of the complex **31** whose ligand (**25**) possessed only non-chiral decyloxy chains was broadly similar to that found in previous examples [5,6], showing a nematic phase from 133–160°C. However, on the introduction of a chiral citronellyl group, the stability of the nematic phase was reduced and the N* phase cleared at 142°C (**32**) or 132°C (**33**). However, the difference in these two complexes was in the stability of the crystal phase and its relation to the nematic. Thus, in **32** in which the citronellyl group was at the *C*-end of the ligand, the crystalline phase melted at 121°C while in **33**, in which the citronellyl group was at the other end of the ligand, the crystal melted at 137°C so that in fact the N* phase was monotropic. Such differences in crystal phase stability for such similar complexes are rather difficult to explain, at least in the absence of crystal structure data. When both terminal chains were citronellyl (**34**), the melting point stayed relatively high at 130°C, but the stability of the N* phase dropped even further than in **32** and **33** and could not be seen before crystallisation set in at around 110°C. The behaviour of **35** in which one citronellyl group was hydrogenated was very similar. Finally, an interesting comparison is that between the behaviour of **36** (in which the imine group was moved towards the end of the molecule as in the first series of ligands and complexes considered in this paper), **32** and **33** (in which the imine group was in the centre of the molecule) and the complexes **21**–**24**. Thus, in **21**–**24** we saw rather high transition temperatures which we attributed to a more efficient packing of complexes when the $[Re(CO)_4]$ fragment is attached to one end of the ligand. In **36**, which possesses longer chains, one of which is chiral, this effect is clearly still present, evident by comparison with the clearing points for **32** and **33** where the N* phase is destabilised by about 16°C.

4. Conclusions

In this systematic study, we have examined how changes in the nature of the ligand have affected the mesomorphism of some complexes of Re(I). It is interesting that we find that many of the trends seen in the ligands are reflected in the behaviour of the complexes, although there are aspects of the ligand design which have a profound effect on the shape of the complex formed which in turn influence the mesomorphism, leading to some synergy between ligand- and complex-derived effects.

5. Experimental

Elemental analyses were determined by the University of Exeter Microanalysis Service. NMR spectra were recorded on either a Bruker ACF-300 or a Bruker DRX-400 spectrometer, where the chemical shifts are reported relative to the internal standard of the deuterated solvent used. Analysis by DSC was carried out on a Perkin–Elmer DSC7 instrument using heating and cooling rates of either 5 or 10 K min^{-1}. Analysis by hot stage microscopy was carried out using an Olympus BH40 microscope equipped with a Link-Am HFS91 hot stage, TMS92 controller and LNP2 cooling unit. Solvents were purified by standard methods before use. 4-Heptylbenzoic acid, 4-hexyloxyaniline and 4-heptylaniline were obtained from Aldrich.

5.1. Preparation 4-decyloxybenzoic acid (1)

Ethyl 4-hydroxybenzoate (8.31 g, 0.05 mol) and 1-bromodecane (16.59 g, 0.075 mol) were added to a suspension of potassium carbonate (27.64 g, 0.2 mol) and dibenzo-18-crown 6 (0.01 g) in butanone (290 cm^3). The solution was heated at reflux for 72 h. Water (250 cm^3) was added and the organic layer extracted with DCM (4×150 cm^3). The combined organic extracts were dried over anhydrous $MgSO_4$, filtered and evaporated under reduced pressure to give a yellow oil. Potassium hydroxide (3.4 g, 0.06 mol) was dissolved in ethanol (200 cm^3, 95%) and added to the yellow liquid, the resulting solution was heated at reflux for 3 h and cooled. Water (200 cm^3) was added, followed by hydrochloric acid (concentrated) until pH 1. The white solid was filtered and recrystallised from ethanol (95%) and dried under vacuum to give a pure white solid. Yield 7.22 g (52%). ^{1}H NMR (400 MHz, $CDCl_3$): δ 0.88 (t, 3, CH_3), 1.24 (m, 14, 7CH_2), 1.81 (q, 2, CH_2CH$_2$O), 4.02 (t, 2, CH_2O), 6.92 (AA′XX′, 2, $J=8.9$ Hz, H12), 8.04 (AA′XX′, 2, $J=8.9$ Hz, H13).

(*S*)-4-Citronellyloxybenzoic acid (**2**) and hexyloxybenzoic acid (**3**) were similarly prepared in yields of 68 and 60%, respectively. Spectroscopic parameters were identical except for details of the NMR in the region of the alkyl chain. ^{1}H and ^{13}C NMR data are given for **2**. ^{1}H NMR (400 MHz, $CDCl_3$): δ 0.97 (d, 3, CH_3CH), 1.26 (m, 2, CH_2CH), 1.40 (m, 1, C*H*CH$_3$), 1.62 (s, 3, CH_3C=), 1.69 (s, 3, CH_3C=), 1.86 (m, 2, CH_2CH$_2$O), 2.03 (m, 2, CH_2), 4.08 (t, 2, CH_2O), 5.11 (m, 1, C*H*=C), 6.94 (AA′XX′, 2, $J=9.0$ Hz, H12), 8.05 (AA′XX′, 2, $J=9.0$ Hz, H13). ^{13}C{^{1}H} NMR (100 MHz, $CDCl_3$): δ 17.7 (C8), 19.5 (C7), 25.4 (C6), 25.7 (C2), 29.5(C1), 35.9 (C9), 37.1 (C5), 66.6 (C10), 114.2 (C12), 121.3 (C14), 124.6 (C4), 131.9 (C3), 132.3 (C13), 163.6 (C11), 171.0 (C15).

5.2. Preparation of 4-decyloxybenzoyloxy-4′-benzoic acid (5)

4-Decyloxybenzoic acid (**1**) (7.22 g, 0.026 mol) was added to a suspension of DCC (5.36 g, 0.026 mol), DMAP (0.015 g) and benzyl 4-hydroxybenzoate (5.93 g, 0.026 mol) in CH_2Cl_2 (300 cm^3) and stirred under nitrogen for 18 h. The off-white precipitate was filtered and the filtrate con-

centrated to an off-white solid. The crude product was purified by column chromatography (SiO_2, eluent CH_2Cl_2) and a colourless solid was obtained after evaporation of the solvent. The solid was dissolved in THF (200 cm^3), then triethylamine (5 cm^3) and a palladium on carbon catalyst (5%) was added to the solution. After saturating with hydrogen gas, the solution was filtered and washed with CH_2Cl_2. The solvent was evaporated and the colourless solid was recrystallised from ethanol (95%) and dried under vacuum to give a pure colourless solid. Yield 4.07 g (39%). ^{1}H NMR (400 MHz, $CDCl_3$): δ 0.90 (t, 3, CH_3), 1.28 (m, 14, 7 CH_2), 1.83 (m, 2, CH_2CH$_2$O), 4.06 (t, 2, CH_2O), 7.00 (AA′XX′, 2, J = 9.00 Hz, H12), 7.35 (AA′XX′, 2, J = 9.00 Hz, H17), 8.16 (AA′XX′, 2, J = 9.00 Hz, H13), 8.20 (AA′XX′, 2, J = 9.00 Hz, H18).

4-Hexyloxybenzoyloxy-4′-benzoic acid (**6**) and 4-heptylbenzoyloxy-4′-benzoic acid (**7**) were similarly prepared in yields of 45 and 42%, respectively. NMR parameters were almost identical to those of **5**, except in the aliphatic region.

5.3. Preparation of (S)-4-citronellyloxybenzaldehyde

(*S*)-(+)-Citronellylbromide (5.0 g, 0.023 mol) and 4-hydroxybenzaldehyde (1.83 g, 0.015 mol) were added to a suspension of potassium carbonate (8.29 g, 0.06 mol) and dibenzo-18-crown 6 (0.01 g) in butanone (150 cm^3). The solution was heated at reflux under nitrogen for 24 h. Water (150 cm^3) was added to the solution and the organic layer extracted with CH_2Cl_2 (200 $cm^3 + 3 \times 100$ cm^3). The combined organic extracts were dried over anhydrous $MgSO_4$, filtered and evaporated to give a yellow oil. The crude product was purified by column chromatography (SiO_2, eluent $CHCl_3$:hexane, 3:1 v/v) and the solvent evaporated to give the pure yellow oil. Yield 2.82 g (72%). IR (NaCl plates): ν_{CO} 1700 cm^{-1}. ^{1}H NMR (400 MHz, $CDCl_3$): δ 0.96 (d, 3, CH_3CH), 1.26 (m, 2, CH_2CH), 1.39 (m, 1, CHCH$_3$), 1.61 (s, 3, CH_3C=), 1.68 (s, 3, CH_3C=), 1.83 (m, 2, CH_2), 2.01 (m, 2, CH_2CH$_2$O), 4.08 (t, 2, CH_2O), 5.10 (m, 1, CHC=), 6.98 (AA′XX′, 2, J = 8.7 Hz, H12), 7.82 (AA′XX′, 2, J = 8.9 Hz, H13), 9.87 (s, 1, CHO). ^{13}C{^{1}H} NMR (100 MHz, $CDCl_3$): δ 17.7 (C8), 19.5 (C7), 25.4 (C6), 25.7 (C2), 29.5 (C1), 35.9 (C9), 37.1 (C5), 66.7 (C10), 114.8 (C12), 124.5 (C4), 129.8 (C14), 131.4 (C3), 132.0 (C13), 164.2 (C11), 190.7 (C15).

5.4. Preparation of 4-decyloxybenzoyloxy-4′-benzaldehyde (*8*)

4-Decyloxybenzoic acid (2.79 g, 0.01 mol) was added to a suspension of DCC (2.06 g, 0.01 mol), 4-hydroxybenzaldehyde (1.22 g, 0.01 mol) and DMAP (0.05 g) in CH_2Cl_2 (200 cm^3) and stirred under nitrogen for 18 h. The colourless precipitate was filtered and the filtrate evaporated to give an off-white solid. The crude product was purified by column chromatography (SiO_2, eluent DCM) and the solvent evaporated to give a pure colourless solid. Yield 3.14 g (82%). *Anal*. Found: C, 75.1; H, 7.3. Calc. for $C_{24}H_{30}O_4$: C, 75.4; H, 7.9%. IR (KBr): ν_{CO2} 1737, ν_{CHO} 1699 cm^{-1}. ^{1}H NMR (400 MHz, $CDCl_3$): δ 0.89 (t, 3, CH_3), 1.28 (m, 14, 7 CH_2), 1.83 (q, 2, CH_2CH$_2$O), 4.05 (t, 2, CH_2O), 6.99 (AA′XX′, 2, J = 9.0 Hz, H12), 7.40 (AA′XX′, 2, J = 8.5 Hz, H17), 7.97 (AA′XX′, 2, J = 8.6 Hz, H18), 8.14 (AA′XX′, 2, J = 8.9 Hz, H13), 10.03 (s, 1, CHO).

4-(*S*)-Citronellyloxybenzoyloxy-4′-benzaldehyde (**9**), 4-decyloxybenzoyloxy-4′-benzoyloxy-4″-benzaldehyde (**10**), 4-hexyloxybenzoyloxy-4′-benzoyloxy-4″-benzaldehyde (**11**) and 4-heptylbenzoyloxy-4′-benzoyloxy-4″-benzaldehyde (**12**) were similarly prepared from **1**, **5**, **6** and **7** in yields of 76, 56, 20 and 50%, respectively.

5.5. Preparation of (S)-citronellyloxy-4-nitrobenzene

(*S*)-(−)-Citronellol (5.0 g, 0.032 mol) was dissolved in dimethylsulfoxide (50 cm^3). To the solution was added *p*-nitrochlorobenzene (5.04 g, 0.032 mol), and the mixture was stirred at 40°C for 10 min. Sodium hydride (0.84 g, 0.032 mol, 80% dispersion in oil) was added and the mixture heated to 70°C for 1.5 h. The green–black solution was quenched with water (30 cm^3) and acidified with HCl (2 mol dm^{-3}). The red solution was extracted with diethyl ether (2 × 30 cm^3) and the combined extracts dried over anhydrous Na_2SO_4. After filtering and evaporating the solvent, a deep red oil was obtained. The crude product was purified by column chromatography (SiO_2, eluent hexane:diethyl ether 5:1 v/v) and the solvent evaporated to give a pure yellow oil. Yield 6.47 g (73%). IR (NaCl plates): $\nu_{NO(asymmetric)}$ 1518 (broad), $\nu_{NO(symmetric)}$ 1380 cm^{-1} (sharp). ^{1}H NMR (400 MHz, $CDCl_3$): δ 0.97 (d, 3, CH_3CH), 1.25 (m, 2, CH_2CH), 1.39 (m, 1, CHCH$_3$), 1.61 (s, 3, CH_3C=), 1.69 (s, 3, CH_3C=), 1.86 (m, 2, CH_2CH$_2$O), 2.01 (m, 2, CH_2CH=), 4.08 (t, 2, CH_2O), 5.10 (m, 1, CHC=), 6.94 (AA′XX′, 2, J = 9.3 Hz, H12), 8.20 (AA′XX′, 2, J = 9.3 Hz, H13). ^{13}C{^{1}H} NMR (100 MHz, $CDCl_3$): δ 17.7 (C8), 19.5 (C7), 25.4 (C6), 25.7 (C2), 29.4 (C1), 35.9 (C9), 37.0 (C5), 67.2 (C10), 114.4 (C12), 124.4 (C4), 125.9 (C13), 129.6 (C14), 131.5 (C3), 164.2 (C11).

5.6. Preparation 4-(S)-citronellyloxybenzoyloxy-4′-nitrobenzene (*14*)

(*S*)-4-Citronellyloxybenzoic acid (**2**) (2.76 g, 0.01 mol) was added to a suspension of DCC (2.06 g, 0.01 mol), *p*-nitrophenol (2.59 g, 0.01 mol)and DMAP (0.02 g) in CH_2Cl_2 (200 cm^3) and stirred under nitrogen for 18 h. The precipitate was filtered and the solvent evaporated to give a yellow oil. The crude product was purified by column chromatography (SiO_2, eluent DCM) and the solvent evaporated to give a pure pale yellow oil. Yield 3.47 g (87%). IR (NaCl plates): ν_{CO} 1740, $\nu_{NO(asymmetric)}$ 1512 (broad), $\nu_{NO(symmetric)}$ 1378 cm^{-1} (sharp). ^{1}H NMR (400 MHz, $CDCl_3$): δ 0.99 (d, 3, CH_3CH), 1.26 (m, 2, CH_2CH), 1.41 (m, 1, CHCH$_3$), 1.62 (s, 3, CH_3C=), 1.70 (s, 3, CH_3C=), 1.88 (m, 2,

CH_2CH_2O), 2.02 (m, 2, CH_2C=), 4.10 (t, 2, CH_2O), 5.12 (m, 1, C*H*C=), 6.99 (AA′XX′, 2, J=9.0 Hz, H12), 7.40 (AA′XX′, 2, J=9.2 Hz, H17), 8.14 (AA′XX′, 2, J=9.0 Hz, H13), 8.31 (AA′XX′, 2, J=9.2 Hz, H18). $^{13}C\{^1H\}$ NMR (100 MHz, $CDCl_3$): δ 17.7 (C8), 19.5 (C7), 25.4 (C6), 25.7 (C2), 29.5 (C1), 35.9 (C9), 37.1 (C5), 66.8 (C10), 114.6 (C12), 120.5 (C15), 122.6 (C17), 124.5 (C4), 125.2 (C18), 131.4 (C3), 132.5 (C13), 145.3 (C19), 156.1 (C14), 163.9 (C16), 164.1 (C11).

4-Decyloxybenzoyloxy-4′-benzoyloxy-4″-nitrobenzene (**13**) was similarly prepared in 80% yield.

*5.7. Preparation of 4-(S)-citronellyloxybenzoyloxy-4′-aniline (**16**)*

To a suspension of 4-decyloxybenzoyloxy-4′-benzoyloxy-4″-nitrobenzene (**14**) (1.7 g, 0.00428 mol) in ethanol (20 cm^3, absolute) were added 5 equiv. of $SnCl_2 \cdot H_2O$ (4.83 g, 0.0214 mol). The mixture was heated to reflux under nitrogen for 18 h, cooled to room temperature and poured onto ice. The pH was adjusted to 8 by addition of NaOH (2 mol dm^{-3}) and the organic layer extracted with ethyl acetate (100 $cm^3 + 2 \times 50$ cm^3). The combined extracts were dried over anhydrous Na_2SO_4, filtered and the filtrate evaporated to give a brown oil. The crude product was purified by column chromatography (SiO_2, eluent diethyl ether:hexane 4:1 v/v) and the solvent evaporated to give a viscous yellow oil. Yield 1.01 g (64%). IR (NaCl plates): ν_{NH} 3458, ν_{NH} 3373, ν_{CO} 1726 cm^{-1}. ^1H NMR (400 MHz, $CDCl_3$): δ 0.98 (d, 3, CH_3CH), 1.26 (m, 2, CH_2CH), 1.40 (m, 1, C*H*CH_3), 1.61 (s, 3, CH_3C=), 1.70 (s, 3, CH_3C=), 1.86 (m, 2, CH_2CH_2O), 2.04 (m, 2, CH_2C=), 3.65 (s, 2, NH_2), 4.09 (t, 2, CH_2O), 5.12 (m, 1, C*H*C=), 6.71 (AA′XX′, 2, J=8.8 Hz, H18), 6.96 (AA′XX′, 2, J=9.0 Hz, H17), 6.99 (AA′XX′, 2, J=8.8 Hz, H12), 8.12 (AA′XX′, 2, J=9.0 Hz, H13). $^{13}C\{^1H\}$ NMR (100 MHz, $CDCl_3$): δ 17.6 (C8), 19.5 (C7), 25.4 (C6), 25.7 (C2), 29.5 (C1), 36.0 (C9), 37.1 (C5), 66.6 (C10), 114.2 (C12), 115.7 (C18), 121.9 (C15), 122.4 (C17), 124.6 (C4), 131.4 (C3), 132.2 (C13), 144.1 (C19), 163.3 (C16), 165.5 (C11).

4-Decyloxybenzoyloxy-4′-aniline (**15**) was similarly prepared in 55% yield.

*5.8. Preparation of the imines: 4-citronellyloxybenzoyloxy-4′-benzylidene-4″-decyloxybenzoyloxy-4‴-aniline (**26**)*

To a suspension of 4-(*S*)-citronellyoxybenzoyloxy-4′-benzaldehyde (**9**) (0.71 g, 0.00187 mol) and 4-decyloxybenzoyloxy-4′-aniline (**15**) (0.69 g, 0.00187 mol) in ethanol (60 cm^3, absolute) and THF (20 cm^3) were added a few drops of acetic acid (glacial). The mixture was heated at reflux under nitrogen for 1 h and then cooled to room temperature. The solid was filtered, crystallised from ethanol (absolute):THF (60:1 v/v) and dried under vacuum to yield a pure off-white solid. Yield 0.74 g (54%). *Anal.* Found: C, 76.7; H, 8.1; N, 2.0. Calc. for $C_{47}H_{57}O_6N$: C, 77.1; H, 7.9; N, 1.9%. IR (KBr): ν_{CO} 1728, $\nu_{C=N}$ 1625 cm^{-1} (weak). ^1H NMR (400 MHz, $CDCl_3$): δ 0.90 (t, 3, CH_3), 0.99 (d, 3, CH_3CH), 1.29 (m, 16, 8 CH_2), 1.47 (m, 1, C*H*CH_3), 1.63 (s, 3, CH_3C=), 1.70 (s, 3, CH_3C=), 1.85 (m, 4, 2 CH_2CH_2O), 2.05 (m, 2, C*H*=C), 4.09 (2 t, 4, $2CH_2O$), 5.12 (m, 1, C*H*=C), 6.98 (AA′XX′, 2, J=9.0 Hz, H28), 6.99 (AA′XX′, 2, J=9.0 Hz, H12), 7.24 (AA′XX′, 2, J=9.0 Hz, H18), 7.29 (AA′XX′, 2, J=9.0 Hz, H17), 7.35 (AA′XX′, 2, J=8.6 Hz, H23), 7.98 (AA′XX′, 2, J=8.6 Hz, H22), 8.16 (AA′XX′, 2, J=9.0 Hz, H27), 8.16 (AA′XX′, 2, J=9.0 Hz, H13), 8.50 (s, 1, –C*H*=N–).

All other imines (**17**–**20** and **25**–**30**) were similarly prepared. Yields and analytical data are collected in Table 3.

*5.9. Preparation of the rhenium(I) complexes: complex **24***

To a suspension of 4-heptylbenzoyloxy-4′-benzoyloxy-4″-benzylidene-4‴-heptylaniline (**20**) (0.050 g, 0.080 mmol) in toluene (20 cm^3) was added pentacarbonylmethylrhenium(I) (0.030 g, 0.088 mmol). The reaction mixture was stirred under reflux for 20 h, under a nitrogen atmosphere, and then was cooled to room temperature and the solvent removed. The yellow solid was dissolved in CH_2Cl_2 and purified by column chromatography on alumina with CH_2Cl_2 as eluent. The solution was concentrated and hexane was added to give the pure yellow solid in 80% yield (0.059 g). ^1H NMR (400 MHz, CD_2Cl_2): δ 0.92 (t, 6, $^3J_{HH}$=7.00 Hz, CH_3), 1.35 (m, 16, CH_2), 1.68 (m, 4, CH_2CH_2Ph), 2.70 (t, 2, $^3J_{HH}$=7.80 Hz, CH_2Ph), 2.75 (t, 2, $^3J_{HH}$=7.80 Hz, CH_2Ph), 7.10 (dd, 1, $^3J_{HH}$=8.00 Hz, $^4J_{HH}$=4.00 Hz, H18),

Table 3
Microanalytical data for the ligands and complexes

Compound	Yield (%)	Calculated (found) (%)		
		C	H	N
Imines				
17	60	75.3 (75.2)	7.0 (7.0)	2.2 (2.1)
18	50	77.5 (77.2)	7.3 (7.3)	2.2 (2.1)
19	60	77.3 (77.3)	7.3 (7.3)	2.2 (2.1)
20	60	79.1 (79.1)	7.6 (7.7)	2.2 (2.1)
25	54	76.9 (76.9)	8.1 (8.2)	1.9 (1.7)
26	54	77.1 (76.8)	7.8 (7.8)	1.9 (1.7)
27	64	77.1 (76.8)	7.8 (7.9)	1.9 (1.7)
28	75	77.3 (77.3)	7.6 (7.8)	1.9 (1.8)
29	43	77.1 (77.3)	7.8 (7.9)	1.9 (1.8)
30	30	77.1 (76.8)	7.8 (7.8)	1.9 (1.7)
Rhenium complexes				
21	43	56.2 (55.9)	4.6 (4.6)	1.5 (1.4)
22	68	57.6 (57.3)	4.8 (4.7)	1.5 (1.4)
23	73	57.6 (57.4)	4.8 (4.7)	1.5 (1.4)
24	80	59.1 (58.8)	5.1 (4.9)	1.5 (1.5)
31	57	59.4 (59.3)	5.7 (5.6)	1.4 (1.3)
32	22	59.5 (59.5)	5.4 (5.4)	1.3 (1.3)
33	75	59.5 (59.3)	5.5 (5.4)	1.4 (1.3)
34	58	59.5 (59.3)	5.5 (5.3)	1.4 (1.2)
35	44	59.6 (59.4)	5.4 (5.4)	1.4 (1.3)
36	28	59.5 (59.4)	5.4 (5.3)	1.3(1.2)

7.28 (2AA′XX′, 4, H25, H8), 7.39 (AA′XX′, 2, $^3J_{HH}$ = 8.40 Hz, H13), 7.44 (AA′XX′, 2H, $^3J_{HH}$ = 8.80 Hz, H24), 7.81 (d, 1, $^3J_{HH}$ = 8.40 Hz, H19), 7.84 (d, 1, $^4J_{HH}$ = 4.00 Hz, H20), 8.14 (AA′XX′, 2, $^3J_{HH}$ = 8.40 Hz, H14), 8.32 (AA′XX′, 2, $^3J_{HH}$ = 8.80 Hz, H9), 8.20 (s, 1, –C*H*=N–).

All other rhenium complexes (**21**–**23** and **31**–**36**) were prepared in the same way. Analytical data are collected in Table 3.

Acknowledgements

The authors would like to thank the EU for a Marie Curie Fellowship (MAG), and EPSRC (ADP), the Leverhulme Trust (SRC) and Dorset (MJD) and Dyfed (SKH) local education authorities for financial support.

References

[1] See e.g. B. Donnio, D.W. Bruce, in: D.M.P. Mingos (Ed.), Structure and Bonding, vol. 95, Springer, 1998, Ch. 5, pp. 193–247.
[2] D.W. Bruce, Adv. Mater. 6 (1994) 699.
[3] D.W. Bruce, X.-H. Liu, J. Chem. Soc., Chem. Commun. (1994) 729.
[4] X.-H. Liu, M.N. Abser, D.W. Bruce, J. Organomet. Chem. 551 (1998) 271.
[5] D.W. Bruce, X.-H. Liu, Liq. Cryst. 18 (1995) 165.
[6] X.-H. Liu, I. Manners, D.W. Bruce, J. Mater. Chem. 8 (1998) 1555.
[7] S. Morrone, G. Harrison, D.W. Bruce, Adv. Mater. 7 (1995) 665.
[8] S. Morrone, D. Guillon, D.W. Bruce, Inorg. Chem. 35 (1996) 7041.
[9] K.E. Rowe, D.W. Bruce, J. Chem. Soc., Dalton Trans. (1996) 3913.
[10] K.E. Rowe, D.W. Bruce, Mol. Cryst. Liq. Cryst. 326 (1999) 15.
[11] J.P. Rourke, D.W. Bruce, T.B. Marder, J. Chem. Soc., Dalton Trans. (1995) 317.
[12] X.-H. Liu, B. Heinrich, I. Manners, D. Guillon, D.W. Bruce, J. Mater. Chem., in press.
[13] X.-H. Liu, Ph.D. Thesis, University of Sheffield, 1996.
[14] In Ref. [7], the crystal smectic phase of related ligands was identified as crystal smectic G on the basis of optical microscopy. However, subsequent X-ray diffraction studies [12] revealed that this phase is in fact a crystal smectic J phase in all related ligands investigated. The crystal smectic J phase is assigned here by analogy.
[15] G.W. Gray, J.W. Goodby, Smectic Liquid Crystals, Textures and Structures, Blackie, Glasgow, 1984.
[16] V. Vill, LiqCryst Database 3.1, LCI, Hamburg, 1999.
[17] J.W. Goodby, J. Mater. Chem. 1 (1991) 307.
[18] See e.g. A. Omenat, M. Ghedini, J. Chem. Soc., Chem. Commun. (1994) 1309.
[19] M.J. Baeña, J. Barbera, P. Espinet, A. Ezcurra, M.B. Ros, J.-L. Serrano, J. Am. Chem. Soc. 116 (1994) 1899.
[20] R. Deschenaux, J. Santiago, Tetrahedron Lett. 35 (1994) 2169.
[21] C. Imrie, C. Loubser, J. Chem. Soc., Chem. Commun. (1994) 2159.

PERGAMON

www.elsevier.nl/locate/poly

Polyhedron 19 (2000) 259–266

POLYHEDRON

Hybrid organic–inorganic multilayer materials: influence of π electrons as magnetic media in a series of bridged-layer compounds $M_2(OH)_{4-x}A_{x/2}$ (M = Cu(II) or Co(II), A = dicarboxylate anion)

C. Hornick, P. Rabu, M. Drillon *

Institut de Physique et Chimie des Matériaux de Strasbourg, UMR 75040, CNRS, 23 rue du Loess, 67037 Strasbourg, France

Received 22 June 1999; accepted 12 August 1999

Abstract

We report the preparation, structure and magnetic properties of a series of multilayer copper(II) hydroxy-dicarboxylates. These are prepared by anion-exchange, starting from copper(II) hydroxy-acetate $Cu_2(OH)_3(OAc)\cdot H_2O$. The acetate ion is substituted for *n*-methylene dicarboxylates $O_2CXCO_2^{2-}$, with $X=(CH_2)_n$ and $n=1$ to 8. Similar exchange reactions are carried out with unsaturated dicarboxylate anions ($X=(CH)_n$, with $n=2$, 4 and $X=C_4H_6$). The compounds, of general formulation $Cu_2(OH)_{4-x}(XC_2O_4)_{x/2}\cdot zH_2O$, exhibit a layered structure with a step-like variation of the basal spacing, according to *n* parity. IR spectroscopy indicates that the carboxylate functions are linked to the metal ions, each aliphatic chain bridging adjacent hydroxide layers. Only compounds with $n=2$, 4 and 8 show a net magnetic moment within copper(II) layers. For the short chain anions, an antiferromagnetic order occurs at low temperature, with a metamagnetic transition in low field, except for the unsaturated dicarboxylate $Cu_2(OH)_{1.92}(C_4H_6C_2O_4)_{1.04}\cdot 0.22H_2O$ which exhibits a long-range ferromagnetic order at $T_C=13$ K. For the long-chain anion, $X=C_8H_{16}$, a ferrimagnetic 3d order is stabilized below $T_C=17$ K. On the basis of structural and magnetic findings, a comparison is made between the saturated and unsaturated aliphatic chain compounds. This study provides new insight on the influence of π electrons on the ordering between magnetic layers. Finally, preliminary results for the cobalt(II) *trans*-hexenedioate analog indicate that a 3d ferromagnet is obtained below $T_C=56.5$ K, thus emphasizing the key role of the in-plane spin–spin correlations on the ordering temperature. ©2000 Elsevier Science Ltd All rights reserved.

Keywords: Hybrid copper(II) compounds; Dicarboxylate-based compounds; Magnetic properties; Layered magnets; Long-range ferromagnetism

1. Introduction

Since the first report by Gamble et al. on superconducting properties of the intercalated compound 2H–TaS_2 [1], the past quarter of a century has witnessed substantial efforts in the development of intercalation chemistry. The combination at the nanometer scale of molecular species and inorganic layered networks has been at the origin of a new class of systems, the organic–inorganic hybrid multilayer compounds. A variety of layered host structures exhibiting structural flexibility such as clays, chalcogenides or layered double hydroxides (LDH) [2–6] have been investigated in view of promoting intercalation reactions. Basically, the ability of these inorganic networks to undergo ionic exchange, or redox or acido-basic reactions, and the resulting effect on electronic properties, has initiated attractive applications in various fields, such as supported catalysis, non-linear optics or therapeutic treatments of trace element deficiencies [7,8].

The studies of hybrid multilayer compounds exhibiting coupled physical properties, i.e. whose properties differ from those of individual assemblies, represent a major challenge today. Striking results have been reported in photo-induced magnetic and conducting materials [9,10], and in systems combining two basic properties, such as conductivity and magnetism or optics and magnetism, for instance [11–14]. Thus, a multi-functional system has been achieved by intercalation of the hyperpolarizable dimethylamino-*N*-methyl stilbazolinium (DAMS) chromophore in between $MnPS_3$ inorganic layers [15,16]. The obtained compound exhibits both a net magnetic moment below 40 K, and remarkable non-linear optical properties (two orders of magnitude those of urea).

A large number of such cation-exchangeable layered compounds are known, in which the intercalated species favor pillared structures, but it can be emphasized that, usually, no real chemical bond exists between the guest and host subnetworks [17,18]. The cohesion is basically due to electro-

* Corresponding author.

0277-5387/00/$ - see front matter ©2000 Elsevier Science Ltd All rights reserved.
PII S0277-5387(99)00355-1

static or van der Waals interactions, and when available to weak hydrogen bond couplings.

In contrast, anion-exchangeable layered compounds are scarce, probably because the anions are usually strongly bonded to the metal ions, and form the framework of the crystal.

Exchange of interlamellar anions by organic species (dicarboxylic acid anions) was first reported by Miyata and Kumura [19]. The interlayer arrangement of anionic surfactant has been extensively studied in layered double hydroxides (LDHs) $[M^{II}_{1-x}M^{II}_{1-x}M^{III}_{x}(OH)_2]^{x+}A_x^-$ consisting of positively charged hydroxide layers, separated by A^- anions counter-balancing the positive charge of the layers [20,21]. In such compounds, the stabilization of two valence states for the metal ions induces a statistic disorder in the inorganic layers.

Basically, the chemistry of simple hydroxides with botallackite-type structure appears to be more adapted for the design of hybrid materials with outstanding magnetic properties. Yamanaka et al. [22] have investigated the exchange reactions in the layered copper(II) compound $Cu_2(OH)_3(CH_3COO)\cdot H_2O$. The acetate anion located in the interlayer space may easily be substituted by halides, NO_3^-, ClO_4^- or MnO_4^- anions, giving 2d triangular arrays of metal ions, with interlayer spacing depending closely on the size of the exchanged anion.

The use of large organic species (i.e. aliphatic chain anions) coordinating the metal ion enables tuning of the basal spacing, and accordingly drastic modification of the magnetic properties [23–27]. Thus, *n*-alkyl chain molecules involving a single anionic function (carboxylate or sulfate anion) have been used to separate basic layers (Fig. 1(a)).

In that case, the organic spacers exhibit a saturated carbon chain, whose length is mediated by the number of carbon atoms, up to 40 Å [23–26,28,29]. The magnetic interaction within layers is highly dependent on the nature of the anionic function and the chain stacking, so that ferro-, ferri- or antiferromagnetic behavior may be stabilized. Clearly, the *n*-alkyl chains do not participate directly in interlayer interaction (they may be viewed as 'neutral' pillars) but they modulate the distance between magnetic sheets, and as a result influence through-space magnetic interactions. We have shown that, owing to dipolar coupling [30], ferromagnetic 3d order is stabilized when the basal spacing becomes large enough (>10 Å). The interaction mechanism between ferromagnetic layers is then mainly driven by the divergence of the in-plane spin–spin correlation length when the temperature is decreased. Such systems appear to be good prototypes of monolayer magnets interacting through classical dipolar interactions.

Similarly, radical-based anions have been grafted onto copper(II) and cobalt(II) hydroxide layers [31–33]. The most interesting results are obtained for imino-nitroxide benzoate (imb) species coordinating cobalt(II) ions, giving $Co_2(OH)_{3.5}(imb)_{0.5}\cdot H_2O$ [31,33]. Such systems are good examples of hybrid multilayer ferromagnets, with a strong coupling between organic and inorganic networks.

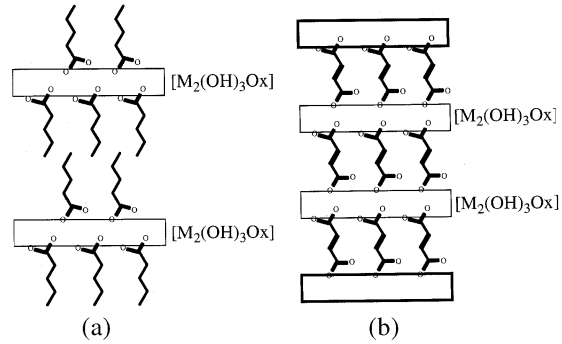


Fig. 1. Structural models showing the packing of aliphatic chains in layered metal hydroxides for (a) mono-carboxylate anions, (b) dicarboxylate anions.

Anionic exchange in divalent metal hydroxide compounds thus appears promising for the design of new multiproperty systems. It is however worthwhile to be able to control the connection between magnetic layers. For this purpose, we have focused on the design of dicarboxylate-based compounds, involving difunctional *n*-methylene, or *n*-alkenylene bridging anions between adjacent magnetic layers (Fig. 1(b)). From the comparison of hybrid systems with saturated and unsaturated aliphatic chains, basic insight is expected to result on the role of π electrons in the interlayer exchange mechanism.

We discuss here the synthesis and structure–property correlations for a series of copper(II)-based dicarboxylates ($n=1$ to 8). On the basis of structural and magnetic findings, a comparison is made with the cobalt(II) analog for the *trans*-hexenedioate anion.

2. Grafting of dicarboxylate anions

2.1. Experimental

The products were characterized by powder X-ray diffraction by using a Siemens D500 diffractometer in the Bragg–Brentano geometry (Co $K\alpha_1$, 1.78897 Å). Thermogravimetric analysis of the compounds was performed with a Setaram TGA 92 thermobalance up to 1000 K under air. Magnetic data ($\chi(T)$, $\chi_{ac}(T)$, $M(H)$) were collected from a Faraday-type equipment (Manics DSM10) and a SQUID magnetometer (Quantum Design MPMS*XL*) covering the temperature and field ranges 2–300 K, 0–5 T. A.c. susceptibility measurements were performed in a ± 3.5 Oe field (20 Hz). Fourier transform IR (FTIR) spectra were obtained in KBr pellets on an ATI-Mattson spectrometer, in the range 400–4000 cm^{-1}.

2.2. Synthesis

A series of copper(II) hydroxy-dicarboxylates has been prepared by anionic exchange. The starting hydroxy-acetate

Table 1
Structural and magnetic characteristics of the compounds

Hybrid compounds	Basal spacing (Å)	Magnetic behavior [a] 2d/3d	θ values [b] (K)	Some characteristic IR bands (cm^{-1})		
				C=O	C–O	γ(OH–O)
Saturated dicarboxylates						
$Cu_2(OH)_{2.84}(CH_2C_2O_4)_{0.58}\cdot 0.23H_2O$	9.20	AF/–	−1.7	577	1432	
$Cu_2(OH)_{2.90}(C_2H_4C_2O_4)_{0.55}\cdot 0.58H_2O$	8.80	F/meta, $T_N = 11.2$ K	+1.7	1536	1421	864
$Cu_2(OH)_{2.76}(C_3H_6C_2O_4)_{0.62}\cdot 1.62H_2O$	11.04	AF/–	−40	1536	1408	
$Cu_2(OH)_{2.08}(C_4H_8C_2O_4)_{0.96}\cdot 0.13H_2O$	10.45	F/meta, $T_N = 15.7$ K	+35	1571	1429	864
$Cu_2(OH)_{2.08}(C_5H_{10}C_2O_4)_{0.96}\cdot 1.47H_2O$	13.20	AF/–	−80	1572	1407	
$Cu_2(OH)_{2.36}(C_6H_{12}C_2O_4)_{0.82}\cdot 0.46H_2O$	13.15	AF/–	−18	1592	1398	
$Cu_2(OH)_{2.36}(C_7H_{14}C_2O_4)_{0.82}\cdot 0.46H_2O$	14.73	AF/–	−126	1563	1408	
$Cu_2(OH)_{1.64}(C_8H_{16}C_2O_4)_{1.18}\cdot 0.45H_2O$	15.60	Ferri/ferri, $T_C = 17$ K	−69	1592	1400	895
Unsaturated dicarboxylates						
$Cu_2(OH)_{2.96}(C_2H_2C_2O_4)_{0.52}\cdot 0.47H_2O$	8.80	AF/–	−26	1584	1383	
$Cu_2(OH)_{1.92}(C_4H_6C_2O_4)_{1.04}\cdot 0.22H_2O$	10.22	F/F, $T_C = 13$ K	+46	1580	1413	873
$Cu_2(OH)_{2.24}(C_4H_4C_2O_4)_{0.88}\cdot 0.44H$	10.38	F/meta, $T_N = 16$ K	+40	1559	1407	884
$Co_7(OH)_{11.6}(C_4H_6C_2O_4)_{1.20}\cdot 5.5H_2O$	13.40	F/F, $T_C = 56.5$ K	+12	1548	1382	

[a] Meta, AF, Ferri, and F hold for the meta-, antiferro-, ferri- and ferromagnetic states, respectively.
[b] The θ values are determined from the high temperature variation of susceptibility, $\chi^{-1} = (T-\theta)/C$.

$Cu_2(OH)_3(OAc)\cdot H_2O$ is synthesized by titration of copper acetate by potassium hydroxide with the OH:Cu = 3:2 molar ratio [23,25,26]. Then, the acetate ions are exchanged for *n*-methylene dicarboxylate anions $XC_2O_4^{2-}$, with $X = (CH_2)_n$ and $n = 1$ to 8. Similar exchange reactions have been achieved with unsaturated dicarboxylate anions by using the fumaric ($X = C_2H_2$), *trans*-hexenedioic ($X = C_4H_6$) and muconic ($X = C_4H_4$) acid salts. Following the usual procedure [23,25,26], $Cu_2(OH)_3(OAc)\cdot H_2O$ powder (1 mmol) is dispersed into 30 ml of an aqueous solution (0.25 M) of the corresponding sodium dicarboxylate ($XC_2O_4Na_2$), at room temperature. After one day, the exchange is completed by repeating once the treatment of the reaction product with a fresh dicarboxylate solution, for two days. The precipitate of green crystal powder is washed with alcohol, then dried at 40°C. The general formulation of the compounds, given in Table 1, is $Cu_2(OH)_{4-x}(XC_2O_4)_{x/2}\cdot zH_2O$, with $1.0 < x < 2.4$ and $0.1 < z < 1.6$.

The cobalt(II) derivative with *trans*-hexenedioate ($X = C_4H_6$) anion is synthesized starting from pink hydroxy-nitrate $Co_2(OH)_3(NO_3)$. The latter is obtained by slow hydrolysis of an aqueous solution (3.5 M) of $Co(NO_3)_2\cdot H_2O$ by KOH (1 M), with OH:Co = 1.3, at 95°C [34]. The exchange reaction is carried out as above, with *trans*-hexenedioic acid salt for a 5:1 molar ratio between the sodium salt and the starting hydroxy-nitrate. The reaction is carried out at 45°C, within 20 h, under argon flux. The pH is set to 7.5 by addition of NaOH at the beginning of the reaction. The bluish-green crystal powder is washed with alcohol and dried at 40°C. The general formulation of the compounds is given in Table 1.

The stoichiometries in dicarboxylate and water of the above compounds agree with C, H and H_2O chemical analysis within less than 0.3 mass per cent. The amount of Cu is determined from the weight loss at 500°C under air (final product, CuO). The amount of Co is determined from the weight loss at 700°C under air (final product, Co_3O_4).

2.3. Structure

All the compounds exhibit a lamellar structure as is evident from their XRD patterns which show, in the low 2θ range, intense 00*l* diffraction lines, up to at least the third harmonic (Fig. 2). This corresponds to the stacking periodicity of the hydroxide-based layers (basal spacing). During the exchange process, the completeness of the reaction is checked by the abrupt change in peak position, by comparison with the starting materials $Cu_2(OH)_3(OAc)\cdot H_2O$ ($d_{001} = 9.3$ Å) or $Co_2(OH)_3(NO_3)$ ($d_{001} = 6.93$ Å). The other reflections (*hkl* with *h* and $k \neq 0$) are much smaller, and exhibit usual enlargement for disordered pillared compounds with turbostratic disorder [35]. Despite the poor quality of crystallographic data, the diffraction patterns may be analyzed using hexagonal or pseudo-hexagonal unit cells, as for the monocarboxylate derivatives [23,25,26]. The similarity of XRD

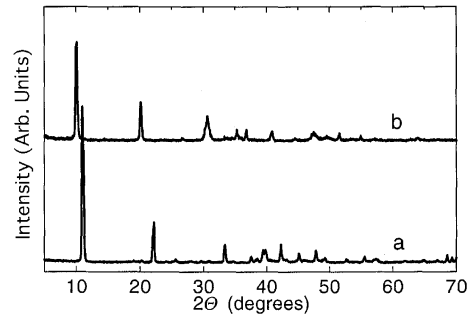


Fig. 2. Powder X-ray diffraction patterns of (a) $Cu_2(OH)_3(OAc)\cdot H_2O$, and (b) $Cu_2(OH)_{1.92}(C_4H_6C_2O_4)_{1.04}\cdot 0.22H_2O$ showing the shift of 00*l* diffraction lines.

patterns to those of $Cu_2(OH)_3(OAc)\cdot H_2O$ or $Co_2(OH)_3(NO_3)$ suggests that the local structure of the hydroxide-based layers remains quasi-unchanged after exchange reaction. In turn, the color change of the cobalt(II) exchanged compound (bluish-green) points to the occurrence of tetrahedral sites for the metal ion, and accordingly a structural modification of the inorganic layers.

The experimental basal spacing (interlayer distance) for copper(II) dicarboxylate compounds is given in Table 1. The variation of d_{001} with the chain length (n) is plotted in Fig. 3 for saturated *n*-methylene dicarboxylate anions. The basal spacing shows a step-like variation, in agreement with *n*-parity, which is related to the systematic change of orientation of the carboxylate groups in each bridging unit. For a given parity, a linear variation of d_{001} is observed, in agreement with the length of the exchanged anion. The slopes of the two straight lines (Fig. 3) are different, indicating a different tilt angle of the molecules with respect to the normal plane defined by the layers. The tilt angles are 42.9 and 25.7° for odd and even n values, respectively. The inorganic layer thickness deduced from the extrapolated values of d to $n=0$ differs by ca. 2 Å between the odd (8.3 Å) and even (6.3 Å) series. The mean value (7.3 Å) is close to the basal spacing reported for the parent compound $Cu_2(OH)_3NO_3$ ($d=6.95$ Å), exhibiting a Brucite-like structure [34,36]. This suggests that the hydroxide-based layers in the exchanged compounds are identical to those of the copper(II) hydroxy-nitrate, showing a quasi-planar triangular array of copper(II) ions in octahedral surrounding. Such a structural model for the inorganic layer is also found for the copper(II) hydroxy-acetate [37,38].

For unsaturated dicarboxylate anions, very close basal spacings are observed (0–0.2 Å step aside), compared to the corresponding saturated derivative.

The cobalt(II) compound is characterized by a basal spacing larger than that of the copper(II) analog by about 3.2 Å. Such a difference, already emphasized for the monocarboxylate series, is due to a larger thickness of the inorganic layer [39]. As noted above, the color change after anion-exchange points to the presence of cobalt(II) ions in tetrahedral surrounding. It can be predicted that the local structure of the metal-based layers is close to that of $Zn_5(OH)_8(NO_3)_2\cdot 2H_2O$ [40] or $Co_7(OH)_{12}(NO_3)_2\cdot zH_2O$ [41]. In these compounds, the inorganic 2d network consists of a median layer of transition metals in OH site, with metal vacancies at the apex of which lie two metal ions in T_d symmetry. The latter are surrounded by three oxygen atoms of the median layer completed by an oxygen atom belonging to nitrate.

In the frame of this model structure for the cobalt(II) compound, the organic anions could be connected through carboxylate moities to the Co(T_d) metal ions, and occupy the space in between the layers with water molecules.

Characteristic IR spectra of the exchanged compounds are displayed in Fig. 4 for representative samples. The presence of a broad feature in the hydroxyl stretching region (3000–3600 cm^{-1}) corresponds to lattice water, according to quantitative analysis (Table 1). A set of superimposed bands (Fig. 4(a)) is attributed to free CuO–H and CO–H hydrogen bonds. The spectra of the quasi-anhydrous compounds (Fig. 4(c)) present only one intense free O–H band at 3560–3570 cm^{-1}. The presence of organic molecules is confirmed by several bands around 2950 cm^{-1} which are attributed to C–H vibrations. The carboxylate doublet is clearly identified at 1530–1580 cm^{-1} and 1400–1430 cm^{-1}. The first one corresponds to the C=O stretch, and may include water for a small contribution (a more or less pronounced shoulder at ca. 1610 cm^{-1} is observed for hydrated compounds). From the position of the band, it is likely that the carboxyl groups are bonded to copper(II). The doublet is unique, indicating that the two carboxylate functions are linked to the layers, according to the charge balance between the organic and inorganic sub-networks. Finally, a relatively strong band around 870 cm^{-1}, attributed to the out-of-plane γ(OH–O) vibration [42], is recorded for five compounds, namely the succinic (864 cm^{-1}), adipic (864 cm^{-1}), *trans*-hexenedioic (873 cm^{-1}), muconic (884 cm^{-1}) and sebacic (895 cm^{-1}) acid derivatives. This particular feature is not observed for the cobalt(II) compound.

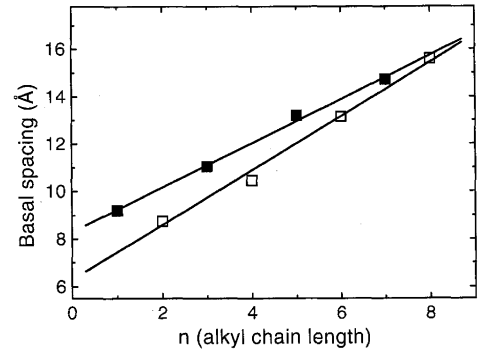


Fig. 3. Variation of the basal spacing as a function of n in copper(II) *n*-methylene dicarboxylates. Linear variations are observed for odd and even series.

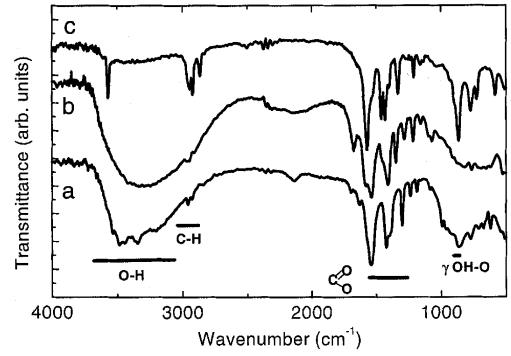


Fig. 4. IR spectra for (a) $Cu_2(OH)_{2.90}(C_2H_4C_2O_4)_{0.55}\cdot 0.58H_2O$, (b) $Cu_2(OH)_{2.76}(C_3H_6C_2O_4)_{0.62}\cdot 1.62H_2O$ and (c) $Cu_2(OH)_{2.08}(C_4H_8C_2O_4)_{0.96}\cdot 0.13H_2O$.

2.4. Magnetic properties

The magnetic properties of the copper(II)-based compounds involving *n*-methylene dicarboxylate bridging anions

are shown to be very sensitive to the spatial extension of the organic chains, as summarized in Table 1, but no clear correlation can be drawn.

Most of the studied compounds exhibit a 2d antiferromagnetic (AF) behavior over the whole temperature range, as illustrated by the continuous decay of the χT product at decreasing temperature (Fig. 5). There is no evidence of bulk ordering in the investigated temperature range. Only compounds with $n=2$, 4 and 8 show ferro or ferrimagnetic 2d behavior, in other words copper(II) layers with a net magnetic moment. For the saturated $n=2$ (succinate) anion, the variation of χT (Fig. 6) is very similar to that of the acetate derivative [23,25,26]. Upon cooling, a constant χT value is obtained down to 50 K, then a slight increase up to 0.95 cm^3 $K\ mol^{-1}$ at 11.2 K, suggesting weak ferromagnetic (F) in-plane interactions. At lower temperature, the drop of χT agrees with interlayer AF interactions, promoting a 3d long-range order. In turn, the unsaturated derivative ($X=C_2H_2$) shows clearly an AF behavior over the whole temperature range. Note that such a variation cannot be explained by a change of the basal spacing, but is due most likely to slight modification in the local structure of the inorganic layer, inducing a change of sign of the exchange coupling. Such a magnetic dependence is well documented for copper(II) systems which appear to be very sensitive to the metal–oxygen–metal bridging angle [43,44].

The most striking results are noticed for the $n=4$ anions with saturated ($X=C_4H_8$) and unsaturated ($X=C_4H_6$ and $X=C_4H_4$) aliphatic chains, noted hereafter **4₀**, **4₁** and **4₂**, respectively. These compounds, which only differ by the number of double bonds of the anionic spacer (0 to 2), are characterized by very close basal spacings (10.45 to 10.22 Å), and as a result have analogous structures.

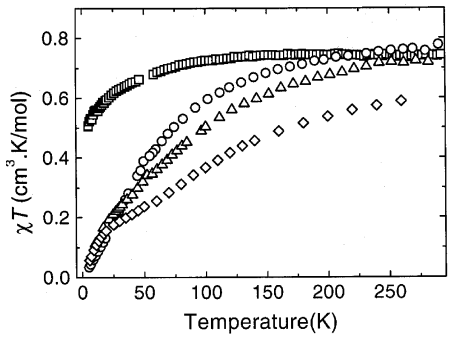


Fig. 5. Temperature dependence of the χT product for copper(II) *n*-methylene dicarboxylates with $n=1$ (□), 3 (○), 5 (△) and 7 (◇).

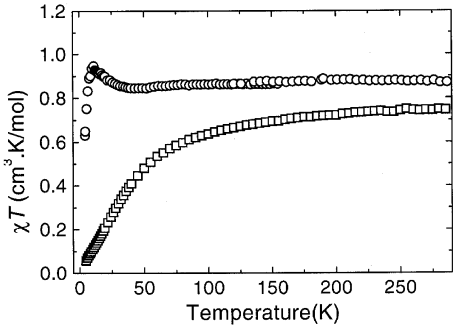


Fig. 6. Temperature dependence of the χT product for the copper(II) dicarboxylates $Cu_2(OH)_3(XC_2O_4)_{0.5}$ with the saturated ($X=C_2H_4$) (○), and unsaturated ($X=C_2H_2$) (□) bridging anions.

A strong and regular increase of χT is observed upon cooling down (Fig. 7), characteristic of significant in-plane ferromagnetic interactions, with a maximum at 15.7 K for **4₀**, 13.0 K for **4₁** and 16.0 K for **4₂**. The main difference occurs at low temperature, since **4₀** and **4₂** show an AF long-range ordering with a metamagnetic transition for $H_C=2250$ and 2040 Oe, respectively (inset of Fig. 7), while **4₁** exhibits a characteristic ferromagnetic transition. This is evidenced from the strong divergence of χT at low temperature (factor 10 with respect to **4₀**), and the variation of a.c. susceptibility (Fig. 8). The T_C value recorded from the maximum of χ'_{ac} is found to be 13.0 K. The variation of magnetization, plotted in the inset of Fig. 8, agrees with a ferromagnetic order between copper(II) layers. The hysteretic effect at 4 K is small (around 100 Oe), indicating that the anisotropy of magnetic moments is weak.

A fit of the magnetic susceptibility has been performed in the paramagnetic regime to determine the in-plane exchange interaction between copper(II) ions. Using the high temperature series expansions [45,46] for the spin-1/2 2d Heisen-

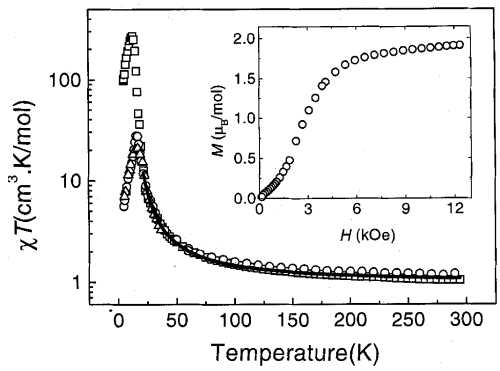


Fig. 7. Temperature dependence of the χT product for the copper(II) dicarboxylates involving the saturated, $X=C_4H_8$ (○), and the unsaturated $X=C_4H_6$ (□) and $X=C_4H_4$ (△) bridging anions. The full line corresponds to the best fit, using HTS expression for the susceptibility [45,46].The inset shows the metamagnetic transition of $M(H)$ for the saturated dicarboxylate.

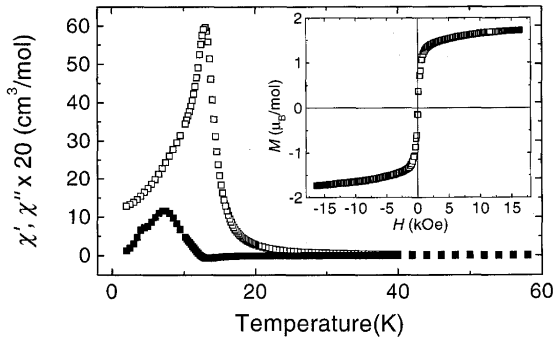


Fig. 8. Temperature dependence of the a.c. susceptibilities of $Cu_2(OH)_{1.92}(C_4H_6C_2O_4)_{1.04}\cdot 0.22H_2O$ involving a π electron bridging anion. The inset shows the $M(H)$ variation at 4 K.

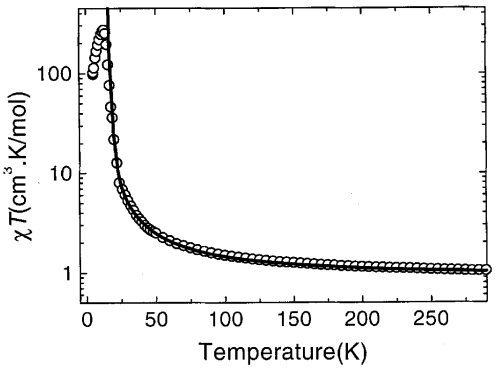


Fig. 9. Best fit of the paramagnetic susceptibility of $Cu_2(OH)_{1.92}(C_4H_6C_2O_4)_{1.04}\cdot 0.22H_2O$ from the sum of Arrhenius-like laws (see text), showing two regimes for the magnetic behavior.

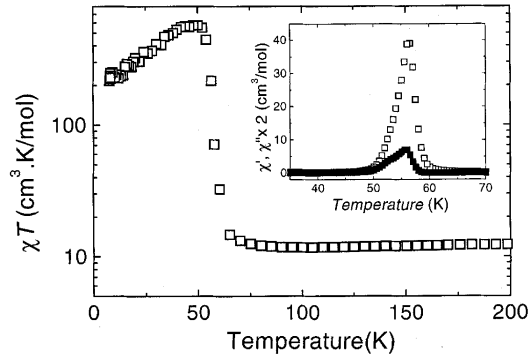


Fig. 10. Temperature dependence of the magnetic susceptibility of $Co_7(OH)_{11.6}(C_4H_6C_2O_4)_{1.20}\cdot 5.5H_2O$. χT is plotted as a function of temperature. The a.c. susceptibilities are shown in the inset.

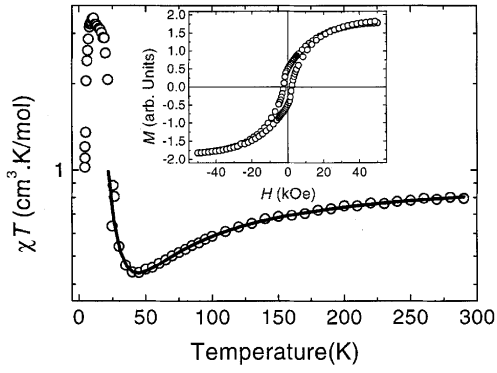


Fig. 11. Temperature dependence of the χT product for the copper(II) dicarboxylate $Cu_2(OH)_{1.64}(C_8H_{16}C_2O_4)_{1.18}\cdot 0.45H_2O$. The full line represents the best fit from the sum of exponential laws (see text). The inset shows the hysteresis of the $M(H)$ curve at 2 K.

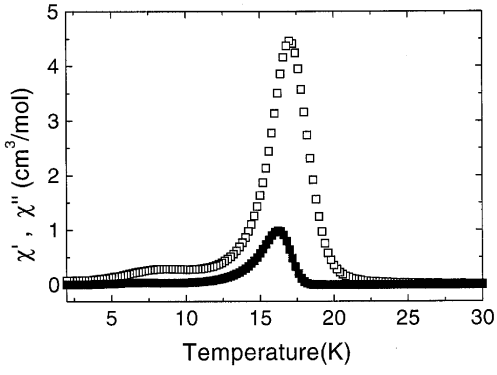


Fig. 12. Temperature dependence of a.c. susceptibilities for $Cu_2(OH)_{1.64}(C_8H_{16}C_2O_4)_{1.18}\cdot 0.45H_2O$.

berg triangular lattice [1], a very good agreement between theory and experimental findings is obtained for $J/k = 27$ K ($H = -J\sum S_iS_j$) (Fig. 7). Note that above T_C, the χT variation is well fitted from the sum of Arrhenius-like contributions, $a\exp(E_1/kT) + 0.86\exp(E_2/kT)$ with $a = 5.10^{-6}$, $E_1/k = 287$ K and $E_2/k = 52.6$ K, (Fig. 9), showing clearly two regimes for the magnetic behavior (0.86 gives the high temperature Curie constant). Thus, above 25 K, χT is well described by an exponential decay whose activation energy corresponds roughly to $2J$. In the vicinity of T_C, the variation of χT is depicted by a rapidly diverging function, with a strong activation energy, indicating that interlayer interactions are no longer negligible.

Preliminary experiments have been performed for the cobalt(II) *trans*-hexenedioic ($X = C_4H_6$) parent compound. The χT plot (Fig. 10) shows a slight decay from room temperature down to 100 K (11.7 cm^3 K mol^{-1}), due to the spin–orbit coupling effect, then a sharp divergence below 65 K with a maximum of 575 cm^3 K mol^{-1}, pointing to a long-range ferromagnetic ordering. A.c. susceptibility measurements confirm the occurrence of a magnetic ground-state with an out-of-phase signal below $T_C = 56.5$ K.

Finally, the long-chain compound $n = 8$ (sebacic acid) exhibits a very different magnetic behavior (Fig. 11). The χT product decreases on cooling from 0.8 cm^3 K mol^{-1} at room temperature down to 0.44 cm^3 K mol^{-1} at 40 K, then displays a very rapid increase below 20 K. As already mentioned for copper(II) *n*-alkyl carboxylate derivatives [23,25,26], such a χT variation is characteristic of a ferrimagnetic low-lying spin-state for copper(II) layers. Owing to the nature of the in-plane exchange pathways, which involve oxygen atoms from OH^- and $O_2CC_8H_8CO_2^{2-}$, it can be stated that the triangular network is likely strongly distorted and ordered sub-networks with uncompensated magnetic ground-state take place. It follows that an antiferromagnetic spin-1/2 triangular model is irrelevant to determine the in-plane exchange constants.

Nevertheless, the paramagnetic behavior is well described by the relationship $a\exp(E_1/kT) + b\exp(E_2/kT)$, with $a = 0.05$, $b = 0.92$, $E_1/k = 64.6$ K and $E_2/k = -62.5$ K, which indicates clearly two competing regimes. At high temperature, the activation energy E_2 agrees with an AF coupling, while in the vicinity of T_C, the E_1 value indicates a ferromag-

[1] $\chi T = \frac{Ng^2\mu_B^2}{k}\sum_n^{\infty}\frac{a_n}{n!}\left(\frac{-J}{4kT}\right)^n$

$a_0 = 0.25$, $a_1 = -1.5$, $a_2 = 12$, $a_3 = -102$, $a_4 = 900$, $a_5 = -10584$, $a_6 = 195432$, $a_7 = -3411504$, $a_8 = 22723392$, $a_9 = 449551104$, $a_{10} = 17698680192$, $a_{11} = -1884636552960$, $a_{12} = 15953277445632$, $a_{13} = 3244354478011392$.

netic alignment of the resulting spins. The overall Curie constant is given by the sum $a+b$.

At low temperature, the transition towards a magnetic ground-state is evidenced from a.c. susceptibility data (Fig. 12). An out-of-phase signal is observed below $T_C = 17$ K, which is slightly higher than for **4_1**.

The occurrence of long-range ferrimagnetic order is confirmed by a characteristic hysteretic effect in the $M(H)$ curve at $T = 4$ K (inset of Fig. 11). On close examination of the remnant value of magnetization, it may be stated, on the basis of the Stoner–Wohlfarth model developed for single-domain particles with uniaxial anisotropy [47], that about half of copper(II) moments are uncompensated at low temperature, owing likely to the presence of two sub-networks.

3. Concluding remarks

The mechanism responsible for the low temperature magnetic behavior of hybrid systems made of metal hydroxide layers separated by large organic spacers, such as *n*-alkyl sulfate or carboxylate, is now well understood [25,26,39]. Owing to the nature of the ligands, the alkyl chains do not participate directly in the interlayer coupling but noticeable change may be induced on the in-plane exchange mechanism, in particular for copper(II) compounds whose behavior is closely related to the structural features [43,44].

Similarly, either F or AF behavior is observed for copper(II) dicarboxylates, without a clear relationship with the value of the basal spacing. Nevertheless, it can be pointed out that some insight on the correlation with the local structure arises from IR spectroscopy. Thus, a band is observed in the range 864–895 cm^{-1} for copper(II) compounds exhibiting ferro or ferrimagnetic layers, only. Further, it is worth noticing that these systems involve aliphatic chains with even parity, i.e. corresponding to a fixed tilt angle of the bridging anion. This condition for stabilizing magnetic copper(II) layers appears to be significant but not sufficient, as illustrated by the AF behavior of the compounds with $X = C_2H_2$ and C_6H_{12}. A small variation of the anion tilt angle is likely responsible for a slight structural modification of the layer itself, and accordingly for the exchange mechanism within copper(II) layers.

Let us focus now on the low temperature behavior of the saturated dicarboxylate compounds with metal layers showing a ferro or ferrimagnetic spin arrangement, in accordance with the χT variation in the paramagnetic regime.

In these systems, the situation depends to a large extent on the interlayer spacing. For $n = 2$ and 4, a very weak interlayer interaction stabilizes a 3d AF order, and a metamagnetic transition occurs in low field, as already mentioned for monocarboxylate compounds [25,26]. When the spacing is made larger ($n = 8$), a spontaneous magnetization is observed, with a characteristic hysteretic effect, which can only be explained by considering dipolar through-space interactions between ferromagnetically coupled layers [30]. Indeed the strength of the dipolar interaction energy between magnetic layers at a distance *r* apart, varies as r^{-1} for the systems under consideration, so that it is by far the driving contribution for distances larger than 10–11 Å [48].

Clearly, this description fails for the unsaturated ($X = C_4H_6$) bridging anion compound, since bulk ferromagnetism is stabilized for a basal spacing $d = 10.22$ Å, very close to that of the saturated analog. Even if it can be claimed that the *d* turning value is about 10–11 Å, a different mechanism, taking into account the polarization by π electrons, must be involved to explain the occurrence of long-range ferromagnetism.

Further, for the conjugated derivative ($X = C_4H_4$), an AF ground-state takes place with a metamagnetic transition in low field, according to the spin polarization in the conjugated π system. The number of double bonds in the bridging anion is thus an essential feature to control the coupling between magnetic layers.

Finally, the magnetic study of this series of hybrid compounds shows that spectacular and unexpected behaviors may be obtained, depending on the basal spacing and the π character of the bridging species. In this respect, these systems differ markedly from the classical layered hybrid compounds, mostly because they provide a new class of multilayer magnets with possible electronic transfers between adjacent layers. Such hybrid systems may be viewed as good candidates for tunneling magnetoresistance effects.

Acknowledgements

The authors are very grateful to S. Angelov for fruitful discussions, A. Derory and R. Poinsot for assistance with magnetic experiments. This work has been partly funded by the European Network 'Molecular Magnetism: from Materials toward Devices' no. ERBFMRXCT980181.

References

[1] F.R. Gamble, F.J. Disalvo, R.A. Klemm, T.H. Geballe, Science 168 (1970) 568.
[2] R. Burch, Pillared clays, Catal. Today 2 (1988) 1.
[3] K. Watanabe, T. Kondow, M. Soma, T. Onishi, K. Tamaru, Proc. R. Soc. London, Ser. A 333 (1973) 51.
[4] M. Meyn, K. Beneke, G. Lagaly, Inorg. Chem. 29 (1990) 5201.
[5] V. Prevot, C. Forano, J.P. Besse, J. Mater. Chem. 9 (1999) 155.
[6] M.L. Occelli, H. Robson (Eds.), Expanded Clays and Other Microporous Solids, Van Nostrand Reinhold, New York, 1992.
[7] T.J. Pinnavaia, ACS Symp. Ser. 192 (1982) 241.
[8] R. Clement, Science 263 (1993) 658.
[9] Y. Sano, M. Tanaka, N. Koga, K. Matsuda, H. Iwamura, P. Rabu, M. Drillon, J. Am. Chem. Soc. 119 (1997) 8246.
[10] K. Inoue, H. Iwamura, J. Am. Chem. Soc. 116 (1994) 3173.
[11] M. Kurmoo, A.W. Graham, P. Day, S. Coles, M.B. Hursthouse, J.L. Caulfield, J. Singleton, F.L. Pratt, W. Hayes, L. Ducasse, P. Guionneau, J. Am. Chem. Soc. 117 (1995) 12209.
[12] P. Gütlich, Mol. Cryst. Liq. Cryst. 305 (1997) 17.

[13] L. Ouahab, Chem. Mater. 9 (1997) 1909.
[14] E. Coronado, J.R. Galan-Mascaros, C. Gimenez-Saiz, C.J. Gomez-Garcia, NATO ASI Ser. C 486 (1996) 28.
[15] R. Clément, P.G. Lacroix, D. O'Hare, J. Evans, Adv. Mater. 6 (1995) 794.
[16] S. Bénard, P. Yu, T. Coradin, E. Rivière, K. Nakatani, R. Clément, Adv. Mater. 9 (1997) 981.
[17] S. Yamanaka, in: Microporous Crystals, vol. 21, Chem. Soc. Jpn., Tokyo, 1994, p. 89.
[18] S. Yamanaka, Y. Inoue, M. Hattori, F. Okumura, M. Yoshikawa, Bull. Chem. Soc. Jpn. 65 (1992) 2494.
[19] S. Miyata, T. Kumura, Chem. Lett. (1973) 843
[20] M. Meyn, K. Beneke, G. Lagaly, Inorg. Chem. 32 (1993) 1209.
[21] M. Bujoli-Doeuff, L. Force, V. Gadet, M. Verdaguer, K. elMalki, A. deRoy, J.P. Besse, J.P. Renard, Mater. Res. Bull. 26 (1991) 577.
[22] S. Yamanaka, T Sako, K. Seki, M. Hattori, Solid State Ionics 53–56 (1992) 127.
[23] M. Drillon, C. Hornick, V. Laget, P. Rabu, F. Romero, S. Rouba, G. Ulrich, R. Ziessel, Mol. Cryst. Liq. Cryst. 273 (1995) 125.
[24] W. Fujita, K. Awaga, Inorg. Chem. 35 (1996) 1915.
[25] P. Rabu, S. Rouba, V. Laget, C. Hornick, M. Drillon, Chem. Commun. (1996) 1107.
[26] V. Laget, C. Hornick, P. Rabu, M. Drillon, J. Mater. Chem. 9 (1999) 169.
[27] M.A. Girtu, C.M. Wynn, W. Fujita, K. Awaga, A.J. Epstein, J. Appl. Phys. 83 (1998) 7378.
[28] V. Laget, S. Rouba, P. Rabu, C. Hornick, M. Drillon, J. Magn. Magn. Mater. 154 (1996) L7.
[29] V. Laget, P. Rabu, C. Hornick, F.M. Romero, R. Ziessel, P. Turek, M. Drillon, Mol. Cryst. Liq. Cryst. 305 (1997) 291.
[30] M. Drillon, P. Panissod, J. Magn. Magn. Mater. 188 (1998) 93.
[31] V. Laget, P. Rabu, C. Hornick, F.M. Romero, R. Ziessel, P. Turek, M. Drillon, Mol. Cryst. Liq. Cryst. 305 (1997) 291.
[32] W. Fujita, Ph.D. Thesis, Tokyo University, 1997.
[33] V. Laget, C. Hornick, P. Rabu, M. Drillon, P. Turek, R. Ziessel, Adv. Mater. 10 (1998) 1024.
[34] P. Rabu, S. Angelov, P. Legoll, M. Belaiche, M. Drillon, Inorg. Chem. 32 (1993) 2463.
[35] R.C. Reynolds, in: D.L. Bish, J.E. Post (Eds.), Modern Powder Diffraction, Reviews in Mineralogy, 1989, p. 20.
[36] H. Effenberger, Z. Kristallogr. 165 (1983) 127.
[37] N. Masciocchi, E. Corradi, A. Sironi, G. Moretti, G. Minelli, P. Porta, J. Solid State Chem. 131 (1997) 252.
[38] W. Fujita, K. Awaga, Inorg. Chem. 36 (1997) 196.
[39] V. Laget, C. Hornick, P. Rabu, M. Drillon, R. Ziessel, Coord. Chem. Rev. 178 (1998) 1533.
[40] W. Stählin, H.R. Oswald, Acta Crystallogr., Sect. B 26 (1970) 860.
[41] L. Markov, K. Petrov, V. Petkov, Thermochim. Acta 106 (1986) 283.
[42] N. Zotov, K. Petrov, M. Dimitrova-Pankova, J. Phys. Chem. Solids 51 (1990) 1199.
[43] V.H. Crawford, H.W. Richardson, J.R. Wasson, D.J. Hodgson, W.E. Hatfield, Inorg. Chem. 15 (1976) 2107.
[44] E. Ruiz, P. Alemany, S. Alvarez, J. Cano, J. Am. Chem. Soc. 119 (1997) 1297.
[45] G.S. Rushbrooke, G.A. Baker, P.J. Wood, in: C. Domb, M.S. Green (Eds.), Phase Transition and Critical Phenomena, vol. 3, Academic Press, 1974.
[46] N. Elstner, R.R.P. Singh, A.P. Young, Phys. Rev. Lett. 71 (1993) 1629.
[47] E.C. Stoner, E.P. Wohlfarth, Philos. Trans. R. Soc. London, Ser. A 240 (1948) 599.
[48] P. Panissod, M. Drillon, to be published.

PERGAMON

www.elsevier.nl/locate/poly

Polyhedron 19 (2000) 267–274

POLYHEDRON

Discotic liquid crystals of transition metal complexes 25: influence of the central metal on columnar mesomorphism and π-acceptor properties of the octa-alkoxy-substituted bis(diphenyldithiolene)metal complexes[1]

Kazuchika Ohta *, Yoshio Inagaki-Oka, Hiroshi Hasebe, Iwao Yamamoto

Department of Functional Polymer Science, Faculty of Textile Science & Technology, Shinshu University, Ueda 386-8567, Japan

Received 20 March 1999; accepted 15 July 1999

Abstract

In order to investigate the influence of the central metal on mesomorphism and π-acceptor properties of the octa-alkoxy-substituted metal complexes, novel homologs, bis[di(*n*-alkoxy)phenyldithiolene]palladium and bis[di(*n*-alkoxy)phenyldithiolene]platinum (*n*-alkoxy = $C_nH_{2n+1}O$, $n=1$ to 12), have been synthesized. The mesophases were established by microscopic observations, DSC, and temperature-dependent X-ray diffraction techniques. As reported previously, the nickel complexes show a Col_h mesophase for $n=5$ to 12. On the other hand, the present palladium and platinum complexes show a Col_h mesophase for $n=4$ to 12 and $n=6$ to 12, respectively. Thus, they give the Col_h mesophase for a shorter length of alkoxy chain in the order Pd, Ni, Pt. For $6 \leq n \leq 12$, the clearing points become higher in the order Pt < Ni < Pd. The intracolumnar stacking distances of these Ni, Pd and Pt complexes were observed at 3.64 ± 0.02, 3.56 ± 0.03, and 3.73 ± 0.02 Å, respectively. Thus, they gave a longer stacking distance in the order Pt > Ni > Pd. Hence, the order of stacking distances is apparently related to the order of clearing points. Moreover, the Pt, Ni and Pd complexes show reduction potentials at -0.09 ± 0.01, -0.055 ± 0.005, and $0.00 \leq 0.01$ V (versus SCE in CH_2Cl_2), respectively. They become better π-acceptors in the order Pt < Ni < Pd. We reveal from the electronic absorption spectra that the LUMO energy level of these metal complexes decreases in the order Pt < Ni < Pd, and that the back donation of electrons from the central metal to the ligand occurs more in the same order Pt < Ni < Pd. This results in better π-acceptor properties in the order Pt < Ni < Pd for the present complexes. ©2000 Elsevier Science Ltd All rights reserved.

Keywords: Discotic complexes; Columnar complexes; Liquid crystals; π-acceptors; Dithiolene

1. Introduction

Since the first organic metal TTF–TCNQ was found in 1972, many organic one-dimensional conductors have been studied [2,3]. The one-dimensional conductors form an infinite columnar structure with stacking of the planar molecules, and an electron-conducting path is formed along the one-dimensional axis. On the other hand, discotic (disk-like) liquid crystals were discovered in 1977 and similarly form a columnar structure, so that the application of disk-like liquid crystals to one-dimensional conductors has been studied [4–11]. In particular, disk-like liquid crystals of organic transition metal complexes form a one-dimensional chain of the central metal in the columnar axis direction which is favorable for high conductivity [12–17].

As shown in Fig. 1, Bélombé suggested in 1983 that a special one-dimensional columnar structure might show high conductivity [18]. In this columnar structure, the π-acceptor dithiolene metal complex and the π-donor glyoximato metal complex are mutually piled up. This special structure not only has the one-dimensional chain of the central metals but also has the mutual arrangement of S and N atoms in the surroundings to form four pseudo $(SN)_x$-like chains. $(SN)_x$ is well known to show superconductivity. Hence, we thought that if these core complexes could be substituted by long chains, they would become columnar liquid crystals and show high conductivity. We previously succeeded in the synthesis of octa-long-chain-substituted π-donor glyoximato metal complexes (M = Ni, Pd, Pt). According to our expectation, these complexes have columnar mesophases [19–23]. The oxida-

* Corresponding author. Tel.: +81-268-21-5492; fax: +81-268-21-5321; e-mail: ko52517@giptc.shinshu-u.ac.jp

[1] For Part 24, see Ref. [1].

0277-5387/00/$ - see front matter ©2000 Elsevier Science Ltd All rights reserved.
PII S0277-5387(99)00356-3

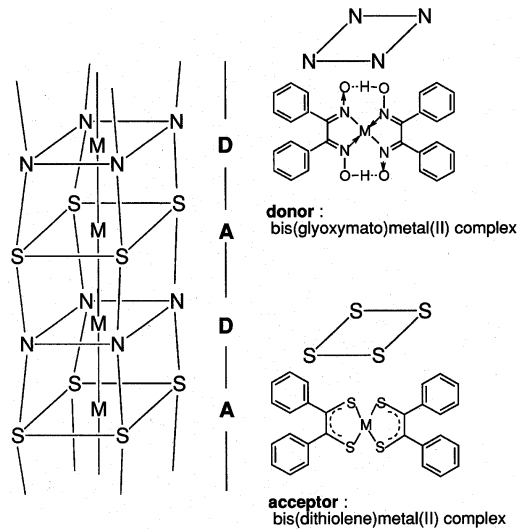


Fig. 1. Schematic representation of the one-dimensional conductor composed of a metal–metal linear chain surrounded by four $(SN)_x$-like chains [18].

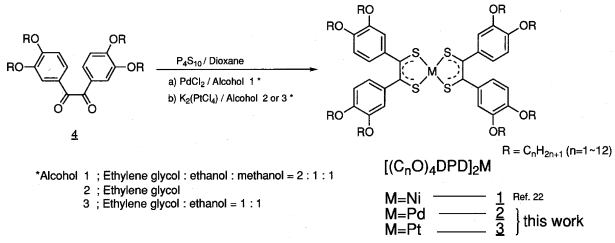


Fig. 2. Synthetic route for the bis[1,2-bis(3′,4′di-*n*-alkoxyphenyl)ethane-1,2-dithiolene]metal complexes.

tion potentials are approximately constant irrespective of the central metal [24]. On the other hand, for the π-acceptor dithiolene metal complexes, only synthesis of the octa-long-chain-substituted bis(diphenyldithiolene)nickel complexes (**1** in Fig. 2) has been successful. These Ni complexes also showed columnar liquid crystalline phases. Their reduction potentials are −0.05 to −0.06 V irrespective of the length of the alkoxy chains [25]. These nickel complexes are the first π-acceptor columnar liquid crystals.

In this study, we have, hence, synthesized novel Pd and Pt complexes **2** and **3** (Fig. 2), to obtain better π-acceptor dithiolene metal complexes in the homologs of octa-long-chain-substituted dithiolene metal complexes. We investigated the influence of central metal species on the π-acceptor and liquid crystal properties. Interestingly, the disk-like Pd and Pt complexes synthesized here exhibit the same Col_h mesophase as the Ni complexes. More interestingly, the Pd complexes exhibit the highest clearing points and the broadest temperature range of the mesophases, and are the best π-acceptor columnar mesogens in these three kinds of metal complexes. We wish to report here the liquid crystal and π-acceptor properties of these interesting octa-long-chain-substituted dithiolene metal complexes.

2. Experimental

2.1. Synthesis

The synthetic route for the $[(C_nO)_4DPD]_2Pd$ ($n=1$ to 12) (**2**) and $[(C_nO)_4DPD]_2Pt$ ($n=1$ to 12) (**3**) complexes is shown in Fig. 2. The detailed procedure of preparation of these complexes is the same as described by us previously, except for the solvent for metal salts [26]. By modification of the solvent (Fig. 2), we succeeded for the first time in syntheses of the target complexes, $[(C_nO)_4DPD]_2Pd$ ($n=1$ to 12) (**2**) and $[(C_nO)_4DPD]_2Pt$ ($n=1$ to 12) (**3**). Tables 1 and 2 summarize the solvents for metal salts, the elemental analysis data, the yields, the recrystallization solvents, and the colors of the virgin state of these complexes. The detailed procedures are described for the representative $[(C_{12}O)_4DPD]_2Pd$ and $[(C_{12}O)_4DPD]_2Pt$ complexes, as follows.

Table 1
Solvent for the metal salt, elemental analysis data, yields, recrystallization solvent, and color (virgin state) of the $[(C_nO)_4DPD]_2Pd$ ($n=1$–12) complexes **2**

n	Solvent for the metal salt	Elemental analysis, found (calc.) (%)		Yield (%)	Recrystallization solvent	Color (virgin state)
		C	H			
1	Alcohol 1 [a]	52.19 (52.01)	4.45 (4.37)	12		dark brown
2	Alcohol 1	56.28 (56.01)	5.59 (5.56)	16	ethyl acetate/CCl_4	black
3	Alcohol 1	59.43 (59.16)	6.61 (6.49)	20	$CHCl_3$/*n*-hexane	black (Cry_1)
4	Alcohol 1	61.70 (61.70)	7.19 (7.25)	10	*n*-hexane	dark brown (Cry_1)
5	Alcohol 1	63.67 (63.80)	7.80 (7.87)	13	*n*-hexane/EtOH [b]	dark brown (Cry_1)
6	Alcohol 1	65.53 (65.56)	8.50 (8.40)	16	*n*-hexane/EtOH	dark brown (Cry_1)
7	Alcohol 1	67.09 (67.05)	8.80 (8.84)	27	*n*-hexane/EtOH	dark brown (Cry_1)
8	Alcohol 1	68.01 (68.34)	9.14 (9.23)	16	*n*-hexane/EtOH	black (Cry_1)
9	Alcohol 1	69.39 (69.47)	9.47 (9.56)	20	*n*-hexane/EtOH	black
10	Alcohol 1	70.40 (70.45)	9.80 (9.85)	12	*n*-hexane/EtOH	black
11	Alcohol 1	71.40 (71.32)	10.14 (10.11)	10	*n*-hexane/EtOH	black (Cry_1)
12	Alcohol 1	72.79 (72.10)	10.26 (10.34)	18	*n*-hexane/EtOH	black

[a] Alcohol 1, ethylene glycol:ethanol:methanol = 2:1:1.
[b] EtOH, ethanol.

Table 2
Solvent for the metal salt, elemental analysis data, yield, recrystallization solvent, and color (virgin state) of the $[(C_nO)_4DPD]_2Pd$ ($n=1$–12) complexes **3**

n	Solvent for the metal salt	Elemental analysis, found (calc.) (%)		Yield (%)	Recrystallization solvent	Color (virgin state)
		C	H			
1	Alcohol 2 [a]	46.83 (47.00)	4.00 (3.94)	42	$CHCl_3$/EtOH [c]	blue
2	Alcohol 2	50.96 (51.20)	5.09 (5.08)	48	Ethyl acetate/CCl_4	black (Cry_1)
3	Alcohol 2	54.31 (54.57)	5.91 (5.99)	45	$CHCl_3$/*n*-hexane	blue
4	Alcohol 2	57.38 (57.35)	6.68 (6.74)	50	*n*-hexane/EtOH	blue (Cry_1)
5	Alcohol 2	59.79 (59.67)	7.37 (7.36)	37	*n*-hexane/EtOH	violet (Cry_1)
6	Alcohol 2	61.92 (61.63)	7.96 (7.89)	30	*n*-hexane/EtOH	violet (Cry_1)
7	Alcohol 2	63.12 (63.32)	8.29 (8.35)	39	*n*-hexane/EtOH	violet
8	Alcohol 2	64.76 (64.79)	8.66 (8.75)	45	*n*-hexane/EtOH	dark blue (Cry_1)
9	Alcohol 2	66.27 (66.08)	9.09 (9.09)	60	*n*-hexane/EtOH	black (Cry_1)
10	Alcohol 2	67.11 (67.21)	9.41 (9.40)	11	*n*-hexane/EtOH	black (Cry*)
11	Alcohol 2	68.21 (69.34)	9.63 (9.67)	30	*n*-hexane/EtOH	black (Cry_1)
12	Alcohol 3 [b]	69.34 (69.13)	9.84 (9.92)	28	*n*-hexane/EtOH	black (Cry_1)

[a] Alcohol 2, ethylene glycol.
[b] Alcohol 3, ethylene glycol:ethanol = 2:1.
[c] EtOH, ethanol.

*2.1.1. Bis[1,2-bis(3′,4′-di-n-dodecyloxyphenyl)ethane-1,2-dithiolene]palladium (**2**)*

To dioxane (86 ml), phosphorus pentasulfide (1.78 g, 4.03 mmol) and 3,3′,4,4′-tetradodecyloxybenzil (**4**) (1.90 g, 2.01 mmol) were added and then the mixture was refluxed for 9 h under a nitrogen atmosphere. The hot reaction mixture was filtrated to remove the precipitates. To the hot filtrate was added palladium(II) chloride (0.18 g, 1.0 mmol) dissolved in about 50 ml of a mixed solvent of ethylene glycol:ethanol:methanol = 2:1:1(v/v/v). The reaction mixture was refluxed for 2 h under a nitrogen atmosphere. After the reflux, about 100 ml of ethanol was added to the reaction mixture. After cooling to room temperature, it was filtered to collect the precipitates. The target complex was the precipitate on the filter paper. Purification was carried out by silica gel column chromatography (*n*-hexane:benzene = 1:1 (v/v), $R_f = 0.67$) and recrystallization from a mixed solvent of *n*-hexane and ethanol to give 0.38 g of **2** as black crystals. Yield 18%.

^{1}H NMR ($CDCl_3$, TMS) δ (ppm): 0.88 (t, $J = 5$ Hz, 24H), 1.12–1.91 (m, 160H), 3.76 (t, $J = 6$ Hz, 8H), 3.99 (t, $J = 6$ Hz, 8H), 6.81–7.25 (m, 12H).

IR (KBr pellet, cm^{-1}): 2920, 2860, 1600, 1510, 1350.

*2.1.2. Bis[1,2-bis(3′,4′-di-n-dodecyloxyphenyl)ethane-1,2-dithiolene]platinum (**3**)*

To dioxane (93 ml), phosphorus pentasulfide (1.88 g, 4.23 mmol) and 3,3′,4,4′-tetradodecyloxybenzil (**4**) (2.00 g, 2.11 mmol) were added and then the mixture was refluxed for 5 h under a nitrogen atmosphere. The hot reaction mixture was filtrated to remove the precipitates. To the hot filtrate was added potassium tetrachloroplatinate(II) (0.44 g, 1.1 mmol) dissolved in 20 ml of a mixed solvent of ethylene glycol:ethanol = 1:1 (v/v). The reaction mixture was refluxed for 2 h under a nitrogen atmosphere. After cooling to room temperature, the precipitates appeared and the reaction mixture was filtered to collect the precipitates. The target complex was the precipitate on the filter paper. Purification was carried out by silica gel column chromatography (*n*-hexane:benzene = 1:1 (v/v), $R_f = 0.67$) and recrystallization from a mixed solvent of *n*-hexane and ethanol to give 0.63 g of **3** as black crystals. Yield 28%.

^{1}H NMR ($CDCl_3$, TMS) δ (ppm): 0.94 (t, $J = 5$ Hz, 24H), 1.09–2.16 (m, 160H), 3.77 (t, $J = 5$ Hz, 8H), 3.99 (t, $J = 5$ Hz, 8H), 6.69–7.12 (m, 12H).

IR (KBr pellet, cm^{-1}): 2920, 2860, 1600, 1510, 1350.

2.2. Measurements

The final products were identified by elemental analysis, ^{1}H NMR and IR spectra using a Perkin–Elmer elemental analyzer 240B, a JEOL JNM-FX90A, and a JASCO A-100, respectively. The phase transition behaviors of these compounds were observed by an OLYMPUS BH2 polarizing microscope equipped with a heating plate controlled by a thermoregulator, Mettler FP80 and FP82, and measured with a Shimadzu DSC-50 differential scanning calorimeter. To establish the mesophases, powder X-ray patterns were measured with Cu Kα radiation using a Rigaku Geigerflex equipped with a hand-made heating plate controlled by a thermoregulator. The electrochemical properties were determined in dichloromethane solutions containing 0.1 M of tetrabutylammonium perchlorate as supporting electrolyte. Cyclic voltammograms were obtained with a hand-made potentiostat and recorded with a Yokogawa Electric Works type 3086X-Y recorder. The measurements were made at a glassy carbon working electrode versus saturated calomel electrode (SCE). Electronic spectra were measured with a Hitachi 330 spectrophotometer.

Table 3
Phase transition temperatures (T) and enthalpy changes (ΔH) of the $[(C_nO)_4DPD]_2Pd$ ($n=1$–12) complexes **2** [a b]

n	Phase $\xrightarrow[\text{[}\Delta H\text{(kJ/mol)]}]{\text{T(°C)}}$ Phase[a] ⇝ relaxation
1	Cry $\xrightarrow{245.9}$ decomposition
2	Cry $\rightleftharpoons^{179.2}$ I (decomposition)
3	$Cry_1 \rightleftharpoons^{134.0}_{[6.00]} Cry_2 \rightleftharpoons^{163.5}_{[54.3]}$ I
4	$Cry_1 \xrightarrow{124.2} Cry_1 \rightleftharpoons^{127.4} Col_h(b) \rightleftharpoons^{145.5}_{[8.04]}$ I
5	$Cry_1 \xrightarrow{105.2}_{[4.17]} Cry_2 \rightleftharpoons^{110.9}_{[33.5]} Col_h(a) \rightleftharpoons^{146.0}_{[10.8]}$ I
6	$Cry_1 \xrightarrow[[13.0]]{54.3} Cry_2 \rightleftharpoons^{90.7}_{[37.7]} Col_h(a) \rightleftharpoons^{136.0}_{[10.6]}$ I
7	$Cry^b \rightleftharpoons^{95.3}_{[34.8]} Col_h(b) \rightleftharpoons^{136.5}_{[12.2]}$ I; Cry ⇌ 75.0 [13.4]
8	$Cry_1 \xrightarrow[[40.5]]{46.2} Cry_3 \rightleftharpoons^{69.9}_{[66.1]} Col_h(d) \rightleftharpoons^{130.5}_{[11.4]}$ I; $Cry_2 \rightleftharpoons^{62.6}_{[0.761]}$
9	Cry $\rightleftharpoons^{68.2}_{[10.2]} Col_h(d) \rightleftharpoons^{130.1}_{[12.4]}$ I
10	Cry $\rightleftharpoons^{68.1}_{[10.4]} Col_h(c) \rightleftharpoons^{126.4}_{[11.9]}$ I
11	$Cry_1 \xrightarrow{52.9} Cry_2 \rightleftharpoons^{61.0} Col_h(c) \rightleftharpoons^{123.3}_{[12.4]}$ I
12	Cry $\rightleftharpoons^{58.7}_{[143]} Col_h(d) \rightleftharpoons^{111.5}_{[11.7]}$ I

[a] Phase nomenclature: Cry = crystal, Col_h = hexagonal columnar mesophase (the order of the stacking disks in the column could be observed as four types, see Fig. 4: a, type a; b, type b; c, type c; d, type d), and I = isotropic liquid.
[b] Several unidentified phase transitions were observed before melting to the mesophase.

Table 4
Phase transition temperatures (T) and enthalpy changes (ΔH) of the $[(C_nO)_4DPD]_2Pt$ ($n=1$–12) complexes **3** [a b c]

n	Phase $\xrightarrow[\text{[}\Delta H\text{(kJ/mol)]}]{\text{T(°C)}}$ Phase[a] ⇝ relaxation
1	Cry $\rightleftharpoons^{267.2}_{[40.9]}$ I
2	$Cry_1 \rightleftharpoons^{179.3}_{[75.2]} Cry_2 \rightleftharpoons^{192.2}_{[60.2]}$ I
3	$Cry^* \rightleftharpoons^{165.8}_{[55.2]}$ I
4	$Cry_1 \rightleftharpoons^{132.8}_{[9.10]} Cry_2 \rightleftharpoons^{138.9}_{[64.7]}$ I
5	$Cry_1 \rightleftharpoons^{32.7}_{[33.4]} Cry_2 \rightleftharpoons^{123.8}_{[51.6]}$ I
6	$Cry_1 \xrightarrow[[10.8]]{53.3} Cry_1 \rightleftharpoons^{105.4} Col_h^c \rightleftharpoons^{109.3}$ I
7	Cry $\rightleftharpoons^{108.2}_{[52.7]} Col_h^c \rightleftharpoons^{113.1}_{[9.10]}$ I
8	Cry_1 (40.7 → Cry_2 [36.1] → Col_h); $Cry_1 \xrightarrow{36.8} Cry_3 \rightleftharpoons^{91.3}_{[47.6]} Col_h(c) \rightleftharpoons^{111.5}_{[10.1]}$ I
9	$Cry_1 \xrightarrow[[5.03]]{43.4} Cry_2 \rightleftharpoons^{65.6}_{[5.57]} Col_h(d) \rightleftharpoons^{112.5}_{[10.5]}$ I
10	$Cry^b \xrightarrow{76.1} Col_h(d) \rightleftharpoons^{110.2}_{[10.7]}$ I; Cry ⇌ 58.3 [5.88]
11	$Cry_1 \xrightarrow[[18.8]]{53.9} Cry_2 \rightleftharpoons^{67.0}_{[53.0]} Col_h(c) \rightleftharpoons^{109.2}_{[10.8]}$ I
12	$Cry_1 \xrightarrow[[4.36]]{46.0} Cry_2 \rightleftharpoons^{62.0}_{[106]} Col_h(c) \rightleftharpoons^{101.0}_{[10.5]}$ I

[a] Phase nomenclature: Cry = crystal, Col_h = hexagonal columnar mesophase (c: type c; d, type d; Fig. 4), and I = isotropic liquid.
[b] Several unidentified phase transitions were observed before melting to the mesophase.
[c] These Col_h phases were identified not by X-ray diffraction but by microscopic observation of the natural textures.

3. Results and discussion

3.1. Mesomorphic properties

As summarized in Tables 3 and 4, some of these compounds have several crystalline phases including metastable phases, whereas the $[(C_nO)_4DPD]_2Pd$ ($n=4$ to 12) and $[(C_nO)_4DPD]_2Pt$ ($n=6$ to 12) complexes have only one enantiotropic columnar mesophase. Each of the $[(C_nO)_4DPD]_2Pd$ ($n=4$ to 12) and $[(C_nO)_4DPD]_2Pt$ ($n=6$ to 12) complexes exhibits a fan-shaped texture when the isotropic liquid is cooled. This texture can usually be observed for a Col_h mesophase.

To establish this mesophase, temperature-dependent X-ray diffraction measurements were carried out. Fig. 3 shows an X-ray diffraction pattern of the mesophase of the $[(C_5O)_4DPD]_2Pd$ complex at 130°C. The X-ray diffraction data are summarized in Table 5. As can be seen from this table, the eight narrow peaks located at the lower angle region agree with a two-dimensional hexagonal lattice; a diffuse band around 4.5 Å ($2\theta \cong 20°$) corresponds to the melting of the alkoxy chains, and another diffuse band centered at 3.38 Å (around $2\theta = 25°$) corresponds to fluctuation of the intermolecular disk distance in the one-dimensional molecular stack. Hence, this mesophase could be identified as a Col_h mesophase. Similarly, each of the mesophases of the other $[(C_nO)_4DPD]_2Pd$ ($n=4$, 6 to 12) and $[(C_nO)_4DPD]_2Pt$ ($n=8$ to 12) complexes could also be identified as a Col_h mesophase by X-ray structural analyses. Since the $[(C_nO)_4DPD]_2Pt$ ($n=6$, 7) complexes in the homologous series show a narrow temper-

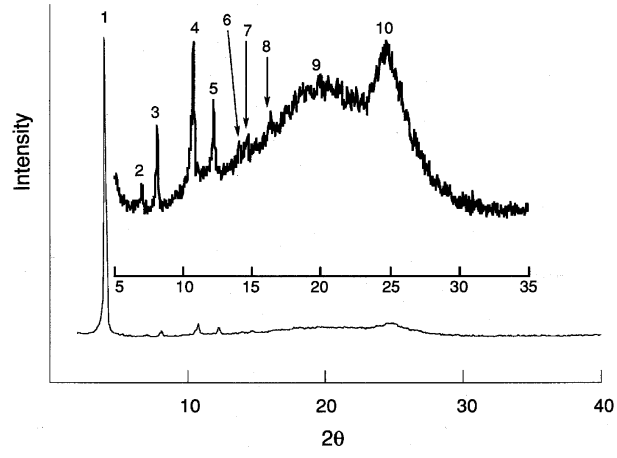


Fig. 3. X-ray diffraction powder pattern of the $[(C_5O)_4DPD]_2Pd$ complex at 130°C.

Table 5
X-ray diffraction data of the $[(C_5O)_4DPD]_2Pd$ complex at 130°C [a]

Peak no.	Spacing (Å)		Miller index (*hkl*)
	d_{obs}	d_{calc}	
1	21.6	21.7	(10)
2	12.6	12.5	(11)
3	10.9	10.9	(20)
4	8.20	8.21	(21)
5	7.25	7.24	(30)
6	6.28	6.27	(22)
7	6.01	6.02	(31)
8	5.41	5.43	(40)
9	~4.5		melting of alkoxy chains
10	3.38		(001)

[a] Col_h: the lattice constant $a = 25.1$ Å.

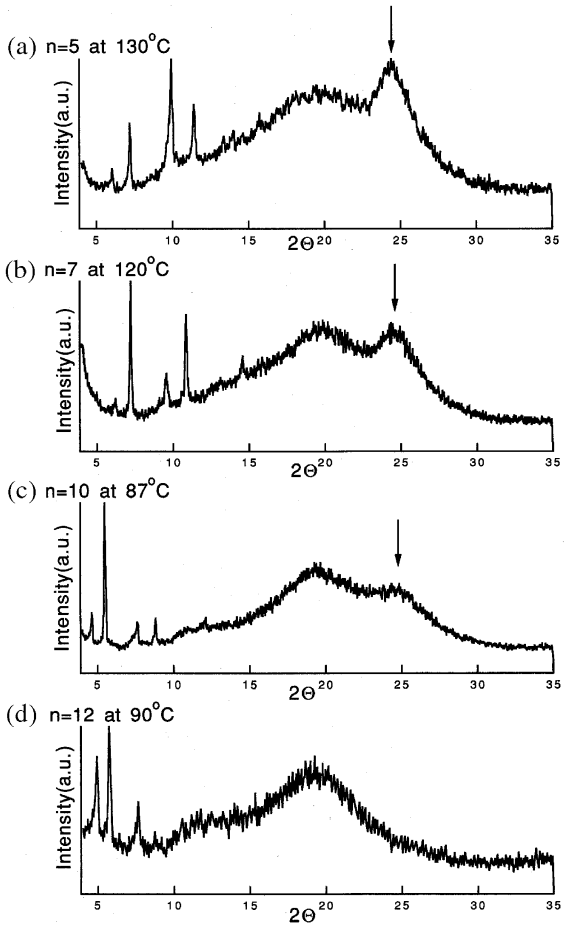


Fig. 4. X-ray diffraction patterns of the Col_h mesophases of the $[(CnO)_4DPD]_2Pd$ complexes ($n = 5$, 7, 10, 12).

ature range for the mesophase, X-ray diffraction measurements were not carried out and these Col_h mesophases were identified only from their fan-shaped textures.

The X-ray diffraction patterns of the Col_h mesophases of $[(C_nO)_4DPD]_2Pd$ ($n = 5$, 7, 10, 12) complexes are shown in Fig. 4. As can be seen from these patterns, the diffraction peak around $2\theta = 25°$ which corresponds to fluctuation of the interdisk distance, becomes broader and smaller with increasing chain length. This means that the order of the interdisk distance is higher for the shorter alkoxy chains, whereas it is lower for the longer chains. It is very interesting that the order decreases gradually and continuously when the chains become longer. Consequently, we could not tell where the disordered columnar phase starts. In our opinion, it is impossible to distinguish clearly between the ordered and disordered columns. Therefore, these present mesophases are only denoted as Col_h.

We have previously reported the liquid crystallinity of the $[(C_nO)_4DPD]_2Ni$ ($n = 1$ to 12) complexes [25]. The phase transition temperatures of the homologous Ni, Pd and Pt complexes, **1**, **2** and **3**, are plotted against the number of carbon atoms (n) in the alkoxy chains in Fig. 5, to investigate the influence of central metal atom on the mesomorphism. For $n = 4$, only the Pd complex gives a Col_h mesophase, and for $n = 5$, the Pd and Ni complexes give the Col_h mesophases but the Pt complex does not. For $n \geq 6$, the Col_h mesophase can be observed for all the Pd, Ni and Pt complexes. Thus, the liquid crystallinity appears more easily in the order Pt, Ni and Pd complexes with shorter chains.

The central metal atoms in these mesogens for $n = 6$ to 12 also influence the clearing points and the temperature range of the mesophase. These clearing points are highest for the Pd complexes, middle for the Ni complexes, and lowest for the Pt complexes. The temperature ranges of the mesophases are widest for the Pd complexes, middle for the Ni complexes

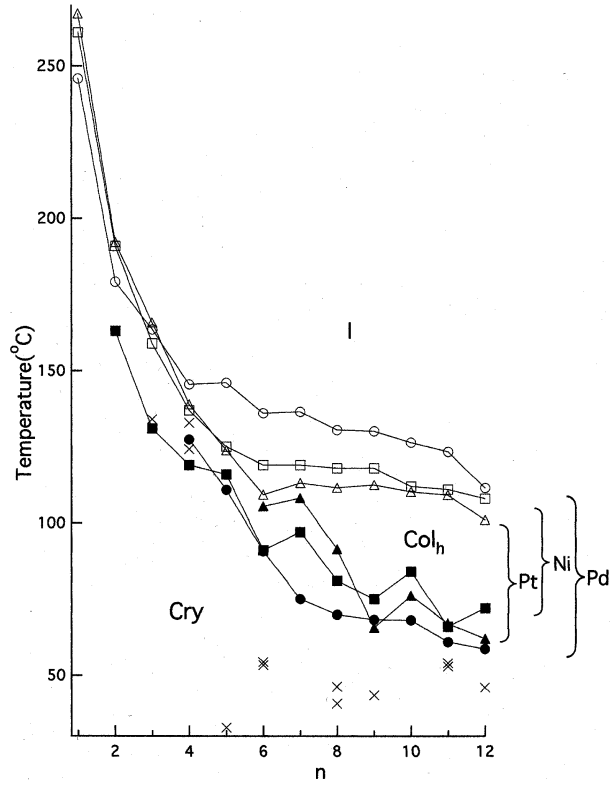


Fig. 5. Phase transition temperatures vs. the number of carbon atoms (n) in the alkoxy chains of the metal complexes **1**–**3**. Nomenclature: Cry = crystal, Col_h = hexagonal columnar mesophase, Ni, Pd, Pt = $[(C_nO)_4DPD]_2M$ ($n = 1$–12, M = Ni, Pd, Pt).

and narrowest for the Pt complexes, in the same order as the clearing points. Hence, the liquid crystallinities are greatly affected by the central metal species.

The lattice constants of the mesophases for the Ni, Pd and Pt complexes are plotted against the number of carbon atoms in the alkoxy chains in Fig. 6. The lattice constants of these three metal complexes gave almost the same linear relationship, irrespective of the central metal atom. Hence, the two-dimensional hexagonal lattice constants are not affected by the central metal species. The interdisk distances could be observed as 3.56 ± 0.03 Å for the Pd complexes, 3.64 ± 0.02 Å for the Ni complexes, and 3.73 ± 0.02 Å for the Pt complexes. Thus, the interdisk distances for the Pd complexes are the narrowest among these three metal complexes. That is to say, the intermolecular interaction in the column is strongest for the Pd complexes, forming the tightest and most stable columns, which may cause the highest clearing points. In contrast, the interdisk distances for the Pt complexes are the widest. The intermolecular interaction in the column is the smallest for the Pt complexes, and the columns can be most easily destroyed into disks, which may cause the lowest clearing points. Hence, the order of these clearing points $Pt < Ni < Pd$ may result from the order of the interdisk distances $Pt > Ni > Pd$.

Thus, contrary to our expectation of a smooth progression for Ni to Pt, the Pd complexes are very special. This reminds us that the calamitic bis(*p*-*n*-alkylstyryl-1,2-dithiolato)-nickel and bis(*p*-*n*-alkylstyryl-1,2-dithiolato)platinum are liquid crystalline but the palladium complexes are not [27].

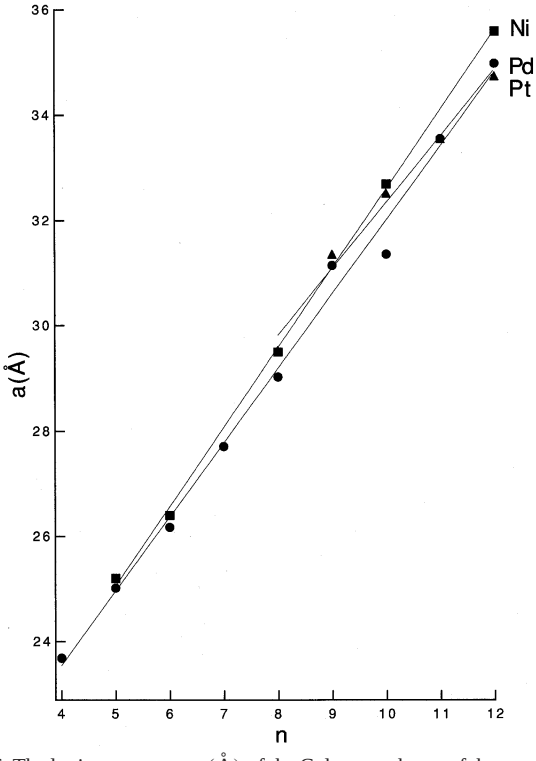


Fig. 6. The lattice constants a (Å) of the Col_h mesophases of the complexes **1**–**3** vs. the number of carbon atoms (n) in the alkoxy chains.

3.2. Electrochemical properties

Each of the cyclic voltammograms of the Pd and Pt complexes for $n = 1$ to 12 was reversible and almost the same. The reduction potentials obtained were -0.09 ± 0.01 V for the Pt complexes, -0.055 ± 0.005 V for the Ni complexes, and 0.00 ± 0.01 V for the Pd complexes. Thus, the values are nearly constant for each of the three metal complexes, irrespective of the chain length. This means that the π-acceptor columnar mesogens can be obtained without impairment of the π-acceptor ability, by introduction of the long chains to each of the bis(dithiolene)metal complexes.

Interestingly, the reduction potentials become more positive in the order $Pt < Ni < Pd$, so that the π-acceptor ability becomes better in the same order. Hence, the Pd complexes are the best π-acceptor columnar mesogens.

The left side of Fig. 7 illustrates the energy levels of the HOMO (Φ_{HOMO}) and LUMO (Φ_{LUMO}) of the dithiolene nickel core complex NiBDT calculated by Herman et al. [28]. Here, E_F, V, e and ΔE_{red} are the constant Fermi level of the counter electrode, an applied voltage, elementary electric charge, and a measured reduction potential, respectively. Eqs. (1) and (2) can be set up as follows:

$$\Phi_{LUMO} = E_F - eV \quad (1)$$

$$\Delta E_{red} = eV \quad (2)$$

So, Eq. (3) can be derived from Eqs. (1) and (2)

$$\Phi_{LUMO} = E_F - \Delta E_{red} \quad (3)$$

Hence, the more positive the reduction potential ΔE_{red} becomes, the more negative the LUMO Φ_{LUMO} becomes. That is to say, the better the π-acceptor ability becomes, the

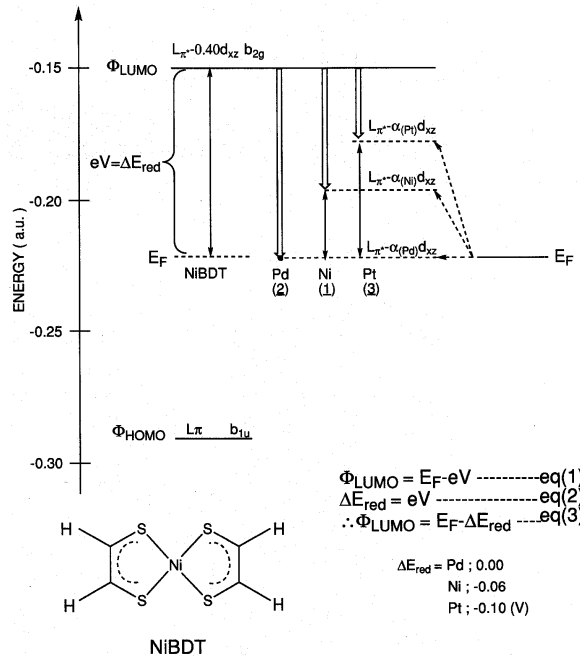


Fig. 7. HOMO and LUMO of NiBDT [26] and the $[(C_nO)_4DPD]_2M$ ($n = 1$–12, M = Ni, Pd, Pt) complexes **1**–**3**.

lower the energy level of the LUMO becomes. To compare the reduction potentials ΔE_{red} of the present metal complexes, the ΔE_{red} values become more positive in the order Pt < Ni < Pd. Hence, it can be derived from Eq. (3) that the Φ_{LUMO} levels become more negative in the order Pt < Ni < Pd, as illustrated on the right side of Fig. 7: the Φ_{LUMO} level against the constant Fermi level is the most positive for the Pt complexes, middle for the Ni complexes and the most negative for the Pd complexes. The Φ_{LUMO} for Pd complexes is situated nearly at the same level as the Fermi level.

This should be dependent on the extent of the contribution from the d_{xz} orbital to the ligand π* orbital which is in the order Pt < Ni < Pd, because the calculation by Herman et al. revealed that the Φ_{LUMO} orbital of NiBDT is formed by mixing of the ligand π* orbital and the central nickel d_{xz} orbital (L_{π^*}–0.40d_{xz}) [28].

3.3. Electronic absorption spectra

Electronic spectra of the [$(C_{12}O)_4$DPD]$_2$M (M = Ni, Pd, Pt) complexes are shown in Fig. 8. These data are listed together with the data for NiBDT in Table 6. Dithiolene metal complexes are well known to have a strong absorption in the near-IR region. The absorption wavelength λ_{max} is easily affected by the substituent groups and the central metals. It has been reported that λ_{max} can be assigned to the allowed HOMO–LUMO transition between the molecular orbitals which spread all over the complex [28–30]. As can be seen from Fig. 8, the absorption bands of the present

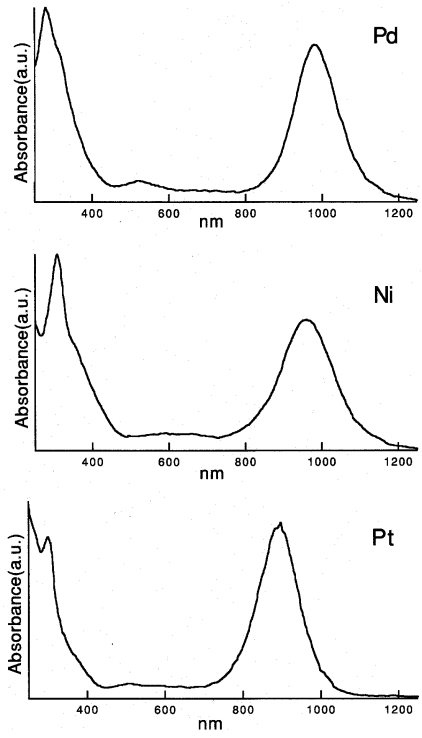


Fig. 8. Electronic absorption spectra of the [$(C_{12}O)_4$DPD]$_2$M complexes in $CHCl_3$: 1.0×10^{-4} M (250–1250 nm), 1 mm cell.

Table 6
Electronic absorption spectral data (λ_{max} (nm) (log ε)) of the NiBDT and [$(C_nO)_4$DPD]$_2$M (M = Ni, Pd, Pt) complexes in $CHCl_3$

Pd	Ni	Pt	NiBDT
			210 (4.30)
			270 (sh [a])
280 (4.79)	309 (4.74)	299 (4.64)	290 (4.42)
319 (sh)	363 (sh)		370 (3.27, broad)
			444 (sh)
517 (3.68)	580 (3.51)	509 (3.42)	550 (3.36)
	647 (sh)		
979 (4.69)	957 (4.55)	898 (4.68)	719 (4.16) [b]
			860 (2.60)

[a] Sh, shoulder.
[b] Ref. [26]. $L_\pi \rightarrow L_{\pi^*}(\pm0.37Spz \pm 0.27Cpz) - 0.40d_{xz}$.

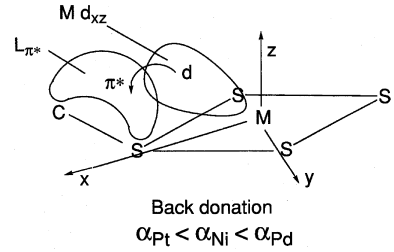


Fig. 9. Back donation of electron from the d_{xz} orbital of the central metal to the π* orbital of the ligand (L_{π^*}) in the [$(C_nO)_4$DPD]$_2$M (n = 1–12, M = Ni, Pd, Pt) complexes **1**–**3**.

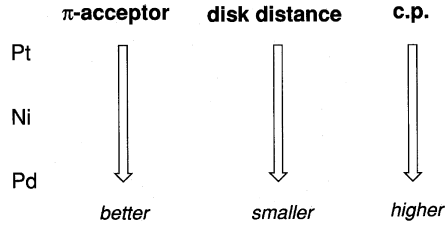
HOMO(L_π) → LUMO(L_{π^*}–αd_{xz}) transition could be observed around 800–1000 nm in the near-IR region. The λ_{max} shifts to longer wavelength in the order of the Pt complex (898 nm), the Ni complex (957 nm), and the Pd complex (979 nm), which means that the energy gap between the HOMO and LUMO levels becomes smaller in this order. Since the HOMO orbital consists only of the ligand π orbital without any contribution from the d orbital as calculated by Herman et al. [28], the HOMO energy levels may be constant. Hence, the decrease in the energy gap shows that the LUMO energy level goes down (Fig. 7). This is consistent with the electrochemical properties mentioned above.

Fig. 9 illustrates the d_{xz} orbital of the central metal (M d_{xz}) and the π* orbital of the ligand (L_{π^*}). The LUMO of the complexes is stabilized by the electron delocalization which originates from the back donation (α) of electron from the d_{xz} orbital of the central metal to the L_{π^*} orbital of the ligand. Hence, the LUMO of these complexes is denoted L_{π^*}–αd_{xz} (Fig. 7). Thus, the LUMO energy level of these metal complexes decreases in the order Pt < Ni < Pd, which implies that the back donation (α_M) of electrons from the central metal to the ligand occurs more in the order M = Pt < Ni < Pd (Fig. 9). Hence, it is apparent that the better the π-acceptor ability, the larger is the back donation occurring.

4. Conclusions

In this study, we have succeeded in the synthesis of the novel π-acceptor columnar liquid crystalline dithiolene Pd

and Pt complexes. All the dithiolene metal complexes with Ni, Pd and Pt as the central metal (**1**, **2** and **3**, respectively) show the same Col_h mesophase. The π-acceptor ability of these metal complexes becomes better in the order Pt < Ni < Pd. It was revealed by electrochemical measurements and electronic spectral measurements that the extent of the back donation of electrons from the central metal to the ligand becomes larger in the same order Pt < Ni < Pd. More interestingly, it was found by X-ray structural analyses that the interdisk distance becomes smaller in the same order Pt > Ni > Pd. This means that the more densely the disks are compacted in the column, the stronger the interdisk interaction in the column becomes in the order Pt < Ni < Pd. This is the reason why the columns are difficult to break up into disks in the order Pt < Ni < Pd when these metal complexes are heated, and why their clearing points become higher in the same order. Hence, apparently there is a good relationship between the intramolecular back donation and the intermolecular disk distance for these metal complexes. The conductivities of these complexes also attract our further interest.



References

[1] K. Ohta, N. Yamaguchi, I. Yamamoto, J. Mater Chem. 8 (1998) 2637.
[2] D.O. Cowan, F.M. Wiygal, Chem. Eng. News 21 (1986) 28.
[3] T.J. Marks, Angew. Chem., Int. Ed. Engl. 29 (1990) 857.
[4] F.D. Saeva, G.A. Reynolds, L. Kaszczuk, J. Am. Chem. Soc. 104 (1982) 3524.
[5] V. Gions, R. Fugnitto, H. Strzelecka, Mol. Cryst. Liq. Cryst. 96 (1983) 215.
[6] V. Gions, H. Strzelecka, M. Veber, Mol. Cryst. Liq. Cryst. 137 (1986) 365.
[7] L.Y. Chiang, J.P. Stokes, C.R. Safinya, A.N. Bloch, Mol. Cryst. Liq. Cryst. 125 (1985) 279.
[8] N. Boden, R.J. Bushby, J. Clements, M.V. Jesudason, P.F. Knowles, G. Williams, Chem. Phys. Lett. 152 (1988) 94.
[9] G.B.M. Vanghan, P.A. Heiney, J.P. McCauley Jr, A.B. Smith III, Phys. Rev. B 46 (1992) 2787.
[10] N. Borden, R.J. Bushby, J. Clements, J. Chem. Phys. 98 (1993) 5920.
[11] N. Borden, R.C. Borner, R.J. Bushby, J. Clements, J. Am. Chem. Soc. 116 (1994) 10807.
[12] C. Piechoki, J. Simon, A. Skoulios, D. Guillon, P. Weber, J. Am. Chem. Soc. 104 (1982) 5245.
[13] J.H. Sluyters, A. Baars, J. Electroanal. Chem. 271 (1989) 41.
[14] Z. Belarbi, J. Phys. Chem. 94 (1990) 7334.
[15] J.F. Van der Pol, M.P. de Haas, J.M. Warman, W. Drenth, Mol. Cryst. Liq. Cryst. 183 (1990) 411.
[16] P.G. Shouten, W. Chen, J.M. Warman, M.P. de Haas, J.F. van der Pol, J.W. Zwikker, Synth. Met. 41–43 (1991) 2665.
[17] P.G. Schouten, J.M. Warman, M.P. de Haas, M.A. Fox, H.-L. Pan, Nature 353 (1991) 736.
[18] M.M. Bélombé, J. Phys. (Paris) 44 (1983) C3–717.
[19] K. Ohta, M. Moriya, M. Ikejima, H. Hasebe, T. Fujimoto, I. Yamamoto, Bull. Chem. Soc. Jpn. 66 (1993) 3553.
[20] K. Ohta, M. Moriya, M. Ikejima, H. Hasebe, T. Fujimoto, I. Yamamoto, Bull. Chem. Soc. Jpn. 66 (1993) 3559.
[21] K. Ohta, M. Ikejima, M. Moriya, H. Hasebe, I. Yamamoto, J. Mater. Chem. 8 (1998) 1971.
[22] K. Ohta, H. Hasebe, M. Moriya, T. Fujimoto, I. Yamamoto, J. Mater. Chem. 1 (1991) 831.
[23] K. Ohta, H. Hasebe, M. Moriya, T. Fujimoto, I. Yamamoto, Mol. Cryst. Liq. Cryst. 208 (1991) 43.
[24] Unpublished results: $[(C_{12}O)_4DPG]_2Ni$ $E_{ox} = 0.85$ V; $[(C_{12}O)_4DPG]_2Pd$ $E_{ox} = 0.85$ V; $[(C_{12}O)_4DPG]_2Pt$ $E_{ox} = 0.89$ V; in CH_2Cl_2 with TBAP versus SCE.
[25] K. Ohta, H. Hasebe, M. Moriya, T. Fujimoto, I. Yamamoto, Mol. Cryst. Liq. Cryst. 208 (1991) 33.
[26] K. Ohta, H. Hasebe, H. Ema, M. Moriya, T. Fujimoto, I. Yamamoto, Mol. Cryst. Liq. Cryst. 208 (1991) 21.
[27] U.T. Mueller-Westerhoff, A. Nazzal, R.J. Cox, A.M. Giroud, Mol. Cryst. Liq. Cryst. 56 (1980) 249.
[28] Z.S. Herman, R.F. Kirchner, G.H. Loew, U.T. Mueller-Westerhoff, A. Nazzal, M.C. Zerner, Inorg. Chem. 21 (1982) 46.
[29] G.N. Schrauzer, Acc. Chem. Rev. 2 (1969) 72.
[30] G.N. Schrauzer, V.P. Mayweg, J. Am. Chem. Soc. 87 (1965) 1483.

PERGAMON

www.elsevier.nl/locate/poly

Polyhedron 19 (2000) 275–289

POLYHEDRON

Synthesis, characterization, and ring-opening polymerization of a novel [1]silaferrocenophane with two ferrocenyl substituents at silicon

Mark J. MacLachlan [a], Juan Zheng [a], Karena Thieme [a], Alan J. Lough [a], Ian Manners [a,*], Carolyn Mordas [b], Robert LeSuer [b], William E. Geiger [b], Louise M. Liable-Sands [c], Arnold L. Rheingold [c]

[a] *Department of Chemistry, University of Toronto, 80 St. George Street, Toronto, M5S 3H6 Ont., Canada*
[b] *Department of Chemistry, University of Vermont, Burlington, VT 05405-0125, USA*
[c] *Department of Chemistry and Biochemistry, University of Delaware, Newark, DE 19716, USA*

Received 30 April 1999; accepted 28 July 1999

Abstract

Reaction of dichlorodiferrocenylsilane, Fc_2SiCl_2 (**4**) (Fc = (η-C_5H_4)Fe(η-C_5H_5)), with dilithioferrocene $fcLi_2 \cdot TMEDA$ (fc = (η-C_5H_4)$_2$Fe, TMEDA = *N*,*N*,*N*,*N*-tetramethylethylenediamine) afforded the novel trimetallic [1]silaferrocenophane **5**, $fcSiFc_2$, in 77% yield. A single crystal X-ray diffraction study of ferrocenophane **5** showed the presence of significant disorder but revealed that the molecule possesses a highly strained structure where the tilt-angle between the planes of the cyclopentadienyl rings of the ferrocenophane is 20–22°, typical of strained silicon-bridged [1]ferrocenophanes. The Fe···Fe distances in **5** are 5.434, 5.537, and 5.687 Å, and metal–metal interactions are evident as redox coupling was detected in the cyclic voltammogram of this species. Differential pulse voltammetry resolved three oxidation waves at 0, 0.22, and 0.45 V relative to the ferrocene/ferrocenium couple. Mössbauer spectroscopy proved useful in corroborating the structure of **5**, as the two distinct Fe environments present were readily resolved ($\delta = 0.424(5)$ mm s^{-1}, d, $\Delta E_q = 2.242(5)$ mm s^{-1}, 2 Fe; $\delta = 0.414(5)$ mm s^{-1}, d, $\Delta E_q = 1.930(5)$ mm s^{-1}, 1 Fe). Further characterization of **5** by IR and Raman spectroscopy was also undertaken. Ring-opening addition of HCl across a strained Si–C bond of **5** afforded chlorotriferrocenylsilane, Fc_3SiCl (**6**), in 81% yield. Subsequent hydrolysis of **6** afforded a silanol Fc_3SiOH (**7**) with three ferrocenyl substituents. Single crystal X-ray diffraction of **7** revealed that the compound crystallizes as hydrogen-bonded dimers. When heated, **5** was found to undergo thermal ring-opening polymerization (ROP) to afford cyclic oligomeric species $[fcSiFc_2]_x$ (**9**$_x$, $x = 2$ or 3) and an insoluble polymeric material $[fcSiFc_2]_n$ (**8**). Copolymers **10** were obtained when **5** was heated in the presence of dimethyl[1]silaferrocenophane, $fcSiMe_2$ (**1a**). ©2000 Elsevier Science Ltd All rights reserved.

Keywords: Ferrocenophane; Inorganic polymers; Silanol; Mössbauer spectroscopy; Ring-opening polymerization

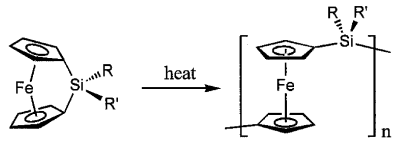
1. Introduction

As a result of recent synthetic advances, polymers that incorporate transition metals in the main chain are attracting renewed attention. Such materials are of considerable interest because of their interesting chemical and physical properties, and in certain cases they may serve as useful precursors to novel ceramic materials (for recent examples of transition metal-based polymeric materials, see, for example [1–8]). Ferrocene, which is cheap, stable, tunable, and possesses very interesting properties, represents a particularly attractive structural moiety to include in a polymer main chain. With this in mind, we have previously shown that strained silicon-bridged [1]ferrocenophanes such as **1a** undergo thermal ring-opening polymerization (ROP) to afford high molecular weight ($M_n > 10^5$) poly(ferrocenylsilanes) (e.g. **2a**) when heated in the melt [9,10] (an atom abstraction ROP route to poly(ferrocenes) with disulfide spacers was published shortly prior to Ref. [9]). Subsequent extensive work has shown that the resulting poly(ferrocenylsilanes) and analogous materials formed by the ROP methodology possess a range of interesting properties [11–14]; for the work of other groups on poly(ferrocenylsilanes) and related materials, see [15–17]. Of particular significance is the observation that these ring-opened poly(ferrocenes) (as exemplified by **2a**) display two reversible oxidation waves (redox coupling, $\Delta E = 0.21$ V) by cyclic voltammetry (CV), which is indicative of

* Corresponding author. Tel.: +1-416-978-3564; fax: +1-416-978-8775

0277-5387/00/$ - see front matter ©2000 Elsevier Science Ltd All rights reserved.
PII S0277-5387(99)00357-5

significant metal–metal interactions along the polymer main chain [9,11,12].



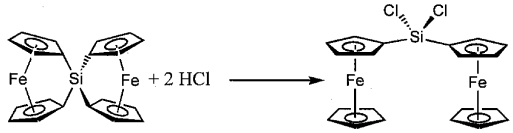
1a (R = R' = CH_3) **2a** (R = R' = CH_3)
1b (R = Fc; R' = CH_3) **2b** (R = Fc; R' = CH_3)

We and Pannell and co-workers have investigated monomer **1b**, fcSiMeFc (Fc = (η-C_5H_4)Fe(η-C_5H_5), fc = (η-C_5H_4)$_2$Fe) with a single ferrocenyl substituent at Si and have shown that thermal ring-opening polymerization (ROP) of this species proceeds to give the high molecular weight poly(ferrocenylsilane) **2b** [18–20]. Cyclic voltammetry of **2b** showed evidence for metal–metal interactions between both skeletal ferrocene units and the ferrocenyl side groups [19,20]. Even more extensive metal–metal interactions would be anticipated in analogous poly(ferrocenes) with two ferrocenyl substituents at silicon. We therefore report in this paper the synthesis, characterization, and ROP of the sterically encumbered [1]silaferrocenophane, fcSiFc$_2$ (**5**). In addition to studies of the ROP of **5** we have also investigated the use of this species as a precursor to compounds with three ferrocenyl substituents via stoichiometric ring-opening reactions.

2. Results and discussion

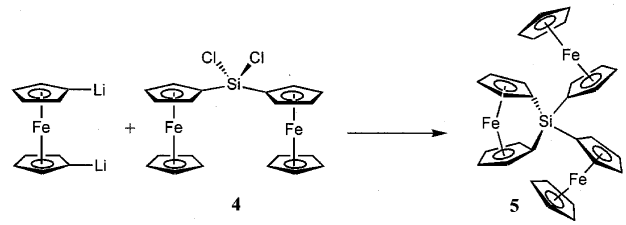
2.1. Synthesis of diferrocenyl[1]silaferrocenophane 5

We have recently shown that the red, air-stable, easily accessible spirocyclic [1]ferrocenophane **3** undergoes ring-opening addition of 2 equiv. of HCl to afford diferrocenyldichlorosilane **4** in very high (ca. 90%) yield [21,22]. Subsequent reactions with **4** have been used to generate a range of interesting species such as siloxanediols and cyclosiloxanes with ferrocenyl substituents at Si [23].



3 **4**

Reaction of **4** with 1 equiv. of fcLi$_2$·TMEDA in THF afforded [1]silaferrocenophane **5** as air-stable, red crystals in 77% yield after work-up (Scheme 1). The ^{13}C NMR data of the product were consistent with the proposed structure for **5**, showing four peaks due to Cp rings of the ferrocenyl substituents and three resonances assigned to the ferrocenophane. The chemical shifts for the resonances assigned to the *ipso* carbon atoms of **5** were observed at 65.4 and 35.0 ppm (C_6D_6). Specifically, the resonance at 65.4 ppm results from the *ipso* carbon atom of the ferrocenyl substituents, while the



4 **5**

Scheme 1.

resonance of the *ipso* carbon atom of the ferrocenophane was observed at 35.0 ppm. The latter value represents a large upfield shift compared to unstrained species, characteristic to [1]ferrocenophanes [24]. In the ^{1}H NMR spectrum of **5**, four pairs of triplets due to Si bound Cp rings and an intense singlet due to the free Cp ring of the ferrocenyl substituents were observed, consistent with the structure. The ^{29}Si chemical shift ($\delta = -15.5$ ppm in $CDCl_3$) is upfield from the resonance observed in **4** (15.2 ppm). The chemical shift for this resonance also lies between the ^{29}Si NMR signals observed for tetraferrocenylsilane ($\delta = -10.1$ ppm) and spirocyclic [1]ferrocenophane **3** ($\delta = -16.6$ ppm) [22]. The additional shielding observed in **3** and **5** might be attributed to a weak dative Fe···Si interaction, and is consistent with the single crystal X-ray structure and Mössbauer data (vide infra) for **5**.

Like other [1]ferrocenophanes, **5** shows a red shift in the λ_{max} in the UV–Vis spectrum relative to analogous ring-opened species. Thus, upon forming the ferrocenophane, the λ_{max} shifts from 448 nm in **4** to 474 nm in **5** (in CH_2Cl_2). This maximum is not as high as for other [1]silaferrocenophanes (e.g. 487 nm for **1a** in CH_2Cl_2), most likely because of the contribution from the superimposed absorption peak of the ferrocenyl substituents. Mass spectrometry of **5** showed the molecular ion ($m/z = 582$) as the major peak.

2.2. X-ray structural determination of 5

To confirm the formation of the [1]ferrocenophane **5**, a single crystal X-ray diffraction study was performed. Red single crystals of **5** were isolated by slow evaporation of a solution of **5** in CH_2Cl_2 under a nitrogen atmosphere. A summary of cell contents and data collection parameters is included in Table 1. A summary of important structural features is provided in Table 2.

[1]Ferrocenophane **5** crystallizes in monoclinic space group $P2_1/c$. Unfortunately, the compound displays static disorder, but the X-ray study does confirm the synthesis of the strained ferrocenophane **5**. A molecular structure showing the disordered structure solution is shown in Fig. 1(a). Primarily two configurations of the ferrocenophane are distributed among the molecular sites in the structure; these are shown separately in Fig. 1(b,c). Bond lengths and bond angles, summarized in Table 2, are reasonable and typical of other ferrocenophanes and ferrocenylsilanes and, in particular, are similar to those for **1b** which was structurally characterized by Pannell et al. [20]. Furthermore, the Cp ligands

Table 1
Crystal data for compounds **5**, **6**, and **7**

	5	**6**	**7**
Empirical formula	$C_{30}H_{26}Fe_3Si$	$C_{30}H_{27}ClFe_3Si$	$C_{30}H_{28}Fe_3OSi$
M_r	582.15	618.61	600.16
Temperature (K)	293(2)	223(2)	100.0(1)
Wavelength (Å)	0.71073	0.71073	0.71073
Crystal system	monoclinic	monoclinic	orthorhombic
Space group	$P2_1/c$	$P2_1/c$	$P2_12_12_1$
a (Å)	17.160(4)	16.2708(2)	11.7739(2)
b (Å)	10.470(2)	11.2324(2)	19.4352(5)
c (Å)	14.178(4)	13.7626(2)	21.6569(6)
α (°)	90	90	90
β (°)	114.21(2)	93.5781(9)	90
γ (°)	90	90	90
V (Å^3)	2323.3(10)	2510.34(4)	4955.7(2)
Z	4	4	8
D_{calc} (g cm^{-3})	1.664	1.637	1.609
μ(Mo Kα) (mm^{-1})	1.918	1.883	1.804
F(000)	1192	1264	2464
Crystal size (mm)	0.22×0.32×0.21	0.40×0.40×0.03	0.15×0.13×0.10
θ Range collected (°)	2.34–27.00	1.25–28.26	4.08–28.29
Total no. of reflections	5022	8326	32631
No. of unique reflections	5013	4662	12236
R_{int}	0.0646	0.0270	0.061
Absorption correction	semi-empirical	none	Denzo-SMN
wR_2 (all data)	0.4489	0.1269	0.0749
R_1 ($I>2\sigma(I)$)	0.1655	0.0359	0.0422
GOF	1.173	1.033	0.988
Absolute structure parameter			0.309(11)
No. of parameters	104	316	634
Residual electron density (e Å^{-3})	1.823, −1.666	0.921, −0.458	0.424, −0.394

Table 2
Selected intramolecular distances (Å) and angles (°) in **5**

Fe(1)···Fe(2)	5.434(1)	Fe(2)···Fe(3)	5.537(1)
Fe(1)···Fe(3)	5.687(1)	Si(1)···Fe(1)	2.726(1)
Si(1)···Fe(2)	3.493(1)	Si(1)···Fe(3)	3.461(1)
average C–C	1.42	average Si–C	1.91
average Fe–C	1.96		
C(1)–Si(1)–C(6)	96.2(3)	C(1*)–Si(1)–C(6*)	92.9(3)
C(1)–Si(1)–C(11)	113.5(3)	C(1*)–Si(1)–C(11*)	116.8(3)
C(1)–Si(1)–C(21)	114.8(3)	C(1*)–Si(1)–C(21*)	106.2(3)
C(6)–Si(1)–C(11)	111.4(3)	C(6*)–Si(1)–C(11*)	111.0(3)
C(6)–Si(1)–C(21)	108.5(3)	C(6*)–Si(1)–C(21*)	113.8(3)
C(11)–Si(1)–C(21)	111.4(3)	C(11*)–Si(1)–C(21*)	114.4(3)

of the ferrocenyl substituents are essentially planar and parallel and the Cp ligands of the ferrocenophane moiety are planar and eclipsed, as expected. The ferrocenophane has a ring tilt of 20–22°, consistent with that observed in other [1]silaferrocenophanes. While the disorder of the C atoms is too large for meaningful comparison, the Si atom and three Fe atoms are not disordered. Surprisingly, these four atoms are coplanar (mean deviations of 0.002 Å from the least-squares plane). As the Fe···Fe distances are only 5.43–5.69 Å in the structure, metal–metal interactions are expected to be detected in the electrochemistry of **5**. The Fe···Si distance for the ferrocenophane in **5** is 2.73 Å, only slightly greater than the sum of the covalent radii of Fe and Si (2.42 Å) [25], suggesting a weak Fe···Si dative interaction.

The molecular arrangement of **5** in the crystal structure is intriguing. The molecules are organized into planes where all of the Si and Fe atoms lie in the *ab* plane. Within that plane, each molecule has six closest neighbours, spaced at 9.12, 10.5, and 11.0 Å (two at each Si···Si distance). For the closest contacts (9.12 Å length), the ferrocenophane moieties are arranged along the Si···Si axis. Fig. 2 shows a picture of the *ab* plane in the structure, illustrating the distribution of the monomers. Between the planes, some of the molecules are separated by only 7.96 Å (Si···Si) with other interplane Si···Si distances of 8.72 and 8.90 Å. Where the separation is only 7.96 Å, the orientation is such that the ferrocenophane moieties are closer to the bridging Si atoms of the other molecule, although the *ipso*-C···Si contacts are still quite long.

*2.3. Electrochemistry of **5***

Recently, several papers have appeared that report the preparation and electrochemical behavior of complexes containing multiple ferrocene moieties [22,23]; for leading references see [26]. These studies contribute to our understanding of how biological systems deliver several electron equivalents to redox sites [27]. For example, it has been

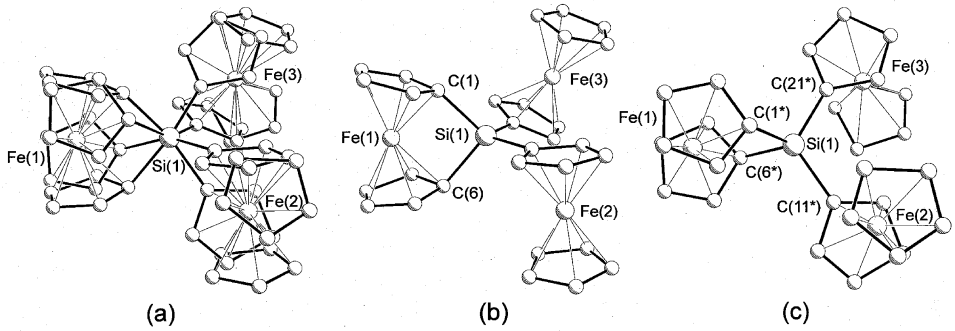


Fig. 1. (a) The structure of the [1]silaferrocenophane **5** shows two independent molecular conformations in the lattice. (b,c) The structure of the two distinct molecules observed in the molecular sites of **5**.

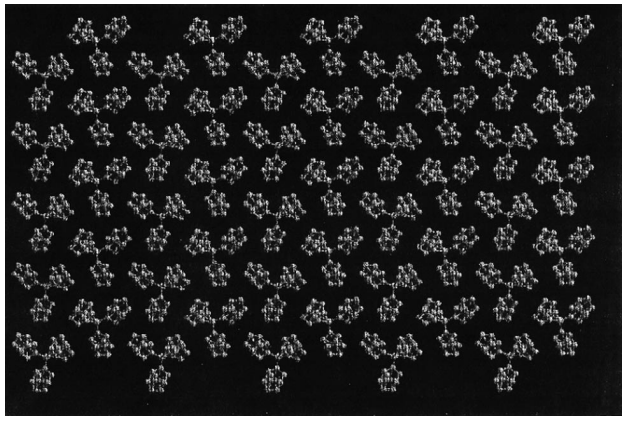


Fig. 2. A projection of the *ab* plane in [1]silaferrocenophane **5**.

demonstrated that the four Fe centers in cytochrome C_3 undergo electron transfer at very similar potentials, the spread of the four Fe^{II}/Fe^{III} $E_{1/2}$ values being only 0.11 V [28]. The electrochemistry of ferrocenophane **5** was investigated by cyclic voltammetry and differential pulse voltammetry (DPV). Owing to precipitation of the tri-oxidized cation in various solvents, the CV was not useful. DPV in dichloromethane, however, showed three oxidation waves as predicted for compound **5**; this is illustrated in Fig. 3. The three oxidation waves were observed at ca. 0, 0.22, and 0.45 V (referenced to the ferrocene/ferrocenium couple), indicating strong electronic interactions between all three metal centers. Thus, after the first Fe is oxidized, the potential required to oxidize the second center is raised. Most likely, the first two

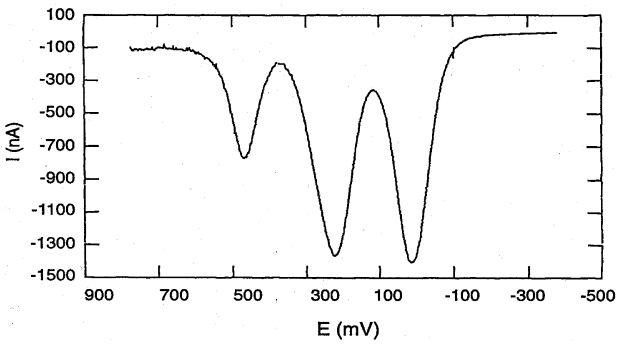


Fig. 3. Differential pulse voltammetry (DPV) of **5** referenced to the ferrocene/ferrocenium couple (dichloromethane).

oxidation waves correspond to oxidation of the ferrocenyl substituents for which the Fe centers would experience the least amount of Coulombic repulsion. Upon oxidizing the third Fe, the tri-oxidized cation precipitated, accounting for the decreased intensity of the third peak relative to the first two.

The spread of the four potentials in tetraferrocenylsilane is 0.42 V, implying appreciable interactions between the ferrocenyl moieties as they are successively oxidized [22]. However, this is less than in compound **5**, where the total spread is 0.45 V. This fact implies that the oxidation of the ferrocenophane imparts a larger amount of Coulombic repulsion upon the other ferrocenyl substituents than oxidation of a ferrocenyl substituent at Si. It may be concluded that single Si bridging atoms allow significant interactions between ferrocenyl substituents in their multiply ferrocenyl-substituted complexes.

2.4. Mössbauer study of 5

The Fe environments of ferrocene and its derivatives have been thoroughly investigated by Mössbauer spectroscopy [29–32]. Studies of [1]ferrocenophanes have indicated a reduced quadrupolar splitting relative to ferrocene (2.37 mm s^{-1}) while the isomer shift is virtually unchanged (0.44 mm s^{-1}) [24]. Silver has postulated that a weak iron-to-heteroatom interaction is the cause of the change in quadrupolar splitting, although the issue is still debated [33]. The Mössbauer spectrum of **5** was obtained at room temperature and is shown in Fig. 4. Clearly, the raw data appear skewed and immediately suggested the presence of more than two peaks in the spectrum. Moreover, the full widths at half-maximum (FWHM) of the peaks (when the spectrum was fitted with only two peaks) were unusually large for crystalline ferrocene derivatives. An automatic peak pick and optimization found two pairs of peaks, as shown in the deconvolution in Fig. 4. The broad doublet has an isomer shift, δ, of 0.424(5) mm s^{-1} and a quadrupolar splitting, ΔE_q, of 2.242(5) mm s^{-1}, similar to ferrocene and unstrained ferrocene derivatives. Thus, the latter absorption is attributed to Fe in the ferrocenyl substituents. On the other hand, the inner doublet has an isomer shift, δ, of 0.414(5) mm s^{-1} and a quadrupolar splitting, ΔE_q, of 1.930(5) mm s^{-1}, consistent

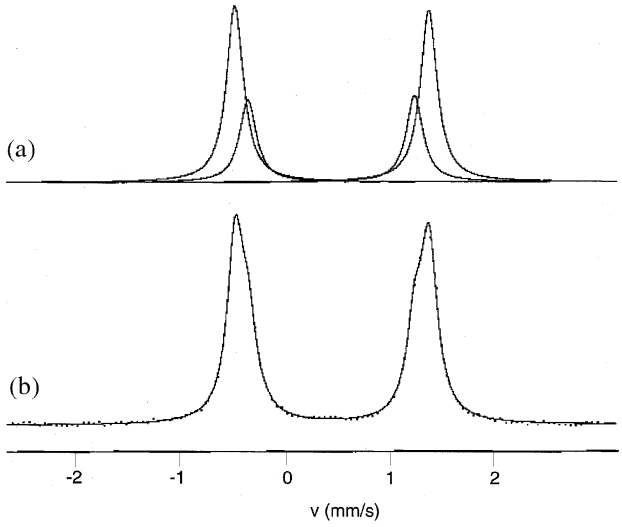


Fig. 4. The Mössbauer spectrum of **5** and fit are shown at the bottom. The deconvolution of the peaks into two quadrupolar doublets is shown on the top. The original data are shown as points.

with a [1]silaferrocenophane [33]. These peaks are attributed to the Fe in the ferrocenophane ring of compound **5**. Furthermore, the intensity of the narrow peaks is half (49.8% total area, 49.3% amplitude) of the broad peaks, as expected for the structure of ferrocenophane **5** (assuming that the recoil free-fractions for the ^{57}Fe in the ferrocenyl substituents and the ferrocenophane are equivalent).

2.5. Vibrational spectra of 5

The vibrational properties of **5** were investigated by IR and Raman spectroscopies. Table 3 lists the observed IR and Raman peaks along with their assignments. Most of the peaks could be assigned by analogy with ferrocene and other ferrocene-containing compounds we have studied. It is worth noting that the Raman spectrum of ferrocenophane **5** resembles the spectra of both compound **3** and tetraferrocenylsilane. A medium intensity, sharp peak observed at 706 cm^{-1} in **5** is also observed in compound **3** (714 cm^{-1}), but not in tetraferrocenylsilane. This may be a νC–Si for the ferrocenophane. In contrast, a medium intensity peak observed at 1161 cm^{-1} in **5** is characteristic of the ferrocenyl substituents as it was observed at 1159 cm^{-1} in tetraferrocenylsilane, but not in compound **3**. Interestingly, the ring breathing modes in **5** were observed at 1106 and 1117 cm^{-1} for the ferrocenyl substituents and ferrocenophane, respectively. For comparison, the same vibration was observed at 1111 cm^{-1} in tetraferrocenylsilane, 1107 cm^{-1} in diferrocenylsilanediol, and 1119 cm^{-1} in spirocyclic [1]silaferrocenophane **3** [21,22].

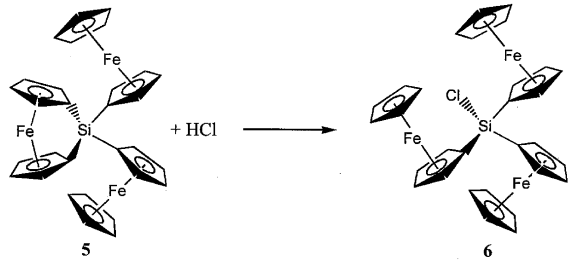
2.6. Addition of hydrogen chloride to 5

When **5** was treated with 1 equiv. of HCl, a single product was isolated (Scheme 2). ^{1}H and ^{13}C NMR spectra and mass spectrometry identified the material as the novel chlorosilane, Fc_3SiCl (**6**). The ^{29}Si NMR spectrum of **6** showed one resonance at 11.5 ppm, substantially deshielded with respect to the starting compound **5** ($\delta = -15.5$ ppm). In addition, the UV–Vis spectrum showed a peak at 456 nm, blue shifted from the starting monomer **5** ($\lambda_{max} = 474$ nm). The product showed the molecular ion as the major peak in the mass

Table 3
IR and Raman peaks of compound **5**

IR [a]	Raman [b]	Assignment [c]
3109 w	3106 s	νC–H
3088 m	3095 s	νC–H
1412 m	1413 m	νC–C
Nujol	1376 m	νC–C
1368 m	1367 m	νC–C
1350 w		
1295 m		
1285 w		
1257 w		
1188 m	1186 w	δC–H_{ip}
1183 s		δC–H_{ip}
1168 s	1161 m	δC–H_{ip}
1117 s	1117 m	asymmetric ring breathing (fc)
1106 s	1106 s	asymmetric ring breathing (Fc)
1063 w	1062 m	δC–H_{oop}
1050 w		
1043 m		
1033 s	1037 w	δC–H_{ip}
1022 s	1017 m	δC–H_{ip}
1004 s		δC–H_{ip}
893 m	886 w	ring distortion
868 m	868 w	
857 w		δC–H_{oop}
848 m		δC–H_{oop}
834 w		δC–H_{oop}
829 w		δC–H_{oop}
811 s		δC–H_{oop}
739 w		
722 w		
705 w	706 m	
683 m		
628 m	625 w	δC–C
599 m		
555 m		
549 s		
532 s		
495 m		
492 s		
475 s		
471 m		
463 w		
458 m		
	435 w	
	404 s	
	393 s	ring tilt (symmetric)
	351 s	νFe–Cp
	327 s	νFe–Cp
	259 m	
	246 s	

[a] Nujol mull.
[b] Crystalline sample.
[c] Legend: ν = stretch; δ = bend; ip = in plane; oop = out of plane; w = weak; m = medium; s = strong.



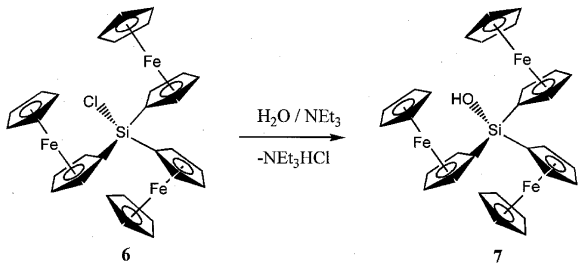
Scheme 2.

spectrum. An IR spectrum of **6** was consistent with the structure, showing the signature of ferrocenyl substituents as well as a Si–Cl stretch at 536 cm^{-1} (νSi–Cl = 552 cm^{-1} for Ph_3SiCl) [34].

2.7. Hydrolysis of *6*

To extend our investigations of silanols with bulky ferrocenyl substituents, we hydrolyzed chlorosilane **6** to give the silanol with three ferrocenyl substituents Fc_3SiOH (**7**) in 80% yield (Scheme 3). NMR data were consistent with the assigned structure, but the chemical shifts were found to be concentration dependent. Resonances in the ^{13}C NMR spectrum of **7** assigned to the cyclopentadienyl ligands attached to Si were observed to vary by up to 0.5 ppm. In addition, small changes in the ^{1}H NMR spectrum were evident, with the proton attributed to the OH group observed at 2.0 ppm in dilute samples and at 2.2 ppm in more concentrated samples.

Interestingly, silanol **7** has been previously claimed as a byproduct in the Friedel–Crafts silylation of ferrocene in 5% yield [35]. The only data reported were the appearance and



Scheme 3.

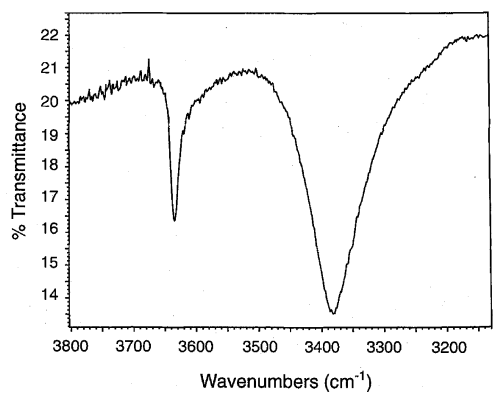


Fig. 5. IR spectrum of silanol **7** in the O–H stretching region.

the melting point (193.5–195°C), which is slightly higher than our observed melting point of 185–186.5°C.

Compound **7** was investigated in the solid-state by IR spectroscopy. In addition to the bands usually observed for Fc substituents, we assign three intense bands to Si–O stretching: 903 (m), 1003 (s), 1031 (s) cm^{-1}. In the O–H stretching region (Fig. 5), two intense peaks were observed: a sharp band at 3635 cm^{-1} and a broader, more intense band at 3382 cm^{-1}. The former is assigned to O–H stretching where the H is not participating in hydrogen bonding. For comparison, $(PhMe_2Si)_3CSiH_2(OH)$ has a band at 3623 cm^{-1} in dilute CCl_4 [36]. The band observed at lower frequency for **7** is attributed to O–H stretching where the H is active in hydrogen bonding; this frequency is usual for hydrogen-bonded OH groups.

2.8. Structural determination of *6*

In order to characterize **6** completely, a single crystal X-ray diffraction study was undertaken. Crystal data and collection parameters are summarized in Table 1. Selected bond lengths and bond angles for **6** are provided in Table 4. Compound **6** crystallizes in the monoclinic space group $P2_1/c$. Fig. 6 illustrates the structure of **6**. The Si–Cl bond length of 2.080(1) Å is normal; for example, the Si–Cl bond length in Ph_3SiCl is 2.077(1) Å [37]. Also, the Si–C bond lengths are normal for ferrocenylsilanes. Although the C–Si–C bond angles (average 111.3°) are significantly larger than the C–

Table 4
Bond lengths (Å) and angles (°) for chlorotriferrocenylsilane **6**

Si–C(5)	1.857(3)	Si–C(15)	1.840(3)
Si–C(25)	1.836(3)	Si–Cl	2.0802(10)
C(5)–Si–C(15)	110.06(13)	C(5)–Si–C(25)	109.03(12)
C(15)–Si–C(25)	114.72(12)	C(5)–Si–Cl	108.45(9)
C(15)–Si–Cl	108.69(9)	C(25)–Si–Cl	105.66(10)

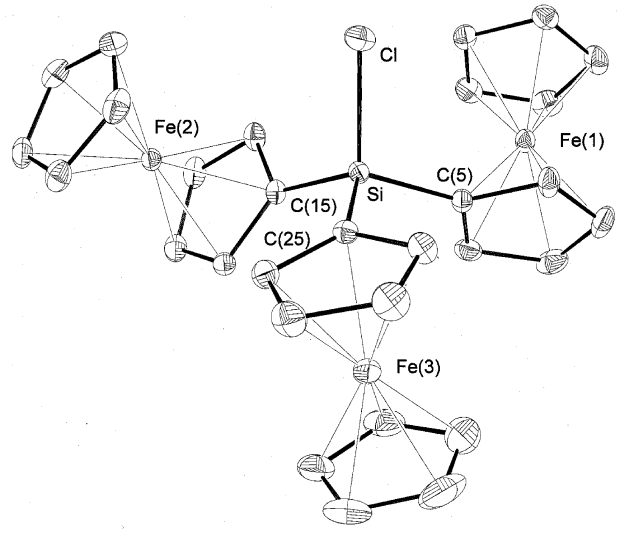


Fig. 6. The structure of chlorotriferrocenylsilane **6** with thermal ellipsoids drawn at the 30% probability level.

Si–Cl bond angles (average 107.6°), the distortion is not caused by the steric hinderance of the ferrocenyl substituents as similar distortions from tetrahedral geometry are observed in Ph_3SiCl [38]. Each of the Cp rings on the ferrocenyl groups is essentially planar and the ferrocenyl groups show very small ring tilts of 0.8, 2.0, and 3.0°. The ferrocenyl groups are separated by only 5.517, 5.969, and 6.208 Å (Fe···Fe distances) in the solid state.

2.9. Structural determination of 7

Hydrogen-bonding in silanols may lead to interesting hydrogen-bonded structures [36]. We have recently reported novel hydrogen-bonding motifs for silanediols and siloxanediols with ferrocenyl substituents on Si [21,23]. Diferrocenylsilanediol crystallizes in hydrogen-bonded dimers which are in turn linked into a chain by hydrogen-bonding between the dimers. Tetraferrocenyldisiloxanediol crystallizes as two stacked hydrogen-bonded chains running parallel to the *c*-axis. When cocrystallized with hexaferrocenylcyclotrisiloxane, tetraferrocenyldisiloxanediol was observed to form hydrogen-bonded helices with dichloromethane. Comparison of the hydrogen-bonding motifs in silanols may also give a measurement of the relative bulkiness of the subsitutents on Si. For example, silanols with highly sterically hindered substituents (e.g. $PhCH_2$, $(PhMe_2Si)_3C$, mesityl, etc.) are often monomeric in the solid state or display weak H–π interactions [36]. As the substituent size changes, a variety of hydrogen-bonded structures are observed, including dimers (e.g. $(Me_3Si)_3CSiPh_2OH$ and (fluorenyl)$SiPh_2OH$), tetramers (e.g. Ph_3SiOH and Bu^t_2SiFOH), and chains (e.g. $(CH_2{=}CH)(OH)CHSiPh_2OH$) [36]. To investigate the solid-state structure of a silanol with three ferrocenyl substituents, a single-crystal structure determination of **7** was undertaken.

Crystals of **7** were grown at −55°C in dichloromethane. Silanol **7** crystallizes in the orthorhombic space group $P2_12_12_1$ with $Z=8$. Crystal data parameters are summarized in Table 1 and selected bond lengths, intramolecular distances, and bond angles are given in Table 5. Fig. 7 shows the structure of the two molecules (A and B) in the asymmetric unit. Silanol **7** crystallizes as isolated dimers which possess one O–H···O hydrogen bond (O···O separation of 2.726(4) Å and O···H···O angle of 177.7°). This agrees with the IR spectroscopy of **7** where vibrations were observed that are attributed to OH groups either participating or not participating in hydrogen-bonding. The silanol $(Me_3Si)_3CSiPh_2OH$ also crystallizes as a dimer with an O–O separation of 2.85(2) Å [39]. In **7**, the Si–O bond lengths of molecules A (1.638(3) Å) and B (1.651(3) Å) are typical of silanols [39].

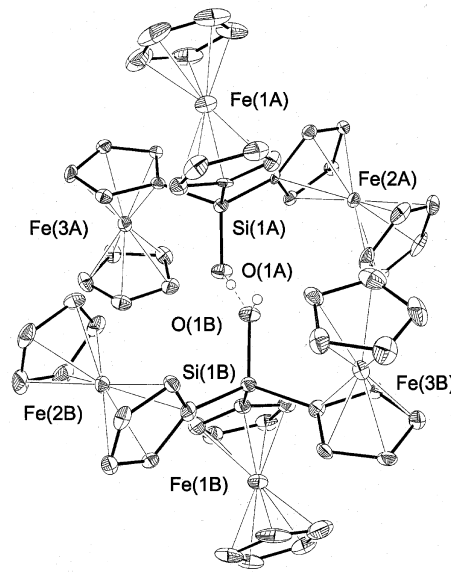


Fig. 7. The structure of the two molecules (A and B) present in the asymmetric unit for silanol **7**. Thermal ellipsoids are drawn at the 50% probability level.

2.10. Thermal ROP of 5

The thermal behavior of **5** was investigated by thermogravimetric analysis (TGA) and differential scanning calorimetry (DSC). The TGA, DTGA (differential thermogravimetric analysis), and DSC traces are shown in Fig. 8. TGA showed a small weight loss at 230°C (ca. 1–2%) followed by a larger weight loss (ca. 52 wt.%) peaking at 425°C (onset 360°C), giving an overall ceramic yield of 46% at 600°C. When examined by DSC at 5°C min^{-1}, **5** undergoes thermal ROP in the solid-state between ca. 150–230°C, peaking at

Table 5
Bond lengths, intermolecular distances (Å), and angles (°) for **7**

Si(1A)–O(1A)	1.638(3)	Si(1B)–O(1B)	1.651(3)
Si(1A)–C(1A)	1.864(4)	Si(1B)–C(1B)	1.844(4)
Si(1A)–C(11A)	1.848(4)	Si(1B)–C(11B)	1.857(4)
Si(1A)–C(21A)	1.865(3)	Si(1B)–C(21B)	1.847(3)
O(1A)···(1B)	2.726(4)		
C(1A)–Si(1A)–O(1A)	108.06(14)	C(1B)–Si(1B)–O(1B)	102.89(15)
C(1A)–Si(1A)–C(11A)	111.67(16)	C(1B)–Si(1B)–C(11B)	113.56(17)
C(1A)–Si(1A)–C(21A)	111.84(15)	C(1B)–Si(1B)–C(21B)	112.90(16)
C(11A)–Si(1A)–O(1A)	111.01(14)	C(11B)–Si(1B)–O(1B)	112.10(15)
C(11A)–Si(1A)–C(21A)	106.70(15)	C(11B)–Si(1B)–C(21B)	107.21(16)
C(21A)–Si(1A)–O(1A)	107.51(15)	C(21B)–Si(1B)–O(1B)	108.12(15)

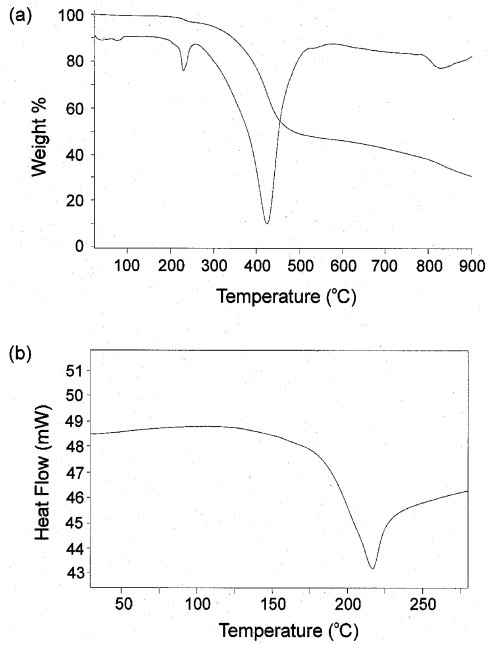
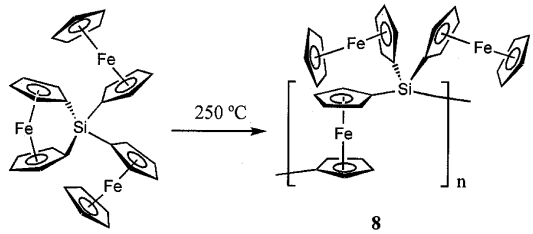


Fig. 8. (a) TGA and DTGA traces (10°C min^{-1}, N_2) and (b) DSC trace of **5** (5°C min^{-1}, N_2).

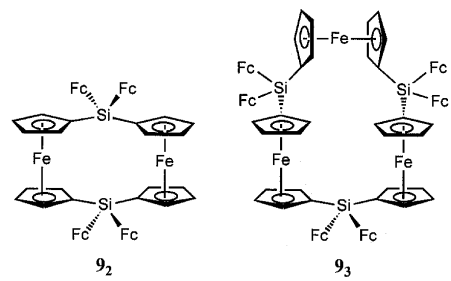
217°C. Although the curve appears unusual, it is reproducible.

When a sample of **5** was heated under vacuum in a Pyrex tube at 250°C, the monomer was consumed and a 37% yield of THF-insoluble material (**8**) was obtained. There was absolutely no evidence of melting during the polymerization as the powder appeared unchanged (except for a slight change in color). Solid-state ^{13}C CP-MAS NMR showed a peak at 68.7 ppm with a shoulder at 71.8 ppm, consistent with Cp ligands. ^{29}Si CP-MAS NMR displayed a single resonance at -11.6 ppm. For comparison, tetraferrocenylsilane, which is a good model for polymerized **5**, shows a single resonance at $\delta = -10.1$ ppm (CD_2Cl_2). Powder X-ray diffraction (PXRD) of the material indicated that it was amorphous, with a single broad halo centered at $2\theta = 17.5°$, $d = 5.06$ Å attributed primarily to diffraction from adjacent Fe atoms. Unfortunately, the solid was insoluble in common organic solvents such as $CHCl_3$, toluene, THF, DMSO, and DMF.



8

The low yield of polymer suggested that there was a substantial amount of oligomeric product formed. Polymerizations were performed from 175 to 240°C to identify the optimal temperature for obtaining oligomeric material. When a sample was sealed under vacuum in a Pyrex tube and heated at 200°C for 24 h, an orange–brown powder was obtained. The powder was completely dissolved in $CHCl_3$ and the resulting solution was filtered through neutral alumina. The dark orange filtrate was then evaporated to dryness, leaving an orange–brown powder in 92% yield. Gel permeation chromatography of the mixture showed a bimodal molecular weight distribution with a peak at $M_w = 5000$ and a small amount of higher molecular weight material ($M_w = 90000$). The material with the lower molecular weight is most likely a mixture of oligomers, for which the molecular weight is highly overestimated as a consequence of the skeletal rigidity relative to the polystyrene calibration standards. Mass spectrometry of the crude mixture showed peaks which could be assigned to $2M^+$ (**9_2**) and $3M^+$ (**9_3**) ($m/z = 582$ for M^+) and logical fragments of those (e.g. $2M^+$–FcH, $3M^+$–FcH). In fact, the dimer **9_2** and trimer **9_3** appear to have similar fragmentation patterns. Fig. 9 shows the mass spectrum obtained from a thermal treatment of **5** at 205°C, where peaks attributed to **9_2**$^+$ and **9_3**$^+$ are observed at $m/z = 1164$ and $m/z \approx 1747$ (note that the mass spectrometer calibration appeared to drift by ± 1 a.m.u. between 1200–2400 a.m.u.). Traces of fragments that would be expected from a cyclic tetramer **9_4** were also observed. ^1H NMR spectra of the oligomeric mixtures were deceptively simple owing to overlapping peaks in the Cp region (4–5 ppm). The ^{13}C NMR spectrum of the oligomeric mixture from the preparation at 205°C showed 2 *ipso*-Cp resonances (67.9, 68.6 ppm), a large resonance due to free Cp ligands at 68.8 ppm, and eight resonances due to CH groups on Cp ligands attached to Si. These resonances are consistent with a mixture of predominantly two cyclic oligomers. Integration of the peaks in the ^{13}C NMR spectrum, assuming the Cp environments are similar, gave an approximate ratio of 3:1 for the quantity of the two products. A single peak was observed in the ^{29}Si NMR spectrum at -11.9 ppm, a reasonable position for cyclic oligomers (cf. $\delta = -11.6$ ppm for the polymer $[fcSiFc_2]_n$). The mixture of oligomers may have the same ^{29}Si NMR chemical shift as the magnetic environments of the Si atoms are very similar (cf. ^{29}Si NMR of **2a** ($\delta = -6.4$ ppm) [9] and $[fcSiMe_2]_2$ ($\delta = -6.5$ ppm) [40]). Furthermore, no end groups were observed in the NMR spectra of the oligomers, consistent wth a cyclic structure. We believe that the combination of mass spectrometry and NMR spectroscopy identifies the soluble oligomers as mainly the cyclic dimer **9_2** and trimer **9_3** in an approximate 3:1 ratio.



9_2 **9_3**

The NMR spectra of the mixture obtained at 200°C were very similar to those of the sample prepared at 205°C, although for the former case a small quantity of an additional

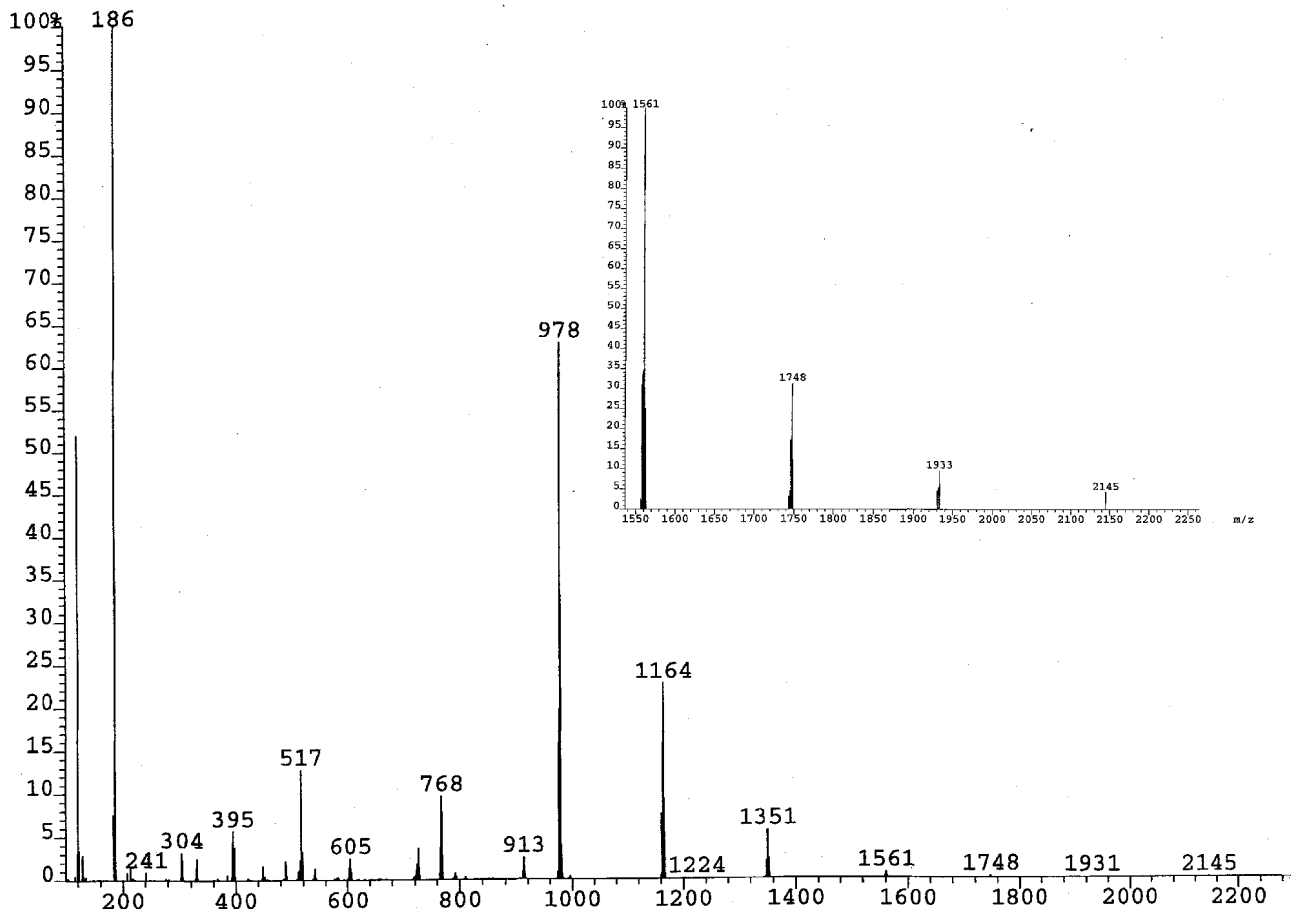


Fig. 9. Mass spectrum (EI) of cyclic oligomers obtained from thermolysis of **5** at 205°C. The inset shows the $m/z = 1500$–2300 portion of the spectrum expanded ca. 100 times.

product was observed in the ^{13}C NMR spectrum, which could be due to larger oligomers. The ^{1}H NMR spectrum was nearly identical and the ^{29}Si NMR spectrum showed only a single resonance at -12.2 ppm. Cyclic oligomers are the major product of the thermal ROP at low (ca. 200°C) temperatures.

This is the first observation of cyclic oligomers in the thermal ROP of a [1]silaferrocenophane. Although transition metal catalyzed ROP of **1a** yields cyclic oligomeric byproducts, only high molecular weight polymer has been previously obtained from the thermal ROP of [1]silaferrocenophanes [41–43]. Our results demonstrate that the polymerization behavior of the [1]ferrocenophane may be altered by incorporating very bulky substituents (i.e. ferrocenyl groups), favoring cyclization over linear polymer formation. This is an important consideration for mechanistic investigations.

The observation of cyclic oligomers from the solid-state thermal ROP of **5** has intriguing possible mechanistic implications for the thermal ROP of [1]silaferrocenophanes. To date, very little is known about the mechanism for the ring-opening polymerization of [1]ferrocenophanes [43]. Experiments have indicated that polymerization of [1]silaferrocenophanes proceeds with cleavage of the strained Si–C bond (instead of the Fe–Cp bond) [43]. It has been suggested that the mechanism may involve a spontaneous Si–C cleavage or possibly involves a small impurity (e.g. water or amine) to facilitate the heterolytic or homolytic cleavage of the Si–C bond. In the present case, the fact that the cyclization occurs in the solid-state suggests that a mechanism in which the transformation proceeds without the aid of a minor impurity is most likely as the diffusion of a trace molecular impurity through the solid would be extremely slow. This does not necessarily apply to other [1]ferrocenophanes, particularly those which undergo thermal ROP in the melt (e.g. **1a**) where an impurity could realistically initiate the polymerization process.

It is worth noting that monomer **5** possesses the bulkiest substituents ever attached to a [1]silaferrocenophane (our study of silanols with ferrocenyl substituents has suggested that the bulkiness of substituents obeys the following order: Mes > Fc ≈ Cy > Ph) [21,23]. These bulky groups would hinder the union of two monomers to form a cyclic, 4-centered $[Si\cdots C]_2$ transition state that would form in a metathesis reaction, where two Si atoms would become 5-coordinate. We feel that a metathesis mechanism is unlikely for the polymerization of **5** in the solid-state.

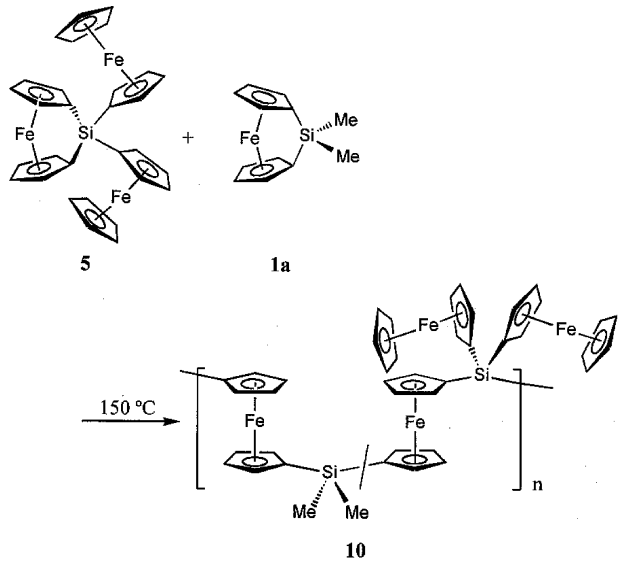
Another interesting observation is that only soluble oligomers were formed in the polymerization performed at

200°C; no insoluble material (**8**) was obtained. If the [1]ferrocenophane spontaneously formed a ring-opened, highly reactive intermediate (via heterolytic or homolytic cleavage of a Si–C bond of the ferrocenophane moiety, for example), reaction with other monomers would be expected to be very slow owing to the steric hinderance at Si in **5**. This would favor the formation of the small cyclic species we have observed at lower temperatures.

From the crystal structure, we have noted that compound **5** is arranged into planes in which the ferrocenophanes each possess two closest intraplanar Si···Si contacts (9.12 Å). Between the layers, dimeric closest contacts (7.96 Å) are present. The bulkiness of the ligands most likely prevents free rotation of the molecule, but may still allow for vibration and translation, particularly at high temperature. If a reactive species spontaneously formed at 200°C by breaking an Si–C bond, the reactive species could undergo a translation within the plane or out of the plane such that it could react with another molecule of **5**. This might explain the prevalence of the cyclic dimer and trimer detected in the oligomerization reactions. Although the intermolecular Si···Si contacts seem very long, the Si···Si separations in the linear pentamer $FcSiMe_2[fcSiMe_2]_3Fc$ are 6.9–7.0 Å [44]. Thus, translation of a ring-opened [1]ferrocenophane by only 1 Å would be necessary to bridge the Si atoms by a ferrocenyl group. The mechanistic ideas we postulate concerning the solid-state ROP of **5** may not be general to [1]silaferrocenophanes which usually undergo thermal ROP in the melt.

2.11. Attempted transition-metal catalyzed polymerizations and thermal copolymerizations of 5

As thermal polymerization gave a mixture of cyclic oligomers, we felt that one may be preferentially formed by a transition-metal catalyzed ROP of **5**. Monomer **5** was treated with several catalysts (Table 6) at different temperatures, but nearly the only substance observed in ^1H and ^{13}C NMR spectra of the crude reaction mixture was unreacted starting material.



5 **1a**

10

Table 6
Reaction conditions for attempted transition-metal catalyzed polymerization reactions for **5**

Catalyst	Solvent	Temperature (°C)	Time (h)
Karstedt's	toluene	reflux	21
Karstedt's	toluene	60	8
$[Rh(1,5\text{-}COD)_2][OTf]$	toluene	80	1.5
$(COD)PdCl_2$	C_6D_6	25	28
$(COD)PdCl_2$	toluene	60	12

Since the homopolymer of **5** was insoluble, we attempted to form soluble copolymers **10** with monomer **1a**. Although **1a** and **5** undergo thermal ROP at significantly different temperatures, we felt that **5** may dissolve in the melt of **1a** and be initiated by reactive chain ends formed during the polymerization. Copolymers were prepared by combining between 10 and 50 mol% of **5** with **1a** in a Pyrex tube and heating for 36 h at 150°C. Upon work-up, soluble material was obtained in each case. Gel permeation chromatography proved the molecular weight distribution of each polymer to be monomodal (e.g. a polymer formed starting with 25 mol% of **5** showed $M_n = 49900$, PDI = 1.97). Unfortunately, because of the long relaxation time for the Si of the $[fcSiFc_2]$ units and the absence of protons nearby (for DEPT), the relative amount of **1a** and **5** incorporated into the polymers could not be determined accurately by ^{29}Si NMR. A sample prepared with 40% of **5** showed two ^{29}Si NMR resonances at -6.5 and -9.7 ppm, consistent with segments derived from **1a** and **5**, respectively. Solid-state ^{29}Si CP-MAS NMR spectroscopy was also used to determine the Si environments present in the samples. Samples prepared with 25% and 40% of **5** showed two ^{29}Si CP-MAS NMR resonances at -6.7 and -12.0 ppm, assigned to segments derived from **1a** and **5**, respectively. In one polymer (11 mol% of **5**), three resonances were present in the solid-state ^{29}Si CP-MAS spectrum, at -7.1, -9.7, and -12.3 ppm; the NMR spectrum of this copolymer is illustrated in Fig. 10. The resonance at $\delta = -7.1$ ppm is assigned to $[fcSiMe_2]$ segments, the resonance at $\delta = -12.3$ ppm is assigned to $[fcSiFc_2]$ segments, and the resonance at $\delta = -9.7$ ppm is assigned to switching groups between the segments. ^{13}C NMR and ^1H NMR provided

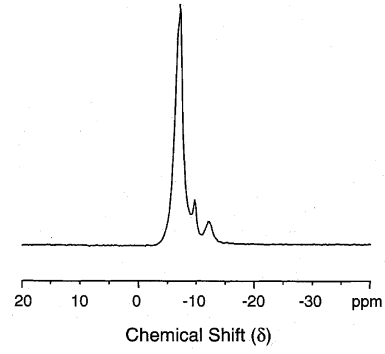


Fig. 10. Solid-state ^{29}Si CP-MAS NMR spectrum of a copolymer **10** prepared with 11 mol% **5**.

evidence that **5** was indeed incorporated into the copolymers. Samples prepared with 15–50% of **5** showed two methyl resonances, at −0.9 ppm and 1.0 ppm in the ^{13}C NMR spectrum, consistent with polymer segments derived from **1a** and switching groups, respectively. Because of the small amount of **5** that was generally incorporated, peaks attributed to segments derived from **5** in the copolymer were not well resolved. In the solution ^{1}H NMR spectrum of the copolymers, additional peaks were certainly present in the Cp region, but also were not well resolved. Two methyl resonances were observed, including a peak due to segments of **2a** at 0.4 ppm and a switching group at 0.05 ppm. Integration of these peaks gave switching group:**2a** ratios of 0.23, 0.46, 0.10, 0.05, and 0.04 for copolymers prepared with 10, 15, 25, 40, and 50 mol% of **5**, respectively. A possible explanation for the decrease in switching groups when the proportion of **5** used exceeded 15 mol% is that more insoluble polymer containing segments derived from **5** (which was removed prior to NMR) were obtained as the initial amount of **5** was increased. Powder X-ray diffraction showed a new amorphous halo present at $2\theta = 17.5°$ when **5** was incorporated, in addition to a broad halo centered at $2\theta = 14.5°$ characteristic of homopolymer **2a**. DSC of the homopolymer **2a** shows a glass transition (T_g) at 33°C and a melt at 120–145°C. None of the copolymers showed the glass transition (T_g) or melt for polymer **2a**, indicating that the copolymers probably possessed random structures, consistent with the observation of a large quantity of switching groups in the copolymer when small (<20 mol%) quantities of **5** were used. However, second-order transitions were observed at 60 and 54°C for copolymers derived from monomer mixtures containing 25% and 50% of **5**, respectively.

Our results indicate that copolymers of **1a** and **5** formed, but much less of **5** was incorporated than expected from the initial ratio of monomers. This is not surprising, considering the bulkiness of **5** relative to **1a**: the reactivity ratios of **1a** and **5** must be very different. The difficulty in ring-opening **5** has already been demonstrated by its resistance to undergo transition-metal catalyzed polymerization. There did not appear to be any correlation between the amount of **5** in the reaction mixture and the amount of **5** incorporated into the polymer. For example, in one sample prepared with 50% of **5**, the soluble material showed no evidence for incorporation of **5** into the polymer. This may be due to insolubility of polymers containing large amounts of **5**. Another difficulty that complicated characterization was that the copolymers became less soluble as they were repeatedly precipitated. This suggests that plasticizing oligomers or impurities (e.g. solvent) facilitate the dissolution of these materials.

3. Conclusions

We have synthesized a novel [1]ferrocenophane with two very bulky ferrocenyl substituents, **5**. Characterization by single crystal X-ray diffraction, NMR spectroscopy, IR, and Raman spectroscopy corroborated the structure. The Mössbauer spectrum of **5** resolved the quadrupole doublets of the ferrocenophane and ferrocenyl substituents. Differential pulse voltammetry of **5** resolved three oxidation waves ($\Delta E = 0.22$, 0.23 V). Ferrocenophane **5** is a convenient precursor to triferrocenylsilane derivatives. Chlorotriferrocenylsilane was synthesized from the ring-opening addition of HCl to **5** and was structurally characterized. Subsequent hydrolysis yielded a silanol with three bulky ferrocenyl substituents on Si. X-ray diffraction revealed that the silanol crystallizes in hydrogen-bonded dimers, characteristic of silanols with very bulky substituents. Ferrocenophane **5** undergoes thermal ring-opening polymerization in the solid state to afford insoluble polymer together with soluble, cyclic oligomers. This represents the first observation of cyclic oligomers from the thermal ROP of a [1]silaferrocenophane and may be associated with the steric hinderance of the ferrocenyl moieties. Copolymers of **5** with dimethyl[1]silaferrocenophane were prepared, but the amount of **5** incorporated into the copolymer **10** could not be controlled due to insolubility of polymer blocks made from **5**. Future work will involve the separation of the cyclic oligomers obtained from thermal ROP of **5** for further characterization.

4. Experimental

4.1. Materials

Dilithioferrocene·TMEDA, dimethyl[1]silaferrocenophane **1a**, and diferrocenyldichlorosilane **4** were prepared by literature methods [9,21,45]. Hydrogen chloride (1.0 M in diethyl ether) was purchased from Aldrich and was used without further purification. Triethylamine was obtained from Aldrich and was distilled from Na prior to use.

4.2. Equipment

All reactions and manipulations were carried out under an atmosphere of prepurified nitrogen using either Schlenk techniques or an inert-atmosphere glovebox (Innovative Technologies) unless otherwise noted. Solvents were dried by standard methods, distilled, and stored under nitrogen. Solution 400 MHz ^{1}H NMR spectra, 100.5 MHz ^{13}C NMR spectra, and 79.5 MHz ^{29}Si NMR spectra were recorded on a Varian Unity 400 spectrometer and were referenced externally to TMS. Molecular weights were estimated by gel permeation chromatography (GPC) using a Water Associates liquid chromatograph equipped with a 510 HPLC pump, U6K injector, ultrastyragel columns with pore sizes of 10^3 and 10^5 Å, and a Waters 410 differential refractometer. A flow rate of 1.0 ml min^{-1} was used and samples were dissolved in a solution of 0.1% NBu_4Br in THF. The GPC was calibrated with nine monodisperse polystyrene standards. Solid-state 79.5 MHz ^{29}Si and 100.5 MHz ^{13}C CP-MAS NMR spectra were obtained on a Bruker DSX 400 spectrometer. Powder

X-ray diffraction patterns were obtained on a Siemens D5000 X-ray diffractometer using Ni-filtered Cu Kα radiation ($\lambda = 1.54178$ Å). UV–Vis spectra were obtained in CH_2Cl_2 (ca. 5×10^{-4} M) on a Perkin–Elmer Lambda 900 UV–Vis/near-IR spectrometer using a 1 cm quartz cuvette. IR spectra were obtained as Nujol mulls or KBr pellets with a Nicolet Magna-IR 550 spectrometer. FT-Raman spectra were collected on a Bomems MB-157 FT-spectrometer with a Spectra Physics diode pumped Nd:YLF laser (1064 nm, 350 kHz repetition rate). The instrument was configured in 180° backscattering mode using sealed glass capillary tubes to hold the neat, crystalline samples. Electron impact (EI) mass spectra were obtained with a VG 70-250S mass spectrometer. As the calibration file used for measuring the mass spectra of the oligomers was an old FAB file and the very high masses are approaching the limit of the instrument, drifts of ± 1 a.m.u. are not surprising. Thermogravimetric analyses were obtained on a Perkin–Elmer TGA-7 analyzer equipped with a TAC-7 instrument controller. Samples were heated at a rate of 10°C min^{-1} under a flow of N_2. Differential scanning calorimetry was performed on a Perkin–Elmer DSC-7 analyzer equipped with a TAC-7 instrument controller. The instrument was calibrated with the melting points of cyclohexane and indium and samples were heated at a rate of 5°C min^{-1}. Differential pulse voltammetry of **5** was performed under ambient conditions under N_2 by analysis of a 0.31 mM solution at a glassy carbon electrode in dichloromethane using a PAR model 174 potentiostat using 1 s drop time and 25 mV modulation amplitude settings. Potentials in this paper are given versus the ferrocene/ferrocenium couple. Room-temperature ^{57}Fe Mössbauer spectra were obtained using a Ranger Scientific Inc. VT-1200 instrument with a MS-1200 digital channel analyzer. The γ-ray source was a 6 mCi ^{57}Co sample supplied by Amersham. The data were collected in a -15.8 to $+15.8$ mm s^{-1} range and referenced to Fe powder. Data were acquired long enough to obtain a suitable fit to standard independent Lorentzian line shapes for sinusoidal baselines. Melting points were determined on a Fisher–Johns hot-stage melting point apparatus and are uncorrected.

*4.3. Synthesis of diferrocenyl[1]silaferrocenophane **5***

A solution of **4** (2.235 g, 4.76 mmol) in ca. 20 ml of THF was added dropwise via cannula to a stirring suspension of dilithioferrocene·TMEDA (1.25 g, 3.98 mmol) in THF (ca. 125 ml) chilled to −78°C under N_2. The mixture was warmed to room temperature over a period of 2 h during which time the color of the solution became darker red. After refluxing the solution at 60–70°C for 1.5 h, the solution was notably darker than before. The solvent was removed under vacuum, leaving an orange and red residue. The crude solid was washed with ca. 20 ml of toluene and the brown mother liquors were discarded (a small amount of hexane soluble compound in the toluene wash was identified by ^{1}H NMR as Fc_3SiCl, a by-product that could be expected if any FcLi was present). Subsequent extraction with dichloromethane (ca. 200 ml) gave a light orange–red solution and a fine white precipitate (LiCl) which was removed by filtration. Recrystallization from dichloromethane afforded 1.480 g (2.54 mmol, 64%) of **5** as an orange powder. An additional 0.312 g (0.536 mmol, 13%) of product was obtained from the supernatant solution, for a total yield of 77% (1.792 g, 3.08 mmol). The product is a red, air stable crystalline solid.

Data for **5**. ^{13}C NMR ($CDCl_3$) $\delta = 77.3$ (Si–Cp), 76.0 (Si–Cp), 74.8 (Si–Cp), 71.3 (Si–Cp), 69.0 (Cp), 64.8 (*ipso*-C), 34.8 (*ipso*-C) ppm. ^{13}C NMR (C_6D_6) $\delta = 77.9$ (Si–Cp), 76.5 (Si–Cp), 75.2 (Si–Cp), 71.6 (Si–Cp), 69.3 (Cp), 65.4 (*ipso*-C), 35.0 (*ipso*-C) ppm. ^{1}H NMR ($CDCl_3$) $\delta = 4.64$ (t, $^3J_{HH} = 1.62$ Hz, 4H, Cp), 4.5–4.6 (m, 8H, Cp), 4.36 (t, $^3J_{HH} = 1.59$ Hz, 4H, Cp), 4.26 (s, 10H, Cp) ppm. ^{1}H NMR (in C_6D_6) $\delta = 4.61$ (t, $^3J_{HH} = 1.69$ Hz, 4H, Cp), 4.55 (t, $^3J_{HH} = 1.61$ Hz, 4H, Cp), 4.39 (t, $^3J_{HH} = 1.61$ Hz, 4H, Cp), 4.36 (t, $^3J_{HH} = 1.67$ Hz, 4H, Cp), 4.20 (s, 10H, Cp) ppm. ^{29}Si NMR ($CDCl_3$) $\delta = -15.5$ ppm. UV–Vis (CH_2Cl_2) $\lambda_{max} = 474$ nm ($\varepsilon = 505$ l mol^{-1} cm^{-1}). MS (EI, 70 eV) m/z (rel. intensity) = 582 (100, M^+), 517 (26, M^+–C_5H_5), 396 (19, M^+–FcH), 340 (18, M^+–FcH–Fe), 186 (68, FcH^+), 121 (36, $C_5H_5Fe^+$). HRMS for $C_{30}H_{26}SiFe_3$: calc. $m/z = 581.9852$; found $m/z = 581.9827$.

*4.4. Synthesis of chlorotriferrocenylsilane **6***

With a syringe, 1.2 ml of HCl (1 M in ether) was added dropwise to a stirred solution of 0.563 g of **5** (0.967 mmol) in 50 ml CH_2Cl_2. The solution changed color from red–orange to yellow–orange. The solvent was removed under vacuum, leaving a yellow solid. After the solid was dissolved in a minimum of warm hexanes/CH_2Cl_2 (ca. 1:3), the solution was filtered to remove oxidized species. Once again, the solvent was removed under vacuum and the product was recrystallized from dichloromethane to give yellow crystals in 81% yield (0.485 g, 0.784 mmol).

Data for **6**. ^{13}C NMR ($CDCl_3$) $\delta = 73.9$ (Si–Cp), 71.2 (Si–Cp), 69.0 (Cp), 68.8 (*ipso*-Cp) ppm. ^{1}H NMR ($CDCl_3$) $\delta = 4.44$ (t, $^3J_{HH} = 1.7$ Hz, 6H, Cp), 4.37 (t, $^3J_{HH} = 1.7$ Hz, 6H, Cp), 4.13 (s, 15H, Cp) ppm. ^{29}Si NMR ($CDCl_3$) $\delta = 11.5$ ppm. UV–Vis (CH_2Cl_2) $\lambda_{max} = 456$ nm ($\varepsilon = 412$ l mol^{-1} cm^{-1}). MS (EI, 70 eV) m/z (rel. intensity) = 618 (100, M^+), 462 (8, M^+–CpFeCl), 397 (53, M^+–FcCl), 367 (9, M^+–FcH–C_5H_5), 331 (8, M^+–FcCl–C_5H_5), 276 (15, M^+–FcCl–FeCp), 186 (12, FcH^+), 121 (11, $CpFe^+$), 93 (13, $CpSi^+$). M.p. 228–229.5°C. IR (KBr pellet) 3088(m), 3082(m), 1411(m), 1381(w), 1356(m), 1350(w), 1300(m), 1190(s), 1179(m), 1166(s), 1107(s), 1055(m), 1034(s), 1022(s), 998(s), 891(w), 867(w), 843(w), 836(s), 821(s), 632(m), 627(m), 618(w), 589(w), 556(m), 542(m), 536(s), 498(m), 483(s), 475(s), 468(s) cm^{-1}. HRMS for $C_{30}H_{27}ClSiFe_3$: calc. $m/z = 617.9619$; found $m/z = 617.9608$.

4.5. Synthesis of triferrocenylsilanol **7**

A solution of 0.177 g (0.286 mmol) of **6** in 50 ml ether was treated with 0.50 ml (3.6 mmol) of triethylamine at room temperature. Using a pipette, 0.5 ml of H_2O (28 mmol) was added dropwise. The solution was then warmed to 40°C in a water bath and maintained there for 30 min. Solvent was removed by rotary evaporation, leaving a yellow residue. The crude product was dissolved in CH_2Cl_2 and the solution was filtered. Large orange crystals were obtained within hours at −55°C. The crystals were isolated on a Buchner funnel, washed with hexanes, and dried under vacuum. Compound **7** was obtained as orange crystals in 80% yield (138 mg, 0.230 mmol).

Data for **7**. ^{13}C NMR ($CDCl_3$) δ=74.2 (Si–Cp), 71.4 (Si–Cp), 69.6 (*ipso*-Cp), 69.0 (Cp) ppm. ^{1}H NMR ($CDCl_3$) δ=4.47 (s, 6H, Cp), 4.40 (s, 6H, Cp), 4.20 (s, 15H, Cp), 2.02 (s, 1H, OH) ppm. ^{29}Si NMR ($CDCl_3$) δ=−2.4 ppm. UV–Vis (CH_2Cl_2) λ_{max}=456 nm (ε=384 l mol^{-1} cm^{-1}). MS (EI, 70 eV) m/z (rel. intensity)=600 (100, M^+), 535 (6, M^+–C_5H_5), 469 (6, MH^+–2(C_5H_5)), 414 (7, M^+–FcH), 349 (28, M^+–FcH–Cp), 305 (16), 186 (5, FcH^+). M.p. 185–186.5°C. *Anal*. Calc.: C, 60.04; H, 4.70; N, 0.00. Found: C, 59.10; H, 4.57; N, 0.14. IR (Nujol mull) 3635(s), 3382(vs), 1367(m), 1349(m), 1299(m), 1189(m), 1167(s), 1105(s), 1054(m), 1031(s), 1003(s), 903(s), 873(m), 859(m), 850(m), 832(m), 820(s), 813(s), 633(m), 557(m), 543(m) cm^{-1}. Raman (crystals) 3106(s), 3084(m), 3077(m), 1411(m), 1382(m), 1367(w), 1187(w), 1164(s), 1106(vs), 1062(m), 1038(m), 1001(w), 398(m), 387(m), 365(w), 326(s), 308(s), 267(w), 229(w), 211(w) cm^{-1}.

4.6. Synthesis of the insoluble homopolymer ***8***

Ferrocenophane **5** (0.35 g, 0.6 mmol) was sealed under vacuum in a Pyrex polymerization tube. The tube was heated for 8 h at 250°C in an oven. After the polymerization tube cooled to room temperature, the contents were stirred overnight in ca. 25 ml of THF. The product was isolated on a Buchner funnel, washed with THF, and dried under vacuum for 12 h at 60°C to yield 0.13 g (37%) of yellow–orange powder.

Data for **8**. ^{13}C{^{1}H} CP-MAS NMR (100.5 MHz, spin rate 6 kHz, recycle delay 3s, contact time 1 ms, ramped contact pulse) δ=71.8 (Si–Cp), 68.7 (Cp) ppm. ^{29}Si{^{1}H} CP-MAS NMR (79.5 MHz, spin rate 6 kHz, recycle delay 10s, contact time 1 ms, ramped contact pulse) δ=−11.6 ppm. PXRD broad halo at 17.5° 2θ, 5.06 Å *d*-spacing (FWHM=2.2°). *Anal*. Calc.: C, 61.90; H, 4.82. Found: C, 61.13; H, 4.78.

4.7. Synthesis of cyclic oligomers ***9***

Ferrocenophane **5** (146 mg, 0.251 mmol) was sealed under vacuum in a Pyrex polymerization tube. The sample was heated at 200°C for 24 h, during which time it changed color from orange–red to orange–brown. Also, a small quantity (ca. 1 mg) of orange crystals were present on the glass. The tube was broken open and the powder was separated from the crystals. The powder dissolved entirely in 20 ml of $CHCl_3$, giving an orange solution, which was then filtered through ca. 5 cm of neutral alumina (~150 mesh). The solvent was removed by rotary evaporation, yielding 134 mg (92%) of orange–brown soluble material. NMR spectroscopy, mass spectrometry, and GPC indicated that the soluble product is primarily cyclic dimer ($\mathbf{9_2}$) and trimer ($\mathbf{9_3}$).

Data for **9** (prepared at 200°C). ^{13}C NMR ($CDCl_3$) δ=74.3 (Si–Cp), 74.1 (Si–Cp), 73.8 (Si–Cp), 72.0 (Si–Cp), 71.0 (Si–Cp), 70.7 (Si–Cp), 70.4 (Si–Cp), 68.9 (Si–Cp), 68.7 (Cp), 67.8 (Si–Cp) ppm. ^{1}H NMR ($CDCl_3$) δ=3.7–4.6 (Cp, m) ppm. ^{29}Si NMR ($CDCl_3$) δ=−12.2 ppm. MS (EI, 70 eV) m/z (rel. intensity)=1558 (1, $\mathbf{9_3}^+$–FcH), 1350 (7, $\mathbf{9_3}^+$–fc_2Si), 1164 (28, $\mathbf{9_2}^+$), 978 (100, $\mathbf{9_2}^+$–FcH), 768 (38, $\mathbf{9_2}^+$–FcH–210), 517 (18, $Fc_2SiCpFe^+$),186 (63, FcH^+).

Data for **9** (prepared at 205°C). ^{13}C NMR ($CDCl_3$) δ=74.8 (Si–Cp), 74.3 (Si–Cp), 73.8 (Si–Cp), 72.6 (Si–Cp), 71.5 (Si–Cp), 71.0 (Si–Cp), 70.7 (Si–Cp), 70.5 (Si–Cp), 68.8 (Cp), 68.6 (Si–Cp), 67.9 (Si–Cp) ppm. ^{1}H NMR ($CDCl_3$) δ=3.7–4.6 (Cp, m) ppm. ^{29}Si ($CDCl_3$) δ=−11.9 ppm. MS (EI, 70 eV) m/z (rel. intensity)=1748 (<1, $\mathbf{9_3}^+$), 1561 (1, $\mathbf{9_3}^+$–FcH), 1351 (7, $\mathbf{9_3}^+$–fc_2Si), 1164 (24, $\mathbf{9_2}^+$), 978 (65, $\mathbf{9_2}^+$–FcH), 768 (12, $\mathbf{9_2}^+$–fc_2Si), 517 (13, $Fc_2SiCpFe^+$), 186 (100, FcH^+).

We tentatively assign the fragments at m/z=768 and 1350–1351 to $\mathbf{9_2}^+$–fc_2Si and $\mathbf{9_3}^+$–fc_2Si, respectively, as fc_2Si is a stable product that could be eliminated during ionization.

4.8. Attempted synthesis of copolymers (***10***) of ***5*** and ***1a***

Copolymers were prepared by a general procedure. Ferrocenophanes **1a** and **5** were ground in an agate mortar and combined in the appropriate ratio to give a sample size of approximately 300 mg. The monomers were sealed under vacuum inside a Pyrex polymerization tube and heated for 36 h at 150°C in an oven. The crude red polymer was dissolved in THF (ca. 10 ml) and the soluble fraction (obtained by filtration) was added dropwise to a stirring solution of 300 ml of hexanes. The polymer was collected in a Buchner funnel and dried under vacuum overnight at 60°C. The polymers were not very soluble, and solution NMR of the soluble fractions showed traces of solvent present in the polymers. However, this solvent was not observed by solid-state NMR spectroscopy, indicating that only a very small amount of solvent was entangled in the polymer chains. We attempted to remove all of the solvent by performing the precipitation into pentanes, but solvent was still detected in the polymer. Samples were prepared using 10, 11, 15, 25, 40, and 50 mol% of **5**. Characterization for three representative preparations are given below.

Data for **10** prepared with 10 mol% of **5** (PFMS=**2a**, PFFS=**8**). ^{13}C NMR ($CDCl_3$) δ=74.3 (Cp), 73.6 (Cp),

73.3 (PFMS–Cp), 72.6 (Cp), 71.6 (Cp), 71.4 (PFMS–Cp), 70.4 (Cp), 68.8 (Cp), 68.0 (*ipso*-Cp), −0.9 (CH_3, PFMS) ppm. ^{1}H NMR ($CDCl_3$) δ = 3.9–4.5 (Cp), 0.42 (s, CH_3, PFMS–Si–PFMS), 0.07 (s, CH_3, PFMS–Si–PFFS) ppm. ^{29}Si NMR ($CDCl_3$) δ = −6.56 (PFMS) ppm. GPC (THF, versus polystyrene) M_n = 23900 (PDI = 1.76).

25 mol% of **5**. ^{13}C NMR ($CDCl_3$) δ = 74.6 (Cp), 73.7 (Cp, PMFS), 72.1 (Cp), 71.9 (Cp, PFMS), 71.0 (Cp), 69.2 (Cp), 1.0 (CH_3, PFMS–Si–PFFS), −0.5 (CH_3, PFMS–Si–PFMS) ppm. ^{1}H NMR ($CDCl_3$) δ = 3.9–4.5 (Cp), 0.45 (s, CH_3, PFMS–Si–PFMS), 0.08 (CH_3, PFMS–Si–PFFS) ppm. ^{29}Si{^{1}H} CP-MAS NMR (79.5 MHz, spin rate 6 kHz, recycle delay 10s, contact time 4 μs) δ = −6.7 (PFMS), −12.0 (PFFS) ppm. GPC (THF, versus polystyrene) M_n = 49900 (PDI = 1.97).

40 mol% of **5**. ^{13}C-NMR (100.5 MHz, $CDCl_3$) δ = 74.4 (Cp), 73.5 (Cp, PMFS), 71.8 (Cp), 71.6 (Cp, PFMS), 70.6 (Cp), 69.0 (Cp), 67.9 (*ipso*-Cp), 1.0 (Cp, CH_3, PFMS–Si–PFFS), −0.9 (s, CH_3, PFMS–Si–PFMS) ppm. ^{1}H NMR ($CDCl_3$) δ = 3.9–4.6 (Cp), 0.42 (s, CH_3, PFMS–Si–PFMS), 0.06 (s, CH_3, PFMS–Si–PFFS) ppm. ^{29}Si-NMR (79.5 MHz, $CDCl_3$) δ = −6.51 (PFMS), −9.68 (PFFS) ppm. ^{29}Si{^{1}H} CP-MAS NMR (79.5 MHz, spin rate 6 kHz, recycle delay 10s, contact time 4 μs) δ = −6.6 (PFMS), −12.0 (PFFS) ppm. GPC (THF, versus polystyrene) M_n = 42100 (PDI = 1.87).

4.9. Attempted transition-metal catalyzed polymerization of 5

Conditions used for the attempts to react **5** with a transition-metal catalyst are listed in Table 6. In a typical preparation, ca. 60–100 mg of **5** were combined with ca. 10–20 ml of solvent and ca. 1% of the transition-metal catalyst (Rh(1,5-COD)$_2$ triflate, (1,5-COD)$PdCl_2$, or Karstedt's catalyst) and treated at 25–110°C. After the appropriate time, the reaction mixture was evaporated to dryness, dissolved in $CDCl_3$, and filtered to remove a brown insoluble material. ^{1}H and ^{13}C NMR spectra of the soluble fraction were consistent with unreacted monomer **5** and, in a few of the attempts, a small amount of a ferrocene-containing by-product which was not further characterized.

4.10. Crystallographic structural determination

Selected crystal, data collection, and refinement parameters for **5**, **6**, and **7** are provided in Table 1. Selected inter- and intramolecular bond distances for **5**, **6**, and **7** are given in Tables 2, 4 and 5, respectively. Crystals of **5**–**7** were each mounted on a glass fiber and coated with epoxy glue.

Intensity data for compound **5** were collected at 293(2) K on a Siemens P4 diffractometer using graphite-monochromated Mo Kα radiation (λ = 0.71073 Å). The ω scan technique was applied with variable scan speeds. Intensities of three standard reflections were measured every 100 reflections; the crystal showed negligible decay (<1%) during the data collection. A semi-empirical absorption correction was applied using the SHELXA-90 routine in SHELXL. The positions of all atoms for **5** were determined by direct methods using Siemens SHELXTL PC [46]. All Fe and Si atoms were refined anisotropically and C and H atoms were refined with isotropic thermal parameters by full-matrix least squares to minimize $\sum w(F_o^2 - F_c^2)^2$. The data showed two distinct orientations of the ferrocenophane (illustrated in Fig. 1(b,c)). Refinement with these two molecules present in equal abundance gave a solution which was chemically and structurally consistent. Bond lengths and angles within the structure display large ESDs as a consequence of the static disorder, but are reasonable when compared with similar structures.

Data for **6** were collected on a Siemens P4 diffractometer equipped with a SMART/CCD detector. The systematic absences in the diffraction data are uniquely consistent for the reported space group. The structure was solved using direct methods, completed by subsequent difference Fourier syntheses and refined by full-matrix least-squares procedures. All non-hydrogen atoms were refined with anisotropic displacement coefficients and the hydrogen atoms were treated as idealized contributions. All software and sources of the scattering factors are contained in the SHELXTL (5.03) program library [46].

Data for **7** were collected on a Nonius Kappa-CCD diffractometer using graphite-monochromated Mo Kα radiation (λ = 0.710 73 Å). The data from 180×1° ϕ scans were integrated and scaled using the Denzo-SMN package [47]. The structure was solved and refined using the SHELXTL package [46]. Refinements were by full-matrix least squares on F^2 using all data (negative intensities included). All hydrogen atoms were included in calculated positions and treated as riding atoms. All non-hydrogen atoms were refined with anisotropic thermal parameters.

Supplementary data

Crystallographic data for **5**–**7** have been deposited with the CCDC (12 Union Road, Cambridge, CB2 1EZ, UK) and are available on request quoting deposition numbers CCDC 132620, 132638, and 132621, respectively.

Acknowledgements

M.J.M. thanks the Natural Sciences and Engineering Research Council of Canada (NSERC) for a Postgraduate Scholarship (1995–1999). I.M. thanks NSERC for an E.W.R. Steacie Fellowship (1997–1999) and the University of Toronto for a McLean Fellowship (1997–2003). Work at the University of Vermont was supported by the National Science Foundation (NSF Grant No. CHE-9705763); C.M. was an NSF-REU participant.

References

[1] C.U. Pittman, C.E. Carraher, M. Zeldin, J.E. Sheats, B.M. Culbertson (Eds.), Metal-Containing Polymeric Materials, Plenum, New York, 1996.
[2] M. Altmann, U.H.F. Bunz, Angew. Chem., Int. Ed. Engl. 34 (1995) 569.
[3] M. Rosenblum, H.M. Nugent, K.S. Jang, M.M. Labes, W. Cahalane, P. Klemarczyk, W.M. Reiff, Macromolecules 28 (1995) 6330.
[4] H.Y. Chen, R.D. Archer, Macromolecules 28 (1995) 1609.
[5] C.E. Stanton, T.R. Lee, R.H. Grubbs, N.S. Lewis, J.K. Pudelski, M.R. Callstrom, M.S. Erickson, M.L. McLaughlin, Macromolecules 28 (1995) 8713.
[6] M.A. Buretea, T.D. Tilley, Organometallics 16 (1997) 1507.
[7] G.E. Southard, M.D. Curtis, Organometallics 16 (1997) 5618.
[8] I. Manners, Angew. Chem., Int. Ed. Engl. 35 (1996) 1602.
[9] D.A. Foucher, B.-Z. Tang, I. Manners, J. Am. Chem. Soc. 114 (1992) 6246.
[10] P.F. Brandt, T.B. Rauchfuss, J. Am. Chem. Soc. 114 (1992) 1926.
[11] I. Manners, Adv. Organomet. Chem. 37 (1995) 131.
[12] I. Manners, Can. J. Chem. 76 (1998) 371.
[13] I. Manners, Chem. Commun. (1999) 857.
[14] M.T. Nguyen, A.F. Diaz, V.V. Dement'ev, K.H. Pannell, Chem. Mater. 5 (1993) 1389.
[15] M. Tanaka, T. Hayashi, Bull. Chem. Soc. Jpn. 66 (1993) 334.
[16] S. Barlow, A.L. Rohl, S. Shi, C.M. Freeman, D. O'Hare, J. Am. Chem. Soc. 118 (1996) 7578.
[17] M. Hmyene, A. Yassar, M. Escorne, A. Percheron-Guegan, F. Garnier, Adv. Mater. 6 (1994) 564.
[18] I. Manners, Adv. Mater. 6 (1994) 68.
[19] D. Foucher, R. Ziembinski, R. Petersen, J. Pudelski, M. Edwards, Y. Ni, J. Massey, C.R. Jaeger, G.J. Vancso, I. Manners, Macromolecules 27 (1994) 3992.
[20] K.H. Pannell, V.V. Dementiev, H. Li, F. Cervantes-Lee, M.T. Nguyen, A.F. Diaz, Organometallics 13 (1994) 3644.
[21] M.J. MacLachlan, M. Ginzburg, J. Zheng, O. Knöll, A.J. Lough, I. Manners, New J. Chem. 22 (1998) 1409.
[22] M.J. MacLachlan, A.J. Lough, W.E. Geiger, I. Manners, Organometallics 17 (1998) 1873.
[23] M.J. MacLachlan, J. Zheng, A.J. Lough, I. Manners, C. Mordas, R. LeSuer, W.E. Geiger, L.M. Liable-Sands, A.L. Rheingold, Organometallics 18 (1999) 1337.
[24] A.G. Osborne, R.H. Whiteley, R.E. Meads, J. Organomet. Chem. 193 (1980) 345.
[25] D.R. Lide (Ed.), CRC Handbook of Chemistry and Physics, CRC Press, Boca Raton, FL, 72nd edn., 1991, p. 9-1.
[26] M.J.L. Tendero, A. Benito, J. Cano, J.M. Lloris, R. Martinez-Manez, J. Soto, A.J. Edwards, P.R. Raithby, M.A. Rennie, Chem. Commun. (1995) 1643.
[27] B. Steiger, C. Shi, F.C. Anson, Inorg. Chem. 32 (1993) 2107.
[28] W.F. Sokol, D.H. Evans, K. Niki, T. Yagi, J. Electroanal. Chem. 108 (1980) 107.
[29] A. Houlton, J.R. Miller, R.M.G. Roberts, J. Silver, J. Chem. Soc., Dalton Trans. (1991) 467.
[30] D.M. Duggan, D.N. Hendrickson, Inorg. Chem. 14 (1975) 955.
[31] R.H. Herber, T.P. Hanusa, Hyperfine Interactions 108 (1997) 563.
[32] R.J. Webb, P.M. Hagen, R.J. Wittebort, M. Sorai, D.N. Hendrickson, Inorg. Chem. 31 (1992) 1791.
[33] R.M.G. Roberts, J. Silver, R.J. Ranson, I.E.G. Morrison, J. Organomet. Chem. 219 (1981) 233.
[34] A.L. Smith, Spectrochim. Acta 23A (1967) 1075.
[35] G.P. Sollott, W.R. Peterson jr, J. Am. Chem. Soc. 89 (1967) 6783.
[36] P.D. Lickiss, Adv. Inorg. Chem. 42 (1995) 147.
[37] É.B. Lobkovskii, V.N. Fokin, K.N. Semenenko, J. Struct. Chem. 22 (1981) 603.
[38] A.I. Al-Mansour, S.S. Al-Juaid, C. Eaborn, P.B. Hitchcock, J. Organomet. Chem. 480 (1994) 139.
[39] E. Lukevics, O. Pudova, R. Sturkovich, Molecular Structure of Organosilicon Compounds, Halsted, Toronto, 1989, pp. 175–179.
[40] D.L. Zechel, D.A. Foucher, J.K. Pudelski, G.P.A. Yap, A.L. Rheingold, I. Manners, J. Chem. Soc., Dalton Trans. (1995) 1893.
[41] Y. Ni, R. Rulkens, J.K. Pudelski, I. Manners, Makromol. Chem. Rapid Commun. 16 (1995) 637.
[42] N.P. Reddy, H. Yamashita, M. Tanaka, J. Chem. Soc., Chem. Commun. (1995) 2263.
[43] I. Manners, Polyhedron 15 (1996) 4311.
[44] R. Rulkens, A.J. Lough, I. Manners, S.R. Lovelace, C. Grant, W.E. Geiger, J. Am. Chem. Soc. 118 (1996) 12683.
[45] M.D. Rausch, D.J. Ciappenelli, J. Organomet. Chem. 10 (1967) 127.
[46] G.M. Sheldrick, SHELXTL/PC, Siemens Analytical X-ray Instruments Inc., Madison, WI, 1994.
[47] Z. Otwinowski, W. Minor, Methods Enzymol. 276 (1997) 307.

PERGAMON

www.elsevier.nl/locate/poly

Polyhedron 19 (2000) 291–295

POLYHEDRON

Bis(ferrocenylsilyl)thiophenes and ferrocenylene(silylene)thiophene oligomers

Keith H. Pannell *, Feng Wang, Hemant K. Sharma, Francisco Cervantes-Lee

Department of Chemistry, The University of Texas at El Paso, El Paso, TX 79968, USA

Received 26 July 1999; accepted 17 August 1999

Abstract

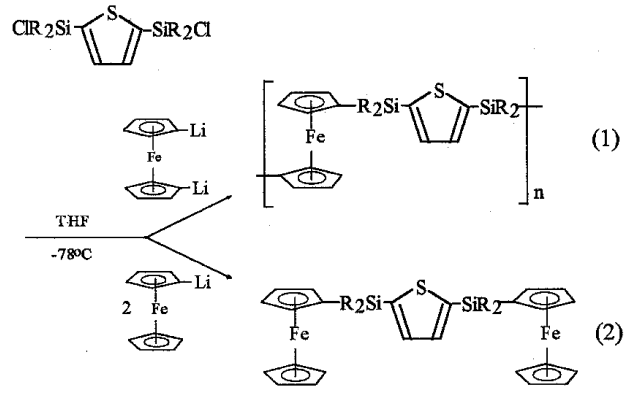
The reaction between 1,1′-dilithioferrocene and 2,5-bis(chlorodimethylsilyl)thiophene (**I**), leads to a series of cyclic oligomers of basic formulation [Fc-$SiMe_2$-TH-$SiMe_2$]$_n$ (**II**); Fc = (η^5-C_5H_4)$_2$Fe, TH = C_4H_2S. The material $n = 2$, **IIa**, has been completely characterized by spectroscopic and single crystal X-ray diffraction. Cyclic voltammetric analysis of **IIa** illustrates two reversible redox processes, indicating a significant interaction between the two ferrocenylene units despite the 5 atom bridge. By comparison, the monomeric analog Fc-$SiMe_2$-TH-$SiMe_2$-Fc (**III**), Fc = (η^5-C_5H_5)Fe(η^5-C_5H_4), prepared from the reaction of mono-lithioferrocene with **I**, exhibits a single redox process, even though there is the same bridge between the two Fe centers. ©2000 Elsevier Science Ltd All rights reserved.

Keywords: Cyclic oligomers; Thiophenes; Ferrocenes

1. Introduction

The interesting properties of polythiophenes are well studied [1] and recently the synthesis and study of thiophene-substituted derivatives of the Group 14 elements has also received attention due to their potential as electroactive materials [2–5]. We have an interest in similar ferrocenyl-substituted Group 14 materials [6–17], and now report studies aimed at the introduction of both the ferrocene and thiophene units into a silicon-containing molecular structure. We hope to produce monomers, oligomers and polymers with interesting structural and electrical properties. As a general procedure for the synthesis of such systems we have used the chemistry outlined in Eqs. (1) and (2) in which either monolithioferrocene or dilithioferrocene is reacted with a 2,5-(chlorosilyl)thiophene (**Ia** R = Me; **Ib** R = Ph).

Whereas the reaction of dilithioferrocene with **I** would, in theory, yield polymeric materials, the use of monolithioferrocene, [Fc]$^-$Li$^+$, was to provide monomers from which the basic optical and electrochemical properties of the system 2,5-bis(ferrocenylsilyl)thiophene could be obtained.



2. Results and discussion

The reaction between 2,5-bis(chlorodimethylsilyl)thiophene, **Ia**, and dilithioferrocene, Eq. (1), resulted in the formation of a series of low molecular weight cyclic oligomers. We attempted to separate these materials by column chromatography and were able to obtain the first of this series, **IIa,** $n = 2$, as pure red crystals. The spectroscopic data for **IIa** are recorded in Table 1 and its structure is presented in Fig. 1, and selected bond angles and lengths in Table 2.

* Corresponding author

0277-5387/00/$ - see front matter ©2000 Elsevier Science Ltd All rights reserved.
PII S0277-5387(99)00358-7

Table 1
NMR [a], UV–Vis, and analytical properties of the new compounds

2,5-bis(hydrodimethylsilyl)thiophene	
^{1}H	0.26 (d, $SiMe_2$); 4.76 (sept. SiH); 7.30 (thiophene)
^{13}C	−2.64 ($SiMe_2$); 136.7 (thiophenyl $C_{3,4}$); 142.8 (thiophenyl $C_{2,5}$)
^{29}Si	−23.3
IR (CCl_4, cm^{-1})	2128.7
2,5-bis(hydrodiphenylsilyl)thiophene	
^{1}H	5.66 (SiH J_{SiH} = 206 Hz); 7.40–7.68 (phenyl, thiophene)
^{13}C	128.1, 130.1, 132.9 (*ipso*), 135.5 (phenyl); 138.9 (thiophene $C_{3,4}$); 140.0 (thiophene $C_{2,5}$)
IR (hexane, cm^{-1})	2136
2,5-bis(chlorodimethylsilyl)thiophene (**Ia**)	
^{1}H	0.76 ($SiMe_2$); 7.52 (thiophene)
^{13}C	3.36 ($SiMe_2$); 136.7 (thiophenyl $C_{3,4}$); 143.3 (thiophenyl $C_{2,5}$)
^{29}Si	15.2
2,5-bis(chlorodiphenylsilyl)thiophene (**Ib**)	
^{1}H	7.42–7.72 (phenyl, thiophene)
^{13}C	128.2, 131.1, 132.4 (*ipso*), 134.9 (phenyl); 139.4 (thiophene $C_{3,4}$); 141.5 (thiophene $C_{2,5}$)
[(ferrocenylenedimethylsilyl)thiophenylene]$_2$ (**IIa**)	
Analysis	Calc.: C, 56.5; H, 5.80. Found: C, 55.9; H, 5.88
^{1}H	0.27 ($SiMe_2$); 3.93, 4.08 (ferrocenylene); 6.91 (thiophene)
^{13}C	0.43 ($SiMe_2$); 70.3, 72.2, 74.2 (ferrocenylene); 136.1 (thiophene $C_{3,4}$); 144.4 (thiophene $C_{2,5}$)
^{29}Si	−9.7
UV–Vis (THF) (nm)	279, 449
[(ferrocenylenedimethylsilyl)thiophenylene]$_n$ (**II*n***)	
^{1}H	0.27, 0.40, 0.54 ($SiMe_2$); 4.08, 4.17 (ferrocenylene); 7.34 (thiophene)
^{13}C	−0.1, 2.1 ($SiMe_2$); 68.7, 70.2, 72.1, 73.8 (ferrocenylene); 135.8 (thiophene $C_{3,4}$); 145.2 (thiophene $C_{2,5}$)
^{29}Si	−4.85, −9.7, −10.4, −10.6, −15.2
UV–Vis (THF) (nm)	279, 449
2,5-bis(ferrocenyldimethylsilyl)thiophene (**III**)	
Analysis	Calc.: C, 59.2; H, 5.67. Found: C, 58.4; H, 5.85
^{1}H	0.57 ($SiMe_2$); 4.01 (C_5H_5), 4.13, 4.19 (C_5H_4), 7.43 (thiophene)
^{13}C	−0.1 ($SiMe_2$); 68.7 (C_5H_5), 69.7 (*ipso*), 71.5, 73.6 (ferrocenyl); 136.0 (thiophene $C_{3,4}$); 145.3 (thiophene $C_{2,5}$)
^{29}Si	−10.6
UV–Vis (THF) (nm)	271, 448
2,5-bis(ferrocenyldiphenylsilyl)thiophene (**IV**)	
Analysis	Calc.: C, 70.6; H, 4.93. Found: C, 69.9; H, 5.50
^{1}H	3.95 (C_5H_5); 4.22, 4.41 (C_5H_4); 7.30–7.60 (phenyl, thiophene)
^{13}C	65.8, 68.8, 71.4, 74.9 (ferrocenyl); 127.7, 129.6, 135.6 (phenyl), 138.7 (thiophene $C_{3,4}$); 141.9 (thiophene $C_{2,5}$)
^{29}Si	−16.9

[a] Spectra were recorded in C_6D_6 with the exception of **IV** which was recorded in $CDCl_3$.

The structure of **IIa** possesses normal bond lengths and angles and the cycle shows no structural sign of ring strain. The two ferrocene groups are completely eclipsed, as noted in Fig. 1(b), and the two thiophene groups are positioned in opposition to each other.

At the present time we have been unable to characterize completely the remainder of the product obtained from the reaction described in Eq. (1). Fast atom bombardment MS indicated the presence of trimeric (m/e = 1147) and tetrameric (m/e = 1529) analogs of **IIa** and the NMR data recorded in Table 1 are consistent with this observation. However, other materials are also present, witness for example the ^{29}Si NMR signals at −15.2 and −4.85 ppm. We continue to study this system.

The reaction outlined in Eq. (2) was satisfactory for the formation of monomeric 2,5-bis(ferrocenyldimethylsilyl)-thiophene, **III**, and the diphenylsilyl analog **IV**, in good yield. The spectroscopic data for **III** and **IV** are in accord with their proposed structures and are recorded in Table 1. The single crystal structure of **III** is recorded in Fig. 2, and representative bond lengths and angles are presented in Table 2. This complex was synthesized to provide baseline data to facilitate the analysis of polymeric and oligomeric analogs.

The related bond lengths and angles of **IIa** can be compared to those of **III** and it is immediately clear that there are no truly significant differences between the two sets. The single exception to this generality are the possibly shorter silicon–thiophene–carbon bond lengths in **IIa** (Si1–C1 = 1.861(3) and Si2–C4a = 1.864(2) Å) compared with those in **III** (Si1–C1 = 1.874(3) and Si2–C1 = 1.872(5) Å). In both structures there are essentially no dihedral angles between the two cyclopentadienyl rings in the ferrocene units, and the thiophene rings are planar with normal bond lengths and angles. The key distinction between the two structures are the

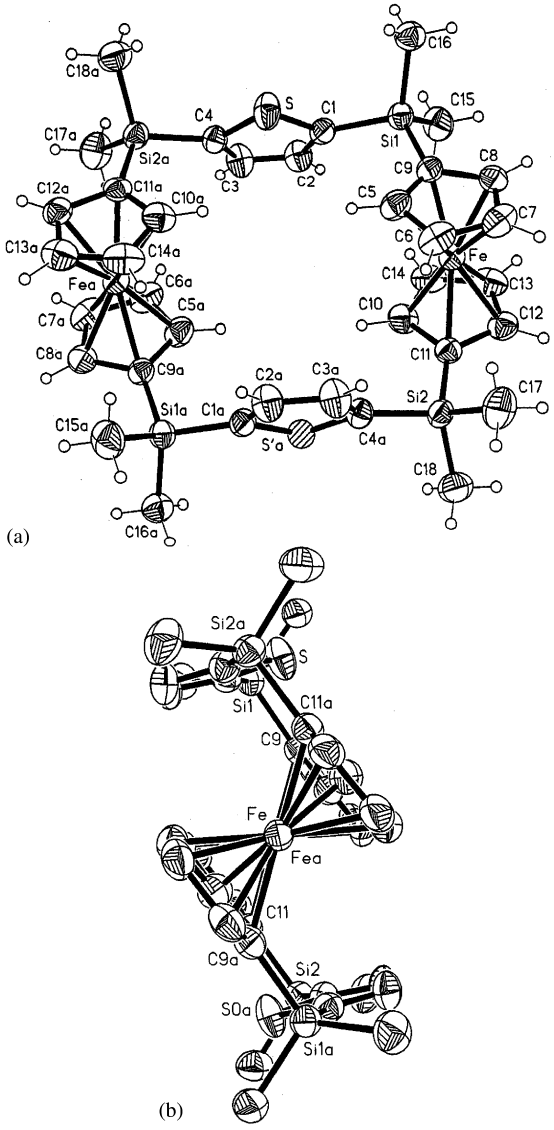


Fig. 1. Crystal structure of **IIa**: (a) regular view, (b) view to show eclipsed ferrocenylene units.

Table 2
Selected bond lengths (Å) and angles (°) for **IIa** and **III**

IIa		**III**	
C9–Si1	1.857(3)	C5–Si1	1.843(5)
C11–Si2	1.856(3)	C15–Si2	1.856(4)
Si1–C1	1.861(3)	Si1–C4	1.874(5)
Si2–C4a	1.864(2)	Si2–C1	1.872(5)
C9–Si1–C1	109.3(1)	C4–Si1–C5	107.7(2)
C11–Si2–C4a	109.1(1)	C1–Si2–C15	111.4(2)
C16–Si1–C15	109.5(1)	C25–Si1–C26	112.0(2)
C18–Si2–C17	111.5(1)	C27–Si2–C28	110.3(2)

two intramolecular Fe···Fe distances. For **IIa** this distance is 7.57 Å, whereas for **III** it is significantly longer at 11.28 Å, and this will impact many properties, vide infra.

One of the diagnostic features of polyferrocenyl and ferrocenylene complexes and materials is their capacity to exhibit more than a single redox process even though the iron containing groups are nominally identical. We have previously noted that in the α, ω diferrocenyl oligosilanes, $Fc(SiMe_2)_nFc$, when the bridging chain is equal or greater than 4, the two ferrocenyl groups do not interact and only a single redox process is observed via cyclic voltammetry [11]. Shorter chains result in two distinct processes: an initial step involving oxidation of alternate Fc groups, and a second step where the presence of a neighboring ferrocenium ion raises the oxidation potential of the remaining ferrocenylene groups. The transmission of the electronic effects from a ferrocenium ion to a neighboring unoxidized Fe center can be a through bond inductive effect, or through space. Silicon atom bridges and acetylenic bridges effectively facilitate such through bond interactions [11,18]. The degree to which the ferrocene groups in **IIa** and **III** can interact in this manner was investigated by cyclic voltammetry. Complex **IIa** exhibited two discrete redox processes when the experiment was performed in CH_2Cl_2; $E_{ox} = 0.51$ V and $E_{ox} = 0.56$ V, $E_{red} = 0.48$ V and $E_{red} = 0.41$ V (relative to Ag/Ag^+). In acetonitrile, a superior coordinating solvent in which the positive charge is better delocalized, only a single process was observed, $E_{ox} = 0.56$ V, $E_{red} = 0.48$ V. By contrast, regardless of the solvent, only a single process was observable when complex **III** was examined, $E_{ox} = 0.56$ V, $E_{red} = 0.46$ V. These results clearly show that the capacity for interaction between the ferrocenium ion and the unoxidized ferrocenylene group can occur through space as well as via an atomic backbone. It is not surprising that in **III**, where the two Fe atoms are separated by >11 Å, the two redox processes are equivalent.

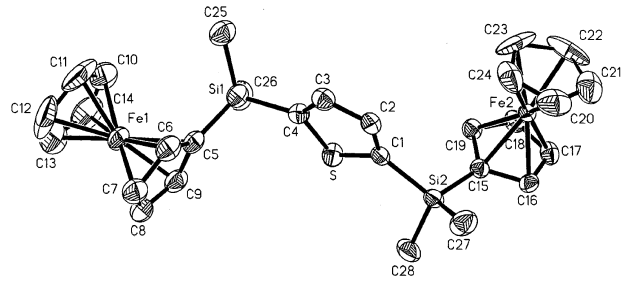


Fig. 2. Crystal structure of **III**.

3. Experimental

All reactions were performed with dry oxygen free solvents in N_2 or Ar atmospheres. Analyses were perfromed by Galbraith Laboratories Inc.; NMR were recorded on a Bruker 250 MHz instrument. LRMS was obtained from the Nebraska Center for Mass Spectrometry. Electrochemical analysis was performed as previously reported, with tetraethylammonium tetrafluoroborate as supporting electrolyte [11].

3.1. Synthesis of 2,5-bis(hydridodimethylsilyl)thiophene [2]

In a 250 ml flask, equipped with a reflux condenser, rubber septum and dropping funnel was added 13.3 g (55 mmol) of

2,5-dibromothiophene in 20 ml of THF to 2.90 g (119 mol) of Mg and 0.4 g I_2 in 100 ml of dry THF. The formation of the Grignard was initiated by mild external heating with a hair dryer and then an exothermic reaction occurred. After complete addition, 3 h, the flask was cooled on an ice bath and 10.4 g (110 mmol) of Me_2SiHCl in 20 ml of THF was added over 20 min. The reaction mixture was stirred overnight and then the solvent removed in vacuo. The crude product was extracted into hexane and filtered. Distillation of the liquid residue after removal of the hexane yielded 6.1 g (30 mmol, 55%) of the title compound, b.p. 90ºC/8 mm Hg.

3.2. Chlorination of 2,5-bis(hydridodimethylsilyl)thiophene [2]

In a 100 ml side-arm flask, 3 g (15 mmol) of 2,5-bis(hydridodimethylsilyl)thiophene was added slowly to a catalytic amount of $PdCl_2$ (0.2 g) in 40 ml of carbon tetrachloride. The reaction was monitored by IR spectroscopy and after 30 min the Si–H stretching frequency at $\sim$2128 cm^{-1} had disappeared. The solvent was removed in vacuo and the liquid product was distilled to yield 2,5-bis(chlorodimethylsilyl)thiophene, (b.p. 125–130ºC/14 mm Hg, 2.12 g, 7.8 mmol, 52%).

3.3. Reaction of 2,5-bis(chlorodimethylsilyl)thiophene with dilithioferrocene

To a 40 ml hexane slurry of 1,1′-dilithioferrocene·tmeda (prepared from ferrocene (3.0 g, 16 mmol), *n*-butyllithium (24.4 ml of a 1.6 M solution) and 5.8 ml of freshly distilled TMEDA in 150 ml of hexane) [19] was added dropwise 2.7 g (10 mmol) of bis-2,5(chlorodimethylsilyl)thiophene at −78°C. The mixture was stirred for 1 h at this temperature and then permitted to warm to room temperature and stirred overnight. After filtration the solvent was removed in vacuo to produce a brown oily material which was dissolved in the minimum of hexane and placed upon a 2×25 cm silica gel column (60–200 mesh). Development with hexane produced two distinct bands. The initial yellow band was collected and after removal of solvents produced 50 mg (0.07 mmol, 14%) of **IIa** as a red powder which was further purified by recrystallization from hexane, m.p. 230–234°C. A second band eluted with hexane yielded an orange–red oil, **II*n***.

*3.4. Synthesis of 2,5-bis(ferrocenyldimethylsilyl)thiophene (**III**)*

A solution of ferrocenyllithium (prepared from the reaction of 9.28 ml of 1.6 M *n*-butyllithium with 1.0 g (2.4 mmol)

Table 3
Crystal and refinement data

	IIa	**III**
Empirical formula	$C_{18}H_{22}Si_2SFe$	$C_{28}H_{32}\cdot Si_2SFe$
Color, habit	orange prism	orange–yellow fragment
Crystal size (mm)	0.32×0.44×0.80	0.60×0.60×0.40
Crystal system	monoclinic	monoclinic
Space group	$P2_1/c$	$P2_1/c$
Unit cell dimensions		
a (Å)	11.734(2)	21.429(5)
b (Å)	11.999(2)	8.775(2)
c (Å)	13.444(2)	14.824(4)
α (°)	90.00	90.00
β (°)	99.14(1)	106.95(2)
γ (°)	90.00	90.00
Volume (Å^3)	1868.8(5)	2666.4(11)
Z	4	4
2θ range (°)	3.5–45	4.0–45
Scan type	ω	ω
Scan speed (° min^{-1})	3–20	3–15
Scan range w (°)	1.40	1.20
Standard reflections	3 measured every 97 reflections	3 measured every 97 reflections
Index ranges		
h	0 to 12	−23 to 22
k	−2 to 12	−9 to 2
l	−14 to 14	−3 to 15
Reflections collected	3189	3794
Independent reflections	2462	3476
Observed reflections	2286 ($F>3.0\sigma(F)$)	3195 ($F>3.0\sigma(F)$)
Absorption correction	Semi-empirical	N/A
Min./max. transmission	0.221/0.254	N/A
Final R indices (observed data)	$R=3.07\%$, $wR=5.07\%$	$R=4.75\%$, $wR=7.32\%$

of FcHgCl) was added dropwise to 1.0 g (3.7 mmol) of 2,5-bis(chlorodimethylsilyl)thiophene in 30 ml of THF at −78°C. The mixture was stirred overnight and then the solvent was removed in vacuo. The product was extracted with hexane, and the solution filtered. After removal of the solvent di-*n*-butylmercury was distilled to leave a gummy residue. This was dissolved in the minimum of hexane and placed upon a 10×2 cm silica gel column (60–200 mesh) and eluted with hexane. An orange band developed and was collected, the solvent removed and the final residue recrystallized from hexane to yield **III**, 1.2 g (2.1 mmol, 57%), m.p. 77°C.

Also prepared by the same general route, in 65% yield, was 2,5-bis(ferrocenyldiphenylsilyl)thiophene (**IV**) from the reaction of ferrocenyllithium and 2,5-bis(chlorodiphenylsilyl)thiophene.

3.5. Structural analysis of *IIa* and *III*

An orange crystal of approximate dimensions 0.32×0.44×0.80 mm (**IIa**) and an orange–yellow crystal approximately 0.60×0.60×0.40 mm in size (**III**) were mounted on glass fibers in a random orientation. Intensity data were collected at room temperature for **IIa** and −100°C for **III**, which decayed under the X-ray beam at room temperature, using a Siemens/Bruker four circle diffractometer with graphite-monochromated Mo Kα radiation, $\lambda = 0.71073$ Å. Unit cell parameters and standard deviations were obtained by least-squares fit of 25 reflections randomly distributed in reciprocal space in the 2θ range of 15–30°. The ω-scan technique was used for intensity measurements in both cases. A range of 1.4° in ω and variable speed of 3.00 to 20.00 ° min^{-1} was used for **IIa** and a 1.2° ω-range and a 3.00 to 15.00° min^{-1} speed for **III**. Background counts were taken with stationary crystal and total background time to scan time ratio of 0.5. Three standard reflections were monitored in both cases every 97 reflections and showed no significant decay for **IIa** and an average intensity decay of 8.2% for **III** even at −100°C. The data were corrected for Lorentz and polarization effects but only **IIa** was corrected semi-empirically for absorption giving a min./max. transmission ratio of 0.221/0.254.

Both structures were solved by direct methods and refined using the PC-version of the SHELXTL PLUS crystallographic software by Siemens. Full-matrix least-squares refinement minimizing $\sum w(F_o - F_c)^2$ was carried out with anisotropic thermal parameters for non-hydrogen atoms. The hydrogen atoms were placed at calculated positions (C–H 0.96 Å; $U_H = 0.08$) during refinements. The weighing scheme has the form $w^{-1} = \sigma^2(F) + gF^2$ and the final R factors the form $R = \sum |F_o - F_c| / \sum F_o$ and $R_w = [w|F_o - F_c|^2 / \sum wF_o^2]^{1/2}$. Relevant crystal and refinement data are provided in Table 3 and selected bond lengths and angles are provided in Table 2. The structures of **IIa** and **III** are illustrated in Figs. 1 and 2, respectively.

4. Supplementary data

Crystallographic data for structures **IIa** and **III** are available from the Cambridge Crystallographic Data Centre, 12 Union Road, Cambridge CB2 1EZ, UK (fax: +44-1223-336033; e-mail: deposit@ccdc.cam.ac.uk or www: http://www.ccdc.cam.ac.uk), quoting the deposition numbers CCDC 140477 (**IIa**) and CCDC 140478 (**III**).

Acknowledgements

This research has been supported by the R.A. Welch Foundation, Houston, TX (grant no. AH-546) and the NSF.

References

[1] J. Roncali, Chem. Rev. 92 (1992) 711.
[2] J. Oshita, D. Kanaya, M. Ishikawa, T. Koike, T. Yamanaka, Macromolecules 24 (1991) 2106.
[3] P. Chicart, R.J.P. Corriu, J.J.E. Moreau, F. Garnier, A. Yassar, Chem. Mater. 3 (1991) 8.
[4] P. Chicart, R.J.P. Corriu, J.J.E. Moreau, F. Garnier, A. Yassar, in: R.M. Laine (Ed.), Inorganic and Organometallic Polymers with Special Properties, Kluwer, 1992, p. 179.
[5] S.K. Riter, R.E. Noftle, Chem. Mater. 4 (1992) 872.
[6] D.A. Foucher, B.-Z. Tang, I. Manners, J. Am. Chem. Soc. 114 (1992) 6246.
[7] D.A. Foucher, R. Ziembinski, B.-Z. Tang, P.M. Macdonald, J. Massey, C.R. Jaeger, G.J. Vancso, I. Manners, Macromolecules 26 (1993) 2878.
[8] I. Manners, Adv. Organomet. Chem. 37 (1995) 131.
[9] M.T. Nguyen, A.F. Diaz, V.V. Dementiev, H.K. Sharma, K.H. Pannell, SPIE Proc. 1910 (1993) 230.
[10] M.T. Nguyen, A.F. Diaz, V.V. Dementiev, K.H. Pannell, Chem. Mater. 5 (1993) 1389.
[11] V.V. Dementiev, F. Cervantes-Lee, L. Párkányi, H.K. Sharma, K.H. Pannell, M.-T. Nguyen, A.F. Diaz, Organometallics 12 (1993) 1983.
[12] M.T. Nguyen, A.F. Diaz, V.V. Dementiev, K.H. Pannell, Chem. Mater. 6 (1994) 952.
[13] K.H. Pannell, V.V. Dementiev, H. Li, F. Cervantes-Lee, M.T. Nguyen, A.F. Diaz, Organometallics 13 (1994) 3644.
[14] M. Tanaka, T. Hayashi, Bull. Chem. Soc. Jpn. 66 (1993) 334.
[15] N.P. Reddy, H. Yamashita, M.J. Tanaka, Chem. Soc., Chem. Commun. (1995) 2263.
[16] M. Hmyene, A. Yasser, M. Escorne, A. Percheron-Guegan, F. Garnier, Adv. Mater. 6 (1994) 564.
[17] K. Mochida, N. Shibayama, M. Goto, Chem. Lett. (1998) 339.
[18] C. Le Vanda, K. Berchgaard, D.O. Cowan, J. Org. Chem. 41 (1976) 2700.
[19] J.J. Bishop, A. Davison, M.L. Katcher, D.W. Lichtenberg, R.E. Merrill, J.C. Smart, J. Organomet. Chem. 27 (1971) 241.

PERGAMON

www.elsevier.nl/locate/poly

Polyhedron 19 (2000) 297–305

POLYHEDRON

Time-resolved, in situ X-ray diffraction studies of intercalation in lamellar hosts

Dermot O'Hare *, John S.O. Evans [1], Andrew Fogg, Stephen O'Brien

Inorganic Chemistry Laboratory, South Parks Road, Oxford OX1 3QR, UK

Received 25 April 1999; accepted 29 August 1999

Abstract

Energy dispersive X-ray diffraction (EDXRD) has been used to perform in situ kinetic studies on the intercalation of a range of guest molecules in layered lattices. The kinetics of the intercalation of cations (K^+, PyH^+ ($Py = C_5H_5N$), NMe_4^+) and the long chain ammonium ions $C_{12}TMA$, $C_{16}TMA$, $C_{18}TMA$ ($C_{12}TMA$ = dodecyltrimethylammonium, $C_{16}TMA$ = hexadecyltrimethylammonium and $C_{18}TMA$ = octadecyltrimethylammonium) into crystals of $MnPS_3$ have been determined. These reactions are very fast, and in some cases novel transient phases are observed. The rate of cobaltocene, $Co(\eta\text{-}C_5H_5)_2$, intercalation in layered metal dichalcogenides ZrS_2, 2H-SnS_2, 2H-$SnSe_2$, 2H-TaS_2, 2H-NbS_2, 1T-TaS_2 and TiS_2 has also been investigated. Integrated intensities of the Bragg reflections have been used to determine the extent of reaction (α) versus time for each of these reactions. A number of kinetic models have been considered, including the Avrami–Erofeyev ($m = 1.5$) deceleratory nuclei-growth model and statistical simulation. The concentration and solvent dependence of the rate of $Co(\eta\text{-}C_5H_5)_2$ intercalation into 2H-SnS_2 has also been determined. Surprisingly, we find that the rate of intercalation is invariant to the initial $Co(\eta\text{-}C_5H_5)_2$ concentration over a wide concentration range. The rate of intercalation of the lithium salts (LiX; X = Cl, Br, NO_3 and OH) into Gibbsite (γ-$Al(OH)_3$) giving the layered double hydroxides $[LiAl_2(OH)_6]X \cdot nH_2O$ (X = Cl, Br, NO_3 and OH) and $[LiAl_2(OH)_6]_2SO_4 \cdot nH_2O$ has been studied. The temperature dependence of the rate of intercalation of LiCl yields an activation energy of 27 kJ mol^{-1}. The reaction was also found to be half order with respect to the initial concentration of LiCl. Time-resolved in situ energy dispersive X-ray powder diffraction (EDXRD) spectra have been recorded following the addition of an aqueous solution of hexadecyltrimethylammonium chloride ($C_{16}H_{33}N^+Me_3Cl^- = C_{16}TMACl$) to kanemite ($NaHSi_2O_5 \cdot 3H_2O$). The diffraction data suggest that initially a layered phase forms due to intercalation of the alkylammonium ions which then transforms into a silicate-organic mesophase which is the precursor to the hexagonal mesoporous silicate, FSM-16. ©2000 Elsevier Science Ltd All rights reserved.

Keywords: In situ X-ray diffraction; Intercalation; Layered compounds; Solid state; Synchrotron radiation

1. Introduction

Some of the earliest and most extensive studies of the kinetics of intercalation reactions were carried out using graphite crystals. For example, classic experiments performed by Hooley and co-workers investigated the gain in weight of a graphite flake under a bromine atmosphere [1,2]. Until recently, only two time-resolved diffraction studies on metal chalcogenide intercalation have been reported [3–7]. The study by Riekel and Schollhorn measured time-resolved neutron diffraction data during the intercalation of 2H-TaS_2 with $NH_3(g)$. However, the available levels of beam flux, whilst high by neutron standards, necessitated either very large sample sizes ($\sim$15 g) or long acquisition times, making a thorough, quantitative study under varying reaction conditions of temperature, concentration and particle size unfeasible. Moreover, because of the large incoherent scattering from hydrogen atoms by neutrons, the samples studied had to be highly deuterated, an expensive and not always achievable prerequisite for other intercalation reactions. Even taking all these previous experiments into consideration, we still have a fairly rudimentary understanding of the intimate mechanism of intercalation reactions. Knowledge of the critical factors which control the rates of these reactions is based on a limited range of experiments. We still commonly use the schematic illustration shown in Fig. 1 to describe these reactions, which undoubtedly greatly oversimplifies the true picture.

In recent years, the technological and experimental advances in energy dispersive powder diffraction (EDXRD) using synchrotron X-ray sources have provided new possi-

* Corresponding author; e-mail: dermot.ohare@chem.ox.ac.uk

[1] Present address: Department of Chemistry, Durham University, Durham DH1 3LE, UK.

0277-5387/00/$ - see front matter ©2000 Elsevier Science Ltd All rights reserved.
PII S0277-5387(99)00359-9

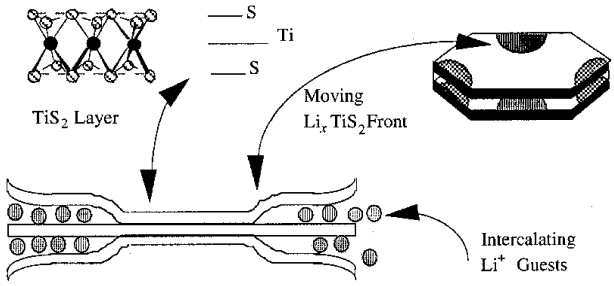


Fig. 1. Schematic representation of the intercalation of a guest into a layered dichalcogenide host lattice.

bilities for the solid state kineticist [8–11]. The markedly higher intensity (several orders of magnitude) over conventional laboratory X-ray sources means that good quality spectra can now be obtained from milligram samples on a time-scale of seconds, making kinetic studies on fast intercalation reactions a realisable goal. We have recently constructed and commissioned a number of environmental cells for measuring time-resolved energy dispersive X-ray diffraction data of intercalation reactions [12–14].

In this paper we will review some of the significant observations we have made to date concerning our investigations into the kinetics of intercalation reactions using in situ, time-resolved X-ray diffraction.

2. Kinetics of intercalation reactions

2.1. Intercalation of cations in metal hexathiohypodiphosphates

The transition metal hexathiohypodiphosphates, MPS_3 (M = Mn, Fe, Ni, Cd), have been shown to intercalate a wide range of guest ions and molecules. In recent years they have been shown by Clement and co-workers to exhibit a unique type of intercalation reaction. MPS_3 (M = Mn, Cd, Fe) reacts spontaneously with aqueous solutions of ionic salts, G^+X^- (where G^+ can range from simple ionic species such as K^+ and NH_4^+ to species as large as, for example, cobaltocenium cations), to give compounds of general formula $Mn_{1-x}PS_3\{G\}_{2x}(H_2O)_y$ [15–17]. In these compounds, charge balance has been maintained by the loss of one Mn^{2+} ion from the intralayer region for every two G^+ ions that are intercalated in the interlayer region.

We have studied the kinetics of K^+, PyH^+ (Py = C_5H_5N), NMe_4^+ and the long chain ammonium ions $C_{12}TMA$, $C_{16}TMA$, $C_{18}TMA$ ($C_{12}TMA$ = dodecyltrimethylammonium, $C_{16}TMA$ = hexadecyltrimethylammonium and $C_{18}TMA$ = octadecyltrimethylammonium) intercalation into sub 90 μm crystals of $MnPS_3$ in water between room temperature and 120°C using time-resolved in situ EDXRD [18]. In a typical experiment, solutions of the appropriate reagents were preheated to the reaction temperature, remotely injected into a 5 ml flask containing the stirred host lattice, and the X-ray diffraction pattern of the resulting suspension monitored as a function of time. Under these conditions the diffraction pattern could be recorded over a 20–4 Å *d*-spacing range in as little as 10 s, allowing the direct observation of the disappearance of the host lattice and growth of the product phase.

Kinetic information was extracted from each experiment by integration of the 001 Bragg reflection using a Gaussian peak fitting routine [19]. The time dependence for pyH^+ intercalation in $MnPS_3$ is shown in Fig. 2. The errors on the integrated areas are small and contained within the data points. The integrated intensities were subsequently converted to the extent of the reaction, α, using the relationship (Eq. (1)):

$$\alpha_{hkl}(t)=\left(\frac{I_{hkl}(t)}{I_{hkl}(t_\infty)}\right) \quad (1)$$

The kinetics of intercalation were analysed following the method of Hulbert, who showed that the general rate expression for nucleation growth reactions developed by Avrami takes the form of Eq. (2) [20–24]. A summary of the least squares fits of such an expression to the experimental data and the rate parameters of the fits are given in Table 1.

$$\ln\frac{1}{1-\alpha}=(kt)^m \quad (2)$$

where α represents the extent of reaction at time *t*.

A number of important conclusions can be drawn from this study. Firstly these intercalation reactions occur extremely rapidly, with half-lives of the order of a minute or less. These exchange intercalation reactions appear to be some of the fastest known molecular intercalation reactions. Secondly the reactions occurred cleanly via a two-phase reactant to product route, and no phenomena such as staging were observed. These systems obey rate expressions similar to those found for the intercalation reactions of other host lattices, and the rate of formation of the product phase and disappearance of the host lattice obey identical rate laws.

The intercalation of dodecyltrimethylammonium bromide ($C_{12}TMABr$) into $MnPS_3$ at 120°C has also been studied using in situ energy dispersive X-ray powder diffraction. The reaction proceeds smoothly and affords a stable crystalline

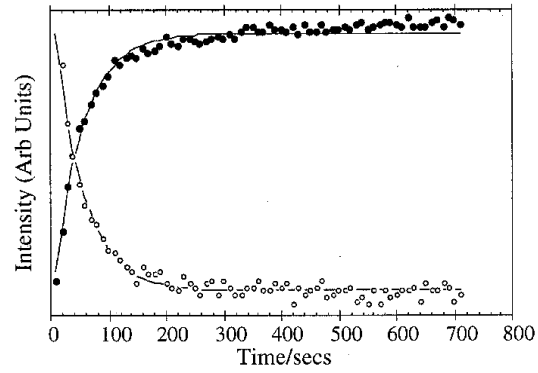


Fig. 2. The time dependence of the intensities of the host (001) (○) and intercalate (001) (●) reflections for the intercalation of pyH^+ by $MnPS_3$ under aqueous conditions at T = 33°C.

Table 1
Kinetic rate parameters for the intercalation of various guest species into some lamellar hosts: experimental rates have been fitted to a rate expression $\alpha = [1 - \exp(-kt)^m]$

Host	Guest	Temperature (°C)	m	k (10^{-3} s^{-1})	$t_{1/2}$ (s)
$MnPS_3$	K^+	33	1.0	12.0	55
$MnPS_3$	pyH^+	33	1.0	20	43
$MnPS_3$	NMe_4^+	51	1.0	88	59
$MnPS_3$	NMe_4^+	60	1.0	20	35
$MnPS_3$	$C_{12}TMA$ [a]	120	1.5	6.3	435

[a] $C_{12}TMA$ = dodecyltrimethylammonium.

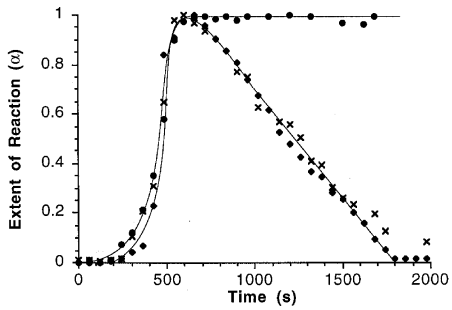


Fig. 3. Plot of extent of reaction (α) vs. time for the following reactions: (●) $C_{12}TMABr$ with $MnPS_3$ in water at 120°C; (×) $C_{16}TMABr$ with $MnPS_3$ in water at 120°C; (♦) $C_{18}TMABr$ with $MnPS_3$ in water at 70°C. $\alpha = I_{hkl}(t)/I_{hkl}(t = I_{max})$ for the (002) Bragg reflection in each case.

compound. The X-ray diffraction pattern of the product can be indexed on a hexagonal unit cell with a *c*-lattice parameter of 11.26 Å. Integration of the (001) Bragg reflection with respect to time is shown in Fig. 3. The half-life for the reaction at 120°C is ca. 400 s with the reaction essentially complete in 700 s. The increase in the interlamellar spacing of 4.77 Å is consistent with the packing of the dodecyltrimethylammonium ions parallel to the planes of the host lattice (Fig. 4). Elemental analysis is consistent with a formulation of this intercalate as $Mn_{0.92}PS_3(C_{12}TMA)_{0.16}$.

However, dramatically different behaviour was observed when we monitored the intercalation of the larger hexadecyl- and octadecyltrimethylammonium bromides ($C_{16}TMABr$ and $C_{18}TMABr$) in $MnPS_3$. For both reactions, we observed the growth of a series of Bragg reflections which can be indexed to a unit cell with *c*-lattice parameters of 33.8 and 36.2 Å for the hexadecyl- and octadecyltrimethylammonium reactions, respectively. These large *c*-lattice parameters correspond to interlayer expansions of ca. 27.3 and 29.7 Å for the hexadecyl- and octadecyltrimethylammonium intercalates, respectively. A plot of the time dependence of the integrated intensities of the Bragg reflections due to these intercalate phases shows that the initial rates of intercalation of all three ammonium cations are essentially equal, suggesting that the rate-determining step in each of these reactions is the separation of the $MnPS_3$ layers. However, for reactions involving the intercalation of $C_{16}TMA^+$ and $C_{18}TMA^+$, the peak intensities of the intercalate phases start

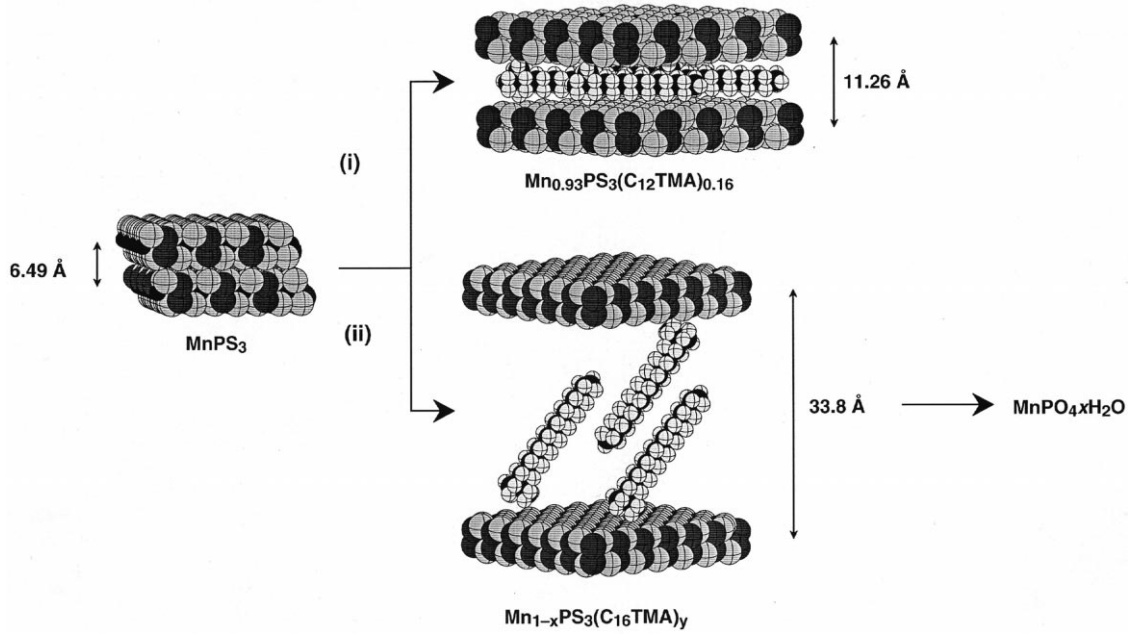


Fig. 4. Synthesis of long chain ammonium intercalates of $MnPS_3$: (i) $MnPS_3$ (150 mg) + $C_{12}TMABr$ (1 mmol) in 5 cm^3 water at 120°C, (ii) $MnPS_3$ (150 mg) + $C_{16}TMABr$ (1 mmol) in 5 cm^3 water at 120°C.

to decrease gradually after ca. 600 s and after approximately 30 min no reflections are observed in the energy window of the detector (Fig. 5). The resulting grey powder which can be collected from the reaction mixtures is identical from both reactions and is poorly crystalline. Both elemental microanalysis and X-ray microprobe analysis suggest that it has composition $MnPO_4 \cdot xH_2O$ although the unit cell dimensions do not match any of the known manganese phosphates or hydrogen phosphates.

Intercalation of the intermediate length tetradecyltrimethylammonium bromide (C_{14}TMABr) in $MnPS_3$ gives rise to a complex reaction. Different behaviour has been observed when the reaction was monitored in situ on three different occasions. The first attempt showed the transient formation of a new phase which could be indexed with a *c*-lattice parameter of 31.6 Å; on a second occasion a different phase was observed with a *c*-lattice parameter of 11.5 Å, which co-formed with a small amount of the previous phase. On another occasion only the phase with a 11.5 Å lattice parameter could be detected. A plot of the unit cell dimension versus the number of carbon atoms for the guest molecule, C_nTMA^+ ($n = 14$, 16, and 18), is linear. The gradient of this plot is 1.15 Å per C. Assuming the guest molecules form a monolayer between the $MnPS_3$ layers, then this suggests that the guest ions are oriented at ca. 65° to the host layers. In addition, it seems reasonable to postulate that the C_{14}TMA cation is just at the critical length where the energy difference between the guests lying parallel to the host layers or at an angle of 65° to the layer plane is very small.

2.2. Kinetics of intercalation of cobaltocene into lamellar metal chalcogenide hosts

Redox-active organometallic compounds can be intercalated into the metal dichalcogenides either by direct reaction, ion-exchange, or by electrochemical routes [25]. This significant reaction was first reported in 1975 when Dines described the intercalation of the metallocenes cobaltocene ($Co(Cp)_2$; $Cp = \eta$-C_5H_5) and chromocene ($Cr(Cp)_2$) into a range of metal disulfides (MS_2: M = Ti, Zr, Nb, Ta and Sn) [26,27]. Since then these materials have been extensively studied due to their fascinating structural and electronic properties. In general, the ability of an organometallic molecule to intercalate in a layered lattice has been based on empirical rules. Therefore we were excited at the possibility of being able to determine quantitatively the kinetics of these reactions and also of being able to investigate whether intermediate novel phases are formed during the course of the reaction.

We have investigated the kinetics of intercalation of $Co(Cp)_2$ into a range of layered metal dichalcogenides using in situ time-resolved EDXRD [19,28]. We were particularly interested to determine whether the variation in the rates of these intercalation reactions could be correlated with the chemical properties of the hosts. Fig. 6 summarises the extent of reaction $\alpha(t)$ versus time (t) for the intercalation of $Co(Cp)_2$ into ZrS_2, SnS_2, $SnSe_2$ and 2H-TaS_2. In each case

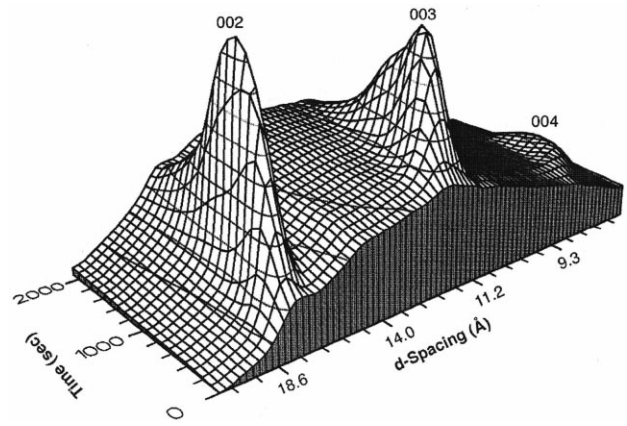


Fig. 5. Time-resolved energy dispersive X-ray diffraction of the reaction of C_{16}TMABr with $MnPS_3$ in H_2O at 120°C.

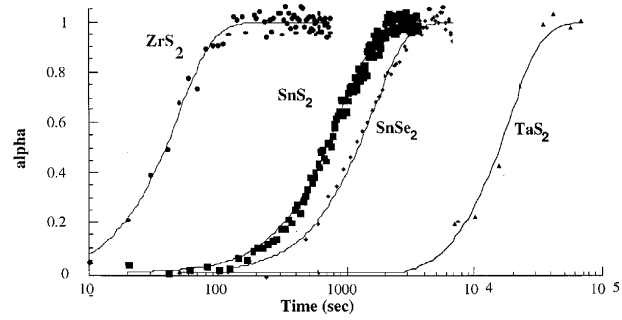


Fig. 6. Extent of reaction (α) vs. time for intercalation of $Co(Cp)_2$ into a range of metal dichalcogenides: ● ZrS_2, 8°C; ■ SnS_2, 20°C; ◆ $SnSe_2$, 50°C; ▲ $TaSe_2$, 120°C. The lines are fits to the Avrami deceleratory nuclei-growth model, $\alpha = 1 - \exp(-k(t - t_0))^{1.5}$.

the reaction yields first stage intercalation compounds of chemical composition $MX_2\{Co(Cp)_2\}_{0.30 \pm 0.05}$. In all cases we observed the smooth growth of intensity of the reflections due to the intercalate phases with increased *c*-lattice constants of 5.35 ± 0.02 Å. No intermediate phases of higher order staging are observed in any of these reactions. What is immediately striking about the data shown in Fig. 6 is the extreme variation in the rate of the reaction for each of the host lattices. For all the reactions, we tried to keep identical conditions; each host was sieved to a particle size distribution between 90–250 mm and the same amount of $CoCp_2$ solution was injected into each sample. Unfortunately, we had to vary the temperature of the reactions in order to collect data on a reasonable timescale. A summary of the rate constants (k_{obs} (s^{-1})) and half-life ($t_{1/2}$) for these reaction is shown in Table 2.

For SnS_2, ZrS_2 and $SnSe_2$ we have also investigated the rate of intercalation as a function of the initial $Co(Cp)_2$ concentration. In each case, varying concentrations of cobaltocene solution (enough volume to provide a 2:1 molar excess with respect to the host) were injected onto 200 mg of the host lattice at a convenient temperature for kinetic analysis. Fig. 7 shows each of the $\alpha(t)$ curves for the intercalation of cobaltocene into SnS_2 at 20°C for a range of initial $Co(Cp)_2$ concentrations.

Table 2
The half-lives and Avrami rate constants for the intercalation of $Co(Cp)_2$ into a range of lamellar metal dichalcogenides at 20 and 120°C (particle size 60–90 μm, in dimethoxyethane)

Host	20°C		120°C	
	Half-life (s)	$k\times10^3/s^{-1.5}$	Half-life (s)	$k\times10^3$ ($s^{-1.5}$)
ZrS_2	23	34.1	<5	400–600 [a]
2H-SnS_2	475	1.64	31	25.3
2H-SnSSe			225	
2H-$SnSe_2$	6730	0.12	410	1.92
2H-TaS_2			16000	0.05
2H-$NbSe_2$			2960	0.26
1T-TaS_2			>16000	<0.05 [b]
TiS_2			>60000	<0.01

[a] At 120°C this is too fast to measure accurately with the time resolution available; the range of values for k is an estimate based on extrapolation of lower temperature results.
[b] Shortage of beam time prevented full analysis. The reaction was significantly slower than that of 2H-TaS_2.

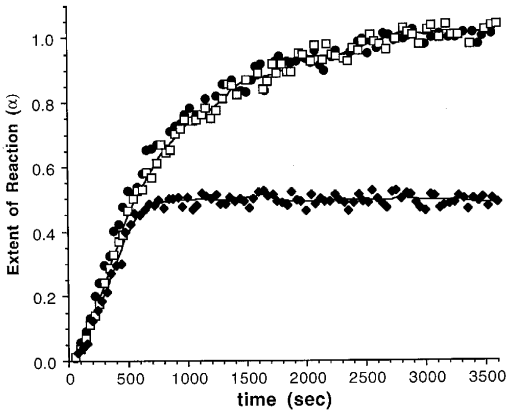


Fig. 7. Extent of reaction vs. time for the intercalation of $CoCp_2$ into SnS_2 at 20°C for a range of guest stoichiometries; the data are extracted from integration of the host (001) reflection such that $\alpha=1$ corresponds to complete loss of coherent diffraction from the host lattice. Data shown are for guest:host molar ratios of 1:1 (●), 0.33:1 (□) and 0.1:1 (♦).

Data could be fitted to Eq. (2) and, for the complete range of initial $Co(Cp)_2$ concentrations studied (10–70 mg cm^{-3}), the measured rate constants and half-lives are invariant within experimental error. Therefore, we conclude that the nucleation and diffusion rate are independent of $Co(Cp)_2$ concentration over the range investigated. The invariance on guest concentration and the congruency of the reaction kinetic curves suggest a number of issues. Firstly, the similarity in the sigmoidal nature of the extent of reaction curve for each system implies a consistent mechanism and a consistent ratio between the rates of nucleation and diffusion. Secondly, the diffusion of guest molecules to the host surface is insignificant with respect to the reaction rate.

If this is an example of a more general phenomenon, this observation has significant practical implications. The zero-order dependence in the guest concentration means that in future experiments it should not be necessary to use a large excess of guest molecules to expedite these reactions. This would be especially useful if the guests are expensive or particularly difficult to synthesise.

2.3. Kinetics of intercalation of lithium salts in aluminium hydroxide

The intercalation of LiCl in Gibbsite (γ-$Al(OH)_3$) is a remarkable example of an intercalation reaction in which both the cation and the anion are simultaneously intercalated in the host lattice [29–32]. The product of the reaction is $[LiAl_2(OH)_6]Cl\cdot H_2O$ which is a layered double hydroxide with a well ordered structure [33–35]. We have studied this reaction using time-resolved in situ EDXRD. In all cases the reactions proceeded directly to the first stage intercalation product and no other crystalline intermediate phases were observed. A typical set of in situ EDXRD spectra for intercalation of LiCl are shown in Fig. 8. The major peak that is observed to grow with time in this energy window corresponds to the (002) Bragg reflection of $[LiAl_2(OH)_6]Cl\cdot H_2O$ at $E=49.1$ keV ($d=7.65$ Å) while the (001) Bragg reflection of Gibbsite at $E=77.0$ keV ($d=4.85$ Å) decays in intensity. We can resolve no changes in the peak position or peak width at half maximum during the growth of the intercalate Bragg peaks. This is probably not too surprising

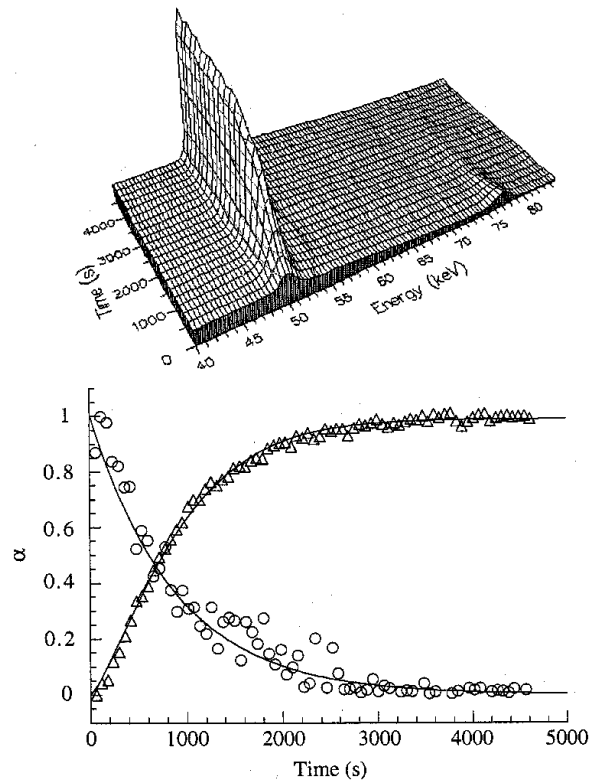


Fig. 8. (a) Time resolved in situ energy dispersive X-ray powder diffraction data showing the course of the reaction between Gibbsite and a 7.5 M aqueous solution of LiCl at 120°C giving $[LiAl_2(OH)_6]Cl\cdot H_2O$. (b) Plot of extent of reaction (α) of the (001) Bragg reflection ($E=77.1$ keV, $d=4.85$ Å) of the Gibbsite (○) and the (002) Bragg reflection of $[LiAl_2(OH)_6]Cl\cdot H_2O$ ($E=49.1$ keV, $d=7.65$ Å) (△) as a function of time.

given that the detector momentum resolution using post sample molybdenum slits is typically $\Delta E/E = 0.0115$.

Kinetic information was extracted from each experiment by integration of the (002) Bragg reflection of $[LiAl_2(OH)_6]Cl \cdot H_2O$. The errors on the integrated areas are small and contained within the data points. The integrated intensities were subsequently converted to the extent of the reaction (α) using the relationship Eq. (1): least-squares fits of the $\alpha(t)$ data are to the Avrami–Erofe'ev rate expression (Eq. (2)). We have investigated the rate of intercalation of LiCl in Gibbsite as a function of both temperature and LiCl concentration.

2.3.1. Effect of temperature

The temperature dependence of the intercalation reaction between a 10 M aqueous solution of LiCl and Gibbsite was investigated over the range 60–140°C. Fig. 9 plots the extent of reaction against time for the temperatures studied and it is clear that the rate of reaction has a marked temperature dependence. In each case the Avrami–Erofe'ev equation (Eq. (2)) has been fitted to the data. Furthermore, plots of reduced time ($t/t_{0.5}$) versus extent of reaction for the different temperatures are superimposable within experimental error, implying a consistent mechanism for the intercalation reaction over the whole temperature range.

The Avrami exponents obtained from the least-squares fits for all the data sets fell in the range 0.8–1.2, though a value of $m = 1.0$ gives a satisfactory fit to the majority of the experimental results. Assuming Avrami–Erofe'ev kinetics to be relevant, this indicates a two-dimensional diffusion controlled nucleation-growth model following instantaneous nucleation. In this case the Avrami–Erofe'ev equation becomes $\alpha = [1 - \exp(-kt)]$.

The validity of Eq. (2) for the whole process can be confirmed by a Sharp–Hancock analysis. In each case this analysis yields a single straight line over the whole reaction, implying that the Avrami–Erofe'ev kinetics discussed above are a good description of this system. Further evidence for this model can be obtained by consideration of the intersection of the host and intercalate curves. The intersection is at $\alpha = 0.5$, implying that loss of coherent diffraction from the host is matched by gain in coherence of the product. In cases where nucleation is random, the rate of loss of coherent diffraction from the host lattice exceeds the rate of growth of the product phase leading to the intersection being at $\alpha < 0.5$.

From the kinetic data obtained from the above analysis, it is possible to extract an activation energy for the intercalation of LiCl into Gibbsite using the Arrhenius expression, $k = A\exp(-E_a/RT)$. A plot of ln k versus $1/T$ yields a value of $E_a = 27$ kJ mol^{-1}. This compares with a value of $E_a = 41$ kJ mol^{-1} obtained from a study of the temperature dependence of the rate of intercalation of cobaltocene ($Co(\eta\text{-}C_5H_5)_2$) in SnS_2.

2.3.2. Effect of concentration

The effect of LiCl concentration on the intercalation reaction was studied at 120°C over the range 4–20 M. The reaction

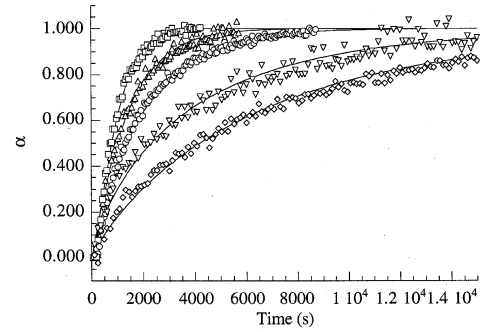


Fig. 9. Extent of reaction (α) against time (t) for the intercalation of LiCl into Gibbsite over a range of temperatures: 140°C (□), 120°C (△), 100°C (○), 80°C (▽) and 60°C (◇). Data for 110°C and 90°C have been omitted for clarity. The data have been fitted using the Avrami–Erofe'ev equation.

with 4 M LiCl did not go to completion in 4 h and no reactions were observed in 2 h for concentrations below this level. From the plots of extent of reaction against time shown in Fig. 10 it can be seen that the reaction rate is strongly dependent on the initial concentration of LiCl. In each case the Avrami–Erofe'ev equation has been fitted to the data. The observation of a dependence of rate of the reaction on the concentration of the guest is in contrast to previous studies on the intercalation of metallocenes into metal dichalcogenides which were found to be zeroth order with respect to the guest concentration. As for the temperature dependence reactions, plots of extent of reaction against reduced time are superimposable within experimental error, suggesting that the same mechanism is occurring in each case. This can be further confirmed by analysis of the Avrami exponents obtained from the curve fitting and from the Sharp–Hancock plots which lie in the range 1.0–1.5 though taking a value of 1.0 again gives a satisfactory fit to the majority of the data. This indicates a two-dimensional diffusion controlled nucleation-growth model following instantaneous nucleation, as was observed for the temperature dependence data. The kinetic parameters are summarised in Table 3.

The order of reaction with respect to LiCl concentration can be determined from a plot of ln k against ln[LiCl] which is shown in Fig. 11. The gradient of this plot is 0.52, indicating

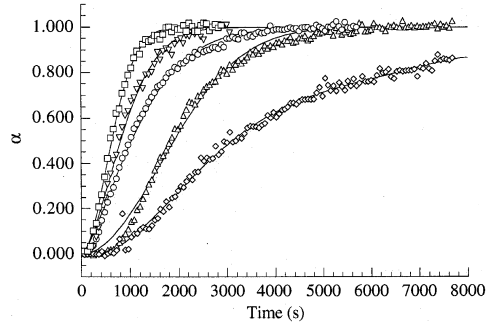


Fig. 10. Extent of reaction (α) against time (t) for the intercalation of LiCl into Gibbsite over a range of initial guest concentrations: 20 M (□), 15 M (▽), 10 M (○), 5 M (△), and 4 M (◇). Data for 12 M and 7.5 M guest solutions have been omitted for clarity.

Table 3
Summary of the kinetic parameters obtained from the Sharp–Hancock analysis of the intercalation of LiCl into Gibbsite for varying initial LiCl concentrations

[LiCl] (mol^{-1})	m [a]	k (s^{-1}) [b]	$t_{0.5}$ (s)
20	1.47	1.21×10^{-3}	600
15	1.40	1.09×10^{-3}	780
12	1.27	9.16×10^{-4}	900
10	1.00	7.40×10^{-4}	960
7.5	1.37	6.86×10^{-4}	1050
5	1.45	6.16×10^{-4}	1830
4	1.26	2.89×10^{-4}	3180

[a] From a least-squares fit to Eq. (2).
[b] From a least-squares fit to $\alpha = [1-\exp(-kT)]$.

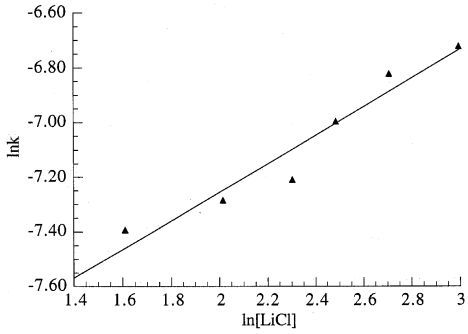


Fig. 11. Plot of ln k vs. ln[LiCl] used to determine the order of reaction with respect to the concentration of LiCl.

that the reaction is half order with respect to [LiCl]. This gives the rate equation as:

$$\text{rate} \propto k[\text{LiCl}]^{0.5}$$

2.4. Intercalation of ammonium ions in the layered silicate kanemite

The synthesis of mesoporous materials has been one of the most topical and rapidly moving fields in solid state chemistry of the last decade. The mechanism of formation of these materials is very poorly understood but is clearly an important issue. The synthetic approach originally reported by Kresge et al. [36] led to the development and investigation of the M41S family of mesoporous molecular sieves [37–39]. The three phases obtained from the M41S synthesis methods are hexagonal (MCM-41), cubic (MCM-48), and lamellar (MCM-50), of which the microscopy and diffraction data are reminiscent of surfactant/water binary systems. Beck et al. initially proposed a liquid crystal template (LCT) mechanism [37]. This mechanistic model served to illustrate the concept of aggregate molecular templating, but was quickly modified to include the role of the silicate anionic species. This model is better described as a process of cooperative assembly, as a result of favourable electrostatic interactions at the inorganic–organic interface [37,40–43].

Another approach, developed by Kuroda and co-workers, takes advantage of the ability of long chain alkyltrimethylammonium cations to intercalate into the single layered polysilicate, kanemite. This was an extension of the intercalation chemistry originally reported by Beneke and Lagaly [44]. Kuroda and co-workers initially reported that the formation of the silicate-surfactant complex [45,46], followed by removal of the surfactant, led to the formation of a hexagonal mesoporous silicate [47,48]. These materials can be tailor made with single size distribution channels in the range 20–40 Å. The mesoporous silicate material denoted FSM-16 is produced by intercalation of hexadecyltrimethylammonium cationic surfactants, and the formation process is representative of the transformation of two-dimensional layers to a three-dimensional framework [49].

We have recorded time-resolved in situ EDXRD spectra following the addition of an aqueous solution of heaxdecyltrimethylammonium chloride ($C_{16}H_{33}N^{+}Me_3Cl^{-}$ = C_{16}TMACl) to kanemite ($NaHSi_2O_5\cdot 3H_2O$) at 70°C over a period of 3 h. The spectra are shown accumulated as a three-

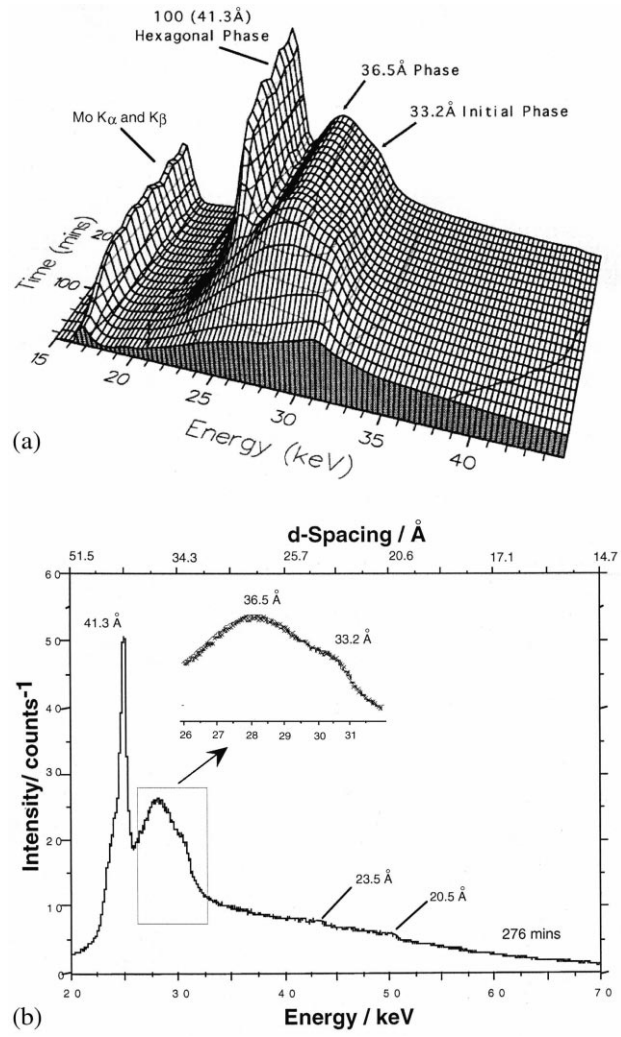


Fig. 12. (a) Three-dimensional stacked plot showing the energy dispersive powder X-ray diffraction spectra recorded following addition of 0.1 M hexadecyl-trimethylammonium chloride ($C_{16}TMA^{+}Cl^{-}$) to kanemite in water at 70°C. (b) The final in situ EDXRD spectrum taken after reaction completion, showing all observable diffraction features.

dimensional stacked plot in Fig. 12(a), along with the final spectrum recorded after 276 min (Fig. 12(b)) which clearly indicate the diffraction peaks present.

The stacked and single spectra can be described as a series of broad Bragg reflections viewed in energy space, that arise due to the growth of 'crystalline' silica-surfactant mesophases from the medium. A stirred suspension of kanemite at this pH and temperature showed only a broad featureless background, thus overwhelming X-ray scattering due to the silicate particles can be ruled out. We expect the coherent X-ray scattering at these low angles (high *d*-spacing) to produce broad Bragg reflections due to the convolution of the small ordered domain size of the silica-surfactant mesophases and the resolution function of the diffractometer setup.

Following the addition of the 0.1 M solution of C_{16}TMACl, a Bragg reflection grows in at a *d*-spacing of ca. 32 Å within 10 min. The *d*-spacing of this reflection increases gradually throughout the course of the reaction, reaching a constant value of 33.2 Å after 30 min. Subsequently, a second even broader Bragg reflection grows in with a *d*-spacing of ca. 36 Å, reaching a maximum after approximately 100 min. Once this Bragg reflection has reached its maximum intensity, we observe the growth of a series of reflections at *d*-spacings of 41.3, 23.5 and 20.5 Å. These reflections can be indexed as the (100), (110) and (200) Bragg reflections corresponding to a hexagonal symmetry mesophase ($a = 47.7$ Å, $2d_{100}/\sqrt{3}$). After pH adjustment with HCl to 8.5 to promote silanol condensation, filtration and calcination, FSM-16 is formed. The in situ diffraction data shown in Fig. 12(a) clearly show that the hexagonal (41 Å) silica-mesophase forms before dissolution of all the crystalline silicates.

It is highly likely that the intermediate phase with *d*-spacing of 33.2 Å has a layered, two-dimensional structure. A series of 00*l* reflections with *c*-lattice constant of 30.5 Å was observed in the laboratory X-ray powder diffraction pattern together with the Bragg reflections of the hexagonal phase from the untreated filtrate isolated after the reaction. It is reasonable to assume that the (00*l*) reflections belong to the lamellar phase observed by in situ EDXRD, and the increased *d*-spacing of the (001) reflection is due to swelling in the reaction medium. This has been observed in the intercalation chemistry of kanemite [50]. An interlayer separation of ca. 30 Å is consistent with intercalated $C_{16}TMA^+$ ions with an estimated length of ca. 23 Å and a silicate layer of approximately 6 Å thick. Lamellar phases appear to be common to all kanemite-surfactant reactions regardless of chain length. Recovery of this lamellar phase from the reaction mixture is possible by filtering the product before the reaction is complete and prior to addition of 1.0 M HCl. However, calcination of this sample led to a condensed amorphous phase, and collapse of any porous structure.

Given the current interest in template assisted crystallisation, these experiments clearly demonstrate the power of time-resolved, in situ diffraction measurements to monitor and help unravel the complex interactions of surfactant molecules with inorganic lattices. In this example, we have not only determined the kinetics of these reactions but also observed novel transient metastable phases that would probably have gone undetected using conventional laboratory procedures.

3. Conclusions

A range of environmental cells are now available to study the kinetics of intercalation into microcrystalline samples using time-resolved X-ray powder diffraction. The use of energy dispersive powder diffraction techniques enables reactions with half-lives of minutes to days to be examined. The design of the experiment allows a wide variety of solid–liquid reactions besides intercalation reactions to be studied with minimal turn-around time and experiments are currently underway to extend these opportunities to other classes of reactions.

Acknowledgements

We would like to thank the Leverhulme Trust, British Council, and the CIBA foundation for financial support and EPSRC for access to the Synchrotron Radiation Source, Daresbury Laboratory. We also thank Dr S.M. Clarke, Daresbury Laboratory and the technical staff at the SRS for helping in the design and construction of the experimental cell.

References

[1] J.G. Hooley, Carbon 11 (1973) 225.
[2] J.G. Hooley, Can. J. Chem. 40 (1962) 749.
[3] C. Riekel, Prog. Solid State Chem. 13 (1980) 89.
[4] C. Riekel, H.G. Reznik, R. Schollhorn, J. Solid State Chem. 34 (1980) 253.
[5] W. Paulus, H. Katzke, R. Schollhorn, J. Solid State Chem. 96 (1992) 162.
[6] C. Riekel, C.O. Fischer, J. Solid State Chem. 29 (1979) 181.
[7] C. Riekel, H.G. Reznik, R. Schollhorn, J. Solid State Chem. 34 (1979) 253.
[8] P. Barnes, Phase Transitions 39 (1992) 1.
[9] D. Hausermann, P. Barnes, Phase Transitions 39 (1992) 99.
[10] P. Barnes, S.M. Clark, D. Hausermann, E. Henderson, C.H. Fentiman, M.N. Muhamad, S. Rashid, Phase Transitions 39 (1992) 117.
[11] A.K. Sheridan, J. Anwar, Chem. Mater. 8 (1996) 1042.
[12] S.M. Clark, P. Irvin, J. Flaherty, T. Rathbone, H.V. Wong, J.S.O. Evans, D. O'Hare, Rev. Sci. Instrum. 65 (1994) 2210.
[13] S.M. Clark, J.S.O. Evans, D. O'Hare, C.J. Nuttall, H.V. Wong, J. Chem. Soc., Chem. Commun. (1994) 809.
[14] S.M. Clark, A. Nield, T. Rathbone, J. Flaherty, C.C. Tang, J.S.O. Evans, R.J. Francis, D. O'Hare, Nucl. Instrum. Methods Beam Interactions Mater. Atoms 97 (1995) 98.
[15] R. Clement, J. Am. Chem. Soc. 103 (1981) 6998.
[16] R. Clement, J.J. Girerd, I. Morgenstern Badarau, Inorg. Chem. 19 (1980) 2852.
[17] R. Clement, J. Chem. Soc., Chem. Commun. (1980) 647.
[18] J.S.O. Evans, D. O'Hare, Adv. Mater. 6 (1994) 646.
[19] J.S.O. Evans, S.J. Price, H.V. Wong, D. O'Hare, J. Am. Chem. Soc 120 (1998) 10837.

[20] S.F. Hulbert, J. Br. Ceram. Soc. 6 (1969) 11.
[21] M. Avrami, J. Chem. Phys. 7 (1939) 1103.
[22] M. Avrami, J. Chem. Phys. 8 (1940) 212.
[23] M. Avrami, J. Phys. Chem. 9 (1941) 177.
[24] B.V. Erofe'ev, C.R. Dokl. Acad. Sci. URSS 52 (1946) 511.
[25] D. O'Hare, in: D.W. Bruce, D. O'Hare (Eds.), Inorganic Intercalation Compounds, Inorganic Materials, Wiley, Chichester, 2nd edn., 1996.
[26] M.B. Dines, F.R. Gamble, B.G. Silbernagel, Bull. Am. Phys. Soc. (1975) 289.
[27] M.B. Dines, Science 188 (1975) 1210.
[28] S.J. Price, J.S.O. Evans, R.J. Francis, D. O'Hare, Adv. Mater. 8 (1996) 2989.
[29] A.P. Nemudry, V.P. Isupov, N.P. Kotsupalo, V.V. Boldyrev, Russ. J. Inorg. Chem. 31 (1986) 651.
[30] K.R. Poeppelmeier, S.-J. Hwu, Inorg. Chem. 26 (1987) 3297.
[31] M. Nayak, T.R.N. Kutty, V. Jayaraman, G. Periaswamy, J. Mater. Chem. 7 (1997) 2131.
[32] C.J. Serna, J.L. Rendon, J.E. Iglesias, Clays Clay Miner. 30 (1982) 180.
[33] I. Sissoko, E.T. Iyagba, R. Sahai, P.J. Biloen, Solid State Chem. 60 (1985) 283.
[34] J.P. Thiel, C.K. Chang, K.R. Poeppelmeier, Chem. Mater. 5 (1993) 297.
[35] A.V. Besserguenev, A.M. Fogg, S.J. Price, J.R. Francis, D. O'Hare, V.P. Isupov, B.P. Tolochko, Chem. Mater. 9 (1997) 241.
[36] C.T. Kresge, M.E. Leonowicz, W.J. Roth, J.C. Vartuli, J.S. Beck, Nature 359 (1992) 710.
[37] J.S. Beck, J.C. Vartuli, W.J. Roth, M.E. Leonowicz, C.T. Kresge, K.D. Schmitt, C.T.W. Chu, D.H. Olson, E.W. Sheppard, S.B. Mccullen, J.B. Higgins, J.L. Schlenker, J. Am. Chem. Soc. 114 (1992) 10834.
[38] J.S. Beck, J.C. Vartuli, G.J. Kennedy, C.T. Kresge, W.J. Roth, S.E. Schramm, Chem. Mater. 6 (1994) 1816.
[39] C.T. Kresge, J.C. Vartuli, W.J. Roth, M.E. Leonowicz, J.S. Beck, K.D. Schmitt, C.T.W. Chu, D.H. Olson, E.W. Sheppard, S.B. Mccullen, J.B. Higgins, J.L. Schlenker, Studies Surf. Sci. Catal. 92 (1995) 11.
[40] A. Firouzi, F. Atef, A.G. Oertli, G.D. Stucky, B.F. Chmelka, J. Am. Chem. Soc. 119 (1997) 3596.
[41] A. Monnier, F. Schüth, Q. Huo, D. Kumar, D. Margolese, R.S. Maxwell, G.D. Stucky, M. Krishnamurty, P. Petroff, A. Firouzi, M. Janicke, B.F. Chmelka, Science 261 (1993) 1299.
[42] Q.S. Huo, D.I. Margolese, U. Ciesla, P.Y. Feng, T.E. Gier, P. Sieger, R. Leon, P.M. Petroff, F. Schüth, G.D. Stucky, Nature 368 (1994) 317.
[43] A. Firouzi, D. Kumar, L.M. Bull, T. Beiser, P. Seiger, Q. Huo, S.A. Walker, J.A. Zasadzinski, C. Glinka, J. Nicol, D. Margolese, G.D. Stucky, B.F. Chmelka, Science 267 (1995) 1138.
[44] K. Beneke, G. Lagaly, Am. Miner. 62 (1977) 763.
[45] T. Yanagisawa, T. Shimizu, K. Kuroda, C. Kato, 56th Natl. Meet. of the Chemical Society of Japan, Tokyo, 1988, Abstract 1,761, No. IXIID42.
[46] T. Yanagisawa, T. Shimizu, K. Kuroda, C. Kato, Bull. Chem. Soc. Jpn. 63 (1990) 988.
[47] S. Inagaki, Y. Fukushima, K. Kuroda, J. Chem. Soc., Chem. Commun. (1993) 680.
[48] S. Inagaki, Y. Koiwai, N. Suzuki, Y. Fukushima, K. Kuroda, Bull. Chem. Soc. Jpn. 69 (1996) 1449.
[49] S. Inagaki, Y. Sakamoto, Y. Fukushima, O. Terasaki, Chem. Mater. 8 (1996) 2089.
[50] K. Kuroda, unpublished results.

PERGAMON

www.elsevier.nl/locate/poly

Polyhedron 19 (2000) 307–313

POLYHEDRON

Influence of the nature of the catalyst on the textural properties of organosilsesquioxane materials

Geneviève Cerveau, Robert J.P. Corriu *, Eric Framery

Laboratoire de Chimie Moléculaire et Organisation du Solide, UMR 5637, Université Montpellier II, cc 007, Place E. Bataillon, 34095 Montpellier Cedex 5, France

Received 27 April 1999; accepted 20 July 1999

Abstract

The hydrolytic sol–gel polymerization of molecular organosilicon precursors with a 'rigid' geometry 1,4-$C_6H_4[Si(OMe)_3]_2$ (**1**) and a 'flexible' geometry 1,4-$C_6H_4[CH_2CH_2Si(OMe)_3]_2$ (**2**) was investigated varying the nature of the catalyst. They were hydrolyzed under nucleophilic catalysis using non-ionic species such as dimethylformamide (DMF), dimethylaminopyridine (DMAP), *N*-methylimidazole (NMI) and hexamethylphosphorotriamide (HMPT) in THF. The effect of the concentrations of both the precursor and the catalyst was studied. Molecular precursor **1** led always to hydrophobic solids with degrees of condensation lying in the range 55–67%. These solids were mainly microporous exhibiting high specific surface areas. The densities lay in the range 1.37–1.42 g cm^{-3}. By contrast, the precursor **2** led to hydrophobic solids with no significant specific surface area. Degrees of condensation ranged between 59 and 74% and the densities between 1.27 and 1.31 g cm^{-3}. The nature of the catalyst (ionic or non-ionic) involved in the hydrolytic sol–gel polymerization of molecular organosilicon precursors appeared to be of great influence on the textural properties of the resulting solids. ©2000 Elsevier Science Ltd All rights reserved.

Keywords: Monophasic hybrid materials; Silsesquioxane gels; Kinetic control; Sol–gel polymerization

1. Introduction

The elaboration of monophasic organic inorganic materials by sol–gel type processes allows the introduction of a wide variety of organic [1–6] or organometallic [7–10] moieties into silica matrices. In such materials both organic and inorganic units are bound through at least two stable Si–C bonds. We have shown that the nature of the organic group has a fundamental influence on the properties of the hybrid solids [11]. Whether the organic group is 'rigid' or 'flexible' drastically influences the arrangement of organic units in the solid: a short-range order has been demonstrated chemically, showing that these monophasic hybrid materials can be nanostructured [2]. Moreover, we have pointed out the importance of all the kinetic parameters involved in the hydrolysis polycondensation reactions: the nature of the catalyst, concentration of the reagents, nature of the hydrolysable group, solvent, etc. [11]. All these parameters have great influence on the textural properties of the resulting xerogels. Although the difficulties encountered in reproducing experiments in sol–gel chemistry have not always been reported by the authors, it is important to point out that the reproducibility depends strongly on a precise control of the kinetic parameters of the hydrolytic polycondensation process. Experiments must be performed very precisely under the same experimental conditions, as is the norm for physico–chemical experiments: very dry solvents, precise control of concentrations, purity of the catalyst, etc. From these observations, we have proposed that the sol–gel type polymerization corresponds to a kinetically controlled process. The macroscopic data which permit the texture of the solid to be described are highly dependent on all of the parameters which control the kinetics of the hydrolytic polycondensation reaction.

In order to support further the argument for kinetic control, we have considered the effect of unusual nucleophilic catalysts. We report here the effect of non-ionic species such as dimethylformamide (DMF), dimethylaminopyridine (DMAP), *N*-methylimidazole (NMI) and hexamethylphosphorotriamide (HMPT). In organosilicon chemistry, these catalysts are known for inducing chemical reactions at silicon by nucleophilic activation [12–14]. However, they are less efficient than F^- and they are not used in sol–gel chemistry. The only exception is the hydrolysis of $Si(OMe)_4$ [15] with the longer gelation times observed in a few experiments.

* Corresponding author. Tel.: +33-467-143-801; fax: +33-467-143-888.

0277-5387/00/$ - see front matter ©2000 Elsevier Science Ltd All rights reserved.
PII S0277-5387(99)00360-5

Since the reactivity of these catalysts is drastically different from the reactivity observed with classical catalysts (acid, bases and F^-), we have studied here the influence of these catalysts on the textural properties of xerogels obtained from two previously explored precursors with respectively a 'rigid' and a 'flexible' geometry [11,16].

2. Experimental

Syntheses of precursors and preparation of the gels were carried out under argon using a vacuum line and Schlenk tube techniques [17]. Solvents and catalysts were dried and distilled before use. Compound 1,4-$C_6H_4[Si(OMe)_3]_2$ (**1**) was prepared according to literature procedures [18], while 1,4-$C_6H_4[CH_2CH_2Si(OMe)_3]_2$ (**2**) was commercial and was purified before use.

Solid state NMR spectra were obtained with a Bruker FTAM 300 spectrometer: ^{13}C CP MAS NMR at 75.47 MHz, recycling delay 5 s and contact time 5 ms; ^{29}Si CP MAS NMR at 59.62 MHz, recycling delay 10 s and contact time 2 ms. The spinning rate was 5000 Hz in all cases. Chemical shifts are given relative to tetramethylsilane.

Specific surface areas, pore volumes and pore size distribution were determined using a Micromeritics Gemini III 2375 apparatus. The density of the materials was determined by a pycnometry measurement with helium using a Micromeritics Accupyc 1330 apparatus.

Elemental analyses were carried out by the Service de Micro-Analyse du CNRS. Oxygen percentages were deduced by difference.

Affinity of xerogels for water ($E_{0.6}$) was determinated by measurement of weight increase of the solid in a 60% humidity atmosphere at 25°C. This atmosphere was obtained with a saturated NaBr solution under vacuum.

Preparation of silsesquioxane gels: The preparation of the gels was carried out according to the following general procedure. The preparation of xerogel **1A1** is given as an example. To 2.86 g (9 mmol) of **1** in 9 ml of THF was added a solution of 6.4 μl (6.57 mg, 90 μmol) of DMF and 486 μl (486 mg, 27 mmol) of water in 8.50 ml of THF. The mixture was warmed to 30°C and after 7 days a monolithic gel had formed. After further ageing for 6 days at 30°C, the solid was collected, then ground and washed twice with ethanol, acetone and diethyl ether. The resulting solid was dried at 120°C in vacuo for 3 h yielding 1.70 g of a white powder **1A1**. The gel time was dependent on concentration of the precursor and on the catalyst (DMF, DMAP, NMI or HMPT), and its concentration. It varied between 1 h and several days. The experimental conditions and the elemental analyses of the xerogels obtained from **1** and **2** are reported in Tables 1 and 2.

3. Results

The molecular precursors **1** and **2** (Scheme 1) containing phenylene units with two different geometries were investigated. The sol–gel polymerization of **1** and **2** was performed in THF at 30°C. Four nucleophilic and non-ionic catalysts were used: DMF, DMAP, NMI and HMPT (Scheme 2). Two concentrations of precursor (0.5 mol l^{-1} and 1.0 mol l^{-1}) were investigated, and in each case the amount of catalyst was 1 mol% and 5 mol%. All of the xerogels obtained were identified by CP MAS NMR spectroscopy and elemental analysis. The texture of the solids was studied by measuring specific surface area, porosity and density.

Table 1
Experimental conditions and elemental analyses of xerogels obtained from **1**

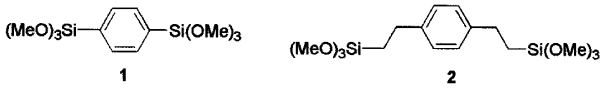
Xerogel	Precursor concentration (mol l^{-1})	Catalyst	Catalyst concentration (mol. equiv.)	Elemental analysis found (%)			Experimental formula [a]
				C	H	Si	
1A1	0.5	DMF	10^{-2}	39.14	4.02	25.61	$C_{7.1}H_{8.7}O_{4.3}Si_{2.0}$
1B1	0.5	DMAP	10^{-2}	39.45	4.18	23.90	$C_{7.7}H_{9.7}O_{4.8}Si_{2.0}$
1C1	0.5	NMI	10^{-2}	39.17	4.06	24.50	$C_{7.5}H_{9.2}O_{4.6}Si_{2.0}$
1D1	0.5	HMPT	10^{-2}	37.67	4.18	25.34	$C_{6.9}H_{9.2}O_{4.5}Si_{2.0}$
1A5	0.5	DMF	5×10^{-2}	37.16	3.90	24.97	$C_{6.9}H_{8.6}O_{4.7}Si_{2.0}$
1B5	0.5	DMAP	5×10^{-2}	38.26	3.72	25.74	$C_{6.9}H_{8.0}O_{4.4}Si_{2.0}$
1C5	0.5	NMI	5×10^{-2}	39.12	4.35	26.55	$C_{6.9}H_{9.1}O_{3.9}Si_{2.0}$
1D5	0.5	HMPT	5×10^{-2}	39.28	4.31	26.10	$C_{7.0}H_{9.2}O_{4.1}Si_{2.0}$
1A1M	1.0	DMF	10^{-2}	39.87	4.13	24.60	$C_{7.4}H_{9.3}O_{4.6}Si_{2.0}$
1B1M	1.0	DMAP	10^{-2}	37.93	3.68	27.55	$C_{6.4}H_{7.4}O_{3.9}Si_{2.0}$
1C1M	1.0	NMI	10^{-2}	38.52	3.82	25.12	$C_{7.2}H_{8.4}O_{4.5}Si_{2.0}$
1D1M	1.0	HMPT	10^{-2}	39.41	4.43	24.53	$C_{7.5}H_{10.0}O_{4.5}Si_{2.0}$
1A5M	1.0	DMF	5×10^{-2}	36.57	4.15	25.70	$C_{6.6}H_{8.9}O_{4.5}Si_{2.0}$
1B5M	1.0	DMAP	5×10^{-2}	37.82	4.06	26.30	$C_{6.7}H_{8.5}O_{4.2}Si_{2.0}$
1C5M	1.0	NMI	5×10^{-2}	38.05	4.14	25.50	$C_{6.9}H_{9.0}O_{4.4}Si_{2.0}$
1D5M	1.0	HMPT	5×10^{-2}	36.30	4.33	23.30	$C_{7.2}H_{10.3}O_{5.5}Si_{2.0}$

[a] Ideal formula $C_6H_4O_3Si_2$.

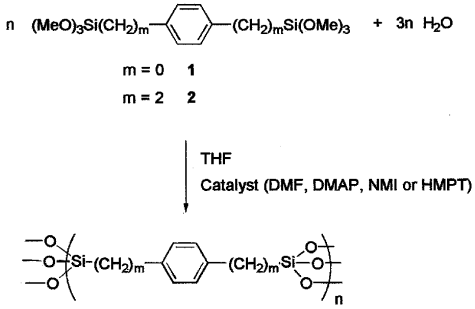
Table 2
Experimental conditions and elemental analyses of xerogels obtained from **2**

Xerogel	Precursor concentration ($mol\ l^{-1}$)	Catalyst	Catalyst concentration (mol. equiv.)	Elemental analysis found (%)			Experimental formula [a]
				C	H	Si	
2A1	0.5	DMF	10^{-2}	48.72	6.22	19.48	$C_{11.7}H_{17.8}O_{4.6}Si_{2.0}$
2B1	0.5	DMAP	10^{-2}	49.35	6.39	20.15	$C_{11.6}H_{17.6}O_{4.1}Si_{2.0}$
2C1	0.5	NMI	10^{-2}	49.76	6.33	24.10	$C_{9.7}H_{14.6}O_{2.9}Si_{2.0}$
2D1	0.5	HMPT	10^{-2}	49.84	6.41	18.00	$C_{12.9}H_{19.8}O_{5.0}Si_{2.0}$
2A5	0.5	DMF	5×10^{-2}	50.19	6.29	21.92	$C_{10.7}H_{15.9}O_{3.5}Si_{2.0}$
2B5	0.5	DMAP	5×10^{-2}	50.49	6.15	20.25	$C_{11.7}H_{16.9}O_{4.0}Si_{2.0}$
2C5	0.5	NMI	5×10^{-2}	50.35	5.96	21.03	$C_{11.2}H_{15.8}O_{3.8}Si_{2.0}$
2D5	0.5	HMPT	5×10^{-2}	49.57	6.04	20.30	$C_{11.4}H_{16.5}O_{4.2}Si_{2.0}$
2A1M	1.0	DMF	10^{-2}	48.30	5.96	20.47	$C_{11.0}H_{16.2}O_{4.3}Si_{2.0}$
2B1M	1.0	DMAP	10^{-2}	49.54	6.10	20.25	$C_{11.4}H_{16.8}O_{4.2}Si_{2.0}$
2C1M	1.0	NMI	10^{-2}	49.87	6.40	19.10	$C_{12.2}H_{18.6}O_{4.5}Si_{2.0}$
2D1M	1.0	HMPT	10^{-2}	49.54	6.17	20.80	$C_{11.1}H_{16.5}O_{4.0}Si_{2.0}$
2A5M	1.0	DMF	5×10^{-2}	49.07	6.14	20.68	$C_{11.1}H_{16.5}O_{4.1}Si_{2.0}$
2B5M	1.0	DMAP	5×10^{-2}	49.11	6.07	21.20	$C_{10.8}H_{15.9}O_{3.9}Si_{2.0}$
2C5M	1.0	NMI	5×10^{-2}	49.02	6.10	20.60	$C_{11.1}H_{16.5}O_{4.1}Si_{2.0}$
2D5M	1.0	HMPT	5×10^{-2}	48.89	5.86	21.50	$C_{10.6}H_{15.2}O_{3.9}Si_{2.0}$

[a] Ideal formula $C_{10}H_{12}O_3Si_2$.



Scheme 1. Molecular precursors.



Scheme 2. Sol–gel process.

*3.1. Sol–gel processing of **1***

The hydrolysis polycondensation of precursor **1** was performed according to the reaction described in Scheme 2. A stoichiometric amount of water was used. In all cases monolithic translucent gels formed within periods of time varying from several hours to several days. The gels were aged for 6 days at 30°C and were then ground and washed with ethanol, acetone and diethyl ether. The resulting powders were dried in vacuo at 120°C for 3 h.

*3.2. Spectroscopic and textural data for xerogels obtained from **1***

NMR data: The ^{13}C and ^{29}Si CP MAS NMR characteristics of the xerogels were determined. In all cases the ^{13}C CPMAS NMR spectra showed the presence of the organic fragment. They displayed two resonances at δ 133.6 ppm (aromatic carbons) and δ 50.7 ppm (residual methoxy groups). The organic fragments were not modified in the solids and the Si–C bonds were not cleaved during the hydrolysis polycondensation process. This was confirmed by the ^{29}Si CP MAS NMR analysis which revealed the absence of signal in the range -90 to -110 ppm corresponding to $SiO_{4/2}$ substructures [19,20]. The ^{29}Si CP MAS NMR spectra exhibited signals indicating that the condensation was incomplete in all cases. Resonances assigned to substructures T^0 (C–Si(OR)$_3$, δ -54.4 ppm), T^1 (C–Si(OR)$_2$(OSi), δ -62.0 ppm), T^2 (C–Si(OR)(OSi)$_2$, δ -69.5 ppm) and T^3 (C–Si(OSi)$_3$, δ -78.0 ppm) were observed in most of the cases. Interestingly, no T^0 substructures were detected when the concentrations of the precursor and the catalyst were 1 mol l^{-1} and 5 mol%, respectively. CP MAS spectroscopy is not quantitative. However, it has been shown [11,21] that single pulse experiments do not reveal any significant variation in relative peak intensity from the CP MAS spectra when there are no hydrogen atoms in the direct vicinity of the studied nucleus. Thus the percentages of the different T^x units, obtained by deconvolution of the spectra have been determined and are reported in Table 3. The degrees of condensation for all of the xerogels obtained from **1** lay in the range 55–67% whatever the catalyst and the concentrations of both the catalyst and the precursor (Table 3). The elemental analyses reported in Table 1 showed that the hybrid gels deviated from the ideal stoichiometry based on totally polycondensed silsesquioxane materials and were in agreement with the degrees of condensation deduced from NMR data. The hybrid network can be described approximately as siloxane chains with bridging units and with average of one uncondensed OH or OMe group per silicon atom.

Hydrophilic character: All the solids obtained from **1** exhibited a moderate to high affinity for water. Weight

Table 3
^{29}Si CP MAS NMR data for xerogels obtained from **1**

Xerogel	^{29}Si CP MAS NMR (%) [a]				Level of condensation
	T^0	T^1	T^2	T^3	
1A1	6	31	32	31	62
1B1	5	30	34	31	64
1C1	9	29	33	29	60
1D1	8	25	43	24	61
1A5		48	38	14	55
1B5		28	42	30	67
1C5	7	31	38	24	59
1D5	6	27	46	21	60
1A1M	7	31	48	14	56
1B1M		33	37	30	65
1C1M	3	29	43	25	63
1D1M	4	35	51	10	56
1A5M		39	54	7	56
1B5M		26	43	31	68
1C5M		22	55	23	67
1D5M		42	53	5	56

[a] Obtained by deconvolution of spectra.

increases in a 60% humidity atmosphere at 25°C ($E_{0.6}$) are reported in Table 4. These values are consistent with the presence of few organic and many hydroxyl groups at the surface.

Texture of the solids: The specific surface areas of the xerogels were determined (Table 4). 35-point adsorption/desorption isotherm plots were used [22]. The specific surface areas were evaluated using the BET equation [23]. Values were very high whatever the catalyst and the concentrations, with the exception of **1C1** and **1D1** which exhibited no significant specific surface areas. The adsorption/desorption isotherms of **1B5M** and **1C5M** are shown in Fig. 1. The shape of the curves was characteristic of microporous solids with different mesoporous contributions [24]. The determination of the porous volume by the BJH method [25] and the evaluation of the microporous volume by analysis of the *t*-plot diagram were performed in each case. The percentages of micropores in the different gels are reported in Table 4. They lay in the range 50–74% depending on the catalyst and the concentrations.

Helium picnometry: The density of the materials was determined by a picnometry measurement with helium. The values of the density are reported in Table 4. They were between 1.37 and 1.42 g cm^{-3}.

3.3. Sol–gel processing of *2*

The organic precursor **2** was hydrolyzed under the same conditions as **1**. Monolithic translucent gels formed in all cases within periods of time varying from several hours to several days. The same processing was used, and xerogels were isolated as white powders.

Table 4
Textural characteristics of hybrid materials obtained from **1**

Xerogel	$E_{0.6}$ (%)	BET (m^2 g^{-1})	μ_{pores} (%)	Density (g cm^{-3})
1A1	19	530	74	1.39
1B1	20	670	63	1.40
1C1	8	<10		1.39
1D1	12	<10		1.39
1A5	13	490	70	1.38
1B5	16	800	63	1.40
1C5	12	430	60	1.39
1D5	11	450	70	1.41
1A1M	13	440	65	1.39
1B1M	27	770	67	1.41
1C1M	20	600	73	1.40
1D1M	18	500	70	1.37
1A5M	14	230	58	1.40
1B5M	24	900	50	1.41
1C5M	17	600	71	1.42
1D5M	12	172		1.39

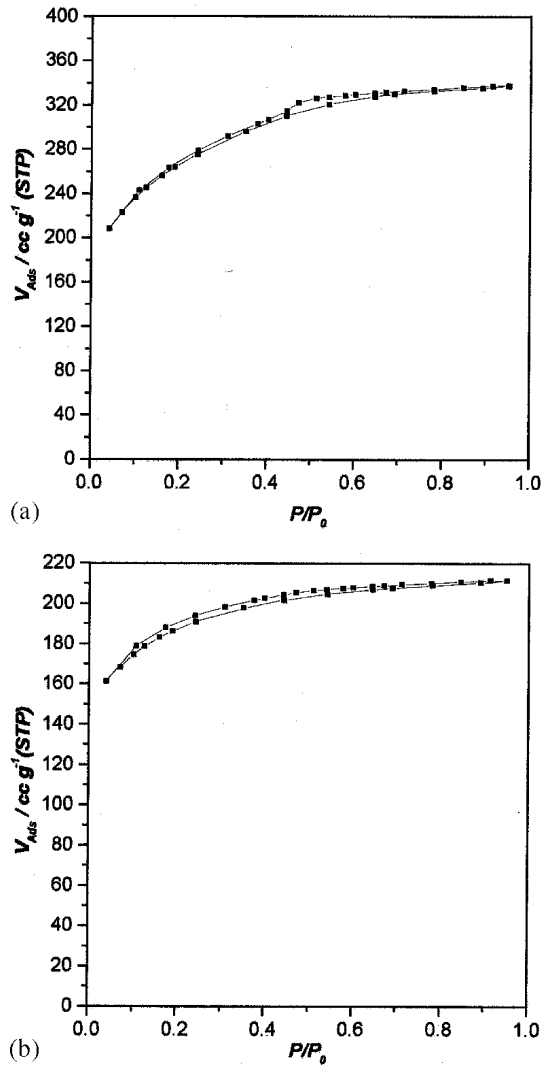


Fig. 1. N_2 adsorption–desorption isotherms of xerogels **1B5M** (a) and **1C5M** (b).

3.4. Spectroscopic and textural data of xerogels obtained from **2**

NMR data: The solid state NMR spectra of xerogels obtained from **2** clearly showed that the Si–C bond was not cleaved during the sol–gel condensation. ^{13}C CP MAS NMR spectra exhibited resonances at δ 143.6 and 127.6 ppm due to aromatic carbons, two at δ 29.1 and 14.8 ppm attributed to CH_2 carbons and one at δ 50.1 ppm corresponding to residual methoxy groups in all cases. When the catalyst was DMAP and NMI, the ^{29}Si CP MAS NMR spectra of xerogels displayed the four resonances assigned to T^0 (δ −42.5 ppm), T^1 (δ −49.6 ppm), T^2 (δ −58.2 ppm), and T^3 (δ −67.5 ppm) substructures whatever the concentrations of catalyst and precursor. Interestingly, when DMF and HMPT were employed, T^0 substructures were not observed. However, the degrees of condensation were evaluated and found to be in the same range (59–74%) whatever the catalyst (Table 5). The hybrid network can be described as siloxane chains with bridging units and with an average of one OR (R = H or Me) group per silicon atom.

Hydrophilic character: The affinity for water of all the xerogels obtained from **2** was very low (Table 6).

Texture of the solids: The nitrogen BET measurements gave no significant specific surface area in any of the samples ($< 10\ m^2\ g^{-1}$).

Helium picnometry: The densities of the gels obtained from **2** are reported in Table 6. The values ranged between 1.27 and 1.31 g cm^{-3}.

Table 5
^{29}Si CP MAS NMR data for xerogels obtained from **2**

Xerogel	^{29}Si CP MAS NMR (%) [a]				Level of condensation
	T^0	T^1	T^2	T^3	
2A1		34	57	9	59
2B1	10	17	35	38	67
2C1	13	15	39	33	64
2D1		30	60	10	60
2A5		25	57	18	64
2B5	6	16	30	48	74
2C5	9	15	35	41	69
2D5		20	55	25	68
2A1M		34	56	10	59
2B1M	7	18	35	40	69
2C1M	13	17	43	27	61
2D1M		23	59	18	65
2A5M		21	44	35	71
2B5M	3	32	31	33	65
2C5M	12	16	42	30	63
2D5M		29	59	12	61

[a] Obtained by deconvolution of spectra.

Table 6
Textural characteristics of hybrid materials obtained from **2**

Xerogel	$E_{0.6}$ (%)	BET ($m^2\ g^{-1}$)	Density (g cm^{-3})
2A1	1.6	< 10	1.27
2B1	2.1	< 10	1.27
2C1	7.3	< 10	1.27
2D1	2.0	< 10	1.28
2A5	2.1	< 10	1.27
2B5	3.6	< 10	1.28
2C5	1.1	< 10	1.27
2D5	2.8	< 10	1.28
2A1M	2.0	< 10	1.31
2B1M	2.1	< 10	1.28
2C1M	2.0	< 10	1.27
2D1M	1.5	< 10	1.28
2A5M	1.1	< 10	1.30
2B5M	0.9	< 10	1.29
2C5M	2.4	< 10	1.28
2D5M	1.5	< 10	1.30

4. Discussion

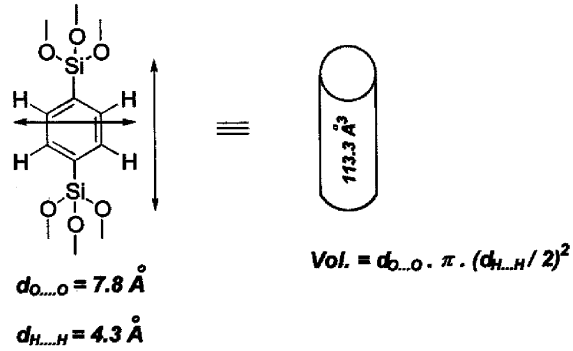
The results presented here show that the nature of the nucleophilic reagent used as catalyst during the hydrolysis polycondensation process has an influence on the textural properties of the resulting silsesquioxane materials. However, the essential parameter is the nature of organic group: 'rigid' or 'flexible' as previously established [11].

The molecular precursor **1** containing a 'rigid' organic group led to solids with similar levels of condensation lying in the range 55–68% whatever the concentrations of the precursor and the catalyst. These values are comparable to those already observed with ionic catalysts (nucleophile, acid or base) in MeOH and in THF. However, the range observed was narrower (63–67%) [16]. In most of the cases, the xerogels obtained from **1** were porous, exhibiting high specific surface areas and absence of narrow pore size distribution. The solids were mainly microporous, the microporous volume being 50–74% of the total porous volume (Table 4), depending on the catalyst and the concentrations. The same xerogels prepared under ionic nucleophile, basic, or acid catalysis exhibited similar microporous volume (50–60%) when the solvent was MeOH, whereas in THF the microporosity was higher (75–82%) [16]. The xerogels obtained from **1** described here exhibited, in almost all cases, an affinity for water lower than the hydrophilicity obtained with a ionic catalyst [16]. The values lay below 20% (8–20%) with the exceptions of **1B1M** and **1B5M** which were 27 and 24%, respectively. In the case of ionic catalysts, the hydrophilicity was always found to be above 20% (20–31%) [11,16]. The densities of the solids obtained from the 'rigid' precursor **1** lay in the range 1.37–1.42 g cm^{-3}. They appeared slightly lower than in the case of ionic catalysts in THF (range 1.39–1.46 g cm^{-3}) [26]. This difference could be attributed to a different distribution of the residual hydroxy or alkoxy groups within the hybrid network although the degrees of condensation were similar (55–68% for non-ionic catalysts and 63–67% for ionic catalysts). In fact the ^{29}Si CP MAS NMR spectra showed resonances corresponding to mainly T^1, T^2 and T^3 substructures. In some cases T^0 units were also

observed. The percentages estimated for the T^1, T^2 and T^3 units were similar in most cases (Table 3). On the other hand, when the hydrolysis was performed in THF with an ionic catalyst, the main substructures were T^2 and T^3 with the major unit T^2 ($\sim$64%) [11]. In this case most of the silicon atoms are C–Si(OR)$(OSi)_2$ whereas with non-ionic catalysts more C–Si$(OR)_2$(OSi) units are present, corresponding to a less dense solid.

When the molecular precursor contained a 'flexible' organic group **2**, the solids obtained had similar levels of condensation lying in the range 59–74% whatever the catalyst (Table 5). These solids appeared less polycondensed when compared to the corresponding solids reported previously [11] and obtained with ionic catalysis in THF (range 73–87%). In all cases the solids obtained from **2** were hydrophobic and had no significant specific surface area. The densities of the xerogels obtained from the 'flexible' precursor **2** lay between 1.27 and 1.31 g cm^{-3} (Table 6). They were lower than those obtained with an ionic catalyst in THF (range 1.32–1.37 g cm^{-3}) [26]. In this case the lower densities observed could be explained by the difference observed for the degrees of condensation: the more the xerogel is polycondensed, the higher is the density. In agreement with ionic catalysts in THF, only T^2 (38%) and T^3 (62%) substructures are observed [11,16] whereas with non-ionic catalysts T^1, T^2 and T^3 (in some cases T^0) substructures are detected (Table 5).

The xerogels obtained from **1** appeared more dense ($d_{av} = 1.39$ g cm^{-3}) than those obtained from **2** ($d_{av} = 1.28$ g cm^{-3}). Furthermore, the volume occupied by the organic group is larger in the solids obtained from **2** than in those obtained from **1**. In the same space, the number of units is lower in the case of **2** and consequently so is the density of the hybrid solid. Using the experimental values of densities, an estimate of the average volume occupied by each organic precursor can be made. The average volume occupied by one moiety is equal to the ratio $(dN/M_W)^{-1}$, where d is the density of the hybrid xerogel, N is Avogadro's number and M_W the molecular weight for $O_{1.5}Si–R–SiO_{1.5}$ [27]. The value obtained for **1** is $V_{exp}^{\mathbf{1}} = 2.15 \times 10^{-22}$ cm^3 and for **2**, $V_{exp}^{\mathbf{2}} = 3.07 \times 10^{-22}$ cm^3. These values can be compared to the volume occupied by the organic moiety calculated by molecular simulation. It was calculated assuming that the unit occupies a space with a cylindrical shape (Scheme 3). The calculated volumes are $V_{calc}^{\mathbf{1}} = 1.13 \times 10^{-22}$ cm^3 and $V_{calc}^{\mathbf{2}} = 1.76 \times 10^{-22}$ cm^3. The experimental volume appeared greater than the calculated volume in both cases. This result indicates that the organic units are not closely packed in the hybrid solid since the rigid spacer occupied 1.9 times the theoretical volume in the hybrid network and 1.75 times for the flexible one. This result may be expected since, in the xerogels obtained from **2**, the organic group is more flexible rendering the solid less compressed and consequently the hybrid network is less organized than with a rigid spacer [28]. Another possibility to explain the difference between calculated and observed volumes could be to take into account the presence of T^0 and T^1 units which might occupy more space than T^2 and T^3 units. It would be of interest to find a possible relationship between the degrees of condensation and the densities. In the case of **1** and **2**, quantitative reliable ^{29}Si SPE MAS NMR spectra have been collected and compared to the ^{29}Si CP MAS NMR spectra [11]. The SPE MAS and CP MAS percentages found for the different T^x units were comparable in both cases. Although the degrees of condensation lay between 55 and 68% in the case of **1** and 59 and 71% for **2**, the densities did not change: 1.38–1.40 g cm^{-3} and 1.27–1.30 g cm^{-3}, respectively. This allows us to eliminate this hypothesis and to consider that the differences between the densities originate from the different organization of organic units within the solid. Moreover, we have shown by chemical methods that the solids obtained from the 'rigid' precursor had a short-range order whereas those obtained from the 'flexible' precursor can be described as solids consisting of cross-linked chains.



Scheme 3. Theoretical calculation of the volume of xerogels obtained from precursor **1**.

5. Conclusions

The results presented here illustrate the close connection between the textural properties of hybrid solids obtained by the sol–gel route and the nature of the catalyst used in the hydrolytic polycondensation. The solids obtained by the sol–gel process are better described as kinetically controlled solids rather than thermodynamically unstable materials [29]. Changing the nature of the nucleophilic catalyst did not modify drastically the main features already established and the determining parameter for the texture of the xerogels is the structure of the organic precursor, 'rigid' or 'flexible'. However, some important differences appeared particularly in the textural properties of the hybrid xerogels when non-ionic catalysts are used. Molecular precursor **1** containing a 'rigid' organic group led to non-porous solids when the catalyst is NMI or HMPT (xerogels **1C1** and **1D1**). These are the only cases where no significant specific surface area has been obtained with this precursor. With non-ionic catalysts both hydrophilicity and densities of the solids were lower than with ionic catalysts. Similar degrees of condensation were obtained. However, T^0 substructures were observed with non-

ionic catalysts. By contrast, when the organic precursor contained a more 'flexible' organic group, the texture, the degree of condensation and the density of the resulting solids were strongly dependent on the nature of the catalyst. In the case of the non-ionic nucleophilic catalysts, the lower densities might correspond to a different arrangement of the organic units within the hybrid network.

The results reported here strengthen the importance of the kinetic control of the solid formation and open new possibilities for controlling the texture of the solids.

References

[1] R.J.P. Corriu, Polyhedron 17 (1998) 925.
[2] G. Cerveau, R.J.P. Corriu, Coord. Chem. Rev. 180 (1998) 1051.
[3] D.A. Loy, K.J. Shea, Chem. Rev. 95 (1995) 1431.
[4] P. Judenstein, C. Sanchez, J. Mater. Chem. 6 (1996) 511.
[5] J.D. Mackenzie, J. Sol–Gel Sci. Technol. 2 (1994) 81.
[6] U. Schübert, N. Hüsing, A. Lorentz, Chem. Mater. 7 (1995) 2010.
[7] G. Cerveau, R.J.P. Corriu, N. Costa, J. Non-Cryst. Solids 163 (1993) 226.
[8] G. Cerveau, R.J.P. Corriu, C. Lepeytre, J. Mater. Chem. 5 (1995) 793.
[9] G. Cerveau, R.J.P. Corriu, C. Lepeytre, Chem. Mater. 9 (1997) 2561.
[10] J.P. Bezombes, C. Chuit, R.J.P. Corriu, C. Reyé, J. Mater. Chem. 8 (1998) 1749.
[11] G. Cerveau, R.J.P. Corriu, C. Lepeytre, P.H. Mutin, J. Mater. Chem. 8 (1998) 2707.
[12] R.J.P. Corriu, G. Dabosi, M. Martineau, J. Organomet. Chem. 154 (1978) 33.
[13] R.J.P. Corriu, G. Dabosi, M. Martineau, J. Organomet. Chem. 186 (1980) 25.
[14] R.J.P. Corriu, C. Guerin, Adv. Organomet. Chem. 20 (1982) 265.
[15] R.J.P. Corriu, D. Leclercq, A. Vioux, M. Pauthe, J. Phalippou, in: J.D. Mackenzie, D.R. Ulrich (Eds.), Ultrastructure Processing of Advanced Ceramics, Wiley, New York, 1988, p. 113.
[16] G. Cerveau, R.J.P. Corriu, C. Fischmeister-Lepeytre, J. Mater. Chem. 9 (1999) 1149.
[17] D.F. Schriver, The Manipulation of Air-Sensitive Compounds, MacGraw-Hill, New York, 1969.
[18] R.J.P. Corriu, J. Moreau, P. Thépot, M. Wong Chi Man, Chem. Mater. 4 (1992) 1217.
[19] M. Mägi, E. Lippmaa, A. Samoson, G. Engelhardt, A.R. Grimmer, J. Phys. Chem. 88 (1984) 1518.
[20] H. Marsmann, in: P. Diehl, E. Fluck, R. Kosfeld (Eds.), ^{29}Si NMR Spectroscopic Results, Springer, Berlin, 1981.
[21] H.W. Oviatt Jr, K.J. Shea, J.H. Small, Chem. Mater. 5 (1993) 943.
[22] S.J. Gregg, S.W. Sing, Adsorption, Surface Area and Porosity, Academic Press, London, 1982.
[23] S. Brunauer, P.H. Emmet, E. Teller, J. Am. Chem. Soc. 60 (1938) 309.
[24] S. Brunauer, L.S. Deming, W.S. Deming, E. Teller, J. Am. Chem. Soc. 62 (1940) 1723.
[25] E. Barett, L. Joyner, P. Halenda, J. Am. Chem. Soc. 73 (1951) 373.
[26] G. Cerveau, R.J.P. Corriu, E. Framery, to be published.
[27] B. Boury, R.J.P. Corriu, V. Le Strat, P. Delord, New J. Chem. 23 (1999) 531.
[28] P. Chevalier, R.J.P. Corriu, P. Delord, J.J.E. Moreau, M. Wong Chi Man, New J. Chem. (1998) 423.
[29] C.J. Brinker, G.W. Scherer, Sol–Gel Science: The Physics and Chemistry of Sol–Gel Processing, Academic Press, San Diego, CA, 1990.

PERGAMON

www.elsevier.nl/locate/poly

Polyhedron 19 (2000) 315–322

POLYHEDRON

Nuclear magnetic resonance techniques for the structural characterization of siloxane–oxide hybrid materials

Florence Babonneau *, Jocelyne Maquet

Chimie de la Matière Condensée, Université Pierre et Marie Curie/CNRS, 4 Place Jussieu, 75252 Paris cedex 05, France

Received 2 August 1999; accepted 9 October 1999

Abstract

The objective of this paper is to discuss the appropriateness of various solution and solid state NMR techniques to describe structural aspects of siloxane–oxide hybrid systems prepared by sol-gel processes. Co-hydrolysis of organosilanes and metallic alkoxides can promote either self-condensation or co-condensation reactions between the different precursors, and this will control the structural homogeneity of the final network. Solution state ^{29}Si and ^{17}O NMR can give unique information on the formation and stability of co-condensing species. In the final gels, solid state ^{29}Si MAS used in conjunction with cross-polarization (CP) and related two-dimensional ^{29}Si–^{1}H heteronuclear NMR correlation techniques, provides detailed information on dipole–dipole coupled ^{29}Si and ^{1}H species among different molecular moieties. Finally, the use of ^{17}O MAS NMR with the newly developed MQ MAS sequence that provides a direct identification of the various oxo bridges will be discussed. ©2000 Elsevier Science Ltd All rights reserved.

Keywords: Sol-gel; NMR; Hybrid materials; Siloxane; Silicon-29; Oxygen-17

1. Introduction

Sol-gel processing of siloxane–oxide hybrid materials [1] is an area of rapid growth due to the wide variety of potential applications of these systems [2]. The flexibility of this synthetic approach — a large variety of precursors and low synthesis temperatures — offers the potential molecular engineering of composition and properties of a diverse range of solid product materials. The intimate mixing of molecular precursors in organic solvents allows organic and inorganic components to be associated at the molecular level, in order to form real organic–inorganic nanocomposites.

These systems are typically prepared from hydrolysis and condensation reactions of molecular precursors, such as organically modified alkoxysilanes $R_xSi(OR')_{4-x}$ ($x=1,2$), and metal alkoxides, $M(OR'')_4$ (M = Si, Ti or Zr) whose reactivities may be different. Both self-condensation (Eq. (1)) and co-condensation (Eq. (2)) reactions can occur, and this will influence the nature of the condensed species formed in solution.

Self-condensation:

$$\equiv Si–OH + RO–M\equiv \rightarrow \equiv Si–O–M\equiv \quad (R=Et, H) \qquad (1)$$

Co-condensation:

$$\equiv Si–OH + RO–Si\equiv \rightarrow \equiv Si–O–Si\equiv \qquad (2)$$

$$\equiv M–OH + RO–M\equiv \rightarrow \equiv M–O–M\equiv$$

A complex series of chemical reactions can occur at each stage of the synthesis procedure, not only in solution (hydrolysis and condensation), but also during aging before gelation, and then during drying. They will thus strongly influence the process of network formation, and the structural properties of the final materials. NMR plays an important role in the characterization of these systems, since local environments of several nuclei can be probed in solution as well as in solid samples.

The objective of this paper is to review the various solution and solid state NMR techniques that have been, or can be, used in this field, and to discuss the type of information they provide, as well as their limitations.

2. Solution NMR techniques

The steps that initiate the formation of the siloxane–oxide hybrid network can be followed by solution NMR techniques. A primary objective is often to characterize the various oxo-bridges formed through either self-condensation (Si–O–Si

* Corresponding author.

0277-5387/00/$ - see front matter ©2000 Elsevier Science Ltd All rights reserved.
PII S0277-5387(99)00361-7

and M–O–M) or co-condensation (Si–O–M) reactions between the organically modified alkoxysilane and the metal alkoxide.

Both ^{29}Si and ^{17}O NMR lend themselves well to such investigations and potentially species M also, if it possesses a NMR active isotope.

^{29}Si is a spin 1/2 species that has a natural abundance of 4.7%; it is 2.1 times more sensitive than ^{13}C, but is usually characterized by long spin relaxation T_1 times [3]. Single-pulse experiments may be quite long, typically 15–30 min for concentrated systems ($c(\mathrm{Si}) \geq 1$ M) such as those used in classical sol-gel preparations, which limits reactions that can be examined.

^{17}O is a spin 5/2 nucleus with a very low natural abundance (0.037%) and low sensitivity compared to ^{13}C (6×10^{-2}), but usually very short T_1 values due to an efficient quadrupolar relaxation mechanism [4]. ^{17}O NMR spectra of concentrated sol-gel systems can be recorded using samples containing ^{17}O in natural abundance, but with typically long measurement times [5]. Moreover, ^{17}O NMR spectra are often dominated by a strong solvent signal (usually from an alcohol), which accounts at least partly for why this technique has not been used extensively until recently, when ^{17}O enriched water has been used as a reactant [6,7]. In addition to the large gain in sensitivity obtained even for relatively low ^{17}O enrichments (10 at.%), selectivity is also enhanced by ^{17}O incorporation preferentially at certain sites, for example in hydroxyl groups (M–*O*H) and oxo bridges (M–*O*–M). This leads to an increase in their detectability compared to the un-enriched R*O*H and M–*O*R groups. As applied specifically to the characterization of siloxane–oxide systems, solution state ^{29}Si and ^{17}O NMR present separate advantages and limitations, mainly depending on the nature of the oxide component.

2.1. Siloxane–silica systems

Siloxane–silica composites are usually prepared from co-hydrolysis in acidic medium of a difunctional $R_2Si(OR')_2$ or trifunctional $RSi(OR')_3$ organosilane and a tetraalkoxysilane, such as tetraethoxysilane (TEOS), $Si(OEt)_4$. The extent of condensation of the network versus time (which represents the number of alkoxy groups which transform in oxo bridges) depends strongly on the nature of the organosilanes as illustrated in Fig. 1. Electronic inductive effects of the organic substituent are responsible for the higher reactivity of organosilanes compared to TEOS under acidic conditions and have already been reported [8,9]. The extremely fast reactions of triethoxysilane (TREOS, $HSi(OEt)_3$) and methyldiethoxysilane (MDES, $MeHSi(OEt)_2$) may be due to additional steric effects: the presence of the very small H-substituent can favor the nucleophilic attack of the water molecule at the Si center [10].

Due to these large differences in reactivities, one might wonder whether co-hydrolysis of two organosilanes, $R_xSi_A(OR')_{4-x}$ and $R_ySi_B(OR')_{4-y}$ would lead to a homogeneous distribution of the Si units. The type of oxo-bridges that should be distinguished and quantified is Si_A–*O*–Si_B. The ^{29}Si NMR experiment seems suitable in this case, since all the metallic sites can be detected, and over a rather large chemical shift range, which renders the technique sensitive to nearest neighbors, next nearest neighbors and cyclic species.

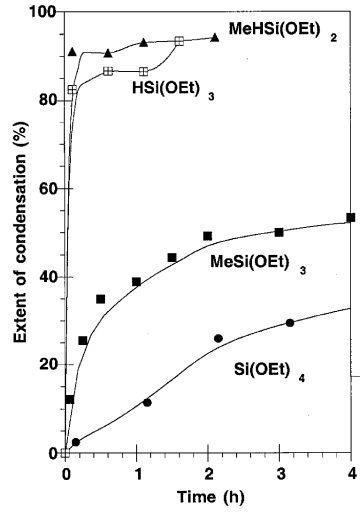


Fig. 1. Extent of condensation of a selected number of organosilanes: $Si(OEt)_4$, $MeSi(OEt)_3$, $HSi(OEt)_3$ and $MeHSi(OEt)_2$ extracted from ^{29}Si in situ solution state NMR. The composition of the starting solutions was: EtOH/Si = 2; H_2O/OEt = 1; pH 2 (HCl).

Several systems have been investigated, mainly using low hydrolysis ratios ($h = H_2O/Si < 0.5$), to prevent extensive condensation, and co-condensed species have been identified in DMDES/TEOS ($Me_2Si(OEt)_2/Si(OEt)_4$) [11], RTES/TEOS ($RSi(OEt)_3/Si(OEt)_4$, R = Me, Et, *n*-Oct, Ph) [12,13], and MDES/TREOS ($MeHSi(OEt)_2/HSi(OEt)_3$) [14] systems. Fig. 2 illustrates the results obtained with a co-hydrolyzed solution of MTES (T units) and TEOS (Q units) in a 1:1 molar ratio. Besides the peaks assigned to monomers (T_0 and Q_0 units) which are not represented in the figure, peaks due to T_1 units are seen at -50.50 and -50.65 ppm

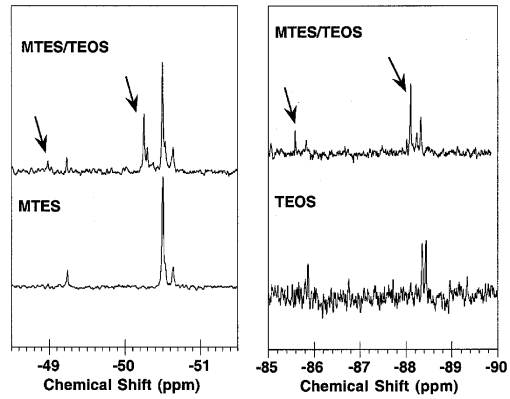


Fig. 2. ^{29}Si solution state NMR spectra of three hydrolyzed solutions of MTES, TEOS and MTES/TEOS in a 1:1 molar ratio (EtOH/Si = 4; H_2O/OEt = 0.1; pH 2 (HCl); aging time 2 days). Arrows indicate signals due to co-condensed species.

(Me*Si*(OEt)$_2$–O–) and at −49.25 ppm (Me*Si*(OEt)(OH)–O–), and due to Q_1 units at −88.35 and −88.44 ppm (*Si*(OEt)$_3$–O–) and at −85.87 ppm (*Si*(OEt)$_2$(OH)–O–). In the co-hydrolyzed system, additional peaks are present due to T–Q species, at −50.25 and −50.29 ppm (Me*Si*(OEt)$_2$–O–), −48.98 ppm (Me*Si*(OEt)(OH)–O, −88.11 and −88.20 ppm (*Si*(OEt)$_3$–O–) and −85.60 ppm (*Si*(OEt)$_2$(OH)–O–). Formation of co-condensed species is accompanied by a lowfield shift, but this never exceeds a few tenths of ppm. These small differences require high spectral resolution in order to identify the various condensed species.

For higher hydrolysis ratios ($h \geq 1$) as reactions proceed, the increasing number of species which are produced leads to a significant number of signals, together with a line broadening [15,16]. Assignments related to the first (*C* or *O* atoms) and second (–*O*R or –*O*–Si groups) nearest neighbors can be safely done, and lead to an estimation of the extent of condensation reactions for the various precursors (Fig. 1). However, definitive conclusions regarding the presence of co-condensed species require sensitivity to the third nearest neighbors, which is difficult to achieve with extensive signal overlap. Unambiguous identification of different Si environments has however been performed recently by using polarization transfer techniques, DEPT [17] and INEPT [18], adapted for systems with multiple heteronuclear coupling constants. More powerful would be two-dimensional ^{29}Si–^{29}Si correlation NMR techniques [19,20], which could describe directly the connectivity existing between different Si sites. But these experiments are very time consuming, mainly due to the low natural abundance of ^{29}Si nuclei, and thus somewhat inappropriate for systems in constant evolution.

Unlike ^{29}Si, the ^{17}O chemical shift range, for such siloxane–silica systems, is short since only Si–*O*–Si bridges are formed. This may prevent clear differentiation between the various oxo bridges. Evidence for co-condensation reactions was unambiguous in the DMDES/TEOS [7,15,21], and MTES/TEOS [7,12,15] systems, but totally obscure in the MDES/TREOS [22] system due to extensive signal overlap, even for low hydrolysis ratio ($H_2O/OEt = 0.1$). Fig. 3 shows the results obtained for a co-hydrolyzed solution of MDES (D^H units) and TEOS. Despite their large difference of reactivities (Fig. 1), a peak due to the formation of oxo bridges between D^H and Q units is shown [10]. Interestingly, no peak due to (Q)–O–(Q) species is present, showing that MDES reacts faster than TEOS, favoring the exclusive formation of (D^H)–O–(D^H) and (D^H)–O–(Q) species. One can notice that the ^{17}O NMR signals are broad, due to the short relaxation times of the quadrupolar ^{17}O nuclei. Variable-temperature experiments have been tried for increasing resolution, but only a modest improvement was obtained on the MTES/TEOS system [12].

In more complex systems with a bulky R group and higher hydrolysis ratio [16], spectral assignment turns out to be very difficult, and conclusions somewhat disappointing. However, co-hydrolysis reactions of MTES/TEOS and DMDES/TEOS have been followed in situ [15], and revealed the formation of co-condensed (D)–O–(Q) and (T)–O–(Q) species, stable with aging time. But in the case of highly reactive organosilanes such as MDES and TREOS, loss of signals can be observed due to the formation of highly condensed species, characterized by long correlation times, τ_c, which shorten even more the relaxation times.

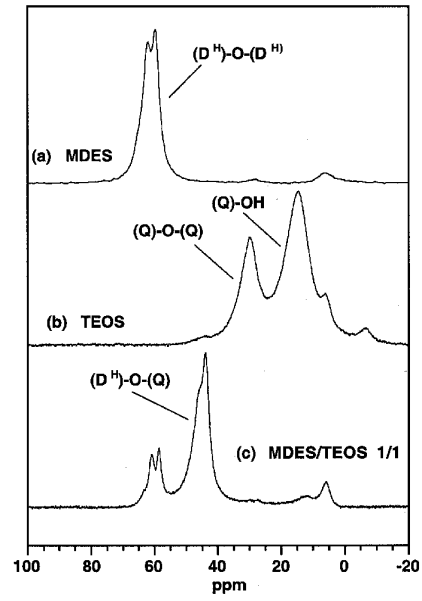


Fig. 3. ^{17}O solution state NMR spectra of three hydrolyzed solutions of (a) MDES, (b) TEOS and (c) MDES/TEOS in a 1:1 molar ratio (EtOH/Si = 4; $H_2O/OEt = 0.1$; pH 2 (HCl); aging time 2 days).

2.2. Siloxane–titania or siloxane–zirconia systems

In this case, the oxo-bridges formed through co-condensation reactions are Si–O–M (M = Ti, Zr). ^{29}Si NMR experiments will only detect the Si sites, and distinction between Si–O–Si and Si–O–M bridges can be subtle. Reaction of titanium isopropoxide [23] or zirconium *n*-propoxide [24] with a pre-hydrolyzed solution of DMDES causes the appearance of new signals in the ^{29}Si NMR spectrum, tentatively but not definitively assigned to the formation of Si–O–M bonds, because of a lack of chemical shift references. Recently, NMR investigations have been performed on several crystalline cyclic titanodiphenylsiloxanes, providing some chemical shift values for Si centers with Si–O–Si and Si–O–Ti bondings [25–27].

For such systems, ^{17}O NMR is a very powerful tool because of the large chemical shift range. This gives interesting clues for the identification of the various oxo-bridges [6,28,29]: 50–70 ppm for Si–*O*–Si, 250–300 ppm for Si–*O*–Ti, 300–400 ppm for μ_4-Ti–*O*–Ti, 500–600 ppm for μ_3-Ti–*O*–Ti, 700–800 ppm for μ_2-Ti–*O*–Ti, 200 ppm for Si–*O*–Zr, 300–350 ppm for μ_4-Zr–*O*–Zr, and 350–400 ppm for μ_3-Zr–*O*–Zr. Introduction of this technique was a real breakthrough in the characterization of siloxane–titania and siloxane–zirconia hybrid systems. It allows the unambiguous identification of Si–O–Ti and Si–O–Zr bond formation in solution, and the

demonstration of their low stability in solution during aging [6,27,30].

3. Solid state NMR techniques

3.1. ^{29}Si CP MAS NMR

The siloxane–oxide hybrid networks, obtained after gelation and drying, can be characterized by solid state NMR techniques. The most commonly used technique is the single-pulse ^{29}Si magic angle spinning (MAS) experiment [31] from which the relative amount of the various Si units and degree of condensation of the siloxane network can be readily extracted. However, for quantitative reliable data, long repetition delays should be used, because of long T_1 relaxation times for most of the units (10–50 s) [32]. Interestingly, addition of paramagnetic chromium ions, even in small amounts, to decrease relaxation times is not recommended if quantitative data are to be obtained, since part of the total NMR signal intensity cannot be detected [32]. In some particular cases, variation of chemical shift versus gel composition can indicate the level of homogeneity of the network, as illustrated in Fig. 4. The D^H and T units in gels prepared from MDES/TEOS and MTES/TEOS mixtures show continuous low field shifts when they are incorporated in a network with an increasing number of Q units: this suggests a progressive change in the nature of the neighboring sites of the observed units, indicative of a large tendency for the two systems to form co-condensed species.

Direct information that relates to the spatial distribution of the various units is more difficult to reach. Two-dimensional ^{29}Si MAS NMR studies have already been performed on crystalline zeolite structures [33], and also on silicate glasses [34]. These experiments provide precise descriptions of the connectivities of silicon sites, but usually require the preparation of ^{29}Si-enriched samples, which is rather expensive. Studies performed in natural abundance were however reported on crystalline samples, Q_8M_8 cubane [35] and zeolites [36], but are time-consuming.

In these systems, the presence of protonated groups directly bonded to some Si units makes the use of ^{29}Si–{^{1}H} cross-polarization (CP) technique very valuable. Based on magnetization transfer between abundant (here ^{1}H) and rare spins, this technique has been largely developed, coupled with MAS and high power proton decoupling [37], to increase the sensitivity of low abundant nuclei (^{13}C, ^{29}Si, ^{15}N). Cross-polarization dynamics is usually described within the framework of spin thermodynamics considering two reservoirs corresponding to the abundant *I*-spin (^{1}H) and the rare *S*-spin (^{29}Si). This model predicts an exponential build-up of *S*-spin magnetization in the rotating frame, characterized by $1/T_{IS}$. Analysis of the variation of peak intensities versus contact time gives access to T_{IS}, the cross-relaxation time, which is directly related to the ^{29}Si–^{1}H dipolar coupling and thus to the ^{29}Si–^{1}H distances [37]. It could thus bring structural information about the proton environment of each detected Si site. The rare spin must be within approximately 10 Å of a proton to facilitate polarization transfer [31]. However, the dipolar coupling can be partially averaged by molecular motions, and direct correlation between T_{IS} and proton environment can thus be made only for rigid networks which is not usually the case for sol-gel derived siloxane–oxide networks. Glass transition temperatures have been reported between 37 and 93°C in the MTES/TEOS system [38], and between −43 and −119°C in the MDES/TREOS system [14]. Quantitative interpretation of the CP dynamics should thus be carried out in these systems with some caution.

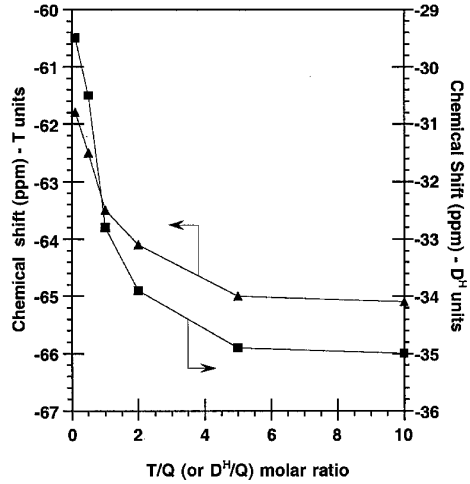


Fig. 4. Variation of chemical shift for the T and D^H units in dried gels prepared from co-hydrolysis of MDES/TEOS and MTES/TEOS in various molar ratios (EtOH/Si = 2; H_2O/OEt = 1; pH 2 (HCl)).

Indeed, the main difficulty encountered in a one-dimensional CP experiment is the uncertain nature of the protons that are actually the source for magnetization transfer. This prevents any definitive conclusions concerning the proximity between ^{1}H and ^{29}Si nuclei. A very elegant application of the CP technique can circumvent this problem: the use of two-dimensional ^{1}H–^{29}Si CP MAS heteronuclear NMR correlation. This experiment was first introduced to characterize surface species on silica and zeolites [39]. Fig. 5 shows the results of the ^{1}H–^{29}Si connectivity experiment carried out on a gel prepared by co-hydrolyzing MDES and TREOS in a 1:1 ratio. One should first note that MAS at 4 kHz gives good resolution on the one-dimensional ^{1}H spectrum. This is related to the presence of motions that can partially average the strong ^{1}H–^{1}H dipolar couplings. It makes possible a clear distinction between the Si–CH_3 (δ = 0.2 ppm) and Si–*H* (δ = 4.6 ppm) signals, and thus allows identification of the sources of polarization transfer. This is why this two-dimensional sequence is so powerful compared to the equivalent one-dimensional experiment: protons responsible for the polarization transfer to a given Si site can be identified, and thus spatial proximity established.

In the present example, at short contact time (50 μs), only correlations between the two types of Si units and the Si–*H*

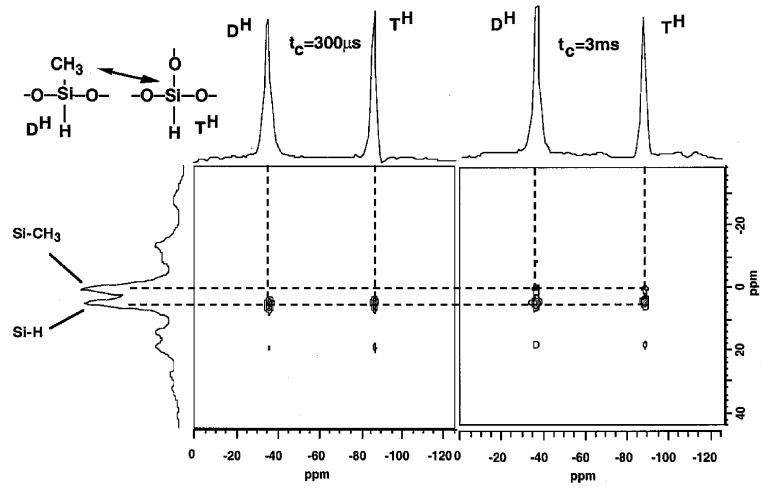


Fig. 5. Contour plot of the two-dimensional ^{1}H–^{29}Si correlation experiment on a gel prepared from co-hydrolysis of MDES and TREOS in a 1:1 molar ratio ($H_2O/OEt = 1$; $EtOH/Si = 2$; pH 2 (HCl)). Experimental parameters are the following: Bruker MSL300 spectrometer; spinning rate 4 kHz; contact time 50 μs and 3 ms; repetition time 5 s; 128 individual experiments with 48 scans each.

proton sources are present, indicating that the polarization transfer to ^{29}Si nuclei occurs only from the directly bonded ^{1}H nuclei. At longer contact times (3 ms), correlations are observed not only between the methyl groups and the D^H units, but also between these methyl groups and the T^H units. The variation in intensity of the correlation peaks with the contact time (Fig. 6) allowed us to extract the cross-relaxation T_{IS} times, characteristic of the ^{29}Si–^{1}H distances: as expected, they are found to be similar and around 100 μs [40] for the correlation peaks between the Si–*H* protons and the two Si sites. More surprisingly, they are also found to be similar (and around 1.5 ms) for the correlation peaks between the Si–CH_3 protons and the two Si units; this suggests a close spatial proximity between the D^H and T^H units.

Similar two-dimensional ^{1}H–^{29}Si heteronuclear NMR correlation experiments have been performed on different siloxane–silica systems prepared from MTES and TEOS [41], or PhTES and TEOS [32], with analogous conclusions: a good distribution of the siloxane and silica units within the hybrid network.

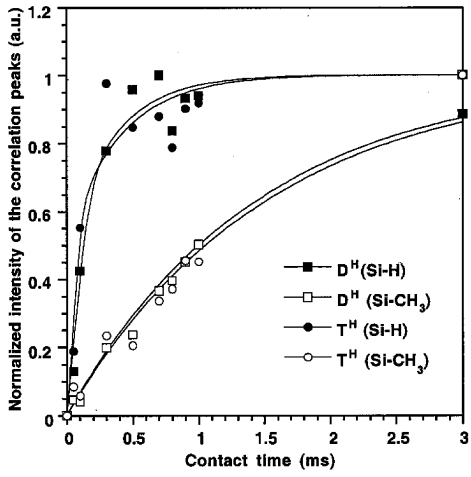


Fig. 6. Variation, with contact time, of the intensity of the correlation peaks observed in the two-dimensional ^{1}H–^{29}Si correlation experiment presented in Fig. 5.

3.2. ^{17}O MAS NMR

3.2.1. Siloxane–titania, siloxane–zirconia and borosiloxane systems

As previously mentioned, the large chemical shift range that can be found for siloxane–titania or siloxane–zirconia systems, makes ^{17}O solid state MAS NMR very attractive to identify the various oxo-bridges present in the hybrid networks.

In the solid state, enrichment of the samples is necessary, at least 10 at.%, but 20 at.% and higher is recommended. But the main problem with a quadrupolar nucleus, such as ^{17}O ($I = 5/2$) is a broadening of the central transition $|-1/2\rangle \leftrightarrow |+1/2\rangle$, due to a partial averaging under MAS of the second-order quadrupolar interaction. This may prevent observation of chemically non-equivalent sites, if their chemical shift difference is too small.

A ^{17}O MAS NMR study on SiO_2–TiO_2 gels has already been reported, showing the presence of the various Si–*O*–Si, Si–*O*–Ti and Si–*O*–Ti bonds [42,43]. Fig. 7 represents the ^{17}O MAS NMR spectrum obtained on a gel prepared from DMDES and $Ti(OPr^i)_4$. The three main signals are respectively assigned to Si–*O*–Si (60 ppm), μ_3-Ti–*O*–Ti (530 ppm), and μ_4-Ti–*O*–Ti (340 ppm) bonds. As already reported [44], the linewidth of the Ti–*O*–Ti resonances is dominated by chemical shift dispersion effects, rather than by quadrupolar effects, allowing the identification of the peak position with the chemical shift. The same is found here for the Si–*O*–Si resonance of the siloxane component, in contrast to the case of the Si–*O*–Si resonance in silica gel, which is characterized by a typical second order quadrupolar pattern ($C_Q \approx 4.7$ MHz) [45]. This suggests a high mobility for the D units in this sample, which may partially average the large quadrupolar interaction. No Si–*O*–Ti resonance, expected

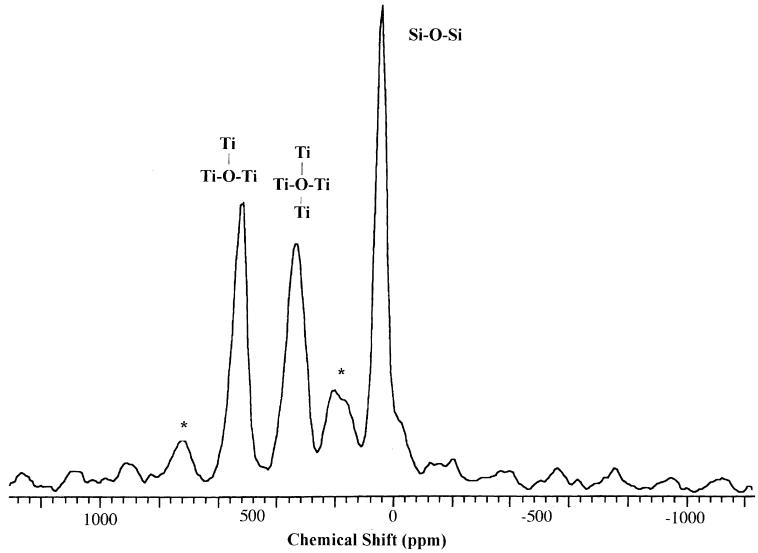


Fig. 7. ^{17}O MAS NMR spectrum of a dried gel prepared from DMDES and $Ti(OPr^i)_4$ (Si/Ti molar ratio 70/30), following a two-step synthetic procedure using 20 at.% enriched $H_2{}^{17}O$ [6]. The spectrum has been recorded on a Chemagnetics CMX-500 spectrometer with a Hahn–Echo sequence, synchronized on the rotor frequency (12.5 kHz). * spinning side bands.

around 300 ppm [44], is clearly present, which suggests a low number, if any, of the corresponding bridges. Indeed, this is in agreement with a solution study, which shows the very low stability of the Si–O–Ti bonds during aging [6]. The gel can thus be described as a nanocomposite with siloxane-rich and titania-rich domains. The ^{29}Si MAS NMR spectrum is characteristic of long polydimethylsiloxane (PDMS) chains [6]. A study using cross-polarization (CP) between ^{29}Si and ^{1}H shows however a low amount of Si units in constrained environment, certainly close to the titania-rich domains [6]. Interestingly, the resonances due to Ti–*O*–Ti bonds are very similar to those obtained on amorphous titania gels, indicating a network formed with μ_3 and μ_4 oxo bridges [29].

^{17}O MAS NMR is really a valuable tool not only to characterize siloxane–titania, but also siloxane–zirconia systems [46–48]. For siloxane–alumina systems, the chemical shift range for the various oxo bridges is quite short, and could prevent signal assignments based on this parameter. But as already reported for aluminosilicates [49], the quadrupolar coupling constant (C_Q) could be the best discriminator of such units. Consequently, the newly developed multiple quantum (MQ) MAS NMR technique [50] offers improved spectral resolution as already demonstrated on an aluminosilicate glass [44], for which complete resolution of Si–O–Si and Si–O–Al fragments has been obtained.

This technique has also been recently extended to borosilicate glasses [51], to distinguish between Si–*O*–Si, Si–*O*–B and B–*O*–B bridges. Similar results have been obtained on polyborosiloxane gel prepared from $EtSi(OEt)_3$ and $B(OEt)_3$ according to a published procedure [52] (Fig. 8). The two-dimensional MQ MAS spectrum [53]shows two peaks on the isotropic dimension at -48 ppm and at -60 ppm. For a spin-5/2 nucleus, the observed resonance frequency in the isotropic dimension of MQ MAS is given by [50]:

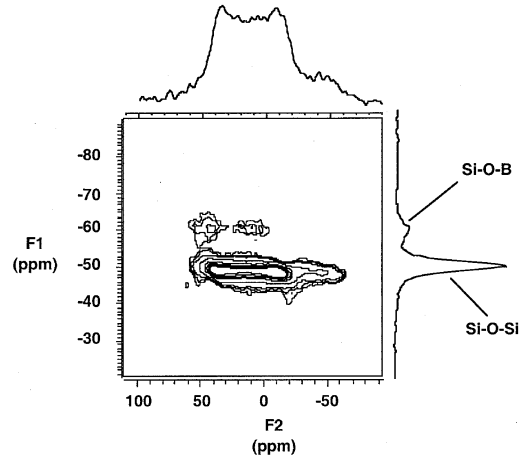


Fig. 8. ^{17}O 3Q MAS NMR spectrum for a polyborosiloxane gel prepared from $EtSi(OEt)_3$ and $B(OEt)_3$ (B/Si = 0.16). The experiment has been recorded on a DSX400 Bruker spectrometer using the shifted echo sequence [53].

$$\delta_{F1} = -\frac{17}{31}\delta_{iso} - \frac{8\times10^6}{93}\frac{\nu_Q^2}{\nu_0^2}\left(1+\frac{\eta^2}{3}\right)$$

with $\nu_Q = 3C_Q/[2I(2I-1)]$ and ν_0 the Larmor frequency of the observed nucleus (54.2 MHz). Simulations of the corresponding MAS projections give the following parameters for the two types of oxo species: Si–O–Si ($\delta_{iso} = 59$ ppm; $C_Q = 4.75$ MHz; $\eta = 0$) and Si–O–B ($\delta_{iso} = 75$ ppm; $C_Q = 4.80$ MHz; $\eta = 0$). No B–O–B species, expected to be at $\delta_{F1} \approx -70$ ppm [51] could be detected in agreement with the ^{11}B MAS NMR study [52].

3.2.2. Siloxane–silica systems

In siloxane–silica systems, the identification of the various oxo-bridges by ^{17}O MAS NMR is not obvious because of a

short chemical shift range for the various Si–*O*–Si species and very similar quadrupolar coupling parameters. For example, (T)–O–(T) units in a gel prepared from MTES are characterized by $\delta_{iso} = 64$ ppm, $C_Q = 4.5$ MHz, $\eta = 0$, while (Q)–O–(Q) units in a TEOS-derived silica gel give $\delta_{iso} = 40$ ppm, $C_Q = 5.1$ MHz, $\eta = 0$ [54]. Nevertheless, the MQ MAS sequence has also been successfully applied to organically modified silicates prepared from various mixtures of MTES and TEOS (Fig. 9) [54]. The isotropic projections for the gels prepared from respectively T and Q units show a peak at $\delta_{F1} = -63$ ppm ((T)–O–(T)) and -51 ppm ((Q)–O–(Q)). In the mixed TQ gels, an additional peak is present at an intermediate position $\delta_{F1} \approx -57$ ppm that corresponds to (T)–O–(Q) bridges. The isotropic chemical shift values and quadrupolar parameters have been extracted from the simulations. $C_Q = 5$ MHz and $\eta = 0$; δ_{iso} varies from 48 to 50 ppm, depending on the composition, and is in good agreement with those found in solution [15]. Quantification of the various oxo-bridges has been extracted by simulating the one-dimensional MAS spectra recorded at two magnetic fields (7 and 9.4 T) [54]: it shows in all samples a large amount of (T)–O–(Q) species, suggesting the excellent homogeneity of these gel networks.

4. Conclusions

This paper has reviewed the use of ^{29}Si and ^{17}O solution and solid state NMR techniques, to characterize the formation and resultant molecular network structures of siloxane–oxide hybrid systems. For siloxane–silica systems, ^{29}Si NMR is generally more sensitive to local structural features and thus is more informative than ^{17}O. Powerful two-dimensional heteronuclear correlation NMR methods (e.g. ^{29}Si–^{1}H) expand significantly the spectral resolution achievable, allowing the spatial proximities of different species (e.g. ^{29}Si and ^{1}H) to be probed especially for organically modified silicates. For siloxane–titania and siloxane–zirconia systems, ^{17}O NMR is generally more informative than ^{29}Si NMR because of the large ^{17}O chemical shift range. In systems for which the characteristic parameters of the various oxo bridges — isotropic chemical shift and quadrupolar coupling constant — are quite similar, such as polyborosiloxanes or polysiloxanes, the newly developed MQ MAS sequence has been successfully used to obtain resolved spectra, and to identify the different oxo species. The coupling with the one-dimensional ^{17}O MAS experiment allows quantification of the various oxo-bridges and a better description of the final network, in terms of phase separation.

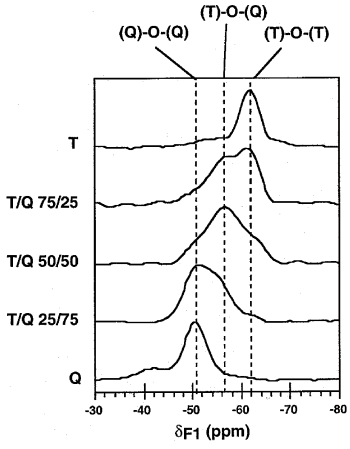


Fig. 9. Isotropic total projections of ^{17}O 3Q MAS spectra for organically modified silica gels prepared from MTES and TEOS in various molar ratios. The experiments have been recorded on a DSX300 Bruker spectrometer using the shifted echo sequence [53].

Acknowledgements

The authors would like to acknowledge C. Gervais, V. Gualandris (CMC, Université Paris 6), P. Florian, D. Massiot (CMRHT-CNRS, Orléans), M. Janicke, B.F. Chmelka (Department of Chemical Engineering, UC Santa Barbara), G.D. Sorarù (Univerity of Trento), M.-N. Rager (ENSCP, Paris) for their valuable contribution to the different studies presented in this manuscript.

References

[1] C. Sanchez, F. Ribot, New J. Chem. 18 (1994) 1007.
[2] H. Schmidt, J. Sol-Gel Sci. Technol. 1 (1994) 217.
[3] L.W. Kelts, N.J. Armstrong, J. Mater. Res. 4 (1989) 423.
[4] J.P. Kintzinger, in: NMR of Newly Accessible Nuclei, vol. 2, Academic Press, 1983, p. 79.
[5] F. Babonneau, L. Bois, J. Livage, Mater. Res. Soc. Symp. Proc. 271 (1992) 237.
[6] F. Babonneau, Mater. Res. Soc. Symp. Proc. 346 (1994) 346.
[7] F. Babonneau, J. Maquet, J. Livage, Chem. Mater. 7 (1995) 1050.
[8] H. Schmidt, H. Scholze, A. Kaiser, J. Non-Cryst. Solids 63 (1984) 1.
[9] L. Delattre, F. Babonneau, Mater. Res. Soc. Symp. Proc. 346 (1994) 365.
[10] V. Gualandris, F. Babonneau, M. Janicke, B.F. Chmelka, J. Sol-Gel Sci. Technol. 12 (1998) 75.
[11] F. Babonneau, Polyhedron 13 (1994) 1123.
[12] S. Prabakar, R.A. Assink, N.K. Raman, S.A Myers, C.J. Brinker, J. Non-Cryst. Solids 202 (1996) 53.
[13] Y. Sugahara, T. Inoue, K. Kuroda, J. Mater. Chem. 7 (1997) 53.
[14] G.D. Sorarù, G. D'Andrea, R. Campostrini, F. Babonneau, J. Mater. Chem. 5 (1995) 1363.
[15] F. Babonneau, V. Gualandris, M. Pauthe, Mater. Res. Soc. Symp. Proc. 435 (1996) 119.
[16] B. Lebeau, J. Maquet, C. Sanchez, F. Beaume, F. Lauprêtre, J. Mater. Chem. 7 (1997) 989.
[17] P. Lux, F. Brunet, J. Virlet, B. Cabane, Magn. Reson. Chem. 34 (1996) 100.
[18] T.M. Alam, R.A. Assink, S. Prabakar, D.A. Loy, Magn. Reson. Chem. 34 (1996) 603.
[19] P. Lux, F. Brunet, H. Desvaux, J. Virlet, Magn. Reson. Chem. 31 (1993) 623.
[20] P. Lux, F. Brunet, J. Virlet, B. Cabane, Magn. Reson. Chem. 34 (1996) 173.
[21] F. Babonneau, C. Toutou, S. Gavériaux, J. Sol-Gel Sci. Technol. 8 (1997) 553.
[22] G.D. Sorarù, G. D'Andrea, R. Campostrini, F. Babonneau, J. Mater. Chem. 5 (1995) 1363.

[23] S. Diré, F. Babonneau, G. Carturan, J. Livage, J. Non Cryst. Solids 147–148 (1992) 62.
[24] F. Babonneau, J. Maquet, S. Diré, Polymer Preprints 34 (1993) 242.
[25] D. Hoebbel, T. Reinert, H. Schmidt, J. Sol-Gel Sci. Technol. 6 (1996) 139.
[26] D. Hoebbel, T. Reinert, H. Schmidt, J. Sol-Gel Sci. Technol. 7 (1996) 217.
[27] D. Hoebbel, M. Nacken, H. Schmidt, V. Huch, M. Veith, J. Mater. Chem. 8 (1998) 171.
[28] V.W. Day, T.A. Eberspacher, W.G. Klemperer, C.W. Park, F.S. Rosenberg, in: L.L. Hench, J.K. West (Eds.), Chemical Processing of Advanced Materials, Wiley, New York, 1992, p. 257.
[29] T.J. Bastow, A.F. Moodie, M.E. Smith, H.J. Whitfield, J. Mater. Chem. 3 (1993) 697.
[30] L. Delattre, M. Roy, F. Babonneau, J. Sol-Gel Sci. Technol. 8 (1997) 567.
[31] R.H. Glaser, G.L. Wilkes, C.E. Bronnimann, J. Non-Cryst. Solids 113 (1989) 73.
[32] M.P.J. Peeters, W.J.J. Wakelkamp, A.P.M. Kentgens, J. Non-Cryst. Solids 189 (1995) 77.
[33] C.A. Fyfe, H. Gies, Y. Feng, J. Am. Chem. Soc. 111 (1989) 7702.
[34] C.T.G. Knight, R.J. Kirkpatrick, E. Oldfield, J. Non-Cryst. Solids 116 (1990) 140.
[35] R. Benn, H. Grondey, C. Brevard, A. Pagelot, J. Chem. Soc., Chem. Commun. (1988) 102.
[36] C.A. Fyfe, H. Gies, H. Grondey, G.T. Kokotailo, J. Am. Chem. Soc. 112 (1990) 3264.
[37] A. Pines, M.G. Gibby, J.S. Waugh, J. Chem. Phys. 59 (1973) 569.
[38] S. Diré, E. Pagani, R. Ceccato, G. Carturan, J. Mater. Chem. 7 (1997) 919.
[39] A.J. Vega, J. Am. Chem. Soc. 110 (1988) 1049.
[40] C. Zhang, F. Babonneau, C. Bonhomme, R.M. Laine, C.L. Soles, H.A. Hristov, A.F. Yee, J. Am. Chem. Soc. 120 (1998) 8380.
[41] C.A. Fyfe, Y. Zhang, P. Aroca, J. Am. Chem. Soc. 114 (1992) 3252.
[42] P.J. Dirken, M.E. Smith, H.J. Whitfield, J. Phys. Chem. 99 (1995) 395.
[43] D.M. Pickup, G. Mountjoy, G.W. Wallidge, R. Anderson, J.M. Cole, R.J. Newport, M.E. Smith, J. Mater. Chem. 9 (1999) 1299.
[44] P.J. Dirken, S.C. Kohn, M.E. Smith, E.R.H. van Eck, Chem. Phys. Lett. 266 (1997) 568.
[45] C. Jäger, R. Dupree, S.C. Kohn, M.G. Mortuza, J. Non-Cryst. Solids 155 (1993) 95.
[46] B. Schaudel, C. Guermeur, C. Sanchez, K. Nakatani, J.A. Delaire, J. Mater. Chem. 7 (1997) 61.
[47] C. Guermeur, J. Lambard, J.F. Gérard, C. Sanchez, J. Mater. Chem. 9 (1999) 769.
[48] D.M. Pickup, G. Mountjoy, G.W. Wallidge, R.J. Newport, M.E. Smith, Phys. Chem. Chem. Phys. 1 (1999) 2527.
[49] J.A. Tossell, Am. Mineral. 78 (1993) 911.
[50] A. Medek, J.S. Harwood, L. Frydman, J. Am. Chem. Soc. 117 (1995) 12779.
[51] S. Wang, J. Stebbins, J. Am. Ceram. Soc. 82 (1999) 1519.
[52] G.D. Sorarù, N. Dallabona, C. Gervais, F. Babonneau, Chem. Mater. 11 (1999) 910.
[53] D. Massiot, B. Touzo, D. Trumeau, J.P. Coutures, J. Virlet, P. Florian, P.J. Grandinetti, Solid State NMR 6 (1996) 73.
[54] V. Gualandris, J. Maquet, F. Babonneau, P. Florian, D. Massiot, Mater. Res. Soc. Symp. Proc., in press.

PERGAMON

www.elsevier.nl/locate/poly

Polyhedron 19 (2000) 323–330

POLYHEDRON

Synthesis of silyl substituted organoboranes by hydroboration of vinylsilanes

Lutz M. Ruwisch, Peter Dürichen, Ralf Riedel *

Technische Universität Darmstadt, Fachbereich Materialwissenschaft, Fachgebiet Disperse Feststoffe, Petersenstrasse 23, 64287 Darmstadt, Germany

Received 1 May 1999; accepted 18 July 1999

Abstract

Hydroboration reactions of dichloroborane-, monochloroborane- and borane-dimethylsulfide with dichloromethylvinylsilane and trichlorovinylsilane were investigated. The proposed structures of the produced organochlorosilylboranes **1**–**4** were verified by NMR spectroscopic measurements and in the case of [α-(dichloromethylsilyl)ethyl]dichloroborane-dimethylsulfide (**4**) the molecular structure was determined by single-crystal X-ray diffraction (L.M. Ruwisch, R. Riedel, U. Klingebiel, M. Noltemeyer, Z. Naturforsch., Teil B 54 (1999) 624). Following the Markovnikov rule, the first addition appears strictly regioselective in the α-position to silicon, producing one chiral methine group between silicon and dichloroborane in compound **4**. The second addition of borane- or monochloroborane-dimethylsulfide at the vinyl groups of dichloromethylvinylsilane and trichlorovinylsilane also takes place in the α-position to silicon, forming a second chiral methine group. In the case of borane-dimethylsulfide the third addition occurs in the β-position (anti-Markovnikov) owing to steric hindrance to boron in tris[(dichloromethylsilyl)ethyl]borane (**1**). A stepwise substitution of chlorine bonded at boron in compounds **2** and **3** using hexamethyldisilazane produces bis[α-(dichloromethylsilyl)ethyl]boryl-trimethylsilylamine (**5**) and bis[α-(trichlorosilyl)ethyl]boryl-trimethylsilylamine (**6**), respectively, under release of chlorotrimethylsilane. The remaining trimethylsilylamine group in **6** can be replaced by further reaction with **3** forming tetrakis[α-(trichlorosilyl)ethyl]diborylamine (**7**). This reaction resembles a selective amino condensation at boron. In a similar condensation reaction of **4** with equivalent amounts of hexamethyldisilazane, tris[α-(dichloromethylsilyl)ethyl]borazine (**8**) can be obtained. ©2000 Elsevier Science Ltd All rights reserved.

Keywords: Hydroboration; Polysilazanes; Precursors; Vinylsilanes; Chloroboranes

1. Introduction

The synthesis of monomeric molecular precursors is one of the major steps in the construction of polymers with definable structural composition as starting materials for the production of novel ceramics with unique properties such as ultra high temperature stability or extraordinary hardness. Depending on the different synthetic pathways applied, the elemental composition of the polymers varies from binary to ternary to quaternary or multinary systems. Nitrogen and/or carbon in addition to main group elements (E = B, P, O, Al, Si) are utilized for the synthesis of a wide range of preceramic polymers with different elemental compositions [1]. Currently, new ceramic materials in the quaternary Si–B–C–N system derived from polymers with outstanding thermal stability in combination with improved crystallization resistance are under investigation by different authors [2,3]. Boron plays an important but still little understood role in enhancing the high temperature characteristics of these boron modified polyorganosilazane derived materials. One first step towards interpretation of the influence of boron is to vary the amount of boron by varying the silicon to boron ratio or to modify the boron environment within the precursors.

Silyl substituted organoboranes produced by hydroboration reactions are generally suitable compounds for the synthesis of polyorganoborosilanes, polyorganosiloxanes [4] and polyorganosilazanes [2,5]. Owing to the functional chlorine attached to silane it is possible to transform the monomeric units into molecules, oligomers and polymers by substitution reactions. Therefore, condensation reactions such as hydrolysis, ammonolysis or aminolysis, and salt elimination such as Wurtz analogue reactions are utilized. The resulting monomers, oligomers, and polymers are defined by the structure and composition of the monomeric building units. Also the silicon to boron ratio of the precursors from which the ceramics will be prepared can be controlled. Nevertheless, owing to the restrictions on the use of BH_3

* Corresponding author. Tel.: +49-6151-166347; fax: +49-6151-166346; e-mail: dg9b@hrzpub.tu-darmstadt.de

0277-5387/00/$ - see front matter ©2000 Elsevier Science Ltd All rights reserved.
PII S0277-5387(99)00362-9

complexes in hydroboration reactions, the resulting Si:B ratios of monomers currently do not change. Only the cocondensation of derived monomers with additional chlorosilanes or the subsequent modification with boranes or boron compounds can be used to adjust higher or lower Si:B ratios in the final polymer. Depending on the different production pathways applied, the elemental compositions of the polymers vary by the amount of secondary modification.

We are currently exploring the Si–B–C–N system in order to develop a precursor concept for ultra high temperature ceramics with extraordinary thermal stability up to 1700°C and above [6]. In this paper we report on the synthesis and characterization of the aforementioned monomolecular species via hydroboration. The selective condensation of the resultant chloro functional boranes with hexamethyldisilazane will be discussed also. Our work is basically focused on the systematic construction of molecules with various Si and B ratios with the aim of studying the influence of the Si:B ratio on the pyrolytic behaviour of the derived polymers and on the high temperature thermal stability of the resulting silicoboron carbonitride ceramics.

2. Experimental

2.1. General

All syntheses were performed under dry (P_4O_{10}) inert atmosphere (argon). The utilized glassware was stored in a drying oven for several hours at 120°C. Toluene was dried with a sodium-benzophenone mixture under reflux. Dichloromethane was dried and stored over pure water-free calcium dichloride. All solvents and chemicals were handled using Schlenk techniques. The commercially available silanes were distilled before use and the boranes were stored at 4°C and used as received by syringe.

^{1}H, ^{13}C, ^{11}B, and ^{29}Si NMR spectroscopy was performed in C_6D_6 or $CDCl_3$ with a Bruker WM 300 spectrometer. Tetramethylsilane was used as an internal standard and trifluoroborane-diethyl ether was used as external standard for ^{11}B NMR. The ^{13}C and ^{29}Si data of compounds **1**–**4** are given in Table 1, and all ^{11}B NMR data are given in Table 2. The mass spectroscopy was performed with a Balzers 429 mass spectrometer. Purification of the reaction products by distil-

Table 1
^{13}C and ^{29}Si NMR data of compounds **1**–**4**

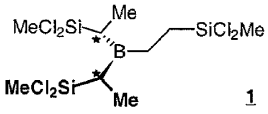
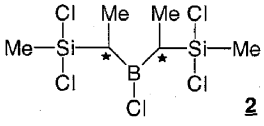
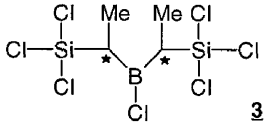
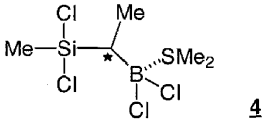
Molecule	Group	^{13}C NMR (ppm)	^{29}Si NMR (ppm)
 **1**	β-*Si*Cl_2–*C*H_3	4.20/4.36/4.44	32.85/33.14/33.36
	α-*Si*Cl_2–*C*H_3	5.73/5.91/6.27	28.06/28.21/28.96
	B(Si)–CH–*C*H_3	10.27/10.45/10.76	
	Si-CH_2–CH_2–B	14.55/15.31/16.61	
	Si–CH_2–*C*H_2–B	16.02/18.61/19.01	
	B(Si)–*C*H–CH_3	28.51/29.84/33.40	
 **2**	α-*Si*Cl_2–*C*H_3	4.96/5.89	27.17/28.08
	B(Si)–CH–*C*H_3	11.13/11.30	
	B(Si)–*C*H–CH_3	31.40/34.53	
 **3**	*Si*Cl_3		4.41, 8.42
	B(Si)–CH–*C*H_3	10.97/11.14	
	B(Si)–*C*H–CH_3	32.78/36.00	
 **4**	α-*Si*Cl_2–*C*H_3	7.93	36.08
	B(Si)–CH–*C*H_3	12.43	
	S$(CH_3)_2$	17.20	
	B(Si)–*C*H–CH_3	20.83	

Table 2
^{11}B NMR data for compounds **1**–**8**

Compound	**1**	**2**	**3**	**4**	**5**	**6**	**7**	**8**
Boron coordination	BC_3	$ClBC_2$	$ClBC_2$	$Cl_2BCS(CH_3)_2$	NBC_2	NBC_2	NBC_2	N_2BC
^{11}B NMR (ppm)	80.0	69.4	68.5	5.8	45.1	43.6	43.8	30.2

lation was avoided because of the thermal instability of the obtained boranes.

2.2. Tris[(dichloromethylsilyl)ethyl]borane (1) [2]

Into a precooled solution of 100 ml (108.5 g, 0.76 mol) dichloromethylvinylsilane dissolved in 50 ml toluene, a mixture of 23.6 ml (19.0 g, 0.25 mol) of borane-dimethylsulfide and 50 ml toluene was added. During the addition of borane and for the first 6 h the temperature should not exceed 10°C. After 30 h of stirring at room temperature the released dimethylsulfide and toluene were removed under reduced pressure (0.02 Torr) at 60°C, and 107 g (98%) of the colourless liquid product were obtained.

Anal. Found: C, 24.3; H, 4.8; Cl, 49.2; Si, 18.1; B, 2.2. Calc.: C, 24.7; H, 4.8; Cl, 48.6; Si, 19.2; B, 2.5%. $\Sigma = 98.6\%$.

Mass spectra (rel. int., %): $C_9H_{21}Cl_6Si_3B$ ($M = 437.1$); 293 (90) $[M–(C_2H_4–SiCl_2CH_3)]^+$.

FT-IR spectra (thin film, KBr, cm^{-1}): ν 3000–2835 (CH_x); 1466 (CH_x); 1261 (Si–CH_x); 1171 (B–C_x); 790 (Si–CH_3); 560, 480 (Si–Cl_2).

NMR (C_6D_6, ppm): ^{1}H δ 0.47, 0.47, 0.48, 0.49, 0.51, 0.55 ($SiCH_3$), 0.86–1.48 (CH_2–CH_2), 1.09–1.13 (CH_3), 1.58–2.03 (CH); ^{11}B δ 80 ($h_{1/2} = 1650$ Hz); ^{13}C and ^{29}Si see Table 1.

2.3. Bis[(α-dichloromethylsilyl)ethyl]chloroborane (2)

A solution of 36 ml (38.1 g, 0.345 mol) chloroborane-dimethylsulfide and 50 ml toluene was added dropwise into a precooled mixture of 90.6 g (98.3 g, 0.70 mol) dichloromethylvinylsilane and 50 ml toluene. The reaction mixture was held below 10°C over 6 h and subsequently warmed to room temperature. After 20 h stirring the side products dimethylsulfide and toluene were removed under vacuum (0.02 Torr) and at 60°C. 110 g (97%) of the colourless liquid **2** were obtained.

Anal. Found: C, 21.5; H, 4.5; Cl, 53.1; Si, 17.7; B, 3.0. Calc.: C, 21.9; H, 4.2; Cl, 55.2; Si, 17.0; B, 3.3%. $\Sigma = 99.8\%$.

Mass spectrum (rel. int., %): $C_6H_{14}Cl_5Si_2B$ ($M = 330.5$); 328 (50) $[M]^+$.

FT-IR spectra (thin film, KBr, cm^{-1}): ν 3000–2840 (CH_x); 1466 (CH_x); 1269 (Si–CH_x); 1179 (B–C_x); 1040 (B–Cl); 802 (Si–CH_3); 560, 480 (Si–Cl_2).

NMR (C_6D_6, ppm): ^{1}H δ 0.48 ($SiCH_3$, 6H), 0.57 ($SiCH_3$, 6H), 1.17 (CH_3, 6H), 1.18 (CH_3, 6H), 1.74 (CH, 2H), 1.97 (CH, 2H); ^{11}B δ 69.4 ($h_{1/2} = 629$ Hz); ^{13}C and ^{29}Si see Table 1.

2.4. Bis[(α-trichlorosilyl)ethyl]chloroborane (3)

The synthesis of **3** was carried out under the same reaction conditions as used for **2**. Into a solution of 87.8 ml (111.5 g, 0.70 mol) trichlorovinylsilane and 50 ml toluene, 36 ml (38.1 g, 0.345 mol) chloroborane-dimethylsulfide were added. After completion of the reaction the solvent toluene and dimethylsulfide were removed under vacuum (0.02 Torr) and 84.5 g (98%) of **3** were obtained as a colourless liquid.

Mass spectrum (rel. int., %): $C_4H_8Cl_7Si_2B$ ($M = 371.3$); 333 (20) $[M–Cl]^+$.

FT-IR spectra (thin film, KBr, cm^{-1}): ν 3000–2875 (CH_x); 1458 (CH_x); 1278 (Si–CH_x); 1161 (B–C_x); 1040 (B–Cl); 625–570, 535–450 (Si–Cl_3).

NMR (C_6D_6, ppm): ^{1}H δ 1.14 (CH_3, 6H), 1.21 (CH_3, 6H), 1.85 (CH, 2H), 2.08 (CH, 2H); ^{11}B δ 68.5 ($h_{1/2} = 495$ Hz); ^{13}C and ^{29}Si see Table 1.

2.5. [(α-Dichloromethylsilyl)ethyl]dichloroborane-dimethylsulfide (4)

Into a solution of 22.5 ml (24.5 g, 0.17 mol) dichloromethylvinylsilane in 50 ml dichloromethane, a homogeneous mixture of 20 ml (25.1 g, 0.17 mol) dichloroborane-dimethylsulfide dissolved in dichloromethane was added. After 6 h stirring at room temperature the reaction mixture was held under reflux for 2 h. Excess solvent was removed under vacuum and 44.9 g (93%) of colourless liquid **4** were obtained.

Mass spectrum (rel. int., %): $C_5H_{13}Cl_4SiBS$ ($M = 285.9$); 222 (60) $[M–S(CH_3)_2]^+$.

FT-IR spectra (thin film, KBr, cm^{-1}): ν 2980–2850 (CH_x); 1460 (CH_x); 1250 (Si–CH_x); 1156 (B–C_x); 1035, 985 (B–Cl_2); 789 (Si–CH_3); 630, 590 ($S(CH_3)_2$); 560, 465 (Si–Cl_2).

NMR (C_6D_6, ppm): ^{1}H δ 0.93 ($SiCH_3$, 3H), 1.25 (CH_3, 3H), 1.57 ($S(CH_3)_2$/CH, 7H); ^{11}B δ 5.8 ($h_{1/2} = 64$ Hz); ^{13}C, ^{29}Si see Table 1.

2.6. Bis[(α-dichloromethylsilyl)ethyl]boryl-trimethylsilylamine (5)

Into 10 ml (12.7 g, 37.8 mmol) of precooled compound **2**, equivalent amounts (8.0 ml, 6.15 g, 38 mmol) of HMDS were added. The reaction mixture was constantly stirred for 2 h at 0°C and the chlorotrimethylsilane produced was removed at 30°C under vacuum (0.02 Torr). Compound **5** was isolated in 14.5 g (98%) yield as a colourless liquid.

Anal. Found: C, 28.0; H, 6.1; Cl, 36.6; Si, 21.5; B, 2.7; N, 3.7. Calc.: C, 28.3; H, 6.3; Cl, 36.7; Si, 22.0; B, 2.9; N, 3.7%. $\Sigma = 98.6\%$.

Mass spectrum (rel. int., %): $C_9H_{24}Cl_4Si_3BN$ ($M = 383.2$); 310 (50) $[M–Si(CH_3)_3]^+$.

NMR ($CDCl_3$, ppm): ^{1}H δ 0.21–0.24 ($Si(CH_3)_3$), 0.75–0.78 ($SiCH_3$, 6H), 1.20–1.25 (CH_3, 6H), 1.34–1.36 (CH, 2H), 4.1 (NH, 1H); ^{11}B δ 45.1 ($h_{1/2} = 792$ Hz); ^{13}C δ 1.54, 1.92 ($Si(CH_3)_3$), 5.7, 5.9 ($SiCH_3$), 9.9, 11.3 (CH_3), 18.1, 23.2 (CH); ^{29}Si δ 5.5 ($Si(CH_3)_3$), 32.3, 33.4 ($SiCl_2CH_3$).

2.7. Bis[(α-trichlorosilyl)ethyl]boryl-trimethylsilylamine (6)

Under the same reaction conditions as described for the synthesis of **5**, 8.0 ml (6.15 g, 38 mmol) HMDS were added

dropwise into 10 ml (13.9 g, 37.7 mmol) of compound **3**. After extraction of chlorotrimethylsilane 15.9 g (99%) of colourless liquid compound **6** were obtained.

Mass spectrum (rel. int., %): $C_7H_{18}Cl_6Si_3BN$ (M = 424.0); 406 (15) $[M–CH_3]^+$.

FT-IR spectra (thin film, KBr, cm^{-1}): ν 3368 (N–H); 2965–2875 (C–H_x); 1617 (N–H); 1456 (C–H_x); 1420–1380 (B–N); 1260 (Si–CH_x); 1155 (B–C_x); 624–575, 500 (Si–Cl_3).

NMR ($CDCl_3$, ppm): ^{1}H δ 0.24–0.27 ($Si(CH_3)_3$), 1.28–1.37 (CH_3, 6H), 1.55–1.63 (CH, 2H), 4.2–4.3 (NH, 1H); ^{11}B δ 43.6 ($h_{1/2}$ = 633 Hz); ^{13}C δ 1.76, 1.86 ($Si(CH_3)_3$), 10.0, 11.6 (CH_3), 21.3, 26.0 (CH); ^{29}Si δ 6.7 ($Si(CH_3)_3$), 11.9, 12.4 ($SiCl_3$).

2.8. Tetrakis[(α-trichlorosilyl)ethyl]-diborylamine (7)

10 ml (13.9 g, 37.7 mmol) of **3** were precooled at 0°C. After addition of 3.9 ml (3.0 g, 18.8 mmol) HMDS the mixture was heated to reflux. The chlorotrimethylsilane formed was removed under vacuum (0.02 Torr) and 12.7 g (99%) of **7** were obtained as a colourless liquid.

Anal. Found: C, 16.5; H, 3.3; N, 2.0; Cl, 58.4; Si, 16.8; B, 2.7. Calc.: C, 16.4; H, 2.5; N, 2.0; Cl, 61.7; Si, 16.3; B, 3.2%. Σ = 99.7%.

FT-IR spectra (thin film, KBr, cm^{-1}): ν 3368 (N–H); 2965–2875 (CH_x); 1617 (N–H); 1450 (CH_x); 1430–1375 (B–N); 1260 (Si–CH_x); 1155 (B–C_x); 624–575, 500 (Si–Cl_3).

NMR ($CDCl_3$, ppm): ^{1}H δ 1.14–1.17 (CH_3, 12H), 1.44–1.57 (CH, 4H), 4.14 (NH, 1H); ^{11}B δ 43.8 ($h_{1/2}$ = 1330 Hz); ^{13}C δ 9.92, 11.50 (CH_3), 21.40, 26.1 (CH); ^{29}Si δ 12.1, 12.6 ($SiCl_3$).

2.9. Tris[(α-dichloromethylsilyl)ethyl]borazine (8)

Into 20 ml (23.7 g, 83.5 mmol) of compound **4**, 18 ml (13.5 g, 85 mmol) HMDS were added. After heat treatment at 30°C for 2 h the chlorotrimethylsilane produced was removed at 0.02 Torr to isolate **8** as a colourless liquid, 13.9 g (98%) yield.

Anal. Found: C, 20.7; H, 4.4; N, 7.3; Cl, 44.1; Si, 14.3; B, n.d. Calc.: C, 21.6; H, 4.8; N, 8.4; Cl, 41.9; Si, 16.8; B, 6.6%.

$C_9H_{24}N_3Si_3Cl_6B_3$ (503.71). FD-MS *m/z* (%): 501 (94) $[M]^+$.

FT-IR spectra (thin film, KBr, cm^{-1}): ν 3437 (N–H); 2965–2868 (CH_x); 1344–1510 (B–N); 1260 (Si–CH_x); 1131 (B–C_x); 792 (Si–CH_3).

NMR ($CDCl_3$, ppm): ^{1}H δ 0.38, 0.47 (s, SiMe), 0.90, 1.06 (m, $CHCH_3$), 4.82 (NH); ^{11}B δ 30.23; ^{13}C δ 4.49, 5.44 (SiMe), 9.10, 9.13 (CH), 31.06, 34.12 (CH_3); ^{29}Si δ 32.7, 33.3.

3. Discussion

The main focus of our work was to alter the silicon to boron ratio within the molecular precursor in a directed way. For this we investigated the hydroboration reactions of borane-, monochloroborane- and dichloroborane-dimethylsulfide adducts with vinylsilanes. The reaction can be categorized according to the number of hydrogen atoms bonded to boron. Therefore the discussion will progress with respect to the borane, i.e. BH_3, $BClH_2$ and BCl_2H.

The appointed ^{13}C and ^{29}Si NMR data of the compounds prepared by these hydroboration reactions are summarized in Table 1, and the ^{11}B NMR shifts of all synthesized molecules are given in Table 2.

3.1. Hydroboration with BH_3

The reaction of borane dimethylsulfide with dichloromethylvinylsilane in toluene results in the formation of tris[(dichloromethylsilyl)ethyl]borane (**1**) (Fig. 1). The respective compound **1** was first prepared by Mikhailev in 1969 [7]. Later Jones et al. investigated several hydroboration reactions of chloromethylsilylalkenes with diborane dissolved in THF, in order to analyse stereochemical effects of primarily generated silyl substituted boranes on further additions of different chlorine functionalized alkenylsilanes [8,9]. The chlorosilylorganoboranes obtained by Jones et al. were not isolated but instead were transformed directly into organosilylboranes, using methylmagnesiumbromide, and subsequently were oxidized smoothly with hydrogen peroxide. The resulting silyl substituted alcohols were analysed by GLC and IR spectroscopy and an isomeric ratio of 90% of 1-silylethanol and 10% of 2-silylethanol was found in the case of compound **1**.

Our investigations on the reaction of 3 equiv. dichloromethylvinylsilane with borane-dimethylsulfide revealed that the first two hydroboration additions take place in the α-position forming dichloromethylvinylsilane. These additions are controlled by a partial negative charge on the α-C atom, resulting from an electron withdrawing effect of silyl chlorine induced by a $(p–\sigma)_\pi$ conjugation of the β-vinylcarbon in $C{=}C–SiCl_2(CH_3)$ [10]. Therefore the reaction of the strong electrophilic Lewis acid borane with vinylsilanes leads to an addition of boron at the α-positioned carbon atom next to silicon. This is in good agreement with results from stereochemical investigations reported by Soderquist et al. [11,12] obtained from similar reactions of borane-dimethylsulfide with 2 equiv. of alkenylsilanes. They describe only α-addition, producing two chiral methine groups between silicon and boron under preservation of the remaining B–H bond.

The third addition is dominated by a steric hindrance caused by the previously added two [α-(dichloromethylsilyl)ethyl] groups. Consequently, the remaining B–H bond reacts in β-addition to silicon, independent of the negative

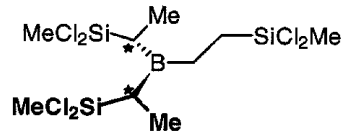


Fig. 1. Structure of **1**.

partial charge at the α-carbon of the silyl substituted vinyl group as mentioned above. This is consistent with analogous results of Soderquist et al. [12] obtained from hydroboration reactions of 9-borabicyclo[3.3.1]nonane and vinylsilanes, which ascertain a high β-regioselectivity of about 99% for dialkylboranes in hydroboration reactions with vinylsilanes.

We were able to confirm the two additions in α-position forming two chiral methine groups and the third hydroboration in β-position producing one ethylene group between boron and silicon by NMR spectroscopic investigations of compound **1**.

Owing to the two chiral methine centres, each connected to silicon, boron, carbon, and hydrogen, four constitutional isomers are formed, one pair of enantiomers (*RR*+*SS*) and the corresponding mesomers (*S*,*R* and *R*,*S*). Thus an A,B,C_2 spectrum should be expected in the ^{1}H, ^{13}C and ^{29}Si NMR. The spectrum is further complicated because of the rotating β-(dichloromethylsilyl)ethyl group. With respect to the planar environment of the central boron atom in **1** this group can be located above (*cis*) or below (*trans*) the *meso* conformations (Fig. 2). This produces an unsymmetrical signal splitting of the *meso* isomers in the ^{29}Si NMR and the corresponding ^{13}C and ^{1}H NMR spectra. In the enantiomeric *RR* and *SS* form the third addition does result in a similar pattern, owing to the resultant symmetrical environment at boron. Therefore, the β-addition produces an A,B,C,C′ spectrum (d+l, *meso*-above and *meso*-below) in the ^{1}H, ^{13}C and ^{29}Si NMR spectra of tris[(dichloromethylsilyl)ethyl]borane (**1**). The determined ^{29}Si NMR resonance of the α-hydroborated silanes are in the range from 28 to 30 ppm. The nearby location of boron effects a shift to high field of α-positioned silicon compared to a hydrogen substituted ethyl group [13]. The β-positioned dichloromethylsilylethyl group produces three ^{29}Si NMR signals between 32 and 34 ppm, according to symmetrical operations at the 1-boryl-2-silyl-substituted ethane. An intensity ratio of 2:1 was found for the α- and β-silicon in the ^{29}Si NMR spectrum. Considering the low ^{29}Si isotope abundance it will be necessary to verify the observed peak intensities by further measurements.

The same intensity ratio of 2:1 is found for the 1,1-ethyl and 1,2-ethylene protons in the ^{1}H NMR spectrum, after normalization by the observed methylsilyl-proton intensities. The appearance of six silyl bonded methyl groups supports the expected peak splitting for three isomers multiplied by two for α and β bonded silyl groups in tris[(dichloromethylsilyl)ethyl]borane (**1**). This finding coincides with ^{13}C (DEPT)-NMR data, which showed six methylene carbon in the shift range from 13 to 19 ppm. Three signals produced by C-bonded methyl groups at 10 ppm and three broad methine signals between 27 and 34 ppm ascertain the expected A,B,C,C′ isomer splitting in compound **1**. The observed peak broadening of the methine carbon originates from the magnetic quadrupole nucleus boron in direct contact to carbon. In ^{11}B NMR measurements the central boron appears at 80 ppm with a peak broadening of $h_{1/2}=1650$ Hz, which can also be caused by the isomer alteration.

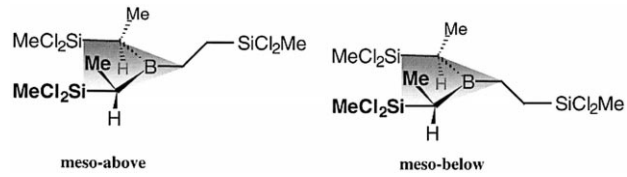


Fig. 2. Enantiomeric forms of **1**.

3.2. Hydroboration with BH_2Cl

In a similar hydroboration reaction of dichloromethylvinylsilane or trichlorovinylsilane with monochloroborane-dimethylsulfide, two organosilyl substituted boranes are formed, bis[(α-dichloromethylsilyl)ethyl]chloroborane (**2**) and bis[(α-trichlorosilyl)ethyl]chloroborane (**3**). Reactions of alkenes with monochloroborane-dimethylsulfide published by Brown et al. [14] resulted in a characteristic high α-regioselectivity of monochloroboranes for silyl substituted alkenes. Comparable investigations of Soderquist et al. [11] on the reaction of borane-dimethylsulfide with different vinylsilanes exhibited the same exclusive α-addition of borane next to silicon. Therefore it is evident that two chiral α-carbon centres are formed via this addition process and an A,B spectrum is expected, the enantiomeric isomers (*RR*+*SS*) and the *meso* form respectively. The ^{29}Si NMR data exhibit the typical C_2SiCl_2 (27.6, 27.2 ppm) **2** and $CSiCl_3$ (6.8, 6.2 ppm) **3** [15] shifts and confirm the A,B-splitting of the chiral methine groups. In ^{13}C-(DEPT) NMR data two broad peaks of the methine C-atoms bonded to boron and silicon are found at 28 and 33 ppm. The corresponding methyl groups appear at 9.4 and 9.5 ppm for bis[(α-dichloromethylsilyl)ethyl]chloroborane (**2**). This is in full agreement with the methine and methyl groups in compound **1**. In the ^{13}C NMR spectra of compound **3** we also found two broad signals at 33 and 35 ppm reflecting the methine groups. The corresponding methyl groups appear at ∼11 ppm. Owing to the exchange of carbon by chlorine, in comparison to compound **1** the boron resonances are shifted to 69.4 ppm in **2** and 68.5 ppm in **3**. From ^{1}H NMR a $^{3}J_{H-H}$ coupling of 6.7 and 6.8 Hz between methine and methyl protons was found in both molecules **2** and **3**. Only the chemical shifts differ in accordance with the silyl substituents. It can be concluded from our investigations that the first two additions of B–H take place strictly in α-position to silicon and are unaffected by the silicon or boron substituents.

3.3. Hydroboration with $BHCl_2$

In contrast to the previously described synthesis of compounds **1**, **2** and **3** in toluene, dichloroborane-dimethylsulfide added to a solution of dichloromethylvinylsilane dissolved in toluene does not lead to the presumed hydroboration forming [(α-dichloromethylsilyl)ethyl]dichloroborane (**4**). The decreased reactivity of dichloroborane-dimethylsulfide compared to borane- and monochloroborane-dimethylsulfide can be attributed to the stronger Lewis acidity of the $HBCl_2$ group. Consequently, dissociation of the dimethylsulfide adduct in

toluene is hampered [16]. Performing the reaction in methylene dichloride as solvent supports the dissociation of dichloroborane and dimethylsulfide and leads to a higher quantity of uncomplexed $HBCl_2$ [17] which can react directly with dichloromethylvinylsilane. During extraction of excess methylene dichloride [(α-dichloromethylsilyl)-ethyl]dichloroborane (**4**) and dimethylsulfide reassemble to form a stable 1:1 adduct with dimethylsulfide bonded to boron. The formed complex precipitates after 1 day at 7°C. From the crystals obtained the structure of **4** was determined by means of single-crystal X-ray diffraction [18]. Corresponding to the discussed regioselectivity the hydroboration of dichloroborane appears only in the α-position to silicon. Owing to the formation of the chiral methine groups, optical isomers *R* and *S* have to be considered. The NMR data again prove the exclusive formation of [(α-dichloromethylsilyl)ethyl]dichloroborane-dimethylsulfide (**4**). ^{13}C-DEPT NMR studies show the α-C atom of the original vinyl group bonded to boron with a signal at 20.83 ppm. The ^{1}H NMR spectrum exhibits a coupling constant of $^{3}J_{H-H} = 7.3$ Hz of the methine proton at 1.25 ppm, appearing as a quartet, and the methyl proton (doublet, superimposed by the peaks of the dimethylsulfide protons) at ~1.57 ppm. The high field shift of the related dimethylsulfide at $\delta = 1.57$ ppm compared to free dissolved dimethylsulfide ($\delta \geq 1.7$ ppm) and a peak broadening verifies the presence of an adduct.

The presented hydroboration reactions are summarized in the scheme given in Fig. 3. It clearly demonstrates the influence of the amount of chlorine in the borane on the composition of the resulting organosilylborane. As can be seen, the Si:B ratio adopts values from 3:1 to 1:1 depending on the borane used. The novel organosilylboranes allow the desired Si:B ratio to be adjusted for further transformations into polymers and ceramics with predefined compositions and properties.

3.4. Stepwise substitution with hexamethyldisilazane (HMDS)

In a second reaction step it is possible to replace selectively chlorine bonded to boron of the previously synthesized chloroboranes **2**, **3** and **4** by trimethylsilylamine using HMDS. Reactions of halogeno boranes with hexamethyldisilazane were investigated by Kulijian [19], and are a source for continued work of Barlos and Noeth [20]. Baldus and Jansen substituted the trimethylsilyl group in trimethyltrichlorodisilazane (TTDS, [21]) by trichloroborane to form trichlorosilylaminodichloroborane (TADB) [3]. Based on this reaction, they synthesized new types of polyborosilazanes as ceramic precursors in the non-oxide systems Si–B–N and Si–B–(C)–N. In an analogous substitution reaction we reacted compounds **2** and **3** with equivalent amounts of HMDS to give bis[(α-dichloromethylsilyl)ethyl]boryl-trimethylsilylamine (**5**) and bis[(α-trichlorosilyl)ethyl]boryl-trimethylsilylamine (**6**) (Fig. 4). The side product chlorotrimethylsilane was removed from the reaction mixture

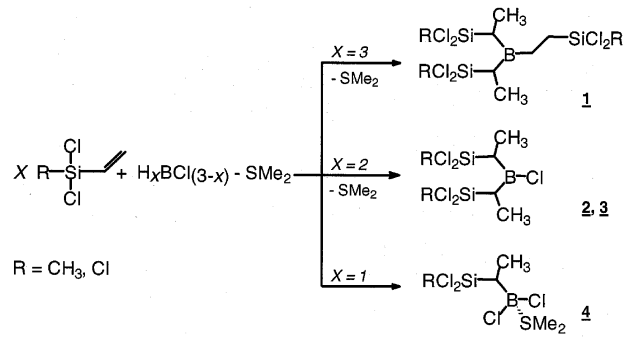


Fig. 3. Summarized reaction scheme for the reaction of chlorovinylsilanes with boranes and chloroboranes (see Section 3).

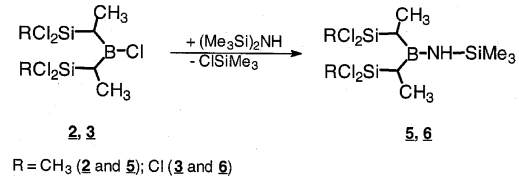


Fig. 4. Substitution reactions of HMDS at **2** and **3**.

by distillation under reduced pressure. Spectroscopic data (NMR, MS and FT-IR) of **5** and **6** reveal the systematic substitution of chlorine bonded to boron by $NH–SiMe_3$. The methine groups of the starting molecules are shifted to higher fields (^{13}C NMR, $\Delta\delta = -10$ to -15 ppm), whereas the connected silyl groups appear shifted slightly to lower magnetic fields compared to compounds **2** and **3** (^{29}Si NMR, $\Delta\delta = 5$ to 7 ppm). These changes are effected by the altered electronic properties of boron in **5** and **6**, compared to **2** and **3**, due to the introduced trimethylsilylamine group. The substitution of chlorine attached to silicon by HMDS was not found. The observed chemical shifts of boron to higher magnetic field in compounds **5** ($\delta = 45.1$ ppm) and **6** ($\delta = 43.6$ ppm) also reflect the exchange of chlorine by trimethylsilylamine and coincide with already published ^{11}B NMR data of $R_2B–NR_2$ (R = alkyl, H) [22].

Similar to the previously discussed substitution of Cl using HMDS to give **6**, bis[(α-trichlorosilyl)ethyl]boryl-trimethylsilylamine (**6**) itself can substitute Cl in bis[(α-trichlorosilyl)ethyl]chloroborane (**3**) leading to the formation of tetrakis[(α-trichlorosilyl)ethyl]diborylamine (**7**) (Fig. 5). The obtained molecule **7** can be described as a symmetrically silyl substituted diborylamine, corresponding to a regioselective condensation of bis[(α-trichlorosilyl)ethyl]chloroborane (**3**) with ammonia. This reaction allows for a selective step by step polymerization of silyl substituted chloroboranes, under prevention of well defined molecular units, and leads to a predictable elemental arrangement in the corresponding polymers. Except for the disappearance of the tri-

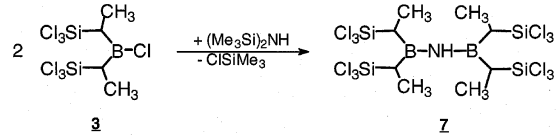


Fig. 5. Synthesis of tetrakis[(α-trichlorosilyl)ethyl]diborylamine (**7**).

methylsilyl group, compared to **6** the peak shifts in ^{11}B, ^{13}C and ^{29}Si NMR measurements were not significantly affected by the second substitution reaction forming compound **7**. The relative peak intensities of the amine protons at 4.1 ppm compared to the ethyl protons change from 1:8 (**6**) to 1:16 (**7**). The FT-IR spectra of compounds **6** and **7** reveal a typical resonance at 1628 cm^{-1}, due to a conjugated >B–NH group system as discussed earlier by Noeth et al. [23]. Independent of the second NH substituents (boron or silicon) the electron lone pair of the amine is part of a fluctuating back-bonding system between boron and nitrogen.

The reaction of [(α-dichloromethylsilyl)ethyl]dichloroborane-dimethylsulfide (**4**) with equivalent quantities of HMDS leads to a complete substitution of the chlorine bonded to boron forming tris[(α-dichloromethylsilyl)-ethyl]borazine (**8**) (Fig. 6). This finding can be explained by the formation of the intermediate [(α-dichloromethylsilyl)ethyl]chloroboryl-trimethylsilylamine which reacts further under intramolecular and/or intermolecular elimination of chlorotrimethylsilane. The silyl-substituted aminochloroborane formed as an intermediate cannot be isolated, although similar organosilylamino-chloroboranes are stable under these conditions for several days [24]. Depending on the B-substituent four-, six- and eight-membered B–N ring systems can be formed, besides minor amounts (< 5%) of polymeric chains [25]. A HCl elimination, described by Nöth and Spargue [26] was not observed. The reaction product **8** was characterized by NMR, and mass spectroscopy. Considering the three chiral methine groups connected to boron, four borazine isomers are formed, respectively two pairs of enantiomers (*RRR*/*SSS*) and (*RSS*/*SRR*). ^{29}Si NMR data show two peaks at 32.7 and 33.3 ppm, confirming the expected peak splitting for the two diastereometric isomers. We also found two separated peaks for the methine groups at 31.7 and 34.1 ppm and the methyl groups bonded to silicon at 4.5 and 5.4 ppm in the ^{13}C NMR spectra. The ^{11}B NMR data reflect the formation of alkyl(silyl) substituted borazine. Obviously the chiral substituents at boron give rise to a slight overlap forming a peak shoulder at 25 ppm, apart from the main peak at 30 ppm.

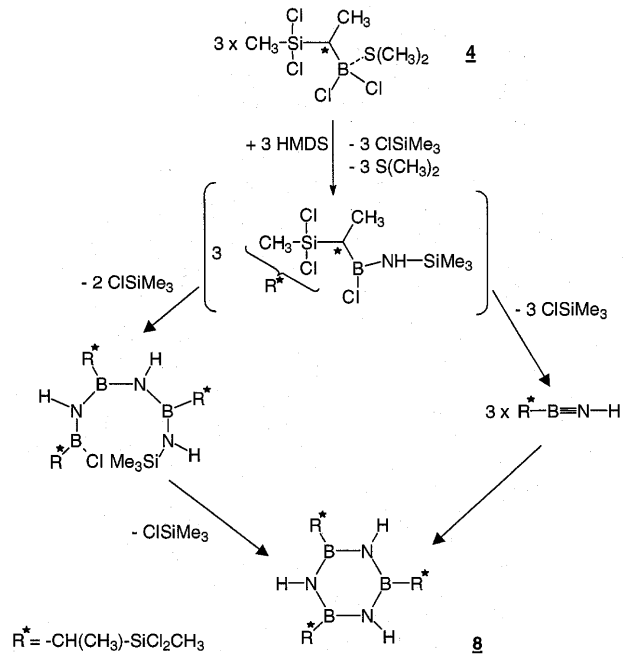


Fig. 6. Intramolecular and intermolecular condensation of **4**.

4. Conclusions and outlook

The hydroboration reaction of unsaturated organosilanes is a promising method for the synthesis of a wide range of single source precursors suitable for the production of preceramic polymers. It was shown that the hydroboration of vinylsilanes with chloroboranes gives access to molecular precursors with Si:B ratios ranging from 3:1 to 1:1. The stepwise substitution of silyl substituted dichloroboranes or monochloroboranes using HMDS or HMDS derivatives can be utilised for further adjustment of the Si:B ratios within these precursors.

The various molecular precursors can be transformed into polyborocarbosilazanes with predefined Si to B ratios by reaction with NH_3 or amines. After a crosslinking step around 300–400°C and pyrolysis at 1000°C, black amorphous ceramics with an unaltered Si:B ratio are obtained which reveal remarkable thermomechanical properties. The materials obtained from **1** and **2** by ammonolysis and subsequent pyrolysis show no further weight loss upon heating to 2000°C [2]. Moreover, a reduced tendency towards crystallization is observed, i.e. the ceramics remain amorphous up to about 1600°C. Other very promising properties are the high stability under oxidizing atmospheres and the very high resistance to creep [27]. Such properties make them potential candidates for applications as fibres and composite materials or as oxidation protective coatings. Interestingly a dependence of the mentioned properties on the elemental ratios as well as the structure of the molecular precursor was found. For example the ceramic prepared from compound **4** is quite unstable compared to that obtained from **1** and **2**. The SiBCN ceramic obtained from **4** exhibits a significant weight loss at $T > 1350$°C [28]. Such different behaviour is the reason for the necessity to prepare molecular precursor with defined elemental ratios. These precursors and the various ceramics prepared therefrom help us to clarify the processes involved during ceramic formation and especially the reasons for different high temperature stabilities of such compounds. In particular, the influence of boron in terms of content and chemical environment on the thermomechanical stability of the ceramics is presently under investigation.

Acknowledgements

We gratefully acknowledge financial support of the DFG (Deutsche Forschungsgemeinschaft/Bonn) and the Fonds der Chemischen Industrie (Frankfurt Germany).

References

[1] J. Bill, F. Aldinger, Adv. Mater. 7 (1995) 775.
[2] R. Riedel, A. Kienzle, W. Dreßler, L. Ruwisch, J. Bill, F. Aldinger, Nature 382 (1996) 796.
[3] H.-P. Baldus, M. Jansen, Angew. Chem. 109 (1997) 338.
[4] R. Riedel, A. Kienzle, G. Petzow, M. Brück, T. Vaahs, German Patent DE4320784-87, 1993.
[5] S.R. Riccitiello, M.T.S. Hsu, T.S. Chen, US Patent 4987201, 1991.
[6] W. Dressler, R. Riedel, Int. J. Refractory Hard Mater. 15 (1997) 13.
[7] B.M. Mikhailev, P.M. Aronovich, Zh. Obshchei Khim. 30 (1969) 3615.
[8] P.R. Jones, J.K. Myers, J. Organomet. Chem. 34 (1972) C9.
[9] P.R. Jones, J.K. Myers, J. Organomet. Chem. 38 (1976) 27.
[10] H.-U. Reißig, Chem. unserer Zeit 2 (1984) 46.
[11] J.A. Soderquist, S.H. Lee, Tetrahedron 44 (13) (1988) 4033.
[12] J.A. Soderquist, I. Rivera, A. Negron, J. Org. Chem. 54 (1989) 4051.
[13] J. Schraml, V. Chvalovsky, M. Mägi, E. Lippmaa, Collect. Czech. Chem. Commun. 44 (1979) 854.
[14] H.C. Brown, N. Ravindran, S.U. Kulkarin, J. Org. Chem. 44 (14) (1979) 2417.
[15] J. Schramml, V. Chvalovsky, M. Mägli, E. Lippmaa, Collect. Czech. Chem. Commun. 44 (1979) 854.
[16] H.C. Brown, N. Ravindran, J. Am. Chem. Soc. 99 (1979) 7097.
[17] H.C. Brown, N. Ravindran, J. Org. Chem. 42 (14) (1977) 2533.
[18] L.M. Ruwisch, R. Riedel, U. Klingebiel, M. Noltemeyer, Z. Naturforsch., Teil B 54 (1999) 624.
[19] A.B. Burg, E.S. Kulijian, J. Am. Chem. Soc. 72 (1950) 3103.
[20] K. Barlos, H. Noeth, Chem. Ber. 110 (1977) 2790.
[21] J.P. Mooser, H. Noeth, W. Tinhof, Z. Naturforsch., Teil B 29 (1974) 166.
[22] Houben-Weyl, Methoden der anorganischen Chemie, Band XIII/3a, 4. Aufl., 1982, p. 491.
[23] K. Jonás, H. Noeth, W. Storch, Chem. Ber. 110 (1977) 2783.
[24] P. Greymeyer, E.G. Rochow, U. Wannagat, Angew. Chem. 76 (1964) 499.
[25] J. Kiesgen, J. Münster, P. Paetzold, Chem. Ber. 126 (1993) 1559.
[26] H. Nöth, M. Spargue, J. Organomet. Chem. 22 (1970) 11.
[27] R. Riedel, L.M. Ruwisch, L. An, R. Raj, J. Am. Ceram. Soc. 81 (1998) 3341.
[28] L. Ruwisch, PhD Thesis, Technical University of Darmstadt, 1998.

PERGAMON

www.elsevier.nl/locate/poly

Polyhedron 19 (2000) 331–341

POLYHEDRON

Surface functionalization of cadmium sulfide quantum confined nanoclusters 6: Evidence of facile electronic communication between remote surface sites[1]

Jonathan G.C. Veinot, Abdiaziz A. Farah, Josie Galloro, Fabio Zobi, Valerie Bell, William J. Pietro *

Department of Chemistry, York University, 4700 Keele Street, Toronto, Ont. M3J 1P3, Canada

Received 30 April 1999; accepted 28 September 1999

Abstract

The preparation and derivatization of a series of surface functionalized ~30 Å cadmium sulfide nanoclusters possessing surfaces of varied electron demand, tethered covalently to an electroactive fluorescent ruthenium polypyridyl complex, are described. Electrochemical analyses of these nanoclusters bearing ruthenium moieties yield a monotonic relationship between the Ru(II/III) oxidation potential and the electron withdrawing nature of the cluster surface, indicating that the electron density at the electroactive ruthenium center is indeed influenced by remote electropositive and electronegative substituents attached to the nanocluster. Further evidence of cluster mediated electronic interactions between remote surface moieties presents itself in the form of a dependence of the integrated ruthenium based MLCT emission intensity on the mole per cent of attached thiolate capping agent possessing an electron withdrawing substituent in the position *para* to the point of cluster attachment. ©2000 Elsevier Science Ltd. All rights reserved.

Keywords: CdS nanoclusters; Ruthenium(II) polypyridyls; Functionalized nanoclusters; Mesophase materials; Molecular devices

1. Introduction

Within the past two decades there have appeared numerous examples of experimental and theoretical investigations focused on semiconductor nanoclusters [2–7]. Many of these studies have been predicated on the future application of these interesting nanoscaled materials to molecular electronic devices [8–10]. The unique optical and electronic properties exhibited by semiconductor nanoclusters arise from the quantum size effect, which results from the splitting of the bulk semiconductor band structure into discrete, albeit closely spaced, electronic energy levels and a concurrent widening of the band gap [7]. This phenomenon becomes manifest when the size of the cluster approaches that of the exciton of the semiconductor, and can be thought of as a shift in the behavior of the conduction electrons from Bloch wave mechanics to particle-in-a-sphere wave mechanics. To date, one fundamental question crucial to the eventual development of such proposed devices (i.e. tunnel, negative resistance and coulomb blockade devices, and single electron diodes and transistors) [11–13] still remains unanswered: will the quantum size effect lead to a loss of ability of the semiconductor to mediate electronic communication between surface groups?

Previously, we demonstrated that the electronic and physical properties of thiolate-capped CdS nanoclusters are influenced significantly by the characteristics of substituents in the position *para* to the point of attachment to the cluster on an aromatic thiolate capping agent [14–17], and we presented evidence for facile surface–core communication of conduction carriers [1]. In this contribution we present the preparation of a ruthenium polypyridyl complex which, when attached covalently to mixed surface nanoclusters via previously reported esterification methods [16], serves as an effective electrochemical and fluorescent probe of cluster

* Corresponding author. Tel.: +1-416-736-5246; fax: +1-416-736-5936; e-mail: pietro@yorku.ca

[1] For part 5 in this series, see Ref. [1].

0277-5387/00/$ - see front matter ©2000 Elsevier Science Ltd. All rights reserved.
PII S0277-5387(99)00363-0

mediated electronic communication between remote surface moieties.

2. Experimental

2.1. Chemicals

Water was purified by passage through a Sybron-Barnstead D8902 mixed-bed ion exchange column followed by a Sybron-Barnstead D8204 activated charcoal filter. Reagent grade dimethylformamide (DMF), acetonitrile and methanol were purchased from Caledon Laboratories (Georgetown, Ont., Canada). DMF was dried over 4 Å molecular sieves for 12 h and filtered prior to use, while acetonitrile and methanol were used as received. All deuterated solvents used for ^{1}H NMR spectroscopy were purchased from Cambridge Isotope Laboratories (Andover, MA) in sealed ampules and used immediately upon opening. $RuCl_3 \cdot xH_2O$, sodium sulfide nonahydrate, isatin (2,3-indolinedione), 2-acetylpyridine, and sucrose were purchased from Sigma-Aldrich and used as received. Cadmium acetate (Aldrich reagent grade) was recrystallized with concurrent dehydration from glacial acetic acid and dried at 100°C in vacuo for 24 h. 4-Hydroxythiophenol was obtained reagent grade from Sigma-Aldrich and distilled at reduced pressure immediately prior to use. 4-Nitrothiophenol and 2,2′-bipyridine were obtained reagent grade from Sigma-Aldrich, recrystallized from absolute ethanol and stored in a nitrogen atmosphere at 5°C until required. Phenolic surface CdS nanoclusters (**1**) were prepared using the kinetic trapping method as described previously [16].

2.2. Mixed surface X%NO_2/Y%OH quantum dot synthesis (**2a–2f**)

The synthesis of **2c** (16% NO_2) will be discussed as a representative sample for all mixed surface 'nitro-phenolic' CdS nanoclusters (**2a**–**2f**). Two solutions were prepared in a 1:1:2 MeOH:MeCN:H_2O (v:v:v) solvent mixture. A 20 ml cadmium acetate solution (1.7 g, 7.4 mmol) was prepared and degassed thoroughly with N_2. A second solution (20 ml) of sodium sulfide nonahydrate (0.7 g, 2.9 mmol), 4-nitrothiophenol (0.2 g, 1.3 mmol) and 4-hydroxythiophenol (1.2 g, 9.5 mmol) was degassed and added to the cadmium acetate solution yielding a yellow precipitate. The precipitate was repeatedly sonicated in water and recovered by centrifugation. The precipitate was then suspended in acetonitrile, reprecipitated upon addition of water, recovered by centrifugation, and dried in vacuo for 12 h.

Yield 0.8 g. ^{1}H NMR (DMSO, ppm): δ 8.6–9.02 (m, 1H), 5.9–7.8 (m, aromatic 5H). FT-IR (KBr, cm^{-1}): 3288 (s, v br, O–H stretch), 1654 (s), 1920, 1750 (w, 1,4-disub-ϕ overtone), 1613 (m), 1576 (m), 1489 (vs, NO_2 asymmetric stretch), 1432 (s, ring C=C), 1331 (vs, NO_2 symmetric stretch), 1090 (s), 822 (m), 745 (m, ϕ C–H out-of-plane), 635 (m). UV–Vis (DMF, nm): 404.

2.3. Preparation of 2-(2-pyridyl)-4-carboxyquinoline sodium salt (**3**)

2-(2-Pyridyl)-4-carboxyquinoline was prepared using a modification of the literature preparation described by Bass and Morgan [18]. 18 g (0.12 mol) of isatin (2,3-indolinedione) and 15 g (0.12 mol) of 2-acetylpyridine were combined and stirred for 30 min. The reaction mixture was subsequently cooled to 5°C and 60 ml of 33% aqueous NaOH was added with stirring. The ensuing reaction mixture was warmed to ~60°C. The addition of 60 ml of ice water yielded a purple–red slurry, which was recovered by filtration and washed with water. The crude product was dissolved in a minimum of hot water and decolorized using NORIT activated carbon pellets. Upon cooling, light purple shiny crystals of the sodium salt were obtained and dried in vacuo.

Yield 18.43 g (67%). M.p. >340°C (literature >300°C).

2.4. Preparation of 2-(2-pyridyl)-4-carboxyquinoline (**4**)

17.3 g of **3** were dissolved in 300 ml of water and titrated, with stirring, to pH 7 using 10% HCl. Off-white crystals were recovered by filtration and dried in vacuo.

Yield 13.71 g. M.p. >300°C (literature >300°C). ^{1}H NMR (DMSO, ppm): δ 8.99 (s, 1H), 8.78 (d, 1H), 8.76 (d, 1H), 8.62 (t, 1H), 8.21 (d, 1H), 8.05 (t, 1H), 7.75 (t, 1H), 7.56 (t, 1H). EI-MS (m/z): 250, 206.

2.5. Preparation of cis-[Ru(bpy)$_2$]Cl$_2$ (**5**)

cis-Ru(bpy)$_2$Cl$_2$ was prepared using a modified literature preparation as outlined by Meyer and coworkers [19]. 2.54 g of $RuCl_3 \cdot xH_2O$, 3.78 g (24.20 mmol) of 2,2′-bipyridine and 6.7 g (0.15 mol) of LiCl were refluxed in DMF (40 ml) under a nitrogen atmosphere for 8 h with vigorous stirring. The reaction mixture was allowed to cool to room temperature and then 200 ml of acetone was added. After standing for 18 h at 4°C, a dark solid was recovered, washed three times with 30 ml portions of water and dried in vacuo. The recovered product was subsequently Soxhlet extracted with methylene chloride for a period of 4 days. The purple methylene chloride solution was concentrated to half its original volume and the resultant shiny dark purple crystals were recovered and dried in vacuo.

Yield 1.61 g, 3.3 mmol, (14%). M.p. >300°C. ^{1}H NMR (DMSO-d_6, ppm): δ 10.00 (d, 2H), 8.30 (d, 2H), 8.13 (d, 2H), 7.91 (dd, 2H), 7.51 (dd, 2H), 7.49 (d, 2H), 6.93 (dd, 2H). UV–Vis (methanol, nm): 364, 524.

2.6. Preparation of [Ru(bpy)$_2$(2-PCQH)]Cl$_2$ (**6a**)

cis-Ru(bpy)$_2$Cl$_2$ (0.25 g, 0.52 mmol) was dissolved in 10 ml of methanol and a methanol solution (10 ml) containing $AgNO_3$ (0.241 g, 1.04 mmol) was added. The reaction mixture was stirred for 2 h yielding an orange solution and white precipitate. The precipitate was removed by filtration and

0.13 g (0.55 mmol) of **4** was added. The reaction mixture was refluxed for 16 h under a N_2 atmosphere. The solvent was removed in vacuo, and the orange–red residue was purified by column chromatography on alumina using a 1:1 methanol:chloroform eluent.

Yield 0.31 g, 0.42 mmol (81%). M.p. 280–282°C (dec.). ^{1}H NMR (DMSO-d_6): δ 8.9 (d, 1H), 8.8 (m, 2H), 8.7 (s, 1H), 8.6 (d, 1H), 8.5 (d, 1H), 8.4 (d, 1H), 8.15 (m, 6H), 8.0 (t, 1H), 7.8 (d, 1H), 7.7 (d, 1H), 7.6 (m, 8H), 7.3 (t, 1H). FT-IR (KBr, cm^{-1}): 3410 (m, br, OH stretch), 3070 (m, br, aromatic C–H stretch), 1610 (s, sharp, C=O stretch). UV–Vis (methanol, nm): 450, 482 shoulder. ES-MS (m/z): 334.0, 333.5, 333.0, 332.5, 332.0, 331.5, 331.0, 330.5, 330.0, 329.5, 329.0.

2.7. Preparation of $[Ru(bpy)_2(2\text{-}PCQH)](PF_6)_2$ (**6b**)

0.2 g (0.27 mmol) of **6a** was dissolved in water and the addition of an aqueous solution of excess of NH_4PF_6 resulted in the precipitation of an orange solid. The precipitate was isolated by centrifugation and washed three times with water.

Yield 0.19 g. M.p. 244–246°C (dec.). ^{1}H NMR (DMSO-d_6): δ 9.0 (d, 1H), 8.9 (m, 2H), 8.7 (m, 4H), 8.2 (m, 5H), 8.0 (m, 2H), 7.6 (m, 11H), 7.3 (t, 1H). ES-MS (m/z): 334.0, 333.5, 333.0, 332.5, 332.0, 331.5, 331.0, 330.5, 330.0, 329.5, 329.0.

2.8. Covalent attachment of **6b** to **1**, **2a–2f** via esterification (**7**, **8a–8f**)

The preparation of **7** will be presented as a representative example of the derivatization of CdS nanoclusters with polypyridyl ruthenium probe through an ester linkage. 30 mg of **6b** were refluxed in $SOCl_2$ (10 ml) under a dry N_2 atmosphere for 3 h to yield a purple solution. The excess solvent was removed in vacuo, and 100 mg of imidazole in 10 ml of toluene were added to the purple residue and refluxed for 1.5 h. The toluene was removed and the residue was heated at 60°C in vacuo to sublime excess imidazole from the reaction flask. All procedures involving nanoclusters were carried out under subdued light. 300 mg of **1** were suspended in 10 ml of DMF with sonication. The DMF suspension was added to the reaction flask containing the imidazole derivative of **6b** and stirred for 1 h. The reaction mixture was quenched with water and the resulting orange solid was isolated by centrifugation and purified through repeated sonication/centrifugation cycles in water, methanol and diethyl ether. The solid was dried in vacuo for 12 h.

Yield 105 mg. ^{1}H NMR (DMSO-d_6, ppm): δ 6.0–9.2 (br M, aromatic and OH protons). FT-IR (KBr, cm^{-1}): 3265 (s, v br, OH stretch) 1874 (w, 1,4-disub-ϕ overtone), 1652 (m), 1582 (m), 1488 (s), 1431 (m), 1383 (w), 1256 (s), 1170 (m), 1092 (w), 821 (m), 763 (w), 635 (w). UV–Vis (DMF, nm): 310 (shoulder), 430, 505.

2.9. Electrochemical analysis of **7**, **8a–8f**

2.9.1. Electrode preparation

A homogeneous conductive carbon paste was prepared by thoroughly mixing 1.2 g of graphite powder with 200 μl of heavy paraffin oil. Electrodes were subsequently constructed by thoroughly mixing 100 mg of the standard paste matrix with 20 mg of the nanocluster to be studied, in subdued light, until a homogeneous mixture was obtained. A $\sim$2 mm thick pellet of the paste was formed in the tip of a 1 ml glass syringe (diameter $\sim$2 mm) and electrical contact was achieved via the compression of a silver powder layer which was in turn addressed with a copper wire.

2.9.2. Differential pulse polarography of **7**, **8a–8f**

Differential pulse polarography was carried out using a Cypress Inc. computer controlled potentiostat system in a 0.1 M $TBAPF_6$ acetonitrile solution with a graphite paste working electrode, platinum wire counter electrode and platinum wire pseudo-reference electrode. All electrochemical measurements were calibrated using an internal ferrocene standard. The pulse height, pulse width, and sample time for all differential pulse polarography measurements were 50 mV, 40.0 ms, and 35.0 ms, respectively. Prior to analysis, all electrolyte solutions were thoroughly degassed with argon and all experiments were carried out in an argon atmosphere.

2.10. Voltammetric analysis of **6a**, **6b**

Cyclic voltammetry was performed with a Princeton Applied Technologies PAR 263 potentiostat/galvanostat using an electrode system which consisted of a platinum disk working electrode (diameter 0.5 mm), a platinum wire counter electrode and platinum wire pseudo-reference electrode which were separated from the bulk solution by a polished graphite frit. Samples were prepared in a stock 0.1 M $TBAPF_6$ solution in electrochemical grade dimethylformamide and degassed with dry argon prior to analysis. All measurements were done at a scan rate of 100 mV s^{-1} and potentials were standardized using an internal ferrocene standard.

2.11. Spectroscopic analyses

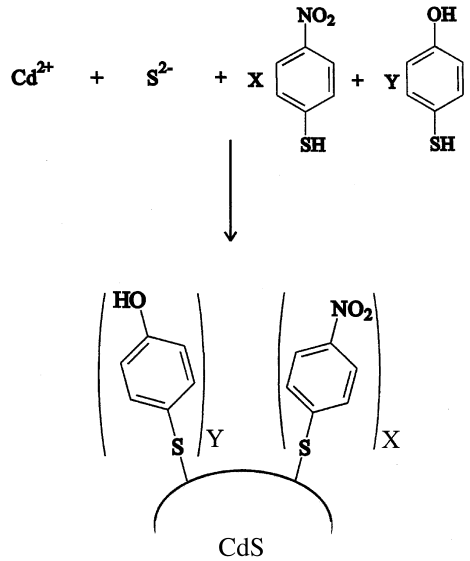
IR spectra were recorded as KBr pellets with a Mattson 3000 Fourier transform IR spectrometer. ^{1}H NMR spectra were performed on a Brucker ARX 400 MHz nuclear magnetic resonance spectrometer. ^{1}H NMR samples were sonicated in DMSO-d_6 and centrifuged prior to analysis. Electronic spectra were performed in 1 cm quartz cuvettes using a Hewlett-Packard 8452 diode array spectrometer. Solutions for fluorescence studies were thoroughly deoxygenated with argon and measurements were made using a Shimadzu RF-551 spectrofluorometric detector driven by PC-551 software.

2.12. Transmission electron microscopy

Transmission electron microscopy (TEM) was performed using a Phillips EM-301 transmission electron microscope. Nanocluster samples were prepared by placing a few drops of freshly sonicated and centrifuged DMF suspension of the desired cluster (2.5 mg of nanocluster in 3 ml of solvent) onto J.B.EM Services (Pointe Claire, Dorval, Que.) JBS-183 300 mesh carbon coated copper grids (cleaned in acetone, chloroform and again in acetone followed by air drying). The excess solvent was drawn off with a piece of filter paper while holding the grid in non-capillary forceps, leaving aggregates as well as individual nanoclusters adhering to the grid surface. Grids were then air dried at room temperature. Size calibration was performed using a precision silicon grid of 21600 lines cm^{-1}.

3. Results and discussion

The covalent attachment of an electroactive transition metal fluorophore to the surface of a semiconductor nanocluster offers an opportunity to probe the electronic interactions between remote surface moieties as mediated by the quantum dot core. All 'parent' CdS nanoclusters were prepared using a modification of the kinetic trapping method (Scheme 1) thus providing control of the cluster size and surface composition while facilitating the introduction of chemically active moieties [1,14–17,20]. We have successfully controlled the electron withdrawing/donating properties of nanocluster organic surface layers through careful consideration of the surface capping agent composition employed in the initial reaction mixture. By incorporating predetermined mole percentages of an electronegative surface moiety (4-nitrothiophenolate) and an electron donating surface moiety (4-hydroxythiophenolate), we have prepared a series of CdS quantum dots (**2a**–**2f**) with varied surface electronic properties as well as surface moieties which are easily derivatized via well established esterification methods [16].



2a) X=0.06, Y=0.94
2b) X=0.07, Y=0.93
2c) X=0.16, Y=0.84
2e) X= 0.51, Y= 0.49
2f) X= 0.97, Y=0.03

Scheme 1.

Proton NMR analyses of **2a**–**2f** show characteristic homogeneous peak broadening with superimposed structure similar to that discussed for other CdS nanocluster systems indicative of the multiple chemical shift environments and slow cluster tumbling on the NMR timescale [1,14,15,21]. Regions of the ^{1}H NMR spectra of **2a**–**2f** can be assigned to aromatic (~6–8 ppm) and phenolic protons (8.5–9.95 ppm). The integration of these broadened regions provides a suitable determination of the relative percentages of 4-hydroxythiophenolate and 4-nitrothiophenolate actually incorporated as surface caps. The ^{1}H NMR spectrum of **2a**, corresponding to 6 mol% 4-nitrothiophenolate, is shown in Fig. 1. For all mixed surface nanoclusters (**2a**–**2f**), ^{1}H NMR integration ratios indicate that the fraction of 4-nitrothiophenolate surface caps is somewhat greater than that defined by the relative solution mercaptan concentrations during cluster synthesis; this is expected considering the relative acidities of 4-nitrothiophenol ($pK_{a(SH)} = 4.5$) [22] and 4-hydroxythiophenol ($pK_{a(SH)} = 6.75$) [23]. A summary of the ^{1}H NMR spectra and surface compositions for **2a**–**2f** are included in Tables 1 and 2, respectively.

All mixed surface nanoclusters prepared in this work (**2a**–**2f**) lie in a 20–30 Å size regime. The diameters of nanoclusters with low percentages of surface tethered ϕ-NO_2 (**2a**) may be determined by applying tight binding band theory analysis to data obtained from electronic spectroscopy as previously described, and are in good agreement with measurements obtained by TEM and X-ray analysis [14–17,24–26]. Unfortunately, the diameters of clusters with surface mole percentages of the 4-nitrothiophenolate exceeding

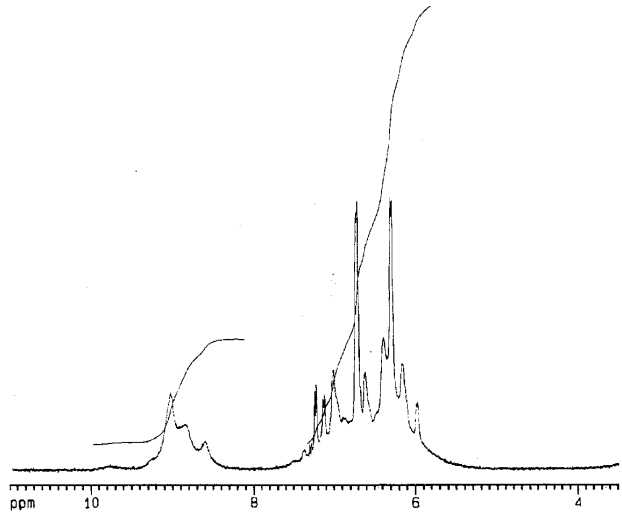


Fig. 1. ^{1}H NMR spectrum of **2a** in DMSO-d_6 showing distinctive signals from aromatic and phenolic protons.

Table 1
Summary of ^{1}H NMR analysis of **2a**–**2f** and **8a**–**8f** in DMSO-d_6

Compound	vs. TMS
2a	8.60–9.05 (br m, 0.94H, OH proton), 6.0–7.3 (br m, 4H, aromatic proton)
2b	8.60–9.01 (br m, 0.93H, OH proton), 6.0–7.8 (br m, 4H, aromatic proton)
2c	8.50–9.60 (br m, 0.84H, OH proton), 6.0–7.7 (br m, 4H, aromatic proton)
2d	8.60–9.20 (br m, 0.78H, OH proton), 5.7–7.8 (br m, 4H, aromatic proton)
2e	8.70–9.21 (br m, 0.49H, OH proton), 5.8–7.8 (br m, 4H, aromatic proton)
2f	9.95 (br m, 0.03H, OH proton), 6.7–8.25 (br m, 4H, aromatic proton)
7	6.0–9.2 (broad and structured, aromatic and phenolic H)
8a	5.9–9.5 (broad and structured, aromatic and phenolic H)
8b	5.5–9.4 (broad and structured, aromatic and phenolic H)
8c	5.7–10.0 (broad and structured, aromatic and phenolic H)
8d	5.8–10.0 (broad and structured, aromatic and phenolic H)
8e	6.0–10.0 (broad and structured, aromatic and phenolic H)
8f	6.5–10 (broad and structured, aromatic)

Table 2
Yield and surface composition data for **2a**–**2f**

Compound	Yield (g)	Theoretical NO_2 [a] (%)	Observed NO_2 [b] (%)
2a	0.63	1	6
2b	0.67	5	7
2c	0.66	10	16
2d	0.64	15	22
2e	0.58	50	51
2f	0.55	90	97

[a] From mole ratio of 4-nitrothiophenol in reaction mixture.
[b] Determined from ^{1}H NMR analysis.

about 7% (**2b**–**2f**) cannot be evaluated reliably using electronic spectroscopy as the excitonic absorption of the CdS cluster is obscured by the intense $n \rightarrow \pi^*$ transition of the ϕ-NO_2 chromophore. For these systems, TEM analysis alone was performed to evaluate cluster dimensions. A summary of spectroscopic and TEM determined diameters for **2a**–**2f** may be found in Table 3.

FT-IR spectra of KBr pellets of **2a**–**2f** show absorptions characteristic of the pendant surface groups. As expected, broad absorptions indicative of phenolic functionalities appear at ca. 3300 cm^{-1} for **2a**–**2f**, while the spectra lack the characteristic –SH stretch at 2580 cm^{-1}, thus confirming exclusive thiolate binding of surface moieties. A complete summary of the FT-IR spectra for **2a**–**2f** appears in Table 4.

Polypyridyl complexes of ruthenium have been widely studied [27], and are well known for their stability, long lived charge transfer excited states, intense phosphorescence and well characterized electrochemical properties. Numerous examples of correlations between metal centered electrochemical potentials and electronic properties of chemical moieties on substituents on ligands exist in the literature. The

Table 3
Electronic spectroscopy and cluster dimension data for **2a**–**2f** and **8a**–**8f**

Compound	λ_{max} (nm)	TBT diameter (Å) [a]	TEM diameter (Å) [b]
2a	340 (shoulder), 410	24	26 ± 7
2b	404		27 ± 7
2c	404		23 ± 7
2d	404		25 ± 7
2e	404		26 ± 7
2f	326, 404		24 ± 7
7	365	27	25 ± 7
8a	340 (shoulder)	24	28 ± 7
8b	404		29 ± 7
8c	404		27 ± 7
8d	404		26 ± 7
8e	404		24 ± 7
8f	326, 404		25 ± 7

[a] Estimated using tight binding band theory.
[b] ± 7 Å represents the resolution of the transmission electron microscope.

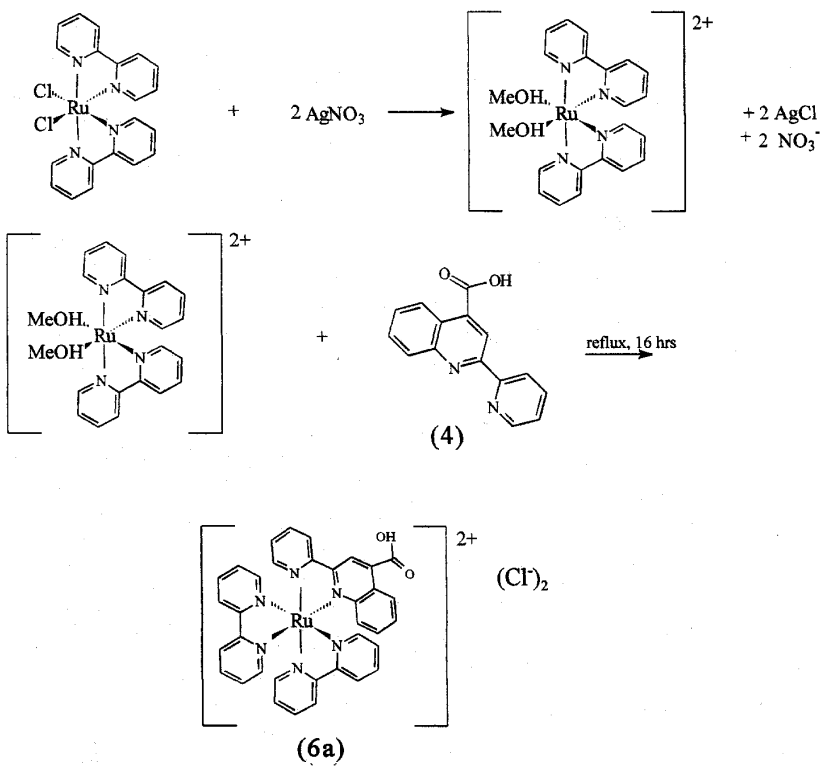
strong dependence of the metal centered oxidation potential upon electron donating and withdrawing properties of substituted fragments affords a means to probe the effectiveness of a ligand (or nanocluster) to mediate the electronic influence of a remote functionality on a metal center. Indeed, Meyer and coworkers [28–31], as well as others [32–35], have demonstrated that a [*cis*-$Ru(bpy)_2$] fragment serves as an effective probe for the electron interaction of a third ligand with the ruthenium metal center.

Although ruthenium polypyridyl species have previously been attached to TiO_2 nanoparticles by Meyer and coworkers [36,37], and although these materials exhibited interesting properties of solar energy conversion with monochromatic efficiencies of 0.30, no detailed discussion of the electrochemical analysis nor the affects of remote substituents on the ruthenium(II/III) oxidation potential was offered. Hence, we endeavored to link covalently an electroactive polypyridyl ruthenium fluorophore to the surface of quantum sized cadmium sulfide where it serves to probe the extent to which the semiconductor core mediates electron demand between surface groups. To facilitate the covalent attachment of a polypyridyl ruthenium complex to a phenolic surface CdS nanocluster, it was necessary to replace a single bipyridine ligand of $[Ru(bpy)_3]^{2+}$ with a polypyridyl analog bearing a carboxylic acid moiety. 2-(2′-Pyridyl)-4-carboxyquinoline (**4**) offers a carboxylic acid group suitable for esterification and was prepared using the coupling reaction of 4-acetylpyridine and isatin (2,3-indolinedione) as described by Bass and Morgan [18].

The 2D-COSY analysis of **4** shows numerous aromatic signals, the most striking of which is a singlet appearing at 9.0 ppm assigned to the proton in the 3 position. The electron impact mass spectrum of **4** shows a parent peak at $m/z = 250$ corresponding to the loss of a proton and a fragmentation pattern including an intense peak at $m/z = 206$ arising from the loss of $–CO_2$. Scheme 2 illustrates the reaction of **4** with

Table 4
A summary of FT-IR assignments of KBr pellets of **2a**–**2f** and **8a**–**8f**

Compound	Wavenumber (cm^{-1})
2a	3272 (s, br, OH stretch), 1870 (vw, 1,4-disub-ϕ overtones), 1582 (m), 1486 (s, NO_2 asymmetric stretch), 1427 (m), 1356 (w), 1231 (s), 1170 (s), 1090 (w), 819 (w), 633 (w)
2b	3250 (s, br, OH stretch), 1875 (vw, 1,4-disub-ϕ overtones), 1578 (s), 1486 (s, NO_2 asymmetric stretch), 1425 (m, ring C=C), 1364 (m), 1169 (s), 1086 (m), 1006 (m), 818 (m), 740 (w, NO_2 symmetric stretch), 630 (w)
2c	3288 (s, v br, O–H stretch) 1654 (s), 1920, 1750 (w, 1,4-disub-ϕ overtone), 1613 (m), 1576 (m), 1489 (vs, NO_2 asymmetric stretch), 1432 (s, ring C=C), 1331 (vs, NO_2 symmetric stretch), 1090 (s), 822 (m), 745 (m, NO_2 symmetric stretch), 635 (m)
2d	3440 (s, br, OH stretch), 1874 (vw, 1,4-disub-ϕ overtones), 1625 (m, br), 1573 (m, br), 1498 (m, NO_2 asymmetric stretch), 1428 (m, ring C=C), 1331 (m, NO_2 symmetric stretch), 1255 (w, br), 1084 (w, br)
2e	3445 (m, br, OH stretch), 3078 (m, br), 1868 (vw, 1,4-disub-ϕ overtones), 1603 (m, sharp), 1573 (m, sharp), 1509 (s, NO_2 asymmetric stretch), 1427 (m, ring C=C) 1338 (s, NO_2 symmetric stretch), 1180 (w, br), 1110 (w, br), 1084 (w, br), 850 (m, shrp), 740 (w, NO_2 symmetric stretch)
2f	3390 (w, br, OH stretch), 3092 (w, aromatic C–H stretch), 1918, 1788 (vw, 1,4-disub-ϕ overtones), 1646 (w), 1509 (s, NO_2 asymmetric stretch), 1432 (m, ring C=C),1340 (s, NO_2 symmetric stretch), 1175 (w), 1104 (w), 1082 (m), 846 (m), 736 (m, NO_2 symmetric stretch), 678 (w), 529 (w)
7	3265 (s, v br, OH stretch) 1874 (w, 1,4-disub-ϕ overtone), 1652 (m, C=O stretch), 1582 (m), 1488 (s, NO_2 asymmetric stretch), 1431 (m, ring C=C), 1383 (w), 1256 (s), 1170 (m), 1092 (w), 821 (m), 763 (w), 635 (w)
8a	3250 (s, v br, OH stretch) 1882 (w, 1,4-disub-ϕ overtone), 1651 (m, C=O stretch), 1579 (m),1489 (s, NO_2 asymmetric stretch), 1429 (m, ring C=C), 1258 (s), 1169 (m), 1090 (w),1009 (w), 823 (m), 763 (m), 635 (m), 512 (w)
8b	3240 (s, v br, OH stretch), 1872 (w, 1,4-disub-ϕ overtone), 1654 (m, C=O stretch), 1578 (m),1489 (s, NO_2 asymmetric stretch), 1431 (m, ring C=C), 1259 (s), 1172 (m), 1090 (w),1009 (w), 823 (m), 762 (m), 635 (m), 512 (w)
8c	3290 (s, v br, OH stretch), 1880 (w, 1,4-disub-ϕ overtone), 1650 (m, C=O stretch), 1578 (m),1490 (s, NO_2 asymmetric stretch), 1428 (m, ring C=C), 1255 (s), 1169 (m), 1088 (w),1006 (w), 822 (m), 753 (m), 635 (m)
8d	3288 (s, v br, OH stretch), 3001 (m, sharp, aromatic C–H stretch), 1878 (w, 1,4-disub-ϕ overtone), 1654 (m, C=O stretch), 1576 (m),1490 (s, NO_2 asymmetric stretch), 1432 (m, ring C=C), 1258 (s), 1170 (m), 1090 (w), 912 (w), 823 (m), 745 (m), 635 (m)
8e	3350 (s, v br, OH stretch) 1870 (w, 1,4-disub-ϕ overtone), 1647 (m, C=O stretch), 1575 (m),1503 (s, NO_2 asymmetric stretch), 1426 (m, ring C=C), 1272 (s), 1175 (m), 1090 (w), 827 (m), 743 (m), 632 (m)
8f	3380 (s, sharp, OH stretch), 3022 (m, sharp, aromatic C–H stretch), 1888 (w, 1,4-disub-ϕ overtone), 1651 (m, C=O stretch), 1572 (m),1406 (s, NO_2 asymmetric stretch), 1429 (m, ring C=C), 1256 (s), 1165 (w), 1090 (m), 1085 (m), 1009 (w), 850 (m), 740 (m), 682 (w), 648 (m), 535 (w)



Scheme 2.

cis-Ru(bpy)$_2$Cl$_2$ yielding ruthenium polypyridyl complex (**6a**) bearing a carboxylic acid functionality which may be exploited as a point of covalent attachment to CdS nanoclusters. The ^{1}H NMR of **6a** is illustrated in Fig. 2, and shows a series of multiplet signals in the aromatic region of the spectrum ($\sim$7.0–10.0 ppm), all of which have been assigned with the aid of 2D NMR. The most striking feature of the ^{1}H NMR spectrum of **6a** is a singlet appearing at 8.67 ppm arising from the unique proton in the 3 position of the 2-2′-pyridylcarboxyquinoline ligand. Peak assignments, chemical shifts, integration ratios and coupling constants for the 2D-COSY spectrum of **6a** are reported in Table 5.

Electrochemical analysis of **6a** shows a well defined reversible Ru(II/III) oxidation process at 1.27 V versus SCE as well as a reversible 2-2′-pyridylcarboxyquinoline reduction at −1.26 V and two reversible bipyridine reductions at −1.57 and −1.93 V versus SCE. In addition, an irreversible chloride oxidation is also observed at 1.18 V versus SCE and will preclude any accurate measurement of changes in the Ru(II/III) oxidation potential of probes tethered to functionalized nanoclusters. Thus, **6a** was converted to the corresponding hexafluorophosphate salt (**6b**) by treatment with excess aqueous NH_4PF_6. The electrochemical analysis of **6b** shows a reversible Ru(II/III) oxidation at 1.27 V versus SCE and three reversible ligand reductions at −1.26, −1.57 and −1.93 V versus SCE, with the chloride oxidation absent.

Electronic and emission spectroscopy of **6a** and **6b** shows the expected MLCT absorptions (450 nm and 482 nm shoulder) and MLCT emission maxima (652 nm), respectively (Fig. 3).

The ^{1}H NMR spectra of all [Ru(bpy)$_2$(PCQ)]$^{2+}$ functionalized CdS nanoclusters (**7**, **8a**–**8f**, Scheme 3) in this

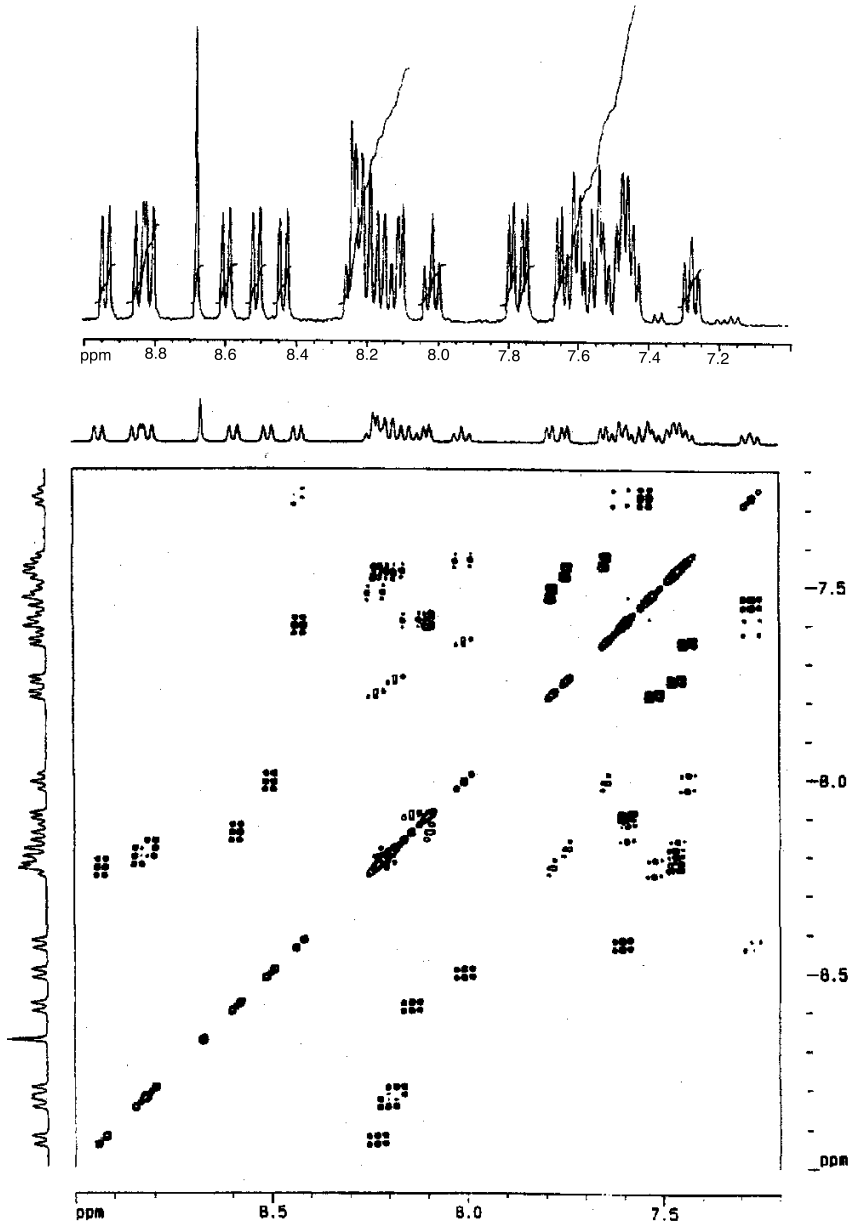


Fig. 2. 1D- and 2D-COSY ^{1}H NMR analysis of **6a**; detailed peak assignments and coupling constants may be found in Table 5.

Table 5
^{1}H NMR-COSY assignments for **6a**

Proton	Chemical shift (δ, ppm vs. TMS)	J_{H-H} (Hz)
3	8.67 (s)	
5	8.44 (d)	8.412
6	~7.6 (t in m)	
7	7.27 (t)	7.628
8	~7.5 (d in m)	
9	~7.5 (d in m)	
10	8.01 (t)	7.840
11	~7.5 (t in m)	
12	~8.2 (m)	
13	8.80 (d)	8.396
14	~8.2 (t in m)	
15	7.5 (t in m)	
16	7.74 (d)	5.564
17	8.2 (d in m)	
18	7.4 (t in m)	
19	~8.2 (t in m)	
20	8.503 (d)	8.160
21	7.837 (d)	5.484
22	7.6 (t in m)	
23	8.2 (t in m)	
24	8.930 (d)	8.188
25	8.589 (d)	8.204
26	~7.6 (t in m)	
27	8.2 (t in m)	
28	8.806 (d)	8.396

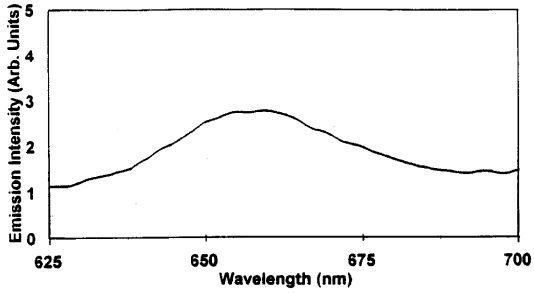
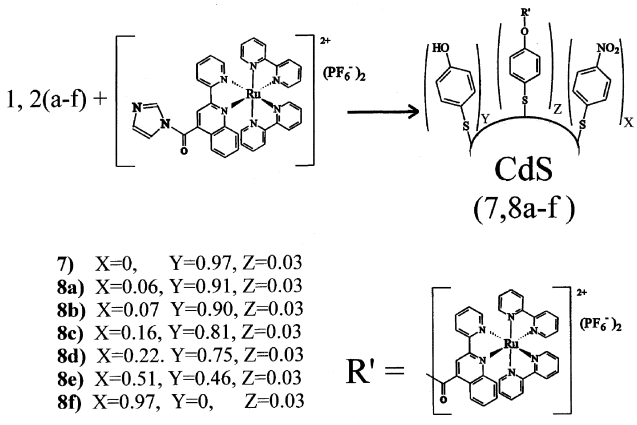


Fig. 3. Emission spectrum of an argon saturated DMF solution of **6b**; $\lambda_{exc} = 430$ nm.



Scheme 3.

work show homogeneously broadened peaks similar to those observed for all nanoclusters discussed previously (**4a**–**4e**), indicating that the cluster core remained intact throughout the derivatization process. The most striking change noted when comparing the ^{1}H NMR spectrum of the ruthenium derivatized CdS functionalized nanoclusters to that of the parent quantum dots is a loss of definition (Fig. 4(b)) between the phenolic and aromatic signal regions previously reported for the corresponding parent nanocluster counterparts (Fig. 4(a)). The increased complexity in the ^{1}H NMR suggests that, as expected, the derivatization process caused an increase in the number of proton environments on the cluster surface. Table 1 summarizes the ^{1}H NMR spectroscopy of **7**, **8a**–**8f**.

FT-IR assignments of KBr pellets of **7** and **8a**–**8f** are summarized in Table 2 The appearance of an absorbance at ~1650 cm^{-1} not present in similar spectra of **1** and **2a**–**2f** confirms the formation of an ester linkage between the phenolic surface functionalities and $[Ru(bpy)_2(PCQ)]^{2+}$. Another significant observation is the appearance of a sharp absorption at 3381 cm^{-1}, characteristic of a non-hydrogen bonded –OH, in the FT-IR spectrum of **8f**, confirming a loss of interaction between surface –OH moieties. Fig. 5 shows the FT-IR spectrum of a KBr pellet of **8f**.

The electronic spectra of CdS quantum dots derivatized with **6b** and bearing low molar percentages of 4-nitrothiophenolate surface caps (**8a**) show the characteristic excitonic shoulder arising from the semiconductor core, while the MLCT absorptions of the pendant ruthenium polypyridyl center are masked by the presence of a weak absorption shoulder arising from the $n \rightarrow \pi^*$ transition of the $-NO_2$. For clusters with greater than about 7 mol% 4-nitrothiophenolate caps, both the excitonic shoulder of the cluster core and the MLCT absorptions of the pendant $[Ru(bpy)_2(PCQ)]^{2+}$ are hidden by the intense absorption attributed to the $n \rightarrow \pi^*$ transition of the $-NO_2$ functionality. The electronic spectrum of **7** is shown in Fig. 6 as a representative example of clusters having surfaces without $-NO_2$ moieties.

For clusters showing excitonic absorptions, **7** and **8a**, it is possible to approximate the core diameter using a tight binding band approach as previously described [24–26]. All of the presented clusters have been found to lie in a size regime of ca. 27 Å. Good agreement was found between tight binding band theory approximations and TEM analyses for clusters **2a**, **7**, and **8a**. A summary of cluster dimensions for **7** and **8a**–**8f** may be found in Table 3.

The properties of the covalently attached ruthenium moieties on **7** and **8a**–**8f** offer two independent methods for the investigation of the electronic processes mediated by the semiconductor core, emission spectroscopy and electrochemistry. All of the presented ruthenium functionalized nanoclusters (**7** and **8a**–**8f**) exhibit MLCT emission characteristic of the tethered ruthenium moiety (**6b**) at ca. 652 nm as shown in Fig. 7. Variation of the mole percentage of 4-nitrothiophenolate surface cap results in a unique relationship between the mole percentage of 4-nitrothiophenolate surface functionality and the integrated fluorescence intensity (Fig. 8(a)). There is an observed rapid decrease in integrated

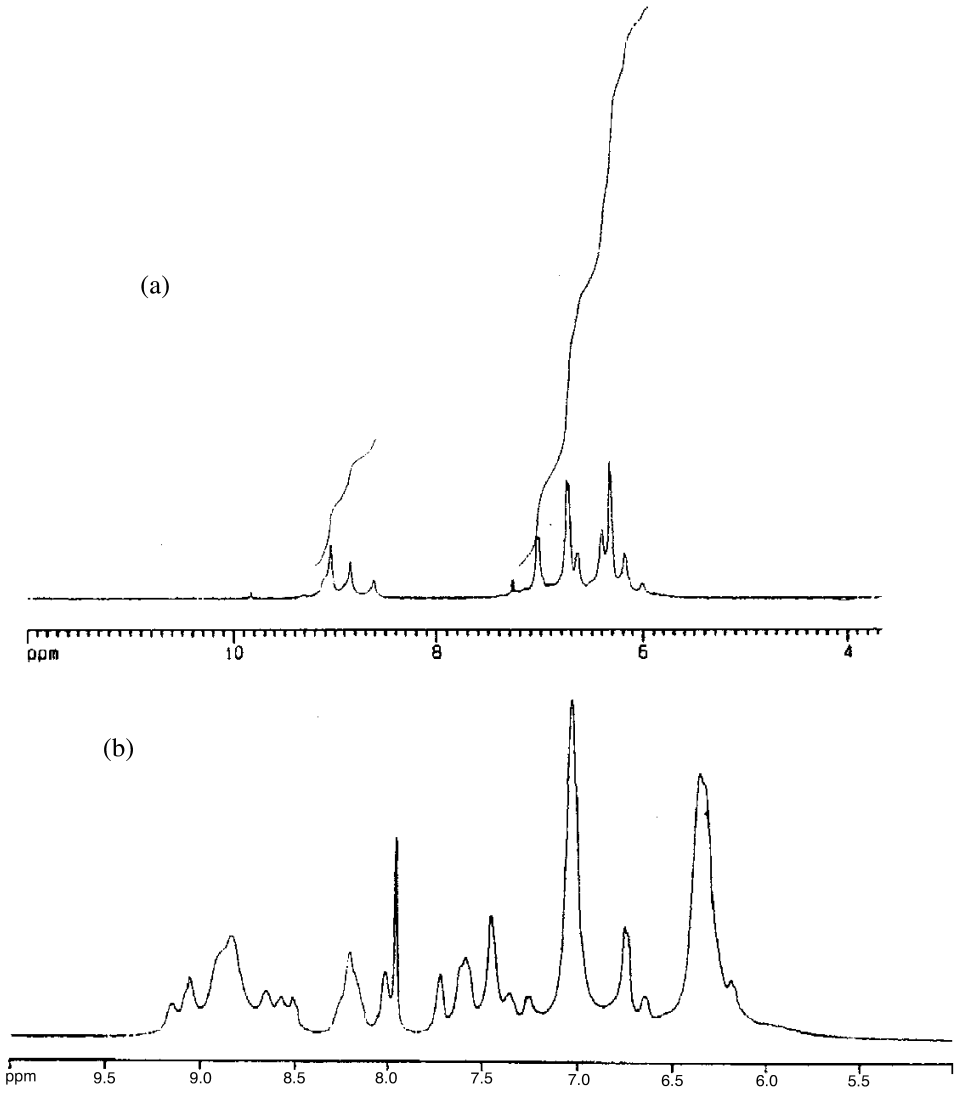


Fig. 4. ^{1}H NMR spectra of DMSO-d_6 suspensions of (a) **1** and (b) **7**.

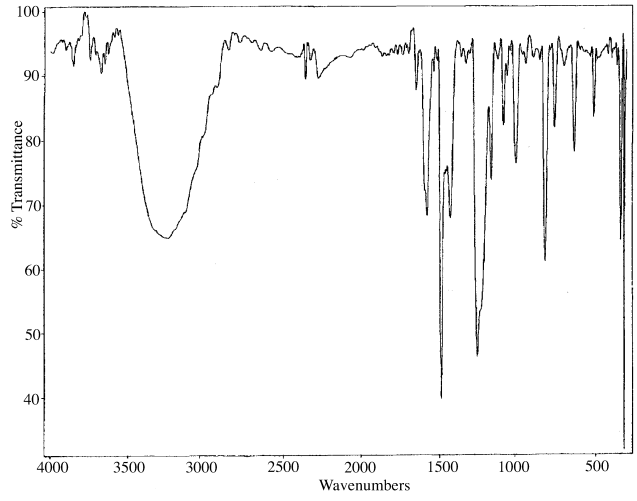


Fig. 5. FT-IR spectrum (KBr pellet) of **8f** showing C=O and OH stretching frequencies at 1651 and 3380 cm^{-1}, respectively; detailed assignments may be found in Table 4.

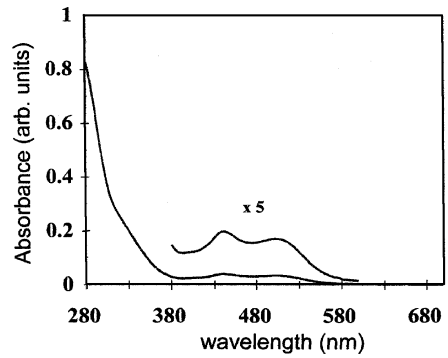


Fig. 6. Characteristic excitonic absorption (310 nm) of a CdS nanocluster and ruthenium based MLCT absorptions (430 and 505 nm) in the electronic spectrum of a suspension of **7** in DMF.

emission intensity as the mole percentage of 4-nitrothiophenolate cap increases from 0 to ~50% followed by a range of slight decrease in intensity for mole percentages between

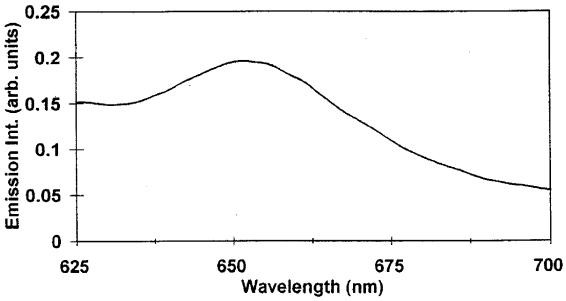


Fig. 7. Emission spectrum of a DMF suspension of **8f**; $\lambda_{exc} = 430$ nm.

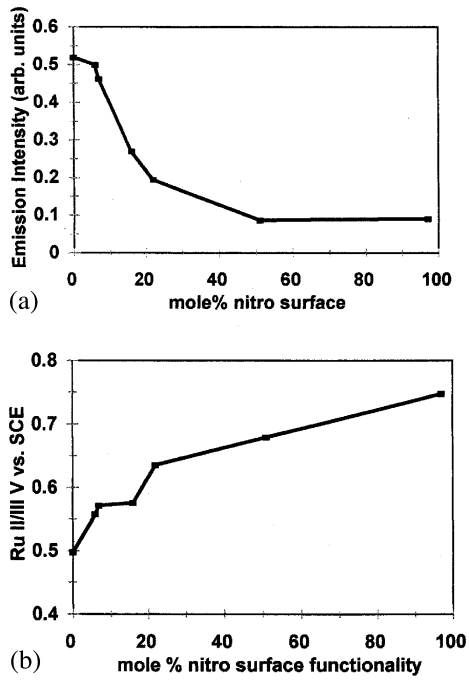


Fig. 8. Observed dependence of (a) ruthenium based MLCT emission integrated intensity and (b) ruthenium(II/III) oxidation potential on mole per cent 4-nitrothiophenolate surface functionality for **7**, **8a**–**8f**.

~50 and ~97%. From this analysis, it is evident that the MLCT emission characteristics are effectively quenched by only a few caps bearing remote electron withdrawing substituents, indicating that electronic communication mediated by the semiconductor core is indeed occurring. Interestingly, electrochemical studies of the same series of ruthenium derivatized nanoclusters exhibit a similar relationship (Fig. 8(b)). Differential pulse polarography of a graphite mull of **7** and **8a**–**8f** shows a broad reversible oxidation process arising from the pendant ruthenium center which shifts between 0.497 and 0.747 V versus SCE with increased mole percentage of 4-nitrothiophenolate surface.

These phenomena may be explained on the basis of a core-mediated electronic inductive effect. The valence and conduction band edges of bulk CdS are 1.36 V and −1.18 V, respectively, relative to an SCE reference [38]. The quantum size effect symmetrically widens the observed band gap of bulk CdS ($E_g = 2.54$ eV) to 3.65 eV for ~30 Å diameter CdS nanoclusters, providing a valence band edge of 1.92 V versus SCE and a conduction band edge at −1.74 V versus SCE at the core interior. However, we have previously shown that changes in the electronic properties of the cluster capping agent, as predicted by the Hammett σ_p parameter, result in an ultimate change in the electronegativity of the cluster surface [1], consequently shifting the positions of the conduction and valence band edges at the cluster core/cap interface, relative to the respective levels in the core interior.

If one considers an electron rich surface (**7**), the valence and conduction bands bend up, rendering the surface relatively electropositive (Fig. 9(a)), which in turn increases the electron density at a pendant ruthenium center via a cluster mediated inductive mechanism, and shifts the Ru(II/III) oxidation potential of the pendant $Ru(bpy)_2(PCQ)$ moiety (1.27 V versus SCE for the free complex; 0.497 V versus SCE for **7**). This dramatic change in Ru(II/III) oxidation potential for cadmium sulfide nanocluster tethered ruthenium polypyridyl probes is comparable to that observed for functionalized TiO_2 clusters [36,37] and is in good agreement with the value of 0.59 V versus SCE determined using the literature analysis of ruthenium based MLCT absorptions as described by Lever and Dodsworth [35].

We report here that as the mole ratio of 4-nitrothiophenolate cap increases from 0 to 0.97, the oxidation potential of the pendant $[Ru(bpy)_2(PCQ)]^{2+}$ moiety increases from

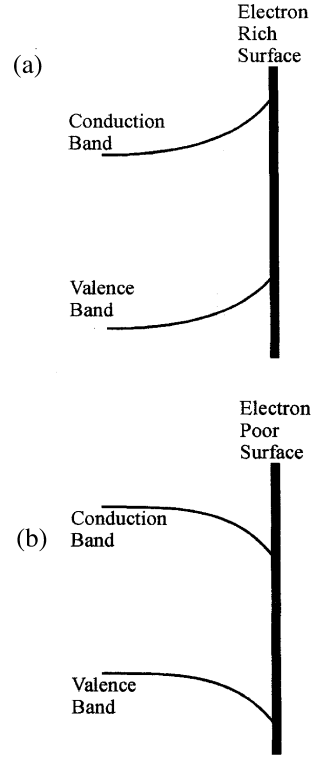


Fig. 9. (a) Electron donating surface caps on Ru-tagged CdS nanoclusters (**7**, **8a**–**8f**) result in an upward bending of the valence and conduction bands, decreasing the cluster surface electronegativity, which in turn results in an increase of electron density at the ruthenium center lowering the Ru(II/III) oxidation potential. (b) Electron withdrawing surface caps cause the conduction and valence bands to bend downward, consequently increasing the cluster surface electronegativity and increasing the Ru(II/III) oxidation potential.

0.497 to 0.747 V versus SCE. Applying the inductive model described above, as the nanocluster surface becomes more electronegative, the valence and conduction bands bend down and the electron density will be depleted at the ruthenium center (Fig. 9(b)), shifting the Ru(II/III) redox couple to higher potentials.

The core-mediated inductive model is also consistent with the observed quenching of the Ru based MLCT emission. In the case of an electron rich surface (**7**), the conduction band edge is bent up above the PCQ π^* level, and the excited π^* electron of $[Ru(bpy)_2(PCQ)]^*$ remains localized within the ligand orbital, ultimately relaxing via MLCT emission. Conversely, for a relatively electronegative surface, the conduction band edge bends below the PCQ π^* level, resulting in electron capture and concurrent fluorescence quenching.

4. Conclusions

We have presented the synthesis and characterization of a series of CdS nanoclusters having controlled surface electron demand, and bearing an electroactive ruthenium polypyridyl fluorophore. Electrochemical and emission studies of these interesting materials have yielded conclusive evidence that electronic communication can indeed be mediated by CdS nanoclusters via a core-mediated inductive mechanism. These results further suggest the possibility that surface functionalized semiconductor nanoclusters may possess device activity.

Acknowledgements

The authors are indebted to Professor A.B.P. Lever, Dr Robert Metcalfe, Dr Scott Fielder and Morey Najman for their useful discussions. They also thank Lisa Nelson and Karen Retheray for assistance with mass spectrometry and transmission electron microscopy, respectively, and the Natural Sciences and Engineering Research Council of Canada (NSERC) for financial support.

References

[1] J.G.C. Veinot, J. Galloro, L. Pugliese, R. Pestrin, W.J. Pietro, Chem. Mater. 11 (1999) 642.
[2] A.P. Alivisatos, J. Phys. Chem. 100 (1996) 13266.
[3] H. Weller, Angew. Chem., Int. Ed. Engl. 32 (1993) 41.
[4] G. Schmid, Chem. Rev. 92 (1992) 1709.
[5] M.L. Steigerwald, L.E. Brus, Acc. Chem. Res. 23 (1990) 183.
[6] A. Henglein, Chem. Rev. 89 (1861) 1989.
[7] M.G. Bawendi, M.L. Steigerwald, L.E. Brus, Annu. Rev. Phys. Chem. 41 (1990) 477.
[8] U. Merkt, Ch. Sikorski, Semiconductor Sci. Technol. 5 (1990) 182.
[9] T.A. Fulton, Nature 346 (1988) 408.
[10] B. Zorman, M.V. Ramakrishna, R.A. Friesner, J. Phys. Chem. 99 (1995) 7649.
[11] D.L. Klien, R. Roth, A.K.L. Lim, A.P. Alivisatos, P.L. McEven, Nature 389 (1997) 699.
[12] M. Moskovits, personal communication, 1997.
[13] M. Moskovits, J.M. Xu, US Patent US 5,581,091, 1996.
[14] H. Noglik, W.J. Pietro, Chem. Mater. 6 (1994) 1593.
[15] H. Noglik, W.J. Pietro, Chem. Mater. 7 (1995) 1333.
[16] J.G.C. Veinot, M. Ginzburg, W.J. Pietro, Chem. Mater. 9 (1997) 2117.
[17] J.G.C. Veinot, J. Galloro, L. Pugliese, V. Bell, R. Pestrin, W.J. Pietro, Special Materials Science Issue, Can. J. Chem. 76 (1998) 1530.
[18] Y. Bass, R.J. Morgan, Synth. Commun. 27 (12) (1997) 2168.
[19] B.P. Sullivan, D.J. Salmon, T.J. Meyer, Inorg. Chem. 17 (1978) 3334.
[20] N. Herron, Y. Wang, H. Eckert, J. Am. Chem. Soc. 112 (1990) 1322.
[21] J.R. Sachleben, E.W. Wooten, L. Emsley, A. Pines, V.L. Covin, A.P. Alivisatos, Chem. Phys. Lett. 198 (1992) 431.
[22] J.I.G. Cadogen, S.V. Ley, G. Pattenden, R.A. Raphael, Dictionary of Organic Compounds, vol. 4, 6th edn., 1996, p. 4161.
[23] J.I.G. Cadogen, S.V. Ley, G. Pattenden, R.A. Raphael, Dictionary of Organic Compounds, vol. 5, 6th edn., 1996, p. 4754.
[24] Y. Wang, N. Herron, Phys. Rev. B 42 (1990) 7253.
[25] Y. Wang, N. Herron, J. Phys. Chem. 95 (1991) 525.
[26] T. Vossmeyer, L. Katsikas, M. Giersig, I.G. Popovic, K. Diesner, A. Chemsddine, A. Eychmuller, H. Weller, J. Phys. Chem. 98 (1994) 7665.
[27] E.A. Seddon, K.R. Seddon, The Chemistry of Ruthenium, Elsevier, 1984.
[28] S.L. Mecklenburg, B.M. Peek, J.R. Schoonover, D.G. McCafferty, C.G. Wall, B.W. Erickson, T.J. Meyer, J. Am. Chem. Soc. 115 (1993) 5479.
[29] B.P. Sullivan, D.J. Salmon, T.J. Meyer, Inorg. Chem. 17 (12) (1978) 3334.
[30] J.V. Caspar, T.J. Meyer, Inorg. Chem. 22 (1983) 2444.
[31] B.A. Moyer, T.J. Meyer, Inorg. Chem. 20 (1981) 436.
[32] M.D. Hossain, M. Haga, H. Monjushiro, B. Gholamkhass, T. Ohno, Chem. Lett. (1997) 573.
[33] P. Ghosh, A. Chakravorty, Inorg. Chem. 23 (1984) 2242.
[34] E.H. Yonemoto, G.B. Saupe, R.H. Schmehl, S.M. Hubig, R.L. Riley, B.L. Iverson, T.E. Mallouk, J. Am. Chem. Soc. 116 (1994) 4786.
[35] E.S. Dodsworth, A.B.P. Lever, Chem. Phys. Lett. 124 (2) (1986) 152.
[36] T.A. Heimer, C.A. Bignozzi, G.J. Meyer, J. Phys. Chem. 97 (1993) 11987.
[37] T.A. Heimer, T. D'Arcangelis, F. Farzad, J.M. Stipkala, G.J. Meyer, Inorg. Chem. 35 (1996) 5319.
[38] P.V. Kamat, N.M. Dimitrijevic, Sol. Energy 44 (2) (1990) 83.

PERGAMON

www.elsevier.nl/locate/poly

Polyhedron 19 (2000) 343–349

POLYHEDRON

Photolithographic deposition of conducting gold films from thin amorphous films of $AuPR_3X$ ($X = NO_3$, RCO_2) on silicon surfaces

J. Pablo Bravo-Vasquez, Ross H. Hill *

Department of Chemistry, Simon Fraser University, Burnaby, BC V5A 1S6, Canada

Received 2 May 1999; accepted 30 July 1999

Abstract

The photochemical reactions of amorphous films of $AuPR_3X$ ($X = NO_3$, RCO_2) on silicon surfaces are presented. In each case these precursors could be used to form amorphous thin films on silicon substrates by spin coating. The photolysis of these films was monitored by FTIR spectroscopy and the products analyzed by Auger electron spectroscopy. The photolysis with 254 nm light led to the loss of the anionic ligand from the film. The phosphine ligand also diffused from the film although far less efficiently. The purity of the contaminated films could be improved by a heat treatment at 150°C. The films following this heat treatment were approximately 90 at.% gold. This process was then used to lithograph gold patterns on silicon surfaces. A feature size of 1.2 μm was demonstrated. ©2000 Elsevier Science Ltd All rights reserved.

Keywords: Photochemistry; Surface chemistry; Photochemical metal organic deposition; Lithography; Gold

1. Introduction

In this paper we outline a method for the deposition of patterned gold films from gold complexes by photochemical metalorganic deposition (PMOD). Gold has properties such as oxidation resistance and high conductivity which make it desirable for use in microelectronics [1]. As the minimum feature size in electronic devices decreases, there is an increasing pressure to use higher conductivity metals as interconnects in the semiconductor industry. This has necessitated the recent change from aluminum to copper for some applications [2]. Gold, like copper, has a higher conductivity than aluminum and its use may be advantageous in some applications.

Metal complexes have been used as precursors to generate thin films of metals and metal oxides by both chemical and photochemical vapor deposition pathways [3–11]. For the production of patterned films, however, photo induced processing is desirable. For gold, considerable work has been done on laser processing by laser induced CVD [12–14]. The laser processing has the disadvantage of high local temperatures during the processing. A photochemical approach has also been taken in processing films consisting of polymers containing metal complexes or particles [15,16]. A related method relies on photolithographed SAMs to transfer the image via metallization yielding patterned gold [17]. The photochemical pathway has the advantage that photolysis through a mask can result in a patterned deposition process. In our research we have utilized thin films of inorganic and organometallic complexes as precursors to metal and metal oxide films [18–27]. In these studies, films of the precursor complexes are converted photochemically in the solid state to thin films of a metal [18,19] or metal oxide [20–27].

Previously we have demonstrated the fabrication of metal and metal oxide structures via photolysis of amorphous films of inorganic precursor through a lithography mask [18–23,25–27]. The amorphous film is formed by spin coating the substrate with a solution of the precursor molecule. This is followed by the irradiation of the surface film through a lithography mask to produce the patterned structures. Generally we find that the product of this reaction in air is the metal oxide. Normally the metal, liberated photochemically, reacts with atmospheric oxygen to yield the metal oxide. In vacuum or an inert atmosphere the metal may be formed directly. Gold presents an opportunity for the direct formation of a metal in air.

2. Results

2.1. Spectroscopic data for the complexes

All the complexes studied here could be cast from methylene chloride solvent as optical quality thin film on both

* Corresponding author. Tel.: +1-604-291-3590; fax: +1-604-291-3765

0277-5387/00/$ - see front matter ©2000 Elsevier Science Ltd All rights reserved.
PII S0277-5387(99)00364-2

silicon chips and CaF_2 optical flats. The FTIR spectral data described in this section were obtained as transmission spectra on CaF_2 substrate. The FTIR spectra of the relevant complexes as thin films are summarized in Table 1.

The nitrate complex $AuPPh_3NO_3$ is characterized by nitrate bands at 1499, 1279 and 979 cm^{-1}. It is worth noting that these bands are not significantly shifted from the energies of 1500, 1270 and 980 cm^{-1} reported for the complex in Nujol mull [28,29]. In this region there are other bands associated with the phosphine ligand at 1437 and 1480 cm^{-1}. The triethylphosphine derivative, $AuPEt_3NO_3$, exhibited absorption bands in the same region characteristic of the nitrate ligand. In addition, to these bands, the CH stretching vibrations of the ethyl groups in the region of 2900 cm^{-1} were also observed.

The FTIR spectra of films formed from the carboxylato complexes are also included in Table 1. The complex $AuPPh_3(OOCCH_3)$ exhibited intense bands characteristic of the symmetric and antisymmetric bands of the coordinated acetate group at 1626 and 1306 cm^{-1}. These bands are consistent with those reported for this complex in a Nujol mull [29] at 1632 and 1310 cm^{-1} and have been interpreted as being associated with a unidentate acetate group. In addition to these bands there are additional absorption bands at 1590 and 1369 cm^{-1}. These weaker bands may be indicative of other coordination modes being present in the amorphous film.

The spectrum of $AuPEt_3(OOCCH_3)$ was very similar to that of the triphenylphosphine derivative. The most intense bands were associated with the symmetric and antisymmetric carboxylate stretches at 1626 and 1310 cm^{-1}. In addition to these, a second pair at 1597 and 1369 cm^{-1} were observed. The only substantial difference was that the stretches associated with the alkyl CH bonds of the triethylphosphine ligand were apparent near 2900 cm^{-1}.

The complex $AuPPh_3(OOCCH(OH)CH_3)$ displayed antisymmetric and symmetric carboxylate stretching modes at 1628 and 1314 cm^{-1}. For this complex the hydroxyl stretch of the lactate ligand was observed at 3443, shifted significantly from the literature value of 3390 cm^{-1} [30]. The triethylphosphine complex exhibited a similar FTIR spectrum. The hydroxyl stretch for this complex was observed at 3455 cm^{-1}. As with the other triethylphosphine complexes, additional bands associated with the CH stretches of the ligand were observed in the region of 2900 cm^{-1}.

Electronic absorption spectra for amorphous films of the pure compounds were obtained from thin films on CaF_2 and the results are summarized in Table 2. The complex $AuPPh_3NO_3$ is characterized by the presence of absorption bands at 200 and 249 nm. Presumably these are associated with charge transfer transitions between the phosphine and nitrate ligands and gold. The intensities of these transitions relative to the FTIR transitions are also given in Table 2. The calibration of the absolute intensities was hampered by problems with partial decomposition of solutions of the gold com-

Table 1
FTIR spectral data for relevant complexes on Si(111)

Complex	Energy (cm^{-1})	Relative intensity	Assignment
$AuPPh_3NO_3$	1497	0.011	$\nu(NO_3)$
	1480	0.0056	$\nu(PPh_3)$
	1437	0.0076	$\nu(PPh_3)$
	1267	0.013	$\nu(NO_3)$
	979	0.0056	$\nu(NO_3)$
$AuPEt_3NO_3$	2970	0.012	$\nu(CH)$
	2922	0.0061	$\nu(CH)$
	2870	0.0045	$\nu(CH)$
	1493	0.034	$\nu(NO_3)$
	1273	0.048	$\nu(NO_3)$
	985	0.0276	$\nu(NO_3)$
$AuPPh_3(OOCCH_3)$	1626	0.086	$\nu_S(CO_2)$
	1597	0.037	$\nu_S(CO_2)$
	1481	0.025	$\nu(PPh_3)$
	1435	0.069	$\nu(PPh_3)$
	1366	0.058	$\nu_S(CO_2)$
	1306	0.10	$\nu_S(CO_2)$
$AuPEt_3(OOCCH_3)$	2965	0.023	$\nu(CH)$
	2933	0.017	$\nu(CH)$
	2906	0.012	$\nu(CH)$
	2878	0.011	$\nu(CH)$
	1626	0.053	$\nu_S(CO_2)$
	1595	0.029	$\nu_S(CO_2)$
	1369	0.046	$\nu_S(CO_2)$
	1310	0.051	$\nu_A(CO_2)$
$AuPPh_3(OOCCH(OH)CH_3)$	3443	0.003	$\nu(OH)$
	1628	0.022	$\nu_S(CO_2)$
	1480	0.0062	$\nu(PPh_3)$
	1435	0.019	$\nu(PPh_3)$
	1309	0.017	$\nu_A(CO_2)$
$AuPEt_3(OOCCH(OH)CH_3)$	3455	0.0091	$\nu(OH)$
	2969	0.015	$\nu(CH)$
	2933	0.013	$\nu(CH)$
	2910	0.0090	$\nu(CH)$
	2876	0.0092	$\nu(CH)$
	1629	0.0239	$\nu_S(CO_2)$
	1315	0.0210	$\nu_S(CO_2)$

Table 2
Electronic spectral data for relevant complexes on Si(111)

Complex	Energy (nm)	Relative intensity
$AuPPh_3NO_3$	200	0.87
	249 sh	0.49
$AuPEt_3NO_3$	200	0.69
	254 sh	0.30
$AuPPh_3(OOCCH_3)$	202	1.71
	252	0.78
$AuPEt_3(OOCCH_3)$	208	0.82
	234	0.56
	252	0.47
$AuPPh_3(OOCCH(OH)CH_3)$	198	2.0
	248	0.65
$AuPEt_3(OOCCH(OH)CH_3)$	200	0.487
	210	0.414
	232	0.213
	252	0.179

plexes. As we will see, these complexes are both light and heat sensitive.

The remaining complexes also have absorptions in this spectral region and the absorption bands are summarized in Table 2. In each case there are intense bands in the UV spectrum near 254 nm. In the following photochemical study of the films we will use 254 nm light to initiate the photochemistry.

2.2. Photochemistry of $AuPPh_3NO_3$ and $AuPEt_3NO_3$

In order to study the photochemistry, an amorphous film of $AuPPh_3NO_3$ was cast on a silicon chip. The initial FTIR spectrum of the complex was obtained as a transmission spectrum through the band gap of silicon. The spectroscopic changes resultant from the photolysis of a thin film of $AuPPh_3NO_3$ were then obtained and are shown in Fig. 1. The bands associated with the nitrate at 1497, 1267 and 979 cm^{-1} all decrease in intensity. This decrease appears to be accompanied by the growth of bands associated with triphenylphosphine oxide at 1200 and 1121 cm^{-1}. The overlap between the bands associated with triphenylphosphine and its oxide do not allow us to determine whether all of the triphenylphosphine is oxidized. The bands associated with the aryl groups bound to phosphorus at 1480 and 1437 cm^{-1} decrease at a much slower rate. Following prolonged photolysis no bands associated with the nitrate ligand are observed within the film. This indicates the loss of all starting material. Bands associated with the aryl groups bound to phosphorus and the phosphine oxide continued to decay although at a much slower rate. Presumably this is associated with the diffusion of the triphenylphosphine out of the film. It is important to note that there must be some interaction between the triphenylphosphine and its oxide and the gold during this process, however, no absorption bands associated with the formation of intermediate gold complexes were observed during the photochemical reaction. This is consistent with the overall photoreaction shown in Eq. (1).

$$AuPPh_3NO_3 \xrightarrow{h\nu} Au + NO_3 + PPh_3 \quad (1)$$

It is notable that in Eq. (1) we depict the photoreaction as

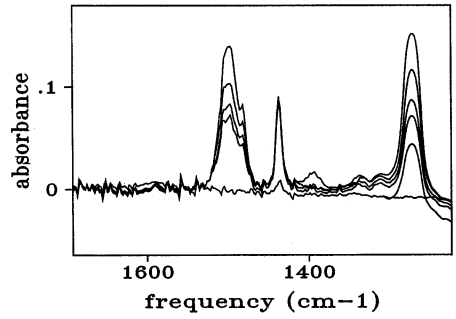


Fig. 1. FTIR spectra associated with the photolysis of an amorphous film of $AuPPh_3NO_3$ for 0, 5, 44, 94, and 200 min followed by thermolysis at 150°C for 1 min.

generating triphenylphosphine directly. The oxidation to the phosphine oxide we believe occurs in a separate unrelated step. Our evidence for this is that the exposure of films of triphenylphosphine in air to the photolytic conditions results in their conversion to the phosphine oxide. This does not rule out other processes also contributing to the formation of the phosphine oxide, but does establish that the proposed mechanism is plausible.

FTIR spectroscopic data following photolysis of the compound indicate loss of all starting material. In order to measure the residual ligand remaining within the films, the resultant films were analyzed by Auger electron spectroscopy. The analysis of films produced from $AuPPh_3NO_3$ is consistent with the loss of NO_3 and some PPh_3 from the film leaving a film composed primarily of gold, phosphorus and carbon (Table 3). The surface layer was removed by sputtering and the composition of the interior of the film is also indicative of the retention of some PPh_3. There is no evidence for oxygen, indicative of triphenylphospine oxide, within the film. The ratio of carbon to phosphorus is higher than expected although this may be indicative of problems associated with some charging of the film during data collection. The key result here is that most of the phosphine is lost from the film. This can be taken as an indication that the photochemistry results in the formation of gold rather than a molecular complex. The gold however retains some phosphine

Table 3
Properties of the films: composition of initial films by FTIR, thickness of the initial films and composition of the final films by Auger analysis

Precursor	Sputter time (s)	Au (%)	P (%)	N (%)	C (%)	O (%)
$AuPPh_3NO_3$	0	2.6	0.9	0	67	0
	10	8.4	2.7	0	89	0
$AuPEt_3NO_3$	0	5	2.0	0	64	28
	10	8	4.0	0	56	32
$AuPPh_3(OOCCH_3)$	0	4	3		71	23
	10	12	5		83	0
$AuPEt_3(OOCCH_3)$	0	6	2		79	13
	10	10	5		73	13
$AuPPh_3(OOCCH(OH)CH_3)$	0	2	2		82	14
$AuPEt_3(OOCCH(OH)CH_3)$	0	4	1		95	0
	10	19	5		76	0

impurity. The results of both the IR and Auger experiments suggest the production of metallic gold as the product film.

Similar experiments were conducted with the triethylphosphine complex $AuPEt_3NO_3$. The results were consistent with the findings for the triphenylphosphine complex. Irradiation resulted in the loss of the ligands from the coordination sphere and the observation of no new IR active products. Once again the bands associated with the nitrate ligand were observed to decay much faster than those associated with the phosphine ligand. In this case the spectra did not provide evidence for the formation of triethylphosphine oxide although it appears reasonable to assume that at least some of the triethylphosphine would oxidize in air. Auger results are indicative of the loss of all the nitrate from the film and some loss of the phosphine ligand. Once again significant organic contamination remained in the film. In this case the amount of carbon and oxygen is suggestive of some external contaminants contributing to the impurity. However, the Auger results indicate that the photochemistry produces an impure gold film rather than a molecular complex. The result of the experiments are all consistent with the photochemistry being that shown in Eq. (2).

$$AuPEt_3NO_3 \xrightarrow{h\nu} Au + NO_3 + PEt_3 \quad (2)$$

2.3. Photochemistry of $AuPPh_3(O_2CCH_3)$, $AuPEt_3(O_2CCH_3)$, $AuPPh_3(O_2CCH(OH)CH_3)$ and $AuPEt_3(O_2CCH(OH)CH_3)$

The spectral changes resulting from the photolysis of an amorphous thin film of $AuPPh_3(O_2CCH_3)$ are summarized in Fig. 2. Photolysis resulted in the loss of absorbance associated with the coordinated carboxylate group at 1626, 1597, 1366 and 1306 cm^{-1}. During the photolysis the relative ratio of these bands remained constant, indicating that no thermally stable intermediate was formed in the photoreaction. The absorption bands associated with the phosphine ligand at 1481 and 1435 cm^{-1} did not change at a proportionate rate but at a much slower rate. These bands are presumably related to the presence of either phosphine or gold phosphine complexes in the film. Also evident from the times given in the caption to Fig. 2 is a slowing of the rate of the photoreaction with time. This decrease in decay rate is at least in part associated with the lessening absorbance of the starting material as the reaction progresses. This effect is expected to be significant since the initial stages of the reaction are occurring under conditions where the starting material absorbs 100% of the incoming light. As the reaction progresses this percentage decreases as a result of the decrease in the amount of starting material remaining and also as a result of competitive absorption (or reflection) by the photoproducts. This effect is expected to be extreme when a gold mirror is on the surface. In order to complete this reaction the surface was heated to 150°C. The result of this heating was the loss of all absorption bands in the FTIR spectrum. For thinner films exhaustive photolysis resulted in the loss of all carboxylate absorption bands.

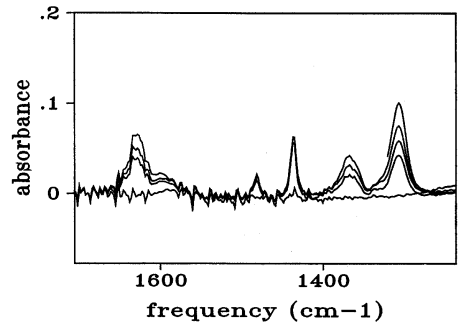


Fig. 2. FTIR spectra associated with the photolysis of an amorphous film of $AuPPh_3(OOCCH_3)$ for 0, 60, 430, and 880 min followed by thermolysis at 150°C for 1 min.

The film produced by the photolytic reaction was examined by Auger electron spectroscopy and the results are summarized in Table 3 (the film used for this study was not subjected to the heat treatment used on the sample of Fig. 2). Clearly the photolysis resulted in the loss of the carboxylate ligand from the film. This is indicated by the lack of oxygen in the film as observed after sputtering. The film has some remaining phosphorus indicative of some triphenylphosphine remaining in the film. The ratio of phosphorus to carbon in the film is consistent with triphenylphosphine being the sole source of carbon contamination. The experimental data are all consistent with the reaction shown in Eq. (3). The detailed analysis of the reaction will be deferred to Section 3.

$$AuPPh_3(O_2CCH_3) \xrightarrow{h\nu} Au + CO_2 + \cdot CH_3 + PPh_3 \quad (3)$$

Similar results were obtained with the triethylphosphine complex $AuPEt_3(O_2CCH_3)$. Photolysis of an amorphous film consisting of this complex resulted in the loss of FTIR bands associated with the starting complex and the formation of a gold film. Once again bands associated with the carboxylate ligand decayed at a much faster rate than those associated with phosphine. The resultant film was subjected to Auger analysis. As can be seen from Table 3 there is a much higher retention of carbon than can be explained on the bases of the phosphine being the sole source of organic impurity. In this sample significant other impurity must be present.

The photochemistry of amorphous thin films of the lactate phosphine complexes was also examined. In all cases the results were similar to those above. Photolysis led to the loss of the carboxylate ligand at a greater rate than the phosphine ligand. Spectroscopic evidence suggested that in the case of $AuPPh_3(O_2CCH(OH)CH_3)$ some of the photoproduced triphenylphosphine was oxidized to the phosphine oxide. Consistent with these results, the Auger was indicative of substantial phosphine or phosphine oxide retention within the product film. In the case of the triethylphosphine containing precursor, only a quarter of the phosphine remained in the film while in the case of the triphenylphosphine containing precursor there was no evidence for loss of the phosphine

from the film. This latter result is however in question as charging made the examination of the surface after sputtering unreliable. The photoreactions of all the carboxylate complexes are summarized in Eq. (4).

$$AuPR_3(O_2CR') \xrightarrow{h\nu} Au + CO_2 + \cdot R' + PR_3 \quad (4)$$

2.4. Thermal chemistry of $AuPR_3(NO_3)$ and $AuPR_3(O_2CR)$

While is was apparent that the chemistry initiated with light could be used to pattern surfaces, the Auger spectroscopy indicated that the films all retained significant impurities. In this section we explore the use of thermal treatment to improve the purity of the surfaces. A brief study of the thermal chemistry of the amorphous films was conducted. A film of $AuPPh_3(NO_3)$ was cast onto a silicon chip and the FTIR spectrum obtained. The sample was heated to 150°C and the FTIR spectrum obtained again. No thermal products were apparent from the spectrum and all bands attributable to the starting material were lost, including those associated with the phosphine ligand. Auger analysis indicated that the film consisted of 90% gold with some remaining phosphorus (1%) and carbon (9%). The resulting film was conductive and a four-point probe measurement yielded a sheet resistance of 40 μΩ cm. This value is significantly higher than the bulk value of 2.8 μΩ cm [1]. One reason for this discrepancy may be the poor signal to noise of our measurement. At high enough current density for measurement the electrodes used were glowing and a deposition of some sort appeared on the surface of the film.

The above results were general and appeared to be insensitive to the phosphine ligand combination chosen. In addition, complexes photolyzed then subjected to thermal treatment gave similar results.

2.5. Lithography

This surface photochemistry is compatible with lithography allowing us to pattern surfaces. This was demonstrated by irradiation of a surface film of $AuPPh_3(O_2CCH_3)$ through a lithography mask. The mask was set up in contact with the surface negating the need for optics. The films were exposed with 254 nm light for 2 h through the mask. The resultant latent image was formed and the surface developed with a methylene chloride rinse. The resultant image is shown in Fig. 3. Clear formation of lines 1.2 μm by 50 μm is visible. Similar results were found for films constructed of the other complexes.

3. Discussion

The complexes studied here all provide useful staring materials for the deposition of gold films. These compounds all spin coat well to yield optical quality amorphous films.

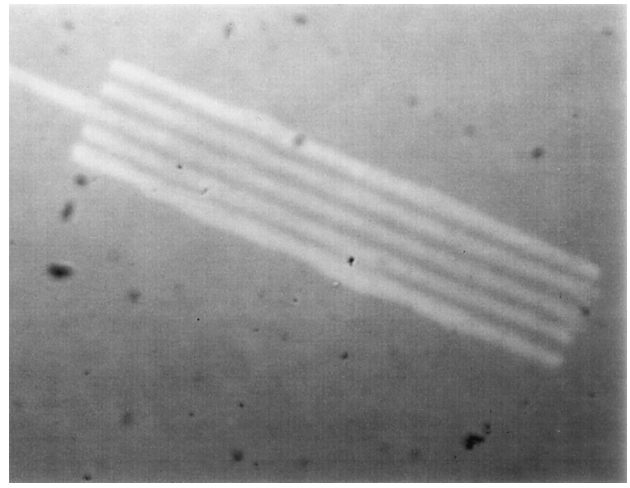


Fig. 3. Optical micrograph of surface obtained by the photolithography of $AuPPh_3(O_2CCH_3)$ on a silicon surface. An internal scale is provided by the 50 μm length of the lines.

The complexes with the films provide FTIR spectral data consistent with their formulation as monomeric complexes within the film entirely analogous to the structure in a mull or in solution.

The photochemical reactions all appear to follow a charge transfer transition. In the case of $AuPPh_3(NO_3)$ this would result in the formation of gold(0) and the nitrate radical. The nitrate radical would then be lost from the film, leaving gold phosphine clusters. Such clusters have been proposed as intermediates in the thermal reactions of gold compounds [30]. These are evidently unstable in the film and gold metal is formed.

The reactions of the carboxylate complexes can be rationalized in a similar fashion. Charge transfer transitions result in the extrusion of carbon dioxide from the carboxylate and the resulting formation of a gold(0) phosphine and an organic radical. The radicals can combine in the film yielding volatile organic fragments. The gold(0) phosphine decomposes to yield an impure gold film. The purity of the film may be enhanced by heating the films following the photochemistry.

The lithographic images presented establish that this process can be used to pattern gold films. This were done by simple contact printing on a laboratory bench and is not meant to imply that we have established limits on the feature size available by this process. The quality of the image does however establish that the optical quality of the film is retained throughout the deposition process. This presumably is the result of self healing of the film during the photoreaction. Surface diffusion of molecules of the precursor from areas of high surface energy to areas of lower surface energy results in the self healing of the film. The quality of the films produced indicates that the rates of surface diffusion of these precursors are acceptable for this surface healing to occur.

4. Conclusions

The studies described here establish that conducting gold films can be deposited by photochemical metal organic dep-

osition. The photoreactions are dependent upon the anionic ligand. For $AuPR_3(OOCR')$ the initial charge transfer transition results in the loss of CO_2 and the formation of an organic radical and $AuPR_3$. Photolysis of $AuPR_3NO_3$ results in the expulsion of the nitrate ligand and the production of $AuPR_3$. In each case the gold containing product is not stable and loses phosphine yielding gold films.

The use of this process for lithographic deposition of gold has been illustrated. The most practical way to achieve lithography in these complexes is with the combination of the thermal and photochemical routes.

5. Experimental

The silicon wafers were obtained from Wafernet. The Si(111) surface was used in these studies and the wafers were p-type silicon cut to the approximate dimensions of 1 cm × 1.5 cm in house. The CaF_2 crystals were obtained from Wilmad Glass Co. Inc.

The FTIR spectra were obtained with 4 cm^{-1} resolution using a Bomem Michelson 120 FTIR spectrophotometer. Electronic absorption spectra were obtained with a HP 8452A diode array spectrometer. The photolysis was conducted with the 254 nm output of a low pressure mercury lamp. Auger spectra were obtained using a PHI double pass CMA at 0.85 eV resolution at the Surface Physics Laboratory, Department of Physics, Simon Fraser University. Optical microscopy was conducted with a Leitz Laborlux 12 MES optical microscope. The chromium plated quartz lithography mask was kindly donated by IBM.

The complexes $AuPPh_3(O_2CCH_3)$ and $AuPPh_3(O_2CCH(OH)CH_3)$ were prepared by literature procedures [29,30]. The remaining complexes, $AuPEt_3NO_3$, $AuPEt_3(O_2CCH_3)$ and $AuPEt_3(O_2CCH(OH)CH_3)$ were prepared by routes analogous to the literature preparations of the PPh_3 complexes [28–30].

5.1. Calibration of absorption on the surface

A solution of $AuPPh_3NO_3$, in methylenechloride was used to spin coat a silicon chip. The resultant sample was mounted in the FTIR spectrometer and the spectrum determined. The spectrum is summarized in Table 1. A similar procedure was used to obtain the spectra of all the complexes studied here.

The electronic absorption spectra were obtained by spin coating samples onto CaF_2 plates. The energies of the electronic transitions are obtained directly while the extinction coefficients were obtained relative to the intensities of the IR transitions. Energies and relative extinction coefficients for all the compounds are reported in Table 2.

5.2. Photolysis of complexes as films on silicon surfaces

An amorphous film of $AuPPh_3(NO_3)$ on a silicon surface was prepared by dispensing a CH_2Cl_2 solution containing the gold complex onto a spinning silicon chip. This resulted in the formation of a uniform, amorphous coating on the chip. The FTIR spectrum of the film deposited on the chip was obtained. The sample was then irradiated for 5 min and another FTIR spectrum was obtained. This procedure was repeated for the following (accumulated) photolysis times: 44, 94 and 200 min. The spectra are presented in Fig. 1.

A sample prepared in a similar fashion was investigated in the scanning Auger microprobe for elemental analysis of the surface. The results are presented in Table 3.

A similar procedure was used to monitor the photoreactions of all the complexes studied here.

5.3. Lithography

A film containing $AuPPh_3(O_2CCH_3)$ was spin coated onto a silicon chip, as described above. This sample was then photolyzed through a mask in contact with the surface. The film was then rinsed with methylene chloride to yield the image shown in Fig. 3.

Acknowledgements

We wish to thank B. Heinrich and K. Myrtle of the Surface Physics Laboratory, Simon Fraser University, for assistance in obtaining the Auger spectra. We thank NSERC (Canada) for financial support.

References

[1] R.C. Weast, Handbook of Chemistry and Physics, CRC Press, Cleveland, OH, 1974.
[2] P.C. Andricacos, The Electrochemical Society Interface Spring 1999, p. 32.
[3] M.J. Almond, D.A. Rice, C.A. Yates, Chem. Br. 24 (1988) 1130.
[4] M.J. Rand, J. Electrochem. Soc. 120 (1973) 686.
[5] R. Kumar, M. Rashidi, R.J. Puddephatt, Polyhedron 8 (1989) 551.
[6] N.H. Dryden, R. Kumar, E. Ou, M. Rashidi, S. Roy, P.R. Norton, R.J. Puddephatt, Chem. Mater. 3 (1991) 677.
[7] H.H. Gilgen, T. Cacouris, P.S. Shaw, R.R. Krchnavek, R.M. Osgood, Appl. Phys. B 42 (1987) 55.
[8] D.K. Liu, R.J. Chin, A.L. Lai, Chem. Mater. 3 (1991) 13.
[9] J.S. Foord, R.B. Jackman, Chem. Phys. Lett. 112 (1984) 190.
[10] V. Borker, K.S. Rane, V.N. Kamat Dalal, J. Mater. Sci. 4 (1993) 241.
[11] G. Frolov, V.S. Zhigalov, S.M. Zharkov, I.R. Yarullin, Phys. Solid State 36 (1994) 526.
[12] T.H. Baum, P.B. Comita, Thin Solid Films 218 (1992) 80.
[13] T.H. Baum, J. Electrochem. Soc. 134 (1987) 2616.
[14] R.B. Klassen, T.H. Baum, Organometallics 8 (1989) 2477.
[15] M.E. Gross, G.J. Fisanick, P.K. Gallagher, K.J. Schnoes, M.D. Fennell, Appl. Phys. Lett. 47 (1985) 923.
[16] Y. Yonesawa, I. Kawabata, T. Sato, Ber. Bunsenges. Phys. Chem. 100 (1996) 39.
[17] J.-F. Liu, L.-G. Zhang, N. Gu, J.-Y. Ren, Y.-P. Wu, Z.-H. Lu, P.-S. Mao, D.-Y. Chen, Thin Solid Films 327–329 (1998) 176.
[18] R.H. Hill, A.A. Avey, S.L. Blair, M. Gao, B.J. Palmer, Mater. Chem. Phys. 43 (1996) 233.
[19] A.A. Avey, R.H. Hill, J. Am. Chem. Soc. 118 (1996) 237.

[20] J.P. Bravo-Vasquez, L.W.C. Ching, W.L. Law, R.H. Hill, J. Photopolymer Sci. Technol. 11 (1998) 589.
[21] L.W.C. Ching, R.H. Hill, J. Vac. Sci. Technol. 16 (1998) 897.
[22] W.L. Law, R.H. Hill, Mater. Res. Bull. 33 (1998) 69.
[23] M. Gao, R.H. Hill, J. Mater. Res. 13 (1998) 1379.
[24] M. Gao, R.H. Hill, J. Photochem. Photobiol. A: Chem. 97 (1996) 73.
[25] C.W. Chu, R.H. Hill, Mater. Chem. Phys. 43 (1996) 135.
[26] C.W. Chu, M.J. Deen, R.H. Hill, J. Electrochem. Soc. 145 (1998) 4219.
[27] S.L. Blair, R.H. Hill, J. Organomet. Chem. 554 (1998) 63.
[28] A.M. Mueting, B.D. Alexander, P.B. Boyle, A.L. Casalnuovo, L.N. Ito, B.J. Johnson, L.H. Pignolet, Inorg. Synth. 29 (1988) 279.
[29] D.I. Nichols, A.S. Charleston, J. Chem. Soc. A (1969) 2581.
[30] J.P. Fackler Jr, Md.N.I. Khan, C. King, R.J. Staples, R.E.P. Winpenny, Organometallics 10 (1991) 2178.

PERGAMON

www.elsevier.nl/locate/poly

Polyhedron 19 (2000) 351–355

POLYHEDRON

Metal–organic chemical vapour deposition of lead scandium tantalate: chemical issues and precursor selection

Anthony C. Jones [a,*], Timothy J. Leedham [a], Hywel O. Davies [b], Kirsty A. Fleeting [b], Paul O'Brien [1,b], Michael J. Crosbie [c], Peter J. Wright [c], Dennis J. Williams [c], Penelope A. Lane [c]

[a] *Inorgtech Limited, 25 James Carter Road, Mildenhall, Suffolk IP28 7DE, UK*

[b] *Department of Chemistry, Imperial College of Science Technology and Medicine, London SW7 2AZ, UK*

[c] *Defence Evaluation and Research Agency, St. Andrews Road, Great Malvern, Worcestershire WR14 3PS, UK*

Received 2 May 1999; accepted 16 June 1999

Abstract

MOCVD is a promising technique for the deposition of the pyroelectric oxide lead scandium tantalate, $Pb(Sc_{0.5}Ta_{0.5})O_3$. In order to exploit the full potential of the method, it is important to identify the optimum combination of precursors so that process parameters and film properties are optimised. In this paper, issues involved in the selection of suitable Pb, Sc and Ta precursors are discussed and the molecular design of new Ta and Sc sources is described. It is shown how the use of carefully matched precursors allows the growth of $Pb(Sc_{0.5}Ta_{0.5})O_3$ in the required perovskite phase at low substrate temperatures. ©2000 Elsevier Science Ltd All rights reserved.

Keywords: Metal–organic chemical vapour deposition; Precursors; Lead scandium tantalate; Ferroelectric oxides

1. Introduction

Thin films of the ferroelectric oxides $Pb(Zr,Ti)O_3$, $Pb(Mg,Nb)O_3$ and $Pb(Sc_{0.5}Ta_{0.5})O_3$ have important applications in pyroelectric [1], and piezoelectric devices [2]. Various techniques have been used for the deposition of such oxides, including reactive sputtering [3], sol–gel deposition [4,5] and metal–organic chemical vapour deposition (MOCVD) [6–8]. Of these techniques, MOCVD offers the most flexible approach, having the advantages of large area deposition capability, good composition control and film uniformity, high film densities and deposition rates, and excellent conformal step coverage at device dimensions less than 2 μm, which is particularly important in microelectronics applications.

An essential requirement for successful MOCVD is the availability of suitable precursors with the appropriate physical properties for transport and reactivity for deposition. There must be an adequate temperature window between precursor vaporisation and decomposition, and for most electronics applications oxide deposition is limited to temperatures in the region of 500°C, to prevent degradation of the underlying silicon circuitry and metal interconnects.

The most accessible and widely used precursors for ferroelectric oxide MOCVD are metal alkoxides and β-diketonates [9], which generally have quite low equilibrium vapour pressures, typically in the order of 1 Torr at 200°C. In order to overcome this inherent involatility, liquid injection MOCVD, in which a solution of the precursor is injected into a heated evaporator, is now widely used [10,11]. This approach minimises thermal degradation of precursors, but leads to the added requirements that the precursor must be stable for long periods in solution, and must not react with other precursors in the solution. Precursor solutions should also evaporate at a common temperature without decomposition, otherwise blockages will eventually occur in the evaporator. Ideally, the separate precursors should also decompose to deposit oxide film in a similar temperature regime in order to optimise film uniformity. Although acceptable MOCVD performance and high quality ferroelectric films can often be obtained using existing precursors, in the case of more complex oxides it is sometimes necessary to 'tailor' the precursor to improve compatibility with other precursors and to optimise process parameters such as precursor evaporation temperature and oxide deposition temperature. In this paper we discuss one approach to the selection

* Corresponding author. Fax: +44-163-871-8259; e-mail: tony@inorgtech.co.uk

[1] Also corresponding author.

0277-5387/00/$ - see front matter ©2000 Elsevier Science Ltd All rights reserved.
PII S0277-5387(99)00365-4

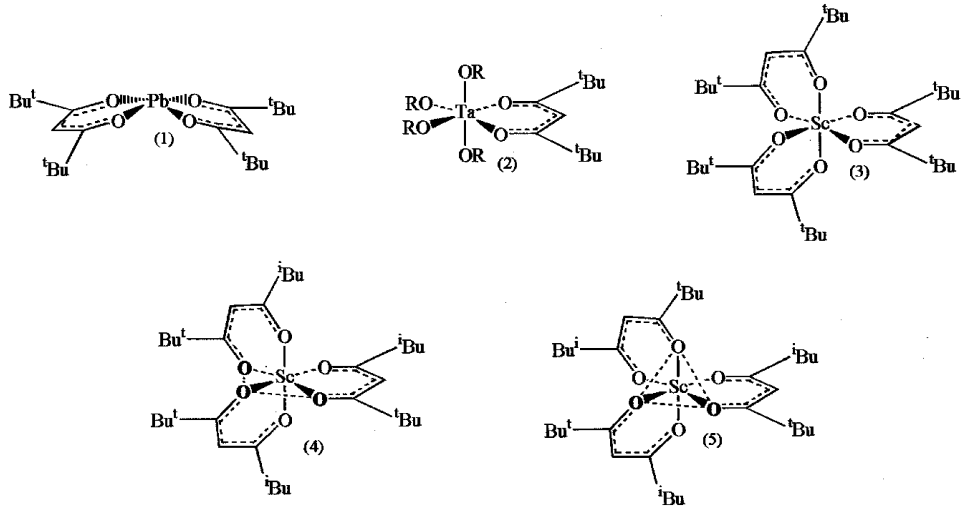


Fig. 1. Molecular structures of some lead, scandium and tantalum compounds used in this study. (1) $Pb(thd)_2$, (2) $Ta(OR)_4(thd)$, (3) $Sc(thd)_3$, (4,5) $Sc(tmod)_3$. In the solid state $Sc(tmod)_3$ exists as a mixture of meridional and facial isomers (4) and (5). In solution the statistically preferred facial isomer predominates.

and design of precursors for the deposition of $Pb(Sc_{0.5}Ta_{0.5})O_3$ by liquid injection MOCVD. $Pb(Sc_{0.5}Ta_{0.5})O_3$ is a sensitive pyroelectric oxide with a high figure of merit which has applications in uncooled thermal imaging, including night sight technologies and fire detection [12].

2. Precursor selection

2.1. Pb precursors

Although PbO and $Pb(Zr,Ti)O_3$ can be deposited using lead alkyls or alkoxides such as tetraethyllead, $PbEt_4$, lead *tert*-butoxide, $Pb(OBu^t)_2$, and triethyllead neopentoxide, $Et_3Pb(OCH_2C(CH)_3)$, their high toxicity and reactivity, coupled with their high volatility, make them difficult to handle and extremely hazardous to use in liquid injection MOCVD.

In contrast, lead β-diketonates are less toxic and have lower vapour pressures, which minimises the toxic release hazard. Therefore the following precursors have all been used in MOCVD: $Pb(thd)_2$ (thd = 2,2,6,6-tetramethyl-3,5-heptanedionate), Pb(acetylacetonate)$_2$, Pb(hexafluoroacetylacetonate)$_2$, $Pb(fod)_2$ (fod = 1,1,1,2,2,3,3-heptafluoro-7,7-dimethyloctane-4,6-dionate) [6]. The fluorine-containing compounds $Pb(hfac)_2$ and $Pb(fod)_2$ can lead to high levels of fluorine contamination in the oxide films, decomposing above 300°C to form a PbF_2 phase [6]. Consequently, the most volatile of the non-fluorine containing precursors $Pb(thd)_2$ is at present the precursor of choice for the MOCVD of lead oxide based ferroelectrics $Pb(Zr,Ti)O_3$ and $Pb(Sc_{0.5}Ta_{0.5})O_3$.

$Pb(thd)_2$ is a monomeric molecule [13], see Fig. 1, which gives it a reasonably high vapour pressure for a β-diketonate compound of 0.1 Torr at 128°C. In liquid injection MOCVD [11], an evaporator temperature of 200°C is sufficient to give acceptable PbO growth rates at substrate temperatures above 400°C, with maximum growth rates occurring in the region 450–500°C [11]. However, at evaporator temperatures greater than 250°C, $Pb(thd)_2$ begins to decompose to deposit an oxide residue, and at substrate temperatures greater than 500°C desorption of PbO from the substrate occurs. Therefore, for the growth of $Pb(Sc_{0.5}Ta_{0.5})O_3$ with good uniformity, it is necessary to identify the Sc and Ta sources which most closely match the evaporation and deposition characteristics of $Pb(thd)_2$.

2.2. Sc precursors

The choice of Sc precursor is more limited than that of Pb, with the available Sc sources being restricted to β-diketonates such as $Sc(thd)_3$. This molecule is monomeric [14] with octahedral coordination at the metal atoms, see Fig. 1, and it deposits oxide films over a conveniently wide temperature regime of 450 to at least 600°C (see Fig. 2), showing reasonable overlap with the $Pb(thd)_2$ oxide deposition zone (450–500°C) [15]. However, $Sc(thd)_3$ is significantly less

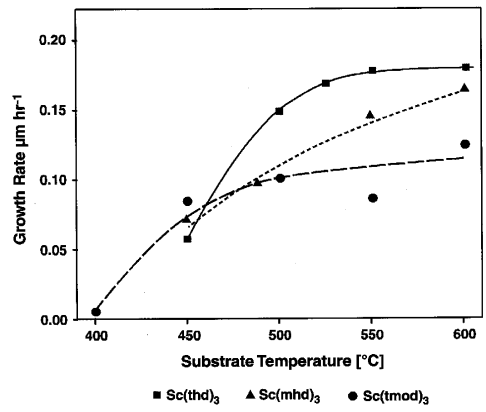


Fig. 2. Variation in oxide growth rate with substrate temperature for $Sc(thd)_3$, $Sc(tmod)_3$ and $Sc(mhd)_3$.

volatile than $Pb(thd)_2$, and consequently the evaporator temperature must be approximately 300°C to obtain adequate Sc_2O_3 growth rates. This can lead to decomposition of the $Pb(thd)_2$ and the Ta alkoxide precursors, and so a more volatile Sc oxide source than $Sc(thd)_3$ would be very desirable.

Asymmetric β-diketonate ligands R′C(O)CHC(O)R″, containing two different R groups, such as tmod (2,2,7-trimethyloctane-3,5-dionate) and mhd (6-methylheptane-2,4-dionate) (see Fig. 3) have been shown to influence significantly the volatility of yttrium β-diketonates [16]. The lack of symmetry and increased disorder associated with the tmod and mhd ligands can be expected to disrupt the molecular packing of the metal β-diketonates, thereby increasing the precursor vapour pressure [16]. We have therefore investigated the sterically hindered scandium β-diketonates $Sc(tmod)_3$ and $Sc(mhd)_3$ as alternatives to $Sc(thd)_3$, and a schematic of the $Sc(tmod)_3$ structure is shown in Fig. 1. TGA data for the various Sc β-diketonates, shown in Fig. 4, indicate that $Sc(tmod)_3$ and $Sc(mhd)_3$ both evaporate at lower temperature than $Sc(thd)_3$. The residues of between 5 and 10 wt.% remaining after the evaporation of $Sc(tmod)_3$ and $Sc(mhd)_3$ are not intrinsic features, and arise from slight sample decomposition due to the presence of trace oxygen and moisture during analysis of very small samples (ca. 10 mg).

Both $Sc(tmod)_3$ and $Sc(mhd)_3$ were shown to deposit oxide over a wide temperature range (Fig. 2), fully compatible with the oxide deposition temperature from $Pb(thd)_2$. In particular, the new $Sc(tmod)_3$ source looks to be ideally suited to the MOCVD of $Pb(Sc_{0.5}Ta_{0.5})O_3$, however the tmodH ligand is significantly more expensive than thdH which may somewhat limit the utility of $Sc(tmod)_3$ as an alternative to $Sc(thd)_3$.

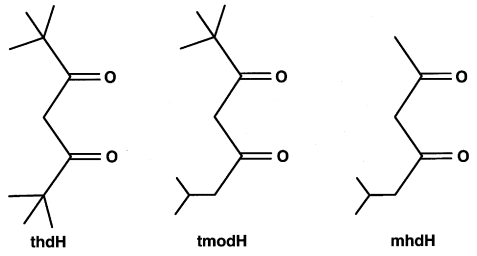


Fig. 3. β-diketone ligands used to influence the volatility of Sc(β-diketonate)$_3$ complexes.

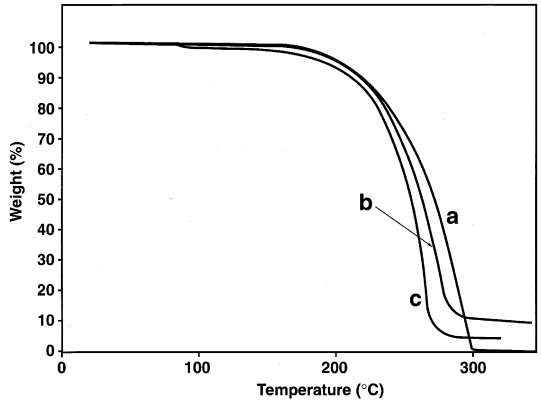


Fig. 4. Typical TGA data for some *tris*-β-diketonates of scandium: (a) [$Sc(thd)_3$], (b) [$Sc(mhd)_3$], (c) [$Sc(tmod)_3$]. Sample weight ca. 10 mg, Pt cell, argon atmosphere, heating rate 20°C min^{-1}.

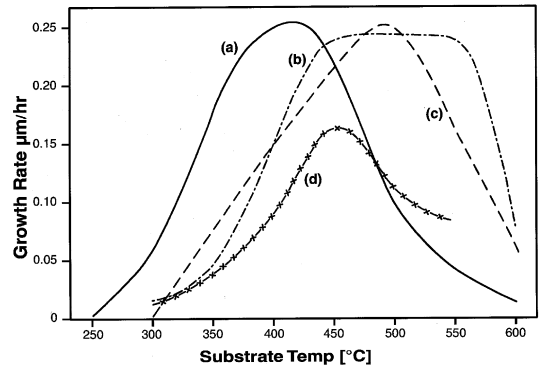


Fig. 5. Variation in growth rate with substrate temperature for Ta alkoxides: (a) $Ta(OEt)_5$, (b) $Ta(OMe)_4(thd)$, (c) $Ta(OEt)_4(thd)$, (d) $Ta(OPr^i)_4(thd)$.

2.3. Ta precursors

The selection of a suitable Ta source presents a major challenge in the MOCVD of $Pb(Sc_{0.5}Ta_{0.5})O_3$. There are no tantalum β-diketonates available, and the simple alkoxide precursor $Ta(OEt)_5$ has a significantly lower thermal stability than $Sc(thd)_3$, which leads to oxide deposition in a different temperature regime, and also gives rise to decomposition of $Ta(OEt)_5$ in the evaporator and reactor inlet pipes at the temperatures used to evaporate $Sc(thd)_3$.

However, the thermal stability of tantalum alkoxide precursors can be increased by the insertion of β-diketonate groups, or by altering the alkoxide group. For instance, the oxide deposition temperature is higher for $Ta(OEt)_4(thd)$ than for $Ta(OEt)_5$ and increases in the order $Ta(OPr^i)_4(thd) < Ta(OEt)_4(thd) < Ta(OMe)_4(thd)$ [17], as shown by the growth rate data in Fig. 5. These precursors are monomeric (Fig. 1) and are less air sensitive than the parent alkoxides. It has also been shown that $Ta(OR)_4(thd)$ compounds undergo significantly less decomposition than $Ta(OEt)_5$ in the evaporator at temperatures greater than 200°C [17]. Therefore $Ta(OEt)_4(thd)$ and $Ta(OMe)_4(thd)$ can be selected as most compatible with $Sc(thd)_3$ and $Pb(thd)_2$ for $Pb(Sc_{0.5}Ta_{0.5})O_3$ growth.

3. MOCVD of $Pb(Sc_{0.5}Ta_{0.5})O_3$

The application of $Pb(Sc_{0.5}Ta_{0.5})O_3$ in pyroelectric devices has been restricted by the high temperatures (>1000°C) usually required to synthesise the desired perovskite phase and to eliminate the pyrochlore phase, with its poor dielectric properties, which tends to form at low temperature. Although $Pb(Sc_{0.5}Ta_{0.5})O_3$ in the perovskite phase has been grown at low temperature by sol-gel techniques

[18,19], there have been relatively few reports of successful MOCVD studies. Early studies [20] reported that a processing temperature of 800°C and a post growth anneal were required to obtain the perovskite phase. More recent studies [21] have shown that $Pb(Sc_{0.5}Ta_{0.5})O_3$ in the perovskite phase can be grown in one step at temperatures as low as 600°C. However, in both of these studies conventional MOCVD was employed, in which the Pb, Sc and Ta precursors were held in bubblers at relatively high source temperatures, leading to the possibility of source decomposition with time.

In order to avoid source decomposition we have employed liquid injection MOCVD, and $Pb(Sc_{0.5}Ta_{0.5})O_3$ films have been successfully grown at substrate temperatures of between 400 and 600°C using a single solution of $Pb(thd)_2$, $Sc(thd)_3$ and $Ta(OEt)_4(thd)$, dissolved in tetrahydrofuran (THF) [22]. This precursor combination was selected initially as the best compromise between precursor availability and cost and MOCVD performance.

At substrate temperatures of 500°C and below the material was found to be a mixture of the perovskite and pyrochlore phases. Increasing the substrate temperature led to increasing amounts of the perovskite phase, and at 600°C the perovskite phase was found to be predominant (see Fig. 6). These low growth temperatures are fully compatible with device fabrication requirements, indicating that the use of liquid injection MOCVD techniques, together with the use of carefully selected precursors, should lead to increased exploitation of this important technology.

4. Conclusions

Careful selection and molecular design of the Pb, Sc and Ta precursors have allowed us to match more closely the physical properties of each precursor, and to achieve oxide growth in a similar temperature regime. The use of the precursor combination $Pb(thd)_2$, $Sc(thd)_3$ and $Ta(OEt)_4(thd)$ has allowed the growth of $Pb(Sc_{0.5}Ta_{0.5})O_3$ in the required perovskite phase at substrate temperatures as low as 600°C.

5. Experimental

5.1. Precursor synthesis

The β-diketones thdH, tmodH and mhdH used in this study were purchased from Lancaster synthesis. $Pb(thd)_2$ was synthesised by the addition of Na(thd) to $PbCl_2$ in aqueous methanol [13]. The Sc β-diketonates $Sc(thd)_3$, $Sc(tmod)_3$ and $Sc(mhd)_3$ were synthesised by the reaction of $Sc(NO_3)_3(H_2O)_x$ with the sodium salts of the respective β-diketonates (3 mol equivalents, prepared in situ by reaction of NaOH with the β-diketone in aqueous methanol) [23]. After isolation of the solid products by filtration, the Sc β-diketonates were dried overnight and then purified by vacuum

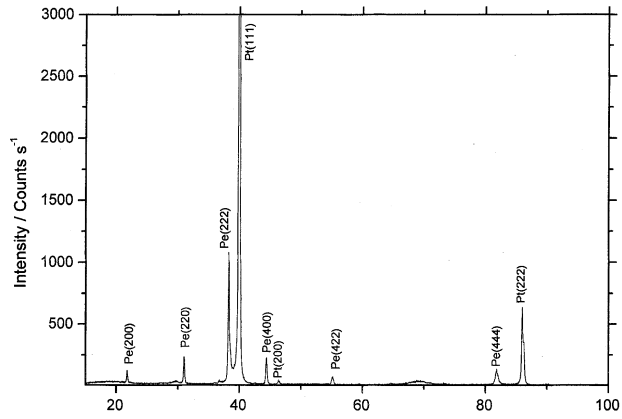


Fig. 6. X ray diffraction data for $Pb(Sc_{0.5}Ta_{0.5})O_3$ grown at 600°C using $Pb(thd)_2$, $Sc(thd)_3$ and $Ta(OEt)_4(thd)$. Pe diffraction peaks from perovskite phase, Pt diffraction peaks from platinum substrate.

sublimation. Each compound was fully characterised by ^1H NMR, $^{13}C\{^1H\}$ NMR, mass spectroscopy, and microanalysis, and full details are given elsewhere [14].

$Ta(OR)_4(thd)$ compounds were prepared from the reaction between $Ta(OR)_5$ and 1 mol equivalent of thdH in *n*-hexane solvent. After removal of the solvent and volatiles in vacuo, the $Ta(OR)_4(thd)$ products were purified by vacuum distillation. The synthesis and characterisation of $Ta(OR)_4(thd)$ compounds are described more fully elsewhere [24].

5.2. Growth of single oxide films

PbO, Sc_2O_3 and Ta_2O_5 films were deposited on Si(100) substrates at 1000mbar, using a liquid injection MOCVD reactor described elsewhere [11]. The films were grown from individual solutions of the Pb, Sc and Ta oxide precursors dissolved in THF. The growth conditions are summarised in Table 1.

5.3. Growth of $Pb(Sc_{0.5}Ta_{0.5})O_3$ films

Thin films of $Pb(Sc_{0.5}Ta_{0.5})O_3$ were deposited onto Pt(111) substrates by the evaporation of a single solution of precursors in THF using an MOCVD reactor described in detail elsewhere [11]. An evaporator temperature of 300°C

Table 1
Growth conditions used for deposition of single metal oxides [a]

Precursor	THF solution concentration (molar)	Injection rate ($cm^3\ h^{-1}$)	Evaporator temperature (°C)
$Pb(thd)_2$	0.16	1	200
$Sc(thd)_3$,	0.1	2	300
$Sc(tmod)_3$	0.1	2	300
$Sc(mhd)_3$	0.1	2	300
$Ta(OR)_4(thd)$	0.1	2	225

[a] Reactor pressure 1000 mbar, substrate Si(100), Ar flow rate 4000 $cm^3\ min^{-1}$, oxygen flow rate 1000 $cm^3\ min^{-1}$.

Table 2
Growth conditions used for deposition of $Pb(Sc_{0.5}Ta_{0.5})O_3$ from a single precursor solution

Reactor pressure (mbar)	1000
Substrate	Pt(111)
THF solution composition (%)	$Pb(thd)_2$ 35.5, $Sc(thd)_3$ 32.25, $Ta(OEt)_4(thd)$ 32.25
Solution injection rate ($cm^3\ h^{-1}$)	2
Argon flow rate ($cm^3\ min^{-1}$)	4000
Oxygen flow rate ($cm^3\ min^{-1}$)	1000
Evaporator temperature (°C)	300
Substrate temperature (°C)	450–600
Film growth rate ($\mu m\ h^{-1}$)	0.1–1

was used to prevent condensation of the least volatile precursor $Sc(thd)_3$, and minimal decomposition of $Pb(thd)_2$ and $Ta(OEt)_4(thd)$ was observed. A full summary of growth conditions is given in Table 2.

Acknowledgements

We gratefully acknowledge the support of the Department of Trade and Industry for a Teaching Company Fellowship to HOD. POB is the Sumitomo/STS Professor of Materials Chemistry. KAF thanks the EPSRC and Inorgtech for support via the CASE scheme.

References

[1] N.M. Shorrocks, S.G. Porter, R.W. Whatmore, A.D. Parsons, J.N. Gooding, D.J. Pedder, Proc. SPIE 1320 (1990) 88.
[2] D.L Polla, Microelectron. Eng. 29 (1995) 51.
[3] S. Krupanidhi, N. Maffeo, M. Sayer, K. El-Assel, J. Appl. Phys. 54 (1983) 6601.
[4] K.D. Budd, S.K. Dey, D.A. Payne, Proc. Br. Ceram. Soc. 36 (1985) 107.
[5] B.A. Tuttle, R.W. Schwartz, MRS Bull. 21 (1996) 49.
[6] C.H. Peng, S.B. Desu, J. Am. Ceram. Soc. 77 (1994) 1799.
[7] M. Okada, K. Tominaga, T. Araki, S. Katayama, Y. Sakashita, Jpn. J. Appl. Phys. 29 (1990) 718.
[8] C.J. Brierly, C. Trundle, L. Considine, R.W. Whatmore, F.W. Ainger, Ferroelectrics 91 (1989) 181.
[9] A.C. Jones, Chem. Vap. Deposition 4 (1998) 169.
[10] W.S. Rees, in: W.S. Rees (Ed.), CVD of Non Metals, VCH, Weinheim, 1996, Ch. 1, Section 1.5, and references therein.
[11] A.C. Jones, T.J. Leedham, P.J. Wright, M.J. Crosbie, P.A. Lane, D.J. Williams, K.A. Fleeting, D.J. Otway, P. O'Brien, Chem. Vap. Deposition 4 (1998) 46.
[12] R.W. Whatmore, S.B. Stringfellow, N.M. Shorrocks, Infrared Technol. XIX (1993) 391.
[13] M.A. Malik, P.O'Brien, M. Motevalli, A.C. Jones, Polyhedron 18 (1999) 1641.
[14] K.A. Fleeting, P.O. Brien, H.O. Davies, A.J.P. White, D.J. Williams, A.C. Jones, T.J. Leedham, Chem. Vap. Deposition 5 (1999) 261.
[15] A.C. Jones, T.J. Leedham, P.J. Wright, M.J. Crosbie, D.J. Williams, P.A. Lane, P. O'Brien, Mater. Res. Soc. Symp. Proc. 495 (1998) 11.
[16] H.A. Luten, W.S. Rees, V.L. Goedken, Chem. Vap. Deposition 2 (1996) 149.
[17] M.J. Crosbie, P.J. Wright, D.J. Williams, P.A. Lane, J. Jones, A.C. Jones, T.J. Leedham, P. O'Brien, H.O. Davies, Paper presented at EURO CVD 12, Sitges, Spain, September 5–10, 1999, J. Phys. IV France 9 (1999) PR8-935.
[18] D. Liu, L. Ma, D.A. Payne, D.D. Viehland, Mater. Lett. 17 (1993) 319.
[19] D. Liu, D.A. Payne, J. Appl. Phys. 77 (1995) 1458.
[20] F.W. Ainger, K. Bass, C.J. Brierly, M.D. Hudson, C. Trundle, R.W. Whatmore, Prog. Cryst. Growth Charact. 22 (1991) 183.
[21] D. Liu, H. Chen, Mater. Lett. 28 (1996) 17.
[22] M.J. Crosbie, P.A. Lane, P.J. Wright, A.C. Jones, T.J. Leedham, D.J. Williams, C.L. Reeves, submitted to J. Cryst. Growth.
[23] K.J. Eisentrout, R.E. Sievers, Inorg. Synth. 11 (1978) 94.
[24] H.O. Davies, T.J. Leedham, A.C. Jones, P. O'Brien, A.J.P. White, D.J. Williams, Polyhedron.

PERGAMON

www.elsevier.nl/locate/poly

Polyhedron 19 (2000) 357–363

POLYHEDRON

Compartmental control of mineral formation: adaptation of a biomineralization strategy for biomedical use

William L. Murphy [1], Phillip B. Messersmith *

Northwestern University, Division of Biological Materials, Departments of Physical Medicine and Rehabilitation, and Biomedical Engineering, 311 East Chicago Avenue, Chicago, IL 60611, USA

Received 8 June 1999; accepted 1 October 1999

Abstract

A common biomineralization strategy is the use of lipid vesicle compartments to sequester ions, control ion transport, and to control the shape and size of inorganic mineral particles deposited within developing tissues. In this paper, we describe an adaptation of this bioinspired strategy for inducing rapid formation of calcium phosphates for potential medical and dental use. Calcium and inorganic phosphate salts were separately loaded into temperature-sensitive liposomes composed of 90% 1,2-bis(palmitoyl)-*sn*-glycero-3-phosphocholine and 10% 1,2-bis(myristoyl)-*sn*-glycero-3-phosphocholine. Leakage of calcium and inorganic phosphate from liposomes stored at room temperature was negligible over a period of several weeks. Calcium-loaded liposomes released entrapped calcium when heated to 36–37°C, while phosphate-loaded liposomes released entrapped inorganic phosphate (P_i) at slightly lower temperatures (33–34°C). Release of entrapped ions at this temperature was due to increased permeability of phospholipid bilayers at the lipid chain melting temperature. Aqueous suspensions containing mixtures of calcium and P_i-loaded liposomes formed calcium phosphate mineral when heated to 37°C, as indicated by a rapid drop in suspension pH from 7 to approximately 5. This result was consistent with diffusion of both calcium and phosphate ions out of the liposomes and their reaction to form calcium phosphate mineral. Such a strategy could be used in medical and dental procedures to induce rapid inorganic mineral formation from an injectable liposome-containing fluid. This was illustrated by applying a liposome suspension to warm human dentin and enamel surfaces, which resulted in deposition of calcium phosphate minerals onto the tissue substrates. ©2000 Elsevier Science Ltd All rights reserved.

Keywords: Calcium phosphates; Biomimetics; Biomineralization; Liposomes

1. Introduction

A ubiquitous biological strategy during mineralized tissue formation is the use of lipid vesicle compartments to sequester ions, control ion transport, and to control the shape and size of inorganic mineral particles deposited within developing tissues [1]. Both lower and higher organisms utilize the compartment of lipid vesicles to exert control over the size, shape, and even orientation of biological inorganic crystals. For example, in the cytoplasm of magnetotactic bacteria, a string of nanosized magnetic iron oxide particles is deposited within pre-existing lipid vesicles [2–4]. The individual magnetite particles (typically 100 nm diameter) are organized with their magnetic axes aligned in the same direction, and the entire construct is believed to be used by the organism to navigate according to the magnetic field of the earth [2–4]. The complex-shaped calcium carbonate exoskeletons (coccoliths) of some marine algae are also believed to be the result of mineralization within a lipid vesicle [1,5–7]. Each coccolith is itself composed of several anvil-shaped subunits, each of which acts as a single crystal (by diffraction) and is formed within an intracellular lipid vesicle [5–7].

Like many of the non-collagenous proteins that are important contributors to mineralized tissue formation [8], phospholipids appear to play an important role in both developing and mature bone, dentin, and enamel (the following reviews and references cited therein discuss the role of phospholipids in mineralization [9,10]). It has been shown that certain phospholipids can only be extracted after acidic decalcification of bone and dentine [11–13]. Ennever and Vogel also observed that demineralized dental calculus and bone matrix did not recalcify in the absence of its lipid components [14,15]. In the form of so-called matrix vesicles, phospholipids may also play a role in ion transport, reagent seques-

* Corresponding author: Tel.: +1-312-503-1789; fax: +1-312-503-2440.; e-mail: philm@nwu.edu

[1] Present Address: University of Michigan, Department of Biomedical Engineering, Ann Arbor, MI 48104, USA.

0277-5387/00/$ - see front matter ©2000 Elsevier Science Ltd All rights reserved.
PII S0277-5387(99)00366-6

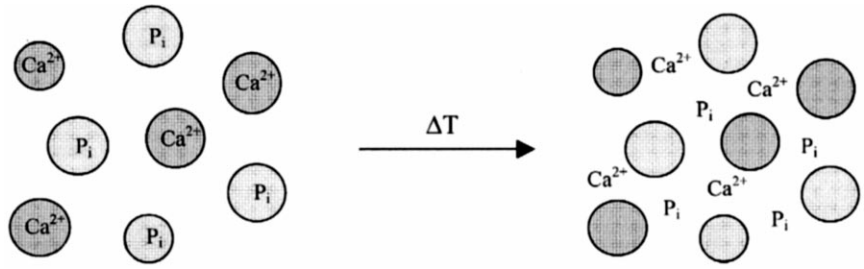


Fig. 1. Schematic illustration of thermally triggered release of Ca^{2+} and P_i from temperature-sensitive liposomes.

tering, and the nucleation of calcium phosphate crystals during the development of dentin and certain types of bone [16–23]. Matrix vesicles are non-cellular lipid vesicles believed to form as a result of budding from plasma membranes, which migrate in the extracellular matrix and accumulate at the calcification front (growth plate) of long bones [16]. It was reported in the late 1960s by Bonucci and Anderson that initial mineral formation during growth plate mineralization occurs within or on the surface of extracellular matrix vesicles [17,18].

Eanes and coworkers utilized synthetic liposomes as tools to model the mineral precipitation sequence believed to occur during matrix vesicle calcification [19–23]. Phosphate-loaded liposomes of size similar to matrix vesicles were prepared by encapsulating aqueous inorganic phosphate (P_i) solutions within liposomes constructed from phosphatidylcholine, dicetyl phosphate, and cholesterol [20,21]. The lipid bilayer, which serves as a barrier to ion transport, isolated extraliposomal Ca^{2+} from entrapped P_i and prevented mineral formation. However, when these liposomes were made permeable to external Ca^{2+} using a calcium ionophore, apatite mineral readily formed inside the liposomes. Mineral also formed outside of vesicles when intraliposomally formed apatite crystals penetrated the surrounding lipid bilayer membrane and seeded crystallization in the external medium. This model system was used to investigate the role of acidic phospholipids such as phosphatidylserine, phosphatidic acid, and phosphatidylinositol in calcium phosphate crystal nucleation and growth [22,23].

Several investigators have utilized lipid vesicles as components for the formation of nanometer-sized inorganic particles [24–30]. Typically, ions encapsulated within the vesicles are allowed to react with suitable ions of opposite charge permeating at a controlled rate through the vesicle membrane. In these studies, the vesicles are used to provide nucleation sites, control reaction kinetics and the size, geometry, and aggregation properties of the products. Nanoscale particles of oxides [25,26,29], hydroxides [27,28], and semiconductor particles [25,26] have been synthesized using this technique.

In our laboratory we recently began to explore the use of vesicles and other three-dimensional assemblies of phospholipids to mediate in situ formation of biomaterials [31–33]. We developed a strategy whereby the protective nature of phospholipid vesicles is exploited to isolate intravesicular Ca^{2+} from extravesicular P_i [31,32]. Using appropriate mixtures of saturated phospholipids, thermally sensitive Ca-loaded liposomes were designed which released entrapped calcium at physiologic temperature (37°C), resulting in rapid mineral formation as a result of reaction with extraliposomal phosphate ions.

In this paper, we extend this strategy to include the use of both Ca- and P_i-loaded vesicles, as depicted in Fig. 1. When heated to physiologic temperature, both Ca- and P_i-loaded liposomes release their contents into the extravesicular aqueous phase, where the ions react to form hydroxyapatite mineral. We also demonstrate how this approach can be used to deposit mineral onto enamel and dentin surfaces.

2. Experimental

2.1. Materials

1,2-bis(palmitoyl)-*sn*-glycero-3-phosphocholine (DPPC, >99%) and 1,2-bis(myristoyl)-*sn*-glycero-3-phosphocholine (DMPC, >99%) were obtained from Avanti Polar Lipids and used as received. Reagent grade $CaCl_2 \cdot 2H_2O$, Na_2HPO_4, ammonium molybdate ($(NH_4)_6Mo_7O_{24} \cdot 4H_2O$), sulfuric acid, citric acid, arsenazo III (AIII) dye, and all other chemicals were obtained from Aldrich Chemical Co. and used as received.

2.2. Preparation and characterization of calcium-loaded liposomes

All liposomes were prepared using the interdigitation-fusion method [34]. Ca^{2+} loaded liposomes were prepared using aqueous $CaCl_2$ (0.2 M, pH 7) from a mixture of DPPC (90 mol%) and DMPC (10 mol%) as described previously [32]. Unentrapped Ca^{2+} was removed from the liposome suspension by washing with aqueous NaCl (0.285 M, pH 7), centrifuging at 20000*g*, and decanting the supernatant. This process was repeated a minimum of five times or until Ca^{2+} could not be detected in the supernatant, using a standard spectrophotometric method [35]. The amount of Ca^{2+} contained in the liposome suspension was then determined by atomic absorption spectroscopy as described previously [31]. Calcium encapsulation efficiency ranged from 60–75% of available calcium.

Temperature-dependent release of Ca^{2+} from liposomes was detected using the Ca^{2+}-sensitive dye AIII, which undergoes a color change from purple to blue upon complexation with Ca^{2+} [35]. Following removal of unencapsulated Ca^{2+}, a 10 μl aliquot of the vesicle suspension was transferred to 4 ml of an AIII solution (0.4 mM AIII in 0.285 M NaCl) buffered to pH 7.4 with HEPES (10 mM). A circulating water bath and a jacketed quartz cuvette were used to heat the suspension at a rate of 1°C min^{-1} during measurement. Release of Ca^{2+} from the liposomes was followed by measuring the absorption intensity of the 650 nm band as a function of temperature. The amount of Ca^{2+} released, expressed as a percentage of total encapsulated Ca^{2+} ($\%Ca_{rel}$), was calculated from:

$$\%Ca_{rel} = \frac{A}{A_{100\%} - A_{0\%}} \times 100 \quad (1)$$

where $A_{100\%}$ and $A_{0\%}$ correspond to the final and initial absorbance at 650 nm, respectively. $A_{100\%}$ was determined by adding a lipid surfactant (20 μl of a 20% solution of Triton X-100) to the suspension following collection of data.

2.3. Preparation and characterization of phosphate-loaded liposomes

P_i loaded liposomes were prepared from 90% DPPC and 10% DMPC using the interdigitation-fusion method by substituting Na_2HPO_4 (0.23 M, pH 9) in place of $CaCl_2$ in the above protocol. Removal of unencapsulated P_i was accomplished as described above by washing with aqueous NaCl (0.285 M), and the amount of entrapped P_i determined using a phosphomolybdate assay [36]. Briefly, a 60 μl aliquot of the liposome suspension was diluted to within the linear range of the UV–Vis instrument and added to a solution containing 2 vol. acetone, 1 vol. sulfuric acid (5N), and 1 vol. ammonium molybdate (10 mM). Immediately following the formation of the phosphomolybdate complex, a small amount of 1.0 M citric acid was added to the solution to stop the reaction and thus avoid interference from acid-labile organic phosphates in the lipid membranes. A calibration curve for absorbance (400 nm) versus [P_i] was obtained using standard solutions of known P_i concentration. Inorganic phosphate encapsulation efficiency ranged from approximately 75–85% of available P_i.

Leakage of P_i from liposomes at room temperature was determined by dispersing 1 ml P_i-loaded liposomes in 14 ml aqueous NaCl (0.285 M, pH 7.4) and storing at room temperature for several weeks. At selected intervals, the suspension was vortexed and a 500 μl aliquot removed from the solution. The aliquot was transferred into a microcentrifuge tube and spun for 3 min at 20 000×g. The amount of P_i in the supernatant was then determined using the phosphomolybdate assay as described above.

Thermally triggered release of P_i from liposomes was detected using a modification of the phosphomolybdate assay described above [36]. Briefly, 20 μl liposomes, 3.2 ml ammonium molybdate (10 mM), and 400 μl sulfuric acid (5N) were combined and immediately transferred to a water-jacketed quartz cuvette. A circulating water bath was used to heat the suspension at a rate of 1°C min^{-1} during measurement. Release of P_i from the liposomes resulted in formation of the phosphomolybdate complex, detected by an increase in absorbance at 400 nm. Absorbance values were converted to percentage P_i release as described above. Control experiments performed using this method indicated that only minimal P_i leakage occurred during the first hour at ambient temperature.

2.4. Thermally triggered mineral formation

Temperature-activated mineral formation in unbuffered liposome suspensions was detected by measuring time-dependent pH changes of suspensions containing Ca^{2+}- and P_i-loaded liposomes held isothermally at various temperatures [32]. In a thin-walled glass tube, one part each of Ca-loaded liposomes, P_i-loaded liposomes, and 0.285 M NaCl were incubated at 20°C for 30 min. Initial pH values of the metastable liposome suspension ranged from 6.8 to 7.0. The liposome suspension was then transferred to a water bath thermostated at 25, 30, 34, or 37°C. A computerized data acquisition system was used to monitor simultaneously the voltage output from a pH electrode, sample temperature, and bath temperature prior to and during immersion. pH values were corrected for temperature changes as described previously [32].

2.5. Mineralization of dentin and enamel

Mineralization of dentin and enamel slabs was investigated as follows. 1 mm thick slabs of human dentin and enamel were cut from non-carious third molars using a diamond cutting wheel. The smear layer was removed by etching in 10% H_3PO_4 for 20 s to expose the tissue surface, after which the slabs were washed in distilled water and stored at room temperature in HEPES (10 mM, pH 7.4). An aluminum cylinder of dimension 2 cm diameter by 3 cm height was immersed in a thermostated water bath to a depth of 2.8 cm. Onto the top surface of the cylinder, which was not submerged, was placed a dentin or enamel slab and the tip of a thermocouple probe was affixed in direct contact with the top surface of the slab. By using a thermal controller to modulate power input to the water bath, the temperature of the slab was maintained at 37°C via heat transfer through the aluminum cylinder. After equilibration at the temperature indicated, 200 μl of a suspension of Ca^{2+}- and P_i-loaded liposomes ([Ca] = [P] = 5–60 mM) suspended in 0.285 M NaCl was pipetted onto the surface of the slab and left unstirred for 20 min. Following this, the slab was removed and washed in room temperature distilled water to remove the liposome suspension. Treated samples were then air dried for 1 h and dried in vacuo for an additional 24 h.

2.6. Electron microscopy

Treated dentin/enamel slabs were mounted on specimen stubs using colloidal graphite and sputter coated with Au/Pd. The surfaces of the treated dentin/enamel slabs were imaged in secondary electron mode using a Cambridge Scanning Electron Microscope (SEM) operating at an accelerating voltage of 25 kV.

3. Results and discussion

The interdigitation-fusion method was used to encapsulate Ca^{2+} and P_i because it results in large unilamellar liposomes with a high encapsulation efficiency [34]. This method takes advantage of the formation of a lamellar interdigitated phase in the presence of low molecular weight alcohols to form large unilamellar vesicles, and was easily adapted for entrapment of Ca^{2+} and P_i. After removal of unentrapped Ca^{2+}, the measured Ca^{2+} concentration of the Ca-loaded liposome suspension was 120 mM. Likewise, the P_i concentration of the P_i-loaded liposomes was 180 mM. Both Ca and P_i-loaded liposomes were stable and highly resistant to leakage when stored at room temperature for several weeks. For example, P_i-loaded liposomes lost less than 2% of entrapped P_i during room temperature storage for 6 weeks (Fig. 2).

The liposomes used in this study were formulated to release their entrapped contents when heated to body temperature, which was accomplished by utilizing a mixture of DPPC (90%) and DMPC (10%) phospholipids. In a previous study, liposomes constructed from this mixture were found to release Ca^{2+} rapidly at 37°C [32]. Thermally triggered release from both Ca-loaded and P_i-loaded liposomes was determined using a spectrophotometric method in which release of liposome-entrapped species was detected photometrically by either a Ca^{2+} sensitive dye [35] or the formation of a phosphomolybdate complex [36]. As shown in Fig. 3, Ca^{2+} was rapidly released from 90% DPPC/10% DMPC liposomes beginning at approximately 36–37°C, which is in agreement with our previous results [32]. Surprisingly, as shown in Fig. 4, P_i release from liposomes of identical composition (90% DPPC/10% DMPC) began at a slightly lower temperature (approximately 33°C). Although the reason for the observed difference in release temperature is not known, it is possible that the low pH conditions ($pH < 2$) necessary to detect photometrically the phosphomolybdate complex [36] may have altered the release behavior of the P_i-loaded liposomes.

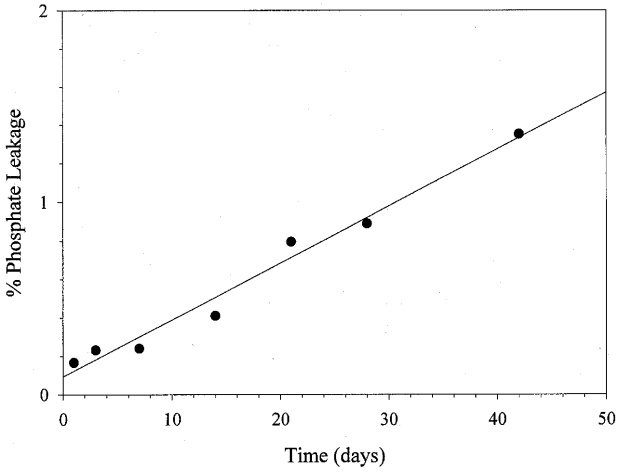


Fig. 2. Time-dependent release of P_i from liposomes during storage at room temperature. Raw absorbance data were converted to percentage P_i release as described in the text.

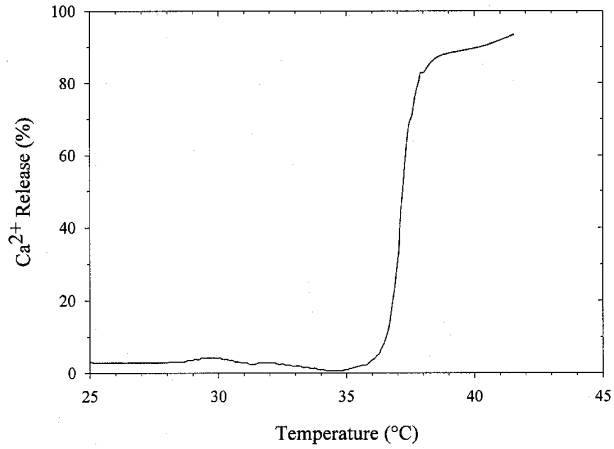


Fig. 3. Detection of thermally triggered release of Ca^{2+} from liposomes. Liposomes were suspended in *iso*-osmotic AIII solution and heated at 1°C min^{-1} while monitoring absorbance of the solution. Raw absorbance data were converted to percentage Ca release as described in the text.

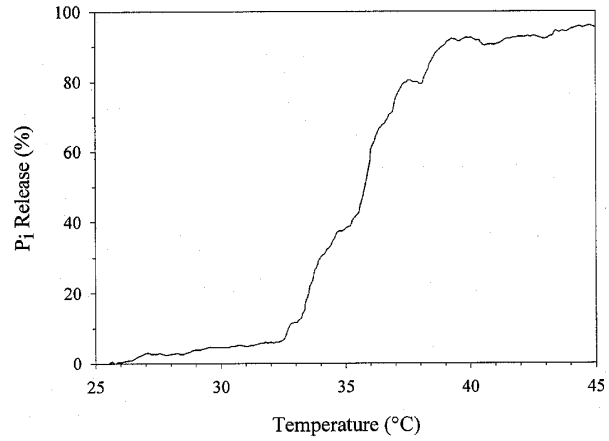


Fig. 4. Detection of thermally triggered release of P_i from liposomes. Liposomes were suspended in ammonium molybdate solution and heated at 1°C min^{-1} while monitoring absorbance of the solution. Raw absorbance data were converted to percentage P_i release as described in the text.

Because of the sequestering of Ca^{2+} and P_i within separate vesicle compartments, liposome suspensions containing very high concentrations of Ca^{2+} and P_i could be made by combining Ca-loaded liposomes with P_i-loaded liposomes. As described previously [32], we used pH as an indicator of the extent of mineral formation in the liposome suspensions, since upon release from the liposomes the Ca^{2+} and P_i ions react to form apatite-like and/or brushite calcium phosphates according to the idealized reactions

$$5CaCl_2 + 3Na_2HPO_4 + H_2O \rightarrow Ca_5(PO_4)_3OH + 6NaCl + 4HCl \quad (2)$$

$$CaCl_2 + NaH_2PO_4 + 2H_2O \rightarrow CaHPO_4 \cdot 2H_2O + NaCl + HCl \quad (3)$$

Mixtures of Ca-loaded liposomes and P_i-loaded liposomes maintained stable neutral pH values for several hours after combining (data not shown). However, rapid pH changes were observed when these suspensions were heated to temperatures above ambient (Fig. 5). For example, when a liposome suspension of concentration $[Ca^{2+}] = [P_i] = 40$ mM was held isothermally at 30°C, there was a slight increase of approximately 0.1 pH unit during the first 2 min, after which the pH remained stable. When the same suspension was heated to 34°C, a slightly larger increase (0.4 pH units) was observed in the first few minutes but again the pH did not change significantly within 30 min. However, when the suspension was heated at 37°C, there was an initial rise in pH after which the pH dropped rapidly to approximately pH 5.

The temperature-dependent behavior of the liposome suspensions can be explained by taking into consideration the differences in temperature release characteristics of the Ca-loaded and P_i-loaded liposomes. The data in Figs. 3 and 4 clearly show that the P_i-loaded liposomes released P_i at a temperature 2–3°C below that of the Ca-loaded liposomes. At 30°C there may have been slow leakage from the P_i-loaded liposomes, and since the pH of the P_i solution was basic (pH 9), there was a slight increase in measured pH of the suspension. At 34°C P_i leakage was more pronounced, leading to a larger pH rise as shown in Fig. 5. Finally, at 37°C both P_i and Ca^{2+} were released from the liposomes. This gave rise to an initial increase in pH due to the basicity of the P_i solution, after which the solution rapidly became highly supersaturated with respect to both apatite and brushite and mineral formation occurred as indicated by the rapid drop in pH as shown in Fig. 5.

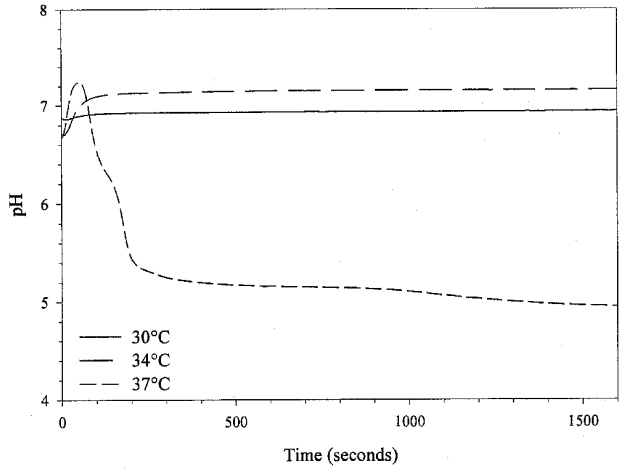


Fig. 5. pH vs. time of liposome suspensions isothermally held at 30, 34, and 37°C. Thin-walled glass tubes containing the liposome suspensions ($[Ca] = 40$ mM; $[P_i] = 60$ mM) were immersed in a thermostated water bath at time 0.

The pH of the reaction medium is likely to have a strong influence on the calcium phosphate phases formed in the liposome suspensions. For example, it is well known that apatitic calcium phosphate forms at neutral to basic pH values, whereas brushite forms under acidic conditions [37]. In the present case, the initial pH of the suspension undergoing mineralization at 37°C was slightly acidic, increased slightly as a result of phosphate release, and then rapidly dropped to approximately 5. Because of this pH fluctuation, it is likely that a combination of both apatite and brushite mineral formed during thermally triggered mineralization. It is also possible that apatite mineral formed during the initial stages of the reaction (at neutral pH), subsequently dissolved as the pH dropped, and reprecipitated as brushite.

The use of thermally triggered mineral formation to deposit mineral onto the surfaces of dentin and enamel tissue was explored by applying liposome suspension (buffered to pH 7.4) to dentin/enamel slabs equilibrated at specific temperatures (Fig. 6), and examining the treated surfaces to detect mineral deposition. As shown in Figs. 7 and 8, treatment of dentin and enamel in this manner at 20°C did not result in detectable mineral formation. However, treatment of dentin/enamel with liposome mineralizing suspension at 37°C resulted in the deposition of mineral particles on both dentin and enamel surfaces. Although the composition of these particles was not determined, the experimental conditions (pH 7.4 and high Ca, P_i concentration) are favorable for the formation of amorphous calcium phosphates, which may gradually transform into poorly crystalline apatite. The appearance of the mineral deposits is consistent with this interpretation.

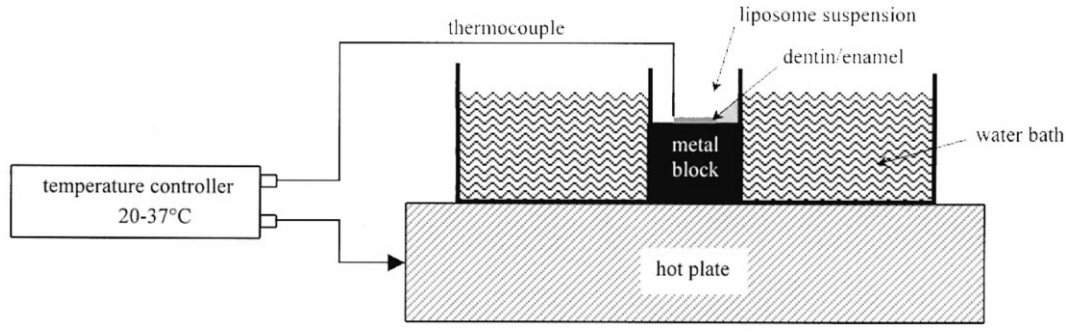


Fig. 6. Experimental apparatus used to control enamel/dentin slab temperature during treatment with liposome suspension.

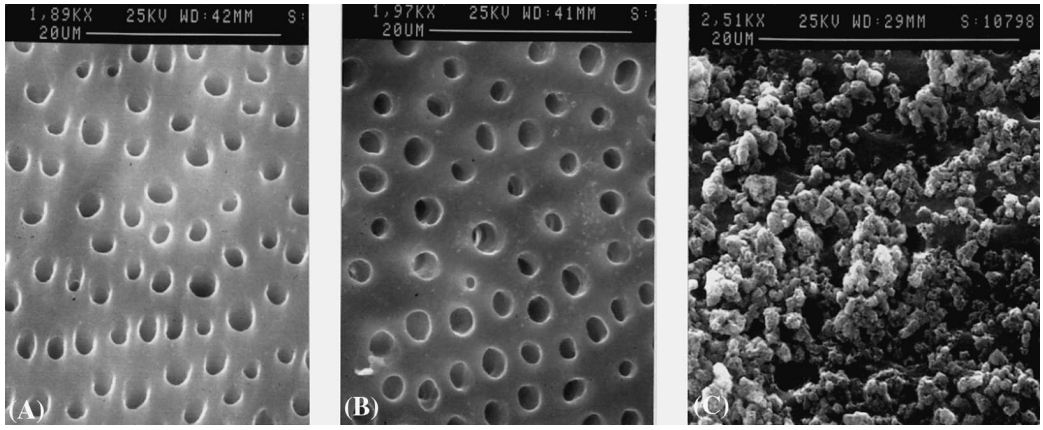


Fig. 7. Scanning electron micrographs of acid etched human dentin surfaces following treatment with liposome suspension ([Ca] = [P] = 40 mM). Dentin slabs were untreated (A) or treated with liposome suspension for 20 min at either 20°C (B) or 37°C (C).

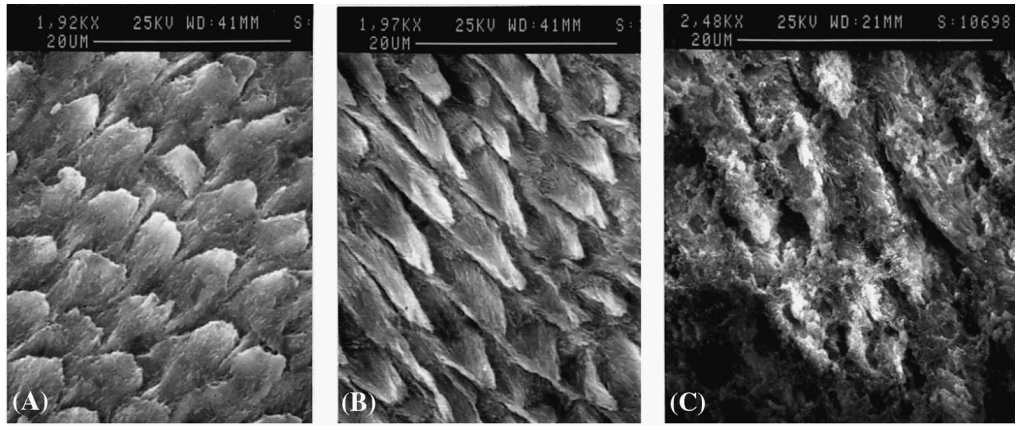


Fig. 8. Scanning electron micrographs of acid etched human enamel surfaces following treatment with liposome suspension ([Ca] = [P] = 40 mM). Enamel slabs were untreated (A) or treated with liposome suspension for 20 min at either 20°C (B) or 37°C (C).

In summary, we have used the biomimetic strategy of compartmentalization to isolate reactive precursors for calcium phosphate mineral formation. Interdigitation-fusion processing yielded liposomes containing highly concentrated solutions of either calcium or phosphate. Leakage of ions from these vesicles was slow when stored at room temperature for a period of several weeks, in spite of the high concentration gradient existing across the liposome membrane. Liposomes were constructed from a mixture of dipalmitoyl and dimyristoyl phosphatidylcholines, which rendered the vesicles permeable to calcium and phosphate ions when heated to body temperature. At this temperature, entrapped calcium and phosphate rapidly diffused out of the liposomes into the aqueous medium where they reacted to form calcium phosphate. This strategy is designed to take advantage of the difference between ambient and body temperature and could be useful for minimally invasive repair or reconstruction of human skeletal tissue. To illustrate this, a room temperature liposome suspension was applied to warm dentin and enamel slabs, and mineral was found to be deposited onto the surface. Potential dental and medical applications of this technology include the remineralization of incipient caries, treatment of hypersensitive dentin, and as a bone substitute material.

Acknowledgements

This research was sponsored by The Whitaker Foundation and NIH grant R29 DE 12599.

References

[1] H.A. Lowenstam, S. Weiner, On Biomineralization, Oxford University Press, Oxford, 1989.
[2] R.P. Blakemore, Science 190 (1975) 377.
[3] Y.A. Gorby, T.J. Beveridge, R.P. Blakemore, J. Bacteriol. 170 (1988) 834.
[4] R.B. Frankel, Annu. Rev. Biophys. Bioeng. 13 (1984) 85.
[5] H.H. Dixon, Proc. R. Soc. London (Biol.) 68 (1900) 305.
[6] P. Westbroek, E.W. de Jong, P. van der Wal, A.H. Borman, E.W. de Vrind-de Jong, Philos. Trans. R. Soc. London, Ser. B 304 (1984) 435.
[7] N. Watabe, Calcif. Tissue Res. 1 (1967) 114.
[8] L.W. Fisher, J.D. Termine, Clin. Orthop. 200 (1985) 362.
[9] A.L. Boskey, in: D.L. Hukins (Ed.), Calcified Tissue, CRC Press, Boca Raton, FL, 1989, p. 215.
[10] J.J. Vogel, B.D. Boylan-Salyers, Clin. Orthop. Relat. Res. 118 (1976) 230.
[11] R.E. Wuthier, J. Lipid Res. 9 (1968) 68.
[12] I.M. Shapiro, Calcif. Tissue Res. 5 (1970) 13.

[13] A.A. Odutuga, R.E.S. Prout, R.J. Hoare, Arch. Oral Biol. 20 (1975) 311.
[14] J. Ennever, J.J. Vogel, L.A. Benson, J. Dent. Res. 52 (1973) 1056.
[15] J. Ennever, J.J. Vogel, B.M. Levy, Proc. Soc. Exp. Biol. (NY) 145 (1974) 1386.
[16] S.Y. Ali, S.W. Sadjera, H.C. Anderson, Proc. Natl. Acad. Sci. USA 67 (1970) 1513.
[17] E. Bonucci, J. Ultrastruct. Res. 20 (1967) 33.
[18] H.C. Anderson, J. Cell Biol. 41 (1969) 59.
[19] E.D. Eanes, B.R. Heywood, in: H.M. Myers (Ed.), New Biotechnology in Oral Research, Karger, San Francisco, CA, 1989, p. 54.
[20] E.D. Eanes, A.W. Hailer, J.L. Costa, Calcif. Tissue Int. 36 (1984) 421.
[21] E.D. Eanes, A.W. Hailer, Calcif. Tissue Int. 37 (1985) 390.
[22] E.D. Eanes, A.W. Hailer, Calcif. Tissue Int. 40 (1987) 43.
[23] E.D. Eanes, A.W. Hailer, B.R. Heywood, Calcif. Tissue Int. 43 (1988) 226.
[24] J.H. Fendler, Chem. Rev. 87 (1987) 877.
[25] S. Mann, R.J.P. Williams, J. Chem. Soc., Dalton Trans. (1983) 311.
[26] S. Mann, J.P. Hannington, J. Colloid Interface Sci. 122 (1988) 326.
[27] S. Bhandarkar, A. Bose, J. Colloid Interface Sci. 135 (1990) 531.
[28] S. Bhandarkar, A. Bose, J. Colloid Interface Sci. 139 (1990) 541.
[29] I.I. Yaacob, S. Bhandarkar, J. Mater. Res. 8 (1993) 573.
[30] E.D. Eanes, B.R. Heywood, in: H.M. Myers (Ed.), New Biotechnology in Oral Research, Karger, San Francisco, CA, 1989, p. 54.
[31] P.B. Messersmith, S. Vallabhaneni, V. Nguyen, Chem. Mater. 10 (1998) 109.
[32] P.B. Messersmith, S. Starke, Chem. Mater. 10 (1998) 117.
[33] H. Cui, P.B. Messersmith, in: I. McCullough, S. Shalaby (Eds.), Tailored Polymeric Materials for Controlled Delivery Systems, ACS Symp. Ser. 709, American Chemical Society, Washington, DC, 1998, p. 203.
[34] P.L. Ahl, L. Chen, W.R. Perkins, S.R. Minchey, L.T. Boni, T.F. Taraschi, A.S. Janoff, Biochim. Biophys. Acta 1195 (1994) 237.
[35] P.M. Sokolove, M.B. Kester, Anal. Biochem. 177 (1989) 402.
[36] J.K. Heinonen, R.J. Lahti, Anal. Biochem. 113 (1981) 313.
[37] R.Z. LeGeros, in: Monographs in Oral Science, Karger, San Francisco, CA, 1991, p. 46.

PERGAMON

www.elsevier.nl/locate/poly

Polyhedron 19 (2000) 367–373

POLYHEDRON

Ethylenimine in the synthetic routes of a new silylating agent: chelating ability of nitrogen and sulfur donor atoms after anchoring onto the surface of silica gel

Luiza N.H. Arakaki, Claudio Airoldi *

Instituto de Química, Universidade Estadual de Campinas, Caixa Postal 6154, 13083-970 Campinas, São Paulo, Brazil

Received 2 July 1999; accepted 29 October 1999

Abstract

Using a heterogeneous route, the precursor silylating agent 3-mercaptopropyltrimethoxysilane (mts) was first grafted onto silica gel and then condensed to one molecule of ethylenimine (etn). In the homogeneous route, mts reacted with etn to yield 3-trimethoxypropylthioethylamine (mptt), which was covalently anchored onto silica gel. In both cases, the new silylating agent displayed a chelating moiety containing nitrogen and sulfur basic centres. The amount of nitrogen immobilized was 1.73 and 1.74 mmol g^{-1} silica for the heterogeneous and homogeneous methods, respectively. In both routes of synthesis ν(N–H) stretching bands appeared at 3361 and 3284 cm^{-1} with the absence of a ν(S–H) stretching band. ^{13}C NMR of the new silylating agent, $(CH_3O)_3SiCH_2CH_2CH_2SCH_2CH_2CH_2NH_2$, showed chemical shifts for methoxy groups at 50.0 ppm and signals at 8.4, 23.0, 34.4, 36.1 and 41.2 ppm for the sequence of carbons from the silicon atom to the NH_2 group at the end of the organic chain. The ^1H NMR spectrum presented a singlet peak which was attributed to methoxy groups at 3.52 ppm; a triplet at 2.76, quintet at 1.64 ppm, multiplet at 2.49 and triplet at 0.65 ppm were assigned to hydrogen atoms bonded to carbons in the same sequence as above. A broad amidic proton peak appeared at 1.08 ppm. ^{13}C NMR–CPMAS (cross-polarization magic-angle spinning) of the immobilized surface gave a series of peaks similar to those of the free silylating agent. Thermal and elemental analyses confirmed the covalent attachment of the organic species onto the silica gel surface. The chelating moiety formed by basic centre atoms of the pendant groups on the silica surface have a pronounced ability to extract divalent copper from aqueous solution. ©2000 Elsevier Science Ltd All rights reserved.

Keywords: Ethylenimine; Immobilization; 3-Mercaptopropyltrimethoxysilane; Silica gels

1. Introduction

Work on the immobilization of molecules on inorganic supports has been intensively revived in the last three decades [1,2], with much attention given to the establishment of a new covalent bond on the desired surface [3,4]. These investigations depend on the substitution reactions between the modifiers and accessible silanol groups distributed on such surfaces. In exploring the advantages of the covalent bond formed, a series of porous adsorbents, such as silica gel [5–12], porous glass [13,14], porous polymers [15,16], alumina [17], titania and zirconia [18], have been investigated as supports.

The systematic application of immobilization has been directed mainly at silica gel, because its surface has been investigated from both physical and chemical aspects and it offers many advantages over organic surfaces: (1) a large variety of silylating agents can be used [1,3,19], allowing a myriad of pendant functional groups to be immobilized on the support; (2) functional groups immobilized on silica gel react more easily than those on an organic support because this matrix has a large number of crosslinking bonds which may require hours to reach equilibrium; (3) silica, as well as other inorganic supports, are unreactive to organic solvents and have a high thermal resistance [20].

Conventional modifiers have been used to establish a link between the molecule and the inorganic support through mono-, di- and trifunctional chlorosilanes or by employing methoxy or ethoxysilane derivatives. Normally, these silylating agents are reacted with the silanol of the surface in a one-step procedure, allowing the function of the organic chain to be explored for various uses. However, for other purposes, agents are synthesized before anchoring, or a simple immobilized molecule reacts in a heterogeneous medium

* Corresponding author. Fax: +55-19-788 3023; e-mail: airoldi@iqm.unicamp.br

0277-5387/00/$ - see front matter ©2000 Elsevier Science Ltd All rights reserved.
PII S0277-5387(99)00347-2

in order to increase the chain to include a variety of organic functions. In coordination chemistry, these agents can be enriched by a diversity of functional groups, which can act as chelating agents, for example, to remove cations from a complex mixture. These anchored supports can also be used in analytical investigations for which a high selectivity is desirable [15,21,22], as well as in several applications, such as chemically bonded phases in chromatography [23–28], extraction of cations from aqueous or non-aqueous solvents [10–12,29,30], in catalytic [1,3,22,31–33] or ion-exchange [3,29,34–36] reactions and also in some biotechnological processes [37–40].

This present paper focuses on the immobilization of the three-member cyclic ethylenimine molecule on the surface of silica gel, using homogeneous and heterogeneous routes as previously proposed [8,9], in order to elucidate and characterize the products of reactions. This new and unusual anchored compound contains sulfur and nitrogen as heteroatoms in the organic chain, and has the ability to extract cations from solution. This synthetic silylating agent was first obtained through a homogeneous method, before immobilization on the silica gel surface. The nitrogen content was established as a good criterion to distinguish the effectiveness of both routes of immobilization.

2. Experimental

2.1. Materials

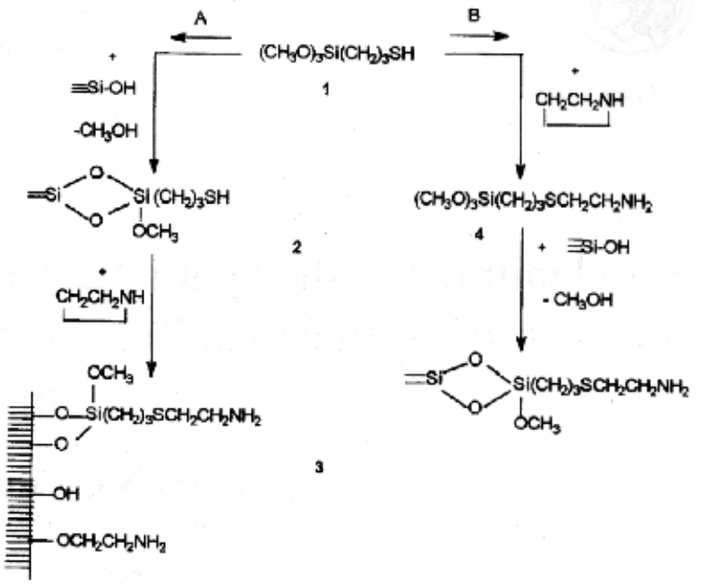
The silylating agent 3-mercaptopropyltrimethoxysilane (mpts) (Aldrich) was used without previous purification. Silica gel (Aldrich), with particle size 70–230 mesh, medium diameter 60 Å and pore volume 0.75 $m^3 g^{-1}$, was stirred with H_2SO_4–HNO_3 (2.0 mol dm^{-3}) in 9:1 proportion. The suspension was left standing for 24 h and the supernatant then decanted. The solid was added to the same acidic solution and the same procedure was repeated. Then, the solid was filtered and extensively washed with bidistilled water until the filtrate had the same pH as water. After this treatment, the silica was activated by heating at 423 K for 8–10 h in vacuo under nitrogen atmosphere. Ethylenimine was synthesized following a described procedure, by reacting 2-amino-hydrogen sulfate (Aldrich) in hot alkali medium [41]. Xylene was firstly treated with metallic sodium and distilled just before use. A solution of divalent copper nitrate was prepared in bidistilled water from reagent grade materials.

2.2. Immobilization of ethylenimine

2.2.1. Reaction with the precursor

Ethylenimine was covalently bonded to the precursor mpts through two distinct routes: heterogeneous (A) or homogeneous (B) [8,9]. Scheme 1 outlines the different procedures.

2.2.1.1. Heterogeneous method. First, 40.0 g of activated silica gel was suspended in 150.0 cm^3 of dry xylene and 15.0



Scheme 1. Distinct routes of immobilizing ethylenimine on a silica gel surface: heterogeneous (A); homogeneous (B).

cm^3 (84.0 mmol) of mpts was slowly added to this suspension. The mixture was mechanically stirred under solvent reflux, in an inert dry nitrogen atmosphere for 72 h [29]. After cooling, the solid was filtered, washed with xylene and acetone until the filtered solution did not test positive for thiol groups [42]. The obtained product, denominated ≡Sil–SH, was dried in vacuo for 8 h at 373 K. In the next stage, 5.0 g of the modified silica was suspended in 30.0 cm^3 of several amounts of xylene. The suspension was maintained under solvent reflux with mechanical stirring; 2.0 cm^3 (38.77 mmol) of liquid etn was added under nitrogen atmosphere and the reflux continued for another 24 h. After cooling, the solid was filtered off, washed with xylene and anhydrous acetone, and dried in vacuo for 12 h.

2.2.1.2. Homogeneous method. A 5.5 cm^3 volume (29.0 mmol) of mpts was reacted with 6.0 cm^3 (116.0 mmol) of etn under reflux at 323 K, with magnetic stirring, under inert dry nitrogen atmosphere for 24 h. Excess etn was eliminated from the cooled solution in vacuo. The resulting compound, 3-trimethoxypropylthioethylamine (mptt), was allowed to react with 5.0 g of activated silica in dry xylene at 343 K and the mixture was mechanically stirred for 72 h. Then, the solid was washed and dried as in the heterogeneous method, to obtain the final product.

2.2.2. Direct immobilization of ethylenimine

An 5.0 g amount of silica was suspended in 50.0 cm^3 of dry toluene and 10.0 cm^3 (193.5 mmol) of ethylenimine in a sealed tube closed under low pressure. The mixture was heated at 353 K for 48 h and was periodically shaken at least three times a day. The solid was filtered and washed with toluene, water and finally ethanol and dried in vacuo for 8 h at room temperature.

The degree of functionalization of the silica that contained an attached amino group or etn molecule was based on nitrogen analyses using the Kjeldhal method. Sulfur elemental

analysis was carried out for the precursor thiol silica ≡Sil–SH (compound **2**; Scheme 1).

2.3. Capacity of modified silicas to adsorb copper

The capacity of the modified silica to extract metal ions from aqueous solution was determined in duplicate using a batchwise process with copper(II) nitrate as follows: about 50.0 mg of the modified silica was suspended in 20.0 cm^3 of an aqueous solution of $Cu(NO_3)_2$ with concentrations varying from 1.0 to 40.0 mmol dm^{-3}. The suspensions were mechanically stirred for 3 h at 298 ± 1 K and separated by centrifugation at 3000 rpm for 10 min [9]. Aliquots of the supernatant solution were pipetted and the cation was determined by EDTA complexometric titration. From these values the adsorption capacities were calculated.

2.4. Physical measurements

Activated silica gel and functionalized silicas were characterized by determination of the surface area using the BET method [43] in a Flowsorb II 2300 Micrometrics apparatus.

Carbon, nitrogen, sulfur and hydrogen contents were determined using a Perkin-Elmer microelemental Model PE 2400 analyser.

Thermogravimetric curves were produced using DuPont model 1090 B apparatus coupled with a thermobalance 951, by heating the samples from room temperature to 1273 K at a heating rate of 0.17 K s^{-1} under argon flow of 1.67 cm^3 s^{-1}, with the sample varying in weight from 15.0 to 30.0 mg.

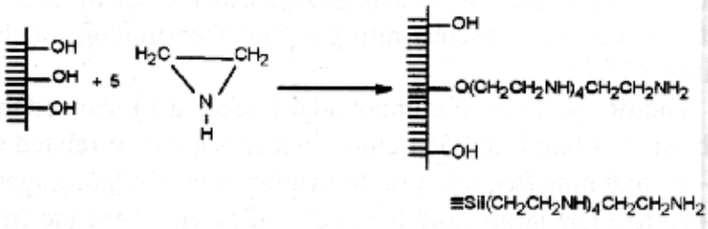
IR spectra of all compounds were obtained with a Fourier transform IR spectrophotometer (MB-Bomem). Liquid samples were obtained using the thin film technique between windows of sodium chloride; solid samples were obtained from KBr pellets.

NMR spectra were obtained on Gemini-300 Varian and AC 300/P Bruker spectrometers. The liquid samples were prepared in carbon tetrachloride for hydrogen and carbon signals. The parameters used for ^1H spectra were: frequency 300 MHz with pulse width 30°, pulse delay 1 s, acquisition time 2.35 s; 64 scans were used. For ^{13}C spectra of liquid samples, frequency at 75.47 MHz, pulse width 45°, pulse delay at 2 s, acquisition time of 0.88 s and 256 scans were used. For solid samples, the carbon signal was obtained on an AC/300P Bruker spectrometer with cross-polarization and magic-angle spinning (CPMAS) at a frequency of 75.47 MHz with acquisition time 0.156 s, pulse delay at 4 s, contact time 1 ms and in the range of 13 663–25 600 scans.

3. Results and discussion

The condensation of ethylenimine molecules on the active sulfur sites of the silica gel surface embracing the derivative precursor ≡Sil–SH gave, by elemental analyses, 2.5% of this element, which corresponds to 0.78 mmol of thiol groups per gram of support. The value found for nitrogen by the Kjeldhal method was 1.73 mmol g^{-1} silica [8,9]. Based on this value, it is supposed that all precursor thiol groups should react with etn molecules. However, the presence of an excess of 0.95 mmol of nitrogen on the surface of the inorganic support beyond the equivalent molar ratio could be due to the reaction of the remaining free silanol groups on the surface with the cyclic compound. On the other hand, the homogeneous route gave 1.74 mmol of nitrogen immobilized per gram of silica. The nitrogen analyses for the immobilized compound obtained from the direct reaction of the cyclic molecule with silica surface gave 3.40 mmol g^{-1} silica. This large value clearly demonstrates the great ability of this cyclic molecule to interact with free silanol groups on the silica gel surface. Thus, this molecule develops a remarkable role in reacting with almost all disposed active acidic centres, as shown in the heterogeneous route. However, the effectiveness of the etn molecule in interacting with the unmodified surface is elucidated by considering the accepted number of free silanol groups, which is proposed to be 4–5 mmol g^{-1} silica [42,44]. Based on the present results it is inferred that this cyclic molecule succeeded in nearly completely covering the available silanol groups.

The immobilization of the cyclic etn molecule on the support was performed by the two proposed routes shown in Scheme 1. In route A, the precursor silylating agent mpts was first immobilized; subsequently, the cyclic molecule was incorporated to increase the original carbonic chain. Based on the determined amount of nitrogen bonded to the organic chains, the result inferred that a parallel reaction occurred between etn molecules and the remaining silanol groups, after anchoring the pendant groups on the silica surface. In attempting to elucidate this fact, a direct reaction of etn molecules with the activated silica gel was made to yield the new modified surface, represented by $\equiv Sil(CH_2CH_2NH)_4CH_2CH_2NH_2$, as shown in reaction 1:



(1)

The main contribution to the knowledge of the distribution of these pendant groups on the silica surface was obtained through ^{13}C NMR in solid state. The spectrum showed an intense peak at 49.2 ppm and a small one at 41.5 ppm, as illustrated in Fig. 1. These peaks in A were deconvoluted using a computer simulation, giving spectrum B, and the correspondent areas gave a 9:1 ratio in C and D. Peak C was assigned to a set of nine non-resolved carbon atoms and peak D to the methylene group bonded to the amine function, in a normal chain of this new immobilized molecule.

The reaction of ethylenimine with mpts in route B was carried out without catalyst or solvent during a reaction period

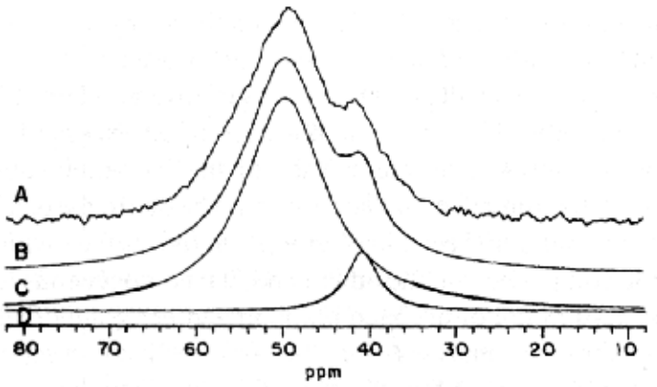
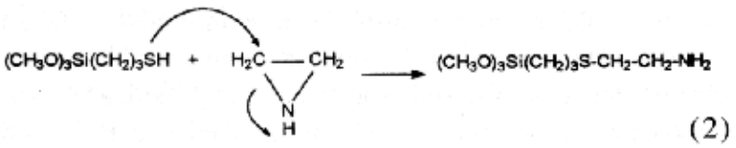


Fig. 1. ^{13}CNMR–CPMAS spectra for $\equiv Sil(CH_2CH_2NH)_4CH_2CH_2NH_2$ (A), computer simulation (B) and the deconvoluted signals (C, D).

of 24 h at 323 K to avoid the possible polymerization of the monomer of the reagent. The proposed mechanism of the reaction process can be illustrated by reaction 2:



(2)

After the synthesis and characterization of the desired compound **4** (Scheme 1), it was grafted onto activated silica to form the same anchored silica as obtained in the preceding route A. However, a better yield on functionalization can be obtained from route B. This procedure has the advantage that the precursor compound can be easily characterized. However, route A is the most useful method due to its operational simplicity [8,9].

The determination of the specific surface area, S_{BET} [43], based on the adsorption of gaseous nitrogen at several pressures at 77 K, gave values of 484, 345, 285 and 21 $m^2\ g^{-1}$ for activated silica, ≡Sil–SH (compound **2**), ≡Sil–SN (compound **3**) and $\equiv Sil(CH_2CH_2NH)_4CH_2CH_2NH_2$, respectively. This decrease in surface area after functionalization is due to the presence of pendant groups which block the access of molecules of gaseous nitrogen into the structure of the silica [43,45].

The IR spectrum of compound **4** (Scheme 1) showed the absence of bands at 2564 cm^{-1}, which should be related to S–H stretching frequency of the original mpts silylating agent [45,46]. The large band located at 3239 cm^{-1} for the free etn molecule, which was attributed to NH stretching vibrational mode of the secondary amine, disappeared after reacting. On the other hand, the appearance of two other new bands at 3361 and 3284 cm^{-1}, characteristic of NH stretching vibrational modes of the primary amine formed during the reaction, were detected. All these features are in agreement with the success of the immobilization, and the IR spectra of the silylating agent (A), the ligand ethylenimine (B) and the formed compound **4** (C) are shown in Fig. 2.

The ^{13}C NMR spectrum of 3-trimethoxypropylthioethylamine, compound **4**, whose formula is shown below, showed a chemical shift for methoxy groups (C-6) at 50.0 ppm [45,46].

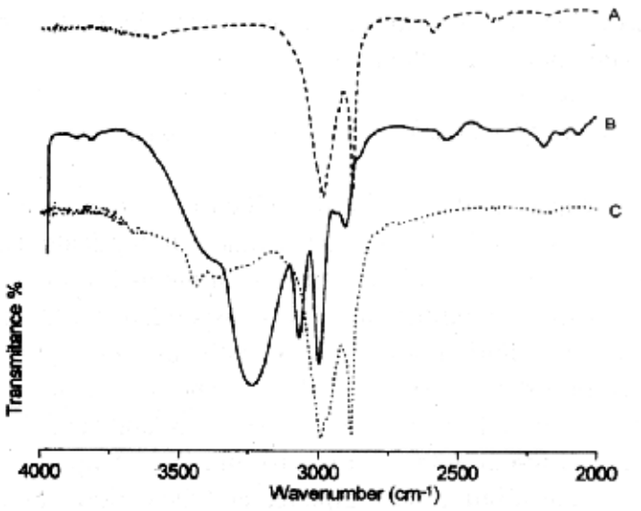


Fig. 2. IR spectra of 3-mercaptopropyltrimethoxysilane (A), ethylenimine (B) and 3-trimethoxypropylthioethylamine (C).

$$(CH_3O)_3Si\ CH_2\ CH_2\ CH_2\ S\ CH_2\ CH_2\ NH_2$$
$$6 \qquad 5 \quad 4 \quad 3 \qquad 2 \quad 1$$

The chemical shifts at 41.2, 36.1, 34.4, 23.0 and 8.4 ppm refer to carbons labelled 1, 2, 3, 4 and 5, respectively, in the above formula; the chemical shift at 96.0 ppm is due to the solvent CCl_4 [8], as shown in Fig. 3. The corresponding signals for protons for this compound can be summarized as follows: methylenes 1 and 5 appeared as triplets at 2.78 and 0.65 ppm, respectively, while protons of carbons 2 and 3 presented a multiplet at 2.48 ppm; the methylene 4 appeared at 1.64 ppm as a quintet; the amidic proton showed a broad peak at 1.08 ppm. Finally, an intense singlet peak at 3.52 ppm is attributed to the presence of the methoxy groups.

The IR spectrum in Fig. 4 showed a large and broad band near 3600 cm^{-1} for the activated silica (A), which corresponds to O–H stretching vibration. Some additional bands are incorporated, as illustrated after anchoring the silylating agent mpts (B) and the subsequent reaction with etn molecule (C). Identical IR spectra of immobilized compound **3**, shown in Fig. 4(C), were obtained by both routes and are

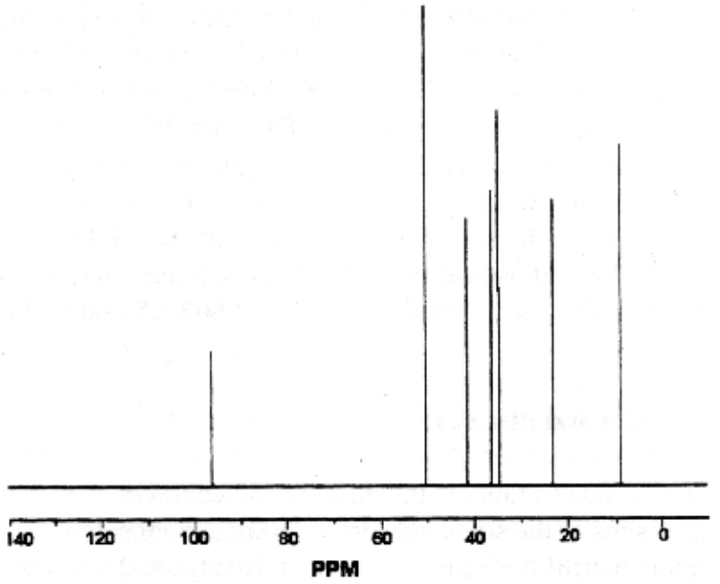


Fig. 3. ^{13}C NMR spectrum of 3-trimethoxypropylthioethylamine.

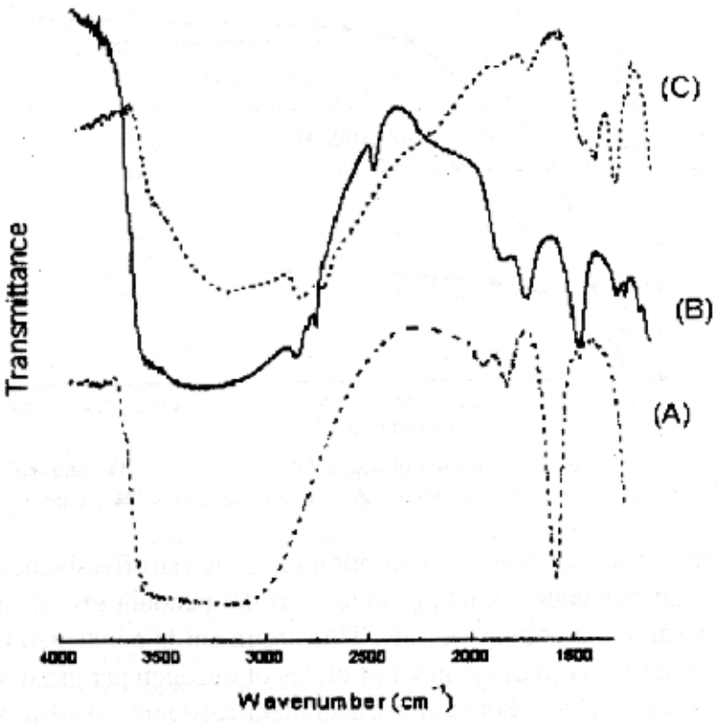


Fig. 4. IR spectra of silica gel (A), ≡Sil–SH (B) and ≡Sil–SN (C).

characterized by the disappearance of the band at 2564 cm^{-1}, which is attributed to S–H stretching vibrational group. This band is clearly observed for the precursor compound, as illustrated in Fig. 4(B). Compounds B and C presented two bands in the range 2950–2850 cm^{-1}, characteristic of CH stretching vibration mode. The CN stretching band belonging to compound 4C is well defined at 1600 cm^{-1}. However, the organofunctionalized surface $\equiv Sil(CH_2CH_2NH)_4CH_2CH_2NH_2$ showed two well-defined bands at 2949 and 2838 cm^{-1} that were attributed to C–H stretching vibration modes [45,46].

The solid state carbon NMR spectrum of the final immobilized surface gave a series of peaks, in the same sequence as observed for the free molecule in liquid phase. Thus, for compound synthesized by homogeneous methods, a weak signal was observed at 50.7 ppm, relative to methoxy carbon groups, and the chemical shift at 13.2; 24.0; 35.8 and 42.1 ppm are attributed to carbons 5, to the equivalent carbons 2 and 3, 4 and 1, respectively, as illustrated in Fig. 5(a). The compound synthesized by the heterogeneous process has a sharp and strong peak at 50.0 ppm, attributed to methoxy carbon groups. This is due to the parallel reaction of the free silanol groups on the silica surface with etn. This molecule is anchored by forming a new oxygen carbon bond, whose chemical shift is the same as those of the methoxy groups. The sequence of peaks is exactly the same as observed in the homogeneous process, with the following chemical shifts: 12.7; 24.3; 35.8 and 42.2 ppm, respectively, as shown in Fig. 5(b).

The thermogravimetric curve of the activated silica gel is shown in Fig. 6(A). An initial 1.0% weight loss at 298–473 K is attributed to the water physically adsorbed water on the surface. The following loss of mass of 2.60% reached at 1170 K is related to the condensation of free silanol groups on the

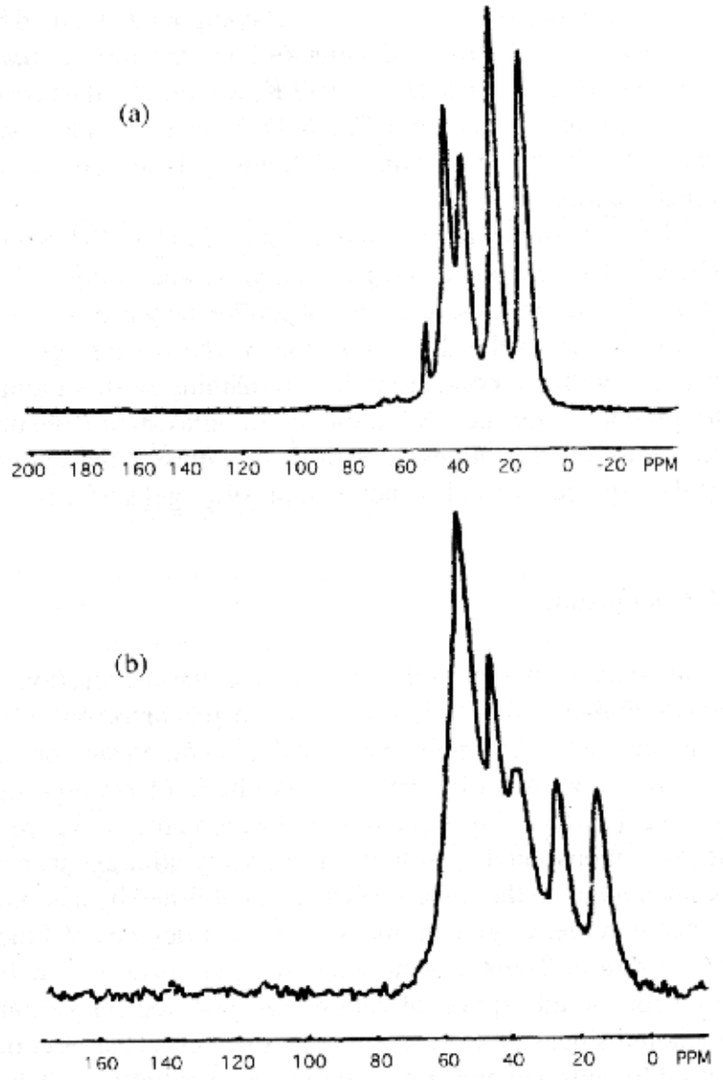


Fig. 5. ^{13}C NMR–CPMAS spectra of ≡Sil–SN obtained by homogeneous (a) and heterogeneous (b) routes.

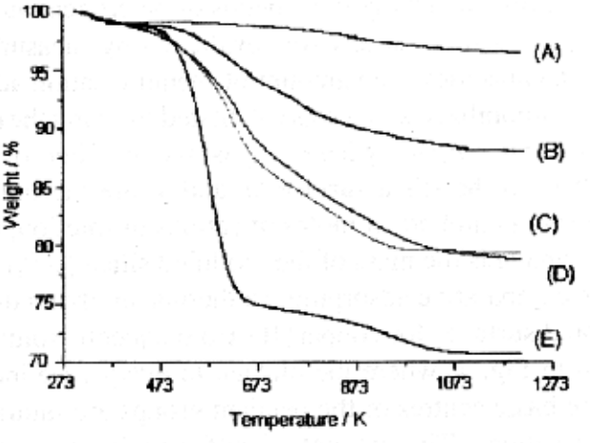


Fig. 6. Thermogravimetric data for silica gel (A), ≡Sil–SH (B) and ≡Sil–SN obtained by the heterogeneous (C) and homogeneous routes (D), and $\equiv Sil(CH_2CH_2NH)_4CH_2CH_2NH_2$ (E).

surface to form siloxane groups [47]. For compound **2** in Scheme 1, referring to the ≡Sil–SH immobilized surface as represented in Fig. 6(B), a first loss of mass of 1.11% between 298 and 473 K, is due to physically adsorbed water. The second loss of mass corresponding to 11.0% at 525–1075 K is due to decomposition of the organic groups covalently bonded on the silica surface. In considering both thermogravimetric data of compound **3**, only one loss of mass is

observed in both cases. Thus, for the compound obtained by the heterogeneous method (Fig. 6(C)), the loss of mass corresponded to 18.0% at 495–973 K, whereas by the homogeneous route (as shown in Fig. 6(D)) the loss of mass was equal to 20.0%, indicating a slightly higher degree of functionalization.

The thermogravimetric curve of the ≡Sil$(CH_2CH_2NH)_4$-$CH_2CH_2NH_2$ anchored surface, as represented in Fig. 6(E), showed a second loss of mass of 24.2% between 493 and 1040 K, due to the decomposition of the organic groups together with the condensation of remaining silanol groups to produce siloxane. All these thermogravimetric results showed a direct relationship of the loss of mass to the amount of the organic molecules anchored on silica gel surfaces.

4. Conclusions

In conclusion, the results demonstrate that the reaction of ethylenimine with a thiol-immobilized precursor on silica was successful in forming a new stable modified support, as was well confirmed by the direct synthesis of etn onto the silica gel surface. The same immobilization process was perfectly demonstrated by isolating the new silylating agent prior to anchorage on the same surface, as established by a homogeneous route, to give surfaces of distinct degrees of functionalization. These organofunctionalized surfaces can be used for the adsorption of cations, as observed for various anchored silicas. In the present case, two basic centres composed by nitrogen and sulfur atoms are potentially available as chelating moieties to complex cations.

The ability of the anchored silicas, ≡Sil–SH and ≡Sil–SN, the latter obtained by homogeneous or heterogeneous methods, in extracting cations was evaluated by measuring the sorption capacities. The amount of metallic cation adsorbed on the immobilized silica was calculated by using the expression $n_{fix} = n_i - n_s/m$, where n_{fix} is the number of moles adsorbed on the silica surface, n_i and n_s are the initial and equilibrium numbers of moles of cations in solution, respectively, and m is the mass of the modified silica [8,9,11].

The comparative adsorption isotherms involving the three anchored surfaces for copper(II) from aqueous solution are shown in Fig. 7, where the plateau in every case indicated that the basic centres of the pendant groups are saturated by copper cations. The amount of sulfur basic centre of 0.78 mmol g^{-1} on precursor ≡Sil–SH extracted 0.40 mmol g^{-1} of cation. However, this value contrasted with 1.50 and 1.60 mmol g^{-1} for the anchored surfaces obtained from heterogeneous and homogeneous methods, respectively. The proximity of the maximum adsorption capacities should be associated with the bidentate chelate centres composed by sulfur and nitrogen atoms. Therefore, a coherence was obtained with the largest values for these last immobilized surfaces, which reflected the elemental analysis of the number of nitrogens bonded in the pendant groups, indicating a slight increase for the surface synthesized by the homogeneous

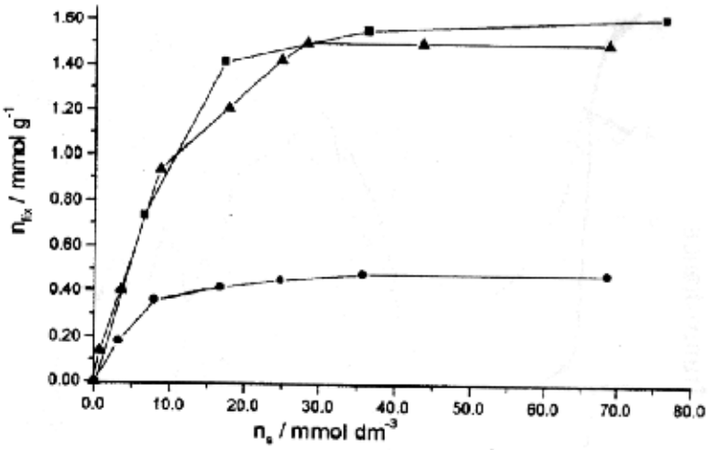


Fig. 7. Isotherms of adsorption of copper(II) by ≡Sil–SH (●) and ≡Sil–SN obtained by the heterogeneous (▲) and homogeneous (■) routes.

route. The increment in adsorption suggested an effectiveness of the bidentate chelating moiety on the pendant groups in coordinating copper cations. This argument is connected to the similarity in the number of moles of nitrogen per gram of silica gel, which should give a near identical degree of adsorption. However, the organofunctionalized surface obtained by the heterogeneous method is also embodied by the amine groups derived from the reaction of the cyclic ethylenimine molecules bonded to silanol groups on the surface, which should be involved in the coordination process [3,4], but in an expected less effective fashion.

These synthetic methods have elucidated the importance of designing appropriate molecules to embrace chelate centres to coordinate cations from aqueous solution through distinct routes, which makes clear the efficiency of the preparative methods.

Acknowledgements

The authors are indebted to CNPq for fellowships, FAPESP for financial support and José A.R. Rodrigues for valuable discussion.

References

[1] B. Buszewski, M. Jezierska, M. Welniak, D. Berek, J. High Resolut. Chromatogr. 21 (1998) 267.
[2] V.Z. Bermudez, L.D. Carlos, L. Alcácer, Chem. Mater. 11 (1999) 569.
[3] H.A. Mottola, J.R. Steimetz, Chemically Modified Surfaces, Elsevier, New York, 1992.
[4] D.E. Leyden, W.T. Collins, Chemically Modified Surface in Science and Industry, Gordon and Breach, London, 1988.
[5] F.R. Hartler, P.N. Vezey, Adv. Organometal. Chem. 15 (1977) 189.
[6] U. Deschler, P. Kleinschmit, P. Panster, Angew. Chem., Int. Ed. Engl. 25 (1986) 236.
[7] B. Pfeiderer, K. Albert, E. Bayer, L. Van de Ven, J. de Haan, C. Cramers, J. Phys. Chem. 94 (1990) 4189.
[8] C. Airoldi, M.R.M.C. Santos, J. Mater. Chem. 4 (1994) 1479.
[9] M.R.M.C. Santos, C. Airoldi, J. Colloid Interface Sci. 183 (1996) 416.

[10] E.F.C. Alcantara, C. Airoldi, O. Nakamura, H. Vargas, F. Paixão, Polyhedron 13 (1992) 1701.
[11] C. Airoldi, E.F.C. Alcantara, J. Chem. Thermodyn. 27 (1995) 623.
[12] A.S. Gonçalves, C. Airoldi, Polyhedron 8 (1989) 2901.
[13] M.T. Dulay, P. Rajan, R.N. Zare, Anal. Chem. 70 (1998) 5103.
[14] E.R. Kiranas, M.I. Karayannis, S.M. Tzouwara-Karayanni, Talanta 45 (1998) 1015.
[15] S. Pegiadou, J.T. Guthrine, M.H. Gill, J. Appl. Polym. Sci. 70 (1998) 211.
[16] L.M. Ferreira, J.M.S. Rocha, M.H. Gil, Radiat. Phys. Chem. 52 (1998) 207.
[17] P.S. Santos, U.A. Lima, H.S. Santos, P.K. Kiyohara, An. Acad. Bras. Cienc. 70 (1998) 23.
[18] C.S. Pundia, N.K. Kucchal, A.K. Bhargava, Biotechnol. Appl. Biochem. 27 (1998) 103.
[19] L.N.H. Arakaki, C. Airoldi, Quim. Nova 22 (1999) 246.
[20] V.I. Lygin, Kinet. Katal. 35 (1994) 480.
[21] D.E. Leyden, Silanes Surfaces and Interfaces, Gordon and Breach, London, 1986.
[22] O. Kröcher, R.A. Köppel, A. Baiker, Chem. Commun. (1996) 1497.
[23] C.R. Silva, I.C.S.F. Jardim, C. Airoldi, J. High Resolut. Chromatogr. 22 (1999) 103.
[24] W. Wasiak, W. Urbaniak, J. Chromatogr. A 757 (1997) 137.
[25] K. Jinno, C. Okamura, M. Taniguchi, Y.L. Chen, Chromatographia 44 (1997) 613.
[26] J. Haginaka, H. Takehira, J. Chromatogr. A 777 (1997) 241.
[27] Y. Wu, M. Krocka, T. Li, J. Chromatogr. A 822 (1998) 11.
[28] Y. Mochida, H. Nishi, K. Nakamura, J. Chromatogr. A 810 (1998) 33.
[29] A.R. Cestari, C. Airoldi, J. Braz. Chem. Soc. 6 (1995) 79.
[30] A.R. Cestari, C. Airoldi, Langmuir 13 (1997) 2681.
[31] A.R. Cestari, E.F.M. Barradas, C. Airoldi, R. Buffon, Braz. J. Chem. Eng. 15 (1998) 146.
[32] J.H. Clark, D.J. Macquarrie, Chem. Commun. (1998) 853.
[33] J.M. Coronado, J.Á. Anderson, J. Mol. Catal. A 138 (1999) 83.
[34] A. Tong, T. Akam, S. Tanaka, Anal. Chim. Acta 230 (1990) 179.
[35] L.A. Ciolino, J.G. Dorsey, J. Chromatogr. A 675 (1994) 29.
[36] Y. Gushiken, W.C. Moreira, Colloids Surf. 25 (1987) 155.
[37] K.M.R. Kallury, W.E. Lee, M. Thompson, Anal. Chem. 65 (1993) 2459.
[38] A.M. Dupraz, J.R. Wijin, S.A.T. Meer, K. de Groot, J. Biomed. Mater. Res. 30 (1996) 231.
[39] R.R. Lee, M. Ogiso, A. Watanabe, K. Ishihara, J. Biomed. 38 (1997) 11.
[40] A. Frey, M.R. Neutra, F.A. Robey, Bioconjugate Chem. 8 (1997) 424.
[41] C.F. Allen, F.W. Spnagler, E.R. Webster, Org. Synth. Coll. 4 (1963) 433.
[42] R.K. Iler, The Chemistry of Silica, Wiley, New York, 1979.
[43] S. Brunauer, P. Emett, E. Teller, J. Am. Chem. Soc. 60 (1938) 309.
[44] K. Unger, N. Becker, P. Roumeliotis, J. Chromatogr. 125 (1976) 115.
[45] A.R. Cestari, C. Airoldi, J. Colloid Interface Sci. 195 (1997) 338.
[46] E.F.S. Vieira, J.A. Simmoni, C. Airoldi, J. Mater. Chem. 7 (1997) 2249.
[47] S. Kutahara, K. Takada, T. Sakata, H. Murashi, J. Colloid Interface Sci. 84 (1981) 519.

PERGAMON

www.elsevier.nl/locate/poly

Polyhedron 19 (2000) 375–380

POLYHEDRON

d^3–d^3 Diolates of dimolybdenum and ditungsten Part 4. [1] Molybdenum derivatives of *S*(−)-1,1-diphenyl-1,2-propanediol, *S*(−)-1,1,2-triphenyl-1,2-ethanediol and (1*R*, 2*R*)-(−)-1,2-dicyclohexyl-1,2-ethanediol

Malcolm H. Chisholm *, Kirsten Folting, John C. Huffman, Hui Li, Ann M. Macintosh, De-Dong Wu

Department of Chemistry and Molecular Structure Center, Indiana University, Bloomington, IN 47405, USA

Received 13 August 1999; accepted 29 October 1999

Abstract

From the reactions between the diols *S*(−)-1,1-diphenyl-1,2-propanediol, *S*(−)-1,1,2-triphenyl-1,2-ethanediol and (1*R*, 2*R*)-(−)-1,2-dicyclohexyldiol and each of $Mo_2(O^tBu)_6$ and $Mo_2(NMe_2)_6$, the compounds $Mo_2(O_2C_{15}H_{15})_3$ (**1**), $Mo_2(O_2C_{20}H_{17})_3$ (**2**) and $Mo_2(O_2C_{14}H_{25})_4$ (**3**) have been isolated and characterized. In the reactions leading to the formation of **1** and **2**, kinetic control leads to highly sterically congested products having six phenyl groups at one end of the Mo–Mo axis. Three methyl groups in compound **1** and three phenyl groups in compound **2** are at the other Mo centers. In compound **3**, four equivalents of the diol are taken up by the Mo_2^{6+} center, two straddle the Mo–Mo triple bond and one chelates at each Mo center. Inspection of the Mo–O and O···O distances in compound **3** reveals the presence of OH groups such that the compound may be considered an alcoholate $Mo_2(O\sim\sim O)_2(O\sim\sim OH)_2$. These results are discussed in terms of crystals engineering an infinite chain of Mo_2 units with parallel Mo–Mo axes wherein a chiral ligand framework imposes a C_3 screw axis.
©2000 Elsevier Science Ltd All rights reserved.

Keywords: Crystal engineering; Dimolybdenum; Dimolybdenum diolates

1. Introduction

The field of crystal engineering rests on a fundamental understanding of intermolecular forces and their use in ordering molecules or aggregates in the solid state [1]. In general it is the weak forces of molecular recognition, such as hydrogen bonding, π–π stacking of aromatic hydrocarbons or dipolar interactions, that are involved in this ordering. The problem of control of architecture in the solid state is, however, complicated by the variety of ways in which such weak forces may act in concert as well as in the molecular design of the subunits to be assembled. Multiple bonds between metal atoms in dinuclear complexes, M_2L_n, are known to have large diamagnetic anisotropies [2,3] and, more recently, have been shown to have large hyperpolarizabilities leading to large third-order non-linear optical responses [4,5]. The measurements of the latter have been made in solution or in the solid state from microcrystalline powders. These measurements of γ represent an isotropic or averaged value and if any application of this phenomenon is to be forthcoming it would be useful to know the value of γ parallel and perpendicular to the M–M axes. From our studies of the liquid crystalline phases of $Mo_2(O_2CR)_4$ compounds, we know that the largest component of the index of refraction for the mesophase is coincident with the columnar axis, which in turn is coincident with the M–M quadruple bond axis, i.e. the mesophase is an optically positive uniaxial material [6]. While we have learnt how to orientate the mesophase in an applied field, it is still simpler in principle to align the M–M axes in the solid state by taking advantage of weak intermolecular peaking forces as in $W_2(O^cC_6H_{11})_6$ or by weak intermolecular metal–ligand interactions as in $W_2(O_2C_2Me_4)_3$, where $O_2C_2Me_4$ is pinacolate [7]. These two structures are shown in Figs. 1 and 2, respectively. In the $W_2(O^cC_6H_{11})_6$ structure the W≡W bonds are aligned in a parallel manner but the shortest intermolecular W to W non-bonding distance is >6 Å, whereas in $W_2(O_2C_2Me_4)_3$, where there are weak

[1] For Part 3 see Ref. [13].

0277-5387/00/$ - see front matter ©2000 Elsevier Science Ltd All rights reserved.
PII S0277-5387(99)00348-4

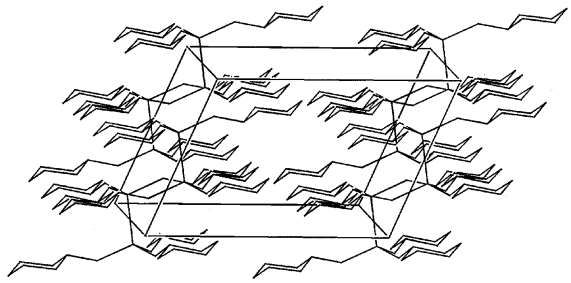


Fig. 1. Drawing depicting the packing of the $W_2(OCy)_6$ molecule. The cyclohexyl rings cause the alignment of the W–W axes without any $\sim W_2\cdots O\cdots W_2\cdots O$ intermolecular bonding.

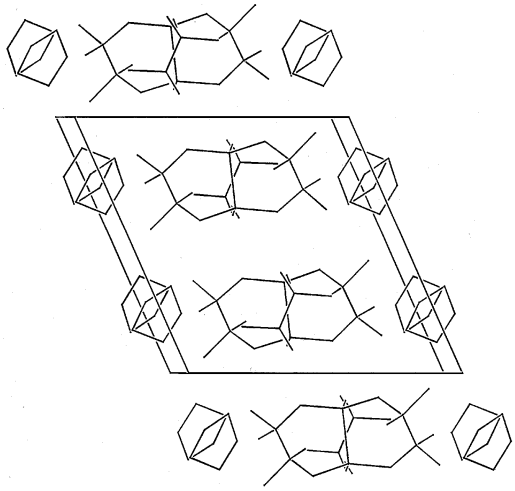


Fig. 2. Drawing of the unit cell of $W_2(O_2C_2Me_4)_6$ THF showing the alignment of the Mo–Mo triple bonds as a result of the weak intermolecular $W_2\cdots O\cdots W_2\cdots O$ interactions. The THF solvate is disordered and not bonded to the W_2 units but is found between the columnar stacks of $[W_2(O_2C_2Me_4)_3]_\infty$.

$(W_2\cdots O\cdots W_2–O–)_\infty$ chains the W to W non-bonded distances are $\sim$3.0 Å. Compounds of this type, wherein the M–M axes are all parallel and are at a unique angle with respect to the crystal growth axis *c*, are ideal for single crystal spectroscopic studies. It seemed plausible that the use of a chiral diolate ligand could impart a helical pitch to the infinite chains in a structure of the type shown in Fig. 2. It was with this in mind that we carried out the present study.

2. Results and discussion

2.1. Synthesis

2.1.1. $[Mo_2(O_2C_{15}H_{15})_3]_2\cdot 2THF$ (1)

The reaction between either $Mo_2(O^tBu)_6$ [8] or $Mo_2(NMe_2)_6$ [9] and (*S*)-(−)-1,1-diphenyl-1,2-propanediol in benzene gave the yellow crystalline compound **1**. The molecular structure of this compound is shown in Fig. 3. It involves two dinuclear units weakly bonded to each other by $Mo_2\cdots O$ interactions of the type seen in Fig. 2 for $W_2(O_2C_2Me_4)_3$. Each terminal Mo is also very weakly ligated by tetrahydrofuran (THF) molecules with Mo–O equal to 2.9 and 3.0 Å. However, it is not these molecules that terminate chain propagation in the solid state but rather that the mechanism of diolate substitution at the M_2^{6+} center leads to an unfavorable steric disposition of ligands. Specifically six phenyl groups are crowded at one Mo center while the three methyl groups are at the other. The dimer of M_2^{6+} units is favored over chain propagation by the linking of the sterically unencumbered Mo atoms through the weak Mo···O bonds, 2.6 and 2.7 Å. The weaker (as evidenced by longer Mo···oxygen THF bonds) are formed at the terminus. Selected bond distances and angles are given in Table 1. Fig. 4 shows a view looking down the M–M axis.

2.1.2. $Mo_2(O_2C_{20}H_{17})_3$ (2)

From a similar reaction between $Mo_2(O^tBu)_6$ [8] or $Mo_2(NMe_2)_6$ [9] and (*S*)-(−)-1,1,2-triphenyl-1,2-propanediol a yellow crystalline product (**2**) was obtained. The ^1H NMR spectrum of this complex implicated a similar substitution pattern, namely six phenyl groups at one Mo end and three at the other (see below). Suitable crystals were not obtained for a single crystal X-ray diffraction study.

2.1.3. $Mo_2(O_2C_{14}H_{24})_2(O_2C_{14}H_{25})_2$ (3)

The reaction between $Mo_2(O^tBu)_6$ [8] and (1*R*, 2*R*)-(−)-1,2-dicyclohexyl-1,2-ethanediol was carried out in benzene with the formation of compound **3**. Cooperative substitution at the Mo_2 center was observed so that no $Mo_2(O_2C_{14}H_{24})_3$ could be obtained. The molecular structure of this compound is shown in Fig. 5. Selected bond distances and angles are given in Table 2. From Fig. 5 one can see that there are two bridging and two chelating diolate ligands. From an inspection of the Mo–O distances one can see two long distances of 2.21 Å, involving the chelate ligands, one at each Mo atom (Mo(1)–O(35) and Mo(2)–O(54)), implying the presence of two OH groups. Inspection of the O···O distances

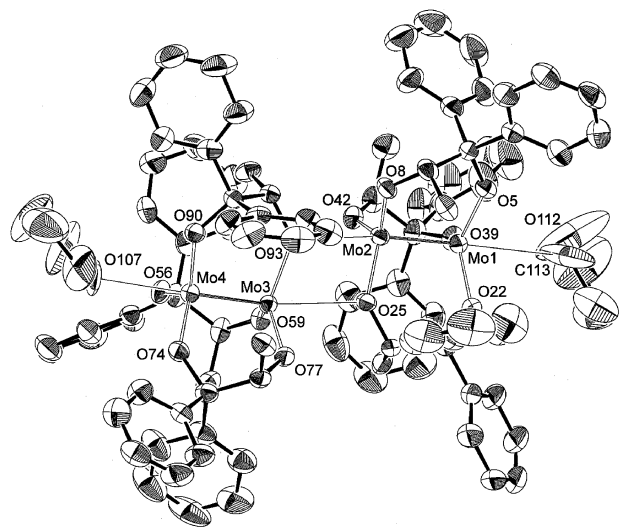


Fig. 3. Molecular structure of the dimeric $(1\cdot THF)_2$ found in the solid state, showing the atom numbering scheme. One THF denoted by C113 and O112 is disordered such that the O and C atoms cannot be distinguished. The $Mo_2\cdots THF$ interactions are extremely weak.

Table 1
Selected bond distances (Å) and angles (°) of compound **1**

Mo(1)–Mo(2)	2.2169(8)
Mo(1)–O(5)	1.904(3)
Mo(1)–O(22)	1.897(3)
Mo(1)–O(39)	1.895(3)
Mo(2)–O(8)	1.903(3)
Mo(2)–O(25)	1.918(3)
Mo(2)–O(42)	1.896(3)
Mo(2)–O(93)	2.641(3)
Mo(3)–Mo(4)	2.2154(7)
Mo(3)–O(25)	2.682(3)
Mo(3)–O(59)	1.896(3)
Mo(3)–O(77)	1.904(3)
Mo(3)–O(93)	1.921(3)
Mo(4)–O(56)	1.908(3)
Mo(4)–O(74)	1.902(3)
Mo(4)–O(90)	1.912(3)
Mo(2)–Mo(1)–O(5)	100.5(1)
Mo(2)–Mo(1)–O(22)	100.6(1)
Mo(2)–Mo(1)–O(39)	100.0(1)
O(5)–Mo(1)–O(22)	120.1(1)
O(5)–Mo(1)–O(39)	115.3(1)
O(22)–Mo(1)–O(39)	115.2(1)
Mo(1)–Mo(2)–O(8)	98.9(1)
Mo(1)–Mo(2)–O(25)	99.9(1)
Mo(1)–Mo(2)–O(42)	99.4(1)
O(8)–Mo(2)–O(25)	117.5(1)
O(8)–Mo(2)–O(42)	118.6(2)
O(25)–Mo(2)–O(42)	116.1(2)
Mo(4)–Mo(3)–O(59)	100.1(1)
Mo(4)–Mo(3)–O(77)	99.6(1)
Mo(4)–Mo(3)–O(93)	99.2(1)
O(59)–Mo(3)–O(77)	118.1(2)
O(59)–Mo(3)–O(93)	113.7(2)
O(77)–Mo(3)–O(93)	119.9(1)
Mo(3)–Mo(4)–O(56)	99.6(1)
Mo(3)–Mo(4)–O(74)	99.9(1)
Mo(3)–Mo(4)–O(90)	100.3(1)
O(56)–Mo(4)–O(74)	115.2(1)
O(56)–Mo(4)–O(90)	118.2(1)
O(74)–Mo(4)–O(90)	117.9(1)

reveals that O(54)···O(38) = 2.50 Å and O(35)···O(51) = 2.51 Å, suggestive of OH···O bonding across the Mo–Mo bond (see Table 2).

2.2. ^{1}H NMR characterization

The ^{1}H NMR spectra of compounds **1** and **2** in toluene-d_8 are entirely consistent with that observed for the substitution pattern as seen for compound **1** in Fig. 3. Thus for compound **1**, aside from the phenyl proton resonances, we observe one Me doublet at δ 0.1 and a quartet for the methine proton signal at δ 5.84. The upfield position of the Me signal and the downfield shift of the methine ^{1}H signal can be attributed to the magnetic anisotropy of the Mo≡Mo bond and the phenyl groups.

For compound **2** only a single methine signal is observed at $\delta \sim 5.2$, consistent with three equivalent methine groups at one end of the molecule.

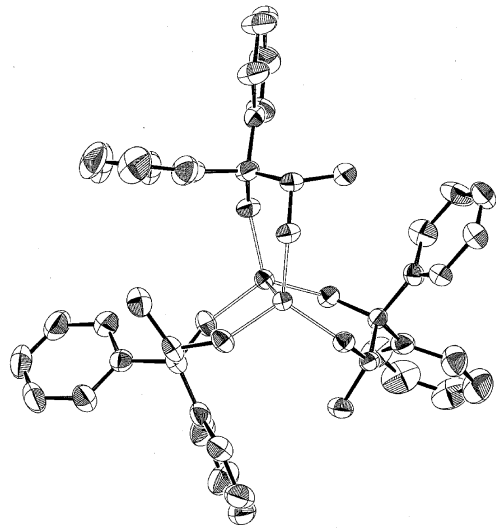


Fig. 4. View looking down the Mo–Mo axis of compound **1** showing the near eclipsed geometry of the Mo_2O_6 skeleton. The O–Mo–Mo–O torsion angles are 9°. The ground state configuration is Δ ($\lambda\lambda\lambda$).

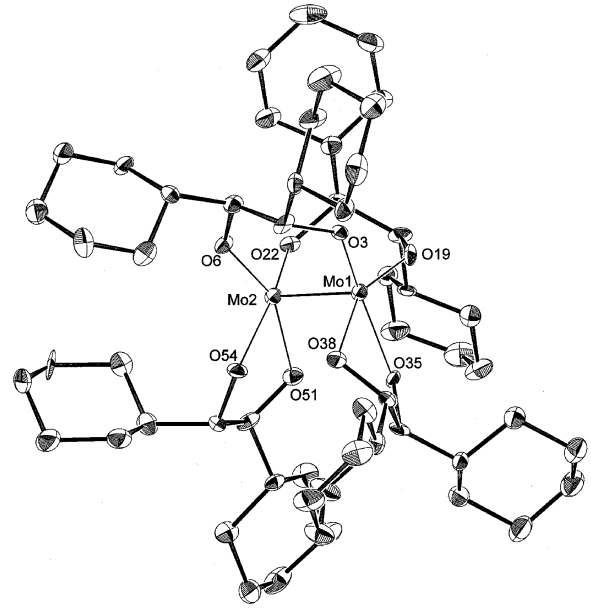


Fig. 5. Drawing of molecule **3** showing the presence of two bridging and two chelating diolate ligands. The Mo–O distances indicate that O(35) and O(54) are protonated and from the O···O distances that they are hydrogen-bonded O(35)–H···O(51) and O(54)–H···O(38).

For compound **3**, which has virtual C_2 symmetry with two chelating and two bridging diolates, we observe three methine signals at $\delta \sim 4.9$, 4.0 and 3.4 in the integral ratio 2:1:1. The most plausible explanation for this would seem to be that the most downfield C*H*O signal arises from the μ-$O_2C_2H_2Cy_2$ ligand because of accidental degeneracy, whereas for the chelate $O_2C_2H_2Cy$ ligands the methine protons are in markedly different orientations with respect to the Mo≡Mo bond, one being proximal and the other distal. The hydroxyl proton is observed at $\delta \sim 4.7$ in toluene-d_8 at 25°C as a somewhat broadened signal. On the ^{1}H NMR time-scale rapid OH···O

Table 2
Selected bond distances (Å) and angles (°) of compound **2**

Mo(1)–Mo(2)	2.1998(9)
Mo(1)–O(3)	1.912(6)
Mo(1)–O(19)	1.887(7)
Mo(1)–O(35)	2.208(6)
Mo(1)–O(38)	2.059(7)
Mo(2)–O(6)	1.917(6)
Mo(2)–O(22)	1.885(6)
Mo(2)–O(51)	2.037(6)
Mo(2)–O(54)	2.211(7)
Mo(2)–Mo(1)–O(3)	100.1(2)
Mo(2)–Mo(1)–O(19)	100.9(2)
Mo(2)–Mo(1)–O(35)	93.9(2)
Mo(2)–Mo(1)–O(38)	94.8(2)
O(3)–Mo(1)–O(19)	107.2(2)
O(3)–Mo(1)–O(35)	158.3(3)
O(3)–Mo(1)–O(38)	90.0(3)
O(19)–Mo(1)–O(35)	86.1(3)
O(19)–Mo(1)–O(38)	154.1(3)
O(35)–Mo(1)–O(38)	72.3(2)
Mo(1)–Mo(2)–O(6)	100.1(2)
Mo(1)–Mo(2)–O(22)	100.9(2)
Mo(1)–Mo(2)–O(51)	94.3(2)
Mo(1)–Mo(2)–O(54)	93.2(2)
O(6)–Mo(2)–O(22)	100.9(3)
O(6)–Mo(2)–O(51)	153.3(3)
O(6)–Mo(2)–O(54)	85.2(2)
O(22)–Mo(2)–O(51)	98.3(3)
O(22)–Mo(2)–O(54)	163.3(3)
O(51)–Mo(2)–O(54)	71.6(2)
Hydrogen bonding	
O(35)···O(51)	2.51
O(38)···O(54)	2.50

transfer clearly makes the chelating diolates oxygen atoms and their attendant methine protons equivalent.

2.3. Isomerization of compound *1* to compound *4*

When a toluene solution of compound **1** is heated in the presence of pyridine, an isomerization occurs to give a compound (**4**) with a much more complex ^{1}H NMR spectrum. However, in the C*Me* region there are simply three sets of doublets of equal intensity and for the C*H* methine signals we observe two resonances of equal integral intensity at δ 4.9 and 4.3, each appearing as quartets (J_{HH} = 6 Hz). The region from δ 6 to 8.8 contains many aromatic resonances and within this region there is concealed the third methine quartet as determined by a COSY spectrum.

There are two possible isomers of compound **1**, namely a $Mo_2(\mu\text{-}O\sim\sim O)(\eta^2\text{-}O\sim\sim O)_2$ complex and a $Mo_2(\mu\text{-}O\sim\sim O)_3$ complex wherein one of the μ-O$\sim\sim$O ligands has 'turned around'. In the latter isomer, one Mo has two OCHMe groups and one $OCPh_2$ and the other two $OCPh_2$ and one OCHMe. In both the chelate and bridged isomers of compound **1** there would be three inequivalent C*Me* and C*H* groups and thus NMR spectroscopy cannot unequivocally distinguish between these isomers. However, from the construction of models we are disinclined to favor the bis-chelate structure because of strain within the five-membered MO_2C_2 rings. Also for the tris-bridged compound we note that one C*H* group is disposed toward the center of the Mo–Mo triple bond. This would cause a significant deshielding [10], resulting in its movement to lower field and as such would explain why it likely appears below 6 ppm.

3. Concluding remarks

The present findings reveal how subtle substitutional preferences at the Mo_2^{6+} center have thwarted our attempts at the 'molecular engineering' of chiral chains of aligned Mo_2 units in the solid state. The kinetic preference for the formation of isomer **1** relative to **4** reveals that substitution at the Mo_2 center is influenced in a cooperative manner. The intermediate $Mo_2(\mu\text{-}OCHMeCPh_2O)(O^tBu)_4$ is preferentially attacked by the next diol at the least sterically hindered Mo atom by the MeHC*OH* moiety and this is again repeated for $Mo_2(\mu\text{-}OCHMeCPh_2O)_2(O^tBu)_2$. Thus ring closure occurs across the Mo≡Mo bond, leading to the most sterically congested isomer having six Ph groups near one Mo atom but only three Me at the other. As in previous studies, such ethane-like isomers are thermally stable and only in the presence of the donor ligand pyridine do we observe the isomerization of compound **1** to compound **4** [11].

4. Experimental

All syntheses were carried out employing thoroughly dried and degassed solvents under a purified N_2 atmosphere. Samples were stored and handled in a Vacuum Atmospheres DriLab system under N_2. The preparation of $Mo_2(NMe_2)_6$ [8] and $Mo_2(O^tBu)_6$ [9] was according to literature methods. The chiral diols employed in this work were obtained from Aldrich and were degassed and stored over 4 Å molecular sieves prior to use.

^{1}H NMR spectra were recorded on a Varian Gemini 300 in benzene-d_6 or toluene-d_8.

4.1. Synthesis of $Mo_2(O_2C_{15}H_{15})_3$ (*1*)

4.1.1. From $Mo_2(O^tBu)_6$

To a solution of $Mo_2(O^tBu)_6$ (0.41 g, 1.8 mmol) dissolved in benzene (10 cm^3) at 25°C was added (*S*)-(−)-1,1-diphenyl-1,2-propanediol (0.40 g, 0.63 mmol) dissolved in benzene (20 cm^3). (The latter required heating for 1 h.) The solution was stirred with the aid of a magnetic stir-bar for 20 h at room temperature. The color gradually darkened from yellow to brown. The solvent and volatile organic components were removed under a dynamic vacuum at room temperature to leave crude $Mo_2(O_2C_{15}H_{15})_3$ (**1**) as a yellow solid. Recrystallization of this solid from benzene–hexane

gave a pale yellow microcrystalline solid (0.39 g, yield 71%). ^{1}H NMR (C_6D_6, 25°C, 30 MHz): δ 7.76 (m, 6H), 6.9–7.3 (m, 24H), 5.85 (d, 3H), 0.10 (d, 9H), with J_{HH} = 6 Hz.

Crystals suitable for single crystal X-ray study were obtained by dispersing hexane in a concentrated solution of compound **1** dissolved in THF. This gave $[Mo_2(O_2C_{15}H_{15})_3]_2 \cdot 2THF$ with the structure shown in Fig. 3.

4.1.2. From $Mo_2(NMe_2)_6$

To a solution of $Mo_2(NMe_2)_6$ (0.4 g, 0.88 mmol) dissolved in benzene (15 cm^3) at room temperature was added (*S*)-(−)-1,1-diphenyl-1,2-propanediol (0.56 g, 2.46 mmol) dissolved in benzene (25 cm^3). (The latter required heating for 1 h to obtain complete dissolution of the diol.) The solution was stirred with the aid of a magnetic follower for 24 h at room temperature. The color changed from yellow to orange–red. The solvent and organic components were removed under a dynamic vacuum at room temperature to yield a yellow powder. Recrystallization from hexane–benzene gave compound **1** as a microcrystalline yellow solid (0.50 g, yield 65%). The ^{1}H NMR data were identical to those reported above.

Compound **1** is air-sensitive and soluble in common hydrocarbon solvents and ethers. It is thermally stable at 100°C for several hours.

4.2. Isomerization of compound *1*

Pure crystalline compound **1** (60 mg) was dissolved in dry and deoxygenated pyridine and heated to 80°C for 15 min. The color changed from yellow to maroon. The pyridine was removed under a dynamic vacuum at room temperature to yield a maroon powder. The ^{1}H NMR spectrum was more complex than that reported above, indicating a lower symmetry. The CH_3 resonance were split into three sets of equal intensity in benzene-d_6: δ 1.95, 1.72 and 1.45, each doublets of equal integral intensity with J_{HH} = 6 Hz. Methine ^{1}H NMR: δ 4.36, 4.94 and 6.18, each quartets of equal integral intensity, J_{HH} = 6 Hz.

4.3. Synthesis of $Mo_2(O_2C_{20}H_{17})_3$ (*2*)

4.3.1. From $Mo_2(O^tBu)_6$

To a Schlenk flask (150 ml), $Mo_2(O^tBu)_6$ (0.80 g, 1.27 mmol) and (*S*)-(−)-1,2,3-triphenyl-1,2-ethanediol were added followed by benzene (3 cm^3). The resultant solution was stirred for 12 h at room temperature and solvent was then removed under a dynamic vacuum to give a yellow microcrystalline powder. The pure compound $Mo_2(O_2C_{20}H_{17})_2$ (**2**) was obtained by recrystallization from a benzene–hexane solution (1.35 g, 67% yield).

^{1}H NMR data (benzene-d_6, 25°C, 300 MHz): δ 7.83 (d, 6H), 6.8–7.2 (m, 39H), 5.15 (s, 3H).

4.3.2. From $Mo_2(NMe_2)_6$

A similar reaction procedure involving $Mo_2(NMe_2)_6$ and the diol (as described in the preparation of compound **1**) yielded compound **2** in 65% yield.

4.4. Synthesis of $Mo_2(O_2C_{14}H_{25})_4$ (*3*)

To a solution of $Mo_2(O^tBu)_6$ (0.25 g, 0.4 mmol) dissolved in benzene (10 cm^3) at room temperature was added (1*R*, 2*R*)-(−)-1,2-dicyclohexyl-1,2-ethanediol (0.35 g, 1.55 mmol) dissolved in benzene (20 cm^{-3}). (The latter required heating to 60°C for 1 h.) The solution was stirred with the aid of a magnetic follower for 24 h at room temperature. The solution darkened from yellow to brown. The solvent was removed under a dynamic vacuum to leave $Mo_2(O_2C_{14}H_{25})_4$ (**3**) as a pale yellow powder. Slow recrystallization of this product from benzene yielded the benzene solvate, $Mo_2(O_2C_{14}H_{25})_4 \cdot 2C_6H_6$ (**3**$\cdot 2C_6H_6$), which was used in the crystallographic study.

Reactions employing $Mo_2(O^tBu)_6$ and 2.5 equivalents of this diol still led to the formation of compound **3** along with unreacted $Mo_2(O^tBu)_6$. Attempts to remove one equivalent of diol from $Mo_2(O_2C_{14}H_{25})_4$ by heating compound **3** under a dynamic vacuum at 55, 70, 85 and 95°C failed, yielding only compound **3**. Above 120°C compound **3** undergoes thermal decomposition.

4.5. Single crystal X-ray studies

General operating procedures have been published previously [12]. A summary of the crystal data is given in Table 3.

Table 3
Summary of crystal data

	3$\cdot 2C_6H_6$	**1**$\cdot 2$THF
Chemical formula	$C_{68}H_{108}Mo_2O_8$	$C_{98}H_{100}Mo_4O_{14}$
Formula weight	1245.48	1885.62
Space group	$P2_1$	$P1$
T (°C)	−168	−168
a (Å)	11.655(2)	13.682(2)
b (Å)	21.018(3)	15.477(2)
c (Å)	13.785(2)	13.326(1)
α (°)	90	114.08(1)
β (°)	99.91(1)	118.25(1)
γ (°)	90	87.22(1)
V (Å^3)	3326.41	2232.62
Z	2	1
ρ_{calc} (g cm^{-3})	1.244	1.402
Wavelength λ (Å)	0.71069	0.71069
μ (cm^{-1})	4.268	5.951
Unique reflections	4494	15 688
Reflections with $F = 3\sigma(F)$	3738	12 886
$R(F)$ [a]	0.0375	0.0317
$R_w(F)$ [b]	0.0347	0.0311

[a] $R = \{||F_o| - |F_c||\}/|F_o|$.
[b] $R = \{w(|F_o| - |F_c|)^2/wF_o^2\}^{1/2}$, where $w = 1[\sigma^2(|F_o|)]$.

Supplementary data

Full crystallographic data have been deposited with the Cambridge Crystallographic Data Centre. For **1**·2THF request CCDC 133551; for **3**·2C_6H_6, request CCDC 133552. Copies of the data can be obtained free of charge on application to the CCDC, Cambridge Crystallographic Data Centre, 12 Union Road, Cambridge CB2 1EZ, UK (fax: +44-1223-336033; e-mail: deposit@ccdc.cam.uk).

Acknowledgements

We thank the National Science Foundation for financial support.

References

[1] G.R. Desiraju, Angew. Chem., Int. Ed. Engl. 34 (1995) 2311.
[2] F.A. Cotton, R.A. Walton, Multiple Bonds Between Metal Atoms, Oxford University Press, Oxford, 2nd ed., 1993.
[3] F.A. Cotton, S. Kitagawa, Polyhedron 7 (1988) 1673.
[4] K. Mashima, M. Tanaka, Y. Kaneda, A. FukuMoto, H. MizoMoto, K. Tami, H. Nakano, A. Nakamura, T. Sakaguchi, K. Kamada, K. Ohta, Chem. Lett. (1997) 411.
[5] M.D. Hopkins, personal communication.
[6] D.V. Baxter, M.H. Chisholm, M.A. Lynn, E.F. Putilina, S.T. Trszska, T. Swager, Chem. Mater. 10 (1998) 1658.
[7] M.H. Chisholm, K. Folting, M.J. Hampden-Smith, Polyhedron 6 (1987) 1747.
[8] M.H. Chisholm, F.A. Cotton, C.A. Murillo, W.W. Reichert, Inorg. Chem. 16 (1977) 1801.
[9] M. Akiyama, M.H. Chisholm, F.A. Cotton, M.W. Extine, D.A. Haitko, D. Little, P.E. Fanwick, Inorg. Chem. 18 (1979) 2266.
[10] T.P. Blatchford, M.H. Chisholm, J.C. Huffman, Polyhedron 6 (1987) 1677.
[11] M.H. Chisholm, J.-H. Huang, J.C. Huffman, I.P. Parkin, Inorg. Chem. 36 (1997) 1642.
[12] M.H. Chisholm, K. Folting, J.C. Huffman, C.C. Kirkpatrick, Inorg. Chem. 23 (1984) 1021.
[13] M.H. Chisholm, K. Folting, W.E. Streib, D. Wu, Inorg. Chem. 37 (1998) 50.

PERGAMON

www.elsevier.nl/locate/poly

Polyhedron 19 (2000) 381–387

POLYHEDRON

Synthesis of diorganotin derivatives containing asymmetric disubstituted bis(pyrazol-1-yl)methanes: X-ray crystal structures of (3-isopropylpyrazol-1-yl-5′-isopropylpyrazol-1-yl)methane diphenyltin(IV) dibromide and bis(5-isopropylpyrazol-1-yl)methane diphenyltin(IV) dibromide

Liang-Fu Tang, Zhi-Hong Wang, Wen-Li Jia, Yu-Ming Xu, Ji-Tao Wang *

Department of Chemistry, Nankai University, Tianjin 300071, People's Republic of China

Received 25 March 1999; accepted 18 November 1999

Abstract

The reaction of 3-*tert*-butylpyrazole with dibromomethane under phase-transfer catalytic conditions afforded a new ligand, bis(3-*tert*-butylpyrazol-1-yl)methane [CH_2(3-Bu^{t}Pz)$_2$]. However, the reaction of 3-isopropylpyrazole with dibromomethane under the same conditions yielded three isomers: bis(5-isopropylpyrazol-1-yl)methane [CH_2(5-iPrPz)$_2$], (3-isopropylpyrazol-1-yl-5′-isopropylpyrazol-1-yl)methane [CH_2(3-iPrPz-5′-iPrPz)] and bis(3-isopropylpyrazol-1-yl)methane [CH_2(3-iPrPz)$_2$]. Although CH_2(5-iPrPz)$_2$ suffered the greatest degree of steric hindrance, this ligand was obtained in highest yield. Upon treating the isomeric mixture with diorganotin halides in petroleum ether (60–90°C), the isomers were isolated in the form of diorganotin derivatives of bis(pyrazol-1-yl)methanes. The crystal structures of CH_2(3-iPrPz-5′-iPrPz)$SnPh_2Br_2$ and CH_2(5-iPrPz)$_2SnPh_2Br_2$ determined by X-ray crystallography indicated that the isopropyl group in the 3-position of the pyrazole ring decreased the coordination ability of CH_2(3-iPrPz-5′-iPrPz), and the average Sn–N distance in CH_2(3-iPrPz-5′-iPrPz)$SnPh_2Br_2$ (2.52 Å) was longer than that in CH_2(5-iPrPz)$_2SnPh_2Br_2$ (2.435 Å). ©2000 Elsevier Science Ltd All rights reserved.

Keywords: Organotin(IV); Poly(pyrazol-1-yl)alkanes; X-ray structure

1. Introduction

Diorganotin complexes containing nitrogen donor ligands have attracted considerable attention in recent years due to their potential antitumor activity against P388 leukemia [1,2]. Many complexes of the type R_2SnX_2(N–N) have been synthesized and tested [3], in which the N–N ligands are symmetric *N*,*N*-chelating agents such as bipyridine-type ligands [4] or asymmetric ones such as 8-aminoquinoline [5]. We have successfully prepared a variety of pentacoordinate organotin(IV) complexes in which the metal was coordinated with tridentate ligands containing nitrogen and oxygen. We find that the Schiff bases of amino acids [6,7], substituted hydrazones [8], semicarbazones and thiosemicarbazones [9] exhibit good coordination activity for organotin(IV) complexes.

Recently, poly(pyrazol-1-yl)alkanes, especially bis(pyrazol-1-yl)alkanes, have also been found to act as good donors to organotin compounds. Pettinari and co-workers have extensively studied the interactions between bis(pyrazol-1-yl)alkanes and tin(IV) and organotin(IV) acceptors [10–13]. The donating ability can be easily controlled by varying the substituents of the pyrazole ring [14]. A survey of the larger number of tin(IV) and organotin(IV) derivatives of poly(pyrazol-1-yl)alkanes showed that poly(pyrazol-1-yl)alkanes in these derivatives are completely symmetric, and no tin(IV) and organotin(IV) derivatives with asymmetric poly(pyrazol-1-yl)alkanes have been reported. An important reason may be that it is difficult to obtain pure asymmetric poly(pyrazol-1-yl)alkane ligands.

In the present work, we report a simple method to obtain organotin(IV) derivatives containing asymmetric poly(pyrazol-1-yl)alkanes and the first determination of their crystal structures. In order to explain the different steric and electronic features of isopropyl and *tert*-butyl groups,

* Corresponding author. Tel.: +86-22-23501735; fax: +86-22-23501735; e-mail: wangjt@sun.nankai.edu.cn

0277-5387/00/$ - see front matter ©2000 Elsevier Science Ltd All rights reserved.
PII S0277-5387(99)00367-8

organotin(IV) derivatives of bis(3-*tert*-butylpyrazol-1-yl)methane have also been synthesized and characterized.

2. Experimental

Melting points were measured with a PHMK melting-point apparatus and were uncorrected. Elemental analyses were carried out on a Perkin-Elmer 240C analyser. The ^{1}H NMR spectra were obtained with a Bruker AC-P 200MHz spectrometer and the ^{119}Sn NMR spectra were recorded on a Bruker AC-P 200MHz spectrometer at 74.63 MHz, using $CDCl_3$ as solvent unless otherwise noted. The chemical shifts were reported in ppm with respect to the references (internal $SiMe_4$ for ^{1}H NMR, external $SnMe_4$ for ^{119}Sn NMR). IR spectral data were obtained from a Nicolet 170SX spectrometer using KBr discs. The conductivity in solution was measured with a DDS-11A conductimeter at room temperature. 3-*tert*-Butylpyrazole [15] and 3-isopropylpyrazole [16] were prepared by published methods. The solvents were dried by standard methods, and all reactions related to Ph_2SnX_2 (X = Cl, Br) were carried out under moisture-free conditions.

*2.1. Bis(3-tert-butylpyrazol-1-yl)methane (**1**)*

3-*tert*-Butylpyrazole (12.4 g, 100 mmol), CH_2Br_2 (8.7 g, 50 mmol), 25 ml of 40% aqueous sodium hydroxide and tetrabutylammonium bromide (1.0 g, 3.1 mmol) were added to benzene (50 ml). The mixture was vigorously stirred and refluxed for 48 h. After cooling, the two layers were separated and the aqueous layer was extracted with benzene (2×30 ml). The organic phases were combined and dried over anhydrous magnesium sulfate. The solvent was removed in vacuo to give an oil. The oil was redissolved in minimum petroleum ether (60–90°C) and cooled to −20°C to yield the crude product, which was recrystallized from petroleum ether to yield colorless plates of CH_2(3-Bu^{t}Pz)$_2$ (**1**) (5.98 g, 46%), m.p. 99–101°C. ν_{max} (cm^{-1}) (pyrazole ring) 1520.2 s. δ_H 1.27 (18H, s, C(CH_3)$_3$), 6.10 (2H, d, H^4), 6.18 (2H, s, CH_2) and 7.45 (2H, d, H^5). *Anal*. Calc. for $C_{15}H_{24}N_4$: C, 69.23; H, 9.23; N, 21.54. Found: C, 69.30; H, 9.39; N, 21.42%.

*2.2. Bis(5-isopropylpyrazol-1-yl)methane (**2**), (3-isopropylpyrazol-1-yl-5′-isopropylpyrazol-1-yl)methane (**3**) and bis(3-isopropylpyrazol-1-yl)methane (**4**)*

3-Isopropylpyrazole (13 g, 118 mmol), CH_2Br_2 (10.3 g, 59 mmol), 40 ml of 40% aqueous sodium hydroxide and tetrabutylammonium bromide (1.1 g, 3.5 mmol) were added to benzene (60 ml). The mixture was vigorously stirred and refluxed for 48 h. After cooling, the two layers were separated and the aqueous layer was extracted with dichloromethane (2×30 ml). The organic phases were combined and dried over anhydrous magnesium sulfate. The solvent was removed in vacuo to yield an oil. Upon treatment of the oil with 30 ml of petroleum ether (60–90°C), a white solid precipitated out. The precipitate was filtered off and discarded. Evaporating the filtrate again yielded a colorless oil. The oil was kept under 1 mmHg at 100°C for several hours to remove all volatile materials to give the mixture of compounds **2**, **3** and **4** (7.4 g, 54%, total yield). The relative amounts were 54% (**2**), 33% (**3**) and 13% (**4**), calculated from ^{1}H NMR of the mixture. δ_H 1.17 (d, CH(CH_3)$_2$ in compound **4**), 1.18 (d, CH(CH_3)$_2$ in compound **2**), 1.20 (d, CH(CH_3)$_2$ in compound **3**), 1.22 (d, CH(CH_3)$_2$ in compound **3**), 2.98 (m, CH(CH$_3$)$_2$ in componds **3** and **4**), 3.33 (septet, CH(CH$_3$)$_2$ in compound **3**), 3.46 (septet, CH(CH$_3$)$_3$ in compound **2**), 6.01 (m, H^4 in compounds **2**, **3** and **4**), 6.04 (s, CH_2 in compound **3**), 6.13 (s, CH_2 in compound **2**), 6.20 (s, CH_2 in compound **4**), 7.26 (d, H^5 in compound **4**), 7.45 (dd, H^3 or H$^{5'}$ in compound **3**), 7.48 (d, H^3 in compound **2**). The assignment was achieved by analyzing the ^{1}H NMR and crystal structures of adducts with Ph_2SnBr_2.

*2.3. Bis(3-tert-butylpyrazol-1-yl)methane diphenyltin(IV) dibromide (**5**)*

A solution of compound **1** (0.26 g, 1 mmol) dissolved in 5 ml of diethyl ether was added dropwise to a stirred diethyl ether solution (15 ml) of Ph_2SnBr_2 (0.433 g, 1 mmol) by syringe. After the mixture was stirred for 2 h at room temperature, the solvent was removed under reduced pressure. The residual was washed with petroleum ether (60–90°C) and dried in vacuo to afford a white powder of CH_2(3-Bu^{t}Pz)$_2$SnPh$_2$Br$_2$ (**5**) (0.52 g, 75%), m.p. 63–65°C. ν_{max} (cm^{-1}) 1523.3 s (pyrazole ring) and 452.1 m (Sn–C). δ_H 1.28 (18H, s, C(CH_3)$_3$), 6.10 (2H, d, H^4), 6.17 (2H, s, CH_2), 7.49 (8H, m, H^5 and C$_6$H$_5$), 7.66 (4H, m, C$_6$H$_5$). ^{119}Sn NMR ($CDCl_3$): δ −157.4. *Anal*. Calc. for $C_{27}H_{34}Br_2N_4Sn$: C, 46.75; H, 4.91; N, 8.08. Found: C, 46.40; H, 4.90; N, 7.80%.

*2.4. Bis(3-tert-butylpyrazol-1-yl)methane diphenyltin(IV) dichloride (**6**)*

This complex was prepared similarly to complex **5**, yielding 0.48 g of a white solid (80%), m.p. 73–75°C. ν_{max} (cm^{-1}) 1523.3 s (pyrazole ring) and 453.9 m (Sn–C). δ_H 1.28 (18H, s, C(CH_3)$_3$), 6.11 (2H, d, H^4), 6.19 (2H, s, CH_2), 7.46 (2H, d, H^3), 7.52 (6H, m, C$_6$H$_5$), 7.69 (4H, m, C$_6$H$_5$). *Anal*. Calc. for $C_{27}H_{34}Cl_2N_4Sn$: C, 53.64; H, 5.63; N, 9.27. Found: C, 53.49; H, 5.56; N, 9.43.%.

*2.5. Bis(5-isopropylpyrazol-1-yl)methane diphenyltin(IV) dibromide (**7**) and (3-isopropylpyrazol-1-yl-5′-isopropylpyrazol-1-yl)methane diphenyltin(IV) dibromide (**8**)*

A mixture of isomers **2**, **3** and **4** (0.232 g, 1 mmol) was added dropwise to a stirred petroleum ether (60–90°C) solution (30 ml) of Ph_2SnBr_2 (0.433 g, 1 mmol) by syringe. The reaction mixture was stirred continuously for 2 h at room

temperature, during which time a white precipitate was gradually formed. The precipitate was filtered off, washed with petroleum ether and recrystallized from dichloromethane–hexane at −20°C to yield colorless crystals of CH_2(5-iPrPz)$_2SnPh_2Br_2$ (**7**) (0.28 g, 78%, based on the ratios **2**:**3**:**4** = 54:33:13), which was identified by X-ray crystallography, m.p. 140–142°C. ν_{max} (cm^{-1}) 1527.8 m (pyrazole ring) and 460.1 s (Sn–C). δ_H 1.15 (12H, d, CH(CH_3)$_2$), 3.51 (2H, septet, CH(CH_3)$_2$), 6.08 (2H, d, H^4), 6.43 (2H, s, CH_2), 7.45 (2H, d, H^3), 7.50 (6H, m, C_6H_5), 7.65 (4H, m, C_6H_5). ^{119}Sn NMR ($CDCl_3$): δ −83.4. *Anal*. Calc. for $C_{25}H_{30}Br_2N_4Sn$: C, 45.11; H, 4.51; N, 8.42. Found: C, 44.95; H, 4.08; N, 8.56%. The mother liquor was concentrated to 5 ml to afford a white solid, which was filtered off, washed with cooled petroleum ether (25 ml) and dried in vacuo to yield a white powder of CH_2(3-iPrPz-5′-iPrPz)$SnPh_2Br_2$ (**8**) (0.12 g, 65%), which was identified by X-ray crystallography, m.p. 96–98°C. ν_{max} (cm^{-1}) 1528.3 m (pyrazole ring) and 456.9 s (Sn–C). δ_H 1.19 (12H, dd, 3- and 5′-CH(CH_3)$_2$), 2.98 (1H, septet, 3- or 5′-CH(CH_3)$_2$), 3.32 (1H, septet, 3- or 5′-CH(CH_3)$_2$), 6.05 (2H, dd, H^4 and $H^{4'}$); 6.22 (2H, s, CH_2), 7.49 (8H, m, H^3 or $H^{5'}$ and C_6H_5), 7.65 (4H, m, C_6H_5). ^{119}Sn NMR ($CDCl_3$): δ −85.0. *Anal*. Calc. for $C_{25}H_{30}Br_2N_4Sn$: C, 45.11; H, 4.51; N, 8.42. Found: C, 44.75; H, 4.34; N, 8.28%.

*2.6. Bis(5-isopropylpyrazol-1-yl)methane diphenyltin(IV) dichloride (**9**) and (3-isopropylpyrazol-1-yl-5′-isopropylpyrazol-1-yl)methane diphenyltin(IV) dichloride (**10**)*

A mixture of isomers **2**, **3** and **4** (0.232 g, 1 mmol) was added dropwise to a stirred petroleum ether (60–90°C) solution (30 ml) of Ph_2SnCl_2 (0.344 g, 1 mmol) by syringe. A white precipitate was formed immediately. The reaction mixture was stirred continuously for 2 h at room temperature to complete the reaction. The precipitate was filtered off, washed with petroleum ether and recrystallized from dichloromethane–hexane at −20°C to yield colorless crystals of CH_2(5-iPrPz)$_2SnPh_2Cl_2$ (**9**) (0.25 g, 81%,), identified by comparing the ^{1}H NMR spectrum with that of complex **7**, m.p. 137–139°C. ν_{max} (cm^{-1}) 1527.4 m (pyrazole ring) and 458.2 s (Sn–C). δ_H 1.25 (12H, d, CH(CH_3)$_2$), 2.98 (2H, septet, CH(CH_3)$_2$), 6.10 (2H, d, H^4), 6.25 (2H, s, CH_2), 7.45 (8H, m, H^3 and C_6H_5), 7.67 (4H, m, C_6H_5). *Anal*. Calc. for $C_{25}H_{30}Cl_2N_4Sn$: C, 52.08; H, 5.21; N, 9.72. Found: C, 51.82; H, 5.44; N, 9.70%. The mother liquor was concentrated to 5 ml to afford a white solid, which was filtered off, washed with cooled petroleum ether (25 ml) and dried in vacuo to yield a white powder of CH_2(3-iPrPz-5′-iPrPz)$SnPh_2Cl_2$ (**10**) (0.11 g, 62%), identified by comparing its ^{1}H NMR with that of complex **8**, m.p. 101–103°C. ν_{max} (cm^{-1}) 1527.6 m (pyrazole ring) and 458.4 s (Sn–C). δ_H 1.19 (12H, dd, 3 and 5′-CH(CH_3)$_2$), 2.94 (1H, septet, 3 or 5′-CH(CH_3)$_2$), 3.31 (1H, septet, 3 or 5′-CH(CH_3)$_2$), 6.04 (2H, dd, H^4 and $H^{4'}$), 6.21 (2H, s, CH_2), 7.50 (2H, dd, H^3 and $H^{5'}$), 7.52 (6H, m, C_6H_5), 7.66 (4H, m, C_6H_5). *Anal*. Calc. for $C_{25}H_{30}Cl_2N_4Sn$: C, 52.08; H, 5.21; N, 9.72. Found: C, 52.41; H, 5.36; N, 10.12%.

2.7. X-ray crystallography

Crystals of compound **7** suitable for crystallographic investigation were grown from slow vaporization of a dichloromethane–hexane solution at room temperature. Intensity data were collected on a CAD4 diffractometer with graphite-monochromated Mo Kα radiation (0.71073 Å) at 299 K using the $\omega/2\theta$ scan technique in the range of $2° \leq \theta \leq 23°$. Correction for empirical absorption (DIFABS) [17] was applied, and the stucture was solved by direct methods [18] and refined by full-matrix least-squares. All non-hydrogen atoms were refined anisotropically. The calculations were performed on a PDP 11/44 computer with the SDP-PLUS program package [19].

Crystals of compound **8** suitable for X-ray analysis were obtained from a dichloromethane–hexane solution at 4°C. The data were collected on a Rigaku AFC7R diffractometer with graphite-monochromated Mo Kα radiation (λ = 0.71069 Å) at 20°C using the $\omega/2\theta$ scan technique to a maximun 2θ value of 50°. An empirical absorption correction was applied, and the structure was solved by direct methods [20] and expanded using Fourier techniques [21]. The non-hydrogen atoms were refined anisotropically. All calculations were performed using the teXsan [22] crystallographic software package. The crystallographic data and data collection parameters for complexes **7** and **8** are summarized in Table 1.

3. Results and discussion

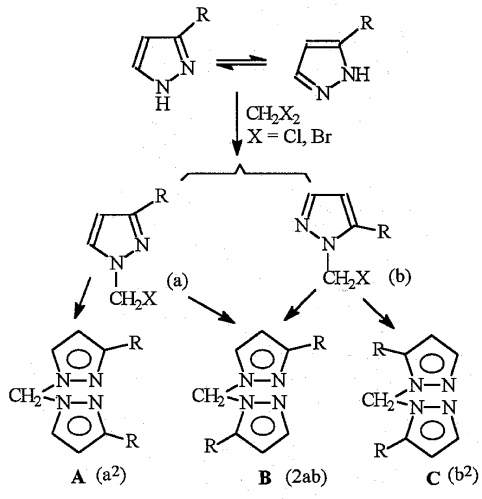
3.1. Synthesis of ligands

Since asymmetric pyrazoles such as 3(5)-methylpyrazole and 3(5)-aminopyrazole can exist in two tautomeric structures in solution, the reaction of asymmetric pyrazoles with alkylation agents such as methylene chloride or methylene bromide in phase-transfer catalytic conditions yields three isomers **A**, **B** and **C** (Scheme 1), in which R is a methyl or amino group. It is of interest that the relative amounts of isomeric bis(pyrazol-1-yl)methanes (**A**:**B**:**C**) correspond to $(a+b)^2$ [23,24]. Recent investigation shows that the reaction of 3-(2-pyridyl)pyrazole with CH_2Br_2 under phase-transfer conditions affords only two isomers **A** and **B**, where R is a 3-(2-pyridyl) group, and the third isomer **C** is not formed [25].

In this work, we find that the reaction of 3-*tert*-butylpyrazole with CH_2Br_2 in analogous conditions gives only isomer **A** (R = Bu^t), which is the result of the strong steric hindrance of *tert*-butyl group. However, when R is an isopropyl group, the reaction of 3-isopropylpyrazole with CH_2Br_2 under the same conditions gives three isomers. It is notable that the relative amount of isomer **C** (R = iPr) with the strongest

Table 1
Crystal data for compounds **7** and **8**

	7	**8**
Formula	$C_{25}H_{30}Br_2N_4Sn$	$C_{25}H_{30}Br_2N_4Sn$
M_r	665.05	665.04
Crystal size (mm)	0.22×0.32×0.52	0.20×0.20×0.30
Crystal system	monoclinic	monoclinic
Space group	$P2_1$	$P2_1/c$
a (Å)	9.667(2)	9.376(1)
b (Å)	15.409(3)	17.368(4)
c (Å)	9.899(2)	16.928(4)
β (°)	115.66(3)	95.82(1)
V (Å^3)	1329(1)	2742.4(10)
Z	2	4
T (K)	299	293
λ (Mo Kα, Å)	0.71073	0.71069
No. reflections measured	2051	4776
No. reflections observed	1751($I \geq 3\sigma(I)$)	3263($I \geq 2.0\sigma(I)$)
No. parameters	288	290
Weighting scheme (w)	$[\sigma^2(F)+0.0001F^2]^{-1}$	$[\sigma^2(F_o)]^{-1}=4F_o^2[\sigma^2(F_o^2)]^{-1}$
Residuals R, R_w	0.044, 0.050	0.029, 0.033



Scheme 1. Compound **1**: **A**, R = C(CH$_3$)$_3$; compound **2**: **C**, R = CH(CH$_3$)$_2$; compound **3**: **B**, R = CH(CH$_3$)$_2$; compound **4**: **A**, R = CH(CH$_3$)$_2$.

steric hindrance is highest (54%), which reflects the characteristics of the isopropyl group [16]. The assignment of ^{1}H NMR spectra of the mixture is achieved by comparision with the ^{1}H NMR spectra of their adducts with $SnPh_2X_2$ (X = Cl, Br) and the crystal structures of their adducts.

3.2. Complexes with diphenyltin(IV) dihalides

Although ligand **1** has a bulky substituent in the 3-position of the pyrazole ring, its reaction with an equimolar amount of Ph_2SnX_2 (X = Cl, Br) in ether afforded 1:1 adducts compounds **5** and **6**. The two complexes were slightly soluble in petroleum ether, and soluble in polar organic solvents such as CH_2Cl_2 and acetone.

The pure isomers **A**, **B** and **C** were obtained by chromatography as described in the literature [23,24], which was time-consuming and resulted in some losses. In our work, the isomers **A**, **B** and **C**, where R = iPr, were easy isolated by taking advantage of the different solubility of their adducts with $SnPh_2X_2$ (X = Cl, Br) in petroleum ether (60–90°C). The reaction of the isomeric mixture with $SnPh_2Br_2$ in petroleum ether precipitated out the adduct of isomer **C** (complex **7**), while the adduct of isomer **B** (complex **8**) and the adduct of isomer **A** remained in solution. The pure complex **8** could be obtained from recrystallizing the mixture of complex **8** and the adduct of isomer **A** with $SnPh_2Br_2$ from dichloromethane–hexane. However, we could not obtain the pure adduct of isomer **A** by recrystallization due to its low yield and its similar solubility to that of complex **7**.

The ^{1}H NMR spectra of complexes **5**, **6**, **7** and **9** indicated that the two methylene protons are equivalent, as are the corresponding pyrazole protons. It may be possible that a fluxional behavior of rapid boat inversion through Sn–N bond breaking [12] could exist, owing to weak interactions between ligands and organotin(IV) (see Section 3.3). Since the pyrazole protons and isopropyl protons in complexes **8** and **10** are non-equivalent, two sets of signals for the pyrazole and isopropyl protons were observed. The ^{119}Sn NMR chemical shifts for complexes **5**, **7** and **8** occurred at −157.4, −83.4 and −85.0 ppm in $CDCl_3$, respectively. These data are comparable with those of related organotin derivatives of poly(pyrazol-1-yl)alkanes [10] and $SnPh_2Br_2$ (−72.9 ppm) determined under the same conditions, which showed that these complexes are also extensively dissociated in chloroform solution. The molar conductances of these complexes (Table 2) were found to be in the range of 4–8 Ω^{-1} cm^2 mol^{-1} in acetone, indicating that they are not electrolytic in acetone. However, all complexes are partly ionized in dimeth-

Table 2
Conductances of complexes **5**–**10**

Compound	Solvent	Concentration [a]	Λ [b]	Solvent	Concentration [a]	Λ [b]
5	Acetone	1.0	6.7	DMSO	1.0	38.5
6	Acetone	1.0	7.1	DMSO	1.0	23.9
6	Acetone	2.0	4.0	DMSO	2.0	17.5
7	Acetone	1.0	6.4	DMSO	1.0	39.4
7				DMSO	0.5	55.0
8	Acetone	1.0	6.1	DMSO	1.0	47.7
8				DMSO	0.5	77.1
9	Acetone	1.0	6.5	DMSO	1.0	25.7
10	Acetone	1.0	6.6	DMSO	1.0	26.6

[a] mol l^{-1} ($\times 10^{-3}$).
[b] Ω^{-1} cm^2 mol^{-1} at room temperature.

ylsulfoxide (DMSO) owing to the strong complexing ability of DMSO.

3.3. Crystal structures of complexes *7* and *8*

Selected distances and angles for complexes **7** and **8** are listed in Tables 3 and 4, respectively. The crystal structure of complex **7** is shown in Fig. 1 and that of complex **8** in Fig. 2; it is clear that the two isopropyl groups in complex **7** are in the 5- and 5′-positions of pyrazole rings, whereas in complex **8** one isopropyl group is in the 3-position of the pyrazole ring and the other in the 5′-position. The tin atoms in complexes **7** and **8** are six-coordinate with a distorted octahedral geometry, a *cis* arrangement of the bromine atoms and a *trans* arrangement of the phenyl groups. The six-membered Sn–N–N–C–N–N metallacycle in complex **7** adopts a slightly distorted boat conformation, which is similar to that in complex **8**.

Table 3
Selected bond lengths (Å) and angles (°) for compound **7**

Sn(1)–Br(1)	2.565(2)	Sn(1)–C(11)	2.143(16)
Sn(1)–Br(2)	2.631(10)	Sn(1)–C(21)	2.158(16)
Sn(1)–N(1)	2.421(8)	N(2)–C(1)	1.441(16)
Sn(1)–N(3)	2.448(11)	N(4)–C(1)	1.458(18)
Br(1)–Sn(1)–Br(2)	100.3(10)	Sn(1)–C(21)–C(22)	121.0(10)
Br(1)–Sn(1)–N(1)	90.6(2)	Sn(1)–C(21)–C(26)	120.0(12)
Br(2)–Sn(1)–N(1)	168.6(2)	Sn(1)–N(3)–N(4)	118.8(7)
Br(1)–Sn(1)–N(3)	168.1(2)	Sn(1)–N(3)–C(41)	123.3(9)
Br(2)–Sn(1)–N(3)	91.6(2)	N(2)–C(1)–N(4)	111.6(12)
N(1)–Sn(1)–N(3)	77.6(3)	Sn(1)–C(11)–C(12)	118.4(11)
Br(1)–Sn(1)–C(11)	94.4(3)	Sn(1)–C(11)–C(16)	120.5(10)
Br(2)–Sn(1)–C(11)	93.0(3)	N(3)–Sn(1)–C(21)	84.9(4)
N(1)–Sn(1)–C(11)	82.9(4)	C(11)–Sn(1)–C(21)	168.2(5)
N(3)–Sn(1)–C(11)	86.0(5)	Sn(1)–N(1)–N(2)	124.2(7)
Br(1)–Sn(1)–C(21)	93.0(3)	Sn(1)–N(1)–C(31)	126.6(8)
Br(2)–Sn(1)–C(21)	94.6(3)	N(1)–Sn(1)–C(21)	87.9(4)

Table 4
Selected bond lengths (Å) and angles (°) for compound **8**

Sn–Br(1)	2.6261(8)	Sn–Br(2)	2.6182(6)
Sn–N(1)	2.455(4)	Sn–N(3)	2.576(4)
Sn–C(14)	2.137(4)	Sn–C(20)	2.144(4)
N(4)–C(4)	1.433(6)	N(2)–C(4)	1.443(6)
Br(1)–Sn–Br(2)	94.68(2)	Br(1)–Sn–N(1)	89.32(9)
Br(1)–Sn–N(3)	167.02(9)	Br(1)–Sn–C(14)	94.9(10)
Br(1)–Sn–C(20)	93.5(10)	Br(2)–Sn–N(1)	175.57(9)
Br(2)–Sn–N(3)	98.14(9)	Br(2)–Sn–C(14)	94.1(10)
Br(2)–Sn–C(20)	96.6(10)	N(1)–Sn–N(3)	77.9(10)
N(1)–Sn–C(14)	83.7(10)	N(1)–Sn–C(20)	85.0(2)
N(3)–Sn–C(14)	86.2(10)	N(3)–Sn–C(20)	83.1(10)
C(14)–Sn–C(20)	165.8(2)	Sn–N(1)–N(2)	125.3(3)
Sn–N(1)–C(1)	126.7(3)	Sn–N(3)–N(4)	119.4(3)
Sn–N(3)–C(7)	131.3(3)	Sn–C(14)–C(19)	121.6(3)
N(2)–C(4)–N(4)	112.8(4)	Sn–C(20)–C(25)	123.1(4)
Sn–C(14)–C(15)	120.4(3)	Sn–C(20)–C(21)	118.3(3)

It is of interest that the two phenyl groups in complexes **7** and **8** bend towards bis(pyrazol-1-yl)methane ligands owing to the repulsion between phenyl groups, bromine atoms and bis(pyrazol-1-yl)methane, and the stronger repulsion of bromine atoms than that of bis(pyrazol-1-yl)methane ligand. The two phenyl planes form a dihedral angle of 104.4° in complex **7** and 91.6° in complex **8**.

Although the angles ∠N–Sn–N and ∠C–Sn–C in complex **7** [∠N(1)–Sn(1)–N(3) = 77.6(3)° and ∠C(21)–Sn(1)–C(11) = 168.2(5)°, respectively] are similar to those in complex **8** [∠N1–Sn–N3 = 77.9(10)°, ∠C14–Sn–C20 = 165.8(2)°], the angles ∠Br–Sn–Br and ∠N1–Sn–Br2 are quite different. The angle ∠Br–Sn–Br in complex **7** (100.3(10)°) is larger than that in complex **8** [94.68(2)°] and the angle ∠N1–Sn–Br2 in complex **7** [168.6(7)°] is smaller than that in complex **8** [175.57(9)°]. It seems that the isopropyl group in the 3-position of the pyrazole ring is responsible for these. The isopropyl group increases the repulsion of phenyl groups in complex **8** and ligand **3** so that the phenyl group (composed of C20, C21, C22, C23, C24, C25) is pushed out to Br2, which leads to increased repulsion between the phenyl group and Br2, making Br2 bend towards Br1. Thus, the angle ∠Br–Sn–Br in complex **8** decreases and the angle ∠N1–Sn–Br2 increases, compared with those in complex **7**. The Sn–C distances are 2.158(16) and 2.143(16) Å in complex **7** and 2.144(4) and 2.137(4) Å in complex **8**, which are within the normal range for such bonds [10]. The average Sn–N distance in complex **7** (2.435 Å) is similar to that in $CH_2(4\text{-MePz})_2SnMe_2Cl_2$ (2.436 Å) [10]. However, the average Sn–N distance in complex **8** is 2.52 Å and con-

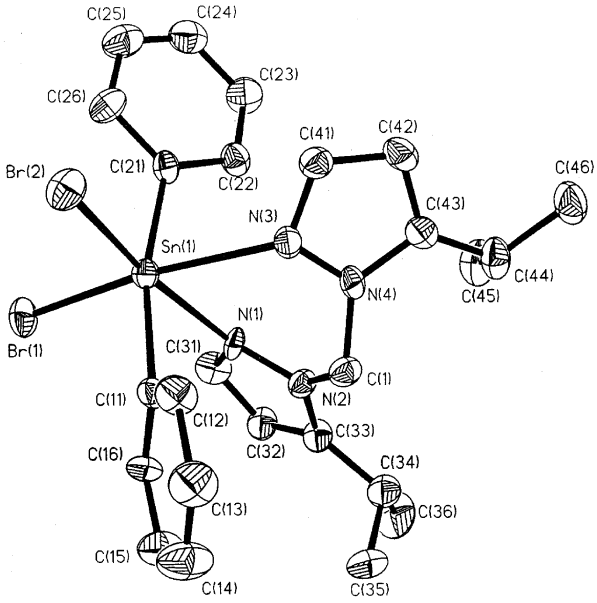


Fig. 1. The molecular structure of compound **7**.

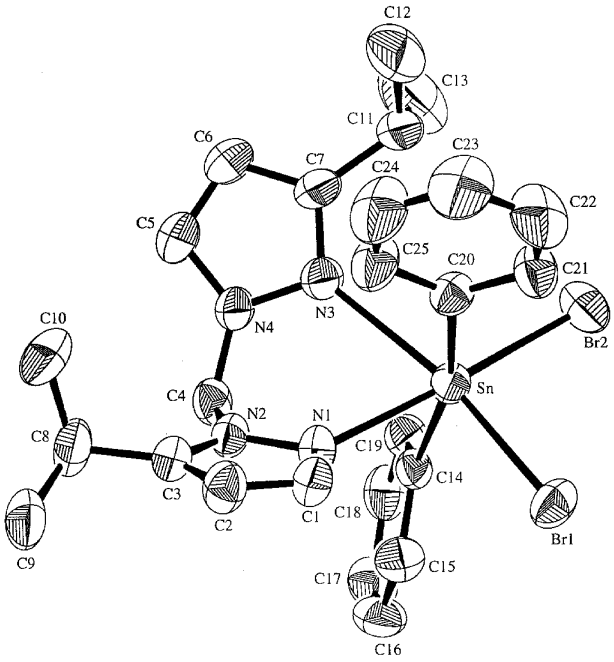


Fig. 2. The molecular structure of compound **8**.

siderably longer than that in complex **7** due to the isopropyl group in the 3-position of the pyrazole ring weakening the interactions between ligand **3** and organotin acceptors.

In conclusion, the bulky substituents in the 3- or 5-position of the pyrazole ring significantly affect the structures of organotin derivatives of poly(pyrazol-1-yl)alkanes. The steric hindrance of substituents reduces the interactions of poly(pyrazol-1-yl)alkanes with organotin acceptors. The Sn–N bonds in complexes **7** and **8** are found to be remarkably longer than the values in the antitumor active compounds [10].

Supplementary data

Atomic coordinates, thermal parameters and bond lengths and angles for complexes **7** and **8** have been deposited at the Cambridge Crystallographic Data Centre (CCDC). Any request to the CCDC for this material should quote the full literature citation and the reference numbers CCDC 114184 and CCDC 114185.

Acknowledgements

This work was supported by the National Natural Science Foundation of China (No. 29902002 and No. 29572055) and the Key Laboratory of Organometallic Chemistry, Shanghai Institute of Organic Chemistry, Chinese Academy of Sciences.

References

[1] A.J. Crowe, P.J. Smith, G. Atassi, Chem. Biol. Interact. 32 (1980) 171.
[2] A.J. Crowe, P.J. Smith, G. Atassi, Inorg. Chim. Acta 93 (1984) 179.
[3] A.K. Saxena, F. Huber, Coord. Chem. Rev. 95 (1989) 109.
[4] P.G. Sammes, G. Yahioglu, Chem. Soc. Rev. (1994) 327.
[5] A. Bengtson, N.K. Goh, A. Hazell, L.E. Khoo, J. Ouyang, K.R. Pedersen, Acta Chem. Scand. 50 (1996) 1020.
[6] J.T. Wang, Y.W. Zhang, Y.M. Xu, Z.W. Wang, Heteroatom Chem. 3 (1992) 599.
[7] J.T. Wang, X.P. Yang, J.P. Cheng, Y.M. Xu, B. Liu, H.G. Wang, D.K. Zhang, J. Chem. Soc., Dalton Trans. (1996) 3889.
[8] J.T. Wang, F.Q. Liu, Y.W. Zhang, R.J. Wang, H.G. Wang, X.K. Yao, J. Organomet. Chem. 375 (1989) 173.
[9] J.T. Wang, Y.W. Zhang, Y.M. Xu, Z.W. Wang, Heteroatom Chem. 6 (1995) 443.
[10] C. Pettinari, A. Lorenzotti, G. Sclavi, A. Cingolani, E. Rivarola, M. Colapietro, A. Cassetta, J. Organomet. Chem. 496 (1995) 69.
[11] G.G. Lobbia, F. Bonati, A. Cingolani, D. Leonesi, A. Lorenzotti, J. Organomet. Chem. 359 (1989) 21.
[12] G.G. Lobbia, A. Cingolani, D. Leonesi, A. Lorenzotti, F. Bonati, Inorg. Chim. Acta 130 (1987) 203.
[13] R. Visalakshi, V.K. Jain, S.K. Kulshreshtha, G.S. Rao, Inorg. Chim. Acta 118 (1986) 119.
[14] C. Pettinari, A. Lorenzotti, M. Pellei, C. Santini, Polyhedron 16 (1997) 3435.
[15] S. Trofimenko, J.C. Calabrese, J.S. Thompson, Inorg. Chem. 26 (1987) 4507.
[16] S. Trofimenko, J.C. Calabrese, P.J. Domaille, J.S. Thompson, Inorg. Chem. 28 (1989) 1091.
[17] N. Walker, D. Stuart, Acta Crystallogr., Sect. A 39 (1983) 158.
[18] SDP-PLUS, B.A. Frenz & Associates, Inc., College Station, TX, and Enraf-Nonius, Delft, The Netherlands, 1982.
[19] SDP Structure Determination Package, Enraf-Nonius, Delft, 1985.
[20] G.M. Sheldrick, SHELXS 86, G. Sheldrick, M.C. Kruger, R. Goddard, Crystallographic Computing 3, 1985, 175 Oxford University Press, Oxford.

[21] P.T. Beurskens, G. Admiraal, G. Beurskens, W.P. Bosman, S. Garcia-Granda, R.O. Gould, J.M.M. Smits, C. Smykalla, DIRDIF92: The DIRDIF Program System, Technical Report of the Crystallography Laboratory, University of Nijmegen, The Netherlands, 1992.
[22] teXsan, Crystals Structures Analysis Package, Molecular Structure Corporation, 1985 and 1992.
[23] S. Julia, P. Sala, J. Mazo, M. Sancho, C. Ochoa, J. Elguero, J.P. Fayet, M.C. Vertut, J. Heterocycl. Chem. 19 (1982) 1141.
[24] R.M. Claramunt, H. Hernandez, J. Elguero, S. Julia, Bull. Soc. Chem. Fr. 2 (1983) 5.
[25] K. Mann, L.V. Jeffery, J.C. McCleverty, J.A.P. Thornton, M.D. Ward, J. Chem. Soc., Dalton Trans. (1998) 89.

PERGAMON

www.elsevier.nl/locate/poly

Polyhedron 19 (2000) 389–397

POLYHEDRON

The electronic structure of planar phosphazene rings

Martin Breza *

Department of Physical Chemistry, Slovak Technical University, SK-812 37 Bratislava, Slovakia

Received 2 August 1999; accepted 22 November 1999

Dedicated to Professor Peter Pelikán on the occasion of his 60th birthday.

Abstract

Using a standard ab initio method, the electronic structure and optimal geometries of cyclo-$(NPX_2)_n$ ($n=2$, 3, 4 and X = H, F, Cl) have been investigated using the DZP basis set. The out-of-plane π bonds as well as the in-plane π' bonds in phosphazenes are dominated by p orbitals, although the bonding interaction between p orbitals on N atoms and d orbitals on P atoms is symmetrically forbidden in rings of D_{nh} symmetry with odd n only. In-plane π' and σ bonds in cyclic planar phosphazenes can be distinguished using Mulliken population analysis of cylindrical atomic orbitals. The d functions on P atoms do not correspond to their d orbitals and can be explained as polarization functions only. ©2000 Elsevier Science Ltd All rights reserved.

Keywords: Ab initio methods; Cyclic phosphazenes; Electronic structures; Group theory

1. Introduction

The phosphazene backbone formally consists of alternating single and double P–N bonds. The electronic structure of phosphazenes has been the subject of much controversy, but the generally accepted 'island model' [1] supposes that the σ bonds in the phosphazenes are formed by sp^3 hybrid orbitals of phosphorus. Out-of-plane π bonds are formed by the nitrogen p_z orbital, the adjacent phosphorus d_{xz} and d_{yz} orbitals being combined into sets of three-centre π molecular orbitals (MOs) which overlap only weakly with one another. The break in conjugation at each phosphorus atom implies that adjacent three-centre π bonds need not be coplanar and that the cyclic phosphazenes are not aromatic. A second set of delocalized electrons that occupy MOs symmetric to reflection in the molecular plane (d_{xy} and $d_{x^2-y^2}$ orbitals on P atoms, p_x and p_y orbitals on N atoms), but which are otherwise generally similar to the MO concerned in π delocalization, is referred to as in-plane π' bonding [2].

The importance of the d orbitals of the central atoms of the main group for bonding in hypervalent tetracoordinate species [3] has been questioned and makes the above model doubtful. Moreover, claims of dsp^3 or d^2sp^3 hybridization in such species are misleading. The d orbitals on the central atom play only a secondary role in π bonding, which occurs mainly through negative hyperconjugation. Using energy criteria (a correlation extra energy per valence shell electron pair) it has been shown [4] that the d functions of the main group elements act as polarizing and correlating functions only.

The above statements cannot assume that the d functions are unnecessary. Many authors have shown their importance for the exact description of the geometry and electronic structure of phosphazenes using various semi-empirical and ab initio treatments [5–18]. It can be concluded that the d orbital must be described using d functions, but that not all d functions describe d orbitals. In the latter sense they improve the flexibility of the incomplete s and p basis sets only.

The most common subjects of theoretical studies are small cyclic phosphazenes (Fig. 1) with planar phosphazene rings of D_{nh} symmetry (despite the fact that IR spectra in vapour and in solution [19] indicate non-vanishing deviations from ring planarity for $n>3$). Ab initio methods [13–18] using good basis sets are able to reproduce the experimental structure data [20–24] satisfactorily (Table 1). The charge distribution is best described as a zwitterionic form because there is a significant amount of charge accumulation on the ring nitrogen. An experimental electron density map was in agreement with the classical 'island' model [25]. Contrary to out-

0277-5387/00/$ - see front matter ©2000 Elsevier Science Ltd All rights reserved.
PII S0277-5387(99)00368-X

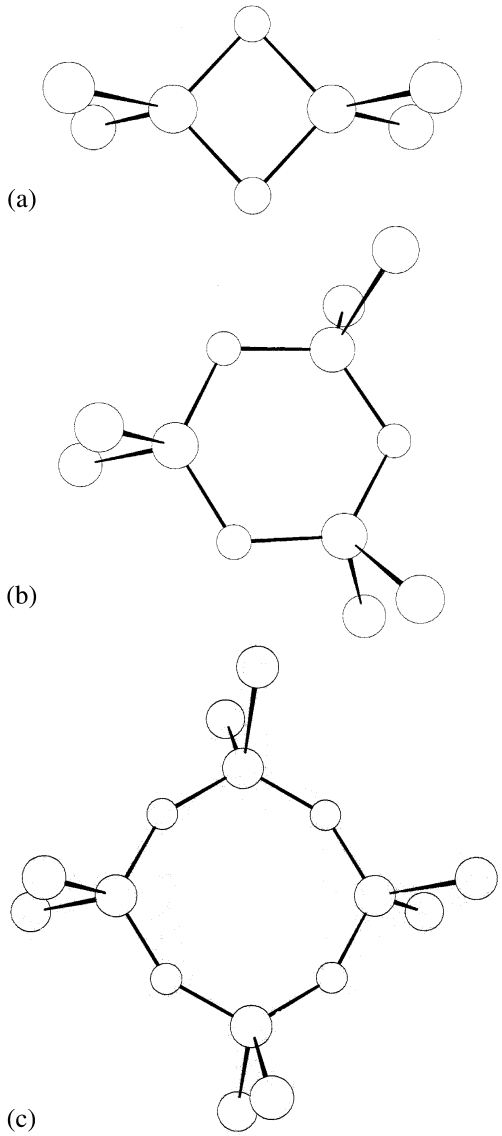


Fig. 1. Molecular structure of planar cyclo-$(NPX_2)_2$ (a), cyclo-$(NPX_2)_3$ (b) and cyclo-$(NPX_2)_4$ (c).

of-plane π bonds (antisymmetric to the ring plane), group theoretical treatment cannot distinguish between in-plane π′ and σ bonds. An attempt to estimate the π′ bond order was based on the d electron population on P atoms [17].

The aim of our present study was a critical reinvestigation of the classical picture of the bonding of phosphazenes in the light of recent ideas of the role of d functions. Using more complex group theoretical analysis accompanied by ab initio calculations, we have attempted to distinguish between in-plane π′ and σ bonds.

2. Group theoretical analysis

The geometry of planar cyclic phosphazenes (Fig. 1) is described by D_{nh} symmetry point groups. The plane of the phosphazene ring is usually denoted as a σ_{xy} or σ_h mirror

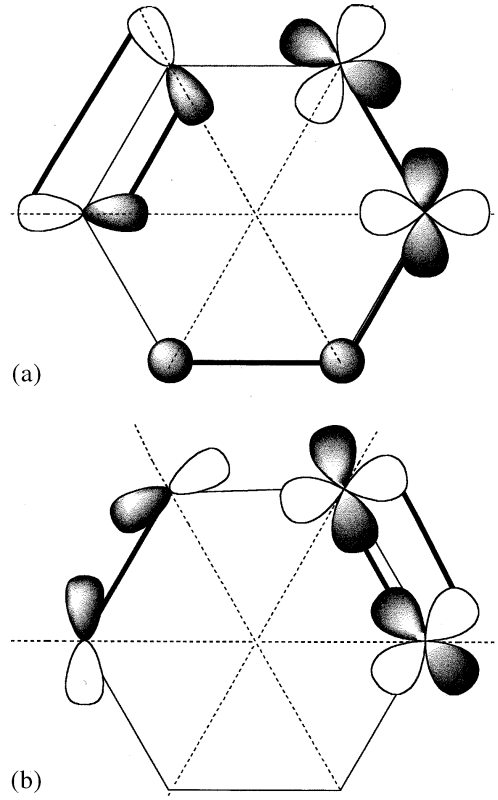


Fig. 2. In-plane bonding in six-membered rings: (a) (from bottom clockwise) σ bonding s–s, non-bonding s–p_r, in-plane π′ bonding p_r–p_r, non–bonding p_r–d_{hr}, σ bonding d_{hr}–d_{hr} and σ bonding d_{hr}–s interactions; (b) σ bonding p_τ–p_τ, non-bonding p_τ–$d_{h\tau}$ and in-plane π′ bonding $d_{h\tau}$–$d_{h\tau}$ interactions.

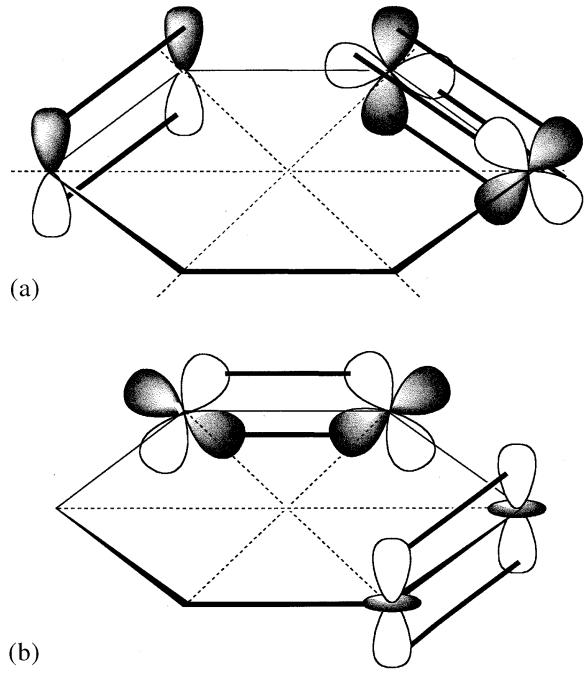


Fig. 3. Out-of-plane π bonding in six-membered rings: (a) bonding p_z–p_z, non-bonding p_z–d_{zr} and bonding d_{zr}–d_{zr} interactions; (b) bonding $d_{z\tau}$–$d_{z\tau}$, non-bonding d_{zt}–d_{z^2} and bonding $d_{z^2-z^2}$ interactions.

plane. The principal symmetry axis and couples of opposite P and/or N atoms define *n* vertical σ_v planes (perpendicular to σ_h planes). In order to describe the bonding ability of individual atomic orbitals (AOs), we have introduced a non-planar tangential τ surface that contains all the ring atoms and is perpendicular to the σ_h and all σ_v mirror planes. This surface shape is something between a cylindrical and *n*-gonal prismatic one; in the atom areas it is tangential to the σ_v planes and between them corresponds to the symmetry plane (perpendicular to σ_h) of the P–N bond. It can be thought of simply as a prismatic surface with (infinitesimally) rounded edges.

For our purposes, it is advantageous to use the cylindrical coordinate system with an origin at the centre of the ring instead of the Cartesian system. As the *z*-axis is equivalent to the principal axis, the AOs of s, p_z and d_{z^2} types are the same in both coordinate systems. Using simple coordinate transformations, the couples of p_x and p_y orbitals are converted into radial p_r and tangential p_τ AOs (see Fig. 2) in the σ_h mirror plane. Analogously, the $d_{x^2-y^2}$ and d_{xy} orbitals in the σ_h plane are transformed into radial d_{hr} and tangential $d_{h\tau}$ orbitals. The remaining d_{xz} and d_{yz} orbitals perpendicular to σ_h are converted into radial d_{zr} and tangential $d_{z\tau}$ orbitals (Fig. 3).

In the linear combination of AOs treatment, the MOs are constructed as symmetry-adapted linear combinations of individual AOs. According to the group theoretical rules, only orbitals with the same symmetry species can contribute to chemical bonding [26]. This means that all AOs in the same MO must be either symmmetric or antisymmetric under the same symmetry operation.

The symmetry properties relating to σ_h and τ elements are crucial for ring P–N bonding. The AOs on the adjacent atoms must be of the same symmetry defined by these elements, otherwise the bonding interactions cannot be formed. Consequently, these orbitals can be grouped as follows (see Table 2 and Figs. 2 and 3):

Table 1
Selected structure data of cyclo-$(NPX_2)_n$

n	X	Distance (10^{-10} m)		Angle (°)			Comments
		P–N	P–X	P–N–P	N–P–N	X–P–X	
2	H	1.840	1.420	86.8	93.2	103.1	DZ basis set [14] [a]
		1.650	1.405	85.8	94.2	101.2	DZd(P,N) basis set [14] [a]
		1.636	1.394	85.0	95.0	101.4	DZP basis set
	F	1.608	1.526	83.7	96.3	98.3	DZP basis set
	Cl	1.623	1.996	84.3	95.7	102.7	DZP basis set
3	H	1.724	1.419	119.8	120.2	103.1	DZ basis set [14] [a]
		1.610	1.401	126.5 (123.6 [b])	113.5 (116.4 [b])	101.2	DZd(P) basis set [14] [a]
		1.597	1.392	123.7	116.6	101.5	DZP basis set [18]
	F	1.560	1.546	127.2	112.8	99.1	6-31G* basis set [13]
		1.557	1.503	123.3	116.7	99.2	LP-21G*$^+$ basis set [16] [a]
		1.574	1.578	122.1	117.9	98.1	LP-31G* basis set [16] [a]
		1.557	1.533	126.8	113.2	99.1	3-21G* basis set [16]
		1.568	1.543	123.2	116.8	98.6	DZP basis set [17]
		1.568	1.529	123.5	116.5	98.7	DZP basis set [18]
		1.570(13)	1.529(4)	120.4(8)	119.6(1)	99.1(1)	[20] [c]
	Cl	1.582	2.008	123.6	116.4	102.4	DZP basis set [17]
		1.579	2.003	123.9	116.1	102.5	DZP basis set [18]
		1.627	2.067	123.1	116.9	102.1	DZ basis set [18]
		1.569	2.001	123.4	116.6	102.1	DZP2d(P) basis set [18]
		1.581(5)	1.993(5)	121.4(2)	118.4(1)	101.4(2)	[21] [c]
4	H	1.576	1.392	148.3	121.7	101.6	DZP basis set
	F	1.538	1.506	148.6	121.4	99.3	LP-21G* basis set [16] [a]
		1.556	1.581	147.0	123.0	98.7	LP-31G* basis set [16] [a]
		1.534	1.536	152.5	117.5	99.2	3-21G* basis set [16]
		1.547	1.533	149.0	121.0	99.3	DZP basis set
		1.507(15)	1.514(15)	147.2(10)	122.7(10)	99.9(10)	[22] [c]
	Cl	1.555	2.010	149.8	120.2	102.8	DZP basis set
		1.570(9)	1.985(4) 1.993(4)	131.3(6)	121.2(4)	102.8(4)	non-planar K-form [23] [c]
		1.559(12)	1.992(4)	133.6(8) 137.6(8)	120.5(7)	103.1(2)	non-planar T-form [24] [c]

[a] Pseudo-potential calculation.
[b] DZd(P,N) basis set.
[c] Monocrystal X-ray structure data.

Table 2
Symmetry description of cylindrical atomic orbitals (see Figs. 2 and 3)

Atomic orbital	Character value			Cartesian analogs	Specification
	τ	σ_h	$n\sigma_v$		
S	+1	+1	+1	s	
P_r	−1	+1	+1	(p_x, p_y)	principal axis in σ_v, nodal plane $\equiv\tau$
p_τ	+1	+1	−1	(p_x, p_y)	nodal plane $\equiv\sigma_v$, principal axis in τ
P_z	+1	−1	+1	p_z	
d_{hr}	+1	+1	+1	($d_{x^2-y^2}$, d_{xy})	two lobes in σ_v, two lobes in τ
$d_{h\tau}$	−1	+1	−1	($d_{x^2-y^2}$, d_{xy})	one nodal plane $\equiv\sigma_v$, one nodal plane $\equiv\tau$
d_{zr}	−1	−1	+1	(d_{xz}, d_{yz})	four lobes in σ_v, one nodal plane $\equiv\tau$
$d_{z\tau}$	+1	−1	−1	(d_{xz}, d_{yz})	one nodal plane $\equiv\sigma_v$, four lobes in τ
d_{z^2}	+1	+1	+1	d_{z^2}	

1. Bonds can be formed by s, p_τ and/or d_{hr} orbitals that are both σ_h and τ symmetric. They are situated in the σ_h plane, contrary to d_{z^2} orbitals which might contribute to the out-of-plane π interactions only (in-plane s–d_{z^2} bonds vanish due to the ring-shaped nodal surface of the d_{z^2} orbitals).
2. In-plane π' bonds can be formed by p_r and/or $d_{h\tau}$ orbitals which are σ_h symmetric and τ antisymmetric.
3. Out-of-plane π bonds can be formed by p_z and/or $d_{z\tau}$ orbitals that are σ_h antisymmetric and τ symmetric.
4. Another set of out-of-plane π bonds might be formed by d_{zr} orbitals that are both σ_h and τ antisymmetric.

As no d orbitals on N atoms are assumed, further simplifications can be concluded:

1. Simple σ bonds can originate in s(P)–s(N), s(P)–p_τ(N), p_τ(P)–s(N), p_τ(P)–p_τ(N), d_{hr}(P)–s(N) and d_{hr}(P)–p_τ(N) orbital interactions only.
2. In-plane π' bonds can originate in p_r(P)–p_r(N) and $d_{h\tau}$(P)–p_r(N) orbital interactions only.
3. Out-of-plane π bonds can originate in p_z(P)–p_z(N) and $d_{z\tau}$(P)–p_z(N) orbital interactions only.

In phosphazene rings of D_{nh} symmetry with odd n, the opposite P and N atoms are situated in the same σ_v mirror planes. Because all atoms of the same type are equivalent, the AOs located on the neighbouring atoms must be either σ_v symmetric or antisymmetric to form the bond. This additional condition (Table 2) causes further reduction of bonding patterns.

Possible N–P bonding interactions in the phosphazene ring may be exclusively of s(P)–s(N), p_τ(P)–p_τ(N) and s(N)–d_{hr}(P) of σ type, p_z(P)–p_z(N) of out-of-plane π type and p_r(P)–p_r(N) of in-plane π' type. These results indicate that the π and the π' bonding between p orbitals on N atoms and d orbitals on P atoms is symmetry forbidden in D_{nh} phosphazene rings with odd n. This statement can also be generalized to all non-phosphazene rings of D_{nh} symmetry with odd n.

The analogous statement on the π or π' bonding between p orbitals on N atoms and d orbitals on P atoms for D_{nh} phosphazene rings with even n cannot be deduced by symmetry arguments. We can verify it only by numerical calculations (see Section 4).

3. Method of calculation

Ab initio molecular orbital calculations of planar cyclo-$(NPX_2)_n$ molecules with $n = 2$, 3, 4 and X = H, F, Cl were performed using a standard HONDO-type [27] computer program within the standard DZP basis set from the HONDO library [27]. For H atoms, a single p function with exponent of 1.0 has been added to the contracted (4s)/[2s] basis set. Single d functions with exponents equal to 0.8 and 0.9 were added to the contracted (9s5p)/[3s2p] basis sets for N and F atoms, respectively. Similarly, the exponents equal to 0.5 and 0.65 were used for additional d functions to the contracted (11s7p)/[6s4p] basis sets for P and Cl atoms, respectively [27].

The geometries of all the systems were optimized within D_{nh} symmetry (see Table 1 and Fig. 1). Electronic structure was evaluated in terms of Mulliken population analysis (MPA; gross or net atomic charges for atoms and overlap populations for bonds) as well as in terms of Roby–Davidson–Heinzmann–Ahlrichs population analysis based on occupation numbers (PABON; atomic charges with multicentre corrections for atoms and shared electron numbers for bonds) [28,29].

4. Results and discussion

The influence of ligand variation on the properties of phosphazenes has been the subject of several theoretical studies [5–18]. Comparison of our results (Tables 1 and 3–5) with optimal geometries calculated using DZ basis sets confirms the necessity of using polarization functions. Neglecting them causes deviations from the experimental data in bond lengths up to 10^{-11} m and in bond angles up to 5°. Use of DZP basis sets gives discrepancies one order lower (Table 1). Inclusion of diffuse functions may slightly change the results for very electronegative atoms. The basis set effect has been studied elsewhere [18]. Nevertheless, it must be mentioned that the symmetry of the experimental structures [20–24] is lower than D_{nh} due to solid state effects (deviations of ca. 10^{-12}

Table 3
Electronic structure data of cyclo-$(NPX_2)_2$

X	MPA			PABON		
	H	F	Cl	H	F	Cl
	Charges			Charges		
N	−0.898	−0.880	−0.779	−0.961	−0.917	−0.901
P	0.978	1.701	1.294	1.157	1.743	1.285
X	−0.040	−0.410	−0.175	−0.098	−0.413	−0.192
	Formal d electron population					
P(d)	0.453	0.678	0.552			
	Overlap populations			Shared electron numbers		
N–P a_g ($\sigma+\pi'$)	0.182	0.180	0.155	0.744	0.752	0.750
b_{1g} (σ)	0.181	0.182	0.171	0.259	0.250	0.239
b_{2g} (π)	0.041	0.045	0.044	−0.051	−0.052	−0.056
b_{3g} (−)	0.001	0.000	0.000	−0.038	−0.022	−0.031
a_u (−)	0.000	0.000	0.000	0.000	0.000	0.000
b_{1u} (π)	0.155	0.162	0.172	0.172	0.218	0.216
b_{2u} (σ)	0.157	0.196	0.175	0.106	0.120	0.097
b_{3u} ($\sigma+\pi'$)	0.186	0.199	0.167	0.190	0.157	0.149
Total	0.903	0.964	0.885	1.382	1.423	1.362
P–X	0.699	0.584	0.613	1.184	0.793	0.933
P–P	−0.369	−0.227	−0.367	0.182	0.260	0.251
N–N	−0.309	−0.318	−0.307	−0.023	−0.029	−0.027

Table 4
Electronic structure data of cyclo-$(NPX_2)_3$

X	MPA			PABON		
	H	F	Cl	H	F	Cl
	Charges			Charges		
N	−0.989	−0.992	−0.859	−1.038	−0.986	−0.951
P	1.069	1.821	1.218	1.224	1.816	1.338
X	−0.040	−0.413	−0.180	−0.093	−0.414	−0.194
	Formal d electron population					
P(d)	0.458	0.668	0.557			
	Overlap populations			Shared electron numbers		
N–P a_1' ($\sigma+\pi'$)	0.110	0.132	0.109	0.400	0.430	0.402
a_2' (σ)	0.126	0.123	0.111	0.189	0.191	0.164
e′ ($\sigma+\pi'$)	0.310	0.316	0.269	0.441	0.398	0.448
e′ (σ)	0.184	0.268	0.218	0.294	0.306	0.263
a_1''(−)	0.000	0.000	0.000	0.000	0.000	0.000
a_2''(π)	0.099	0.102	0.110	0.122	0.128	0.147
e″ (π)	0.084	0.115	0.115	0.001	0.021	0.017
e″ (−)	0.001	0.001	0.001	−0.045	−0.027	−0.040
Total	0.914	1.056	0.933	1.403	1.447	1.401
P–X	0.765	0.605	0.672	1.218	0.820	0.953
P–P	−0.079	−0.064	−0.084	0.017	0.055	0.037
N–N	−0.128	−0.138	0.018			

m). Moreover, both forms of cyclo-$(NPCl_2)_4$ exhibit significant deviations from planarity (up to 0.4×10^{-10} m) that might be of intrinsic origin [19,23,24]. However, the planarity of model systems is necessary for group theoretical analysis of π bonding. According to our results for the series of planar cyclo-$(NPX_2)_n$ molecules, the P–N bond length decreases with increasing *n* (due to a decrease in ring strain) compared with the nearly constant P–X bond lengths and X–P–X bond angles. These trends are in agreement with experimental data [20–24].

Electronic structure data such as charges on X and P atoms or P–X bond strength are ordered according to the electronegativity of the X ligands (Tables 3–5). The values of the remaining parameters are complex functions of the size (or

Table 5
Electronic structure data of cyclo-$(NPX_2)_4$

X	MPA			PABON		
	H	F	Cl	H	F	Cl
	Charges			Charges		
N	−1.023	−1.074	−0.922	−1.058	−0.999	−0.962
P	1.116	1.912	1.303	1.243	1.804	1.356
X	−0.046	−0.419	−0.190	0.092	−0.402	−0.197
	Formal d electron population					
P(d)	0.478	0.679	0.576			
	Overlap populations			Shared electron numbers		
N–P a_{1g} ($\sigma+\pi'$)	0.081	0.113	0.089	0.241	0.266	0.242
a_{2g} (σ)	0.096	0.097	0.088	0.138	0.138	0.108
b_{1g} (σ)	0.061	0.104	0.083	0.145	0.146	0.144
b_{2g} ($\sigma+\pi'$)	0.104	0.088	0.080	0.149	0.136	0.167
e_g (π)	0.070	0.102	0.099	0.065	0.073	0.088
e_g (−)	0.001	0.000	0.001	−0.029	−0.021	−0.029
a_{1u} (−)	0.000	0.000	0.000	0.000	0.000	0.000
a_{2u} (π)	0.064	0.068	0.073	0.089	0.080	0.104
b_{1u} (π')	0.027	0.029	0.030	−0.028	−0.020	−0.028
b_{2u} (−)	0.001	0.000	0.001	−0.022	−0.011	−0.018
e_u (σ)	0.203	0.174	0.152	0.280	0.266	0.267
e_u ($\sigma+\pi'$)	0.150	0.246	0.190	0.369	0.387	0.362
Total	0.858	1.021	0.886	1.398	1.439	1.406
P–X	0.801	0.612	0.702	1.225	0.852	0.956
P–P	−0.067	−0.059	−0.088	−0.013		
N–N	−0.116	−0.122	−0.123	−0.010	−0.010	−0.010

Table 6
Cylindrical AO contributions (gross Mulliken populations) to molecular orbitals of cyclo-$(NPX_2)_2$

X		s(N)	s(P)	p_r(N)	p_r(P)	p_τ(N)	p_τ(P)	d_{hr}(P)	$d_{h\tau}$(P)
H	a_g ($\sigma+\pi'$)	1.88 (1.88) [a]	2.58	0.62 (0.42)	1.45			0.05	
	b_{1g} (σ)					0.55	1.43		0.02
	b_{2u} (σ)		2.64		1.33	0.51		0.06	
	b_{3u}($\sigma+\pi'$)	1.83 (1.75)		0.85 (0.90)			1.23		0.08
F	a_g ($\sigma+\pi'$)	1.88 (1.89)	2.38	0.59 (0.39)	1.36			0.08	
	b_{1g} (σ)					0.59	1.42		0.04
	b_{2u} (σ)		2.47		1.18	0.52		0.08	
	b_{3u}($\sigma+\pi'$)	1.83 (1.75)		0.84 (0.86)			1.28		0.12
Cl	a_g ($\sigma+\pi'$)	1.89 (1.92)	2.49	0.59 (0.40)	1.44			0.06	
	b_{1g} (σ)					0.54	1.49		0.03
	b_{2u} (σ)		2.60		1.26	0.48		0.06	
	b_{3u} ($\sigma+\pi'$)	1.84 (1.79)		0.84 (0.87)			1.31		0.10
		p_z(N)	p_z(P)	d_{zr}(P)	$d_{z\tau}$(P)	d_{z^2}(P)			
H	a_g (−)					0.01			
	b_{2g} (π)	0.94 (0.96)			0.06				
	b_{3g} (−)		1.40	0.04					
	b_{1u} (π)	0.68	1.52	0.13					
F	a_g (−)					0.02			
	b_{2g} (π)	0.93 (0.96)			0.08				
	b_{3g} (−)		1.16	0.06					
	b_{1u} (π)	0.66	1.38	0.15					
Cl	a_g (−)					0.02			
	b_{2g} (π)	0.93 (0.95)			0.07				
	b_{3g} (−)		1.25	0.04					
	b_{1u} (π)	0.63	1.48	0.13					

[a] Numbers in parentheses correspond to net Mulliken populations.

Table 7
Cylindrical AO contributions (gross Mulliken populations) to molecular orbitals of cyclo-$(NPX_2)_3$

X		s(N)	s(P)	p_r(N)	p_r(P)	p_τ(N)	p_τ(P)	d_{hr}(P)	$d_{h\tau}$(P)
H	a_1' ($\sigma+\pi'$)	1.23 (1.24) [a]	1.68	0.47 (0.32)	0.95			0.04	
	a_2' (σ)					0.39	0.93		0.01
	e′ ($\sigma+\pi'$)	2.39 (2.25)	3.50	1.12 (1.12)	1.83			0.08	
	e′ (σ)					0.69	1.69		0.09
F	a_1' ($\sigma+\pi'$)	1.22 (1.20)	1.55	0.46 (0.31)	0.89			0.07	
	a_2' (σ)					0.40	0.93		0.03
	e′ ($\sigma+\pi'$)	2.40 (2.25)	3.21	1.10 (1.08)	1.68			0.12	
	e′ (σ)					0.73	1.72		0.12
Cl	a_1' ($\sigma+\pi'$)	1.24 (1.24)	1.61	0.46 (0.31)	0.95			0.05	
	a_2' (σ)					0.36	0.99		0.03
	e′ ($\sigma+\pi'$)	2.39 (2.33)	3.38	1.10 (1.09)	1.79			0.10	
	e′ (σ)					0.68	1.78		0.11
		p_z(N)	p_z(P)	d_{zr}(P)	$d_{z\tau}$(P)	d_{z^2}(P)			
H	a_1' (−)					0.01			
	e′ (−)					0.01			
	a_2'' (π)	0.48	1.00	0.07					
	e″ (π)	1.19	1.90	0.08					
	e″ (−)				0.07				
F	a_1' (−)					0.02			
	e′ (−)					0.03			
	a_2'' (π)	0.48	0.91	0.08					
	e″ (π)	1.17	1.62	0.10					
	e″ (−)				0.09				
Cl	a_1' (−)					0.02			
	e′ (−)					0.03			
	a_2'' (π)	0.45	0.98	0.07					
	e″ (π)	1.16	1.75	0.08					
	e″ (−)				0.08				

[a] Numbers in parentheses correspond to net Mulliken populations.

proton number) and the electronegativity of these ligands (cf. [11]). Only P atoms possess non-vanishing formal d electron populations. Intra-ring P–P and N–N interactions are vanishing or antibonding (as implied by MPA).

Group theoretical analysis shows that there is no bonding between d orbitals on P atoms and p orbitals on N atoms in cyclic phosphazenes of D_{nh} symmetry with odd n. Consequently, in-plane π' bond order cannot be estimated using the formal d electron population on P atoms as in Ref. [17]. The possibility to extend these conclusions to all D_{nh} rings is tested by ab initio calculations and the results are compared in Tables 6–8 ($n=2$, 3 and 4). Our results show that d_{hr} functions are always included in the same MOs as the s and p_r functions. The same holds for $d_{h\tau}$ and p_τ as well as for d_{zr} and p_z. As these polarization d functions do not describe d orbitals, they might be understood as flexibility complements to corresponding s and/or p orbitals. Moreover, the out-of-plane π bonding between p_z(N) and d_{zr}(P) AOs is forbidden due to their different symmetry to the τ surface. The same holds for in-plane bonding between p_r(N) and d_{hr}(P) as well as p_τ(N) and $d_{h\tau}$(P) AOs (Table 9). Analogously, a polarization d_{z^2} function might represent the out-of-plane flexibility complement to σ bonds as its symmetry does not allow any bonding interactions within phosphazene rings. The problem of interpretation arises for a $d_{z\tau}$ function without any symmetry counterpart among s and p orbitals of P atoms.

The analysis of phosphazene MOs by bonding type is based on the symmetry properties of individual AOs (deduced from gross orbital populations of MPA). As N atoms are bonded only to P atoms, the difference between gross and net orbital populations on nitrogens (proportional to P–N overlap population) may be helpful to deduce the relative strength of in-plane π' and σ bonds within MOs of the same symmetry.

In cyclo-$(NPX_2)_2$ molecules of D_{2h} symmetry (Table 6), the fully symmetric a_g MO includes AOs that enable σ bonding s(N)–s(P) (with possibly s(N)–d_{hr}(P) also) and in-plane π' bonding p_r(N)–p_r(P) interaction as well. As the gross population on s(N) is equal to or lower than the net population (i.e. no bonding or antibonding character), this MO corresponds exclusively to in-plane π' bonding. MOs of b_{1g} and b_{2u} types describe σ bonds mediated by p_τ(N)–p_τ(P) and p_τ(N)–s(P) (with allowed p_τ(N)–d_{hr}(P)) bonding interactions, respectively. An MO of b_{3u} symmetry corresponds to σ bonding s(N)–p_τ(P) interaction, whereas possible in-plane π' bonding via p_r(N)–$d_{h\tau}$(P) interaction does not occur (also due to a negative difference between the gross and net p(N) population). Possible out-of-plane π bonding via p_z(N)–$d_{z\tau}$(P) interaction of b_{2g} type is questionable not only because of the purely polarizing character of d orbitals

Table 8
Cylindrical AO contributions (gross Mulliken populations) to molecular orbitals of cyclo-$(NPX_2)_4$

X		s(N)	s(P)	p_r(N)	p_r(P)	p_τ(N)	p_τ(P)	d_{hr}(P)	$d_{h\tau}$(P)
H	a_{1g} ($\sigma+\pi'$)	0.91 (0.91) [a]	1.25	0.39 (0.28)	0.69			0.04	
	a_{2g} (σ)					0.29	0.70		0.01
	b_{1g} (σ)		1.34		0.69	0.22			
	b_{2g} ($\sigma+\pi'$)	0.88 (0.84)		0.46 (0.50)			0.61		
	e_u (σ)					0.53	1.30		0.05
	e_u ($\sigma+\pi'$)	1.79 (1.70)	2.58	0.83 (0.78)	1.37			0.07	
F	a_{1g} ($\sigma+\pi'$)	0.90 (0.86)	1.15	0.38 (0.28)	0.65			0.06	
	a_{2g} (σ)					0.29	0.71		0.03
	b_{1g} (σ)		1.23		0.62	0.25			
	b_{2g} ($\sigma+\pi'$)	0.89 (0.86)		0.47 (0.53)			0.61		0.06
	e_u (σ)					0.56	1.28		0.07
	e_u ($\sigma+\pi'$)	1.79 (1.79)	2.36	0.83 (0.77)	1.31			0.11	
Cl	a_{1g} ($\sigma+\pi'$)	0.91 (0.89)	1.20	0.38 (0.28)	0.69			0.05	
	a_{2g} (σ)					0.26	0.75		0.02
	b_{1g} (σ)		1.29		0.66	0.23		0.03	
	b_{2g} ($\sigma+\pi'$)	0.88 (0.86)		0.46 (0.52)			0.63		0.05
	e_u (σ)					0.52	1.37		0.06
	e_u ($\sigma+\pi'$)	1.79 (1.73)	2.48	0.83 (0.78)	1.36			0.08	
		p_z(N)	p_z(P)	d_{z^2}(P)	$d_{z\tau}$(P)	d_{z^2}(P)			
H	a_{1g} ($-$)					0.01			
	e_g (π)	0.86	1.43	0.07					
	e_g ($-$)				0.04				
	a_{2u} (π)	0.38	0.73	0.05					
	b_{1u} (π)	0.46 (0.47)			0.04				
	b_{2u} ($-$)		0.71	0.04					
F	a_{1g} ($-$)					0.02			
	e_g (π)	0.85	1.25	0.08					
	e_g ($-$)				0.05				
	a_{2u} (π)	0.39	0.66	0.05					
	b_{1u} (π)	0.46 (0.47)			0.05				
	b_{2u} ($-$)		0.59	0.03					
Cl	a_{1g} ($-$)					0.02			
	e_g (π)	0.83	1.34	0.04					
	e_g ($-$)				0.07				
	a_{2u} (π)	0.36	0.71	0.05					
	b_{1u} (π)	0.46 (0.47)			0.04				
	b_{2u} ($-$)		0.64	0.02					

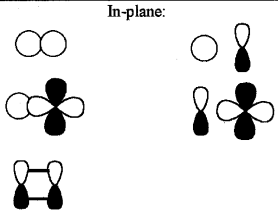
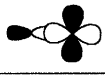
[a] Numbers in parentheses correspond to net Mulliken populations.

but also because of the discrepancy between MPA and PABON description (weakly bonding or antibonding? — see Table 3). The absence of electron density on N atoms implies the P–N non-bonding character of b_{3g} MO. Thus, only b_{1u} MO forms an out-of-plane π bond via p_z(N)–p_z(P) interaction. According to our results, the in-plane π' bond is comparable with the out-of-plane π bond and its strength corresponds to about one-fifth of the total bond strength in cyclic diphosphazenes.

In cyclo-$(NPX_2)_3$ molecules of D_{3h} symmetry (Table 7), the fully symmetric a_1' MO enables analogous σ and in-plane π' bonding such as the a_g MO of cyclic diphosphazenes. Similarly, a_2' and a_2'' MOs are analogues of the b_{1g} and b_{1u} MOs in cyclic dimers, respectively. The degenerate e′ MO has two components. The first includes bonding similar to that of the a_1' MO except that comparison of gross and net orbital populations on s(N) and p(N) AOs indicates σ rather than in-plane π' bonds. The second e′ component is analogous to a σ bonding a_2' MO. The first component of degenerate e″ MO exhibits an out-of-plane π bond like an a_2'' MO, whereas the second component is non-bonding (only $d_{z\tau}$(P) polarizing functions). There is no bonding between p_z(N) and $d_{z\tau}$(P) AOs because they are included in MOs of different symmetries. The same holds for p_τ(N) and d_{hr}(P) as well as for p_r(N) and $d_{h\tau}$(P) AOs. Our results indicate that out-of-plane π bond strength corresponds to about one-fifth of the total bond strength and the in-plane π' bond is about two times weaker than the π bond in cyclic triphosphazenes.

In cyclo-$(NPX_2)_4$ molecules of D_{4h} symmetry (Table 8), the a_{1g} and a_{2g} MOs are completely analogous to a_g and b_{1g} of cyclic diphosphazenes, respectively. In b_{1g} MO, p_τ(N)–s(P) bonding interaction of σ type exists. MOs of b_{2g} and e_u symmetries are analogous to b_{3u} MO in cyclic dimer and e′ MO in cyclic trimer (with the exception of comparable σ and

Table 9
Summary of bonding schemes in planar phosphazene rings

Bonds	Interactions		Ring symmetry		
	bonding	non-bonding	D_{2h}	D_{3h}	D_{4h}
	In-plane:				
$\sigma + \pi'$			a_g	a_1', e'	a_{1g}, e_u
σ			b_{1g}	a_2', e'	a_{2g}, e_u
σ			b_{2u}	-	b_{1g}
$\sigma + \pi'$			b_{3u}	-	b_{2g}
	Out-of-plane:				
π			b_{2g}	-	b_{1u}
π			b_{1u}	a_2'', e''	e_g, a_{2u}

in-plane π' bond strengths), respectively. Similarly, e_g and a_{2u} MOs are completely analogous to e″ MO in cyclic trimer and b_{1u} MO in cyclic dimer, respectively. A possible out-of-plane π bond of b_{1u} MO is questionable (Table 5) in the same way as for b_{2g} MO of diphosphazene. The lack of electron density on N atoms causes the P–N non-bonding character of b_{2u} MO. According to our results, the in-plane π' bond strength corresponds to about one-quarter of the total bond strength and the out-of-plane π bond is somewhat weaker in cyclic phosphazene tetramers.

It is evident that there are only some bonding patterns in planar phosphazene rings (Table 9) that would be preserved in larger cyclic systems. We have shown that in-plane π' and σ bonds in cyclic phosphazenes can be distinguished using MPA and group theory treatment. Although d_π–p_π bonding is symmetry forbidden in cyclic phosphazenes of D_{nh} symmetry with odd n only, it also does not play any significant role in cyclic phosphazenes of D_{nh} symmetry with even n. Both π bonding and π' bonding is dominated by p atomic orbitals. This is in agreement with the idea that the d functions on P atoms do not correspond to their d orbitals but cause increased flexibility of the basis set used. Nevertheless, neglecting them causes non-vanishing discrepancies in electronic structure and geometry.

Acknowledgements

The work reported in this paper has been funded by the Slovak Grant Agency, Project No. 1/4205/97.

References

[1] M.J.S. Dewar, E.A.C. Lucken, M.A. Whitehead, J. Chem. Soc. (1960) 2423.
[2] D.P. Craig, N.L. Paddock, J. Chem. Soc. (1962) 4118.
[3] A.E. Reed, P.v.R. Schleyer, J. Am. Chem. Soc. 112 (1990) 1434 and references therein.
[4] E. Magnusson, J. Am. Chem. Soc. 115 (1993) 1051 and references therein.
[5] J.P. Faucher, J. Devanneux, C. Leibovici, J.F. Labarre, J. Mol. Struct. 10 (1971) 439.
[6] D.R. Armstrong, G.H. Longmuir, P.G. Perkins, J. Chem. Soc., Chem. Commun. (1972) 446.
[7] J.P. Faucher, J.F. Labarre, J. Mol. Struct. 17 (1973) 159.
[8] J.P. Faucher, J.F. Labarre, R.A. Shaw, J. Mol. Struct. 25 (1975) 109.
[9] J.P. Faucher, J.F. Labarre, R.A. Shaw, Z. Naturforsch., Teil B: Anorg. Chem. Org. Chem. 31 (1976) 677.
[10] J.F. Labarre, Struct. Bonding 35 (1985) 1.
[11] M. Breza, Mod. Chem. 135 (1998) 931.
[12] L. Noodleman, K.A.R. Mitchell, Inorg. Chem. 17 (1978) 2709.
[13] R.C. Haddon, Chem. Phys. Lett. 120 (1985) 372.
[14] G. Trinquier, J. Am. Chem. Soc. 108 (1986) 568.
[15] K.F. Ferris, P. Friedman, D.M. Friedrich, Int. J. Quantum Chem., Quantum Chem. Symp. 22 (1988) 207.
[16] K.F. Ferris, C.B. Duke, Int. J. Quantum Chem., Quantum Chem. Symp. 23 (1989) 397.
[17] M. Breza, S. Biskupič, J. Mol. Struct. 309 (1994) 305.
[18] M. Breza, J. Mol. Struct. (in press).
[19] A.C. Chapman, N.L. Paddock, J. Chem. Soc. (1962) 635.
[20] W.M. Daugill, J. Chem. Soc. (1963) 3211.
[21] G.I. Bullen, J. Chem. Soc., A (1971) 1450.
[22] H.McD. McGeachin, F.R. Tromans, J. Chem. Soc. (1961) 4777.
[23] R. Hazekamp, T. Migchelsen, A. Vos, Acta Crystallogr. 15 (1962) 539.
[24] A.J. Wagner, A. Vos, Acta Crystallogr., Sect. B 24 (1968) 707.
[25] T.S. Cameron, B. Borecka, W. Kwiatkowski, J. Am. Chem. Soc. 116 (1994) 1211.
[26] P.W. Atkins, Physical Chemistry, 6th edition, Oxford University Press, Oxford, 1998, p. 427.
[27] M. Dupuis, J.D. Watts, H.O. Villar, G.J.B. Hunt, Program HONDO/7, QCPE 544 (1988).
[28] M. Haser, R. Ahlrichs, J. Comput. Chem. 10 (1989) 104.
[29] R. Ahlrichs, M. Bar, M. Haser, H. Horn, C. Kolmel, Chem. Phys. Lett. 162 (1989) 165.

PERGAMON

www.elsevier.nl/locate/poly

Polyhedron 19 (2000) 399–405

POLYHEDRON

Structures of bis-ethylmaltolatodichloro-tin(IV) and -titanium(IV) and of trichloro(1-methyl-2-ethyl-3-hydroxy-4*H*-pyridin-4-onato)-aquatin(IV)

Saad Alshehri [1], John Burgess *, John Fawcett, Simon A. Parsons [2], David R. Russell

Chemistry Department, University of Leicester, Leicester LE1 7RH, UK

Received 12 August 1999; accepted 15 November 1999

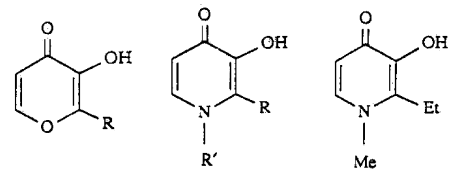
Abstract

The structures of solvates of the bis-ethylmaltolatodichloro-metal(IV) complexes $M(etma)_2Cl_2$, with M = Sn and Ti, and of trichloro(1-methyl-2-ethyl-3-hydroxy-4*H*-pyridin-4-onato)aquatin(IV), $Sn(mepp)Cl_3(H_2O)$, have been established by single crystal X-ray diffraction methods. $Sn(etma)_2Cl_2$ crystallised with one molecule of dichloromethane, $Ti(etma)_2Cl_2$ with one molecule of tetrahydrofuran, and $Sn(mepp)Cl_3(H_2O)$ with one molecule of acetone, from their respective recrystallisation media. Both ethylmaltol complexes $M(etma)_2Cl_2$ are *cis*-octahedral. The coordination around the tin atom in $Sn(mepp)Cl_3(H_2O)$ approximates to octahedral, with the three chloride ligands in *fac* geometry. The tin(IV)–water bond distance in this pyridinone complex is discussed in relation to this distance in other aquatin(IV) complexes. The effects of coordinating tin(IV) on the geometry of the coordinated pyridinone are considered. ©2000 Elsevier Science Ltd All rights reserved.

Keywords: Crystal structures; 2-Ethyl-3-hydroxy-4-pyranonate; Ethylmaltol; 1-Methyl-2-ethyl-3-hydroxy-4-pyridinonate; Tin(IV); Titanium(IV)

1. Introduction

Pyranone and pyridinone ligands and complexes are currently of considerable interest in view of their actual and potential usefulness in clinical diagnosis and chemotherapy, and as agents for controlling metal levels in the body [1,2]. A number of iron(III) complexes have been tested for administration for the amelioration of anaemia [3–5], and, complementarily, a number of these ligands have been tested as orally administrable agents for the control of iron [6] and aluminium [7,8] overload. ^{67,68}Ga and ^{111}In derivatives [9] have been assessed for imaging and chemotherapy. These ligands also form complexes with metal(IV) centres of the type $M(LL)_2X_2$, where X = halide or alkoxide [10–14]. In view of the promise of complexes of this general type, particularly of budotitane, $Ti(bzac)_2(OEt)_2$ [12,13], as antitumour agents, we have been interested in synthesising a series of complexes $M(LL)_2X_2$, where LLH is a 3-hydroxy-4-pyranone such as maltol (maH) or ethylmaltol (etmaH) (**1**) with R = Me or Et, respectively, or a 3-hydroxy-4-pyridinone (**2**). Ethylmaltolate complexes currently appear particularly attractive [14], so we have synthesised a series of complexes $M(etma)_2Cl_2$, where M = Si, Ge, Zr, Hf, V and Mo. These complement our earlier syntheses of series of titanium [15] and tin [16] complexes $M(LL)_2Cl_2$, where LLH is ethylmaltol, several 3-hydroxy-4-pyridinones, or related ligands. Our attempts to synthesise an analogous complex from tin tetrachloride and 1-methyl-2-ethyl-3-hydroxy-4-pyridinone (mepp, **3**) resulted in the isolation of $Sn(mepp)Cl_3(H_2O)$, whose structure combines the interest of the effect of coordination of tin(IV) on bond distances in the coordinated mepp ligand with a tin(IV)–water bond, a fairly uncommon species.



1 **2** **3**

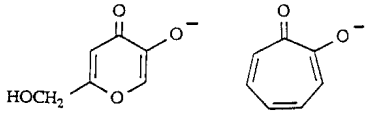
Structures have been reported for several 3-hydroxy-4-pyranones and 3-hydroxy-4-pyridinones [17–20], and for

[1] Permanent address: College of Science, King Saud University, P.O. Box 2455, Riyadh 11451, Saudi Arabia.

[2] Present address: School of Water Sciences, Cranfield University, Cranfield MK43 0AL, UK.

0277-5387/00/$ - see front matter ©2000 Elsevier Science Ltd All rights reserved.
PII S0277-5387(99)00371-X

several of their tris-ligand–metal(III) complexes [21–25]. The coordination of M^{3+} to ligands of this type has small but significant effects on bond distances, especially those that form part of the chelate rings in the complexes [26] — a topic most fully documented for closely related hydroxamato-iron(III) and -gallium(III) complexes [27]. A number of ternary complexes of the type $M^{IV}(LL)_2X_2$ (X = halide or alkoxide) containing these ligands bonded to metals in oxidation state 4+ have been prepared and characterised, but only a very few crystal structure determinations (e.g. that of $Sn(ma)_2Cl_2$ [11,28]) of such a compounds have been published. However, structures have been determined for a number of related complexes of the type $M^{IV}(LL)_2X_2$, including $Sn(acac)_2Cl_2$ [29], $Sn(bzac)_2Cl_2$ [30], $Sn(kojate)_2Me_2$ {as MeOH solvate; kojate = **4**} [31], and $Sn(trop)_2Me_2$ {trop = **5**} [31,32]. In the present paper we report the results of X-ray diffraction determinations of the crystal structures of $Ti(etma)_2Cl_2$ (**I**), $Sn(etma)_2Cl_2$ (**II**) and Sn(mepp)-$Cl_3(H_2O)$ (**III**). We discuss and compare structures for compounds of the type $M^{IV}(LL)_2X_2$, and examine the effects of coordinating Sn^{IV} ion on bond distances in coordinated 1-methyl-2-ethyl-3-hydroxy-pyridin-4-one.



4 **5**

2. Experimental

2.1. Materials

Bis-ethylmaltoldichloro-titanium(IV) and -tin(IV) were obtained from the respective tetrachlorides. Ethylmaltol (2.8 g, 20 mmol) was stirred in 30 ml of anhydrous tetrahydrofuran (THF) at room temperature. Titanium tetrachloride (1.9 g, 10 mmol) was added dropwise to the solution, giving an orange precipitate. The mixture was stirred at room temperature for 30 min, then filtered. The product was washed with anhydrous diethyl ether, and recrystallised from 50/50 dichloromethane/40–60 petroleum ether. The yield of dark orange crystals was 3.8 g (95%). Slow recrystallisation of a portion of product from THF gave crystals suitable for structure determination. The preparation of $Sn(etma)_2Cl_2$ was similar, i.e. reaction of 1.4 g (10 mmol) of ethylmaltol and 1.3 g (5 mmol) of tin tetrachloride giving 2.05 g (87% yield) of pale yellow product. Crystals suitable for X-ray structure determination were obtained by slow evaporation of a dichloromethane solution of this complex. Trichloro(1-methyl-2-ethyl-3-hydroxy-4*H*-pyridin-4-onato)aquatin(IV) was obtained from the reaction of 0.154 g (1 mmol) of the pyridinone, prepared from ethylmaltol as described elsewhere [33], with 0.26 g (1 mmol) of tin tetrachloride in wet acetone; 0.14 g (36%) of product was obtained, in the form of white crystals, upon slow crystallisation of the reaction mixture. The products gave satisfactory CH(N) analyses, and ^1H and ^{13}C NMR spectra were identical with previously characterised samples {for the $M(etma)_2Cl_2$ compounds}.

2.2. X-ray crystallography

Crystals of compounds **I**, **II** and **III** suitable for X-ray crystallographic analysis were obtained as detailed in Section 2.1. Crystal data, and a summary of the data collection and structure refinement parameters, are given in Table 1. Data for compounds **I**, **II** and **III** were measured at 290 K using graphite monochromated Mo Kα radiation ($\lambda = 0.7107$ Å) using omega (ω) scans. Crystals were glued onto glass fibres. Unit cell dimensions for compounds **I** and **II** were determined by least-squares refinement of ω values for different layers, and for compound **III** by least-squares refinement of optimised setting angles. The data were corrected for Lorentz and polarisation effects; analytical absorption corrections were applied to compounds **II** and **III**. The structures were solved by Patterson methods (SHELX86), and refined by full-matrix least-squares using SHELXL96. Hydrogen atoms were included in calculated positions (C–H = 0.96 Å) with the exception of those of the coordinated water molecule in compound **III** which were located from a difference Fourier map. All hydrogen atoms had isotropic displacement parameters fixed at 1.2 U_{eq} of the bonded atom. All non-hydrogen atoms except the THF solvent of compound **I** were refined with anisotropic displacement parameters.

3. Results and discussion

All three complexes are basically octahedral, but with significant distortions of angles at the central metal atom from the ideal 90° and 180°, presumably arising from the impossibility of the two oxygens of the coordinating hydroxypyranone or hydroxypyridinone ligands subtending angles as large as 90° at the metals. The structures of the three complexes are shown in Figs. 1–3; selected bond distances and bond angles are given in Tables 2–4.

The complexes $M(etma)_2Cl_2$ (**6**) are octahedral, with the chlorides in *cis* positions, the hydroxy-oxygens *trans* to each other and the keto-oxygens *cis* to each other. The ethylmaltolate ligand bite angles (∠O–M–O) at 79.0 and 79.8° for the tin compound are slightly smaller than the value of 78.4° (both ligand molecules) for the titanium compound. This is not consistent with the slightly smaller steric constraint imposed by the larger tin atom; ionic radii for Sn^{4+} and Ti^{4+} are 0.71, 0.68 Å [34,35] and 0.83, 0.75 Å [36,37], respectively (differences that are compatible with differences in appropriate pairs of M–O bond distances in Table 2). There is a reasonably good correlation between ∠O–M–O and ionic radii for M^{2+} and M^{3+} complexes with this type of ligand [38], but Sn^{4+} and Ti^{4+} apparently do not fit this pattern. We are unable to offer an explanation for this exceptional

Table 1
Crystallographic data for compounds **I**, **II** and **III**

	I	**II**	**III**
Formula	$C_{14}H_{14}Cl_2O_6Ti \cdot C_4H_8O$	$C_{14}H_{14}Cl_2O_6Sn \cdot CH_2Cl_2$	$C_8H_{12}Cl_3NO_3Sn \cdot C_3H_6O$
Molecular weight	433.59	552.79	453.32
Lattice	monoclinic	orthorhombic	triclinic
Space group	$C2/c$	$Pna2_1$	$P1$
a (Å)	14.24(2)	13.293(9)	9.904(2)
b (Å)	12.01(2)	9.160(2)	10.518(1)
c (Å)	13.68(1)	17.498(12)	9.756(1)
α (°)	90	90	72.15(1)
β (°)	111.77(4)	90	61.46(1)
γ (°)	90	90	87.57(1)
V (Å^3)	2173(6)	2131(3)	843.2(3)
Z	4	4	2
Cell refinement (reflections)	172	496	32
Crystal size (mm)	0.72×0.20×0.16	0.56×0.36×0.28	0.45×0.41×0.40
Crystal colour, shape	colourless, needle	pale yellow, block	colourless, block
Diffractometer	Stoe Stadi-2	Stoe Stadi-2	Siemens P4
Scan width (°)	1.3+0.7sin μ/tan(ups)	1.8+0.7sin μ/tan(ups)	0.94+0.372tan θ
Scan type	omega	omega	omega
Scan range (°)	$3.5<\theta<26$	$3.5<\theta<27$	$5<\theta<25$
Scan index limits (h; k; l)	−17, 16; 0, 14; 0, 15	−12, 16; −7, 11; 0, 22	−12, 13; −13, 14; 0, 13
Absolute correction (T_{min}, T_{max})	not applied	0.41, 0.68	0.476, 0.602
Data collected	3045	4636	5573
Unique data	2029	2229	4737
Goodness-of-fit on F^2	1.041	1.107	1.172
a, b [a] in weighting scheme	0.0884, 1.96	0.5, 0.05	0.835, 0.16
R_{int}	0.017	0.021	0.021
Observed data [$I>2\sigma(I)$]	1294	1805	4382
$R1$ [b]	0.068	0.043	0.032
$wR2$ (all data)	0.182	0.097	0.121
Parameters (n)	125	235	187
ΔF (e Å^{-3})	+0.49/−0.34	+0.385/−0.514	+1.28/−1.34
Δ/σ	0.01	0.026	0.002

[a] $w=1/[\sigma^2(F_o^2)+(aP)^2+bP]$, where $P=(F_o^2-F_c^2)/3$.
[b] $R1=\sum||F_o|-|F_c||/\sum|F_o|$, $wR2=[w(F_o^2-F_c^2)^2/(F_o^2)^2]^{1/2}$, goodness-of-fit $s=[\sum w(F_o^2-F_c^2)^2/(n-p)]^{1/2}$, where n is number of reflections and p is total number of parameters.

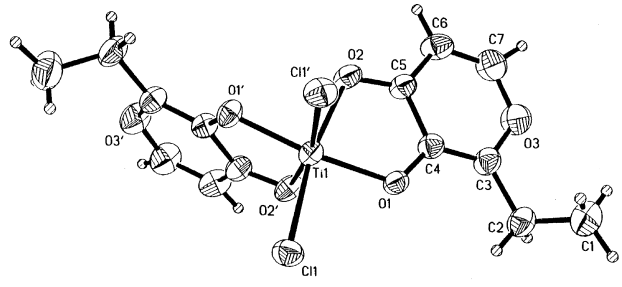


Fig. 1. The molecular structure of compound **I** showing 30% displacement ellipsoids. Hydrogen atoms are represented by circles of arbitrary radius. Primed atoms are generated by symmetry (two-fold axis through $-x$, y, $1\frac{1}{2}-z$). Solvent THF molecules are omitted.

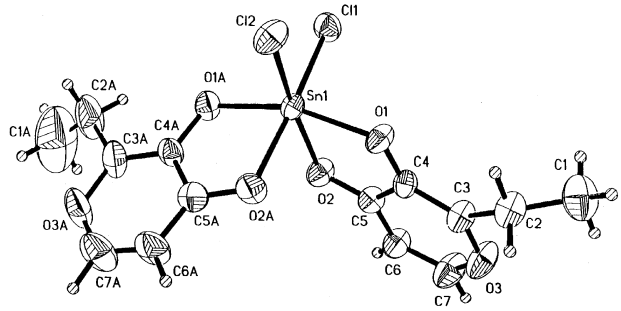


Fig. 2. The molecular structure of compound **II** showing 30% displacement ellipsoids. Hydrogen atoms are represented by circles of arbitrary radius. Solvent dichloromethane molecules are omitted.

behaviour, especially as bond distances in the coordinated ligands cannot here provide clues (see Section 3.5).

Despite the difference in ethylmaltolate ligand bite angles, the Cl–M–Cl angles in $Sn(etma)_2Cl_2$ and $Ti(etma)_2Cl_2$ are identical. The Cl–Sn–Cl angle in $Sn(etma)_2Cl_2$ is exactly the same as in $Sn(bzac)_2Cl_2$, slightly smaller than in $Sn(acac)_2Cl_2$ (96.8°). The ligand bite angles in $Sn(etma)_2Cl_2$ are intermediate between those of $Sn(acac)_2Cl_2$ and $Sn(bzac)_2Cl_2$ (87.0, 87.3 and 86.2, 86.4°) on the one hand and $Sn(kojate)_2Me_2$ and $Sn(trop)_2Me_2$ (71.4, 72.5 and 72.5, 73.2°) on the other.

The coordination environment of the tin in trichloro(1-methyl-2-ethyl-3-hydroxy-4*H*-pyridin-4-onato)aquatin(IV), $Sn(mepp)Cl_3(H_2O)$, is also approximately octahedral, as shown in structure **7**. Angles between pairs of *cis* donor atoms range from 79.3° {the two pyridinone-oxygen donors; the

Table 2
Selected bond lengths (Å) for $M(etma)_2Cl_2$, complexes **I** (M = Ti) and **II** (M = Sn)

I		**II**			
Ti–O(1)	1.911(3)	Sn–O(1)	2.052(6)	Sn–O(1A)	2.043(6)
Ti–O(2)	2.075(3)	Sn–O(2)	2.136(5)	Sn–O(2A)	2.115(7)
Ti–Cl(1)	2.293(2)	Sn–Cl(1)	2.357(3)	Sn–Cl(2)	2.362(2)
O(1)–C(4)	1.333(6)	O(1)–C(4)	1.315(9)	O(1A)–C(4A)	1.342(11)
O(2)–C(5)	1.281(6)	O(2)–C(5)	1.285(10)	O(2A)–C(5A)	1.306(13)
C(1)–C(2)	1.492(9)	C(1)–C(2)	1.49(2)	C(1A)–C(2A)	1.27(3)
C(2)–C(3)	1.489(7)	C(2)–C(3)	1.525(13)	C(2A)–C(3A)	1.47(2)
C(3)–C(4)	1.348(6)	C(3)–C(4)	1.356(12)	C(3A)–C(4A)	1.345(14)
C(4)–C(5)	1.430(6)	C(4)–C(5)	1.439(10)	C(4A)–C(5A)	1.431(14)
C(5)–C(6)	1.412(7)	C(5)–C(6)	1.411(11)	C(5A)–C(6A)	1.40(2)
C(6)–C(7)	1.334(8)	C(6)–C(7)	1.349(14)	C(6A)–C(7A)	1.28(2)
C(7)–O(3)	1.343(7)	C(7)–O(3)	1.296(12)	C(7A)–O(3A)	1.35(2)
O(3)–C(3)	1.354(6)	O(3)–C(3)	1.363(12)	O(3A)–C(3A)	1.360(14)

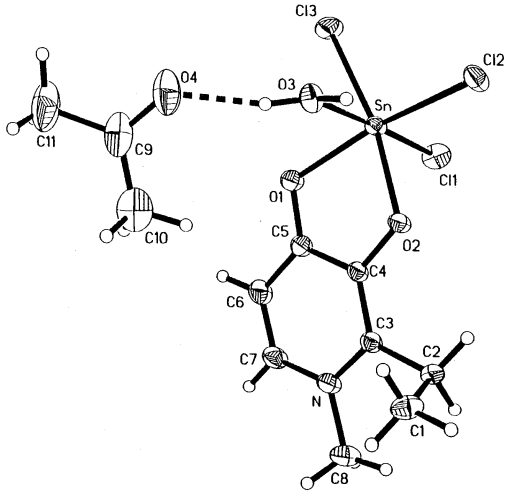
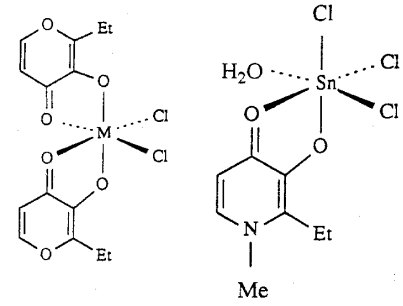


Fig. 3. The molecular structure of compound **III** showing 30% displacement ellipsoids. Hydrogen atoms are represented by circles of arbitrary radius. The dashed line indicates an O–H···O hydrogen bond (O···O < 2.9 Å).

Table 3
Selected bond lengths (Å) for $Sn(mepp)Cl_3(H_2O)Cl_3(H_2O)$, complex **III**

Sn–O(1)	2.050(2)	Sn–Cl(1)	2.378(1)
Sn–O(2)	2.089(2)	Sn–Cl(2)	2.342(1)
Sn–O(3)	2.132(3)	Sn–Cl(3)	2.346(1)
C(1)–C(2)	1.520(5)	C(7)–N(1)	1.346(5)
C(2)–C(3)	1.493(4)	N(1)–C(3)	1.370(4)
C(3)–C(4)	1.366(4)		
C(4)–C(5)	1.412(4)	N(1)–C(8)	1.462(4)
C(5)–C(6)	1.388(4)		
C(6)–C(7)	1.364(5)		

bite here is the same as the mean for $Sn(etma)_2Cl_2$} to 101.5° (two of the chlorides). The three chlorides are mutually *fac*, as in a number of similar compounds, although the Cl–Sn–Cl angles are all considerably greater than 90°. The aqua ligand is *trans* to one of the chlorides, although the angle O–Sn–Cl of 169.3° indicates the marked deviation from collinearity of these *trans* ligands.



6 **7**

3.1. Tin–chlorine distances

The tin–chlorine distances in all the ternary complexes listed in Table 5, and also in $Sn(mepp)Cl_3(H_2O)$, are shorter than tin–chlorine in the hexachlorostannate(IV) anion [39]. The Sn–Cl bond distances appear to decrease as the affinity of the bidentate two-oxygen donor ligands for the metal increases. Thus the shortest Sn–Cl distance is in the bis-acetylacetonate complex, and the Sn–Cl distances of 2.342 and 2.345 Å in the 3-hydroxy-4-pyridinonate complex $Sn(mepp)Cl_3(H_2O)$ are significantly shorter than the Sn–Cl distances in the ethylmaltolate and maltolate complexes shown in Table 5. However, Sn–Cl distances in $Sn(mepp)Cl_3(H_2O)$ actually span 2.34–2.38 Å, and thus the average is very close to the mean Sn–Cl bond distances in the two maltol complexes.

3.2. Tin–water distances

The tin(IV) to water-oxygen distance in $Sn(mepp)Cl_3(H_2O)$ of 2.132 Å is comparable to analogous distances in other tin(IV) complexes containing coordinated water (Table 6) [40–45]. There is little evidence for simple Sn^{4+} aq, either in crystal hydrates or in aqueous solution [46], apart from some rather unconvincing ^1H and ^{119}Sn NMR evidence for a hydration number of six [47], even though

Table 4
Selected bond angles (°) for complexes **I**, **II** and **III**

	I		**II**		**III**	
Ligand bite angles	O(1)–Ti–O(2)	78.40(13)	O(1)–Sn–O(2) O(1A)–Sn–O(2A)	79.0(2) 79.8(3)	O(1)–Sn–O(2)	79.26(9)
cis-Chloride angles	Cl(1)–Ti–Cl(1)	95.40(10)	Cl(1)–Sn–Cl(2)	95.20(14)	Cl(1)–Sn–Cl(2) Cl(2)–Sn–Cl(3) Cl(1)–Sn–Cl(3)	96.14(4) 101.48(4) 93.31(4)

Table 5
Metal–ligand bond lengths (Å) in tin and titanium complexes $M(LL)_2Cl_2$

Tin(IV) compounds	M–Cl distances	Mean	M–O distances [a]	Δ	Titanium(IV) compounds	M–Cl distance	Ti–O distances
cis-$Sn(etma)_2Cl_2$	2.357, 2.362	2.360	2.048, 2.126	0.078	$Ti(etma)_2Cl_2$	2.293	1.911, 2.075
cis-$Sn(ma)_2Cl_2$ [b]	2.351, 2.358	2.355	2.046, 2.142	0.096			
Cis-$Sn(trop)_2Cl_2$	2.347, 2.359	2.353	2.059 to 2.101	(0.042)	$Ti(bzbz)_2Cl_2$	2.16, 2.33	1.89 to 2.05
Cis-$Sn(acac)_2Cl_2$	2.335, 2.344	2.340	2.051, 2.064	0.013	$Ti(dpm)_2Cl_2$	2.27	1.91 to 2.01
Cis-$Sn(bzbz)_2Cl_2$	2.345	2.345	2.062 to 2.074	(0.012)	$[Ti(acac)Cl_3)]_2$	2.21, 2.25	1.89, 1.97
$SnCl_6^{2-}$	2.409, 2.421	2.415			$TiCl_6^{2-}$	2.33 to 2.35	
Trans-$Sn(koj)_2Me_2$ [c]			2.108, 2.378	0.270	$Ti(acac)_2(OC_6H_3{}^iPr_2)_2$		1.99, 2.05
cis-$Sn(trop)_2Me_2$ [d,e]			2.140 to 2.193	(0.053)	$Ti(acac)_3^+$		1.92 to 1.96
cis-$Sn(trop)_2Me_2$ [d,f]			2.143 to 2.203	(0.060)			

[a] Mean distances to carbonyl-oxygen and hydroxyl-oxygen, and their difference, Δ (or range where bracketed).
[b] Values given here are from [11]; both M–Cl = 2.370 and M–O = 2.056, 2.129 (Δ = 0.063) are given in [28].
[c] Formally *trans*; C–Sn–C angle is only 148°.
[d] C–Sn–C angle is 180–109°.
[e] From [31].
[f] From [32].

Table 6
Tin to water-oxygen distances (Å) in aquatin(IV) complexes

Compound	Sn–O (Å)	Ref.
$[SnCl_3(OH)(H_2O)]_2$	2.06	[40]
$[Sn(edta)(H_2O)]$	2.12	[41]
$[SnCl_2Et(OH)(H_2O)]_2$	2.35	[42]
$[SnCl_3(OH)(H_2O)]_2\cdot 4H_2O$ [a]	2.16	[43]
$[SnCl_3(OH)(H_2O)]_2\cdot 4H_2O$ [a]	2.14	[44]
$[SnCl_2Me_2(H_2O)_2]\cdot 4$ purine [b]	2.24	[45]
$[SnCl_3(OH)(H_2O)]_2\cdot 3$ dioxan [a]	2.13	[43]
$[SnCl_3(OH)(H_2O)]_2\cdot 4$ cineole [a]	2.10	[43]
$[SnBr_3(OH)(H_2O)]_2\cdot 4$ cineole [a]	2.16	[43]
$[SnCl_4(H_2O)_2]\cdot 3H_2O$ [c]	2.10	[43]

[a] *fac* trichloro compounds.
[b] *trans*-,*trans*-,*trans*-configuration at tin.
[c] i.e. $SnCl_4\cdot 5H_2O$.

$[Sn(OH)_6]^{2-}$ seems to be long established in the solid state [48]. The tin(II) to water-oxygen distance is 2.21–2.34 Å in Sn^{2+} aq [46].

3.3. Tin to pyranone-oxygen distances

Differences between Sn–O distances in the various complexes $Sn(LL)_2Cl_2$ (see Table 5) are generally too small to merit detailed discussion. However, it is apparent that these Sn–O distances are markedly shorter than in the methyl analogues $Sn(LL)_2Me_2$, and that the differences between tin to carbonyl-oxygen and tin to hydroxyl-oxygen distances (Δ in Table 5) are considerably smaller for the two *cis*-Sn(maltolate)$_2$L$_2$ compounds than for *trans*-$Sn(kojate)_2Me_2$, reflecting the strong *trans* influence of the methyl groups. Elsewhere such differences between metal to carbonyl-oxygen and to hydroxyl-oxygen distances have proved useful in assessing relative extents of delocalisation in chelate rings of hydroxy-pyranonate and hydroxy-pyridinonate complexes, but here the small but significant differences between the two metal–oxygen distances even to symmetrical bidentate ligands ($acac^-$, $trop^-$ and $bzbz^-$) precludes a meaningful assessment of chelate ring delocalisation in these unsymmetrical ternary *cis* complexes by this means.

3.4. Titanium to chlorine and oxygen distances

Similar comments apply to the metal–ligand bond distances in $Ti(etma)_2Cl_2$ as to those in $Sn(etma)_2Cl_2$. The Ti–Cl distance is significantly less than in $TiCl_6^{2-}$ [49–52], but similar to those in the β-diketonate analogues $Ti(\beta\text{-dik})_2Cl_2$ (β-dik = dibenzoylmethane, bzbz [53], or dipivaloylmethane, dpm [54]) and $[Ti(acac)Cl_3]_2$ [55]. All the Ti–Cl distances in octahedral species are markedly longer than in tetrahedral $TiCl_4$, where Ti–Cl = 2.18 Å (electron diffraction [56]; an X-ray examination of solid $TiCl_4$ [57] established lattice constants but not bond distances); Ti–Cl = 2.18 Å in

the Et_4N^+ salt of square-pyramidal $TiOCl_4^{2-}$, where the four chlorides are all equatorial [58].

The Ti–O bond distances in $Ti(etma)_2Cl_2$ are similar to those in the β-diketonate analogues $Ti(\beta\text{-dik})_2Cl_2$ [53,54], in $Ti(acac)_3^+$ [59] and in $Ti(OCH_2CH_2O)_3^{2-}$ [60]. They are slightly shorter than the equivalent Ti–O distances in $Ti(acac)_2$(2,6-diisopropylphenoxide)$_2$ [61] and those in $Cs_4[TiO(ox)_2]_2\,3H_2O$ [62]. All the Ti–O bond distances to chelating O,O′ ligands are longer than those in rutile (1.94, 1.99 Å [63]), in tetrahedral TiO_4^{4-} (1.79–1.84 Å [64,65]) and the axial Ti–O bond in the square-pyramidal $TiOCl_4^{2-}$ [58]. Comparison with Ti–O in Ti^{4+} aq is hardly possible in view of the lack of any firm evidence for the existence of this species, or indeed of the often-invoked TiO^{2+} aq [66], but comparison may be made with Ti–O = 2.01 Å in the organometallic aqua ion $[(\eta^5\text{-}C_5H_5)_2Ti(H_2O)_2]^{2+}$ [67] or, perhaps better, with Ti–O = 2.10, 2.11 Å in the cation $[(tmtaa)Ti(H_2O)_2]^{2+}$, where the macrocyclic ligand tmtaa is a tetra-azatetradecine derivative [68]. Further Ti–O bond distances may be traced through references cited elsewhere [60]; they may be compared with the 'expected distance' of 1.81 Å claimed for a single titanium(IV)–oxygen bond [62].

3.5. Coordinated ligand geometry

Comparison of bond distances in the chelate ring of a complex with analogous bond distances in the free ligand can sometimes give insight into the extent of delocalisation in the chelate ring. Unfortunately we cannot reach any conclusions with regard to the $M(etma)_2Cl_2$ complexes in the present study since the bond distances in the free ligand vary too much between the three polymorphs so far characterised by X-ray diffraction [69].

Bond distances in the chelate ring of $Sn(mepp)Cl_3(H_2O)$ are compared in Fig. 4 with those in the free mepp ligand [19], and with mean values for the three non-identical rings in $Al(mepp)_3$ [70]; other bond distances in the ligand are not significantly affected on coordination to aluminium or tin. It is noteworthy that the C–C distance in the chelate ring is not significantly changed on coordination to tin(IV), since for a number of metal(III) complexes this bond has been found to be significantly shortened on chelation. This C–C distance in the closely related ligand 1,2-dimethyl-3-hydroxy-4*H*-pyridin-4-one (compound **3** with R = R′ = Me; variously called L1, CP20, or deferiprone) is 1.435 Å [17], but in the tris-chelate complexes $[Fe(L1)_3]$ [23] and $[Co(L1)_3]$ [71] has decreased to 1.408 and 1.412 Å, respectively. The difference between the two C–O bond distances is probably the best measure of delocalisation in chelate rings in this type of complex. The C–O distances are significantly affected by coordination to the tin, reflecting delocalisation in the chelate ring. The difference between the two C–O distances is 0.075 Å in the free ligand and 0.026 Å in the complex. The analogous difference for $Al(mepp)_3$ is 0.032 Å. It is tempting to point out the slightly smaller effect for coordination to aluminium(III) than to tin(IV), but the uncertainties in the two values involved do not permit this conclusion to be drawn safely.

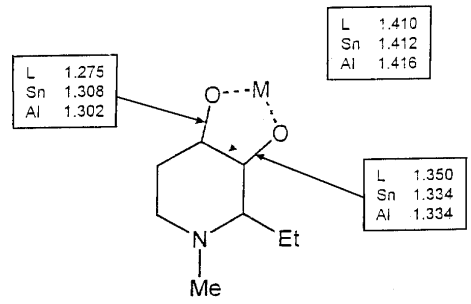


Fig. 4. Comparison of intraligand bond distances in the chelate rings of 3-hydroxy-1-methyl-2-ethyl-4-pyridinonate (mepp) complexes of tin and of aluminium with analogous distances in tris–ligand metal(III) and in the free ligand. L represents free ligand, Sn represents $Sn(mepp)Cl_3(H_2O)$, Al represents $Al(mepp)_3$.

One significant difference between the tin and titanium compounds $M(etma)_2Cl_2$ lies in the shape of the chelate rings. In the tin compound the chelate rings are essentially planar, with a mean deviation from the plane of only 0.005 Å, but the chelate rings in the titanium analogue are puckered, with a mean deviation from the plane of 0.64 Å.

3.6. Solvent of crystallisation

All three compounds crystallised as 1:1 solvates, with dichloromethane, THF and acetone, respectively. In both of the $M(etma)_2Cl_2$ compounds the solvent of crystallisation occupies spaces in the structure and does not interact strongly with surrounding molecules of complex. The dichloromethane in $Sn(etma)_2Cl_2\cdot CH_2Cl_2$ is in sites defined by orthogonal pyran rings in adjacent complex molecules. The tetrahydrofuran in $Ti(etma)_2Cl_2\cdot$THF is end-to-end disordered, and occupies sites in the lattice such that THF-oxygen to titanium distances are well over the limit for significant bonding interaction. By way of contrast, the acetone in $Sn(mepp)Cl_3(H_2O)\cdot C_3H_6O$ is hydrogen-bonded to the coordinated water. The acetone-oxygen to water-oxygen (O_3–O_4) distance is 2.633(4) Å, the H_1 to O_4 distance is 1.856 Å, and the O···H–O angle is 156.4°, all signifying relatively strong hydrogen bonding. It is interesting that it is the water, the very minor component in the solvent medium, that coordinates to the tin, rather than the major component, acetone. However, such strong preferential hydration of a metal centre is normal for metal cations M^{n+} in acetone–water mixtures [72]. It should be added that the methanol of crystallisation in $Sn(kojate)_2Me_2\cdot$MeOH is hydrogen-bonded to coordinated kojate ligands [31].

4. Supplementary data

All other crystallographic data can be obtained from the Cambridge Crystallographic Data Centre, where CIF files have been deposited (deposition numbers 132461 for compound **I**, 132462 for compound **II**, and 132463 for compound

III). Copies of this information can be obtained from The Director, CCDC, 12 Union Road, Cambridge CB2 1EZ, UK (fax: +44-1223-336033; e-mail: deposit@ccdc.cam.uk).

Acknowledgements

S.A. is grateful to the King Khalid Military Academy for leave of absence.

References

[1] J.B. Porter, E.R. Huehns, R.C. Hider, Baillière's Clin. Haematol. 2 (1989) 257.
[2] R.C. Hider, A.D. Hall, Prog. Med. Chem. 28 (1991) 41.
[3] D.A. Brown, M.V. Chidambaran, J.J. Clarke, D.M. McAlleese, Bioinorg. Chem. 9 (1978) 3.
[4] R.C. Hider, G. Kontoghiorghes, J. Silver, M.A. Stockham, UK Patent Application GB 2 136 806 A (1984).
[5] R.C. Hider, G. Kontoghiorghes, M.A. Stockham, European Patent Application 0 107 458 (1984).
[6] G.J. Kontoghiorghes, J.G. Goddard, A.N. Bartlett, L. Sheppard, Clin. Pharmacol. Ther. 48 (1990) 255.
[7] G.J. Kontoghiorghes, J. Barr, First International Symposium on Chelation, London, 1989, p. 19.
[8] G.J. Kontoghiorghes, Analyst 120 (1995) 845.
[9] E. Beatty, J. Burgess, M.S. Patel, Can. J. Chem. 72 (1994) 1370 (numerous references to uses of these isotopes can be traced through references cited herein).
[10] J. Otera, Y. Kawasaki, T. Tanaka, Inorg. Chim. Acta 1 (1967) 294.
[11] C.I.F. Denekamp, D.F. Evans, A.M.Z. Slawin, D.J. Williams, C.Y. Wong, J.D. Woolins, J. Chem. Soc., Dalton Trans. (1992) 2375.
[12] B.K. Keppler, A. Diez, V. Siegfried, Arzneim.-Forsch./Drug Res. 35 (1985) 12.
[13] M.H. Heim, H. Flechtner, B.K. Keppler, Prog. Clin. Biochem. Med. 10 (1989) 217.
[14] J.B. Porter, R.C. Hider, E.R. Huehns, Semin. Haematol. 27 (1990) 95.
[15] J. Burgess, S.A. Parsons, Appl. Organomet. Chem. 7 (1993) 343.
[16] J. Burgess, S.A. Parsons, Polyhedron 12 (1993) 1959.
[17] R.C. Hider, P.D. Taylor, M. Walkinshaw, J.L. Wang, D. van der Helm, J. Chem. Res., Synop. 316 (1990).
[18] R.C. Hider, P.D. Taylor, M. Walkinshaw, J.L. Wang, D. van der Helm, J. Chem. Res., Miniprint 2520 (1990).
[19] J. Burgess, J. Fawcett, M.S. Patel, D.R. Russell, J. Chem. Res., Synop. 50 (1993).
[20] J. Burgess, J. Fawcett, M.S. Patel, D.R. Russell, J. Chem. Res., Miniprint 0214 (1993).
[21] W.O. Nelson, S.J. Rettig, C. Orvig, J. Am. Chem. Soc. 109 (1987) 4121.
[22] M.T. Ahmet, C.S. Frampton, J. Silver, J. Chem. Soc., Dalton Trans. (1988) 1159.
[23] J. Charalambous, A. Dodd, M. McPartlin, S.O.C. Matondo, N.D. Pathirana, H.R. Powell, Polyhedron 7 (1988) 2235.
[24] L. Simpson, S.J. Rettig, J. Trotter, C. Orvig, Can. J. Chem. 69 (1991) 893.
[25] Z. Zhang, S.J. Rettig, C. Orvig, Inorg. Chem. 30 (1991) 509.
[26] G. Xiao, D. van der Helm, R.C. Hider, P.S. Dobbin, J. Chem. Soc., Dalton Trans. (1992) 3265.
[27] A. Dietrich, K.A. Fidelis, D.R. Powell, D. van der Helm, D.L. Eng-Wilmot, J. Chem. Soc., Dalton Trans. (1991) 231.
[28] S. Bhattacharya, N. Seth, V.D. Gupta, H. Nöth, K. Polborn, M. Thomann, H. Schwenk, Chem. Ber. 127 (1994) 1895.
[29] G.A. Miller, E.O. Schlemper, Inorg. Chim. Acta 30 (1978) 131.
[30] D. Searle, P.J. Smith, N.A. Bell, L.A. March, I.W. Nowell, J.D. Donaldson, Inorg. Chim. Acta 162 (1989) 143.
[31] T.P. Lockhart, F. Davidson, Organometallics 6 (1987) 2471.
[32] I. Waller, T. Halder, W. Schwarz, J. Weidlein, J. Organomet. Chem. 232 (1982) 99.
[33] G. Kontoghiorghes, L.N. Sheppard, European Patent Application 0 335 745 (1989).
[34] R.C. Evens, An Introduction to Crystal Chemistry, Cambridge University Press, Cambridge, 1966, p. 38.
[35] B.R. Eggins, Chemical Structure and Reactivity, Macmillan, London, 1972, p. 85.
[36] R.D. Shannon, C.T. Prewitt, Acta Crystallogr., Sect. B 25 (1969) 925.
[37] D.M. Adams, Inorganic Solids, Wiley, London, 1974, p. 32.
[38] S.I. Ahmed, J. Burgess, J. Fawcett, S.A. Parsons, D.R. Russell, Polyhedron 19 (2000) 129.
[39] J.A. Lerbscher, J. Trotter, Acta Crystallogr., Sect. B 32 (1976) 2671.
[40] N.W. Isaacs, C.H.L. Kennard, J. Chem. Soc. A (1970) 1257.
[41] F.P. van Remoortere, J.J. Flynn, F.P. Boer, Inorg. Chem. 10 (1971) 2313.
[42] C. Lecomte, J. Protas, M. Devaud, Acta Crystallogr., Sect. B 32 (1976) 923.
[43] J.C. Barnes, H.A. Sampson, T.J.R. Weakley, J. Chem. Soc., Dalton Trans. (1980) 949.
[44] T.S. Cameron, O. Knop, B.R. Vincent, Can. J. Chem. 63 (1985) 759.
[45] G. Valle, G. Plazzogna, R. Ettorre, J. Chem. Soc., Dalton Trans. (1985) 1271.
[46] H. Ohtaki, T. Radnai, Chem. Rev. 93 (1993) 1157.
[47] A. Fratiello, S. Peak, R.E. Schuster, D.D. Davis, J. Phys. Chem. 74 (1970) 3730.
[48] R. Scholder, G. Brauer, Handbook of Preparative Inorganic Chemistry, vol. 2, Academic Press, New York, 2nd edn., 1965, p. 1677.
[49] G. Engel, Z. Kristallogr. 90 (1935) 341.
[50] J. Wernet, Z. Anorg. Allg. Chem. 272 (1953) 279.
[51] J.A. Bland, S.N. Flengas, Can. J. Phys. 39 (1961) 941.
[52] E. Hey, U. Müller, Z. Naturforsch., Teil B 36 (1981) 135.
[53] K. Matilainen, I. Mutikainen, M. Leskela, Acta Chem. Scand. 50 (1996) 755.
[54] C. Glidewell, G.M. Turner, G. Ferguson, Acta Crystallogr., Sect. C 52 (1996) 11.
[55] N. Serpone, C.H. Bird, A. Somogyvari, D.G. Bickley, Inorg. Chem. 16 (1977) 2381.
[56] M.W. Lister, L.E. Sutton, Trans. Faraday Soc. 37 (1941) 393.
[57] P. Brand, H. Sackmann, Z. Anorg. Allg. Chem. 321 (1963) 262.
[58] W. Haase, H. Hoppe, Acta Crystallogr., Sect. B 24 (1968) 282.
[59] U. Thewalt, T. Adam, Z. Naturforsch., Teil B 33 (1978) 142.
[60] P.H. Bird, A.R. Fraser, C.F. Lau, Inorg. Chem. 12 (1973) 1322.
[61] G.J. Gainsford, T. Kemmitt, C. Lensink, N.B. Milestone, Inorg. Chem. 34 (1995) 746.
[62] W.H. Baur, Acta Crystallogr. 9 (1956) 515.
[63] J.R. Günter, G.B. Jameson, Acta Crystallogr., Sect. C 40 (1984) 207.
[64] D.T. Richens, The Chemistry of Aqua Ions, Wiley, Chichester, 1997, p. 212.
[65] T. Miyanaga, I. Watanabe, S. Ikeda, Bull. Chem. Soc. Jpn. 63 (1990) 3282.
[66] H.-P. Klein, U. Thewalt, Z. Anorg. Allg. Chem. 476 (1981) 62.
[67] A. Fester, W. Bensch, M. Trömel, Inorg. Chim. Acta 193 (1992) 99.
[68] C.E. Housmekerides, D.L. Ramage, C.M. Kretz, J.T. Shontz, R.S. Pilato, G.L. Geoffroy, A.L. Rheingold, B.S. Haggerty, Inorg. Chem. 31 (1992) 4453.
[69] S.D. Brown, J. Burgess, J. Fawcett, S.A. Parsons, D.R. Russell, E. Waltham, Acta Crystallogr., Sect. C 51 (1995) 1335.
[70] J. Burgess, J. Fawcett, M.S. Patel, L.J.S. Prouse, D.R. Russell (unpublished results).
[71] J. Burgess, J. Fawcett, M.A. Llewellyn, S.A. Parsons, D.R. Russell, Transition Met. Chem. (in press).
[72] J. Burgess, Metal Ions in Solution, Ellis Horwood, Chichester, 1978, Chapter 6.

PERGAMON

www.elsevier.nl/locate/poly

Polyhedron 19 (2000) 407–412

POLYHEDRON

The X-ray crystal structures of (*O*,*O*-2,3-dimethylbutylene and *O*,*O*-2-dimethylpropylene dithiophosphato)diphenyltellurium(IV) derivatives, $Ph_2Te[S_2POCMe_2CMe_2O]_2$ and $2Ph_2Te[S_2POCH_2CMe_2CH_2O]_2 \cdot 2Ph_2TeCl_2 \cdot CS_2$ and those of (*O*,*O*-2,3-dimethylbutylene and *O*,*O*-2-dimethylpropylene dithiophosphoric acids, $HS_2POCMe_2CMe_2O$ and $HS_2POCH_2CMe_2CH_2O$

John E. Drake *, Layla N. Khasrou, Anil G. Mislankar [1], Raju Ratnani [2]

Chemistry and Biochemistry. School of Physical Sciences, University of Windsor, Windsor, Ont. N9B 3P4, Canada

Received 6 July 1999; accepted 18 November 1999

Abstract

The immediate environment about tellurium in $Ph_2Te[S_2POCMe_2CMe_2O]_2$ (**1**) and $2Ph_2Te[S_2POCH_2CMe_2CH_2O]_2 \cdot 2Ph_2TeCl_2 \cdot CS_2$ (**2**) is essentially that of a saw-horse structure in which the lone-pair is apparently stereochemically active and occupying an equatorial position in a distorted trigonal bipyramid. However, when the second sulfur atom of the unsymmetrical bidentate ligand is included in the coordination sphere, the arrangement about tellurium in compound **1** is better described as distorted octahedral and that in $Ph_2Te[S_2POCH_2CMe_2CH_2O]_2$ as distorted pentagonal pyramidal. An intermolecular association involving a chlorine atom of Ph_2TeCl_2 results in a pentagonal bipyramidal arrangement. Sulfur and chlorine bridges between the Te atoms of $Ph_2Te[S_2POCH_2CMe_2CH_2O]_2$ and Ph_2TeCl_2 indicate pseudo dimers or Te_2S_2Cl cages. The isolation of this mixed species rather than $Ph_2TeCl[S_2POCH_2CMe_2CH_2O]$ was most unexpected. There is no indication of hydrogen bonding in $HS_2POCMe_2CMe_2O$ (**3**) and $HS_2POCH_2CMe_2CH_2O$ (**4**); even the shortest S–S internuclear distance, which is in compound **3**, is 3.556(2) Å. In both acids, the P–SH bond is significantly longer than the P=S terminal bond. ©2000 Elsevier Science Ltd All rights reserved.

Keywords: *O*,*O*-Alkylene dithiophosphate acids and ligands; Organotellurium(IV)

1. Introduction

Diphenyltellurium(IV) *O*,*O*-alkylene dithiophosphates of the type $Ph_2Te[S_2POGO]_2$ (where G = –CMe_2CMe_2–, –CHMeCHMe–, –$CH_2CMe_2CH_2$–, –$CH_2CEt_2CH_2$– and –$CHMeCH_2CMe_2$–) have been reported in the literature [1]. A report of the corresponding dimethyltellurium(IV) compounds of the type $Me_2Te[S_2POGO]_2$ includes the crystal structures of $Me_2Te[S_2POCMe_2CMe_2O]_2$ and $Me_2Te[S_2POCH_2CEt_2CH_2O]_2$ [2]. In the course of attempting to prepare fully substituted GeL_4 compounds, where L = $S_2POCMe_2CMe_2O$ and $S_2POCH_2CMe_2CH_2O$, X-ray quality crystals of $HS_2POCMe_2CMe_2O$ and $HS_2POCH_2CMe_2CH_2O$ were obtained, presumably as a result of hydrolysis. This provides an opportunity to report on the structures of these acids along with the corresponding diphenyltellurium derivatives of these cyclic dithiophosphates, $Ph_2Te[S_2POCMe_2CMe_2O]_2$ and $2Ph_2Te[S_2POCH_2CMe_2CH_2O]_2 \cdot 2Ph_2TeCl_2CS_2$. The latter was formed fortuitously while attempting the synthesis of halo derivatives of the type $Ph_2TeCl[S_2POGO]$. Comparisons are made with the related dimethyltellurium(IV)dithio derivatives [2], which generally show greater stability than their diphenyl counterparts as well as less tendency to undergo reductive elimination to the diligand and diorganotellurium(II) [3].

[1] Present address: Information Technology, Celestica Inc., Toronto, Ont. M3C 1V7, Canada.

[2] Present address: Department of Applied Chemistry & Chemical Technology, MDS University, Ajmer, India.

0277-5387/00/$ - see front matter ©2000 Elsevier Science Ltd All rights reserved.
PII S0277-5387(99)00372-1

2. Experimental

$TeCl_4$ and Ph_4Sn were obtained from Aldrich. Ph_2TeCl_2 was prepared by the reaction of $TeCl_4$ and Ph_4Sn in toluene at 60°C under reflux [4]. Sodium/ammonium salts of alkylene dithiophosphates were prepared by literature methods [5]. $Ph_2Te[S_2\overline{POCMe_2CMe_2O}]_2$ (**1**) was synthesized on the basis of the method given earlier [1] by the reaction of Ph_2TeCl_2 with a greater than two-fold excess of $NH_4[S_2\overline{POCMe_2CMe_2O}]$. Reactions with equimolar amounts of Ph_2TeCl_2 and $NH_4[S_2\overline{POCMe_2CMe_2O}]$ or $NH_4[S_2\overline{POCH_2CMe_2CH_2O}]$ were carried out in carbon disulfide to attempt the preparation of the partially substituted derivatives, $Ph_2TeCl[S_2\overline{POCMe_2CMe_2O}]$ and $Ph_2TeCl[S_2\overline{POCH_2CMe_2CH_2O}]$, but the only crystals that were isolated were those of $2Ph_2Te[S_2\overline{POCH_2CMe_2CH_2O}]_2 \cdot 2Ph_2TeCl_2CS_2$. The acids were originally formed by the fortuitous in situ hydrolysis of GeL_4, where $L = S_2\overline{POCMe_2CMe_2O}$ or $S_2\overline{POCH_2CMe_2CH_2O}$, but can of course also be obtained by more conventional methods.

2.1. Crystal structure determination

The procedures for data collection, structure solution and refinement were as described previously [6] and relevant information is in Table 1.

The structures were solved by direct methods [7]. The non-hydrogen atoms were refined anisotropically and the hydrogen atoms were included in their idealized positions with C–H set at 0.95 Å and with isotropic thermal parameters set at 1.2 times that of the carbon atom to which they were attached. For compounds **3** and **4**, the H atom attached to S was located from difference maps and treated isotropically, with positional parameters fixed at the observed values from the penultimate least-squares cycle to ensure convergence. All calculations were performed using the TEXSAN [8] crystallographic software package of Molecular Structure Corp.

3. Results and discussion

$Ph_2Te[S_2\overline{POCMe_2CMe_2O}]_2$ (**1**) crystallizes in the space group $P2_1/n$ and $2Ph_2Te[S_2\overline{POCH_2CMe_2CH_2O}]_2 \cdot 2Ph_2TeCl_2 \cdot CS_2$ (**2**) in the space group $C2/c$. The ORTEP diagrams (Fig. 1) illustrate that, for both dithiophosphate derivatives, as well as for Ph_2TeCl_2, the immediate environment about tellurium can be described as the saw-horse structure typical of tellurium(IV) compounds in which the lone-pair is apparently stereochemically active and occupying an equatorial position in a distorted trigonal bipyramid, approximately in the position of the Te labels. For the two phenyl groups occupying the other two equatorial positions in $Ph_2Te[S_2\overline{POCMe_2CMe_2O}]_2$ and $Ph_2Te[S_2\overline{POCH_2CMe_2CH_2O}]_2$, the average Te–C bond lengths

Table 1
Crystallographic data for $Ph_2Te[S_2\overline{POCMe_2CMe_2O}]_2$ (**1**), $2Ph_2Te[S_2\overline{POCH_2CMe_2CH_2O}]_2 \cdot 2Ph_2TeCl_2 \cdot CS_2$ (**2**), $HS_2\overline{POCMe_2CMe_2O}$ (**3**) and $HS_2\overline{POCH_2CMe_2CH_2O}$ (**4**)

	1	**2**	**3**	**4**
Crystal	yellow, block	yellow, needle	yellow, needle	yellow, needle
Size (mm)	0.45×0.40×0.36	0.48×0.28×0.26	0.50×0.20×0.20	0.47×0.19×0.17
Molecular formula	$C_{24}H_{34}O_4S_4P_2Te$	$C_{69}H_{80}O_8S_{10}P_4Cl_4Te_4$	$C_6H_{13}O_2S_2P$	$C_5H_{11}O_2S_2P$
Crystal system	monoclinic	monoclinic	monoclinic	monoclinic
Space group	$P2_1/n$	$C2/c$	$P2_1/n$	$C2/c$
a (Å)	12.139(6)	39.168(6)	6.436(5)	9.949(2)
b (Å)	15.830(4)	12.388(7)	15.189(7)	9.131(3)
c (Å)	16.710(7)	18.170(5)	10.913(5)	20.606(2)
β (°)	103.54(4)	97.51(2)	99.65(5)	92.17(1)
V (Å^3)	3121(2)	8740(5)	1052(1)	1870.7(7)
Z	4	4	4	8
ρ_{calc} (g cm^{-3})	1.50	1.62	1.34	1.41
Diffractometer	Rigaku AFC6S			
Scan technique	$\omega-2\theta$			
$2\theta_{max}$ (°)	50	50	50	50
μ (Mo Kα) (cm^{-1})	13.5	18.04	6.14	6.85
Transmission factors	0.79–1.00	0.67–1.00	0.81–1.00	0.89–1.00
Temperature (°C)	23	23	23	23
Total reflections measured	6010	8243	2118	1864
Unique data used [$I_o \geq 3\sigma(I_o)$], N_o	3496	2064	1049	957
No. parameters refined, N_p	316	254	100	91
Largest shift/e.s.d. in final cycle	0.001	0.001	0.001	0.001
Largest residual electron density (e Å^{-3})	0.75	0.64	0.27	0.31
$R = \Sigma \lvert \lvert F_o \rvert - \lvert F_c \rvert \rvert / \Sigma \lvert F_o \rvert$	0.0534	0.0592	0.0398	0.0362
$R_w = [\Sigma w(\lvert F_o \rvert - \lvert F_c \rvert)^2 / \Sigma w(F_o)^2]^{1/2}$	0.0502	0.0475	0.0305	0.028
Gain of function, $S = [\Sigma(\lvert F_o \rvert - \lvert F_c \rvert)/\sigma]/(N_o - N_p)$	1.98	1.82	1.88	1.7

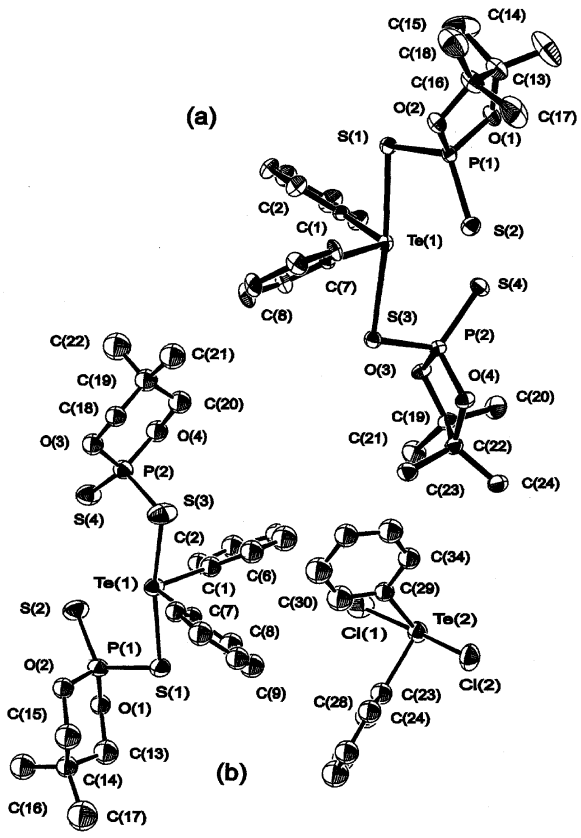


Fig. 1. ORTEP plots of the molecules (a) $Ph_2Te[S_2\overline{POCMe_2CMe_2O}]_2$ (**1**) and (b) $2Ph_2Te[S_2\overline{POCH_2CMe_2CH_2O}]_2 \cdot 2Ph_2TeCl_2 \cdot CS_2$ (**2**). Atoms are drawn with 30% probability ellipsoids and spheres, with hydrogen atoms and CS2 omitted for clarity.

2.130(4) and 2.135(21) Å, respectively, are marginally longer than those in $Me_2Te[S_2\overline{POCMe_2CMe_2O}]_2$ and $Me_2Te[S_2\overline{POCH_2CEt_2CH_2O}]_2$ (2.121(7) Å) [2], and longer than that in Ph_2TeCl_2 (2.095(7) Å) in the asymmetric unit of compound **2** (Table 2).

In $Ph_2Te[S_2\overline{POCMe_2CMe_2O}]_2$, as was found in the analogous non-cyclic dithiophosphate derivatives $Ph_2Te[S_2P(OMe)_2]_2$ [9] and $Ph_2Te[S_2P(OEt)_2]_2$ [10], both Te–S bonds in the axial positions (S–Te–S bond angle of 173.78(7)°) are of similar length, the average value of 2.630(9) Å being close to the overall average for most bisdithio derivatives R_2TeL_2. By contrast, in $Ph_2Te[S_2\overline{POCH_2CMe_2CH_2O}]_2$, one of the Te–S bonds is significantly longer than the other (2.657(6) and 2.615(6) Å), as was also found for $Me_2Te[S_2\overline{POCMe_2CMe_2O}]_2$ and $Me_2Te[S_2\overline{POCH_2CEt_2CH_2O}]_2$ [2]. However, there are no obvious Te–S intermolecular interactions involving S(1) or S(3) in compound **2** to rationalize this difference.

As was found for the other dithiophosphates [2,9,10], the terminal sulfur atoms are oriented towards the tellurium atom at distances of 3.323(3) and 3.402(3) Å in compound **1** and 3.637(7) and 3.479(7) Å in compound **2**; such distances are significantly shorter than the sum of the van der Waals radii of Te and S [11]. The inclusion of the second sulfur atom of these anisobidentate ligands in the coordination sphere of tellurium results in a bi-capped trigonal bipyramid for $Ph_2Te[S_2P(OEt)_2]_2$ [10] and a distorted octahedron for $Me_2Te[S_2\overline{POCMe_2CMe_2O}]_2$ and $Me_2Te[S_2\overline{POCH_2CEt_2CH_2O}]_2$ [2]. The description of a distorted octahedron is also apt for compound **1** (Fig. 2a), but a distorted pentagonal pyramid is more appropriate for the dithiophosphate in compound **2** (Fig. 2b). Thus in compound **1**, C(1), Te(1), S(1) and S(2) are approximately coplanar (mean deviation from plane is 0.123 Å) with the second phenyl carbon atom attached to tellurium, C(7), out of the plane by 2.13(1) Å. Similarly, C(7), Te(1), S(3) and S(4) are approximately coplanar (mean deviation of 0.137 Å) with the C(1) out of the plane by 2.12(1) Å. The dihedral angle between the planes Te(1), S(1), S(2) and Te(1), S(3), S(4) is 71.5(2)° with the aniso-bonded atoms *cis* to one another. The dihedral angle is similar to that in $Me_2Te[S_2\overline{POCMe_2CMe_2O}]_2$ (77.0(2)°). By contrast, in compound **2**, Te(1), S(1), S(2), S(3), S(4) and C(7) are approximately coplanar (mean deviation from plane is 0.157 Å) with the second phenyl carbon atom attached to tellurium, C(1), out of this plane by 2.14(1) Å. The difference in the orientation of the ligands is emphasized by noting that the dihedral angle between the planes Te(1), S(1), S(2) and

Table 2
Important distances (Å) and angles (°) for $Ph_2Te[S_2\overline{POCMe_2CMe_2O}]_2$ (**1**)

Te(1)–S(1)	2.636(2)	Te(1)–S(3)	2.624(2)
Te(1)–C(1)	2.127(8)	Te(1)–C(7)	2.132(8)
S(1)–P(1)	2.047(3)	S(3)–P(2)	2.055(3)
S(2)–P(1)	1.938(3)	S(4)–P(2)	1.921(3)
P(1)–O(1)	1.591(6)	P(2)–O(3)	1.588(6)
P(1)–O(2)	1.586(6)	P(2)–O(4)	1.601(6)
O(1)–C(13)	1.45(1)	O(3)–C(19)	1.486(9)
O(2)–C(16)	1.45(1)	O(4)–C(22)	1.47(1)
Te(1)···S(2)	3.323(3)	Te(1)···S(4)	3.402(3)
S(1)···S(2)	3.348(3)	S(3)···S(4)	3.358(3)
P(1)···C(15)	3.24(1)	P(2)···C(20)	3.25(1)
P(1)···C(14)	3.76(1)	P(2)···C(21)	3.80(1)
P(1)···C(17)	3.22(1)	P(2)···C(23)	3.25(1)
P(1)···C(18)	3.78(1)	P(2)···C(24)	3.80(1)
S(1)–Te(1)–S(3)	173.78(7)	C(1)–Te(1)–C(7)	97.2(3)
S(1)–Te(1)–C(1)	86.6(2)	S(3)–Te(1)–C(1)	90.7(2)
S(1)–Te(1)–C(7)	89.4(2)	S(3)–Te(1)–C(7)	85.3(2)
Te(1)–S(1)–P(1)	97.5(1)	Te(1)–S(3)–P(2)	99.2(1)
S(1)–P(1)–S(2)	114.3(1)	S(3)–P(2)–S(4)	115.2(1)
S(1)–P(1)–O(1)	109.8(2)	S(3)–P(2)–O(3)	104.4(2)
S(1)–P(1)–O(2)	105.6(2)	S(3)–P(2)–O(4)	108.5(2)
S(2)–P(1)–O(1)	113.2(3)	S(4)–P(2)–O(3)	116.2(3)
S(2)–P(1)–O(2)	115.6(3)	S(4)–P(2)–O(4)	113.5(3)
O(1)–P(1)–O(2)	96.8(3)	O(3)–P(2)–O(4)	97.1(3)
P(1)–O(1)–C(13)	113.0(5)	P(2)–O(3)–C(19)	111.9(5)
P(1)–O(2)–C(16)	112.0(5)	P(2)–O(4)–C(22)	111.3(5)
O(1)–C(13)–C(16)	105.6(8)	O(3)–C(19)–C(22)	101.8(6)
O(2)–C(16)–C(13)	106.9(8)	O(4)–C(22)–C(19)	103.2(6)
S(1)–Te(1)···S(2)	67.22(7)	S(3)–Te(1)···S(4)	66.27(6)
S(1)–Te(1)···S(4)	119.62(7)	S(3)–Te(1)···S(2)	116.52(7)
S(2)···Te(1)–C(1)	151.0(2)	S(4)···Te(1)–C(7)	148.3(2)
S(2)···Te(1)–C(7)	95.0(2)	S(4)···Te(1)–C(7)	96.9(2)
S(2)···Te(1)···S(4)	86.06(7)		

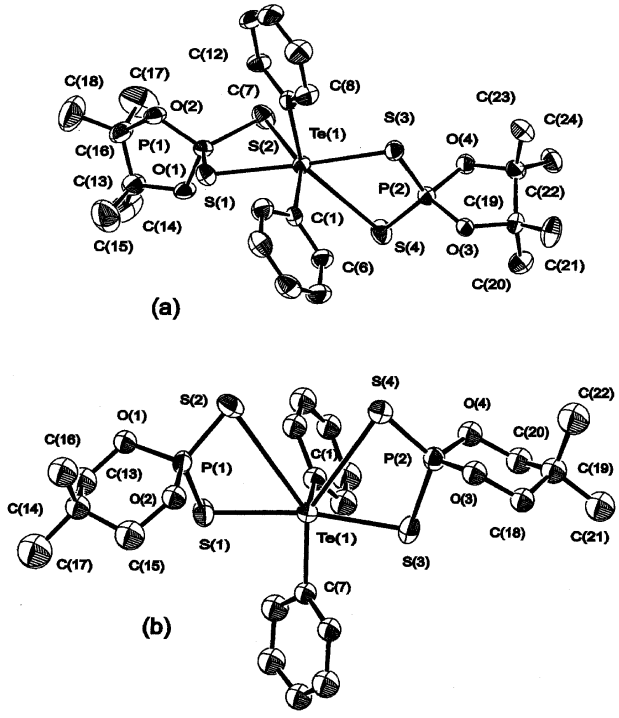


Fig. 2. ORTEP plots of the molecules showing the stereochemistry about tellurium when the intramolecular interactions leading to unsymmetrical bidentate ligands are included for $Ph_2Te[S_2POCMe_2CMe_2O]_2$ (**1**) and (b) $Ph_2Te[S_2POCH_2CMe_2CH_2O]_2$ (**2**). The atoms are drawn with 30% probability ellipsoids and spheres. Hydrogen atoms are omitted for clarity.

Te(1), S(3), S(4) is now 172.5(2)°. There is also an intermolecular interaction in compound **2** involving a chlorine atom of Ph_2TeCl_2 which results in a Te(1)···Cl(2)′ distance of 3.531(7) Å and a C(1)–Te(1)···Cl(2)′ angle of 175.0(6)°. Thus the complete extended environment about tellurium is a seven-coordinate distorted pentagonal bipyramid.

The bite angles of 67.22(7) and 66.27(6)° in compound **1** and 62.4(2) and 65.1(2)° in compound **2**, and bite lengths of 3.348(3) and 3.358(3) Å in compound **1** and 3.368(9) and 3.36(1) Å in compound **2**, reflect the slightly longer Te(1)–S(2) and Te(1)–S(4) distances in compound **2**, which in turn could arise from additional intermolecular associations in compound **2**, as discussed below.

The TeS–P bonds, which average 2.051(6) Å in compound **1** and 2.043(13) Å in compound **2**, are longer than the terminal or aniso-bonded P=S bonds, which average 1.93(1) Å in compound **1** and 1.912(13) Å in compound **2**. These distances are comparable to those reported for $Me_2Te[S_2POCMe_2CMe_2O]_2$ and $Me_2Te[S_2POCH_2CEt_2CH_2O]_2$ and the related non-cyclic derivatives, as are the S–P–S bond angles that average 114.8(6)° in compound **1** and 116.6(4)° in compound **2**. The O–P–O bond angles average 97.0(2)° in compound **1** and 103.9(6)° in compound **2**, which are essentially identical to those in the five- and six-membered rings of $Me_2Te[S_2POCMe_2CMe_2O]_2$ and $Me_2Te[S_2POCH_2CEt_2CH_2O]_2$ [2]. However, the comparable angles in the two derivatives containing the non-cyclic dimethoxy and diethoxy dithiophosphates [9,10] range from 93.6(5) to 96.2(5)°, indicating that the larger O–P–O angle is related to the constraints imposed by the ring systems. The bond lengths and angles within the ring systems are as expected and essentially as observed and described in detail for $Me_2Te[S_2POCMe_2CMe_2O]_2$ and $Me_2Te[S_2POCH_2CEt_2CH_2O]_2$ [2].

The bond lengths and angles around Te in Ph_2TeCl_2 in compound **2** (Table 3) are essentially the same as in the pure orthorhombic compound [12]. One Te–Cl bond is longer than the other, 2.515(7) and 2.466(6) Å in compound **2** and 2.529(2) and 2.482(2) Å in orthorhombic Ph_2TeCl_2, and the Cl–Te–Cl angles are 174.9(2) and 175.5(1)°, respectively. In orthorhombic Ph_2TeCl_2, the longer Te–Cl bond is associated with the only secondary interaction with a Te atom of an adjacent Ph_2TeCl_2 molecule. In compound **2** the longer Te–Cl bond in Ph_2TeCl_2 is associated with the tellurium atom of the closest $Ph_2Te[S_2POCH_2CMe_2CH_2O]_2$ molecule, as mentioned above. The Te···Cl′ partial bond (3.677(2) Å) in orthorhombic Ph_2TeCl_2 is essentially *trans* to a C–Te bond (Cl′···Te–C = 164.1(2)°), resulting in a distorted octahedral arrangement about Te with the position *trans* to the second Te–C bond being vacant [12]. In compound **2**, this interaction is replaced by the Te(2)···S(2)′ partial bond (3.641(8) Å) *trans* to the C(29)–Te(2) bond (S(2)′···Te(2)–C(29) = 157.3(5)°). There is also a weak interaction with the second pendant (or aniso) atom of $Ph_2Te[S_2POCH_2CMe_2CH_2O]_2$ with Te(2)···S(4)′ (3.783(7) Å) *trans* to the C(23)–Te(2) bond (S(4)′···Te(2)–C(23) = 162.1(5)°). Thus the extended environment about Te(2) is distorted octahedral and the additional intermolecular interactions in compound **2** are consistent with the longer Te···S intramolecular interactions in compound **2** relative to compound **1**. $Ph_2Te[S_2POCH_2CMe_2CH_2O]_2$ and Ph_2TeCl_2 can also be considered as pseudo dimers in a Te_2S_2Cl cluster. The core atoms around each tellurium atom are shown in Fig. 3. The two aniso sulfur atoms and one of the chlorine atoms form bridges between the two tellurium atoms to give a Te(1)···Te(2)′ distance of 4.340(2) Å.

$HS_2POCMe_2CMe_2O$ (**3**) crystallizes in the space group $P2_1/n$ and $HS_2POCH_2CMe_2CH_2O$ (**4**) in the space group $C2/c$, the same space groups as the corresponding tellurium derivatives just reported. The ORTEP diagrams are shown in Fig. 4. The S–H bond lengths and H–S–P angles of 1.12 Å and 90.9° in compound **3** and 1.21 Å and 90.5° in compound **4** (Table 4) compare well with the gas phase structure of H_2S of 1.33 Å and 92° (for H–S–H). There is no evidence of hydrogen bonding in compound **3** or compound **4**.

The HS–P bonds, 2.052(2) Å in compound **3** and 2.082(2) Å in compound **4** are longer than the terminal P=S bonds, 1.923(2) Å in compound **3** and 1.908(2) Å in compound **4**. These distances are very similar to those reported above for $Ph_2Te[S_2POCMe_2CMe_2O]_2$ and $Ph_2Te[S_2POCH_2CMe_2CH_2O]_2$, as are the S–P–S bond angles 112.78(8)° in compound **3** and 115.64(8)° in compound **4**,

Table 3
Important distances (Å) and angles (°) for $2Ph_2Te[S_2\overline{POCH_2CMe_2CH_2O}]_2 \cdot 2Ph_2TeCl_2 \cdot CS_2$ (**2**) [a]

Te(1)–S(1)	2.657(6)	Te(1)–S(3)	2.615(6)
Te(1)–C(1)	2.15(2)	Te(1)–C(7)	2.12(2)
S(1)–P(1)	2.033(9)	S(3)–P(2)	2.052(9)
S(2)–P(1)	1.920(9)	S(4)–P(2)	1.901(9)
P(1)–O(1)	1.57(1)	P(2)–O(3)	1.57(1)
P(1)–O(2)	1.59(2)	P(2)–O(4)	1.58(1)
O(1)–C(13)	1.47(2)	O(3)–C(18)	1.45(3)
O(2)–C(15)	1.48(3)	O(4)–C(20)	1.46(2)
Te(1)···S(2)	3.637(7)	Te(1)···S(4)	3.479(7)
S(2)···Te(2)′	3.641(8)	S(4)···Te(2)′	3.737(7)
S(1)···S(2)	3.368(9)	S(3)···S(4)	3.36(1)
Te(1)···Cl(2)′	3.531(7)	Te(1)···Te(2)′	4.340(2)
P(1)···C(16)	3.68(3)	P(2)···C(22)	3.68(3)
P(1)···C(17)	4.43(3)	P(2)···C(21)	4.45(3)
C(35)–S(5)	1.46(2)		
Te(2)–Cl(1)	2.466(6)	Te(2)–Cl(2)	2.515(7)
Te(2)–C(23)	2.10(2)	Te(2)–C(29)	2.09(2)
S(1)–Te(1)–S(3)	168.3(2)	C(1)–Te(1)–C(7)	97.8(8)
S(1)–Te(1)–C(1)	87.0(6)	S(3)–Te(1)–C(1)	90.9(6)
S(1)–Te(1)–C(1)	86.1(6)	S(3)–Te(1)–C(1)	82.7(6)
Te(1)–S(1)–P(1)	98.2(3)	Te(1)–S(3)–P(2)	100.0(3)
S(1)–P(1)–S(2)	116.8(4)	S(3)–P(2)–S(4)	116.3(4)
S(1)–P(1)–O(1)	106.5(6)	S(3)–P(2)–O(3)	105.2(7)
S(1)–P(1)–O(2)	106.7(6)	S(3)–P(2)–O(4)	105.4(7)
S(2)–P(1)–O(1)	112.3(7)	S(4)–P(2)–O(3)	112.4(7)
S(2)–P(1)–O(2)	109.4(7)	S(4)–P(2)–O(4)	113.0(7)
O(1)–P(1)–O(2)	104.3(8)	O(3)–P(2)–O(4)	103.4(4)
P(1)–O(1)–C(13)	116(1)	P(2)–O(3)–C(18)	117(1)
P(1)–O(2)–C(15)	118(1)	P(2)–O(4)–C(20)	120(1)
O(1)–C(13)–C(14)	111(2)	O(3)–C(18)–C(19)	113(2)
O(2)–C(15)–C(14)	110(2)	O(4)–C(20)–C(19)	111(2)
S(1)–Te(1)···S(2)	62.4(2)	S(3)–Te(1)···S(4)	65.1(2)
S(1)–Te(1)···S(4)	126.5(2)	S(3)–Te(1)···S(2)	129.3(2)
S(2)···Te(1)–C(1)	96.8(6)	S(4)···Te(1)–C(1)	92.4(6)
S(2)···Te(1)–C(7)	144.4(6)	S(4)···Te(1)–C(7)	146.4(6)
S(2)···Te(1)···S(4)	64.6(2)	Cl(2)···Te(1)–C(1)	175.0(6)
Cl(1)–Te(2)–Cl(2)	174.9(2)	C(23)–Te(2)–C(29)	100.7(9)
Cl(1)–Te(2)–C(23)	89.3(7)	Cl(2)–Te(2)–C(23)	89.0(7)
Cl(1)–Te(2)–C(29)	88.2(6)	Cl(2)–Te(2)–C(29)	87.3(6)
S(2)–Te(2)′–C(29)′	157.3(5)	S(4)–Te(2)′–C(23)′	162.1(5)

[a] Symmetry equivalent position $(x, y-1, z)$ given by prime.

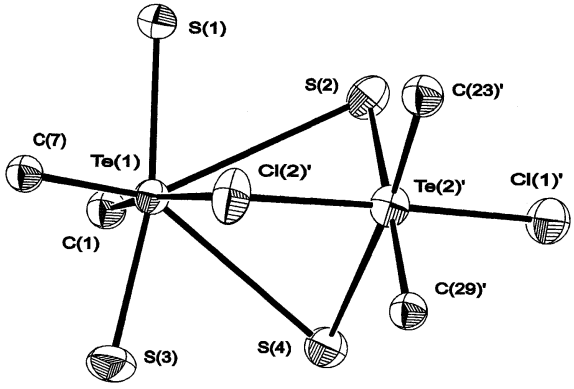


Fig. 3. The immediate environment about the tellurium atoms in $2Ph_2Te[S_2\overline{POCH_2CMe_2CH_2O}]_2 \cdot 2Ph_2TeCl_2 \cdot CS_2$ (**2**).

and the S(1)–S(2) distances 3.311(3) and 3.378(2) Å for compounds **3** and **4**, respectively. Thus the 'bite' of the ligand is essentially unaffected whether attached to Te or H. In both

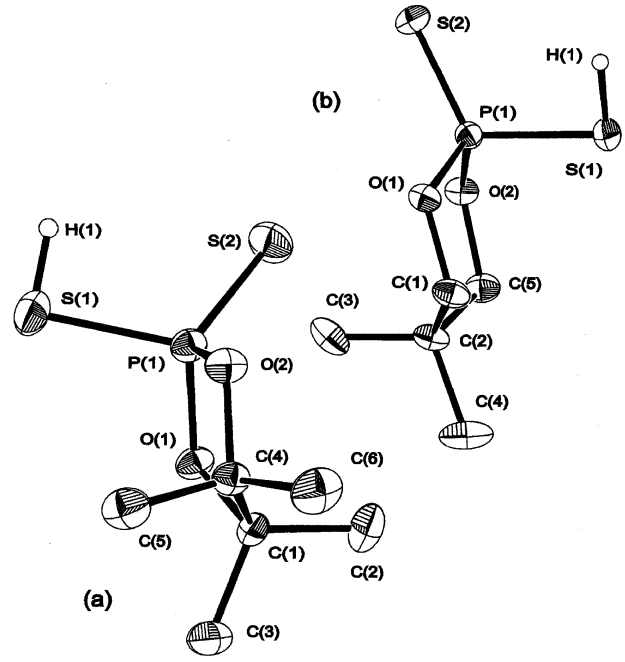


Fig. 4. ORTEP plots of the molecules (a) $HS_2\overline{POCMe_2CMe_2O}$ (**3**) and (b) $HS_2\overline{POCH_2CMe_2CH_2O}$ (**4**). Atoms are drawn with 30% probability ellipsoids and spheres, with hydrogen atoms, other than that attached to sulfur, omitted for clarity.

Table 4
Important distances (Å) and angles (°) for $HS_2\overline{POCMe_2CMe_2O}$ (**3**) and $HS_2\overline{POCH_2CMe_2CH_2O}$ (**4**) [a]

Compound **3**		Compound **4**	
S(1)–H(1)	1.12	S(1)–H(1)	1.21
S(1)–P(1)	2.052(2)	S(1)–P(1)	2.082(2)
S(2)–P(1)	1.923(2)	S(2)–P(1)	1.908(2)
P(1)–O(1)	1.594(3)	P(1)–O(1)	1.583(3)
P(1)–O(2)	1.589(3)	P(1)–O(2)	1.582(3)
O(1)–C(1)	1.482(5)	O(1)–C(1)	1.468(4)
O(2)–C(4)	1.488(4)	O(2)–C(5)	1.469(4)
S(1)···S(2)	3.311(3)	S(1)···S(2)	3.378(2)
S(1)···S(1)′	3.556(3)	S(1)···S(2)″	3.833(2)
P(1)···C(2)	3.269(5)	P(1)···C(3)	3.656(5)
P(1)···C(3)	3.787(4)	P(1)···C(4)	4.449(5)
P(1)···C(5)	3.295(5)		
P(1)···C(6)	3.775(5)		
S(1)–P(1)–H(1)	90.9	S(1)–P(1)–H(1)	90.5
S(1)–P(1)–S(2)	112.78(8)	S(1)–P(1)–S(2)	115.64(8)
S(1)–P(1)–O(1)	103.4(1)	S(1)–P(1)–O(1)	106.5(1)
S(1)–P(1)–O(2)	110.1(1)	S(1)–P(1)–O(2)	102.7(1)
S(2)–P(1)–O(1)	118.5(1)	S(2)–P(1)–O(1)	112.7(1)
S(2)–P(1)–O(2)	113.1(1)	S(2)–P(1)–O(2)	113.1(1)
O(1)–P(1)–O(2)	97.6(2)	O(1)–P(1)–O(2)	105.1(1)
P(1)–O(1)–C(1)	111.4(2)	P(1)–O(1)–C(1)	117.4(2)
P(1)–O(2)–C(4)	111.9(2)	P(1)–O(2)–C(5)	119.1(2)
O(1)–C(1)–C(4)	103.4(3)	O(1)–C(1)–C(2)	110.8(3)
O(2)–C(4)–C(1)	103.3(3)	O(2)–C(5)–C(2)	112.2(3)

[a] Symmetry equivalent position $(1-x, 2-y, 1-z)$ given by prime and $(0.5+x, 0.5+y, z)$ given by double prime.

compound **3** and compound **4**, the hydrogen atom attached to sulfur is not in the S_2P plane. The dihedral angles defined by H(1), S(1), P(1) and H(1), S(2), P(1) are essentially identical (157 and 156°, respectively, for compound **3** and compound **4**) but very different from the corresponding angles involving Te, S, P planes in compounds **1** and **2**, which is to be expected because of the secondary interactions involved in the tellurium derivatives. However, the structural features of the dithiophosphate ring systems in the acids and tellurium derivatives are similar. The O–P–O bond angle is smaller, 97.6(2)°, in the five-membered ring of compound **3** than in the six-membered ring, 105.1(1)° of compound **4**. The twist in the five-membered ring in compound **3** is the same as in compound **1** as is demonstrated by the fact that the two carbon atoms in the ring are above and below the P(1), O(1), O(2) plane, with C(1) 0.33 Å above and C(4) 0.24 Å below. Also, as in compound **1**, a view down the C(1)–C(4) bond shows that the four methyl groups are in the staggered configuration so that two methyl groups are oriented above and below the approximate plane of the distorted five-membered ring at an average distance of 3.28(2) Å from P. The second pair of methyl groups are oriented away from phosphorus, at an average distance of 3.78(1) Å. In compound **4**, as with compound **2**, the six-membered ring has the chair conformation as demonstrated by P(1) and C(2) being 0.59 and 0.69 Å above and below the O(1), O(2), C(1), C(5) plane. The orientation within the ring again results in one of the methyl groups being oriented away from phosphorus and the other towards it to give two very different distances; 3.656(5) and 4.449(5) Å for P(1)–C(3) and P(1)–C(4), respectively.

The isolation of the mixed species compound **2**, rather than $Ph_2TeCl[S_2POCH_2CMe_2CH_2O]$, was most unexpected in view of the number of halo-dimethyl and -diphenyl derivatives whose structures have been reported by us, including $Me_2TeI[(SPPh_2)_2N]$, $Me_2TeBr[S_2CN(CH_2)_3CH_2]$, $Me_2TeCl[S_2COEt]$ [13–15], $Ph_2TeBr[S_2CNEt_2]$ [16] and most recently $Me_2TeCl[S_2POCMe_2CMe_2O]$ [17].

Supplementary data

Additional material available from the Cambridge Data Centre comprises the final atomic coordinates of the non-hydrogen atoms, hydrogen-atom coordinates, thermal parameters and all of the bond lengths and angles. Crystal structure codes are as follows: $Ph_2Te[S_2POCMe_2CMe_2O]_2$ (132699), $2Ph_2Te[S_2POCH_2CMe_2CH_2O]_2 \cdot 2Ph_2TeCl_2CS_2$ (132700), $HS_2POCMe_2CMe_2O$ (132701) and $HS_2POCH_2CMe_2CH_2O$ (132702). Structure factors tables are available from the authors.

Acknowledgements

We thank the Natural Sciences and Engineering Research Council of Canada for financial support.

References

[1] T.N. Srivastava, J.D. Singh, S.K. Srivastava, Polyhedron 9 (1990) 943.
[2] J.E. Drake, L.N. Khasrou, A.G. Mislankar, R. Ratnani, Can. J. Chem. 72 (1994) 1328.
[3] D. Dakternieks, R.D. Giacomo, R.W. Gable, B.F. Hoskins, J. Am. Chem. Soc. 110 (1988) 6762.
[4] R.C. Paul, K.K. Bhasin, R.K. Chadha, J. Inorg. Nucl. Chem. 37 (1975) 2337.
[5] H.P.S. Chauhan, C.P. Bhasin, G. Srivastava, R.C. Mehrotra, Phosphorus Sulfur 15 (1983) 99.
[6] A. Silvestru, J.E. Drake, J. Yang, Polyhedron 16 (1997) 4113.
[7] G.M. Sheldrick, Acta Crystallogr., Sect. A. 46 (1990) 467.
[8] TEXSAN-TEXRAY Structure Analysis Package, Molecular Structure Corporation, Woodlands, TX, 1985.
[9] R.K. Chadha, J.E. Drake, N.T. McManus, B.A. Quinlan, B. Sarkar, Organometallics 6 (1987) 813.
[10] D. Dakternieks, R.D. Giacomo, R.W. Gable, B.F. Hoskins, J. Organomet. Chem. 349 (1988) 305.
[11] A. Bondi, J. Phys. Chem. 68 (1964) 441.
[12] N.W. Alcock, W.D. Harrison, J. Chem. Soc., Dalton Trans. (1982) 251.
[13] J.E. Drake, R.J. Drake, A. Silvestru, J. Yang, Can. J. Chem. 77 (1999) 356.
[14] J.E. Drake, J. Yang, Inorg. Chem. 36 (1997) 1890.
[15] J.E. Drake, R.J. Drake, L.N. Khasrou, R. Ratnani, Inorg. Chem. 35 (1996) 2831.
[16] J.H.E. Bailey, J.E. Drake, M.L.Y. Wong, Can. J. Chem. 69 (1991) 1948.
[17] J.E. Drake, R.J. Drake, L.N. Khasrou, R. Ratnani, Inorg. Chem. 38 (1999) 3994.

PERGAMON

www.elsevier.nl/locate/poly

Polyhedron 19 (2000) 413–416

POLYHEDRON

Molecular structure of *N*-tosylimido-*meso*-tetraphenylporphyrinatozinc(II), Zn(N-NTs-tpp)

Yu-I Li [a], Chen-Shing Chang [b], Jo-Yu Tung [b], Cheng-Hsi Tsai [b], Jyh-Horung Chen [b,*], Feng-Ling Liao [c], Sue-Lein Wang [c]

[a] *Chia Nan College of Pharmacy and Science, Tainan 71743, Taiwan, ROC*
[b] *Department of Chemistry, National Chung-Hsing University, Taichung 40227, Taiwan, ROC*
[c] *Department of Chemistry, National Tsing-Hua University, Hsin-Chu 30043, Taiwan, ROC*

Received 13 September 1999; accepted 29 November 1999

Abstract

The crystal structure of *N*-tosylimido-*meso*-tetraphenylporphyrinatozinc(II), Zn(N-NTs-tpp), was determined. The zinc is tetracoordinated with the nitrogen atoms of only three pyrrole bases and with an extra nitrogen atom of the nitrene fragment. The porphyrin ring is severely distorted, the pyrrole ring bonded to the NTs ligand making a large dihedral angle of 29.1° with the plane containing the three pyrrole nitrogens bonded to the zinc (i.e. the (3N) plane) and the other pyrroles making smaller angles of 13.8, 7.6 and 5.9°. The zinc atom lies out of the (3N) plane by 0.39 Å and the extra nitrogen N(4) by 1.54 Å on the same side as the zinc. ©2000 Elsevier Science Ltd All rights reserved.

Keywords: Bridged structures; Crystal structures; Heteronuclear multiple bond coherence; *N*-Tosyl ligands; Zinc porphyrin complexes

1. Introduction

Metalloporphyrins with a bridged structure between the central metal and one of the four pyrrole nitrogens have drawn much attention recently. Bridged metalloporphyrins with a metal–N–N linkage (metal = Zn, Ni, Fe, Hg) [1–6] have been reported. Callot et al. [1] described X-ray structure investigations of the metallation of *N*-tosylamido-*meso*-tetraphenylporphyrin [N-NHTs-Htpp] (NHTs = tosylamido, tpp = di-anion of *meso*-tetraphenylporphyrin, Ts = tosyl) [7] leading to mononuclear complexes of *N*-tosylimido-*meso*-tetraphenylporphyrinatonickel(II) [Ni(N-NTs-tpp)] (NTs = tosylimido) [1]. The nickel in Ni(N-NTs-tpp) is tetracoordinated with nitrogen atoms of only three pyrrole bases and with the extra nitrogen atom of the nitrene fragment. The title compound, *N*-tosylimido-*meso*-tetraphenylporphyrinatozinc(II), Zn(N-NTs-tpp), is a homolog of Ni(N-NTs-tpp). Zn(N-NTs-tpp) is also a four-coordinate zinc(II) porphyrin complex. It is noted that the ionic radius increases from 0.69 Å for Ni^{2+} in Ni(N-NTs-tpp) to 0.74 Å for Zn^{2+} in Zn(N-NTs-tpp) [8]. In addition, the ^{13}C chemical shifts of β-pyrrole carbon (C_β) provide a complementary method to investigate the distortion of the *N*-pyrrole ring via the insertion of the nitrene moiety into the Zn(1)···N bond in Zn(N-NTs-tpp).

However, until now there were no X-ray structural data available for Zn(N-NTs-tpp). In this paper we report (1) the X-ray structure determination of Zn(N-NTs-tpp), which establishes definitively the Zn^{II}-NTs-N structure, and (2) the ^{13}C chemical shifts of the C_β, to investigate the distortion in the porphyrin macrocycle for Zn(N-NTs-tpp).

2. Experimental

2.1. Preparation of Zn(N-NTs-tpp)

The title compound was prepared as described elsewhere [1]. Crystals were grown by diffusion of ether vapor into a CH_2Cl_2 solution. The complex was dissolved in $CDCl_3$ (99.8%; from Aldrich) at 24°C for the ^1H and ^{13}C NMR measurements. ^1H NMR (400.13 MHz; Fig. 1b): 9.00 (d, $^3J_{H-H} = 4.7$ Hz, $H_\beta(4,15)$), where $H_\beta(a,b)$ represents the two equivalent β-pyrrole protons attached to carbons a and b, respectively; 8.90 (d, $^3J_{H-H} = 4.7$ Hz, $H_\beta(5,14)$); 8.82 (s, $H_\beta(9,10)$); 7.40 (s, $H_\beta(19,20)$); 8.47 (d, $^3J_{H-H} = 7.3$ Hz),

* Corresponding author. Fax: +886-4-2862547; e-mail: jhchen@mail.nchu.edu.tw

0277-5387/00/$ - see front matter ©2000 Elsevier Science Ltd All rights reserved.
PII S0277-5387(99)00375-7

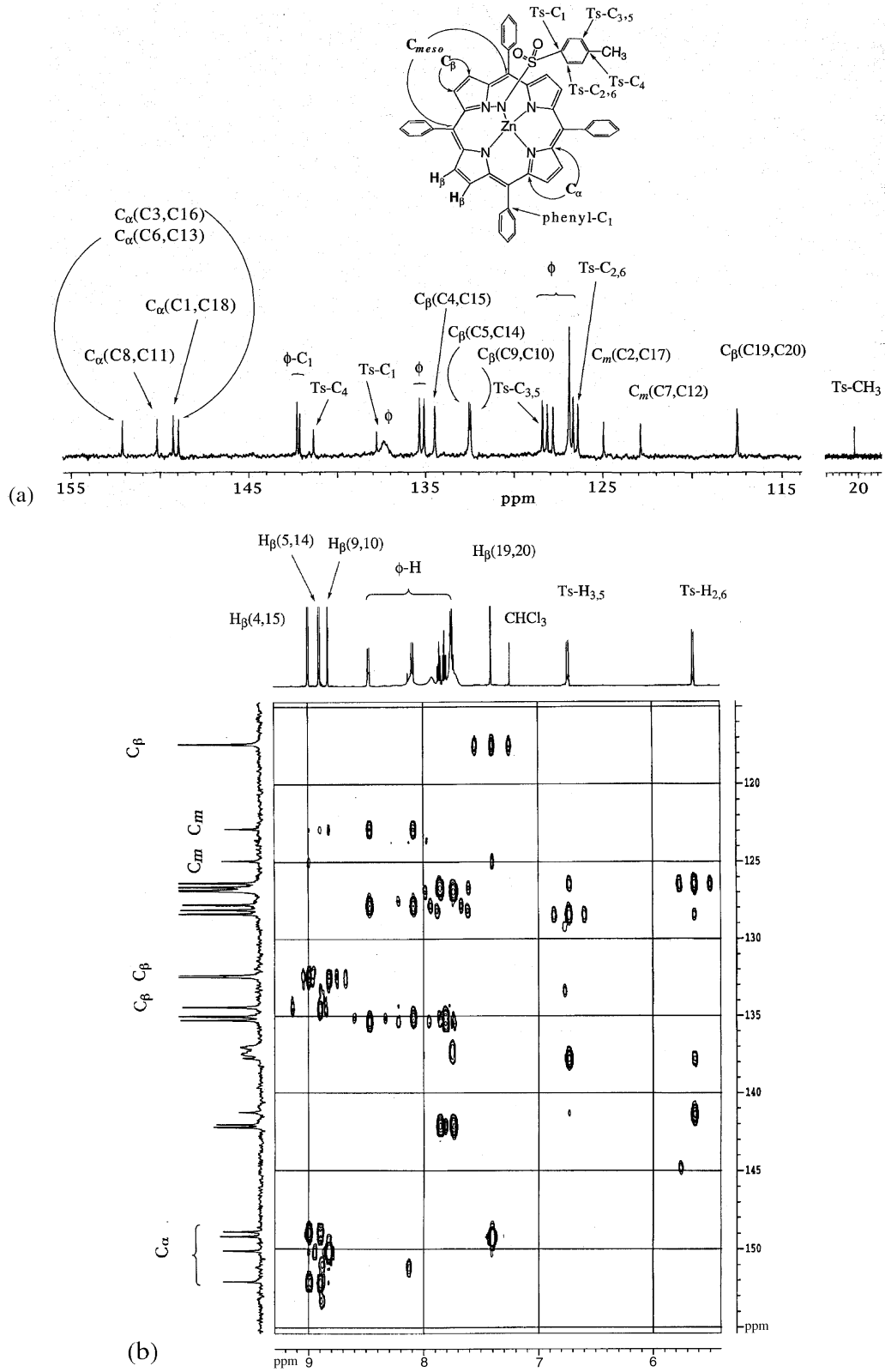


Fig. 1. (a) ^{13}C broad-band (50.33 MHz) and (b) HMBC [600.16 MHz (^{1}H), 150.92 (^{13}C)] NMR spectra for Zn(N-NTs-tpp) in $CDCl_3$ at 24°C, where ϕ-C_1 represents the phenyl-C_1 carbons, ϕ represents the phenyl-$C_{2,6}$, $C_{3,5}$ and C_4 carbons, and ϕ-H represents the phenyl protons.

8.09 (d, $^{3}J_{H-H} = 7.4$ Hz) and 7.72–7.85 (m) for *ortho*-, *meta*- and *para*-phenyl protons (*o*-, *m*-, *p*-H); 6.73 (d, $^{3}J_{H-H} = 8.0$ Hz, tosyl-$H_{3,5}$); 5.64 (d, $^{3}J_{H-H} = 8.1$ Hz, tosyl-$H_{2,6}$); 2.23 (s, tosyl-CH_3). ^{13}C NMR (100.61 MHz; Fig. 1a): 152.2 (s, C_α(C6, C13)); 149.0 (s, C_α(C3, C16)); 149.3 (s, C_α(C1, C18)); 150.2(s, C_α(C8, C11)); 142.3 (s) and 142.1 (s) for

phenyl-C_1(C33, C27) and phenyl-C_1(C39, C21)); 117.5 (s, C_β(C19, C20)); 132.4 (s, C_β(C9, C10)); 132.5 (s, $C_{\beta?}$(C5, C14)); 134.5 (s, C_β(C4, C15)); 125.0 (s, C_m(C2, C17)); 122.9 (s, C_m(C7, C12)); 141.3 (s, tosyl-C_4); 137.8 (s, tosyl-C_1); 128.4 (s, tosyl-$C_{3,5}$); 126.4 (s, tosyl-$C_{2,6}$); 21.2 (s, tosyl-CH_3); 135.3 (s), 135.1 (s), 128.2 (s), 127.8 (s), 126.9 (s) and 126.7 (s) for phenyl-$C_{2,6}$, $C_{3,5}$, C_4.

2.2. Spectroscopy

Proton and ^{13}C NMR spectra in $CDCl_3$ (99.8%; from Aldrich) were recorded at 400.13 (or 600.16) and 100.61 (or 150.92) MHz, respectively, on a Bruker AM-400 (or Bruker DMX-600) spectrometer locked on solvent deuterium, and referenced to the solvent peak. ^1H and ^{13}C NMR are relative to $CDCl_3$ at 7.24 and the central line of $CDCl_3$ at 77.0, respectively. ^1H–^{13}C correlation spectroscopy was used to correlate protons and carbon through one-bond coupling and heteronuclear multiple-bond coherence (HMBC) for two- and three-bond proton–carbon coupling.

2.3. Crystallography

Table 1 presents the crystal data and other information for Zn(N-NTs-tpp). Measurements were taken on a Siemens SMART CCD diffractometer using monochromatized Mo Kα radiation ($\lambda = 0.71073$ Å). Empirical absorption corrections were applied. The structures were solved by direct methods (SHELXTL PLUS) and refined by full-matrix least-squares. All non-hydrogen atoms were refined with anisotropic thermal parameters, whereas all hydrogen atom positions were calculated using a riding model and included in the structure factor calculation. Table 2 lists selected bond distances and angles.

3. Results and discussion

3.1. Molecular structures of Zn(N-NTs-tpp)

Fig. 2 illustrates the skeletal framework of the complex Zn(N-NTs-tpp). This structure has a four-coordinate zinc with three nitrogen atoms of the porphyrins and the extra nitrogen atom (N(4)) from the nitrene fragment. Zn(N-NTs-tpp) appears as the *N*-tosyl moiety being inserted into a Zn–N bond of *meso*-tetraphenylporphyrinatozinc(II), Zn(tpp). The most interesting distances and angles from Zn(II) atoms to the ligand are summarized in Table 2.

The pyrrole nitrogen N(5) is no longer bonded to the zinc as shown by the large Zn(1)···N(5) distance of 2.588(2) Å. Consequently, the Zn(1)–N(2) bond *trans* to the N(4) position is somewhat shorter than the other two Zn(1)–N distances [1.929(2) Å for Zn(1)–N(2) versus 2.044(2) Å for Zn(1)–N(1) and 2.049(2) Å for Zn(1)–N(3)]. Fig. 3 shows the porphyrin skeleton departures from the mean plane containing the three pyrrole nitrogens N(1), N(2) and N(3)

Table 1
Crystal data for Zn(N-NTs-tpp)

Empirical formula	$C_{51}H_{35}N_5O_2Zn$
Formula weight	847.27
Space group	$P\bar{1}$
Crystal system	triclinic
a (Å)	11.0485(9)
b (Å)	11.7484(9)
c (Å)	17.943(1)
α (°)	108.976(1)
β (°)	94.460(1)
γ (°)	106.377(1)
V (Å^3)	2075.9(3)
Z	2
F(000)	876
D_c (g cm^{-3})	1.356
μ(Mo Kα) (cm^{-1})	6.90
S	1.036
Crystal size (mm)	0.50×0.25×0.20
$2\theta_{max}$ (°)	56.2
T (K)	296(2)
No. reflections measured	20340
No. reflections observed	9097
R [a] (%)	4.08
Rw [b] (%)	11.22

[a] $R = [\Sigma||F_o| - |F_c||/\Sigma|F_o|]$.
[b] $Rw = [\Sigma w(||F_o| - |F_c||)^2/\Sigma w(|F_o|)^2]^{1/2}$, $w = A/(\sigma^2 F_o + BF_o^2)$.

Table 2
Selected bond distances (Å) and angles (°) for Zn(N-NTs-tpp)

Zn(1)–N(1)	2.044(2)	N(4)–S(1)	1.609(2)
Zn(1)–N(2)	1.929(2)	S(1)–O(1)	1.430(2)
Zn(1)–N(3)	2.049(2)	S(1)–O(2)	1.432(2)
Zn(1)–Zn(4)	1.951(2)	S(1)–C(45)	1.762(3)
N(4)–N(5)	1.404(3)		
Zn(1)–N(4)–N(5)	99.6(1)	N(1)–Zn(1)–N(2)	95.12(7)
Zn(1)–N(4)–S(1)	144.7(1)	N(1)–Zn(1)–N(3)	153.54(8)
O(1)–S(1)–O(2)	119.8(1)	N(1)–Zn(1)–N(4)	91.12(8)
N(4)–S(1)–C(45)	107.7(1)	N(2)–Zn(1)–N(3)	94.54(7)
N(4)–S(1)–O(1)	104.2(1)	N(2)–Zn(1)–N(4)	155.53(8)
N(4)–S(1)–O(2)	111.5(1)	N(3)–Zn(1)–N(4)	90.20(7)

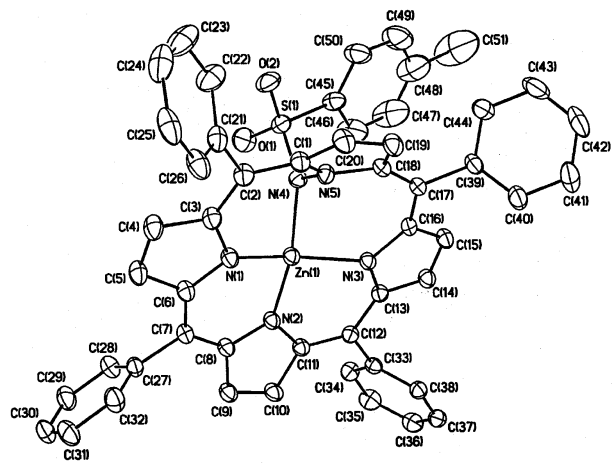


Fig. 2. Molecular configuration and atom-labeling scheme for Zn(N-NTs-tpp), with ellipsoids drawn at 30% probability. Hydrogen atoms are omitted for clarity.

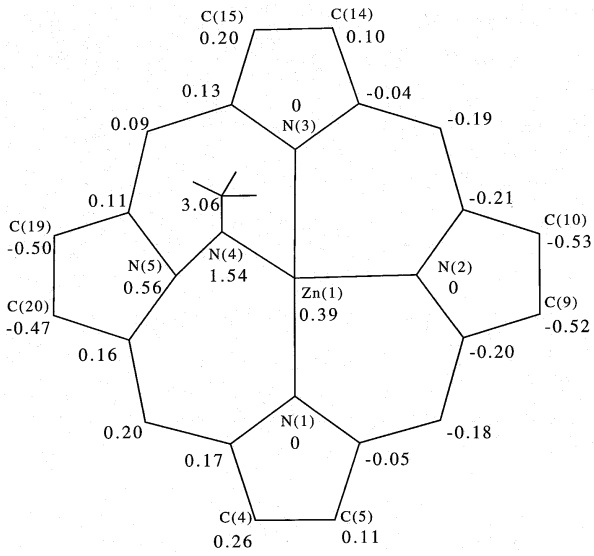


Fig. 3. Diagram of the porphyrinato core ($C_{20}N_4$, Zn and NTs) of Zn(N-NTs-tpp) showing the displacement (in Å) of the atoms from the mean plane of 3N [i.e. N(1), N(2) and N(3)].

bonded to the zinc (i.e. the (3N) plane). The tosyl nitrogen N(4) is considerably removed from the (3N) plane; its displacement of 1.54 Å is in the same direction as that of the zinc atom itself displaced by 0.39 Å (Fig. 3). The porphyrin macrocycle is severely distorted as a result of the *N*-tosyl group. Thus, the pyrrole N(5) bearing the *N*-tosyl group deviates most from the (3N) plane, making a dihedral angle of 29.1°, whereas small angles of 7.6, 13.8 and 5.9° occur with pyrrole N(1), N(2) and N(3). The extent of this large deviation from planarity for pyrrole N(5) is observed from the upfield shift of approx. −15.6 ppm for C_β (C19, C20) at 117.5 ppm relative to 134.5 ppm for C_β (C4, C15), 132.5 ppm for C_β (C5, C14) and 132.4 ppm for C_β (C9, C10). The distortion for Zn(N-NTs-tpp) is, however, less important than that present in the Ni(N-NTs-tpp) complex in which the dihedral angle between the mean plane of one pyrrole ring and mean plane of the four pyrrole nitrogens (4N) is as large as 40.5° [1]. The plane (P) defined by Zn(1), N(4), N(5) and the sulfur atom S(1) is almost perpendicular to the (3N) plane (87.8°). The tosyl group (T) defined by C(45)–C(50) is bound to N(4) such that it lies above the macrocycle making a dihedral angle of 18.9° with the (3N) plane. The dihedral angles between the mean plane of the skeleton (3N) and the planes of the phenyl group are 58.9° (C(27)), 52.1° (C(33)), 61.1° (C(39)) and 63.3° (C(21)).

In comparing the four-coordinate structure of Ni(N-NTs-tpp) [1], we adopt the mean plane of the four pyrrole nitrogens N(1), N(2), N(3) and N(5) as a reference plane (i.e. the (4N) plane). Because the larger size of the Zn^{2+}, Zn and N(4) lie 0.29 Å and 1.23 Å further above the (4N) plane in Zn(N-NTs-tpp) [cf. the corresponding displacement of 0.21 Å for Ni and 0.94 Å for the nitrogen atom of the nitrene fragment in Ni(N-NTs-tpp)] [1].

3.2. ^1H and ^{13}C NMR for Zn(N-NTs-tpp) in $CDCl_3$

Zn(N-NTs-tpp) was characterized by ^1H and ^{13}C NMR spectroscopy. In solution, where the phenyl and *N*-tosyl groups are free to rotate, the molecule has effective C_s symmetry with the mirror plane running through the N(2)–Zn(1)–N(4)–N(5) unit. In this case there are four distinct β-pyrrole protons, H_β, four β-pyrrole carbons C_β, four α-pyrrole carbons C_α, two different *meso* carbons C_{meso} and two phenyl-C_1 carbons. ^1H NMR reveals that the aromatic protons of the tosyl group appear as doublets at 6.73 (tosyl-$H_{3,5}$) and 5.64 ppm (tosyl-$H_{2,6}$) for Zn(N-NTs-tpp). All tosylimido protons are shifted upfield compared to those of free NHTs, presumably due to the porphyrin ring current effect. The ^1H NMR showed four different chemical shifts of H_β: the doublet at 9.00 ppm is assigned as H_β(4, 15), the doublet again at 8.90 ppm is assigned as H_β(5,14), the singlet at 8.82 ppm is assigned as H_β(9, 10) and the singlet again at 7.40 ppm is assigned as H_β(19, 20). The distinction of the two doublets is via HMBC. As shown in the HMBC of Zn(N-NTs-tpp) (Fig. 1), the correlation between C_m(C7, C12) (122.9 ppm) and H_β at 8.90 ppm, and between C_m(C2, C17) (125.0 ppm) and H_β at 9.00 ppm supports our assignment of the 8.90 ppm as H_β(5, 14) and 9.00 ppm as H_β(4, 15).

Zn(N-NTs-tpp) is the second X-ray structure of the metal M^{II}-NTs-N linkage in the porphyrin complex with four coordinate geometry. Disregarding the phenyl protons and carbons, the unambiguous assignment of ^1H and ^{13}C NMR data for Zn(N-NTs-tpp) in $CDCl_3$ is reported in this work.

Acknowledgements

Financial support from the National Research Councils of the ROC under Grant NSC 89-2113-M-005-014 is gratefully acknowledged.

References

[1] H.J. Callot, B. Chevrier, R. Weiss, J. Am. Chem. Soc. 100 (1978) 4733.
[2] H.J. Callot, Tetrahedron 35 (1979) 1455.
[3] K. Ichimura, Bull. Chem. Soc. Jpn. 51 (1978) 1444.
[4] J.P. Mahy, P. Battioni, D. Mansuy, J. Am. Chem. Soc. 108 (1986) 1079.
[5] J.P. Mahy, P. Battioni, G. Bedi, D. Mansuy, J. Fishcher, R. Weiss, I. Morgenstern-Badarau, Inorg. Chem. 27 (1988) 353.
[6] H.J. Callot, B. Chevrier, R. Weiss, J. Am. Chem. Soc. 101 (1979) 7729.
[7] S.M. Au , W.H. Fung, M.C. Cheng, C.M. Che, S.M. Peng. Chem. Commun. (1997) 1655.
[8] J.E. Huheey, E.A. Keiter, R.L. Keiter, Inorganic Chemistry, Harper Collins College, New York, 4th edn., 1993, p. 114.

PERGAMON

www.elsevier.nl/locate/poly

Polyhedron 19 (2000) 417–423

POLYHEDRON

Electron paramagnetic resonance and potentiometric studies of the interactions of Cr(VI) and Cr(V) with D-ribose 5-phosphate and nucleotides[1]

Marcela Rizzotto [a], Virtudes Moreno [b], Sandra Signorella [a], Verónica Daier [a], Luis F. Sala [a,*]

[a] *Area Química Inorgánica, UNR, Suipacha 531,2000 Rosario, Argentina*

[b] *Departamento de Química Inorgánica, UB, Diagonal 647, Barcelona, Spain*

Received 8 July 1999; accepted 15 November 1999

Abstract

Cr(VI) and Cr(V) interaction with D-ribose 5′-monophosphate (R5P), adenosine 5′-monophosphate (AMP), cytidine 5′-monophosphate (CMP) and 2′-deoxythymidine 5′-monophosphate (dTMP) was studied by electron paramagnetic resonance (EPR) spectroscopy (Cr(V)) and potentiometry (Cr(VI)) in aqueous solutions. The EPR spectra showed a narrow but composed signal. The Cr(V) signals showed experimental g_{iso} and ^{53}Cr A_{iso} values that are typical of five-coordinate oxochromate(V) complexes. Potentiometric studies of CMP and AMP in the presence and absence of potassium dichromate allow us to suggest the presence of three species of S–Cr(VI), differing in their degree of protonation. ©2000 Elsevier Science Ltd All rights reserved.

Keywords: Carcinogenic; Chromium; Nucleotides

1. Introduction

The carcinogenicity and mutagenicity of chromium(VI) has been established in many different compounds [1–6]. Chromate causes a variety of damage to DNA, such as single-strand breaks (SSB), induction of apurinic/apyrimidinic sites (AP-sites), alkali-labile sites and DNA–protein cross-links both in vivo and in cultured cells [7]. The observation that both lesions (induction of AP-sites and SSB in isolated DNA) are formed with equal probability and follow a similar time course suggests that they might arise from attack by a reactive species at C4′ of the DNA sugar moiety [8].

Although well-established as carcinogens, the way in which Cr(VI) compounds exert their carcinogenic, mutagenic and DNA-damaging potential remains obscure [9], but this oxidation state is not considered to be responsible for the DNA lesions associated with the observed carcinogenic activity [10]. Reduction of Cr(V) to lower oxidation states by cellular reductants is an important step [11] and has been observed with a wide variety of naturally occurring cellular reductants such as ascorbate, cysteine and glutathione (GSH). The chromium oxidation state that is responsible for producing a particular DNA lesion and the mechanism by which the lesion is produced are not unknown. However, there is a general belief that Cr(V) and Cr(IV), acting either directly or through reactive oxygen species produced from molecular oxygen or hydrogen peroxide, are responsible for much of the oxidative stress and DNA damage observed in biological systems [10,12]. Relatively long-lived Cr(V) intermediates have been detected in the reduction of Cr(VI) both in vitro and in vivo [10]. Farrell et al. initially postulated that direct binding of Cr(V) to DNA led to oxidation and DNA strand breakage [13], and, recently, studies of the genotoxicity of Cr(V) complexes in mammalian cells supported other evidence that Cr(V) may be important in Cr-induced cancers [14]. This intermediate oxidation state is frequently stabilized by the formation of complexes with ligands that possess two oxygen atoms able to form five-member chelate rings about the metal atom, such as 1,2-diols and α-hydroxy-acids [15]. For this reason, sugars and their derivatives may play an important role in the chemistry of Cr(VI) [16]. Although studies have been performed about Cr(V) species with small molecular weight reductants (ascorbate, GSH, etc.) [7,9], few of them related to nucleotides [10,15]. Nucleosides and nucleotides have, in their sugar moiety,

* Corresponding author. Fax: +54-341-4350214; e-mail: inquibir@satlink.com

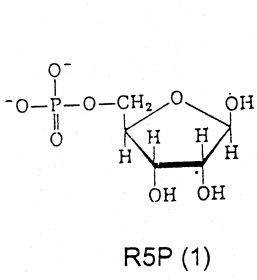
[1] Part of this work was presented at the 3rd International Conference of the Pan-African Environmental Mutagen Society (PAEMS '99), Harare, Zimbabwe, 1–5 March 1999.

0277-5387/00/$ - see front matter ©2000 Elsevier Science Ltd All rights reserved.
PII S0277-5387(99)00378-2

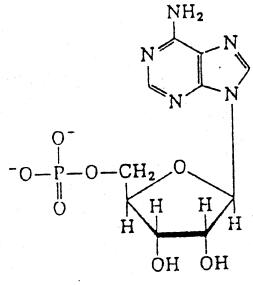
hydroxyl groups with the correct geometry for stabilizing Cr(V) [15].

As most of the known Cr(V) compounds are EPR-active at room temperature due to their d^1 electronic configuration, EPR spectroscopy has become the most powerful technique for studying Cr(V) chemistry [17].

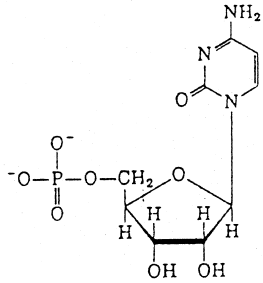
In previous work, we found several Cr(V)–sugar species formed during the Cr(VI) reduction by aldoses (D-mannose [18], D-ribose [19]), deoxyaldoses (L-rhamnose [18], 2-deoxy-D-glucose (2DG) [20,21], 2-deoxy-D-ribose (2DR) [19]) and aldonic acids [22,23]. The previous data have been employed to understand the interaction of Cr(VI) and/or Cr(V) with D-ribose 5′-monophosphate (R5P), adenosine 5′-monophosphate (AMP), cytidine 5′-monophosphate (CMP) and 2′-deoxythymidine 5′-monophosphate (dTMP) in vitro as simple bioinorganic models. Potentiometric studies of the chromic esters of nucleotides provided the stoichiometric relationship between Cr(VI) and ligand, and EPR spectroscopy of the ligand-exchange reaction of the substrates with $[Cr(ehba)_2O]^-$ (**I**) allowed the characterization of Cr(V) intermediates in these systems.



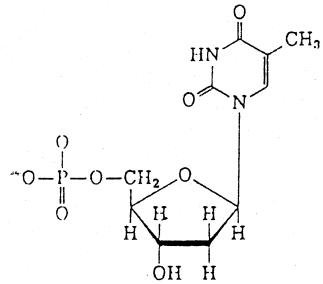
R5P (1)



AMP (2)



CMP (3)



dTMP (4)

2. Experimental

Caution: Cr(VI) compounds are human carcinogens and the Cr(V) complexes are mutagenic and potential carcinogens [1–6]. Appropriate precautions should be taken to avoid skin contact and inhalation of Cr(VI) and Cr(V) solutions and dusts.

2.1. Reagents

Potassium dichromate (from BDH), AMP, CMP, dTMP and D-ribose 5-phosphate sodium salt (Sigma) were used as received. $Na[Cr(ehba)_2O]\cdot H_2O$ (ehba = 2-ethyl-2-hydroxybutyric acid) was synthesized from 2-ethyl-2-hydroxybutanoic acid (Aldrich; 99%) and sodium dichromate in acetone [24].

2.2. EPR spectroscopy

X-band EPR spectra were recorded as the first derivative of absorption on a Bruker spectrometer operating at room temperature. Spectral parameters were: 100 kHz field modulation, 0.25–5.0 G modulation amplitude, ≈9.78 GHz microwave frequency, 1×10^5 receiver gain, centre field = 3525 G. Measurements were done on samples of ≈0.1 ml, drawn into a capillary tube that was sealed at one end with high-vacuum grease. Typically 1024 points were accumulated per spectrum. The complexes of Cr(V) with R5P, AMP, CMP and dTMP were generated: (1) in situ by mixing stock solutions of $K_2Cr_2O_7$ and each substrate; (2) by dissolving $Na[Cr(O)(ehba)_2]$ (typically 1 mmol dm^{-3}) in aqueous solutions of each substrate.

In all these cases the mole ratio [S]/[Cr(V)] was ≥100/1; the excess of organic substrate shifted the equilibrium toward the ligand-exchange products. The reactions and spectra were made at room temperature. The stock solutions of both aqueous reagents were kept at 5°C before mixing, in order to minimize the redox reaction.

2.3. Potentiometric measurements

Potentiometric studies of CMP and AMP, in the absence and presence of Cr(VI) (as potassium dichromate), were carried out with a Corning 350 pH meter equipped with glass combination electrodes calibrated with HCl to read $-\log[H^+]$ = pH. The temperature was maintained at 25.0°C and the experimental solutions, adjusted to 0.10 M ionic strength (μ) by addition of KCl, were titrated with 0.100 M standard CO_2-free NaOH.

Potentiometric studies were carried out on 50.00 ml of experimental solution in a thermostated cell, purged with CO_2-free nitrogen; 30–40 points were acquired per pH profile, providing in general at least ten pairs of data (volume base, pH) per neutralization equivalent. All stability constants and the standard deviations in the refined constant were determined using procedures outlined in detail in the literature, with the aid of BEST [25] and random error analysis in the determination of equilibrium constants [26]. Log K_w for the system, defined in terms of $\log([H^+][OH^-])$, was maintained fixed at −13.78 during the refinements [25]. For the determinations of species distributions, the program SPE was used [25]. Different relationships [S]/[Cr(VI)] were tried. These experiments were done only with AMP and CMP, because no redox reaction took place between the nucleotide and Cr(VI) during the time of performing the potentiometric measurements.

2.4. ^{31}P NMR

$^{31}P\{^{1}H\}$ NMR measurements were recorded on a Bruker WM-250 spectrometer at 20°C. Spectra of 0.03 M aqueous solution of the substrates R5P, AMP, CMP and dTMP and of the reaction mixtures S–Cr(VI) at molar ratio [S]/[Cr(VI)] = 3/1 and S–**I** at molar ratio [S]/[CrV)] = 30/1 were recorded at $t = 3$ min after mixing ($[Cr(VI)]_o = 0.01$ M and $[Cr(V)]_o = 0.001$ M). Typical data acquisition conditions were as follows: sweep width 300 (±150) and 30 (±15) ppm, with 85% orthophosphoric acid as external reference, with complete proton decoupling; acquisition time for the spectrum was 100 s. The reagents were stored at 4°C before the reactions were initiated in order to decrease the oxidation rate.

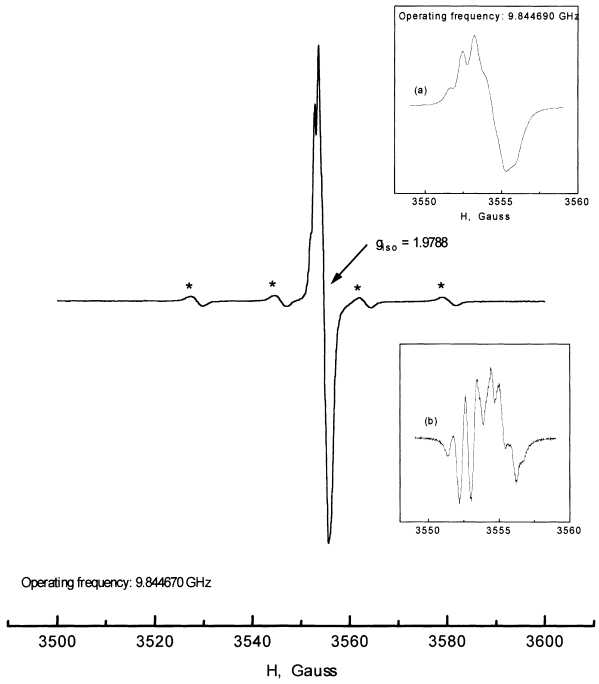


Fig. 1. X-band EPR spectrum of the Cr(V) species generated in the reaction of potassium dichromate with R5P; reaction time 6 h. * ^{53}Cr hyperfine coupling. Other conditions as in Table 1. (a) Details of the shf structure; modulation amplitude 0.25 G. (b) Second-derivative plot of (a), filtered.

Table 1
Isotropic spin hamiltonian parameters for the Cr(V) species generated in the systems Cr(VI)–substrate [a]

Substrate	g_{iso}	$\Delta H_{p\text{-}p}$ (G)	A_{iso} ^{53}Cr (G)
R5P	1.9788	2.03	17.42
AMP	1.9789	1.87	17.37
CMP	1.9789	1.81	17.35
dTMP	1.9790	2.00	ND [b]

[a] Room temperature, pH 7.5, reaction time 5–6 h, $[substrate]_o = 0.37$ M, $[Cr(VI)]_o = 0.037$ M.
[b] ND, not determined. The ^{53}Cr hyperfine signals were too weak to allow accurate determination of A_{iso} values.

2.5. Geometry optimizations

Geometry optimizations were carried out with HYPERCHEM modelling software using a personal computer.

3. Results and discussion

3.1. EPR determination of Cr(V) complexes on R5P/Cr(VI) and nucleotide/Cr(VI) systems

EPR spectra of aqueous solution of R5P/Cr(VI) (mole ratio 10:1), pH 7.5, at room temperature were acquired 5–6 h after mixing. The spectrum was dominated by a sharp signal ($\Delta H_{p\text{-}p} = 2.03$ G) with a g_{iso} mean value of 1.9788 (Fig. 1), with four ^{53}Cr (9.55% abundance, $I = 3/2$) hyperfine coupling lines (Table 1).

The spectra of the nucleotide/Cr(VI) systems showed a similar pattern to that observed for R5P, dominated by a narrow signal with a g_{iso} value of ≈1.979 and the minor peaks that arise from the ^{53}Cr hyperfine coupling (Fig. 2). Signals were detected more than 1 h after mixing AMP or CMP with Cr(VI).

EPR spectra of the Cr(V)–AMP species showed the same pattern of Cr(V)–adenosine EPR spectra. This experience

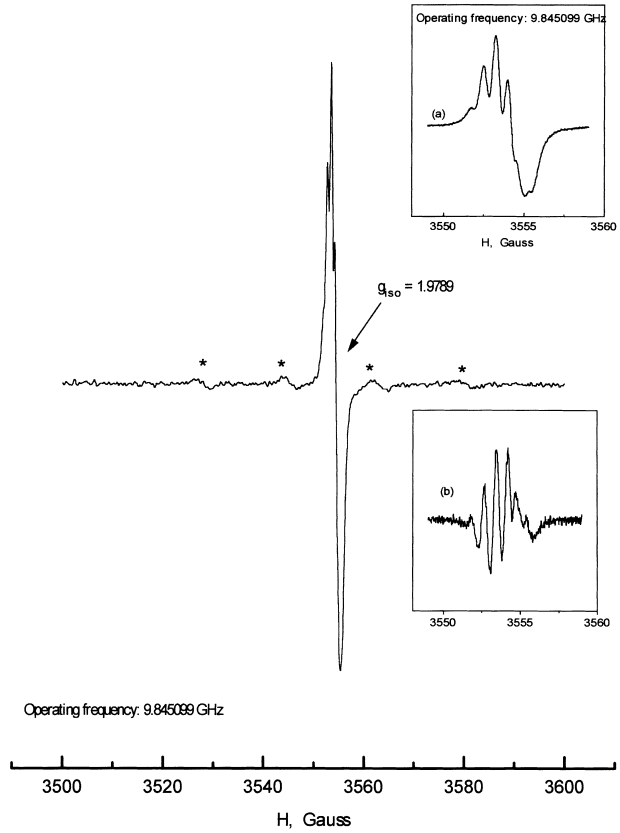


Fig. 2. X-band EPR spectrum of the Cr(V) species generated in the reaction of potassium dichromate with AMP; reaction time 6 h. * ^{53}Cr hyperfine coupling. Other conditions as in Table 1. (a) Details of the shf structure; modulation amplitude 0.25 G. (b) Second-derivative plot of (a), filtered.

was made in order to compare substrates with and without phosphate group [27].

Table 1 summarizes the experimentally observed isotropic values for g and A ^{53}Cr for the Cr(V) species in the systems R5P/Cr(VI) and nucleotides/Cr(VI) at room temperature and pH 7.5.

3.2. Ligand-exchange reactions of $[Cr(O)(ehba)_2]^-$ (I) with R5P and with nucleotides

Cr(V) may undergo rapid ligand exchange reactions in the presence of suitable reductants; hence, it may be possible to use pre-existing Cr(V) complexes as starting materials in the generation of new complexes. Normally, these reactions are rapid compared to the subsequent reduction of Cr(V) by organic substrates, or disproportionation of Cr(V) to Cr(VI) and Cr(III) [28]. The relatively stable Cr(V) complex $Na[Cr(O)(ehba)_2]$(I) was used for ligand exchange reactions in the presence of large excess of the substrates ($[S]/[I] \geq 100/1$), in aqueous solutions.

The splitting of the ^{53}Cr hyperfine coupling bands 2 min after mixing compound **I** with R5P (Fig. 3b), suggested that more than one species of Cr(V) was present, which might imply that the exchange of the ehba ligands was taking place. Such splitting was not observed in the EPR spectrum of $[Cr(O)(ehba)_2]^-$ under the experimental conditions employed in this work (Fig. 3a)) The observed superhyperfine (shf) pattern of the ligand-exchange reaction between compound **I** and R5P changed through time (Fig. 4), and it

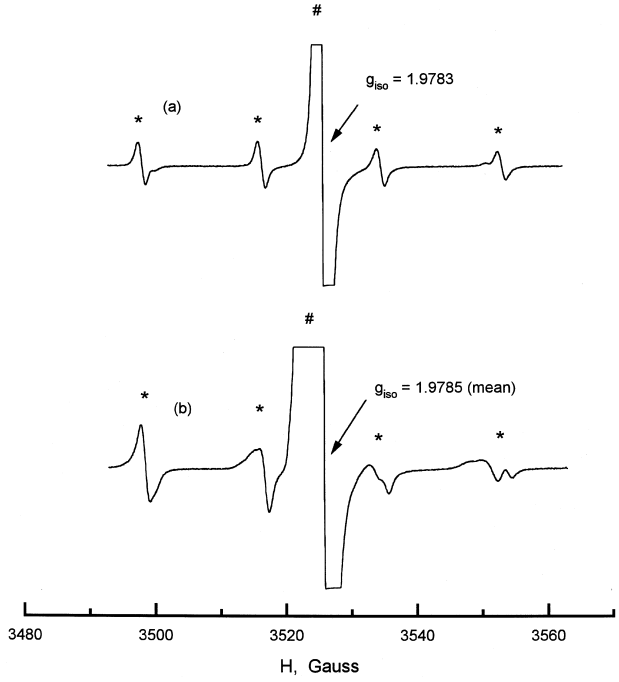


Fig. 3. X-band spectrum of compound **I** (a) and of the ligand-exchange reaction of compound **I** with R5P (b) 2 min after mixing. $T = 25$°C, $[\mathbf{I}] = 1$ mM, $[R5P] = 0.28$ M, pH 10. Assignment of peaks: # ^{52}Cr, $I = 0$; * ^{53}Cr, $I = 3/2$ hyperfine coupling, showing a different pattern in (a) than in (b). Modulation amplitude 1.603 G. Receiver gain 5e+004. Operating frequencies (GHz): (a) 9.779522; (b) 9.780355.

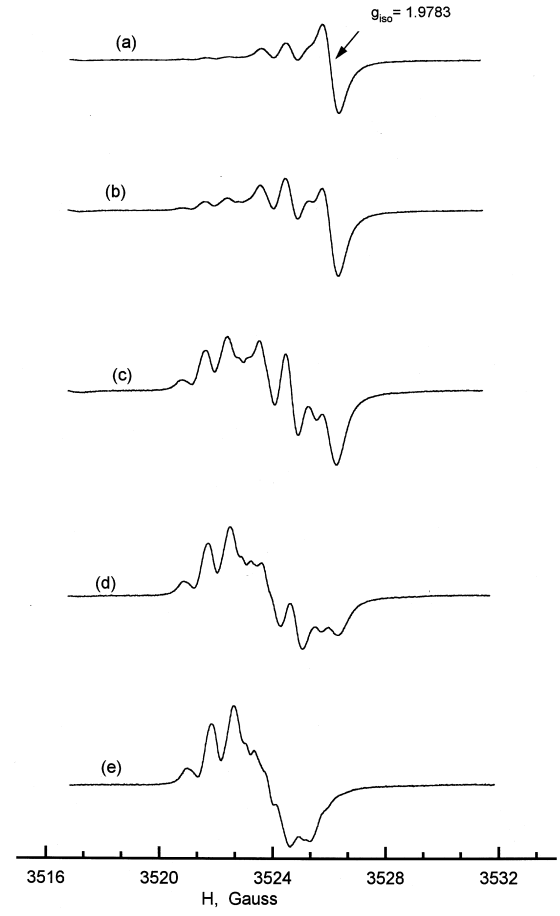


Fig. 4. X-band spectra of the ligand-exchange reaction of compound **I** with R5P. $T = 25$°C, $[\mathbf{I}] = 1$ mM, $[R5P] = 0.28$ M, pH 10; modulation amplitude 0.285 G. Operating frequencies (GHz) and times of reaction: (a) 9.780661, 2 min; (b) 9.780681, 3 min; (c) 9.780170, 5 min; (d) 9.780748, 7 min; (e) 9.780658, 14 min.

showed a very different pattern when the ehba ligand began to be exchanged and when the exchange was practically finished. The single peak due to compound **I** ($g_{iso} = 1.9783$) [29], which dominated the spectrum at $t = 2$ min, decreased in intensity with a simultaneous increase of signals of the complex species Cr(V)–R5P. After 14 min the spectrum look similar to that observed for a mixed solution of R5P–Cr(VI) (Fig. 1a). In the system Cr(V)–D-ribose, the EPR pattern observed was not so complex compared with the that of the system Cr(V)–R5P (Fig. 5). In general, the EPR spectra in the systems **I**–nucleotide (Fig. 6) and **I**–dTMP (a deoxynucleotide, Fig. 7) retained the same pattern as those with R5P. The second derivative plots of the spectra of central Cr signal (Figs. 1b, 2b, 6e and 7d) were unsymmetric, which suggests the presence of more than one species.

3.3. Structure of the Cr(V)–S complexes

All the A_{iso} ^{53}Cr and all the g_{iso} (mean) values experimentally observed were assignable to five-coordinate complexes with all oxygen donors [17]. As the g_{iso} and A_{iso} values are not consistent with a six-coordinate geometry [17,30], hence

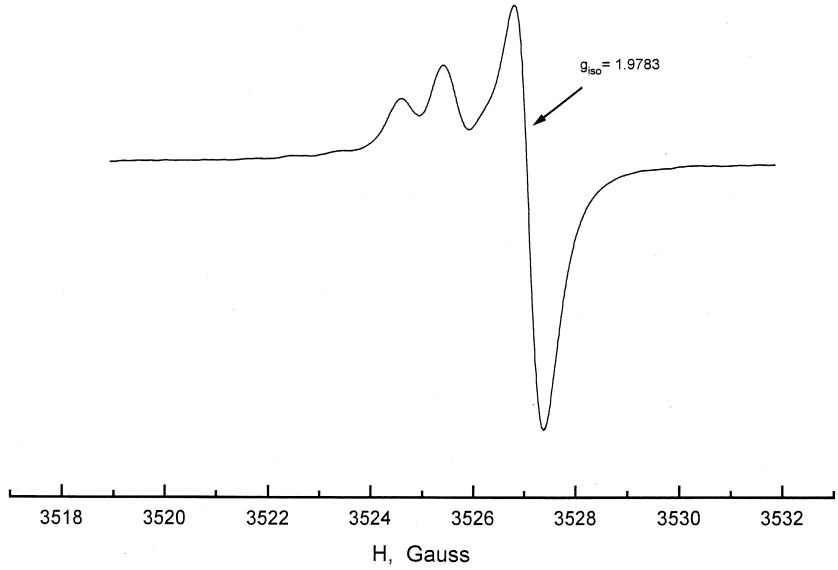


Fig. 5. Observed X-band EPR spectrum of the Cr(V) species generated in the ligand-exchange reaction of $[Cr(O)(ehba)_2]^-$ with D-ribose. $[Cr(O)(ehba)_2]^-$ concentration = 1 mM, [D-ribose] = 120 mM, pH 5.5, t = 15 min, T = 25°C, modulation amplitude = 0.285 G, operating frequency = 9.781895 GHz.

EPR spectral results need to be rationalized in the context of a five-coordinate geometry; thus, the structures of these complexes are most likely to be square-pyramidal $[Cr{=}O]^{3+}$ species [30]. Neither superhyperfine coupling due to two phosphorus atoms nor to nitrogen atoms nor hyperfine coupling of ^{53}Cr with N donors [31–33] were observed.

The g_{iso} values of $\approx$1.980 observed for all central Cr signals let us suggest species of $(CrO)^{3+}$ coordinated with four RO^- groups [17], at C2′ and C3′ of the ribose unit of two nucleotide moieties [15]. The second derivative plots of the spectra were more complicated when the ligand was R5P than with nucleotides. Possibly, R5P acts as a tridentate ligand [17] bound to Cr(V) at the hydroxyl groups of C1, C2 and C3, or C1, C2 and the phosphate group, or C2, C3 and the phosphate group. All of these coordination modes are possible according to the molecular mechanics force field method Hyperchem. Besides the other species to be considered are mono- or bis-chelates with donor sites at the hydroxyl groups of C1 and C2, and C2 and C3.

Additionally, $^{31}P\{^1H\}$ NMR spectra were recorded in aqueous solution of the substrates and in the reaction mixtures S–Cr(VI) and S–**I**. Employing molar ratios of [S]/[Cr(VI)] = 3/1 ([Cr(VI)] = 0.01 M) and [S]/[Cr(V)] = 30/1 ([Cr(V)] = 0.001 M), at t = 3–4 min after mixing, all these systems showed little change in ^{31}P chemical shift relative to the free substrates [34], indicating a weak interaction with the phosphate group [35,36].

The presence of phosphate modifies sterically and electronically the donor ability of the polyalkoxide moiety of the sugar. Phosphate itself affords an additional binding site [37].

The result is a different and more complex EPR pattern with a larger number of signals, which means a mixture of species with very close g values. A simpler EPR pattern was observed for nucleotides, as a consequence of a lower number of linkage isomers involving only three coordination sites — phosphate group, C2′OH and C3′OH — compared with four binding sites available in a ligand such as R5P.

Table 2
Log values of protonation constants of Cr(VI), AMP (L) and CMP (L), and their binding constants with chromate (Cr) at 25.0°C, μ = 0.10 M (KCl)

Equilibrium quotient	Cr(VI)		AMP		CMP	
	This work	Others [a]	This work	Others [a]	This work	Others [a]
$[HCrO_4^-]/[CrO_4^{2-}][H^+]$	6.10	6.09				
$[Cr_2O_7^{2-}]/[CrO_4^{2-}]^2[H^+]^2$	13.62	13.9				
$[HL^-]/[L^{2-}][H^+]$			6.17	6.19	6.19	6.3
$[H_2L]/[L^{2-}][H^+]^2$			9.96	9.99	10.51	10.8
$[LCrO_4^{2-}]/[CrO_4^{2-}][L^{2-}]$			2.32 ± 0.07 [b]		2.64 ± 0.14 [b]	
$[HLCrO_4^{2-}]/[CrO_4^{2-}][L^{2-}][H^+]$			8.67 ± 0.04 [b]		8.80 ± 0.26 [b]	
$[H_2LCrO_4]/[CrO_4^{2-}][L^{2-}][H^+]^2$			14.30 ± 0.13 [b]		14.55 ± 0.39 [b]	

[a] Smith and Martell [40].
[b] Obtained as mean values from potentiometric determinations in the systems AMP–Cr(VI) and CMP–Cr(VI) with the following concentrations: [Cr(VI)] = 0.00196 M; [AMP] = 0.00135, 0.00293, 0.00593 M; [CMP] = 0.00182, 0.00357, 0.00708 M.

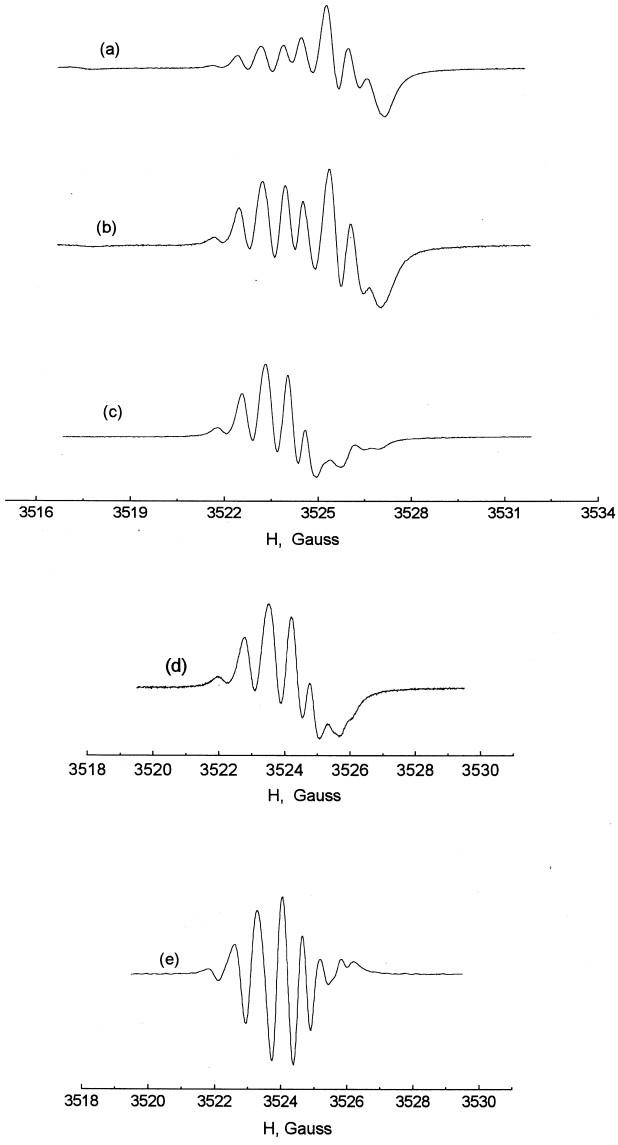


Fig. 6. X-band spectra of the ligand-exchange reaction of compound **I** with CMP (a–c). $T = 25°C$, aqueous solution, [**I**] = 1 mM, [CMP] = 0.096 M. Operating frequencies (GHz) and time of reaction: (a) 9.782007, 2 min; (b) 9.782016, 3 min; (c) 9.782028, 10 min. (d) X-band spectrum of the Cr(V) species generated in the reaction of potassium dichromate with CMP. Operating frequency 9.782746 GHz, time of reaction 2 h. (e) Second-derivative plot of (d), filtered.

It is very difficult to ascertain the number and structures of the species present in solution due to the overlapping of shf coupling ^{31}P ($I = 1/2$) [17,38] and ^{1}H, even with simulation software [39]. Work is in progress to elucidate the species present in these systems.

3.4. Potentiometric studies

The protonation constants of chromate, AMP and CMP and the formation constant of dichromate were calculated from titration data under the present experimental conditions. The potentiometric titration curve for a mixture of CMP and potassium dichromate in a molar ratio [CMP]/[Cr(VI)] = 1/1 is shown in Fig. 8, together with the curve of CMP. The curves were analyzed, and species with stoichiometry LM, HLM and H_2LM were found, where L is the deprotonated nucleotide ($H_2L = [C_{10}O_7N_5PH_{12}]^{2-}$ for AMP and $[C_9O_8N_3PH_{12}]^{2-}$ for CMP) [40] and M represents chromate. Similar curves were obtained for the system AMP–potassium dichromate. The values of the equilibrium constants obtained at different relationship [S]/[Cr(VI)] are reported in Table 2, and Fig. 9 shows the species distribution for the system Cr(VI)–CMP. Similar curves were obtained for the system AMP–potassium dichromate. In all cases the σ_{fit} values [25] were less than 0.030, and the analysis of random error [26] gave a very satisfactory result for each constant.

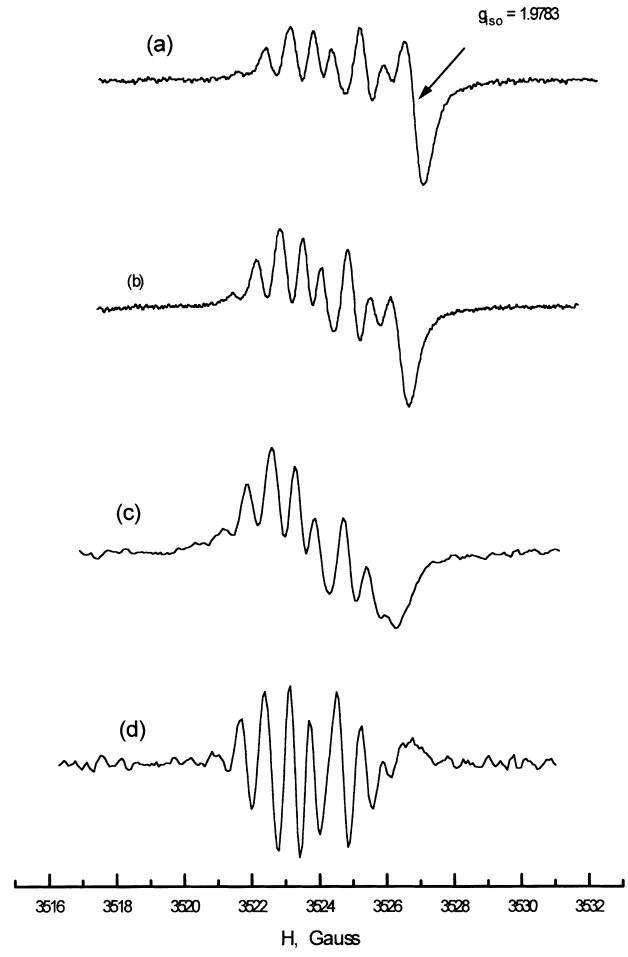


Fig. 7. X-band spectra of the ligand-exchange reaction of compound **I** with dTMP. $T = 25°C$, pH 10, [**I**] = 1 mM, [dTMP] = 0.1 M. Operating frequencies (GHz) and times of reaction: (a) 9.780587, 3 min; (b) 9.780598, 4 min; (c) 9.780617, 11 min. (d) Second-derivative plot of (c), filtered.

Although three species could be found between each nucleotide (AMP or CMP) and chromate, with different degrees of protonation, the concentration of di- and monoprotonated species decreased with the decrease of pH. In all relationships [S]/[Cr(VI)] the non-protonated species, LM, reached the maximum percentage. Thus, the nucleotide diprotonated would not form a stable complex with chromate. These results seem to indicate that the first step leading to the electron

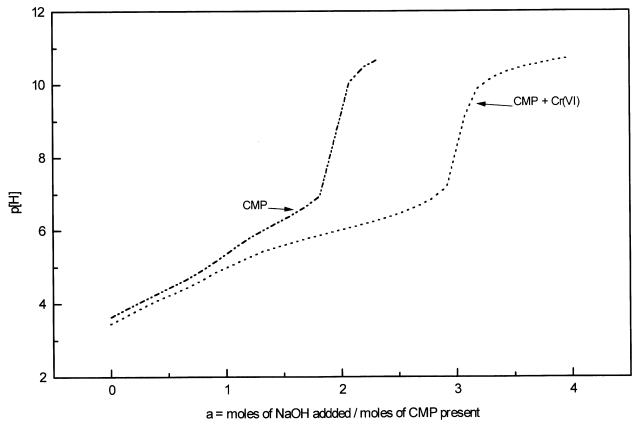


Fig. 8. Potentiometric tritration curves of CMP with and without potassium dichromate. [CMP] = 1.8 mM, [Cr(VI)] = 1.96 mM, [NaOH] = 0.1245 M, T = 25°C, μ = 0.1 M (KCl).

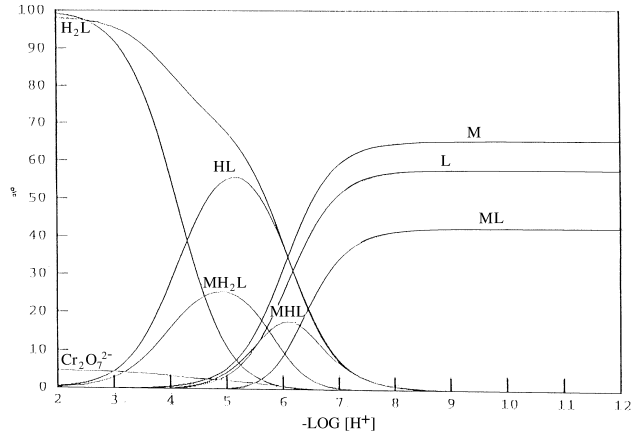


Fig. 9. Species distribution curves of a 1:1 molar ratio CMP–Cr(VI) as a function of $-\log[H^+]$ for a solution initially containing CMP 1.82 mM and chromate 1.96 mM. μ = 0.1 M (KCl), T = 25°C. L, CMP; M, chromate.

transfer reaction should be the chromate monochelate formed with the deprotonate nucleotide.

Acknowledgements

We thank the National Research Council of Argentina (CONICET), the National University at Rosario, and the International Foundation for Sciences (IFS) for financial support. V. Daier thanks CONICET for a fellowship. We thank Dr Nuria Clós (Barcelona University, Spain) for the registration of the EPR spectra. M. Rizzotto thanks Professor Peter Lay for useful comments.

References

[1] International Agency for Research on Cancer Chromium, Nickel and Welding, IARC Monographs on the Evaluation of Carcinogenic Risk to Human 49 (1990) 49.
[2] A. Standeven, K. Wetterhahn, J. Am. Coll. Toxicol. 7 (1989) 1275.
[3] V. Ramana, K. Sastry, J. Inorg. Biochem. 56 (1994) 87.
[4] S. Katz, H. Salem, The Biological and Environmental Chemistry of Chromium, VCH, New York, 1994.
[5] S. De Flora, K. Wetterhahn, Life Chem. Rep. 7 (1989) 169.
[6] M. Costa, A. Zhitkovich, P. Toniolo, E. Taioli, T. Popov, A. Lukanova, Environ. Health Perspect. 104 (1996) 917.
[7] L. Zhang, P. Lay, J. Am. Chem. Soc. 118 (1996) 12624, and references cited therein.
[8] A. Kortenkamp, M. Casadevall, P. Da Cruz Fresco, Ann. Clin. Lab. Sci. 26 (1996) 160.
[9] A. Kortenkamp, M. Casadevall, S. Faux, A. Jenner, R. Shayer, N. Woodbridge, P. O'Brien, Arch. Biochem. Biophys. 329 (1996) 199.
[10] K. Sudgen, K. Wetterhahn, J. Am. Chem. Soc. 118 (1996) 10811.
[11] D. Stearns, L. Kennedy, K. Courtney, P. Giangrande, L. Phieffer, K. Wetterhahn, Biochemistry 34 (1995) 910.
[12] P. Lay, A. Levina, J. Am. Chem. Soc. 120 (1998) 6704.
[13] R. Farrell, R. Judd, P. Lay, N. Dixon, R. Baker, A. Bonin, Chem. Res. Toxicol. 2 (1989) 227.
[14] C. Dillon, P. Lay, A. Bonin, M. Cholewa, G. Legge, T. Collins, K. Kostka, Chem. Res. Toxicol. 11 (1998) 119.
[15] M. Quiros, D. Goodgame, Polyhedron 11 (1992) 1.
[16] M. Branca, A. Dessi, H. Kozlowsky, G. Micera, J. Swiatk, J. Inorg. Biochem. 39 (1990) 217.
[17] G. Barr-David, M. Charara, R. Codd, R. Farrell, J. Irwing, P. Lay, R. Bramley, S. Brumby, Ji Ji-Ying, G. Hanson, J. Chem. Soc., Dalton Trans. 91 (1995) 1207.
[18] L.F. Sala, S. Signorella, M. Rizzotto, M. Frascaroli, F. Gandolfo, Can. J. Chem. 70 (1992) 2046.
[19] V. Daier, S. Signorella, M. Rizzotto, M.I. Frascaroli, C. Palopoli, C. Brondino, J.M. Salas-Peregrin, L.F. Sala, Can. J. Chem. 77 (1999) 57.
[20] M. Rizzotto, S. Signorella, M. Frascaroli, V. Daier, L.F. Sala, J. Carbohydr. Chem. 14 (1995) 45.
[21] S. Signorella, M. Rizzotto, V. Daier, M. Frascaroli, C. Palopoli, D. Martino, A. Bousseckson, L.F. Sala, J. Chem. Soc., Dalton Trans. (1996) 1607.
[22] S. Signorella, M. Santoro, M. Mulero, L.F. Sala, Can. J. Chem. 72 (1994) 398.
[23] S. Signorella, S. García, L.F. Sala, Polyhedron 16 (1997) 701.
[24] M. Krumpolc, J. Rocek, J. Am. Chem. Soc. 101 (1979) 3206.
[25] A. Martell, R. Motekaitis, Determination and Use of Stability Constants, 2nd edn., VCH, New York, 1992.
[26] A. Olivieri, G. Escandar, Anal. Lett. 30 (1997) 1967.
[27] L.F. Sala et al., to be published.
[28] R.P. Farrell, P. Lay, Comments Inorg. Chem. 13 (1992) 133.
[29] R. Bramley, J.-Y. Ji, J. Judd, P. Lay, Inorg. Chem. 29 (1990) 3089.
[30] R. Bramley, J.Y. Jing, P. Lay, Inorg. Chem. 30 (1991) 1557.
[31] K. Srinivasan, J. Kochi, Inorg. Chem. 24 (1985) 4671.
[32] D. Goodgame, P. Hayman, D. Hathway, Polyhedron 1 (1982) 497.
[33] H. Fujii, T. Yoshimura, H. Kamada, Inorg. Chem. 36 (1997) 1122.
[34] M. Rizzotto et al. (unpublished results).
[35] V. Rodríguez-Bailey, M. Clarke, Inorg. Chem. 36 (1997) 1611.
[36] R. Bose, R. Viola, R. Cornelius, J. Am. Chem. Soc. 106 (1984) 3336.
[37] K. Sugden, K. Wetterhahn, Inorg. Chem. 35 (1996) 3727.
[38] R.V. Parish, NMR, NQR, EPR and Mössbauer Spectroscopy in Inorganic Chemistry, Ellis Horwood, Chichester, 1990.
[39] WinSIM EPR Calculations for MS-Windows, Version 0.96. National Institute of Environmental Health Sciences, 1995.
[40] R. Smith, A. Martell, Critical Stability Constants, vol. 6, Plenum, New York, 1989.

PERGAMON

www.elsevier.nl/locate/poly

Polyhedron 19 (2000) 425–429

POLYHEDRON

Electrochemistry and strong near-IR absorption of the $[Ni(dphdt)_2]^n$ complexes ($n = -1, 0$; dphdt = 5,6-diphenyl-1,4-dithiin-2,3-dithiolate); X-ray crystal structure of $(Ph_4P)[Ni(dphdt)_2](CH_2Cl_2)$

Ha-Jin Lee, Dong-Youn Noh *

Department of Chemistry, Seoul Women's University, Seoul 139-774, South Korea

Received 17 March 1999; accepted 6 December 1999

Abstract

Nickel bisdithiolene complexes $C_x[Ni(dphdt)_2]$ ($x = 1$ or 0.1, C = tetrabutylammonium (n-Bu_4N^+); $x = 1$, C = tetraphenylphosphonium (Ph_4P^+); dphdt = 5,6-diphenyl-1,4-dithiin-2,3-dithiolate) have been synthesized and characterized. The molecular structure of $(Ph_4P)[Ni(dphdt)_2](CH_2Cl_2)$ was determined by X-ray analysis. $Ni(S_2C_2S_2)_2$ core is planar and stacking along the *c*-axis and the shortest intra-stack S···S distance is 4.529 Å. According to the cyclic voltammetry of (n-Bu_4N)$[Ni(dphdt)_2]$, two phenyl groups on the dphdt ligand decrease the electron density on the $Ni(S_2C_2S_2)_2$ core and increase the oxidation potentials compared to those of the (n-Bu_4N)$[Ni(dddt)_2]$ complex (dddt = 5,6-dihydro-1,4-dithiin-2,3-dithiolate). Near-IR spectra of the complexes show that phenyl substitution on the ligand does not give rise to the evident change in transition energy due to the lack of coplanarity with the $Ni(S_2C_2S_2)_2$ core. ©2000 Elsevier Science Ltd All rights reserved.

Keywords: Crystal structures; Cyclic voltammetry; Nickel bisdithiolenes; Strong near-IR absorption

1. Introduction

Metal bisdithiolene complexes have received considerable attention in the area of developing new materials due to their versatile properties such as electrical conductivity, strong near-IR absorption, molecular magnetism and catalytic behaviour [1–3]. In order to obtain better properties, many new ligands have been designed, prepared and utilized in preparing metal complexes [4–15]. Recently, we have been intensively involved in developing new dithiolene ligands and their metal complexes with those properties [4–13]. One of those ligands is diphenyl-containing dphdt (5,6-diphenyl-1,4-dithiin-2,3-dithiolate) as shown in Scheme 1, which was prepared by [2 + 4] cycloaddition reaction followed by oxo transformation using $Hg(OAc)_2$ [9]. $Ni(dphdt)_2$ complex in which dPhEDT-DTO (4,5-diphenylethylenedithio-1,3-dithiole-2-one) is used as a ligand precursor, is one of the analogues of $Ni(dddt)_2$ complex (dddt = 5,6-dihydro-1,4-dithiin-2,3-dithiolate) [16–18] which is regarded as a promising metal dithiolene because its molecular structure is closely similar to that of ET (bis(ethylenedithio)tetrathiafulvalene). Other analogues include $Ni(phdt)_2$ (phdt = 5-phenyl-6-hydro-1,4-dithiin-2,3-dithiolate) [7,14] and $Ni(medt)_2$ (medt = 5-methyl-6-hydro-1,4-dithiin-2,3-dithiolate) [15] which contain one phenyl and one methyl substituent per ligand, respectively. Compared to the phdt ligand containing one phenyl substituent, dphdt contains two symmetrically substituted phenyls.

In this paper, we describe the molecular structure and crystal packing of $(Ph_4P)[Ni(dphdt)_2](CH_2Cl_2)$. The strong near-IR absorption and electrochemical behaviour of the $Ni(dphdt)_2$ complexes are also explained and compared with those of $Ni(dddt)_2$ and $Ni(phdt)_2$ complexes.

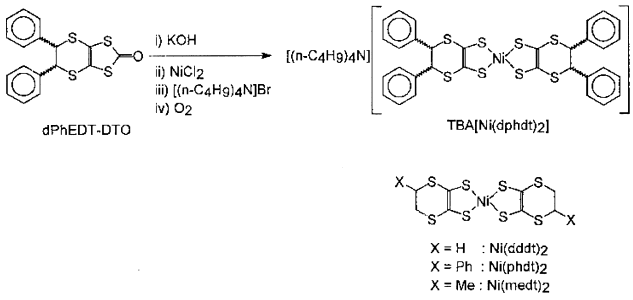
2. Experimental

2.1. Synthesis

All reactions were carried out under nitrogen atmosphere. Ligand precursors (dPhEDT-DTO and PhEDT-DTO) were prepared by the [2 + 4] cycloaddition reaction as fully explained in the previous report [9]. The nickel complexes prepared in this study were recrystallized from CH_2Cl_2–ethyl acetate, the synthesis of which [7] is outlined in Scheme 1.

* Corresponding author. Tel.: +82-2-970-5656; fax: +82-2-970-5660; e-mail: dynoh@swu.ac.kr

0277-5387/00/$ - see front matter ©2000 Elsevier Science Ltd All rights reserved.
PII S0277-5387(99)00379-4



Scheme 1.

2.1.1. (n-Bu$_4$N)[Ni(dphdt)$_2$]

To a methanol solution of dPhEDT-DTO (0.5 mmol) treated with KOH (1 mmol) were added $NiCl_2$ (0.25 mmol) and n-$Bu_4N\cdot Br$ (0.5 mmol) successively in the presence of air. Elemental analysis data for (n-Bu_4N)[Ni(dphdt)$_2$]-(CH_2Cl_2)$_{0.5}$: Calc.: C, 57.84; S, 25.42. Found: C, 57.59; S, 25.73%. FT-IR (KBr, cm^{-1}): 1489.1, 1452.5 (C=C), 1369.5, 1179.8 (C–S).

2.1.2. (Ph$_4$P)[Ni(dphdt)$_2$]

This complex was synthesized by mixing (n-Bu_4N)-[Ni(dphdt)$_2$] and excess $Ph_4P\cdot Br$ in CH_3CN. Elemental analysis data for (Ph_4P)[Ni(dphdt)$_2$](CH_2Cl_2): Calc.: C, 59.74; S, 22.34. Found: C, 59.96; S, 21.82%. FT-IR (KBr, cm^{-1}): 1489.4, 1436.3 (C=C), 1364.6, 1182.2 (C–S).

2.1.3. (n-Bu$_4$N)$_{0.1}$[Ni(dphdt)$_2$]

This complex was prepared by the reaction of (n-Bu_4N)-[Ni(dphdt)$_2$] and excess iodine in CH_3CN. Elemental analysis data for (n-Bu_4N)$_{0.1}$[Ni(dphdt)$_2$](CH_2Cl_2): Calc.: C, 52.22; S, 32.17. Found: C, 51.65; S, 31.98%. FT-IR (KBr, cm^{-1}): 1226.7 (br).

2.1.4. (n-Bu$_4$N)[Ni(phdt)$_2$], (Ph$_4$P)[Ni(phdt)$_2$], [Ni(phdt)$_2$]

Ni(phdt)$_2$ complexes were prepared using the PhEDT-DTO ligand precursor following the method for Ni(dphdt)$_2$ complexes, and fully analyzed as reported previously [7].

2.2. General methods

Infrared spectra were measured by the KBr method on a MIDAC FT-IR spectrometer and UV–Vis–Near-IR spectra in CH_2Cl_2 on a Shimadzu UV-3100 instrument. Cyclic voltammetry was measured at room temperature on a BAS CW50W system in tetrahydrofuran (THF; 2 ml) containing 0.1 M n-$Bu_4N\cdot BF_4$ as a supporting electrolyte, Ag/Ag^+ as a reference electrode, glassy carbon working electrode, and platinum wire as a counter electrode ($E_{1/2}=0.2$ V for the Fc/Fc^+ couple).

2.3. X-ray structure determination

X-ray crystallographic data of (Ph_4P)[Ni(dphdt)$_2$]-(CH_2Cl_2) were collected on an Enraf-Nonius CAD-4 automatic diffractometer with graphite-monochromated Mo Kα radiation ($\lambda=0.71073$ Å) at 293(2) K. Intensities of 3827 ($R_{int}=0.0275$) independent reflections within the θ range 1.23–23.96° were measured using $\omega/2\theta$ scan mode for the range $0\le h\le 11$, $0\le k\le 26$, $-26\le l\le 26$. A total of 3462 reflections were considered [$I>2\sigma(I)$] and used in calculations performed on an IBM PC using SHELXS-86 and SHELXL-93 [19,20]; atomic scattering factors for all non-hydrogen atoms were supplied by the SHELXS-86 system. Crystal parameters and procedural information corresponding to data collection are given in Table 1.

Table 1
Crystal data and structure refinement for (Ph_4P)[Ni(dphdt)$_2$](CH_2Cl_2)

Empirical formula	$C_{57}H_{46}Cl_2NiPS_8$
Formula weight	1148.00
Temperature (K)	293(2)
Wavelength (Å)	0.71073
Crystal system	monoclinic
Space group	$P2_1/n$ (no. 14)
a (Å)	10.395(5)
b (Å)	23.154(5)
c (Å)	23.554(5)
β (°)	90.47(3)
Volume (Å^3)	5669(3)
Z	4
Density (calculated) (Mg m^{-3})	1.345
Absorption coefficient (mm^{-1})	0.796
$F_{(000)}$	2372
θ range for data collection (°)	1.23–23.96
Index ranges	$0\le h\le 11$, $0\le k\le 26$, $-26\le l\le 26$
No. reflections collected	4014
No. independent reflections	3827 ($R_{int}=0.0275$)
Refinement method	full-matrix least-squares on F^2
Data/restraints/parameters	3462/0/615
Goodness-of-fit on F^2	0.904
Final R indices [$I>2\sigma(I)$]	$R1=0.0799$, $wR2=0.2200$
R indices (all data)	$R1=0.0878$, $wR2=0.2308$
Largest difference peak and hole (e Å^{-3})	0.811 and −0.519

3. Results and discussion

3.1. X-ray crystal structure

The molecular structure of (Ph_4P)[Ni(dphdt)$_2$] grown in CH_2Cl_2–CH_3OH solvent pair by slow diffusion was solved by X-ray single crystal analysis. The structure of [Ni(dphdt)$_2$]$^{1-}$ with the atom numbering scheme is shown in Fig. 1, and the selected bond distances and angles are listed in Table 2. The bond distances of C1–C2 and C17–C18 are within 1.33–1.34 Å, corresponding to the typical distance of a C=C bond in alkene [21], and very close to those of [Ni(dddt)$_2$]$^{1-}$ (1.339 Å) [18] as shown in Table 3. They are, however, quite different from those of [Ni(phdt)$_2$]$^{1-}$ (1.384 Å) [14] which corresponds to a C···C bond distance in benzene (1.39 Å) [21]. This could be attributed to the inductive effect together with the structural effect based upon

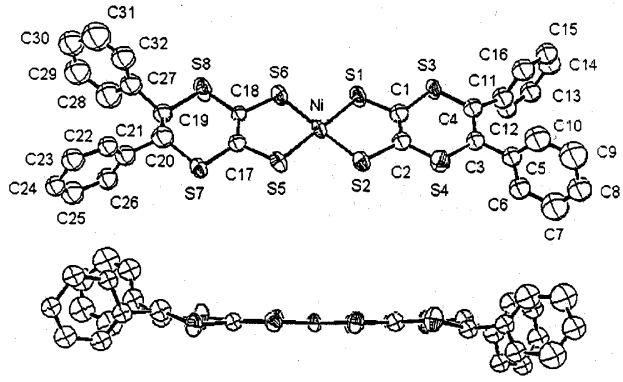


Fig. 1. ORTEP view of $[Ni(dphdt)_2]^{1-}$ with atom numbering scheme: top view (top) and side view (bottom). Hydrogen atoms are omitted for clarity.

Table 2
Selected bond lengths (Å) and angles (°) for $(Ph_4P)[Ni(dphdt)_2]\cdot(CH_2Cl_2)$

Ni–S(1)	2.144(4)	Ni–S(5)	2.151(4)
Ni–S(6)	2.141(5)	Ni–S(2)	2.161(5)
S(1)–C(1)	1.752(15)	S(2)–C(2)	1.749(13)
S(3)–C(1)	1.773(14)	S(3)–C(4)	1.87(3)
S(4)–C(2)	1.715(16)	S(4)–C(3)	1.79(3)
S(5)–C(17)	1.745(15)	S(6)–C(18)	1.748(13)
S(7)–C(17)	1.736(14)	S(7)–C(20)	1.85(3)
S(8)–C(18)	1.769(15)	S(8)–C(19)	1.92(3)
C(1)–C(2)	1.34(2)	C(3)–C(4)	1.50(4)
C(3)–C(5)	1.56(3)	C(4)–C(11)	1.62(3)
C(17)–C(18)	1.335(19)	C(19)–C(20)	1.45(4)
C(19)–C(27)	1.54(4)	C(20)–C(21)	1.55(3)
S(1)–Ni–S(5)	178.41(18)	S(1)–Ni–S(6)	87.26(16)
S(5)–Ni–S(6)	91.28(16)	S(1)–Ni–S(2)	91.74(16)
S(5)–Ni–S(2)	89.74(16)	S(6)–Ni–S(2)	177.78(19)
C(1)–S(1)–Ni	103.4(5)	C(2)–S(2)–Ni	104.8(6)
C(1)–S(3)–C(4)	99.6(10)	C(2)–S(4)–C(3)	106.2(10)
C(17)–S(5)–Ni	105.1(5)	C(18)–S(6)–Ni	104.0(5)
C(17)–S(7)–C(20)	104.6(10)	C(18)–S(8)–C(19)	99.2(11)
C(2)–C(1)–S(1)	122.0(11)	C(2)–C(1)–S(3)	127.6(11)
S(1)–C(1)–S(3)	110.4(9)	C(1)–C(2)–S(4)	127.0(11)
C(1)–C(2)–S(2)	117.9(12)	S(4)–C(2)–S(2)	115.1(9)
C(4)–C(3)–S(4)	111(2)	C(3)–C(4)–S(3)	111(2)
C(18)–C(17)–S(7)	127.9(11)	C(18)–C(17)–S(5)	118.3(11)
S(7)–C(17)–S(5)	113.6(9)	C(17)–C(18)–S(6)	121.2(11)
C(17)–C(18)–S(8)	127.0(11)	S(6)–C(18)–S(8)	111.7(8)
C(20)–C(19)–S(8)	109(2)	C(19)–C(20)–S(7)	112(2)

Table 3
Bond distances (Å) of chelate five-membered ring of $[NiL_2]^{1-}$ complexes

L	Ni–S	S–C	C=C	Ref.
dphdt [a]	2.149	1.749	1.34	This work
phdt [b]	2.126	1.706	1.384	[14]
dddt [b]	2.148	1.735	1.339	[18]

[a] Tetraphenylphosphonium salt.
[b] Tetrabutylammonium salt.

the fact that dphdt and dddt ligands have two identical substituents (two phenyls and two hydrogens, respectively) symmetrically linked to the peripheral sp^3 carbons, whereas

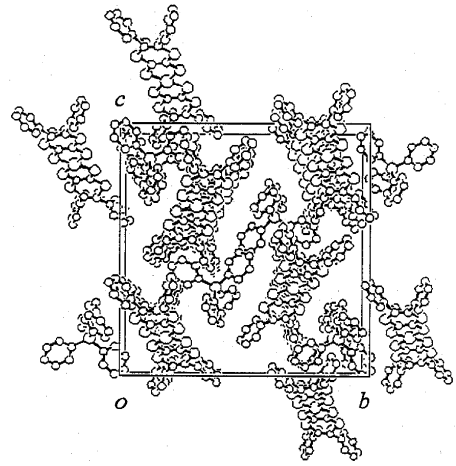


Fig. 2. Crystal structure of $(Ph_4P)[Ni(dphdt)_2]$ viewed along the *a*-axis.

phdt ligand has two different substituents (one phenyl and one hydrogen) (Scheme 1). The similarity in bond distances between $[Ni(dphdt)_2]^{1-}$ and $[Ni(dddt)_2]^{1-}$ can also be observed in the Ni–S and S–C bonds as shown in Table 3.

The $[NiS_4]$ core yields complete square-planar geometry with four S–Ni–S angles adding up to 360° (Table 2). The $S_2C{=}CS_2$ units in dphdt ligand are also planar as the sum of three angles around C1, C2, C17 and C18 are 360°, respectively. Therefore, the $Ni(S_2C_2S_2)_2$ unit is planar and, moreover, external (Ph)CH–CH(Ph) units are not bent so much from the central $Ni(S_2C_2C_2)_2$ plane as can be seen in the molecular side view (Fig. 1). This planar geometry of metal–bisdithiolene complex is one of the requirements for intermolecular close contact and is thus of high electrical conductivity [2,3]. Owing to the planar geometry, $[Ni(dphdt)_2]^{1-}$ units can be stacked along the *a*-axis and make columns which are separated from one another by tetraphenylphosphonium cation (Ph_4P^+) as shown in Fig. 2. The shortest intermolecular S···S interaction occurs within a stacking column with the distance of 4.529 Å between S4 and S7, which is much longer than the sum of van der Waals radii of sulfur atoms (3.7 Å) [22]. This is not surprising if we consider the geometry of $[Ni(dphdt)_2]^{1-}$ units: four phenyl groups connected to the periphery of the ligand are nearly perpendicular to the central $Ni(S_2C_2C_2)_2$ plane (Fig. 1) and would prohibit the close contact of molecules.

3.2. Cyclic voltammetry

Cyclic voltammograms of microcrystalline $(n\text{-}Bu_4N)[Ni(dphdt)_2]$, $(n\text{-}Bu_4N)[Ni(phdt)_2]$ and $(n\text{-}Bu_4N)[Ni(dddt)_2]$ complexes were measured in THF and compared in order to verify the effect of substituted phenyl groups on the redox properties of nickel complexes. Three voltammograms are quite similar in overall shape and redox potentials, implying that the redox processes are not so different for the three complexes.

Upon scanning from about −0.4 V (denoted by an asterisk in Fig. 3), $Ni(dphdt)_2$ complex exhibits two reversible waves

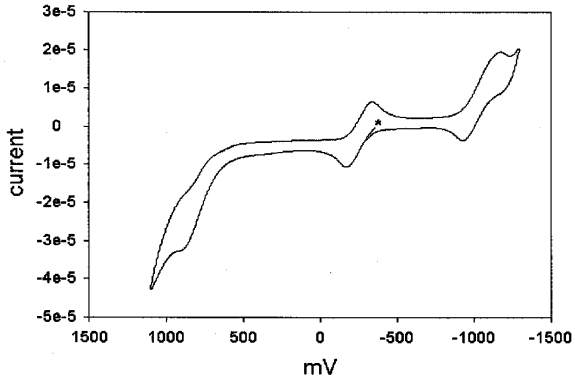


Fig. 3. Cyclic voltammogram recorded at a glassy carbon electrode on a THF solution containing $(n\text{-}Bu_4N)[Ni(dphdt)_2]$ (0.01 mol dm^{-3}) and $n\text{-}Bu_4N\cdot BF_4$ as supporting electrolyte. Scan rate 0.05 V s^{-1}. * Starting potential value.

with the half-wave potentials ($E_{1/2}$) of -0.25 and -1.05 V, respectively, along with the irreversible oxidation peak at around 0.9 V. Based on the redox process of $(n\text{-}Bu_4N)[Ni(dddt)_2]$ reported [16], the wave centred at -1.05 V is undoubtedly due to the $[Ni(dphdt)_2]^{2-} \rightleftharpoons [Ni(dphdt)_2]^{1-}$ process and the wave centred at -0.25 V can be attributed to the formation of neutral complex from $[Ni(dphdt)_2]^{1-}$. It is noteworthy that these potentials are almost the same as those of the $Ni(phdt)_2$ complex (-0.26 and -1.05 V) but comparatively different from those of the $Ni(dddt)_2$ complex (-0.29 and -1.07 V). The potential difference between $Ni(dddt)_2$ and $Ni(dphdt)_2$ complexes can be explained by the acceptor property of phenyl substituents [14]: the stronger the acceptor property of substituent is (phenyl is a stronger acceptor than H), the less electron density is expected on the $Ni(S_2C_2S_2)_2$ core. In consequence, the oxidation potential of the complex becomes higher due to the introduction of phenyl groups. The multielectron irreversible oxidation peak at the higher potential (0.9 V) can be assigned to the formation of cationic complex $[Ni(dphdt)_2]^0 \rightarrow [Ni(dphdt)_2]^{\delta+}$, if we suppose that the redox behaviour of $Ni(dphdt)_2$ and $Ni(dddt)_2$ complexes is not so very different [16].

3.3. Near-IR spectra

The characteristic strong near-IR absorption bands are found in the electronic spectra of nickel complexes prepared in this study. The absorbance and absorption maxima of the complexes are collected in Table 4. Monoanionic $Ni(dphdt)_2$ complexes show absorption maxima at 1158 nm ($\varepsilon \approx 13\,000$ M^{-1} cm^{-1}), which is not so very different from those of $[Ni(phdt)_2]^{1-}$ and $[Ni(dddt)_2]^{1-}$ (20 nm or 14 cm^{-1}) in energy even though the influence of solvent is not ruled out completely. In the simple MO diagram of Ni–dithiolene [1] the frontier orbitals are shifted in energy by the presence of the electron acceptor/donor substituted on the Ni–dithiolene core. Therefore, the highest occupied molecular orbital (HOMO) level ($2b_{1u}$) is expected to be stabilized by the electron-accepting substituent and thereby the transition

Table 4
Near-IR spectral data of the nickel complexes

Complex	λ_{max} (nm)	ε (M^{-1} cm^{-1})	Solvent	Ref.
$(n\text{-}Bu_4N)[Ni(dphdt)_2]$	1158	12 900	CH_2Cl_2	this work
$(Ph_4P)[Ni(dphdt)_2]$	1158	13 100	CH_2Cl_2	this work
$(n\text{-}Bu_4N)_{0.1}[Ni(dphdt)_2]$	1029	24 600	CH_2Cl_2	this work
$(n\text{-}Bu_4N)[Ni(phdt)_2]$	1178	11 300	CH_2Cl_2	this work
	1172	15 000	CH_3CN	[14]
$(Ph_4P)[Ni(phdt)_2]$	1157	9 400	CH_2Cl_2	this work
$[Ni(phdt)_2]$	1012	68 700	CH_2Cl_2	this work
	1028	43 000	C_6H_6	[14]
$(n\text{-}Bu_4N)[Ni(dddt)_2]$	1175	15 600	CH_3CN	[14]

energy (ΔE_{NIR}) between HOMO ($2b_{1u}$) and lowest unoccupied molecular orbital (LUMO) ($3b_{2g}$) levels will increase. In our complex, however, the phenyl substituents are not effectively conjugated with the $Ni(S_2C_2S_2)_2$ core due to the lack of coplanarity, as can be seen in its molecular structure (Fig. 1), and that the substituent effect is not evident. This is comparable to the phenyl-substituted bis[1,2-ethylenedithiolato(2−)-S,S′]nickel complexes in which the phenyl substituents are almost coplanar to the Ni–dithiolene core [23]: bis[1-phenylethene-1,2-dithiolato(2−)-S,S′]-nickel (810 nm) and bis[1,2-diphenylethene-1,2-dithiolato(2−)-S,S′]nickel (865 nm) complexes show an electronic transition energy difference of 55 nm (785 cm^{-1}), which is much bigger than our case (14 cm^{-1}).

Solution near-IR spectrum of $(n\text{-}Bu_4N)[Ni(dphdt)_2]$ is demonstrated in Fig. 4 together with that of $(n\text{-}Bu_4N)_{0.1}[Ni(dphdt)_2]$. While the monocationic complex shows broad absorption ($\lambda_{max} = 1158$ nm) with a shoulder at the high energy region, the partially oxidized complex gives a relatively narrow absorption band at a higher energy region ($\lambda_{max} = 1029$ nm) with more intense absorbance ($\varepsilon = 24\,600$ M^{-1} cm^{-1}) than that of the monocationic one ($\varepsilon \approx 13\,000$ M^{-1} cm^{-1}). This behaviour is also observed in the spectra of $Ni(phdt)_2$ complexes along with the solvent dependency

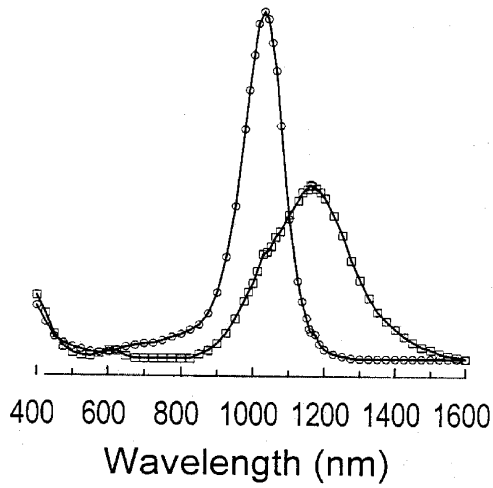


Fig. 4. Near-IR absorption spectra of $(n\text{-}Bu_4N)[Ni(dphdt)_2]$ (□) and $(n\text{-}Bu_4N)_{0.1}[Ni(dphdt)_2]$ (○).

of absorption maxima (Table 4). It can be rationalized by the fact that oxidation of monocationic complex can change HOMO from b_{1u} to b_{3g} of Ni–dithiolene core, for example, and therefore increase the electronic transition energy (ΔE_{NIR}). Consequently, a hypsochromic shift of 129 nm (108 cm^{-1}) results from the oxidation of (n-Bu_4N)-[Ni(dphdt)$_2$] with more intense absorbance.

4. Conclusions

The crystal structure of (Ph_4P)[Ni(dphdt)$_2$](CH_2Cl_2) was solved by X-ray structural analysis. The selected bond distances in this complex such as Ni–S, S–C and C=C are quite close to those of (n-Bu_4N)[Ni(dddt)$_2$] but quite different from those of (n-Bu_4N)[Ni(phdt)$_2$] because of the substituent effect on the ligand: dddt and dphdt ligands are symmetric but phdt is not. Due to the electron-withdrawing effect of substituted phenyl groups, higher oxidation potentials in the cyclic voltammogram are observed in $[Ni(dphdt)_2]^{1-}$ and $[Ni(phdt)_2]^{1-}$ complexes. However, the electronic transition energy of (n-Bu_4N)[Ni(dphdt)$_2$] in the near-IR range (ΔE_{NIR}) is not so very different from that of the (n-Bu_4N)[Ni(phdt)$_2$] complex.

Supplementary data

Full crystallographic details have been deposited at the Cambridge Crystallographic Data Centre (CCDC). Supplementary data are available from the CCDC, 12 Union Road, Cambridge CB2 1EZ, UK, on request, quoting the deposition number 116572.

Acknowledgements

The authors wish to acknowledge the financial support of the Korea Research Foundation made in the program year of 1997. We gratefully thank Professor W.S. Shin (Department of Chemistry, Sogang University, Korea) for helpful discussion.

References

[1] U.T. Mueller-Westerhoff, B. Vance, Comp. Coord. Chem. 2 (1987) 595.
[2] R.-M. Olk, B. Olk, W. Dietzsch, R. Kirmse, E. Hoyer, Coord. Chem. Rev. 117 (1992) 99.
[3] P. Cassoux, L. Valade, H. Kobayashi, A. Kobayashi, R.A. Clark, A.E. Underhill, Coord. Chem. Rev. 110 (1991) 115.
[4] H.-J. Lee, Y.-Y. Kim, D.-Y. Noh, Bull. Korean Chem. Soc. 19 (1998) 1011.
[5] H.-J. Lee, D.-Y. Noh, Bull. Korean Chem. Soc. 19 (1998) 340.
[6] D.-Y. Noh, A.E. Underhill, M.B. Hursthouse, Chem. Commun. (1997) 2211.
[7] D.-Y. Noh, H.-J. Lee, A.E. Underhill, Synth. Met. 86 (1997) 1837.
[8] D.-Y. Noh, M. Mizuno, D.-K. Kim, J.-B. Yoon, J.-H. Choy, Polyhedron 16 (1997) 1351.
[9] D.-Y. Noh, H.-J. Lee, J. Hong, A.E. Underhill, Tetrahedron Lett. 37 (1996) 7603.
[10] D.-Y. Noh, M.-J. Kang, H.-J. Lee, J.-H. Kim, J.-H. Choy, Bull. Korean Chem. Soc. 17 (1996) 46.
[11] D.-Y. Noh, J.-H. Choy, Synth. Met. 70 (1995) 1059.
[12] D.-Y. Noh, M. Mizuno, N.H. Hur, D.-K. Kim, J.-H. Choy, Synth. Met. 70 (1995) 1057.
[13] D.-Y. Noh, M. Mizuno, J.-H. Choy, Inorg. Chim. Acta 216 (1994) 147.
[14] J.-L. Zuo, T.-M. Yao, F. You, X.-Z. You, H.-K. Fun, B.-C. Yip, J. Mater. Chem. 6 (1996) 1633.
[15] T.-M. Yao, J.-L. Zuo, X.-Z. You, X.-Y. Huang, Polyhedron 14 (1995) 1487.
[16] C. Faulman, P. Cassoux, E.B. Yagubskii, L.V. Vetoshkina, New J. Chem. 17 (1993) 385.
[17] V.E. Shklover, S.S. Nagapetyan, Y.T. Struchkov, Russ. Chem. Rev. 59 (1990) 1179.
[18] C.T. Vance, R.D. Bereman, J. Bordner, W.E. Hatfield, J.H. Helms, Inorg. Chem. 24 (1985) 2905.
[19] G.M. Sheldrick, SHELXS-86: A Program for Structure Determination, University of Göttingen, Germany, 1986.
[20] G.M. Sheldrick, SHELXS-93: A Program for Structure Refinement, University of Göttingen, Germany, 1993.
[21] R.T. Morrison, R.N. Boyd, Organic Chemistry, 4th ed., 1983, Allyn and Bacon, Boston.
[22] A. Bondi, J. Phys. Chem. 68 (1964) 441.
[23] C.S. Winter, S.N. Oliver, R.J. Mannig, J.D. Rush, C.A.S. Hill, A.E. Underhill, J. Mater. Chem. 2 (1992) 443.

PERGAMON

www.elsevier.nl/locate/poly

Polyhedron 19 (2000) 431–435

POLYHEDRON

Synthesis, characterization and crystal structures of the cobalt(II) and iron(II) complexes with an octadentate ligand, 1,4,7,10-tetrakis(2-pyridylmethyl)-1,4,7,10-tetraazacyclododecane (**L**), $[M\mathbf{L}]^{2+}$

Xian-He Bu* [1, a], Shou-Liang Lu [a], Ruo-Hua Zhang* [2,a], He Liu [a], Hong-Ping Zhu [b], Qiu-Tian Liu [b]

[a] *Department of Chemistry, Nankai University, Tianjin 300071, People's Republic of China*

[b] *State Key Laboratory of Structure Chemistry, Fujian Institute of Research on the Structure of Matter, Chinese Academy of Science, Fuzhou 350002, People's Republic of China*

Received 19 July 1999; accepted 14 December 1999

Abstract

The potential octadentate ligand, 1,4,7,10-tetrakis(2-pyridylmethyl)-1,4,7,10-tetraazacyclododecane (**L**), gives iron(II) and cobalt(II) complexes of general formula $[M\mathbf{L}](ClO_4)_2 \cdot nH_2O$ ($n = 1$ or 0.5). The crystal and molecular structures of the complexes have been determined by single-crystal X-ray analysis. The complex $[Fe\mathbf{L}](ClO_4)_2 \cdot H_2O$ can be considered as octacoordinated with two semicoordinated bonds. The complex $[Co\mathbf{L}](ClO_4)_4 \cdot 0.5H_2O$ is six-coordinated with approximate octahedral geometry. ©2000 Elsevier Science Ltd All rights reserved.

Keywords: Crystal structures; Cobalt(II) complexes; Iron(II) complexes; Octadentate ligands

1. Introduction

The coordination properties toward metal ions of macrocyclic ligands bearing pendant donor groups have recently attracted much interest, mainly because the study of such systems may provide a basis for a better understanding of the metal environment in some metalloenzymes and metalloproteins [1,2]. A number of derivatives of tetraazamacrocycles (cyclen and cyclam) have been prepared by substituting the hydrogen on the amine group with alkyl substituents having pendant arms containing functional groups such as carboxylic acids, alcohols, pyridyl and other donor groups [3–5]. 1,4,7,10-Tetrakis(2-pyridylmethyl)-1,4,7,10-tetraazacyclododecane (**L**) (Chart 1), a potential octadentate ligand, can bond to transition metals to form a variety of stable complexes utilizing all eight donor atoms or fewer donor atoms to form binuclear and mononuclear complexes. In previous publications, we reported 1,4,7,10-tetraazacyclododecane (cyclen) with four pyridyl groups connected to the macrocycle through methylene chains, and the nickel(II), copper(II), zinc(II) and lanthanide complexes [6–9]. The metal ion is always bound to the four nitrogen atoms of the macrocycle, whose central cavity is too small to accommodate cations, and its coordination sphere is completed by two to four additional nitrogen atoms from the pendant groups.

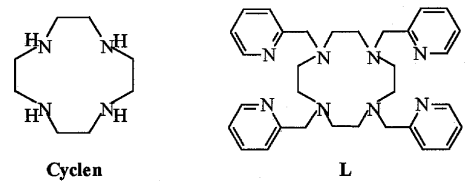


Chart 1

We report here the synthesis, characterization and crystal structure of the iron(II) and cobalt(II) complexes with 1,4,7,10-tetrakis(2-pyridylmethyl)-1,4,7,10-tetraazacyclododecane (**L**). One of the title complexes, $[Fe(\mathbf{L})](ClO_4)_2 \cdot H_2O$ (**1**), is an encapsulated complex. The study of such systems may also provide a basis for a better understanding of the environment in some metalloenzymes and metalloproteins [2].

[1] *Corresponding author.

[2] *Corresponding author. Tel.: +86-22-23502809; fax: +86-22-23530850; e-mail: buxh@nankai.edu.cn

0277-5387/00/$ - see front matter ©2000 Elsevier Science Ltd All rights reserved.
PII S0277-5387(99)00381-2

2. Experimental

2.1. Materials and methods

All reagents were of reagent grade; the intermediate compound 1,4,7,10-tetraazacyclododecane (cyclen) was prepared according to a literature method [10], 2-(chloromethyl)pyridine hydrochloride was purchased from Aldrich and used without further purification, and 1,4,7,10-tetrakis(2-pyridylmethyl)-1,4,7,10-tetraazacyclododecane (**L**) was prepared by a literature method [7]. Hydrated metal perchlorates were prepared by standard methods.

IR spectra were recorded on a 170SX (Nicolet) IR spectrometer in the range 4000–400 cm^{-1} using KBr pellets. UV–Vis spectra were recorded on a Shimadzu UV-240 spectrometer. Magnetic susceptibilities were measured on a Faraday balance at room temperature and Mohr's salt was used for calibration. Variable temperature magnetic susceptibilities were measured on a vibrating sample model CF-1 magnetometer. The effective magnetic moment was calculated using the equation $\mu_{eff} = 2.828(\chi_m T)^{1/2}$, where χ_m is the magnetic susceptibility corrected for diamagnetism of the constituting atoms using Pascal's constants. Elemental analysis was performed on a P-E 240C analyzer.

2.2. Synthesis of the complexes

2.2.1. [Fe**L**](ClO4)2·H2O (**1**)

The ligand **L** (107 mg, 0.2 mmol) in acetonitrile (10 ml) and an aqueous solution (10 ml) of $FeCl_2 \cdot 4H_2O$ (40 mg, 0.2 mmol) in 1:1 molar ratio was mixed at room temperature for 0.5 h. The reaction mixture was filtered to remove small solids and the filtrate treated with a solid sample of $NaClO_4 \cdot H_2O$ (100 mg). The colorless crystalline product suitable for X-ray analysis was obtained from the solution. Yield: 80 mg (49%). *Anal*. Calc. for $C_{32}H_{42}Cl_2N_8O_9Fe$: C, 47.3; H, 5.2; N, 13.8. Found: C, 47.0, H, 4.9, N, 13.4%. Selected IR (cm^{-1}): 2859 (CH_2), 1607, 1571 (py ring), 1090, 623 (ClO_4^-).

2.2.2. [Co**L**](ClO4)2·0.5H2O (**2**)

The above-mentioned procedure was repeated using $Co(ClO_4)_2 \cdot 6H_2O$ (73.2 mg, 0.2 mmol) as starting material. Pink crystals were obtained from the pink reaction solution. Yield: 84 mg (52%). *Anal*. Calc. for $C_{32}H_{41}Cl_2N_8O_{8.5}Co$: C, 47.8; H, 5.1; N, 13.9. Found: C, 47.3, H, 4.9, N, 13.6%. Selected IR (cm^{-1}): 2874 (CH_2), 1608, 1594, 1571 (py ring), 1091, 623 (ClO_4^-).

2.3. Crystallography

Crystal data were measured on an Enraf-Nonius CAD diffractometer with Mo Kα radiation ($\lambda = 0.71073$ Å). The intensities of reflections were measured in the $\omega/2\theta$ scan mode at room temperature with $\theta \leq 25°$ for the Fe(II) complex and $\theta \leq 23°$ for the Co(II) complex. All data were corrected for empirical absorption. The structure was solved by MolEN or SHELXS-86. The final refinement by full-matrix least-squares method with anisotropic thermal parameters for non-hydrogen atoms converged with unweighted and weighted (unit weights for all observed reflections) agreement factors of 0.0624 and 0.0678 for the Fe complex and 0.0594 and 0.0639 for the Co complex.

Table 1 contains the crystal data and further details of the X-ray structural determinations. Selected bond distances and angles are listed in Tables 2 and 3.

Table 1
The crystal structure parameters of the complexes

	[Fe**L**](ClO4)2·H2O	[Co**L**](ClO4)2·0.5H2O
Formula	$FeCl_2O_9N_8C_{32}H_{42}$	$CoCl_2O_{8.5}N_8C_{32}H_{41}$
FW	809.49	803.57
Crystal system	triclinic	triclinic
Space group	*P*-1	*P*-1
a (Å)	9.553	9.590
b (Å)	10.7274	10.651
c (Å)	18.4055	18.531
α (°)	82.86	82.48
β (°)	75.17	75.06
γ (°)	77.64	77.45
V (Å^3)	1776	1780
Z	2	2
D_{calc} (g cm^{-3})	1.51	1.50
No. measured reflections	6237	5077
No. independent reflections	6237	4558
No. observed reflections ($I \geq 3\sigma(I)$)	4019	3496
Parameters	469	456
R	0.0624	0.0594
R_w	0.0678	0.0693
S	1.28	1.30
Maximum residual peak (e Å^{-3})	0.62	0.51

Table 2
Selected bond distances (Å) and angles (°) for [FeL](ClO4)2·H2O

Fe–N(1)	2.344(5)	Fe–N(11)	3.108(5)
Fe–N(2)	2.317(5)	Fe–N(22)	2.226(4)
Fe–N(3)	2.314(6)	Fe–N(33)	2.998(5)
Fe–N(4)	2.302(5)	Fe–N(44)	2.233(6)
N(1)–Fe–N(2)	75.6(2)	N(3)–Fe–N(11)	155.4(2)
N(1)–Fe–N(3)	124.1(2)	N(3)–Fe–N(22)	94.9(2)
N(1)–Fe–N(4)	77.5(2)	N(3)–Fe–N(33)	60.8(2)
N(1)–Fe–N(11)	59.2(1)	N(3)–Fe–N(44)	125.1(2)
N(1)–Fe–N(22)	122.4(2)	N(4)–Fe–N(11)	125.2(2)
N(1)–Fe–N(33)	156.1(2)	N(4)–Fe–N(22)	159.0(2)
N(1)–Fe–N(44)	92.9(2)	N(4)–Fe–N(33)	81.8(2)
N(2)–Fe–N(3)	77.8(2)	N(4)–Fe–N(44)	74.2(2)
N(2)–Fe–N(4)	121.8(2)	N(11)–Fe–N(22)	68.3(2)
N(2)–Fe–N(11)	80.1(2)	N(11)–Fe–N(33)	127.9(1)
N(2)–Fe–N(22)	73.6(2)	N(11)–Fe–N(44)	76.2(2)
N(2)–Fe–N(33)	126.4(2)	N(22)–Fe–N(33)	77.3(1)
N(2)–Fe–N(44)	156.3(2)	N(22)–Fe–N(44)	96.4(2)
N(3)–Fe–N(4)	76.5(2)	N(33)–Fe–N(44)	69.8(2)

Table 3
Selected bond distances (Å) and angles (°) for $[CoL](ClO_4)_2 \cdot 0.5H_2O$

Co(1)–N(1)	2.258(3)	Co(1)–N(11)	2.192(4)
Co(1)–N(2)	2.337(4)	Co(1)–N(13)	2.198(3)
Co(1)–N(3)	2.260(4)	Co(1)–N(12)	3.206(4)
Co(1)–N(4)	2.295(5)	Co(1)–N(14)	3.157(4)
N(1)–Co–N(2)	77.7(1)	N(3)–Co–N(11)	155.9(1)
N(1)–Co–N(3)	122.5(1)	N(4)–Co–N(11)	123.7(1)
N(2)–Co–N(3)	76.2(1)	N(1)–Co–N(13)	158.2(1)
N(1)–Co–N(4)	76.9(1)	N(2)–Co–N(13)	121.7(1)
N(2)–Co–N(4)	126.3(1)	N(3)–Co–N(13)	75.2(1)
N(3)–Co–N(4)	78.9(1)	N(4)–Co–N(13)	96.0(1)
N(1)–Co–N(11)	75.2(1)	N(11)–Co–N(13)	92.6(1)
N(2)–Co–N(11)	93.7(1)		

3. Results and discussion

3.1. Synthesis of the complexes

The reaction of the octadentate ligand **L** with Fe(II) or Co(II) salt in equimolar ratios gave crystalline compounds having the general formula $[ML](ClO_4)_2 \cdot nH_2O$ ($n = 1$ or 0.5). The electronic spectra of the complexes were recorded in methanol solution. Absorption maxima in the 200–800 nm region are listed in Table 4 together with the values of magnetic moment. The spectrum of the iron complex exhibited two strong absorption bands in the 200–300 nm region, which can be assigned to the $\pi \rightarrow \pi^*$ intraligand transitions, and two absorptions at 363 and 350 nm, which correspond to the charge transitions between ligand and metal. The spectrum of the colorless iron(II) complex is essentially featureless in the range 400–800 nm, and d–d transitions are hardly observable. The visible spectrum of the cobalt(II) complex is indicative of a MN_6 coordination sphere, giving two bands at 479 and 565 nm which correspond to the transitions $^4T_{1g(F)} \rightarrow {}^4T_{1g(P)}$ and $^4T_{1g(F)} \rightarrow {}^4A_{2g(F)}$ [11].

3.2. Structure of $[FeL](ClO_4)_2 \cdot H_2O$

The crystal structure consists of a packing of discrete $[FeL]^+$ cations, ClO_4^- anions and H_2O molecules, as illustrated in Fig. 1. The iron(II) ion in the cation is in an eight-coordinate environment (FeN_6N_2'), being coordinated by all eight nitrogen atoms (N(1), N(2), N(3), N(4) and N(11), N(22), N(33), N(44)) of the ligand **L**. The four nitrogen atoms (N(1), N(2), N(3), N(4)) of the macrocyclic ring and the four pyridyl nitrogens (N(11), N(22), N(33), N(44)) of the ligand **L** are arranged at the corners of a square prism with the basal faces rotated about the pseudo-fourfold axis. These nitrogen atoms thus fully encapsulate the Fe(II) ion which lies 1.135 and 1.620 Å from the basal planes in the above order; the two planes form an angle of 2.75° with each other.

Such a high coordination number is achieved at the expense of two long Fe–N(pyridyl) distances (Fe–N(11) = 3.108(5) Å and Fe–N(33) = 2.998(5) Å), which can be considered as semicoordinate. In addition, the four Fe–N(macrocyclic ring) (2.302(5)–2.344(5) Å) and two Fe–N(pyridine pendants in non-adjacent positions) (2.226(4) and 2.233(6) Å) are normal Fe–N bonds. If both semi-bonds are ignored, the coordination stereochemistry of the remaining FeN_6 can be considered as distorted octahedral. The nitrogen atoms (N(22) and N(44)) of coordinated pyridyl groups in non-adjacent positions are in *cis*-positions.

In the unit cell, the two perchlorate ions are linked together by the water molecule through hydrogen bonding.

3.3. Crystal structure of $[CoL](ClO_4)_2 \cdot 0.5H_2O$

The structure of the cobalt(II) complex consists of $[CoL]^{2+}$, ClO_4^- anions and H_2O molecules. The cobalt atom is six-coordinated, with approximate octahedral geometry, by the four nitrogen atoms of the macrocyclic ring and two pyridyl nitrogens (N(11), N(13)) belonging to non-adjacent arms of the ligand (Fig. 2). In the cation, the cobalt atom is constrained to lie on the least-squares plane defined by atoms N(1), N(3), N(13) and N(11), which deviate by ≤ 0.03 Å from that plane, but it is highly displaced, by ca. 1.067 Å, from the four basal nitrogens (of cyclen) of the macrocyclic ligand.

The Co–N distances formed by the pyridyl nitrogens are shorter than those formed by the amine nitrogens, in agreement with what is generally observed [7]. The bond distances Co–N(1) and Co–N(3) are slightly shorter than the distances Co–N(2) and Co–N(4), indicating weaker coordination of

Table 4
Electronic spectra and effective magnetic moments of the complexes

Complex	λ_{max} (nm) (ε (M^{-1} cm^{-1}))	μ_{eff} (BM)
$[FeL](ClO_4)_2 \cdot H_2O$	208, 262, 363 (664.5), 350 (631.0)	5.46
$[CoL](ClO_4)_2 \cdot 0.5H_2O$	266, 251, 479 (16.3), 565 (41.3)	5.31

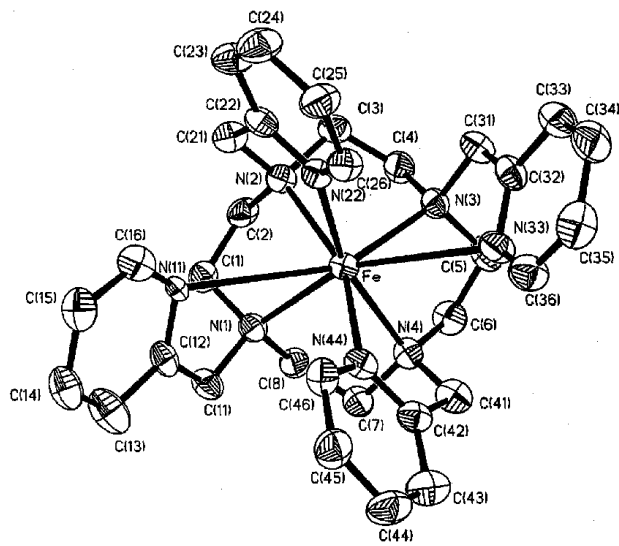


Fig. 1. Perspective view of the cationic entity of the complex $[FeL]^{2+}$.

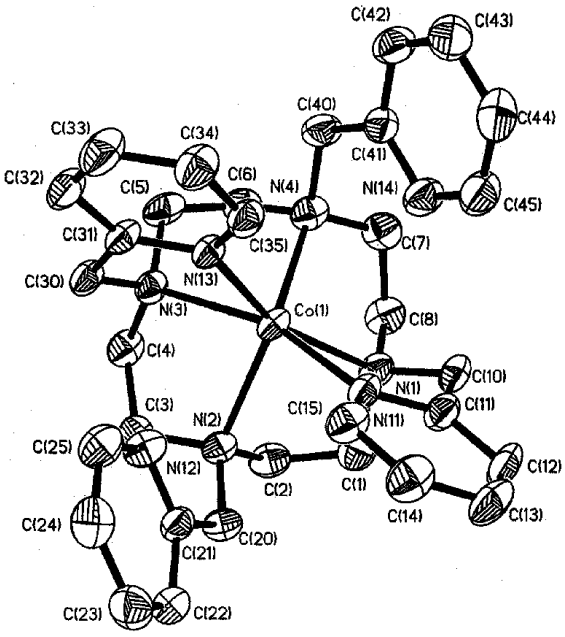


Fig. 2. Perspective view of the cationic entity of the complex $[Co\mathbf{L}]^{2+}$.

the macrocyclic nitrogens connected to the uncoordinated methylpyridines, possibly for relieving steric strain within the macrocycle and minimizing repulsion among the coordinated methylpyridine groups. It is worth noting that the N atoms of uncoordinated methylpyridines are oriented such that they make close contact to Co(II) at Co···N(12) = 3.206 Å and Co···N(14) = 3.157 Å. The presence of Co···N (N(12) and N(14)) contacts of such lengths can be considered to indicate a weak reaction between the central metal atom and the N atoms.

The unit cell contains two molecular units, and hydrogen bonds are not formed between the H_2O molecule and other atoms.

The structures of **1** and **2** may be compared with that of the corresponding Ni(II) complex [7]. The ability of the ligand to adapt to such changes in the dimensions of the cage about the metal ion for a given coordination geometry, as well as its ability to yield six- to eight-coordinate complexes, are indicative of considerable flexibility. In these complexes, the macrocycle takes a *trans*-I configuration in which all the lone pairs in the four basal nitrogens are oriented on the same side of the macrocyclic plane [12] and the 12-membered ring is folded by the coordination of the metal atom; the degrees of folding from the Fe complex to the Ni complex are presented by an increase in the N(2)–M–N(4) angles and a decrease in the N(1)–M–N(3) angles (Table 5). All metal ions are high above the mean plane formed by the four basal macrocyclic nitrogens by ca. 0.900 Å for Ni^{2+}, 1.067 Å for Co^{2+} and 1.135 Å for Fe^{2+}. Four nitrogen atoms of the macrocyclic ring and a pair of nitrogen atoms of coordinated pyridyl groups in non-adjacent positions are bonded to metal ions in normal coordination, and the other nitrogens of pyridyl groups in non-adjacent positions are in uncoordination or semicoordination. The distances between uncoordinated or semicoordinated nitrogen of the pyridine group and M(II) are in the order Fe(II) < Co(II) < Ni(II) in these complexes. The structure of the Co complex is similar to that of the Fe complex, while it is notably different from the Ni complex with respect to the bond angles involving the metal and nitrogens of the macrocyclic ring and the M···N distances formed by the uncoordinated or semicoordinated pyridyl nitrogens (Table 5).

3.4. Magnetic properties of the complexes

The effective magnetic moments of $[Fe\mathbf{L}](ClO_4)_2 \cdot H_2O$ and $[Co\mathbf{L}](ClO_4)_2 \cdot 0.5H_2O$ are 5.46 and 5.31 BM (293 K), corresponding to an $S = 2$ and an $S = 3/2$ state with an appreciable orbital contribution. A variable-temperature (4.2–300 K) study of the magnetic susceptibility was undertaken for **1**. The magnetic properties of **1** are shown in Fig. 3 in the form of effective magnetic moment versus temperature plot. The magnetic moment of 5.37 BM at 298 K decreases steadily with decreasing temperature, reaching a value of 5.06 BM at 21 K, and then it starts to decrease very rapidly, reaching a value of 3.33 BM at 4.5 K. The rapid decrease in the magnetic moment below 21 K may be attributed to an intermolecular antiferromagnetic interaction and/or a zero-field splitting of the iron(II) ion. It was also found that within the temperature range from 21 to 300 K, the susceptibilities may be approximated by the Curie–Weiss law: $\chi_m = C/(T-\theta)$, where $\theta = -6.4$ K.

Table 5
Selected X-ray data for Fe(II), Co(II) and Ni(II) complexes

Angle (°) or distance (Å)	Fe	Co	Ni
N(1)–M–N(3)	124.1	122.5	105.3
N(2)–M–N(4)	121.8	126.3	153.7
M···N(33) [a]	2.998	3.206	5.211
M···N(11) [a]	3.108	3.157	5.288
Deviation of M atom from the basal plane of macrocyclic nitrogens	1.135	1.067	0.900

[a] N(12) and N(14) for Co(II) and Ni(II) complexes.

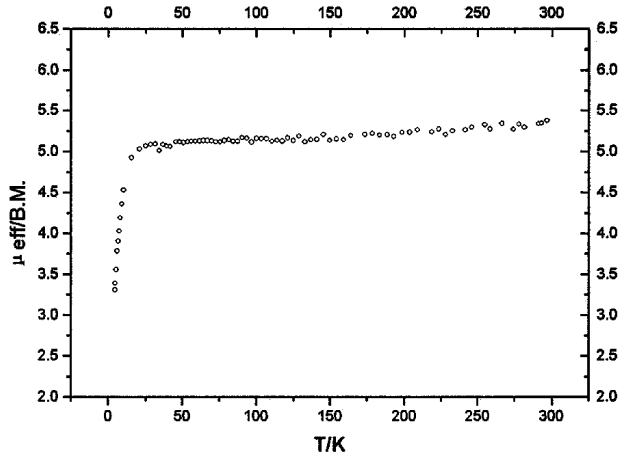


Fig. 3. Plot of μ_{eff} (BM) vs. T for $[Fe\mathbf{L}](ClO_4)_2 \cdot H_2O$.

3.5. Mössbauer studies of [Fe**L**](ClO)$_2$·H$_2$O

The Mössbauer spectrum of solid complex **1** at room temperature is a symmetrical doublet and yields an isomer shift $\delta = 1.007$ mm s^{-1} and quadrupole splitting $\Delta E = 3.20$ mm s^{-1}, corresponding to typical high-spin Fe(II) ($S = 2$) [13]. The values of the isomer shifts indicate a pronounced difference for $FeCl_2$ ($\Delta\delta = -0.1081$ mm s^{-1}, $\Delta(\Delta E) = 0.5$ mm s^{-1}). In addition, there is a small peak in the spectrum indicating the presence of a small amount of Fe(III) impurity in the sample of the Fe(II) complex.

Supplementary data

Supplementary data are available from the CCDC, 12 Union Road, Cambridge CB2 1EZ, UK on request, quoting the deposition numbers 127379 and 127380.

Acknowledgements

This work was financially supported by the National Natural Science Foundation of China (No. 19771022), the National Science Foundation of Tianjin, China, and the Trans-Century Talents Training Programme Foundation by the State Education Ministry of China (to X.-H. Bu).

References

[1] V. Alexandra, Chem. Rev. 95 (1995) 273.
[2] G. de M. Norante, M. Di Vaira, F. Mani, S. Mazzi, P. Stoppioni, Inorg. Chem. 29 (1990) 2822.
[3] U. Bossek, D. Hanke, K. Wieghardt, B. Nuber, Polyhedron 12 (1993) 1.
[4] C.-M. Che, W.-T. Tang, T.C.W. Mak, J. Chem. Soc., Dalton Trans. (1988) 2879.
[5] M. Di Vaira, F. Mani, P. Stoppioni, J. Chem. Soc., Dalton Trans. (1992) 1127.
[6] X.-H. Bu, X.-C. Cao, W.-Q. Zhang, R.H. Zhang, T. Clifferd, Transition Met. Chem. 22 (1997) 513.
[7] X.-H. Bu, X.-C. Cao, W. Chen, R.-H. Zhang, T. Clifferd, Polyhedron 17 (1998) 289.
[8] X.-H. Bu, X.-C. Cao, M.-X. Yuan, X.-B. Wan, R.-T. Chen, Chin. J. Struct. Chem. 15 (1996) 499.
[9] X.-H. Bu, S.-L. Lu, R.-H. Zhang, H.-M. Wang, Synth. React. Inorg. Met.-Org. Chem. 28 (1998) 1127.
[10] J.E. Richman, T.J. Alkins, J. Am. Chem. Soc. 96 (1974) 2268.
[11] M.S. Islam, M. Begum, H.N. Roy, Synth. React. Inorg. Met.-Org. Chem. 25 (1995) 293.
[12] V.J. Thöm, C.C. Fox, J.C.A. Boeyens, R.D. Hancock, J. Am. Chem. Soc. 106 (1984) 5947.
[13] N.N. Greenwood, T.C. Gibb, Mössbauer Spectroscopy, Chapman and Hall, London, 1971.

PERGAMON

www.elsevier.nl/locate/poly

Polyhedron 19 (2000) 437–439

POLYHEDRON

Tetrahedral chalcogeno thiocyanate cluster complexes $[Re_4Q_4(SCN)_{12}]^{4-}$ (Q = S, Se, Te): synthesis and crystal structures

Yuri V. Mironov [1] *

Lehstuhl für Analytische Chemie, Ruhr-Universität Bochum, D-44780 Bochum, Germany

Received 21 July 1999; accepted 9 December 1999

Abstract

The $[Re_4Q_4(SCN)_{12}]^{4-}$ (Q = S, Se, Te) anions were obtained by the reactions of neutral molecular clusters $Re_4Q_4Cl_8(TeCl_2)_4$, Q = S, Se, Te, with melting KSCN. Crystal structures were determined for the isostructural compounds $(Ph_4P)_4Re_4S_4(SCN)_{12}$ (**1**), $(Ph_4P)_4Re_4Se_4(SCN)_{12}$ (**2**) and $(Ph_4As)_4Re_4Te_4(SCN)_{12}$ (**3**). Each contains an Re_4Q_4 cubane-like cluster core with Re–Re distances in the ranges 2.762(3)–2.768(2) Å (**1**), 2.799(2)–2.803(2) Å (**2**) and 2.864(2)–2.877(2) Å (**3**). The faces of the Re_4 units are symmetrically capped by triply bridging chalcogenide ligands Q^{2-} (Q = S, Se, Te). ©2000 Elsevier Science Ltd All rights reserved.

Keywords: Rhenium; Metal clusters; Sulfur; Selenium; Tellurium; Crystal structures

1. Introduction

Re_4 tetrahedral cluster compounds have been studied intensively in recent years. At the present time a number of well characterized chalcogeno halide clusters are known: $Re_4Q_4Te_4X_{16}$ (Q = S, Se, Te; X = Cl, Br) [1,2] and $(Pr_4N)_2Re_4Q_4(CH_3CONH)_2Cl_8$ (Q = S, Se) [3], chalcogeno cyanide clusters $[Re_4Q_4(CN)_{12}]^{4-}$ [4–6], the mixed rhenium thiotelluride $Re_4S_4Te_4$ [7] and thio complexes $[Re_4S_4(\mu\text{-}S_3)_6]^{4-}$ [8,9]. We have now successfully extended this work to allow the isolation of the first such rhenium clusters with thiocyanate ligands, which display the ionic structures $(Ph_4P)_4Re_4Q_4(SCN)_{12}$, Q = S, Se, and $(Ph_4As)_4Re_4Te_4(SCN)_{12}$.

2. Experimental

All manipulations were performed under air. $Re_4Q_4Te_4Cl_{16}$ (Q = S, Se, Te) was prepared as described previously [1]. IR spectra were recorded as KBr discs on a Perkin-Elmer 1760X spectrometer. Elemental analyses were performed on an elemental analyzer system Vario E1.

2.1. Synthesis of $(Ph_4P)_4Re_4S_4(SCN)_{12}$ (1)

$Re_4S_4Te_4Cl_{16}$ (50 mg, 0.026 mmol) and KSCN (200 mg, 2.06 mmol) were heated up to the melting point of KSCN, left at this temperature for 5 min and then cooled down. The solid product was dissolved in 10 ml of water and PPh_4Cl (100 mg, 0.267 mmol) was added to this solution. The resulting precipitate was filtered off, dried and recrystallized from the solvent mixture CH_3CN–$(C_2H_5)_2O$ to afford dark red crystals of $(Ph_4P)_4Re_4S_4(SCN)_{12}$; yield 35 mg (46%). *Anal*. Found: C, 43.9; H, 2.6; N, 5.6; S, 17.1. Calc. for $C_{108}H_{80}N_{12}P_4Re_4S_{16}$: C, 44.3; H, 2.75; N, 5.7; S, 17.5%. IR (cm^{-1}): 2085 ν(CN) (cationic bands are omitted).

2.2. Synthesis of $(Ph_4P)_4Re_4Se_4(SCN)_{12}$ (2)

50 mg of $(Ph_4P)_4Re_4Se_4(SCN)_{12}$ were obtained from $Re_4Se_4Te_4Cl_{16}$ (50 mg, 0.023 mmol) and KSCN (200 mg, 2.06 mmol) by a procedure similar to that described for **1**. Yield 69%. *Anal*. Found: C, 41.0; H, 2.65; S, 11.9. Calc. for $C_{108}H_{80}N_{12}P_4Re_4S_{12}Se_4$: C, 41.6; H, 2.59; S, 12.3%. IR (cm^{-1}): 2089 ν(CN) (cationic bands are omitted).

2.3. Synthesis of $(Ph_4As)_4Re_4Te_4(SCN)_{12}$ (3)

48 mg of $(Ph_4As)_4Re_4Te_4(SCN)_{12}$ were obtained from $Re_4Te_8Cl_{16}$ (60 mg, 0.026 mmol) and KSCN (200 mg, 2.06 mmol) in a manner as described for **1**, using Ph_4AsCl instead

* Tel.: +7-3832-344489; fax: +7-3832-344253; e-mail: m_yuri@hotmail.com

[1] On leave from Institute of Inorganic Chemistry of RAS, Lavrent'ev pr. 3, 630090 Novosibirsk, Russia.

0277-5387/00/$ - see front matter ©2000 Elsevier Science Ltd All rights reserved.
PII S0277-5387(99)00382-4

Table 1
Crystal data for compounds **1**, **2** and **3**

	1	**2**	**3**
Formula	$C_{108}H_{80}N_{12}P_4Re_4S_{16}$	$C_{108}H_{80}N_{12}P_0Re_4S_{12}Se_4$	$C_{108}H_{80}As_4N_{12}Re_4S_{12}Te_4$
Formula weight	2927.48	3115.08	3485.44
Crystal system	tetragonal	tetragonal	tetragonal
Space group	$I4(1)/a$	$I4(1)/a$	$I4(1)/a$
a (Å)	28.235(7)	28.191(3)	28.286(6)
c (Å)	14.297(6)	14.353(2)	14.615(3)
V (Å^3)	11397(6)	11406(2)	11694(4)
Z	4	4	4
ρ (Mg m^{-3})	1.706	1.814	1.980
Crystal size (mm)	0.25×0.08×0.04	0.26×0.18×0.10	0.4×0.02×0.02
Diffractometer	Siemens P4	Siemens P4	Siemens P4
Radiation	Mo Kα	Mo Kα	Mo Kα
Scan mode	ω	ω	ω
θ Range (°)	2.04–22.5	2.04–22.55	2.04–25.01
μ (mm^{-1})	4.636	5.835	6.494
Temperature (K)	293(2)	293(2)	293(2)
Data/restraints/parameters	3711/0/206	3716/12/139	5136/12/206
Reflections with $I>2\sigma(I)$	1357	1528	2018
$R_1[I>2\sigma(I)]$	0.0920	0.0870	0.0869
wR_2	0.1063	0.1288	0.1150
Goodness-of-fit on F^2	1.033	1.051	0.989

Table 2
Selected bond distances (Å) for compounds **1**, **2** and **3**

	1	**2**	**3**
Re(1)–Re(1)#1 [a]	2.762(3)	2.799(2)	2.864(2)
Re(1)–Re(1)#2	2.768(2)	2.803(2)	2.877(2)
Re(1)–Re(1)#3	2.768(2)	2.803(2)	2.877(2)
Re(1)–N(1)	2.07(3)	2.13(3)	2.09(2)
Re(1)–N(2)	2.14(2)	2.18(2)	2.11(2)
Re(1)–N(3)	2.12(3)	2.07(3)	2.14(2)
Re(1)–Q	2.378(7)	2.448(3)	2.628(2)
Re(1)–Q#1	2.353(8)	2.443(3)	2.626(2)
Re(1)–Q#2	2.356(7)	2.447(3)	2.628(2)
Q–Re(1)#1	2.353(8)	2.443(3)	2.626(2)
Q–Re(1)#3	2.356(7)	2.447(3)	2.628(2)
S(1)–C(1)	1.63(3)	1.64(3)	1.61(2)
C(1)–N(1)	1.11(3)	1.06(3)	1.13(2)
S(2)–C(2)	1.63(3)	1.56(3)	1.59(3)
N(2)–C(2)	1.07(3)	1.06(3)	1.10(3)
S(3)–C(3)	1.62(3)	1.64(3)	1.61(3)
C(3)–N(3)	1.07(3)	1.08(3)	1.11(2)

[a] Symmetry transformations used to generate equivalent atoms: #1, $-x+1-1$, $-y+1/2$, $z+1-1$; #2, $y-1/4$, $-x+1/4$, $-z+1/4$; #3, $-y+1/4$, $x+1/4$, $-z+1/4$.

of Ph_4PCl. Yield 53%. *Anal*. Found: C, 37.1; H, 2.37; S, 10.7. Calc. for $C_{108}H_{80}N_{12}P_4Re_4S_{16}Te_4$: C, 37.2; H, 2.31; S, 11.0%. IR (cm^{-1}): 2092 ν(CN) (cationic bands are omitted).

2.4. X-ray structural analyses

Crystals used in the crystallographic study were mounted on glass fibres. Intensity data were collected at room temperature on a Siemens P4 diffractometer. Graphite-monochromated Mo Kα radiation ($\lambda=0.71073$ Å) was utilized. SHELXS-86 [10] was employed for structure solution by direct methods and SHELXL-93 [11] for refinement by full-matrix least-squares. DIFABS [12] (compound **1**) and semi-empirical absorption corrections based on ψ scan data (compounds **2** and **3**) were applied to the intensity data. Hydrogen atoms were included at calculated positions [13]. Crystal data for compounds **1**, **2** and **3** are given in Table 1, selected bond distances are given in Table 2.

3. Result and discussion

Treatment of molecular clusters $Re_4Q_4Cl_8(TeCl_2)_4$, Q = S, Se, with molten KSCN leads to the formation of chalcogeno thiocyanate complexes with tetra anions $Re_4Q_4(SCN)_{12}^{4-}$, Q = S, Se, Te. During the reaction, exchange of all terminal ligands, Cl^- and $TeCl_2$, by thiocyanate ligands is observed. The final products may be obtained as salts with different tetraalkylammonium counter cations, such as Me_4N^+, Et_4N^+, Pr_4N^+ or with Ph_4X^+ (X = P, As). Although all of these compounds were tested for suitability, only the Ph_4X^+ (X = P, As) forms were found to be of adequate though poor scattering power for X-ray analysis. Their mediocre quality may be gauged by the relatively low number of reflections with $I>2\sigma(I)$ which varies between 36.5% (for **1**) and 39.3% (for **3**). As a result the reliability indices R_1 and wR_2 in Table 1 are rather high and with the exception of the bond distances to Re, metrical aspects of the structures will not, therefore, be discussed in detail.

The structures of all three compounds $(Ph_4P)_2Re_4S_4(SCN)_{12}$ (**1**), $(Ph_4P)_2Re_4Se_4(SCN)_{12}$ (**2**) and $(Ph_4P)_2Re_4Te_4(SCN)_{12}$ (**3**) were determined by single-

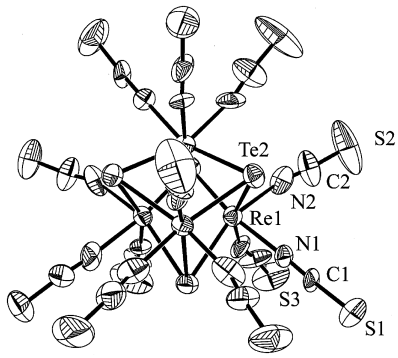


Fig. 1. The crystal structure of the anion $Re_4Te_4(SCN)_{12}^{4-}$.

crystal X-ray analysis. A view of the cluster anion is shown in Fig. 1. Compounds **1**, **2** and **3** are isostructural and possess crystallographic S_4 symmetry. Each contains an Re_4Q_4 cubane-like core formed from a nearly regular Re_4 tetrahedron with Re–Re distances in the range 2.762(3)–2.768(2) Å for **1**, 2.799(2)–2.803(2) Å for **2** and 2.864(2)–2.877(2) Å for **3**. Each triangular face of the Re_4 tetrahedron is capped symmetrically by triply bridging chalcogenide ions with Re–Q distances of respectively 2.353(8)–2.378(7) Å (**1**), 2.443(3)–2.448(3) Å (**2**), and 2.626(2)–2.628(2) Å (**3**). These values are in good agreement with those reported for other Re_4 cluster compounds [1]. Each Re atom is ligated by the N atoms of three terminal SCN^- ligands with Re–N distances lying in the ranges 2.07(3)–2.14(2) Å for **1**, 2.07(3)–2.18(2) Å for **2**, and 2.09(2)–2.14(2) Å for **3**. This type of coordination mode was also observed for the SCN^- ligand in previously characterized cluster complexes of Mo and W [13–15].

The most interesting feature of this reaction lies in the preservation of the cluster units $[Re_4Q_4]$ (Q = Se, Te) in the presence of KSCN, as a potential source of sulfur atoms. This state of affairs is in accordance with a high kinetic stability of these fragments under the chosen reaction conditions. Treatment of Re with S and Te at high temperature leads to the formation of $[Re_4S_4]Te_4$ [7], indicating that $[Re_4S_4]$ clusters are thermodynamically more stable than those of the heavier Group 16 congener. It was also previously found for W and Nb, that the reactions of selenium-rich cluster complexes with molten KSCN under similar conditions always lead to exchange of Se by S atoms from the thiocyanate source [16]. The only known selenothiocyanate cluster $(Me_2NH_2)_6[(SCN)_9W_3Se_4SnCl_3]\cdot 0.5H_2O$ was obtained by the reaction of $[W_3Se_4(H_2O)_9]^{4+}$ in aqueous HCl solution with $SnCl_2\cdot 2H_2O$ in the presence of Me_2NH_2Cl and NaSCN [17].

$[Re_4Te_4(SCN)_{12}]^{4-}$ is the first example of a tellurothiocyanate cluster anion.

Supplementary data

Supplementary data are available from the Cambridge Crystallographic Data Center, 12 Union Road, Cambridge CB2 1EZ, UK (fax: +44-1223-336033; e-mail: deposit@ccdc.cam.uk) on request, quoting the deposition numbers CCDC 132396 (**1**), 132397 (**2**) and 132398 (**3**).

Acknowledgements

I am grateful to the Alexander von Humboldt foundation for a fellowship and to Professor W.S. Sheldrick for helpful discussions.

References

[1] Y.V. Mironov, T.E. Albrecht-Schmitt, J.A. Ibers, Inorg. Chem. 36 (1997) 944.
[2] E.S. Lang, U. Abram, J. Strähle, Z. Anorg. Allg. Chem. 622 (1996) 251.
[3] Y.V. Mironov, Eur. J. Inorg. Chem. (1999) 997.
[4] M. Laing, P.M. Kiernan, W.P. Griffith, J. Chem. Soc., Chem. Commun. (1977) 221.
[5] V.P. Fedin, M.R.J. Elsegood, W. Clegg, A.G. Sykes, Polyhedron 15 (1996) 485.
[6] Y.V. Mironov, T.E. Albrecht-Schmitt, J.A. Ibers, Z. Krist.-New Cryst. Struct. 212 (1997) 308.
[7] V.E. Fedorov, Y.V. Mironov, V.P. Fedin, H. Imoto, T. Saito, Acta Crystallogr., Sect. C 52 (1996) 1065.
[8] A. Müller, E. Krickemeyer, H. Bögge, Angew. Chem., Int. Ed. Engl. 25 (1986) 272.
[9] A. Müller, E. Krickemeyer, H. Bögge, Z. Anorg. Allg. Chem. 554 (1987) 61.
[10] G.M. Sheldrick, SHELXS-86, Acta Crystallogr., Sect. A 46 (1990) 467.
[11] G.M. Sheldrick, SHELXL-93, Universität Göttingen, Germany, 1993.
[12] N. Walker, P. Stuart, Acta Crystallogr., Sect. A 39 (1983) 158.
[13] V.P. Fedin, M.N. Sokolov, A.V. Virovets, N.V. Podberezskaya, V.E. Fedorov, Polyhedron 11 (1992) 2395.
[14] V.P. Fedin, M.N. Sokolov, A.V. Virovets, N.V. Podberezskaya, V.E. Fedorov, Polyhedron 11 (1992) 2973.
[15] A. Müller, V.P. Fedin, E. Diemann, H. Bögge, E. Krickemeyer, D. Sölter, A.M. Giuliani, R. Barbieri, P. Adler, Inorg. Chem. 33 (1994) 2243.
[16] V.P. Fedin, A. Müller, E. Krickemeyer, M.N. Sokolov, V.E. Fedorov, Zh. Neorg. Khim. 39 (1994) 1663 (in Russian).
[17] V.P. Fedin, M.N. Sokolov, A.V. Virovets, N.V. Podberezskaya, V.E. Fedorov, Inorg. Chim. Acta 269 (1998) 292.

PERGAMON

www.elsevier.nl/locate/poly

Polyhedron 19 (2000) 441–451

POLYHEDRON

Synthesis, spectroscopic and cyclic voltammetry studies of copper(II) complexes with open chain, cyclic and a new macrocyclic thiosemicarbazones

Eva Franco [a], Elena López-Torres [a], Mª Antonia Mendiola [a,*], Mª Teresa Sevilla [b]

[a] *Departamento de Química Inorgánica, Universidad Autónoma, Cantoblanco, 28049 Madrid, Spain*

[b] *Departamento de Química Analítica y Análisis Instrumental, Universidad Autónoma, Cantoblanco, 28049 Madrid, Spain*

Received 28 October 1999; accepted 10 December 1999

Abstract

New copper complexes have been prepared from benzilbisthiosemicarbazone (L^1H_6) and from the cyclic 6-methoxi-1,6-diphenyl-4-thio-3,4,5,6-tetrahydro-2,3,5-triazine (L^2H_2). The complexes were characterized by mass spectrometry, IR, electronic and electron paramagnetic resonance spectra. Complexes from L^1H_6 (**1**–**5**) present 1:1 stoichiometry and show different characteristics with a variable grade of deprotonation in the ligand, depending on the salt used (chloride, nitrate or sulfate) and the presence of acid in the medium. A macrocyclic Schiff base, 3,4,9,10-tetraphenyl-1,2,5,6,8,11-hexaazacyclododeca-7,12-dithione-3,4,9,10-tetraene (L^3H_2), containing thiosemicarbazone moieties is readily prepared and characterized for the first time, with fairly good yield, from the mesocycle (L^2H_2) in methanol with copper chloride as template. Near quantitative synthesis of the precursor, L^2H_2, which is a potential chemotherapeutic agent against cancer, has been achieved by reacting benzil and thiosemicarbazide in the absence of metal salt and using a high dilution technique. Macrocyclic complexes **6** and **7** containing thiosemicarbazone moieties were obtained from L^2H_2 and copper nitrate and sulfate. Direct reaction between the copper salt and the macrocyclic thiosemicarbazone (L^3H_2) gave similar complexes but with a lower grade of purity. Macrocyclic complexes **6** and **7** present metal–ligand ratios of 1:2 and 1:1 and the ligand is in a deprotonated form. The redox behaviour was explored by cyclic voltammetry. L^1H_6 complexes show Cu(II)/Cu(I) couples and quasireversible waves associated with the Cu(III)/Cu(II) process. The reduction/oxidation potential depends on the structure and conformation of the central atom in the coordination compounds. ©2000 Elsevier Science Ltd All rights reserved.

Keywords: Thiosemicarbazones; Macrocyclic ligands; Electrochemistry; Copper complexes; Dithio-Schiff base complexes

1. Introduction

Schiff base macrocyclic ligands based on thiosemicarbazones and their complexes have received considerable attention since, because of their pharmacological properties, they have numerous applications, for example as antibacterial and anticancer agents [1–3]. They can yield mono- or polynuclear complexes, some of which are biologically relevant [4–7]; for example, some copper complexes can serve as models for enzymes such as galactose oxidase and may be used as effective oxidant and redox catalysts [8,9]. Furthermore, they allow selective complexation and extraction of metallic cations and anions of biochemical and environmental importance [10–13]. The number and relative position of donor atoms and the cavity size in the macrocyclic compounds give these molecules special reactivity. For a particular dicarbonyl and diamine as precursors, control of the reaction conditions allows the condensation product formed to be determined: [1+1], [1+2] and [2+2] condensation products, with open chain and cyclic structures. Alternatively, the high dilution technique is a good method to obtain macrocyclic Schiff bases [14]. The most important factors are the solvent, pH, temperature and the presence of metal ions. Metal salts have been used as templating agents to yield macrocyclic Schiff bases from diamine and dicarbonyl as precursors [15,16], but transition metals such as copper and nickel, which have been used in the preparation of aza crowns, are surprisingly absent [17]. If the metal is present, the size, charge and favourable geometries of the metal have to be considered.

Biological activities may be related to the redox properties of complexes. For some copper(II) compounds a lower reduction potential seems to be related to an increased anti-

0277-5387/00/$ - see front matter ©2000 Elsevier Science Ltd All rights reserved.
PII S0277-5387(99)00383-6

fungal activity [1,3]. Some copper complexes exhibit the abilities of superoxide dismutase (SOD) and chemical nucleases [18,19]. Moreover, copper is also toxic in elevated concentration so many investigations have attempted to develop sensors to determine its presence with high selectivity. Potentiometric measurements with copper ion-selective electrodes (ISE) allow the free ion concentration to be determined directly in water samples. The possible biomimetic activity and the potential application as sensors for copper complexes can be evaluated from the electrochemical behaviour and visible and EPR spectra.

The redox properties include oxidation and reduction of the central metal ion, various oxidation and reduction reactions of the ligand, and processes which involve both the central atom and the ligand [20]. The redox potentials of the Cu(III)/Cu(II) and Cu(II)/Cu(I) couples have been shown to be markedly affected by the nature of the solvent, background electrolyte and by the structure of the chelating ligand and of the complex as a whole. Redox potentials of Cu(II)–Cu(I) systems depend on the relative thermodynamic stabilities of the two oxidation states in a given ligand environment. The factors influencing the metal-located redox properties of the copper systems have been extensively studied. The influence of various structural features has been gauged, including ring size, degree and arrangement of unsaturation and alkyl substitution [21–23].

In previous work, we obtained different condensation products from the reaction of benzil and thiosemicarbazide depending on the reaction conditions: open chain molecule, benzilbisthiosemicarbazone L^1H_6, and a cyclic [1+1] molecule L^2H_2. Both compounds were obtained in the absence of metal salts (nickel, copper or iron), because in the presence of these salts the product isolated was always a thiosemicarbazide complex, even when working with high dilution conditions [24]. However, the reaction between the open chain molecule and iron chloride in methanol and in the presence of lithium hydroxide gave an iron complex of a macrocyclic species, but it is not possible to obtain the free macrocycle from this complex [25]. We have prepared metal complexes from L^1H_6 with several metal salts [24,26]. Redox properties of cobalt(II) and nickel(II) complexes have been explored [26]. Some copper derivatives have shown that the changes in the coordination sphere are connected with the halfwave potential values for the Cu(II)/Cu(I) redox couple, and these results and the spectral data on solution agree with the superoxide dismutase (SOD) mimetic activity [27]. Moreover, carbon paste ion selective electrodes based on thiohydrazone and thiosemicarbazone complexes exhibit rapid response, adequate sensitivity and selectivity for copper ions [28].

As a part of our work involving the preparation of free iminomacrocyclic compounds and their metal complexes, we are interested in obtaining the free [2+2] condensation product from benzil and thiosemicarbazide. The aim of our work is to compare the reactivity of different macroligands containing the same functional group, but with variable number and different structure, with a particular metal ion. In addition, we are trying to determine the best conditions to control the nature of copper complexes, since the different structures can improve their potential applications. Therefore, we report the reactions of an open chain ligand, benzilbisthiosemicarbazone L^1H_6, a cyclic molecule 6-methoxi-1,6-diphenyl-4-thio-3,4,5,6-tetrahydro-2,3,5-triazine L^2H_2 (Fig. 1) with copper(II) chloride, nitrate and sulfate in variable work conditions. Since a new free macrocycle 3,4,9,10-tetraphenyl-1,2,5,6,8,11-hexaazacyclododeca-7,12-dithione-3,4,9,10-tetraene L^3H_2 (Fig. 1) has been obtained from the reaction of L^2H_2 with copper chloride, we have studied its interactions with copper nitrate and sulfate. We have studied the electrochemical behaviour of complexes by cyclic voltammetry, because their applications as SOD mimetic complexes and as copper sensors are related to the redox properties.

2. Experimental

2.1. Reagents

Copper salts were commercial products of highest chemical grade (Fluka). Solvents were purified according to standard procedures.

2.2. Synthesis of the organic molecules

Benzilbisthiosemicarbazone, L^1H_6, was prepared following the procedure previously reported [24].

L^2H_2 was prepared by modifying the published procedure [25]. A solution of thiosemicarbazide (1.14 g, 12.5 mmol) in methanol (150 cm^3), a solution of hydrochloric acid (25 cm^3, 2 M), 1 cm^3 of HCl (12 M) and a solution of benzil (2.63 g, 12.5 mmol) in methanol (100 cm^3) were added alternately dropwise and slowly with strong stirring to 75 cm^3 of methanol. After completion of the addition of all reactants, the mixture was heated for 8 h. Overnight a crystalline solid was formed, which was filtered off, washed and dried in vacuo (yield 95%).

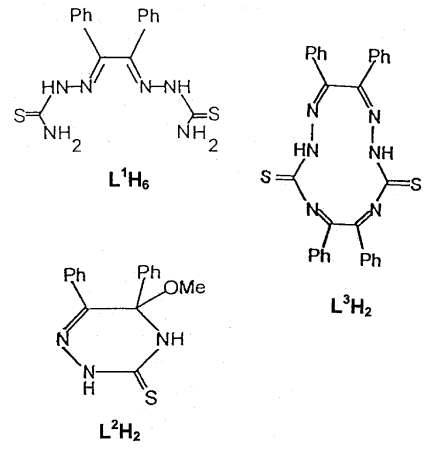


Fig. 1. Structures proposed for the organic molecules.

A solution of copper chloride dihydrate (0.23 g, 1.40 mmol) in methanol (50 cm^3) was added to a solution of L^2H_2 (0.41 g, 1.40 mmol) in methanol (50 cm^3). The mixture was stirred for 2 h at room temperature. The cream solid L^3H_2 formed was filtered off, washed several times with methanol and dried in vacuo (yield 79%), m.p. 205°C. *Anal*. Calc. for $C_{30}H_{22}N_6S_2$: C, 67.92; H, 4.15; N, 15.85; S, 12.07. Found: C, 67.82; H, 4.28; N, 15.75; S, 12.13%. Selected spectroscopic data: *m/z* (FAB) 529.1 ($C_{30}H_{21}N_6S_2$, 100%). ^{13}C NMR (DMSO, 300 MHz): 166.90 (CS), 156.57, 155.97 (CN), 134.89, 134.54, 131.31, 129.79, 129.47, 128.67, 128.57 (Ph).

2.3. Synthesis of the complexes from L^1H_6 and copper(II) chloride dihydrate

To L^1H_6 (0.20 g, 0.56 mmol) in methanol (25 cm^3) was added a solution of copper(II) chloride dihydrate (0.10 g, 0.56 mmol) in methanol (40 cm^3). The mixture was stirred for 5 h at room temperature, heated under reflux for 5 h or heated under reflux for 5 h in the presence of LiOH. In all cases a brown solid **1** was formed, which was filtered off, washed with methanol and dried in vacuo (yield 40%).

To L^1H_6 (0.20 g, 0.56 mmol) in methanol (25 cm^3) was added a solution of copper(II) chloride dihydrate (0.05 g, 0.28 mmol) in methanol (20 cm^3). The mixture was stirred for 12 h at room temperature. The reddish solid **2** formed was filtered off, washed with methanol and dried in vacuo (yield 20%).

A solution of copper(II) chloride dihydrate (0.24 g, 1.40 mmol) and hydrochloric acid (50 cm^3, 12 M) in methanol (50 cm^3), was added to L^1H_6 (0.50 g, 1.40 mmol) in methanol (100 cm^3). The mixture was refluxed for 3 h with stirring. The green solid **3** formed was filtered off, washed with methanol and dried in vacuo (yield 85%).

The same solid was obtained if the acid (2 M) was added dropwise.

A suspension of L^1H_6 (0.75 g, 2.10 mmol) in dichloromethane (25 cm^3) was mixed with a suspension of copper(II) chloride dihydrate (0.36 g, 2.10 mmol) in the same solvent (20 cm^3). The mixture was refluxed for 2 h with stirring. The green solid formed was filtered under nitrogen and dried in vacuo. The solid decomposes very quickly in the presence of air.

The reaction was carried out using toluene and cyclohexane as solvent with the same results described above.

A solution of copper(II) chloride dihydrate (0.10 g, 0.58 mmol) in methanol (50 cm^3) was added to a suspension of L^1H_6 (0.20 g, 0.58 mmol) and benzil (0.12 g, 0.58 mmol) in methanol (60 cm^3). The mixture was refluxed for 4 h with stirring. The brown solid formed was filtered off, washed with methanol and dried in vacuo (yield 45%).

2.4. Synthesis of complexes from L^1H_6 and copper(II) nitrate trihydrate

A solution of copper(II) nitrate trihydrate (0.36 g, 1.50 mmol) in methanol (20 cm^3) was added to L^1H_6 (0.53 g, 1.50 mmol) in methanol (20 cm^3). The mixture was stirred for 3 h at room temperature. The brown solid **4** formed was filtered off, washed with methanol and dried in vacuo (yield 65%).

A solution of copper(II) nitrate trihydrate (0.36 g, 1.50 mmol) in methanol (20 cm^3) and 50 cm^3 of nitric acid (15 M) was added to L^1H_6 (0.53 g, 1.50 mmol) in methanol (20 cm^3). The mixture was stirred for 2 h at room temperature. The green oil formed was concentrated in a rotary evaporator to half the initial volume and then the solvent was evaporated slowly at room temperature. Finally needle shaped yellow crystals were separated.

Identical results were obtained adding the acid (2 M) dropwise.

2.5. Synthesis of complexes from L^1H_6 and copper(II) sulfate pentahydrate

To a suspension of L^1H_6 (0.10 g, 0.30 mmol) in methanol (40 cm^3) was added a solution of copper(II) sulfate pentahydrate (0.06 g, 0.28 mmol) in methanol (40 cm^3). The mixture was stirred for 6 h at room temperature. The reddish solid formed was filtered off, washed with methanol and dried in vacuo (yield 20%).

To a suspension of L^1H_6 (0.10 g, 0.30 mmol) in methanol (40 cm^3) were added three drops of sulfuric acid (18 M) and then a solution of copper(II) sulfate pentahydrate (0.07 g, 0.28 mmol) in methanol (40 cm^3). The mixture was stirred for 12 h at room temperature. On slow diffusion of ether through the dark blue oil formed, a crystalline dark blue solid **5** was obtained. The solid was filtered off, washed with ether and dried in vacuo (yield 51%).

2.6. Synthesis of complexes derived from L^2H_2

A solution of copper(II) nitrate trihydrate (0.15 g, 0.63 mmol) in methanol (20 cm^3) was added to a suspension of L^2H_2 (0.37 g, 1.26 mmol) in methanol (20 cm^3). The mixture was stirred for 12 h at room temperature. The brown solid **6** formed was filtered off, washed with methanol and dried in vacuo (yield 27%).

A solution of copper(II) sulfate pentahydrate (0.10 g, 0.40 mmol) in methanol (20 cm^3) was added to a suspension of L^2H_2 (0.24 g, 0.80 mmol) in methanol (20 cm^3). The mixture was stirred for 12 h at room temperature. The orange–brown solid **7** formed was filtered off, washed with methanol and dried in vacuo (yield 37%).

2.7. Synthesis of complexes from L^3H_2

A solution of copper(II) chloride dihydrate (0.02 g, 0.23 mmol) in dried methanol (10 cm^3) was added to a suspension of L^3H_2 (0.11 g, 0.23 mmol) in dried methanol (10 cm^3). The mixture was heated under reflux with stirring for 2 h. The red solid **8** formed was filtered off, washed with methanol and dried in vacuo (yield 27%).

A solution of copper(II) nitrate trihydrate (0.02 g, 0.90 mmol) in methanol (20 cm^3) was added to a suspension of L^3H_2 (0.05 g, 0.90 mmol) in methanol (20 cm^3). The mixture was heated under reflux with stirring for 2 h. The clear brown solid **9** formed was filtered off, washed with methanol and dried in vacuo (yield 47%).

2.8. Physical measurements

Microanalyses were carried out using a Perkin-Elmer 2400 II CHNS/O elemental analyser. Copper was analysed on a Hitachi Z-8200 atomic absorption spectrophotometer.

IR spectra in the 4000–400 cm^{-1} range were recorded as KBr pellets on a Bomen-100 spectrophotometer and in the range 550–200 cm^{-1} on a Bruker IFS 66V spectrophotometer. UV–Vis spectra in solution were registered on an Ati-Unicam UV2 spectrophotometer and the solid reflectance spectra on a Pye-Unicam SP-8-100 spectrophotometer. Conductivity data were measured using freshly prepared DMF solutions (ca. 10^{-3} M) at 25°C with a Metrohm Herisau model E-518 instrument. ^1H and ^{13}C NMR spectra were recorded on a Bruker AMX-300 spectrophotometer using dimethylsulfoxide-d_6 as solvent and TMS as internal reference. EPR spectra in the solid state were run on a Bruker ER 200D X-band spectrophotometer.

Fast atom bombardment mass spectra were recorded on a VG Auto Spec instrument using Cs as the fast atom and *m*-nitrobenzylalcohol (*m*NBA) as the matrix.

Electrochemical measurements were performed with a BAS CV 27 voltammograph and a BAS A-4 XY register using a glassy carbon (ϕ 5 mm) working electrode, a platinum wire as auxiliary, and a double junction, with porous ceramic wick, Ag/AgCl reference electrode, standardized for the redox couple ferricinium/ferrocene ($E_{1/2} = +0.400$ V, $\Delta E_p = 60$ mV). Cyclic voltammetry studies of ligands and complexes were carried out on 0.01 M solutions in dimethylsulfoxide (L^1H_6 complexes) and dichloromethane (L^2H_2 derivatives) containing 0.1 M $[NBu_4][PF_6]$ as supporting electrolyte. The range of potential studied was between +1 and −1.5 V. All solutions were purged with nitrogen steam for 5 min before measurement and the working electrode was polished before each experiment with diamond paste. The procedure was performed at room temperature and a nitrogen atmosphere was maintained over the solution during the measurements.

3. Results and discussion

The reaction of L^2H_2 with copper chloride in methanol at room temperature yields a cream solid. The analytical data show the modification of the reactant. The mass spectrum shows a peak at 529 amu corresponding to the macrocyclic species $[C_{30}H_{21}N_6S_2]^+$. The ^1H NMR spectrum in DMSO confirms the absence of methanol inserted or as a crystallization molecule. The ^{13}C NMR spectrum shows signals corresponding to one thio group, seven phenyl carbons and two imine carbons, confirming the proposed structure. The absorption bands observed in the IR spectrum are consistent with the functional groups present in the molecule.

The reaction of compound L^2H_2 with copper chloride, under the described conditions, is the first direct procedure to isolate a free macrocycle L^3H_2 containing thiosemicarbazone moieties. The copper chloride acts as a selective template in the reaction from the mesocycle. This effect is original because the template usually acts from diamine and dicarbonyl as precursors, but with benzil and thiosemicarbazide the condensation reaction does not work [24].

The direct reaction, using the high dilution technique, improves the yield of the cyclic ligand L^2H_2, which could be useful in the future since this molecule is a potential anticancer agent and it is being currently tested against the full panel of 60 human tumours (NSC no. 711635-Y) by the National Cancer Institute (USA).

The complexes characterized are stable to air and moisture. The analytical data of complexes are consistent with the stoichiometries proposed which are summarized in Table 1.

3.1. L^1H_6 complexes

Complexes from L^1H_6 present different formulae and variable grades of deprotonation depending on the halide and/or the working conditions, in particular the presence of protons.

From the copper chloride reactions, three type of complexes with the same stoichiometry are obtained. In methanol as solvent, complexes **1**, **2** and **3** are isolated; the last compound appears only in the presence of hydrochloric acid. Working in a molar ratio 1:2, the complex **2** is obtained. This product had been obtained previously in ethanol under reflux [24]. The reaction in the presence of benzil yields complex **1**.

The reactions with nitrate give only the complex **4** because by working in the presence of nitric acid only a ligand breakdown product is obtained. However, with sulfate two different complexes are obtained, **5** and **2**, depending on whether or not protons are present in the medium.

The analytical data of complexes are in agreement with the ligand acting as a monoanion in complexes **1** and **4**, a dianion in complex **2** and a neutral molecule in complexes **3** and **5**. The mass spectra of complexes show a peak at 418 amu corresponding to $[C_{16}H_{15}N_6S_2Cu]^+ + 1$ and in addition for complex **4** the spectrum exhibits the peak corresponding to the molecular mass.

The conductivity data in DMF indicate that the complexes are non-electrolyte compounds, but complex **5** is a 1:1 electrolyte [29]. Therefore chloride and nitrate are bonded to the copper ion, while the sulfate ion is outside the metal coordination sphere.

3.1.1. IR spectra

The most significant IR bands, useful for determining the ligand mode of coordination, are listed in Table 2. The most important bands of the ligand were assigned according to published data [24].

Table 1
Analytical data and some physical properties of complexes

	$CuC_{16}H_{15}N_6S_2Cl$ (**1**)	$CuC_{16}H_{14}N_6S_2$ (**2**)	$CuC_{16}H_{16}N_6S_2Cl_2$ (**3**)	$CuC_{16}H_{15}N_6S_2NO_3$ (**4**)	$CuC_{16}H_{16}N_6S_2SO_4\cdot H_2SO_4\cdot 2CH_3OH$ (**5**)	$Cu(C_{30}H_{21}N_6S_2)_2CH_3OH$ (**6**)	$CuC_{30}H_{20}N_6S_2$ (**7**)
C (%) found	41.64	45.70	38.82	39.63	33.76	62.20	57.90
Calc.	41.29	45.98	39.14	39.95	31.97	63.45	60.86
N (%) found	18.32	19.15	16.74	20.77	12.79	14.48	13.42
Calc.	18.50	20.12	17.12	20.39	12.39	14.56	14.20
H (%) found	3.31	3.38	3.59	2.98	3.48	3.32	3.13
Calc.	3.30	3.55	3.33	3.12	3.83	3.98	3.38
S (%) found	13.80	15.16	12.92	13.02	19.56	10.88	11.05
Calc.	13.97	15.32	13.05	13.31	18.89	11.09	10.81
Cu (%) found	14.13	15.12	11.53	13.22	7.35	5.77	10.80
Calc.	13.98	15.19	12.94	13.22	9.37	5.50	10.73
pf (°C)	228	210	230	208	> 260	184	> 260
Colour	brown	red	green	brown	blue	brown	orange–brown

The absence of any bands in the 2600–2800 cm^{-1} region of the IR spectra of L^1H_6 and its complexes suggests the absence of any thiol tautomer in the solid state [30].

The spectrum of complex **2** shows three bands in the 3500–3000 cm^{-1} region, which indicate the total deprotonation of the ligand. Spectra of complexes **3** and **5** exhibit a larger number of bands in the amine stretching region, which confirms that the neutral form of the ligand is bonded in these complexes. Spectra of complexes **1** and **4** show an intermediate situation, more bands than complex **2** and less than complex **3**, which agrees with a partial loss of the acidic hydrogens present in L^1H_6. These conclusions are according to the analytical data of complexes and the mass spectrum of complex **4**.

The IR spectra of the complexes, except complex **5**, show the band assigned to the azomethine nitrogen shifted to lower wavenumber [31]. Coordination of these nitrogens is confirmed with the presence of new bands assignable to ν(Cu–NC) in the spectra of complexes (Table 2) [32].

In the spectra of complexes **3** and **5**, in which the ligand acts in its neutral form, the band assigned to $\delta(NH_2)$ remains in the same position as in the free ligand, so the primary amines are not bonded to the copper ion. In addition, coordination via the sulfur atoms is indicated by a decrease in the frequency of the thioamide band. The presence of a new band assignable to ν(CuS) confirms that the sulfur atoms are involved in the coordination.

The spectrum of complex **4** shows bands corresponding to the nitrate anion coordinated to the copper. Except for these bands, this spectrum is very similar to the spectra of **1** and **2** in the 1700–700 cm^{-1} region so the ligand coordination modes must be the same. The three spectra show a band at 1634 cm^{-1}, which could be related to the $\delta(NH_2)$ shifted because of bonding to copper or the new CN group since the ligand is deprotonated. The new bands appearing below 500 cm^{-1} confirm that the primary amines are bonded to the metal ion. Therefore L^1H_6 acts as a tetradentate ligand through four nitrogen atoms.

From the IR spectra data, one can deduce that the coordinative behaviour of L^1H_6 depends on whether it is deprotonated or acts in its neutral form. In complexes **1**, **2**, and **4**, which contain the ligand in deprotonated form, it is bonded to the copper through four nitrogen atoms (provided by the imine and the primary amine groups). However, in complexes **3** and **5**, in which L^1H_6 acts as a neutral molecule, the sulfur atoms participate in the coordination. The copper coordination sphere is completed by the anions present in complexes **1**, **3** and **4**.

3.1.2. Electronic and EPR spectra

The significant electronic absorption bands in the spectra of complexes recorded in solution and in solid state are presented in Table 3.

The reflectance spectra of complexes **3**, **4** and **5** present bands in the same region, so the copper will have the same environment, with a distorted octahedral geometry around

Table 2
Relevant IR spectral data and assignament of L^1H_6 complexes (cm^{-1})

	$\nu(NH)+\nu(NH_2)$	$\nu(C{=}N)+\delta(NH_2)$	Thioamide I	Thioamide IV	$\nu(Cu–N)/\nu(Cu–S)$	$\nu(Cu–X)$
L^1H_6	3420 [a], 3330 [a], 3250, 3090	1610, 1585	1465 [a]	837		
$CuC_{16}H_{15}N_6S_2Cl$ (**1**)	3443, 3240 [a], 3084 [a]	1626, 1611, 1575	1445, 1527	848	447, 427	329
$CuC_{16}H_{14}N_6S_2$ (**2**)	3343, 3271, 3102	1626, 1600, 1569	1467, 1427	836	449, 428	
$CuC_{16}H_{16}N_6S_2Cl_2$ (**3**)	3333, 3240 [a], 3084	1609, 1575	1535, 1446 [a]	768	427, 297	284
$CuC_{16}H_{15}N_6S_2NO_3$ (**4**)	3438 [a], 3406 [a], 3269, 3082	1634, 1608, 1575	1551, 1532, 1447	848	447, 428	335, 350
$CuC_{16}H_{16}N_6S_2SO_4\cdot 2CH_3OH$ (**5**)	3308 [a], 3140, 3100 [a]	1653, 1632	1560	784	292	

[a] Several bands.

Table 3
Electronic spectra (nm) and EPR data for L^1H_6 complexes

Complex	Diffuse reflectance	Solution				EPR		
	Solid	DMF	DMSO	MeOH	DMF + HX	$g_\parallel$	$g_\perp$	g_0
1	372, 466, 666(sh) [a]	500, 550(sh)	500, 550(sh)	483		2.17	2.07	2.10
2	420, 490, 540(sh)	500, 550(sh)	500, 550(sh)	484		2.14	2.05	2.08
3	424, 590–690	500, 550(sh)	500, 550(sh)	484	694, 767	2.18	2.07	2.11
4	600–520	500, 550(sh)	500, 504	500, 544(sh)		2.15	2.06	2.09
5	580	500, 550(sh)	500, 550(sh)	483	694, 767			2.07

[a] sh shoulder.

the metal ion [33]. Therefore, the nitrate ion acts as a bidentate ligand in complex **4**. The spectrum of complex **2** agrees with a quasiplanar disposition for the copper ion. The spectrum of complex **1** is different from the others, the number and positions of the absorption bands suggest a pentacoordinated geometry.

Structures for each coordination number are illustrated in Fig. 2, where we have plotted the output of the calculation carried out using the Hyperchem program (semiempirical method, ZINDO/1).

The solution spectra of all complexes in DMSO, DMF and methanol present the same absorption bands (solutions are red), so the solvent molecules partially replace the anion in the coordination sphere of copper, giving a quasiplanar environment in all complexes. The spectrum of complex **2** does not change in solution because the disposition in the solid state was already quasiplanar.

For complexes **3** and **5** the spectra in DMF were registered after the addition of hydrochloric acid (2 M). An important change was observed: the solution colour changes to green and the position of the band indicates a significant modification in the copper coordination sphere giving a pseudo-octahedral geometry for the copper ion as in the complexes in the solid state (Fig. 3) [33].

We studied the variation of UV–Vis spectra of 10^{-3} M copper(II) chloride dihydrate solution in DMSO after successive additions of 10^{-3} M L^1H_6 solution in the same solvent with the total volume constant and in the presence of $[NBu_4][PF_6]$ to maintain the ionic force. The visible spectra were recorded and the absorbance variations represented versus the molar fraction of ligand added/Cu (Fig. 4).

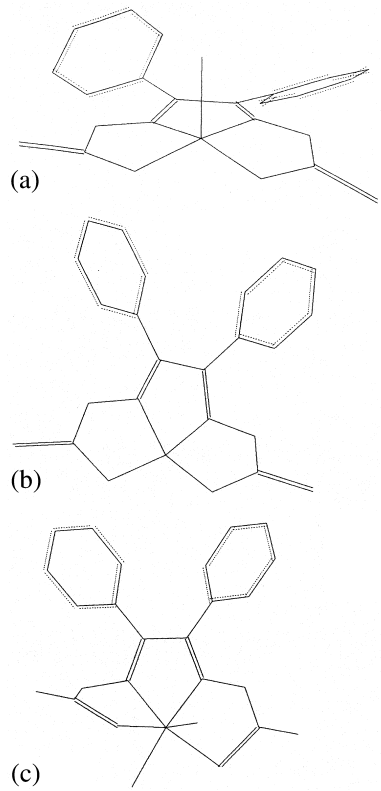


Fig. 2. Possible structures for L^1H_6 complexes: (a) complex **1**, (b) complex **2**, (c) complex **3**.

From the first addition, a new band appears at 448 nm in the visible spectrum whose absorbance increases lineally until a 2 molar fraction; after that the value is constant.

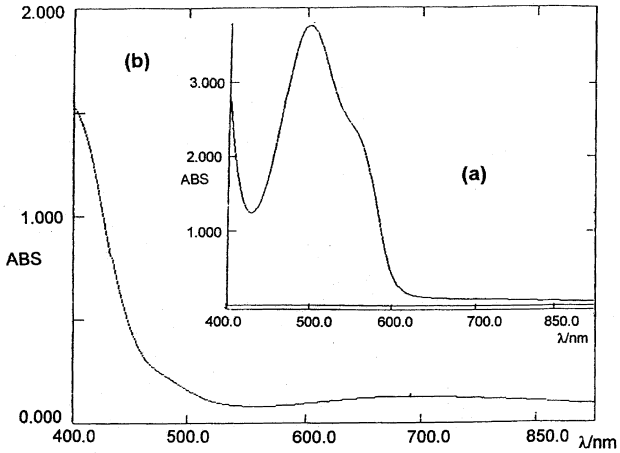


Fig. 3. UV–Vis spectra of complex **3** [$CuL^1H_6Cl_2$]: (a) DMF solution; (b) DMF + HCl (2 M).

The spectra were registered after 2 days, and the position of the band is shifted to 500 nm (identical position to that in the isolated complexes in DMSO solutions). The absorbance increases until a 1.5 molar fraction and then is constant (Fig. 4). Therefore, in DMSO a 1:1 molar ratio complex is formed but in this solvent an excess of the ligand is necessary.

The EPR parameters observed for complexes in the solid state (300 K) are presented in Table 3. In Fig. 5 the spectrum of complex **1** is shown.

The EPR spectra, which do not show hyperfine coupling, confirm the copper oxidation state and the mononuclear nature for the complexes. Complexes **1**, **2**, **3** and **4** give typical axial spectra, but complex **5** has a slightly axial isotropic spectrum. Values of $g_\parallel$ and $g_\perp$ are in the range for this kind of complexes. In all of the complexes, $g_\parallel > g_\perp > 2$ values are consistent with a $d_{x^2-y^2}$ state. Complex **2** presents a lower $g_\parallel$

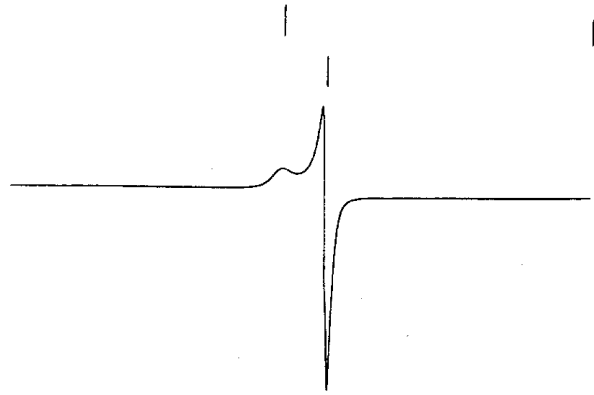


Fig. 5. Solid state EPR spectrum of complex **1**.

value, which agrees with the L^1H_6 being tetradentate dianion and pseudo-planar, while the higher value is presented for complex **3** in which the ligand is neutral and the copper is hexacoordinated [8,30,34].

3.2. Complexes derived from L^2H_2

Reactions of the mesocyclic ligand L^2H_2 with copper(II) nitrate and sulfate hydrate give stable solids in air and moisture. The colour, melting point and analytical data are included in Table 1. The formulae of complexes depend on the metal salt used.

Reaction with nitrate gives complex **6**, whose analytical data and mass spectra indicate that the complex contains the deprotonated macrocyclic ligand L^3H. The mass spectrum shows a peak at 529 amu corresponding to the macrocycle molecular mass $[C_{30}H_{21}N_6S_2]^+$ and a peak corresponding to the fragment $[CuC_{30}H_{21}N_6S_2CH_3OH]^+$. From the reaction with sulfate the complex **7** was obtained. Its analytical

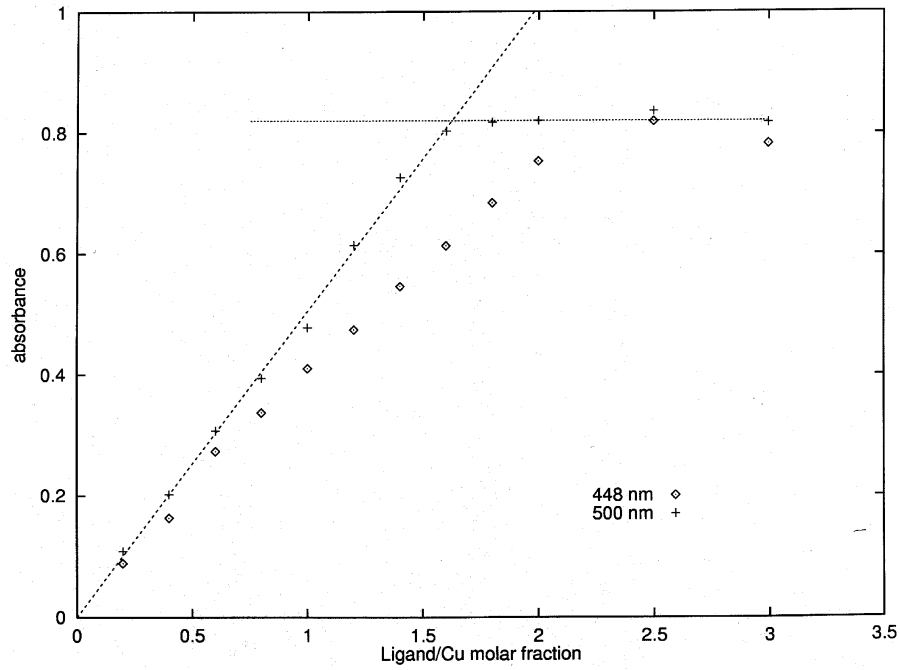


Fig. 4. Absorbance evolution of the L^1H_6 copper complex, in DMSO solution, versus ligand/Cu molar fraction; (◇) direct measurements; (+) after 24 h.

Table 4
Relevant IR spectral data and assignment of L^2H_2 complexes (cm^{-1})

	ν(N–H)	ν(C=N)	Thioamide I	Thioamide IV	ν(Cu–N)/ν(Cu–S)
L^2H_2	3184, 3131	1608	1550	846	
$L^3H_2C_{30}H_{22}N_6S_2$	3057	1599, 1581	1480	866	
$Cu(C_{30}H_{21}N_6S_2)_2CH_3OH$ (**6**)	3053	1601, 1583, 1575, 1550	1485	865	439
$CuC_{30}H_{20}N_6S_2$ (**7**)	3053	1600, 1582, 1575, 1550	1488	878, 866	436

data suggest a 1:1 deprotonated ligand:copper ratio. The mass spectrum confirms the macrocyclation of the ligand. In addition, in both reactions L^3H_2 is isolated from the reaction liquor. Therefore, the macrocyclic ligand is formed in all reactions where the copper ion acts as template. The characteristics of the final product depend on the salt used. A free macrocycle is obtained in the reaction with copper chloride, while complexes were isolated from the reaction with nitrate and sulfate.

3.2.1. IR spectra

The IR spectrum of complex **6** shows only a band assignable to ν(NH), the thioamide I slightly shifted to higher frequencies and four bands in the region of stretching vibration of the imine group (Table 4). These modifications suggest that the L^3H_2 ligands are partially deprotonated and two equivalent imine groups of each ligand are bonded to the copper ion.

The spectrum of complex **7** exhibits the presence of water and the deprotonation of the ligand. The bands are slightly shifted with respect to the L^3H_2, indicating that the ligand is bonded to the copper ion through four nitrogen atoms.

3.2.2. Electronic spectra

The electronic spectra of complexes in the solid state are very similar. Both of them show a band at a position which agrees with a pentacoordination for the copper, so the solvent molecules are bonded to the copper ion.

3.3. Complexes derived from L^3H_2

Direct reactions of the macrocyclic ligand with copper chloride and nitrate give complexes **8** and **9**, respectively. The analytical and spectroscopic data indicate that they are adulterated with the ligand, although it was necessary to work under stronger conditions than with the mesocyclic ligand L^2H_2, probably owing to its inherent rigidity.

3.4. Cyclic voltammetry

The study of the electrochemical behaviour of the complexes was carried out in the range from +1 to −1.5 V. In the positive range, +1 to 0 V, the oxidation processes Cu(III)/Cu(II) can be observed. Cyclic scanning between 0 and −1.5 V permits study of the copper reduction centred processes and the ligand reductions; the potential reduction of the Cu(II)/Cu(I) process is related to the potential SOD mimetic activity. Both ranges of potentials were studied independently. The electrochemical response in the total range studied (Figs. 6–8) showed a pattern that can be considered as the sum of the individual responses.

The cyclic voltammogram of L^1H_6 in DMSO shows irreversible reduction waves in the more negative region (Fig. 9(b)) [26,35].

The voltammetric response of all L^1H_6 complexes exhibits oxidation and reduction metal centred processes, as for complexes previously published [27]. Cyclic voltammograms between +1 and 0.0 V show a redox couple associated with the Cu(III)/Cu(II) process (Table 5). In addition, in the range 0.0 to −1.5 V, peaks which can be assigned to Cu(II)/Cu(I) and Cu(I)/Cu(0) processes appear [1].

Cyclic scanning of complex **1** (Fig. 6(a)) between +1 and 0 V shows in the cathodic scan a peak at +0.625 V. In the forward scan a poorly defined wave at +0.410 V can be observed and an anodic peak at +0.680 V associated with

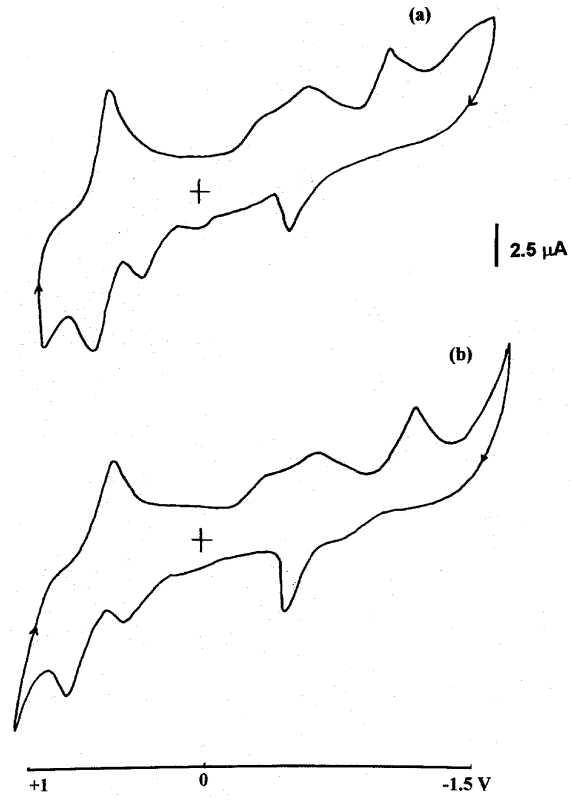


Fig. 6. Cyclic voltammograms for complexes: (a) complex **1**, $[CuL^1H_5Cl]$; (b) complex **3**, $[CuL^1H_6Cl_2]$; $\nu = 100$ mV s^{-1}.

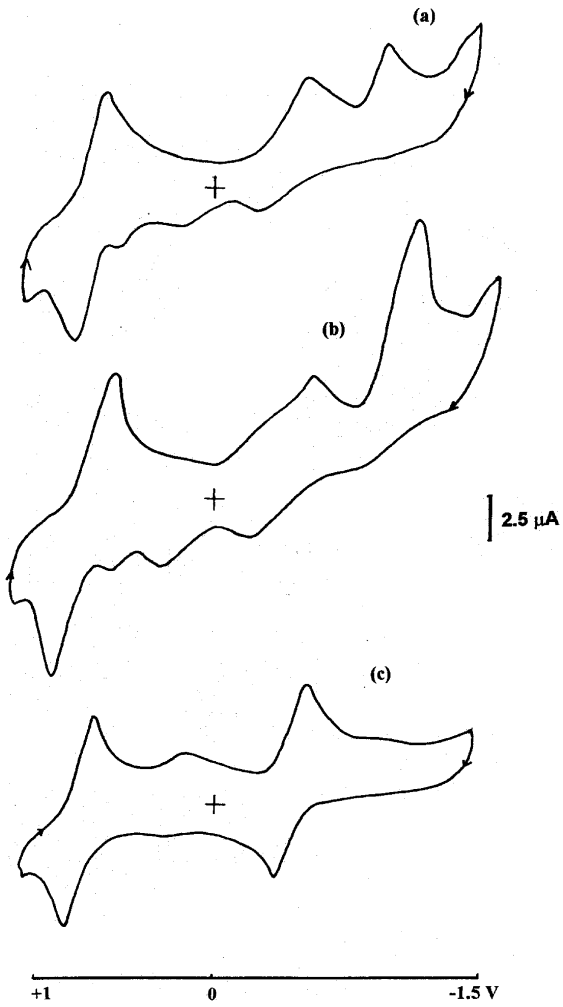


Fig. 7. Cyclic voltammograms for (a) complex **4**, $[CuL^1H_5NO_3]$, (b) complex **5**, $[CuL^1H_6CH_3OH]SO_4$, (c) complex **2**, $[CuL^1H_4]$, $\nu = 100$ mV s^{-1}.

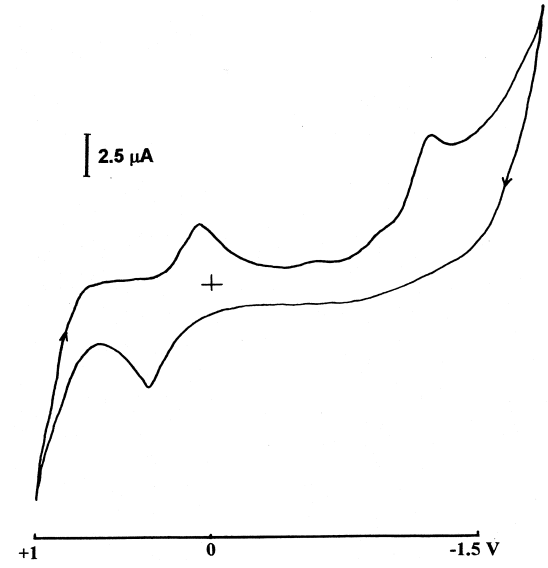


Fig. 8. Cyclic voltammogram of complex **3**, $[CuL^1H_6Cl_2]$, in DMSO after the addition of HCl (2 M), $\nu = 100$ mV s^{-1}.

the cathodic peak at +0.625 V. The ΔE_p values fall in the range 50–70 mV, when the scan rate is varied between 100–800 mV s^{-1}, with peak current ratio constant (0.8). Also the ratio between the cathodic peak current and the square root of the scan rate ($I_{pc}/\nu^{1/2}$) is practically constant. All of these data are diagnostic of a quasireversible one-electron transfer controlled by diffusion following the equation

$$[Cu(III)L] + e^- \Leftrightarrow [Cu(II)L]$$

Cyclic scans of **1** in the range 0 to −1.5 V reveal peaks at −0.470 and −0.930 V in the cathodic scan and in the forward scan a peak at −0.390 V associated with the more negative cathodic peak. These peaks can be assigned to successive Cu(II) reduction processes.

The voltammogram of complex **3** (Fig. 6(b)) is very similar to that of complex **1**. The cyclic voltammogram of **3** shows, between +1.5 and 0 V, a cathodic peak at +0.680 V and an anodic peak at +0.740 V associated with the cathodic peak. The ΔE_p and the current peak ratio of this couple of peaks are as expected for a quasireversible Cu(III)/Cu(II) process.

In the cathodic scan, in the range 0 to −1.5 V, peaks at −0.400 V and −1.030 V are observed. In the anodic scan there is a peak at −0.380 V, associated with the more negative cathodic peak. The first wave is attributed to Cu(II)/Cu(I) reduction and the other peaks correspond to the Cu(II)/Cu(0) reduction processes.

Cyclic voltammograms of complexes **4** and **5** (Fig. 6(a,b)) are very similar. The electrochemical response of complex **4** in the cathodic scan shows a peak at +0.600 V and in the reverse scan an anodic peak at +0.675 V associated with the cathodic peak. The variation of the redox parameters of the redox couple is indicated in Table 6, so it is associated with a quasireversible Cu(III)/Cu(II) process. The voltammogram between 0 and −1.5 V shows peaks at −0.520 V and −0.960 V, which can be attributed to the reductions Cu(II)/Cu(I) and Cu(I)/Cu(0), respectively. The electrochemical parameters for complex **5** are included in Table 6.

The cyclic voltammogram of complex **2** (Fig. 7(c)) shows a different electrochemical response and it is close to that published previously [27]. The most important characteristic is the quasireversible waves associated with the Cu(II)/Cu(I) process (Table 6).

For all complexes, redox processes associated with oxidation to Cu(III) are observed, probably because the L^1H_6 is

Table 5
Oxidation potential values (V) of L^1H_6 complexes

Compound	$E_{1/2}$ [a] Cu(III)/Cu(II)
$C_{16}H_{15}N_6S_2CuCl$ (**1**)	0.652
$C_{16}H_{14}N_6S_2Cu$ (**2**)	0.645
$C_{16}H_{16}N_6S_2CuCl_2$ (**3**)	0.710
$C_{16}H_{15}N_6S_2CuNO_3$ (**4**)	0.635
$CuC_{16}H_{16}N_6S_2SO_4 \cdot 2CH_3OH$ (**5**)	0.640

[a] $E_{1/2} = (E_{pa} + E_{pc})/2$, $\nu = 100$ mV s^{-1}.

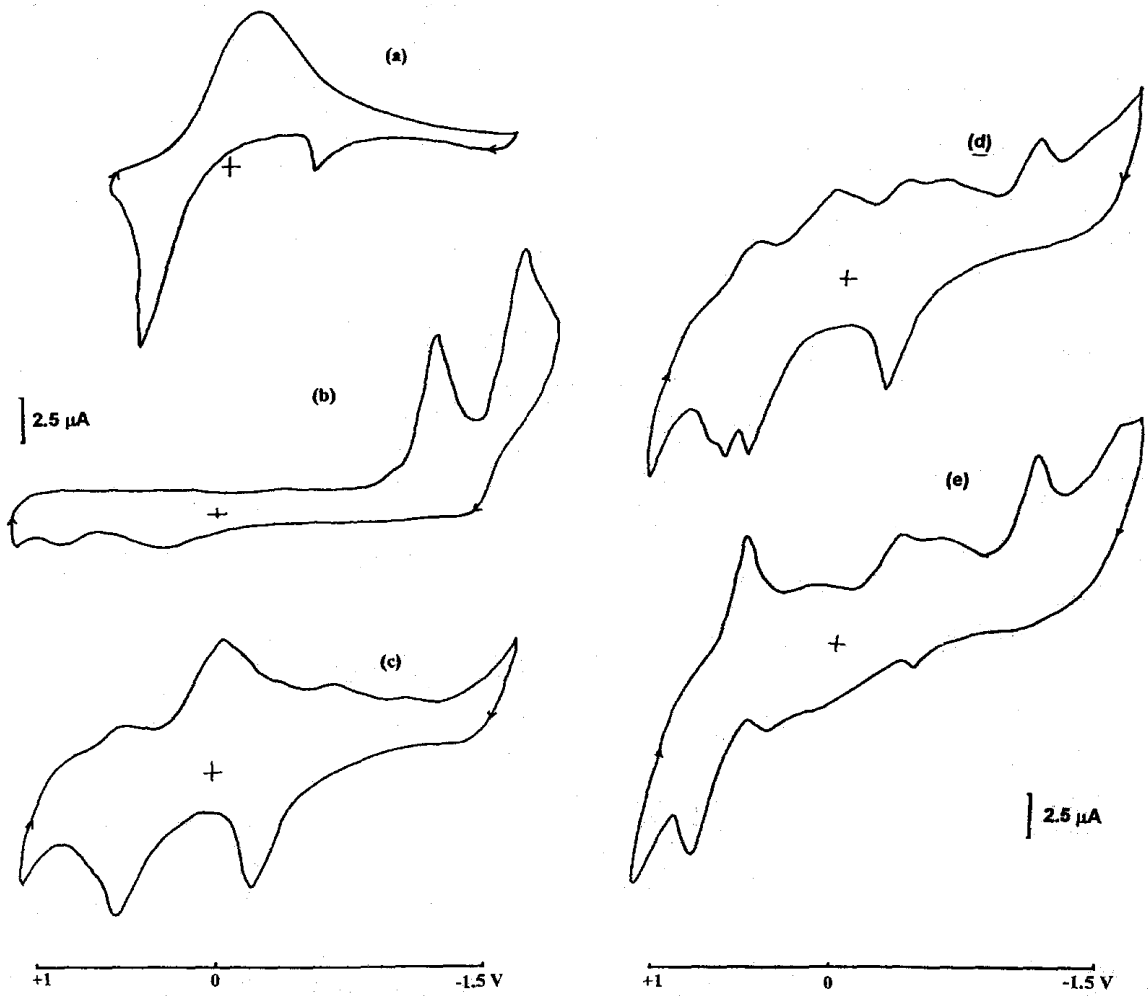


Fig. 9. Evolution of the cyclic voltammogram of $CuCl_2 \cdot 2H_2O$ in DMSO (a); with successive additions of L^1H_6 (b); after 0.4 ml (c); after 1.4 ml (d); after 2.4 ml (e).

Table 6
Summary of electrochemical data for complexes [a]

Complex	+1.5 to 0 V				0 to −1.5 V		
	E_{pc}	E_{pa}	ΔE_p	I_{pc}/I_{pa} [b]	E_{pc}	E_{pa}	E_{pc}
1	0.625	0.680	0.055	0.800	−0.470	−0.390	−0.930
2	0.620	0.670	0.050	0.860	−0.600	−0.500	
3	0.680	0.740	0.060	1.000	−0.400	−0.380	−1.030
4	0.600	0.675	0.075	0.980	−0.520		−0.960
5	0.610	0.670	0.060	0.820	−0.510		−0.990

[a] Redox potential (V) at 298 K, scan rate 100 mV s^{-1}. Cyclic voltammograms registered in the range from +1 to −1.5 V.
[b] Scan rate in the range 100–800 mV s^{-1}.

an open chain ligand and in its complexes the oxidation of copper is favoured since this ligand can adopt a different conformation to fit the small copper(III). The change from the Cu(II) to the Cu(III) state (d^8 low spin) involves a drastic reduction of the metal ion radius. In addition, this process does not involve changes in the geometries of the copper(II) complexes in DMSO solution. The oxidation values in Table 5 agree with that, because more positive values and more difficulty in stabilizing the copper(III) oxidation state are observed for complexes **1** and **3** [36,37].

On the other hand, the values of the reduction potential fall in the range −0.400 to −0.520 V, indicating difficulty in reducing the copper(II) ion in these complexes. This fact can be interpreted in terms of less favourable fitting of the Cu(II)/Cu(I) ion, because this reduction is related to the level of tetrahedral distortion in the complexes and in our

case in solution they seem to be almost planar. In accordance with these reduction potentials and the electronic spectra of L^1H_6 complexes, they do not seem to be suitable SOD mimetics.

The electrochemical response of complexes **1** and **3** with successive additions of hydrochloric acid (2 M) was also studied. The voltammogram changes immediately with the first addition, the more positive potential peaks are modified and a new peak couple arises. These changes increase with the successive additions of acid or with time until 1 cm^3 is added. The voltammogram (Fig. 8) now shows two peaks at $+0.280$ and -1.00 V in the cathodic scan and an anodic peak at $+0.360$ V associated with $+0.280$ V, indicating a significant change in the complex structure under these conditions. These results agree with those from the visible spectra in the same solvent described in the previous section.

Reaction of copper(II) chloride with L^1H_6 in DMSO was studied by cyclic voltammetry. Cyclic voltammograms of $CuCl_2 \cdot 2H_2O$ solutions in DMSO, in which L^1H_6 was added gradually until a 1:3 molar ratio was reached, were recorded (Fig. 9(a,b)). Changes in the colour and in the electrochemical response were shown from the first addition. The changes increase when the ligand proportions increase (Fig. 9(c,d)), but the cyclic voltammogram does not reproduce the cyclic voltammogram of isolated complex until a 1:2.5 molar ratio. These results indicate that the complexation reaction is slow. The donor character of the solvent may be the reason for that, owing to the difficult substitution by the ligand as was shown for the visible spectra of complexes.

Cyclic voltammograms of macrocyclic complexes **6** and **7** are very different to those of the open chain complexes. They do not show waves corresponding to a Cu(III)/Cu(II) process; this agrees with the behaviour of similar copper macrocyclic complexes [27]. The voltammograms only exhibit reduction waves at negative potentials which could be related to the reduction process of the copper ion and the unsaturation of the ligand [38].

Acknowledgements

We thank Professor J. Borrás (Universitat de Vàlencia) for EPR spectra and the Comunidad Autónoma de Madrid (Spain) for financial support (project: 6M/041/96).

References

[1] D.X. West, E. Liberta, S.B. Padhye, R.C. Chikate, P.B. Sonawane, A.S. Kumbar, R.S. Yeranda, Coord. Chem. Rev. 123 (1993) 49 and Refs. therein.
[2] D.X. West, S.B. Padhye, P.B. Sonawane, Struct. Bonding 76 (1991) 1.
[3] Y. Haiduc, A. Silvestru, Coord. Chem. Rev. 99 (1990) 253.
[4] O.E. Ichiro, D. Busch, H. Shull (Eds.), Bionorganic Chemistry, Allym and Bacon, Boston, MA, 1977.
[5] R.W. Hay, J.R. Dilworth, K.B. Nolan, in: Bioinorganic Chemistry, vol. 1, JAI Press, London, 1991.
[6] V.W.-W. Yam, Y.-L. Pui, W.-P. Li, K.K.-W. Lo, K.-K. Cheung, J. Chem. Soc., Dalton Trans. (1998) 3615.
[7] M.R. Malachowski, B.T. Dorsey, M.J. Parker, M.E. Adams, R.S. Kelly, Polyhedron 17 (1998) 1289.
[8] B.J. Hathaway, in: G. Wilkinson, R. Gillard, J.A. McCleverty (Eds.), Comprehensive Coordination Chemistry, Pergamon, Oxford, 1987.
[9] D.W. Margerum, G.D. Owens, in: H. Sigel (Ed.), Metal Ions in Biological Systems, Marcel Dekker, New York, 1981.
[10] B. Dietrich, Pure Appl. Chem. 65 (1993) 1457.
[11] R.M. Izatt, K. Pawlak, J.S. Bardshaw, Chem. Rev. 95 (1995) 2529.
[12] K. Kalcher, J.M. Kauffman, J. Wank, I. Svancare, K. Vitras, C. Neuhal, Z. Yang, Electroanalysis 7 (1995) 5.
[13] M.A.T. Gilmartin, J.P. Hart, Analyst 120 (1995) 1029.
[14] B. Dietrich, P. Viout, J.M. Lehn (Eds.), Macrocyclic Chemistry, VCH, Weinheim, 1993.
[15] E.C. Constable, Metals and Ligand Reactivity, VCH, Weinheim, 1996.
[16] A.L. Vance, N.W. Alcock, D.H. Busch, J.A. Heppert, Inorg. Chem. 36 (1997) 5132.
[17] S.M. Nelson, Pure Appl. Chem. 52 (1980) 69.
[18] C.M. Liu, G. Xiong, X.Z. You, Y.J. Liu, Polyhedron 15 (1996) 4565.
[19] Z. Duracková, J. Labuda, J. Inorg. Biochem. 58 (1995) 297.
[20] J.A. Streeky, D.G. Pillsburg, D.H. Busch, Inorg. Chem. 19 (1980) 3148.
[21] A.A. Isse, A. Gennaro, E. Vianello, J. Chem. Soc., Dalton Trans. (1993) 2091.
[22] H. Yokoi, A.W. Addison, Inorg. Chem. 16 (1977) 1341.
[23] F. Lovecchio, E.S. Gore, D.H. Busch, J. Am. Chem. Soc. (1974) 96.
[24] P. Souza, M.A. Mendiola, A. Arquero, V. Fernández, E. Gutiérrez-Puebla, C. Ruíz-Valero, Z. Naturforsch., Teil B 49 (1994) 263.
[25] A. Arquero, M. Cañadas, M. Martínez-Ripoll, M.A. Mendiola, A. Rodríguez, Tetrahedron 54 (1998) 11271.
[26] A. Arquero, M.A. Mendiola, P. Souza, M.T. Sevilla, Polyhedron 15 (1996) 165.
[27] Z. Duracková, M.A. Mendiola, M.T. Sevilla, A. Valent, Bioelectrochem. Bioenerg. 48 (1999) 109.
[28] J. Gismera, M.A. Mendiola, J.R. Procopio, M.T. Sevilla, Anal. Chim. Acta 385 (1999) 143.
[29] W.J. Geary, Coord. Chem. Rev. 7 (1971) 81.
[30] D.E. Fenton, D.H. Cook, J. Chem. Soc., Chem. Commun. (1977) 724.
[31] G.A. Bain, D.X. West, J. Krejci, J. Valdés-Martínez, S. Hernández-Ortega, R.A. Toscano, Polyhedron 16 (1997) 855 and Refs. therein.
[32] J. Valdés-Martínez, R.A. Toscano, A. Zentella-Dehesa, M.M. Salberg, G.A. Bain, D.X. West, Polyhedron 15 (1996) 427 and Refs. therein.
[33] A.B.P. Lever, Inorganic Electronic Spectroscopy, Elsevier, Amsterdam, 2nd edn., 1984.
[34] B.A. Goodman, J.B. Raynor, Adv. Inorg. Chem. Radiochem. 13 (1970) 135.
[35] E. Eisner, Karowa-Eisner, in: A.J. Bard, H. Lund (Eds.), Encyclopedia of Electrochemistry of the Elements, 1979, p. 13.
[36] F.P. Bossu, K.L. Chellapa, D.W. Margerum, J. Am. Chem. Soc. (1977) 2195.
[37] X.H. Bu, X.Ch. Cao, D.L. An, R.H. Zhang, C. Thomas, E. Kimura, J. Chem. Soc., Dalton Trans. (1998) 433.
[38] Y. Sunatsuki, T. Matsumoto, Y. Fukashima, M. Minura, M. Hirota, N. Natsumoto, F. Kai, Polyhedron 17 (1998) 1943.

PERGAMON

www.elsevier.nl/locate/poly

Polyhedron 19 (2000) 453–456

POLYHEDRON

Synthesis and crystal structure of lanthanide sandwich complexes with mixed cyclooctatetraenyl and chelating ether side chain-cyclopentadienyl ligands: crystal structures of $(\eta^5\text{-MeOCH}_2\text{CH}_2\text{Cp})\text{Nd}(\eta^8\text{-C}_8\text{H}_8)(\text{THF})$ and $(\eta^5\text{-C}_4\text{H}_7\text{OCH}_2\text{C}_5\text{H}_4)\text{La}(\eta^8\text{-C}_8\text{H}_8)(\text{THF})$

Qiancai Liu [a], Xiaoqiang Shen [a], Jiling Huang [a], Yanlong Qian [a,*], Albert Sun-Chi Chan [b], Wing-Tak Wong [c]

[a] *Laboratory of Organometallic Chemistry, East China University of Science and Technology, P.O. Box 421, 130 Meilong Road, Shanghai 200237, People's Republic of China*

[b] *Department of Applied Biology and Chemistry, Hong Kong Polytechnic University, Hong Kong, People's Republic of China*

[c] *Department of Chemistry, The University of Hong Kong, Hong Kong, People's Republic of China*

Received 5 January 1999; accepted 17 December 1999

Abstract

$LnCl_3$ reacted with $K_2C_8H_8$ in THF in the ratio 1:1 at room temperature and formed $(C_8H_8)LnCl\cdot n$THF, which was then treated with RCpK–THF ($RCp = MeOCH_2CH_2C_5H_4$ or $C_4H_7OCH_2C_5H_4$) to yield the title complexes $(\eta^5\text{-RCp})Ln(\eta^8\text{-}C_8H_8)(THF)$ (Ln = Nd (**1**) and Sm (**2**), $RCp = MeOCH_2CH_2C_5H_4$; Ln = La (**3**), Nd (**4**) and Sm (**5**), $RCp = C_4H_7OCH_2C_5H_4$). The crystal structures of complexes **1** and **3** were determined by X-ray diffraction and revealed that the oxygen atoms of the ether group on the cyclopentadienyl ring is coordinated to the central metal atom. The central lanthanum atom is in a distorted tetrahedral geometry. The average bond distances Nd–C(η^8) and Nd–C(η^5) are 2.697(2) and 2.749(2) Å, respectively, while the Nd–O(THF) and Nd–O(η^1) distances are 2.580(1) and 2.619(1) Å, respectively. The average bond lengths La–C(η^5) and La–C(η^8) are 2.842(7) and 2.740(8) Å, respectively. The La–O(THF) and La–O(η^1) distances are 2.607(4) and 2.633(4) Å. ©2000 Elsevier Science Ltd All rights reserved.

Keywords: Organolanthanide complexes; Ether-side chain cyclopentadienyl; Cyclooctatetraenyl; Crystal structures

1. Introduction

Cyclooctatetrene and its derivatives are important backbones for the construction of organolanthanide sandwich complexes [1–4]. Hayes and Thomas initially synthesized cyclooctatetraenyl complexes [5], and Jamerson et al. reported the synthesis of $(\eta^5\text{-}C_5H_5)Sm(\eta^8\text{-}C_8H_8)(THF)$, leading to the wide use of cyclooctatetraenyl (COT) as a ligand in organolanthanide chemistry [6]. In 1989, Schumann and coworkers reported a series of cyclopentadienyl and cyclooctatetraenyl lanthanide complexes such as $(\eta^5\text{-}C_5Me_5)Lu(\eta^8\text{-}C_8H_8)$ and $(\eta^5\text{-}C_5(CH_2Ph)_5)Lu(\eta^8\text{-}C_8H_8)$ [7,8]. Furthermore, Chen and coworkers reported the crystal structures of $(\eta^5\text{-}C_5H_5)Pr(\eta^8\text{-}C_8H_8)(THF)_2$ and $(\eta^5\text{-}C_9H_7)Pr(\eta^8\text{-}C_8H_8)(THF)$ [9], $(\eta^5\text{-}2,4\text{-}Me_2C_5H_3)Sm(\eta^8\text{-}C_8H_8)$ and a trinuclear $[(\eta^8\text{-}C_8H_8)_3(\eta^5\text{-}C_6H_5CH_2C_5H_4)\text{-}Nd_2K(THF)_3]$ [10,11].

Recently, Porema et al. reported the synthesis of silylated cyclooctatetraenyl lanthanide complexes [12]. Chen and coworkers reported acyclic pentadienyl and cyclooctatetraenyl lanthanide complexes [13]. Cyclopentadiene ligands with ether side chains have been widely used as ligands to synthesize organolanthanocene complexes [14,15], so we are interested in investigating the synthesis of lanthanide complexes with both cyclooctatetraenyl and substituted cyclopentadienyl as ligands. In this paper we wish to report our recent progress: the synthesis and crystal structure of the title complexes.

2. Experimental

All manipulations were carried out under dry argon using Schlenk techniques. The solvents were dried with sodium

* Corresponding author. Tel./fax: +86-21-6470-2573; e-mail: qianling@online.sh.cn

0277-5387/00/$ - see front matter ©2000 Elsevier Science Ltd All rights reserved.
PII S0277-5387(99)00384-8

wires and distilled from sodium benzophenone ketyl before use. Anhydrous $LnCl_3$ was prepared by Taylor's method [16]. Potassium methoxyethyl cyclopentadienide and tetrahydrofurfuryl cyclopentadienide were prepared as previously reported [14]. The mass spectra were obtained on a HP 5989A mass spectrometer using EI method (70 eV). The elemental analyses were performed at the micro-analytical laboratory, Shanghai Institute of Organic Chemistry, Chinese Academy of Sciences.

*2.1. Synthesis of (η^5-$MeOCH_2CH_2Cp$)Nd(η^8-C_8H_8)(THF) (**1**)*

Complex **1** was synthesized as follows. To a well mixed suspension of $NdCl_3$ (1.94 g, 7.74 mmol) in THF (40 cm^3), $K_2C_8H_8$ (8.20 mmol) in THF (13 cm^3) was added with stirring. The mixture turned to pale green initially, then to pale yellow and finally to blue–green. The suspension was stirred for a further 24 h and $MeOCH_2CH_2CpK$ (7.74 mmol) in THF (13 cm^3) was added with a color change to brown, and the reaction was continued for a further 24 h. After centrifugation, the residual was washed twice with THF (2×20 cm^3); the combined solution was concentrated to dryness to give a green crystalline solid which was recrystallized in THF to form violet–green prism crystals (1.41 g, 41%), m.p. 138°C (dec.). *Anal.* Calc. for $C_{20}H_{27}NdO_2$: C, 54.14; H, 6.13. Found: C, 53.85; H, 6.06%. EI-MS: 369 (M^+–THF, 7.80%), 246 (Nd(COT), 1.6%), 267 (Nd($MeOCH_2CH_2Cp$), 1.9%), 104 (C_8H_8, 13%), 91 ($C_5H_4CH_2CH_2^+$, 100%).

*2.2. Synthesis of (η^5-$MeOCH_2CH_2Cp$)Sm(η^8-C_8H_8)(THF) (**2**)*

This complex was prepared from $SmCl_3$ (1.61 g, 6.27 mmol), $K_2C_8H_8$ (6.27 mmol) and $MeOCH_2CH_2CpK$ (6.27 mmol) in THF (40 cm^3) using the procedure above. Purple–brown crystals were obtained (1.31 g, 46.5%), m.p. 110°C (dec.). *Anal.* Calc. for $C_{20}H_{27}SmO_2$: C, 53.40; H, 6.05. Found: C, 53.26; H, 6.21%. EI-MS: 379 (M^+–THF, 5.5%), 275 (($MeOCH_2CH_2Cp$)–Sm, 16.4%), 256 (Sm(COT), 0.55%), 104 (C_8H_8, 17.3%), 92 ($CpCH_2CH_2^+$, 53.4%).

*2.3. Synthesis of (η^5-$C_4H_7OCH_2C_5H_4$)La(η^8-C_8H_8)(THF) (**3**)*

This complex was prepared from $LaCl_3$ (1.83 g, 7.46 mmol) in THF (40 ml), and $K_2C_8H_8$ (7.5 mmol) in THF (12 ml). The pale blue reaction mixture was stirred for 24 h with the color changing to pale yellow. Then a 6.8 ml THF solution of potassium tetrahydrofurfuryl cyclopentadienide $C_4H_7OCH_2C_5H_4K$ (7.44 mmol) was added and the resulting suspension was stirred for 3 days. After work-up, the resulting pale yellow crystalline solid was dissolved in THF and set in a refrigerator to obtain yellow prism crystals (2.08 g, 60.2%), m.p. 164°C (dec.). *Anal.* Found: C, 57.03; H, 6.27. Calc. for $C_{22}H_{29}LaO_2$: C, 56.90; H, 6.29%. EI-MS: 392 (M^+–THF, 100%), 288 (La($C_4H_7OCH_2C_5H_4$), 16%), 243 (La(COT), 23%).

*2.4. Synthesis of (η^5-$C_4H_7OCH_2C_5H_4$)Nd(η^8-C_8H_8)(THF) (**4**)*

Complex **4** was prepared analogously to **3** from $NdCl_3$ (1.13 g, 4.51 mmol), and $K_2C_8H_8$ (4.51 mmol in 7 ml THF) in 30 ml THF, which was then reacted with $C_4H_7OCH_2C_5H_4K$ (4.51 mmol in 4.0 ml THF). Blue–green crystals were obtained (0.891 g, 42.0%), m.p. 148°C (dec.). *Anal.* Found: C, 55.91; H, 6.05. Calc. for $C_{22}H_{29}NdO_2$: C, 56.27; H, 6.22%. EI-MS: 466 (M^+, 10%), 394 (M^+–THF, 88.8%), 291 (Nd($C_4H_7OCH_2C_5H_4$), 24.7%), 246 (Nd(C_8H_8), 22.5%), 150 ($C_4H_7OCH_2C_5H_4$, 11%), 104 (C_8H_8, 9.7%).

*2.5. Synthesis of (η^5-$C_4H_7OCH_2C_5H_4$)Sm(η^8-C_8H_8)(THF) (**5**)*

Complex **5** was prepared analogously to **3** from $SmCl_3$ (1.20 g, 4.67 mmol), and $K_2C_8H_8$ (4.66 mmol in 7.5 ml THF) in 30 ml THF, which was then reacted with $C_4H_7OCH_2C_5H_4K$ (4.97 mmol in 4.5 ml THF). Purple–black crystals were obtained (1.05 g, 47.2%), m.p. 135°C (dec.). *Anal.* Found: C, 55.11; H, 5.99. Calc. for $C_{22}H_{29}O_2Sm$: C, 55.55; H, 6.14%. EI-MS: 404 (M^+, 23.6%), 301 (Sm($C_4H_7OCH_2C_5H_4$), 100%), 257 (Sm(C_8H_8), 5.5%), 149 ($C_4H_7OCH_2C_5H_4$, 4.7%), 104 (C_8H_8, 11.2%).

*2.6. Structure determination of (η^5-$MeOCH_2CH_2Cp$)Nd(η^8-C_8H_8)(THF) (**1**) and (η^5-$C_4H_7OCH_2Cp$)La(η^8-C_8H_8)(THF) (**3**)*

Blue–green crystals of **1** and yellow prismatic crystals of **3** were sealed and mounted on a Siemens P4 four-circle diffractometer (for **3**, Rigaku AFC7R diffractometer). Crystal data were collected at ambient temperature using Mo Kα radiation ($\lambda = 0.71069$ Å for **1** and $\lambda = 0.71073$ Å for **3**). The data were corrected for Lorentz and polarization and empirical absorption. The structure was solved by heavy-atom Patterson methods and expanded Fourier techniques. The structure was refined by full-matrix least-squares. All of the hydrogen atoms were found from difference Fourier maps connecting analysis of geometric positions. All coordination parameters for atoms were refined, anisotropic thermal parameters for non-hydrogen atoms and isotropic parameters for hydrogen atoms. The molecular structures of **1** and **3** are shown in Figs. 1 and 2. Crystal data, selected bond lengths and angles for complexes **1** and **3** are given in Tables 1–3, respectively.

3. Results and discussion

Using well established ester-substituted cyclopentadienyl ligands, one can synthesize a series of lanthanocene com-

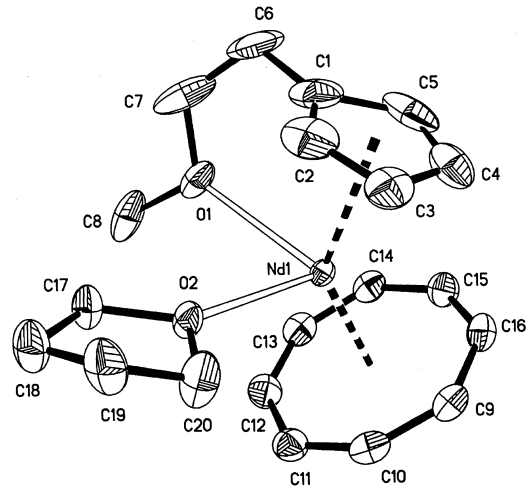


Fig. 1. Molecular structure of $(\eta^5\text{-MeOCH}_2\text{CH}_2\text{Cp})\text{Nd}(\eta^8\text{-C}_8\text{H}_8)(\text{THF})$ (**1**).

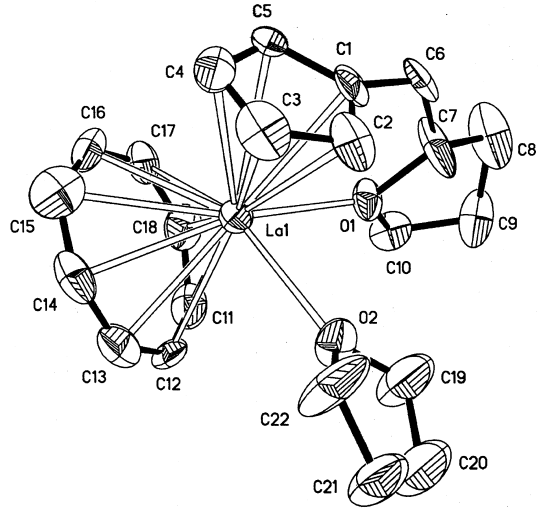
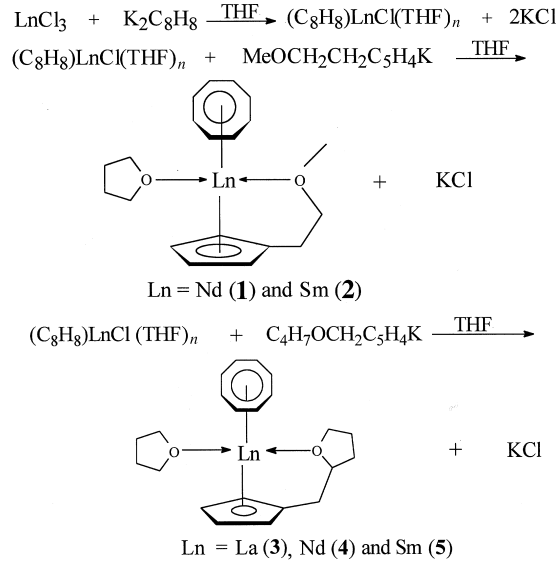


Fig. 2. Molecular structure of $(\eta^5\text{-C}_4\text{H}_7\text{OCH}_2\text{Cp})\text{La}(\eta^8\text{-C}_8\text{H}_8)(\text{THF})$ (**3**).

plexes [15,17,18]. The crystal structures determined for these complexes indicate that the oxygen atoms of the ligands can have intramolecular coordination to lanthanide metal ions, and can also satisfy the coordination requirement of the lanthanide centers even in the cases of early lanthanocene halide complexes. Anhydrous $LnCl_3$ was reacted with potassium salt of cyclooctatetraenyl, and then treated with the potassium salt of methoxyethyl cyclopentadienide or tetrahydrofurfuryl cyclopentadienide in THF. This led to isolation of the title complexes **1**–**5**. They may have one THF fragment in the crystals. However, the THF fragments were not observed in MS spectra of complexes **1**–**5**. This indicates that coordination between the lanthanide center and solvent THF of **1** and **5** is weak, which can be further proved by drying the above complexes under reduced pressure for more than 1 h with the loss of THF. Elemental analyses and mass spectra suggested that the title complexes were successfully synthesized, and X-ray determination confirmed the molecular structures. These results can be indicated as follows:

Table 1
Crystal data for complexes **1** and **3**

	$C_{20}H_{27}NdO_2$ (**1**)	$C_{22}H_{29}LaO_2$ (**3**)
Formula weight	443.66	464.38
Crystal system	orthorhombic	monoclinic
Space group	$P2_12_12_1$	$P2_1/c$
a (Å)	8.306(2)	8.474(4)
b (Å)	14.769(3)	17.629(3)
c (Å)	15.291(3)	14.021(3)
β (°)	90	102.25(3)
V (Å^3)	1875.8(7)	2047(1)
Z	4	4
D_{calc} (g cm^{-3})	1.571	1.51
μ (cm^{-1})	27.75	20.9
$F(000)$	892	936
Temperature (K)	293(2)	293(2)
Crystal dimensions (mm)	0.28×0.26×0.22	0.30×0.20×0.20
2θ limits (°)	$1.92<2\theta<25.50$	$18.31<2\theta<25.90$
No. of collected reflections	6301	3996
No. of unique reflections	3442	3733
No. of parameters	202	227
Largest difference peak and hole (e Å^{-3})	max. 0.487, min. −0.688	max. 0.70, min. −0.90
R	0.0324	0.035
R_w	0.0341	0.042



Single crystal X-ray determinations of **1** and **3** gave further evidence (Figs. 1 and 2). In these complexes, the central atom is bonded to a substituted cyclopentadienyl ring, a cyclooctatetraenyl ring and two oxygens (from the substituted Cp ring and THF) to form a distorted tetrahedron and the coordination number of the central atom is 9.

In complex **1**, the bond lengths Nd–C(η^8) range from 2.679(2) to 2.717(2) Å and the average Nd(1)–C(η^8) length is 2.697(2) Å which is similar to the bond lengths of $[(\eta^8\text{-C}_8\text{H}_8)_3(\eta^5\text{-C}_6\text{H}_5\text{CH}_2\text{C}_5\text{H}_4)\text{Nd}_2\text{K}(\text{THF})_3]$ (2.690(4) and 2.737(4) Å) [11], $[(\eta^8\text{-C}_8\text{H}_8)\text{Nd}(\text{THF})_2][(\eta^8\text{-C}_8\text{H}_8)_2\text{Nd}]$ (2.68(1) and 2.79(4) Å) and $(\eta^8\text{-C}_8\text{H}_8)\text{-Nd}(\eta^5\text{-2,4-C}_7\text{H}_{11})(\text{THF})$ (2.65(7) Å) [13]; the bond

Table 2
Selected bond lengths (Å) and bond angles (°) for complex **1**

Nd(1)–C(1)	2.747(3)	Nd(1)–C(12)	2.702(2)
Nd(1)–C(2)	2.755(3)	Nd(1)–C(13)	2.720(2)
Nd(1)–C(3)	2.749(2)	Nd(1)–C(14)	2.692(2)
Nd(1)–C(4)	2.759(2)	Nd(1)–C(15)	2.681(2)
Nd(1)–C(5)	2.743(2)	Nd(1)–C(16)	2.708(2)
Nd(1)–C(9)	2.702(2)	Nd(1)–O(1)	2.618(2)
Nd(1)–C(10)	2.685(2)	Nd(1)–O(2)	2.577(1)
Nd(1)–C(11)	2.711(2)		
O(1)–Nd(1)–O(2)	77.71(4)	Nd(1)–O(1)–C(7)	126.80(12)
C(1)–Nd(1)–C(2)	29.4(6)	C(10)–Nd(1)–C(11)	30.39(5)
C(2)–Nd(1)–C(3)	26.8(7)	C(11)–Nd(1)–C(12)	29.91(6)
C(3)–Nd(1)–C(4)	29.8(6)	C(12)–Nd(1)–C(13)	29.92(6)
C(4)–Nd(1)–C(5)	29.4(5)	C(13)–Nd(1)–C(14)	28.80(5)
C(5)–Nd(1)–C(1)	30.0(5)	C(14)–Nd(1)–C(15)	29.45(5)
C(9)–Nd(1)–C(10)	29.17(5)	C(15)–Nd(1)–C(16)	29.42(6)
C(9)–Nd(1)–C(16)	31.18(6)	Nd(1)–O(1)–C(8)	124.66(10)

Table 3
Selected bond lengths (Å) and angles (°) for complex **3**

La–O(1)	2.607(4)	La–O(2)	2.633(4)
La–C(1)	2.751(7)	La–C(3)	2.717(8)
La–C(2)	2.691(7)	La–C(4)	2.731(8)
La–C(5)	2.743(9)	La–C(6)	2.744(8)
La–C(7)	2.771(8)	La–C(8)	2.774(8)
La–C(9)	2.843(6)	La–C(10)	2.867(7)
La–C(11)	2.839(7)	La–C(12)	2.827(7)
La–C(13)	2.832(6)	O(1)–C(15)	1.380(9)
O(1)–C(18)	1.450(7)	O(2)–C(19)	1.40(1)
O(2)–C(22)	1.37(1)		
O(1)–La–O(2)	76.1(1)	O(1)–La–C(1)	81.2(2)
O(1)–La–C(2)	96.2(4)	O(1)–La–C(3)	121.8(4)
O(1)–La–C(4)	149.4(4)	O(1)–La–C(5)	161.0(3)
O(1)–La–C(6)	134.9(4)	O(1)–La–C(7)	106.6(3)
O(1)–La–C(8)	86.2(2)	O(1)–La–C(9)	77.9(2)
O(1)–La–C(10)	105.3(2)	O(1)–La–C(11)	108.2(2)
O(1)–La–C(12)	82.5(2)	O(1)–La–C(13)	62.2(2)

lengths Nd–C(η^5) range from 2.743(2) to 2.759(2) Å and the average length is 2.749(2) Å which is shorter than the relative value in $(MeOCH_2CH_2Cp)_3Nd$ (2.807 Å) [17] and in $[(\eta^8\text{-}C_8H_8)_3(\eta^5\text{-}C_6H_5CH_2C_5H_4)Nd_2K(THF)_3]$ (2.838(4) Å) [13] because of the steric effect of cyclooctatetraenyl and the ether group on the side chain. The bond length Nd–O(THF) is 2.580(1) Å, similar to that of $(\eta^8\text{-}C_8H_8)Nd(\eta^5\text{-}2,4\text{-}C_7H_{11})(THF)$ (2.55(9) Å) [13], and the Nd–O(η^1) distance is 2.619(1) Å, slightly shorter than that of $(MeOCH_2CH_2Cp)_3Nd$ (2.782 Å) [17].

In complex **3**, the La–C(η^5) bond distances range from 2.827(7) to 2.867(7) Å, the average La–C(η^5) distance is 2.842(7) Å, similar to those of $(MeOCH_2CH_2Cp)_3La$ (2.860 Å) [17] and $[(MeOCH_2CH_2Cp)_2LaCl]_2$ (2.836 Å) [18]. However, it is longer than the La–C(η^5) distance of $(C_8H_8)La(C_5Me_4H)(THF)_2$ (2.573(2) Å) [19]. The La–COT(η^8) bond distances range from 2.691(8) to 2.774(8) Å, and the average La–C(η^8) distance is 2.740(8) Å, which is longer than that of $(C_8H_8)La(C_5Me_4H)(THF)_2$ (2.094(3) Å). While La–O(THF) is 2.607(4) Å, comparable to those of $La(C_5H_5)_3(THF)$ (2.47 Å) and La–O(η^1) (2.633(4) Å) in itself and La–O of $(\eta^8\text{-}C_8H_8)La(C_5Me_4H)(THF)_2$ (2.681(3) Å), it is shorter than the relative La–O average distances in $[(MeOCH_2CH_2Cp)_2LaCl]_2$ (2.720(2) Å) [18] and $(MeOCH_2CH_2Cp)_3La$ (2.806(6) Å) [17]. The bond angle O(1)–La–O(2) is 76.1(1)°.

The average bond distances Nd–C(η^8) (2.697(2) Å) and Nd–C(η^5) (2.749(2) Å) in complex **1** are slightly shorter than those of La–C(η^8) (2.842(7) Å) and La–C(η^5) (2.740(8) Å) in complex **3**, which can be considered as the result of the different radii of the central ions.

Supplementary data

All of the parameters for atomic coordinates, isotropic thermal parameters, bond lengths and angles have been deposited at CCDC (CCDC numbers 108612 for **1** and 112642 for **3**).

Acknowledgements

Financial support for this work from the National Natural Science Foundation of China (NNSF) and Sino-Pec (29734145), and NNSF (29871010), The Research Fund for The Doctoral Program of Higher Education (RFDP), The State Key Laboratory of Coordination Chemistry, Nanjing, and Shanghai Postdoctoral Research Foundation (98BSH1423) is gratefully acknowledged.

References

[1] H. Schumann, J.A. Meese-Marhtscheffel, L. Esser, Chem. Rev. 95 (1995) 865.
[2] C. Schaverian, Adv. Organomet. Chem. 155 (1994) 1.
[3] F.T. Edelmann, in: E.W. Abel, F.G.A. Stone, G. Wilkinson (Eds.), Comprehensive Organometallic Chemistry II, vol. 4, Pergamon, 1995, p. 11.
[4] F.T. Edelmann, New J. Chem. 19 (1995) 535.
[5] R.G. Hayes, J.L. Thomas, J. Am. Chem. Soc. 91 (1969) 6876.
[6] J.D. Jamerson, A.P. Masino, J. Takats, J. Organomet. Chem. 65 (1974) C33.
[7] H. Schumann, R.D. Kohn, F.W. Reier, A. Dietrich, J. Pickardt, Organometallics 8 (1989) 1388.
[8] H. Schumann, C. Janiak, R.K. Kohn, J. Lobel, A. Dietrich, J. Organomet. Chem. 365 (1989) 137.
[9] K. Wen, Z. Jin, W. Chen, J. Chem. Soc., Chem. Commun. (1991) 680.
[10] J. Jin, Z. Jin, W. Chen, J. Chem. Soc., Chem. Commun. (1991) 1328.
[11] J. Xia, X. Zhuang, Z. Jin, W. Chen, Polyhedron 15 (1996) 3399.
[12] P. Porema, U. Reiβmann, M. Noltemeyer, H.G. Schmidt, W. Bruser, F.T. Edelmann, J. Organomet. Chem. 544 (1997) 1.
[13] S. Zhang, J. Jin, G. Wei, W. Chen, J. Liu, J. Organomet. Chem. 483 (1994) 57 and refs. therein.
[14] Q. Huang, Y. Qian, Synthesis (1987) 910.
[15] B. Wang, D. Deng, C. Qian, New J. Chem. 19 (1995) 515.
[16] M.P. Taylor, C.P. Carter, J. Inorg. Nucl. Chem. 24 (1962) 387.
[17] C. Qian, B. Wang, D. Deng, J. Sun, F.E. Hahn, J. Chen, P. Zheng, J. Chem. Soc., Dalton Trans. (1996) 955.
[18] C. Qian, B. Wang, D. Deng, J. Hu, J. Chen, G. Wu, G. Zheng, Inorg. Chem. 33 (1994) 3382.
[19] H. Schumann, M. Glanz, J. Winterfeld, H. Hemling, J. Organomet. Chem. 456 (1993) 77.

PERGAMON

www.elsevier.nl/locate/poly

Polyhedron 19 (2000) 457–463

POLYHEDRON

Comparison of theophyllinato Cu(II) complexes of ethanolamine and diethanolamine
Part 2. Structure and thermal study of the dimeric complex with diethanolamine[1]

János Madarász [a,*], Petra Bombicz [b], Mátyás Czugler [b], György Pokol [a]

[a] *Institute of General and Analytical Chemistry, Technical University of Budapest, H-1521 Budapest, Hungary*

[b] *Institute of Chemistry, Chemical Research Center, Hungarian Academy of Sciences, POB 17, H-1525 Budapest, Hungary*

Received 23 September 1999; accepted 15 December 1999

Abstract

There is now much evidence that anticancer drugs exert biological action by preferred binding of a transition metal to the N7 sites of the guanine residues of DNA. In our series of theophyllinato copper(II) complexes containing amine ligands, the structural effect of changing from ethanolamine to diethanolamine is examined. A new mixed ligand copper(II) complex, bis(μ-2-(2-hydroxyethyl)aminoethanolato-*O,N,O′*)bis(theophyllinato-N7)dicopper(II) ($C_{22}H_{34}N_{10}O_8Cu_2$) (**1**) has been synthesized as model compound from aqueous solutions of $CuSO_4$, theophylline, and diethanolamine (dea). Its distinct $Me_2L_2L'_2$ structure has been determined by single crystal X-ray diffraction. The centrosymmetric binuclear complex contains two strongly distorted square pyramidally (or pseudo-octahedrally) coordinated copper ions bound together by two alkoxo-bridges. The bridging O is a deprotonated oxygen of the monoalcoholate formed from diethanolamine. Both of the theophyllinate anions take part in N7/O6 chelation in the complex **1**, while only one of the theophyllinate anions is able to perform it in the mononuclear complex (SPY-5-12)-(2-aminoethanol-N)(2-aminoethanol-*N,O*)bis(theophyllinato-N7)copper(II) dihydrate (**2**). The two copper(II) centres in **1** are found to be antiferromagnetically coupled. The combined thermogravimetric and evolved gas detection shows that the tridentate alcoholate anions are fragmented and evolved between 125 and 275°C, whilst the degradation of theophyllinate anions begins at 350°C. Structural, spectroscopic and thermal comparison to the previously published analogous monoethanolamine Cu(II) complex (**2**) is presented. ©2000 Elsevier Science Ltd All rights reserved.

Keywords: Dialkoxo-bridged binuclear Cu(II) complexes; Model of metal–guanine interaction; Single crystal structures; Thermal decomposition; Theophylline; Diethanolamine(2,2′-iminodiethanol)

1. Introduction

The synthesis and structural study of transition metal complexes containing theophylline still draw considerable attention because of the potential antitumour activity of these complexes [2–4]. They are used as models of direct interactions and associations between various transition metal ions and the chain-bonded guanine base of oligonucleotides and DNA [5], especially to model binding of the antitumour drug *cis*-platin (*cis*-$Pt(NH_3)_2Cl_2$), through its *cis*-diammineplatinum(2+) form to the N7 site of guanine residues of DNA [3,4].

Metal complexes isolated from non-alkaline medium bind theophylline as a neutral ligand, while other complexes which are obtained from alkaline solutions show the presence of theophyllinate anions [6,7]. Single crystal data prove that theophylline moieties are regularly bound to the metal centre through the N7 nitrogen atom [8].

Special theophyllinato metal complexes can be prepared using aqueous solutions of ammonia, various amines or aminoalcohols, also incorporating these amine type molecules as ligands [9–11]. Nevertheless, the structures of such complexes depend on the type of transition metal and amine as well. There are a few single crystal data reported on complexes chelated with diamines or triamines. Ethylenediaminebis(theophyllinato)zinc(II) [12] has tetrahedral coordination, while bis(theophyllinato)diethylenetriaminecopper(II) dihydrate [13] is found to be pentacoordi-

[1] For Part 1, see Ref. [1].

0277-5387/00/$ - see front matter ©2000 Elsevier Science Ltd All rights reserved.
PII S0277-5387(99)00386-1

nated, whilst theophyllinatochlorobis(ethylenediamine)-cobalt(III) salts have basically octahedral arrangements [14,15].

Recently we have found that there are two distinguishable ethanolamine molecules in bis(ethanolamine)bis(theophyllinato)copper(II) dihydrate [1]. One behaves as a monodentate, while the other behaves as a bidentate ligand within the same square pyramidal structure. Furthermore, a secondary interaction between the copper cation and one of the theophylline carbonyl oxygens (O6) occurs. Such an interaction had been postulated earlier to be an advantageous structural feature for potential antitumour activity. In addition, a strong correlation has been observed between the binding strength and the thermal escape sequence of the variably bonded ligands of this complex [1].

As a part of our ongoing research on the binding interactions in theophyllinato complexes incorporating various amines or aminoalcohols [16], we report here the synthesis, single crystal structure and thermal decomposition scheme of a new theophyllinato copper complex containing diethanolamine (2,2′-iminodiethanol). The structural and thermal features of the obtained bis(μ-2-(2-hydroxyethyl)aminoethanolato)bis(theophyllinato)dicopper(II) (**1**) are compared to those of the (SPY-5-12)-(2-aminoethanol-N)-(2-aminoethanol-*N,O*)bis(theophyllinato-N7)copper(II) dihydrate (**2**) building up from neutral monoethanolamine (2-aminoethanol) [1] (Fig. 1). Characterization of **1** was completed with FTIR spectroscopy, powder X-ray diffraction (XRD), electron spin resonance (ESR) and magnetic susceptibility measurements.

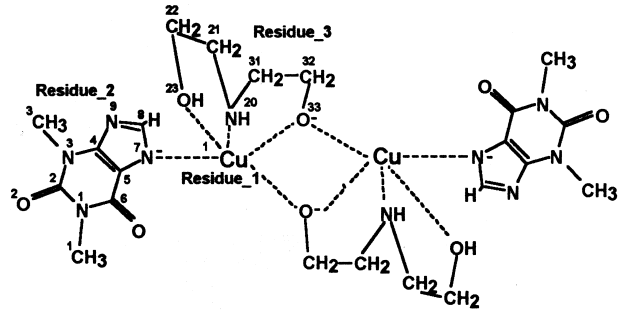
2. Experimental

2.1. Synthesis of *1*

A clear solution was obtained from $CuSO_4 \cdot 5H_2O$ (0.25 g, 1.00 mmol) in 20 cm^3 of water with 2 cm^3 (17.3 mmol) of diethanolamine. It was added to 20 cm^3 of aqueous solution of theophylline (0.40 g, 2.02 mmol) dissolved also by the addition of 1 cm^3 (8.7 mmol) of diethanolamine. The reaction mixture was heated in a water bath for 2 h. The blue precipitate was allowed to crystallize in its mother liquor. After slow cooling it was placed in a refrigerator at 4°C for 2 weeks. Finally, the blue columns of single crystals were filtered (yield 90% based on $CuSO_4 \cdot 5H_2O$).

2.2. Elemental analysis

C, H, and N analysis of the crystals of **1** was carried out by the Microanalytical Laboratory, Roland Eötvös University of Budapest, Hungary. Found: C, 38.1; H, 4.9; N, 19.7%. Calc. for $Cu_2(C_7H_7N_4O_2)_2(C_4H_{10}NO_2)_2$ (**1**): C, 38.1; H, 4.9; N, 20.2%.



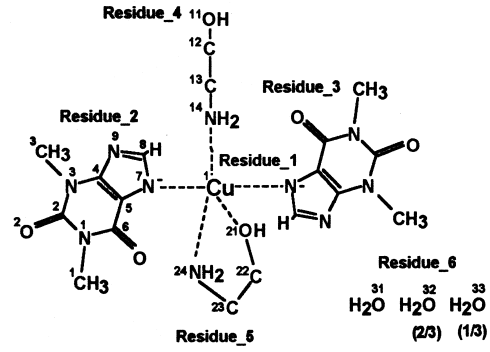


Fig. 1. Formulae diagrams of bis(μ-2-(2-hydroxyethyl)aminoethanolato)bis(theophyllinato)dicopper(II), $[Cu_2(dea)_2(th)_2]$ (**1**) and (SPY-5-12)-(2-aminoethanol-N)(2-aminoethanol-*N,O*)bis(theophyllinato-N7)-copper(II) dihydrate (**2**).

2.3. Thermal and FTIR studies

Thermal behaviour of **1** was studied by a DuPont 990 instrument equipped with model 951 thermobalance. A sample size of 5–6 mg and heating rate of 10°C min^{-1} were used. The measurements were carried out in dynamic air atmosphere at a flow rate of 10 l h^{-1}.

Evolved gas detection (EGD) study was carried out with a DuPont 916 thermal evolution analyzer. For measurement of organic volatile products a hydrogen flame ionization detector was applied in this instrument. Samples of 4–6 mg were heated in a nitrogen flow of 1.8 l h^{-1} up to 350°C at a heating rate of 8°C min^{-1}.

FTIR spectroscopy was used to study **1** and the solid intermediates during its decomposition. The FTIR spectra were obtained in the range 400–4000 cm^{-1} with a Perkin Elmer IR 2000 instrument in KBr pellets.

2.4. X-ray diffraction

Determination of the unit cell parameters and collection of reflections of **1** were performed on an Enraf-Nonius CAD4 single crystal diffractometer using graphite-monochromated Cu Kα radiation (1.54184 Å) at 293(2) K. A blue needle-like single crystal with size $0.30 \times 0.14 \times 0.08$ mm was mounted on a glass fibre. The unit cell dimensions of the monoclinic crystal ($a = 12.847(2)$, $b = 7.288(1)$, $c = 14.865(2)$ Å; $\beta = 95.12(3)°$) were calculated using 25

reflections observed in the θ range from 36.97 to 39.76°. $Cu_2(C_7H_7N_4O_2)_2(C_4H_{10}NO_2)_2$ (**1**) crystallizes in the space group $P2_1/n$, $Z=2$. The calculated density is 1.662 g cm^{-3}. 3073 reflections were collected between 4.36 and 74.85° θ angles within the index ranges $0 \le h \le 16$, $0 \le k \le 9$, $-18 \le l \le 18$. 2838 intensity data were found to be independent ($R_{int} = 0.0091$). Data reduction was carried out using the program XCAD4 [17], while the empirical absorption correction (ψ-scan method) was carried out using MolEN [18]. The maximum and minimum transmissions were 1.000 and 0.863, respectively. The initial structure model was found by direct methods (SHELXS86 [19]), while the structure refinement was done by SHELXL93 [20]. Anisotropic displacement parameters were refined for all of the non-hydrogen atoms. All non-carbon hydrogen atoms and H82 were located on the difference Fourier map. CH_3 hydrogen atoms were introduced into calculated positions and refined riding on the respective carbon atoms.

The full-matrix least-squares refinement on F^2 with 2740/199 data/parameter ratio resulted in R values ($I > 2\sigma(I)$) of $R_{obs} = 0.0300$, $R_w = 0.0918$ and $R_{wtot} = 0.0954$. The goodness of fit was 1.079. The largest diffraction peak and hole in the final difference map were 0.590 e Å^{-3} and -0.477 e Å^{-3}, respectively. Neutral atomic scattering factors were taken from the International Tables for X-ray Crystallography, vol. C [21].

X-ray powder patterns for the complex **1** and the decomposition products were recorded by an FPM HZG4 and a Philips PW 3710 powder diffractometer using Cu Kα radiation (Ni filter and graphite monochromator were used, respectively).

3. Results and discussion

*3.1. FTIR analysis of **1**: indication of anionic ligands*

The FTIR spectrum of **1** shows two carbonyl stretching absorption bands at 1691 cm^{-1} for O2 and 1657 cm^{-1} for O6. These are at lower wavenumbers than those observed in the spectra of pure theophylline (1716 and 1667 cm^{-1}) or in complexes of neutral theophylline ligands (in the range 1702–1715 and 1662–1681 cm^{-1}) [6]. (The corresponding bands of **2** containing monoethanolamine occur at 1691 cm^{-1} for O2 and 1643 cm^{-1} for O6 [1].) These wavenumber shifts are due to deprotonation and coordination of the theophylline moiety at the N7 nitrogen. We can suppose that the larger is the shift observed towards lower wavenumbers, the stronger is the secondary interaction of the O6 oxygen atom with the metal.

The very sharp and intense band at 3272 cm^{-1} corresponds to the ν_{NH} stretching vibration of the metal-bonded secondary amine group of diethanolamine, while a weak sharp band at 1582 cm^{-1} is an NH deformation frequency of the same amine. Broad bands centred at 3421 and 3152 cm^{-1} are probably due to weaker and stronger H-bonded OH stretching vibrations. An unusual splitting of CH stretching absorption bands observed in the 2800–3000 cm^{-1} region and even the occurrence of one branch of them at 2855 cm^{-1} indicates the presence of the alcoholate/ethanolate functional group, which can belong to a partially deprotonated diethanolamine.

*3.2. Thermal analysis of **1**: indication of the dimeric structure*

The thermogravimetric curve of **1** measured in an air stream (Fig. 2) is found to be completely different from that of **2** [1]. The first thermal change of **1** between 125 and 275°C (mass loss 31%) seems to be a rather complex change. It consists of several slow continuous processes and a rapid but overlapping mass loss process, whilst in the case of **2** two well separated and stoichiometric releases of mono- and bidentate neutral ethanolamine ligands were observed [1]. The final step of the air decomposition of **1** (350–400°C) corresponds to the rapid oxidative degradation of the theophyllinato moieties, causing local heat evolution in the surroundings of the sample. The thermocouple indicates this is a strong exothermic process. The recorded temperature overtakes the programmed temperature value and cools only later. Meanwhile a rapid change in the mass also takes place. If the rate of mass change (time derivative of the recorded mass curve TG) is redrawn as a function of recorded temperature (DTG curve), a curiously skewed peak corresponds to the sudden exothermic decomposition, which in this case leads to the formation of CuO. The residue was checked by powder XRD (JCPDS card No. 41-254, CuO). The percentage of

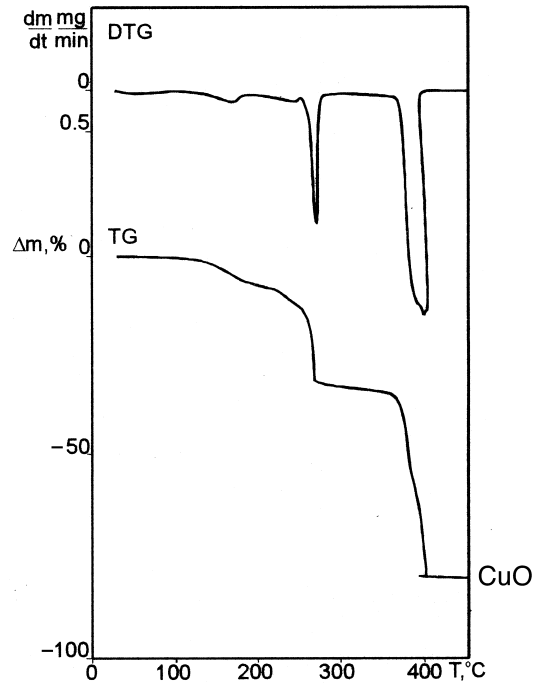


Fig. 2. TG (Δm vs. T) and DTG ($d(\Delta m)/dt$ vs. T) curves of $[Cu_2(dea)_2(th)_2]$ (**1**) in air flow of 10 l h^{-1}, at a heating rate of 10°C min^{-1}; initial weight is 5.78 mg.

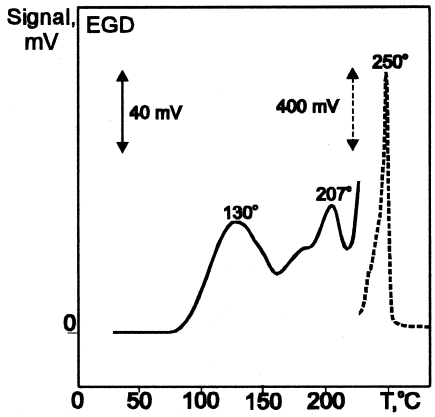


Fig. 3. Evolution rate of organic volatile substances from $[Cu_2(dea)_2(th)_2]$ (**1**) in nitrogen flow of 1.8 l h^{-1}, at a heating rate of 8°C min^{-1}; an initial weight of 5.03 mg was used during the evolved gas detection (EGD).

CuO residue (22%) was found to be about twice as large as that of the corresponding value for **2** (ca. 11%).

This high copper content was the first indication of a possible binuclear structure of **1**. A dimeric composition requires all of the ligands to be in deprotonated anionic form in order to compensate for the four positive charges of two copper(II) cations. The participation of two 2-(2-hydroxyethyl)-aminoethanolates (monoalcoholate of diethanolamine) and two theophyllinate anions in the dimeric composition of **1** has been found to be in good agreement with data obtained from both elemental analysis and air decomposition in the thermal balance.

The following explanation of the TG process of **1** can be given. First the monoalcoholate anions are degraded and evolved thermally (the theoretical mass loss is 30.31%). The complexity of chemical degradation of the alcoholate ligands may explain the overlapping mass changes up to 275°C. The rate of evolved organic gaseous species observed by hydrogen flame ionization detector (Fig. 3) shows also that organic volatile fragments are released parallel to the mass loss (Fig. 2, DTG curve). Above 300°C the more stable theophyllinate anion also begins to decompose. The process is accelerated above 360°C and it is accompanied by oxidative processes of the decomposition products in air.

3.3. Single crystal X-ray structure

The asymmetric unit contains half of the dialkoxo-bridged copper complex (Fig. 4). An inversion centre is located between the two Cu^{2+} ions. The bridging oxygen atoms and the copper atoms form a centrosymmetric planar Cu_2O_2 core (Fig. 5). The relevant bond distances and angles are listed in Tables 1 and 2. The N72, N203, O233 and O62 atoms deviate by −0.6423(3), 0.213(2), 2.310(2) and −2.7895(1) Å from the Cu_2O_2 plane. The Cu1···Cu1a distance of 3.004(1) Å agrees well with the distances found in other dimeric alkoxo-bridged Cu(II) complexes [22,23]. The Cu_2O_2 core and the theophylline frame has a dihedral angle of 56.70(4)°.

Two nitrogen atoms, one from the theophyllinato anion (N72···Cu1 1.973(2) Å) and the other from diethanolamine (N203···Cu1 2.023(2) Å), and the deprotonated oxygen atom from the anion of diethanolamine (O333···Cu1 1.926(2) Å) with its symmetry related pair (O33a···Cu1 1.932(2) Å) form a distorted square planar coordination geometry around the copper ion. The planes O333···Cu1···O33a and N72···Cu1···N203 are at an angle of 19.2(2)°. The inner coordination sphere of the copper cation is completed to a square pyramid with the hydroxyl oxygen atom of the tridentate diethanolamine anion (O233···Cu1 2.457(1) Å).

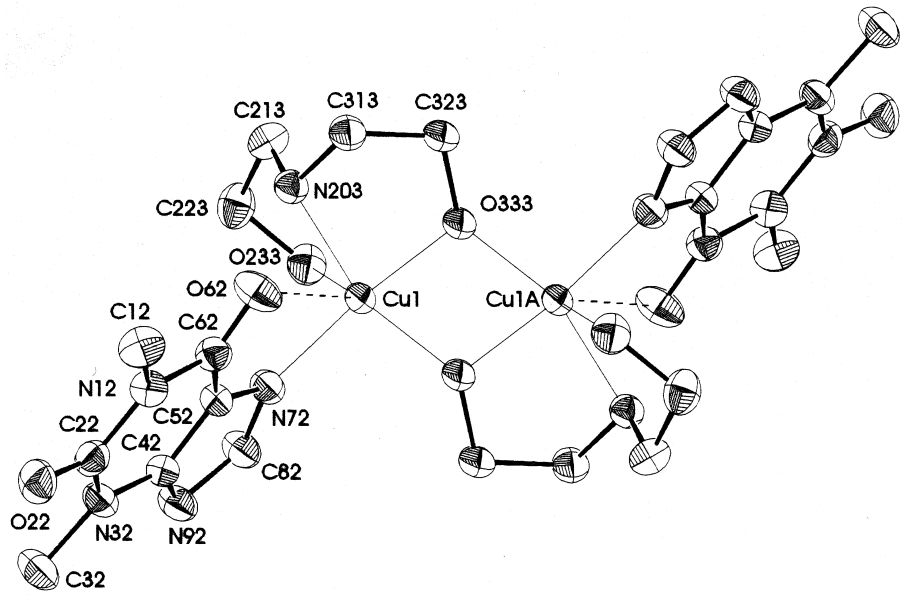


Fig. 4. ZORTEP [27] diagram of the molecule $[Cu_2(dea)_2(th)_2]$ (**1**) showing atomic displacement parameters at 50% probability level and atomic numbering. The asymmetric unit contains half of the complex molecule. The inversion centre is placed between the two Cu^{2+} ions. The symmetry operator to generate equivalent atoms is $-x+1, -y, -z+1$.

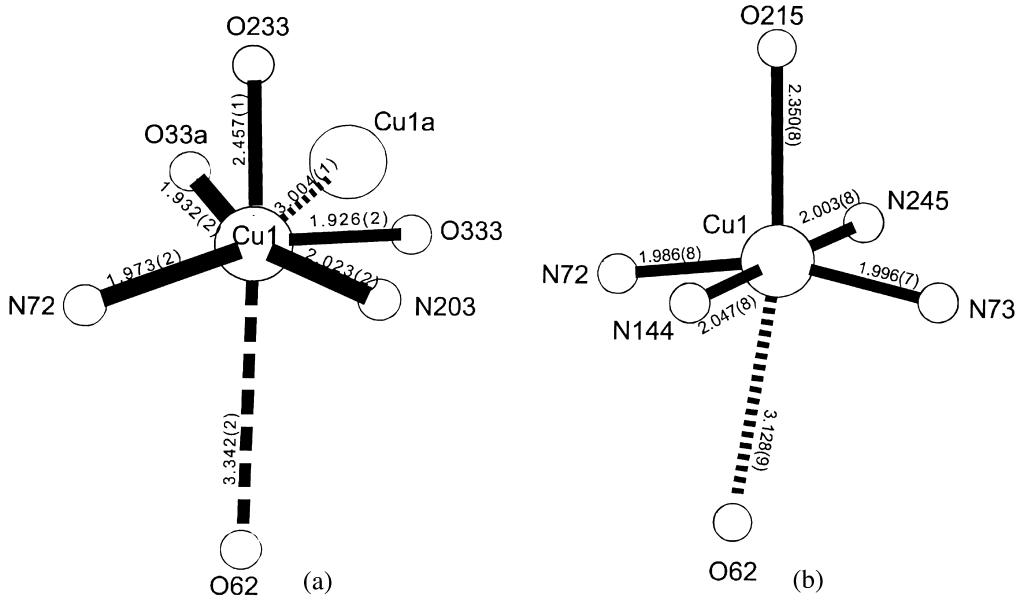


Fig. 5. Square pyramidal or pseudooctahedral coordination around Cu^{2+} in (a) $[Cu_2(dea)_2(th)_2]$ (**1**) and (b) $[Cu(ea)_2(th)_2 \cdot 2H_2O]$ (**2**). The inversion centre organizes the atoms denoted by 'a' in **1**. The octahedron is repeated around Cu1a upside-down.

Table 1
Selected bond lengths (Å) in $[Cu_2(dea)_2(th)_2]$ (**1**)

C82–N92	1.354(3)	N72–C82	1.328(3)
Cu1–N72	1.973(2)	Cu1–N203	2.023(2)
Cu1–O233	2.457(1)	Cu1–O62	3.342(2)
Cu1–O333	1.926(2)	Cu1–O33a	1.932(2)
Cu1–Cu1#1	3.004(1)		

Table 2
Selected bond angles (°) of the Cu^{2+} coordination spheres in the structure of $[Cu_2(dea)_2(th)_2]$ (**1**) and $[Cu(ea)_2(th)_2 \cdot 2H_2O]$ (**2**)

1		**2** [a]	
N72–Cu1–O33a	99.4(1)	N72–Cu1–N144	89.3(6)
N72–Cu1–N203	100.5(1)	N72–Cu1–N245	90.4(6)
O333–Cu1–O33a	77.7(1)	N73–Cu1–N144	89.4(6)
O333–Cu1–N203	83.3(1)	N73–Cu1–N245	90.5(6)
N72–Cu1–O233	91.3(1)	N72–Cu1–O215	95.7(5)
O333–Cu1–O233	107.8(1)	N73–Cu1–O215	101.9(5)
O33a–Cu1–O233	102.2(1)	N144–Cu1–O215	99.8(5)
N203–Cu1–O233	77.8(1)	N245–Cu1–O215	81.2(5)
O62–Cu1–O233	130.5(1)	O62–Cu1–O215	160.7(4)

[a] Ref. [1].

The copper ions can increase their coordination by association with oxygen anions forming dimeric, tetrameric or infinite chain species [23]. Dimeric complex formation is realized in **1** because of the presence of the hydroxide group in the diethanolamine ligand (O233···Cu1 2.457(1) Å) and the exocyclic oxygen atom of the theophyllinato anion (O62···Cu1 3.342(2) Å) near to the open apical position of the primer pyramidal coordination sphere. This O62···Cu1 distance is longer than bonds formed usually by oxygen atoms in an inner coordination sphere but it is shorter than the average Cu···O6 distance (3.75 Å) [8] in related structures, where the carbonyl O6 is involved in a hydrogen bond to a neighbouring ligand. No hydrogen bond of O6 is found in the crystal structure of **1**. Considering potential antitumour activity, an opportunity for N7/O6 chelation to the metal centre is postulated to be useful, whilst competitive interligand interactions to O6 in the form of, for example, hydrogen bonds is suggested to be injurious [8].

The crystal structure of (SPY-5-12)-(2-aminoethanol-N)-(2-aminoethanol-*N*,*O*)bis(theophyllinato-N7)copper(II) dihydrate (**2**) [1] gives the opportunity to compare the copper coordination sphere (Fig. 5, Tables 1 and 2, see also Fig. 1). Two theophyllinato anions, one 2-ethanolamine as bidentate and one 2-ethanolamine as monodentate ligand, form the square pyramidal arrangement of Cu^{2+} in the mononuclear **2**. One of the theophyllinato ligands has an exocyclic oxygen atom closer to the copper in **2** (O62···Cu1 3.128(9) Å) than in **1** (O62···Cu1 3.342(2) Å) at the open apical direction in the sixth coordination site. This means that only one of the theophyllinate anions can take part in N7/O6 chelation in the mononuclear complex **2**, whilst both of the theophyllinate anions form a similar, but weaker, N7/O6 chelation in the complex **1**.

The slightly distorted square pyramidal arrangement around the copper cation in **2** becomes a more distorted arrangement in **1**. An apical elongation can be observed, while three of the four bonds in the square plane are shortened because of the more favourable dialkoxo-bridging binuclear complexation. The fourth coordination bond becomes longer in **1**, as N203 also takes part in an interligand hydrogen bond. The bond angles in the pentahedron also characterize the distortion: the angles in the square plane of **1** are strongly different from 90°, nevertheless their sum is 360.3°. The exocyclic O62 of the theophyllinato ligand is also farther and in a more deviating position in **1** compared to **2**. These distor-

tions make possible the spatial adjustment of the two symmetry related pseudo-octahedra around Cu1 and Cu1a. The well-defined coordination of the bidentate theophylline and tridentate diethanolamine ligands yields low thermal motion.

The dimeric molecules of **1** are ordered into columns along the crystallographic *a* axis (Fig. 6). The theophylline rings in the column are 3.41(1) Å apart showing π···π stacking interaction between their purine rings. Intermolecular hydrogen bonds of N203···O22 (2.897(5) Å) in the column and N92···O233 (2.787(4) Å) between the columns stabilize the crystal.

3.4. Magnetic and ESR measurements

A sharp electron spin resonance signal proves the presence of unpaired electrons of the copper(II) centres, while the magnetic susceptibility is very small and measured with great standard deviation at various temperatures. In the literature various hydroxy and alkoxy bridged copper Cu_2O_2 type dimers have been studied, in order to find correlations between their structural and magnetic features [24,25]. Crawford et al. [26] have found a rather strong linear relationship between the Cu–O–Cu bridge angle and the magnetic exchange parameter 2*J* for a series of μ-hydroxo bridged planar dimers. In the same series, plots of the 2*J* values versus copper–copper distance were also found to be linear. Our planar compound does not seem to be a member of this series, for rather different $2J = -360\ cm^{-1}$ ($\phi_{Cu-O-Cu} = 102.3(1)°$) and $2J = -510\ cm^{-1}$ ($d_{Cu-Cu} = 3.004(1)$ Å) values of the exchange parameter could be estimated from the two correlation lines given there. Although we were not able to deduce the experimental 2*J* value, the above estimates indicate the antiferromagnetic nature of **1**. Antiferromagnetic behaviour was also reported for several structurally closely related dialkoxo bridged Cu dimeric compounds [22,23].

4. Summary

Bis(μ-2-(2-hydroxyethyl)aminoethanolato-*O,N,O′*)bis-(theophyllinato-N7)dicopper(II) (**1**) has been synthesized from aqueous solutions of $CuSO_4$, theophylline and excess diethanolamine in order to examine the structural effect of changing one of the ligands from ethanolamine to diethanolamine in theophyllinato copper complexes. The FTIR spectrum showed the presence of both anionic ligands (theophyllinate and aminoalcoholate). The thermal decomposition of the crystalline material indicated a composition for **1** consisting of one to one ratio of both anions to the copper cation. Single crystal studies proved that **1** has a dialkoxo-bridged binuclear structure with planar Cu_2O_2 core. The bridging O is the deprotonated oxygen of the monoalcoholato ligand formed from diethanolamine. The 2-(2-hydroxyethyl)aminoethanolate anion is found to be a tridentate ligand. It is bonded to one of the copper cations through its amino, hydroxo and alcoholate group. The theophyllinato ligand is bonded to the copper atom through the N7 nitrogen atom, while its O6 oxygen also has a weak secondary interaction with the centre. Such a coordination predicts only potentially medium antitumour activity. According to the ESR and magnetic measurements the two copper atoms are antiferromagnetically coupled.

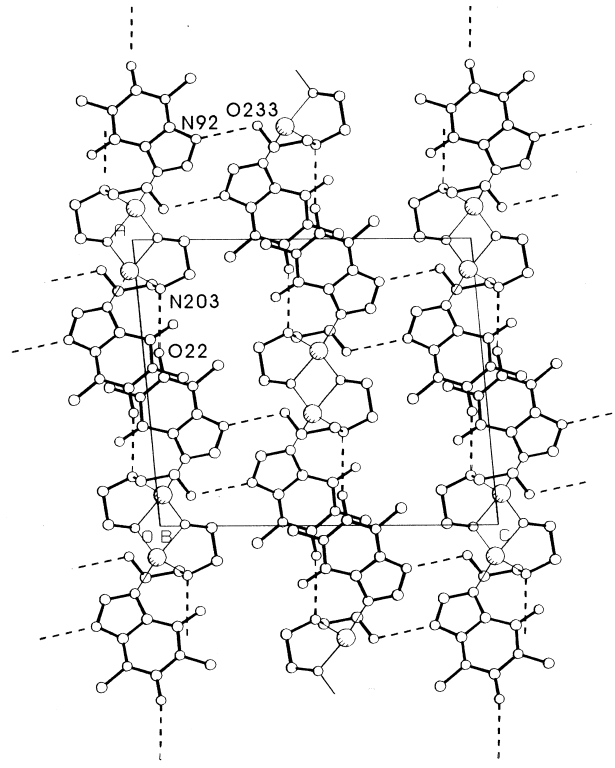


Fig. 6. The packing motif in the unit cell of $[Cu_2(dea)_2(th)_2]$ (**1**) shows the parallel arrangement of the columns of complexes and their hydrogen-bonding interligand interactions viewed from the direction of the crystallographic *b* axis.

Supplementary data

Crystallographic data (final atomic coordinates with anisotropic displacement parameters, full list of interatomic distances, interbond angles, torsion angles together with least square plane data, and F_o/F_c values, excluding structure factors) for the structure in this paper have been deposited at the Cambridge Crystallographic Data Centre as supplementary data deposition no. CCDC 127826. Copies of the data can be obtained, free of charge, on application to CCDC, 12 Union Road, Cambridge CB2 1EZ, UK (fax: +44-1223-336033; e-mail: deposit@ccdc.cam.ac.uk). Measured and calculated powder diffraction patterns are available from the authors.

Acknowledgements

The authors thank Mr Csaba Kertész, Dr László Korecz and Dr Imre Labádi for the measurement of the single crystal X-ray, ESR and magnetic data, respectively. Many thanks to

Dr Vladislav Izvekov for the valuable discussion on the IR spectra. This work was supported by the National Scientific Research Foundation of Hungary (OTKA, Grant No. F 025664). Dr Edit Forizs is also thanked for her inspiration on this work.

References

[1] P. Bombicz, J. Madarász, E. Forizs, I. Foch, Polyhedron 16 (1997) 3601.
[2] B. Song, G. Oswald, M. Bastian, H. Sigel, B. Lippert, Metal Based Drugs 3 (1996) 131.
[3] M.J. Bloemink, J. Reedijk, Met. Ions Biol. Syst. 32 (1996) 641.
[4] J.P. Whitehead, S.L. Lippard, Met. Ions Biol. Syst. 32 (1996) 678.
[5] S.B. Howell (Ed.), Platinum and Other Metal Coordination Compounds in Cancer Chemotherapy, Plenum, New York, 1991.
[6] C.M. Mikulski, M.K. Kurlan, S. Grossman, M. Bayne, M. Gaul, N.M. Karayannis, J. Coord. Chem. 15 (1987) 347.
[7] P. Umpathy, R.A. Skaikh, J. Indian Chem. Soc. 62 (1985) 103.
[8] N.S. Begum, H. Manohar, Polyhedron 13 (1994) 307 and refs. therein.
[9] M.S. Zitzman, R.R. Krebs, J. Birdsall, J. Inorg. Nucl. Chem. 40 (1978) 571.
[10] W.J. Birdsall, M.S. Zitzman, J. Inorg. Nucl. Chem. 41 (1979) 117.
[11] S.D. Rothenberger, M.S. Zitzman, W.J. Birdsall, J. Inorg. Nucl. Chem. 43 (1981) 1673.
[12] M.J. Gardner, F.X. Smith, E. Shefter, J. Pharm. Sci. 72 (1983) 148.
[13] T. Sorrell, L.G. Marzilli, T.J. Kistenmacher, J. Am. Chem. Soc. 98 (1976) 2181.
[14] T.J. Kistenmacher, Acta Crystallogr., Sect. B 31 (1975) 85.
[15] T.J. Kistenmacher, Acta Crystallogr., Sect. B 31 (1975) 90.
[16] S. Gál, J. Madarász, E. Forizs, I. Labádi, V. Izvekov, G. Pokol, J. Therm. Anal. Cal. 53 (1998) 343.
[17] K. Harms, XCAD4, Program for Data Reduction of CAD4 Output, 1996.
[18] MolEN, Structure Determination System, Enraf-Nonius, 1990.
[19] G.M. Sheldrick, Acta Crystallogr., Sect. A 46 (1990) 467.
[20] G.M. Sheldrick, SHELXL93, Program for the Refinement of Crystal Structures, University of Göttingen, Germany, 1993.
[21] International Tables for Crystallography, vol. C, Kluwer, Dordrecht, 1992.
[22] J. Valo, M. Klinga, I. Mutikainen, M. Näsäkkälä, Acta Chem. Scand. 49 (1995) 248.
[23] L. Walz, H. Paulus, W. Haase, J. Chem. Soc., Dalton Trans. (1985) 913 and refs. therein.
[24] D.J. Hodgson, Prog. Inorg. Chem. 19 (1975) 173.
[25] R.J. Doedens, Prog. Inorg. Chem. 21 (1976) 209.
[26] H.V. Crawford, H.W. Richardson, J.R. Wasson, D.J. Hodgson, W.E. Hatfield, Inorg. Chem. 15 (1976) 2107.
[27] L. Zsolnai, H. Pritzkow, ORTEP Program for Personal Computer, Original Modified in University Heidelberg, 1994, Version July 1996.

PERGAMON

www.elsevier.nl/locate/poly

Polyhedron 19 (2000) 465–469

POLYHEDRON

Chiral macrocyclic Nd(III) and Tm(III) complexes

Jerzy Lisowski *, Przemysław Starynowicz

Department of Chemistry, University of Wrocław, 14 F. Joliot-Curie, 50-383 Wrocław, Poland

Received 21 July 1999; accepted 15 December 1999

Abstract

The two new chiral macrocyclic complexes obtained in a template condensation of *R,R*-1,2-diaminocyclohexane and 2,6-diformylpyridine, $[NdL](NO_3)_3$ and $[TmL](NO_3)_3$, have been synthesized and their X-ray crystal structures have been determined. The lanthanide(III) ions in both complexes are coordinated by a helically twisted hexadentate macrocycle and two bidentate nitrate anions. The $[NdL](NO_3)_3$ and $[TmL](NO_3)_3$ complexes have been studied also by ^1H and ^{13}C NMR spectroscopy. The signal assignment was based on COSY, NOESY and HMQC measurements. The spectra of the investigated compounds in methanol–chloroform solution confirm the D_2-symmetrical helical conformation of the ligand. ©2000 Elsevier Science Ltd All rights reserved.

Keywords: Macrocycles; Lanthanide complexes; Chiral complexes; NMR of paramagnetic compounds

1. Introduction

The Schiff bases obtained in a template 2 + 2 condensation of diamines and 2,6-diformylpyridine or 2,6-diacetylpyridine are particularly suitable for the coordination of relatively large metal ions [1]. The complexes of these hexaazamacrocyles with lanthanide(III) ions have attracted a lot of attention owing to their unique properties. For instance, they have been shown to be efficient catalysts for cleavage of the phosphate ester bond [2–4]. The Gd(III) complexes have been studied also as potential MRI contrast agents [5].

When the chiral precursor *R,R*-1,2-diaminocyclohexane is used in the above template reaction, chiral lanthanide(III) complexes $[LnL](NO_3)_3 \cdot nH_2O$ (where Ln is the lanthanide(III) ion and L = 4(*R*),9(*R*),19(*R*),24(*R*)-3,10,18,25,31,35-hexaazapentacyclo[25.3.1.1^{12,24}.0^{4,9}.0^{19,24}]-dotriaconta-1(31),2,10,12,14,16(32),17,25,27,29-decaene, Fig. 1) are formed [6,7]. The coordination of the lanthanide(III) ion in a chiral macrocyclic environment leads to interesting properties of these compounds. Thus the $[TbL](NO_3)_3$ and $[EuL](NO_3)_3$ complexes have been shown to exhibit circularly polarized luminescence [6] and the paramagnetic $[EuL](NO_3)_3$ and $[YbL](NO_3)_3$ complexes have been shown to form diastereoisomeric complexes with D- and L-amino acids [7].

^1H NMR and ^{13}C NMR study of the La(III), Ce(III), Eu(III) and Yb(III) complexes has indicated a D_2-symmetrical helical conformation of the ligand in solution [7]. In contrast, the solid state X-ray crystal structure of related racemic $[GdL(H_2O)_3]Cl_3 \cdot 3H_2O$ shows lower symmetry of the complex with the twist-bent conformation of the ligand and unsymmetrical coordination of the axial water molecules [8]. In this report we show that the two new members of this

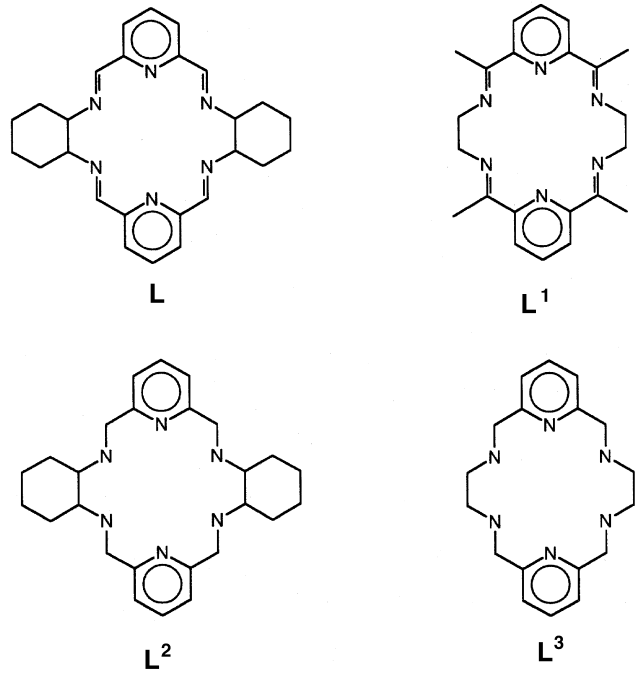


Fig. 1. The general structure of the macrocycle L and related ligands.

* Corresponding author. Tel.: +48-71-320-4252; fax: +48-71-328-2348; e-mail: jurekl@wchuwr.chem.uni.wroc.pl

0277-5387/00/$ - see front matter ©2000 Elsevier Science Ltd All rights reserved.
PII S0277-5387(99)00387-3

family of complexes, $[NdL](NO_3)_3$ and $[TmL](NO_3)_3$, also maintain the symmetrical structure of the ligand in the solid state.

2. Experimental

2.1. Synthesis

The $[NdL](NO_3)_3$ and $[TmL](NO_3)_3$ complexes have been prepared in the same way as earlier complexes [6,7]. Thus, 1 mmol (114.2 mg) of *R,R*-1,2-diaminocyclohexane, 1 mmol (135.1 mg) of 2,6-diformylpyridine, and 0.5 mmol of appropriate lanthanide nitrate hydrate were refluxed for 3 h in 15 ml of methanol. The white precipitates were filtered, recrystallized from methanol and dried in vacuo to give $[NdL](NO_3)_3$ or $[TmL](NO_3)_3$ in 48 and 65% yields, respectively. Both compounds gave satisfactory C, H, N analyses.

2.2. Methods

The NMR spectra were taken on a Bruker AMX 300 spectrometer. The chemical shifts were referenced to the residual solvent signal or TMS. The magnitude COSY spectra were acquired using 512 data points in both dimensions. The data were processed using a square sine bell window in both dimensions and zero filled to a $1K \times 1K$ matrix. The phase-sensitive (TPPI) NOESY spectra were recorded using mixing times varying from 15 to 400 ms and shifted square sine function. HMQC spectra were recorded using BIRD preparation period and 512×512 data points. A square sine function was used for apodization in both dimensions. T_2 relaxation times were evaluated from the linewidths. Elemental analyses were obtained from the elemental analysis facility in this department.

2.3. X-ray data collection

Crystals of both $[NdL](NO_3)_3 \cdot CH_3OH$ and $[TmL](NO_3)_3 \cdot CH_3OH$ were grown by slow evaporation of chloroform–methanol solutions of $[NdL](NO_3)_3$ and $[TmL](NO_3)_3$. The obtained crystalline compounds lose solvent molecules and decompose when exposed to vacuum. Crystals of approximate size $0.4 \times 0.4 \times 0.2$ mm for $[NdL](NO_3)_3 \cdot CH_3OH$ and $0.5 \times 0.4 \times 0.2$ mm for $[TmL](NO_3)_3 \cdot CH_3OH$ were mounted on a Kuma KM4 diffractometer equipped with a CCD counter and an Oxford Cryosystem low-temperature appliance. The measurement was performed at 100 K. The structure was solved with direct

Table 1
Crystal data and structure refinement details

	Nd compound	Tm compound
Empirical formula	$C_{27}H_{34}N_9NdO_{10}$	$C_{27}H_{34}N_9O_{10}Tm$
Formula weight	788.87	813.56
Temperature (K)	100(2)	100(2)
Wavelength (Å)	0.71073	0.71073
Crystal system	monoclinic	monoclinic
Space group	*C*2	*C*2
Unit cell dimensions		
a (Å)	17.294(3)	17.253(3)
b (Å)	8.834(2)	8.754(2)
c (Å)	22.441(5)	22.562(5)
β (°)	95.24(3)	96.00(3)
Volume (Å^3)	3414.1(12)	3388.9(12)
Z	4	4
Density (calculated) (Mg m^{-3})	1.535	1.595
Absorption coefficient (mm^{-1})	1.586	2.683
F(000)	1596	1632
Crystal size (mm)	$0.4 \times 0.4 \times 0.2$	$0.5 \times 0.4 \times 0.2$
θ range for data collection (°)	2.8–28.8	2.7–28.9
Index ranges	$-22 \le h \le 22,\ -8 \le k \le 11,\ -30 \le l \le 30$	$-22 \le h \le 23,\ -10 \le k \le 11,\ -30 \le l \le 29$
Reflections collected	11082	9944
Independent reflections	5788 ($R_{int} = 0.0295$)	6073 ($R_{int} = 0.0325$)
Absorption correction	empirical	empirical
Max. and min. transmission	1.1802 and 0.5897	2.0914 and 0.7514
Refinement method	full-matrix least-squares on F^2	full-matrix least-squares on F^2
Data, restraints, parameters	5788, 1, 426	6073, 1, 426
Goodness-of-fit on F^2	5.170	4.080
Final *R* indices ($I > 2\sigma(I)$)	$R(F) = 0.0545$, $R_w(F^2) = 0.1139$	$R(F) = 0.0490$, $R_w(F^2) = 0.0969$
R indices (all data)	$R(F) = 0.0553$, $R_w(F^2) = 0.1141$	$R(F) = 0.0500$, $R_w(F^2) = 0.0972$
Absolute structure parameter	0.00(2)	0.024(15)
Largest difference peak and hole (e Å^{-3})	2.394 and −1.709	2.703 and −2.205

methods with SHELXS-97 [9] and refined with SHELXL-97 [10]. The absorption corrections were applied with a locally written program [11]. Since the two compounds are isomorphic, the parameters obtained for $[NdL](NO_3)_3 \cdot CH_3OH$ were used as the starting values for the refinement of the $[TmL](NO_3)_3 \cdot CH_3OH$ structure. The positions of C-bonded hydrogen atoms, with the exception of the CH_3 group of the methanol molecule, were placed geometrically, and their positions were constrained to the relevant C atoms, while their temperature factors were set at 1.2 times the trace of the C atoms. No attempt to localize the methanol hydrogens was made. The enantiomorph was selected on the basis of the value of Flack parameter. Details of the data collection and the refinement are presented in Table 1.

3. Results and discussion

3.1. X-ray crystal structures

The two structures are isomorphous and are composed of relevant macrocyclic complexes, nitrate anions and methanol molecules of solvation. The metal cations are decacoordinate; their coordination environments are composed of four nitrate oxygen atoms, and six nitrogen atoms belonging to the macrocyle: two from pyridine and four from the Schiff base fragments. The distances are unexceptional (see Table 2). The planes of the coordinated nitrate anions (N10, O11, O12, O13 and N20, O21, O22, O32) are twisted at angles of 72.2 and 72.8° in the case of the $[NdL](NO_3)_3 \cdot CH_3OH$ and $[TmL](NO_3)_3 \cdot CH_3OH$, respectively. Generally, the macrocyclic ligand is more twisted in the case of the Tm(III) complex: the angle between the least-squares mean planes of the cyclohexyl fragments (C7, C8, C9, C10, C11, C12 and C20, C21, C22, C23, C24, C25) is 75.2°, whereas the analogous angle is 64.6° for the Nd compound. The angles between the pyridine rings (C1, C2 C3, C4, C5, N1 and C14, C15, C16, C17, C18, N4) are 23.8 and 28.0° for the Nd(III) and Tm(III) compounds, respectively. The Cremer and Pople ring puckering parameters [12], calculated with the PUCK2 program [13], for the cyclohexyl rings C7, C8, C9, C10, C11, C12 are $Q = 0.558(10)$ Å, $\theta = 4.3(10)°$ for $[NdL](NO_3)_3 \cdot CH_3OH$ and $Q = 0.573(10)$ Å, $\theta = 8.7(10)°$ for $[TmL](NO_3)_3 \cdot CH_3OH$. The parameters for the C20, C21, C22, C23, C24, C25 rings are the following: $Q = 0.575(11)$ Å, $\theta = 4.2(11)°$ for the Nd compound and $Q = 0.609(12)$ Å, $\theta = 9.0(11)°$ for the Tm compound (the ϕ angle, which is rather meaningless for the case of low θ values, is omitted). Thus all the rings display fairly good chair conformations. The structure is held together by van der Waals interactions and hydrogen O···O bonds. An ORTEP [14] view of the complexed macrocycle is presented in Fig. 2.

The X-ray molecular structures of both $[NdL](NO_3)_3 \cdot CH_3OH$ and $[TmL](NO_3)_3 \cdot CH_3OH$ confirm the conclusion reached on the basis of solution NMR study [7], that the macrocycle L in $[LnL](NO_3)_3$ complexes adopts a helical structure of D_2 symmetry. In contrast, the X-ray crystal structure of the related racemic compound $[GdL(H_2O)_3]Cl_3 \cdot 3H_2O$ shows lower symmetry of the complex with the twist-bent conformation of the ligand and unsymmetrical coordination of the axial water molecules [8]. Thus the different axial ligation of lanthanide(III) ions complexed by the ligand L brings about a rather profound change of conformation of this macrocycle. In fact the bent structure observed for $[GdL(H_2O)_3]Cl_3 \cdot 3H_2O$ is characteristic [1] for complexes of hexaazatetraimine macrocycles, e.g. that of ligand L^1, and is observed also for the La(III) complex [15] of L^2 (a saturated tetraamine analogue of L). On the other hand, the helical structure is observed in the case of Zn(II) and Cd(II) complexes of the related tetraamine ligands L^2 and L^3 [15–17]. In these complexes, however, the twisting of the macrocyclic ligand is much more pronounced, as compared with that observed for $[LnL](NO_3)_3$ complexes. The extent of helical twisting of the discussed macrocyclic ligands can be measured by the dihedral angle between the N_3 donor sets derived from the two pyridine fragments. This angle is equal to 22.1° for $[NdL](NO_3)_3 \cdot CH_3OH$ and is slightly larger (27.7°) for $[TmL](NO_3)_3 \cdot CH_3OH$, as expected for

Table 2
Selected bond lengths (Å)

	Ln = Nd	Ln = Tm
Ln–O(11)	2.536(9)	2.393(10)
Ln–O(12)	2.506(7)	2.392(8)
Ln–O(21)	2.491(7)	2.380(7)
Ln–O(22)	2.506(8)	2.393(9)
Ln–N(1)	2.669(6)	2.621(6)
Ln–N(2)	2.672(7)	2.598(7)
Ln–N(3)	2.675(10)	2.623(12)
Ln–N(4)	2.664(6)	2.599(5)
Ln–N(5)	2.639(8)	2.587(11)
Ln–N(6)	2.656(8)	2.586(8)

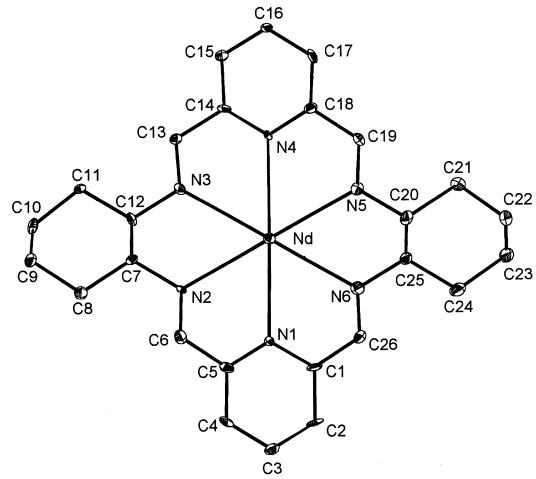


Fig. 2. View of the complex cation $[NdL]^{3+}$ together with the atom numbering scheme. The nitrate anions have been omitted for clarity.

the smaller lanthanide(III) ion. Both values are considerably smaller than that observed [15] for $[ZnL^1]^{2+}$ (103.4°) and $[CdL^1]^{2+}$ (69.0°). In this way the $[NdL](NO_3)_3 \cdot CH_3OH$ and $[TmL](NO_3)_3 \cdot CH_3OH$ complexes constitute examples of relatively planar, moderately twisted hexaazamacrocyclic complexes.

3.2. NMR spectroscopy

The investigated compounds give rise to eight signals in their ^{1}H NMR spectra and seven signals in ^{13}C spectra (Fig. 3), which is consistent with the presence of diastereotopic cyclohexane protons and indicates the effective D_2 symmetry of the $[LnL](NO_3)_3$ complexes in the investigated solutions. This symmetry is in accord with the helical twist conformation of the macrocyclic ligand, similar to observations in the case of analogous La(III), Ce(III), Eu(III) and Yb(III) complexes [7].

The signals of both complexes are strongly affected by the additional shift, called the isotropic shift δ_{iso}, that arises from the interaction of the nuclear and electronic spins (for NMR of paramagnetic complexes, see refs. [18–22]). The magnitude of this shift is difficult to predict and prevents assignment of spectra based on the values of chemical shifts.

In the case of the solution of the $[NdL](NO_3)_3$ complex in CD_3OD–$CDCl_3$ 1:2 v/v the signal **a** at 11.84 ppm (see the labelling scheme, Fig. 3) can be easily found on the basis of integration (intensity 2H, in contrast to signals of intensity 4H of other positions). This signal shows both COSY and NOESY cross peaks to the pyridine signal **b** at 12.95 ppm. The HMQC spectrum (Fig. 3) shows a pair of geminal protons of the cyclohexane ring at 3.08 and 2.69 ppm and another pair at 3.08 and 1.59 ppm, each pair correlated to one carbon signal. The integration of the signal at 3.08 ppm confirms that it corresponds to two overlapped resonances. As expected, these three signals at 3.08, 2.69 and 1.59 ppm are correlated to each other in COSY and NOESY spectra. Additionally, the signal at 2.69 ppm is COSY correlated to another signal at 3.54 ppm. This latter signal must then correspond to the remaining cyclohexane proton **d**. It follows that the pair of signals at 2.69 and 3.08 ppm belongs to the protons **e′** and **e**, while the pair of signals at 3.08 and 1.59 ppm belongs to the geminal protons **f** and **f′**. The remaining signal at 25.64 ppm has to correspond to the imino proton **c**.

The assignment of the ^{1}H NMR spectrum of $[Tm](NO_3)_3$ was based on analysis of the linewidths. In the case of a dominant dipolar and/or Curie relaxation mechanism, the relaxation times of protons in a paramagnetic metal complex should be proportional to the sixth power of proton–metal ion distances [9]. The ratio of relaxation times equal to 39.9:17.0:4.3:1:11.4:11.9:61.8:24.1 for the positions **a**, **b**, **c**, **d**, $\mathbf{e_{eq}}$, $\mathbf{e_{ax}}$, $\mathbf{f_{eq}}$, $\mathbf{f_{ax}}$, respectively, can be calculated on the basis of proton–lanthanide(III) ion distances. Since linewidths are inversely proportional to the T_2 relaxation times, it is clear that the linewidths of the $[LnL](NO_3)_3$ complexes should increase in the following order: **f**, **f′**, **a** < **b**, **e**, **e′** < **c** < **d**. This information, together with identification of pairs of geminal signals **e**, **e′** and **f**, **f′** on the basis of HMQC correlations as well as the integration of signal a to 2H, allows for the assignment of protons **a**, **b**, **c**, **d**, **e**, **e′**, **f**, **f′** to the signals at −8.86, −13.03, −16.69, 38.27, 7.81, 6.02, 8.10 and 5.70 ppm, respectively.

The HMQC spectra allow for the assignment of ^{13}C NMR spectra of $[NdL](NO_3)_3$ and $[TmL](NO_3)_3$ complexes on

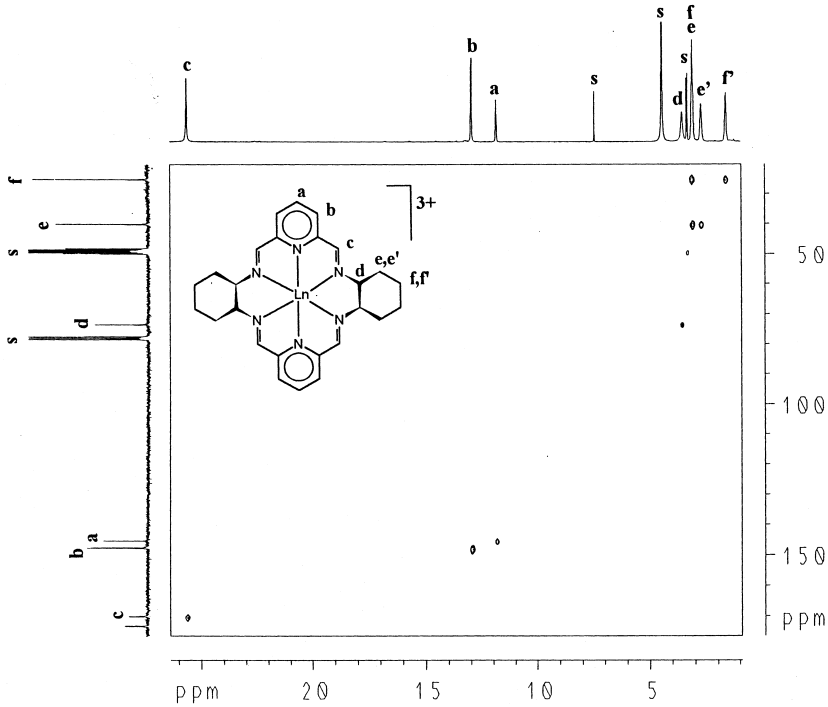


Fig. 3. The HMQC spectrum and labelling scheme of $[NdL](NO_3)_3$ (CD_3OD–$CDCl_3$ 1:2 v/v solution, 294 K); s solvent and HDO signals.

the basis of ^{1}H NMR assignments. The carbon atoms **a**, **b**, **c**, **d**, **e**, f, and the quaternary carbon **q** give rise to signals at 145.36, 147.70, 170.13, 73.36, 40.01, 25.22 and 173.32 ppm, respectively, in the case of the $[NdL](NO_3)_3$ complex, and to signals at 116.63, 89.56, 109.50, 41.41, 33.28, 30.04 and 81.22 ppm, respectively, in the case of the $[TmL](NO_3)_3$ complex.

In summary, we have shown that the $[LnL](NO_3)_3$ complexes exhibit symmetrical helical structure both in solution and in the solid state. The influence of different axial ligands on the symmetry of the macrocycle L complexed to lanthanide(III) ions is presently under investigation.

Supplementary data

Supplementary data for $[NdL](NO_3)_3 \cdot CH_3OH$ and $[TmL](NO_3)_3 \cdot CH_3OH$ structures are available from the Cambridge Crystallographic Data Centre, 12 Union Road, Cambridge CB2 1EZ, UK (fax: +44-1223-336033; e-mail: deposit@ccdc.cam.uk) on request, quoting the deposition numbers CCDC 130630 and CCDC 130631, respectively.

Acknowledgements

This work was supported by KBN grant 3 T09A 02812.

References

[1] V. Alexander, Chem. Rev. 95 (1995) 273.
[2] J.R. Morrow, L.A. Butterey, V.M. Shelton, K.A. Berback, J. Am. Chem. Soc. 114 (1903) 1992.
[3] N. Hayashi, N. Takeda, T. Shiiba, M. Yashiro, K. Watanabe, M. Komiyama, Inorg. Chem. 32 (1993) 5899.
[4] R.W. Hay, N. Govan, Polyhedron 24 (1997) 4233.
[5] P.H. Smith, J.R. Brainard, D.E. Morris, G.D. Jarvinen, R.R. Ryan, J. Am. Chem. Soc. 111 (1989) 7437.
[6] T. Tsubomura, K. Yasaku, T. Sato, M. Morita, Inorg. Chem. 31 (1992) 447.
[7] J. Lisowski, Magn. Reson. Chem. 37 (1999) 287.
[8] S.W.A. Bligh, N. Choi, W.J. Cummins, E.G. Evagorou, J.D. Kelly, M. McPartlin, J. Chem. Soc., Dalton Trans. (1994) 3369.
[9] G.M. Sheldrick, Acta Crystallogr., Sect. A 46 (1990) 467.
[10] G.M. Sheldrick, SHELXL-97, Program for Structure Refinement, University of Göttingen, Germany, 1997.
[11] P. Starynowicz, unpublished data, 1998.
[12] D. Cremer, J.A. Pople, J. Am. Chem. Soc. 97 (1975) 1354.
[13] P. Luger, R. Bülow, J. Appl. Crystallogr. 16 (1985) 183.
[14] C.K. Johnson, ORTEPII, Report ORNL-5138, Oak Ridge National Laboratory, Oak Ridge, TN, 1976.
[15] S.W.A. Bligh, N. Choi, E.G. Evagorou, W.-S. Li, M. McPartlin, J. Chem. Soc., Chem. Commun. (1994) 2399.
[16] L.H. Bryant Jr., A. Lachgar, S.C. Jackels, Inorg. Chem. 34 (1995) 4230.
[17] L.H. Bryant Jr., A. Lachgar, K.S. Coates, S.C. Jackels, Inorg. Chem. 33 (1994) 2219.
[18] G.N. La Mar, W. De W. Horrocks Jr., R.H. Holm (Eds.), NMR of Paramagnetic Molecules, Academic Press, New York, 1973.
[19] I. Bertini, C. Luchinat, NMR of Paramagnetic Molecules in Biological Systems, Benjamin/Cummings, Menlo Park, CA, 1986.
[20] I. Bertini, P Turano, A.J. Vila, Chem. Rev. 93 (1993) 2833.
[21] I. Bertini, C. Luchinat, Coord. Chem. Rev. 150 (1996) 1.
[22] A.D. Sherry, C.F.G.C. Geraldes, in: J.-C.G. Bunzli (Ed.), Lanthanide Probes in Life, Chemical and Earth Sciences: Theory and Practice, Elsevier, Amsterdam, 1989, Chapter 4.

PERGAMON

www.elsevier.nl/locate/poly

Polyhedron 19 (2000) 471–474

POLYHEDRON

Synthesis and characterization of 1-aza-allyl complexes of aluminum, gallium and bismuth

Chunming Cui, Haijun Hao, Mathias Noltemeyer, Hans-Georg Schmidt, Herbert W. Roesky *

Institut für Anorganische Chemie der Universität Göttingen, Tammannstrasse 4, D-37077 Göttingen, Germany

Received 13 August 1999; accepted 16 December 1999

Abstract

Bis(1-aza-allyl) aluminum compounds of formula R'_2AlY (Y = Cl (**1**), Me (**2**); R′ = $N(SiMe_3)C(Bu^t)CH(SiMe_3)$) were obtained in good yields by the reaction of $(LiR')_2$ with equivalent amounts of $AlCl_3$ and $AlMeCl_2$, respectively, in diethyl ether. The reaction of compound **1** with one equivalent of $AlCl_3$ in toluene afforded the ionic species $[R'_2Al][AlCl_4]$ (**3**). Treatment of RLi·THF ($R = N(SiMe_3)C(Ph)C(SiMe_3)_2$) with $GaCl_3$ and $BiBr_3$ yielded mono(1-aza-allyl) complexes $RGaCl_2$ (**4**) and $RBiBr_2$ (**5**), respectively. Complexes **1**, **2**, **4** and **5** have been characterized by multinuclear NMR spectroscopy, mass spectroscopy and elemental analysis. The characterization of compound **3** is based on multinuclear NMR spectroscopy and physical properties, whereas single crystal X-ray diffraction data are provided for compound **1**. ©2000 Elsevier Science Ltd All rights reserved.

Keywords: Aluminum complexes; 1-Aza-allyl; Bismuth complexes; Crystal structures; Gallium complexes

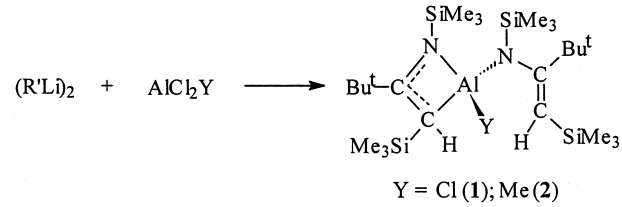
1. Introduction

1-Aza-allyl lithium salts RLi·THF ($R = N(SiMe_3)C(Ph)C(SiMe_3)_2$) and $(R'Li)_2$ ($R' = N(SiMe_3)C(Bu^t)CH(SiMe_3)$), first prepared by Lappert and co-workers [1–3], have been successfully used as ligand transfer reagents for preparing a variety of transition metal and main group element complexes [4]. One of the most interesting features of these ligands is their diversified bonding modes, including η^3 chelating, η^2 bridging, and η^1 enamido, depending greatly on the metal centers, substituents on the ligand backbone and the other ligands on the metal atom. It seems that this type of ligand is suitable for fundamental studies of the relationship between ligand structure and metal coordination geometry due to the variation of the substituents on the ligand backbone. The known 1-aza-allyl complexes include a few main group elements (K, Li, Na, Pb, Sn) [1–3,5] and transition metal (Cu, Hg, Zr, Sm, Yb, Th) [6–11] compounds. Recently we reported on a general route for preparing mono(1-aza-allyl) aluminum compounds of formula $RAlX_2$ (X = halogen, alkyl; $R = N(SiMe_3)C(Ph)C(SiMe_3)_2$) [12]. Here we describe bis(1-aza-allyl) aluminum derivatives and the related gallium and bismuth compounds.

2. Results and Discussion

*2.1. Syntheses of the bis(1-aza-allyl) aluminum complexes **1**, **2** and **3***

Reaction of the 1-aza-allyl lithium salt $(R'Li)_2$ ($R' = N(SiMe_3)C(Bu^t)CH(SiMe_3)$) with $AlCl_3$ or $AlMeCl_2$ in diethyl ether afforded the bis(1-aza-allyl) aluminum complex R'_2AlCl (**1**) or R'_2AlMe (**2**) in good yield (Scheme 1). Compounds **1** and **2** were fully characterized by ^1H, ^{13}C and ^{29}Si NMR, mass spectroscopy and elemental analyses. Spectroscopic data for compound **1** indicate that two ligands are coordinated to the aluminum center in different bonding modes: one is η^3 chelating and the other is η^1 amido. NMR spectra for compound **2** are rather complicated due to rapid exchange of ligands in solution compared to compound **1** with a more polarized Al–Cl bond. Mass spectra indicate that both compounds **1** and **2** are monomers in the



Scheme 1.

* Corresponding author. Tel.: +49-551-393001; fax: +49-551-393373; e-mail: hroesky@gwdg.de

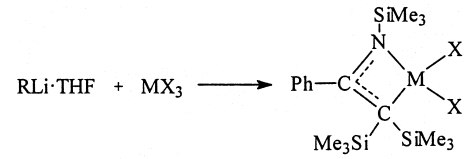
0277-5387/00/$ - see front matter ©2000 Elsevier Science Ltd All rights reserved.
PII S0277-5387(99)00390-3

gas phase. Initial efforts to examine reactivities of the two compounds showed that compound **2** does not react with the fluorinating reagent Me_3SnF in CH_2Cl_2 or toluene to give the corresponding fluoride, and that compound **1** cannot be reduced by alkali metals (Na and K) in hydrocarbon solvents even at elevated temperatures as indicated by recovery of 70–80% of compound **1** after refluxing for 24 h in n-hexane. Treatment of compound **1** with the Lewis acid $AlCl_3$ in toluene afforded a yellow oil that deposited from the solvent. Obviously a liquid clathrate (an oil containing compound **3** and solvent) is formed like many of the aluminum ionic compounds which exhibit two-phase liquid behavior in aromatic solvents [13,14]. A white solid of compound **3** can be obtained after treating the crude product with pentane. The solid is extremely air-sensitive and unstable in tetrahydrofuran (THF) and CH_2Cl_2. Crystallization of the solid from THF or CH_2Cl_2 leads to the formation of $AlCl_3(THF)_2$ [15,16] and compound **1** or decompostion of compound **3** into $AlCl_3$ and compound **1**. The formation of $AlCl_3(THF)_2$ from compound **3** in THF is particularly noteworthy since the direct interaction of aluminum chloride (Al_2Cl_6) and THF has been shown to give the ionic compound $[AlCl_2(THF)_4][AlCl_4]$ [17,18]. The mechanism might involve the initial interaction of the cation R'_2Al^+ with THF, which is in contrast to the related cation $[(2\text{-}C(SiMe_3)_2Py)_2Al]^+$, which could be crystallized from THF [19,20]. The different stabilities may be due to the flexibility of the 1-aza-allyl ligand. Compound **3** can be dissolved in CD_2Cl_2, and the solution is stable for a few days, which allows easy characterization of the product by NMR spectroscopy. The ^1H NMR spectrum of compound **3** contains four singlets (δ 0.30, 0.42, 1.39, 3.03 ppm) which are assigned to $NSiMe_3$, $SiMe_3$, Bu^t and CH, respectively. The chemical shift for CH indicates that the ligand is coordinated to the aluminum atom in an η^3 fashion due to the high field signal, compared with those found for the protons of normal C=C double bonds. Further evidence for the formation of cationic species was provided by the ^{27}Al NMR spectrum, in which two signals are observed: one at 103 ppm is typical for $AlCl_4^-$ [21]; the second (111 ppm) is assigned to R_2Al^+, which is in the typical range for a four-coordinated aluminum center.

Attempts to synthesize bis(1-aza-allyl) aluminum compounds containing the more bulky ligand R (R= $N(SiMe_3)C(Ph)C(SiMe_3)_2$) in solvents such as diethyl ether, n-hexane, THF and toluene were unsuccessful, even under reflux conditions.

2.2. Synthesis and characterization of complexes *4* and *5*

Reaction of RLi·THF with $GaCl_3$ and $BiBr_3$ in toluene–n-hexane afforded the corresponding mono(1-aza-allyl) gallium dichloride $RGaCl_2$ (**4**) and bismuth dibromide $RBiBr_2$ (**5**), respectively (Scheme 2). The two compounds have been characterized by MS, multinuclear NMR and elemental analysis. Mass spectra of compounds **4** and **5** indicate that the two compounds are monomers. The ^1H and ^{29}Si NMR



M = Ga, X=Cl (**4**); M = Bi, X=Br (**5**)

Scheme 2.

spectra of compounds **4** and **5** contain only one singlet for $SiMe_3$ (see Section 3), indicating that R is coordinated to the central atom in an η^3 chelating mode. It should be mentioned that $RAlCl_2$ has been characterized by X-ray single-crystal diffraction analysis, in which R is coordinated to Al in an η^3 chelating mode [12]. Compounds **4** and **5** have similar NMR patterns comparable to $RAlCl_2$. Compound **4** is soluble in hydrocarbon solvents while compound **5** has only a very limited solubility in n-hexane and is soluble in aromatic solvents. Compound **5** is not stable in solution, and slowly decomposes even under an inert atmosphere. Reduction of compound **5** with potassium in toluene afforded a slightly yellow oil, which we were not able to characterize completely. Compounds **4** and **5** represent the first known 1-aza-allyl compounds of gallium and bismuth. Further investigation of the chemistry of 1-aza-allyl gallium and bismuth compounds is in progress.

2.3. Molecular structure of compound *1*

Single crystals of **1** were obtained from n-hexane solution at −30°C. Selected bond lengths and angles are given in Table 1. The structure of compound **1** with the atom labeling scheme is shown in Fig. 1. Compound **1** adopts a distorted tetrahedral structure with aluminum bonded to C(3), Cl(1), N(1) and N(4); thus one ligand R is coordinated to the aluminum atom in an η^3 chelating fashion with the acute core angle N(1)–Al(1)–C(3) (71.44(6)°). The other ligand acts as amide ligand only, with the N(4) being coordinated to the aluminum atom. The different bonding modes of the ligand can be further realized when selected bond parameters are compared to each other. The Al(1)–N(1) distance (1.9701(15) Å) is longer than the Al(1)–N(4) distance (1.8194(15) Å); moreover the C(2)–C(3) bond length (1.478(2)Å) is longer than the C(5)–C(6) bond length (1.349(2) Å) while the N(1)–C(2) bond length (1.321(2) Å) is shorter than the N(4)–C(5) bond length (1.450(2)

Table 1
Selected bond lengths (Å) and angles (°) for compound **1**

Al(1)–N(1)	1.9701(15)	Al(1)–N(4)	1.8194(15)
Al(1)–C(3)	2.003(2)	Al(1)–Cl(1)	2.1504(8)
C(2)–C(3)	1.478(2)	C(5)–C(6)	1.349(2)
N(1)–C(2)	1.321(2)	N(4)–C(5)	1.450(2)
N(1)–Al(1)–C(3)	71.44(6)	N(1)–Al(1)–N(4)	115.59(7)
N(4)–Al(1)–C(3)	119.93(7)	N(1)–C(2)–C(3)	111.82(14)
N(4)–Al(1)–Cl(1)	108.81(5)	N(1)–Al(1)–Cl(1)	116.66(5)
N(4)–Al(1)–C(2)	116.87(6)	C(6)–C(5)–N(4)	119.2(2)

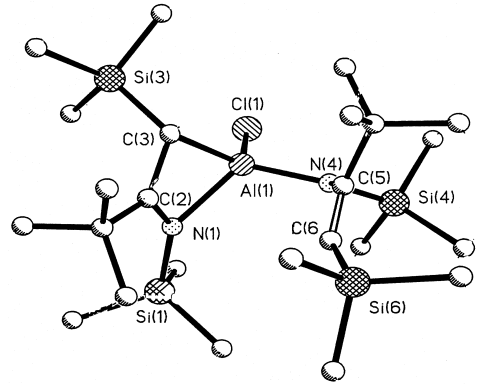


Fig. 1. Molecular structure of compound **1** in the crystal; hydrogen atoms have been omitted for clarity.

Å) due to electron delocalization in the η^3 ligand backbone. The bond angle C(3)–C(2)–N(1) (111.82(14)°) reflects an sp^3 hybrid of C(2) while the angle N(4)–C(5)–(C(6) (119.2(2)°) indicates an sp^2 hybrid of C(5). These data are in agreement with the different bonding modes of the ligand. The ^{1}H NMR spectrum of compound **1** clearly shows two sets of signals for the R′ group, indicating that the solid-state structure is maintained in C_6D_6 solution at room temperature. The singlets (δ 2.33 and 4.94 ppm) in the ^{1}H NMR spectrum also demonstrate different bonding modes of the ligand and can be used to identify the bonding interactions in the compounds incorporating this ligand.

3. Experimental

3.1. General

All manipulations were carried out under a purified nitrogen atmosphere using standard Schlenk techniques. Solvents were distilled from drying agents and degassed prior to use. The ^{1}H NMR (250.130 MHz), ^{13}C NMR (100.600 MHz), ^{29}Si NMR (79.460 MHz) and ^{27}Al NMR spectra (104.245 MHz) were recorded using Bruker AM 200 and Bruker AM 250 spectrometers. The chemical shifts were externally referenced to $SiMe_4$ (^{1}H, ^{13}C, ^{29}Si NMR) and $AlCl_3$ (^{27}Al NMR). EI (70 eV) mass spectra were measured on a Finnigan MAT 8230 or a Varian MAT CH5 instrument. Elemental analysis was performed by the analytical laboratory of the Institute of Inorganic Chemistry at the University of Göttingen. Melting points were measured in sealed glass tubes and were not corrected.

3.2. Preparations

3.2.1. [{N(SiMe$_3$)C(Bu^t)CH(SiMe$_3$)}$_2$AlCl] (1)

(LiR′)$_2$ (0.75 g, 1.5 mmol) in diethyl ether (20 ml) was added to a suspension of $AlCl_3$ (0.40 g, 1.5 mmol) in diethyl ether (10 ml) at −78°C. The reaction mixture was allowed to warm to room temperature and then stirred for 18 h. The volatiles were removed in vacuo and the residual was extracted with pentane (3×20 ml). The extract was concentrated and stored at −30°C overnight to afford colorless crystals of compound **1** (0.72 g, 88%). M.p.: 136–137°C. MS: *m/z* (%): 531 [M−Me]$^+$ (8%), 489 [M−Bu^t]$^+$ (81%), 304 [M−R′]$^+$ (100%). ^{1}H NMR (C_6D_6): δ 0.25, 0.29 (s, 9H, NSiMe$_3$), 0.36, 0.47 (s, 9H, SiMe$_3$), 1.07, 1.30 (s, 9H, Bu^t), 2.33, 4.94 (s, 1H, CH). ^{13}C NMR (C_6D_6): δ 1.99, 2.93 (s, NSiMe$_3$), 3.51, 4.12 (s, SiMe$_3$), 29.04, 31.83 (s, Bu^t), 39.22, 42.38 (s, Bu^t), 119.1, 47.4 (s, CH), 172.8, 222.0 (s, CN). ^{29}Si NMR (C_6D_6): δ −14.6, 0.81 (s, SiMe$_3$), 3.20, 3.49 (s, NSiMe$_3$). *Anal*. Found: C, 52.40; H, 10.17; N, 5.05%. Calc. for $C_{24}H_{56}AlClN_2Si_4$: C, 52.65; H, 10.31; N, 5.11%.

3.2.2. [{N(SiMe$_3$)C(Bu^t)CH(SiMe$_3$)}$_2$AlMe] (2)

This compound was prepared using (LiR′)$_2$ (2.00 g, 4 mmol) and $AlMeCl_2$ (3 ml, 1 M in n-hexane, 4 mmol) as described for compound **1**. After work-up, colorless crystals (1.90 g, 90%) were obtained. M.p.: 115–116°C. MS: *m/z* (%) 526 M$^+$ (5%), 511 [M−Me]$^+$ (20%), 469 [M−Bu^t]$^+$ (56%), 284 [M−R′]$^+$ (100%). ^{1}H NMR (C_6D_6, 295 K): δ −0.12 (s, 3 H, AlMe), 0.25–0.37 (m, SiMe$_3$), 1.07–1.29 (m, Bu^t), 2.32, 4.95(s, CH). ^{13}C NMR (C_6D_6, 300 K): δ −3.57 (s, AlMe), 1.37, 2.01, 2.25, 2.95, 3.53, 3.72, 4.13 (s, NSiMe$_3$ and SiMe$_3$), 29.25, 31.04 (s, Bu^t), 45.88, 42.39, 45.88 (s, Bu^t), 116.64 (s, CH), 174.4, 222.0 (s, CN). *Anal*. Found: C, 56.16; H, 11.44; N, 5.46%. Calc. for $C_{25}H_{59}AlN_2Si_4$: C, 56.95; H, 11.29; N, 5.32%.

3.2.3. [({N(SiMe$_3$)C(Bu^t)CH(SiMe$_3$)}$_2$Al)][AlCl$_4$] (3)

A mixture of compound **1** (0.55 g, 1 mmol) and $AlCl_3$ (0.13 g, 1.0 mmol) in toluene (10 ml) was stirred at room temperature for 2 h. Two phases (a yellowish oil deposited) were formed with the complete consumption of $AlCl_3$. The volatiles were removed to leave a semi-solid product, which was washed with pentane (2×5 ml) to give compound **3** as a white solid (0.47 g, 69%). ^{1}H NMR (CD_2Cl_2): δ 0.30 (s, 18H, NSiMe$_3$), 0.42 (s, 18H, SiMe$_3$), 1.39 (s, 18H, Bu^t), 3.03 (s, 2H, CH). ^{27}Al NMR (CD_2Cl_2): δ 103.0 (s, $AlCl_4^-$), 111.8 (br, R′$_2$Al$^+$).

3.2.4. [{N(SiMe$_3$)C(Ph)C(SiMe$_3$)$_2$}GaCl$_2$] (4)

A solution of RLi·THF (0.83 g, 2 mmol) in toluene (15 ml) was added to a stirred suspension of $GaCl_3$ (0.35 g, 2 mmol) in n-hexane (10 ml) at −78°C. The mixture was allowed to warm to room temperature and stirred for 15 h and then filtered. The filtrate was concentrated and stored at −30°C for 2 days to afford colorless crystals (0.62 g, 65%). M.p.: 165°C. MS: *m/z* (%) 475 M$^+$ (90%), 460 [M−Me]$^+$ (100%). ^{1}H NMR (C_6D_6): δ −0.01 (s, 9H, NSiMe$_3$), 0.24 (s, 18H, SiMe$_3$), 6.82–7.00 (m, 5H, Ph). ^{13}C NMR (C_6D_6): δ 0.69 (s, NSiMe$_3$), 2.55 (s, SiMe$_3$), 63.6 (s, CSi$_2$), 126.4, 128.7, 130.8 (s, Ph), 139.3 (s, *ipso*-C), 207.3 (s, CN). ^{29}Si NMR (C_6D_6): δ −0.42 (s, SiMe$_3$), 9.73 (s, NSiMe$_3$). *Anal*. Found: C, 42.69; H, 6.48; N, 2.98%. Calc. for $C_{17}H_{32}Cl_2GaNSi_3$: C, 42.90; H, 6.78; N, 2.94%.

*3.2.5. [{N(SiMe$_3$)C(Ph)C(SiMe$_3$)$_2$}BiBr$_2$] (**5**)*

A solution of RLi·THF (0.83 g, 2 mmol) in toluene (20 ml) was added to a suspension of $BiBr_3$ (0.90 g, 2.0 mmol) in n-hexane (10 ml) at −78°C. The mixture was allowed to warm to room temperature, stirred for 20 h and then filtered. The filtrate was concentrated and stored at −30°C overnight to give orange crystals (0.97 g, 69%). M.p.: 90°C(dec.). MS: *m/z* (%) 703 M^+ (4%), 624 $[M-Br]^+$ (90%), 73 $[SiMe_3]^+$ (100%). ^{1}H NMR (C_6D_6): δ −0.08 (s, 9H, $SiMe_3$), 0.33 (s, 18H, $SiMe_3$), 6.82–7.00 (m, 5H, Ph). ^{29}Si NMR (C_6D_6): δ −2.17 (s, $SiMe_3$), 4.00 (s, $NSiMe_3$). *Anal.* Found: C, 29.81; H, 4.88; N, 2.33%. Calc. for $C_{17}H_{32}BiBr_2NSi_3$: C, 29.03; H, 4.59; N, 1.99%.

3.3. X-ray structure determination and refinement

Data for crystal structure of compound **1** were collected on a Stoe-Siemens four circle diffractometer using Mo Kα radiation (λ = 0.71073 Å). The structure was solved by direct methods (SHELXS-96) [22] and refined against F^2 using SHELXL-97 [23]. All heavy atoms were refined anisotropically. Hydrogen atoms were included using the riding model with U_{iso} tied to the U_{iso} of the parent atom. Crystal data, data collection details and refinement are summarized in Table 2.

Table 2
Crystallographic data for compound **1**

Formula	$C_{24}H_{56}AlClN_2Si_4$
M	547.50
T (K)	150(2)
Crystal system	Monoclinic
Space group	$P2_1/n$
a (Å)	11.3848(13)
b (Å)	20.020(3)
c (Å)	15.355(2)
α (°)	90
β (°)	102.647(12)
γ (°)	90
V (Å^3)	3414.9(9)
Z	4
d (g cm^{-3})	1.065
μ (mm^{-1})	0.292
F(000)	1200
Crystal size (mm)	1.00×1.00×0.70
θ range (°)	3.56–25.02
Ranges of *h*, *k*, *l*	−13 to 13, −7 to 23, −18 to 18
No. reflections collected	8721
No. independent reflections	6010 (R_{int} = 0.0231)
Data, restraints, parameters	6001, 0, 307
Goodness of fit on F^2	1.068
Final *R* indices [$I > 2\sigma(I)$]	$R1$ = 0.0343, $wR2$ = 0.0854
R indices(all data)	$R1$ = 0.0410, $wR2$ = 0.0937
Largest difference peak and hole (e Å^{-3})	0.333 and −0.259

Supplementary data

Crystallographic data (excluding structure factors) for the structure of compound **1** have been deposited with the Cambridge Crystallographic Data Centre as supplementary publication no. CCDC-133327. Copies of the data can be obtained free of charge on application to CCDC, 12 Union Road, Cambridge CB2 1EZ, UK (fax: +44-1223-336033; e-mail: deposit@ccdc.cam.ac.uk).

Acknowledgements

We thank the Deutsche Forschungsgemeinschaft for financial support and Witco GmbH for chemicals.

References

[1] P.B. Hitchcock, M.F. Lappert, D.-S. Liu, J. Chem. Soc., Chem. Commun. (1994) 2637.
[2] P.C. Andrews, D.R. Armstrong, M. MacGregor, R.E. Mulvey, D. Reed, J. Chem. Soc., Chem. Commun. (1989) 1341.
[3] D.R. Armstrong, W. Clegg, L. Dunbar, S.T. Liddle, M. MacGregor, R.E. Mulvey, D. Reed, S.A. Quinn, J. Chem. Soc., Dalton Trans. (1998) 3431.
[4] M.F. Lappert, D.-S. Liu, J. Organomet. Chem. 500 (1995) 203.
[5] P.B. Hitchcock, M.F. Lappert, M. Layh, Inorg. Chim. Acta 269 (1998) 181.
[6] P.B. Hitchcock, J. Hu, M.F. Lappert, M. Layh, J. Severn, Chem. Commun. (1997) 1189.
[7] P.B. Hitchock, M.F. Lappert, D.-S. Liu, J. Chem. Soc., Chem. Commun. (1994) 1669.
[8] P.B. Hitchcock, M.F. Lappert, M. Layh, Chem. Commun. (1998) 1619.
[9] P.B. Hitchcock, M.F. Lappert, S. Tian, J. Organomet. Chem. 549 (1997) 1.
[10] P.B. Hitchcock, S.A. Holmes, M.F. Larppert, S. Tian, J. Chem. Soc., Chem. Commun. (1994) 2691.
[11] P.B. Hitchcock, J. Hu, M.F. Lappert, S. Tian, J. Organomet. Chem. 536 (1997) 473.
[12] C. Cui, H.W. Roesky, M. Noltemeyer, M.F. Lappert, H.-G. Schmidt, H. Hao, Organometallics 18 (1999) 2256.
[13] J.L. Atwood, J.E.D. Davies, D.D. MacNicol, Inclusion Compounds, vol. 1, Academic Press, London, 1984, p. 375.
[14] E. Ihara, V.G. Young Jr., R.F. Jordon, J. Am. Chem. Soc. 120 (1998) 8277.
[15] $AlCl_3(THF)_2$ has been characterized by X-ray crystal analysis; C. Cui, H.W. Roesky, unpublished result.
[16] $AlCl_3(THF)_2$ was formed from the adduct $(Me_2N)_3SiCl·AlCl_3$; see A.H. Cowley, M.C. Cushner, R.E. Davis, P.E. Riley, Inorg. Chem. 20 (1981) 1179.
[17] N.C. Means, C.M. Means, S.G. Bott, J.L. Atwood, Inorg. Chem. 26 (1987) 1466.
[18] J. Derouault, M.T. Forel, Inorg. Chem. 16 (1977) 3207.
[19] L.M. Engelhardt, U. Kynast, C.L. Raston, A.H. White, Angew. Chem. 99 (1987) 702.
[20] L.M. Engelhardt, U. Kynast, C.L. Raston, A.H. White, Angew. Chem., Int. Ed. Engl. 26 (1987) 681.
[21] J. Derouault, P. Granger, M.T. Forel, Inorg. Chem. 16 (1977) 3214.
[22] G.M. Sheldrick, Acta Crystallogr. Sect. A 46 (1990) 467.
[23] G.M. Sheldrick, SHELXL, Program for Crystal Structure Refinement, University of Göttingen, Germany, 1997.

PERGAMON

www.elsevier.nl/locate/poly

Polyhedron 19 (2000) 475–485

POLYHEDRON

Synthesis and X-ray crystal structures of several dinuclear ruthenium cymene complexes based on the tetradentate ligand, 2,2′-(1*H*-pyrazole-3,5-diyl)bis(6-methylpyridine) (Me_2DppzH)

Vincent J. Catalano *, Tegan J. Craig

Department of Chemistry, University of Nevada, Reno, NV 89557, USA

Received 12 July 1999; accepted 6 December 1999

Abstract

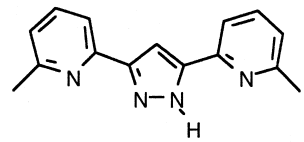
The complexes $[Ru_2(6,6'\text{-}Me_2dppz)(\eta^6\text{-}p\text{-cymene})_2Cl_2]^+$ (**1**), $[Ru_2(6,6'\text{-}Me_2dppz)(\eta^6\text{-}p\text{-cymene})_2(NO_3)_2]^+$ (**2**), $[Ru_2(6,6'\text{-}Me_2dppz)(\eta^6\text{-}p\text{-cymene})_2(OH_2)_2]^{3+}$ (**3**), $[Ru_2(6,6'\text{-}Me_2dppz)(\eta^6\text{-}p\text{-cymene})_2(NO_2)_2]^+$ (**4**), $[Ru_2(6,6'\text{-}Me_2dppz)(\eta^6\text{-}p\text{-cymene})_2(CH_3CN)_2]^{3+}$ (**5**) and $[Ru_2(NO_2\text{-}6,6'\text{-}Me_2dppz)(\eta^6\text{-}p\text{-cymene})_2Cl_2]^+$ (**6**), where 6,6′-Me_2dppzH is 2,2′-(1*H*-pyrazole-3,5-diyl)-bis(6-methylpyridine) and NO_2-6,6′-Me_2dppzH is 2,2′-(1*H*-4-nitropyrazole-3,5-diyl)bis(6-methylpyridine), were synthesized and characterized by ^{1}H NMR and UV–Vis spectroscopy, X-ray crystallography and elemental analysis. Compounds **2** and **4** were additionally characterized by IR spectroscopy. Reaction of compound **1** with an aqueous silver ion produces the corresponding aquo complex **3**. Complex **3** can be isolated or further reacted with $NaNO_2$ to form the N-bound nitrite complex **4**. Complex **1** can also be reacted with an acetonitrile solution of HPF_6 to produce the acetonitrile species (**5**). Reaction of compound **1** with an excess of $NOBF_4$ produces the corresponding chloro complex with nitration at the pyrazole carbon atom. Attempts to isomerize the geometry of complex **1** from the 'anti-facial' geometry to the 'syn' geometry were unsuccessful using either chemical or photochemical means. All efforts to convert the bound nitro group to the nitrosyl were futile, resulting in either ligand substitution or alteration of the ligand backbone. ©2000 Elsevier Science Ltd All rights reserved.

Keywords: Cymene; Nitration; Pyrazolyl; Ruthenium; Structure; Synthesis

1. Introduction

Mononuclear ruthenium polypyridyl complexes are known to perform a variety of inorganic [1–4] and organic transformations [5,6]. Their ease of synthesis, high catalytic performance under relatively mild reaction conditions, high selectivity and easily modified ligand systems make these complexes particularly well suited for this purpose. For example, the terpyridine-containing complex $[Ru(trpy)(bpy)(NO_2)]^+$ (where trpy is 2,2′:6′,2″-terpyridine and bpy is 2,2′-bipyridine) is capable of interconverting a bound nitrite ligand to a nitrosyl moiety using simple acid–base chemistry, and further to an ammonia ligand by electrochemical methods [7]. Further, the closely related Ru(IV)=O complexes, $[Ru(trpy)(diimine)O]^{2+}$, are used extensively as catalysts for the oxidation of organic substrates [5,6,8–14].

It has been postulated that this catalytic behavior could be enhanced by coupling two adjacent metals, thus allowing for strong communication between the metals and perhaps a cooperative catalytic or redox behavior [15,16]. Meyer et al. have reported a dinuclear ruthenium oxo-bridged catalyst that homogeneously transforms water into dioxygen. This dimer is also capable of many other substrate oxidations [17–19]. Although the reactivity of the dimeric form is high, instability renders the complex less effective as a catalyst. However, incorporation of a multidentate ligand as a chelating backbone can alleviate this problem by stabilizing the dimeric form [15,20–24].



6,6′-Me_2dppzH

The dipyridylpyrazolate ligand (6,6′-dppzH) is one such candidate. Deprotonation of this ligand provides an open coordination pocket that allows for dimetallic complex formation, forcing the two ruthenium centers into close proximity. This arrangement allows a halide or small molecule to

* Tel.: +1-775-7841329; fax: +1-775-7846804; e-mail: vjc@unr.edu

0277-5387/00/$ - see front matter ©2000 Elsevier Science Ltd All rights reserved.
PII S0277-5387(99)00391-5

bridge between the metals [25] and allows both metals to influence the reactivity of the bridging molecule. Further, methyl groups in the 6 and 6′ positions add moderate steric congestion to the complex, directing incoming substrate molecules towards the center of the complex. Herein is reported the synthesis, characterization and reactivity of a series of new dimetallic ruthenium compounds based on the dipyridylpyrazolate ligand.

2. Results

2.1. Synthesis

The synthesis of the 2,2′-(1*H*-pyrazole-3,5-diyl)bis(6-methylpyridine) (6,6′-Me_2dppzH) ligand was modified from the literature procedure [25–27], and $Ru_2Cl_4(\eta^6$-*p*-cymene$)_2$ was prepared according to a literature procedure [28]. Reaction of the 6,6′-Me_2dppzH ligand with one equivalent of $Ru_2Cl_4(\eta^6$-*p*-cymene$)_2$ produced complex **1** as a bright orange, microcrystalline solid in 90% yield (Eq. (1)).

$$6,6'\text{-Me}_2\text{dppzH} + \text{Ru}_2\text{Cl}_4(\eta^6\text{-}p\text{-cymene})_2 \rightarrow [\text{Ru}_2(6,6'\text{-Me}_2\text{dppz})(\eta^6\text{-}p\text{-cymene})_2\text{Cl}_2]\text{Cl} + \text{HCl} \quad (1)$$

As shown in Fig. 1, the crystal structure (see below) of complex **1** has an 'anti-facial' geometry in which the cymene ligands are directed away from one another. This geometry likely results from a minimization of the steric hindrance caused by the bulky arene ligands. The reaction to form complex **1** also produced a minor product (less than 10%), which might be an isomer of complex **1**. This impurity could not be removed by recrystallization or chromatographic techniques.

According to Scheme 1, complex **1** can be treated with excess $AgNO_3$ in acetone–H_2O to produce the monodentate nitrate species (**2**) as a yellow solid. Complex **1** can also be reacted with $NOBF_4$ dissolved in CH_2Cl_2 to form complex **6**, in which the ligand backbone has been nitrated. Reaction of complex **1** in acetone with an aqueous solution of $AgBF_4$ or $AgClO_4$ produces the aquo species (**3**). This can be isolated or further reacted with $NaNO_2$ to form species **4** as a yellow solid. The IR spectrum (KBr pellet) of compound **4** displays two stretches at 1367 and 1311 cm^{-1} along with a bending mode at 845 cm^{-1}, consistent with an N-bound nitro group [29]. Dissolution of complex **4** in acetonitrile and further treatment with HPF_6 produces the solvato species (**5**). Substitution chemistry of complex **1** to form complexes **2**, **3** and **5** eliminates the aforementioned impurity. All of the complexes reported here have been studied by X-ray diffraction and have analogous structures with the 'anti-facial' geometry and non-bridging small molecule ligands.

2.2. NMR spectroscopy studies

General ^{1}H NMR assignments were made for each of the complexes, and the chemical shift data are presented in Section 5. Analyses of the 1D and 2D ^{1}H NMR and ^{13}C{^{1}H} NMR experiments provide for nearly complete assignment of protons for complex **5,** while 1D experiments were used for the remaining complexes. The ^{1}H NMR spectra for complexes **1**–**6** further support the geometry of the complexes. The pyrazole proton resonances for each of the complexes appears between 7.65 and 7.89 ppm and are not significantly influenced by changes in ligation at the metal centers. Each complex also shows the appropriate aromatic resonances for the ligand backbone between 8.11 and 7.57 ppm, again with little shift upon ligand substitution. The cymene ring protons are also unaffected by substitution at the ruthenium centers,

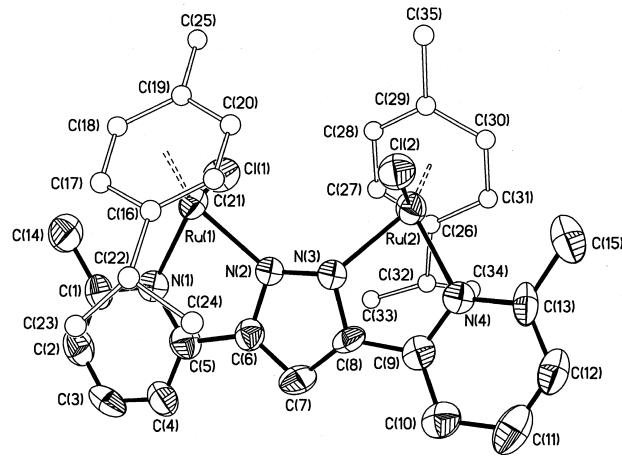
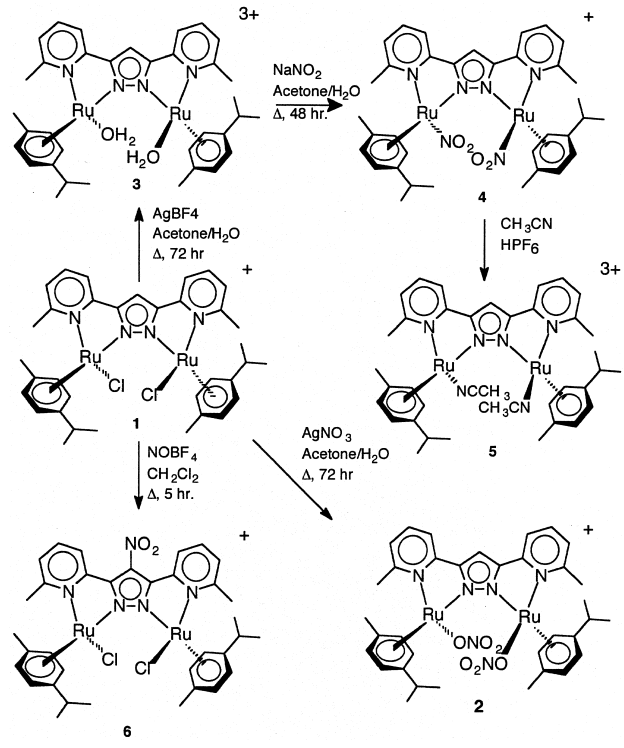


Fig. 1. Crystal structure drawing for the cation of $[Ru_2(6,6'\text{-Me}_2\text{dppz})(\eta^6\text{-}p\text{-cymene})_2Cl_2](PF_6)$ (**1**) with 40% probability ellipsoids. Cymene carbon atoms are shown as arbitrarily sized circles and hydrogen atoms are removed for clarity.



Scheme 1.

giving rise to four resonances in the aromatic region of the spectra between 6.64 and 5.67 ppm. The methyl groups in the 6 and 6′ positions provide a distinct spectroscopic handle in the ^{1}H NMR spectra. The characteristic 6,6′-Me_2dppz methyl resonance for complex **1** appears at 3.26 ppm. Substitution of the chloride for NO_3^- shifts the resonance downfield to 3.41 ppm. This resonance moves upfield to 3.10 and 3.11 ppm for NO_2^- and CH_3CN, respectively. For complex **6** the resonance appears at 3.31 ppm, and for the aquo species (in D_2O) the resonance appears at 3.28 ppm. The aliphatic portions of the cymene ligands are resolved and appear between 2.71 and 0.57 ppm, as expected.

2.3. Electronic absorption spectra

The electronic absorption spectra of compounds **1**–**6** (CH_3OH) are similar. All six complexes show intense $\pi-\pi^*$ absorptions in the UV portion of the spectrum. For compound **1** this band appears at 327 nm. Substitution in complexes **2**–**6** shifts the band to slightly higher energy to 319, 322, 326, 320 and 317 (shoulder) nm, respectively. Complex **6** also exhibits a shoulder at 302 nm. Each complex also exhibits a broad band in the visible region of the spectrum. This band can be assigned to a metal-to-ligand charge transfer (MLCT) process and appears at 430 nm for compound **1**. The MLCT band shifts slightly upon substitution of the chloride for nitrate to 425 nm for compound **2**. For compounds **3** and **5** this band shifts to higher energy, to 407 and 400 nm, as expected for the substitution of an anionic ligand for a neutral species. The poor donor property of the monodentate nitrate moiety in compound **4** is exemplified with a MLCT band shift at 398 nm. Upon nitration of the ligand backbone the MLCT band appears at 407 nm for compound **6**. As expected, this energy is higher than that of compound **1**.

3. Structural analyses

3.1. Structure of [Ru_2(6,6′-Me_2dppz)(η^6-*p*-cymene)$_2Cl_2$](PF_6)·0.5CH_3OH (**1**)

The asymmetric unit of complex **1** contains the cation, one disordered hexafluorophosphate counterion, and one-half of a molecule of methanol. There are no unusual contacts between these moieties. A view of the cation is presented in Fig. 1. Selected bond distances and angles are given in Table 1, and atomic coordinates and complete crystallographic details are provided in the section on supplementary data. The structure of compound **1** shows each Ru atom in a roughly octahedral environment with the η^6-*p*-cymene ligand coordinated in a facial fashion. The 6,6′-Me_2dppz ligand is bound in a chelate fashion to both ruthenium centers. The chloride atom is positioned in a manner as to prohibit bridging between the two ruthenium centers. The ruthenium atoms are on opposite sides of the bridging ligand backbone, and the η^6-*p*-cymene ligands are directed away from one another in an 'anti-facial' geometry. The cymene methyl groups are directed on the same side as the chloro ligands with the cymene isopropyl groups pointing opposite to the chloro groups, possibly to remove any steric hindrance from the large chloride ligand. The steric encumbrance of the 6,6′-Me_2dppz methyl groups is manifested in the Ru–N separations. The Ru(1)–N(1) and Ru(2)–N(4) distances of 2.129(12) and 2.160(12) Å are longer than the Ru(1)–N(2) and Ru(2)–N(3) distances of 2.090(10) and 2.089(11) Å, respectively. The distance between the two metal centers is long at 4.445 Å. The average Ru–C bond distance is normal [30–32] at 2.20 Å with the average Ru–$C_{centroid}$ length of 1.691 Å, while both Ru(1)–Cl(1) and Ru(2)–Cl(2) distances of 2.402(5) and 2.386(4) Å are typical for a ruthenium(II)–chloro complex [5,32,33]

Table 1
Selected bond distances (Å) and angles (°) for compounds **1** and **6**

	1	**6**
Ru(1)–Cl(1)	2.402(5)	2.399(3)
Ru(2)–Cl(2)	2.386(4)	2.400(3)
Ru(1)–N(1)	2.129(12)	2.132(8)
Ru(1)–N(2)	2.090(10)	2.101(7)
Ru(2)–N(3)	2.089(11)	2.098(7)
Ru(2)–N(4)	2.160(12)	2.161(8)
Ru(1)–$C_{centroid}$	1.688	1.689
Ru(2)–$C_{centroid}$	1.694	1.710
C(7)–N(5)		1.459(13)
N(5)–O(1)		1.169(11)
N(5)–O(2)		1.243(12)
Ru(1)–N(1)–C(1)	130.0(11)	127.1(7)
N(1)–C(1)–C(14)	116.9(15)	119.4(9)
Ru(2)–N(5)–C(13)	126.7(11)	127.1(7)
N(5)–C(13)–C(15)	118.5(16)	119.6(10)
Cl(1)–Ru(1)–N(1)	84.7(3)	85.3(2)
Cl(1)–Ru(1)–N(2)	89.5(3)	88.9(2)
Cl(2)–Ru(2)–N(3)	88.9(3)	89.2(2)
Cl(2)–Ru(2)–N(4)	84.9(3)	84.9(2)
N(1)–Ru(1)–N(2)	76.5(4)	76.5(3)
Ru(1)–N(2)–N(3)	135.5(9)	133.1(6)
N(3)–Ru(2)–N(4)	76.3(4)	76.5(3)
Ru(2)–N(3)–N(2)	132.04(9)	133.3(6)
C(7)–N(5)–O(1)		120.3(11)
C(7)–N(5)–O(2)		115.3(10)
O(1)–N(5)–O(2)		124.4(11)

3.2. Structure of [Ru_2(6,6′-Me_2dppz)(η^6-*p*-cymene)$_2$-(NO_3)$_2$](PF_6)·0.5(CH_3)$_2$CO (**2**)

The structure of compound **2** is analogous to that of compound **1**. The asymmetric unit of compound **2** contains the cation, one disordered hexafluorophosphate counterion and one-half of an acetone solvate molecule, with no unusual contacts between any of these species. A drawing of the cation is shown in Fig. 2, and selected bond distances and angles are given in Table 2. Complete crystallographic data are provided in the section on supplementary data. The structure of

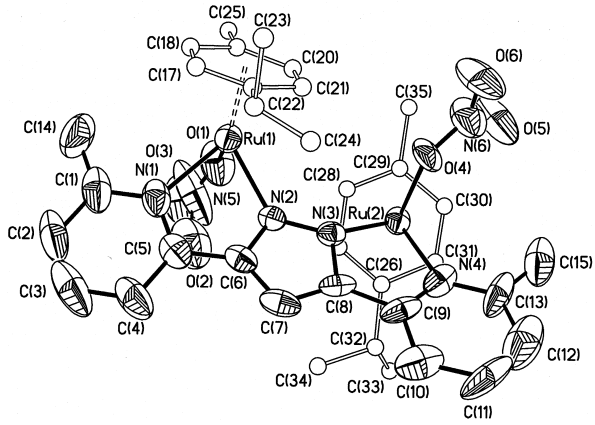


Fig. 2. Thermal ellipsoid plot (40% probability) for the cation of $[Ru_2(6,6'\text{-}Me_2dppz)(\eta^6\text{-}p\text{-cymene})_2(NO_3)_2](PF_6)$ (**2**). Cymene carbon atoms are shown as arbitrarily sized circles and hydrogen atoms are removed for clarity.

Table 2
Selected bond distances (Å) and angles (°) for compounds **2** and **4**

	2	**4**
Ru(1)–N(1)	2.151(10)	2.144(5)
Ru(1)–N(2)	2.071(8)	2.089(5)
Ru(2)–N(3)	2.100(8)	2.085(5)
Ru(2)–N(4)	2.139(9)	2.130(6)
$Ru(1)–C_{centroid}$	1.697	1.717
$Ru(2)–C_{centroid}$	1.692	1.731
Ru(1)–O(1)	2.070(9)	
O(1)–N(5)	1.134(15)	1.193(8)
O(2)–N(5)	1.36(2)	1.136(7)
O(3)–N(5)	1.183(15)	
Ru(2)–O(4)	2.112(7)	
O(4)–N(6)	1.246(12)	1.227(8)
O(5)–N(6)	1.244(13)	
O(6)–N(6)	1.176(12)	
Ru(1)–N(5)		2.155(5)
Ru(2)–N(6)		2.091(6)
O(3)–N(6)		1.205(8)
Ru(1)–N(1)–C(1)	128.1(11)	128.6(5)
N(1)–C(1)–C(14)	119.6(15)	120.7(7)
Ru(2)–N(5)–C(13)	127.5(12)	128.9(5)
N(5)–C(13)–C(15)	120.8(16)	119.9(7)
N(1)–Ru(1)–N(2)	76.6(4)	78.0(2)
Ru(1)–N(2)–N(3)	133.4(6)	137.0(4)
N(3)–Ru(2)–N(4)	76.6(4)	77.8(2)
Ru(2)–N(3)–N(2)	132.2(6)	137.8(4)
Ru(1)–O(1)–N(5)	140.8(11)	
O(1)–N(5)–O(2)	107.5(16)	123.7(7)
O(1)–N(5)–O(3)	139.5(17)	
O(2)–N(5)–O(3)	107.3(18)	
Ru(2)–O(4)–N(6)	128.7(8)	
O(4)–N(6)–O(5)	120.0(12)	
O(4)–N(6)–O(6)	121.0(13)	
O(5)–N(6)–O(6)	119.0(13)	
Ru(1)–N(5)–O(1)		116.9(5)
Ru(1)–N(5)–O(2)		119.1(5)
Ru(2)–N(6)–O(3)		120.0(5)
Ru(2)–N(6)–O(4)		120.2(5)
O(3)–N(6)–O(4)		119.7(7)

compound **2** is similar to that of compound **1**. As seen in compound **1**, the ruthenium centers of compound **2** lie on opposite faces of the 6,6′-Me_2dppz ligand backbone. Again, the cymene methyl groups are directed towards the monodentate nitrate ligand. The Ru(1)–O(1)–N(5) and Ru(2)–O(4)–N(6) angles are larger than the ideal 120°, at 140.8(11) and 128.7(8)°, respectively. The O(1)–N(5)–O(2) and O(4)–N(6)–O(5) angles are 107.5(16) and 120.0(12)°, while the O(1)–N(5)–O(3), O(2)–N(5)–O(3), O(4)–N(6)–O(6) and O(5)–N(6)–O(6) angles are 139.5(17), 107.3(18), 121.0(13) and 119.0(13)°. Again, the steric encumbrance of the methyl groups of the Me_2dppz ligand forces the metal–pyridine bond to elongate relative to that of the metal–pyrazole; the Ru(1)–N(1) and Ru(2)–N(4) distances are 2.151(10) and 2.139(9) Å, compared with the Ru(1)–N(2) and Ru(2)–N(3) distances of 2.071(8) and 2.100(8) Å, respectively. The Ru···Ru separation of 4.420 Å and the average $Ru–C_{centroid}$ bond distance of 1.695 Å are similar to those of compound **1**. The average Ru–O distance is 2.091 Å.

*3.3. Structure of $[Ru_2(6,6'\text{-}Me_2dppz)(\eta^6\text{-}p\text{-cymene})_2(H_2O)_2](ClO_4)_3\cdot 2CH_3CH_2COCH_3$ (**3**)*

The structure of complex **3** contains the cation, three-disordered perchlorate counterions and two molecules of disordered 2-butanone solvent in the asymmetric unit. There are no unusual contacts between any of these moieties. A view of the cation is given in Fig. 3. Selected bond distances and angles are given in Table 3, while complete crystallographic details are provided in the section on supplementary data. The 'anti-facial' geometry is again present in complex **3**, with the methyl groups of the cymene ligands pointed in the same direction as the coordinated water molecule. The Ru(1)–N(1) distance of 2.170(6) Å is longer than the Ru(1)–N(2) distance of 2.091(5) Å. Similar to the above compounds, the Ru···Ru separation is 4.456 Å, and the average $Ru–C_{centroid}$ bond distance is 1.679 Å. The Ru(1)–O(1) bond distance is

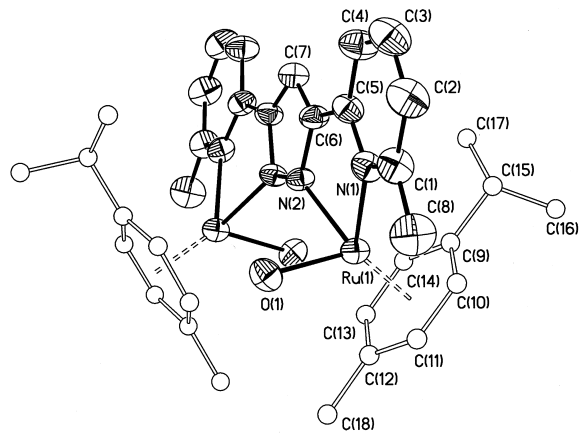


Fig. 3. Crystal structure drawing for the cation of $[Ru_2(6,6'\text{-}Me_2dppz)(\eta^6\text{-}p\text{-cymene})_2(H_2O)_2](BF_4)_3$ (**3**) with 40% probability ellipsoids. Cymene carbon atoms are shown as arbitrarily sized circles and hydrogen atoms are removed for clarity.

Table 3
Selected bond distances (Å) and angles (°) for compounds **3** and **5**

	3	**5**
Ru(1)–N(1)	2.170(6)	2.156(7)
Ru(1)–N(2)	2.091(5)	2.076(7)
Ru(2)–N(3)		2.092(7)
Ru(2)–N(4)		2.134(8)
Ru(1)–$C_{centroid}$	1.679	1.695
Ru(2)–$C_{centrois}$		1.709
Ru(1)–O(1)	2.153(5)	
Ru(1)–N(5)		2.071(9)
N(5)–C(36)		1.120(13)
C(36)–C(37)		1.51(2)
Ru(2)–N(6)		2.050(8)
N(6)–C(38)		1.113(12)
C(38)–C(39)		1.49(2)
Ru(1)–N(1)–C(1)	127.1(5)	128.0(7)
N(1)–C(1)–C(8)	121.2(7)	
N(1)–C(1)–C(14)		120.5(10)
Ru(2)–N(4)–C(13)		128.3(7)
N(5)–C(13)–C(15)		120.5(10)
N(2)–Ru(1)–O(1)	84.9(2)	
N(1)–Ru(1)–O(1)	85.3(2)	
N(1)–Ru(1)–N(2)	76.7(2)	77.2(3)
Ru(1)–N(2)–N(3)		132.4(5)
N(3)–Ru(2)–N(4)		77.4(3)
Ru(2)–N(3)–N(2)		134.7(5)
N(1)–Ru(1)–N(5)		83.5(3)
N(2)–Ru(1)–N(5)		91.8(3)
N(3)–Ru(2)–N(6)		91.0(3)
N(4)–Ru(2)–N(6)		84.5(3)
Ru(1)–N(5)–C(36)		170.5(9)
N(5)–C(36)–C(37)		174.9(14)
Ru(2)–N(6)–C(38)		172.6(9)
N(6)–C(38)–C(39)		177.2(14)

2.153(5) Å, which is a typical length for ruthenium(II) aquo complexes [34].

*3.4. Structure of [Ru_2(6,6′-Me_2dppz)(η^6-p-cymene)$_2$-(NO_2)$_2$](ClO_4)·0.5(CH_3)$_2$CO (**4**)*

The solid-state structure of complex **4** contains the cation, one disordered perchlorate counterion and one-half of an acetone solvate molecule in the asymmetric unit. There are no unusual contacts between these species. A drawing of the cation is presented in Fig. 4. The complete crystallographic data are provided in the section on supplementary data, and selected bond distances and angles are given in Table 2. Complex **4** also maintains the 'anti-facial' geometry, with the cymene methyl groups pointed in a similar direction as the nitrite ligands. The solid state structure confirms the N-bound geometry of the nitrite group with the Ru(1)–N(5) and Ru(2)–N(6) separations of 2.155(5) and 2.091(6) Å, respectively. The average Ru–N–O angle is 119.0°, and the O(1)–N(5)–O(2) and O(3)–N(6)–O(4) angles are 120.2(5) and 119.7(7)°. These angles are typical of ruthenium(II)–nitrite complexes [35]. As above, the Ru(1)–N(1) and Ru(2)–N(4) distances of 2.144(5) and 2.130(6) Å are longer than the Ru(1)–N(2) and Ru(2)–N(3) distances of 2.089(5) and 2.085(5) Å, respectively. The Ru···Ru separation is 4.468 Å, and the Ru–$C_{centroid}$ distances are 1.717 and 1.731 Å, slightly longer than those of compound **1**. The average Ru–C bond distance is 2.226 Å for compound **4**.

*3.5. Structure of [Ru_2(6,6′-Me_2dppz)(η^6-p-cymene)$_2$-(CH_3CN)$_2$](PF_6)$_2$(BF_4)·0.5(CH_3)$_2$CO (**5**)*

The asymmetric unit of compound **5** contains the cation, two hexafluorophosphate counterions (one of which is slightly disordered), one tetrafluoroborate counterion and one-half of a molecule of acetone solvent. There are no unusual contacts between any of these species. Fig. 5 displays the structure of the cation. Selected bond distances and angles are given in Table 3, and complete crystallographic data are provided in the section on supplementary data. Like the above structures, the geometry of complex **5** is 'anti-facial', with

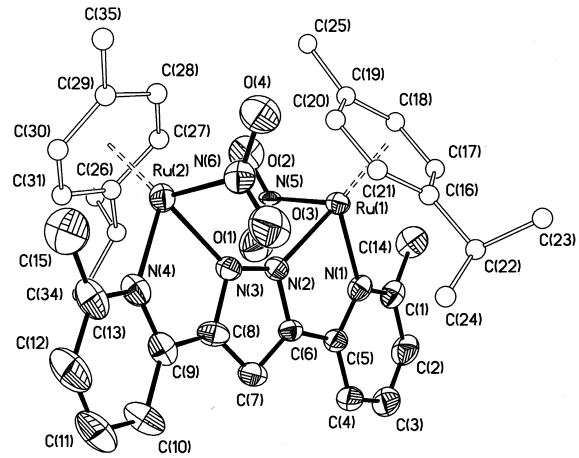


Fig. 4. Thermal ellipsoid plot (40% probability) for the cation of [Ru_2(6,6′-Me_2dppz)(η^6-*p*-cymene)$_2$(NO_2)$_2$](PF_6) (**4**). Cymene carbon atoms are shown as arbitrarily sized circles and hydrogen atoms are removed for clarity.

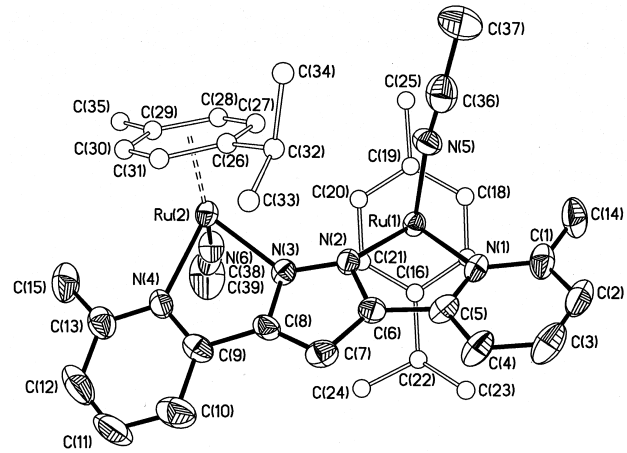


Fig. 5. Crystal structure drawing for the cation of [Ru_2(6,6′-Me_2dppz)(η^6-*p*-cymene)$_2$(CH_3CN)$_2$](BF_4)$_3$ (**5**) with 40% probability ellipsoids. Cymene carbon atoms are shown as arbitrarily sized circles and hydrogen atoms are removed for clarity.

the cymene methyl groups pointed in the same direction as the coordinated acetonitrile molecules. In agreement with complex **1**, the Ru(1)–N(1) and Ru(2)–N(4) bond distances are 2.156(7) and 2.134(8) Å, and the Ru(1)–N(2) and Ru(2)–N(3) distances are 2.076(7) and 2.092(7) Å, respectively. Similar to compound **1**, the Ru···Ru distance is 4.482 Å and the average Ru–$C_{centroid}$ bond distance is 1.702 Å. The Ru(1)–N(5) and Ru(2)–N(6) distances are 2.071(9) and 2.050(8) Å, typical for this type of complex [5,36].

*3.6. Structure of [Ru_2(NO_2-6,6′-Me_2dppz)(η^6-p-cymene)$_2$-Cl_2](PF_6)·0.25CH_2Cl_2 (**6**)*

The asymmetric unit of complex **6** contains the cation, one disordered hexafluorophosphate counterion and one-quarter of a dichloromethane solvate molecule, with no unusual contacts between these species. A view of the cation is presented in Fig. 6. Selected bond distances and angles are given in Table 1, while atomic coordinates and complete crystallographic details are provided in the section on supplementary data. As seen in all the above structures, complex **6** has an 'anti-facial' geometry. The cation of complex **6** resembles that of compound **1** with many similar bond distances and angles. The Ru(1)–N(1) and Ru(2)–N(4) bond distances are 2.132(8) and 2.161(8) Å, and the Ru(1)–N(2) and Ru(2)–N(3) distances are 2.101(7) and 2.098(7) Å, respectively. Similar to compound **1**, the Ru···Ru distance is 4.418 Å, the average Ru–C bond distance is 1.700 Å and the average Ru–Cl distance is 2.400 Å. The striking feature of this structure is the nitrated pyrazole group. The nitro group is significantly canted with respect to the pyrazole ring, with a dihedral angle defined by the nitro group and the pyrazole ring of 117.6°. The O(1)–N(5)–O(2) angle is 124.4(11)°, while the N(5)–O(1) and N(5)–O(2) separations are 1.169(11) and 1.243(12) Å and the C(7)–N(5) distance is 1.459(13) Å.

3.7. Electrochemistry

In acetonitrile, complex **1** exhibits a reversible oxidation at 1.5 V and an irreversible reduction past −1.3 V relative to Ag/AgCl. Nitration of the ligand backbone in compound **6** shifts the potential anodically with a reversible oxidation at 1.6 V and a quasi reversible reduction at −0.9 V. Given the strong electronic coupling expected between the two metals, these are likely one-electron processes. Compounds **2**, **3** (in H_2O), **4** and **5** did not exhibit reversible electrochemical behavior in the range of +1.8 to −1.8 V.

4. Discussion

All of the complexes described here possess the 'anti-facial' geometry with respect to the 6,6′-Me_2dppz ligand backbone. The preference for this arrangement is likely

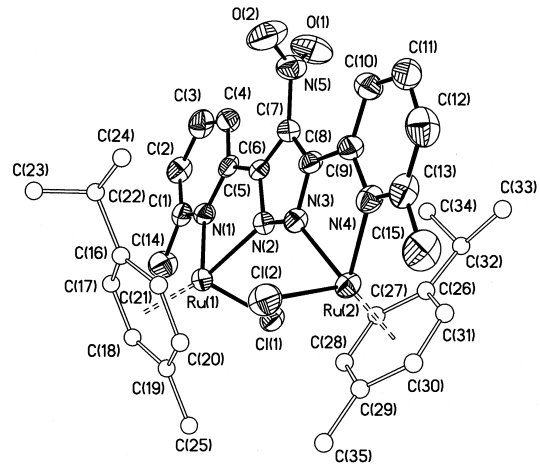
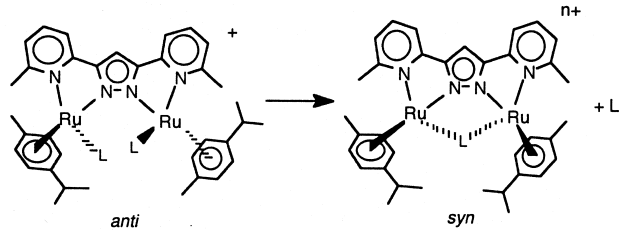


Fig. 6. Thermal ellipsoid plot (40% probability) for the cation of [Ru_2(NO_2-6,6′-Me_2dppz)(η^6-*p*-cymene)$_2Cl_2$](PF_6) (**6**). Cymene carbon atoms are shown as arbitrarily sized circles and hydrogen atoms are removed for clarity.

related to the large steric bulk of the coordinated arene. Interestingly, the analogous benzene derivative of compound **1** shows the same 'anti-facial' arrangement, indicating that the [Ru(arene)]$^{n+}$ fragment is sufficiently large to block one side of the 6,6′-Me_2dppz ligand, preventing the second metal center from entering 'syn' to the first group [37]. The lack of bridging in this arrangement precludes concerted chemistry at the small molecule site, and much effort was therefore directed at isomerizing these complexes to the 'syn' isomer (Eq. (2)):



(2)

Simple thermal isomerization of compounds **1**, **3** or **5** proved unfruitful, as did an attempted photochemical isomerization of compound **5**. Reactions to induce isomerization of compound **1** by introducing a bridging group (as in compound **2** or **4**) produced the 'anti' geometry as the only product. Further, the reactions of compound **1** with other bridging groups, including CO_3^{2-}, oxalate and N_3^-, showed either no reaction or resulted in decomposition. Alternatively, substitution reactions of the arene were also unfruitful. Unlike many Ru(II)–cymene complexes, compound **1** did not react with phosphines, pyridine or dimethylsulfoxide (DMSO) under forcing conditions and extended reaction times. Instead, only starting materials were recovered.

This lack of reactivity is in part attributed to the presence of the Me_2dppz ligand whose strong sigma donor properties stabilize the Ru–cymene bonding. The competition for π-bonding between the cymene and the Me_2dppz further explains the sluggish substitution chemistry observed for displacement of the anionic, π-basic chloride ligand in com-

pound **1**. The highly anodic Ru(III)/Ru(II) couples further reflect this property. For comparison, the loosely related $[Ru(cymene)Cl(PPh_2R)(NCCH_3)]^+$ (R = allyl or vinyl) complexes have Ru(III)/Ru(II) couples between 1.46 and 1.63 V [38]. With their good σ-donating phosphines these complexes are expected to be more electron-rich.

Another manifestation of the electron-poor nature of complexes **1**–**6** resides in their inability to form a stable nitrosyl complex. Polypyridine Ru(II)–NO_2 complexes are well known to undergo nitrite to nitrosyl conversion effectively upon protonation (Eq. (3)).

$$[Ru-NO_2]^{n+} \underset{-H^+,\ +H_2O}{\overset{+2H^+,\ -H_2O}{\rightleftharpoons}} [Ru-NO]^{n+2} \quad (3)$$

However, replacement of the polypyridine groups with the π-acidic cymene ligand likely prevents the effective backbonding necessary to stabilize a nitrosyl ligand. For example, treatment of compound **4** with HCl regenerated the chloro species (**1**), while reaction of compound **4** with aqueous $HClO_4$ produced compound **3**, and reaction of compound **4** with an acetonitrile solution of HPF_6 formed compound **5**. In each case the nitrosyl may have formed but was ultimately displaced by better donor molecules present in solution. Similarly, direct reaction of the aquo species (**3**) with NO(g) also did not produce a bound NO ligand. Lastly, reaction of compound **1** with $NOBF_4$ did not produce the anticipated nitrosyl complex, but it nitrated the 4 position of the pyrazole ring instead, leaving the metal unchanged to form compound **6**. A control reaction between Me_2dppz and $NOBF_4$ produced no reaction, indicating that the formation of compound **6** must be metal-assisted. There is precedence for formation of Ru(II)–nitrosoarene complexes [39]; however, since the corresponding Ru–nitrosyl complex could not be formed in our system, the mechanism likely resembles an electrophilic aromatic substitution by NO^+ followed by oxidation to the nitro species [40].

4.1. Conclusion

The complexes reported here show a remarkable preference for the 'anti' geometry with respect to the Me_2dppz ligand and are remarkably resistant to both isomerization and to arene substitution. Furthermore, unlike many Ru(II) complexes, conversion of the nitro ligand to nitrosyl was not achieved, nor was the attempted introduction of a NO ligand from NO(g) or NO^+.

5. Experimental

5.1. Materials

Silver tetrafluoroborate (99%) and 60% hexafluorophosphoric acid were from Acros; nitrosonium tetrafluoroborate was from Aldrich; 97.6% sodium nitrite was from Fisher; 50% *R*-(−)-α-phellandrene was from Fluka Chemika; silver nitrate was from Mallinckrodt; $RuCl_3 \cdot 3H_2O$, 99.5% ammonium hexafluorophosphate, 98% sodium tetrafluoroborate and 99% silver perchlorate monohydrate were from Strem Chemical. All chemicals were used without further purification.

^{1}H NMR spectra were obtained on a Varian Unity Plus 500 MHz spectrometer, and all spectra were referenced to tetramethyl silane. UV–Vis spectra were recorded using a HP845 diode array instrument with Teflon-stoppered quartz cells having a 1.0-cm path length. IR spectra were obtained using a Perkin-Elmer FT-IR spectrometer. Elemental analyses were carried out by Desert Analytics, Tucson, AZ. The irradiation study was carried out using a 300-W Xe lamp.

All electrochemical experiments were performed with a Bioanalytical Systems (BAS) model CV50-W electrochemical analyzer. Cyclic voltammetry (CV) was performed at 20 ± 3°C with a normal three-electrode configuration consisting of a highly polished glassy-carbon working electrode and an AgCl/Ag reference electrode containing 1.0 M KCl. The working compartment of the electrochemical cell was separated from the reference compartment by a modified Luggin capillary. All three compartments contained a 0.1 M solution of supporting electrolyte. Acetonitrile (Burdick and Jackson) was distilled from CaH_2 before use. Tetrabutylammonium hexafluorophosphate ($TBA^+PF_6^-$, from Southwest Analytical) was used as received.

5.2. Preparations

$Ru_2Cl_4(\eta^6$-*p*-cymene$)_2$ [28] and 2,2′-(1*H*-pyrazole-3,5-diyl)bis(6-methylpyridine) (6,6′-Me_2dppzH) [25–27] were synthesized according to literature procedures.

Caution: perchlorate salts are potentially explosive and should be handled with proper precautions.

*5.2.1. [Ru_2(6,6′-Me_2dppz)(η^6-*p*-cymene)$_2Cl_2$](PF_6) (1)*

$Ru_2Cl_4(\eta^6$-*p*-cymene$)_2$ (0.245 g, 0.400 mmol) and 2-Me_2dppz (0.100 g, 0.400 mmol) were refluxed under a nitrogen atmosphere with magnetic stirring for 60 h in 50 ml of 95% ethanol. The solvent was removed by rotary evaporation. The orange residue was dissolved in 20 ml of absolute ethanol, added to 10 equivalents of 99.5% NH_4PF_6 (0.655 g, 4.000 mmol), and stirred for 30 min. The mixture was cooled in an ice bath, and the orange microcrystalline precipitate was collected on a sintered-glass funnel. The solid was washed with 2-propanol and dried with diethyl ether. Recrystallization was accomplished by slowly cooling a hot acetone–2-propanol solution of the compound. Yield: 0.337 g, 90%. ^{1}H NMR [$(CD_3)_2CO$]: δ = 8.03 (apparent t, $^3J_{(HH)}$ = $^3J_{(HH)}$ = 7.5 Hz, 2H, H2), 7.89 (unresolved dd, $^3J_{(HH)}$ = 7.5 Hz, 2H, H1), 7.75 (s, 1H, H4), 7.57 (unresolved dd, $^3J_{(HH)}$ = 7.5 Hz, 2H, H3), 6.64 (unresolved dd, $^3J_{(HH)}$ = 6.0 Hz, 2H, cymene ring H), 6.20 (unresolved dd, $^3J_{(HH)}$ = 6.0 Hz, 2H, cymene ring H), 6.12 (unresolved dd, $^3J_{(HH)}$ = 6.0 Hz, 2H, cymene ring H), 5.80 (unresolved dd, $^3J_{(HH)}$ = 6.0

Hz, 2H, cymene ring H), 3.26 (s, 6H, H5), 2.64 (s, 6H, H11), 1.96 (apparent septet, $^3J_{(HH)} = {}^3J_{(HH)} = 7.0$ Hz, 2H, H6), 0.69 (d, $^3J_{(HH)} = 7.0$ Hz, 6H, cymene isopropyl H), 0.59 (d, $^3J_{(HH)} = 7.0$ Hz, 6H, cymene isopropyl H). UV–Vis [λ_{max} (nm), ε_{max} (dm^3 mol^{-1} cm^{-1})] (in CH_3OH): 430 (2.2×10^3), 327 (2.3×10^4). $C_{35}H_{41}Cl_2F_6N_4PRu_2\cdot 0.5C_8H_{18}O$ (1007.85): Calc. C, 46.77; H, 5.05; N, 5.60. Found: C, 47.01; H, 4.97; N, 6.02%.

*5.2.2. [Ru_2(6,6′-Me_2dppz)(η^6-p-cymene)$_2$(NO_3)$_2$](PF_6) (**2**)*

[Ru_2(6,6′-Me_2dppz)(η^6-*p*-cymene)$_2Cl_2$](PF_6) (0.100 g, 0.107 mmol) and 10 equivalents of $AgNO_3$ (0.364 g, 2.140 mmol) were refluxed under a nitrogen atmosphere with magnetic stirring for 72 h in 50 ml of acetone–water (4:1, v/v). The yellow–gray solution was filtered over Celite, and the filtrate was evaporated to dryness. The yellow residue was dissolved in dichloromethane and filtered over Celite to remove insoluble materials. The filtrate was evaporated to dryness. The residue was dissolved in 10 ml of methanol and added to 10 equivalents of 99.5% NH_4PF_6 (0.175 g, 1.070 mmol). The methanol was removed by rotary evaporation, the residue was dissolved in dichloromethane, and the mixture was filtered. To the filtrate was added 20 ml of 2-propanol, and the solution was reduced in volume to remove the dichloromethane. The mixture was cooled in an ice bath. The yellow precipitate was collected on a sintered-glass funnel, washed with cold 2-propanol, and dried with diethyl ether. Yield: 0.0836 g, 79%. ^{1}H NMR [$(CD_3)_2CO$]: $\delta = 8.09$ (apparent t, $^3J_{(HH)} = {}^3J_{(HH)} = 7.5$ Hz, 2H, H2), 7.94 (unresolved dd, $^3J_{(HH)} = 7.5$ Hz, 2H, H1), 7.81 (s, 1H, H4), 7.66 (dd, $^3J_{(HH)} = 7.5$ Hz, 2H, H3), 6.45 (unresolved dd, $^3J_{(HH)} = 6.0$ Hz, 2H, cymene ring H), 6.28 (unresolved dd, $^3J_{(HH)} = 6.0$ Hz, 2H, cymene ring H), 6.17 (unresolved dd, $^3J_{(HH)} = 6.0$ Hz, 2H, cymene ring H), 6.10 (unresolved dd, $^3J_{(HH)} = 6.0$ Hz, 2H, cymene ring H), 3.41 (s, 6H, H5), 2.51 (unresolved dq, 6H, H11), 0.78 (unresolved d, 6H, cymene isopropyl H), 0.66 (unresolved d, 6H, cymene isopropyl H). UV–Vis [λ_{max} (nm), ε_{max} (dm^3 mol^{-1} m^{-1})] (in CH_3OH): 425 (1.8×10^3), 319 (2.2×10^4). IR [29] (KBr): $\nu_{as}(NO_2) = 1484$ cm^{-1} (s), $\nu_s(NO_2) = 1271$ cm^{-1} (vs), $\nu(NO) = 842$ cm^{-1} (vs) (m). $C_{38}H_{46}F_6N_6O_7Cl_5PRu_2\cdot(CH_3)_2CO\cdot CHCl_3\cdot CH_2Cl_2$ (1223.18): Calc.: C, 37.3; H, 3.8; N, 6.9. Found: C, 37.07; H, 4.25; N, 6.33%.

*5.2.3. [Ru_2(6,6′-Me_2dppz)(η^6-p-cymene)$_2$(H_2O)$_2$](BF_4)$_3$ (**3**)*

This complex was prepared by the analogous procedure of Gerli et al. [6]. [Ru_2(6,6′-Me_2dppz)(η^6-*p*-cymene)$_2$-$(Cl)_2$](PF_6) (0.100 g, 0.107 mmol) and 10 equivalents of 99% $AgBF_4$ (0.421 g, 2.140 mmol) were refluxed under a nitrogen atmosphere with magnetic stirring for 72 h in 50 ml of acetone–water (4:1, v/v). The gray solution was filtered over Celite, and the solvent was removed by rotary evaporation at 30°C. The yellow–gray residue was dissolved in 20 ml of methanol, added to 10-fold excess of 98% $NaBF_4$ (0.360 g, 3.210 mmol) and evaporated to dryness. The residue was dissolved in CH_2Cl_2 and filtered over Celite to remove insoluble materials. The filtrate was added to 20 ml of 2-propanol, and the solution was reduced in volume to remove the CH_2Cl_2. To the mixture was added 30 ml of diethyl ether, and the flask was stored at 0°C for 30 min. The light yellow solid was collected on a sintered-glass funnel and dried with diethyl ether. Yield: 0.0912 g, 84%. ^{1}H NMR (D_2O): $\delta = 8.09$ (apparent t, $^3J_{(HH)} = {}^3J_{(HH)} = 8.0$ Hz, 2H, H2), 7.91 (unresolved dd, $^3J_{(HH)} = 8.0$ Hz, 2H, pyridyl H), 7.68 (unresolved dd, $^3J_{(HH)} = 8.0$ Hz, 2H, pyridyl H), 7.65 (s, 1H, H4), 6.29 (unresolved dd, $^3J_{(HH)} = 6.0$ Hz, 2H, cymene ring H), 6.18 (unresolved dd, $^3J_{(HH)} = 6.0$ Hz, 2H, cymene ring H), 6.15 (unresolved dd, $^3J_{(HH)} = 6.0$ Hz, 2H, cymene ring H), 5.67 (unresolved dd, $^3J_{(HH)} = 6.0$ Hz, 2H, cymene ring H), 3.28 (s, 6H, H5), 2.63 (s, 6H, H11), 1.80 (unresolved dq, 2H, H6), 0.73 (unresolved d, 6H, cymene isopropyl H), 0.60 (unresolved d, 6H, cymene isopropyl H). UV–Vis [λ_{max} (nm), ε_{max} (dm^3 mol^{-1} cm^{-1})] (in CH_3OH): 407 (2.6×10^3), 322 (2.0×10^4). $C_{35}H_{45}Cl_3N_4O_{14}Ru_2$ (1054.25): Calc.: C, 39.87; H, 4.30; N, 5.31. Found: C, 39.98; H, 4.75; N, 5.20%. The above compound as a perchlorate salt has also been prepared by an analogous procedure with $AgClO_4\cdot H_2O$.

*5.2.4. [Ru_2(6,6′-Me_2dppz)(η^6-p-cymene)$_2$(NO_2)$_2$](PF_6) (**4**)*

[Ru_2(6,6′-Me_2dppz)(η^6-*p*-cymene)$_2Cl_2$](PF_6) (0.100 g, 0.107 mmol) and 10 equivalents of 99% $AgBF_4$ (0.421 g, 2.140 mmol) were refluxed under a nitrogen atmosphere with magnetic stirring for 72 h in 50 ml of acetone–water (4:1, v/v). The yellow–brown solution was filtered over Celite, and the solvent was removed by rotary evaporation at 30°C. The yellow–gray residue was dissolved in 40 ml of acetone and filtered over Celite to remove insoluble materials. The yellow solution was added to 10 equivalents of $NaNO_2$ (0.151 g, 2.14 mmol) dissolved in 10 ml of water. The solution was refluxed under a nitrogen atmosphere with magnetic stirring for 48 h. The yellow–gray solution was filtered over Celite, and the solvent was removed by rotary evaporation. The yellow residue was dissolved in dichloromethane and filtered over Celite to remove insoluble materials. The filtrate was evaporated to dryness, and the residue was dissolved in methanol and added to 10 equivalents of 99.5% NH_4PF_6 (0.175 g, 1.070 mmol). The methanol was removed by rotary evaporation. The residue was dissolved in dichloromethane and filtered. To the filtrate was added 20 ml of 2-propanol, and the dichloromethane was removed by rotary evaporation. The yellow precipitate was collected on a sintered-glass funnel. The solid was washed with cold 2-propanol and dried with diethyl ether. Yield: 0.0879 g, 86%. ^{1}H NMR [$(CD_3)_2CO$]: $\delta = 8.07$ (apparent t, $^3J_{(HH)} = {}^3J_{(HH)} = 8.0$ Hz, 2H, H2), 7.98 (dd, $^3J_{(HH)} = 8.0$ Hz, $^4J_{(HH)} = 1.0$ Hz, 2H, H1), 7.89 (s, 1H, H4), 7.60 (dd, $^3J_{(HH)} = 8.0$ Hz, $^4J_{(HH)} = 1.0$ Hz, 2H, H3), 6.34 (unresolved dd, $^3J_{(HH)} = 6.0$ Hz, 2H, H9′), 6.16 (unresolved dd, $^3J_{(HH)} = 6.0$ Hz, 2H, H10), 6.12 (unresolved dd, $^3J_{(HH)} = 6.0$ Hz, 2H, H10′), 6.03 (unresolved dd, $^3J_{(HH)} = 6.0$ Hz, 2H, H9), 3.10 (s, 6H, H5), 2.71 (s, 6H, H11), 1.85 (unresolved dq, 2H, H6), 0.67 (unre-

solved d, 6H, cymene isopropyl H), 0.57 (unresolved d, 6H, cymene isopropyl H). UV–Vis [λ_{max} (nm), ε_{max} (dm^3 mol^{-1} cm^{-1})] (in CH_3OH): 398 (2.2×10^3), 326 (2.5×10^4). IR [29] (KBr): $\nu_{as}(NO_2)=1367$ cm^{-1} (s), $\nu_s(NO_2)=1311$ cm^{-1} (s), $\delta(ONO)=845$ cm^{-1} (s). $C_{35}H_{41}F_6N_6O_4PRu_2$ (956.85): Calc.: C, 43.93; H, 4.32; N, 8.78. Found: C, 43.88; H, 4.47; N, 8.61%. The above compound as a perchlorate salt has also been prepared by an analogous procedure with $AgClO_4\cdot H_2O$.

*5.2.5. [Ru_2(6,6′-Me_2dppz)(η^6-p-cymene)$_2$(CH_3CN)$_2$](BF_4)$_3$ (**5**)*

[Ru_2(6,6′-Me_2dppz)(η^6-*p*-cymene)$_2$(NO_2)$_2$](PF_6) (0.100 g, 0.105 mmol) was dissolved in 5 ml CH_3CN and 1 ml 60% HPF_6 was added to the solution dropwise. The solution was stirred for 5 min with gentle heating, cooled in an ice bath, and poured into 100 ml of diethyl ether. The precipitate was collected, redissolved in acetone and filtered. The filtrate was evaporated to dryness, and the residue was dissolved in a 5 ml CH_3CN. Diethyl ether was added to the filtrate to precipitate a light-yellow solid. The solid was filtered and washed with diethyl ether. Yield: 0.0699 g, 63%. ^{1}H NMR [$(CD_3)_2CO$]: $\delta=8.06$ (apparent t, $^3J_{(HH)}=$ $^3J_{(HH)}=7.8$ Hz, 2H, H2), 7.97 (dd, $^3J_{(HH)}=7.8$ Hz, $^4J_{(HH)}=1.1$ Hz, 2H, H1), 7.86 (s, 1H, H4), 7.59 (dd, $^3J_{(HH)}=7.8$ Hz, $^4J_{(HH)}=1.1$ Hz, 2H, H3), 6.31 (unresolved dd, $^3J_{(HH)}=6.0$ Hz, 2H, H9′), 6.17 (unresolved dd, $^3J_{(HH)}=6.3$ Hz, 2H, H10), 6.09 (unresolved dd, $^3J_{(HH)}=6.0$ Hz, 2H, H10′), 6.05 (unresolved dd, $^3J_{(HH)}=6.3$ Hz, 2H, H9), 3.11 (s, 6H, H5), 2.72 (s, 6H, H11), 1.91 (unresolved dq, 2H, H6), 0.70 (unresolved d, 6H, cymene isopropyl H), 0.64 (unresolved d, 6H, cymene isopropyl H). UV–Vis [λ_{max} (nm), ε_{max} (dm^3 mol^{-1} cm^{-1})] (in CH_3OH): 400 (2.3×10^3) and 320(2.1×10^4). $C_{39}H_{47}F_{18}N_6P_3Ru_2\cdot CHCl_3$ (1355.97): Calc.: C, 35.39; H, 3.58; N, 6.19. Found: C, 34.96; H, 3.79; N, 6.83%.

*5.2.6. [Ru_2(NO_2-6,6′-Me_2dppz)(η^6-p-cymene)$_2$$Cl_2$]($PF_6$) (**6**)*

[Ru_2(6,6′-Me_2dppz)(η^6-*p*-cymene)$_2$$Cl_2$]($PF_6$) (0.100 g, 0.107 mmol) and 3 equivalents of $NOBF_4$ (0.075 g, 0.642 mmol) were refluxed under a nitrogen atmosphere with magnetic stirring for 5 h in 20 ml of dichloromethane. The yellow solution was rotavapped to dryness, and the residue was dissolved in methanol and added to 10 equivalents of 99.5% NH_4PF_6 (0.175 g, 1.070 mmol). The solution was evaporated to dryness. The residue was dissolved in CH_2Cl_2–acetone and filtered. To the filtrate was added 15 ml of 2-propanol, and the CH_2Cl_2 was removed by rotary evaporation. The solution was cooled and the yellow precipitate was filtered and washed with diethyl ether. Yield: 0.0652 g, 62%. ^{1}H NMR [$(CD_3)_2CO$]: $\delta=8.13$ (apparent t, $^3J_{(HH)}=$ $^3J_{(HH)}=8.0$ Hz, 2H, H2), 7.83 (unresolved dd, $^3J_{(HH)}=8.0$ Hz, $^4J_{(HH)}=1.0$ Hz, 2H, pyridyl H), 7.77 (dd, $^3J_{(HH)}=8.0$ Hz, $^4J_{(HH)}=1.0$ Hz, 2H, pyridyl H), 6.48 (unresolved dd, $^3J_{(HH)}=6.0$ Hz, $^4J_{(HH)}=1.3$ Hz, 2H, cymene ring H), 6.43 (unresolved dd, $^3J_{(HH)}=6.0$ Hz, $^4J_{(HH)}=1.3$ Hz, 2H, cymene ring H), 6.26 (unresolved dd, $^3J_{(HH)}=6.0$ Hz, $^4J_{(HH)}=1.3$ Hz, 2H, cymene ring H), 5.83 (dd, $^3J_{(HH)}=6.0$ Hz, $^4J_{(HH)}=1.3$ Hz, 2H, cymene ring H), 3.32 (s, 6H, H5), 2.85 (singlet, 6H, H11), 2.12 (apparent septet, $^3J_{(HH)}=$ $^3J_{(HH)}=7.0$ Hz, 2H, H6), 0.79 (d, $^3J_{(HH)}=7.0$ Hz, 6H, cymene isopropyl H), 0.66 (d, $^3J_{(HH)}=7.0$ Hz, 6H, cymene isopropyl H). UV–Vis [λ_{max} (nm), ε_{max} (dm^3 mol^{-1} cm^{-1})] (in CH_3OH): 407 shoulder (4.5×10^3), 317 shoulder (1.5×10^4), 302 (1.9×10^4). $C_{38}H_{46}Cl_2F_6N_5O_3PRu_2\cdot0.5C_3H_6O$ (1019.77): Calc.: C, 43.90; H, 4.47; N, 6.73. Found: C, 44.38; H, 4.30; N, 7.29%.

5.3. X-ray structure and solution

Crystals were grown by slow diffusion of di-n-butyl ether into an acetone solution of compound **1**, **2** or **5**, a 2-butanone solution of compound **3** or **4** or a dichloromethane solution of compound **6**. Suitable crystals were coated with epoxy cement, mounted on a glass fiber and placed on the goniometer of a Siemens P4 diffractometer. Unit cell parameters were determined by least-squares analysis of 40 reflections with $5.15°<\theta<12.45°$ for compound **1**, 42 reflections with $4.8°<\theta<12.5°$ for compound **2**, 28 reflections with $4.83°<\theta<12.54°$ for compound **3**, 27 reflections with $5.33°<\theta<12.47°$ for compound **4**, 47 reflections with $4.83°<\theta<12.5°$ for compound **5** and 28 reflections with $4.83°<\theta<12.54°$ for compound **6**. A total of 6268 reflections were collected between $3.5°<2\theta<45°$ yielding 5054 unique reflections ($R_{int}=0.0603$) for compound **1**, while for compound **2** 6999 reflections were collected with $3.5°<2\theta<45.0°$, producing 5729 ($R_{int}=0.0327$) unique data. For compound **3**, 5497 reflections were collected with $3.5°<2\theta<45.0°$, yielding 4568 unique reflections ($R_{int}=0.0384$), and for compound **4** 8095 reflections were collected, generating 6873 unique ($R_{int}=0.0438$) reflections with $3.5°<2\theta<50.0°$. A total 10 538 data were collected for compound **5** with $3.5°<2\theta<50.0°$, producing 8784 unique data ($R_{int}=0.0571$), and 6365 data were collected with $3.5°<2\theta<45.0°$ for compound **6**, yielding 5167 unique data ($R_{int}=0.0343$).

The data were corrected for Lorentz and polarization effects. Crystal data are given in Table 4. Scattering factors and corrections for anomalous dispersion were taken from a standard source [41].

Calculations were performed using Siemens SHELXTL PLUS, version 5.03, system of programs refining on F^2. The structures were solved by direct methods. Each complex contained a positionally disordered counterion typical of room temperature structures. Simple models of all of this disorder provided satisfactory refinements. Each structure contains a solvent of crystallization. Complex **1** contains one-half of a methanol solvate, while complexes **2**, **4** and **5** each contain one-half of an acetone molecule. Complex **3** contains a methyl ethyl ketone solvate. Complex **6** contains one-quarter of a dichloromethane solvate. An absorption correction was applied using an empirical model derived from ψ scans.

Table 4
Crystallographic data for compounds **1–6** [a,b]

	1·0.5CH_3OH	**2**·0.5$(CH_3)_2CO$	**3**·2$CH_3COCH_2CH_3$	**4**·0.5$(CH_3)_2CO$	**5**·0.5$(CH_3)_2CO$	**6**·0.25CH_2Cl_2
Formula	$C_{35.5}H_{43}Cl_2F_6N_4O_{0.5}PRu_2$	$C_{36.5}H_{44}F_6N_6O_{6.5}PRu_2$	$C_{43}H_{61}Cl_3N_4O_{16}Ru_2$	$C_{36.5}H_{44}ClN_6O_{8.5}Ru_2$	$C_{40.5}H_{44}BF_{16}N_6O_{0.5}P_2Ru_2$	$C_{35.25}H_{40.5}Cl_{2.5}F_6N_5O_2PRu_2$
M (g mol^{-1})	951.75	1017.89	1198.10	940.37	1201.71	1001.97
a (Å)	15.287(2)	16.7,53(2)	16.935(2)	36.102(4)	13.864(3)	15.1002(11)
b (Å)	16.190(2)	15.481(2)	15.147(2)	10.5210(10)	21.882(3)	16.4380(13)
c (Å)	16.832(2)	17.1094(15)	20.294(2)	23.091(2)	16.989(2)	17.1379(18)
β (°)	110.677(8)	99.484(12)	95.910(10)	117.220(10)	104.380(10)	111.800(7)
V (Å^3)	3897.4(8)	4376.8(8)	5178.0(10)	7799.3(13)	4992.5(14)	3949.7(6)
ρ (g cm^{-3})	1.619	1.545	1.511	1.597	1.599	1.684
Z	4	4	4	8	4	4
Crystal system	monoclinic	monoclinic	monoclinic	monoclinic	monoclinic	monoclinic
Space group	$P2_1/n$	$P2_1/c$	$C2/c$	$C2/c$	$P2_1/n$	$P2_1/n$
μ (Mo Kα) (mm^{-1})	1.014	0.802	0.806	0.902	0.766	1.042
λ (Å)	0.71073	0.71073	0.71073	0.71073	0.71073	0.71073
Crystal size (mm)	0.10×0.54×0.10	0.26×0.48×0.44	0.48×0.08×0.38	0.18×0.42×0.39	0.08×0.62×0.42	0.06×0.80×0.22
Temperature (K)	293(2)	298(2)	293(2)	293(2)	293(2)	298(2)
Scan range (θ) (°)	1.80–22.50	1.79–22.50	1.81–24.99	1.80–25.00	1.78–25.01	1.78–22.50
No. measured reflections	6268	6999	5497	8095	10538	6356
No. unique reflections	5094	5729	4568	6873	8794	5167
No. observed reflections	4237	5095	4049	6218	7555	5167
No. refined parameters	499	588	375	533	685	569
$R1$ [$I>2\sigma(I)$]	0.0784	0.0633	0.0617	0.0575	0.0694	0.0580
$R1$ for all	0.1717	0.1121	0.1124	0.0999	0.1423	0.1022
Goodness-of-fit	1.017	1.054	1.086	1.007	1.076	1.051

[a] $wR2 = \{\sum[w(F_o^2 - F_c^2)^2] / \sum[w(F_o^2)^2]\}^{0.5}$.
[b] $R1 = \sum |F_o| - |F_c| / \sum |F_o|$.

Tuesday Mar 07 03:41 PM StyleTag -- Journal: POLY (Polyhedron) Article: 3366

Hydrogen atom positions were calculated using a riding model with a C–H distance fixed at 0.96 Å and a thermal parameter 1.2 times that of the host carbon atom. The largest peaks in the final difference maps were all small and could be ignored.

Supplementary data

Crystallographic data (excluding structure factors) for the structures reported in this paper have been deposited with the Cambridge Crystallographic Data Centre as supplementary publications CCDC 121429–121434. Copies can be obtained free of charge on application to CCDC, 12 Union Road, Cambridge CB2 1EZ, UK (fax: +44-1223-336033; e-mail: deposit@ccdc.cam.ac.uk).

Acknowledgements

Acknowledgement is made to the National Science Foundation for their generous financial support (CHE-9624281).

References

[1] F.R. Keene, D.J. Salmon, J.L. Walsh, H.D. Abruña, T.J. Meyer, Inorg. Chem. 19 (1980) 1896.
[2] D. Ooyama, N. Nagao, H. Nagao, Y. Miura, A. Hasegawa, K. Ando, F.S. Howell, M. Mukaida, K. Tanaka, Inorg. Chem. 34 (1995) 6024.
[3] C.R. Hecker, P.E. Fanwick, D.R. McMillin, Inorg. Chem. 30 (1991) 659.
[4] D.W. Pipes, T.J. Meyer, Inorg. Chem. 23 (1984) 2466.
[5] V.J. Catalano, R.A. Heck, C.E. Immoos, A. Öhman, M.G. Hill, Inorg. Chem. 37 (1998) 2150.
[6] A. Gerli, J. Reedijk, M.T. Lakin, A.L. Spek, Inorg. Chem. 34 (1995) 1836.
[7] W.R. Murphy Jr., K. Takeuchi, M.H. Barley, T.J. Meyer, Inorg. Chem. 25 (1986) 1041.
[8] A.M. El-Hendawy, A.H. Al-Kubaisi, H.A. Al-Mafada, Polyhedron 16 (1997) 3039.
[9] C.-M. Che, C.-K. Li, W.-T. Tang, W.-Y. Yu, J. Chem. Soc., Dalton Trans. (1992) 3153.
[10] W.P. Griffith, Chem. Soc. Rev. 21 (1992) 179.
[11] C.-M. Che, C. Ho, T.-C. Lau, J. Chem. Soc., Dalton Trans. (1991) 1901.
[12] W.K. Seok, T.J. Meyer, J. Am. Chem. Soc. 110 (1988) 7358.
[13] M.S. Thompson, W.F. De Giovani, B.A. Moyer, T.J. Meyer, J. Org. Chem. 49 (1984) 4972.
[14] M.S. Thompson, T.J. Meyer, J. Am. Chem. Soc. 104 (1982) 5070.
[15] A.E.M. Boelrijk, T.X. Neenan, J. Reedijk, J. Chem. Soc., Dalton Trans. (1997) 4561.
[16] E.L. Dias, R.H. Grubbs, Organometallics 17 (1998) 2758.
[17] S.J. Raven, T.J. Meyer, Inorg. Chem. 27 (1988) 4478.
[18] J.A. Gilbert, D.S. Eggleston, W.R. Murphy Jr., D.A. Geselowitz, S.W. Gersten, D.J. Hodgson, T.J. Meyer, J. Am. Chem. Soc. 107 (1985) 3855.
[19] S.W. Gersten, G.J. Samuels, T.J. Meyer, J. Am. Chem. Soc. 104 (1982) 4029.
[20] F. Meyer, A. Jacobi, B. Nuber, P. Rutsch, L. Zsolnai, Inorg. Chem. 37 (1998) 1213.
[21] A.E.M. Boelrijk, M.M. VanVelzen, T.X. Neenan, J. Reedijk, H. Kooijman, A.L. Spek, J. Chem. Soc., Chem. Commun. (1995) 2465.
[22] R. Hage, J.G. Haasnoot, J. Reedijk, R. Wang, J.G. Vos, Inorg. Chem. 30 (1991) 3263.
[23] J.-P. Collin, A. Jouaiti, J.-P. Suavage, W.C. Kaska, M.A. McLoughlin, N.L. Keder, W.T.A. Harrison, G.D. Stucky, Inorg. Chem. 29 (1990) 2238.
[24] R. Hage, J.G. Haasnoot, H.A. Nieuwenhuis, J. Reedijk, D.J.A. De Ridder, J.G. Vos, J. Am. Chem. Soc. 112 (1990) 9245.
[25] J. Pons, X. López, E. Benet, J. Casabó, F. Teixidor, F.J. Sánchez, Polyhedron 9 (1990) 2839.
[26] G. Black, E. Depp, B.B. Corson, J. Org. Chem. 14 (1949) 14.
[27] H.B. Amin, R. Taylor, J. Chem. Soc., Perkin Trans. II (1979) 624.
[28] M.A. Bennett, A.K. Smith, J. Chem. Soc., Dalton Trans. (1974) 233.
[29] K. Nakamoto, Infrared Spectra of Inorganic and Coordination Compounds, Wiley, New York, 2nd ed., 1970.
[30] S. Bhambri, D.A. Tocher, J. Chem. Soc., Dalton Trans. (1997) 3367.
[31] R.S. Bates, M.J. Begley, A.H. Wright, Polyhedron 9 (1990) 1113.
[32] F.B. McCormick, D.D. Cox, W.B. Gleason, Organometallics 12 (1993) 610.
[33] D. Sellmann, K. Engl, T. Gottschalk-Gaudig, F.W. Heinemann, Eur. J. Inorg. Chem. (1999) 333.
[34] Y. Sun, N.J. Taylor, A.J. Carty, Inorg. Chem. 32 (1993) 4457.
[35] C.A. Bessel, R.F. See, D.L. Jameson, M.R. Churchill, J. Chem. Soc., Dalton Trans. (1993) 1563.
[36] O.Y. Carreón, M.A. Leyva, J.M. Fernández-G., A. Pénicaud, Acta Crystallogr., Sect. C 53 (1997) 301.
[37] Unpublished results.
[38] K.D. Redwine, H.D. Hansen, S. Bowley, J. Isbell, D. Vodak, J.H. Nelson, Synth. React. Inorg. Met.-Org. Chem. (in press).
[39] W.L. Bowden, W.F. Little, T.J. Meyer, J. Am. Chem. Soc. 96 (1974) 5605.
[40] H.E. Smith, P. Satai, The Chemistry of Amino, Nitroso and Nitro Compounds and Their Derivatives, Wiley, New York, 1982, p. 999
[41] International Tables for X-Ray Crystallography, Kynoch Press, Birmingham, vol. 4, 1974.

PERGAMON

www.elsevier.nl/locate/poly

Polyhedron 19 (2000) 487–493

POLYHEDRON

Water as hydride source in the reduction of nitrobenzene to aniline catalyzed by *cis*-[Rh(CO)$_2$(2-picoline)$_2$](PF$_6$) in aqueous 2-picoline under CO atmosphere: kinetics study

Clementina Longo* [1, a], Juan Alvarez [b], María Fernández [b], Alvaro J. Pardey* [2, b], Sergio A. Moya [c], Pablo Baricelli [d], Millan M. Mdleleni [e]

[a] *Centro de Investigación y Desarrollo de Radiofármacos, Facultad de Farmacia, Universidad Central de Venezuela, Caracas, Venezuela*
[b] *Escuela de Química, Facultad de Ciencias, Universidad Central de Venezuela, Caracas, Venezuela*
[c] *Departamento de Química Aplicada, Facultad de Química y Biología, Universidad de Santiago de Chile, Casilla 307-2, Santiago, Chile*
[d] *Centro de Investigaciones Químicas, Facultad de Ingeniería, Universidad de Carabobo, Valencia, Venezuela*
[e] *Department of Chemistry, University of California, Santa Barbara, CA 93106, USA*

Received 10 November 1999; accepted 9 December 1999

Abstract

The *cis*-[Rh(CO)$_2$(2-picoline)$_2$](PF$_6$) complex is active for the catalytic reduction of nitrobenzene to aniline in aqueous 2-picoline solution under water gas shift reaction conditions. The catalytic activities for this system were studied as functions of the reaction parameters (P(CO), [Rh]$_{tot}$, and T). The nitrobenzene reduction rate displays a first-order dependence on CO pressure, P(CO), over the range 0–1.9 atm at 80, 100 and 120°C. The kinetics behavior with respect to P(CO) leads to the proposal that addition of CO to the catalytic species precedes the rate-limiting step. The catalytic activity proved to be non-linear in total rhodium concentration, [Rh]$_{tot}$, over the range 5–60 mM. This observation was interpreted in terms of the presence of active mononuclear and polynuclear rhodium species in the system, the mononuclear species being the more active for nitrobenzene reduction. In situ FT-IR spectroscopic study confirms the presence of rhodium species with terminal and bridging carbonyls. ©2000 Elsevier Science Ltd All rights reserved.

Keywords: Nitrobenzene catalytic reduction; Rhodium complexes; 2-picoline; Water gas shift reaction

1. Introduction

The reduction of nitroarenes catalyzed by transition metal complexes under CO/H$_2$O (Eq. (1)) has been reported in the literature [1–14]. This reaction has been proposed to proceed via a multi-step catalytic scheme [15]. However, a detailed kinetics study has not yet been carried out.

$$\text{R-NO}_2 + 3\text{CO} + \text{H}_2\text{O} \rightarrow \text{R-NH}_2 + 3\text{CO}_2 \quad (1)$$

The rhodium(I) complexes of *cis*-[Rh(CO)$_2$(amine)$_2$](PF$_6$) (amine = 4-picoline, 2-picoline, pyridine, or 2,6-lutidine) in aqueous amine, 2/8, v/v, [Rh] = 10 mM, and P(CO) = 0.9 atm at 100°C catalyzed the water gas shift reaction [16] (WGSR, Eq. (2)). Proposed mechanisms for these systems involve the formation of rhodium hydride intermediates (Rh-H), which were confirmed by in situ ^{1}H NMR spectroscopic studies. So, it should be possible to intercept this Rh-H species by reaction with nitrobenzene to generate rhodium nitrobenzene intermediates. Under WGSR conditions, the latter would expect to react further to give aniline.

$$\text{CO} + \text{H}_2\text{O} \rightleftarrows \text{CO}_2 + \text{H}_2 \quad (2)$$

Furthermore, research in our group [14] demonstrated the selective reduction of nitrobenzene to aniline by rhodium(I) complexes, *cis*-[Rh(CO)$_2$(amine)$_2$](PF$_6$) (amine = 4-picoline, 3-picoline, 2-picoline, pyridine, 3,5-lutidine or 2,6-lutidine), dissolved in aqueous amine, under WGSR conditions. In addition, the role of amine was examined and the formation of aniline (yield in mmol, after 3 h) followed the order 2-picoline (0.52) > 2,6-lutidine (0.46) > 3,5-lutidine (0.44) > 3-picoline (0.35) > 4-picoline (0.13) > pyridine (0.08). Reaction conditions were as follows: 10 ml of amine/H$_2$O, 2/8, v/v, 0.26 ml of nitrobenzene (2.5×10^{-3} mol), [Rh] = 10 mM, and P(CO) = 0.9 atm at 100°C.

[1] *Corresponding author. Fax: +582-605 2707; e-mail: clongo@sagi.ucv.edu.ve
[2] *Corresponding author. Fax: +582-605 2240; e-mail: apardey@strix.ciens.ucv.ve

0277-5387/00/$ - see front matter ©2000 Elsevier Science Ltd All rights reserved.
PII S0277-5387(99)00392-7

In this report, quantitative studies are described on the effect of variation of the carbon monoxide pressure $P(CO)$, rhodium concentration [Rh], and temperature T on the reduction of nitrobenzene to aniline catalyzed by *cis*-$[Rh(CO)_2(2\text{-picoline})_2](PF_6)$ dissolved in aqueous 2-picoline under water gas shift reaction conditions. Also, these data are discussed in terms of a possible mechanism.

2. Experimental

2.1. Materials

2-Picoline (2-pic) was obtained from Aldrich and distilled from KOH. Nitrobenzene (RNO_2) was distilled in H_2SO_4 (1 M) and redistilled in $CaCl_2$ before use. Double distilled water was used for the preparation of solutions. The gas mixtures CO/CH_4 (95.8/4.2%, v/v), He/H_2 (91.4/8.6%) and $CO/CH_4/CO_2/H_2$ (84.8/5.1/5.3/4.8%, v/v) were purchased from BOC Gases. *Cis*-$[Rh(CO)_2(2\text{-pic})_2](PF_6)$ was prepared by the method reported by Denise and Pannetier [17].

2.2. Instrumentation

Infrared spectra were recorded on a Perkin-Elmer 1760X-FT spectrophotometer. Analyses of gas samples from kinetics runs were performed as described previously [18] on a Hewlett-Packard 5890 series II programmable (ChemStation) gas chromatograph (GC) fitted with a thermal conductivity detector. The column used was Carbosieve-B (80-100) mesh obtained from Hewlett-Packard. The column temperature was programmed from 60–175°C at a flow rate of 50 $ml \cdot min^{-1}$ using a He/H_2 mixture as the carrier gas. Calibration curves were prepared periodically for H_2, CO, CO_2, and CH_4. The individual analyses were found to be accurate and reproducible to within less than 10%.

Liquid phase reaction products were analyzed using a Hewlett-Packard 5890 series II programmable gas chromatograph fitted with 3% OV-10N Supelcoport (mesh 80-100) column and flame ionization detector using *ortho*-xylene as an internal standard, and identified by co-injection on a Hewlett-Packard 5890 series II programmable gas chromatograph-mass spectrometer fitted with Pona capillary column (50 m).

2.3. Batch reactor procedures

Kinetics runs were conducted in an all-glass reactor vessel described in detail in a previous publication [18]. In a typical kinetics experiment, a given amount (typically 0.1 mmol) of *cis*-$[Rh(CO)_2(2\text{-pic})_2](PF_6)$ and 10 ml of 80% aqueous 2-picoline were added to the glass reactor vessel, then the solution was degassed by three freeze–pump–thaw cycles. The reaction vessel was charged with CO/CH_4 mixture at the desired CO partial pressure (typically 0.9 atm), then suspended in a circulating thermostated glycerol oil bath set at a desired temperature (typically 100°C). The specified reaction temperatures were maintained at ± 0.5°C by continuous stirring of the oil bath and the reaction mixture which was provided with a Teflon-coated magnetic stirring bar.

After reaching a constant WGSR activity [16], a given amount (typically 0.26 ml, 2.4×10^{-3} mol) of nitrobenzene was added to the reaction vessel. Subsequent to addition of nitrobenzene, the glass reactor vessel was charged with CO/CH_4 at the desired CO pressure and placed in the heated oil bath for a given time and at a given temperature. At the end of the desired reaction time, gas samples (1.0 ml) were removed from the reactor vessel in a manner similar to that described previously for the WGSR catalytic test [16] and analyzed by GC. Also, liquid samples were removed and analyzed by GC and GC-MS. The CH_4 was used as internal standard to allow calculation of absolute quantities of CO consumed and CO_2 produced, during a time interval. In addition, calibration curves were prepared periodically for CO, CH_4, H_2, and CO_2, and their validities were checked by analyzing known gas mixtures.

3. Results and discussion

3.1. Catalysis study of the nitrobenzene reduction

The rhodium(I) complex *cis*-$[Rh(CO)_2(2\text{-pic})_2](PF_6)$ in 80% aqueous 2-picoline generates a system that shows higher catalytic activity for nitrobenzene reduction than those found for the other ligand and solvent systems studied (pyridine, 4-picoline, 3-picoline, 2,6-lutidine or 3,5-lutidine) under the same reaction conditions. Also, the effect of varying the ratio $[RNO_2]/[Rh]$ was examined in the range 2500 to 25 at $P(CO) = 0.9$ atm and $T = 100$°C and the reaction rate was found to be almost independent of the initial concentration of nitrobenzene within this range [14]. Furthermore, aniline formation (the only organic product detected by analyzing the catalysis liquid phase) and CO_2 formation (the only gas product detected by analyzing the catalysis gas phase) were equal stoichiometrically (within experimental uncertainty) as required by Eq. (1) [14]. For example, analyses of liquid samples using *ortho*-xylene as internal standard were carried out to check the consistency of these results and showed that there was no statistically significant difference between both GC methods for a confidence level of 95% [19].

Control experiments show catalytic inactivity toward both WGSR and nitrobenzene reduction when 10 ml of 80% aqueous 2-picoline solution under $P(CO) = 0.9$ atm at 100°C for 3 h is tested in the absence of the *cis*-$[Rh(CO)_2(2\text{-pic})_2](PF_6)$ complex. Also, this Rh/2-pic catalytic system exhibits no WGSR activity (i.e. no molecular hydrogen is formed) in the presence of nitrobenzene. Fig. 1 shows a plot of turnover number (moles aniline/moles Rh) versus reaction time for $[Rh] = 10$ mM and $P(CO) = 0.9$ atm at 100°C.

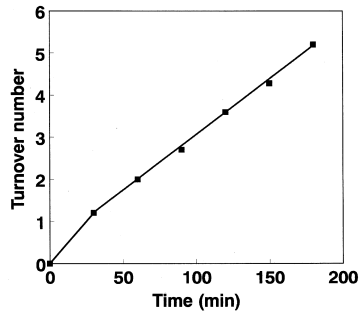


Fig. 1. Plot of turnover number (mol aniline formed/mol Rh) vs. reaction time. Reaction conditions: 0.26 ml of nitrobenzene, [Rh] = 10 mM, [nitrobenzene]/[Rh] = 25, $P(CO) = 0.9$ atm, at 100°C and 10 ml of 2-picoline/water, 8/2, v/v. (Line drawn for illustrative purposes only).

The total turnover as a function of time increased from 1.2 (5% conversion) at 30 min to 5.2 (20% conversion) at 3 h.

3.2. FT-IR characterization

The FT-IR spectrum of an active Rh/2-pic catalyst solution ([Rh] = 100 mM), in the presence of nitrobenzene, after being exposed to CO (0.9 atm) and heated at 100°C for 1 h, displays six bands in the ν_{CO} region at 2083(m), 2009(s), 1998(s), 1990(vs), 1964(m, sh), 1932(m) cm^{-1} characteristic of CO coordinated terminally to Rh, and one band at 1813(s) cm^{-1} characteristic of bridging CO.

Furthermore, the IR spectrum, both in pyridine solution and in the solid state, of the well characterized polynuclear anionic rhodium(−I), $[Rh_5(CO)_{13}(py)_2]^-$ complex shows five bands in the CO stretching region at 2040(m), 2011(m), 1980(vs) 1818(m), and 1756(m) cm^{-1}. The X-ray structure of this compound shows five Rh atoms at the vertices of a trigonal bipyramid, seven terminal and six edge-bridging carbonyls and two coordinated pyridine molecules to one Rh [20]. In addition, Fachinetti et al. [21] demonstrated that this complex was accumulated during catalysis of the WGSR by *cis*-$[Rh(CO)_2(py)_2](PF_6)$ or $RhCl_3 \cdot 3H_2O$/80% aqueous pyridine systems.

On the other hand, the solid state IR spectrum of mononuclear cationic rhodium(I), *cis*-$[Rh(CO)_2(2\text{-pic})_2](PF_6)$ complex presents two bands in the CO stretching region at 2080(s) and 2010(s) cm^{-1} characteristic of CO coordinated terminally to Rh(I) [17]. Also, the solid state IR spectrum of rhodium(I), $[Rh(CO)(py)_3](PF_6)$ complex presents one band in the CO stretching region at 1993 cm^{-1} characteristic of a CO coordinated terminally to Rh(I) [20].

Thus, based on analysis of the number as well as the position of the CO stretching bands of the Rh/2-pic catalytic active solution, we suggest the presence of mononuclear cationic *cis*-$[Rh(CO)_2(2\text{-pic})_2]^+$ (bands at 2083 and 2009 cm^{-1}), $[Rh(CO)(2\text{-pic})_3]^+$ (band at 1998 cm^{-1}) and polynuclear anionic rhodium(−I) complexes of the type $[Rh_5(CO)_x(2\text{-pic})_y]^-$ (bands at 1990, 1964, 1932, and 1814 cm^{-1}) with bridging carbonyls as reaction intermediates. These assignments are consistent with the reported results of Fachinetti et al. [20,21] and Denise and Pannetier [17].

3.3. Kinetics study of the nitrobenzene reduction

For this highly active Rh/2-pic system the effects of varying the carbon monoxide pressure $P(CO)$, the rhodium concentration [Rh], and the temperature T on the nitrobenzene reduction were explored. Owing to simplicity and speed of analysis of gaseous samples, TF(aniline) kinetics data reported in Tables 1 and 2 and Figs. 2–4 are based on CO_2 production. These were confirmed periodically by analyzing the liquid phase. The results of Table 1 represent the average value of duplicate runs performed under identical experimental conditions. The calculated kinetics activity defined as TF(aniline) (TF(aniline) = mol aniline (mol Rh 24 h)$^{-1}$) was reproducible to within less than 10% for a series of experimental runs. In addition, the TF(aniline) for the kinetics runs were determined for short periods (3 h or less) where $P(CO)$, $[H_2O]$ and [nitrobenzene] were essentially constant, diminishing by less than 20% overall. Hence, possible shifts in $P(CO)$-, $[H_2O]$- and [nitrobenzene]-dependent equilibria among the catalyst component during a run were minimized owing to the near constancy of $P(CO)$, $[H_2O]$ and [nitrobenzene]. On the other hand, the highest value

Table 1
Effect of carbon monoxide pressure on nitrobenzene reduction catalysis by *cis*-$[Rh(CO)_2(2\text{-pic})_2](PF_6)$ in aqueous 2-picoline under CO/H_2O [a]

$P(CO)$ (atm)	T (°C)	CO_2 [b] (mmol)	Aniline [c] (mmol)	TF (aniline) [d]
0.5	80	0.35	0.11	14
0.7	80	0.57	0.19	22
0.9	80	0.86	0.29	34
1.2	80	1.03	0.34	41
1.5	80	1.04	0.35	56
1.7	80	0.80	0.26	62
1.9	80	0.95	0.32	75
0.5	100	0.63	0.21	18
0.7	100	0.96	0.32	27
0.9	100	1.59	0.53	41
1.2	100	1.68	0.56	47
1.5	100	2.04	0.68	65
1.9	100	2.97	0.90	85
0.5	120	0.31	0.15	26
0.7	120	0.49	0.64	40
0.9	120	0.69	0.23	57
1.2	120	0.98	0.33	79
1.5	120	1.25	0.42	101
1.7	120	1.41	0.47	114
1.9	120	1.66	0.55	132

[a] [nitrobenzene]/[Rh] = 25, 0.26 ml of nitrobenzene, [Rh] = 10 mM, 8 ml of 2-picoline and 2 ml of H_2O.
[b] Yield of CO_2 formed after 3 h or less of continuous heating in order to keep the conversion less than 20%.
[c] Selectivity > 99%. Based on CO_2 formed.
[d] TF(aniline) = mol aniline (mol Rh 24 h)$^{-1}$. Experimental uncertainty < 10%.

Table 2
Effects of rhodium concentration and temperature on nitrobenzene reduction catalysis by *cis*-[Rh(CO)$_2$(2-pic)$_2$](PF$_6$) in aqueous 2-picoline under CO/H$_2$O [a]

[Rh] (mM)	T (°C)	Nitrobenzene (ml)	CO_2 [b] (mmol)	Aniline [c] (mmol)	TF(aniline) [d]
5	100	0.13	1.35	0.45	72
10	100	0.26	1.59	0.53	41
20	100	0.52	2.46	0.82	33
30	100	0.78	2.58	0.86	23
40	100	1.04	2.70	0.90	18
50	100	1.30	2.82	0.94	15
60	100	1.56	3.01	1.00	13
10	70	0.26	0.87	0.29	32
10	80	0.26	1.32	0.44	35
10	90	0.26	1.44	0.48	39
10	100	0.26	1.59	0.53	41
10	110	0.26	1.74	0.58	46
10	120	0.26	2.10	0.70	56
10	130	0.26	2.46	0.82	65
5	130	0.13	3.82 [e]	1.28 [e]	200 [e]

[a] [nitrobenzene]/[Rh] = 25, 8 ml of 2-picoline, 2 ml of H_2O and $P(CO) = 0.9$ atm.
[b] Yield of CO_2 formed after 3 h or less of continuous heating in order to keep the conversion less than 20%.
[c] Selectivity > 99%. Based on CO_2 formed.
[d] TF(aniline) = mol aniline (mol Rh 24 h)$^{-1}$. Experimental uncertainty < 10%.
[e] $P(CO) = 1.9$ atm.

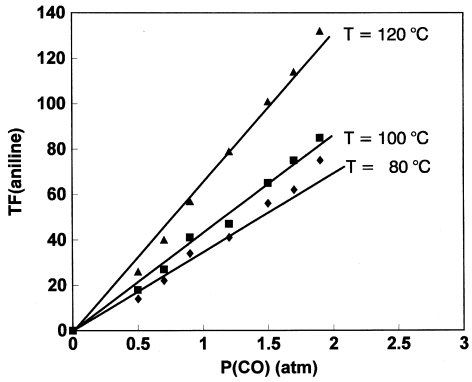


Fig. 2. Effect of carbon monoxide pressure. Reaction conditions: 0.26 ml of nitrobenzene, [Rh] = 10 mM, [nitrobenzene]/[Rh] = 25, at T = 80, 100 and 120°C and 10 ml of 2-picoline/water, 8/2, v/v. (Lines drawn for illustrative purposes only).

TF(aniline) = 200 day^{-1} (89% conversion) was achieved under optimal conditions, e.g. [Rh] = 5 mM, $P(CO) = 1.9$ atm at 130°C for 3 h (Table 2).

3.3.1. Effect of carbon monoxide pressure

Fig. 2 is a plot of TF(aniline) versus $P(CO)$ for [Rh] = 10 mM at 80, 100 and 120°C (Table 1). A linear dependence of TF(aniline) on $P(CO)$ variation in the range of the study was noted, indicating that the reaction is first order in [CO]. In addition, this was confirmed by plotting log TF(aniline) versus log $P(CO)$ in which slopes with values of 1.2, 1.1 and 1.2 were observed at 80, 100 and 120°C, respectively. This clearly establishes a first-order dependence on $P(CO)$ in the range 0–1.9 atm. Similar first-order [CO] behavior was reported in the catalysis of the WGSR by Baker et al. [22] and by Pardey and Ford [16].

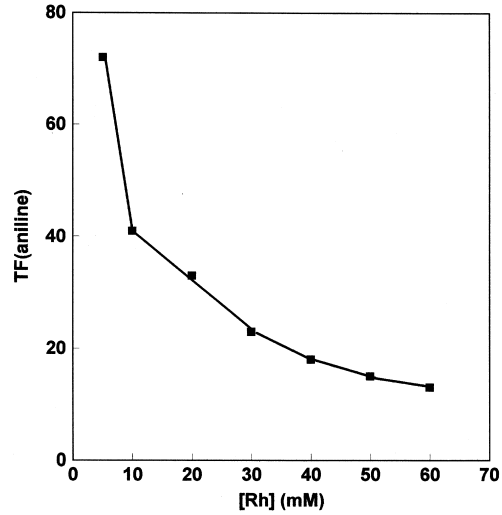


Fig. 3. Effect of rhodium concentration. Reaction conditions: 0.13–1.56 ml of nitrobenzene, [nitrobenzene]/[Rh] = 25, $P(CO) = 0.9$ atm at 100°C and 10 ml of 2-picoline/water, 8/2, v/v. (Line drawn for illustrative purposes only).

Based on the first order in [CO] we suggest a possible mechanism in that the rate-limiting step (k_2) is preceded by coordination of CO, e.g.

$$[RNO_2\text{-Rh}]^+ + CO \overset{k_1}{\rightarrow} [RNO_2\text{-Rh-CO}]^+ \overset{k_2}{\rightarrow} [Rh]^+ + \text{products} \quad (3)$$

The rate law ($r_{aniline}$) for such behavior would be:

$$r_{aniline} = k_1 k_2 P(CO)[Rh]_{tot} \quad (4)$$

where $[Rh]_{tot} = [RNO_2\text{-Rh}]^+ + [RNO_2\text{-Rh-CO}]^+$ and k_1

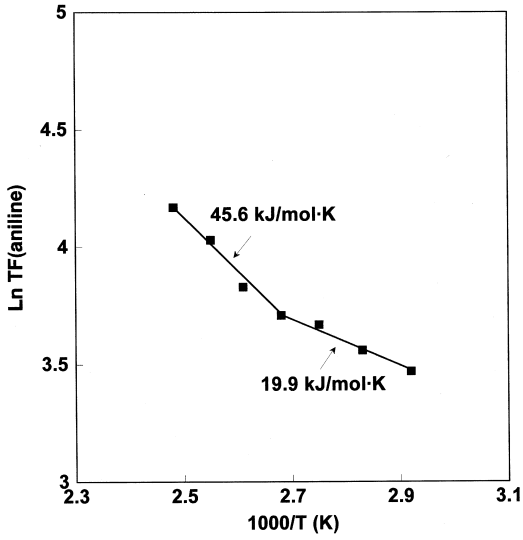


Fig. 4. Arrhenius plot for nitrobenzene reduction. Reaction conditions: 0.26 ml of nitrobenzene, [Rh] = 10 mM, [nitrobenzene]/[Rh] = 25, $P(CO) = 0.9$ atm and 10 ml of 2-picoline/water, 8/2, v/v.

includes $[RNO_2]$ and the solubility of CO in the medium. The above expression (Eq. (4)) can be reduced to:

$$TF(\text{aniline}) = k_1 k_2 P(CO) \quad (5)$$

For this kinetics model, plots of *TF*(aniline) versus $P(CO)$ should be linear with slopes of k_1k_2 and zero intercept. Indeed, these plots are linear at 80, 100 and 120°C with nearly zero intercept value as predicted by Eq. (5).

3.3.2. Effect of rhodium concentration

Runs were carried out for a series of different rhodium concentrations over the range 5–60 mM. The amount of nitrobenzene was varied from 0.13 at [Rh] = 5 mM to 1.56 ml at [Rh] = 60 mM in order to keep the ratio [nitrobenzene]/[Rh] = 25 in all runs (Table 2).

A typical kinetics run involved determining the reaction rate defined as turnover frequency *TF*(aniline) as a function of [Rh] under $P(CO) = 0.9$ atm at 100°C. Fig. 3 is a plot of the *TF*(aniline) values versus [Rh]. An increase in [Rh] from 5 to 40 mM resulted in a decrease in *TF*(aniline), followed by nearly constant values at higher [Rh]. The results indicate that the reaction rate is not first order in the [Rh] range 5–60 mM, and suggest that the active species may be present in several forms having different nuclearities (mononuclear and polynuclear) with mononuclear species being the more active. This suggestion is strongly supported by the in situ FT-IR data discussed above and by similar results reported for the homogeneous WGSR catalysts *cis*-$[Rh(CO)_2(4\text{-pic})_2](PF_6)$ and $RhCl_3 \cdot 3H_2O$ both dissolved in aqueous 4-picoline. The dependence of the rates on [Rh] complex in both batch [16] and continuous flow reactors [23] suggested the presence of at least two different active species in solution; in situ ^{13}C NMR and IR spectral analyses were consistent with this explanation. Based on their results, Ford and co-workers concluded that the active species were mononuclear and polynuclear in equilibrium, where the mononuclear species showed a higher activity. Furthermore, Fachinetti et al. in their study of WGSR catalysis by *cis*-$[Rh(CO)_2(py)_2](PF_6)$ and $RhCl_3 \cdot 3H_2O$, both dissolved in aqueous pyridine, proposed a catalytic cycle where the mononuclear *cis*-$[Rh(CO)_2(py)_2]^+$ and the polynuclear $[Rh_5(CO)_{13}(py)_2]^-$ are the active species [21].

3.3.3. Effect of temperature

In order to determine the activation parameters for the reduction of nitrobenzene catalyzed by *cis*-$[Rh(CO)_2(2\text{-pic})_2](PF_6)$ in 80% aqueous 2-picoline, *TF*(aniline) values were measured at various temperatures (Table 2). Fig. 4 displays a plot of ln *TF*(aniline) versus $1/T$ for [Rh] = 10 mM at $P(CO) = 0.9$ atm. This Arrhenius plot is concave in the 70–130°C range and can be fitted with two curves. A lower activation energy ($E_{a1} = 19.9$ kJ mol^{-1} K^{-1}) was calculated at temperatures below 100°C; temperatures greater than 100°C gave a higher energy ($E_{a2} = 45.6$ kJ mol^{-1} K^{-1}). Arrhenius plots which are concave upwards suggest a change in the rate-limiting step between two competitive reaction pathways, with the reaction path with the higher activation energy being favored at high temperatures and the reaction path with the lower activation energy being predominant at low temperatures [24].

It was suggested from the rhodium concentration studies that an equilibrium between the two kinds of rhodium active species, mononuclear and polynuclear, was established under the reaction conditions. It can also be envisioned that upwards segmentation of the Arrhenius plot could result when the nitrobenzene reduction is catalyzed by both mononuclear and polynuclear rhodium species with different activation energy pathways, as observed in the present study. If the polynuclear species are favored at low temperatures, a possible explanation is that E_{a1} represents the catalytic pathway with these species at low temperatures.

Non-linear Arrhenius plots similar to that reported here have previously been observed for the WGSR catalyzed by $RhCl_3 \cdot 3H_2O$ in 80% aqueous 4-picoline [20]. Recently Ford and co-workers [25] reported the hydrogenation and hydroformylation of alkenes catalyzed by polymer-anchored rhodium complexes under WGSR conditions. The temperature dependence also follows a segmented Arrhenius plot.

Furthermore, other factors such as variation in the oxidation state of these rhodium complexes may be responsible for curvatures in the Arrhenius plot. For example, the rate-limiting step of catalysis between these two competitive cationic mononuclear Rh and anionic polynuclear Rh complexes may not be the same owing to the different charge of these complexes [26].

3.4. Mechanistic consideration

The evaluation of the mechanism for aniline formation by solutions prepared from *cis*-$[Rh(CO)_2(2\text{-pic})_2](PF_6)$ in 80% aqueous 2-picoline and nitrobenzene in CO shows some

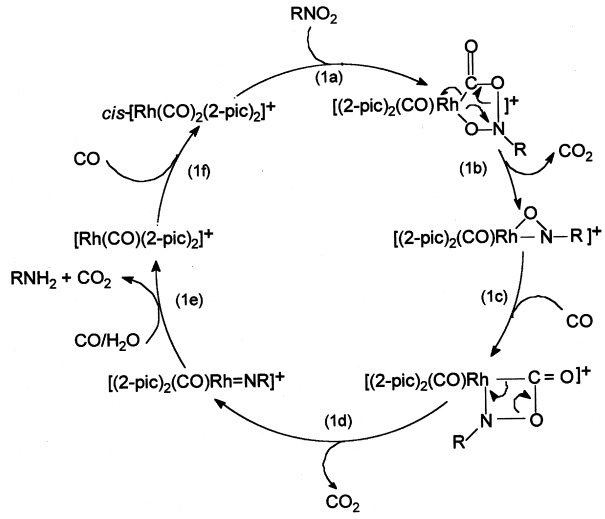
key features. First, aniline was the only organic product detected. Second, IR spectroscopy studies of the catalytic solution point to the presence of both cationic mononuclear and anionic polynuclear rhodium complexes as the predominant species. Third, kinetics study indicates that the reaction is first order in [CO] and pseudo-first order in [RNO_2]. Fourth, the rhodium concentration and temperature studies suggest a mononuclear–polynuclear equilibrium between active rhodium species, under nitrobenzene reduction conditions. Fifth, catalytic schemes for the reduction of nitrobenzene to aniline have been proposed in which nitrobenzene cycloaddition to a metal carbonyl complex is an important first step [15]. In addition, kinetics study related to the reaction between nitroarenes and [Ru(dppe)$(CO)_3$] where dppe = 1,2-bis(diphenylphosphino)ethane show a first-order reaction on each reagent. An intermediate identified as [Ru(dppe)$(CO)_2(\eta^2$-ONR)] was reported [27]. Given the above, the reaction mechanism depicted in Scheme 1 is proposed for the reduction of nitrobenzene to aniline catalyzed by the most active mononuclear Rh species.

In Scheme 1, the cycloaddition (1a) of the nitro group to the Rh–CO bond followed by elimination of CO_2 leads to the formation of rhodium nitrosobenzene [Rh(CO)$(2\text{-pic})_2(\eta^2$-ONR)]$^+$ complex (1b) [27]. Insertion of one CO molecule to the Rh–O bond (1c) forms the [Rh(CO)$(2\text{-pic})_2(\eta^2$-O(CO)NR)]$^+$ complex.

The formation of [Rh(CO)$(2\text{-pic})_2(\eta^2$-O(CO)NR)]$^+$ specie as the rate-limiting step (1c) would rationalize the first-order dependence of *TF*(aniline) on *P*(CO). Decarboxylation of the rhodium [Rh(CO)$(2\text{-pic})_2(\eta^2$-O(CO)-NR)]$^+$ (1d) generates a rhodium-nitrene complex [Rh(CO)$(2\text{-pic})_2$(NR)]$^+$ and CO_2. Hydrogenation (1e) of this rhodium-nitrene species, probably by the Rh-H species formed under conditions similar to the WGSR, affords aniline, CO_2 and the coordinatively unsaturated [Rh(CO)$(2\text{-pic})_2$]$^+$ complex. Coordination of CO to the latter would give the *cis*-[Rh$(CO)_2(2\text{-pic})_2$]$^+$ complex to close the catalytic cycle (1f). An analogous cycle may be proposed for the polynuclear Rh complexes.

4. Conclusions

The following conclusions have been drawn from catalytic studies of the reduction of nitrobenzene by *cis*-[Rh$(CO)_2(2\text{-pic})_2$](PF_6) dissolved in aqueous 2-picoline under conditions analogous to those for the WGSR. The FT-IR and kinetics study of the Rh/(2-pic) system suggest the presence of rhodium carbonyl compounds with different nuclearities and different oxidation state numbers as reaction intermediates. The Rh/(2-pic) system shows a first-order dependence of the rate on *P*(CO) and non-linear dependence of the rate on Rh concentration. Finally the effect of variation of Rh concentration and temperature on catalytic activity can be explained on the basis of the presence of at least two kinds of rhodium species with different nuclearities and oxidation states.



Scheme 1.

Acknowledgements

CDCH-UCV (Proy. 06.10.3401.96 and AI. 03.12. 4232.98) and CONICIT-Venezuela (S1-95001662 and S1-2435, GC) provided financial support for this research. SAM thanks FONDECYT-Chile and PB thanks CODECIHT-UC for support.

References

[1] Y. Shvo, D. Czarkie, J. Organomet. Chem. 368 (1989) 357.
[2] K. Nomura, M. Ishino, M. Hazama, J. Mol. Catal. 66 (1991) L19.
[3] K. Nomura, M. Ishino, M. Hazama, J. Mol. Catal. 78 (1993) 273.
[4] K. Nomura, J. Mol. Catal. 73 (1992) L1.
[5] K. Kaneda, H. Kuwahara, T. Imanaka, J. Mol. Catal. 88 (1994) L267.
[6] V. Macho, L. Vojeek, M. Schmidtova, M. Harustiak, J. Mol. Catal. 88 (1994) 177.
[7] A. Ben Taleb, G. Jenner, J. Mol. Catal. 91 (1994) L149.
[8] M.M. Mdleleni, R.G. Rinker, P.C. Ford, J. Mol. Catal. 89 (1994) 283.
[9] F. Ragaini, M. Pizzotti, S. Cenini, A. Abbotto, G.A. Pagani, F. Demartin, J. Organomet. Chem. 489 (1995) 107.
[10] S.A. Moya, R. Sariego, P. Aguirre, R. Sartori, P. Dixneuf, Bull. Soc. Chim. Belg. 104 (1995) 19.
[11] K. Nomura, J. Mol. Catal. A 95 (1995) 203.
[12] F. Ragaini, S. Cenini, J. Mol. Catal. A 105 (1996) 145.
[13] C. Linares, M. Mediavilla, A.J. Pardey, C. Longo, P. Baricelli, S.A. Moya, Bol. Soc. Chil. Quím. 43 (1998) 55.
[14] C. Linares, M. Mediavilla, A.J. Pardey, P. Baricelli, C. Longo-Pardey, S.A. Moya, Catal. Lett. 50 (1998) 183.
[15] K. Nomura, J. Mol. Catal. A 130 (1998) 1.
[16] A.J. Pardey, P.C. Ford, J Mol. Catal. 53 (1989) 247.
[17] B. Denise, G. Pannetier, J. Organomet. Chem. 63 (1973) 423.
[18] M. Mediavilla, D. Pineda, F. López, D. Moronta, C. Longo, S.A. Moya, P. Baricelli, A.J. Pardey, Polyhedron 17 (1998) 1621.
[19] J.C. Miller, J.N. Miller, Statistics for Analytical Chemistry, Wiley, New York, 1984.
[20] G. Fachinetti, T. Funaioli, P.F. Zanazzi, J. Organomet. Chem. 460 (1993) C34.

[21] G. Fachinetti, G. Fochi, T. Funaioli, Inorg. Chem. 33 (1994) 1719.
[22] E.C. Baker, D.E. Hendriksen, R. Eisenberg, J. Am. Chem. Soc. 102 (1980) 1020.
[23] B.S. Lima Neto, K.H. Ford, A.J. Pardey, R.G. Rinker, P.C. Ford, Inorg. Chem. 30 (1991) 3837.
[24] J.R. Hulett, Q. Rev. Chem. Soc. 18 (1964) 227.
[25] M.M. Mdleleni, R.G. Rinker, P.C. Ford, Inorg. Chim. Acta 270 (1998) 345.
[26] A.J. Pardey, C. Longo-Pardey, P. Baricelli, Rev. Soc. Venez. Quím. 18 (1995) 10.
[27] S.J. Skoog, J.P. Campbell, W.L. Gladfelter, Organometallics (1994) 4137.

PERGAMON

www.elsevier.nl/locate/poly

Polyhedron 19 (2000) 495–498

POLYHEDRON

A new synthesis of a potentially versatile ligand 2,2′-bi-(1,10-phenanthroline): crystal structure and complexation chemistry

Craig R. Rice *, Kirsty M. Anderson

School of Chemistry, University of Bristol, Cantock's Close, Bristol BS8 1TS, UK

Received 13 September 1999; accepted 3 January 1999

Abstract

Coupling of 2-chloro-1,10-phenanthroline with a source of Ni(0) affords the tetradentate ligand 2,2′-bi-(1,10-phenanthroline). This ligand and a resulting Ni(II) complex were characterised by X-ray crystallography. ©2000 Elsevier Science Ltd All rights reserved.

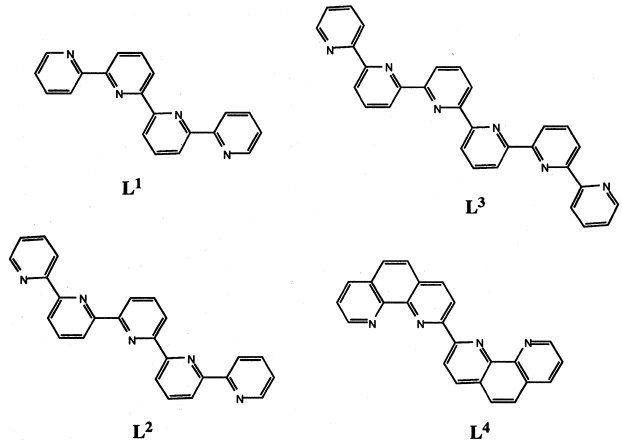
Keywords: Crystal structures; Complexation chemistry; 1,10-Phenanthroline

1. Introduction

The chemistry of 2,2′:6′2″:6″,2‴-quaterpyridine (**L**^{1}) and its higher analogues such as 2,2′:6′,2″:6″,2‴:6‴,2⁗-quinquepyridine (**L**^{2}) and 2,2′:6′,2″:6″,2‴:6‴,2⁗:6⁗,2⁗′-sexipyridine (**L**^{3}) have been extensively studied [1]. Unlike their smaller 2,2′-bipyridine and 2,2′:6′,2″-terpyridine [2,3] analogues which form mainly mononuclear complexes, ligands **L**^{1}–**L**^{3} can, under the right conditions, form polynuclear helical complexes [4–8]. Examples of such complexes, which have been examined crystallographically, include $[Cu^{I}_{2}(L^{1})_{2}]$ [9], $[Ag^{I}_{2}(L^{1})_{2}]$ [9], $[Cu^{I}_{2}L^{2}]$ [4–8], $[Ni^{II}Cu^{I}(L^{2})_{2}]$ [10], $[Ni^{II}_{2}(L^{2})_{2}]$ [11] and $[Co^{II}Ag^{I}(L^{2})_{2}]$ [12]. However, one related class of ligand that has been largely ignored is the poly-phenanthrolines. In this paper we describe the synthesis and solid state structure of 2,2′-bi-(1,10-phenathroline) (**L**^{4}) as the free ligand and as a nickel(II) complex.

2. Results and discussion

2,2′-Bi-(1,10-phenanthroline) was first reported by Case in 1964 [13] and was prepared by Ullman coupling of 2-chloro-phenanthroline with copper, although surprisingly no further reports have appeared in the literature. 2,2′-Bi-(1,10-phenanthroline) is a desirable ligand owing to its rigidity and extended π-system and also once formed, the ligand can undergo further reactivity by oxidation of the inter-pyridine ethylene bridge. Herein we describe the preparation of 2,2′-bi-(1,10-phenanthroline) (**L**^{4}) directly from phenanthroline



in four steps (Scheme 1), the final step requiring coupling of 2-chloro-1,10-phenanthroline employing the method of Iyoda et al. [14].

Thus reaction of the chloro derivative (**4**) with a catalytic amount of nickel(0), generated in situ by reaction of $[NiCl_{2}(PPh_{3})_{2}]$ with excess Zn in thf yielded, after refluxing for 24 h, 2,2′-bi-(1,10-phenanthroline) (**L**^{4}) as a crude material which was purified by recrystallisation from chloroform. It is important to note that the final step of coupling 2-chloro-1,10-phenanthroline is highly dependent upon the purity of the chloro-substituted precursor (**4**) and before coupling was attempted, great care had to be taken to remove any remaining halogenated solvent. Furthermore, as long as this purification

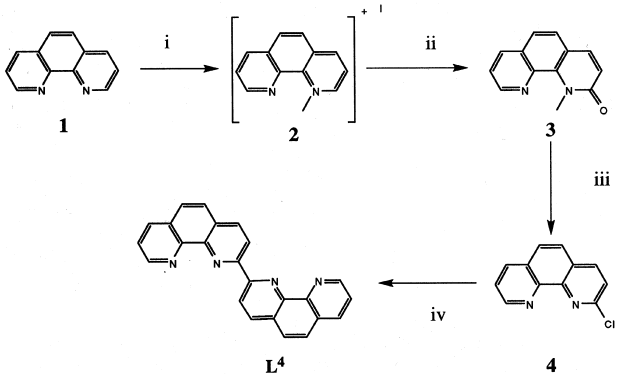
* Corresponding author. Tel.: +44-117-954-6332; fax: +44-117-929-0509; e-mail: c.r.rice@bristol.ac.uk

0277-5387/00/$ - see front matter ©2000 Elsevier Science Ltd All rights reserved.
PII S0277-5387(00)00292-8

procedure is adhered to, this preparation has proven to be, at least in our hands, more robust than that reported by Case.

The crystal structure of **L⁴** (Fig. 1) as a chloroform solvate shows that the structure is almost planar with an angle of 10.0(2)° between the least-square planes of the two phenanthroline units, thereby maximising the π-bonding. Nitrogens N(2) and N(3) exhibit *transoid* geometries similar to those found in the other polypyridines such as bipyridine [15–17] and quaterpyridine [18]. This conformation is observed as it minimises the nitrogen lone pair–lone pair interactions. However, owing to the constraints of the phenanthroline geometry, nitrogens N(1)–N(2) and N(3)–N(4) necessarily lie mutually *cis* to one another. No π-stacking is observed in the crystal, unlike in quaterpyridine [18], presumably owing to the presence of three chloroform molecules of crystallisation.

Reaction of **L⁴** with 1 equiv. of $NiCl_2 \cdot 6H_2O$, in methanol gave a complex characterised as $[Ni(\mathbf{L^4})Cl(H_2O)]Cl \cdot H_2O$ by X-ray crystallography (Fig. 2). The ligand (**L⁴**) acts in a tetradentate manner with all four nitrogens virtually co-planar (with an angle of 5.6(1)° between the least-square planes of the two phenanthroline units), with the remaining two sites (mutually *trans*) occupied by the chlorine and the water molecules (Ni–Cl 2.419(1) and Ni–O 2.066(3) Å with the Cl–Ni–O angle close to linearity at 172.09(8)°). The internal coordinating site of **L⁴** (N(2)–Ni–N(3) 75.9(1)°, N(2)–Ni 2.026(3), N(3)–Ni 2.020(3) Å) is comparable with that found in the related quaterpyridine compound $[Ni(NCMe)_2(L^1)]^{2+}$ [18] (N(1)–Ni–N(1A) 77.6(2)°, N(1)–Ni



Scheme 1. Reagents and conditions: i, MeI, $PhNO_2$; ii, $K_3Fe(CN)_6$, NaOH(aq); iii, $POCl_3$, PCl_5; iv, $[NiCl_2(PPh_3)_2]$, Zn, thf.

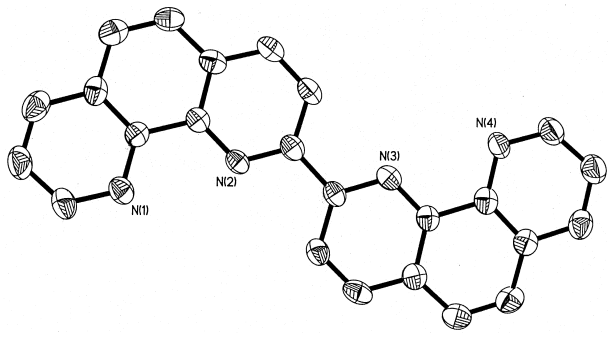


Fig. 1. Molecular structure of **L⁴** (ellipsoids shown at 50% probability).

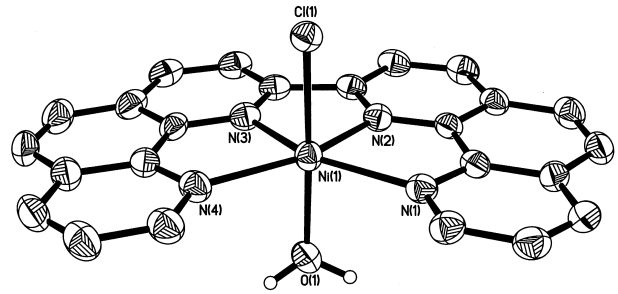


Fig. 2. Molecular structure of the cation $[Ni(\mathbf{L^4})Cl(H_2O)]$ (ellipsoids shown at 50% probability). Selected bond lengths and angles: Ni(1)–N(1) 2.200(3), Ni(1)–N(2) 2.026(3), Ni(1)–N(3) 2.020(3), Ni(1)–N4 2.172(3), Ni(1)–O(1) 2.066(3) and Ni(1)–Cl(1) 2.419(1) Å; N(1)–Ni(1)–N(4) 128.0(1), O(1)–Ni(1)–Cl(1) 172.09(8), N(2)–Ni(1)–N(3) 75.9(1), N(1)–Ni–N(2) 77.4(1), N(3)–Ni(1)–N(4) 78.3(1), N(2)–Ni(1)–N(4) 154.0(1) and N(1)–Ni(1)–N(3) 153.1(1)°.

2.004(3) Å). The two outermost coordination sites N(1) and N(4) have longer Ni–N bonds (N(1)–Ni 2.200(3), N(4)–Ni 2.172(3) Å; c.f. Ni(L^1), N(2)–Ni 2.106(4) Å), similar to that observed for **L¹**, although for **L⁴** the geometry is constrained, unlike that of **L¹** which can, at least in theory, rotate away from the metal centre.

One of the main objectives of the synthesis of 2,2′-bi-(1,10-phenanthroline) was to produce polynuclear helical species as found for the polypyridyls, although all such attempts have so far been fruitless. The inability to form such dinuclear complexes may be a result of the constrained terminal pyridine groups found in **L⁴**, unlike that of **L¹** in which all the pyridine groups can rotate freely. However, molecular modelling [19] of $[Ag_2(\mathbf{L^4})_2]^{2+}$ shows that the corresponding helical complex is only slightly more strained than that of the analogous quaterpyridine helicate $[Ag_2(L^1)_2]^{2+}$, thus indicating that helical complexes of **L⁴** are, at least in principle, feasible.

Further work will focus upon formation of polynuclear helical complexes and derivatising 2,2′-bi-(1,10-phenanthroline) by oxidation of the inter-pyridine ethylene bridge.

3. Experimental

^{1}H NMR spectra were recorded on a JEOL Λ-300 MHz spectrometer. Mass spectra were obtained on a VG-Autospec instrument (EI) and on a VG-Quattro mass spectrometer (ESI). Starting materials were obtained from either Aldrich or Lancaster Synthesis and used without further purification, apart from thf which was distilled from sodium wire under an atmosphere of nitrogen.

3.1. Synthesis

N-methyl-1,10-phenanthrolinium iodide (**2**) [20]. M.p. 209–211°C (lit. 210–213°C [20]). *Anal*. Found: C, 48.9; H, 3.5; N, 9.0. $C_{13}H_{11}N_2I$ requires: C, 48.5; H, 3.4; N, 8.7%. ^{1}H NMR (300 MHz, $(CD_3)_2SO$): δ 9.57 (H^2, dd, 1H, $J^{2,3}=5.9$, $J^{2,4}=1.0$ Hz), 9.38 (H^4, dd, 1H, $J^{4,3}=8.2$, $J^{4,2}=1.0$ Hz),

9.30 (H^9, dd, 1H, $J^{9,8}=4.4$, $J^{9,7}=0.8$ Hz), 8.78 (H^7, dd, 1H, $J^{7,8}=8.2$, $J^{7,9}=0.8$ Hz), 8.42 (H^3, dd, 1H, $J^{3,4}=8.2$, $J^{3,2}=5.9$ Hz), 8.41 (H^5, d, 1H, $J^{5,6}=8.8$ Hz), 8.37 (H^6, d, 1H, $J^{6,5}=8.8$ Hz), 8.04 (H^8, dd, 1H, $J^{8,7}=8.2$, $J^{8,9}=4.4$ Hz), 5.26 (CH_3, s, 3H).

N-Methyl-1,10-phenanthrolin-2(1H)-one (**3**) [20]. To a vigorously stirred solution of $K_3[Fe(CN)_6]$ (7.0 g, 21.2 mmol) in water, solutions of saturated NaOH and *N*-methyl-1,10-phenanthrolinium iodide (2.9 g, 9.0 mmol) in water (10 cm^3) were added dropwise, adding approximately three times the amount of alkali to phenanthroline. It was important to make sure that the *N*-methyl-1,10-phenanthrolinium iodide solution was completely dissolved, which required periodic heating. After addition was complete, the solution was allowed to stir for 45 min after which extraction with CH_2Cl_2 (3×50 cm^3), drying ($MgSO_4$) and solvent removal by vacuum afforded crude *N*-methyl-1,10-phenanthrolin-2(1H)-one as a brown oil. This oil was then dissolved in the minimum amount of hot toluene, treated with decolorising charcoal, filtered and cooled to give pure *N*-methyl-1,10-phenanthrolin-2(1H)-one as yellow crystals. Yield 1.4 g, 74%. M.p. 123–124°C (lit. 120–121°C [20]). *Anal*. Found: C, 74.0; H, 4.4; N, 13.1. $C_{13}H_{10}N_2O$ requires: C, 74.3; H, 4.8; N, 13.3%. ^{1}H NMR (300 MHz, $CDCl_3$): δ 8.92 (H^9, dd, 1H, $J^{9,8}=4.2$, $J^{9,7}=1.8$ Hz), 8.16 (H^7, dd, 1H, $J^{7,8}=8.3$, $J^{7,9}=1.8$ Hz), 7.75 (H^3, d, 1H, $J^{3,4}=9.1$ Hz), 7.55 (H^5, d, 1H, $J^{5,6}=8.4$ Hz), 7.51 (H^6, d, 1H, $J^{6,5}=8.4$ Hz), 7.48 (H^8, dd, 1H, $J^{8,7}=8.3$, $J^{8,9}=4.2$ Hz), 6.89 (H^4, d, 1H, $J^{4,3}=9.1$ Hz), 4.46 (N–CH_3, s, 3H). Mass spectrum: *m/z* 210 (M^+ 79%).

2-Chloro-1,10-phenanthroline (**4**) [20]. To a suspension of *N*-methyl-1,10-phenanthrolin-2(1H)-one (6.0 g, 28.0 mmol) in $POCl_3$ (54 cm^3), PCl_5 (7.2 g, 34.0 mmol) was added and the reaction refluxed for 8 h. The solvent was then removed by vacuum and ice added carefully and the resulting solution poured onto ammonia solution (0.88 sp.gr., 150 cm^3). Upon addition, a precipitate formed which was isolated by filtration and washed with water (4×10 cm^3). The precipitate was then redissolved in CH_2Cl_2 (30 cm^3) washed with water (2×10 cm^3) and dried ($MgSO_4$). Removal of all the volatiles by vacuum afforded a solid which was then dissolved in the minimum amount of hot toluene, treated with decolorising charcoal, filtered and cooled to give pure title compound as pale yellow crystals. Further purification was achieved by dissolving in the minimum amount of $CHCl_3$ from which large colourless crystals were deposited over a period of a few days. Yield 4.1 g, 68%. M.p. 127–128°C (lit. 129–130°C [20]). *Anal*. Found: C, 67.4; H, 3.3; N, 13.2. $C_{12}H_7N_2Cl$ requires: C, 67.1; H, 3.3; N, 13.0%. ^{1}H NMR (300 MHz, $CDCl_3$): δ 9.26 (H^9, dd, 1H, $J^{9,8}=4.4$, $J^{9,7}=1.7$ Hz), 8.31 (H^7, dd, 1H, $J^{7,8}=8.1$, $J^{7,9}=1.7$ Hz), 8.22 (H^4, d, 1H, $J^{4,3}=8.3$ Hz), 7.85 (H^5, d, 1H, $J^{5,6}=8.8$ Hz), 7.81 (H^6, d, 1H, $J^{6,5}=8.8$ Hz), 7.70 (H^8, dd, 1H, $J^{8,7}=8.1$, $J^{8,9}=4.4$ Hz), 7.65 (H^3, d, 1H, $J^{3,4}=8.3$ Hz). Mass spectrum: *m/z* 214 (M^+ 90%, correct isotope pattern).

2,2′-Bi-(1,10-phenanthroline) (**L^4**). To a round-bottomed flask charged with $[NiCl_2(PPh_3)_2]$ (0.22 g, 0.33 mmol), $[Et_4N]I$ (0.84 g, 3.3 mmol) and zinc dust (0.32 g, 4.9 mmol) under an atmosphere of argon, thf (20 cm^3) was added and the reaction stirred until a dark brown colour had formed (approximately 45 min). To this reaction mixture a solution of 2-chloro-1,10-phenanthroline (0.70 g, 3.3 mmol) in thf (10 cm^3) was then added and the reaction refluxed for 12 h. After this time the solvent was removed by vacuum and ammonia solution (0.88 sp.gr., 100 cm^3) added and the reaction stirred for a further 12 h. After this time the suspension was extracted with CH_2Cl_2 (3×75 cm^3) and dried ($MgSO_4$). Removal of all the volatiles by vacuum afforded a yellow oil, which was suspended in Et_2O and the resulting solid isolated by filtration. Dissolving in the minimum amount of chloroform and cooling gave pure 2,2′-bi-(1,10-phenanthroline) as yellow crystals, which lost solvent rapidly. Yield 0.18 g, 30%. M.p. $<$300°C (lit. 365–366°C [13]). *Anal*. Found: C, 63.7; H, 3.1; N, 11.0. $C_{24}H_{14}N_4\cdot CHCl_3$ requires: C, 62.8; H, 3.2; N, 11.7%. ^{1}H NMR (300 MHz, $CDCl_3$): δ 9.50 (H^4, d, 1H, $J^{4,3}=8.4$ Hz), 9.34 (H^9, dd, 1H, $J^{9,8}=4.4$, $J^{9,7}=1.6$ Hz), 8.51 (H^3, d, 1H, $J^{3,4}=8.4$ Hz), 8.34 (H^7, dd, 1H, $J^{7,8}=8.1$, $J^{7,9}=1.6$ Hz), 7.94 (H^5, d, 1H, $J^{5,6}=8.8$ Hz), 7.85 (H^6, d, 1H, $J^{6,5}=8.8$ Hz), 7.70 (H^8, dd, 1H, $J^{8,7}=8.1$, $J^{8,9}=4.4$ Hz). Mass spectrum: *m/z* 358 (M^+ 100%). HRMS: $C_{24}H_{14}N_4$ requires 358.12184, found 358.12184.

$[Ni(\mathbf{L^4})Cl(H_2O)]Cl\cdot H_2O$. To a solution of $NiCl_2\cdot6H_2O$ (0.010 g, 0.04 mmol) in MeOH (1 cm^3) a suspension of 2,2′-bi-(1,10-phenanthroline) (0.015 g, 0.04 mmol) in MeOH (1 cm^3) was added and the solution filtered. Cooling at -29°C for several days gave a brown precipitate which was collected by filtration and washed with Et_2O (1 cm^3) and dried in vacuo. Yield 0.015 g, 71%. *Anal*. Found: C, 55.9; H, 2.6; N, 10.4. $C_{24}H_{14}N_4NiCl_2\cdot2H_2O$ requires: C, 55.0; H, 3.5; N, 10.7%. ESI mass spectrum: *m/z* 451 ($[C_{24}H_{14}N_4NiCl]^+$, 10%).

3.2. Crystallography

The structures were solved by direct methods and refined by least-squares on F^2 values for all reflections. All non-hydrogen atoms were assigned anisotropic displacement parameters and refined without positional constraints. All hydrogen atoms (excepting those on the water molecules of $[Ni(\mathbf{L^4})Cl(H_2O)Cl\cdot H_2O$, H(1–6), which were located in the electron density difference map, assigned isotropic displacement parameters and refined without positional constraints) were constrained to ideal geometries and refined with fixed isotropic displacement parameters. Absorption correction was carried out using the SADABS [21] absorption correction software (Table 1).

Within $[Ni(\mathbf{L^4})Cl(H_2O)]Cl\cdot H_2O$ the cation is ordered, with a hydrogen bond between H(6) and Cl(1) (H(6)···Cl(1) 2.247(24) Å). However, the chloride counterion Cl(2) is disordered over two sites. The major site Cl(2) has an occupancy of 0.879(3) and contains a free

Table 1
Crystal data [a] and details of measurements for $\mathbf{L^4}$ and $[Ni(\mathbf{L^4})Cl(H_2O)]Cl\cdot H_2O$

Compound	$\mathbf{L}^4$	$[Ni(L^4)Cl(H_2O)]Cl\cdot H_2O$
Colour and habit	yellow block	dark brown block
Size (mm)	0.5×0.2×0.1	0.4×0.2×0.1
Formula	$C_{24}H_{14}N_4.3CHCl_3$	$C_{24}H_{19.76}Cl_2N_4NiO_{2.88}$
M	716.50	539.85
Crystal system	triclinic	monoclinic
Space group	$P\bar{1}$ (no. 2)	$P2_1/c$ (no. 14)
Z	2	4
a (Å)	9.678(3)	11.194(2)
b (Å)	13.156(2)	14.218(2)
c (Å)	13.861(3)	14.421(3)
α (°)	63.162(13)	90
β (°)	74.548(12)	101.07(2)
γ (°)	86.70(2)	90
U (Å^3)	1513.8(5)	2252.6(8)
Temperature (K)	173(2)	173(2)
μ(Mo Kα) (mm^{-1})	0.859	1.134
F(000)	720	1108
Measured reflections	13135	14287
Unique reflections	5317	3962
R_{int}	0.0544	0.0373
$2\theta_{max}$ (°)	50	50
Completeness to 2θ (%)	97	92
No. of parameters	361	341
Effective transmission coefficients (min., max.)	1.000000, 0.680516	0.778495, 0.495504
R_1 (on F, $I>2\sigma(I)$)	0.0477	0.0371
wR_2 (on F^2, all data)	0.1181	0.1016

[a] The crystal structures of both compounds were determined from data collected on a Siemens SMART diffractometer ($\lambda = 0.71073$ Å). Both compounds are air stable and were mounted on a glass fibre with vacuum grease.

chloride ion together with a water molecule of the same occupancy (O(3)) which is hydrogen bonded to O(1) (H(2)···O(3) 1.91(2) Å). H(3) is also hydrogen bonded to Cl(2) (H(3)···Cl(2) 2.194(23) Å). The minor site has an occupancy of 0.121(3) and contains a chloride ion Cl(2′) weakly hydrogen-bonded to H(2) (Cl(2′)···H(2) 2.73(2) Å).

Supplementary data

Supplementary data are available on request from the Cambridge Crystallographic Data Centre, 12 Union Road, Cambridge CB2 1EZ, UK (fax: +44-1223-336033; e-mail: deposit@ccdc.cam.uk), CCDC 133855/CCDC 133856.

Acknowledgements

We thank E.P.S.R.C. for support. We would also like to thank Professor A.G. Orpen, Dr M.D. Ward and Dr N.C. Norman for their advice and support and Mr J. Starbuck for his help with the crystallography and molecular modelling.

References

[1] E.C. Constable, Tetrahedron 48 (1992) 10013.
[2] E.C. Constable, Adv. Inorg. Chem. Radiochem. 30 (1986) 69.
[3] E.C. Constable, Adv. Inorg. Chem. Radiochem. 31 (1986) 1.
[4] M. Barley, E.C. Constable, S.A. Corr, M.G.B. Drew, R.C.S. McQueen, J.C. Nutkins, M.D. Ward, J. Chem. Soc., Dalton Trans. (1988) 2655.
[5] E.C. Constable, M.G.B. Drew, M.D. Ward, J. Chem. Soc., Chem. Commun. (1987) 600.
[6] E.C. Constable, M.G.B. Drew, G.A. Forsyth, M.D. Ward, Polyhedron 8 (1989) 2551.
[7] E.C. Constable, Nature 346 (1990) 314.
[8] E.C. Constable, Chem. Ind. (1994) 57.
[9] E.C. Constable, S.M. Elder, M.J. Hannon, A. Martin, P.R. Raithby, D.A. Tocher, J. Chem. Soc., Dalton Trans. (1996) 2423.
[10] E.C. Constable, A.J. Edwards, P.R. Raithby, D.R. Smith, J.V. Walker, L. Whall, J. Chem. Soc., Chem. Commun. (1996) 2551.
[11] E.C. Constable, M.A.M. Daniels, M.G.B. Drew, D.A. Tocher, J.V. Walker, P.D. Wood, J. Chem. Soc., Dalton Trans. (1993) 1947.
[12] E.C. Constable, A.J. Edwards, P.R. Raithby, J.V. Walker, Angew. Chem., Int. Ed. Engl. 32 (1993) 1465.
[13] F.H. Case, Heterocyclic Chem. 1 (1964) 112.
[14] M. Iyoda, H. Otsuka, K. Sato, N. Nisato, M. Oda, Bull. Chem. Soc. Jpn. 63 (1990) 80.
[15] L.L. Merritt Jr., E.D. Schroeder, Acta Crystallogr. 9 (1956) 801.
[16] K. Nakatsu, H. Yoshioka, M. Matsui, S. Koda, S. Ooi, Acta Crystallogr., Sect. A 28 (1972) S24.
[17] M.H. Chisholm, J.C. Huffman, I.P. Rothwell, P.G. Bradley, N. Kress, W.H. Woodruff, J. Am. Chem. Soc. 103 (1981) 4945.
[18] E.C. Constable, S.M. Elder, J. Healy, D.A. Tocher, J. Chem. Soc., Dalton Trans. (1990) 1669.
[19] Molecular modelling studies were performed on CERIUS Molecular Modelling Software, MSI/BIOSYM Inc., Cambridge, UK.
[20] B.E. Halcrow, W.O. Kermack, J. Chem. Soc. (1946) 155.
[21] SADABS Absorption Correction Software, Siemens Analytical X-ray Instruments Inc., Madison, WI, 1994.

PERGAMON

www.elsevier.nl/locate/poly

Polyhedron 19 (2000) 499–502

POLYHEDRON

The preparation and characterisation of platinum and palladium phosphine thiocarbonate complexes $M(PR_3)_2(CS_3)$ and $Pt(PR_3)_2(CSeS_2)$

Steven A. Aucott, Alexandra M.Z. Slawin, J. Derek Woollins *

Department of Chemistry, University of St Andrews, St Andrews, Fife KY16 9ST, UK

Received 15 October 1999; accepted 4 January 2000

Abstract

Reaction of CS_2 with NH_3(liq) gives the $(CS_3)^{2-}$ dianion which undergoes in situ reaction with $MCl_2(PR_3)_2$ to give $M(PR_3)_2(CS_3)$. X-ray analysis of four examples (M = Pt, PR_3 = PMe_3, PMe_2Ph, PPh_3, dppp) reveals square planar coordination with the $[CS_3]^{2-}$ dianion being effectively in the same plane as the coordination sphere. The first example of a $[CSeS_2]^{2-}$ complex is also reported. ©2000 Elsevier Science Ltd All rights reserved.

Keywords: Platinum; Palladium; Phosphine thiocarbonates

1. Introduction

Sulfur donor ligands have been investigated by a number of groups for both academic and industrial reasons including their use in lubricant additives [1], metal specific coordination [2] and bioinorganic chemistry [3]. Although there is a wide range of organosulfur systems [4], and more recently S–P–N–P–S systems [5–8], there is surprisingly little information [9–12] on perhaps the simplest anionic sulfur chelate, $[CS_3]^{2-}$. We have been interested in the incorporation of sulfur-rich ligands into complexes for a number of reasons [13,14], and the thiocarbonate ligand has the attraction of giving complexes with exocyclic sulfur atoms which could be important in the formation of molecular metals as a result of weak interactions to other species in the solid state [15]. There was a recent report on the synthesis of (diphosphine)platinum(II) carbonate complexes [16] and this has prompted us to describe our work on the related thiocarbonate compounds. In this work we describe a facile synthesis of $[CS_3]^{2-}$ together with the formation of a range of $M(PR_3)_2(CS_3)$ (M = Pd, Pt) complexes. The complexes have been characterised by NMR and vibrational spectroscopy; in addition, the X-ray structures of selected examples are reported.

* Corresponding author. Tel.: +44-1334-463861; fax: +44-1334-463384; e-mail: jdw3@st-and.ac.uk

2. Experimental

2.1. General

Diethyl ether, petroleum ether (60–80°C) and tetrahydrofuran were purified by reflux over sodium and distillation under nitrogen. Dichloromethane was heated to reflux over powdered calcium hydride and distilled under nitrogen. Chemicals were purchased from Aldrich and Lancaster and were used as received. The compounds $[PdCl_2cod]$ and $[PtCl_2cod]$ [17] were prepared using literature procedures.

Infrared spectra were recorded from KBr discs on a Perkin-Elmer system 2000 spectrometer; ^{31}P NMR spectra were recorded on a Jeol FX90Q operating at 36.21 MHz; ^{1}H, ^{13}C and ^{31}P NMR spectra were recorded on Bruker instruments operating at 250, 62.9 and 101.3 MHz, respectively. Fast atom bombardment mass spectra were obtained by the Swansea Mass Spectrometer service.

2.2. Synthesis of *1–8*

Carbon disulfide (5–10 ml) was placed into a Schlenk tube and cooled to −78°C. NH_3 was bubbled into the cooled CS_2 until two distinct layers were formed (ca. 10 min), a clear bottom layer and a blood red top layer containing the CS_3^{2-} anion. MCl_2(bis-phosphine), M = Pd, Pt (100–130 mg) was added as a solid and the mixture was stirred magnetically for

0277-5387/00/$ - see front matter ©2000 Elsevier Science Ltd All rights reserved.
PII S0277-5387(00)00295-3

2 h at −78°C and then slowly warmed to room temperature with continual stirring until the excess NH_3 had evaporated. The resulting bright orange residue was placed under vacuum for 1 h then extracted with 3×20 ml portions of dichloromethane. The combined extracts were reduced in volume to approximately 10 ml, and 60–80 petroleum ether (ca. 40 ml) was added slowly to the stirred solution to precipitate the product. The bright yellow solid was collected by suction filtration, washed with a small amount of methanol (5 ml) and diethyl ether (1 ml), and dried overnight in vacuo. Yield 70–90% based on metal used.

2.3. Synthesis of **9** and **10**

Tetrabutylammonium borohydride (0.144 g, 0.560 mmol) and elemental selenium (0.022 g, 0.279 mmol) were heated to 40°C under a nitrogen atmosphere in dry thf (50 cm^3) for 4 h or until the reaction mixture was colourless. The mixture was then cooled to −78°C (cardice/acetone) and 11.9 cm^3 of a 1.78×10^{-3} M solution of CS_2 in thf (0.021 g, 0.276 mmol) was added and the solution stirred for 30 min, resulting in a bright red coloured solution. To this was added solid $PtCl_2(PMe_2Ph)_2$ (0.151 g, 0.278 mmol) and the mixture was stirred for 1 h at −78°C and 1 h at room temperature, giving a bright orange solution containing a light colourless precipitate. The precipitate was removed by filtration through celite and the filtrate was evaporated to dryness leaving an oily dark orange residue. The crude product was taken up into a small volume of dichloromethane (1.5–2 cm^3) and diethyl ether (40 cm^3) was added with stirring to give an orange precipitate. The product was collected by suction filtration, washed with ice cold methanol (2 cm^3) followed by diethyl ether (2×5 cm^3) and dried in vacuo. Yield 0.091 g, 52%.

2.4. X-ray crystallography

Details of the structure determination of **1**–**5** are given in Table 1. X-ray diffraction measurements were made with graphite-monochromated Mo Kα X-radiation ($\lambda=0.71073$ Å) using a Siemens SMART diffractometer or with Cu Kα radiation and a Rigaku AFC7S serial diffractometer. For the SMART data, intensity data were collected using 0.3° or 0.15° width ω steps accumulating area detector frames spanning a hemisphere of reciprocal space for all structures (data were integrated using the SAINT [18] program) and for the Rigaku AFC7S data were collected by ω scans over a single quadrant of reciprocal space. All data were corrected for Lorentz, polarisation and long-term intensity fluctuations. Absorption effects were corrected on the basis of multiple equivalent reflections or by empirical methods. Structures were solved by direct methods and refined by full-matrix least-squares against F (teXsan) or F^2 (SHELXTL) for all data with $I>3\sigma(I)$ with weights w set equal to $(\sigma_c^2(F_o^2)+(aP)^2+bP]^{-1}$, where $P=[\max(F_o^2,0)+2F_c^2]/3$. The parameter x, of the form $k[1+0.001xF_c^2\lambda^3/\sin(2q)]^{0.25}$ was refined for the SMART/SHELXTL [19] structures; the weighting scheme for the Rigaku/teXsan [20] was as previously reported [21]. All hydrogen atoms were assigned isotropic displacement parameters and were constrained to idealised geometries. Refinements converged to residuals given in Table 1. High electron densities in the final difference maps were located close to the heavy metal centre in all the determinations. In **10** the S/Se disorder of the metal bonded sites in the $[CSeS_2]^{2-}$ was refined using 50% occupancy, using anisotropic refinements with the sulfur and selenium atoms on each site sharing common coordinates. There was no indication of any contribution from a selenium occupancy for the terminal sulfur atom. All calculations were made with SHELXTL [19] or teXsan [20].

Table 1
Details of the crystal data and refinements

	1	**3**	**4**	**5**
Empirical formula	$C_7H_{18}P_2PtS_3$	$C_{17}H_{22}P_2PtS_3$	$C_{37.5}H_{31}ClP_2PtS_3$	$C_{28}H_{26}P_2PtS_3$
Formula weight	455.4	579.6	870.3	715.7
Crystal system	monoclinic	triclinic	triclinic	triclinic
Space group	$P2_1/c$	P-1	P-1	P-1
a (Å)	9.0048(5)	11.108(1)	11.0763(2)	10.665(1)
b (Å)	11.0771(6)	11.427(2)	13.6100(2)	12.675(2)
c (Å)	15.2897(8)	9.053(1)	13.7719(1)	10.505(1)
α (°)		104.33(1)	81.936(1)	102.03(1)
β (°)	105.32(1)	110.86(1)	86.775(1)	103.05(1)
γ (°)		85.27(1)	66.92(1)	85.55(1)
Volume (Å^3)	1471	1040	1891	1352
Z	4	2	2	2
Density (calc.) (g cm^{-3})	2.057	1.850	1.53	1.76
μ (mm^{-1})	10.15	16.3 [a]	4.05	12.7*
F(000)	864	560	858	700
Independent reflections/observed reflections	2094/1633	3101/2635	5388/4565	4021/3547
Final R_1/wR_2	0.0662/0.1863	0.050/0.047	0.0374/0.0905	0.047/0.049

[a] Cu radiation. Pt(dppp)(CS_2Se), space group $P2_1/n$, $a=10.842(1)$, $b=15.713(1)$, $c=15.257(1)$ Å, $\beta=106.37(1)°$.

3. Results and discussion

The $(CS_3)^{2-}$ dianion is well established but not particularly well investigated. Typically the dianion is prepared by reaction of a base such as KOH with CS_2 in an inert solvent such as dimethylformamide [9]. We have found liquid ammonia to be a very useful solvent for a range of reactions [22]. Here we report a simple reaction for the preparation of $(NH_4)_2(CS_3)$ as well as for a range of $M(PR_3)_2(CS_3)$ complexes (M = Pd, Pt). Furthermore, we have determined the X-ray crystal structures of four $Pt(PR_3)_2(CS_3)_2$ complexes for comparison with the $(CO_3)^{2-}$ complex which was recently reported [16].

The new $[CS_3]^{2-}$ complexes were obtained by reaction of CS_2 with excess NH_3(liq) followed by the appropriate $MCl_2(PR_3)_2$ species. All of the compounds gave satisfactory microanalyses and FAB mass spectra (with the expected isotopomer distributions, Table 2). In **1**–**8** (Tables 3 and 4) the ν(C=S) vibrations were observed at ca. 1050, and the ν(M–S) all lie close to 337 cm^{-1} which is in accord with previous observations for related systems [10]. In the ^{31}P NMR spectra the platinum complexes have δ values which are ca. 8 ppm to higher frequency than the analogous carbonate complexes [16].

The $^1J(^{31}P–^{195}Pt)$ coupling constants observed for the $Pt(PR_3)_2(CS_3)$ complexes lie in the range 2590–3145 Hz for the dppm and PPh_3 complexes, respectively and as such are generally ca. 500 Hz smaller in magnitude than those observed for the analogous carbonate complexes. The values observed here are relatively high for sulfur donor systems though there are few dianionic examples that are directly comparable.

X-ray analysis of four $Pt(PR_3)_2(CS_3)$ complexes reveals (Table 5, Fig. 1) the expected square planar geometry at platinum. The Pt–S distances appear independent of the *trans* phosphine (range 2.336(3)–2.358(2) Å), though as expected the Pt–P distances vary with the nature of the phosphine, with the PPh_3 complex having the longest Pt–P bond length. Interestingly, in Pt(dppp)(CS_3) (**5**) the Pt–P bond lengths (2.263(3), 2.266(3) Å) are substantially longer than those [16] in Pt(dppp)(CO_3) (2.216(5), 2.2149(5) Å).

Table 2
Microanalytical data (expected values in parentheses) and mass spectral data for **1**–**8**

Complex	C	H	*m/z*
1 $[Pt(PMe_3)_2\{CS_3\}]$	18.6 (18.5)	3.9 (4.0)	455
2 $[Pt(PEt_3)_2\{CS_3\}]$	29.4 (28.9)	5.4 (5.6)	540
3 $[Pt(PMe_2Ph)_2\{CS_3\}]$	36.7 (36.2)	3.9 (3.8)	580
4 $[Pt(PPh_3)_2\{CS_3\}]$	53.9 (53.7)	3.8 (3.7)	828
5 [Pt(dppp){CS_3}]	46.6 (47.0)	3.4 (3.7)	715
6 [Pt(dppm){CS_3}]	44.9 (45.4)	3.3 (3.2)	688
7 [Pd(dppe){CS_3}]	52.6 (52.9)	3.7 (3.9)	611
8 $[Pd(PEt_3)_2\{CS_3\}]$	32.8 (34.6)	6.6 (6.7)	451
9 $[Pt(PMe_2Ph)_2\{CS_2Se\}]$	32.4 (32.6)	3.6 (3.5)	627
10 [Pt(dppp){CS_2Se}]	44.4 (44.0)	3.2 (3.4)	763

Table 3
$^{31}P\{^1H\}$ NMR (36.2 MHz) and selected IR data for **1**–**8**

Complex	δ_P (ppm)	^1J(P–Pt) (Hz)	ν(C=S) (cm^{-1})	ν(M–S) (cm^{-1})
1	−29.4	2969	1052(vs)	395(w), 337(w)
2	5.2	3013	1057(vs)	385(w), 336(w)
3	−19.1	3018	1060(vs)	387(w), 339(w)
4	17.9	3145	1061(vs)	386(w), 339(w)
5	−4.2	2881	1050(vs)	387(w), 339(w)
6	−51.7	2590	1047(vs)	386(w), 338(w)
7	52.0		1047(vs)	390(w), 337(w)
8	18.6		1039(vs)	375(w), 332(w)

Table 4
$^{31}P\{^1H\}$ NMR (36.2 MHz) and selected IR data for **9** and **10**

Complex	Chemical shift (ppm)		Coupling constant (Hz)		
	$\delta(P_A)$	$\delta(P_B)$	^1J(Pt–P_A)	^1J(Pt–P_B)	^2J(P_A–P_B)
9	−19.5	−17.8	3005	3028	23
10	2.8	3.4	2865	2886	33

Table 5
Selected bond lengths (Å) and angles (°) for $[Pt(PR_3)\{CS_3\}]$ complexes

	PMe_3 **1**	PMe_2Ph **3**	PPh_3 **4**	dppp **5**
Pt–P(1)	2.263(3)	2.265(3)	2.303(2)	2.263(3)
Pt–P(2)	2.2669(4)	2.265(3)	2.280(2)	2.266(3)
Pt–S(1)	2.342(4)	2.336(3)	2.358(2)	2.47(3)
Pt–S(2)	2.354(4)	2.349(4)	2.337(2)	2.346(3)
S(1)–C(1)	1.70(2)	1.69(1)	1.731(8)	1.76(1)
S(2)–C(1)	1.756(12)	1.71(1)	1.762(7)	1.71(1)
S(3)–C(1)	1.655(12)	1.67(1)	1.630(7)	1.64(1)
S(1)–Pt–S(2)	73.8(2)	73.3(1)	73.74(7)	73.6(1)
P(1)–Pt–P(2)	98.7(1)	95.4(1)	98.99(6)	93.2(1)
S(1)–C(1)–S(3)	127.7(8)	125.4(8)	126.9(5)	125..7(6)
S(2)–C(1)–S(3)	123.1(9)	124.1(8)	125.6(5)	126.1(6)
S(1)–C(1)–S(2)	109.2(7)	110.5(7)	107.5(4)	108.1(5)
Pt–S(1)–C(1)	89.3(4)	88.6(4)	89.3(2)	88.6(3)
Pt–S(2)–C(1)	87.6(5)	87.6(5)	89.2(3)	89.7(3)

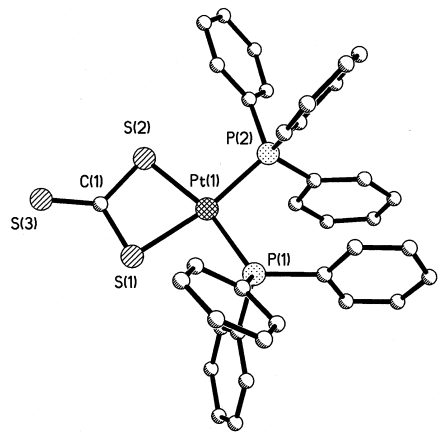


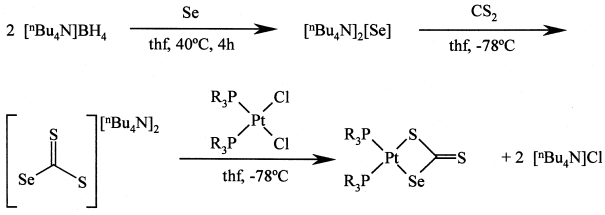
Fig. 1. The X-ray structure of $Pt(PPh_3)_2(CS_3)$ (**4**).

This is presumably a consequence of the greater electronegativity of the carbonate ligand that enables the dppp to behave as a better σ donor; the same effect would also explain the difference in the $^1J(^{31}P–^{195}Pt)$ coupling constants. The S–Pt–S angle in **5** (73.6(1)°) is significantly less strained than the O–Pt–O angle (65.3(5)°) in the carbonate complex [16]. The C–S bond lengths in the $[CS_3]^{2-}$ ligand are longer for the coordinated sulfur atoms than for the exocyclic sulfur which is as anticipated. Within the PtS_2C rings the Pt–S–C and S–C–S angles are in the range 87.6(5)–89.7(3)° and 107.5(4)–110.5(7)°, respectively, reflecting the ability that sulfur has to adapt to greater angular distortion. In all of the structures the $(CS_3)^{2-}$ ligand is effectively coplanar with the coordination plane (maximum deviation for S(3) 0.29 Å in **4**). There are no significant intermolecular interactions in the solid state for any of the structures.

We have also developed a synthesis of the previously unknown $[CS_2Se]^{2-}$ dianion according to Scheme 1. We made no attempt to isolate the $[Bu_4N]_2[CS_2Se]$ but used it in situ to form complexes **9** and **10**. The NMR of **9** and **10** are the expected AB type with $^1J(^{31}P–^{195}Pt)$ couplings which are appropriate for the *trans* coordination of sulfur or selenium. Although very similar, the δ values can be assigned to phosphorus *trans* to sulfur and selenium by comparison with the δ values/coupling constants in complexes **3** and **5**. The X-ray diffraction studies on **10** clearly indicate the presence of a 50% disordered $[CS_2Se]^{2-}$ group with the selenium being bound to the platinum; however, no meaningful bond lengths and angles can be derived because of the disorder.

Supplementary data

Atomic coordinates, thermal parameters and bond lengths and angles have been deposited at the Cambridge Crystallographic Data Centre, 12 Union Road, Cambridge, CB2 1EZ, UK (fax: +44-1223-336033; e-mail: deposit@ccdc.cam.ac.uk or www:http://www.ccdc.cam.ac.uk. Any request to CCDC for this material should quote the full literature citation and the reference number 135551–135554.



Scheme 1. Synthesis of platinum (II) selenodithiocarbonate complexes.

Acknowledgements

We are grateful to the JREI for an equipment grant.

References

[1] J.R. Phillips, J.C. Poat, A.M.Z. Slawin, D.J. Williams, P.T. Wood, J.D. Woollins, J. Chem. Soc., Dalton Trans. (1995) 2369.
[2] D. Cupertino, R.W. Keyte, A.M.Z. Slawin, D.J. Williams, J.D. Woollins, Inorg. Chem. 35 (1996) 2695.
[3] J.D. Woollins, Inorganic sulfur chemistry. In: S. Mitchell (Ed.), Biological Interactions of Sulfur Compounds, Taylor and Francis, 1996, pp. 1–19.
[4] R.P. Burns, F.P. McCullogh, C.A. McAuliffe, Adv. Inorg. Radiochem. 23 (1980) 211.
[5] R. Cea-Olivares, J. Novosad, J.D. Woollins, A.M.Z. Slawin, V. García-Montalvo, G. Espinosa-Pérez, P. García y García, Chem. Commun. (1996) 519.
[6] J.D. Woollins, J. Chem. Soc., Dalton Trans. (1996) 2893.
[7] D. Cupertino, R.W. Keyte, A.M.Z. Slawin, J.D. Woollins, D.J. Williams, Polyhedron 15 (1996) 4441.
[8] J.R. Phillips, A.M.Z. Slawin, A.J.P. White, D.J. Williams, J.D. Woollins, J. Chem. Soc., Dalton Trans. (1995) 2467.
[9] J.P. Fackler Jr., D. Coucouvanis, J. Am. Chem. Soc. 88 (1966) 3913.
[10] J.M. Burke, J.P. Fackler Jr., Inorg. Chem. 11 (1972) 2744.
[11] A. Muller, P. Christopliemk, I. Tossidis, C.K. Jorgensen, Z. Anorg. Allg. Chem. 401 (1973) 274.
[12] J. Novosad, D.J. Williams, J.D. Woollins, Z. Anorg. Allg. Chem. 620 (1994) 495.
[13] V.C. Ginn, P.F. Kelly, J.D. Woollins, J. Chem. Soc., Dalton Trans. (1992) 2129.
[14] V.C. Ginn, P.F. Kelly, A.M.Z. Slawin, C. Papadimitriou, D.J. Williams, J.D. Woollins, J. Chem. Soc., Dalton Trans. (1993) 1805.
[15] J.D. Martin, E. Canadell, J.C. Fitzmaurice, A.M.Z. Slawin, D.J. Williams, J.D. Woollins, J. Chem. Soc., Dalton Trans. (1994) 1995.
[16] M.A. Andrews, G.L. Gould, W.T. Klooster, K.S. Koenig, E.J. Voss, Inorg. Chem. 35 (1996) 5478.
[17] D. Drew, J.R. Doyle, Inorg. Synth. 28 (1992) 346.
[18] SAINT (Siemens Area Detector INTegration) program, Siemens Analytical X-Ray, Madison, WI, 1995.
[19] Siemens SHELXTL, Revision 5.03, Siemens Analytical X-Ray, Madison, WI, 1995.
[20] teXsan Crystal Structure Analysis Package, Molecular Structure Corporation, 1985, 1992.
[21] A.M.Z. Slawin, M.B. Smith, J.D. Woollins, J. Chem. Soc., Dalton Trans. (1996) 3659.
[22] P.F. Kelly, A.M.Z. Slawin, D.J. Williams, J.D. Woollins, Chem. Soc. Rev. (1992) 245.

PERGAMON

www.elsevier.nl/locate/poly

Polyhedron 19 (2000) 503

POLYHEDRON

Author Index of Volume 19/4

Airoldi, C., 367
Alshehri, S., 399
Alvarez, J., 487
Anderson, K.M., 495
Arakaki, L.N.H., 367
Aucott, S.A., 499

Baricelli, P., 487
Bombicz, P., 457
Breza, M., 389
Bu, X.-H., 431
Burgess, J., 399

Catalano, V.J., 475
Chan, A.S.-C., 453
Chang, C.-S., 413
Chen, J.-H., 413
Chisholm, M.H., 375
Craig, T.J., 475
Cui, C., 471
Czugler, M., 457

Daier, V., 417
Drake, J.E., 407

Fawcett, J., 399
Fernández, M., 487
Folting, K., 375
Franco, E., 441

Hao, H., 471
Huang, J., 453
Huffman, J.C., 375

Jia, W.-L., 381

Khasrou, L.N., 407

Lee, H.-J., 425
Li, H., 375
Li, Y.-I., 413
Liao, F.-L., 413
Lisowski, J., 465
Liu, H., 431
Liu, Q., 453
Liu, Q.-T., 431
Longo, C., 487
López-Torres, E., 441
Lu, S.-L., 431

Macintosh, A.M., 375
Madarász, J., 457
Mdleleni, M.M., 487
Mendiola, A., 441
Mironov, Y.V., 437
Mislankar, A.G., 407
Moreno, V., 417
Moya, S.A., 487

Noh, D.-Y., 425
Noltemeyer, M., 471

Pardey, A.J., 487
Parsons, S.A., 399
Pokol, G., 457

Qian, Y., 453

Ratnani, R., 407
Rice, C.R., 495
Rizzotto, M., 417
Roesky, H.W., 471
Russell, D.R., 399

Sala, L.F., 417
Schmidt, H.-G., 471
Sevilla, T., 441
Shen, X., 453
Signorella, S., 417
Slawin, A.M.Z., 499
Starynowicz, P., 465

Tang, L.-F., 381
Tsai, C.-H., 413
Tung, J.-Y., 413

Wang, J.-T., 381
Wang, S.-L., 413
Wang, Z.-H., 381
Wong, W.-T., 453
Woollins, J.D., 499
Wu, D.-D., 375

Xu, Y.-M., 381

Zhang, R.-H., 431
Zhu, H.-P., 431

Elsevier Science Ltd.

PERGAMON

www.elsevier.nl/locate/poly

Polyhedron 19 (2000) 505–507

POLYHEDRON

Organometallic chemistry at the interface with materials science

Jeffrey Schwartz *, Ellen S. Gawalt, Gang Lu, Delia J. Milliron, Kathleen L. Purvis, Steven J. Woodson, Steven L. Bernasek, Andrew B. Bocarsly, Susan K. VanderKam

Department of Chemistry, Princeton University, Princeton, NJ 08544-1009, USA

Received 4 October 1999; accepted 29 November 1999

Abstract

Surface hydroxyl groups of indium tin oxide (ITO) react with zirconium or tin alkoxides to give surface metal alkoxide complexes, which can be converted to surface metallic complexes of carboxylates or phenoxides. These latter surface complexes can be used to modify electrode properties of the ITO. ©2000 Elsevier Science Ltd All rights reserved.

Keywords: Indium tin oxide; Surface modification; Alkoxides; Interfaces

Organometallic materials play an important role as essential components of modern optoelectronic devices, for example of organic light emitting diodes (OLEDs). In one OLED process, 'holes' are injected from an inorganic anode into an organic 'hole transport layer (HTL)' material; typically, the anode is a mixed oxide of indium and tin (ITO), and the HTL is an aromatic hydrocarbon derivative (Fig. 1) [1–3]. 'Hole injection' into (oxidation of) the HTL is often inefficient, perhaps owing to poor molecular contact at the interface between the hydrophilic ITO and the hydrophobic HTL; this inefficiency results in device failure after only short utilization times [1,4,5]. Until the surface chemistry of ITO is better understood, it is unlikely that precisely designed interfaces can be developed for applications in microelectronic devices. Fortunately, surface hydroxyl groups can provide a chemical 'handle' with which to accomplish ITO surface modification in a well controlled, systematic way, and because they react with surface OH groups, organometallic species seem perfectly set up to enhance, on the molecular level, the interface between an oxide-based inorganic electrode and an organic overlayer.

Metal alkoxides react with OH groups of metal oxides to give surface organometallic complexes by protolytic loss of one or more alkoxide ligands [6–10]. Alkoxide ligands remaining in the coordination sphere of the metal following 'chemisorption' can react by ligand metathesis to give families of new surface-bound complexes from a common precursor [11–16]. Tetra(*tert*-butoxy)zirconium (**1**) is a particularly useful 'linker' to interface metal oxide surfaces with organic materials. Reaction of **1** with ITO/glass was accomplished both in ultrahigh vacuum (UHV) and under 'normal' laboratory conditions (10^{-2}–10^{-4} Torr). Products were determined in UHV using reflectance–absorbance IR spectroscopy (FT-RAIRS), X-ray photoelectron spectroscopy (XPS), and thermally programmed desorption mass spectrometry (TDS), all of which indicated the presence of *tert*-butoxy ligation. Chemisorption involves protolytic loss primarily of one *tert*-butoxide ligand to give **2**; a small amount of **2′**, formed by a second protonolysis step, may also be present at room temperature. A similar deposition stoichiometry is to be expected for reaction of **1** with ITO/glass under 'normal' laboratory conditions (Scheme 1).

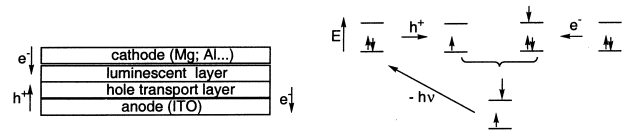
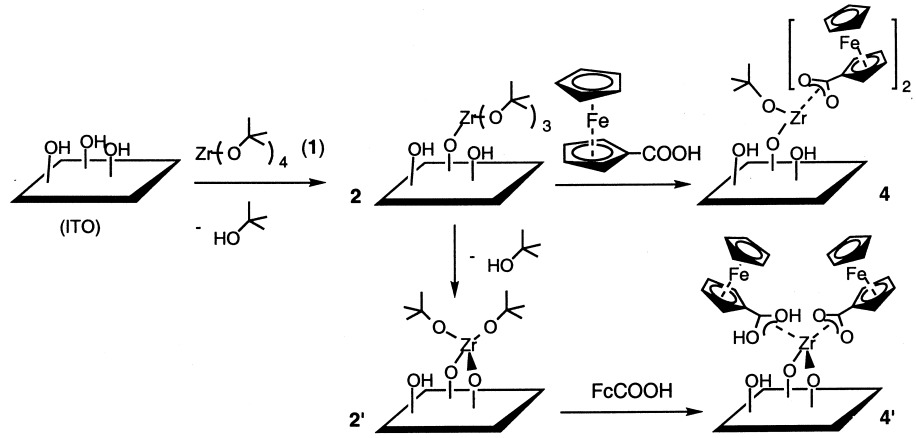


Fig. 1. Schematic diagram of a simple OLED.

Ligand metathesis of **2**/**2′** with simple carboxylic acids [16] was modeled in UHV using Al-bound Zr alkoxide complexes [11]. Carboxylate-for-alkoxide exchange was accomplished by repetitive dosing of the substrate with butanoic acid at 170 K, followed by heating to 300 K. FT-RAIRS analysis after one cycle of treatment of **1** with 0.6×10^{-6} Torr-sec. of butanoic acid showed both alkoxide and carboxylate ligands. Even after eleven further 'dose–desorb' cycles, FT-RAIRS showed only two *tert*-butoxy ligands had been exchanged for butanoate ligands, to give butanoate com-

* Corresponding author. Tel.: +1-609-258-3926; fax: +1-609-258-2383; e-mail: jschwartz@chemvax.princeton.edu

0277-5387/00/$ - see front matter ©2000 Elsevier Science Ltd All rights reserved.
PII S0277-5387(99)00395-2

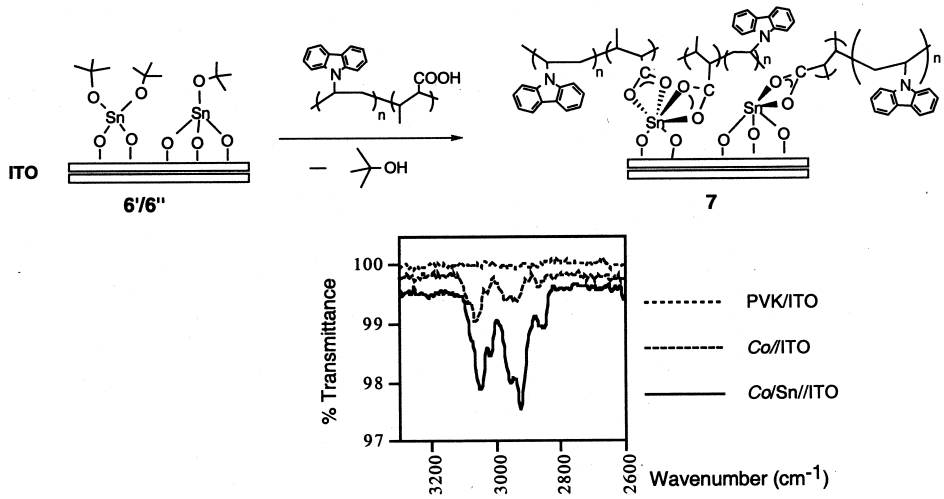


Scheme 1. Synthesis of surface organometallic complexes on ITO.

plexes **3**/**3**′. Reaction of **3**′ with a third equivalent of carboxylic acid may be sterically unfavorable.

Surface hydroxylated ITO/glass was treated with vapor of **1** to give **2**/**2**′; slides were then sprayed with an aerosol of a 1 mM solution of ferrocenecarboxylic acid (FcCOOH) in ether, dried, washed, and dried again, to give **4** and **4**′ [15]. ITO/glass electrodes coated with **4**/**4**′ were rinsed thoroughly and subjected to electrochemical analysis. The cyclic voltammogram of the **4**/**4**′-modified ITO electrode showed a redox peak at $E_{1/2} = 0.55$ V versus SCE, which is reasonable for a surface bound carboxyferrocene derivative [17,18]. The loading density of surface-bound ferrocene carboxylate ligands of **4**/**4**′ onto ITO was determined by chronocoulometry [19] to be 1.01×10^{-10} mol cm^{-2}. Assuming that there are two ferrocenecarboxylate ligands in **4**/**4**′, then the amount of **4**/**4**′ on the surface per nominal unit area is ca. 5×10^{-11} mol cm^{-2}, comparable to the amount reported by 'self-assembly' of elaborated ferrocenyl derivatives on ITO [18,20–22]. Importantly, our studies show that the redox properties of the FcCOOH-derived reagent have not been changed significantly by its incorporation into a surface organometallic complex: The surface complex does not constitute an insulating barrier.

Tin interfaces are attractive for ITO surface modification, in that their use does not entail introduction of a new metallic species, such as Zr. UHV stoichiometric determination for reaction products of ITO/glass and tetra(*tert*-butoxy)tin (**5**) indicated a mixture of tin analogs of **2**/**2**′ (**6**/**6**′/**6**″), similar to that found for deposition of **5** onto hydroxylated Ti [10]. It is interesting that both on ITO and on oxidized metals, Sn alkoxides are more reactive toward multiple chemisorption than are Zr analogs [7]. Polyvinylcarbazole (PVK) is an HTL material of significance for polymer-based OLEDs [23], but PVK does not adhere well to untreated ITO. We prepared a co-polymer of polyvinylcarbazole and crotonic acid, which incorporates a low level of the acidic component, by polymerizing a large excess of vinylcarbazole (relative to crotonic acid) using AIBN initiation [24]. The co-polymer adhered [14] better to ITO than did PVK, but it adhered even better in the presence of **6**′/**6**″, which gives **7** (see Scheme 2). Using typical spin-coating techniques, we were able to prepare a simple OLED with **7**. Analysis of current versus voltage for this simple device indicated much higher carrier mobility compared with a device prepared simply by spin-coating a solution of PVK onto untreated ITO.



Scheme 2. Preparation of PVK co-polymer/ITO via an Sn interface.

An interesting model to facilitate 'hole injection' from ITO into an HTL material involves the organization of a dipole at the surface of the ITO [3,25]. Phenols are acidic compared to *tert*-butanol, and we find that **2**/**2′** react with phenols from the gas phase to give products of ligand metathesis in which *tert*-butoxy ligands are replaced by phenoxides [13]. A series of substituted phenolic compounds was reacted with **2**/**2′** to give a family of similar phenoxyzirconium complex surface materials. An analogous series was made using **6′**/**6″**. Surface phenoxides were structurally elucidated though a combination of FT-RAIRS, XPS and TPD measurements. Functional studies of Zr and Sn phenoxides on ITO are now underway.

In conclusion, we have shown that covalently binding a metallic complex interface to the surface of ITO can enhance interactions between generally hydrophobic organic materials and the hydrophilic oxide substrate surface. In conventional cases, the interaction between such organic materials and the oxide surface would depend on either hydrogen bonding effects or Lewis acid/Lewis base interactions. However, for an oxide such as ITO which is not heavily hydroxylated, and for tertiary amines such as are present in PVK, hydrogen bonding and Lewis acid/Lewis base interactions will likely be weak. In marked contrast, using the metallic interface, strong covalent bonding can be effected irreversibly between the substrate and the organic material.

References

[1] S.R. Forrest, P.E. Burrows, M.E. Thompson, Laser Focus World 31 (1995) 99.
[2] P.E. Burrows, G. Gu, V. Bulovic′, Z. Shen, S.R. Forrest, M.E. Thompson, Achieving Full-Color Organic Light Emitting Devices for Lightweight, Flat-Panel Displays, vol. 44, Institute of Electrical and Electronics Engineers, New York, 1997.
[3] C.W. Tang, S.A. VanSlyke, Appl. Phys. Lett. 51 (1987) 913.
[4] N.C. Greenham, S.C. Moratti, D.D.C. Bradley, R.H. Friend, A.B. Holmes, Nature 365 (1993) 628.
[5] H. Antoniadis, J.N. Miller, D.B. Roitman, I.H. Cambell, IEEE Trans. Electron Devices 44 (1997) 1289.
[6] G. Lu, K.L. Purvis, J. Schwartz, S. Bernasek, Langmuir 13 (1997) 5791.
[7] G. Lu, J. Schwartz, S.L. Bernasek, Langmuir 14 (1998) 1532.
[8] J.B. Miller, J. Schwartz, S.L. Bernasek, J. Am. Chem. Soc. 115 (1993) 8239.
[9] J.B. Miller, S.L. Bernasek, J. Schwartz, J. Am. Chem. Soc. 117 (1995) 4037.
[10] K.L. Purvis, G. Lu, J. Schwartz, S.L. Bernasek, Langmuir 15 (1999) 7092.
[11] K.L. Purvis, G. Lu, J. Schwartz, S.L. Bernasek, Langmuir 14 (1998) 3720.
[12] E.S. Gawalt, G. Lu, S.L. Bernasek, J. Schwartz, Langmuir 15 (1999) 8929.
[13] S.K. VanderKam, G. Lu, S.L. Bernasek, J. Schwartz, J. Am. Chem. Soc. 119 (1997) 11639.
[14] S.K. VanderKam, A.B. Bocarsly, J. Schwartz, Chem. Mater. 10 (1998) 685.
[15] S.K. VanderKam, E.S. Gawalt, J. Schwartz, A.B. Bocarsly, Langmuir 15 (1999) 6598.
[16] Y.G. Aronoff, B. Chen, G. Lu, C. Seto, J. Schwartz, S.L. Bernasek, J. Am. Chem. Soc. 119 (1997) 259.
[17] M.S. Wrighton, M.C. Palazzotto, A.B. Bocarsly, J.M. Bolts, A.B. Fischer, L. Nadjo, J. Am. Chem. Soc. 100 (1978) 7264.
[18] T.J. Gardner, C.D. Frisbie, M.S. Wrighton, J. Am. Chem. Soc. 117 (1995) 6927.
[19] F.C. Anson, R.A. Osteryoung, J. Chem. Ed. 60 (1983) 293.
[20] K. Chen, B.R. Herr, E.T. Singewald, C.A. Mirkin, Langmuir 8 (1992) 2585.
[21] B.R. Herr, C.A. Mirkin, J. Am. Chem. Soc. 116 (1994) 1157.
[22] G. Zotti, G. Schiavon, S. Zecchin, A. Berlin, G. Pagani, A. Canavesi, Langmuir 13 (1997) 2964.
[23] J. Kido, H. Shionoya, K. Nagai, Appl. Phys. Lett. 16 (1995) 2281.
[24] S.J. Woodson, S.K. VanderKam, J. Schwartz, unpublished results, 1998.
[25] R.W. Zehner, B.F. Parsons, R.P. Hsung, L.R. Sita, Langmuir 15 (1999) 1121.

PERGAMON

www.elsevier.nl/locate/poly

Polyhedron 19 (2000) 509–512

POLYHEDRON

Sol–gel entrapped heteronuclear transition metal catalysts

Jochanan Blum [a,*], Faina Gelman [a], Raed Abu-Reziq [a], Irena Miloslavski [a], Herbert Schumann [b], David Avnir [a]

[a] *Department of Organic Chemistry, Hebrew University, Jerusalem 91904, Israel*
[b] *Institut für Anorganische und Analytische Chemie, Technische Universität Berlin, D-10623 Berlin, Germany*

Received 4 October 1999; accepted 17 November 1999

Abstract

The heteronuclear complexes $[(CO)_4Fe(\mu\text{-}PPh_2)Pd(\mu\text{-}Cl)_2]_2$, $[Et_4N][FeCo_3(CO)_{12}]$ and $Rh_2Co_2(CO)_{12}$ were physically entrapped in SiO_2–sol–gel matrices. The doped materials, so formed, were utilized as recyclable catalysts for (a) selective isomerization of 1-octene, (b) selective dimerization of norbornadiene to 'binor-S', and (c) hydrogenation and hydrogenolysis of styrene, nitrobenzene and 1-chloronaphthalene, respectively. During the hydrogenation of the nitrobenzene and of chloronaphthalene, the dodecacarbonylbis(cobalt)dirhodium was converted into sol–gel entrapped carbonyl-free nanoparticles that efficiently catalyze the reduction of the aromatic C–C bonds.
©2000 Elsevier Science Ltd All rights reserved.

Keywords: Heteronuclear catalysts; Immobilization; Nanoparticles; Sol–gel matrices

1. Introduction

Recent studies on heterogenizing of homogeneous transition metal catalysts revealed that physical entrapment of a wide range of mono- and homobimetallic complexes in SiO_2–sol–gel matrices does not only permit facile recycling of the encapsulated catalysts, but often also increases their stability and improves their catalytic properties [1]. In recent years, heteropolynuclear catalysts have become of particular interest. Synergistic effects that may exist in such compounds are responsible for their unusually high catalytic potency and/or their ability to promote unique organic processes [2]. However, under homogeneous conditions, many mixed-metal complexes tend to dissociate or to disproportionate and to yield either mononuclear or homopolynuclear species. With the objective of overcoming this discrepancy, we have now investigated the immobilization of three model heterobimetallic complexes by their entrapment in sol–gel glasses, and studied some of the catalytic properties of the resulting hybrid materials.

2. Experimental: entrapment of mixed-metal complexes in sol–gel matrices

2.1. (2Fe–Pd)octacarbonyl[μ-(di-μ-chlorodipalladio)-bis(μ-diphenylphosphino)]diiron

A Schlenk tube was charged under Ar atmosphere with 30 mg of $[(CO)_4Fe(\mu\text{-}PPh_2)Pd(\mu\text{-}Cl)]_2$ [3] in 4 ml of dry THF. To the clear stirred solution were injected 3.2 ml of degassed *tert*-BuOH and 2.0 ml of $SiCl_4$. Stirring was continued until gelling occurred (4 h). The gel was left for aging for 24 h and dried at 1 mm for 24 h. The sol–gel material was treated under exclusion of air for 1 h with 20 ml of boiling CH_2Cl_2, sonicated in the same solvent at room temperature, and dried at 1 mm to constant weight (3 h).

2.2. Tetraethylamminium(3Co–Co)(3Co–Fe)tricarbonyl-(tri-μ-carbonylhexacarbonyltricobaltate)ferrate(1−)

A flask was charged under N_2 with 1.2 ml of HCl solution of pH 1.9, 2.5 ml of $Si(OMe)_4$ and 3.5 ml of MeOH. The mixture was stirred magnetically for 20 min and the pH was raised by addition of 0.44 ml of 0.1 N aqueous NH_3. To the mixture was added at once a solution of 30 mg of $[Et_4N][FeCo_3(CO)_{12}]$ [4] in 4 ml of dry THF. Stirring was continued until complete gelation (4–5 h). The gel was left

* Corresponding author. Tel.: +972-2-658 5329; fax: +972-2-651 3832; e-mail: jblum@chem.ch.huji.ac.il

0277-5387/00/$ - see front matter ©2000 Elsevier Science Ltd All rights reserved.
PII S0277-5387(99)00396-4

for aging for 2 days, dried at 1 mm, washed thoroughly with 20 ml of CH_2Cl_2 and sonicated for 30 min in the same solvent. Finally, the glass was dried to constant weight.

2.3. (Co–Co)(4Co–Rh)(Rh–Rh)tri-μ-carbonyltetracarbonyl(pentacarbonyldicobalt)dirhodium

To a stirred solution of 19.8 mg of $Rh_2Co_2(CO)_{12}$ [5] in 1 ml of benzene was added under N_2 2.5 ml of MeOH. After a further 5 min, 2.4 ml of water were added. The mixture was then treated with 3.5 ml of $Si(OMe)_4$ and the stirring was continued until gelation occurred (usually 2–3 h). The sol–gel material, so formed, was dried at 0.1 mm for 20 h, washed and sonicated twice with 20 ml of benzene and dried again for 2 h at 0.1 mm.

3. Results and discussion

Each of the three mixed metal complexes was entrapped in a sol–gel matrix in a different way. The water sensitive isomerization catalyst $[(CO)_4Fe(\mu\text{-}PPh_2)Pd(\mu\text{-}Cl)]_2$ [6] was immobilized by a non-hydrolytic process in which the complex was added to a polycondensation reaction mixture of $SiCl_4$ and *tert*-BuOH in THF. Although the interaction of *tert*-butanol and silicon halides is a known procedure for the preparation of sol–gel materials [7], to the best of our knowledge it has not yet been used for molecular entrapment of metallic complexes. FT-IR measurements indicated that during the entrapment all eight CO groups were eliminated. Continuous Soxhlet extraction of the heterogenized complex with CH_2Cl_2 (48 h) gave a paramagnetic mixture whose FAB mass spectrum consisted of the molecular ions of the starting material less 8-CO ($m/z = 762$–768) as well as of THF adducts (up to $m/z \sim 1340$). When a mixture of the entrapped complex and 1-octene (catalyst:substrate molar ratio 1:330) was heated under N_2 at 90°C for 6.5 h most of the alkene was converted into *cis*- and *trans*-2-octene.

$$CH_3(CH_2)_5CH{=}CH_2 \rightarrow$$

$$cis + trans\text{-}CH_3(CH_2)_4CH{=}CHCH_3$$

The seven isomeric octenes could be separated on a 25 m × 0.25 mm CP-Sil 5 capillary column between 50 and 150°C, programmed for a temperature increase of 2°C min^{-1}. Although the heterogenized catalyst was shown to be leach proof and recyclable, its selectivity decreased in the second run owing to clogging of some pore entrances [8]. Reopening of the pores was accomplished by initial sonication with CH_2Cl_2 (30 min) followed by treatment with hot water (80°C, 30 min) and drying. After such treatment the activity and selectivity of the catalyst did not change further. A representative set of experiments of the [Fe–Pd]-catalyzed isomerization of 1-octene is summarized in Table 1. Unlike the isomerization by the homogeneous complex [9], the heterogenized catalyst did not require the presence of MeOH.

It is remarkable that after the entrapment of the bimetallic catalyst it became insensitive to water. Under 40 atm of CO at 100°C and a catalyst:substrate ratio of 1:50 it even promoted the hydration of acetylenes in aqueous dioxane containing 10% of H_2O:

$$C_6H_5C{\equiv}CH + H_2O \xrightarrow[63\%]{10\ h} C_6H_5COCH_3$$

The entrapment of the norbornadiene dimerization catalyst $[Et_4N][FeCo_3(CO)_{12}]$ [10] in a sol–gel matrix was best accomplished by a two-step process, in which $Si(OMe)_4$ was first hydrolyzed at low pH to polysilicic acids which in turn were treated with aqueous NH_3 and a THF solution of the mixed metal complex [11].

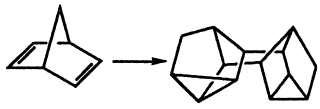
FT-IR studies revealed that upon this encapsulation of the cluster in the sol–gel matrix, no considerable structural changes in the complex took place. The homogeneous and the entrapped catalyst, before and after application (vide infra), showed *the same* C–O stretching vibrations (KBr pellets) at 2061, 2010, 1992, 1965, 1924 and 1815 cm^{-1} (cf. [4]). When a mixture of norbornadiene (2.97 mmol), $BF_3 \cdot OEt$ (0.49 mmol), the encapsulated catalyst (containing 0.1 mmol of the Fe–Co complex) and 2 ml of acetone was heated for 1 h at 48°C, a quantitative yield of dodecahydro-1,2,4:5,6,8-dimetheno-*s*-indecene ('binor-S') free of any other norbornadiene dimer was isolated. Under the same conditions a quantitative yield of 'binor-S' was obtained also in the second run, but the catalysis slowed down in the third and

Table 1
Isomerization of 1-octene by the sol–gel entrapped [Fe–Pd] catalyst [a]

Run	Composition of reaction mixture after 6.5 h (%)				
	1-octene	*cis*-2-octene	*trans*-2-octene	*trans*-3-octene	*trans*-4-octene
1	1	17	48	27	7
2 [b]	10	17	38	25	10
3	8	19	49	18	6
4	8	19	49	18	6
5	8	19	49	18	6

[a] Reaction conditions: 9.9 mmol of 1-octene, 3×10^{-2} mmol catalyst, 90°C.
[b] After the second run the catalyst was treated with water at 80°C.

fourth runs (conversions after 1 h were 93 and 88%, respectively) owing to partial pore clogging in the hybrid catalyst.



The complex $Rh_2Co_2(CO)_{12}$ [5] could be entrapped in sol–gel matrices by the conventional method in which a benzene solution of the tetranuclearic cluster was added to a reaction mixture of $Si(OMe)_4$, H_2O and MeOH during the 'one-step' polycondensation process [11]. Unlike the homogeneous complex which tends to disproportionate in various media into rhodium and cobalt carbonyls [12,13], the sol–gel entrapped version seems to preserve its original structure. Thus, the C–O bonds of the non-entrapped compounds (in pentane) at 1855, 1871, 1885, 1910, 1920, 2038, 2059, 2064 and 2074 cm^{-1} [5] were shifted only slightly (KBr pellets) to 1857, 1869, 1888, 1908, 1919, 1941, 2040, 2055 and 2069 cm^{-1}. When the immobilized catalyst was employed in the hydrogenation of styrene (1.7 mmol substrate, 0.015 mmol catalyst, 3.4 atm H_2, 10 ml hexane, 30°C, 22 h) a quantitative yield of ethylbenzene was obtained.

$$C_6H_5CH{=}CH_2 + H_2 \rightarrow C_6H_5CH_2CH_3$$

During the next five runs the results did not change but the metal carbonyl peaks gradually became weaker. The reaction could be enhanced by increasing the temperature to 60°C. (Under the same conditions at 30°C the non-encaged cluster yielded only 62% of ethylbenzene.) Nitrobenzene reacted with hydrogen only above 60°C. The mixture of products in the first four runs consisted, after 22 h, of the following respective amounts of aniline and of aminocyclohexane: first run 96 and 4%; second run 64 and 36%; third run 16 and 84%; fourth run 2 and 98%.

$$C_6H_5NO_2 + H_2 \rightarrow C_6H_5NH_2 + C_6H_{11}NH_2$$

A similar change in product distribution was observed during the hydrogenation of 1-chloronaphthalene. Under the above conditions the chloroarene was transferred in the first three runs of 22 h to 5-chlorotetralin, *cis*-decaline and *trans*-decaline in the following respective amounts: first run 29, 58 and 8%; second run 11, 72 and 12%; third run 6, 82 and 12%.

$$1\text{-}ClC_{10}H_7 + H_2 \rightarrow 5\text{-}ClC_{10}H_{11} + \textit{cis}\text{-}C_{10}H_{12} + \textit{trans}\text{-}C_{10}H_{12}$$

High resolution transition electron microscopy (TEM) studies of the hybrid catalyst before and after the hydrogenation processes revealed that during the catalyses of nitrobenzene and 1-chloronaphthane (but not during the reaction of styrene), metallic nanoparticles of 2–3 nm diameter are formed (see Fig. 1). Energy dispersive X-ray microanalysis (EDX), which was used in conjunction with TEM, failed to indicate the presence of metal lattices in the particles, which suggests that the particles are composed of a Rh–Co alloy [14].

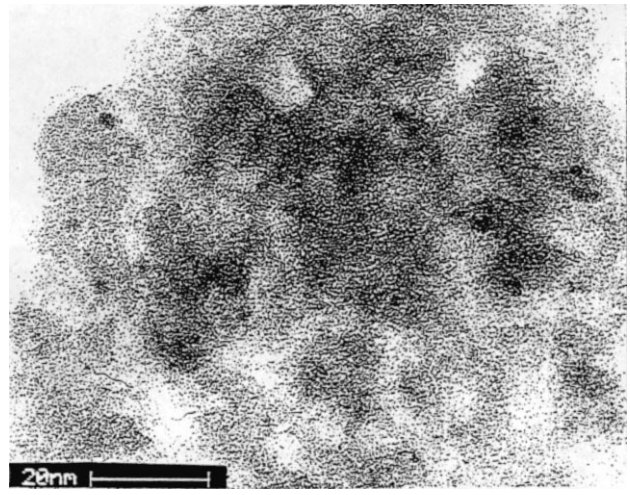


Fig. 1. Transmission electron micrograph of sol–gel entrapped $Rh_2Co_2(CO)_{12}$ after its use as catalyst for hydrogenation of nitrobenzene (fourth run).

While the sol–gel entrapped nanoparticles catalyze the hydrogenation of aromatic C–C bonds in nitroarenes and chloroarenes, they fail to promote the reduction of the aromatic ring in styrene. In fact, the presence of styrene during the hydrogenation of nitrobenzene leads only to the formation of aniline. However, after the consumption of the styrene in a hydrogenation process, the used catalyst promotes the transformation of nitrobenzene to aminocyclohexane. Phenylacetylene, like styrene, is reduced (at 60°C) to ethylbenzene rather than to ethylcyclohexane.

4. Conclusions

The results of this study show that sol–gel entrapped heteronuclear clusters preserve the unique catalytic properties of the homogeneous compounds. The encaging process can be accomplished under hydrolytic or non-hydrolytic conditions and may be associated with extrusion of CO ligands. Further transformation of the encaged mixed-metal carbonyl complexes to catalytically active nanoparticles occurs during ring hydrogenation of nitroarenes and chloroarenes.

Acknowledgements

We thank the German–Israel Foundation for Scientific Research and Development (GIF), the US–Israel Binational Science Foundation and the Israel Science Foundation for financial support of this study. DA also thanks the Israel Ministry of Science for an Infrastructure fund.

References

[1] J. Blum, D. Avnir, H. Schumann, Chemtech. 29 (2) (1999) 32.
[2] P. Braunstein, J. Rose, in: E.W. Abel, F.G.A. Stone, G. Wilkinson, R.D. Adams (Eds.), Comprehensive Organometallic Chemistry II,

vol. 10, Pergamon, Oxford, 1995, pp. 351–385 and refs. cited therein.
[3] B.C. Benson, R. Jackson, K.K. Joshi, D.T. Thompson, J. Chem. Soc., Chem. Commun. (1968) 1506.
[4] A.A. Low, J.W. Lauher, Inorg. Synth. 27 (1990) 188.
[5] S. Martinengo, P. Chini, V.G. Albano, F. Cariati, T. Salvatori, J. Organomet. Chem. 59 (1973) 379.
[6] D.T. Thompson, Platinum Met. Rev. 19 (1975) 88.
[7] R.J.P. Corriu, D. Ledercq, P. Lefèvre, P.H. Mutin, A. Vioux, J. Non-Cryst. Solids 146 (1992) 301.
[8] A. Rosenfeld, D. Avnir, J. Blum, J. Chem. Soc., Chem. Commun. (1993) 583.
[9] G.A. Catton, F.C. Jones, M.J. Mays, J.A.S. Howell, Inorg. Chim. Acta 20 (1976) L41.
[10] C.J. Brinker, K.D. Keefer, D.W. Schaefer, C.S. Ashley, J. Non-Cryst. Solids 48 (1982) 47.
[11] A. Rosenfeld, J. Blum, D. Avnir, J. Catal. 164 (1996) 363.
[12] I.T. Horváth, G. Bohr, M. Garland, P. Pino, Organometallics 5 (1986) 1441.
[13] I.T. Horváth, M. Garland, G. Bohr, P. Pino, J. Organomet. Chem. 358 (1988) C17.
[14] N. Toshima, T. Yonezawa, New J. Chem. (1998) 1179, and Refs. cited therein.

PERGAMON

www.elsevier.nl/locate/poly

Polyhedron 19 (2000) 513–515

POLYHEDRON

Stereoselective hydroformylation, cuprate addition and domino reactions with the aid of a catalyst directing group

Bernhard Breit *, Stephan K. Zahn

Organisch-Chemisches Institut, Ruprecht-Karls-Universität Heidelberg, Im Neuenheimer Feld 270, D-69120 Heidelberg, Germany

Received 4 October 1999; accepted 1 November 1999

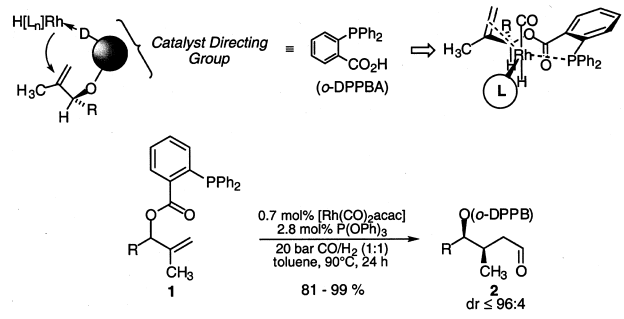
Abstract

Stereoselective hydroformylation and stereoselective conjugate addition to enoates has been achieved in a synthetic sequence employing a substrate-bound catalyst directing the *o*-DPPB group (*o*-DPPB = *ortho*-diphenylphosphanyl benzoate). Furthermore, a stereoselective domino process combining hydroformylation, Wittig olefination and a transition metal catalyzed hydrogenation is described. ©2000 Elsevier Science Ltd All rights reserved.

Keywords: Hydroformylation; Organocopper reagents; Catalysis; Asymmetric synthesis; Domino reactions

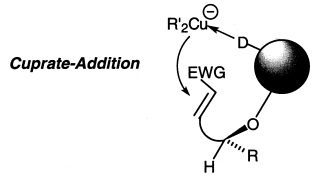
Hydroformylation of olefins is an industrially important homogenously catalyzed C–C bond forming process; for recent reviews, see Refs. [1–4]. However, this important reaction has not found many applications in organic synthesis (for exceptions see Refs. [5–8]). This may be due to the difficulty in controlling stereoselectivity in the course of this reaction; for reviews see Refs. [9–11]. Although some recently developed chiral rhodium catalysts allow for enantioselective and diastereoselective hydroformylation of certain specific classes of alkenes [12–18], only very little is known on the diastereoselective hydroformylation of acyclic olefins (for substrate directed diastereoselective hydroformylation of cyclic systems, see Refs. [19–21]).

We recently devised a solution to this problem making efficient use of substrate direction employing a substrate bound catalyst directing group (CDG) [22–24]. The principles which guided the design of an efficient CDG were as follows: (i) reversible coordination of the catalytically active transition metal center under hydroformylation conditions, (ii) ease of introduction into and removal from the substrate, and (iii) correct geometry to pass a cyclic transition state for the stereochemistry defining step.



A system which proved to be in accord with these criteria is the *ortho*-diphenylbenzoyl group (*o*-DPPB). Introduction of this CDG enabled a stereoselective hydroformylation of methallylic and homomethallylic alcohol derivatives, with high levels of acyclic stereocontrol (**1**→**2**) [22–26].

In order to optimize the CDG concept, it was decided to employ the specifically introduced *o*-DPPB group in a second step, again as a stereochemistry control unit. In this context, the conjugate addition of cuprates to acyclic enoates became of interest.

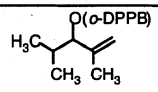
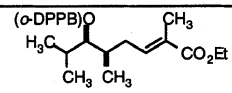
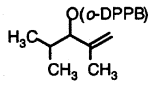
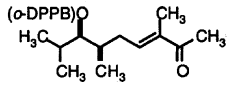
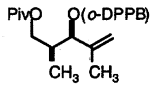
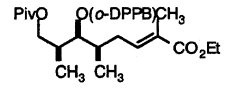
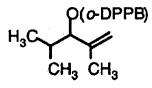
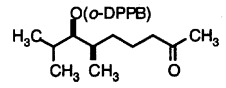
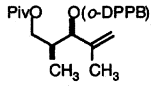
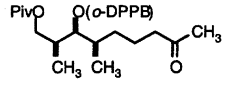
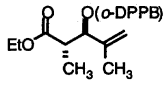
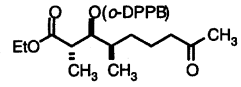
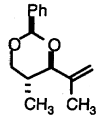
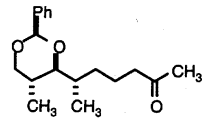
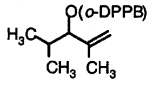
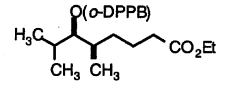
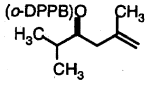
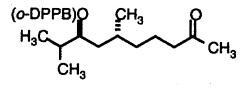


Starting from methallylic *o*-DPPB esters **1**, *o*-DPPB directed hydroformylation (→**2**), HWE olefination (→**3**),

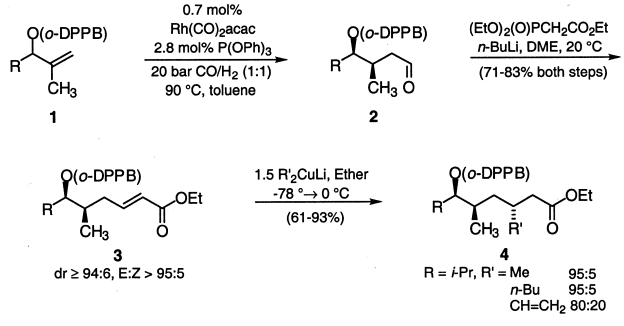
* Corresponding author. Tel.: +49-6221-54-6207; fax: +49-6221-54-4205; e-mail: bernhard.breit@urz.uni-heidelberg.de

0277-5387/00/$ - see front matter ©2000 Elsevier Science Ltd All rights reserved.
PII S0277-5387(99)00397-6

Table 1
Diastereoselective domino-hydroformylation-Wittig and domino-hydroformylation-Wittig-hydrogenation reactions

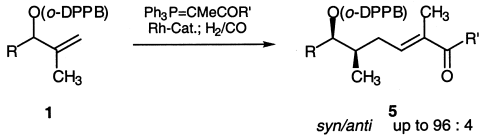
entry	alkene	ylid	major diastereomer	yield (%)	dr (*syn*:*anti*)
1		$Ph_3P{=}CMeCO_2Et$		75	96:4
2		$Ph_3P{=}CMeCOMe$		78	92:8
3		$Ph_3P{=}CMeCO_2Et$		60	92:8
4		$Ph_3P{=}CHCOMe$		70	92:8
5		$Ph_3P{=}CHCOMe$		68	92:8
6		$Ph_3P{=}CHCOMe$		60	90:10
7		$Ph_3P{=}CHCOMe$		78[d]	> 98:2
8		$Ph_3P{=}CHCO_2Et$		36	92:8
9		$Ph_3P{=}CHCOMe$		82	91:9

followed by an *o*-DPPB directed cuprate addition gave the corresponding *anti*-conjugate adducts **4** in good yield and diastereoselectivity. Control experiments indicated that the *o*-DPPB group controls both the reactivity and diastereoselectivity [27].

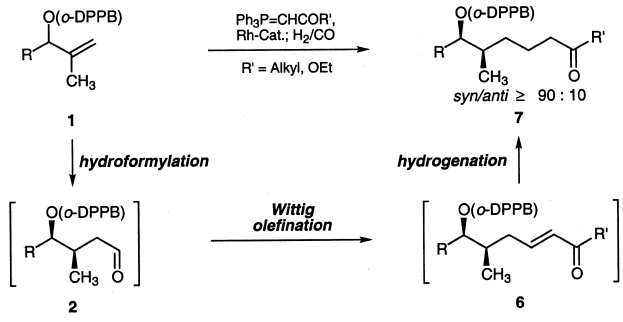


Combining, *o*-DPPB directed hydroformylation, HWE olefination, and *o*-DPPB directed cuprate addition gave access to building blocks with up to four stereogenic centers.

In order to improve the synthetic efficiency of an *o*-DPPB directed hydroformylation reaction, one may want to employ this reaction as a part of sequential transformations. In this regard the hydroformylation should be ideally suited, since a synthetically most valuable aldehyde functionality is generated under mild reaction conditions. This aldehyde may be reacted with carbon nucleophiles to allow for further skeleton extending processes in a one-pot operation. Thus, hydroformylation of methallylic *o*-DPPB esters **1** in the presence of disubstituted Wittig-ylids furnished the trisubstituted alkenes **5** in good yield and diastereoselectivity. These are the first examples of a domino-hydroformylation-Wittig reaction (see Table 1) [28–31].



Interestingly, when using mono-substituted Wittig-ylids the saturated derivatives **7** were obtained (see Table 1). These compounds result from three sequential reactions: step 1 is the hydroformylation reaction to give the aldehyde **2** which is olefinated in step 2 with the Wittig-ylid present ($\rightarrow$**6**); finally, a transition metal catalyzed hydrogenation of the alkene finishes the sequence of reactions and provides the saturated products **7** in good yield and diastereoselectivity.



Since the hydroformylation is the stereochemistry defining step, one could make use of both 1,2- and 1,3-asymmetric induction employing the CDG concept (entries 1–6, 8, 9, Table 1). Alternatively, one could employ substrate control via conformational constraints to give an all-*anti* stereotriad building block (entry 7).

As a result of its mild nature, this domino process may allow the coupling of any two given complex building blocks within the context of a convergent synthesis strategy.

Acknowledgements

This work was supported by the Fonds der Chemischen Industrie (fellowship to S.K.Z.), the Deutsche Forschungsgemeinschaft (SFB 260, Philipps-Universität Marburg) and the Otto Röhm Gedächtnisstiftung. We thank BASF and Degussa for their gift of chemicals.

References

[1] J.A. Moulijn, P.W.N.M. van Leeuwen, R.A. van Sauten, Catalysis — An Integrated Approach to Homogenous, Heterogenous and Industrial Catalysis, Elsevier, Amsterdam, 1995, p. 199.
[2] C.D. Frohning, C.W. Kohlpaintner, in: B. Cornils, W.A. Herrmann (Eds.), Applied Homogeneous Catalysis with Organometallic Compounds, VCH, Weinheim, 1996, p. 29.
[3] M. Beller, B. Cornils, C.D. Frohning, C.W. Kohlpaintner, J. Mol. Catal. A 104 (1995) 17.
[4] J.K. Stille, in: B.M. Trost, I. Fleming (Eds.), Comprehensive Organic Synthesis, vol. 4, Pergamon, Oxford, 1991, p. 913.
[5] S.D. Burk, J.E. Cobb, K. Takeuchi, J. Org. Chem. 55 (1990) 2138.
[6] T. Takahashi, K. Machida, Y. Kido, K. Nagashima, S. Ebata, T. Doi, Chem. Lett. (1997) 1291.
[7] B. Breit, S.K. Zahn, Tetrahedron Lett. 39 (1998) 1901.
[8] I. Ojima, E.S. Vidal, J. Am. Chem. Soc. 63 (1998) 7999.
[9] P. Eilbracht, in: G. Helmchen, R.W. Hoffmann, J. Mulzer, E. Schaumann (Eds.), Houben-Weyl, Methods of Organic Synthesis, E 21c, Stereoselective Synthesis, Thieme, Stuttgart, 1995, p. 2488.
[10] F. Agbossou, J.-F. Carpentier, A. Mortreux, Chem. Rev. 95 (1995) 2485.
[11] S. Gladiali, J.C. Bayón, C. Claver, Tetrahedron Asymm. 6 (1995) 1453.
[12] N. Sakai, S. Mano, K. Nozaki, H. Takaya, J. Am. Chem. Soc. 115 (1993) 7033.
[13] N. Sakai, K. Nozaki, H. Takaya, J. Chem. Soc., Chem. Commun. (1994) 395.
[14] K. Nozaki, N. Sakai, T. Nanno, T. Higashijima, S. Mano, T. Horiuchi, H. Takaya, J. Am. Chem. Soc. 119 (1997) 4413.
[15] T. Horiuchi, T. Ohta, E. Shirakawa, K. Nozaki, H. Takaya, Tetrahedron 53 (1997) 7795.
[16] K. Nozaki, W. Li, T. Horiuchi, H. Takaya, Tetrahedron Lett. 38 (1997) 4611.
[17] T. Horiuchi, T. Ohta, E. Shirakawa, K. Nozaki, H. Takaya, J. Org. Chem. 62 (1997) 4285.
[18] J.E. Babin, G.T. Todd, Union Carbide, IPN: WO93/03839.
[19] S.D. Burke, J.E. Cobb, Tetrahedron Lett. 27 (1986) 4237.
[20] W.R. Jackson, P. Perlmutter, E.E. Tasdelen, J. Chem. Soc., Chem. Commun. (1990) 763.
[21] T. Doi, H. Komatsu, K. Yamamoto, Tetrahedron Lett. 37 (1996) 6877.
[22] B. Breit, Angew. Chem. 108 (1996) 3021; Angew. Chem., Int. Ed. Engl. 35 (1996) 2835.
[23] B. Breit, Liebigs Ann. (1997) 1841.
[24] B. Breit, M. Dauber, K. Harms, Chem. Eur. J. 5 (1999) 2819.
[25] B. Breit, Chem. Commun. (1997) 591.
[26] B. Breit, Eur. J. Org. Chem. (1998) 1123.
[27] B. Breit, Angew. Chem. 110 (1998) 535.
[28] B. Breit, Angew. Chem., Int. Ed. Engl. 37 (1998) 525.
[29] B. Breit, S.K. Zahn, Angew. Chem. 111 (1999) 1022.
[30] B. Breit, Angew. Chem., Int. Ed. Engl. 38 (1999) 969.
[31] B. Breit, Tetrahedron Lett. 39 (1998) 5163.

PERGAMON

www.elsevier.nl/locate/poly

Polyhedron 19 (2000) 517–520

POLYHEDRON

The Heck reaction: mechanistic insights and novel ligands

Michael Casey *, John Lawless, Colette Shirran

Chemistry Department, University College Dublin, Belfield, Dublin 4, Ireland

Received 4 October 1999; accepted 6 December 1999

Abstract

The kinetics of the Heck reaction of aryl iodides with methyl acrylate using phosphane ligands were studied. Triphenylphosphane strongly inhibited the reaction when used in excess over the Pd(0) precatalyst. The rate of reaction was found to be weakly dependent on the concentrations of both the aryl iodide and the alkene. The results indicate that the migratory insertion step is turnover limiting, with the oxidative addition to the aryl iodide being faster but not negligible. Phosphane sulfane hemilabile ligands were found to give good yields and good catalyst stability in Heck reactions. ©2000 Elsevier Science Ltd All rights reserved.

Keywords: Heck reactions; Palladium; Phosphane; Sulfane; Ligands; Mechanism

1. Introduction

The Heck reaction has developed into an extremely important synthetic method [1–4]. Nevertheless, there is scope for further improvement, for example in developing catalysts which give greater reactivity or enantioselectivity. We were interested in studying ligands containing sulfur donors because, despite their extensive coordination chemistry [5,6], such ligands have not often been applied in transition metal catalysis [7–13]. Phosphane ligands are frequently employed in the Heck reaction, so we decided initially to carry out a semiquantitative kinetic comparison of our new ligands with triphenylphosphane. Surprisingly, although the individual steps of the catalytic cycle have been studied in detail [14–17], very few studies of the kinetics of the Heck reaction using phosphorus ligands have been reported [18–20]. We now report our preliminary observations on the kinetics of Heck reactions of aryl iodides.

2. Experimental

Kinetics runs were carried out by adding a freshly prepared solution of $Pd_2dba_3 \cdot CHCl_3$ or $Pddba_2$ (0.02–0.05 mmol) in DMF (1 ml) to the reaction mixture consisting of iodobenzene (1 mmol), methyl acrylate (1.2 equiv.), ligand (0.02–0.08 equiv.), DIPEA (5 equiv.) and pentamethylbenzene (internal standard for GC analysis), in dry DMF (5–20 ml), at room temperature. After stirring for 10 min, the mixture was heated to the required temperature. All steps were performed under an atmosphere of nitrogen. Samples were withdrawn periodically and analysed by GC. All kinetics experiments were carried out at least twice.

3. Results and discussion

The model Heck reaction studied was the addition of iodobenzene to methyl acrylate to give methyl cinnamate (Fig. 1). Use of $Pd_2dba_3 \cdot CHCl_3$ and $Pddba_2$ as precatalysts gave essentially identical results. Early runs at 50°C, using 4% Pd and 8% ligand, revealed an induction period, during which the rate was negligible. During this phase the reaction mixtures remained pale yellow in colour, but they darkened quickly once product formation had begun, to give wine coloured solutions. When the reactions got underway the decay of iodobenzene and the formation of methyl cinnamate appeared to be roughly exponential, but the rates decreased substantially towards the end. All of the PhI was consumed, but only ca. 65% yields of product were obtained.

The length of the induction period correlated strongly with the initial ratio of PPh_3 to Pd, varying from ca. 700 min for a 4:1 ratio to ca. 30 min for a 1.1:1 ratio. Addition of CuI, which is known to bind to PPh_3 [21], caused a significant reduction in the induction period. When $Pd(OAc)_2/2PPh_3$ was the catalyst precursor, only a short induction period was observed (ca. 30 min). Presumably, 1 equiv. of PPh_3 was

* Corresponding author. Tel.: +353-1-706-2420; fax: +353-3-706-2127; e-mail: mike.casey@ucd.ie

0277-5387/00/$ - see front matter ©2000 Elsevier Science Ltd All rights reserved.
PII S0277-5387(99)00398-8

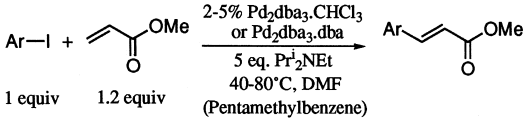


Fig. 1. The model Heck reaction.

consumed in reducing the $Pd(OAc)_2$ [22], so that the initial PPh_3:Pd(0) ratio was 1:1. When an additional 0.5 equiv. of PPh_3 relative to Pd was added to a reaction mixture after ca. 40% product formation, the reaction stopped completely for 155 min, after which it continued to completion, albeit at a slower rate. These experiments showed that when the PPh_3:Pd ratio exceeds 1:1 the reaction is *strongly* inhibited. With higher initial ratios, the PPh_3 is slowly oxidised by traces of air, until most of the excess is destroyed, and the overall rate then increases dramatically. We thought that catalyst decomposition might be responsible for the observed curvature of the graphs of product concentration against time. The amount of Pd was therefore increased from 4% to 10%, only 11% of PPh_3 was employed to keep the induction period to a minimum, and the temperature was reduced to 40°C. GC analysis produced straight line graphs of product concentration versus time, with tailing at the end (Fig. 2). Virtually no induction period was observed, but again only ca. 60% yield of methyl cinnamate was obtained. The results suggested that the reaction was proceeding with pseudo zero order kinetics (constant [Pd]). The reactions of 4-iodotrifluoromethylbenzene and 4-fluoroiodobenzene with methyl acrylate, and the reaction of iodobenzene with styrene, which were slower than the model reaction, also showed linear behaviour.

A series of experiments was performed using 10% Pd and 11% PPh_3 at 40°C, varying the initial concentrations of substrates. The rate of reaction in the initial linear phase was calculated in each case, but we were unable to obtain quantitatively reproducible rates. To minimise sources of error, the reactions were then carried out in batches of three, prepared by dividing one solution of catalyst, ligand, base and one substrate in three, and adding different quantities of the second substrate. The three reactions were then treated identically. Although the rate constants still showed some variability, the trends observed within these series of triple

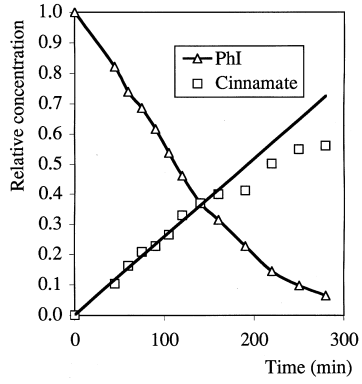


Fig. 2. Product concentration vs. time.

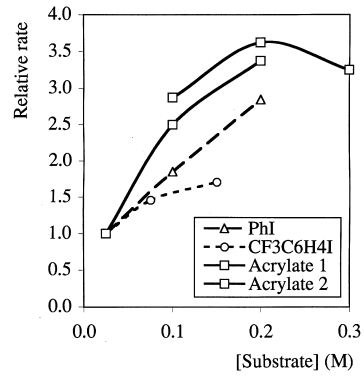


Fig. 3. Relative rate of the reaction vs. substrate concentration.

experiments were reproducible (Fig. 3). The initial rate was found to be weakly dependent on the concentration of iodobenzene, with a ca. three-fold rate increase on an eight-fold increase in [PhI]. A weaker dependence of rate on aryl iodide concentration was observed for the reaction of 4-iodotrifluoromethylbenzene with methyl acrylate at 75°C. The initial rate increased by a factor of ca. 2 on increasing [acrylate] by a factor of eight and the dependence was suggestive of saturation behaviour. The weak dependence on substrate concentration is consistent with the approximate straight line kinetics depicted in Fig. 2, with curvature at high conversions.

In these model reactions only ca. 60% yields of methyl cinnamate were obtained even though virtually all the iodobenzene had been consumed. Benzene seemed a likely by-product as there are reports of reduction of aryl halides under Heck conditions [23,24]. Indeed, GC showed that benzene was formed and ^{19}F NMR analysis of a 4-fluoroiodobenzene reaction showed that fluorobenzene was the only significant by-product. The reduction can be accounted for by coordination of DIPEA to the PhPdI oxidative addition complex, and β-H elimination of the amine [25,26], thus forming a hydridopalladium(II) species such as **6**, which gives benzene by reductive elimination (Fig. 4). To confirm the proposal, bases which cannot undergo β-elimination were tested. With 2,2,6,6-tetramethylpiperidine, DABCO [27] or quinuclidine, reaction continued to only ca. 30% conversion but the yields of methyl cinnamate based on iodobenzene consumed were excellent.

Based on these results, we propose a mechanism for the model Heck reaction that focuses on the ligation of the oxidative addition product (Fig. 4). Initially, the Pd(0) bistriphenylphosphane complex **1** is formed from the $Pd(dba)_2$ [28]. This species is in equilibrium with other Pd(0) complexes formed by coordination of other ligands such as dba [28], acrylate, trialkylamine [29] and iodide [30]. Reaction with iodoarene then gives bisphosphane complex **2** ($P=D=PPh_3$) [28] and the alkene coordination step is unfavourable and turnover limiting due to the difficulty of displacing PPh_3. The reaction proceeds, if at all at these low temperatures, by a slow catalytic cycle. When the phosphane to Pd ratio is reduced to <2:1 by air oxidation, the oxidative addition products may be substitutionally labile *mono*phos-

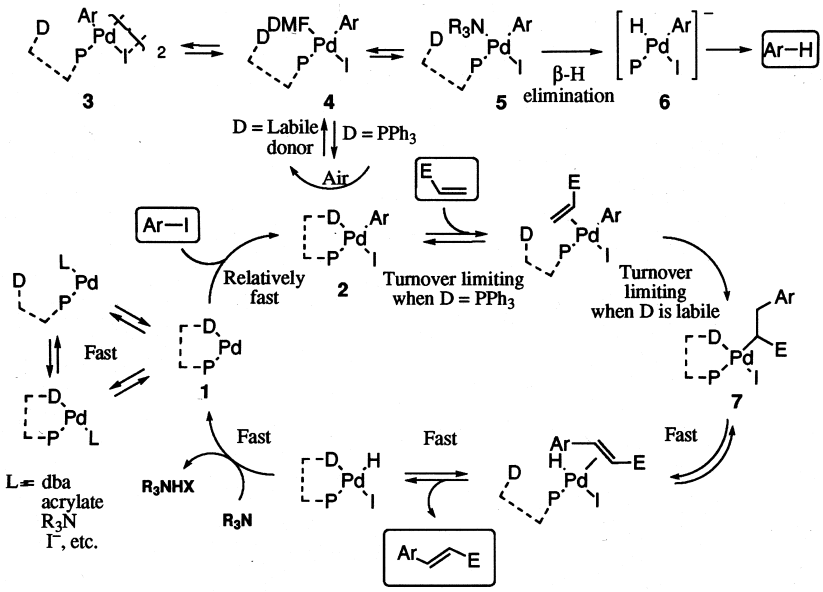
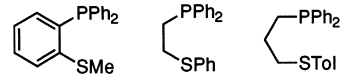


Fig. 4. Proposed mechanism for the model Heck reaction.

phane complexes such as **3**, **4**, and **5** [19,31] in which one phosphane is replaced by more weakly coordinating ligands. Alkene coordination is now fast and the equilibrium favours the alkene complex **7**. The approximate pseudo zero order kinetics are consistent with this, and prove also that oxidative addition is a relatively fast step (although it seems to be sufficiently slow to influence the rate weakly). Any of the other steps may be turnover limiting, but the migratory insertion is likely to be the slowest of these. As the reaction nears completion, continued phosphane oxidation and catalyst decomposition may be contributing to the departure from linearity. To our knowledge, this is the first detailed study of the kinetics of this prototypical Heck reaction using phosphane ligands at atmospheric pressure. *It indicates that for aryl iodides, alkene coordination is turnover limiting with ≥2 equiv. of PPh_3, whereas migratory insertion is turnover limiting with 1 equiv. of phosphane.* The mechanistic proposal is consistent with previous work, especially with its emphasis on the need for a weak ligand/vacant site to facilitate alkene coordination [14,19]. An induction period in the Heck reaction [23] and inhibition by phosphane have been reported [20,32,33]. A fast reaction cycle involving monoligated complexes has also been invoked in a very recent paper by van Leeuwen and co-workers [19], but with their very bulky phosphorus amidite ligand the reaction was first order with respect to alkene (styrene).

We also studied the kinetics of reactions using tri-*o*-tolylphosphane, which Heck showed to be the ligand of choice in many cases [34]. The use of 1–4 equiv. of $P(o\text{-Tol})_3$ with both iodobenzene (40°C) and 4-iodotrifluoromethylbenzene (70°C) gave high conversion, with no more than a brief induction period, and pseudo zero order kinetics up to 60% conversion. The contrast with PPh_3 is striking and the results suggest that $Pd[P(o\text{-Tol})_3]_2$ forms sterically hindered oxidative addition complexes (**2**, $P=D=P(o\text{-Tol})_3$) in which one phosphane is readily displaced by other ligands including alkene [31,34].



8 **9** **10**

With these mechanistic insights, we decided to study a series of heterobidentate phosphane/sulfane ligands **8**–**10**. We hoped that these hemilabile ligands [35] would form active catalysts, as alkene coordination could take place by displacement of a weakly coordinating sulfane rather than a strongly coordinating phosphane. Ligand **8** was tested using a 1:1 Pd:ligand ratio at 80°C. Product formation clearly followed pseudo zero order kinetics until the conversion reached ca. 75% and the yield was ca. 100%. Ligand **9** gave very similar results under the same conditions (Fig. 5), although an induction period of ca. 95 min was observed. Ligand **10** gave much faster reaction, but the yield of cinnamate was only ca. 65%.

Clearly PS ligands are viable in the Heck reaction. The reactions were relatively fast, high conversions were achieved and yields of methyl cinnamate were high, except for ligand

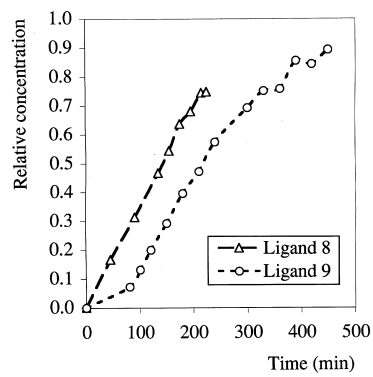


Fig. 5. Product concentration vs. time for the ligands **8** and **9**.

10 with the propane backbone. When the catalyst is a palladium complex containing PS ligands, the sulfur donor atom of the oxidative addition product (**2**, PD = chelating phosphanosulfane) is easily displaced by the alkene. The ligands give better catalyst stability and higher yields than PPh_3, presumably because the dissociated S moiety of the hemilabile ligand can recoordinate to stabilise the other complexes in the cycle, and to prevent competitive coordination of the amine. Ligand **10** gives faster reactions and lower yields than ligands **8** and **9**, presumably because it gives a less stable six-membered chelate. Reactions using these ligands are not as fast as those using 1 equiv. PPh_3 or $P(o\text{-Tol})_3$, where the concentration of the Pd-alkene complex should be the highest. To our knowledge, the use of hemilabile ligands in the Heck reaction has not been reported, although they have been used in related reactions involving insertion of alkenes [36,37]. Ligand **9** seemed to give the best results so it was investigated further. The reaction of styrene, in the presence of ligand **9**, was performed at 90°C. An induction period of ca. 90 min was observed, the reaction rate was slow (ca. 1000 min to reach completion) and excellent pseudo zero order kinetics were observed. High conversion was obtained (ca. 95%) but the yield was relatively low (ca. 70%), albeit much higher than using PPh_3. Bromobenzene was reacted with methyl acrylate employing **9** as ligand (2.4 equiv.) at the higher temperature of 110°C. The reaction was slow (ca. 20 h at 110°C), it ceased at 40% consumption of PhI, and the yield of methyl cinnamate was only 35%. Although these preliminary results are not as impressive as others reported recently [19], we believe that PS ligands offer considerable potential and deserve further investigation.

Acknowledgements

We are very grateful to Enterprise Ireland for financial support (Basic Research Project No. SC/1996/435), and to Johnson-Matthey for a gift of palladium salts.

References

[1] R.F. Heck, Org. React. 27 (1982) 345.
[2] T. Jeffery, Adv. Met.-Org. Chem. 5 (1996) 152.
[3] A. de Meijere, F.E. Meyer, Angew. Chem., Int. Ed. Engl. 33 (1994) 2379.
[4] M. Shibasaki, C.D.J. Boden, A. Kojima, Tetrahedron 53 (1997) 7371.
[5] S.G. Murray, F.R. Hartley, Chem. Rev. 81 (1981) 365.
[6] H.B. Kagan, B. Ronan, Rev. Heteroatom. Chem. 7 (1992) 92.
[7] D.A. Evans, K.R. Campos, J.S. Tedrow, F.E. Michael, M.R. Gange, J. Org. Chem. 64 (1999) 2994.
[8] E. Hauptman, P.J. Fagan, W. Marshall, Organometallics 18 (1999) 2061.
[9] K. Hiroi, Y. Suzuki, I. Abe, Tetrahedron Asymm. 10 (1999) 1173.
[10] M. Hiraoka, A. Nishikawa, T. Morimoto, K. Achiwa, Chem. Pharm. Bull. 46 (1998) 704.
[11] B. Koning, A. Meetsma, R.M. Kellogg, J. Org. Chem. 63 (1998) 5533.
[12] J.C. Anderson, D.S. James, J.P. Mathias, Tetrahedron Asymm. 9 (1998) 753.
[13] A. Chesney, M.R. Bryce, R.W.J. Chubb, A.S. Batsanov, J.A.K. Howard, Tetrahedron Asymm. 8 (1997) 2337.
[14] G.T. Crisp, Chem. Soc. Rev. 27 (1998) 427 and Refs. cited therein.
[15] C. Amatore, A. Jutand, J. Organomet. Chem. 576 (1999) 254.
[16] A. Ashimori, B. Bachand, M.A. Calter, S.P. Govek, L.E. Overman, D.J. Poon, J. Am. Chem. Soc. 120 (1998) 6488.
[17] F.C. Rix, M. Brookhart, P.S. White, J. Am. Chem. Soc. 118 (1996) 2436.
[18] S. Hillers, O. Reiser, Chem. Commun. (1996) 2197.
[19] G.P.F. van Strijdonck, M.D.K. Boele, P.C.J. Kamer, J.G. deVries, P.W.N.M. van Leeuwen, Eur. J. Inorg. Chem. (1999) 1073.
[20] F.Y. Zhao, B.M. Bhanage, M. Shirai, M. Arai, J. Mol. Catal. A, Chem. 142 (1999) 383.
[21] V. Farina, S Kapadia, B. Krishnan, C. Wang, L.S. Liebeskind, J. Org. Chem. 59 (1994) 5905.
[22] C. Amatore, E. Carré, A. Jutand, M.A. M'Barki, Organometallics 14 (1995) 1818.
[23] A. Spencer, J. Organomet. Chem. 258 (1983) 101.
[24] S. Kirschbaum, H. Waldmann, J. Org. Chem. 63 (1998) 4936.
[25] R. Benhaddou, S. Czernecki, G. Ville, J. Chem. Soc., Chem. Commun. (1988) 247.
[26] A.F. Shmidt, A. Khalaika, Kinet. Catal. 39 (1998) 803.
[27] C. Chen, D.R. Lieberman, R.D. Larsen, T.R. Verhoeven, P.J. Reider, J. Org. Chem. 62 (1997) 2676.
[28] C. Amatore, A. Jutand, F. Khalil, M.A. M'Barki, L. Mottier, Organometallics 12 (1993) 3168.
[29] R. Benhaddou, S. Czernecki, G. Ville, A. Zegar, Organometallics 7 (1988) 2435.
[30] C. Amatore, A. Jutand, A. Suarez, J. Am. Chem. Soc. 115 (1993) 9531.
[31] J.F. Hartwig, Synlett (1997) 329.
[32] L.F. Tietze, T. Nöbel, M. Spescha, J. Am. Chem. Soc. 120 (1998) 8971.
[33] C.S. Cho, S. Motofusa, K. Ohe, S. Uemura, S.C. Shim, J. Org. Chem. 60 (1995) 883.
[34] C.B. Ziegler Jr, R.F. Heck, J. Org. Chem. 43 (1978) 2941.
[35] C.S. Slone, D.A. Weinberger, C.A. Mirkin, Prog. Inorg. Chem. 48 (1999) 233.
[36] M.J. Green, G.J.P. Britovsek, K.J. Cavell, B.W. Skelton, A.H. White, Chem. Commun. (1996) 1563.
[37] W. Keim, H. Maas, S. Meeking, Z. Naturforsch., Teil B 50 (1995) 430.

PERGAMON

www.elsevier.nl/locate/poly

Polyhedron 19 (2000) 521–523

POLYHEDRON

The catalytic transformation of thiiranes to cyclic disulfides by tungsten carbonyl complexes

Richard D. Adams *, Joseph L. Perrin

Department of Chemistry and Biochemistry, University of South Carolina, Columbia, SC 29208, USA

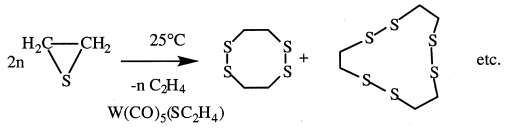
Received 4 October 1999; accepted 8 November 1999

Abstract

This report reviews our recent studies of the catalytic transformations of thiiranes and vinylthiiranes by tungsten pentacarbonyl complexes. Whereas the thiranes yield only macrocyclic polydisulfides, the latter reactions yield only the cyclic monodisulfides known as 3,6-dihydro-1,2-dithiins. ©2000 Elsevier Science Ltd All rights reserved.

Keywords: Thiiranes; Dihydrodithiins; Tungsten carbonyls

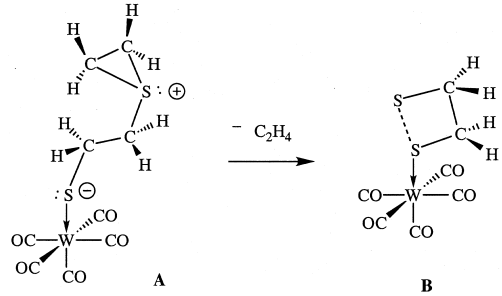
In recent studies we have discovered novel transformations of thiiranes into macrocyclic polydisulfides by carbonyl complexes of tungsten, Eq. (1) [1,2].



(1)

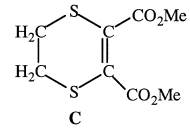
Two equivalents of thiirane are consumed in the formation of each disulfide group. One equivalent of alkene is also formed. The thiirane molecule is activated by coordination of its sulfur atom to the tungsten atom. In one case, a thiirane-tungsten complex, $W(CO)_5$(*cis*-SCHMeCHMe)), was isolated and characterized structurally by single crystal X-ray diffraction methods [1,2]. The sulfur atom from a second molecule of thiirane is then added to one of the carbon atoms of the thiirane ligand of the complex in a ring opening step. This leads to the formation of a zwitterionic intermediate **A** containing a thiiranium-thiolate ligand that subsequently eliminates an olefin from the thiiranium group to yield a reactive alkene disulfide containing tungsten species **B**, Scheme 1.

The nature of the bond between the sulfur atoms in **B** has not been established. The alkene disulfide ligand in **B**, also known as 1,2-dithietane, has not yet been synthesized and isolated as a free molecule by any procedures. The dithietane ligands from two or more molecules then combine to form the cyclic polydisulfides and regenerate catalytically active



Scheme 1.

'$W(CO)_5$' groupings. Evidence for the existence of the dithietane ligand in **B** was obtained by trapping experiments using dimethylacetylene dicarboxylate (DMAD) which yielded the product 1,4-dithia-2,3-bis(methoxycarbonyl)-cyclohexene (**C**). Compound **C** is not formed from mixtures of the macrocyclic polydisulfides and DMAD.



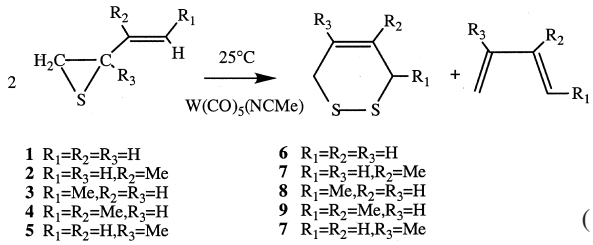
C

$W(CO)_5$(NCMe) is as good a catalyst precursor for these reactions, but $W(CO)_6$, which has no labile ligands, is not catalytically active.

We have also found that vinylthiirane (**1**) and the methyl-substituted vinylthiiranes **2**–**5** can be effectively transformed into 3,6-dihydro-1,2-dithiin (**6**) and a series of new methyl-substituted 3,6-dihydro-1,2-dithiins **7**–**9** by tungsten carbonyl compounds such as $W(CO)_5$(NCMe), Eq. (2) [3,4].

* Corresponding author. Tel.: +1-803-7777187; fax: +1-803-7776781; e-mail: adams@mail.chem.sc.edu

0277-5387/00/$ - see front matter ©2000 Elsevier Science Ltd All rights reserved.
PII S0277-5387(99)00399-X



1 $R_1=R_2=R_3=H$
2 $R_1=R_3=H, R_2=Me$
3 $R_1=Me, R_2=R_3=H$
4 $R_1=R_2=Me, R_3=H$
5 $R_1=R_2=H, R_3=Me$
6 $R_1=R_2=R_3=H$
7 $R_1=R_3=H, R_2=Me$
8 $R_1=Me, R_2=R_3=H$
9 $R_1=R_2=Me, R_3=H$
7 $R_1=R_2=H, R_3=Me$

(2)

These reactions are accompanied by the formation of the corresponding butadiene and essentially 100% conversion is obtained when they are performed at 25°C. Turnover frequencies (TOFs) range from a low of 2 h^{-1} to a high of 29 h^{-1}, see Table 1. The reaction is inhibited by methyl groups on the thiirane ring, but is accelerated when methyl groups are placed on the vinyl group. The reaction is insensitive to the atmosphere over it and similar turnover frequencies were obtained when the reactions were performed under nitrogen, in air and even under CO.

The tungsten complex $W(CO)_5(\overline{SSCH_2CH{=}{=}CHCH_2})$ (**10**) was isolated from the vinylthiirane reaction and was structurally characterized [3,4]. The molecule contains a dihydrodithiin ligand coordinated to the tungsten atom through one of the sulfur atoms. This complex was shown to be a component in the catalytic cycle, see Scheme 2.

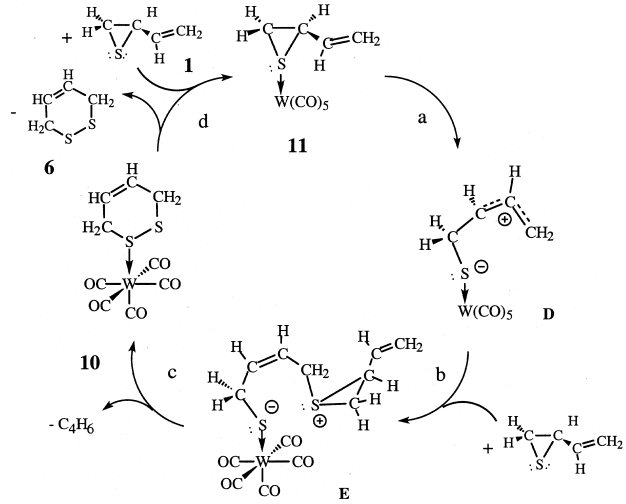
$W(CO)_5(NCMe)$ is a good catalyst precursor, but is not a component in the catalytic cycle. ^{13}C NMR studies of catalytically active solutions showed that **10** is converted to vinylthiirane containing tungsten complexes **11** (two isomers which differ depending on which of the two lone pairs of electrons on the sulfur atom is coordinated) in the course of the catalysis. Unlike the reactions of the simple thiiranes, it was proposed that the thiirane ring opening occurs spontaneously in the complexes **11** (Scheme 2, step a), to give an allylium-thiolate intermediate **D**. This could explain the enhancement of the reaction by methyl substituents on the vinyl group. Intermediate **D** then rapidly adds a second equivalent of vinylthiirane, step b, to yield a thiiranium-thiolate species **E** that eliminates butadiene, step c, to yield the stable dihydrodithiin complex **10**. Vinylthiirane is capable of displacing the dihydrodithiin ligand to release the six-membered ring product **6** and also to complete the catalytic cycle, step d.

Interestingly, it has been shown that the catalysis is significantly increased when a phosphine ligand is substituted for

Table 1
Results of catalytic transformations of vinylthiiranes to dihydrodithiins by $W(CO)_5(NCMe)$ [3,4]

Reagent	Product	Yield (%) [a]	TON (24 h)	TOF (h^{-1})
1	**6**	86	212	15
2	**7**	84	141	29
3	**8**	86	149	24
4	**9**	80	146	19
5	**7**	34	53	2

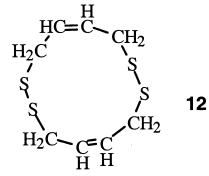
[a] Isolated yields after 24 h.



Scheme 2.

CO on the tungsten atom. For example, the turnover frequency for the catalytic formation of **6** from **1** by $W(CO)_4(PPh_3)(NCMe)$ is 47 h^{-1}, nearly three times the rate of that of $W(CO)_5(NCMe)$. The increase can be attributed to steric crowding effects that promote the spontaneous ring opening step, Scheme 2, step a.

Since the monodisulfides **6**–**9** contain relatively stable six-membered rings, few if any macrocyclic polydisulfides are formed in these reactions. However, these disulfides do possess some torsional ring strain at the S–S bond [5] and concentrated solutions of them will yield polymers in the presence of stimulation by light. Interestingly, the macrocyclic 12-membered bis-disulfide 1,2,7,8-tetrathiacyclododeca-4,10-diene (**12**) (a dimer of **6**) can be isolated from solutions of **6** during the course of these polymerizations [3,4]. Compound **6** reacts with $Os_3(CO)_{10}(NCMe)_2$ by insertion into the S–S bond to yield a series of osmium cluster complexes containing the butadienedithiolate ligand [6].



12

Dihydrodithiins have been prepared by other methods, most notably the addition of S_2 to butadienes [7–9], but the catalytic procedure described above appears to be superior by far.

Acknowledgements

These studies were supported by the Division of Chemical Sciences of the Office of Basic Energy Sciences of the US Department of Energy.

References

[1] R.D. Adams, J.H. Yamamoto, A. Holmes, B.J. Baker, Organometallics 16 (1997) 1430.
[2] R.D. Adams, J.A. Queisser, J.H. Yamamoto, J. Am. Chem. Soc. 118 (1996) 10674.
[3] R.D. Adams, J.L. Perrin, J. Am. Chem. Soc. 121 (1999) 3984.
[4] R.D. Adams, J.W. Long IV, J.L. Perrin, J. Am. Chem. Soc. 120 (1998) 1922.
[5] J.A. Burns, G.M. Whitesides, J. Am. Chem. Soc. 112 (1990) 6296.
[6] R.D. Adams, J.L. Perrin, J. Organomet. Chem. 582 (1999) 9.
[7] D.N. Harpp, J.G. MacDonald, J. Org. Chem. 53 (1988) 3812.
[8] S.L. Tardif, A.Z. Rys, C.B. Abrams, I.A. Abu-Yousef, P.B.F. Leste-Lasserre, E.K.V. Schultz, D.N. Harpp, Tetrahedron 53 (1997) 12225.
[9] A.Z. Rys, D.N. Harpp, Tetrahedron Lett. 38 (1997) 4931.

PERGAMON

www.elsevier.nl/locate/poly

Polyhedron 19 (2000) 525–528

POLYHEDRON

Palladium-catalyzed asymmetric reactions enantiocontrolled by chiral organosulfur functionality

Kunio Hiroi *, Yoshio Suzuki, Yoko Kaneko, Fumiko Kato, Ikuko Abe, Ryoko Kawagishi

Department of Synthetic Organic Chemistry, Tohoku Pharmaceutical University, 4-4-1 Komatsushima, Aoba-ku, Sendai, Miyagi 981-8558, Japan

Received 4 October 1999; accepted 6 December 1999

Abstract

Participation of chiral sulfinyl functionality in palladium-catalyzed asymmetric reactions is demonstrated by using chiral sulfoxides as chiral ligands or chiral substrates. New chiral ligands, *o*-(phosphinoamino)phenyl and *o*-phosphinophenyl sulfoxides, have been developed. The structure of an intermediary palladium complex was determined by X-ray crystallographic analysis. The palladium-catalyzed asymmetric 1,3-rearrangements of (1,3-butadienyl)cyclopropanes bearing chiral sulfinyl groups to cyclopentenes are described. The participation of the chiral sulfinyl group to the palladium catalyst is described. ©2000 Elsevier Science Ltd All rights reserved.

Keywords: Asymmetric alkylation; Asymmetric rearrangements; Chiral ligands; Chiral sulfoxides; Palladium catalysts

The organosulfur functionality has been widely used in organic synthesis as a stereo- and enantiocontrollable element, and the high efficiency of the selectivity, especially the enantioselectivity by chiral sulfinyl groups, has received much attention in recent years. We wish to demonstrate here the usefulness of chiral sulfinyl functionality as a ligand or a chiral source in the substrate in palladium-catalyzed asymmetric reactions such as nucleophilic substitutions of chiral π-allylpalladium complexes and 1,3-rearrangements in olefinic cyclopropanes bearing chiral sulfinyl groups.

There have been published some issues related to asymmetric synthesis using chiral ligands involving organosulfur functions; however, few reports have appeared concerning asymmetric synthesis with chiral ligands bearing chiral organosulfur groups [1–7] such as sulfinyl [8–10] and sulfoximine [11] functions as the sole chiral source. Hitherto, we have studied asymmetric synthesis using chiral sulfoxide ligands as the sole chiral source.

A chiral sulfinyl group forms a chiral chelate of palladium by coordination of the sulfinyl sulfur atom. The design and development of chiral efficient ligands along this line provided new ligands bearing chiral sulfinyl groups as sole chiral sources, and other coordinatable heteroatoms such as nitrogen and phosphorus (Scheme 1).

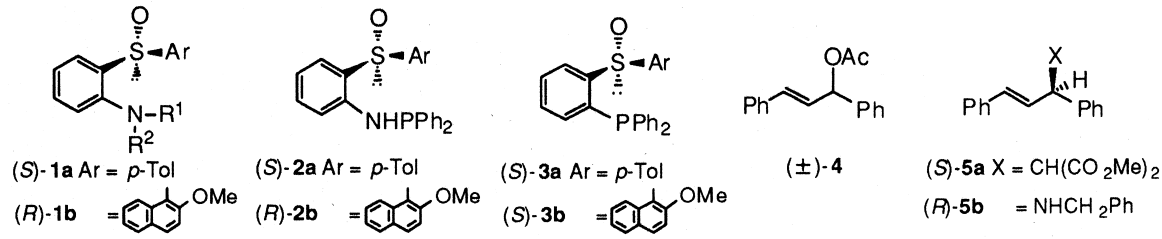
Use of chiral *o*-aminophenyl *p*-tolyl sulfoxides (*S*)-**1** [12,13] as ligands in the palladium-catalyzed reaction of compound **4** with sodium malonate provided compound (*S*)-**5a** with moderate enantiomeric excess (e.e.). The reactions proceed via chiral π-allylpalladium chelate **6** (Scheme 2). Chelate **6B** would be sterically preferred to chelate **6A** because of the existence of steric hindrance between the *p*-tolyl and the phenyl group in the allylic systems in compound **6A**. Therefore, the nucleophile (malonate sodium enolate) would attack the allylic site (c) in compound **6B** from the back side of the palladium to produce compound (*S*)-**5a**.

Use of chiral *o*-(phosphinoamino)phenyl sulfoxides as ligands improved the enantioselectivity. The palladium-catalyzed reactions of compound (±)-**4** with sodium malonate using compound (*R*)-**2b** produced compound (*R*)-**5a** with 97% e.e. Thus, the existence of vicinal phosphinoamino groups in the chiral sulfinyl ligands was essential for the improvement of the enantioselectivity. This high enantioselectivity presumably arises from the formation of a sterically controllable six-membered transition state [14].

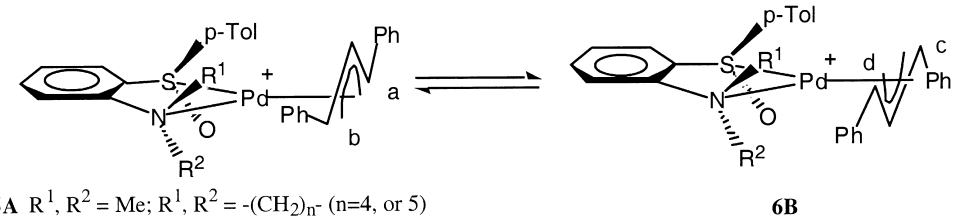
The phosphorus and sulfur atoms in the chiral ligands (*S*)-**2a** have rather strong coordination ability to palladium catalysts, forming six-membered π-allylpalladium intermediates (**7**) (Scheme 3). The nucleophile (malonate carbanion) would preferentially attack the allylic site *trans* to the phosphorus group in the conformationally most preferred π-allylpalladium complex (**7Ba**), producing compound (*S*)-**5a**.

* Corresponding author. Tel.: +81-22-2344181; fax: +81-22-2752013; e-mail: khiroi@tohoku-pharm.ac.jp

0277-5387/00/$ - see front matter ©2000 Elsevier Science Ltd All rights reserved.
PII S0277-5387(99)00400-3



Scheme 1.



Scheme 2.

With compound (*R*)-**2b** as a ligand, the nucleophile would attack the allyl terminus *syn* to the phosphorus group because of steric interference by the bulky naphthyl substituent in complex **7Bb**.

In contrast to (*R*)-2-(diphenylphosphino)ethyl *p*-tolyl sulfoxide, chiral *o*-phosphinophenyl sulfoxides were obtained with retention of the chirality on the sulfonyl functions.

The chiral sulfoxide (*S*)-**3b** was concluded to be very stable in tetrahydrofuran (THF) at room temperature, with complete retention of the chirality without conversion into the phosphine oxide. However, upon heating in refluxing THF, a more rapid irreversible transformation of compound (*S*)-**3b** into compound **8** was observed with almost complete retention (>96% e.e.) of the chirality (Scheme 4). This is shown in Fig. 1, which was plotted from HPLC analysis with Chiralpak AD in relation to the elapse of the reaction time [15].

A chiral sulfinyl compound, (*S*)-**3b**, with a bulky substituent was demonstrated to serve as a highly efficient chiral ligand in the palladium-catalyzed reactions, providing an extremely high degree of asymmetric induction. The reactions of compound (±)-**4** with sodium malonate were carried out in THF at −20°C in the presence of $PdCl_2(CH_3CN)_2$ (0.03 equiv.) and compound (*S*)-**3b** (0.06 equiv.) to afford compound (*S*)-**5a** in good yields with 82% e.e.

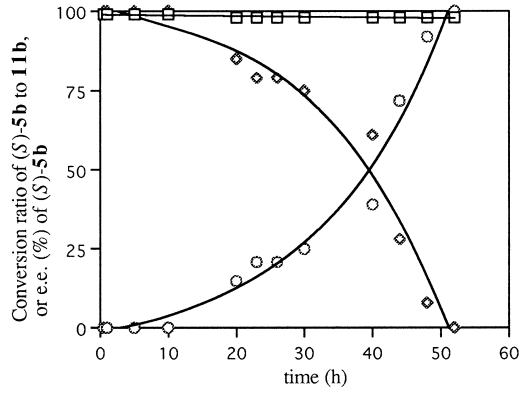
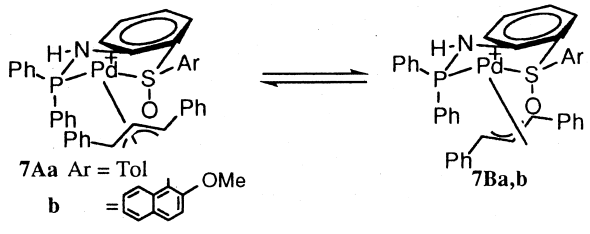
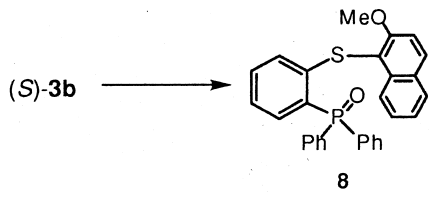


Fig. 1. The conversion ratio of compound **3b** to compound **8**, showing enantiomeric excess (e.e.) (%) of compounds (*S*)-**3b** (□), (*S*)-**3b** (◇) and **8** (○).



Scheme 3.



Scheme 4.

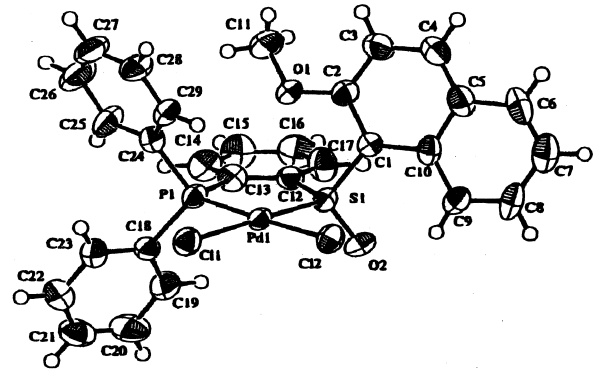
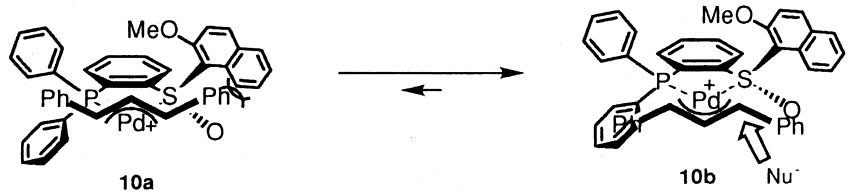
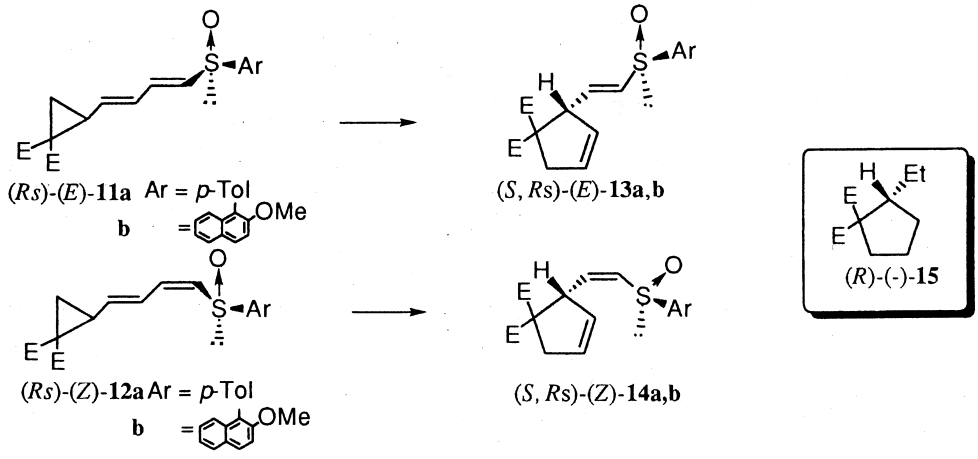


Fig. 2. Molecular structure (ORTEP drawing) of compound **9**. Selected bond distances (Å) and angles (°) are: Pd(1)–S(1) 2.221(2), Pd(1)–P(1) 2.229(2), Pd(1)–Cl(1) 2.313(2), Pd(1)–Cl(2) 2.356(2), S(1)–Pd(1)–P(1) 88.88(8), S(1)–Pd(1)–Cl(2) 89.13(8), P(1)–Pd(1)–Cl(1) 87.85(8).



Scheme 5.



Scheme 6.

The intermediary palladium complex derived from compound (*S*)-**3b** and $PdCl_2(CH_3CN)_2$ was isolated by recrystallization from CH_2Cl_2–Et_2O. The structure as determined by X-ray crystallographic analysis is shown in Fig. 2. The palladium-catalyzed reactions of compound (±)-**4** with sodium malonate using the isolated palladium complex **9** as a catalyst gave the same result as that obtained under the normal reaction conditions.

As the crystallographic data clearly show, a five-membered chelated palladium complex is formed by coordination of the phosphino group and the sulfinyl sulfur function to palladium. In the conformational equilibrium (Scheme 5), the conformer **10b** would be preferred to compound **10a** because of the existence of steric interference between the large substituent (*p*-tolyl or 2-methoxy-1-naphthyl) on the chiral sulfoxide and the phenyl group in the allyl terminus in compound **10a**. Therefore, the nucleophile (sodium malonate or benzylamine) attacks preferentially the allyl terminus in compound **10b** *trans* to the better π-acceptor, which is the phosphine group in the current case, despite the steric effect by the bulky substituent (2-methoxy-1-naphthyl), affording compounds (*S*)-**5a** and (*R*)-**5b** in a highly enantioselective fashion.

The unequivocal participation of the chiral sulfinyl functionality was observed in palladium-catalyzed 1,3-rearrangements of 1,3-butandienylcyclopropanes bearing chiral sulfinyl groups [16].

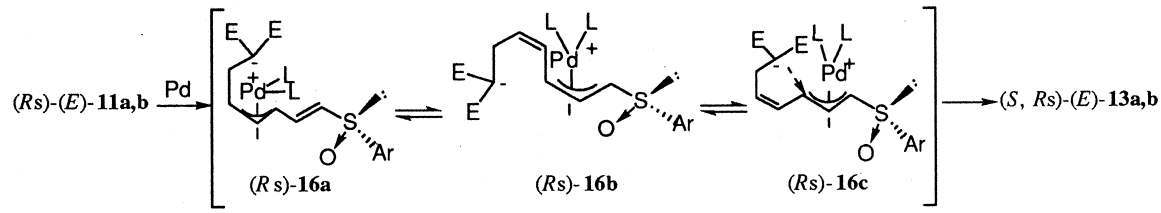
The palladium-catalyzed reaction of compound (*R*s)-(*E*)-**11a,b** was carried out in toluene at room temperature for 18 h in the presence of $Pd_2(dba)_3 \cdot CHCl_3$ (0.1 equiv.) and phosphine ligands (0.2 equiv.) to give compound (*S*,*R*s)-(*E*)-**13a,b** with high diastereomeric excess (d.e.) (90–94%) (Scheme 6). A similar reaction of compound (*R*s)-(*Z*)-**12a,b** was carried out under the same reaction conditions to produce compound (*S*,*R*s)-(*Z*)-**14a,b** with high d.e., with unexpected retention of the (*Z*)-geometry of the starting olefin.

The absolute configuration of the newly asymmetric carbon center was determined to be the (*S*)-configuration by chemical correlation to compound **15**.

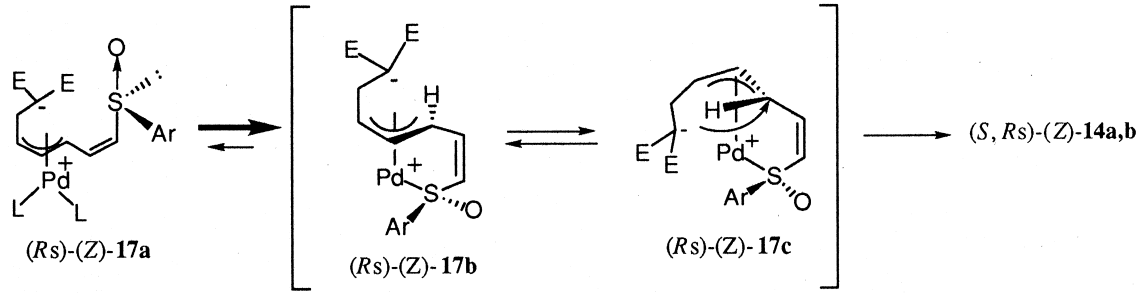
The mechanism for the asymmetric induction in these palladium-catalyzed rearrangements is rationalized on the basis of the stereochemical outcome observed.

The initially formed π-allylpalladium complex (*R*s)-**16a** derived from complex (*R*s)-(*E*)-**11a,b** would be equilibrated into the more stable π-allyl system (*R*s)-**16b,c**; in the most preferred π-allyl system, (*R*s)-**16c**, with the *syn* arylsufinyl group at C1 and the *syn* substituent at C3, the palladium–phosphine moiety is orientated at the sterically less crowded upper side (the lone pair side of the sulfinyl group) in the electronically most advantageous conformation with the sulfinyl sulfur–oxygen bond coplanar to the π-allyl system, as designated in compound **16c**. The intramolecular substitution of the carbanion in compound (*R*s)-**16c** occurs at the C3 allyl site from the opposite side of the palladium in a highly stereoselective fashion to afford compound (*S*,*R*s)-(*E*)-**13a,b** with high d.e. (Scheme 7).

In the case of compound (*R*s)-(*Z*)-**12a,b**, the direct participation of the chiral sulfinyl group to the palladium should be crucial for the rationalization of the stereochemical results; the initially formed π-allylpalladium complex (*R*s)-(*Z*)-**17a** would be stabilized by the coordination of the sulfinyl group to the palladium. It is certainly assumed that the formation of the conformationally more stable π-allylpalladium complex



Scheme 7.



Scheme 8.

(*Rs*)-(*Z*)-**17c** with the retained (*Z*)-configuration of the olefin, presumably by the coordination of the sulfinyl sulfur atom to the palladium, followed by intramolecular nucleophilic substitution from the opposite side of the palladium, provided compound (*S*,*Rs*)-(*Z*)-**14a,b** in a highly stereoselective fashion (Scheme 8).

Supplementary data

Supplementary data are available from the CCDC, 12 Union Road, Cambridge CB2 1EZ, UK (fax: +44-1223-336033; e-mail: deposit@ccdc.cam.ac.uk) on request, quoting deposition number 136433.

Acknowledgements

The present work was supported by a Grant-in-Aid for Scientific Research from the Ministry of Education, Science, Sports, and Culture, Japan.

References

[1] C.G. Frost, J.M.J. Williams, Tetrahedron Lett. 34 (1993) 2015.
[2] G.J. Dawson, C.J. Martin, J.M.J. Williams, S.J. Coote, Tetrahedron Lett. 14 (1993) 7793.
[3] C.G. Frost, J.M.J. Williams, Tetrahedron: Asymmetry 4 (1993) 1785.
[4] C.G. Frost, J.M.J. Williams, Synlett (1994) 551.
[5] J. Kang, J.I. Yu, H.G. Cho, Bull. Korean Chem. Soc. 16 (1995) 439.
[6] T. Morimoto, K. Tachibana, K. Achiwa, Synlett (1997) 783.
[7] J.C. Anderson, D.S. James, J.P. Mathias, Tetrahedron: Asymmetry 9 (1988) 753.
[8] J.V. Allen, J.F. Bower, J.M.J. Williams, Tetrahedron: Asymmetry 5 (1994) 1895.
[9] R. Tokunoh, M. Sodeoka, K. Abe, M. Shibasaki, Tetrahedron Lett. 36 (1995) 8035.
[10] C. Bolm, D. Kaufmann, M. Zehnder, M. Neuburger, Tetrahedron Lett. 37 (1996) 3985.
[11] G. Chelucci, D. Berta, A. Saba, Tetrahedron 53 (1997) 3843.
[12] K. Hiroi, Y. Suzuki, Heterocycles 77 (1997) 46.
[13] K. Hiroi, Y. Suzuki, I. Abe, Y. Hasegawa, K. Suzuki, Tetrahedron: Asymmetry 9 (1998) 3797.
[14] K. Hiroi, Y. Suzuki, Tetrahedron Lett. 39 (1998) 6499.
[15] K. Hiroi, Y. Suzuki, R. Kawagishi, Tetrahedron Lett. 40 (1999) 715.
[16] K. Hiroi, Y. Yoshida, Y. Kaneko, Tetrahedron Lett. 40 (1999) 3431.

PERGAMON

www.elsevier.nl/locate/poly

Polyhedron 19 (2000) 529–531

POLYHEDRON

Silylcupration of acylimidazolides: a new synthesis of α-aminoacylsilanes and their synthetic applications

Bianca Flavia Bonini, Mauro Comes-Franchini *, Mariafrancesca Fochi, Germana Mazzanti, Alfredo Ricci, Greta Varchi

Dipartimento di Chimica Organica 'A. Mangini', Università di Bologna, Via Risorgimento 4, I-40136 Bologna, Italy

Received 4 October 1999; accepted 22 November 1999

Abstract

Several new *N*-Boc-protected α-aminoacylsilanes from L-phenylalanine and L-isoleucine are synthesized via silylcupration of the corresponding imidazolides. The addition reaction of nucleophiles to the carbonyl moiety gives satisfactory yields of highly functionalized β-amino alcohols and statine analogues. The diastereoselectivity ranges from 30 to 98% and depends upon the nature of the C-nucleophile, on the structure of the starting amino acid as well as on the chelating properties of the Lewis acid employed. ©2000 Elsevier Science Ltd All rights reserved.

Keywords: α-Aminoacylsilanes; β-Amino alcohols; Lewis acid; Silylcupration; Statine analogues

1. Introduction

The synthesis of enantiopure β-amino alcohols is currently the subject of enormous interest, mainly due to their applications as peptidomimetics, as building blocks for pharmaceuticals and also as ligands for asymmetric catalysis. Diastereoselective addition to α-amino aldehydes [1,2] has emerged as one of the most efficient and versatile methods available for preparing functionalized β-amino alcohols [3,4]. However, it is well known that most of the nitrogen-protected α-amino aldehydes are relatively unstable both chemically and configurationally and they must be used immediately after their preparation. Another problem is the low degree of stereoselectivity often encountered in the addition step.

Homochiral α-aminoacylsilanes [5,6], obtained from natural α-amino acids, can be used as stable synthetic equivalents of α-amino aldehydes for the diastereoselective synthesis of optically active β-amino alcohols. This approach is based on the possibility of replacing the silyl group stereospecifically with a proton in the α-hydroxysilanes initially formed. Moreover, the use of acylsilanes as synthetic equivalents of the corresponding aldehydes has the advantage of increasing the degree of stereoselectivity in the addition of nucleophiles, due to the bulkiness of the silyl group.

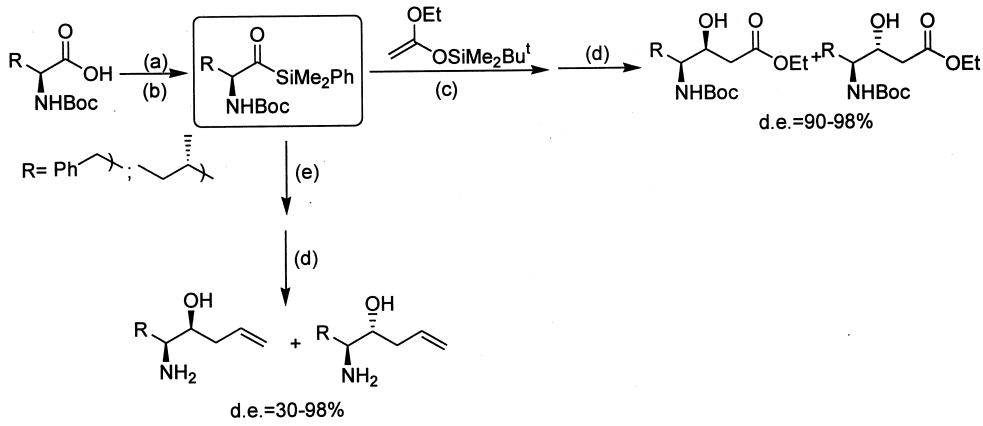
2. Results and discussion

We have previously reported that the allylation reaction under Hosomy–Sakurai conditions of *N*-Pht- and *NH*-Ts-protected α-aminoacylsilanes derived from L-phenylalanine occurs with good chemical yields and high diastereoselectivity [5,6]. The degree of diastereoselectivity during the nucleophilic addition depends on both the nitrogen protecting group and the reagents. Diastereomeric excess (de) values ranging between 96 and 98% were obtained in the $TiCl_4$-promoted allylation of the *N*-Pht-aminoacylsilanes and of the *NH*-Ts-aminoacylsilane with allyltrimethylsilane. Lower de values were obtained in the $Sc(OTf)_3$-catalysed allylation with tetra-allyltin.

In the formation of the homoallylic alcohols the harsh reaction conditions required for deprotection–desylilation made these steps problematic. This led us to consider as more suitable candidates for these reactions *NH*-Boc aminoacylsilanes in which the Boc group could be removed under much milder conditions. To this end *NH*-Boc L-phenylalanine and *NH*-Boc L-isoleucine were converted in good yields into the corresponding α-aminoacylsilanes by reaction with carbon-

* Corresponding author. Tel.: +39-051-209 3626; fax: +39-051-209 3654; e-mail: comes@ms.fci.unibo.it

0277-5387/00/$ - see front matter ©2000 Elsevier Science Ltd All rights reserved.
PII S0277-5387(99)00401-5



Scheme 1. (a) CDI, THF, room temperature (RT), 45 min, 97–98%; (b) $(PhMe_2Si)_2CuCNLi_2$, −78°C, 1 h, 50–55%. (c) $BF_3 \cdot Et_2O$, CH_2Cl_2, −78°C, 10–48 h, 61–67%. (d) TBAF, THF, RT, 24 h, 63–65%. (e) $(CH_2{=}CHCH_2)_4Sn$, $Sc(OTf)_3$ (7% mol), CH_2Cl_2, RT, 24 h, 60–61%; or $CH_2{=}CHCH_2Br$, In, THF, RT, 15 h, 95–96%. (d) TBAF, THF, RT, 24 h, 80–90%. (f) 4 N HCl–dioxan, 1 h, RT, 63–95%.

yldiimidazole, followed by treatment of the acylimidazolides with $(Me_2PhSi)_2CuCNLi_2$ (Scheme 1).

A systematic three-carbon and two-carbon stereoselective elongation of the carbon skeleton of the two α-aminoacylsilanes was performed via allylation and aldol reactions, respectively.

Since the allylation under Hosomi–Sakurai conditions led to extensive decomposition of the starting materials because of the incompatibility of $TiCl_4$ with the *NH*-Boc moiety, and to avoid racemization at C-2 induced by more basic allylic metals, $Sc(OTf)_3$-catalysed allylation [7] with tetra-allyltin and In-mediated [8] allylation with allyl bromide under Barbier conditions were employed. Both these reactions afforded the expected homoallylic alcohols in satisfactory to good yields and with de values ranging between 30 and 98%.

The α-hydroxysilanes thus formed were then subjected to stereospecific protiodesilylation with TBAF to give the enantiopure β-amino alcohols, and the subsequent deprotection of the *NH*-Boc group took place under normal conditions affording the isomerically pure free amino alcohols in high yields.

The significant differences in diastereoselectivities appear to be related to the structure of the starting amino acid. The observation that, under the same allylation conditions only the isoleucine leads to very high *syn* selectivity, suggests that factors other than chelation are likely to play a major role in determining the stereochemical outcome.

Stereoselective two-carbon elongation of the carbon skeleton of the two α-aminoacylsilanes was performed by introducing an acetic acid moiety. The aldol reaction of *O*-ethyl-*O*-*tert*-butyldimethylsilyl ketene acetal proceeded smoothly in the presence of $BF_3 \cdot Et_2O$ to give the expected addition products in good yields and with high diastereoselectivity in favour of the *syn* adduct. The stereochemistry of the adducts was determined after desilylation of the compounds with TBAF by comparing the spectroscopic data with those reported in the literature. A set of important biologically active statine analogues with natural configurations [9] (3*S*,4*S*) can thus be prepared by this four-step highly *syn*-diastereoselective sequence. In summary, the methodology outlined here, based on three-carbon and two-carbon elongation of the carbon chain of several new *N*-Boc-protected α-aminoacylsilanes via nucleophilic addition to the carbonyl moiety, constitutes a convenient and reliable means for the stereoselective synthesis of functionalized β-amino alcohols.

3. Experimental

3.1. Silylcupration: general procedure

Phenyldimethylsilyl lithium [10] 0.85 M (35.5 ml, 30.17 mmol) was added to a suspension of CuCN (1.25 g, 15.07 mmol) in tetrahydrofuran (THF) (70 ml) at 0°C. The reaction mixture was stirred for 20 min under argon and then slowly transferred by cannula to a suspension of (2*S*)-2-[*N*-(*tert*-butoxycarbonyl)amino]-1-imidazol-1-yl-3-phenylpropan-1-one (4.31 g, 13.7 mmol) in THF (90 ml) at −78°C. Stirring was continued at this temperature for a further 30 min. A saturated solution of NH_4Cl was then added and the mixture was allowed to warm to room temperature; it was then extracted three times with diethyl ether (3×30 ml). The organic extracts were separated and dried on Na_2SO_4. After removal of the solvent in vacuo the crude extract was purified by column chromatography on silica gel (light petroleum–Et_2O, 4:1), affording 2.62 g (50%) of pure (2*S*)-3-phenyl-2-[*N*-(*tert*-butoxycarbonyl)amino]-propanoyl-dimethylphenylsilane as a light yellow oil. $[\alpha]_D^{24}$ +19.3 (*c* 2.00, $CHCl_3$). IR (cm^{-1}): 3420, 1715, 1650, 1240. MS (EI): *m/z* 383 (M^+), 298, 221, 164, 135, 91, 57. ^1H NMR (200 MHz): δ 0.55 (s, 6H), 1.40 (s, 9H), 2.50 (dd, 1H, *J* = 14.0 , 7.4 Hz), 2.95 (dd, 1H, *J* = 14.0 , 5.8 Hz), 4.70 (bq, 1H, *J* = 7.6 Hz), 4.95 (d, 1H, *J* = 9.9 Hz), 6.80–6.95 (m, 2H), 7.20–7.80 (m, 8H). ^{13}C NMR (50.3 MHz): δ

−4.6, −4.4, 28.2, 35.6, 64.2, 79.5, 126.5, 128.3, 128.3, 129.3, 130.1, 134.0, 134.1, 136.0, 154.8, 241.6. *Anal*. Calc. for $C_{22}H_{29}NO_3Si$: C, 68.90; H, 7.63; N, 3.65. Found: C, 68.82; H, 7.58; N, 3.61%.

(2*S*,3*S*)-3-Methyl-2-[*N*-(*tert*-butoxycarbonyl)amino]-pentanoyl-dimethylphenylsilane was prepared following the above procedure, using (2*S*,3*S*)-2-[*N*-(*tert*-butoxycarbonyl)amino]-1-imidazol-1-yl-3-methyl-pentan-1-one (4.2 g, 15.0 mmol) and 16.5 mmol of bis-dimethylphenylsilyl lithium cyanocuprate. Silica gel chromatography (light petroleum–Et_2O, 6:1) gave 2.88 g (55%) of (2*S*,3*S*)-3-methyl-2-[*N*-(*tert*-butoxycarbonyl)amino]-pentanoyl-dimethylphenylsilane as a pale yellow oil. $[\alpha]_D^{24}$ +62.6 (*c* 2.00, $CHCl_3$). IR (cm^{-1}): 3440, 1730, 1650, 1240. MS (EI): *m/z* 349 (M^+), 232, 220, 186, 135, 86, 57. ^1H NMR (300 MHz): δ 0.48–0.87 (m, 12H), 1.45–1.85 (m, 12H), 4.50 (dd, 1H, J=8.9, 3.2 Hz), 5.05 (bd, 1H, J=8.3 Hz), 7.30–7.60 (m, 5H). ^{13}C NMR (50.3 MHz): δ −4.4, 11.3, 16.4, 23.0, 28.3, 34.8, 68.7, 79.3, 128.2, 130.0, 132.9, 133.9, 155.8, 243.0. *Anal*. Calc. for $C_{19}H_{31}NO_3Si$: C, 65.29; H, 8.95; N, 4.01. Found: C, 65.27; H, 8.93; N, 4.00%.

Acknowledgements

This work was supported by the University of Bologna (Funds for Selected Research Topics, A.A. 1999-01) and by the National Project 'Stereoselezione in Sintesi Organica. Metodologie ed Applicazioni'.

References

[1] M.T. Reetz, Angew. Chem., Int. Ed. Engl. 30 (1991) 1531.
[2] J. Jurczak, A. Gobielowsky, Chem. Rev. 89 (1989) 149.
[3] A. Dondoni, D. Perrone, P. Merino, J. Org. Chem. 60 (1995) 8074.
[4] F. D'Aniello, A. Mann, M. Matii, M. Taddei, J. Org. Chem. 59 (1994) 3762.
[5] B.F. Bonini, M. Comes-Franchini, G. Mazzanti, A. Ricci, M. Sala, J. Org. Chem. 61 (1996) 7242.
[6] B.F. Bonini, M. Comes-Franchini, M. Fochi, J. Gawronsky, G. Mazzanti, A. Ricci, G. Varchi, Eur. J. Org. Chem. (1999) 437.
[7] S. Kobayashi, Synlett (1994) 689.
[8] L. Paquette, T.M. Mitzel, M.B. Isaac, C.F. Crasto, W.W. Schomer, J. Org. Chem. 62 (1997) 4293.
[9] R.V. Hoffmann, J. Tao, J. Org. Chem. 62 (1997) 2292.
[10] L.M. Harwood, C.J. Moodie, J.K. Taylor, Organocopper Reagents, Oxford University Press, Oxford, 1994, p. 260.

PERGAMON

www.elsevier.nl/locate/poly

Polyhedron 19 (2000) 533–535

POLYHEDRON

Organometallic reagents and protocols for synthesis

Alex G. Fallis *, Pat Forgione, Simon Woo [1], Stephanie Legoupy [2], Sandrine Py [3], Curtis Harwig [4], Tanya Rietveld

Department of Chemistry, University of Ottawa, 10 Marie Curie, Ottawa, Ont. K1N 6N5, Canada

Received 4 October 1999; accepted 8 November 1999

Abstract

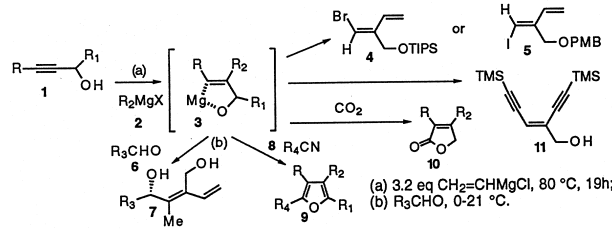
The addition of vinyl, aryl and alkynyl Grignard reagents to propargyl alcohols for the direct synthesis of dihydroxydienes (**7**), furans (**9**), butenolides (**10**) and enediyne alcohols (**11**) from a one-pot reaction involving a putative magnesium chelate intermediate (**3**) is described. Treatment of 5-bromo-1,3-pentadiene with indium metal in the presence of carbonyl compounds resulted in γ-pentadienylation to generate 1,4-dienes (**30**). Dehydration afforded cross-conjugated trienes (**31**) for tandem Diels–Alder reactions, while the alcohol product (**34**) from an unsaturated aldehyde after oxy-Cope rearrangement afforded the 1,4-diene product (**35**) and ultimately hydrindane (**36**). ©2000 Elsevier Science Ltd All rights reserved.

Keywords: Cycloadditions; Dienes; Indium; Magnesium; Trienes

Our interest in the synthesis of taxoids required the development of diverse organometallic reagents and protocols for the preparation of key intermediates and building blocks [1–3]. This included routes to stereodefined dienes by the direct addition of vinyl Grignard reagents to propargyl alcohols (**1**) [4–14]. Thus generation of the magnesium chelate (**3**) (or a closely related species) provides a direct synthesis of the family illustrated in Scheme 1. This includes the halodienes (**3**, **4**) [15], plus diene-diols (**7**), furans (**9**), 2(5*H*)-furanones (butenolides) (**10**) and enediynes (**11**) [16,17].

Direct condensation of the diene unit with carbonyl compounds was more efficient in cyclohexane due to the increased nucleophilicity of the Grignard complex in a less polar solvent. Table 1 lists representative examples for the preparation of compound **7**. It is of interest that the presence of the silyl ether is sufficient to inhibit the reaction of compound **14** (Table 1, entry e).

Furans comprise an important class of oxygen heterocycles for which new preparative routes continue to be developed [18–21]. Following the protocol developed above, substituted furans (**9**) can be synthesized directly upon reaction of (**3**) with dimethylformamide (DMF) followed by acidification. Alternatively, reaction with aryl nitriles provides C-2 substitution. The vinyl furan systems contain useful functionality for the construction of more complex skeletons



Scheme 1. Compounds from carbometallation of compound **1**.

Table 1
Synthesis of dihydroxydienes (**7**)

Entry	Substrate R—≡—CH_2OH	Reactant	Yield (%)	
			C_6H_{12}	THF
a	**12**, R = Me	PhCHO	80	50
b	**12**, R = Me [a]	PhCHO	68	44
c	**12**, R = Me [b]	PhCHO	100	
d	**13**, R = TMS	PhCHO	78	94
e	**14**, R = CH_2OTBS	PhCHO	0	0

[a] 2.1 equiv. CH_2=CHMgCl.
[b] 0.5 equiv. MeCCCH_2OH plus PhCHOHCH=CH_2.

* Corresponding author. Tel.: +1-613-562-5732; fax: +1-613-562-5170; e-mail: afallis@science.uottawa.ca
[1] Present address: AstraZeneca, St. Laurent, PQ, Canada.
[2] Present address: Department of Chemistry, University of Le Mans, Le Mans, France.
[3] Present address: LEDSS, Université Joseph Fourier, Grenoble Cedex, France.
[4] Present address: Anormed Inc., Vancouver, BC, Canada.

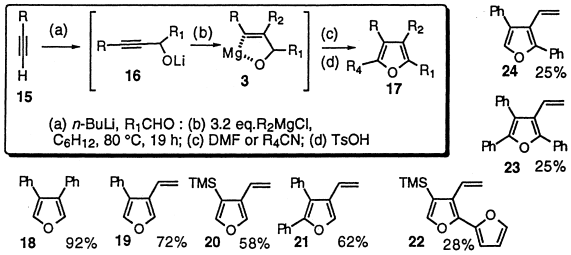
0277-5387/00/$ - see front matter ©2000 Elsevier Science Ltd All rights reserved.
PII S0277-5387(99)00402-7

via a double Diels–Alder strategy and also may be used as monomers. The versatility and scope of this furan synthesis was extended by in situ generation of the intermediate chelate compound **3** via lithium–magnesium transmetallation, as illustrated in Scheme 2. Thus, modification of the standard protocol permitted the control of the substitution pattern at all the ring positions. Various examples are listed, including the bis-furanyl system (**23**). Thus, depending upon the substrate–reagent–reactant combination selected, a large number of substituted furans can be prepared in a straightforward manner.

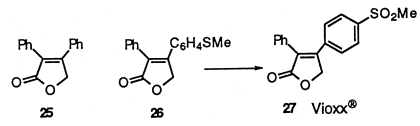
The study and synthesis of enyne and enediyne chromophores are of current interest because of their challenging structures and biological activity as antibiotics and antitumor agents [22–24]. An additional application of the synthetic utility of this carbometallation method is the facile preparation of these building blocks [25–28]. Thus the enediyne alcohol (**11**) [29] was prepared easily with trimethylsilylacetylene magnesium chloride.

Early examples of dialkyl butenolides from the condensation of species related to compound **3** with carbon dioxide have been reported [30,31], and other methods are available [32,33]. However, there is medicinal interest in preparing 3,4-diaryl-2(5*H*)-furanones. Thus, phenylpropargyl alcohol plus phenylmagnesium chloride or 4-thiomethylphenylmagnesium chloride followed by carbon dioxide afforded lactones **25** and **26** (Scheme 3). Oxidation of the sulfide with *m*-chloroperoxybenzoic acid gave the new Merck anti-inflammatory drug Vioxx® (**27**) in quantitative yield.

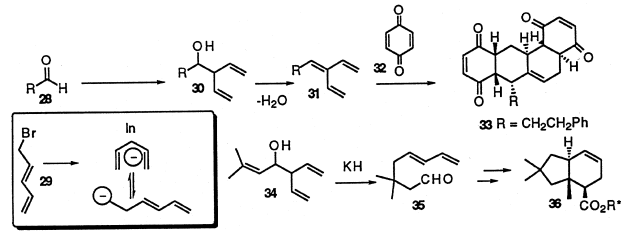
Li and Chan [34] have demonstrated the utility of allylindium species for addition to carbonyl compounds where the tin and zinc reagents failed [35–37]. For many metal pentadienyl systems condensation is not regioselective, and the delocalized anion may react at either the α or γ position (Scheme 4). However, the reagent generated from 5-bromo-1,3-pentadiene [38] and indium metal adds in a regioselective manner to give non-conjugated compounds of type **30** [39]. During our investigations, Araki and co-workers [40] reported related studies. Recently, Chan and Yang [41] have established that allylindium additions to ketones proceed via



Scheme 2. Synthesis of furans.



Scheme 3. Butenolide products.



Scheme 4. Pentadienyl indium addition and [4+2] cycloadditions.

the formation of an indium(I) species rather than indium(III). A parallel process involving metal surface-mediated allyl radical anions is also possible. In view of the close structural similarity between pentadienyl and allylindium species, the mechanisms are probably closely related.

Dehydration of these diene products (**30**) under Mitsunobu-type conditions (Ph_3P, diethylazodicarboxylate (DEAD), C_6H_6, 80°C) generated the corresponding trienes (**31**). These trienes facilitate diene-transmissive tandem Diels–Alder reactions [42] such as the reaction with compound **32** to give compound **33**. The alcohol product (**34**) from an unsaturated aldehyde is a surrogate for the Michael addition product. Thus oxy-Cope rearrangement afforded the 1,4-diene product (**35**). Subsequent cycloaddition with the Oppolzer chiral auxiliary [43,44] completed an enantioselective route to the hydrindane (**36**) [45].

In summary, the carbometallation protocols described above provide direct access to a number of useful unsaturated systems that can be employed for a variety of synthetic objectives. In addition, the organoindium reagent derived from 5-bromo-1,3-pentadiene and indium metal reacts with excellent regioselectivity and after further manipulation affords rapid entry to complex multicyclic skeletons from various [4+2] cycloadditions.

Acknowledgements

We are grateful to the Natural Sciences and Engineering Research Council of Canada, the Canadian Breast Cancer Research Initiative (NCI, Canada) and the Saunders-Matthey Foundation for Breast Cancer Research for financial support of this research. P. Forgione thanks Torcan Chemical Ltd. and the Government of Ontario for an OGSST Fellowship, S. Py thanks the Association Française pour la Recherche Thérapeutique for a Postdoctoral Fellowship and S. Woo thanks NSERC for a Postdoctoral Fellowship. C.W. Harwig and T. Rietveld thank NSERC for Postgraduate Scholarships.

References

[1] A.G. Fallis, Acc. Chem. Res. 32 (1999) 464.
[2] A.G. Fallis, Can. J. Chem. 77 (1999) 159.
[3] A.G. Fallis, Pure Appl. Chem. 69 (1997) 495.
[4] H.G. Richey Jr., F.W. Von Rein, J. Organomet. Chem. 20 (1969) 32.
[5] F.W. Von Rein, H.G. Richey Jr., Tetrahedron Lett. (1971) 3777.

[6] L. Labaundinière, J. Hanaizi, J.-F. Normant, J. Org. Chem. 57 (1992) 6903.
[7] I. Creton, I. Marek, J.-F. Normant, Tetrahedron Lett. 36 (1995) 7451.
[8] E. Negishi, Y. Zhang, F.E. Cederbaum, M.B. Webb, J. Org. Chem. 51 (1986) 4080.
[9] B. Jousseaume, J.-G. Duboudin, J. Organomet. Chem. 91 (1975) C1.
[10] J.G. Duboudin, B. Jousseaume, J. Organomet. Chem. 168 (1979) 1.
[11] J.G. Duboudin, B. Jousseaume, A. Bonakdar, J. Organomet. Chem. 168 (1979) 227.
[12] J.H. Merkley, J.E. Gallo, J. Org. Chem. 44 (1979) 587.
[13] J.J. Eisch, J.H. Merkley, J. Organomet. Chem. 20 (1969) 37.
[14] S. Ma, E. Negishi, J. Org. Chem. 62 (1997) 784.
[15] T. Wong, N.W. Tjepkema, H. Audrain, P.D. Wilson, A.G. Fallis, Tetrahedron Lett. 37 (1996) 755.
[16] P. Forgione, A.G. Fallis, Tetradedron Lett. 41 (2000) 11.
[17] P. Forgione, P.D. Wilson, A.G. Fallis, Tetrahedron 41 (2000) 17.
[18] T.L. Gilchrist, Contemp. Org. Syn. 1 (1994) 205.
[19] T.L. Gilchrist, J. Chem. Soc., Perkin Trans. I (1998) 615.
[20] E. Bures, P.G. Spinazze, G. Beese, I.R. Hunt, C. Rodgers, B.A. Keay, J. Org. Chem. 62 (1997) 8741.
[21] P. Wipf, L.T. Rahman, S.R. Rector, J. Org. Chem. 63 (1998) 7132.
[22] D.B. Borders, T.W. Doyle, Enediyne Antibiotics as Antitumor Agents, Marcel Dekker, New York, 1995.
[23] H. Lhermitte, D.S. Grierson, Contemp. Org. Syn. 3 (1996) 41.
[24] H. Lhermitte, D.S. Grierson, Contemp. Org. Syn. 3 (1996) 43.
[25] Y.F. Lu, C.W. Harwig, A.G. Fallis, J. Org. Chem. 58 (1993) 4202.
[26] Y.F. Lu, C.W. Harwig, A.G. Fallis, Can. J. Chem. 73 (1995) 2253.
[27] C.W. Harwig, S. Py, A.G. Fallis, J. Org. Chem. 62 (1997) 7902.
[28] S. Py, C.W. Harwig, S. Banerjee, D.L. Brown, A.G. Fallis, Tetrahedron Lett. 39 (1998) 6139.
[29] A.G. Meyers, P.M. Harrington, E.Y. Kuo, J. Am. Chem. Soc. 113 (1991) 694.
[30] R. Mornet, L. Gouin, Bull. Soc. Chim. Fr. (1977) 737.
[31] J.-G. Duboudin, B. Jousseaume, J. Organomet. Chem. 168 (1979) 233.
[32] S. Ma, Z. Shi, J. Org. Chem. 63 (1998) 6387.
[33] S. Ma, Z. Shi, Tetrahedron Lett. 40 (1999) 2393.
[34] C.J. Li, T.H. Chan, Tetrahedron Lett. 32 (1991) 7017.
[35] T.H. Chan, C.J. Li, M.C. Lee, Z.Y. Wei, Can. J. Chem. 72 (1994) 1181.
[36] C.J. Li, Chem. Rev. 93 (1993) 2023.
[37] P. Cintas, Synlett (1995) 1087.
[38] C. Prevost, P. Miginiac, L. Miginiac-Groizeleau, Bull. Soc. Chim. Fr. (1964) 2485.
[39] S. Woo, N. Squires, A.G. Fallis, Org. Lett. 1 (1999) 573.
[40] T. Hirashita, S. Inoue, H. Yamamura, M. Kawai, S. Araki, J. Organomet. Chem. 549 (1997) 305.
[41] T.H. Chan, Y. Yang, J. Am. Chem. Soc. 121 (1999) 3228.
[42] J.D. Winkler, Chem. Rev. 96 (1996) 167.
[43] W. Oppolzer, D. Dupuis, Tetrahedron Lett. 26 (1985) 5437.
[44] W. Oppolzer, D. Dupuis, G. Poli, T.M. Raynham, G. Bernardinelli, Tetrahedron Lett. 26 (1988) 5885.
[45] A.G. Melekhov, A.G. Fallis, Tetrahedron Lett. 40 (1999) 7862.

PERGAMON

www.elsevier.nl/locate/poly

Polyhedron 19 (2000) 537–539

POLYHEDRON

The first catalytic enantioselective Nozaki–Hiyama–Kishi reaction

Marco Bandini, Pier Giorgio Cozzi* [1], Achille Umani-Ronchi* [2]

Dipartimento di Chimica G. Ciamician, Università di Bologna, Via Selmi 2, 40126 Bologna, Italy

Received 4 October 1999; accepted 4 January 2000

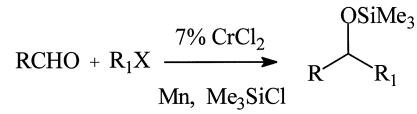
Abstract

Herein we report the first example of a catalytic enantioselective Nozaki–Hiyama–Kishi reaction performed with a catalytic amount of chiral chromium complex. A large variety of non-stereogenic and stereogenic reactive halides can be added to aldehydes to afford the corresponding alcohols with excellent stereoselectivity using a catalytic amount of chiral chromium complex ©2000 Elsevier Science Ltd All rights reserved.

Keywords: Chromium; Salen; Manganese; Catalysis; Enantioselection; Nozaki–Hiyama–Kishi reaction

In recent years catalytic redox reactions have become increasingly important in organic synthesis as processes which are environmentally friendly. Titanium [1], samarium [2], vanadium [3] and chromium [4] catalytic redox processes have recently been applied in C–C bond forming reactions. Among these, the Nozaki–Hiyama–Kishi (NHK) reaction [5] reported by Fürstner and Shi [6], with catalytic amounts of chromium, is of considerable interest (Scheme 1). In fact, Cr(II) or Cr(II)/Ni(II) mediated reactions are unique in scope and chemoselectivity.

The wide compatibility with different functional groups in both reaction partners and the low basicity make the organochromium complexes the best reagents for the synthesis of sensitive and polyfunctional compounds. The driving force of the chromium reaction arises from the formation of stable O–Cr(III) bonds. For this reason stoichiometric NHK reactions require almost 2 mol of Cr(II) per 1 mol of organic halide. The key features of Fürstner's modification are based on the addition of an oxophilic additive such as trimethyl silyl chloride as the scavenger and driving force for the chemical catalytic reaction [7], and on the use of Mn which reduces the Cr(III) to Cr(II). In fact, the main advantage is that the Mn is not capable of reacting with the substrates in the reaction mixture, and the Mn(II) salt obtained is a weak Lewis acid. We have carried out the first catalytic enantioselective Nozaki–Hiyama–Kishi reaction, catalytic both in chromium and in ligand. Our enantioselective process requires the use



Scheme 1. Carbon–carbon bond forming redox processes promoted by a catalytic amount of $CrCl_2$.

of the inexpensive and commercially available chiral Salen ligand (Fig. 1).

Chiral chromium(III)–Salen complexes were reported to mediate interesting transformations [8,9]. The chiral Cr–Salen complex was prepared in situ according to Jacobsen and co-workers by adding anhydrous $CrCl_2$ to a THF solution of Salen. The further addition of allyl bromide affords the organometallic allylchromium reagent which was used in a catalytic amount (10%) in the presence of manganese, TMSCl, and benzaldehyde at room temperature (Scheme 2). However, under these conditions the desired silylated homoallylic alcohol was only obtained in low yields (15%, 21% enantiomeric excess), with the main product being the pinacol.

We optimized the reaction conditions for the preparation of the Cr–Salen complex by adding a base (20%) capable of

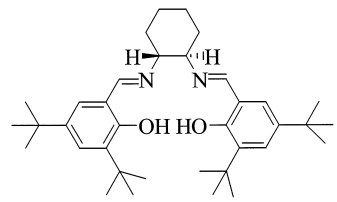
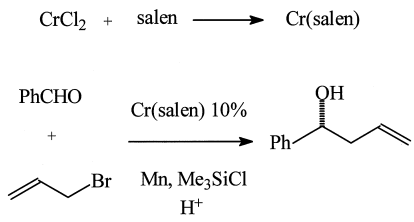


Fig. 1. (*R*,*R*)-(−)-Salen = (*R*,*R*)-(−)-*N*,*N*′-bis(3,5-di-*tert*-butyl-salicylidene)-1,2-cyclohexane-diamine.

[1] *Corresponding author. Tel.: +39-051-2099-511; fax: +39-051-2099-456; e-mail: pgcozzi@ciam.unibo.it

[2] *Corresponding author. E-mail: umani@ciam.unibo.it

0277-5387/00/$ - see front matter ©2000 Elsevier Science Ltd All rights reserved.
PII S0277-5387(00)00290-4



Scheme 2. Allylation reaction of the PhCHO promoted by Cr(Salen) complex in THF.

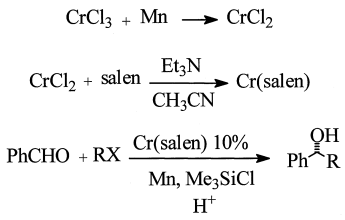
deprotonating the Salen ligand in acetonitrile, where the pinacol coupling was minimized. The procedure was improved further on avoiding the manipulation of the highly sensitive Cr(II) salt by the reduction in situ of anhydrous $CrCl_3$ with Mn in CH_3CN. The Cr(II) salt was complexed to the Salen ligand by the addition of Et_3N (20 mol%). The resulting Cr(II)–Salen, used in catalytic amount (10%), promoted the addition of several allyl, propargyl, and benzyl halides to benzaldehyde in the presence of Me_3SiCl (Scheme 3).

As summarized in Table 1 a large variety of reactive halides can be used, however a high enantiomeric excess was only obtained with allyl chloride (Table 1, entry 1). Vinyl or aryl halides, where the presence of a catalytic amount of nickel salt in the NHK reaction is necessary, are under investigation.

As reported in Table 2, the results obtained with several aliphatic and aromatic aldehydes show the generality of the method. Different silylating agents do not exhibit any significant influence on the asymmetric induction of the reaction, while the dependence on the enantioselection of the chromium salts and halides employed was observed [10].

Unfortunately in all cases, by-products derived from the pinacol coupling (20–40%) or derived from the reduction of the aldehyde (with aliphatic aldehydes) were isolated.

Several Schiff bases were synthesized to improve the enantiomeric excess of the homoallylic alcohols. However, all the



Scheme 3. Schematic representation of the optimized protocol for the catalytic enantioselective addition of organohalides to PhCHO promoted by Cr(Salen) complex.

Table 1
Results for reactive halides

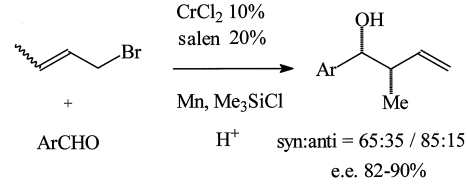
Entry	RX	Yield (%)	Enantiomeric excess (%)
1	C_3H_5Cl	65	84
2	C_3H_5Br	64	52
3	C_3H_5I	70	0
4	$PhCH_2Cl$	67	30
5	$CNCH_2Cl$	53	24
6	C_3H_3Cl	65	54

new Schiff bases screened in allylation reaction performed with the standard protocol have shown lower enantioselectivity than Salen. Stereogenic allylhalides were also employed with our method. After several attempts, we discovered that the amount of ligand is crucial for achieving good results. In fact, high diastereoisomeric and enantiomeric excesses were obtained with the addition of crotyl bromide to aromatic aldehydes, when the reaction was performed with an excess of Salen ligand (Scheme 4). The addition of crotyl chromium reagent to aromatic aldehydes shows a *syn* simple diastereoselection. This is an important result which indicates the possibility of modifying selectively the diastereoselection of organometallic reactions when macrocyclic ligands are involved.

The reaction performed in the presence of the Salen ligand is unique because normally reactions of aldehydes with stereogenic allylchromium reagents afford homoallylic alcohols with an excellent degree of *anti* selectivity. This selectivity is thought to be due to a cyclic Zimmermann–Traxler transition state. In fact, using the catalytic conditions described by Fürstner for the addition of crotylbromide to aromatic

Table 2
Results for aliphatic and aromatic aldehydes

Entry	R-CHO	Yield (%)	Enantiomeric excess (%)
1	*p*-Ph-C_6H_4CHO	54	82
2	*p*-Me-C_6H_4CHO	67	78
3	*p*-F-C_6H_4CHO	41	77
4	$PhCH_2CH_2CHO$	45	77
5	c-$C_6H_{11}CHO$	42	89



Scheme 4. *Syn* diastereoselective addition of crotyl bromide to aromatic aldehydes promoted by chiral Cr(Salen) complex.

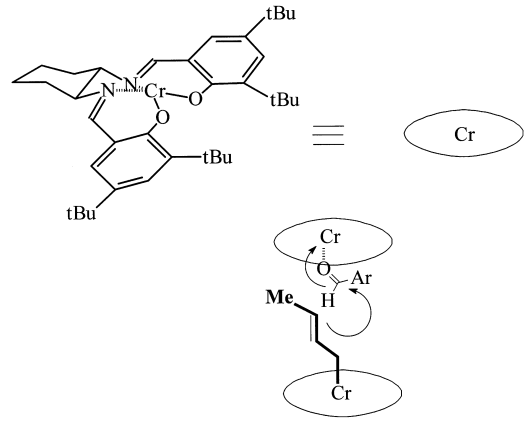


Fig. 2. Hypothetical open transition state for the addition of crotyl bromide to ArCHO.

aldehydes, the *anti* diastereoisomer was always obtained in larger amount [6]. This intriguing result may suggest a mechanism for the Cr–Salen mediated NHK reactions in which two molecules of Cr–Salen complexes are involved in the transition state (Fig. 2) [11].

In conclusion, the catalytic enantioselective NHK reaction described here represents the first example of an effective enantioselective reaction mediated by a catalytic amount of Cr salt, opening the way to rational design of new redox catalytic enantioselective reactions. Work on this project is currently under investigation in our laboratory.

1. Typical experimental procedure

$CrCl_3$ (16 mg, 0.1 mmol) and Mn (166 mg, 3 mmol) were added to anhydrous CH_3CN (5 ml) and the mixture was kept for about 5–10 min, then the reaction mixture was stirred until a green–white precipitate was observed. The Salen ligand (54 mg, 0.1 mmol) was introduced followed by dried triethylamine (30 μl, 0.2 mmol) and the resulting brown solution was stirred at room temperature for 1 h. The solution was treated with allylchloride (116 μl, 1.5 mmol) and the resulting red solution was stirred for 1 h at room temperature. Finally, PhCHO (100 μl, 1 mmol) and Me_3SiCl (190 μl, 1.5 mmol) were added and the mixture was stirred until complete consumption of the aldehyde. After quenching with a saturated solution of $NaHCO_3$, the reaction mixture was filtered on a celite© bed, and the CH_3CN was evaporated under reduced pressure. The residue was extracted with Et_2O and the organic phases were collected and evaporated under reduced pressure. The oil obtained was dissolved in THF (3 ml) and treated with 1 ml of HCl 1 N. The mixture was stirred to complete desilylation (checked by TLC). After evaporation of THF, the residue was extracted with Et_2O. The organic phases were collected, dried over Na_2SO_4 and concentrated in vacuo to give a brown residue purified by flash chromatography (silica gel, cyclohexane/Et_2O 4/1, $R_f = 0.3$). The (*R*)-1-phenyl-3-buten-1-ol was isolated as a light yellow oil (100 mg, 67% yield) in 84% enantiomeric excess.

References

[1] A. Gansäuer, Synlett (1998) 801.
[2] R. Nomura, T. Matsuno, T. Endo, J. Am. Chem. Soc. 116 (1996) 11666.
[3] B. Hatano, A. Ogawa, T. Hirao, J. Org. Chem. 63 (1998) 9421.
[4] A. Svantoš, W. Boland, Synlett (1998) 549.
[5] A. Fürstner, Chem. Rev. 99 (1999) 991.
[6] A. Fürstner, N. Shi, J. Am. Chem. Soc. 118 (1996) 12349.
[7] A. Fürstner, Chem. Eur. J. 4 (1998) 567.
[8] J.F. Larrow, S.E. Schaus, E.N. Jacobsen, J. Am. Chem. Soc. 118 (1996) 7420.
[9] S.E. Schaus, J. Brånalt, E.N. Jacobsen, J. Org. Chem. 63 (1998) 403.
[10] M. Bandini, P.G. Cozzi, P. Melchiorre, A. Umani-Ronchi, Angew. Chem., Int. Ed. Engl. 38 (1999) 3357.
[11] R.G. Konsler, J.K. Karl, E.N. Jacobsen, J. Am. Chem. Soc. 120 (1998) 10780.

PERGAMON

www.elsevier.nl/locate/poly

Polyhedron 19 (2000) 541–543

POLYHEDRON

A new quinazoline-containing axially chiral ligand for asymmetric catalysis

Mary McCarthy, Patrick J. Guiry *

Department of Chemistry, University College Dublin, Belfield, Dublin 4, Ireland

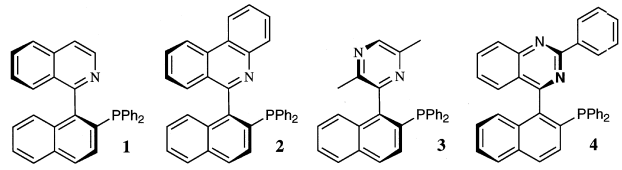
Received 4 October 1999; accepted 8 November 1999

Abstract

The rationale behind the design of an axially chiral quinazoline-containing phosphinamine ligand, 2-phenyl-Quinazolinap, is described. Its synthesis had two metal-catalysed couplings as the key steps. Enantiopure ligand was obtained after resolution and afforded up to 66% enantiomeric excess (ee) in Pd-catalysed allylic alkylation. η^3-Allyl Pd complexes were investigated by ^{1}H NMR in an attempt to explain the sense of enantioselection observed, which was opposite to that of related ligands. Rhodium-catalysed enantioselective hydroboration of a variety of substituted styrenes was achieved with excellent conversions, good regioselectivities and ee values of up to 91% with 2-phenyl-Quinazolinap as the ligand. ©2000 Elsevier Science Ltd All rights reserved.

Keywords: Allylic alkylation; Axially chiral phosphinamine; Hydroboration; Quinazolines

Recently, interest in non-C_2-symmetric axially chiral phosphinamine bidentate ligands has increased [1–4]. The first axially chiral phosphinamine to be reported was Quinap (**1**) and it was applied in Rh-catalysed hydroboration and Pd-catalysed allylic substitution [5–7]. Mechanistic studies suggested that the 3H of the isoquinoline unit takes up a region in space leading to steric interactions that are important for asymmetric induction [7]. This observation was the design principle behind the vaulted analogue Phenap (**2**), which in turn gave high enantioselectivities in Rh-catalysed hydroboration [8] and Pd-catalysed allylic substitution [9]. In a recent study we prepared and resolved 1-(3,6-dimethylpyrazin-2-yl)(2-naphthyl)diphenylphosphine (**3**), but this was found to racemise at room temperature [10]. As an extension to these studies we designed diphenyl[1-(2-phenylquinazolin-4-yl)(2-naphthyl)]phosphine (**4**), which has the acronym 2-phenyl-Quinazolinap. (We have prepared a series of substituted diphenyl[1-quinazolin-4-yl)(2-naphthyl)]phosphines and we find this acronym useful as it follows directly from the Binap, Quinap and Phenap acronyms [11].) The 2-phenylquinazoline unit was chosen as we predicted that the naphthalene–quinazoline pivot would be essentially inert to racemisation and, once resolved, we could investigate the effect on enantioselection relative to compounds **1** and **3** of the increased steric bulk at the 2-position of compound **4** (equivalent to the 3-position of compound **1**). In this communication the synthesis and resolution of ligand **4** and its preliminary application in asymmetric catalysis is described.

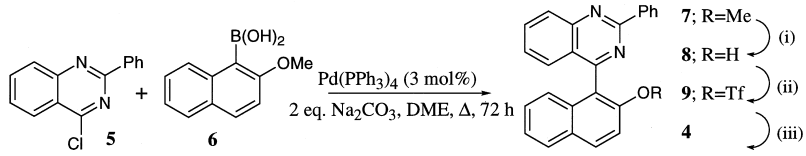


The synthesis of compound **4**, similar to that previously reported for ligands **1**–**3**, has the metal-catalysed reactions of biaryl coupling and formation of the naphthyl–phosphorus bond as the two key steps. The electrophilic component of the Pd-catalysed cross-coupling was 4-chloro-2-phenylquinazoline (**5**), while the nucleophilic component was 2-methoxy-1-naphthylboronic acid (**6**) Scheme 1. This gave 2-methoxy-1-(2-phenylquinazolin-4-yl)naphthalene (**7**) in 53% yield. The next two steps involved the conversion of the methyl ether into 1-(2-phenylquinazolin-4-yl)-2-naphthyl(trifluoromethyl)sulfonate (**9**) by demethylation and triflation of the resultant alcohol (**8**) in 81 and 46% yields, respectively. Nickel(II)-catalysed coupling of compound **9** with diphenylphosphine gave 2-phenyl-Quinazolinap (**4**) as a racemate in 74% yield.

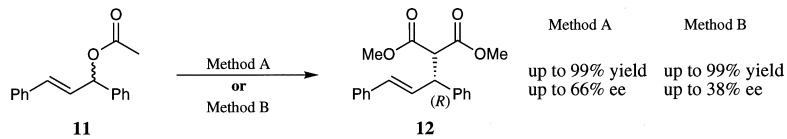
Ligand **4** was successfully resolved by the separation of diastereomeric complexes derived from compound **4** and (+)-di-μ-chlorobis{(*R*)-dimethyl[1-(1-naphthyl)ethyl]-

* Corresponding author. Tel.: +353-1-7062309; fax: +353-1-7062127; e-mail: p.guiry@ucd.ie

0277-5387/00/$ - see front matter ©2000 Elsevier Science Ltd All rights reserved.
PII S0277-5387(99)00403-9

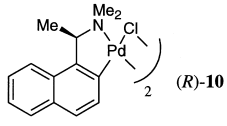


Scheme 1. Reagents: (i) BBr_3, CH_2Cl_2; (ii) $(TfO)_2O$, DMAP, CH_2Cl_2; (iii) Ph_2PH, $NiCl_2$dppe, DABCO, DMF.



Scheme 2. Method A: $[Pd(C_3H_5)Cl]_2$, (*R*)-**4** (2 mol%), $NaCH(CO_2Me)_2$. Method B: $[Pd(C_3H_5)Cl]_2$, (*R*)-**4** (2 mol%), $CH_2(CO_2Me)_2$; BSA, KOAc.

aminato-C_2,*N*}dipalladium(II) (**10**), a resolving agent that has been successful in the resolution of a wide range of phosphorus-containing ligands [12–14].



The initial precipitate from the reaction in MeOH was the (*R*,*R*)-diastereomer; the (*S*,*R*)-diastereomer was isolated from the filtrate [15]. Enantiopure ligand was generated after decomplexation of the appropriate diastereomer by the addition of dppe. The enantiopurity was tested by recomplexing with (*R*)-**10** and observing only one diastereomer by ^1H and ^{31}P NMR. We then wished to test its metal complexes in asymmetric catalysis.

Pd-catalysed allylic alkylation is an asymmetric transformation that has proved to be a useful testing ground for new ligands and for gaining mechanistic insights into organopalladium chemistry [16–19]. The standard test reaction in allylic substitution is between 1,3-diphenylpropenyl acetate (**11**) and the soft nucleophile derived from dimethyl malonate. The results of our preliminary investigations using (*R*)-**4** are summarised in Scheme 2. The key points are that the conversions are good (up to 99% yield) but the enantioselectivities are moderate (optimised to 66%) and show the *opposite* sense of asymmetric induction compared to ligands **1** and **2**; i.e. (*R*)-**1** and (*R*)-**2** afford an excess of (*S*)-**12** whereas (*R*)-**4** gives (*R*)-**12** in excess.

As the major structural difference between compounds **1**, **2** and **4** is the presence of the 2-phenyl substituent on the quinazoline, this substituent must cause steric interactions which lead to lowered and opposite asymmetric induction. From ^1H NMR solution studies of cationic 1,1,3-triphenylallyl palladium complexes of ligand **4** it was determined that the CPh_2 group was *trans* to nitrogen in the major diastereomer [20]. Inspection of molecular models is also useful in coming to the same conclusion to explain the formation of the (*R*)-enantiomer in excess. Unambiguous NOE (nuclear Overhauser effect) assignments were not possible for complexes **13** and **14**, but we infer attack *trans* to phosphorus at the *endo* isomer (**13**) being disfavoured due to the 2-phenyl substituent inhibiting the required rolling of the allyl [21] (Scheme 3). Attack *trans* to phosphorus at the *exo* isomer (**14**) gives *R* product in a favoured process as now the rolling alleviates potential steric interactions between the phenyl groups. There is, therefore, a mismatch between the *R* axial chirality and the presence of a bulky 2-substituent and in this case the latter steric interaction predominates.

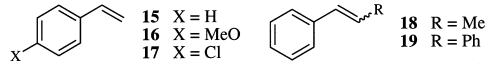
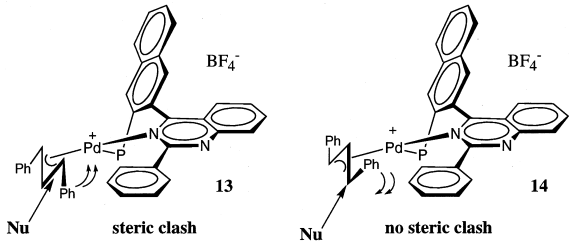


Table 1
Rhodium-catalysed hydroboration of olefins **15**–**19** with (*R*)-2-phenyl-Quinazolinap (**4**)

Entry	Olefin	Temperature	Conversion (%) [a]	α:β [b]	ee (%) [c] (configuration)
1	**15**	RT [d]	100	68:32	63 (*R*)
2	**15**	0°C	100	80:20	79 (*R*)
3	**16**	RT	100	75:25	77 (*R*)
4	**17**	0°C	100	78:22	46 (*R*)
5	(*E*)-**18**	RT	100	91:9	93 (*R*)
6	(*Z*)-**18**	RT	100	92:8	91 (*R*)
7	(*E*)-**19**	RT	–	–	–
8	(*Z*)-**19**	RT	100	–	59 (*R*)

[a] Conversions determined by ^1H NMR.
[b] α:β ratios (α refers to the benzylic position) determined by ^1H NMR.
[c] Enantiomeric excesses (ee) determined by GC (β-Dex®120 column, 30 m × 0.25 mm, 0.25-μm film thickness).
[d] Room temperature.



Scheme 3.

Axially chiral diphosphine [22] and phosphinamine ligands have also been applied in the Rh-catalysed hydroboration of alkenes [7,8,23]. A summary of the preliminary Rh-catalysed hydroboration results that we have obtained using ligand **4** with a range of variously substituted styrenes (**15**–**19**) is given in Table 1.

Our reactions were carried out with catecholborane in tetrahydrofuran (THF) using 1 mol% of a catalyst prepared in situ from adding trimethylsilsyl (TMS) triflate to a solution of (1,5-cyclooctadiene)(2,4-pentanedionato)rhodium(I) and compound **4**. These results demonstrate that we have an extremely enantioselective catalyst system which affords high enantioselectivities for substituted styrenes and stilbenes. This is in marked contrast to Rh complexes of BINAP where (*Z*)-**19** gave only 16% enantiomeric excess (ee) [22]. We explain these results by inferring that the increased steric demand of the olefin is more easily accommodated by our less sterically demanding ligand **4**.

In conclusion, this communication reports a new quinazoline-containing axially chiral ligand and its preliminary applications in asymmetric catalysis.

Acknowledgements

We thank Enterprise Ireland for a Basic Research Award (SC/94/565) to support this work and an Enterprise Ireland Research Scholarship (BR/94/158) to M.McC. The award of the 1997 BOC Gases Postgraduate Bursary to M.McC is gratefully acknowledged. We thank Johnson Matthey for a gift of Pd salts, Patrick Lacey for a critical reading of this manuscript and UCD for an award to P.J.G. to attend OMCOS 10.

References

[1] Y. Imai, W. Zhang, T. Kida, Y. Nakatsuji, I. Ikeda, Tetrahedron Lett. 39 (1998) 4343.
[2] M. Ogasawara, K. Yoshida, H. Kamei, K. Kato, Y. Uozumi, T. Hayashi, Tetrahedron: Asymmetry 9 (1998) 1779.
[3] S. Vyskocil, M. Smrcina, V. Hanus, M. Polasek, P. Kocovsky, J. Org. Chem. 63 (1998) 7738.
[4] M. McCarthy, P.J. Guiry, Tetrahedron (in preparation).
[5] N.W. Alcock, J.M. Brown, D.I. Hulmes, Tetrahedron: Asymmetry 4 (1993) 743.
[6] J.M. Brown, D.I. Hulmes, T.P. Layzell, Chem. Commun. (1993) 1673.
[7] J.M. Brown, D.I. Hulmes, P.J. Guiry, Tetrahedron 50 (1994) 4493.
[8] J.-M. Valk, G.A. Whitlock, T.P. Layzell, J.M. Brown, Tetrahedron: Asymmetry 6 (1995) 2593.
[9] J.-M. Valk, T.D.W. Claridge, J.M. Brown, D. Hibbs, M.B. Hursthouse, Tetrahedron: Asymmetry 6 (1995) 2597.
[10] M. McCarthy, P.J. Guiry, Tetrahedron 55 (1999) 3061.
[11] M. McCarthy, P. Lacey, C. Saunders, J. Commiskey, C. McDonnell, P.J. Guiry (unpublished results).
[12] P.G. Kerr, P.-H. Leung, S.B. Wild, J. Am. Chem. Soc. 109 (1987) 4321.
[13] P. Leung, S. Loh, K.F. Mok, A.J.P. White, D.J. Williams, Tetrahedron: Asymmetry 7 (1996) 45.
[14] P. Leung, S. Loh, K.F. Mok, A.J.P. White, D.J. Williams, Chem. Commun. (1996) 591.
[15] M. McCarthy, R. Goddard, P.J. Guiry, Tetrahedron: Asymmetry 10 (1999) 2797.
[16] T. Hayashi, I. Ojima, Catalytic Asymmetric Synthesis, VCH, Weinheim, 1993, p. 325.
[17] C.G. Frost, J. Howarth, J.M.J. Williams, Tetrahedron: Asymmetry 3 (1992) 1089.
[18] B.M. Trost, D.L. van Vranken, Chem. Rev. 96 (1996) 395.
[19] J.P. Cahill, P.J. Guiry, Tetrahedron: Asymmetry 9 (1998) 4302 and references cited therein.
[20] M. McCarthy, P.J. Guiry (in preparation).
[21] S. Ramdeehul, P. Dierkes, R. Aguado, P.C. Kamer, P.W.N.M. van Leeuwen, J.A. Osborn, Angew. Chem., Int. Ed. Engl. 37 (1998) 3118.
[22] T. Hayashi, Y. Matsumoto, Y. Ito, Tetrahedron: Asymmetry 2 (1991) 601.
[23] H. Doucet, E. Fernandez, T.P. Layzell, J.M. Brown, Chem. Eur. J. 5 (1999) 1320.

PERGAMON

www.elsevier.nl/locate/poly

Polyhedron 19 (2000) 545–548

POLYHEDRON

Addition of the alkenyl C–H bond of enamines to η^3-allenyl/propargyl complexes leading to the formation of pyrrole derivatives

An-Chi Yeh, Shang-I Chen, Ai-Jan Chen, Gene-Hsiang Lee, Yu Wang, Jwu-Ting Chen *

Department of Chemistry, National Taiwan University, Taipei, 106 Taiwan, Republic of China

Received 4 October 1999; accepted 24 November 1999

Abstract

The reactions of enamines (ROC)HC=CMe(NH^{i}Pr) with η^3-allenyl/propargyl complexes $[M(PPh_3)_2(\eta^3\text{-}C_3H_3)]^+$ (M = Pd, Pt) result in the formation of pyrrole derivatives. Such reactions involve the intermediates of central-carbon-substituted η^3-allyl complexes $\{M(PPh_3)_2(\eta^3\text{-}CH_2C[C(COR)=CMe(NH^iPr)]CH_2)\}^+$ which are formed by hydroalkenylation to the C_3H_3 moiety. ©2000 Elsevier Science Ltd All rights reserved.

Keywords: Enamine; Alkenylation; Pyrrole

1. Introduction

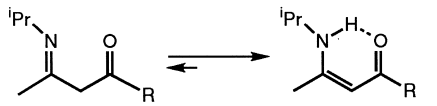
The addition of an olefinic C–H bond across an unsaturated carbon–carbon bond is highly interesting from the viewpoint of synthetic methodology [1]. The involvement of transition metal complexes in such processes is often crucial, particularly for the development of novel ways of C–C bond formation [2]. We and other groups have discovered that cationic η^3-allenyl/propargyl complexes generally behave as good carbon electrophiles and are subject to the addition with a wide variety of nucleophiles containing O, S, Se, N, P or C donor [3–7]. Meanwhile, such complexes exhibit keen chemical selectivity. For instance, tertiary amine such as Et_3N can be added to $[Pt(PPh_3)_2(\eta^3\text{-}C_3H_3)]^+$ (**3**) via C–N bond formation to give a platinacyclobutene adduct [8]. In contrast, compound **3** activates a phenyl C–H bond in NMe_2Ph to allow arylation, yielding an arylallyl complex [9].

We have chosen to use enamines that are known to contain both active N–H as well as C–H bonds to react with η^3-allenyl/propargyl complexes. Our studies lead to the discovery of the first examples of hydroalkenylation of metal complexes of allenyl/propargyl. The insertion of η^3-C_3H_3 to an enamine C–H bond affords a diene 'skeleton' which allows incorporation of an amino functionality to form the pyrrole derivatives.

* Corresponding author. Tel: +886-2-2366-0352; fax: +886-2-2363-6359; e-mail: jtchen@ccms.ntu.edu.tw

2. Results and discussion

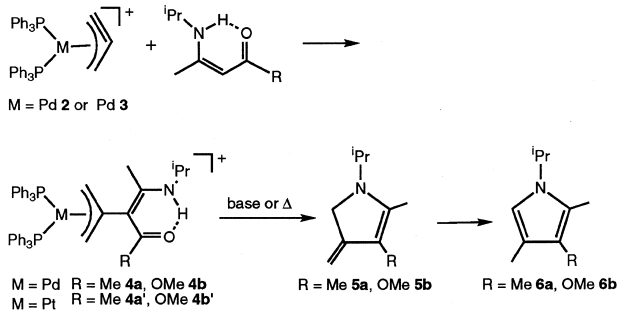
The enamines Me(NH^{i}Pr)C=CHR [R = COMe (**1a**), CO_2Me (**1b**)] have been prepared by the reactions of α,γ-diketone or ketoester methane, respectively, with ^{i}PrNH$_2$ [10]. The NMR data for compounds **1a** and **1b** indicate that tautomerization overwhelmingly inclines to the enamine form, which is presumably stabilized by hydrogen bonding between N–H and the keto group:



R = Me **1a**, OMe **1b** (1)

Previous studies have shown that amines and amino derivatives with active hydrogen are prone to undergo regioselective hydroamination to $[M(PPh_3)_2(\eta^3\text{-}C_3H_3)]^+$ [M = Pd (**2**), Pt (**3**)], yielding azatrimethylenemethane (N-TMM) complexes and their derivatives (N-TMM represents the azatrimethylenemethane complexes $M[CH_2C(NR)CH_2]$) [11]. However, heating a mixture of compounds **2** and **1b** at 50°C was found to generate the pyrrole derivatives. Further investigation shows that reactions of equimolar amounts of compound **2** and enamine at 25°C undergo unprecedented hydroalkenylation. The regioselective C–C coupling takes place between the central carbon of the C_3H_3 and the β-olefinic carbon of the enamine, and results in enamine–allyl complexes of the formula of $Pd(PPh_3)_2\{\eta^3\text{-}CH_2C$-

0277-5387/00/$ - see front matter ©2000 Elsevier Science Ltd All rights reserved.
PII S0277-5387(99)00404-0



Scheme 1.

$[C(COR)CMe(NH^iPr)]CH_2\}^+$ [R = Me (**4a**), OMe (**4b**)] with yields of over 75%. Complexes **4a** and **4b** were characterized mainly by NMR techniques and elemental analysis. By heating the reaction solutions of complexes **4a** and **4b** to 50°C, or treating them with base, yielded the pyrrole derivatives **6a** and **6b**, respectively (Scheme 1).

The analogous reactions of $[Pt(PPh_3)_2(\eta^3\text{-}C_3H_3)](BF_4)$ (**3**) with compound **1a** or **1b** produced $\{Pt(PPh_3)_2(\eta^3\text{-}CH_2C[C(COR)=CMe(NH^iPr)]CH_2)\}(BF_4)$ [R = Me (**4a′**), OMe (**4b′**)], also in very good yields. The enamine–allyl platinum complexes could alternatively be formed from the reactions of *trans*-$Pt(Br)(PPh_3)_2(\eta^1\text{-}CHCCH_2)$ and enamine at 25°C, but with longer reaction time. Single-crystal X-ray crystallography provides the authentic molecular structure of **4b′**. Fig. 1 shows its ORTEP drawing. The length of C2–C4 is 1.46(2) Å, a typical C_{sp^2}–C_{sp^2} single bond. The dihedral angle between the C1–C2–C3 and C1–Pt–C2 planes is 68(1)° and ∠C1–C2–C3 is 113(1)°, which is consistent with the η^3-allyl characteristic and somewhat approaches that of the η^3-trimethylenemethane species [7,12]. This indicates that there is significant electronic delocalization in the planar N–C5–C4–C10–O1 moiety of enamine. The distance between N and O1 atoms is 2.52 Å, which is suitable for hydrogen bonding in the vicinity. However, the generated amino hydrogen points out of the enamine plane with ∠O1–H–N = 116(7)°. The single crystals of compound **4b′** were obtained by recrystallization in CH_2Cl_2–Et_2O solution. Crystal data: orthorhombic $P2_12_12_1$ $a = 11.100(5)$ Å, $b = 17.764(4)$ Å, $c = 21.951(4)$ Å, $V = 4328(2)$ Å^3, Mo Kα radiation $\lambda = 0.7107$ Å, $Z = 4$, $\mu = 3.398$ mm^{-1}, 5490 total reflections, 3032 observed reflections ($I > 2.0\sigma(I)$), $R = 0.044$, $R_w = 0.036$.

Ring closure in compounds **4a** and **4b** could be accomplished by heating or treating with base as well, except that cyclization of compound **4b** first generates a dihydropyrrole derivative (**5b**). Upon chromatographing on a silica gel column, **5b** would isomerize to the stable pyrrole product (**6b**). Such a reaction is mechanistically comparable to furan formation from an enolate–allyl complex [13].

3. Conclusions

The regioselective addition of enamine to η^3-allenyl/propargyl complexes demonstrates a new type of 'alkene–alkyne' coupling which affords new enamine–allyl complexes and leads to the formation of pyrrole derivatives.

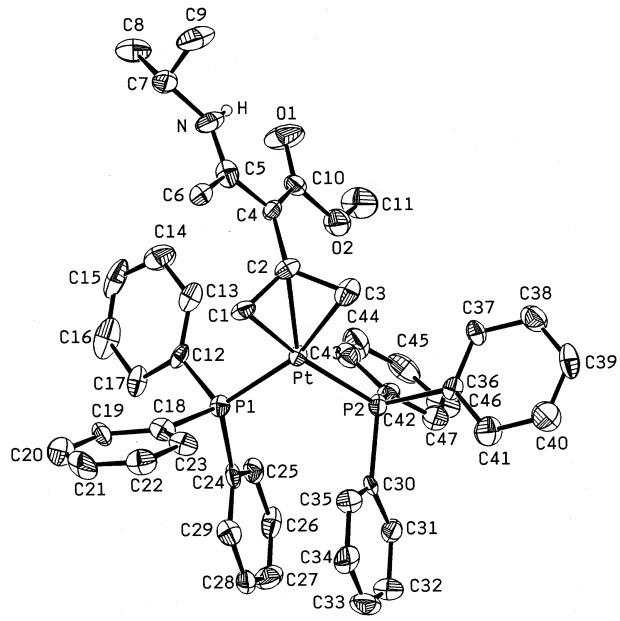


Fig. 1. ORTEP drawing of $\{Pt(PPh_3)_2(\eta^3\text{-}CH_2C[C(CO_2Me)\text{-}CMe(NH^iPr)]CH_2)\}(BF_4)$ (**4b′**) with 50% probability ellipsoids. All hydrogen atoms except the N-bound one are omitted for clarity. Selected bond distances (Å) and angles (°): Pt–P1 2.298(4), Pt–P2 2.300(3), Pt–C1 2.17(1), Pt–C2 2.24(1), Pt–C3 2.19(1), C1–C2 1.40(2), C2–C3 1.45(2), C2–C4 1.46(2), C4–C5 1.44(2), C4–C10 1.41(2), C5–N 1.32(2), C10–O1 1.22(2); ∠P1–Pt–P2 100.3(1), ∠C1–Pt–C3 66.2(5), ∠C1–C2–C3 113(1), ∠C1–C2–C4 122(1), ∠C3–C2–C4 125(1), ∠C5–C4–C10 116(1), ∠C5–C4–C2 118(1), ∠C2–C4–C10 126(1), ∠C4–C5–N 120(1), ∠C4–C10–O1 130(1).

4. Experimental

4.1. General

Commercially available reagents were purchased and used without purification unless necessary. Solvents were dried using standard procedures. All reactions and other manipulations were carried out under a nitrogen atmosphere, using standard Schlenk techniques. The IR spectra were recorded on a Bio-Rad FTS-40 spectrophotometer. The NMR spectra were run on either a Bruker AC-200 or ACE-300 spectrometer. For the ^{31}P NMR spectra, the spectrometer frequency at 81.015 or 121.49 MHz was employed, and the chemical shifts are given in ppm (δ) relative to 85% H_3PO_4 in $CDCl_3$. Values upfield of the standard are defined as negative. The corresponding frequencies for ^{13}C NMR spectra were at 75.47 MHz, respectively. Mass spectrometric (MS) data were collected on a JEOL SX-102A spectrometer. Elemental analyses were done on a Perkin-Elmer 2400 CHN analyzer.

4.2. Synthesis and characterization

4.2.1. $\{Pd(PPh_3)_2(\eta^3\text{-}CH_2C[C(COMe)=CMe(NH^iPr)]\text{-}CH_2)\}(BF_4)$ (**4a**)

The reaction of compound **2** (300 mg, 0.39 mmol) and (MeOC)HC=CMe(NH^iPr) (**1a**) (55 μl, 0.039 mmol) was

carried out in 20 ml of predried CH_2Cl_2 at −30°C. After stirring for 90 min, the solution was concentrated to 2 ml. Addition of 20 ml of dried Et_2O gave a yellow solid product. Recrystallization resulted in compound **4a** in 76% isolated yield (260 mg). ^{31}P NMR ($CDCl_3$, 300 MHz): δ 23.8. ^{1}H NMR ($CDCl_3$, 300 MHz): δ 1.21, 1.24 (3H, 3H, s, s, CH_3), 2.00 (6H, d, J_{HH} = 6.9 Hz, CH(CH_3)$_2$), 3.50 (2H, m, br, H_{anti}), 3.69 (1H, m, CH(CH$_3$)$_2$), 4.12 (2H, br, H_{syn}), 7.02–7.73 (30H, m, phenyl H), 12.6 (1H, d, J_{HH} = 2.2 Hz, NH). ^{13}C NMR (CD_3CN, 300 MHz): δ 18.4, 23.7 (*C*H$_3$), 30.5 (*C*H$_2$), 46.2 (CO*C*H$_3$), 80.1 (t with virtual coupling, J_{CP} = 15.4 Hz, C_t), 104.2 (C_γ), 129–134 (phosphino phenyl C), 146.1 (C_c), 165.0 (N*C*=C), 193.7 (*C*OMe). MS (FAB, *m*/*z*): 810 ($M^+ - BF_4$). *Anal*. Calc. for $PdC_{47}H_{48}NOP_2BF_4$: C, 62.86; H, 5.38; N, 1.56. Found: C, 62.30; H, 5.04; N, 1.25%.

*4.2.2. {Pd(PPh$_3$)$_2$(η^3-CH$_2$C[C(CO$_2$Me)=CMe(NH^{i}Pr)]-CH$_2$)}(PF$_6$) (**4b**)*

Refer to compound **4a** for the procedure. The reaction of compounds **2** (100 mg, 0.12 mmol) and **1b** (20 mg, 0.15 mmol) gave a yellow solid product in 76% isolated yield (90 mg). IR (KBr) (cm^{-1}): ν_{CO} 1638. ^{31}P NMR ($CDCl_3$, 300 MHz): δ 24.53. ^{1}H NMR ($CDCl_3$, 300 MHz): δ 1.15 (6H, d, J_{HH} = 6.4 Hz, CH(CH_3)$_2$), 2.04 (3H, CH_3), 3.14 (3H, s, OCH_3), 3.68 (5H, m, br, CH_2(allyl), CH(CH$_3$)$_2$), 6.82–7.64 (30H, m, phenyl H), 10.09 (1H, d, J_{HH} = 2.0 Hz, NH). ^{13}C NMR ($CDCl_3$, 300 MHz): δ 17.7 (*C*H$_3$), 23.5 (s, (*C*H$_3$)$_2$CH), 45.3 ((CH$_3$)$_2$*C*H), 50.9 (O*C*H$_3$), 78.5 (t, J_{CP} = 15.7 Hz, C_t), 91.2 (MeC=*C*), 128.7, 128.9, 130.1, 130.7, 131.1, 133.7 (phosphino phenyl C), 141.5 (C_c), 164.0 (Me*C*=C), 168.8 (*C*O$_2$Me). MS (FAB, *m*/*z*): 826 ($M^+ - PF_6$). *Anal*. Calc. for $PdC_{47}H_{48}NO_2P_3F_6.CH_2Cl_2$: C, 55.43; H, 4.75; N, 1.35. Found: C, 54.01; H, 4.63; N, 1.11%.

*4.2.3. {Pt(PPh$_3$)$_2$(η^3-CH$_2$C[C(COMe)=CMe(NH^{i}Pr)]-CH$_2$)}(PF$_6$) (**4a′**)*

The reaction of compound **3** (240 mg, 0.28 mmol) and an equimolar amount of compound **1a** produced compound **4a′** in 82% yield (220 mg). ^{31}P NMR ($CDCl_3$, 300 MHz): δ 18.1 (J_{PPt} = 3828 Hz). ^{1}H NMR ($CDCl_3$, 300 MHz): δ 2.00 (6H, d, J_{HH} = 6.9 Hz, CH(CH_3)$_2$), 2.13, 2.15 (3H, 3H, s, s, CH_3), 3.33 (2H, br, H_{syn}), 3.45 (2H, dd, J_{HP} = 8 Hz, J_{HPt} = 40.8 Hz, H_{anti}), 3.77 (1H, m, CH(CH$_3$)$_2$), 7.03–7.76 (30H, m, phenyl H), 12.5 (1H, d, J_{HH} = 2.2 Hz, NH). ^{13}C NMR ($CDCl_3$, 300 MHz): δ 15.2, 23.4 (*C*H$_3$), 30.6 (*C*H$_2$), 45.4 (CO*C*H$_3$), 69.6 (d, J_{CP} = 34 Hz, J_{CPt} = 105 Hz, C_t), 103.7 (J_{CPt} = 30 Hz, C_γ), 128.0–133.9 (phosphino phenyl C), 143.5 (t, J_{CP} = 4 Hz, J_{CPt} = 20.2 Hz, C_c), 165.1 (N*C*=C), 192.4 (*C*OMe). MS (FAB, *m*/*z*): 899 ($M^+ - BF_4$). *Anal*. Calc. for $PtC_{47}H_{48}NOP_2BF_4$: C, 57.20; H, 4.90; N, 1.42. Found: C, 56.78; H, 4.04; N, 1.20%.

*4.2.4. {Pt(PPh$_3$)$_2$(η^3-CH$_2$C[C(CO$_2$Me)=CMe(NH^{i}Pr)]-CH$_2$)}(BF$_4$) (**4b′**)*

Complex **3** was first prepared from *trans*-Pt(Br)(PPh$_3$)$_2$(η^3-CHCCH$_2$) (300 mg, 0.36 mmol) and $AgBF_4$ (69 mg, 0.36 mmol) in situ. The reaction of compounds **3** and **1b** (0.36 mmol) basically followed the procedure used for the preparation of compound **4a** and produced **4b′** in 77% isolated yields (272 mg). Colourless single crystals were obtained by recrystallization from CH_2CH_2–benzene. IR (KBr) (cm^{-1}): ν_{CO} 1634, $\nu_{C=C}$ 1580. ^{31}P NMR ($CDCl_3$, 300 MHz) δ 19.6 (J_{PPt} = 3845 Hz,). ^{1}H NMR ($CDCl_3$, 300 MHz): δ 1.24 (6H, d, J_{HH} = 6.3 Hz, CH(CH_3)$_2$), 2.20 (3H, J_{HPt} = 7.2 Hz, CH_3), 3.10 (2H, d, J_{HH} = 8.6 Hz, J_{HPt} = 42 Hz, H_{anti}), 3.20 (3H, s, OCH_3), 3.63 (2H, br, H_{syn}), 3.77 (1H, dhep, J_{HH} = 6.3, 8.0 Hz, CH(CH$_3$)$_2$), 7.0–7.6 (30H, m, phenyl H), 10.4 (1H, d, J_{HH} = 8.0 Hz, NH). ^{13}C NMR ($CDCl_3$, 300 MHz): δ 15.1 (*C*H$_3$), 22.6 (s, (*C*H$_3$)$_2$CH), 45.4 (dd, J_{CP} = 5.8, 14.2 Hz, (CH$_3$)$_2$*C*H), 50.9 (O*C*H$_3$), 67.6 (d, J_{CP} = 32 Hz, J_{CPt} = 100 Hz, C_t), 91.6 (J_{CPt} = 27 Hz, MeC=*C*), 128.4–133.4 (phosphino phenyl C), 140.6 (t, J_{CP} = 2.9 Hz, J_{CPt} = 18.4 Hz, C_c), 165.0 (J_{CPt} = 19.0 Hz, Me*C*=C), 169.1 (J_{CPt} = 11 Hz, *C*O$_2$Me). *Anal*. Calc. for $PtC_{47}H_{48}NO_2P_2BF_4$: C, 56.29; H, 4.83; N, 1.40. Found: C, 55.74; H, 4.91; N, 1.12%.

*4.2.5. 3-Carboxymethyl-2-methyl-4-methylene-N-isopropyldihydropyrrole (**5b**)*

^{1}H NMR (C_6D_6, 200 MHz): δ 1.13 (6H, d, J_{HH} = 6.5 Hz, CH_3), 2.31 (3H, s, CH_3), 3.61 (3H, s, OCH_3), 4.01 (1H, m, J_{HH} = 6.5 Hz, CH), 4.18 (2H, t, J_{HH} = 3.4 Hz, CH_2), 4.52, 5.10 (1H, 1H, dt, J_{HH} = 1.5, 3.4 Hz, =CH_2).

*4.2.6. 3-Acetyl-2,4-dimethyl-N-isopropyldihydropyrrole (**6a**)*

A solution that contained compound **4a** (30 mg) in 2 ml of chloroform was heated at 50°C for 24 h. The solution was then chromatographed on alumina and eluted with Et_2O. Compound **6a** was obtained in 75% yield. ^{1}H NMR ($CDCl_3$, 200 MHz): δ 1.34 (6H, d, J_{HH} = 6.6 Hz, CH(CH_3)$_2$), 2.38, 2.47 (3H, s, s, CH_3), 4.28 (1H, m, J_{HH} = 6.6 Hz, CH(CH$_3$)$_2$), 6.38 (1H, s, =CH).

*4.2.7. 3-Carboxymethyl-2,4-dimethyl-N-isopropylpyrrole (**6b**)*

^{1}H NMR ($CDCl_3$, 200 MHz): δ 1.34 (6H, d, J_{HH} = 6.6 Hz, CH_3), 2.19 (3H, s, CH_3), 2.48 (3H, s, CH_3), 3.76 (3H, s, OCH_3), 4.27 (1H, m, J_{HH} = 6.6 Hz, CH_2), 6.38 (1H, s, =CH). ^{13}C NMR ($CDCl_3$, 300 Hz): 11.1, 12.8, 23.2, 46.6, 50.3, 114.0, 120.4, 128.4, 132.0, 166.9. HRMS: calc. for $C_{11}H_{17}NO_2$ (M^+) 194.1181; found 194.1180.

4.3. X-ray crystallographic analysis

Diffraction data were measured at 298 K on a Nonius CAD-4 diffractometer with graphite-monochromatized Mo Kα radiation. Cell parameters were determined by a least-squares fit on 25 reflections. Intensity data were corrected for absorption on the basis of an experimental ψ rotation curve. The refinement procedure was by a full-matrix least-squares

method including all the non-hydrogenic atoms anisotropically. Hydrogen atoms were fixed at the ideal geometry and the C–H distance of 1.0 Å; their isotropic thermal parameters were fixed to the values of the attached carbon atoms at the convergence of the isotropic refinement. Atomic scattering factors were taken from international tables [14]. Computing programs are from the NRCC SDP VAX package [15]. Detailed data of compound **4b′**are supplied in the supplementary material.

Supplementary data

Supplementary data are available from the CCDC, 12 Union Road, Cambridge CB2 1EZ, UK (fax: +44-1223-336033; e-mail: deposit@ccdc.cam.ac.uk), on request, quoting deposition number 135924.

Acknowledgements

We thank the National Science Council, Taiwan, ROC, for financial support.

References

[1] J. March, Advanced Organic Chemistry, Reactions, Mechanisms, and Structure 4th ed. Wiley, New York, 1992.
[2] C.P. Casey, C.S. Yi, J. Am. Chem. Soc. 114 (1992) 6597.
[3] T.-M. Huang, J.-T. Chen, G.-H. Lee, Y. Wang, J. Am. Chem. Soc. 115 (1993) 1170.
[4] V. Plantevin, P.W. Blosser, J.C. Gallucci, A. Wojcicki, Organometallics 13 (1994) 3651.
[5] T.-M. Huang, R.-H. Hsu, C.-S. Yang, J.-T. Chen, G.-H. Lee, Y. Wang, Organometallics 13 (1994) 3657.
[6] F.-Y. Tsai, R.-H. Hsu, J.-T. Chen, G.-H. Lee, Y. Wang, J. Organomet. Chem. 520 (1996) 85.
[7] J.-T. Chen, Coord. Chem. Rev. 190/192 (1999) 1143 and references therein.
[8] J.-T. Chen, Y.-C. Cheng, Y.-K. Chen, T.-M. Huang, C.-I. Yu, G.-H. Lee, Y. Wang, Organometallics 17 (1998) 2953.
[9] J.-T. Chen, R.-H. Hsu, A.-J. Chen, J. Am. Chem. Soc. 120 (1998) 3243.
[10] J.L. Chiara, A. Gómez-Sánchez, Z. Rappoport, The Chemistry of Enamines, Wiley, New York, 1994, p. 353.
[11] A.-J. Chen, C.-C. Su, F.-Y. Tsai, J.-J. Lee, T.-M. Huang, C.-S. Yang, J.-T. Chen, G.-H. Lee, Y. Wang, J. Organomet. Chem. 569 (1998) 39 and references therein.
[12] A. Wojcicki, New J. Chem. 21 (1997) 733.
[13] K. Ohe, H. Matsuda, T. Moromoto, S. Ogoshi, N. Chatani, S. Murai, J. Am. Chem. Soc. 116 (1994) 4125.
[14] International Tables for X-Ray Crystallography IV (1974) Kynoch Press, Birmingham .
[15] E.J. Gabe, Y. LePage, J.-P. Charland, F.L. Lee, P.S. White, J. Appl. Crystallogr. 22 (1989) 384.

PERGAMON

www.elsevier.nl/locate/poly

Polyhedron 19 (2000) 549–551

POLYHEDRON

Indium-mediated monoallylation of carbonyl compounds with allylic chlorides and bisallylation of 2-pyridyl carboxylates with allylic halides in aqueous media

Jehyeon Yoo, Kyung Eun Oh, Gyochang Keum, Soon Bang Kang, Youseung Kim *

Biochemicals Research Center, Korea Institute of Science and Technology, Cheongryang, P.O. Box 131, Seoul 130-650, Korea

Received 4 October 1999; accepted 15 November 1999

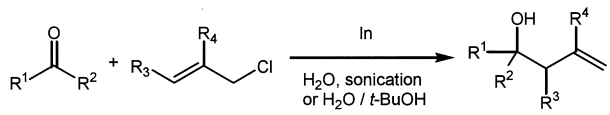
Abstract

Allylic chlorides are efficient reagents in the indium-mediated Barbier-type allylation reaction with various aldehydes and ketones in pure water under sonication or in a 1:1 mixture of H_2O and t-BuOH. Also indium is effective in bisallylation reactions of the 2-pyridyl esters with allyl halides in pure water. ©2000 Elsevier Science Ltd All rights reserved.

Keywords: Allylation; Aqueous reactions; Esters; Indium; Indium compounds; Pyridines

Recently, organic reactions that can be carried out in aqueous media or water have become one of the most challenging areas in organic synthesis due to environmental benefits and favorable effects of water on organic transformations [1]. In particular, reactions mediated by indium in aqueous media are of current interest because of its exceptional stability to air and water compared to other metals and considerable applications in organic synthesis [2,3]. Since indium has special properties in water, the application of indium for other chemical transformation will be of great interest. Here we report the indium-mediated allylation reaction of carbonyl compounds with allylic chlorides and bisallylation of 2-pyridyl carboxylate with allyl halides.

The allylation reaction of carbonyl compounds with allylic halides to afford the homoallylic alcohols is probably the most widely used of the many indium-mediated reactions in organic synthesis [4]. Allylic bromide and iodide have been used effectively in this reaction, but allylic chloride, a cheaper and more stable reagent, has rarely been used because of low yields, even in other metal-mediated reactions [5,6]. We report here that allylic chlorides are efficient reagents in indium-mediated Barbier-type allylation reactions in aqueous media [7].



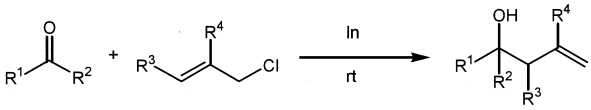
* Corresponding author. Tel: +82-2-9585138; fax: +82-2-9585189; e-mail: yosekim@kistmail.kist.re.kr

A variety of aldehydes and ketones can be sucessfully allylated with allylic chlorides using indium metal in pure water under sonication or in a 1:1 mixture of H_2O and t-BuOH to afford the corresponding homoallylic alcohols in good to excellent yields. The results are summarized in Table 1. A mixture of carbonyl compounds (1 mmol), allyl chloride (2 mmol) and indium powder (1 mmol) was stirred at room temperature in water (2 ml) (method A), under sonication (method B) or in a 1:1 mixture of H_2O and t-BuOH (method C). Using method A, the reaction required a longer reaction time and gave poorer yields in most cases. The reactions with the addition of NH_4Cl or using a mixed solvent of water and THF were unsatisfactory too. As can be seen in Table 1, the reaction using method B or method C gave good yield irrespective of the substituents on aromatic aldehydes; in particular, the yield of 4-carboxybenzaldehyde increased dramatically when method C was used, probably due to its solubility (entry 12). The reaction of crotyl chloride using method B was γ-regioselective (entries 5, 6) and gave a diastereomeric mixture in the raio of 2.8:1 in moderate yield, whereas β-substitution did not affect the yield (entry 7). Even low boiling aliphatic aldehydes can be effectively allylated in these conditions (entry 13). In the case of ketone, acetophenone and β-keto ester were reacted in method C to give moderate and excellent yields, respectively (entries 16, 17).

Although the indium-mediated allylation of carbonyl compounds such as aldehydes and ketones has been explored

0277-5387/00/$ - see front matter ©2000 Elsevier Science Ltd All rights reserved.
PII S0277-5387(99)00405-2

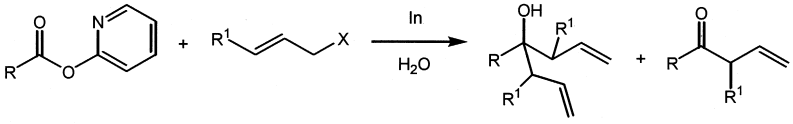
Table 1
Indium-mediated Barbier-type allylations of allylic chlorides [a]



Entry	R^1	R^2	R^3	R^4	Time (h) A/B/C	Yield		
						A	B	C
1	$4CH_3CH_2–C_6H_4–$	H	H	H	17/6	31	89	
2	$4CH_3O–C_6H_4–$	H	H	H	17/5	38	85	
3	$4CH_3S–C_6H_4–$	H	H	H	17/8	54	96	
4	$4F–C_6H_4–$	H	H	H	17/6	15	95	
5	$2CH_3–C_6H_4–$	H	CH_3	H	9		65 [b]	
6	$4F–C_6H_4–$	H	CH_3	H	6		75 (2.8:1) [c]	
7	$4F–C_6H_4–$	H	H	CH_3	20/9	41	96	
8	$C_6H_5–$	H	H	H	17/6/16	47	84	89
9	$2CH_3–C_6H_4–$	H	H	H	5/7/41	73	95	97
10	$4HO–C_6H_4–$	H	H	H	44/9/71	59	92	82
11	$4Cl–C_6H_4–$	H	H	H	17/12/41	70	88	98
12	$4HO_2C–C_6H_4–$	H	H	H	66/15/41	10	5	94
13	$CH_3(CH_2)_2–$	H	H	H	20/8/16	46	25	91
14	$(CH_3)_3C–$	H	H	H	–/6/10		95	73
15		H	H	H	39/–/17	62		93
16	$C_6H_5–$	CH_3	H	H	17/72/26	trace	trace	50
17	$CH_3–$	CH_2CO_2Et	H	H	20/8/10	38	70	95

[a] Reaction conditions: A, H_2O; B, H_2O, sonication; C, H_2O–t-BuOH (1:1).
[b] GC yield.
[c] Diastereomeric ratio was determined by ^1H NMR.

Table 2
Indium-mediated bisallylation of 2-pyridyl esters [a]

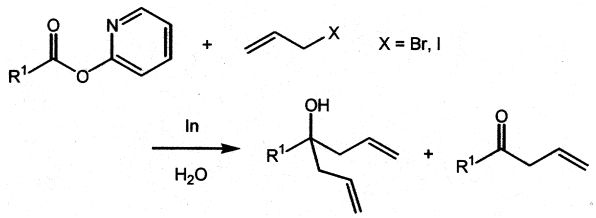


Entry	R	R^1	X	Time (h)	Yield [b] (%)	
					Tertiary alcohol	Ketone
1 [c]	$C_6H_5–$	H	Br	20	60	0
2	$C_6H_5–$	H	Br	10	86	0
3 [d]	$C_6H_5–$	H	I	5	80	6
4 [e]	$2ClC_6H_4–$	H	I	3	55	12
5	$C_6H_5–$	Br	Br	9	82 [f]	0
6	$CH_3(CH_2)_8–$	H	Br	2	35	1
7	$C_6H_5–$	CH_3	Br	12	3	26
8	$3BrC_6H_4–$	CH_3	Br	16	0	37
9	$C_6H_5–$	Ph	Br	4	0	83

[a] Reactions were carried out with ester (1 equiv), allyl halide (1 equiv) and indium (3 equiv) at 10°C.
[b] Isolated yield.
[c] Ratio of 2-pyridyl ester–allyl halide–indium is 1.5:1:3.
[d] At 0°C.
[e] 1 equiv of NH_4Cl was added.
[f] Debrominated product was obtained.

extensively, the reaction with carboxylic ester compounds has never been reported. Among the indium-mediated reactions with carboxylic acid derivatives, only the indium-mediated allylations of cyclic acid anhydrides in DMF [7] and acyloyl-imidazoles and pyrazoles in water [8] have been reported. Our continuous efforts in the area of indium [9,10]

lead us to determine that indium is effective in bisallylation of the 2-pyridyl carboxylate with allyl halides.



Various 2-pyridyl esters were reacted with indium metal and allylic halides in water at 10°C to give the corresponding bisallylated alcohols in moderate to good yields together with a small amount of homoallyl ketones, as shown in Table 2. The reactions with allyl bromides and iodides were all successful and the ester hydrolysis was increased at higher temperature or with a longer reaction time. In these bisallylation reactions the optimized ratio of ester, allyl halide and indium was 1:1:3 in spite of various trials for increasing the yields by changing the ratio of reactants. In the case of γ-methyl-substituted crotyl bromide (entry 7), the reaction was γ-regioselective and the major product was the homoallyl ketone due to the steric bulkiness. More bulky cinnamyl bromide afforded exclusively the corresponding ketone in a good yield (entry 9). Interestingly, 3-pyridyl or 4-pyridyl carboxylates did not react under these conditions.

A typical procedure is as follows. To a mixture of 2-pyridyl benzoate (0.5 mmol) and allyl bromide (0.5 mmol) in 2 ml of water was added indium powder (1.5 mmol) in one portion. The reaction mixture was stirred vigorously for 10 h in an ice-bath while the progress of the reaction was monitored by TLC. The reaction was stopped by the addition of 1 N HCl, and then the mixture was extracted with ethyl acetate (3×10 ml). The combined organic phase was washed with brine, dried over magnesium sulfate and concentrated in vacuo. The bisallylated alcohol was obtained in 86% yield after purification by flash column chromatography on silica gel using a 10:1 mixture of hexane and ethyl acetate as eluent.

In conclusion, allylic chlorides have been successfully employed in indium-mediated Barbier-type allylation reactions with various carbonyl compounds in aqueous media to afford the homoallylic alcohols in good to excellent yields. Also we have demonstrated that the 2-pyridyl ester compounds can be converted to bisallylated alcohols mediated by indium with allyl halides in pure water.

References

[1] C.J. Li, T.H. Chan, Organic Reactions in Aqueous Media, Wiley, New York, 1997.
[2] A.S.K. Hashmi, J. Prakt. Chem. 340 (1998) 84.
[3] P. Cintas, Synlett (1995) 1087.
[4] C.J. Li, Tetrahedron 52 (1996) 5643.
[5] M. Wada, H. Ohki, K. Akiba, Bull. Chem. Soc. Jpn. 63 (1990) 1738.
[6] C.J. Li, T.H. Chan, Tetrahedron Lett. 32 (1991) 7017.
[7] S. Araki, N. Katsumura, H. Ito, Y. Butsugan, Tetrahedron Lett. 30 (1989) 1581.
[8] V.J. Bryan, T.H. Chan, Tetrahedron Lett. 38 (1997) 6493.
[9] H.J. Lim, G. Keum, S.B. Kang, B.Y. Chung, Y. Kim, Tetrahedron Lett. 39 (1998) 4367.
[10] H.J. Lim, G. Keum, S.B. Kang, B.Y. Chung, Y. Kim, Tetrahedron Lett. 40 (1999) 1547.

PERGAMON

www.elsevier.nl/locate/poly

Polyhedron 19 (2000) 553–555

POLYHEDRON

Structure and reactivity of cyanocuprates containing the monoanionic C,N-chelating aminoaryl ligand $[C_6H_4CH_2NMe_2\text{-}2]^-$

Claudia M.P. Kronenburg, Johann T.B. H. Jastrzebski, Gerard van Koten *

Debye Institute, Department of Metal-Mediated Synthesis, Utrecht University, Padualaan 8, 3584 CH Utrecht, The Netherlands

Received 4 October 1999; accepted 6 December 1999

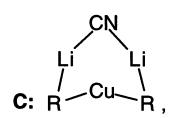
Abstract

The 2:1 cyanocuprate $[Ar_2Cu(CN)Li_2(THF)_4]_\infty$ (**1**, Ar = $[C_6H_4CH_2NMe_2\text{-}2]^-$) is obtained as the only product in the reaction of two equivalents of ArLi with one equivalent of CuCN in tetrahydrofuran (THF) at −78°C. The X-ray crystal structure reveals an ionic polymeric chain consisting of consecutive $[Ar_2Cu]^-$ and $[(THF)_2LiCNLi(THF)_2]^+$ units. Its composition in THF solution has been investigated.
©2000 Elsevier Science Ltd All rights reserved.

Keywords: Cryoscopy; Cyanocuprates; Ionic; Reactivity; Structures

The application of cyanocuprates of general formula $[R_nCu(CN)Li_n]$ ($n = 1$ or 2) to organic synthesis by Lipshutz et al. [1] in 1981 led to a lively discussion on their possible structure in the solid state and in solution in the following years. Depending on the stoichiometry of the reaction of alkyl- or aryllithiums (one or two molar equivalents) with copper(I) cyanide, two types of cyanocuprates can be formed: the so-called 1:1 cyanocuprates of type $[RCu(CN)Li]$, or the 2:1 cyanocuprates with formula $[R_2Cu(CN)Li_2]$. According to the initial proposal by Lipshutz, the high reactivity of the latter type of cyanocuprates is due to bond formation between the cyano anion and the copper(I) center, thereby forming a dianionic species of type $[R_2Cu(CN)]^{2-}$ (**A**) [2]. In addition to this proposal, three other structures were also postulated: a monoanionic copper species (**B**) [3,4], a neutral monomeric copper species (**C**) [5,6] and a 'cyano-Gilman' cuprate (**D**) [7].

A: $[R_2Cu(CN)]^{2-}$ $2[Li]^+$, **B:** $[R_2Cu]^-$ $[Li_2(CN)]^+$,



C: , **D:** $R_2CuLi + LiCN$

The discussion on the structural aspects of 2:1 cyanocuprates has mainly been focused on proposals **C** and **D**, although arguments were put forward to support each of the four structures [8]. Moreover, recent spectroscopic studies (EXAFS [9–11] and NMR [12–14]) and molecular weight determinations [15] seemed also to support the structural proposals **C** and **D**.

Unambiguous proof of the structure of the thermodynamically most stable form of 2:1 cyanocuprates in the solid state has been obtained by crystal structure determinations. In 1998 both our group [15] and the group of Boche [16] reported the crystal structure of a 2:1 cyanocuprate. Remarkably, both structures, one alkyl- and one arylcyanocuprate, support proposal **B**. We reported on the synthesis, isolation and structural characterization of the bisarylcyanocuprate $[Ar_2CuLi_2(CN)(THF)_4]_\infty$ (**1**, Ar = $[C_6H_4CH_2NMe_2\text{-}2]^-$) (see Fig. 1). The solid state structure of this 2:1 cyanocuprate comprises a linear polymeric chain, consisting of alternating $[ArCu]^-$ anionic units and $[Li_2CN(THF)_4]^+$ cationic units. These are linked via intermolecular coordination by the nitrogen donor atom of the aryl ligand. The CN^- acts as a bridging C,N-coordinating ligand for two Li^+ to form a very stable $[Li_2CN]^+$ with a linear LiNCLi arrangement. Furthermore, the X-ray structure determinations of [t-BuCu(CN)Li] [16] and $[Li(THF)_2\{Cu(CN)C_6H_3\text{-}2,6\text{-}Trip_2\}]_2$ (Trip = C_6H_2-2,4,6-iPr_3) have been reported [17].

To study the aggregation behaviour of cuprates in solution we measured the molecular weights by cryoscopy of various cuprates in tetrahydrofuran (THF) in collaboration with the group of Professor Krause (Table 1) [6]. Although for an anion/cation pair a calculated value of the aggregation state

* Corresponding author. Tel.: +31-30-2531813; fax: +31-30-2523615; e-mail: g.vankoten@chem.uu.nl

0277-5387/00/$ - see front matter ©2000 Elsevier Science Ltd All rights reserved.
PII S0277-5387(99)00406-4

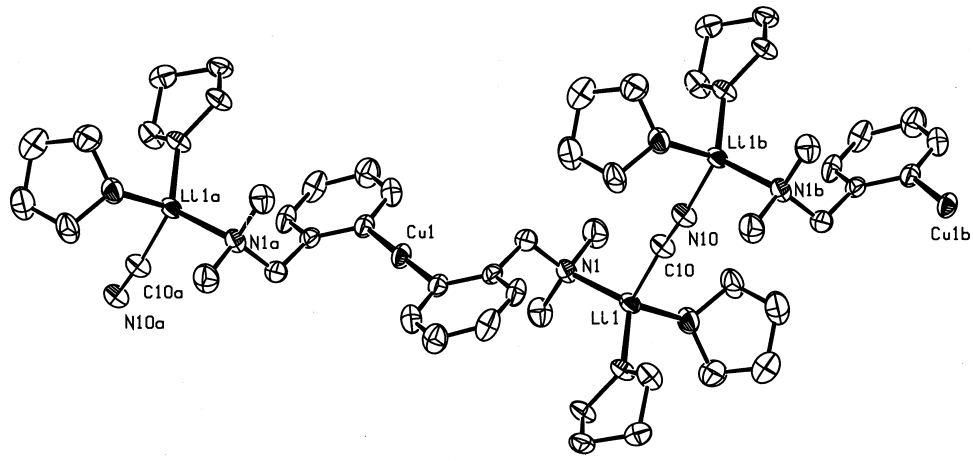


Fig. 1. ORTEP drawing (50% probability level) of $[Ar_2Cu(CN)Li_2(THF)_4]_\infty$ (**1**). C(1a)–Cu–C(1) 180°; Li(1)–C(10)–N(10) 175.6(3)°, C(10)–N(10) 1.156 Å. For X-ray structural data and tables of fractional coordinates, thermal parameters, bond distances and angles see [15].

Table 1
Cryoscopic data for cuprate compounds in THF

Entry	Cuprate	C_{nom} (mmolal)	$n = C_{nom}/C_{exp}$
1	$[Me_2CuLi_2(CN)]_n$	35.2–72.9	1.1–1.2
2	$[t\text{-}Bu_2CuLi_2(CN)]_n$	46.0–75.7	0.7–0.8
3	$[t\text{-}BuCu(CN)Li]_n$	70.4	1.1
4	$[Ph_2CuLi_2(CN)]_n$	25.5	1.2
5	$[PhCu(CN)Li]_n$	88.2	2.0
6	$[Ar_2CuLi_2(CN)]_n$	14.8–73.6	0.7–0.9
7	$[ArCu(CN)Li]_n$	79.9–147.2	0.9–1.4
8	$[Ar_2CuLi]_n$	24.8–84.2	2.0–1.7

of 0.5 is expected, the measured values for the 2:1 cyanocuprates (entries 2 and 6) range from $n = 0.7$ to 0.9. This suggests the presence of a trinuclear $CuLi_2$ species, structure **C**, which can be regarded as a neutral cuprate complex comprising an anionic $[R_2Cu]^-$ and a cationic $[Li_2CN]^+$ unit. However, for the other cuprates described in Table 1, discrete monomeric or dimeric species are found.

It is noted that cryoscopic results may be deceptive, as association of anionic and cationic species to higher aggregates (ion-pair formation) [18] might occur. As a result of such association, a virtual aggregation state of almost 1 could be calculated.

The higher reactivity of the 2:1 cyanocuprates in most of the substitution reactions was ascribed to the fact that the CN^- was bound to copper. [The idea of using a CN group as a 'non-transferable' ligand was first introduced by Gorlier et al. [19].] In order to further test the hypothesis that the active species contains $[R_2Cu]^-$ in solution, we studied the influence of the nature of the various cuprate reagents on the outcome of a substitution reaction of a primary halide with such cuprate reagents (Table 2). These preliminary results (see Table 2) show that in the given reaction time (1 h) the 2:1 cyanocuprates (entries 1 and 2) transfer 50% of the R groups to the substrate, while the other Cu^I species tested are not reactive (entries 3–5).

Table 2
Results of the investigation of organocopper, -cuprates and -cyanocuprates with Ar as a ligand in the substitution reaction with a primary halide

Entry	[Rcu] [a]	Substrate	Product	Yield (%)
1	$[(Ar)_2CuLi_2(CN)]$	Octyl-Br	Ar-octyl	53
2	$[Ph_2CuLi_2(CN)]$	Octyl-Br	Ph-octyl	40
3	$[ArCu(CN)Li]$	Octyl-Br	Ar-octyl	10
4	$[(Ar)_4Cu_2Li_2]$ [b]	Octyl-Br	Ar-octyl	10
5	[ArCu] [c]	Octyl-Br	Ar-octyl	<1

[a] R:substrate = 1:1. Reaction conditions: THF, −78°C → RT, 1 h.
[b] van Koten and Noltes [20].
[c] van Koten et al. [21].

The fact that only 50% of the R groups of the 2:1 cyanocuprate (see entries 1 and 2) is transferred suggests that the remaining cyanocuprate species, after transfer of the R group, assembles into a stable, and unreactive, 1:1 cyanocuprate (entry 3).

In conclusion, it can be stated that the solid-state structure of a 2:1 cyanocuprate of type $[Ar_2CuLi_2CN]_\infty$ has revealed the presence of ionic structural motifs. In addition, more insight into the apparent structure of some specific cyanocuprates in solution has been provided by cryoscopic measurements in THF.

Supplementary data

X-ray structural data for compound **1** are available from the CCDC, 12 Union Road, Cambridge CB2 1EZ, UK (fax: +44-1223-336033; e-mail: deposit@ccdc.cam.ac.uk) on request, quoting the deposition number SITYEZ.

Acknowledgements

We thank Professor N. Krause and Dr A. Gerold for the collaboration in the field of the cryoscopic measurements and helpful discussions.

References

[1] B.H. Lipshutz, R.S. Wilhelm, D.M. Floyd, J. Am. Chem. Soc. 103 (1981) 7672.
[2] B.H. Lipshutz, Synthesis (1987) 325.
[3] S.H. Bertz, J. Am. Chem. Soc. 112 (1990) 4031.
[4] T.A. Mobley, F. Müller, S. Berger, J. Am. Chem. Soc. 120 (1990) 1333.
[5] J.P. Snyder, D.P. Spangler, J.R. Behling, J. Org. Chem. 59 (1994) 2665.
[6] A. Gerold, J.T.B.H. Jastrzebski, C.M.P. Kronenburg, N. Krause, G. van Koten, Angew. Chem., Int. Ed. Engl. 36 (1997) 755.
[7] S.H. Bertz, G. Miao, M. Eriksson, Chem. Commun. (1996) 815.
[8] N. Krause, A. Gerold, Angew. Chem., Int. Ed. Engl. 36 (1997) 186 (review).
[9] T.L. Stemmler, T.M. Barnhart, J.E. Penner-Hahn, C.E. Tucker, P. Knochel, M. Böhme, G. Frenking, J. Am. Chem. Soc. 117 (1995) 12489.
[10] T.M. Barnhart, H. Huang, J.E. Penner-Hahn, J. Org. Chem. 60 (1995) 4310.
[11] T. Stemmler, J.E. Penner-Hahn, P. Knochel, J. Am. Chem. Soc. 115 (1993) 348.
[12] B.H. Lipshutz, S. Sharma, E.L. Elsworth, J. Am. Chem. Soc. 112 (1990) 4032.
[13] B.H. Lipshutz, B. James, J. Org. Chem. 59 (1994) 7585.
[14] S.H. Bertz, K. Nilsson, O. Davidsson, J.P. Snyder, Angew. Chem., Int. Ed. Engl. 37 (1998) 314.
[15] C.M.P. Kronenburg, J.T.B.H. Jastrzebski, A.L. Spek, G. van Koten, J. Am. Chem. Soc. 120 (1998) 9688.
[16] G. Boche, F. Bosold, M. Marsch, K. Harms, Angew. Chem. 110 (1998) 1779.
[17] C.-S. Hwang, P.P. Power, J. Am. Chem. Soc. 120 (1998) 6409.
[18] M. Szwarc, Ions and Ion Pairs in Organic Reactions, Wiley-Interscience, New York, 1967 (chapter 1).
[19] J.-P. Gorlier, L. Hamon, J. Levisalles, J. Wagnon, J. Chem. Soc., Chem. Commun. (1973) 88.
[20] G. van Koten, J.G. Noltes, J. Chem. Soc., Chem. Commun. (1972) 940.
[21] G. van Koten, A.J. Leusink, J.G. Noltes, J. Chem. Soc., Chem. Commun. (1970) 1107.

PERGAMON

www.elsevier.nl/locate/poly

Polyhedron 19 (2000) 557–561

POLYHEDRON

Iridium complex-catalyzed allylic alkylation

Ryo Takeuchi *

Department of Environmental Science, Faculty of Science, Yokohama City University, 22-2 Seto, Kanazawa-ku, Yokohama 236-0027, Japan

Received 4 October 1999; accepted 9 November 1999

Abstract

An iridium complex was found to be an efficient catalyst for allylic alkylation of allylic acetates with a stabilized carbon nucleophile. Two unique features of iridium complex catalysis are found. (1) Regioselective alkylation at the substituted allylic terminus: the reaction of (*E*)-2-alkenyl acetates or 1-substituted 2-propenyl acetates with sodium salt of diethyl malonate in the presence of a catalytic amount of $[Ir(COD)Cl]_2/P(OPh)_3$ ($P/Ir = 1–2$) gave products alkylated at the substituted allylic terminus with 95–99% selectivities. ^{31}P NMR and ^{13}C NMR revealed that a catalytically active species is $Ir(COD)(P(OPh)_3)Cl$. The π-acceptor property of $P(OPh)_3$ promotes a carbonium ion character at the substituted allylic terminus. Therefore, the nucleophile is directed to this position. (2) Retention of *Z* geometry in the allylic alkylation of (*Z*)-2-alkenyl acetates; the reaction of (*Z*)-2-alkenyl acetates gave a product alkylated at the unsubstituted allylic terminus with the retention of *Z* geometry predominantly. Retention of *Z* geometry in allylic alkylation is also possible by iridium catalysis. ©2000 Elsevier Science Ltd All rights reserved.

Keywords: π-Allyl complexes; Allylic substitutions; Iridium; Regioselectivity; Stereoselectivity; Phosphites

1. Introduction

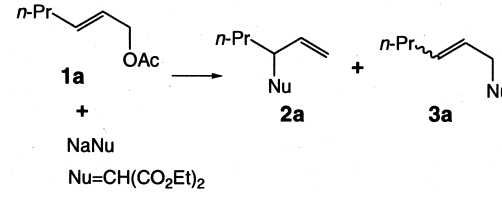
The use of iridium complexes for organic synthesis is relatively unexplored. Since Crabtree reported that a cationic iridium complex is a highly active catalyst for hydrogenation of alkenes [1], iridium complexes have received much attention as efficient hydrogenation catalysts. In contrast to its utility in hydrogenation, the iridium complex-catalyzed carbon–carbon bond forming reaction was not developed until the 1990s. Recently, synthetically useful carbon–carbon bond forming reactions have been reported [2–5].

One of the most important carbon–carbon bond forming reactions catalyzed by transition metal complexes is allylic alkylation, which is widely used for constructing complex organic molecules. The control of regioselectivity in allylic alkylation is important. When the π-allyl intermediate is terminally monosubstituted, palladium complexes generally lead to a preferential alkylation at the unsubstituted allylic terminus [6–8]. On the other hand, molybdenum [9,10], tungsten [11], ruthenium [12] and platinum [13–15] complexes tend to lead to a preferential alkylation at the substituted allylic terminus. Complete regiocontrol of alkylation at the substituted allylic terminus is a challenging problem. A new catalyst is required for the realization of such selectivity. We have found an iridium complex that is a new and efficient catalyst for allylic alkylation [16,17]. Based on our results, iridium complex-catalyzed asymmetric allylic alkylation has been reported [18,19].

2. Results

2.1. Regioselective allylic alkylation at the substituted allylic terminus

The reaction of (*E*)-2-hexenyl acetate (**1a**) with sodium salt of diethyl malonate in the presence of a catalytic amount of $[Ir(COD)Cl]_2$ and ligand gave compounds **2a**, (*E*)-**3a** and (*Z*)-**3a** (Eq. (1)).



(1)

Added phosphorus ligand had a substantial effect on the selectivity and yield of the products. Results are summarized in Table 1. $P(OPh)_3$ was found to be the most efficient ligand. The reactions using 1 or 2 equivalents of $P(OPh)_3$ to Ir

* Tel./fax: +81-45-7872218; e-mail: rtakeuch@yokohama-cu.ac.jp

0277-5387/00/$ - see front matter ©2000 Elsevier Science Ltd All rights reserved.
PII S0277-5387(99)00407-6

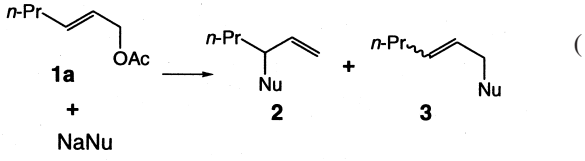
Table 1
Effect of ligand on allylic alkylation of compound **1a** with sodium salt of diethyl malonate [a]

Entry	Ligand	P/Ir	Conditions	Yield (%) [b]	Ratio [c] **2a**:**3a** (*E*/*Z*)
1	$P(OPh)_3$	1	room temperature, 3 h	90	96:4 (78/22)
2	$P(OPh)_3$	2	room temperature, 3 h	89	96:4 (81/19)
3	$P(O4\text{-}MeC_6H_4)_3$	2	room temperature, 8 h	81	95:5 (73/27)
4	$P(O4\text{-}FC_6H_4)_3$	2	room temperature, 23 h	55	94:6 (94/6)
5	$P(OEt)_3$	2	reflux 3 h	81	59:41 (90/10)
6	PPh_3	2	reflux 16 h	6	24:76 (63/37)
7	dppe	2	reflux 16 h	18	39:61 (94/6)

[a] A mixture of compound **1a** (2 mmol), $NaCH(CO_2Et)_2$ (4 mmol), $[Ir(COD)Cl]_2$ (0.04 mmol), ligand and THF (10 ml) was stirred under argon.
[b] Isolated yield.
[c] Determined by GLC.

proceeded at room temperature to give an excellent yield of products (entries 1 and 2). The selectivity of compound **2a** was 96%. The use of $P(O4\text{-}MeC_6H_4)_3$ and $P(O4\text{-}FC_6H_4)_3$ as a ligand gave an excellent selectivity for compound **2a**, but the reactions required a longer reaction time compared to that using $P(OPh)_3$ (entries 3 and 4). With $P(OEt)_3$, the reaction gave compound **2a** in a much decreased selectivity (entry 5). Reaction using a more electron-donating phosphorus ligand such as PPh_3 and dppe gave products in poor yields (entries 6 and 7).

Reaction of compound **1a** with various stabilized carbon nucleophiles was examined (Eq. (2)).

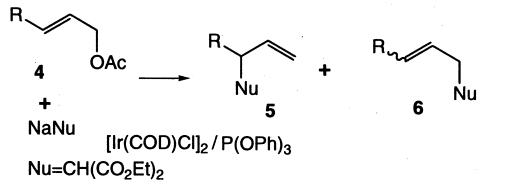


(2)

b	$Nu=CH(CO_2Me)_2$	room temp. 3 h	90%	97 : 3 (E/Z=79/21)
c	$Nu=CHAcCO_2Et$	THF reflux 7 h	85%	93 : 7 (E/Z=80/20)
d	$Nu=CMe(CO_2Et)_2$	THF reflux 1 h	87%	29 : 71 (E/Z=90/10)

The reaction of compound **1a** with various stabilized carbon nucleophiles gave product **2a**–**c** in 93–97% selectivities. Increasing the steric bulk of carbon nucleophile reversed the regioselectivity. The reaction with sodium salt of diethyl ethyl malonate gave product **3d** in 71% selectivity.

We examined the reaction of a series of acyclic allylic acetates (**4**) with sodium salt of diethyl malonate in the presence of a catalytic amount of $[Ir(COD)_2Cl]_2/P(OPh)_3$ (P/Ir=2) (Eq. (3)).

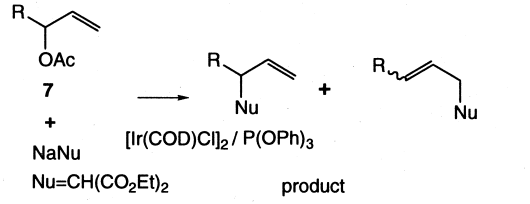


(3)

a	R= Me	room temp. 2 h	77%	97 : 3
b	R= Ph	room temp. 3 h	98%	99 : 1 (E/Z=100/0)
c	R= *n*-Hex	room temp. 5 h	99%	95 : 5 (E/Z=66/34)
d	R= *n*-Oct	room temp. 5 h	95%	95 : 5 (E/Z=69/31)

Highly regioselective alkylation at the substituted allylic terminus was achieved. All reactions proceeded at room temperature to give compound **5** in 95–97% selectivities.

Regioisomeric acetate **7** was used as a substrate (Eq. (4)).



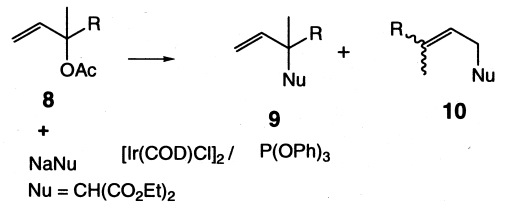
(4)

product

a R= *n*-Pr	room temp. 3 h	86%	**2a: 3a**	95 : 5	(E/Z=78/22)
b R= Ph	room temp. 3 h	91%	**5b: 6b**	99 : 1	(E/Z=79/21)
d R= *n*-Oct	room temp. 3 h	95%	**5d: 6d**	95 : 5	(E/Z=78/22)

Reactions with sodium salt of diethyl malonate gave the same product distribution to that of compounds **1a**, **4b** and **4d**. The result strongly suggests the intermediacy of a π-allyl iridium complex.

The most unique feature of iridium complex catalysis was demonstrated for the reaction of compound **8**. The reactions occurred with perfect regioselectivity at the tertiary allylic terminus to give a product (**9**) bearing a quaternary carbon center exclusively (Eq. (5)).

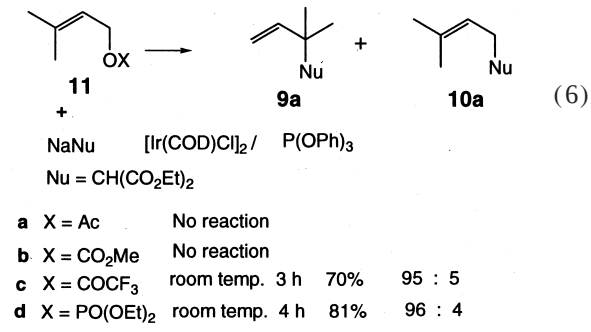


(5)

a	R= Me	room temp. 2 h	80%	100 : 0
b	R= *n*-Bu	room temp. 16 h	80%	100 : 0
c	R= $CH_2CH_2C=Me_2$	room temp. 5 h	85%	100 : 0

Iridium complex-catalyzed allylic alkylation provides an efficient method for the construction of a quaternary carbon center which is a feature of broad range of natural products. Several transition metal complex-catalyzed reaction of compound **8** have been reported [20]. Iridium complex only led to the exclusive formation of a product bearing a quaternary carbon center.

3-Methyl-2-butenyl acetate (**11**) failed to react with sodium salt of diethyl malonate under refluxing dioxane for 24 h. The corresponding product was not obtained at all. 3-Substituted 2-alkenyl acetate was much less reactive than that of 2-alkenyl acetate. Changing the leaving group enhanced the reactivity of the substrate (Eq. (6)).

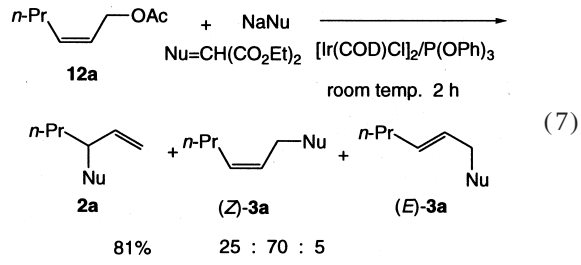


(6)

The reaction of compounds **11c** and **11d** with sodium salt of diethyl malonate proceeded at room temperature to give compound **9a** in 96 and 95% selectivity, respectively.

2.2. Retention of Z geometry in the allylic alkylation

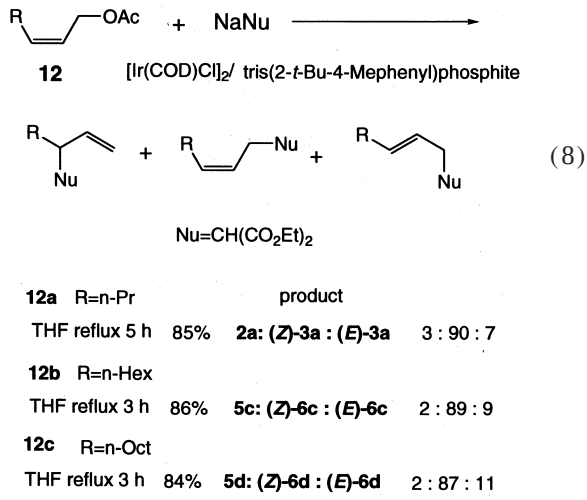
The geometry of the carbon–carbon double bond in the allyl system affected the regiochemistry of the allylic alkylation. The reaction of compound **12a** with sodium salt of diethyl malonate at room temperature gave products in 81% yield (Eq. (7)).



(7)

The major product was (*Z*)-**3a**, resulting from the alkylation at the unsubstituted allylic terminus. Regioselectivity was opposite to that of compound **1a**. This result showed that the alkylation occurred prior to *syn–anti* isomerization and the regioselectivity of alkylation to the *syn* π-allyl iridium complex was different from that to the *anti* π-allyl iridium complex.

Palladium complex-catalyzed allylic alkylation of (*Z*)-2-alkenyl acetate resulted in a loss of *Z* geometry [21], because the *anti* π-allyl palladium complex easily isomerized to the thermodynamically more stable *syn* π-allyl palladium complex [22]. The reaction of compound **12a** with sodium salt of diethyl malonate gave compound (*Z*)-**3a** as a major product. The ratio (*Z*)-**3a**/(*E*)-**3a** was 93/7. *Syn–anti* isomerization of a terminally monosubstituted π-allyl iridium complex is quite slow compared to that of a terminally monosubstituted π-allyl palladium complex. Iridium catalysis provides a possibility of (*Z*)-selective allylic alkylation. However, in the reaction of (*Z*)-2-alkenyl acetate, the regioselectivity of alkylation at the unsubstituted allylic terminus is not satisfactory. To improve the selectivity of (*Z*)-alkene, alkylation must be directed to the unsubstituted allylic terminus. A bulky phosphite ligand is expected to increase such regioselectivity. We examined the reaction of (*Z*)-2-alkenyl ester with sodium salt of diethyl malonate using a bulky phosphite ligand (Eq. (8)).



(8)

The reaction using 1 equivalent of tris(2-*tert*-butyl-4-methylphenyl)phosphite to iridium under refluxing THF for 3 h gave the product in 85% yield (entry 2). The selectivity of compound (*Z*)-**3a** was increased to 90%. The reaction of compounds **12b** and **12c** with sodium salt of diethyl malonate gave compounds (*Z*)-**6c** and (*Z*)-**6d** in 89 and 87% selectivity, respectively.

3. Discussion

As mentioned above, triphenylphosphite is an essential ligand for regioselective alkylation at the substituted allylic terminus. To clarify the catalytically active species, we monitored the reaction of $[Ir(COD)Cl]_2$ with $P(OPh)_3$ in THF-d_8 by ^{31}P NMR. The spectra are shown in Fig. 1. The spectrum at $P/Ir = 1$ showed a singlet (δ 86.9). No free $P(OPh)_3$ was detected. It indicated the formation of a monophosphite species (species A). The ^{13}C NMR spectra of species A showed two sets of doublets (δ 54.7, $J = 2.4$ Hz; 106.4 $J = 19.5$ Hz). Species A was identified as $IrCl(COD)(P(OPh)_3)$ by comparing these chemical shifts values and their coupling constants with those in the literature [23].

Increasing the amount of $P(OPh)_3$ led to the appearance of a new set of signals. The reaction of $[Ir(COD)Cl]_2$ with 2 equivalents of $P(OPh)_3$ formed three species (species A, B and C). The spectrum at $P/Ir = 2$ showed a singlet (δ 86.9; species A), three sets of doublets (δ 71.7, 86.1 and 95.9, $J = 30$, 24 Hz; species B) and two sets of doublets (δ 96.3 and 101.8, $J = 24$ Hz; species C) in the ratio 42:42:16. The

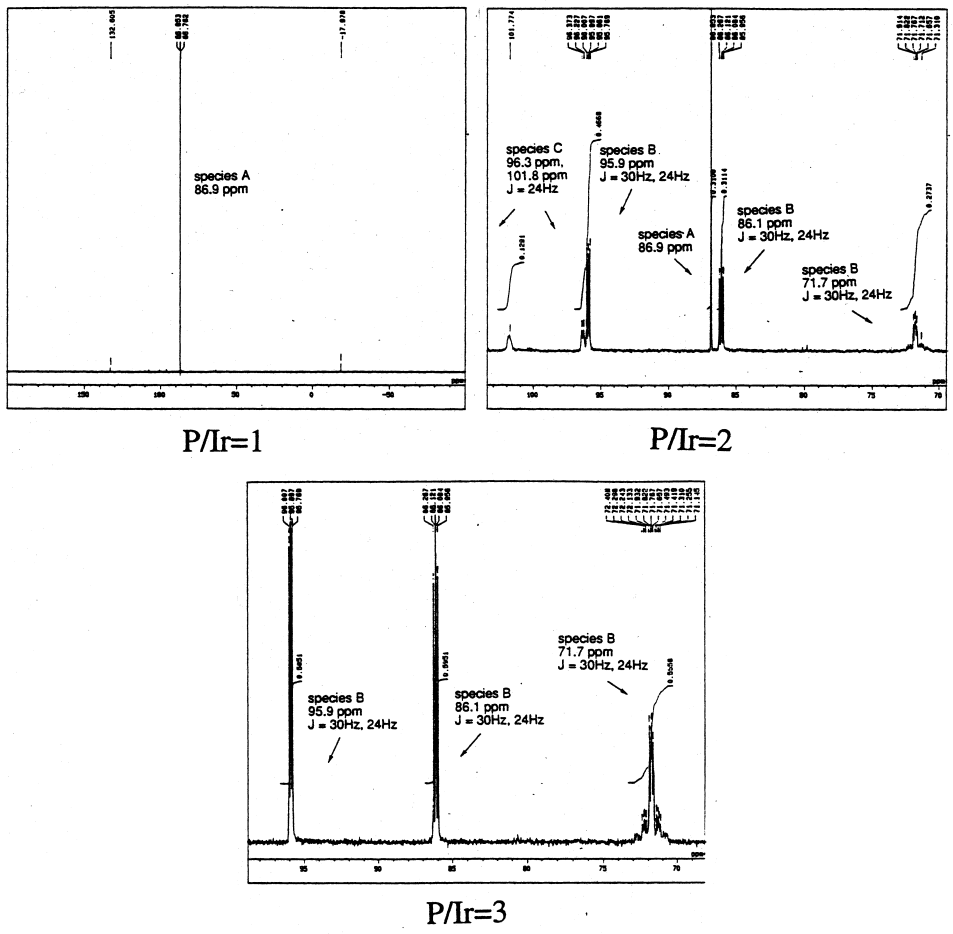
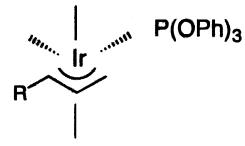


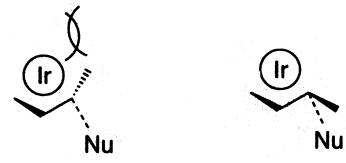
Fig. 1. ^{31}P NMR spectra of the reaction of $[Ir(COD)Cl]_2$ with $P(OPh)_3$.

spectra at $P/Ir = 3$ showed three sets of doublets (δ 71.7, 86.1 and 95.9, $J = 30$, 24 Hz; species B). Signals of species A and C disappeared. The allylic alkylation was highly regioselective at the ratios $P/Ir = 1$ and 2 (Table 1; entries 1 and 2). It is clear that a catalytically active species is species A. Triphenylphosphite coordinates with the metal *trans* to the substituted allylic terminus to avoid steric repulsion. Since $P(OPh)_3$ is a better π-acceptor, it promotes a carbonium ion character at the substituted allylic terminus and directs the nucleophilic attack to this position (Scheme 1). In agreement with this, when a ligand with weaker acceptor properties was used, such as $P(OEt)_3$, the reaction was much less selective (Table 1; entry 5).

The regioselectivity of the reaction of (*Z*)-2-alkenyl acetate is different from that of (*E*)-2-alkenyl acetate. The difference is explained as follows. Nucleophilic attack at the substituted allylic terminus in *anti* π-allyl iridium intermediate would bring the *anti* substituent close to the iridium moiety. The steric interaction gives an unfavorable transition state. On the other hand, such steric interaction does not occur in the alkylation at the substituted allylic terminus of the *syn* π-allyl iridium intermediate. Thus, alkylation at the unsubstituted allylic terminus is favored in the case of (*Z*)-2-alkenyl acetate (Scheme 2).



Scheme 1.



Scheme 2.

In conclusion, iridium complex was found to be a new and efficient catalyst for allylic alkylation. The selectivities described here complement palladium complex catalysis. These unique features will make iridium complexes a useful tool for the carbon–carbon bond forming reaction.

References

[1] R.H. Crabtree, Acc. Chem. Res. 12 (1979) 331.
[2] H. Takaya, T. Naota, S.-I. Murahashi, J. Am. Chem. Soc. 120 (1998) 4244.

[3] M. Murakami, K. Itami, M. Ubukata, I. Tsuji, Y. Ito, J. Org. Chem. 63 (1998) 4.
[4] N. Chatani, S. Ikeda, K. Ohe, S. Murai, J. Am. Chem. Soc. 114 (1992) 9710.
[5] J.B. Wakefield, J.M. Stryker, J. Am. Chem. Soc. 113 (1991) 7057.
[6] J. Tsuji, Palladium Reagents and Catalysts, Wiley, New York, 1995, p. 290.
[7] R. Pretot, A. Pfaltz, Angew. Chem., Int. Ed. Engl. 37 (1998) 323.
[8] R. Pretot, G.C. Lloyd-Jones, A. Pfaltz, Pure Appl. Chem. 70 (1998) 1035.
[9] B.M. Trost, I. Hachiya, J. Am. Chem. Soc. 120 (1998) 1104.
[10] B.M. Trost, C.A. Merlic, J. Am. Chem. Soc. 112 (1990) 9590.
[11] G.C. Lloyd-Jones, A. Pfaltz, Angew. Chem., Int. Ed. Engl. 34 (1995) 462.
[12] S. Zhang, T. Mitsudo, T. Kondo, Y. Watanabe, J. Organomet. Chem. 450 (1993) 197.
[13] J.M. Brown, J.E. Maclntyre, J. Chem. Soc., Perkin Trans. 2 (1985) 961.
[14] A.J. Blacker, M.L. Clark, M.S. Loft, J.M.J. Williams, Chem. Commun. (1999) 913.
[15] A.J. Blacker, M.L. Clark, M.S. Loft, M.F. Mahon, J.M.J. Williams, Organometallics 18 (1999) 2867.
[16] R. Takeuchi, M. Kashio, J. Am. Chem. Soc. 120 (1998) 8647.
[17] R. Takeuchi, M. Kashio, Angew. Chem., Int. Ed. Engl. 36 (1997) 263.
[18] J.P. Janssen, G. Helmchen, Tetrahedron Lett. 38 (1997) 8025.
[19] B. Bartels, G. Helmchen, Chem. Commun. (1999) 741.
[20] T. Cuvigny, M. Julia, C. Roland, J. Organomet. Chem. 285 (1985) 395.
[21] B.M. Trost, T.R. Verhoeven, J. Am. Chem. Soc. 102 (1980) 4730.
[22] J.W. Faller, M.E. Thomsen, M.J. Mattina, J. Am. Chem. Soc. 93 (1971) 2642.
[23] R.H. Crabtree, G.E. Morris, J. Organomet. Chem. 135 (1977) 395.

PERGAMON

www.elsevier.nl/locate/poly

Polyhedron 19 (2000) 563–566

POLYHEDRON

Synthesis and reactivity of polymetallated olefins and functionalized metalloalkynes

Julia Kaftanov, Claudia Averbuj, Natalia Vais-Morlender, Annie Liard, Ilan Marek *

Department of Chemistry and Institute of Catalysis Science and Technology, Technion-Israel Institute of Technology, Technion City, 32 000 Haifa, Israel

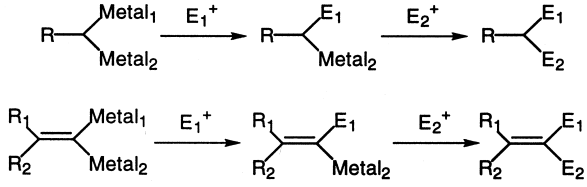
Received 4 October 1999; accepted 19 November 1999

Abstract

The first straightforward synthesis of tris-metallated olefins and functionalized metallated alkynes is reported via the use of low-valent titanium derivatives. ©2000 Elsevier Science Ltd All rights reserved.

Keywords: Alkynes; Functionalized metalloalkynes; Olefins; Polymetallated olefins; Titanium

The development of new strategies in organic syntheses with a minimum of chemical steps is becoming increasingly necessary for the efficient assembly of complex molecular structures [1], and then the combination of multiple reactions in a single operation represents a particularly efficient approach. Among different strategies [2], the synthesis and reactivity of geminated organobismetallics is becoming increasingly useful for the synthesis of molecules with complex architecture [3].



One particular example is the preparation of polysubstituted olefins in a single-pot operation from polymetallated olefins. Indeed, several 1,1-dimetalloalkenes with a large variety of metals (dilithium [4], aluminum and titanium [5,6], aluminum and zirconium [5,6], zinc and zirconium [7,8], zinc and boron [9], copper and boron [9], copper and zirconium [7,8], lithium and boron [10,11] and boron and zirconium [12–14]) have been used as a source of polysubstituted carbon–carbon double bonds with variable stereochemical purities. In this context, we have already reported that the allylmetallation of alkynyl metals [15–18] leads to sp^2 1,1-bis-metallic derivatives in good overall yield [19,20]. These geminated bis-anions react selectively with two different electrophiles and can be a source of chiral α,α'-disubstituted alkynes [19–21] (Scheme 1).

However, the major drawback of this strategy is the necessary incorporation of the allyl moiety on the carbon skeleton. Also we needed a more general preparation of sp^2 polymetallated derivatives allowing the access to a wide variety of carbon skeletons. To answer this requirement, we thought that some organometallic derivatives might behave, to a certain extent, like a carbon atom. If this assumption is correct, it should then be possible to prepare an organometallic derivative on an already metallated carbon center. In order to test this new concept, we used the pioneering work of Sato and co-workers [22], who demonstrated that various disubstituted alkynes react with diisopropoxy(η^2-propene)-titanium (**1**), readily generated by the reaction of $Ti(OiPr)_4$ with 2 equivalents of iPrMgX, to give the corresponding titanacyclopropene derivatives as described in Scheme 2, path A.

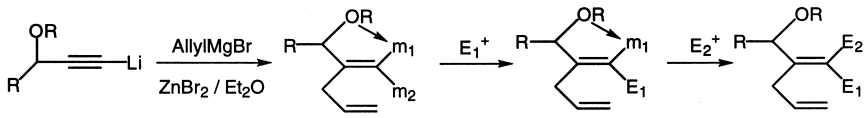
As terminal alkynes failed to participate in the present reaction (path B versus path A), the Sato reagent was ideal for testing this new concept: can a metallated alkyne behave like a disubstituted alkyne (path C identical to path A) and so an organometallic moiety like a carbon atom?

Our initial attempts were to add alkynyl metal derivatives to the preformed Ti(II) complex (**1**) as described in Scheme 3.

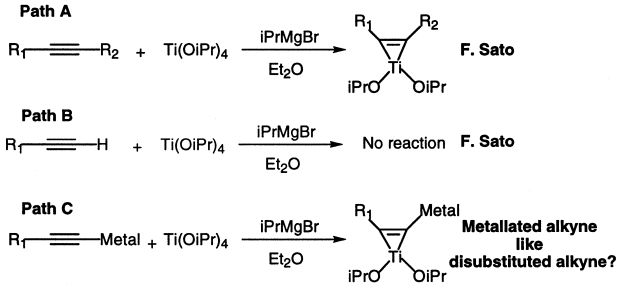
The metallated titanacyclopropenes were effectively obtained with moderate chemical yield for $MX_{n-1}=$

* Corresponding author. Tel.: +972-4-8293709; fax: 972-4-8233735; e-mail: chilanm@tx.technion.ac.il

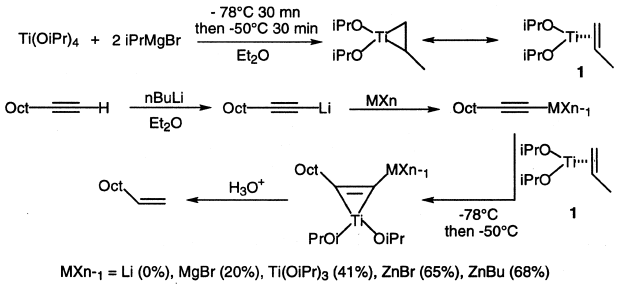
0277-5387/00/$ - see front matter ©2000 Elsevier Science Ltd All rights reserved.
PII S0277-5387(99)00408-8



Scheme 1.

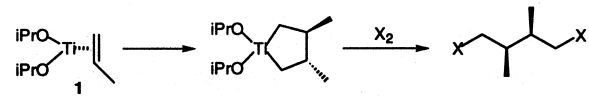


Scheme 2.



Scheme 3.

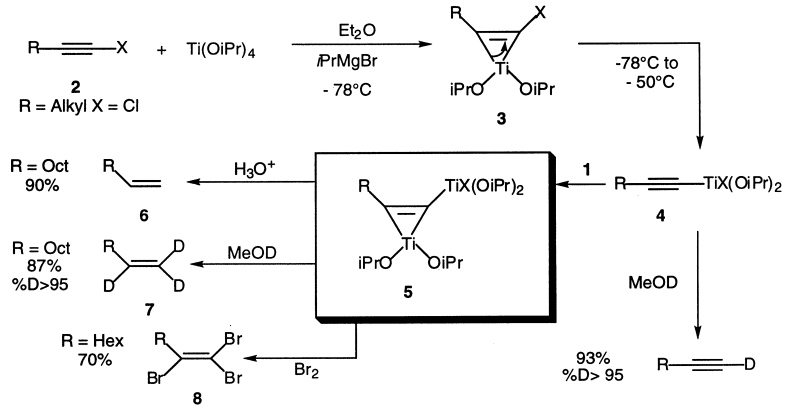
$Ti(OiPr)_3$, ZnBr or ZnBu. However, it was very difficult, in our hands, to get reproducible results (for example, the yield of the alkynylzinc bromide varied from 25 to 70%). These fluctuations were attributed to the possible instability of the preformed low-valent titanium alkoxide (**1**) in these Grignard experimental conditions [Grignard conditions (formation of the organometallic derivative and then introduction of the electrophile) as compared to Barbier conditions (formation of the organometallic derivative in the presence of the electrophile)], and also to the rearrangement of compound **1** into the corresponding cyclic product (*meso*/*dl* = 99/1) (Scheme 4).



Scheme 4.

In order to overcome these chemical yield fluctuations, it was then necessary to prepare compound **1** in the presence of the alkyne (Barbier conditions, see above). However, the addition of iPrMgBr to the mixture of alkynylzinc bromide and $Ti(OiPr)_4$ in ether at low temperature in Barbier conditions did not give the expected product, but more probably the alkynyldiisopropyl zincate. So, the transmetallation between iPrMgBr and the alkynylzinc bromide was faster than the reaction between the same Grignard and the titanium(IV). Finally, we found that treatment of chloroalkyne (**2**) with 2.5 equivalents of the combination $Ti(OiPr)_4$–2iPrMgBr in Et_2O gives, in a single-pot operation at $-50°C$, the desired titanotitanacyclopropene (**5**) in high chemical yield as described in Scheme 5.

Then, the in situ formed diisopropoxy(η^2-propene)-titanium (**1**) reacts with the chloroalkyne (**2**) to give as unstable intermediate, the chlorotitanacyclopropene (**3**). This latter undergoes a fast β-elimination at low temperature to give the alkynyltitanium derivative (**4**). The second equivalent of compound **1** present in the reaction mixture reacts with compound **4** to give the metallated titanacyclopropene (**5**). After hydrolysis, the alkene (**6**) is obtained in high chemical yield. The presence of three carbon–metal bonds was proven by the reaction of compound **5** with MeOD or with Br_2 to give, respectively, the trideuterated olefin (**7**) in 87% yield (D > 95%) or the tribromo derivative in 70%



Scheme 5.

Table 1
Generalization for the synthesis of metallated titanacyclopropenes

Entry	R	X	Compound	Yield (%) [a]
1	oct	Cl	**6**	90
2	hex	Br	**9**	75
3	hex	I	**10**	65
4	hex	SPh	**11**	70
5	tolyl	Cl	**12**	95
6	tert-*O*-amyl$(CH_2)_2$	Cl	**13**	93

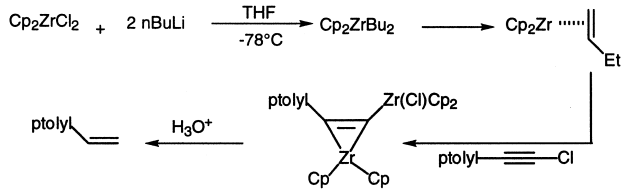
[a] Isolated yields after hydrolysis.

yield. The scope of this reaction is broad, as described in Table 1, since alkyl as well as aromatic groups on the alkyne give the polymetallated olefins whatever the nature of the leaving group (compare entries 1, 2 and 3).

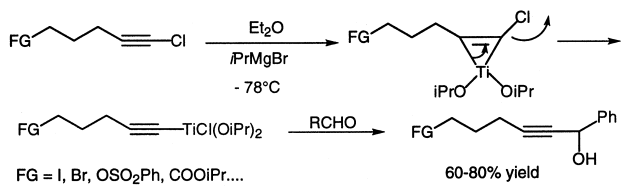
The reactivity of zirconocenes [23] and titanocenes [24] was also studied in this process and we found that only the combination zirconocenes/aromatic halogenoalkynes gave good results (Scheme 6).

In a parallel study, we have also investigated the reactivity of tribromo olefins such as compound **8** (see Scheme 5) and found that this compound can undergo specific coupling reaction with various organometallics in the presence of a catalytic amount of transition metal [25].

We finally turned our attention to the new preparation of metalloalkyne (**4**) (Scheme 5) via diisopropoxy(η^2-propene)titanium (**1**). Indeed, it is known that triisopropoxyalkynyl titanium derivatives react chemoselectively with carbonyl compounds to give the corresponding carbinols in high yield [26]. However, and to the best of our knowledge, these metallated alkynes were always prepared by transmetallation between alkynyl lithium and $ClTi(OiPr)_3$, which precludes the presence of sensitive moieties on the carbon skeleton [27]. It then appeared to us that this new methodology established for the synthesis of **4** could be an interesting alternative for the formation of chlorodiisopropoxyalkynyl titanium possessing sensitive groups [28]. This was effectively the case, as described in Scheme 7.



Scheme 6.



Scheme 7.

The metallated alkyne (**14**) shows a remarkable functional group tolerance, and several classical functional organic moieties can be present during the formation of the chlorodiisopropoxyalkynyl titanium derivatives.

In conclusion, this new concept (organometallic derivative can behave like a carbon atom) enabled us to describe the first and straightforward preparation of tris-metallated olefins in high chemical yield. Moreover, during the preparation of the latter, we found a new preparation of metallated alkynes possessing functional groups.

Acknowledgements

I.M. is the Holder of the Lawrence G. Horowitz Career Development Chair, is a Ygal Alon Fellow and Evelyn and Salman Grand Academic Lectureship — USA. This research was supported in part by The Israel Science Foundation founded by The Academy of Sciences and Humanities (No. 060-471) and by the fund for the promotion of research at the Technion. Acknowledgment is also made to the donors of The Petroleum Research Fund, administered by the ACS, for partial support of this research (PRF 33747-AC1). The authors thank also P. and E. Nathan Research Fund, N. Haar and R. Zinn Research Fund. J.K. thanks the Ministry of Immigrant Absorption for financial support.

References

[1] E.J. Corey, X. Cheng, The Logic of Chemical Synthesis (1989) Wiley-Interscience, New York.
[2] Frontiers in Organic Synthesis, Chem. Rev. 1 (1996) 96.
[3] I. Marek, J.F. Normant, Chem. Rev. 96 (1996) 3241.
[4] J. Barluenga, M.A. Rodriguez, P.J. Campos, G. Asensio, J. Am. Chem. Soc. 110 (1988) 5567 and references cited therein.
[5] T. Yoshida, E.I. Negishi, J. Am. Chem. Soc. 103 (1981) 1276.
[6] E.I. Negishi, Pure Appl. Chem. 53 (1981) 2333.
[7] C.E. Tucker, P. Knochel, J. Am. Chem. Soc. 113 (1991) 9888.
[8] C.E. Tucker, B. Greve, W. Klein, P. Knochel, Organometallics 13 (1994) 94.
[9] J.R. Waas, A.R. Sidduri, P. Knochel, Tetrahedron Lett. 33 (1992) 3717.
[10] A. Pelter, E.M. Colclough, Tetrahedron 51 (1995) 811 and references cited therein.
[11] M.P. Cooke Jr., J. Org. Chem. 59 (1994) 2930.
[12] M. Srebnik, L. Deloux, M. Sabat, J. Org. Chem. 69 (1995) 3276.
[13] L. Deloux, M. Srebnik, J. Org. Chem. 59 (1994) 6871.
[14] L. Deloux, E. Skrzypczak-Jankun, B.V. Cheesman, M. Srebnik, M. Sabat, J. Am. Chem. Soc. 116 (1994) 10302.
[15] M. Gaudemar, C.R. Acad. Sci., Ser. C 273 (1971) 1669.
[16] Y. Frangin, M. Gaudemar, C.R. Acad. Sci., Ser. C 278 (1974) 885.
[17] Y. Frangin, M. Gaudemar, Synthesis (1977) 205.
[18] J. Auger, G. Courtois, L. Miginiac, J. Organomet. Chem. 133 (1977) 285.
[19] I. Creton, I. Marek, J.F. Normant, Tetrahedron Lett. 36 (1995) 7451.
[20] I. Creton, I. Marek, J.F. Normant, Synthesis (1996) 1499.
[21] I. Creton, H. Rezaei, I. Marek, J.F. Normant, Tetrahedron Lett. 40 (1999) 1899.

[22] K. Harada, H. Urabe, F. Sato, Tetrahedron Lett. 36 (1995) 3203.
[23] E.I. Neghishi, T. Takahashi, Bull. Chem. Soc. Jpn. 71 (1998) 755 for the use of dialkylzirconocenes in synthesis.
[24] S.L. Buchwald, R.B. Nielsen, Chem. Rev. 88 (1988) 1047 for the use of dialkyltitanocenes in synthesis.
[25] A. Liard, I. Marek, unpublished results.
[26] N. Krause, D. Seebach, Chem. Ber. 120 (1987) 1845.
[27] M. Reetz, M. Schlosser, Organometallics in Synthesis, 1998, Wiley, New York, p. 195.
[28] N. Morlender-Vais, J. Kaftanov, I. Marek, in preparation.

PERGAMON

www.elsevier.nl/locate/poly

Polyhedron 19 (2000) 567–568

POLYHEDRON

Stereodivergent hydrosilylation of 1-alkynes catalyzed by $RhI(PPh_3)_3$ leading to (*E*)- and (*Z*)-alkenylsilanes and the application to polymer synthesis

Atsunori Mori *, Eisuke Takahisa, Hiroshi Kajiro, Yasushi Nishihara, Tamejiro Hiyama

Research Laboratory of Resources Utilization, Tokyo Institute of Technology, 4259 Nagatsuta, Yokohama 226-8503, Japan

Received 4 October 1999; accepted 15 November 1999

Abstract

Hydrosilylation of 1-alkynes catalyzed by $RhI(PPh_3)_3$ gives (*E*)- and (*Z*)-alkenylsilanes in a stereodivergent manner by switching the reaction conditions and the order of the addition of the reagents. The reaction is also applied to the synthesis of silicon-containing polymers with (*E*) and (*Z*) main-chain structures via polyaddition. ©2000 Elsevier Science Ltd All rights reserved.

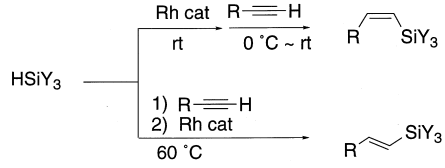
Keywords: Alkenylsilanes; Hydrosilylation; $RhI(PPh_3)_3$; Polyaddition; Stereodivergent

Hydrosilylation serves as one of the most fundamental reactions in organosilicon chemistry. The reaction proceeds by the catalysis of a variety of transition metals, and the control of the reactivity and the selectivity in the hydrosilylation have been of major concern in synthetic organic chemistry as well as in organometallic chemistry [1,2]. The hydrosilylation of a terminal alkyne with a hydrosilane, for example, would form regio- and stereochemical isomers.

We found that the use of $RhI(PPh_3)_3$ as a catalyst for the hydrosilylation of a terminal alkyne furnishes *E*- and *Z*-alkenylsilanes in stereochemically divergent manners by switching the order of the addition of the reagents and reaction conditions [3,4].

The process is illustrated in Scheme 1. When an alkyne was added to a pretreated mixture of a hydrosilane and the rhodium catalyst at room temperature for 2 h, (*Z*)-alkenylsilane was obtained in a good yield (>99%) with an excellent stereoselectivity (>99:1). On the other hand, reaction of the mixture of a hydrosilane, an alkyne and the catalyst at 60°C lead to the (*E*)-product (>99% yield, >99% selectivity).

The results on the stereodivergent hydrosilylation leading to *E*- and *Z*-alkenylsilanes are summarized in Table 1. The hydrosilylation is effective for a variety of hydrosilanes, namely those with heteroatom substituent(s) such as a siloxy or an alkoxy group. This is in contrast to most of the previous rhodium-catalyzed hydrosilylations which have been examined with the use of triethylsilane [1].



Scheme 1.

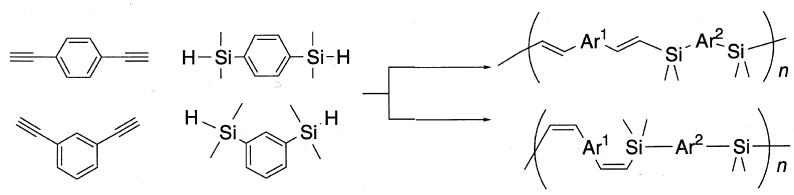
Table 1
Stereoselective hydrosilylation of 1-alkynes leading to *Z*- and *E*-alkenylsilanes

Alkyne	$HSiY_3$	Condition [a]	Temperature (°C), time (h)	Ratio *E*:*Z*
PhC≡CH	$HSiMe_2OSiMe_3$	A	RT, 2	0:100
		B	60, 1	100:0
	$HSiMe(OEt)_2$	A	60, 48 [b]	2:98
		B	60, 1	100:0
4-$MeOC_6H_4C$≡CH	$HSiMe_2OSiMe_3$	A	RT, 2	2:98
4-$MeOC_6H_4C$≡CH	$HSiMe_2OSiMe_3$	B	60, 2	100:0
n-$C_6H_{13}C$≡CH	$HSiMe(OEt)_2$	A	80, 48 [c]	3:97

[a] Condition A: pretreatment of a hydrosilane with 0.1 mol% of the rhodium catalyst at room temperature (RT) for 2 h followed by addition of alkyne. Condition B: reaction with a mixture of a hydrosilane, an alkyne and the catalyst.
[b] The amount of the rhodium catalyst was 0.01 mol%.
[c] The amount of the rhodium catalyst was 0.005 mol%.

* Corresponding author. Tel.: +81-45-9245-231; fax: +81-45-9245-224; e-mail: amori@res.titech.ac.jp

0277-5387/00/$ - see front matter ©2000 Elsevier Science Ltd All rights reserved.
PII S0277-5387(99)00409-X



Scheme 2.

The obtained alkenylsilanes were successfully subjected to transformation reactions of the carbon–silicon bond to a carbon–carbon bond via palladium-catalyzed cross-coupling reaction with retention of the stereochemistry [5].

Then the stereodivergent hydrosilylation was applied to bis-alkynes with bis-hydrosilanes via polyaddition to afford the poly[(phenylene)-((*E*), or (Z)-vinylene)-(silylene)]s. The reactions proceeded in a highly stereospecific manner as shown in Scheme 2, with the ratios higher than 90%. The molecular weights and the molecular weight distributions were estimated by SEC analyses in the range 6000–20000 and 2.4–5.5, respectively. UV absorption and emission spectra of the polymers were also measured [6].

References

[1] I. Ojima, S. Patai, Z. Rappoport, The Chemistry of Organic Silicon Compounds, Wiley, New York, 1989, p. 1479.
[2] T. Hiyama, T. Kusumoto, B.M. Trost, I. Fleming, Comprehensive Organic Synthesis, vol. 8, Pergamon, Oxford, 1991, p. 763.
[3] K. Hirabayashi, E. Takahisa, Y. Nishihara, A. Mori, T. Hiyama, Bull. Chem. Soc. Jpn. 71 (1998) 2409.
[4] A. Mori, E. Takahisa, H. Kajiro, K. Hirabayashi, Y. Nishihara, T. Hiyama, Chem. Lett. (1997) 443 (preliminary communication).
[5] Y. Hatanaka, T. Hiyama, Pure Appl. Chem. 66 (1994) 1471.
[6] R.M. Chen, K.-M. Chien, K.-T. Wong, B.-Y. Jin, T.-Y. Luh, J.-H. Hou, W. Fann, J. Am. Chem. Soc. 119 (1997) 11321 related studies on spectroscopy of silicon-containing polymers.

PERGAMON

www.elsevier.nl/locate/poly

Polyhedron 19 (2000) 569–571

POLYHEDRON

X-ray crystallographic proof of regioselectivity in a nitrosobenzene cycloaddition, and development of a novel in situ heterocycloaddition trap for use during decomplexation of tricarbonyliron diene complexes in hippeastrine synthesis

Christopher E. Anson [1], Sascha Hartmann, Richard D. Kelsey, G. Richard Stephenson *

School of Chemical Sciences, University of East Anglia, Norwich NR4 7TJ, UK

Received 4 October 1999; accepted 18 November 1999

Abstract

The heterocycloaddition reaction between nitrosobenzene and 2-methylcyclohexa-1,3-diene preferentially affords the regioisomer with the N–Ph group next to the methyl substituent, and this product has been characterised by X-ray crystallography. As a model study for a tricarbonyliron mediated route to the alkaloid hippeastrine, a 2-methyl-6-phenylcyclohexadiene analogue has been prepared from tricarbonyl(η^5-3-methylcyclohexadienyl)iron(1+) hexafluorophosphate(1−) and has been examined in the heterocycloaddition reaction. A novel in situ heterocycloaddition trapping procedure has been developed based on this chemistry. Tricarbonyl(η^4-2-methyl-6-phenylcyclohexadiene)iron(0) can be converted directly into the cycloadduct in this way by reaction with trimethylamine *N*-oxide in the presence of nitrosobenzene. ©2000 Elsevier Science Ltd All rights reserved.

Keywords: Nitrosobenzene cycloaddition; Regioselectivity; Organoiron compounds; Decomplexation; Heterocycloaddition trap; Alkaloid synthesis

Our investigation of the use of tricarbonyliron complexes as electrophilic intermediates in alkaloid synthesis aims to demonstrate the intrinsic flexibility of this approach, by addressing synthetic targets with common structural features that are arranged differently around a central portion of the molecule. In the case of the *Amaryllidaceae* alkaloids [1] lycoramine and hippeastrine, this central feature contains an aromatic and saturated (or partially-saturated) six-membered ring, joined at a chiral centre. Because of their shared biogenesis from tyrosine, these alkaloids also contain a two-carbon alkylamine (CH_2–CH_2–X) side-chain, but this appears at the chiral centre in the aryl-substituted ring junction in lycoramine, and opposite the point of arene attachment in hippeastrine. Tricarbonyliron complexes used in these syntheses serve as powerful electrophiles and give complete stereocontrol in reactions with nucleophiles, and our general approach is based on the concept of a central 'C_{12} building block' [2] comprising an aryl-substituted chiral cyclohexadienyliron complex. We have reported [3] a formal total synthesis of lycoramine based on this approach and employing a sequence of two organoiron-mediated nucleophile addition steps at the same carbon atom. Analysis of the requirements for regiocontrol [4] (Fig. 1) in the manipulation of the tricarbonyliron complexes shows this to be a '1,1' pattern, because both of the nucleophile addition steps occur at the same carbon atom. This is achieved by developing an OMe leaving group at the C-1 position in the electrophile, the centre at which the first nucleophile adds. For hippeastrine, a '1,2' regiocontrol pattern is needed, and for this the leaving group needs to be located at C-6. We have demonstrated that in this way, a sequence of nucleophile addition, reactivation by extraction of the leaving group, and an intramolecular second nucleophile addition step can form the ABC ring system of the hippeastrine target [5], and since both nucleophiles react under control of the iron centre, *cis* relative stereochemistry at the BC ring junction is assured in this approach. We have also shown that biotechnology can afford from arenes a simple enantioselective entry to suitably substituted chiral diene complexes equipped with correctly placed leaving groups [6].

In this communication, we present results that relate to the CD ring section of hippeastrine, where our objective is to use

* Corresponding author. Tel.: +44-1603-592019; fax: +44-1603-592710; e-mail: g.r.stephenson@uea.ac.uk

[1] Present address: Institut für Anorganische Chemie, Universität Karlsruhe, Engesserstrasse Geb. 30.45, 76131 Karlsruhe, Germany.

0277-5387/00/$ - see front matter ©2000 Elsevier Science Ltd All rights reserved.
PII S0277-5387(99)00410-6

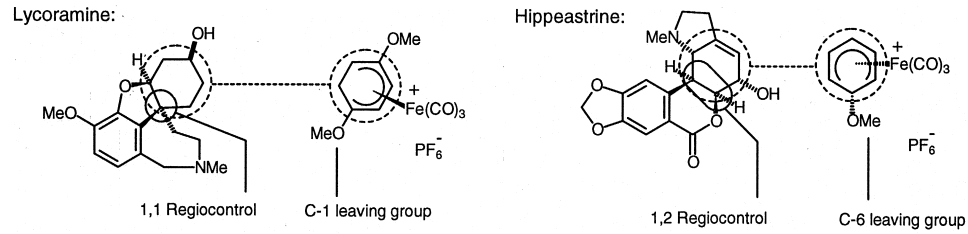


Fig. 1. Identification of 1,1 and 1,2 regiocontrol patterns needed for syntheses of *Amaryllidaceae* alkaloids such as lycoramine and hippeastrine, using alkoxy-substituted cyclohexadienyliron complexes.

aryl, acyl, or α-chloroalkylnitroso compounds as heterodienophiles to trap the diene at the decomplexation step in the iron-mediated synthesis. Intermediates for hippeastrine that combine a 1,3-diene in ring C with the lactone in ring B are prone to aromatisation by opening of the lactone [7], but we have developed a novel in situ procedure for heterocycloaddition in the presence of reagents for the oxidative detachment of the tricarbonyliron group. This should offer good prospects for use with sensitive intermediates in our synthetic route.

The cycloaddition chemistry of nitroso complexes has been studied in detail and has the advantage of proceeding at low temperature (room temperature, or even below [8]), but regiocontrol with unsymmetrical dienes [9–11] has not been so extensively defined as is the case with classic Diels–Alder cycloadditions. For our purpose, we require the nitrogen atom of the nitroso reagent to add to the carbon adjacent to the 'CH_2–CH_2–X' alkyl substituent on the cyclohexadiene, so that the D ring can ultimately be formed by cyclisation of CH_2–X to the nitrogen introduced in the dienophile. This is known [11] to be the preferred regioselectivity of reaction of nitrosobenzene with 2-methylbutadiene. We began by preparation of the known [12] 2-methylcyclohexa-1,3-diene (**1**) and an examination of its reaction with commercially available nitrosobenzene. An excess of the nitroso compound was mixed with the diene and stored at −20°C for 1 week. After chromatography, the major product **2** was recrystallised from ethanol–water, and we were able to prove by X-ray crystallography [13] (Fig. 2) that the correct regioisomer had been formed. The substituted end of the heterodienophile adds to the more hindered end of the diene, suggesting that the reaction is initiated by approach of the oxygen terminus of the Ph–N=O unit to the most accessible site for reaction.

A substrate for use in a model study of in situ trapping of the diene was easily prepared from tricarbonyl(η^5-3-methylcyclohexadienyl)iron hexafluorophosphate (**3**). Excellent results were obtained by reaction with Ph_2CuLi in THF. The *exo*-substituted product **4** was obtained in 91% yield. This complex has the same relative position of alkyl and aryl components as the proposed 'C_{12} + CH_2–CH_2–X' [2] building block for our route to hippeastrine. Attempted direct reaction of the tricarbonyliron complex with an excess of nitrosobenzene resulted only in recovery of the starting material, but by pre-mixing the complex and nitrosobenzene in DMA at 0°C, then adding trimethylamine *N*-oxide and allowing the mixture to warm to room temperature, the cycloadduct **5** was obtained in 68% yield. The same cycloadduct could be formed by a conventional stepwise procedure, detaching the metal first with trimethylamine *N*-oxide, and taking the crude diene (ca. 50% yield, mixed with products from aromatisation) on into the cycloaddition step (Scheme 1). TLC analysis of the products of the cycloaddition reaction using a

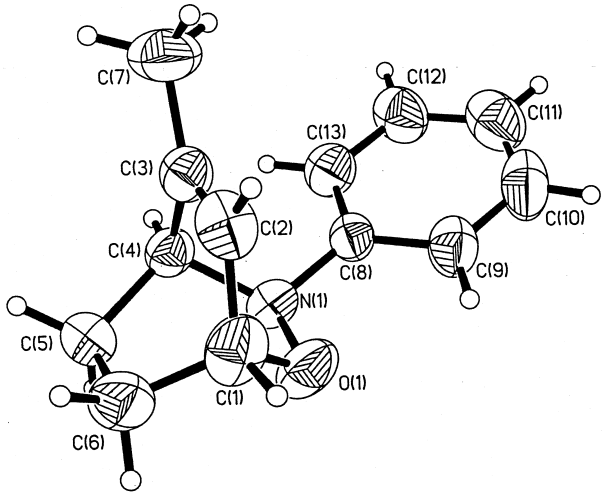
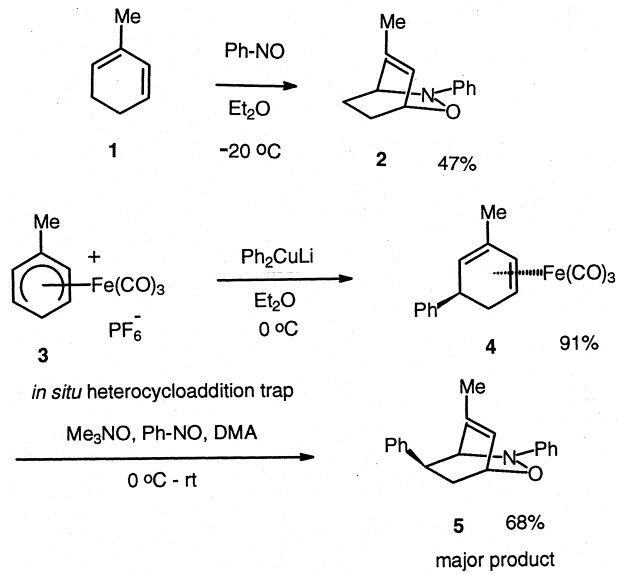


Fig. 2. X-ray structure of the major regioisomer (**2**) from the heterocycloaddition reaction between 2-methylcyclohexadiene and nitrosobenzene. Selected bond lengths for **2**: C2–C3 1.309(4), N1–O1 1.445(3), N1–C4 1.449(4), O1–C1 1.479(4), N1–C8 1.423(4) Å.



Scheme 1.

phosphomolybdic acid stain produces characteristic purple spots, and in this way it was demonstrated that although several cycloaddition products are formed in this reaction, one predominates to a large extent. Minor reaction pathways to alternative stereo- and regioisomers can account for this observation, but at this stage only the major diastereoisomer has been isolated and characterised (HRMS, ^{1}H NMR, COSY, ^{13}C NMR, DEPT). To date, attempts to obtain crystals to confirm the relative stereochemistry by X-ray crystallography have been unsuccessful, but the NMR data are consistent with the expected product, which corresponds to the approach of the heterodienophile to the unsubstituted face of the diene, and the structure is provisionally assigned on that basis.

In summary, we have developed a novel low temperature trapping procedure to intercept sensitive substituted diene products during the metal removal step, which when applied in our organoiron-mediated approach to hippeastrine shows promise as a convenient and efficient method to introduce the C–N and C–O substituents on the C ring. Cycloaddition ensures that these two features are *cis* to one another, and approach of the dienophile to the open face of the structure, and with the unsubstituted end of the nitroso compound bonding preferentially to the less hindered end of the diene, would lead to the formation of the required regio- and stereoisomer as the major product. By the in situ trapping method, the decomplexation reaction becomes a 'working step' [14] in the synthesis, and the metal-mediated construction of the 'C_{12}' aryl-substituted cyclohexadiene complex described here is suitable to allow easy preparation of more representative model structures containing the methylenedioxy and CH_2–CH_2–X features that will figure in the natural product synthesis itself. The scope of the in situ trapping method with more highly substituted dienes and with heterodienophiles that can easily be converted into NMe substituents by reduction of the N–O bond [15] in the cycloaddition product, is currently under investigation.

Supplementary data

Supplementary data are available from the Cambridge Crystallographic Data Centre, 12 Union Road, Cambridge CB2 1EZ, UK (fax: +44-1223-336 033; e-mail: deposit@ccdc.cam.ac.uk) upon request, quoting the deposition number CCDC -132482.

Acknowledgements

RDK thanks the EPSRC for financial support and we thank the EPSRC National Mass Spectrometry Service Centre, University of Wales Swansea for high resolution mass spectrometric measurements.

References

[1] O. Hoshino, in: G.A. Cordell (Ed.), The Alkaloids, Academic Press, 1998, pp. 51, 323.
[2] A.V. Malkov, A. Auffrant, C. Renard, E. Rose, F. Rose-Munch, D.A. Owen, E.J. Sandoe, G.R. Stephenson, Inorg. Chim. Acta 296 (1999) 139.
[3] E.J. Sandoe, G.R. Stephenson, S. Swanson, Tetrahedron Lett. 37 (1996) 6283.
[4] G.R. Stephenson, S.T. Astley, I.M. Palotai, P.W. Howard, D.A. Owen, S. Williams, in: K.H. Dotz, R.W. Hoffmann (Eds.), Organic Synthesis via Organometallics, Vieweg, Braunschweig, 1991, p. 169.
[5] S.T. Astley, G.R. Stephenson, Synlett (1992) 507.
[6] S.T. Astley, M. Meyer, G.R. Stephenson, Tetrahedron Lett. 34 (1993) 2035.
[7] S.T. Astley, G.R. Stephenson, unpublished results, 1993.
[8] Y.A. Arbuzov, T.A. Mastryukova, Izv. Akad. Nauk SSSR Otdel. Kim. Nauk (1952) 665.
[9] S.M. Weinreb, R.R. Staib, Tetrahedron 38 (1982) 3087.
[10] G. Kresze, A. Mavromatis, Tetrahedron 34 (1978) 697.
[11] M. Shibusaki, M. Sodeoka, Y. Ogawa, J. Org. Chem. 49 (1984) 4098, see also Ref. 14 for an example applied to alkaloid synthesis.
[12] R.P. Gregson, R.N. Mirrington, Aust. J. Chem. 29 (1976) 2049.
[13] Crystallographic details for **2**: $C_{13}H_{15}NO$; colourless block, $0.3\times0.3\times0.2$ mm. Monoclinic, $P2_1/n$, $Z=4$, $a=8.964(3)$, $b=7.624(1)$, $c=16.312(6)$ Å, $\beta=98.21(3)°$, $U=1103.4(4)$ Å^3, $F(000)=432$. Mo Kα, $\lambda=0.71073$ Å, $\mu=0.076$ mm^{-1}. 2075 data (ω-scans, $2\theta_{max}=50°$) measured on Rikagu AFC7R, corrected for absorption (ψ-scans, $0.915<T<0.995$), 1941 unique ($R_{int}=0.0534$). Full-matrix refinement on F^2 (all data, 197 parameters; xyz and U_{iso} refined for all H), wR_2(all data) = 0.1394, $R_1(I>2\sigma(I))=0.0377$.
[14] A 'working step' advances a synthesis by the formation of at least one new bond present in the target. G.R. Stephenson, in: G.R. Stephenson (Ed.), Advanced Asymmetric Synthesis, Blackie 1996, p. 313.
[15] For an example of the use of acyl nitroso compounds in cycloaddition reactions with cyclohexadiene, and reduction of the products with AlHg, directed towards the synthesis of lycoricidine and narciclasine, see G.E. Keck, S. Flemming, D. Nickell, P. Weider, Synth. Commun. 9 (1979) 281.

PERGAMON

www.elsevier.nl/locate/poly

Polyhedron 19 (2000) 573–576

POLYHEDRON

Synthesis of dimethyl carbonate from carbon dioxide: catalysis and mechanism

Toshiyasu Sakakura *, Jun-Chul Choi, Yuko Saito, Takeshi Sako

National Institute of Materials and Chemical Research, 1-1 Higashi, Tsukuba, Ibaraki 305-8565, Japan

Received 4 October 1999; accepted 7 December 1999

Abstract

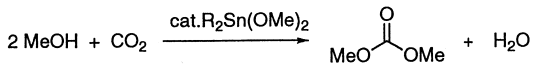
The turnover number of the catalytic production of dimethyl carbonate from CO_2 and methanol is restricted by thermodynamics as well as catalyst decomposition. The catalytic efficiency is remarkably improved using an acetal as the starting material in methanol. The catalytic activity and selectivity also depend strongly on the CO_2 pressure. A possible catalytic cycle involving transformation of CO_2 to dimethyl carbonate is postulated based on mechanistic studies at a molecular level. ©2000 Elsevier Science Ltd All rights reserved.

Keywords: Carbon dioxide; Dimethyl carbonate; Homogeneous catalysis; Mechanism; Supercritical conditions

1. Introduction

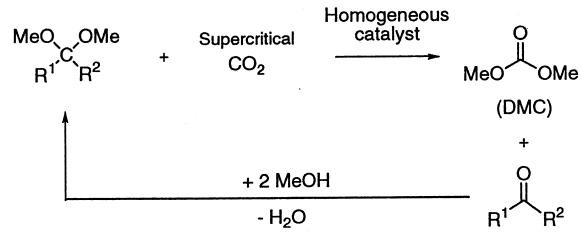
There is no need to discuss the importance of carbon dioxide as a C_1 feedstock (for recent reports of CO_2 conversion by homogeneous catalysis, see Refs. [1–6]). In particular, the utilization of supercritical carbon dioxide has recently attracted much interest from the viewpoint of Green Chemistry [7] for the following reasons. (i) The environmentally friendly nature of CO_2 (non-toxic and inflammable) is attractive for solvent-free processes and as a substitute for toxic chemicals such as phosgene and CO. (ii) Physical properties such as polarity, solubility etc. can be varied by changing the pressure and temperature. (iii) The reactivity of CO_2 itself is often improved dramatically under supercritical conditions [8,9]. (iv) Separation from the reaction mixture is easy.

One of the most interesting synthetic targets starting from CO_2 is dimethyl carbonate (DMC) [10–12]. The possible organotin-catalyzed formation of DMC from CO_2 was first proposed by Japanese groups (Eq. (1)) [13,14]. Kizlink et al. have paid much attention to improving the catalytic activities of this reaction although the turnover number (TON) is still far from satisfactory [15–18].



(1)

Previously, we reported the organotin-catalyzed synthesis of DMC from orthoesters and CO_2 [19–21]. However, this procedure has the disadvantages of high cost of the starting material and the co-production of methyl ester. This article discloses an improved procedure, the synthesis of DMC from acetals and CO_2 (Eq. (2)) [22,23]. Since the co-produced carbonyl compounds are easily recycable, the process can be regarded as a formal DMC synthesis from methanol and CO_2.



(2)

2. Results and discussion

2.1. Catalytic reaction

As for the synthesis of DMC from methanol and CO_2 only (Eq. (1)), there are two factors that restrict the amount of DMC: (i) thermodynamics and (ii) deactivation of the catalyst by water. Although both factors are important, the former is more notable. Indeed, the yield of DMC does not depend significantly on the amount of catalyst (Fig. 1). In other words, the turnover number decreases sharply with increasing amount of catalyst (Fig. 2).

* Corresponding author. Tel: +81-298-54-4719; fax: +81-298-54-4511; e-mail: sakakura@home.nimc.go.jp

0277-5387/00/$ - see front matter ©2000 Elsevier Science Ltd All rights reserved.
PII S0277-5387(99)00411-8

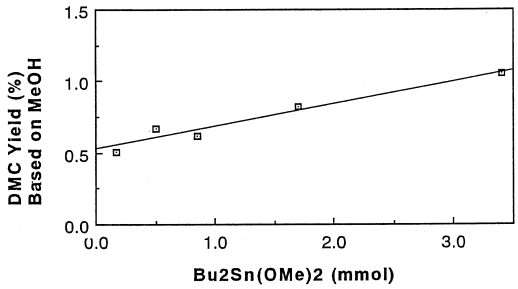


Fig. 1. Effect of amount of catalyst on the yield of DMC. Reaction conditions: $Bu_2Sn(OMe)_2$, MeOH (8.1 cm^3), 180°C, 300 atm, 24 h.

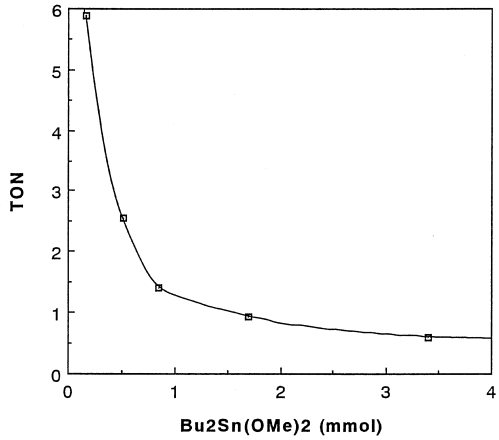


Fig. 2. Effect of amount of Sn on catalyst efficiency. Reaction conditions: $Bu_2Sn(OMe)_2$, MeOH (8.1 cm^3), 180°C, 300 atm, 24 h.

Owing to the limitations stated above, the amount of DMC becomes constant during the initial stage of the reaction of Eq. (1) (black squares in Fig. 3). On the other hand, we have found that the DMC yield increased steadily with a longer reaction time in the presence of dimethyl acetals (white squares). Namely, the addition of acetals is an effective way to overcome the thermodynamic limitation.

Another important factor in achieving high DMC yields is the CO_2 pressure. Higher DMC yields were obtained by applying a higher CO_2 pressure [22,23]. Interestingly, the

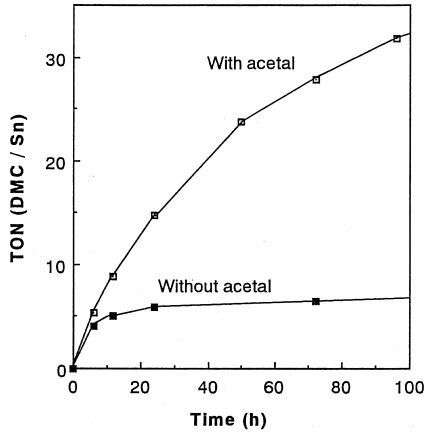


Fig. 3. Time dependence of DMC synthesis. Reaction conditions: 2,2-dimethoxypropane (10 mmol or 0 mmol), $Bu_2Sn(OMe)_2$ (0.17 mmol), MeOH (8.1 cm^3), 180°C, 300 atm.

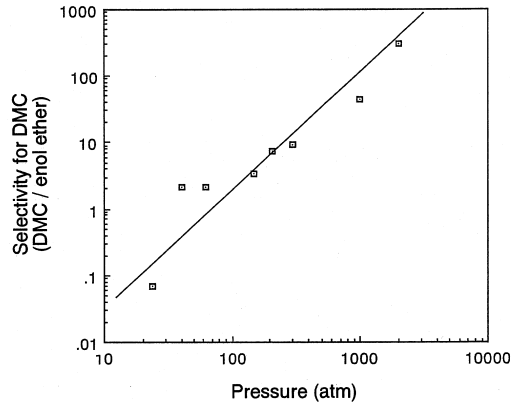
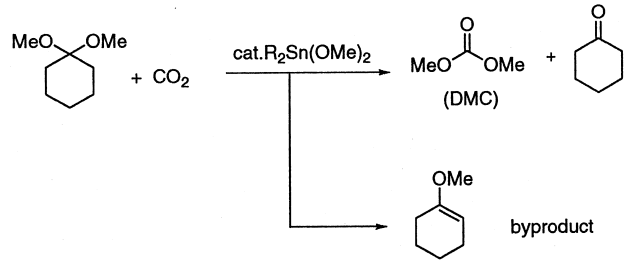


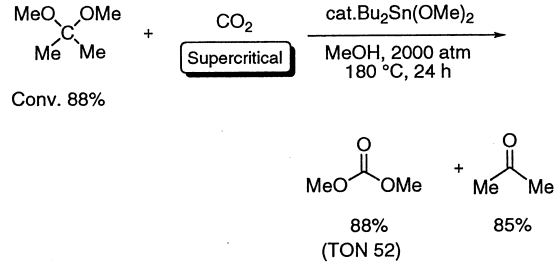
Fig. 4. Effect of pressure on the selectivity. Reaction conditions: 1,1-dimethoxycyclohexane (10 mmol), $Bu_2Sn(OMe)_2$ (0.17 mmol), MeOH (8.1 cm^3), 180°C, 24 h. Selectivity: DMC/enol ether.

selectivity, DMC/(enol ether) ratio, is also improved under higher CO_2 pressure (Eq. (3), Fig. 4).



(3)

After rough optimization, a nearly 90% yield and 100% selectivity were realized by carrying out the reaction at 2000 atm using 2,2-dimethoxypropane as the substrate (Eq. (4)).



(4)

The phase behavior of the reaction mixture was studied using an autoclave with sapphire windows. Two phases were observed at a low CO_2 pressure such as 25 atm. The gas phase became smaller as the CO_2 pressure increased, and finally vanished around 150 atm (Fig. 5). The reaction mixture was completely homogeneous above 300 atm. The phase behavior and the enhancement of the DMC yield at high pressures [22,23] are presumably attributable to the increase in CO_2 density. The densities of pure CO_2 at 180°C are calculated to be 0.200, 0.417, and 1.025 g cm^{-3} under 150, 300, and 2000 atm, respectively (CO_2 densities were calculated according to the literature method, see Ref. [24]).

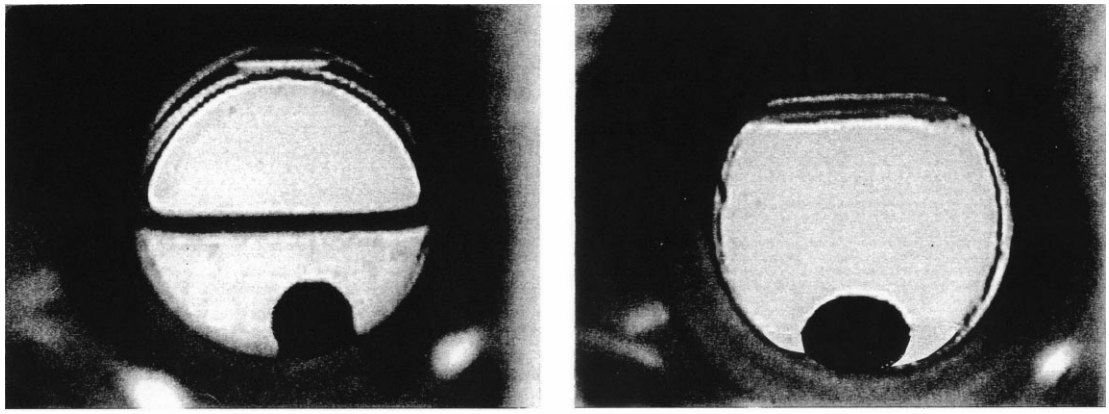
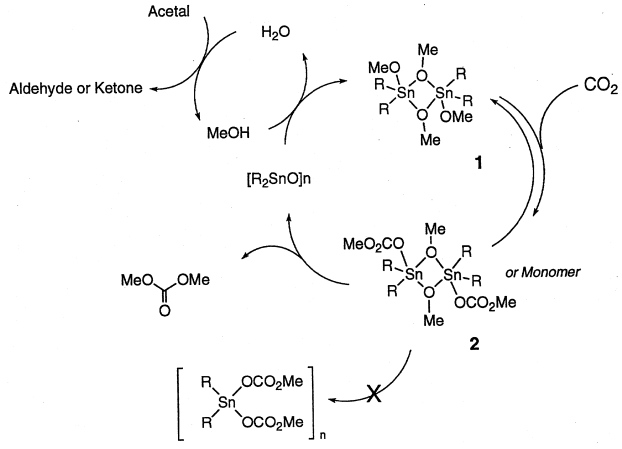


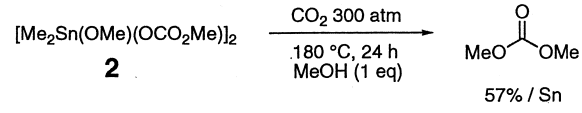
Fig. 5. Phase behavior of $Bu_2Sn(OMe)_2$-catalyzed synthesis of DMC from CO_2 and acetal. The black bar at the bottom is a stirring magnet. Reaction conditions: 1,1-dimethoxycyclohexane (10 mmol), $Bu_2Sn(OMe)_2$ (0.17 mmol), MeOH (8.1 cm^3), 180°C, 24 h.

2.2. Possible mechanism

A possible catalytic cycle of the tin-based system is shown in Scheme 1. $R_2Sn(OMe)_2$ (**1**) has a methoxo-bridged dinuclear structure. Carbon dioxide inserts only into the non-bridging methoxo groups of **1** to give a dinuclear carbonato complex (**2**) [25](see also Ref. [13]). The second CO_2 insertion into **2** did not occur even at a high CO_2 pressure (60 atm), as confirmed by ^1H, ^{13}C, and ^{119}Sn NMR studies [26]. The thermolysis of **2** resulted in the formation of DMC in a reasonable yield (Eq. (5)). On the other hand, the carbonato complex **2** readily loses CO_2 under an N_2 atmosphere even at room temperature to regenerate **1**. In addition, the equilibrium between **1** and **2** should shift in the direction of CO_2 release at higher temperatures. Hence, at the reaction temperature (180°C), a high pressure would be required to generate **2** in a fair concentration. This may be one reason for the remarkable acceleration of Eq. (2) under high CO_2 pressure. The role of acetals in realizing high turnover numbers is presumably as H_2O scavengers rather than as reactants in the catalytic cycle.

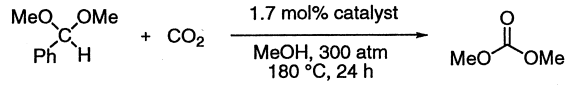


Scheme 1. Possible catalytic cycle.



(5)

Dialkyltin oxide (or its oligomer) is a key intermediate in Scheme 1. Hence, the catalytic activity of $Bu_2Sn{=}O$ was examined using dimethoxyphenylmethane as a substrate. As expected, $Bu_2Sn{=}O$ exhibited almost the same catalytic activity as $Bu_2Sn(OMe)_2$ (Eq. (6)). Although $Bu_2Sn{=}O$ was insoluble in the reaction mixture at room temperature, a clear solution was obtained at 180°C. Thus, each step of Scheme 1 seems plausible.



Catalyst	Yield (%)
$Bu_2Sn{=}O$	14
$Bu_2Sn(OMe)_2$	14
none	0

(6)

In summary, we have achieved formal DMC synthesis from CO_2 and methanol catalyzed by organotin complexes. This work demonstrates the promising prospect of using carbon dioxide, especially under supercritical conditions, as a non-toxic and cheap C_1 building block in molecular catalysis.

3. Experimental

Moisture sensitive complexes were handled using Schlenk and/or glovebox techniques under argon or carbon dioxide. 2,2-Dimethoxypropane, 1,1-dimethoxycyclohexane, dimethoxyphenylmethane, dibutyltin dimethoxide, dibutyltin oxide, and carbon dioxide (purity over 99.9%, water content less than 0.01%) were all commercially available. Dimethyltin dimethoxide was synthesized according to the litera-

ture [27]. Reaction products were analyzed by GC using capillary columns and further characterized by GC-MS.

A typical high pressure reaction was carried out as follows. In a stainless steel autoclave (20 cm^3 inner volume), carbon dioxide (liquid, 65 atm) was added to a mixture of dimethyl acetal (10 mmol), a tin complex (0.17 mmol), and methanol (8.1 cm^3) at room temperature. The autoclave was then heated in an oil bath and the initial pressure was adjusted to 300 atm at 180°C. After cooling, 1,3,5-trimethylbenzene (50 μl) was added to the reaction mixture as the internal standard for the GC analysis.

Caution. All high-pressure experiments need sufficient safety considerations although CO_2 itself is non-toxic.

References

[1] P.G. Jessop, T. Ikariya, R. Noyori, Science 269 (1995) 1065.
[2] P.G. Jessop, T. Ikariya, R. Noyori, Chem. Rev. 95 (1995) 259.
[3] W. Leitner, Angew. Chem., Int. Ed. Engl. 34 (1995) 2207.
[4] D.A. Morgenstern, R.M. LeLacheur, D.K. Morita, S.L. Borkowsky, S. Feng, G.H. Brown, L. Luan, M.F. Gross, M.J. Burk, W. Tumas, in: P.T. Anastas, T.C. Williamson (Eds.), Green Chemistry, ACS Symp. Ser. 626, American Chemical Society, Washington, DC, 1996, p. 132.
[5] M. Cheng, E.B. Lobkovsky, G.W. Coates, J. Am. Chem. Soc. 120 (1998) 11018.
[6] D.J. Darensbourg, M.W. Holtcamp, G.E. Struck, M.S. Zimmer, S.A. Niezgoda, P. Rainey, J.B. Robertson, J.D. Draper, J.H. Reibenspies, J. Am. Chem. Soc. 121 (1999) 107.
[7] P.T. Anastas, J.C. Warner, Green Chemistry, Theory and Practice, Oxford University Press, Oxford, 1998.
[8] R. Noyori, Special issue on supercritical fluids, Chem. Rev. 99 (2) (1999) 1.
[9] P.G. Jessop, W. Leitner (Eds.), Chemical Synthesis using Supercritical Fluids, Wiley-VCH, Weinheim, 1999.
[10] M.A. Pacheco, C.L. Marshall, Energy Fuels 11 (1997) 2.
[11] M. Aresta, E. Quaranta, CHEMTECH (1997) 32.
[12] A.-A. Shaikh, S. Sivaram, Chem. Rev. 96 (1996) 951.
[13] S. Sakai, T. Fujinami, T. Yamada, S. Furusawa, Nippon Kagaku Kaishi (1975) 1789.
[14] N. Yamazaki, S. Nakahama, F. Higashi, Rep. Asahi Glass Found. Ind. Technol. 33 (1978) 31.
[15] J. Kizlink, I. Pastucha, Collect. Czech. Chem. Commun. 60 (1995) 687.
[16] J. Kizlink, I. Pastucha, Collect. Czech. Chem. Commun. 59 (1994) 2116.
[17] J. Kizlink, Collect. Czech. Chem. Commun. 58 (1993) 1399.
[18] S. Fang, K. Fujimoto, Appl. Catal. A 142 (1996) L1.
[19] T. Sakakura, K. Ishiguro, T. Sako, 9th IUPAC Symposium for Organometallic Chemistry Directed towards Organic Synthesis, Göttingen, Germany, 20–25 July 1997, IUPAC, Abstract SL-25.
[20] T. Sakakura, Y. Saito, M. Okano, J.-C. Choi, T. Sako, J. Org. Chem. 63 (1998) 7095.
[21] M. Cheong, S.-C. Kim, J.B. Park, New J. Chem. 21 (1997) 1143.
[22] A part of the work was presented by T. Sakakura, M. Okano, T. Sako, 11th Int. Symp. on Homogeneous Catalysis, St. Andrews, 12–17 July 1998, Royal Society of Chemistry, Abstract C6.
[23] T. Sakakura, J.-C. Choi, Y. Saito, T. Masuda, T. Sako, T. Oriyama, J. Org. Chem. 64 (1999) 4506.
[24] F.-H. Huang, M.-H. Li, L.L. Lee, K.E. Starling, F.T.H. Chung, J. Chem. Eng. Jpn. 18 (1985) 490.
[25] J.-C. Choi, T. Sakakura, T. Sako, J. Am. Chem. Soc. 121 (1999) 3793.
[26] J.-C. Choi, T. Sakakura, T. Saka, 76th Annual Meeting of Japan Chemical Society, Yokohama, Japan, 28–31 March 1999, Abstract 2B 316.
[27] D.L. Alleston, A.G. Davies, J. Chem. Soc. (1962) 2050.

PERGAMON

www.elsevier.nl/locate/poly

Polyhedron 19 (2000) 577–579

POLYHEDRON

Role of halide ions in palladium(II) catalyzed nucleophile alkyne-α,β-unsaturated carbonyl coupling reactions

Xiyan Lu *, Zhong Wang

Shanghai Institute of Organic Chemistry, Chinese Academy of Sciences, 354 Fenglin Lu, Shanghai 200032, People's Republic of China

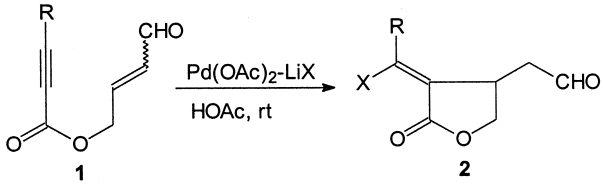
Received 4 October 1999; accepted 22 November 1999

Abstract

The integral role of halide ions as a ligand in divalent palladium catalyzed nucleophile alkyne-α,β-unsaturated carbonyl coupling reactions as well as in the stoichiometric reaction of arylpalladium reagents with acrolein was studied. Excess of halide ions can effectively inhibit the β-hydride elimination of a (2-oxoalkyl)palladium intermediate, giving preferentially the protonolysis product in acidic media. ©2000 Elsevier Science Ltd All rights reserved.

Keywords: Palladium catalyzed reactions; Halide ions; Coupling reactions; Protonolysis

In our ongoing studies of divalent palladium catalyzed reactions, we have established a series of efficient methods for synthesizing α-alkylidene-γ-butyrolactone derivatives using halopalladation–cyclization–deheteropalladation as the key step [1–3]. While studying the scope and synthetic application of this protocol, we discovered serendipitously an intramolecular Pd-catalyzed conjugate addition reaction, which was applied to the formal synthesis of (+)-pilocarpine [4]. In this reaction, an aldehydic enyne ester **1** was cyclized under the catalysis of Pd(II) to give the aldehydic γ-lactones **2**.

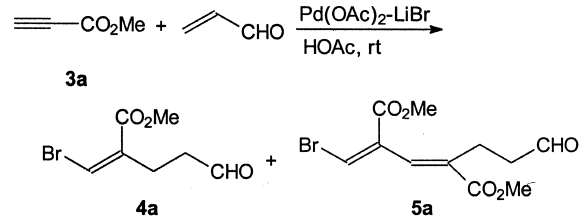


1 **2**

Based on this intramolecular version, we developed the tandem halopalladation-conjugate addition [5] and tandem oxypalladation-conjugate addition reactions [6] which allow efficient and highly stereoselective synthesis of multifunctional carbonyl compounds.

1. Tandem halopalladation-conjugate addition to γ,δ-unsaturated carbonyls [5]

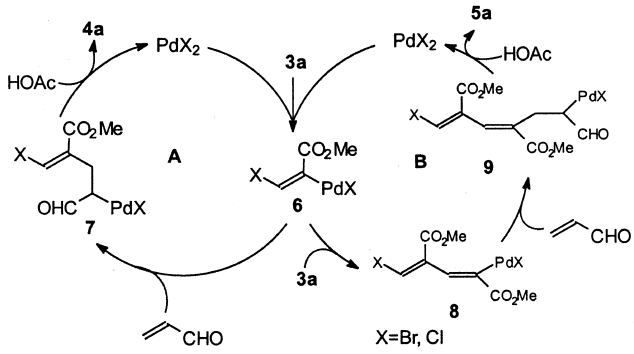
When methyl propynoate **3a** (1.0 mmol) was treated with acrolein (5.0 mmol) in the presence of $Pd(OAc)_2$ (0.02 mmol) and LiBr (4.0 mmol) in acetic acid, two products **4a** and **5a** were isolated.



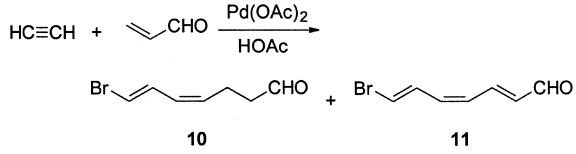
Compound **4a** was the 1:1 codimerization product and **5a** was the 2:1 cotrimerization product. The formation of these two products was rationalized by the mechanism shown in the following. Vinylpalladium intermediate **6** was first formed by *trans*-halopalladation of **3a** in HOAc, followed by acrolein insertion (path A) or subsequent alkyne and acrolein insertion (path B). The competing alkyne insertion may be ascribed to the higher reactivity of acetylenes than olefins. Both reaction paths involved the protonolysis of the carbon–palladium bond to regenerate the catalytic Pd(II) species, giving **4a** and **5a**, respectively.

* Corresponding author. Tel.: +86-21-64163300; fax: +86-21-64166128; e-mail: xylu@pub.sioc.ac.cn

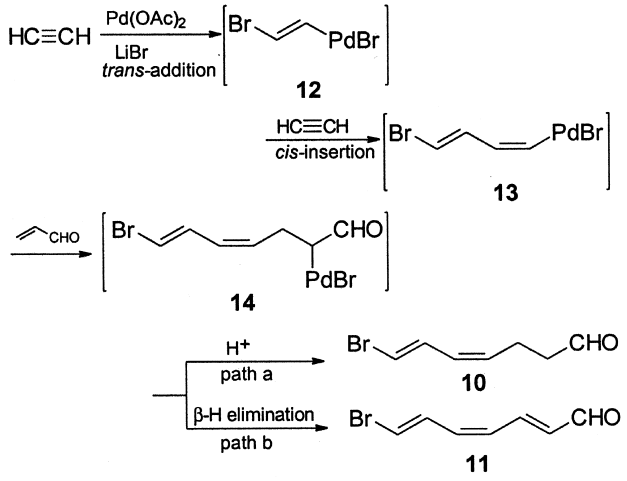
0277-5387/00/$ - see front matter ©2000 Elsevier Science Ltd All rights reserved.
PII S0277-5387(99)00412-X



The reaction of acetylene with α,β-unsaturated electron-deficient alkenes in the presence of a palladium catalyst was attempted to explore the possibility of developing new methods for (*E,Z*)-diene synthesis [7]. The reaction afforded the expected dienal **10** together with the α,β-unsaturated trienal **11** in 220 and 80% yield, respectively (yields are calculated on the basis of $Pd(OAc)_2$). Compound **10** could be purified carefully by column chromatography and its NMR data show unambiguously the (*E,Z*)-configuration of the molecule.



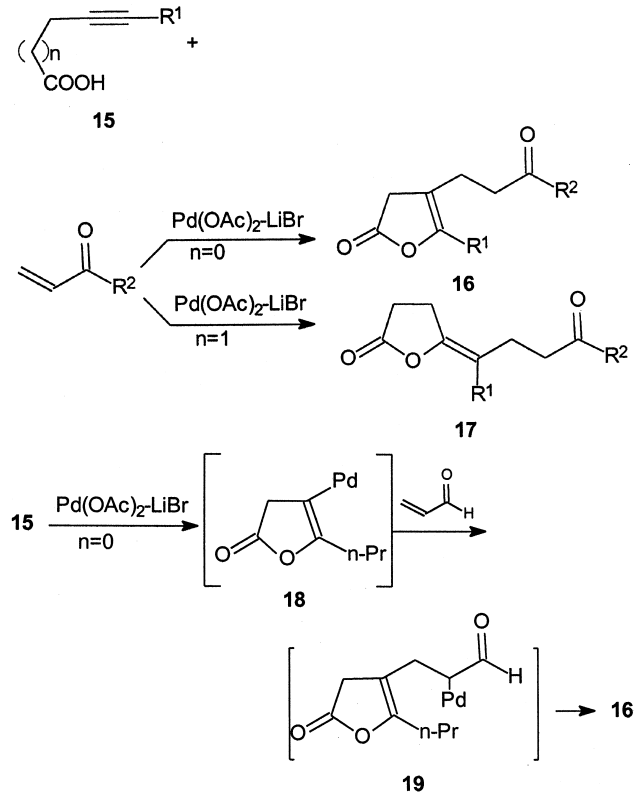
The formation of **10** and **11** could be explained with the following mechanism which also rationalizes the stereoselectivity:



Preliminary results showed that polar solvents, high acetylene concentration, high halide concentration and low temperature favor the formation of **10**.

2. Nucleophile alkyne-α,β-unsaturated carbonyl coupling [6]

Using $Pd(OAc)_2$ as the catalyst, 4-substituted 3-butynoic acid (**15**, $n=0$) and 5 equiv. of acrolein in the presence of excess LiBr (2 equiv.) in HOAc gave the cyclized acrolein coupling products **16** in high yield [6]. The reaction of 4-alkynoic acids (**15**, $n=1$) with acrolein afforded γ-alkylidene-γ-butyrolactone derivatives **17** in good yield and stereoselectivity.



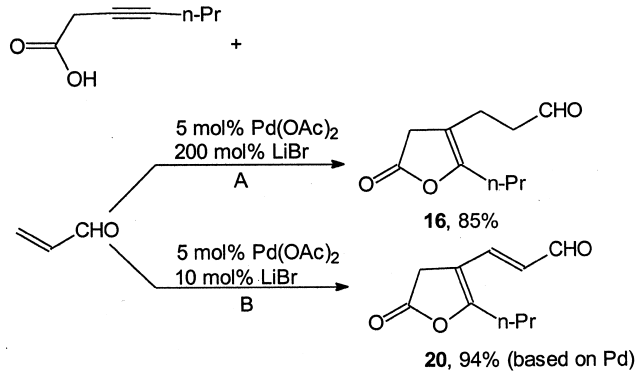
3. Role of halide ions

The key step to form the products and regenerate the Pd(II) catalytic species in the above reactions is the protonolysis of the carbon–palladium bond in **7**, **9**, **14** and **19**. Vinylpalladium species usually react with α,β-unsaturated carbonyls to give vinylation products through β-hydride elimination of the insertion intermediate rather than addition products through protonolysis. There are a few reports concerning the quenching of carbon–palladium bonds by acid hydrolysis [8,9], but the formation of addition products was influenced by many factors [10].

Inhibition of the normal β-hydride elimination pathway was achieved by addition of excess phosphine, but this inhibited the insertion step as well. In the reaction of preparation of (*E,Z*)-dienes, while pure **10** could be obtained in high concentration of LiBr, the reaction afforded the expected dienal **10** together with the trienal **11** in 220 and 80% yield (based on Pd), respectively, with a low concentration of LiBr. We found that the LiBr:Pd ratio has a great impact on the reaction: when the LiBr:Pd ratio was increased from 10:1 to 200:1, the catalyst activity was enhanced dramatically and the reaction yield went up from 550 to 3980% (based on Pd),

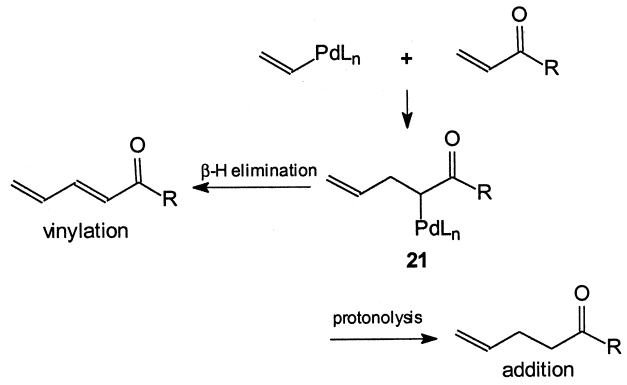
respectively. This can be accounted for by the predominant complexation of halide ions on palladium which favors protonolysis over β-H elimination.

While a high yield of lactone **16** was obtained by the oxypalladation procedure in a high concentration of LiBr, in the presence of less LiBr **20** was produced by β-hydride elimination and obtained in 94% yield (based on Pd) together with precipitated palladium black [6]. This, again, demonstrated the significant role of halide in the present reaction.



In order to explore the mechanism of protonolysis, a stoichiometric reaction of a palladium complex with acrolein in the absence or presence of the halide ion was studied as a model reaction of the role of halide ions. The reaction shows that with no extra anionic ligand or with ClO_4^- or OAc^- only the β-H elimination product is formed, while reactions with Cl^-, Br^- or I^- afford exclusively the protonolysis product. This indicates that the anions play a critical role in determining the reaction outcome.

It is significant that by simply applying metal halides, the reaction pathway of an alkylpalladium intermediate can be cleanly switched from the normal β-H elimination (Heck-type reaction) to heterolytic C–Pd bond cleavage processes, i.e. protonolysis, when the forming carbanion is stabilized by an electron-withdrawing group.



Acknowledgements

We thank the National Natural Sciences Foundation of China and the Chinese Academy of Sciences for financial support.

References

[1] S. Ma, G. Zhu, X. Lu, J. Org. Chem. 58 (1993) 3692.
[2] X. Lu, G. Zhu, Z. Wang, S. Ma, J. Ji, Z. Zhang, Pure Appl. Chem. 69 (1997) 553.
[3] X. Lu, G. Zhu, Z. Wang, Synlett (1998) 115.
[4] Z. Wang, X. Lu, Tetrahedron Lett. 38 (1997) 5213.
[5] Z. Wang, X. Lu, Chem. Commun. (1996) 535.
[6] Z. Wang, X. Lu, J. Org. Chem. 61 (1996) 2254.
[7] Z. Wang, X. Lu, A. Lei, Z. Zhang, J. Org. Chem. 63 (1998) 3806.
[8] W. Cabri, I. Candiani, Acc. Chem. Res. 28 (1995) 2.
[9] S. Cacchi, Pure Appl. Chem. 62 (1990) 713.
[10] A. Arcadi, S. Cacchi, G. Fabrizi, F. Marinelli, P. Pace, Synlett (1996) 568.

PERGAMON

www.elsevier.nl/locate/poly

Polyhedron 19 (2000) 581–586

POLYHEDRON

Synthesis of porphyrins: models of natural hemoproteins and impressive catalysts for asymmetric epoxidation of olefins

E. Rose [a,*], M. Quelquejeu [a], R.P. Pandian [a], A. Lecas-Nawrocka [a], A. Vilar [a], G. Ricart [b], J.P. Collman [c], Z. Wang [c], A. Straumanis [c]

[a] *Laboratoire de Synthèse Organique et Organométallique, UMR 7611, Université P. et M. Curie, BP 181, 4 place Jussieu, 75252 Paris Cedex 5, France*
[b] *Laboratoire de Spectrochimie de Masse, Bâtiment C4, USTL, Cité Scientifique, 59655 Villeneuve d'Asq Cedex, France*
[c] *Department of Chemistry, Stanford University, Stanford, CA 94305, USA*

Received 4 October 1999; accepted 6 December 1999

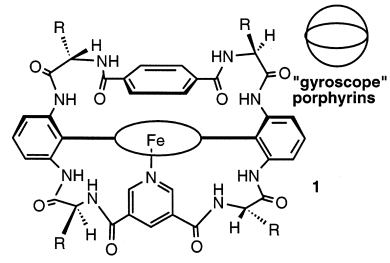
Abstract

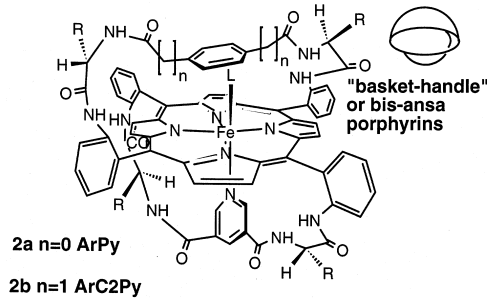
Porphyrins, with two chiral binaphthyl handles, efficiently catalyze the epoxidation of terminal olefins to give epoxides with high enantiomeric excess and turnover number. ©2000 Elsevier Science Ltd All rights reserved.

Keywords: Porphyrins; Hemoprotein models; Chiral catalysts; Epoxidation; Olefins

Porphyrins play an important role in a bewildering array of proteins [1]. Their functions include O_2 storage (myoglobin Mb), O_2 transport (hemoglobin Hb), oxidation of unactivated carbon–hydrogen bonds (cytochrome P_{450}), and oxygen reduction (cytochrome *c* oxidase.) In the case of Mb and Hb, the axial ligand is the nitrogen atom of a histidine residue, whilst in the case of cytochrome P_{450}, the axial ligand is the sulfur atom of a cysteinate. The diversity of functions of these natural hemoproteins is mainly dictated by the number and the nature of the axial ligands, the spin and the oxidation state of the metal center, the nature of the polypeptide chain, and the geometry of the porphyrin ring.

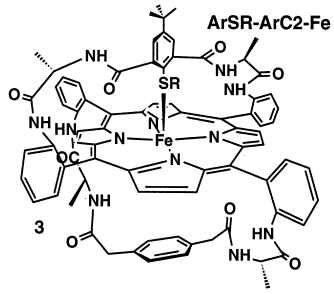
In the presence of O_2, synthetic iron(II) porphyrins, which are not protected on both faces, tend to be oxidized irreversibly and give μ-oxo Fe(III) dimers [2]. To avoid this, several models with protected faces have been developed [3–5]. For instance, we have prepared 'gyroscope' porphyrins **1** [4,6], which have two different handles: one pyridinic handle which is able to coordinate the iron atom of the porphyrin and one terephthalic handle which protects the active site. We have also prepared 'basket handle' porphyrins **2**, with the same handles or with a homologated terephthalic handle. It is worth noting that **2b** discriminates carbon monoxide and oxygen in a similar way to Mb and Hb [7,8]. Indeed, we observed a partition coefficient $M = 105$ (M is the ratio between O_2 and CO affinity), which is similar to the values described in the case of natural hemoproteins. Similarly, we prepared cytochrome P_{450} models **3** [4] and **4** [9] bearing handles or pickets which contain sulfur derivatives.

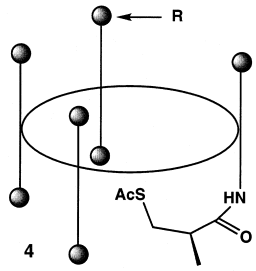




* Corresponding author. Tel.: +33-1-44-27-62-35; fax: +33-1-44-27-55-04; e-mail: rose@ccr.jussieu.fr

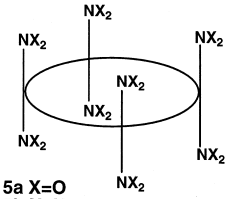
0277-5387/00/$ - see front matter ©2000 Elsevier Science Ltd All rights reserved.
PII S0277-5387(99)00413-1

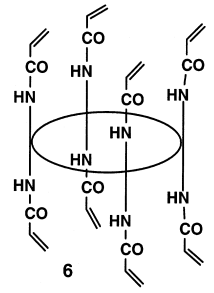


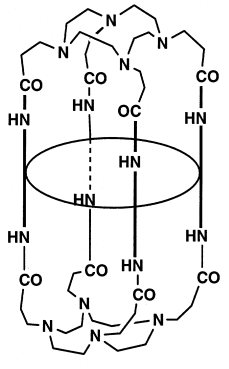


R=-NH-C(O)-C*(OMe)(CF_3)(C_6H_5)

More recently, we prepared an octa nitrophenyl porphyrin **5a** by condensing pyrrole with 2,6-dinitro-4-*tert*-butylbenzaldehyde and correspondingly the octa aminophenyl porphyrin **5b**. Condensation of acryloyl chloride with **5b** gave the octa-Michael acceptor **6** which reacts with cyclen to give a porphyrin that we called a 'barrel' porphyrin **7** [9].



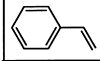
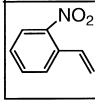




In parallel, we developed a new class of catalysts for asymmetric epoxidation of olefins based on cytochrome P_{450} models. Indeed, it is well known that by using a strong oxidant, it is possible to oxidize the iron atom to a high oxidation state able to epoxidize olefins [10]. We undertook the mixed condensation of pyrrole with two aldehydes, namely pentafluorobenzaldehyde and 2,6-dinitro-4-*tert*-butylbenzaldehyde [11]. The first aldehyde was used to obtain catalysts with robust pentafluoro phenyl groups while the *tert*-butylbenzaldehyde was selected in order to increase the solubility of the catalyst. Thus, we obtained porphyrins **14**, **15** and **17** with two, four and six nitro or amino groups respectively ($R = NO_2$, NH_2), Table 2. Condensation of different chiral acylchlorides with the amino-porphyrins allowed us to prepare porphyrins **15** and **17** (R = –NH–C(O)–C*(CF_3)-(C_6H_5)(OMe)) [11]. Unfortunately, epoxidations conducted with porphyrins bearing Mosher pickets only gave low enantiomeric excess, Table 2.

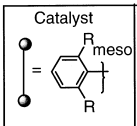
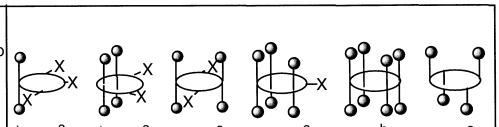
Other chiral porphyrins have been obtained by condensing a chiral binap diacid chloride with aminophenyl porphyrin. The iron-porphyrin **8** called a 'seat' porphyrin, was used to epoxidize different terminal olefins in the presence of iodosylbenzene. We respectively obtained 59% and 85% enantiomeric excesses for styrene and pentafluorostyrene [18].

Table 1
Type I system: single-faced protected ansa porphyrins. Summary of percentages of enantiomeric excess obtained with catalysts **1**–**13** and styrene and *ortho*-nitrostyrene

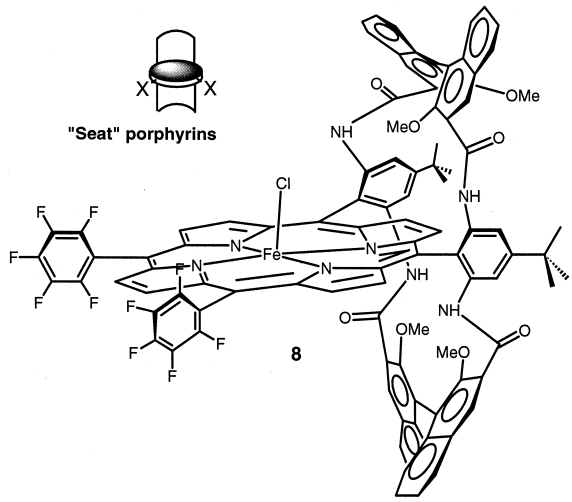
Catalyst	 **10**[a]	 **11**[b]	 **12**[c]	 **13**[d]
Substrate 	50	39	69	69
NO_2 	-	37	74	74

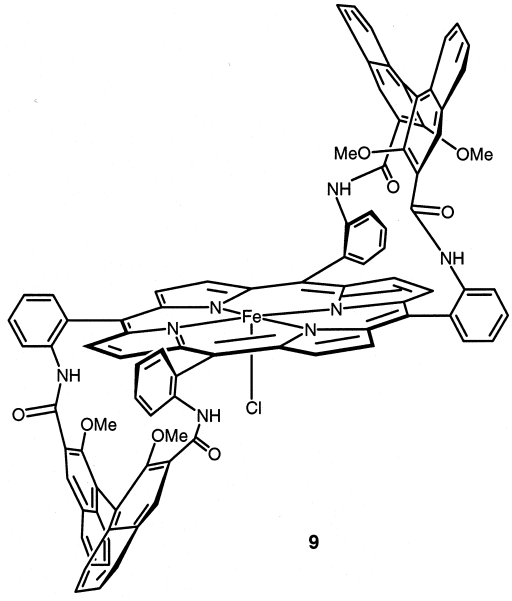
[a] Refs. [21,22].
[b] Refs. [23].
[c] Refs. [24,25].
[d] Ref. [26].

Table 2
Type II system: double-faced protected picket porphyrins. Summary of percentages of enantiomeric excess obtained with catalysts **14**–**19** and styrene

Catalyst 	 **14**[a] **15**[a] **16**[a] **17**[a] **18**[b] **19**[c] R=-NH-C(O)-C*(OMe)(CF_3)(C_6H_5)
Substrate 	6 3 d 1 d,e 20-48

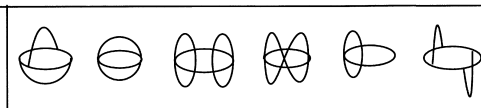
[a] Ref. [11].
[b] Refs. [11–14] (see also Refs. [15–17]).
[c] Refs. [27–33].
[d] In preparation.
[e] Too bulky with R=–NH–C(O)–C*(OMe)(CF_3)(C_6H_5).





These results can be compared with those obtained using a similar catalyst **9** which is prepared by condensing the same binap diacylchloride with the $\alpha^2\beta^2$ atropoisomer of tetrakis-2-aminophenylporphyrin. This atropoisomer is obtained in 92% yield by heating the statistical mixture ($\alpha\beta\alpha\beta/\alpha\alpha\alpha\alpha/\alpha^2\beta^2/\alpha^3\beta = 1/1/2/4$) of tetrakis-2-nitrophenyl Zn porphyrin atropoisomers in naphthalene [19]. Interestingly, with the bis-binaphthylporphyrin **9**, we obtained 83% and 88% enantiomeric excess for the epoxidation of styrene and pentafluorostyrene [20]. The best enantiomeric excess yet ever observed with our porphyrin catalyst was obtained in the case of *tert*-butylethylene with a 92% enantiomeric excess. Surprisingly, we observed an increase of the enantiomeric excess during the initial period of the styrene epoxidation using **9**. Indeed, enantiomeric excess values raised from 65% at 10 turnovers to 83% at 200 turnovers. From 100 to 2000 turnovers, the reaction maintains 83% enantiomeric excess. The complex catalyzes the epoxidation at a rate of 2400 turnovers per hour if iodosylbenzene is added portionwise to the reaction mixture. Indeed, after 5000 turnovers the enantiomeric excess is still about 75%. We believe that oxidative demethylation of the binap strap occurs during the initial reaction corresponding to the transformation to a quinone-like structure. Probably, the quinone-type catalyst is less hindered than the original methoxy catalyst, allowing easier access of the olefin to the active site with a good facial discrimination.

Table 3
Type III system: double-faced protected ansa porphyrins. Summary of percentages of enantiomeric excess obtained with catalysts **20**–**23**, **8** and **9** and styrene and *ortho*-nitrostyrene

Catalyst						
	20[a]	**21**[b]	**22**[c]	**23**[d]	**8**[e]	**9**[f]
Substrate 	48	-	54	28	59	83
	-	-	89	54	70	88

[a] Refs. [7,8,34–36].
[b] Refs. [6,8].
[c] Refs. [37–40].
[d] Refs. [37–41].
[e] This work.
[f] Refs. [18,20].

At this stage, we can compare the properties of the different catalysts described in the literature (Tables 1–3). A classification of the catalysts into three structure-types can be proposed:

type I systems correspond to single-faced protected ansa porphyrins,
type II systems are bis-faced picket porphyrins,
type III systems are bis-faced protected ansa porphyrins.

In the case of type I porphyrins, enantiomeric excess can reach 58% with catalyst **10** [21,22] for the epoxidation of indene with PhIO in the presence of different imidazoles as blocking ligands (Fig. 1). When the handle of the catalyst **12** is too far from the metal center, a low 13% enantiomeric excess is obtained for the epoxidation of styrene [24,25]. Using Mn-'threitol' porphyrins with a small strap **13c**, the enantiomeric excess can reach 74% with *ortho*-nitrostyrene. However, the numbers of turnovers remain low when the unhindered face of the porphyrin is blocked with a bulky imidazole ligand, (Table 1, Fig. 1) [23,26].

In the case of type II catalysts, the Mn catalyst **18b** shows 76% enantiomeric excess for the epoxidation of *cis*-β-methylstyrene [13]. Catalysts **18c**, **18d** give 70% enantiomeric excess of the R epoxide of styrene [14]. In the particular cases of catalysts **19a**–**19c**, low turnovers and enantiomeric excess are obtained. With the catalyst **19d**, the turnover is good but not the enantiomeric excess [27]. An improvement has been described by Marchon and co-workers using Mn

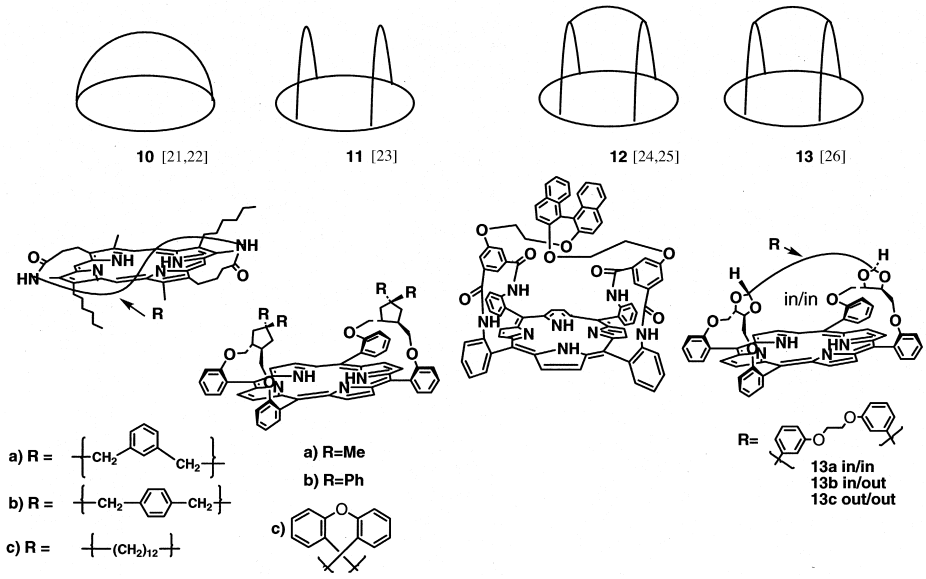


Fig. 1. Type I system: single-faced protected ansa porphyrins.

chiroporphyrins **19f** [31–33]. Indeed, they obtained 86% enantiomeric excess with the bulky porphyrin **19f** for the epoxidation of 1,2-dihydronaphthalene (Fig. 2, Table 2) [31].

With type III catalysts, the enantiomeric excess can reach 72% for the epoxidation of *cis*-β-methylstyrene with the bis-ansa derivative **20c**, but the turnover barely reaches 300 [36] and is only 2 in the case of catalyst **20b** [34]. The enantiomeric excess can be improved using staggered and eclipsed catalysts **22** and **23** (twin-coronet porphyrins) [37–40]; an enantiomeric excess of up to 54% in the case of styrene (Fig. 3, Table 3) [37–41] can be obtained but yields for the preparation of the catalysts are low. However, the enantiomeric excess can reach 96% for the epoxidation of the electron-deficient 3,5-dinitrostyrene [37–40].

In conclusion, we have prepared chiral bis-handle porphyrins that are good models of Mb in terms of discriminating between CO and O_2. We have also prepared *C*2-symmetric chiral porphyrins bearing binaphthyl handles. These are efficient catalysts for olefin epoxidation giving high enantiomeric excess and turnover numbers. In particular, catalyst **9** gives the highest enantiomeric excess ever obtained for the

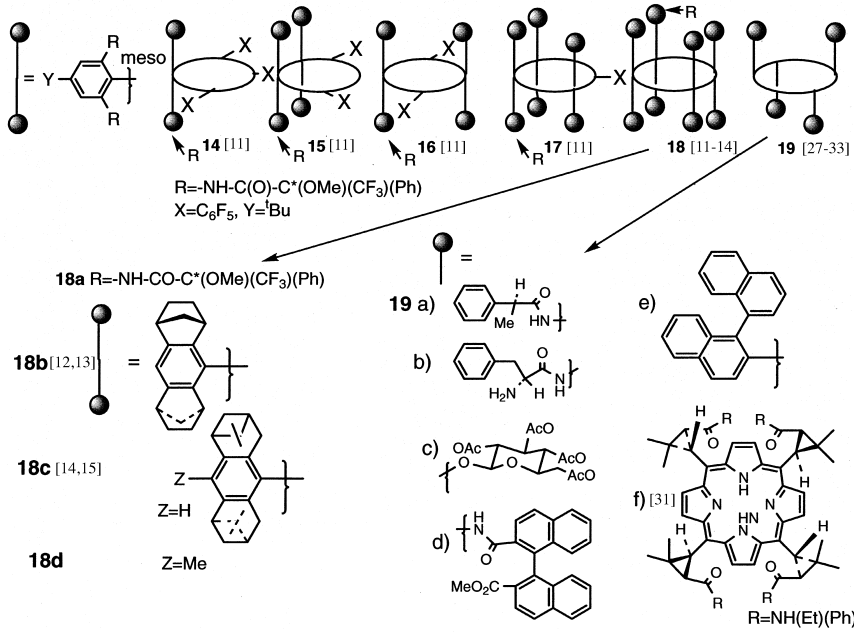


Fig. 2. Type II system: double-faced protected picket porphyrins.

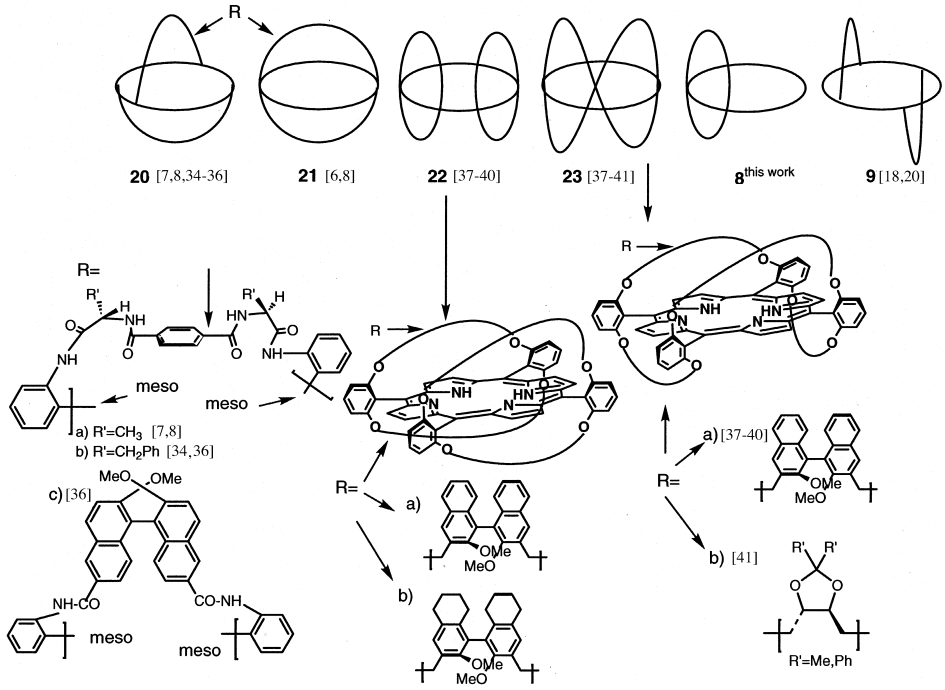


Fig. 3. Type III system: double-faced protected ansa porphyrins.

epoxidation of aliphatic olefins, 92% enantiomeric excess for the epoxidation of *tert*-butylethylene, and the turnovers are unexpectedly high!

Acknowledgements

We thank NATO (Grant No. 960485), the NSF (Grant No. CHE-9612725) and CNRS for financial support (RPP).

References

[1] J.A. Shelnutt, X.-Z. Song, J.-G. Ma, S.-L. Jia, W. Jentzen, C. Medforth, J. Chem. Soc. Rev. 27 (1998) 31.
[2] J.P. Collman, R.R. Gagne, C.A. Reed, T.R. Halbert, G. Lang, W.T. Robinson, J. Am. Chem. Soc. 97 (1975) 1427.
[3] M. Momenteau, Models of hemoprotein active sites. In: A.D. Hamilton (Ed.), Supramolecular Control of Structure and Reactivity, Wiley, New York, 1996, pp. 155–223.
[4] E. Rose, A. Lecas, M. Quelquejeu, A. Kossanyi, B. Boitrel, Coord. Chem. Rev. 178–180 (1998) 1407.
[5] C. Kalodimos, I. Gerothanassis, E. Rose, G.E. Hawkes, R. Pierattelli, J. Am. Chem. Soc. 121 (1999) 2903.
[6] B. Boitrel, A. Lecas, Z. Renko, E. Rose, J. Chem. Soc., Chem. Commun. (1985) 1820.
[7] E. Rose, B. Boitrel, M. Quelquejeu, A. Kossanyi, Tetrahedron Lett. 34 (1993) 7267.
[8] B. Boitrel, A. Lecas, Z. Renko, E. Rose, New J. Chem. 13 (1989) 73.
[9] E. Rose, A. Kossanyi, M. Quelquejeu, M. Soleilhavoup, F. Duwavran, N. Bernard, A. Lecas, J. Am. Chem. Soc. 118 (1996) 1567.
[10] J.T. Groves, Y. Watanabe, J. Am. Chem. Soc. 108 (1986) 507.
[11] E. Rose, M. Soleilhavoup, L. Christ-Tommasino, G. Moreau, J.P. Collman, M. Quelquejeu, A. Straumanis, J. Org. Chem. 63 (1998) 2042.
[12] R.L. Halterman, S. Jan, J. Org. Chem. 56 (1991) 5253.
[13] R.L. Halterman, S.T. Jan, H.L. Nimmons, D.J. Standlee, M.A. Khan, Tetrahedron 53 (1997) 11257.
[14] J.F. Barry, L. Campbell, D.W. Smith, T. Kodadek, Tetrahedron 53 (1997) 7753.
[15] R. Zhang, W-Y. Yu, T-S. Lai, C-M. Che, Chem. Commun. (1999) 1791.
[16] L.A. Campbell, T. Kodadek, J. Mol. Catal. A. 113 (1996) 293.
[17] K.S. Suslick, S. Van Deusen-Jeffries, in: J.L. Atwood, J.E.D. Davies, D.D. MacNicol, F. Vögtle, J.M. Lehn (Eds.), Comprehensive Supramolecular Chemistry, vol. 5, Elsevier, Oxford, 1996, p. 141.
[18] E. Rose, manuscript in preparation.
[19] E. Rose, A. Cardon-Pilotaz, M. Quelquejeu, N. Bernard, A. Kossanyi, B. Desmazières, J. Org. Chem. 60 (1995) 3919.
[20] J.P. Collman, Z. Wang, A. Straumanis, M. Quelquejeu, E. Rose, J. Am. Chem. Soc. 121 (1999) 460.
[21] K. Konoshi, K. Oda, K. Nishida, T. Aida, S. Inoue, J. Am. Chem. Soc. 114 (1992) 1313.
[22] S. Inoue, T. Aida, K. Konoshi, J. Mol. Catal. 74 (1992) 121.
[23] J.P. Collman, V.J. Lee, C.J. Kellen-Yuen, X. Zhang, J.A. Ibers, J.I. Brauman, J. Am. Chem. Soc. 117 (1995) 692.
[24] J.P. Collman, J.I. Brauman, J.P. Fitzgerald, P.D. Hampton, Y. Naruta, J.W. Sparapany, J.A. Ibers, J. Am. Chem. Soc. 110 (1988) 3477.
[25] J.P. Collman, X. Zhang, R.H. Hembre, J.I. Brauman, J. Am. Chem. Soc. 112 (1990) 5356.
[26] J.P. Collman, V.J. Lee, X. Zhang, J.A. Ibers, J.I. Brauman, J. Am. Chem. Soc. 115 (1993) 3834.
[27] J.T. Groves, R.S. Myers, J. Am. Chem. Soc. 105 (1983) 5791.
[28] S. O'Malley, T. Kodadek, J. Am. Chem. Soc. 111 (1989) 9116.
[29] S. Licoccia, M. Paci, P. Tagliatesta, R. Paolesse, S. Antonaroli, T. Boschi, Magn. Res. Chem. 29 (1991) 1084.
[30] P. Maillard, J.L. Guerquin-Kern, M. Momenteau, Tetrahedron Lett. 32 (1991) 4901.
[31] C. Pérrollier, J. Pécaut, R. Ramasseul, J.C. Marchon, Inorg. Chem. 38 (1999) 3758.
[32] C. Pérrollier, J. Pécaut, R. Ramasseul, R. Bau, J.C. Marchon, Chem. Commun. (1999) 1597.

[33] M. Veyrat, O. Maury, F. Faverjon, D.E. Over, R. Ramasseul, J.C. Marchon, I. Turowska-Tyrk, W.R. Scheidt, Angew. Chem., Int. Ed. Engl. 33 (1994) 220.
[34] D. Mansuy, P. Battioni, J.P. Renaud, P. Guerin, J. Chem. Soc., Chem. Commun. (1985) 155.
[35] J.P. Collman, X. Zhang, V.J. Lee, J.I. Brauman, J. Chem. Soc., Chem. Commun. (1992) 1647.
[36] J.T. Groves, P. Viski, J. Org. Chem. 55 (1990) 3628.
[37] Y. Naruta, F. Tani, N. Ishihara, K. Maruyama, J. Am. Chem. Soc. 113 (1991) 6865.
[38] Y. Naruta, F. Tani, K. Maruyama, Chem. Lett. (1989) 1269.
[39] Y. Naruta, N. Ishihara, F. Tani, K. Maruyama, Bull. Chem. Soc. Jpn. 66 (1993) 158.
[40] Y. Naruta, N. Ishihara, F. Tani, K. Maruyama, Chem. Lett. (1991) 1933.
[41] Z. Gross, S. Ini, J. Org. Chem. 62 (1997) 5514.

PERGAMON

www.elsevier.nl/locate/poly

Polyhedron 19 (2000) 587–589

POLYHEDRON

Asymmetric synthesis of trisubstituted pyrrolidines via boronic esters

Donald S. Matteson *, Rajendra P. Singh, Jianhui Lu, Jingjing Yang, Philip S. Pharazyn

Department of Chemistry, Box 644630, Washington State University, Pullman, WA 99164-4630 USA

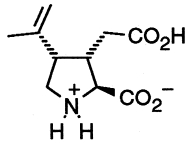
Received 4 October 1999; accepted 23 November 1999

Abstract

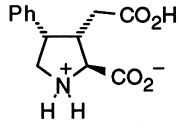
Attempts to synthesize kainic acid and analogous kainoids via asymmetric boronic ester chemistry are described. Problems involving functional group and steric interactions have been encountered, and most have been solved. The way to completion now appears clear.
©2000 Elsevier Science Ltd All rights reserved.

Keywords: Kainoids; Boronic esters; Asymmetric synthesis; Pyrrolidine

Kainic acid (**1**) and related compounds such as the phenyl analog **2** are of interest as agonists at glutamate receptor sites in the brain [1].



1



2

The relative stereochemistry of these trisubstituted pyrrolidines is the same as that produced by successive chain extensions of boronic esters with (dichloromethyl)lithium, but the polar functional groups involved impose new problems for this method of asymmetric synthesis [2].

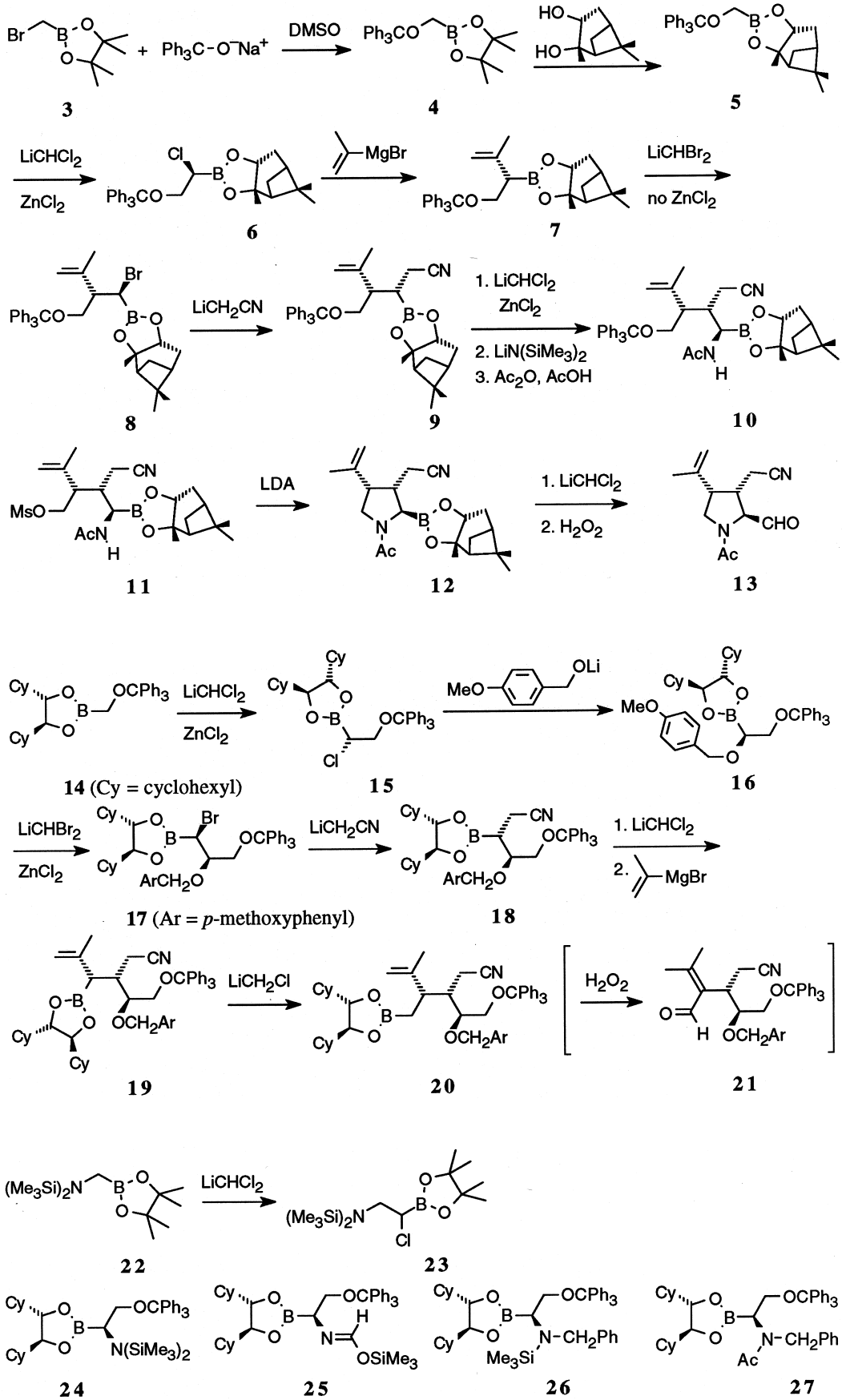
Several attempts to complete syntheses of **1** or **2** have fallen short. Our first approach began with the unusual reaction of sodium trityl oxide with bromomethyl boronic ester **3** to form trityloxy boronic ester **4**, which was converted to the pinanediol ester **5** prior to asymmetric reaction with (dichloromethyl)lithium to generate **6** [3]. Isopropenylation of **6** to **7** was routine [4]. Chain extension of **7**, done without the usual zinc chloride promoter in order to avoid allylic isomerization, yielded crystalline bromo intermediate **8** plus ~10% diastereomer. Conversion of **8** to cyano compound **9**, chain extension to acetamido boronic ester **10**, and further conversions to **11** and **12** followed. This sequence eventually foundered because the reaction of the very polar amido boronic ester **12** with (dichloromethyl)lithium proved inefficient, and insufficient amounts of the pyrrolidine aldehyde **13** were obtained to allow further progress toward **1** [4].

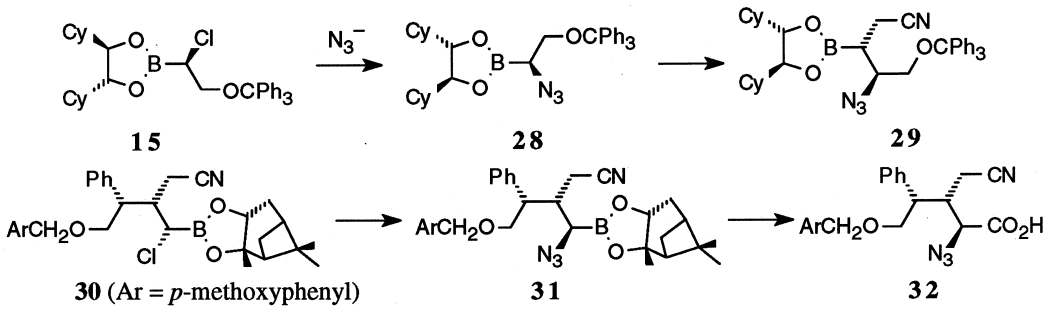
We also tried approaching the molecule from the opposite direction starting from **14**, which utilizes (*R*,*R*)-1,2-dicyclohexylethane-1,2-diol as the chiral director [5]. Possible precursor **20**, which contains all of the stereocenters corresponding to kainic acid (**1**) but only oxygen and carbon linked substituents, was easily synthesized via intermediates **15**–**19**. A single attempt at deboronation of **20** to the alcohol resulted in an oxidative rearrangement to α,β-unsaturated aldehyde **21**, but replacement of the boron in a useful manner could no doubt be achieved with further study. Completion of this route would require cleavage of the trityl ether of **20** and oxidation of the hydroxymethyl group to carboxyl, as well as replacement of the *p*-methoxybenzyl protected hydroxyl group of **20** by an amine, accompanied by some means of double inversion to achieve the correct diastereomer.

Because of the inherent number of steps required for any possible route from **20** to kainic acid (**1**), we have attempted to revise this synthesis to incorporate the carbon–nitrogen bond from the start. Initially encouraged by the successful chain extension of [bis(trimethylsilyl)aminomethyl]-boronic ester **22** to α-chloro boronic ester **23**, we made **24**–**27** from **15** and tested their reactions with (dichloromethyl)lithium [6]. NMR evidence indicated that yields of up to 30–50% of chain extended α-chloro boronic esters were obtained from **24** and **25**, but efficient conversions were never achieved. Intermediates **26** and **27** did not yield any detectable chain extension products, although based on proton NMR spectra it appeared that **27** did form the expected borate complex with (dichloromethyl)lithium.

* Corresponding author. Tel.: +1-509-335-3365; fax: +1-509-335-8867; e-mail: dmatteson@wsu.edu

0277-5387/00/$ - see front matter ©2000 Elsevier Science Ltd All rights reserved.
PII S0277-5387(99)00414-3


DMSO
LiCHCl2
ZnCl2
MgBr
LiCHBr2
no ZnCl2
LiCH2CN
1. LiCHCl2
ZnCl2
2. LiN(SiMe3)2
3. Ac2O, AcOH
LDA
1. LiCHCl2
2. H2O2
LiCH2Cl
H2O2
14 (Cy = cyclohexyl)
17 (Ar = p-methoxyphenyl)



In work in progress, we have investigated the use of azido boronic esters as intermediates for the synthesis of **1** or **2** [7]. The first problem was to find satisfactory conditions to convert α-chloro boronic esters such as **15** to the corresponding azides. These details will be published later. Azido boronic ester **28** was prepared and converted to **29** in the usual manner. Attempts to carry out chain extension of **29** with (dichloromethyl)lithium or (dibromomethyl)lithium yielded erratic results.

Our most nearly completed synthesis, in progress as this is written, closely resembles the route from **3** to **10**, but with *p*-methoxybenzyl in place of trityl, phenyl in place of isopropenyl, and conversion of chloro boronic ester **30** to the azido derivative **31**. Chain extension of **31** to azido acid **32** was carried out by the same method as that used in our published amino acid synthesis [8]. Further conventional transformations of **32** have brought us to within one or two steps of our objective.

Acknowledgements

We thank the National Science Foundation, grants CHE9303074 and CHE9613857, and the National Institutes of Health, grant GM50298, for support.

References

[1] A.F. Parsons, Tetrahedron 52 (1996) 4149.
[2] D.S. Matteson, Tetrahedron 54 (1998) 10555.
[3] H. Ho, R. Soundararajan, J. Lu, D.S. Matteson, Z. Wang, X. Chen, M. Wei, R.D. Willett, Organometallics 14 (1995) 2855.
[4] D.S. Matteson, J. Lu, Tetrahedron: Asymmetry 9 (1998) 2423.
[5] D.S. Matteson, J.-J. Yang, Tetrahedron: Asymmetry 8 (1997) 3855.
[6] D.S. Matteson, R.P. Singh, C.H. Sutton, J.D. Verheyden, J. Lu, Heteroatom. Chem. 8 (1997) 487.
[7] D.S. Matteson, R.P. Singh, P.S. Pharazyn, unpublished results, 1998–1999.
[8] D.S. Matteson, E.C. Beedle, Tetrahedron Lett. 28 (1987) 4499.

PERGAMON

www.elsevier.nl/locate/poly

Polyhedron 19 (2000) 591–592

POLYHEDRON

A general method for the synthesis of *E* and/or *Z* oligoisoprenoids based on Pd-catalyzed homoallyl-alkenyl and homopropargyl-alkenyl cross coupling and Zr-catalyzed carboalumination

Ei-ichi Negishi *, Show-Yee Liou, Caiding Xu, Shouquan Huo

Department of Chemistry, Purdue University, West Lafayette, IN 47907, USA

Received 4 October 1999; accepted 15 November 1999

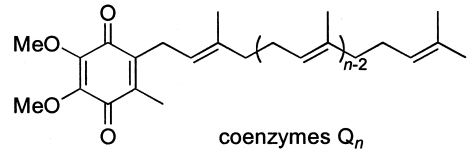
Abstract

A truly general, versatile, and highly regioselective and stereoselective methodology for the synthesis of terpenoids containing 1,5-diene units of *E* and/or *Z* geometry critically involves (a) Pd-catalyzed homoallyl-alkenyl and homopropargyl-alkenyl coupling and (b) Zr-catalyzed carboalumination of alkynes. In each introduction of an *E* or *Z* trisubstituted C_5 alkene unit, the yield is excellent, and the regioselectivity and stereoselectivity level is >98%. As such, this appears to represent the first general synthetic method accommodating *Z* alkene units in >95% regioselectivity and stereoselectivity. Its application to some representative terpenoids of both natural and unnatural geometries is discussed. ©2000 Elsevier Science Ltd All rights reserved.

Keywords: 1,5-diene; Cross coupling; Terpenoids; Carboalumination; Palladium

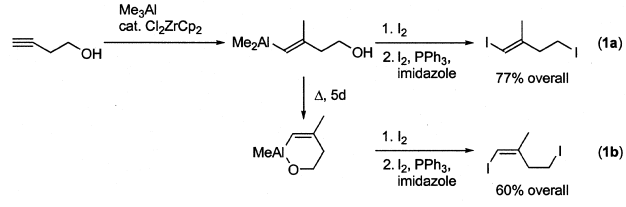
Herein reported is an unprecedentedly general, efficient, and selective methodology for the synthesis of geometrically defined 1,5-dienes and 1,5-oligoenes, especially of terpenoid origins. This methodology is based on (i) carbometallation [1,2] of hetero-substituted alkynes [3] for the preparation of **1a**, (ii) chelation-promoted synthesis of **1b** [4], (iii) exceedingly clean, high-yielding, and selective lithiation of primary alkyl iodides [5] applicable to lithiation of homoallyl iodides, and (iv) Pd-catalyzed homoallyl-alkenyl and homopropargyl-alkenyl cross coupling involving homoallylzinc and homopropargylzinc derivatives [6–8] (Schemes 1–3).

Elongation of 1,5-diene containing isoprenoids by an (*E*)- or (*Z*)-C_5 unit as shown in Schemes 2 and 3 can be achieved in one pot in ≥98% stereoselectivity, and these processes can be used both iteratively and convergently. In these manners, various natural and/or unnatural isomers of farnesol, geranylgeraniol, and coenzymes Q_n have been synthesized. Capping the tail end of isoprenoids in the form of allylic alcohols can be achieved by Zr-catalyzed carboalumination-hydroxymethylation for the *E* isomer [9] and by Sato's Ti-catalyzed hydromagnesiation-methylation of propargylic alcohols for the *Z* isomer [10].

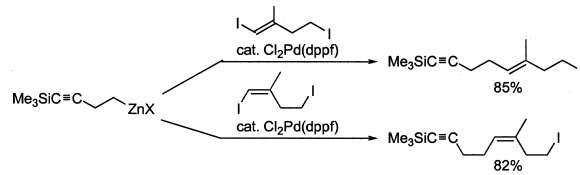


coenzymes Q_n

The details of these transformations are discussed orally. To the best of our knowledge, a recently reported multistep homologation of isoprenoids requiring several steps in up to 90% stereoselectivity [11] represented the state of the art for the synthesis of isoprenoids containing (*Z*)-trisubstituted



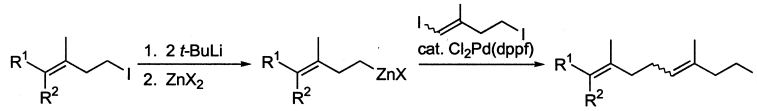
Scheme 1.



Scheme 2.

* Corresponding author. Tel.: +1-765-494-5301; fax: +1-765-494-0239; e-mail: negishi@purdue.edu

0277-5387/00/$ - see front matter ©2000 Elsevier Science Ltd All rights reserved.
PII S0277-5387(99)00415-5



Scheme 3.

alkene units in the middle of an isoprenoid chain. In contrast, the present methodology permits one-pot homologation in $\geq 98\%$ stereoselectivity, either *E* and/or *Z*, in both iterative and convergent manners.

Acknowledgements

We thank NSF, NIH, and Purdue University for support of this research.

References

[1] D.E. Van Horn, E. Negishi, J. Am. Chem. Soc. 100 (1978) 2252.
[2] E. Negishi, D.E. Van Horn, T. Yoshida, J. Am. Chem. Soc. 107 (1985) 6639.
[3] C.L. Rand, D.E. Van Horn, M.W. Moore, E. Negishi, J. Org. Chem. 46 (1981) 4093.
[4] S. Ma, E. Negishi, J. Org. Chem. 62 (1997) 784.
[5] E. Negishi, D.R. Swanson, C.J. Rousset, J. Org. Chem. 55 (1990) 5406.
[6] E. Negishi, L.F. Valente, M. Kobayashi, J. Am. Chem. Soc. 102 (1980) 3298.
[7] M. Kobayashi, E. Negishi, J. Org. Chem. 45 (1980) 5223.
[8] For a review, see E. Negishi, F. Liu, in: P.J. Stang, F. Diederich (Eds.), Cross Coupling Reactions, Wiley-VCH, Weinheim, 1998, p. 1.
[9] N. Okukado, E. Negishi, Tetrahedron Lett. (1978) 2357.
[10] F. Sato, H. Ishikawa, H. Watanabe, T. Miyake, M. Sato, J. Chem. Soc., Chem. Commun. (1981) 718.
[11] N.Ya. Grigorieva, O.A. Pinsker, A.M. Moiseenkov, Mendeleev Commun. (1994) 129.

PERGAMON

www.elsevier.nl/locate/poly

Polyhedron 19 (2000) 593–596

POLYHEDRON

Synthesis of carbocycles and heterocycles by the titanocene(II)-promoted reactions of thioacetals

Takeshi Takeda *, Md. Abdur Rahim, Mayumi Takamori, Kenjirou Yanai, Tooru Fujiwara

Department of Applied Chemistry, Tokyo University of Agriculture and Technology, Koganei, Tokyo 184-8588, Japan

Received 4 October 1999; accepted 14 December 1999

Abstract

The preparation of carbocyclic and heterocyclic compounds by the low-valent titanium species-promoted intramolecular reactions of thioacetals was studied. The cyclization of thioacetals having an olefin moiety proceeded with the loss of terminal olefin carbon to produce the corresponding five-, six-, and seven-membered cycloalkenes when they were treated with the low-valent titanium species $Cp_2Ti[P(OEt)_3]_2$. This method has been successfully applied to the syntheses of cyclic unsaturated amines and ethers. When *S*-[3,3-bis(phenylthio)propyl] thioalkanoates were treated with the low-valent titanium species, the intramolecular carbonyl olefination proceeded to produce 5-substituted 2,3-dihydrothiophenes. ©2000 Elsevier Science Ltd All rights reserved.

Keywords: Thioacetal; Titanocene(II); Ring-closing metathesis; Intramolecular carbonyl olefination; Cycloalkenes; Heterocyclic compounds

1. Introduction

Recently we found the first practical method for the preparation of organotitanium species which serve as carbene complexes by the desulfurization of thioacetals with the low-valent titanium complex $Cp_2Ti[P(OEt)_3]_2$ (**1**). Since thioacetals are easily prepared from carbonyl compounds or through alkylation, this method enables us to utilize various types of titanium-carbene complexes in organic synthesis. We found that these organotitanium compounds react with organic molecules having a carbon–oxygen [1–5] or carbon–carbon multiple bond [6–8]. It was also found that the organotitanium species formed by the reaction of *gem*-dichlorides with **1** are useful for the Wittig-like olefination of carbonyl compounds [9,10].

The construction of cyclic molecules is of fundamental importance in organic synthesis, and many carbon–carbon bond forming reactions have been employed for this purpose. Because a variety of functionalized thioacetals are easily available, we have studied the preparation of carbocyclic and heterocyclic compounds by titanocene(II)-promoted intramolecular reactions.

* Corresponding author. Tel. and fax: +81-42-388-7034; e-mail: takeda-t@cc.tuat.ac.jp

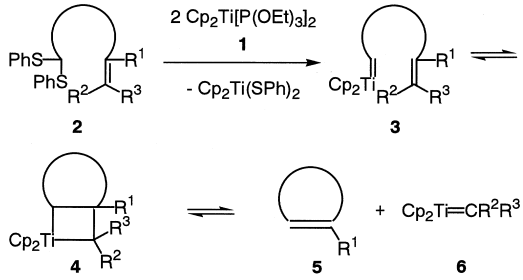
2. Ring-closing metathesis of thioacetals having a carbon–carbon double bond

The transition metal catalyzed ring-closing metathesis (RCM) of dienes is a useful method for the preparation of cyclic compounds [11,12]. Ruthenium, molybdenum, and tungsten carbene complexes have been employed as catalysts for such transformations. Nicolaou et al. recently reported the preparation of cyclic ethers from unsaturated esters by the successive carbonyl methylenation and RCM using the Tebbe or Petasis reagent. An alkylidenetitanocene is suggested to serve as an intermediate in this reaction [13].

Since the titanocene(II)-promoted reaction of thioacetals with trialkylallylsilanes afforded the metathesis products, γ-substituted allylsilanes [8], we expected that thioacetals could be employed as starting materials for RCM. We then studied the preparation of cycloalkenes **5** from thioacetals **2** having a carbon–carbon double bond via the formation of titanium-carbene complexes **3** as shown in Scheme 1.

First the thioacetal **2b** was treated with the low valent titanium species prepared from Cp_2TiCl_2 (4 equiv.), magnesium turnings (4.4 equiv.), and $P(OEt)_3$ (8 equiv.) at room temperature, and then the reaction was quenched with D_2O (Scheme 2). The formation of the dideuterio compound **7** suggests that this reaction proceeds via the titanacyclobutane intermediate **4**. The RCM product **5a** was obtained in

0277-5387/00/$ - see front matter ©2000 Elsevier Science Ltd All rights reserved.
PII S0277-5387(99)00388-5

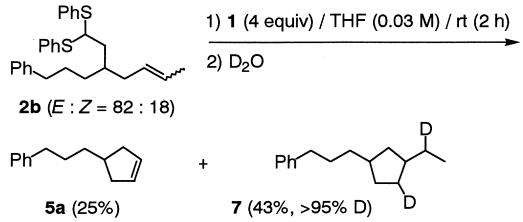


Scheme 1.

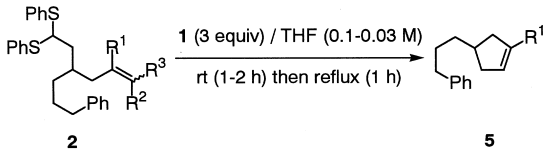
good yield when the reaction mixture was refluxed after the treatment of **2b** with **1** at room temperature. The reaction of thioacetal **2a** having a terminal olefin also produced the cyclopentene **5a** in comparable yield. In contrast to these results, only a small amount of cyclopentene **5a** was produced from the thioacetal **2c** having two methyl groups at a terminal sp2 carbon atom. In the case that a trisubstituted olefin was formed, metathesis proceeded smoothly to produce the methyl group substituted cyclopentene **5b** in high yield (Scheme 3, Table 1). These substituent effects are explained well by the extent of the formation of the titanacyclobutane intermediate **4** and the extent of the retrograde reaction between the RCM product **5** and the alkylidenetitanocene **6**.

Under similar conditions, the reactions of various thioacetals **2** were performed, and the six- and seven-membered cycloalkenes were obtained in good yields [14]. Some representative examples are provided in Scheme 4.

This RCM can be employed for the synthesis of various heterocyclic compounds (Scheme 5). The cyclic ethers **9** were produced by the simple treatment of the acyclic ethers **8** having a thioacetal and an olefin moiety. Using the unsaturated amines **10** as starting materials, the cyclic amines **11** were obtained [15]. Monocyclic seven- and eight-membered amines, the formation of which would be a conformationally less favorable process than the formation of a cyclic amine fused with a benzene ring, are produced in good yields by this reaction. In the case of the preparation of eight-membered rings, the slow addition of thioacetals to a THF solution of **1** over 3 h increased the yields of RCM products.



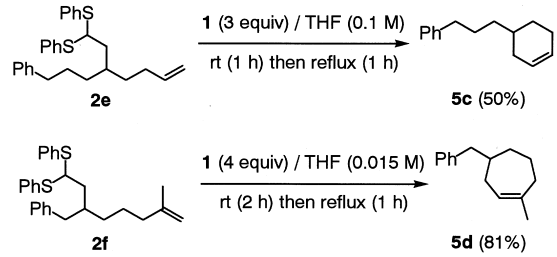
Scheme 2.



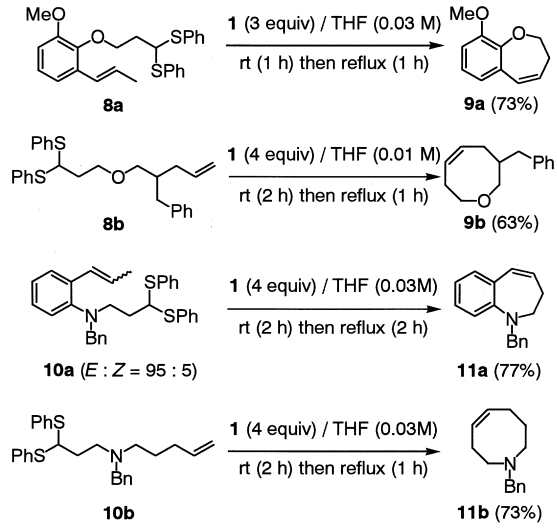
Scheme 3.

Table 1
Preparation of cyclopentenes **5**

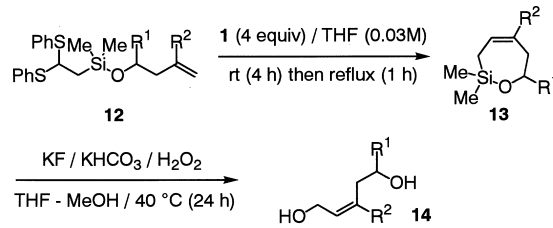
Thioacetal **2**	**5**	Yield (%)
2a: $R^1=H$, $R^2=H$, $R^3=H$	**5a**	71
2b: $R^1=H$, $R^2=H$, $R^3=Me$	**5a**	67
2c: $R^1=H$, $R^2=Me$, $R^3=Me$	**5a**	8
2d: $R^1=Me$, $R^2=H$, $R^3=H$	**5b**	87



Scheme 4.



Scheme 5.



Scheme 6.

Table 2
Preparation of *Z*-olefinic diols **14**

Silyl ether **12**	Overall yield **12**→**14** (%)
12a: $R^1=Ph$, $R^2=H$	68
12b: $R^1=Ph(CH_2)_2$, $R^2=H$	54
12c: $R^1=Ph(CH_2)_2$, $R^2=Me$	61
12d: $R^1=Me(CH_2)_8$, $R^2=H$	51

An interesting application of RCM using thioacetal is the preparation of unsaturated diols **14**. When the silyl ethers **12** were treated with the low-valent titanium species **1** at room temperature and then at the reflux temperature, the cyclic allylsilanes **13** were obtained. The oxidation of **13** under the conditions developed by Tamao et al. [16] produced the *Z*-diols **14** in good overall yields (Scheme 6, Table 2) [17].

The stereoselective preparation of *Z*-olefinic dihydroxy compounds by the transition metal-alkylidene catalyzed RCM of silicon-connected dienes followed by oxidative ring cleavage was reported by Chang and Grubbs [18]. Similar preparations of silicon-containing oxygen heterocycles were also reported [19,20]. It should be noted that the present method provides an alternative synthetic route to the olefinic diols.

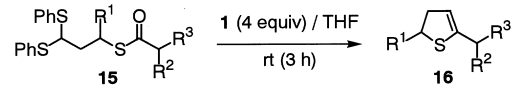
3. Intramolecular carbonyl olefination

Another useful application of titanocene(II)-promoted reaction of thioacetals to the synthesis of heterocyclic compounds is the intramolecular carbonyl olefination of carboxylic acid derivatives. This idea was substantiated when *S*-[3,3-bis(phenylthio)propyl] thioalkanoates **15** were treated with 4 equiv. of the low-valent titanium species **1** in THF at room temperature giving the intramolecular olefination products, 5-substituted 2,3-dihydrothiophenes **16** in good yields (Scheme 7, Table 3) [21].

2,3-Dihydrothiophene is one of the most fundamental sulfur-containing heterocycles and several methods have been developed for its preparation [22–28]. Paquette et al. reported the synthesis of 5-hydroxymethyl-2,3-dihydrothiophenes by the reaction of 5-lithio-2,3-dihydrothiophene with aldehydes [29], and the improved procedure using 5-tributylstannyl-2,3-dihydrothiophene was reported by O'Neil et al. [30]. The chemistry of 5-substituted 2,3-dihydrothiophenes, however, has not been fully explored yet. During this study, we found an interesting isomerization reaction. 5-Substituted 2,3-dihydrothiophenes **16** obtained by this reaction were susceptible to sunlight, and easily isomerized to exocyclic olefins **17** by a brief irradiation with a high pressure mercury lamp under air (Scheme 8, Table 4) [21].

4. Conclusions

We have developed the intramolecular reactions of titanium carbene complexes formed from thioacetals with carbon–carbon or carbon–oxygen double bonds. The results described above indicate that these reactions are useful for the construction of a variety of carbocyclic and heterocyclic compounds. Recently we found that the treatment of titanium-alkylidenes with trialkylsilanes or related Group 14 metal hydrides affords the corresponding Group 14 organometallic compounds [31], and the vinylcarbene complexes react with *tert*-alkyl halides to form terminal olefins [32].

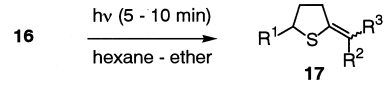


Scheme 7.

Table 3
Preparation of 2,3-dihydrothiophenes **16** [a]

Thiol ester **15**	Product	Yield (%)
15a: R^1 = H, R^2 = H, R^3 = $Me(CH_2)_6$	**16a**, **17a**	57 [b]
15b: R^1 = H, R^2 = Et, R^3 = Bu	**16b**	68
15c: R^1 = H, R^2 = $PhCH_2$, R^3 = $PhCH_2$	**16c**	55
15d: R^1 = Me, R^2 = R^3 = $(CH_2)_5$	**16d**	62

[a] The thioacetal was added slowly to a THF solution of **1** over 20 min.
[b] **16a**:**17a** = 95:5.



Scheme 8.

Table 4
Isomerization of 2,3-dihydrothiophenes **16** by photoirradiation

2,3-Dihydrothiophene **16**	Thiophene recovered (%)	**17**:**16**
16a	62	74:26
16b	71	94:6
16c	69	>99:<1
16d	71	80:20

These results suggest that the organotitanium species would be reactive toward various organic molecules in addition to olefins and carbonyls. Further study of the reactions of organotitanium species formed from thioacetals and their application to the synthesis of cyclic compounds is now in progress.

Acknowledgements

This work was supported by a Grant-in-aid for Scientific Research from the Ministry of Education, Science, Sports and Culture, Japan.

References

[1] Y. Horikawa, M. Watanabe, T. Fujiwara, T. Takeda, J. Am. Chem. Soc. 119 (1997) 1127.
[2] T. Takeda, M. Watanabe, N. Nozaki, T. Fujiwara, Chem. Lett. (1998) 115.
[3] M.A. Rahim, H. Taguchi, M. Watanabe, T. Fujiwara, T. Takeda, Tetrahedron Lett. 39 (1998) 2153.
[4] T. Takeda, M. Watanabe, M.A. Rahim, T. Fujiwara, Tetrahedron Lett. 39 (1998) 3753.
[5] T. Fujiwara, N. Iwasaki, T. Takeda, Chem. Lett. (1998) 741.
[6] Y. Horikawa, T. Nomura, M. Watanabe, T. Fujiwara, T. Takeda, J. Org. Chem. 62 (1997) 3678.

[7] T. Takeda, H. Shimokawa, Y. Miyachi, T. Fujiwara, Chem. Commun. (1997) 1055.
[8] T. Fujiwara, M. Takamori, T. Takeda, Chem. Commun. (1998) 51.
[9] T. Takeda, R. Sasaki, T. Fujiwara, J. Org. Chem. 63 (1998) 7286.
[10] T. Takeda, Y. Endo, A.C.S. Reddy, R. Sasaki, T. Fujiwara, Tetrahedron 55 (1999) 2475.
[11] M. Schuster, S. Blechert, Angew. Chem., Int. Ed. Engl. 36 (1997) 2036.
[12] R.H. Grubbs, S. Chang, Tetrahedron 54 (1998) 4413.
[13] K.C. Nicolaou, M.H.D. Postema, C.F. Claiborne, J. Am. Chem. Soc. 118 (1996) 1565.
[14] T. Fujiwara, T. Takeda, Synlett (1999) 354.
[15] T. Fujiwara, Y. Kato, T. Takeda, Heterocycles 52 (2000) 147.
[16] K. Tamao, N. Ishida, Y. Ito, M. Kumada, Org. Synth. 69 (1990) 96.
[17] T. Fujiwara, M. Takamori, K. Yanai, T. Takeda, to be published.
[18] S. Chang, R.H. Grubbs, Tetrahedron Lett. 38 (1997) 4757.
[19] C. Meyer, J. Cossy, Tetrahedron Lett. 38 (1997) 7861.
[20] T.R. Hoye, M.A. Promo, Tetrahedron Lett. 40 (1999) 1429.
[21] M.A. Rahim, T. Fujiwara, T. Takeda, Synlett (1999) 1029.
[22] S.F. Birch, D.T. McAllan, J. Chem. Soc. (1951) 2556.
[23] G. Sosnovsky, Tetrahedron 18 (1962) 903.
[24] M.A. Gianturco, M.A. Friedel, V. Flanagan, Tetrahedron Lett. 23 (1965) 1847.
[25] L.A. Cohen, J.A. Steele, J. Org. Chem. 31 (1966) 2333.
[26] P.Y. Johnson, E. Koza, R.E. Kohrman, J. Org. Chem. 38 (1973) 2967.
[27] N.N. Sauer, R.J. Angelici, Y.C.J. Huang, W.S. Trahanovsky, J. Org. Chem. 51 (1986) 113.
[28] P.A. Delaney, R.A.W. Johnstone, J. Chem. Soc, Perkin Trans. 1 (1986) 1861.
[29] L.A. Paquette, B.M. Branan, D. Friedrich, S.D. Edmondson, R.D. Rogers, J. Am. Chem. Soc. 116 (1994) 506.
[30] I.A. O'Neil, K.M. Hamilton, J.A. Miller, Synlett (1995) 1053.
[31] T. Takeda, N. Nozaki, T. Fujiwara, Tetrahedron Lett. 39 (1998) 3533.
[32] T. Takeda, N. Nozaki, N. Saeki, T. Fujiwara, Tetrahedron Lett. 40 (1999) 5353.

PERGAMON

www.elsevier.nl/locate/poly

Polyhedron 19 (2000) 597–598

POLYHEDRON

Catalyzed and non-catalyzed addition reactions to the triple bond

I.P. Beletskaya *, M.A. Kazankova

Moscow State University, Moscow 119899, Russia

Received 4 October 1999; accepted 1 December 1999

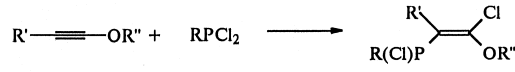
Abstract

New addition reactions of the E–Hal bond (E = Hg, P(III), P(V), Si, Ge, Sn) to electron-enriched alkynes leading to trisubstituted and tetrasubstituted alkenes with carbon–heteroatom bonds are considered. ©2000 Elsevier Science Ltd All rights reserved.

Keywords: Alkoxyalkynes; Aminoalkynes; Addition reactions; Organophosphorus halides; Organosilane halides; Organogermane halides; Pd-catalyzed cross-coupling reactions

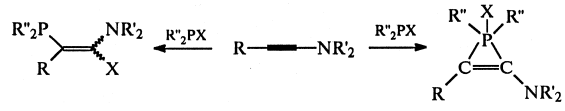
In recent years our laboratory in Moscow State University has studied different types of addition reactions to alkynes. These reactions include the following. (1) Electrophilic addition reactions of the E–Hal bond to alkoxyalkynes and aminoalkynes to give functionalized trisubstituted or tetrasubstituted olefines with nucleophilic and electrophilic centers. (2) Nucleophilic addition reactions catalyzed by Pd(II) and, more unusually, by Pt(IV) complexes. The reaction of terminal alkynes in the system I^-–I_2–MeOH catalyzed by $Na_2PtCl_6 \cdot 6H_2O$ leads to *trans*,*trans*-1,4-diiododienes ICH=C(R)–C(R)=CHI [1]. The intermediate Pt(IV) complex was isolated and characterized by X-ray analysis [2] and the diene was introduced in a variety of cross-coupling reactions. (3) Reactions of E–H addition (E = Si) to cyclopropylacetylenes and dicyclopropylacetylenes catalyzed by Rh(I) and Pd(0) complexes leading to disubstituted and trisubstituted olefines [3,4], and silaformylation of alkynes catalyzed by a very efficient Rh(I) complex $[(C_4H_6)_2RhCl]_2$ [5]. (4) The addition of $HP(O)(OR)_2$ to various terminal alkynes using a modified Tanaka procedure [6,7] and further asymmetric hydrogenation of vinylphosphonates formed [7]. (5) The addition of Ph_2PH or Ph_2PSiMe_3 to alkynes catalyzed by Pd(0) or Ni(0) complexes [8].

In this report we concentrate on reactions of the first type. These are less known in spite of the fact that they proceed very easily and lead to interesting and useful olefines. The example of this reaction is the addition of $HgCl_2$ to terminal or internal alkoxyacetylenes with the formation of anti-addition products in quantitative yield. The addition of P–Cl bond of PCl_3 and $RPCl_2$ proceeds in the same manner to give in the case of $R^1 = EMe_3$ tetrasubstituted olefines with C–E and C–P bonds at the same carbon center.

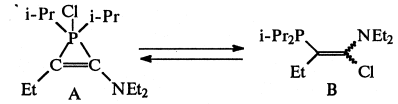


R=Cl, Alk; R'=Alk, Me_3Si, Me_3Ge, R"=Alk

The addition of dialkyl(aryl)chlorophosphines to internal alkoxyacetylenes revealed the formation of cyclic phosphacyclopropene-phosphirene as a stable compound. In the same reaction with aminoacetylenes both products, stable phosphirenium halides and non-cyclic addition product, can be formed depending on the nature of R, R′, R″, Hal, and solvent employed.



The tautomeric equilibrium with 1:1 ratio between these two forms in benzene is shifted to the cyclic form in dichloromethane and to the open form in hexane, as observed for the first time [9].

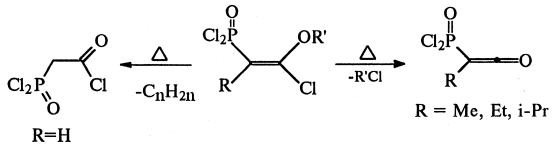


hexane A : B = 10 : 90 benzene A : B = 53 : 47 CH_2Cl_2 A 100%

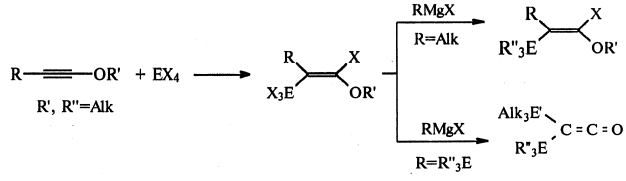
* Corresponding author. Tel. and fax: +7-95-939-3618; e-mail: beletska@org.chem.msu.ru

0277-5387/00/$ - see front matter ©2000 Elsevier Science Ltd All rights reserved.
PII S0277-5387(99)00416-7

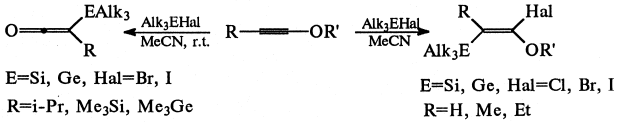
The products of the addition of phosphorus pentachloride to alkoxyalkynes or aminoalkynes were transformed into many useful compounds, for example $(R_2N)_2P(O)C(R)=C(NEt_2)(NR_2)$ [10]. 2-Alkoxy-2-chloroalkenyldichlorophosphonate under heating was converted to phosphorylated ketene for R = Alk and to α-phosphorylated acid chloride for R = H.



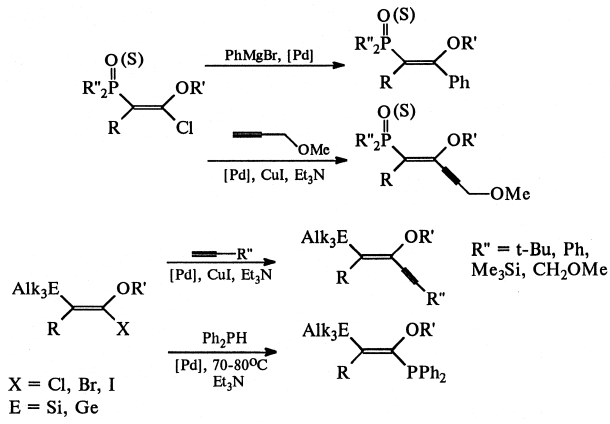
The addition of $EHal_4$ (E = Si, Ge, Sn; Hal = Cl, Br) to alkoxyacetylenes proceeds very smoothly with terminal and internal alkoxyalkynes and in the case of element containing alkoxyacetylene gives tetrasubstituted olefines with two C–E bonds at the same carbon center. Treating these compounds with RMgX leads to dielement substituted ketenes.



Alk_3EHal (E = Si, Ge; Hal = Br, I) can also be added to alkoxyacetylenes but in the case of bulky substituents in acetylene the reaction affords element substituted ketenes, probably owing to rearrangement.



Owing to the high lability of the halogen (even chlorine) atom in the α-position to alkoxy or dialkylamino groups, all compounds obtained can be easily introduced in different types of Pd-catalyzed cross-coupling reactions. We illustrate this here by several examples [11,12].



Acknowledgements

The contributions of co-workers and post-graduate students and financial support by INTAS grant N 97-1874, RFBR grant N 97-03-33035, 96-15-97484, Integration grant N 234 are gratefully acknowledged.

References

[1] S.A. Mitchenko, V.P. Ananikov, I.P. Beletskaya, Yu.A. Ustynyuk, Mendeleev Commun. (1997) 130.
[2] V.P. Ananikov, S.A. Mitchenko, I.P. Beletskaya, S.E. Nefedov, I.L. Eremenko, Inorg. Chem. Commun. (1998) 411.
[3] N.A. Donskaya, B.A. Lukovskii, R.A. Mishechkin, N.M. Yurieva, I.P. Beletskaya, Zh. Org. Khim. 33 (1997) 965.
[4] A.G. Bessmertnykh, K.A. Blinov, Yu.K. Grishin, N.A. Donskaya, E.V. Tveritinova, N.M. Yurieva, I.P. Beletskaya, J. Org. Chem. 62 (1997) 6069.
[5] N.A. Donskaya, N.M. Yurieva, A.S. Sigeev, T.I. Voevodskaya, I.P. Beletskaya, V.F. Tretyakov, Mendeleev Commun. (1995) 220.
[6] L.-B. Han, M. Tanaka, J. Am. Chem. Soc. 118 (1996) 1571.
[7] J.-C. Henry, D. Lavegne, V. Ratovelomanana-Vidal, J.-P. Genet, I.P. Beletskaya, T.M. Dolgina, Tetrahedron Lett. 39 (1998) 3473.
[8] M.A. Kazankova, A.N. Kochetkov, I.V. Efimova, I.P. Beletskaya, Tetrahedron Lett. in press.
[9] N.V. Lukashev, P.E. Zhichkin, M.A. Kazankova, I.P. Beletskaya, Tetrahedron Lett. 34 (1993) 1331.
[10] I.G. Trostyanskaya, S.V. Lutsenko, I.V. Efimova, M.A. Kazankova, I.P. Beletskaya, Zh. Org. Khim. 32 (1996) 1054.
[11] M.A. Kazankova, E.A. Chirkov, I.V. Efimova, I.P. Beletskaya, Tetrahedron Lett. 40 (1999) 573.
[12] M.A. Kazankova, I.G. Trostyanskaya, S.V. Lutsenko, I.P. Beletskaya, Tetrahedron Lett. 40 (1999) 569.

PERGAMON

www.elsevier.nl/locate/poly

Polyhedron 19 (2000) 601–606

POLYHEDRON

Spectral and structural characterization of copper(I) halide, nitrate and perchlorate complexes of pyrazine carboxamide (pyza) and X-ray crystal structure of polymeric $[Cu(pyza)_2I]_n$ complex

Mohamed A.S. Goher [a,*], Franz A. Mautner [b]

[a] *Department of Chemistry, Faculty of Science, Kuwait University, P.O. Box 5969, Safat, 13060 Kuwait*
[b] *Institut für Physikalische und Theoretische Chemie, Technische Universität Graz, A-8010 Graz, Austria*

Received 2 June 1999; accepted 29 November 1999

Abstract

Copper(I) salts form with pyrazine carboxamide (pyza) complexes of the type $Cu(pyza)_2X$ for X = Cl, Br, I, NO_3 and ClO_4, $Cu_2(pyza)_3X_2$ for X = Cl and Br, Cu(pyza)X for X = Cl, Br and I, and $Cu(pyza)I \cdot H_2O$. The complexes were characterized by elemental analysis and infrared, Raman and electron spectroscopy. The overall physical measurements suggest that pyza behaves as a monodentate ligand in all complexes, except the 1:1 bromide which contains *N*-, and *N*,*O*-pyza molecules, whereas the halide, nitrate and perchlorate complexes behave as bridging ligands giving rise to polymeric structures. The structural determination of $Cu(pyza)_2I$ reveals that the Cu and I atoms are arranged alternately to form a polymeric zigzag chain with an approximately tetrahedral copper(I) environment. These chains are connected via hydrogen bonds of the type N–H···O between two pyza molecules to form two-dimensional systems. The bromide and iodide complexes of all types display visible emission in the 640–675 nm region when irradiated in the UV, whereas the other complexes do not fluoresce at room temperature. ©2000 Elsevier Science Ltd All rights reserved.

Keywords: Copper(I) complexes; Crystal structures; Electronic spectra; Emission spectra; Pyrazine carboxamide complexes; Vibrational spectra

1. Introduction

Hoskins and Robson [1] have proposed that infinite-ordered frameworks may be formed by linking together tetrahedral or octahedral metal centres through rod-like connecting ligands, such as pyrazine. These coordination polymers [1–4] present potential utility in host–guest chemistry, ion exchange and heterogeneous catalysis. Thus, numerous examples of pyrazine-bridged derivatives of copper(II) complexes have been prepared and structurally characterized in order to study the ability of the pyrazine bridge to mediate interactions in novel one- [5,6] and two-dimensional [7,8] materials. Pyrazine carboxamide (otherwise known as pyrazine amide (**I**), hereafter abbreviated as pyza), while keeping the rod-like nature of pyrazine, adds two coordination centres (namely –CO and $–NH_2$ groups), thereby increasing the coordination ability of pyza as a ligand. It has been pointed out [9] that pyza acts as a bidentate ligand with coordination via the O atom and N α-hetero atom of the ring in $M(OAc)_2(pyza)_2$ (M = Mn or Ni), whereas it acts as a monodentate ligand with coordination through the N β-hetero atom and carbonyl O atom in the corresponding Cu and Hg complexes, respectively. Complexes of pyza with many transition metal ions, including Ni(II), Co(II) [10], Fe(II), Cu(II), Zn(II), Cd(II), Hg(II) and Pd(II) [11,12], as well as with Ti(IV) and Zr(IV) [13], have been studied. Variable-temperature magnetic susceptibility studies of $CuX_2(pyza)_2$ suggested a one-dimensional chain structure for these complexes [14]. Crystal structures have been determined for $ZnCl_2(pyza)_2$ [15] and $Cu(pyza)_2(ClO_4)_2$ [16]. The zinc centre is tetrahedrally coordinated in $ZnCl_2(pyza)_2$, whereas the copper centre, which is chelated by the amide O atom and α-N atom of two ligand molecules, is weakly bonded to other N atoms of the pyrazine rings of two neighbouring complex molecules in $Cu(pyza)_2(ClO_4)_2$ [16]. To the best of our knowledge no copper(I) complex of pyza has been reported in the literature. In the present paper we report the synthesis and characterization of such copper(I) complexes, together with the X-ray structure determination of the title iodide complex, the first to have been reported.

* Corresponding author; e-mail: mohame_goher@yahoo.com

0277-5387/00/$ - see front matter ©2000 Elsevier Science Ltd All rights reserved.
PII S0277-5387(99)00374-5

2. Experimental

Pyrazine carboxamide (pyza) was purchased from Aldrich; other chemicals are of analytical grade quality.

2.1. Preparation of complexes

2.1.1. $Cu(pyza)_2X$ ($X = Cl, Br, I$)

L-(+)-Ascorbic acid was added to an aqueous solution mixture of $Cu(NO_3)_2 \cdot 3H_2O$ (0.48 g, 2 mmol) and NaX (in 1:1 molar ratio with respect to copper). A saturated solution of NaX was then added dropwise until a clear solution was obtained. Upon addition of an ethanol solution of pyza (0.83 g, 6 mmol) and boiling, a clear yellow solution was produced. The final mixture was allowed to stand for several days to yield red crystals of the complexes.

2.1.2. $Cu_2(pyza)_3X_2$ ($X = Cl, Br$)

These complexes were prepared according to the above method except that the amount of pyza added was in a molar ratio of 2:1 to copper.

2.1.3. $Cu(pyza)I \cdot H_2O$

This complex was prepared as above except that the molar ratio of pyza to copper was 1:1. The final mixture was allowed to stand in the open air for several days to yield the complex.

2.1.4. $Cu(pyza)X$ ($X = Cl, Br, I$)

These complexes were prepared by mixing a suspension of CuX (2 mmol) in water with a boiled aqueous solution of pyza (0.27 g, 2 mmol). The complexes were deposited as powder samples after several minutes.

2.1.5. $Cu(pyza)_2X$ ($X = NO_3$ or ClO_4)

These complexes were prepared by the addition of L-(+)-ascorbic acid to a mixture of $Cu(NO_3)_2 \cdot 3H_2O$ or $Cu(ClO_4)_2 \cdot 6H_2O$ and pyza in a molar ratio of 1:2.5, in aqueous ethanol medium. The final mixture was boiled, cooled and allowed to stand for several hours.

2.2. Elemental analysis

Elemental analysis results and some physical properties of the isolated complexes are listed in Table 1.

2.3. Spectral measurements

The IR and Raman spectral data for some complexes are given in Table 2. The experimental procedures and instruments used for different physical measurements are as described previously [17].

2.4. X-ray structural analyses

$[Cu(pyza)_2I]_n$, $C_{10}H_{10}IN_6O_2$, fw = 436.68, monoclinic, space group $P2_1/m$ (no. 11), $a = 4.1192(13)$, $b = 26.493(7)$, $c = 6.177(2)$ Å, $\beta = 97.16(2)°$, $V = 668.9(3)$ Å^3, $Z = 2$; $d_c = 2.168$ Mg m^{-3}. The X-ray single crystal data were collected on a modified STOE four circle diffractometer. Crystal size: $0.11 \times 0.08 \times 0.05$ mm. Graphite-monochromatized

Table 1
Analytical data for isolated copper(I) complexes of pyrazine carboxamide

Complex	Colour	Analysis (%): Found (Calc.)				
		C	H	N	Cu	X
$Cu(pyza)_2Cl$ (**1**)	red fine needle-like crystals	34.5 (34.8)	3.0 (2.9)	20.0 (20.4)	17.9 (18.4)	10.4 (10.2)
$Cu(pyza)_2Br$ (**2**)	red needle-like crystals	30.2 (30.8)	2.7 (2.6)	21.4 (21.6)	16.5 (16.3)	20.1 (20.5)
$Cu(pyza)_2I$ (**3**)	red crystals	27.4 (27.4)	2.6 (2.3)	18.9 (19.2)	14.2 (14.5)	28.7 (29.1)
$Cu_2(pyza)_3Cl_2$ (**4**)	red-orange fine needles	31.9 (31.8)	2.9 (2.7)	22.0 (22.2)	11.5 (11.2)	12.0 (12.5)
$Cu_2(pyza)_3Br_2$ (**5**)	red-orange fine crystals	27.6 (27.4)	2.4 (2.3)	19.0 (19.2)	19.1 (19.3)	25.3 (25.8)
$Cu(pyza)Cl$ (**6**)	brown microcrystalline powder	26.6 (27.0)	2.4 (2.3)	19.0 (18.9)	28.8 (28.6)	15.7 (16.0)
$Cu(pyza)Br$ (**7**)	yellow powder	22.5 (22.5)	2.0 (1.9)	15.3 (15.8)	23.2 (23.8)	30.5 (30.0)
$Cu(pyza)I \cdot H_2O$ (**8**)	red-orange fine needles	17.8 (18.1)	2.4 (2.1)	12.9 (12.7)	19.8 (19.2)	38.0 (38.3)
$Cu(pyza)I$ (**9**)	yellow powder	19.7 (19.2)	1.8 (1.6)	12.9 (13.4)	19.7 (20.2)	40.0 (40.5)
$Cu(pyza)_2ClO_4$ (**10**)	dark-brown microcrystalline powder	28.2 (29.3)	2.6 (2.9)	20.3 (20.5)	15.9 (15.5)	
$Cu(pyza)_2NO_3$ (**11**)	yellow fine needles	31.9 (32.3)	2.9 (2.7)	26.2 (26.4)	16.8 (17.1)	

Table 2
IR and Raman spectral data for pyza and some of its copper(I) complexes [a]

pyza		Complex **3**		Complex **7**		
IR	Raman	IR	Raman	IR	Raman	Assignments
3414vs	3429vw	3433s	3400vw	3378s	3410vw	$\nu_{as}(NH_2)$
3290m		3386ms		3312ms		
3162s		3288m	3167s			$\nu_{s}(NH_2)$
	3065ms		3080s			
1714s	1672wm	1709s	1673w	1708vs	1673m	$\nu(C=O)$
				1673s		
1610s		1602ms		1605m		$\nu(NH_2)$
1581ms	1576s	1595m	1583s	1588m	1583s	ν_{8a}, ring
1521m	1523m	1515m	1514ms	1517w	1514ms	ν_{8b}, ring
1478m	1487m	1475w	1478m	1497w	1478m	ν_{19a}, ring
				1474w		
1438m	1451ms	1438m	1447m	1435m	1447m	
1378vs	1380wm	1379vs	1383w	1381*vs	1383wm	amide
	1295wm			1322m		
1182m	1179m	1184wm	1179m	1185m	1179m	$\delta(CH)$
1162ms	1165vw	1154wm	1166m	1165wm	1166m	ν_{14}, ring
				1141*m		
1085m	1079m	1082w	1088m	1096m	1088m	$\delta(NH_2)$
1054ms	1051s	1059w	1059s	1061m	1059vs	$\delta(CH)$
1024s	1022vs	1021ms	1022vs	1024s	1022vs	ν_{12}, ring
870ms	867w	873m	874m	877m	874m	$\gamma(CH)$
787m	805s	803m,br	812s	819m,br	812s	$\delta(OH)$def. + ν_1, ring
761w	776wm			759m		ν_4, ring
670ms	659w	670m	661s	674m	661s	$\omega(NH_2)$
619wm	616w	634ms	633s	640m	633s	ν_{6a} or ν_{6b}
544s	534m	545sh	536ms	567*m	530m	$\delta(OCN)$
432s	412m	455ms	447wm	449s	447m	ν_{16b}, ring

[a] v, very; w, weak; m, medium; s, strong; sh, shoulder; *split band.

Mo Kα radiation ($\lambda = 0.71069$ Å) with the ω-scan technique was used to collect the data set. The accurate unit-cell parameters were determined from automatic centering of 47 reflections ($3.7° < \theta < 15.6°$) and refined by least-squares methods; 2040 reflections (1480 independent reflections, $R_{int} = 0.0306$) were collected in the range $3.08° < \theta < 26.97°$. Corrections were applied for Lorentz polarization effects, and for absorption using the DIFABS [18] computer program (range of normalized transmission coefficients 0.340–1.000). The structure was solved by direct methods and refined by full-matrix least-squares methods on F^2 (i.e. squared), using the SHELXTL/PC V 5.03 [19] program package. All non-hydrogen atoms were refined anisotropically. The hydrogen atoms were assigned isotropic displacement factors and included in the final refinements cycles by use of geometrical restraints. The final R indices are 0.0454 (R_1) and 0.1083 (wR_2) [$I > 2\sigma(I)$]. Goodness-of-fit on F^2 is 1.193. Number of refined parameters is 102. Maximum and minimum peaks in the final difference Fourier synthesis were 1.253 [in vicinity of I(1)] and −1.288 e Å^{-3}. Selected bond parameters are given in Table 3.

Table 3
Selected bond lengths (Å) and angles (°) for $[Cu(pyza)_2I]_n$ [a]

Cu(1)···Cu(1B)	4.119(2)	Cu(1)–N(1A)	2.026(5)
Cu(1)–N(1)	2.026(5)	Cu(1)–I(1B)	2.656(2)
Cu(1)–I(1)	2.741(2)	I(1)–Cu(1C)	2.656(2)
N(1)–C(4)	1.325(8)	N(1)–C(1)	1.343(8)
C(1)–C(2)	1.374(9)	C(2)–N(2)	1.335(8)
C(2)–C(5)	1.514(9)	N(2)–C(3)	1.332(9)
C(3)–C(4)	1.396(9)	C(5)–O(1)	1.234(8)
C(5)–N(3)	1.313(8)	N(3)···O(1D)	2.870(8)
H(5)···O(1D)	2.05(3)		
N(1A)–Cu(1)–N(1)	133.0(3)	N(1A)–Cu(1)–I(1B)	106.2(2)
N(1)–Cu(1)–I(1B)	106.2(2)	N(1A)–Cu(1)–I(1)	103.6(2)
N(1)–Cu(1)–I(1)	103.6(2)	I(1B)–Cu(1)–I(1)	99.49(5)
Cu(1C)–I(1)–Cu(1)	99.49(5)	N(3)–H(5)···O(1D)	161(7)

[a] Symmetry codes: (A) $x, -y+\frac{1}{2}, z$; (B) $x+1, y, z$; (C) $x-1, y, z$; (D) $-x, -y+1, -z+2$.

3. Results and discussion

The reactions between pyza and copper(I) halide, nitrate and perchlorate or the reduction of copper(II)–pyrazine carboxamide complex in the presence of these anions afforded the complexes given in Table 1. All the complexes are coloured and stable against air oxidation when well-dried. The copper(I) halide, nitrate and perchlorate complexes are insoluble in many non-polar solvents (e.g. benzene, carbontetrachloride, toluene) and polar solvents (e.g. water, alcohols, acetone), which is an indication of their polymeric nature.

3.1. IR and Raman spectra

The IR and Raman (R) spectral results for pyrazine carboxamide and some of its copper(I) complexes are given in Table 2. The assignments given are in accordance with those reported previously [17] for the parent ligand. The spectra of these complexes show a very strong band around 1700 cm^{-1} (IR) and 1670 cm^{-1} (R), suggesting that the carbonyl group does not participate in the coordination bond with copper(I). In case of the yellow 1:1 bromide complex two bands are observed at 1706 and 1662 cm^{-1} (IR), suggesting the existence of two types of pyza molecules; in one of them the carbonyl group coordinates the metal atom whereas it does not in the other. The small shift of the carbonyl band from 1714 cm^{-1} in the spectrum of free ligand may be due to hydrogen bonding. The bands due to the amino group in the 3400–2800 cm^{-1} region and around 1610 cm^{-1} are little influenced by coordination, and this again may be due to N–H···O hydrogen bonding. The spectrum of complex **8** shows a broad band of medium to strong intensity around 3450 cm^{-1} due to the hydrogen-bonded water molecule. A broad band of medium intensity appears in the IR spectra of all complexes, except in the region 800–815 cm^{-1} for complex **7** and at 805 cm^{-1} in free pyza, which exists as dimers formed by hydrogen bonds between carboxamide groups. This band is assigned to the OH out-of-plane deformation of the system, similar to that reported for dimers formed by hydrogen bonds between carboxylic groups [20]. In the 1600–400 cm^{-1} region (pyrazine nucleus vibrations) the bands at 1581, 1054, 787 cm^{-1} (IR) and at 1576, 1051, 867, 805, 616 cm^{-1} (R) are slightly shifted; those at 619, 432 cm^{-1} (IR) and at 412 and 379 cm^{-1} (R) experience substantial shifts to higher frequencies, whereas the other bands are not affected or are slightly shifted to lower wave numbers upon complexation. Similar results have been reported for other metal complexes of pyrazine [21]. These results suggest that pyza may act as a *N*-monodentate ligand in all but one of the isolated copper(I) complexes. In the yellow 1:1 bromide complex one pyza acts as a *N*-monodentate whereas the other acts as a *N*,*O*-bidentate ligand. Further evidence for the presence of two different pyza molecules in the above complex comes from the splitting and appearance of a large number of peaks (Table 2). In the far IR region we could not locate any absorption band due to νCu–Cl or Cu–Br above 200 cm^{-1}, the region where these vibrations are expected [22]. This suggests that the halide atoms act as bridging ligand in these complexes. The spectra of the 1:2 copper(I) perchlorate complex show three peaks at 1144, 1112 and 1087 cm^{-1} and two peaks at 636 and 628 cm^{-1} (IR), and at 1096, 1068 and 1037 cm^{-1} and at 673, 658 and 620 cm^{-1} (R), due to ν_3 and ν_1 modes of the perchlorate, a result which indicates a bridging bidentate perchlorate group [22]. Likewise the appearance of strong bands at 1313 and 1436 cm^{-1} due to ν_5 and ν_1 (IR), respectively, of the NO_3^- group is suggestive of a bridging bidentate nitrate group in the respective complex. The above conclusions are confirmed by crystal structure determination of the 1:2 copper(I), bromide (**3**) and iodide (**4**) complexes.

3.2. Structure of $[Cu(pyza)_2I]_n$

The structural determination of $[Cu(pyza)_2I]_n$ confirms the presence of pyza dimers as inferred by the IR spectral results given above. Cu^+ and I^- occupy special positions on mirror planes with multiplicity 2; thus the asymmetric unit (Fig. 1) corresponds exactly to 2:1 pyza–CuI stoichiometry. The copper and iodide ions are arranged alternately to form a polymeric zigzag chain [I–Cu–I = 99.49(5)°, Cu–I–Cu = 99.49(5)°] extending along the *a*-axis. The almost planar hydrogen-bonded pyza dimeric unit [mean deviation from planarity = 0.034 Å; torsion angle C(5D)–O(1D)···N(3)–C(5) = −2.7°] is diagonally linked, through the nitrogen atoms, N(1), to two metal centres belonging to adjacent $(CuI)_n$ chains (Fig. 2). The coordination geometry about the copper(I) atom is thus approximately tetrahedral (Table 3), and the resulting crystal structure comprises layers parallel to the *ab* set of planes.

The present structure is very similar to that of the previously reported $CuCl(HNA)_2$ complex (HNA is nicotinic acid) [23], having tetrahedral copper(I) atoms and zigzag $(CuCl)_n$ chains. While the measured Cu–N bond distances (Table 3) lie within the range of 2.00–2.05 Å for copper(I) complexes with pyridine and substituted pyridine ligands [24], the Cu–I bonds are longer than those found [2.475(4), 2.611(4) Å] in the structure of $[Cu(s\text{-collidine})I]_n$ containing trigonal planar copper(I) [25]. Complexes of stoichiometry L_2CuX, where L = pyridine or substituted pyridine and X = halogen, commonly exist as bis(μ-halo)-bridged $[L_2CuX]_2$ dimers with a cyclic Cu_2X_2 core [26–28]. When steric crowding of the ligand prevents dimerization, a mononuclear, pseudo-trigonal planar L_2CuX complexes are produced, as found in the structures of $(2,6\text{-}Me_2py)_2 \cdot CuX$, X = Cl, Br [29] or I [27]. The present structure is an example of the rare polymeric structure of L_2CuX stoichiometry, the existence of which may be ascribed to the stabilizing influence of the hydrogen-bonded pyrazine carboxamide.

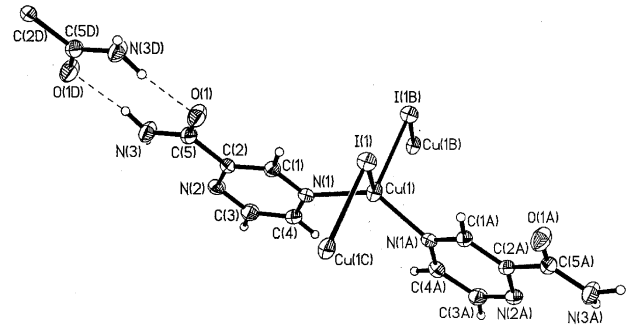


Fig. 1. Molecular geometry and atom labelling scheme of $[Cu(pyza)_2I]_n$. Symmetry codes are according to Table 3. Hydrogen bonds are indicated as broken lines.

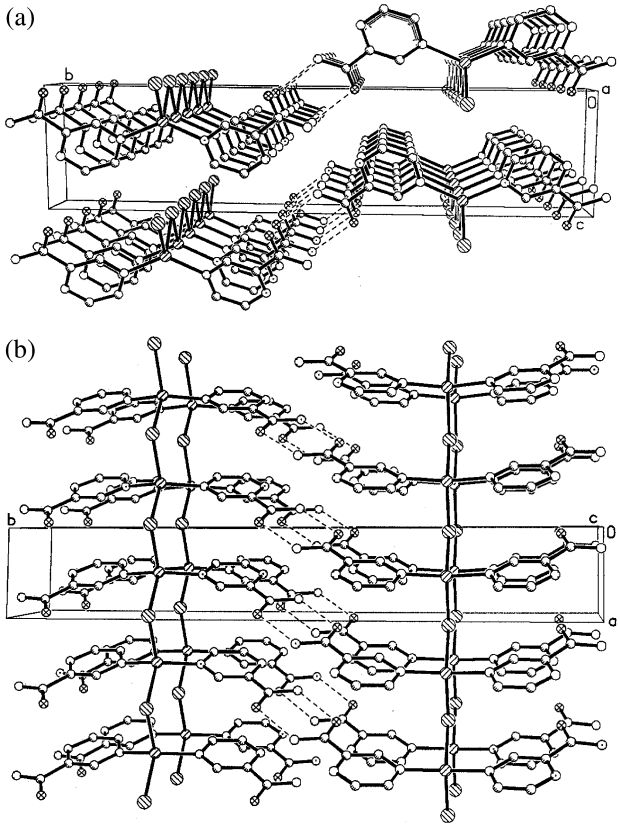


Fig. 2. Packing view of $[Cu(pyza)_2I]_n$ (a) along the *a*-axis and (b) along the *c*-axis of the unit cell.

3.3. Electronic spectra

The electronic spectra (Table 4, Fig. 3) of the solid copper(I) complexes mulled in Nujol exhibit strong absorption bands in the visible region, which are due to metal-to-ligand charge transfer (MLCT) from Cu^I d^{10} to an empty π^* orbital on the pyza molecule. The brown to black complexes (**2**–**6**, **10**), however, show two such MLCT bands. A similar situation occurs in the copper(I)–pyrazinic acid complexes [30], in the bis(arylazo-oximates) of copper(I) [31,32] and in bis[(2-phenylazo)-pyridine]copper(I) complexes [33], except that the two bands appear at 700–780 nm and 550–580 nm, in the latter two cases, respectively. In a tetrahedral molecular environment, the metal valence d orbitals split into two sublevels, t_2 and e. If the two MLCT bands observed in the spectra of some of the present complexes are due to t_2–π^* (516–618 nm) and e–π^* (400–428 nm), the energy gap between them lies in the range 7100–6500 cm^{-1}. This difference is comparable to that observed for the above pyrazinic acid complexes, but much greater than that for arylazo-oximate or phenylazopyridine–copper(I) complexes. Copper(I) complexes of bipyridine and related ligands exhibit the lowest energy charge-transfer band near 450 nm [34,35], whereas those of pyridine and related ligands show an MLCT band around 300–500 nm [36–38]. In grossly planar and unsaturated macrocyclic environments for copper(I), an allowed transition is documented [39,40] near 700 nm.

3.4. Emission spectra

The results of the room temperature emission spectra of the solid copper(I) complexes are given in Table 4. The bromide and iodide complexes display emission spectra at room temperature with λ_{max} in the range 640–675 nm, whereas the chlorides of all types, the nitrate and the perchlorate complexes do not emit. The spectrum of each of the emitting compounds consists of a single slightly asymmetric band, as seen in Fig. 4. The luminescence spectra of all of the emitting compounds proved to be independent of the exci-

Table 4
Electronic [a] and emission [b] spectral data

Complex	λ_{max} (nm)	
	MLCT [c]	Emission
$Cu(pyza)_2Cl$	300–540	no emission
$Cu(pyza)_2Br$	414, 516 br	671
$Cu(pyza)_2I$	408, 540 br	660
$Cu_2(pyza)_3Cl_2$	400, 596 br	no emission
$Cu_2(pyza)_3Br_2$	409, 542 br	651
$Cu(pyza)Cl$	412, 618 br	no emission
$Cu(pyza)Br$	300–450	642
$Cu(pyza)I \cdot H_2O$	300–530	645
$Cu(pyza)I$	280–440	650
$Cu(pyza)_2ClO_4$	428, 618 br	no emission
$Cu(pyza)_2NO_3$	440	no emission

[a] Measured as Nujol mull.
[b] Measured at room temperature.
[c] Metal-to-ligand charge transfer.

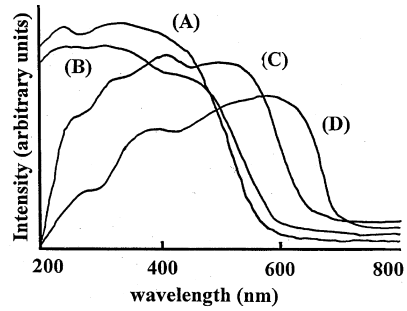


Fig. 3. Electronic spectra of solid complexes: (A) Cu(pyza)Br, (B) $Cu(pyza)_2(NO_3)$, (C) $Cu(pyza)_2Br$, (D) Cu(pyza)Cl.

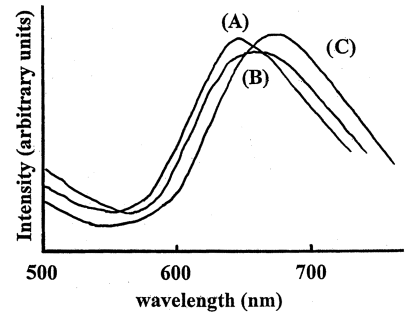


Fig. 4. Room temperature emission spectra of solid complexes: (A) Cu(pyza)I, (B) $Cu(pyza)_2I$, (C) $Cu(pyza)_2Br$.

tation wavelength, and their excitation spectra are very similar.

The emission spectra of copper(I) halide complexes of pyridine and pyridine derivatives have been extensively studied [41–47] and found to display high-energy (HE; 430–540 nm) and low-energy (LE; 620–698 nm) bands. The HE band was attributed to MLCT or halide-to-metal charge transfer (XMCT) [47], and the LE band to the metal centre in the Cu_4X_4 core with Cu···Cu distances less than 2.8 Å [46]. It is clear from Table 4 that the λ_{max} changes from 671 for the 1:2 bromide to 660 nm for the corresponding iodide, a result that is consistent with what has been observed previously [48], namely that the emission bands for the chloride clusters occur at lower energy than the HE bands of the respective iodide clusters. As these complexes do not possess the Cu_4X_4 core structure, the LE bands are not expected, and therefore the emitting state in the present copper(I) halide complexes of pyza would be triplet MLCT or XLCT excited states. The results given in Table 4 suggest that the emission spectra of the complexes of pyza experience a substantial shift to lower energies when compared with corresponding complexes of pyridine [46–50], which reflects the influence of the substituent in the skeleton of the aromatic ring itself.

Supplementary data

Supplementary data are available from CCDC, 12 Union Road, Cambridge CB2 1EZ, UK (fax: +44-1223-336033; e-mail: deposit@ccdc.cam.ac.uk), on request, quoting deposition number CCDC 123608.

Acknowledgements

M.A.S. Goher acknowledges the financial support by the Kuwait University Research Administration Project (no. SC 097) and the Department of Chemistry General Facility Projects (Analab). F.A. Mautner thanks Professors Kratky and Belaj (Graz University) for the use of the STOE diffractometer.

References

[1] B.F. Hoskin, R. Robinson, J. Am. Chem. Soc. 112 (1990) 1546.
[2] R.W. Gabe, B.F. Hoskins, R. Robson, J. Chem. Soc., Chem. Commun. (1990) 1677.
[3] B.F. Abraham, M. Hardie, B.F. Hoskins, R. Robson, E.E. Sutherland, J. Chem. Soc., Chem. Commun. (1994) 1049.
[4] L. Carlucci, G. Ciani, D.M. Proserpio, S. Sironi, J. Chem. Soc., Chem. Commun. (1994) 2755.
[5] T. Otieno, S.J. Retting, R.C. Thompson, J. Trotter, Can. J. Chem. 67 (1989) 1964.
[6] T. Otieno, S.J. Retting, R.C. Thompson, J. Trotter, Can. J. Chem. 68 (1990) 1901.
[7] S. Kitagawa, M. Munakato, T. Taminura, Inorg. Chem. 32 (1992) 1214.
[8] M.M. Turnbull, G. Pon, R.D. Willett, Polyhedron 10 (1991) 1835.
[9] T.A. Azizov, O.F. Khdzhaev, N.A. Parpiev, Koord. Khim. 4 (1978) 1234 [Chem. Abstr. 89, 190194z].
[10] P.P. Singh, J.N. Seth, J. Inorg. Nucl. Chem. 37 (1975) 593.
[11] G.S. Sanyal, A.B. Mudak, A.K. Mudi, Indian J. Chem. 21A (1982) 1044.
[12] P.P. Singh, U.P. Shukla, J.N. Seth, Indian J. Chem. 14A (1975) 158.
[13] S.C. Jain, M.S. Gill, G.S. Rao, J. Indian Chem. Soc. 53 (1976) 537.
[14] R.P. Eckberg, W.E. Hatfield, J. Chem. Soc., Dalton Trans. (1975) 616.
[15] A. Pajunen, A. Tenhunen, Suom. Kemistil. B45 (1976) 81 [Chem. Abstr. 76, 146159z].
[16] M. Sekizaki, Acta Crystallogr., Sect. B 29 (1973) 227.
[17] M.A.S. Goher, T.C.W. Mak, Polyhedron 17 (1998) 3485.
[18] N. Walker, D. Stuart, Acta Crystallogr., Sect. A 39 (1983) 158.
[19] SHELXTL/PC v. 5.03, Siemens Analytical Automation Inc., Madison, WI, 1995.
[20] N.B. Colthup, L.H. Daley, S.W. Wilberlay, Introduction to Infrared and Raman Spectroscopy, Academic Press, New York, 1964, p. 259.
[21] M.J.M. Delgado, F. Marquez, M.I. Suero, J.I. Marcos, Spectrosc. Lett. 21 (1988) 841.
[22] K. Nakamoto, Infrared Spectra of Inorganic and Coordination Compounds, 2nd ed., Wiley, New York, 1978, and references therein.
[23] M.A.S. Goher, T.C.W. Mak, Inorg. Chim. Acta 127 (1987) L13.
[24] E.W. Ainscough, E.N. Baker, A.M. Brodie, N.G. Larsen, N.G.J. Brown, J. Chem. Soc., Dalton Trans. (1981) 1746.
[25] J.A. Campbell, C.L. Raston, A.H. White, Aust. J. Chem. 30 (1977) 1937.
[26] W. Hiller, P.M. Garrick, Acta Crystallogr., Sect. C 149 (1986) 42.
[27] P.C. Healy, C. Pakawatchai, A.H. White, J. Chem. Soc., Dalton Trans. (1983) 1917.
[28] J.C. Dyason, L.M. Engelhardt, P.C. Healy, C. Pakawatchai, A.H. White, Inorg. Chem. 24 (1985) 1950.
[29] J.C. Dyason, P.C. Healy, C. Pakawatchai, V. Patrick, A.H. White, Inorg. Chem. 24 (1985) 1957.
[30] M.A.S. Goher, T.C.W. Mak, Polyhedron 14 (1995) 2587.
[31] S. Gupta, K. Kalia, A. Chakaravorty, Inorg. Chem. 10 (1971) 1534.
[32] M.H. Dickman, R.J. Doedens, Inorg. Chem. 19 (1980) 3112.
[33] D. Datta, A. Chakravorty, Inorg. Chem. 22 (1983) 1085.
[34] S. Kitagawa, M. Munakata, Inorg. Chem. 20 (1981) 2261.
[35] G.F. Smith, W.H. McCurdy Jr., Anal. Chem. 24 (1952) 371.
[36] S. Kitagawa, M. Munakata, A. Higashei, Inorg. Chim. Acta 59 (1982) 219.
[37] M.A.S. Goher, Can. J. Chem. 53 (1975) 2657.
[38] T.C.W. Mak, M.A.S. Goher, A.K. Hafez, Inorg. Chim. Acta 146 (1988) 103.
[39] D. Katovic, L.T. Taylor, F.L. Urbach, W.H. White, D.H. Busch, Inorg. Chem. 11 (1972) 429.
[40] R.R. Gagne, J.L. Allison, R.S. Gall, C.A. Koval, J. Am. Chem. Soc. 99 (1977) 7170.
[41] A. Voglar, H. Kunkley, J. Am. Chem. Soc. 108 (1986) 7211.
[42] K.R. Kyle, J. DiBenedetto, P.C. Ford, J. Chem. Soc., Chem. Commun. (1989) 714.
[43] K.R. Kyle, P.C. Ford, J. Am. Chem. Soc. 111 (1989) 5005.
[44] K.R. Kyle, W.E. Palke, P.C. Ford, Coord. Chem. Rev. 97 (1990) 35.
[45] K.R. Kyle, C.K. Ryu, P.C. Ford, J. Am. Chem. Soc. 113 (1991) 2934.
[46] N.P. Rath, E.M. Holt, K. Tanimura, Inorg. Chem. 24 (1985) 3934.
[47] M. Vitale, W.E. Palke, P.C. Ford, J. Phys. Chem. 96 (1992) 3329.
[48] C.K. Ryu, K.R. Kyle, P.C. Ford, Inorg. Chem. 30 (1991) 3982.
[49] C.K. Ryu, M. Vitale, P.C. Ford, Inorg. Chem. 32 (1993) 869.
[50] N.P. Rath, R. Holt, J. Chem. Soc., Dalton Trans. (1986) 2303.

PERGAMON

www.elsevier.nl/locate/poly

Polyhedron 19 (2000) 607–613

POLYHEDRON

Synthesis and characterization of a series of copper(II) complexes with azo-linked salicylaldimine Schiff base ligands. Crystal structure of Cu5PHAZOSALTN·$CHCl_3$

A.A. Khandar *, K. Nejati

Department of Inorganic Chemistry, Faculty of Chemistry, Tabriz University, Tabriz, Iran

Received 5 August 1999; accepted 6 December 1999

Abstract

Complexes of copper (II) with Schiff bases obtained by condensation of 5-phenylazo salicylaldehyde with di-or tri-amines have been synthesized and characterized by their infrared spectra and elemental analysis. The copper(II) chelates investigated are [bis(5-phenylazo salicylaldehyde)ethylene diiminato]copper(II) (Cu5PHAZOSALEN) **(I)**, [bis(5-phenylazo salicylaldehyde)*O*-phenylene diiminato]-copper(II) (Cu5PHAZOSALOPHEN) **(II)**, [bis(5-phenylazo salicylaldehyde)trimethylen diiminato]copper(II) (Cu5PHAZOSALTN) (**III**) and [bis(5-phenylazo salicylaldehyde)diethylene triiminato]copper(II) (Cu5PHAZOSALDETA) (**IV**). The single-crystal X-ray diffraction is reported for Cu5PHAZOSALTN·$CHCl_3$. The copper atom lies in a near square-planar coordination with Cu–N bond lengths of 1.962(7) and 1.949(7) Å and Cu–O lengths of 1.903(5) and 1.931(6) Å. Cyclic voltammetry indicates that copper complexes **III** and **IV** have a quasi-reversible redox behaviour and complexes **I** and **II** undergo irreversible and reversible reduction (at a scan rate 0.05 V s^{-1}), respectively, under the experimental conditions. ©2000 Elsevier Science Ltd All rights reserved.

Keywords: Schiff bases; Copper complexes; X-ray structure; 5-Phenylazosalicylaldehyde; Cyclic voltammetry

1. Introduction

Schiff base complexes containing different central metal atoms such as Cu, Ni, Co and Pd have been studied in great detail for their various crystallographic features, enzymatic reactions, steric effects [1–4], structure–redox relationships [5], mesogenic characteristics [6–9], catalysis, magnetic properties [10,11] and their important role in the understanding of the coordination chemistry of transition metal ions [12]. CuN_2O_2 coordination is very common in copper chemistry and the redox behaviour of a wide series of mononuclear copper(II) Schiff base complexes was reviewed some years ago in relation to their structural changes [5]. We report here the synthesis, characterization and cyclic voltammetry of copper(II) complexes of a series of Schiff base ligands derived from condensation of 5-phenylazo salicylaldehyde with di-or tri-amines (Scheme 1). We also report the crystal structure of [bis(5-phenylazo salicylaldehyde)trimethylen diiminato]-copper(II) (Cu5PHAZOSALTN) (**III**) as determined by single-crystal X-ray diffraction.

* Corresponding author. Tel.: +98-41-348917; fax: +98-41-340191; e-mail: tabrizumail@ark.tabrizu.ac.ir

2. Experimental

2.1. Reagents

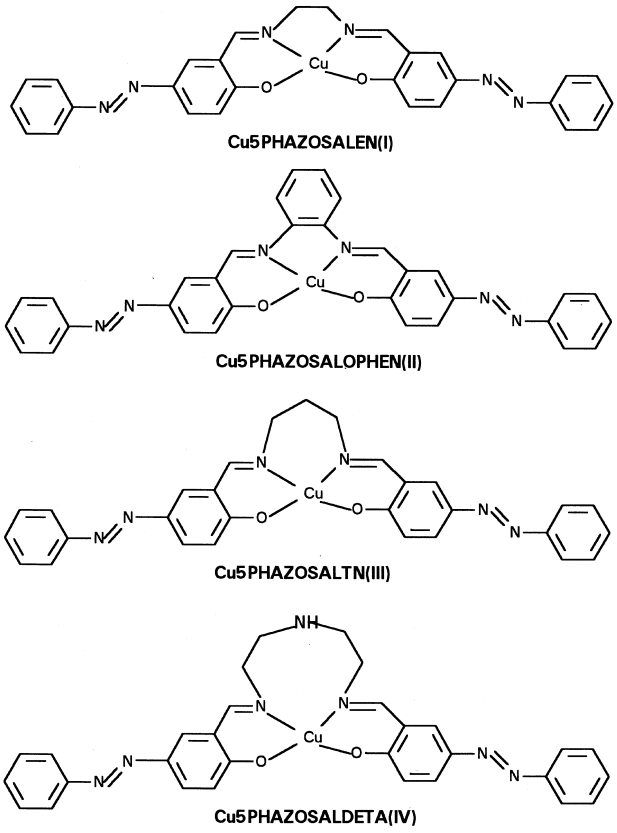
All reagents and solvents were used as supplied by Merck.

2.2. Physical measurements

Elemental (C, H and N) analyses were made on a Perkin-Elmer Model 240B automatic analyser. Electron impact (70 eV) mass spectra were recorded on a Finnigan-mat GC-MS-DS spectrometer Model 8430. Infrared (IR) spectra were recorded on an IR-408 Shimadzu 568. The redox properties of the complexes were studied by cyclic voltammetry. The voltammetric experiments were carried out in deaerated (with purged nitrogen) dimethylformamide (DMF) solutions of the complexes containing 0.1 M tetrabutylammonium perchlorate (TBAP) as supporting electrolyte. Spectroscopic grade DMF was distilled and dried on 0.4-nm molecular sieves. TBAP was dried in an oven and used without further purification.

Cyclic voltammograms were performed using an AMEL Instruments Model 2053 as potentiostat connected with a

0277-5387/00/$ - see front matter ©2000 Elsevier Science Ltd All rights reserved.
PII S0277-5387(99)00380-0



Scheme 1.

function generator (AMEL Model 568).When an iR drop (ohmic drop) was compensated a multipurpose instrument from EG&G was used, comprising potentiostat/galvanostat Model 273 coupled with an IBM personal computer connected to an Epson Model FX-850 printer. In all electrochemical experiments, an aqueous saturated calomel electrode (SCE) was used as reference electrode and all potential cited are given versus SCE. A platinum wire was used as counter electrode and a glassy carbon disc with a diameter of 3 mm was used as working electrode. The ferricinium/ferrocene (Fc^+/Fc) couple was used as an internal standard; the ferrocene solution concentration was 1 mM. All experiments were carried out at room temperature. NMR spectra were measured in $CDCl_3$ on a Brucker ACE-300 NMR spectrometer, 300.133 MHz. All chemical shifts are reported in δ units downfield from Me_4Si.

2.2.1. X-ray crystallography

Crystallographic data for complex **III** are given in Table 1 as a typical example. Single crystals of complex were acquired by slow evaporation from a chloroform–ethanol (5:1) solution at room temperature and mounted in sealed glass capillaries. Diffraction data were collected on a Siemens P3/PC diffractometer (four-circle geometry) at 293 K. Intensity data were obtained using Mo Kα radiation (0.7107 Å) monochromatized from graphite; the ω–2θ scan mode was used to a maximum 2θ value of 47.97. The data were reduced and the structure was solved by direct methods using the program SHELXTL Plus, version 5, and refined by the full-matrix least-squares method. In subsequent refinements, the function $\Sigma w(|F_o|-|F_c|)^2$ was minimized, where F_o and F_c are the observed and calculated structure factor amplitudes. The agreement indices $R=\Sigma||F_o|-|F_c||/\Sigma|F_o|$ and $R_w=[\Sigma w(|F_o|-|F_c|)^2/\Sigma w|F_o|)^2]^{1/2}$ were used to evaluate the results. Atomic scattering factors are from the international tables for X-ray crystallography. Hydrogen atoms were introduced at theoretical positions with a C–H distance of 0.95 Å for the aromatic H atoms and 0.99 Å for methylene groups.

2.3. Materials [1]

2.3.1. 5-Phenylazo salicylaldehyde

5-Phenylazo salicylaldehyde was obtained as described elsewhere [13].

2.3.2. Ligands

All ligands were prepared in a similar manner. First, 0.013 mole of related amine and 0.026 mole of 5-phenylazo salicylaldehyde were condensed by refluxing in 80 ml of absolute ethanol for 1 h. The solution was left at room temperature. Bis(5-phenylazo salicylaldehyde)ethylene diimine (5PHAZOSALEN) and bis(5-phenylazo salicylaldehyde)trimethylen diimine (5PHAZOSALTN) were obtained as yellow microcrystals, and bis(5-phenylazo salicylaldehyde)*O*-phenylene diimine (5PHAZOSALOPHEN) and

Table 1
Crystallographic data for Cu5PHAZOSALTN·$CHCl_3$ (**III**)

Empirical formula	$C_{29}H_{24}CuN_6O_2\cdot CHCl_3$
Formula weight	671.45
Temperature (K)	293(2)
Space group	$P\bar{1}$ (No. 2)
Unit cell dimensions	
a (Å)	9.646(4)
b (Å)	10.961(5)
c (Å)	15.791(6)
α (°)	82.12
β (°)	84.68(3)
γ (°)	64.54(3)
Volume (Å^3)	1492.0(11)
Z	2
Density (calc.) (Mg m^{-3})	1.495
Absorption coefficient (mm^{-1})	1.040
$F(000)$	686
Crystal size (mm)	0.1×0.4×3
θ Range for data collection (°)	2.07 to 23.96
Limiting indices	$0\le h\le 10,\ -11\le k\le 11,\ -17\le l\le 17$
Reflections collected	4079
Independent reflections	3760 ($R_{int}=0.0436$)
Reflections observed	1980
Data/restraints/parameters	3745/0/388
Goodness-of-fit on F^2	1.099
Final R indices [$I>2\sigma(I)$]	0.0758
R_w	0.1653
Largest difference peak and hole (e Å^{-3})	0.484 and −0.454

Friday Mar 31 02:15 PM

Table 2
Physical and characterization data for ligands

	Compound				
	5-Phenylazo salicylaldehyde	5PHAZOSALEN	5PHAZOSALOPHEN	5PHAZOSALTN	5PHAZOSALDETA
Formula	$C_{13}H_{10}N_2O_2$	$C_{28}H_{24}N_6O_2$	$C_{32}H_{24}N_6O_2$	$C_{29}H_{26}N_6O_2$	$C_{30}H_{29}N_7O_2$
Yield (%)	65	93.5	84.5	86	92
M.p. (°C)	128	229	208.6	144.3	126
IR (cm^{-1})					
ν(O–H)	3250	3450	3450	3450	3450
ν(N–H)					3250
ν(C–H) (aromatic)	3050	3050	3050	3050	3050
ν(C–H) (aliphatic)		2900–2950		2900–2950	2900–2950
ν(C=O)	1666				
ν(C=N)		1640	1610	1635	1635
^{1}H NMR (δ)		13.8 (br s, 2H, OH) 8.5 (s, 2H, CH=N,s) 7.96–7.99 (2H, aromatic) 7.85–7.92 (6H, aromatic) 7.44–7.53 (6H, aromatic) 7.057.08 (d, 2H, aromatic, J=9 Hz) 4.04 (s, 4H, CH_2, s)	13.6 (br s, 2H, OH) 8.78 (s, 2H, CH=N,s) 8.03–8.06 (4H, aromatic) 7.87–7.90 (4H, aromatic) 7.15–7.53 (10H, aromatic) 6.86–6.90 (2H, aromatic)	14 (br s, 2H, OH) 8.48 (s, 2H, CH=N, s) 7.97–8.01 (2H, aromatic) 7.85–7.91 (6H, aromatic) 7.40–7.51 (6H, aromatic) 7.07 (d, 2H, aromatic, J=8.8 Hz) 3.78 (t, 4H, CH_2, s, J=6.6 Hz) 2.18 (p, 2H, CH_2, J=6.6 Hz)	14.01 (br s, 2H, OH) 8.43 (br s, 2H, CH=N, s) 7.92–7.95 (2H, aromatic) 7.83–7.86 (6H, aromatic) 7.42–7.50 (6H, aromatic) 7.00 (d, 2H, aromatic, J=8.9 Hz) 3.74 (br s, 4H, =N–CH_2–, s) 3.03 (br s, 4H, =N–C–CH_2–) 1.25 (br s, 1H, NH)
Mass (m/e) (fragment, intensity %)	227 (M+1, 12)		525 (M+1, 7)		
	226 (M, 25) 121 (M−$C_6H_5N_2$, 25) calc.: 226.2		524 (M, 18) 314 (M−2* $C_6H_5N_2$, 78.6) calc.: 524.6		

StyleTag -- Journal: POLY (Polyhedron) Article: 3331

bis(5-phenylazo salicylaldehyde)diethylene triimine (5PHAZOSALTEDA) were obtained as red microcrystals; the microcrystals were filtered off, washed with 10 ml of absolute ethanol and then recrystallized from ethanol–chloroform (1:3, v/v).

2.3.3. Complexes

All complexes were prepared in a similar manner. A solution of 0.004 mole of $Cu(CH_3COO)_2 \cdot 4H_2O$ in 10 ml of ethanol was added to an ethanol–chloroform (1:1, v/v) solution containing 0.004 mole of ligand and refluxed for 1 h. The obtained brown solution was left at room temperature and brown microcrystals were collected by filtration, washed with 15 ml of ethanol and then recrystallized from ethanol–chloroform (2:1, v/v).

3. Results and discussion

3.1. Syntheses

The 5-phenylazo salicylaldehyde (pre-ligand), Schiff base ligands and related copper complexes were obtained in good yield and purity. The pre-ligand and Schiff base ligands were characterized by ^{1}H NMR and IR and mass spectroscopy.

Copper complexes were characterized by elemental analysis and IR spectroscopy. All physical and characterization data for the ligands and complexes are given in Tables 2 and 3, respectively. In the mass spectra of 5-phenylazo salicylaldehyde and the related Schiff base (5PHAZOSALOPHEN), $[M+1]$, M and $[M-C_6H_5N_2]$ for aldehyde and $[M-2{*}C_6H_5N_2]$ for Schiff base were observed. For the IR spectra of the four title complexes, ν(C=N) shifted to a lower wavenumber by 10–30 cm^{-1} upon coordination. On the other hand, the disappearance of the OH band of free ligands in copper(II) complexes indicates that the OH group has been deprotonated and bonded to the metal ions as $-O^-$.

On the basis of these results it can be deduced that in complexes **I**, **II** and **III** the Schiff bases are coordinated to copper atom as tetradentate ONNO ligands. The IR spectra of complex **IV** shows no shift for N–H bond in comparison to the IR spectra of the ligand. Therefore complex **IV** is also four-coordinate via ONNO of the ligand atoms.

*3.2. Crystal structure of [bis(5-phenylazo salicylaldehyde)-trimethylen diiminato]copper(II) (Cu5PHAZOSALTN) (**III**)*

The crystal structure and unit cell diagram of complex **III** are illustrated in Figs. 1 and 2, respectively. The selected bond distances and angles are given in Table 4.

The coordination geometry around copper can be described as a near square-planar. The Cu–O(1) and Cu–O(1′) distances of 1.903(5) and 1.931(6) Å are similar to the corresponding value [Cu–O(2), 1.915(7) Å] in *N*,*N*′-trimethylene bis(salicylaldehyde imine)copper(II), Cu(sal$_2$tn), as reported by Xiong et al. [12], and the differences are not significant, but the differences between Cu–O(1) and Cu–O(1′) with Cu–O(1) [1.840(9)Å] in Cu(sal$_2$tn) are probably just significant.

The Cu–N(1) and Cu–N(1′) distances are 1.949(7) and 1.962(7) Å. The corresponding values of complex Cu(sal$_2$tn) are 1.954(7) and 1.995(8) Å.

The bond angles O(1′)–Cu–O(1), N(1′)–Cu–N(1), N(1)–Cu–O(1′) and N(1′)–Cu–O(1) are 79.8(2), 95.7(3), 171.9(3) and 171.8(3)°, respectively. The two former bond angles are similar to the values in Cu(sal$_2$tn) [79.8(4) and 95.5(4)°], but on the basis of the two latter bond angles [(171.9(3) and 171.8(3)°] we can conclude that the coordination geometry around copper in the title complex is near to square-planar in comparison to Cu(sal$_2$tn), which has corresponding values of 159.7(4) and 158.2(4)°, respectively. The central carbon atom in the trimethylene diamine chelate ring (labelled C(1) and C(1′); see Fig. 1) is disordered over two positions, one of which is above and another below the coordination plane. The disorder is quite common and is observed, for example, in some of the transition metal complexes with Schiff base ligands [14].

Complex **III** has been prepared and recrystallized in ethanol solution. The elemental analysis confirms the formulation of the complex. Recrystallization of complex **III** for preparing a single crystal was carried out in ethanol–chloroform. The crystal structure shows the presence of a $CHCl_3$

Table 3
Physical and characterization data for complexes

	Compound			
	I	**II**	**III**	**IV**
Formula	$C_{28}H_{22}CuN_6O_2$	$C_{32}H_{22}CuN_6O_2$	$C_{29}H_{24}CuN_6O_2$	$C_{30}H_{27}CuN_7O_2$
Yield (%)	94	92	94	92
IR (cm^{-1})				
ν(C=N)	1630	1600	1605	1625
ν(N–H)				3250
Anal.: found (calc.) (%)				
C	62.3 (62.50)	65.4 (65.58)	62.8 (63.09)	61.8 (62.01)
H	4.0 (4.09)	3.7 (3.75)	4.3 (4.35)	4.6 (4.65)
N	15.5 (15.62)	14.1 (14.34)	15.1 (15.23)	16.7 (16.88)

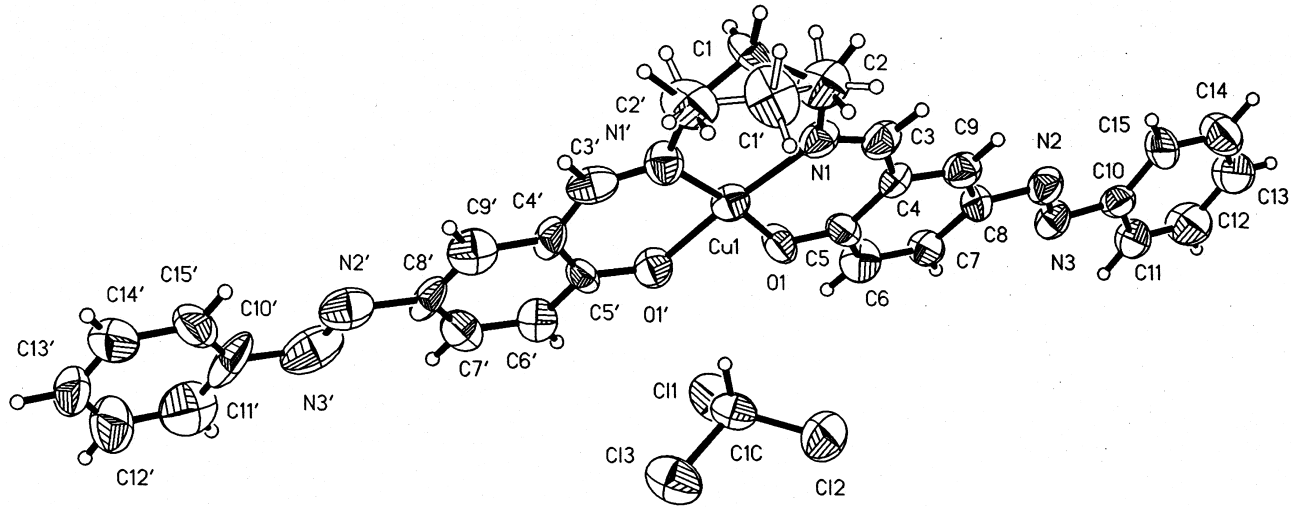


Fig. 1. Structure of Cu5PHAZOSALTN·$CHCl_3$ (**III**).

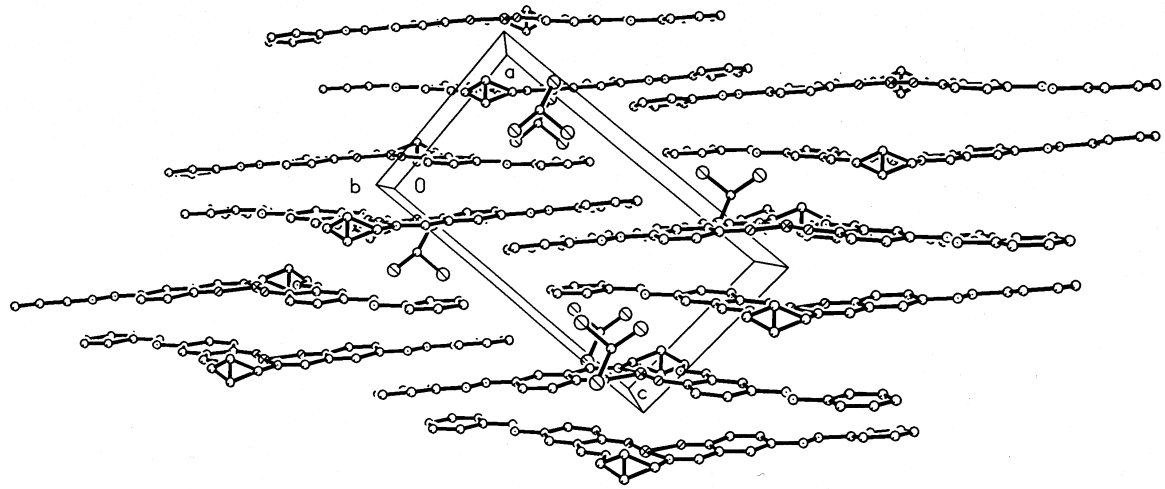


Fig. 2. Stereoview of the unit cell of the Cu5PHAZOSALTN·$CHCl_3$ (**III**).

Table 4
Selected bond lengths (Å) and angles (°) for Cu5PHAZOSALTN·$CHCl_3$ (**III**)

Cu(1)–O(1)	1.903(5)	Cu(1)–O(1′)	1.931(6)
Cu(1)–N(1′)	1.949(7)	Cu(1)–N(1)	1.962(7)
N(1)–C(2)	1.482(10)	N(1′)–C(2′)	1.459(10)
C(2)–C(1)	1.44(2)	C(2)–C(1′)	1.36(3)
C(2′)–C(1)	1.46(3)	C(2′)–C(1′)	1.36(3)
O(1)–Cu(1)–O(1′)	79.8(2)	O(1)–Cu(1)–N(1′)	171.8(3)
O(1′)–Cu(1)–N(1′)	92.4(3)	O(1)–Cu(1)–N(1)	92.1(3)
O(1′)–Cu(1)–N(1)	171.9(3)	N(1′)–Cu(1)–N(1)	95.7(3)
C(5)–O(1)–Cu(1)	130.5(5)	C(3)–N(1)–Cu(1)	124.8(6)
C(2)–N(1)–Cu(1)	123.3(6)	C(5′)–O(1′)–Cu(1)	130.6(5)
C(3′)–N(1′)–Cu(1)	123.4(6)	C(2′)–N(1′)–Cu(1)	124.4(6)

molecule in the crystal structure, with the empirical formula $C_{29}H_{24}CuN_6O_2 \cdot CHCl_3$ (formula weight 671.45).

3.3. Cyclic voltammetry

The cyclic voltammograms recorded (without iR compensation) for complexes **I–IV** are shown in Fig. 3 and the corresponding characteristic data are given in Table 5. Note that the free ligands are electroinactive in the working potential region.

On the basis of the cyclic voltammograms in Fig. 3, complex **I** undergoes an irreversible reduction process under the experimental condition (Fig. 3a). The peak separations ΔE ($=E_{pa}-E_{pc}$) for complexes **II**, **III** and **IV** were 82, 103 and 227 mV, respectively, at a scan rate of 0.05 V s^{-1}, and decreased to 62, 78 and 204 mV when the iR drop was compensated by the cyclic voltammetry set-up; thus the redox process for complex **II** is reversible and quasi-reversible for complexes **III** and **IV** [15]. Note that when a similar iR compensation is applied to the cell, the ferrocene behaved ideally and the peak separation for the ferricinium/ferrocene couple was at 60 mV, which can be used as a criterion for electrochemical reversibility in the present experimental conditions.

As seen in Table 5, the peak:current ratio decreases with increasing scan rate, indicating a weak adsorption of the reactants on the electrode [16]. For N_2O_2 Schiff base complexes of copper the redox potential is correlated with the degree of

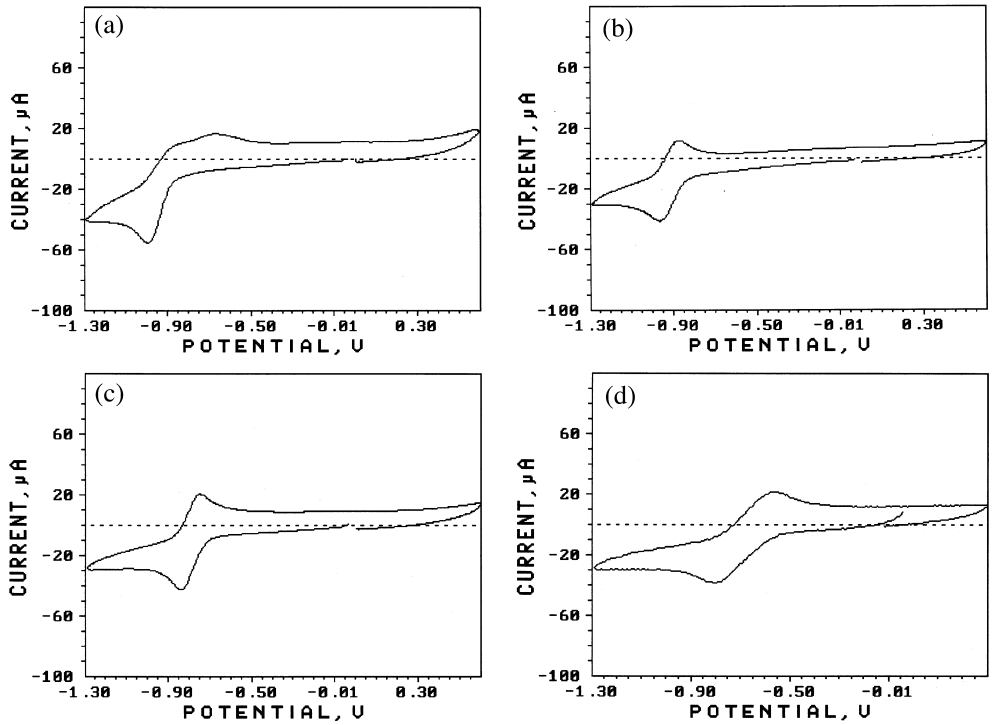


Fig. 3. Cyclic voltammograms (recorded without iR compensation) for (a) Cu5PHAZOSALEN (**I**), (b) Cu5PHAZOSALOPHEN (**II**), (c) Cu5PHAZOSALTN (**III**), (d) Cu5PHAZOSALDETA (**IV**) in DMF (0.002 M) with 0.1 M TBAP as supporting electrolyte at a scan rate 0.1 V s^{-1}.

Table 5
Cyclic voltammetry data (without iR compensation) for complexes **I–IV**

Scan rate (V s^{-1})	E_c (V)	E_a (V)	ΔE	I_c (μA)	I_a (μA)	I_a/I_c
Cu5PHAZOSALEN (**I**)						
0.05	−0.991			30		
0.1	−1.005			42		
0.2	−1.009			57		
0.3	−1.015			69		
0.4	−1.021			78		
0.5	−1.031			84		
Cu5PHAZOSALOPHEN (**II**)						
0.05	−0.970	−0.888	0.082	25.4	19.3	0.77
0.1	−0.974	−0.871	0.103	30.8	23.1	0.75
0.2	−0.981	−0.865	0.116	42.5	30.8	0.72
0.3	−0.993	−0.856	0.137	51.9	36.9	0.71
0.4	−1.005	−0.848	0.157	60.1	41.6	0.69
0.5	−1.025	−0.840	0.185	66.2	44.7	0.67
Cu5PHAZOSALTN (**III**)						
0.05	−0.851	−0.748	0.103	28.6	22.6	0.79
0.1	−0.863	−0.733	0.130	38.6	29.3	0.76
0.2	−0.873	−0.725	0.148	50.5	37.9	0.75
0.3	−0.881	−0.718	0.163	59.8	43.9	0.73
0.4	−0.890	−0.710	0.180	67.8	47.9	0.71
0.5	−0.900	−0.701	0.199	77.1	51.9	0.67
Cu5PHAZOSALDETA (**IV**)						
0.05	−0.785	−0.558	0.227	23.9	21.3	0.89
0.1	−0.798	−0.553	0.245	33.2	28.6	0.86
0.2	−0.820	−0.549	0.271	43.9	37.2	0.85
0.3	−0.825	−0.541	0.284	51.9	43.9	0.85
0.4	−0.852	−0.531	0.321	58.5	47.9	0.82
0.5	−0.860	−0.511	0.349	67.8	53.2	0.78

tetrahedral distortion of the copper coordination environment [17,18]. The more tetrahedral geometries correspond to less negative redox potential for Cu(II)/Cu(I) couples, whereas more planar geometries give rise to more negative potentials.

Complexes **I** and **II** can be assumed to be planar complexes [5]. The angles N(1′)–Cu–O(1) 171.8° and N(1)–Cu–O(1′) 171.9 in complex **III** indicate that the copper coordination environment is near square-planar; therefore the redox potential of this complex is less negative than the planar analogue. On the basis of the redox potential, we conclude that complex **IV** has a structure deviating from square-planar with N_2O_2 and not N_3O_2 coordination [5,19].

Supplementary data

Supplementary crystallographic data are available from the CCDC, 12, Union Road, Cambridge CB2 1EZ, UK (fax. +44-1223-336033; e-mail: deposit@ccdc.cam.ac.uk) on request, quoting the deposition number CCDC 120858.

Acknowledgements

We thank Professor A.I. Yanovsky, Russian Academy of Science, Moscow, for X-ray structure determination, Professor M.H. Pournaghi Azar for useful discussions on cyclic voltammetry investigations and Dr Pakdel, Laval University, Quebec, Canada, for ^{1}H NMR spectra.

References

[1] S.C. Bhatia, J.M. Bindlish, A.R. Saini, P.C. Jain, J. Chem. Soc., Dalton Trans. (1981) 1773.
[2] J.M. Bindlish, S.C. Bhatia, P.C. Jain, Indian J. Chem. 13 (1975) 81.
[3] R.P. Kashyap, J.M. Bindlish, P.C. Jain, Indian J. Chem. 11 (1973) 388.
[4] J.M. Bindlish, S.C. Bhatia, P. Gautam, P.C. Jain, Indian J. Chem., Sect. A 16 (1978) 279.
[5] I. Bernal, in: I. Bernal (Ed.), Stereochemical Control, Bonding and Steric Rearrangements, Elsevier, Amsterdam, 1990, Chapter 3.
[6] A.M. Giroud, P.M. Maitlis, Angew. Chem., Int. Ed. Engl. 30 (1991) 375.
[7] P. Espinet, M.A. Esteruelas, L.A. Oro, J.L. Serrano, E. Sola, Coord. Chem. Rev. 117 (1992) 215.
[8] S.A. Hudson, P.M. Maitlis, Chem. Rev. 93 (1993) 861.
[9] J.L. Serrano, J.L. Serrano, Metallomesogens, Syntheses, Properties and Applications, VCH, Weinheim, 1996.
[10] K.K. Chaturvedl, J. Inorg. Nucl. Chem. 39 (1977) 901.
[11] R.D. Archer, B. Wang, Inorg. Chem. 29 (1990) 39.
[12] R.-G. Xiong, B.-L. Song, J.-Z. Zuo, X.-Z. You, Polyhedron 15 (1996) 903.
[13] A.A. Khandar, Z. Rezvani, Polyhedron 18 (1998) 129.
[14] C.A. Root, J.D. Hoeschele, C.R. Cornman, J.W. Kampt, V.L. Pecoraro, Inorg. Chem. 32 (1993) 3855.
[15] A.J. Bard, L.R. Faulkner, Electrochemical Methods, Fundamentals and Applications, Wiley, New York, 1980, p. 230.
[16] A.J. Bard, L.R. Faulkner, Electrochemical Methods, Fundamentals and Applications, Wiley, New York, 1980, p. 530.
[17] G.S. Patterson, R.H. Holm, Bioinorg. Chem. 7 (1975) 257 and references cited therein.
[18] C. Fraser, B. Bosnich, Inorg. Chem. 33 (1994) 338.
[19] E.D. Mckenzie, S.J. Selvey, Inorg. Chim. Acta 18 (1976) L1.

PERGAMON

www.elsevier.nl/locate/poly

Polyhedron 19 (2000) 615–621

POLYHEDRON

Synthesis, structural and spectroscopic study of polymeric copper(I) thiocyanato complexes $[Cu(NCS)L]_n$ (L = methyl nicotinate and ethyl nicotinate) and $[HL][Cu(NCS)_2]$ (HL = H-ethyl isonicotinate)

Mohamed A.S. Goher [a,*], Qing-Chuan Yang [b], Thomas C.W. Mak [b]

[a] *Department of Chemistry, Faculty of Science, Kuwait University, P.O. Box 5969, Safat 13060, Kuwait*

[b] *Department of Chemistry, The Chinese University of Hong Kong, Shatin, New Territories, Hong Kong, People's Republic of China*

Received 17 June 1999; accepted 10 December 1999

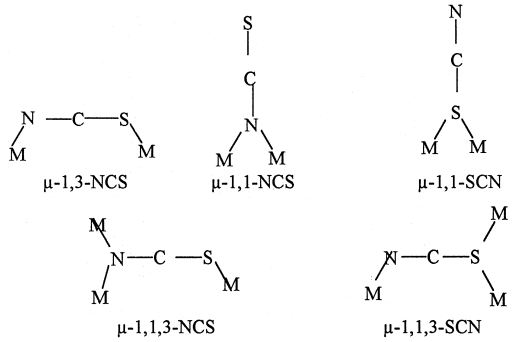
Abstract

Three new copper(I) thiocyanato complexes $[Cu(NCS)L]_n$ (L = methyl nicotinate **1**, ethyl nicotinate **2**), and $[HL][Cu(NCS)_2]$ (HL = H-ethyl isonicotinate **3**), have been prepared and characterized by spectroscopic and crystallographic methods. All three complexes display MLCT transitions in the visible region, as well as visible solid state emission spectra at room temperature. Their IR spectra are measured and discussed. In the structure of **1** each copper atom links two S atoms from two μ-S,S,N thiocyanato ligands and two nitrogen atoms from a pyridine nucleus and from a third μ-S,S,N thiocyanate group; the two S atoms bind another copper atom forming a Cu_2S_2 cyclic unit. The ladder propagates along the *a* axis of the unit cell. The structure of **2** features CuS_2N_2 coordination with approximate tetrahedral environment, μ-S,S,N bridging thiocyanate groups giving rise to corrugated layers at $y = 1/4$. Complex **3** consists of an N-protonated ethyl isonicotinate cation and a polymeric $[Cu(NCS)_2]^-$ anion. Each trigonal planar copper atom in the anion is coordinated by two S atoms from a μ-S,N thiocyanate bridge and a terminal S-thiocyanate group, and the third site is occupied by the end nitrogen of a μ-S,N thiocyanate bridge. The terminal NCS group forms a hydrogen bond of the type N–H···N with an N–H group of the $[HL]^+$ cation. The planar ribbon which runs in the *a* direction is further stabilized by N–H···O hydrogen bonds. ©2000 Elsevier Science Ltd All rights reserved.

Keywords: Copper(I) thiocyanate complexes; Methyl nicotinates; Ethyl nicotinates; Ethyl isonicotinate complexes; Crystal structures; Trigonal planar anions

1. Introduction

The pseudohalide NCS^- is known to coordinate to metals in both terminal and bridging modes. As bridging ligand the thiocyanate can link a pair of metal centers in either an end-on (μ-1,1-NCS, μ-1,1-SCN) or end-to-end (μ-1,3-NCS) configuration. The thiocyanate ion may link a third metal atom giving rise to a μ-1,1-3 (μ-N,N,S or μ-S,S,N) mode:



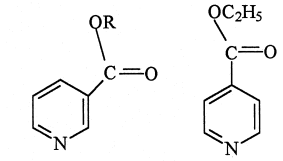
Binuclear, and polynuclear copper thiocyanate systems are of considerable interest owing to the broad range of their structural and magnetic properties [1,2]. However, the vast majority of studies have focused on copper(II) thiocyanate complexes [3,4]. On the other hand, reports on copper(I) thiocyanate complexes are relatively few. For example, only two structures, namely that of $[Cu_2L(\mu\text{-}1,1\text{-}SCN)_2]$ (L = macrocyclic Schiff base) [5] and $[Cu_2(\mu\text{-}Ph_2Ppypz)_2(\mu\text{-}1,1\text{-}SCN)][ClO_4]$ (Ph_2Ppypz = 2-(diphenylphosphino)-6-(pyrazol-1-yl)pyridine] [6] which exhibit μ-1,1-SCN bridges have been established.

Previously we have shown that when a mixture of CuNCS and 2-benzoylpyridine stands in an ethanol medium for about 2 weeks in contact with air, the intramolecular oxidative cyclization of 2-benzoylpyridine occurs with the formation of [9-oxo-indolo[1,2-*a*]pyridinium]$^+$[$Cu(NCS)_2$]$^-$, whereas CuCN and 2-benzoylpyridine under the same conditions lead to the formation of a polymeric 1:1 copper(I) complex [7]. Also, we have shown that copper(I) azide dissolved in excess NaN_3 interacts with pyrazinecarboxamide

* Corresponding author.

0277-5387/00/$ - see front matter ©2000 Elsevier Science Ltd All rights reserved.
PII S0277-5387(99)00385-X

in ethanol giving a novel polymeric copper(I) complex containing an unusual μ-1,1,3-N_3 bridge, and we have established that such methodology is a potentially versatile approach to the construction of uncharged inorganic coordination networks [8]. We have used this approach for the preparation of the copper(I) thiocyanato complexes of methyl nicotinate and ethyl nicotinate (**I**) and ethyl isonicotinate (**II**). In the present paper we describe the synthesis and characterization of the title complexes as elucidated by spectroscopic and crystallographic methods.



2. Experimental

Methyl nicotinate, ethyl nicotinate and ethyl isonicotinate were obtained from Aldrich; the other chemicals were of analytical grade quality.

2.1. Preparation of the complexes

2.1.1. Polymeric [CuNCS(methyl nicotinate)]$_n$ (*1*)

This complex was prepared by mixing aqueous solutions of $Cu(NO_3)_2 \cdot 3H_2O$ (0.48 g, 2 mmol) and NaNCS (0.164 g, 2 mmol) in the presence of excess L(+) ascorbic acid. To the precipitated CuSCN obtained by decantation of the aqueous layer, a concentrated aqueous solution of NaSCN was added until complete dissolution, and any impurities filtered off. An ethanol solution of methyl nicotinate (0.548 g, 4 mmol) was added to the clear solution, and the final mixture allowed to stand in an open beaker over several days until pale yellow needle-like crystals of the complex deposited. Yield 20% (with respect to copper). *Anal*. Found: C, 37.0; H, 2.8; N, 10.9; S, 12.1; Cu, 24.7. Calc. for $C_8H_7CuN_2O_2S$: C, 37.13; H, 2.73; N, 10.82; S, 12.37; Cu, 24.55%.

2.1.2. Polymeric [CuNCS(ethyl nicotinate)]$_n$ (*2*)

This complex was prepared according to the above procedure except that an ethanol solution of ethyl nicotinate was added to the clear aqueous solution of CuNCS dissolved in concentrated solution of NaNCS. The final mixture was allowed to stand over several days to produce yellow crystals of the complex. Yield 25% (with respect to copper). *Anal*. Found: C, 39.8; H, 2.4; N, 10.1, S, 11.6; Cu, 23.4. Calc. for $C_9H_9CuN_2O_2S$: C, 39.62; H, 3.73; N, 10.26; S, 11.73; Cu, 23.29%.

2.1.3. [(Ethyl isonicotinate)H][Cu(NCS)$_2$] (*3*)

A concentrated aqueous solution of NaNCS was added to a suspension of CuSCN (3 mmol) until complete dissolution, followed by addition of an ethanol solution of ethyl isonicotinate (3 mmol), upon which the solution turned yellow.

This clear solution mixture was allowed to stand in open air over 2–3 weeks to yield yellow crystals of the complex. *Anal*. Found: C, 36.3; H, 3.2; N, 12.4; S, 19.1; Cu, 19.3. Calc. for $C_{10}H_{10}CuN_3O_2S_2$: C, 36.19; H, 3.04; N, 12.65; S, 19.28; Cu, 19.15%.

2.2. Physical measurements

The experimental procedures and instruments used for different physical measurements are as described previously [9].

2.3. X-ray crystallography

Information concerning crystallographic data and structure refinement of the three complexes is summarized in Table 1. Data collection was performed on a Siemens R3m/V diffractometer in the variable ω-scan mode [10] using Mo Kα radiation ($\lambda = 0.71073$ Å). Unit cell parameters were calculated from least-squares fitting of 2θ angles. The raw data were processed with a learnt-profile procedure [11], and empirical absorption corrections based on ω-scan data were also applied.

All calculations were performed on a PC 486 computer with the SHELXTL/PC program package [12]. Each crystal structure was solved with the Patterson superposition method. The non-hydrogen atoms were refined anisotropically. All hydrogen atoms were generated geometrically, assigned fixed isotropic thermal parameters and included in the structure factor calculations. Analytical expressions of neutral-atom scattering factors were employed [13], and anomalous dispersion corrections were incorporated.

3. Results and discussion

The reactions between aqueous copper(I) thiocyanate dissolved in excess sodium thiocyanate with the esters of nicotinic and isonicotinic acids in ethanol afforded copper(I) complexes of the type Cu(NCS)L for L = methyl nicotinate and ethyl nicotinate and an ionic complex [LH][Cu(NCS)$_2$] when L is ethyl isonicotinate. Using this procedure allowed us to avoid the isolation of any Cu^{II} impurities, and single crystals of the above complexes were obtained. The three complexes are yellow, diamagnetic and sufficiently stable against air-oxidation when well dried. They are insoluble or slightly soluble in many common non-polar and polar solvents, e.g. benzene, toluene, water, methanol, ethanol, acetone, etc.

Table 1
Crystal data and structure refinement for complexes **1**, **2** and **3**

	1	**2**	**3**
Empirical formula	$C_8H_7CuN_2O_2S$	$C_9H_9CuN_2O_2S$	$C_{10}H_{10}CuN_3O_2S_2$
Formula weight	258.76	272.78	331.87
Temperature (K)	296(2)	293(2)	293(2)
Crystal system	monoclinic	monoclinic	orthorhombic
Space group	$P2_1/n$	$P2_1$	*Pnma*
Unit cell dimensions			
a (Å)	5.822(1)	3.896(1)	7.8426(9)
b (Å)	12.448(3)	10.732(3)	6.7134(8)
c (Å)	13.298(3)	12.423(9)	26.207(3)
α (°)	90	90	90
β (°)	93.36(3)	93.12(2)	90
γ (°)	90	90	90
Volume (Å^3)	962.1(3)	518.7(4)	1379.8(3)
Z	4	2	4
D_{calc} (Mg m^{-3})	1.786	1.747	1.598
Absorption coefficient	2.458	2.285	1.881
$F(000)$	520	276	672
Crystal size (mm)	0.58×0.39×0.27	0.30×0.14×0.12	0.28×0.15×0.13
θ Range for data collection (°)	2.24–28.32	2.51–25.07	1.55–28.30
Reflections collected	6819	1391	9222
Independent reflections	2394 (R_{int} = 0.0185)	1319 (R_{int} = 0.000)	1857 (R_{int} = 0.0408)
Max. and min. transmission	1.0000, 0.7453	1.128, 0.806	1.0000, 0.6583
Data/restraints/parameters	2394/0/156	1391/1/146	1857/0/110
Goodness-of-fit on F^2	1.064	1.078	0.987
Final R indices ($I>2\sigma(I)$)	R_1 = 0.0272	R_1 = 0.0667	R_1 = 0.0321
	wR_2 = 0.0726	wR_2 = 0.1832	wR_2 = 0.0721
R indices (all data)	R_1 = 0.0351	R_1 = 0.0692	R_1 = 0.0544
	wR_2 = 0.0758	wR_2 = 0.1854	wR_2 = 0.0785
Largest difference peak and hole	0.399, 0.662	1.036, −0.616	0.236, −0.333

3.1. Structures

3.1.1. [Cu(NCS)(methyl nicotinate)]$_n$ (1)

Fig. 1 illustrates the principle structural features of complex **1**, along with the atom numbering scheme; bond lengths and bond angles are given in Table 2. Each copper atom, Cu(1), coordinates two nitrogen atoms, from a methyl nicotinate and a thiocyanato ligand. The other two coordination sites are occupied by two sulfur atoms from two thiocyanato ligands, giving rise to an approximate tetrahedral environment around the copper atom. The two sulfur atoms further link a second copper atom, Cu(1A), forming a Cu_2S_2 cyclic unit. Thus the thiocyanate groups function as tridentate μ-S,S,N bridges connecting three different metal centers, resulting in a ladder extended along the *a* axis of the unit cell (Fig. 2). The Cu–N(L) bond length of 2.013(2) Å is within the range of 2.00–2.05 Å found for copper(I) complexes with pyridine and substituted pyridines [14,15]. While the Cu–N(NCS) of 1.944(2) Å match very well, the Cu–S distances are significantly longer than corresponding distances found in the structure of polymeric [$Cu_2(NCS)_2$(pyrazine)]$_n$ (Cu–N = 1.940(4) and Cu–S = 2.249(2), 2.338(2) Å) [16]. The pyrazine complex, however, contains μ-N,S thiocyanate bridges.

3.1.2. [Cu(NCS)(ethyl nicotinate)]$_n$ (2)

The most relevant feature of the structure of complex **2** is the disposition of Cu(I) ions in a two-dimensional lattice. Within each layer the metal ions are bridged by two sulfur atoms from two thiocyanate bridges and two nitrogen atoms from a thiocyanate bridge and from an ethyl nicotinate ligand. Thus each copper atom is tetra-coordinated, giving rise to a CuS_2N_2 chromophore. A view of the chromophore along with the atom labeling scheme is given in Fig. 3, while selected bond lengths and bond angles are listed in Table 2. Within the coordination polyhedron the Cu–N(L) of 2.033(4) Å is slightly longer than the corresponding distance, whereas the Cu–N(NCS) and Cu–S distances are within the ranges found in complex **1**. As seen from Fig. 4, each thiocyanate group functions in the μ-1,1,3-SCN mode as found in the structure of complex **1**. The structure of complex **2**, however, differs from that of **1**. In complex **1** two sulfur atoms from two thiocyanate groups link the same two copper atoms giving rise to a cyclic Cu_2S_2 unit, but in complex **2** the sulfur atoms of two thiocyanate ligands bind three different metal centers, giving rise to corrugated layers at $z = 1/2$, and hence the structure does not contain the Cu_2S_2 cyclic units.

3.1.3. [(Ethyl isonicotinate)H][Cu(NCS)$_2$] (3)

The principle structural features of complex **3** are illustrated in Fig. 5; bond lengths and bond angles are given in

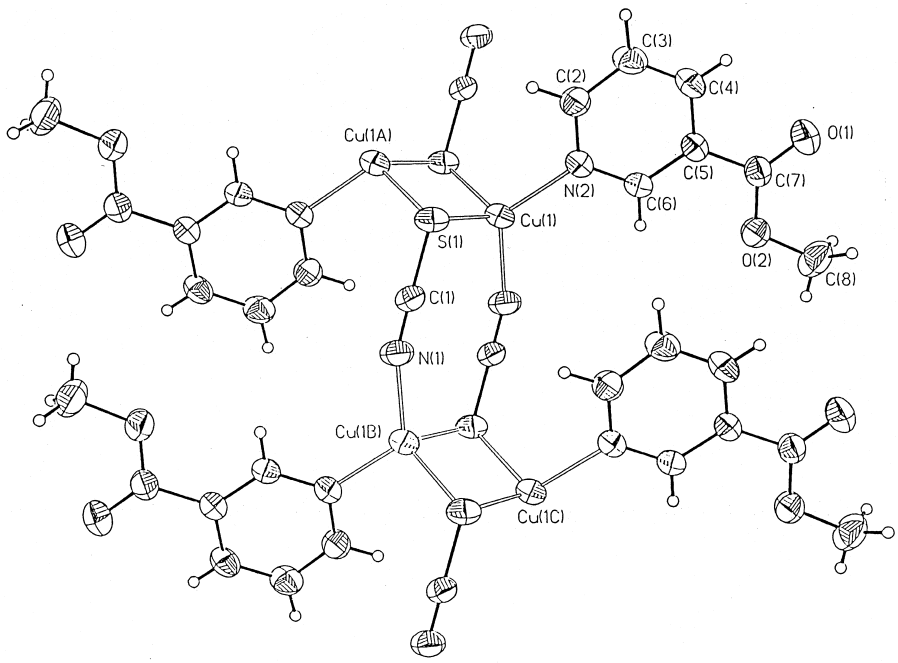


Fig. 1. Atom labeling and principle structural features of polymeric [Cu(SCN)(methyl nicotinate)]$_n$ (**1**).

Table 2
Selected bond lengths (Å) and bond angles (°) for complexes **1**, **2** and **3**

Complex **1** [a]			
Cu(1)–N(1)#1	1.944(2)	Cu(1)–N(2)	2.013(2)
Cu(1)–S(1)#2	2.3576(9)	Cu(1)–S(1)	2.5245(7)
Cu(1)–Cu(1)#2	2.8465(7)	S(1)–C(1)	1.654(2)
S(1)–Cu(1)#2	2.3576(9)	N(1)–C(1)	1.155(3)
N(1)–Cu(1)#1	1.944(2)		
N(1)#1–Cu(1)–N(2)	122.69(7)	N(1)#–Cu(1)–S(1)#2	108.10(6)
N(2)–Cu(1)–S(1)#2	109.39(5)	N(1)#1–Cu(1)–S(1)	103.56(5)
N(2)–Cu(1)–S(1)	103.46(5)	S(1)#2–Cu(1)–S(1)	108.77(2)
C(1)–S(1)–Cu(1)	94.75(7)	Cu(1)#2–S(1)–Cu(1)	71.23(2)
C(1)–N(1)–Cu(1)#1	159.9(1)	C(2)–N(2)–Cu(1)	121.4(1)
C(6)–N(2)–Cu(1)	120.8(1)	N(1)–C(1)–S(1)	178.9(2)
Complex **2** [b]			
Cu(1)–N(1)#1	1.944(4)	Cu(1)–N(2)	2.033(4)
Cu(1)–S(1)#2	2.373(1)	Cu(1)–S(1)	2.452(1)
S(1)–C(1)	1.648(4)	N(1)–C(1)	1.159(5)
N(1)#1–Cu(1)–N(2)	120.2(1)	N(1)#1–Cu(1)–S(1)#2	106.0(1)
N(2)–Cu(1)–S(1)#2	113.2	N(1)#1–Cu(1)–S(1)	108.5(1)
N(2)–Cu(1)–S(1)	100.6(1)	S(1)#2–Cu(1)–S(1)	107.68(5)
C(1)–S(1)–Cu(1)#3	107.0(1)	C(1)–S(1)–Cu(1)	102.6(1)
C(1)–N(1)–Cu(1)#4	175.3(3)	C(6)–N(2)–Cu(1)	123.2(3)
C(5)–N(2)–Cu(1)	120.1(3)	N(1)–C(1)–S(1)	178.7(3)
Complex **3** [c]			
Cu(1)–N(1)#1	1.893(3)	Cu(1)–S(2)	2.2587(9)
Cu(1)–S(1)	2.2640(9)	S(1)–C(1)	1.648(3)
C(1)–N(1)	1.152(4)	S(2)–C(2)	1.654(3)
C(2)–N(2)	1.154(4)		
N(1)#1–Cu(1)–S(2)	121.83(9)	N(1)#1–Cu(1)–S(1)	125.19(9)
S(2)–Cu(1)–S(1)	112.97(3)	C(1)–S(1)–Cu(1)	97.5(1)
N(1)–C(1)–S(1)	179.7(3)	C(2)–S(2)–Cu(1)	94.4(1)
N(2)–C(2)–S(2)	179.1(3)		

[a] Symmetry transformations used to generate equivalent atoms: #1 $-x+1, -y, -z$; #2 $-x, -y, -z$.
[b] Symmetry transformation used to generate equivalent atoms: #1 $-x+1, y-12, -z+1$; #2 $x+1, y, z$; #3 $x-1, y, z$; #4 $-x+1, y+1/2, -z-1$.
[c] Symmetry transformation used to generate equivalent atoms: #1 $x-1/2, y, -z+1/2$.

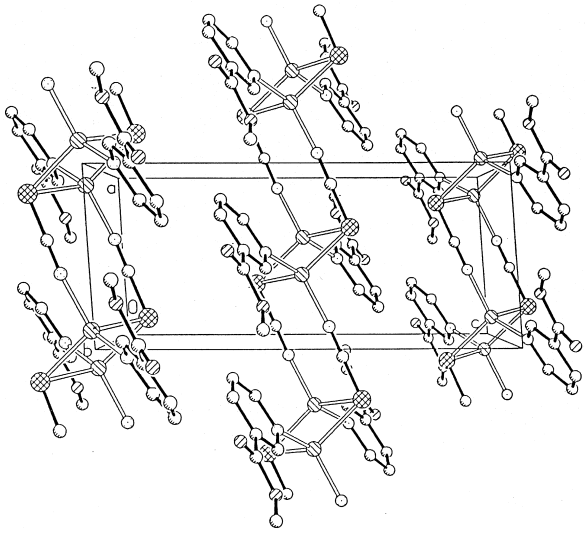


Fig. 2. Stereoview of the crystal structure of polymeric [Cu(SCN)(methyl nicotinate)]$_n$ (**1**).

Table 2. The structure of this complex consists of a packing of N-protonated ethyl isonicotinate cations and polymeric $[Cu(NCS)_2]^-$ species. Ethyl isonicotinate thus differs from methyl nicotinate, or ethyl nicotinate in that its nitrogen atom is protonated and does not enter in the coordination sphere of the copper atom. In the polymeric $[Cu(NCS)_2]^-$ species, each copper atom is coordinated by two sulfur atoms (Cu–S = 2.2587(9) and 2.2640(9) Å) and one nitrogen atom (Cu–N = 1.893(3) Å) from three different thiocyanate ligands, giving rise to approximate trigonal planar geometry around the copper centers. It is clear from Fig. 5 that one independent thiocyanato group S(1)–C(1)–N(1) functions as a μ-1,3-NCS bridging bidentate ligand, giving rise to a planar ribbon at $y = 1/4$ running in the *a* direction of the unit cell. The other independent thiocyanate group acts as a monodentate ligand with S(2) linked to a copper atom; S-coordinated ligands of this type protrude on both sides of each layer and serve as partitions for adjacent heterocyclic cations arranged in rows parallel to the *c* axis. The nitrogen atom, N(2), of the monodentate thiocyanate ligand forms a hydrogen bond of the type N–H···N with the N–H group of the N-protonated ethyl isonicotinate molecule. The structure of the compound is further consolidated by another hydrogen bond of the type C–H···O between the C(7)–H and oxygen atom, O(1), of two adjacent protonated ethyl isonicotinate molecules. Both thiocyanate groups are linear (angles 179.1(3) and 179.7(3)°) within experimental error.

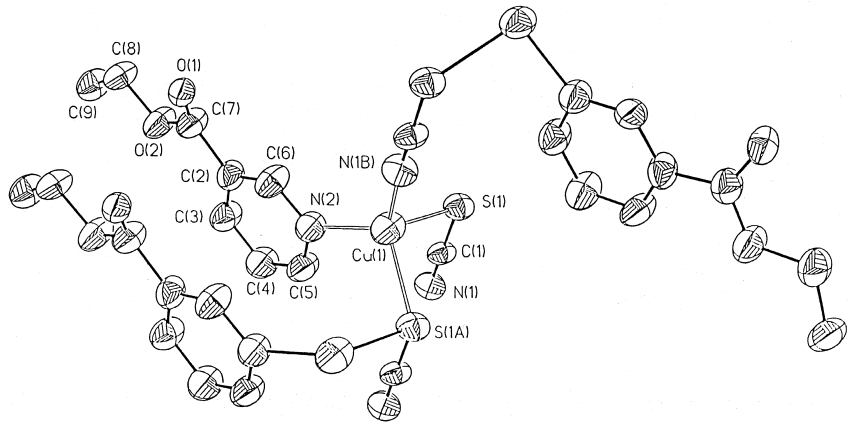


Fig. 3. Atom labeling and principle structural features of polymeric [Cu(SCN)(ethyl nicotinate)]$_n$ (**2**).

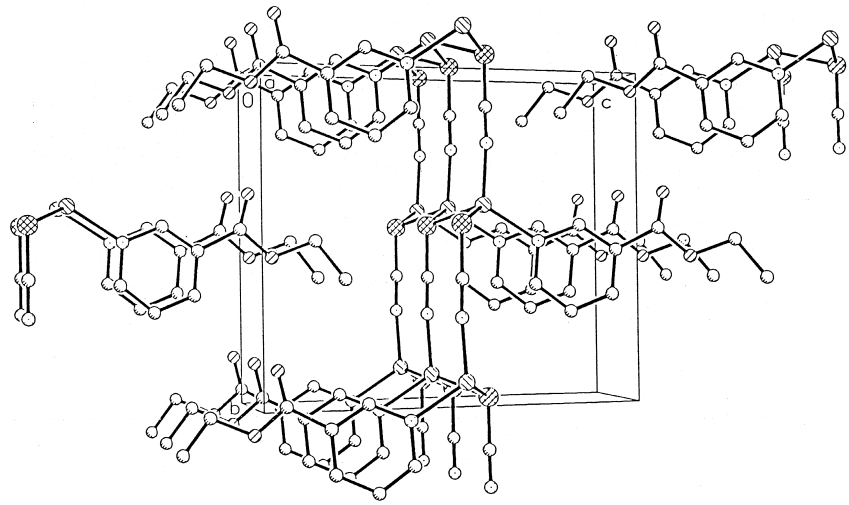


Fig. 4. Stereoview of the crystal structure of polymeric [Cu(SCN)(ethyl nicotinate)]$_n$ (**2**).

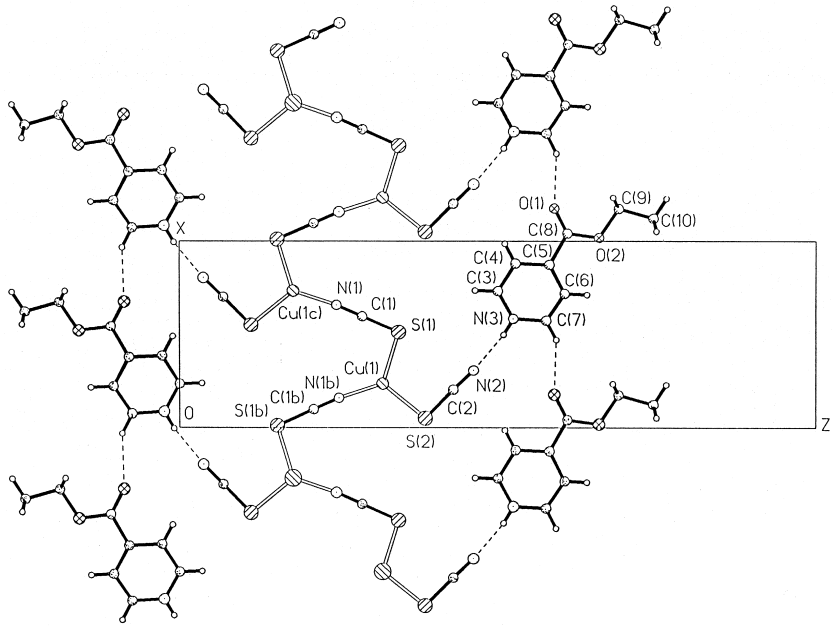


Fig. 5. The coordination environment of the copper(I) atom and the cation in the complex [(ethyl isonicotinate)H][$Cu(SCN)_2$] (**3**). Hydrogen bonds are represented by broken lines.

The structure of the present $[Cu(NCS)_2]^-$ species differs from that of the corresponding species found in the structure of [9-oxo-indolo[1,2-*a*]pyridinium]$^+[Cu(NCS)_2]^-$, although both are polymeric. In the latter species, each copper atom is tetrahedrally coordinated by two nitrogen atoms (Cu–N(av) = 1.947 Å) and two sulfur atoms (Cu–S = 2.373(2) and 2.471(2) Å). This species contains an independent μ-1,1,3-SCN bridging tridentate ligand in which the sulfur atom links two different copper atoms, whereas the nitrogen atom binds a third copper center, giving rise to a puckered layer; the other thiocyanate group acts as an N-monodentate ligand [7].

3.2. Electronic and IR spectra

The electronic spectra of solid samples of the three copper(I) complexes exhibit strong broad absorption bands over the range 300–450 nm (Table 3) due to MLCT transitions in complexes **1** and **2**. For complex **3**, however, L is protonated rather than coordinated, and the charge transfer therefore could not be of the above type. It is possible that the charge transfer in this case is due to XLCT (X = anion).

Table 3
Electronic, IR and emission spectral data

	1	**2**	**3**
Electronic spectra [a]			
λ_{max} (MLCT) (nm)	300–380s	300–400s	300–450s
IR (cm^{-1})			
ν(CN)	2111vs, 2070m	2119vs, 2085m	2117vs, 2076ms
ν(CS)	756m, 696m	755m, 694wm	757m, 689wm
ν(C=O)	1728vs	1722vs	1723vs
ν(N–H···H+)			3420m,br
ν(C–H···O)			3097, 2990m
Emission spectra [b]			
λ_{max} (nm)	499	498	575

[a] Samples measured as solids mulled in Nujol.
[b] Excitation wavelength 358 nm.

The IR spectra (Table 3) of complexes **1**–**3** show two strong absorption peaks above and below 2100 cm^{-1}, associated with the ν(CN) mode of the thiocyanato ligands, in addition to two weak to medium bands due to the ν(CS) mode. These results, while suggesting bridging thiocyanato ligands, cannot distinguish between μ-1,3 and μ-1,1,3 thiocyanate bridges. This result, however, is not uncommon. For example, the IR spectrum of [9-oxo-indolo[1,2-*a*]-[pyridinium][$Cu(NCS)_2$], which contains μ-1,1,3-SCN and terminal NCS groups also exhibits two ν(CN) peaks at 2105 and 2075 cm^{-1} [7]. Bands due to hydrogen bonds are observed in the region 3450–2800 cm^{-1}, in the spectrum of complex **3** only. The small shift of the ν(C=O) band in the spectrum of complex **3** to a lower frequency compared with that of free ligand (1735 cm^{-1}) is due to hydrogen bonding, N–H···O formation with the N–H group of an adjacent molecule. The N-protonation of ethyl isonicotinate manifests itself in a large shift [17] of the vibration bands related to the pyridine ring to higher frequencies (1633, 1605, 1557 cm^{-1}) when compared with those of free ligand (1600, 1570 cm^{-1}) or with other copper(I) complexes of the same ligand [18].

3.3. Emission spectra

The results of the emission spectra of complexes **1**–**3** in the solid state at room temperature are given in Table 3 and Fig. 6. The three compounds fluoresce in the solid state and their emission spectra exhibit a single band, slightly asym-

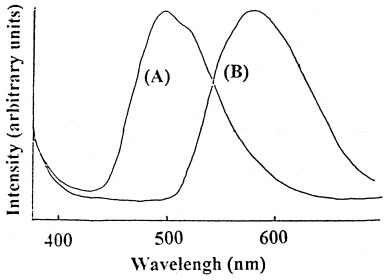


Fig. 6. Emission spectra of solid complexes at room temperature: (A) [Cu(SCN)(methyl nicotinate)]$_n$ (**1**); (B) [(ethyl isonicotinate)H]-[Cu(SCN)$_2$] (**3**).

metric for complex **3**, but with a pronounced shoulder on the lower energy side for both complexes **1** and **2**. While the λ_{max} of the main band appears at 498 and 499 nm for **1** and **2**, respectively, complex **3** shows λ_{max} at 575 nm. The luminescence spectra of these complexes proved independent of the excitation wavelength at room temperature. Previous studies [19–22] of the emission spectra of copper(I) halides of pyridine and pyridine derivatives have shown that these complexes display a high energy (HE) band (430–540 nm) attributed to metal-to-ligand charge transfer (MLCT) or XLCT, and a low energy (LE) band (620–698 nm) related to the metal center in complexes with Cu···Cu distance of less than 2.8 Å. The energies of the former band are quite sensitive to the substituent on the pyridine; the electron-withdrawing substituent shifts these bands to lower energy values. The results given in Table 3 suggest that the emission observed in the present complexes **1** and **2** is attributed to the MLCT transition states. In the case of complex **3**, the emission is substantially due to XLCT (X = anion) transition since the ligand L is protonated and not coordinated to the copper atom. That the λ_{max} of the emission band observed for complex **3** is shifted to lower energy compared to those for **1** and **2**, which reflects the difference between the source of the emission in both cases, is also consistent with what has been observed previously [23,24], and suggests that the HE emission band (MLCT) is not only sensitive to the nature of the substituent group, but is also sensitive to its position in the pyridine ring.

Supplementary data

Supplementary data are available from the CCDC, 12 Union Road, Cambridge CB2 1EZ, UK (fax: +44-1223-336033; e-mail: deposit@ccdc.cam.ac.uk) on request, quoting the deposition numbers; CCDC 121740, 121741 and 121744, for **1**, **2** and **3**, respectively.

Acknowledgements

M.A.S.G. thanks the Department of Chemistry, Faculty of Science, Kuwait University (Analab) for performing some measurements. T.C.W.M. acknowledges the Hong Kong Research Grants Council Earmarked Grant Ref. No. CUHK 4022/98P.

References

[1] J.L.R. Larramendi, J.L. Mesa, R. Cortes, T. Rojo, M.K. Urtiaga, M.I. Arriortua, Polyhedron 11 (1992) 623.
[2] M.I. Arriortua, J.L. Mesa, T. Rojo, T. Debaerdemaeker, D. Beltrain, H. Stratemeier, D. Reinen, Inorg. Chem. 27 (1988) 2976.
[3] J.P. Cornelissen, R.A.G. De Graaff, J.G. Haasnoot, R. Prins, J. Reedijk, M. Biagini-Cingi, A.M. Manotti-Lanfredi, A. Tiripicchio, Polyhedron 8 (1989) 2313.
[4] J.G. Haasnoot, W.L. Driessen, J. Reedijk, Inorg. Chem. 23 (1984) 2803.
[5] S.M. Nelson, F.S. Esho, M.G.B. Drew, J. Chem. Soc., Chem. Commun. (1981) 388.
[6] S.-M. Kuang, Z.-Z. Zhang, Q.-G. Wang, T.C.W. Mak, J. Chem. Soc., Dalton. Trans. (1997) 4477.
[7] M.A.S. Goher, R.-J. Wang, T.C.W. Mak, J. Coord. Chem. 38 (1996) 151.
[8] M.A.S. Goher, F.A. Mautner, J. Chem. Soc., Dalton Trans. (1999) 1535.
[9] M.A.S. Goher, T.C.W. Mak, Polyhedron 17 (1998) 3485.
[10] R.A. Sparks, in: F.R. Ahmed (Ed.), Crystallographic Computing Techniques, Munksgaard, Copenhagen, 1976, p. 452.
[11] G. Kopfmann, R. Huber, Acta Crystallogr., Sect. A 24 (1968) 348.
[12] G.M. Sheldrick, in: G.M. Sheldrick, C. Kruger, R. Goddard (Eds.), Crystallographic Computing 3: Data Collection, Structure Determination, Proteins and Databases, Oxford University Press, New York, 1985, p. 175.
[13] G.M. Sheldrick, SHELXL 93, a Program for the Refinement of Crystal Structure, University of Göttingen, Germany, 1993.
[14] A.H. Lewin, R.J. Michl, P. Ganis, U. Lepore, G. Avitabile, J. Chem. Soc., Chem. Commun. (1971) 1400.
[15] E.W. Ainscough, A.G. Bingham, A.E. Brodie, K.L. Brown, J. Chem. Soc., Dalton Trans. (1984) 989.
[16] A.J. Blake, N.R. Champess, M. Crew, L.R. Hanton, S. Parsons, M. Schröder, J. Chem. Soc., Dalton Trans. (1998) 1533.
[17] P.C.H. Mitchell, J. Inorg. Nucl. Chem. 21 (1961) 382.
[18] M.A.S. Goher, M. Dratovsky, J. Inorg. Nucl. Chem. 38 (1976) 1269.
[19] K.R. Kyle, P.C. Ford, Coord. Chem. Rev. 97 (1990) 35.
[20] K.R. Kyle, C.K. Ryu, P.C. Ford, J. Am. Chem. Soc. 113 (1991) 2954.
[21] N.P. Rath, E.M. Holt, K. Tanimura, Inorg. Chem. 24 (1985) 3934.
[22] N.P. Rath, R. Holt, J. Chem. Soc., Dalton Trans. (1986) 2303.
[23] C.K. Ryu, M. Vitale, P.C. Ford, Inorg. Chem. 32 (1993) 869.
[24] F.A. Mautner, M.A.S. Goher, Polyhedron 19 (1999) 553.

PERGAMON

www.elsevier.nl/locate/poly

Polyhedron 19 (2000) 623–626

POLYHEDRON

Crystal structure of a copper stabilized hydrate of di-2-pyridyl ketone

O. Jerry Parker *, Sheryl L. Aubol, Gary L. Breneman

Department of Chemistry and Biochemistry, Eastern Washington University, Cheney, WA 99004, USA

Received 14 May 1999; accepted 6 December 1999

Abstract

The addition of a yellow ethanolic solution of di-2-pyridyl ketone to a blue–green aqueous solution of copper(II) bromide produces an exothermic reaction and a brilliant purple solution. Brilliant purple single crystals were obtained from the solution by solvent evaporation and were subjected to a crystal structure determination. The structure of the isolated *gem*-diol compound stabilized by a transition metal contains two di(2-pyridyl)methanediol ligands bonded to the central copper atom in a distorted octahedral arrangement providing four nitrogen atoms at relatively short bond distances and two oxygen atoms at longer bond distances. In the solid state, both oxygen atoms on each of the *gem*-diol ligands are protonated. ©2000 Elsevier Science Ltd All rights reserved.

Keywords: Copper; *gem*-Diol,di-2-pyridyl ketone; Di(2-pyridyl)methanediol; Crystal structures

1. Introduction

The reversible addition of water to carbonyl compounds yielding hydrates (*gem*-diol compounds) has been a subject of considerable interest [1–7]. The hydration reaction has been extensively studied as the mechanistic prototype for many reactions at carbonyl centers. Most *gem*-diol compounds are too unstable or too labile to isolate for determination of the crystal or molecular structure. Predominant examples of stable hydrated ketones are polyhaloginated ketones and cyclic compounds such as chloral hydrate and the hydrate of cyclopropanone. The fluorinated alcohol hexafluoropropane-2,2-diol, $(CF_3)_2C(OH)_2$, forms *gem*-diol complexes with many metals such as Cu^{2+}, Ni^{2+}, Co^{3+}, Mn^{2+} and Pt^{2+} in a variety of structures with at least three different modes of coordination [8–10]. Recent interest in di-2-pyridyl ketone as a ligand has shown that several different types of structures are possible. Di-2-pyridyl ketone can function as a bidentate ligand with bonding through the two nitrogens or as a tridentate ligand with bonding through the oxygen and two nitrogen atoms [11]. Mononuclear and polynuclear transition metal complexes with ligands of di-2-pyridyl ketone that has undergone hydrolysis and alcoholysis have been reported [12–17]. The title compound is a copper(II) complex that has two stable *gem*-diol ligands in the solid state and presumably in the aqueous solution from which it was prepared. The stability of the crystalline state is enhanced by a system of hydrogen bonding involving both hydroxy groups of the hydrated di-2-pyridyl ketone ligands through water molecules. The hydrated di-2-pyridyl ketone ligands are stabilized by modifying the angles about the carbon to the normal tetrahedral angles while preserving a square planar configuration about the copper. The complex has a molecular composition represented by $[Cu(dpydiol)_2]$-$Br_2 \cdot 4H_2O$, where dpydiol = di(2-pyridyl)methanediol, and an empirical formula of $[Cu(C_{11}H_{10}N_2O_2)_2]Br_2 \cdot 4H_2O$. The presence of two bromide anions for each $[Cu(dpydiol)_2]^{2+}$ cation shows that both oxygen atoms on each di(2-pyridyl)methanediol ligand are protonated in the solid state. The dimensions of the ligand and the tetrahedral angle about the *gem*-diol carbon requires that the six-membered ring formed by this carbon, two additional carbons and two nitrogens from each pyridyl ring, and the center copper atom be stable in either a chair or boat type configuration. The observed boat configuration places one of the oxygen atoms on the *gem*-diol carbon close to the fifth position of an octahedral stereochemistry about the copper atom. The second di(2-pyridyl)menthanediol ligand furnishes two of the nitrogen atoms and an oxygen atom from one of the two hydroxy groups on the *gem*-diol to complete the distorted octahedral arrangement around the central copper atom.

* Corresponding author. Tel.: +1-509-359-6521; fax: +1-509-359-6973; e-mail: jparker@ewu.edu

0277-5387/00/$ - see front matter ©2000 Elsevier Science Ltd All rights reserved.
PII S0277-5387(99)00393-9

2. Results and discussion

2.1. Crystal and molecular structure of $[Cu(dpydiol)_2]Br_2 \cdot 4H_2O$

A summary of the crystal data is given in Table 1. Selected bond distances and bond angles are presented in Table 2. A thermal ellipsoid plot of the structure and atom numbering scheme with hydrogen atoms omitted is shown in Fig. 1. Fig. 2 shows the hydrogen bonding network between molecules. Fig. 3 shows a unit cell packing diagram.

The X-ray structure of the complex (Fig. 1) contains a copper atom positioned at a center of inversion. The nitrogens from the two di(2-pyridyl)methanediol ligands surround the copper atom in a square planar arrangement with Cu–N1 and Cu–N2 bond distances of 2.011(4) Å and an N1–Cu–N2 angle of 87.8(1)°. The crystallographic symmetry demands that the N1–Cu–N1′ angle be 180°. The fifth and sixth positions which form a distorted octahedral arrangement about the copper atom are occupied by an oxygen atom of one of the two hydroxy groups on each di(2-pyridyl)methanediol ligand. The Cu–O2 distance is 2.464(3) Å with O2–Cu–N1 and O2–Cu–N2 angles of 74.9(1) and 73.6(1)° respectively. The bond distances are very similar to those reported for $[Cu\{C_{11}H_8N_2(OH)_2\}_2](ClO_4)_2$ with Cu–N1 of 2.009(2) Å and Cu–N2 of 2.010(2) Å and the Cu1–O1 distance is 2.454(3) Å [17]. The structure and bond distances are very similar to those reported for $[Cu\{C_{11}H_8N_2(OH)_2\}_2]$-$Cl_2 \cdot 4H_2O$, with Cu–N1 of 2.006(5) Å and Cu–N2 of 1.994(5) Å and the Cu–O1 distance is 2.465(5) Å, and for the compound $Cu\{C_{11}H_8N_2(OH)_2\}_2](NO_3)_2 \cdot 2H_2O$ with Cu–N1 of 1.990(5) Å and Cu–N2 of 2.036(5) Å and the Cu–O1 distance is 2.464(4) Å [12].

The Cu–O distance of 2.464(3) Å is very similar to the long Cu–O distance of 2.43 Å in $Cu(DMG)_2$, where DMG = dimethylglyoxime [18], and 2.397(8) Å for anhydrous copper(II) formate [19]. The O1 atom of the hydroxy group that does not occupy an octahedral position about the copper atom is slightly distorted from the expected tetrahedral angles about the C6 atom as seen in Table 1. Both hydroxy groups on each di(2-pyridyl)methanediol ligand are hydro-

Table 1
Crystallographic data for the molecule $[Cu(dpydiol)_2]Br_2 \cdot 4H_2O$

Empirical formula	$CuBr_2O_8N_4C_{22}H_{28}$
Cell dimensions	
a (Å)	14.771(4)
b (Å)	12.396(3)
c (Å)	14.893(5)
β (°)	91.45(2)
V (Å^3)	2725(1)
Z (molecule per cell)	4
Molecular weight	699.84
Space group	$C2/c$
T (°C)	22
Wavelength (Å)	0.71073
d_{calc} (g cm^{-3})	1.706
Linear absorption coefficient (mm^{-1})	3.76
$R(F)$	0.038
$R_w(F)$	0.056

Table 2
Selected bond distances (Å) and angles (°) for $[Cu(dpydiol)_2]Br_2 \cdot 4H_2O$

Cu–N(1)	2.011(4)	N(1)–Cu–N(2)	87.8(1)
Cu–N(2)	2.011(4)	O(2)–Cu–N(1)	74.9(1)
Cu–O(2)	2.464(3)	O(2)–Cu–N(2)	73.6(1)
C(5)–C(6)	1.533(7)	O(1)–C(6)–O(2)	113.2(4)
C(6)–C(7)	1.536(7)	O(1)–C(6)–C(5)	107.9(4)
C(6)–O(1)	1.381(5)	O(1)–C(6)–C(7)	113.0(4)
C(6)–O(2)	1.418(6)	O(2)–C(6)–C(5)	108.9(4)
		O(2)–C(6)–C(7)	105.1(3)
		C(5)–C(6)–C(7)	108.6(4)

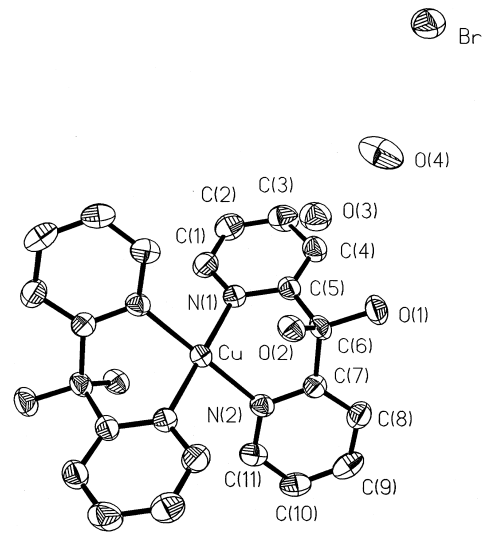


Fig. 1. Thermal ellipsoid (50% probablility) plot of $[Cu(dpydiol)_2]$-$Br_2 \cdot 4H_2O$ showing the atom numbering scheme. H atoms have been omitted.

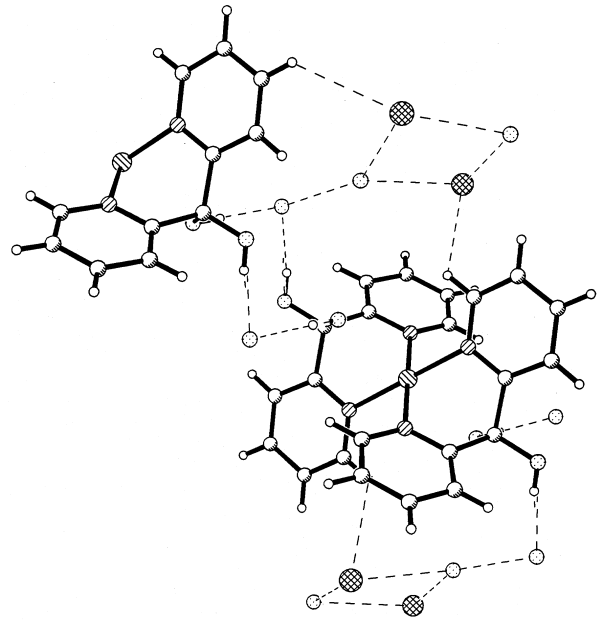


Fig. 2. H-bond network from the $[Cu(dpydiol)_2]^{2+}$ ion to water molecules and bromide ions.

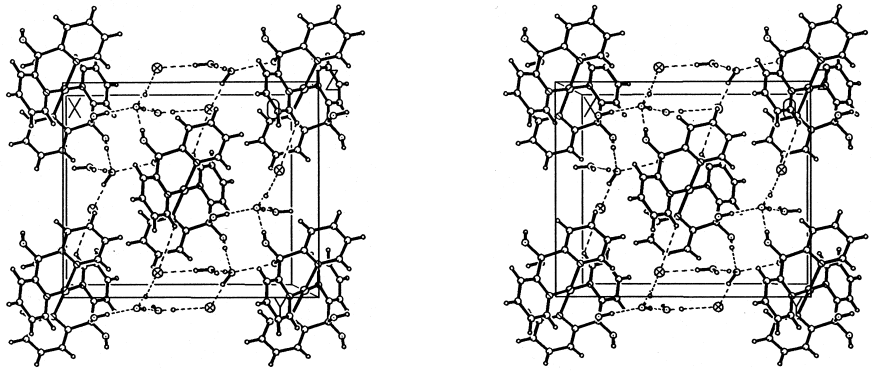


Fig. 3. Stereo packing diagram for $[Cu(dpydiol)_2]Br_2 \cdot 4H_2O$.

gen bonded through two water molecules to the crystallographically related hydroxy groups on a di(2-pyridyl)-methanediol ligand of a neighboring $[Cu(dpydiol)_2]^{2+}$ cation. Two additional water molecules are associated through hydrogen bonding to the two bromide counter ions present in the crystal packing.

3. Experimental

3.1. Preparation

The reaction of copper(II) bromide (0.447 g, 2 mmol) in water with di-2-pyridyl ketone (0.737 g, 4 mmol) in ethyl alcohol resulted in an exothermic reaction which produced a brilliant purple solution. Deep purple crystals were obtained by the evaporation of solvent for the structural determination. The compound and crystals were stable at room temperature.

3.2. Single-crystal X-ray determination

$[Cu(dpydiol)_2]Br_2 \cdot 4H_2O$. A summary of crystal data is given in Table 1. All data were collected on an Enraf Nonius CAD4 diffractometer using monochromated Mo Kα radiation. Diffraction symmetry ($2/m$) and systematic extinctions (hkl, $h+k$ odd; $h0l$, l odd) indicated monoclinic Cc or $C2/c$ as the choices for the space group. Successful solution and refinement in $C2/c$ proved this to be the correct space group. An approximately $0.15 \times 0.20 \times 0.70$ mm crystal was mounted in a glass capillary for data collection on the CAD4 diffractometer using a 1.6° θ–2θ scan. Cell dimensions were determined by least-squares refinement of 25 reflections in the range $19.9 < \theta < 22.4°$. One standard reflection was monitored periodically and showed no systematic variation. Psi scan absorption corrections were made. The structure was solved using direct methods and subsequent cycles of structure-factor calculations and difference synthesis. Non-hydrogen atoms were refined anisotropically. H atom positions were calculated and left riding the non-hydrogen atoms during refinement to $R = 0.038$ and $wR = 0.056$ using $w^{-1} = \sigma^2(F_o) + 0.0004|F_o|^2$, $\sum w(|F_o| - |F_c|)^2$ minimized. All data reduction was executed using MolEN [20] on a VAX 6410 computer. Structure solution and graphics were done using SHELXTL/PC [21] on a Pentium based PC.

Supplementary data

Crystallographic data (excluding structure factors) for the structure in this paper have been deposited with the Cambridge Crystallographic Data Centre as supplementary publication no. CCDC 135311. Copies of the data can be obtained, free of charge, on application to CCDC, 12 Union Road, Cambridge CB2 1EZ, UK (fax: +44-1223-336033; e-mail: deposit@ccdc.cam.ac.uk).

Acknowledgements

We gratefully acknowledge financial support for this study by a M.J. Murdock Charitable Trust Award of Research Corporation.

References

[1] J.M. Sayer, J. Org. Chem. 40 (1975) 2545.
[2] F.C. Kokesh, J. Org. Chem. 41 (1976) 3593.
[3] J. Hine, L.R. Green, P.C. Meng Jr., V. Thiagarajan, J. Org. Chem. 41 (1976) 3343.
[4] P. Greenzaid, Z. Luz, D. Samuel, J. Am. Chem. Soc. 89 (1967) 749.
[5] P. Greenzaid, Z. Luz, D. Samuel, J. Am. Chem. Soc. 89 (1967) 756.
[6] C.A. Lewis Jr., R. Wolfenden, J. Am. Chem. Soc. 95 (1973) 6685.
[7] I.H. Williams, D. Spangler, D.A. Femec, G.M. Maggiora, R.L. Schowen, J. Am. Chem. Soc. 105 (1983) 31.
[8] R. Hynes, N.C. Payne, C.J. Willis, J. Chem. Soc., Chem. Commun. (1990) 745.
[9] P. Bradford, R.C. Hynes, N.C. Payne, C.J. Willis, J. Am. Chem. Soc. 112 (1990) 2647.
[10] R. Hynes, C.J. Willis, N.C. Payne, Acta Crystallogr., Sect. C 48 (1992) 42.
[11] A.C. Deveson, S.L. Heath, C.J. Harding, A.K. Powell, J. Chem. Soc., Dalton Trans. (1996) 3173.
[12] S.L. Wang, J.W. Richardson, S.J. Briggs, R.A. Jacobson, Inorg. Chim. Acta 111 (1986) 67.

[13] S.O. Sommerer, J.D. Baker, W.P. Jensen, A. Hamza, R.A. Jacobson, Inorg. Chim. Acta 210 (1993) 173.
[14] A.N. Papadopoulos, V. Tongoulis, C.P. Raptopoulou, A. Terzis, D.P. Kessissoglou, Inorg. Chem. 35 (1996) 559.
[15] V. Tangoulis, C.P. Raptopoulou, A. Terzis, S. Paschalidou, S.P. Perlepes, E.G. Bakalbassis, Inorg. Chem. 36 (1997) 3996.
[16] S.R. Breeze, S. Wang, J.E. Greedan, N.P. Raju, Inorg. Chem. 35 (1996) 6944.
[17] G. Yang, M.-L. Tong, X.-M. Chen, S.W. Ng, Acta Crystallogr., Sect. C 54 (1998) 732.
[18] E. Frasson, R. Bardi, B. Bezzi, Acta Crystallogr. 12 (1959) 201.
[19] G.A. Barclay, C.H.L. Kennard, J. Chem. Soc. (1961) 3289.
[20] C.K. Fair, MolEN, An interactive structure solution procedure, Enraf-Nonius, Delft, The Netherlands, 1990.
[21] Siemens Crystallographic Research, SHELXTL/PC 1990, Release 4.1, Siemens Crystallographic Research Systems, Madison, WI, USA.

PERGAMON

www.elsevier.nl/locate/poly

Polyhedron 19 (2000) 627–632

POLYHEDRON

Synthesis of oxonium derivatives of the dodecahydro-*closo*-dodecaborate anion $[B_{12}H_{12}]^{2-}$. Tetramethylene oxonium derivative of $[B_{12}H_{12}]^{2-}$ as a convenient precursor for the synthesis of functional compounds for boron neutron capture therapy

Igor B. Sivaev [a,b,*], Andrei A. Semioshkin [a], Bernd Brellochs [c], Stefan Sjöberg [b], Vladimir I. Bregadze [a]

[a] *A.N. Nesmeyanov Institute of Organo-Element Compounds, Russian Academy of Sciences, Vavilov Street 28, 117813 Moscow, Russia*
[b] *Institute of Chemistry Department of Organic Chemistry, Uppsala University, P.O. Box 531, S-75121 Uppsala, Sweden*
[c] *Institut für Anorganische Chemie der Universität München, Meiserstrasse 1, 80333 Munich, Germany*

Received 28 October 1999; accepted 4 January 2000

Abstract

Direct synthesis of oxonium derivatives of the dodecahydro-*closo*-dodecaborate anion is described and the reaction mechanism is discussed. Various derivatives of the $[B_{12}H_{12}]^{2-}$ anion containing hydroxyl, amine, acid, and amino acid functions were prepared by ring opening reactions of the tetramethylene oxonium derivative $[B_{12}H_{11}O(CH_2)_4]^-$ with different nucleophiles. This approach is suitable for the development of compounds to be used in tumour selective boron neutron capture therapy (BNCT) and as linkers for the attachment of radioactive halogen labels for radioimmunodetection and radioimmunotherapy. ©2000 Elsevier Science Ltd All rights reserved.

Keywords: *closo*-Dodecaborate; Oxonium derivatives; Functional derivatives; Amino acids; Boron neutron capture therapy

1. Introduction

Water-soluble functionalised derivatives of the dodecahydro-*closo*-dodecaborate anion $[B_{12}H_{12}]^{2-}$ are promising candidates for boron neutron capture therapy (BNCT) for cancer [1]. The traditional approach for the functionalisation of the $[B_{12}H_{12}]^{2-}$ anion consists of the introduction of a primary substituent (reactive centre) such as an amino [2–4], mercapto [5–7], or hydroxy [8–10] group into the boron cage, followed by the attachment of a side chain containing a functional group.

Here, we describe the direct synthesis of various oxonium derivatives of the dodecahydro-*closo*-dodecaborate anion and the use of one of these, the tetramethyleneoxonium derivative $[B_{12}H_{11}O(CH_2)_4]^-$, as a convenient precursor for the synthesis of various functional derivatives of the $[B_{12}H_{12}]^{2-}$ anion for BNCT, namely the $[B_{12}H_{11}O(CH_2)_4Z]^{2-}$ (Z = OH, NH_2, C(O)H, COOH, $CH(NH_2)COOH$) derivatives. The key step in the synthesis of these derivatives is a nucleophilic ring opening reaction.

* Corresponding author. Fax: +7-95-135-5085; e-mail: sivaev@kemi.uu.se

2. Experimental

2.1. General

The ^1H, ^{11}B, and ^{13}C NMR spectra were collected using a Bruker ACP-200, a Varian Gemini 200 or a Varian Unity 400 spectrometer with TMS as internal or $BF_3 \times OEt_2$ as external standard. Infrared spectra were obtained on a Perkin Elmer 1760 FTIR spectrometer. Elemental analyses were performed in the Laboratory of Microanalysis of the Institute of Organo-Element Compounds (Moscow).

2.1.1. $(Me_4N)[B_{12}H_{11}OEt_2]$

2.70 g (1.2 mmol) *p*-nitrobenzoyl chloride dissolved in 10 ml diethyl ether were added slowly during 2 h at room temperature to a solution of 1.90 g (10.0 mmol) $Na_2[B_{12}H_{12}]$ in 20 ml acetone, and the reaction mixture was stirred for 1 h. The reaction mixture was filtered and the filtrate was evaporated to dryness. The residue was treated with 70 ml water and stirred in air for 12 h. Then the solution was filtered and the filtrate was treated with 2.18 g (20.0 mmol) Me_4NCl dissolved in 30 ml water. The precipitate formed was filtered

0277-5387/00/$ - see front matter ©2000 Elsevier Science Ltd All rights reserved.
PII S0277-5387(00)00293-X

off, washed with a few small portions of cold water and with ether and dried in air, giving 2.68 g (92%) of the product. ^{1}H NMR (MeCN-d_3, ppm): 4.48 (4H, q, –OCH_2CH$_3$), 3.09 (12H, s, N–CH_3), 1.39 (6H, t, –OCH$_2$CH_3). ^{13}C NMR (MeCN-d_3, ppm): 78.2 (–OCH$_2$CH$_3$), 56.2 (t, Me_4N^+), 13.4 (–OCH$_2$CH$_3$). ^{11}B NMR (MeCN-d_3, ppm): 8.3 (1B, s), −16.3 (5B, d), −16.8 (5B, d), −19.3 (1B, d). *Anal.* Calc. for $C_8H_{33}B_{12}NO$: C, 33.21; H, 11.51; N, 4.84. Found: C, 33.04; H, 11.26; N, 4.88%.

2.1.2. (Me$_4$N)[B$_{12}$H$_{11}$O(CH$_2$)$_4$]

0.7 ml (0.78 g, 5.5 mmol) $BF_3\times Et_2O$ was added to a stirred solution of 0.95 g (5.0 mmol) $Na_2[B_{12}H_{12}]$ in 25 ml of dry tetrahydrofuran and the reaction mixture was stirred at room temperature for 12 h. The reaction mixture was filtered and the solvent was distilled off from the filtrate. The residue was dissolved in 70 ml water and treated with a solution of 1.54 g (10.0 mmol) Me_4NBr in 30 ml water. The precipitate formed was filtered and dried in air, giving 1.25 g (86%) of the product. ^{1}H NMR (MeCN-d_3, ppm): 4.38 (4H, t, –O(CH_2CH$_2$)$_2$), 3.09 (12H, s, N–CH_3), 2.07 (4H, t, –O(CH$_2$CH_2)$_2$). ^{13}C NMR (MeCN-d_3, ppm): 81.6 (–O(CH_2CH$_2$)$_2$), 56.3 (Me_4N^+), 25.7 (–O(CH$_2$CH_2)$_2$). ^{11}B NMR (MeCN-d_3, ppm): 7.2 (1B, s), −16.6 (10B, d, J_{B-H} = 131.0 Hz), −19.4 (1B, d, J_{B-H} = 131.0 Hz). *Anal.* Calc. for $C_8H_{31}B_{12}NO$: C, 33.44; H, 10.88; N, 4.88. Found: C, 32.95; H, 10.76; N, 4.78%.

2.1.3. (Bu$_4$N)[B$_{12}$H$_{11}$O(CH$_2$)$_4$]

In another experiment the aqueous solution of crude Na[$B_{12}H_{11}O(CH_2)_4$] prepared as described above was treated with a solution of Bu_4NBr in water. The precipitate formed was filtered off, dried in air and recrystallised from methanol, giving the crystalline product in 88% yield. ^{1}H NMR ($CDCl_3$, ppm): 4.52 (4H, dt, –O(CH_2CH$_2$)$_2$), 3.21 (8H, m, Bu_4N^+), 2.15 (4H, dt, –O(CH$_2$CH_2)$_2$), 1.62 (8H, m, Bu_4N^+), 1.44 (8H, q, Bu_4N^+), 0.98 (12H, t, Bu_4N^+).

2.1.4. (Ph$_3$PMe)[B$_{12}$H$_{11}$O(CH$_2$CH$_2$)$_2$O]

0.7 ml (0.78 g, 5.5 mmol) $BF_3\times Et_2O$ was added to a stirred solution of 0.95 g (5.0 mmol) $Na_2[B_{12}H_{12}]$ in 70 ml 1,4-dioxane and the reaction mixture was stirred at room temperature for 1 week. The reaction mixture was filtered and the solvent was distilled off from the filtrate. The residue was dissolved in 70 ml water and treated with 4.05 g (10.0 mmol) Ph_3PMeI dissolved in 130 ml water. The precipitate formed was filtered, washed with water, and dried, giving 0.98 g (38%) of the product. ^{1}H NMR (MeCN-d_3, ppm): 7.7 (15H, t, *Ph*$_3$PMe$^+$), 4.47 (4H, t, –O(CH_2CH$_2$)$_2$O), 3.83 (4H, t, –O(CH$_2$CH_2)$_2$O), 2.8 (3H, d, Ph$_3$P*Me*$^+$). ^{13}C NMR (MeCN-d_3, ppm): 136.1 (d, *Ph*$_3$PMe$^+$), 134.2 (d, *Ph*$_3$PMe$^+$), 131.2 (d, *Ph*$_3$PMe$^+$), 120.0 (d, *Ph*$_3$PMe$^+$), 82.0 (–O(*C*H$_2$CH$_2$)$_2$O), 65.8 (–O(CH$_2$*C*H$_2$)$_2$O), 8.3 (d, Ph$_3$P*Me*$^+$). ^{11}B NMR (MeCN-d_3, ppm): 6.0 (1B, s), −16.7 (5B, d), −17.9 (5B, d), −22.7 (1B, d). *Anal.* Calc. for $C_{23}H_{37}B_{12}O_2P$: C, 54.52; H, 7.37. Found: C, 53.71; H, 7.75%.

2.1.5. Cs$_2$[B$_{12}$H$_{11}$OBu]

0.28 ml (0.31 g, 2.2 mmol) $BF_3\times Et_2O$ was added to a stirred suspension of 1.25 g (2.0 mmol) $(Bu_4N)_2[B_{12}H_{12}]$ in 100 ml tetrahydrofuran and the reaction mixture was refluxed overnight. The solution formed was evaporated to dryness. The residue was treated with 20 ml 1 M aqueous solution Na_2CO_3 and extracted with 100 ml dichloromethane. The residue was redissolved in 30 ml methanol and treated with 0.36 g (2.4 mmol) CsF in 10 ml methanol. The precipitate formed was filtered, washed with methanol and dichloromethane and dried in air, giving 0.75 g (78%) of the product. ^{1}H NMR (DMSO-d_6, ppm): 3.22 (2H, m, –OCH_2CH$_2$CH$_2$CH$_3$), 1.40–1.10 (4H, m, –OCH$_2$-CH_2CH_2CH$_3$), 0.82 (3H, t, –OCH$_2$CH$_2$CH$_2$CH_3). ^{13}C NMR (DMSO-d_6, ppm): 68.0 (–O*C*H$_2$CH$_2$CH$_2$CH$_3$), 34.0 (–OCH$_2$*C*H$_2$CH$_2$CH$_3$), 19.1 (–OCH$_2$CH$_2$*C*H$_2$CH$_3$), 14.3 (–OCH$_2$CH$_2$CH$_2$*C*H$_3$).

2.1.6. (Ph$_4$P)$_2$[B$_{12}$H$_{11}$O(CH$_2$)$_4$OMe]

0.29 g (1.0 mmol) $(Me_4N)[B_{12}H_{11}O(CH_2)_4]$ was stirred in 200 ml 2 M NaOH solution in aqueous methanol (3:1) overnight. The solution formed was neutralised with 2 M HCl, concentrated to 70 ml and treated with 0.90 g (2.4 mmol) Ph_4PCl in 20 ml water. The precipitate formed was filtered, washed with water and dried in vacuo, giving 0.80 g (87%) of the product. ^{1}H NMR (DMSO-d_6, ppm): 8.0–7.6 (40H, m, Ph_4P^+), 3.20 (4H, m, –OCH_2CH$_2$CH$_2$CH_2OCH$_3$), 3.13 (3H, s, –OCH$_2$CH$_2$CH$_2$CH$_2$OCH_3), 1.33 (4H, m, –OCH$_2$CH_2CH_2CH$_2$OCH$_3$). ^{13}C NMR (DMSO-d_6, ppm): 135.5 (d, Ph_4P^+), 135.1 (d, Ph_4P^+), 130.6 (d, Ph_4P^+), 117.7 (d, Ph_4P^+), 72.4, 67.8, 57.7, 28.5, 26.1.

2.1.7. (Ph$_4$P)$_2$[B$_{12}$H$_{11}$O(CH$_2$)$_4$OH]

0.29 g (1.0 mmol) $(Me_4N)[B_{12}H_{11}O(CH_2)_4]$ in 70 ml 2 M aqueous NaOH was stirred with heating to 60°C for 4 h. The solution formed was neutralised with 2 M HCl and treated with 0.90 g (2.4 mmol) Ph_4PCl in 20 ml water. The precipitate formed was filtered, washed with water and dried in vacuo, giving 0.88 g (97%) of the product. ^{1}H NMR (DMSO-d_6, ppm): 8.0–7.6 (40H, m, Ph_4P^+), 4.57 (1H, t, –OCH$_2$CH$_2$CH$_2$CH$_2$O*H*), 3.4–3.1 (4H, m, –OCH_2-CH$_2$CH$_2$CH_2OH), 1.32 (4H, m, –OCH$_2$CH_2CH_2CH$_2$OH). ^{13}C NMR (DMSO-d_6, ppm): 135.4 (d, Ph_4P^+), 134.6 (d, Ph_4P^+), 130.5 (d, Ph_4P^+), 117.7 (d, Ph_4P^+), 68.1, 61.2, 30.3, 29.0. ^{11}B NMR (DMSO-d_6, ppm): 6.4 (1B, s), −16.8 (5B, d), −18.3 (5B, d), −23.2 (1B, d). IR (Nujol, cm^{-1}): 3519 (ν_{OH}), 2472 (ν_{BH}).

2.1.8. (Me$_4$N)$_2$[B$_{12}$H$_{11}$O(CH$_2$)$_4$N(CO)$_2$C$_6$H$_4$]

0.22 g (1.2 mmol) potassium phthalimide was added to a solution of 0.46 g (1.0 mmol) $(Bu_4N)[B_{12}H_{11}O(CH_2)_4]$ in 40 ml dimethylformamide and the reaction mixture was stirred overnight. The solvent was distilled off in vacuo and the residue was dissolved in 30 ml methanol. The solution was filtered and added to a solution 0.24 g (2.2 mmol) Me_4NCl in 10 ml methanol. The precipitate formed was fil-

tered, washed with methanol and dichloromethane and dried in air, giving 0.39 g (77%) of the product. ^{1}H NMR (DMSO-d_6, ppm): 7.83 (4H, m, C_6H_4), 3.52 (2H, t), 3.21 (2H, t), 3.08 (24H, s, Me_4N^+), 1.50 (2H, m), 1.30 (2H, m). ^{13}C NMR (DMSO-d_6, ppm): 168.0, 134.3, 131.6, 123.0, 67.5, 54.4 (t, Me_4N^+), 37.8, 29.5, 25.3.

2.1.9. $(Bu_4N)[B_{12}H_{11}O(CH_2)_4NH_3]$

1.0 ml hydrazine hydrate was added to a solution of 0.25 g (0.5 mmol) $(Me_4N)_2[B_{12}H_{11}O(CH_2)_4N(CO)_2C_6H_4]$ in 50 ml water and the reaction mixture was heated under reflux overnight. The reaction mixture was allowed to cool to room temperature and a solution of 0.64 g (2.0 mmol) Bu_4NBr in 20 ml water was added. The solution was then concentrated to 30 ml under vacuum at room temperature. The precipitate formed was filtered, washed with water and dried in air, giving 0.15 g (65%) of the crystalline product. ^{1}H NMR (DMSO-d_6, ppm): 7.67 (3H, s, $-OCH_2CH_2CH_2CH_2NH_3$), 3.29 (2H, t, $-OCH_2CH_2CH_2CH_2NH_3$), 3.15 (8H, m, Bu_4N^+), 2.69 (2H, t, $-OCH_2CH_2CH_2CH_2NH_3$), 1.56 (12H, m, $-OCH_2CH_2CH_2CH_2NH_3 + Bu_4N^+$), 1.29 (8H, q, Bu_4N^+), 0.92 (12H, t, Bu_4N^+). ^{13}C NMR (DMSO-d_6, ppm): 67.7, 57.5 (Bu_4N^+), 30.1, 26.8, 23.1 (Bu_4N^+), 19.7 (Bu_4N^+), 13.5 (Bu_4N^+). ^{11}B NMR (DMSO-d_6, ppm): 5.5 (1B, s), −16.9 (5B, d), −17.8 (5B, d), −22.3 (1B, d). IR ($CHCl_3$, cm^{-1}): 3179 (ν_{NH}), 2479 (ν_{BH}), 1621 (δ_{NH}). *Anal*. Calc. for $C_{20}H_{58}B_{12}N_2O$: C, 50.85; H, 12.37; B, 27.46; N, 5.93. Found: C, 50.97; H, 12.0; B, 27.28; N, 5.93%.

2.1.10. $Cs_2[B_{12}H_{11}O(CH_2)_4CHS_2(CH_2)_3]$

0.6 ml (1.5 mmol) 2.5 M solution of *n*-butyllithium in hexane was added at −30°C to a stirred solution of 0.10 g (0.8 mmol) 1,3-dithiane in 50 ml tetrahydrofuran and the solution was stirred at −30°C for 2 h. 0.23 g (0.5 mmol) $(Bu_4N)[B_{12}H_{11}O(CH_2)_4]$ was added and the reaction mixture was stirred at −30°C for 1 h and then at room temperature overnight. The solvent was distilled off in vacuo and the residue was dissolved in 30 ml methanol. The solution was filtered and treated with 0.18 g (1.2 mmol) CsF in 10 ml methanol. The precipitate formed was filtered, washed with methanol, dried in air, and dissolved in 10 ml water. The solution was then filtered, evaporated to half its volume, and treated with 70 ml methanol. The precipitate was collected by filtration, washed with methanol and ether, giving 0.22 g (73%) of the product. ^{1}H NMR (DMSO-d_6, ppm): 4.08 (1H, t, $-O(CH_2)_4CHS_2(CH_2)_3$), 3.18 (2H, m, $-OCH_2CH_2CH_2CH_2CHS_2(CH_2)_3$), 2.95–2.65 (4H, m, $-O(CH_2)_4CHS_2(CH_2)_2CH_2$), 2.10–1.60 (2H, m, $-O(CH_2)_4CHS_2(CH_2)_2CH_2$), 1.60–1.25 (6H, m, $-OCH_2CH_2CH_2CH_2CHS_2(CH_2)_3$). ^{13}C NMR (DMSO-$d_6$, ppm): 69.0 ($-OCH_2CH_2CH_2CH_2CHS_2(CH_2)_3$), 47.5 ($-O(CH_2)_4CHS_2(CH_2)_3$), 35.9 ($-OCH_2CH_2CH_2CH_2CHS_2(CH_2)_3$), 31.6 ($-OCH_2CH_2CH_2CH_2CHS_2(CH_2)_3$), 30.3 ($-O(CH_2)_4CHS_2(CH_2)_2CH_2$), 26.4, 23.7.

2.1.11. $(Bu_4N)_2[B_{12}H_{11}O(CH_2)_4CN]$

A solution of 0.23 g (0.5 mmol) $(Bu_4N)[B_{12}H_{11}O(CH_2)_4]$ and 0.16 g (0.5 mmol) tetrabutylammonium bromide in 50 ml dichloromethane was added to a solution of 0.05 g (1.0 mmol) sodium cyanide in 25 ml 1 M aqueous sodium hydroxide and the reaction mixture was stirred vigorously at room temperature overnight. The organic layer was separated, washed with water, dried over anhydrous $MgSO_4$, and evaporated to dryness, giving 0.35 g (97%) of the product. ^{1}H NMR ($CDCl_3$, ppm): 3.70 (2H, t, $-OCH_2CH_2CH_2CH_2CN$), 3.25 (16H, m, Bu_4N^+), 2.44 (2H, t, $-OCH_2CH_2CH_2CH_2CN$), 1.60 (20H, m, $-OCH_2CH_2CH_2CH_2CN + Bu_4N^+$), 1.43 (16H, q, Bu_4N^+), 0.97 (24H, t, Bu_4N^+). ^{13}C NMR ($CDCl_3$, ppm): 121.1 ($-OCH_2CH_2CH_2CH_2CN$), 67.6 ($-OCH_2CH_2CH_2CH_2CN$), 58.8 (Bu_4N^+), 30.0, 24.1 (Bu_4N^+), 22.6, 19.7 (Bu_4N^+), 16.7, 13.7 (Bu_4N^+). ^{11}B NMR ($CDCl_3$, ppm): 6.3 (1B, s), −16.3 (5B, d), −17.7 (5B, d), −22.3 (1B, d). IR ($CHCl_3$, cm^{-1}): 2470 (ν_{BH}), 2246 (ν_{CN}).

2.1.12. $(Bu_4N)_2[B_{12}H_{11}O(CH_2)_4COOH]$

A solution of 10.0 g potassium hydroxide in 25 ml water was added to a solution of 0.29 g (0.4 mmol) $(Bu_4N)_2[B_{12}H_{11}O(CH_2)_4CN]$ in 50 ml methanol and the reaction mixture was refluxed overnight. The solution was cooled to room temperature and adjusted to pH 3 by addition of hydrochloric acid. The reaction mixture was evaporated to dryness. The residue was treated with 200 ml of water and extracted twice with 200 ml of dichloromethane. The organic layer was dried over $MgSO_4$ and the solvent was distilled off, giving 0.26 g (88%) of the product. ^{1}H NMR ($CDCl_3$, ppm): 3.76 (2H, t, $-OCH_2CH_2CH_2CH_2COOH$), 3.24 (16H, m, Bu_4N^+), 2.63 (2H, t, $-OCH_2CH_2CH_2CH_2COOH$), 1.60 (20H, m, $-OCH_2CH_2CH_2CH_2COOH + Bu_4N^+$), 1.43 (16H, q, Bu_4N^+), 0.97 (24H, t, Bu_4N^+). ^{13}C NMR ($CDCl_3$, ppm): 177.2 ($-OCH_2CH_2CH_2CH_2COOH$), 69.7 ($-OCH_2CH_2CH_2CH_2COOH$), 58.7 (Bu_4N^+), 34.8, 27.6, 25.5, 24.1 (Bu_4N^+), 19.7 (Bu_4N^+), 13.7 (Bu_4N^+). ^{11}B NMR ($CDCl_3$, ppm): 5.7 (1B, s), −16.4 (5B, d), −17.6 (5B, d), −22.1 (1B, d). IR ($CHCl_3$, cm^{-1}): 2475 (ν_{BH}), 1717 (ν_{CO}).

2.1.13. $Cs_2[B_{12}H_{11}O(CH_2)_4C(COOEt)_2NHCOMe]$

0.26 g (1.2 mmol) diethyl acetamidomalonate, 0.46 g (1.0 mmol) $(Bu_4N)[B_{12}H_{11}O(CH_2)_4]$, 0.32 g (1.0 mmol) Bu_4NBr, and 0.70 g (5.0 mmol) K_2CO_3 in 50 ml acetonitrile was refluxed overnight. The reaction mixture was cooled and filtered. The solvent was distilled off in vacuo, the residue was dissolved in 15 ml methanol and treated with 0.36 g (2.4 mmol) CsF in 10 ml methanol. The precipitate formed was filtered, washed with methanol and ether, giving 0.55 g (79%) of yellowish product. ^{1}H NMR (DMSO-d_6, ppm): 8.23 (1H, s, $NHCOCH_3$), 4.11 (4H, q, $COOCH_2CH_3$), 3.39 (2H, t, $-OCH_2CH_2CH_2CH_2C(NHCOMe)(COOEt)_2$), 2.00 (2H, t, $-OCH_2CH_2CH_2CH_2C(NHCOMe)(COOEt)_2$), 1.24 (4H, m, $-OCH_2CH_2CH_2CH_2C(NHCOMe)(COOEt)_2$),

1.13 (6H, t, $COOCH_2CH_3$). IR (Nujol, cm^{-1}): 3379 (ν_{NH}), 2477 (ν_{BH}), 1735 ($\nu_{CO(ester)}$), 1665 ($\nu_{CO(amide)}$).

2.1.14. Cs[$B_{12}H_{11}O(CH_2)_4CH(NH_3)COOH$]

0.21 g (0.3 mmol) was dissolved in 40 ml 2 M hydrochloric acid and the solution was refluxed overnight. The solvent was distilled off to dryness in vacuo and the residue was washed with methanol giving 0.08 g (63%) of the product. ^1H NMR (D_2O, ppm): 3.87 (1H, t, $–OCH_2(CH_2)_3CH(NH_3)COOH$), 3.52 (2H, t, $–OCH_2(CH_2)_3CH(NH_3)COOH$), 1.82 (2H, m), 1.71 (2H, m), 1.45 (2H, m). ^1H NMR (DMSO-d_6, ppm): 8.30 (3H, s, $–OCH_2(CH_2)_3CH(NH_3)COOH$), 3.87 (1H, t, $–OCH_2(CH_2)_3CH(NH_3)COOH$), 3.63 (2H, t, $–OCH_2(CH_2)_3CH(NH_3)COOH$), 1.74 (4H, m), 1.4 (2H, m). ^{11}B NMR (DMSO-d_6, ppm): 3.3 (1B, s), −16.4 (5B, d), −17.5 (5B, d), −22.3 (1B, d). IR (Nujol, cm^{-1}): 3218 (ν_{NH}), 2494 (ν_{BH}), 1730 (ν_{CO}), 1620 (δ_{NH}).

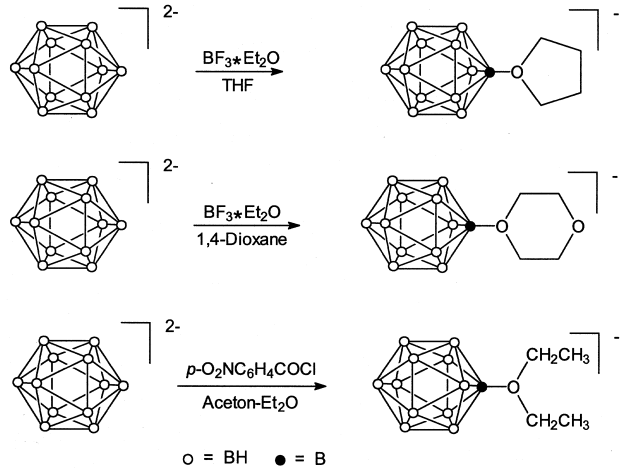
3. Results and discussion

The formation of stable oxonium charge-compensated derivatives seems to be one of the characteristic features of the chemistry of polyhedral boron hydrides. At present, a number of such compounds with side and cage-bridging oxonium atoms have been described, such as $[B_{12}H_{11}O(CH_2)_5]^-$ [8], [8-O(CH_2CH_2)$_2$O-3,3′-Co(1,2-$C_2B_9H_{10}$)(1′,2′-$C_2B_9H_{11}$)] [11], [8-X-8′-O(CH_2CH_2)$_2$O-3,3′-Co(1,2-$C_2B_9H_{10}$)$_2$] (X = Br, I) [12,13], [3-(CO)$_2$-3-(η^3-C_3H_5)-8-Et_2O-3,1,2-$MoC_2B_9H_{10}$], [1,2-Me_2-3-(CO)$_2$-3-(η^3-C_3H_5)-8-Et_2O-3,1,2-$MC_2B_9H_8$] (M = Mo, W), [1,2-Me_2-3-(CO)$_2$-(η^3-C_3H_5)-8-O(CH_2)$_4$-3,1,2-$MoC_2B_9H_8$] [14], [3-(CO)$_3$-8-O(CH_2)$_4$-3,1,2-$MnC_2B_9H_{10}$] [15], ($Et_2C_2B_4H_4$)Co($Et_4C_4B_8H_7O(CH_2)_4$) [16], [1,1′-(μ-H)-2,2′-(μ-OR)-($B_{10}H_8$)$_2$]$^{2-}$ (R = Et, $O(CH_2)_4OMe$, $O(CH_2)_4O(CH_2)_2CHMe_2$) [17,18], [8,8′-(μ-OR)-3,3′-Co(1,2-$C_2B_9H_{10}$)$_2$] (R = Me, Et) [19], and [6,6′-μ-MeO-2,2′-Co(1,7-$C_2B_9H_{10}$)$_2$] [20].

In the literature until now, the only known oxonium derivative of the dodecahydro-*closo*-dodecaborate anion, $[B_{12}H_{11}O(CH_2)_5]^-$, has been obtained by alkylation of $[B_{12}H_{11}OH]^{2-}$ with 1,5-dibromopentane [8]. The formation of this oxonium derivative was supposed to favour the six-membered ring closing and no oxonium derivatives form in alkylation of $[B_{12}H_{11}OH]^{2-}$ with other alkyl halides [8,10].

Most known oxonium derivatives of polyhedral boron hydrides have not been prepared by the alkylation reaction, but by the solvent molecule addition.

We here report that oxonium derivatives of the $[B_{12}H_{12}]^{2-}$ anion can also be obtained by the 'solvent addition' reaction. The reaction of $Na_2[B_{12}H_{12}]$ with boron trifluoride etherate in tetrahydrofuran at room temperature results in the formation of tetramethyleneoxonium derivative in high yield (Scheme 1).



Scheme 1.

We suppose that boron trifluoride in this reaction acts as a Lewis acid and abstracts hydride ion from the $[B_{12}H_{12}]^{2-}$ anion, giving $[HBF_3]^-$ [21] and $[B_{12}H_{11}]^-$ intermediates which react with the solvent molecule.

$$[B_{12}H_{12}]^{2-} \xrightarrow[-HBF_3^-]{BF_3*Et_2O} [B_{12}H_{11}]^- \xrightarrow{THF} [B_{12}H_{11}O(CH_2)_4]^-$$

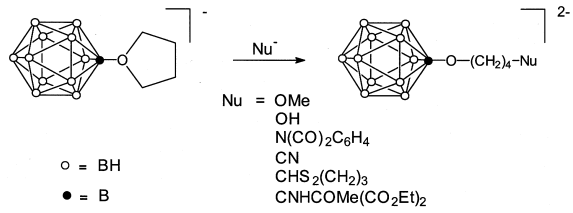
The possibility of formation of the $[B_{12}H_{11}]^-$ intermediate was mentioned earlier by Knoth et al. [22], and its formation in acid-assisted substitution reactions from the $[B_{12}H_{12}]^{2-}$ anion is supported by calculations [23]. This mechanism is close to the 'electrophile-induced nucleophilic substitution' (EINS) mechanism [24], which is characterised by the following processes: (i) the electrophile removes the terminal hydrogen from the B–H vertex; (ii) the transient vacancy at this B-vertex is then filled by the best nucleophile or by the most abundant nucleophile present in the reaction medium.

The reaction of $(Bu_4N)_2[B_{12}H_{12}]$ with $BF_3 \times Et_2O$ in refluxing tetrahydrofuran did not give the tetramethyleneoxonium derivative, but the butoxy derivative. Formation of the butoxy derivative could be due to the initial formation of the tetramethyleneoxonium derivative followed by attack with $[HBF_3]^-$ at high temperature.

The reaction of $Na_2[B_{12}H_{12}]$ with $BF_3 \times Et_2O$ in 1,4-dioxane also leads to the corresponding oxonium derivative $[B_{12}H_{11}O(CH_2CH_2)_2O]^-$, but its yield is much lower because of the cluster decomposition during the reaction (Scheme 1).

The diethyloxonium derivative $[B_{12}H_{11}OEt_2]^-$ was prepared by reaction of $Na_2[B_{12}H_{12}]$ with *p*-nitrobenzoylchloride in acetone–diethyl ether mixture (Scheme 1). A possible reaction mechanism includes electrophilic attack of $[B_{12}H_{12}]^{2-}$ with *p*-$NO_2C_6H_4CO^+$ which results in the formation of $[B_{12}H_{11}]^-$ and the corresponding aldehyde and subsequent reaction of $[B_{12}H_{11}]^-$ with the solvent molecule. It was shown earlier that in the absence of diethyl ether the main product of the reaction is $[B_{12}H_{11}C(O)R]^{2-}$ [25].

Little is known about the reactivity of oxonium derivatives of polyhedral boranes. It has been shown that the treatment



Scheme 2.

of $[1,2\text{-}Me_2\text{-}3\text{-}(CO)_2\text{-}3\text{-}(\eta^3\text{-}C_3H_5)\text{-}8\text{-}Et_2O\text{-}3,1,2\text{-}MC_2B_9H_8]$ (M = Mo, W) with K-Selectride in dichloromethane results in the loss of one ethyl group with formation of the corresponding ethoxy derivatives [14]. The ring openings in $[B_{12}H_{11}O(CH_2)_5]^-$ under nucleophilic attack with hydroxide and fluoride ions [26], in $[8\text{-}I\text{-}8'\text{-}O(CH_2CH_2)_2O\text{-}3,3'\text{-}Co(1,2\text{-}C_2B_9H_{10})_2]$ under treatment with $C_5H_{11}ONa$ [13], in $[1,2\text{-}Me_2\text{-}3\text{-}(CO)_2\text{-}(\eta^3\text{-}C_3H_5)\text{-}8\text{-}O(CH_2)_4\text{-}3,1,2\text{-}MoC_2B_9H_8]$ with fluoride ions [14], and in $[3\text{-}(CO)_3\text{-}8\text{-}O(CH_2)_4\text{-}3,1,2\text{-}MnC_2B_9H_{10}]$ under treatment with Lewis bases (PPh_3, NEt_3, 4-MePy) and iodide ions [15], have been reported. Considering $[B_{12}H_{11}O(CH_2)_4]^-$ as a possible synthon for the synthesis of various derivatives of the *closo*-dodecaborate anion via ring opening, we investigated its reactions with different nucleophiles. We found that attack of strong nucleophilic agents results in the ring opening reaction, giving $[B_{12}H_{11}O(CH_2)_4Nu]^{2-}$ derivatives, where $Nu^- = OMe^-$, OH^-, $N(CO)_2C_6H_4^-$, $(CH_2)_3S_2CH^-$, CN^-, $C(COOEt)_2NHCOMe^-$ (Scheme 2).

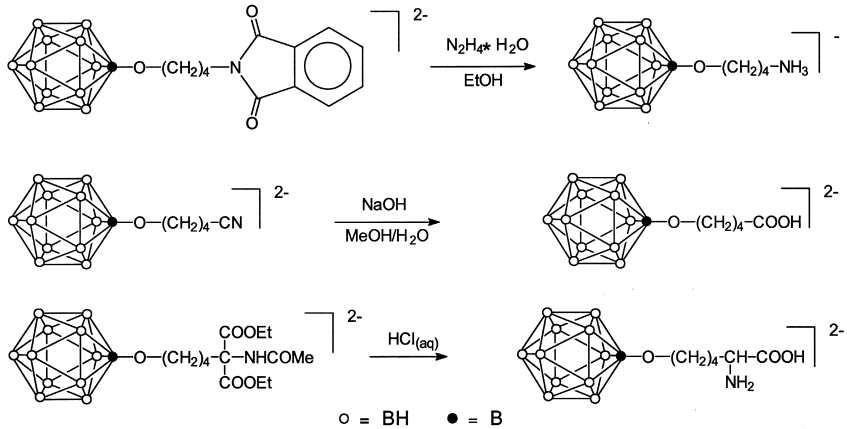
It should be noted that treatment of $[B_{12}H_{11}O(CH_2)_4]^-$ with 2-lithio-1,3-dithiane in tetrahydrofuran at room temperature does not give the desired product and that 95% of the starting material was recovered. Refluxing of the reaction mixture gives the desired ring-opened product in less than 20% yield. However, the reaction of $[B_{12}H_{11}O(CH_2)_4]^-$ with 2,2-dilithio-1,3-dithiane proceeds smoothly at room temperature, giving the corresponding protected aldehyde in high yield. It is known that the lithium atom in 2-lithio-1,3-dithiane occupies the equatorial postion (the preference for the equatorial conformer is largely thermodynamically controlled) [27,28] and the unshared electron pairs of the sulfur atoms can prevent attack with sterically hindered electrophiles such as $[B_{12}H_{11}O(CH_2)_4]^-$. Heating increases the amount of the more reactive axial conformer, but at the same time results in destruction of the organolithium compound. Use of the dilithium derivative of 1,3-dithiane overcomes these sterical restrictions and results in the desired product in high yield.

An initial attempt at ring opening with cyanide in dimethylsulfoxide at 90°C [29] failed; however, the reaction under phase transfer conditions (method used earlier to open 1,2-epoxides [30]) using sodium cyanide and an equimolar amount of tetrabutylammonium bromide at room temperature was successful and gave the nitrile required, which can be readily converted to the coresponding acid by alkaline hydrolysis (Scheme 3).

Deprotection of $[B_{12}H_{11}O(CH_2)_4N(CO)_2C_6H_4]^{2-}$ with hydrazine hydrate gave unexpectedly the protonated amino derivative $[B_{12}H_{11}O(CH_2)_4NH_3]^-$ isolated at pH 8 (Scheme 3). The protonated form obtained can be considered as an inner salt stabilised by formation of the intramolecular hydrogen bond between the ammonium proton and the oxygen atom or the intramolecular B–H···H–N dihydrogen bond similar to the corresponding dihydrogen bonds found in ammonium salts of the dodecahydro-*closo*-dodecaborate anion [31,32].

The first amino acid derived from the *closo*-dodecaborate anion was prepared by the ring-opening reaction with diethyl acetamidomalonate (glycine anion equivalent for amino acid synthesis) in acetonitrile in the presence of potassium carbonate, a variation of the classical Sörensen synthesis of amino acids, followed by acidic hydrolysis and decarboxylation.

The synthesis described here of the tetramethylene oxonium derivative of the *closo*-dodecaborate $[B_{12}H_{11}\text{-}O(CH_2)_4]^-$ anion followed by ring opening under nucleophilic attack is a powerful instrument for the synthesis of various functional derivatives and synthetic building blocks on the basis of the $[B_{12}H_{12}]^{2-}$ anion. The compounds prepared can be used not only for boron neutron capture therapy, but also as carriers of radioactive halogen labels for radioimmunodetection and for radioimmunotherapy [33–35].



Scheme 3.

Acknowledgements

The authors thank the Royal Swedish Academy of Sciences, the Swedish Cancer Society (3009-B97-08XBB), and the Russian Foundation for Basic Research (99-03-33073) for financial support.

References

[1] M.F. Hawthorne, Angew. Chem., Int. Ed. Engl. 32 (1993) 950.
[2] I.B. Sivaev, A.B. Bruskin, V.V. Nesterov, M.Yu. Antipin, V.I. Bregadze, S. Sjöberg, Inorg. Chem. 38 (1999) 5887.
[3] T. Peymann, E. Lork, M. Schmidt, H. Nöth, D. Gabel, Chem. Ber. 130 (1997) 795.
[4] B. Grüner, B. Bonnetot, H. Mongeot, Collect. Czech. Chem. Commun. 62 (1997) 1185.
[5] K. Nagasawa, M. Narisada, Tetrahedron Lett. 31 (1990) 4029.
[6] D. Gabel, D. Moller, S. Harfst, J. Röesler, H. Ketz, Inorg. Chem. 32 (1993) 2276.
[7] D.H. Swenson, B.H. Laster, R.L. Metzger, J. Med. Chem. 35 (1996) 1540.
[8] T. Peymann, E. Lork, D. Gabel, Inorg. Chem. 35 (1996) 1355.
[9] A.A. Semioshkin, P.V. Petrovskii, I.B. Sivaev, E.G. Balandina, V.I. Bregadze, Russ. Chem. Bull. 45 (1996) 683.
[10] I.B. Sivaev, S. Sjöberg, V.I. Bregadze, D. Gabel, Tetrahedron Lett. 40 (1999) 3451.
[11] J. Plesek, S. Hermanek, A. Franken, I. Cisarova, C. Nachtigal, Collect. Czech. Chem. Commun. 62 (1997) 47.
[12] J. Plesek, B. Stibr, S. Hermanek, Collect. Czech. Chem. Commun. 49 (1984) 1492.
[13] P. Selucky, J. Plesek, J. Rais, M. Kyrs, L. Kadlecova, J. Radioanal. Nucl. Chem. 149 (1991) 131.
[14] D. Mullica, E.L. Sappenfield, F.G.A. Stone, S.F. Woollam, Organometallics 13 (1994) 157.
[15] M. Gomez-Saso, D.F. Mullica, E. Sappenfield, F.G.A. Stone, Polyhedron 15 (1996) 793.
[16] Z.-T. Wang, E. Sinn, R.N. Grimes, Inorg. Chem. 24 (1985) 834.
[17] F. Li, K. Shelly, R.R. Kane, C.B. Knobler, M.F. Hawthorne, J. Am. Chem. Soc. 118 (1996) 6506.
[18] F. Li, K. Shelly, R.R. Kane, C.B. Knobler, M.F. Hawthorne, Angew. Chem., Int. Ed. Engl. 35 (1996) 2646.
[19] J. Plesek, S. Hermanek, K. Base, L.J. Todd, W.F. Wright, Collect. Czech. Chem. Commun. 41 (1976) 3509.
[20] J. Plesek, B. Gruner, J. Holub, Collect. Czech. Chem. Commun. 62 (1997) 884.
[21] J. Goubeau, R. Bergmann, Z. Anorg. Chem. 263 (1950) 69.
[22] W.H. Knoth, J.C. Sauer, D.C. England, W.R. Hertler, E.L. Muetterties, J. Am. Chem. Soc. 86 (1964) 3973.
[23] A.M. Mebel, O.P. Charkin, K.A. Solntsev, N.T. Kuznetsov, Russ. J. Inorg. Chem. 34 (1989) 813.
[24] J. Jelínek, B. Štíbr, F. Mares, J. Plesek, S. Hermanek, Polyhedron 6 (1987) 1740.
[25] A.A. Semioshkin, P.V. Petrovskii, D. Gabel, B. Brellochs, V.I. Bregadze, Russ. Chem. Bull. 47 (1998) 950.
[26] T. Peymann, K. Kück, D. Gabel, Inorg. Chem. 36 (1997) 5138.
[27] E.L. Eliel, A.A. Hartmann, A.G. Abatjoglou, J. Am. Chem. Soc. 96 (1974) 1807.
[28] A.G. Abatjoglou, E.L. Eliel, L.F. Kuyper, J. Am. Chem. Soc. 99 (1977) 8262.
[29] I. Friedman, H. Shechter, J. Org. Chem. 25 (1960) 877.
[30] D. Mitchell, T.M. Koenig, Tetrahedron Lett. 33 (1992) 3281.
[31] E.A. Malinina, L.V. Goeva, K.A. Solntsev, N.T. Kuznetsov, Russ. J. Inorg. Chem. 36 (1991) 1361.
[32] A.M. Orlova, V.N. Mustyatsa, L.V. Goeva, S.B. Katser, V.L. Lagun, K.A. Solntsev, N.T. Kuznetsov, Russ. J. Inorg. Chem. 41 (1996) 1599.
[33] V. Tolmachev, H. Lundqvist, J. Carlsson, I. Sivaev, A. Orlova, A. Sundin, J. Labelled Compd. Radiopharmaceut. 40 (1997) 125.
[34] V. Tolmachev, J. Koziorowski, I. Sivaev, H. Lundqvist, J. Carlsson, A. Orlova, L. Gedda, P. Olsson, S. Sjöberg, A. Sundin, Bioconjugate Chem. 10 (1999) 338.
[35] A. Orlova, O. Lebeda, V. Tolmachev, S. Sjöberg, J. Carlsson, H. Lundquist, Suppl. 1, J. Labelled Compd. Radiopharmaceut. 42 (1999) 735.

PERGAMON

www.elsevier.nl/locate/poly

Polyhedron 19 (2000) 633–639

POLYHEDRON

Crystal of *meso-p*-tolyl-porphyrinato copper(II) Cu(tptp) and di-cation ion-pair complex $[H_4tptp]^{2+}[CF_3SO_3]_2^-$ formation during the reaction of $Cu(CF_3SO_3)_2$ with *meso-p*-tolyl-porphyrin in $CDCl_3$

Cheng-Hsi Tsai [a], Jo-Yu Tung [a], Jyh-Horung Chen [a,*], Feng-Ling Liao [b], Sue-Lein Wang [b], Shin-Shin Wang [c], Lian-Pin Hwang [d], Chie-Bein Chen [e]

[a] *Department of Chemistry, National Chung-Hsing University, Taichung 40227, Taiwan*
[b] *Department of Chemistry, National Tsing-Hua University, Hsin-Chu 30043, Taiwan*
[c] *Union Chemical Laboratories, Hsin-Chu 30043, Taiwan*
[d] *Department of Chemistry, National Taiwan University and Institute of Atomic and Molecular Sciences, Academia Sinica, Taipei 10764, Taiwan*
[e] *Department of Business Administration, Ming Chuan University, Taipei, Taiwan*

Received 16 May 1999; accepted 4 January 2000

Abstract

In the NMR and ESR time-scale of this experiment, an attempt was made to prepare the copper sitting-atop (SAT) species $[Cu(H_2tptp)]^{2+}$ by the reaction of $Cu(CF_3SO_3)_2$ with *meso-p*-tolyl-porphyrin (H_2tptp) in $CDCl_3$; however, this led to the formation of *meso-p*-tolyl-porphyrinatocopper(II) Cu(tptp) and the protonated porphyrin $[H_4tptp]^{2+}[CF_3SO_3]_2^-$ (**2a**). Previous researchers might have misinterpreted the SAT $[Cu(H_2tpp)]^{2+}$ complex as being a single component instead of a mixture of $[H_4tpp]^{2+}[CF_3SO_3]_2^-$ (**1**) and Cu(tpp) for a similar reaction between 5,10,15,20-tetraphenylporphyrin H_2tpp and $Cu(CF_3SO_3)_2$ in CH_3CN. This work determines the crystal structure of Cu(tptp) and its hyperfine constants $a_{Cu} = 94.0$ G and $a_N = 15.8$ G using ESR. The crystal structure of $[H_4tptp]^{2+}[CH_3SO_3]_2^-$ (**3**) is reported and employed to simulate the groupings of $[H_4tptp]^{2+}$ and $CF_3SO_3^-$ in the di-cation ion-pair complex **2a**. ©2000 Elsevier Science Ltd All rights reserved.

Keywords: Crystal structures; Cu^{2+} porphyrin complexes; Protonated porphyrins; SAT complexes; Electron spin resonance; Nuclear magnetic resonance

1. Introduction

Previously, Inada et al. [1,2] reported on the formation of the 'sitting-atop' (SAT) complex $[Cu(H_2tpp)]^{2+}$ via the reaction of $Cu(CF_3SO_3)_2$ with 5,10,15,20-tetraphenylporphyrin (H_2tpp) in acetonitrile under a dry nitrogen atmosphere. We have not been successful in synthesizing the complex $[Cu(H_2tpp)]^{2+}$ by repeating the previous work [1] using the same solvent acetonitrile. According to their suggestion, the reaction of $Cu(CF_3SO_3)_2$ with H_2tpp in $CHCl_3$ in the absence of a strong base should be easily arrested at the formation of the SAT complex because of the low donor number (DN) of $CHCl_3$. It is known that the donor number of chloroform (DN = −) is less than that of acetonitrile (DN = 14.1) [3]. Hence, we did not investigate the reaction in the same solvent, i.e. chloroform. However, the SAT complex $[Cu(H_2tpp)]^{2+}$ is not detected in the reaction of $Cu(CF_3SO_3)_2$ with H_2tpp in $CDCl_3$ under a dry N_2 atmosphere; instead, a mixture (A) consisting of Cu(tpp) and $[H_4tpp]^{2+}[CF_3SO_3]_2^-$ (**1**) is observed. The proton NMR spectrum (^{1}H NMR) for the Cu(tpp) in mixture A in $CDCl_3$ shows a broad multiplet at 7.50 ppm for *meta*-hydrogens and at 7.64 ppm for *para*-hydrogens (see Fig. 1 and Table 1). The ^{1}H NMR values are quite close to those of 7.48 ppm (*meta*-H) and 7.62 ppm (*para*-H) for the compound Cu(tpp) reported by Godziela and Goff [4]. The ^{1}H NMR data for **1** in mixture A in $CDCl_3$ at 24°C (see Fig. 1 and Table 1) showed a singlet at 8.73 ppm (8H) for β-pyrrole protons, a doublet at 8.61 ppm (8H) for *ortho*- protons and a multiplet at 8.00 ppm (12H) for *meta*- and *para*- protons, and a singlet at −1.84 ppm (with 4H) for the N-H protons. Our interpretation of these data differs from that of Inada et al. [1,2]. Inada et al. [1,2] might have misinterpreted the mixture A as the SAT complex $[Cu(H_2tpp)]^{2+}$. The ^{1}H NMR data for their SAT complex in CD_3CN at room temperature (see Table 1) showed a singlet at 8.77 ppm (4H)

* Corresponding author. Fax: +886-4-2862574; e-mail: jhchen@mail.nchu.edu.tw

0277-5387/00/$ - see front matter ©2000 Elsevier Science Ltd All rights reserved.
PII S0277-5387(00)00294-1

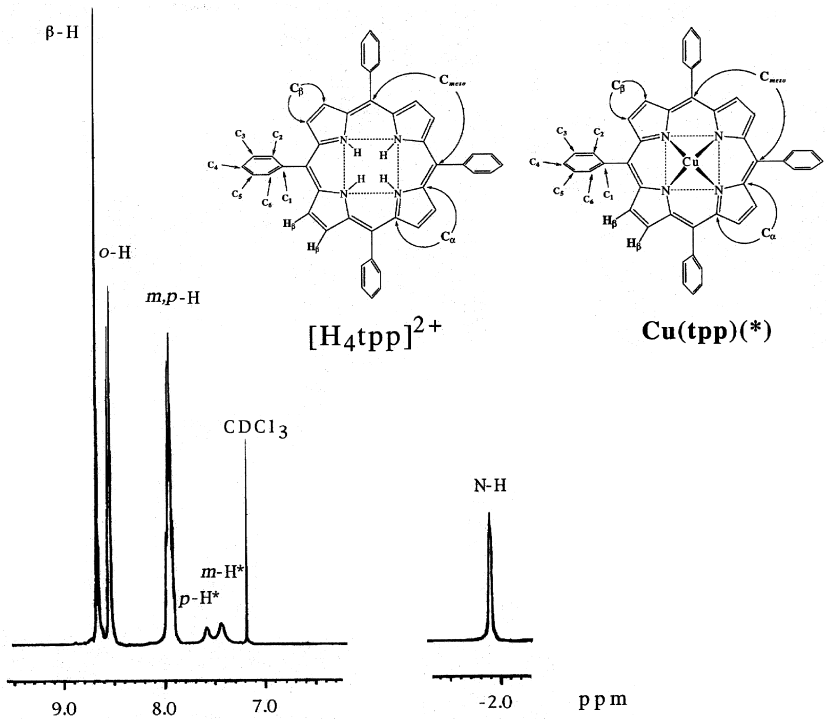


Fig. 1. 400.13 MHz ^{1}H NMR spectrum for the mixture A consists of Cu(tpp) and $[H_4tpp]^{2+}[CF_3SO_3]_2^-$ (**1**) in $CDCl_3$ at 24°C. Resonances due to Cu(tpp) are labeled with an asterisk (*).

Table 1
Proton chemical shifts (δ) for copper and protonated porphyrins in $CDCl_3$ at 24°C

Porphyrin	β-H	*o*-H	*m*-H	*p*-H	*p*-CH_3	NH	CH_3SO_3
H_2tptp	8.84	8.08 (7.8) [a]	7.54 (7.7)		2.69	−2.79	
$[H_4tptp]^{2+}[CH_3SO_3]_2^-$ (**3**) [b]	8.71	8.60 (7.6)	7.86 (7.2)		2.77	−2.22	2.65
$[H_4tptp]^{2+}[CF_3SO_3]_2^-$ (**2b**) [c]	8.68	8.50 (8)	7.83 (8)		2.78	−1.74	
Cu(tptp)[4]		7.48	7.30		2.52		
2a in mixture B [d]	8.66	8.48 (6.1)	7.62 (6.0)		2.77	−1.76	
Cu(tptp) in mixture B			7.30		2.53		
Free ionic $CH_3SO_3^-$ [19]							2.80
H_2tpp	8.89	8.25–8.27	7.74–7.81			−2.73	
$[H_4tpp]^{2+}[CF_3SO_3]_2^-$ (**1**) [c]	8.74	8.60 (7.2)	8.00 (m) [f]			−1.84	
Cu(tpp)[4]			7.48	7.62			
$[Cu(H_2tpp)]^{2+}$ in CD_3CN[1]	8.66(NH) 8.77(N)	8.10–8.12	7.31–7.50			−2.05	
1 in mixture A [e]	8.73	8.61 (6.9)	8.00 (m)			−1.84	
Cu(tpp) in mixture A			7.50	7.64			

[a] ^3J(H–H) coupling constant.
[b] Compound **3** was obtained by protonation of H_2tptp with CH_3SO_3H.
[c] Compound **2b** (or **1**) was obtained by protonation of H_2tptp (or H_2tpp) with CF_3SO_3H.
[d] Mixture B = **2a** + Cu(tptp).
[e] Mixture A = **1** + Cu(tpp).
[f] m = multiplet.

for the coordinating β-pyrrole protons, a doublet at 8.66 ppm (4H) for the uncoordinating β-pyrrole protons, one multiplet at 8.10–8.12 ppm for *ortho*-phenyl protons and another multiplet at 7.31–7.50 ppm for the *meta*- and *para*-phenyl protons, and a singlet at −2.05 ppm (2H) for pyrrole N-H [1,2]. If the doublet centered at 8.61 ppm is due to the long-range

coupling of β-protons with a nitrogen-bonded proton of the same pyrrole ring, the ^4J(H–H) coupling constant should be less than 4 Hz [5,6]. However, the coupling constant of 6.9 Hz is reasonably assigned to adjacent ^{1}H–^{1}H coupling, ^3J(H–H). Furthermore, the doublet at 8.61 ppm remains unchanged on irradiating the NH proton at δ −1.84 ppm. In addition, the doublet for the *ortho*- protons becomes a singlet on irradiating the *meta*- and *para*-phenyl protons at 8.00 ppm. Thus the ^{1}H NMR spectral data support the composition of mixture A proposed by us and disagree with the SAT complex reported previously [1,2].

When the porphyrin group (tpp) was substituted using *meso-p*-tolyl-porphyrin (tptp), a mixture B consisting of *meso-p*-tolyl-porphyrinatocopper(II) Cu(tptp) and the protonated porphyrin $[H_4tptp]^{2+}[CF_3SO_3]_2^-$ (**2a**) was formed via the reaction of $Cu(CF_3SO_3)_2$ with H_2tptp in $CDCl_3$. Cu(tptp) was crystallized out in mixture B and its X-ray structure is reported here. Both Cu(tptp) and **2a** in mixture B were characterized using ESR, ^{1}H, ^{13}C and ^{19}F NMR methods.

2. Experimental

2.1. Preparation of mixture B consisting of Cu(tptp) and $[H_4tptp]^{2+}[CF_3SO_3]_2^-$ (2a)

H_2tptp (0.5 mmol) and $Cu(CF_3SO_3)_2$ (1 mmol, from TCI) were dissolved in $CDCl_3$ (15 cm^3, 99.8% from Aldrich) under a nitrogen atmosphere and the mixture was stirred at room temperature for 12 h. After the removal of unreacted $Cu(CF_3SO_3)_2$ through filtration, the filtrate consisting of Cu(tptp) and **2a** (i.e. the mixture B) was studied using NMR (Fig. 2) and ESR (Fig. 3) spectroscopy. Meanwhile, a blue–purple crystal of Cu(tptp) was grown by slow evaporation of $CDCl_3$ from the solution of mixture B.

2.2. Preparation of $[H_4tptp]^{2+}[CH_3SO_3]_2^-$ (3) and $[H_4tptp]^{2+}[CF_3SO_3]_2^-$ (2b)

Compound **3** (or **2b**) was obtained by protonation of H_2tptp (1 mmol) with 3 mmol of CH_3SO_3H (or CF_3SO_3H) in $CHCl_3$. Compound **3** was dissolved in $CHCl_3$ and layered with benzene. After 2 weeks, blue–green and equant shape crystals of complex **3** were obtained for single-crystal X-ray analysis. ^{1}H (or ^{13}C, or ^{19}F) NMR data for **2b** and **3** are shown in Table 1 (or Table 2), respectively.

2.3. NMR spectra

^{1}H and ^{13}C NMR spectra in $CDCl_3$ were recorded at 400.13 and 100.61 MHz, respectively, on a Bruker AM-400 spectrometer. The ^{19}F NMR spectra were measured in $CDCl_3$ at 376.76 or 282.40 MHz, on a Varian Mercury-400 or Bruker MSL-300 spectrometer. The reference peaks in ^{1}H NMR and ^{13}C NMR are relative to $CHCl_3$ at 7.24 ppm and the center line of $CDCl_3$ at 77.0 ppm, respectively. ^{19}F data are externally relative to $CFCl_3$.

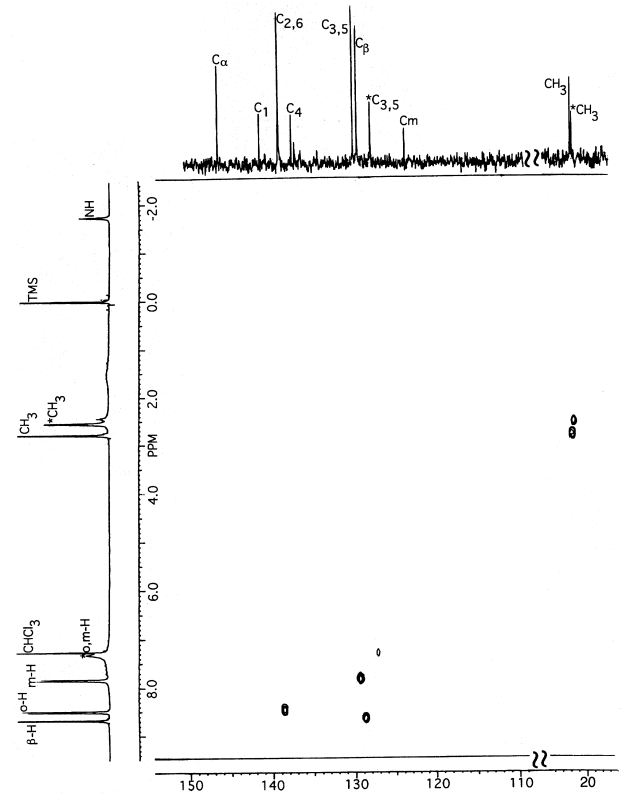


Fig. 2. The C-H COSY spectrum for the mixture B consists of Cu(tptp) and complex **2a** in $CDCl_3$ at 24°C. Resonances due to Cu(tptp) are labeled with an asterisk (*).

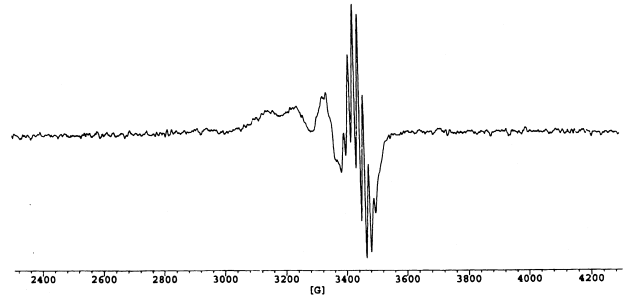


Fig. 3. The first derivative ESR spectrum for Cu(tptp) of mixture B in $CDCl_3$ at 24°C.

2.4. ESR spectra

ESR spectra were obtained with a Bruker EMX-10 X-band spectrometer system operating at 9.726 GHz with 100 kHz field modulation.

2.5. Crystallography

Table 3 presents crystal data and other information for Cu(tptp) and $[H_4tptp]^{2+}[CH_3SO_3]_2^- \cdot 2CHCl_3$ (**3**·2$CHCl_3$). Measurements were taken on a Siemens SMART CCD diffractometer using monochromatic Mo Kα radiation

Table 2
^{13}C and ^{19}F NMR chemical shifts (δ) for $[H_4tptp]^{2+}[CF_3SO_3]_2^-$ (**2a**) and Cu(tptp) in mixture B in $CDCl_3$ at 24°C

Porphyrin	C_α	C_1	C_4	$C_{2,6}$	C_β	$C_{3,5}$	C_m	*p*-CH_3	CF_3SO_3	CH_3SO_3	CF_3SO_3 (^{19}F)
H_2tptp		139.4	137.4	134.6	131.1	127.4	120.1	21.5			
$[H_4tptp]^{2+}[CH_3SO_3]_2^-$ (**3**) [a]	145.8	141.0	136.9	139.0	128.5	129.4	123.1	21.6		38.0	
$[H_4tptp]^{2+}[CF_3SO_3]_2^-$ (**2b**) [a]	145.8	140.9	137.0	138.6	128.7	129.3	122.9	21.6	116.9 (320)		−81.1
2a in mixture B [b]	145.9	140.9	137.1	138.7	128.8	129.3	123.0	21.6	116.2 [c] (318) [d]		−81.2
Cu(tptp) in mixture B						127.1		21.4			
Free ionic $CF_3SO_3^-$ [19]									121.0 (321)		−78.7
Free ionic $CH_3SO_3^-$ [19]										41.3	

[a] The preparation of compounds **3** and **2b** is shown in Table 1.
[b] Mixture B = **2a** + Cu(tptp).
[c] Measured at −50°C.
[d] ^1J(C–F) coupling constant.

Table 3
Crystal data for Cu(tptp) and **3**·2$CHCl_3$

Empirical formula	$C_{48}H_{36}CuN_4$	$C_{52}H_{48}Cl_6N_4O_6S_2$
FW	732.3	1101.8
Space group	$P2_1/n$	$P4_32_12$
Crystal system	monoclinic	tetragonal
Crystal color, habit	black lamellar	blue equant
a (Å)	9.9271(4)	17.6633(3)
b (Å)	9.2107(4)	
c (Å)	20.9383(5)	16.8444(4)
β (°)	98.533(2)	
V (Å^3)	1893.3(6)	5255(1)
Z	2	4
D_{calc} (g cm^{-3})	1.285	1.392
μ(Mo Kα) (cm^{-1})	6.16	4.59
S	1.03	1.08
Crystal size (mm)	0.07×0.08×0.31	0.19×0.25×0.30
$2\theta_{max}$ (°)	56.0	55.8
T (K)	296	296
No. reflections measured	5636	19092
No. reflections observed ($I \geq 3.0\sigma(I)$)	1544	2916
R (%) [a]	4.57	5.27
R_w (%) [b]	4.95	5.55

[a] $R = [\sum||F_o| - |F_c||/\sum|F_o|]$.
[b] $R_w = [\sum w(|F_o| - |F_c|)^2/\sum w(|F_o|)^2]^{1/2}$; $w = A/(\sigma^2F_o + BF_o^2)$.

($\lambda = 0.71073$ Å). Next, absorption corrections were based on 3191 (or 13717) symmetry-equivalent reflections using the SHELXTL-PC program package with $T_{min} = 0.481$, $T_{max} = 0.962$ or $T_{min} = 0.786$, $T_{max} = 0.942$ for Cu(tptp) and **3**·2$CHCl_3$, respectively. The structures were solved by direct methods (SHELXTL PLUS) and refined using full-matrix least-squares. All non-hydrogen atoms were refined with anisotropic thermal parameters, whereas all hydrogen-atom positions were located on a difference map (or were calculated using a riding model) and included in the structure factor calculation for Cu(tptp) and **3**·2$CHCl_3$. Table 4 outlines selected bond distances and angles for both complexes.

Table 4
Selected bond distances (Å) and angles (°) for Cu(tptp) and **3**·2$CHCl_3$

Cu(tptp)	
Cu(1)–N(1)	2.000(4)
Cu(1)–N(2)	1.994(4)
Cu(1)–N(1)–C(2)	127.2(3)
Cu(1)–N(1)–C(5)	127.4(4)
Cu(1)–N(2)–C(7)	127.4(4)
Cu(1)–N(2)–C(10)	126.9(3)
N(1)–Cu(1)–N(1a)	180.0(1)
N(1)–Cu(1)–N(2)	90.0(2)
3·2$CHCl_3$	
S(1)–C(30)	1.748(8)
S(1)–O(1)	1.442(5)
S(1)–O(2)	1.433(5)
S(1)–O(3)	1.463(4)
N(2)–C(7)	1.390(7)
N(2)–C(10)	1.367(6)
N(1)–C(2)	1.390(7)
N(1)–C(5)	1.370(6)
C(30)–S(1)–O(1)	106.3(3)
C(30)–S(1)–O(2)	106.1(3)
C(30)–S(1)–O(3)	106.4(3)
O(1)–S(1)–O(2)	114.5(3)
O(1)–S(1)–O(3)	111.8(3)
O(2)–S(1)–O(3)	111.2(3)
C(7)–N(2)–C(10)	110.6(4)
N(2)–C(10)–C(11)	127.2(5)
N(2)–C(10)–C(9)	106.5(4)
N(2)–C(7)–C(6)	126.6(4)
N(2)–C(7)–C(8)	105.4(4)
C(7)–C(6)–C(5)	123.3(5)
C(7)–C(6)–C(16)	120.4(4)

3. Results and discussion

3.1. Molecular structure of Cu(tptp)

Crystals of Cu(tptp) were obtained by slow evaporation of $CDCl_3$ from the mixture B. Fig. 4(a) illustrates the skeletal framework of complex Cu(tptp), with $P2_1/n$ symmetry. This

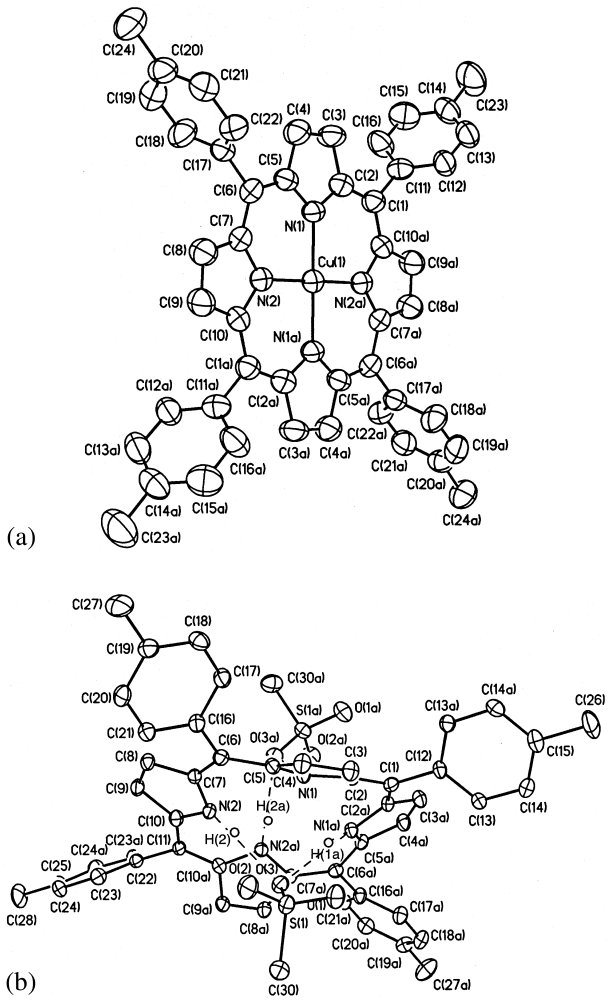


Fig. 4. Molecular configuration and atom-labeling scheme for (a) Cu(tptp) and (b) $\mathbf{3}\cdot 2CHCl_3$, with ellipsoids drawn at 20% probability. The refined positions of the hydrogen atoms bonded to the pyrrole nitrogens are shown for $\mathbf{3}\cdot 2CHCl_3$; all other hydrogen atoms for both compounds and solvents C(29)H(29a)Cl(1)Cl(2)Cl(3) for $\mathbf{3}\cdot 2CHCl_3$ are omitted for clarity.

structure has a four-coordinate copper with four nitrogen atoms of the porphyrinato group. Bond distances are Cu(1)–N(1) = 2.000(4) and Cu(1)–N(2) = 1.994(4) Å. The $C_{20}N_4$ core is essentially planar. The Cu(1) sits at the inversion center, so the angles N(1)–Cu(1)–N(1a) and N(2)–Cu(1)–N(2a) are 180.0(1)°. The dihedral angles between the mean plane of the skeleton ($C_{20}N_4$) and the planes of the phenyl groups are 68.4° (C(14)) and 87.5° (C(20)).

The radius of the central hole ($C_{t'}\cdots N$, the distance from the geometrical center $C_{t'}$ of the mean plane of the 24-atom core to the porphyrinato-core N atoms) is 1.997 Å (or ~2.00 Å) which is similar to the value of ~2.01 Å suggested by Collins and Hoard [7]. Hence, the copper(II) atom is bonded and centered in a porphyrinato core ($C_{20}N_4$) with 'radial strain' being minimized. The average distance of 1.997 Å in Cu(tptp) is comparable with the observed Cu–N distances of 1.981 Å in Cu(tpp) [8], 1.998 Å in Cu(oep) (H_2oep = octaethylporphyrin) [9], 1.997 Å in Cu(oetpp) (H_2oetpp = octaethyltetraphenylporphyrin) [10], 1.984 Å in CutTEtpp (H_2tTEtpp = 2,3,12,13-tetraethyl-5,10,15,20-tetraphenylporphyrin), 1.975 Å in CucTEtpp (H_2cTEtpp = 2,3,7,8-tetraethyl-5,10,15,20-tetraphenylporphyrin) and 1.980 Å in CuHEtpp (H_2HEtpp = 2,3,7,8,12,13-hexaethyl-5,10,15,20-tetraphenylporphyrin) [11]. Interestingly, the structure of Cu(tptp) is also isomorphic to that of *meso-p*-tolyl-porphyrinatozinc(II) Zn(tptp) [12].

3.2. The crystal structure of $[H_4tptp]^{2+}[CH_3SO_3]_2^-\cdot 2CHCl_3$ ($\mathbf{3}\cdot 2CHCl_3$)

Each porphyrin nucleus is associated with two complex anions $CH_3SO_3^-$ (Fig. 4(b)). First, the contacts between the porphyrin nitrogen atoms N(2) (or N(1a)) and O(3) of the anion are 2.866 (or 2.927 Å), and these are short enough to permit hydrogen bonding of the type N–H···O. The mean N···O distance in these types of hydrogen bonds is calculated as 2.90 Å. Second, the H···O distances (based on the refined hydrogen atom positions) are 1.94 Å for O(3)···H(2) and 1.98 Å for O(3)···H(la). The mean H···O distance in hydrogen bonds is calculated as 2.60 Å. Third, the values of N–H···O angles are close to linear values with 171.5° for N(2)–H(2)···O(3) and 163.2° for N(la)–H(1a)···O(3). All these results indicate that two triflate anions are hydrogen bonded to the pyrrole hydrogens in a monodentate bridging fashion, with one O(3) (or O(3a)) bonded to two opposite N-H protons, i.e. H(2) and H(la) (or H(1) and H(2a)), on the same face of the porphyrin [13]. The four phenyl group–porphyrin dihedral angles in $\mathbf{3}\cdot 2CHCl_3$ are 35.4° (C(15)), and 31.4° (C(19a)), 40.0° (C(25)) and 31.4° (C(l9)). These dihedral angles are quite acute, averaging only 34.6°. They are slightly larger than the average 27° in $[H_2tpp][ClO_4]_2$ but smaller than 63° (or 75°) in $[H_4tmp][ClO_4]_2$ [14]. The distortion ($C_{20}N_4$) of $\mathbf{3}\cdot 2CHCl_3$ is saddle shaped. Fig. 5 depicts the displacement (in Å) of each atom of the

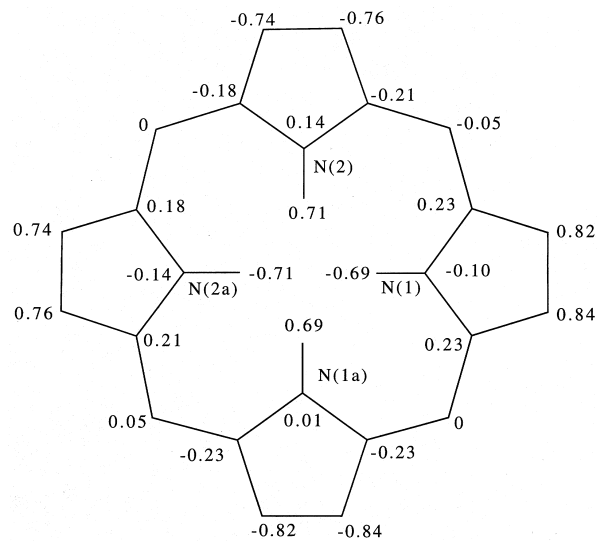
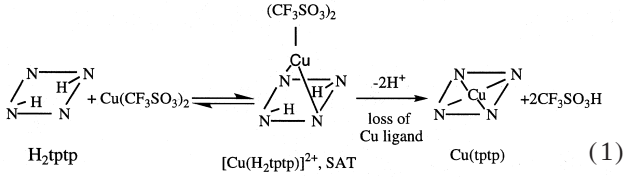


Fig. 5. Schematic diagram of the porphyrin core ($C_{20}N_4$) and four inner hydrogen atoms of $\mathbf{3}\cdot 2CHCl_3$ in which each atom symbol is replaced by a number showing the displacement (in Å) of that atom from the mean plane of the porphyrin ($C_{20}N_4$) with a typical esd of 0.003 Å.

porphyrin from the porphyrin mean plane ($C_{20}N_4$) as well as displacements of the four central hydrogen atoms. The pyrrole NH protons are alternately displaced above and below the 24-atom mean plane by −0.69 Å for H(1), 0.71 Å for H(2), −0.71 Å for H(2a), and 0.69 Å for H(1a). The out-of-plane displacements of the inner hydrogen atoms help to relieve steric strain [15]. The groupings of $[H_4tptp]^{2+}$ and $CH_3SO_3^-$ of **3** in $CDCl_3$ retain their basic properties when bonded together by hydrogen bonds called an ion-pair. Although the structures of Cu(tpp) [8], Cu(oep) [9], Cu(oetpp) [10], CutTEtpp [11], CucTEtpp [11], CuHEtpp [11] and the di-cation of tetraarylporphyrin species $[H_4por](ClO_4)_2$ [14], $[H_4por](TFA)_2$ (TFA = trifluoroacetate) [15], and $[H_4por](OAc)_{3/2}(TFA)_{1/2}$ [15] (por = tpp, oep, oetpp) have already been published, Cu(tptp) and **3** are two new crystal structures with different porphyrin (tptp) and counter ion ($CH_3SO_3^-$).

*3.3. NMR spectra of Cu(tptp) and $[H_4tptp]^{2+}[CF_3SO_3]_2^-$ (**2a**) in mixture B*

The net reaction of $Cu(CF_3SO_3)_2$ with H_2tptp in $CDCl_3$ is known by Eqs. (1) and (2), where **2a** is a di-cation ion-pair complex [16].



(1)

$$H_2tptp + 2CF_3SO_3H \rightarrow [H_4tptp]^{2+}[CF_3SO_3]_2^- \quad (2)$$
(**2a**)

The SAT complex $[Cu(H_2tptp)]^{2+}$ has been proposed as an intermediate. Loss of the N-H protons and $CF_3SO_3^-$ ligand produces Cu(tptp) and CF_3SO_3H. Finally, protonation of the remaining H_2tptp produces the ion-pair complex **2a** between the *meso*-*p*-tolyl-porphyrin di-cation $[H_4tptp]^{2+}$ and triflate ($CF_3SO_3^-$). Only Cu(tptp) and complex **2a** are observed by ^1H NMR in our system. The ^1H NMR spectrum for Cu(tptp) in mixture B in $CDCl_3$ (see Table 1 and Fig. 2) shows *m*-phenyl signals at 7.30 ppm and methyl protons at 2.53 ppm. These values are quite close to the corresponding signals at 7.30 ppm for the *m*-phenyl protons and 2.52 ppm for the methyl protons in complex Cu(tptp) reported by Godziela and Goff [4]. The N-H signals are downfield shifted by ~1.03 ppm from −2.79 (for H_2tptp) to −1.76 ppm for complex **2a** by protonation. The similar downfield shift due to protonation is also reflected by observing a 4.2–4.7 ppm downfield shift of N-H at −2.588 and −2.672 ppm for H_2Cttp (**4**) (2-aza-21-carba-5,10,15,20-tetra-*p*-tolylporphyrin), compared to 2.034, 1.877 and 1.612 ppm for $[\mathbf{4}\text{-}H_2]^{2+}$ [17]. In complex **2a**, the integrated peak areas are 8:8:8:4 for the β-pyrrole:*o*-phenyl:*m*-phenyl:N-H protons, respectively. Owing to the paramagnetic copper(II) ion in Cu(tptp), the ^{13}C NMR spectrum of Cu(tptp) (see Fig. 2 and Table 2) shows only two peaks at 127.1 ($C_{3,5}$) and 21.4 ppm (*p*-CH_3). The ^{13}C, ^{19}F and ^1H NMR data for **2a** in mixture B shown in Tables 1 and 2 are consistent with those of $[H_4tptp]^{2+}[CF_3SO_3]_2^-$ (**2b**) obtained by protonation of H_2tptp using CF_3SO_3H. Notably, these consistencies suggest that complex **2a** is **2b**. Furthermore, the ^{13}C (or ^{19}F) resonance of $CF_3SO_3^-$ for compound **2a** at $\delta = 116.2$ ppm with ^1J(C–F) coupling constant 318 Hz (or −81.2 ppm) is different from that of free ionic $CF_3SO_3^-$, i.e. $Bu_4N^+CF_3SO_3^-$, with $\delta = 121.0$ and ^1J(C–F) = 321 Hz (or −78.7 ppm) at room temperature [18,19]. Hence, the mutual geometric arrangement of the $[H_4tptp]^{2+}$, $CF_3SO_3^-$ and the solvent $CDCl_3$ in complex **2a** is explained as ion pairs. The intramolecular electric fields in the ion-pair complex **2a** cause considerable upfield shifts of −4.8 ppm (from 121.0 to 116.2 ppm) for the triflate carbon and about −2.5 ppm (from −78.7 to −81.2 ppm) for the ^{19}F resonance in the same complex [20]. When the CF_3^- of **2a** was replaced by a CH_3^- group, the complex **2a** became $[H_4tptp]^{2+}[CH_3SO_3]_2^-$ (**3**). In the absence of the crystal structure of **2a**, the close resemblance of ^{13}C and ^1H data (shown in Tables 1 and 2) for the di-cation $[H_4tptp]^{2+}$ of **2b** and **3** indicates a similar structure for these two complexes. Two $CH_3SO_3^-$ anions axial and hydrogen-bonded to the pyrrole hydrogen in **3** (shown in Fig. 4(b)) suggest that two $CF_3SO_3^-$ might be located on the axial position of the porphyrin ring ($C_{20}N_4$) of **2a**. The upfield shift of about −3.3 ppm (from 41.3 (obtained from free $CH_3SO_3^-$, i.e. $Cs^+CH_3SO_3^-$) [19] to 38.0 ppm) for carbon of CH_3SO_3 in **3** is due to the same electric field as in complex **2a**. Nevertheless, the ^1H chemical shift of CH_3SO_3 in **3** experienced an upfield shift of −0.15 ppm from 2.8 (obtained from free $CH_3SO_3^-$) [19] to 2.65 ppm, being controlled by the ring current effect.

3.4. ESR spectra for Cu(tptp) in mixture B

Cu(tptp) are paramagnetic because of the d^9 configuration of Cu(II). The unpaired electron resides in the $d_{x^2-y^2}$ orbital, which leads to characteristic EPR spectra for Cu(tptp): four peaks due to the nuclear spin ($I = 3/2$) of the Cu and super-hyperfine interaction with the four nitrogens ($I = 1$) of the porphyrin. Cu(tptp) in $CDCl_3$ exhibits a typical Cu(II) porphyrin EPR spectrum as shown in Fig. 3. The experimental spectrum yields $a_{Cu} = 94.0$ G and four nitrogens with $a_N = 15.8$ G. These data are similar to those reported, $a_{Cu} = 90.5$ G and $a_N = 15.8$ G for Cu(tpp) [21], $a_{Cu} = 90$ G and $a_N = 15$ G for Cu(oep) [9], or $a_{Cu} = 86.5$ G and $a_N = 14.4$ G for Cu(oetpp) [10].

4. Conclusions

Inada postulated that in the reaction of Cu(II) with H_2tpp in CH_3CN, an intermediate complex species forms,

$[Cu(H_2tpp)]^{2+}$, in which the metal stays above the tetra-aza plane. We have repeated the reaction using a slightly different porphyrin (H_2tptp) in less basic solvent $CDCl_3$, and have crystallized from the solution the Cu(tptp) and the doubly protonated ligand $[H_4tptp]^{2+}[CF_3SO_3]^-$ (**2a**), which demonstrates that the H_2tptp acts simultaneously as Cu^{2+} complexation and as a proton receptor.

Acknowledgements

The authors would like to thank the National Science Council of the Republic of China for financially supporting this work under Contract No. NSC 88-2113-M-005-017.

References

[1] Y. Inada, Y. Sugimoto, Y. Nakano, S. Funahashi, Chem. Lett. (1996) 881.
[2] Y. Inada, Y. Sugimoto, Y. Nakano, Y. Itoh, S. Funahashi, Inorg. Chem. 37 (1998) 5519.
[3] J.E. Huheey, Inorganic Chemistry, Harper & Row, Singapore, 3rd edn., 1983, p. 340.
[4] G.M. Godziela, H.M. Goff, J. Am. Chem. Soc. 108 (1986) 2237.
[5] C.B. Storm, Y. Teklu, J. Am. Chem. Soc. 94 (1972) 1745.
[6] M. Tsutsui, C.P. Hrung, D. Ostfeld, T.S. Srivastava, D.L. Cullen, E.F. Meyer, J. Am. Chem. Soc. 97 (1975) 3952.
[7] D.M. Collins, J.L. Hoard, J. Am. Chem. Soc. 92 (1970) 3761.
[8] E.B. Fleischer, C.K. Miller, L.E. Webb, J. Am. Chem. Soc. 86 (1964) 2342.
[9] R. Pak, W.R. Scheidt, Acta Crystallogr., Sect. C 47 (1991) 431.
[10] M.W. Renner, K.M. Barkigia, Y. Zhang, C.J. Medforth, K.M. Smith, J. Fajer, J. Am. Chem. Soc. 116 (1994) 8582.
[11] M.O. Senge, W.K. Kalisch, Inorg. Chem. 36 (1997) 6103.
[12] P. Dastidar, I. Goldberg, Acta Crystallogr., Sect. C 52 (1996) 1976.
[13] M.O. Senge, T.P. Forsyth, L.T. Nguyen, K.M. Smith, Angew. Chem., Int. Ed. Engl. 33 (1994) 2485.
[14] B. Cheng, O.Q. Munro, H.M. Marques, W.R. Scheidt, J. Am. Chem. Soc. 119 (1997) 10732.
[15] E. Cetinkaya, A.W. Johnson, M.F. Lappert, G.M. Mclaughlin, K.W. Muir, J. Chem. Soc., Dalton Trans. (1974) 1236.
[16] K. Letts, R.A. Mackey, Inorg. Chem. 14 (1975) 2993.
[17] P.J. Chmielewski, L. Latos-Grazynski, K. Rachlewicz, T. Glowiak, Angew. Chem., Int. Ed. Engl. 33 (1994) 779.
[18] A.D. Boersma, H.M. Goff, Inorg. Chem. 21 (1982) 581.
[19] C.J. Pouchert, J. Behnke, The Aldrich Library of ^{13}C and ^{1}H FT NMR Spectra, vol. I, Aldrich, Milwaukee, 1st edn., 1993, pp. 1431 (A, B), 1427 (A,B).
[20] E. Breitmaier, W. Voelter, Carbon-13 NMR Spectroscopy, VCH, New York, 3rd edn., 1990, pp. 116, 121.
[21] P.F. Richardson, C.K. Chang, L.K. Hanson, L.D. Spaulding, J. Fajer, J. Phys. Chem. 83 (1979) 3420.

PERGAMON

www.elsevier.nl/locate/poly

Polyhedron 19 (2000) 641–647

POLYHEDRON

Amine-oxide-mediated oxidative methanolysis of metal–metal bonds in $[MM'(CO)_{10}]$ (M = Mn, Re; M′ = Re) and $[Os_3(CO)_{12}]$: crystal structure of *fac*-$[Re\{OC(O)OMe\}(CO)_3(\eta^2\text{-dppf})]$

Yaw-Kai Yan [a,*], Wendy Koh [b], Chenghua Jiang [b], Weng Kee Leong [b], T.S. Andy Hor [b]

[a] *Division of Chemistry, National Institute of Education, Nanyang Technological University, 469 Bukit Timah Road, Singapore 259756, Singapore*

[b] *Department of Chemistry, National University of Singapore, Kent Ridge, Singapore 119260, Singapore*

Received 20 October 1999; accepted 15 December 1999

Abstract

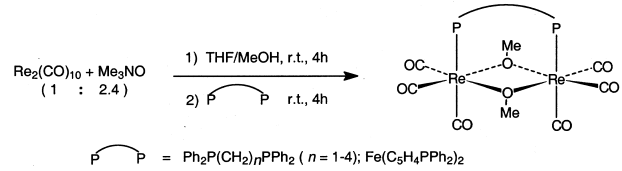
The reaction of 1,1′-bis(diphenylphosphino)ferrocene (dppf) with a mixture of $[MnRe(CO)_{10}]$, MeOH and Me_3NO afforded the complexes *fac*-$[MnH(CO)_3(\eta^2\text{-dppf})]$ and $[Re_2(\mu\text{-OMe})_2(\mu\text{-dppf})(CO)_6]$. In the one-pot reaction of $[Re_2(CO)_{10}]$ with Me_3NO, MeOH and dppf, the major mononuclear Re species isolated was the CO_2-inserted complex *fac*-$[Re\{OC(O)OMe\}(CO)_3(\eta^2\text{-dppf})]$, the crystal structure of which was determined. The coordination sphere of the rhenium atom is roughly octahedral, consisting of an oxygen atom from the methyl carbonate ligand, two phosphorus atoms from a chelating dppf ligand, and three carbon atoms from a facial arrangement of three terminally bonded carbonyls. Analogous Me_3NO-mediated methoxylation reactions involving $[Os_3(CO)_{12}]$ were also investigated. With a $[Me_3NO]:[Os_3(CO)_{12}]$ ratio of 2:1, the major product is $[Os_3(CO)_{10}(\mu\text{-H})(\mu\text{-OMe})]$. With three molar equivalents of Me_3NO, significant quantities of $[Os_3(CO)_{10}(\mu\text{-OMe})_2]$ are also obtained. ©2000 Elsevier Science Ltd All rights reserved.

Keywords: Amine oxide; Methanolysis; Rhenium; Osmium; Carbonyl; Methylcarbonate

1. Introduction

Transition-metal carbonyl hydroxides and alkoxides have been proposed as intermediates in a number of important reactions, such as metal-catalysed hydrogenation of CO [1], the water-gas shift reaction [2], and carboalkoxylation of olefins [3]. They are also molecular models of silica-anchored $M(CO)_n$ species, the only structural difference between alkoxy and surfaced anchored complexes being that the –OR group is replaced by an –OSi≡ group [4].

We have reported the facile synthesis of a series of dimethoxo-bridged complexes $[Re_2(\mu\text{-OMe})_2(\mu\text{-PP})(CO)_6]$ (PP = dppf (1,1′-bis(diphenylphosphino)ferrocene) or $Ph_2P(CH_2)_nPPh_2$, $n = 1$–4) by the addition of diphosphines to a mixture obtained from the reaction of $[Re_2(CO)_{10}]$ with Me_3NO in THF–MeOH mixture at room temperature (Scheme 1) [5,6]. The facile rupture of the Re–Re bond under such mild conditions is in sharp contrast to the general observation that metal–metal bonds are quite resistant to thermal cleavage [7,8] and that Re–Re bond alcoholysis requires rather drastic conditions, such as refluxing in methanolic KOH [9].

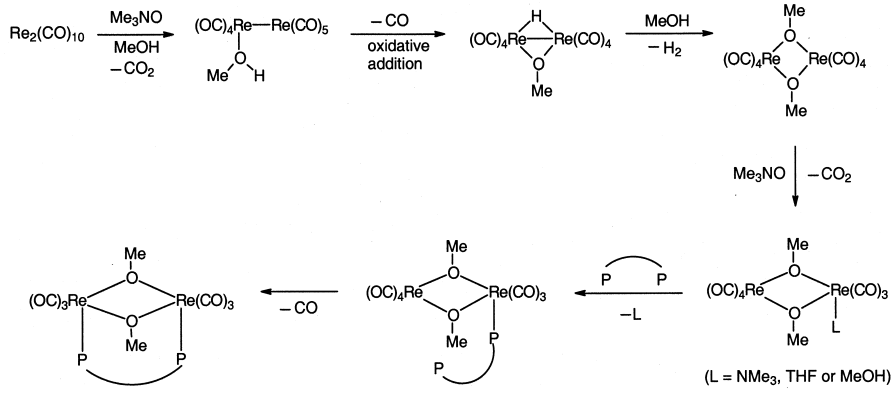


Scheme 1.

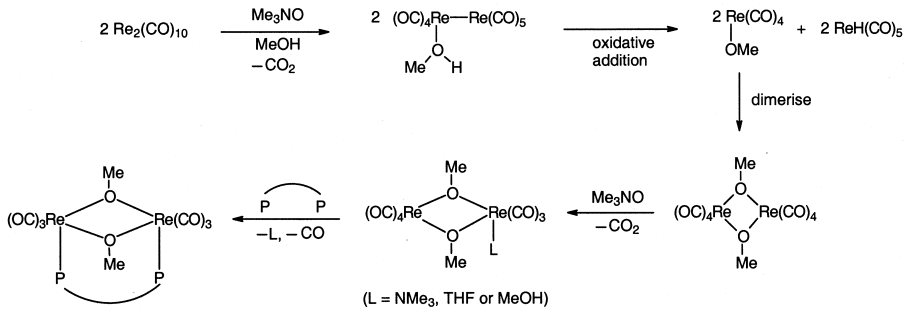
At first, a mechanism for the Me_3NO-aided oxidative methoxylation reaction in which the originally bonded Re atoms in $[Re_2(CO)_{10}]$ remain paired in the same molecule of the product $[Re_2(\mu\text{-OMe})_2(\mu\text{-PP})(CO)_6]$ (Scheme 2) seemed plausible [10]. We then extended our investigations to the reaction of $[Re_2(CO)_{10}]$ with Me_3NO and phenol, which yielded the complexes $[Re_3(\mu\text{-H})(CO)_{14}]$ and $[Re_2(\mu\text{-OPh})_3(CO)_6]^-$ [11]. This suggested a mechanism involving the separation of the Re atoms of $[Re_2(CO)_{10}]$ into mononuclear hydrido and phenoxo species, followed by dimerisation of the phenoxo species to form the bis(phenoxo)-bridged intermediate $[Re_2(\mu\text{-OPh})_2(CO)_8]$ [11]. It seemed probable that the oxidative methoxylation reaction also follows a similar pathway involving Re–Re

* Corresponding author. Tel.: +65-4605180; fax: +65-4698952; e-mail: ykyan@nie.edu.sg

0277-5387/00/$ - see front matter ©2000 Elsevier Science Ltd All rights reserved.
PII S0277-5387(00)00296-5



Scheme 2.



Scheme 3.

bond heterolysis, but we have not been able to observe any rhenium hydrido species in this reaction. The reaction of $[Re_2(CO)_{10}]$ with Me_3NO and methanol (without diphosphine) yields $[Me_3NH]^+[Re_3(\mu_3\text{-}OMe)(\mu\text{-}OMe)(\mu\text{-}OH)_2(CO)_9]^-$ as the only isolable product [11].

In an effort to throw more light onto the mechanism of Me_3NO-aided oxidative methoxylation, we studied the reaction of dppf with the mixture of $[MnRe(CO)_{10}]$, MeOH and Me_3NO. The products of this reaction should indicate whether the Re and Mn atoms are separated during the reaction. Formation of the homometallic complexes $[Re_2(\mu\text{-}OMe)_2(\mu\text{-dppf})(CO)_6]$ and/or $[Mn_2(\mu\text{-}OMe)_2(\mu\text{-dppf})(CO)_6]$ would support the M–M bond heterolysis mechanism. The results of this study are reported in this paper. We also report a similar amine-oxide mediated methoxylation of Os–Os bonds in the cluster $[Os_3(CO)_{12}]$ to form $[Os_3(\mu\text{-}H)(\mu\text{-}OMe)(CO)_{10}]$ and $[Os_3(\mu\text{-}OMe)_2(CO)_{10}]$. These methoxo clusters were first reported in 1968 [12], but to date no convenient one-pot synthesis giving high yields of these clusters from $[Os_3(CO)_{12}]$ has been reported [4,13–16].

2. Results and discussion

2.1. Reaction of dppf with $MnRe(CO)_{10}$, MeOH and Me_3NO

The reaction of dppf with the mixture of $[MnRe(CO)_{10}]$, MeOH and Me_3NO afforded the complexes *fac*-$[MnH(CO)_3(\eta^2\text{-dppf})]$ (8%), $[Re_2(\mu\text{-}OMe)_2(\mu\text{-dppf})(CO)_6]$ (26%) and a trace amount of *fac*-$[ReCl(CO)_3(\eta^2\text{-dppf})]$. These results confirm the occurrence of metal–metal bond cleavage and the formation of metal hydride intermediates in the reaction. The mechanism for the formation of $[Re_2(\mu\text{-}OMe)_2(\mu\text{-dppf})(CO)_6]$ from the reaction of dppf with $[Re_2(CO)_{10}]$, MeOH and Me_3NO is therefore proposed as shown in Scheme 3.

Interestingly, the complexes $[Mn_2(\mu\text{-}OMe)_2(\mu\text{-dppf})(CO)_6]$ and $[ReH(CO)_3(\eta^2\text{-dppf})]$ are not observed as products of the reaction, probably because these complexes are unstable under the conditions of the reaction and isolation of products. The complex $[ReCl(CO)_3(\eta^2\text{-dppf})]$ is likely to be produced from the reaction of initially formed $[ReH(CO)_3(\eta^2\text{-dppf})]$ with CH_2Cl_2 used during the isolation of products by TLC [17]. We have also not been able to synthesise $[Mn_2(\mu\text{-}OMe)_2(\mu\text{-dppf})(CO)_6]$ via the reaction of dppf with the mixture of $[Mn_2(CO)_{10}]$, Me_3NO and MeOH.

2.2. One-pot reaction of $[Re_2(CO)_{10}]$ with Me_3NO, MeOH and dppf

In an attempt to trap the $[Re(OMe)(CO)_4]$ intermediate in the reaction of $[Re_2(CO)_{10}]$ with Me_3NO and MeOH, the one-pot reaction of $[Re_2(CO)_{10}]$ with Me_3NO, MeOH and dppf has been carried out [11]. The major mononuclear Re complex formed in this reaction (**1**) was mistakenly identified as the terminal methoxo complex *fac*-$[Re(OMe)(CO)_3(\eta^2\text{-dppf})]$ in Ref. [11]. We have subsequently determined the crystal structure of **1** (see below), and iden-

tified it as the methyl carbonate complex *fac*-[Re{OC(O)OMe}(CO)$_3$(η^2-dppf)].

Complex **1** is most probably formed by the insertion of CO_2 into the intermediate complex *fac*-[Re(OMe)(CO)$_3$(η^2-dppf)] resulting from the reaction of dppf with [Re(OMe)(CO)$_4$]. The CO_2 needed for the insertion reaction is probably produced by the decarbonylation of [Re_2(CO)$_{10}$] by Me_3NO. The facile CO_2-insertion reactions of the complexes *fac*-[Re(OR)(CO)$_3$(η^2-PP)] (R = Me, Et, CF_3CH_2; PP = 1,2-bis(diphenylphosphino)ethane (dppe), 1,3-bis(diphenylphosphino)propane) with atmospheric CO_2 has been reported [18].

2.3. Crystal structure of fac-[Re{OC(O)OMe}(CO)$_3$(η^2-dppf)] (1)

The crystal structure of **1** (Fig. 1) is similar to that of *fac*-[Mn{OC(O)OMe}(CO)$_3$(η^2-dppe)] [18]. The coordination sphere of the rhenium atom is roughly octahedral, consisting of an oxygen atom from the methyl carbonate ligand (taken to occupy an axial position), two phosphorus atoms from a chelating dppf ligand, and three carbon atoms from a facial arrangement of three terminally bound carbonyls. The P–Re–P angle in **1** (Table 1) is larger than the P–Mn–P angle in *fac*-[Mn{OC(O)OMe}(CO)$_3$(η^2-dppe)] (84.1(1)°), probably owing to the greater steric demand of dppf compared to dppe. The Re–CO(eq) distances (average 1.943(7) Å) are longer than the Re–CO(ax) distance (1.890(7) Å). Correspondingly, the C–O bond length of the axial carbonyl (1.154(8) Å) is longer than the lengths of 1.131(7) and 1.138(7) Å observed for the equatorial carbonyls. This can be attributed to the greater extent of M → CO backbonding experienced by the axial carbonyl, which is *trans* to the π-donating methyl carbonate ligand. The Re–O(1) bond to the methyl carbonate ligand has a length of 2.150(4) Å, which is comparable to the Re–O bond lengths of 2.150(4) Å in *fac*-[Re(OPh)(CO)$_3$(η^2-dppe)] [19], 2.162(6) Å (average) in [Re_2(μ-OMe)$_2$(μ-dppf)(CO)$_6$] [5], and 2.143(8) Å (average) in [Re_2(μ-OMe)$_2$(μ-dppm)(CO)$_6$] [6].

2.4. Reactions of [Os$_3$(CO)$_{12}$] with Me$_3$NO and MeOH

Reaction of [Os_3(CO)$_{12}$] with Me_3NO (1.2 molar equivalents) in refluxing THF–methanol (7:1) mixture for 4 h gave the complex [Os_3(μ-H)(μ-OMe)(CO)$_{10}$] (**2**) in 71% yield. Increasing the amount of amine oxide (2.4 molar equivalents) and methanol (THF:MeOH 4:1) did not significantly increase the yield of **2** (73%). The same cluster has been prepared in 10% yield by direct reaction of [Os_3(CO)$_{12}$] with methanol at 170°C for 38 h in vacuo in a steel-lined autoclave [13]. It can also be prepared via multi-step processes involving [Os_3(CO)$_{10}$(cyclohexa-1,3-diene)] [14], [Os_3(CO)$_{10}$(cyclooctene)$_2$] [15], [Os_3(CO)$_{10}$(CH_3CN)$_2$] [15], or [Os_3(μ-H)(μ-NCHNMe_2)(CO)$_{10}$] [16] as intermediates. However, since three or four steps are required starting from [Os_3(CO)$_{12}$], overall yields are never more than 50%. More recently, the reaction of methanol with the silica-anchored cluster [Os_3(μ-H)(μ-OSi≡)(CO)$_{10}$] (prepared by refluxing an *n*-octane solution of [Os_3(CO)$_{12}$] with silica for 10 h) was reported to give complex **2** in 52% yield (starting from [Os_3(CO)$_{12}$]) [4]. An alternative route involving the reaction of methanol with [Os_3(μ-H)(μ-OH)(CO)$_{10}$] (prepared by heating a suspension of [Os_3(μ-H)(μ-OSi≡)(CO)$_{10}$] in a water–toluene mixture at 95°C for 5 h) gives complex **2** in 82% overall yield from [Os_3(CO)$_{12}$] [4]. Compared with the reported syntheses of **2**, the present method is much more attractive since it is a high-yield one-pot synthesis over 4 h, starting directly from [Os_3(CO)$_{12}$], under relatively mild conditions.

When the molar ratio of Me_3NO to [Os_3(CO)$_{12}$] is increased to 3.3:1, the bis(methoxo) cluster [Os_3(μ-OMe)$_2$(CO)$_{10}$] (**3**) is obtained in 11% yield, while complex **2** is obtained in 33% yield. The yield of **3** is increased to 17% when 4.3 molar equivalents of amine oxide are used, while the yield of **2** remains essentially unchanged. As far as we are aware, the highest-yield synthesis for **3** reported thus far involves direct reaction of [Os_3(CO)$_{12}$] with methanol at 170°C for 38 h in vacuo in a steel-lined autoclave, which

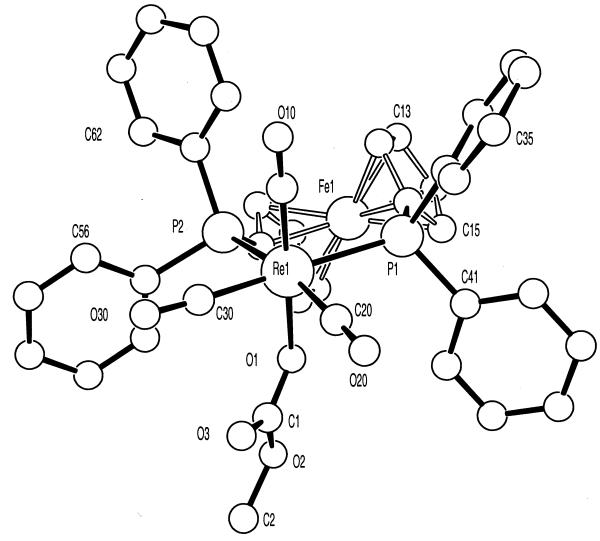


Fig. 1. Crystal structure of *fac*-[Re{OC(O)OMe}(CO)$_3$(η^2-dppf)] (**1**). Hydrogen atoms are omitted for clarity.

Table 1
Bond lengths (Å) and angles (°) for *fac*-[Re{OC(O)OMe}(CO)$_3$(η^2-dppf)] (**1**)

Re(1)–P(1)	2.508(2)	C(20)–O(20)	1.131(7)
Re(1)–P(2)	2.505(2)	C(30)–O(30)	1.138(7)
Re(1)–O(1)	2.150(4)	C(1)–O(1)	1.300(7)
Re(1)–C(10)	1.890(7)	C(1)–O(2)	1.244(8)
Re(1)–C(20)	1.946(7)	C(1)–O(3)	1.224(7)
Re(1)–C(30)	1.940(7)	O(2)–C(2)	1.438(8)
C(10)–O(10)	1.154(8)		
P(1)–Re(1)–P(2)	96.18(5)	O(1)–C(1)–O(3)	124.1(7)
Re(1)–O(1)–C(1)	125.6(4)	C(1)–O(2)–C(2)	118.1(6)
O(1)–C(1)–O(2)	112.3(5)	O(2)–C(1)–O(3)	123.6(7)

gives **3** in 13% yield and **2** in 10% yield (see above) [13]. The present one-pot synthesis for **3** is comparatively more convenient and gives a similar yield of the cluster.

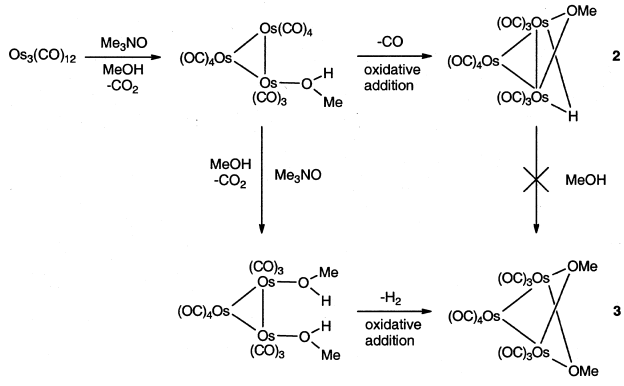
*2.5. Proposed mechanism for the formation of clusters **2** and **3***

A plausible mechanism for the formation of clusters **2** and **3** is given in Scheme 4. As in the proposed mechanism for the formation of $[Re_2(\mu\text{-}OMe)_2(\mu\text{-}dppf)(CO)_6]$ from $[Re_2(CO)_{10}]$, the first step involves Me_3NO-assisted substitution of a CO ligand by methanol. Oxidative addition of MeO–H across the M–M bond does not, however, result in the formation of two separate mononuclear species $[OsH(CO)_3]$ and $[Os(OMe)(CO)_3]$, since the two $[Os(CO)_3]$ fragments are still bonded to the third osmium atom, which keeps them in close proximity. The oxidative addition reaction therefore results preferentially in the hydrido- and methoxo-bridged cluster $[Os_3(\mu\text{-}H)(\mu\text{-}OMe)(CO)_{10}]$ (**2**), with three Os–Os bonds. The loss of the second CO ligand which accompanies the oxidative addition presumably does not require Me_3NO, since there is no significant difference in the yield of **2** whether 1.2 or 2.4 molar equivalents of amine oxide is used.

The cluster $[Os_3(\mu\text{-}OMe)_2(CO)_{10}]$ (**3**) is probably formed by the oxidative addition of methanol and elimination of H_2 from the disubstituted intermediate $[Os_3(CO)_{10}(MeOH)_2]$. The formation of $[Os_3(CO)_{10}(MeOH)_2]$ from $[Os_3(CO)_{11}(MeOH)]$ probably requires Me_3NO and is slow compared to the conversion of $[Os_3(CO)_{11}(MeOH)]$ to $[Os_3(\mu\text{-}H)(\mu\text{-}OMe)(CO)_{10}]$. Hence cluster **3** is only formed in significant quantities when excess amine oxide is used. The higher concentration of Me_3NO probably increases the rate of formation of $[Os_3(CO)_{10}(MeOH)_2]$, enabling this process to compete more effectively against the formation of $[Os_3(\mu\text{-}H)(\mu\text{-}OMe)(CO)_{10}]$. Cluster **3** is unlikely to be formed from the secondary reaction of **2** with excess methanol since **2** remains unchanged when refluxed in methanol for 4 h.

Interestingly, Deeming et al. reported that $[Ru_3(CO)_{12}]$ reacts with $Me_3NO\cdot 2H_2O$ (5.8 molar equivalents) in the presence of (*R*)-BINAP (2,2′-bis(diphenylphosphino)-1,1′-binaphthyl) to give an 80% yield of the dihydroxo complex $[Ru_3(\mu\text{-}OH)_2(CO)_8\{\mu\text{-}(R)\text{-}BINAP\}]$ [20]. Although the authors identified $Me_3NO\cdot 2H_2O$ as the probable source of the hydroxo ligands, they did not propose any mechanism for the formation of $[Ru_3(\mu\text{-}OH)_2(CO)_8\{\mu\text{-}(R)\text{-}BINAP\}]$. We believe that the mechanism is similar to that proposed above for the formation of $[Os_3(\mu\text{-}OMe)_2(CO)_{10}]$. The complex $[Ru_3(\mu\text{-}OH)_2(CO)_{10}]$ is probably formed, and is further decarbonylated by the excess Me_3NO present to give an unsaturated intermediate which reacts with BINAP to form $[Ru_3(\mu\text{-}OH)_2(CO)_8\{\mu\text{-}(R)\text{-}BINAP\}]$. It is noteworthy that when dppm (bis(diphenylphosphino)methane) was added to the mixture resulting from the reaction of $[Os_3(CO)_{12}]$ with 4.3 molar equivalents of Me_3NO in THF–MeOH, a product tentatively identified as $[Os_3(\mu\text{-}H)(\mu\text{-}OMe)(\mu\text{-}dppm)(CO)_8]$ could be isolated.

So far, we have not observed products where two or more Os–Os bonds have been methoxylated.



Scheme 4.

3. Summary and conclusions

The reaction of dppf with the mixture of $MnRe(CO)_{10}$, MeOH and Me_3NO gives the complexes *fac*-$[MnH(CO)_3(\eta^2\text{-}dppf)]$ and $[Re_2(\mu\text{-}OMe)_2(\mu\text{-}dppf)(CO)_6]$, confirming that mononuclear alkoxo and hydrido intermediates are formed during the reaction. Reaction of $[Os_3(CO)_{12}]$ with Me_3NO (1–2 molar equivalents) and methanol gives $[Os_3(\mu\text{-}H)(\mu\text{-}OMe)(CO)_{10}]$ in good yield. With 3 molar equivalents of Me_3NO, significant quantities of $[Os_3(\mu\text{-}OMe)_2(CO)_{10}]$ are also obtained. No further methoxylation of Os–Os bonds occurs when the $[Me_3NO]$:$[Os_3(CO)_{12}]$ ratio is increased to 4:1.

4. Experimental

All reactions were performed under pure dry argon using standard Schlenk techniques. Solvents used were of reagent grade and were dried by published procedures and freshly distilled under argon before use. Unless otherwise stated, all reagents and starting materials used were of AR grade and were obtained from commercial sources and used as supplied. Precoated silica plates of layer thickness 0.25 mm were obtained from Merck. ^1H and $^{31}P\{^1H\}$ NMR spectra were recorded at ca. 300 K on a Bruker ACF 300 MHz spectrometer. ^1H and ^{31}P chemical shifts are quoted in ppm downfield of tetramethylsilane and external 80% H_3PO_4, respectively. Infrared spectra were recorded on either a Perkin Elmer 1600 or a Bio-Rad FTS165 FT-IR spectrophotometer. Elemental analyses were performed by the Microanalytical Laboratory, Department of Chemistry, National University of Singapore.

4.1. Preparation of $[MnRe(CO)_{10}]$

The reported method [21,22] for the preparation of $[MnRe(CO)_{10}]$ was used with slight modification. A

degassed solution of $[Mn_2(CO)_{10}]$ (0.235 g, 0.60 mmol) in freshly dried THF (10 cm^3) was transferred into a Schlenk flask (cooled in an ice bath) containing sodium amalgam (3% Na by weight) ($\sim$1 g). The resultant suspension was stirred under argon at 0°C for 1 h, then at room temperature for another 1 h. The solution was then filtered under argon into a flask containing a stirred solution of $[ReBr(CO)_5]$ (0.406 g, 1.0 mmol) in THF (10 cm^3). Reaction was continued at room temperature under argon for 4 h. Solvent was removed under reduced pressure and the resultant residue was exposed in air for 1 week to oxidise any unreacted $[Mn_2(CO)_{10}]$. The orange solid obtained was then sublimed at 55°C, 0.3 mmHg. The compound $[MnRe(CO)_{10}]$ was obtained as an orange solid with a yield of 0.40 g (77% based on Re).

The purity of the $[MnRe(CO)_{10}]$ obtained was ascertained by IR spectroscopy and elemental analysis. ν_{max}(CO): 2054s, 2017 vs,1978s cm^{-1} (cyclohexane) (none of the IR absorption peaks of $[Mn_2(CO)_{10}]$ and $[Re_2(CO)_{10}]$ were detected). *Anal*. $C_{10}MnO_{10}Re$ requires: C, 23.0. Found: C, 23.4%.

4.2. Reaction of dppf with [MnRe(CO)$_{10}$], MeOH and TMNO

The solution of $Me_3NO\cdot 2H_2O$ (0.062 g, 0.56 mmol) in THF–MeOH (1:1, 20 cm^3) was transferred into a Schlenk flask containing a stirred solution of $[MnRe(CO)_{10}]$ (0.120 g, 0.23 mmol) in THF (10 cm^3) at room temperature. This solution was stirred in vacuo for 4 h at room temperature. Solid dppf (0.128 g, 0.23 mmol) was added and the orange solution so formed was stirred in vacuo for 1 h. It was then evaporated to half its volume and stirred for 3 h. The solvent was then removed and the residue was redissolved in a minimum amount of CH_2Cl_2 and chromatographed on silica TLC plates (CH_2Cl_2:hexane 2:3). From the main bands the complexes *fac*-$[MnH(CO)_3(\eta^2\text{-dppf})]$ ($R_f = 0.57$) and $[Re_2(\mu\text{-OMe})_2(\mu\text{-dppf})(CO)_6]$ ($R_f = 0.47$) were isolated with yields of 0.012 g (8%) and 0.035 g (26%), respectively. A trace amount of *fac*-$[ReCl(CO)_3(\eta^2\text{-dppf})]$ ($R_f = 0.13$) was also isolated.

The complex *fac*-$[MnH(CO)_3(\eta^2\text{-dppf})]$ was recrystallised from CH_2Cl_2–MeOH mixture at 0°C. *Anal*. Found: C, 63.5; H, 4.3; P, 8.8. $C_{37}H_{29}O_3P_2FeMn$ (FW 694) requires: C, 64.0; H, 4.2; P, 8.9%. ν_{max}(CO): 1998s, 1920m(sh), 1903m ($CHCl_3$); 1996s, 1917m(sh), 1903m (CH_2Cl_2); 1997s, 1922m(sh), 1906m cm^{-1} (THF). δ_H ($CDCl_3$) 7.7–7.4 (m) (20H, Ph), 4.38 (s, 2H, CpH), 4.29 (s, 2H, CpH), 4.18 (s, 2H, CpH), 4.08 (s, 2H, CpH), -6.18 (t, 1H, hydride), $J_{(P-Mn-H)}$ 50 Hz; δ_p ($CDCl_3$) 64.8. The complexes $[Re_2(\mu\text{-OMe})_2(\mu\text{-dppf})(CO)_6]$ and *fac*-$[ReCl(CO)_3(\eta^2\text{-dppf})]$ were identified by IR, ^1H and ^{31}P NMR spectroscopy [5,23].

4.3. Preparation of fac-[Re{OC(O)OMe}(CO)$_3$(η^2-dppf)] (1)

A solution of $Re_2(CO)_{10}$ (0.151 g, 0.23 mmol) in THF (20 cm^3) was transferred into a stirred solution of $Me_3NO\cdot 2H_2O$ (0.062 g, 0.56 mmol) and dppf (0.128 g, 0.23 mmol) in a mixture of MeOH (10 cm^3) and THF (20 cm^3). The resultant solution was stirred under partial vacuum at room temperature for 4 h. The solvent was removed under reduced pressure and the residue was redissolved in a minimum amount of THF and chromatographed on silica TLC plates (acetone:hexane 1:4). The complex *fac*-$[Re\{OC(O)OMe\}(CO)_3(\eta^2\text{-dppf})]$ (**1**) was isolated from the chrome-yellow band at $R_f = 0.23$. Air-stable orange prismatic crystals of **1** were obtained by cooling a solution of **1** in benzene–hexane–MeOH mixture to -10°C. Yield 0.016 g (4%). The crystals have the composition $[Re\{OC(O)OMe\}(CO)_3(\eta^2\text{-dppf})](C_6H_6)_{0.5}$. *Anal*. $C_{42}H_{34}FeO_6P_2Re$ (FW 938.7) requires: C, 53.7; H, 3.6; P, 6.5. Found: C, 53.8; H, 3.7; P, 6.4%. ν_{max}(CO) 2037vs, 1948m, 1899s (C_6H_6); 2033vs, 1951s, 1900s (acetone); 2029s, 1947s, 1895s cm^{-1} (KBr); ν(C=O methyl carbonate ligand) 1678m cm^{-1} (KBr). δ_H (C_6D_6) 7.94–7.82 (m), 7.17–7.02 (m) (20H, C_6H_5), 5.06 (s, 2H, CpH), 4.32 (s, 2H, CpH), 3.90 (s, 2H, CpH), 3.81 (s, 2H, CpH), 3.59 (s, 3H, OCH_3); δ_P (C_6D_6) 7.23 (s).

4.4. Reaction of [Os$_3$(CO)$_{12}$] with MeOH and one molar equivalent of Me$_3$NO

Tetrahydrofuran (60 cm^3) and $[Os_3(CO)_{12}]$ (0.0365 g, 0.040 mmol) were placed in a 250 ml three-neck round-bottom flask fitted with a reflux condenser, an argon inlet, and a 100 ml pressure-equalising dropping funnel. The reaction mixture was stirred and heated to reflux (oil bath temperature maintained at 80°C). A solution of $Me_3NO\cdot 2H_2O$ (0.0052 g, 0.047 mmol) in THF–methanol (1:1) mixture (20 cm^3) was then added dropwise over an hour. The resultant solution was refluxed for a further 3 h. The yellow solution obtained was then cooled to room temperature and filtered through silica. The silica was washed with THF until the washings were colourless. The combined filtrate and washings was rotary evaporated to obtain an oily residue. The residue was redissolved in a minimum amount of CH_2Cl_2 and chromatographed on silica TLC plates, eluting with CH_2Cl_2–hexane (5:95) mixture. A major yellow band ($R_f = 0.72$) was obtained and extracted with CH_2Cl_2 to give $[Os_3(\mu\text{-H})(\mu\text{-OMe})(CO)_{10}]$ (**2**). Yield 0.0251 g (71%). The identity of this compound was confirmed by IR and ^1H NMR spectroscopy [12].

4.5. Reaction of [Os$_3$(CO)$_{12}$] with MeOH and two molar equivalents of Me$_3$NO

The procedure adopted was similar to that for the reaction with one molar equivalent of Me_3NO except for the relative

amounts of reagents used: $[Os_3(CO)_{12}]$ 0.0352 g, 0.039 mmol; $Me_3NO \cdot 2H_2O$ 0.0103 g, 0.093 mmol; dissolved in THF–methanol (1:1) mixture (40 cm^3). Yield of **2** was 0.0249 g (73%).

4.6. Reaction of $[Os_3(CO)_{12}]$ with MeOH and three molar equivalents of Me_3NO

The amounts of reagents used were as follows: $[Os_3(CO)_{12}]$ 0.0356 g, 0.039 mmol; $Me_3NO \cdot 2H_2O$ 0.0143 g, 0.129 mmol; dissolved in THF–methanol (1:1) mixture (60 cm^3). TLC on silica plates (CH_2Cl_2:hexane 1:9) gave two main yellow bands: **2** ($R_f = 0.87$, 0.0173 g, 49%) and **3** $[Os_3(\mu\text{-OMe})_2(CO)_{10}]$ ($R_f = 0.71$, 0.0039 g, 11%). The identity of compound **3** was confirmed by IR and ^1H NMR spectroscopy [12].

4.7. Reaction of $[Os_3(CO)_{12}]$ with MeOH and four molar equivalents of Me_3NO

The amounts of reagents used were as follows: $[Os_3(CO)_{12}]$ 0.0335 g, 0.037 mmol; $Me_3NO \cdot 2H_2O$ 0.0178 g, 0.160 mmol; dissolved in THF–methanol (1:1) mixture (80 cm^3). Yields: **2** (0.0103 g, 32%); **3** (0.0056 g, 17%).

4.8. Reaction of $[Os_3(CO)_{12}]$ with MeOH, four molar equivalents of Me_3NO, and one equivalent of bis(diphenylphosphino)methane (dppm)

The compounds $[Os_3(CO)_{12}]$ (0.0556 g, 0.061 mmol), $Me_3NO \cdot 2H_2O$ (0.0294 g, 0.265 mmol, dissolved in THF–methanol (1:1) mixture (80 cm^3)) were allowed to react as above. After 4 h, dppm (0.0243 g, 0.093 mmol) was added. The solution was stirred for another 30 min, during which the colour of the solution darkened somewhat. The solution was filtered through silica and the filtrate was rotary evaporated to obtain an oily residue. The residue was dissolved in CH_2Cl_2 and loaded onto a silica column. Elution with CH_2Cl_2–hexane mixture (1:4) yielded a major yellow band which gave IR and ^1H NMR spectra consistent with the formulation $[Os_3(\mu\text{-H})(\mu\text{-OMe})(\mu\text{-dppm})(CO)_8]$. $\nu_{max}(CO)$ 2086vw, 2074m, 2048w, 2038vw, 2003vs, 1990sh, 1941m cm^{-1} (hexane). δ_H ($CDCl_3$) 7.3–7.5 (m) (20H, Ph), 3.4 (s) (3H, OCH_3), 3.1 (dt) (1H, CH_2), 2.9 (dt) (1H, CH_2), −11.2 (t) (1H, hydride), $J_{(H-P)}$ 12 Hz; δ_P ($CDCl_3$) −8.4 (s).

4.9. X-ray crystallography of fac-[Re{OC(O)OMe}-$(CO)_3(\eta^2\text{-dppf})$] (**1**)

Data were collected on a crystal of dimensions $0.17 \times 0.30 \times 0.40$ mm using a Siemens P4 diffractometer in the θ–2θ mode, with graphite-monochromated Mo Kα radiation ($\lambda = 0.71073$ Å). Crystal data: $C_{39}H_{31}FeO_6P_2Re \cdot 0.5(C_6H_6)$, monoclinic, $P2_1/n$, a = 9.670(2), b = 18.983(4), c = 20.823(5) Å, β = 92.58(1)°, V = 3819(2) $Å^3$, Z = 4. Data were collected at 297 K to a maximum 2θ value of 55.0°. A total of 9993 reflections were measured, of which 8004 were unique ($R_{int} = 0.034$). The number of data used for structure solution and refinement was 5303 ($I > 2.0\sigma(I)$). Empirical ψ corrections were made; the minimum and maximum transmission factors were 0.7130 and 0.9560 respectively. The structure was solved by direct methods. All non-hydrogen atoms (except those of the disordered solvate molecule) were refined anisotropically by the full-matrix least-squares method (on F^2). Hydrogen atoms were introduced in calculated positions and refined isotropically (riding model) in the final cycles of least-squares refinement. The disordered benzene solvate is located about a crystallographic inversion centre. The unique half of the benzene molecule was modelled isotropically in terms of two overlapping C_3 fragments of half occupancy each (C(100)–C(300)) and (C(101)–C(301)), with the constraint C–C = 1.390 ± 0.002 Å. The C(100)···C(300) and C(101)···C(301) distances were constrained to be 2.400 ± 0.002 Å to fix the C–C–C angles at 120°. The last least-squares cycle was calculated with 466 parameters and 7950 reflections (all of the unique reflections except very negative ones), and converged with R_1 = 0.040 and $wR_2 = 0.080$ (for reflections with $I > 2.0\sigma(I)$) ($R_1 = \sum||F_o| - |F_c||/\sum|F_o|$, $wR_2 = [\sum w(F_o^2 - F_c^2)^2/\sum w(F_o^2)^2]^{1/2}$). The weighting function used was $w^{-1} = \sigma^2(F_o^2) + (0.0400P)^2$, where $P = (F_o^2 + 2F_c^2)/3$. In the last difference map the deepest hole was −0.605 e $Å^{-3}$, and the highest peak was 0.677 e $Å^{-3}$. Computations were carried out on a Pentium PC using the SHELXTL PLUS software package [24].

Supplementary data

Crystallographic data for the structural analysis have been deposited with the Cambridge Crystallographic Data Centre, 12 Union Road, Cambridge CB2 1EZ, UK (fax: +44-1223-336033; e-mail: deposit@ccdc.cam.ac.uk), CCDC no. 135934.

Acknowledgements

Financial support by the National Institute of Education, Singapore and the National University of Singapore (NUS) is gratefully acknowledged. C.J. thanks NUS for the award of a research scholarship.

References

[1] D. Milstein, J. Am. Chem. Soc. 108 (1986) 3525.
[2] M.A. Bennett, T.W. Matheson, in: G. Wilkinson, F.G.A. Stone, E.W. Abel (Eds.), Comprehensive Organometallic Chemistry, vol. 4, Pergamon, Oxford, 1st edn., 1982.
[3] H. E. Bryndza, W. Tam, Chem. Rev. 88 (1988) 1163.

[4] D. Roberto, E. Lucenti, C. Roveda, R. Ugo, Organometallics 16 (1997) 5974.
[5] Y.K. Yan, H.S.O. Chan, T.S.A. Hor, K.L. Tan, L.K. Liu, Y.S. Wen, J. Chem. Soc., Dalton Trans. (1992) 423.
[6] P.M.N. Low, Y.L. Yong, Y.K. Yan, T.S.A. Hor, S.-L. Lam, K.K. Chan, C. Wu, S.C.F. Au-Yeung, Y.-S. Wen, L.-K. Liu, Organometallics 15 (1996) 1369.
[7] C.C. Grimm, P.E. Brotman, R.J. Clark, Organometallics 9 (1990) 1119.
[8] N.J. Coville, A.M. Stolzenberg, E.L. Mutterties, J. Am. Chem. Soc. 105 (1983) 2499.
[9] G. Ciani, G. D'Alfonso, M. Freni, P. Romiti, A. Sironi, J. Organomet. Chem. 152 (1978) 85.
[10] T.S.A. Hor, C.F. Lam, Y.K. Yan, Bull. Sing. Natl. Inst. Chem. 19 (1991) 115.
[11] C. Jiang, Y.-S. Wen, L.-K. Liu, T.S.A. Hor, Y.K. Yan, J. Organomet. Chem. 543 (1997) 179.
[12] B.F.G. Johnson, J. Lewis, P.A. Kilty, J. Chem. Soc. A (1968) 2859.
[13] K.A. Azam, A.J. Deeming, R.E. Kimber, P.R. Shukla, J. Chem. Soc., Dalton Trans. (1976) 1853.
[14] E.G. Bryan, B.F.G. Johnson, J. Lewis, J. Chem. Soc., Dalton Trans. (1977) 1328.
[15] M. Tachikawa, J.R. Shapley, J. Organomet. Chem. 124 (1977) C19.
[16] J. Banford, M.J. Mays, P.R. Raithby, J. Chem. Soc., Dalton Trans. (1985) 1355.
[17] M. Freni, D. Ginsto, P. Romiti, J. Inorg. Nucl. Chem. 33 (1971) 4093.
[18] S.K. Mandal, D.M. Ho, M. Orchin, Organometallics 12 (1993) 1714.
[19] S.K. Mandal, J. Feldman, M. Orchin, J. Coord. Chem. 33 (1994) 219.
[20] A.J. Deeming, D.M. Speel, M. Stchedroff, Organometallics 16 (1997) 6004.
[21] M.D. Michels, H.J. Svec, Inorg. Chem. 20 (1981) 3445.
[22] N. Flicroft, D.K. Huggins, H.D. Kaesz, Inorg. Chem. 3 (1964) 1123.
[23] T.M. Miller, K.J. Ahmed, M.S. Wrighton, Inorg. Chem. 28 (1989) 2347.
[24] G.M. Sheldrick, SHELXTL PC, Version 5.03, Siemens Analytical X-ray Instruments Inc., Madison, WI, 1994.

PERGAMON

www.elsevier.nl/locate/poly

Polyhedron 19 (2000) 649–653

POLYHEDRON

Complexation of lead(II) by L-aspartate: crystal structure of polymeric Pb(aspH)(NO_3)

Laura Gasque [a,*], Sylvain Bernès [b], Rosana Ferrari [a], Cecilia R. de Barbarín [c], Ma. de Jesús Gutiérrez [a], Guillermo Mendoza-Díaz [d]

[a] *Departamento de Química Inorgánica, Facultad de Química, Universidad Nacional Autónoma de México, Ciudad Universitaria, México D.F. 04510, Mexico*

[b] *Unidad de Servicios de Apoyo a la Investigación, Facultad de Química, Universidad Nacional Autónoma de México, Ciudad Universitaria, México D.F. 04510, Mexico*

[c] *Facultad de Ciencias Químicas, Universidad Autónoma de Nuevo León, Monterrey N.L., Mexico*

[d] *Facultad de Química, Universidad de Guanajuato, Noria Alta s/n, Guanajuato Gto. 36050, Mexico*

Received 1 September 1999; accepted 10 January 2000

Abstract

Two lead compounds containing the aspartate ligand are described, with compositions Pb(aspH)NO_3 and Pb(asp). The crystal structure of the first shows it is a three-dimensional polymer in which each lead atom is coordinated to six oxygen atoms, five from carboxyl groups and one from a nitrate ion. For Pb(asp), spectroscopic data suggest the presence of Pb–NH_2 interaction. ©2000 Elsevier Science Ltd All rights reserved.

Keywords: Lead(II); Aspartate; Structures

1. Introduction

Knowledge of the toxicity of lead goes back to ancient times. Recent clinical studies have established that it affects several organs such as the kidneys and the brain, and also that it interferes with many steps in the biosynthesis of heme [1–3]. However, the critical interactions of this metal with specific biomolecules have not yet been elucidated. For instance, it is known that it binds strongly to sulfhydryl groups, acting as a soft acid, but also that it accumulates in the oxygen rich sites of bone, where it replaces calcium, a typical hard acid, and that its toxic effects are more serious for patients who are calcium deficient [4,5]. Recent studies strongly suggest that Pb(II) finds its way into the organism by binding to a calcium transport protein known as ICBP or calbindine [6]. The amino acid sequence of this protein has been determined and it is known that the calcium binding site is rich in aspartic and glutamic residues. This fact, together with the lack of studies of interactions of lead with simple biomolecules, motivated the present work, in which two different lead complexes with aspartate were obtained, Pb(aspH)(NO_3) (**I**) and Pb(asp) (**II**). Since lead can present a wide variety of coordination numbers and geometries [7] and since the crystal structures of several metal complexes with aspartate [8–12] show the coordination versatility of this ligand, the structural analysis of this pair of complexes proved to be interesting in itself.

2. Experimental

Lead nitrate and lead oxide (litharge) were purchased from Merck, L-aspartic acid and L-aspartic acid monosodium salt hydrate were from Sigma Chemical Co., and all were used without further purification. Elemental analyses were carried out by Desert Analytics, Tucson, AZ. IR spectra were recorded in the 4000–400 cm^{-1} region using both KBr pellets and HCBD suspension in a Nicolet 540 spectrophotometer. The far IR spectra were recorded in a Nicolet 740 FTIR in the 700–70 cm^{-1} region using polyethylene pellets. Amino group protons were interchanged by deuterium by soaking samples in D_2O for 24 h.

The ^{13}C CP-MAS spectra were recorded on a Varian Unity-plus 300 MHz spectrometer operating at 75.429 MHz, and 30° pulse was used. A 7 mm diameter silicon nitride rotor

* Corresponding author. Tel. and fax: +525-641-5084; e-mail: gasquel@servidor.unam.mx

0277-5387/00/$ - see front matter ©2000 Elsevier Science Ltd All rights reserved.
PII S0277-5387(00)00299-0

with kel-F caps was used. The rotor spin rate was kept between 3.5 and 4.5 kHz for all experiments, with a delay time of 7 s, and between 128 and 516 transients accumulated. Adamantane was used as external reference.

2.1. Preparation of Pb(aspH)(NO_3) (I)

3.31 g (10 mmol) of lead nitrate were dissolved in 50 ml water and combined with 1.55 g (10 mmol) of monosodium aspartate hydrate also in 50 ml of water. The pH was adjusted to 4.0 with 0.1 M NaOH and the solution left to crystallise. Colourless needles were collected the next day. *Anal*. Calc. for Pb($C_4H_6O_4N$)(NO_3): C, 11.97; H, 1.49; N, 6.98. Found: C, 12.11, H, 1.55, N, 6.84%.

2.2. Preparation of Pb(asp) (II)

1.33 g (10 mmol) aspartic acid were dissolved in 300 ml water. To this solution, 2.23 g PbO powder (litharge) were added. The reaction vessel was placed in an ultrasound bath for 15 min during which the yellow powder dissolved and a white precipitate formed. *Anal*. Calc. for Pb($C_4H_5O_4N$): C, 14.20, H, 1.47, N, 4.1. Found: C, 14.10; H, 1.42, N, 3.98%.

2.3. Crystallography

Pertinent crystal data are collected in Table 1, and complete crystallographic information is deposited as a CIF file. The structure was solved and refined using standard procedures [13–15]. On the final difference map, a maximum peak of 1.81 e $Å^{-3}$ close to the heavy atom was attributed to the fact that the crystal was larger than the X-ray beam and to the difficulty in applying a suitable absorption correction. H atoms were omitted because of their small contribution to the structure factors.

Table 1
Crystal data

Empirical formula	$C_4H_6N_2O_7Pb$
Formula weight	401.30
Crystal system	Orthorhombic
Colour, habit	colourless, regular needle
Crystal size (mm)	$0.74\times0.16\times0.06$
Space group	$P2_12_12_1$
Unit cell dimensions	
a (Å)	4.5894(5)
b (Å)	11.6164(9)
c (Å)	15.476(2)
Z	4
Absorption coefficient (mm^{-1})	20.467
Radiation	Mo Kα ($\lambda=0.71073$ Å)
2θ Range (°)	3–55
Reflections collected	1472
Independent reflections [a]	1335 ($R_{int}=3.33\%$)
Transmission factors (min., max.)	0.0113, 0.0373
Final R indices (1269 $I>2\sigma(I)$) (%)	$R_1=3.83$, $wR_2=9.77$
Final R indices (all data) (%)	$R_1=4.27$, $wR_2=10.76$
Goodness-of-fit, S	1.175
Data-to-parameters ratio	1335/128

[a] R_{int}, R_1, wR_2 and S are defined as follows:

$$R_{int}=\frac{\sum|F_o^2-\langle F_o^2\rangle|}{\sum F_o^2},\quad R_1=\frac{\sum||F_o|-|F_c||}{\sum|F_o|},$$

$$wR_2=\sqrt{\frac{\sum w(F_o^2-F_c^2)^2}{\sum w(F_o^2)^2}},\quad S=\sqrt{\frac{\sum w(F_o^2-F_c^2)^2}{m-n}}.$$

3. Results and discussion

3.1. Spectroscopic results

3.1.1. IR spectra

For the free ligand, in its monosodium salt form, asymmetric and symmetric stretching absorptions of the carboxylate group appear at 1582 and 1415 cm^{-1} respectively, while for the lead complex **I**, the first absorption shifts to 1560 cm^{-1} and the second is obscured by the nitrate ion absorption, which displays a quite intense band at 1385 cm^{-1}. Even though the crystal structure shows each lead atom has a nitrate ion coordinated in unidentate mode, the IR spectrum displays the characteristic band of free nitrate, which appears practically at the same wavenumber in Pb(NO_3)$_2$, suggesting a rather weak interaction, mainly of electrostatic nature. To rule out the possibility that coordination of nitrate to lead had been broken during the fabrication of the KBr pellet, the spectrum was recorded in HCBD, which is transparent in the 1565–1170 cm^{-1} region, and showed no difference. In the N–H region, three weak bands in the 2920–3150 cm^{-1} interval are consistent with the presence of the –NH_3^+ group.

The IR spectrum for complex **II**, however, is very different in the latter region. It has two very well defined bands with moderate intensity at 3301 and 3233 cm^{-1}, indicative of a coordinated –NH_2 group [16,17]. The assignment of these two bands was confirmed by deuterium exchange upon which they shift towards 2464 and 2379 cm^{-1} respectively.

The asymmetric stretching absorption of the carboxylate in this complex is located at 1532 cm^{-1}, 28 cm^{-1} lower than for the Pb(aspH)NO_3 complex. The symmetric stretching absorption can be observed in complex **II** at 1347 cm^{-1}. The difference ($\Delta\nu$) between ν_a and ν_s is 185 cm^{-1}, which is very close to the $\Delta\nu$ of the free amino acid or its sodium salt (vide supra, 167 cm^{-1}), and this is in agreement with a bridging carboxylate [16,17].

3.1.2. Far IR spectra

Pb(asp) has an important band at 325 cm^{-1}, not present in the far IR spectrum of Pb(aspH)NO_3. Since it shifts to 313 cm^{-1} in the deuterated sample, it could be indicative of a Pb–NH_2 vibration.

3.1.3. NMR spectra

Table 2 shows chemical shifts in ^{13}C solid state NMR for both the reported complexes as well as for the acid and monobasic forms of the ligand. While δ (ppm) values for aliphatic carbon atoms in both lead complexes are very sim-

Table 2
^{13}C NMR chemical shifts (ppm)

Nucleus	$AspH_2$	NaAspH	Pb(AspH)NO_3	Pb(Asp)
COOα	176.32	174.24	181.54	188.7
CH	54.11	48.9	56.80	56.60
CH_2	38.26	34.85	44.02	42.34
COOβ	175.25	174.24	177.48	181.8

ilar, those for the carboxylate groups of Pb(asp) are significatively shifted to lower fields, suggesting a qualitatively different interaction with lead atoms.

Further experiments were carried out to measure ^1H relaxation times by observing the change in signal intensity for cross-polarisation ^{13}C solid state spectra, as a function of time [18,19] (Fig. 1(a,b)). For Pb(AspH)NO_3 a value of 3.60 ± 0.16 s was obtained, whereas for Pb(asp) the value was 12.37 ± 0.68 s. Since these values are a measure of the rigidity of the molecules, the latter is consistent with the chelate formation suggested by the IR spectrum. For both forms of the ligand, relaxation times are assumed to be less than 1 s, which is the minimum waiting time allowed by the apparatus, since signal intensity was constant at all times measured up to 70 s.

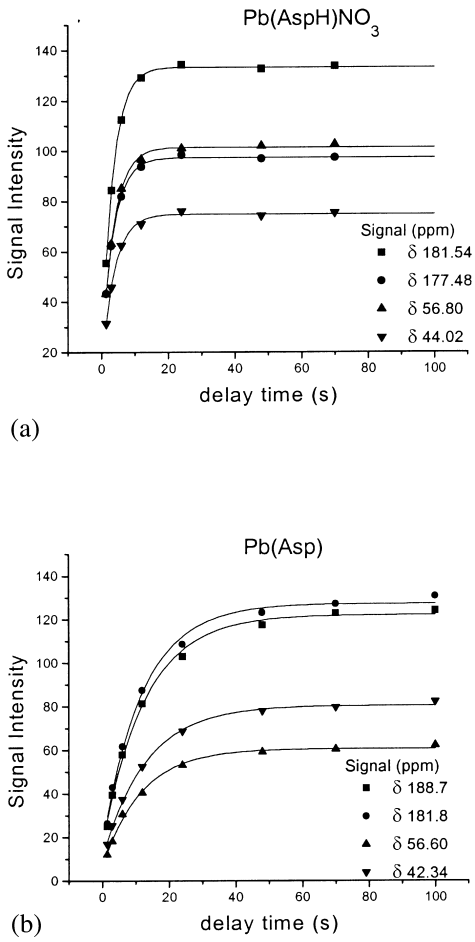


Fig. 1. Determination of ^1H relaxation times for (a) Pb(aspH)(NO_3) and (b) Pb(asp).

3.2. Crystal structure

The crystal structure shows this compound forms a three-dimensional network, owing to the nature of the aspartate ligand which can coordinate to two different lead atoms through each carboxylate, together with the fact that a single oxygen atom in a carboxylate can bridge two metal atoms. The three-dimensional network has chains running along the three axes of the orthorhombic cell. A remarkable feature is the formation of 18-membered rings containing three Pb ions and three ligand molecules with weak metal–metal interactions: Pb···Pb 4.589 and 4.706 Å (Fig. 2).

The overall geometry around each Pb can be considered a distorted square pyramid, with the apex occupied by the two oxygen atoms from the chelating β-carboxylic group (Fig. 3) with a bite angle O1–Pb–O2 = 49.8° and with bond lengths C1–O1 = 1.264(19) and C1–O2 = 1.24(2) Å. The difference in the two Pb–O distances for this group, Pb–O1 = 2.706(12) and Pb–O2 = 2.500(11) Å, is consistent with the

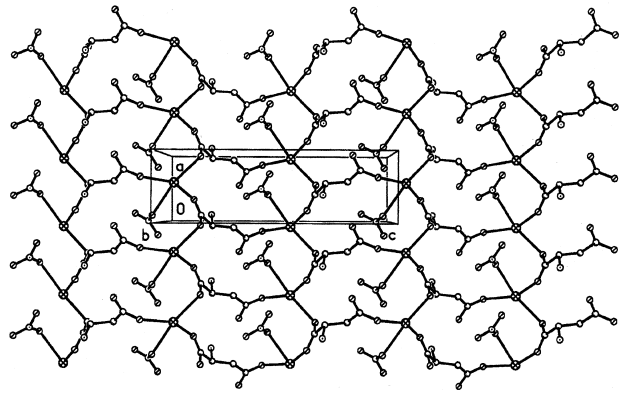


Fig. 2. 18-membered rings containing three Pb ions and three ligand molecules.

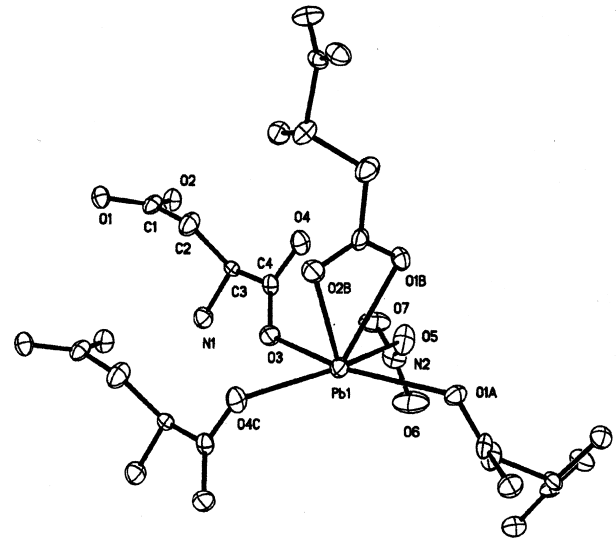


Fig. 3. The coordination environment of lead atoms in Pb(aspH)(NO_3) with the labelling scheme. Symmetry codes used to generate equivalent atoms are the following: A $-x-1/2$, $-y+2$, $z+1/2$; B $-x-1$, $y-1/2$, $-z+3/2$; C $x+1$, y, z. Thermal ellipsoids are at 30% probability level. H atoms were not included in the refinement.

bridging role of O1 between two symmetry related Pb ions (Table 3).

The lead atom lies 0.13 Å above the base of the pyramid, which is defined by four oxygen atoms from four different ligand moieties. Two of these oxygen atoms are from α-carboxylates in two symmetry related ligands, with similar distances, Pb–O3 = 2.493(12) and Pb–O4′ = 2.563(12) Å.

The third position in the base of the pyramid is occupied by the oxgen atom O1A, which forms part of a β-carboxylate that chelates a neighbouring Pb atom. An oxygen atom from the nitrate anion is coordinated at the fourth position in the base of this pyramid in unidentate mode, with the expected distance Pb1–O5 = 2.730(17) Å, only slightly shorter than the Pb–O distance in lead nitrate (2.81 Å [20]), which is in agreement with the apparent ionic behaviour of this nitrate observed in the IR spectrum.

The α-carboxylic groups are disymmetric, as noted from bond lengths C4–O3 = 1.20(2) and C4–O4 = 1.257(19) Å, in line with a localisation of the negative charge on O3. This is confirmed by the fact that Pb–O3 is the shortest coordination distance (2.493(12) Å).

This geometry leaves a wide space below the base of the pyramid containing the lead atom, which can be thought of as occupied by the 'inert pair' of electrons on Pb(II).

The possible stereochemical activity of the lone pair in divalent lead compounds has recently been discussed by Shimoni-Livny et al. based on a thorough review of crystal data available in the Cambridge Structural Database (CSD) [7]. They classify lead complex coordination as holodirected or hemidirected. Holodirected refers to complexes in which the bonds to ligand atoms are directed throughout the surface of an encompassing sphere, while hemidirected refers to those cases in which the bonds to ligand atoms are directed throughout only part of the coordination sphere, leaving a void or gap in the distribution of bonds to the ligand. The latter, present in all Pb(II) compounds with coordination numbers 2 to 5, is quite common in Pb(II) complexes with coordination numbers 6, 7 and 8, and does not exist in lead complexes with higher coordination numbers, where holodirected geometry is the rule. For the structure described here, coordination around the lead atoms is hemidirected with a significant void *trans* to the chelating β-carboxylate, quite similar to what Clegg et al. found for lead crotonate [21].

The coordination chemistry of Pb(II) in aqueous media has not yet been widely explored, but at the present time both solution equilibria and structural studies suggest a low affinity of lead for nitrogen donors, particularly aliphatic amines. In most cases, pH values needed to deprotonate these donors promote metal hydrolysis and precipitation of $Pb(OH)_2$, which is why the compound Pb(asp) described in this work cannot be found in aqueous solution. This suggests that under physiological conditions, amine residues in proteins or

Table 3
Bond lengths (Å) and bond angles (°) for complex **I**

Pb(1)–O(3)	2.493(12)	Pb(1)–O(2)#1 [a]	2.500(11)
Pb(1)–O(4)#2	2.536(12)	Pb(1)–O(1)#1	2.706(12)
Pb(1)–O(5)	2.730(17)	Pb(1)–O(1)#3	2.743(10)
C(1)–O(2)	1.24(2)	C(1)–O(1)	1.264(19)
C(1)–C(2)	1.53(2)	C(2)–C(3)	1.52(2)
C(3)–N(1)	1.47(2)	C(3)–C(4)	1.56(2)
C(4)–O(3)	1.20(2)	C(4)–O(4)	1.257(19)
O(1)–Pb(1)#4	2.706(11)	O(1)–Pb(1)#5	2.743(10)
O(2)–Pb(1)#4	2.500(11)	O(4)–Pb(1)#6	2.536(12)
N(2)–O(6)	1.19(2)	N(2)–O(7)	1.25(2)
N(2)–O(5)	1.289(19)		
O(3)–Pb(1)–O(2)#1	91.4(4)	O(3)–Pb(1)–O(4)#2	79.2(4)
O(2)#1–Pb(1)–O(4)#2	77.8(4)	O(3)–Pb(1)–O(1)#1	99.2(4)
O(2)#1–Pb(1)–O(1)#1	49.8(4)	O(4)#2–Pb(1)–O(1)#1	127.6(4)
O(3)–Pb(1)–O(5)	73.5(4)	O(2)#1–Pb(1)–O(5)	112.9(5)
O(4)#2–Pb(1)–O(5)	150.7(3)	O(1)#1–Pb(1)–O(5)	68.3(4)
O(3)–Pb(1)–O(1)#3	155.3(4)	O(2)#1–Pb(1)–O(1)#3	99.0(4)
O(4)#2–Pb(1)–O(1)#3	124.8(4)	O(1)#1–Pb(1)–O(1)#3	71.7(3)
O(5)–Pb(1)–O(1)#3	81.8(4)		
O(2)–C(1)–O(1)	123.0(15)	O(2)–C(1)–C(2)	119.8(14)
O(1)–C(1)–C(2)	117.1(16)	C(3)–C(2)–C(1)	113.0(14)
N(1)–C(3)–C(2)	110.0(13)	N(1)–C(3)–C(4)	112.5(14)
C(2)–C(3)–C(4)	107.5(13)	O(3)–C(4)–O(4)	128.5(14)
O(3)–C(4)–C(3)	117.2(14)	O(4)–C(4)–C(3)	114.3(13)
C(1)–O(1)–Pb(1)#4	88.3(10)	C(1)–O(1)–Pb(1)#5	122.9(9)
Pb(1)#4–O(1)–Pb(1)#5	119.5(4)	C(1)–O(2)–Pb(1)#4	98.7(9)
C(4)–O(3)–Pb(1)	117.6(11)	C(4)–O(4)–Pb(1)#6	122.3(9)
O(6)–N(2)–O(7)	122.0(18)	O(6)–N(2)–O(5)	119.5(18)
O(7)–N(2)–O(5)	118.0(17)	N(2)–O(5)–Pb(1)	127.9(12)

[a] Symmetry transformations used to generate equivalent atoms: #1 $-x-1, y-1/2, -z+3/2$; #2 $x+1, y, z$; #3 $-x-1/2, -y+2, z+1/2$; #4 $-x-1, y+1/2, -z+3/2$; #5 $-x-1/2, -y+2, z-1/2$; #6 $x-1, y, z$.

peptides do not contribute in a significant manner to lead assimilation.

Supplementary data

Crystallographic data have been deposited at the Cambridge Crystallographic Data Centre, 12 Union Road, Cambridge CB2 1EZ, UK (fax: +44-1223-336033; e-mail: deposit@ccdc.cam.ac.uk), deposition number CCDC 133354.

Acknowledgements

L.G. thanks Professor Sigfrido Escalante for motivating this work, Conacyt for sponsoring it (Grant 4913-E9406), and Gerardo Medina for his assistance on IR spectra of deuterated samples. L.G., R.F. and G.M.D. also thank UNAM's Academic Interchange Office.

References

[1] H.G. Seiler (Ed.), Handbook on Toxicity of Inorganic Compounds, Chap. 31, Marcel Dekker, New York, 1988.
[2] R.G. Feldman, Occupational and Environmental Neurotoxicology, Chap. 4, Lippincott Williams and Willkins, Philadelphia, PA, 1998.
[3] C. Castellino, P. Casellino, N. Sannolo, Inorganic Lead Exposure: Metabolism and Intoxication, Lewis, Boca Raton, FL, 1994.
[4] C.S. Fullmer, Environ. Res. 54 (1991) 159.
[5] J.D. Bodgen, S.B. Sheldon, S. Christakos, F.W. Kemp, Z. Yang, S.R. Katz, C. Chu, J. Nutr. 122 (1992) 1351.
[6] C.S. Fullmer, S. Edlstein, R. Wasserman, J. Biol. Chem. 260 (1985) 6816.
[7] L. Shimoni-Livny, J.P. Glusker, C.W. Bock, Inorg. Chem. 37 (1998) 1853.
[8] H. Schmidbaur, I. Bach, D.L. Wilkinson, G. Müller, Chem. Ber. 122 (1989) 1427.
[9] H. Schmidbaur, G. Müller, J. Riede, G. Manninger, J. Helbing, Angew. Chem., Int. Ed. Engl. 25 (1986) 1013.
[10] L. Kryger, S.E. Rasmussen, J. Helbing, Acta Chem. Scand. 27 (1973) 2674.
[11] H. Schmidbaur, I. Bach, D.L. Wilkinson, G. Müller, Chem. Ber. 122 (1989) 1445.
[12] H. Schmidbaur, I. Bach, J. Riede, G. Müller, J. Helbing, G. Hopf, Chem. Ber. 120 (1987) 867.
[13] J. Fait, XSCANS Users Manual, Siemens Analytical X-ray Instruments Inc., Madison, WI, 1991.
[14] G.M. Sheldrick, SHELXTL-plus, release 5.03, Siemens Analytical X-ray Instruments Inc., Madison, WI, 1995.
[15] G.M. Sheldrick, SHELX97 Users Manual, University of Göttingen, Germany, 1997.
[16] K. Nakamoto, Infrared and Raman Spectra of Inorganic and Coordination Compounds, Part B, Wiley, New York, 5th edn., 1997.
[17] L. Antolini, G. Marcotrigiano, L. Menaube, G.C. Pellacani, M. Saladini, Inorg. Chem. 21 (1982) 2263.
[18] H.O. Kalinowski, S. Berger, S. Braun, Carbon-13 NMR Spectroscopy, Wiley, Chichester, UK, 1988, p. 228.
[19] A.D. Irwin, C.D. Chendler, R. Assink, M.J. Hampden-Smith, Inorg. Chem. 33 (1994) 1005.
[20] R.W. Wyckoff, Crystal Structures, vol. 2, Wiley-Interscience, New York, 1964, p. 480.
[21] W. Clegg, I.R. Little, B.P. Straughan, Acta Crystallogr., Sect. C 42 (1986) 1319.

PERGAMON

www.elsevier.nl/locate/poly

Polyhedron 19 (2000) 655–664

POLYHEDRON

Electrochemical and X-ray studies of nickel(II) Schiff base complexes derived from salicylaldehyde. Structural effects of bridge substituents on the stabilisation of the +3 oxidation state

I.C. Santos [a], M. Vilas-Boas [a], M.F.M. Piedade [c,d], C. Freire [a,*], M.T. Duarte [b,d], B. de Castro [a]

[a] *CEQUP/Departamento de Química, Faculdade de Ciências, Universidade do Porto, Rua do Campo Alegre 687, P-4169-007 Porto, Portugal*

[b] *Instituto Superior Técnico, Universidade Técnica de Lisboa, Lisbon, Portugal*

[c] *Departamento de Química e Bioquímica, Faculdade de Ciências, Universidade de Lisboa, Lisbon, Portugal*

[d] *Centro de Química Estrutural, I.S.T, Lisbon, Portugal*

Received 10 August 1999; accepted 13 January 2000

Abstract

The oxidative chemistry of three Ni(II) complexes with Schiff base ligands derived from salicylaldehyde and diamines with different steric demands, *N*,*N*′-2-methylpropane-2,3-diyl-bis(salicylideneiminate)nickel(II) (**1**), *N*,*N*′-1,2-cyclohexyl-1,2-dyil-bis(salicylideneiminate)-nickel(II) (**2**) and *N*,*N*′-2,3-dimethylbutane-2,3-diyl-bis(salicylideneiminate)nickel(II) (**3**), was studied by cyclic voltammetry and chronoamperometry in *N*,*N*′-dimethylformamide and $(CH_3)_2SO$. The electrogenerated species were characterised by EPR spectroscopy. All three complexes exhibited metal-centred oxidised processes and the oxidised products were low-spin six-coordinate Ni(III) species (d_{z^2} ground state) with two solvent molecules axially coordinate. Addition of pyridine resulted in the replacement of solvent molecules with no changes in the ground state. The crystal structures of compounds **1** and **3** were determined from single crystal X-ray diffraction data, and the crystal packing for any of the complexes did not show any systematic parallel orientation of any part of the molecules. X-ray structural data for the Ni(II) complexes provided a rationale for the $E_{1/2}$ values obtained in the oxidation processes and for the relative energy of the low-lying excited duplets of the electrogenerated Ni(III) species. ©2000 Elsevier Science Ltd All rights reserved.

Keywords: Crystal structures; Electrochemistry; EPR; Nickel(II)/(III) complexes; Schiff base complexes

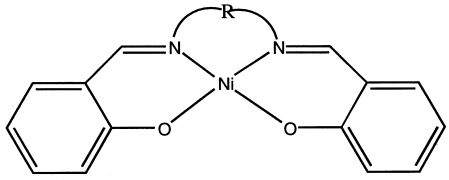
1. Introduction

Nickel(II) complexes with N_2O_2 Schiff base ligands derived from salicylaldehyde have long been used as homogeneous catalysts [1–3]. More recently, the ease of preparation of metal salen-based modified electrodes by oxidative electropolymerisation of metal complexes in poor coordinating solvents has prompted their use in heterogeneous electrocatalysis [4]. Knowledge of the role played by structural/electronic effects to control the redox chemistry of these metal complexes may prove to be critical in the design of new catalysts.

We have been studying the oxidative chemistry of Ni(II) complexes with N_2O_2 Schiff base ligands in solvents with different coordinating strength and have found the oxidation products to be solvent dependent [5–15]. Nickel(II) complexes with salicylaldehyde-based ligands (L) are oxidised in dimethylformamide (DMF) and $(CH_3)_2SO$ by a one-electron metal-centred process to six-coordinate Ni(III) species, formulated as $[Ni^{III}L(solv)_2]^+$ (where solv stands for a solvent molecule) [5–9]. However, in CH_3CN the complexes are oxidatively polymerised at the electrode surface to generate electroactive films [10–15], for which the oxidative behaviour has been shown to be associated with a ligand-centred process of the surface redox couple [11–13]. The complexes [Ni(salen)] and [Ni(saltMe)] (see Scheme 1 for an explanation of the abbreviations used) exhibit in strong coordinating solvents (DMF and $(CH_3)_2SO$) a quasi-reversible diffusion-controlled one-electron transfer process [8], in which the value of $E_{1/2}$ of [Ni(salen)] is less positive (approximately 0.07 V in DMF and 0.09 V in $(CH_3)_2SO$) than that of [Ni(saltMe)], a behaviour suggested to arise

* Corresponding author. Tel: +351-22-608 2890; fax: +351-22-608 2959; e-mail: acfreire@fc.up.pt

0277-5387/00/$ - see front matter ©2000 Elsevier Science Ltd All rights reserved.
PII S0277-5387(00)00300-4



R= -C(CH$_3$)$_2$CH$_2$- [Ni(saldMe)] (1)
R= cyclo-C$_6$H$_{10}$ [Ni(salhd)] (2)
R= -C(CH$_3$)$_2$C(CH$_3$)$_2$- [Ni(saltMe)] (3)
R= -CH$_2$CH$_2$- [Ni(salen)] (4)

Scheme 1.

from steric repulsions imposed on axial binding by the axially oriented methyl groups of the imine bridge [8].

In CH_3CN the electrogenerated polymers exhibit, in the oxidative redox switching, quite different properties in terms of stabilisation; poly[Ni(saltMe)] reveals high stability/durability, and conductivity in CH_3CN (even for very thick polymers) and for a wide potential window [11], a behaviour to be contrasted with that of poly[Ni(salen)], a poor conducting polymer with very low stability [10]. Since these two nickel complexes differ in four methyl substituents of the ethylenimine bridge, we decided to investigate the effect of a smooth increase in the bulkiness of the imine bridge substituents on the solution redox properties of salen-based Ni(II) complexes in $(CH_3)_2SO$ and DMF, and on the redox properties of their electrogenerated polymers in CH_3CN.

The work presented here describes the redox characterisation of [Ni(saldMe)] (**1**) and of [Ni(salhd)] (**2**) in CH_3SO and DMF; the results in CH_3CN will be published elsewhere. The ligand, H_2saldMe, has only two methyl groups in the imine bridge, albeit on the same carbon atom, and the ligand H_2salhd, has the nitrogen atoms bound to two consecutive carbons of a cyclohexane (Scheme 1). These ligands provide intermediate situations between those of H_2salen and H_2saltMe. Cyclic voltammetry and chronoamperometry were used to characterise electrochemically the complexes; chronoamperometric data are also included for [Ni(saltMe)] (**3**). The molecular and crystal structures of [Ni(saldMe)] and [Ni(saltMe)] have been solved and are reported here. Cyclic voltammetric data for [Ni(saltMe)] have been published elsewhere [8], but a brief description of the key features are included to provide a complete and coherent framework for the overall study reported here.

2. Experimental

2.1. Reagents, solvents, ligands and complexes

The solvents for syntheses were of reagent grade and those for electrochemical studies were of analytical grade; all were used as received. All reagents (nickel acetate tetrahydrate, salicylaldehyde, 2-methyl-2,3-propanediamine, 1,2-cyclohexanediamine) were obtained from Aldrich and used as received. Tetraethylammonium perchlorate (TEAP; Fluka, puriss) was kept in an oven at 60°C prior to use. **Caution**: perchlorates are hazards and may explode.

The ligands H_2saldMe, *N*,*N*′-2-methylpropane-2,3-dyil-bis(salicylideneimine), and H_2salhd, *N*,*N*′-1,2-cyclohexyl-1,2-dyil-bis(salicylideneimine), and the respective Ni(II) complexes were prepared by standard methods [16]; in H_2salhd the cyclohexane in the imine bridge exists as a mixture of the *cis* and the *trans* isomers. The synthesis, spectroscopic and cyclic voltammetric studies in DMF and $(CH_3)_2SO$ of the Ni(II) complex with *N*,*N*′-2,3-dimethylbutane-2,3-diyl-bis(salicylideneiminate), [Ni(saltMe)], have been published previously [8]. X-ray quality crystals of [Ni(saldMe)] and [Ni(saltMe)] were obtained by slow evaporation of solutions of the corresponding complexes in CH_3CN–CH_3Cl.

[Ni(saldMe)], $C_{18}H_{18}N_2O_2Ni$. *Anal*. Calc.: C, 61.2; H, 5.1; N, 7.9. Found: C, 61.6; H, 5.2; N, 7.8%. ^{1}H NMR ($CDCl_3$, 298 K, δ): 7.41 (2H, =CH), 7.27–7.01 (6H, aromatic H), 6.59–6.50 (2H, aromatic H), 3.26 (2H, –CH_2), 1.50 (6H, –C(CH_3)$_2$. Electronic spectra (800–250 nm), λ_{max} (ε, mol^{-1} dm^3 cm^{-1}): in $(CH_3)_2SO$, 558 (133), 444 (2460), 410 (5900), 388 (3318), 342 (7146), 321 (7482); in DMF, 559 (137), 444 (3317), 411 (6545), 386 (3614), 344 (7911), 324 (8455).

[Ni(salhd)], $C_{20}H_{20}N_2O_2Ni$. *Anal*. Calc.: C, 63.3; H, 5.3; N, 7.4. Found: C, 63.3; H, 5.2; N, 7.4%. ^{1}H NMR (DMSO-d_6, 298 K, δ): 7.71 (2H, =CH), 7.38–7.34 (2H, aromatic H), 7.20–7.11 (2H, aromatic H), 6.70–6.66 (2H, aromatic H), 6.53–6.50 (2H, aromatic H), 3.11 (4H, –C_6H_{10}), 1.77 (2H, –C_6H_{10}), 1.25 (4H, –C_6H_{10}). Electronic spectra (700–250 nm), λ_{max} (ε, mol^{-1} dm^3 cm^{-1}): in $(CH_3)_2SO$, 557 (133), 443 (3227), 410 (6588), 390 (4152), 345 (7410), 324 (7914); in DMF, 557 (127), 444 (2509), 412 (5717), 392 (3264), 345 (6528), 322 (7443).

Details on the electrosynthesis of Ni(III) complexes and the preparation of their pyridine adducts have been described elsewhere [5,8].

2.2. Physical measurements

Elemental analyses (C, H and N) were performed at the Departamento de Química, Universidade de Aveiro, Portugal. ^{1}H NMR spectra were recorded with a Bruker AC 200 spectrometer at 25°C, using $SiMe_4$ as internal reference. Electronic spectra of Ni(II) complexes were recorded with a Unicam UV2 spectrophotometer at room temperature, in a standard 1-cm quartz cuvette, using solutions of the ligands (1×10^{-5} mol dm^{-3}) or of the metal complexes (1×10^{-3} and 1×10^{-5} mol dm^{-3}) in DMF and $(CH_3)_2SO$. EPR spectra were obtained with a Bruker ESP 300 spectrometer (X-band) at 120 K; the magnetic field was calibrated by using Mn^{2+} in MgO and diphenylpicrylhydrazyl was used as internal reference (dpph; $g=2.0037$). The reported EPR parameters were obtained by spectral simulation using the program WinEPR Simfonia (Bruker) and assuming rhombic

spin hamiltonians; line widths were typically in the range 0.05–0.20 mT.

Electrochemical measurements were performed using an Autolab PGSTAT20 potentiostat/galvanostat. The electrochemical cell used in cyclic voltammetry and in double potential step chronoamperometry was a closed standard three-electrode cell connected to a solution reservoir through a Teflon tube. A Pt disk electrode with an area of 0.0314 cm^2 was used as the working electrode, a Pt gauze electrode as the counter electrode and an Ag/AgCl (1 mol dm^{-3} NaCl) as reference electrode. The ferrocene/ferrocinium (Fc/Fc) redox couple was used as internal standard: under the experimental conditions used, $E_{1/2}$ for the Fc/Fc^+ couple was 0.48 and 0.45 V in DMF and $(CH_3)_2SO$, respectively. Prior to use, the Pt working electrode was polished with an aqueous suspension of 0.05-μm alumina (Buehler) on a Master-Tex (Buehler) polishing pad, then rinsed with water and acetone and dried in an oven. All solutions were de-areated and delivered to the cell by a stream of argon. For cyclic voltammetry, scan rates in the interval 0.005–1.0 V s^{-1} were used, and the potential limits were 0.0 and 1.3 V. For chronoamperometry the potential was stepped from 0.0 V to E_1 and back to 0.0 V. After each step the potential was held for 20 s. The applied potentials E_1 were the same for all complexes in DMF and equal to 1.0 V; in $(CH_3)_2SO$ they were 0.93, 0.90 and 1.0 V for [Ni(saldMe)], [Ni(salhd)] and [Ni(saltMe)], respectively.

Electrolysis were carried out at controlled potential, at a value 0.1 V higher than the anodic peak potential. A three-electrode cell was used, with a Pt gauze as the working electrode, a Pt foil as counter electrode and an Ag/AgCl (1 mol dm^{-3} NaCl) as reference electrode.

2.3. Crystallography

Data were collected at room temperature for [Ni(saldMe)] on an Enraf Nonius TURBOCAD4 diffractometer with a copper rotating anode and for [Ni(saltMe)] on an Enraf Nonius MACH3 diffractometer with Mo graphite monochromatised radiation. Data reduction, Lorentz, polarisation and empirical absorption corrections were made using the CAD4 software package.

For both complexes the positions of the nickel atoms were obtained from a three-dimensional Patterson synthesis. Three molecules were found in the asymmetric unit of compound [Ni(saltMe)], while only one molecule was refined in complex [Ni(saldMe)]. All the non-hydrogen atoms were located in subsequent difference Fourier maps, and were refined, on F^2, with anisotropic thermal motion parameters. The hydrogen atoms were inserted in calculated positions and refined isotropically riding with the parent carbon atom. Details for data collection and for structure refinement are presented in Table 1.

Structure solution and refinement were done with SHELXS-86 [17] and SHELX-97 [18], and all molecular diagrams were drawn with the program ORTEP III [19]. Atomic scattering factors and anomalous scattering terms

Table 1
Crystal data and structure refinement for [Ni(saldMe)] and [Ni(saltMe)]

Identification code	[Ni(saldMe)]	[Ni(saltMe)]
Empirical formula	$C_{18}H_{18}N_2NiO_2$	$C_{20}H_{22}N_2NiO_2$
Formula weight	353.09	381.11
Temperature (K)	293(2)	293(2)
Wavelength (Å)	1.54184	0.71069
Crystal system	orthorhombic	monoclinic
Space group	*Pcab*	$P2_1/a$
Unit cell dimensions		
a (Å)	11.521(3)	11.1850(10)
b (Å)	15.973(4)	21.640(3)
β (°)		91.040(10)
c (Å)	17.414(4)	22.245(2)
Volume ($Å^3$)	3204.6(14)	5383.4(10)
Z	8	12
Calc. density (Mg m^{-3})	1.464	1.411
Absorption coefficient (mm^{-1})	1.671	1.096
$F(000)$	1472	2400
Theta range for data collection (°)	5.08–72.60	1.83–27.00
Index ranges	$-14 \le h \le 0$; $-19 \le k \le 0$; $-21 \le l \le 0$	$-14 \le h \le 14$; $-27 \le k \le 1$; $-28 \le l \le 28$
Reflections collected/unique	3182/3182 ($R_{int} = 0.0000$)	24706/11732 ($R_{int} = 0.0609$)
Completeness to 2θ (%)	72.60, 96.5	27.00, 97.2
Refinement method	full-matrix least-squares on F^2	full-matrix least-squares on F^2
Data/restraints/parameters	3182/0/205	11732/0/739
Goodness-of-fit on F^2	1.105	1.033
Final R indices [$I > 2\sigma(I)$]	$R1 = 0.0535$; $wR2 = 0.1494$	$R1 = 0.0586$; $wR2 = 0.1034$
R indices (all data)	$R1 = 0.0679$; $wR2 = 0.1674$	$R1 = 0.1278$; $wR2 = 0.1344$
Largest difference peak and hole (e $Å^{-3}$)	0.272 and −1.003	0.925 and −0.644

were taken from International Tables for Crystallography [20].

3. Results and discussion

3.1. Spectroscopic characterisation

Ni(II) complexes with the ligands H_2saldMe and H_2salhd show electronic spectra in DMF and $(CH_3)_2SO$ that are very similar to those of [Ni(saltMe)] and of other Ni(II) Schiff base complexes derived from salicylaldehyde, both in solution and in solid. They are characteristic of square planar low-spin Ni(II) complexes [21]; typically the spectra exhibit a low-intensity broad brand at $\lambda_{max} \approx 550$–560 nm ($\varepsilon \approx 125$–135 mol^{-1} dm^3 cm^{-1}) assigned to transitions from the four low-lying orbitals, which is superimposed on a group of high-intensity charge transfer bands at higher energies ($\lambda <$ 440 nm, $\varepsilon \approx 2500$–500 mol^{-1} dm^3 cm^{-1}). The similarity between the spectra in both solvents and in the solid indicates that no effective coordination of solvent molecules took place in any of the solvents.

3.2. Molecular structure

Molecular structure of complexes [Ni(saldMe)] and [Ni(saltMe)] are depicted in Figs. 1 and 2; relevant bond lengths and bond angles and the most relevant torsion angles are listed in Table 2. The same numbering scheme was used for the three independent molecules of [Ni(saltMe)].

In both compounds the coordination geometry around the nickel atom is roughly square planar, with the ligands bound through two nitrogen and two oxygen atoms in a *cis* configuration, but with the four N_2O_2 atoms distorted in a tetrahedral fashion.

The maximum deviation from planarity of the coordinated atoms in [Ni(saltMe)] are 0.074(2), 0.084(2) and 0.099(2) Å for molecules A, B and C, respectively, while the nickel atom is 0.018(2) Å out of that plane for molecule A, and 0.016(2) Å for molecules B and C. In [Ni(saldMe)], the coordination atoms are more distorted towards a tetrahedron, with a maximum deviation from planarity of 0.124(1) Å and with the nickel atom 0.013(1) Å out of the plane. The values of maximum deviation from planarity compare with those found for the two independent molecules of [Ni(1*R*,2*R*(-)salhd)] [22], which are 0.057 Å for molecule 1 and 0.088 Å for molecule 2; however, in this molecule the nickel atom lies practically within the coordination plane (−0.0096 and −0.0042 Å, respectively). The values of maximum deviation from planarity also compare with those found for *N*,*N*′-1,2-*cis*-cyclohexane-1,2-diyl-bis(2-hydroxyacetophenonylidene-iminate)nickel(II), [Ni(α,α′-Me_2-salhd)], for which the deviation is 0.076 Å and the nickel atom is 0.018 Å out of the plane [7]. It must be pointed that [Ni(salhd)] exists in solution as a mixture of isomers and it is to be expected that they present a comparable deviation

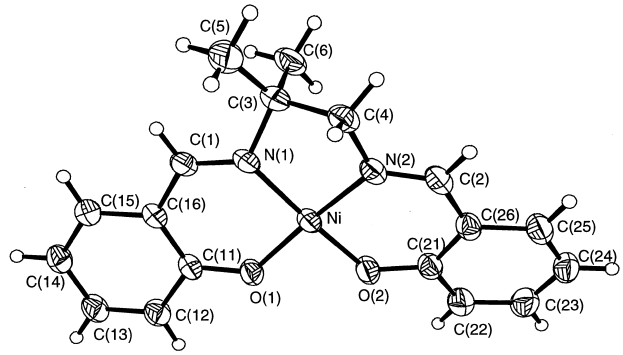


Fig. 1. Molecular diagram with atomic labelling scheme for [Ni(saldMe)]. Ellipsoids at 40% probability level [19,38].

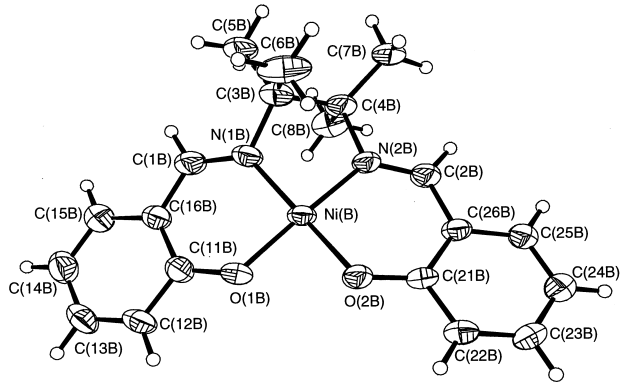


Fig. 2. Molecular diagram with atomic labelling scheme for molecule B of [Ni(saltMe)]. Ellipsoids at 40% probability level [19,38].

from planarity. In contrast, the structure of the compound with no substituents in the imine bridge, [Ni(salen)], is almost planar; maximum deviation from planarity of 0.023 Å and with the nickel atom 0.0056 Å out of the plane [23].

The configuration of the three independent molecules of [Ni(saltMe)] is asymmetric umbrella, with NCCN torsion angles of 20(1)° for molecule A, −43.9(6)° for molecule B and −46.7(5)° for molecule C; the conformations of the imine bridge are thus *cis*, *gauche* and *gauche*, respectively. Deviations of the imine bridge atoms, C3 and C4, from the NiN_2O_2 plane are −0.02(1) and −0.19(1) Å (molecule A), −0.619(8) and 0.097(7) Å (molecule B) and −0.300(7) and 0.507(7)° (molecule C). The values of the torsion angle for molecules B and C are of the same order of magnitude as those observed in the homologous ligand derived from naphthaldehyde, [Ni(naptMe)], for which the value is 47.5(5)° [6].

The configuration of the [Ni(saldMe)] molecules is an asymmetric umbrella but with the two aldehyde moieties twisted. The NCCN torsion angle is 39.6(5)°, smaller than those found in the two crystallographic independent molecules in the similar complex *N*,*N*′-2-methylpropane-2,3-diyl-bis(3-hydroxysalicylideneiminate)nickel(II), [Ni(3-HO-saldMe)], [24], which are 44(1) and 45(1)°. The two carbon atoms, C3 and C4, in [Ni(saldMe)] are below and above the NiO_2N_2 coordination plane with a quasi-symmetric displacement, −0.365(5) and +0.341(5) Å, respectively.

Table 2
Selected bond lengths (Å), bond angles (°) and torsion angles for [Ni(saldMe)] and [Ni(saltMe)]

	[Ni(saldMe)]	[Ni(saltMe)]		
		A molecule	B molecule	C molecule
Ni–O(1)	1.836(2)	1.844(3)	1.844(3)	1.829(3)
Ni–O(2)	1.845(2)	1.839(3)	1.842(3)	1.835(3)
Ni–N(2)	1.847(2)	1.837(4)	1.846(4)	1.842(4)
Ni–N(1)	1.853(3)	1.843(4)	1.838(4)	1.858(4)
N(1)–C(1)	1.291(4)	1.290(6)	1.290(6)	1.279(6)
N(1)–C(3)	1.502(4)	1.494(6)	1.494(6)	1.499(6)
O(1)–C(11)	1.310(4)	1.297(5)	1.305(6)	1.307(6)
N(2)–C(2)	1.292(4)	1.287(6)	1.278(6)	1.301(6)
N(2)–C(4)	1.462(4)	1.502(7)	1.523(6)	1.498(6)
O(2)–C(21)	1.318(4)	1.297(5)	1.302(5)	1.317(6)
C(1)–C(16)	1.434(4)	1.418(7)	1.427(6)	1.425(7)
C(3)–C(4)	1.517(5)	1.298(9)	1.479(8)	1.544(7)
C(3)–C(6)	1.524(5)	1.875(10)	1.601(8)	1.545(7)
C(3)–C(5)	1.525(5)	1.477(7)	1.521(7)	1.521(7)
C(2)–C(26)	1.422(5)	1.429(6)	1.427(6)	1.433(7)
O(1)–Ni–O(2)	84.41(10)	83.85(14)	84.64(14)	83.79(16)
O(1)–Ni–N(2)	173.07(11)	174.3(2)	173.80(17)	174.75(17)
O(2)–Ni–N(2)	94.77(11)	95.61(16)	95.42(15)	95.17(17)
O(1)–Ni–N(1)	95.34(10)	95.76(16)	94.62(16)	95.60(16)
O(2)–Ni–N(1)	171.63(12)	176.46(17)	175.72(18)	172.88(17)
N(2)–Ni–N(1)	86.47(11)	85.13(18)	85.77(17)	86.07(17)
C(1)–N(1)–C(3)	119.2(3)	120.3(4)	121.4(4)	121.4(4)
C(1)–N(1)–Ni	126.1(2)	125.7(3)	126.9(3)	125.0(4)
C(3)–N(1)–Ni	114.0(2)	113.8(3)	111.5(3)	113.2(3)
C(11)–O(1)–Ni	127.52(19)	126.7(3)	126.1(3)	127.8(3)
C(2)–N(2)–C(4)	120.1(3)	122.3(4)	120.9(4)	122.4(5)
C(2)–N(2)–Ni	126.8(2)	125.1(3)	125.3(3)	125.2(4)
C(4)–N(2)–Ni	112.7(2)	112.6(4)	112.8(3)	112.4(3)
C(21)–O(2)–Ni	127.4(2)	126.4(3)	126.8(3)	126.0(4)
N(1)–C(1)–C(16)	125.0(3)	125.9(5)	124.3(5)	126.5(5)
C(11)–C(16)–C(1)	121.9(3)	121.5(4)	121.5(5)	121.5(5)
O(1)–C(11)–C(16)	123.7(3)	123.8(4)	124.3(4)	123.6(5)
O(1)–C(11)–C(12)	118.8(3)	118.7(4)	118.5(5)	118.4(5)
C(16)–C(11)–C(12)	117.5(3)	117.5(4)	117.1(5)	118.1(5)
N(1)–C(3)–C(4)	103.8(3)	112.1(5)	103.9(4)	103.9(4)
N(1)–C(3)–C(6)	107.0(3)	99.9(5)	107.8(5)	108.0(4)
C(4)–C(3)–C(6)	111.3(3)	86.9(7)	105.7(5)	110.6(4)
N(1)–C(3)–C(5)	113.6(3)	115.6(5)	114.0(5)	112.2(4)
C(4)–C(3)–C(5)	109.5(3)	127.1(6)	113.7(5)	113.7(4)
C(6)–C(3)–C(5)	111.4(3)	105.5(6)	111.0(5)	108.2(5)
N(2)–C(2)–C(26)	125.3(3)	126.0(4)	125.5(4)	125.2(5)
C(21)–C(26)–C(2)	121.5(3)	120.7(4)	121.7(4)	121.7(5)
O(2)–C(21)–C(22)	118.2(3)	119.4(4)	119.7(4)	118.2(6)
O(2)–C(21)–C(26)	123.8(3)	124.3(4)	123.6(4)	123.5(5)
N(2)–C(4)–C(3)	108.7(3)	112.9(6)	106.0(4)	103.1(4)
N(1)–C(3)–C(4)–N(2)	39.6(3)	19.6(13)	−43.9(6)	−46.7(5)

The maximum deviation from planarity of the coordinated atoms (and the distance of the nickel atom to the equatorial plane) in similar molecules which have ethylene-based bridges without substituents or aromatic bridges are 0.033 Å (0.0073 Å) in [Ni(α,α′-Me_2salen)] [7], 0.023 Å (0.0056 Å) in [Ni(salen)] [23], 0.013 Å in [Ni(saloph)] [25], 0.039 Å (0.0078 Å) in [Ni(3,5-Cl_2salophen)] [7] and 0.01 Å in [Ni(napen)] [26]. We can conclude, when comparing the above values with those of [Ni(saldMe)], [Ni(1*R*,2*R*-(-)salhd)] and [Ni(saltMe)], that the observed distortions are mainly due to the bulkiness of the substituents in the imine bridge. The presence of these bulky substituents imposes severe steric requirements due to interactions between the hydrogen atoms, and consequently the three molecules [Ni(saldMe)], [Ni(saltMe)] and [Ni(salhd)] are quite distorted.

Another key result that emerged from the molecular structures is that one methyl group in [Ni(saldMe)] is oriented perpendicular to the equatorial plane, and that two methyl groups in [Ni(saltMe)] are oriented perpendicular to the

equatorial plane and in opposite directions. No crystal structure is known for [Ni(salhd)] with the cyclohexane in the *cis* form, but recalling that of [Ni(α,α′-Me_2salhd)] it is to be expected the ring to be also axially oriented.

Regarding the Ni–O and Ni–N bonding distances (Table 2), they are comparable to those observed in Schiff base complexes with identical coordination spheres [6,7,23–29] and are within the average values found in a Cambridge Structural Database search [28,29] for compounds having two carbon atoms in the imine bridge. The relative values of Ni–O and Ni–N bond lengths do not follow any pattern and no trend could be established between their values and any of the parameters used to characterise molecular distortion.

3.3. Crystal packing

The packing of both [Ni(saldMe)] and [Ni(saltMe)] do not show any Ni···Ni intermolecular distance below 3.5 Å. In the packing of [Ni(saldMe)] the shorter Ni···Ni interaction is 4.463 Å, and for [Ni(saltMe)] the existence of three independent molecules with such different orientations in the asymmetric unit prevents shorter interactions in the crystal packing. The shorter ones, 5.561 and 6.471Å, are between the nickel atom of molecule A and the nickel atoms of molecules B and C. Actually, the close intermolecular interactions between molecule A and the surrounding molecules in the unit cell explain the different conformation found for this molecule.

3.4. Cyclic voltammetry

3.4.1. Ligands

The three ligands, H_2saldMe, H_2salhd and H_2saltMe, are irreversibly oxidised in both solvents; the respective anodic peak potentials (scan rate 0.01 V s^{-1}) are approximately 1.22, 1.26 and 0.88 V in DMF, and 1.17, 1.15 and 0.84 V in $(CH_3)_2SO$. With increasing scan rates all ligands show a positive peak potential shift, as well as an increase in current intensity. Although no comparison between the potential peak values of the three ligands can be made due to the irreversible nature of charge transfer, it should be noted that the peak potential pattern for H_2saltMe is quite different from that of the other ligands.

3.4.2. Nickel complexes

Cyclic voltammetric data are summarised in Table 3. The results for [Ni(saltMe)] have been published elsewhere [8], and this complex shows in both solvents a quasi-reversible oxidation of Ni(II) to Ni(III). The cyclic voltammograms of [Ni(saldMe)] and [Ni(salhd)] are solvent dependent; in DMF in the potential range used they exhibit one anodic peak and the corresponding cathodic peak. The values of $E_{1/2}$ (vs. Ag/AgCl) are very similar and the anodic–cathodic peak potential separations, for the lowest scan rates used, are comparable to that of Fc^+/Fc couple, but somewhat higher for fast sweep rates. The ratio i_{pc}:i_{pa} was found to decrease with increasing scan rates.

The behaviour of [Ni(saldMe)] and [Ni(salhd)] in $(CH_3)_2SO$ is more intricate, since the voltammograms are dependent on scan rate. At low scan rates (0.005–0.02 V s^{-1}), two anodic waves, E_{pa}(I) and E_{pa}(II), but only one cathodic wave, which is related to the first anodic process (E_{pc}(I)), could be detected (Fig. 3 and Table 3). As the scan rate increases, a positive shift in E_{pa}(I) and E_{pa}(II) (larger for the latter process) and an increase in peak current (smaller for the latter process) are observed; furthermore, for scan rates faster than 0.05 V s^{-1} only the first anodic wave and the corresponding cathodic wave could be observed, as shown in Fig. 3. The ratio i_{pc}:i_{pa} (Table 3) for the first process is somewhat larger than 1 for low scan rates, but smaller than 1 for the highest scan rates.

For [Ni(saldMe)] and [Ni(salhd)] in the two solvents, the dependence of i_p with $\nu^{1/2}$ was found to be linear at low scan rates, but to deviate from linearity with increasing sweep rate. By coupling these results with the observations that, with increasing scan rate, the ratios i_{pc}:i_{pa} become smaller than 1 and the anodic–cathodic peak potential separation (ΔE) becomes larger than the values for Fc^+/Fc, it becomes clear that the rate of the electron transfer, relative to that of the mass transport, is insufficient to maintain the nernstian

Table 3
Cyclic voltammetric data for Ni(II) complexes in DMF and $(CH_3)_2SO$ (0.1 mol dm^{-3} TEAP) [a]

Complex	ν (V s^{-1})	In DMF					In $(CH_3)_2SO$					
		E_{pa}	E_{pc}	ΔE	$E_{1/2}$	i_{pc}:i_{pa}	E_{paI}	E_{paII}	E_{pcI}	ΔE	$E_{1/2}$	i_{pc}:i_{pa} [b]
[Ni(salhd)]	0.01	0.87	0.78	0.08	0.83	1.02	0.77	0.91	0.69	0.08	0.73	1.05
	1	0.92	0.73	0.19	0.82	0.68	0.87	[c]	0.39	0.48	[d]	0.65
[Ni(saldMe)]	0.01	0.85	0.78	0.07	0.82	1.02	0.76	0.88	0.70	0.06	0.73	1.05
	1	0.89	0.74	0.15	0.82	0.75	0.81	[c]	0.63	0.18	[d]	0.80
[Ni(saltMe)]	0.01	0.94	0.84	0.10	0.89	1.00	0.86	–	0.78	0.08	0.82	0.93
	1	0.94	0.85	0.09	0.90	0.97	0.89	–	0.75	0.14	0.82	0.78

[a] All potentials are referred to Ag/AgCl (1 mol dm^{-3} NaCl).
[b] Refers to process denoted as (I).
[c] The anodic wave is not detected at high scan rates.
[d] Electrochemical process with a high degree of irreversibility.

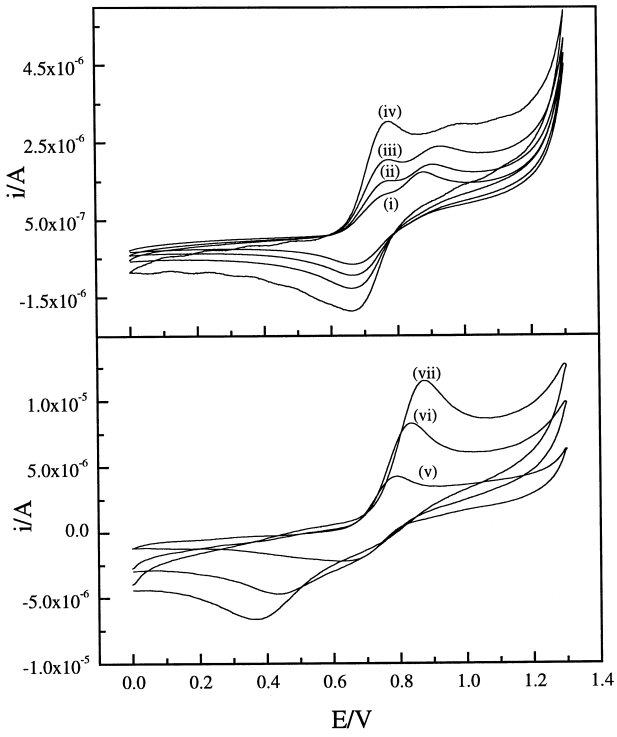


Fig. 3. Cyclic voltammograms of [Ni(salhd)] in 0.1 mol dm^{-3} TEAP–$(CH_3)_2SO$ between 0.00 and 1.30 V at different scan rates: (i) 0.005, (ii) 0.010, (iii) 0.020, (iv) 0.050, (v) 0.100, (vi) 0.500, (vii) 1.00 V s^{-1}.

equilibrium at the electrode surface. The one-electron charge transfer process is thus reversible and diffusion controlled at low scan rates, whereas at high scan rates a transition to a quasi-reversible mixed (kinetic and diffusion) controlled process must take place [30].

The oxidation of several N_2O_2 salicylaldehyde-derived Schiff base Ni(II) complexes has been shown to occur with a concomitant axial coordination of solvent molecules, and this step proved to be decisive in the overall charge transfer process, as it controls the final oxidised products and the $E_{1/2}$ values [5–15]. A similar solvent dependence is also operative in the oxidation process of [Ni(salhd)] and [Ni(saldMe)], as can be gathered by noting that their $E_{1/2}$ values are less positive in $(CH_3)_2SO$, the strong coordinating solvent used.

The $E_{1/2}$ values for [Ni(salhd)] and [Ni(saldMe)] in each solvent are similar, albeit slightly more positive than that of [Ni(salen)] [$E_{1/2}$ (DMF) = 0.81 V and $E_{1/2}$ ($(CH_3)_2SO$) = 0.70 V; scan rate 0.01 V s^{-1}] and less positive than that of [Ni(saltMe)]. To account for this behaviour, it must be pointed out that introduction of substituents in the imine bridge not only affects the electronic properties of the complex, but also may impose steric constraints on axial coordination. Electron-donating substituents (methyl groups and the cyclohexyl) are expected to decrease the values of $E_{1/2}$, and as such their $E_{1/2}$ values would be expected to be less positive than those of [Ni(salen)]. However, the values obtained were more positive, an indication that steric constraints play a more important role than electronic effects in the solution stability of the electrogenerated Ni(III) species. The X-ray structure of [Ni(saldMe)] shows one methyl group oriented towards one axial position which thus will interact directly with one axially bound solvent molecule in the oxidised species, weakening the bond to the metal with the consequent destabilisation of Ni(III) complexes. This explanation also holds for [Ni(saltMe)], for which two methyl groups of the imine bridge are directed towards two opposite axial positions thus weakening axial coordination of the two solvent molecules in the Ni(III) complexes. Therefore [Ni(saltMe)] exhibits, as expected, the more positive $E_{1/2}$ values for the series of complexes studied. Although no crystal structure for the *cis* isomer of [Ni(salhd)] is known, the preceding discussion suggests that in this isomer the cyclohexane ring must hinder axial coordination and must influence markedly its electrochemical responses.

A caveat to the above discussion is that structural data were obtained in the solid state. In solution, where solid states effects are absent, it is not possible to rule out the existence of other conformations of [Ni(saldMe)] and [Ni(salhd)], and thus the two anodic processes observed at low scan rates in $(CH_3)_2SO$ may be due to the oxidation of complexes in different conformations, one of which does not allow stabilisation of Ni(III) species.

3.5. Chronoamperometry

In both solvents the current–time responses in chronoamperometric experiments for [Ni(saldMe)], [Ni(salhd)] and [Ni(saltMe)], depicted as i versus $t^{-1/2}$ (Cottrell representation [30]), are straight lines that exhibit small deviations from linearity for long periods, particularly in the reduction step (typically longer than 6 s for the oxidation and 2 s for the reverse step). These deviations from linearity suggest a change from a diffusion-controlled process to a mixed controlled process [30], as has been inferred from cyclic voltammetry in $(CH_3)_2SO$. By using the linear region of the Cottrell equation, the diffusion coefficients for oxidation ($D_{CA}{}^{oxi}$) and the reverse step ($D_{CA}{}^{red}$) were calculated and are summarised in Table 4. The values for $D_{CA}{}^{oxi}$ are of the same magnitude as those obtained for the oxidation of [Ni(salen)] and [Co(salen)] using the Randles–Sevcik equation [31].

Table 4
Values of D_{CA} obtained using the Cottrell equation

Complex	$(CH_3)_2SO$		DMF	
	Step (V)	$10^6 D_{CA}$ (cm^2 s^{-1})	Step (V)	$10^6 D_{CA}$ (cm^2 s^{-1})
[Ni(saldMe)]	0.0→0.93	4.00	0.0→1.0	9.20
	0.93→0.0	3.66	1.0→0.0	8.91
[Ni(salhd)]	0.0→0.90	3.68	0.0→1.0	8.91
	0.90→0.0	3.10	1.0→0.0	8.58
[Ni(saltMe)]	0.0→1.0	2.98	0.0→1.0	8.35
	1.0→0.0	2.65	1.0→0.0	7.35

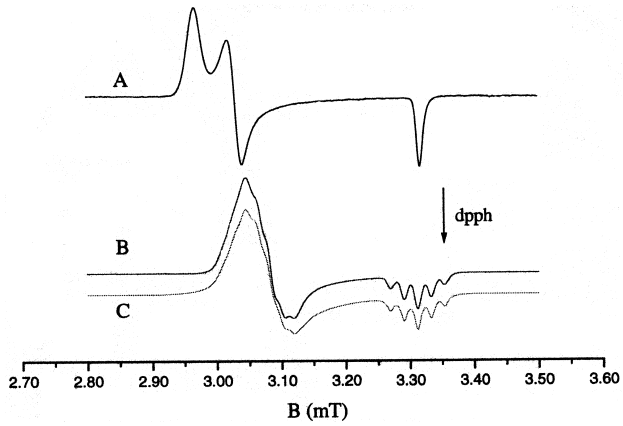


Fig. 4. Frozen-solution X-band EPR spectra at −140°C of (A) an electrochemically oxidised solution of [Ni(saldMe)] in DMF, (B) the corresponding pyridine adduct, and its simulation (C).

Analysis of D_{CA} shows that: (1) the values in DMF are higher than those obtained in $(CH_3)_2SO$, and (2) the values decrease in both solvents in the order [Ni(saldMe)] > [Ni(salhd)] > [Ni(saltMe)]. Solvent dependence can easily be accounted for by differences in solvent viscosity [30,31]: the complexes have smaller D_{CA} values in the solvent with higher viscosity, $(CH_3)_2SO$. No straightforward explanation can be invoked for the differences in D_{CA} for the complexes; we note, however, that the smallest value is obtained for the complex with the longest axial bonds ($[Ni(saltMe)(solv)_2]^+$ (see EPR section, below), and that the average size of the Ni(III) complexes may be the key factor in controlling diffusion.

3.6. Electrolysis and EPR characterisation of the oxidised solutions

Electrochemical oxidation of [Ni(saldMe)] and [Ni(salhd)] in DMF and $(CH_3)_2SO$ proceeds as that of [Ni(saltMe)] and [Ni(salen)] [8], with a solution colour change from reddish to dark brown. Frozen-solution EPR spectra of electrolytically generated nickel complexes are similar in both solvents, and show the rhombic symmetry and the large *g* tensor anisotropy typically associated with metal-centred oxidised species (Fig. 4A). The spectra exhibit no hyperfine splittings and are similar to those of oxidised solutions of [Ni(saltMe)], [Ni(salen)] [8] and other electrogenerated Ni(III) Schiff base complexes derived from salicylaldehyde [5–7]. The oxidised complexes can thus be formulated as six-coordinate, with two solvent molecules bound axially, $[Ni(L)(solv)_2]^+$, and with the metal centre in a low-spin $^2A_1$ (d_{z^2}) ground state. In the absence of EPR crystal data for the Ni(III) complexes studied, the observed similarity between their *g* features and those of analogous Ni(III) compounds [5–9] can be extended to support the following orientation scheme for the tensor axes of the nickel complexes: $g_1 = g_x$, $g_2 = g_y$, $g_3 = g_z$, where g_1 an g_3 refer to the lowest and highest magnetic field *g* values, respectively. EPR data for Ni(III) species in DMF and $(CH_3)_2SO$ are summarised in Table 5; for comparison the values for $[Ni(salen)(X)_2]^+$ and $[Ni(saltMe)(X)_2]^+$ are also included.

In order to obtain more information on the effect of the imine bridge substituents on the electronic properties of six-coordinate Ni(III) species, the EPR characterisation was extended to compounds with axially bound pyridine molecules. Upon addition of pyridine to freshly prepared solutions of electrogenerated Ni(III) complexes in DMF at temperatures just above the softening point of the frozen glass, new Ni(III) species are formed, as can be inferred from their frozen-solution EPR spectra (Fig. 4B). These are of rhombic type, although with less rhombicity than the parent complexes, have smaller values of g_{av} (2.140–2.144) and exhibit hyperfine couplings in all *g* regions. The existence of one

Table 5
EPR parameters for $[Ni(L)(X)_2]^+$ complexes

Complex	Experimental values					Coefficients [a]			Energy of excited state (cm^{-1})		
	g_x	g_y	g_z	g_{av} [b]	Δ_{xy}	C_1	C_2	C_3	$\Delta(^2B_1)$	$\Delta(^2A_2)$	ΔQ [c]
$[Ni(salen)(dmf)_2]^+$ [d]	2.266	2.222	2.021	2.170	0.044	0.0343	0.0424	0.1075	11465	9275	3658
$[Ni(salen)(Me_2SO)_2]^+$ [d]	2.256	2.216	2.020	2.164	0.040	0.0334	0.0399	0.1045	11774	9856	3763
$[Ni(salen)(py)_2]^+$ [d]	2.201	2.172	2.021	2.131	0.029	0.0251	0.0298	0.1096	15667	13196	3588
$[Ni(salhd)(dmf)_2]^+$	2.267	2.220	2.027	2.171	0.047	0.0330	0.0405	0.1202	11930	9707	3273
$[Ni(salhd)(Me_2SO)_2]^+$	2.264	2.223	2.026	2.171	0.041	0.0336	0.0402	0.1181	11700	9780	3330
$[Ni(salhd)(py)_2]^+$	2.208	2.182	2.030	2.140	0.026	0.0257	0.0299	0.1236	15310	13150	3181
$[Ni(saldMe)(dmf)_2]^+$	2.268	2.220	2.027	2.172	0.048	0.0330	0.0407	0.1202	11930	9667	3271
$[Ni(saldMe)(Me_2SO)_2]^+$	2.263	2.223	2.026	2.171	0.040	0.0336	0.0400	0.1180	11700	9821	3332
$[Ni(saldMe)(py)_2]^+$	2.213	2.190	2.030	2.144	0.023	0.0271	0.0309	0.1230	14270	12740	3196
$[Ni(saltMe)(dmf)_2]^+$ [d]	2.265	2.224	2.020	2.170	0.041	0.0348	0.0414	0.1053	11300	9499	3734
$[Ni(saltMe)(Me_2SO)_2]^+$ [d]	2.254	2.226	2.020	2.167	0.028	0.0351	0.0396	0.1047	11204	9931	3756
$[Ni(saltMe)(py)_2]^+$ [d]	2.214	2.186	2.022	2.141	0.028	0.0278	0.0324	0.1060	14146	12137	3710

[a] Obtained from McGarvey equations; see text.
[b] The value of g_{av} was calculated as $(g_x + g_y + g_z)/3$.
[c] Difference between the average energy of the quartet states and the ground state.
[d] From [8].

Table 6
^{14}N superhyperfine coupling constants and spin densities for $[NiL(py)_2]^+$ complexes

Complex	Experimental superhyperfine coupling [a]					Anisotropic superhyperfine tensor		Spin densities on ^{14}N			λ^2
	A_x	A_y	A_z	$A_\perp$ [b]	A_{iso} [c]	$A_{xx,yy}$	A_{zz}	C^2_{2s}	C^2_{2p}	Total [d] (%)	
$[Ni(salen)(py)_2]^+$ [e]	1.65	1.76	2.14	1.71	1.85	−0.15	0.28	0.033	0.084	23.4	2.5
$[Ni(salhd)(py)_2]^+$	1.70	1.65	2.13	1.68	1.83	−0.15	0.29	0.033	0.088	24.1	2.7
$[Ni(saldMe)(py)_2]^+$	1.85	1.75	2.15	1.80	1.92	−0.12	0.22	0.034	0.067	20.2	1.9
$[Ni(saltMe)(py)_2]^+$ [e]	1.82	1.63	2.14	1.72	1.86	−0.14	0.27	0.033	0.080	22.7	2.4

[a] The A values are expressed in mT.
[b] $A_\perp$ was calculated as $(A_x+A_y)/2$.
[c] A_{iso} could not be obtained for the adducts; instead it was calculated from $(A_x+A_y+A_z)/3$.
[d] Spin density delocalized onto the two axial nitrogen atoms.
[e] From [8].

well-resolved quintuplet ($A=2.15$–2.13 mT) in the region of higher magnetic field and of two non-resolved quintuplets in the other g regions, implies that solvent molecules have been substituted by two pyridines (^{14}N; $I=1$) and that the resulting Ni(III) complexes have unequivocally a low-spin $^2A_1$ (d_{z^2}) ground state. The similarity between the g pattern of these species with those of the parent complex supports the same orientation scheme for the g tensor of the pyridine adducts.

No EPR signals were detected in fluid solutions of pyridine–DMF or in frozen solution of pyridine adducts in $(CH_3)_2SO$, as has also been observed for the homologous complexes with H_2salen and H_2saltMe ligands, a consequence of the very fast decomposition rate of the pyridine adducts in fluid solutions [5,8,9,32]. EPR parameters for $[Ni(L)py_2]^+$ are summarised in Tables 5 and 6; values for similar complexes with salen and saltMe are also included.

3.7. Electronic structure of the Ni(III) species

Analysis of the EPR parameters using the model developed by McGarvey for d^7 systems with an $^2A_1$ (d_{z^2}) ground state [33], in conjunction with the approximation suggested by Labause and Raynor [34,35], can provide information on the electronic structure of Ni(III) species. A full description of this analysis is described elsewhere [5,8,9] and its application allows an estimate of the energy of excited doublet states $\Delta(^2B_1)$ and $\Delta(^2A_2)$ and the average energy of the quartet states ΔQ, provided the values of complex spin orbit coupling constants (ξ) are known. We have used the ξ values of $[Ni(saltMe)((CH_3)_2SO)_2]^+$ and $[Ni(salen)((CH_3)_2SO)_2]^+$, which were found to be 55% of the free ion [8,36]. In Table 5 are included the values for $\Delta(^2B_1)$, $\Delta(^2A_2)$ and ΔQ for $[Ni(L)(DMF)_2]^+$, $[Ni(L)((CH_3)_2SO)_2]^+$ and $[Ni(L)(py)_2]^+$.

Analysis of data in Table 6 failed to reveal any correlation between the energy of the excited quartets and axial ligation. The energy of the doublet states does not change significantly when the solvent is varied from DMF to $(CH_3)_2SO$, but the axial coordination of pyridine induces a significant increase in the energy of the doublets, as a result of the strong interaction of the pyridine lone pair with the d_{z^2} orbital. This increase lowers the value of the McGarvey coefficients, C_2 and C_1, and using the g factor equations neglecting second-order terms, $g_x=2.0023+6C_2$ and $g_y=2.0023+6C_1$ [5,8,9], a decrease in g_x and g_y is predicted, as was actually observed.

Analysis of data in Table 5 reveals also that for the same axial coordinate molecule (X = DMF, $(CH_3)_2SO$ and py), the energy of the excited doublets decreases in the order $[Ni(salen)(X)_2]^+ > [Ni(salhd)(X)_2]^+ \geq [Ni(saldMe)(X)_2]^+ > [Ni(saltMe)(X)_2]^+$. This ordering reflects the strength of the axial ligation/axial bond length and thus we can deduce that axial bond lengths in the Ni(III) complexes with saltMe are the weakest (longest), and that those of salen complexes are the strongest (shortest), with the other complexes exhibiting intermediate and similar bond lengths. These observations correlate with the sequence of $E_{1/2}$ values, and reflects mainly, as mentioned above, steric interactions of the imine bridge substituents with the axially bound molecules in Ni(III) complexes.

3.7.1. Nitrogen hyperfine tensor and spin density on nitrogen atoms of axial bound pyridines

The 2s and 2p spin densities, the ratio p:s ($\lambda^2=C^2_{2p}/C^2_{2s}$) and the total spin density delocalised onto the axially bounded pyridine have been calculated by procedures described elsewhere [5,8,9,37] and are reported in Table 6. The values of C^2_{2s} are practically insensitive to changes in the equatorial ligand, whereas those of C^2_{2p} show larger variations. Thus changes in total spin density and in λ^2 reflect primarily changes in values of C^2_{2p}. The two new complexes exhibit values for the latter quantities that are in the range observed for pyridine adducts of Ni(III) complexes with ligands derived from salicylaldehyde and aliphatic diamines, but no correlation with the bulkiness of the aliphatic imine bridge could be extracted from the data, probably due to the limited number of complexes studied.

4. Concluding remarks

The oxidation of [Ni(saldMe)] and [Ni(salhd)] in DMF and $(CH_3)_2SO$ (strong donor solvents) was shown to proceed through oxidation of the metal centre and with concomitant axial coordination of solvent molecules, as has been observed for [Ni(salen)] and [Ni(saltMe)], giving Ni(III) complexes formulated as $[Ni(L)(solv)_2]^+$, where L is a Schiff base and solv a solvent molecule.

X-ray structure of the complexes revealed that in [Ni(saltMe)] two methyl groups of the imine bridge are perpendicular to the equatorial plane and directed towards the two axial coordination positions, whereas in [Ni(saldMe)] only one methyl group is directed towards one axial position. It is to be expected also that in the *cis* isomer of [Ni(salhd)] the cyclohexane group is directed towards one of the axial positions. Thus the required axial coordination of solvent molecules in these electrogenerated Ni(III) species is hindered sterically when compared with [Ni(salen)] and the main result is that the sequence observed for the $E_{1/2}$ values, [Ni(salen)] < [Ni(salhd)] ≤ [Ni(saldMe)] < [Ni(saltMe)], parallels the hindrance on axial coordination. Thus, bulky substituents in the imine bridge tend to render less accessible the +3 oxidation state in Ni(II) complexes with the N_2O_2 Schiff base ligands.

Supplementary data

Crystallographic data (excluding structure factors) for the structures in this paper have been deposited with the Cambridge Crystallographic Data Centre as supplementary publications nos. CCDC 133149 {[Ni(saldMe)]} and CCDC 133150 {[Ni(saltMe)]}. Copies of the data can be obtained, free of charge, on application to CCDC, 12 Union Road, Cambridge CB2 1EZ, UK, (fax: +44-1223-336033 or e-mail: deposit@ccdc.cam.ac.uk).

Acknowledgements

This work was partially supported by the 'Fundação para a Ciência e Tecnologia' (F.C.T.) through project PBIC/QUI/2137/95. M.V.-B. thanks the FCT/Praxis XXI for a fellowship.

References

[1] C. Gosden, K.P. Healy, D. Pletcher, J. Chem. Soc., Dalton Trans. (1978) 972.
[2] K.P. Healy, D. Pletcher, J. Organomet. Chem. 186 (1980) 401.
[3] C. Gosden, J.B. Kerr, D. Pletcher, R. Rosas, J. Electroanal. Chem. Interfacial Electrochem. 117 (1981) 101.
[4] C.E. Dahm, D.G. Peters, J. Electroanal. Chem. Interfacial Electrochem. 406 (1996) 119.
[5] B. Castro, C. Freire, Inorg. Chem. 29 (1990) 5113.
[6] M.A.A.F. de C.T. Carrondo, B. Castro, A.M. Coelho, D. Domingues, C. Freire, J. Morais, Inorg. Chim. Acta 205 (1993) 157.
[7] F. Azevedo, M.A.A.F. de C.T. Carrondo, B. Castro, M. Convery, D. Domingues, C. Freire, M.T. Duarte, K. Nielsen, I.C. Santos, Inorg. Chim. Acta 219 (1994) 43.
[8] C. Freire, B. Castro, J. Chem. Soc., Dalton Trans. (1998) 1491.
[9] C. Freire, B. Castro, Polyhedron 17 (1998) 4227.
[10] M. Vilas-Boas, C. Freire, B. Castro, A.R. Hillman, P.A. Christensen, Inorg. Chem. 36 (1997) 4929.
[11] M. Vilas-Boas, C. Freire, B. Castro, A.R. Hillman, J. Phys. Chem. B 102 (1998) 8533.
[12] K.A. Goldsby, J. Coord. Chem. 19 (1988) 83.
[13] K.A. Goldsby, L.A. Hoferkamp, Chem. Mater. 1 (1989) 348.
[14] P. Audebert, P. Capdevielle, M. Maumy, New J. Chem. 15 (1991) 235.
[15] P. Audebert, P. Capdevielle, M. Maumy, New J. Chem. 16 (1992) 697.
[16] R.H. Holm, G.W. Everett, A. Chakravorty, Prog. Inorg. Chem. 7 (1966) 183.
[17] G.M. Sheldrick, in: G.M. Sheldrick, C. Kurger, R. Goddard (Eds.), Crystallographic Computing 3, Oxford University Press, Oxford, 1985, p. 175.
[18] G.M. Sheldrick, A Computer Program for Refinement of Crystal Structures (SHELXL-97), University of Göttingen.
[19] M.N. Burnett, C.K. Johnson, ORTEP III: Oak Ridge Thermal Ellipsoid Plot Program for Crystal Structure Illustrations, Oak Ridge National Laboratory Report ORNL-6895, 1996.
[20] International Tables for X-Ray Crystallography, vol. IV, Kynoch Press, Birmingham, 1974.
[21] G. Maki, J. Chem. Phys. 28 (1958) 651.
[22] A. Wojtczak, E. Szlyk, M. Jaskólski, E. Larson, Acta Chem. Scand. 51 (1997) 274.
[23] A.G. Manfredotti, C. Guastini, Acta Crystallogr., Sect. C 39 (1983) 863.
[24] U. Casellato, P. Guerriero, S. Tamburini, P.A. Vigato, C. Benelli, Inorg. Chim. Acta 207 (1993) 39.
[25] A. Radha, M. Seshasayee, K. Ramalingam, G. Aravamudan, Acta Crystallogr., Sect. C 41 (1985) 1169.
[26] F. Akhtar, Acta Crystallogr., Sect. B 37 (1981) 84.
[27] M. Calligaris, G. Nardin, L. Randaccio, Coord. Chem. Rev. 7 (1972) 385.
[28] F.H. Allen, O. Kennard, R. Taylor, Acc. Chem. Res. 16 (1983) 146.
[29] F.H. Allen, J.E. Davies, J.J. Galloy, O. Johnson, O. Kennard, C.F. Macrae, G.F. Mitchell, G.F. Mitchell, J.M. Smith, D.G. Watson, J. Chem. Inf. Comput. Sci. 31 (1987) 187.
[30] A.J. Bard, L.R. Faulkner, Electrochemical Methods, Wiley, New York, 1980.
[31] A. Kapturkiewicz, B. Behr, Inorg. Chim. Acta 69 (1983) 247.
[32] B. Castro, C. Freire, E. Pereira, J. Chem. Soc., Dalton Trans. (1994) 571.
[33] B.R. McGarvey, Can. J. Chem. 53 (1975) 2498.
[34] G. Labause, J.B. Raynor, J. Chem. Soc., Dalton Trans. (1980) 2388.
[35] G. Labause, J.B. Raynor, J. Chem. Soc., Dalton Trans. (1981) 590.
[36] A.H. Maki, N. Edelstein, A. Davison, R.H. Holm, J. Am. Chem. Soc. 86 (1964) 4580.
[37] B.A. Goodman, J.B. Raynor, Adv. Inorg. Chem. Radiochem. 13 (1970) 135.
[38] P. McArdle, J. Appl. Crystallogr. 28 (1995) 65.

PERGAMON

www.elsevier.nl/locate/poly

Polyhedron 19 (2000) 665–672

POLYHEDRON

Divalent transition metal complexes of alkylpyridyl derivatized dmit ligands

Jan Becher [a], Alan Hazell [b], Christine J. McKenzie [a,*], Claus Vestergaard [a]

[a] *Department of Chemistry, University of Southern Denmark, Odense University, DK-5230 Odense M, Denmark*
[b] *Department of Chemistry, Aarhus University, DK-8000 Aarhus C, Denmark*

Received 20 October 1999; accepted 13 January 2000

Abstract

The two new bis-alkylpyridyl substituted dmit ligands, 4,5-bis(2-pyridylmethylsulfanyl)-1,3-dithiole-2-thione (bpmdmit) and 4,5-bis(2-pyridylethylsulfanyl)-1,3-dithiole-2-thione (bpedmit), and some of their transition metal complexes have been prepared. Two basic structural types for the complexes MX_2L (M = Ni, Co, Cu, Pd; L = bpmdmit or bpedmit; X = Cl or Br) were determined by X-ray crystallography. The cobalt(II) and the nickel(II) complexes $CoBr_2$(bpmdmit) and $NiCl_2$(bpmdmit) show octahedral geometries around the metal ions with coordination to the metal ions by the pyridyl nitrogen atoms and the thioether sulfur atoms of the ligand and *cis* coordination of the halide ions. By contrast, only the pyridyl nitrogen atom of the ligands in the copper(II) and the palladium(II) complexes, $CuCl_2$(bpedmit) and $PdCl_2$(bpedmit), are coordinated to the metal ions to give essentially square planar metal environments. The copper complex was isolated as both green and purple crystals. However, the X-ray structures of both forms are similar, and show a dimeric arrangement with bis-μ-chloride bridges between the copper ions in the dimeric units. The green crystals contain two molecules of acetonitrile in the unit cell, however these do not interact with the metal ions. The geometry of the copper ions in the green form deviates most from centrosymmetric square planar geometry and this is consistent with the observed colour. Apart from the colour, the solids can be distinguished in the solid state by EPR spectroscopy since they give different rhombic signals. UV–Vis and EPR spectroscopy show that in solution the structures of the purple and green forms of $CuCl_2$(bpedmit) are identical, as expected. ©2000 Elsevier Science Ltd All rights reserved.

Keywords: Copper; Cobalt; Nickel; Palladium; dmit; 4,5-bis(2-pyridylmethylsulfanyl)-1,3-dithiole-2-thione; 4,5-bis(2-pyridylethylsulfanyl)-1,3-dithiole-2-thione

1. Introduction

4,5-Disulfanyl-1,3-dithiole-2-thionate ($dmit^{2-}$) has been used extensively for the preparation of mononuclear bis-dmit and tris-dmit complexes of transition and main group metals [1–3]. These sulfur-rich molecules have the potential for novel electronic properties owing to the extensive π overlap of the sulfur and metal-based d orbitals. Several examples of thiolate functionalized dmit compounds have been reported [4] but to our knowledge none of these have been used as ligands for metal ions. The work reported here describes the attachment of alkylpyridyl moieties to the thiolate sulfur atoms of $dmit^{2-}$, to give chelating groups containing thioether and pyridyl donor groups (Chart 1). The thioether groups are not expected to be strong donors to other than soft metal ions; however, as part of a chelating system thioether groups are known to coordinate to metal ions [5–9]. In this study complexation reactions with various metal(II) salts were investigated. Only reactions with chloride salts gave tractable products and the structures of these have been determined.

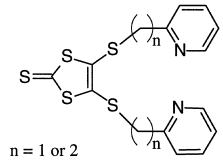


Chart 1

2. Experimental

NMR spectra were recorded on either a Varian Gemini 300 MHz spectrometer or a Bruker AC-250 MHz spectrometer. UV–Vis measurements were recorded using a Shimadzu UV-3100 UV–Vis–near-IR spectrophotometer. IR spectra were recorded as KBr pellets with a Perkin-Elmer 1720 IRFT spec-

* Corresponding author. Tel.: +45-6557-2518; fax: +45-6615-8780; e-mail: chk@chem.sdu.dk

0277-5387/00/$ - see front matter ©2000 Elsevier Science Ltd All rights reserved.
PII S0277-5387(00)00301-6

trometer. FAB mass spectra were recorded on a Kratos MS50TC. Electron spin resonance (ESR) measurements at X-band frequencies were obtained using a Bruker ESP-380E FT-EPR spectrometer. Cyclic voltammograms were measured using a locally constructed three-electrode potentiostat using acetonitrile solutions containing $^{n}Bu_4NPF_6$ (0.1 M) and a scan rate of 0.100 V s^{-1}. The working electrode was a BAS platinum electrode, with an Ag/AgCl electrode as reference electrode and a counter electrode of platinum. $^{n}Bu_4PF_6$ was used as electrolyte ($\approx$0.1 M). In this set-up ferrocene was used as an internal standard for which a halfwave potential at 105 mV was recorded. Elemental analyses were carried out at the microanalytical laboratory of the H.C. Ørsted Institute, Copenhagen. TLC was carried out on Merck Silicagel 60 F_{254} coated aluminium foil; the same type of silica was used for columns. Where necessary, solvents were dried according to standard literature methods [10]. $(Et_4N)_2$-$(Zn(dmit)_2)$ [11] and 4,5-bis(benzoylsulfanyl)-1,3-dithiole-2-thione [12] were prepared by literature methods.

2.1. Syntheses

2.1.1. 4,5-Bis(2-pyridylmethylsulfanyl)-1,3-dithiole-2-thione (bpmdmit)

4,5-Bis(benzoylsulfanyl)-1,3-dithiole-2-thione (3.173 g, 7.80 mmol) was suspended in 80 cm^3 anhydrous methanol and purged with nitrogen for 25 min. Sodium (0.73 g, 31.75 mmol) dissolved in anhydrous methanol (50 cm^3) was added over a period of 30 min. After the addition the suspension was stirred for a further 15 min, by which time it became a deep red colour and all of the thione dissolved. 2-Picolylchloride hydrochloride (2.56 g, 15.61 mmol) was added over a period of 90 min and the solution stirred overnight. The resulting red solution was concentrated in vacuo and the residue dissolved in EtOAc. A small amount of precipitate was removed by filtration. The filtrate was concentrated and purified by column chromatography using EtOAc as eluent. The product was obtained as a TLC- and NMR-pure dark brown oil. Raw yield, 1.771 g (60%). The oil was dissolved in boiling hexane (50 cm^3) and a yellow powder obtained by scratching the glass vessel while cooling. Yield, 0.569 g (19%); m.p. 52–53°C (hexane). *Anal*. Found: C, 47.83; H, 3.27; N, 6.94. Calc. for $C_{15}H_{12}N_2S_5$: C, 47.34; H, 3.18; N, 7.36%. ^{1}H NMR (250 MHz, $CDCl_3$): δ 4.13 (s, 4H, CH_2), 7.18–7.24 (m, 4H, Py-H4,5), 7.63 (dt, J=2/8 Hz, 2H, Py-H3), 8.55–8.57 (d, J=5 Hz, 2H, Py-H6). ^{13}C NMR (62.5 MHz, $CDCl_3$): δ 42.38 (CH_2), 122.60 (Py-C3/5), 123.09 (Py-C3/5), 136.72 (Py-C4), 137.26 (C=C), 149.74 (Py-C6), 155.68 (Py-C2) and 211.22 (C=S). IR (KBr): 1060, 1435, 1475, 1568, 1594 cm^{-1}. UV–Vis (CH_3OH): λ_{max} (log ε) 266 (4.05), 377 nm (4.06).

2.1.2. 4,5-Bis(2-pyridylethylsulfanyl)-1,3-dithiole-2-thione (bpedmit)

$(Et_4N)_2(Zn(dmit)_2)$ (10.619 g, 14.79 mmol) and 2-vinylpyridine (9.774 g, 93 mmol) were mixed in $CHCl_3$/AcOH (3:1, 200 cm^3) and heated under reflux overnight. The solution was filtered and washed with water (200 cm^3), sat. aq. $NaHCO_3$ (2×200 cm^3) (caution!), sat. aq. NaCl (200 cm^3), water (200 cm^3), dried ($MgSO_4$) and concentrated in vacuo. The residue was dissolved in acetone and a small amount of sticky precipitate was discarded. The solution was concentrated and purified by column chromatography with EtOAc/hexane (2:1) as eluent. The product was recovered as an oil, R_f=0.24 (EtOAc/hexane, 2:1). After 3 h in an open flask the oil solidified. The solid was pulverized and dried. Yield, 6.956 g (58%); m.p. 37–38.5°C. *Anal*. Found: C, 49.95, H, 3.94, N, 6.88. Calc. for $C_{17}H_{16}N_2S_5$: C, 49.97; H, 3.95; N, 6.86%. ^{1}H NMR (300 MHz, $CDCl_3$): δ 3.15 (t, J=7 Hz, 4H, SCH_2), 3.34 (t, J=7 Hz, 4H, CH_2Py), 7.15–7.20 (m, 4H, Py-H4,5), 7.63 (dt, J=2/8 Hz, 2H, Py-H3), 8.55 (d, J=4 Hz, 2H, Py-H6). ^{13}C NMR (75 MHz, $CDCl_3$): δ35.71 (SCH_2), 38.01 (CH_2Py), 121.89 (Py-C3/5), 123.42 (Py-C3/5), 136.55 (Py-C4), 136.61 (C=C), 149.64 (Py-C6), 158.43 (Py-C2), 211.39 (C=S). IR (KBr): 1062, 1435, 1473, 1569, 1592 cm^{-1}. UV–Vis (CH_3OH): λ_{max} (log ε) 263 (4.18), 381 nm (4.13).

2.1.3. 4,5-Bis(2-pyridylmethylsulfanyl)-1,3-dithiole-2-thione cobalt(II) bromide, $CoBr_2$(bpmdmit) (**1**)

Bpmdmit (35.7 mg, 0.094 mmol) and cobalt(II) bromide hexahydrate (31.4 mg, 0.096 mmol) were dissolved in CH_3CN (20 cm^3) to give a blue–green solution. After 2 h red/green pleochroic crystals began to precipitate. Yield, 39 mg (69%). *Anal*. Found: C, 30.06; H, 2.02; N, 4.67. Calc. for $C_{15}H_{12}Br_2CoN_2S_5$: C, 30.49; H, 1.87; N, 4.82%. FABMS: *m/z* 598 (M^+), 519 ([M−Br]$^+$), 381 ([ligand+H]$^+$). IR (KBr): 1072, 1438, 1482, 1568, 1601 cm^{-1}. UV–Vis (CH_3OH): λ_{max} (log ε): 267 (4.24), 377 nm (4.16).

2.1.4. 4,5-Bis(2-pyridylmethylsulfanyl)-1,3-dithiole-2-thione nickel(II) chloride, $NiCl_2$(bpmdmit) (**2**)

Bpmdmit (43.6 mg, 0.115 mmol) and nickel(II) chloride hexahydrate (33.6 mg, 0.141 mmol) were mixed in CH_3CN:H_2O (25:1, 25 cm^3) to give a green solution. Green crystals deposited after 24 h. Yield, 35 mg (60%). *Anal*. Found: C, 34.08, 34.16; H, 2.34, 2.36; N, 5.32, 5.37. Calc. for $C_{15}H_{12}Cl_2N_2NiS_5 \cdot H_2O$: C, 34.11; H, 2.67; N, 5.30%. FABMS: *m/z* 551 ([ligand+NiCl+DMSO]$^+$), 473 ([ligand+NiCl]$^+$), 438 ([ligand+Ni]$^+$), 381 ([ligand+H]$^+$). IR (KBr): 1072, 1439, 1482, 1568, 1601 cm^{-1}. UV–Vis (CH_3OH): λ_{max} (log ε): 266 (5.09), 377 nm (5.08).

2.1.5. 4,5-Bis(2-pyridylethylsulfanyl)-1,3-dithiole-2-thione copper(II) chloride, $CuCl_2$(bpedmit)·$2CH_3CN$ (**3a**)

Bpedmit (58.8 mg, 0.144 mmol) and copper(II) chloride dihydrate (25.2 mg, 0.15 mmol) were dissolved in CH_3CN (5 cm^3) to give a green solution. On standing, **3a** as green needles and a small amount of **3b** as purple needles precipitated from the solution. Combined yield, 70.2 mg (79–92%). The crystals were separated manually to obtain the elemental

analysis and spectroscopic data for **3a** and the crystal used for X-ray crystallography. *Anal*. Found: C, 40.16; H, 3.48; N, 8.64. Calc. for $C_{17}H_{16}Cl_2CuN_2S_5 \cdot 2CH_3CN$: C, 40.35; H, 3.55; N, 8.96%. IR (KBr): 1062, 1440, 1485, 1570, 1605, 2244 cm^{-1}. FABMS: *m/z* 541 ($[ligand + CuCl_2]^+$), 506 ($[ligand + CuCl]^+$), 471 ($[ligand + Cu]^+$), 409 ($[ligand + H]^+$). UV–Vis (CH_3OH): λ_{max} (log ε): 263 (4.78), 380 (4.64), 611 nm (2.81). UV–Vis (CH_3CN): λ_{max} (log ε) 263 (4.09), 384 nm (4.06).

*2.1.6. 4,5-Bis(2-pyridylethylsulfanyl)-1,3-dithiole-2-thione copper(II) chloride, $CuCl_2$(bpedmit) (**3b**)*

4,5-Bis(2-pyridylethylsulfanyl)-1,3-dithiole-2-thione (bpedmit) (98.6 mg, 0.241 mmol) dissolved in ethanol (15 cm^3) and copper(II) chloride dihydrate (51.2 mg, 0.300 mmol) dissolved in ethanol (10 cm^3) were mixed, effecting an immediate colour change from yellow to green. The product precipitated as purple block like crystals. Yield, 120 mg (92%). *Anal*. Found: C, 37.70, 37.80; H, 2.88, 2.89; N, 5.13, 5.18. Calc. for $C_{17}H_{16}Cl_2CuN_2S_5$: C, 37.60; H, 2.97; N, 5.16%. IR (KBr): 1064, 1439, 1485, 1570, 1605 cm^{-1}. FABMS: *m/z* 541 ($[ligand + CuCl_2]^+$), 506 ($[ligand + CuCl]^+$), 471 ($[ligand + Cu]^+$), 409 ($[ligand + H]^+$). UV–Vis (CH_3OH): λ_{max} (log ε): 263 (3.55), 381 (3.47), 606 nm (2.44). UV–Vis (CH_3CN): λ_{max} (log ε): 263 (4.00), 383 (3.99).

*2.1.7. 4,5-Bis(2-pyridylethylsulfanyl)-1,3-dithiole-2-thione palladium(II) chloride, $PdCl_2$(bpedmit) (**4**)*

Bpedmit (89.0 mg, 0.218 mmol) and $Pd(CH_3CN)_2Cl_2$ (63.5 mg, 0.245 mmol) dissolved in CH_3CN (45 cm^3) were mixed to give a turbid yellow solution. The solution was filtered and red crystals deposited. Yield, 51.0 mg (40%). *Anal*. Found: C, 35.14; H, 2.53; N, 5.41. Calc. for $C_{17}H_{16}Cl_2N_2PdS_5$: C, 34.85; H, 2.75; N, 4.78%. ^1H NMR (250 MHz, $(CD_3)_2SO$): δ 3.59–3.66 (m, 4H, SCH_2), 4.27–4.34 (4H, m, CH_2Py), 7.45–7.50 (m, 4H, Py-H4,5), 7.98 (dt, 2H, Py-H3), 9.04 (d, 2H, Py-H6). IR (KBr): 1064, 1445, 1488, 1569, 1604, 2249 cm^{-1}. UV–Vis (CH_3OH): λ_{max} (log ε): 264 (3.71), 371 nm (3.10).

2.2. X-ray crystal structure determinations

The structures of complexes **1** and **3a** were determined with data measured using a four-circle diffractometer. Cell dimensions were determined from the setting angles of selected reflections measured at $\pm 2\theta$. Intensity data were corrected for background, Lorentz and polarization effects using the programs in the KRYSTAL system [13]. The structures of complexes **2**, **3b** and **4** were determined with data measured using an area detector [14]; data were processed using SAINT [14] and SADABS [15]. The structures were determined using SIR92 [16] and refined using the local modification [13] of ORFLS [17]. Non-hydrogen atoms were refined with anisotropic displacement parameters, hydrogen atoms were kept fixed in calculated positions (C#H = 0.95 Å) except for those of the acetonitrile molecules of **3a** where the hydrogen atom coordinates were refined. Hydrogen atoms were given isotropic displacement parameters 20% larger than those of the atoms to which they were attached. Atomic scattering factors were taken from Ref. [18]. Crystal data and details of the structure determinations are given in Table 1.

3. Results and discussion

3.1. Synthesis

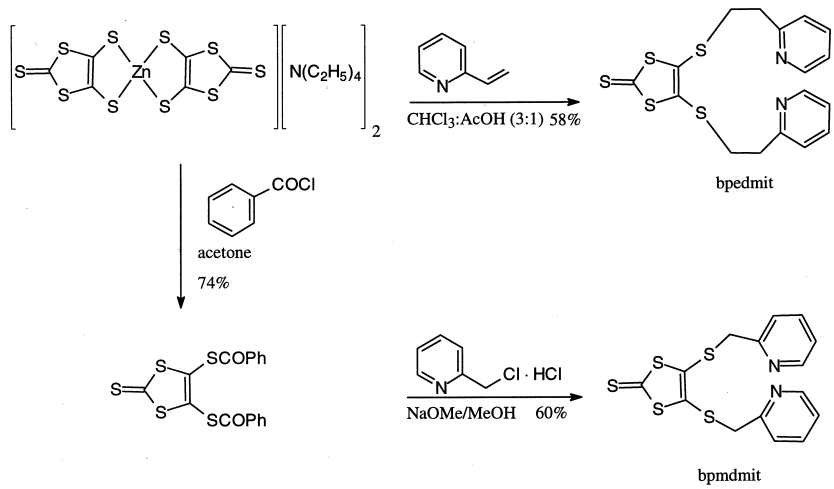
Two potentially tetradentate ligands containing dmit and pyridyl units 4,5-bis(2-pyridylmethylsulfanyl)-1,3-dithiole-2-thione (bpmdmit) and 4,5-bis(2-pyridylethylsulfanyl)-1,3-dithiole-2-thione (bpedmit), Chart 1, have been prepared using the zinc salt of $dmit^{2-}$, $[Et_4N]_2[Zn(dmit)_2]$, as starting material, as depicted in Scheme 1. Bpedmit was obtained by the direct reaction of $[Et_4N]_2[Zn(dmit)_2]$ with 2-vinylpyridine in chloroform:acetic acid (3:1). Bpmdmit was obtained by a two-step synthesis; first $[Et_4N]_2[Zn(dmit)_2]$ was reacted with benzoyl chloride in acetone to obtain the benzoyl protected dmit which was subsequently deprotected using sodium methoxide. The resulting dithiolate was alkylated using picolyl chloride.

Reaction of bpmdmit and bpedmit with the halide salts of the divalent metal ions Co^{2+}, Ni^{2+}, Cu^{2+} and Pd^{2+} has given a series of five complexes, all of which have been characterized by X-ray crystallography. Reactions of bpmdmit or bpedmit with non-halide salts of the same metal ions did not lead to solid products. Two basic structural types for complexes with the MLX_2 (L = bpmdmit or bpedmit; X = Cl or Br) formulation have been found. (i) Complexes in which the metal coordination geometry is octahedral and the thioether sulfur atoms and the pyridyl nitrogen atoms are coordinated leaving two *cis* oriented coordination sites. (ii) Square planar complexes in which only the pyridyl nitrogen atoms are used as *trans*-orientated donor atoms and halide ions complete the coordinations sphere of the metal. The complexes of the ligand with the pyridylmethyl arms (bpmdmit) show the octahedral coordination geometry, while the complexes of the homologous ligand, bpedmit, are the square planar complexes. Whether or not the coordination geometries observed are controlled by the choice of ligand or of metal ion has not been established, however, the geometries observed are those expected for the respective metal ions. Attempted preparations of bpedmit complexes of Ni^{2+} and Co^{2+} and bpmdmit complexes of Cu^{2+} and Pd^{2+} did not lead to tractable products.

The crystal structures of the cobalt(II) and nickel(II) of bpmdmit complexes **1** and **2** are depicted in Figs. 1 and 2. Complex **1** crystallizes with two almost identical molecules in the asymmetric unit (Fig. 1). Both molecules have approximate two-fold symmetry with the cobalt atom coordinated to two *cis* bromide atoms (Co1–Br 2.514(1), 2.496(1) Å;

Table 1
Crystallographic data for [(bpmdmit)$CoBr_2$] (**1**), [(bpmdmit)$NiCl_2$] (**2**), [(bpedmit)$CuCl_2$]·$2CH_3CN$ (**3a**), [(bpedmit)$CuCl_2$] (**3b**) and [(bpedmit)$PdCl_2$] (**4**)

	1	**2**	**3a**	**3b**	**4**
Chemical formula	$C_{15}H_{12}N_2S_5CoBr_2$	$C_{15}H_{12}N_2S_5NiCl_2$	$C_{21}H_{22}N_4S_5CuCl_2$	$C_{17}H_{16}N_2S_5CuCl_2$	$C_{17}H_{16}N_2S_5PdCl_2$
FW	599.31	510.19	625.18	543.08	585.93
Space group	$P2_1/a$ (no. 14)	$P2_1/c$ (no. 14)	$P\bar{1}$ (no. 2)	$P\bar{1}$ (no. 2)	*Pnma* (no. 62)
Crystal system	monoclinic	monoclinic	triclinic	triclinic	orthorhombic
a (Å)	13.932(3)	8.7895(1)	13.881(2)	8.0902(5)	8.3326(2)
b (Å)	20.903(4)	16.7011(1)	10.134(1)	8.4337(6)	15.2094(3)
c (Å)	14.419(2)	13.9928(2)	12.131(2)	16.649(1)	16.6240(4)
α (°)	90	90	123.366(6)	96.123(1)	90
β (°)	97.286(10)	105.343(1)	96.290(8)	100.393(1)	90
γ (°)	90	90	105.339(8)	103.498(1)	90
U (Å^3)	4165(1)	1980.88(4)	1303.9(3)	1073.3(1)	2106.82(8)
Z	8	4	2	2	4
Temperature (K)	294	295	294	295	295
Habit	plate	plate	needle	plate	plate
Colour	violet	green	green	purple	orange–red
Crystal dimensions (mm)	0.50×0.30×0.15	0.45×0.40×0.275	0.42×0.23×0.18	0.24×0.10×0.05	0.34×0.20×0.11
$F(000)$	2344	1032	638	550	1168
μ(Mo Kα) (mm^{-1})	5.165	1.778	1.462	1.759	1.637
Transmission	0.271–0.482	0.504–0.631	0.716–0.786	0.426–0.857	0.59–0.709
Radiation	Mo Kα	Mo Kα	Mo Kα	Mo Kα	Mo Kα
Wavelength (Å)	0.71073	0.71073	0.71073	0.71073	0.71073
Index ranges	$-16 \le h \le 16$	$-12 \le h \le 11$	$0 \le h \le 18$	$-9 \le h \le 10$	$-11 \le h \le 11$
	$0 \le k \le 24$	$-23 \le k \le 20$	$-13 \le k \le 12$	$-11 \le k \le 10$	$-14 \le k \le 20$
	$0 \le l \le 17$	$-18 \le l \le 10$	$-16 \le l \le 15$	$-21 \le l \le 15$	$-22 \le l \le 22$
θ Range for data collection (°)	1.7–25.0	1.9–29.4	1.6–28.0	1.3–29.0	1.8–29.6
Reflections measured	5964	13274	6785	7418	13388
Unique reflections	5582	5019	6303	5201	2853
Significant data ($I > 3\sigma(I)$)	4290	4345	4642	3004	2458
No. of variables	452	227	323	245	131
R	0.034	0.023	0.033	0.041	0.021
R'	0.044	0.031	0.045	0.049	0.030
GOF	0.935	1.741	1.075	1.238	1.412
Δ/σ max	0.00055	0.00149	0.0053	0.00052	0.00164
Δ/σ mean	0.00007	0.00023	0.0002	0.00005	0.00015
$\Delta\rho$ max	0.59(9)	0.35(5)	0.39(7)	0.68(8)	0.35(6)
$\Delta\rho$ min	−0.53(9)	−0.31(5)	−0.59(7)	−0.66(8)	−0.52(6)



Scheme 1.

Co2–Br 2.509(1), 2.488(1) Å), two *trans* pyridyl nitrogen atoms (Co1–N 2.195(5), 2.169(5) Å; Co2–N 2.168(5), 2.171(5) Å), and to the two sulfanyl sulfur atoms (Co1–S 2.596(2), 2.522(2) Å; Co2–S 2.543(2), 2.551(2) Å). The dmit unit is coplanar with the $CoBr_2$ moiety. Complex **2** crystallizes with only one molecule in the asymmetric unit, and the coordination geometry is similar to that of complex **1** with the nickel atom coordinated to two chloride atoms

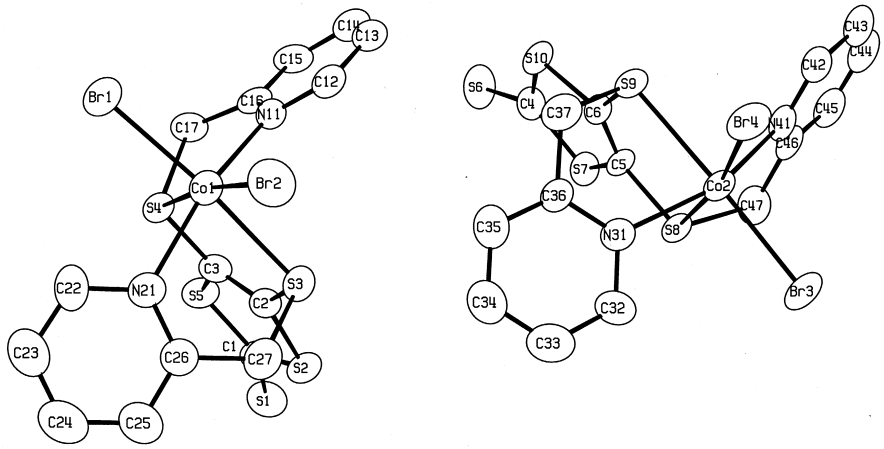


Fig. 1. The atomic arrangement for the two molecules of $CoBr_2$(bpmdmit) (**1**) together with the numbering scheme. Ellipsoids are drawn at the 50% probability level.

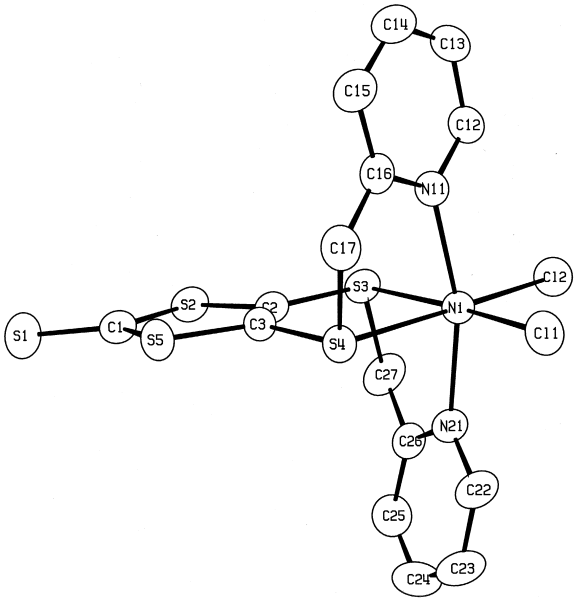


Fig. 2. The atomic arrangement for $NiCl_2$(bpmdmit) (**2**) together with the numbering scheme. Ellipsoids are drawn at the 50% probability level.

(Ni–Cl 2.3435(5), 2.3683(4) Å), two pyridyl nitrogen atoms (Ni–N 2.103(1), 2.106(1) Å), and to the two sulfanyl sulfur atoms (Ni–S 2.4620(4), 2.4763(4) Å). Selected bond distances and angles for complexes **1**, **2**, **3a**, **3b** and **4** are listed in Tables 2 and 3, respectively.

The complex obtained from the reaction of copper chloride with bpedmit gives two distinct crystalline products: green needles (**3a**) and dark purple crystals (**3b**) from acetonitrile solutions, and dark purple crystals (**3b**) only from ethanol solutions. On no occasion was **3a** isolated from acetonitrile solution free of **3b**. The colour difference prompted solid state studies of both crystalline types, however, the structures are similar with no solvent coordination. Both complexes are bis(μ-chloro)-bridged dimers. The structure of **3a** is shown in Fig. 3. In contrast to the Co and Ni complexes described above, the thioether sulfur atoms are not coordinated to the metal ions in either of these complexes. The coordination geometries around the copper atom in these complexes are approximately square pyramidal with the two pyridine nitrogen atoms (Cu–N 2.040(2), 2.041(2) Å) and two chloride ions (Cu–Cl 2.324(1), 2.226(1) Å) in the square plane. A long bond to the chloride ion bound to an adjacent copper atom forms the apical bond. The Cu–N and Cu–Cl distances are significantly shorter than the corresponding distances found for the octahedral Ni and Co complexes. The ligand is folded sharply at the thioether sulfur atoms and there are no Cu···S interactions shorter than 5 Å. The structure of complex **3a** shows approximate mirror symmetry. Pairs of centrosymmetrically related complexes are linked by weak Cu···Cl interactions, Cu···Cl1 2.858(1) Å, to form dimers with a Cu···Cu distance of 3.864(1) Å. The Cu–Cl bond of the

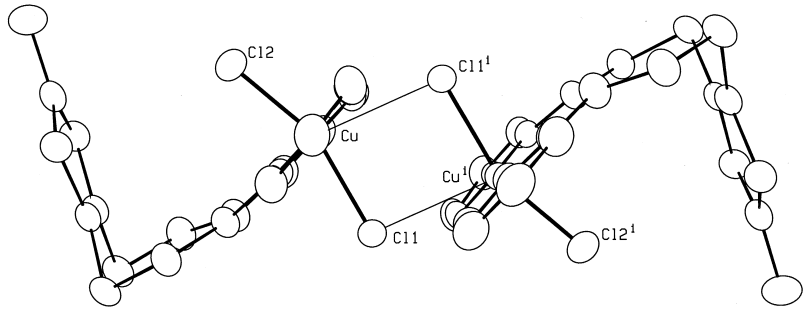


Fig. 3. The atomic arrangement for $CuCl_2$(bpedmit)·$2CH_3CN$ (**3a**) together with the numbering scheme and showing the weak Cu···Cl interactions. The symmetry code is $1-x, -y, 1-z$. Ellipsoids are drawn at the 50% probability level.

Table 2
Selected bond distances (Å) for the metal–ligand donor bonds for complexes **1**, **2**, **3a**, **3b** and **4**

	1 molecule 1	**1** molecule 2	**2**	**3a**	**3b**	**4**
M	Co	Co	Ni	Cu	Cu	Pd
X	Br	Br	Cl	Cl	Cl	Cl
M–X1	2.514(1)	2.509(1)	2.3435(5)	2.324(1)	2.274(1)	2.317(1)
M–X2	2.496(1)	2.488(1)	2.3683(4)	2.266(1)	2.238(1)	2.299(1)
M–S3	2.596(2)	2.543(2)	2.4763(5)			
M–S3A	2.522(2)	2.551(2)	2.4620(4)			
M–N1	2.195(5)	2.168(5)	2.103(1)	2.041(2)	2.022(3)	2.038(2)
M–N1A	2.169(5)	2.171(5)	2.106(1)	2.040(2)	2.016(3)	2.038(2)
M···X1′				2.858(1)	3.178(1)	
M···M′				3.864(1)	4.178(1)	
S1–C1	1.640(7)	1.633(7)	1.640(2)	1.643(3)	1.626(6)	1.646(3)
S2–C1	1.737(8)	1.737(7)	1.739(2)	1.734(3)	1.723(6)	1.734(2)
S2A–C1	1.723(7)	1.736(8)	1.734(2)	1.727(3)	1.750(6)	1.734(2)
S2–C2	1.741(6)	1.743(6)	1.742(2)	1.752(3)	1.736(6)	1.750(2)
S2A–C2A	1.730(7)	1.740(6)	1.740(2)	1.756(3)	1.749(5)	1.750(2)
S3–C2	1.764(7)	1.767(6)	1.764(2)	1.755(3)	1.763(6)	1.759(2)
S3A–C2A	1.764(6)	1.748(7)	1.763(2)	1.750(3)	1.753(5)	1.759(2)
S3–C3	1.801(7)	1.807(7)	1.815(2)	1.824(3)	1.819(6)	1.840(2)
S3A–C3A	1.813(6)	1.807(8)	1.814(2)	1.824(3)	1.798(5)	1.840(2)
C2–C2A	1.350(9)	1.357(8)	1.351(2)	1.351(4)	1.336(7)	1.341(4)

chloride bridge is 0.058 Å longer than that to the terminal Cl. The acetonitrile molecules are not involved in bonding to the complex. The purple form of complex **3b** crystallizes without lattice acetonitrile and the structure is similar to that of **3a**, with Cu–N 2.016(3), 2.022(3) Å and Cu–Cl 2.238(1), 2.274(1) Å. However the apical Cu···Cl interactions (Cu···Cl1 3.178(1) Å) are weaker and consequently the copper–copper separation (Cu···Cu 4.178(1) Å) of the dimer is longer. The crystal structures show that the square plane of the metal ion of the green form (**3a**) has a slight tetrahedral distortion with N–Cu–N_A 177.71(7)° and Cl1–Cu–Cl2 159.87(3)°. The crystal structure of the purple form **3b** is closer to square planar with differences in the metal ligand bonds in the *xy* plane less than those for **3a** and its four strong bonds quite close to planar with N–Cu–N_A 171.5(1)° and Cl1–Cu–Cl2 176.02(7)°. As well, there is a significantly shorter apical Cu···Cl interaction for **3a** compared to **3b**, further distorting the Cu environment in **3a**. This is consistent with the observed colour differences: deviation from the centrosymmetric square planar geometry allows a forbidden transition to occur, with the consequence that yellow is mixed with the blue giving the observed green colour. A similar dimeric arrangement was observed in the the structures of the blue Cu(2-methylpyridine)$_2$Cl$_2$ [19]. The bond lengths in Cu(2-methylpyridine)$_2$Cl$_2$ are Cu–Cl 2.21, 2.26 Å and Cu–N 1.98, 2.02 Å, an apical Cu···Cl distance of 3.37 Å and a Cu···Cu distance in the dimer of 4.41 Å. For the Cu–Cl bonds, one bond is longer than the other and the Cu···Cl distance is significantly longer. The distance between the two metal ions in Cu(2-methylpyridine)$_2$Cl$_2$ is longer than in **3a** and **3b**, owing to the longer apical Cu···Cl bonds, and is consistent with the colour variation in the series of compounds, **3a** (green), **3b** (purple) and Cu(2-methylpyridine)$_2$Cl$_2$ (blue) [19].

The structural arrangement in the palladium complex **4** is similar to that found for the copper complexes with a square planar geometry about the palladium ion with Pd–N 2.038(2) Å and Pd–Cl 2.299(1), 2.317(1) Å (Fig. 4). However, by contrast to the copper complexes the complex is monomeric in the solid state. There are no significant metal···sulfur interactions. Complex **4** crystallizes with the molecule across a crystallographic mirror plane so that the molecule itself has exact mirror symmetry.

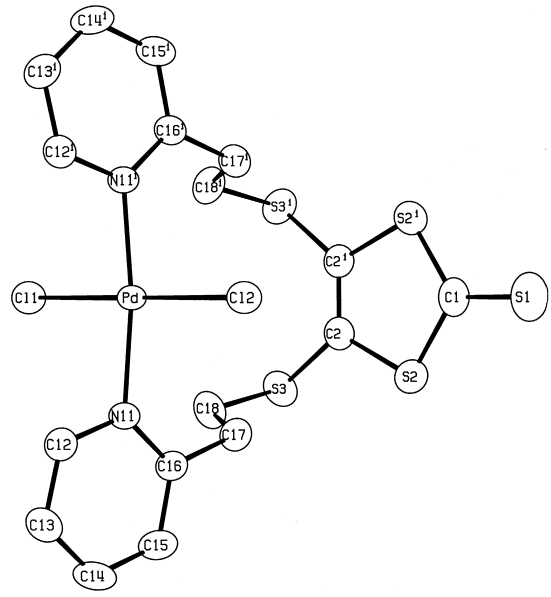


Fig. 4. The atomic arrangement for $PdCl_2$(bpedmit) (**4**) together with the numbering scheme. The symmetry code is $x, 1/2-y, z$. Ellipsoids are drawn at the 50% probability level.

Table 3
Selected angles and torsion angles (°) for **1**, **2**, **3a**, **3b** and **4**

	1 molecule 1	**1** molecule 2	**2**	**3a**	**3b**	**4**
M	Co	Co	Ni	Cu	Cu	Pd
X	Br	Br	Cl	Cl	Cl	Cl
X1–M–S3	167.38(5)	170.17(5)	173.23(2)			
X2–M–S3A	171.11(6)	172.19(5)	172.42(2)			
X1–M–S3A	83.95(5)	85.58(5)	86.78(2)			
X2–M–S3	87.74(5)	87.74(5)	86.18(2)			
S3–M–N1	77.9(2)	78.7(1)	82.09(4)			
S3–M–N1A	85.6(1)	82.5(1)	88.23(4)			
S3A–M–N1	82.6(2)	81.8(1)	85.02(4)			
S3A–M–N1A	79.9(1)	78.7(1)	82.08(4)			
X1–M–N1	100.3(2)	100.5(1)	97.70(4)	91.21(6)	91.7(1)	92.11(4)
X2–M–N1A	100.5(1)	101.9(1)	99.49(4)	90.00(6)	88.62(9)	92.11(4)
X1–M–N1A	92.3(1)	94.9(1)	90.46(4)	90.06(6)	90.70(9)	87.98(4)
X2–M–N1	94.6(2)	95.2(1)	92.18(4)	88.15(6)	89.5(1)	87.98(4)
X1–M–X2	104.87(4)	102.08(4)	100.59(2)	159.87(3)	176.02(7)	178.53(4)
S3–M–S3A	83.43(6)	84.61(6)	86.46(1)			
N1–M–N1A	157.1(2)	154.1(2)	164.32(5)	177.71(7)	171.5(1)	171.48(8)
X1–M···X1				84.13(3)	81.29(4)	
X2–M···X1′				115.99(3)	94.88(4)	
N1A–M···X1′				91.77(6)	95.9(1)	
N1–M···X1′				90.25(6)	92.5(1)	
M–X1···M′				95.87(3)	98.71(4)	
S1–C1–S2	123.8(4)	123.6(5)	123.7(1)	122.7(2)	124.5(3)	124.18(8)
S1–C1–S2A	123.2(5)	123.9(4)	123.5(1)	124.8(2)	123.7(4)	124.18(8)
S2–C1–S2A	113.0(4)	112.5(4)	112.79(9)	112.5(2)	111.8(3)	111.6(2)
C1–S2–C2	97.0(3)	97.3(3)	97.18(8)	98.0(1)	98.3(3)	98.1(1)
C1–S2A–C2A	97.4(3)	97.8(3)	97.47(8)	97.8(1)	97.5(3)	98.1(1)
S2–C2–C2A	116.0(5)	116.5(5)	116.4(1)	115.6(2)	116.6(4)	115.88(7)
S2A–C2A–C2	116.6(5)	115.6(5)	116.2(1)	116.0(2)	115.8(4)	115.88(7)
S2–C2–S3	118.2(4)	117.7(4)	118.96(9)	119.3(2)	117.6(3)	117.3(1)
S3A–C2A–S2A	118.0(4)	117.8(4)	118.13(9)	120.4(2)	118.5(3)	117.3(1)
S3–C2–C2A	125.7(5)	125.4(5)	124.6(1)	125.0(2)	125.7(5)	126.75(7)
S3A–C2A–C2	125.0(5)	126.3(5)	125.3(1)	123.5(2)	125.1(5)	126.75(7)
C2–S3–C3	101.7(3)	103.0(3)	102.31(9)	100.0(1)	100.3(3)	102.14(9)
C2A–S3A–C3A	102.8(3)	102.6(3)	102.97(8)	100.6(1)	103.9(2)	102.14(9)
S2–C2–C2A–S2A	−1.7(7)	−0.8(7)	−0.2(5)	0.7(3)	−1.3(5)	0.0
S3–C2–C2A–S3A	−13.0(9)	11.6(9)	−11.0(2)	3.4(4)	−5.7(7)	0.0
S2–C2–C2A–S3A	170.3(4)	−175.0(3)	171.9(1)	−174.7(1)	169.8(3)	−176.9(1)
S3–C2–C2A–S2A	175.1(4)	174.2(3)	176.8(1)	178.7(2)	−176.8(3)	176.9(1)
C2A–C2–S3–C3	106.8(6)	−106.0(6)	103.6(1)	125.0(2)	−120.5(5)	−94.5(1)
C2–C2A–S3A–C3A	107.5(6)	−105.5(6)	107.6(1)	−128.4(2)	126.6(4)	94.5(1)

3.2. ESR spectroscopy

ESR spectra of the copper complexes **3a** and **3b** were recorded in powder form (room temperature) and in frozen glass solution (methanol/DMF,100 K). The two solid state forms of $CuCl_2$(bpedmit) **3a** and **3b** can be distinguished by the observation of slightly different rhombic signals; for **3a** with $g_x = 2.034$, $g_y = 2.066$ and $g_z = 2.249$ and for **3b** with $g_x = 2.034$, $g_y = 2.056$ and $g_z = 2.223$. The solution ESR spectra of **3a** and **3b** are identical as expected, giving an axial signal with $g_\perp = 2.074$, $g_{||} = 2.398$ and $A_{||} = 121$ G. This is corroborated by identical solution UV–Vis spectra for **3a** and **3b** in methanol.

3.3. Cyclic voltammetry

Irreversible oxidation peaks at 1.017 and 1.252 V for the free ligands bpmdmit and bpedmit were obtained respectively. These peaks originate from the dmit moieties of the ligands since an irreversible peak is observed for the simpler dimethyl derivatized dmit (4,5-bis(methylsulfanyl)-1,3-dithiole-2-thione, i.e. there are no pyridyl groups) at 871 mV. The peaks are absent in the voltammograms of the complexes, thus irreversible ligand oxidation is, not unexpectedly, suppressed by complexation to a dipositive metal ion. The cobalt complex **1** was the only complex to give an electrochemical response in the range available. For **1** a reversible peak assigned to a Co(II)/(III) process with a halfwave potential at 576 mV versus Ag/AgCl was recorded.

4. Conclusions

This work describes the first reported transition metal complexes of the thiolate-functionalized dmit-containing ligands

4,5-bis(2-pyridylmethylsulfanyl)-1,3-dithiole-2-thione (bpmdmit) and 4,5-bis(2-pyridylethylsulfanyl)-1,3-dithiole-2-thione (bpedmit). Complexes with the formulation MX_2L (M = Ni, Co, Cu, Pd; L = bpmdmit or bpedmit; X = Cl or Br) have been crystallographically characterized. The thioether sulfur atoms are coordinated to the metal ions in the octahedral Ni and Co complexes but not in the square planar Cu and Pd complexes. Oxidation of the dmit units of the ligands is suppressed by coordination to the metal ions in these complexes.

Supplementary data

Crystallographic data (excluding structure factors) for the structures in this paper have been deposited with the Cambridge Crystallographic Data Centre as supplementary publication nos. CCDC 136158, CCDC 136159, CCDC 136160, CCDC 136161, CCDC 136162. Fractional atomic coordinates for **1**, **2**, **3a**, **3b**, **4** (STables 1–5); complete listing of bond distances, angles and selected torsion angles (STables 6–10). Copies of the data can be obtained, free of charge, on application to CCDC, 12 Union Road, Cambridge CB2 1EZ, UK (fax: +44-1223-336033; e-mail: deposit@ccdc.cam.ac.uk).

Acknowledgements

We acknowledge support from the Danish Natural Science Council (grant no. 28808 to C.J.M.) and a Ph.D. grant to C.V. from University of Southern Denmark, Odense University, and Jens Zacho Pedersen for recording the ESR spectra. A.H. is grateful for access to the Siemens SMART diffractometer at The Technical University of Denmark.

References

[1] R.-M. Olk, B. Olk, W. Dietzsch, R. Kirmse, E. Hoyer, Coord. Chem. Rev. 117 (1992) 99.
[2] P. Cassoux, L. Valade, H. Kobayashi, A. Kobayashi, R.A. Clark, A. Underhill, Coord. Chem. Rev. 110 (1991) 115.
[3] D.W. Bruce, D. O'Hare (Eds.), Inorganic Materials, Wiley, Chichester, 1992, pp. 1–58.
[4] R.-M. Olk, B. Olk, W. Dietzsch, R. Kirmse, E. Hoyer, Coord. Chem. Rev. 117 (1992) 11 Table 11.
[5] H. Endres, Z. Naturforsch., Teil B 41 (1988) 1351.
[6] K. Brunn, H.Z. Endres, J. Weiss, Z. Naturforsch., Teil B 43 (1988) 224.
[7] X. Gan, M. Munakata, T. Kuroda-Sowa, M. Maekawa, Y. Misaki, Polyhedron 14 (1995) 1343.
[8] X. Gan, M. Munakata, T. Kuroda-Sowa, M. Maekawa, M. Yamamoto, Polyhedron 14 (1995) 1647.
[9] M. Munakata, T. Kuroda-Sowa, M. Maekawa, A. Hirota, S. Kitagawa, Inorg. Chem. 34 (1995) 2705.
[10] D.D. Perrin, W.L.F. Armarego, Purification of Laboratory Chemicals, Pergamon, Oxford, 1988.
[11] G. Steimecke, R. Kirmse, E. Hoyer, Z. Chem. 15 (1975) 28.
[12] G. Steimecke, H.-J. Sieler, R. Kirmse, E. Hoyer, Phosphorus Sulfur 7 (1979) 49.
[13] A. Hazell, KRYSTAL, Integrated System of Crystallographic Programs, Aarhus University, Denmark, 1995.
[14] SMART and SAINT, Area-Detector Control and Integration Software, Siemens Analytical X-Ray Instruments Inc., Madison, WI, 1995.
[15] SADABS, Empirical Absorption (and Other) Corrections, Siemens Analytical X-Ray Instruments Inc., Madison, WI, 1995.
[16] A. Altomare, G. Cascarano, C. Giacovazzo, A. Guagliardi, M.C. Burla, G. Polidori, M. Camalli, J. Appl. Crystallogr. 27 (1994) 435.
[17] W.R. Busing, K.O. Martin, H.A. Levy, ORFLS, Rep. ORNL-TM-305, Oak Ridge National Laboratory, Oak Ridge, TN, 1962.
[18] International Tables for Crystallography, vol. C, 1992.
[19] V.F. Duckworth, N.C. Stephenson, Acta Crystallogr., Sect. B 25 (1969) 1795.

PERGAMON

www.elsevier.nl/locate/poly

Polyhedron 19 (2000) 673–680

POLYHEDRON

Synthesis of Zn *N*-salicylidene-L-aminoacidatos: X-ray structure of [(*N*-salicylidene-L-alaninato)(aqua)zinc(II)]·0.25H_2O and [(*N*-salicylidene-L-valinato)(aqua)zinc(II)]

Angel García-Raso [a,*], Juan J. Fiol [a], Adela López-Zafra [a], Ignasi Mata [b], Enrique Espinosa [b], Elies Molins [b]

[a] *Departament de Química, Universitat de les Illes Balears, 07071 Palma de Mallorca, Spain*
[b] *Institut de Ciència de Materials de Barcelona (CSIC), Campus de la Universitat Autònoma, 08193 Cerdanyola, Spain*

Received 8 November 1999; accepted 13 January 2000

Abstract

The synthesis in aqueous ethanol solution of eight Zn(II) compounds of salicylaldehyde-amino acid Schiff bases together with their spectral characterisation is reported. Two of the complexes, [(*N*-salicylidene-L-alaninato)(aqua)zinc(II)]·0.25H_2O (**1**) and [(*N*-salicylidene-L-valinato)(aqua)zinc(II)] (**2**), have been obtained in the form of crystals suitable for X-ray crystallography. The coordination geometry about the zinc in both structures is between distorted trigonal bipyramidal and distorted square pyramidal with the iminic nitrogen N(4) (**1** = 2.020(3) and **2** = 2.015(7) Å), the phenolic O(8) (**1** = 1.991(2) and **2** = 1.997(6) Å) and the carboxylic O(1) (**1** = 2.160(2) and **2** = 2.156(5) Å) of the *N*-salicylidene-aminoacidato base ligand. Another carboxylic O(1)* of an adjacent unit (**1** = 2.033(2) and **2** = 2.033(5) Å), curiously shorter than the bond from the ligand itself, and a water molecule (**1** = 2.006(3) and **2** = 1.999(6) Å) comprise the fourth and fifth coordination positions. The crystals are constituted by polymeric [(*N*-salicylidene-L-aminoacidato)zinc(II)] moieties forming helical arrays about three-fold screw axes. To our knowledge these are the first two structures of binary complexes of the type [(*N*-salicylidene-L-aminoacidato)Zn(II)]. The NMR studies, in DMSO, agree with a general *endo* disposition between the side chain of the amino acid and the aromatic ring of the salicylidene moiety. ©2000 Elsevier Science Ltd All rights reserved.

Keywords: Schiff base complexes; *N*-Salicylidene derivatives; X-ray structures; Zn(II) complexes

1. Introduction

Transition metal complexes of salicylaldehyde-amino acid Schiff bases are non-enzymatic models for pyridoxal-amino acid systems which are of considerable importance as key intermediates in many metabolic reactions of amino acids catalysed by enzymes which require pyridoxal as a cofactor [1–6]. Considerable effort has been devoted to the preparation and structural characterisation of Schiff base Cu(II) complexes derived from salicylaldehyde and amino acids such as Gly [7–9], β-Ala [10], Val [11,12], Ser [13], Thr [14], Met [15], Glu [16,17], Phe [18,19], Tyr [20], Trp [21] and α-aminoisobutyrato [22] and reduced salicylidene amino acids [23]. Although the syntheses of several *N*-salicylideneaminoacidato zinc(II) complexes have been reported in the literature [24–26], most of them have been carried out in solution [25,27–30] and single-crystal X-ray diffraction studies on *N*-salicylidene-aminoacidato Zn(II) complexes are very limited [31–34].

As part of a continuing study of complexes formed by metal(II) ions and Schiff base amino acids [13,21], we have synthesised and characterised spectroscopically eight new zinc(II) complexes with *N*-salicylidene amino acids (Scheme 1). Moreover, the first X-ray structures of binary Zn(II) *N*-salicylidenealaninato and valinato, Zn(Sal-L-ala) and Zn(Sal-L-val), are described.

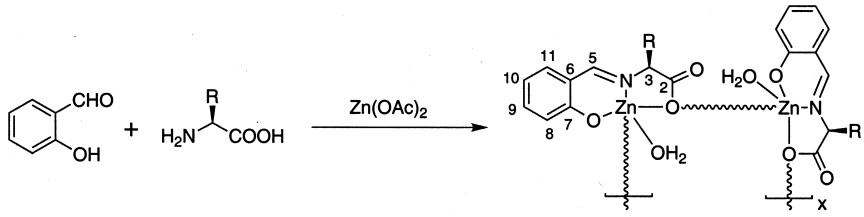
2. Experimental

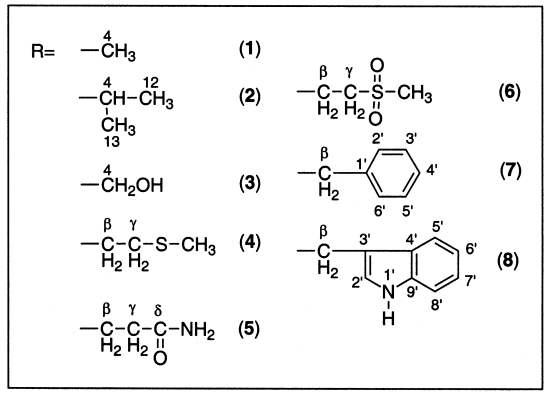
2.1. Analysis and physical measurements

IR spectra were measured in the solid state (KBr pellets) on a PE 683 with an IR data station PE 1600 and the electronic spectra were registered on a PE 552 spectrophotometer. Ther-

* Corresponding author. Tel.: +34-971-173263; fax: +34-971-173426; e-mail: dquagr0@clust.uib.es

0277-5387/00/$ - see front matter ©2000 Elsevier Science Ltd All rights reserved.
PII S0277-5387(00)00302-8





Scheme 1.

mogravimetric data in the temperature range from 30 to 700°C were recordered in a flowing nitrogen atmosphere (heating rate 10°C min^{-1}) on a PE TGA-2 thermobalance. 1D and 2D ^1H and ^{13}C NMR spectra were recorded on a Bruker AMX 300. Proton and carbon chemical shifts in DMSO-d_6 were referenced to DMSO-d_6 (^1H NMR, $\delta_{(DMSO)} = 2.60$ ppm; ^{13}C NMR, $\delta_{(DMSO)} = 43.5$ ppm). Unequivocal assignments were made by 2D NMR experiments, HMQC [35] and HMBC [36], or by comparison of spectra of other related products. Satisfactory C, H and N analyses were obtained for all compounds and carried out with a Carlo Erba model 1106 microanalyser. NOE studies were performed by 2D NMR experiments (ROESY) [37]. The 2D spectra were processed using commercial Bruker software and experimental characteristics presented below.

^1H-Detected heteronuclear multiple quantum coherence spectroscopy (HMQC). The one-bond ^1H–^{13}C shift correlation spectra resulted from a 502×2048 data matrix with 48 scans (preceded by 16 dummy scans) per t_1 value. Pre-delay was 1.0 s and a 10.3 μs, 90° ^{13}C pulse width was used. A sine bell squared filter was used prior to Fourier transformation in the t_2 and t_1 dimensions.

^1H-Detected multiple-bond heteronuclear multiple quantum coherence spectroscopy (HMBC). The multiple-bond ^1H–^{13}C shift correlation spectra resulted from a 246×2048 data matrix with 128 scans (preceded by 8 or 16 dummy scans) per t_1 value. Pre-delay was 1.0 s and a 10.3 μs, 90° ^{13}C pulse width was used. The delay between the first and the second 90° ^{13}C pulses was 75 ms. A sine bell squared filter was used prior to Fourier transformation in the t_2 and t_1 dimensions.

Rotating frame Overhauser effect spectroscopy (ROESY). The ^1H–^1H shift correlation spectra resulted from a 250×2048 data matrix with 64 scans (preceded by 8 or 16 dummy scans) per t_1 value. Pre-delay was 2.0 s and a 5.1 μs, 90° ^1H pulse width and 2.3 kHz (23 dB) of ^1H r.f. power and 107.5 μs, 90° ^1H pulse width were used. Mixing time was 500–600 ms. A sine bell squared filter was used prior to Fourier transformation in the t_2 and t_1 dimensions.

Salicylaldehyde, amino acids and zinc(II) acetate monohydrate were purchased from Aldrich and used without further purification.

2.2. Crystallographic studies

Crystals were selected and mounted on an Enraf-Nonius CAD-4 four-circle diffractometer with graphite-monochromated Mo Kα radiation at room temperature. Unit cell parameters were determined from the automatic centring of 25 reflections (in the ranges $12 < \theta < 31°$ and $10 < \theta < 32°$ for **1** and **2**, respectively) and refined by least-squares methods. In both cases, intensities were collected using the ω–2θ scan technique. Three standard reflections were measured every hour as intensity controls during data collections; no significant intensity decay was observed in any case. Lorentz polarization and Ψ-scan absorption corrections (maximum and minimum transmissions factors for **1** and **2**: $T_{max} = 0.998$, $T_{min} = 0.906$ and $T_{max} = 0.999$, $T_{min} = 0.967$) were applied using the MolEN package [38]. Additional crystallographic data are presented in Table 1. The structures were solved by direct methods with the SHELXS-86 [39] computer program and refined by full-matrix least-squares methods using the SHELXL-93 [40] computer program. Thermal motions of non-hydrogen atoms were refined anisotropically. H-atoms were positioned at calculated positions and refined with two global isotropic thermal factors in each case. The refinement processes converged at $R_1 = 0.046$ and 0.038 and $wR_2 = 0.083$ and 0.080 ($I > 2\sigma(I)$) for **1** and **2**, respectively. In both cases

Table 1
Selected crystallographic data for [(*N*-salicylidene-L-alaninato)(aqua)zinc(II)]·0.25H_2O (**1**) and [(*N*-salicylidene-L-valinato)(aqua)zinc(II)] (**2**)

	1	**2**
Empirical formula	$C_{10}H_{11}NO_4Zn$	$C_{12}H_{15}NO_4Zn$
Crystal size (mm)	0.55×0.16×0.09	0.42×0.15×0.15
Crystal system	trigonal	trigonal
Space group	*P*31	*P*31
Molecular weight	274.57	302.62
Unit cell dimensions		
a (Å)	12.317(2)	12.815(3)
b (Å)	12.317(2)	12.815(3)
c (Å)	6.8200(10)	6.8020(10)
Volume (Å^3)	896.0(2)	967.4(3)
Z	3	3
Density (calc.) (Mg m^{-3})	1.526	1.558
Absorption coefficient (mm^{-1})	2.053	1.909
θ Range (°)	3.31–30.43	3.18–30.39
Reflections collected	10816	1177
Independent reflections	3616 (R_{int} = 0.0986)	1177
Final *R* indices ($I > 2\sigma(I)$) (all data)	R_1 = 0.0459, wR_2 = 0.0742	R_1 = 0.0378, wR_2 = 0.0799
R indices (all data)	R_1 = 0.0834, wR_2 = 0.0859	R_1 = 0.1261, wR_2 = 0.0933
Largest difference peak (e Å^{-3})	0.346	0.231
Largest difference hole (e Å^{-3})	−0.521	−0.275

the minimised function was $\sum w(|F_o|^2 - |F_c|^2)$, with respectively $w = [\sigma^2(|F_o|^2) + (0.0574P)^2]^{-1}$ and $w = [\sigma^2(|F_o|^2) + (0.0393P)^2]^{-1}$, $P = [(|F_o|^2 + 2|F_c|^2)/3]$. Scattering factors were taken from International Tables for X-ray Crystallography [41] except for those of the H-atoms [42]. A summary of the refinements is shown in Table 1. Selected bond distances and angles for **1** and **2** are listed in Table 2.

2.3. Preparation of the complexes: general procedure

To a warm solution (60–70°C) of the corresponding amino acid (**1**–**8**) (5 mmol) (Scheme 1) in 10 ml of water (or ethanol for compound **8**), 5 mmol (0.61 g) of salicylaldehyde in 10 ml of ethanol were added. The resulting solution was stirred for 0.5 h. A solution of zinc(II) acetate monohydrate (5 mmol, 1.00 g) dissolved in a minimum quantity of water was added dropwise. During the addition, the pH was adjusted to 7 by addition of 0.5 M KOH. The solution was stirred for 1 h and the yellowish precipitate obtained was filtered, washed with water and air dried. The resulting solid was crystallised from either methanol or DMSO.

2.3.1. [(N-Salicylidene-L-alaninato)(aqua)zinc(II)]·0.25H_2O (*1*)

47% yield. White crystals from MeOH. Exhibits a mass decrease (found 6.66; calc. 6.56) between 142 and 200°C corresponding to the loss of one water molecule per formula unit. *Anal*. Found: C, 43.04; H, 3.95; N, 5.02. Calc. for $C_{10}H_{11}NO_4Zn \cdot 0.25H_2O$: C, 43.03; H, 4.12; N, 5.02%. IR (cm^{-1}): 3301m, 2975m, 2934m, 1647s, 1607s, 1542s, 1470s, 1448s, 1381m, 1362s, 1338s, 1290s, 1260m, 1193m, 1157m, 1135m, 1115m, 1062w, 1041w, 987w, 937w, 913m, 873w, 859w, 799m, 763s, 746m, 681w, 648w, 601w, 540m, 508w, 487w, 437w, 403w, 340w. UV–Vis (DMSO): λ 370 (ε 6.5×10^3), 258 nm (9.1×10^3 dm^3 mol^{-1} cm^{-1}). ^{1}H NMR (DMSO-d_6, 293 K): δ 8.45s (1H, H(5)), 7.25d+t (2H, H(11)+H(9)), 6.80bd (1H, H(8)), 6.57t (1H, H(10), *J* = 7.1 Hz), 3.81q (1H, H(3), *J* = 7.1 Hz), 1.41d (1H, CH_3, *J* = 7.1 Hz). ^{13}C-NMR (DMSO-d_6, 293K): δ 180.3 (C(2)), 173.0 (C(7)), 171.8 (C(5)), 139.0 (C(11)), 137.3 (C(9)), 126.5 (C(8)), 123.4 (C(6)), 117.7 (C(10)), 66.7 (C(3)), 25.1 (CH_3). Λ_M (Ω^{-1} cm^2 mol^{-1}) (10^{-3} mol dm^{-3} in DMSO, 23.5°C) 3.0.

2.3.2. [(N-Salicylidene-L-valinato)(aqua)zinc(II)] (*2*)

84% yield. White crystals from DMSO. Exhibits a mass decrease (found 6.11; calc. 5.95) between 128 and 160°C (−0.5H_2O) and 232 and 265°C (−0.5H_2O) corresponding to the loss of one water molecule per formula unit. *Anal*. Found: C, 47.67; H, 5.07; N, 4.64. Calc. for $C_{12}H_{17}NO_5Zn$: C, 47.62; H, 4.96; N, 4.63%. IR (cm^{-1}): 3302m, 2966m, 1632s, 1605s, 1542s, 1471s, 1449s, 1414w, 1338s, 1313m, 1279w, 1253w, 1193m, 1157m, 1134w, 1099w, 1066w, 1039w, 996w, 978w, 966w, 942w, 924w, 902w, 871m, 857w, 846w, 831w, 804m, 787w, 761m, 746m, 694w, 635w, 603w, 546m, 507w, 462w, 425w, 406w, 339w, 282w, 251w, 231w. UV–Vis (DMSO): λ 371 (ε 8.8×10^3), 258 nm (1.5×10^4 dm^3 mol^{-1} cm^{-1}). ^{1}H NMR (DMSO-d_6, 325 K): δ 8.36s (1H, H(5)), 7.27d+t (2H, H(11)+H(9)), 6.87bd (1H, H(8), $J_{estimated}$ = 7.7 Hz), 6.60t (1H, H(10), *J* = 7.2 Hz), 3.49d (1H, H(3), *J* = 5.0 Hz), 2.14dhp (1H, H(4), *J* = 5.0 and 6.9 Hz), 1.10d (3H, CH_3, *J* = 6.9 Hz), 0.98d (1H, CH_3, *J* = 6.9 Hz). ^{13}C NMR (DMSO-d_6, 325 K): δ 178.8 (C(2)), 172.3 (C(5)), 172.1 (C(7)), 139.0 (C(11)), 137.3 (C(9)), 126.5 (C(8)), 123.6 (C(6)), 118.7 (C(10)), 78.8

Table 2
Bond lengths (Å) and angles (°) for [(*N*-salicylidene-L-alaninato)-(aqua)zinc(II)]·0.25H_2O (**1**) and [(*N*-salicylidene-L-valinato)(aqua)-zinc(II)] (**2**)

[(*N-salicylidene-L-alaninato*)(*aqua*)*zinc*(*II*)]·0.25H_2O (***1***)			
Zinc coordination sphere			
Zn–O(8)	1.991(2)	Zn–O(1)* [a]	2.033(2)
Zn–O(W)	2.006(3)	Zn–O(1)	2.160(2)
Zn–N(4)	2.020(3)	O(1)–Zn**	2.033(2)
O(8)–Zn–O(W)	103.34(11)	O(8)–Zn–O(1)*	91.25(10)
O(8)–Zn–N(4)	91.70(11)	O(W)–Zn–O(1)*	106.22(11)
O(W)–Zn–N(4)	105.42(12)	N(4)–Zn–O(1)*	146.59(11)
O(8)–Zn–O(1)	168.37(9)	O(W)–Zn–O(1)	84.98(9)
N(4)–Zn–O(1)	78.11(10)	O(1)–Zn–O(1)*	94.22(10)
Zn**–O(1)–Zn	129.31(11)		
Ligand			
O(1)–C(2)	1.280(4)	C(6)–C(7)	1.408(5)
C(2)–O(2)	1.239(4)	C(6)–C(11)	1.410(5)
C(2)–C(3)	1.509(6)	C(7)–O(8)	1.318(4)
C(3)–N(4)	1.474(4)	C(7)–C(8)	1.422(5)
C(3)–C(4)	1.535(8)	C(8)–C(9)	1.367(6)
N(4)–C(5)	1.279(5)	C(9)–C(10)	1.383(8)
C(5)–C(6)	1.446(5)	C(10)–C(11)	1.357(7)
O(2)–C(2)–O(1)	121.8(11)	C(2)–O(1)–Zn	113.0(2)
O(2)–C(2)–C(3)	119.5(3)	C(2)–O(1)–Zn**	108.3(2)
O(1)–C(2)–C(3)	118.4(3)	C(5)–N(4)–Zn	124.8(2)
N(4)–C(3)–C(2)	109.8(3)	C(3)–N(4)–Zn	116.0(2)
N(4)–C(3)–C(4)	110.6(4)	C(7)–O(8)–Zn	126.8(2)
C(2)–C(3)–C(4)	110.5(4)	O(8)–C(7)–C(8)	118.2(3)
C(5)–N(4)–C(3)	119.2(3)	C(6)–C(7)–C(8)	117.6(3)
N(4)–C(5)–C(6)	126.4(3)	C(9)–C(8)–C(7)	120.8(4)
C(7)–C(6)–C(11)	119.0(3)	C(8)–C(9)–C(10)	121.5(4)
C(5)–C(6)–C(7)	124.8(3)	C(11)–C(10)–C(9)	118.9(4)
C(11)–C(6)–C(5)	116.1(3)	C(10)–C(11)–C(6)	122.2(5)
O(8)–C(7)–C(6)	124.2(3)		
[(*N-salicylidene-L-valinato*)(*aqua*)*zinc*(*II*)] (***2***)			
Zinc coordination sphere			
Zn–O(8)	1.997(6)	Zn–O(1)*	2.033(5)
Zn–O(W)	1.999(6)	Zn–O(1)	2.156(5)
Zn–N(4)	2.015(7)	O(1)–Zn**	2.033(5)
O(8)–Zn–O(W)	104.0(3)	O(8)–Zn–O(1)*	92.0(2)
O(8)–Zn–N(4)	91.2(3)	O(W)–Zn–O(1)*	103.2(3)
O(W)–Zn–N(4)	109.9(3)	N(4)–Zn–O(1)*	144.9(3)
O(8)–Zn–O(1)	167.7(2)	O(W)–Zn–O(1)	84.7(2)
N(4)–Zn–O(1)	77.5(2)	O(1)–Zn–O(1)*	94.5(2)
Zn**–O(1)–Zn	130.5(3)		
Ligand			
O(1)–C(2)	1.291(9)	C(6)–C(7)	1.396(12)
C(2)–O(2)	1.236(9)	C(6)–C(11)	1.400(12)
C(2)–C(3)	1.517(12)	C(7)–O(8)	1.307(10)
C(3)–N(4)	1.472(10)	C(7)–C(8)	1.412(12)
C(3)–C(4)	1.546(13)	C(8)–C(9)	1.376(14)
N(4)–C(5)	1.300(11)	C(9)–C(10)	1.37(2)
C(5)–C(6)	1.428(12)	C(10)–C(11)	1.40(2)
C(4)–C(12)	1.45(2)	C(4)–C(13)	1.50(2)
O(2)–C(2)–O(1)	121.2(7)	C(2)–O(1)–Zn	113.4(5)
O(2)–C(2)–C(3)	121.6(7)	C(2)–O(1)–Zn**	107.4(5)
O(1)–C(2)–C(3)	117.2(5)	C(5)–N(4)–Zn	123.4(6)
N(4)–C(3)–C(2)	109.1(6)	C(3)–N(4)–Zn	117.2(5)
N(4)–C(3)–C(4)	112.1(7)	C(7)–O(8)–Zn	126.4(6)
C(2)–C(3)–C(4)	112.7(9)	O(8)–C(7)–C(8)	118.6(8)
C(5)–N(4)–C(3)	118.8(8)	C(6)–C(7)–C(8)	118.1(8)
N(4)–C(5)–C(6)	125.9(8)	C(9)–C(8)–C(7)	121.9(10)
C(7)–C(6)–C(11)	119.0(9)	C(8)–C(9)–C(10)	120.5(10)
C(5)–C(6)–C(7)	126.2(7)	C(11)–C(10)–C(9)	118.7(10)
C(11)–C(6)–C(5)	114.8(9)	C(10)–C(11)–C(6)	121.8(11)
O(8)–C(7)–C(6)	123.3(8)	C(12)–C(4)–C(13)	117.9(13)
C(12)–C(4)–C(3)	113.8(10)	C(13)–C(4)–C(3)	111.7(10)

[a] Symmetry transformations used to generate equivalent atoms. For **1**: * $-y+1, x-y+1, z+1/3$; ** $-x+y, -x+1, z-1/3$. For **2**: * $1-x+y, 1-x, z-1/3$; ** $1-y, x-y, z+1/3$.

(C(3)), 37.4 (C(4)), 22.8 (CH_3), 22.3 (CH_3). Λ_M (Ω^{-1} cm^2 mol^{-1}) (10^{-3} mol dm^{-3} in DMSO, 23.5°C) 3.0.

*2.3.3. [(N-Salicylidene-L-serinato)(aqua)zinc(II)]·1.5H_2O (**3**)*

72% yield. White crystals from methanol. Exhibits a mass decrease (found 13.88; calc. 14.18) between 110 and 115°C ($-1.5H_2O$) and 150 and 230°C ($-1H_2O$) corresponding to the loss of two and a half water molecules per formula unit. *Anal*. Found: C, 37.75; H, 4.27; N, 4.41. Calc. for $C_{10}H_{11}NO_5Zn\cdot 1.5H_2O$: C, 37.81; H, 4.41; N, 4.41%. IR (cm^{-1}): 3400–3100bs, 1646s, 1608s, 1554s, 1478s, 1448s, 1414m, 1362s, 1332m, 1318m, 1283s, 1259m, 1227w, 1202m, 1160s, 1143m, 1118m, 1080m, 1045w, 1034m, 991w, 971m, 949w, 932w, 850w, 765m, 684w, 657w, 554m, 518w, 479w, 454w, 419w, 400w, 364w, 343w, 261m. UV–Vis (DMSO): λ 367 (ε 6.5×10^3), 258 nm (8.3×10^3 dm^3 mol^{-1} cm^{-1}). ^{1}H NMR (DMSO-d_6, 319 K): δ 8.43s (1H, H(5)), 7.29d+t (2H, H(11)+H(9)), 7.03bd (1H, H(8), $J_{estimated}=8.5$ Hz), 6.65t (1H, H(10), $J=7.3$ Hz), 4.96bs (1H, OH), 3.97dd (1H, Hβ_1, $J=10.5$ and 3.7 Hz), 3.85dd (1H, H(3), $J=8.2$ and 3.7 Hz), 3.97bt (1H, Hβ_2). ^{13}C NMR (DMSO-d_6, 319 K): δ 177.2 (C(2)), 172.5 (C(7)), 172.3 (C(5)), 138.8 (C(11)), 136.9 (C(9)), 126.2 (C(8)), 123.2 (C(6)), 117.8 (C(10)), 74.7 (C(3)), 67.5 (C(4)). Λ_M (Ω^{-1} cm^2 mol^{-1}) (10^{-3} mol dm^{-3} in DMSO, 23.5°C) 2.0.

*2.3.4. [(N-Salicylidene-L-methioninato)(aqua)zinc(II)] (**4**)*

77% yield. White solid. Exhibits a mass decrease (found 6.11; calc. 5.38) between 150 and 180°C corresponding to the loss of one water molecule per formula unit. *Anal*. Found: C, 43.02; H, 4.55; N, 4.20. Calc. for $C_{12}H_{15}NO_4SZn$: C, 43.06; H, 4.49; N, 4.19%. IR (cm^{-1}): 3280bm, 2971m, 2938m, 2910s, 1632s, 1589s, 1545s, 1473s, 1449s, 1437s, 1417m, 1377s, 1339s, 1303s, 1272w, 1222w, 1198s, 1176m, 1164s, 1134m, 1093m, 1046w, 994w, 975m, 959w, 943w, 916w, 890m, 857m, 797m, 769s, 741s, 725s, 692m, 638w, 551m, 506w, 482m, 454m, 403w, 358m, 322w, 284w, 260m. UV–Vis (DMSO): λ 368 (ε 7.5×10^3), 257 nm (1.1×10^4 dm^3 mol^{-1} cm^{-1}). ^{1}H NMR (DMSO-d_6): δ 8.42s (1H, H(5)), 7.27d+t (2H, H(11)+H(9)), 6.83bd (1H, H(8)), 6.58t (1H, H(10), $J=7.1$ Hz), 3.81t (1H, H(3), $J=6.1$ Hz), 2.54t (2H, Hγ, $J=7.7$ Hz), 2.12s (3H, SCH_3, $J=6.9$ Hz), 2.04m (2H, Hβ). ^{13}C NMR (DMSO-d_6): δ 178.6 (C(2)), 173.6 (C(7)), 172.8 (C(5)), 139.1 (C(11)),

137.3 (C(9)), 126.5 (C(8)), 123.2 (C(6)), 117.3 (C(10)), 71.2 (C(3)), 38.6 (Cβ), 33.2 (Cγ), 18.6 (SCH_3). Λ_M (Ω^{-1} cm^2 mol^{-1}) (10^{-3} mol dm^{-3} in DMSO, 23.5°C) 2.0.

2.3.5. [(N-Salicylidene-L-glutaminato)(aqua)zinc(II)] · H_2O (5)

77% yield. White crystals from DMSO. Exhibits a mass decrease (found 5.00; calc. 5.15) between 180 and 200°C corresponding to the loss of one water molecule per formula unit. *Anal*. Found: C, 40.82; H, 4.50; N, 7.91. Calc. for $C_{12}H_{14}N_2O_5Zn \cdot H_2O$: C, 41.21; H, 4.58; N, 8.01%. IR (cm^{-1}): 3473m, 3352m, 3201w, 2906w, 1660s, 1641s, 1605s, 1544m, 1475s, 1449s, 1413w, 1392w, 1367s, 1339s, 1309m, 1296m, 1259w, 1240w, 1198m, 1162s, 1136m, 1090w, 1047w, 1043w, 970w, 944w, 901w, 881w, 860w, 799m, 770s, 750m, 735m, 631w, 580w, 565w, 553m, 532w, 509w, 479w, 447w, 402w, 354w, 301w, 264w. UV–Vis (DMSO): λ 369 (ε 5.9×10^3), 272 nm (1.4×10^4 dm^3 mol^{-1} cm^{-1}). ^{1}H NMR (DMSO-d_6, 320 K): δ 8.43s (1H, H(5)), 7.29d + t (2H, H(11) + H(9)), 7.00bd (1H, H(8), $J_{estimated}$ = 8.1 Hz), 6.64t (1H, H(10), J = 7.3 Hz), 3.81t (1H, H(3), J = 6.1 Hz), 2.26m (2H, Hγ), 2.15m (1H, $H\beta_1$), 2.05m (1H, $H\beta_2$). ^{13}C NMR (DMSO-d_6, 320 K): δ 178.7 (C(2)), 177.7 *C*ONH_2), 172.8 (C(7)), 171.6 (C(5)), 138.7 (C(11)), 137.0 (C(9)), 126.2 (C(8)), 123.1 (C(6)), 117.6 (C(10)), 71.7 (C(3)), 35.0 (Cγ), 34.8 (Cβ). Λ_M (Ω^{-1} cm^2 mol^{-1}) (10^{-3} mol dm^{-3} in DMSO, 25.9°C) 2.3.

2.3.6. [(N-Salicylidene-L-methioninato sulfone)(aqua)-zinc(II)] · 0.25H_2O (6)

80% yield. White solid. Exhibits a mass decrease (found 6.11; calc. 6.07) between 170 and 200°C corresponding to the loss of 1.25 water molecules per formula unit. *Anal*. Found: C, 39.03; H, 4.27; N, 3.89. Calc. for $C_{12}H_{15}NO_6SZn \cdot 0.25H_2O$: C, 38.82; H, 4.18; N, 3.77%. IR (cm^{-1}): 3280bm, 3005m, 2974w, 2937m, 1634s, 1594s, 1546s, 1477s, 1452s, 1425w, 1376s, 1343m, 1337m, 1325m, 1300s, 1283s, 1261w, 1247w, 1198m, 1178m, 1162s, 1130s, 1097m, 1064w, 1045w, 1034w, 1003w, 974w, 961m, 943w, 917w, 890w, 856m, 797m, 770s, 747m, 736m, 691w, 637w, 554m, 520m, 481m, 448m, 398w, 358w, 310w, 280w, 262w. UV–Vis (DMSO): λ 371 (ε 7.5×10^3), 272 (7.7×10^3), 256 nm (7.4×10^3 dm^3 mol^{-1} cm^{-1}). ^{1}H NMR (DMSO-d_6): δ 8.45s (1H, H(5)), 7.26d + t (2H, H(11) + H(9)), 6.76bd (1H, H(8)), 6.57t (1H, H(10), J = 7.1 Hz), 3.85t (1H, H(3), J = 6.1 Hz), 3.27m (1H, $H\gamma_1$), 3.16m (1H, $H\gamma_2$), 3.08s (3H, SO_2CH_3), 2.22m (2H, Hβ). ^{13}C NMR (DMSO-d_6): δ 178.2 (C(2)), 173.6 (C(7)), 172.8 (C(5)), 139.2 (C(11)), 137.5 (C(9)), 126.5 (C(8)), 123.2 (C(6)), 117.5 (C(10)), 70.0 (C(3)), 54.3 (Cγ), 44.2 (SO_2CH_3), 31.5 (Cβ). Λ_M (Ω^{-1} cm^2 mol^{-1}) (10^{-3} mol dm^{-3} in DMSO, 23.5°C) 2.0.

2.3.7. [(N-Salicylidene-L-phenylalaninato)(aqua)zinc(II)] · 0.25H_2O (7)

77% yield. White solid. Exhibits a mass decrease (found 6.11; calc. 6.34) between 140 and 240°C corresponding to the loss of 1.25 water molecules per formula unit. *Anal*. Found: C, 53.97; H, 4.20; N, 3.96. Calc. for $C_{16}H_{15}NO_4Zn \cdot 1.25H_2O$: C, 54.10; H, 4.37; N, 3.94%. IR (cm^{-1}): 1610br s, 1525s, 1450s, 1440s, 1411s, 1380s, 1340m, 1318m, 1270m, 1240w, 1180m, 1152m, 1140m, 1120m, 1078w, 1050m, 1020m, 1008s, 955s, 898w, 840w, 802m, 748m, 730m, 699m, 602w, 580m, 520m, 450w, 420w, 392w, 340w, 318w, 253w. UV–Vis (DMSO): λ 372 (ε 3.3×10^3), 270 nm (2.9×10^4 dm^3 mol^{-1} cm^{-1}). ^{1}H NMR (DMSO-d_6, 325 K): δ 7.62s (1H, H(5)), 7.31m (3H, H(4′) and H(3′) + H(5′)), 7.20m (3H, H(9) and H(2′) + H(6′)), 6.81bd (1H, H(11)), 6.78bd (1H, H(8)), 6.46t (1H, H(10), J = 7.3 Hz), 3.90dd (1H, H(3), J = 9.4 and 3.8 Hz), 3.39dd (1H, $H\beta_1$, J = 13.5 and 3.8 Hz), 2.95dd (1H, $H\beta_2$, J = 13.5 and 9.4 Hz). ^{13}C NMR (DMSO-d_6, 325 K): δ 177.8 (C(2)), 173.6 (C(7)), 170.9 (C(5)), 141.5 (C(1′)), 138.1 (C(11)), 136.6 (C(9)), 133.5 (C(2′) + C(6′)), 131.7 (C(3′) + C(5′)), 129.9 (C(4′)), 126.1 (C(8)), 122.5 (C(6)), 116.6 (C(10)), 73.7 (C(3)), 44.3 (Cβ). Λ_M (Ω^{-1} cm^2 mol^{-1}) (10^{-3} mol dm^{-3} in DMSO, 23.2°C) 2.9.

2.3.8. [(N-Salicylidene-L-tryptophanato)(aqua)-zinc(II)] · 0.25H_2O (8)

61% yield. White solid. Exhibits a mass decrease (found 5.90; calc. 5.71) between 170 and 210°C corresponding to the loss of 1.25 water molecules per formula unit. *Anal*. Found: C, 54.94; H, 4.23; N, 7.24. Calc. for $C_{18}H_{16}N_2O_4Zn \cdot 0.25H_2O$: C, 54.84; H, 4.19; N, 7.11%. IR (cm^{-1}): 3345s, 3057m, 2956m, 2982m, 1636s, 1577s, 1546s, 1472s, 1449s, 1422w, 1381s, 1357m, 1338m, 1321m, 1299m, 1266w, 1257w, 1241w, 1200m, 1160m, 1132m, 1110w, 1096w, 1043w, 1018w, 986w, 976w, 933w, 912w, 879w, 847w, 802m, 792m, 754m, 738s, 728s, 608w, 588w, 553m, 533w, 507w, 482w, 440w, 425w, 345w, 324w, 284w, 256w. UV–Vis (DMSO): λ 366 (ε 7.2×10^3), 275 nm (1.2×10^4 dm^3 mol^{-1} cm^{-1}). ^{1}H NMR (DMSO-d_6, 325 K): δ 10.71s (1H, NH), 7.67d (1H, H(5′), J = 7.8 Hz), 7.61s (1H, H(5)), 7.44d (1H, H(8′), J = 8.0 Hz), 7.20m (2H, H(9) and H(7′)), 7.07m (2H, H(2′) + H(6′)), 6.87d (1H, H(8), J = 8.5 Hz), 6.75dd (1H, H(11), J = 7.7 and 1.7 Hz), 6.46t (1H, H(10), J = 7.3 Hz), 3.98dd (1H, H(3), J = 9.2 and 3.5 Hz), 3.55dd (1H, $H\beta_1$, J = 14.4 and 3.5 Hz), 3.10 dd (1H, $H\beta_2$, J = 14.4 and 9.2 Hz). ^{13}C NMR (DMSO-d_6, 325 K): δ 178.5 (C(2)), 173.8 (C(7)), 170.5 (C(5)), 140.1 (C(9′)), 137.9 (C(11)), 136.3 (C(9)), 131.0 (C(4′)), 127.9 (C(2′)), 126.0 (C(8)), 124.5 (C(7′)), 122.7 (C(6)), 122.0 (C(5′) + C(6′)), 116.8 (C(10)), 114.9 (C(8′)), 113.8 (C(3′)), 72.6 (C(3)), 34.2 (Cβ). Λ_M (Ω^{-1} cm^2 mol^{-1}) (10^{-3} mol dm^{-3} in DMSO, 23.5°C) 3.0.

3. Results and discussion

3.1. Crystal structures

The ORTEP drawings of the structural units of **1** and **2** are shown in Figs. 1 and 2. The coordination geometry about the zinc in both structures **1** and **2** is between distorted trigonal bipyramid and distorted square pyramidal with the iminic nitrogen N(4) (**1** = 2.020(3) and **2** = 2.015(7) Å), the phenolic O(8) (**1** = 1.991(2) and **2** = 1.997(6) Å) and the carboxylic O(1) (**1** = 2.160(2) and **2** = 2.156(5)) of *N*-salicylidene-aminoacidato base ligand, another O(1)* carboxylic of other unit (**1** = 2.033(2) and **2** = 2.033(5) Å) and a water molecule (**1** = 2.006(3) and **2** = 1.999(6)) occupying the five coordination positions. The Zn–N(4) and Zn–O(8) distances are similar to that corresponding to [(methoxysalicylidene-L-aminoacidato)(pyridine)$_2$zinc(II)], where the amino acid is methionine [31], valine [32] or serine [33] (2.030–2.035 and 1.992–2.010 Å, respectively) but the Zn–O(1) varies significantly (2.087–2.133 Å). Moreover, the [(*N*-salicylidene-ethanolaminato)zinc(II)] [34] presents slightly shorter Zn–N(4) (2.007 Å) and clearly shorter Zn–O(8) (1.938 Å) distances. The polymeric structure results from the repetition of [Zn**–O(1)–Zn–O(1)*]$_n$ (Zn**–O(1) and Zn–O(1)*, **1** = 2.033(2) and **2** = 2.033(5) Å; Zn–O(1), **1** = 2.160(2) and **2** = 2.156(5) Å). The crystals are constituted by polymeric [(*N*-salicylidene-L-aminoacidato)zinc(II)] moieties forming helical arrays about three-fold screw axes (Fig. 3).

To our knowledge these are the first structures of binary complexes of the type [(*N*-salicylidene-L-aminoacidato)-zinc(II)]. Only the pyridine complexes of [*N*-methoxysalicylidene-L-(methioninato, valinato or serinato)(pyridine)$_2$zinc(II)] [31–33] and the binary complex of [(*N*-salicylidene-ethanolaminato)zinc(II)] [34] have been described until now.

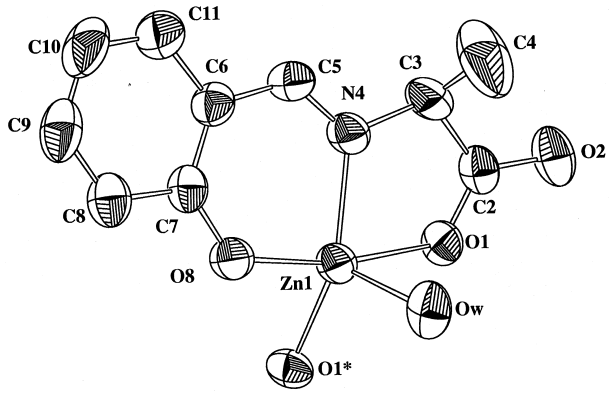


Fig. 1. ORTEP drawing of [(*N*-salicylidene-L-alaninato)(aqua)-zinc(II)]·0.25H_2O (**1**).

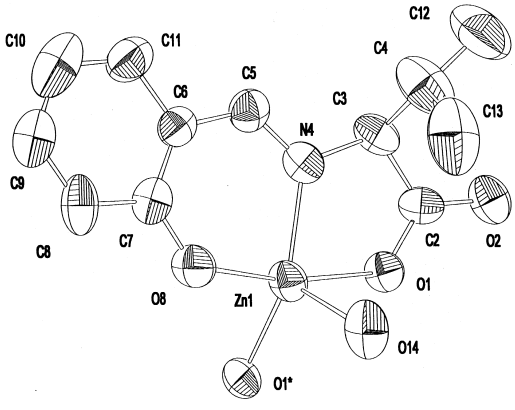


Fig. 2. ORTEP drawing of [(*N*-salicylidene-L-valinato)(aqua)zinc(II)] (**2**).

3.2. Infrared spectra

The Schiff base structure of the salicylidene-aminoacidato moiety of the obtained compounds is confirmed by the presence of strong imine ν(C=N) bands occurring in the range 1624–1647 cm^{-1} of the IR spectra [13,43,44]. The strong band at 1660 cm^{-1} in **5** is assigned to the carbonyl group of the glutamine lateral chain [45].

The ν_{as}(COO) is related to the strong band appearing in the spectra of the complexes between 1577 and 1608 cm^{-1}, whereas the ν_s(COO) is attributed to the medium–strong peaks appearing in the 1339–1392 cm^{-1} region. This gives rise to a $\Delta\nu$ (ν_{as}(COO) − ν_s(COO)) of 196–266 cm^{-1} characteristic of monodentate coordination of the carboxylate group [46]. According to X-ray structural analysis in com-

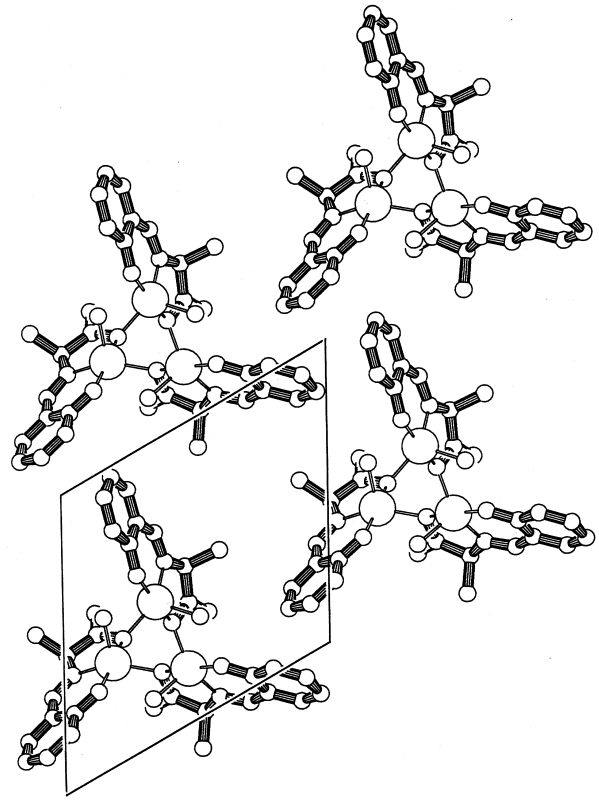


Fig. 3. View of the crystal structure of [(*N*-salicylidene-L-alaninato)-(aqua)zinc(II)]·0.25H_2O (**1**) showing the helical arrays about three-fold screw axes. (The view is through the C3 axis and the apparent trimers are really polymeric pillars.)

Table 3
Selected ^{1}H and ^{13}C NMR values of [(*N*-salicylidene-L-aminoacidato)zinc(II)] complexes

	L-alanine **1**	L-valine **2**	L-serine **3**	L-methionine **4**	L-glutamine **5**	L-methionine sulfone **6**	L-phenylalanine **7**	L-tryptophan **8**
C(5)–H	8.45	8.36	8.43	8.42	8.43	8.45	7.62	7.61
C(11)–H	7.25	7.27	7.29	7.27	7.29	7.26	6.81	6.75
C(9)–H	7.25	7.27	7.29	7.27	7.29	7.26	7.20	7.20
C(8)–H	6.80	6.87	7.03	6.83	7.00	6.76	6.78	6.87
C(10)–H	6.57	6.60	6.58	6.58	6.64	6.57	6.46	6.46
C(3)–H	3.81	3.49	3.85	3.81	3.81	3.85	3.90	3.98
C(2)	180.3	178.8	177.2	178.6	178.7	178.2	177.8	178.5
C(7)	173.0	172.1	172.5	173.6	172.8	173.6	173.6	173.8
C(5)	171.8	172.3	172.3	172.8	171.6	172.8	170.9	170.5
C(11)	139.0	139.0	138.8	139.1	138.7	139.2	138.1	137.9
C(9)	137.3	137.3	136.9	137.3	137.0	137.5	136.6	136.3
C(8)	126.5	126.5	126.2	126.5	126.2	126.5	126.1	126.0
C(6)	123.4	123.6	123.2	123.2	123.1	123.2	122.5	122.7
C(10)	117.7	118.7	117.3	117.3	117.6	117.5	116.6	116.8
C(3)	66.7	78.8	74.7	71.2	71.7	70.0	73.7	72.6

plexes **1** and **2**, the bridging carboxylate group is bound 'via only one oxygen' to two Zn(II) ions. This coordination mode has been described and discussed in other $RCOO^-$ anions and similar systems, i.e. NO_2^- [47] but has not been discussed in the extensive IR studies performed on metal complexes of carboxylic acids [46]. The shape, intensity and frequency of the two ν(COO) bands in complexes **3** and **5** are very similar to those of **1** and **2**, the $\Delta\nu$ values being very close to 240 cm^{-1} which could be indicative of the same type of carboxylate bridge although the presence of the terminal donor groups of the lateral chain in **3** and **5** can change the coordination sphere of the Zn(II) and the way in which the monomeric units are linked.

3.3. NMR spectra

^{1}H NMR and ^{13}C NMR were unequivocally assigned via bidimensional techniques (HMQC and HMBC) and by comparison with other similar spectra (Table 3). As can be seen, in **7** and **8**, a relative *endo* disposition between the two aro-

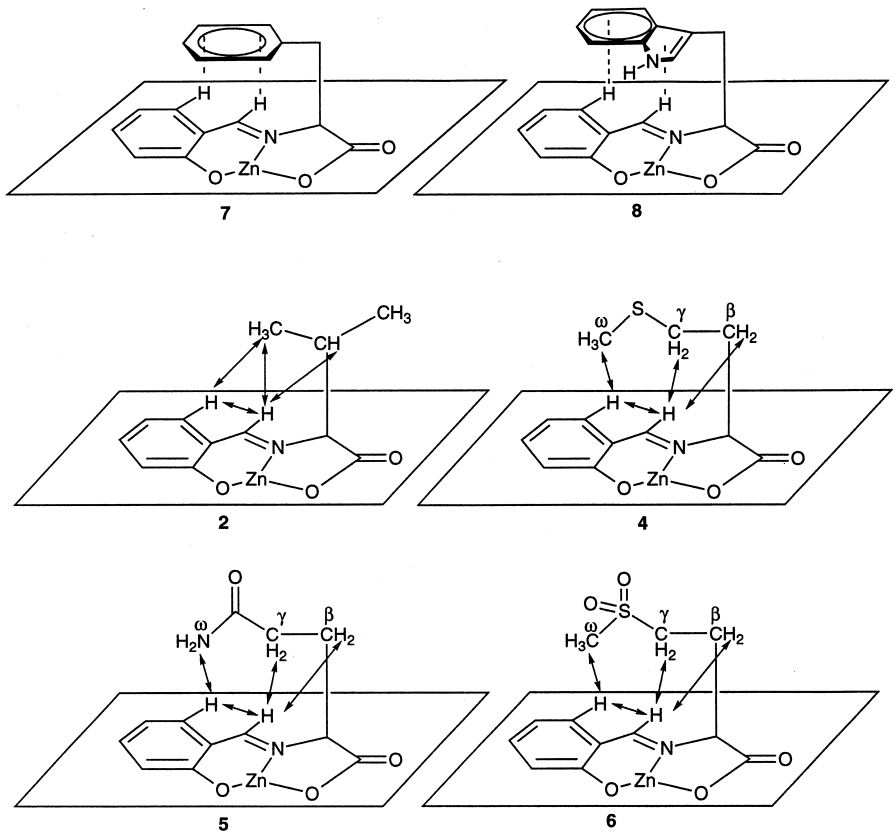


Fig. 4. Relative disposition of the lateral chain of different Schiff bases in DMSO solution (selected NOEs).

matic systems of the complex is necessary in order to explain the observed downfield shift in ^{1}H NMR for C(5)–H (standard value for non-aromatic amino acids is 8.40 ± 0.05 versus 7.60 ppm) and C(11)–H (standard value for non-aromatic amino acids is 7.27 ± 0.02 versus 6.78 ± 0.03) that can be assigned to the anisotropic behaviour of the aromatic rings of the lateral chain of these two amino acids towards methylene and *ortho* carbons of the Schiff base. On the other hand, NOEs presented in the ROESY between the *ortho* C(11)–H and the ω-Hs and between the iminic C(5)–H and the γ-Hs of the lateral chain of the amino acids show, if aggregates do not exist in solution, a general tendency for the *endo* disposition. Fig. 4 shows the NOEs presented in **2**–**8**. Moreover, ROESY results obtained for compound **2** indicate that the disposition of the lateral chain in DMSO solution is not the same as that in the crystal structure (see Figs. 2 and 4). This characteristic could be presumably extended to the remaining Zn(II) complexes since these compounds are probably monomers in solution, whereas in the crystal they are present as polymeric structures. On the other hand, the Λ_M (10^{-3} mol dm^{-3}) values in DMSO at 23–26°C (between 2.0 and 3.0 Ω^{-1} cm^2 mol^{-1}) imply the presence of non-electrolyte species [48].

Supplementary data

Supplementary data are available from Cambridge Crystallographic Data Centre, 12 Union Road, Cambridge CB2 1EZ, UK (fax: +44-1223-336033; e-mail: deposit@ccdc.cam.ac.uk) on request, quoting the deposition numbers 136497 (**1**) and 136496 (**2**).

Acknowledgements

This work was supported financially by the Vicerrectorat d'Investigació de la Universitat de les Illes Balears (UIB), and Spanish Project PB98-0123.

References

[1] J.B. Longenecker, E.E. Snell, J. Am. Chem. Soc. 79 (1956) 142.
[2] E.E. Snell, P.M. Fasella, A. Braunstein, A. Ross-Fanelli, Chemical and Biological Aspects of Pyridoxal Catalysis, McMillan, New York, 1963.
[3] E.E. Snell, A. Braunstein, E.S. Severin, V.M. Torchinsky, Pyridoxal Catalysis: Enzymes and Model Systems, Interscience, New York, 1968.
[4] V.M. Doctor, J. Oro, Biochem. J. 112 (1969) 691.
[5] Y. Bkouche-Waksman, J.M. Barbe, A. Kvick, Acta Crystallogr., Sect. B 44 (1988) 595.
[6] J. Krätsmar-Smogrovic, M. Blahovà, V. Kettmann, Chirality 3 (1991) 503.
[7] T. Ueki, T. Ashida, V. Sasada, K. Kakudo, Acta Crystallogr., Sect. B 25 (1969) 328.
[8] T. Ueki, T. Ashida, V. Sasada, K. Kakudo, Acta Crystallogr. 22 (1967) 870.
[9] Y. Bkouche-Waksman, J.M. Barbe, A. Kvick, Acta Crystallogr., Sect. B 44 (1988) 595.
[10] P.E. Werner, A. Valent, V. Adelskold, O. Svajlenová, Acta Chem. Scand. Ser. A 37 (1983) 51.
[11] K. Korhonen, R. Hämäläinen, Acta Chem. Scand. Ser. A 33 (1979) 569.
[12] H.M. Dawes, J.M. Waters, T.N. Waters, Inorg. Chim. Acta 66 (1982) 29.
[13] A. García-Raso, J.J. Fiol, A. López-Zafra, A. Cabrero, I. Mata, E. Molins, Polyhedron 18 (1999) 871.
[14] K. Korhonen, R. Hämäläinen, U. Turpeinen, Acta Crystallogr., Sect. B 37 (1981) 829.
[15] M.S. Palacios, E. Medina, F.G. Manrique, M.T. do P. Gambardella, R.H. de A. Santos, M.L. Rodriguez, J.M. Dance, Polyhedron 8 (1989) 2131.
[16] J. Krätsmar-Smogrovic, F. Pavelcik, J. Soldánová, J. Sivy, V. Seressová, M. Zemlicka, Z. Naturforsch., Teil B 46 (1991) 1323.
[17] K. Korhonen, R. Hämäläinen, U. Turpeinen, Acta Crystallogr., Sect. C 40 (1984) 1175.
[18] R. Hämäläinen, U. Turpeinen, M. Ahlgrén, M. Rantala, Acta Chem. Scand. Ser. A 32 (1978) 549.
[19] J.E. Davies, Acta Crystallogr., Sect. C 40 (1984) 903.
[20] R. Hämäläinen, M. Ahlgrén, U. Turpeinen, M. Rantala, Acta Chem. Scand. Ser. A 32 (1978) 235.
[21] A. García-Raso, J.J. Fiol, F. Bádenas, M. Quirós, Polyhedron 15 (1996) 4407.
[22] H. Fujimaki, I. Oonishi, F. Muto, A. Nakahara, Y. Komiyama, Bull. Chem. Soc. Jpn. 44 (1971) 28.
[23] L.L. Koh, J.O. Ranford, W. Robinson, J.O. Svensson, A.L.C. Tan, D. Wu, Inorg. Chem. 35 (1996) 6466 and Refs. therein.
[24] G.N. Weinstein, M.J. O'Connor, R.H. Holm, Inorg. Chem. 9 (1970) 2104.
[25] L. Casella, M. Gullotti, J. Am. Chem. Soc. 103 (1981) 6338.
[26] R.K. Mehta, S.P. Rao, R.C. Kapoor, Indian J. Chem. 7 (1969) 933.
[27] L. Casella, M. Gullotti, J. Am. Chem. Soc. 105 (1983) 803.
[28] B.E. Leach, D.L. Leussing, J. Am. Chem. Soc. 93 (1971) 3377.
[29] K.S. Bai, D.L. Leussing, J. Am. Chem. Soc. 89 (1967) 6126.
[30] D. Hopgood, D.L. Leussing, J. Am. Chem. Soc. 91 (1969) 3740.
[31] S-L. Li, D-X. Liu, J-H. Zhou, F-Q. Meng, Z-H. Yang, Huaxue Xuebao (Acta Chim. Sinica) 53 (1995) 343 Cambridge Database compound ZOGMOX.
[32] Y-J. Kang, D-X. Liu, S-L. Li, Z-H. Li, L. Liu, Z-H. Yang, Huaxue Xuebao (Acta Chim. Sinica) 54 (1996) 893 Cambridge Database compound NEZFAZ.
[33] D-X. Liu, Y-J. Kang, S-L. Li, L. Liu, Z-H. Yang, Huaxue Xuebao (Acta Chim. Sinica) 54 (1996) 1114 Cambridge Database compound NOTGIM.
[34] T. Akimoto, M. Maeda, Y. Itaka, Chem. Pharm. Bull. 27 (1979) 424.
[35] A. Bax, S. Subramanian, J. Magn. Reson. 67 (1986) 565.
[36] A. Bax, M.F. Summers, J. Am. Chem. Soc. 108 (1986) 2093.
[37] A. Bax, D.G. Davis, J. Magn. Reson. 63 (1985) 207.
[38] C.K. Fair, MolEN, an interactive intelligent system for crystal structure analysis, Enraf-Nonius, Delft, 1990.
[39] G.M. Sheldrick, Acta Crystallogr., Sect. A 46 (1990) 467.
[40] G.M. Sheldrick, SHELXL-93, A computer program for crystal structure refinement, University of Göttingen, Germany, 1993.
[41] D.T. Cromer, J.T. Waber, in: T. Hahn (Ed.), International Tables for X-Ray Crystallography, vol. IV, Kynoch, Birmingham, 1974.
[42] R.F. Stewart, E.R. Davidson, W.T. Simpson, J. Chem. Phys. 42 (1965) 3175.
[43] A. Mederos, F.G. Manrique, A. Medina, Anal. Química 77 (1980) 206.
[44] G.O. Carlisle, A. Syamal, K.K. Ganguli, L.J. Theriot, J. Inorg. Nucl. Chem. 34 (1972) 2761.
[45] R.S. Krishnan, V.N. Sankaranarayanan, K. Krishnan, J. Indian Inst. Sci. 55 (1973) 66.
[46] K. Nakamoto, Infrared and Raman Spectra of Inorganic and Coordination Compounds, Wiley, New York, 1986.
[47] D.M.L. Goodgame, M.A. Hitchman, D.F. Marsham, P. Phavanantha, D. Rogers, J. Chem. Soc., Chem. Commun. (1969) 1383.
[48] W.J. Geary, Coord. Chem. Rev. 7 (1971) 81.

PERGAMON

www.elsevier.nl/locate/poly

Polyhedron 19 (2000) 681–688

POLYHEDRON

^{13}C NMR and FT-IR spectra of thiocyanogen, $S_2(CN)_2$, selenocyanogen, $Se_2(CN)_2$, and related compounds

F. Cataldo *

Progega snc, Via Casilina 1626/A, 00133 Rome, Italy

Received 9 November 1999; accepted 13 January 2000

Abstract

The pseudohalogens thiocyanogen [$(SCN)_2$], sulfur dicyanide [$S(CN)_2$], selenocyanogen [$(SeCN)_2$], selenium dicyanide [$Se(CN)_2$] and selenium diselenocyanate [$Se(SeCN)_2$] have been prepared and studied by ^{13}C NMR spectroscopy for the first time. The ^{13}C NMR results confirm the structure previously assigned to these compounds on the basis of vibrational spectroscopy. Thiocyanogen, sulfur dicyanide, selenocyanogen and selenium dicyanide have been also studied as liquid film on KBr plate in the solid state (KBr pellet) by FT-IR spectroscopy and the data collected have been compared and discussed with previous results recorded on solutions in organic solvents. Good agreement with early results has been obtained. It has been confirmed by solid state ^{13}C NMR–MAS that under mild conditions selenocyanogen disproportionates into selenium dicyanide and selenium diselenocyanate. By heating selenocyanogen above 180°C it polymerizes irreversibly into a brown polymer known as paraselenocyanogen whose FT-IR spectrum is surprisingly very similar to that of parathiocyanogen or polythiocyanogen, the product of self-polymerization of thiocyanogen. ©2000 Elsevier Science Ltd All rights reserved.

Keywords: Pseudohalogens; Selenocyanogen; Thiocyanogen

1. Introduction

The chemistry of pseudohalogens has always been a fascinating and rather briefly treated subject in textbooks of inorganic chemistry [1–4]. Thiocyanogen [$S_2(CN)_2$] was discovered by Soderback 81 years ago [1,5], whereas selenocyanogen [$Se_2(CN)_2$] was prepared in pure form only in 1925 [1,6,7].

Infrared (IR) and Raman spectra of thiocyanogen [8–10] strongly suggest structure **1**, which has a disulfide bridge, NC–S–S–CN, rather than structure **2**, which has the isothiocyanate form S=C=N–N=C=S, even though, according to certain authors [9], on the basis of the position of the IR band due to a –SCN or –NCS group, structure **2** is favoured in polar solvents such as ether while structure **1** is largely predominant in non-polar aprotic solvents. This consideration is not negligible because the addition of thiocyanogen to ethylenic double bonds of organic substrates involves the addition of both –SCN and –NCS groups [11]:

$$R–CH=CH–R + S_2(CN)_2 \rightarrow$$

$$NC–S–C(R)–C(R)–S–CN \ (\mathbf{3})$$

$$+ NC–S–C(R)–C(R)–N=C=S \ (\mathbf{4})$$

However, in contrast to the above suggestion, the product with structure **4** can be formed in both polar and non-polar solvents [11,12]. Recently, the matter has been rationalized [12], and it has been shown that the IR band shift of thiocyanogen observed previously in ether could reasonably be due to a charge-transfer interaction of thiocyanogen with solvent rather than to the presence of isomer **2**.

Moreover, it has been pointed out [12] that the heat of formation of thiocyanogen found experimentally coincides with the value theoretically calculated for isomer **1** rather than compound **2** [13], and similar conclusions were obtained from the gas-phase UV spectrum of thiocyanogen, in agreement with theoretical calculations [14].

Thus, to explain the different addition behaviour which leads simultaneously to structures **3** and **4**, it is possible that the thiocyanogen radical derived from S–S homolysis has a bifunctional behaviour, as has been previously postulated [11,15–17]:

* Tel.: +39-06-205 5084; fax: +39-06-205 0800; e-mail: cdcata@flashnet.it

0277-5387/00/$ - see front matter ©2000 Elsevier Science Ltd All rights reserved.
PII S0277-5387(00)00304-1

•S–CN (**5**) ↔ •N=C=S (**6**)

Bhatnagar et al. [18] have shown by magnetic susceptibility measurements that freshly prepared solutions of thiocyanogen in carbon disulfide and other solvents are diamagnetic but that on standing they become paramagnetic. In certain solvents such as cyclohexane, thiocyanogen is less stable and paramagnetism is observed also in freshly prepared solutions. The paramagnetism can be attributed to the formation of thiocyanogen radicals due to homolysis of S–S bonds during solution ageing. Probably these radicals induce the irreversible self-polymerization of thiocyanogen to a brick-red solid known as parathiocyanogen or polythiocyanogen whose structure seems to be very peculiar [15–17,19].

Selenocyanogen [$Se_2(CN)_2$] was isolated for the first time in 1925 thanks to the work of Birkenback and Kellermann ([6,7]). Fundamental studies of the structure of selenocyanogen and related compounds have already been published [20,21] and are based on IR spectroscopy; some short reviews on selenocyanogen and related compounds are also available [22–24]. Selenocyanogen and related compounds belong to the class of pseudohalides and are the selenium analogues of the thiocyanogen family of compounds. In comparison to thiocyanogen, selenocyanogen and its homologues have received much less attention by investigators, but the available data show that the selenocyanogen family has the same chemical structure as the thiocyanogen family of compounds.

Some unexpected differences between thiocyanogen and selenocyanogen can be immediately outlined here. While thiocyanogen is unstable and cannot be isolated in the pure state unless special conditions at low temperatures are adopted, selenocyanogen is rather more stable and can be isolated at room temperature as a yellow powder; it can also be re-crystallized from CH_2Cl_2 solutions and remains unchanged for months if stored in a closed flask at $+5$°C in the absence of humidity or solvent impurities. Thiocyanogen heated above 0°C or isolated by solvent evaporation at room temperature quickly turns into a brick-red solid [17]; however, selenocyanogen when heated in solution with carbon disulfide undergoes a unique disproportionation reaction as follows [21–24]:

$$2Se_2(CN)_2 \rightarrow Se(CN)_2 + Se_3(CN)_2 \quad (1)$$

When heated at higher temperatures, selenocyanogen liberates a sublimate (see below) and is polymerized into a brownish material. Practically nothing is known about the selenocyanogen polymerization products or about the strong sensitivity of selenocyanogen to certain molecules and solvents which cause its polymerization to a deep-red solid [25].

The difference in stability between thiocyanogen and selenocyanogen is quite striking notwithstanding that the two molecules should have the same geometrical structure, and in general it is expected that the S–S bond strength is comparable to that of the Se–Se bond strength. However, the dissociation energy of a Se–Se bond in diselenides is about 73 kcal mol^{-1} [24], which is larger than that for a S–S bond, which requires 63 kcal mol^{-1} [26]; in any case, these data should be considered only as approximations. Taking into account the rich organic chemistry of selenium [23,24], the C–Se bond should be as stable as the C–S bond; moreover, the Pauling electronegativity of selenium is slightly lower than that of sulfur [24], thus the C–Se bond should have at least the same degree of covalency as the C–S bond.

2. Experimental

^{13}C NMR spectra in $CDCl_3$ solution were performed with a Bruker AMX-600 spectrometer operating at 150.9 MHz; 7 s relaxation delay with 0.7 s of acquisition time and 90° pulse angle were applied. Spectra were obtained with 64 000 words. All reagents and solvents used were from Aldrich or Fluka.

Solid state ^{13}C MAS–NMR spectra were recorded at room temperature on a Bruker AC-200 spectrometer, equipped with an HP amplifier, ^1H 200 MHz, 120 W continuous wave and a pulse amplifier M3205. Samples were packed into 4-mm zirconia rotors and sealed with Kel-F caps. The spin rate was 8 kHz. Spectra were obtained with 512 words in the time domain, zero-filled and Fourier-transformed with a size of 1024 words; 20 000 scans were performed.

FT-IR spectra were recorded on a Perkin-Elmer 1710 spectrometer. Samples were studied embedded in KBr pellets. All reagents and solvents were from Aldrich or Fluka and were used as received.

2.1. Lead thiocyanate preparation

Lead thiocyanate was prepared by adding ammonium thiocyanate solution to an aqueous solution of lead(II) nitrate in stoichiometric amounts. The white precipitate was collected by filtration, washed with water and dried in an oven at 105°C.

2.2. Silver cyanide preparation

Similarly, silver cyanide was prepared by precipitation from silver nitrate and sodium cyanide in stoichiometric amounts. The white precipitate was collected by filtration, protected totally from light and dried in a desiccator under dynamic vacuum.

2.3. Thiocyanogen preparation

Thiocyanogen [$S_2(CN)_2$] was prepared as previously reported [17], by suspending 6.8 g of dry lead(II) thiocyanate in 50 ml of $CDCl_3$ (deuterated chloroform) by magnetic stirring and adding dropwise 3.36 g of bromine. The freshly prepared thiocyanogen solution was decanted and immediately used to record the ^{13}C NMR spectrum. On standing the

solution polymerized to the insoluble and brick-red solid polythiocyanogen [15–17].

2.4. Sulfur dicyanide preparation

Sulfur dicyanide [$S(CN)_2$] was prepared by suspending 4.5 g of silver cyanide in 50 ml of $CDCl_3$ by vigorous stirring and by adding dropwise 1.0 ml of sulfur dichloride (SCl_2). The mixture was stirred for 30 min at room temperature and then the silver chloride formed was separated by decantation. The $CDCl_3$ solution of $S(CN)_2$ was used to record the ^{13}C NMR spectrum.

2.5. Preparation of silver selenocyanate

Silver selenocyanate was prepared by adding a solution of potassium selenocyanate to a solution of silver nitrate in stoichiometric amounts. The precipitate formed was collected by filtration, washed with water and dried into a desiccator under dynamic vacuum. Care should be taken to avoid exposure to light.

2.6. Preparation of selenocyanogen

Selenocyanogen was prepared by suspending 13.5 g of silver selenocyanate [Ag(SeCN)] in 100 ml of dichloromethane with vigorous stirring. Then an iodine solution in dichloromethane was added (6.0 g of iodine per 160 ml of dichloromethane). Very rapid discolouration of the iodine was observed. The mixture was stirred for 2 h at +13°C and then it was decanted. The silver iodide collected was yellow while the $Se_2(CN)_2$ solution was orange. Dichloromethane was then distilled off under reduced pressure in a water-bath to leave a canary-yellow powder. Yield: 2.77 g (55.9% over iodine used).

Selenocyanogen was dissolved in $CDCl_3$ to record the ^{13}C NMR spectrum in solution immediately after preparation. The solid-state ^{13}C NMR spectrum was recorded 3 weeks after preparation.

2.7. Stability of selenocyanogen

Selenocyanogen is rather stable when stored in closed flasks in the dark at +5°C. When stored in this way no decomposition can be observed (visually and by IR spectroscopy) even after months. However, humidity, heat and certain solvents greatly accelerate the decomposition and polymerization of selenocyanogen [10].

2.8. Preparation of selenium dicyanide and paraselenocyanogen

Selenocyanogen (0.217 g) was mixed with 15 ml of decalin and heated in a oil-bath for 2 h at 210°C and 1 h at 180°C. The initially yellow decalin solution quickly became orange and then during heating turbid and brown. In the refrigerator, a discrete crystalline sublimate was deposited; this was collected and identified as selenium dicyanide by its IR spectrum. The dark-brown precipitate formed in the flask was easily separated from decalin by settling and decantation. The collected precipitate was washed several times with dichloromethane and then dried in air. The precipitate was paraselenocyanogen or polyselenocyanogen.

2.9. Stability of selenium dicyanide

The white and tabular crystals of selenium dicyanide are stable for months when stored in a tightly closed flask at room temperature. Exposure to light causes the formation of an orange colour. Also moisture and certain solvents cause a change in colour.

3. Results and discussion

In previous work we have concentrated our efforts on the study of the structure of parathiocyanogen or polythiocyanogen [$(SCN)_x$], the inorganic polymer resulting from spontaneous polymerization of thiocyanogen [15–17]. In these studies we reported evidence about the peculiar and probably linear structure of parathiocyanogen. With FT-IR and electronic spectroscopy we have also studied thiocyanogen [$(SCN)_2$] with the aim of understanding some aspects of its spontaneous polymerization [17].

3.1. ^{13}C NMR spectrum of thiocyanogen

The ^{13}C NMR spectrum of freshly prepared thiocyanogen (see Table 1) is characterized by a sharp singlet at 107.36 ppm. The thiocyanate ion of potassium thiocyanate is reported to show a ^{13}C NMR signal at about 133.3 ppm [27,28], but alkyl thiocyanates such as methyl-, ethyl- and butylthiocyanate give an NMR signal at higher fields, namely at 113.5, 112.1 and 112.1 ppm, respectively [27]. On the other hand, organic isothiocyanates are detected at 128–136 ppm [27,28], in the same range where the inorganic thiocyanate ion of KSCN gives an NMR signal, hence at considerably lower fields than organic thiocyanates (see Table 1).

Based on these data, it can be concluded that thiocyanogen has structure **1**, with a disulfide bridge connecting the two cyanide groups because its NMR signal is comparable to that of alkylthiocyanates. In fact, for isomer **2** of 'isothiocyanogen' we should expect a singlet NMR signal at 128–132 ppm, while for isomer **7** of 'thiocyanogen–isothiocyanogen' (NC–S–N=C=S) we would expect two different signals, one due to the thiocyanate group at about 107 ppm and the other due to the isothiocyanate group at 128–132 ppm. Since we observe a unique signal at 107.36 ppm we can conclude that structure **1** is the correct structure of thiocyanogen.

Additionally, our NMR spectrum does not show any evidence for the presence of thiocyanate (**5**) and isothiocyanate

Table 1
^{13}C NMR synopsis

Compound name	Structure (see text)	NMR signal (ppm)	Reference
Thiocyanogen	**1**	107, 36 (singlet, in $CDCl_3$)	this work
Sulfur dicyanide	**8**	126 (singlet, in $CDCl_3$)	this work
Selenocyanogen	**10**	89, 92 (singlet, in $CDCl_3$)	this work
Selenium dicyanide	see Eq. (2)	130 (broad, solid-state MAS–NMR)	this work
Selenium diselenocyanate	see Eq. (2)	98,3 (broad, solid-state MAS–NMR)	this work
Potassium thiocyanate	KSCN	133.3	[27,28]
Methyl thiocyanate	Me–SCN	113.5	[27]
Ethyl thiocyanate	Et–SCN	112.1	[27]
Potassium cyanide	KCN	168.5	[28]
Alkyl nitrile	R–CN	112–126	[28]
Alkyl isonitrile	R–N=C	157–167	[27,28]
Alkyl isothiocyanate	R–N=C=S	128–136	[27,28]

(**6**) radicals, which means that these radicals are only present at very low concentrations in our system.

Ageing of thiocyanogen solution in $CDCl_3$ causes the formation of an orange-coloured solution, and also a brick-red precipitate starts to appear in suspension and at the bottom of the solution. As mentioned in Section 1, Bhatnagar et al. [18] have shown that freshly prepared thiocyanogen solutions are diamagnetic but become paramagnetic upon ageing due to free radical formation. The ^{13}C NMR spectrum of aged thiocyanogen solution still shows the signal at 107 ppm due to thiocyanogen but a new feature at 169.6 ppm starts to appear. We have already shown [17] that thiocyanogen polymer (polythiocyanogen) has a unique feature at 186 ppm in dimethylformamide (DMF) solution, where it has some degree of solubility; however, polythiocyanogen is not soluble in chloroform. Thus the signal at 169.6 ppm (in $CDCl_3$) could be due to a low molecular weight and soluble oligomer of thiocyanogen.

Other possible interpretations involve the presence of isothiocyanate ion, which we suppose should absorb in this field from the observation that isocyanides give NMR signals at 157–165 ppm (see Table 1). If the assignment of the feature at 169.6 ppm to the isothiocyanate group is correct, we have the first direct indication that thiocyanogen undergoes the scission of its S–S bond followed by a rearrangement to an isothiocyanate group. This could explain the simultaneous N and S addition to the double bonds of organic substrates (see structures **3** and **4**). However, a simpler and more convincing explanation exists for the feature at 169.6 ppm. In fact, cyanide ion absorbs at 168.5 ppm (see Table 1); hence, instead of scission of the S–S bond, we have evidence of scission of the C–S bond which leads to the cyanide group. Scission of the C–S bond of thiocyanogen would imply the formation of thiocyanate ion and free sulfur. Unfortunately, there is no evidence of the presence of free thiocyanate in our NMR spectrum because no signal at 113.5 ppm was observed. Thus, the NMR spectroscopy data suggest that the degradation of thiocyanogen in chloroform involves the formation of cyanide ions and free sulfur.

3.2. ^{13}C NMR spectrum of sulfur dicyanide

We have also studied by ^{13}C NMR spectroscopy the lower thiocyanogen homologue sulfur dicyanide, which has the structure NC–S–CN (**8**) (V-shaped, not linear), which was assigned on the basis of vibrational spectroscopy and X-ray studies [22,23], rather than NC–N=C=S (**9**) or other possible structures.

Freshly prepared sulfur dicyanide shows a unique and sharp singlet at about 126 ppm (see Table 1) in $CDCl_3$ solution. Even if the ^{13}C NMR signal of this molecule appears at lower fields than that observed for thiocyanogen, we can immediately exclude structure **9**, which requires two different signals at lower fields, namely one at least at 157 ppm [27,28] for the isocyanide group, which was not observed, and the other above 130 ppm for the isothiocyanide group [27,28]. Since only one signal was detected we can conclude that structure **8** is the correct structure of sulfur dicyanide. To explain why the signal of sulfur dicyanide appears at 126 ppm and that of thiocyanogen at 107 ppm we must assume that some conjugation between the triple bonds of the two cyano groups occurs through the sulfur bridge in the case of sulfur cyanide, while this is absent in the case of thiocyanogen, which has two sulfur atoms per bridge. Therefore, conjugation causes an NMR signal closer to the thiocyanate ion in the case of sulfur dicyanide (133.3 ppm for thiocyanate versus 126 ppm for sulfur dicyanide), while for thiocyanogen the NMR signal at 107 ppm is comparable to that of organic alkyl thiocyanates which in fact absorb in that region [20,21]. The general observation that sulfur dicyanide is more stable than thiocyanogen could be ascribed to the fact that the former is stabilized also by conjugation while the latter is not. In fact, sulfur dicyanide can be isolated in the form of crystals by sublimation [22], whereas thiocyanogen can be isolated in crystal form only under more complex conditions at $-50°C$ [10] and at temperatures above 0°C shows a certain stability only in solution. When thiocyanogen in solution is concentrated by evaporating the solvent at room temperature under reduced pressure, it polymerizes very quickly [17], sometimes with detonation [17]. Upon prolonged ageing in solu-

tion at room temperature, sulfur dicyanide begins self-polymerization. The ^{13}C NMR spectrum shows a resonance at 129 ppm, but also a new line appears at 124 ppm and complicated resonances are observed in the 147–165 ppm region with the main peak at 155.5 ppm. Additional features are observed in the 171–182 ppm region. These aged spectra will be interpreted and discussed elsewhere [25].

3.3. ^{13}C NMR spectra of selenocyanogen and selenium dicyanide

As reported in Table 1, the ^{13}C NMR spectrum of freshly prepared selenocyanogen [$Se_2(CN)_2$] in $CDCl_3$ solution shows a sharp singlet at 89.92 ppm. The presence of a unique singlet is in complete agreement with the fact that the correct structure of selenocyanogen is analogous to that assigned to thiocyanogen, NC–Se–Se–CN (**10**).

All other possible structures involving isoselenocyanide, Se=C=N–N=C=Se (**11**), and selenocyanide isoselenocyanide, Se=C=N–Se–CN (**12**), can be excluded completely. What is somewhat surprising is that the resonance of selenocyanogen appears at higher fields than that of thiocyanogen (89.92 ppm for the former versus 107.36 ppm for the latter), notwithstanding that these two compounds have the same general structure and that selenium and sulfur are very close in their chemical properties. At present we have no clear explanation for this difference, but it may be that if the Se–Se–C angle is different from the S–S–C angle this difference could affect the electronic shielding of the carbon nucleus leading to a difference in chemical shift.

As mentioned in Section 1, selenocyanogen is relatively stable at room temperature and we have tried to record also its solid-state ^{13}C NMR spectrum. This spectrum (see Table 1), was recorded only 3 weeks after selenocyanogen preparation. It is characterized by two main resonance peaks, one lying at 98.3 ppm and a doublet at about 130 ppm. Since only one resonance was detected in freshly prepared selenocyanogen solution, it is likely that some disproportionation or decomposition occurred in the solid during the 3 weeks after the preparation so that the solid-state spectrum now shows at least two resonance peaks. Since the well-known disproportionation reaction of selenocyanogen described in the literature [22–24] involves the reaction (Eq. (1)) showing that selenocyanogen is transformed into selenium dicyanide and selenium diselenocyanate in mild conditions, we tentatively assign the resonance due to selenium diselenocyanate the peak at 98.3 ppm, while the peak at about 130 ppm is assigned to selenium dicyanide by observing that sulfur dicyanide has a ^{13}C NMR signal (in solution) at 126 ppm.

3.4. FT-IR spectra of thiocyanogen and sulfur dicyanide

As shown in Table 2, the strong thiocyanogen band due to antisymmetric stretching of the –CN group has been observed

Table 2
Infrared band summary; values in cm^{-1}

Thiocyanogen film on KBr plate [a]	Thiocyanogen solution in carbon tetrachloride [b]	Thiocyanogen solution in carbon disulfide [b]	Thiocyanogen solution in ether [b]	Sulfur dicyanide [c]	Sulfur dicyanide (KBr pellet) [d]
2162 vs	2175 s	2171 s	2177 ms	2179 s (with 2188 sh)	2180 s
2073 m	1990 m		2030 m		
	1735 vw, br				
1660 s					
1415 mw					
	1350 vw, br				
1300 sh					
1220 m					
					1140 br
1060 mw					
780 sh					790 mw
					740 mw
670 m	668 s	673 s		684 s	685 m
600 w		667 s		665 vs	
				635 m	620 m
					600 w
					550 w
					525 w
440 vw		490 mw		499 vvw	465 w
					420 vw
	368 w	359 vw		374 w	
				329 w	

[a] From [17].
[b] From [9,10].
[c] From [8].
[d] This work.

in the range 2171–2177 cm^{-1} by various authors when the pseudohalogen was dissolved in organic solvents. By leaving some drops of thiocyanogen solution in CH_2Cl_2 to evaporate onto a KBr disk, it is possible to record the spectrum of almost 'dry' and still not polymerized thiocyanogen [17]. Under these special conditions, the strong band due to antisymmetric stretching appears at 2162 cm^{-1} while the band presumably due to symmetric stretching is detected at 2073 cm^{-1}. This is at a significantly higher frequency than the value detected in CCl_4 solution (1990 cm^{-1}) and in ether solution (2030 cm^{-1}) reported by other authors [9,10]. This suggests that this band is very sensitive to the nature of the solvent in which the molecule is dissolved [12]. The intense band at about 670 cm^{-1} is due to a C–S stretching band, confirming structure **1**.

An alternative and reasonable interpretation suggests that the band at 2073 cm^{-1} could be assigned to cyanide ion. In fact, sodium cyanide shows an IR band at 2060 cm^{-1} [15]. This assignment seems to confirm the NMR interpretation we have given in the preceding section about the decomposition of thiocyanogen in chloroform.

Table 2 shows also that the FT-IR spectrum of sulfur dicyanide is in reasonable agreement with previously published spectra. In particular, only one nitrile stretching band is observed at 2180 cm^{-1} in the solid state (KBr pellet). Thermodynamic calculations using the group increment method [29] give for thiocyanogen $\Delta G_f^o = 63.7$ kcal mol^{-1} and $\Delta H_f^o = 69.8$ kcal mol^{-1} (literature experimental data: $\Delta H_f^o = 74.3$ kcal mol^{-1}). Sulfur dicyanide is a slightly less endothermic compound, with $\Delta G_f^o = 61.4$ kcal mol^{-1} and $\Delta H_f^o = 64.0$ kcal mol^{-1}.

3.5. FT-IR spectra of selenocyanogen and selenium dicyanide

The IR spectrum of selenocyanogen in solution has been studied by several authors [20,21,23]. In this work we have recorded for the first time the FT-IR spectrum of selenocyanogen in KBr pellet. As shown in Table 3, there is generally good agreement between the main bands of $Se_2(CN)_2$ measured in solution and in the solid state. The nitrile stretching band of selenocyanogen was reported at 2152 cm^{-1} when measured in organic solvents [20], while it is shifted to 2143 cm^{-1} in KBr pellet followed by a weaker band at 1992 cm^{-1}. If the former stronger band is assigned to nitrile antisymmetric stretching then the weaker band at lower frequency is assignable to nitrile symmetric stretching. There are no indications about the presence of an isoselenocyanate group, since it is characterized by out-of-phase stretching at 2182 cm^{-1} and in-phase stretching mode at 983 cm^{-1} [30], which are completely absent from our spectra. The symmetric Se–C(N) stretching is reported as a strong band at 521 cm^{-1} in organic solvents whereas in KBr pellet it appears at 505 cm^{-1}; in the solid state we observe also another band at 580 cm^{-1} which could be due to antisymmetric Se–C(N) stretching. In the solid state we were able to observe also Se–CN bending at 436 cm^{-1}. Additionally, we have recorded other intense bands in the FT-IR spectrum of selenocyanogen in KBr. These bands were never reported previously because the spectra were recorded in organic solvents so that some spectral regions were buried by the intense absorption of the solvent, or at the time of the early measurements certain spectral regions were not accessible to the spectrophotometers or were not considered by the researchers. In fact, we observe additional bands at 3650, 3540 and 3434 cm^{-1}; these bands are strong and may be are only overtones or combination bands, but additionally we observe other two bands at 1640 and 1610 cm^{-1} which, however, remain unassigned. There are several other weak and very weak infrared bands (see Table 1) which were detected for the first time but which could also be due to impurities.

Also for selenium dicyanide (see Table 1), for the IR spectrum (in KBr) recorded on the sublimate formed by thermal decomposition of selenocyanogen there is a good general agreement between early reported spectra and the FT-IR reported here. The nitrile stretching appears in KBr pellet as a sharp peak at 2181 cm^{-1}, hence at higher frequency than selenocyanogen, in agreement with previous values reported at 2171 and 2183 cm^{-1} [20,21]. In agreement with previous measurements [20,21] we observe the antisymmetric C–Se stretching at 605 cm^{-1} and the symmetric C–Se stretching at 507 cm^{-1}. At 462 and 436 cm^{-1} we observe the C–Se bending mode. Again also in the case of selenium dicyanide we observe new IR bands never reported before, namely at 3649, 3589, 3581, 3453, 2922, 2851 cm^{-1} and at 1638, 1612 cm^{-1}. These bands remain unassigned; some of them could be due to impurities.

3.6. FT-IR spectrum of paraselenocyanogen

Concerning paraselenocyanogen or polyselenocyanogen there are no precise data available in the literature. In Section 2 we have shown that selenocyanogen undergoes a thermal decomposition reaction when heated at high temperature with liberation of a sublimate which was identified as selenium dicyanide by IR spectroscopy as just discussed, and the formation of a dark-brown insoluble product which is paraselenocyanogen and can be described by the general formula of $[Se_y(CN)_2]_x$ with $0 < y < 3$ and x very large. We will examine in more detail the paraselenocyanogen formation mechanism and its structural aspects elsewhere [25]. However, here we would like to report that the IR spectrum of paraselenocyanogen is very peculiar and is very similar to the spectrum of parathiocyanogen [17].

In fact, the spectrum of paraselenocyanogen is characterized by a very intense and broad band at 1200 cm^{-1} with a shoulder at 1263 cm^{-1}, two medium bands at 1444 and 1412 cm^{-1} and medium-weak bands at 1619 and 881 cm^{-1}. Weak bands are detectable at 801, 638, 609, 525 cm^{-1} as well as at 2262, 2184 and 2148 cm^{-1}. Since selenium diselenocyanate $[Se_3(CN)_2]$ has only three main IR lines (see Table 3) which do not coincide at all with the spectrum of para-

Table 3
Infrared band summary; values in cm^{-1}

Selenium diselenocyanate (KBr) [a]	Selenocyanogen (KBr pellet) [b]	Selenocyanogen (chloroform) [a]	Selenium dicyanide (KBr pellet) [b]	Selenium dicyanide [a]	Selenium dicyanide [c]
	3650 ms		3649 vs		
	3625 sh		3627 sh		
	3583 sh		3589 vs		
	3540 vs		3544 sh		
			3518 vs		
	3434 vs		3435 m		
	2935 mw		2922 vs		
	2867 w		2851 ms		
	2656 w				
	2523 vw				
	2500 vw				
			2181 s	2171 s (KBr) [d]	2183
2131 ms	2143 vs	2152 vs			
	1992 br				
	1721 sh				
	1640 m		1638 m		
	1610 s		1612 vs		
	1503 vw				
	1460 vw		1449 ms		
			1345 w		
			1308 w		
	1280 m, br		1260 w		
			1228 w		
	1120 vw		1140 w		
	1080 vw		1055 w		
	1020 w		1020 w		
	990 sh		973 mw		
			925 mw		
	870 sh				
			839 mw		
	745 vw				
	580 br		605 br	608 m	608
513 s	505 vvs	521 vs	507 vvs	516 vs	516
			462 w		
	436 mw		436 w	436 w	
364 and 360 w	412 w	357 w		345 w	345
		333 w		336 w	
				312 w	310
				302 w	

[a] From [20].
[b] This work.
[c] From [21].
[d] In acetonitrile the bands are resolved at 2183 (sh) and 2175 (m).

selenocyanogen, we can conclude that the disproportionation reaction (Eq. (1)) happens under very mild conditions, while under strong heating the decomposition reaction of selenocyanogen is as follows:

$$2x\mathrm{Se}_2(\mathrm{CN})_2 \rightarrow x\mathrm{Se}(\mathrm{CN})_2 + [\mathrm{Se}_y(\mathrm{CN})_2]_x + x\mathrm{Se} \quad (2)$$

(with $0<y<3$)

The coincidence between the FT-IR spectra of paraselenocyanogen and parathiocyanogen shows only that selenocyanogen polymerizes like thiocyanogen by forming a polymer which should have the same structure of parathiocyanogen. Since we have proposed [15–17] that parathiocyanogen could have a linear structure rather than a triazine-based structure, we can conclude that paraselenocyanogen also has a linear structure because its spectrum is impressively similar to that of parathiocyanogen.

Acknowledgements

We wish to thank Dr Donatella Capitani from Istituto di Chimica Nucleare, CNR, Monterotondo Stazione, Rome, for assistance in recording the ^{13}C NMR spectra.

References

[1] H.J. Emeleus, J.S. Anderson, Modern Aspects of Inorganic Chemistry, Routledge & Kegan, London, 1960, chapter 13.
[2] A.K. Holliday, G. Hughes, S.M. Walker, J.C. Bailar, H.J. Emeleus, R. Nyholm, A.F. Trotman-Dickenson, Comprehensive Inorganic Chemistry, vol. 1, Pergamon, Oxford, 1973, p. 1247.
[3] N.N. Greenwood, A. Earnshaw, Chemistry of the Elements, Pergamon, Oxford, 1984, chapter 8.
[4] P. Brun, A. Fontaine, P. Pascal, Nouveau Traité de Chimie Minérale, vol. 8, Masson, Paris, 1961, p. 973.
[5] E.E. Soderback, Liebigs Ann. Chem. 419 (1919) 217.
[6] L. Birkenback, K. Kellermann, Chem. Ber. 58 (1925) 786.
[7] L. Birkenback, K. Kellermann, Chem. Ber. 58 (1925) 2377.
[8] F. Seel, E. Muller, Chem. Ber. 88 (1955) 1747.
[9] J.M. Nelson, A.D. Pullin, J. Chem. Soc. (1960) 604.
[10] C.E. Vanderzee, A.S. Quist, Inorg. Chem. 5 (1966) 1238.
[11] R.J. Maxwell, L.S. Silbert, J.R. Russell, J. Org. Chem. 42 (1977) 1510.
[12] E.V. Skorobogatova, V.R. Karthashov, Russian Chem. Rev. 67 (1998) 423.
[13] B. Ruscic, J. Berkowitz, J. Chem. Phys. 101 (1994) 7975.
[14] D.C. Frost, C. Kirby, W.M. Lau, C.B. Macdonald, C.A. Mcdowell, M.P.C. Westwood, Chem. Phys. Lett. 69 (1980) 1.
[15] F. Cataldo, Polyhedron 11 (1992) 79.
[16] F. Cataldo, P. Fiordiponti, Polyhedron 12 (1993) 279.
[17] F. Cataldo, J. Inorg. Organomet. Polym. 7 (1997) 35.
[18] S.S. Bhatnagar, H.B. Dunncliff, A. Mohammad, J. Indian Chem. Soc. 17 (1940) 529.
[19] I.V. Krivoishei, V.M. Skorobogatov, Russian Chem. Rev. 50 (1981) 397.
[20] E.E. Aynsley, N.N. Greenwood, M.J. Sprague, J. Chem. Soc. (1964) 704.
[21] G. Cauquis, G. Pierre, C.R. Acad. Sci., Ser. C 269 (1969) 740.
[22] H. Lumbroso, in: P. Pascal (Ed.), Nouveau Traité de Chimie Minérale, vol. 8, Masson, Paris, 1961, p. 1867.
[23] Gmellins Handbuch der Anorganischen Chemie, 8th ed., System C14, Part D6, 1975, p. 233.
[24] J.C. Bailar, H.J. Emeleus, R. Nyholm, A.F. Trotman-Dickenson, Comprehensive Inorganic Chemistry, vol. 2, Pergamon, Oxford, p. 944; see also pp. 967, 992.
[25] F. Cataldo, to be published.
[26] D. Kondepudi, I. Prigogine, Modern Thermodynamics, Wiley, New York, 1998, p. 57.
[27] E. Pretsch, T. Clerc, J. Seibl, W. Simon, Tables of Spectral Data for Structure Determination of Organic Compounds, 2nd ed., Springer, Berlin, 1989.
[28] G.C. Levy, R.L. Lichter, G.L. Nelson, Carbon-13 Nuclear Magnetic Resonance for Organic Chemists, 2nd ed., Wiley, New York, 1980.
[29] D.W. Van Krevelen, Properties of Polymers, 3rd ed., Elsevier, Amsterdam, 1990, chapter 20.
[30] D. Lin-Vien, N.B. Colthup, W.G. Fateley, J.G. Grasselli, The Handbook of Infrared and Raman Frequencies of Organic Molecules, Academic Press, San Diego, 1991, p. 112; see also p. 220.

PERGAMON

www.elsevier.nl/locate/poly

Polyhedron 19 (2000) 689–693

POLYHEDRON

Ni(II) and Cu(II) complexes with the dianionic N,N,O-tridentate Schiff base 6-amino-5-formyl-1,3-dimethyluracil-benzoylhydrazone. Crystal structure of the monodimensionally hydrogen-bonded aqua-(6-amino-1,3-dimethyl-uracilato-benzoylhydrazone(2-)-N^6,N^{51},O^{52}]-copper(II) hydrate

Francisco Hueso-Ureña [a], Nuria A. Illán-Cabeza [a], Miguel N. Moreno-Carretero [a,*], Antonio L. Peñas-Chamorro [a], René Faure [b]

[a] *Departamento de Química Inorgánica y Orgánica, Universidad de Jaén, 23071 Jaén, Spain*

[b] *Département Chimie Analytique 2, Université 'Claude Bernard'-Lyon I, 69622 Villeurbanne Cedex, France*

Received 26 October 1999; accepted 18 January 2000

Abstract

From the reaction between Cu(II) and Ni(II) salts and the Schiff base 6-amino-5-formyl-1,3-dimethyluracil-benzoylhydrazone (H_2BEZDO), in dimethylformamide (DMF)–water and ammonia media, the complexes Ni(BEZDO)·H_2O·NH_3, Cu(BEZDO)·H_2O·NH_3 and [Cu(BEZDO)(H_2O)]·H_2O containing the dianionic organic ligand have been obtained. These compounds have been studied by IR, electronic and EPR spectroscopy and magnetic measurements. The structure of [Cu(BEZDO)(H_2O)]·H_2O has been solved by means of X-ray diffraction methods. The coordination environment around the Cu(II) may be described as a square-plane structure in which the Schiff base acts as tridentate ligand through the N(6), N(51) and O(52) atoms, making two five- and six-membered chelate rings. The coordination sphere is completed with the oxygen atom of a water molecule; any additional interactions with potential donor atoms in the axial direction have not been found. The crystal structure is formed by infinite hydrogen-bonded monodimensional chains, in which the nearest metal centres are at distances of 4.511 and 3.585 Å. ©2000 Elsevier Science Ltd All rights reserved.

Keywords: Crystal structures; Nickel complexes; Copper complexes; Schiff bases; Uracil

1. Introduction

Biological activity of complexes derived from hydrazones has been widely studied and contrasted, acting in processes such as antibacterial, antitumoral, antiviral, antimalarial and antituberculosis effects [1]. The antitumoral and antiviral activities of a lot of complexes derived from hydrazones such as thiosemicarbazones have also been reported [2–5]. Often, these compounds show an N,N,S-coordinating pattern; however, there is very little information about O,N,O- or N,N,O-coordinated hydrazone compounds in the literature. We are studying the structure of several complexes with hydrazones derived from uracil, in which O,N,O- [6] and N,N,O-chelating systems [7–9] are present.

This paper focuses on the structural study of three new Ni(II) and Cu(II) complexes with the dianion of 6-amino-5-formyl-1,3-dimethyluracil-benzoylhydrazone, which seems to possess some important structural features related to the thiosemicarbazone complexes with biological activity. Thus, the molecular structure displays a global planar character with a local square plane around the metal ion and a N,N,O-tridentate system which may allow coordination of metal ions with a stronger acid character than the N,N,S-thiosemicarbazone chelating systems [10].

2. Experimental

2.1. Synthesis

2.1.1. Preparation of the ligand

The Schiff base ligand 6-amino-5-formyl-1,3-dimethyluracil-benzoylhydrazone (H_2BEZDO) was prepared by con-

* Corresponding author. Tel.: +34-953-212150; fax: +34-953-212186; e-mail: mmoreno@ujaen.es

0277-5387/00/$ - see front matter ©2000 Elsevier Science Ltd All rights reserved.
PII S0277-5387(00)00309-0

densation, in EtOH medium containing a few drops of glacial acetic acid, of equimolar amounts of 6-amino-5-formyl-1,3-dimethyluracil with benzoylhydrazine. Yield 85%. *Anal.* Found: C, 55.7; H, 5.1; N, 23.3%. Calc. for $C_{14}H_{15}N_5O_3$: C, 55.8; H, 5.1; N, 23.2%. IR (cm^{-1}): 3311, 3243, ν(N–H); 1705, 1646, ν(C=O); 1615, ν(C=N) + ν(C=C); 1456, 1289, ν(C=C) + ν(C–N); 1554, *Amide II*; 927, ν(N–N).

*2.1.2. Preparation of Ni(BEZDO)·H_2O·NH_3 (**1**)*

Equimolar amounts (0.5 mmol) of the ligand and the corresponding nitrate salt were mixed in 100 ml of concentrated aqueous ammonia. The resulting suspension was stirred and strongly heated for several hours; an orange powdery material was obtained, which was filtered off, washed with ethanol and diethyl ether and air dried. Yield 72%. *Anal.* Found: C, 42.8; H, 4.6; N, 21.3; $NH_3 + H_2O$, 9.4%. Calc. for $C_{14}H_{18}N_6O_4Ni$: C, 42.8; H, 4.6; N, 21.4; $NH_3 + H_2O$, 8.9%; loss of water and ammonia between 50 and 320°C (DSC peaks at 82 and 263°C). IR (cm^{-1}): 3455, 3405, ν(N–H); 1690, ν(C=O); 1615, 1592, ν(C=N) + ν(C=C); 1473, 1311, ν(C=C) + ν(C–N); 1555, *Amide II*; 971, ν(N–N); 435, ν(Ni–N). $\Lambda_M = 4$ ohm^{-1} cm^2 mol^{-1}.

*2.1.3. Preparation of Cu(BEZDO)·H_2O·NH_3 (**2**)*

The same procedure as that for complex **1** was used. Yield 60%. *Anal.* Found: C, 42.2; H, 4.4; N, 21.0; $NH_3 + H_2O$, 9.1%. Calc. for $C_{14}H_{18}N_6O_4Cu$: C, 42.3; H, 4.5; N, 21.1; $NH_3 + H_2O$, 9.0%; loss of water and ammonia between 50 and 300°C (DSC peaks at 97 and 235°C). IR (cm^{-1}): 3326, 3171, ν(N–H); 1693, ν(C=O); 1616, 1592, ν(C=N) + ν(C=C); 1474, 1301, ν(C=C) + ν(C–N); 1546, *Amide II*; 964, ν(N–N); 431, ν(Cu–N). $\Lambda_M = 2$ ohm^{-1} cm^2 mol^{-1}.

*2.1.4. Preparation of [Cu(BEZDO)(H_2O)]·H_2O (**3**)*

The synthesis of this complex was carried out by mixing equimolar amounts (0.5 mmol) of the ligand and $Cu(NO_3)_2 \cdot 3H_2O$ in 30 ml of DMF–water (1:1). The resulting solution was stirred and strongly heated for several hours; then, in order to make the solvent evaporate very slowly, the flask was covered with a plastic layer containing small holes. Some days later, a small amount of crystals suitable for X-ray diffraction studies was obtained; these crystals were filtered off, washed with ethanol and diethyl ether and air dried. Yield 65%. *Anal.* Found: C, 42.1; H, 4.3; N, 17.8; H_2O, 9.2%. Calc. for $C_{14}H_{17}N_5O_5Cu$: C, 42.2; H, 4.3; N, 17.6; H_2O, 9.0%; loss of water between 50 and 260°C (DSC peaks at 132 and 198°C). IR (cm^{-1}): 3436, 3387, ν(N–H); 1698, ν(C=O); 1621, 1598, ν(C=N) + ν(C=C); 1313, ν(C=C) + ν(C–N); 1559, *Amide II*; 970, ν(N–N); 434, ν(Cu–N). $\Lambda_M = 2$ ohm^{-1} cm^2 mol^{-1}.

2.2. Crystallographic studies

Crystal data: $C_{14}H_{17}N_5O_5Cu$; $M = 398.88$; monoclinic; $P2_1/c$; $a = 7.708(1)$, $b = 28.080(1)$, $c = 8.004(1)$ Å, $\beta = 115.812(1)°$, $V = 1559.6(5)$ Å^3 (from 25 random reflections); $T = 293$ K; graphite-monochromated Mo Kα radiation ($\lambda = 0.71073$ Å); $Z = 4$; $D_c = 1.699$ Mg m^{-3}; $F(000) = 820$; black cube ($0.1 \times 0.1 \times 0.1$ mm); $\mu = 14.971$ mm^{-1}; KappaCCD diffractometer, ω scans, data range $3.00 < \theta < 27.12°$, $0 \le h \le 8$, $0 \le k \le 36$, $-10 \le l \le 9$, 3530 reflections were measured, 2130 with $I > 3\sigma(I)$ were used in the refinement. Non-hydrogen atoms were located in successive difference Fourier maps and refined anisotropically by full-matrix least-squares on *F*. All the hydrogen atoms were located from ΔF series, but were not refined. The weighting scheme was $1/[\sigma^2(F_o) + 0.03F_o]$. The final *wR* [$I > 3\sigma(I)$] was 0.047 for 297 parameters, goodness-of-fit was 1.542, maximum and minimum residuals in the ΔF map were +0.35 and −0.57 e Å^{-3}. All calculations were made with the MaXus system (MacScience, Japan) and drawings were performed using the PLUTON 94 system.

2.3. Physical measurements

Microanalyses of C, H and N were performed on a Fisons EA1108 apparatus. The loss of water and ammonia was determined from the TG and DSC plots (Shimadzu TGA-50). Conductivity measurements were carried out using 10^{-3} M freshly prepared DMF solutions on a Hanna HI8820 instrument. IR were measured on a Perkin-Elmer FT-IR 1760-X (KBr pellets, 4000–400 cm^{-1}) and FT-IR Bruker Vector-22 spectrophotometers (polyethylene pellets, 600–220 cm^{-1}). Reflectance diffuse spectra (240–1500 nm) were recorded on a Perkin-Elmer UV–Vis–near-IR Lambda-19 machine using a $BaSO_4$ pellet as reference. The EPR spectra were obtained in the X-band at room temperature on a Bruker ESP 300E apparatus, with a microwave frequency of 9.79 GHz and a modulation frequency of 100 kHz. Magnetic measurements (77–290 K) were carried out on a Manics DSM-8 system.

3. Results and discussion

3.1. Description of the structure

In Fig. 1 a view of the molecular structure of the complex [Cu(BEZDO)(H_2O)]·H_2O (**1**) is depicted. The bond

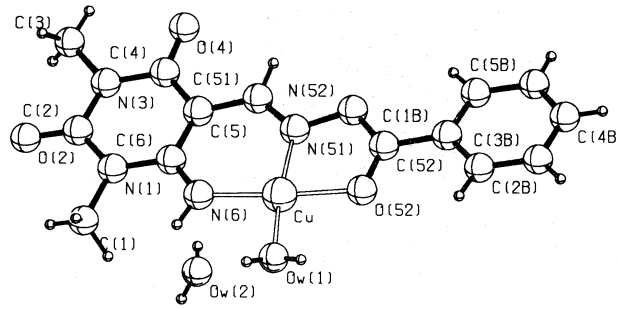


Fig. 1. Molecular drawing and numbering scheme for the monomeric unit of [Cu(BEZDO)(H_2O)]·H_2O.

Table 1
Bond lengths (Å) and angles (°) around the copper in the asymmetric unit of $[Cu(BEZDO)(H_2O)]\cdot H_2O$

Cu–N(51)	1.900(4)	N(6)–Cu–O(W1)	95.4(2)
Cu–N(6)	1.917(4)	N(51)–Cu–O(W1)	170.2(2)
Cu–O(52)	1.922(3)	O(52)–Cu–O(W1)	90.5(2)
Cu–O(W1)	1.980(4)	C(51)–N(51)–Cu	127.7(3)
N(51)–Cu–N(6)	92.5(2)	N(52)–N(51)–Cu	114.9(3)
N(51)–Cu–O(52)	81.8(2)	C(52)–O(52)–Cu	110.7(3)
N(6)–Cu–O(52)	173.9(2)	C(6)–N(6)–Cu	128.1(3)

Table 2
Hydrogen bonds in the structure of $[Cu(BEZDO)(H_2O)]\cdot H_2O$

D–H···A	D···A (Å)	H···A (Å)	∠D–H···A (°)
O(W1)–H···O(W2) [a]	2.673(5)	1.898	174
O(W1)–H···O(4) [b]	2.699(5)	1.941	175
O(W2)–H···N(52) [c]	2.865(5)	2.082	169
O(W2)–H···O(4) [d]	2.841(5)	1.983	177

[a] $1-x, -y, 2-z$.
[b] $1+x, y, 1+z$.
[c] $-x, -y, 1-z$.
[d] $x, y, 1+z$.

length and angles around the metal centre are given in Table 1. The coordination sphere around the metal displays a square-based geometry with the tridentate ligand $BEZDO^{2-}$ coordinated through the N(6), N(51) and O(52) atoms and an oxygen atom of a water molecule, at distances of between 1.9 and 2.0 Å. The assignment of the N(6) as metal-binding site, instead of its pseudo-related O(4) atom (through the pseudo-two-fold axis passing through O(2)–C(2)–C(5)–C(51)), was carried out on the basis of two facts: (1) the location of one hydrogen, H(6), attached to the N(6) donor atom; and (2) the larger C(6)–N(6) distance (1.310(6) Å) compared with the C(4)–O(4) distance (1.261(5) Å) [6–9]. The remaining water molecule is joined to the structure through three hydrogen bonds. There is no other potential donor atom above or below the coordination plane, which allows us to suggest a coordination number bigger than four.

The molecular unit rings are virtually planar, with average torsion angles from 0.9 (benzene ring) to 4.2° (uracil ring). The uracil ring is almost coplanar with both chelates, with dihedral angles near to 4°. However, the benzene ring is angled by 10.4° with the uracil ring, and this angle is smaller than that of the free ligand (38.2°) . Thus, the molecular unit is formed by three adjacent rings, the two chelates and the uracil ring, almost coplanar with each other, which must contribute to the stability of the structure.

Geometrical details of the hydrogen bonding are given in Table 2. The establishment of hydrogen bonds makes chains that are monodimensionally extended through the 101 direction (Fig. 2). The molecules are joined through the hydrogen bonds O(W1)–H···O(W2), O(W1)–H···O4 and O(W2)–H···N(52); these bonds make a chain in which the coordination planes are roughly perpendicular to the $10\bar{1}$ direction. Each chain is paired with an analogous one through two hydrogen bonds O(W2)–H···O(4), in such a way that the molecular units are mutually related by symmetry centres. In the structure, the shorter distances between two copper atoms are Cu–Cu $(1-x, -y, 1-z)$ 4.511 Å and Cu–Cu $(1-x, -y, 2-z)$ 3.585 Å.

In order to analyse the possible different tautomeric forms of the ligand $HBEZDO^{2-}$ in this complex, the bond distances near the donor atoms have been compared (see Table 3) with those in the free ligand structure and in other complexes in which this ligand appears undeprotonated [6] and monodeprotonated [8,11]. The possible forms in which the negative charges lie near to the donor atoms, i.e. N(6), N(51) and O(52), are given in Fig. 3. In forms I–III, the negative charge of the N(6) atom moves near the donor atoms. The forms

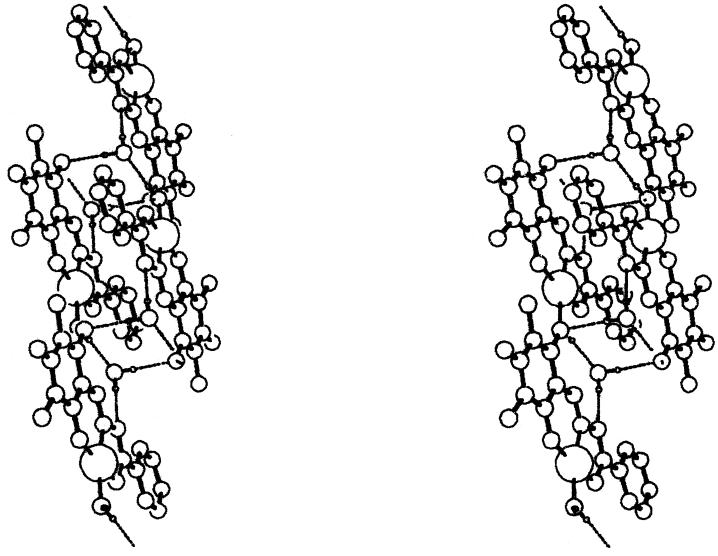


Fig. 2. Stereoview of the hydrogen-bonded chains in the crystal structure of $[Cu(BEZDO)(H_2O)]\cdot H_2O$. The chain grows following the [101] direction and the coordination planes are roughly perpendicular to the $10\bar{1}$ direction.

Table 3
Selected bond lengths (Å) in H_2BEZDO

Bond	Free [a]	Coordinated to Cu(II)		
		Neutral [b] (O4, N51, O52)	Monoanion [c] (N6, N51, O52)	Dianion [d] (N6, N51, O52)
C(4)–O(4)	1.24	1.258	1.226(6)	1.261
C(6)–N(6)	1.32	1.329	1.303(5)	1.310
C(5)–C(51)	1.434	1.418	1.40(1)	1.412
C(51)–N(51)	1.283	1.245	1.29(1)	1.295
N(51)–N(52)	1.39	1.393	1.390(2)	1.405
N(52)–C(52)	1.335	1.333	1.328(6)	1.310
C(52)–O(52)	1.23	1.26	1.259(3)	1.311

[a] In H_2BEZDO·0.5EtOH.
[b] In [Cu(H_2BEZDO)(H_2O)(ClO_4)]ClO_4.
[c] Mean values from compounds [Cu(HBEZDO)(H_2O)(MeOH)]NO_3, [Cu(HBEZDO)(H_2O)(EtOH)]NO_3, [Cu(HBEZDO)(DMF)Cl] and [Cu(HBEZDO)Br]·2H_2O; in parentheses, standard deviation.
[d] In [Cu(BEZDO)(H_2O)]·H_2O (this work).

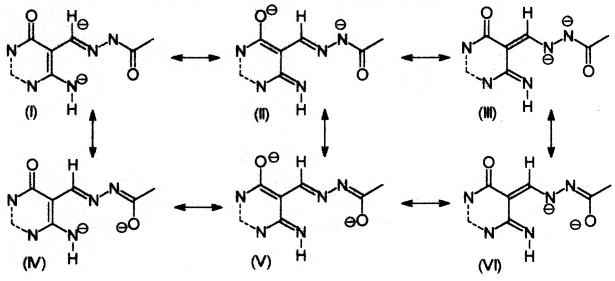


Fig. 3. Structure of the possible tautomeric forms for the dianion $BEZDO^{2-}$.

IV–VI may be explained by the ceto-imine equilibrium which displaces the negative charge from the N(52) atom to the O(52) atom.

The C(52)–O(52) bond distance is clearly longer in the dianion than in the others. This indicates that there is an important contribution of any of forms IV–VI. The C(4)–O(4) bond distance becomes longer due to involvement of the oxygen atom in the hydrogen bonds. The C(6)–N(6) and C(5)–C(51) bond distances become shorter, as in the monoanionic form of the ligand. C(51)–N(51) becomes a little longer than in the monoanion, and N(51)–N(52) and N(52)–C(52) become longer and shorter, respectively, with respect to their lengths in the monoanionic form. Therefore, it may be suggested there is a main contribution to the structure of the dianion by forms III and VI. The proximity of the two negative charges in form III may explain the lengthening of the N(51)–N(52) bond (1.405 Å), whereas the double bond N(52)=C(52), present in form VI, could justify the shortening of this distance (1.310 Å) compared with the monoanion (≈1.33 Å). Finally, the C(52)–O(52) bond is double in form III and single in form VI, which is in accordance with the intermediate bond distance experimentally found (1.311 Å). However, some contribution of form IV must be taken into account in order to explain the intermediate single–double character of the C(6)–N(6) bond (1.310 Å).

3.2. Spectral and magnetic properties

The comparative study of the infrared spectra of the complexes and the free ligand is very difficult because of the large number of bands, and only general remarks can be made. A general displacement is observed due to the coordination and deprotonation processes. These shifts agree with those found in the literature for similar compounds [12–16]. In all cases, as observed in other related complexes, the band assigned to the ν(N–N) mode is shifted to a higher wavenumber, which could be explained by the more electronic delocalization due to the O52 coordination to the metal. Also, the far-IR spectra show a band at around 430 cm^{-1} assignable to the ν(M–N) mode [17].

The Ni(II) complex (**1**) is diamagnetic, although when diamagnetic corrections were done $\mu_{eff} \approx 0.5$ BM was found, which is in accordance, together with the orange colour of the compound, with a square-plane structure. Magnetic susceptibility measurements at different temperatures in the two Cu(II) complexes have been successfully fitted to the Curie–Weiss law ($1/\chi_m = (T-\theta)/C$) (**2**, $C = 0.299(5)$ ucgs K mol^{-1}, $\theta = 16(5)$ K, $r = 0.9969$, $\mu_{eff} = 1.85(5)$ BM; **3**, $C = 0.325(6)$ ucgs K mol^{-1}, $\theta = 16(6)$ K, $r = 0.9960$, $\mu_{eff} = 1.91(5)$ BM) and the effective magnetic moments are in accordance with diluted monomeric units.

The X-band EPR spectrum on polycrystalline samples of the two Cu(II) complexes looks like an axial doublet with $g_\perp = 2.03$ and $g_\parallel = 2.19$ (**1**), $g_\perp = 2.05$ and $g_\parallel = 2.21$ (**2**). The observed pattern $g_\parallel > g_\perp > 2.0$ is indicative of a copper(II) $d_{x^2-y^2}$ orbital ground state in agreement with the square-plane environment of the copper.

The electronic spectra show bands assignable to tetragonally surrounded Ni(II) and Cu(II) ions. Thus, in the spectrum of the Ni(II) complex, only a single absorption is observed at 20900 cm^{-1}, as a consequence of the eight electrons of Ni(II) paired in the four low-lying d orbitals; these orbitals are often so close together in energy that individual transitions therefrom to the upper d level cannot be distinguished [18]. The copper complexes display a broad and poorly defined band centred at 17600 (**2**) and 16600 cm^{-1} (**3**); the bathochromic shift of the maximum is in accordance with the existence of a coordinated ammonia and a water molecule, respectively.

From these data, a similar structure to that found for complex **3** can be proposed for complexes **1** and **2**, but in these compounds the square-planar coordination around the metals must be completed with an ammonia molecule, instead of a water molecule as in compound **3**.

Supplementary data

Supplementary data are available from the Cambridge Crystallographic Data Centre, 12 Union Road, Cambridge CB2 1EZ, UK (fax: +44-1223-336033; e-mail: deposit@ccdc.cam.ac.uk) on request, quoting deposition number CCDC 119505.

Acknowledgements

The authors are indebted to Dirección General de Enseñanza Superior e Investigación Científica (MEC, Spain) for financial support through the project PB97-0786-C03-03.

References

[1] D.X. West, A.E. Liberta, S.B. Padhye, P.B. Chikate, A.S. Sonawane, O. Kumbhar, R.G. Yerande, Coord. Chem. Rev. 123 (1993) 49.
[2] D. Kovala-Demertzi, A. Domopoulou, M. Demertzis, C. Raptopoulou, A. Terzis, Polyhedron 13 (1994) 1917.
[3] D.X. West, M.A. Lockwood, A. Castiñeiras, Transition Met. Chem. 22 (1997) 447.
[4] D.X. West, H. Gebremedhin, R.J. Butcher, J.P. Jasinski, Transition Met. Chem. 20 (1995) 84.
[5] D. Kovala-Demertzi, A. Domopoulou, M.A. Demertzis, G. Valle, A. Papageorgiou, J. Inorg. Biochem. 68 (1997) 147.
[6] F. Hueso-Ureña, M.N. Moreno-Carretero, A.L. Peñas-Chamorro, J.M. Amigó, V. Esteve, T. Debaerdemaeker, Polyhedron 18 (1999) 2205.
[7] F. Hueso-Ureña, M.N. Moreno-Carretero, A.L. Peñas-Chamorro, M. Quirós-Olozábal, J.M. Salas-Peregrín, Polyhedron 18 (1999) 351.
[8] F. Hueso-Ureña, M.N. Moreno-Carretero, A.L. Peñas-Chamorro, J.M. Amigó, V. Esteve, T. Debaerdemaeker, Polyhedron 18 (1999) 3629.
[9] F. Hueso-Ureña, M.N. Moreno-Carretero, A.L. Peñas-Chamorro, M. Quirós-Olozábal, J.M. Salas-Peregrín, J. Chem. Crystallogr. 29 (1999) 283.
[10] F. Hueso-Ureña, N.A. Illán-Cabeza, M.N. Moreno-Carretero, A.L. Peñas-Chamorro, R. Faure, Inorg. Chem. Commun. 2 (1999) 323.
[11] F. Hueso-Ureña, M.N. Moreno-Carretero, A.L. Peñas-Chamorro, J.M. Amigó, V. Esteve, T. Debaerdemaeker, Z. Kristallogr. NCS 215 (2000) 155.
[12] D.X. West, J.S. Ives, J. Krejci, M.M. Salberg, T.L. Zumbahlen, G.A. Bain, A.E. Liberta, J. Valdés-Martínez, S. Hernández-Ortiz, R.A. Toscano, Polyhedron 14 (1995) 2189.
[13] D.X. West, R.M. Makeever, G. Ertem, J.P. Scovill, L.K. Pannell, Transition Met. Chem. 11 (1986) 131.
[14] D. Kovala-Demertzi, A. Domopoulou, M.A. Demertzis, G. Valle, A. Papageorgiou, J. Inorg. Biochem. 68 (1997) 147.
[15] D. Lin-Vien, N.B. Colthup, W.G. Fateley, J.G. Grasselli, The Handbook of Infrared and Raman Characteristic Frequencies of Organic Molecules, Academic Press, London, 1991.
[16] G. Socrates, Infrared Characteristic Group Frequencies, Wiley, Chichester, 1994.
[17] J.R. Ferraro, Low-Frequency Vibrations of Inorganic and Coordination Compounds (1971) Plenum Press, New York .
[18] A.B.P. Lever, Inorganic Electronic Spectroscopy 2nd edn., (1984) Elsevier, Amsterdam .

PERGAMON

www.elsevier.nl/locate/poly

Polyhedron 19 (2000) 695–704

POLYHEDRON

New *E*-unidentate $[Ph_2P(O)NP(E)Ph_2]^-$ (E = S or Se) complexes of palladium(II) and platinum(II)

Martin B. Smith* [1,a], Alexandra M.Z. Slawin* [2,b]

[a] *Department of Chemistry, Loughborough University, Loughborough, Leics. LE11 3TU, UK*
[b] *School of Chemistry, University of St. Andrews, St. Andrews, Fife KY16 9ST, UK*

Received 27 October 1999; accepted 21 January 2000

Abstract

Metathesis of the monochloro metal(II) complexes [MCl(dien)]Cl (M = Pd or Pt; dien = diethylenetriamine) with $K[Ph_2P(O)NP(E)Ph_2]$ (E = S or Se) or $K[Ph_2P(O)NPPh_2]$ (prepared in situ from $Ph_2P(O)NHPPh_2/KOBu^t$) in methanol gave the cationic, mononuclear compounds $[M\{Ph_2P(O)NP(E)Ph_2\text{-}E\}(dien)]^+$ or $[M\{Ph_2P(O)NPPh_2\text{-}P\}(dien)]^+$, isolated as their hexafluorophosphate salts. Ligand substitution reactions of the dichlorometal(II) precursors $[MCl_2(N\sim N)]$ (M = Pd or Pt; N∼N = ethane-1,2-diamine, 1,2-diaminocyclohexane) with $K[Ph_2P(O)NP(E)Ph_2]$ or $K[Ph_2P(O)NPPh_2]$ gave the neutral bis substituted compounds $[M\{Ph_2P(O)NP(E)Ph_2\text{-}E\}_2(N\sim N)]$ or $[M\{Ph_2P(O)NPPh_2\text{-}P\}_2(N\sim N)]$ in high yields (63–89%). Reaction of the unsymmetrical palladium(II) compound $[PdCl_2(ampy)]$ (ampy = 2-aminomethylpyridine) with $K[Ph_2P(O)NP(E)Ph_2]$ gave $[Pd\{Ph_2P(O)NP(E)Ph_2\text{-}E\}_2(ampy)]$, analogous to the recently described compound $[Pd\{Ph_2P(O)NP(E)Ph_2\text{-}E\}_2(en)]$, in which both $[Ph_2P(O)NP(E)Ph_2]^-$ ligands are exclusively *E*-monodentate bound. In contrast, transmetallation of $K[Ph_2P(O)NP(E)Ph_2]$ with $[PdCl_2(tmeda)]$ (tmeda = *N,N,N′,N′*-tetramethylethylenediamine) gave only the *O,E*-chelate monocationic complexes $[Pd\{Ph_2P(O)NP(E)Ph_2\text{-}O,E\}(tmeda)]PF_6$ and not $[Pd\{Ph_2P(O)NP(E)Ph_2\text{-}E\}_2(tmeda)]$. Under similar reaction conditions the symmetrical anions $[Ph_2P(E)NP(E)Ph_2]^-$ (E = S or Se) gave, without exception, the known bis homoleptic complexes $[M\{Ph_2P(E)NP(E)Ph_2\text{-}E,E'\}_2]$ (M = Pd or Pt) with displacement of all chloride and amine ligands. All new compounds have been characterised by a combination of multinuclear NMR (^1H, $^{31}P\{^1H\}$, $^{195}Pt\{^1H\}$), IR spectroscopy and elemental analyses. Furthermore, the X-ray crystal structures of five compounds have been determined and reveal a range of intermolecular and intramolecular hydrogen bonding contacts. There is also evidence for π-delocalisation within the E–P–N–P–O and P–N–P–O backbones of the *E*-ligating or *O,E*-chelating ligand. ©2000 Elsevier Science Ltd All rights reserved.

Keywords: Palladium(II) complexes; Platinum(II) complexes; Chloride metathesis; X-ray crystallography; Heterodifunctional ligands

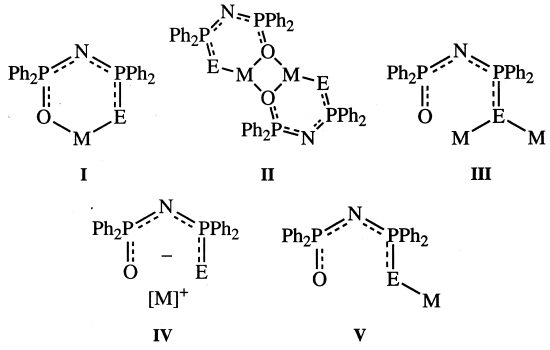
1. Introduction

The coordination chemistry of phosphorus containing ligands with inorganic backbones, for example R_2PNHPR_2 [1–4], $[R_2PNPR_2]^-$ [5,6], $R_2P(E)NHPR_2$ [7,8], $[R_2P(E)NPR_2]^-$ [7,8] and $[R_2P(E)NP(E)R_2]^-$ (E = O, S or Se) [9–17], has been the topic of much interest especially over the last three years. Specifically $[Ph_2P(E)NP(E)Ph_2]^-$, which coincidentally is closely related to $acac^-$ (acetylacetonate), is an excellent ligand for complexing numerous metal ions and furthermore has found important uses as selective metal extractants [18], NMR shift reagents [19] and more recently in catalysis [20]. This class of ligand displays a wide range of ligation modes reminiscent to that of $acac^-$ and its derivatives [21]. In contrast, the coordinating ability of the unsymmetrical ligands $[Ph_2P(O)NP(E)Ph_2]^-$ (E = S or Se), bearing a mismatch in donor atoms, has been remarkably poorly studied, especially towards transition-metal ions [22–26]. Furthermore, sparse examples of compounds with $[Ph_2P(O)NP(E)Ph_2]^-$ and a central s- [27] or p-block [28–30] element have only recently been reported. Of those examples documented, the *O,E*-chelating mode of binding (**I**) is most prevalent [22,25,26,28–30]. One very unusual example is the complex *cis*-$[Pd\{Ph_2P(O)NP(Se)Ph_2\text{-}O,Se\}_2]$ in which both six-membered Pd–O–P–N–P–Se rings adopt distinctly different ring geometries (X-ray evidence) [26]. Silvestru and coworkers recently described the synthesis and X-ray crystal structure of the dimeric compound $[Na\{Ph_2P(O)NP(S)Ph_2\}\cdot 2C_4H_8O]_2$ in which each $[Ph_2P(O)NP(S)Ph_2]^-$ behaves simultaneously as an *O,S*-chelating and *O*-bridging ligand (**II**) [27]. In

[1] *Corresponding author. Tel.: +44-1509-222553; fax: +44-1509-223925; e-mail: m.b.smith@lboro.ac.uk
[2] *Corresponding author.

0277-5387/00/$ - see front matter ©2000 Elsevier Science Ltd All rights reserved.
PII S0277-5387(00)00311-9

contrast the 'soft' *E*-donor of $[Ph_2P(O)NP(E)Ph_2]^-$ can bridge two late transition-metal centres (**III**), as observed in $[\{Pd(\eta^3\text{-}C_3H_5)[\mu\text{-}Ph_2P(O)NP(Se)Ph_2\text{-}Se]\}_2]$, forming a central Pd_2Se_2 core with two pendant $-P(O)Ph_2$ groups [23]. The $[Ph_2P(O)NP(E)Ph_2]^-$ can also behave as a non-coordinating anion (**IV**) as exemplified by the unusual salt $[Pt(Ph_2PC_6H_4NH_2\text{-}P,N)(Ph_2PC_6H_4NH\text{-}P,N)][Ph_2P(O)\text{-}NP(E)Ph_2]$ (E = S or Se) [22]. We described in a recent preliminary communication [24] the synthesis and characterisation of $[Pd\{Ph_2P(O)NP(E)Ph_2\text{-}E\}_2(en)]$ and $[Au\{Ph_2P(O)NP(E)Ph_2\text{-}E\}\{Ph_2P(O)NHPPh_2\text{-}P\}]$ which are the first reported examples in which $[Ph_2P(O)NP\text{-}(E)Ph_2]^-$ adopts an *E*-monodentate coordination mode (**V**). This mode of ligation is especially noteworthy since $[Ph_2P(O)NP(E)Ph_2]^-$ are ambidentate ligands capable of binding through either O or E donor atoms depending on whether the metal centre is 'soft' or 'hard' in character. Furthermore in these rare examples there is a strong propensity for hydrogen bonding between the 'dangling' $-P(O)Ph_2$ group and the ancillary amine ligand [en, $Ph_2P(O)NHPPh_2$] in the metal coordination sphere.



An understanding of the binding capabilities of these extremely versatile, readily synthesised, ligands towards precious metals and their subsequent reactivity is important given that complexes of acac are useful in several metal complex catalysed reactions. Furthermore, there is considerable interest in *cis*-$[PtCl_2(amine)_2]$ for their cytotoxic activity and their reactivity with various sulfur containing ligands. To elucidate further the complexing properties of $[Ph_2P(O)NP(E)Ph_2]^-$ (E = S or Se), their reactions with selected metal(II) amine complexes have been investigated. We present here our work regarding the synthesis and characterisation of a series of square-planar palladium(II) and platinum(II) complexes with didentate and tridentate amine and monodentate *E*-bound $[Ph_2P(O)NP(E)Ph_2]^-$ ligands. For comparison we have extended the scope of these reactions to the preparation of related complexes with *P*-bound $[Ph_2P(O)NPPh_2]^-$ ligands. The new compounds have been characterised by multinuclear NMR (^1H, $^{31}P\{^1H\}$, $^{195}Pt\{^1H\}$), IR spectroscopy and elemental analyses. Moreover, the molecular structures of five compounds are reported and confirm, in three cases, that $[Ph_2P(O)NP(E)Ph_2]^-$ adopts an *E*-unidentate mode of bonding and also a range of intramolecular and intermolecular hydrogen bonding motifs.

2. Experimental

2.1. General

Unless otherwise stated manipulations were carried out in air with no special precaution taken regarding the use of dry/distilled solvents. The potassium salts $K[Ph_2P(O)\text{-}NP(E)Ph_2]$ (E = S or Se) [26] and $K[Ph_2P(E)NP(E)Ph_2]$ (E = S or Se) [8,31] were prepared according to known procedures whilst $K[Ph_2P(O)NPPh_2]$ was prepared in situ from $Ph_2P(O)NHPPh_2$/KOBu^t. The compounds $[PdCl_2\text{-}(en)]$, $[PdCl_2(tmeda)]$, $[PtCl_2(C_6H_{14}N_2)]$ ($C_6H_{14}N_2$ = 1,2-diaminocyclohexane), $[PtCl_2(py)_2]$, $[NH_4][PF_6]$ and KOBu^t were purchased from Aldrich Chemical Co. and used without further purification. [MCl(dien)]Cl (M = Pd or Pt) and $[PdCl_2(ampy)]$ were prepared by previous reported methods [32–34].

Infrared spectra were recorded as KBr pellets in the range 4000–220 cm^{-1} on a Perkin-Elmer system 2000 Fourier-transform spectrometer. ^1H NMR spectra (250 MHz) were recorded on a Bruker AC250 FT spectrometer with chemical shifts δ in ppm to high frequency of $Si(CH_3)_4$ and coupling constants *J* in Hz; $^{31}P\{^1H\}$ NMR spectra (36.2 MHz) were recorded on a JEOL FX90Q spectrometer with chemical shifts δ in ppm to high frequency of 85% H_3PO_4 and coupling constants *J* in Hz; $^{195}Pt\{^1H\}$ NMR spectra (53.7 MHz) were recorded on a Bruker AC250 FT NMR spectrometer with δ referenced to external H_2PtCl_6 (in D_2O/HCl). All spectra were measured in $CDCl_3$ unless otherwise stated. Elemental analyses (Perkin-Elmer 2400 CHN elemental analyser) were performed by the Loughborough University Analytical Service within the Department of Chemistry.

Precious metal salts were provided on loan by Johnson Matthey plc.

2.2. Preparations

2.2.1. Preparation of $[Pd\{Ph_2P(O)NP(S)Ph_2\text{-}S\}(dien)]PF_6$ (1)

To the solids [PdCl(dien)]Cl (0.029 g, 0.103 mmol) and $K[Ph_2P(O)NP(S)Ph_2]$ (0.051 g, 0.108 mmol) was added CH_3OH (1 cm^3). After stirring at ambient temperature for ca. 2 h, the yellow solution was filtered to remove trace amounts of solid, and a methanolic solution (ca. 0.5 cm^3) of $[NH_4][PF_6]$ (0.041 g, 0.252 mmol) was added. The solution was stirred for 15 min and distilled water was added dropwise to afford a yellow precipitate. The mixture was stirred for an additional 20 min and the solid **1** isolated by suction filtration and dried in vacuo. Yield 0.071 g, 88%. FAB^+ MS: *m/z* 641 $(M\text{–}PF_6)^+$. IR: 3641 (ν_{OH}), 3319, 3268, 3202, 3112 (ν_{NH}), 1243 (ν_{PNP}), 562 (ν_{PS}). ^1H NMR (CD_3OD): 7.99–7.29 (arom. H), 2.89–2.54 (dien). In a similar manner the following complexes were prepared: $[Pd\{Ph_2P(O)NP(Se)\text{-}Ph_2\text{-}Se\}(dien)]PF_6$ (**2**) (85%). FAB^+ MS: *m/z* 689 $(M-PF_6)^+$. IR: 3639 (ν_{OH}), 3316, 3268, 3203, 3115 (ν_{NH}), 1236 (ν_{PNP}), 558 (ν_{PSe}). ^1H NMR (CD_3OD): 7.96–7.34

(arom. H), 2.90–2.55 (dien). [Pt{$Ph_2P(O)NP(S)Ph_2$-*S*}(dien)]PF_6 (**3**) (83%). FAB^+ MS: *m/z* 730 ($M-PF_6$). IR: 3640 (ν_{OH}), 3306, 3214 (ν_{NH}), 1223 (ν_{PNP}), 559 (ν_{PS}). ^1H NMR (CD_3OD): 7.95–7.35 (arom. H), 3.06–2.48 (dien). [Pt{$Ph_2P(O)NP(Se)Ph_2$-*Se*}(dien)]PF_6 (**4**) (85%). FAB^+ MS: *m/z* 777 $(M-PF_6)^+$. IR: 3651, 3636 (ν_{OH}), 3303, 3204, 3113 (ν_{NH}), 1239 (ν_{PNP}), 558 (ν_{PSe}). ^1H NMR (CD_3OD): 7.97–7.36 (arom. H), 3.18–2.46 (dien). [Pd{$Ph_2P(O)NPPh_2$-*P*}(dien)]PF_6 (**5**) (71%). FAB^+ MS: *m/z* 609 $(M-PF_6)^+$. IR: 3334, 3280, 3193 (ν_{NH}), 1165, 1155 (ν_{PNP}). ^1H NMR (CD_3OD): 8.03–7.38 (arom. H), 3.08–2.63 (dien).

Crystals of **1** and **2** suitable for X-ray crystallography were grown by slow diffusion of Et_2O into a CH_3OH solution over ca. 4 days.

Reaction of [MCl(dien)]Cl (M = Pd or Pt) with K[$Ph_2P(E)NP(E)Ph_2$] (E = S or Se, 1:1 or 1:2 molar ratio) under analogous conditions to those described above gave the known homoleptic complexes [M{$Ph_2P(E)NP(E)Ph_2$-*E,E′*}$_2$] [42]. The ^{31}P NMR shifts were identical to those previously reported.

2.2.2. Preparation of [Pd{$Ph_2P(O)NPPh_2$-*P*}$_2$(en)] (*6*)

To the solids [$PdCl_2$(en)] (0.024 g, 0.101 mmol) and $Ph_2P(O)NHPPh_2$ (0.084 g, 0.209 mmol) was added CH_3OH (1.5 cm^3). To this slurry was added $KOBu^t$ (0.025 g, 0.223 mmol) and the mixture was stirred for ca. 4 h. The solid was filtered under reduced pressure, washed with CH_3OH (ca. 0.5 cm^3) and dried in vacuo. Yield 0.062 g, 63%. FAB^+ MS: *m/z* 967 (M^+). IR: 3650 (ν_{OH}), 3313, 3294, 3194 (ν_{NH}), 1188, 1173 (ν_{PNP}). ^1H NMR: 8.18–6.90 (arom. H), 2.80, 1.76 (CH_2, NH_2).

Crystals of **6** suitable for X-ray crystallography were grown by slow evaporation of a $CDCl_3/Et_2O$ solution over ca. 30 days.

2.2.3. Preparation of [Pt{$Ph_2P(O)NP(S)Ph_2$-*S*}$_2$($C_6H_{14}N_2$)] (*7*)

A slurry of [$PtCl_2(C_6H_{14}N_2)$] (0.020 g, 0.0526 mmol) and K[$Ph_2P(O)NP(S)Ph_2$] (0.050 g, 0.106 mmol) in CH_3OH (10 cm^3) was refluxed, under a nitrogen atmosphere, for 5 h. The yellow solution was evaporated to dryness under reduced pressure, the residue taken up in CH_2Cl_2 (5 cm^3) and passed through a Celite pad. The volume was reduced to ca. 1 cm^3 and petroleum ether (b.p. 60–80°C, 10 cm^3) added to precipitate the product **7** which was collected by suction filtration and dried in vacuo. Yield 0.050 g, 81%. FAB^+ MS: *m/z* 1175 (M^+). IR: 3287, 3262, 3201 (ν_{NH}), 1282, 1249, 1235 (ν_{PNP}), 560 (ν_{PS}). ^1H NMR: 7.89–7.24 (arom. H), 5.46, 4.40, 1.80–0.80 ($C_6H_{14}N_2$). In a similar manner [Pt{$Ph_2P(O)NP(Se)Ph_2$-*Se*}$_2$($C_6H_{14}N_2$)] (**8**) was prepared in 89% yield. FAB^+ MS: *m/z* 1269 (M^+). IR: 3293, 3266, 3205 (ν_{NH}), 1243 (ν_{PNP}), 545 (ν_{PSe}). ^1H NMR: 7.91–7.26 (arom. H), 5.35, 4.40, 1.81–0.86 ($C_6H_{14}N_2$). Attempts to prepare [Pt{$Ph_2P(O)NP(E)Ph_2$-*E*}$_2$($py)_2$] under similar conditions gave several phosphorus containing species (^{31}P NMR evidence).

2.2.4. Preparation of [Pd{$Ph_2P(O)NP(S)Ph_2$-*S*}$_2$(ampy)] (*9*)

To the solids [$PdCl_2$(ampy)] (0.017 g, 0.070 mmol) and K[$Ph_2P(O)NP(S)Ph_2$] (0.070 g, 0.148 mmol) was added CH_3OH (1 cm^3). The solids dissolved slowly within ca. 10 min whereupon product **9** deposited. The mixture was stirred for a further 2 h and the solid collected by suction filtration and dried in vacuo. Yield 0.058 g, 77%. FAB^+ MS: *m/z* 1079 (M^+). IR: 3227, 3176 (ν_{NH}), 1287, 1266, 1232 (ν_{PNP}), 564 (ν_{PS}). ^1H NMR: 8.90–6.76 (arom. H), 5.21, 3.78 (NH_2, CH_2). In a similar manner [Pd{$Ph_2P(O)NP(Se)Ph_2$-*Se*}$_2$(ampy)] (**10**) was prepared in 87% yield. FAB^+ MS: *m/z* 1174 (M^+). IR: 3231, 3189 (ν_{NH}), 1283, 1259, 1225 (ν_{PNP}), 560, 549, 540 (ν_{PSe}). ^1H NMR: 9.23–6.87 (arom. H), 4.83, 3.75 (NH_2, CH_2). The solids **9** and **10** could be recrystallised from CH_2Cl_2/OEt_2.

Crystals of **9** suitable for X-ray crystallography were grown by slow diffusion of petroleum ether (b.p. 60–80°C) into a $CDCl_3$ solution over the course of ca. 4 days.

Reaction of [$PdCl_2$(ampy)] with 2 equiv. of K[$Ph_2P(E)NP(E)Ph_2$] (E = S or Se) gave [Pd{$Ph_2P(E)NP(E)Ph_2$-*E,E′*}$_2$] in 87% (E = S) and 63% (E = Se) yields respectively.

2.2.5. Preparation of [Pd{$Ph_2P(O)NP(S)Ph_2$-*O,S*}(tmeda)]PF_6 (*11*)

To the solids [$PdCl_2$(tmeda)] (0.029 g, 0.099 mmol) and K[$Ph_2P(O)NP(S)Ph_2$] (0.049 g, 0.104 mmol) was added CH_3OH (1 cm^3). After stirring for 2 h, the solution was filtered and a methanolic (ca. 0.5 cm^3) solution of [NH_4][PF_6] (0.040 g) was added to afford a yellow precipitate. The product was collected by suction filtration and dried in vacuo. Yield 0.073 g, 92%. FAB^+ MS: *m/z* 654 $(M-PF_6)^+$. IR: 1230 (ν_{PNP}), 581 (ν_{PS}). ^1H NMR: 7.90–7.38 (arom. H), 2.76 (CH_2), 2.63, 2.39 [$N(CH_3)_2$]. In a similar manner [Pd{$Ph_2P(O)NP(Se)Ph_2$-*O,Se*}(tmeda)]PF_6 (**12**) was prepared (95%). FAB^+ MS: *m/z* 702 $(M-PF_6)^+$. IR: 1230 (ν_{PNP}), 539 (ν_{PSe}). ^1H NMR: 7.92–7.38 (arom. H), 2.76 (CH_2), 2.60, 2.46 [$N(CH_3)_2$].

Crystals of **11** suitable for X-ray crystallography were grown by slow diffusion of diethyl ether into a CH_3OH/CH_2Cl_2 solution over the course of ca. 3 days.

Microanalytical and spectroscopic data are given in Tables 1 and 2.

2.3. X-ray crystallography

The crystal structures of complexes **1**, **2**, **6**, **9** and **11** were determined using either a Rigaku AFC7S serial diffractometer with graphite-monochromated (Cu Kα) radiation (λ = 1.541 78 Å) and ω-scans or a Bruker SMART diffractometer with graphite-monochromated (Mo Kα) radiation (λ = 0.710 37 Å). Details of the crystal data collections and

Table 1
Microanalytical data for compounds **1**–**12** [a]

Compound	C	H	N
1 [b]	41.70 (41.70)	4.25 (4.55)	7.25 (6.85)
2 [c]	39.40 (40.20)	3.80 (4.00)	5.95 (6.45)
3	38.00 (38.40)	3.60 (3.80)	6.05 (6.40)
4	36.15 (36.45)	3.55 (3.60)	5.95 (6.05)
5	44.45 (44.55)	4.45 (4.40)	7.05 (7.40)
6 [d]	60.90 (60.95)	4.85 (5.15)	5.55 (5.70)
7	55.00 (55.25)	4.85 (4.65)	4.60 (4.75)
8	51.20 (51.15)	4.35 (4.30)	4.10 (4.40)
9 [d]	58.95 (59.10)	4.45 (4.60)	5.00 (5.10)
10 [d]	54.15 (54.45)	4.10 (4.25)	4.35 (4.70)
11	44.85 (45.05)	4.30 (4.55)	5.70 (5.25)
12	42.50 (42.55)	4.25 (4.30)	4.95 (4.95)

[a] Calculated values in parentheses.
[b] As $H_2O \cdot 0.5CH_3OH$ solvate.
[c] As CH_3OH solvate.
[d] As H_2O solvate.

Table 2
Selected NMR data for compounds **1**–**12**

Compound	$\delta(P_E)$ [a]	$J(PtP_E)$	$J(PSe)$	$\delta(P_O)$	$J(PP)$	$\delta(Pt)$
1	29.1 [b]			16.5		
2	14.6 [b]		497	17.3		
3	26.4 [b]	96.8		16.6		−3084
4	11.5 [b]	101.2	484	17.4		−3135
5	32.1			21.7	19.8	
6	35.5			18.2	17.6	
7	25.9	94.5		15.0		−3226
8	10.4	105.6	514	15.6		−3399
9	28.1, 27.4			15.1, 10.3		
10	14.0, 13.3		488, 519	16.3, 11.7		
11	34.8 [b]			37.6		
12	20.2 [b]		475	38.9		

[a] E = S or Se.
[b] Recorded in $CDCl_3/CH_3OH$.

refinements are given in Table 3. For the SMART data, intensities were collected using 0.3° or 0.15° width ω steps accumulating area detector frames spanning a hemisphere of reciprocal space for all structures (data were integrated using the SAINT [35] program) and for the Rigaku AFC7S data collections by ω scans over a single quadrant of reciprocal space. All data were corrected for Lorentz, polarisation and long-term intensity fluctuations. Absorption effects were corrected on the basis of multiple equivalent reflections or by empirical methods [36].

Structures were solved by direct methods and refined by full-matrix least-squares against F (TEXSAN [37]) or F^2 (SHELXTL [38]) for all data with $I > 2\sigma(I)$. Standard SHELXTL weighting scheme was used for **2**, **6**, **9** and **11** whilst in the case of **1** the weighting scheme for the Rigaku/TEXSAN structure was as previously reported [26]. For **1** the O–H hydrogen atoms on both the H_2O and CH_3OH solvent molecules were located from ΔF maps. In compound **2** the N(3)–H hydrogen atom was not located. For **6** the hydro-

Table 3
Details of the X-ray data collections and refinements for compounds **1**, **2**, **6**, **9** and **11**

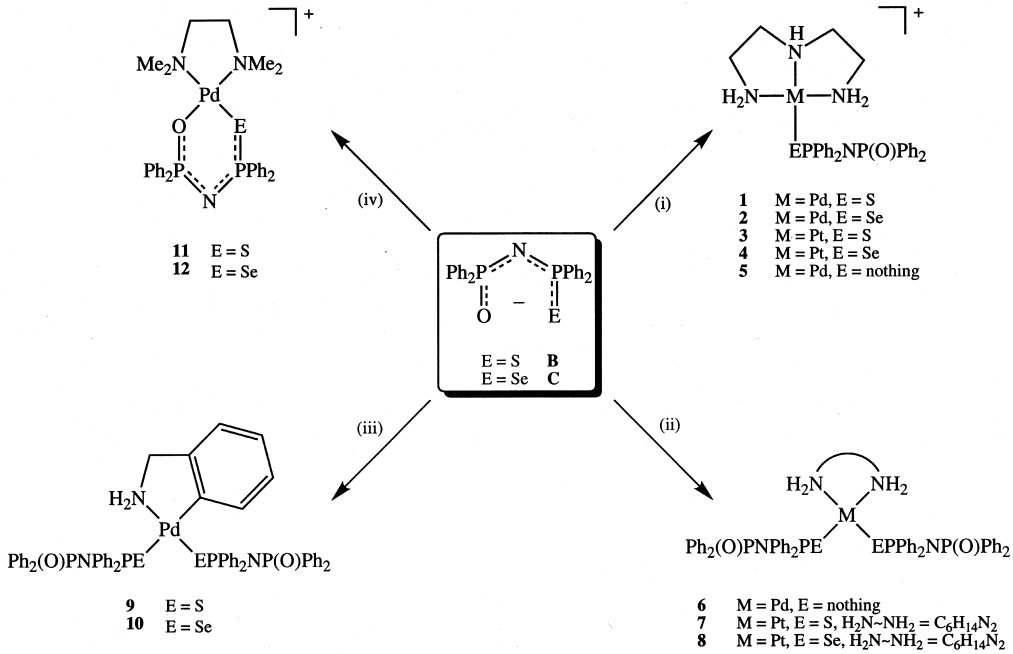
	1	**2**	**6**	**9**	**11**
Empirical formula	$C_{28}H_{33}F_6N_4OP_3PdS \cdot H_2O \cdot 0.5CH_3OH$	$C_{28}H_{33}F_6N_4OP_3PdSe \cdot CH_3OH$	$C_{50}H_{48}N_4O_2P_4Pd \cdot H_2O$	$C_{54}H_{48}N_4O_2P_4PdS_2 \cdot H_2O$	$C_{30}H_{36}F_6N_3OP_3PdS$
M	821.0	865.9	985.22	1097.38	799.99
Crystal system	monoclinic	orthorhombic	triclinic	triclinic	monoclinic
Space group	$P2_1/a$	$P2_12_12_1$	$P\bar{1}$	$P\bar{1}$	Cc
a (Å)	23.070(4)	13.348(1)	12.159(1)	17.893(1)	10.680(1)
b (Å)	11.341(3)	13.802(1)	13.844(1)	18.416(1)	15.548(1)
c (Å)	27.015(2)	20.237(1)	16.441(1)	18.433(1)	20.682(1)
α (°)			77.41(1)	79.28(1)	
β (°)	96.38(1)		73.56(1)	64.03(1)	92.73(1)
γ (°)			64.72(1)	71.09(1)	
U (Å^3)	7024(2)	3728(1)	2385(1)	5159(1)	3430(1)
T (K)	293	293	293	298	293
Z	8 [a]	4	2	4 [a]	4
μ (mm^{-1})	6.70	1.66	0.57	0.61	0.80
Measured reflections	11413	15864	11373	20897	7490
Independent reflections ($R_{int.}$)	11103 (0.089)	5384 (0.2699)	6815 (0.0165)	13846 (0.0544)	4304 (0.0178)
Observed reflections ($I > 2.0\sigma(I)$)	3736	3943	5893	6366	4160
Final R, R'	0.053, 0.060	0.056, 0.093	0.026, 0.067	0.061, 0.14	0.019, 0.048

[a] Two independent molecules.

gen atoms on the H_2O solvent molecule were located from ΔF maps with these hydrogen atoms and those on N(49) and N(50) refined isotropically. One mole of H_2O for each independent molecule of **9** (two H_2O molecules in the asymmetric unit) was located and all O–H hydrogen atoms found. In all structures the remaining hydrogen atoms (including those on the solvent molecules in **1** and **2**) were assigned isotropic displacement parameters and were constrained to idealised geometries. The chirality of **2** was tested by a Flack parameter refinement which refined to −0.007(13) indicating the correct absolute stereochemistry. Refinements converged to residuals given in Table 3. All calculations were made with programs of the TEXSAN [37] or SHELXTL [38] systems.

3. Results and discussion

The cationic compounds [MCl(dien)]Cl (M = Pd, Pt) are useful precursors in which the tridentate dien ligand leaves a single vacant coordination site for ligand exchange reactions as illustrated by the recent synthesis of [Pt(O_2CCH_2SMe-*S*)(dien)]Cl (**A**) [39]. Hence metathesis of [MCl(dien)]-Cl with 1 equiv. of K[$Ph_2P(O)NP(E)Ph_2$] (E = S **B**; E = Se **C**) in CH_3OH, followed by addition of methanolic [NH_4][PF_6] and precipitation with water, gave the following series of metal(II) complexes (Scheme 1): [M{Ph_2P-(O)NP(E)Ph_2-*E*}(dien)]PF_6 (M = Pd, E = S **1**; M = Pd, E = Se **2**; M = Pt, E = S **3**; M = Pt, E = Se **4**). Compounds **1**–**4** were isolated in good yields (83–88%) as air-stable, yellow (**1** and **2**) or white (**3** and **4**) solids, insoluble in hydrocarbons (e.g. toluene) and water but appreciably soluble in CH_2Cl_2 and CH_3OH. The pertinent spectroscopic and microanalytical data for these compounds are given in Tables 1 and 2 and Section 2. Particularly informative was $^{31}P\{^1H\}$ NMR which showed single metal complexes as inferred by resonances at $\delta(P_S)$ 29.1 (for **1**) and 26.4 ppm (for **3**) and $\delta(P_{Se})$ 14.6 (for **2**) and 11.5 ppm (for **4**). In the case of **3** (and **4**) the P_S and P_{Se} resonances were flanked by ^{195}Pt satellites (^1J(PtP) coupling constant of ca. 100 Hz). Furthermore $\delta(P_O)$ was observed at ca. 17 ppm and implied that the phosphoryl group was not involved in coordination with the metal(II) centre. These observations are consistent with **B** and **C** adopting an *E*-monodentate mode of binding through either the 'soft' S or Se donor atom. Pasini and coworkers recently described a series of related complexes of formula [Pt(L-*S*)(dien)]$^+$ (L = methylsulfanyl- and methylsulfinyl-acetate, benzoate and phenolate ligands) and confirmed by NMR and IR the absence of any carboxylate interaction with the metal centre [39,40]. The $^{195}Pt\{^1H\}$ NMR spectra of **3** (and **4**) appeared as broad, poorly resolved signals at ca. δ(Pt) −3100 ppm and in the range anticipated for complexes with a PtN_3S core [40,41]. The ^1H NMR spectra for **1**–**4** (recorded in CD_3OD) have chemical shifts that lie in a very similar range, indicating congruous structures. Treatment of **1** in $CDCl_3/CH_3OH$ with concentrated HCl resulted in smooth conversion to the parent acid $Ph_2P(O)NHP$-(S)Ph_2 and [PdCl(dien)]Cl ($^{31}P\{^1H\}$ NMR evidence). The corresponding reaction with the symmetrical ligands K[$Ph_2P(E)NP(E)Ph_2$] (E = S or Se) gave only the known neutral metal(II) complexes [M{$Ph_2P(E)NP(E)Ph_2$-*E*,*E*′}$_2$] [42]. The compound [Pd{$Ph_2P(O)NPPh_2$-*P*}-(dien)]PF_6 (**5**) was likewise prepared from [PdCl-(dien)]Cl and K[$Ph_2P(O)NPPh_2$] in 71% yield and the spectroscopic data are in full agreement with the structure proposed. The $^{31}P\{^1H\}$ NMR spectrum showed a pair of doublets centred at 32.1 and 21.7 ppm ($^2J(PP_O)$ 19.8 Hz)



Scheme 1. (i) [MCl(dien)]Cl, [NH_4][PF_6], (ii) [MCl_2(N~N)], (iii) [$PdCl_2$(ampy)], (iv) [$PdCl_2$(tmeda)], [NH_4][PF_6].

indicating two non-equivalent phosphorus environments. Attempts to prepare the platinum(II) compound [Pt{$Ph_2P(O)NPPh_2$-*P*}(dien)]PF_6 from [PtCl(dien)]Cl have so far proved unsuccessful.

The crystal structure of **1** (Fig. 1, Table 4) reveals an approximate square planar environment around the palladium(II) metal centre (N(3)–Pd(1)–N(4) 85.0(5), N(2)–Pd(1)–N(3) 85.3(5), S(1)–Pd(1)–N(4) 94.5(3), S(1)–Pd(1)–N(2) 95.0(4)°, molecule 1; N(33)–Pd(31)–N(34) 84.5(5), N(32)–Pd(31)–N(33) 84.9(5), S(31)–Pd(31)–N(32) 94.8(3), S(31)–Pd(31)–N(34) 95.8(3)°, molecule 2) with the Pd lying 0.08 (molecule 1) and 0.05 Å (molecule 2) out of the plane of its four donor centres. The ligand adopts an *E*-monodentate coordination mode with long P–S and short P–N bonds consistent with some degree of delocalisation. There is extensive hydrogen bonding in **1**, consisting of (i) intramolecular PO···HN hydrogen bonding (O(2)···N(2) 3.04, O(2)···H(2A) 2.30 Å, O(2)···H(2A)–N(2) 139°, molecule 1; O(32)···N(32) 2.84, O(32)···H(32A) 1.81 Å, O(32)···H(32A)–N(32) 175°, molecule 2), (ii) intermolecular hydrogen bonding to CH_3OH and H_2O solvate molecules (O(2)···O(60) 2.70, O(2)···H(60) 1.64 Å, O(2)···H(60)–O(60) 157°, N(3)···O(60*) 2.84, O(60*)···H(3) 1.87 Å, O(60*)···H(3)–N(3) 146°, N(4)···O(33) 2.95, N(4)···H(33A) 2.11 Å, N(4)···H(33A)–O(33) 164°, molecule 1; O(32)···O(36) 2.68, O(32)···H(36A) 1.89 Å, O(32)···H(36A)–O(36) 122°, O(36)···N(33) 2.82, O(36)···H(33) 1.82 Å, O(36)···H(33)–N(33) 143°, molecule 2).

The X-ray structure of **2** (Fig. 2, Table 4) shows the palladium metal centre to be roughly square planar (N(3)–Pd(1)–N(4) 83.5(2), N(2)–Pd(1)–N(3) 84.2(2), N(2)–Pd(1)–Se(1) 90.67(14), N(4)–Pd(1)–Se(1) 102.16(14)°). The PdN_3Se core embraces a tridentate dien ligand and an Se-bound [$Ph_2P(O)NP(Se)Ph_2$]$^-$ ligand with the palladium lying approximately in the plane of its four

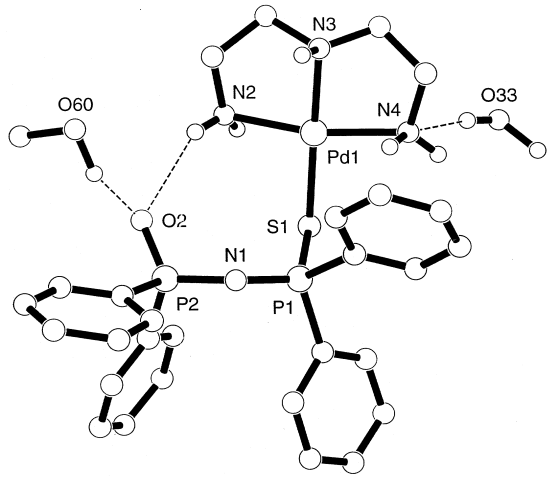


Fig. 1. Crystal structure of [Pd{$Ph_2P(O)NP(S)Ph_2$-*S*}(dien)]PF_6·H_2O·0.5CH_3OH showing one of the independent cations (PF_6^- anion and CH protons omitted for clarity). Hydrogen bonding is indicated by thin dashed lines.

Table 4
Selected bond distances (Å) and angles (°) for compounds **1** and **2**

	1 (E = S) [a]	**2** (E = Se)
Pd(1)–E(1)	2.315(4) [2.334(4)]	2.4475(7)
E(1)–P(1)	2.053(5) [2.046(5)]	2.215(2)
P(1)–N(1)	1.57(1) [1.55(1)]	1.604(6)
N(1)–P(2)	1.58(1) [1.59(1)]	1.599(5)
P(2)–O(2)	1.516(9) [1.512(9)]	1.515(5)
Pd(1)–N(2)	2.05(1) [2.05(1)]	2.058(6)
Pd(1)–N(3)	2.03(1) [2.03(1)]	2.061(5)
Pd(1)–N(4)	2.07(1) [2.06(1)]	2.058(6)
Pd(1)–E(1)–P(1)	100.6(2) [98.3(2)]	109.20(5)
E(1)–P(1)–N(1)	118.8(5) [117.7(4)]	119.2(2)
P(1)–N(1)–P(2)	137.9(9) [137.6(8)]	129.8(3)
N(1)–P(2)–O(2)	116.3(6) [115.6(5)]	119.0(3)
E(1)–Pd(1)–N(2)	95.0(4) [94.8(3)]	90.67(14)
E(1)–Pd(1)–N(3)	178.1(4) [179.7(4)]	172.6(2)
E(1)–Pd(1)–N(4)	94.5(3) [95.8(3)]	102.16(14)
N(2)–Pd(1)–N(3)	85.3(5) [84.9(5)]	84.2(2)
N(2)–Pd(1)–N(4)	168.2(4) [168.1(4)]	165.6(2)
N(3)–Pd(1)–N(4)	85.0(5) [84.5(5)]	83.5(2)

[a] Equivalent parameters for the second molecule are given in square brackets.

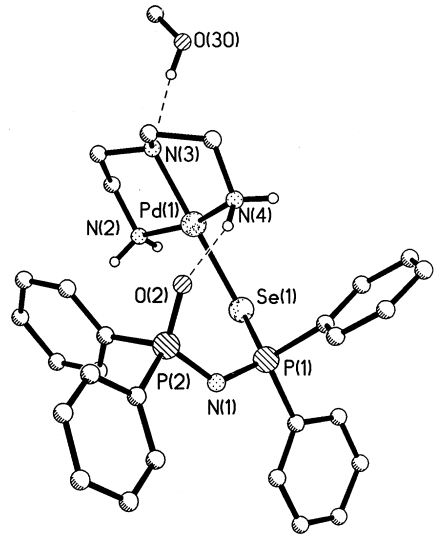


Fig. 2. Crystal structure of [Pd{$Ph_2P(O)NP(Se)Ph_2$-*Se*}(dien)]PF_6·CH_3OH (PF_6^- anion and CH protons omitted for clarity). Hydrogen bonding is indicated by thin dashed lines.

N_3Se-donor atoms. The Pd(1)–Se(1) distance of 2.4475(7) Å is similar to that observed in other complexes with [$Ph_2P(O)NP(Se)Ph_2$]$^-$, e.g. [{Pd(η^3-C_3H_5)[μ-Ph_2P-(O)NP(Se)Ph_2-*Se*]}]$_2$ (Pd–Se 2.477(2), 2.475(2) Å) [23] but longer than that observed in *cis*-[Pd{Ph_2P-(O)NP(Se)Ph_2-*O*,*Se*}$_2$] (Pd–Se 2.381(7), 2.383(8) Å) [26]. A comparison of bond distances and angles within the Se(1)–P(1)–N(1)–P(2)–O(2) backbone is especially noteworthy. The Se(1)–P(1), P(1)–N(1) and N(1)–P(2) bond lengths indicate some degree of delocalisation within the [$Ph_2P(O)NP(Se)Ph_2$]$^-$ ligand and are similar to those reported for [{Pd(η^3-C_3H_5)[μ-$Ph_2P(O)NP(Se)Ph_2$-*Se*]}]$_2$ [23], [Pd{$Ph_2P(O)NP(Se)Ph_2$-*Se*}$_2$(en)] [24] and

cis-[Pd{$Ph_2P(O)NP(Se)Ph_2$-*O*,*Se*}$_2$] [26], whilst the P–N–P angle (129.8(3)°) is smaller in magnitude compared with **1** (137.9(9)° for molecule 1; 137.6(8)° for molecule 2). The P(2)–O(2) bond length (1.515(5) Å) in **2** is similar to that observed for $Ph_2P(O)NHP(S)Ph_2$ (average P–O 1.503(4) Å) which exists in the solid state as a hydrogen-bonded polymeric chain [27]. There is a CH_3OH solvate which displays a close contact with N(3) of the coordinated dien ligand (N(3)···O(30) 2.93, N(3)···H(30) 2.22 Å, N(3)···H(30)–O(30) 144°). There is also an intramolecular hydrogen bond between the PO functionality and N(4)–H(4b) (N(4)···O(2) 2.85, H(4b)···O(2) 1.99 Å, N(4)–H(4b)···O(2) 160°) and an intermolecular N(2)–H(2b)···O(2*) hydrogen bond (N(2)···O(2*) 2.84, H(2b)···O(2*) 1.96 Å, N(2)–H(2b)···O(2*) 166°).

We recently described the preparation and characterisation of [Pd{$Ph_2P(O)NP(E)Ph_2$-*E*}$_2$(en)] [24] containing two *E*-monodentate bound [$Ph_2P(O)NP(E)Ph_2$]$^-$ ligands. Using this metathetical procedure we have synthesised the complex [Pd{$Ph_2P(O)NPPh_2$-*P*}$_2$(en)] (**6**) from [$PdCl_2$(en)] and 2 equiv. of K[$Ph_2P(O)NPPh_2$] in methanol. The $\delta(P_O)$ chemical shift for **6** is similar to that for **5** and the previously reported values for the mixed P^{III}/P^{V} ligand $Ph_2P(O)NHPPh_2$ ($\delta(P_O)$ 21.4 ppm) and $Ph_2P(O)NHP(O)Ph_2$ ($\delta(P_O)$ 20.7 ppm), suggesting no phosphoryl interaction with the Pd^{II} metal centre [43].

In the X-ray structure of **6** (Table 5, Fig. 3) the palladium centre is bound by two terminal [$Ph_2P(O)NPPh_2$]$^-$ ligands and a didentate $H_2NCH_2CH_2NH_2$ ligand in a slightly distorted square planar geometry with coordination angles in the range 81.11(8)–98.19(2) and 170.47(6)–172.39(6)°. The Pd–P distances in **6** (2.264(1) and 2.272(1) Å) are at the higher end of the range found in the corresponding complexes [Pd(*o*-$C_6H_4CH_2NMe_2$-*C*,*N*)-{$Ph_2P(O)NPPh_2$-*P*,*O*}]·CH_3OH (2.242(1) Å) and [PdCl{$Ph_2P(O)NPPh_2$-*P*,*O*}(Ph_2POCH_3)]·0.5CH_2Cl_2 (2.255(3) Å) [44] but shorter than that found in [{Pd(η^3-C_3H_5)[μ-$Ph_2P(O)NPPh_2$-*P*,*O*]}$_2$] (2.293(1) Å) [45]. The P–N bond lengths in **6** (P(1)–N(1) 1.601(2), N(1)–P(2) 1.604(2), P(3)–N(3) 1.593(2), N(3)–P(4) 1.599(2) Å) are similar to those described previously for metal complexes with [$Ph_2P(O)NPPh_2$]$^-$ and indicate some degree of delocalisation within the P–N–P backbone. The P(1)–O(1) and P(3)–O(3) bond lengths (1.492(2) and 1.499(2) Å) are similar in magnitude to that observed for $Ph_2P(O)NHPPh_2$ (1.508(2) Å) which exists in the solid state as a hydrogen-bonded dimer pair [43]. Both [$Ph_2P(O)NPPh_2$]$^-$ ligands are involved in intramolecular N–H···OP hydrogen bonding with $H_2NCH_2CH_2NH_2$ (N(49)···O(1) 2.85, H(49A)···O(1) 1.92 Å and N(49)–H(49A)···O(1) 158°; N(50)···O(3) 2.80, H(50B)···O(3) 1.85 Å and N(50)–H(50B)···O(3) 162°). This leads to a spirocyclic arrangement composed of two seven-membered rings about a central palladium(II) metal centre. An intermolecular O–H···O hydrogen bond is observed between O(3) and H(60A) of a water molecule (O(3)···O(60) 2.77, O(3)···H(60A) 1.79 Å and O(3)···H(60A)–O(60) 176°).

Table 5
Selected bond distances (Å) and angles (°) for compound **6**

Pd(1)–P(2)	2.2644(6)
Pd(1)–P(4)	2.2721(6)
P(2)–N(1)	1.604(2)
N(1)–P(1)	1.601(2)
P(1)–O(1)	1.492(2)
P(4)–N(3)	1.599(2)
N(3)–P(3)	1.593(2)
P(3)–O(3)	1.499(2)
Pd(1)–N(49)	2.145(2)
Pd(1)–N(50)	2.144(2)
Pd(1)–P(2)–N(1)	116.88(8)
P(2)–N(1)–P(1)	126.89(14)
N(1)–P(1)–O(1)	119.64(11)
Pd(1)–P(4)–N(3)	116.61(8)
P(4)–N(3)–P(3)	130.88(14)
N(3)–P(3)–O(3)	119.92(11)
N(50)–Pd(1)–N(49)	81.11(8)
N(50)–Pd(1)–P(2)	172.39(6)
N(49)–Pd(1)–P(2)	91.30(6)
N(50)–Pd(1)–P(4)	89.41(6)
N(49)–Pd(1)–P(4)	170.47(6)
P(2)–Pd(1)–P(4)	98.19(2)

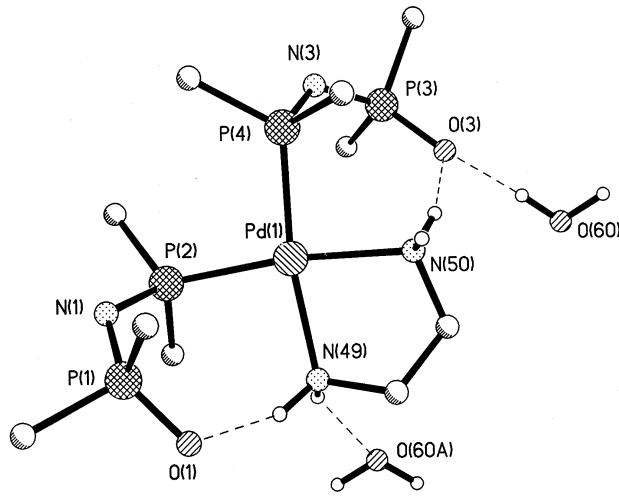


Fig. 3. Crystal structure of [Pd{$Ph_2P(O)NPPh_2$-*P*}$_2$(en)]·H_2O (only the *ipso* and methylene carbons and solvent are shown for clarity). Hydrogen bonding is indicated by thin dashed lines.

A second intermolecular N–H···O hydrogen bond is also observed between H(49B) and an adjacent water molecule (N(49)···O(60A) 3.15, H(49B)···O(60A) 2.29 Å and N(49)–H(49B)···O(60A) 146°).

Using more forcing conditions (reflux, 5 h) we were able to prepare the platinum(II) complexes [Pt{$Ph_2P(O)NP(E)Ph_2$-*E*}$_2$($C_6H_{14}N_2$)] (E = S **7**; E = Se **8**) [3] whereas attempts to obtain analogues with [$Ph_2P(E)NP(E)Ph_2$]$^-$ gave only [M{$Ph_2P(E)NP(E)Ph_2$-*E*,*E*′}$_2$]. Reaction of **B** with [$PtCl_2(py)_2$] (2:1 molar ratio) in refluxing CH_3OH

[3] Crystals of **7** have also been isolated but refinement of the X-ray data only resulted in a value of $R = 13.2\%$. Nevertheless the refinement again indicated an *S*-bound arrangement of the [$Ph_2P(O)NP(S)Ph_2$]$^-$ ligands.

gave, after solvent evaporation, a solid whose $^{31}P\{^{1}H\}$ NMR spectrum clearly showed a mixture of phosphorus containing species. Two major compounds identified were $[Pt\{Ph_2P(O)NP(S)Ph_2\text{-}O,S\}_2(py)_2]$ ($\delta(P_S)$ 25.7 ppm, $^{1}J(PtP)$ 88 Hz; $\delta(P_O)$ 11.3 ppm, $^{2}J(P_SP_O)$ 5 Hz) and $Ph_2P(O)NHP(S)Ph_2$, but attempts to isolate the platinum(II) complex by recrystallisation have so far proved unyielding.

The reaction of $[PdCl_2(ampy)]$ with **B** (and **C**) was of particular interest since it has previously been shown that, depending on the choice of $[PdCl_2(amine)_2]$, different products were obtained. Hence when $[PdCl_2(bipy)]$ was employed the *O,E*-chelate complexes $[Pd\{Ph_2P(O)NP(E)Ph_2\text{-}O,E\}(bipy)]PF_6$ were isolated in high yields, but in contrast $[PdCl_2(en)]$ gave $[Pd\{Ph_2P(O)NP(E)Ph_2\text{-}O,E\}_2(en)]$ with *E*-monodentate ligands [24,25]. Transmetallation of **B** (or **C**) with $[PdCl_2(ampy)]$ in methanol gave the neutral compounds $[Pd\{Ph_2P(O)NP(E)Ph_2\text{-}O,E\}_2(ampy)]$ (E = S **9**; E = Se **10**) and hence the reactivity seen here resembles that of $[PdCl_2(en)]$. Four ^{31}P resonances were observed in the $^{31}P\{^{1}H\}$ NMR spectra of **9** (and **10**) consistent with four unique phosphorus environments (i.e. two *E*-monodentate $[Ph_2P(O)NP(E)Ph_2]^-$ ligands *trans* to the divergent nitrogen donor atoms of ampy). Furthermore $\delta(P_O)$ was indicative of a 'dangling' PO functionality (Table 2).

The X-ray structure of **9** (Fig. 4, Table 6) reveals two independent molecules and shows the palladium metal centres to be roughly square planar (N(3)–Pd(1)–N(4) 82.2(3), N(4)–Pd(1)–S(1) 90.7(2), S(1)–Pd(1)–S(3) 91.74(8), N(3)–Pd(1)–S(3) 95.5(2)°, molecule 1; N(63)–Pd(2)–N(64) 82.1(3), N(64)–Pd(2)–S(61) 90.1(2), S(61)–Pd(2)–S(63) 92.85(8), N(63)–Pd(2)–S(63) 94.9(2)°, molecule 2). The PdN_2S_2 core is composed of a didentate 2-aminomethylpyridine ligand and two *S*-bound $[Ph_2P(O)NP(S)Ph_2]^-$ ligands with the palladium lying essentially in the plane of its four constituents (for both independent molecules). The Pd(1)–N(3) distance (2.070(7) for molecule 1; 2.071(7) Å for molecule 2) is longer than that reported for $[Pd(cbdca)(ampy)]\cdot 2H_2O$ (1.989(12) Å) (cbdca = cyclobutane-1,1-dicarboxylate) whereas the Pd(1)–N(4) bond length (2.030(6) for molecule 1; 2.048(6) Å for molecule 2) is similar to that in $[Pd(cbdca)(ampy)]\cdot 2H_2O$ (2.024(12) Å) [34]. The Pd–S distances of 2.304(2) and 2.324(2) Å (molecule 1) and 2.299(2) and 2.314(2) Å (molecule 2) are similar to those in **1** (2.315(4), molecule 1; 2.334(4), molecule 2) and **11** (2.3315(8) Å). Within the S–P–N–P–O backbone there is evidence for some electron delocalisation with long S–P and short P–N/N–P bonds. The P–O bond lengths (1.494(5), 1.485(5) Å, molecule 1; 1.499(5), 1.495(5) Å, molecule 2) are similar to that observed in $Ph_2P(O)NHP(S)Ph_2$ [27]. One of the $[Ph_2P(O)NP(S)Ph_2]^-$ ligands is involved in intramolecular hydrogen bonding with $H_2NCH_2C_5H_3N$ (N(4)···O(2) 2.85, H(4C)···O(2) 1.97 Å, N(4)–H(4C)···O(2) 164°, molecule 1; N(64)···O(62) 2.85, H(64C)···O(62) 1.96 Å, N(64)–H(64C)···O(62) 166°, molecule 2) forming a pseudo eight-membered ring. This may account for the enlarged P(3)–N(2)–P(4) (137.2(4), molecule 1; 138.4(4)°, molecule 2) angle with respect to P(1)–N(1)–P(2) (132.6(5), molecule 1; 135.7(5)°, molecule 2). There is also additional intermolecular hydrogen bonding with a water solvent molecule (N(4)···O(71) 3.06, H(4B)···O(71) 2.21 Å, N(4)–H(4B)···O(71) 156°, molecule 1; N(64)···O(72) 3.03, H(64B)···O(72) 2.15 Å, N(64)–H(64B)···O(72) 166°, molecule 2).

We have also attempted to prepare *E*-monodentate analogues of $[PdCl_2(tmeda)]$ but were only able to isolate the *O,E*-chelate complexes $[Pd\{Ph_2P(O)NP(E)Ph_2\text{-}O,E\}$-

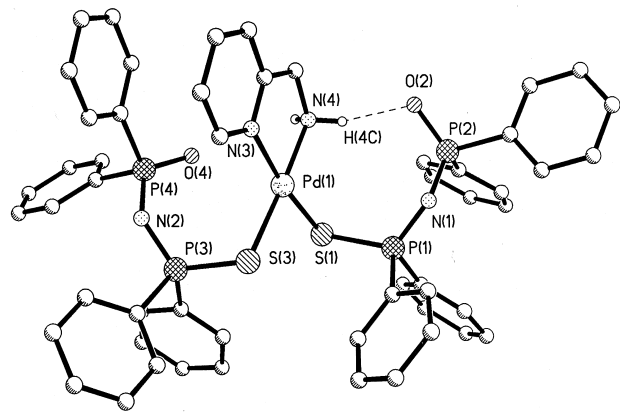


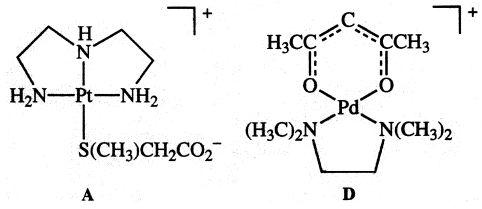
Fig. 4. Crystal structure of $[Pd\{Ph_2P(O)NP(S)Ph_2\text{-}S\}_2(ampy)]\cdot H_2O$ showing one of the independent molecules (solvent and CH protons omitted for clarity). Hydrogen bonding is indicated by thin dashed lines.

Table 6
Selected bond distances (Å) and angles (°) for compound **9** [a]

Pd(1)–S(1)	2.304(2) [2.299(2)]
Pd(1)–S(3)	2.324(2) [2.314(2)]
S(1)–P(1)	2.039(3) [2.028(3)]
S(3)–P(3)	2.042(3) [2.032(3)]
P(1)–N(1)	1.590(6) [1.579(6)]
P(3)–N(2)	1.575(6) [1.557(6)]
N(1)–P(2)	1.602(6) [1.596(6)]
N(2)–P(4)	1.589(6) [1.600(6)]
P(2)–O(2)	1.494(5) [1.499(5)]
P(4)–O(4)	1.485(5) [1.495(5)]
Pd(1)–N(3)	2.070(7) [2.071(7)]
Pd(1)–N(4)	2.030(6) [2.048(6)]
Pd(1)–S(1)–P(1)	103.86(12) [102.45(12)]
Pd(1)–S(3)–P(3)	104.53(11) [104.24(12)]
S(1)–P(1)–N(1)	119.9(3) [118.8(3)]
S(3)–P(3)–N(2)	118.7(3) [121.1(3)]
P(1)–N(1)–P(2)	132.6(5) [135.7(5)]
P(3)–N(2)–P(4)	137.2(4) [138.4(4)]
N(1)–P(2)–O(2)	117.0(3) [117.5(3)]
N(2)–P(4)–O(4)	121.0(4) [120.6(3)]
N(3)–Pd(1)–N(4)	82.2(3) [82.1(3)]
N(3)–Pd(1)–S(1)	172.4(2) [172.2(2)]
N(3)–Pd(1)–S(3)	95.5(2) [94.9(2)]
N(4)–Pd(1)–S(1)	90.7(2) [90.1(2)]
N(4)–Pd(1)–S(3)	177.2(2) [176.9(2)]
S(1)–Pd(1)–S(3)	91.74(8) [92.85(8)]

[a] Equivalent parameters for the second molecule are given in square brackets.

(tmeda)]PF_6 (E = S **11**; E = Se **12**) in high yields (>90%). López and coworkers recently described the synthesis of the cationic complex $[Pd(acac)(tmeda)]^+$ (**D**) from the hydroxo palladium dimer $[\{Pd(\mu\text{-}OH)(tmeda)\}_2]^{2+}$ and the protic acid Hacac [46]. The $^{31}P\{^1H\}$ NMR spectra of **11** and **12** showed that $\delta(P_O)$ was shifted downfield by ca. 20 ppm with respect to **1**–**4**, **7**–**10**, suggesting an *O,E*-chelation mode of binding. This was further corroborated by ^1H NMR which showed two well resolved $N(CH_3)_2$ resonances at 2.63, 2.39 (for **11**) and 2.60, 2.46 ppm (for **12**). Furthermore, the IR spectra of **11** and **12** showed the absence of ν_{PdCl} (326 cm^{-1}) for $[PdCl_2(tmeda)]$, consistent with metathesis of both Pd–Cl ligands by an *O,E*-chelating $[Ph_2P(O)NP(E)Ph_2]^-$ anion. The reaction of $[PdCl_2$-(tmeda)] with 2 equiv. of **B** in CH_3OH was monitored by $^{31}P\{^1H\}$ NMR spectroscopy and showed that both **11** and unreacted **B** were present with no evidence for a neutral complex such as $[Pd\{Ph_2P(O)NP(S)Ph_2\text{-}S\}_2(tmeda)]$. This difference in reactivity may be ascribed to the use of a more sterically hindered diamine, the absence of suitable centres for hydrogen bonding or a combination of both factors. Attempts to prepare a corresponding complex from $[PdCl_2(tmeda)]$ and $K[Ph_2P(O)NPPh_2]$ (1:1 molar ratio) gave instead the known bis homoleptic compound *cis*-$[Pd\{Ph_2P(O)NPPh_2\text{-}P,O\}_2]$ [43].



The X-ray structure of **11** (Fig. 5, Table 7) shows the palladium metal centre to be surrounded by a chelating $Me_2NCH_2CH_2NMe_2$ and $[Ph_2P(O)NP(S)Ph_2]^-$ ligand in a slightly distorted square planar geometry with coordination angles in the range 85.89(12)–96.05(7) and 171.52(7)–172.09(12)°. The palladium lies 0.05 Å out of the plane of its four N_2OS donor constituents. The Pd(1)–N bond lengths reflect the nature of the *trans* donor atom (Pd(1)–N(25) 2.055(3), P *trans* to O; Pd(1)–N(26) 2.104(3) Å, P *trans* to S). Furthermore Pd(1)–N(25) is at the lower end of the range previously reported for the aryl- and alkoxide complexes *cis*-$[Pd(CH_3)(OR)(tmeda)]$ (2.060(5) (R = *p*-$C_6H_4NO_2$) to 2.080(2) Å (R = $CH(CF_3)_2$)) [47]. The six-membered Pd–O–P–N–P–S ring conformation in **11** can be most readily described as pseudo-boat with S(1) at the prow (0.88 Å above the plane) and P(2) at the stern (0.21 Å above the plane) of the 'boat'. In **11** the Pd(1)/P(1)/N(1)/O(2) atoms are approximately coplanar (maximum deviation from the mean plane 0.2 Å for N(1)). Within the $PdOP_2NS$ metallacycle the bond lengths are consistent with a fair degree of delocalisation.

We have shown that new complexes of palladium(II) and platinum(II) with *E*-monodentate $[Ph_2P(O)NP(E)Ph_2]^-$ ligands are readily accessible via transmetallation reactions. In contrast the use of symmetrical anions $[Ph_2P(E)$-$NP(E)Ph_2]^-$ leads exclusively to the formation of $[M\{Ph_2P(E)NP(E)Ph_2\text{-}E,E'\}_2]$ with displacement of all chloride and amine ligands. This disparity can presumably be traced to the dissimilar donor properties of the asymmetrical ligands. In this context the rare coordination mode displayed by $[Ph_2P(O)NP(E)Ph_2]^-$ may well mean that these ligands have a role in catalysis and in the synthesis of heterobimetallic compounds.

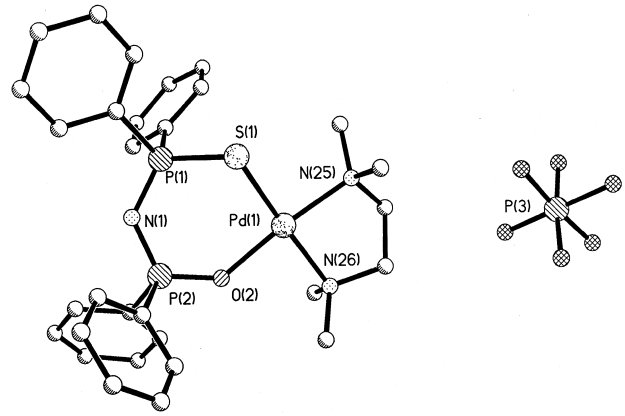


Fig. 5. Crystal structure of $[Pd\{Ph_2P(O)NP(S)Ph_2\text{-}O,S\}(tmeda)]PF_6$ (CH protons omitted for clarity).

Table 7
Selected bond distances (Å) and angles (°) for compound **11**

Pd(1)–S(1)	2.3315(8)
Pd(1)–O(2)	2.027(3)
S(1)–P(1)	2.0359(10)
P(1)–N(1)	1.573(3)
N(1)–P(2)	1.587(3)
P(2)–O(2)	1.529(3)
Pd(1)–N(25)	2.055(3)
Pd(1)–N(26)	2.104(3)
Pd(1)–S(1)–P(1)	104.35(4)
S(1)–P(1)–N(1)	116.96(11)
P(1)–N(1)–P(2)	128.0(2)
N(1)–P(2)–O(2)	118.58(14)
P(2)–O(2)–Pd(1)	134.2(2)
O(2)–Pd(1)–N(25)	172.09(12)
O(2)–Pd(1)–N(26)	87.22(10)
N(25)–Pd(1)–N(26)	85.89(12)
O(2)–Pd(1)–S(1)	96.05(7)
N(25)–Pd(1)–S(1)	91.31(10)
N(26)–Pd(1)–S(1)	171.52(7)

Supplementary data

Crystallographic data (excluding structure factors) for the structures in this paper have been deposited with the Cambridge Crystallographic Data Centre as supplementary publication nos. CCDC 136068 (for **1**), 136069 (for **2**), 136070 (for **6**), 136071 (for **9**) and 136072 (for **11**). Copies of the data can be obtained, free of charge, on application to CCDC,

12 Union Road, Cambridge, CB2 1EZ, UK (fax: +44-1223-336033; e-mail: deposit@ccdc.cam.ac.uk).

Acknowledgements

We should like to thank the EPSRC for support and the EPSRC Mass Spectrometry Service Centre at Swansea.

References

[1] I. Bachert, P. Braunstein, M.K. McCart, F. Fabrizi de Biani, F. Laschi, P. Zanello, G. Kickelbick, U. Schubert, J. Organomet. Chem. 573 (1999) 47.
[2] F.A. Cotton, A. Yokochi, M.J. Siwajek, R.A. Walton, Inorg. Chem. 37 (1998) 372.
[3] J. Geicke, I.-P. Lorenz, M. Engel, K. Polborn, Inorg. Chim. Acta 269 (1998) 157.
[4] C.S. Browning, R.A. Burrow, D.H. Farrar, H.A. Mirza, Inorg. Chim. Acta 271 (1998) 112.
[5] M. Knorr, C. Strohmann, Eur. J. Inorg. Chem. (1998) 495.
[6] A. Winkler, W. Bauer, F.W. Heinemann, V. Garcia-Montalvo, M. Moll, J. Ellermann, Eur. J. Inorg. Chem. (1998) 437.
[7] A.M.Z. Slawin, M.B. Smith, J.D. Woollins, J. Chem. Soc., Dalton Trans. (1996) 4567.
[8] P. Bhattacharyya, A.M.Z. Slawin, D.J. Williams, J.D. Woollins, J. Chem. Soc., Dalton Trans. (1995) 2489, 3189.
[9] S.W. Magennis, S. Parsons, A. Corval, J.D. Woollins, Z. Pikramenou, Chem. Commun. (1999) 61.
[10] M. Arca, A. Garau, F.A. Devillanova, F. Isaia, V. Lippolis, G. Verani, G.L. Abbati, A. Cornia, Z. Anorg. Allg. Chem. 625 (1999) 517.
[11] G. Kräuter, S.K. Sunny, W.S. Rees Jr., Polyhedron 17 (1998) 391.
[12] C. Silvestru, R. Rösler, J.E. Drake, J. Yang, G. Espinosa-Pérez, I. Haiduc, J. Chem. Soc., Dalton Trans. (1998) 73.
[13] V. García-Montalvo, J. Novosad, P. Kilian, J.D. Woollins, A.M.Z. Slawin, P. García y García, M. López-Cardoso, G. Espinosa-Pérez, R. Cea-Olivares, J. Chem. Soc., Dalton Trans. (1997) 1025.
[14] C. Papadimitriou, P. Veltsistas, J. Novosad, R. Cea-Olivares, A. Toscano, P. García y García, M. López-Cardosa, A.M.Z. Slawin, J.D. Woollins, Polyhedron 16 (1997) 2727.
[15] U. Abram, E. Schulz Lang, S. Abram, J. Wegmann, J.R. Dilworth, R. Kirmse, J.D. Woollins, J. Chem. Soc., Dalton Trans. (1997) 623.
[16] M. Geissinger, J. Magull, Z. Anorg. Allg. Chem. 623 (1997) 755.
[17] E.N.-M. Ho, W.-T. Wong, J. Chem. Soc., Dalton Trans. (1997) 915.
[18] O. Navrátil, E. Herrmann, G. Grossmann, J. Teply, Collect. Czech. Chem. Commun. 55 (1990) 364.
[19] L. Barkaoui, M. Charrouf, M.-N. Rager, B. Denise, N. Platzer, H. Rudler, Bull. Soc. Chim. Fr. 134 (1997) 167.
[20] H. Rudler, B. Denise, J.R. Gregorio, J. Vaissermann, Chem. Commun. (1997) 2299.
[21] S. Kawaguchi, Coord. Chem. Rev. 70 (1986) 51.
[22] A.M.Z. Slawin, M.B. Smith, New. J. Chem. 23 (1999) 777.
[23] P. Bhattacharyya, A.M.Z. Slawin, M.B. Smith, J. Chem. Soc., Dalton Trans. (1998) 2467.
[24] A.M.Z. Slawin, M.B. Smith, J.D. Woollins, J. Chem. Soc., Dalton Trans. (1998) 1537.
[25] A.M.Z. Slawin, M.B. Smith, J.D. Woollins, Polyhedron 17 (1998) 4465.
[26] A.M.Z. Slawin, M.B. Smith, J.D. Woollins, J. Chem. Soc., Dalton Trans. (1996) 3659.
[27] J. Yang, J.E. Drake, S. Hernandez-Ortega, R. Rösler, C. Silvestru, Polyhedron 16 (1997) 4061.
[28] J.E. Drake, A. Silvestru, J. Yang, I. Haiduc, Inorg. Chim. Acta 271 (1998) 75.
[29] R. Rösler, J.E. Drake, C. Silvestru, J. Yang, I. Haiduc, J. Chem. Soc., Dalton Trans. (1996) 391.
[30] V. García-Montalvo, R. Cea-Olivares, G. Espinosa-Pérez, Polyhedron 15 (1996) 829.
[31] I. Haiduc, in: J.D. Woollins (Ed.), Inorganic Experiments, VCH, Weinheim, 1994.
[32] G. Annibale, M. Brandolisio, B. Pitteri, Polyhedron 14 (1995) 451.
[33] F.L. Wimmer, S. Wimmer, P. Castan, Inorg. Synth. 29 (1992) 185.
[34] T. Rau, M. Shoukry, R. van Eldik, Inorg. Chem. 36 (1997) 1454.
[35] SAINT (Siemens Area Detector INTegration) program, Siemens Analytical X-ray, Madison, WI, 1995.
[36] N.G. Walker, D. Stuart, DIFABS, Acta Crystallogr., Sect. A 39 (1983) 158.
[37] TEXSAN, Crystal Structure Analysis Package, Molecular Structure Corporation, The Woodlands, TX, 1985, 1992.
[38] Siemens SHELXTL, Revision 5.03, Siemens Analytical X-Ray, Madison, WI, 1995.
[39] A. Pasini, M. Moroni, J. Chem. Soc., Dalton Trans. (1997) 1093.
[40] A. Pasini, C. Fiore, Inorg. Chim. Acta 285 (1999) 249.
[41] C.D.W. Fröhling, W.S. Sheldrick, Chem. Commun. (1997) 1737.
[42] P. Bhattacharyya, J. Novosad, J. Phillips, A.M.Z. Slawin, D.J. Williams, J.D. Woollins, J. Chem. Soc., Dalton Trans. (1995) 1607.
[43] P. Bhattacharyya, A.M.Z. Slawin, M.B. Smith, J.D. Woollins, Inorg. Chem. 35 (1996) 3675.
[44] A.M.Z. Slawin, M.B. Smith, J.D. Woollins, J. Chem. Soc., Dalton Trans. (1996) 1283.
[45] M.B. Smith, A.M.Z. Slawin, J.D. Woollins, Polyhedron 15 (1996) 1579.
[46] G. Sánchez, J.L. Serrano, J. García, G. López, J. Pérez, E. Molins, Inorg. Chim. Acta 287 (1999) 37.
[47] G.M. Kapteijn, A. Dervisi, D.M. Grove, H. Kooijman, M.T. Lakin, A.L. Spek, G. van Koten, J. Am. Chem. Soc. 117 (1995) 10939.

PERGAMON

www.elsevier.nl/locate/poly

Polyhedron 19 (2000) 705–711

POLYHEDRON

Scandium alkoxides: the first mixed-ligand alkoxides containing the $[M_5O(OR)_8]$ core, scandium alkoxoaluminates

Evgeniya P. Turevskaya [a,*], Alexander I. Belokon' [b], Zoya A. Starikova [b], Alexander I. Yanovsky [b], Evgeniy N. Kiruschenkov [a], Nataliya Ya. Turova [a]

[a] *Chemistry Department, Moscow State University, 119899 Moscow, Russia*

[b] *A.N. Nesmeyanov Institute of Organoelement Compounds of Russian Academy of Sciences, 117813 Moscow, Russia*

Received 9 September 1999; accepted 24 January 2000

Abstract

The electrochemical synthesis of $Sc(OMe)_3$ (**1**), $Sc(OEt)_3$ (**2**) and $Sc_5O(OPr^i)_{13}$ (**3**) was carried out via anodic oxidation of scandium metal in aliphatic alcohols. X-ray single crystal study showed **3** to be analogous to the known isopropoxides of Y, Er, Yb and In. The interaction of **3** with excess ROH (R = Me, Et, Bu^n, Bu^s, Bu^t) gives non-volatile amorphous **1**, **2** and $Sc(OBu^n)_3$ (**4**), and volatile $Sc_5O(OBu^s)_{13}$ (**5**) and $Sc_5O(OPr^i)_8(OBu^t)_5$ (**6**). Oxoalkoxides $Sc_5O(OPr^i)_8(OR)_5$ (R = Bu^n **7**, Me **8**) were obtained on reaction of **3** with n-ROH in 1:5 ratio. The mass spectral study shows **5** is an individual compound, whereas **6**–**8** in the gas phase consist of a number of aggregates with different extents of substitution for OPr^i groups, $Sc_5O(OR)_n(OPr^i)_{13-n}$: for R = Bu^t $n \leq 5$, for R = Bu^n $n \leq 8$, and for R = Me $n \leq 12$. The maximal intensity in the spectrum of **6** is observed for $Sc_5O(OPr^i)_{10}(OBu^t)_2^+$, and in the spectra of **7** and **8** for $Sc_5O(OPr^i)_{12-n}(OBu^n)_n^+$, $n = 4$, 5, and $Sc_5O(OPr^i)_9(OMe)_3^+$ respectively. The presence of the $Sc_5O(OMe)_{12}^+$ ion in the spectrum of **8** indicates the possibility of replacing all the OPr^i in the pentanuclear core and demonstrates the existence of a 'volatile scandium methoxide' in the gas phase. Study of the complex formation of $Sc(OR)_3$ with $Al(OR)_3$ has shown that **2** and **4** form volatile $Sc[Al(OR)_4]_3$, R = Et **9**, Bu^n **10**, while **3** does not react under these conditions. $Sc[Al(OPr^i)_4]_3$ (**11**) can be obtained only on exchange reaction of $ScCl_3$ with $KAl(OPr^i)_4$. The results obtained indicate rather high stability of the $[Sc_5O(OR)_8]$ core for primary and secondary R. ©2000 Elsevier Science Ltd All rights reserved.

Keywords: Scandium; Alkoxides; Crystal structures; Volatility

1. Introduction

The scandium alkoxides are the least studied among the analogous derivatives of the rare earth elements. The methoxide **1**, ethoxide **2** [1,2], isopropoxide **3** [2–4], n- **4** and *tert*-butoxides [1,2] have been described, and also a volatile derivative of a fluorinated alcohol $\{Sc[OCH(CF_3)_2]_3\}_2$, its solvate $\{Sc[OCH(CF_3)_2]_3(NH_3)_2\}_2$-*trans* [5], and a sterically overcrowded phenoxide $Sc(OC_6H_2Me\text{-}4\text{-}Bu^t_2\text{-}2,6)_3$ [6].

The aliphatic derivatives are formed by an exchange reaction of $ScCl_3$ with alcohols in the presence of ammonia [1] or with NaOR [3,4], and also, according to patent data, on interaction of $Sc(RCOO)_3$ with the corresponding alkoxides of Li, Na or K [2]. The described reactions (as well as other syntheses of this kind) are complicated by the formation of rather stable intermediate alkoxide halides or carboxylates. The preparation of **3** was achieved via alcoholysis of $Sc[N(SiMe_3)_2]_3$, and also by interaction of metal with alcohol in the presence of mercury salts as catalysts [3,4]. The disadvantages of this method include a very low reaction rate and the possibility of partial thermolysis in the presence of $HgCl_2$ [7]. The direct electrochemical synthesis of **3** appeared therefore rather more simple and efficient [4].

According to the literature, **1** is an insoluble polymer, and **4** is a viscous oil that crystallizes slowly on storage [1]. Bradley et al. [3] have shown using mass spectral and ^1H NMR data that **3** has a molecular structure analogous to that of indium and ytterbium isopropoxides, i.e. $M_5(\mu_5\text{-}O)(\mu_3\text{-}OPr^i)_4(\mu\text{-}OPr^i)_4(OPr^i)_5$. The molecules of the latter are $[M_5]$ tetragonal pyramids, centered by a μ_5-oxoatom and supported by four μ_3-OR groups situated over the side faces and by four μ-OR groups over the edges of the basal plane. Crystalline **3** can be sublimed in vacuo (150 and 220°C, 10^{-2} Torr [3,4]), its thermal decomposition begins at about 300°C.

* Corresponding author; e-mail: turevsk@inorg.chem.msu.ru

0277-5387/00/$ - see front matter ©2000 Elsevier Science Ltd All rights reserved.
PII S0277-5387(00)00312-0

The present work is devoted to the development of the electrochemical synthesis of different $Sc(OR)_3$ homologs and the study of reactions of alcohol interchange for **3** and also the complex formation of scandium and aluminum alkoxides.

2. Results and discussion

2.1. Conditions for the formation of scandium alkoxides

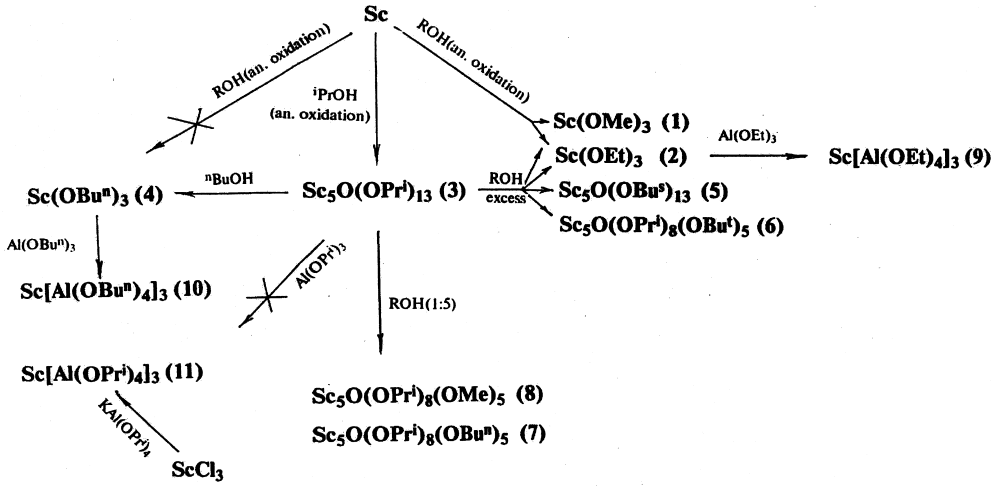
Scandium alkoxides have been prepared using two methods.

(a) The anodic oxidation of metal, which at present is a common route for the preparation of III–VIII group alkoxides [8]. The electrolysis in MeOH occurred with a high rate and was accompanied by precipitation of **1**. The synthesis of **2** was complicated by a continuous decrease in current and extinguishing of the process. The isolated soluble product contained residual amounts of chlorine. The conditions used for the preparation of **3** in the present work did not differ substantially from those described earlier [4], however the more accessible LiCl was used instead of $[Bu_4N]Br$. The rate of anodic dissolution in n-, s- and t-BuOH was so low, even at rather high concentrations of electrolyte (>0.1 M), that it became impossible to use it for the preparation of butoxides. The electrochemical method therefore was attractive in the case of insoluble **1** and in that of **3**, which crystallizes from solution at room temperature.

(b) Alcohol interchange reactions starting from the isopropoxide The alcohol interchange reactions starting from the isopropoxide have been used for the preparation of numerous homologs of different rare-earth metals. Taking into account the fact that scandium isopropoxide is an oxoderivative, it appeared to be of interest to determine the nature of other homologs formed via alcohol interchange reactions starting from it. Relationships between products, described in the present work, are summarized in Scheme 1.

The action of considerable excess of ROH (R = Me, Et, Bu^n, Bu^s, Bu^t) on solution of **3** in toluene only led instantly to precipitation in the case of R = Me, while the reaction products were soluble in other cases. Isolated from solutions (see Section 3) they were solids (R = Et, Bu^t) or liquids ($R = Bu^n$, Bu^s). The microanalysis data indicate that only $Sc(OMe)_3$ (**1**) does not contain oxoligands. $Sc(OEt)_3$ (**2**) and $Sc(OBu^n)_3$ (**4**) did possess a lower oxocontent than the initial **3**. The derivatives of n-alcohols, **1**, **2** and **4**, were not volatile, while the products formed by the action of different ramified ROH were transferred into the gas phase under the conditions of the mass-spectral experiment. The products of alcohol interchange with ^{s}BuOH and ^{t}BuOH turned out to be $Sc_5O(OBu^s)_{13}$ (**5**) and $Sc_5O(OPr^i)_8(OBu^t)_5$ (**6**), according to mass spectral and microanalysis data. Both **3** and **5**, the derivatives of the secondary alcohols, appear therefore to have the same composition and structure. Only 5 out of 13 OPr^i groups in **6** could be substituted. It might be supposed that these groups are terminal in the molecule of **3** (taking into account its structure).

We then tried to replace five OPr^i groups in **3** with other radicals on the action of ROH (R = Me, Bu^n) on **3** in a 5:1 molar ratio. Thus the soluble products of composition $Sc_5O(OPr^i)_8(OR)_5$ ($R = Bu^n$ **7** or R = Me **8**) were obtained. In the mass spectra of the partial substitution products **6**–**8**, in contrast to the individual complexes **3** and **5**, the series of ions (Fig. 1) of composition $Sc_5O(OPr^i)_{12-n}(OR)_n^+$ were observed. The number of substituted OPr^i groups *n* varied from 1 to 5 for $R = Bu^t$, from 1 to 8 for $R = Bu^n$, and from 2 to 12 for R = Me. The depth of substitution is higher when a smaller ligand is applied. The maximal intensity was observed for the ions with $n = 2$ for $R = Bu^t$, $n = 4$, 5 for $R = Bu^n$ and $n = 3$ for R = Me. The observed series of ions could not result from the fragmentation under electron impact. Ions differed in *m/z* by 14 ($R = Bu^n$, Bu^t) or 28 (R = Me), which corresponds to CH_2 and C_2H_4 groups. The loss of CH_2 groups by an OBu^n ligand or C_2H_4 groups by an OPr^i ligand appears to have a low probability. The results



Scheme 1.

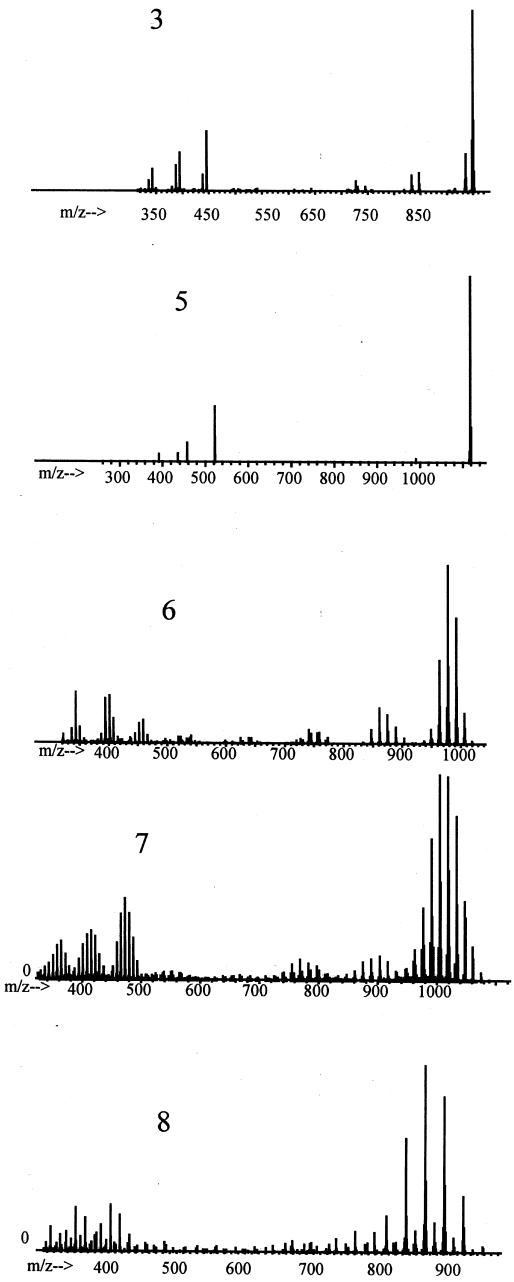


Fig. 1. Mass spectra: $Sc_5O(OPr^i)_{13}$ (**3**), $Sc_5O(OBu^s)_{13}$ (**5**), $Sc_5O(OPr^i)_8(OBu^t)_5$ (**6**), $Sc_5O(OPr^i)_8(OBu^n)_5$ (**7**), $Sc_5O(OPr^i)_8(OMe)_5$ (**8**).

obtained indicate that $Sc_5O(O^iPr)_{13-n}(OR)_n$ molecules, with different extents of substitution for OPr^i groups, exist not only in the gas but even in the condensed phase.

In the mass spectra of **5**–**8**, as well as in that of **3** (Fig. 2), the first ions correspond to the loss of one alkoxide group with the formation of $Sc_5O(OR)_{12}^+$ ($R = Pr^i$, Bu^s) or $Sc_5O(O^iPr)_{12-n}(OR)_n^+$ ($R = Bu^t$, Bu^n, Me). Then they all undergo (except **8**) the elimination of ethers R_2O ($R = Pr^i$,Bu^s) and ^iPrOR ($R = Bu^n$, Bu^t) with the formation of $Sc_5O_2(O^iPr)_{10-n}(OR)_n^+$.

The mass spectral data indicate thus that the introduction of 5 equiv. of alcohol (which is supposed to affect only the terminal groups) affects actually also the ligands that belong

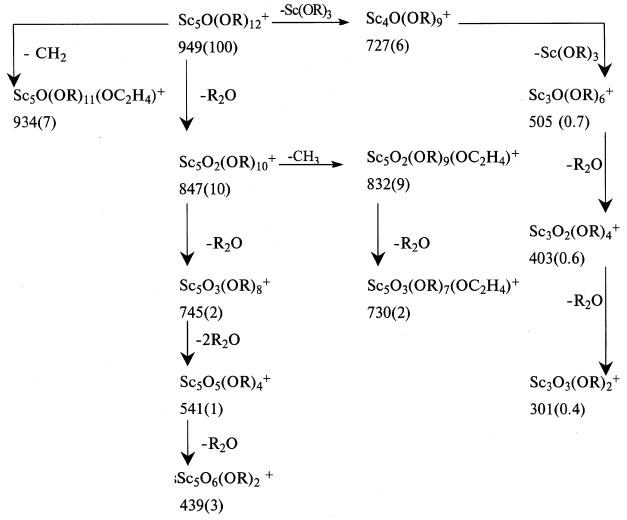


Fig. 2. Fragmentation scheme for $Sc_5O(OPr^i)_{13}$ (**3**).

to the 'core', up to three bridging OR groups in the case of ^{n}BuOH and seven in the case of MeOH. The presence of the mixed-ligand species in the mass spectra of **7** and **8** (up to $Sc_5O(OMe)_{12}^+$, which can be considered as the fragmentation product of the 'volatile' methoxide) is of special interest. As was noted, the action of the considerable excess of n-ROH in the course of the preparation of $Sc(OR^n)_3$ leads to destruction of the pentanuclear core of **3** and the formation of polymeric, non-volatile products. The prepared complexes **6**–**8** are the first mixed-ligand complexes of rare earth elements containing different alkoxide groups.

In conclusion we can identify two types of reaction of **3** with alcohols: (1) complete or partial substitution of the terminal and bridging groups with conservation of the $[Sc_5O(OR)_8]$ core, which keeps the products volatile **6**–**8**; (2) decomposition of the pentanuclear core on action of the most acidic and least sterically demanding n-ROH with the formation of disordered aggregated structures of '$Sc(OR)_3$' **1**, **2**, **4**. It should be taken into account that the alcohol interchange products of **3** (as well as those of the other rare earth isopropoxides) do contain oxoligands. Therefore the data on the possibility of preparation of various homologs of the $Ln(OR)_3$ [9–12] series using this route should be questioned. This method can be used successfully for the preparation of homoleptic alkoxides only in cases where the product formed is insoluble (as for **1**) or crystallizes easily from the reaction mixture (as, for example, for $[Y(OC_2H_4OMe)_3]_{10}$ or $\{Y[OCH(CF_3)_2]_3Thf_3\}$ [13,14]). In both latter cases the complexes containing a higher number of oxogroups than the initial isopropoxides remain in the parent solution. The reaction products obtained on complete evacuation of the solvent (as for samples **2** and **4**), should undoubtedly contain an amount of oxogroups equal to or surpassing that in the initial isopropoxide.

2.2. Crystal structure

The X-ray single crystal study of **3** (the selected bond distances and angles are given in Table 1) shows that its

Table 1
Selected bond distances (Å) and angles (°) in **3**

Sc(1)–O(3)	1.873(6)	Sc(3)–O(1)	2.193(7)
Sc(1)–O(13)	2.154(7)	Sc(3)–O(12)	2.281(7)
Sc(1)–O(11)	2.155(7)	Sc(3)–O(11)	2.304(6)
Sc(1)–O(1)	2.159(6)	Sc(4)–O(6)	1.890(8)
Sc(1)–O(14)	2.162(7)	Sc(4)–O(10)	2.077(8)
Sc(1)–O(12)	2.179(7)	Sc(4)–O(8)	2.092(7)
Sc(2)–O(2)	1.878(8)	Sc(4)–O(1)	2.169(6)
Sc(2)–O(9)	2.086(8)	Sc(4)–O(11)	2.300(7)
Sc(2)–O(7)	2.095(7)	Sc(4)–O(13)	2.317(7)
Sc(2)–O(1)	2.165(6)	Sc(5)–O(5)	1.875(8)
Sc(2)–O(12)	2.282(7)	Sc(5)–O(10)	2.075(8)
Sc(2)–O(14)	2.287(7)	Sc(5)–O(9)	2.084(7)
Sc(3)–O(4)	1.884(7)	Sc(5)–O(1)	2.181(7)
Sc(3)–O(8)	2.061(7)	Sc(5)–O(13)	2.272(7)
Sc(3)–O(7)	2.074(7)	Sc(5)–O(14)	2.277(7)
Sc(1)–Sc(3)	3.183(3)	Sc(2)–Sc(5)	3.059(3)
Sc(1)–Sc(5)	3.186(3)	Sc(2)–Sc(3)	3.067(3)
Sc(1)–Sc(2)	3.189(3)	Sc(3)–Sc(4)	3.078(3)
Sc(1)–Sc(4)	3.203(3)	Sc(4)–Sc(5)	3.069(3)
O(3)–Sc(1)–O(1)	179.3(3)	C(1)–O(2)–Sc(2)	172.8(10)
O(2)–Sc(2)–O(1)	171.9(3)	C(4)–O(3)–Sc(1)	174.2(10)
O(4)–Sc(3)–O(1)	173.1(3)	C(7)–O(4)–Sc(3)	171.1(9)
O(6)–Sc(4)–O(1)	173.7(3)	C(10)–O(5)–Sc(5)	175.3(10)
O(5)–Sc(5)–O(1)	170.1(3)	C(13)–O(6)–Sc(4)	170.9(12)

structure is analogous to those of the known Yb [5], In [5], Y [15] and Er [16] isopropoxides (Fig. 3).

2.3. Complexation with $Al(OPr^i)_3$

The problem of stability of the $[Ln_5O(OPr^i)_8]$ core has been discussed repeatedly in the literature, and is exemplified by the reaction of complex formation of 'isopropoxides' with $Al(OPr^i)_3$. The compounds of the general formula $M[Al(OPr^i)_4]_3$, (where M = Sc, Y, Ln) were synthesized and investigated by Mehrotra et al. [17,18]. The majority of these volatile complexes, including $Sc[Al(OPr^i)_4]_3$, were obtained by an exchange reaction of the corresponding metal chlorides with $K[AlOPr^i]_4$.

According to Hubert-Pfalzgraf and coworkers, no interaction was observed on prolonged reflux of the solutions prepared from $Al(OPr^i)_3$ and the crystalline $[Y_5O(OPr^i)_{13}]$ or $[Nd_5O(OPr^i)_8(^iPrOH)_2]$. At the same time, the reaction of $Al(OPr^i)_3$ with the sample of '$Y(OPr^i)_3$', obtained by reaction of metal with alcohol or with rather unstable $[Nd(OPr^i)_3(^iPrOH)]_4$, led to the formation of volatile $Ln[Al(OPr^i)_4]_3$ [9,19]. However, Westin et al. [16] observed the formation of $Ln[Al(OPr^i)_4]_3$, (Ln = Er, Y), using crystalline $[M_5O(OPr^i)_{13}]$ as reactants. We have studied the complex formation with three scandium alkoxides, **2**, **4** and **3**. Crystalline **3** as well as its yttrium analog [15] did not react with $Al(OPr^i)_3$ on prolonged heating. It was **3** that crystallized from the reaction mixture on heating and the mass spectrum of the residue after evacuation contained only the fragmentation patterns of the components. At the same time the reaction products of **2** or **4** with corresponding $Al(OR)_3$

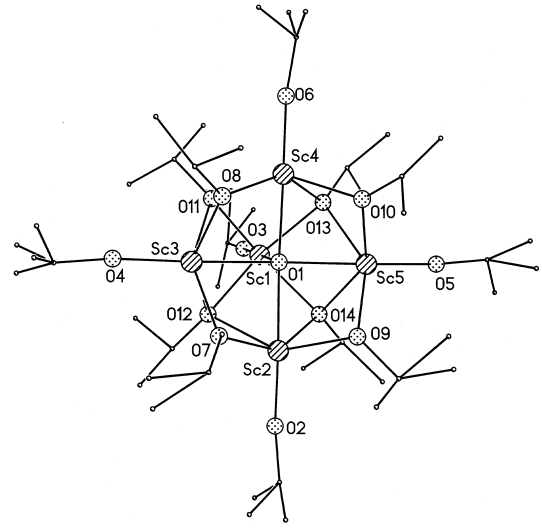


Fig. 3. Stereoscopic ORTEP drawing of non-hydrogen atoms in **3**, showing atom labeling of inner coordination sphere. Unlabeled atoms are carbon.

were the $ScAl_3(OR)_{12}$ bimetallic species, R = Et **9** (amorphous solid), Bu^n **10** (vax). The most intensive peaks in their mass spectra corresponded to $[ScAl_3(OR)_{11}]^+$, which decomposed further under electron impact mainly via elimination of ethers (Fig. 4). $Sc[Al(OPr^i)_4]_3$ (**11**) could be prepared only using the method proposed by Mehrotra et al. [17]. These results indicate the high stability and low reactivity of $[M_5O(OPr^i)_{13}]$ molecules (existing not only in the crystal structure but also in the gas phase). Samples of **2** and **4**, incorporating oxogroups in particles of different size and structure, react easily with the aluminum alkoxides and form rather stable scandium alkoxoaluminates. The possibility of preparation of **11** by an exchange reaction of $ScCl_3$ with $KAl(OPr^i)_4$ is presumably due to the fact that **3** is not formed as an intermediate in this reaction. The fragmentation patterns in the spectra of **9**–**11** correspond to that described for $La[Al(OPr^i)_4]_3$ [20]. The mass spectrum of **10** contains in combination with the ions of the complex itself (their intensity is considerably lower than for the corresponding ones in the spectra of **8** and **11**) the ions corresponding to the fragmentation of the components. This fact can indicate either the lower stability of **10**, or the incompleteness of the complexation in case of n-butoxides.

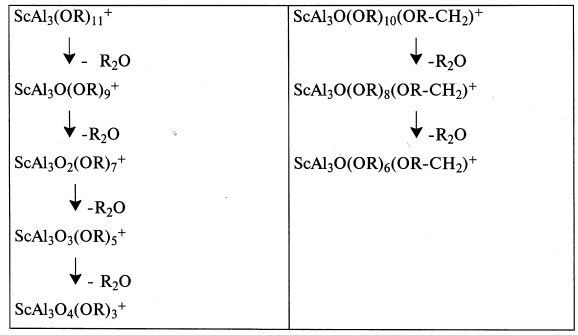


Fig. 4. Fragmentation scheme for $Sc[Al(OR)_4]_3$ (**9**–**11**).

3. Experimental

All compounds described in this work are sensitive to moisture and therefore all operations were carried out using a dry-box. Dehydration of alcohols used was performed by boiling them under reflux over magnesium (MeOH, ^{n}BuOH, ^{s}BuOH), calcium (EtOH), aluminum (^{i}PrOH) alkoxides and zeolite (^{t}BuOH) with subsequent distillation. Toluene and hexane were refluxed with sodium and then distilled over $LiAlH_4$. The carbon and hydrogen contents of the samples were determined using the conventional combustion technique. The scandium content was determined from the incombustible residue.

Infrared spectra were registered with a UR-20 for Nujol or hexachlorobutadiene mulls. Crystalline solids were identified using powder diffractometry (DRON 3M). Mass spectra were measured with a MI 1201 spectrometer (direct insertion of substance, 70 eV, 250°C).

$Al(OPr^i)_3$ was obtained by dissolution of metal in ^{i}PrOH on reflux and purified by distillation. $Al(OR)_3$ ($R = Et, Bu^n$) were obtained from $Al(OPr^i)_3$ by alcohol interchange [21].

3.1. Synthesis and isolation of the products obtained

The anodic oxidation of Sc in different alcohols was carried out in a standard cell with an undivided cathodic and anodic space, supplied with water cooling [4]. A Sc cylinder was used as an anode, a stainless steel plate was used as a cathode. Solutions of LiCl in MeOH (0.001 M) and EtOH, ^{i}PrOH (0.05 M) were used as electrolytes. (LiCl was previously dried in vacuo at 80–100°C.) The process was performed under direct current ($V = 110$ V, $I = 0.4$–1 A) [4].

3.2. $Sc(OMe)_3$ (1)

(a) The anodic dissolution in MeOH occurred much faster than in other alcohols. The current remained constant during the whole reaction time. Some minutes after the start of the electrolysis, a white sediment began to precipitate, continuing in the course of the process. When the synthesis was finished (after 2 h) the sediment was separated by centrifugation, washed twice with MeOH and dried in vacuo. White powder. Yield 2.3 g, 98% (in relation to metal dissolved). *Anal*. Found: C, 25.4; H, 7.3; Sc, 31.8. Calc. for $C_3H_9O_3Sc$: C, 26.1; H, 6.5; Sc, 32.6%. IR (cm^{-1}): 1170 m, 1070 s, 1040 sh, 465 s(br).

(b) MeOH (3.95 g, 123 mmol) was added to the solution of **3** (0.5 g, 0.5 mmol) in 10 ml of toluene. The precipitate formed was separated from the solution (the latter still contained a certain amount of alkoxide). 10 ml of MeOH were added to the precipitate and the mixture was subjected to reflux for 15 min. The solution was then removed and a new portion of MeOH was added. The procedure was repeated twice and the residual solid was dried in vacuo. Its composition was found to be $Sc(OMe)_{2.9}(OPr^i)_{0.1}$. Yield 0.24 g (70%). *Anal*. Found: C, 27.7; H, 6.7; Sc, 31.4. Calc. for $C_{3.2}H_{9.4}O_3Sc$: C, 27.2; H, 6.7; Sc, 31.9%.

3.3. $Sc(OEt)_3$ (2)

(a) The electrochemical synthesis was carried out during 12–15 h. In order to separate the product, the electrolyte was evacuated and hexane was added to the white solid residue. Its major part dissolved with formation of a yellow solution. Evaporation of the hexane extract gave a white powder that contained about 3% Cl. On addition of EtOH, in order to purify it by recrystallization, there occurred initially a complete dissolution of the solid and then a slow precipitation of a snow-white powder, which was then separated and dried in vacuo. It also contained a chlorine admixture (1.99%). Yield 1.5 g (51%). *Anal*. Found: C, 39.5; H, 8.6; Sc, 24.6. Calc. for $C_6H_{15}O_3Sc$: C, 40.0; H, 8.3; Sc, 25.0%.

(b) EtOH (3.95 g, 86 mmol) was added to the solution of **3** (0.5 g, 0.5 mmol) in 10 ml of toluene and then the mixture was evacuated. When the volume of the solution diminished to a few milliliters the procedure was repeated. Once the operation had been carried out 3–4 times the solvent was evacuated completely. The composition of the white powder obtained corresponded to $ScO_{0.1}(OEt)_{2.8}$. Yield 0.43 g (100%). *Anal*. Found: C, 38.9; H, 7.3; Sc, 25.8. Calc. for $C_{5.6}H_{14}O_{2.9}Sc$: C, 38.9; H, 8.1; Sc. 26.1%. IR (cm^{-1}): 1170 vs, 1110 s, 1070 vs, 900 m, 525 s, 515 vs.

3.4. $Sc_5O(OPr^i)_{13}$ (3)

(a) The current remained constant (1 A) in the course of the synthesis. The crystals precipitating on cooling of the parent solution were separated and recrystallized twice from ^{i}PrOH and dried in vacuo. Colorless crystals. Yield 0.95 g (95%). *Anal*. Found: C, 46.5; H, 9.26; Sc, 21.9. Calc. for $C_{39}H_{91}O_{14}Sc_5$: C, 46.4; H, 9.0; Sc, 22.3%. IR (cm^{-1}): 1175 vs, 1158 sh, 1130 s, 1060 m, 1022 s, 985 m, 955 m, 899 vw, 847 w, 730 w, 565 s, 520 s, 490 m, 465 vw, 455 m, 428 m. EI-mass spectrum, *m/z*: 949 (100), 934 (7), 847 (10), 832 (9), 745 (2), 730 (2), 727 (6), 541 (1), 505 (0.7), 439 (3), 403 (0.6), 301 (0.4) (Fig. 2).

3.5. $Sc(OBu^n)_3$ (4)

(b) Same as **2**. The composition of the liquid corresponded to $ScO_{0.05}(OBu^n)_{2.9}$. Yield 0.65 g (100%). *Anal*. Found: C, 53.8; H, 10.0; Sc, 17.7. Calc. for $C_{11.6}H_{26.1}O_{2.95}Sc$: C, 54.0; H, 10.1; Sc, 17.5%. IR (cm^{-1}): 1160 vs, 1110 (s),1085 vs, 1005 s, 970 m, 910 m, 860 w, 810 w, 640 s, 585 s, 480 s.

3.6. $Sc_5O(OBu^s)_{13}$ (5)

(b) Same as **2**. Dry foam. Yield 0.59 g (100%). *Anal*. Found: C, 52.8; H, 10.8; Sc, 17.5. Calc. for $C_{52}H_{117}O_{14}Sc_5$: C, 52.4; H, 9.8; Sc, 18.9%. IR (cm^{-1}): 1115 vs, 1070 vs,

1005 s, 970 m, 930 m, 855 w, 770 w. EI-mass spectrum, *m/z*: 1117 (100, M^+–OR), 987 (1.7, M^+–OR–R_2O).

3.7. $Sc_5O(OPr^i)_8(OBu^t)_5$ (6)

(b) Same as **2**. White crystalline powder. Yield 0.53 g (99%). *Anal*. Found: C, 48.6; H, 9.1; Sc, 20.0. Calc. for $C_{44}H_{101}O_{14}Sc_5$: C, 49.0; H, 9.4; Sc, 20.9%. X-ray powder, *d*, $E(I/I_0)$: 13.22 (32), 10.10 (100), 9.574 (46), 6.209 (27), 4.160 (26). IR (cm^{-1}): 1170 s, 1135 s, 1020 vs, 970 m, 955 m, 915 w, 850 w, 780 vw, 650 w, 620 w, 565 s, 520 s, 450 m, 427 w. EI-mass spectrum, *m/z*: $Sc_5(OPr^i)_{12-n}(OBu^t)_n^+$ 1019 (2.1), $n=5$; 1005 (19), $n=4$; 991 (71), $n=3$; 977 (100) $n=2$; 963 (45), $n=1$; $Sc_5O_2(OPr^i)_{10-n}(OBu^t)_n^+$ 903 (3), $n=4$; 889 (9) $n=3$; 875 (16), $n=2$; 861 (16), $n=1$.

3.8. $Sc_5O(OPr^i)_8(OBu^n)_5$ (7)

(b) ^{n}BuOH (0.19 g, 2.5 mmol) was added to the solution of **3** (0.5 g, 0.5 mmol) in 10 ml of toluene; the solution was refluxed for 15 min and the product was isolated by evacuation. Foamy solid. Yield 0.53 g (100%). *Anal*. Found: C, 49.4; H, 10.2; Sc, 18.7. Calc. for $C_{44}H_{101}O_{14}Sc_5$: C, 49.0; H, 9.4; Sc, 20.9%. IR (cm^{-1}): 1080 vs, 1020 s, 980 m, 905 w, 845 m, 575 vs, 460 s. EI-mass spectrum, *m/z*: $Sc_5(OPr^i)_{12-n}(OBu^n)_n^+$ 1061 (10), $n=8$; 1047 (33), $n=7$; 1033 (71), $n=6$; 1019 (98), $n=5$; 1005 (100), $n=4$; 991 (82), $n=3$; 977 (49), $n=2$; 963 (20), $n=1$; $Sc_5O_2(OPr^i)_{10-n}(OBu^n)_n^+$ 945 (0.9), $n=7$; 931 (2.5), $n=6$; 917 (5.2), $n=5$; 903 (3), $n=4$; 889 (9), $n=3$; 875 (16), $n=2$; 861 (16), $n=1$.

3.9. $Sc_5O(OPr^i)_8(OMe)_5$ (8)

(b) MeOH (0.16 g, 5 mmol) was added to the solution of **3** (1 g, 1 mmol) in 10 ml of toluene; the solution was refluxed for 15 min and the product was isolated by evacuation. Viscous liquid. Yield 0.86 g (100%). *Anal*. Found: C, 40.9; H, 9.3; Sc, 24.5. Calc. for $C_{29}H_{71}O_{14}Sc_5$: C, 40.1; H, 8.2; Sc, 25.9%. IR (cm^{-1}): 1165 s, 1140 s, 1080 vs, 1030 m, 960 w, 890 vw, 860 w, 625 m, 570 m, 420 w. EI-mass spectrum, *m/z*: $Sc_5(OPr^i)_{12-n}(OMe)_n^+$ 893 (60), $n=2$; 865 (100), $n=3$; 837 (60), $n=4$; 809 (50), $n=5$; 781 (44), $n=6$; 753 (42), $n=7$; 725 (30), $n=8$; 697 (25), $n=9$; 669 (18), $n=10$; 641 (9), $n=11$; 613 (6.5), $n=12$.

3.10. $ScAl_3(OEt)_{12}$ (9)

$Sc(OEt)_3$ (0.5 g, 2.8 mmol) and $Al(OEt)_3$ (1.36 g, 8.4 mmol) were dissolved in 10 ml of EtOH, refluxed for 30 min and dried in vacuo. White powder. Yield 1.85 g (100%). *Anal*. Found: C, 43.4; H, 8.7; $Al_2O_3+Sc_2O_3$, 33.1. Calc. for $Al_3C_{24}H_{60}O_{12}Sc$: C, 43.2; H, 9.0; $Al_2O_3+Sc_2O_3$, 33.3%. IR (cm^{-1}): 1070 s, 920 w, 900 w, 620 m, 600 m, 525 m(br). EI-mass spectrum, *m/z*: 621 (75, M^+–OR), 547 (100, M^+–OR–R_2O), 473 (2, M^+–OR–$2R_2O$), 399 (7, M^+–OR–$3R_2O$), 325 (5, M^+–OR–$4R_2O$), 251 (22, M^+–OR–$5R_2O$), 607 (20, M^+–OR–CH_2), 533 (4, M^+–OR–CH_2–R_2O), 459 (19, M^+–OR–CH_2–$2R_2O$), 385 (27, M^+–OR–CH_2–$3R_2O$).

3.11. $ScAl_3(OBu^n)_{12}$ (10)

$Sc(OBu^n)_3$ (0.5 g, 1.9 mmol) and $Al(OBu^n)_3$ (1.40 g, 5.7 mmol) were dissolved in 10 ml ^{n}BuOH, refluxed for 30 min and dried in vacuo. White powder. Yield 1.89 g (100%). *Anal*. Found: C, 56.6; H, 9.7; $Al_2O_3+Sc_2O_3$, 20.8. Calc. for $Al_3C_{48}H_{108}O_{12}Sc$: C, 57.5; H, 10.8; $Al_2O_3+Sc_2O_3$, 22.1%. IR (cm^{-1}): 1080 s, 1010 w, 975 vw, 910 vw, 880 vw, 840 vw, 675 m, 640 m, 575 m, 475 w. EI-mass spectrum, *m/z*: 929 (13, M^+–OR), 799 (6.5, M^+–OR–R_2O), 669 (1, M^+–OR–$2R_2O$), 540 (0.3, M^+–OR–$3R_2O$), 901 (2.5, M^+–OR–CH_2), 785 (4.8, M^+–OR–CH_2–R_2O), 655 (0.4, M^+–OR–CH_2–$2R_2O$).

3.12. $ScAl_3(OPr^i)_{12}$ (11)

$Al(OPr^i)_3$ (3.07 g, 15 mmol) was dissolved in 50 ml ^{i}PrOH and K metal (0.58 g, 15 mmol) was added. An $ScCl_3$ (0.76 g, 5 mmol) solution in 20 ml of ^{i}PrOH was added dropwise to the $K[Al(OPr^i)_4]$ solution obtained. The viscous liquid obtained by evacuation of the solution after the removal of KCl solidified at 0°C on storage. Yield 4.18 g (100%). White powder. *Anal*. Found: C, 51.2; H, 10.7; $Al_2O_3+Sc_2O_3$, 26.1. Calc. for $Al_3C_{36}H_{84}O_{12}Sc$: C, 51.8; H, 10.1; $Al_2O_3+Sc_2O_3$, 26.6%. IR (cm^{-1}): 1470 s, 1380 s, 1180 vs, 1140 s, 1080 s, 1030 s, 970 s, 900 w, 850 s, 675 s, 595 s. EI-mass spectrum, *m/z*: 775 (100, M^+–OR), 673 (45, M^+–OR–R_2O), 571 (18, M^+–OR–$2R_2O$), 469 (27, M^+–OR–$3R_2O$), 367 (34, M^+–OR–$4R_2O$), 761 (45, M^+–OR–CH_2), 659 (9, M^+–OR–CH_2–R_2O), 557 (2, M^+–OR–CH_2–$2R_2O$).

3.13. Crystallography

X-ray quality crystals of **3** were grown in ^{i}PrOH at −10°C. The crystals were placed in glass capillaries, and sealed under an inert atmosphere. Complex **3**, $C_{39}H_{91}O_{14}Sc_5$, $M=1008.92$, monoclinic, space group $P2_1/n$, $a=12.537(6)$, $b=21.253(12)$, $c=20.720(11)$ Å, $\beta=90.35(4)°$, $V=5547(5)$ Å^3, $Z=4$, $D_c=1.208$ g cm^{-3}, $F(000)=2168$, $\mu=6.32$ cm^{-1}, crystal size $0.6\times0.5\times0.3$ mm.

3.14. Crystal structure determination

The X-ray crystal data were collected at 143 K using a Siemens P3/PC diffractometer equipped with graphite-monochromated Mo Kα radiation, ($\lambda=0.71073$ Å), θ–2θ scan mode (θ range 1.4–22.5°). The total of 6187 reflections were averaged to produce 5199 unique data. The structure was solved by direct methods and refined by full-matrix least-squares in the anisotropic approximation for non-hydrogen atoms with the exception of the carbon atoms of some dis-

ordered ^{i}Pr groups. The H atoms were placed geometrically and included in the refined rigid model approximation. The refinement converged to $wR_2 = 0.2467$ (on F_{hkl}^2 for all 5110 reflections, 480 variables) with $R_1 = 0.0807$ (on F_{hkl} for 2835 reflections with $I > 2\sigma(I)$). The highest peak in the final difference Fourier map had a height of 0.58 e Å^{-3}. The maximum negative peak in the final difference electron density synthesis was -0.37 e Å^{-3}. All calculations were performed on an IBM PC using the SHELXTL PLUS 5 program package [22].

Supplementary data

Supplementary data are available from the Cambridge Crystallographic Data Centre, 12 Union Road, Cambridge CB2 1EZ, UK (fax: +44-1223-336033; e-mail: deposit@ccdc.cam.ac.uk) on request, quoting the deposition number 117908.

Acknowledgements

The authors are indebted to Dr V. Kessler at the Department of Chemistry, Swedish University of Agricultural Sciences for assistance with discussion of the results. This work was supported by the Program Universities of Russia, Grant 54-80. The authors are indebted to the Russian Foundation for Basic Research for its financial support (Project No. 97-03-33783a) and for covering the License Fee for the use of the Cambridge Structural Database which was used for analysis of the structural results discussed in the present paper (Project No. 96-07-89187).

References

[1] H. Funk, B. Kohler, Z. Anorg. Allg. Chem. 325 (1963) 67.
[2] Y. Ozaki, K. Kaneko, French Patent, 2529.884 (1984); US Patent, 4507.245 (1985).
[3] D.C. Bradley, H. Chudzynska, D.M. Frigo, M.E. Hammond, M.B. Hursthouse, M.A. Mazid, Polyhedron 9 (1990) 719.
[4] N.I. Kozlova, N.Ya. Turova, E.P. Turevskaya, Soviet J. Coord. Chem. 8 (1982) 339.
[5] D.C. Bradley, H. Chudzynska, M.E. Hammond, M.B. Hursthouse, M. Motevalli, W. Ruowen, Polyhedron 11 (1992) 375.
[6] P.B. Hitchcock, M.F. Lappert, A. Singh, J. Chem. Soc., Chem. Commun. (1983) 1499.
[7] L.M. Brown, K.S. Mazdiyasni, Inorg. Chem. 9 (1970) 2783.
[8] N.Ya. Turova, E.P. Turevskaya, M.I. Yanovskaya, V.G. Kessler, D.E. Tcheboukov, Polyhedron 17 (1998) 899.
[9] K.S. Mazdiyasni, C.T. Lynch, J.S. Smith, Inorg. Chem. 5 (1966) 342.
[10] S.N. Misra, T.N. Misra, R.N. Kapoor, R.C. Mehrotra, Chem. Ind. (1963) 120.
[11] B.S. Sankhla, R.N. Kapoor, Aust. J. Chem. 20 (1967) 2013.
[12] J.M. Batwara, U.D. Tripathi, R.K. Mehrotra, R.C. Mehrotra, Chem. Ind. (1966) 1379.
[13] O. Poncelet, L.G. Hubert-Pfalzgraf, J.C. Daran, R. Astier, J. Chem. Soc., Chem. Commun. (1989) 1846.
[14] F. Labrize, L.G. Hubert-Pfalzgraf, Polyhedron 14 (1995) 881.
[15] O. Poncelet, W.J. Sartain, L.G. Hubert-Pfalzgraf, K. Folting, K.G. Caulton, Inorg. Chem. 28 (1989) 263.
[16] G. Westin, M. Kritikos, M. Wijk, J. Solid State Chem. 141 (1998) 149.
[17] R.C. Mehrotra, M.M. Agrawal, A. Mehrotra, Synth. Inorg. Met. Org. Chem. 3 (2) (1973) 181.
[18] R.C. Mehrotra, A. Mehrotra, Proc. Indian Nat. Sci. Acad. A 40 (1974) 215.
[19] G. Helgesson, S. Jagner, O. Poncelet, L.G. Hubert-Pfalzgraf, Polyhedron 10 (1991) 1559.
[20] J.G. Oliver, I.J. Worrall, J. Chem. Soc. A (1979) 845.
[21] N.Ya. Turova, N.I. Kozlova, M.I. Yanovskaya, Soviet J. Coord. Chem. 6 (1980) 509.
[22] W. Robinson, G.M. Sheldrick, in: Crystallographic Computing Techniques and New Technologies, Oxford University Press, Oxford, 1988, p. 366.

PERGAMON

www.elsevier.nl/locate/poly

Polyhedron 19 (2000) 713–718

POLYHEDRON

Chemical reactivity of $[(\mu\text{-RSe})(\mu\text{-S})\{Fe_2(CO)_6\}_2(\mu_4\text{-S})]^-$: synthesis and characterization of $(\mu\text{-RSe})(\mu\text{-R'S})\{Fe_2(CO)_6\}_2(\mu_4\text{-S})$ and $(\mu_3\text{-S})_2Fe_3(CO)_8[Se(Ph)Fe(CO)_2Cp]$

Huai-Ben Zheng [a], Shao-Bin Miao [a], Zhong-Xia Wang [a,*], Zhong-Yuan Zhou [b], Xiang-Ge Zhou [b]

[a] *Department of Chemistry, University of Science and Technology of China, Hefei, Anhui 230026, People's Republic of China*

[b] *Chengdu Institute of Organic Chemistry, Chinese Academy of Science, Chengdu 610041, People's Republic of China*

Received 27 October 1999; accepted 28 January 2000

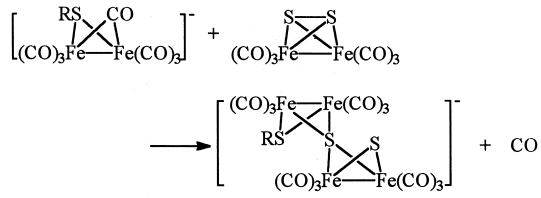
Abstract

The reaction of $(\mu\text{-S}_2)Fe_2(CO)_6$ with $[(\mu\text{-RSe})(\mu\text{-CO})Fe_2(CO)_6]^-$ gives the anionic complexes $[(\mu\text{-RSe})(\mu\text{-S})\{Fe_2(CO)_6\}_2(\mu_4\text{-S})]^-$ (**1**). Reactions of **1** with electrophiles such as alkyl halides, acid chlorides and PhN_2BF_4 form neutral complexes $(\mu\text{-RSe})(\mu\text{-R'S})[Fe_2(CO)_6]_2(\mu_4\text{-S})$ (R = Ph, R' = Me **2a**; R = Ph, R' = $PhCH_2$ **2b**; R = Et, R' = Me **2c**; R = Ph, R' = $CH_3C(O)$ **3a**; R = Ph, R' = PhC(O) **3b**; R = Et, R' = PhC(O) **3c**; R = R' = Ph **4**). Treatment of **1** with $Cp(CO)_2FeI$ affords pentanuclear iron complexes $(\mu\text{-RSe})[\mu\text{-Cp}(CO)_2FeS][Fe_2(CO)_6]_2(\mu_4\text{-S})$ (R = Ph **5a**; R = Et **5b**). From the reaction mixture of **1** (R = Ph) and $Cp(CO)_2FeI$, $(\mu_3\text{-S})_2Fe_3(CO)_8[Se(Ph)Fe(CO)_2Cp]$ (**6**) was also obtained. The structure of complex **6** was determined by single-crystal X-ray analysis.
©2000 Elsevier Science Ltd All rights reserved.

Keywords: Iron; Selenium; Sulfur; Synthesis; Reaction

1. Introduction

The chemical reactivities of $[(\mu\text{-RS})(\mu\text{-CO})Fe_2(CO)_6]^-$ and $[(\mu\text{-RSe})(\mu\text{-CO})Fe_2(CO)_6]^-$ have been studied extensively [1–17]. However, most studies concentrated mainly on reactions with organic reagents. Studies of the reactivities toward organometallic compounds, especially cluster complexes, are relatively rare. Available examples include the reactions with organomercury [3–5], organogold [15], organoiridium [16], organorhenium and organomanganese [17] compounds. Recently we reported the reaction of $[(\mu\text{-RS})(\mu\text{-CO})Fe_2(CO)_6]^-$ with $(\mu\text{-S}_2)Fe_2(CO)_6$, yielding anionic complexes $[(\mu\text{-RS})(\mu\text{-S})\{Fe_2(CO)_6\}_2(\mu_4\text{-S})]^-$ (see Eq. (1)) [18], which reacted readily with electrophiles to form neutral complexes of the type $(\mu\text{-RS})(\mu\text{-R'S})[Fe_2(CO)_6]_2(\mu_4\text{-S})$. To compare the reactivity of $[(\mu\text{-RSe})(\mu\text{-CO})Fe_2(CO)_6]^-$ with that of $[(\mu\text{-RS})(\mu\text{-CO})Fe_2(CO)_6]^-$, we have investigated the reaction of $[(\mu\text{-RSe})(\mu\text{-CO})Fe_2(CO)_6]^-$ with $(\mu\text{-S}_2)Fe_2(CO)_6$, and the reactivity of the resulting complexes $[(\mu\text{-RSe})(\mu\text{-S})\{Fe_2(CO)_6\}_2(\mu_4\text{-S})]^-$ toward electrophiles. Herein we report the results.



(1)

2. Experimental

All reactions were carried out under nitrogen using standard Schlenk techniques. Tetrahydrofuran (THF) and diethyl ether were distilled from sodium benzophenone ketyl. PhSeH [19], PhN_2BF_4 [20], $Fe_3(CO)_{12}$ [21], $Cp(CO)_2FeI$ [22] and $(\mu\text{-S}_2)Fe_2(CO)_6$ [23] were prepared by published procedures. The solution of $[(\mu\text{-RSe})(\mu\text{-CO})Fe_2(CO)_6]^-$ (R = Ph, Et) was prepared by the method described in the literature [8,14]. The progress of all reactions was monitored by thin-layer chromatography. Infrared spectra (KBr disk) were obtained using a VECTOR22 spectrometer. ^1H NMR spectra were recorded on either a Varian EM360L or a JEOL FX-90Q spectrometer. Elemental analyses were performed with a 240C analyzer.

* Corresponding author. Tel.: +86-551-3603301; fax: +86-551-3631760; e-mail: zxwang@ustc.edu.cn

0277-5387/00/$ - see front matter ©2000 Elsevier Science Ltd All rights reserved.
PII S0277-5387(00)00317-X

2.1. Preparation of (μ-PhSe)(μ-R^1S)[$Fe_2(CO)_6$]$_2$(μ$_4$-S) (**2a**, R^1 = Me; **2b**, R^1 = $PhCH_2$)

A solution of the triethylammonium salt of [(μ-PhSe)(μ-CO)$Fe_2(CO)_6$]$^-$ was generated by reacting 0.65 g (1.29 mmol) of $Fe_3(CO)_{12}$, 0.14 ml (1.32 mmol) of PhSeH and 0.19 ml (1.36 mmol) of Et_3N in 30 ml of THF at room temperature under nitrogen. The solution was cooled to −78°C, and 0.27 g (0.78 mmol) of (μ-S_2)$Fe_2(CO)_6$ was added with stirring for 30 min at −78°C. Subsequently 0.12 ml (1.93 mmol) of iodomethane was syringed. The mixture was warmed to room temperature and stirred overnight. The solvent was removed at reduced pressure and the residue extracted with petroleum ether. After removal of the solvent, the material remaining was subjected to filtration chromatography (silica gel) using petroleum ether as eluent. The first band gave 0.10 g (26% based on (μ-S_2)$Fe_2(CO)_6$) of (μ$_3$-S)$_2$$Fe_3(CO)_9$ as dark purple crystals. The second band gave 0.02 g (5% based on $Fe_3(CO)_{12}$) of dark red crystalline (μ-PhSe)$_2$$Fe_2(CO)_6$ and the third main band afforded 0.16 g (26% based on (μ-S_2)$Fe_2(CO)_6$) of red crystalline **2a**, m.p. 142–144°C. *Anal*. Found: C, 28.50; H, 0.89. Calc. for $C_{19}H_8Fe_4O_{12}S_2Se$: C, 28.72; H, 1.01%. ^{1}H NMR (CCl_4): δ (ppm) 2.20 (s, 3H, Me), 7.26 (s, 5H, Ph). IR: ν (cm^{-1}) 2083m, 2056s, 2031vs, 1993s, 1973s (Fe–CO).

A similar reaction was carried out, in which 1.30 mmol of benzyl chloride was added to a solution of anion **1** prepared from 1.43 mmol of $Fe_3(CO)_{12}$, 1.51 mmol of PhSeH and 1.50 mmol of Et_3N followed by addition of 1.28 mmol of (μ-S_2)$Fe_2(CO)_6$ giving, after similar work-up, 0.08 g (13% based on (μ-S_2)$Fe_2(CO)_6$) of (μ$_3$-S)$_2$$Fe_3(CO)_9$, 0.19 g (25% based on $Fe_3(CO)_{12}$) of (μ-PhSe)$_2$$Fe_2(CO)_6$ and 0.14 g (13% based on (μ-S_2)$Fe_2(CO)_6$) of dark red crystals of **2b**, m.p. 110°C (dec.). *Anal*. Found: C, 34.33; H, 1.13. Calc. for $C_{25}H_{12}Fe_4O_{12}S_2Se$: C, 34.48; H, 1.39%. ^{1}H NMR (CCl_4): δ (ppm) 3.60 (s, 2H, CH_2), 7.03–7.23 (m, 10H, Ph). IR: ν (cm^{-1}) 2082m, 2054vs, 2036vs, 2010s, 1999vs, 1990vs (Fe–CO).

2.2. Preparation of (μ-EtSe)(μ-MeS)[$Fe_2(CO)_6$]$_2$(μ$_4$-S) (**2c**)

A Schlenk tube was charged with 0.16 g (2.03 mmol) of selenium powder, 30 ml of THF and 2.00 mmol of EtMgBr in Et_2O. The mixture was stirred at room temperature for 20 min. To the solution was added 0.90 g (1.78 mmol) of $Fe_3(CO)_{12}$ and stirring was continued for 20 min, resulting in a brown–red solution of [MgBr][(μ-EtSe)(μ-CO)-$Fe_2(CO)_6$]. The solution was cooled to −78°C, and 0.55 g (1.60 mmol) of (μ-S_2)$Fe_2(CO)_6$ was added with stirring for 30 min at −78°C. Subsequently 0.20 ml (3.21 mmol) of iodomethane was syringed. The mixture was warmed to room temperature and stirred for 3 h. Work-up as described in Section 2.1 gave 0.11 g (14% based on (μ-S_2)$Fe_2(CO)_6$) of (μ$_3$-S)$_2$$Fe_3(CO)_9$ and 0.13 g (11% based on (μ-S_2)-$Fe_2(CO)_6$) of red crystalline complex **2c**, m.p. 143–146°C. *Anal*. Found: C, 24.41; H, 1.32. Calc. for $C_{15}H_8Fe_4O_{12}S_2Se$: C, 24.13; H, 1.08%. ^{1}H NMR (CCl_4): δ (ppm) 1.50 (t, J = 7 Hz, 3H, Me), 2.16 (s, 3H, Me), 2.67 (q, J = 7.5 Hz, 2H, CH_2). IR: ν (cm^{-1}) 2083m, 2057s, 2035vs, 2006s, 1992s, 1969s (Fe–CO).

2.3. Preparation of (μ-PhSe)[μ-R^2C(O)S]-[$Fe_2(CO)_6$]$_2$(μ$_4$-S) (**3a**, R^2 = Me; **3b**, R^2 = Ph)

To a cooled solution of [Et_3NH][(μ-PhSe)(μ-CO)-$Fe_2(CO)_6$] generated from 0.82 g (1.61 mmol) of $Fe_3(CO)_{12}$, 0.18 ml (1.70 mmol) of PhSeH and 0.24 ml (1.71 mmol) of Et_3N in about 30 ml of THF was added 0.44 g (1.28 mmol) of (μ-S_2)$Fe_2(CO)_6$ with stirring for 30 min at −78°C. Subsequently 0.20 ml (1.82 mmol) of acetyl chloride was syringed. The mixture was warmed to room temperature and stirred overnight. Work-up as described in Section 2.1 gave 0.08 g (13% based on (μ-S_2)$Fe_2(CO)_6$) of (μ$_3$-S)$_2$$Fe_3(CO)_9$, 0.22 g (46% based on $Fe_3(CO)_{12}$) of (μ-PhSe)$_2$$Fe_2(CO)_6$ and 0.08 g (8% based on (μ-S_2)-$Fe_2(CO)_6$) of **3a** as red crystals, m.p. 130°C (dec.). *Anal*. Found: C, 29.38; H, 1.12. Calc. for $C_{20}H_8Fe_4O_{13}S_2Se$: C, 29.20; H, 0.98%. ^{1}H NMR (CCl_4): δ (ppm) 2.54 (s, 3H, Me), 7.20 (s, 5H, Ph). IR: ν (cm^{-1}) 2085m, 2054s, 2036vs, 1999s, 1988s, 1976s (Fe–CO); 1732w (MeCO).

A similar reaction, in which 0.16 ml (1.38 mmol) of benzoyl chloride was added to a cooled solution of anion **1** (prepared from 1.57 mmol of $Fe_3(CO)_{12}$, 1.61 mmol of PhSeH and 1.64 mmol of Et_3N and then 1.37 mmol of (μ-S_2)$Fe_2(CO)_6$), gave 0.11 g (16% based on (μ-S_2)$Fe_2(CO)_6$) of (μ$_3$-S)$_2$$Fe_3(CO)_9$, 0.08 g (17% based on $Fe_3(CO)_{12}$) of (μ-PhSe)$_2$$Fe_2(CO)_6$ and 0.26 g (21% based on (μ-S_2)$Fe_2(CO)_6$) of red crystals of **3b**, m.p. 140°C (dec.). *Anal*. Found: C, 34.06; H, 1.29. Calc. for $C_{25}H_{10}Fe_4O_{13}S_2Se$: C, 33.94; H, 1.14%. ^{1}H NMR ($CDCl_3$): δ (ppm) 7.18 (s, 5H, Ph), 7.34–7.46 (m, 3H, Ph), 7.97–8.09 (m, 2H, Ph). IR: ν (cm^{-1}) 2085m, 2052s, 2039vs, 2000s (Fe–CO); 1681m (PhCO).

2.4. Preparation of (μ-EtSe)[μ-Ph C(O)S]-[$Fe_2(CO)_6$]$_2$(μ$_4$-S) (**3c**)

The solution of [MgBr][(μ-EtSe)(μ-S){$Fe_2(CO)_6$}$_2$-(μ$_4$-S)] was prepared according to the same procedure and scale as described in Section 2.2. To the cooled solution was added 0.19 ml (1.64 mmol) of benzoyl chloride. The mixture was warmed to room temperature and stirred overnight. Work-up as described in Section 2.1 gave 0.07 g (9% based on (μ-S_2)$Fe_2(CO)_6$) of (μ$_3$-S)$_2$$Fe_3(CO)_9$ and 0.14 g (10% based on (μ-S_2)$Fe_2(CO)_6$) of red crystalline **3c**, m.p. 140°C (dec.). *Anal*. Found: C, 30.41; H, 1.38. Calc. for $C_{21}H_{10}Fe_4O_{13}S_2Se$: C, 30.14; H, 1.20%. ^{1}H NMR ($CDCl_3$): δ (ppm) 1.53 (t, J = 7 Hz, 3H, Me), 2.70 (q, J = 7 Hz, 2H, CH_2), 7.30–7.70 (m, 3H, Ph), 7.90–8.25 (m, 2H, Ph). IR: ν (cm^{-1}) 2085m, 2057s, 2036vs, 2000s, 1989vs (Fe–CO); 1681w (PhCO).

2.5. Preparation of (μ-PhSe)(μ-PhS)[$Fe_2(CO)_6$]$_2$(μ$_4$-S) (**4**)

To a cooled solution of [Et_3NH][(μ-PhSe)(μ-CO)-$Fe_2(CO)_6$] generated from 0.78 g (1.53 mmol) of $Fe_3(CO)_{12}$, 0.17 ml (1.61 mmol) of PhSeH and 0.23 ml (1.64 mmol) of Et_3N in about 30 ml of THF was added 0.42 g (1.22 mmol) of (μ-S_2)$Fe_2(CO)_6$ and the mixture was stirred for 30 min at −78°C. Subsequently 0.24 g (1.25 mmol) of PhN_2BF_4 was added. The mixture was warmed to room temperature and stirred overnight. Work-up as described in Section 2.1 gave 0.08 g (14% based on (μ-S_2)$Fe_2(CO)_6$) of (μ_3-S)$_2Fe_3(CO)_9$, 0.23 g (50% based on $Fe_3(CO)_{12}$) of (μ-PhSe)$_2Fe_2(CO)_6$ and 0.07 g (7% based on (μ-S_2)$Fe_2(CO)_6$) of red crystals of **4**, m.p. 175°C (dec.). *Anal*. Found: C, 33.35; H, 1.35. Calc. for $C_{24}H_{10}Fe_4O_{12}S_2Se$: C, 33.64; H, 1.18%. ^{1}H NMR (CCl_4): δ (ppm) 7.22–7.62 (m, 10H, Ph). IR: ν (cm^{-1}) 2081m, 2057s, 2037vs, 1996s, 1976m (Fe–CO).

2.6. Preparation of (μ-PhS)[μ-Cp(CO)$_2$FeS]-[$Fe_2(CO)_6$]$_2$(μ$_4$-S) (**5a**) and (μ_3-S)$_2Fe_3(CO)_8$-[PhSeFe(CO)$_2$Cp] (**6**)

To a cooled solution of [Et_3NH][(μ-PhSe)(μ-CO)-$Fe_2(CO)_6$] generated from 0.86 g (1.69 mmol) of $Fe_3(CO)_{12}$, 0.19 ml (1.80 mmol) of PhSeH and 0.25 ml (1.79 mmol) of Et_3N in 30 ml of THF was added 0.46 g (1.34 mmol) of (μ-S_2)$Fe_2(CO)_6$ and the mixture was stirred for 30 min at −78°C. Subsequently 0.41 g (1.35 mmol) of Cp(CO)$_2$FeI was added. The reaction mixture was warmed to room temperature and stirred overnight. Solvent was removed at reduced pressure and the residue extracted with CH_2Cl_2:petroleum ether (1:9 v/v). After removal of the solvent, the material remaining was subjected to filtration chromatography (silica gel). Petroleum ether eluted a purple band which gave 0.05 g (8% based on (μ-S_2)$Fe_2(CO)_6$) of (μ_3-S)$_2Fe_3(CO)_9$. The second band gave 0.05 g (10% based on $Fe_3(CO)_{12}$) of (μ-PhSe)$_2Fe_2(CO)_6$. Further elution with 2:8 v/v CH_2Cl_2:petroleum ether gave 0.19 g (15% based on (μ-S_2)$Fe_2(CO)_6$) of complex **5a** as black crystals and 0.10 g (9% based on (μ-S_2)$Fe_2(CO)_6$) of black crystalline complex **6**. **5a**: m.p. 150°C (dec.). *Anal*. Found: C, 31.38; H, 1.32. Calc. for $C_{25}H_{10}Fe_5O_{14}S_2Se$: C, 31.39; H, 1.05%. ^{1}H NMR ($CDCl_3$): δ (ppm) 5.08 (s, 5H, Cp), 7.20 (s, 5H, Ph). IR: ν (cm^{-1}) 2076m, 2051s, 2027vs, 1973s (Fe–CO). **6**: m.p. 87–88°C. *Anal*. Found: C, 31.63; H, 1.24. Calc. for $C_{21}H_{10}Fe_4O_{10}S_2Se$: C, 31.98; H, 1.28%. ^{1}H NMR ($CDCl_3$): δ (ppm) 4.90 (s, 5H, Cp), 7.20 (s, 5H, Ph). IR: ν (cm^{-1}) 2066s, 2039s, 2017vs, 1997vs, 1954m, 1947m (Fe–CO).

2.7. Preparation of (μ-EtS)[μ-Cp(CO)$_2$FeS]-[$Fe_2(CO)_6$]$_2$(μ$_4$-S) (**5b**)

The solution of [MgBr][(μ-EtSe)(μ-S){$Fe_2(CO)_6$}$_2$-(μ$_4$-S)] was prepared according to the same procedure and scale as described in Section 2.2. To the solution was added 0.50 g (1.64 mmol) of Cp(CO)$_2$FeI at −78°C with stirring. The mixture was warmed to room temperature and stirred overnight. Solvent was removed at reduced pressure and the residue extracted with CH_2Cl_2:petroleum ether (1:9 v/v). After removal of the solvent, the material remaining was subjected to filtration chromatography (silica gel). Petroleum ether eluted a purple band which gave 0.09 g (12% based on (μ-S_2)$Fe_2(CO)_6$) of (μ_3-S)$_2Fe_3(CO)_9$. Further elution with 2:8 v/v CH_2Cl_2:petroleum ether gave 0.13 g (9% based on (μ-S_2)$Fe_2(CO)_6$) of complex **5b** as black crystals, m.p. 142°C (dec.). *Anal*. Found: C, 28.27; H, 1.37. Calc. for $C_{21}H_{10}Fe_5O_{14}S_2Se$: C, 27.76; H, 1.11%. ^{1}H NMR ($CDCl_3$): δ (ppm) 1.50 (t, J = 7.5 Hz, 3H, Me), 2.53 (q, J = 7.5 Hz, 2H, CH_2), 5.10 (s, 5H, Ph). IR: ν (cm^{-1}) 2074m, 2050s, 2026vs, 1996s, 1982s, 1967vs (Fe–CO).

2.8. Crystal data and structure determination of complex **6**

Black crystals of complex **6** were grown from a petroleum ether–CH_2Cl_2 solution at 0°C. Data were collected on a Siemens P4 four-circle diffractometer using graphite-monochromated Mo Kα radiation. Absorption correction was applied using SADABS. The structure was solved by the direct method and refined by full-matrix least-squares on F^2 with anisotropic thermal parameters for non-hydrogen atoms on a PC using SHELXS-86 and SHELXL-97 software packages, respectively [24,25]. A summary of crystal data and refinement parameters is given in Table 1. Selected bond distances and angles are listed in Table 2.

Table 1
Crystal data and refinement parameters for complex **6**

Formula	$C_{21}H_{10}Fe_4O_{10}S_2Se$
M	788.77
Crystal system	triclinic
Space group	$P\bar{1}$ (no. 2)
a (Å)	10.5626(10)
b (Å)	10.6168(10)
c (Å)	13.4368(12)
α (°)	75.686(2)
β (°)	70.409(2)
γ (°)	75.352(2)
U (Å^3)	1351.5(2)
Z	2
Crystal size (mm)	0.18×0.16×0.16
Radiation λ (Å)	0.71073
Temperature (K)	294(2)
Scan type	ω–2θ
$2\theta_{max}$ (°)	55.06
Total reflections	6109
Independent reflections	6106 (R_{int} = 0.0000)
Reflections with $I > 2\sigma(I)$	4884
Goodness-of-fit on F^2	0.679
Final R indices ($I > 2\sigma(I)$)	
R_1 [a]	0.0282
wR_2 [b]	0.0814
Largest differences peak and hole (e Å^{-3})	0.441, −0.375

[a] $R_1 = \Sigma||F_o| - |F_c||/\Sigma|F_o|$.
[b] $wR_2 = [\Sigma w(F_o^2 - F_c^2)^2/\Sigma wF_o^4]^{1/2}$.

Table 2
Selected bond distances (Å) and angles (°) for complex **6**

Se(1)–C(16)	1.9415(19)	Fe(2)–S(2)	2.2545(6)
Se(1)–Fe(4)	2.4134(4)	Fe(2)–S(1)	2.2569(6)
Se(1)–Fe(1)	2.4433(3)	Fe(2)–Fe(3)	2.5728(5)
Fe(1)–S(1)	2.2080(6)	Fe(3)–S(1)	2.2416(6)
Fe(1)–S(2)	2.2351(5)	Fe(3)–S(2)	2.2516(5)
Fe(1)–Fe(2)	2.6291(4)	Fe(4)–Cent [a]	1.714
C(16)–Se(1)–Fe(4)	99.76(6)	S(2)–Fe(2)–S(1)	78.91(2)
C(16)–Se(1)–Fe(1)	112.89(6)	S(2)–Fe(2)–Fe(3)	55.130(15)
Fe(4)–Se(1)–Fe(1)	114.556(13)	Fe(3)–Fe(2)–Fe(1)	81.516(14)
S(1)–Fe(1)–S(2)	80.36(2)	S(1)–Fe(3)–S(2)	79.29(2)
S(1)–Fe(1)–Se(1)	158.195(18)	S(1)–Fe(3)–Fe(2)	55.396(17)
S(2)–Fe(1)–Se(1)	85.752(15)	S(2)–Fe(3)–Fe(2)	55.236(16)
S(1)–Fe(1)–Fe(2)	54.792(16)	Fe(1)–S(1)–Fe(3)	99.51(2)
S(2)–Fe(1)–Fe(2)	54.499(15)	Fe(1)–S(1)–Fe(2)	72.138(17)
S(1)–Fe(2)–Fe(3)	54.836(18)	Fe(3)–S(1)–Fe(2)	69.768(17)
S(2)–Fe(2)–Fe(1)	53.812(14)	Fe(1)–S(2)–Fe(3)	98.40(2)
S(1)–Fe(2)–Fe(1)	53.070(15)	Fe(1)–S(2)–Fe(2)	71.689(18)
Se(1)–Fe(1)–Fe(2)	103.412(13)	Fe(3)–S(2)–Fe(2)	69.634(18)

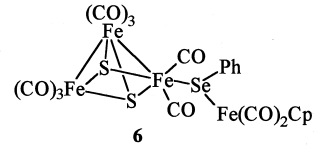
[a] Cent is the centroid of the Cp ring composed of carbon atoms C(11)–C(15).

3. Results and discussion

The synthesis and reactions of $[(\mu\text{-RSe})(\mu\text{-S})\{Fe_2(CO)_6\}_2(\mu_4\text{-S})]^-$ are summarized in Scheme 1. Both $[Et_3NH][(\mu\text{-PhSe})(\mu\text{-CO})Fe_2(CO)_6]$ and $[MgBr][(\mu\text{-EtSe})(\mu\text{-CO})Fe_2(CO)_6]$ were prepared by reported methods [12,14] and reacted readily with $(\mu\text{-S}_2)Fe_2(CO)_6$ at −78°C, as indicated by gas evolution. Treatment of the reaction mixture with electrophiles such as alkyl halides, acid chlorides and PhN_2BF_4 gave neutral complexes of the type $(\mu\text{-RSe})(\mu\text{-R}'\text{S})[Fe_2(CO)_6]_2(\mu_4\text{-S})$ (R′ = alkyl, acyl or phenyl). Thus the expected anions **1** were formed. Similarly to the reaction between $[(\mu\text{-RS})(\mu\text{-CO})Fe_2(CO)_6]^-$ and $(\mu\text{-S}_2)Fe_2(CO)_6$, the sulfur–sulfur bond of $(\mu\text{-S}_2)Fe_2(CO)_6$ is cleaved by the iron-centered anions and the μ-CO ligand of $[(\mu\text{-RSe})(\mu\text{-CO})Fe_2(CO)_6]^-$ is replaced by one of the sulfur atoms of $(\mu\text{-S}_2)Fe_2(CO)_6$. It is noteworthy that the yields of $(\mu\text{-RSe})(\mu\text{-R}'\text{S})[Fe_2(CO)_6]_2(\mu_4\text{-S})$ were low and, for R = Ph, the oxidation product $(\mu\text{-PhSe})_2Fe_2(CO)_6$ was formed in low to moderate yield. In addition, $(\mu_3\text{-S})_2Fe_3(CO)_9$ was also obtained in each reaction. Treatment of the reaction mixture of $[(\mu\text{-RSe})(\mu\text{-CO})Fe_2(CO)_6]^-$ and $(\mu\text{-S}_2)Fe_2(CO)_6$ with $Cp(CO)_2FeI$ afforded pentanuclear complexes **5a** and **5b**. For R = Ph, an unexpected product, $(\mu_3\text{-S})_2Fe_3(CO)_8[Se(Ph)Fe(CO)_2Cp]$ (**6**), was also isolated. The formation of complex **6** may arise from the reaction of $(\mu_3\text{-S})_2Fe_3(CO)_9$ with $PhSeFe(CO)_2Cp$ produced from $Cp(CO)_2FeI$ and excess $Et_3NH^+SePh^-$ (Scheme 2).

$$Et_3NH^+SePh^- + Cp(CO)_2FeI \longrightarrow Cp(CO)_2FeSePh$$

$(\mu_3\text{-S})_2Fe_3(CO)_9$ →

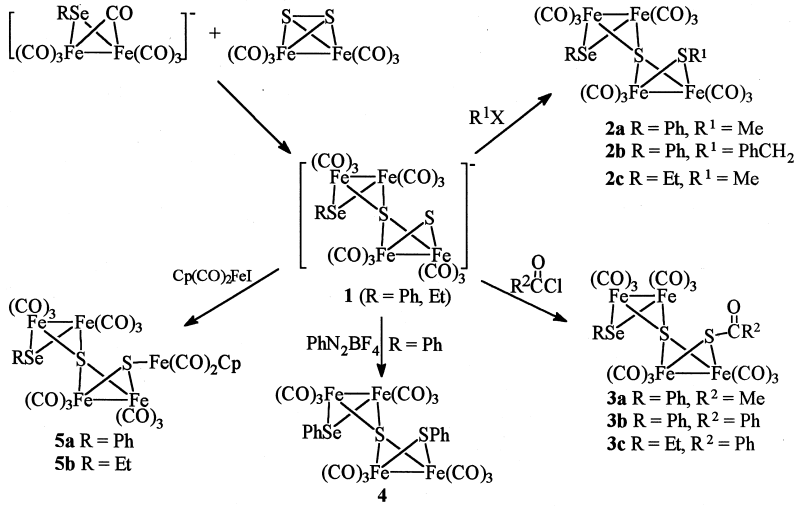


6

Scheme 2.

Both complexes $(\mu_3\text{-S})_2Fe_3(CO)_9$ and $(\mu\text{-PhSe})_2Fe_2(CO)_6$ are known and were identified by elemental analyses and by comparison of their melting points, IR and ^1H NMR (for the latter) spectra with those of authentic samples [26,27].

Complexes **2**–**4** are red solids and **5a** and **5b** are black solids. They are air stable in the solid state, but slightly air sensitive in solution. The new complexes **2**–**5** were characterized by elemental analyses, IR and ^1H NMR spectra. Their IR spectra showed four to six terminal carbonyl absorption bands in the range 2085–1969 cm^{-1}. For complexes **3a**–**3c** the absorption bands of thiocarboxylato groups were also observed. Their ^1H NMR spectra all exhibited respective organic group resonance signals. It is worthy of note that complexes **2**–**5** can exist as only one isomer in which the two substituents are bonded to the bridged Se and S atoms with an equatorial type of bond. This is because the μ_4-S atom of **2**–**5** utilizes two axial bonds to attach both (μ-RSe)-



Scheme 1.

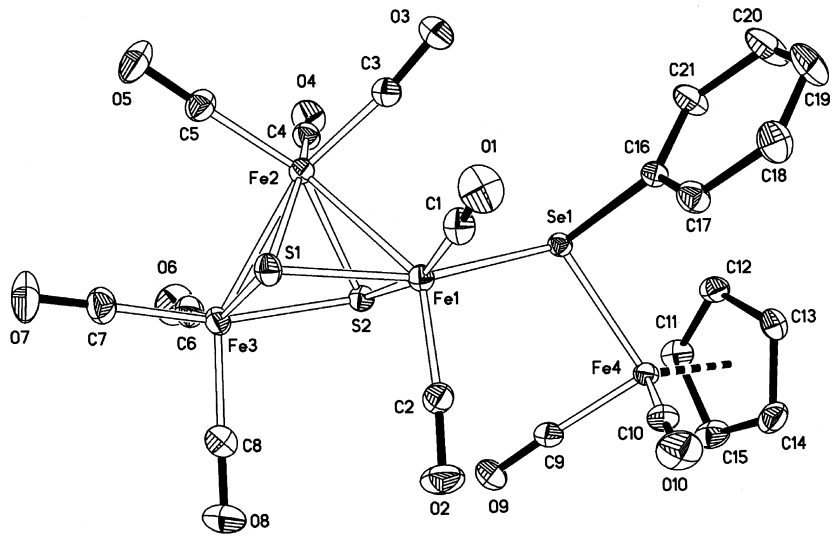


Fig. 1. ORTEP representation of the molecular structure of complex **6**. The thermal ellipsoids are drawn at the 20% probability level.

$Fe_2(CO)_6$ and $(\mu\text{-}R'S)Fe_2(CO)_6$ units, respectively, and because there are larger non-bonded repulsions between the axial R (or R′) group and axial $Fe(CO)_3$ group [28]. This deduction can be verified by some of the ^1H NMR spectra. For example, the ^1H NMR spectrum of **2c** showed one quartet at δ 2.67 ppm for $SeCH_2$ [29] and one singlet at δ 2.16 ppm for SCH_3 [28]; the $CH_3C(O)$ group of **3a** showed one singlet at δ 2.54 ppm [30] and the CH_2Se group of **3c** showed one quartet at δ 2.70 ppm [29].

Complex **6** was isolated as a black solid. Its IR spectrum exhibited terminal carbonyl absorption bands and the ^1H NMR spectrum showed the presence of phenyl and cyclopentadienyl groups. The C/H analytical data agree closely with the calculated values for complex **5**. From these analytical results it seems as if complex **6** was an isomer of complex **5**. However, the chemical shift of the ^1H NMR spectrum for the Cp group (δ 4.90 ppm) was close to that of an axial $Fe(CO)_2Cp$ [31]. This would involve considerable non-bonded repulsion between two axial groups. For this reason, a single-crystal X-ray diffraction study was undertaken. The result showed that complex **6** is a mono-substituted product of $(\mu_3\text{-}S)_2Fe_3(CO)_9$ by $Se(Ph)Fe(CO)_2Cp$ (Fig. 1). The skeletal structure is very similar to that of $(\mu_3\text{-}S)_2Fe_3(CO)_9$ [32], i.e. it consists of an open triangle of iron atoms (Fe(1)Fe(2)Fe(3)) capped on each side by the two sulfur ligands, and S_2Fe_3 is a distorted square pyramid.

$Se(Ph)Fe(CO)_2Cp$ replaces the carbonyl at the basal position and the orientation of $Se(Ph)Fe(CO)_2Cp$ is axial. This is consistent with $(\mu_3\text{-}S)_2Fe_3(CO)_8[P(OMe)_3]$ [33] and $(\mu_3\text{-}S)_2Fe_3(CO)_8[P(SPh)_3]$ [34]. The bond lengths Fe–Fe and Fe–S are comparable with the corresponding values in $(\mu_3\text{-}S)_2Fe_3(CO)_8[P(OMe)_3]$ [33] and $(\mu_3\text{-}S)_2Fe_3(CO)_8[P(SPh)_3]$ [34]. The Se–Fe bond length (2.4433(3) and 2.4134(4) Å, respectively) is close to those found in $Fe_4(CO)_{10}(\mu\text{-}CO)(\mu_4\text{-}Se)$ (average 2.428 Å) [35], but a little longer than those in $(\mu\text{-}PhSe)(\mu\text{-}PhCH_2SC{=}S)\text{-}Fe_2(CO)_6$ (average 2.374 Å) [8] and $(\mu\text{-}Se_2)Fe_2(CO)_6$ (average 2.364 Å) [36].

Supplementary data

Supplementary data are available from the Cambridge Crystallographic Data Centre, 12 Union Road, Cambridge CB2 1EZ, UK (fax: +44-1223-336033; e-mail: deposit@ccdc.cam.ac.uk) on request, quoting the deposition number CCDC 134795.

Acknowledgements

We thank the Chinese Academy of Science and the Educational Ministry of China for financial support.

References

[1] D. Seyferth, G.B. Womack, J.C. Dewan, Organometallics 4 (1985) 508.
[2] D. Seyferth, J.B. Hoke, J.C. Dewan, Organometallics 6 (1987) 895.
[3] D. Seyferth, L.L. Anderson, W.M. Davis, J. Organomet. Chem. 459 (1993) 271.
[4] D. Seyferth, D.P. Ruschke, W.M. Davis, M. Cowie, A.D. Hunter, Organometallics 13 (1994) 3834.
[5] D. Seyferth, L.L. Anderson, F. Villafane, M. Cowie, R.W. Hilts, Organometallics 11 (1992) 3262.
[6] L.-C. Song, Q.-M. Hu, J. Organomet. Chem. 414 (1991) 219.
[7] L.-C. Song, Chem. J. Chin. Univ. 17 (1996) 575.
[8] L.-C. Song, C.-G. Yan, Q.-M. Hu, R.-J. Wang, T.C.W. Mak, Organometallics 14 (1995) 5513.
[9] L.-C. Song, C.-G. Yan, Q.-M. Hu, X.-Y. Huang, J. Organomet. Chem. 505 (1995) 119.
[10] D. Seyferth, J.B. Hoke, D.R. Wheele, J. Organomet. Chem. 341 (1988) 421.
[11] L.-C. Song, C.-G. Yan, Q.-M. Hu, R.-J. Wang, T.C.W. Mak, X.-Y. Huang, Organometallics 15 (1996) 1535.

[12] D. Seyferth, G.B. Womack, C.M. Archer, J.C. Dewan, Organometallics 8 (1989) 430.
[13] L.-C. Song, C.-G. Yan, Q.-M. Hu, B.-M. Wu, T.C.W. Mak, Organometallics 16 (1997) 632.
[14] L.-C. Song, G.-L. Lu, Q.-M. Hu, X.-D. Qin, C.-X. Sun, J. Yang, J. Sun, J. Organomet. Chem. 571 (1998) 55.
[15] E. Delgado, E. Hernández, O. Rossell, M. Seco, E.G. Puebla, C. Ruiz, J. Organomet. Chem. 455 (1993) 177.
[16] J. Chen, C.L. Day, R.A. Jacobson, R.J. Angelici, J. Organomet. Chem. 522 (1996) 21.
[17] Z. Qin, J. Sun, J. Chen, Organometallics 17 (1998) 600.
[18] Z.-X. Wang, C.-S. Jia, Z.-Y. Zhou, X.-G. Zhou, J. Organomet. Chem. 580 (1999) 201.
[19] D.G. Foster, Organic Synthesis, Coll. vol. 3, Wiley, New York, 1955, p. 771.
[20] D.T. Flood, Organic Synthesis, Coll. vol. 2, Wiley, New York, 1955, p. 295.
[21] R.B. King, Organometallic Synthesis, vol. 1, Academic Press, New York, 1965, p. 95.
[22] R.B. King, Organometallic Synthesis, vol. 1, Academic Press, New York, 1965, p. 175.
[23] L.E. Bogan Jr., D.A. Lesch, T.B. Ranchfuss, J. Organomet. Chem. 250 (1983) 429.
[24] G.M. Sheldrick, SHELXS-86, Program for X-ray Crystal Structure Determination, University of Göttingen, Germany, 1986.
[25] G.M. Sheldrick, SHELXL-97, Program for X-ray Crystal Structure Refinement, University of Göttingen, Germany, 1986.
[26] R. Havlin, G.R. Knox, J. Organomet. Chem. 4 (1965) 247.
[27] E.D. Schermer, W.H. Baddley, J. Organomet. Chem. 30 (1971) 67.
[28] D. Seyferth, R.S. Henderson, L.-C. Song, Organometallics 1 (1982) 125.
[29] L.-C. Song, R.-J. Wang, Y. Li, H.-G. Wang, J.-T. Wang, Acta Chim. Sinica 48 (1990) 867.
[30] L.-C. Song, Z.-Y. Zhao, J.-T. Wang, Youji Huaxue 2 (1987) 119.
[31] L.-C. Song, R.-G. Liu, J.-T. Wang, Acta Chim. Sinica 45 (1987) 1138.
[32] C.H. Wei, L.F. Dahl, Inorg. Chem. 4 (1965) 493.
[33] T.M. Bockman, J.K. Kochi, J. Am. Chem. Soc. 109 (1987) 7725.
[34] Q.-W. Liu, B.-F. Wu, X. Hu, S.-T. Liu, X.-Y. Yan, J.-Q. Shi, Acta Chim. Sinica 50 (1992) 778.
[35] P. Mathur, Md.M. Hossain, R.S. Rashid, J. Organomet. Chem. 467 (1994) 254.
[36] C.F. Campana, F.Y.-K. Lo, L.F. Dahl, Inorg. Chem. 18 (1979) 3060.

PERGAMON

www.elsevier.nl/locate/poly

Polyhedron 19 (2000) 719–724

POLYHEDRON

Synthesis and properties of $[CuLCl_2]$ and $[CuL(N_3)(OClO_3)]\cdot H_2O$ (L = α,α′-bis(pyrazolyl)-*m*-xylene): X-ray structure of $[CuLCl_2]_2$

Rajeev Gupta, Rabindranath Mukherjee *

Department of Chemistry, Indian Institute of Technology, Kanpur 208 016, India

Received 21 July 1999; accepted 28 January 2000

Abstract

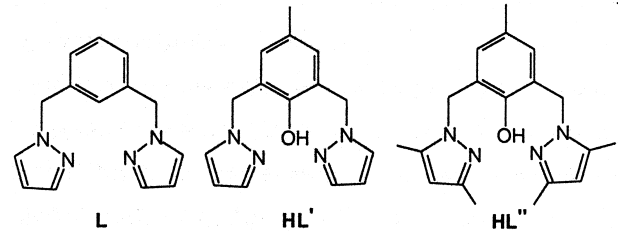
Using an *m*-xylyl based dinucleating ligand α,α′-bis(pyrazolyl)-*m*-xylene (L), providing only one pyrazole nitrogen coordination to each copper(II) centre, two copper(II) complexes $[CuLCl_2]$ (**1**) and $[CuL(N_3)(OClO_3)]\cdot H_2O$ (**2**) have been synthesized. Complex **1** has been structurally characterized, revealing that the coordination sphere of each copper(II) ion is distorted square pyramidal. Two pyrazole nitrogens from two different ligands and two chloride ions form the equatorial plane and an additional weak bonding interaction by a chloride ion from an adjacent layer provide axial coordination. The dimeric repeat unit $[CuLCl_2]_2$ having a Cu_2Cl_2 bridging unit gives rise to an extended network. Based on physicochemical studies, a similar structure has been proposed for **2**; however, in **2** one azide ion and a coordinating perchlorate ion are in the equatorial plane. Magnetic susceptibility measurements (25–300 K) reveal that the two copper(II) centres in each 'pseudo dicopper(II) unit' are weakly antiferromagnetically coupled, with the relevant 2*J* values of $\approx -10\ cm^{-1}$ for **1** and $\approx -9\ cm^{-1}$ for **2**. The square pyramidal stereochemistry of the copper(II) centres is revealed by absorption and EPR spectral properties. ©2000 Elsevier Science Ltd All rights reserved.

Keywords: α,α′-Bis(pyrazolyl)-*m*-xylene; Copper(II) complexes; X-ray structure; Network structures; Absorption spectroscopy; Electron spin resonance

1. Introduction

During the past few years we have investigated [1–13] the coordination chemistry of pyrazole-based chelating ligands. Recently, we have initiated a programme [14–16] to investigate the reactivity properties of binuclear Cu(I) complexes with dioxygen and pinpoint the effect of ligand topology on arene hydroxylation, using *m*-xylyl based ligands capable of providing only two N-coordination to each copper site. As part of this activity, using 4-methyl-2,6-bis(pyrazol-1-ylmethyl)phenol (HL′) and its 3,5-dimethyl pyrazole derivative (HL′′), we have synthesized and characterized two diphenoxo-bridged copper(II) complexes $[Cu_2(L'/L'')_2(OClO_3)_2]$ and the complex $[Cu_2(L')_2(OClO_3)_2]$ has been structurally characterized. The copper(II) centres in these complexes are strongly antiferromagnetically coupled [17].

With the aim of synthesizing and studying the magnetic properties of dichloro- and diazido-bridged copper(II) complexes, similar to diphenoxo-bridged copper(II) complexes $[Cu_2(L'/L'')_2(OClO_3)_2]$, we have investigated the reaction between $CuCl_2\cdot 2H_2O$ and $Cu(ClO_4)_2\cdot 6H_2O/NaN_3$ and L. Here we present the properties of two dimeric copper(II) complexes $[Cu^{II}LCl_2]_2$ (**1**) and $[Cu^{II}_2(L)_2(N_3)_2(OClO_3)_2]\cdot 2H_2O$ (**2**). We also present the molecular structure of **1** and comparative spectroscopic and temperature-dependent magnetic properties of **1** and **2**.



2. Experimental

2.1. Materials

All chemicals and reagents were obtained from commercial sources and used as received, unless otherwise stated. Purification of methanol was achieved by distillation from $Mg(OMe)_2$. DMF was stored over BaO and distilled under

* Corresponding author: Tel.: +91-512-597437; fax: +91-512-597436; e-mail: rnm@iitk.ac.in

0277-5387/00/$ - see front matter ©2000 Elsevier Science Ltd All rights reserved.
PII S0277-5387(00)00318-1

inert atmosphere. Dichloromethane was washed thoroughly with aqueous solution of Na_2CO_3 followed by distilled water before final reflux and distillation over anhydrous $CaCl_2$. 2,6-bis(1-bromomethyl)benzene was prepared following a reported procedure [18].

2.2. Synthesis of ligand α,α′-bis(pyrazolyl)-m-xylene (L)

The methodology followed to prepare this ligand (which does not require phase-transfer catalysed conditions such as that reported [19]) is adapted from Sorrell et al. [20].

Pyrazole (0.26 g, 3.8 mmol) was added to a suspension of sodium hydride (0.24 g, 10.0 mmol) in DMF (7 cm^3), under a dry dinitrogen atmosphere. The mixture was then stirred for 1 h. To this was added 2,6-bis(1-bromomethyl)benzene in DMF (4 cm^3) dropwise, anaerobically. The resulting mixture was stirred magnetically for 4 days at 298 K. Addition of water (5 cm^3) followed by solvent evaporation under reduced pressure afforded a slurry, to which was added 10% sodium hydroxide solution (5 cm^3). The ligand was extracted with CH_2Cl_2 and the organic layer washed with water, followed by drying over anhydrous Na_2SO_4. Solvent removal under reduced pressure afforded a thick yellowish-brown oil (yield ca. 90%). ^{1}H NMR (80 MHz, $CDCl_3$): δ 7.5 (2H, s, aromatic protons), 7.3 (2H, d, aromatic protons), 7.10–6.73 (4H, m, aromatic protons), 6.30 (2H, t, aromatic protons), 5.30 (4H, s, $PhCH_2$) [19].

2.3. Synthesis of [$Cu^{II}LCl_2$]

A methanolic solution (8 cm^3) of L (0.1 g, 0.42 mmol) was added to a solution of $CuCl_2 \cdot 2H_2O$ (0.072 g, 0.42 mmol) in methanol (4 cm^3), under magnetic stirring at 298 K and a green mixture resulted. After 2 h, the solution was filtered to remove some yellow precipitate. On concentration of the filtrate a dark green crystalline material precipitated out. The crystalline product was collected by filtration, washed with methanol and dried in vacuo (yield ca. 64%). Single crystals suitable for X-ray diffraction studies were obtained from the filtrate within a day. *Anal*. Found: C, 45.4; H, 3.7; N, 15.3; Cl, 19.3. Calc. for $C_{14}H_{14}N_4Cl_2Cu$: C, 45.1; H, 3.8; N, 15.0, Cl 19.1%. Absorption spectrum (DMF solution): λ_{max} (nm) (ε ($dm^3\ mol^{-1}\ cm^{-1}$)) 434 (560), 945 (160).

2.4. Synthesis of [$Cu^{II}(L)(N_3)(OClO_3)] \cdot H_2O$

A methanolic solution (8 cm^3) of L (0.1 g, 0.42 mmol) was added to a solution of $Cu(ClO_4)_2 \cdot 6H_2O$ (0.156 g, 0.42 mmol) in methanol (4 cm^3), followed by solid NaN_3 (0.027 g, 0.42 mmol). The resulting brownish-green mixture was stirred for 2 h at 298 K. The diethyl ether was added to the filtrate, resulting in the formation of a dark green crystalline material. The product was collected by filtration, washed with methanol and dried in vacuo. Recrystallization from MeCN–$(C_2H_5)_2O$ afforded microcrystalline solid (yield ca. 77%). *Anal*. Found: C, 36.6; H, 3.4; N, 20.6. Calc. for $C_{14}H_{16}N_7O_5ClCu$: C, 36.4; H, 3.5; N, 21.3%. IR (KBr, cm^{-1}, selected peaks): 2080 ($\nu[N_3^-]$); 1100, 1060, 630, 625 ($\nu[ClO_4^-]$). Absorption spectrum (DMF solution): λ_{max} (nm) (ε ($dm^3\ mol^{-1}\ cm^{-1}$)) 417 (2200), 655 (290).

2.5. Measurements

Elemental analysis was obtained from the Indian Association for the Cultivation of Science, Calcutta. Solution electrical conductivity measurements were carried out with an Elico (Hyderabad, India) type CM-82 T conductivity bridge. Spectroscopic data were obtained using the following instruments: IR spectra, Perkin-Elmer M-1320; electronic spectra, Perkin-Elmer Lambda 2; X-band EPR spectra, Varian E-109 C; ^{1}H NMR spectra, Bruker WP-80 (80 MHz) NMR spectrometer. Variable-temperature (25–300 K) solid-state magnetic susceptibility measurements were recorded by the Faraday technique using a locally built magnetometer. The setup [21,22] consists of an electromagnet with constant gradient pole caps (Polytronic Corporation, Mumbai, India), Sartorius M25-D/S balance (Germany), a closed cycle refrigerator and a Lake Shore temperature controller (Cryo Industries, USA). All measurements were made at a fixed main field strength of $\approx$10 kG. Susceptibility was corrected for diamagnetic contribution using Pascal constants [23].

2.6. Structure determination and refinement

A green crystal of [$CuLCl_2$] (dimensions $0.2 \times 0.1 \times 0.05$ mm) was used for data collection. Diffracted intensities were collected on an Enraf Nonius CAD4-Mach diffractometer using graphite-monochromated Mo Kα radiation ($\lambda = 0.710\ 73$ Å). The data were collected at 298 K using θ–2θ scan techniques to a maximum 2θ value of 45.0°. 5810 reflections were measured of which 2614 were unique and 1376 reflections with $I > 3\sigma(I)$ were used in the structure refinement. The cell parameters were obtained from least-squares analyses of 25 machine-centred reflections in the range $16.02 \leq 2\theta \leq 27.18°$. Three standard reflections were measured at every hour to monitor instrument and crystal stability.

2.6.1. Crystal data

$C_{14}H_{14}N_4Cl_2Cu$, $M = 372.55$, monoclinic, space group $P2_1/c$, $a = 7.797(1)$, $b = 22.328(7)$, $c = 8.699(9)$ Å, $\beta = 101.77(5)°$, $V = 1482.8(2)$ Å^3, $Z = 4$, $D_c = 1.670$ g cm^{-3}, $\mu = 18.3\ cm^{-1}$, $F(000) = 756$.

Intensity data were corrected for Lorentz and polarization effects; analytical absorption corrections were applied. The structures were solved by the direct method and successive difference Fourier syntheses. All non-H atoms were refined anisotropically and H atoms were included at their calculated positions but not refined. All non-hydrogen atoms were refined with anisotropic thermal parameters. All refinements were performed by full-matrix least-squares procedures on F where the function minimized was $\sum w(F_o - F_c)^2$ where

Table 1
Selected bond distances (Å) and angles (°) for $[CuLCl_2]_2$

Cu–N(2)	2.003(6)	N(2)–Cu–N(3)	162.8(2)
Cu–N(3)	1.987(7)	Cl(1)–Cu–Cl(2)	178.8(1)
Cu–Cl(1)	2.281(2)	Cl(1)–Cu–N(2)	89.5(2)
Cu–Cl(2)	2.325(2)	Cl(1)–Cu–N(3)	90.1(2)
Cu–Cl(2a)	2.778(2)	Cl(2)–Cu–N(2)	91.3(2)
		Cl(2)–Cu–N(3)	89.5(2)

$w = 1/\sigma(F)$. The final cycle of refinement included 190 variable parameters and converged with $R = 0.046$, $R_w = 0.036$ ($I > 3\sigma(I)$), $S = 1.892$, final difference Fourier synthesis: $-0.92 \le \Delta\rho \le 0.88$ e Å^{-3}. All calculations were performed using the XTAL3.2 crystallographic software package [24]. Selected bond lengths and angles are given in Table 1.

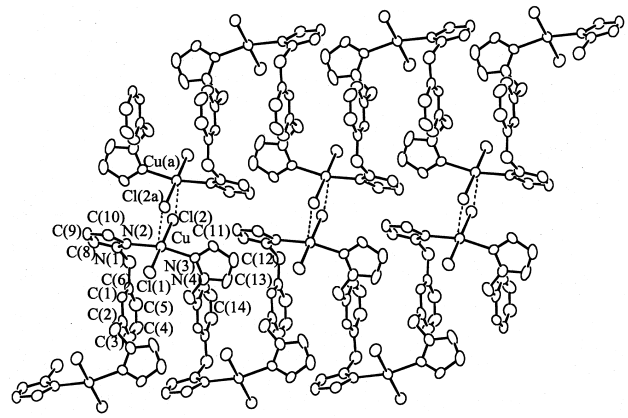


Fig. 1. View of the repeat unit of $[CuLCl_2]_2$. Hydrogen atoms are omitted for clarity. Unlabelled atoms are related to labelled atoms by the crystallographic centre of inversion.

3. Results and discussion

3.1. Synthesis

The ligand L was prepared from the reaction between 2,6-bis(1-bromomethyl)benzene and sodium pyrazolate in DMF. A straightforward reaction between L and $CuCl_2 \cdot 2H_2O$ (1:1 mole ratio) in methanol afforded a dark green complex of composition $[CuLCl_2]$. A single-crystal structural analysis (vide infra) revealed its dimeric nature $[CuLCl_2]_2$ (**1**). A similar reaction using $Cu(ClO_4)_2 \cdot 6H_2O$, L and NaN_3 (1:1:1 mole ratio) afforded a brownish-green solid of composition $[Cu(L)(N_3)(OClO_3)] \cdot H_2O$. The IR spectrum of this complex clearly demonstrated the presence of azide ion [25], coordinated perchlorate ion [17] and water of crystallization. The electrical conductivity data of complex **1** in DMF ($\Lambda_M = 50\ \Omega^{-1}\ cm^2\ mol^{-1}$) revealed that it behaves as a 1:1 electrolyte (expected range for a 1:1 electrolyte: 65–90 Ω^{-1} cm^2 mol^{-1} [26]), implying that the chloride ions are partially dissociated in solution, i.e. in solution the copper(II) centre is bound by only one chloride ion with additional DMF coordination (vide infra). Complex **2** behaves almost as a 1:2 electrolyte in DMF ($\Lambda_M = 130\ \Omega^{-1}\ cm^2\ mol^{-1}$; expected range 130–170 Ω^{-1} cm^2 mol^{-1} [26]), implying that both the anions are dissociated in solution. Based on physicochemical properties (vide infra) the azido complex has been proposed to be a dimer $[Cu(L)(N_3)(OClO_3)]_2 \cdot 2H_2O$ (**2**). Microanalytical, IR (for **2**), and absorption spectral behaviour (vide infra) are in conformity with the suggested formulations for **1** and **2**.

3.2. Description of the structure of $[CuLCl_2]_2$

Fig. 1 provides a perspective view of **1**. The dimeric unit sits on a crystallographically imposed inversion centre. Each copper(II) centre is coordinated by two pyrazole nitrogens from two L and two chloride ions. Interestingly, an additional bonding interaction exists at 2.778 Å, provided by a Cl atom of an adjacent layer (Cl(2a)). However, from each CuN_2Cl_2 moiety only one chloride ion is engaged in this type of interaction. Hence each copper(II) ion is present in a five-coordinate environment. The Cu···Cu separation between the two successive layers (Cu–Cu(a)) is 3.798(2) Å and within a layer (Cu–Cu′) is 8.112(3) Å. The separation between Cl(2) and Cl(2a) is 3.20(6) Å. The angles Cu–Cl(2)–Cu(a) and Cu–Cl(2a)–Cu(a) are 86.78(4) and 75.29(3)°, respectively. The average Cu–N(pyrazole) distance of 1.995 Å is in line with the metric parameters of copper(II) complexes of pyrazole-based chelating ligands [1]. The average Cu–Cl distance in the equatorial plane is 2.303 Å. The N(2)–Cu–N(3) angle is 162.8(2)°, which is appreciably smaller than the expected 180° for a linear arrangement of two pyrazole nitrogens to a copper centre having a perfect square planar geometry. However, the Cl(1)–Cu–Cl(2) angle (178.77(8)°) is close to 180°. From this equatorial plane the Cu(II) ion is displaced towards a chloride ion of an adjacent layer by 0.1357 Å. The Addison structural distortion index parameter τ [27] is 0.266. Therefore the coordination environment for each copper(II) centre is best described as distorted square pyramidal.

3.3. Electronic properties

3.3.1. Absorption spectroscopy

In the solid state (dispersed in mineral oil) compound **1** exhibits a peak at ~680 nm along with a low energy shoulder at ~950 nm, typical of square pyramidal geometry around the copper(II) centre [28]. However, in going from solid to solution (DMF), a red shift of the main absorption band was observed, which is known to occur as a result of increased coordination around the metal centre (tetragonal geometry) [13]. Thus this complex exhibits a d–d transition at 945 nm with an additional band at 434 nm. The latter band could be due to $Cl^- \rightarrow Cu(II)$ charge transfer. In the solid state, complex **2** also shows a low energy band centred at 705 nm; however, a blue shift has been observed in the DMF solution (655 nm). This result implies that for **2** in the solid state a

'pseudo dimeric structure' exists [13], due to weak coordination of one azide ion of a Cu(II) centre to a nearby Cu(II) centre. We note that the extent of DMF coordination is more in **1** than in **2**. For **2** the band at 417 nm could be assigned as $N_3^- \rightarrow Cu(II)$ charge-transfer transition.

3.3.2. EPR spectroscopy

In the polycrystalline state (77 K), the complex **1** exhibits an axial EPR spectrum with $g_\parallel = 2.171$, $g_\perp = 2.066$ and $A_\parallel = 105$ G. The position of the high-field signal ($g > 2.04$) is consistent with a $d_{x^2-y^2}$ ground state [28]. In frozen DMF solution, superhyperfine interaction with chlorine atoms on the $g_\perp$ component is clearly observable; however, the resolution is not sufficient to extract any meaningful information. Otherwise, the spectral parameters remain almost unaltered with slightly diminished signal intensity. Complex **2** is EPR silent in the solid state both at 300 K and at 77 K. This could be due to concentration broadening caused by magnetic dipolar interaction. However, in frozen DMF solution it exhibits a typical axial spectrum with $g_\parallel = 2.396$, $g_\perp = 2.077$ and $A_\parallel = 120$ G.

3.4. Magnetic properties

To study (i) whether any magnetic exchange interaction exists between two copper(II) centres in **1** and (ii) to substantiate the proposed structure of **2** (unsymmetrical azide bridging), we investigated the temperature-dependent (25–300 K) magnetic susceptibility behaviour. The μ_{eff}/Cu values at 300 K and at 25 K vary from 1.83 to 1.60 μ_B for **1** and 1.85 to 1.68 μ_B for **2**. The magnetic behaviour (Fig. 2) is typical of a very weak antiferromagnetic interaction. If we assume that the observed magnetic curve is intrinsic to the binuclear entity then χ_M may be expressed as [15–17]

$$\chi_M = \frac{2N\beta^2 g^2}{kT}[3+\exp(-2J/kT)]^{-1} + 2N_\alpha \qquad (1)$$

where the symbols have their usual meanings. Keeping the temperature-independent paramagnetism ($2N_\alpha$) fixed at 120×10^{-6} cm^3 mol^{-1}, the parameters J (the singlet–triplet energy gap is expressed in terms of $2J$) and g were determined by looking for the minimum of $R = \Sigma(\chi_M^{obsd} - \chi_M^{calc})^2/\Sigma(\chi_M^{obsd})^2$. Non-linear regression analysis of the data using Eq. (1) gave good data fits (Fig. 2): $J = -4.9$ cm^{-1}, $g = 2.00$, $R = 1.45\times10^{-6}$ for **1** and $J = -4.4$ cm^{-1}, $g = 2.103$, $R = 1.60\times10^{-6}$ for **2**. Inclusion of a corrective term for non-coupled copper(II) impurity gave no improvement in the fit.

Incorporation of a corrective term (θ) for interdimer interactions [29] in **1** and hence using Eq. (2),

$$\chi_M = \frac{2N\beta^2 g^2}{k(T-\theta)}[3+\exp(-2J/kT)]^{-1} + 2N_\alpha \qquad (2)$$

a similar data analysis gave rise to the following parameters: $J = -4.67$ cm^{-1}, $g = 1.977$ ($2N_\alpha = 120\times10^{-6}$ cm^3 mol^{-1}, fixed), $\theta = -0.055$ K, and R is then equal to 9.37×10^{-7}, which corresponds to an excellent agreement between observed and calculated magnetic data. The very small θ value, however, indicates that intermolecular exchange effects are essentially non-existent. The observed behaviour is again pointing towards the weak nature of antiferromagnetic coupling betwen two copper centres.

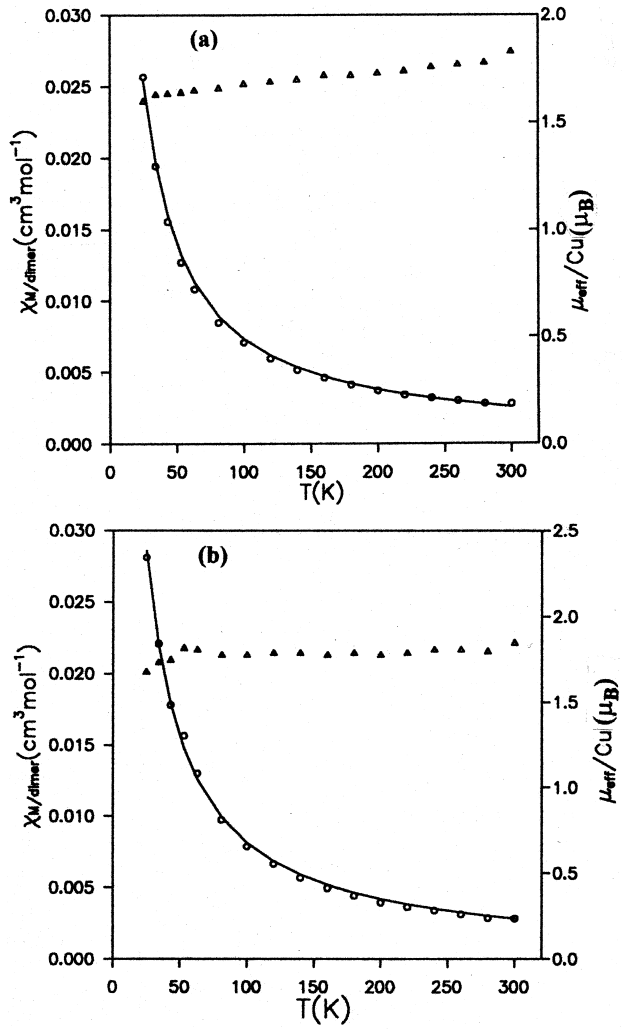
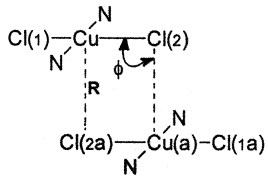


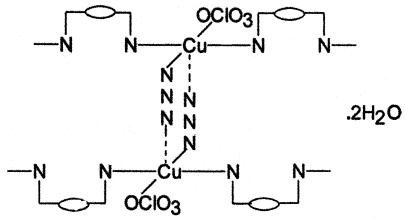
Fig. 2. Plot of magnetic susceptibility (left scale) per dimer and effective magnetic moment (right scale) per metal vs. temperature for polycrystalline samples of (a) $[CuLCl_2]_2$ (**1**) and (b) $[CuL(N_3)(OClO_3)]_2\cdot2H_2O$ (**2**). The solid line represents theoretical fits using Eq. (1), as described in the text.

In the solid state of compound **1** (Fig. 1) one Cl atom at each Cu site occupies the fifth coordination of the Cu centre of an adjacent layer, resulting in a long intermolecular Cu···Cl contact. However, the optimized $2J$ parameter for this compound does not follow the empirical Hodgson correlation between structural parameter ϕ/R and the coupling constant J [30,31]. Here ϕ is the Cu–Cl(2)–Cu(a) bridging angle and R is the longer Cu–Cl(2a) separation. The dihedral angle between the planes Cu–Cl(2)–Cu(a) and Cu–Cl(2a)–Cu(a) is 87.92°, revealing that the four-membered ring Cu–

Cl(2)–Cu(a)–Cl(2a) is non-planar. This could be the reason behind its deviation from this empirical correlation.



With asymmetric end-to-end azido bridges, with a short and a long Cu–N(azide) bond, it is well documented that the magnetic interaction is negligible when the geometry around the copper(II) ion is square pyramidal [32,33]. The observed magnetic behaviour of **2** is in line with this bonding interaction. In fact, in **2** the geometry around the copper centre is square-based pyramidal (vide absorption spectra). Two nitrogen atoms from two ligands are bonded to the Cu(II) ion; one oxygen atom from a perchlorate ion and a bridging azide ion are coordinated in the basal plane. The two copper(II) atoms are linked via one end-to-end bridging azide. The situation is very similar to what we have observed in **1**. Thus the structure of compound **2** can be proposed as shown below.



4. Conclusions

Using an *m*-xylyl based pyrazole ligand L two dimeric copper(II) complexes $[CuLCl_2]_2$ and $[CuL(N_3)(OClO_3)]_2 \cdot 2H_2O$ have been synthesized. The presence of a dimeric structure containing a $\{Cu_2Cl_2\}^{2+}$ structural unit, with an interacting Cl^- ion from an adjacent layer affording a network structure, is clearly established by a crystal structural analysis of one such complex **1**. The structure reveals that two L ligands are not capable of accommodating two copper centres at a distance capable of providing a discrete $Cu_2L_2Cl_2$ bridged structure. The X-ray structure of the dicopper(I) complex of the 3,5-dimethylpyrazole derivative of L behaved similarly (each copper(I) centre had two pyrazole coordination from two ligands with a Cu···Cu separation of 6.350 Å) [34]. Temperature-dependent magnetic measurements reveal very similar structures for **1** and **2**, exhibiting weak antiferromagnetic exchange coupling.

Supplementary data

Full tables of bond lengths and angles, tables of non-hydrogen and hydrogen atomic coordinates, anisotropic thermal parameters for non-hydrogen atoms as well as hydrogen atom parameters are available as supplementary material from the Cambridge Crystallographic Data Centre, 12 Union Road, Cambridge CB2 1EZ, UK (fax: +44-1223-336033; e-mail: deposit@ccdc.cam.ac.uk), on request (CCDC deposition number 129652).

Acknowledgements

This work is supported by grants from the Council of Scientific and Industrial Research (CSIR) and Department of Science and Technology (DST), Government of India, New Delhi. R.G. gratefully acknowledges the award of SRF by CSIR. The financial assistance of the National X-ray diffractometer facility by DST at this department is gratefully acknowledged.

References

[1] R. Mukherjee, Coord. Chem. Rev. (2000) in press.
[2] S. Mahapatra, N. Gupta, R. Mukherjee, J. Chem. Soc., Dalton Trans. (1991) 2911.
[3] S. Mahapatra, D. Bhuniya, R. Mukherjee, Polyhedron 11 (1992) 2045.
[4] S. Mahapatra, R. Mukherjee, J. Chem. Soc., Dalton Trans. (1992) 2337.
[5] S. Mahapatra, R. Mukherjee, Indian J. Chem., Sect. A 32 (1993) 64.
[6] S. Mahapatra, R. Mukherjee, Indian J. Chem., Sect. A 32 (1993) 428.
[7] S. Mahapatra, T.K. Lal, R. Mukherjee, Polyhedron 12 (1993) 1477.
[8] S. Mahapatra, R. Mukherjee, Polyhedron 12 (1993) 1603.
[9] Z. Shirin, R. Mukherjee, J.F. Richardson, R.M. Buchanan, J. Chem. Soc., Dalton Trans. (1994) 465.
[10] S. Mahapatra, R.J. Butcher, R. Mukherjee, J. Chem. Soc., Dalton Trans. (1993) 3723.
[11] T.K. Lal, R. Mukherjee, Polyhedron 16 (1997) 3577.
[12] T.K. Lal, J.F. Richardson, M.S. Mashuta, R.M. Buchanan, R. Mukherjee, Polyhedron 16 (1997) 4331 and Refs. therein.
[13] T.K. Lal, R. Gupta, S. Mahapatra, R. Mukherjee, Polyhedron 18 (1999) 1743 and Refs. therein.
[14] D. Ghosh, T.K. Lal, S. Ghosh, R. Mukherjee, Chem. Commun. (1996) 13.
[15] R. Gupta, R. Mukherjee, Inorg. Chim. Acta 263 (1997) 133.
[16] D. Ghosh, R. Mukherjee, Inorg. Chem. 37 (1998) 6597.
[17] R. Gupta, S. Mukherjee, R. Mukherjee, J. Chem. Soc., Dalton Trans. (1999) 4025.
[18] W. Wenner, J. Org. Chem. 17 (1952) 523.
[19] C.M. Hartshorn, P.J. Steel, Aust. J. Chem. 48 (1995) 1587.
[20] T.N. Sorrell, C.J. O'Connor, O.P. Anderson, J.H. Reibenspies, J. Am. Chem. Soc. 107 (1985) 4199.
[21] M. Ray, D. Ghosh, Z. Shirin, R. Mukherjee, Inorg. Chem. 36 (1997) 3568.
[22] A.K. Patra, R. Mukherjee, Polyhedron 18 (1999) 1317.
[23] C.J. O'Connor, Prog. Inorg. Chem. 29 (1982) 203.
[24] S.R. Hall, H.D. Flack, J.M. Stewart, The XTAL 3.2 Reference Manual, Universities of Western Australia, Geneva, and Maryland, 1992.
[25] S.S. Tandon, L.K. Thompson, M.E. Manuel, J.N. Bridson, Inorg. Chem. 33 (1994) 5555.
[26] W.J. Geary, Coord. Chem. Rev. 7 (1971) 81.
[27] A.W. Addison, T.N. Rao, J. Reedijk, J. van Rijn, G.C. Verschoor, J. Chem. Soc., Dalton Trans. (1984) 1349.

[28] B.J. Hathaway, in: G. Wilkinson, R.D. Gillard, J.A. McCleverty (Eds.), Comprehensive Coordination Chemistry, vol. 5, Pergamon, Oxford, 1987, p. 533.
[29] L.K. Thompson, S.K. Mandal, S.S. Tandon, J.N. Bridson, M.K. Park, Inorg. Chem. 35 (1996) 3117 and Refs. therein.
[30] W.E. Marsh, K.C. Patel, W.E. Hatfield, D.J. Hodgson, Inorg. Chem. 22 (1983) 511.
[31] K.-S. Bürger, P. Chaudhuri, K. Wieghardt, Inorg. Chem. 35 (1996) 2704 and Refs. therein.
[32] S. Sikorav, I. Bkouche-Waksman, O. Kahn, Inorg. Chem. 23 (1984) 490 and Refs. therein.
[33] P. Chaudhuri, K. Oder, K. Wieghardt, B. Nuber, J. Weiss, Inorg. Chem. 25 (1986) 2818.
[34] T.N. Sorrell, D.L. Jameson, J. Am. Chem. Soc. 104 (1982) 2053.

PERGAMON

www.elsevier.nl/locate/poly

Polyhedron 19 (2000) 725–730

POLYHEDRON

New Cu(II) and Zn(II) complexes of benzolamide with diethylenetriamine: synthesis, spectroscopy and X-ray structures

Gloria Alzuet [a], Sacramento Ferrer-Llusar [a], Joaquín Borrás [a,*], Ramón Martínez-Mánez [b]

[a] *Departamento de Química Inorgánica, Facultad de Farmacia, Universidad de Valencia, Avda. Vicent Andrés Estelles s/n, 46100 Burjassot, Spain*
[b] *Departamento de Química, Universidad Politécnica de Valencia, Camino de Vera s/n, 46071 Valencia, Spain*

Received 24 November 1999; accepted 28 January 2000

Abstract

New benzolamide (H_2bz, 5-phenylsulfonamide-1,3,4-thiadiazole-2-sulfonamide) zinc(II) and copper(II) complexes with diethylenetriamine were synthesized and characterized. The crystal structures of the [M(Hbz)$_2$(dien)] (M = Cu(II), Zn(II); dien = diethylenetriamine) complexes were determined. The metal centre adopts a near regular square pyramidal geometry. The benzolamidate anion acts as a monodentate ligand through the thiadiazole N atom contiguous to the deprotonated sulfonamido group. Spectroscopic properties are in good agreement with the crystal structures. The EPR and electronic spectroscopic studies showed that the copper(II) species doped into the zinc(II) complex adopts a near square planar geometry. The energy and composition of the SOMO of [Cu(Hbz)$_2$(dien)] and of copper substituted [Zn(Hbz)$_2$(dien)] were studied. ©2000 Elsevier Science Ltd All rights reserved.

Keywords: Divalent metals; Zinc; Copper; Benzolamide; Diethylenetriamine; Ternary complexes

1. Introduction

There are many areas of considerable potential interest for sulfonamide coordination chemistry. Metal complexes of 2-sulfanilamidopyrimidine (sulfadiazine) have been used to prevent bacterial infections of burns, and many of these complexes have been structurally characterized [1,2]. A tungsten complex of the bis-sulfonamide of 2,6-bis(aminomethyl)-pyridine catalyses cleavage of N–N bonds and is therefore of interest as a model for fixation of nitrogen [3]. More recently, a chiral zinc-sulfonamide complex has been demonstrated to be a relevant catalyst in enantioselective cyclopropanations [4]. Moreover, aromatic and heteroaromatic sulfonamides are well known as inhibitors of carbonic anhydrase (CA) and they have been extremely useful in the study of molecular properties and of the catalytic mechanisms of zinc-containing carbonic anhydrases [5].

A part of our investigation is focused on the study of these heteroaromatic sulfonamides as ligands. Neutral sulfonamides are expected to be poor ligands because of the withdrawal of the electron density from the nitrogen atom onto the electronegative oxygen atoms. However, if the sulfonamide N atom bears a dissociable hydrogen atom, this same electron-withdrawing effect increases its acidity and in the deprotonated form sulfonamide anions are effective sigma-donor ligands. Our previous studies on the interaction of sulfonamides with metal ions (Zn(II), Co(II), Ni(II) and Cu(II)) have shown that these can bind in several ways and not only as unidentate anions through the sulfonamide N atom [6–11]. Recently, as a continuation of our investigation, we initiated the study of the coordination behaviour of benzolamide (H_2bz, 5-phenylsulfonamide-1,3,4-thiadiazole-2-sulfonamide). Benzolamide (Fig. 1) contains two dissociable protons and affords potentially chelating thiadiazole and sulfonamide N donor binding sites, hence different coordination possibilities can be expected.

We have reported ternary zinc and copper benzolamide complexes with amines (ammomia, diethylenetriamine (dien), dipropylenetriamine (dpt) and tris(2-benzimidazolyl-methylamine) (L)) [12,13]. In these complexes the coordination behaviour of the benzolamide was different. Thus, in Cu(bz)(NH$_3$)$_4$, Cu(bz)(dien)·H_2O and Cu(bz)(dpt)·H_2O the dideprotonated sulfonamide coordinates the metal ion through the N atom of the free sulfonamido

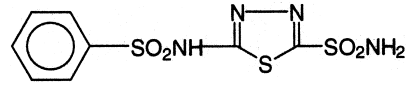


Fig. 1. Benzolamide.

* Corresponding author. Tel.: +34-6-3864530; fax: +34-6-3864960; e-mail: Joaquin.Borras@uv.es

0277-5387/00/$ - see front matter ©2000 Elsevier Science Ltd All rights reserved.
PII S0277-5387(00)00319-3

group, whereas in the polymer $\{[Zn_2(bz)_2(NH_3)_4]\cdot 2H_2O\}_\infty$ the dinegative benzolamide anion acts as a bridge, linking two metal centres through the N atom of the free sulfonamido group and the thiadiazole N closest to the substituted sulfonamido moiety. In the $[Zn(Hbz)L]ClO_4\cdot H_2O$ compound the monodeprotonated benzolamide interacts via thiadiazole N contiguous to the substituted sulfonamido moiety [13]. In this paper, as a part of our continuing interest in the coordination behaviour of benzolamide, we report the synthesis, structure and spectroscopic properties of the new benzolamide $M(Hbz)_2(dien)$ (M = Cu(II) and Zn(II)) complexes in which the sulfonamide in its monodeprotonated form interacts through one of the thiadiazole N atoms.

2. Experimental

2.1. Materials

Benzolamide (H_2bz, 5-phenylsulfonamide-1,3,4-thiadiazole-2-sulfonamide) was provided by Professor C.T. Supuran (University of Florence, Italy). All reagents were of the highest grade commercially available and used without further purification.

2.2. Methods

IR spectra were recorded on a Perkin-Elmer 843 instrument. Samples were prepared using the KBr technique. Electronic spectra were registered on a Shimadzu UV 2101PC spectrophotometer. EPR spectra were carried out with a Bruker ER 200 D spectrometer. Magnetic susceptibility measurements at room temperature were taken with a fully automated AZTEC DSM8 pendulum-type susceptometer. Mercury tetrakis(thiocyanato)cobaltate(II) was used as a susceptibility standard. Corrections for diamagnetism were estimated from Pascal's constants.

2.3. Synthesis

2.3.1. Cu(Hbz)$_2$(dien)

0.25 mmol of diethylenetriamine was added with continuous stirring to 40 ml of an ethanolic solution containing 0.25 mmol of $Cu(NO_3)_2\cdot 3H_2O$ and 0.5 mmol of benzolamide. Immediately, a little amount of a blue solid was formed. It was separated by filtration and the filtrate was left to stand at 4°C. After a few days prismatic blue crystals suitable for X-ray measurements were obtained. The crystals were filtered, washed with cooled ethanol and dried under vacuum. Yield 40%. *Anal*. Found: C, 29.45; H, 3.28; N, 19.23. Calc. for $C_{20}H_{27}CuN_{11}O_8S_6$: C, 29.83; H, 3.35; N, 19.14%.

2.3.2. Zn(Hbz)$_2$(dien)

The synthesis procedure is similar to that described above but $Zn(ClO_4)_2\cdot 6H_2O$ was used and no solid was obtained after the addition of diethylenetriamine. After 3–4 days prismatic colourless crystals were obtained from the resulting solution at room temperature. Yield 30%. *Anal*. Found: C, 29.57; H, 3.31; N, 19.32. Calc. for $C_{20}H_{27}ZnN_{11}O_8S_6$: C, 29.76; H, 3.34; N, 19.10%.

2.3.3. Doped Zn,Cu(Hbz)(dien)

0.25 mmol of dien was added to 40 ml of an ethanolic solution containing 0.225 mmol of $Zn(ClO_4)_2\cdot 6H_2O$ and 0.025 of $Cu(ClO_4)_2\cdot 6H_2O$ under stirring. The solution turned dark blue and then 0.5 mmol of benzolamide was added. It was stirred for about half an hour and then was left to stand at room temperature. Slow evaporation of the solvent gives a violet precipitate. Yield 65%.

2.4. Crystal data and structure refinement

A well-shaped blue crystal of $[Cu(Hbz)_2(dien)]$ ($0.22\times0.25\times0.27$ mm) and a colourless crystal of $[Zn(Hbz)_2(dien)]$ ($0.17\times0.18\times0.18$ mm) were mounted on a Siemens P4 four circle diffractometer coupled to Mo Kα radiation. The unit cell dimensions were determined from the angular settings of 25 reflections with $1.88<\theta<22.5°$ for the Cu(II) compound and $1.87<\theta<22.5°$ for the Zn(II) complex. A total of 4376 and 4415 reflections were measured for $[Cu(Hbz)_2(dien)]$ and $[Zn(Hbz)_2(dien)]$, respectively, of which 4130 ($R_{int}=0.0248$) and 4161 ($R_{int}=0.0452$) were unique ($0\le h\le 12$, $-12\le k\le 11$, $-14\le l\le 14$). Semi-empirical absorption corrections from ψ scans were applied for $[Zn(Hbz)_2(dien)]$ and no absorption corrections were applied for $[Cu(Hbz)_2(dien)]$. Each structure was solved by direct methods [14] and refined by full-matrix least-squared analysis on F^2. Largest peak and hole in the final difference map were $+0.767$ and -0.664 e Å^{-3} (Cu(II) compound) and 0.415 and -0.563 e Å^{-3} (Zn(II) complex). Other relevant parameters of crystal structure determination are collected in Table 1.

2.5. EHMO calculations

All calculations were performed using the Package of Programs for Molecular Orbital Analysis by Mealli and Proserpio [15] based on CDNT (atom Cartesian coordinate calculations), ICON (extended Hückel method with the weighted *Hij* formula) and FMO (fragment molecular orbital), including the drawing program CACAO (computer aided composition of atomic orbitals).

The extended Hückel parameters are as follows. *Hij*: Cu 4s, −11.40 eV; Cu 4p, −6.06 eV; Cu 3d, −14.00 eV; Zn 4s, −12.41 eV; Zn 4p, −6.53 eV; N 2s, −26.00 eV; N 2p, −13.40 eV; S 3s, −20.00 eV; S 3p, −13.30 eV; O 2s, −32.30 eV; O 2p, −14.80 eV; C 2s, −21.40 eV; C 2p, −11.40 eV; H 1s, −13.60 eV. Orbital exponents (contraction coefficients in double-ξ expansion given in parentheses): Cu 4s, 4p, 2.200; Cu 3d, 5.950 (0.5933), 2.300 (0.5744); Zn 4s, 2.010; Zn 4p, 1.700; N 2s, 2p, 1.950; S 3s, 3p, 1.817; O 2s, 2p, 2.275; C 2s, 2p, 1.625; H 1s, 1.300.

Table 1
Crystal data and structure refinement

	[Cu(Hbz)$_2$(dien)]	[Zn(Hbz)$_2$(dien)]
Formula	$C_{20}H_{27}CuN_{11}O_8S_6$	$C_{20}H_{27}ZnN_{11}O_8S_6$
Formula weight	805.43	806.25
Symmetry, space group	triclinic, $P\bar{1}$	triclinic, $P\bar{1}$
a (Å)	11.284(2)	11.256(5)
b (Å)	11.790(2)	11.827(5)
c (Å)	13.359(2)	13.405(2)
α (°)	103.582(10)	102.82(3)
β (°)	100.939(13)	101.58(4)
γ (°)	105.225(13)	105.41(3)
U (Å^3)	1606.0(4)	1612.2(12)
Z	2	2
D_c (g cm^{-3})	1.666	1.663
$F(000)$, μ (cm^{-1})	826, 11.33	828, 12.13
Refined parameters	415	416
GOF	1.077	0.973
R ($I>2\sigma(I)$) [a]	$R_1=0.0489$, $wR_2=0.1310$	$R_1=0.0600$, $wR_2=0.1401$
R (all data)	$R_1=0.0748$, $wR_2=0.1531$	$R_1=0.1137$, $wR_2=0.17524$

[a] $R=\Sigma(|F_o|-|F_c|)/\Sigma|F_o|$, $R_w=[\Sigma w(F_c^2)/\Sigma wF_o^4]^{1/2}$.

3. Results and discussion

3.1. Synthesis of the complexes

The ternary complexes [M(Hbz)$_2$(dien)] were obtained by reaction of the metal salt, the triamine and benzolamide in a molar ratio 1:1:2. The ratio of reagents is important to obtain the compounds described here since the addition of an equimolecular amount of triamine and benzolamide leads to the formation of the previously reported [M(bz)(dien)]·H_2O compounds in which the benzolamide is present in its dideprotonated form [12].

3.2. Description of the crystal structures

A drawing of [Cu(Hbz)$_2$(dien)] including the atomic numbering scheme is shown in Fig. 2. Interatomic distances and angles relevant to the coordination sphere for the [Cu(Hbz)$_2$(dien)] and [Zn(Hbz)$_2$(dien)] complexes are given in Table 2.

The metal ion is pentacoordinated by five N atoms, the structure being best described as a regular square pyramid. The three N atoms (N(5), N(6) and N(7)) of the dien ligand occupy equatorial positions. The remaining two M(II) square pyramidal coordination sites are occupied by two benzolamidate anions that interact through the thiadiazole N atom contiguous to the deprotonated sulfonamido group (N(3), N(9)). The Cu–N(dien) bond distances are in the narrow range from 2.014(5) to 2.035(5) Å and the Zn–N(dien) lengths range from 2.082(7) to 2.202(7) Å. As expected from the ionic radii of the divalent metal ions, the average of these Zn–N bond distances is considerably longer than those involving Cu. Both MN_5 chromophores are essentially square pyramidal but with significant differences in the local molecular stereochemistry. In particular, in the Zn complex the Zn–N(6) (2.202(7) Å) is the longest bond distance while in the Cu compound the Cu–N(6) (2.035(5) Å) distance is one of the shorter distances. Moreover, the equatorial Cu–N(thiadiazole) (Cu–N(3), 2.070(5) Å) is markedly shorter than the axial Cu–N(thiadiazole) distance (Cu–N(9), 2.233(5) Å) but the equatorial Zn–N(thiadiazole) (Zn–N(3), 2.188(7) Å) is longer than the axial Zn–N(thiadiazole) distance (Zn–N(9), 2.042(7) Å). The equatorial Cu–N(thiadiazole) is found to be comparable to the corresponding bond in Cu(II) complexes with related sulfonamides [7,9] and the equatorial Zn–N(thiadiazole) is comparable to the same distance in the [Zn(Hbz)L]ClO_4·H_2O compound (L = tris(2-benzimidazolyl-methylamine)) [13]. The axial Cu–N(thiadiazole) length is ca. 0.23 Å shorter than that of the Cu(Hacm)$_2$(en)$_2$ complex (H_2acm = acetazolamide, en = ethylenediamine) [8]. The

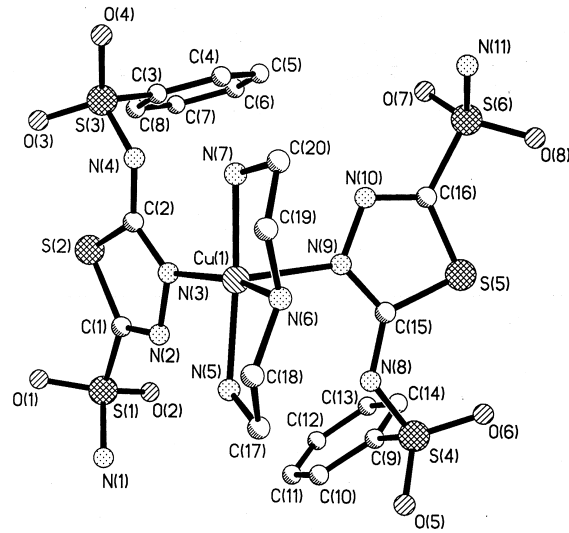


Fig. 2. Drawing of the [Cu(Hbz)$_2$(dien)] complex.

Table 2
Selected bond lengths (Å) and angles (°) with e.s.d.s in parentheses

[Cu(Hbz)$_2$(dien)]		[Zn(Hbz)$_2$(dien)]	
Cu(1)–N(5)	2.014(5)	Zn(1)–N(5)	2.093(7)
Cu(1)–N(6)	2.035(5)	Zn(1)–N(6)	2.202(7)
Cu(1)–N(9)	2.233(5)	Zn(1)–N(9)	2.045(7)
Cu(1)–N(7)	2.017(5)	Zn(1)–N(7)	2.082(8)
Cu(1)–N(3)	2.070(5)	Zn(1)–N(3)	2.188(7)
N(5)–Cu(1)–N(7)	163.4(2)	N(7)–Zn(1)–N(5)	149.8(3)
N(5)–Cu(1)–N(6)	82.8(2)	N(5)–Zn(1)–N(6)	80.1(3)
N(7)–Cu(1)–N(6)	83.8(2)	N(7)–Zn(1)–N(6)	80.2(3)
N(5)–Cu(1)–N(3)	90.8(2)	N(5)–Zn(1)–N(3)	88.7(3)
N(5)–Cu(1)–N(9)	100.8(2)	N(9)–Zn(1)–N(5)	109.2(3)
N(6)–Cu(1)–N(9)	94.6(2)	N(9)–Zn(1)–N(6)	99.5(3)
N(6)–Cu(1)–N(3)	162.3(2)	N(3)–Zn(1)–N(6)	153.4(3)
N(7)–Cu(1)–N(3)	99.2(2)	N(7)–Zn(1)–N(3)	98.9(3)
N(7)–Cu(1)–N(9)	90.8(2)	N(9)–Zn(1)–N(7)	96.5(3)
N(3)–Cu(1)–N(9)	102.8(2)	N(3)–Zn(1)–N(9)	107.0(3)

Cu–N(dien) bond distances are similar to those in other Cu(II) complexes with dien [16–19].

The in-plane angular distortions described by the ratio τ represent a percentage trigonal distortion of a square pyramidal geometry (1 for perfect trigonal bipyramidal, 0 for perfect square pyramidal). The calculated τ value from bond angles of 0.02 for the Cu(II) compound and of 0.06 for the Zn(II) complex clearly indicates a quasi regular pyramidal geometry [20]. For the two structures the major changes in the angles subtended at the metal centre are found in N(5)–M–N(7) and N(6)–M–N(3) which expand from 149.8(3) and 153.4(3)° [$Zn(Hbz)_2(dien)$] to 163.4(2) and 162.3(2)° [$Cu(Hbz)_2(dien)$]. The *cis* equatorial N–M–N bond angles differ from 90° owing to the presence of a chelate ring that produces rhombic in-plane effects [21].

In the copper compound the atoms that constitute the equatorial plane deviate 0.050 Å from planarity and those of the zinc complex deviate 0.006 Å. The copper atom is displaced 0.2543 Å from the equatorial plane towards the apical position and the zinc ion is situated at 0.4876 Å from this plane.

It is also interesting to note that the copper compound presents a square pyramidal geometry since of the dien complexes structurally characterized, very few contain dien and a monodentate ligand [17] and these adopt six-coordinate tetragonally elongated octahedral geometries, with both ligands located equatorially and anions weakly bound axially [17]. Square pyramidal geometries are found only in copper dien complexes with bidentate ligands [22]. This geometry is also exhibited by Cu(II) compounds with pentamethyldiethylenetriamine and a monodentate ligand, but in these cases a third ligand (either solvent or anion) binds in the axial position [23–25].

The uninegative benzolamidate anions behave as monodentate ligand through the thiadiazole N atom (N(3), N(9)) contiguous to the deprotonated sulfonamido group. This coordination behaviour is also exhibited by the monodeprotonated benzolamide in the $[Zn(Hbz)L]ClO_4 \cdot H_2O$ compound (L = tris(2-benzimidazolyl-methylamine)) [13]. In these complexes the coordination mode of the benzolamide is determined by the fact that the deprotonation takes place on the substituted sulfonamido moiety. This makes the thiadiazole N closest to this sulfonamido group the best donor atom. However, it differs from that found in $[Cu(bz)(NH_3)_4]$ [12] where the dideprotonated benzolamide acting as monodentate ligand binds the metal ion through the free sulfonamide N atom. Although it is difficult to rationalize the coordination behaviour of benzolamide, our investigation of its coordination properties has demonstrated that in the monodeprotonated form it behaves as a monodentate ligand coordinating the metal through the thiadiazole N atom closest to the substituted sulfonamido group. When dideprotonated it shows a more variable coordination behaviour, acting as a bridge through the thiadiazole and free sulfonamido N atoms [13] or as monodentate via free sulfonamido N atom [12].

It is interesting to compare the coordination behaviour of benzolamide and the structurally related acetazolamide (H_2acm, 5-acetamido-1,3,4-thiadiazole-2-sulfonamide) when both are monodeprotonated. Although both sulfonamides offer the same donor sites, a N thiadiazole atom and a N sulfonamido, the coordination behaviour of acetazolamide in the previously reported $[Cu(Hacm)(dien)] \cdot H_2O$ and $[Cu(Hacm)(dpt)] \cdot H_2O$ compounds [26] contrasts with that of benzolamide. Acetazolamide in these complexes acts as a monodentate ligand through the N sulfonamido atom.

3.3. IR spectra

In Table 3 are collected the most significant IR data for the complexes reported here. For comparison the IR data for related compounds are also included.

The modifications of the characteristic bands of the benzolamide ligand give some information about its coordination and/or its deprotonation. It is found that the changes in the asymmetric and symmetric stretching modes of the SO_2 group afford some evidence of the deprotonated nature of the benzolamide. When monodeprotonated, two bands are associated with each vibration, whereas when dideprotonated, one band for each vibration is observed. These bands show some splitting in the $[Zn(Hbz)_2(dien)]$ complex that probably arises from hydrogen bonding or crystal packing effects. Moreover, it is noteworthy that in all the complexes, the ν(C=N) vibration is strongly modified. Since the changes occur in the complexes where the benzolamide is monodeprotonated and in the complexes where the benzolamide is

Table 3
IR selected bands (cm^{-1}) [a]

Compound	$\nu(C{=}N)_{ring}$	$\nu(SO_2)_{asym}$	$\nu(SO_2)_{sym}$	ν(S–N)
Benzolamide(H_2bz)	1580–1570d, 1500	1360, 1320	1180, 1140	940, 910
$[Cu(Hbz)_2(dien)]$	1460	1360,1270	1180, 1150	940, 920
$[Zn(Hbz)_2(dien)]$	1480–1465d	1360–1350d, 1280–1260d	1170, 1140	930, 915
$Cu(bz)(deta)(H_2O)$ [b]	1430	1275	1140	970, 950
$Cu(bz)(dpt)(H_2O)$ [b]	1430	1300–1280d	1140–1130d	950–940d
$[Zn(Hbz)L]ClO_4 \cdot H_2O$ [c]	1475	1356,1275	1160, 110	920

[a] d doublet.
[b] From Ref. [12].
[c] From Ref. [13].

dideprotonated, this fact could be attributed to the modifications that take place on the thiadiazole π-system upon deprotonation of the substituted sulfonamido group.

3.4. Magnetic susceptibility, electronic and EPR spectra

The [Cu(Hbz)$_2$(dien)] compound exhibits a normal value of magnetic moment for an orbitally non-degenerate ground state, 1.76 BM.

The solid electronic spectrum of [Cu(Hbz)$_2$(dien)] is in agreement with the crystallographic data. It presents a single broad ligand field absorption with a maximum at 630 nm as expected for copper(II) complexes having a square pyramidal geometry [27].

At room temperature the solid-state EPR spectrum of [Cu(Hbz)$_2$(dien)] is axial with the parallel component poorly resolved. The calculated EPR parameters are $g_\parallel \approx 2.30$ and $g_\perp = 2.13$. The EPR of the copper doped into its zinc counterpart is also axial in nature. The low-field region shows the quartet hyperfine structure from Cu ($I = 3/2$). The ground state parameters extracted from the experimental spectrum by simulation [28] are $g_\parallel = 2.21$, $g_\perp = 2.05$ and $A_\parallel = 191 \times 10^{-4}$ cm^{-1}. This $A_\parallel$ value of the complex diluted in the isomorphous zinc lattice is larger than the values expected for a five-coordinated geometry. It is well known that Cu(II) square planar and octahedral complexes with tetragonal elongation lead to a large parallel Cu hyperfine coupling. Further, the quotient $g_\parallel/A_\parallel$ lies in the range 105–135 cm, supporting a square planar geometry [29]. So, it seems that the Cu(II) assumes a stereochemistry much more close to that of a planar CuN_4 chromophore [30]. This change in the geometry is supported by the mull spectrum of the copper(II) complex doped in the corresponding zinc complex that exhibits a shift from 630 nm in the pure copper to 575 nm.

In acetonitrile the EPR spectrum of the [Cu(Hbz)$_2$(dien)] displayed axial anisotropy with some rhombic perturbation. The EPR features obtained from simulation are $g_\parallel \approx 2.29$, $g_\perp = 2.13$ and $A_\parallel = 185 \times 10^{-4}$ cm^{-1}. They are indicative of a square planar based structure. The UV–Vis spectrum shows a d–d band at ca. 600 nm ($\varepsilon = 130$ mol^{-1} cm^{-1}) which agrees well with a square planar arrangement around the copper ion. Apart from the d–d transition, the spectrum displays an intense absorption at 300 nm ($\varepsilon = 29120$ mol^{-1} cm^{-1}) and a less intense absorption at 245 nm ($\varepsilon = 16990$ mol^{-1} cm^{-1}) associated with ligand π–π* transitions. Both EPR and electronic spectra indicate that the geometry of the copper ion in solution is, like in the doped compound, nearer to square planar with weak apical interactions.

3.5. Extended Hückel molecular orbitals calculations

The crystal structures of the isomorphous [Cu(Hbz)$_2$(dien)] and [Zn(Hbz)$_2$(dien)] complexes have shown that both compounds present some differences in their local molecular stereochemistry. The most significant differences are found in the M–N(9) (2.233(5) (Cu) and 2.045(7) Å (Zn)), in the M–N(6) (2.035(5) (Cu) and 2.202(7) Å (Zn)) bond lengths and in the *trans* angles N(5)–M–N(7) and N(6)–M–N(3), which expand from 149.8(3) and 153.4(3)° [Zn(Hbz)$_2$(dien)] to 163.4(2) and 162.3(2)° [Cu(Hbz)$_2$(dien)]. Moreover, the [Cu(Hbz)$_2$(dien)] complex presents electronic properties (see Section 3.4) different to those of the copper doped compound that suggests that when the Cu(II) substitutes the Zn(II) ion does not adopt the geometry observed in the pure copper compound. In order to understand how these structural differences can affect the energy and composition of the relevant molecular orbitals of the complexes we have undertaken extended Hückel molecular orbital (EHMO) calculations by means of the CACAO program [15]. These calculations have been performed using the crystallographic coordinates derived from the crystal structures of the [Cu(Hbz)$_2$(dien)] compound and [Zn(Hbz)$_2$(dien)] in which the Zn(II) has been replaced by Cu(II) as a 'model' of the copper doped compound.

The SOMO of the [Cu(Hbz)$_2$(dien)] presents an energy of −11.049 eV (Fig. 3). The contribution of metal d orbitals to the SOMO is 39% ($d_{x^2-y^2}$ (28%), d_{xz} (8%), d_{xy} (2%) and d_{z^2} (1%)). The atomic orbitals of the ligands that participate in SOMO formation are the three N atoms of the dien (N(5), px 12%, py 2%; N(6), py 18%; N(7), px 10%, pz 3%) and one N thiadiazole atom (N(3), py 9%) from one of the benzolamidate ligands.

When these calculations are performed on the 'model' copper doped compound, a SOMO with an energy of −11.649 eV is obtained (Fig. 4). The overall contribution of the copper d atomic orbitals to this MO is 34% ($d_{x^2-y^2}$ (25%), d_{xz} (7%) d_{xy} (1%) and d_{yz} (1%)), although the ligand orbitals involved are the same as in Cu(Hbz)$_2$(dien) their contribution is slightly different (N(5), px 12%; N(6), py 21%; N(7), px 7%, pz 5%; N(3), py 9%).

The electronic and EPR spectra of the [Cu(Hbz)$_2$(dien)] and of the copper doped compound suggest a change of geometry for the Cu(II) ion when it replaces the Zn(II) ion in the [Zn(Hbz)$_2$(dien)] complex. The EHMO calculations have

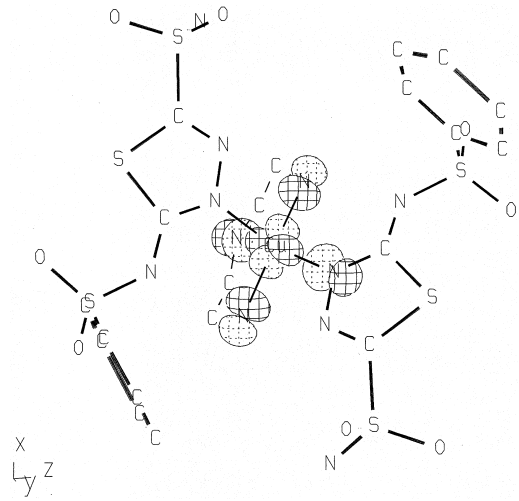


Fig. 3. SOMO of the [Cu(Hbz)$_2$(dien)] complex.

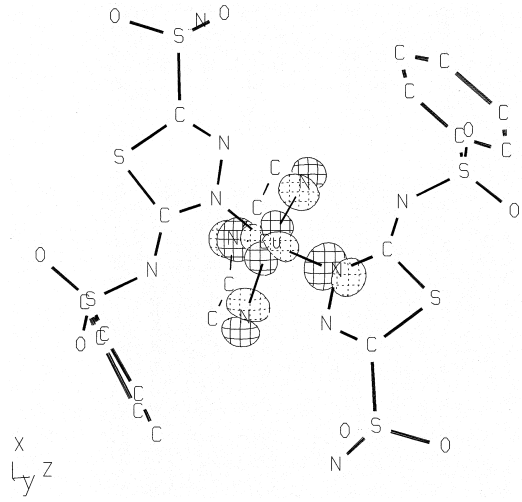


Fig. 4. SOMO of the copper substituted [Zn(Hbz)$_2$(dien)] complex.

shown that the energy difference between the SOMOs of both compounds, 0.6 eV (ca. 5000 cm^{-1}), could explain the variances found in their electronic properties.

Supplementary data

Supplementary crystallographic data are available from the Cambridge Crystallographic Data Centre, 12 Union Road, Cambridge CB2 1EZ, UK (fax: +44-1223-336033; e-mail: deposit@ccdc.cam.ac.uk) on request, deposition numbers CCDC 132907/CCDC 132908.

Acknowledgements

The authors acknowledge financial support from the Spanish CICYT (PM97-0105-C02-01). We thank Professor C.T. Supuran for providing us the benzolamide.

References

[1] C.J. Brown, D.S. Cook, L. Sengier, Acta Crystallogr., Sect. C 43 (1987) 2332.
[2] N.C. Baenziger, A.W. Struss, Inorg. Chem. 15 (1976) 1807.
[3] S. Cai, R.R. Schrock, Inorg. Chem. 30 (1991) 4105.
[4] S.E. Denmark, S.P. O'Connor, S.R. Wilson, Angew. Chem., Int. Ed. Engl. 37 (8) (1998) 1149.
[5] T. Koike, E. Kimura, I. Nakamura, Y. Hashimoto, M. Shiro, J. Am. Chem. Soc. 114 (1992) 7338.
[6] S. Ferrer, J. Borrás, C. Miratvilles, A. Fuertes, Inorg. Chem. 28 (1989) 160.
[7] S. Ferrer, J. Borrás, C. Miratvilles, A. Fuertes, Inorg. Chem. 29 (1990) 206.
[8] S. Ferrer, J.G. Haasnoot, R.A.G. de Graaff, J. Reedijk, J. Borrás, Inorg. Chim. Acta 192 (1992) 129.
[9] J.C. Pedregosa, J. Casanova, G. Alzuet, J. Borrás, S. García-Granda, M.R. Díaz, A. Gutierrez-Rodriguez, Inorg. Chim. Acta 232 (1995) 117.
[10] S.L. Sumulan, J. Casanova, G. Alzuet, J. Borrás, A. Castiñeiras, C.T. Supuran, J. Inorg. Biochem. 62 (1996) 31.
[11] P. Borja, G. Alzuet, J. Casanova, J. Server-Carrió, J. Borrás, M. Martínez-Ripoll, C.T. Supuran, Main Group Met. Chem. 21 (1998) 279.
[12] G. Alzuet, J. Casanova, J. Borrás, S. García Granda, A. Gutiérrez-Rodríguez, C.T. Supuran, Inorg. Chim. Acta 273 (1998) 334.
[13] G. Alzuet, S. Ferrer-Llusar, J. Borrás, J. Server-Carrió, R. Martínez-Mánez, J. Inorg. Biochem. 75 (1999) 189.
[14] SHELXTL, Program version 5.03, Siemens Analytical X-Ray Instruments, Madison, WI, 1994.
[15] C. Mealli, D. Proserpio, Computer Aided Composition of Atomic Orbitals (CACAO program), PC version, July 1992. See also: J. Chem. Educ. 67 (1990) 399.
[16] G. Druhan, B. Hathaway, Acta Crystallogr., Sect. B 35 (1979) 344.
[17] K. Miki, S. Kaida, M. Saeda, K. Yamatoya, N. Kasai, M. Sato, J.-I. Nakaya, Acta Crystallogr., Sect. C 42 (1986) 1004.
[18] M.J. Begley, P. Hubberastey, J. Stroud, Polyhedron 16 (1997) 805.
[19] B-H. Ye, L-N. Ji, F. Xue, T.C.W. Mak, Polyhedron 17 (1998) 2687.
[20] A.W. Addison, T.N. Rao, J. Reedijk, J. van Rijn, G.C. Verschoor, J. Chem. Soc., Dalton. Trans. (1984) 1349.
[21] S. Siddiqui, R.E. Shepherd, Inorg. Chem. 25 (1986) 3869.
[22] N. Shintani, E. Nukui, H. Miyamae, Y. Fukuda, K. Sone, Bull. Chem. Soc. Jpn. 67 (1994) 1828.
[23] P.J. van Koningsbruggen, J.W. van Hal, E. Müller, R.A.G. de Graaff, J.G. Haasnoot, J. Reedijk, J. Chem. Soc., Dalton Trans. (1993) 1371.
[24] M.J. Scott, L.C. Lee, R.H. Holm, Inorg. Chem. 33 (1994) 4651.
[25] M.J. Scott, L.C. Lee, R.H. Holm, J. Am. Chem. Soc. 116 (1994) 11357.
[26] G. Alzuet, L. Casella, A. Perotti, J. Borrás, J. Chem. Soc., Dalton Trans. (1994) 2347.
[27] J.-L. Pierre, P. Chautemps, S. Refaif, C. Beguin, A. El Marzouki, G. Serratrice, E. Saint-Aman, P. Rey, J. Am. Chem. Soc. 117 (1995) 1965.
[28] WINEPR-Simfonia 1.25, Bruker Analytik GmbH, Karlsruhe, 1994–1996.
[29] U. Sakaguchi, A.W. Addison, J. Chem. Soc., Dalton Trans. (1979) 600.
[30] M. Velayutham, B. Varghese, S. Subramanian, Inorg. Chem. 37 (1998) 5983.

PERGAMON

www.elsevier.nl/locate/poly

Polyhedron 19 (2000) 733–738

POLYHEDRON

Synthesis, crystal structure and bonding features of a trinuclear cluster $[Mo_3X(S_2)_3(dtp)_3I_3]$ (X = O, S) with layer-like packing

Ying Peng, Shao-Fang Lu *, Hong-Jun Fan, Qiang-Jin Wu, Rong-Min Yu, Jian-Quan Huang

State Key Laboratory of Structural Chemistry, Fujian Institute of Research on the Structure of Matter, Chinese Academy of Sciences, Fuzhou, Fujian 350002, People's Republic of China

Received 20 October 1999; accepted 10 January 2000

Abstract

The reaction of $Mo_3OS_3(dtp)_4(H_2O)$ ($dtp = S_2P(OC_2H_5)_2$) with CuI yielded the new trimolybdenum cluster $[Mo_3(\mu_3\text{-}X)(\mu_2\text{-}S_2)_3(dtp)_3I_3]$ (X = 58%O + 42%S). Crystal structure analysis showed that the compound has a $[Mo_3X(S_2)_3]^{4+}$ cluster core, and the I_3^- group functions as a two-way coordinated ligand which links the three out-of-$\{Mo_3\}$ plane S atoms in the cluster core at one end (I–S ~ 3.3 Å) and two adjacent trinuclear clusters at the other (I···S ~ 3.6 Å), thus forming a $[Mo_3X(S_2)_3]$ cluster layer. The bonding features of the cluster characteristic of a semiconductor are demonstrated by energy band and density functional calculations. ©2000 Elsevier Science Ltd All rights reserved.

Keywords: Mo–S clusters; Crystal structures; Electronic structures; Layer-like packing

1. Introduction

Cluster compounds with a $[Mo_3S_7]^{4+}$ core have been widely studied in the last two decades owing to their potential applications in biological inorganic chemistry and new materials research. For example, $(NH_4)_2[Mo_3(\mu_3\text{-}S)(\mu\text{-}S_2)_3(S_2)_3]$ may be used as a good hydrodesulfurition catalyst [1]. Many clusters with different ligands and anions have been synthesized using a variety of methods, including the reduction of some Mo(V) complexes, and the oxidation of some Mo(III) compounds in solution or by solid state reaction [2–6]. Since 1980 we have obtained a series of M_2-type clusters [7–10] of the general formula $[Mo_3X(S_2)_3L_3Y]$ (X = O, S; $L = S_2P(OC_2H_5)_2^-$ (dtp), $S_2CN(C_2H_5)_2^-$, $S_2CNC_4H_8^-$, $S_2P(OC_3H_7)_2^-$, $S_2C_6H_3CH_3^{2-}$, Cl; Y = Cl, I, $S_2P(OC_3H_7)_2^-$). However, a cluster of this type containing the I_3^- anion has not yet been reported. Herein, the synthesis and crystal structure of the cluster $[Mo_3X(S_2)_3(dtp)_3(I_3)]$ (X = 58%O + 42%S) are described together with a discussion of the formation mechanism and bonding features.

2. Experimental

All the reactions and manipulations were carried out under the atmosphere with CP or AR grade reagents. CuI was used as purchased, and the compound $[Mo_3OS_3(dtp)_4(H_2O)]$ was prepared according to the literature procedure [11].

2.1. Preparation of the title compound

A mixture of 0.1 g (0.09 mmol) $Mo_3OS_3(dtp)_4(H_2O)$ and 0.02 g (0.1 mmol) CuI was dissolved in 25 ml CH_3COOEt with stirring, and then 0.2 ml DMF was added to the resulting solution. The solution was stirred for 2 h at room temperature and filtered. The filtrate was evaporated in air. Well shaped black crystals (0.03 g) were obtained after 1 month. The crystals were isolated, washed with EtOH and petroleum ether, and then dried in air (yield 23%).

2.2. X-ray structural characterization

Information concerning crystallographic data and structure refinement is summarized in Table 1.

Intensity data were collected using a crystal of dimensions 0.4 × 0.4 × 0.1 mm on a Rigaku AFC5R diffractometer with graphite-monochromatized Mo Kα radiation ($\lambda = 0.71069$ Å). The structure was solved by direct methods, and all non-hydrogen atoms were refined with anisotropic thermal parameters except for the carbon atoms and X atom. The hydrogen atoms were placed in idealized geometries and their contributions were added to the structure factor calculations. Full-

* Corresponding author. Tel.: +86-591-3711368; fax: +86-591-3714946; e-mail: LSF@ms.fjirsm.ac.cn

0277-5387/00/$ - see front matter ©2000 Elsevier Science Ltd All rights reserved.
PII S0277-5387(00)00298-9

Table 1
Summary of crystal data and structure refinement parameters

Empirical formula	$C_{12}H_{30}I_3Mo_3O_{6.58}P_3S_{12.42}$
Crystal colour	black
Crystal size (mm)	0.40×0.40×0.10
Temperature (K)	293(2)
Wavelength (Å)	0.71069
Crystal system	monoclinic
Space group	$P2_1/n$
Unit cell parameters	
a (Å)	14.016(3)
b (Å)	19.762(4)
c (Å)	15.403(3)
β (°)	96.92(3)
Volume (Å^3)	4235(2)
Z	4
D_{calc} (Mg m^{-3})	2.257
θ Range for data collection (°)	1.68–26.01
Limiting indices	$0\le h\le 17$, $0\le k\le 24$, $-18\le l\le 18$
Reflections collected	7310
Independent reflections (R_{int})	7036 (0.0225)
Absorption correction	semi-empirical absorption
Max. and min. transmission	1.0000 and 0.6892
Refinement method	full-matrix least-squares on F^2
Data/restraints/parameters	7034/0/297
Goodness-of-fit on F^2	1.113
Final R indices ($I>2\sigma(I)$) [a]	$R_1=0.0429$, $wR_2=0.1127$
R indices (all data)	$R_1=0.0774$, $wR_2=0.1168$
Largest difference peak, hole (e Å^{-3})	1.804 (close to X atom), −1.088
Max. shift $(\Delta/\sigma)_{max}$ in final cycle	−0.002

[a] $R=\sum||F_o|-|F_c||/\sum|F_o|$, $wR=[\sum w(F_o^2-F_c^2)^2/\sum w(F_o^4)]^{1/2}$, $w=[\sigma^2(F_o^2)+(aP)^2+bP]^{-1}$, $P=(2F_c^2+F_o^2)/3$.

matrix least-squares refinement was based on F^2 with the SHELXTL-5 program [12].

Selected bond lengths and angles are listed in Table 2.

3. Results and discussion

3.1. Description of the molecular structure

An ORTEP drawing of the molecular structure of $[Mo_3X(S_2)_3(dtp)_3I_3]$ is shown in Fig. 1, and a packing diagram is shown in Fig. 2.

Fig. 1 shows that the title compound has a typical M_2 type structure, in which three Mo atoms form an approximately equilateral triangle with Mo–Mo bond distances of 2.657(1), 2.663(1) and 2.663(1) Å. The average Mo–Mo bond distance (2.661 Å) is between those of the clusters $[Mo_3S_7(dtp)_3I]$ and $[Mo_3OS_6(dtp)_3I]$, whose average Mo–Mo bond distances are 2.723 and 2.626 Å, respectively [9]. The μ_3-X atom with O/S statistical distribution (X=58%O+42%S) is above the $\{Mo_3\}$ triangle. Each pair of Mo atoms is bridged by a (S_2) group, and each Mo atom is coordinated further by a terminal dtp ligand; thus a pentagonal bipyramidal coordinated geometry of the Mo atom is formed by six S atoms and a μ_3-X atom. The most specific feature of this structure is that three out-of-plane S atoms are connected with the I_3^- anion at S–I bond distances of 3.270(2), 3.307(2) and 3.364(3) Å (average 3.314 Å), which are much shorter than the corresponding van der Waals

Table 2
Selected bond lengths (Å) and angles (°)

Mo(1)–X	2.196(5)	I(1)–I(2)	2.824(1)
Mo(1)–S(2)	2.399(2)	I(1)···S(1)$^{\#1}$ [a]	3.530(2)
Mo(1)–S(6)	2.414(2)	I(1)···S(3)$^{\#2}$	3.641(2)
Mo(1)–S(1)	2.472(2)	I(1)···S(10)$^{\#2}$	3.648(2)
Mo(1)–S(5)	2.480(2)	I(2)–I(3)	3.039(1)
Mo(1)–S(8)	2.492(2)	I(3)–S(2)	3.270(2)
Mo(1)–S(7)	2.549(2)	I(3)–S(4)	3.307(2)
Mo(1)–Mo(2)	2.656(1)	I(3)–S(6)	3.364(2)
Mo(1)–Mo(3)	2.663(1)	P(1)–O(2)	1.554(7)
Mo(2)–X	2.207(5)	P(1)–O(1)	1.577(9)
Mo(2)–S(2)	2.410(2)	P(1)–S(7)	1.968(4)
Mo(2)–S(4)	2.415(2)	P(1)–S(8)	1.998(4)
Mo(2)–S(1)	2.482(2)	P(2)–O(4)	1.557(7)
Mo(2)–S(3)	2.484(2)	P(2)–O(3)	1.570(7)
Mo(2)–S(10)	2.502(2)	P(2)–S(9)	1.989(3)
Mo(2)–S(9)	2.547(2)	P(2)–S(10)	2.001(3)
Mo(2)–Mo(3)	2.663(1)	P(3)–O(5)	1.565(7)
Mo(3)–X	2.205(5)	P(3)–O(6)	1.566(7)
Mo(3)–S(4)	2.409(2)	P(3)–S(12)	1.990(3)
Mo(3)–S(6)	2.410(2)	P(3)–S(11)	2.007(3)
Mo(3)–S(3)	2.471(2)	S(1)–S(2)	2.044(3)
Mo(3)–S(5)	2.480(2)	S(3)–S(4)	2.060(3)
Mo(3)–S(11)	2.503(2)	S(5)–S(6)	2.036(3)
Mo(3)–S(12)	2.552(2)		
X–Mo(1)–S(2)	109.27(14)	S(3)–Mo(3)–S(5)	171.42(7)
X–Mo(1)–S(6)	108.94(13)	X–Mo(3)–S(11)	79.75(13)
S(2)–Mo(1)–S(6)	86.21(8)	X–Mo(3)–S(12)	157.84(14)
X–Mo(1)–S(1)	85.77(14)	S(11)–Mo(3)–S(12)	78.10(8)
S(6)–Mo(1)–S(1)	135.58(8)	Mo(1)–Mo(3)–Mo(2)	59.84(4)
X–Mo(1)–S(5)	86.09(14)	I(2)–I(1)–S(1)$^{\#1}$	91.06(4)
S(2)–Mo(1)–S(5)	135.21(8)	I(2)–I(1)–S(3)$^{\#2}$	115.82(4)
S(1)–Mo(1)–S(5)	171.76(7)	S(1)$^{\#1}$–I(1)–S(3)$^{\#2}$	150.86(5)
X–Mo(1)–S(8)	79.04(14)	I(2)–I(1)–S(10)$^{\#2}$	172.59(4)
X–Mo(1)–S(7)	157.28(14)	S(1)$^{\#1}$–I(1)–S(10)$^{\#2}$	95.18(5)
S(8)–Mo(1)–S(7)	78.24(8)	S(3)$^{\#2}$–I(1)–S(10)$^{\#2}$	57.29(5)
Mo(2)–Mo(1)–Mo(3)	60.09(3)	I(1)–I(2)–I(3)	174.01(3)
X–Mo(2)–S(2)	108.52(14)	I(2)–I(3)–S(2)	140.27(4)
X–Mo(2)–S(4)	108.79(13)	I(2)–I(3)–S(4)	81.37(4)
S(2)–Mo(2)–S(4)	86.80(8)	S(2)–I(3)–S(4)	60.54(5)
X–Mo(2)–S(1)	85.29(13)	I(2)–I(3)–S(6)	92.56(4)
S(4)–Mo(2)–S(1)	135.95(7)	S(2)–I(3)–S(6)	59.43(5)
X–Mo(2)–S(3)	85.23(14)	S(4)–I(3)–S(6)	59.03(6)
S(2)–Mo(2)–S(3)	136.21(7)	Mo(1)–X–Mo(3)	74.5(2)
S(1)–Mo(2)–S(3)	170.38(7)	Mo(1)–X–Mo(2)	74.2(2)
X–Mo(2)–S(10)	80.55(14)	Mo(3)–X–Mo(2)	74.3(2)
X–Mo(2)–S(9)	158.72(14)	Mo(1)–S(1)–Mo(2)	64.86(6)
S(10)–Mo(2)–S(9)	78.19(8)	Mo(1)–S(2)–Mo(2)	67.06(6)
Mo(1)–Mo(2)–Mo(3)	60.07(3)	S(1)–S(2)–I(3)	173.57(10)
X–Mo(3)–S(4)	109.08(14)	Mo(3)–S(3)–Mo(2)	65.02(6)
X–Mo(3)–S(6)	108.78(14)	Mo(3)–S(4)–Mo(2)	67.01(6)
S(4)–Mo(3)–S(6)	85.99(8)	S(3)–S(4)–I(3)	172.02(11)
X–Mo(3)–S(3)	85.61(14)	Mo(1)–S(5)–Mo(3)	64.95(6)
S(6)–Mo(3)–S(3)	135.67(8)	Mo(3)–S(6)–Mo(1)	66.99(6)
X–Mo(3)–S(5)	85.90(14)	S(5)–S(6)–I(3)	171.58(11)
S(4)–Mo(3)–S(5)	135.01(8)		

[a] Symmetry transformations used to generate equivalent atoms: #1 $x+1/2$, $-y+1/2$, $z+1/2$; #2 $-x+1/2$, $y-1/2$, $-z+1/2$; I(1)···S(1), I(1)···S(3) and I(1)···S(10) are the intermolecular interactions.

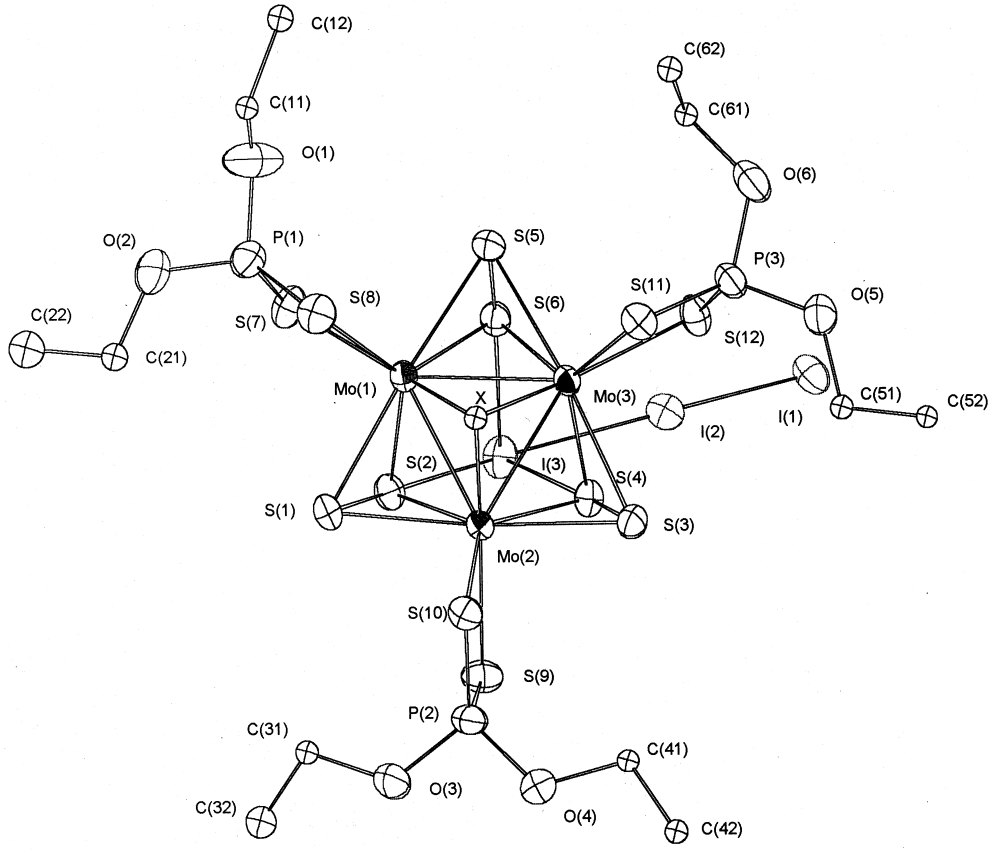


Fig. 1. Structure of the cluster $[Mo_3X(S_2)_3(dtp)_3(I_3)]$ (X = O, S).

contact ($\sim$4.00 Å) [13], showing weak bonding interaction between the S and I atoms. The I–I bond lengths of the I_3^- anion are 2.824(1) and 3.040(1) Å, which are comparable with the corresponding values found in the dinuclear cluster $[Mo_2(NTO)_2(dtp)_2S(O_2CMe)(SI_3)]_n$ reported by Jun et al. [14]. Another important feature lies in the packing structure. As shown in Fig. 2, the other terminal atom of I_3^- connects with the S(1), S(3) and S(10) atoms of two adjacent cluster molecules at S···I distances of 3.530(2), 3.641(2) and 3.648(2) Å, respectively. Thus three cluster molecules are joined together through the I_3^- anion, and a layer-like structure corresponding approximately to the (101) plane is formed in the unit cell. This is the first example of such M_2 type clusters.

3.2. About the formation mechanism

The title compound is an unexpected product according to the following reaction scheme:

$$Mo_3OS_3(dtp)_4\cdot H_2O + CuI \xrightarrow{\text{EtOAc, DMF, air}} Mo_3(X)(S_2)_3(dtp)_3\cdot I_3$$

In this sulfur-addition reaction, the source of the S atoms may come from the disruption of parts of the starting cluster $[Mo_3OS_3(dtp)_4\cdot H_2O]$, and the $(S_2)^{2-}$ groups are formed by the oxidative dimerization $2S^{2-} \rightarrow (S_2)^{2-}$ in air. Such reactions have been observed previously in our reaction system [15]. The I_3^- group may originate from the oxidation of CuI in air. Some capping O atoms were also substituted by S atoms during the reaction. As a result, two kinds of molecules, i.e. $Mo_3OS_6(dtp)_3(I_3)$ and $Mo_3S_7(dtp)_3(I_3)$ were cocrystallized at 58 and 42% occupancies, respectively.

3.3. Energy band structure

In order to study the electronic structure of the cluster with layer-like packing structure, we used the tight-binding method within the extended Hückel scheme [16,17] to calculate the energy band, which is shown in Fig. 3. Analysis of the composition of the bands shows that the bands around E_f consist mainly of the contributions of I, Mo and S atoms. There are many bands near E_f, and the band gap is very narrow; furthermore, there is a band crossing through several bands while bending to E_f, which shows that the crystal is a typically anisotropic semiconductor. The main compositions of this band are the components of I and S atoms, indicating that it is the I···S interaction that causes the charge transfer between the clusters.

3.4. Density functional calculation

DFT calculations have been performed on this cluster compound using the Amsterdam Density Functional package

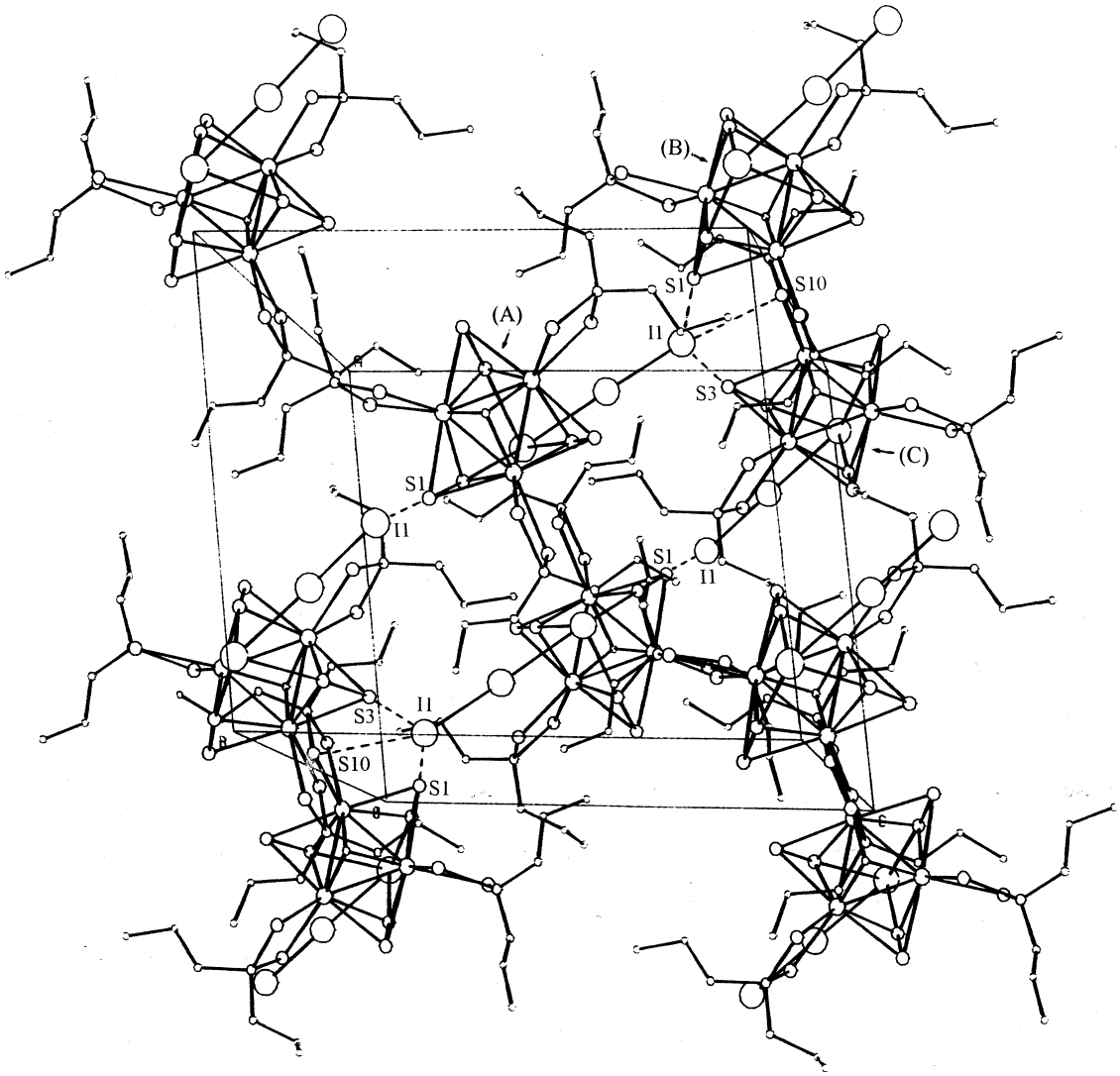


Fig. 2. Packing diagram of $[Mo_3X(S_2)_3(dtp)_3(I_3)]$.

(ADF) developed by Baerends et al. [18]. An uncontracted double-ξ STO basis set has been used for 5s, 5p, and 4d orbitals of molybdenum atoms, for 5s, 5p orbitals of iodine atoms, and for ns, np of S, P, O, C atoms. The calculations have been performed on the LSD level, and the VWN [19] approximation with Becke [20] and Perdew's [21] non-local corrections has been used.

The electronic structures of $[Mo_3S_7]^{4+}$ and $[Mo_3S_7(dtc)_3]^{+}$ have been carefully studied using ADF by Mayor-Lopez et al. [22]. In their work the electronic structure of $[Mo_3OS_6]^{4+}$ which is very similar to those of $[Mo_3S_7]^{4+}$ and $[Mo_3S_7(dtc)_3]^{+}$ was calculated, and so we do not describe it here but will focus on the interaction between I_3 and the cluster. As the oxygen component is the major component of the μ_3-X atom in the cluster $[Mo_3X(S_2)_3(dtp)_3I_3]$, we use $[Mo_3O(S_2)_3(dtp)_3I_3]$ in the study of the electronic structure.

From the crystal cell packing diagram of the cluster we can see that each I_3^- connects with three cluster molecules A, B and C in different ways. I(3) connects with molecule A by three intramolecular I–S_{ax} distances at 3.270(2), 3.307(2) and 3.364(2) Å. I(1) connects with two adjacent cluster molecules: one by I(1)···S(1) with molecule B at 3.530(2) Å, and the other by I(1)···S(3) and I(1)···S(10) with molecule C at 3.641(2) and 3.648(2) Å. Thus we calculated four structures: I_3^- with molecule A, I_3^- with molecule B, I_3^- with molecule C, and the cluster core $[Mo_3O(S_2)_3]$ itself. In order to reduce the computing time, we substituted $O(CH_3)_2$ for the group $O(CH_2CH_3)_2$, which is not expected to influence the electronic structure of the I_3^- and $[Mo_3OS_6]$ moieties significantly.

The calculated total binding energies (E_b) between I_3 and clusters are listed in Table 3 ($E_b = E(\text{cluster and } I_3) - E(\text{cluster}) - E(I_3)$).

From Table 3 we can see that the binding energy between I_3 and molecule A is much larger than that of a common hydrogen bond (about 10–20 kcal mol^{-1}) and the binding energy between I_3 and molecule B (or C), but is less than a

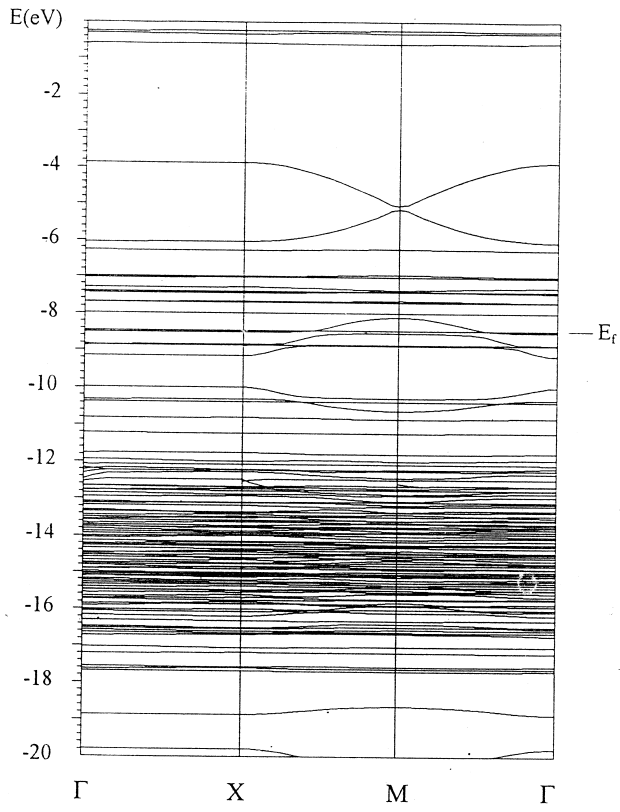


Fig. 3. Band structure of $[Mo_3X(S_2)_3(dtp)_3(I_3)]$.

normal covalent bond. The interactions between I_3 and molecule B, I_3 and molecule C are also stronger than the hydrogen bond. Thus we believe that there exist relatively strong interactions between I_3 and its adjacent molecules, and the cluster cores are connected to form a layer-like structure through I_3. The order of the binding energies between I_3 and the three molecules is the same as that of the distances between I_3 and the adjacent S atoms among the clusters.

Table 3
Binding energies between I_3 and the cluster molecules

	Molecule A and I_3	Molecule B and I_3	Molecule C and I_3
E_b (kcal mol^{-1})	55.690	45.682	40.47
HOMO–LUMO gap (eV)	0.915	0.139	0.029

Now we describe the electronic structure of the clusters. The main constitution of the frontier orbitals of the calculated structures is displayed in Tables 4–6. The frontier occupied orbitals are mainly from I and S, and the unoccupied orbitals are from Mo and S. Here the S atoms denote those in $[Mo_3OS_6]$, while the S atoms of the ligand contribute little to the frontier orbitals. By a more detailed analysis we find that the occupied orbitals are p–π* (p orbital of I with π* of Mo_3OS_6), p–σ* (p orbital of I with σ* of Mo_3OS_6) and σ bonds within I_3, while the unoccupied orbitals are all from Mo_3OS_6. The overlap between the orbitals of I_3 and molecule A is much larger than those between the orbitals of I_3 and molecule B (or C). The HOMO–LUMO gaps of the three calculated complexes are very narrow (see Table 3), and the orbitals of S and I overlap each other, just like the results of EHT calculation. The DFT calculation also supports the conclusion that the crystal may be a semiconductor (conduction by I–S charge transfer).

4. Conclusions

The reaction of $Mo_3OS_3(dtp)_4 \cdot H_2O$ with CuI yielded a novel cluster $[Mo_3X(S_2)_3(dtp)_3(I_3)]$ (X = O, S) in which I_3^- can be viewed as an intermediary of the trinuclear unit aggregation. The energy band and density functional calcu-

Table 4
Constitution of frontier orbitals (the HOMO is orbital 105): molecule A and I_3

	101	102	103	104	105	106	107	108	109	110
Mo	1.7	2.1	1.5	0.9	0.4	50.4	52.1	70.3	54.5	25.2
Cap-O	0.2	0.4	0.3	0.0	0.0	6.3	6.6	0.0	0.0	0.6
$S_{eq,ax}$	15.8	6.2	6.7	2.7	1.1	28.9	26.5	26.5	38.2	52.3
Lig-S	1.8	1.5	1.2	0.4	0.1	7.8	7.8	3.0	1.8	8.4
I	80.1	89.7	90.3	95.7	98.4	0.5	0.3	0.1	0.7	10.1

Table 5
Constitution of frontier orbitals (the HOMO is orbital 105): molecule B and I_3

	101	102	103	104	105	106	107	108	109	110
Mo	0.7	0.4	0.7	1.4	0.1	16.6	44.5	50.4	66.9	60.0
Cap-O	0.1	0.0	0.0	0.1	0.0	1.1	4.8	5.9	0.2	0.6
$S_{eq,ax}$	10.2	0.5	1.1	9.2	0.2	72.8	40.6	23.1	29.73	32.7
Lig-S	1.2	0.9	2.3	0.6	0.1	5.4	5.2	10.5	2.9	2.0
I	86.6	96.7	94.8	88.3	99.2	2.1	0.3	3.5	0.0	0.2

Table 6
Constitution of frontier orbitals (the HOMO is orbital 105): molecule C and I_3

	101	102	103	104	105	106	107	108	109	110
Mo	0.5	0.8	0.4	1.2	0.4	18.5	43.1	48.5	66.1	59.8
Lig-O	0.1	0.3	0.2	0.1	0.1	0.7	0.8	0.9	0.0	1.5
$S_{eq,ax}$	9.3	0.7	1.8	7.2	0.3	71.1	42.6	25.2	30.7	32.6
Lig-S	0.9	2.2	1.0	0.5	0.2	5.1	4.9	11.1	2.8	2.3
I	88.7	95.0	96.2	90.7	98.9	1.5	0.2	3.0	0.0	0.1

lations showed that this crystal possesses semiconducting properties.

Supplementary data

Crystallographic data have been deposited with the Cambridge Crystallographic Data Centre, 12 Union Road, Cambridge, CB2 1EZ, UK (fax: +44-1223-336033; e-mail: deposit@ccdc.cam.ac.uk) and are available on request quoting the deposition number CCDC 134349.

Acknowledgements

This study was supported by the National Natural Science Foundation of China, the NSF of Fujian Province and the State Key Laboratory of Structural Chemistry. The authors would like to thank Li-Min Wu, Xiang Lin, Zi-Xiang Huang and Jin Chen for their kind help in the preparation of this manuscript.

References

[1] A. Müller, E. Diemann, A. Branding, F.W. Baumann, M. Breysse, M. Vrinat, Appl. Catal. 62 (1990) 13.
[2] K. Hegetschweiler, T. Keller, H. Zimmermann, W. Schneider, H. Schmalle, E. Dubler, Inorg. Chim. Acta 169 (1990) 235.
[3] H. Zimmermann, K. Hegetschweiler, T. Keller, V. Gramlich, H.W. Schmalle, W. Petter, W. Schneider, Inorg. Chem. 30 (1991) 4336.
[4] K. Hegetschweiler, T. Keller, M. Bäumle, G. Rihs, W. Schneider, Inorg. Chem. 30 (1991) 4342.
[5] V.P. Fedin, M.N. Sokolov, O.A. Geras'ko, A.V Virovets, N.V. Podberezskaya, V.Ye. Fedorov, Inorg. Chim. Acta 187 (1991) 81.
[6] V.P. Fedin, M.N. Sokolov, A.V. Virovets, N.V. Podberezskaya, V.Ye. Fedorov, Inorg. Chim. Acta 194 (1992) 195.
[7] J.-L. Huang, M.-Y. Shang, J.-Q. Huang, H.-H. Zhuang, S.-F. Lu, J.-X. Lu, Chin. J. Struct. Chem. 2 (1982) 1.
[8] J.-L. Huang, J.-Q. Huang, M.-Y Shang, J.-X. Lu, Adv. Sci. China Chem. 3 (1990) 155.
[9] S.-F. Lu, J.-Q. Huang, Y.-H. Lin, J.-L. Huang, Acta Chim. Sinica 45 (1987) 842.
[10] S.-F. Lu, Q.-J. Wu, H.-B. Chen, R.-M. Yu, J.-Q. Huang, Chin. J. Struct. Chem. 13 (1994) 389.
[11] S.-F. Lu, M.-Y. Shang, J.-Q. Huang, J.-L. Huang, J.-X. Lu, Sci. Sinica Ser. B 31 (1988) 147.
[12] G.M. Sheldrick, SHELXTL Version 5 Reference Manual, Siemens Analytical X-ray Instruments, Madison, WI, 1995.
[13] F.A. Cotton, G.W. Wilkinson, Advanced Inorganic Chemistry, Wiley, New York, 1972.
[14] Q.-L. Jun, L.S. Mickael, F.R. John, E.N. Mark, Inorg. Chem. 34 (1995) 5055.
[15] J.-Q. Huang, J.-L. Huang, S.-F. Lu, H.-H. Zhuang, X.-T. Lin, D.-M. Wu, R.-M. Yu, H.-B. Chen, Q.-H. Chen, Z.-X. Huang, Chin. J. Struct. Chem. 14 (1995) 180.
[16] M.-H. Whangbo, R. Hoffmann, J. Am. Chem. Soc. 100 (1978) 6093.
[17] M.-H. Whangbo, R. Hoffmann, R.B. Woodward, Proc. R. Soc. London, Ser. A 366 (1979) 23.
[18] ADF 1.15 Department of Theoretical Chemistry, Vrije Universteit, Amsterdam, 1995.
[19] S.H. Vosko, L. Wilk, M. Nusair, Can. J. Phys. 58 (1980) 1200.
[20] A.D. Becke, Phys. Rev. A 38 (1998) 1908.
[21] J.P. Perdew, Phys. Rev. B 33 (1986) 8822.
[22] M.J. Mayor-Lopez, J. Weber, K. Hegetschweiler, M.D. Meienberger, F. Joho, S. Leoni, R. Nesper, G.J. Reiss, W. Frank, B.A. Kolesov, V.P. Fedin, V.E. Fedorov, Inorg. Chem. 37 (1998) 2633.

PERGAMON

www.elsevier.nl/locate/poly

Polyhedron 19 (2000) 739–742

POLYHEDRON

Synthesis of a polymetallic Pt, Sn complex containing square planar and trigonal bipyramidal platinum centres. Crystal and molecular structure of bis{chlorotriethylphosphinoplatinum(II)}μ-2,3,5,6-tetrakis(α-pyridyl)-pyrazinetetrakis(trichlorostannyl)triethylphosphinoplatinate(II)

Wagner M. Teles [a], Nivaldo L. Speziali [b], Carlos A.L. Filgueiras [c,*]

[a] *Departamento de Química, ICEx, Universidade Federal de Minas Gerais, 31270-901 Belo Horizonte, MG, Brazil*
[b] *Departamento de Física, ICEx, Universidade Federal de Minas Gerais, 30123-970 Belo Horizonte, MG, Brazil*
[c] *Departamento de Química Inorgânica, IQ, Universidade Federal do Rio de Janeiro, C.P. 68563, 21945-970 Rio de Janeiro, RJ, Brazil*

Received 15 September 1999; accepted 6 December 1999

Abstract

Reaction between 2,3,5,6-tetrakis(α-pyridyl)pyrazine (TPP) and the dimer $[Pt_2(PEt_3)_2Cl_4]$ yielded an ionic complex of formula $[\{Pt(PEt_3)Cl\}_2\mu\text{-}(TPP)][Pt(PEt_3)Cl_3]_2$ (**1**), in which TPP behaves as a bis(bidentate) ligand between the two Pt atoms of the cation. Insertion of $SnCl_2$ into the Pt–Cl bonds of this compound led to an unusual rearranged product, $[\{Pt(PEt_3)Cl\}_2\mu\text{-}(TPP)][Pt(SnCl_3)_4(PEt_3)]$ (**2**), with a rare example of a pentacoordinate Pt(II) species in the anionic moiety, where Pt is at the centre of a trigonal bipyramid, in addition to two other square planar Pt atoms in the cationic moiety. ©2000 Elsevier Science Ltd All rights reserved.

Keywords: Insertion reactions; Platinum(II) complexes; Platinum–tin bimetallics; 2,3,5,6-Tetrakis(α-pyridyl)pyrazine

1. Introduction

Platinum(II) complexes containing trichlorostannyl groups are widely studied due to their ability to behave as homogeneous catalysts in olefin hydroformylation, hydrogenation and carbonylation, especially when the Sn:Pt ratio is large [1–4]. $SnCl_3^-$ groups are also important in the stabilization of a few unusual pentacoordinate Pt compounds [5–8], such as $[Pt(SnCl_3)_5]^{3-}$, $[Pt(SnCl_3)_4H]^{3-}$ and $[Pt(SnCl_3)_3L_2]^-$, where L = PEt_3 or $AsEt_3$.

The ligand 2,3,5,6-tetrakis(α-pyridyl)pyrazine (TPP) has been used as a bridge to prepare several bimetallic complexes, in which TPP is bis-tridentate [9–14]. However, there is no example of a bis-bidentate coordination mode for this ligand. Reaction between the $[Pt(PEt_3)Cl_2]_2$ bridging dimer and TPP led to the isolation of $[\{Pt(PEt_3)Cl\}_2\mu\text{-}(TPP)]$-$[Pt(PEt_3)Cl_3]_2$. $SnCl_2$ insertion was performed on this complex, for the following reasons: in addition to having a large cation, which is an essential requisite for stabilizing large anionic complexes, our precursor complex provided a means of having different kinds of Pt–Cl bonds into which $SnCl_2$ insertion might be attempted. Only the anionic part was attacked, however, leading to a change in coordination number and the formation of a pentacoordinate anionic cluster, $[Pt(SnCl_3)_4(PEt_3)]^{2-}$, which was stabilized by the $[\{Pt(PEt_3)Cl\}_2\mu\text{-}(TPP)]^{2+}$ cation.

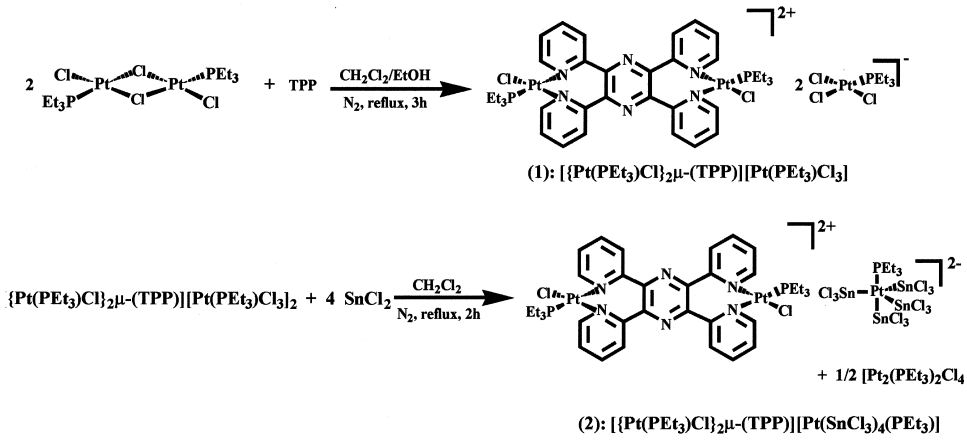
The present study allowed a series of correlations to be undertaken, namely between the molecular structure of the final product, on the one hand, and multinuclear NMR ($^{31}P\{^1H\}$, ^{119}Sn and ^{195}Pt) studies of both this complex and its precursor, on the other, which clearly established the nature of the novel heptametallic complex.

2. Experimental

All the reactions were carried out under N_2 in Schlenk glassware, with solvents purified by standard methods. 2,3,5,6-Tetrakis(α-pyridyl)pyrazine and $[Pt_2(PEt_3)_2Cl_4]$ were prepared according to the literature [15,16]. Scheme 1 shows the reactions from which the complexes **1** and **2** were prepared.

* Corresponding author. E-mail: calf@iq.ufrj.br

0277-5387/00/$ - see front matter ©2000 Elsevier Science Ltd All rights reserved.
PII S0277-5387(99)00394-0



Scheme 1.

2.1. Synthesis of [{Pt(PEt$_3$)Cl}$_2$μ-(TPP)][Pt(PEt$_3$)Cl$_3$]$_2$ (1)

A 10-ml volume of a CH_2Cl_2 solution of [$Pt_2(PEt_3)_2Cl_4$] (301 mg, 0.392 mmol) was added under N_2 to 15 ml of an EtOH solution of TPP (76 mg, 0.196 mmol). The mixture was refluxed for 3 h, followed by reduction to one-quarter its original volume. Addition of n-hexane caused precipitation of a yellow product. This was filtered off and dried in vacuo. The solid was recrystallised from a 1:1 mixture of CH_2Cl_2–n-hexane. Yield 86%, m.p. 179–180°C. *Anal*. Found: C, 30.3; H, 3.9; N, 4.2; Pt, 40.5. Calc. for $C_{48}H_{76}N_6P_4Cl_8Pt_4$: C, 30.0; H, 4.0; N, 4.4; Pt, 40.5%.

2.2. Synthesis of [{Pt(PEt$_3$)Cl}$_2$μ-(TPP)][Pt(SnCl$_3$)$_4$(PEt$_3$)] (2)

Solid $SnCl_2$ (118 mg, 0.622 mmol) was added under N_2 to 11 ml of a CH_2Cl_2 solution of [{Pt(PEt_3)Cl}$_2$μ-(TPP)][Pt(PEt_3)Cl_3]$_2$ (299 mg, 0.156 mmol). After a 2 h reflux, during which the solution changed colour from yellow to brick, reduction to one-quarter of the initial volume, followed by addition of n-hexane, a red precipitate was formed. This was filtered off, washed with tetrahydrofuran (THF) and dried in vacuo. Attempts to obtain single crystals at this stage led to decomposition of the complex. Good crystals were later fortuitously obtained from the CD_3NO_2 solution used in the $^{31}P\{^1H\}$ NMR experiment. Yield 78%, m.p. 200°C (dec.). *Anal*. Found: C, 21.6; H, 2.3; N, 3.5; Pt, 26.0; Sn, 21.0. Calc. for $C_{42}H_{61}N_6P_3Cl_{14}Pt_3Sn_4$: C, 21.9; H, 2.7; N, 3.7; Pt, 25.5; Sn, 20.7%.

$^{31}P\{^1H\}$, ^{195}Pt and ^{119}Sn NMR spectra were obtained in different solvents using a DRX400 Bruker Avance instrument, with 85% H_3PO_4, K_2PtCl_4 and Me_4Sn, respectively, as external references. The pertinent NMR data are shown in Table 1. Red prismatic single crystals of [{Pt(PEt_3)Cl}$_2$μ-(TPP)][Pt($SnCl_3$)$_4$(PEt_3)] were collected from a CD_3NO_2 solution previously used in NMR studies, and the crystallographic data collection was performed on a Siemens P4 diffractometer equipped with graphite monochromator Mo Kα radiation ($\lambda = 0.71073$ Å), using XSCANS software [17]. Several well-formed red crystals were selected by optical analyses in a polarized light microscope and mounted on glass fibre using epoxy glue. The crystals were optically centred in the X-ray beam and rotation photographics and peak profiles of representative reflections were used to choose the best crystal, which was then used in subsequent data collection. The molecular structure of [{Pt(PEt_3)Cl}$_2$μ-(TPP)]-[Pt($SnCl_3$)$_4$(PEt_3)] is shown in Fig. 1.

Crystal data: $C_{42}H_{61}N_6P_3Cl_{14}Pt_3Sn_4$, $M = 2299.21$, triclinic space group $P\bar{1}$, $a = 9.994(2)$, $b = 18.839(3)$, $c = 20.772(3)$ Å; $\alpha = 66.02(1)$, $\beta = 85.62(1)$, $\gamma = 78.90(1)°$; $V = 3506.5(10)$ Å^3; $Z = 2$; $D_c = 2.178$ Mg m^{-3}; $\mu = 7.997$ mm^{-1}. The structure of the crystal ($0.15 \times 0.15 \times 0.20$ mm) was solved by direct methods and analysis of Fourier difference map. Hydrogen atoms were placed in calculated positions. Full-matrix least-squares methods were employed in

Table 1
Multinuclear NMR data [a]

Complex	δ ^{31}P	δ ^{195}Pt	δ ^{119}Sn	$^1J_{PtP}$	$^1J_{PtSn}$	$^2J_{SnP}$	$^2J_{SnSn}$
[{Pt(PEt_3)Cl}$_2$μ-(TPP)][Pt(PEt_3)Cl_3]$_2$ [b]	5.42	−3448 d		3350			
	4.25	−3522 d		3707			
[{Pt(PEt_3)Cl}$_2$μ-(TPP)][Pt($SnCl_3$)$_4$(PEt_3)] [c]	5.95	−3459 d	−84.7 Sn_{eq}	3299	19328 Pt–Sn_{eq}	230 Sn_{eq}–P	15800 Sn_{eq}–Sn_{eq}
	7.82	−5560 d	−173.6 Sn_{ax}	2377	5967 Pt–Sn_{ax}	2439 Sn_{ax}–P	1330 Sn_{ax}–Sn_{eq}

[a] Coupling constants are given in Hz; d refers to doublet.
[b] Spectra obtained in CD_2Cl_2.
[c] Spectra obtained in CD_2Cl_2–CD_3NO_2.

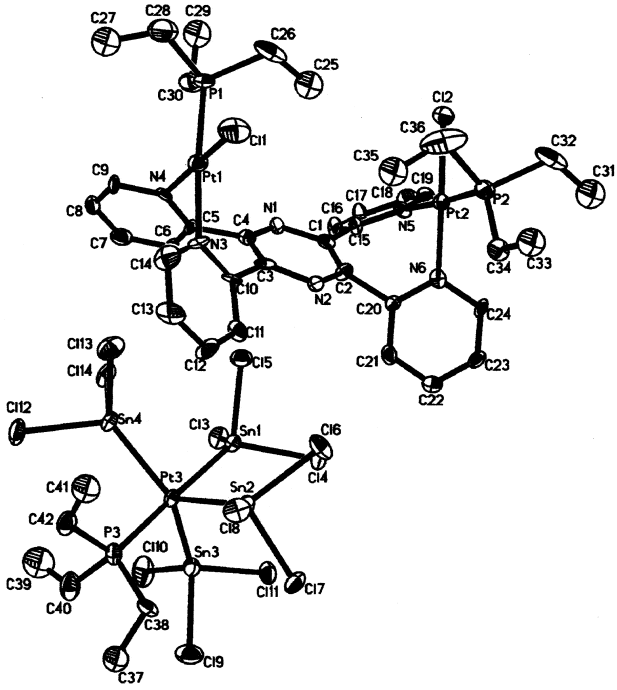


Fig. 1. Molecular structure of $[\{Pt(PEt_3)Cl\}_2\mu\text{-}(TPP)][Pt(SnCl_3)_4(PEt_3)]$ (**2**) with atomic numbering scheme. Hydrogen atoms are omitted for clarity.

the refinements using 7161 independent reflections, 5686 with $F_o > 4\sigma(F_o)$, from a set of 8996 collected ones; SHELX97 software was used in the refinements [18]. Anisotropic displacement factors were used for Pt, Sn, P, Cl, N and the aromatic carbons, and isotropic ones were used for the aliphatic carbons and hydrogen atoms. Final refinements converged to $R = 0.065$, $wR2 = 0.132$. Selected bond distances and angles are given in Table 2.

Table 2
Selected bond distances and angles for $[\{Pt(PEt_3)Cl\}_2\mu\text{-}(TPP)][Pt(SnCl_3)_4(PEt_3)]$ (**2**)

Bond distances (Å)		Bond angles (°)	
Pt(1)–N(3)	2.083(7)	P(1)–Pt(1)–N(3)	175.3(5)
Pt(1)–N(4)	1.993(14)	Cl(1)–Pt(1)–N(4)	174.0(5)
Pt(1)–Cl(1)	2.283(7)	N(3)–Pt(1)–N(4)	85.3(7)
Pt(1)–P(1)	2.243(7)	P(1)–Pt(1)–Cl(1)	90.1(3)
Pt(2)–N(5)	2.102(17)	N(3)–Pt(1)–Cl(10)	90.1(3)
Pt(2)–N(6)	2.000(16)	N(4)–Pt(1)–P(1)	95.0(5)
Pt(2)–Cl(2)	2.272(6)	P(2)–Pt(2)–N(5)	177.8(5)
Pt(2)–P(2)	2.237(6)	Cl(2)–Pt(2)–N(6)	174.7(5)
Pt(3)–Sn(1)	2.580(2)	N(5)–Pt(2)–N(6)	86.0(6)
Pt(3)–P(3)	2.304(6)	P(2)–Pt(2)–Cl(2)	88.9(2)
Pt(3)–Sn(2)	2.601(16)	N(5)–Pt(2)–Cl(2)	89.0(5)
Pt(3)–Sn(3)	2.592(17)	N(6)–Pt(2)–P(2)	96.1(4)
Pt(3)–Sn(4)	2.578(16)		

3. Results and discussion

A complex formulated as $(Et_4N)_2[Pt(SnCl_3)_4(PEt_3)]$ has been described in the literature; its structure was suggested on the basis of an NMR study [19]. In our case, both the molecular structure and NMR analysis are presented. The present case also differs from previous examples in the literature in that we have a complex anion of a complex bimetallic cation.

Table 1 shows the NMR data for compounds **1** and **2**. Complex **1** shows two $^{31}P\{^1H\}$ signals at δ 5.42 and 4.25, with two sets of satellites, corresponding to $^1J_{PtP}$ values of 3350 and 3707 Hz, respectively. The former was assigned to the less shielded phosphorus *trans* to nitrogen in the cationic moiety of compound **1**, whereas the latter was associated with phosphorus *trans* to chloride in the anionic species. The $^1J_{PtP}$ values are consistent with this assignment [20], since the Pt–N bond is stronger than the Pt–Cl bond, implying less PtP coupling in the cationic moiety compared with the anionic part of complex **1**. Complex **2** also shows two P signals, at δ 5.95 and 7.82, with $^1J_{PtP}$ values of 3299 and 2377 Hz, respectively. The cationic part hardly changed in both chemical shift and $^1J_{PtP}$, whereas the anionic species became more shielded and underwent a considerable decrease in its $^1J_{PtP}$, which can be accounted for by its being *trans* to the very strong $SnCl_3^-$ π acceptor.

Table 1 also shows the ^{195}Pt NMR data for compounds **1** and **2**. Complex **1** presents two doublets at δ –3448 and –3522, with $^1J_{PtP}$ values of 3368 and 3702 Hz, respectively. The first of these absorptions corresponds to the cation Pt atoms, with the signals somewhat broadened as a result of the fact that the Pt atoms are bound to N atoms, which exhibit a quadrupolar nuclear effect. The PtP couplings are the same, within experimental error, as those observed in the $^{31}P\{^1H\}$ NMR measurements.

Complex **2** also shows two doublets, relative to two types of Pt atoms in totally different chemical environments. The doublet centred at δ −3459, with $^1J_{PtP} = 3299$ Hz, was assigned to the tetracoordinate cationic Pt atoms, whereas the doublet at δ −5560, with $^1J_{PtP} = 2378$ Hz, was assigned to the pentacoordinate anionic Pt atom. One can see that for the tetracoordinate Pt atoms the values of both δ and $^1J_{PtP}$ remained very similar to those of complex **1**, as expected. It is important to note how the presence of the strong $SnCl_3^-$ π-acceptor groups affects $^1J_{PtP}$ of the pentacoordinate moiety, dramatically lowering its value (from 3702 to 2378 Hz), compared to that of complex **1**. The great downward change in chemical shift between the ^{195}Pt signals shown by the anionic parts of complexes **1** and **2** reflects the much enhanced shielding shown by the Pt nucleus in the latter. It was not possible here to observe the ^{119}Sn satellites in the ^{195}Pt NMR spectrum, even after the temperature was lowered to −50°C, and the coupling between Pt and Sn could only be observed in the ^{119}Sn spectrum.

The ^{119}Sn NMR spectrum of complex **2** was obtained at −90°C, and allowed us to distinguish two types of Sn atoms in a 3:1 ratio. The signal at δ −84.7 presents $^2J_{SnP} = 230$ Hz, and ^{195}Pt satellites with $^1J_{PtSn} = 19328$ Hz; this was assigned to the equatorial Sn atoms. In contrast, the signal at δ −173.6,

with $^2J_{SnP} = 2439$ Hz and $^1J_{PtSn} = 5967$ Hz, was assigned to the axial Sn atom. Of course, equatorial $SnCl_3^-$ groups will produce much greater SnPt coupling constants than axial groups, taking into account the enhanced Pt–Sn back-donation in the former compared to the latter. As expected also, $^2J_{SnP}$ values follow an inverse order; that is, the equatorial Sn atoms, which are approximately at a 90° angle to the P atom, show lower $^2J_{SnP}$ values than the axial Sn atom, which is at an angle of approximately 180° to the P atom. Finally, the ^{119}Sn NMR spectrum also gives the $^2J_{SnSn}$ couplings; as the data in Table 1 show, two equatorial Sn atoms present a much higher $^2J_{SnSn}$ value (15800 Hz) than an equatorial and the apical Sn atom (1330 Hz).

Fig. 1 shows the molecular structure of complex **2**, and Table 2 gives a selected number of bond distances and angles. One can see that there is an excellent agreement between the NMR results and the crystallographic data; that is, the complex retains its solid-state structure when dissolved. The Pt(1) and Pt(2) sites in the cationic part of the complex are joined by the TPP ligand and coordinated in a bidentate mode to the pyridine nitrogens in a slightly distorted square planar geometry. It is interesting to note in the cationic part of the complex that the Pt(1)–N(3) and Pt(2)–N(5) bond distances are significantly longer than Pt(1)–N(4) and Pt(2)–N(6), respectively, as a result of the more efficient Pt–P bonding as compared to Pt–Cl. As a consequence, the bonds *trans* to the phosphorus atoms will be weakened, hence their longer distances.

The structure of the cationic moiety also shows that the two PEt_3 groups are in a *sym–trans* configuration, probably due to steric requirements in the solid state.

The anionic site presents a distorted trigonal bipyramidal geometry, in which the phosphine occupies an axial position *trans* to Sn(1). The Sn(2), Sn(3) and Sn(4) atoms lie on the equatorial plane, from which Pt(3) is 0.169 Å away, towards P(3). In spite of this position of Pt(3), on the average, the Pt(3)–Sn_{eq} bonds are longer than Pt(3)–Sn(1). This is in accordance with the expectation that in d^8 TBP transition metal complexes the metal–axial ligand bonds ought to be shorter than the metal–equatorial ligand bonds [21]. In addition, the fact that any Pt(3)–Sn bond is significantly shorter than the sum of the covalent radii (≈ 2.80 Å) suggests some degree of multiple bonding in Pt–Sn, including a considerable π Pt → Sn back-bonding [22–24]. This is corroborated by the greater Pt(3)–P(3) bond distance compared to Pt(1)–P(1) and Pt(2)–P(2), consistent with the strong *trans* influence provided by the $SnCl_3^-$ group (and also shown in the respective $^1J_{PtP}$ coupling constants).

Supplementary data

Crystallographic data have been deposited at the Cambridge Crystallographic Data Centre, 12 Union Road, Cambridge CB2 1EZ, UK (fax: +44-1223-336033; e-mail: deposit@ccdc.cam.ac.uk). The deposition number for this compound is CCDC 12390.

Acknowledgements

The authors are grateful to the agencies CNPq and Fapemig for financial support.

References

[1] M. Gómez, G. Muller, D. Sainz, J. Sales, X. Solans, Organometallics 10 (1991) 4036.
[2] A. Scrivanti, A. Berton, L. Toniolo, C. Botteghi, J. Organomet. Chem. 314 (1986) 369.
[3] E. Farkas, L. Kollár, M. Moret, A. Sioni, Organometallics 15 (1996) 1345.
[4] G.K. Anderson, C. Billard, H.C. Clark, J.A. Davies, C.S. Wong, Inorg. Chem. 22 (1983) 439.
[5] R.D. Cramer, R.V. Lindsey Jr., C.T. Prewitt, U.G. Stolberg, J. Am. Chem. Soc. 87 (1965) 658.
[6] J.H. Nelson, N.W. Alcock, Inorg. Chem. 21 (1982) 1196.
[7] P.S. Pregosin, H. Rügger, Inorg. Chim. Acta 86 (1984) 55.
[8] A. Albinati, R. Nägeli, H. Rügger, P.S. Pregosin, Angew. Chem., Suppl. (1982) 755.
[9] R.R. Runinski, C. Letner, Inorg. Chim. Acta 162 (1989) 175.
[10] R.R. Ruminski, J. Kiplinger, Inorg. Chem. 29 (1990) 4581.
[11] M. Graf, B. Greaves, H. Stoeckli-Evans, Inorg. Chim. Acta 204 (1993) 239.
[12] L.M. Vogler, B. Scott, K.J. Brewer, Inorg. Chem. 32 (1993) 898.
[13] J.-P. Collin, P. Lainé, J.-P. Launay, J.-P. Sauvage, A. Sour, J. Chem. Soc., Chem. Commun. (1993) 434.
[14] M. Graf, H. Stoeckli-Evans, A. Escuer, R. Vicente, Inorg. Chim. Acta 257 (1997) 89.
[15] H.A. Godwin, F. Lions, J. Am. Chem. Soc. 81 (1959) 6415.
[16] F.R. Hartley, Organometal. Chem. Rev. A 6 (1970) 119.
[17] Siemens XSCANS Users Manual, Siemens Analytical X-Ray Instruments, Madison, WI, 1994.
[18] G.M. Sheldrick, SHELX97, Program for the Refinement of Crystal Structures, University of Göttingen, Germany, 1997.
[19] A. Albinati, P.S. Pregosin, H. Rügger, Inorg. Chem. 23 (1984) 3223.
[20] W.M. Teles, N.G. Fernandes, A. Abras, C.A.L. Filgueiras, Transition Met. Chem. 24 (1999) 321.
[21] A.R. Rossi, R. Hoffmann, Inorg. Chem. 14 (1975) 365.
[22] W.M. Teles, C.A.L. Filgueiras, A. Abras, Hyperfine Interact. (in press).
[23] W.R. Rocha, W.B. de Almeida, Int. J. Quantum Chem. 65 (1997) 643.
[24] W.R. Rocha, W.B. de Almeida, Organometallics 17 (1998) 1961.

PERGAMON

www.elsevier.nl/locate/poly

Polyhedron 19 (2000) 743–749

POLYHEDRON

Synthesis, spectroscopic and structural characterisation of copper, silver and gold complexes of the mixed P/O-donor ligand $Ph_2P(CH_2)_2O(CH_2)_2O(CH_2)_2PPh_2$

Bjorn Heuer, Simon J.A. Pope, Gillian Reid *

Department of Chemistry, University of Southampton, Highfield, Southampton SO17 1BJ, UK

Received 8 September 1999; accepted 3 January 2000

Abstract

Reaction of L^1 ($L^1 = Ph_2P(CH_2)_2O(CH_2)_2O(CH_2)_2PPh_2$) with $[Cu(MeCN)_4]PF_6$ or $AgBF_4$ in CH_2Cl_2 solution yields the complexes $[Cu(L^1)]PF_6$ and $[Ag(L^1)]BF_4$ respectively as white solids. Spectroscopic measurements are consistent with coordination via the P-donors and the crystal structure of $[Ag(L^1)]BF_4$ confirms that L^1 acts as a *trans*-chelate giving an unusual example of approximately linear P_2-coordination at Ag(I) ($\angle$P–Ag–P = 164.66(4)°) and, despite the availability and proximity of the ether O atoms, these remain essentially uncoordinated (Ag···O = 2.95 Å), thus reflecting the low affinity of the soft Ag(I) ion for hard O-donor ligands. $[AuCl(tht)]$, L^1 and $TlPF_6$ react in a 1:1:1 molar ratio in MeCN solution to yield the analogous Au(I) species $[Au(L^1)]PF_6$, the structure of which also shows linear P_2-coordination and once again the O-donors are non-coordinating, at a distance of ca. 3.16 Å from Au(I). The neutral dinuclear species $[(AuCl)_2(L^1)]$ is readily formed by reaction of $[AuCl(tht)]$ with L^1 in a 2:1 molar ratio in MeCN. Confirmation of the coordinated Cl ligands comes from IR spectroscopy, ν(Au–Cl) = 324 cm^{-1}, and $\delta(^{31}P)$ which is indicative of a PCl donor set at Au(I). This arrangement is confirmed in the solid state from the crystal structure. The related phosphathia complex $[(AuBr)_2(L^2)]$ ($L^2 = Ph_2P(CH_2)_2S(o\text{-}C_6H_4)S(CH_2)_2PPh_2$) is prepared similarly from $[AuBr(tht)]$ and L^2 in MeCN solution and its structure reveals the AuBr units each coordinated to one P-donor and directed to the same side as the *o*-C_6H_4 unit. ©2000 Elsevier Science Ltd All rights reserved.

Keywords: Copper complexes; Silver complexes; Gold complexes

1. Introduction

Our interest in multidentate mixed P/S-, P/N- and P/O-donor ligands, in which the phosphine functions are located at the termini, stems mainly from the fact that complexes of these ligands offer a wide structural diversity, and incorporation of two different donor types within a single ligand may lead to unusual properties. Phosphine ligation may enhance the binding properties of the poorer thioether functions or of the hard amine or ether functions or, alternatively, these functions may simply act as spacers between the phosphines. To date, our work has mainly focused on the phosphathia ligands and we have shown, for example, that $Ph_2P(CH_2)_2S(CH_2)_2S(CH_2)_2PPh_2$ (L^3) coordinates to Pt(II) and Pt(IV) via both the P and the S donor atoms in $[Pt(L^3)]^{2+}$ and $[PtX_2(L^3)]^{2+}$, generating square planar and octahedral species respectively [1]. In contrast, in the Au(I) species $[Au(L^3)]PF_6$ we observe primary P_2-coordination, with weak interactions to the thioether donors at ca. 3.0 Å. L^3 can also act as a bridging ligand, e.g. in $[Au_2(L^3)_2]Cl_2$, which adopts a helical metallocyclic cavity which hosts one of the Cl^- anions [2–4]. In view of the unusual structures adopted by these phosphathia ligand complexes we were interested to investigate the effect of substituting the thioether functions for the much harder ether functions, since the combination of hard and soft donors may lead to other unusual characteristics. A variety of transition metal complexes of the mixed P/O-donor ligand $Ph_2P(CH_2)_2O(CH_2)_2O(CH_2)_2PPh_2$ (L^1) are known, including *cis*- and *trans*-$[MX_2(L^1)]$ (M = Ni, Pd or Pt, X = Cl, Br or I) [5–7], and the Rh(I) species $[Rh(L^1)(EtOH)(CO)]PF_6$ [8]. Gray and co-workers have also investigated metallocyclic species containing the related P_2O_n-donor ligands L ($L = Ph_2P\{(CH_2)_2O\}_n(CH_2)_2PPh_2$, n = 3–5), e.g. *cis*-$[Mo(CO)_4(L)]$ [9], which involve bidentate P_2-coordination with the O-donors non-coordinating. The Pt(II) species $[PtX_2(L)]$ also show P_2-coordination and treatment of these species with a halide abstractor affords the species $[Pt(H_2O)(L)]^{2+}$, which involve coordination of L

* Corresponding author. Tel.: +44-1703-593609; fax: +44-1703-593781; e-mail: gr@soton.ac.uk

0277-5387/00/$ - see front matter ©2000 Elsevier Science Ltd All rights reserved.
PII S0277-5387(00)00291-6

to Pt(II) via both P-donor atoms and one ether O-donor [10]. The closely related metallocrown ether complex $[PdX_2\{Ph_2P(CH_2CH_2O)_4CH_2CH_2PPh_2\text{–}P,P'\}]_n$ (X = Cl or I) shows a unique and reversible mode of molecular recognition in which PdX_2 units are incorporated into the metallocrown ether ring via a ring-expansion [11].

We describe herein the preparation and characterisation of a series of transition metal complexes incorporating the mixed P/O-donor ligand L^1, including the crystal structures of $[Ag(L^1)]BF_4$, $[Au(L^1)]PF_6$ and $[(AuCl)_2(L^1)]$. The crystal structure of the phosphathia ligand complex $[(AuBr)_2(L^2)]$ is also included.

2. Results and discussion

The ligand L^1 was prepared using a modification of the literature procedure [6]. $LiPPh_2$ was generated in situ by reaction of Li metal with PPh_3 in thf solution. The LiPh byproduct was then destroyed by addition of ^tBuCl and $Cl(CH_2)_2O(CH_2)_2O(CH_2)_2Cl$ was added. The resulting mixture was refluxed for 1 h. After work-up and recrystallisation of the product from CH_2Cl_2/hexane, L^1 was obtained in good yield. When the reaction was attempted without refluxing, $^{31}P\{^1H\}$ NMR studies showed considerable amounts of starting material, along with some mono-substituted product and traces of L^1.

Treatment of $[Cu(MeCN)_4]PF_6$ with one molar equivalent of L^1 in CH_2Cl_2 solution, followed by precipitation with Et_2O, yields a white solid. Electrospray mass spectrometry shows peaks at 549 and 551 indicative of $[^{63/65}Cu(L^1)]^+$, with no significant peaks at higher *m/z*. The IR spectrum shows no evidence for any remaining coordinated MeCN, but peaks corresponding to coordinated L^1 and free PF_6^- are clearly evident. ^1H NMR spectroscopy and microanalyses are consistent with the formulation $[Cu(L^1)]PF_6$ for the product. The $^{31}P\{^1H\}$ NMR spectrum shows a singlet at −16.2 ppm (broadened owing to direct bonding to quadrupolar $^{63/65}Cu$) arising owing to the coordinated L^1 and a septet due to the PF_6^- anion centred at −146 ppm. The NMR spectra were recorded using thoroughly degassed solvents, since upon the introduction of air to the solution the $^{31}P\{^1H\}$ NMR spectrum also shows a resonance at +29.5 due to oxidised phosphine. These data indicate the formulation $[Cu(L^1)]PF_6$ for the product, and suggest that coordination to Cu(I) is via the P-donors.

The corresponding Ag(I) species, $[Ag(L^1)]BF_4$, was obtained as a white, light-sensitive solid by reaction of $AgBF_4$ with L^1 in MeCN in a foil-wrapped flask, followed by concentration of the solution and addition of Et_2O. The IR spectrum shows peaks indicative of coordinated L^1 as well as peaks at ca. 1053 and 525 cm^{-1}, corresponding to free BF_4^- anion. The APCI mass spectrum shows peaks at *m/z* 593 and 595, corresponding to $[^{107/109}Ag(P_2O_2)]^+$. These data, together with ^1H NMR spectroscopic and microanalytical data, indicate the formulation $[Ag(L^1)]BF_4$ for the product. The $^{31}P\{^1H\}$ NMR spectrum of this species shows (Fig. 1) two doublets at −3.4 ppm with $^1J(^{109}Ag\text{–}P) = 601$ Hz and $^1J(^{107}Ag\text{–}P) = 523$ Hz. These data are consistent with coordination of L^1 to Ag(I) via the two P-donor atoms [12]. The coupling constants for this species are larger than those observed for the phosphathia ligand analogues, e.g. $[Ag\{Ph_2P(CH_2)_2S(CH_2)_2S(CH_2)_2PPh_2\}]^+$ which gave $^1J(^{109}Ag\text{–}P) = 510$ Hz and $^1J(^{107}Ag\text{–}P) = 445$ Hz [2–4], although the $^1J(^{107}Ag\text{–}P)$:$^1J(^{109}Ag\text{–}P)$ ratio of 0.87 is the same, and this is consistent with the ratio expected from the respective nuclear magnetic moments of the two nuclei. $^1J(^{107}Ag\text{–}P)$ for the two-coordinate species $[Ag\{P(tol)_3\}]_2PF_6$ and $[Ag(P^tBu_3)_2]BF_4$ are reported as 496 and 444 Hz respectively [12,13], while the crystallographically authenticated two-coordinate $[Ag\{P(NMe_2)_3\}_2]$-BPh_4 shows $^1J(^{107}Ag\text{–}P) = 610$ Hz [14].

In order to confirm the 1:1 Ag:L^1 stoichiometry and to establish unequivocally the coordination mode of L^1 to Ag(I), a single crystal structure determination was undertaken. The crystal structure of $[Ag(L^1)]BF_4$ confirms (Fig. 2, Table 1) that L^1 functions essentially as a *trans*-chelating ligand, giving an approximately linear arrangement at Ag(I) with $d(Ag\text{–}P) = 2.402(1)$ Å, and with a P–Ag–P angle of 164.66(4)°. The Ag···O distances of ca. 2.95 Å are possibly indicative of very weak interactions, but are probably simply a consequence of the bite angle of the diphosphine unit in L^1. Both the large P–Ag–P angle and the observation that the P, O and Ag atoms are approximately co-planar, provide strong evidence that the O-donor atoms are not coordinating. L^1 is expected to be sufficiently flexible to accommodate a distortion towards the tetrahedral geometry usually favoured by four coordinate Ag(I). Both the cation and the BF_4^- anion have crystallographic two-fold symmetry, with the Ag and B atoms sitting on two-fold axes. Although Ag(I) has a much greater affinity for soft donor atoms such as phosphines rather

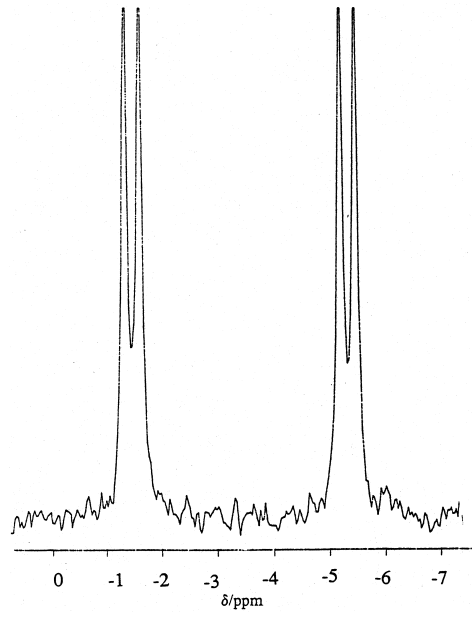


Fig. 1. $^{31}P\{^1H\}$ (145.8 MHz, $CDCl_3$) NMR spectrum of $[Ag(L^1)]BF_4$.

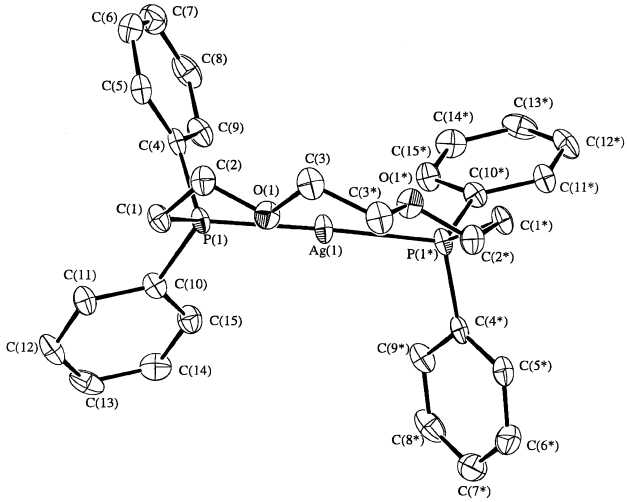


Fig. 2. View of the structure of $[Ag(L^1)]^+$ with the numbering scheme adopted. Atoms marked * are related by a crystallographic two-fold axis. Ellipsoids are drawn at the 40% probability level and H atoms are omitted for clarity.

Table 1
Selected bond lengths (Å) and angles (°) for $[Ag(L^1)]BF_4$

Ag(1)–P(1)	2.402(1)
P(1)–Ag(1)–P(1*)	164.66(4)
Ag(1)–P(1)–C(1)	113.9(1)
Ag(1)–P(1)–C(4)	109.0(1)
Ag(1)–P(1)–C(10)	116.8(1)

than hard ether functions, significant Ag–O(ether) interactions have been observed, for example, in the mixed thia/oxa macrocyclic species $[Ag_n([15]aneS_2O_3)_n](PF_6)_n$ ([15]aneS_2O_3 = 1,4,7-trioxa-10,13-dithiacyclopentadecane) (Ag–O = 2.492(4)–2.690(4) Å) [15] and $\{[Ag_2([18]aneS_2O_4)_2]_2\}(PF_6)_4$ ([18]aneS_2O_4 = 1,4,7,10-tetraoxa-13,16-dithiacyclohexadecane) (Ag–O = 2.458(7)–2.661(6) Å) [16], hence there is no inherent reason for the O-donors not interacting with the Ag(I) ion. Only two mononuclear Ag(I) complexes involving genuine P_2-coordination have been structurally characterised previously, [Ag(trimesitylphosphine)$_2$]PF_6 (P–Ag–P = 179.4(5)°, Ag–P = 2.461(6) Å) [17,18] and $[Ag\{P(NMe_2)_3\}_2]BPh_4$ (P–Ag–P = 166.9(1)°, Ag–P = 2.395(2), 2.393(2) Å) [14]. Several bis(phosphine)–silver(I) species involving ClO_4^- or NO_3^- are known, although these also involve coordination via the O-donors of the anions and this results in a much smaller P–Ag–P angle, e.g. $[Ag\{PPh_2(C_5H_9)\}_2]ClO_4$, Ag–P = 2.397(2)–2.432(2) Å, Ag···O = 2.662(5), 2.709(5) Å, ∠P–Ag–P = 145.1(1), 153.0(1)° [19], $[Ag(PCy_3)_2(NO_3)]$, Ag–P = 2.440(3), 2.445(3) Å, Ag–O = 2.45(1), 2.73(1) Å, ∠P–Ag–P = 139.04(9)° [20], $[Ag(PCy_3)_2]ClO_4$, Ag–P = 2.429(1), 2.432(1) Å, Ag···O = 2.720(7) Å, ∠P–Ag–P = 147.34(3)° [20].

Reaction of L^1 with [AuCl(tht)] in a 2:1 molar ratio in MeCN gave the neutral dinuclear species $[(AuCl)_2(L^1)]$ which was isolated by precipitation with Et_2O from a concentrated solution. The IR spectrum confirms the presence of L^1 and a peak at 327 cm^{-1} is attributed to ν(Au–Cl). This compares with 324 cm^{-1} for $[(AuCl)_2(L^2)]$ [2–4]. The APCI mass spectrum shows peaks with the correct isotopic distribution at *m/z* 915, corresponding to $[Au_2(L^1)Cl]^+$. Further peaks at lower *m/z* correspond to loss of Cl or Au from the complex. The $^{31}P\{^1H\}$ NMR spectrum shows a single resonance at +23.3 ppm, which is comparable with $\delta(^{31}P)$ for the previously synthesised $[(AuCl)_2(L^2)]$ (25.3 ppm) [2–4].

The crystal structure of $[(AuCl)_2(L^1)]$ shows (Fig. 3, Table 2) each gold atom coordinated to one P-donor from L^1 and one Cl ligand, giving essentially linear coordination, with no interaction between the Au centres and the O-donor atoms. The Cl–Au–P angles are 174.2(2) and 174.1(3)°. The L^1 backbone adopts a twisted conformation with the AuCl units pointing in the same direction.

We have reported previously the preparation and spectroscopic characterisation of the species $[(AuCl)_2(L)]$ ($L = L^2$, L^3 or L^4) ($L^4 = Ph_2P(CH_2)_2S(CH_2)_3S(CH_2)_2PPh_2$) although their structures were not authenticated crystallographically [2–4]. In order to provide a comparison with

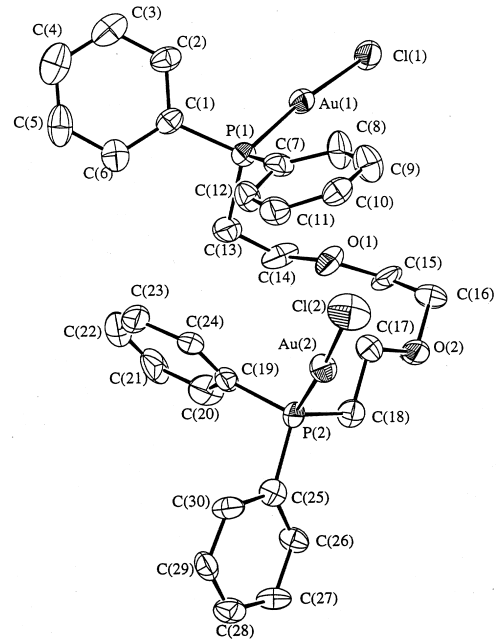


Fig. 3. View of the structure of $[(AuCl)_2(L^1)]$ with numbering scheme adopted. Ellipsoids are drawn at 40% probability and H atoms are omitted for clarity.

Table 2
Selected bond lengths (Å) and angles (°) for $[(AuCl)_2(L^1)]$

Au(1)–Cl(1)	2.295(5)	Au(1)–P(1)	2.231(5)
Au(2)–Cl(2)	2.279(5)	Au(2)–P(2)	2.219(5)
Cl(1)–Au(1)–P(1)	174.2(2)	Cl(2)–Au(2)–P(2)	174.1(3)
Au(1)–P(1)–C(1)	113.7(6)	Au(1)–P(1)–C(7)	112.9(8)
Au(1)–P(1)–C(13)	110.8(8)	Au(2)–P(2)–C(19)	110.7(7)
Au(2)–P(2)–C(18)	113.4(7)		
Au(2)–P(2)–C(25)	115.5(6)		

$[(AuCl)_2(L^1)]$ above, we have prepared the species $[(AuBr)_2(L^2)]$ similarly from L^2 and [AuBr(tht)] in MeCN. The Au–Br stretching vibration occurs at 315 cm^{-1} for this species and $\delta(^{31}P)$ occurs as a singlet at 28.0 ppm, consistent with coordination of an AuBr fragment to each P-donor of L^2. A single crystal X-ray structure determination was also undertaken on a weakly diffracting crystal of $[(AuBr)_2(L^2)]$. The structure shows (Fig. 4) a dinuclear molecule with each Au(I) ion coordinated linearly to one P-donor from L^2 and one Br atom, with the S-donor atoms remaining non-coordinating. The molecule has crystallographic C_2 symmetry and the Au–P distances of 2.16(1) Å are slightly shorter than those in $[(AuCl)_2(L^1)]$ above, although since the structure quality is rather poor, geometric parameters should be treated with caution. The P–Au–Br angle is 177.5(4)°. The L^2 backbone adopts an approximately planar arrangement and the AuBr units lie on the same side of the backbone as the *o*-phenylene unit.

The 1:1 Au:L^1 complex, $[Au(L^1)]PF_6$ was prepared readily by treatment of [AuCl(tht)] with one molar equivalent of L^1 and $TlPF_6$ in MeCN to give a white precipitate (TlCl) and a colourless solution. Following removal of the TlCl by filtration through Celite, concentration of the solution and addition of Et_2O, a white precipitate was obtained. The IR spectrum of this product provides evidence for the presence of L^1 and PF_6^- (840, 555 cm^{-1}), and there is no evidence for an Au–Cl stretching vibration. The highest mass peak in the APCI mass spectrum appears at *m/z* 683, corresponding to $[Au(L^1)]^+$. These data, together with ^1H NMR spectroscopic and microanalytical data, suggest the formulation $[Au(L^1)]PF_6$ for the product. The $^{31}P\{^1H\}$ NMR resonance due to the coordinated L^1 occurs at 32.5 ppm, i.e. a higher frequency than that for $[(AuCl)_2(L^1)]$, and is indicative of a P_2-donor set at Au(I). The septet due to the PF_6^- anion occurs at −146.0 ppm.

This crystal structure of $[Au(L^1)]PF_6$ shows (Fig. 5, Table 3) L^1 acting as a *trans*-chelating ligand, bonded to Au(I) by the two P-donors (Au–P = 2.308(2), 2.311(2) Å), with the Au···O distances ca. 3.15 Å indicating no interaction, and demonstrating the indifference of Au(I) towards the hard O-donor atoms. Thus, this geometry is similar to that observed for $[Ag(L^1)]^+$ above. The Au–P distances in this cation are slightly shorter than the Ag–P distances in $[Ag(L^1)]^+$ and the P–Au–P angle of 171.85(9)° is larger than the corresponding P–Ag–P angle in the analogous Ag(I) species. Schmidbaur and co-workers have previously demonstrated that for the isomorphous species [Ag(trimesitylphosphine)$_2$]BF_4 and [Au(trimesitylphosphine)$_2$]BF_4, d(Ag–P) > d(Au–P) by almost 0.1 Å [18]; a similar trend is observed here. The structure of the analogous phosphathia complex $[Au(L^2)]PF_6$ shows similar primary Au–P interactions of 2.284(7) and 2.302(7) Å, although in this case long-range, weak Au···S interactions of ca. 3.0 Å are also observed in the solid state [2–4].

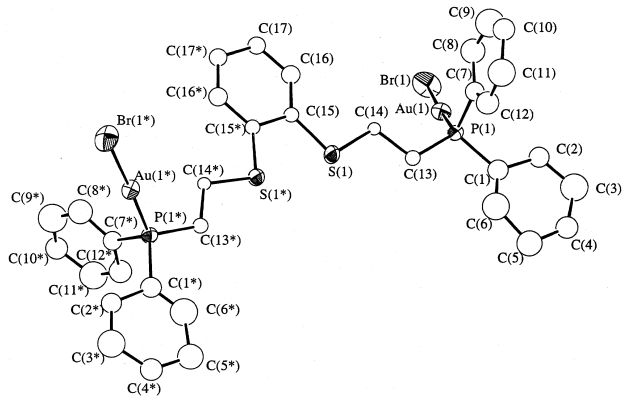


Fig. 4. View of the structure of $[(AuBr)_2(L^2)]$ with numbering scheme adopted. Ellipsoids are drawn at 40% probability. Atoms marked * are related by a crystallographic two-fold axis and H atoms are omitted for clarity. Au(1)–P(1) = 2.16(1) Å, ∠P(1)–Au(1)–Br(1) = 177.5(4)°.

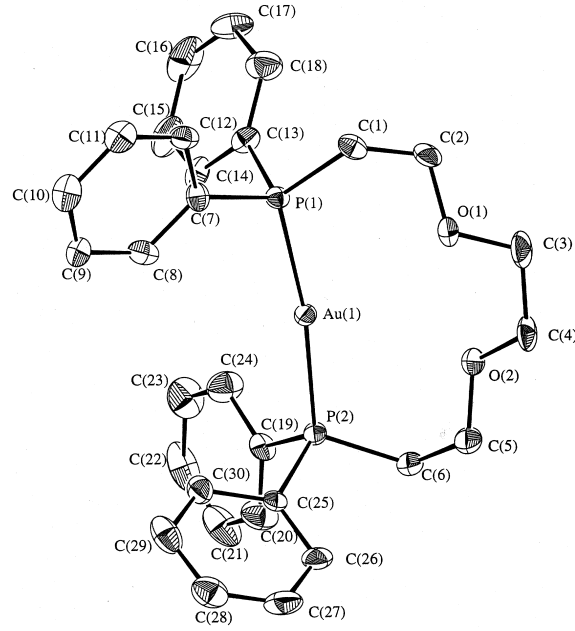


Fig. 5. View of the structure of $[Au(L^1)]^+$ with numbering scheme adopted. Ellipsoids are drawn at 40% probability and H atoms are omitted for clarity.

Table 3
Selected bond lengths (Å) and angles (°) for $[Au(L^1)]PF_6$

Au(1)–P(1)	2.308(2)	Au(1)–P(2)	2.311(2)
P(1)–Au(1)–P(2)	171.85(9)	Au(1)–P(1)–C(1)	117.4(3)
Au(1)–P(1)–C(7)	113.5(3)	Au(1)–P(1)–C(13)	107.9(3)
Au(1)–P(2)–C(6)	115.5(3)	Au(1)–P(2)–C(19)	114.3(3)
Au(1)–P(2)–C(25)	109.2(3)		

3. Experimental

Infrared spectra were recorded as KBr or CsI disks using a Perkin-Elmer 983 spectrometer over the range 4000–200 cm^{-1}. Mass spectra were run by positive electrospray or by APCI (atmospheric pressure chemical ionisation) in MeCN solution using a VG Biotech platform. ^1H and $^{13}C\{^1H\}$ NMR spectra were recorded in $CDCl_3$ using a Bruker AM300 spec-

trometer. $^{31}P\{^{1}H\}$ NMR spectra were recorded in CH_2Cl_2 containing ca. 10–15% $CDCl_3$ using a Bruker AM360 spectrometer operating at 145.8 MHz and are referenced to 85% H_3PO_4. Microanalyses were performed by the University of Strathclyde microanalytical service. L^2 was prepared according to the literature procedure [6].

3.1. Preparations

L^1: PPh_3 (30 g, 114 mmol) was dissolved in dry, degassed thf (300 cm^3) and freshly crushed Li (3 g, 432 mmol) was added in small pieces at room temperature. This reaction mixture was stirred for 12 h, before the remaining pieces of lithium were filtered off. ^{t}BuCl (9.9 cm^3, 91 mmol) was added dropwise and the mixture was stirred for 1 h at room temperature. $Cl((CH_2)_2O)_2(CH_2)_2Cl$ (7.5 cm^3, 0.4 equiv., 46 mmol) was added slowly and the mixture was heated to reflux for 1 h until it decolourised and a white precipitate formed. After cooling, degassed water (30 cm^3) was added dropwise. The organic layer was separated, the aqueous layer was washed with Et_2O and the combined organic extracts were dried over $MgSO_4$. The $MgSO_4$ was filtered off under nitrogen and the solvent was removed in vacuo. The residue was taken up in a small amount of CH_2Cl_2, then hexane was added. The mixture was stirred for a few minutes and subsequent cooling yielded a white precipitate which was filtered and dried in vacuo. Yield 10.7 g, 39%. *Anal*. Calc. for $C_{30}H_{32}O_2P_2$: C, 74.1; H, 6.6. Found: C, 73.7; H, 6.9%. ^{1}H NMR: δ 7.41–7.52 (m, 20H, Ph), 3.58 (m, 4H, OCH_2), 3.51 (s, 4H, OCH_2), 2.40 (m, 4H, CH_2P) ppm. $^{13}C\{^{1}H\}$ NMR: δ 28.9 (CH_2P), 68.7 (*C*H_2CH$_2$P), 70.2 (OCH_2CH_2O), 128.6 (*para*-C), 128.8 (*meta*-C), 132.8 (*ortho*-C), 138.5 (*ipso*-C) ppm. $^{31}P\{^{1}H\}$ NMR: δ −21.3.

$[Cu(L^1)]PF_6$: L^1 (0.100 g, 0.206 mmol) was dissolved in CH_2Cl_2 (30 cm^3) and $[Cu(CH_3CN)_4]PF_6$ (0.077 g, 0.206 mmol) was added in one portion. The mixture was stirred for 1 h and the volume was reduced to ca. 2 cm^3 in vacuo. Et_2O was then added to afford a white solid which was collected by filtration and dried in vacuo. Yield 0.085 g, 60%. *Anal*. Calc. for $C_{30}H_{32}O_2P_3F_6Cu$: C, 51.8; H, 4.6. Found: C, 52.4; H, 4.6%. ^{1}H NMR: δ 7.17–7.49 (m, 20H, Ph), 3.62–3.77 (m, 8H, CH_2), 2.59 (m, 4H, CH_2) ppm. $^{31}P\{^{1}H\}$ NMR: δ −16.2 (s, L^1), −146.2 (spt, PF_6^-) ppm. APCI mass spectrum: found *m/z* 551, 549, 487; calc. for $[^{65}Cu(L^1)]^+$ *m/z* 551, $[^{63}Cu(L^1)]^+$ 549, $[L^1]^+$ 486. IR spectrum (CsI disk): 3058w, 2985w, 2922w, 2873w, 1574w, 1485m, 1438s, 1403w 1360m, 1310w, 1161m, 1133s, 1101s, 999m, 841vs, 744s, 696s, 558m, 508m, 478m cm^{-1}.

$[Ag(L^1)]BF_4$: To a degassed solution of L^1 (0.100 g, 0.206 mmol) in MeCN (20 cm^3) at 0°C was added $AgBF_4$ (0.040 g, 0.206 mmol) and the resulting mixture was stirred for 1 h at room temperature in a foil-wrapped flask. The solution was then concentrated in vacuo to ca. 5 cm^3 and Et_2O was added to afford a white solid which was filtered, washed with Et_2O and dried in vacuo. Yield 0.096 g, 69%. *Anal*. Calc. for $[C_{30}H_{32}AgBF_4O_2P_2]$: C, 52.9; H, 4.7. Found: C, 52.6; H, 4.4%. Electrospray mass spectrum (MeCN): found *m/z* 595, 593, 487; calc. for $[^{109}Ag(L^1)]^+$ *m/z* 595, $[^{107}Ag(L^1)]^+$ 593, $[L^1]^+$ 486. ^{1}H NMR: δ 7.4–7.7 (m, Ph, 20H), 3.7 (m, CH_2O, 8H), 2.8 (m, CH_2P, 4H). $^{31}P\{^{1}H\}$ NMR: δ –3.4 (d, $^1J^{109}(Ag–^{31}P) = 601$ Hz, d, $^1J^{107}(Ag–^{31}P) = 523$ Hz). IR spectrum (CsI disk): 3055w, 2960w, 2917w, 2869w, 1572w, 1481m, 1461w, 1434m, 1410w, 1365m, 1350m, 1309w, 1284w, 1099s, 1053s, 1005s, 998s, 976w, 885m, 856m, 790w, 760s, 746s, 712m, 698s, 692s, 673w, 525m cm^{-1}.

$[Au(L^1)]PF_6$: To a solution of L^1 (0.100 g, 0.206 mmol) in degassed MeCN (20 cm^3) was added [AuCl(tht)] (0.066 g, 0.206 mmol). After stirring this mixture for 15 min, $TlPF_6$ (0.072 g, 0.206 mmol) was added and the reaction mixture was stirred for ca. 12 h. The resulting white precipitate (TlCl) was removed by filtration and the filtrate was concentrated in vacuo. Addition of Et_2O gave a white precipitate which was filtered, washed with Et_2O and dried in vacuo. Yield 0.054 g, 32%. *Anal*. Calc. for $[C_{30}H_{32}AuF_6O_2P_3]$: C, 43.5; H, 3.9. Found: C, 43.5; H, 3.6%. Electrospray mass spectrum (MeCN): found *m/z* 683, 487; calc. for $[Au(L^1)]^+$ *m/z* 683, $[L^1]^+$ 486. ^{1}H NMR: δ 7.5–7.8 (m, Ph, 20H), 3.8 (m, CH_2O, 4H), 3.6 (s, CH_2O, 4H), 2.9 (m, CH_2P, 4H). $^{31}P\{^{1}H\}$ NMR: δ 32.5 (s, L^1), −146.0 (spt, PF_6^-). IR spectrum (CsI disk): 3061w, 2980w, 2925w, 2866w, 1560w, 1482m, 1458w, 1435s, 1406w, 1362m, 1227w, 1186w, 1134s, 1114m, 1104s, 1063m, 1012m, 836vs, 789m, 744m, 713s, 696s, 690s, 558s, 529m, 509m 463m, 438w cm^{-1}.

$[(AuCl)_2(L^1)]$: To a solution of L^1 (0.100 g, 0.206 mmol) in degassed MeCN (30 cm^3) was added [AuCl(tht)] (0.130 g, 0.411 mmol). The mixture was stirred for 1 h before being concentrated in vacuo. Et_2O was then added to yield a white solid which was filtered, washed with Et_2O and dried in vacuo. Yield 0.060 g, 31%. *Anal*. Calc. for $[C_{30}H_{32}Au_2Cl_2O_2P_2]$: C, 37.9; H, 3.4. Found: C, 38.0; H, 3.4%. Electrospray mass spectrum (MeCN): found *m/z* 915, 683, 487; calc. for $[Au_2{}^{35}Cl(L^1)]^+$ *m/z* 915, $[Au(L^1)]^+$ 683, $[L^1]^+$ 486. ^{1}H NMR: δ 7.4–7.8 (m, Ph, 20H), 3.8 (m, CH_2O, 4H), 3.5 (s, CH_2O, 4H), 2.8 (m, CH_2P, 4H). $^{31}P\{^{1}H\}$ NMR: δ +23.3 (s, L^1). IR spectrum (CsI disk): 3049w, 2945w, 2911w, 2857w, 1560w, 1482m, 1433s, 1395w, 1368m, 1351m, 1289w, 1158w, 1129s, 1100s, 1009m, 998w, 980m, 905w, 864w, 763m, 744s, 698s, 690s, 544m, 525m, 487m, 476w, 327m cm^{-1}.

$[(AuBr)_2(L^2)]$: To a solution of L^2 (0.08 g, 0.0141 mmol) in degassed MeCN (30 cm^3) was added [AuBr(tht)] (0.103 g, 0.242 mmol). The resulting mixture was stirred for 1 h. The reaction volume was concentrated to 2 cm^3 in vacuo and Et_2O was added to give a white solid. Yield 0.115 g, 73%. *Anal*. Calc. for $[C_{34}H_{32}Au_2Br_2P_2S_2]\cdot Et_2O$: C, 38.1; H, 3.3. Found: C, 37.8; H, 3.0%. Electrospray mass spectrum (MeCN): found *m/z* 763, 566; calc. for $[Au(L^2)]^+$ *m/z* 763, $[L^2]^+$ 566. ^{1}H NMR: δ 7.1–7.7 (m, aromatic H, 24H), 2.6–3.2 (m, CH_2S, 8H). $^{31}P\{^{1}H\}$ NMR: δ 28.0 (s, L^1). IR spectrum (Nujol mull): 315 cm^{-1}.

Table 4
Crystallographic data

	$[Ag(L^1)]BF_4$	$[Au(L^1)]PF_6$	$[(AuCl)_2(L^1)]$	$[(AuBr)_2(L^2)]\cdot 2CH_2Cl_2$
Formula	$C_{30}H_{32}AgBF_4O_2P_2$	$C_{30}H_{32}AuF_6O_2P_3$	$C_{30}H_{32}Au_2Cl_2O_2P_2$	$C_{36}H_{32}Au_2Br_2Cl_4P_2S_2$
M	681.20	828.46	951.37	1286.27
Crystal system	monoclinic	triclinic	monoclinic	monoclinic
Space group	$C2/c$	$P\text{-}1$	Pn	$C2$
a (Å)	15.822(7)	10.670(3)	9.285(2)	13.203(5)
b (Å)	13.157(7)	15.458(4)	11.905(2)	13.038(4)
c (Å)	15.76(1)	10.135(3)	14.276(1)	12.250(6)
α (°)	90	107.97(2)	90	90
β (°)	118.11(5)	97.75(3)	96.54(1)	95.02(3)
γ (°)	90	75.39(2)	90	90
U (Å^3)	2894(3)	1535.6(8)	1567.8(5)	2100(1)
Z	4	2	2	2
μ(Mo Kα) (cm^{-1})	8.58	50.27	96.16	93.64
Transmission factors (max. and min.)	1.000, 0.850	1.000, 0.667	1.000, 0.490	1.000, 0.499
Unique observed reflections	5112	5400	2917	3973
R_{int} (based on F^2)	0.075	0.050	0.064	0.170
Observed reflections with $I_o > n\sigma(I_o)$	4469, $n=2$	4191, $n=2$	2169, $n=2$	1118, $n=2$
No. of parameters	182	379	343	117
R [a]	0.053	0.045	0.035	0.063
R_w [b]	0.073	0.057	0.040	0.069

[a] $R = \sum(|F_{obs}|_i - |F_{calc}|_i)/\sum|F_{obs}|_i$.
[b] $R_w = \sqrt{[\sum w_i(|F_{obs}|_i - |F_{calc}|_i)^2/\sum w_i|F_{obs}|_i^2]}$.

3.2. X-Ray crystallography

Details of the crystallographic data collection and refinement parameters are given in Table 4. The crystals were grown by vapour diffusion of diethyl ether onto solutions of the complexes in CH_2Cl_2 at ca. −15°C or by slow evaporation from a solution of the complex in CH_2Cl_2/EtOH ($[Ag(L^1)]BF_4$). Data collection used a Rigaku AFC7S four-circle diffractometer equipped with an Oxford Systems open-flow cryostat operating at 150 K, using graphite-monochromated Mo Kα X-radiation ($\lambda = 0.71073$ Å). The structures were solved by heavy atom methods [21] and developed by iterative cycles of full-matrix least-squares and difference Fourier synthesis [22]. The weighting scheme $w^{-1} = \sigma^2(F)$ gave satisfactory agreement analyses.

$[Ag(L^1)]BF_4$: During data collection an 8.2% decrease in the intensity of the standard reflections was observed and hence a linear decay correction was applied. The initial cell was triclinic, and was solved to reveal one $[Ag(L^1)]^+$ cation and one BF_4^- anion occupying general positions. However, further analysis suggested a C-centred monoclinic cell, which was solved to reveal a half $[Ag(L^1)]^+$ cation and half BF_4^- anion, both with crystallographic two-fold symmetry. Although the final residuals for the monoclinic version are slightly higher ($R = 0.053$ versus 0.045) than for the triclinic solution, it does appear that the correct solution is as monoclinic C-centred. All non-H atoms were refined anisotropically while H-atoms were placed in fixed, calculated positions. Selected bond lengths and angles are given in Table 1.

$[Au(L^1)]PF_6$: All non-H atoms were refined anisotropically while H-atoms were placed in fixed, calculated positions. Selected bond lengths and angles are given in Table 3.

$[(AuCl)_2(L^1)]$: All non-H atoms were refined anisotropically and H atoms were included in fixed, calculated positions. Selected bond lengths and angles are given in Table 2.

$[(AuBr)_2(L^2)]\cdot 2CH_2Cl_2$: The data were collected from a weakly diffracting crystal, hence the structure quality is not as high as normal. The molecule possesses crystallographic C_2 symmetry and hence only half the molecule is present in the asymmetric unit. A CH_2Cl_2 solvent molecule was also identified in the asymmetric unit. At isotropic convergence a DIFABS [23] absorption correction was applied. In view of the weak data, only the Au, Br, S and P atoms were refined anisotropically. The H atoms were included in fixed, calculated positions.

Supplementary data

Supplementary data are available from the Cambridge Crystallographic Data Centre, 12 Union Road, Cambridge CB2 1EZ, UK (fax: +44-1223-336033; e-mail: deposit@ccdc.cam.ac.uk) on request, quoting the deposition numbers 134142–134145.

Acknowledgements

We thank the EPSRC and the University of Southampton for support and Johnson Matthey plc for generous loans of gold salts. We also thank the crystallographic referee for suggesting the higher symmetry cell for $[Ag(L^1)]BF_4$.

References

[1] J. Connolly, R.J. Forder, G. Reid, Inorg. Chim. Acta 264 (1997) 137.
[2] A.M. Gibson, G. Reid, J. Chem. Soc., Dalton Trans. (1996) 1267.
[3] A.R.J. Genge, A.M. Gibson, N.K. Guymer, G. Reid, J. Chem. Soc., Dalton Trans. (1996) 4099.
[4] C.L. Doel, A.M. Gibson, G. Reid, C.S. Frampton, Polyhedron 14 (1995) 3139.
[5] P. Dapporto, L. Sacconni, J. Chem. Soc. A (1971) 1914.
[6] W.E. Hill, J.G. Taylor, C.A. McAuliffe, K.W. Muir, L. Manojlovic-Muir, J. Chem. Soc., Dalton Trans. (1982) 833.
[7] W.E. Hill, J.G. Taylor, C.P. Falshaw, T.J. King, B. Beagley, D.M. Tonge, R.G. Pritchard, C.A. McAuliffe, J. Chem. Soc., Dalton Trans. (1986) 2289.
[8] N.W. Alcock, J.M. Brown, J.C. Jeffrey, J. Chem. Soc., Dalton Trans. (1976) 583.
[9] A. Varshney, G.M. Gray, Inorg. Chem. 30 (1991) 1748.
[10] A. Varshney, M.L. Webster, G.M. Gray, Inorg. Chem. 31 (1992) 2580.
[11] D.C. Smith, C.H. Lake, G.M. Gray, Chem. Commun. (1998) 2771.
[12] E.L. Muetterties, C.W. Alegranti, J. Am. Chem. Soc. 94 (1972) 6386.
[13] R.G. Goel, P. Pilon, Inorg. Chem. 17 (1978) 2876.
[14] S.M. Socol, R.A. Jacobson, J.G. Verkade, Inorg. Chem. 23 (1984) 88.
[15] A.J. Blake, G. Reid, M. Schröder, J. Chem. Soc., Chem. Commun. (1992) 1074.
[16] A.J. Blake, R.O. Gould, C. Radek, M. Schröder, J. Chem. Soc., Chem. Commun. (1994) 985.
[17] E.C. Alyea, G. Ferguson, A. Smogyvari, Inorg. Chem. 21 (1982) 1369.
[18] A. Bayler, A. Schier, G.A. Bowmaker, H. Schmidbaur, J. Am. Chem. Soc. 118 (1996) 7006.
[19] A. Baiada, F.H. Jardine, R.D. Willett, Inorg. Chem. 29 (1990) 3042.
[20] M. Camalli, F. Caruso, Inorg. Chim. Acta 144 (1988) 205.
[21] P.T. Beurskens, G. Admiraal, G. Beurskens, W.P. Bosman, S. Garcia-Granda, R.O. Gould, J.M.M. Smits, C. Smykalla, PATTY, The DIRDIF Program System, Technical Report of the Crystallography Laboratory, University of Nijmegen, The Netherlands, 1992.
[22] TeXsan, Crystal Structure Analysis Package, Molecular Structure Corporation, TX, 1995.
[23] N. Walker, D. Stuart, Acta Crystallogr., Sect. A 39 (1983) 158.

PERGAMON

www.elsevier.nl/locate/poly

Polyhedron 19 (2000) 751–756

POLYHEDRON

The reactions of $[M(dppe)_2]$ (M = Pd, Pt) with elemental selenium or tellurium: preparation and structure of the platinum polyselenide $[PtSe_4(dppe)]$

Mark R. Lewtas [a], Christopher P. Morley [a,*], Massimo Di Vaira [b]

[a] *Department of Chemistry, University of Wales Swansea, Singleton Park, Swansea SA2 8PP, UK*

[b] *Dipartimento di Chimica, Università degli Studi di Firenze, Via Maragliano 75/77, 50144 Florence, Italy*

Received 1 November 1999; accepted 14 January 2000

Abstract

Reaction of $[Pt(dppe)_2]$ (dppe = 1,2-bis(diphenylphosphino)ethane) with elemental selenium in toluene under reflux, or of $[PtCl_2(dppe)]$ with lithium polyselenide in tetrahydrofuran, leads in good yield to the complex $[PtSe_4(dppe)]$ whose structure has been determined by X-ray crystallography. Reaction of $[Pt(dppe)_2]$ with elemental tellurium, followed by treatment with dichloromethane, leads to isolation of the salt $[Pt_3(\mu_3\text{-}Te)_2(dppe)_3]Cl_2$. $[Pd(dppe)_2]$ reacts with elemental selenium to give $[Pd_2(\mu\text{-}Se)_2(dppe)_2]$ or $[Pd_3(\mu_3\text{-}Se)_2(dppe)_3]Cl_2$, depending on the conditions. ©2000 Elsevier Science Ltd All rights reserved.

Keywords: Palladium; Platinum; Selenium; Tellurium

1. Introduction

Investigations of the reactions of low-valent transition metal compounds with elemental selenium or tellurium are rare [1,2]. We are interested in the use of such reactions for the preparation of metal polychalcogenides, and the reactivity of the products towards activated alkynes to yield diselenolenes or ditellurolenes. These are the selenium and tellurium analogues of dithiolenes, which already have a variety of applications in materials chemistry [3]. The incorporation of heavier chalcogen atoms is an attractive synthetic target since this should lead to a smaller HOMO–LUMO gap, and an increase in the strength of intermolecular interactions in the solid state.

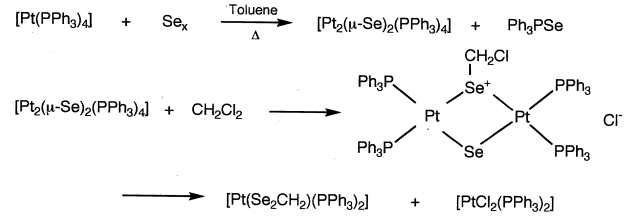
The platinum(0) and palladium(0) complexes $[M(PPh_3)_4]$ and $[M(dppe)_2]$ react with sulfur at room temperature, to yield both tetrasulfides $[MS_4L_2]$ and dinuclear disulfides $[M_2S_2L_4]$, depending on the conditions (Eq. 1) [4,5].

$$[Pt(PPh_3)_4] + S_8 \xrightarrow[RT]{\text{Benzene}} [Pt_2(\mu\text{-}S)_2(PPh_3)_4] + [PtS_4(PPh_3)_2] \quad (1)$$

Further treatment of $[PtS_4(PPh_3)_2]$ with dimethylacetylene dicarboxylate leads to the dithiolene $[Pt\{S_2C_2(CO_2Me)_2\}(PPh_3)_2]$ (Eq. 2) [6].

$$[PtS_4(PPh_3)_2] + MeO_2CC{\equiv}CCO_2Me \xrightarrow[\Delta]{CH_2Cl_2} [Pt\{S_2C_2(CO_2Me)_2\}(PPh_3)_2] \quad (2)$$

We have previously reported the results of the reactions of $[M(PPh_3)_4]$ with selenium. Whilst only decomposition was observed for M = Pd, when M = Pt the product is the dinuclear diselenide $[Pt_2(\mu\text{-}Se)_2(PPh_3)_4]$ [7], which reacts further with dichloromethane to yield a novel methanediselenolate complex (Eq. 3) [8]. No reaction was observed between $[M(PPh_3)_4]$ (M = Pd, Pt) and tellurium.



(3)

We have now studied the analogous reactions of $[M(dppe)_2]$ (M = Pd, Pt) and find significant differences from our work with $[M(PPh_3)_4]$.

* Corresponding author. Tel.: +44-1792-295273; fax: +44-1792-295747; e-mail: c.p.morley@swan.ac.uk

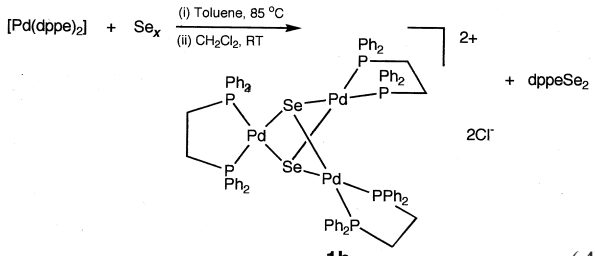
0277-5387/00/$ - see front matter ©2000 Elsevier Science Ltd All rights reserved.
PII S0277-5387(00)00303-X

2. Results and discussion

Heating a toluene solution containing $[Pd(dppe)_2]$ with an excess of powdered vitreous selenium to reflux overnight leads to dissolution of some of the selenium, and formation of a brown–black precipitate. This may be isolated by filtration and purified by treatment with triphenylphosphine, which reacts with any selenium still present. The residue is insoluble in all common organic solvents, but, on the basis of microanalysis, infrared and visible spectroscopy may be identified as $[Pd_2(\mu\text{-}Se)_2(dppe)_2]$ (**1a**), or a polymeric form thereof (Eq. 4a). It is notable that compound **1a**, unlike the analogous compound containing platinum and triphenylphosphine (see above), does not appear to react with dichloromethane.

Carrying out the reaction of $[Pd(dppe)_2]$ with selenium at lower temperature (85°C) leads to a different product. Filtration of the reaction mixture and extraction of the residue with dichloromethane leads to the isolation of compound **1b**, which has been identified as the salt $[Pd_3(\mu_3\text{-}Se)_2(dppe)_3]Cl_2$ (Eq. 4b).

$$[Pd(dppe)_2] + Se_x \xrightarrow[\Delta]{\text{Toluene}} \underset{\mathbf{1a}}{[Pd_2(\mu\text{-}Se)_2(dppe)_2]} + dppeSe_2 \qquad (4a)$$



(4b)

Sulfido species of the type $[M_3(\mu_3\text{-}S)_2(PR_3)_6]^{2+}$ have been reported for: M = Ni, $R_3 = Et_3$ [9]; M = Pd, $R_3 = Me_3$ or $MePh_2$ [10]; M = Pt, $R_3 = Me_2Ph$ [4,11]. Analogous selenides are known only for M = Ni [12,13]. They are usually prepared, either directly or indirectly, via nucleophilic attack of the bridging chalcogenide ligands in $[M_2(\mu\text{-}E)_2(PR_3)_4]$ (E = S or Se) on *cis*-$[MCl_2(PR_3)_2]$. In the case of compound **1b**, the mechanism is presumably similar, with the $[PdCl_2(dppe)]$ being generated in situ by the action of dichloromethane on an unidentified intermediate.

Compound **1b** has been characterised by microanalysis, NMR, UV–Vis and IR spectroscopy, and by mass spectrometry. It is a brown microcrystalline air-stable solid, readily soluble in polar organic solvents. An intense cluster of peaks is observed in the FAB mass spectrum, corresponding to the ion $[Pd_3(\mu_3\text{-}Se)_2(dppe)_3Cl]^+$. The ^{77}Se resonance is at unusually high field (−41 ppm), but chemical shifts for triply bridging selenides are known to cover a wide range, i.e. from 796 ppm for $[CoFe_2(\mu_3\text{-}Se)(\eta\text{-}C_5H_5)(CO)_6]$ [14] to −483 ppm for $[Fe_2Pt(\mu_3\text{-}Se)(CO)_6(PPh_3)_2]$ [15]. Coupling to ^{31}P could not be resolved. Compound **1b** behaves as a 1:2 electrolyte in dichloromethane solution.

The platinum compound $[Pt(dppe)_2]$ reacts with vitreous selenium in a visually similar manner. The product isolated after extraction of the residue with dichloromethane is, however, in this case the polyselenide $[PtSe_4(dppe)]$ (**2**) (Eq. 5).

$$[Pt(dppe)_2] + Se_x \xrightarrow[\Delta]{\text{Toluene}} \underset{\mathbf{2}}{[PtSe_4(dppe)]} + dppeSe_2 \qquad (5)$$

The crystal structure of compound **2** has been determined by X-ray diffraction (Fig. 1). One molecule of the recrystallisation solvent (dichloromethane) was incorporated per four formula units. Selected bond lengths and angles are listed in Table 1. The platinum atom is approximately square planar coordinated. There is, however, a significant distortion of the coordination geometry towards tetrahedral, as indicated by the deviations of the donor atoms from the least-squares plane through the $PtSe_2P_2$ unit: Se(1), −0.04 Å; Se(4), +0.04 Å; P(1), +0.30 Å; P(2), −0.27 Å. This is presumably in part brought about by the need to accommodate the obtuse angle subtended by the polyselenide ligand at the Pt atom, Se(1)–Pt–Se(2) (98.1°), the bite angle of the chelating diphosphine being relatively fixed. A similar distortion has been noted in $[Pt(Se_4)_2]^{2-}$ [16]. Preliminary extended Hückel calculations indicate that electronic factors (relating to the bonding in the Se_4^{2-} fragment) are also important in determining the observed geometry. The Pt–Se and Pt–P bond lengths are similar to those reported previously: e.g.

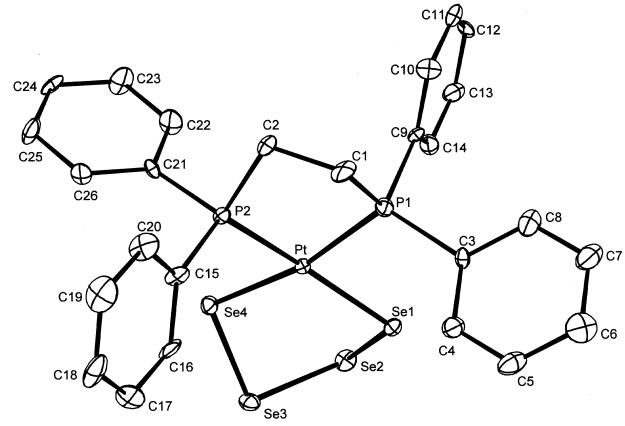


Fig. 1. Molecular stucture of compound **2** in $[PtSe_4(dppe)]\cdot 0.25CH_2Cl_2$.

Table 1
Selected bond lengths (Å) and angles (°) for $[PtSe_4(dppe)]\cdot 0.25CH_2Cl_2$

Pt–P(1)	2.246(5)	Pt–P(2)	2.242(5)
Pt–Se(1)	2.445(3)	Pt–Se(4)	2.448(2)
Se(1)–Se(2)	2.352(3)	Se(2)–Se(3)	2.303(4)
Se(3)–Se(4)	2.338(4)		
P(1)–Pt–Se(1)	89.19(16)	Se(1)–Pt–Se(4)	98.09(8)
Se(4)–Pt–P(2)	87.69(15)	P(2)–Pt–P(1)	86.31(20)
Pt–Se(1)–Se(2)	105.93(10)	Se(1)–Se(2)–Se(3)	97.13(12)
Se(2)–Se(3)–Se(4)	97.50(13)	Se(3)–Se(4)–Pt	104.34(11)

2.426 (av.) Å and 2.282 (av.) Å, respectively, in $[Pt(Se_2CH_2)(PPh_3)_2]$ [8]. There is an alternation amongst the Se–Se distances in the polyselenide ligand, with Se(2)–Se(3) being the shortest (by about 0.04 Å). This is a common feature in the structures of tetraselenide complexes [17].

Compound **2** is a red crystalline, air-stable solid, soluble in a wide range of organic solvents. It has been further characterised by microanalysis, NMR, UV–Vis and IR spectroscopy, and by mass spectrometry. The colour of compound **2** is associated with the tail of an intense UV absorption ($\lambda_{max} = 260$ nm) which has significant intensity up to a wavelength of approximately 470 nm.

Only a single broad resonance at 640 ppm is observed in the ^{77}Se NMR spectrum. This is surprising, as α-Se and β-Se generally have quite different chemical shifts in tetraselenide complexes. For example, the ^{77}Se NMR spectrum of $[Pt(Se_4)_2]^{2-}$ has peaks at 680 and 790 ppm [16]. It may be that the resonance for the metal-bound selenium atoms in compound **2** is not observed as a result of the broadening due to coupling to ^{31}P and ^{195}Pt. The satellite structure of the ^{31}P resonance for compound **2** is shown in Fig. 2(a). The inner lines are due to coupling to ^{13}C. It has not been possible to analyse this spectrum completely, as too few of the eight lines expected for each AA′X pattern have been observed, but the presence of coupling to at least one ^{77}Se is clear.

Compound **2** may also be prepared by the action of a polyselenide solution on $[PtCl_2(dppe)]$ (Eq. 6). This method avoids the formation of dppe diselenide, which must be separated from the product in the reaction of $[Pt(dppe)_2]$ with selenium, and proceeds in comparable yield. A tetrafuran (THF) solution of lithium polyselenide does not, however, react with $[PdCl_2(dppe)]$ under the same conditions, the starting material being recovered largely unchanged in this case.

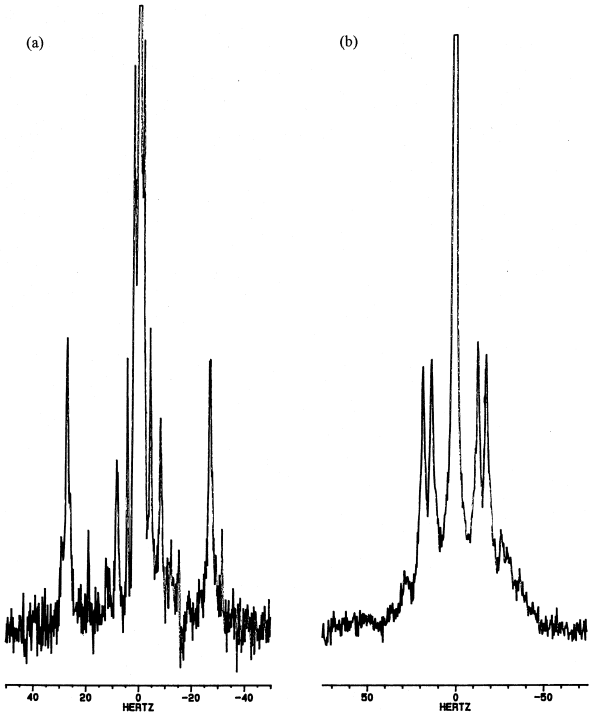
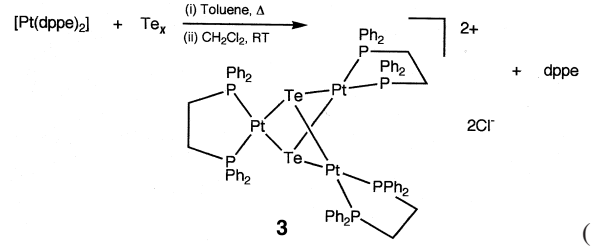


Fig. 2. Satellite structure of ^{31}P resonance for compounds **2** (a) and **3** (b).

$$[PtCl_2(dppe)] + Li_2Se_x \xrightarrow[\Delta]{THF} \underset{\mathbf{2}}{[PtSe_4(dppe)]} + LiCl \qquad (6)$$

Tellurium is not as reactive as selenium in this system. No change is observed on heating a mixture of $[Pd(dppe)_2]$ and tellurium powder for a prolonged period in toluene under reflux. $[Pt(dppe)_2]$ does react with tellurium, but a tetratelluride analogous to compound **2** is not formed. Treatment of a toluene solution of $[Pt(dppe)_2]$ with an excess of powdered tellurium leads to the eventual precipitation of a yellow solid. Filtration of the reaction mixture and extraction of the residue with dichloromethane yields compound **3**, identified as $[Pt_3(\mu_3\text{-}Te)_2(dppe)_3]Cl_2$ (Eq. 7).



(7)

Compound **3** is analogous to the triethylphosphine derivative $[Pt_3(\mu_3\text{-}Te)_2(PEt_3)_6][PF_6]_2$, previously reported by Dahl and co-workers [18]. It is presumably formed by the same mechanism as the tripalladium diselenide (**1b**) via $[Pt_2(\mu\text{-}Te)_2(dppe)_2]$ and $[PtCl_2(dppe)]$. Compound **3** is a yellow microcrystalline solid, readily soluble in polar organic solvents. It has been characterised by microanalysis, NMR, UV–Vis and IR spectroscopy, and by mass spectrometry. The electronic spectrum of compound **3** is similar to that of compound **2** in having three absorption maxima in the ultraviolet region; the difference in colour arises because absorption attenuates more rapidly at higher wavelengths. An intense cluster of peaks is observed in the FAB mass spectrum, corresponding to the ion $[Pt_3(\mu_3\text{-}Te)_2(dppe)_3Cl]^+$, and, like compound **1b**, it behaves as a 2:1 electrolyte in dichloromethane solution. In contrast to the selenium-containing compound, however, compound **3** is prone to decomposition in solution, depositing tellurium after a few hours at room temperature or above.

The satellite structure of the ^{31}P resonance for compound **3** is shown in Fig. 2(b). Coupling to ^{125}Te is clearly visible. The spectrum is, however, deceptively simple. This is the A and A′ part of an $A_3A'_3X$ system: simulation using estimated values for the coupling constants (based on data for comparable compounds) shows that it consists of a total of 46 lines. The ^{31}P resonance is significantly further upfield ($\delta = 41.4$ ppm), and the platinum–phosphorus coupling constant (3147 Hz) much greater than those for the mononuclear tetrachalcogenides $[PtE_4(dppe)]$ (E = S: $\delta = 49.6$ ppm, $^1J(^{195}Pt–^{31}P) = 2809$ Hz; E = Se (**2**): $\delta = 47.1$ ppm,

$^1J(^{195}Pt–^{31}P) = 2805$ Hz). The same trend is also evident from a comparison of the chemical shifts of the tripalladium diselenide (**1b**) (50.9 ppm) and [PdS_4(dppe)] (57.2 ppm). The magnitude of $^1J(^{195}Pt–^{31}P)$ for compound **3** is similar to that observed in the analogous complexes [$Pt_3(\mu_3$-$Te)_2(PEt_3)_6][PF_6]_2$ (3238 Hz) [18] and [$Pt_3(\mu_3$-$S)_2$-$(PMe_2Ph)_6][BF_4]_2$ (3202 Hz) [11].

The reactions of the polyselenide (**2**) with activated alkynes to yield diselenolenes are currently under study and the results will be reported separately [19].

3. Experimental

All reactions were performed using standard Schlenk techniques and pre-dried solvents under an atmosphere of dinitrogen. ^1H and ^{13}C NMR spectra: Bruker AC400, tetramethylsilane as internal standard. ^{31}P and ^{77}Se NMR spectra: Bruker WM250, 85% phosphoric acid or dimethyl selenide as external standard. IR spectra: Perkin-Elmer 1725X. UV–Vis spectra: Perkin-Elmer Lambda 9. Mass spectra were recorded by the EPSRC Mass Spectrometry Centre, using fast atom bombardment (FAB). Values of m/z quoted are for isotopomers containing ^{35}Cl, ^{80}Se, ^{106}Pd, or ^{195}Pt as appropriate; expected isotope distribution patterns were observed. Elemental analyses were performed by the Analytical Service of the University of Wales, Cardiff.

Bis[bis(diphenylphosphino)ethane]palladium [20,21] and -platinum [22] and [bis(diphenylphosphino)ethane]-dichloroplatinum [23] were prepared by literature procedures.

3.1. Bis[bis(diphenylphosphino)ethane]di-μ_2-selenidodipalladium (*1a*)

A mixture of [Pd(dppe)$_2$] (0.45 g, 0.5 mmol) and powdered vitreous selenium (0.40 g, 5.0 mmol) in toluene (50 cm^3) was heated under reflux for 18 h. After this time a microcrystalline brown–black solid had been formed. This was collected by filtration and purified by treatment with triphenylphosphine (13.1 g, 50 mmol) in toluene under reflux for 2 days. The product was a brown–black solid, insoluble in all common solvents.

Yield 0.24 g, 82%. M.p. 300°C (dec.). *Anal*. Found: C, 51.9; H, 4.11. $C_{52}H_{48}P_4Pd_2Se_2$ requires: C, 53.5; H, 4.14%. Vis (diffuse reflectance), absorption across the whole of the visible region apart from 435–450, 480–495 and 585–700 nm. IR (KBr disk) (cm^{-1}): ν 3044m, 2963m, 2920s, 2851m, 1637m, 1436m, 1401w, 1385m, 1262w, 1188s, 1102vs, 1052m, 879w, 818m, 694m, 569w, 531s, 490w.

3.2. Tris[bis(diphenylphosphino)ethane]di-μ_3-selenidotripalladium dichloride (*1b*)

A mixture of [Pd(dppe)$_2$] (0.09 g, 0.1 mmol) and powdered vitreous selenium (0.79 g, 1.0 mmol) in toluene (50 cm^3) was heated to 85°C for 18 h. The product was collected by filtration, washed with toluene and extracted into dichloromethane. Removal of the solvent by evaporation under reduced pressure left a crystalline brown solid.

Yield: 0.03 g, 52%. M.p. 342°C. *Anal*. Found: C, 50.7; H 4.21. $C_{78}H_{72}Cl_2P_6Pd_3Se_2$ requires: C, 53.7; H, 4.16%. ^1H NMR: δ 7.34 (m, 36H), 7.07 (m, 24H), 2.49 (m, 12H). ^{13}C NMR: δ 132.9 [$J(^{13}C–^{31}P)$ not resolved], 131.7, 129.6 [average $J(^{13}C–^{31}P)$ 23 Hz], 128.9 [$J(^{13}C–^{31}P)$ not resolved], 26.6 [$J(^{13}C–^{31}P)$ not resolved]. ^{31}P NMR: δ 50.9. ^{77}Se NMR: δ −41 [$J(^{77}Se–^{31}P)$ not resolved]. UV–Vis (CH_2Cl_2), λ_{max} (ε, $dm^3\ cm^{-1}\ mol^{-1}$): 230 (55000), 280 (35000), 300 (31000), 360 (20000), 370 (16000), 470 (1500) nm. IR (KBr disk) (cm^{-1}): ν 3056s, 2960m, 2928s, 1620m, 1482m, 1434vs, 1307w, 1186w, 1101s, 1026m, 998m, 876m, 820m, 746m, 705s, 691vs, 531vs, 480s. MS: *m/z* 1707 [{M − Cl}$^+$].

3.3. Bis(diphenylphosphino)ethane(tetraselenido-Se, Se)-platinum (*2*)

(a) A mixture of [Pt(dppe)$_2$] (0.25 g, 0.25 mmol) and powdered vitreous selenium (0.20 g, 2.5 mmol) in toluene (50 cm^3) was heated under reflux for 5 h. After cooling overnight, the product was collected by filtration, washed with toluene and extracted into dichloromethane. Removal of the solvent by evaporation under reduced pressure left a crystalline red solid. Yield: 0.16 g (70%).

(b) A mixture of $LiBEt_3H$ (3.0 cm^3 of a 1 M solution in THF, 3.0 mmol) and powdered vitreous selenium (0.43 g, 5.4 mmol) in THF (150 cm^3) was heated under reflux for 1 h. A hot suspension of [$PtCl_2$(dppe)] (0.66 g, 1.0 mmol) in THF (150 cm^3) was added to the purple solution of Li_2Se_x thus formed, and the mixture was heated under reflux for a further 2 h. The solvent was removed by evaporation under reduced pressure. The black residue was Soxhlet extracted with dichloromethane to yield an orange solution. Removal of the solvent in vacuo left a red crystalline solid, which was washed with cold toluene and dried. Yield: 0.64 g (70%).

M.p. 207°C (dec.). *Anal*. Found: C, 34.1; H, 2.83. $C_{26}H_{24}P_2PtSe_4$ requires: C, 34.3; H, 2.66%. ^1H NMR: δ 7.71 (m, 8H), 7.43 (m, 12H), 2.41 (m, 4H). ^{13}C NMR: δ 133.2 [average $J(^{13}C–^{31}P)$ 6 Hz], 131.7, 129.9 [average $J(^{13}C–^{31}P)$ 31 Hz], 128.8 [average $J(^{13}C–^{31}P)$ 6 Hz], 29.0 [eight peaks]. ^{31}P NMR: δ 47.1 [$J(^{195}Pt–^{31}P)$ 2805 Hz]. ^{77}Se NMR: δ 640 [$J(^{77}Se–^{31}P)$ not resolved]. IR (KBr disk) (cm^{-1}): ν 3050m, 2963m, 2927m, 1639m, 1618m, 1483m, 1435s, 1408m, 1385m, 1308w, 1262m, 1187w, 1160w, 1103s, 1027m, 998w, 879w, 820m, 749m, 715m, 706m, 691s, 657w, 617w, 533vs, 484m, 405w. UV–Vis (CH_2Cl_2), λ_{max} (ε, $dm^3\ cm^{-1}\ mol^{-1}$) 230 (36000), 250 (7500), 260 (7000) nm. MS: *m/z* 913 [M$^+$].

3.4. Tris[bis(diphenylphosphino)ethane]di-μ_3-telluridotriplatinum dichloride (*3*)

A mixture of [Pt(dppe)$_2$] (0.25 g, 0.25 mmol) and tellurium powder (0.32 g, 2.5 mmol) in toluene (50 cm^3) was

heated under reflux for 3 h. The solution became deep red in colour and some of the tellurium gradually dissolved. After cooling overnight, a yellow solid had been deposited. The product was collected by filtration, washed with toluene and extracted into dichloromethane to yield an orange solution. Removal of the solvent by evaporation under reduced pressure left a yellow oily solid, which could be further purified by passage of a dichloromethane solution through a bed of Celite. The product was unstable in solution and decomposed after a few hours at room temperature with the deposition of tellurium.

Yield: 0.09 g, 51%. M.p. 168°C (dec.). *Anal*. Found: C, 53.4; H 3.11. $C_{78}H_{72}Cl_2P_6Pt_3Te_2$ requires: C, 44.5; H, 3.44%. ^{1}H NMR: δ 7.43 (m, 12H), 7.35 (m, 24H), 7.18 (m, 24H), 2.54 (m, 12H). ^{13}C NMR: δ 132.8 [average $J(^{13}C–^{31}P)$ 5 Hz], 131.8, *ipso*-C not observed, 128.8 [average $J(^{13}C–^{31}P)$ 5 Hz], 27.7 [average $J(^{13}C–^{31}P)$ 20 Hz]. ^{31}P NMR: δ 41.4 [$J(^{195}Pt–^{31}P)$ 3147 Hz]. UV–Vis (CH_2Cl_2), λ_{max} (ε, dm^3 cm^{-1} mol^{-1}): 230 (21000), 250 (13000), 260 (11000) nm. IR (KBr disk) (cm^{-1}): ν3056s, 2960m, 2928s, 1637vs, 1619vs, 1435m, 1385m, 1262w, 1103s, 803w, 749m, 692vs, 669s, 618s, 534vs, 483vs. MS: m/z 2071 [$\{M-Cl\}^+$].

3.5. X-ray crystallography

Details of the crystal structure determination of compound **2** are given in Table 2. Measurements were carried out at room temperature with an Enraf-Nonius CAD4 diffractometer, using graphite-monochromated Mo Kα radiation. Crystals diffracted poorly; the sample used for the final data collection was cut from a bigger piece. Lattice parameters were determined from the settings of 24 reflections at $12 \le \theta \le 14$. No decay of intensities was observed at data collection time. An empirical correction for absorption was applied to the data, with DIFABS [24] (correction factors range 0.677–1.419). Structure solution was by direct methods with SIR97 [25], and Fourier cycles with SHELXL-93 [26], which was also used for structure refinements. The final refinement cycles were performed against F^2 with all non-hydrogen atoms anisotropic and with hydrogen atoms in calculated positions. Phenyl rings were treated as rigid groups with idealized geometry; refinement of the light atoms parameters suffered from the poor quality of the data (probably caused in part by disordered solvent) and from the presence of heavy atoms. The presence of dichloromethane solvate molecules disorderly arranged about a 2-fold axis was suggested by difference Fouriers. The occupancy factor of the site was assigned based on the results of refinements in which the solvent molecule, geometrically constrained throughout, was applied an overall temperature factor.

Table 2
Crystallographic data for $[PtSe_4(dppe)]\cdot 0.25CH_2Cl_2$ (**2**)

Formula	$C_{26.25}H_{24.50}Cl_{0.50}P_2PtSe_4$
M	930.55
Crystal system	orthorhombic
Space group	*Pbnb* (alternative setting of *Pccn*, no. 56)
a (Å)	15.513(6)
b (Å)	17.881(8)
c (Å)	20.442(14)
U (Å^3)	5670(5)
Z	8
D_c (g cm^{-3})	2.180
Crystal size (mm)	0.30×0.40×0.60
μ (mm^{-1})	10.26
Radiation	Mo Kα (λ = 0.71069 Å)
Data collected	$h \ge 0$, $k \ge 0$, $-1 \le l \le 20$
Scan type	ω–2θ
2θ Range (°)	5–50
Reflections collected	4435
Unique reflections	4084 (R_{int} = 0.035)
Unique observed reflections, with $I > 2\sigma(I)$	2123
No. parameters	278 (201 restraints)
R1 (observed reflections)	0.059
R1 (all unique reflections)	0.169
wR2	0.144
Goodness of fit	1.046
Largest features (max., min.) in final ΔF map (e Å^{-3})	1.00, −1.65

Supplementary data

Crystallographic data for compound **2** have been deposited with the Cambridge Crystallographic Data Centre, 12 Union Road, Cambridge, CB2 1EZ, UK (fax: +44-1223-336033; e-mail: deposit@ccdc.cam.ac.uk), and are available on request quoting the deposition number CCDC 136385.

Acknowledgements

We thank EPSRC for the provision of a research studentship to M.R.L., Johnson Matthey plc for the gift of palladium and platinum salts, and the Ministero dell'Università e della Ricerca Scientifica e Tecnologica for financial support to M.d.V.

References

[1] S.M. Stuczynski, Y.U. Kwon, M.L. Steigerwald, J. Organomet. Chem. 449 (1993) 167.
[2] S.J. Hibble, D.A. Rice, M.J. Almond, K.A.H. Mohammed, S.P. Pearse, J.R. Sagar, J. Mater. Chem. 2 (1992) 1237.
[3] U.T. Müller-Westerhoff, B. Vance, in: G. Wilkinson (Ed.), Comprehensive Coordination Chemistry, vol. 2, Pergamon, Oxford, 1988, p. 595.
[4] J. Chatt, D.M.P. Mingos, J. Chem. Soc., Sect. A (1970) 1243.
[5] R.R. Gukathasan, R.H. Morris, A. Walker, Can. J. Chem. 61 (1983) 2490.
[6] D.S. Dudis, C. King, J.P. Fackler Jr., Inorg. Chim. Acta 181 (1991) 99.
[7] A. Bencini, M. Di Vaira, R. Morassi, P. Stoppioni, F. Mele, Polyhedron 15 (1996) 2079.
[8] P.K. Khanna, C.P. Morley, M.B. Hursthouse, K.M.A. Malik, O.W. Howarth, Heteroat. Chem. 6 (1995) 519.

[9] C.A. Ghilardi, S. Midollini, L. Sacconi, Inorg. Chim. Acta 31 (1978) L431.
[10] H. Werner, W. Bertleff, U. Schubert, Inorg. Chim. Acta 43 (1980) 199.
[11] G.W. Bushell, K.R. Dixon, R. Ono, A. Pidcock, Can. J. Chem. 62 (1984) 696.
[12] F. Cecconi, C.A. Ghilardi, S. Midollini, Inorg. Chem. 22 (1983) 3802.
[13] K. Matsumoto, N. Saiga, S. Tanaka, S. Ooi, J. Chem. Soc., Dalton Trans. (1991) 1265.
[14] P. Mathur, P. Sekar, C.V.V. Satyanarayana, M.F. Mahon, Organometallics 14 (1995) 2115.
[15] W.A. Herrmann, H.-J. Kneuper, J. Organomet. Chem. 348 (1988) 193.
[16] J.A. McConnachie, M.A. Ansari, J.A. Ibers, Inorg. Chem. 32 (1993) 3250.
[17] M.A. Ansari, C.H. Mahler, G.S. Chorghade, Y.-J. Lu, J.A. Ibers, Inorg. Chem. 29 (1990) 3832.
[18] A.G. Ma, J.B. Thoden, L. Dahl, J. Chem. Soc., Chem. Commun. (1992) 1516.
[19] S. Ford, M.R. Lewtas, C.P. Morley, M. Di Vaira, Eur. J. Inorg. Chem. (in press).
[20] B.M. Trost, T.A. Runge, L.N. Jungheim, J. Am. Chem. Soc. 102 (1980) 2840.
[21] D.R. Coulson, Inorg. Synth. 13 (1974) 121.
[22] K.R. Laing, S.D. Robinson, M.F. Uttley, J. Chem. Soc., Dalton Trans. (1974) 1205.
[23] G. Booth, J. Chatt, J. Chem. Soc., Sect. A (1966) 634.
[24] N. Walker, D. Stuart, Acta Crystallogr., Sect. A 39 (1983) 158.
[25] A. Altomare, M.C. Burla, M. Camalli, G.L. Cascarano, C. Giacovazzo, A. Guagliardi, A.G.G. Moliterni, G. Polidori, R. Spagna, J. Appl. Crystallogr. 32 (1999) 115.
[26] G.M. Sheldrick, SHELXL-93, Program for Crystal Structure Refinement, University of Göttingen, Germany, 1993.

PERGAMON

www.elsevier.nl/locate/poly

Polyhedron 19 (2000) 757–764

POLYHEDRON

Diphenylphosphinoacetate, nicotinate and thiophenoxyacetate as bridging ligands in heterometallic complexes involving bis(η-cyclopentadienyl)titanium(IV) and group 10 or 11 metal chlorides. Crystal structures of $[(\eta\text{-}C_5H_5)_2Ti\{OC(O)CH_2PPh_2\}_2]$ and $[(\eta\text{-}C_5H_5)_2Ti\{\mu\text{-}OC(O)CH_2PPh_2\}_2PdCl_2]$

Dennis A. Edwards *, Mary F. Mahon, Timothy J. Paget

Department of Chemistry, University of Bath, Bath BA2 7AY, UK

Received 1 November 1999; accepted 17 January 2000

Abstract

Heterobi- and tri-metallic compounds containing a $Cp_2Ti(IV)$ unit linked via nicotinate, thiophenoxyacetate or diphenylphosphinoacetate ligands to Pd, Pt, Cu, Ag or Au centres have been isolated. They are of the types $[Cp_2Ti\{\mu\text{-}OC(O)R\}_2MCl_2]$ (M = Pd, R = *m*-C_5H_4N, CH_2SPh and CH_2PPh_2; M = Pt, R = *m*-C_5H_4N or CH_2PPh_2), $[Cp_2Ti\{\mu\text{-}OC(O)CH_2PPh_2\}_2(M'Cl)_2]$ (M′ = Cu or Au) and $[Cp_2Ti\{\mu\text{-}OC(O)CH_2PPh_2\}_2AgCl]$. The diphenylphosphinoacetate products arise both from methane elimination reactions of $[Cp_2TiMe_2]$ with either $[MCl_2(Ph_2PCH_2CO_2H)_2]$ or $[M'Cl(Ph_2PCH_2CO_2H)]$ and from reactions of $[Cp_2Ti\{OC(O)CH_2PPh_2\}_2]$ with metal complexes containing labile ligands. Crystal structures of $[Cp_2Ti\{OC(O)CH_2PPh_2\}_2]$ and $[Cp_2Ti\{\mu\text{-}OC(O)CH_2PPh_2\}_2PdCl_2]$ are discussed. The latter compound contains diphenylphosphinoacetate groups which are O-unidentate with respect to titanium and P-unidentate with respect to palladium, the result being the formation of a ten-atom heterobimetallic ring system. ©2000 Elsevier Science Ltd All rights reserved.

Keywords: Bis(η-cyclopentadienyl)titanium(IV); Crystal structures; Diphenylphosphinoacetate; Heterometallics; Nicotinate; Thiophenoxyacetate

1. Introduction

Compounds containing $Cp_2Ti(IV)$ units linked to late transition metal centres are representatives of a broad class of heterometallic species, interest in which has been stimulated by, for example, their potential catalytic [1], biological [2,3] or medicinal [4] applications. The combination of an oxophilic early transition metal centre with electron-rich late transition metal centres may lead to products with properties considerably different than bimetallic species containing identical or closely related metals. This topic has been comprehensively reviewed by Stephan [5,6], whose group has made major advances in the application of early transition metal complexes functionalised to act as metalloligands for late transition metals.

Bridging ligands that have been employed to link the $Cp_2Ti(IV)$ fragment to late transition metals include μ-η^1:η^2-carbonyl [7] and anions such as phosphino [8], thiolato [9], selenolato [10] and η^1,η^6-benzoate [11]. Crystallographic results and extended Hückel or Fenske–Hall molecular orbital calculations are consistent with the presence of direct early–late transition metal interactions in a number of such compounds, for example, in $[Cp_2Ti(SCH_2CH_2SCH_2)_2CH_2Cu][PF_6]$ [12] and $[Cp_2Ti(SCH_2CH_2CH_2PPh_2)_2Ni]$ [13].

Of particular relevance to the results reported here, is a recent communication [14] reporting the self-assembly of two heterobimetallic early–late metallomacrocycles from the iso-nicotinate $[Cp_2Ti\{OC(O)C_5H_4N\text{-}p\}_2]$ [15] and the Pt(II) triflate complexes *cis*-$[Pt(OSO_2CF_3)_2L_2]$ [L = PEt_3 or $0.5Ph_2P(CH_2)_3PPh_2$]. The products, $[Cp_2Ti\{\mu\text{-}OC(O)C_5H_4N\text{-}p\}_2PtL_2]_2[CF_3SO_3]_4$, were held to be cationic and tetranuclear with a 28-atom ring based on NMR and, for the PEt_3 complex, liquid SIMS evidence. No X-ray crystal-

* Corresponding author. Tel.: +44-1225-826444; fax: +44-1225-826231; e-mail: chsdae@bath.ac.uk

0277-5387/00/$ - see front matter ©2000 Elsevier Science Ltd All rights reserved.
PII S0277-5387(00)00305-3

lographic evidence was available but molecular modelling was used to illustrate the shape of the complex and its cavity based on square planar platinum and distorted tetrahedral titanium as corner units.

We report here on a wider variety of related heterometallic compounds containing $Cp_2Ti(IV)$ carboxylate units linked to late transition metals synthesised by employing functionalised carboxylates containing additional nitrogen (nicotinate, *m*-$C_5H_4NCO_2^-$ [16]), sulfur (thiophenoxyacetate, $PhSCH_2CO_2^-$) or phosphorus (diphenylphosphinoacetate, $Ph_2PCH_2CO_2^-$) donor sites. Unlike the cationic, tetranuclear iso-nicotinate complexes [14], the products are non-ionic and either binuclear macrocycles involving a $Cp_2Ti(IV)$ unit assembled with one group 10 (Pd or Pt) or group 11 (Ag) metal, or trinuclear acyclic complexes in which the $Cp_2Ti(IV)$ unit is linked to two group 11 (Cu or Au) metals. The majority of the investigation has employed diphenylphosphinoacetate as the bridging carboxylate and it has been shown that most of the products can be prepared equally well either from methane elimination reactions of $[Cp_2TiMe_2]$ with our recently reported [17] complexes $[MCl_2(Ph_2PCH_2CO_2H)_2]$ (M = Pd or Pt) and $[M'Cl(Ph_2PCH_2CO_2H)]$ (M = Cu or Au) or from reactions which employ the new O-unidentate carboxylate $[Cp_2Ti\{OC(O)CH_2PPh_2\}_2]$ as a metalloligand in reactions with late transition metal complexes containing labile ligands. An X-ray crystallographic structure determination shows one of the products, $[Cp_2Ti\{OC(O)CH_2PPh_2\}_2PdCl_2]$, to contain a ten-atom heterobimetallocyclic ring.

2. Experimental

Diphenylphosphinoacetic acid was prepared and characterised as before [17], nicotinic and thiophenoxyacetic acids being used as supplied (Aldrich). The compound $[Cp_2TiMe_2]$ was prepared from the chloride (Aldrich) and methyllithium in diethyl ether. Bis(benzonitrile)Pd(II) or Pt(II) dichlorides were obtained by dissolving the metal chlorides in hot benzonitrile and isolating the crystalline products by filtration of the cooled solutions. Solvents were dried by distillation from appropriate reagents (sodium–benzophenone, calcium hydride or molecular sieves) before use and all reactions and manipulations were carried out under dry nitrogen.

Microanalyses were carried out using a Carlo-Erba microanalysis system. JEOL GX 270 and EX 400 spectrometers were used to obtain ^1H, ^{13}C and ^{31}P NMR spectra. Infrared spectra were recorded as Nujol or hexachlorobutadiene mulls (NaCl or CsI windows) using Nicolet 510P or Perkin-Elmer 597 spectrophotometers. Only selected bands are reported here. Positive and negative ion FAB mass spectra were recorded in 3-nitrobenzyl alcohol matrices using a VG Autospec instrument. The *m*/*z* values reported are based on ^{35}Cl, ^{48}Ti, ^{63}Cu and ^{197}Au isotopes and intensities are expressed relative to the strongest metal-containing fragment.

2.1. Bis(cyclopentadienyl)bis(O-nicotinato)titanium(IV) (1)

Sodium nicotinate (1.00 g, 6.9 mmol), prepared by reaction of the acid with sodium ethoxide in absolute alcohol, and $[Cp_2TiCl_2]$ (0.50 g, 2.0 mmol) were reacted in refluxing tetrahydrofuran (25 cm^3) under nitrogen for 1 h. After cooling, sodium salts were removed by filtration and the orange filtrate was treated with hexane to produce orange crystals on standing in an ice-bath (0.125 g, 15%). *Anal*. Found (calc. for $C_{22}H_{18}N_2O_4Ti$): C, 62.9 (62.6); H, 4.30 (4.30); N, 6.66 (6.63)%. IR (cm^{-1}): 3106s, 3049w (Cp), 1634vs (ν_{asym} CO_2), 1423m (Cp), 1350vs, 1306vs (ν_{sym} CO_2), 1028m (Cp), 824s (Cp). ^1H NMR ($CDCl_3$): δ 6.66 (s, 5H, Cp), 7.42 (dd, 1H, pyridyl), 8.28 (dt, 1H, pyridyl), 8.76 (dd, 1H, pyridyl), 9.21 (d, 1H, pyridyl). $^{13}C\{^1H\}$ NMR ($CDCl_3$): δ 118.8 (Cp), 123.2, 129.2, 137.2, 151.0, 152.0 (pyridyl), 170.1 (CO_2). FAB-MS (*m*/*z*): 344 (50% $[M-C_5H_4N]^+$), 300 (100% $[M-C_5H_4NCO_2]^+$).

2.2. Bis(cyclopentadienyl)bis(O-thiophenoxyacetato)-titanium(IV) (2)

A solution of $[Cp_2TiMe_2]$ (0.44 g, 2.1 mmol) in tetrahydrofuran (3 cm^3) was added dropwise to a suspension of thiophenoxyacetic acid (0.71 g, 4.2 mmol) in tetrahydrofuran (12 cm^3) resulting in a vigorous evolution of methane. After stirring for 1 h, removal of the solvent gave the required product, recrystallised from tetrahydrofuran–hexane as bright red cubes (1.00 g, 93%). *Anal*. Found (calc. for $C_{26}H_{24}O_4S_2Ti$): C, 60.6 (60.9); H, 4.73 (4.72)%. IR (cm^{-1}): 3108m (Cp), 1661s, 1632vs (ν_{asym} CO_2), 1437sh (Cp), 1337s, 1302vs (ν_{sym} CO_2), 1022m (Cp), 824s (Cp). ^1H NMR ($CDCl_3$): δ 3.61 (s, 2H, CH_2), 6.27 (s, 5H, Cp), 7.09 (m, 1H, Ph), 7.22 (m, 2H, Ph), 7.35 (m, 2H, Ph). $^{13}C\{^1H\}$ NMR ($CDCl_3$): δ 37.8 (CH_2), 118.5 (Cp), 125.8, 128.1, 128.8, 136.4 (Ph), 174.1 (CO_2). FAB-MS (*m*/*z*): 447 (7% $[M-Cp]^+$), 345 (100% $[M-PhSCH_2CO_2]^+$), 178 (16% $[Cp_2Ti]^+$).

2.3. Bis(cyclopentadienyl)bis(O-diphenylphosphino-acetato)titanium(IV) (3)

A solution of $[Cp_2TiMe_2]$ (0.33 g, 1.6 mmol) in dichloromethane (6 cm^3) was added dropwise to a solution of diphenylphosphinoacetic acid (0.77 g, 3.2 mmol) in dichloromethane (4 cm^3). After evolution of methane, the mixture was stirred for 6 h, then the solvent was removed to produce a solid which was recrystallised from dichloromethane layered with hexane to give bright orange cubes suitable for an X-ray crystal structure determination (1.01 g, 95%). *Anal*. Found (calc. for $C_{38}H_{34}O_4P_2Ti$): C, 67.6 (67.7); H, 5.13 (5.17)%. IR (cm^{-1}): 3100w, 3056vw (Cp), 1649m, 1618s (ν_{asym} CO_2), 1433w (Cp), 1325s, 1285s (ν_{sym} CO_2), 1019w (Cp), 824m (Cp). ^1H NMR ($CDCl_3$): δ 2.96 (s, 2H, CH_2), 6.01 (s, 5H, Cp), 7.10 (m, 6H, Ph), 7.29 (m, 4H, Ph). $^{13}C\{^1H\}$ NMR ($CDCl_3$): δ 37.6 (d, $^1J_{C,P}$ = 17.6 Hz,

CH_2), 118.2 (s, Cp), 128.3 (d, $^2J_{C,P}$ = 6.6 Hz, C_{meta}), 128.6 (s, C_{para}), 132.6 (d, $^1J_{C,P}$ = 19.8, C_{ipso}), 138.4 (d, $^2J_{C,P}$ = 15.4 Hz, C_{ortho}), 175.4 (d, $^2J_{C,P}$ = 8.8 Hz, CO_2). $^{31}P\{^1H\}$ ($CDCl_3$): δ −17.6. FAB-MS (m/z): 599 (5% $[M-Cp]^+$), 522 (9%, $[M-Cp-Ph]^+$), 421 (100%, $[M-Ph_2PCH_2CO_2]^+$), 344 (29%, $[M-Ph_2PCH_2CO_2-Ph]^+$).

2.4. Adduct of compound **1** with $PdCl_2$

A solution of $[PdCl_2(NCPh)_2]$ (0.045 g, 0.12 mmol) in tetrahydrofuran (5 cm^3) was added dropwise with stirring to a solution of compound **1** (0.050 g, 0.12 mmol) in tetrahydrofuran (10 cm^3) to give an orange precipitate. After stirring for 24 h the product was obtained by filtration and washed with tetrahydrofuran (0.099 g, 69%). *Anal*. Found (calc. for $C_{22}H_{18}Cl_2N_2O_4PdTi$): C, 44.0 (44.1); H, 3.41 (3.03); N, 4.57 (4.67)%. IR (cm^{-1}): 3108w (Cp), 1642vs (ν_{asym} CO_2), 1462m (Cp), 1319vs (ν_{sym} CO_2), 1019w (Cp), 828s (Cp), 358m (ν PdCl).

2.5. Adduct of compound **1** with $PtCl_2$

This compound was prepared in a similar manner to the above palladium complex using $[PtCl_2(NCPh)_2]$ (0.034 g, 0.07 mmol) and compound **1** (0.030 g, 0.07 mmol) in dichloromethane (5 cm^3). Yield: 0.018 g, 37%. *Anal*. Found (calc. for $C_{22}H_{18}Cl_2N_2O_4PtTi$): C, 37.0 (38.4); H, 2.79 (2.64); N, 4.40 (4.07)%.

2.6. Adduct of compound **2** with $PdCl_2$

A similar method to that above using $[PdCl_2(NCPh)_2]$ (0.070 g, 0.18 mmol) dissolved in dichloromethane (5 cm^3) and compound **2** (0.089 g, 0.18 mmol) in dichloromethane (3 cm^3) gave a bright orange precipitate which was filtered and washed with dichloromethane before drying in vacuo. Yield: 0.090 g, 72%. *Anal*. Found (calc. for $C_{26}H_{24}Cl_2O_4PdS_2Ti$): C, 44.2 (45.3); H, 3.46 (3.51)%. IR (cm^{-1}): 3112m (Cp), 1626vs (ν_{asym} CO_2), 1443s (Cp), 1319vs (ν_{sym} CO_2), 1024m (Cp), 828s (Cp), 358w, 324m (ν PdCl).

2.7. Adduct of compound **3** with $PdCl_2$

2.7.1. Method A

Complex **3** was generated in situ from $[Cp_2TiMe_2]$ (0.19 g, 0.90 mmol) and diphenylphosphinoacetic acid (0.44 g, 1.80 mmol) in dichloromethane (6 cm^3). Addition of a solution of $[PdCl_2(NCPh)_2]$ (0.35 g, 0.90 mmol) in dichloromethane (2 cm^3) gave a red solution which, on standing, deposited large red crystals which were collected by filtration (0.43 g, 43%).

2.7.2. Method B

A solution of $[Cp_2TiMe_2]$ (0.034 g, 0.17 mmol) in dichloromethane (2 cm^3) was added to a suspension of *trans*-$[PdCl_2(Ph_2PCH_2CO_2H)_2]$ [17] (0.11 g, 0.17 mmol) in dichloromethane (2 cm^3). Slow evolution of methane was observed. After 2 h the solvent was removed to give an orange solid. *Anal*. Found (calc. for $C_{38}H_{34}Cl_2O_4P_2PdTi$): C, 52.1 (54.2); H, 3.90 (4.07)%. IR (cm^{-1}): 3087w (Cp), 1651vs (ν_{asym} CO_2), 1435s (Cp), 1312vs (ν_{sym} CO_2), 1019m (Cp), 818s (Cp), 339m, 307m (ν PdCl). ^1H NMR ($CDCl_3$): δ 3.53 (t, 2H, J = 4.4 Hz, CH_2), 6.30 (s, 5H, Cp), 7.22 (m, 6H, Ph), 7.59 (m, 4H, Ph). $^{31}P\{^1H\}$ ($CDCl_3$): δ +13.8.

2.8. Adduct of compound **3** with $PtCl_2$

2.8.1. Method A

The desired compound was prepared as for the palladium analogue using $[Cp_2TiMe_2]$ (0.05 g, 0.24 mmol), $Ph_2PCH_2CO_2H$ (0.117 g, 0.48 mmol) and $[PtCl_2(NCPh)_2]$ (0.12 g, 0.24 mmol) in dichloromethane (3 cm^3).

2.8.2. Method B

A solution of $[Cp_2TiMe_2]$ (0.052 g, 0.25 mmol) in dichloromethane (0.5 cm^3) was added to a suspension of *cis*-$[PtCl_2(Ph_2PCH_2CO_2H)_2]$ [17] (0.166 g, 0.25 mmol) in toluene–dichloromethane (5:1, 6 cm^3). A further 0.5 cm^3 of dichloromethane was added and the mixture stirred for 24 h. The orange precipitate was filtered and washed with dichloromethane (0.071 g, 23%). A further crop of orange crystals was obtained by concentration of the filtrate (0.123 g, 40%). *Anal*. Found (calc. for $C_{38}H_{34}Cl_2O_4P_2PtTi$): C, 48.6 (49.1); H, 3.60 (3.68)%. IR (cm^{-1}): 3088w (Cp), 1647s, 1593s (ν_{asym} CO_2), 1439s (Cp), 1312s (ν_{sym} CO_2), 1028w (Cp), 822w (Cp), 322m, 310m (ν PtCl).

2.9. Adduct of compound **3** with 2CuCl

2.9.1. Method A

Cu(I) chloride (0.10 g, 1.00 mmol) and complex **3** (0.34 g, 0.50 mmol) were stirred in dichloromethane (5 cm^3) for 72 h to give a dark red solution. Filtration followed by concentration of the filtrate in vacuo gave an orange powder (0.40 g, 93%).

2.9.2. Method B

A solution of $[Cp_2TiMe_2]$ (0.061 g, 0.29 mmol) in dichloromethane (2 cm^3) was added with stirring to a suspension of $[\{CuCl(Ph_2PCH_2CO_2H)\}_4]$ [17] in dichloromethane (2 cm^3). Evolution of methane was observed. After standing for 72 h, concentration of the solution gave an orange solid (0.17 g, 68%). *Anal*. Found (calc. for $C_{38}H_{34}Cl_2Cu_2O_4P_2Ti$): C, 52.4 (52.9); H, 3.93 (3.97)%. IR (cm^{-1}): 3050w (Cp), 1634s (ν_{asym} CO_2), 1435s (Cp), 1310s (ν_{sym} CO_2), 1017w (Cp), 828s (Cp). ^1H NMR ($CDCl_3$): δ 3.48 (br s, 2H, CH_2), 6.23 (s, 5H, Cp), 7.40 (m, 6H, Ph), 7.68 (m, 4H, Ph). $^{13}C\{^1H\}$ NMR ($CDCl_3$): δ 37.3 (s, CH_2), 118.9 (s, Cp), 128.9 (s, Ph), 130.3 (s, Ph), 132.3 (d, J = 15.5 Hz, Ph), 132.7 (t, J = 7.7, Ph), 172.5 (s, CO_2). $^{31}P\{^1H\}$ NMR ($CDCl_3$): δ −12.4 (s). FAB-MS (m/z) 827

(16% $[M-Cl]^+$), 762 (21% $[M-CuCl]^+$), 727 (100% $[762-Cl]^+$), 662 (74% $[727-Cp]^+$).

2.10. Adduct of compound **3** with AgCl

2.10.1. Method A

Compound **3** (0.050 g, 0.08 mmol) and silver chloride (0.011 g, 0.08 mmol) were stirred in dichloromethane (4 cm^3) for 72 h. Filtration followed by concentration of the filtrate gave a bright orange solid. The same product resulted from similar reactions employing two or four molar equivalents of AgCl, but in these cases an excess of AgCl had to be removed by filtration.

2.10.2. Method B

Silver(I) diphenylphosphinoacetate (0.60 g, 1.70 mmol), prepared from $AgNO_3$ and $Ph_2PCH_2CO_2Na$, and $[Cp_2TiCl_2]$ (0.21 g, 0.85 mmol) were stirred in dichloromethane (10 cm^3) for 24 h. Filtration removed AgCl and the orange filtrate was evaporated and the solid product crystallised from dichloromethane to give an orange crystalline solid (0.53 g, 77%). *Anal*. Found (calc. for $C_{38}H_{34}AgClO_4P_2Ti$): C, 55.3 (56.5), H, 4.49 (4.24)%. IR (cm^{-1}): 3050w (Cp), 1642vs (ν_{asym} CO_2), 1435s, (Cp), 1310sh, 1273vs (ν_{sym} CO_2), 1017m (Cp), 828s (Cp). ^1H NMR ($CDCl_3$): δ 3.51 (s, 2H, CH_2), 6.10 (s, 5H, Cp), 7.37 (m, 6H, Ph), 7.66 (m, 4H, Ph). $^{13}C\{^1H\}$ NMR ($CDCl_3$): δ 37.9 (d, $^1J_{C,P}=8.3$ Hz, CH_2), 118.9 (s, Cp), 129.0 (d, $^2J_{C,P}=5.0$ Hz, C_{meta}), 130.5 (s, C_{para}), 131.9 (d, $^1J_{C,P}=12.9$ Hz, C_{ipso}), 132.8 (d, $^2J_{C,P}=8.3$ Hz, C_{ortho}), 171.7 (s, CO_2). $^{31}P\{^1H\}$ NMR ($CDCl_3$): δ −1.84 ($^1J^{107}$Ag, $^{31}P=439.3$ Hz; $^1J^{109}$Ag, $^{31}P=506.4$ Hz). FAB-MS (m/z): 773 (100% $[M-Cl]^+$), 709 (77% $[M-Cl-Cp]^+$).

2.11. Adduct of compound **3** with 2AuCl

A solution of $[Cp_2TiMe_2]$ (0.050 g, 0.24 mmol) in dichloromethane (1 cm^3) was added slowly with stirring to a suspension of $[AuCl(Ph_2PCH_2CO_2H)]$ [17] (0.23 g, 0.48 mmol) in dichloromethane (2 cm^3). After stirring overnight, concentration of the solution in vacuo gave an orange–yellow solid (0.22 g, 81%). *Anal*. Found (calc. for $C_{38}H_{34}Au_2Cl_2O_4P_2Ti$): C, 40.1 (40.4); H, 2.92 (3.03)%. IR (cm^{-1}): 3058w (Cp), 1634vs (ν_{asym} CO_2), 1439s (Cp), 1325s, 1292vs (ν_{sym} CO_2), 1017m (Cp), 824s (Cp), 335ms (ν AuCl). ^1H NMR ($CDCl_3$): δ 4.11 (d, 2H, $^2J_{P,H}=13.4$ Hz, CH_2), 6.24 (s, 5H, Cp), 7.49 (m, 6H, Ph), 7.84 (m, 4H, Ph). $^{13}C\{^1H\}$ NMR ($CDCl_3$): δ 37.8 (d, $^1J_{C,P}=33.1$ Hz, CH_2), 119.0 (s, Cp), 129.1 (d, $^2J_{C,P}=11.0$ Hz, Ph), 129.9 (s, Ph), 131.9 (s, Ph), 133.3 (d, $^1J_{C,P}=14.4$ Hz, Ph), 170.6 (d, $^2J_{C,P}=2.2$ Hz, CO_2). $^{31}P\{^1H\}$ NMR ($CDCl_3$): δ +24.9 (s). FAB-MS (m/z) 1129 (3% $[M]^+$), 1093 (13% $[M-Cl]^+$), 1028 (13% $[M-Cl-Cp]^+$), 917 (14% $[Au_2Cl(Ph_2PCH_2CO_2H)_2]^+$), 441 (100% $[Au(Ph_2PCH_2CO_2H)]^+$).

2.12. X-ray crystallography

Crystal data, collection and refinement details for $[Cp_2Ti\{OC(O)CH_2PPh_2\}_2]$ (crystals from dichloromethane solution layered with hexane) and for $[Cp_2Ti\{\mu\text{-}OC(O)CH_2PPh_2\}_2PdCl_2]\cdot 3CH_2Cl_2$ (crystals from dichloromethane solution; method A above) are given in Table 1.

Selected bond lengths and angles are reported in Tables 2 and 3, respectively. Diagrams of the molecular structures produced using ORTEX [18] are shown in Figs. 1 and 2.

Data were collected using an Enraf-Nonius CAD4 diffractometer using graphite-monochromated Mo Kα 0.71069 Å radiation. Data for both compounds were corrected for Lorentz and polarisation effects and those for the $PdCl_2$ adduct also corrected for absorption. The structures were solved using SHELX 86 and refined using SHELX 93 [19,20]. For $[Cp_2Ti\{OC(O)CH_2PPh_2\}_2]$, in the final least-squares cycles all atoms were allowed to vibrate anisotropically. Hydrogen atoms were included at calculated positions. Data for $[Cp_2Ti\{\mu\text{-}OC(O)CH_2PPh_2\}_2PdCl_2]\cdot 3CH_2Cl_2$ were collected at 170(2) K, the crystals not being of a very high quality and crystal mounting was not without difficulty due to solvent loss. As a result, satisfactory anisotropic refinement of all atoms was not achieved. In the final least-squares cycles, atoms O(3), C(13), C(29) and C(37) were treated isotropically whereas all other atoms were allowed to vibrate anisotropically. Hydrogen atoms were included at calculated positions.

3. Results and discussion

Two new bis(η-cyclopentadienyl)titanium(IV) bis(*O*-carboxylates), $[Cp_2Ti\{OC(O)R\}_2]$ with $R=CH_2SPh$ (thiophenoxyacetate) and CH_2PPh_2 (diphenylphosphinoacetate) and the previously known [16] analogue with $R=C_5H_4N$-*m* (nicotinate) have been shown to act as S-, P- or N-donor metalloligands to various transition metal centres. Products contain Ti(IV) linked to either group 10 d^8 (Pd or Pt) or group 11 d^{10} (Cu, Ag or Au) metal chlorides via bridging carboxylate moities which are O-unidentate with respect to titanium and S-, P- or N-unidentate with respect to the group 10 or group 11 metal. Most of the work reported here focuses on the use of the diphenylphosphinoacetate in this manner.

The carboxylates have been prepared from $[Cp_2TiCl_2]$ and sodium nicotinate or from $[Cp_2TiMe_2]$ and thiophenoxyacetic or diphenylphosphinoacetic acids, the latter reactions proceeding with the smooth elimination of methane. Analytical, NMR (^1H, ^{13}C and ^{31}P), partial IR and mass spectrometric data for the three compounds are given in Section 2 and, being unexceptional, are not discussed further except to note that in the mass spectra the most abundant fragment in each case is that of the parent ion having lost one carboxylate group.

Table 1
Crystal data and data collection details for $[Cp_2Ti\{OC(O)CH_2PPh_2\}_2]$ and $[Cp_2Ti\{\mu\text{-}OC(O)CH_2PPh_2\}_2PdCl_2]\cdot 3CH_2Cl_2$

	$[Cp_2Ti\{OC(O)CH_2PPh_2\}_2]$	$PdCl_2\cdot$Adduct$\cdot 3CH_2Cl_2$
Empirical formula	$C_{38}H_{34}O_4P_2Ti$	$C_{41}H_{40}Cl_8O_4P_2PdTi$
Molecular formula	664.49	1096.57
Temperature (K)	293(2)	170(2)
Crystal system	triclinic	monoclinic
Space group	$P\bar{1}$ (no. 2)	$P2_1/n$ (no. 14)
a (Å)	11.664(3)	12.350(3)
b (Å)	11.847(3)	22.037(4)
c (Å)	14.191(4)	16.770(5)
α (°)	95.09(2)	
β (°)	101.18(3)	102.04(2)
γ (°)	117.33(2)	
U (Å^3)	1673.1(8)	4463.7(19)
Z	2	4
D_c (Mg m^{-3})	1.319	1.632
μ (mm^{-1})	0.391	1.173
$F(000)$	692	2208
Crystal size (mm)	0.2×0.2×0.3	0.4×0.35×0.2
θ Range for data collection (°)	2.03–22.00	2.09–21.99
hkl ranges	−13 to 0, −12 to 13, −15 to 16	−13 to 12, 0 to 23, 0 to 17
Reflections collected	4374	5451
Independent reflections (R_{int})	4123 (0.0360)	5451 (0.0790) [a]
Data, restraints, parameters	3967, 0, 404	5432, 18, 496
Goodness of fit on F^2	1.042	1.141
Final R_1, wR_2 indices [$I>2\sigma(I)$]	0.0656, 0.1310	0.0740, 0.1221
All data	0.1505, 0.1775	0.1563, 0.1636
Largest residuals (e Å^{-3})	0.601 and –0.267	1.261 and −0.873
Weighting scheme, w	$1/[\sigma^2(F_o^2)+(0.0610P)^2+2.5766P]$, where $P=(F_o^2+2F_c^2)/3$	$1/[\sigma^2(F_o^2)+(0.0000P)^2+58.8248P]$, where $P=(F_o^2+2F_c^2)/3$

[a] Pre-DIFABS R_{int}.

Table 2
Selected bond lengths (Å) and angles (°) for $[Cp_2Ti\{OC(O)CH_2PPh_2\}_2]$

Ti(1)–O(1)	1.972(4)	Ti(1)–O(3)	1.925(5)
O(1)–C(11)	1.282(8)	O(3)–C(25)	1.300(7)
O(2)–C(11)	1.216(8)	O(4)–C(25)	1.189(8)
C(11)–C(12)	1.516(9)	C(25)–C(26)	1.502(9)
C(12)–P(1)	1.856(6)	C(26)–P(2)	1.830(7)
Average Ti(1)–C(1–5)	2.372(7)	Average Ti(1)–C(6–10)	2.360(8)
Average C–C in Cp ring C(1)–C(5)	1.382(10)	Average C–C in Cp ring C(6)–C(10)	1.362(13)
O(1)–Ti(1)–O(3)	91.5(2)		
Ti(1)–O(1)–C(11)	136.1(5)	Ti(1)–O(3)–C(25)	143.4(4)
O(1)–C(11)–O(2)	125.0(7)	O(3)–C(25)–O(4)	123.3(7)
O(1)–C(11)–C(12)	115.2(7)	O(3)–C(25)–C(26)	113.6(6)
O(2)–C(11)–C(12)	119.8(7)	O(4)–C(25)–C(26)	122.9(7)
C(11)–C(12)–P(1)	109.5 (5)	C(25)–C(26)–P(2)	110.4(5)

To provide a comparison with one of the metal halide adducts, an X-ray single-crystal structure determination of $[Cp_2Ti\{OC(O)CH_2PPh_2\}_2]$ has been carried out (Fig. 1). This confirms the presence of a distorted tetrahedral environment around the metal with two O-unidentate carboxylate groups [Ti–O 1.972(4) and 1.925(5) Å] in accord with the large IR [$\nu_{asym}-\nu_{sym}$ CO_2] difference of 333 cm^{-1}. Taking the centroids of the cyclopentadienyl rings as Z, the distortion from regular geometry is evident from the Z–Ti–Z angle of 132.4° and the O(1)–Ti–O(3) angle of 91.5(2)°. The two carboxylate oxygens, O(2) and O(4), not bonded to the titanium, are more than 3 Å from the metal, and the two phosphorus atoms, which could potentially donate, are more than 5 Å from the titanium with the phosphine units so arranged that the lone pairs are directed away from each other. Unidentate carboxylate coordination is also indicated by the significant differences in C–O bond lengths depending on whether the oxygen is coordinated to titanium [1.282(8), 1.300(7) Å] or not [1.216(8), 1.189(8) Å]. The two diphenylphoshinoacetate groups are bonded to the titanium in a somewhat inequivalent manner, one carboxylate having a longer Ti–O (difference 0.047 Å), a smaller Ti–O–C angle

Table 3
Selected bond lengths (Å) and angles (°) for $[Cp_2Ti\{\mu\text{-}OC(O)CH_2PPh_2\}_2PdCl_2]\cdot 3CH_2Cl_2$

Ti(1)–O(1)	1.971(8)	Ti(1)–O(3)	1.959(8)
O(1)–C(11)	1.286(14)	O(3)–C(13)	1.291(14)
O(2)–C(11)	1.197(14)	O(4)–C(13)	1.213(14)
C(11)–C(12)	1.53(2)	C(13)–C(14)	1.52(2)
C(12)–P(1)	1.824(13)	C(14)–P(2)	1.830(13)
Pd(1)–P(1)	2.259(4)	Pd(1)–P(2)	2.277(4)
Pd(1)–Cl(1)	2.348(4)	Pd(1)–Cl(2)	2.339(4)
Average Ti(1)–C(1–5)	2.35(2)	Average Ti(1)–C(6–10)	2.37(2)
Average C–C in Cp ring C(1)–C(5)	1.36(2)	Average C–C in Cp ring C(6)–C(10)	1.38(2)
O(1)–Ti(1)–O(3)	89.4(3)		
Ti(1)–O(1)–C(11)	143.2(8)	Ti(1)–O(3)–C(13)	142.1(8)
O(1)–C(11)–O(2)	125.8(13)	O(3)–C(13)–O(4)	126.4(12)
O(1)–C(11)–C(12)	114.3(11)	O(3)–C(13)–C(14)	115.0(11)
O(2)–C(11)–C(12)	119.6(12)	O(4)–C(13)–C(14)	118.6(11)
C(11)–C(12)–P(1)	116.3(10)	C(13)–C(14)–P(2)	116.3(9)
C(12)–P(1)–Pd(1)	112.8(5)	C(14)–P(2)–Pd(1)	111.6(4)
P(1)–Pd(1)–P(2)	103.93(13)	P(2)–Pd(1)–Cl(1)	172.36(13)
P(1)–Pd(1)–Cl(1)	83.12(13)	P(2)–Pd(1)–Cl(2)	84.63(13)
P(1)–Pd(1)–Cl(2)	170.63(13)	Cl(1)–Pd(1)–Cl(2)	88.15(12)

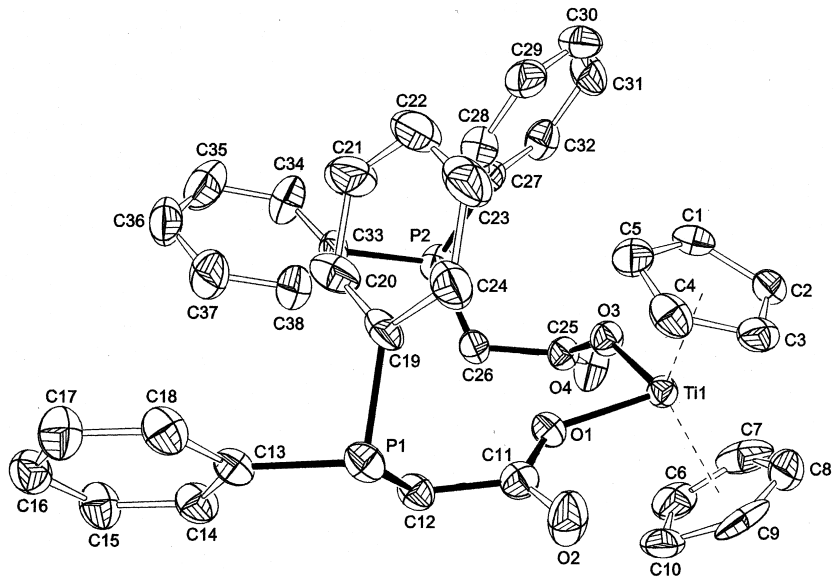


Fig. 1. ORTEX plot of the molecular structure of $[Cp_2Ti\{OC(O)CH_2PPh_2\}_2]$ (**3**) showing the labelling scheme. Hydrogen atoms are omitted for clarity. Thermal ellipsoids are at the 30% probability level.

(difference 7.3°) and a shorter C–O bond length (difference 0.018 Å) than the other. This may imply the presence of a differing extent of Ti–O π interaction supporting the primary σ bonding for the two carboxylate ligands. Such differences have been noted previously, for example in the orthorhombic form of $[Cp_2Ti\{OC(O)Ph\}_2]$ [21,22], which shows Ti–O, Ti–O–C and C–O differences between the two benzoates of 0.101 Å, 33.5° and 0.025 Å, respectively. This has been ascribed to the presence of a strong Ti–O π bond supplementing the Ti–O σ bond for one of the benzoates, thus giving an effective 18-electron count rather than a formal 16-electron count for the valence electrons. However, structure determinations of some other $[Cp_2Ti\{OC(O)R\}_2]$ compounds show very near equivalence of the carboxylate groups, e.g. R = H [23] or CH_2CN [24], presumably resulting from some additional Ti–O π bonding for both carboxylate groups, as indicated by EHMO calculations on the formate [25]. The average Ti–C and C–C bond lengths and C–C–C angles of the cyclopentadienyl groups agree well with such values from structure determinations of other $[Cp_2TiX_2]$ compounds [25]. Finally, it is noted that the present structure determination appears to be the first in which the diphenylphosphinoacetate anion acts solely as a unidentate ligand, the usual coordination mode being O,P-chelating as in, for example, *cis*-$[Pd\{OC(O)CH_2PPh_2\}_2]$ [26].

The compound $[Cp_2Ti\{OC(O)CH_2PPh_2\}_2]$ has been used both as a P-donor chelate metalloligand to assemble neutral bimetallic macrocyclic complexes in which the two phosphorus atoms bond to one group 10 (Pd or Pt) or group 11 (Ag) metal centre and as a P-donor bridging metalloligand

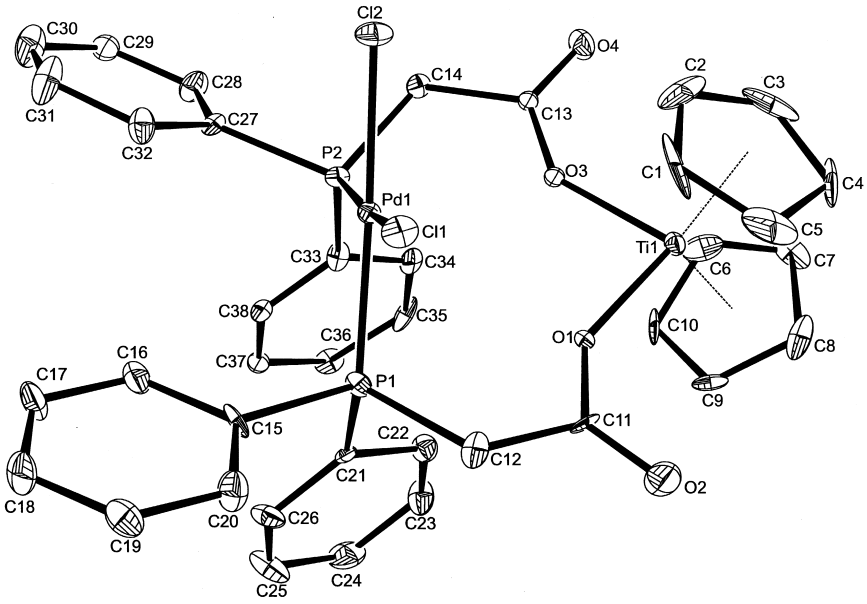


Fig. 2. ORTEX plot of the molecular structure of the 1:1 adduct of compound **3** and $PdCl_2$ solvated with $3CH_2Cl_2$ showing the labelling scheme. The dichloromethane molecules and hydrogen atoms are omitted for clarity. Thermal ellipsoids are at the 30% probability level.

forming neutral trimetallic acyclic complexes by bonding to two group 11 (Cu or Au) metal centres. In each case, the diphenylphosphinoacetate ligands remain O-unidentate with respect to the titanium. These products are therefore related to, but quite distinct in type from, the cationic tetranuclear $[Cp_2Ti\{\mu\text{-}OC(O)C_5H_4N\text{-}p\}_2PtL_2]_2[CF_3SO_3]_4$ complexes (L = PEt_3 or 0.5 dppp) isolated by Stang and Persky [14] from *cis*-$[PtL_2(OSO_2CF_3)_2]$ and $[Cp_2Ti(\text{iso-nicotinate})_2]$. The binuclear complexes $[Cp_2Ti\{\mu\text{-}OC(O)CH_2PPh_2\}_2MCl_2]$ (M = Pd or Pt) have been prepared from $[MCl_2(NCPh)_2]$ and the trinuculear $[Cp_2Ti\{\mu\text{-}OC(O)CH_2PPh_2\}_2(CuCl)_2]$ directly from Cu(I) chloride. One significant feature concerning the syntheses of these compounds is that they can be prepared at least equally well, and often better, from methane elimination reactions of $[Cp_2TiMe_2]$ with the neutral P-donor diphenylphosphinoacetic acid complexes $[MCl_2(Ph_2PCH_2CO_2H)_2]$ (M = Pd or Pt) and $[M'Cl(Ph_2PCH_2CO_2H)]$ (M′ = Cu or Au) that we have reported previously [17]. For the complexes involving group 11 metals, the silver complex has a 1:1 Ti:Ag stoichiometry whereas the copper and gold products both have 1:2 Ti:M′ stoichiometries. The silver complex $[Cp_2Ti\{\mu\text{-}OC(O)CH_2PPh_2\}_2AgCl]$ has been prepared both from the direct reaction of AgCl with $[Cp_2Ti\{OC(O)CH_2PPh_2\}_2]$ and from the reaction of silver diphenylphosphinoacetate with $[Cp_2TiCl_2]$.

The silver complex has a large IR ($\nu_{asym} - \nu_{sym}\ CO_2$) separation of around 370 cm^{-1}, indicative of the expected O-unidentate bonding of the carboxylates to Ti(IV). The single ^{31}P NMR resonance and the magnitude of the ^{107}Ag–^{31}P and ^{109}Ag–^{31}P coupling constants are reasonable for a silver–bisphosphine complex [27]. These results coupled with the mass spectrometric data, which show no significant fragments of mass above that of $[Cp_2Ti\{\mu\text{-}OC(O)CH_2PPh_2\}_2Ag]^+$, suggest that the complex is a bimetallocyclic three-coordinate silver species. For the copper and gold complexes $[Cp_2Ti\{\mu\text{-}OC(O)PPh_2\}_2(M'Cl)_2]$, the gold product certainly contains linear two-coordinate PAuCl moieties with both an IR ν(AuCl) and a ^{31}P NMR chemical shift almost identical to those of the structurally characterised [17] $[AuCl(Ph_2PCH_2CO_2H)]$ (IR ν(AuCl) 335 cm^{-1}; ^{31}P NMR δ +25 ppm). The mass spectrum contains a parent ion supporting this proposal, other fragments involving loss of chloride and/or cyclopentadienyl units. On the other hand, the copper complex is unlikely to contain two-coordinate Cu(I). If it did, an IR ν(CuCl) at around 400 cm^{-1} may be expected but no such band could be assigned. The ^{31}P NMR δ of −12.4 ppm is very similar to that of $[CuCl(Ph_2PCH_2CO_2H)]$ (δ of −13.3 ppm) which was suggested [17] to be tetrameric with a cubane or step structure. The present complex could be similar. The ^{31}P NMR δ values of the group 11 metal complexes are all downfield of that of the parent $[Cp_2Ti\{OC(O)CH_2PPh_2\}_2]$ as a result of the additional bonding from phosphorus. The coordination shifts, $\Delta\delta$, increase significantly on progressing from copper through to gold ($\Delta\delta$ values of 5.2, 15.8 and 42.5 ppm for the copper, silver and gold complexes, respectively).

The square planar palladium and platinum complexes $[Cp_2Ti\{\mu\text{-}OC(O)CH_2PPh_2\}_2MCl_2]$ have been isolated from both preparative routes but are less soluble than the group 11 metal complexes, the very low solubility of the platinum complex in suitable solvents precluding the acquisition of NMR data. For the palladium complex, the ^{31}P NMR chemical shift is close to that of $[PdCl_2(Ph_2PCH_2CO_2H)_2]$ [17]. These two complexes, as confirmed by the X-ray crystal structure determination of the palladium complex, involve *cis*-$[MCl_2P_2]$ geometry with ten-atom $\overline{TiOCCPMPCCO}$ rings. The precursor $[PdCl_2(Ph_2PCH_2CO_2H)_2]$ has [17] a

trans square planar geometry when crystallised from aqueous ethanol so that in its reaction with $[Cp_2TiMe_2]$ to produce $[Cp_2Ti\{\mu\text{-}OC(O)CH_2PPh_2\}_2PdCl_2]$ a rearrangement of the ClPdCl and PPdP arrays from *trans* to *cis* must occur. Large IR ($\nu_{asym} - \nu_{sym}$ CO_2) differences for both complexes confirm the expected O-unidentate coordination of the carboxylates to titanium and the detection of two IR (νMCl) stretches supports the presence of *cis*-$[MCl_2P_2]$ arrangements.

A crystal structure determination of the palladium complex, as a tris(dichloromethane) solvate, confirms that the titanium has a distorted tetrahedral environment comprising two cyclopentadienyl and two O-unidentate carboxylate ligands (Fig. 2). The distortion can be assessed by considering the centroids, Z, of the cyclopentadienyl rings, the Z–Ti–Z angle being 131.6° and the O(1)–Ti–O(3) angle 89.4(3)°. The carboxylates are also P-bonded to the palladium to produce the ten-atom ring mentioned above. The Ti···Pd distance across the ten-atom ring is 4.18 Å indicating the absence of direct metal–metal interaction, unlike, for example, the square planar Rh(I) complex $[Cp_2Ti(SCH_2CH_2CH_2PPh_2)_2Rh][BF_4]$ in which the Ti···Rh distance is only 3.127(2) Å [28]. The *cis*-$[PdCl_2P_2]$ square planar arrangement is distorted, the P–Pd–P angle opening to 103.93(13)° and the Cl–Pd–P angles closing to 83.12(13) and 84.63(13)°. The Pd–P bond lengths [2.259(4), 2.277(4) Å] are slightly shorter than those found [17] for the three independent molecules in *trans*-$[PdCl_2(Ph_2PCH_2CO_2H)_2]\cdot 0.33H_2O\cdot 0.33EtOH$ [2.326(1), 2.309(1), 2.337(2) Å]. Conversely, the Pd–Cl bond lengths are longer [2.348(4), 2.339(4) Å] when compared to those of the above solvated diphenylphosphinoacetic acid complex [2.305(1), 2.303(1), 2.295(1) Å]. Some comparisons and contrasts with the structure of the parent $[Cp_2Ti\{OC(O)CH_2PPh_2\}_2]$ are instructive. The markedly inequivalent diphenylphosphinoacetate ligands of $[Cp_2Ti\{OC(O)CH_2PPh_2\}_2]$, as illustrated by Ti–O and C–O bond length and Ti–O–C bond angle differences, become essentially equivalent in the palladium complex with respect to the titanium centre, the Ti–O and C–O bond length differences being 0.01 Å or less and the Ti–O–C angles showing only a difference of 0.7°. The average Ti–C (ring) distances of 2.35(2) and 2.37(2) Å are in good agreement with those of $[Cp_2Ti\{OC(O)CH_2PPh_2\}_2]$, [2.372(7), 2.360(8) Å], and many other bis(cyclopentadienyl)Ti(IV) compounds [25].

Finally, we have illustrated the versatility of this type of reaction by using the potentially N- and S-donor carboxylates, nicotinate and thiophenoxyacetate, in place of the P-bonding diphenylphosphinoacetate but in a more restricted range of examples. In this manner, analogous $[Cp_2Ti\{\mu\text{-}OC(O)C_5H_4N\text{-}m\}_2MCl_2]$ (M = Pd and Pt) and $[Cp_2Ti\{\mu\text{-}OC(O)CH_2SPh\}_2PdCl_2]$ complexes have been isolated as orange, rather insoluble, solids from reactions of the appropriate $[Cp_2Ti\{OC(O)R\}_2]$ with $[MCl_2(NCPh)_2]$. These products will similarly possess ten-atom TiOCCEMECCO rings (E = N or S).

Supplementary data

Crystallographic data are available from CCDC, 12 Union Road, Cambridge CB2 1EZ, UK (fax: +44-1223-336033; e-mail: deposit@ccdc.cam.ac.uk), on request, quoting the deposition numbers CCDC 136188 and CCDC136189.

Acknowledgements

We thank EPSRC for a maintenance grant to T.J.P.

References

[1] F. Lindenberg, T. Shribman, J. Sieler, E. Hey-Hawkins, M.S. Eisen, J. Organomet. Chem. 515 (1996) 19.
[2] A. Muller, E. Krahn, Angew. Chem., Int. Ed. Engl. 34 (1995) 1071.
[3] K.D. Demadis, D. Coucouvanis, Inorg. Chem. 34 (1995) 436.
[4] M. Berardini, T.J. Emge, J.G. Brennan, Inorg. Chem. 32 (1993) 2724.
[5] D.W. Stephan, Coord. Chem. Rev. 95 (1989) 41.
[6] D.W. Stephan, T.T. Nadasdi, Coord. Chem. Rev. 147 (1996) 147.
[7] D.G. Dick, Z. Hou, D.W. Stephan, Organometallics 11 (1992) 2378.
[8] T.S. Targos, R.P. Rosen, R.R. Whittle, G.L. Geoffroy, Inorg. Chem. 24 (1985) 1375.
[9] T.T. Nadasdi, D.W. Stephan, Inorg. Chem. 33 (1994) 1532.
[10] M. Sato, T. Yoshida, J. Organomet. Chem. 94 (1975) 403.
[11] H.-M. Gau, C.-T. Chen, T.T. Jong, M.-Y. Chien, J. Organomet. Chem. 448 (1993) 99.
[12] Y. Huang, R.J. Drake, D.W. Stephan, Inorg. Chem. 32 (1993) 3022.
[13] G.S. White, D.W. Stephan, Organometallics 7 (1988) 903.
[14] P.J. Stang, N.E. Persky, Chem. Commun. (1997) 77.
[15] S.C. Dixit, R. Sharan, R.N. Kapoor, Inorg. Chim. Acta 158 (1989) 109.
[16] S.C. Dixit, R. Sharan, R.N. Kapoor, Inorg. Chim. Acta 133 (1987) 251.
[17] D.A. Edwards, M.F. Mahon, T.J. Paget, Polyhedron 17 (1998) 4121.
[18] P. McArdle, J. Appl. Crystallogr. 27 (1994) 438.
[19] G.M. Sheldrick, Acta Crystallogr., Sect. A 46 (1990) 467.
[20] G.M. Sheldrick, A Computer Program for Crystal Structure Refinement, University of Göttingen, 1993.
[21] K. Doppert, H.-P. Klein, U. Thewalt, J. Organomet. Chem. 303 (1986) 205.
[22] C.R. Lucas, E.J. Gabe, F.L. Lee, Can. J. Chem. 66 (1988) 429.
[23] D.H. Gibson, Y. Ding, J.F. Richardson, M.S. Mashuta, Acta Crystallogr., Sect. C 52 (1996) 1614.
[24] D.A. Edwards, M.F. Mahon, T.J. Paget, Polyhedron 16 (1997) 25.
[25] D.M. Hoffmann, N.D. Chester, R.C. Fay, Organometallics 2 (1983) 48.
[26] S. Civis, J. Podlahova, J. Loub, J. Jecny, Acta Crystallogr., Sect. B 36 (1980) 1395.
[27] E.L. Muetterties, C.W. Alegranti, J. Am. Chem. Soc. 94 (1972) 6386.
[28] G.S. White, D.W. Stephan, Organometallics 6 (1987) 2169.

PERGAMON

www.elsevier.nl/locate/poly

Polyhedron 19 (2000) 765–770

POLYHEDRON

Polymerization of aniline on copper phosphonate materials

Gary B. Hix [a,b], Victoria C. Maddocks [b], Kenneth D.M. Harris [b,*]

[a] *School of Chemistry, University of St Andrews, St Andrews, Fife KY16 9ST, UK*
[b] *School of Chemistry, University of Birmingham, Edgbaston, Birmingham B15 2TT, UK*

Received 19 April 1999; accepted 13 January 2000

Abstract

We report the use of layered copper phosphonate materials for the oxidative polymerization of aniline. The use of copper carboxyethylphosphonate results in the formation of the perinigraniline form of polyaniline in the interlayer region of the host structure, giving rise to an increase in the interlayer spacing by 10.2 Å. For copper phenylphosphonate, the emeraldine form of polyaniline is generated, although there is no evidence for intercalation within the interlayer region of the host material. Copper methylphosphonate is destroyed during the process of polymerization of aniline, yielding bulk copper metal as the only solid product. The results demonstrate the diversity of behaviour that may result from the use of structurally related, although chemically different, host materials for the polymerization of aniline. ©2000 Elsevier Science Ltd All rights reserved.

Keywords: Aniline polymerization; Copper phosphonates; Intercalation compounds

1. Introduction

Polyaniline (PANI) has been much studied as a conducting polymer [1–6], and may be described by the general formula $\{[-(C_6H_4)-NH-(C_6H_4)-NH-]_{1-x}[-(C_6H_4)-N=(C_6H_4)=N-]_x\}_n$, where the value of x ($0 \leq x \leq 1$) defines the oxidation state of the polymer [7]. The forms with $x \neq 0$ have the capacity to be protonated by non-oxidizing acids, with protonation occurring on the imine (–N=) nitrogen atoms [8]. The formation of polyaniline chains separated (insulated) from each other by microporous dielectric host materials has received considerable attention in recent years [9–13]. As a result of such confinement of the polymer chains, the polymer may display quantum-size effects in its electrical and optical properties [14]. As a consequence, formation and confinement of a given polymer in different host materials may allow the physical properties to be controlled and optimized for specific applications of the material.

A number of layered host materials have been reported [9,10,15–21] to catalyse the polymerization of aniline, including montmorillonite, vanadium pentoxide, iron oxychloride, copper-exchanged α-zirconium phosphate, zirconium phosphonates and copper-containing layered double hydroxide materials. Previous reports [9,10,19–21] of the formation of PANI using layered copper-containing materials indicate that the polymer can be formed either in the interlayer region or on the external surfaces of the material [9,10]. In general, in these preparations, the PANI is produced in the emeraldine base form (with $x = 0.5$). The presence of Cu(II) is thought to enhance the oxidation of aniline by ambient O_2, as a consequence of the accessible Cu(I) oxidation state [9]. In a number of these systems, however, complete reduction to produce bulk copper metal has been observed.

This paper reports the use of layered copper phosphonate materials to bring about the polycondensation of aniline. Copper phosphonates, $Cu(O_3PR)\cdot H_2O$, are layered materials in which layers of five-coordinate copper atoms are linked via $-PO_3$ pyramids. The phosphorus atom is tetrahedrally coordinated, and the fourth vertex is occupied by an organic functional group R [22]. As a variety of groups R can be used, there is considerable scope for fine-tuning both the structural and chemical properties of these materials. In particular, chemical reactions in which the interlayer region is accessed by the reactant molecules may be influenced significantly by the nature of the host material. For copper phosphonates, the presence of a redox active metal leads to the possibility of electron transfer between the intercalated guest species and the host material, with potentially important implications concerning electronic conductivity. The copper phosphonate materials chosen for this study were copper methylphosphonate ($R = CH_3$), copper phenylphosphonate ($R = C_6H_5$) and copper carboxyethylphosphonate ($R = CH_2CH_2CO_2H$).

* Corresponding author. Fax: +44-121-414-7473; e-mail: k.d.m.harris@bham.ac.uk

0277-5387/00/$ - see front matter ©2000 Elsevier Science Ltd All rights reserved.
PII S0277-5387(00)00307-7

2. Experimental

2.1. Synthetic aspects

Copper carboxyethylphosphonate (abbreviated CuCEP) was synthesized following the method of Drumel et al. [23]. Copper nitrate hydrate and 2-carboxyethylphosphonic acid (molar ratio 1:1) were placed in a solution of 5% deionized water in acetone, which was then kept at 60°C for 5 days. The solid was recovered by centrifugation, washed with deionized water and dried in air at 60°C.

Copper phenylphosphonate (abbreviated CuPhP) was synthesized using the method of Hayashi and Hudson [24]. Basic copper nitrate was prepared by adding copper oxide (8.0 g, 0.1 mol) to an aqueous solution of copper nitrate (100 cm^3, 2.4 mol dm^{-3}) with vigorous stirring at ambient temperature. After 16 h, the dark green solid was filtered off, washed with deionized water and ethanol, and then dried in air at 60°C. This solid (1 g) was then suspended in an aqueous solution of phenylphosphonic acid (160 cm^3, 0.1 mol dm^{-3}) and the pH adjusted to 6 by addition of NaOH solution (1 mol dm^{-3}). The suspension was maintained at 65°C and stirred for 16 h. Copper phenylphosphonate was recovered by filtration, washed with deionized water, and then dried in air at 60°C.

Copper methylphosphonate (abbreviated CuMeP) was prepared following a synthetic method that we have published previously [25]. Copper hydroxide and methylphosphonic acid were mixed in a 1:1 molar ratio. This mixture was placed in a sealed glass tube and heated at 100°C for 48 h. After cooling, the product was washed with deionized water and dried in air at 60°C.

2.2. Polymerization of aniline

A quantity (typically 0.5 g) of the copper phosphonate materials was placed in a flask with 50 cm^3 of pure aniline, and the mixture was refluxed overnight (at 184°C). The resulting solutions were black in colour. The solid residues were recovered from these solutions by filtration, and washed with acetone prior to drying in air at ambient temperature. The black colour of the solutions is probably due to colloidal copper (perhaps with some contribution from any oligomers of PANI present in the solution), although here we focus on the solid products recovered by filtration rather than the remaining liquid (colloidal) phase.

2.3. Characterization

Powder X-ray diffraction patterns were recorded using Cu $K\alpha_1$ radiation on a Siemens D5000 diffractometer, operating in transmission mode with a primary beam Ge monochromator. Fourier transform IR (FTIR) spectra were recorded on a Perkin Elmer Paragon 1000 FTIR spectrometer at a spectral resolution of 2 cm^{-1}; the samples were prepared as KBr pellets (containing approximately 1% sample). Thermogravimetric analysis (TGA) was carried out on a TA Instruments SDT 2960 simultaneous DTA-TGA thermogravimetric analyser. Samples were heated (at a rate of 10°C min^{-1}) in an alumina crucible to a maximum temperature of 1200°C in an atmosphere of flowing oxygen (100 ml min^{-1}). Recalcined alumina was used as the reference material. For the materials containing PANI (CuPhP–PANI and CuCEP–PANI, see Section 3.1), the copper content was measured using a Philips PU9400X atomic absorption spectrometer. The solutions for analysis were prepared by digesting the samples in concentrated HNO_3 (Analar). The solutions were gently warmed to aid dissolution; after cooling, the solutions were made up to the required volume with distilled water. Standards of 5.0 ppm, 2.5 ppm and 0.5 ppm were prepared by dilution of a commercial copper solution standard.

3. Results and discussion

3.1. General observations

Refluxing the copper phosphonate materials in aniline resulted in the formation of viscous black solutions in which solid products were suspended. This colour change is indicative of polymerization of aniline in each of the reactions carried out. In each case, the solid products were separated by filtration, and we focus here on characterization of these materials. The nature of the recovered solids was different for each of the copper phosphonates considered. For the preparation involving CuMeP, the only crystalline solid recovered (as identified from powder X-ray diffraction) was bulk copper metal. Any other solid residues are presumably either amorphous (and not directly evident from powder X-ray diffraction) or have particle sizes sufficiently small that they are not collected in the filtration procedure. The solid (denoted CuCEP–PANI) recovered from the preparation involving CuCEP was violet in colour. The solid (denoted CuPhP–PANI) recovered from the preparation involving CuPhP was dark green in colour.

The colour of the solid products gives some indication of the oxidation state of the PANI, and the reported [26] colours of different forms of PANI are given together with their classical names in Table 1. The most frequently reported form of PANI resulting from reactions of this type [9,10] is the emeraldine base, which is dark blue in colour and becomes green on protonation.

The dark green colour of CuPhP–PANI suggests that the protonated emeraldine form of polyaniline has been formed. Indeed, this assignment is supported by the fact that, on subsequently suspending the material in a dilute solution of NaOH, a colour change from green to blue is observed (corresponding to deprotonation).

The CuCEP–PANI sample is particularly interesting, as the violet colour suggests that the PANI is produced in the fully oxidized perinigraniline form (note that the colour of this form does not change on protonation). Further reaction

Table 1
Colours and nomenclature for different forms of PANI; in each case the colour of the protonated form is given in brackets

	Colour	Name
$\{-(C_6H_4)-NH-(C_6H_4)-NH-\}_n$	yellow	leucoemeraldine base
$\{[-(C_6H_4)-NH-(C_6H_4)-NH-]_{0.75}[-(C_6H_4)-N=(C_6H_4)=N-]_{0.25}\}_n$	blue (light green)	protoemeraldine base
$\{[-(C_6H_4)-NH-(C_6H_4)-NH-]_{0.5}[-(C_6H_4)-N=(C_6H_4)=N-]_{0.5}\}_n$	dark blue (green)	emeraldine base
$\{[-(C_6H_4)-NH-(C_6H_4)-NH-]_{0.25}[-(C_6H_4)-N=(C_6H_4)=N-]_{0.75}\}_n$	blue–black (blue)	nigraniline base
$\{-(C_6H_4)-N=(C_6H_4)=N-\}_n$	violet (violet)	perinigraniline base

of CuCEP–PANI with dilute hydrochloric acid and dilute NaOH did not result in any colour change. As discussed below, we believe that the PANI is in the interlayer region in CuCEP–PANI, which probably renders it inaccessible to external reagents. To our knowledge, the perinigraniline form of PANI has not been reported previously to be obtained from a reaction of this type.

3.2. Sample analyses

For CuCEP–PANI, on the initial assumption that the sample contains only CuCEP and PANI, the CHN analysis (Table 2) leads to the composition $[Cu(O_3PCH_2CH_2CO_2H)] \cdot [C_6H_4N]_{0.95}$. However, while this accounts for the relative values of the percentages of C, H and N, it does not account for the absolute values of these percentages. Furthermore, this stoichiometry suggests that the residue ($Cu_2P_2O_7$) in the TGA experiments should represent 50.0% of the original mass (whereas the actual residue is 64.7% of the original mass), and suggests that the copper content is 16.4% (whereas the actual copper content found from analysis is 40.0%). These discrepancies are due to the presence of bulk copper metal (as evident from powder X-ray diffraction) in addition to CuCEP and PANI. During the TGA experiment, the bulk copper metal is oxidized to CuO, accounting for a mass increase centred around 550°C. On this basis, the residue from the TGA experiment (after heating to 1200°C) comprises $Cu_2P_2O_7$ (from the CuCEP) and CuO (from the bulk copper metal). In summary, the overall stoichiometry of the recovered product is $[Cu(O_3PCH_2CH_2CO_2H)] \cdot [C_6H_4N]_{0.95}[Cu]_{1.3}$.

For CuPhP–PANI, similar analysis (Table 2) leads to the following overall stoichiometry of the recovered product: $[Cu(O_3PC_6H_5)] \cdot [C_6H_4N]_{1.1}[Cu]_{0.1}$. In this case, the amount of bulk copper metal within the sample is substantially smaller than for the CuCEP–PANI sample discussed above. The presence of some bulk copper metal in CuPhP–PANI is again evident from powder X-ray diffraction, although this amount is apparently not sufficient to give an observable mass increase in the TGA experiment.

The TGA trace for CuPhP–PANI shows two major mass losses centred at 185 and 385°C, implying that the organic material in CuPhP–PANI is lost in two steps. These mass losses may be attributed to the loss of PANI (see also Section 3.3) and the organic part of CuPhP respectively. On the other hand, the TGA trace for CuCEP–PANI shows only one major mass loss centred at 378°C, suggesting that all the organic material (PANI and the organic part of CuCEP) is lost in one step. In both cases, there is a further mass loss at ca. 640°C, arising from the final oxidation to yield $Cu_2P_2O_7$.

3.3. Powder X-ray diffraction

The powder X-ray diffraction patterns for all the solid materials contain peaks characteristic of bulk copper metal. For the experiment involving CuMeP, bulk copper metal is the only crystalline product, whereas for the experiments involving CuCEP and CuPhP, bulk copper metal is not the major product. The powder X-ray diffraction patterns for CuCEP–PANI and CuPhP–PANI have an intense series of $(00l)$ peaks, suggesting that the layered nature of the host materials is retained during the formation of PANI. However, as now discussed, significant changes in the positions of these peaks indicate changes in the interlayer spacing. For CuCEP–PANI, no peaks with $h \neq 0$ or $k \neq 0$ are discernible above the noise level in the powder X-ray diffraction pattern, whereas for CuPhP–PANI, only very few peaks with $h \neq 0$ or $k \neq 0$ are discernible.

Table 2
Results of analyses of CuPhP–PANI and CuCEP–PANI; the experimental errors are ca. 0.3% in the CHN analysis and ca. 0.5% in the Cu analysis; the TGA residue represents $Cu_2P_2O_7 + CuO$

	CuPhP–PANI	CuCEP–PANI
C (%)	46.7	26.9
H (%)	4.2	2.3
N (%)	4.8	3.4
Cu (%)	23.7	40.0
TGA residue (theoretical)	42.9 (48.5%)	64.7 (66.5%)
Composition	$[Cu(O_3PC_6H_5)] \cdot [C_6H_4N]_{1.1}[Cu]_{0.1}$	$[Cu(O_3PC_2H_4CO_2H)] \cdot [C_6H_4N]_{0.95}[Cu]_{1.3}$

For CuCEP–PANI, powder X-ray diffraction (Fig. 1) shows that the formation of PANI is associated with an increase in the interlayer spacing of the CuCEP host material, providing direct evidence that the PANI is located within the interlayer region. The increase in the interlayer spacing is 10.2 Å. It is reported that inclusion of PANI within layered host materials leads to an increase in the interlayer spacing of ca. 4.2 Å if the phenyl rings are oriented parallel to the host layers [9] and ca. 8.6 Å if the phenyl rings are oriented perpendicular to the host layers [10]. On this basis, we deduce that the PANI included within CuCEP has a perpendicular orientation of the rings with respect to the layers of the host material.

In contrast, powder X-ray diffraction (Fig. 2) for CuPhP–PANI shows no evidence for an increase in the interlayer spacing, but instead a slight decrease from 14.5 to 12.7 Å is observed (note that powder X-ray diffraction patterns recorded at lower diffraction angles (higher *d*-spacing) than those shown in Fig. 2 confirm that no new peaks appear at very low diffraction angle (such peaks would indicate an increase in the interlayer spacing)). The slight decrease in the interlayer spacing in CuPhP–PANI suggests that some

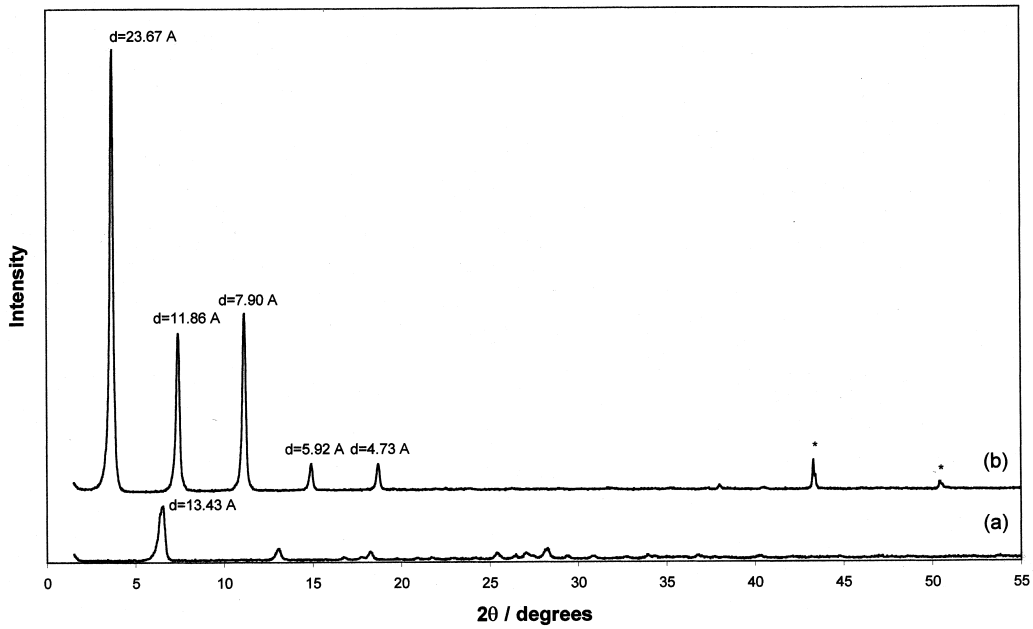


Fig. 1. Powder X-ray diffraction patterns (Cu Kα_1 radiation) for (a) CuCEP and (b) CuCEP–PANI. The *d*-spacings for selected (00*l*) peaks due to the layered metal phosphonate material are indicated. Peaks marked with an asterisk are due to bulk copper metal.

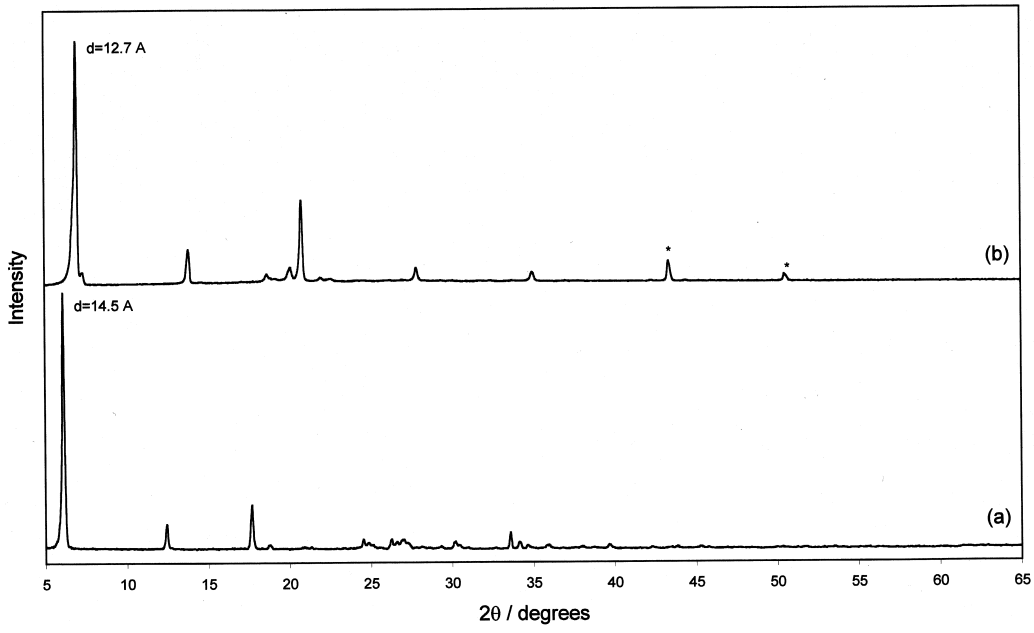


Fig. 2. Powder X-ray diffraction patterns (Cu Kα_1 radiation) for (a) CuPhP and (b) CuPhP–PANI. The *d*-spacings for selected (00*l*) peaks due to the layered metal phosphonate material are indicated. Peaks marked with an asterisk are due to bulk copper metal.

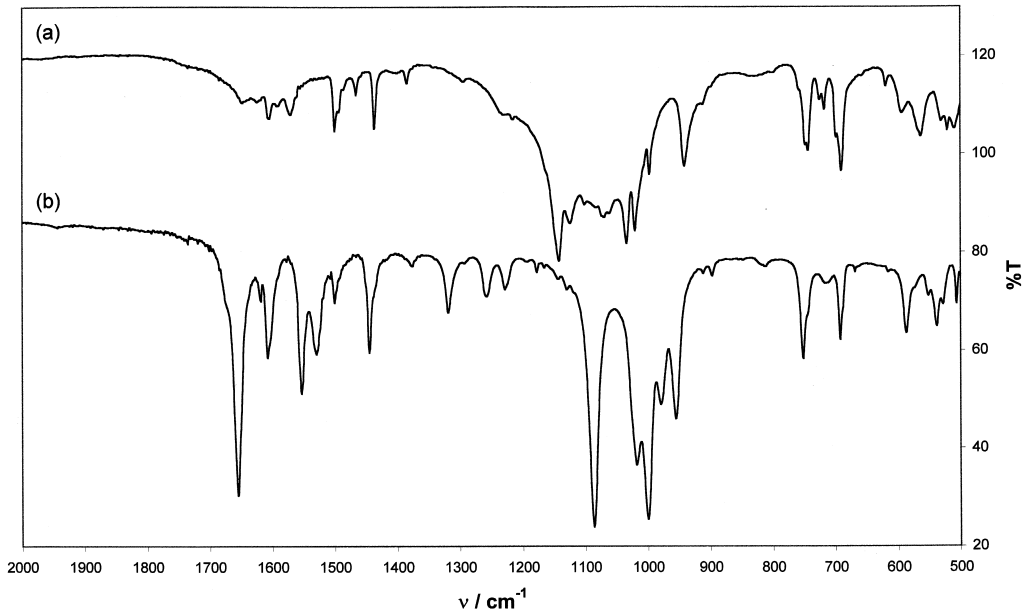


Fig. 3. FTIR spectra for (a) CuPhP–PANI and (b) CuCEP–PANI.

structural rearrangement of the parent host material (perhaps resulting from loss of water) is associated with the polymerization reaction. Our observations suggest that the formation of PANI in this system does not actually involve intercalation of PANI within the interlayer region, but may instead occur on the external surface of the CuPhP particles. Presumably some amount of PANI may be retained on the external surfaces of the CuPhP particles (giving rise to the colour of the solid product). However, the relative amount of PANI in the CuPhP–PANI sample recovered (see Section 3.2) implicates the presence of an additional phase of PANI (i.e. in addition to PANI on the external surfaces of the CuPhP particles). As there is no evidence from powder X-ray diffraction for any crystalline phase other than CuPhP, we may conclude that the excess PANI is present as an amorphous phase.

3.4. Infrared spectroscopy

Infrared spectroscopy has been used previously [8,10] to assign the oxidation state of PANI. The assignment relies on the relative intensities of peaks at ca. 1500 and 1600 cm^{-1}, which are associated with phenyl and quinoid ring vibrations respectively. The IR spectrum of the fully reduced form (leucoemeraldine) of PANI exhibits only a very weak peak at ca. 1600 cm^{-1}, and this peak becomes apparent as the level of oxidation of PANI increases (i.e. as the proportion of quinoid units increases). For CuPhP–PANI and CuCEP–PANI, peaks are observed in both regions ca. 1500 and ca. 1600 cm^{-1} (Fig. 3, Table 3). Other bands characteristic of the formation of PANI are at ca. 1290 cm^{-1} (medium) and ca. 820 cm^{-1} (weak), and are assigned as ring breathing and out-of-plane CH bending respectively. In addition, two sharp peaks observed in the ranges 770–730 cm^{-1} and 710–630 cm^{-1} are characteristic of five adjacent ring hydrogens (representing the chain end of the polymer). The fact that these bands are observed may indicate that the PANI is present as short oligomers. No bands characteristic of aniline or protonated aniline are observed for either CuPhP–PANI or CuCEP–PANI.

Table 3
Diagnostic vibration frequencies observed in FTIR spectra of CuPhP–PANI and CuCEP–PANI

CuPhP–PANI	CuCEP–PANI	Assignment
	1654	C=O carboxylic acid
1603	1607	ring mode (quinoid)
1499	1499	ring mode (phenyl)
1033	1085	ν(P–O) XPO_3 stretching mode
1019	1017	ν(P–O) XPO_3 stretching mode
996	998	ν(P–O) XPO_3 stretching mode
745	751	δ(C–H) out-of-plane 5 adjacent H atoms
690	692	δ(C–H) out-of-plane 5 adjacent H atoms
592	585	aromatic ring deformation
508	506	aromatic ring deformation

Bands associated with the layered copper phosphonate host materials are also observed in the region 1150–990 cm^{-1}, representing P–O stretching modes of the phosphonate group. The peak at 1654 cm^{-1} in the spectrum of CuCEP–PANI arises from the C=O group of the carboxylic acid. This frequency is slightly lower than that expected for a free carboxylic acid (ca. 1700 cm^{-1}) and may constitute evidence for an interaction between the carboxylic acid group and PANI in the interlayer region.

4. Conclusions

In summary, all three copper phosphonate materials used in this work give rise to polymerization of aniline. It is thought

that copper aids the oxidation of aniline by atmospheric oxygen, but in doing so, the copper phosphonate material is itself destroyed in the process. Reduction of Cu(II) to bulk copper metal is evident in the powder X-ray diffraction patterns of all the samples recovered. For CuMeP, bulk copper metal is the only crystalline product isolated following the polymerization reaction. For CuCEP and CuPhP, PANI is formed with retention (at least partially) of the layered copper phosphonate host material. For CuPhP–PANI, the emeraldine form of PANI is produced, but formation on the surfaces of the CuPhP particles (rather than within the interlayer region) is implicated. As such there is little change in the powder X-ray diffraction pattern of the layered copper phosphonate host material, and, as shown by the analyses, a relatively small quantity of bulk copper metal is produced. For CuCEP–PANI, the PANI is present as the perinigraniline form, and powder X-ray diffraction provides direct evidence that the PANI is retained within the layered copper phosphonate host material. The higher oxidation state of the PANI is reflected by the larger quantity of bulk copper metal produced (with the implication that the reduction of copper is associated with oxidation of PANI). In conclusion, the results reported here provide new insights concerning preparative aspects of PANI through reactions in constrained solid state environments, and demonstrate the diversity of behaviour that may result from the use of structurally related, although chemically different, host materials for this reaction. Ultimately, the observed differences in the course of the reactions in the three different copper phosphonate materials reflect, inter alia, the differing relative stabilities of these materials as well as the differing relative accessibilities of the metal centres to the aniline guest molecules. Clearly a future programme of experimental research, including the use of both in situ and ex situ probes of the structural and chemical evolution of the system as a function of reaction progress, should shed further light on mechanistic aspects of the reactions to produce PANI as well as the concomitant structural degradation of the copper phosphonate materials.

Acknowledgements

We thank Professor J. Rozière and Dr D. Jones for useful discussions and Mrs Sylvia Williamson (University of St Andrews) for sample analyses. We are grateful to EPSRC for financial support.

References

[1] A.G. MacDiarmid, J.C. Chiang, A.F. Richter, A.J. Epstein, Synth. Met. 18 (1987) 285.
[2] J.C. Chiang, A.G. MacDiarmid, Synth. Met. 13 (1986) 193.
[3] F. Wudl, R.O. Angus Jr., F.L. Lu, P.M. Allemand, D.F. Vachon, M. Nowak, Z.X. Lui, A.J. Heeger, J. Am. Chem. Soc. 109 (1987) 3677.
[4] D.F. Vachon, R.O. Angus Jr., F.L. Lu, M. Nowak, Z.X. Lui, H. Shaffer, F. Wudl, A.J. Heeger, Synth. Met. 18 (1987) 297.
[5] E.M. Genies, M. Lapowski, C. Santier, E. Viell, Synth. Met. 18 (1987) 631.
[6] S. Ghosh, G.A. Bowmaker, R. Cooney, J. Mater. Chem. 7 (1997) 597.
[7] G.E. Asturias, A.G. MacDiarmid, R.P. Mccall, A.J. Epstein, Synth. Met. 29 (1989) E157.
[8] L.W. Shacklette, J.F. Wolf, S. Gould, R.H. Baughman, J. Chem. Phys. 88 (1988) 3955.
[9] G.L. Rosenthal, J. Caruso, S.G. Stone, Polyhedron 13 (1994) 1311.
[10] T. Challier, R.C.T. Slade, J. Mater. Chem. 4 (1994) 367.
[11] P. Enzel, T. Bein, J. Phys. Chem. 93 (1989) 6270.
[12] C.-G. Wu, T. Bein, Science 264 (1994) 1757.
[13] C.-G. Wu, T. Bein, J. Mater. Chem. 6 (1994) 1109.
[14] V. Mehrotra, E.P. Giannelis, Solid State Commun. 77 (1991) 155.
[15] P. Cloos, A. Moreale, C. Broers, C. Badot, Clay Miner. 14 (1979) 307.
[16] T.C. Chang, S.Y. Ho, K.J. Chao, J. Chinese Chem. Soc. 39 (1992) 209.
[17] M.G. Kanatzidis, C.G. Wu, H.O. Marcy, D.C. DeGroot, C.R. Kannewurf, J. Am. Chem. Soc. 111 (1989) 4139.
[18] M.G. Kanatzidis, C.G. Wu, H.O. Marcy, D.C. DeGroot, C.R. Kannewurf, A. Kostikas, V. Papaefthymiou, Adv. Mater. 2 (1990) 364.
[19] D.J. Jones, R. El Mejjad, J. Rozière, in: T. Bein (Ed.), Supramolecular Architecture: Synthetic Control in Thin Films and Solids, ACS Symp. Ser., vol. 499, ACS, Washington, DC, 1992, p. 220.
[20] B. Bonnet, R. El Mejjad, M.H. Herzog, D.J. Jones, J. Rozière, Mater. Sci. Forum 91–93 (1992) 177.
[21] P. Maireles-Torres, P. Olivera-Pastor, E. Rodríguez-Castellon, A. Jiménez-López, J. Inclusion Phenom. Mol. Recog. Chem. 14 (1992) 327.
[22] Y. Zhang, A. Clearfield, Inorg. Chem. 31 (1992) 2821.
[23] S. Drumel, P. Janvier, P. Barboux, M. Bujoli-Doeuff, B. Bujoli, Inorg. Chem. 34 (1995) 148.
[24] H. Hayashi, M.J. Hudson, J. Mater. Chem. 5 (1995) 115.
[25] G.B. Hix, K.D.M. Harris, J. Mater. Chem. 8 (1998) 579.
[26] W.-S. Huang, B.D. Humphrey, A.G. MacDiarmid, J. Chem. Soc., Faraday Trans. 82 (1986) 2385.

PERGAMON

www.elsevier.nl/locate/poly

Polyhedron 19 (2000) 771–777

POLYHEDRON

Optical spectroscopy of neodymium(III) complexes with diethylenetriaminepentaacetic acid in solution and in $[C(NH_2)_3]_2[Nd(dtpa)(H_2O)]\cdot 7H_2O$ single crystal

Anna Mondry *, Przemysław Starynowicz

Faculty of Chemistry, University of Wrocław, Joliot-Curie 14, 50-383 Wrocław, Poland

Received 8 November 1999; accepted 3 January 2000

Abstract

The crystal structure of $[C(NH_2)_3]_2[Nd(dtpa)(H_2O)]\cdot 7H_2O$ (H_5dtpa = diethylenetriaminepentaacetic acid) has been determined. Electronic absorption spectra of a single crystal of the $[C(NH_2)_3]_2[Nd(dtpa)(H_2O)]\cdot 7H_2O$ compound were measured at room and liquid helium temperatures. In order to investigate the formation and structure of Nd^{III}–dtpa species occurring in solution, the spectral results for the crystal were compared with those of the Nd^{III}–dtpa (1:1) complex in solution. The analysis of spectral properties of this system may be applied for solutions of coordination chemistry problems encountered in lanthanide polyaminopolycarboxylates. ©2000 Elsevier Science Ltd All rights reserved.

Keywords: Contrast agents; Crystal structures; Diethylenetriaminepentaacetate; Lanthanides; Neodymium

1. Introduction

Our previous studies based on electronic absorption spectroscopy of lanthanide complexes with multidonor ligands in solution and single crystals have proved the usefulness of this method in the elucidation of such problems as the structure of complexes, the coordination environment of the Ln^{III} ion and the role of ligand polarizability [1–3]. Among lanthanide chelates with acyclic polyaminopolycarboxylates, the coordination chemistry of the Ln^{III} complexes with diethylenetriaminepentaacetic acid (H_5dtpa) is well recognized both in solution [4–25] and in the solid state [25–30]. The majority of investigations concern, however, the Gd^{III}–dtpa complex [19–27,31,32]. This compound has for many years been approved clinically as a contrast enhancing agent in magnetic resonance imaging (MRI).

Studies of Ln^{III} ion complexation in solution with the dtpa ligand were carried using various NMR techniques [13–24]. However, the application of those techniques may sometimes be problematic, particularly in cases when two or more species with different coordination modes are in equilibrium. To ascertain how the coordination properties of the Ln^{III}–dtpa system determined by different physical methods will influence its optical behaviour, we decided to study the Nd^{III}–dtpa complex using electron absorption spectroscopy both in the single crystal and in solution.

The aim of this paper is to report the solid-state X-ray structure and UV–Vis absorption spectroscopic results of the $[C(NH_2)_3]_2[Nd(dtpa)(H_2O)]\cdot 7H_2O$ crystal in order to compare its spectral properties with those of the Nd^{III}–dtpa (1:1) system in solution.

2. Experimental

2.1. Materials and sample preparation

A stock solution of neodymium perchlorate was prepared from Nd_2O_3 (99.9%; Merck). The Nd^{III} ion concentration was determined complexometrically using xylenol orange as indicator. The stock solution of H_5dtpa (98%; Aldrich) was prepared by half-neutralization with NaOH. The NaOH solution was also used to adjust the pH of investigated solutions. All measured solutions were prepared with the same ionic strength (0.5 M $NaClO_4$).

Crystals of $[C(NH_2)_3]_2[Nd(dtpa)(H_2O)]\cdot 7H_2O$ were prepared by a slightly changed method described by Ruloff

* Corresponding author. Tel.: +48-71-3204370; fax: +48-71-3282348; e-mail: anm@wchuwr.chem.uni.wroc.pl

0277-5387/00/$ - see front matter ©2000 Elsevier Science Ltd All rights reserved.
PII S0277-5387(00)00308-9

et al. [27]. The molar ratio of Nd_2O_3, H_5dtpa and $[C(NH_2)_3]_2CO_3$ was 1:2:2. After dissolution of the substrates, the solution was alkalized with $[C(NH_2)_3]_2CO_3$ to the final pH 5 and left to crystallization. Large well-formed violet crystals were obtained. The Nd^{III} ion concentration in these crystals was determined by inductively coupled plasma atomic emission spectroscopy (2.185 M). *Anal*. Found: C, 24.6; H, 6.2; N, 16.1; Nd, 19.1. Calc. for $[C(NH_2)_3]_2$-$[Nd(dtpa)(H_2O)]\cdot 7H_2O$: C, 24.1; H, 5.8; N, 15.8; Nd, 18.1%.

The refractive index (n) of the crystal was assumed to be 1.50 and that of the measured solutions − 1.33.

2.2. Crystallography

A suitable crystal was cut from a larger one, placed in a capillary and mounted on a Kuma KM4 diffractometer with κ geometry and a graphite monochromator. The unit cell parameters were determined from angular settings of 37 reflections with 2θ between 18 and 23°. The stability of data collection was monitored with three control reflections remeasured every 100 intensities. The data were corrected for Lorentz and polarization factors, but not for extinction. The position of the neodymium ion was found from a Patterson map; other atoms were found from subsequent difference Fourier syntheses. The C- and N-bonded hydrogen atoms were placed from geometry, and some of the water hydrogen atoms were found from a difference Fourier synthesis. The absorption corrections were calculated with the locally modified ABSORB program [33]. The structure was refined with the full-matrix least-squares method with all non-hydrogen atoms anisotropic and hydrogen atoms isotropic with common temperature factors (separately for C-, N- and O-bonded atoms). The positions of the hydrogen atoms were geometrically constrained (the C- and N-bonded ones) or restrained (the O-bonded ones). The calculations were performed with SHELXS-97 [34] and SHELXL-97 [35] programs with commonly used atom scattering factors and anomalous dispersion corrections [36]. Other details of data collection and the structure refinement are given in Table 1.

Table 1
Crystallographic data for $[C(NH_2)_3]_2[Nd(dtpa)(H_2O)]\cdot 7H_2O$

Empirical formula	$[C(NH_2)_3]_2[Nd(C_{14}H_{18}N_3O_{10})(H_2O)]\cdot 7H_2O$
Colour	violet
Crystal size (mm)	0.5×0.4×0.3
Crystal system	monoclinic
Space group	$P2_1/n$
a (Å)	12.797(7)
b (Å)	16.062(9)
c (Å)	16.390(11)
β (°)	107.90(6)
V (Å^3)	3206(3)
Z	4
M	796.86
D_m (g cm^{-3})	1.63 (by flotation in CH_3Cl–CH_3Br)
D_c (g cm^{-3})	1.651
Absorption coefficient (mm^{-1})	1.706
$F(000)$	1636
λ (Å) (Mo Kα)	0.71073
Scan type	$\omega/2\theta$
θ Range for data collection (°)	2–25
Index ranges h; k; l	0–15; 0–19; −19–18
Reflections collected	5899
Independent reflections	4070 ($R_{int}=0.0496$)
Observed reflections	4070 [$I\geq 3\sigma(I)$]
Quantity minimized	$s=\sum w(F_o^2-F_c^2)^2$
Weighting scheme	$w=1/\sigma^2(F^2)$
No. parameters refined	430
Final R [a]	0.0342
Final R' [b]	0.0753
Goodness-of-fit	3.040
Max., min. residual ρ (e Å^{-3})	0.688, −0.703

[a] $R=\sum|F_o-F_c|/\sum|F_c|$.
[b] $R'=[\sum w(F_o^2-F_c^2)^2/\sum w(F_o^2)^2]^{1/2}$.

2.3. Spectroscopic measurements and calculations

All absorption spectra were recorded on a Cary 5 UV–Vis–near-IR spectrophotometer which was equipped with an Oxford CF 1204 continuous flow helium cryostat for single crystal measurements in the 293–4 K temperature range. The intensities of the 4f–4f transitions (P) and values of the Ω_λ parameters were calculated from the Judd–Ofelt [37,38] relation:

$$P=\chi\,\frac{8\pi^2 mc\sigma}{3h(2J+1)}\sum_{\lambda=2,4,6}\Omega_\lambda(f^n\psi J\|U^{(\lambda)}\|f^n\psi' J')^2 \qquad (1)$$

where P denotes the oscillator strength, $\chi=(n^2+2)^2/9n$, n is the refractive index, J is the total quantum number of the ground state, $(f^n\psi J\|U^{(\lambda)}\|f^n\psi' J')$ is the reduced matrix element of the unit tensor operator $U^{(\lambda)}$ tabulated by Carnall et al. [39] and Ω_λ are empirical least-squares fitted parameters.

3. Results and discussion

3.1. Crystal structure

The geometry of the first coordination sphere of the Nd^{III} ion is presented in Table 2. The structure consists of the complex anion, guanidinium cations and water of hydration. The Nd^{III} ion is nine-coordinate. Its environment consists of three nitrogen, five carboxylate oxygen atoms and a water molecule. The shortest Nd···Nd distance is 8.720(5) Å. The coordination figure of the lanthanide cation may be defined as a distorted capped square antiprism (CSA). In the best fitted figure the non-capped base is spanned by N(1), N(2), N(3) and O(9), whereas O(3), O(1), O(5) and O(7) form the capped one, and OW(1) is the cap. The parameter Δ (defined as $\Sigma d_i^2/9$, i=1–9, where d_i is the distance between ith atom and the relevant vertex of the ideal least-squares fitted polyhedron [40]) was 0.123 Å^2. On the other hand, none of the fitted tricapped trigonal prisms had Δ less than

Table 2
Selected bond lengths (Å) and angles (°) for $[C(NH_2)_3]_2$-$[Nd(dtpa)(H_2O)]\cdot 7H_2O$

Nd–O(9)	2.387(4)	Nd–O(7)	2.467(4)
Nd–O(1)	2.420(4)	Nd–N(1)	2.686(5)
Nd–O(5)	2.426(4)	Nd–N(2)	2.732(5)
Nd–OW1	2.449(4)	Nd–N(3)	2.751(5)
Nd–O(3)	2.454(4)		
O(9)–Nd–O(1)	134.2(2)	OW1–Nd–N(1)	122.8(2)
O(9)–Nd–O(5)	131.06(14)	O(3)–Nd–N(1)	62.6(2)
O(1)–Nd–O(5)	73.37(14)	O(7)–Nd–N(1)	149.4(2)
O(9)–Nd–OW1	138.3(2)	O(9)–Nd–N(2)	83.9(2)
O(1)–Nd–OW1	75.2(2)	O(1)–Nd–N(2)	73.9(2)
O(5)–Nd–OW1	79.5(2)	O(5)–Nd–N(2)	64.47(14)
O(9)–Nd–O(3)	75.30(14)	OW1–Nd–N(2)	137.7(2)
O(1)–Nd–O(3)	88.7(2)	O(3)–Nd–N(2)	129.57(14)
O(5)–Nd–O(3)	153.59(13)	O(7)–Nd–N(2)	126.56(14)
OW1–Nd–O(3)	77.2(2)	N(1)–Nd–N(2)	67.1(2)
O(9)–Nd–O(7)	84.5(2)	O(9)–Nd–N(3)	63.2(2)
O(1)–Nd–O(7)	140.68(14)	O(1)–Nd–N(3)	134.9(2)
O(5)–Nd–O(7)	85.9(2)	O(5)–Nd–N(3)	70.20(14)
OW1–Nd–O(7)	68.3(2)	OW1–Nd–N(3)	121.9(2)
O(3)–Nd–O(7)	96.8(2)	O(3)–Nd–N(3)	133.8(2)
O(9)–Nd–N(1)	69.0(2)	O(7)–Nd–N(3)	61.32(14)
O(1)–Nd–N(1)	65.49(14)	N(1)–Nd–N(3)	115.31(14)
O(5)–Nd–N(1)	122.8(2)	N(2)–Nd–N(3)	66.9(2)

0.3 Å^2. An ORTEP [41] view of the complex anion is presented in Fig. 1. There are two independent guanidinium cations in the structure. One of them forms hydrogen bonds with five water molecules and only one hydrogen bond to a carboxylate oxygen atom, O(4), from the complex anion. The other guanidinium cation links two symmetry related complex anions with two pairs of hydrogen bonds, and also forms bonds with two water molecules. In general, the structure is held together by a network of O···O and N···O hydrogen bonds.

It may be mentioned that in the case of crystals with bulky anions the countercations can markedly influence structural geometries around the metal ion because of their role in the formation of hydrogen bond network. Thus, comparing the crystal structures of the $[Nd(dtpa)(H_2O)]^{2-}$ anion in the barium [28] and in guanidinium salt, one can notice that for the first one, the Nd^{III}–$O(H_2O)$ distance is equal to 2.616 Å and is situated between the Nd^{III}–$O(COO^-)$ and Nd^{III}–N distances. For the $[C(NH_2)_3][Nd(dtpa)(H_2O)]\cdot 7H_2O$ compound this distance is equal to 2.449 Å and is comparable with Nd^{III}–$O(COO^-)$ bond lengths. The average Nd^{III}–dtpa distances for these crystals are 2.566 and 2.540 Å, respectively.

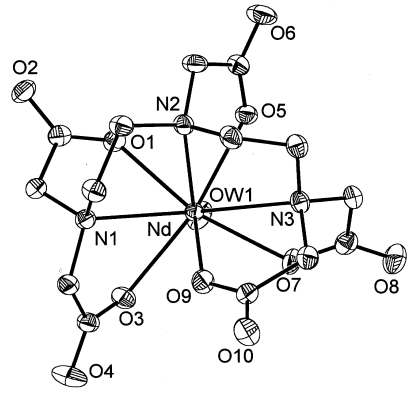


Fig. 1. An ORTEP view of the complex anion, together with the atom numbering scheme. The thermal ellipsoids are drawn at 30% probability. The labels of carbon atoms have been omitted for the sake of clarity. The OW(1) atom is eclipsed by Nd.

3.2. Spectral results

Absorption spectra of the Nd^{III}–dtpa (1:1) system were examined in aqueous solution over a wide pH range (1.5–13) at room temperature and for the $[C(NH_2)_3]_2$-$[Nd(dtpa)(H_2O)]\cdot 7H_2O$ single crystal at 293 and 4 K.

The assignment of the f–f transitions of the investigated complexes in the 300–2000 nm region is shown in Fig. 2. One can observe a good correspondence between the absorption spectra for these two phases. The number of Stark components of the excited states observed in the 4 K spectra for the crystal is in agreement with the expected splitting of levels predicted by the group theory for a single Nd^{III} ion site with the C_1 symmetry. The appearance of a single, sharp peak of the $^4I_{9/2}\rightarrow{}^2P_{1/2}$ transition at 23283 cm^{-1} with a half-width of 5 cm^{-1}, as well as a splitting of the $^2H_{11/2}$ into six optical lines (16071, 16029, 16000, 15962, 15928, 15914 cm^{-1}), the $^4F_{9/2}$ into five lines (14874, 14846, 14798, 14744, 14717 cm^{-1}) and the $^4F_{3/2}$ into two lines (11549, 11459 cm^{-1}) is indicative of a single Nd^{III} site, consistent with the X-ray analysis.

In order to compare the spectral properties of the single crystal with those in solution, the influence of pH on the UV–Vis spectra of 1:1 Nd^{III}–dtpa solutions was studied. The effect of pH on the shape of the two most characteristic transitions of the Nd^{III} ion, namely the $^4I_{9/2}\rightarrow{}^2P_{1/2}$ and the $^4I_{9/2}\rightarrow{}^4G_{5/2}$, $^2G_{7/2}$ for a 1:1 Nd^{III}–dtpa solution, is shown in Fig. 3. The shape and intensity of the absorption bands of the f–f transitions, especially of these two mentioned above, change up to a pH of about 3. A further increase of pH gives no changes in the absorption spectra. It indicates that even at pH ≈ 3 (which is lower than the third pK_a value of the H_5dtpa acid [42]), the inner coordination sphere of Nd^{3+} is not affected by protonation. It may suggest that the proton is attached to a non-coordinated atom of the carboxylate group.

The $^4I_{9/2}\rightarrow{}^2P_{1/2}$ transition can indicate the number of species of different coordination geometry around the Nd^{III} ion existing in equilibrium in solution, because the excited $^2P_{1/2}$ state is a Kramer's doublet and does not split in the ligand field of any symmetry. At low pH, around 2, two well-resolved peaks of this transition are observed. The energy of the first component corresponds to that observed for the aquoion (23406 cm^{-1}) and disappears when the pH of the investigated solutions increases, whereas the position of the second peak at 23276 cm^{-1} remains constant in all examined solutions. With the pH increases up to 3 it becomes only

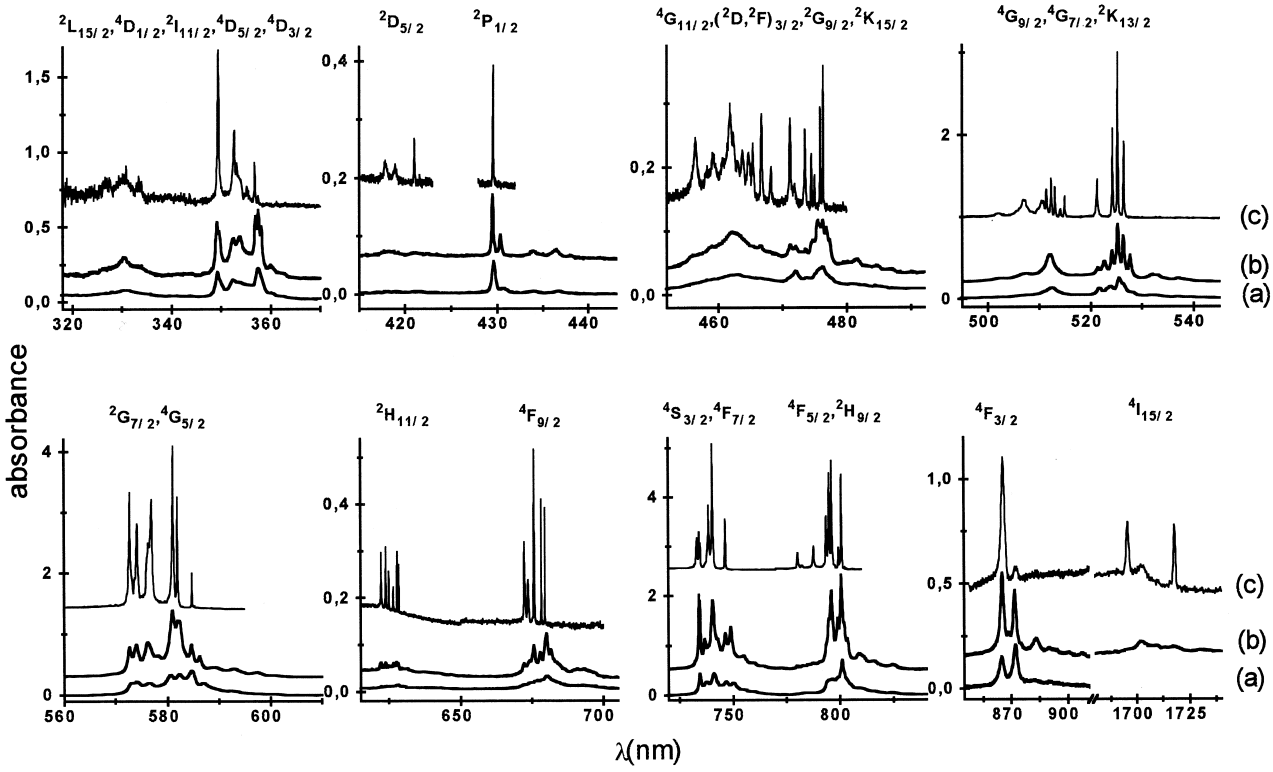


Fig. 2. Absorption spectra of Nd^{III}–dtpa complexes in solution (a) and for the crystal of $[C(NH_2)_3]_2[Nd(dtpa)(H_2O)]\cdot 7H_2O$ at 293 K (b) and 4 K (c). For solution: $c_{Nd}=1.827\times10^{-2}$ M, $c_{dtpa}=2.403\times10^{-2}$ M, pH = 8.61, $d=2$ cm. For crystal: $c_{Nd}=2.185$ M, $d=0.053$ cm.

narrower and more intense. Its width at the half-height is equal to 33 and 24 cm^{-1} at pH 1.85 and at pH ≥ 3, respectively, while the half-width of the relevant peak of the $[C(NH_2)_3]_2[Nd(dtpa)(H_2O)]\cdot 7H_2O$ crystal at 23283 cm^{-1} is equal to 13 cm^{-1} at 293 K.

Since the excited $^2P_{1/2}$ state is a Kramer's doublet, we were able to deduce the energies of the components of the $^4I_{9/2}$ ground multiplet, which amount: 0, 60, 235, 378 cm^{-1} for solutions at pH above 3 (the fifth level was not identified) and 0, 47 (45), 240 (239), 372 (374), 453 (459) cm^{-1} for the crystal. The values of the energy sublevels given in parentheses were found from the splitting of the $^4I_{9/2}\rightarrow{}^4F_{3/2}$ transition.

The hypersensitive $^4I_{9/2}\rightarrow{}^4G_{5/2}$, $^2G_{7/2}$ transition shows among all f–f transitions the strongest intensity variations depending on the changes of the nearest surrounding of the Nd^{III} ion. It has to be pointed out that when the equilibrium between species is reached (pH ≈ 3), the intensity and shape of the band does not change any more. Absorption spectra of this transition for the aquoion and the $[C(NH_2)_3]_2$-$[Nd(dtpa)(H_2O)]\cdot 7H_2O$ crystal are for comparison purposes also presented in Fig. 3b. A good agreement between the crystal field energies, but not between intensities of particular crystal field components, in the hypersensitive transition of these two phases is observed. This may indicate that the similarity between the coordination polyhedra of species found for the crystal and those existing in solution is not satisfied.

Analysing the $^4I_{9/2}\rightarrow{}^2P_{1/2}$ transition spectra shown in Fig. 3a, one may observe that even in the solution with a very low pH value (≈2), for which exists the equilibrium between the aquoion and hydrated species of the Nd^{III}–dtpa complex, the arrangements of donor atoms around the Nd^{III} ion are very similar to that of the fully deprotonated Nd^{III}–dtpa chelate. Probably in the case when the dtpa is still highly protonated, the number of water molecules is about three, as was shown from the luminescence decay lifetime measurements for the Tb^{III}–dtpa complex [12]. Nevertheless, the characteristic peak energy of the Nd^{III}–dtpa complex is unchangeable as well for the hydrated protonated species as for the deprotonated species. This means that this large polyaminopolycarboxylate molecule imposes the coordination environment around the Nd^{III} ion even at very low pH values, by encapsulating hydrated species of the Nd^{III} ion. When the carboxylate groups become deprotonated, the coordinated water molecules are substituted.

The appreciable broadening of the peak of the $^4I_{9/2}\rightarrow{}^2P_{1/2}$ transition at 23276 cm^{-1} in the solution spectra as compared to that in the crystal may be a result of stronger vibronic interactions in the solution and/or of the presence of species which differ very slightly from each other. It seems likely that it can be caused by the mutual interconversion of two species which occur in the middle O_2CCH_2N branch of the dtpa ligand [18].

It should be pointed out that the energy of the highest peak in the $^4I_{9/2}\rightarrow{}^2P_{1/2}$ transition is shifted to the UV region in

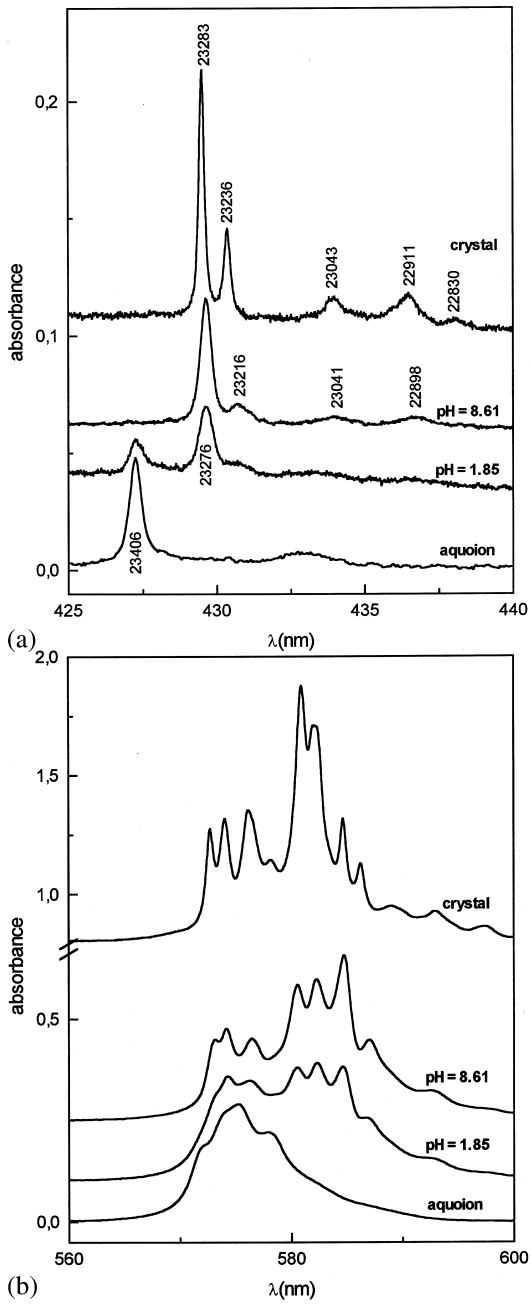


Fig. 3. Absorption spectra of the $^4I_{9/2} \rightarrow {}^2P_{1/2}$ (a) and $^4I_{9/2} \rightarrow {}^4G_{5/2}, {}^2G_{7/2}$ (b) transitions of the aquoion and Nd^{III}–dtpa systems. For solution: $c_{Nd} = 1.827 \times 10^{-2}$ M, $c_{dtpa} = 2.403 \times 10^{-2}$ M, $d = 2$ cm. For crystal: $c_{Nd} = 2.185$ M, $d = 0.053$ cm.

the spectrum of the crystal compared to that in solution. However, one should notice that the energy of this transition in the crystal spectra may depend on the size and electrostatic properties of the used counter-cations. As has been shown by the X-ray investigations of the barium [28] and guanidinium salts, these counter-cations form a different hydrogen bond network with the hydration water molecules and the oxygen atoms from the ligand molecules. The rigid hydrogen bond network in the solid state, contrary to that in the solution, to some degree may affect the geometry around the Ln^{III} ion, which influences the position of the $^4I_{9/2} \rightarrow {}^2P_{1/2}$ transition.

It is interesting to compare the spectral intensities of all f–f transitions as well as the Ω_λ parameters for the studied Nd^{III}–dtpa complexes in solutions and in the single crystal. These results together with that for the aquoion are presented in Table 3. A large decrease in intensity of almost all transitions in the single crystal is observed when the temperature is lowered from 293 to 4 K. Because of the high J manifolds of the Nd^{III} ion in the ground and excited states it is difficult to establish which part of the intensity changes is related to 'hot' transitions from the ground state and which to the vibronic transitions.

The oscillator strength values of the f–f transitions of the $[Nd(dtpa)(H_2O)]^{2-}$ complex in the crystal at 293 K resemble much more those of the aquoion than those calculated for solutions. This is especially well seen for the most intense transitions of the Nd^{III} ion like the $^4I_{9/2} \rightarrow {}^4G_{5/2}, {}^2G_{7/2}$ hypersensitive transition, the $^4I_{9/2} \rightarrow {}^4F_{7/2}$, $^4S_{3/2}$ and $^4I_{9/2} \rightarrow {}^4F_{5/2}$, $^2H_{9/2}$ transitions, which play a significant role in the Judd-Ofelt intensity analysis.

According to Mason [43], the ligand polarization mechanism is important mainly for hypersensitive transitions and influences the Ω_2 parameter values, while the crystal field mechanism contributes mostly to the Ω_6 values. In the case of Nd^{III} compounds, the Ω_6 parameters depend particularly on intensities of the $^4I_{9/2} \rightarrow {}^4F_{7/2}$, $^4S_{3/2}$ and $^4I_{9/2} \rightarrow {}^4F_{5/2}$, $^2H_{9/2}$ transitions for which the $U^{(6)}$ matrix elements have the highest values [39]. In the Nd^{III}–dtpa solution spectrum, the values of the oscillator strengths of these transitions, the hypersensitive one as well as the Ω_λ parameters have higher values than those for the crystal spectrum. This may indicate that in solution various species differing in both symmetry and total polarizability of ligands are present.

A similar phenomenon, connected with much higher oscillator strength values of the $^4I_{9/2} \rightarrow {}^4F_{7/2}$, $^4S_{3/2}$ and $^4I_{9/2} \rightarrow {}^4F_{5/2}$, $^2H_{9/2}$ transitions for solution as compared to the crystal, was earlier reported for the $[Nd(dpa)_3]^{3-}$ complex [1], where dpa^{2-} is a dipicolinate anion. This distinct intensity increase was explained to be caused by a high structural dynamics between $[Nd(N_3O_6)]^{3-}$ species, which in solution exist as a racemic mixture [44,45].

It is noteworthy that, in the solid state, the oscillator strengths of the $^4I_{9/2} \rightarrow {}^4F_{7/2}$, $^4S_{3/2}$ and $^4I_{9/2} \rightarrow {}^4F_{5/2}$, $^2H_{9/2}$ transitions, which are higher than those of the aquoion but similar to those observed for Nd^{III}–dtpa (1:1) and $[Nd(dpa)_3]^{3-}$ complexes in solution, were obtained for a dimeric crystal of the Nd^{III} complex with triethylenetetraaminehexaacetic acid [3]. In this crystal both Nd^{III} centres are very similar, though not strictly equivalent. This confirms a significant contribution of the crystal field mechanism on the Ω_6 parameter value.

The presented results establish a certain parallelism to earlier investigations of lanthanide polyaminocarboxylates, and therefore will be of use while studying similar systems for which other methods are difficult to apply.

Table 3
Oscillator strength (P) and Ω_λ parameters for Nd^{III} complexes with dtpa in solution at 293 K and for the $[C(NH_2)_3]_2[Nd(dtpa)(H_2O)]\cdot 7H_2O$ crystal at 293 and 4 K [a]

	Solution, 293 K			Crystal	
	Aquoion	Nd^{III}dtpa		293 K	4 K
	pH 3.08	pH 1.85	pH 8.61		
Transition(s) $^4I_{9/2}\rightarrow$	$10^8 P_{exp}$	$10^8 P_{exp}$	$10^8 P_{exp}$	$10^8 P_{exp}$	
$^4F_{3/2}$	219.30	292.77	282.36	189.24	89.64
$^4F_{5/2}$, $^2H_{9/2}$	871.92	1071.09	1163.24	917.24	605.48
$^4F_{7/2}$, $^4S_{3/2}$	878.09	1129.00	1276.81	992.75	447.66
$^4F_{9/2}$	59.47	72.37	87.62	70.68	28.88
$^2H_{11/2}$	16.47	20.94	24.49	18.20	12.74
$^4G_{5/2}$, $^2G_{7/2}$	927.02	1409.83	1584.87	935.82	647.44
$^2K_{13/2}$, $^4G_{7/2}$, $^4G_{9/2}$	656.20	832.96	958.61	649.24	372.47
$^2K_{15/2}$, $^2G_{9/2}$, (^2D, $^2F)_{3/2}$, $^4G_{11/2}$	190.21	222.59	246.44	187.42	171.37
$^2P_{1/2}$	34.84	51.16	43.82	22.24	6.46
$^2D_{5/2}$	8.18	17.57	12.84	7.73	9.57
$^4D_{3/2}$, $^4D_{5/2}$, $^2I_{11/2}$, $^4D_{1/2}$, $^2L_{15/2}$	945.70	1078.30	1231.83	804.43	517.86
$10^{20}\,\Omega_2$ (cm^2)	1.08 ± 0.36	2.87 ± 0.46	3.24 ± 0.53	1.40 ± 0.32	
$10^{20}\,\Omega_4$ (cm^2)	4.38 ± 0.33	4.97 ± 0.43	5.65 ± 0.49	3.18 ± 0.29	
$10^{20}\,\Omega_6$ (cm^2)	7.89 ± 0.47	10.12 ± 0.59	11.27 ± 0.67	7.88 ± 0.40	
rms $\times 10^7$	6.49	8.24	9.43	6.35	

[a] In solution: $c_{Nd}=1.827\times10^{-2}$ M, $c_{dtpa}=2.403\times10^{-2}$ M, $d=2$ cm. In crystal: $c_{Nd}=2.185$ M, $d=0.053$ cm.

Supplementary data

The X-ray crystallographic data for the structure of the $[C(NH_2)_3]_2[Nd(dtpa)(H_2O)]\cdot 7H_2O$ compound have been deposited with the Cambridge Crystallographic Data Centre, 12 Union Road, Cambridge CB2 1EZ, UK (fax: +44-1223-336033; e-mail: deposit@ccdc.cam.ac.uk) as supplementary publication no. CCDC 136710.

Acknowledgements

The authors would like to thank Professor K. Bukietyńska for valuable discussions and Dr L.B. Jerzykiewicz for help in performing the X-ray measurement. This work was supported by the Polish Committee of Scientific Research.

References

[1] A. Mondry, P. Starynowicz, J. Alloys Compd. 225 (1995) 367.
[2] A. Mondry, P. Starynowicz, Inorg. Chem. 36 (1997) 1176.
[3] A. Mondry, P. Starynowicz, J. Chem. Soc., Dalton Trans. (1998) 859.
[4] N.A. Kostromina, Zh. Neorg. Khim. 19 (1974) 665.
[5] R.B. Gayhart, T. Moeller, J. Inorg. Nucl. Chem. 39 (1977) 49.
[6] E. Brücher, G. Laurenczy, J. Inorg. Nucl. Chem. 43 (1980) 2089.
[7] C.C. Bryden, C.N. Reilley, Anal. Chem. 54 (1982) 610.
[8] L. Spaulding, H.G. Brittain, Inorg. Chem. 22 (1983) 3486.
[9] M. Albin, W. DeW. Horrocks Jr., Inorg. Chem. 24 (1985) 895.
[10] A. Mondry, J.P. Riehl, Acta Phys. Polon., A 84 (1993) 969.
[11] S.T. Frey, W. DeW. Horrocks Jr., Inorg. Chim. Acta 229 (1995) 383.
[12] C.A. Chang, H.G. Brittain, J. Telser, M.F. Tweedle, Inorg. Chem. 29 (1990) 4468.
[13] G.R. Choppin, P.A. Baisden, S.A. Khan, Inorg. Chem. 18 (1979) 1330.
[14] B.M. Alsaadi, F.J.C. Rosotti, R.J.P. Williams, J. Chem. Soc., Dalton Trans. (1980) 2151.
[15] B.G. Jenkins, R.B. Lauffer, J. Magn. Reson. 80 (1988) 328.
[16] B.J. Jenkins, R.B. Lauffer, Inorg. Chem. 27 (1988) 4730.
[17] S. Aime, M. Botta, Inorg. Chim. Acta 177 (1990) 101.
[18] J.A. Peters, Inorg. Chem. 27 (1988) 4686.
[19] R.B. Lauffer, Chem. Rev. 87 (1987) 901.
[20] M.F. Tweedle, in: J.-C.G. Bünzli, G.R. Choppin (Eds.), Lanthanide Probes in Life, Chemical and Earth Sciences, Theory and Practice-Elsevier, Amsterdam, 1989, p. 93.
[21] H.G. Brittain, G.R. Choppin, P.P. Barthelemy, J. Coord. Chem. 26 (1992) 143.
[22] K. Micskei, L. Helm, E. Brücher, A.E. Merbach, Inorg. Chem. 32 (1993) 3844.
[23] D.H. Powell, O.M. Ni Dhubhghaill, D. Pubanz, L. Helm, Y.S. Lebedev, W. Schlaepfer, A.E. Merbach, J. Am. Chem. Soc. 118 (1996) 9333.
[24] J.W. Chen, R.L. Belford, R.B. Clarkson, J. Phys. Chem. A 102 (1998) 2117.
[25] S. Bénazeth, J. Purans, M.-C. Chalbot, M. Kim Nguyen-van Duong, L. Nicolas, F. Keller, A. Gaudemer, Inorg. Chem. 37 (1998) 3667.
[26] H. Gries, H. Miklautz, Physiol. Chem. Phys. Med. NMR 16 (1984) 105.
[27] R. Ruloff, T. Gelbrich, E. Hoyer, J. Sieler, L. Beyer, Z. Naturforsch., Teil B 53 (1998) 955.
[28] J.J. Stezowski, J.L. Hoard, Isr. J. Chem. 24 (1984) 323.
[29] M.B. Inoue, M. Inoue, Q. Fernando, Inorg. Chim. Acta 232 (1995) 203.
[30] N. Sakagami, J.-I. Homma, T. Konno, K.-I. Okamoto, Acta Crystallogr., Sect. C 53 (1997) 1378.
[31] R. Fossheim, S.G. Dahl, Acta Chem. Scand. 44 (1990) 698.
[32] U. Cosentino, G. Moro, D. Pitea, A. Villa, P.C. Fantucci, A. Maiocchi, F. Uggeri, J. Phys. Chem., A 102 (1998) 4606.
[33] F. Ugozzoli, Comput. Chem. 11 (1987) 109.

[34] G.M. Sheldrick, Acta Crystallogr., Sect. A 46 (1990) 467.
[35] G.M. Sheldrick, SHELXL-97, Program for Crystal Structure Refinement, University of Göttingen, Germany, 1994.
[36] A.J.C. Wilson (Ed.), International Tables for X-ray Crystallography, C 1992, Kluwer, Dordrecht, The Netherlands.
[37] B.R. Judd, Phys. Rev. 127 (1962) 750.
[38] G.S. Ofelt, J. Chem. Phys. 37 (1962) 511.
[39] W.T. Carnall, P.R. Fields, K. Rajnak, J. Phys. Chem. 49 (1968) 4424.
[40] M.G.B. Drew, Coord. Chem. Rev. 24 (1977) 179.
[41] C.K. Johnson, ORTEPII, Report ORNL-5138, Oak Ridge National Laboratory, Oak Ridge, TN, 1976.
[42] T.F. Gritmon, M.P. Goedken, G.R. Choppin, J. Inorg. Nucl. Chem. 39 (1977) 2021.
[43] S.F. Mason, Inorg. Chim. Acta 94 (1984) 313.
[44] G.L. Hilmes, J.P. Riehl, Inorg. Chem. 25 (1986) 2617.
[45] D.H. Metcalf, S.W. Snyder, J.N. Demas, F.S. Richardson, J. Am. Chem. Soc. 112 (1990) 469.

PERGAMON

www.elsevier.nl/locate/poly

Polyhedron 19 (2000) 779–783

POLYHEDRON

Synthesis, crystal structure and fluorescence emission of complexes of lanthanide picrates with 2,2′-[1,2-phenylenebis(oxy)]-bis(*N*,*N*-diphenylacetamide) (PBD)

Liyan Fan [a], Weisheng Liu [a,*], Xinmin Gan [a], Ning Tang [a], Minyu Tan [a], Weihua Jiang [a], Kaibei Yu [b]

[a] *Department of Chemistry, Lanzhou University, Lanzhou 730000, People's Republic of China*
[b] *Chengdu Center of Analysis and Measurement, Academia Sinica, Chengdu 610041, People's Republic of China*

Received 9 August 1999; accepted 7 January 2000

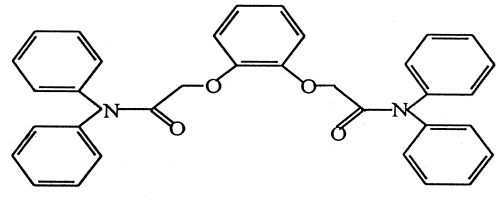
Abstract

Solid complexes of lanthanide picrates with 2,2′-[1,2-phenylenebis(oxy)]bis(*N*,*N*-diphenylacetamide) (PBD) have been prepared in ethanol. These complexes have been characterized by elemental analysis, conductivity measurements, IR, electronic and ^{1}H NMR spectroscopies. The crystal and molecular structures of $[Y(pic)_3(PBD)]\cdot 3.8CH_3CN$ have been determined. The crystal structure shows that the Y(III) ion is coordinated to four oxygen atoms of PBD, four oxygen atoms of one bidentate and two unidentate picrates. The coordination number of yttrium is eight. The structure reveals that PBD acts as a tetradentate ligand, forming a ring-like coordination structure similar to those of crown compounds. The Eu(III) complex shows strong emission when excited with 260 nm radiation in the solid state. The intensity ratio $^5D_0$–$^7F_2$/$^5D_0$–$^7F_1$ is 21.5. ©2000 Elsevier Science Ltd All rights reserved.

Keywords: Lanthanide picrates; PBD; Fluorescence; Crystal structures

1. Introduction

Acyclic polyethers offer many advantages over the use of crown ethers in the extraction and analysis (ion-selective electrodes) of rare earths [1–6]. Ding et al. have reported that *N*,*N*,*N*′,*N*′-tetraphenyl-3,6-dioxaoctanedimide (TDD) has the largest separation factor of five derivatives of glycol-*O*,*O*′-diacetamide, and both the separation factor and distribution ratio of lighter lanthanide ions for TDD are larger than those for dicyclohexyl-18-crown-6, if the picrate is used as accompanying ion [4]. In order to further investigate the affect of the variety of skeleton on the properties and structures of compounds, the group $–CH_2–CH_2–$ of TDD was changed to phenylene, i.e. 2,2′-[1,2-phenylenebis(oxy)]-bis(*N*,*N*-diphenylacetamide) (PBD). PBD has been used as a neutral carrier of sodium ion-selective electrodes [7], however solid complexes with PBD have rarely been investigated. We report here the synthesis, characterization and structure of complexes of lanthanide picrates with PBD.



2,2'-[1,2-phenylenebis(oxy)]bis(*N*,*N*-diphenylacetamide) (PBD)

2. Experimental

2.1. Materials

Lanthanide picrates [8] and PBD [7] were prepared according to the literature methods. All commercially available chemicals were reagent grade and were used without further purification.

2.2. General preparation of the complexes

A solution of lanthanide picrate (0.1 mmol) in 15 ml of anhydrous ethanol was added dropwise to a solution of PBD

* Corresponding author. Tel.: +86-931-8912552; fax: +86-931-8912582; e-mail: liuws@lzu.edu.cn

0277-5387/00/$ - see front matter ©2000 Elsevier Science Ltd All rights reserved.
PII S0277-5387(00)00313-2

Table 1
Crystal data and structure refinement for the complex [Y(pic)$_3$(PBD)]

Empirical formula	$C_{57.63}H_{42.44}N_{13.81}O_{25}Y$
Temperature (K)	295(2)
Formula weight	1417.33
Crystal color	yellow
Crystal size (mm)	0.48×0.48×0.40
Space group	$P\bar{1}$
Unit cell dimensions	
a (Å)	10.582(2)
b (Å)	13.285(2)
c (Å)	23.373(4)
α (°)	88.20(1)
β (°)	89.49(1)
γ (°)	72.81(1)
V (Å^3)	3137.5(9)
Z	2
Density (calculated) (g cm^{-3})	1.500
F(000)	1448
Radiation, graphite-monochromatized, λ (Å)	Mo Kα, 0.71073
Reflections collected	12322
Independent reflections	10910
No. of reflections used	5929
θ Range for data collection	1.60–2.50
Index range	$0 \le h \le 12$ $-15 \le k \le 15$ $-27 \le l \le 27$
Goodness-of-fit on F^2	0.794
Final R indices ($I > 2\sigma(I)$) [a]	$R_1 = 0.0416$, $wR_2 = 0.0711$
R indices (all data)	$R_1 = 0.0954$, $wR_2 = 0.1110$
Largest difference peak and hole (e Å^{-3})	0.362, −0.419

[a] $w = 1/[\sigma^2(F_o^2) + (0.0337P)^2]$; $P = (F_o^2 + F_c^2)/3$.

(0.1 mmol) in 10 ml of anhydrous ethanol. The mixture was stirred at room temperature for 2 h. The precipitated solid complex was filtered, washed with ethanol and dried in vacuo over P_4O_{10} for 48 h. All the complexes are yellow powders and stable in air. Single crystals of the yttrium complex were grown and recrystallized from MeCN with slow evaporation in a desiccator over $CaCl_2$ at room temperature. After ca. 3 weeks, transparent yellow crystals were formed from the solution.

2.3. Chemical and physical measurement

The lanthanide(III) ion was determined by EDTA titration using xylenol orange as an indicator. C, H, N were determined using a vario-EL elemental analyzer. Conductivity was determined using a conductivity bridge with 10^{-3} mol dm^{-3} in CH_3COCH_3 at 25°C. Thermal analyses (TG and DTA) were performed on a Beijing Optical Instrument Factory PCT-2 precision thermobalance analyzer in air at a heating rate of 5°C min^{-1}. The IR spectra were recorded on a Nicolet 170 SX FT-IR instrument using KBr disks in the 220–4000 cm^{-1} region. ^{1}H NMR spectra were recorded on a Bruker AC 80 spectrometer in CD_3COCD_3 solution, with TMS as internal standard. Electronic spectra were recorded with a UV-260 Shimadzu spectrophotometer in acetonitrile solution. Fluorescence spectra were obtained on a Hitachi M-850 fluorescence spectrophotometer.

2.4. X-ray crystallography

For the yttrium complex, X-ray measurements were performed on a P4 four-circle diffractometer with graphite-monochromatized Mo Kα radiation at 295 ± 2 K. A summary of crystallographic data and details of the structure refinements are listed in Table 1. The structure was solved by direct methods and refined by full-matrix least-squares techniques with all non-hydrogen atoms treated anisotropically. Theoretical models fixed the hydrogen atoms of the compounds. All calculations were performed on an Eclipse S/140 computer with the program package SHELXTL.

3. Results and disscussion

Analytical data for the complexes (presented in Table 2) conform to a 1:3:1 metal-to-picrate-to-PBD stoichiometry, Ln(pic)$_3$(PBD), together with 1 mol C_2H_5OH and 1 mol H_2O. All the complexes are soluble in polar organic solvents, DMSO, acetone, methanol and MeCN etc., and are slightly soluble in ethanol and AcOEt. They are sparingly soluble in benzene, Et_2O and cyclohexane. The molar conductance values of the complexes in acetone (Table 2) indicate the presence of a non-electrolyte [9].

DTA analyses of the complexes of Sm(III) and Y(III) show that they lose one ethanol molecule at 71 and 80°C and lose one water molecule at 148 and 154°C respectively, corresponding to endothermic peaks. The weight losses of these complexes are in agreement with the calculated values.

Table 2
Analytical data and molar conductance values for [Ln(pic)$_3$(PBD)]·C_2H_5OH·H_2O (Ln = La, Nd, Sm, Eu, Er, Y)

Complex	C (%) found (calc.)	H (%) found (calc.)	N (%) found (calc.)	Ln (%) found (calc.)	Λ_m (S cm^2 mol^{-1})
[La(pic)$_3$(PBD)]·C_2H_5OH·H_2O	45.24 (45.80)	3.02 (2.99)	10.79 (10.88)	9.54 (9.81)	22.16
[Nd(pic)$_3$(PBD)]·C_2H_5OH·H_2O	45.61 (45.63)	2.77 (2.98)	10.62 (10.84)	9.89 (10.15)	25.69
[Sm(pic)$_3$(PBD)]·C_2H_5OH·H_2O	45.56 (45.44)	2.96 (2.97)	10.56 (10.80)	10.41 (10.54)	21.83
[Eu(pic)$_3$(PBD)]·C_2H_5OH·H_2O	45.40 (45.38)	2.97 (2.96)	10.57 (10.78)	10.35 (10.64)	20.23
[Er(pic)$_3$(PBD)]·C_2H_5OH·H_2O	44.74 (44.90)	2.67 (2.93)	10.58 (10.67)	11.21 (11.58)	19.12
[Y(pic)$_3$(PBD)]·C_2H_5OH·H_2O	47.96 (47.48)	3.06 (3.10)	10.97 (11.28)	6.74 (6.51)	20.98

3.1. IR spectra

The IR spectrum of free PBD shows bands at 1677 and 1078 cm^{-1} assigned to ν(C=O) and ν(C–O–C). In the complexes of La, Sm and Y, the bonds shift by ca. 60 and 50 cm^{-1} towards lower wave numbers, thus indicating that the C=O and ether O-atoms take part in coordination to the metal ions. The large shifts for ν(C=O) in the spectra of the complexes suggest that the Ln–O(carbonyl) bond is stronger than the Ln–O(ether) bond.

The OH out-of-plane bending vibration of the free Hpic at 1151 cm^{-1} disappears in the spectra of the complexes, indicating that the H-atom of the OH group is replaced by Ln(III). The vibration ν(C–O) at 1265 cm^{-1} is shifted toward higher frequency by ca. 5 cm^{-1} in the complexes. This is due to the following two effects. First, the hydrogen atom of the OH group is replaced by Ln(III), increasing the π-bond character in the C–O bond. Secondly, coordination of the oxygen atom of PBD to Ln(III) causes the π-character to weaken. The free Hpic has $\nu_{as}(NO_2)$ and $\nu_s(NO_2)$ at 1555 and 1342 cm^{-1} respectively, which split into two bands at ca. 1581, 1542 cm^{-1} and ca. 1331, 1361 cm^{-1}, respectively, in the complexes. This indicates that some nitronyl O-atoms take part in coordination [10].

3.2. ^{1}H NMR spectra

The ^{1}H NMR spectra of the free ligand PBD and its lanthanum and yttrium complexes were determined in CD_3COCD_3. The spectrum of PBD exhibits two unsolved multiplets at ca. 7.41 and 6.66 ppm and a singlet at 4.62 ppm, assigned to $-C_6H_5-$, $-C_6H_4-$, $-C(O)-CH_2-$ respectively. Upon coordination, the signals of $-C(O)CH_2-$ are shifted by 0.3 ppm and those of $-C_6H_4-$ protons by only 0.03 ppm. This is probably due to the inductive effect of Ln–O(PBD) bands and a change in the conformation of the ligand in the complexes. The larger shift for $-C(O)-CH_2-$ protons than for $-C_6H_4-$ protons indicates that the Ln–O(C=O) bond is stronger than the Ln–O(C–O–C) bond [11].

The ^{1}H signal of the OH group in free Hpic disappears in the complexes, indicating that the H-atom of the OH group is replaced by Ln(III).The benzene ring protons of the free Hpic exhibit a singlet at 9.12 ppm. Upon coordination, the signal moves to higher field. Only one singlet is observed for the benzene ring protons of the three coordination picrate groups, indicating fast exchange among the groups in solution [12].

In addition, the spectra of these complexes also exhibit a triplet at ca. 3.5 ppm and a quadruplet at ca. 1.2 ppm assigned to $-CH_2-$ and $-CH_3$ of CH_3CH_2OH. There is a singlet at ca. 3 ppm assigned to H_2O which disappeared after D_2O was added.

3.3. Electronic spectra

The electronic spectra in the visible region of the Nd(III) and Er(III) complexes exhibit alternations in intensity and shifts in position of the absorption bands relative to the corresponding Ln(III) aquo ions. The shift has been attributed by Jørgensen to the effect on the crystal field of interelectronic repulsion between the 4f electrons, and is related to the covalent character of the metal–ligand bond, assessed by Sinha's parameter (δ), the nephelauxetic ratio (β) and the bonding parameter ($b^{1/2}$) [13–15]. The relative energies and J level assignments are given in Table 3; the values of covalent parameters are also presented.

The values of β, which are less than unity, and positive values of δ and $b^{1/2}$ support the existence of partial covalent bonding between metal and ligand [16]. The comparatively small magnitude of $b^{1/2}$ values also shows the involvement of the 4f orbital metal–ligand bond to be very small. Moreover, the magnitudes of covalency and bonding parameters increase from Nd(III) to Er(III), indicating that the extent of covalent character of the metal–ligand bond increases with atomic number (in agreement with the lanthanide contraction).

3.4. Electronic fluorescence

Only the Eu(III) complex shows strong emission when excited with 260 nm radiation in the solid state at room temperature. Excitation around 260 nm causes a strong emission of the Eu(III) complex, in which the luminescence band of the ligand does not appear, suggesting that energy transfer from ligand-centered to metal-centered levels takes place [17]. The most intense band at 616 nm is assigned to a $^5D_0$–$^7F_2$ transition, while the two relatively weak bands at 592 and 699 nm are assigned to $^5D_0$–$^7F_1$ and $^5D_0$–$^7F_4$ transitions,

Table 3
Electronic spectral data and covalent parameters

Complex	Frequency (cm^{-1})	Assignment	Covalent parameters
Nd(pic)$_3$(PBD)	11473	$^4I_{7/2}$–$^4F_{3/2}$	$\beta = 0.9992$
	12497	–$^4F_{5/2}$	$\delta = 0.0801$
	13426	–$^4F_{7/2}$	$b^{1/2} = 0.0200$
	13624	–$^4S_{3/2}$	
	14758	–$^4F_{9/2}$	
	16015	–$^2H_{11/2}$	
	17212	–$^4G_{5/2}$	
	19040	–$^2K_{13/2}$	
	19577	–$^4G_{9/2}$	
Er(pic)$_3$(PBD)	15291	$^4I_{15/2}$–$^4F_{9/2}$	$\beta = 0.9991$
	18450	–$^4S_{3/2}$	$\delta = 0.0901$
	19172	–$^2H_{11/2}$	$b^{1/2} = 0.0212$

Table 4
Electronic fluorescence spectral data for the solid Eu complex

Electron transition	Peak (nm)	Relative intensity
$^5D_0$–$^7F_1$	592	0.65
$^5D_0$–$^7F_2$	616	14.05
$^5D_0$–$^7F_4$	699	0.89

respectively (Table 4). The exceptionally high value for the intensity ratio η ($^5D_0$–$^7F_2$/$^5D_0$–$^7F_1$) of 21.5 indicates that the central Eu(III) ion does not lie in a centrosymmetric coordination site [18], in agreement with the crystal structure analysis.

3.5. X-ray crystal structure

Fig. 1 shows the structure and the atomic numbering schemes for the yttrium complex, and Fig. 2 shows the molecular packing arrangement in the unit cell. Selected bond lengths and angles are given in Table 5.

The crystal structure is composed of [Y(pic)$_3$(PBD)] and 3.8CH_3CN linked by van der Waals' force. The Y(III) ion is eight-coordinated by four oxygen atoms of PBD and four oxygen atoms of one bidentate and two unidentate picrates. The coordination polyhedron is a distorted dodecahedron. The PBD molecule wraps around the metal ion with its oxygen atoms and forms a ring-like coordination structure together with the yttrium atom. The four oxygen atoms of PBD (O(1), O(2), O(3), O(4)) are not quite coplanar, their deviation from the mean plane being in the range 0.021–0.064 Å. The mean absolute deviation is 0.051 Å from the mean plane. The yttrium atom lies out of this plane by 0.096 Å.

The average distance between the yttrium atom and the coordinated oxygen atoms is 2.347 Å, where the Y–O(19) distance is the shortest, owing probably to the higher electron density on the oxygen anion of the picrate. The Y–O(C=O) distances (mean 2.283 Å) are significantly shorter than the Y–O(C–O–C) distances (mean 2.460 Å). This suggests that the Er–O(C=O) bond is stronger than the Y–O(C–O–O) bond, in agreement with the ^{1}H NMR and IR spectral data.

Compared with crystallographic data of Y(pic)$_3$TDD [19], the average Y–O(C=O) bond length of the present

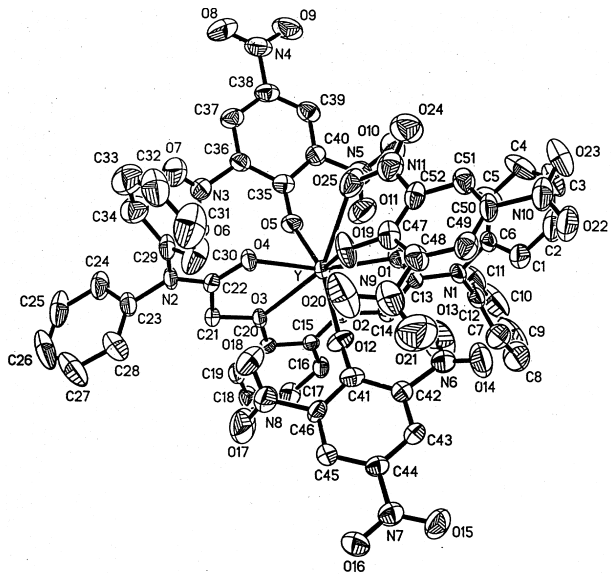


Fig. 1. Molecular structure of [Y(pic)$_3$(PBD)] · 3.8CH_3CN.

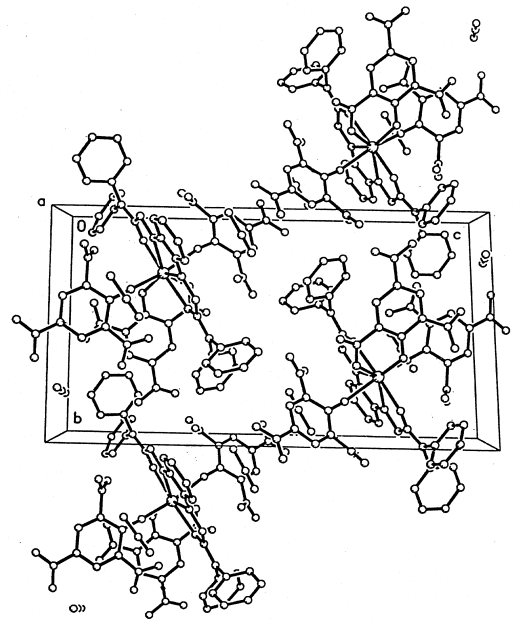


Fig. 2. The molecular packing arrangement in the unit cell.

Table 5
Selected bond lengths (Å) and angles (°) for the Y complex

Y–O(1)	2.290(2)	Y–O(2)	2.451(2)
Y–O(3)	2.468(2)	Y–O(4)	2.276(2)
Y–O(5)	2.226(2)	Y–O(12)	2.223(2)
Y–O(19)	2.209(2)	Y–O(25)	2.630(2)
O(1)–Y–O(2)	65.86(7)	O(4)–Y–O(12)	99.08(8)
O(1)–Y–O(3)	129.30(7)	O(4)–Y–O(19)	80.35(8)
O(1)–Y–O(4)	163.74(7)	O(4)–Y–O(25)	96.57(8)
O(1)–Y–O(5)	92.78(7)	O(5)–Y–O(12)	152.88(8)
O(1)–Y–O(12)	92.09(8)	O(5)–Y–O(19)	127.04(9)
O(1)–Y–O(19)	90.17(8)	O(5)–Y–O(25)	69.21(8)
O(1)–Y–O(25)	67.28(8)	O(12)–Y–O(19)	79.59(9)
O(2)–Y–O(3)	63.47(6)	O(12)–Y–O(25)	136.59(8)
O(2)–Y–O(4)	128.25(6)	O(19)–Y–O(25)	63.53(9)
O(2)–Y–O(5)	81.38(7)	C(13)–O(1)–Y	125.7(2)
O(2)–Y–O(12)	76.36(8)	C(14)–O(2)–Y	120.0(2)
O(2)–Y–O(19)	144.96(8)	C(15)–O(2)–Y	122.8(2)
O(2)–Y–O(25)	122.31(7)	C(20)–O(3)–Y	122.2(2)
O(3)–Y–O(4)	65.18(7)	C(21)–O(3)–Y	120.4(2)
O(3)–Y–O(5)	78.34(7)	C(22)–O(4)–Y	127.7(2)
O(3)–Y–O(12)	77.96(7)	C(35)–O(5)–Y	147.5(2)
O(3)–Y–O(19)	134.70(8)	C(41)–O(12)–Y	165.3(2)
O(3)–Y–O(25)	144.75(7)	C(47)–O(19)–Y	130.1(2)
O(4)–Y–O(5)	82.67(7)	N(11)–O(25)–Y	129.4(2)

complex is a little shorter than that of Y(pic)$_3$TDD, but the Y–O(C–O–C) bond length is longer than that of Y(pic)$_3$ TDD. The existence of phenylene in the PBD skeleton causes a noticeable difference in the conformations of these two crystal structures. The relevant torsion angle is O_2–C_{15}–C_{20}–$O_3 = 0.5(4)°$, which is smaller than that of Y(pic)$_3$TDD (O_2–C_{15}–C_{16}–$O_3 = -53.0(8)°$).

In conclusion, the PBD molecule acts as a multidentate ligand forming a ring-like coordination structure. Because of

its flexibility, PBD exhibits a stable conformation that provides a cavity. The internal cavity formed by the coordination oxygen atoms is suited for the uptake of a cation. Because of its rigid structure, it has a relatively fixed cavity. This enables PBD to be more sensitive to the variation of radius of the lanthanide ion. So it is expected to have a better selectivity than TDD.

Supplementary data

Supplementary data are available from the Cambridge Crystallographic Data centre, 12 Union Road, Cambridge, CB2 1EZ, UK (fax: +44-1223-336033; e-mail: deposit@ccdc.cam.ac.uk).

Acknowledgements

We are grateful to the National Natural Science Foundation of China (project 29571014), the Youth Scientific and Technology Foundation of Gansu Province (project ZQ-95-003) and Key Youth Academic Foundation of Lanzhou University.

References

[1] J.C.G. Bünzli, Handbook on the Physics and Chemistry of Rare Earths, North-Holland, 1987.
[2] J.C.G. Bünzli, J.M. Pfefferlé, B. Ammann, G. Chapuis, F.J. Zuniga, Helv. Chim. Acta 67 (1984) 1121.
[3] Y.S. Yang, Y.Z. Ding, G.Z. Tan, J.Z. Xu, Z.Q. Yiao, F.S. Zhang, J. Nucl. Radiochem. 6 (1984) 196.
[4] Y.Z. Ding, J.C. Lu, Y.S. Yang, G.Z. Tan, J.Z. Xu, Huaxue Shiji 8 (1986) 201.
[5] Y.S. Yang, S.H. Cai, Huaxue Shiji 6 (1984) 133.
[6] Y. Gao, J.Z. Ni, J. Nucl. Radiochem. 5 (1983) 146.
[7] W. Zhang, H.W. Hu, Nanjing Daxue Xuebao 21 (1985) 662.
[8] Y.C. Tia, Y.Q. Liang, J.Z. Ni, Chem. J. Chin. Univ. 9 (1988) 113.
[9] W.J. Geary, Coord. Chem. Rev. 7 (1971) 81.
[10] Y.C. Tian, Y.Q. Liang, J.Z. Ni, Chin. Univ. Chem. J. 9 (1988) 113.
[11] S.X. Liu, W.S. Liu, M.Y. Tan, K.B. Yu, J. Coord. Chem. 10 (1996) 391.
[12] X. Mao, L.F. Shen, J.Z. Ni, Bopuxuezazhi 1 (1985) 201.
[13] C.K. Jørgenson, Prog. Inorg. Chem. 4 (1962) 73.
[14] S.P. Sinha, Spectrochim. Acta 22 (1966) 57.
[15] D.E. Henrie, G.R. Choppin, J. Chem. Phys. 49 (1968) 477.
[16] A.K. Solanki, A.M. Bhandaka, J. Inorg. Nucl. Chem. 41 (1979) 1311.
[17] V. Balzani, E. Berghnans, J.M. Lehn, N. Sabbatini, R. Teröde, R. Ziessel, Helv. Chim. Acta 73 (1990) 2083.
[18] W.S. Liu, M.Y. Tan, X. Wang, S.Y. Zhang, Acta Chim. Sinica 48 (1990) 1090.
[19] W.S. Liu, S.X. Liu, M.Y. Tan, K.B. Yu, Sci. China 40 (1997) 323.

PERGAMON

www.elsevier.nl/locate/poly

Polyhedron 19 (2000) 785–790

POLYHEDRON

Syntheses, spectroscopic properties and X-ray crystal structures of tris(tfacacmetacyclophane)(bpy)europium(III) and piperidinium tetrakis(*p*-tolutfacac)europate(III) complexes

Tetsuji Moriguchi* [1, a], Kazuaki Uchiyama [a], Mikio Yasutake [b], Teruo Shinmyozu [b], Kazunori Sakata [a], Akihiko Tsuge* [2,a]

[a] *Department of Applied Chemistry, Faculty of Engineering, Kyushu Institute of Technology, 1-1 Sensui-cho, Tobata-ku, Kitakyushu 804-8550, Japan*

[b] *Institute for Fundamental Research of Organic Chemistry (IFOC), Kyushu University, 6-10-1 Hakozaki, Higashi-ku, Fukuoka 812-8581, Japan*

Received 13 October 1999; accepted 25 January 2000

Abstract

1-Trifluoromethyl-3-[2.2]metacyclophanyl-1,3-propanedione (HtfacacMCP) which has a non-planar conjugated π system and 1-trifluoromethyl-3-(*p*-tolyl)-1,3-propanedione (*p*-tolutfacacH) as the referential ligand were prepared. Complexation of these ligands with europium(III) chloride in the presence of bipyridine (bpy) gave (tfacacMCP)$_3$(bpy)Eu(III) and piperidinium[(*p*-tolutfacac)$_4$Eu(III)] complexes respectively. The X-ray crystal structure of (tfacacMCP)$_3$(bpy)Eu(III) revealed an eight-coordinate configuration with two N atoms of bpy and six O atoms of HtfacacMCP. On the other hand, piperidinium[(*p*-tolutfacac)$_4$Eu(III)] was found to be an eight-coordinate complex surrounded by eight O atoms of *p*-tolutfacacH. The former contains bpy, but the latter contains no bpy. ©2000 Elsevier Science Ltd All rights reserved.

Keywords: Crystal structures; Europium(III) complexes; Non-planar conjugated ligands; Fluorescence spectra

1. Introduction

Europium(III) complexes of β-diketone type give a narrow-band emission from the europium ion under near-UV excitation, and some of these complexes exhibit laser action when dissolved in organic solvents [1,2]. The absorbed pump energy is transferred intramolecularly to the europium ion via a triplet state (by intersystem crossing). Since this intramolecular energy transfer from the triplet state to the resonance level of an europium ion is of a spin-forbidden type, the energy is transferred by the resonant exchange interaction in which the role of the triplet state is very important. It has been concluded by many researchers that the excitation energy could not be transferred from the ligand to the europium ion if the triplet state of the ligand was below the resonance level of the europium ion [3]. On the other hand, the through-space interaction in small-sized metacyclophane (MCP) compounds has attracted great interest by organic and organophysical chemists [4–7]. The spectral properties of these MCP compounds are particularly interesting because there is transannular interaction between the π electrons of two aromatic rings and the non-planar π conjugated system formed [8]. In the past, experimental and theoretical studies of the fluorescence behavior of these MCP compounds were scarcely investigated because of difficulties in synthesizing MCPs in a large amount and calculation of the energy level of the non-planar π conjugated system in the MCPs. In this paper, we report the preparation of [2.2]MCP having a β-diketone moiety as a ligand and its complexation with an europium ion in the presence of bipyridine and piperidine. Furthermore, the europium(III) complex with 1-trifluoromethyl-3-(*p*-tolyl)-1,3-propanedione (*p*-tolutfacacH) was prepared under the same conditions. Structures of these complexes were analyzed by X-ray structure analyses. ^{1}H NMR, FT-IR, UV and fluorescence spectra of the complexes were recorded in order to determine the relationship between the π electron systems in the ligands and the spectral properties.

[1] *Corresponding author. Tel.: +81-93-884-3330; fax: +81-93-884-3300; e-mail: moriguch@che.kyutech.ac.jp

[2] *Corresponding author.

0277-5387/00/$ - see front matter ©2000 Elsevier Science Ltd All rights reserved.
PII S0277-5387(00)00314-4

2. Experimental

2.1. Materials and methods

All chemicals were of reagent grade and were used without further purification. All solvents except for ethanol were used without further purification. Absolute ethanol was used in the complexation reaction. Reactions were carried out in an apparent flask under argon atmosphere. 8,16-Dimethyl-[2.2]MCP and *p*-tolutfacacH were prepared according to the literature [9,10].

All melting points were recorded on a Yanako hot-stage microscope apparatus and are uncorrected. FT-IR spectra in the region 400–4000 cm^{-1} were taken on a Nippon Bunko JASCO IR-700 spectrophotometer at room temperature. The KBr technique was employed. Ultraviolet and visible spectra covering the 14000–37000 cm^{-1} range were recorded on a Shimadzu UV-200S double beam spectrophotometer for chloroform solutions at room temperature. ^1H NMR measurement were taken on a Nippon Densi α-500 spectrometer operating in Fourier transform mode. The NMR spectra were run in $CDCl_3$ and chemical shifts are given in ppm relative to tetramethylsilane as an internal reference standard. Mass spectra were recorded with a Nippon Densi JMS-SX102A spectrometer using a direct inlet system for EI measurement and in a glycerin matrix for FAB measurement. Elemental analyses were determined with a Yanaco CHN corder MT-3.

2.2. Synthesis of 5-acetyl-8,16-dimethyl[2.2]MCP

To a solution of 8,16-dimethyl[2.2]MCP (4.0 g, 17 mmol) in CS_2 (200 ml) were added acetic anhydride (300 mg, 5.6 mmol) and $TiCl_4$ (3.8 ml), and then the mixture was stirred for 3 h at room temperature. The reaction mixture was poured into water and the organic layer was washed with water and dried over anhydrous magnesium sulfate. Solvents were removed under reduced pressure and the residue was chromatographed on a silica gel column with toluene–chloroform (1:1 vol/vol) as an eluent to give 5-acetylMCP as colorless needles (1.98 g, 42%). M.p. 134–135°C (hexane). *Anal.* Calc. for $C_{20}H_{22}O$: C, 86.29; H, 7.97. Found: C, 86.33; H, 7.91%. ^1H NMR ($CDCl_3$, 500 MHz): 0.49 (s, 3H), 0.53 (s, 3H), 2.56 (s, 3H), 2.70–3.05 (m, 8H), 6.93 (t, 1H, $J=7.32$ Hz), 7.13 (d, 2H, $J=7.32$ Hz), 7.75 (s, 2H). IR (KBr, cm^{-1}): 2569(m), 1672(s), 1585(m), 1353(m), 1282(s), 1184(m), 775(w), 728(w). MS (EI): 278 (M^+).

2.3. Synthesis of 1-trifluoromethyl-3-[2.2]metacyclophanyl-1,3-propanedione (HtfacacMCP)

To a solution of 5-acetyl-8,16-dimethyl[2.2]MCP (1.01 g, 3.6 mmol) in THF (350 ml) was added sodium methoxide (1.06 g, 19.6 mmol) and the mixture was stirred for several minutes at room temperature. Then, methanol (5 ml) and ethyltrifluoroacetate (1.2 ml, 6.02 mmol) were added to the mixture which was stirred for a further 18 h under reflux. Solvents were removed under reduced pressure and the resulting residue was dissolved in chloroform. The solution was washed with water and dried with anhydrous sodium sulfate. Solvents were removed by diminished pressure and the residue was chromatographed on a silica gel column with toluene–chloroform (1:1 vol/vol) as an eluent to give HtfacacMCP as pale-yellow prisms (600 mg, 45%). M.p. 147–149°C (hexane). *Anal.* Calc. for $C_{22}H_{21}O_2F_3$: C, 70.58; H, 5.65. Found: C, 70.48; H, 5.65%. ^1H NMR ($CDCl_3$, 500 MHz): 0.57 (s, 3H), 0.68 (s, 3H), 2.75–3.10 (m, 8H), 6.54 (s, 1H), 6.96 (t, 1H, $J=7.32$ Hz), 7.14 (d, 2H, $J=7.32$ Hz), 7.75 (s, 2H), 15.70 (br s, 1H). IR (KBr, cm^{-1}): 2932(m), 1617(br s), 1585(m), 1452(s), 1286(br s), 1140(s), 799(m), 727(m). MS (EI): 374 (M^+).

2.4. Synthesis of (tfacacMCP)$_3$(bpy)Eu(III)·CH_2Cl_2

To a solution of HtfacacMCP (1.0 g, 2.68 mmol) and bipyridine (280 mg, 19.6 mmol) in absolute ethanol (350 ml) was added a solution of $EuCl_3 \cdot 6H_2O$ (200 mg, 0.55 mmol) in absolute ethanol (20 ml) and piperidine (2.0 ml), and then the solution was stirred for 24 h at room temperature. Solvent was condensed in vacuo and a pale-yellow solid precipitated. The solid was filtered, washed with absolute ethanol and then dried under reduced pressure. Recrystallization from dichloromethane–hexane gave the complex (490 mg, 92%). M.p. 295–297°C. *Anal.* Calc. for $EuC_{76}H_{68}N_2O_6F_9$: C, 63.91; H, 4.80; N, 1.96. Found: C, 63.78; H, 4.97; N, 2.07%. ^1H NMR ($CDCl_3$, 500 MHz): −0.10 (s, 9H), 0.89 (s, 9H), 2.50–3.10 (m, 24H), 2.75 (3H, br s), 5.25 (s, 2H), 6.75 (br s, 6H), 6.84 (t, 3H, $J=7.30$ Hz), 7.06 (d, 6H, $J=7.30$ Hz), 7.10–7.25 (m, 8H). IR (KBr, cm^{-1}): 2935(m), 1611(s), 1585(m), 1583(s), 1299(s), 1183(s), 1134(s), 790(m), 761(m). MS (POS-FAB): 1055 ([$M-$(tfacacMCP)]$^+$).

2.5. Synthesis of piperidinium(t-tolutfacac)$_4$Eu(III)

To a solution of *p*-tolutfacacH (100 mg, 0.27 mmol) and bipyridine (50 mg, 0.32 mmol) in absolute ethanol (100 ml) were added a solution of $EuCl_3 \cdot 6H_2O$ (35 mg, 0.10 mmol) in absolute ethanol (20 ml) and piperidine (2.0 ml), and then the reaction solution was stirred for 24 h at room temperature. Solvent was condensed in vacuo and a pale-yellow solid precipitated. The solid was filtered, washed with absolute ethanol and then dried under reduced pressure. Recrystallization from dichloromethane–hexane gave the complex (106 mg, 92%). M.p. 229–232°C. *Anal.* Calc. for $EuC_{76}H_{68}N_1O_8F_{12}$: C, 50.96; H, 3.84; N, 1.21. Found: C, 50.53; H, 3.80; N, 1.38%. ^1H NMR ($CDCl_3$, 500 MHz): 2.70 (s, 12H), 2.15 (s, 4H), 3.39 (br s, 2H), 4.05 (br s, 4H), 4.87 (br s, 4H), 7.22 (d, 8H, $J=7.94$ Hz), 7.99 (d, 8H, $J=7.94$ Hz), 8.00 (br s, 2H). IR (KBr, cm^{-1}): 2945(m), 1615(s), 1568(m), 1536(s), 1316(s), 1186(s), 1146(s), 783(m), 691(m). MS (POS-FAB): 1055 ([$M-$(*p*-tolutfacac)]$^+$).

2.6. X-ray crystal structure determination of (tfacacMCP)$_3$(bpy)Eu(III)·CH_2Cl_2 and piperidinium-[(p-toluacac)$_4$Eu(III)]

Crystals of (tfacacMCP)$_3$(bpy)Eu(III)·CH_2Cl_2 and piperidinium[(*p*-tolutfacac)$_4$Eu(III)] suitable for X-ray work were obtained from a mixed solution of dichloromethane and hexane. X-ray data were collected with a Rigaku AFC7R diffractometer using Cu Kα radiation at 298 K for (tfacacMCP)$_3$(bpy)Eu(III)·CH_2Cl_2 and with a Rigaku RAXIS-IV diffractometer using Mo Kα radiation at 298 K for piperidinium[(*p*-tolutfacac)$_4$Eu(III)]. Cell parameters and an orientation matrix for data collection were obtained from least-squares refinement, using the setting angles of 25 reflections. Crystallographic data for these complexes are summarized in Table 1. The intensities of three standard reflections of each sample were recorded every 3 h upon X-ray exposure and showed no systematic change. All calculations were carried out with a teXsan crystallographic software package of Molecular Structure Corporation. The intensity data were corrected for Lorentz and polarization effects and empirical absorption corrections (DI-FABS) were also applied. The structures were solved by a combination of Patterson and difference Fourier methods for (tfacacMCP)$_3$(bpy)Eu(III)·CH_2Cl_2 and SHELXS86 and difference Fourier methods for piperidinium[(*p*-tolutfacac)$_4$Eu(III)], and refined by full-matrix least-squares methods. All non-hydrogen atoms were refined anisotropically. The positions and isotropic B factors of hydrogen atoms were refined during least-squares calculation. The final cycle of refinement on *F* converged to the agreement indexes given in Table 1.

3. Results and discussion

3.1. Synthesis and characterization of (tfacacMCP)$_3$(bpy)Eu(III)·CH_2Cl_2 and piperidinium-[(p-tolutfacac)$_4$Eu(III)]

8,16-Dimethyl[2.2]MCP (**1**) [9] was reacted with acetic anhydride in the presence of $TiCl_4$ as a Lewis acid catalyst to give 5-acetyl-8,16-dimethyl[2.2]MCP (**2**) in 68% yield. Reaction of compound **2** with ethyltrifluoroacetate led to compound **3** (48%) (Scheme 1). *p*-TolutfacacH can be prepared from 4′-methylacetophenone in the same manner. Both compound **2** and *p*-tolutfacacH exist in the enol form according to ^{1}H NMR data which are described in Table 2. Complexation of compound **3** with Eu(III)Cl_3·$6H_2O$ in methanol in the presence of bipyridine [10] and piperidine afforded (tfacacMCP)$_3$(bpy)Eu(III)·CH_2Cl_2 (**3**) in 92% yield. On the other hand, complexation of *p*-tolutfacacH with

Table 1
Crystallographic data for (tfacacMCP)$_3$(bpy)Eu·CH_2Cl_2 and piperidinium[(*p*-tolutfacac)Eu]

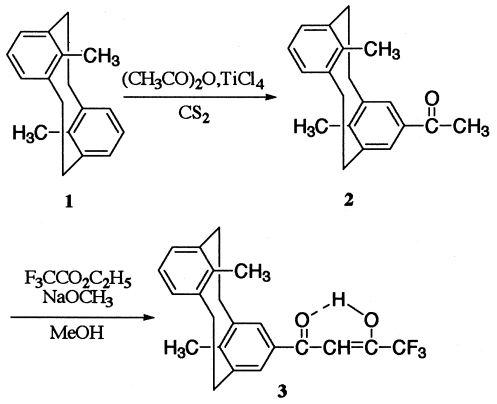
	(tfacacMCP)$_3$(bpy)Eu·CH_2Cl_2	Piperidinium[(*p*-tolutfacac)Eu]
Empirical formula	$EuC_{77}H_{70}N_2O_6F_9C_{l2}$	$EuC_{49}H_{44}NO_8F_{12}$
Formula weight	1513.28	1154.83
Crystal system	triclinic	monoclinic
Space group	$P\bar{1}$ (no. 2)	$P2/n$ (no. 13)
a (Å)	14.710(3)	13.85(3)
b (Å)	24.969(6)	11.83(2)
c (Å)	10.994(5)	15.73(2)
α (°)	99.91(3)	90
β (°)	103.56(3)	101.85(5)
γ (°)	96.33(2)	90
V (Å^3)	3818(2)	2521.8899
Z	2	2
D_{calc} (g cm^{-3})	1.316	1.521
Crystal size (mm)	0.20×0.20×0.40	0.40×0.40×0.50
μ (cm^{-1})	71.03 (Cu Kα)	13.36 (Mo Kα)
Data collection instrument	AFC7R Rigaku	RAXIS-IV
Radiation monochromated in incident beam	1.54178 (Cu Kα)	0.71070 (Mo Kα)
Temperature (°C)	20	20
Scan speed	ω–2θ	imaging plate
Data collection range, $2\theta_{max}$ (°)	120	55.6
No. unique data, total for $F_o^2 > 3\sigma(F_o^2)$	11347, 9072	5176, 4570
No. parameters refined	944	344
R [a]	0.079	0.046
R_w [b]	0.128	0.044
Goodness of fit indicator [c]	4.00	1.37
Largest shift/e.s.d., final cycle	0.40	0.03

[a] $R = \sum||F_o| - |F_c||/\sum|F_o|$.
[b] $R_w = [\sum w(|F_o| - |F_c|)^2/\sum w|F_o|^2]1/2$, $w = 1/\sigma^2(|F_o|)$.
[c] Goodness of fit $[\sum w(|F_o| - |F_c|)^2/(N_{obs} - N_{param})]^{1/2}$.

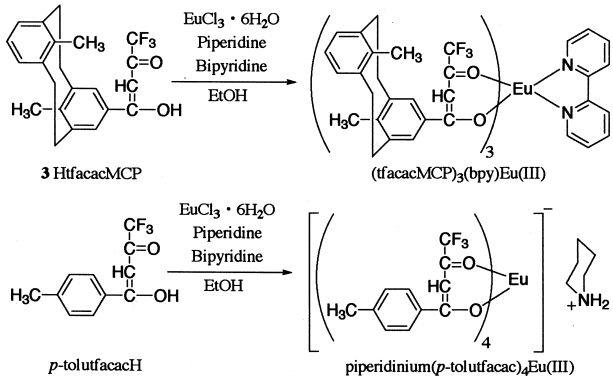
Table 2
Selected ^{1}H NMR data for HtfacacMcP, (tfacacMCP)$_3$(bpy)Eu·CH_2Cl_2, *p*-tolufacacH and piperidinium[(*p*-tolutfacac)Eu] [a]

Compound	Aromatic	Methine (–CH=)	Enol (OH)	Methyl (–CH_3)
HtfacacMCP	6.94–7.75(m)	6.54(s)	15.70(br s)	0.57(s), 0.68(s)
(tfacacMCP)$_3$(bpy)Eu·CH_2Cl_2	6.75–7.25(m)	2.75(s)		−0.10(s), 0.89(s)
p-TolufacacH	7.31(d), 7.84(d)	6.15(s)	15.50(br s)	2.44(s)
Piperidinium[(*p*-tolutfacac)Eu]	7.25(d), 7.99(d)	2.70(s)		2.15(s)

[a] Chemical shifts are given in ppm for TMS. Measured in $CDCl_3$. The multiplicity of a proton signal is given in parentheses after the δ value: s singlet; d doublet; m multiplet.



Scheme 1.



Scheme 2.

Eu(III)$Cl_3 \cdot 6H_2O$ was treated under the same conditions, however, piperidinium[(*p*-tolutfacac)$_4$Eu(III)] was obtained (Scheme 2). In this complex, bipyridine did not coordinate but a piperidinium ion ($C_5H_{12}N$) exists as a counter cation. This result can be explained by the bulkiness of HtfacacMCP.

In order to confirm the structures of their complexes some physical measurements were carried out. Selected ^{1}H NMR spectral data of (tfacacMCP)$_3$(bpy)Eu(III)·CH_2Cl_2 and piperidinium[(*p*-tolutfacac)$_4$Eu(III)] are summarized in Table 2. The signals of some protons in the tfacacMCP and the *p*-tolutfacac ligands are extremely upfield shifted because of the paramagnetic effect of the europium ion.

Elemental analyses of these complexes are summarized in Section 2. Found values of (tfacacMCP)$_3$(bpy)Eu(III)·CH_2Cl_2 were different from calculated values because a molecule of dichloromethane was lost. On the other hand, piperidinium[(*p*-tolutfacac)$_4$Eu(III)] showed good agreement with the expected composition. The europium complexes indicate clusters of ions corresponding to $[M-(\text{tfacacMCP})]^+$ and $[M-(p\text{-tolutfacac})]^+$, respectively, which are the base peak in FAB mass spectra. When the complexes are analyzed with a FAB method, the molecular ions are not obtained.

3.2. Crystal structure of the complexes

The perspective views of the molecular units of (tfacacMCP)$_3$(bpy)Eu(III)·CH_2Cl_2 and piperidinium[(*p*-tolutfacac)$_4$Eu(III)] are shown in Figs. 1 and 2, respectively. The selected bond lengths and bond angles are also given in Tables 3 and 4, respectively. Fig. 1 shows that the structure unit of (tfacacMCP)$_3$(bpy)Eu(III)·CH_2Cl_2 consists of one complex molecule and one dichloromethane molecule. The europium(III) is coordinated through six O atoms of

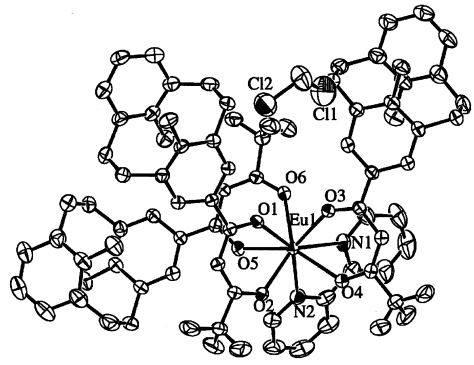


Fig. 1. ORTEP drawing of (tfacacMCP)$_3$(bpy)Eu·CH_2Cl_2.

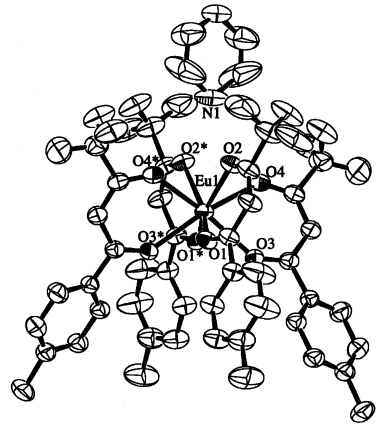


Fig. 2. ORTEP drawing of piperidinium[(*p*-tolutfacac)Eu].

Table 3
Selected bond lengths (Å) and bond angles (°) for $(tfacacMCP)_3(bpy)Eu\cdot CH_2Cl_2$

Eu–O(1)	2.353(10)	Eu–O(2)	2.375(9)
Eu–O(3)	2.330(9)	Eu–O(4)	2.400(10)
Eu–O(5)	2.388(9)	Eu–O(6)	2.351(10)
Eu–N(1)	2.61(1)	Eu–N(2)	2.58(1)
O(1)–Eu–O(2)	72.3(3)	O(1)–Eu–O(3)	73.4(3)
O(1)–Eu–O(4)	115.4(4)	O(1)–Eu–O(5)	78.2(3)
O(1)–Eu–O(6)	79.6(3)	O(2)–Eu–O(3)	119.6(3)
O(2)–Eu–O(4)	81.7(3)	O(2)–Eu–O(5)	76.4(3)
O(2)–Eu–O(6)	140.8(3)	O(3)–Eu–O(4)	70.5(3)
O(3)–Eu–O(5)	139.7(3)	O(3)–Eu–O(6)	75.8(3)
O(4)–Eu–O(5)	149.2(3)	O(4)–Eu–O(6)	136.0(3)
O(5)–Eu–O(6)	71.5(3)	O(1)–Eu–N(1)	148.7(4)
O(1)–Eu–N(2)	145.7(4)	O(2)–Eu–N(1)	138.4(4)
O(2)–Eu–N(2)	81.4(4)	O(3)–Eu–N(1)	82.5(4)
O(3)–Eu–N(2)	140.3(4)	O(4)–Eu–N(1)	73.2(4)
O(4)–Eu–N(2)	81.0(4)	O(5)–Eu–N(1)	110.4(4)
O(5)–Eu–N(2)	74.5(4)	O(6)–Eu–N(1)	75.2(4)
O(6)–Eu–N(2)	110.2(4)	N(1)–Eu–N(2)	62.7(4)

Table 4
Selected bond lengths (Å) and bond angles (°) for piperidinium-[(*p*-tolutfacac)Eu]

Eu–O(1)	2.378(5)	Eu–O(2)	2.441(4)
Eu–O(3)	2.366(3)	Eu–O(4)	2.376(4)
O(1)–Eu–O(2)	71.7(1)	O(1)–Eu–O(3)	70.5(1)
O(1)–Eu–O(4)	120.9(1)	O(2)–Eu–O(3)	98.4(1)
O(2)–Eu–O(4)	70.0(2)	O(3)–Eu–O(4)	72.6(1)
O(1)–Eu–O(1*)	130.4(2)	O(1)–Eu–O(2*)	152.7(1)
O(1)–Eu–O(3*)	78.8(1)	O(1)–Eu–O(4*)	83.5(2)
O(2)–Eu–O(2*)	93.6(2)	O(2)–Eu–O(3*)	135.7(1)
O(2)–Eu–O(4*)	71.9(1)	O(3)–Eu–O(3*)	102.0(2)
O(3)–Eu–O(4*)	154.0(1)	O(4)–Eu–O(4*)	123.1(2)

tfacacMCP and two N atoms of bpy. The average bond lengths Eu–O and Eu–N are 2.366(6) and 2.60(1) Å, respectively. The longest bond length Eu–O is 2.400(10) Å and the shortest length is 2.330(9) Å. The longest bond length Eu–N is 2.61(1) Å and the shortest length is 2.58(1) Å. On the other hand, Fig. 2 shows that the structure unit of piperidinium[(*p*-tolutfacac)$_4$Eu(III)] is composed of one complex molecule and a piperidinium ion. In the complex, the Eu(III) is coordinated through eight O atoms of *p*-tolutfacac ligands. The average bond length Eu–O for piperidinium[(*p*-tolutfacac)$_4$Eu(III)] is 2.390 Å. The longest bond length Eu–O is 2.441(4) Å and the shortest length is 2.366(3) Å, respectively.

3.3. Absorption spectra

The absorption spectral data of the ligands and their Eu(III) complexes are shown in Table 5. These absorption properties are characteristic of β-diketone type compounds, but the maximum absorption of HtfacacMCP shows ca. 34 nm longer shifts than that of *p*-tolutfacacH. This can be explained by the enhanced π system existing between two aromatic rings of an MCP moiety. Maximum absorption of $[(tfacacMCP)_3(bpy)Eu(III)]\cdot CH_2Cl_2$ indicates ca. 28 nm longer shifts than that of piperidinium[(*p*-tolutfacac)$_4$Eu(III)]. This tendency can also be explained by the effect described above.

3.4. Fluorescence spectra

Emission spectral data and charts of these two complexes in solution are given in Table 5, and Fig. 3 for $(tfacacMCP)_3(bpy)Eu(III)\cdot CH_2Cl_2$ and in Fig. 4 for piperidinium[(*p*-tolutfacac)$_4$Eu(III)], respectively. In piperidinium[(*p*-tolutfacac)$_4$Eu(III)], the strong metal-centered emission was observed at 615 nm but the emission from ligands was not observed when the excitation wavelength was 366 nm. This strong emission can be assigned to a $^5D_0$–$^7F_2$ energy level transition of the 4f orbital on the europium ion. Furthermore, another weak emission ($^5D_0$–^7F_n, $n=1,4$) was observed. The corrected excitation spectrum of piperi-

Table 5
Absorption and fluorescence spectral data for tfacacMCP, *p*-tolutfacac, $(tfacacMCP)_3(bpy)Eu\cdot CH_2Cl_2$ and piperidinium[(*p*-tolutfacac)Eu] [a]

Compound	λ_{max} (nm) (ε)	λ_{EM} (nm) (relative intensity)
tfacacMCP	373 (25400)	438 (8.36) [b]
p-Tolutfacac	339 (19000)	453 (6.35) [c]
$(tfacacMCP)_3(bpy)Eu\cdot CH_2Cl_2$	356 (66400)	615 (58.0) [b]
Piperidinium[(*p*-tolutfacac)Eu]	328 (70800)	451 (1.02), 615 (0.09) [c]

[a] In $CHCl_3$.
[b] $\lambda_{EX}=366$ nm.
[c] $\lambda_{EX}=366$ nm.

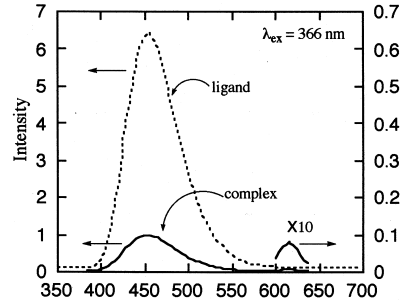


Fig. 3. Emission spectral chart of tfacacMCP and $(tfacacMCP)_3(bpy)Eu(III)$ in $CHCl_3$ at room temperature.

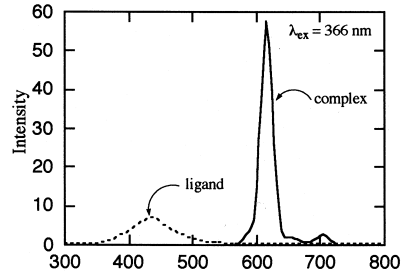


Fig. 4. Emission spectral chart of *p*-tolutfacac and piperidinium(*p*-tolutfacac)$_4$Eu(III) in $CHCl_3$ at room temperature.

dinium[(*p*-tolutfacac)$_4$Eu(III)] (λ_{EM} = 615 nm) shows exactly the same pattern as its absorption spectrum. This means that light absorption in the ligands is followed by energy transfer to the emitting $^5D_0$ excited state of the europium ion. In [(tfacacMCP)$_3$(bpy)Eu(III)]·CH_2Cl_2, the intensity of the metal-centered emission was much weaker than that of the ligand emission from the MCPtfacac moiety. Although the corrected excitation spectrum of [(tfacacMCP)$_3$(bpy)Eu(III)]·CH_2Cl_2 (λ_{EM} = 615 nm) shows exactly the same pattern as its absorption spectrum, the excited energy almost seems to be relaxed on the MCP ligand. That is to say, a part of the excited energy is transferred from the ligands to the europium ion. This phenomenon is perhaps due to the excited energy level of the triplet state in the MCP skeleton existing in the vicinity of the $^5D_0$ energy level of the 4f orbital on the europium ion.

Supplementary data

Further details of crystal structure determinations can be ordered from the Cambridge Crystallographic Data Centre, 12 Union Road, Cambridge CB2 1EZ, UK (fax: +44-1223-336033; e-mail: deposit@ccdc.cam.ac.uk) on request, quoting the deposition numbers 116595 for [(tfacacMCP)$_3$-(bpy)Eu(III)]·CH_2Cl_2 and 116030 for piperidinium[(*p*-tolutfacac)$_4$Eu(III)], respectively.

Acknowledgements

We are grateful to the Center for Instrumental Analysis, Kyushu Institute of Technology for elemental analyses, mass spectra and NMR spectra.

References

[1] M.L. Bhaumik, C.L. Telk, J. Opt. Soc. Am. 54 (1964) 1211.
[2] H. Samelson, A. Lempiki, C. Brecher, V. Brophy, Appl. Phys. Lett. 5 (1964) 173.
[3] R.G. Charles, E.P. Riedel, J. Inorg. Chem. 28 (1966) 527.
[4] P.M. Keehn, S.M. Rosenfeld (Eds.), Cyclophanes, vols. I and II, Academic Press, New York, 1983.
[5] V. Boekelheide, in: F.L. Boschke (Ed.), Topics in Current Chemistry, Springer, Berlin, 1987.
[6] F. Diederich, Cyclophanes, The Royal Society of Chemistry, Cambridge, 1989.
[7] J.F. Stoddart (Ed.), Monographs in Supramolecular Chemistry, vol. 1, The Royal Society of Chemistry, Cambridge, 1989.
[8] A. Tsuge, T. Moriguchi, S. Mataka, M. Tashiro, J. Org. Chem. 60 (1995) 4930.
[9] M. Tashiro, T. Yamato, J. Org. Chem. 46 (1981) 1543.
[10] S. Sato, M. Wada, Jpn. J. Appl. Phys. 7 (1968) 7.

PERGAMON

www.elsevier.nl/locate/poly

Polyhedron 19 (2000) 791–799

POLYHEDRON

Stereochemistry of chiral, substituted η^3-butadienyl molybdenum(II) complexes

Annabelle G.W. Hodson *, Rupinder K. Thind

Faculty of Applied Sciences, University of the West of England, Bristol BS16 1QY, UK

Received 1 November 1999; accepted 25 January 2000

Abstract

Chiral complexes of general type $[MoCl(CO)_2(\eta^3\text{-}CH_2C(COX)C{=}CH_2)(phen)]$ (phen = 1,10-phenanthroline) containing optically active substituents X have been prepared by reaction of the chlorocarbonyl (**1**) with esters of L-valine, L-alanine, L-phenylalanine, L-cysteine, L- and DL-serine or with amino alcohols (*S*)-(+)-1-amino-2-propanol and (*S*)-(+)-2-amino-1-propanol, and their diastereomers have been investigated by ^{1}H NMR spectroscopy. Reaction of compound **1** with diamines containing one (L-lysine) or two (L-cystine) stereogenic centres gives rise to dimeric complexes containing dibutadienyl bridging ligands, and these have been identified by a combination of synthetic and computer modelling methods. The probable spectra and structures of the corresponding poly-L-lysine derivatives are discussed.
©2000 Elsevier Science Ltd All rights reserved.

Keywords: Bridging ligands; Butadienyl; Chiral substituents; Molybdenum

1. Introduction

The synthesis and reactivity of η^3-allyl transition metal complexes have been widely investigated, both experimentally and theoretically, in part because of their relevance to allylic alkylation and coupling reactions of commercial importance [1,2]. By comparison, the chemistry of related η^3-butadienyl complexes has received limited attention. During the past decade several synthetic routes have been discovered which provide access to these complexes containing a range of substituents at C1, C2 or C3 positions of the C1C2C3=C4 unit [3–5], and the organic fragment has been examined crystallographically [6,7]. However, theoretical and mechanistic studies of η^3-butadienyl transition metal complexes are rare, and their reactivity has not been systematically explored. In addition, whilst there are many known examples of complexes containing the allyl unit acting as a bridging ligand between metal centres [8], only a very limited number of bridging butadienyl systems have been described [9–11]. In an attempt to explore some of these issues, the authors and others have been investigating the formation and reactivity of complexes of the general type $[MCl(CO)_2(\eta^3\text{-}CH_2C(COX)C{=}CH_2)(L_2)]$ (M = Mo,W; L_2 = 2,2′-bipyridyl, 1,10-phenanthroline) containing various substituents X at C2. The ester, amide and thioester (X = OR, NRR′, SR) complexes have been characterised by spectroscopic and crystallographic methods, and mechanisms of formation for the chlorocarbonyl (X=Cl) and ester substituted complexes have been discussed [12–14]. The asymmetry of the metal-bound substituted butadienyl unit leads to an expectation that isomers of this type of complex should be accessible; however, to date they have not been observed in either solution or solid states. In this study, a series of mono- and diamines containing one or more stereogenic centres has been used to explore the stereochemistry of chiral mono- and dimeric η^3-butadienyl complexes and to predict the structures of long-chain polymeric systems.

2. Experimental

2.1. Materials and physical methods

All chemicals were purchased from Sigma-Aldrich and used without further purification. Solvents and liquid reagents were dried with molecular sieves and degassed with dinitrogen prior to use. All reactions were carried out under an atmosphere of this gas at room temperature unless specified otherwise. The starting material (**1**) was freshly prepared from 1,4-dichloro-2-butyne and $Ph_4P[MoCl(CO)_3(phen)]$

* Corresponding author. Tel.: +44-117-9656261; fax: +44-117-9763871; e-mail: annabelle.hodson@uwe.ac.uk

0277-5387/00/$ - see front matter ©2000 Elsevier Science Ltd All rights reserved.
PII S0277-5387(00)00315-6

by the published method [12] and recrystallised from dichloromethane–petrol mixtures. Infrared spectra were recorded on a Perkin-Elmer 781 spectrometer using samples prepared as Nujol mulls on sodium chloride discs. The ^{1}H NMR spectra were obtained for solutions in dichloromethane-d_2 or dimethylsulfoxide-d_6 (DMSO-d_6) and referenced to tetramethylsilane (TMS) as internal standard. Molecular modelling was carried out using Hyperchem software (HyperChem™ version 5.1 uses molecular mechanics computations to predict new structures based on X-ray diffraction data of known complexes), and the structure of [Mo($O_2CC_3F_7$)(CO)$_2$(η^3-CH_2C(CONHMe)C=CH_2)-(2,2′-bipyridine)] was accessed from the Cambridge Crystallographic Database, UK.

2.2. Preparation of the complexes

2.2.1. Synthesis of monomeric complexes (2–6, 9, 10)

A solution of glycine ethyl ester hydrochloride or the methyl ester hydrochlorides of L-serine, L-valine, L-alanine, L-phenylalanine, L-cysteine (5.0 mmol) or L-lysine (1.0 mmol) in 2-propanol (50 cm^3) was stirred with excess potassium hydrogen carbonate (6.0 mmol, 0.600 g) for 1 h. To this was added triethylamine (1.0 mmol, 0.14 cm^3) and freshly prepared complex **1** (1.0 mmol, 0.483 g), and the mixture was stirred for a further 2 h. The solvent was removed under vacuum, the residue was extracted three times with aqueous dichloromethane (15 cm^3, 35%, v/v) and the organic phase finally dried over sodium sulfate. Chromatography on silica gel (60–120 mesh) using 5%, v/v methanolic dichloromethane, followed by addition of petrol and storage at low temperature yielded the products as orange powders, which were recrystallised from dichloromethane–petrol mixtures with yields of 30–55%.

2.2.2. Synthesis of aminopropanol derivatives (7, 8)

A solution of compound **1** (0.5 mmol, 0.2415 g) in dichloromethane (25 cm^3) was stirred with excess triethylamine (0.5 cm^3). To this was added dropwise (*S*)-(+)-2-amino-1-propanol or (*S*)-(+)-1-amino-2-propanol (0.5 mmol) and the mixture stirred for 2 h. The filtered solution was mixed with petrol and stored at low temperature. The crude solid which precipitated was recrystallised as described above, and gave the products as bright orange, microcrystalline powders in yields of 57 and 76%.

2.2.3. Synthesis of N(α)-acetyl-L-lysine product (11)

N(α)-Acetyl-L-lysine methyl ester hydrochloride (0.46 mmol, 0.108 g) was stirred with excess potassium hydrogen carbonate (1.0 mmol) in 2-propanol (20 cm^3) and then reacted with compound **1** (0.46 mmol, 0.222 g) and triethylamine (0.14 cm^3) as described in Section 2.2.1. Yield: 60%.

2.2.4. Synthesis of dimeric complexes (12, 13)

A suspension of excess potassium hydrogen carbonate (3.0 mmol, 0.300 g) in 2-propanol (20 cm^3) was stirred with the dimethyl ester dihydrochloride of L-cystine or methyl ester hydrochloride of L-lysine (0.5 mmol) for 1 h, and this mixture was then combined with triethylamine (1.0 mmol, 0.14 cm^3) and complex **1** (1.0 mmol, 0.483 g). After stirring for 2 h, the mixture was treated as described in Section 2.2.1, and the dried dichloromethane solution (15 cm^3) was chromatographed on silica gel (60–120 mesh) using dichloromethane followed by 5%, v/v methanol–dichloromethane as eluant. The alcoholic solution was collected, the solvent removed by vacuum and the residue recrystallised from dichloromethane–petrol. Yields: 20%, 31%.

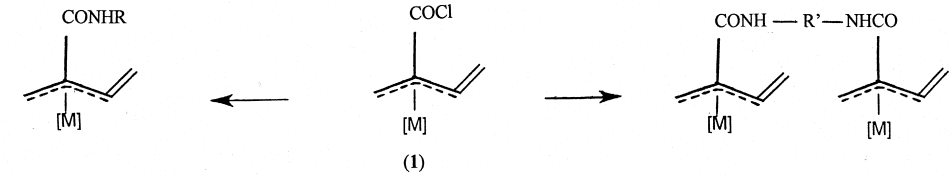
2.2.5. Synthesis of poly-L-lysine derivative (14)

Poly-L-lysine hydrobromide of approximate molecular weight 1000 (0.1 mmol, 0.100 g) was stirred with potassium hydrogen carbonate (0.7 mmol, 0.707 g) in 2-propanol (20 cm^3) for 60 min, and this was added to a stirred mixture of excess triethylamine (0.5 cm^3) and compound **1** (0.5 mmol, 0.2415 g). Filtration after 2 h gave a dark orange–brown residue, which was washed with dichloromethane to remove unreacted compound **1**, and dried in vacuo. Yield: 10%.

3. Results and discussion

3.1. Synthesis and structure of monomeric complexes

Reaction of compound **1** with a series of L-amino esters or L-aminopropanols under basic conditions gave rise to substi-



(**1**)

R = CH_2CO_2Et (**2**), HC(Me)CO_2Me (**3**),
HC(CH_2Ph)CO_2Me (**4**), HC(^{i}Pr)CO_2Me (**5**),
HC(CH_2OH)CO_2Me (**6**), HC(Me)CH_2OH (**7**),
CH_2C(OH)(H)Me (**8**), HC(CH_2SH)CO_2Me (**9**),
$(CH_2)_4$HC(NH_2)CO_2Me (**10**), $(CH_2)_4$HC(NHCOMe)CO_2Me (**11**)

R' = HC(CO_2Me)CH_2SSCH_2HC(CO_2Me) (**12**),
R' = HC(CO_2Me)$(CH_2)_4$ (**13**)

[M] = MoCl(CO)$_2$(phen)

Scheme 1.

tuted 2-amido η^3-butadienyl complexes (Scheme 1, **2**–**10**), and these were characterised by IR and NMR spectroscopy and by elemental analysis (Tables 1 and 2). The ^{1}H NMR spectra of complexes **3**–**6**, produced from methyl esters of L-alanine, L-phenylalanine, L-valine and L-serine, and of complexes **7** and **8**, obtained from (*S*)-(+)-2-amino-1-propanol and (*S*)-(+)-1-amino-2-propanol, respectively, all showed evidence of diastereomers in solution; however, that of complex **2**, derived from glycine ethyl ester, did not. This can be understood by considering the probable structures of the chlorocarbonyl precursor **1** and its amide derivatives. These can be predicted with some confidence based upon the ^{1}H NMR evidence, the existing X-ray data obtained by the authors and others for [Mo($O_2CC_3F_7$)(CO)$_2$(η^3-CH_2C(CONHMe)-C=CH_2)(2,2′-bipyridine)] [15] and the use of molecular modelling methods. Crystallographic analysis of the bipyridyl complex did not locate the amide hydrogen atom, and during refinement this was placed at an idealised position which approximated to sp^3 hybridisation at nitrogen. The structure revealed a *trans* arrangement of CO and NH and an essentially planar CO–NC unit. This is in accord with a high degree of double bond character between the carbonyl carbon and nitrogen atom of the amide, and predicts a high barrier to rotation about this bond. The double bond terminus of the η^3-butadienyl unit was orientated away from the carbonyl of the amide, and a similar structural unit in this part of the molecule in the new complexes **2**–**10** can be expected. A mechanism has been proposed for reaction of Ph_4P-[MoCl(CO)$_3$(phen)] and 1,4-dichloro-2-butyne in dichloromethane which is consistent with the production of compound **1** as an enantiomeric pair (Fig. 1, A and B). These give rise to a single set of proton NMR resonances due to the highly symmetrical nature of the (CO)$_2$Mo(phen) unit and to the magnetically equivalent environments of the two butadienyl groups. On reaction with an achiral amine such as glycine, the amide-substituted analogues of each isomer are formed. These are indistinguishable from their ^{1}H NMR spectra, because the butadienyl, NH and ester substituent for each isomer continue to exist in magnetically equivalent environments. For a chiral amine, however, reaction with the two isomers of compound **1** gives rise to a pair of diastereomers with amide substituents in inequivalent magnetic fields, and these can be differentiated from their ^{1}H NMR spectra as described below.

Spectra for complexes **3**–**7** all exhibited two sets of signals which could be assigned to a diasteromeric pair. However, pairs of resonances for the 1-amino-2-propanol derivative (**8**) were all superimposed with the exception of H''_{syn} of the butadienyl terminal double bond and the methyl group at C_α of the substituent. Thus increasing distance between the metal-bound phenanthroline moiety and $C_\alpha H$ of the chiral amine decreases the observable magnetic inequivalence of the diastereomeric pair. There was no evidence for the formation of dimeric complexes arising from reaction of compound **1** at hydroxyl groups of serine ester or the amino alcohols during production of compounds **6**–**8**, the more basic amine reacted preferentially in each case. Both L-serine (**6**) and DL-serine methyl ester products (DL-**6**) were prepared from compound **1**, and their ^{1}H NMR spectra were compared. Both complexes produced two sets of resonances, and almost identical peak positions and $^3J_{NH-CH}$ coupling constants were observed for compounds **6** and DL-**6**. This arises because the pair of diastereomers for L-**6** shows an enantiomeric relationship to a diastereomeric pair for D-**6**. Consider the pairs C/F and D/E shown in Fig. 2, which represent the pairs of diastereomers arising from L-serine and D-serine products, respectively. The symmetrical nature of the (CO)$_2$Mo(phen) unit gives rise to a similar magnetic environment for the $C_\alpha H$

Table 1
Selected infrared and analytical data for monomeric and polymeric butadienyl complexes

Complex	Reactant amine	Infrared data (cm^{-1})			Found (calc.) (%)		
		ν(C≡O) [a]	ν(C=O) [a]	ν(XH) [e]	C	H	N
2	glycine ester	1902, 1978	1640, 1732	3420	50.24 (50.22)	3.67 (3.63)	7.41 (7.64)
3	L-alanine ester	1890, 1968	1643, 1748	3411	49.98 (50.22)	3.38 (3.63)	7.47 (4.64)
4	L-phenylalanine ester	1893, 1962	1648, 1733	3398	55.36 (55.63)	3.82 (3.83)	7.08 (6.71)
5	L-valine ester	1893, 1968	1650, 1733	3425	51.90 (51.94)	4.16 (4.15)	7.21 (7.27)
6	L-serine ester	1893, 1971	1633, 1739	3430, 3398	48.40 (48.80)	3.65 (3.53)	7.50 (7.42)
7	2-amino-1-propanol	1891, 1976	1621	3390–3410br	47.92 (47.87)	3.82 (3.72)	7.77 (7.44) [c]
8	1-amino-2-propanol	1895, 1966	1649	3424, 3393	47.87 (47.87)	3.35 (3.72)	7.16 (7.44) [c]
9	L-cysteine ester	1901, 1974	1643, 1736	3410		[d]	
10	L-lysine ester	1892, 1970	1644, 1734	3405	46.45 (46.85)	3.84 (4.19)	7.69 (8.09) [b]
11	*N*(α)-acetyl-L-lysine ester	1874, 1970	1642br, 1738	3303br	50.82 (50.81)	4.44 (4.47)	8.42 (8.63)
12	L-cystine diester	1899, 1973	1646, 1738	3380	44.60 (45.26)	3.95 (3.21)	7.02 (6.74)
13	L-lysine ester	1898, 1973	1648, 1738	3418	48.31 (48.50)	4.10 (3.51)	7.03 (7.38) [b]
14	poly-L-lysine	1913, 1984	1624, 1700	3300–3450br		[d]	

[a] Bands strong.
[b] CH_2Cl_2 calculated.
[c] $0.5CH_2Cl_2$ calculated.
[d] Non-reproducible analysis.
[e] X = N or O. Weak.

Table 2
^{1}H NMR data for monomeric and polymeric complexes **2**–**13** [a]

	H'_{anti} H'_{syn}	H''_{anti} H''_{syn}	NH	Aliphatic CH_2/XH [c]	CH_3	OCH_3	Aromatics
2 [b]	2.04 (s, H), 3.84 (s, H)	5.80 (d, 2.02, H), 6.31 (d, 2.20, H)	5.52 (d, 5.60, H)	1.92 (dd, 4.22, 18.69, H), 2.95 (dd, 5.67, 18.50, H), 3.97 (q, 6.96, 2H)	1.14 (t, 7.14, 3H)		7.90 (m, 4H), 8.43 (d, 8.24, H), 8.52 (d, 8.25, H), 9.12 (d, 5.13, H), 9.19 (d, 4.95, H)
3 [b]	2.14 (s, H), 2.16 (s, H), 3.97 (s, H), 4.03 (s, H)	5.92 (d, 2.20, 2H), 6.43 (d, 2.19, H), 6.46 (d, 2.20, H)	5.89 (d, 5.22, H), 6.00 (d, 5.22, H)	2.64–2.69 (m, 2H)	−0.15 (d, 6.96, 3H), 0.93 (d, 6.96, 3H)	3.62 (s, 3H), 3.65 (s, 3H)	7.76–8.07 (m, 8H), 8.46 (d, 8.24, H), 8.56–8.64 (m, 3H), 9.21 (d, 4.13, H), 9.23–9.31 (m, 3H)
4 [b]	2.03 (s, H), 2.05 (s, H), 3.86 (s, H), 3.90 (s, H)	5.68 (d, 2.20, H), 5.77 (d, 2.13, H), 6.05 (d, 2.20, H), 6.16 (d, 2.13, H)	5.62 (d, 5.63, H), 5.64 (d, 5.22, H)	1.67 (m, 2H), 2.57 (m, 2H), 3.04 (m, 2H)		3.36 (s, 3H), 3.43 (s, 3H)	6.67 (m, H), 6.79 (m, H), 7.16 (m, 4H), 7.24 (m, 4H), 7.70–7.98 (m, 8H), 8.32 (d, 8.24, H), 8.47 (d, 8.24, H), 8.53 (m, 2H), 9.03 (d, 4.88, H), 9.15 (d, 6.10, H), 9.19 (d, 4.19, 2H)
5 [b]	2.04 (s, 2H), 3.89 (s, H), 3.93 (s, H)	5.79 (d, 2.57, H), 5.80 (d, 2.38, H), 6.30 (d, 2.20, H), 6.35 (d, 2.38, H)	5.85 (d, 5.23, H), 5.88 (d, 5.23, H)	0.73 (m, H), 1.61 (m, H), 2.88 (dd, 2.58, 3.48, H), 3.13 (dd, 4.22, 3.48, H)	−0.15 (d, 6.78, 3H), 0.18 (d, 6.96, 3H), 0.53 (d, 3.66, 3H), 0.56 (d, 3.85, 3H)	3.45 (s, 3H), 3.51 (s, 3H)	7.74–7.88 (m, 8H), 8.43 (d, 8.25, H), 8.43–8.49 (m, 3H), 9.09 (d, 4.95, H), 9.13–9.18 (m, 3H)
6	1.94 (s, H), 1.95 (s, H), 3.85 (s, H), 3.88 (s, H)	5.65 (s, H), 5.80 (s, H), 6.28 (d, 2.19, H), 6.32 (d, 2.01, H)	6.00 (d, 7.51, H), 6.04 (d, 6.59, H)	2.44 (m, H), 2.64 (m, H), 3.04 (d, 3.30, H), 4.70 (t, 5.30, H) [d], 4.77 (t, 5.32, H) [d]		3.42 (s, 3H), 3.49 (s, 3H)	7.97–8.10 (m, 4H), 8.14 (s, 2H), 8.16 (s, 2H), 8.74–8.83 (m, 4H), 9.17 (m, 2H), 9.25 (m, 2H)
7	1.86 (s, H), 1.90 (s, H), 3.90 (s, H), 3.92 (s, H)	5.74 (d, 1.83, H), 5.77 (d, 1.80, H), 6.24 (d, 2.01, H), 6.30 (d, 2.01, H)	5.61 (d, 7.14, H), 5.79 (d, 7.51, H)	1.79 (m, H), 2.17 (m, H), 2.36 (m, H), 2.56 (m, H), 2.68 (m, H), 2.80 (m, H), 4.27 (t, 5.31, H) [d], 4.47 (t, 5.31, H) [d]	−0.41 (d, 6.59, 3H), 0.38 (d, 6.60, 3H)		8.03 (m, 4H), 8.16 (s, 2H), 8.17 (s, 2H), 8.81 (m, 4H), 9.14 (d, 4.03, H), 9.17 (d, 3.85, H), 9.25 (d, 4.03, H), 9.27 (d, 4.03, H)
8	1.91 (s, 2H), 3.86 (s, 2H)	5.81 (d, 2.20, 2H), 6.30 (d, 2.28, H), 6.32 (d, 2.28, H)	5.84 (m, 2H)	2.51 (d, 7.26, H), 2.56 (d, 8.24, H), 2.69 (d, 3.27, H), 2.74 (d, 3.11, H), 2.87 (m, 4.20 (m, H) [d], 4.81 (m, H) [d]	0.49 (d, 6.23, 3H), 0.56 (d, 6.23, 3H)		8.01 (m, 4H), 8.17 (s, 4H), 8.82 (d, 5.04, 4H), 9.13 (d, 4.77, 2H), 9.24 (d, 4.40, 2H)

(*continued*)

Thursday Apr 13 09:53 AM StyleTag -- Journal: **POLY** *(Polyhedron)* Article: **3391**

Thursday Apr 13 09:53 AM

Table 2 (*continued*)

	H'_{anti} H'_{syn}	H''_{anti} H''_{syn}	NH	Aliphatic CH_2/XH [c]	CH_3	OCH_3	Aromatics
10	1.91 (s, H), 3.90 (s, H)	5.77 (s, 2H), 6.26 (s, 2H)	6.15 (m, 2H), 7.78 (m, 2H)	0.22 (m, 4H), 0.83 (m, 4H), 1.24 (m, 4H), 1.59 (m, 4H), 3.38 (m, 2H)		3.43 (s, 6H)	8.00 (m, 4H), 8.13 (m, 4H), 8.78 (m, 4H), 9.11 (m, 2H), 9.24 (m, 2H)
11	1.84 (s, 2H), 3.86 (s, 2H)	5.75 (s, 2H), 6.28 (s, 2H)	3.61 (d, 4.58, 2H), 6.07 (m, 2H)	0.11 (m, 4H), 0.70 (m, 4H), 1.27(m, 4H), 1.66 (m, 2H), 1.84 (m, 2H), 4.01 (m, 2H)	1.85 (s, 6H)	3.38 (s, 6H)	8.01 (m, 4H), 8.14 (m, 4H), 8.79 (d, 8.06, 4H), 9.13 (d, 4.94, 2H), 9.25 (d, 4.58, 2H)
12	1.92 (s, H), 1.97 (s, H), 3.62 (s, 3H), 3.67 (s, 3H)	5.76 (s, H), 5.79 (s, H), 6.25 (s, H), 6.32 (s, H)	6.49 (m, 2H)	0.84 (m, 2H), 2.08 (m, 2H), 2.83 (m, 2H)		3.62 (s, H), 3.67 (s, H)	8.00 (m, 4H), 8.14 (m, 4H), 8.78 (m, 4H), 9.16 (m, 2H), 9.25 (m, 2H)
13	1.85 (s, H), 1.91 (s, H), 1.94 (s, 2H), 3.86 (s, 2H), 3.90 (s, H), 3.93 (s, H)	5.72 (m, H), 5.77 (m, 2H), 5.91 (m, H), 6.13 (m, H), 6.26 (m, 2H), 6.32 (m, H)	5.91–6.15 (m, 4H)	0.23 (m, 2H), 0.83 (m, 4H), 1.15 (m, 2H), 1.23 (m, 2H), 1.49 (m, 2H), 1.66 (m, 2H), 2.40 (m, H), 2.62 (m, H), 3.44 (m, 2H)		3.36 (s, 6H)	7.87–8.26 (m, 16H), 8.54–8.67 (m, 2H), 8.75–8.80 (m, 4H), 8.81–8.91 (m,2 H), 9.09–9.15 (m, 4H), 9.25–9.31 (m, 4H)

[a] Data are reported in ppm, multiplicity, coupling constant (Hz) and number of protons. Spectra were recorded in DMSO-d_6 except where indicated.
[b] Recorded in dichloromethane-d_2.
[c] X = C.
[d] X = O.

StyleTag -- Journal: **POLY** *(Polyhedron)* Article: **3391**

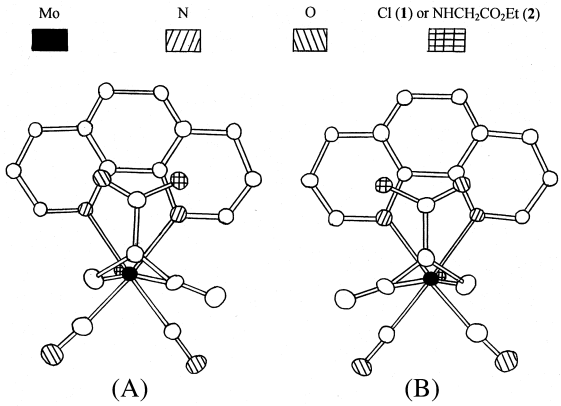


Fig. 1. Enantiomers of compounds **1** and **2** (hydrogen atoms are omitted for clarity).

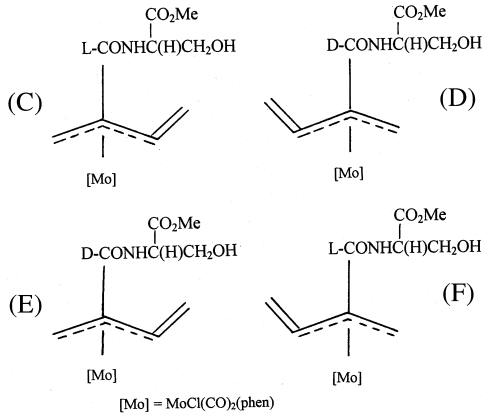


Fig. 2. Enantiomers of complexes L-**6** and D-**6**.

group and substituent R in the pair C/D, and thus this enantiomeric pair gives rise to one set of resonances. Similarly, the magnetic environments of these groups in the pair E/F are equivalent, and this pair also produces a single set of resonances. Thus the spectra of L-, D- and racemic DL-serine products are all expected to show two sets of very similar resonances, and this was confirmed by experiment. (Data for the L-serine derivative are given in Table 2.)

The relative positions of ester, $C_\alpha H$ and R groups within the (η^3-$CH_2C(CONHC_\alpha H(R)CO_2Me)C{=}CH_2$) unit in complexes **3**–**6** can be predicted using both a comparison of ^1H NMR resonances for the free and reacted amino acid ester and the Karplus relationship for vicinal protons based on $^3J_{NH-CH}$ coupling constants [16]. Singlets arising from the methyl ester in the metal complexes were found close to the free amino ester positions of approx. 3.5 ppm, and these two resonances for any pair of diastereomers were separated by less than 0.07 ppm. In contrast, resonances due to the R group at $C_\alpha H$ in the complexes were shifted significantly upfield compared to the free positions, and signals for a particular component of R in one complex differed by up to 1.08 ppm between the two diastereomers. For example, the two diastereomers of the L-alanine complex **3** gave rise to two singlets at 3.62 and 3.65 ppm due to the methyl ester and two doublets at −0.15 and 0.93 ppm due to the C_α methyl group. This implies that for both isomers the ester is distant from, and unaffected by, the anisotropic ring system, and that the C_α substituents have differing, but greater proximity to phenanthroline. Using the Karplus relationship, the $^3J_{NH-CH}$ value of 5.22 Hz for both isomers of compound **3** was found to be consistent with torsion angles of approximately 27 or 123°. The probable structure of compound **3** was modelled, based upon the known structure of [$Mo(O_2CC_3F_7)(CO)_2$(η^3-$CH_2C(CONHMe)C{=}CH_2$)(2,2′-bipyridine)], by replacing the heptafluorobutyrate with a chlorine atom, changing bipyridyl to phenanthroline and substituting the amide methyl group by L-alanine methyl ester. Geometry optimisation was carried out using a molecular mechanics programme, and gave a minimum energy conformation whose dihedral angles were consistent with the observed NMR coupling constants. Viewed along the HN–C_α bond, the two isomers may be represented by G and H in Fig. 3, in which the two methyl groups at C_α are orientated towards different regions of the phenanthroline ring system. Similar arguments pertain to the structures of the diastereomers of L-serine derivative **6**; however, the $^3J_{NH-CH}$ constants are noticeably different for this pair at 6.59 and 7.51 Hz. Construction of molecular models of compound **6** shows that hydrogen bonding between NH and the C_α hydroxyl controls the NH–CH torsion angle, and the resultant approach of OH to phenanthroline accounts for the large upfield shift of the hydroxyl signal, from a broad peak at 8.6 ppm in the free amine to a pair of triplets at 4.70 and 4.77 ppm in the two isomers of the complex. As discussed above, the proton NMR spectra of DL-serine and L-serine derivatives are identical, and by analogy the spectrum of (*S*)-(+)-aminopropanol derivative (**7**) should be magnetically equivalent to the (*R*)-(−) derivative. This permits direct comparison of spectra for compounds **6** and **7**, which both contain CH_2OH groups at C_α of the butadienyl substituent. The two spectra exhibited similar resonance positions for methine, methylene and hydroxyl groups at the C_α substituent, and $^3J_{NH-CH}$ constants were comparable. However, whilst the signal due to the methyl ester in compound **6** was almost identical to that for free serine ester, the C_α methyl group of (*S*)-(+)-aminopropanol shifted resonance position from 1.00 for the free amine to 0.38 and −0.41 ppm in the two isomers of complex **7**. It is likely, therefore, that the structures of compounds **6** and **7** are related, but that the absence of a carboxy group in compound **7** results in the C_α methyl moving within the sphere of influence of the phen system.

The cysteine product (**9**) was identified by the position of the amide carbonyl stretching frequency and SH absorption

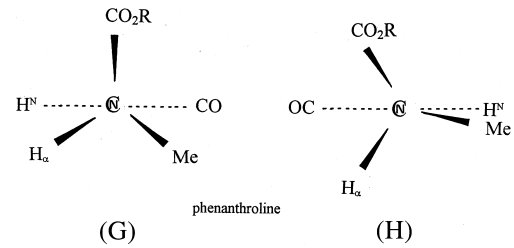


Fig. 3. Relative positions of amide substituents in compound **3**.

in the IR spectrum. This product proved to be unstable in solution over several days (oxidation of the thiol group by traces of atmospheric O_2 leads to formation of the dimeric disulfide, probably by way of thioxy radicals or sulfenic acid derivatives), and this led to non-repeating elemental analyses. In addition, the ^{1}H NMR spectrum of compound **9** was very broad, and signals attributable to the dimeric cystine derivative (**12**) were identified by comparison (see Section 3.2).

Combination of L-lysine ester, which contains two primary amine groups of pK_a 9.2 and 10.8, with compound **1** in a 1:1 mole ratio may result in the acyl chloride reacting at either C_α or C_ε positions only to give a monomeric complex, or the reaction may occur at both positions leading to a dimeric product and unreacted amino ester. Only one set of ^{1}H NMR signals for the phen ring system, the termini of the butadienyl unit and the amino ester substituent in the resultant complex (**10**) was observed. Comparison of the integrals for signals due to the lysine unit and the butadienyl termini revealed the presence of a monomeric species only, and this was supported by the elemental analysis results. Synthesis of the *N*(α)-acetyl-L-lysine ester derivative (**11**) for comparison was informative. This complex gave rise to one set of signals in its ^{1}H NMR solution spectrum, in accord with a diastereomeric pair having C_α distal from the metal–phen unit. Two signals attributable to NH could be identified at 3.61 and 6.07 ppm. The latter is within the range of 5.61–6.04 ppm found for complexes **3**–**6** and can be assigned to $CON_\varepsilon H$, which is adjacent to the butadienyl group. The ^{1}H NMR spectrum of lysine monomer **10** also showed a single set of signals, and comparison of integrals for phen and the $N_\varepsilon H(CH_2)_4$-$C(H)N_\alpha H$ unit confirmed a preferential reaction of the acyl chloride at $N_\varepsilon H$, the amine of higher pK_a.

3.2. Synthesis and structure of polymeric complexes

Mixing compound **1** with L-cystine dimethyl ester in 2:1 mole ratio under basic conditions gave rise to complex **12**, which was identified from elemental analysis and IR and NMR evidence as a dimeric species having two metal-bound η^3-butadienyl units bridged by the bis-amido disulfide unit. The ^{1}H NMR spectrum of compound **12** showed only two sets of broad signals despite the presence of two stereogenic centres, suggesting that the magnetic environments of the possible diastereomers are not sufficiently dissimilar to differentiate all the possible forms. Some peaks attributable to compound **12** could be identified in the spectrum of compound **9**, and refluxing compound **12** with 2-mercaptoethanol gave compound **9** by cleavage of the disulfide bond. Attempts to separate the isomers of compound **12** by fractional crystallisation or chromatography were not successful.

Reaction of L-lysine methyl ester and compound **1** in 1:2 mole ratio yielded complex **13**, whose ^{1}H NMR spectrum was highly complex. It has been demonstrated that two sets of signals due to diastereomers may be observed when $C_\alpha H$ is adjacent to the butadienyl amide substituent and that increasing distance of $C_\alpha H$ from the butadienyl amide group leads to overlapping of these signals. Thus if both the amine at $C_\alpha H$ ($N_\alpha H$) and the terminal amine ($N_\varepsilon H$) have reacted with the chlorocarbonyl group to give a dimeric complex, then the two diastereomers of compound **13** should give rise to a total of three magnetically distinct sets of signals, integrating in the ratio 1:1:2. Whilst this was observed for the butadienyl terminal protons, detailed interpretation was not possible, since the three peaks for the amide and those of the ester were each broad and overlapping and the multiplets due to aromatic and methylene protons gave rise to highly complex patterns. By comparison of the integrals for multiplet peaks arising from the phenanthroline unit, the methyl ester and for NH with those due to the $(CH_2)_4$ chain it was possible to support a dimeric formulation for compound **13**, and this was confirmed by the elemental analyses. Reaction of long-chain polyamines and excess compound **1** would give increasingly complex spectra; however, some general observations can be made on their probable structure. Poly-L-amino acids can exist naturally in either α-helix or β-pleated sheet forms, and the preferred construction is dependent upon the degree and extent of inter- and intra-molecular hydrogen bonding. Under laboratory conditions of pH 12 and above the α-helix stucture is adopted, and thus mixing a basic solution of excess compound **1** and poly-L-lysine (approximate molecular weight 1000) may be predicted to give rise to a short helical chain having butadienyl groups at some or all of the peripheral $N_\varepsilon H$ groups and/or at the $N_\alpha H$ terminus. Whilst the IR spectrum of this product (**14**) confirmed the presence of metal–carbonyl, C=O amide and NH groups, the low solubility of the solid in common organic solvents resulted in poor elemental analyses and also prevented investigation by NMR solution spectroscopy. This was unfortunate, since the small size of $^3J_{HN-C\alpha H}$ coupling constants can be used as a hallmark characteristic of α-helix secondary structure [17], and torsion angle constraints can be calculated from their associated empirical Karplus relations [18,19]. An average degree of polymerisation for the polylysine of six might be used as a model system. It has been shown that compound **10** gives rise to one set of NMR signals due to attachment of the butadienyl at $N_\varepsilon H$ only, and that compound **13** gives a complex pattern in which signals due to three diastereomers may be identified. The spectra and elemental analysis of compound **13** suggest that, in the presence of excess compound **1**, terminal and pendant amino groups of polylysine will all react, and a total of six pendant and one terminal butadienyl group will be present in the product **14**. The resultant ^{1}H NMR spectrum can be expected to be highly complex, although some simplification may occur if magnetic equivalence of pendant butadienyl groups is present.

3.3. Infrared spectroscopy

All complexes gave rise to a pair of strong absorptions between 1980 and 1890 cm^{-1}, and these can be assigned to the stretching modes of a *cis*-metal–dicarbonyl unit. A band

of medium intensity near 1735 cm^{-1} resulted from the carbonyl of the alkyl ester functionality in complexes **2**–**6** and **9**–**13**, and weak absorptions at about 1675 cm^{-1} due to the vinylic double bond could be identified for some complexes. Signals due to NH were found in the region 3425–3303 cm^{-1}, and, with the exception of spectra for compounds **2**, **4** and **9** which each exhibited a single sharp peak, these absorptions were broad and weak. For the poly-L-lysine derivative **14**, the terminal carboxylic acid group gave rise to a broad peak centred at 1700 cm^{-1} (carbonyl), and signals due to OH, NH(amide) and NH (primary amine) were combined in a very wide, shallow band across the range 3650–3300 cm^{-1}. It has been demonstrated [12] that the position of the carbonyl absorption due to ester, amide and thioester substitutents in the butadienyl unit of $[WCl(CO)_2(\eta^3\text{-}CH_2C(COX)C{=}CH_2)(phen)]$ (X = OMe, NEt_2, SBu) reflects the differing electronegativities of the group X. In accord with these observations, a carbonyl stretching absorption for the amide appeared near 1645 cm^{-1} for all the complexes, and supported reaction at the more basic amine rather than the hydroxyl in 1-amino-2-propanol and 2-amino-1-propanol. A weak absorption near 2600 cm^{-1} for SH of the freshly prepared cysteine complex **9** was absent from the cystine complex **12**.

3.4. ^1H NMR spectroscopy

The poor solubilities of the complexes in common organic solvents precluded measurement of ^{13}C NMR spectra, however proton NMR spectra of complexes in dichloromethane-d_2 and DMSO-d_6 were recorded where possible, and pertinent data are presented in Table 2. The glycine derivative (**2**) gave rise to a pair of doublets (coupling constants ca. 2.2 Hz) at 5.80 ppm (H_{anti}) and 6.31 ppm (H_{syn}) due to the vinylic protons of the butadienyl and to singlets at 2.04 ppm (H_{anti}) and 3.84 ppm (H_{syn}) arising from the allylic protons. This is in accord with previous observations for a transoid butadienyl in which the uncoordinated carbon–carbon bond is unconjugated with respect to the π-delocalisation of the η^3-allyl unit [12]. Peaks assigned to the alkyl groups of the ethyl ester were shifted slightly upfield compared to the free amine due to the anisotropic effect of the phenanthroline ring system. The methylene protons adjacent to NH produced two multiplets due to their differing magnetic environments, and coupling of NH to the two protons was dissimilar. The hydrogen at higher field can be expected to be closer to the phenanthroline ligand, and this gives rise to a smaller coupling constant (4.22 Hz) than for the lower field signal (5.67 Hz). There were no minor peaks present in the spectrum to suggest isomers were present, and there was no alteration of the spectrum in the temperature range −50 to +25°C to indicate dynamic behaviour in solution.

Spectra for complexes derived from the esters of alanine, phenylalanine, valine, serine (**3**–**6**) and from 2-amino-1-propanol and 1-amino-2-propanol (**7**, **8**) all showed doubling of peaks across the whole ppm range, although some overlapping of signals was observed for the latter complex. The relative intensities of these pairs were dependent upon the length of time between completion of reaction of compound **1** with the amine and filtration of the precipitated product after addition of petrol, implying fractional crystallisation of two diastereomers was occurring. For example, the spectrum of the L-phenylalanine derivative (**4**) filtered after 24 h was dominated by one set of peaks which was shadowed by a second set as a 5% component (by integration). On filtration after 7 days the intensity of the minor set had increased to almost equal that of the second set of peaks. The two sets of signals could be assigned to two independent isomeric forms. Fig. 4 shows illustrative regions of this spectrum. The vinylic protons of the butadienyl gave rise to four doublets between 5.6 and 6.2 ppm with two pairs of coupling constants of 2.13 and 2.20 Hz. Comparison of integrals showed the total sum of the lower field pair was equivalent to the higher field pair, and each pair of minor or major doublets were of equal integration. An obscured pair of doublets due to the NH proton occurred near 5.64 ppm. The two sets of signals for vinylic protons and the NH both integrated in the ratio 2:2:2, and indicated the presence of two diastereoisomers of compound **4** in solution. The allylic protons occurred as two pairs of singlets near 2.04 and 3.88 ppm, and the methyl ester signal appeared as a pair of singlets near 3.40 ppm. For each isomer, the methylene group of the α-carbon substituent gave rise to two AB quartets, which were centred near 1.67 and 2.57 ppm. Signals due to phenanthroline were unexceptional and appeared as distinct sets for the two isomers. Inequivalence of the protons of the benzyl ring was apparent, with four multiplets centred at 6.67, 6.79, 7.16 and 7.24 ppm integrating in the ratio 1:1:4:4, and was in accord with two diastereoisomers, each having one *ortho* proton of the ring directed towards the anisotropic phen ligand.

Both the lysine derivative (**10**) and its *N*(α)-acetyl model (**11**) gave one set of ^1H NMR signals only in accord with $C_\alpha H$ being distant from the butadienyl amide substituent. Attachment of the butadienyl unit to $N_\varepsilon H$ in both complexes was supported by peak positions of 6.15 and 6.07 ppm, respectively, and the free $N_\alpha H$ signal at 7.78 ppm for compound **10** appeared slightly upfield from the free lysine ester position of 8.40 ppm due to the proximity of phen in the complex. Although the spectra for cystine and lysine deriv-

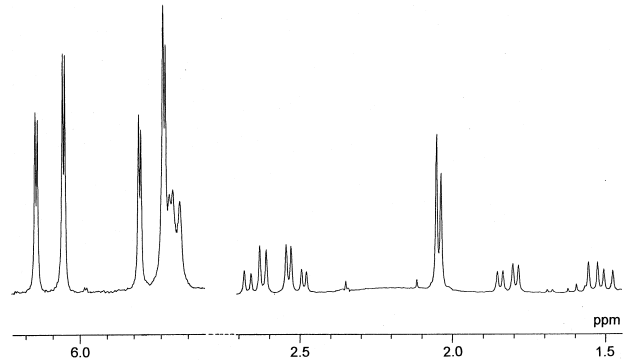


Fig. 4. Part of the ^1H NMR spectrum of compound **4**.

atives **13** and **14** were broad, individual peaks due to the terminal protons of the butadienyl could be identified, and for the latter complex these appeared in the ratio 1:1:2, as predicted for a dimeric species. Comparison of integration of peaks across the full spectral width supported dimeric formulae in each case.

4. Conclusions

Reaction of chiral L-amino esters or (*S*)-(+)-amino alcohols with [$MoCl(CO)_2(\eta^3$-$CH_2C(COCl)C{=}CH_2)(phen)$] yields monomeric complexes containing an amide substituent, and these optical isomers can be identified by ^1H spectroscopy. Both dibasic L-cystine and L-lysine may react with the chlorocarbonyl substituent to give dimeric complexes containing two metal centres bridged by linked butadienyl groups. However, equimolar reactions of L-lysine and the chlorocarbonyl complex result in reaction at the amine of higher pK_a preferentially. The chemistry of these complexes is currently under investigation.

Acknowledgements

Elemental analyses were carried out by the Analysis Centre, University of Kent; NMR spectra were recorded by the University of Portsmouth.

References

[1] M.P.T. Sjogren, H. Frisell, B. Akermark, P. Norrby, L. Erikkson, A. Vitagliano, Organometallics 16 (1997) 942.
[2] M.T.P. Sjogren, S. Hansson, B. Akermark, A. Vitagliano, Organometallics 13 (1994) 1963.
[3] B.J. Brisdon, R.A. Walton, Polyhedron 14 (1995) 1259.
[4] H. Werner, R. Wiedemann, P. Steinart, J. Wolf, Chem. Eur. J. 3 (1997) 127.
[5] N.A. Vinson, C.S. Day, M.E. Welker, Organometallics 18 (1999) 1824.
[6] C. Slugovc, K. Mereiter, R. Schmid, K. Kirchner, J. Am. Chem. Soc. 120 (1998) 6175.
[7] C.S. Yi, N. Liu, A.L. Rhiengold, L.M. Liable-Sands, Organometallics 16 (1997) 3910.
[8] J.P. Collman, L.S. Hegedus, J.R. Norton, R.G. Finke, Principles and Applications of Organotransition Metal Chemistry, University Science Books, Mill Valley, CA, 1987.
[9] C.P. Casey, W.H. Miles, P.J. Fagan, K.J. Haller, Organometallics 4 (1985) 559.
[10] D. Nucciarone, N.J. Taylor, A.J. Carty, A. Tiripicchio, M.T. Camellini, E. Sappa, Organometallics 7 (1988) 118.
[11] E. Baralt, C.M. Lukehart, A.T. McPhail, D.R. McPhail, Organometallics 10 (1991) 516.
[12] A.G.W. Hodson, G. Conole, Organometallics 17 (1998) 5347.
[13] A.G.W. Hodson, S.M. Saunders, J. Organomet. Chem. 525 (1996) 207.
[14] A.G.W. Hodson, J. Organomet. Chem. 547 (1997) 343.
[15] B.J. Brisdon, R.J. Deeth, A.G.W. Hodson, C.M. Kemp, M.F. Mahon, K.C. Molloy, Organometallics 10 (1991) 1107.
[16] M.J. Karplus, J. Phys. Chem. 30 (1959) 11.
[17] A. Pardi, M. Billeter, K. Wuthrich, J. Mol. Biol. 180 (1984) 741.
[18] J. Cavanagh, W.J. Fairbrother, A.G. Palmer, N.J. Skelton, Protein NMR Spectroscopy: Principles and Practices, Academic Press, San Diego, CA, 1996.
[19] R. Weisemann, H. Ruterjans, H. Schwalbe, H. Schleucher, W. Bermal, C. Griesinger, J. Biomol. NMR 4 (1994) 231.

PERGAMON

www.elsevier.nl/locate/poly

Polyhedron 19 (2000) 801–808

POLYHEDRON

Ruthenium dithiophosphates: synthesis, X-ray crystal structure, spectroscopic and electrochemical properties

Prateek U. Jain [a], Pradip Munshi [a], Mrinalini G. Walawalkar [a], Sankar Prasad Rath [b], Kajal Krishna Rajak [b], Goutam Kumar Lahiri [a,*]

[a] *Department of Chemistry, Indian Institute of Technology, Bombay, Powai, Mumbai 400076, India*
[b] *Department of Inorganic Chemistry, Indian Association for the Cultivation of Science, Jadavpur, Calcutta 700032, India*

Received 8 November 1999; accepted 26 January 2000

Abstract

The reactions of ammonium salts of dialkyldithiophosphate ligands, $(RO)_2PS_2^-NH_4^+$ (R = Me/Et), with $Ru^{III}Cl_3 \cdot 3H_2O$ in methanol solvent and under N_2 atmosphere result in one-electron paramagnetic tris complexes $\{(RO)_2PS_2\}_3Ru^{III}$ (**1**) in the solid state. The molecular structures of both complexes were determined by single-crystal X-ray diffraction. This shows the expected pseudo-octahedral geometry with reasonable strain due to the presence of a four-membered chelate ring. The reflectance spectra of the solid complexes display two bands in the range 596–476 nm and in the solid state the complexes exhibit one isotropic EPR signal at 77 K. Although the complexes **1** are stable in the solid state, in solution the complexes are transformed selectively into the diamagnetic and electrically non-conducting sulfur-bridged dimetallic species $[\{(RO)_2PS_2\}_2Ru^{IV}(\mu\text{-}S)_2Ru^{IV}\{S_2P(OR)_2\}_2]$. The formation of dimeric species in the solution state is authenticated by the electrospray mass spectrum of one representative complex where R = Et (**1b**). In dichloromethane solution the complexes show two moderately strong sulfur to ruthenium charge-transfer transitions in the range 514–419 nm, and two strong ligand based transitions in the UV region. The complexes exhibit two successive reversible reductions in the ranges $1.01 \rightarrow 0.91$ V and $-0.44 \rightarrow -0.49$ V versus SCE corresponding to Ru^{IV}–Ru^{IV}/Ru^{III}–Ru^{III} and Ru^{III}–Ru^{III}/Ru^{II}–Ru^{II} couples respectively. Electrochemically or chemically generated first step reduced complexes $[\{(RO)_2PS_2\}_2Ru^{III}(\mu\text{-}S)_2Ru^{III}\{S_2P(OR)_2\}_2]^{2-}$ display two ligand to metal charge-transfer transitions in the visible region and in the complexes the two one-electron paramagnetic metal centers (low-spin Ru^{III}, t_{2g}^5, $S = 1/2$) are antiferromagnetically coupled. The second step reduced species $[\{(RO)_2PS_2\}_2Ru^{II}(\mu\text{-}S)_2Ru^{II}\{S_2P(OR)_2\}_2]^{4-}$ are observed to be very unstable. ©2000 Elsevier Science Ltd All rights reserved.

Keywords: Ruthenium; Phosphates; X-ray crystal structures

1. Introduction

Although the ruthenium chemistry of dithioacid based ligands such as dithiocarbamate and dithiocarbonate has been the subject of continuous study [1–24], the corresponding ruthenium dithiophosphate chemistry has not been developed much [25–29]. The versatile bonding, structural features as well as fascinating chemical and electrochemical reactivities of ruthenium dithiocarbamate and dithiocarbonate complexes have prompted us to make a systematic study of ruthenium dialkyldithiophosphate complexes. The present study indicates that the reactions of ammonium salts of dialkyldithiophosphates, $(RO)_2P(S)S^-NH_4^+$, with $RuCl_3 \cdot 3H_2O$ result in tris complexes $\{(RO)_2PS_2\}_3Ru^{III}$ (**1**) in the solid state, whereas in solution the complexes **1** exist predominantly in the dimeric form of type $[\{(RO)_2PS_2\}_2Ru^{IV}(\mu\text{-}S)_2\text{-}Ru^{IV}\{S_2P(OR)_2\}_2]$. Herein we report the solid state characterization of the tris complexes **1**, including the single-crystal X-ray structure and the solution spectroscopic and electron-transfer properties of the complexes.

2. Experimental

2.1. Materials

Commercial ruthenium trichloride (S.D. Fine Chemicals, Bombay, India) was converted into $RuCl_3 \cdot 3H_2O$ by repeated evaporation to dryness with concentrated hydrochloric acid. The ligands NH_4L^{1-2} were synthesized according to the reported method [30]. Other chemicals and solvents were

* Corresponding author. Tel.: +91-22-576-7159; fax: +91-22-578-3480; e-mail: lahiri@ether.chem.iitb.ernet.in

0277-5387/00/$ - see front matter ©2000 Elsevier Science Ltd All rights reserved.
PII S0277-5387(00)00316-8

reagent grade and were used as received. Silica gel (60–120 mesh) used for chromatography was of BDH quality. For spectroscopic and electrochemical studies, HPLC grade solvents were used. Commercial tetraethyl ammonium bromide was converted into pure tetraethyl ammonium perchlorate by following an available procedure [31].

2.2. Physical measurements

UV–Vis spectra were recorded using a Shimadzu-160 spectrophotometer. FT-IR spectra were taken on a Nicolet spectrophotometer with samples prepared as KBr pellets. Solution electrical conductivity was checked using a Systronic 305 conductivity bridge. Magnetic susceptibility was checked with a PAR vibrating sample magnetometer. NMR spectra were obtained with a 300 MHz Varian Fourier transform spectrometer. Cyclic voltammetric, differential pulse voltammetric and coulometric measurements were carried out using a PAR model 273A electrochemistry system. Platinum wire working and auxiliary electrodes and an aqueous saturated calomel reference electrode (SCE) were used in a three-electrode configuration. The supporting electrolyte was $[NEt_4]ClO_4$ and the solute concentration was 10^{-3} M. The half-wave potential E^0_{298} was set equal to $0.5(E_{pa}+E_{pc})$, where E_{pa} and E_{pc} are the anodic and cathodic cyclic voltammetric peak potentials respectively. A platinum wire-gauze working electrode was used in coulometric experiments. All experiments were carried out under a dinitrogen atmosphere and were uncorrected for junction potentials. The electrospray mass spectra were recorded on a Micromass Quattro II triple quadrupole mass spectrometer. The elemental analyses were carried out with a Carlo Erba (Italy) elemental analyzer. The EPR measurements were made with a Varian model 109C E-line X-band spectrometer fitted with a quartz Dewar for measurements at 77 K (liquid nitrogen). The spectra were calibrated using tetracyanoethylene (tcne) ($g=2.0023$).

2.3. Preparation of complexes

The complexes (**1a** and **1b**) were synthesized by following a general procedure. Details are given for the complex **1a**. Yields vary in the range 70–75%.

2.3.1. Tris(dimethyldithiophosphate)ruthenium(III) (*1a*)

$RuCl_3\cdot 3H_2O$ (100 mg, 0.38 mmol) was dissolved in 15 ml of methanol solvent and a stream of nitrogen gas was flushed through the solution for a period of 15 min. The ligand NH_4L^1, 266 mg (1.52 mmol), was added and the reaction mixture was stirred magnetically under nitrogen atmosphere for 12 h. The solvent was removed under reduced pressure and the solid product thus obtained was purified using a silica gel column. On elution with benzene one pink colored band was separated out, leaving behind a dark mass at the top of the column which did not move even on using methanol. On removal of benzene under reduced pressure, dark crystalline solid complex **1a** was obtained in the pure state. Yield 190 mg (72%).

2.4. X-ray structure determination

Single crystals of complexes **1a** and **1b** were grown by slow diffusion of dichloromethane solution of the complexes into hexane followed by slow evaporation.

Cell parameters were determined by least-squares fit of 25 ($2\theta=10$–$17°$) and 30 ($2\theta=15$–$30°$) machine centered reflections for **1a** and **1b** respectively. Data were collected by the ω-scan technique in the ranges $4\le 2\theta\le 50°$ and $3\le 2\theta\le 48°$ on a Nonius MACH 3 and Siemens R3m/V four-circle diffractometer for **1a** and **1b** respectively with graphite-monochromated Mo Kα radiation ($\lambda=0.71073$ Å) at 293 K. Significant crystal data and data collection parameters are listed in Table 1. The check reflections were measured after every 100 reflections during data collection to monitor crystal stability. No significant intensity reduction was observed during exposure to X-ray radiation. Absorption correction was done by performing psi-scan measurements for **1a** and for **1b** all data were corrected for Lorentz polarization effects and empirical absorption corrections were done on the basis of azimuthal scans of six reflections [32]. For **1a**, data reduction was done using MAXUS and structure solution and refinement were done using the programs SHELXS-97 and SHELXL-97 respectively [33,34]. For **1b**, all calculations for data reduction, structure solution and refinement were done using the program SHELXTL Version 5.03 [33,34]. The metal atom was located from the Patterson map and the other non-hydrogen atoms emerged from successive Fourier synthesis and the structure was refined by full-matrix least-squares on F^2. All non-hydrogen atoms were refined anisotropically. Hydrogen atoms were included in calculated positions. The numbers of variable parameters were 198 and

Table 1
Crystallographic data for complexes **1a** and **1b**

	1a	**1b**
Formula	$C_6H_{18}O_6P_3S_6Ru$	$C_{12}H_{30}O_6P_3S_6Ru$
FW	572.54	656.70
Crystal symmetry	monoclinic	monoclinic
Space group	*Cc*	*C*2/*c*
a (Å)	14.121(6)	14.267(6)
b (Å)	11.191(10)	13.569(3)
c (Å)	12.978(7)	14.316(6)
β (°)	97.11(10)	90.33(3)
U (Å^3)	2035.4(2)	2771(2)
Z	4	4
D_c (Mg m^{-3})	1.868	1.574
μ(Mo Mα) (mm^{-1})	1.638	1.214
R_1 [a]	0.0221	0.0378
wR_2 [b]	0.0565	0.0985

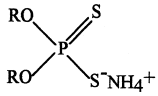
[a] $R_1=\sum||F_o|-|F_c||/\sum|F_o|$.
[b] $wR_2=[\sum\{w(F_o^2-F_c^2)^2\}/\sum\{w(F_o^2)^2\}]^{1/2}$; $w^{-1}=\sigma^2(F_o^2)+(ap)^2+bp$, where $p=(F_o^2+2F_c^2)/3$ and *a* and *b* are respectively 0.0389, 0.0551 and 1.6585, 5.2552 for **1a** and **1b**, constant adjusted by the program.

128, affording data-to-parameter ratios of 9.47:1 and 17.05:1 for **1a** and **1b** respectively. The refinement converged to $R_1 = 0.0221$, $wR_2 = 0.0565$ and $R_1 = 0.0378$, $wR_2 = 0.0985$ and goodness of fit 1.070 and 1.064 with the largest difference peak of 0.399 and 0.559 e $Å^{-3}$ near the metal atom for **1a** and **1b** respectively.

3. Results and discussion

3.1. Synthesis

Two dialkyldithiophosphate ligands were used for the present study and are abbreviated as NH_4L^1 and NH_4L^2.



R= Me, NH_4L^1
R= Et, NH_4L^2

The reaction of NH_4L with $RuCl_3 \cdot 3H_2O$ in methanol solvent under N_2 atmosphere at room temperature for 12 h results in a dark solution. Chromatographic purification of the dark solution on silica gel column, using benzene as eluant, yields pure tris complexes, $Ru^{III}\{S_2P(OR)_2\}_3$ (**1**) (R = Me **1a**, R = Et **1b**) in the solid state, Eq. (1).

$$Ru^{III}Cl_3 \cdot 3H_2O + (RO)_2PS_2NH_4 \rightarrow Ru^{III}\{S_2P(OR)_2\}_3 + NH_4Cl + H_2O \quad (1)$$

3.2. Solid state characterization

The complexes **1a** and **1b** are stable in the solid state. Microanalytical data of the complexes are in good agreement with the calculated values (Table 2). The complexes are one-electron paramagnets (Table 2), as expected for low-spin Ru^{III} complexes (low spin d^5, $S = 1/2$) [35].

The molecular structures of both the complexes were determined by single-crystal X-ray diffraction. The crystal structures are shown in Figs. 1 and 2. Selected bond lengths and angles are listed in Table 3. The complexes are monomeric and the lattice consists of one type of molecule where the

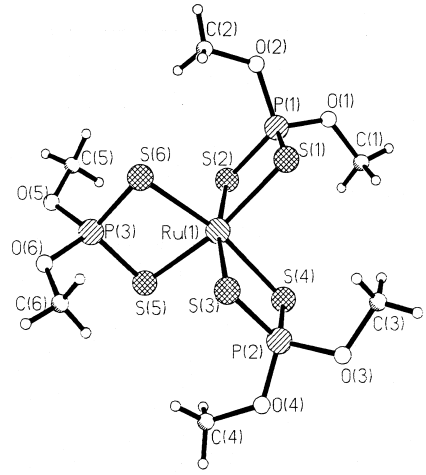


Fig. 1. An ORTEP plot for complex **1a**.

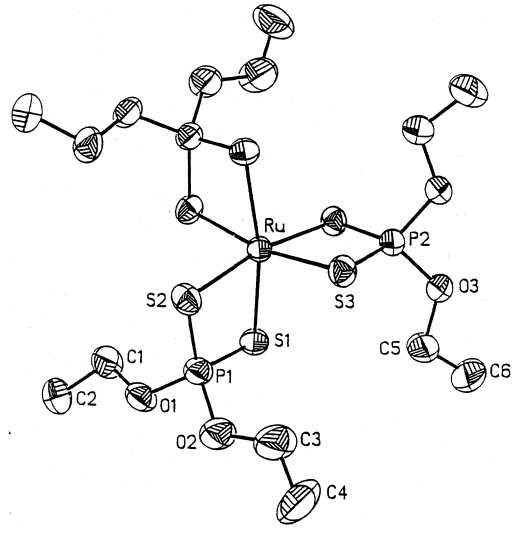


Fig. 2. An ORTEP plot for complex **1b**.

dialkyldithiophosphate ligands are in bidentate *S,S* mode. For **1b**, Ru and P_2 atoms are in special positions and a mirror plane passes through them (Fig. 2). The RuS_6 coordination sphere is distorted octahedral as can be seen from the angles subtended at the metal (Table 3). The observed distortion from the perfect octahedral symmetry originates from the constraints due to the four-membered chelate rings in which the average S–Ru–S bite angles are 81.54(8)° and 81.84(6)° for **1a** and **1b** respectively (Table 3). A similar effect of ring

Table 2
Microanalytical [a], reflectance [b], magnetic moment [c] and EPR data [d] for complexes **1**

Compound	Elemental analysis (%)		Reflectance λ (nm)	Magnetic moment μ_M (BM)	EPR (g)
	C	H			
1a	12.49 (12.59)	3.19 (3.15)	580, 476	2.059	2.030
1b	22.14 (21.95)	4.53 (4.57)	596, 476	1.916	1.865

[a] Calculated values are in parentheses.
[b] In the solid state.
[c] In the solid state at 298 K.
[d] In the solid state at 77 K.

Table 3
Selected bond distances (Å) and angles (°) and their estimated standard deviations for **1a** and **1b**

	1a	**1b**	
Ru–S(1)	2.433(3)	2.407(2)	
Ru–S(2)	2.402(3)	2.4249(14)	
Ru–S(3)	2.419(3)	2.4011(13)	
Ru–S(4)	2.452(3)		
Ru–S(5)	2.395(3)		
Ru–S(6)	2.408(3)		
S(1)–P(1)	1.994(5)	1.996(2)	
S(2)–P(1)	2.011(4)	1.997(2)	
S(3)–P(2)	1.987(4)	2.000(2)	
P(1)–O(1)	1.525(9)	1.564(3)	
P(1)–O(2)	1.618(8)	1.569(4)	
P(2)–O(3)	1.624(8)	1.571(3)	
S(1)–Ru–S(2)	81.62(10)	S(1)–Ru–S(2)	81.63(5)
S(3)–Ru–S(4)	81.17(10)	S(3)#1–Ru–S(3)	82.06(7)
S(5)–Ru–S(6)	81.83(4)	S(1)#1–Ru–S(2)	91.01(5)
S(5)–Ru–S(2)	90.74(11)	S(2)–Ru–S(2)#1	95.84(7)
S(2)–Ru–S(6)	98.67(13)	S(3)–Ru–S(1)	98.32(5)
S(5)–Ru–S(3)	96.65(12)	S(1)–Ru–S(1)#1	169.04(7)
S(2)–Ru–S(3)	169.32(4)	S(3)#1–Ru–S(2)#1	91.73(5)
S(6)–Ru–S(3)	90.03(11)	S(3)#1–Ru–S(2)	168.76(5)
S(5)–Ru–S(1)	168.98(12)	S(3)–Ru–S(1)#1	89.97(5)
S(6)–Ru–S(1)	91.43(12)	P(1)–S(2)–Ru	86.62(6)
S(3)–Ru–S(1)	92.04(11)	P(1)–S(1)–Ru	87.13(6)
S(5)–Ru–S(4)	91.20(11)	P(2)–S(3)–Ru	86.97(7)
S(6)–Ru–S(4)	168.10(12)	S(1)–P(1)–S(2)	104.53(8)
S(1)–Ru–S(4)	96.84(4)	S(3)–P(2)–S(3)#1	104.00(10)
S(2)–Ru–S(4)	91.01(11)	O(1)–P(1)–O(2)	94.9(2)
		O(3#1)–P(2)–O(3)	96.2(3)

constraints on the molecular geometry has been also observed earlier [36–39].

The Ru–S distances are unequal, the longer and shorter distances are respectively 2.452(3) and 2.395(3) Å for **1a** and 2.425(14) and 2.401(13) Å for **1b**. The Ru^{III}–S distances in the present complexes are reasonably longer than the corresponding Ru^{III}–S distances, 2.376(4) and 2.383(6) Å (mean Ru^{III}–S distances) in the tris-ruthenium dithiocarbamate complexes $Ru^{III}(S_2CNEt_2)_3$ and $Ru^{III}\{S_2C(CN)(CH_2)_4O\}_3$ respectively [40,41] (the only two other structurally characterized tris-ruthenium(III) dithioacid complexes).

The distances within the dithiophosphate ligands agree well with those found in structurally characterized dithiophosphate complexes of other metal ions [42–44].

It may be noted that the present work demonstrates the first crystal structure of a ruthenium complex incorporating the dithiophosphate ligand.

The reflectance spectra of the solid complexes **1** exhibit two broad bands in the visible region (Fig. 3, Table 2). The band profiles look similar for both complexes, but the lowest energy band maxima are observed to be sensitive to the nature of the R groups.

Consistent with the low-spin configuration, the complexes $[Ru^{III}L_3]$ (low-spin d^5 Ru^{III}, $S=1/2$) display one isotropic

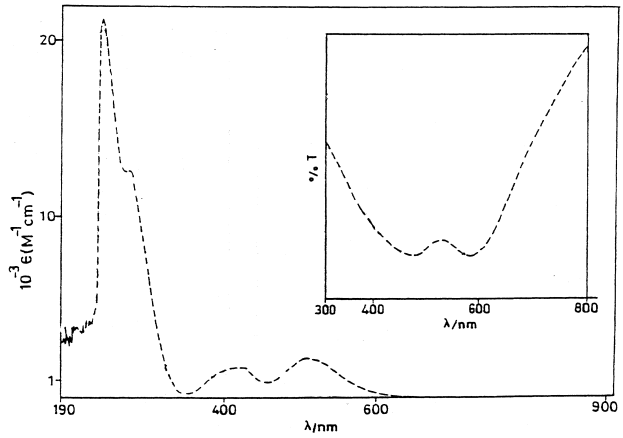


Fig. 3. Electronic spectrum of **1a** in dichloromethane. The inset shows the reflectance spectrum of **1a**.

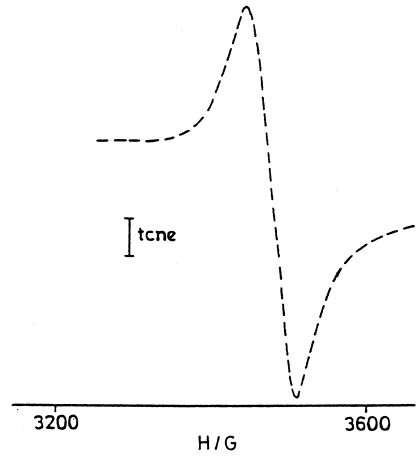


Fig. 4. X-band EPR spectrum of **1b** in the solid state at 77 K.

broad EPR signal (Table 2, Fig. 4) [45,46]. No anisotropic pattern has been observed even at liquid N_2 temperature (77 K).

3.3. Solution properties of the complexes

The solid complexes **1** are fairly soluble in non-polar solvents such as dichloromethane, chloroform and benzene, but are sparingly soluble in polar solvents such as acetonitrile, *N*,*N*-dimethylformamide and dimethylsulfoxide. In dichloromethane and acetonitrile the complexes **1** are non-conducting, diamagnetic and consequently EPR silent even at chloroform–toluene glass temperature (77 K, liquid N_2). The change in magnetic behavior of the complexes while moving from the solid to solution state implies that the one-electron paramagnetic solid complexes **1** undergo molecular reorganization in the solution state which eventually leads to the formation of diamagnetic complexes.

The electrospray mass spectrum of a representative complex (**1b**) was recorded in dichloromethane solvent. The maximum molecular peak is observed at *m/z* 1006 (Fig. 5) which corresponds to the molecular ion $[\{(EtO)_2PS_2)\}_2Ru^{IV}(\mu\text{-}S)_2Ru^{IV}\{S_2P(OEt)_2\}_2]$ (calculated molecular

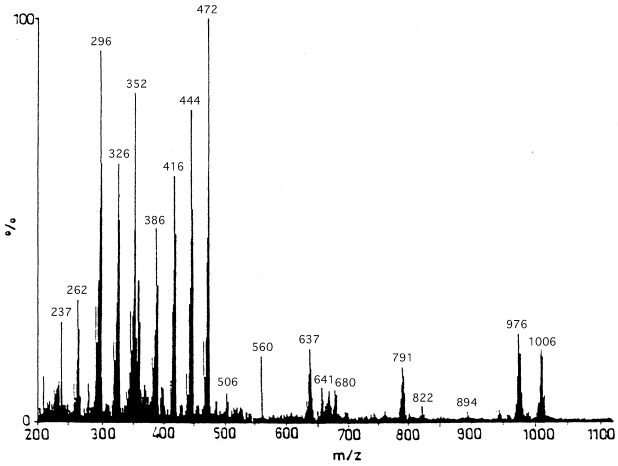
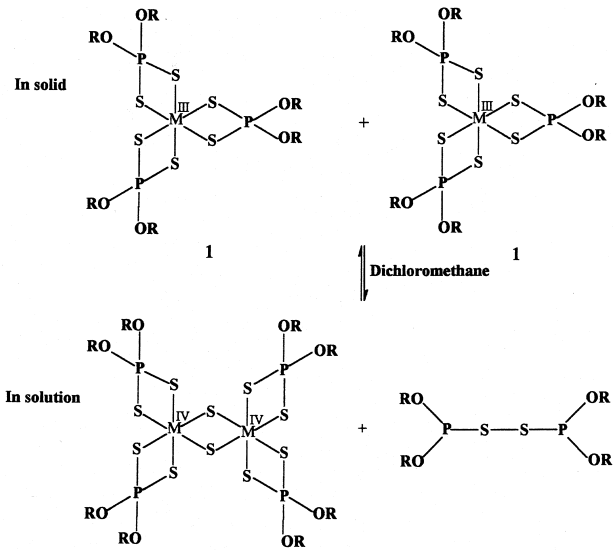


Fig. 5. Electrospray mass spectrum of $[\{(EtO)_2PS_2\}_2Ru^{IV}(\mu\text{-}S)_2\text{-}Ru^{IV}\{S_2P(OEt)_2\}_2]$ (**1b**) in dichloromethane.

weight 1006.2). Thus the tris complexes **1** in the solid state have been transformed into the sulfur bridged dinuclear species as shown in Scheme 1. The conversion of solid tris complexes **1** to the dimeric complexes in the solution state can account for the change in magnetic behavior (one-electron paramagnetic in the solid state and diamagnetic in the solution state) and overall electron balancing.

It may be noted that the tris dithiophosphate cobalt complex $Co^{III}(L)_3$ is also known to liberate one L^- from the tris core in the solution state and the liberated L^- subsequently dimerizes to the disulfide species [47].

^{1}H NMR spectra of the ligands NH_4L^{1-2} and the complexes were recorded in D_2O and $CDCl_3$ respectively. The representative spectra are shown in Fig. 6. The ^{1}H NMR spectrum of NH_4L^1 exhibits two singlets at 3.663 and 3.615 ppm due to two inequivalent $-OCH_3$ groups and similarly NH_4L^2 exhibits two quartets (3.93 and 3.76 ppm) and two triplets (1.17 and 1.12 ppm) due to two inequivalent $-OC_2H_5$ groups. The ^{1}H NMR spectrum of the $R = CH_3$ complex exhibits one



Scheme 1.

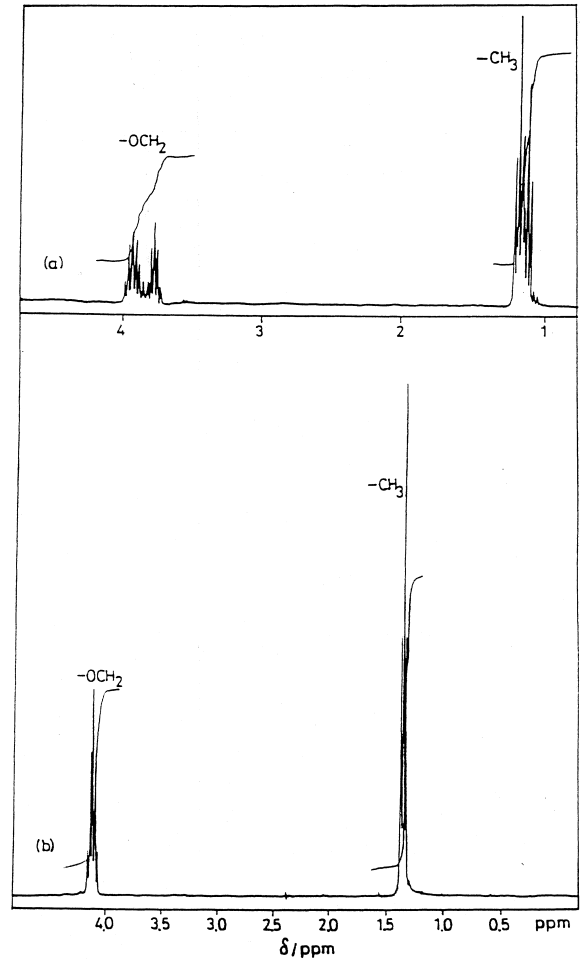


Fig. 6. ^{1}H NMR spectra of (a) NH_4L^2 in D_2O and (b) **1b** in $CDCl_3$.

singlet corresponding to $-OCH_3$ groups at 3.70 ppm and for the $R = C_2H_5$ complex one quartet at 4.18 and one triplet at 1.28 ppm due to $-OC_2H_5$ groups as internal symmetry makes all the ligands equivalent.

Although the decoupled ^{31}P NMR spectra of the ligands (NH_4L^{1-2}) in D_2O exhibit one signal as expected, the complexes in $CDCl_3$ solvent display two signals near 85 and 100 ppm having an intensity ratio of approximately 1:2 due to the presence of more than one type of phosphorus center in the solution state. This may provide support in favor of the presence of disulfide species along with the dimeric complex as proposed in Scheme 1.

In dichloromethane the violet colored complexes exhibit multiple transitions in the UV–Vis region. In the visible region the complexes display two moderately intense bands and the higher energy band is associated with a shoulder at a further higher energy part of the spectra (Table 4, Fig. 3). Since the ruthenium ion is in the +4 oxidation state in the complexes, the bands may therefore be assigned as ligand to metal charge-transfer transitions from sulfur to the metal ion [48–52]. The direct comparisons of the solid state reflectance spectra of **1** with the solution absorption spectra (Fig. 3, Tables 2 and 4) reveal that the bands have been reasonably blue shifted while moving from the solid to solution state.

Table 4
Electronic spectral [a] and electrochemical [b] data

Compound	λ (nm) (ε (M^{-1} cm^{-1}))	M^{IV}–M^{III} couple E^0_{298} (V) (ΔE_p (mV))	n [c]	M^{III}–M^{II} couple E^0_{298} (V) (ΔE_p (mV))
1a	510 (2231), 419 (1930), 277 (12748), 248 (21167)	1.01 (120)	1.93	−0.44(120)
1b	514 (2038), 422 (1680), 278 (11423), 246 (19455)	0.91 (122)	2.11	−0.49(100)
1a^{2-}	613, 400, 266			
1b^{2-}	600, 350, 243			

[a] In dichloromethane at 298 K.
[b] Conditions: solvent, dichloromethane; supporting electrolyte, NEt_4ClO_4; reference electrode, SCE; solute concentration, 10^{-3} M; working electrode, platinum. Cyclic voltammetric data: scan rate, 50 mV s^{-1}; $E^0_{298} = 0.5(E_{pc} + E_{pa})$ where E_{pc} and E_{pa} are the cathodic and anodic peak potentials respectively.
[c] $n = Q/Q'$ where Q' is the calculated Coulomb count for a two-electron transfer and Q that found after exhaustive electrolysis of $\sim 10^{-2}$ mol of solute.

The observed shift in band maxima on switching from solid to solution state supports the existence of different species in the solution state as shown in Scheme 1.

The strong bands in the UV region (Fig. 3) may be due to ligand centered transitions as the free ligands also exhibit a strong band in the same region (NH_4L^1, 236 nm and NH_4L^2, 237 nm in H_2O).

Electron-transfer properties of the complexes were studied in dichloromethane solvent by cyclic voltammetry using a platinum working electrode in the range ± 2.0 V versus a saturated calomel electrode (SCE) (tetraethyl ammonium perchlorate as electrolyte, 298 K). Representative voltammograms are shown in Fig. 7 and the reduction potentials are given in Table 4. The complexes display two reversible reductive couples and the separation between the two $E_{1/2}$ values is found to be ~ 1.4 V (Fig. 7, Table 4). The two-electron nature of the first couple (Fig. 7, couple I) is confirmed with the help of constant-potential coulometry (Table 4). The two-electron nature of the second couple (Fig. 7, couple II) at the negative side of SCE is determined by direct comparison of its differential pulse voltammogram peak height with that of the previous two-electron process (confirmed by coulometric experiment). The reduction potentials are observed to be lower for the complex having the ethoxy group (**1b**) as compared to the methoxy complex (**1a**).

The responses at positive and negative potentials are respectively assigned to ruthenium(IV)–ruthenium(III) and ruthenium(III)–ruthenium(II) couples as in Eqs. (2) and (3).

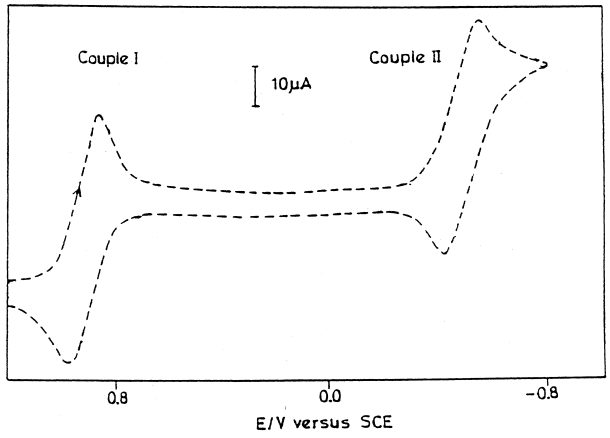


Fig. 7. Cyclic voltammograms of **1b** in dichloromethane at 298 K.

$$[\{(RO)_2PS_2\}_2Ru^{IV}(\mu\text{-}S)_2Ru^{IV}\{S_2P(OR)_2\}_2] + 2e^- \rightleftharpoons [\{(RO)_2PS_2\}_2Ru^{III}(\mu\text{-}S)_2Ru^{III}\{S_2P(OR)_2\}_2]^{2-} \quad (2)$$

$$[\{(RO)_2PS_2\}_2Ru^{III}(\mu\text{-}S)_2Ru^{III}\{S_2P(OR)_2\}_2]^{2-} + 2e^- \rightleftharpoons [\{(RO)_2PS_2\}_2Ru^{II}(\mu\text{-}S)_2Ru^{II}\{S_2P(OR)_2\}_2]^{4-} \quad (3)$$

It may be noted that the free ligands (NH_4L^{1-2}) do not show any redox activities within the specified potential range. Here the difference in potential between the two successive reduction processes is found to be ~ 1.4 V (Table 4) which is in good agreement with the earlier observed potential differences (1.3–1.4 V) between the two successive reduction processes $Ru^{IV/III}$–$Ru^{III/II}$ in other complexes [53–55].

Electrochemical reductions (constant-potential coulometry) of the complexes at 0.5 V versus SCE in dichloromethane solvent using a platinum gauze working electrode under a dinitrogen atmosphere result in a sharp color change from pink to greenish yellow. The observed Coulomb counts correspond to two-electron transfer (Table 4). The resulting reduced $[\{(RO)_2PS_2\}_2Ru^{III}(\mu\text{-}S)_2Ru^{III}\{S_2P(OR)_2\}_2]^{2-}$ species display voltammograms which are superposable on those of the corresponding starting complexes, which imply that the reductions here may be stereoretentive in nature [56]. When the same reduced solutions are reoxidized coulometrically at a potential 100 mV positive to the corresponding E_{pa} of the M^{III}/M^{IV} couple, the starting violet colored tetravalent complexes are formed quantitatively. The reduced species are not stable enough to be isolated in the solid state even at 273 K, however, we have managed to check the EPR spectra of the reduced complexes at 77 K and to record the qualitative electronic spectra. Since the reduced complexes are observed to be EPR silent even at 77 K, it may therefore be assumed that the two ruthenium(III) centers in the complexes are antiferromagnetically coupled [57]. In dichloromethane solvent, the complexes display two sulfur to metal charge transfer transitions in the visible region (Fig. 8, Table 4) and one ligand based transition in the UV region (Table 4).

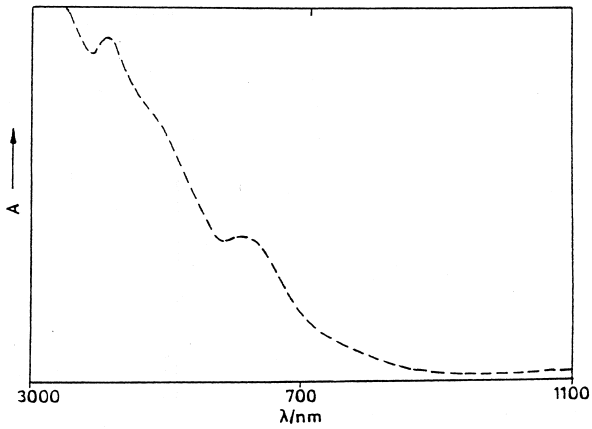


Fig. 8. Electronic spectrum of coulometrically reduced complex of $[\{(MeO)_2PS_2\}_2Ru^{III}(\mu\text{-}S)_2Ru^{III}\{S_2P(OMe)_2\}_2]^{2-}$ (**1a**$^{2-}$) in dichloromethane.

Coulometric reductions of the ruthenium complexes at −0.7 V versus SCE result in light blue colored reduced species. The resulting reduced complexes $[\{(RO)_2PS_2\}_2Ru^{II}(\mu\text{-}S)_2\,Ru^{II}\{S_2P(OR)_2\}_2]^{4-}$ are very unstable. On contact with a small amount of air, the complexes are oxidized immediately to the trivalent species, therefore no further study was made in this direction. The low $Ru^{III/II}$ potentials (~ -0.5 V) and the tetraanionic nature of the second reduced species might be responsible for their spontaneous aerial oxidation to the higher congeners.

The complexes can also be reduced chemically to the trivalent congeners by hydrazine hydrate. Although the greenish-yellow colored first step reduced species $[\{(RO)_2PS_2\}_2Ru^{III}(\mu\text{-}S)_2Ru^{III}\{S_2P(OR)_2\}_2]^{2-}$ are stable on the coulometric time scale and can even be generated by chemical means, all our attempts to isolate the first step reduced species in the pure solid state have failed. Further investigations are in progress in the direction of developing the first step reduced species, $[\{(RO)_2PS_2\}_2Ru^{III}(\mu\text{-}S)_2Ru^{III}\{S_2P(OR)_2\}_2]^{2-}$, particularly in the absence of any disulfide product in order to obtain direct evidence in favor of dimer formation.

4. Conclusions

We have observed that the reactions of dialkyldithiophosphate ligands with $RuCl_3\cdot 3H_2O$ result in paramagnetic tris ruthenium complexes $\{(RO)_2PS_2\}_3Ru^{III}$ (**1**) in the solid state, however, in solution the complexes exist predominantly in the dimeric form, $[\{(RO)_2PS_2\}_2Ru^{IV}(\mu\text{-}S)_2Ru^{IV}\{S_2P(RO)_2\}_2]$. The tetravalent dinuclear complexes are susceptible to facile stereoretentive electrochemical reductions to the corresponding trivalent and bivalent dinuclear congeners $[\{(RO)_2PS_2\}_2Ru^{III}(\mu\text{-}S)_2Ru^{III}\{S_2P(RO)_2\}_2]^{2-}$ and $[\{(RO)_2PS_2\}_2Ru^{II}(\mu\text{-}S)_2Ru^{II}\{S_2P(RO)_2\}_2]^{4-}$ respectively. The bivalent species are found to be unstable whereas the trivalent complexes are stable on the coulometric time scale but isolation in the pure solid state has not been successful.

Supplementary data

Supplementary data are available from the Cambridge Crystallography Data Centre, 12 Union Road, Cambridge CB2 1EZ, UK (fax: +44-1223-336033; e-mail: deposit@ccdc.cam.ac.uk) on request, quoting the deposition numbers 136793 and 136794 for compounds **1a** and **1b** respectively.

Acknowledgements

Financial support received from the Department of Science and Technology, New Delhi, India, is gratefully acknowledged. The X-ray structural studies of **1a** and **1b** were carried out at the National Single Crystal Diffractometer Facilities, Indian Institute of Technology, Bombay and Department of Inorganic Chemistry, Indian Association for the Cultivation of Science, Calcutta, India respectively. Special acknowledgement is made to the Regional Sophisticated Instrumental Center, RSIC, Indian Institute of Technology, Bombay for providing NMR and EPR facilities.

References

[1] D.J. Duffy, L.H. Pignolet, Inorg. Chem. 13 (1974) 2045.
[2] K.W. Given, B.M. Mattson, L.H. Pignolet, Inorg. Chem. 15 (1976) 3152.
[3] B.M. Mattson, L.H. Pignolet, Inorg. Chem. 16 (1977) 488.
[4] L.H. Pignolet, D.J. Duffy, L. Que Jr., J. Am. Chem. Soc. 95 (1973) 289.
[5] L.J. Mathew, L.H. Pignolet, Inorg. Chem. 18 (1979) 3626.
[6] A.M. Bond, L. Martin, Coord. Chem. Rev. 54 (1984) 23.
[7] D. Coucouvanis, Prog. Inorg. Chem. 26 (1979) 301.
[8] K.W. Given, B.M. Mattson, G.L. Miessler, L.H. Pignolet, J. Inorg. Nucl. Chem. 39 (1977) 1309.
[9] C.L. Raston, A.W. White, J. Chem. Soc., Dalton Trans. (1975) 2418.
[10] J.V. Kingston, G. Wilkinson, J. Inorg. Nucl. Chem. 28 (1966) 2709.
[11] A.R. Hendrickson, J.M. Hope, R.L. Martin, J. Chem. Soc., Dalton Trans. (1976) 2032.
[12] C.L. Raston, A.W. White, J. Chem. Soc., Dalton Trans. (1975) 2405.
[13] C.L. Raston, A.W. White, J. Chem. Soc., Dalton Trans. (1975) 2422.
[14] A. Pramanik, N. Bag, G.K. Lahiri, A. Chakravorty, J. Chem. Soc., Dalton Trans. (1990) 3823.
[15] A. Pramanik, N. Bag, G.K. Lahiri, A. Chakravorty, Inorg. Chem. 30 (1991) 410.
[16] K.D. Keerthi, B.K. Santra, G.K. Lahiri, Polyhedron 17 (1998) 1387.
[17] G.A. Thakur, K. Narayanaswamy, G.K. Lahiri, Indian J. Chem. 35A (1996) 379.
[18] B.K. Santra, G.K. Lahiri, J. Chem. Soc., Dalton Trans. (1997) 129.
[19] A. Pramanik, N. Bag, G.K. Lahiri, A. Chakravorty, J. Chem. Soc., Dalton Trans. (1992) 101.
[20] N. Bag, G.K. Lahiri, A. Chakravorty, J. Chem. Soc., Dalton Trans. (1990) 1557.
[21] A. Pramanik, N. Bag, D. Ray, G.K. Lahiri, A. Chakravorty, J. Chem. Soc., Chem. Commun. (1991) 139.
[22] P.S. Rao, G.A. Thakur, G.K. Lahiri, Indian J. Chem. 35A (1996) 946.

[23] B.K. Santra, G.A. Thakur, P. Ghosh, A. Pramanik, G.K. Lahiri, Inorg. Chem. 35 (1996) 3050.
[24] B.K. Santra, P. Munshi, G. Das, P. Bharadwaj, G.K. Lahiri, Polyhedron 18 (1999) 617.
[25] S.S. Kulkarni, B.K. Santra, P. Munshi, G.K. Lahiri, Polyhedron 17 (1998) 4365.
[26] C.K. Jorgensen, Acta Chem. Scand. 16 (1962) 1048.
[27] M. Schroder, T.A. Stephenson, in: G. Wilkinson (Ed.), Comprehensive Coordination Chemistry, vol. 4, Pergamon, 1987, p. 430.
[28] W.P. Griffith, in: G. Wilkinson (Ed.), Comprehensive Coordination Chemistry, vol. 4, Pergamon, 1987, p. 603.
[29] M. Schroder, in: R.B. King (Ed.), Encyclopedia of Inorganic Chemistry, vol. 5, Wiley, New York, 1994, p. 2837.
[30] J.L. Lefferts, K.C. Mollouy, J.J. Zuckerman, I. Haituc, C. Guta, D. Ruse, Inorg. Chem. 19 (1980) 1662.
[31] D.T. Sawyer, A. Sobkowick, J.L. Roberts Jr., Electrochemistry for Chemists, Wiley, New York, 2nd edn., 1995.
[32] A.C.T. North, D.C. Phillips, F.S. Mathews, Acta Crystallogr., Sect. A 24 (1968) 351.
[33] G.M. Sheldrick, SHELXTL, Version 5.03, Siemens Analytical X-ray Instruments Inc., Madison, WI, 1994.
[34] C.K. Johnson, ORTEP, Report ORNL-5138, Oak Ridge National Laboratory, Oak Ridge, TN, 1976.
[35] N. Bag, G.K. Lahiri, S. Bhattacharya, L.R. Falvello, A. Chakravorty, Inorg. Chem. 27 (1988) 4396.
[36] B.K. Santra, M. Menon, C.K. Pal, G.K. Lahiri, J. Chem. Soc., Dalton Trans. (1997) 1387.
[37] S.L. Lawton, Inorg. Chem. 10 (1971) 328.
[38] D.F. Lewis, S.J. Lippard, J.A. Zubieta, Inorg. Chem. 11 (1972) 823.
[39] S.R. Fletcher, A.C. Skapski, J. Chem. Soc., Dalton Trans. (1972) 635.
[40] C.L. Raston, A.W. White, J. Chem. Soc., Dalton Trans. (1975) 2405.
[41] L.H. Pignolet, Inorg. Chem. 13 (1974) 2051.
[42] S.L. Lawton, G.T. Kakotailo, Inorg. Chem. 8 (1969) 2410.
[43] J.F. McConnell, V. Kastalsky, Acta Crystallogr. 22 (1967) 853.
[44] K. Kirschbaum, U. Bonnighausen, E. Gesing, K. Greiwe, U. Kuhlmann, H. Strasdeit, B. Krebs, G. Henkel, Z. Naturforsch., Teil B 45 (1990) 245.
[45] G.K. Lahiri, S. Bhattacharya, B.K. Ghosh, A. Chakravorty, Inorg. Chem. 26 (1987) 4324.
[46] R. Hariram, B.K. Santra, G.K. Lahiri, J. Organomet. Chem. 540 (1997) 155.
[47] L.L. Costanzo, I. Fragala, S. Giuffrida, G. Condorelli, Inorg. Chim. Acta 28 (1978) 19.
[48] N. Bag, A. Pramanik, G.K. Lahiri, A. Chakravorty, Inorg. Chem. 31 (1992) 40.
[49] M. Haga, E.S. Dodsworth, A.B.P. Lever, Inorg. Chem. 25 (1986) 447.
[50] A.B.P. Lever, P.R. Auburn, E.S. Dodsworth, M. Haga, W. Liu, M. Melnik, W.A. Nevin, J. Am. Chem. Soc. 110 (1988) 8076.
[51] B.K. Santra, G.K. Lahiri, J. Chem. Soc., Dalton Trans. (1997) 1883.
[52] A. Bharath, B.K. Santra, P. Munshi, G.K. Lahiri, J. Chem. Soc., Dalton Trans. (1998) 2643.
[53] B.M. Holligan, J.C. Jeffery, M.K. Norgett, E. Schatz, M.D. Ward, J. Chem. Soc., Dalton Trans. (1992) 3345.
[54] P. Ghosh, A. Pramanik, N. Bag, G.K. Lahiri, A. Chakravorty, J. Organomet. Chem. 454 (1993) 273.
[55] D.A. Bradwell, J.C. Jeffery, E. Schatz, E.E.M. Tilley, M.D. Ward, J. Chem. Soc., Dalton Trans. (1995) 825.
[56] R. Samanta, P. Munshi, B.K. Santra, N.A. Lokanath, M.A. Sridhar, J.S. Prasad, G.K. Lahiri, J. Organomet. Chem. 581 (1999) 311.
[57] B.K. Santra, G.K. Lahiri, J. Chem. Soc., Dalton Trans. (1998) 139.

PERGAMON

www.elsevier.nl/locate/poly

Polyhedron 19 (2000) 809–812

POLYHEDRON

Synthesis and characterisation of platinum(II) complexes containing heterobidentate *S*,*N*-chelating ligands: X-ray crystal structure of *cis*-[Pt{SPPh$_2$N=C(Me)NH-*S*,*N*}(PMe$_2$Ph)$_2$]Cl

Pravat Bhattacharyya, Alexandra M.Z. Slawin, J. Derek Woollins *

Department of Chemistry, University of St Andrews, St Andrews, Fife, Scotland KY16 9ST, UK

Received 30 November 1999; accepted 21 January 2000

Abstract

Deprotonation of the terminal amino group in the *N*-thiophosphoryl compounds Me$_2$P(S)N=C(NH$_2$)$_2$ (HL^1), Ph$_2$P(S)N=C(Me)NH$_2$ (HL^2) or Ph$_2$P(S)N=C(NH$_2$)$_2$ (HL^3) using potassium *tert* butoxide in thf, followed by treatment with *cis*-[PtCl$_2$(PR$_3$)$_2$] (PR$_3$ = PMe$_2$Ph or $\frac{1}{2}$dppe) generates monocationic complexes *cis*-[Pt(L^n-*S*,*N*)(PR$_3$)$_2$]Cl (**1**–**6**), which have been characterised by ^{31}P{^{1}H} NMR, IR and FAB$^+$ mass spectroscopies, and for *cis*-[Pt(L^2-*S*,*N*)(PMe$_2$Ph)$_2$]Cl (**2**) by single crystal X-ray diffraction. The molecular structure of **2** reveals bidentate coordination of the platinum(II) centre by a bidentate *S*,*N*-chelating [Ph$_2$P(S)N=C(Me)NH]$^-$ anion, giving a six-membered platinacycle, which adopts a chaise-longue conformation, with a strong hydrogen-bonding interaction between the chloride counterion and the nitrogen-bound proton. ©2000 Elsevier Science Ltd All rights reserved.

Keywords: Thiophosphoryl guanidines; Platinum complexes; Crystal structures

1. Introduction

Ourselves [1,2] and others [3–8] have studied the coordination chemistry of imidodiphosphinate anions [R$_2$P(E)NP(E′)R′$_2$]$^-$ (R, R′ = alkyl, aryl or alkoxy; E, E′ = oxygen, sulfur or selenium), generated from the weak acids HN(R$_2$PE)(R′$_2$PE′), regarded as 'inorganic' analogues of the more ubiquitous β-diketonates such as acetylacetonate. Bidentate *E*,*E*′ chelation of imidodiphosphinate ligands at d- and p-block metal centres produces hexa-atomic metallacycles; crystallographic analyses of several such metal complexes indicate substantial flexibility within the E–P–N–P–E′ backbone which enables the adoption of a variety of chelate ring conformations in the solid state, although planarity is rarely observed. The facile construction of imidodiphosphinate ligands, generally by the base-catalysed clipping together of R$_2$P(E)NH$_2$ and R′$_2$P(E′)Cl precursors or via oxidation of the parent diphosphine R$_2$PNHPR′$_2$ using elemental chalcogen or hydrogen peroxide, has led to applications for such ligands as metal extraction agents, NMR shift reagents and recently in a catalytic function in the aerobic co-oxidation of alkenes and aldehydes [7–10].

As a class of potentially chelating bidentate ligands, the phosphorus(V) derivatised guanidines and amidines R$_2$P(E)N=C(X)NH$_2$ (R = alkyl or aryl; E = oxygen or sulfur; X = NH$_2$ or alkyl) have been known for some time, but their coordination chemistry does not appear to have been well explored [11–16]. The presence in these molecules of an ionisable nitrogen-bound proton coupled with the potential for delocalisation of the resulting uninegative charge through the π-system of the anion suggests a high degree of similarity with both imidodiphosphinate and β-diketonate ligands. The combination of chalcogen and nitrogen donor atoms offered by these molecules is, however, rarely encountered in their P–N–P or carbon-backboned counterparts.

Here, we describe our studies on the coordination chemistry of the monoanions derived from Me$_2$P(S)N=C(NH$_2$)$_2$ (HL^1) and Ph$_2$P(S)N=C(X)NH$_2$ (X = Me (HL^2) or NH$_2$ (HL^3)) at platinum(II) centres, including one representative crystal structure.

2. Results and discussion

Deprotonation of the amine nitrogen atom in HN(R$_2$PE)(R′$_2$PE) gives π-delocalised imidodiphosphinate anions [R$_2$P(E)NP(E′)R′$_2$]$^-$ which have great propen-

* Corresponding author. Tel.: +44-1334-463861; fax: +44-1334-463384; e-mail: jdw3@st-and.ac.uk

0277-5387/00/$ - see front matter ©2000 Elsevier Science Ltd All rights reserved.
PII S0277-5387(00)00320-X

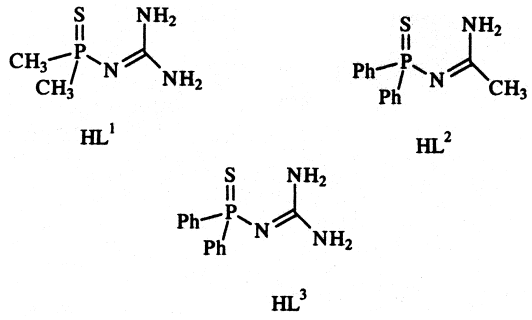


Fig. 1. Structures of the ligands $HL^{1–3}$.

sity towards bidentate *E,E′* chelation at metal centres [1–6]. We believed that the *N*-thiophosphoryl amidine (HL^2) and guanidines ($HL^{1,3}$) (Fig. 1) could in a similar way function as monobasic acids and undergo coordination to metal ions, to give chelates using a heterobidentate *S,N* donor array. To test our hypothesis we attempted to prepare platinum(II) complexes using the anions derived from $HL^{1–3}$.

Treatment of thf solutions of $HL^{1–3}$ with potassium *tert*-butoxide followed by a stoichiometric quantity of *cis*-$[PtCl_2(PR_3)_2]$ ($PR_3 = PMe_2Ph$ or $\frac{1}{2}$dppe) proceeds smoothly at reflux with displacement of the chloro ligands from the metal coordination sphere and chelation of the $(L^n)^-$ anion to give cationic complexes *cis*-$[Pt(L^n\text{-}S,N)(PR_3)_2]Cl$ (**1**–**6**) isolable in moderate yields (39–65%) from dichloromethane–diethyl ether, Eq. (1).

$$cis\text{-}[PtCl_2(PR_3)_2] + KL^n \rightarrow cis\text{-}[Pt(L^n\text{-}S,N)(PR_3)_2]Cl + KCl \quad (1)$$

The platinum(II) complexes **1**–**6** are colourless (**1**, **2**) or pale yellow (**3**–**6**) solids, tolerant to air and moisture, and are highly soluble in chlorinated solvents and thf. In their FAB^+ mass spectra all of the complexes give intense peaks which correspond to an ion of composition $[PtL(PR_3)_2]^+$. The $^{31}P\{^1H\}$ NMR spectra for **1**–**6** (Table 1) contain extensive information on ^{195}Pt–^{31}P and ^{31}P–^{31}P coupling constants and are in accord with their structures; the complexes exhibit first-order AMX spin systems with platinum-195 satellites. The ^1J(Pt–P) coupling constants for the phosphine co-ligands P(2), P(3) lie in the ranges 2917–3004 Hz (P(3) *trans* sulfur) and 3234–3371 Hz (P(2) *trans* nitrogen) in accord with the weaker *trans* influence of N versus S. A similar variation in ^1J(Pt–P) values as a function of the *trans* donor atom has been observed in *cis*-$[Pt(S_2N_2)(PR_3)_2]$ and *cis*-$[Pt(S_2N_2H)(PR_3)_2]^+$, in which the sulfur–nitrogen anions are *S,N*-bidentate at platinum(II) [17,18]. The ^2J(Pt–P) couplings for the phosphorus(V) atom P(1) of the chelate in **1**–**6** (85–102 Hz) are somewhat larger than the values we have reported in the dithio-imidodiphosphinate complexes *cis*-$[Pt\{(SPPh_2)_2N\}(PR_3)_2]Cl$ (60–64 Hz for monodentate phosphines, 79 Hz for dppe) which contain *S,S′*-chelating $[(SPPh_2)_2N]^-$ anions [19]. The *cis* $^2J(P^{III}\text{–}Pt\text{–}P^{III})$ couplings for the $PhMe_2P$ complexes **1**–**3** (20–25 Hz) are larger in magnitude compared with the dppe complexes (5–10 Hz), in which there is an additional ^3J(P–P) component through the ligand backbone of opposite sign. Each of the *cis* or *trans* $^3J(P^{III}\text{–}Pt\text{–}S\text{–}P^{V})$ couplings for **1**–**6** have comparable magnitudes, being between 4 and 11 Hz. Upon deprotonation and chelation the phosphorus atom P(1) of the chelate experiences modest shielding, moving ca. 15 ppm to low frequency from the free ligand value (δ_P 48.3 and 42.2 for HL^1 and HL^2 (*d*-chloroform), 42.5 for HL^3 (d_4-methanol)). Formation of the *S,N* chelate is exclusive in these instances; there is no evidence from $^{31}P\{^1H\}$ NMR spectroscopy for the formation of isomeric complexes of $(L^1)^-$ or $(L^3)^-$ in which the $[R_2P(S)NC(NH_2)NH]^-$ anion functions as an *N,N′* bidentate chelate to platinum(II) by the amino groups at the imine carbon.

In their IR spectra **1**–**6** exhibit several strong bands in the region 1400–1700 cm^{-1}; the ν_{NH} vibrations (broad bands of medium intensity between 3400–3100 cm^{-1}) and the ν_{PS} bands (ca. 562 cm^{-1} for **1** and **4**, ca. 588 cm^{-1} for **2**, **3**, **5** and **6**) are shifted only marginally from the values in the uncomplexed molecules $HL^{1–3}$ (HL^1 3377, 3142 (ν_{NH}) and 558 (ν_{PS}); HL^2 3361, 3285, 3230 (ν_{NH}) and 575 (ν_{PS}); HL^3 3437, 3350, 3299, 3201 (ν_{NH}) and 586 (ν_{PS})).

The molecular structure of *cis*-$[Pt\{SPPh_2N{=}C(Me)NH\text{-}S,N\}(PMe_2Ph)_2]Cl$ (**2**) has been determined by single crystal X-ray diffraction, Fig. 2. The coordination sphere at the metal atom Pt(1) comprises two mutually *cis* dimethylphenylphosphine ligands, bound through P(2) and P(3), and $(L^2)^-$ ligand bound via the terminal sulfur and nitrogen atoms S(1) and N(14) to form a six-membered Pt(1)–

Table 1
$^{31}P\{^1H\}$ NMR spectral data for $[Pt(L^n\text{-}S,N)(PR_3)_2]Cl$ (**1**–**6**) [a]

	δ_P			^1J(Pt–P)/Hz			J(P–P)/Hz		
	P(1)	P(2)	P(3)	Pt–P(1)	Pt–P(2)	Pt–P(3)	P(1)–P(2)	P(1)–P(3)	P(2)–P(3)
$[Pt(L^1\text{-}S,N)(PMe_2Ph)_2]Cl$ (**1**)	32.2	−7.7	−22.6	92	3273	2930	11	4	22
$[Pt(L^2\text{-}S,N)(PMe_2Ph)_2]Cl$ (**2**)	25.2	−7.7	−23.5	88	3371	2913	10	6	20
$[Pt(L^3\text{-}S,N)(PMe_2Ph)_2]Cl$ (**3**)	28.2	−7.6	−22.5	102	3332	2938	10	[b]	25
$[Pt(L^1\text{-}S,N)(dppe)]Cl$ (**4**)	48.9	38.5	30.3	3234	2997	85	6	6	10
$[Pt(L^2\text{-}S,N)(dppe)]Cl$ (**5**)	52.1	37.8	24.0	3247	3003	87	10	5	5
$[Pt(L^3\text{-}S,N)(dppe)]Cl$ (**6**)	50.4	38.8	26.7	3262	3004	90	8	8	8

[a] $CDCl_3$ solutions. P(1) = PS, P(2) *trans* nitrogen and P(3) *trans* sulfur.
[b] Not resolved.

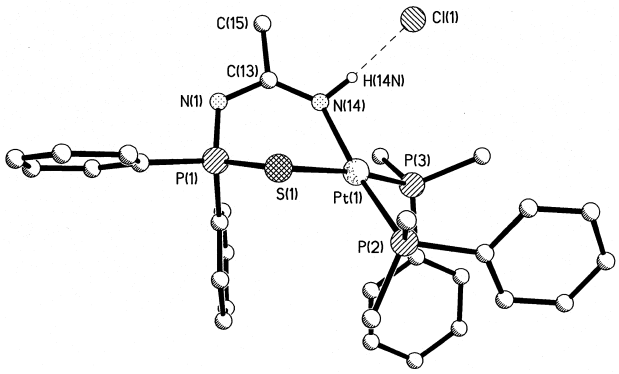


Fig. 2. X-ray crystal structure of *cis*-[Pt{SPPh$_2$N=C(Me)NH-*S*,*N*}-(PMe$_2$Ph)$_2$]Cl (**2**) (hydrogen atoms bound to carbon omitted for clarity). Selected bond lengths (Å) and angles (°): Pt(1)–S(1) 2.403(2), Pt(1)–P(2) 2.284(2), Pt(1)–P(3) 2.289(2), Pt(1)–N(14) 2.060(8), P(1)–S(1) 2.036(4), P(1)–N(1) 1.604(8), N(1)–C(13) 1.335(12), C(13)–N(14) 1.314(12); P(3)–Pt–P(2) 96.17(9), P(2)–Pt(1)–S(1) 85.57(9), S(1)–Pt(1)–N(14) 90.8(3), N(14)–Pt(1)–P(3) 89.1(3), Pt(1)–S(1)–P(1) 91.75(12), P(1)–N(1)–C(13) 121.5(7), S(1)–P(1)–N(1) 115.3(3), N(1)–C(13)–N(14) 127.5(9), C(13)–N(14)–Pt(1) 134.5(7).

S(1)–P(1)–N(1)–C(13)–N(14) platinacycle. There is a hydrogen-bonding interaction between the chloride counterion Cl(1) and the remaining amine proton H(14n) at N(14) (H(14n)···Cl(1) 2.34 Å, N(14)–H(14n)···Cl(1) 164°). Within the chelate ring, the atoms of the Pt(1)–N(14)–C(13)–N(1)–P(1) chain are coplanar, S(1) being displaced by 1.27 Å from this plane. There are deviations from square planarity at the metal centre; the angles between *cis* atoms are in the range 85.6–96.2°, moreover the P(2)–Pt(1)–P(3) and N(14)–Pt(1)–S(1) planes are twisted by 13° relative to each other. The Pt–P and Pt–N distances in **2** (Pt(1)–P(2) 2.284(2), Pt(1)–P(3) 2.289(2) and Pt(1)–N(14) 2.060(8) Å) correspond closely with the parameters for [Pt(S$_2$N$_2$)(PMe$_2$Ph)$_2$] (Pt–P 2.271(4) and 2.265(3) Å, Pt–N 2.081(8) Å) although the Pt–S distance is somewhat longer in the $(L^2)^-$ complex (Pt–S 2.403(2) Å in **2**, c.f. 2.270(5) Å for the $(S_2N_2)^{2-}$ complex) [17].

In summary *S*,*N* bidentate chelates can be readily formed at platinum(II) by *N*-thiophosphoryl derivatives of guanidines and amidines upon prior deprotonation using potassium *tert*-butoxide. Efforts are underway to extend the range of metal complexes which can be obtained using the anions derived from HL[1–3].

3. Experimental

Complexation reactions were performed under an atmosphere of oxygen-free nitrogen; subsequent work-up and recrystallisations were in air. Dichloromethane and thf were dried and distilled from calcium hydride and sodium respectively, *cis*-[PtCl$_2$(PR$_3$)$_2$] (PR$_3$ = PMe$_2$Ph or $\frac{1}{2}$dppe) was prepared by the addition of stoichiometric quantities of PR$_3$ to *cis*-[PtCl$_2$(cycloocta-1,5-diene)] in dichloromethane, potassium *tert*-butoxide (Aldrich) and other solvents employed were unpurified. ^{31}P{^{1}H} NMR (36.2 MHz, referenced to external 85% phosphoric acid (δ 0)) and IR spectra (pressed KBr discs) were recorded on JEOL FX90Q NMR and Perkin-Elmer System 2000 NIR FT-Raman spectrometers respectively. Elemental analyses (PE 2400 CHN elemental analyser) were performed by the University of Loughborough Analytical Service, FAB mass spectra (positive ionisation mode, 3-nitrobenzyl alcohol matrix) were carried out by the EPSRC National Mass Spectrometry Service Centre, Swansea.

The platinum(II) complexes *cis*-[Pt(L^n-*S*,*N*)(PR$_3$)$_2$]Cl (**1**–**6**) were prepared by the same general procedure.

To a solution of the ligand HL^n (0.2 mmol) and potassium *tert*-butoxide (0.25 mmol) in thf (5 cm^3) was added *cis*-[PtCl$_2$(PR$_3$)$_2$] (0.2 mmol) as a solid in one portion. The resulting yellow mixture was heated at reflux for 2 h and then cooled to room temperature. The solvent was removed in vacuo, the crude product was extracted in dichloromethane (5 cm^3) and the solution filtered through a plug of glass wool-Celite. The dichloromethane filtrate was concentrated under reduced pressure to ca. 2 cm^3; vapour diffusion of diethyl ether into the solution over several days gave the complexes *cis*-[Pt(L^n-*S*,*N*)(PR$_3$)$_2$]Cl (**1**–**6**) as either colourless (**1**, **2**) or pale yellow (**3**–**6**) solids. Conversion is quantitative by ^{31}P{^{1}H} NMR spectroscopy, isolated yields of the complexes were typically 39–65% based on Pt.

[Pt(L^1-*S*,*N*)(PMe$_2$Ph)$_2$]Cl (**1**). *Anal.* Found: C, 33.40; H, 4.70; N, 6.10. Calc. for C$_{19}$H$_{31}$N$_3$P$_3$ClPtS: C, 34.73; H, 4.76; N, 6.40%. FAB$^+$ MS: *m/z* 621 ($M^+ - $Cl). IR (cm^{-1}): 3302, 3156 (ν_{NH}), 562 (ν_{PS}).

[Pt(L^2-*S*,*N*)(PMe$_2$Ph)$_2$]Cl (**2**). *Anal.* Found: C, 45.51; H, 4.58; N, 3.49. Calc. for C$_{30}$H$_{36}$N$_2$P$_3$ClPtS: C, 46.18; H, 4.65; N, 3.59%. FAB$^+$ MS: *m/z* 744 ($M^+ - $Cl). IR (cm^{-1}): 3123 (ν_{NH}), 588 (ν_{PS}).

[Pt(L^3-*S*,*N*)(PMe$_2$Ph)$_2$]Cl (**3**). *Anal.* Found: C, 45.78; H, 4.78; N, 5.75. Calc. for C$_{29}$H$_{35}$N$_3$P$_3$ClPtS: C, 44.59; H, 4.52; N, 5.38%. FAB$^+$ MS: *m/z* 746 ($M^+ - $Cl). IR (cm^{-1}): 3439, 3264, 3203 (ν_{NH}), 588 (ν_{PS}).

[Pt(L^1-*S*,*N*)(dppe)]Cl (**4**). *Anal.* Found: C, 39.41; H, 4.69; N, 6.17. Calc. for C$_{29}$H$_{34}$N$_3$P$_3$ClPtS: C, 44.64; H, 4.39; N, 5.39%. FAB$^+$ MS: *m/z* 743 ($M^+ - $Cl). IR (cm^{-1}); 3329, 3163 (ν_{NH}), 562 (ν_{PS}).

[Pt(L^2-*S*,*N*)(dppe)]Cl (**5**). *Anal.* Found: C, 50.96; H, 4.77; N, 3.06. Calc. for C$_{40}$H$_{39}$N$_2$P$_3$ClPtS: C, 53.19; H, 4.35; N, 3.10%. FAB$^+$ MS: *m/z* 866 ($M^+ - $Cl). IR (cm^{-1}): 3340 (ν_{NH}), 585 (ν_{PS}).

[Pt(L^3-*S*,*N*)(dppe)]Cl (**6**). *Anal.* Found: C, 50.57; H, 4.42; N, 4.98. Calc. for C$_{39}$H$_{38}$N$_3$P$_3$ClPtS: C, 51.80; H, 4.24; N, 4.65%. FAB$^+$ MS: *m/z* 867 ($M^+ - $Cl). IR (cm^{-1}); 3346, 3148 (ν_{NH}), 588 (ν_{PS}).

3.1. X-ray crystallography

X-ray diffraction studies on crystals of *cis*-[Pt(L^2-*S*,*N*)(PMe$_2$Ph)$_2$]Cl (**2**) grown from dichloromethane–hexane by solvent diffusion, were performed using a Bruker SMART diffractometer with graphite-monochromated Mo

Kα radiation ($\lambda = 0.71073$ Å). The structure was solved by direct methods, the non-hydrogen atoms were refined with anisotropic displacement parameters; hydrogen atoms bound to carbon were idealised and fixed (C–H 0.95 Å); the NH proton H(14n) associated with N(14) was located by a ΔF map and allowed to refine anisotropically. Structural refinements were by the full-matrix least-squares method on F^2 using the program SHELXTL-PC [20]. $C_{30}H_{36}N_2P_3ClPtS$, colourless needles, $0.08 \times 0.12 \times 0.15$ mm, $M = 780.12$, monoclinic, $a = 9.9790(2)$, $b = 29.4825(4)$, $c = 10.9449(2)$ Å, $\beta = 90.835(1)°$, $U = 3219.7(1)$ Å^3, $T = 293$ K, space group $P2_1/n$, $Z = 4$, μ(Mo Kα) = 4.677 mm^{-1}. Of 13959 measured data 4587 were unique reflections ($R_{int} = 0.0421$) to give $R_1 = 0.0414$ ($I > 2\sigma(I)$, 3680 observed) and $wR_2 = 0.0881$.

Supplementary data

Full lists of structure refinement data, atomic coordinates, bond lengths and angles, anisotropic displacement parameters and hydrogen atom parameters have been deposited as supplementary material, no. 137216, at the Cambridge Crystallographic Data Centre, 12 Union Road, Cambridge CB2 1EZ, UK (fax: +44-1223-336033; e-mail: deposit@ccdc.cam.ac.uk).

Acknowledgements

We are grateful to the EPSRC for funding (P.B.), Johnson Matthey plc for the loan of platinum salts and to Professor Alfred Schmidpeter, University of Munich, for the generous gift of samples of HL[1–3].

References

[1] A.M.Z. Slawin, M.B. Smith, J.D. Woollins, J. Chem. Soc., Dalton Trans. (1998) 1537.
[2] D.J. Birdsall, A.M.Z. Slawin, J.D. Woollins, Inorg. Chem. 38 (1999) 4152.
[3] J. Novosad, M. Necas, J. Marek, P. Veltsistas, C. Papadimitriou, I. Haiduc, M. Watanabe, J.D. Woollins, Inorg. Chim. Acta 290 (1999) 256.
[4] R. Rossi, A. Marchi, L. Marvelli, L. Magon, M. Peruzzini, U. Casellato, R. Graziani, J. Chem. Soc., Dalton Trans. (1993) 723.
[5] R. Cea-Olivares, G. Espinosa-Perez, I. Haiduc, R. Rösler, C. Silvestru, Inorg. Chem. 34 (1995) 3352.
[6] J. Ellermann, P. Gabold, F.A. Knoch, M. Moll, A. Schmidt, M. Schutz, Z. Naturforsch., Teil B 51 (1996) 201.
[7] L. Barkoui, M. Charrouf, M.-N. Rager, B. Denise, N. Platzer, H. Rudler, Bull. Chim. Soc. Fr. 134 (1997) 167.
[8] H. Rudler, B. Denise, J.R. Gregario, J. Vaissermann, J. Chem. Soc., Chem. Commun. (1997) 2299.
[9] E. Herrmann, O. Navratil, P. Sladek, Phosphorus Sulfur Silicon Relat. Elem. 109–110 (1996) 201.
[10] G. Grossmann, E. Herrmann, O. Navratil, Collect. Czech. Chem. Commun. 55 (1990) 364.
[11] N. Inguimbert, L. Jäger, M. Taillefer, H.J. Cristau, J. Organomet. Chem. 529 (1997) 257.
[12] J. Münchenberg, O. Böge, A.K. Fischer, P.G. Jones, R. Schmutzler, Phosphorus Sulfur Silicon Relat. Elem. 86 (1994) 103.
[13] A. Schmidpeter, J. Ebeling, Angew. Chem. 70 (1967) 534.
[14] M.A.R. Khayat, F.S. Al-Isa, J. Prakt. Chem. 331 (1988) 149.
[15] R. Appel, Chem. Ber 105 (1972) 2476.
[16] G. Capozzi, P. Haake, J. Am. Chem. Soc. 94 (1972) 3249.
[17] P.F. Kelly, J.D. Woollins, J. Chem. Soc., Dalton Trans. (1988) 1053.
[18] P.A. Bates, M.B. Hursthouse, P.F. Kelly, J.D. Woollins, J. Chem. Soc., Dalton Trans. (1986) 2367.
[19] J.R. Phillips, A.M.Z. Slawin, D.J. Williams, J.D. Woollins, Polyhedron 15 (1996) 3175.
[20] G.M. Sheldrick, SHELXTL, Version 5.03, program for crystal structure solution, University of Göttingen, Germany, 1994.

PERGAMON

www.elsevier.nl/locate/poly

Polyhedron 19 (2000) 813–819

POLYHEDRON

Reaction of the diethyltin(IV) cation with pyridoxine (PN, vitamin B_6) in the presence of various anionic species: the crystal structure of $[SnEt_2(PN–H)]Cl$

José S. Casas [a], Alfonso Castiñeiras [a], Félix Condori [a], María D. Couce [b], Umberto Russo [c], Agustín Sánchez [a], José Sordo [a,*], José M. Varela [a]

[a] *Departamento de Química Inorgánica, Universidade de Santiago de Compostela, 15706 Santiago de Compostela, Galicia, Spain*
[b] *Departamento de Química Inorgánica, Universidade de Vigo, Vigo, Galicia, Spain*
[c] *Dipartimento di Chimica Inorganica, Metallorganica ed Analitica, Università di Padova, Padua, Italy*

Received 1 November 1999; accepted 28 January 2000

Abstract

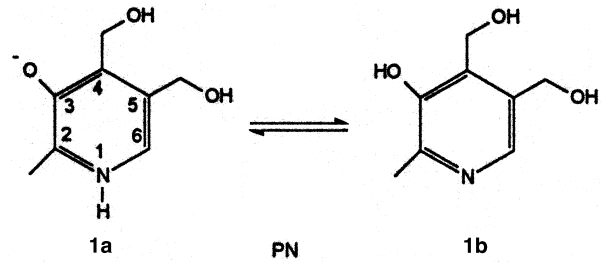
The reaction of the diethyltin(IV) cation with pyridoxine (PN, vitamin B_6) in 80:20 (v/v) ethanol–water mixtures containing NO_3^- and Cl^-, NO_3^- and AcO^- or Cl^- and AcO^- ions in various molar ratios was investigated. The compounds $[SnEt_2(PN–H)]Cl$ (**1**), $[SnEt_2(PN–H)](NO_3)\cdot 2H_2O$ (**2**) and $[SnEt_2(PN–2H)]$ (**3**) were isolated. These compounds were characterized by IR, Raman and Mössbauer spectroscopy and EI and FAB mass spectrometry. The structure of compound **1**, determined by X-ray diffraction, consists of dimeric $[SnEt_2(PN–H)]_2^{2+}$ units (in which two bridging-chelating hydrogen pyridoxinate anions link Sn atoms with coordination number five) and hydrogen-bonded Cl^- ions. The behaviour of these compounds in DMSO-d_6 and DMF-d_7 was studied by NMR spectroscopy. ©2000 Elsevier Science Ltd All rights reserved.

Keywords: Crystal structures; Diethyltin; Pyridoxine

1. Introduction

The wide range of industrial applications of organotin compounds [1] has led to increasing concern about their presence in the environment and, as a consequence, to an increase in research aimed at determining the species generated by their hydrolysis [2–5]. Also, biological considerations such as the possible use of organotin compounds as antitumour agents [6] have led to increased study of the interactions of their cations with ligands of biological significance in water or mixtures of water and organic solvents [7–13]. Although most work on the hydrolysis and thermodynamics of organotin has concerned the dimethyltin(IV) cation [2–5,7–13], recent studies have used the diethyl and dibutyl cations [14–17], finding that for a given ligand the stability of the species present in solution depends on the nature of R in SnR_2^{2+}.

As part of our work on the interactions of diorganotin compounds with vitamins in aqueous or organo-aqueous media [18,19], we have previously studied [20] the interaction of the dimethyltin(IV) cation with pyridoxine (2-methyl-3-hydroxy-4,5-bis(hydroxymethyl)pyridine, PN), one of the recognized forms of vitamin B_6 [21], in ethanol–water containing NO_3^- and Cl^-, NO_3^- and AcO^- or Cl^- and AcO^- in various molar ratios; the presence of these anions enabled us to prepare complexes of $SnMe_2^{2+}$ with both di- and mono-deprotonated pyridoxine, Cl^- and NO_3^- acting as counterions in the latter case. We now report the results of an analogous study using the diethyltin(IV) cation, and describe the crystal structure of one of the compounds isolated, $[SnEt_2(PN–H)]Cl$.



* Corresponding author. Tel.: +34-981-594-636; fax: +34-981-594-912; e-mail: qijsordo@usc.es

0277-5387/00/$ - see front matter ©2000 Elsevier Science Ltd All rights reserved.
PII S0277-5387(00)00321-1

2. Experimental

2.1. Material and methods

Pyridoxine hydrochloride (Aldrich), pyridoxine (Aldrich), diethyltin dichloride (Aldrich), silver nitrate (Merck) and silver acetate (Probus) were used as received. Elemental analysis was performed with a Fisons 1108 microanalyser. Melting points were determined with a Büchi apparatus. Mass spectra were recorded on a Kratos MS50TC spectrometer connected to a DS90 system and operating under EI conditions (direct insertion probe, 70 eV, 250°C) and FAB (*m*-nitrobenzyl alcohol, Xe, 8 eV; ca. 1.28×10^{-15} J); ions were identified by DS90 software and values for the metallated peaks were calculated using the isotope ^{120}Sn. IR spectra (KBr pellets or Nujol mulls) and Raman spectra (polycrystalline samples) were recorded on a Bruker IFS66V FT-IR spectrometer equipped with an FRA-106 Raman accessory and are reported in Section 2.2 using the following abbreviations: vs very strong, s strong, m medium, w weak, sh shoulder, br broad. ^{1}H NMR spectra in DMSO-d_6 or DMF-d_7 were recorded at room temperature on a Bruker AMX 300 operating at 300.14 MHz, using 5 mm o.d. tubes; chemical shifts are reported relative to TMS. ^{119}Sn NMR spectra in DMSO-d_6 were run on a Bruker AMX 500 instrument using 5 mm o.d. tubes, and referred to external neat tetramethyltin. The conductivities of 10^{-3} M solutions were measured in a Crison MicroCM2202 conductivity meter. Mössbauer spectra were recorded at 80.0 K in a Harwell cryostat; the $Ca^{119m}SnO_3$ source (15 mCi, NEN) was kept at room temperature and moved with a triangular velocity wave form; suitable computer programs were employed to fit Lorentzian lineshapes to the experimental data.

2.2. Synthesis of the compounds

2.2.1. [$SnEt_2$(PN–H)]Cl (**1**)

Solid NaOH (0.40 g, 10 mmol) was added to a solution of PN·HCl (2.06 g, 10 mmol) in ethanol–water (80:20 v/v, 50 ml) (solution A). Solid Ag(AcO) (1.67 g, 10 mmol) was added to a solution of $SnEt_2Cl_2$ (1.23 g, 5 mmol) in the same solvent (25 ml), and the AgCl formed upon stirring was filtered out to leave solution B. Solution B was added with stirring to solution A, and stirring was continued for 1 day (final pH 5.5). After 12 h standing, the appearance of well formed crystals was observed. *Anal*. Found: C, 38.0; N, 3.7; H, 5.2. Calc. for [$SnEt_2$(PN–H)]Cl: C, 37.8; N, 3.7; H, 5.2%. M.p. 218°C. Yield (first batch) 65%. The main metallated signals in the EI spectrum are at *m/e* (ion, intensity): 327 ([$SnEt_2$(PN–2H–OH)], 60.95); 268 ([$SnEt_2$-(PN–2H–2CH_2OH–CH_3)], 73.8); 240 ([SnEt(PN–H–2CH_2OH–CH_3)], 35.7); 195 ([$SnEt_2$OH], 12.5); 149 ([SnEt], 27.1), 120 ([Sn], 29.8). The FAB spectrum shows a signal at 344 ([$SnEt_2$(PN–2H)], 100). Infrared (Raman) cm^{-1}: 1622w (1622w, 1607w), 1530vs (1538w), 1455m (1456m), ν(ring); 1020vs, 1012vs, ν(CO); 528m (524w), ν_{asym}(Sn–C); 478sh (482vs), ν_{sym}(Sn–C). Mössbauer: δ 1.61, ΔE_Q 3.83, Γ 1.04, $A_{2/1}$ 1.02. Λ_M (DMF, 10^{-3} M solution), 23.8 S cm^2 mol^{-1}.

The same product was obtained in media with Cl^- and AcO^- in 3:1 molar ratio, with Cl^- and NO_3^- in 3:1 molar ratio, and with Cl^- alone (see Table 1).

2.2.2. [$SnEt_2$(PN–H)](NO_3)·2H_2O (**2**)

To a solution of PN·HCl (2.06 g, 10 mmol) in ethanol–water (80:20 v/v, 50 ml) were added solid NaOH (0.40 g, 10 mmol) and solid $AgNO_3$ (1.70 g, 10 mmol). The AgCl formed upon stirring was filtered out, a solution of $SnEt_2Cl_2$ (1.23 g, 5 mmol) in the same solvent (25 ml) was added with stirring, and stirring was continued for 1 day (final pH 5.5). Slow concentration of the solution afforded a crystalline solid. *Anal*. Found: C, 31.6; N; 6.2; H, 5.5. Calc. for [$SnEt_2$(PN–H)](NO_3)·2H_2O: C, 32.5; N, 6.3; H; 5.4%. M.p. 220°C. Yield (first batch) 51%. The main metallated signals in the EI spectrum are at *m/e* (ion, intensity): 327 ([$SnEt_2$(PN–2H–OH)], 57.4); 298 ([$SnEt_2$(PN–H–CH_2OH–OH)], 12.89); 268 ([$SnEt_2$(PN–2H–2CH_2OH–CH_3)], 68.1); 240 ([SnEt(PN–H–2CH_2OH–CH_3)], 39.7); 195 ([$SnEt_2$OH], 11.8); 149 ([SnEt], 33.4), 120 ([Sn], 48.1). The FAB spectrum has a signal at 344 ([$SnEt_2$(PN–2H)], 100). Infrared (Raman), cm^{-1}: 1630w (1641w, 1625w), 1527vs, 1474m ν(ring); 1026m, 995vs, ν(CO); 1383vs, ν_{asym}(NO_3^-); 1040sh (1046vs), ν_{sym}(NO_3^-);

Table 1
Molar quantities of NO_3^-, Cl^- and AcO^- present in reactions affording the compound shown, relative to the quantity of SnR_2^{2+}

[SnR_2]	[PN]	[NO_3^-]	[Cl^-]	[AcO^-]	Compound prepared
1	2	0	4	0	[$SnEt_2$(PN–H)]Cl (**1**)
1	2	1	3	0	[$SnEt_2$(PN–H)]Cl (**1**)
1	2	2	2	0	[$SnEt_2$(PN–H)](NO_3)·2H_2O (**2**)
1	2	3	1	0	[$SnEt_2$(PN–H)](NO_3)·2H2O (**2**)
1	2	4	0	0	[$SnEt_2$(PN–H)](NO_3)·2H_2O (**2**)
1	2	0	2	2	[$SnEt_2$(PN–H)]Cl (**1**)
1	2	0	3	1	[$SnEt_2$(PN–H)]Cl (**1**)
1	2	2	0	2	[$SnEt_2$(PN–2H)] (**3**)
1	2	3	0	1	[$SnEt_2$(PN–H)](NO_3)·2H_2O (**2**)

539m (537w), ν_{asym}(Sn–C); 482sh (485vs), ν_{sym}(Sn–C). Mössbauer: δ 1.63, ΔE_Q 3.90, Γ 0.93, $A_{2/1}$ 1.08. Λ_M (DMF, 10^{-3} M solution), 39.8 S cm^2 mol^{-1}.

The same product was obtained in media with NO_3^- and Cl^- in 3:1 molar ratio, with NO_3^- and AcO^- in 3:1 molar ratio, and with NO_3^- alone (see Table 1).

*2.2.3. [$SnEt_2$(PN–2H)] (**3**)*

To a solution of PN·HCl (2.06 g, 10 mmol) in ethanol–water (80:20 v/v, 50 ml) were added solid NaOH (0.40 g, 10 mmol) and $AgNO_3$ (1.70 g, 10 mmol), and the AgCl formed after stirring was filtered out to leave solution A. To a solution of $SnEt_2Cl_2$ (1.23 g, 5 mmol) in the same solvent (25 ml) was added solid Ag(OAc) (1.67g, 10 mmol) and the AgCl formed after stirring was filtered out to leave solution B. Solution B was added with stirring to solution A and stirring was continued for 1 day (final pH 5). After standing for 2 days, crystals of **3** were observed. *Anal*. Found: C, 41.6; N, 4.2; H, 5.5. Calc. for [$SnEt_2$(PN–2H)]: C, 41.8; N, 4.1; H, 5.5%. M.p. 275°C. Yield (first batch) 68%. The main metallated signals in the EI spectrum are at *m/e* (ion, intensity): 327 ([$SnEt_2$(PN–2H–OH)], 41.3); 268 ([$SnEt_2$-(PN–2H–2CH_2OH–CH_3)], 55.7); 240 ([SnEt(PN–H–2CH_2OH–CH_3)], 27.5); 195 ([$SnEt_2$OH], 9.5); 149 ([SnEt], 28.7) and 120 ([Sn], 50.4). The FAB spectrum has signals at 344 ([$SnEt_2$(PN–2H)], 100) and 688 ([{$SnEt_2$(PN–2H)}$_2$], 23). Infrared (Raman), cm^{-1}: 1556m (1557w), 1463sh (1454w), 1404m, ν(ring); 1018s (1022w), 982s, ν(CO); 517m (525w), ν_{asym}(Sn–C); 490sh (488,476vs), ν_{sym}(Sn–C). Mössbauer: δ 1.44, ΔE_Q 3.07, Γ 0.96, $A_{2/1}$ 1.01.

2.3. Crystal structure determination

2.3.1. X-ray data collection and reduction

A colourless prismatic crystal of **1** was mounted on a glass fibre for data collection in an Enraf-Nonius MACH3 automatic diffractometer [22]. Cell constants and an orientation matrix for data collection were obtained by least-squares refinement of the diffraction data for 25 reflections in the range $10.63 < \theta < 18.12°$. Data were collected at 293 K using Mo Kα radiation ($\lambda = 0.71073$ Å) and the ω scan technique, and were corrected for Lorentz and polarization effects [23]. An empirical absorption correction (DIFABS) [24] was also made.

2.3.2. Structure solution and refinement

The structure was solved by direct methods [25] and subsequent Fourier maps, and refined on F^2 by a full-matrix least-squares procedure using anisotropic displacement parameters [26]. All hydrogen atoms were located from difference Fourier maps and were refined isotropically. Atomic scattering factors were taken from International Tables for X-ray Crystallography [27]. Molecular graphics were generated with PLATON98 [28]. The crystal data, experimental details and refinement results are summarized in Table 2.

Table 2
Crystal data, data collection and structure refinement parameters

Compound	[$SnEt_2$(PN–H)]Cl (**1**)
Empirical formula	$C_{24}H_{40}Cl_2N_2O_6Sn_2$
Formula weight	760.86
Temperature (K)	293(2)
Wavelength (Å)	0.71073
Crystal system	monoclinic
Space group	$P2_1/c$ (no. 14)
Unit cell dimensions	
a (Å)	9.4266(3)
b (Å)	12.3347(11)
c (Å)	13.0787(7)
β (°)	94.275(4)
V (Å^3)	1516.49(16)
Z	2
D_c (Mg m^{-3})	1.666
F(000)	760
μ (mm^{-1})	1.861
Crystal size (mm)	0.55×0.15×0.15
θ Range for data collection (°)	2.27 to 26.28
Index ranges	$-11 \le h \le 0$
	$-0 \le k \le 15$
	$-16 \le l \le 16$
Reflections collected	3264
Unique reflections	3075 ($R_{int} = 0.0180$)
Absorption correction	DIFABS
Maximum, minimum transmission	0.7677, 0.4276
Data, restraints, parameters	3075, 0, 244
Goodness of fit on F^2	1.053
Final R indices ($I > 2\sigma(I)$)	$R_1 = 0.0212$, $wR_2 = 0.0540$
R indices (all data)	$R_1 = 0.0306$, $wR_2 = 0.0570$
Largest difference peak, hole (e Å^{-3})	0.420, −0.309

3. Results and discussion

3.1. Synthesis

The crystal of **1** used for X-ray diffraction studies was synthesized as described in Section 2. Additionally, compound **1** and other compounds were prepared using other quantities of $AgNO_3$ and/or Ag(OAc) in solutions A and B so as to procure other relative amounts of NO_3^-, Cl^- and AcO^- in the reaction mixture; as previously [20], PN was used in excess to promote its deprotonation. Table 1 lists the reactions affording products that were characterized successfully by chemical analysis and by IR and ^{1}H NMR spectrometry. In each case, after the first batch of solid was separated from the mother liquor, further concentration led to the formation of impure solids.

As in the case of the methyl derivatives [20], the solids isolated from asymmetric NO_3^-/Cl^- systems contain the major anion of the solution; and whereas the 2:2 Cl^-/AcO^- solutions afforded a solid with monodeprotonated pyridoxine, the ligand was dideprotonated in the solid obtained with 2:2 NO_3^-/AcO^- solution. However, when the NO_3^-:Cl^- molar ratio was 2:2 the nitrate was obtained, whereas the methyl derivative obtained under the same conditions contained random amounts of Cl^- and NO_3^- [20].

3.2. Structure of [$SnEt_2$(PN–H)]Cl (**1**)

The crystal is composed of chloride ions and dimeric $[Sn_2Et_4(PN–H)_2]^{2+}$ units in which the Sn atoms are linked as shown in Fig. 1 by two bridging-chelating hydrogen pyridoxinate anions derived from **Ia** (see Section 1) by deprotonation of the C(4)–CH_2OH group. Selected bond distances and angles are listed in Tables 3 and 4. In each dimeric unit, each tin atom coordinates to two ethyl C atoms (the unremarkable Sn–C bond distances are close to those found in other diethyltin(IV) complexes [29]), to the O(2) of a deprotonated phenolic hydroxyl group, to the O(1) of a deprotonated C(4)–CH_2OH group and to the similarly deprotonated O(1)[a] of the other pyridoxinate anion, leading to a coordination polyhedron that is closer to a square pyramid than a trigonal bipyramid [30]. No other atoms lie nearer the tin atom than 3.70 Å, the sum of the van der Waals radii of tin and oxygen [31].

Like $[SnMe_2(PN–H)](NO_3)\cdot 2H_2O$ and $[SnMe_2(H_2O)(PN–H)]Cl\cdot H_2O$, the two previously characterized diorganotin complexes of monodeprotonated pyridoxine [20], $[SnEt_2(PN–H)]Cl$ contains dimeric $[SnR_2(PN–H)]_2^{2+}$ units. The following similarities and differences deserve comment.

In $[SnEt_2(PN–H)]Cl$ the tin atom is pentacoordinated, whereas in the methyl compounds it is hexacoordinated, the sixth position being occupied by one of the C(5)–CH_2OH oxygens of a neighbouring unit in the nitrate and by the oxygen of an H_2O molecule in the chloride. Nevertheless, the difference in coordination environment does not significantly change the structural parameters of either the planar Sn_2O_2 ring (in which distances and angles are very close to those found in the dimethyltinpyridoxinatenitrate) or the SnR_2 unit (the C–Sn–C angle, 152.77(13)°, is only slightly narrower than the angle of 159.9(1)° found in the methyltin chloride derivative, in which the tin atom has distorted octahedral coordination).

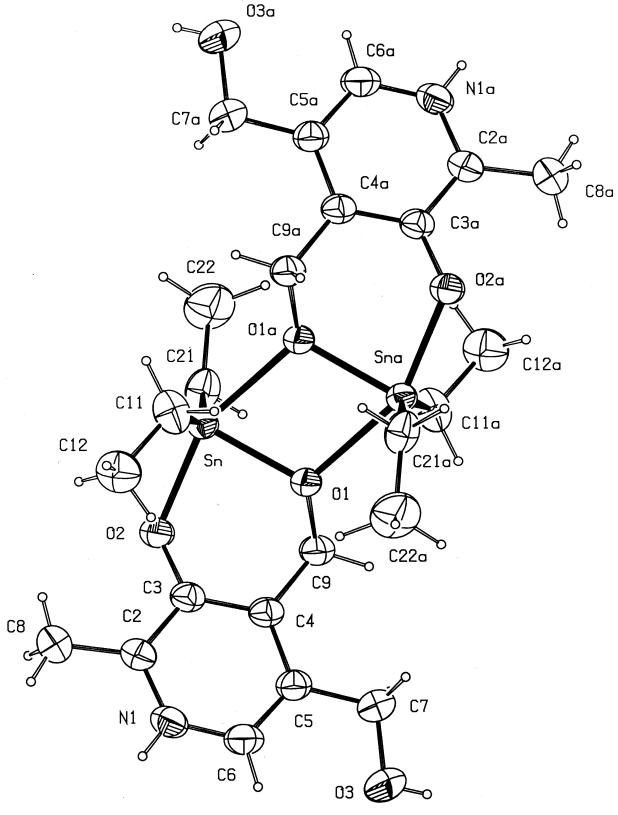


Fig. 1. The crystal structure of $[SnEt_2(PN–H)]Cl$ (**1**), showing the numbering scheme (chloride ions have been omitted).

Table 3
Bond distances (Å) and angles (°) in $[SnEt_2(PN–H)]Cl$ (**1**), with e.s.d.s in parentheses [a]

Tin environment			
Sn–O(1)	2.0875(16)	Sn–O(1)#1	2.2937(15)
Sn–O(2)	2.1109(17)	Sn–Sn#1	3.5711(3)
Sn–C(21)	2.126(3)	Sn–C(11)	2.135(3)
O(1)–Sn–O(2)	83.93(6)	O(1)–Sn–C(21)	102.68(9)
O(2)–Sn–C(21)	95.77(10)	C(3)–O(2)–Sn	125.75(15)
O(1)–Sn–C(11)	101.41(11)	C(22)–C(21)–Sn	115.9(2)
O(2)–Sn–C(11)	99.23(10)	C(21)–Sn–Sn#1	96.70(8)
C(21)–Sn–C(11)	152.77(13)	C(11)–Sn–Sn#1	94.74(9)
O(2)–Sn–O(1)#1	154.81(6)	O(1)–Sn–O(1)#1	70.90(7)
C(21)–Sn–O(1)#1	88.97(10)	C(9)–O(1)–Sn	119.70(15)
C(11)–Sn–O(1)#1	87.05(9)	C(9)–O(1)–Sn#1	123.11(14)
Sn–O(1)–Sn#1	109.10(7)	C(12)–C(11)–Sn	115.4(2)
Pyridoxine ligand			
O(1)–C(9)	1.426(3)	N(1)–C(2)	1.335(3)
O(3)–C(7)	1.404(4)	N(1)–C(6)	1.344(4)
O(1)–O(1)#1	2.547(3)	C(2)–C(8)	1.491(4)
O(2)–C(3)	1.316(3)	C(4)–C(5)	1.401(3)
C(2)–C(3)	1.409(3)	C(5)–C(6)	1.377(4)
C(3)–C(4)	1.407(3)	C(11)–C(12)	1.511(4)
C(4)–C(9)	1.501(3)	C(21)–C(22)	1.499(5)
C(5)–C(7)	1.508(4)		
C(2)–N(1)–C6)	124.9(2)	N(1)–C(2)–C(3)	118.1(2)
N(1)–C(2)–C(8)	118.9(3)	O(2)–C(3)–C(4)	122.9(2)
O(2)–C(3)–C(2)	118.4(2)	C(4)–C(3)–C(2)	118.7(2)
C(5)–C(4)–C(3)	120.0(2)	C(5)–C(4)–C(9)	122.2(2)
C(3)–C(4)–C(9)	117.8(2)	C(6)–C(5)–C(4)	119.0(2)
C(6)–C(5)–C(7)	119.3(2)	C(4)–C(5)–C(7)	121.7(2)
N(1)–C(6)–C(5)	119.3(3)	O(3)–C(7)–C(5)	109.1(3)
O(1)–C(9)–C(4)	111.1(2)	C(3)–C(2)–C(8)	123.0(3)
C(9)–O(1)–O(1)#1	153.92(18)		

[a] Symmetry operations: #1 $-x+1, -y, -z+1$.

Table 4
Hydrogen bond distances and angles [a]

D–H···A	*d*(D–H)	*d*(H···A)	*d*(D···A)	∠DHA
N(1)–H(10)···Cl#2	0.81(3)	2.27(3)	3.080(2)	177(3)
O(3)–H(30)···Cl#3	0.77(5)	2.39(5)	3.143(3)	164(5)

[a] Symmetry operations: #2 $-x, y-1/2, -z+1/2$; #3 $x, -y-1/2, z+1/2$.

The main geometrical features of the (PN–H) ligand are similar to those found previously in the methyl derivatives; for example, the C(2)–N(1)–C(6) angle (124.9(2)°) is in all three compounds practically identical to that found in PN·HCl [32] (124.7(2)°). Nevertheless, C(8), O(2),

C(9) and C(7) lie somewhat farther from the plane of the pyridine ring than in the methyl derivatives (O(2), for example, is 0.093 Å from the plane, as against 0.05 Å in the methyltin nitrate). The conformation of the C(5)–CH_2OH group, with O(3) near C(6) (the torsion angle C(4)–C(5)–C(7)–O(3) is $-170.3(3)°$), resembles that found in the methyltin chloride compound, whereas O(3) is closer to C(9) in the methyltin nitrate.

The absence of water from the lattice of the ethyl derivative makes its hydrogen bond system simpler than in the methyl derivatives, the only such bonds being those of the N–H and C(5)–CH_2OH groups with the Cl^- ions (Tables 3 and 4).

3.3. Vibrational spectra

Besides the bands indicated in Section 2, the IR spectra of compounds **1** and **2** exhibit medium-strong bands at 3346 and 3404 cm^{-1} respectively (the latter contributed to by ν(OH) of the lattice water), and also a set of medium-strong bands centred on 2900 cm^{-1} (2981, 2970, 2952, 2918, 2866 and 2811 cm^{-1} in the case of [$SnEt_2$(PN–H)]Cl) and attributed to ν(C–H), ν(O–H) of the C(5)–CH_2OH group and ν(N–H) of the N–H group. In the spectrum of **3** the latter region shows only three bands, at 2957, 2925 and 2871 cm^{-1}. The range 1650–1450 cm^{-1} shows the pyridine ring bands and, in the spectra of the compounds with protonated N(py), the expected [33] strong IR band at about 1530 cm^{-1} (probably contributed to by ν(C–O) of the coordinated phenolato group) and two weak Raman bands near 1600 cm^{-1}. In the spectra of **3** these two bands do not appear and the IR band at 1530 cm^{-1} is only a shoulder. The strong bands close to 1000 cm^{-1} have been attributed [34] to ν(C–O) of the C(5)–CH_2OH group, and the other bands near this position may be produced jointly by the coordinated C(4)–CH_2O^- group and the pyridine ring. The non-linearity of the C–Sn–C fragment is shown by the presence of ν_{asym}(Sn–C) and ν_{sym}(Sn–C) in the IR and Raman spectra of all three compounds.

3.4. Mössbauer spectra

All the Mössbauer spectra consist of well resolved, slightly asymmetric doublets with isomer shift and quadrupole splitting values that reflect the coordination geometries around the tin centres and the charges of the ligand. The isomer shift is larger for compounds **1** and **2**, in which the ligand is monoanionic, than for compound **3**, in which it is a dianion; since δ is positively correlated with the electron density on the tin centre, this may be attributed to the metal drawing more charge from the monoanion than from the dianion.

Owing to the pronounced deviation of **1** from ideal trigonal bipyramidal geometry, only the contribution of the covalently bonded organic groups has been taken into account in using the point charge model to calculate ΔE_Q. The simplified formula [35]:

$$\Delta E_Q = -4[R]\left(1-\tfrac{3}{4}\sin^2\theta\right)^{1/2} \quad (1)$$

together with the experimental C–Sn–C bond angle, 152.77°, yields a ΔE_Q value of 3.45 or 4.16 mm s^{-1} depending on whether the p.q.s. used is appropriate for organic moieties in tba positions (0.94 mm s^{-1}) or tbe positions (-1.13 mm s^{-1}). Although both these ΔE_Q values are within the usually accepted margin of error, a value of 3.81 mm s^{-1} in much better agreement with the experimental 3.83 mm s^{-1} is obtained if the p.q.s. is -1.03 mm s^{-1}, half way between the tba and tbe values, in consonance with the C–Sn–C bond angle being half way between those of the apical and equatorial positions (180 and 120°, respectively).

The parameters of compound **2** are very close to those of compound **1** and so the same coordination structure can be proposed. This supports the hypothesis that the water in **2** is occluded in the lattice, not coordinated to tin atoms.

3.5. Studies in solution

In DMSO, the PN signal that is most affected by deprotonation and complexation is that of H(6), which shifts to higher field in the complexes of both dimethyltin(IV) [20] and diethyltin(IV) derivatives (Table 5). This shift seems to be increased by di-deprotonation and the formation of PN–2H derivatives in which N(1) is deprotonated as well as O(2) being deprotonated and coordinated. The other PN protons are at most only slightly shielded when [SnR_2(PN–H)]$^+$ forms in the presence of Cl^-, but are slightly or significantly deshielded in the presence of NO_3^-. Note that the nature of the counterion also affected the synthesis of the complexes. The coordination of O(1) in compounds **2** and **3** is confirmed by the singlet associated with C(9)H_2 being flanked by two satellites due to the coupling of these protons with the tin atom. Like the organometallic methyl protons of the dimethyltin(IV) derivatives [20] (and like H(6)), the ethyl methylene protons of the $(CH_3CH_2)_2Sn^{2+}$ complexes are more shielded with the dideprotonated than with the monodeprotonated ligand. The same effect seems also to be shown, though less strongly, by the protons of the methyl group, the $^3J(^1H–^{119}Sn)$ coupling constant decreasing with increasing shielding like $^2J(^1H–^{119}Sn)$ does in the dimethyltin(IV) derivatives [20] ($^2J(^1H–^{119}Sn)$ could not be calculated for the diethyltin(IV) complexes).

There are significant differences between the ligand regions of the spectra of the diethyltin(IV) and dimethyltin(IV) derivatives of PN–$2H^{2-}$. The signals of [$SnEt_2$(PN–2H)] appear at higher field, the H(6) proton being shielded by ca. 0.6 ppm relative to the free ligand, as it is in the dibutyltin(IV) complex [36].

These differences may be due to the presence of an additional ligand (a water molecule) in the coordination sphere of the dimethyltin(IV) cation in [$SnMe_2$(PN–2H)(H_2O)] [20], but other structural and/or coordination factors cannot be ruled out since the coordination kernel observed in the solid state may be modified upon solution in DMSO.

Table 5
^{1}H and ^{119}Sn NMR data obtained for SnR_2^{2+} complexes of pyridoxine in DMSO-d_6 and DMF-d_7 [a]

	H(6)	H(O3)	H(9)	H(7)	H(8)	Sn–**CH$_2$**–CH$_3$	Sn–CH$_2$–**CH$_3$**	^3J(^{1}H–Sn)	^{119}Sn	Reference
DMSO-d_6										
PN	8.17s (1)	5.21s,b (1)	4.76s (2)	4.50s (2)	2.34s(3)					[20]
[SnMe$_2$(H$_2$O)(PN–H)]Cl·H$_2$O	7.76s (1)	5.14s,b (1)	4.75s (2)	4.49s (2)	2.33s(3)					[20]
[SnEt$_2$(PN–H)]Cl	7.81s (1)	5.11s,b (1)	4.75s (2)	4.47s (2)	2.32s (3)	1.45b (4)	1.23t (6)	165/158	− 220.4	this work
[SnMe$_2$(PN–H)](NO$_3$)·2H$_2$O	7.83s (1)	5.50s,b (1)	4.83s (2)	4.56s (2)	2.40s (3)					[20]
[SnEt$_2$(PN–H)(NO$_3$)·2H$_2$O	7.81s (1)	5.43s,b (1)	4.91s (2) $^3J=44$	4.53s (2)	2.42s (3)	1.31b (4)	1.15t (6)	132	− 303.7	this work
[SnMe$_2$(H$_2$O)(PN–2H).0.5H$_2$O	7.73s (1)	5.25s,b (1)	4.83s (2)	4.49s (2)	2.34s (3)					[20]
[SnEt$_2$(PN–2H)]	7.59s (1)	4.95t (1)	4.79s (2) $^3J=40$	4.37d (2)	2.28s (3)	1.26b (4)	1.15t (6)	127	− 251.5	this work
[SnBu$_2$(PN–2H)]	7.60s (1)	4.94s,b (1)	4.79s (2)	4.38d (2)		2.26s (3)				[36]
DMF-d_7										
PN	7.96s (1)		5.04s (2)	4.63s (2)	2.42s (3)					
[SnEt$_2$(PN–H)]Cl	7.91s (1)		5.00s (2)	4.61s (2)	2.41s (3)	1.60m (4)	1.32t (6)	157/150		
[SnEt$_2$(PN–H)](NO$_3$)·2H$_2$O	8.02s (1)		5.04s (2)	4.77s (2)	2.54s (3)	1.55c (4)	1.24t (6)	144		
[SnEt$_2$(PN–2H)]	7.88s (1)		4.99s (2)	4.59s (2)	2.38s (3)	1.41m (4)	1.22t (6)	146		

[a] Chemical shifts in ppm (δ); J in Hz; s singlet; b broad; t triplet; d doublet. In parentheses, relative numbers of protons calculated by integration.

Table 5 also lists the ^{1}H NMR data for PN and its complexes in DMF-d_7. In this solvent the signal corresponding to H(O3) disappears, probably owing to fast exchange of this proton with the deuterated solvent. In [SnEt$_2$(PN–H)]Cl the ligand protons are hardly shielded at all relative to PN, while in the nitrate complex most are deshielded. Only in [SnEt$_2$(PN–2H)] do the proton signals clearly lie at higher field than in the spectrum of pyridoxine.

Finally, ^{119}Sn chemical shifts in DMSO-d_6 are also listed in Table 5. Though also influenced by other factors [37], these shifts depend largely on the coordination number of the tin atom. The values obtained for our compounds are in the range −90 to −330 reported [38] for pentacoordinated tin compounds, but are nevertheless sufficiently negative for it not to be possible to rule out the possibility of a DMSO molecule bringing the coordination number up to six, especially in the case of the nitrate complex.

Supplementary data

Crystallographic data have been deposited at the Cambridge Crystallographic Data Centre, 12 Union Road, Cambridge CB2 1EZ, UK (fax: +44-1223-336033; e-mail: deposit@ccdc.cam.ac.uk), deposition number CCDC 135673.

Acknowledgements

We wish to thank the Xunta de Galicia, Spain, for financial support.

References

[1] C.J. Evans, S. Karpel, Organotin Compounds in Modern Technology, Elsevier, Amsterdam, 1985.
[2] M.M. McGrady, R.S. Tobias, Inorg. Chem. 3 (1964) 1157.
[3] G. Arena, R. Purrello, E. Rizzarelli, A. Gianguzza, L. Pellerito, J. Chem. Soc., Dalton Trans. (1989) 773.
[4] R. Barbieri, A. Silvestri, Inorg. Chim. Acta 188 (1991) 95.
[5] T. Natsume, S. Aizawa, K. Hatano, S. Funahashi, J. Chem. Soc., Dalton Trans. (1994) 2749.
[6] M. Gielen, H. Dalil, D. de Vos, M. Biesemans, R. Willem, Metal-Based Drugs 5 (1998) 265.
[7] G. Arena, A. Gianguzza, L. Pellerito, S. Musumeci, R. Purrello, E Rizzarelli, J. Chem. Soc., Dalton Trans. (1990) 2603.
[8] G. Arena, A. Contino, S. Musumeci, R. Purrello, J. Chem. Soc., Dalton Trans. (1990) 3383.
[9] F. Capolongo, A.M. Giuliani, M. Giomini, U. Russo, J. Inorg. Biochem. 49 (1993) 275.
[10] G. Arena, R. Cali, A. Contino, A. Musumeci, S. Musumeci, R. Purrello, Inorg. Chim. Acta 237 (1995) 187.
[11] C. De Stefano, C. Foti, A. Gianguzza, M. Martino, L. Pellerito, S. Sammartano, J. Chem. Eng. Data 41 (1996) 511.
[12] C. De Stefano, A. Gianguzza, M. Marrone, D. Piazzese, Appl. Organomet. Chem. 11 (1997) 683.
[13] M.M. Shoukry, E.M. Khairy, M.M.A. Mohamed, Talanta 44 (1997) 1149.

[14] N. Buzás, T. Gajda, E. Kuzmann, L. Nagy, A. Vértes, K. Burger, Main Group Met. Chem. 18 (1995) 641.
[15] B. Gyurcsik, N. Buzás, T. Gajda, L. Nagy, E. Kuzmann, A. Vértes, K. Burger, Z. Naturforsch., Teil B 50 (1995) 515.
[16] M.M. Shoukry, Talanta 43 (1996) 177.
[17] M.M. Shoukry, M.M.H. Mohamed, Main Group Met. Chem. 20 (1997) 281.
[18] J.S. Casas, M.V. Castaño, M.S. García-Tasende, T. Perez Alvarez, A. Sánchez, J. Sordo, J. Inorg. Biochem. 61 (1996) 97.
[19] J.S. Casas, A. Castiñeiras, M.D. Couce, G. Martínez, J. Sordo, J.M. Varela, J. Organomet. Chem. 517 (1996) 165.
[20] J.S. Casas, E.E. Castellano, F. Condori, M.D. Couce, A. Sánchez, J. Sordo, J.M. Varela, J.J. Zuckerman-Schpector, J. Chem. Soc., Dalton Trans. (1997) 4421.
[21] E.E. Snell, in: D. Dolphin, R. Poulson, O. Avramovic (Eds.), Vitamin B_6 Pyridoxal Phosphate, Wiley, New York, 1986, Part A, Chap. 1, p. 6.
[22] B.V. Nonius, CAD4-Express Software, Version 5.1/1.2, Enraf-Nonius, Delft, The Netherlands, 1994.
[23] M. Kretschmar, GENHKLK, Program for the reduction of CAD4 diffractometer data, University of Tübingen, Germany, 1997.
[24] N. Walker, D. Stuart, Acta Crystallogr., Sect. A 39 (1983) 158.
[25] G.M. Sheldrick, Acta Crystallogr., Sect. A 46 (1990) 467.
[26] G.M. Sheldrick, SHELX-97, Program for the refinement of crystal structures, University of Göttingen, Germany, 1997.
[27] International Tables for X-ray Crystallography, vol. C, Kluwer, Dordrecht, 1995.
[28] A.L. Spek, Acta Crystallogr., Sect. A 46 (1990) C34.
[29] J.S. Casas, A. Castiñeiras, M.D. Couce, N. Playá, U. Russo, A. Sánchez, J. Sordo, J.M. Varela, J. Chem. Soc., Dalton Trans. (1998) 1513.
[30] A.W. Addison, N.T. Rao, J. Reedijk, J. Van Rijn, G.C. Verschoor, J. Chem. Soc., Dalton Trans. (1984) 1349.
[31] J.E. Huheey, E.A. Keiter, R.L. Keiter, Inorganic Chemistry: Principles of Structure and Reactivity, Harper Collins, New York, 4th edn., 1993, pp. 292, 1513.
[32] G.E. Bacon, J.S. Plant, Acta Crystallogr. 36 (1980) 1130.
[33] T.A. Franklin, M.F. Richardson, Inorg. Chim. Acta 46 (1980) 191.
[34] N.A. Drobinskaya, L.V. Inova, M.Ya. Karpeiskii, V.L. Florent'ev, Chem. Heterocycl. Comp. (Engl. Translation) 7 (1973) 330.
[35] R.V. Parish, Structure and bonding in tin compounds, in: G.L. Long (Ed.), Mössbauer Spectroscopy Applied to Inorganic Chemistry, Plenum, New York, 1984.
[36] F. Kayser, M. Biesemans, M. Gielen, R. Willem, Magn. Res. Chem. 32 (1994) 358.
[37] R.K. Harris, J.D. Kennedy, W. McFarlane, in: R.K. Harris, B.E. Mann (Eds.), NMR and the Periodic Table, Academic Press, London, 1978, p. 342.
[38] J. Otera, J. Organomet. Chem. 221 (1981) 57.

PERGAMON

www.elsevier.nl/locate/poly

Polyhedron 19 (2000) 821–827

POLYHEDRON

Crystal structures of three [bis(1,3-dithiole-2-thione-4,5-dithiolato)zincate]$^{2-}$ salts: $[Q]_2[Zn(dmit)_2]$ (Q = 1,4-Me_2-pyridinium or NEt_4) and $[PPh_4]_2[Zn(dmit)_2]\cdot DMSO$. Comparison of the dianion packing arrangements in $[Q]_2[Zn(dmit)_2]$

William T.A. Harrison [a], R. Alan Howie [a], James L. Wardell [a,*], Solange M.S.V. Wardell [a], Nadia Maria Comerlato [b], Luiz Antônio Sodré Costa [b], Alexandre Carneiro Silvino [b], Ana Isabel de Oliveira [c], Rosalice Mendonca Silva [c]

[a] *Department of Chemistry, University of Aberdeen, Meston Walk, Old Aberdeen, Aberdeen, AB24 3UE, Scotland, UK*
[b] *Instituto de Quimica, Universidade Federal do Rio de Janeiro, C.P. 68563, 21945-970 Rio de Janeiro, RJ, Brazil*
[c] *Departamento de Quimica, Universidade Federal de Minas Gerais, 31279-901 Belo Horizonte, MG, Brazil*

Received 22 November 1999; accepted 28 January 2000

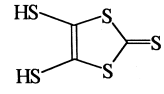
Abstract

$[Zn(dmit)_2]^{2-}$ dianions in $[Q]_2[Zn(dmit)_2]$ complexes (**2**: Q = 1,4-Me_2-pyridinium ($C_7H_{10}N$) or NEt_4), and $[PPh_4]_2[Zn(dmit)_2]\cdot DMSO$ ((**2**: Q = PPh_4)·DMSO) have distorted tetrahedral geometries, as a result of the 94.49(3) to 95.27(3)° range of the bite angle of the dmit ligands; H_2-dmit = 4,5-dimercapto-1,3-dithiole-2-thione, $H_2C_3S_5$. The Zn–S bond lengths are in the range from 2.3285(8) to 2.3520(9) Å. In (**2**: Q = $C_7H_{10}N$) and (**2**: Q = NEt_4), both the cations and the dianions are found in alternating layers, which form columns and sheets. Whereas in (**2**: Q = $C_7H_{10}N$), there are no S···S contacts less than the sum of the van der Waals radii, 3.70 Å, S···S contacts at 3.5792(13) and 3.6605(12) Å, within dianion layers, are found in (**2**: Q = NEt_4). In ((**2**: Q = PPh_4)·DMSO), the steric bulk of the $[PPh_4]^+$ cations is such that the dianions cannot be distributed in well-defined sheets: no S···S contacts less than 4.0 Å are found in ((**2**: Q = PPh_4)·DMSO). The structures are compared with those reported for other $[Q]_2[Zn(dmit)_2]$ compounds. ©2000 Elsevier Science Ltd All rights reserved.

Keywords: 1,3-dithiole-2-thione-4,5-dithiolates; dmit complexes; Zinc dmit compounds; Zincates

1. Introduction

Derivatives of 4,5-dimercapto-1,3-dithiole-2-thione (H_2-dmit **1**) have been extensively studied as heterocyclic compounds [1], coordination compounds [2–4], precursors of tetrathiafulvalene derivatives [1,5–8] and electronic conducting materials [9]. Both transition and main group metal–dmit coordination compounds have attracted considerable attention in recent times [2–4]. Of the main group metal complexes, $[Zn(dmit)_2]^{2-}$ salts have a pivotal role as stable dmit precursors for use with other metals and in the syntheses of heterocyclic compounds [1–4].



Dmit derivatives have a tendency to associate in the solid state, particularly via S···S contacts, at distances less than the sum of the van der Waals radii of two sulfur atoms, 3.70 Å [10]. This is illustrated generally in the dmit compounds listed in the Cambridge Crystallographic Data Base [11,12]. The nature and extent of the intermolecular S···S contacts, and the arrays generated, depend on the dmit compound. For example, the inter-dianionic S···S interactions in $[Q]_2[Sn(dmit)_3]$ compounds vary with the cation Q; the connectivity is three-dimensional for the smallest cations Q = 1,4-dimethylpyridinium and NMe_4, in chains for the somewhat larger cation NEt_4, and is absent for the still larger

* Corresponding author. Tel.: +44-1224-272930; Fax: +44-1224-272921; e-mail: j.wardell@abdn.ac.uk

0277-5387/00/$ - see front matter ©2000 Elsevier Science Ltd All rights reserved.
PII S0277-5387(00)00322-3

PPh_4 cation [13]. Variable S···S contacts are also indicated in three reported structures of $[Q]_2[Zn(dmit)_2]$ (**2**) compounds, namely $[NEt_4]_2[Zn(dmit)_2]\cdot MeOH$ ((**2**: $Q = NEt_4)\cdot MeOH$) [14], [(ferrocenylmethyl)trimethyl)-ammonium]$_2[Zn(dmit)_2]$ (**2**: $Q = FcCH_2NMe_3$) [14], and $[NBu_4]_2[Zn(dmit)_2]$ (**2**: $Q = NBu_4$) [15]. To investigate further the effect of the cation on inter-dianionic interactions of $[Zn(dmit)_2]^{2-}$ salts, the crystal structures of unsolvated $[NEt_4]_2[Zn(dmit)_2]$ (**2**: $Q = NEt_4$) and [1,4-Me_2-pyridinium]$_2[Zn(dmit)_2]$ (**2**: $Q = C_7H_{10}N$) as well as the solvated salt $[PPh_4]_2[Zn(dmit)_2]\cdot DMSO$ ((**2**: $Q = PPh_4)\cdot DMSO$) have been determined and are now reported.

2. Results and discussion

The cations in the three $[Zn(dmit)_2]^{2-}$ salts have their usual geometries and are not futher discussed.

2.1. Dianion structures

Atom arrangements for the dianions in (**2**: $Q = C_7H_{10}N$ or NEt_4) and ((**2**: $Q = PPh_4)\cdot DMSO$) are shown in Fig. 1; Zn–S bond lengths and S–Zn–S angles are listed in Tables 1–3. The dmit bite angles, between 94.49(3) and 95.27(3)°, lead to distorted tetrahedral zinc geometries. These angles are similar to those previously reported for (**2**: $Q = NBu_4$) [15], NEt_4 [14] and $FcCH_2NMe_3$ [14], see Table 4. While the Zn–S bond lengths (Table 4) and geometric parameters within each dmit ligand (Table 5) of all six $[Q]_2[Zn(dmit)_2]$ salts vary little, there is a noticeable difference between the interplanar dmit angle in ((**2**: $Q = NEt_4)\cdot MeOH$) of 69.9(5)° [14] and those of the other compounds, which are between 79.53(3) and 84.72(2)°; the dianion in ((**2**: $Q = NEt_4)\cdot MeOH$) is thus somewhat flattened compared to the other complexes. The reference dmit plane is taken as the plane through the central C=C bond and the attached S atoms. The thione atoms, C=S, and the metal atom, M, in metal–dmit complexes, e.g. the $[Sn(dmit)_s]^{2-}$ complexes, are frequently out of this reference plane, providing either boat or chair shaped MSCSCSCS eight-membered rings, see Fig. 2. However, in only three of the ten distinct $[Zn(dmit)_2]^{2-}$ fragments in the six $[Q]_2[Zn(dmit)_2]$ complexes are the Zn atoms appreciably out (i.e. > 0.1 Å) of the dmit reference plane, see Table 4; these three $[Zn(dmit)_2]^{2-}$ fragments are present, one in each of the two independent dianions in (**2**: $Q = NEt_4$) and in the dianion of (**2**: $Q = PPh_4$). The thione S atoms, in these three cases, are just out of the reference dmit plane, by between 0.0961(17) and 0.1381(15) Å, on the same side as the Zn atoms. These fragments, thus, have flattened boat conformations; all others have near planar conformations. There are no apparent correlations between the conformations and other geometric parameters, including the asymmetry in the Zn–S bond lengths to each dmit ligand.

Table 1
Zn–S bond lengths (Å) and S–Zn–S angles (°) in (**2**: $Q = C_7H_{10}N$)

Zn1–S1	2.3373(11)	Zn1–S1^{i}	2.3373(11)
Zn1–S2	2.3419(11)	Zn1–S2^{i}	2.3419(11)
S1–Zn1–S2	95.22(3)	S2^{i}–Zn1–S1	122.52(4)
S1^{i}–Zn1–S2^{i} [a]	95.22(3)	S1–Zn1–S1^{i}	110.21(6)
S1^{i}–Zn1–S2	122.52(4)	S2–Zn1–S2^{i}	113.35(6)

[a] i = $-x, y, -z+1/2$.

Table 2
Zn–S bond lengths (Å) and S–Zn–S angles (°) in (**2**: $Q = NEt_4$)

Molecule 1		Molecule 2	
Zn1–S1	2.3383(9)	Zn2–S11	2.3448(10)
Zn1–S2	2.3405(10)	Zn2–S12	2.3520(9)
Zn1–S6	2.3484(10)	Zn2–S16	2.3355(9)
Zn1–S7	2.3522(10)	Zn2–S17	2.3477(10)
S1–Zn1–S2	95.12(3)	S11–Zn2–S12	94.49(3)
S6–Zn1–S7	94.77(3)	S16–Zn2–S17	95.27(3)
S1–Zn1–S6	115.90(3)	S16–Zn2–S12	116.72(3)
S2–Zn1–S6	120.15(4)	S17–Zn2–S12	119.45(3)
S1–Zn1–S7	120.71(4)	S16–Zn2–S11	119.58(3)
S2–Zn1–S7	112.11(3)	S11–Zn2–S17	113.17(4)

Table 3
Zn–S bond lengths (Å) and S–Zn–S angles (°) in ((**2**: $Q = PPh_4)\cdot DMSO$)

Zn1–S1	2.3356(8)	Zn1–S6	2.3285(8)
Zn1–S2	2.3473(8)	Zn1–S7	2.3376(8)
S1–Zn1–S2	95.05(3)	S2–Zn1–S6	113.68(3)
S6–Zn1–S7	95.06(3)	S1–Zn1–S7	111.54(3)
S1–Zn1–S6	122.95(3)	S2–Zn1–S7	120.67(3)

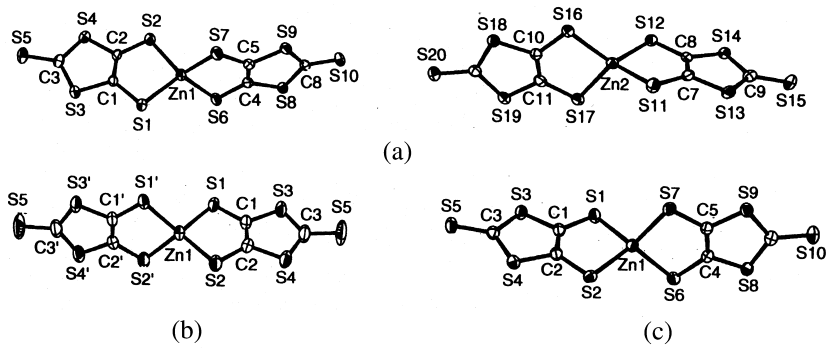


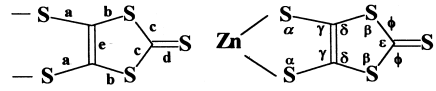
Fig. 1. Atom arrangements and numbering systems for the dianions of **2**.

Table 4
Selected geometric parameters in $[Q]_2[Zn(dmit)_2]$

Cation Q	Zn–S (Å)	Dmit bite angle (°)	Angle between dmit planes (°)	Zn out of dmit plane [a] (Å) (ZnOOP)	Thione S out of dmit plane [a] (Å) (SOOP)	Reference
1,4-Me_2-pyridinium	2.3373(11), 2.3419(11)	95.22(3)	79.53(3)	+0.0171(18)	−0.069(3)	this study
	2.3373(11), 2.3419(11)	95.22(3)		+0.0171(18)	−0.069(3)	
NEt_4						this study
Molecule 1	2.3383(9), 2.340510)	95.12(3)	82.77(2)	+0.0044(14)	+0.0548(18)	
	2.3484(9), 2.3522(10)	94.77(3)		−0.3690(14)	−0.1315(16)	
Molecule 2	2.3448(10), 2.3520(9)	94.49(3)	84.72(2)	−0.0139(13)	+0.0637(13)	
	2.3355(9), 2.3477(10)	95.27(3)		−0.3425(13)	−0.0961(17)	
$NEt_4 \cdot MeOH$	2.346(2), 2.346(2)	94.01(8)	69.5(5)	0.0	0.0	[14]
	2.350(2), 2.350(2)	93.43(9)		0.0	0.0	
$FcCH_2NMe_3$	2.3311(12), 2.3445(12)	93.67(4)	83.2(5)	0.0739(5)	0.0254(5)	[14]
	2.3311(12), 2.3445(12)	93.67(4)				
NBu_4	2.330(5), 2.345(3)	95.0(1)	79.8(5)	0.0999(5)	0.0006(5)	[15]
	2.330(5), 2.345(3)	95.0(1)				
$PPh_4 \cdot DMSO$	2.3356(8), 2.3473(8)	95.05(3)	81.70(2)	−0.2631(12)	−0.1381(15)	this study
	2.3285(8), 2.3376(8)	95.06(3)		−0.0977(11)	−0.0453(15)	

[a] The dmit plane is taken as the plane through the C=C and the attached S atoms.

Table 5
Ranges of bond lengths (Å) and angles (°) within the dmit ligands in complexes **2**



a	1.735(3)–1.748(4)	α	94.83(11)–97.02(14)
b	1.743(4)–1.761(3)	β	98.07(16)–98.89(15)
c	1.710(5)–1.732(5)	γ	125.9(3)–127.6(2)
d	1.652(4)–1.666(3)	δ	114.7(2)–116.0(3)
e	1.343(6)–1.365(4)	ε	111.84(18)–112.7(2)
		ϕ	122.6(2)–124.8(2)

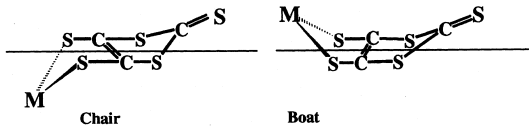


Fig. 2. Chair and boat conformations of MSCSCSCS eight-membered rings in metal–dmit fragments.

2.2. Dianion packing

In (**2**: Q = $C_7H_{10}N$) and (**2**: Q = NEt_4), both the cations and the dianions are found in distinct layers which alternate throughout the structures, see Figs. 3 and 4. In (**2**: Q = $C_7H_{10}N$), the layers are perpendicular to [102]. They are extended in the direction of *b* (perpendicular to the plane of the drawing in Fig. 3) purely by cell translations thus forming columns. For the dianions, these columns are related to one another by crystallographic centres of symmetry thus forming sheets. Within a single dianionic sheet, all the dianions are identical in geometry and orientation. Adjacent dianion sheets are related by crystallographic centres of symmetry (and the *c*-glide plane), thus producing inversion of the atomic arrangement from one sheet to the next. This last general arrangement applies also to the sheets of cations but here there is the additional complication that two crystallographically distinct type of cations are present.

While this general description is also applicable to (**2**: Q = NEt_4), the detailed description is very different. First of all, the sheets are now perpendicular to $[\bar{1}02]$, see Fig. 4. Two crystallographically distinct dianions are present in the asymmetric unit and the operation of a 2_1 axis together with cell translations transforms each of these into a dianionic column. Since the individual dianions are crystallographically distinct (discounting the strong pseudosymmetry of the structure discussed further below) so too are the columns which they form. The cationic sheets are also more complex because no fewer than four crystallographically distinct species are present.

In the final stages of the structure refinement of (**2**: Q = NEt_4) in the preferred space group, $P2_1$, the refinement

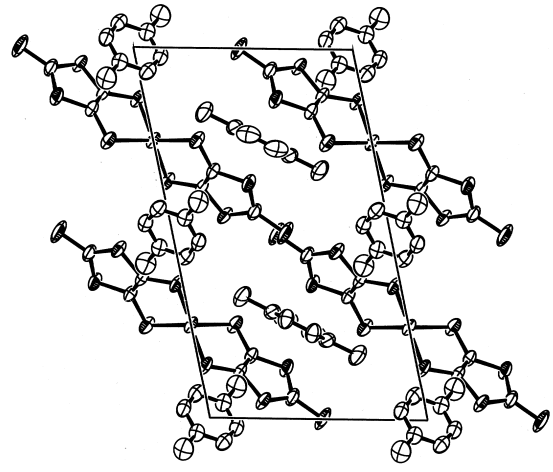


Fig. 3. The cell of (**2**: Q = $C_7H_{10}N$) projected on 010 with *a* across and *b* down into the page. Non-H atoms are shown as 50% ellipsoids and H atoms have been omitted for clarity.

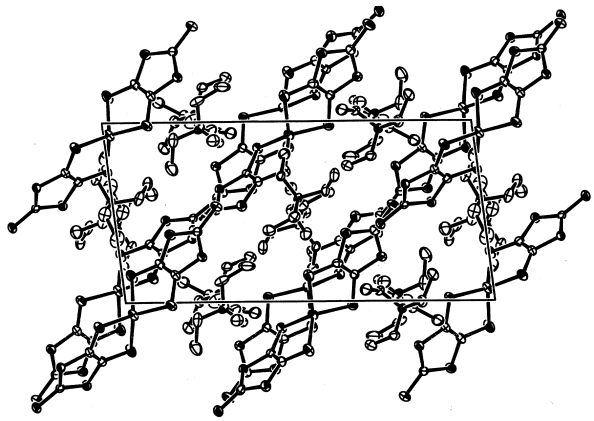


Fig. 4. The cell of (**2**: Q = NEt_4) projected on 010 with *c* across and *b* up out of the page. Non-H atoms are shown as 50% ellipsoids and H atoms have been omitted for clarity.

program (SHELXL97) indicated twin refinement. In response to this, the introduction of the TWIN and BASF instructions resulted in the refined value of the Flack *x* parameter, representing the fraction of the minor twin component, of 0.306(7). The absolute structure of this compound is therefore to this extent indeterminate. The success of the twin refinement of the structure of (**2**: Q = NEt_4) prompts the question how and why is it twinned? It is evident from the unit cell contents of (**2**: Q = $C_7H_{10}N$) and (**2**: Q = NEt_4), see Figs. 3 and 4, that the two structures almost verge on the isostructural, despite the differences in their unit cells and space groups. The cell content of (**2**: Q = $C_7H_{10}N$), with $b = 8.8467(7)$ Å, can be thought of as a single layer, which is replicated purely by cell translation in the direction of *b* to complete the structure. For (**2**: Q = NEt_4), with $b = 17.8699(2)$ Å, the cell content consists of two layers, which are related by the operation of a crystallographic twofold screw axis. As a direct consequence, the dianion layers in (**2**: Q = NEt_4) are more buckled than they are in (**2**: Q = $C_7H_{10}N$), owing to the greater bulk of the NEt_4 cation compared to the 1,4-Me_2-pyridinium cation.

As noted above, adjacent dianion layers of (**2**: Q = $C_7H_{10}N$), parallel to *b*, are related to one another by a crystallographic centre of symmetry. In the space group $P2_1$, this is not precisely possible for the dianion layers of (**2**: Q = NEt_4), but if it were approximately true, this would account for the pseudosymmetry detected by ADDSYM. Further, if in the structure of (**2**: Q = NEt_4) the occasional (roughly 1 in 3) dianion layer was incorporated in the inverted configuration, this would account for the success of the twin refinement. Note that if the structure of (**2**: Q = NEt_4) were truly in the centrosymmetric space group $P2_1/c$, half of the NEt_4 cations would have to lie on centres of symmetry and would be highly disordered. It is concluded therefore that it is ordering the NEt_4 cations which reduces the space group symmetry to $P2_1$ and disorder in the dianionic layers, which is responsible for the twinning.

In ((**2**: Q = PPh_4) · DMSO), the phosphorus atoms in the cations are associated more or less in planes perpendicular to

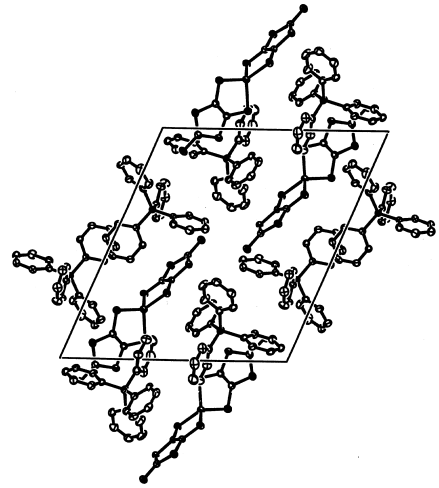


Fig. 5. The cell of ((**2**: Q = PPh_4) · DMSO) viewed down *a* with *b** across the (landscape) page. Non-H atoms are shown as 50% ellipsoids. H-atoms and DMSO solvate atoms have been omitted for clarity.

$[0\bar{1}1]$. However, the bulk of the phenyl groups is such that the dianions cannot be distributed in well-defined sheets, see Fig. 5.

2.3. Interanion S···S contacts in (2: Q = $C_7H_{10}N$ or NEt_4) and ((2: Q = PPh_4) · DMSO)

In (**2**: Q = $C_7H_{10}N$), there are no S···S contacts less than the sum of the van der Waals radii; the closest contacts involve (a) S4···S4′ (symmetry operation: $-x-1$, y, $-z+1/2$; S(ring)···S(ring), between adjacent dianionic sheets) at 3.876(2) Å and (b) S4···S5′ (symmetry operation: $-x-1$, $-y$, $-z+1$; S(ring)···S(thione), within a dianionic sheet) at 3.876(2) Å.

Short S···S contacts are present in (**2**: Q = NEt_4). With the notation that the ligands on Zn1 are ligand A (S1, S5 etc.) and ligand B (S6, S10 etc.) and ligands on Zn2 are ligand C (S11, S15 etc.) and ligand D (S16, S20 etc.), then contacts involve SB(ring)···SC(thione) (S8···S15′ = 3.5792(13) Å (symmetry operation: $x+1$, y, z)) and SB(thione)··· SD(ring) (S10···S19′ = 3.6605(12) Å (symmetry operation: $-x+1, y-1/2, -z+1$)). No sulfur atoms of ligand A are involved in any of these contacts: the shortest contacts are S3···S20′ (SA(ring)···SD(thione)) at 3.8236(12) Å and S5···S13′ (SA(thione)···SC(ring)) at 3.8324(12) Å. All of the contacts are within a dianion layer. There are no contacts between adjacent dianion layers.

There are no S···S contacts in ((**2**: Q = PPh_4) · DMSO) less than 4.0 Å.

2.4. Comparison with other $[Q]_2[Zn(dmit)_2]$ salts

Distinction between the structures of the $[Q]_2$-$[Zn(dmit)_2]$ salts (Q = $C_7H_{10}N$, NEt_4, NBu_4, $FcCH_2NMe_3$ and PPh_4) can be made on the basis of the cation size, and the effect that this has on the layering of the dianions.

The structures of the salts with the smallest cations, $C_7H_{10}N$ and NEt_4 (**2**: Q = $C_7H_{10}N$ or NEt_4) and ((**2**: Q = NEt_4)·MeOH) [14], are in the form of well-defined and alternating cation and dianion layers. While the layers are aligned differently in the three compounds (parallel to 102, $\bar{1}02$ and 001, respectively), the dianion layers are similar and can be described in terms of dianions stacked end to end in rows and side by side in columns. Adjacent columns are staggered with respect to one another and interpenetrate to differing extents; Fig. 6 illustrates the situation with ((**2**: Q = NEt_4)·MeOH) [14], in which the interpenetration of the columns is greatest. Interestingly, this complex also contains the anomalously flattened dianions. The MeOH solvate molecules occupy sites within the dianion layers. The interpenetration of columns is least in (**2**: Q = $C_7H_{10}N$), where the thione S atoms are more or less aligned.

Layers of dianions are also discernable in (**2**: Q = $FcCH_2NMe_3$) [14], but here the dianions are tilted with respect to the direction of propagation of the rows, see Fig. 7(a), and the layers themselves are also markedly corrugated, see Fig. 7(b). Some corrugation, but to a much smaller extent, occurs in (**2**: Q = NEt_4) also. The corrugation in (**2**: Q = $FcCH_2NMe_3$) is particularly apparent when viewed along the length of the rows of dianions and cations, Fig. 7(b): interanionic S3···S3′ contacts of 3.519(2) Å form chains running diagonally through the dianion layers, while the S4···S4′ contacts of 3.696(2) Å interconnect these layers. A striking feature of the structure of (**2**: Q = $FcCH_2NMe_3$) is the pairs of cation rows lying in channels defined by six rows of dianions, see Fig. 7(b).

In (**2**: Q = NBu_4) [15], the physical bulk of the cations prevents the formation of layers of dianions. Here instead the dianions are found stacked side by side in columns parallel to *b* but separated by the cell translation (8.954 Å) and therefore essentially unassociated.

With the still bulkier tetraphenylphosphonium cation in (**2**: Q = PPh_4), there is still less association of the dianions, which exist in loosely associated pairs in cavities between the cations (Fig. 5). Other cavities are occupied by dimethyl sulfoxide solvate molecules.

3. Experimental

Compounds $[Q]_2[Zn(dmit)_2]$ (**2**: Q = NEt_4, 1,4-Me_2-pyridinium or PPh_4) were obtained by a general procedure, from Na, CS_2 and [Q]X ([Q]X = [NEt_4]Br, [1,4-Me_2-pyridinium]I or [PPh_4]Cl) [14]. The ^{1}H NMR spectrum in Me_2CO-d_6 of the sample of (**2**: Q = PPh_4), grown from DMSO solution and with m.p. 198–201°C, indicated the presence of approximately 1 mol of DMSO per mole of (**2**: Q = PPh_4); elemental analytical data were in between those expected for unsolvated and mono-solvated species. *Anal.* Found: C, 55.8; H, 3.7. Calc. for $C_{54}H_{40}P_2S_{10}Zn$ ($C_{56}H_{46}OP_2S_{11}Zn$): C, 57.0 (55.3); H, 3.5 (3.8)%. Conformation of the DMSO solvate came from the X-ray studies, see later. The analytical analyses for (**2**: Q = NEt_4), m.p. 186–188°C, and (**2**: Q = $C_7H_{10}N$), m.p. 232–233°C (both obtained from Me_2CO/isopropanol solutions), were as expected for unsolvated species.

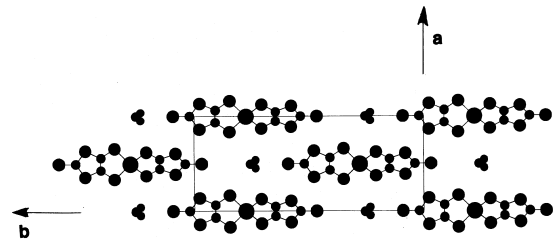


Fig. 6. A portion of the dianion layer of ((**2**: Q = NEt_4)·MeOH) projected on 001. The atoms, with $-0.125 < z < 0.125$ are shown as spheres of arbitrary radius. Atoms of incomplete dianions have not been drawn. The disordered MeOH solvate molecules are also indicated.

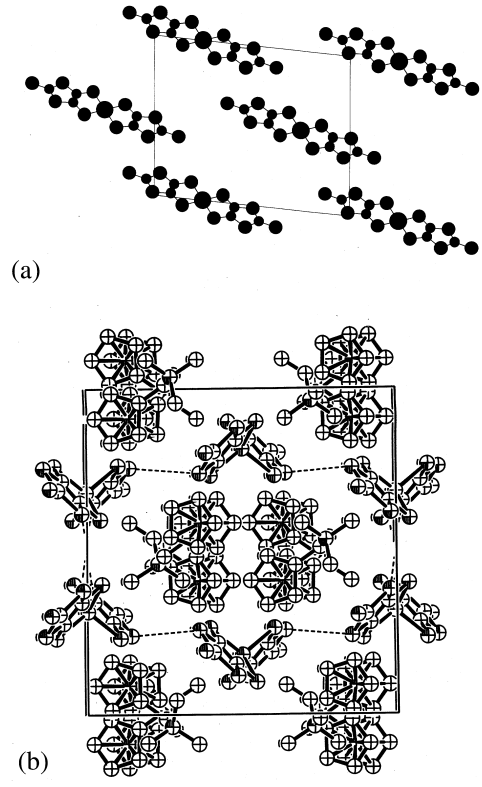


Fig. 7. (a) A portion of the dianion layer of (**2**: Q = $FcCH_2NMe_3$) projected on 010, with *a* vertically up the page. Atoms have *z* coordinates in the range $0 < z < 0.5$. Atoms are shown as spheres of arbitrary radius and atoms of incomplete dianions have not been drawn. (b) The cell of (**2**: Q = $FcCH_2NMe_3$) viewed down *c*, i.e. showing the rows of dianions and cations end-on. The reciprocal *b** axis is across the (landscape) page. Non-H atoms are shown as 50% ellipsoids and H atoms have been omitted for clarity.

3.1. Crystal structure determinations

3.1.1. Compounds ((2: Q = PPh_4)·DMSO) and (2: Q = NEt_4)

Data for (**2**: Q = NEt_4) and ((**2**: Q = PPh_4)·DMSO) were obtained at 150 K, at the National Data Collection Centre of the EPSRC at Southampton on an Enraf Nonius KappaCCD area detector with an Enraf Nonius FR591 rotating anode as

X-ray source. The ϕ–ω scan mode, filling the Ewald sphere, was employed. Data collection, and cell refinement and data reduction were accomplished with COLLECT [16] and DENZO [17]. An empirical correction for absorption was applied by means of SORTAV [18,19]. The structure was solved by direct methods, SHELXS-97 [20], and completed and refined with SHELXL-97 [21]. All non-H atoms were refined anisotropically and H atoms were placed in calculated positions and refined with a riding model.

In (**2**: Q = NEt_4) the asymmetric unit consists of two complete dianions and no fewer than four complete cations. In this case the ADDSYM component of the checkcif facility of the IUCr is at pains to point out the possible existence of an additonal symmetry element (which turns out to be a putative *c*-glide) and, as a result, a crystallographic centre of symmetry. A careful re-examination of this structure in the space group $P2_1/c$ does indeed provide some sort of a solution for the structure but attempted refinement of this alternative model resulted in an extremely high final *R*-factor and very poor estimates of bond lengths and angles and in addition provoked an extreme degree of disorder in one of the cations. It is concluded that the extra symmetry is merely an accidental approximation and not crystallographic in nature and may be neglected.

In ((**2**: Q = PPh_4)·DMSO), the phosphorus atoms in the cations are associated more or less in planes perpendicular to $[0\bar{1}1]$. However, the bulk of the phenyl groups is such that the dianions cannot be distributed in well-defined sheets. In the later stages of refinement, several quite large features (C*n*S, *n* = 1 to 7) were found in a difference map and included in the refinement simply as C atoms with SOF = 1 and refined isotropically. These 'atoms', and the bonds and angles which they provide, were commented out of the final cif at which point the PLATON element of checkcif indicated the presence in the structure of solvent accessible voids of 264 $Å^3$. The additional electron density, which is found (in subsequent calculations) to be equivalent to ca. $28e^-$ summed over the seven C*n*S atoms and to ca. $38e^-$ when other small peaks $>1e^-$ are included, is considered to arise from the presence of a highly disordered DMSO solvent molecule. These molecules, one per Zn atom, occur as centrosymmetrically related pairs in the voids revealed by PLATON.

Table 6
Crystal data and structure refinement for $[Q]_2[Zn(dmit)_2]$

	Q = 1,4-Me_2-pyridinium	Q = NEt_4	Q = PPh_4·(DMSO)
Empirical formula	$C_{20}H_{20}N_2S_{10}Zn$	$C_{22}H_{40}N_2S_{10}Zn$	$C_{54}H_{40}P_2S_{10}Zn.(C_2H_6OS)$
Formula weight	674.35	718.53	1136.77
Temperature (K)	293(2)	150(2)	150(2)
Wavelength (Å)	0.71073	0.71073	0.71073
Crystal system; space group	monoclinic; $P2_1/c$	monoclinic; $P2_1$	triclinic; $P\bar{1}$
Unit cell dimensions			
a (Å)	9.6784(8)	9.57220(10)	9.80970(10)
b (Å)	8.8467(7)	17.8699(2)	16.7811(3)
c (Å)	16.6274(14)	19.4194(2)	18.9519(3)
α (°)	90	90	65.5651(8)
β (°)	102.250(2)	97.1592(6)	79.0773(10)
γ (°)	90	90	80.5986(10)
Volume ($Å^3$)	1391.3(2)	3295.87(6)	2791.19(7)
Z	2	4	2
Calculated density (Mg m^{-3})	1.610	1.448	1.353
Absorption coefficient (mm^{-1})	1.648	1.395	0.906
F(000)	688	1504	1168
Crystal color	dark orange–brown	red	red
Crystal size (mm)	0.2×0.2×0.2	0.25×0.18×0.18	0.20×0.20×0.10
θ Range for data collection (°)	2.15–28.48	1.55–30.53	1.19–27.46
Index ranges	$-12 \le h \le 9$ $-11 \le k \le 11$ $-21 \le l \le 21$	$-13 \le h \le 13$ $-25 \le k \le 25$ $-27 \le l \le 27$	$-12 \le h \le 12$ $-21 \le k \le 20$ $-24 \le l \le 24$
Reflections collected/unique	7972/3145 (R_{int} = 0.0422)	68335/19801 (R_{int} = 0.0890)	47791/12758 (R_{int} = 0.0438)
Completeness to 2θ (%)	28.48, 84.0	30.53, 99.2	27.46, 99.7
Absorption correction	empirical	empirical	empirical
Refinement method	full-matrix least-squares on F^2	full-matrix least-squares on F^2	full-matrix least-squares on F^2
Data, restraints, parameters	3145, 0, 151	19801, 1, 648	12758, 0, 632
Goodness-of-fit on F^2	1.044	1.018	1.045
T_{max}, T_{min}		0.7873, 0.7217	0.914, 0.873
Final *R* indices ($I > 2\sigma(I)$)	R_1 = 0.0563, wR_2 = 0.1104	R_1 = 0.0469, wR_2 = 0.0920	R_1 = 0.0478, wR_2 = 0.1233
R indices (all data)	R_1 = 0.0993, wR_2 = 0.1261	R_1 = 0.0716, wR_2 = 0.1013	R_1 = 0.0650, wR_2 = 0.1349
Absolute structure parameter	n/a	0.306(7)	n/a
Extinction coefficient	0.0033(11)		
Largest difference peak and hole (e $Å^{-3}$)	0.484 and −0.484	0.733 and −0.530	1.371 and −1.136

*3.1.2. Compound (**2**: Q = $C_7H_{10}N$)*

Data were obtained at 293 K on a Siemens SMART automated CCD diffractometer (graphite-monochromated Mo Kα radiation). Preliminary scans indicated a primitive monoclinic unit cell. Raw frame data were collected in narrow-slice ω-scan mode. Data collection and cell refinement, and data reduction utilised the programs, SMART and SAINT [22]. Duplicate data, collected at the end of the experiment, indicated that no significant crystal decay or movement had occurred. An absorption correction was applied with SADABS [23] on the basis of multiple and symmetry-equivalent reflections. The structure was solved by direct methods, SHELXS-97 [20], and completed and refined with SHELXL-97 [21]. All non-H atoms were refined anisotropically and H atoms were placed in calculated positions and refined with a riding model.

Every ion sits on a crystallographic symmetry element. The zinc atom of the dianion lies on a crystallographic two-fold axis and therefore, in addition to Zn, only a single but complete dmit ligand (S1–S5 and C1–C3) is present in the asymmetric unit. The centroid of one of the cations (C4, C5/N1, C6 and C7) coincides with a crystallographic centre of symmetry. The other cation (C8, C9/N2, C10 and C11) lies on a crystallographic two-fold axis passing through the midpoints of the C8–C8′ and C10–C10′ bonds (symmetry operation: $-x-1, y, -z+3/2$). Thus for both of these cations, only one half is present in the asymmetric unit. Furthermore, the atom pairs C5/N1 and C9/N2 must be completely disordered to comply fully with the crystallographic symmetry. It is for these reasons that they have been refined in pairs with SOF values fixed at 0.5 and coordinates and thermal vibration parameters constrained to be exactly equal within the pair.

Diagrams were obtained with ORTEP-3 for Windows [24] and ATOMSV4.1 [25]. Crystal data and structure refinement details are listed in Table 6.

Supplementary data

Supplementary data are available from the Cambridge Crystallographic Data Centre, 12 Union Road, Cambridge CB2 1EZ, UK (fax: +44-1223-336033; e-mail: deposit@ccdc.cam.ac.uk) on request, quoting the deposition numbers CCDC 137189 to 137191 for (**2**: Q = $C_7H_{10}N$), (**2**: Q = NEt_4) and ((**2**: Q = PPh_4)·DMSO), respectively.

Acknowledgements

The authors thank the EPSRC Crystallography Service, based at the University of Southampton, UK for data collection for the compounds (**2**: Q = NEt_4) and ((**2**: Q = PPh_4)·DMSO). The agencies CAPES, CNPq and Fapemig, are thanked for their support.

References

[1] N. Svenstrup, J. Becher, Synthesis (1995) 215.
[2] R.-M. Olk, B. Olk, W. Dietzsch, R. Kirmse, E. Hoyer, Coord. Chem. Rev. 117 (1992) 99.
[3] A.E. Pullen, R.-M. Olk, Coord. Chem. Rev. 188 (1999) 211.
[4] G.E. Matsubayashi, Trends Inorg. Chem. 4 (1996) 79.
[5] S.K. Kumar, H.B. Singh, J.P. Jasinski, E.S. Paight, R., J. Butcher, J. Chem. Soc., Perkin Trans. 1 (1991) 3341.
[6] H. Muller, Y. Ueba, Synthesis (1991) 853.
[7] S.B. Wilkes, I.R. Butler, A.E. Underhill, M.B. Hursthouse, D.E. Hibbs, K.M.A. Malik, J. Chem. Soc., Dalton Trans. (1995) 897.
[8] M.R. Bryce, J. Mater. Chem. 5 (1995) 1481.
[9] P. Cassoux, L. Valade, H. Kobayashi, R.A. Clark, A.E. Underhill, Coord. Chem. Rev. 110 (1991) 115.
[10] J.E. Huheey, E.A. Keiter, R.L. Keiter, Inorganic Chemistry, Principles of Structure and Reactivity, Harper Collins, New York, 4th edn., 1993.
[11] F.H. Allen, O. Kennard, Chem. Des. Automation News 8 (1993) 1, 31.
[12] D.A. Fletcher, R.F. McMeeking, D. Parkin, J. Chem. Inf. Comput. Sci. 36 (1996) 746.
[13] F. de Assis, Z.H. Chohan, R.A. Howie, A. Khan, J.N. Low, G.M. Spencer, J.L. Wardell, S.M.S.V. Wardell, Polyhedron 18 (1999) 3533.
[14] Z.H. Chohan, R.A. Howie, J.L. Wardell, R. Wilkens, S.M.S.V. Doidge-Harrison, Polyhedron 16 (1997) 2689.
[15] H. Wang, D. Zhu, N. Zhu, H. Fu, Wuli Huaxue Xuebao 35 (1986) 378.
[16] R. Hooft, COLLECT: data collection software, Nonius BV, 1998.
[17] Z. Otwinowski, W. Minor, in: C.W. Carter, R.M. Sweet (Eds.), Methods in Enzymology, 1997, vol. 276, Macromolecular Crystallography, Part A, Academic Press, New York, 1997 pp. 307–326.
[18] R.H. Blessing, Acta Crystallogr., Sect. A 51 (1995) 33.
[19] R.H. Blessing, J. Appl. Crystallogr. 30 (1997) 421.
[20] G.M. Sheldrick, Acta Crystallogr., Sect. A 46 (1990) 467.
[21] G.M. Sheldrick, SHELXL-97, Program for crystal structure refinement, University of Göttingen, Germany, 1997.
[22] SMART and SAINT Software for area-detector diffractometers, Siemens Analytical X-ray Systems, Madison, WI, 1997.
[23] G.M. Sheldrick, SADABS, Program for scaling and correction of area detector data, University of Göttingen, Germany, 1997.
[24] L.J. Farrugia, J. Appl. Crystallogr. 30 (1997) 565.
[25] ATOMS V4.1 For Windows, Shape Software, 521 Hidden Valley Road, Kingsport, TN, 1998.

PERGAMON

www.elsevier.nl/locate/poly

Polyhedron 19 (2000) 829–833

POLYHEDRON

Liquid-mediated metathetical synthesis of binary and ternary transition-metal pnictides

Claire J. Carmalt, Daniel E. Morrison, Ivan P. Parkin *

Department of Chemistry, Christopher Ingold Laboratories, University College London, 20 Gordon Street, London WC1H 0AJ, UK

Received 30 November 1999; accepted 28 January 2000

Abstract

Nickel and cobalt pnictides have been synthesised using a liquid-mediated metathetical reaction of transition-metal dihalides with the appropriate sodium pnictide Na_3E (E = P, As, Sb) in refluxing toluene for 48 h. Binary and ternary compounds have been prepared. Products were analysed by powder X-ray diffraction, scanning electron microscopy, energy dispersive analysis by X-rays, FT-IR, Raman and vibrating sample magnetometry. ©2000 Elsevier Science Ltd All rights reserved.

Keywords: Antimonides; Arsenides; Metathesis; Phosphides

1. Introduction

Nickel and cobalt phosphides, arsenides and antimonides have various uses and characteristics as advanced materials. However, few synthetic methods for these materials can be found in the literature.

Amorphous NiP shows anomalous magnetisation temperature characteristics [1]. NiP has been evaluated as a catalyst for oxidative dehydrogenation of ethylbenzene [2] and as an underlayer for magnetic recording media and computer hard drives. There has been an extensive effort into understanding its magnetic properties [3] and crystallisation behaviour [4]. NiP/Sn multilayers have been investigated because of their unique properties [5]. NiP is used as an interlayer between particles and matrix in aluminium-matrix composites [6]. Nickel and cobalt phosphides have been synthesised as thin films by plasma arc spraying [7], ion implantation [8,9], galvanic and electrodeposition [10,11]. NiP, NiAs and NiSb have been synthesised by electroplating [12]. CoP and CoAs have been synthesised by single- and dual-source chemical vapour deposition [13] and molecular organic chemical vapour deposition [14]. Bulk transition-metal phosphides, arsenides and antimonides have been synthesised by the high-temperature hydrogen reduction of phosphates, arsenates and antimonates [15], by direct combination of the elements, typically at 1000°C and by solid state metathesis reactions at 550°C in sealed ampoules [16].

Phosphorus was thought to form a metal phosphide with all metals in the periodic table with the exception of antimony and bismuth [17]. However, recent work has suggested the existence of BiP and SbP [18]. A wide range of stoichiometries are known for metal phosphides, from M_4P to MP_{15}. For nickel, eight stoichiometric phosphide phases are known and have been cystallographically characterised: Ni_3P, Ni_5P_2, $Ni_{12}P_5$, NiP_2, Ni_5P_4, NiP, NiP_2 and NiP_3. The corresponding nickel and cobalt arsenide and antimonide chemistry is also extremely rich with a multitude of well characterised phases [17].

We report here the low temperature synthesis of amorphous and crystalline cobalt and nickel phosphides, arsenides and antimonides via a convenient liquid-mediated metathetical route.

2. Experimental

All manipulations were performed under an inert N_2 atmosphere using either Schlenk techniques or a Saffron Scientific inert atmosphere glove box. Toluene was dried over sodium and distilled from sodium under nitrogen prior to use. Distilled water was degassed with nitrogen prior to use and absolute ethanol (Aldrich, 99.5%) was dried over 3 Å molecular sieves. $NiBr_2$ (98%), $NiCl_2$ (98%) and $CoCl_2$ (98%) were purchased from Aldrich Chemicals and used as received. Na_3P, Na_3As and Na_3Sb were prepared by a modification of the literature procedure [19,20] from the reaction of sodium

* Corresponding author. Fax: +44-171-380-7463; e-mail: i.p.parkin@ucl.ac.uk

0277-5387/00/$ - see front matter ©2000 Elsevier Science Ltd All rights reserved.
PII S0277-5387(00)00323-5

metal with the appropriate chalcogenide in refluxing toluene under an inert atmosphere for 48 h. Precursor identity was verified by powder X-ray diffraction. Thermolysis studies were performed in a Lenton Thermal Designs tubular furnace, the samples were sealed in evacuated glass ampoules and annealed at 500°C for 48 h. Some selected samples were annealed at 800°C in evacuated silica ampoules. Powder X-ray diffraction measurements were recorded on a Siemens D5000 transmission diffractometer using germanium monochromated Cu $K\alpha_1$ radiation ($\lambda = 1.5406$ Å). Samples were mounted between two pieces of adhesive tape. Scanning electron microscope (SEM) micrographs were taken and energy dispersive analysis by X-rays (EDAX) was performed on an Hitachi S570 scanning electron microscope with a Link Analytical EDAX detector attachment. The EDAX system had an elemental detection limit of 0.2 atom% and a quantitative accuracy of 2 atom%. Polished elemental samples were used to calibrate the system. The EDAX excitation volume was typically of the order of 1 μm^3, sufficiently small that individual grains of the product could, in most cases, be investigated. Vibrating sample magnetometry (VSM) was performed on an Aerosonic 3001 magnetometer at room temperature. IR spectra were recorded on a PE 205 grating spectrometer from 4000 to 250 cm^{-1} and Raman spectra on a Dilor XY spectrometer.

2.1. Liquid-mediated metathesis reactions of MX_2 and Na_3E ($M = Ni, Co$; $E = P, As, Sb$; $X = Br$ for all reactions save $NiCl_2 + Na_3P$)

MX_2 (3.00 mmol) and Na_3E (2.00 mmol) were separately ground in a mortar and pestle. Na_3E was placed in a Schlenk flask to which 20 ml of dried, degassed toluene was added. MX_2 was added to the Schlenk flask with stirring and the resultant mixture was heated and allowed to reflux under stirring for 48 h. The resulting slurry was allowed to settle and the toluene was syringed off. The solid was washed with ethanol (2×20 ml), followed by distilled water (3×20 ml) and ethanol (2×20 ml). The remaining powder was dried in vacuo (yield 75%). The resulting powders were analysed by X-ray powder diffraction (Table 1), SEM, EDAX and VSM. Selected samples were analysed by Raman, IR and UV measurements.

3. Results

The reaction of a stirred suspension of sodium pnictide and metal(II) halide in refluxing toluene for 48 h results, after trituration with ethanol and distilled water, in the formation of amorphous metal pnictides (Eq. (1)). Powders obtained from evaporation of the water and ethanol washings showed them to be sodium halide by X-ray diffraction.

$$3MX_2 + 2Na_3E \rightarrow 2ME + 6NaX + M \quad (1)$$

(M = Ni, Co; E = P, As, Sb; X = Cl, Br)

Neither starting material had any detectable solubility in refluxing toluene. However, a fine suspension of the reactants did form. A slow colour change of the suspended solids was observed during the course of the reaction. The colours of the two individual precursors were seen to become less and less distinct as the reaction proceeded and a fine black powder product became more apparent.

The powder X-ray diffraction patterns of all the as-formed triturated samples revealed them to be X-ray amorphous. Analysis of the evaporated washings by X-ray powder diffraction showed crystalline NaBr or NaCl. The amorphous triturated pnictide powders were annealed at 500°C for 48 h. The annealing results are summarised in Table 1 and the unit cell dimensions of the samples that crystallised are collected in Table 2, and in the case of NiAs represented in Fig. 1.

Vibrating sample magnetometry shows either no response or a very weak ferromagnetic signal on the as-formed pnictides. This indicates that the as-formed pnictide powders did not contain any significant quantity of free metal. SEM analysis of these powders showed ca. 2–5 μm amorphous particles (Fig. 2). Spot EDAX analysis using an approximately 1-μm^3 excitation volume shows consistent metal to pnictide ratios over a number of spots with no evidence of sodium, chlorine or bromine (ca. 0.2% detection limit). These data taken together indicate that an amorphous, but, on the 1-μm scale, a chemically homogeneous powder is formed. This

Table 1
Compound description and data from the reaction of MX_2 and Na_3E in refluxing toluene for 48 h [a]

Reaction	Product colour	Phase detected by XRD (after annealing)	EDAX results as prepared	EDAX results after annealing
$3NiCl_2 + 2Na_3P$	black	Ni_3P (800°C/24 h)	2:1: Ni:P	1:1 Ni:P; 2:1 Ni:P (500°C/72 h)
$3NiBr_2 + 2Na_3As$	black	NiAs	1:1 Ni:As	1:1 Ni:As
$3NiBr_2 + 2Na_3Sb$	black	NiSb	1:1 Ni:Sb	1:1 Ni:Sb
$3NiCl_2 + Na_3As + Na_3Sb$	black	amorphous	2:1:1 Ni:As:Sb	2:1:1 Ni:As:Sb
$3NiCl_2 + 0.5Na_3As + 1.5Na_3Sb$	black	amorphous	4:1:3 Ni:As:Sb	4:1:3 Ni:As:Sb
$3CoCl_2 + 2Na_3P$	black	amorphous	3:2 Co:P	3:2 Co:P
$3CoCl_2 + 2Na_3As$	black	CoAs	3:2 Co:As	3:2 Co:As
$3CoCl_2 + 2Na_3Sb$	black	CoSb	3:2 Co:Sb	3:2 Co:Sb
$3CoCl_2 + Na_3As + Na_3Sb$	black	amorphous	3:1:1 Co:As:Sb	3:1:1 Co:As:Sb

[a] Annealing was performed at 500°C for 48 h unless otherwise stated.

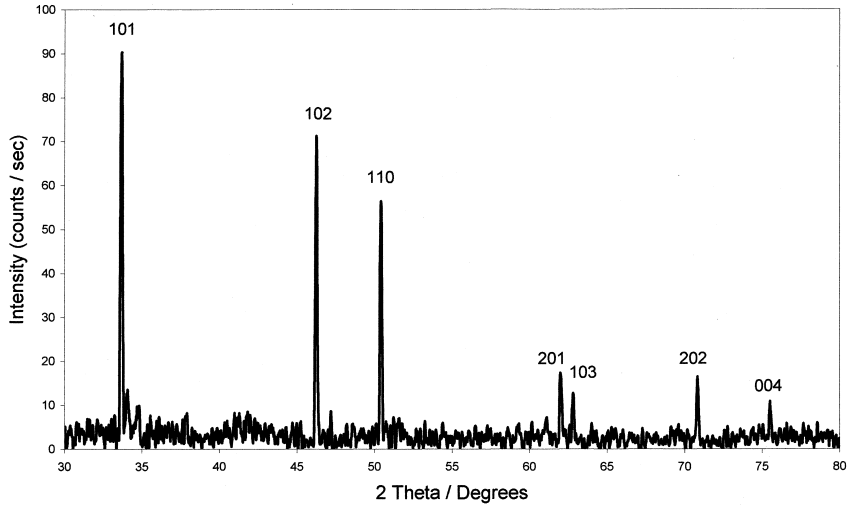


Fig. 1. X-ray powder diffraction pattern of NiAs prepared from the reaction of $NiBr_2$ and Na_3As in refluxing toluene for 48 h, followed by annealing at 500°C for 48 h.

Table 2
Compound description and X-ray powder diffraction data from the reaction of MX_2 (M = Ni, Co) and Na_3E in refluxing toluene for 48 h

Reaction	Phase	Unit cell parameters (Å)	
		Literature values [21]	Observed (±0.01)
$NiBr_2 + Na_3As$	hexagonal NiAs	$a = 3.62$, $c = 5.01$	$a = 3.63$, $c = 5.01$
$NiBr_2 + Na_3Sb$	hexagonal NiSb	$a = 3.93$, $c = 5.13$	$a = 3.92$, $c = 5.12$
$CoCl_2 + Na_3As$	orthorhombic CoAs	$a = 3.46$, $b = 5.87$, $c = 5.29$	$a = 3.45$, $b = 5.85$, $c = 5.29$
$CoCl_2 + Na_3Sb$	hexagonal CoSb	$a = 3.88$, $c = 5.19$	$a = 3.86$, $c = 5.18$

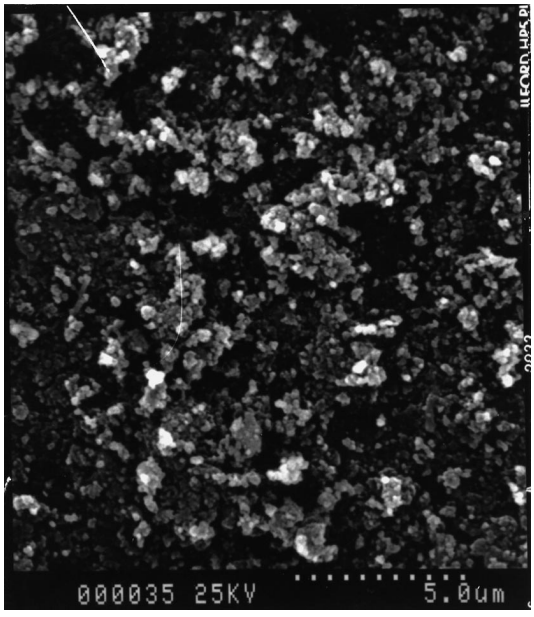


Fig. 2. Scanning electron micrograph of product of the reaction of $CoCl_2$ and Na_3P in refluxing toluene for 48 h.

powder contains little if any free metal. It should be noted that this is counter-intuitive to that speculated in Eq. (1) and is commented upon in the discussion below.

IR spectroscopy of the unannealed products showed spectra consistent with the formation of transition-metal phosphides, arsenides and antimonides with broad IR signals between 250 and 600 cm^{-1}. The Raman spectrum shown in Fig. 3 is that from the reaction of $CoCl_2$ and Na_3P. The spectrum obtained is different from that of free phosphorus and cobalt metal. To our knowledge CoP has no reported Raman spectra.

4. Discussion

Nickel and cobalt pnictides are known to have a large number of phases with different stoichiometries, the majority of which are thermodynamically stable at room temperature. In this work all of the reactions were salt balanced such that all of the sodium and halide in the starting materials can be eliminated as sodium halide. This necessitates that the formally expected phase in all the reactions would be M_3E_2. However, in the reactions involving nickel(II) bromide and sodium antimonide and sodium arsenide the products were invariably the NiE (E = As, Sb) phase with no evidence for the formation of free nickel metal in the product by magnetometry, X-ray powder diffraction or SEM/EDAX analysis. It is anticipated that in this case the excess free nickel metal indicated by Eq. (1) is removed in the washing stage of the reaction, possibly as a soluble hydroxide. Nickel was detected by chemical analysis in the washings from the reaction, but was not quantified, but was of the appropriate magnitude. In reactions involving cobalt halides and sodium pnictides the products after trituration showed a stoichiometry of Co_3E_2 by EDAX.

The as-formed products in all of the reactions were shown to be X-ray amorphous. The products were inferred to be

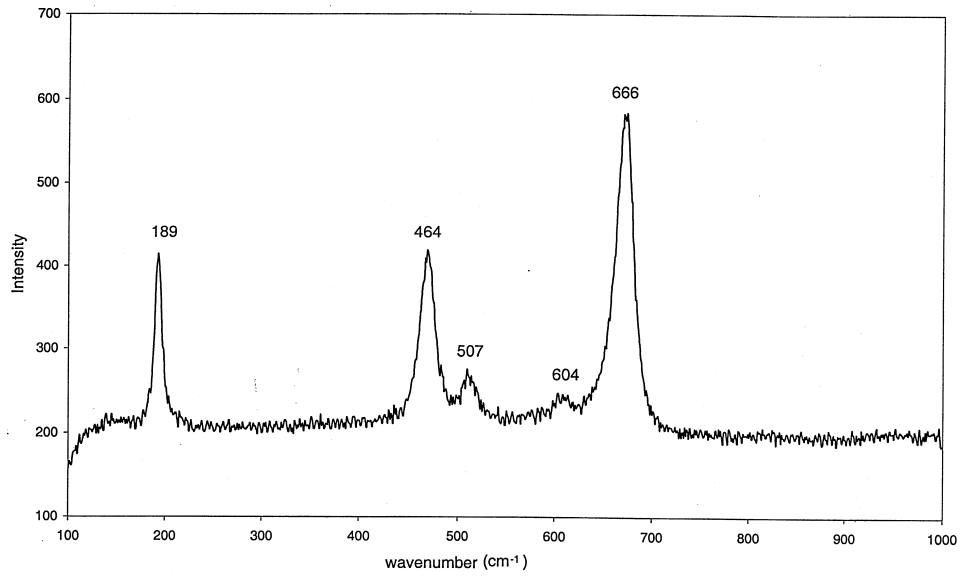


Fig. 3. Raman spectrum for product of the reaction of $CoCl_2$ and Na_3P in refluxing toluene for 48 h, as prepared.

amorphous metal pnictides by the consistent spot EDAX analysis across the samples, the absence of any free metal as evidence by the VSM signature and the formation of sodium halide. Further, the products in all reactions were black, fine grained powders with IR and Raman signatures corresponding to the formation of amorphous metal pnictides.

Annealing the amorphous metal pnictide powders at 500°C for 24 h induced crystallinity for both the nickel and cobalt arsenide and antimonides. The crystalline phases obtained were the binary ME phases (Table 2). These materials indexed well and gave lattice parameters within error limits of those reported in the literature [21]. No X-ray powder diffraction, EDAX or VSM evidence was seen for the presence of free metal in the annealed samples.

Ternary $NiAs_{0.5}Sb_{0.5}$ and $NiAs_{0.25}Sb_{0.75}$ phase could be readily made by reacting the appropriate ratios of sodium arsenide and sodium antimonide with nickel bromide. These phases were found to contain the appropriate elemental ratios by EDAX both before and after annealing over a number of spots. However, it was found difficult to initiate crystallisation in the ternary compounds. Even at higher temperatures (800°C or 1000°C) for prolonged periods, only amorphous X-ray powder diffraction patterns were obtained. EDAX data, the presence of sodium halide in the water washings (Eq. (1)) and the lack of crystalline binary compounds observed in the X-ray powder diffraction pattern suggest that the ternary compounds were obtained.

The reaction of $NiBr_2$ with Na_3P gave a product which by EDAX showed a 2:1 Ni:P atomic ratio over a number of spots. The X-ray powder diffraction pattern of the as-prepared sample showed it to be X-ray amorphous. After annealing at 500°C for 72 h a low-intensity X-ray powder diffraction pattern was observed which corresponded to that of Ni_2P. SEM/EDAX data on the annealed material showed two distinct forms: rounded particles with a corresponding 2:1 Ni:P atomic ratio and angular block-shaped particles corresponding to a 1:1 Ni:P atomic ratio. Thus, the reaction of nickel chloride with sodium phosphide is unlike the corresponding arsenide and antimonide reactions in that the as-formed product has a higher nickel content. Annealing of the sample produces a mixture of Ni_2P and NiP, this probably means that no nickel is lost in this particular case during the initial washing stage. Annealing of the nickel phosphide sample in vacuo at 800°C shows an X-ray powder diffraction pattern corresponding to Ni_3P. It has been observed previously that heating Ni_2P and NiP at 800°C under vacuum eliminates phosphorus producing Ni_3P [19,20].

The reaction of $CoCl_2$ with Na_3P gave a product which by EDAX showed a 3:2 elemental ratio of Co:P, the initial starting ratio. After annealing at 550°C the atomic ratio was still found to be 3:2 by EDAX and X-ray amorphous. The reaction of Na_3As and Na_3Sb with $CoBr_2$ gave a product that analysed as Co_3E_2 by EDAX both before and after annealing. However, X-ray powder diffraction showed only a single crystalline phase after annealing that indexed as CoE. This presents a problem in explaining the difference between the EDAX and X-ray powder diffraction analyses. This can be accounted for by the product being a biphasic mixture of CoE and E (E = As, Sb). If this is the case, the scale of intermixing would have to be submicrometre, the free pnictide be X-ray amorphous, and no preferential sublimation was observed under the annealing conditions employed.

The 1:1 ratio found for the reactions with nickel of Ni:E as compared to the 3:2 ratio of Co:E deserves noting. The cobalt products reflect more accurately the 3:2 elemental ratio of the reactants, while NiAs and NiSb are found solely in a 1:1 ratio. This may be because the NiE forms have a particularly high thermodynamic stability and do not readily incorporate excess nickel into these structures. In the phosphide case the surplus nickel (Eq. (1)) is being incorporated into an amorphous Ni_2P structure. VSM data strongly suggests that there is appreciably less free nickel than Eq. (1) would

suggest, since free nickel would give a much stronger ferromagnetic response than was observed. This is also supported by EDAX data which shows a 2:1 Ni:P ratio in the as-synthesised product as well as in the product annealed at 500°C. Annealing causes some separation of the amorphous as-prepared product into a Ni_2P phase and an amorphous NiP phase.

Liquid phase metathesis routes have been reported previously by Kehr and Wells for the formation of a range of gallium and indium pnictides [22]. In a number of these reactions the as-formed pnictides were nanocrystalline with particle sizes ranging from 3 to 36 nm. These materials gave typically broadened X-ray diffraction spectra. No evidence was seen in the nickel and cobalt reactions reported here for the formation of nanocrystalline products. Despite this, the solution phase metathesis is important in determining the phase of product isolated. The refluxing toluene solution acts as a heat sink in the reaction. The corresponding solid state metathesis reaction, in the absence of a solvent produces temperatures ranging from 1000 to 1400°C. This has a direct effect on the phase of material isolated. For example, the reaction of $NiCl_2$ and Na_3As produces a mixture of crystalline $Ni_{11}As_8$ and Ni_5As_2 by solid state metathesis. Similarly, the corresponding solid state metathesis reaction of $CoCl_2$ and Na_3As produces crystalline mixture of CoAs and Co_2As. The solvent-mediated metathesis reactions have a vast excess of toluene solvent which can absorb reaction enthalpy, lower the reaction temperature to the boiling point of the solvent and enable isolation of amorphous pnictides. The corresponding solid state metathesis reactions are self-sustaining, proceed with a thermal flash, complete in 1–2 s and produce products that are invariably crystalline and fused. The phase differences observed between the solid-state and solvent-mediated routes are a consequence of the temperatures reached in the reactions. If the solvent-mediated metathesis products are heated to 1400°C it is likely that the same (thermodynamic phases) would be formed. The role of the refluxing solvent is also crucial, as it enables large surface areas of the insoluble powders to react. By refluxing and stirring the suspension, fresh reactants are continually brought together thus helping to alleviate the solid state diffusion barrier. The solvent-mediated reactions are completed over a longer time scale than the equivalent solid state metathesis reaction but do enable the isolation of significantly different phases. The surprising feature of this chemistry is that the reactions can be made to proceed at significantly lower temperatures (110°C) than that required to initiate the corresponding solid-state reactions (550–800°C).

5. Conclusions

Binary and ternary nickel and cobalt pnictides have been synthesised successfully using the liquid-mediated metathetical reaction of the transition-metal dihalide with the appropriate sodium pnictide, Na_3E, in refluxing toluene for 48 h. The nickel products form NiE (E = As, Sb) and a mixture of NiP and Ni_2P while cobalt forms Co_2E_3 (E = P, As, Sb). The solution phase metathesis reactions form amorphous products that in certain cases can be readily annealed to form crystalline ME (M = Co, Ni; E = As, Sb). Solvent-mediated metathesis reactions allow access to phases unaccessable from the equivalent solid state metathesis reactions.

Acknowledgements

D.E.M. thanks the CVCP for an ORS award, C.J.C. thanks the Royal Society for a Dorothy Hodgkin Fellowship. Amanda Hardy and Professor R.J.H. Clark are thanked for assistance with the Raman spectra. Dr Q.A. Pankhurst is thanked for assistance with the VSM measurements.

References

[1] K. Iida, J. Magn. Magn. Mater. 35 (1983) 226.
[2] Z. Dziewiecki, M. Jagiello, Przem. Chem. 68 (1989) 401.
[3] R. Ranjan, S. Kaja, J. Magn. Magn. Mater. 79 (1989) 242.
[4] M. Yamamoto, K. Shirai, K. Hiramatsu, Jpn. J. Appl. Phys. 30 (1991) L1036.
[5] G. Wouters, J.P. Celis, J.R. Roos, J. Electrochem. Soc. 140 (1993) 3639.
[6] P. Trespaillebarrau, M. Suery, Mater. Sci. Techn. 10 (1994) 497.
[7] W.M. Macdonald, C.L. Reynolds, A.C. Anderson, Scripta Metall. 15 (1981) 891.
[8] L. Thome, H. Bernas, P. Heubes, M. Diecher, E. Recknagel, Nucl. Instrum. Methods Phys. Res. 199 (1982) 431.
[9] J.H. Hamlyn-Harris, D.H. St. John, D.K. Sood, Mater. Sci. Eng., A 147 (1991) 201.
[10] C.A. Ross, L.M. Goldman, F. Spaepen, J. Electrochem. Soc. 140 (1993) 91.
[11] U. Pittermann, S. Ripper, Phys. Status Solidi A 93 (1986) 131.
[12] M. Robbins, J.J. Hauser, J.T. Plewes, J. Electrochem. Soc. 133 (1986) C323.
[13] Y. Senzaki, W.L. Gladfelter, Abstr. Papers Am. Chem. Soc. 206 (1993) 27-INOR.
[14] F.R. Klingan, A. Miehr, R.A. Fischer, W.A. Herrmann, Appl. Phys. Lett. 67 (1995) 822.
[15] J. Gopalakrishnan, S. Pandey, K.K. Rangan, Chem. Mater. 9 (1997) 2113.
[16] I.P. Parkin, Chem. Soc. Rev. 6 (1994) 2056.
[17] N.N. Greenwood, E.A. Earnshaw, Chemistry of the Elements, Pergamon, Oxford, 1984, p. 559.
[18] G.C. Allen, C.J. Carmalt, A.H. Cowley, A.L. Hector, S. Kamepalli, Y.G. Lawson, N.C. Norman, I.P. Parkin, L.K. Pickard, Chem. Mater. 9 (1997) 1385.
[19] P.S. Kumar, P.K. Nair, J. Mater. Proc. Tech. 156 (1996) 511.
[20] H.X. Li, H.Y. Chen, S.H. Dong, J.S. Yang, J.F. Deng, Appl. Surf. Sci. 125 (1998) 115.
[21] PDF-2 Database, International Centre for Diffraction Data, Swarthmore, PA, 1990.
[22] S.S. Kher, R.L. Wells, Chem. Mater. 6 (1994) 2056.

PERGAMON

www.elsevier.nl/locate/poly

Polyhedron 19 (2000) 835–839

POLYHEDRON

Tetrahydropoxen: 2,2′-(1,2-ethanediylbis(iminomethylene)) bis(pyridine N-oxide) and its complexes. X-ray structure of $[Cu(H_4\text{-poxen})H_2O](ClO_4)_2\cdot H_2O$ and $[Co(poxen)H_2O](ClO_4)_2$

Roman Boča [a,*], Monika Nemečková [a], Martina Vrbová [a], Peter Baran [a], Ingrid Svoboda [b], Hartmut Fuess [b]

[a] *Department of Inorganic Chemistry, Slovak Technical University, SK-812 37 Bratislava, Slovakia*
[b] *Materialwissenschaft, Darmstadt University of Technology, D-64287 Darmstadt, Germany*

Received 23 November 1999; accepted 1 February 2000

Abstract

The condensation reaction of 2-pyridinecarboxaldehyde N-oxide with ethylenediamine yields the tetradentate ligand L^1 = poxen. Hydrogenation then produces tetrahydropoxen, $L^2 = H_4$-poxen, which has been isolated in a free form. Several metal complexes of the formula $[M(H_4\text{-poxen})](ClO_4)_2\cdot nH_2O$ have been prepared (M = Mn, Cu and Zn) and investigated. The X-ray structure of $[Cu(H_4\text{-poxen})H_2O](ClO_4)_2\cdot H_2O$ shows that the copper atom is pentacoordinate, the poxen ligand forming a base of the tetragonal pyramid; the aqua ligand is situated in the apical position inside the cavity formed by the ligand arms. In contrast, in the case of $[Co(poxen)H_2O](ClO_4)_2$, the apical aqua ligand is situated outside the 'cavity' formed by the dehydrogenated ligand arms. ©2000 Elsevier Science Ltd All rights reserved.

Keywords: Pyridine N-oxides; Metal complexes; Hydrogenation; Structures

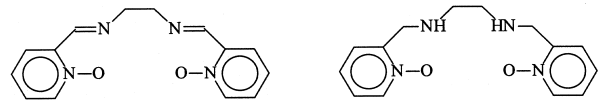
1. Introduction

The condensation of (substituted) salicylaldehyde with ethylenediamine is a Schiff reaction which results in the well known salen, and its derivatives. The coordination chemistry of this class of tetradentate, Schiff-base ligands with transition metal atoms is well investigated, and dozens of examples have been structurally characterized.

Of recent interest are the hydrogenated derivatives of the salen-type ligands, H_4-salen, and their complexes with transition metal ions [1–6]; among these, an X-ray structure of $[Ni(H_4\text{-Bu}^t\text{-salen})]$ has been reported [7].

The Schiff condensation, however, is not restricted to salicylaldehyde derivatives. It proceeds on other aromatic aldehydes, exemplified for instance by 2-pyridinecarboxaldehyde N-oxide. The condensation results in the ligand L^1 abbreviated as poxen (Scheme 1).

The principal difference between salen and poxen lies in the fact that $[M^{II}(salen)]$ complexes are electroneutral whereas $[M^{II}(poxen)]^{2+}$ complexes require the presence of counter anions.



Scheme 1. Sketch of L^1 = poxen (left) and $L^2 = H_4$-poxen (right).

Although the isolation of the free ligand L^1 has not been reported so far, several complexes of the general formula $[M(L^1)]X_2$ have been prepared and structurally characterized [8,9], for example $[Ni(L^1)(H_2O)_2](ClO_4)_2$ and $[Cu(L^1)(H_2O)](ClO_4)_2$ in which the L^1 ligand is tetradentate. In the tetranuclear complex $[ZnCl_4][Cu(L^1)]_2[ZnCl_4]$ the ligand L^1 is pentadentate owing to its bridging functionality [10].

Reports on the hydrogenated analogues of poxen-type ligands are, to our knowledge, absent in the literature. Therefore we focused our attempt to prepare and isolate the free ligand L^2 first. Then a series of metal complexes of formula $[M(L^2)]X_2$ was prepared. Finally the X-ray structure of $[Cu(H_4\text{-poxen})H_2O](ClO_4)_2\cdot H_2O$ was determined and compared with that of $[Co(poxen)H_2O](ClO_4)_2$.

* Corresponding author. Tel.: +421-7-59325-610; fax: +421-7-52493-198; e-mail: boca@cvtstu.cvt.stuba.sk

0277-5387/00/$ - see front matter ©2000 Elsevier Science Ltd All rights reserved.
PII S0277-5387(00)00324-7

2. Experimental

2.1. Ligands

The ligand poxen and its hydrogenated product were synthesized according to Scheme 2.

17.7 g (144 mmol) of 2-pyridinecarboxaldehyde N-oxide in 200 cm^3 of methanol were combined with 3 cm^3 (44.8 mmol) of freshly distilled 1,2-diaminoethane in 10 cm^3 of methanol. The mixture was boiled for 5 min and left to cool. A yellow product was filtered off, washed by ethanol and left to dry. The final product, L^1, was recrystallized from methanol. Yield 14.3 g (74%).

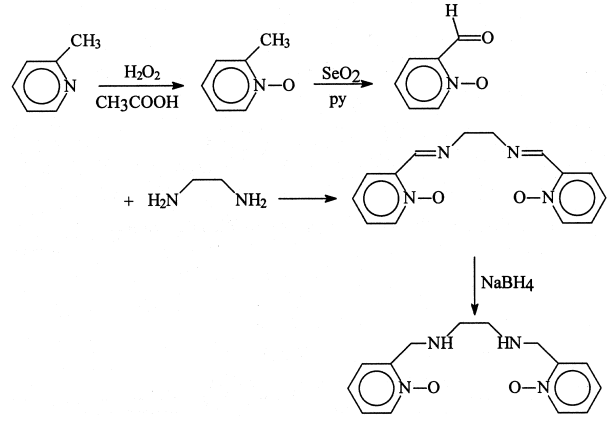
7.6 g (28.1 mmol) of L^1 in 200 cm^3 of methanol were boiled in a water bath and slowly (within 45 min) 3.2 g (84.6 mmol) of $NaBH_4$ were added. The pH of the mixture was then reduced from 11 to 1 by adding conc. HCl and subsequently raised to 10 by adding conc. NaOH. The product was extracted into chloroform (three times 150 cm^3). The extract was dried over Na_2SO_4 and $CHCl_3$ was distilled under reduced pressure. The final product, L^2, was liberated in the form of cream–yellow crystals. Yield 5.6 g (74%). *Anal*. Found: C, 59.9; H, 6.5; N, 19.8. Calc. for $C_{14}H_{18}N_4O_2 \cdot H_2O$: C, 59.3, H, 6.7; N, 19.8%. Melting point 125°C.

The presence of the water molecules as a monohydrate was confirmed by IR spectra (broad stretching bands at 3450 and 3540 cm^{-1}; deformation bands at 1685 and 1655 cm^{-1}). Stretching N–O vibration at 1210 cm^{-1} confirms the presence of the pyridine N-oxide unit.

2.2. Complexes

Complexes of the type $[CuL^2](ClO_4)_2 \cdot nH_2O$ with a variable amount of water were obtained for different conditions of complexation.

1. A blue anhydrous product $[CuL^2](ClO_4)_2$ precipitates when the ethanol solution of L^2 is added slowly to the ethanol solution of $Cu(ClO_4)_2 \cdot 6H_2O$ in the molar ratio $x(L^2{:}Cu) = 1{:}1$. *Anal*. Found: C, 31.3, H, 3.4; N, 10.4; Cu, 12.2; Cl, 13.2. Calc. for $C_{14}H_{18}N_4O_{10}CuCl_2$: C, 31.3; H, 3.4; N, 10.4; Cu, 11.8; Cl, 13.2%.
2. An ethanol solution of $Zn(ClO_4)_2 \cdot 6H_2O$ was added slowly to the ethanol solution of L^2; then the ethanol solution of $CuCl_2 \cdot 2H_2O$ was added so that $x(L^2{:}Zn{:}Cu) = 1{:}1{:}2$. A blue hemihydrate $[CuL^2](ClO_4)_2 \cdot 0.5H_2O$ crystallizes within a week from the blue solution. *Anal*. Found: C, 31.1; H, 3.6; N, 10.2. Calc. for $C_{14}H_{18}N_4O_{10}CuCl_2 \cdot 0.5H_2O$: C, 30.8; H, 3.5; N, 10.3%.
3. An ethanol solution of $Cu(ClO_4)_2 \cdot 6H_2O$ was added slowly to the ethanol solution of L^2; then the ethanol solution of $ZnCl_2 \cdot 2H_2O$ was added so that $x(L^2{:}Zn{:}Cu) = 1{:}2{:}1$. A blue dihydrate $[CuL^2](ClO_4)_2 \cdot 2H_2O$ crystallizes within a week from the blue solution. *Anal*. Found: C, 29.2; H, 3.7; N, 9.6; Cu, 11.5. Calc. for $C_{14}H_{18}N_4O_{10}CuCl_2 \cdot 2H_2O$: C, 29.4; H, 3.9; N, 9.8; Cu, 11.1%.



Scheme 2. Synthetic route for poxen and H_4-poxen.

Complexes of the formula $[ML^2](ClO_4)_2 \cdot nH_2O$ for M = Mn (yellow–green) and M = Zn (pale yellow) were synthesized by adding the ethanol solution of L^2 to the ethanol solution of $M(ClO_4)_2 \cdot 6H_2O$ in the molar ratio $x(L^2{:}M) = 1{:}1$. Elemental analysis confirms the composition of these complexes. *Anal*. Found: C, 31.7; H, 4.0; N, 10.4. Calc. for $C_{14}H_{18}N_4O_{10}MnCl_2 \cdot 0.5H_2O$: C, 31.3; H, 3.6; N, 10.4%. Found: C, 29.5; H, 3.9; N, 9.6. Calc. for $C_{14}H_{18}N_4O_{10}ZnCl_2 \cdot 2H_2O$: C, 29.3; H, 3.9; N, 9.7%.

Attempts to prepare $[ML^2](ClO_4)_2 \cdot nH_2O$ for M = Fe, Co and Ni failed; no acceptable elemental analyses were achieved, probably owing to air sensitivity.

The $[Co(poxen)H_2O](ClO_4)_2$ complex precipitated as a Bordeaux–brown powder from the 1:1 mixture of the ethanol solution of the ligand and the ethanol solution of the cobalt(II) perchlorate. *Anal*. Found: C, 30.0, H, 3.2; N, 9.9. Calc. for $C_{14}H_{14}N_4O_{10}CoCl_2 \cdot H_2O$: C, 30.8; H, 3.0; N, 10.3%.

2.3. X-ray structure determination

Suitable single crystals were mounted on an Enraf-Nonius CAD-4 diffractometer. The cell parameters were determined on the basis of 25 reflections by applying the least-squares method. The intensities were determined by the ω–2θ scan, using Mo Kα radiation with a graphite monochromator. The experimental data are collected in Table 1. The intensities were corrected for Lorentz polarization and an empirical correction for absorption was applied via the ψ-scan technique.

The structure was solved by direct methods [11] allowing determination of the positions of all non-hydrogen atoms. The structure was refined by full-matrix least-squares on F^2 [12]. The hydrogen atoms were situated in the calculated positions except those belonging to water. These were determined from the difference Fourier map and refined. The function minimized for the refinement was $\Sigma w(|F_o| - |F_c|)^2$; the weights were determined using the formulae $w = 1/[\sigma^2(F_o^2) + (0.0868P)^2 + 1.72P]$ for **1** and $w = 1/[\sigma^2(F_o^2) + (0.0807)^2 + 2.95P]$ for **2**, where $P = (F_o^2 + 2F_c^2)/3$.

Table 1
Crystal data and structure refinement for **1** and **2**

Empirical formula	$C_{14}H_{21}Cl_2CuN_4O_{12}$	$C_{14}H_{16}Cl_2CoN_4O_{11}$
Formula weight	571.83	546.17
Temperature (K)	298(2)	297(2)
Wavelength (Å)	0.71093	0.71093
Crystal system	orthorhombic	orthorhombic
Space group	*Pnma*	$P2_12_12_1$
Unit cell dimensions		
a (Å)	8.181(2)	7.937(2)
b (Å)	22.485(5)	9.677(3)
c (Å)	12.203(2)	26.106(3)
$\alpha=\beta=\gamma$ (°)	90	90
Volume (Å^3)	2244.7(8)	2005.1(8)
Z	4	4
Density (calculated) (Mg m^{-3})	1.692	1.809
Absorption coefficient (mm^{-1})	1.205	1.111
$F(000)$	1168	1108
Crystal size (mm)	$0.30\times0.28\times0.18$	$0.40\times0.33\times0.28$
Theta range for data collection (°)	1.81–22.98	1.56–22.95
Index ranges	$-5\le h\le 8,\ -16\le k\le 24,\ -8\le l\le 13$	$-1\le h\le 8,\ -1\le k\le 10,\ -1\le l\le 28$
Reflections collected	2466	2233
Independent reflections	1606 ($R_{int}=0.0227$)	2046 ($R_{int}=0.0362$)
Max. and min. transmission	0.679 and 0.591	0.699 and 0.581
Data/restraints/parameters	1606/24/233	2030/22/334
Goodness-of-fit on F^2	0.958	1.084
Final R indices ($I>2\sigma(I)$)	$R_1=0.0410$, $wR_2=0.1106$	$R_1=0.0382$, $wR_2=0.1082$
R indices (all data)	$R_1=0.0681$, $wR_2=0.1271$	$R_1=0.0510$, $wR_2=0.1579$
Largest difference peak and hole (e Å^{-3})	0.409 and −0.289	0.477 and −0.314

3. Results and discussion

The structure of $[Cu(H_4\text{-poxen})H_2O](ClO_4)_2\cdot H_2O$ (**1**) consists of isolated mononuclear dications, perchlorate anions and a molecule of crystal water. The copper(II) atom is pentacoordinate: four donor atoms of the ligand form a tetragonal base above which at 0.30 Å the central atom is situated. The distances within the *cis*-{CuN_2O_2O'} chromophore are Cu–N2 = 2.003 and Cu–O1 = 1.950 Å towards the basal atoms and Cu–O′ = 2.176 Å for the apical aqua ligand (Table 2).

Table 2
Selected bond lengths (Å) and angles (°) for **1** and **2**

Complex **1** [a]		Complex **2**	
N(1)–O(1)	1.343(4)	N(1)–O(1)	1.331(8)
N(2)–Cu(1)	2.003(4)	N(2)–Co(1)	1.936(6)
O(1)–Cu(1)	1.950(3)	N(3)–Co(1)	1.934(7)
Cu(1)–O(2)	2.176(5)	N(4)–O(2)	1.343(8)
O(2)–O(3)	2.778(7)	O(1)–Co(1)	1.932(5)
		O(2)–Co(1)	1.925(5)
		Co(1)–O(3)	2.489(7)
C(7)–N(2)–Cu(1)	110.6(8)	C(7)–N(2)–Co(1)	113.4(5)
C(6)–N(2)–Cu(1)	111.9(3)	C(9)–N(3)–Co(1)	126.4(6)
C(7A)–N(2)–Cu(1)	99.7(6)	C(6)–N(2)–Co(1)	126.1(5)
N(1)–O(1)–Cu(1)	117.5(2)	C(8)–N(3)–Co(1)	111.5(5)
O(1)#1–Cu(1)–O(1)	85.7(2)	N(1)–O(1)–Co(1)	125.0(4)
O(1)#1–Cu(1)–N(2)#1	92.21(14)	N(4)–O(2)–Co(1)	124.7(4)
O(1)–Cu(1)–N(2)#1	162.5(2)	O(2)–Co(1)–O(1)	89.9(2)
O(1)#1–Cu(1)–N(2)	162.5(2)	O(2)–Co(1)–N(3)	91.7(2)
O(1)–Cu(1)–N(2)	92.21(14)	O(1)–Co(1)–N(3)	177.7(3)
N(2)#1–Cu(1)–N(2)	84.5(2)	O(2)–Co(1)–N(2)	174.6(2)
		O(1)–Co(1)–N(2)	93.4(2)
		N(3)–Co(1)–N(2)	84.9(3)

[a] Symmetry transformations used to generate equivalent atoms: #1 x, $-y+1/2$, z.

A few fragments of the structure are noticeable (Fig. 1): (i) the oxygen atoms of the crystal water and the aqua ligand occupy special positions; (ii) the perchlorate group is disordered; (iii) the ethylene bridge is disordered since for the carbon atoms two equivalent positions exist.

The ligand as a whole is far from the planar arrangement. The planes of the pyridine N-oxide make an angle of 44°;

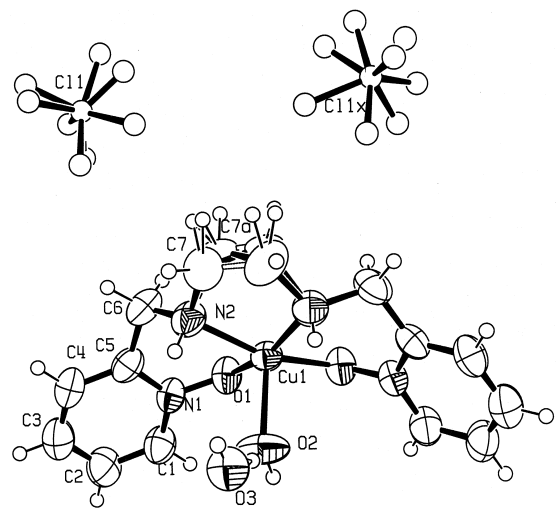


Fig. 1. ORTEP plot for **1**.

their dihedral angles with respect to the basal plane N_2O_2 are 34°. The butterfly-like arms form a cavity inside which the aqua ligand is situated. The bond length Cu–O2 = 2.176 Å is anomalously short compared, for instance, with Cu–O2 = 2.519 Å in the dehydrogenated analogue $[Cu(poxen)H_2O](ClO_4)_2 \cdot H_2O$ [9]. The dihedral angle of the pyridine N-oxide planes in the latter compound is only 16° and, moreover, the apical aqua ligand is situated outside the 'cavity'.

The crystal water molecule forms a hydrogen bond towards the aqua ligand: O2–O3 = 2.778 Å (and angle O2–H2B–O3 = 158°). The perchlorate groups do not show any hydrogen bonding.

The structure of $[Co(poxen)H_2O](ClO_4)_2$ (**2**), shows some similarities to the corresponding salen-type complexes (Fig. 2). The cobalt(II) atom is pentacoordinate: the central atom is situated only 0.05 Å above a tetragonal base formed of four donor atoms. The distances within the *cis*-$\{CoN_2O_2O'\}$ chromophore are Co–N = 1.934 and 1.936 Å and Co–O = 1.925 and 1.932 Å. The apical aqua ligand is situated at Co–O3 = 2.489 Å (Table 2).

The ligand arms are only slightly bent (the angle of the pyridine rings is 29°); the dihedral angles with respect to the basal plane N_2O_2 are 11 and 19°, respectively. The apical aqua ligand is situated outside the 'cavity' formed by the ligand arms. In this respect the structure of $[Co(poxen)H_2O](ClO_4)_2$ is quite similar to that of $[Cu(poxen)H_2O](ClO_4)_2 \cdot H_2O$ [9]. One perchlorate group shows a static disorder.

The copper(II) complex of the H_4-poxen ligand is stable against oxygen both in the solid state and in solution. This property is analogous to Cu(salen)- and Cu(poxen)-type complexes. In all these cases the unpaired electron occupies the in-plane molecular orbital, predominantly of d_{xy} character (*x*-axis bisecting the angle O–M–O). This orbital is well screened against attack from the molecular oxygen. In contrast, in planar Co(II) complexes the unpaired electron occupies an out-of-plane orbital (predominanly of either d_{yz} or d_{z^2} character) which has been confirmed by ESR spectroscopy [13]. Therefore effective interaction with the attacking dioxygen is possible and this leads to the formation of the end-on superoxo-like adduct $Co(III)-(O_2^-)$ [14]. The dioxygen activated in this way potentially acts as a strong oxidation agent able to subtract $H^{\bullet}$ radicals from organic substrates. In the hydrogenated ligands, like H_4-salen and H_4-poxen, there are some hydrogen atoms just sterically available owing to the distorted structure of the corresponding complex; they can be removed by the activated dioxygen and therefore the $[Co(H_4\text{-salen})]$ and $[Co(H_4\text{-poxen})]$ type complexes are air unstable.

In order to support these predictions a molecular-orbital model was calculated. The geometry of the $[Co(poxen)]^{2+}$ complex was optimized first using the ZINDO/1-UHF method [15]. Figs. 3 and 4 show drawings of the spin density in the corresponding complexes (contours of 0.015 e). It can be seen that in $[Cu(poxen)]^{2+}$ the spin density is situated in-plane and delocalized over the donor set. On the contrary, in $[Co(poxen)]^{2+}$ the spin density is situated out-of-plane and highly localized. These data support the hypothesis that the in-plane spin density in $[Cu(H_4\text{-poxen})]^{2+}$ prevents appreciable interaction with the oxygen molecule and thus secures its air stability.

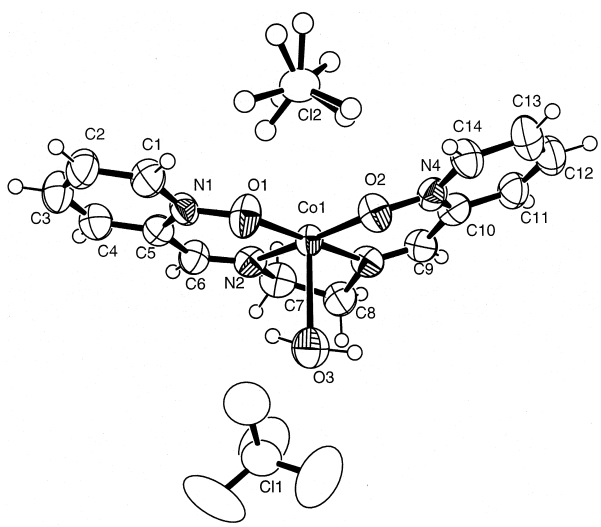


Fig. 2. ORTEP plot for **2**.

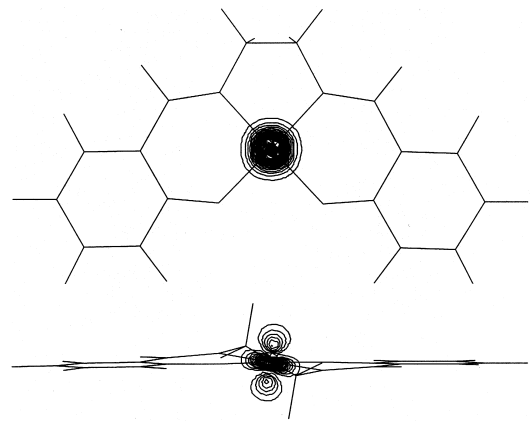


Fig. 3. Contours of the spin density in $[Co(poxen)]^{2+}$; top and side views.

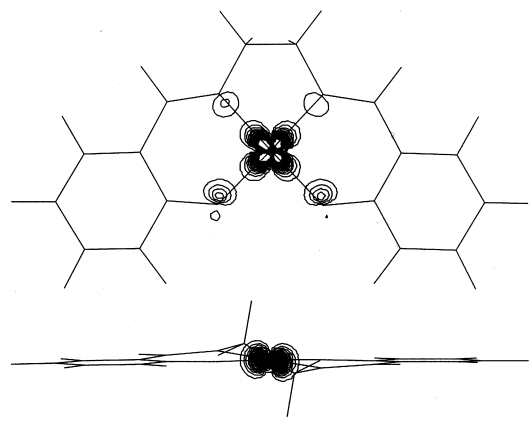


Fig. 4. Contours of the spin density in $[Cu(poxen)]^{2+}$; top and side views.

Supplementary data

Supplementary X-ray structure data and final atomic coordinates are available from the Cambridge Crystallographic Data Centre, 12 Union Road, Cambridge CB2 1EZ, UK (fax: +44-1223-336033; e-mail: deposit@ccdc.cam.ac.uk) on request; the deposition numbers are 136714 and 136715 for **1** and **2**, respectively.

References

[1] L. Borel, L. Thalken, C. Ceccarelli, M. Glick, J. Hua Zhang, W.M. Reiff, Inorg. Chem. 22 (1983) 1719.
[2] P. Baran, A. Böttcher, H. Elias, W. Haase, M. Hüber, H. Fuess, H. Paulus, Z. Naturforsch. 476 (1992) 1681.
[3] A. Böttcher, H. Elias, A. Hüber, L. Müller, in: D.H. Barton, A.E. Martell, D.T. Sawyer (Eds.), The Activation of Dioxygen and Homogeneous Catalytic Oxidation, Plenum, New York, 1993, p. 395.
[4] A. Böttcher, H. Elias, E.-F. Jäger, H. Langfelderová, M. Mazúr, L. Müller, H. Paulus, P. Pelikán, M. Rudolph, M. Valko, Inorg. Chem. 32 (1993) 4131.
[5] M. Valko, R. Klement, P. Pelikán, R. Boča, L. Dlháň, A. Böttcher, H. Elias, L. Müller, J. Phys. Chem. 99 (1995) 137.
[6] M. Valko, R. Boča, R. Klement, J. Kožíšek, M. Mazúr, P. Pelikán, H. Morris, H. Elias, L. Müller, Polyhedron 16 (1997) 903.
[7] A. Böttcher, H. Elias, L. Müller, H. Paulus, Angew. Chem., Int. Ed. Engl. 31 (1992) 623.
[8] Zh. Yin, G. Wang, L. Yei, F. Wang, Y. Fan, Nanjing Univ. Dax. Xuebao Zir. Kex. 26 (1990) 256.
[9] Y. Zang, Q. Lu, Zh. Yin, Ch. Zeng, A. Dai, Zh. Zhou, Gaodeug Xuexiao Huaxue Xuebao (Chem. J. Chim. Univ.) 10 (1989) 1; Cambridge Crystallographic Data Base code: VEHJOH.
[10] Y. Zang, Zh. Yin, G. Wang, Ch. Zeng, A. Dai, Zh. Zhou, Inorg. Chem. 29 (1990) 560.
[11] G.M. Sheldrick, SHELXS-86, Program for the solution of crystal structures, University of Göttingen, Germany, 1986.
[12] G.M. Sheldrick, SHELXL-93, Program for crystal structure determination, University of Göttingen, Germany, 1993.
[13] C. Daul, C.W. Schläpfer, A. von Zelewsky, Struct. Bonding 26 (1979) 129.
[14] R. Boča, Coord. Chem. Rev. 50 (1972) 1.
[15] Program HyperChem, Hypercube, 1993.

PERGAMON

www.elsevier.nl/locate/poly

Polyhedron 19 (2000) 841–847

POLYHEDRON

Structural and spectral studies of a heterocyclic N(4)-substituted bis(thiosemicarbazone), $H_2$2,6Achexim·H_2O, its heptacoordinated tin(IV) complex [Bu_2Sn(2,6Achexim)], and its binuclear zinc(II) complex [Zn(2,6Achexim)]$_2$

Gerimário F. de Sousa [a], Douglas X. West [b,*], Christine A. Brown [b], John K. Swearingen [b], Jesús Valdés-Martínez [c], Rubén A. Toscano [c], Simon Hernández-Ortega [c], Manfredo Hörner [d], Adaílton J. Bortoluzzi [d]

[a] *Instituto de Química, Universidade de Brasília, 70919.900 Brasília, D.F, Brazil*
[b] *Department of Chemistry, Illinois State University, Normal, IL 61790-4160, USA*
[c] *Instituto de Química, Universidad Autónoma de México, Circuito Exterior, Ciudad Universitaria, Coyoacán 04510, D.F. México*
[d] *Departamento de Química, Universidade Federal de Santa Maria, Santa Maria, 97119.900, Rio Grande do Sul, R.S, Brazil*

Received 16 August 1999; accepted 26 January 2000

Abstract

The multidentate ligand, 2,6-diacetylpyridine bis(3-hexamethyleneiminylthiosemicarbazone) monohydrate, $H_2$2,6Achexim·H_2O, crystallizes with one thiosemicarbazone moiety in an intramolecular hydrogen bonded, bifurcated *E′* form. The other thiosemicarbazone moiety is *E* and is not involved in intramolecular hydrogen bonding, but is involved in hydrogen bonding with the hydrate water molecule. The dianion (loss of N3a and N3b hydrogens) of $H_2$2,6Achexim acts as a pentadentate ligand, 2,6Achexim, in a planar conformation to a central tin(IV) ion, and as a bridging tetradentate ligand with the two thiosemicarbazone moieties of 2,6Achexim coordinating to different zinc atoms. The tin(IV) is heptacoordinate in a distorted pentagonal dipyramidal configuration, with the five SNNNS donor atoms of 2,6Achexim in the pentagonal plane and the two *n*-butyl groups in the axial positions. The binuclear zinc complex has two equivalent tetrahedral zinc centers, with the pyridyl nitrogens of the two ligands not coordinated. ©2000 Elsevier Science Ltd All rights reserved.

Keywords: Heterocyclic bis(thiosemicarbazone); Heptacoordinate complexes; Organotin(IV) complexes; Binuclear zinc complexes

1. Introduction

Considerable interest has been shown in 2,6-diacetylpyridine bis(thiosemicarbazone), and its metal complexes [1]. Crystal structures have been reported for three different zinc complexes, and two are binuclear [2]. Of the two binuclear complexes, one features distorted octahedral zinc atoms that are nearly equivalent, and the second binuclear complex contains a distorted octahedral and a tetrahedral zinc center. More recently, the former of these binuclear complexes has been prepared under different conditions and a new crystal structure reported [3]. De Sousa et al. reported the crystal structures of heptacoordinate tin(IV) complexes, namely [MeSnCl(H2,6Ac4DH)]Cl·MeOH [4] and [Ph_2Sn(H2,6-Ac4DH)]Cl [5], where $H_2$2,6Ac4DH = 2,6-diacetylpyridine bis(thiosemicarbazone). Other reports on $H_2$2,6Ac4DH complexes include the following: a third tin(IV) heptacoordinate complex [Ph_2Sn(2,6Ac4DH)]·2DMF [6], the structure of a manganese(II) complex [7], and the structures of several indium(III) complexes [8]. Although spectral and biological studies have been carried out on metal complexes of 2,6-diacetylpyridine bis(N(4)-substituted thiosemicarbazones) [9,10], no structural information has been provided even though the N(4)-substituent in other types of thiosemicarbazones, including bis(thiosemicarbazones), has been shown to affect their biological activity [11].

X-ray studies [12–14] have previously shown that 2-formyl-, 2-acetyl- and 2-benzoylpyridine N(4)-substituted thiosemicarbazones exist in the solid state in at least four different

* Corresponding author. Tel.: +1-309-438-7019; fax: +1-309-438-5538; e-mail: dxwest@ilstu.edu

0277-5387/00/$ - see front matter ©2000 Elsevier Science Ltd All rights reserved.
PII S0277-5387(00)00326-0

structural modifications: *E* isomers without hydrogen bonding by N3H to the pyridine nitrogen, two forms of hydrogen bonding *Z* isomers, and as a bifurcated hydrogen bonded *E′* isomer. The four modifications are shown in Fig. 1 and can be described as follows: (a) *E* with respect to the imine function of the thiosemicarbazone [12] without hydrogen bonding to the pyridyl nitrogen; (b) hydrogen bonding to the pyridyl nitrogen by N3H, *Z* with respect to the imine function of the thiosemicarbazone and *Z* with respect to the N3–C8 bond [12–14]; (c) hydrogen bonding to the pyridyl nitrogen by the N3H, *Z* with respect to the imine function of the thiosemicarbazone, but *E* with respect to the N3–C8 bond [13]; (d) the bifurcated *E′* tautomer in which the N3 hydrogen has shifted to the imine nitrogen, N2, and is hydrogen bonding to both the pyridyl nitrogen and sulfur of the thiosemicarbazone moiety [12,15]. A representation of $H_2$2,6Achexim showing that one thiosemicarbazone moiety is *E* and the other is *E′* is included in Fig. 1.

Since tin(IV) [16] and zinc(II) complexes [1,17] have significant pharmacological activity and little research has been done on N-heterocyclic bis(thiosemicarbazones), we report in this work the X-ray crystal structures of $H_2$2,6Achexim·H_2O, [Bu_2Sn(2,6Achexim)], and [Zn(2,6-Achexim)]$_2$.

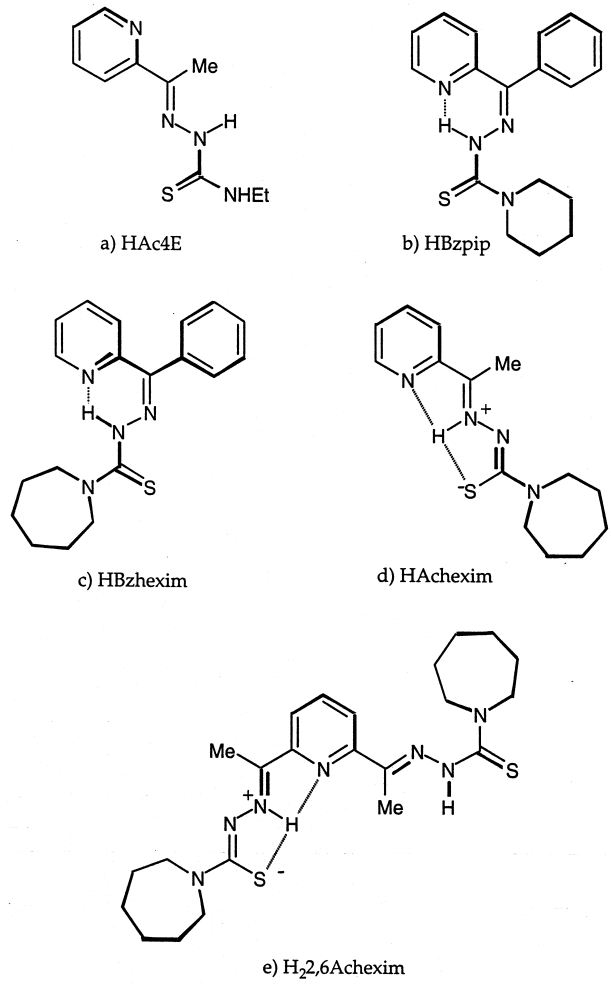


Fig. 1. (a) A representation of an *E* isomer of 2-acetylpyridine N(4)-ethylthiosemicarbazone, HAc4E; (b) a representation of a *ZZ* isomer of 2-benzoylpyridine 3-piperidylthiosemicarbazone, HBzpip; (c) a representation of a *ZE* isomer of 2-benzoylpyridine 3-hexamethyleneiminylthiosemicarbazone, HBzhexim; (d) a representation of an *E′* isomer of 2-acetylpyridine 3-hexamethylene-iminylthiosemicarbazone, HAchexim; (e) 2,6-diacetylpyridine bis(3-hexamethyleneimylthiosemicarbazone), $H_2$2,6Achexim.

2. Experimental

2.1. Materials

Solvents were purified and dried according to standard procedures. 2,6-Diacetylpyridine (Aldrich), di-*n*-butyltin(IV)dichloride (Aldrich) and zinc acetate were used without further purification. IR spectra were recorded on a Nicolet 5ZDX-FT spectrophotometer in the 4000–400 cm^{-1} range using KBr pellets. NMR spectra were obtained with a Varian 300 MHz Gemini spectrometer using [$^2H_6$]DMSO or $CDCl_3$ as the solvents with chemical shifts reported in parts per million downfield from Me_4Si.

2.2. Preparation of $H_2$2,6Achexim·H_2O, [Bu_2Sn(2,6Achexim)] and [Zn(2,6Achexim)]$_2$

The bright yellow bis(thiosemicarbazone), $H_2$2,6-Achexim·H_2O, was prepared by refluxing a 2:1 molar mixture of hexamethyleneiminylthiosemicarbazide (1.73 g, 10 mmol) [18] with 2,6-diacetylpyridine (0.82 g, 5 mmol) in absolute EtOH (50 ml). The tin(IV) complex was obtained by mixing $H_2$2,6Achexim·H_2O (0.10 g, 0.20 mmol) and the acid n-Bu_2SnCl_2 (0.15 g, 0.21 mmol) in 15 ml of EtOH, and slow evaporation of the solvent led to the appearance of a crystalline product suitable for X-ray structure analysis. The zinc complex was prepared by refluxing zinc acetate dihydrate (0.22 g, 1 mmol) and $H_2$2,6Achexim·H_2O (0.5 g, 1 mmol) in 40 ml of EtOH for 2 h. The resulting orange solid was filtered, washed with anhydrous Et_2O and dried on a warm plate. $H_2$2,6Achexim·H_2O, yield 60%; m.p. = 167–169°C. *Anal.* Found: C, 55.4; H, 7.5; N, 19.4. Calc.: C, 55.6; H, 7.4; N, 19.6%. [Bu_2Sn(2,6Achexim)], yield 74%; m.p. = 261–264°C. *Anal.* Found: C, 52.7; H, 7.3; N, 13.9. Calc.: C, 52.6; H, 7.1; N, 13.7%. [Zn(2,6Achexim)]$_2$, yield, 67%, m.p. = 266–268°C (dec.).

2.3. X-ray crystallography

Crystals of $H_2$2,6Achexim·H_2O, [Bu_2Sn(2,6Achexim)] and [Zn(2,6Achexim)]$_2$ were grown by evaporation of EtOH solutions and mounted on glass fibers. The structures were solved with direct methods and missing atoms were found by difference-Fourier synthesis. All non-hydrogen atoms were refined with anisotropic temperature factors, and all hydrogens were found on the difference Fourier map. The

Table 1
Crystallographic data for $H_2$2,6Achexim·H_2O, [Bu_2Sn(2,6Achexim)] and [Zn(2,6Achexim)]$_2$

	$H_2$2,6Achexim·H_2O	[Bu_2Sn(2,6Achexim)]	[Zn(2,6Achexim)]$_2$
Formula	$C_{23}H_{37}N_7OS_2$	$C_{31}H_{51}N_7S_2Sn$	$C_{23}H_{33}N_7S_2Zn$
Formula weight	491.7	704.6	537.1
Crystal system	orthorhombic	orthorhombic	monoclinic
Crystal color, habit	yellow, laminar	red, prism	orange, prism
Z	8	4	4
Space group	*Pbcn*	*Pnma*	$P2/c$
Crystal dimensions (mm)	0.38×0.30×0.18	0.40×0.25×0.20	0.40×0.24×0.12
T (K)	293	193	293
a (Å)	33.071(2)	10.183(2)	10.617(2)
b (Å)	8.915(2)	15.197(3)	13.443(2)
c (Å)	17.608(2)	22.509(5)	18.635(2)
β (°)	90	90	106.42(2)
V (Å^3)	5191.3(4)	3483.3(12)	2551.1(5)
D_{calc} (g cm^{-3})	1.258	1.340	1.398
Index ranges	$0 \le h \le 35$	$0 \le h \le 12$	$0 \le h \le 12$
	$0 \le k \le 9$	$-1 \le k \le 18$	$0 \le k \le 15$
	$0 \le l \le 18$	$-1 \le l \le -26$	$-22 \le l \le 21$
F(000)	2112	1472	1128
Diffractometer	Siemens P4/PC	Nonius CAD-4	Siemens P4/PC
Absorption coefficient (mm^{-1})	2.088	0.884	1.152
Radiation	Cu Kα	Mo Kα	Mo Kα
Wavelength (Å)	1.54178	0.71073	0.71073
Reflections collected	6274	3633	4758
Observed reflections	3361 ($F > 4.0\sigma(F)$)	2024 ($I > 2.0\sigma(I)$)	2316 ($F > 3.0\sigma(F)$)
Goodness-of-fit	1.26	1.031	1.02
R (%)	6.80	5.40	5.27
Rw (%)	10.05	11.24	5.22
Largest difference peak/hole (e Å^{-3})	0.45/−0.48	0.831/−0.734	0.40/−0.37

H atoms attached to carbons were allowed to ride on the C atoms and assigned a fixed isotropic temperature factor, $U = 0.06$ Å^2 ($U = 0.08$ Å^2 for [Bu_2Sn(2,6Achexim)]). Only the coordinates of the H atoms attached to nitrogens and oxygen were refined. Both seven-membered rings of $H_2$2,6Achexim·H_2O display conformational disorder such that atoms C13A and C11B split into two alternative positions with complementary occupancy factors (0.65 and 0.35).

Owing to the site symmetry of [Bu_2Sn(2,6Achexim)] the atoms N1, C4, Sn and the carbon atoms of the *n*-butyl groups are located in special crystallographic positions, with $y/b = 0.25$ and site multiplicity 0.50. One of the *n*-butyl groups is apparently disordered (C31–C34) while the other group (C41–C44) does not show any sign of disorder. The C32 atom is split between two positions related by the mirror plane, and the C31, C33 and C34 atoms show largely elongated displacement ellipsoids perpendicular to the mirror plane also indicating disorder. Attempts to refine C32 with the two positions did not cause any decrease in R values, however. The alternative structure solution involving the space group $Pn2_1$[a], one maximal non-isomorphic subgroup of *Pmna*, was also possible and all non-hydrogen atoms were found by subsequent Fourier difference synthesis and refined isotropically. However, the molecule with site symmetry 1 shows one *n*-butyl group (C31–C34) that is chemically incorrect. The crystallographic experimental details are given in Table 1 and selected bond lengths and angles for $H_2$2,6Achexim·H_2O and the complexes are reported in Tables 2 and 3, respectively.

Table 2
Selected bond distances (Å) for $H_2$2,6Achexim·H_2O, [Bu_2Sn(2,6-Achexim)] and [Zn(2,6Achexim)]$_2$

$H_2$2,6Achexim		[Bu_2Sn(2,6Achexim)]		[Zn(2,6Achexim)]$_2$	
		Sn–N1	2.415(6)		
		Sn–N2a	2.437(5)	Zn1–N2a	2.053(5)
		Sn–N2b	2.437(5)	Zn1–N2b	2.050(6)
		Sn–S1	2.6924(16)	Zn1–S1	2.352(2)
		Sn–S2	2.6924(16)	Zn1–S2	2.363(2)
		Sn–C31	2.148(10)		
		Sn–C41	2.170(8)		
S1–C8a	1.716(6)		1.744(6)		1.732(7)
S2–C8b	1.689(7)		1.744(6)		1.728(7)
N3a–C8a	1.364(7)		1.350(8)		1.348(9)
N3b–C8b	1.359((7)		1.350(8)		1.349(12)
N4a–C8a	1.346(7)		1.369(7)		1.345(9)
N4b–C8b	1.337(9)		1.369(7)		1.348(11)
N2a–N3a	1.347(6)		1.375(6)		1.378(8)
N2b–N3b	1.372(7)		1.375(6)		1.358(9)
N2a–C7a	1.291(6)		1.330(7)		1.299(8)
N2b–C7b	1.313(7)		1.330(7)		1.306(10)
C7a–C2	1.471(7)		1.491(8)		1.454(10)
C7b–C6	1.474(7)		1.491(8)		1.456(10)

Table 3
Selected bond angles (°) for $H_2$2,6Achexim·H_2O, [Bu_2Sn(2,6Achexim)] and [Zn(2,6Achexim)]$_2$

$H_2$2,6Achexim		[Bu_2Sn(2,6Achexim)] [a]		[Zn(2,6Achexim)]$_2$	
		N2a–Sn–S1	71.62(11)	N2a–Zn1–S1	83.6(2)
		N2a–Sn–S2	154.5(7)	N2a–Zn1–S2	105.5(2)
		N2a–Sn–N2b	133.3(2)	N2a–Zn1–N2b	159.2(2)
		N2a–Sn–N1	66.88(10)		
		N2a–Sn–C31	87.36(18)		
		N2a–Sn–C41	89.31(15)		
		N2b–Sn–S1	154.5(7)	N2b–Zn1–S1	110.6(2)
		N2b–Sn–S2	71.62(11)	N2b–Zn1–S2	82.9(2)
		N2b–Sn–N1	66.88(10)		
		N2b–Sn–C31	87.36(18)		
		N2b–Sn–C41	89.31(15)		
		N1–Sn–S1	138.19(4)		
		N1–Sn–S2	138.19(4)		
		N1–Sn–C31	90.7(4)		
		N1–Sn–C41	80.9(3)		
		S1–Sn–S2	83.34(7)	S1–Zn1–S2	114.6(1)
		S1–Sn–C31	92.4(3)		
		S1–Sn–C41	93.91(16)		
		C31–Sn–C41	171.6(4)		
		Sn–S1–C8a	98.6(2)	Zn1–S1–C8a	94.7(2)
				Zn1–S2–C8b	94.8(3)
		Sn–N2a–N3a	124.03(3)	Zn1–N2a–N3a	120.8(4)
				Zn1–N2b–N3b	121.7(5)
		Sn–N2a–C7a	123.0(2)	Zn1–N2a–C7a	122.9(5)
				Zn1–N2b–C7b	122.9(5)
C2–C7a–N2a	117.0(5)		115.3(5)		115.5(6)
C6–C7b–N2b	113.6(5)				116.0(6)
N3a–N2a–C7a	123.0(4)		115.1(5)		115.6(3)
N3b–N2b–C7b	117.1(5)				115.3(6)
N2a–N3a–C8a	112.4(4)		114.8(5)		114.4(5)
N2b–N3b–C8b	126.6(5)				114.7(6)
N3a–C8A–N4a	113.1(5)		114.4(5)		115.2(6)
N3b–C8b–N4b	121.5(6)				114.9(6)
N3a–C8a–S1	124.1(4)		128.4(5)		126.2(5)
N3b–C8b–S2	115.1(5)				125.7(6)
N4a–C8a–S1	122.7(4)		117.3(5)		118.6(5)
N4b–C8b–S2	123.4(5)				119.4(6)

[a] The two thiosemicarbazone moieties of [Bu_2Sn(2,6Achexim)] are equivalent.

3. Results and discussion

3.1. Molecular structure of $H_2$2,6Achexim·H_2O

The molecular structure of $H_2$2,6Achexim·H_2O is shown in Fig. 2. Much of $H_2$2,6Achexim·H_2O is planar, except for the hexamethyleneimine rings, which are tilted in opposite directions from the plane of the molecule and make dihedral angles of 8.2(1) and 8.0(1)° with the pyridine ring (Fig. 3 is a stereoview of $H_2$2,6Achexim·H_2O). $H_2$2,6Achexim·H_2O, like its tin(IV) complex [Bu_2Sn(2,6Achexim)], crystallizes in the orthorhombic system, in contrast to 2-acetylpyridine 3-hexamethyleneiminylthiosemicarbazone, HAchexim [12], which is monoclinic. However, both ligands possess the bifurcated *E′* structure with the N1 atom of the pyridyl ring and the S1 atom of the moiety hydrogen bonded intramolecularly to the N2a hydrogen (Fig. 1(d,e)). Intermolecular hydrogen bonds between the H_2O molecule and the N3b hydrogen and S2 atoms helps to cause differences in bond distances and angles between the two thiosemicarbazone moieties of $H_2$2,6Achexim·H_2O (Tables 2 and 3).

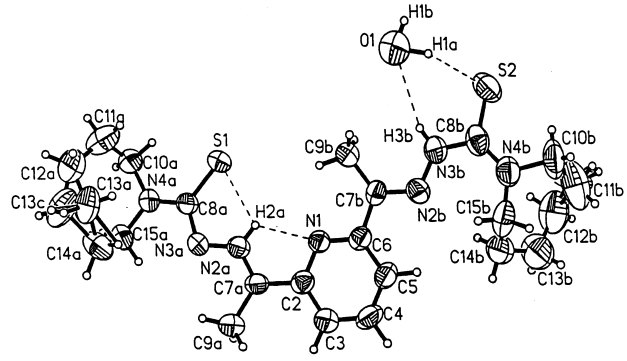


Fig. 2. Perspective view of $H_2$2,6Achexim·H_2O showing the atom numbering scheme.

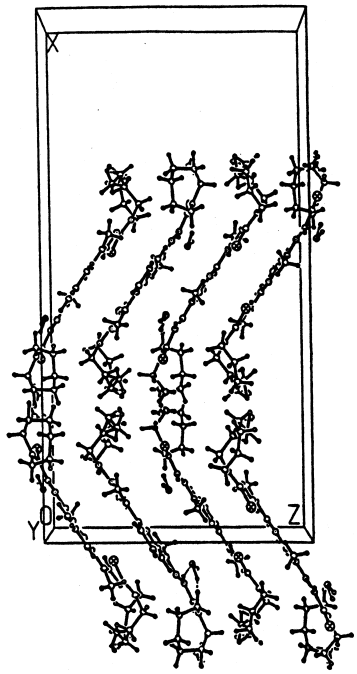


Fig. 3. Stereoview of the unit cell packing of $H_2$2,6Achexim·H_2O.

The *E* arm has a S2–C8b distance of 1.689(7) Å and is intermediate between typical C–S single- and double-bond lengths [5]. This agrees well with the N3b–C8b (1.359(7) Å) and N4b–C8b (1.337(9) Å) bond distances, which indicate partial double-bond character for both bonds. The N2b–C7b bond, 1.313(7) Å, is significantly shorter than a N–C single bond, as expected for a thiosemicarbazone. The *E′* arm S1–C8a distance, 1.716(6) Å, is longer than S2–C8b of the *E* arm, 1.689(7) Å, which is consistent with its involvement in the bifurcated hydrogen bonding resulting in a formal single C–S bond, and similar to that found for HAchexim, 1.70(1) Å [12]. Other bonds in the *E′* thiosemicarbazone moiety of $H_2$2,6Achexim·H_2O and HAchexim are as follows: N2a–C7a, 1.291(6) and 1.29(1) Å; N2a–N3a, 1.347(6) and 1.37(1) Å; N3a–C8a, 1.364(7) and 1.36(2) Å; N4a–C8a, 1.346(7) and 1.36(1) Å. The similarity in bond distances of the two *E′* forms of the two compounds is also true for their bond angles. In summary, the bonding in $H_2$2,6Ahexim·H_2O has considerable delocalization of the electron density along both moieties, and although conventional bonding theory makes the two thiosemicarbazone moieties appear different, the bond distances between the two do not differ greatly. Far greater differences occur in the bond angles with the greatest differences being N2a–N3a–C8a, 112.4(4) and N2b–N3b–C8b, 126.6(5)°; N3a–C8a–S1, 124.1(4) and N3b–C8b–S2, 115.1(5)°; N3a–N2a–C7a, 123.0(4) and N3b–N2b and C7b, 117.1(5)°. This difference in bond angles may be due to the requirements of the thiolato/thione sulfur's difference in hydrogen bonding interactions; the intramolecular H2a···S1 has a distance of 2.38(6) Å and the hydrogen bond involving the water molecule, H1a···S2, has a distance of 2.29(6) Å (Fig. 2).

3.2. Molecular structure of [Bu_2Sn(2,6Achexim)]

The heptacoordinate neutral complex, [Bu_2Sn(2,6-Achexim)], has approximately pentagonal dipyramid stereochemistry, with the bis(thiosemicarbazone) ligand lying in the equatorial plane as shown in Fig. 4. As a result of chelation to the metal center, both five-membered rings and therefore also their symmetry related counterparts, are almost planar Sn–S1–C8–N3–N2 (RMS plane deviation 0.093 Å) and Sn–N2–C7–C2–N1 (RMS plane deviation 0.0548 Å), respectively. As a consequence, the sums of the respective internal angles, 537.4 and 538.4°, are in good agreement with the ideal value of 540°. The observed angle of 8.0(6)° between these rings and the angle between the ring Sn–N2′–C7′–C2′–N1′ and its symmetry related ring Sn–N2′–C7′–C2′–N1′ of 6.14(16) underline the planarity of the pentagonal ring S–N2–N1–N2′–S′ (RMS deviation 0.0751 Å) from which the tin(IV) ion is moved away by 0.008(3)°.

Owing to the geometric requirements of the thiosemicarbazonato moieties, the pentagon is not regular; the angle subtended at tin(IV) by the two sulfur atoms is significantly enlarged to 83.31(7)° from that in an idealized pentagonal bipyramid (72°), while the other equatorial angles range from 66.86(11) to 71.65(11)°. The axial butyl groups also contribute to the observed distortion since they have a C–Sn–C angle of 171.6(4)°. The bond distances Sn–S1 2.6921(17), Sn–N2a 2.436(5), Sn–N1 2.417(6), Sn–C31 2.145(11), and Sn–C41 2.171(8) Å are in good agreement with the bond distances Sn–S 2.593(1) and 2.603(1), Sn–N(imine) 2.427(4) and 2.421(4), Sn–N(py) 2.368(3), and Sn–C 2.178(4) and 2.179(4) Å, found in [Ph_2Sn(2,6-Ac4DH)]·2DMF (2,6Ac4DH is the dianion of 2,6-diacetylpyridine bis(thiosemicarbazone)), another heptacoordinated pentagonal dipyramidal diorganotin(IV) deriva-

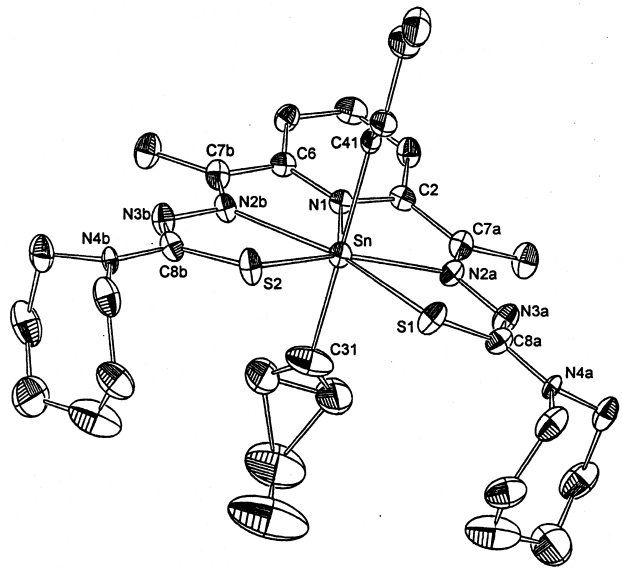


Fig. 4. ORTEP plot with atom-labeling scheme of [Bu_2Sn(2,6Achexim)], displacement ellipsoids at the 30% probability level. Atoms labeled with a and b are related by the symmetry operation $x, -y+1/2, z$.

tive containing a quinquedentate thiosemicarbazone ligand in the pentagonal girdle [6]. Coordination to the tin(IV) center by the imine nitrogen and the thiolato sulfur lengthens N2a–C7a and N2b–C7b to 1.331(7) Å, as well as S1–C8a and S2–C8b to 1.746(7) Å, from an average of 1.302(7) and 1.703(7) Å, respectively, in $H_2$2,6Achexim·H_2O. Therefore, as a result of their coordination, both bonds lose substantial π-character. The bond angles of the entire thiosemicarbazone moiety, which lose the amide hydrogen on coordination, show substantial changes compared to the angles in $H_2$2,6Achexim·H_2O, and the changes are greater for [Bu_2Sn(2,6Achexim)] than for [Zn(2,6Achexim)$]_2$, Table 3. The butyl group bonded to Sn by C31 shows considerable disorder and contributes to the relatively high *R* value for [Bu_2Sn(2,6Achexim)].

3.3. Molecular structure of [Zn(2,6Achexim)$]_2$

The bonding in [Zn(2,6Achexim)$]_2$, Fig. 5, is best described as distorted tetrahedral stereochemistry about the two zinc centers, which are equivalent. As expected, the Zn–S bonds, 2.352(2) and 2.363(2) Å, are longer than the Zn–N2a (and Zn–N2b) bonds, 2.053(5) and 2.050(6) Å. In the octahedral-tetrahedral binuclear zinc complex of 2,6-diacetylpyridine bis(thiosemicarbazone), $H_2$2,6Ac4DH, the tetrahedral Zn center has Zn–S bond distances of 2.317(3) and 2.327(4) Å, shorter than in [Zn(2,6Achexim)$]_2$, and both Zn–N bond distances of 2.07(1) Å [2]. The longer Zn–S bond distances, which likely contribute to the shorter Zn–N distances for [Zn(2,6Achexim)$]_2$, probably result from the bulkiness of the hexamethyleneiminyl rings.

The distortion from tetrahedral symmetry is substantial; the largest bond angle is N(imine)–Zn–N(imine), 159.2(2)°, the S–Zn–S angle with the two largest donor atoms is 114.6(1)°, and the smallest is a chelating S–Zn–N(imine), 82.9(2)°. The smallness of the latter angle is due to the requirements of the chelating thiosemicarbazonato moiety. For the octahedral-tetrahedral binuclear complex [Zn(2,6Ac4DH)$]_2$, the angles around the tetrahedral zinc center are as follows: N(imine)–Zn–N(imine), 140.8(4)°, the S–Zn–S angle is 118.3(2)° and the smallest is a chelating S–Zn–N(imine), 83.8(4)°. The chelating S–Zn–N(imine) angles are essentially the same, but the other two angles show significant differences. Differences are not surprising since in [Zn(2,6Ac4DH)$]_2$ the two arms are from different 2,6Ac4DH ligands, as is the case for 2,6Achexim, but both ligands in [Zn(2,6Ac4DH)$]_2$ coordinate their pyridyl nitrogens to the octahedral zinc center while the pyridyl nitrogens are uncoordinated in [Zn(2,6Achexim)$]_2$.

3.4. IR spectra

The most significant difference which emerges from a comparison of the vibrational spectra of $H_2$2,6Achexim·H_2O and its complexes is the disappearance of the band ν(N–H) at 3221 cm^{-1} as a consequence of the dianionic nature it assumes upon coordination. Assignment of ν(C=N) is complicated by the differences in the thiosemicarbazone moieties (i.e. the bifurcated *E′* and the *E* arm, which is involved in hydrogen bonding to the hydrate water molecule), as well as the partial double bond character possessed by all of the C–N bonds of the molecule. In the bifurcated *E′* arm N3a–C8a is formally a double bond and the bond distances C8a–N4a and C8b–N4b suggest considerable double bond character. The spectrum of $H_2$2,6Achexim·H_2O has bands at 1574 and 1561 cm^{-1} that are likely due to ν(C=N). When two bands are present in the spectra of coordinated anionic thiosemicarbazones that are assignable to ν(C=N), one is usually at lower energy, e.g. C7=N2, and one at higher energy, e.g. N3=C8, compared to ν(C=N) of the uncoordinated neutral thiosemicarbazone [12–15]. The spectrum of [Zn(2,6-Achexim)$]_2$ has bands at 1591 and 1564 cm^{-1} that we suggest are due to ν(C=N) for N3=C8 and C7=N2, respectively. Although the bands at ca. 1272, 1100 and 836 cm^{-1} in the spectrum of $H_2$2,6Achexim·H_2O have a significant contribution from ν(C=S), only the first absorption is shifted to lower frequency (1213 cm^{-1}) in the spectrum of [Bu_2Sn(2,6Achexim)] and the third absorption to lower frequency (739 cm^{-1}) in the spectrum of [Zn(2,6Achexim)$]_2$.

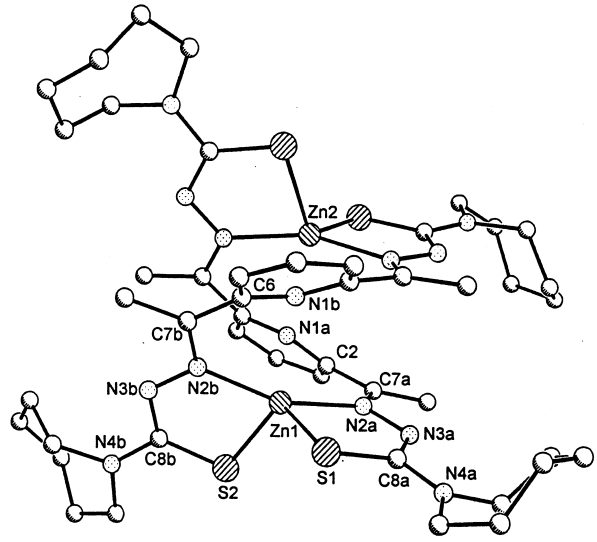


Fig. 5. Perspective view of [Zn(2,6Achexim)$]_2$ showing the atom numbering scheme.

3.5. NMR spectra

The ^{1}H NMR spectrum ($CDCl_3$) of $H_2$2,6Achexim·H_2O shows the two different thiosemicarbazone arms with the *E′* arm having NH3a at 15.18 ppm and NH3b for the *E* arm at 8.52 ppm. Its ^{13}C NMR spectrum shows two peaks for thione carbons, C8a and C8b, at 184.3 and 180.9 ppm, and for imine carbons, C7a and C7b, 147.6 and 147.4 ppm, but we are not able to assign these to a specific carbon atom with certainty. The ^{1}H NMR spectrum ($CDCl_3$) of [Bu_2Sn(2,6Achexim)] shows no peaks assignable to N3aH (or N3bH), but shows a triplet at 8.17 and a doublet at 7.85 ppm for pyridyl protons,

two singlets for N=C–CH_3 protons at 2.83 and 2.57 ppm, two doublets at 3.86, 1.54 ppm and a singlet at 1.79 ppm for the magnetically non-equivalent hexamethyleneiminyl protons. The Sn–CH_2–CH_2–CH_2– protons appear as a complicated multiplet centered at about 0.99 ppm, while the n-bu–CH_3 protons appear as a triplet at 0.60 ppm. In $CDCl_3$ [Zn(2,6Achexim)]$_2$ shows a triplet centered at 7.93 ppm and a doublet at 7.30 ppm for the pyridyl protons, a singlet at 2.53 ppm for N=C–CH_3, and a multiplet centered at 3.69 ppm and broads singlets at 1.85 and 1.59 ppm for the hexametheneiminyl protons.

3.6. Biological activity

Although other bis(thiosemicarbazones) derived from 2-acetylpyridine have shown antitumor activity when tested by the National Cancer Institute, $H_2$2,6Achexim·H_2O showed insufficient activity against 60 tumor lines and showed no activity in the HIV test. In antifungal tests $H_2$2,6-Achexim·H_2O shows no activity against *Aspergillus niger* and modest activity at a concentration of 10^3 mg ml^{-1} against *Paecilomyces variotii*.

Supplementary data

Crystallographic data (excluding structure factors), a complete listing of the atomic positions, bond distances, bond angles and anisotropic thermal parameters, for the structures reported in this paper have been deposited with the Cambridge Crystallographic Data Center as supplementary publication CCDC 118877. Copies of available material can be obtained, free of charge, on application to the Director, CCDC, 12 Union Road, Cambridge CB2 1EZ, UK (fax: +44-1223-336033; e-mail: deposit@ccdc.cam.ac.uk).

Acknowledgements

The authors thank the CNPq, CAPES/PROBRAL for financial support, and Professor Ademir Neves and Professor Ivo Vencato (UFSC, Florianópolis, Brazil) and Professor Joachim Strähle (University of Tübingen, Germany) for the diffractometer facilities.

References

[1] M. Mohan, P. Sharma, M. Kumar, N.K. Jha, Inorg. Chim. Acta 9 (1986) 9.
[2] A. Bino, N. Cohen, Inorg. Chim. Acta 210 (1993) 11.
[3] M.C. Rodriguez-Argeulles, M.B. Ferrari, G.G. Fava, C. Pellizi, P. Tarasconi, R. Albertini, P.P. Dallagio, P. Lunghi, S. Pinneli, J. Inorg. Biochem. 58 (1995) 157.
[4] G.F. de Sousa, C.A.L. Filgueiras, A. Abras, S.S. Al-Juaid, P.B. Hitchcock, J.F. Nixon, Inorg. Chim. Acta 218 (1993) 139.
[5] P.C. Moreno, R.H.P. Francisco, M.P. do, P. Gambardella, G.F. de Sousa, A. Abras, Acta Crystallogr., Sect. C 53 (1997) 1411.
[6] J.S. Casas, A. Castiñeiras, A. Sánches, J. Sordo, A. Vásquez-Lópes, M.C. Argüelles, U. Russo, Inorg. Chim. Acta 221 (1994) 61.
[7] A.H. Othman, K.-L. Lee, H.-K. Fun, B.-C. Yip, Acta Crystallogr., Sect. C 52 (1996) 602.
[8] S. Abram, C. Maichle-Mössmer, U. Abram, Polyhedron 17 (1998) 131.
[9] M. Mohan, A. Agarawal, N.K. Jha, J. Inorg. Biochem. 34 (1998) 41.
[10] M. Maji, S. Ghosh, S.K. Chattopadhyay, Transition Met. Chem. 23 (1998) 81.
[11] A.E. Liberta, D.X. West, Biometals 5 (1992) 121.
[12] D.X. West, G.A. Bain, R.J. Butcher, J.P. Jasinski, R.Y. Pozdniakiv, Y. Lee, J. Valdés-Martínez, R.A. Toscano, S. Hernández-Ortega, Polyhedron 15 (1996) 665.
[13] J. Valdés-Martínez, S. Hernández-Ortega, D.X. West, A.M. Stark, G.A. Bain, J. Chem. Crystallogr. 26 (1996) 861.
[14] J. Valdés-Martínez, S. Hernández-Ortega, D.X. West, J.S. Ives, G.A. Bain, Z. Krystallogr. 213 (1998) 246.
[15] D.X. West, P. Ahrweiler, G. Ertem, J.P. Scovill, D.L. Klayman, J.L. Flippen-Anderson, R. Gilardi, C. George, L.K. Pannell, Transition Met. Chem. 10 (1985) 264.
[16] A.K. Saxena, Appl. Organomet. Chem. 1 (1987) 39.
[17] M.A. Ali, C.M. Haroon, M. Nazimuddin, S.M.M. Majumbder, M.T.H. Tarafder, M.A. Khair, Transition Met. Chem. 17 (1992) 133.
[18] J.P. Scovill, Phosphorus Sulfur Silicon 60 (1991) 15.

PERGAMON

www.elsevier.nl/locate/poly

Polyhedron 19 (2000) 849–853

POLYHEDRON

Bismuth(III) thioether chemistry: synthesis and structure of a coordination polymer derived from $BiCl_3$ and $MeSi(CH_2SMe)_3$

Hing W. Yim [a], Kin-Chung Lam [b], Arnold L. Rheingold* [1,b], Daniel Rabinovich* [2,a]

[a] *Department of Chemistry, The University of North Carolina at Charlotte, 9201 University City Boulevard, Charlotte, NC 28223, USA*

[b] *Department of Chemistry and Biochemistry, The University of Delaware, Newark, DE 19716, USA*

Received 25 October 1999; accepted 20 January 2000

Abstract

The bismuth(III) halides BiX_3 (X = Cl, Br) react readily with the tridentate thioether $MeSi(CH_2SMe)_3$ to give complexes of composition $Bi_2\{MeSi(CH_2SMe)_3\}_2X_6$, which have been characterized analytically, spectroscopically and, for the chloro derivative, by single-crystal X-ray diffraction. In contrast to the mononuclear derivatives formed in the reactions of $BiCl_3$ with crown thioethers, $Bi_2\{MeSi(CH_2SMe)_3\}_2Cl_6$ exhibits in the solid state an extended chain structure with bridging unidentate/bidentate thioether ligands. ©2000 Elsevier Science Ltd All rights reserved.

Keywords: Bismuth; Thioether; Coordination polymers; Crystal structures; Electrospray

1. Introduction

We recently reported the synthesis of the new tridentate thioether $MeSi(CH_2SMe)_3$ (Chart 1) and prepared and structurally characterized its group 6 metal carbonyl derivatives $\{MeSi(CH_2SMe)_3\}M(CO)_3$ (M = Cr, Mo, W) [1] as well as a number of polymeric copper(I) complexes, including $Cu_3L_2X_3$ (X = Cl, Br) and $[LCu(NCMe)]PF_6$ [2].

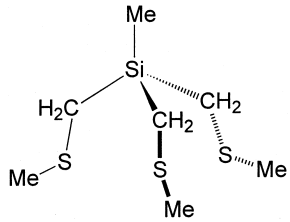


Chart 1

Seeking to extend our survey of the coordination chemistry of this ligand to the main group metals, we set out to explore its reactivity towards bismuth(III) halides. Bi(III), a 'borderline' metal ion according to Pearson's HSAB Principle [3,4] forms coordination complexes with both 'hard' (N, O) and 'soft' (S) Lewis bases [5,6]. While a variety of sulfur ligands, including thioureas $[(R_2N)_2CS]$, thiolates (RS^-), xanthates ($ROCS_2^-$), and dithiocarbamates ($R_2NCS_2^-$), have been extensively used in the context of bismuth chemistry, thioether derivatives are surprisingly uncommon. In this regard, other than a handful of macrocyclic or 'crown' thioether complexes such as (15S5)$BiCl_3$ and (18S6)$BiCl_3$ [7–9], only the dinuclear anion $[Bi_2I_8(SMe_2)_2]^{2-}$ [10] and a polymeric compound of stoichiometry $Bi_4\{MeS(CH_2)_3SMe\}_4Cl_{12}$ [11] have been reported. It is also interesting to note that compounds of bismuth, the heaviest non-radioactive element in the periodic table, have a fascinating array of applications, ranging from organic synthesis [12] to biology and medicine [13–16]. The synthesis and complete characterization of two new thioether complexes of bismuth(III) are described in this paper.

2. Results and discussion

The reaction of equimolar amounts of the bismuth(III) halides BiX_3 (X = Cl, Br) and $MeSi(CH_2SMe)_3$ in dichloromethane or acetonitrile affords yellow (X = Cl) or yellow–orange (X = Br) complexes of elemental composition $Bi\{MeSi(CH_2SMe)_3\}X_3$, isolated in 60–80% yield after appropriate work-up (Eq. (1)).

$$BiCl_3 + MeSi(CH_2SMe)_3 \rightarrow Bi\{MeSi(CH_2SMe)_3\}Cl_3 \quad (1)$$

The products are diamagnetic, slightly air-sensitive solids, soluble in polar solvents such as acetonitrile, dimethylsulf-

[1] *Corresponding author. E-mail: arnheim@udel.edu

[2] *Corresponding author. Tel.: +1-704-547-4442; fax: +1-704-547-3151; e-mail: Drabinov@email.uncc.edu

0277-5387/00/$ - see front matter ©2000 Elsevier Science Ltd All rights reserved.
PII S0277-5387(00)00328-4

oxide (DMSO), or tetrahydrofuran (THF) but insoluble in aliphatic, aromatic, or chlorinated hydrocarbons.

The new complexes were characterized by a combination of analytical and spectroscopic techniques. Their ^{1}H NMR spectra (in CD_3CN) are very similar and display three singlet resonances in the ratio 3:2:1, assigned to the methylthio, methylene, and methylsilyl protons, respectively, all of which are only slightly downfield shifted (ca. 0.1–0.2 ppm) relative to the free ligand in the same solvent. These observations are consistent with the presence in acetonitrile solution of a fairly symmetrical complex bearing a tridentate thioether ligand (e.g. $LBiX_3$) or, alternatively, the existence of two or more highly fluxional species that are rapidly equilibrated in the NMR time scale (e.g. L_2BiX_3). Similarly, the ^{13}C NMR spectra of both compounds consist of only three signals, with approximate chemical shifts δ 21.2, 18.7, and -4.8 ppm, corresponding to the MeS, CH_2, and MeSi groups, respectively.

Electrospray ionization mass spectrometry (ESI-MS) [17,18] was used to investigate the nature of the new complexes in solution. The positive ion mass spectra of dilute acetonitrile solutions of both complexes (Fig. 1) exhibit peaks corresponding to the $[LBiX_2]^+$ (X = Cl, m/z = 505; X = Br, m/z = 595) and $[L_2BiX_2]^+$ (X = Cl, m/z = 731; X = Br, m/z = 821) fragments, all of which show the correct isotopic distributions. It is worth noting that loss of a halide is the most common ionization pathway for transition metal coordination complexes containing halide ligands [19]. This observation is in agreement with the formation of cationic complexes derived from both $LBiX_3$ and L_2BiX_3, and provides indirect evidence for the existence of a fast equilibrium of at least these two species in acetonitrile solution. In addition, a set of peaks centered at m/z = 517, tentatively assigned to the $[LBi(NCMe)_2]^+$ species, was also observed for the chloro complex. Interestingly, both spectra show an intense peak corresponding to the BiS^+ ion (m/z = 241), a species previously observed in the electron ionization (EI) and atmospheric pressure chemical ionization (APCI) mass spectra of some dithiabismuth(III) heterocyclic compounds [20] and an indication of significant thermal decomposition of the thioether complexes during ionization.

Single crystals suitable for an X-ray diffraction study of the chloro derivative were obtained by slow evaporation at room temperature of a saturated acetonitrile solution of $Bi\{MeSi(CH_2SMe)_3\}Cl_3$ (Fig. 2). Selected bond lengths and angles given in Table 1. The compound exhibits in the solid state with an extended chain structure, with each asymmetric unit consisting of a dinuclear Bi_2Cl_6 group and two bridging unidentate/bidentate (μ-η^1:η^2) thioether ligands. We have also observed this binding mode of $MeSi(CH_2SMe)_3$ in the aforementioned Cu(I) coordination polymers [2], a phenomenon that underscores the enhanced flexibility of our thioether ligand relative to that of related crown thioethers such as 9S3 (1,4,7-trithiacyclononane). The two six-coordinate bismuth centers are linked by a single chloro ligand so that the complex could also be envisioned as a

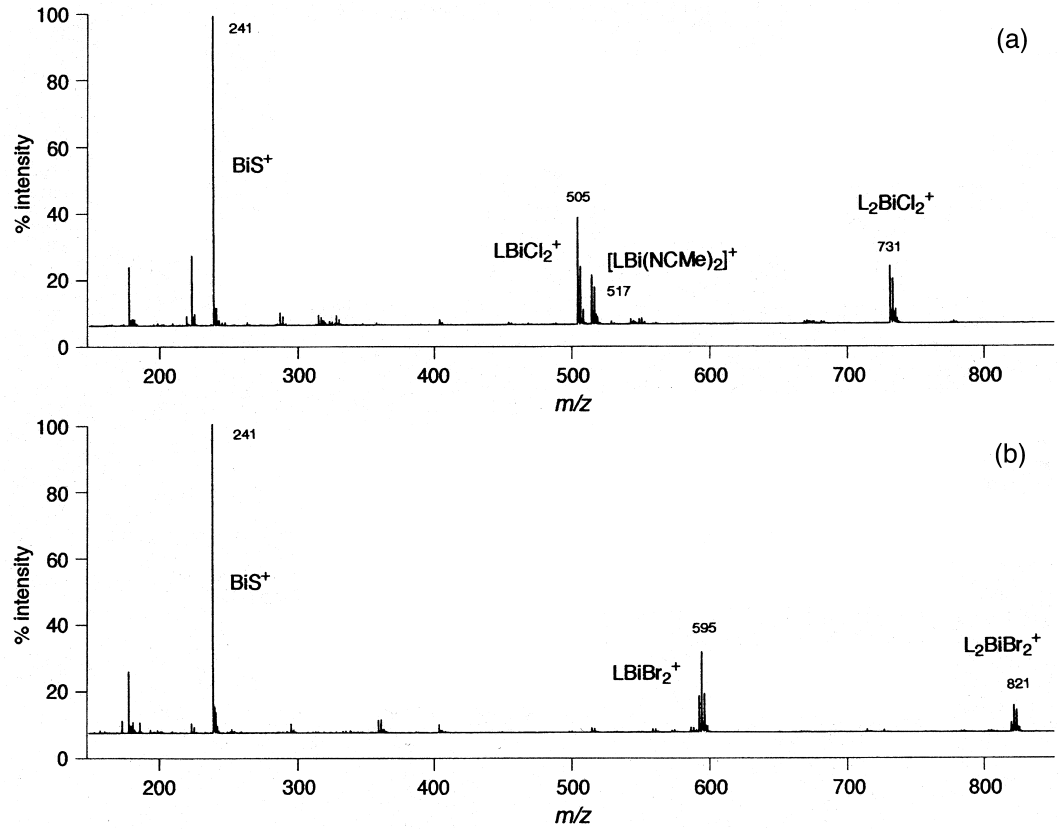


Fig. 1. Positive ion ESI mass spectra (cone voltage 80 V) of acetonitrile solutions of (a) $Bi_2\{MeSi(CH_2SMe)_3\}_2Cl_6$ and (b) $Bi_2\{MeSi(CH_2SMe)_3\}_2Br_6$.

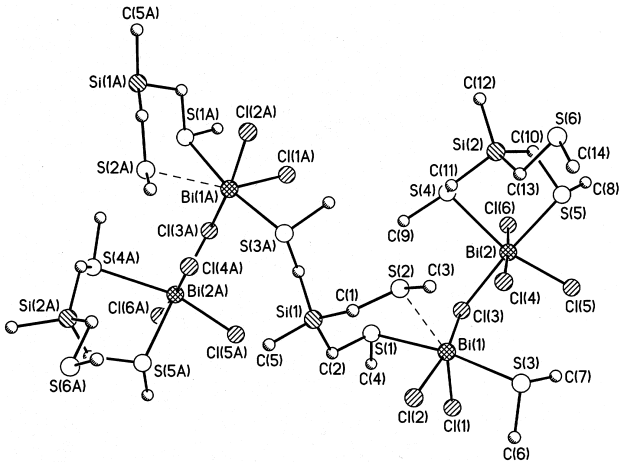


Fig. 2. Two repeating units of the extended structure of $Bi_2\{MeSi(CH_2SMe)_3\}_2Cl_6$ with hydrogen atoms omitted for clarity.

Table 1
Selected bond lengths (Å) and angles (°) for $Bi_2\{MeSi(CH_2SMe)_3\}_2Cl_6$

Bi(1)–Cl(1)	2.545(2)	Bi(2)–Cl(3)	2.729(3)
Bi(1)–Cl(2)	2.549(2)	Bi(2)–Cl(4)	2.810(2)
Bi(1)–Cl(3)	2.980(3)	Bi(2)–Cl(5)	2.579(2)
Bi(1)–S(1)	2.956(2)	Bi(2)–Cl(6)	2.576(3)
Bi(1)···S(2)	3.180(2)	Bi(2)–S(4)	3.051(2)
Bi(1)–S(3)	2.872(2)	Bi(2)–S(5)	2.896(2)
Cl(1)–Bi(1)–Cl(2)	90.56(8)	Cl(1)–Bi(1)–S(3)	84.76(7)
Cl(2)–Bi(1)–S(3)	82.71(7)	Cl(1)–Bi(1)–S(1)	88.81(7)
Cl(2)–Bi(1)–S(1)	91.70(7)	S(3)–Bi(1)–S(1)	171.42(6)
Cl(1)–Bi(1)–Cl(3)	80.49(8)	Cl(2)–Bi(1)–Cl(3)	162.52(8)
S(3)–Bi(1)–Cl(3)	111.11(8)	S(1)–Bi(1)–Cl(3)	73.25(7)
Cl(6)–Bi(2)–Cl(5)	92.82(9)	Cl(6)–Bi(2)–Cl(3)	96.49(8)
Cl(5)–Bi(2)–Cl(3)	96.09(9)	Cl(6)–Bi(2)–Cl(4)	175.78(8)
Cl(5)–Bi(2)–Cl(4)	91.33(8)	Cl(3)–Bi(2)–Cl(4)	83.79(7)
Cl(6)–Bi(2)–S(5)	93.42(8)	Cl(5)–Bi(2)–S(5)	81.97(8)
Cl(3)–Bi(2)–S(5)	170.00(8)	Cl(4)–Bi(2)–S(5)	86.44(7)
Cl(6)–Bi(2)–S(4)	83.68(8)	Cl(5)–Bi(2)–S(4)	164.94(8)
Cl(3)–Bi(2)–S(4)	98.85(8)	Cl(4)–Bi(2)–S(4)	92.12(7)
S(5)–Bi(2)–S(4)	83.62(6)	Bi(2)–Cl(3)–Bi(1)	103.70(8)

dinuclear derivative of stoichiometry $Bi_2\{MeSi(CH_2SMe)_3\}_2Cl_6$. It is noteworthy that complexes containing neutral Bi_2Cl_6 groups supported exclusively by additional donor ligands are extremely rare. The bipyridine derivative $Cl_2(bipy)_2Bi(\mu\text{-}Cl)Bi(bipy)Cl_3$ [21], which exhibits both hexa- and heptacoordinate metal centers, appears to be the only other such complex to have been structurally characterized. Both bismuth atoms in $Bi_2\{MeSi(CH_2SMe)_3\}_2Cl_6$ display distorted octahedral geometries, with 'trans' Cl(S)–Bi–Cl(S) angles in the range 162.5 to 175.8°. There are two distinctive coordination environments for the bismuth centers: (i) BiS_3X_3, with one arm of a thioether ligand and two from another bonded to a $BiCl_3$ center, as for Bi(1), and (ii) BiS_2X_4, with two arms of a thioether ligand and the bridging Cl atom attached to the other $BiCl_3$ moiety, as in Bi(2).

Four of the five terminal Bi–Cl bonds (Bi(1)–Cl(1), Bi(1)–Cl(2), Bi(2)–Cl(5), and Bi(2)–Cl(6)) are almost identical in length (ca. 2.56 Å) and are similar to those

Table 2
Summary of observed Bi(III)–S(thioether) bond lengths

Complex	d(Bi–S) (Å)	Reference
$(12S4)BiCl_3$	2.987(3)–3.206(3)	[7]
$(15S5)BiCl_3$	3.057(7)–3.433(7)	[7]
$(18S6)BiCl_3$	3.146(4), 3.225(4)	[8]
$(24S8)(BiCl_3)_2$	3.134(2)–3.313(2)	[9]
$(SMe_3)_2[Bi_2I_8(SMe_2)_2]$	3.054(8)	[10]
$Bi_4\{MeS(CH_2)_3SMe\}_4Cl_{12}$	2.857(7), 2.977(7)	[11]
$(LBiCl)_2$ [a]	2.849(5)	[20]
$(LBiSCH_2CH_2)_2S$ [a]	3.071(5)–3.197(5)	[20]
$Bi_2\{MeSi(CH_2SMe)_3\}_2Cl_6$	2.872(2)–3.180(2)	this work

[a] L = η^3-$S(CH_2)_2S(CH_2)_2S$.

observed in other bismuth chloride derivatives. For example, the mean terminal Bi–Cl bond length for compounds contained in the Cambridge Structural Database [22] is 2.616 Å. In contrast, the terminal Bi(2)–Cl(4) bond length (2.810(2) Å) is closer to the mean value for bridging Bi–μ-Cl bond lengths (2.936 Å) found in the same database. While the asymmetry of the bridging Bi–Cl–Bi group (Bi(1)–Cl(3) = 2.980(3) Å, Bi(2)–Cl(3) = 2.729(3) Å) could be ascribed to the contribution of a charge-separated complex $[Bi(S)_3Cl_2]^+[Bi(S)_2Cl_4]^-$ (S = thioether donor group) to the overall bonding scheme, we also note that its geometry is similar to that observed for such bridging units in other polynuclear bismuth complexes, including $[Bi_2Cl_{10}]^{4-}$ [23,24], Ph_2BiCl [25], $PhBi(THF)Cl_2$ [26], $[Bi_2Cl_8(THF)_2]^{2-}$ [27], and $Bi_2(bipy)_3Cl_6$ [20]. The Bi–S bond lengths vary between 2.872(2) and 3.180(2) Å and are within the range of values reported for other bismuth(III) thioether complexes (Table 2). While the observed Bi–S distances exceed the sum of covalent radii of bismuth and sulfur (2.56 Å) [28], they are significantly shorter than the sum of their van der Waals radii (4.25 Å) [28]. All the remaining interatomic distances (i.e. S–C and Si–C bond lengths) appear to be normal [29].

3. Conclusions

In contrast to the mononuclear seven-, eight- or nine-coordinate complexes obtained from $BiCl_3$ and crown thioethers, the corresponding reaction with $MeSi(CH_2SMe)_3$ results in the formation of a polymeric product with hexacoordinate bismuth centers. $Bi_2\{MeSi(CH_2SMe)_3\}_2Cl_6$ is only the second coordination polymer of Bi(III) to be structurally characterized, a reflection of the enhanced coordinative flexibility of $MeSi(CH_2SMe)_3$, at least relative to that of crown thioethers. ESI-MS studies revealed that the mono- and bis(thioether) complexes $[LBiX_2]^+$ and $[L_2BiX_2]^+$ are the two main species present in acetonitrile solutions of $Bi_2\{MeSi(CH_2SMe)_3\}_2X_6$ and that bismuth(III) sulfide or perhaps the sulfohalides Bi(S)X readily form upon thermal decomposition of these complexes. Finally, it is interesting to note that all the thioether complexes of bismuth that have

been isolated and structurally characterized to date are adducts of BiX_3 (X = Cl, I), an observation that has stimulated our current interest in the preparation of thioether derivatives of some organobismuth compounds.

4. Experimental

4.1. General considerations

All reactions were performed under dry oxygen-free nitrogen in an Innovative Technology System One-M-DC glove box or under argon using a combination of high-vacuum and Schlenk techniques [30–32]. Solvents were purified and degassed by standard procedures and all commercially available reagents were used as received. $MeSi(CH_2SMe)_3$ was prepared as reported [1].

^1H and ^{13}C NMR spectra were obtained on General Electric QE 300 or Varian Gemini (300 MHz) FT spectrometers. Chemical shifts (δ) are reported in parts per million relative to $SiMe_4$ ($\delta = 0$ ppm) and were referenced internally with respect to the residual protio or ^{13}C solvent resonances (δ 1.94 for CD_2HCN, δ 1.39 for CD_3CN); coupling constants are given in hertz (Hz). IR spectra were recorded as KBr pellets on a Midac Collegian FT spectrophotometer and are reported in cm^{-1}; relative intensities of the absorptions are indicated in parentheses (vs very strong, s strong, m medium, w weak). Electrospray ionization mass spectra were obtained on a PerSeptive Biosystems Mariner ESI-TOF mass spectrometer by direct infusion using acetonitrile solutions and a flow rate of 10 μl min^{-1}. Elemental analyses were determined by Desert Analytics (Tucson, AZ).

4.2. Synthesis of $Bi\{MeSi(CH_2SMe)_3\}Cl_3$

A stirred suspension of $BiCl_3$ (1.00 g, 3.17 mmol) in dichloromethane (20 ml) was treated with $MeSi(CH_2SMe)_3$ (0.64 ml, 3.22 mmol), resulting in an immediate color change from off-white to yellow. After stirring for 2 h at room temperature, the suspension was concentrated under reduced pressure to ca. 5 ml, and pentane (15 ml) was added. The yellow microcrystalline product was isolated by filtration, washed with pentane (2 × 10 ml), and dried in vacuo for 1 h (1.03 g, 60%). NMR data in CD_3CN: ^1H δ 0.21 (s, 3H, CH_3Si), 1.98 (s, 6H, CH_2), 2.18 (s, 9H, SCH_3); ^{13}C δ −4.8 (q, $^1J_{C–H} = 121$, 1C, CH_3Si), 18.5 (t, $^1J_{C–H} = 132$, 3C, CH_2), 20.9 (q, $^1J_{C–H} = 140$, 3C, SCH_3). IR data: 2964 (w), 2911 (w), 2878 (w), 2825 (w), 1420 (m), 1381 (w), 1314 (w), 1254 (m), 1141 (w), 961 (m), 813 (vs). *Anal*. Calc. for $C_7H_{18}BiCl_3S_3Si$: C, 15.5; H, 3.4. Found: C, 15.4; H, 3.1%.

4.3. Synthesis of $Bi\{MeSi(CH_2SMe)_3\}Br_3$

A stirred suspension of $BiBr_3$ (1.00 g, 2.23 mmol) in dichloromethane (30 ml) was treated with $MeSi(CH_2SMe)_3$ (0.48 ml, 2.42 mmol), resulting in an immediate color change from yellow to yellow–orange. After stirring for 1 h at room temperature, the suspension was concentrated under reduced pressure to ca. 10 ml, and pentane (40 ml) was added. The yellow–orange microcrystalline product was isolated by filtration, washed with pentane (3 × 30 ml), and dried in vacuo for 1 h (1.20 g, 80%). NMR data in CD_3CN: ^1H δ 0.25 (s, 3H, CH_3Si), 2.11 (s, 6H, CH_2), 2.31 (s, 9H, SCH_3); ^{13}C δ −4.7 (q, $^1J_{C–H} = 121$, 1C, CH_3Si), 18.8 (t, $^1J_{C–H} = 132$, 3C, CH_2), 21.6 (q, $^1J_{C–H} = 140$, 3C, SCH_3). IR data: 2956 (w), 2911 (w), 2876 (w), 1414 (m), 1374 (m), 1256 (m), 1143 (m), 961 (s), 811 (vs). *Anal*. Calc. for $C_7H_{18}BiBr_3S_3Si$: C, 12.5; H, 2.7. Found: C, 12.1; H, 2.6%.

Table 3
Crystallographic data for $Bi_2\{MeSi(CH_2SMe)_3\}_2Cl_6$

Formula	$C_{14}H_{36}Bi_2Cl_6S_6Si_2$
Formula weight	1083.63
Crystal system	monoclinic
Space group	$P2_1/n$ (no. 14)
Temperature (K)	173(2)
a (Å)	9.2715(2)
b (Å)	25.6859(2)
c (Å)	14.7164(2)
β (°)	99.0449(2)
V (Å^3)	3461.08(5)
Z	4
ρ (calc.) (g cm^{-3})	2.080
μ (Mo Kα) (mm^{-1})	11.056
θ_{max} (°)	26
No. of data	6638
No. of parameters	271
R_1 ($I > 2\sigma(I)$) [a]	0.0399
wR_2 ($I > 2\sigma(I)$) [a]	0.1326

[a] $R_1 = \Sigma(|F_o| - |F_c|)/\Sigma|F_o|$; $wR_2 = \{\Sigma[w(F_o^2 - F_c^2)^2]/\Sigma[w(F_o^2)^2]\}^{1/2}$.

4.4. X-ray structure determination

Crystal data collection and refinement parameters are given in Table 3. A crystal suitable for data collection was selected and mounted in a nitrogen-flushed, thin-walled capillary. Data were collected on a Siemens P4 diffractometer equipped with a SMART/CCD detector using Mo Kα radiation ($\lambda = 0.71073$ Å). The systematic absences in the diffraction data were uniquely consistent with the reported space group. The structure was solved using direct methods, completed by subsequent difference Fourier synthesis, and refined by full-matrix least-squares procedures. An empirical absorption correction was applied to the data set using DIFABS [33]. All non-hydrogen atoms were refined with anisotropic displacement coefficients and all hydrogen atoms were treated as idealized contributions. All software and sources of the scattering factors are contained in the SHELXTL (version 5.10) program library [34].

Supplementary data

Crystallographic data (excluding structure factors) for $Bi_2\{MeSi(CH_2SMe)_3\}_2Cl_6$ have been deposited with the Cambridge Crystallographic Data Centre, 12 Union Road,

Cambridge CB2 1EZ, UK (fax: +44-1223-336033; e-mail: deposit@ccdc.cam.ac.uk), CCDC No. 134940.

Acknowledgements

We thank the Camille and Henry Dreyfus Foundation Faculty Start-Up Grant Program for Undergraduate Institutions, Research Corporation for a Cottrell College Science Award, the donors of the Petroleum Research Fund, administered by the American Chemical Society, and The University of North Carolina at Charlotte for support of this research. We also gratefully acknowledge the National Science Foundation for the purchase of the mass spectrometry instrumentation (Grant No. CHE-9871160) and Professor Brian T. Cooper (UNC Charlotte) for helpful discussions regarding the ESI-MS experiments.

References

[1] H.W. Yim, L.M. Tran, E.D. Dobbin, D. Rabinovich, L.M. Liable-Sands, C.D. Incarvito, K.-C. Lam, A.L. Rheingold, Inorg. Chem. 38 (1999) 2211.
[2] H.W. Yim, L.M. Tran, E.E. Pullen, D. Rabinovich, L.M. Liable-Sands, T.E. Concolino, A.L. Rheingold, Inorg. Chem. 38 (1999) 6234.
[3] R.G. Pearson, Science 151 (1966) 172.
[4] R.G. Pearson, Chemical Hardness, Wiley-VCH, New York, 1997, Ch. 1 and Refs. therein.
[5] C.A. McAuliffe, in: G. Wilkinson, R.D. Gillard, J.A. McCleverty (Eds.), Comprehensive Coordination Chemistry, vol. 3, Pergamon, Oxford, 1987, Ch. 28, p. 279.
[6] S.M. Godfrey, C.A. McAuliffe, A.G. Mackie, R.G. Pritchard, in: N.C. Norman (Ed.), Chemistry of Arsenic, Antimony, and Bismuth, Blackie, London, 1998, Ch. 4, p. 186.
[7] G.R. Willey, M.T. Lakin, N.W. Alcock, J. Chem. Soc., Dalton Trans. (1992) 591.
[8] G.R. Willey, M.T. Lakin, N.W. Alcock, J. Chem. Soc., Dalton Trans. (1992) 1339.
[9] A.J. Blake, D. Fenske, W.-S. Li, V. Lippolis, M. Schröder, J. Chem. Soc., Dalton Trans. (1998) 3961.
[10] W. Clegg, N.C. Norman, N.L. Pickett, Polyhedron 12 (1993) 1251.
[11] A.R.J. Genge, W. Levason, G. Reid, Chem. Commun. (1998) 2159.
[12] H. Suzuki, T. Ikegami, Y. Matano, Synthesis (1997) 249.
[13] U. Dittes, E. Vogel, B.K. Keppler, Coord. Chem. Rev. 163 (1997) 345.
[14] H. Sun, H. Li, P.J. Sadler, Chem. Ber./Recueil 130 (1997) 669.
[15] P.J. Sadler, H. Li, H. Sun, Coord. Chem. Rev. 185–186 (1999) 689.
[16] G.G. Briand, N. Burford, Chem. Rev. 99 (1999) 2601.
[17] W. Henderson, B.K. Nicholson, L.J. McCaffrey, Polyhedron 17 (1998) 4291.
[18] C.L. Gatlin, F. Turecek, in: R.B. Cole (Ed.), Electrospray Ionization Mass Spectrometry, Wiley, New York, 1997, Ch. 15, p. 527.
[19] W. Henderson, C. Evans, Inorg. Chim. Acta 294 (1999) 183.
[20] L. Agocs, N. Burford, T.S. Cameron, J.M. Curtis, J.F. Richardson, K.N. Robertson, G.B. Yhard, J. Am. Chem. Soc. 118 (1996) 3225.
[21] G.A. Bowmaker, F.M.M. Hannaway, P.C. Junk, A.M. Lee, B.W. Skelton, A.H. White, Aust. J. Chem. 51 (1998) 325.
[22] F.H. Allen, O. Kennard, Chem. Des. Automation News 8 (1993) 1 CSD version 5.17, April 1999.
[23] F. Bigoli, M. Lanfranchi, M.A. Pellinghelli, Inorg. Chim. Acta 90 (1984) 215.
[24] S. Jarraya, R.B. Hassen, A. Daoud, Acta Crystallogr., Sect. C 51 (1995) 2537.
[25] R. Hillwig, F. Kunkel, K. Harms, B. Neumüller, K. Dehnicke, Z. Naturforsch., Teil B 52 (1997) 149.
[26] W. Clegg, R.J. Errington, G.A. Fisher, R.J. Flynn, N.C. Norman, J. Chem. Soc., Dalton Trans. (1993) 637.
[27] S.C. James, N.C. Norman, A.G. Orpen, M.J. Quayle, Acta Crystallogr., Sect. C 53 (1997) 1024.
[28] J. Emsley, The Elements, Oxford University Press, New York, 3rd edn., 1998, pp. 36, 198.
[29] F.H. Allen, O. Kennard, D.G. Watson, L. Brammer, A.G. Orpen, R. Taylor, J. Chem. Soc., Perkin Trans. II (1987) S1.
[30] R.J. Errington, Advanced Practical Inorganic and Metalorganic Chemistry, Blackie, London, 1997.
[31] A.L. Wayda, M.Y. Darensbourg (Eds.), Experimental Organometallic Chemistry, American Chemical Society, Washington, DC, 1987.
[32] D.F. Shriver, M.A. Drezdzon, The Manipulation of Air-Sensitive Compounds, Wiley-Interscience, New York, 2nd edn., 1986.
[33] N. Walker, D. Stuart, Acta Crystallogr., Sect. A 39 (1983) 158.
[34] G.M. Sheldrick, Siemens XRD, Madison, WI.

PERGAMON

www.elsevier.nl/locate/poly

Polyhedron 19 (2000) 855–862

POLYHEDRON

Cobalt(II) complexes with pyrazole-derived ligands: crystal structure of {bis[3-phenyl-5-(2-pyridyl) pyrazole]aquachlorocobalt(II)}chloride monohydrate

Arafa Chadghan [a], Josefina Pons [a,*], Amparo Caubet [b], Jaume Casabó [a], Josep Ros [a], Angel Alvarez-Larena [c], Joan Francesc Piniella [c]

[a] *Departament de Química, Unitat de Química Inorgànica, Universitat Autònoma de Barcelona, 08193 Bellaterra, Barcelona, Spain*
[b] *Departament de Química Inorgànica, Universitat de Barcelona, Martí i Franquès s/n, 08028 Barcelona, Spain*
[c] *Departament de Geologia, Unitat de Cristal.lografia, Universitat Autònoma de Barcelona, 08193 Bellaterra, Barcelona, Spain*

Received 3 October 1999; accepted 3 January 2000

Abstract

The synthesis of the new pyrazole-derived ligands 3-phenyl-5-(2-pyridyl) pyrazole (HL^0) and 3-phenyl-5-(6-methyl-(2-pyridyl))pyrazole (HL^1) and their Co(II) complexes is reported. Elemental analyses, conductivity measurements and IR and UV–Vis spectroscopies defined all complexes. ^1H and ^{13}C NMR spectroscopies were also used in the characterization of ligands. The crystal and molecular structures of $[Co(HL^0)_2Cl(H_2O)]Cl\cdot H_2O$, consisting of discrete ions and water molecules linked by hydrogen bonds, are also reported. The hexacoordinated metal atom is bonded to two pyridinic nitrogens, two pyrazolic nitrogens (one of each nitrogen belonging to two different ligands), one chlorine atom and one water molecule, forming a distorted octahedral environment. The ligands are not exactly planar and the arrangement of ligands is *cis*, with a dihedral angle between the two mean planes of ligands of 89.21(6)°. The degree of distortion from regular octahedral geometry is compared to that of closely related structures. ©2000 Elsevier Science Ltd All rights reserved.

Keywords: Cobalt complexes; Crystal structures

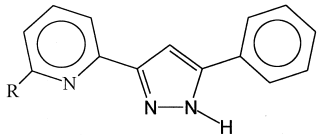
1. Introduction

Since the first review of pyrazole-derived ligands appeared in 1972 [1], the coordination chemistry of pyrazole and its derivatives has strongly evolved over the last two decades [2]. La Monica and Ardizzoia published an extensive review in 1997, which covers the years 1985–1995, and updates the work of Trofimenko [3]. Recent studies have shown the high catalytic activity, under mild conditions, of some polynuclear heterobridged pyrazolate complexes, thus encouraging the exploration of the unusual and specific features of the pyrazolate ligands [1,2]. Some authors have suggested that the nucleophilicity of N2 (sp^2) and the acid character of pyrazole may be modified by introducing appropriate substituents at the positions 3, 4 or 5 of the heterocyclic ring [4,5]. We have described the preparation of the ligands 3,5-bis(2-pyridyl)pyrazole (HL), 2-(6-methyl)pyridyl-2-pyridyl-3,5-pyrazole (HL′) and 3,5-bis-2-(6-methylpyridyl)pyrazole (HL″), where the pyrazole ring is attached to nitrogen heterocycles at the positions 3 and 5. We elsewhere [6,7] have also studied a series of HL complexes with the divalent metal ions Ni(II), Co(II), Zn(II) and Cu(II) [6–9]. Structural data on the Ni(II) [6] and Cu(II) [8] complexes have shown that this tetradentate nitrogen donor has a marked preference for the formation of dinuclear complexes, in which the ligand (itself) exhibits a strictly planar bridging mode with the axial coordination sites of the metal ions occupied by additional solvent molecules. In 1995 Munakata et al. [10] reported three HL complexes, two of Ag(I), and one of Cu(II).

Here, following the research on 3,5-disubstituted pyrazole ligands, we report the synthesis of the new pyrazole ligands 3-phenyl-5-(2-pyridyl)pyrazole (HL^0) and 3-phenyl-5-(6-methyl-(2-pyridyl))pyrazole (HL^1) (Fig. 1) and of some Co(II) complexes of formula $Co(HL^0)_2X_2$ (X = NO_3 (**1**), Cl (**2**), Br (**3**)), $Co(HL^1)_2X_2$ (X = NO_3 (**4**), Cl (**5**), Br (**6**)), $Co(HL^0)Cl_2$ (**7**), $Co(HL^1)X_2$ (X = Cl (**8**), Br (**9**),

* Corresponding author. Tel.: +34-93-581-2895; fax: +34-93-581-3101; e-mail: josefina.pons@uab.es

0277-5387/00/$ - see front matter ©2000 Elsevier Science Ltd All rights reserved.
PII S0277-5387(00)00330-2



R = H, CH_3

Fig. 1. Pyrazole-derived ligands: R = H, CH_3.

and $Co(HL^0)Cl(OH)$ (**10**). The crystal structure of $[Co(HL^0)_2Cl(H_2O)]Cl\cdot H_2O\cdot 0.2CH_3CN$ (**2**) is described and compared to those of closely related structures.

2. Experimental

2.1. General methods

Preparations were performed using usual Schlenk techniques. All reagents were commercial grade materials and were used without further purification. All solvents (ethanol, tetrahydrofurane THF) were dried and distilled by standard methods and previously deoxygenated in a vacuum line.

Analyses (C, N, H) were performed in our analytical laboratory on a Perkin-Elmer 240-B instrument. Conductivity measurements were performed at room temperature in 10^{-3} M methanolic solutions employing a Radiometer CDM-3 conductimeter. Infrared spectra were recorded from KBr discs or Nujol films on a Perkin-Elmer 2000 spectrometer in the region 4000–100 cm^{-1}. The ^1H and $^{13}C\{^1H\}$ NMR spectra were obtained in $CDCl_3$ or acetone-d_6 solutions on a Bruker AC-250 MHz instrument and referenced to TMS. In all cases chemical shifts (δ) are given in ppm. Mass spectra were obtained on a HP 5989A apparatus. Electronic spectra in solution were run on a Kontron-Uvikon 860 in different solvents and in solid state (KBr pellets, diffuse reflectance) were obtained on a Kontron-Tegimenta, Rotkreuz, Switzerland.

2.2. Materials

Methyl 2-picolinate and methyl 6-methyl-2-picolinate were prepared by previously reported procedures [11,12].

2.3. Synthesis of the ligands

2.3.1. Preparation of 1-phenyl-3-(2-pyridyl)-1,3-propanodione

Under a dinitrogen atmosphere, a 250 ml Schlenk flask was charged with sodium (0.68 g, 29.6 mmol). Deoxygenated absolute ethanol (20 ml) was added and the mixture was stirred until all the sodium was consumed. The ethanol was eliminated in vacuo to yield a white solid. Dry toluene (25 ml), methyl-2-picolinate (4.05 g, 32.4 mmol) and acetophenone (4.83 g, 45.0 mmol) were added in this order, slowly, to the white residue of sodium ethanolate. Upon stirring the mixture overnight, a pale orange compound precipitated, which was filtered and dried. The resulting solid was slowly added to a vigorously stirred solution of acetic acid (30 ml), water (30 ml) and ice (100 g), yielding a white solid, which was filtered and dried in vacuo. Yield: 6.2 g, 85.0%. Melting point: 85–86°C. IR (KBr, cm^{-1}): $\nu(C–H)_{ar}$ 3098, $\nu(C=O)$, $\nu(C=C)$ 1602, $\nu(C=N)$ 1549, $\delta(C–H)_{OOP}$ 775. ^1H NMR (250 MHz, acetone-d_6, ppm): δ 4.84 (s, 1H, $H_2C(C=O)_2$), 7.5–7.7 (m, 4H, H–ph, H–py), 8.0–8.2 (m, 4H, H–ph, H–py), 8.75 (d, 1, H–py). ^{13}C NMR: (62.75 MHz, acetone-d_6, ppm): δ 49.7 (H_2C), 94.5 (C–py), 120.0, 128.0, 129.1, 130.0, 131.2, 135.5, 136.0, 137.3, 152.0 (C–py, C–ph), 153.6 (C–py), 185, 186.0 (C=O). MS (CI, CH_4) *m/z*: 225 (MH^+, 95), 105 ($PhCO^+$, 97), 78 (py, 79), 77 (ph, 83), 51 ($C_4H_4^+$, 100). *Anal*. Found: C, 74.6; H, 5.1; N, 6.2. Calc. for $C_{14}H_{11}NO_2$: C, 74.6, H, 4.9; N, 6.2%.

2.3.2. Preparation of 3-phenyl-5-(2-pyridyl) pyrazole (HL^0)

A 100 cm^3 Schlenk flask connected to a Dean-Stark apparatus was charged with 1-phenyl-3-(2-pyridyl)-1,3-propanodione (1 g, 4.4 mmol) and hydrazine (0.27 g, 5.4 mmol). Dry toluene (20 ml) was added, and the mixture was refluxed for 18 h, allowed to cool to room temperature and then filtered. Yield: 0.50 g, 51%. Melting point: 167–168°C. IR (KBr, cm^{-1}): ν(N–H) 3244, $\nu(C–H)_{ar}$ 3062, ν(C=C), ν(C=N) 1598–1565, $\delta(C–H)_{OOP}$ 759. ^1H NMR (250 MHz, $CDCl_3$, ppm): δ 7.2–7.4 (m, 5H, H–ph, H–py), 7.8–7.9 (m, 4H, H–ph, H–py), 8.57 (d, 1H, H–py), 11.0 (b, 1H, H–N(pz)). ^{13}C NMR (62.75 MHz, $CDCl_3$, ppm): δ 100.3 (C–pz), 120.1, 124.0, 126.0, 128.2, 129.3, 132.6, 137.0, 144.6, 148.0, 149.1, 152.0 (C–py, C–ph), 207.4 (C–pz). MS (CI, CH_4) *m/z*: 221 (MH^+,100), 192 ($MH^+–N_2H$, 64), 78 (py, 37), 77 (ph, 31), 51 ($C_4H_4^+$). *Anal*. Found: C, 74.3; H, 5.1; N, 18.6. Calc. for $C_{14}H_{11}N_3\cdot 1/4H_2O$: C, 74.5, H, 5.1, N, 18.6%.

2.3.3. Preparation of 1-phenyl-3-(6-methyl-(2-pyridyl))-1,3-propanodione

Under a dinitrogen atmosphere, a 250 ml Schlenk flash was charged with sodium (0.68 g, 29.0 mmol). Ethanol (20 ml) was added and the mixture was stirred until all the sodium was consumed. The ethanol was eliminated in vacuo. Dry toluene (25 ml), methyl-6-methyl-2-picolinate (4.05 g, 27.0 mmol) and acetophenone (4.83 g, 45.0 mmol) were added in this order, slowly, to the white residue of sodium ethanolate. The mixture was stirred until a yellowish precipitate appeared (ca. 1 h), then it was gently warmed for 12 h until the sodium salt of the β-diketone was formed. The salt was filtered and dried. The resulting solid was slowly added to a vigorously stirred solution of acetic acid (30 ml), water (30 ml) and ice (100 g), yielding a solid, which was filtered off and dried in vacuo. Yield: 4.90 g, 76.4%. Melting point: 50–52°C. IR (KBr, cm^{-1}): $\nu(C–H)_{ar}$ 3095, ν(C=O), ν(C=C) 1601, ν(C=N) 1561, $\delta(CH_3)$ 1448, $\delta(C–H)_{OOP}$ 773. ^1H NMR (250 MHz, $CDCl_3$, ppm): δ 2.70 (s, 3H, CH_3–py), 4.74 (s, 1H, $H_2C(C=O)_2$), 7.4–7.6 (m, 5H, H–ph), 7.66 (t, 1H, H–py), 7.91 (d, 1H, H–py), 8.03 (d, 1, H–py). ^{13}C

NMR (62.75 MHz, $CDCl_3$, ppm): δ 24.2 (CH_3–py), 48.2 (H_2C), 93.3, 118.9 (C–py), 124.0, 125,2, 126.0, 132.2, 137.0 (C–py, C–ph), 151.6 (C–py), 183.8, 185.8 (C–pz), 195.0, 196.0 (C=O). MS (CI, CH_4) *m/z*: 239 (MH^+, 62), 162 (MH^+–Ph, 18), 105 ($PhCO^+$, 100), 93 (2-Mepy, 97), 77 ($PhCO^+$–CO, 84). *Anal*. Found: C, 75.1; H, 5.7; N, 5.8. Calc. for $C_{15}H_{13}NO_2$: C, 75.3; H, 5.8; N, 5.5%.

2.3.4. Preparation of 3-phenyl-5-(6-methyl-(2-pyridyl))-pyrazole (HL^1)

A 100 cm^3 Schlenk flask connected to a Dean-Stark apparatus was charged with 1-phenyl-3-(6-methyl-2-(pyridyl)-1,3-propanodione (1 g, 4.2 mmol) and hydrazine (0.27 g, 5.4 mmol). Toluene (20 ml) was added, then the mixture was refluxed for 18 h, allowed to cool to room temperature and then filtered. Yield: 0.99 g, 50%. Melting point: 158–160°C. IR (KBr, cm^{-1}): ν(N–H) 3283, $\nu(C–H)_{ar}$ 3058, ν(C=C), ν(C=N) 1598–1564, $\delta(C–H)_{OOP}$ 789. ^1H NMR (250 MHz, $CDCl_3$, ppm): δ 2.30 (s, 3H, CH_3–py), 7.03 (s, 1H, H–pz), 7.04 (d, 1H, H–ph), 7.3–7.6 (m, 6H, H–py, H–ph), 7.84 (d, 1H, H–py), 9.8 (b, 1H, H–N(pz)). ^{13}C NMR (62.75 MHz, $CDCl_3$, ppm): δ 24.4 (CH_3–py), 100.2 (C–pz), 117.1, 122.5, 128.7, 132.8, 137.1, 144.7, 151.6, 158.4 (C–py, C–ph), 200.0 (C–pz). MS (CI, CH_4) *m/z*: 235 (MH^+, 100), 207 (MH^+–N_2, 10), 206 (MH^+– N_2H, 36), 92 (2-Mepy, 5), 65 (C_5H_5, 10). *Anal*. Found: C, 76.2; H, 5.5; N, 17.8. Calc. for $C_{15}H_{13}N_3$: C, 76.6; H, 5.6; N, 17.9%.

2.4. Synthesis of the metal complexes

2.4.1. Complexes $Co(HL)_2(NO_3)_2 \cdot xH_2O$ with $HL = HL^0$ (1), HL^1 (4)

The reactions were carried out under anaerobic conditions. The appropriate ligand (HL^0, HL^1) (0.45 mmol: HL^0, 0.10 g; HL^1, 0.11 g) was added to a solution of the $Co(NO_3)_2 \cdot 6H_2O$ (0.06 g, 0.21 mmol) in THF (10 ml). Upon addition no appreciable change in colour was observed, but after 24 h crystalline solids were obtained, which were filtered off and dried in vacuo.

1: IR (KBr, cm^{-1}): ν(N–H) 3122, $\nu(C–H)_{ar}$ 3068, ν(C=C), ν(C=N) 1612, 1574, $\nu(NO_3)$ 1385, $\delta(C–H)_{OOP}$ 763, ν(Co–N) 414, ν(Co–O) 284, ν(Co–N) 256. IR (Nujol, cm^{-1}): $\nu(NO_3)$ 1769, 1741. UV–Vis (methanol 1.23×10^{-3} M, nm): λ (ε) 614 (6), 471 (57). Solid state (KBr, nm): λ 706, 506.

4: IR (KBr, cm^{-1}): ν(N–H) 3143, $\nu(C–H)_{ar}$ 3063, ν(C=C), ν(C=N) 1614, 1571, $\nu(NO_3)$ 1387, $\delta(C–H)_{OOP}$ 766, ν(Co–N) 374, ν(Co–O) 274. IR (Nujol, cm^{-1}): $\nu(NO_3)$ 1767. UV–Vis (methanol 2.27×10^{-3} M, nm): λ (ε) 1606 (40), 489 (49). Solid state (KBr, nm): λ 698, 591, 518.

2.4.2. Complexes $Co(HL)_2X_2 \cdot xH_2O$ with HL^0 and X = Cl (2), and X = Br (3), or HL^1 and X = Cl (5), and X = Br (6)

0.25 mmol of the appropriate metal salt ($CoCl_2 \cdot 6H_2O$, 0.059 g; $CoBr_2 \cdot 6H_2O$, 0.082 g) was added to a solution of 0.45 mmol of the ligand (HL^0, 0.10 g; HL^1, 0.11 g) in ethanol (99%, 40 ml). The mixture was heated with stirring for 20 h, concentrated until a crystalline precipitate appeared, which was filtered off, washed with ethanol (5 ml) and diethyl ether (5 ml) and vacuum dried.

2: IR (KBr, cm^{-1}): ν(N–H) 3183, $\nu(C–H)_{ar}$ 3058, ν(C=C), ν(C=N) 1609, 1573, $\delta(C–H)_{OOP}$ 764, ν(Co–N) 410, ν(Co–Cl) 280. UV–Vis (methanol 1.16×10^{-3} M, nm): λ (ε) 614 (8), 477 (40). (CH_3CN 1.00×10^{-3} M, nm): λ (ε) 685 (119), 589 (95). Solid state (KBr, nm): λ 712, 506.

3: IR (KBr, cm^{-1}): ν(N–H) 3178, $\nu(C–H)_{ar}$ 3081, ν(C=C), ν(C=N) 1609, 1572, $\delta(C–H)_{OOP}$ 763, ν(Co–N) 412, ν(Co–Br) 278, ν(Co–N) 238. UV–Vis (methanol 1.20×10^{-3} M, nm): λ (ε) 614 (6), 464 (112). (CH_3CN 0.98×10^{-3} M, nm): λ (ε) 697 (134), 618 (105). Solid state (KBr, nm): λ 698, 498.

5: IR (KBr, cm^{-1}): ν(N–H) 3112, $\nu(C–H)_{ar}$ 3059, ν(C=C), ν(C=N) 1612, 1570, $\delta(C–H)_{OOP}$ 765, ν(Co–N) 372, ν(Co–Cl) 296, ν(Co–N) 258. UV–Vis (methanol 3.86×10^{-3} M, nm): λ (ε) 1612 (23), 640 (5), 500 (29). (CH_3CN 0.29×10^{-3} M, nm): λ (ε) 664 (530), 570 (363). Solid state (KBr, nm): λ 666, 590, 518.

6: IR (KBr, nm): ν(N–H) 3201, $\nu(C–H)_{ar}$ 3058, ν(C=C), ν(C=N) 1612, 1569, $\delta(C–H)_{OOP}$ 765, ν(Co–N) 372, ν(Co–Br) 280, 260. UV–Vis (methanol 3.67×10^{-3} M, nm): λ (ε) 1612 (19), 497 (28). (CH_3CN 0.29×10^{-3} M, nm): λ (ε) 664 (370), 590 (199). Solid state (KBr, nm): λ 666, 591, 518.

2.4.3. Complexes $Co(HL)X_2 \cdot xH_2O$ with HL^0 and X = Cl (7) or HL^1 and X = Cl (8), and X = Br (9)

The reactions were carried out under a dinitrogen atmosphere. To a Schlenk flask containing deoxygenated warm THF (20 ml) was added, in this order, 3-phenyl-5(2-pyridyl)pyrazole (0.10 g, 0.45 mmol), and $CoX_2 \cdot 6H_2O$ (0.45 mmol). The resulting solution was stirred at room temperature for 24 h and concentrated on a vacuum line to one-fifth of the initial volume. After standing at room temperature for a few hours, crystalline solids were obtained, which were filtered off and dried in vacuo, washed with THF and vacuum dried.

7: IR (KBr, cm^{-1}): ν(N–H) 3192, $\nu(C–H)_{ar}$ 3061, ν(C=C), ν(C=N) 1611, 1572, $\delta(C–H)_{OOP}$ 765, ν(Co–N) 412, ν(Co–Cl) 296, ν(Co–N) 236. UV–Vis (methanol 1.55×10^{-3} M, nm): λ (ε) 614 (5), 493 (26). (CH_3CN 1.30×10^{-3} M, nm): λ (ε) 684 (341), 588 (263). Solid state (KBr, nm): λ 700, 641.

8: IR (KBr, nm): ν(N–H) 3158, $\nu(C–H)_{ar}$ 3066, ν(C=C), ν(C=N) 1615, 1566, $\delta(C–H)_{OOP}$ 764, ν(Co–N) 372, ν(Co–Cl) 280, 268. UV–Vis (methanol 4.44×10^{-3} M, nm): λ (ε) 1608 (28), 494 (87). (CH_3CN 0.90×10^{-3} M, nm): λ (ε) 668 (256), 572 (129). Solid state (KBr, nm): λ 662, 591.

9: IR (KBr, nm): ν(N–H) 3162, $\nu(C–H)_{ar}$ 3065, ν(C=C), ν(C=N) 1615, 1565, $\delta(C–H)_{OOP}$ 763, ν(Co–N)

Table 1
Physical and analytical data for the complexes

Compound	Colour	Yield (%)	Analysis [a]			Conductivity (Ω^{-1} cm^2 mol^{-1})
			C (%)	N (%)	H (%)	
$Co(HL^0)_2(NO_3)_2\cdot H_2O$ (**1**)	pink	87	(52.3) 52.8	(17.4) 17.4	(3.8) 3.7	154 [b]
$Co(HL^1)_2(NO_3)_2\cdot H_2O$ (**4**)	pink	80	(53.6) 53.5	(16.7) 16.7	(4.2) 4.1	109 [b]
$Co(HL^0)_2Cl_2\cdot 2H_2O$ (**2**)	pink	90	(55.3) 55.6	(13.8) 14.0	(4.3) 4.0	110 [b], 55 [c]
$Co(HL^1)_2Cl_2\cdot EtOH$ (**5**)	pink	91	(59.4) 59.1	(13.0) 12.8	(4.9) 4.8	90 [b], 47[c]
$Co(HL^0)_2Br_2\cdot 3H_2O$ (**3**)	pink	77	(47.0) 47.2	(11.7) 11.7	(3.9) 3.9	154 [b], 115 [c]
$Co(HL^1)_2Br_2\cdot H_2O$ (**6**)	pink	70	(50.9) 51.0	(11.9) 11.6	(4.0) 3.8	110 [b], 68 [c]
$Co(HL^0)Cl_2\cdot 2H_2O$ (**7**)	blue	83	(43.4) 43.7	(10.8) 10.6	(3.9) 3.6	135 [b], 71 [c]
$Co(HL^1)Cl_2\cdot H_2O$ (**8**)	blue	55	(47.0) 47.1	(11.0) 10.9	(3.9) 3.3	90 [b], 19 [c]
$Co(HL^1)Br_2\cdot 1/2H_2O$ (**9**)	green	41	(38.9) 38.9	(9.1) 9.1	(3.0) 2.6	125 [b], 56 [c]
$Co(HL^0)(OH)Br\cdot H_2O$ (**10**)	blue	73	(42.5) 42.9	(10.6) 10.5	(3.6) 2.9	148 [b], 68 [c]

[a] Calculated analytical values are given in parentheses.
[b] 10^{-3} M in methanol.
[c] 10^{-3} M in acetonitrile.

374, ν(Co–Br) 288, 266. UV–Vis (methanol 3.67×10^{-3} M, nm): λ (ε) 1610 (27), 492 (52). (CH_3CN 0.43×10^{-3} M, nm): λ (ε) 670 (519), 594 (244). Solid state (KBr, nm): λ 666, 593.

2.4.4. Complex $Co(HL^0)(OH)Br\cdot H_2O$ (**10**)

The procedure was the same as given above (using bromide salt instead of chloride) but concentration of the reagent mixture almost to dryness was necessary in order to obtain crystalline solid. This was filtered off, washed with THF, and dried in vacuo.

10: IR (KBr, nm): ν(N–H) 3194, ν(C–H)$_{ar}$ 3065, ν(C=C), ν(C=N) 1610, 1572, δ(C–H)$_{OOP}$ 764, ν(Co–N) 414, ν(Co–Br) 282, 271. UV–Vis (methanol 1.52×10^{-3} M, nm): λ (ε) 614 (7), 478 (30). (CH_3CN 1.26×10^{-3} M, nm): λ (ε) 696 (205), 617 (136). Solid state (KBr, nm): λ 725, 702, 665.

Table 1 shows the analytical and physical data for all complexes.

2.5. X-ray crystal structure analysis

Suitable crystals for X-ray diffraction experiments of the compound $[Co(HL^0)_2Cl(H_2O)]Cl\cdot H_2O$ were obtained by crystallization from acetonitrile. One crystal was mounted on an Enraf-Nonius CAD4 diffractometer. Intensities were collected using the ω–2θ scan mode to $2\theta_{max}=50°$. Graphite-monochromated Mo Kα radiation was used. The structure was solved by direct methods (SHELXS-86) [13] and refined by full-matrix least-squares methods on F^2 for all reflections (SHELXL-97) [14]. The final $R(F)$ and $R_w(F^2)$ values as well as the number of parameters refined and other details concerning the refinement of the crystal structure are presented in Table 2. The weight was $w^{-1}=\sigma^2(F_o^2)+(0.064P)^2+0.1183P$ where $P=(F_o^2+2F_c^2)/3$.

Table 2
Crystal data and structure refinement

Compound	$[Co(HL^0)_2ClH_2O]Cl\cdot H_2O\cdot 0.2CH_3CN$
Empirical formula	$C_{28.4}H_{26.6}Cl_2CoN_{6.2}O_2$
Formula weight	616.59
Temperature (K)	293(2)
Wavelength	0.71069
Crystal system, space group	triclinic, $P\bar{1}$ (no. 2)
a (Å)	10.466(4)
b (Å)	10.918(5)
c (Å)	13.436(4)
α (°)	74.99(3)
β (°)	78.02(3)
γ (°)	72.77(4)
Volume (Å^3)	1402.0(9)
Z, calculated density (Mg m^{-3})	2, 1.461
Absorption coefficient (mm^{-1})	0.841
Crystal size (mm)	$0.50\times0.40\times0.36$
Unique data/restraints/parameters	4936/8/376
Goodness-of-fit on F^2	1.062
Final R indices ($I>2\sigma(I)$)	$R(F)=0.0337$, $R_w(F^2)=0.0939$
R indices (all data)	$R(F)=0.0418$, $R_w(F^2)=0.0954$
Largest difference peak and hole (e Å^{-3})	0.269 and −0.602

3. Results and discussion

3.1. The synthesis and spectroscopic properties of the complexes

The β-diketone compounds 1-phenyl-3-(2-pyridyl)-1,3-propanodione and 1-phenyl-3-(6-methyl-(2-pyridyl))-1,3-propanodione have been synthesized following a Claisen condensation of the appropriate ketones and esters. Further treatment of these β-diketone compounds with hydrazine in toluene yielded the expected pyrazole-derived ligands 3-phenyl-5-(2-pyridyl)pyrazole and 3-phenyl-5-(6-methyl-(2-pyridyl))pyrazole (Fig. 2).

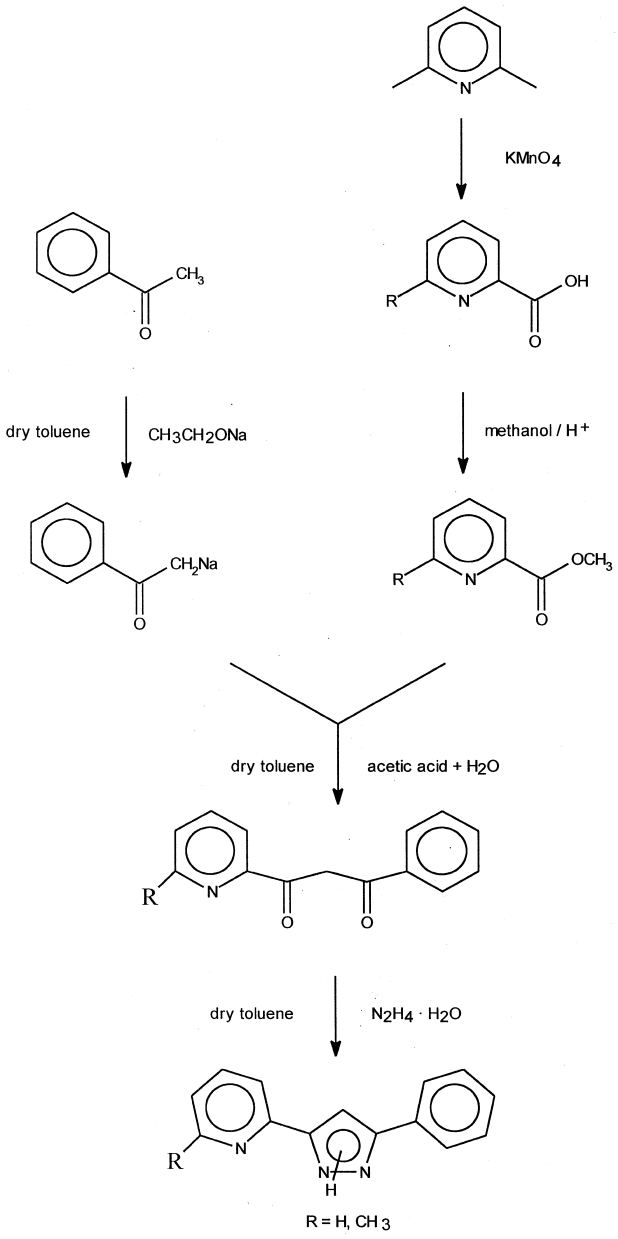


Fig. 2. Scheme of synthesis of the ligands.

In chloroform, the β-diketones here described are in equilibrium with the corresponding ketoenol forms, in the ratio 5% β-diketone to 95% ketoenol (quantified by NMR).

The complexes $Co(HL)X_2$ and $Co(HL)_2X_2$ were obtained by reacting the appropiate metal salt with the corresponding pyrazole ligand in an M:L ratio of 1:1 and 1:2, respectively.

The conductivity of the complexes was measured (Table 1). The values of the nitrate complexes are high enough to assess the non-coordinated nature of the nitrate anion. As for the complexes of formula $Co(HL)X_2$, $Co(HL)_2X_2$ and Co(HL)(OH)Br, different values were found, depending on the solvent. The conductivity in methanol was 90–150 Ω^{-1} cm^2 mol^{-1} (consistent with 1:1 electrolyte) whereas that in acetonitrile was 20–150 Ω^{-1} cm^2 mol^{-1} (in agreement with the non-electrolytic nature of the complexes). The reported values for 1:1 and 1:2 electrolytes in methanol are 80–115 and 160–220 Ω^{-1} cm^2 mol^{-1}, respectively and, in acetonitrile, the values are 120–160 and 220–300 Ω^{-1} cm^2 mol^{-1}, respectively [15,16].

The IR spectra of the nitrate containing complexes are a valuable tool in elucidation of their stereochemistry. Such studies are frequently based on the behaviour of the $\nu_3(E', D_{3h})$ band, which is very sensitive to the coordination mode of the nitrate group. Several bands are attributable to the organic ligands in the N–O stretching mode region, which hinders the analysis of the ν_3 band. Lever and Montovani [17] have shown that the $\nu_1 + \nu_3(E', D_{3h})$ combination band is useful for structural purposes. This band, near 1750 cm^{-1}, is generally not overlapped by other ligand bands. The results of the analysis of the IR absorptions in the $(\nu_1 + \nu_3)$ combination band region of the complexes synthesized were as follows: the complex $Co(HL^0)_2(NO_3)_2$ (**1**) exhibits the typical two bands (1769, 1741 cm^{-1}) of a monodentate nitrate group [18,19]. However, in spite of the band at 1769 cm^{-1}, other ionic nitrate groups cannot be ruled out. In addition, the compound exhibits two bands in the N–O stretching mode region at 1448 and 1284 cm^{-1}, as in monodentate nitrate groups [20].

The complex $Co(HL^1)_2(NO_3)_2$ (**4**) shows one single band at 1767 cm^{-1}, which is consistent with the ionic behaviour of the nitrate group.

The IR spectra of halide complexes in the region 400–100 cm^{-1} were also studied. The complexes $Co(HL)Cl_2$ (**7**, **8**) and $Co(HL)_2Cl_2$ (**2**, **5**) display two well-defined ν(Co–Cl) bands each at 326, 268 cm^{-1} and 296, 258 cm^{-1}, respectively. The bromide derivatives $Co(HL)Br_2$ (**9**) and $Co(HL)_2Br_2$ (**3**, **6**) show two bands ν(Co–Br), at 288 and 260 cm^{-1}, respectively. ν(Co–N(pz)) bands are in the range 414–220 cm^{-1} [21,22]. For the complex $Co(HL^0)(OH)Br$ (**10**) no bands are attributable to OH.

Electronic spectra for the synthesized complexes were measured in methanol, in acetonitrile, and in KBr pellets (reflectance diffuse).

The spectra of Co(II) compounds in methanolic solution show one band in the visible region between 580 and 450 nm (ε = 25–112 mol^{-1} cm^{-1} l), as in octahedral Co(II) complexes [23–25]. The Co(II)-halide complexes in acetonitrile show two bands between 700–660 nm (ε = 120–530 mol^{-1} cm^{-1} l) and 620–550 nm (ε = 95–363 $mol^{-1}cm^{-1}$ l), respectively. The position and intensity of the bands between 700–660 nm are indicative of the $^4A_2 \rightarrow {}^4T_1(P)$ transition of the d^7 ion in a tetrahedral field [26,27], while the bands at 620–550 nm agree with of the transition of the d^7 ion in an octahedral field $^4T_{1g}(F) \rightarrow {}^4T_{1g}(P)$ [7,28]. The presence of two types of absorption is consistent with the coexistence of tetrahedral and octahedral species in solution[24]. The Co(II)-nitrate compounds are insoluble in acetonitrile.

The spectra of the Co(II) complexes were also measured following diffuse reflectance methods. The complexes $Co(HL)X_2$ show one broad band from 750 to 575 nm, in the visible region, which can be assigned to the $^4A_2 \rightarrow {}^4T_1(P)$

transition of the d^7 ion in a tetrahedral field [24,25,29]. The compounds $Co(HL)_2X_2$ show two bands: one weak band between 712 and 690 nm and a broad intense band between 506 and 498 nm. This spectrum suggests that the complexes have a distorted octahedral geometry [24,25,29].

3.2. Crystal structure of $[Co(HL^0)_2Cl(H_2O)]Cl \cdot H_2O \cdot 0.2CH_3CN$ (2)

The molecular structure of the complex (Fig. 3) consists of discrete $[Co(HL^0)_2Cl(H_2O)]^+$ cations, Cl^- anions and solvent molecules (H_2O, MeCN). The cation complex is mononuclear. Table 3 lists selected bond distances and angles.

In the cation, the metal atom, with a distorted octahedral geometry, is coordinated to one Cl atom, one H_2O molecule and two pairs of nitrogen atoms, which correspond to two HL^0 ligands. Each ligand uses only two of its three nitrogen atoms, the pyridinic nitrogen and one of the two pyrazolic nitrogens, acting as a bidentate ligand and forming a five-membered metallocycle.

Three structures with a $Co(II)N_4ClO$ core have been described, two with Cl and O in *cis* arrangement [30,31] and one with Cl and O in *trans* arrangement [32].

The Co–Cl distance, in compound **2** is in the range observed for the *cis* structures (2.400–2.379 Å), and is significantly shorter than the distance found in the *trans* structure (2.617 Å). Likewise, the Co–O bond length is similar to those found in the *cis* complexes (2.319–2.084 Å) and shorter than that found in the *trans* compound (2.341 Å). The O–Co–Cl angle 94.20(6)° is also in the range observed for the reported structures (90–103°). The Co–Npy bond distances (0.06 Å average) are clearly longer than those of Co–Npz. The Co–Npy bond distances are consistent with described values (1.927–2.343 Å) [33].

Twelve structures with Co(II) containing pyrazol ligands have been described. The most common coordination for Co(II) in these structures is tetrahedral, except in four cases, where the coordination is octahedral [34–37]. The Co–Npz bond distances of compound **2** are similar to those found in these four structures.

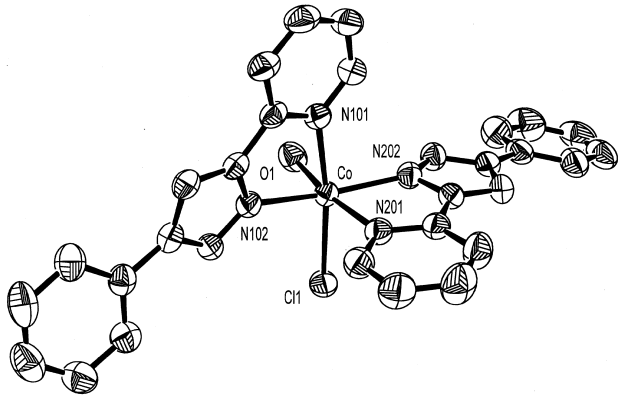


Fig. 3. An ORTEP view of the structure of $[Co(HL^0)_2Cl(H_2O)]^+$. The thermal ellipsoids enclose 50% probability.

The N(102)–Co–N(101) and N(202)–Co–N(201) bite angles, 75.51(8) and 75.31(7)° respectively, are similar to those found in dinuclear nickel(II) and copper(II) compounds with the related ligand 3,5-bis(2-pyridyl) pyrazole (hereafter abbreviated as Hbpypz): 77.8(1)° in $[Ni_2(bpypz)_2(MeOH)_4]Cl_2 \cdot 2H_2O$ (**4**), 79.8(2)° in $[Cu_4(bpypz)_4(H_2O)_4](NO_3)_4 \cdot 4H_2O$ [8], 80.3(2)° in $[Cu_4(bpypz)_4(ClO_4)_4] \cdot 2H_2O$ [10] and in a mononuclear Ag(I) compound 70.7(4)° [10].

The ligand HL^0 is not completely planar. The pyridyl and phenyl groups are slightly twisted with respect to the pyrazole ring with different dihedral angles for the two ligands: in ligand 1, the py–pz angle is 3.87(9)°, the ph–pz angle is 18.60(9)° and the py–ph angle is 14.92(9)°; while in ligand 2, the py–pz angle is 9.18(8)°, the ph–pz angle is 7.50(9)° and the py–ph angle is 16.48(8)°. The dihedral angle between ligand mean planes is 89.21(6)° and 94.88(9)° between pz1 and pz2. The phenyl rings are on opposite sites of the coordination sphere.

Two cations, related by an inversion centre, are linked by two NH–Cl hydrogen bonds and OH–OH–Cl additional hydrogen bonds involving two non-coordinated water molecules. These dimers and two non-coordinating Cl ions are also bonded by hydrogen bonds, yielding infinite chains parallel to the crystallographic vector *a* (Table 4, Fig. 4).

Table 3
Selected bond lengths (Å) and angles (°)

Co–O(1)	2.0845(18)		
Co–N(102)	2.1035(19)		
Co–N(202)	2.1141(19)		
Co–N(101)	2.169(2)		
Co–N(201)	2.1831(19)		
Co–Cl(1)	2.3987(12)		
O(1)–Co–N(102)	95.81(7)	N(202)–Co–N(201)	75.31(7)
O(1)–Co–N(202)	95.08(7)	N(101)–Co–N(201)	89.27(7)
N(102)–Co–N(202)	163.71(7)	O(1)–Co–Cl(1)	94.20(6)
O(1)–Co–N(101)	90.99(8)	N(102)–Co–Cl(1)	93.70(6)
N(102)–Co–N(101)	75.51(8)	N(202)–Co–Cl(1)	97.55(6)
N(101)–Co–Cl(1)	168.47(5)	N(202)–Co–N(101)	92.23(8)
N(201)–Co–Cl(1)	87.33(6)	O(1)–Co–N(201)	170.39(6)
N(102)–Co–N(201)	93.56(7)		

Table 4
Distances and angles related to hydrogen bonding

	D–H	A···H	D···A	D–H···A
O2–H22···Cl2 [a]	0.85(2)	2.34(2)	3.189(3)	172(2)
O1–H11···O2^{i} [b]	0.86(2)	1.87(2)	2.720(3)	168(2)
O1–H12···Cl2^{ii}	0.85(2)	2.28(2)	3.107(2)	162(2)
N203–H23···Cl2^{ii} [a]	0.860(2) [c]	2.317(1)	3.088(3)	149.4(1)
N103–H13···Cl1^{iii}	0.860(2) [c]	2.520(1)	3.202(2)	136.9(1)
O2–H21···Cl1^{iv}	0.88(2)	2.35(2)	3.198(3)	161(2)

[a] O2 is the non-coordinated water molecule and Cl2 is the non-coordinated Cl atom.
[b] (i) $x, y+1, z$; (ii) $-x, -y+1, -z+1$; (iii) $-x+1, -y+2, -z+1$; (iv) $-x+1, -y+1, -z+1$.
[c] N–H distances have been fixed.

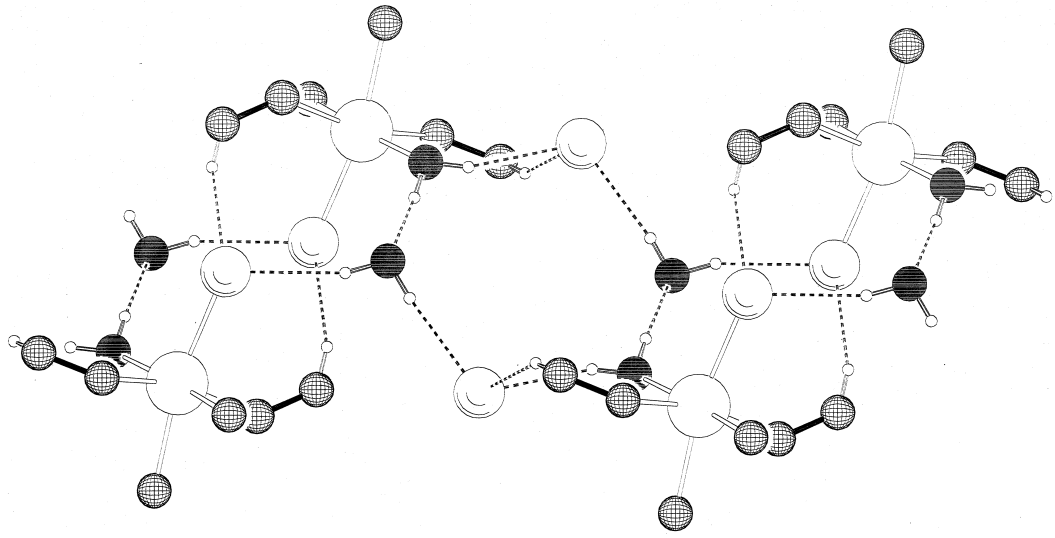


Fig. 4. A partial view of the infinite chain formed by the different units of $[Co(HL^0)_2Cl(H_2O)]Cl \cdot H_2O$ bonded by hydrogen bonds.

4. Conclusions

The study of the coordination of 3-phenyl-5-(2-pyridyl)pyrazole (HL^0) and 3-phenyl-5-(6-methyl-(2-pyridyl)pyrazole (HL^1) to Co(II) has revealed the formation of $Co(HL)X_2$ and $Co(HL)_2X_2$ compounds.

The conductivity measurements and spectroscopic data of the complexes are consistent with mononuclear structures where neutral HL pyrazole ligands coordinate the metal centre in a bidentate form. The electronic spectra of the compounds in methanol suggest that the geometry of the complexes is octahedral, whereas experiments in acetonitrile agree with the coexistence of tetrahedral and octahedral species in solution. Diffuse reflectance spectra have shown that $Co(HL)X_2$ complexes are tetrahedral and that $Co(HL)_2X_2$ are octahedral in the solid state. The X-ray structure of the compound $[Co(HL^0)_2Cl(H_2O)]Cl$ indicates that the coordination of metal in $Co(HL)_2X_2$ complexes is octahedral and that the anions which can be replaced by solvent molecules in the coordination sphere of Co(II) are labile, in agreement with the conductivity results. These results reveal that the ligands HL^0 and HL^1 are appropriate candidates for studies on the coordination of Zn^{2+} centres in order to provide models of zinc metalloenzymes. The geometry of Zn^{2+} in biological systems has proved to be crucial for its biological activity [38].

Supplementary data

Additional material, consisting of fractional atomic coordinates, displacement parameters, observed and calculated structure factors and complete lists of bond distances and bond angles are available from the CCDC, deposition number 134331. Copies of the data can be obtained free of charge on application to Cambridge Crystallographic Data Centre, 12 Union Road, Cambridge CB2 1EZ, UK (fax: +44-1223-336033; e-mail: deposit@ccdc.cam.ac.uk).

Acknowledgements

We thank CICYT (MAT91-0952) and DGICYT (PB96-1146) for financial support. A.C. is grateful for a grant from Ministerio de Asuntos Exteriores: Agencia Española de Cooperación Internacional (Instituto de cooperación con el mundo árabe).

References

[1] S. Trofimenko, Chem. Rev. 72 (1972) 497.
[2] S. Trofimenko, Progress in Inorganic Chemistry, vol. 34, Wiley-Interscience, New York, 1986, p. 115.
[3] G. La Monica, G.A. Ardizzoia, Progress in Inorganic Chemistry, vol. 46, Wiley-Interscience, New York, 1997, p. 151.
[4] J. Catalán, J.L.M. Abboud, J. Elguero, Adv. Heterocycl. Chem. 41 (1987) 187.
[5] J.G. Vos, W.C. Groeneveld, Inorg. Chim. Acta 26 (1978) 71.
[6] J. Casabó, J. Pons, K. Siddiqi, F. Teixidor, E. Molins, C. Miravitlles, J. Chem. Soc., Dalton Trans. (1989) 1401.
[7] J. Pons, X. López, E. Benet, J. Casabó, F. Teixidor, F.J. Sánchez, Polyhedron 9 (1990) 2839.
[8] J. Pons, X. López, J. Casabó, F. Teixidor, A. Caubet, J. Rius, C. Miravitlles, Inorg. Chim. Acta 195 (1992) 61.
[9] J. Pons, F. J. Sánchez, A. Labarta, J. Casabó, F. Teixidor, A. Caubet, Inorg. Chim. Acta 208 (1993) 167.
[10] M. Munakata, L.P. Wu, M. Yamamoto, T. Kurodasowa, M. Maekawa, S. Kawata, S. Kitagawa, J. Chem. Soc., Dalton Trans. (1995) 4099.
[11] A.I. Vogel, Textbook of Practical Organic Chemistry, Longman, London, 4th edn., 1978.
[12] G. Black, E. Depp, B.B. Corson, J. Org. Chem. 14 (1949) 14.
[13] G.M. Sheldrick, SHELXS-86, Program for crystal structure determination, University of Göttingen, Germany, 1986.
[14] G.M. Sheldrick, SHELXL-97, Program for crystal structure refinement, University of Göttingen, Germany, 1997.
[15] W.J. Geary, Coord. Chem. Rev. 7 (1971) 81.
[16] L.K. Thompson, F.L. Lee, E.J. Gabe, Inorg. Chem. 27 (1988) 39.
[17] A.B.P. Lever, E. Montovani, Inorg. Chem. 10 (1971) 817.
[18] M. Shakir, S.P. Varkey, Polyhedron 13 (1994) 791.
[19] M.A.S. Goher, M.A.M. Abu-Youssef, F.A. Mautner, Polyhedron 15 (1996) 453.

[20] C.C. Addison, D. Sutton, Progress in Inorganic Chemistry, vol. 8, Wiley-Interscience, New York, 1967, p. 195.
[21] K. Nakamoto, Infrared Spectra of Inorganic and Coordination Compounds, Wiley, New York, 4th edn., 1986.
[22] J.H. Clark, C.S. Williams, Inorg. Chem. 4 (1965) 350.
[23] D. Sutton, Electronic Spectra of Transition Metal Complexes, McGraw-Hill, UK, 1st edn., 1975.
[24] F.A. Cotton, G. Wilkinson, Advanced Inorganic Chemistry, Wiley, New York, 5th edn., 1988.
[25] J.C. Bailar, H.J. Emeléus, S.R. Nythorm, A.F.T. Dickenson, Comprehensive Inorganic Chemistry Board, Pergamon, Oxford, 1st edn., 1973.
[26] J.C. Plakatouras, S.P. Perlepes, D. Mentzafos, A. Terzis, T. Bakas, V. Papaefthymiou, Polyhedron 11 (1992) 2657.
[27] K. Nakashiro, Y. Or, Bull. Chem. Soc. Jpn. 66 (1993) 9.
[28] L. Rosenberg, L. K. Thompson, E. J. Gabe, F. L. Lee, J. Chem. Soc., Dalton Trans. (1986) 625.
[29] J. Ferguson, Progress in Inorganic Chemistry, vol. 12, Wiley-Interscience, New York, 1970, p. 159.
[30] A.Yu. Kon, I.F. Burshtein, N.N. Proskina, M.A. Simonov, Koord. Khim. 8 (1982) 225.
[31] A. Monge, M. Martínez-Ripoll, E. Gutierrez-Puebla, S. García-Blanco, Acta Crystallogr., Sect. B 35 (1979) 3062.
[32] A. Ceulemans, B. Coninckx, M. Vanhecke, Th. Zeegers-Huyskens, G.S.D. King, Inorg. Chim. Acta 202 (1992) 101.
[33] F.A. Allen, J.E. Davies, J.J. Galloy, O. Johnson, O. Kennard, C.F. Macrae, E.M. Mitchell, G.F. Mitchell, J.M. Smith, D.G. Watson, J. Chem. Inf. Comput. Sci. 31 (1991) 187.
[34] G. Hanggi, H. Schmalle, E. Dubler, Inorg. Chem. 27 (1988) 3131.
[35] G. Hanggi, H. Schmalle, E. Dubler, Acta Crystallogr., Sect. C 44 (1988) 1560.
[36] G. Hanggi, H. Schmalle, E. Dubler, Inorg. Chem. 32 (1993) 6095.
[37] V.Kh. Kravtsov, O.A. Bologa, Yu.A. Simonov, V.I. Lozan, N.V. Gerbeleu, T.I. Malinovski, Koord. Khim. 21 (1995) 549.
[38] C. Bergquist, G. Parkin, Inorg. Chem. 38 (1999) 422 and Refs. therein.

PERGAMON

www.elsevier.nl/locate/poly

Polyhedron 19 (2000) 863–870

POLYHEDRON

Synthesis, structure and spectroscopy of rare earth hypophosphites: 3. Ytterbium hypophosphite [1]

Peter A. Tanner [a,*], Chris S.K. Mak [a], Thomas C.W. Mak [b]

[a] *Department of Biology and Chemistry, City University of Hong Kong, Tat Chee Avenue, Kowloon Hong Kong SAR, People's Republic of China*
[b] *Department of Chemistry, The Chinese University of Hong Kong, Shatin, New Territories, Hong Kong SAR, People's Republic of China*

Received 13 October 1999; accepted 14 February 2000

Abstract

$Yb(H_2PO_2)_3$ crystallizes in space group $C2/m$. Planar rectangular arrays of Yb^{3+} ions are doubly bridged by hypophosphite ions in the *b* direction and singly bridged in the *c* direction, giving rise to a stacking of corrugated layers in the crystal structure. The YbO_6 site symmetry is C_{2h}, but not far from D_{4h}. The vibrational spectra of the hypophosphite anion have been interpreted in detail using unit cell group analysis and are shown to be consistent with the crystallographic data. The 10 K electronic absorption spectrum confirms the presence of two non-equivalent Yb^{3+} ions situated at centrosymmetric sites in the unit cell. For the first time, the two-centre transitions in the vibronic sidebands have been assigned to the excitation of individual unit cell group modes, showing a one-to-one correspondence with the vibrational spectra. The importance of moiety mode–hypophosphite mode couplings, and of Yb^{3+}–hypophosphite interactions of the type quadrupole–dipole, or higher, is indicated in the interpretation of the intensities of the cooperative vibronic transitions. ©2000 Elsevier Science Ltd All rights reserved.

Keywords: Infrared spectroscopy; Raman spectroscopy; Electronic absorption spectroscopy; Crystal structures; Hypophosphite complexes; Cooperative vibronic transitions; Two-centre transitions

1. Introduction

We have recently reported the syntheses, crystal structures and spectroscopic behaviour of anhydrous and hydrated lanthanide hypophosphite complexes $Ln(H_2PO_2)_3$ (Ln = La, Pr, Nd) and $Ln(H_2PO_2)_3 \cdot H_2O$ (Ln = La, Pr) [1,2]. In both series of compounds, the lanthanide ion is eight-coordinate and hypophosphite ions bridge adjacent metal ions to give infinite chains, with additional one-oxygen atom bridges linking the chains in the former series. The structures of the hydrated Ln = La, Eu complexes have in fact been reported some time ago [3,4]. More recently, Seddon et al. [5,6] found that the reactions between $Ln(NO_3)_3$ and NaH_2PO_2 give, with controlled oxidation, the formation of $[Ln(H_2PO_2)(HPO_3)(H_2O)_n] \cdot nH_2O$. These authors reported two distinct types of anhydrous lanthanide hypophosphite: $Pr(H_2PO_2)_3$ type [5], with the lanthanide ion exhibiting eight-coordination as in $La(H_2PO_2)_3$; $Dy(H_2PO_2)_3$ type [6], with six-coordination for the smaller Ln^{3+} ion. Although the space group of $Dy(H_2PO_2)_3$ was equivalent to that previously reported for $Er(H_2PO_2)_3$ [7], there were important differences between the two determinations, such as large disparities between the Er(1)–O axial and equatorial bond distances (2.32 and 2.08 Å), as opposed to fairly similar Dy(1)–O bond distances (2.243 and 2.246 Å). We therefore decided to investigate the structure of the anhydrous lanthanide hypophosphite at the end of the series, which is expected to have the smallest Ln–O bond distances, $Yb(H_2PO_2)_3$ (hereafter, $Yb(hyp)_3$), in order to attempt to resolve these discrepancies. In addition, the spectral characteristics expected for the structural type $Yb(hyp)_3$, which are different from those of earlier members of $Ln(H_2PO_2)_3$ (Ln = La, Nd, Pr [2]), were of particular interest to us. The vibrational and electronic spectra of $Pr(H_2PO_2)_3$ have been assigned in detail [2], and both the different coordination geometry and the presence of non-equivalent Yb^{3+} ions in the unit cell of $Yb(hyp)_3$ would be expected to provide spectral manifestations. $Pr(H_2PO_2)_3$ was not found to be a suitable system for the investigation of vibronic transitions in the electronic spectra of lanthanide ions [2] because of overlapping electronic transitions, and the presence of obscuring impurity bands due to Nd^{3+}. The simple energy level structure of Yb^{3+}, together

* Corresponding author. Tel.: +852-2788-7840; fax: +852-2788-7406; e-mail: bhtan@cityu.edu.hk

[1] For part 1 of this series, see Ref. [2].

0277-5387/00/$ - see front matter ©2000 Elsevier Science Ltd All rights reserved.
PII S0277-5387(00)00333-8

with the ability to obtain large single crystals of $Yb(hyp)_3$, enabled a more detailed study to be undertaken herein of two-centre vibronic transitions.

2. Experimental

2.1. Synthesis of $Yb(hyp)_3$

$Yb(hyp)_3$ was prepared by dissolving 1 g (0.0025 mol) Yb_2O_3 (Strem Chemicals, 99.9%) in 9 cm^3 of 37% hydrochloric acid (Riedel-de Haën, RG) with heating and stirring in a 100 cm^3 beaker. After complete dissolution, 10 cm^3 of 50% hypophosphorous acid (Riedel-de Haën, RG) was added into the solution. The solution was then placed inside a desiccator for crystallization to occur at room temperature. Large crystals, up to several centimetres in length, and small needles were obtained from different preparations, and both were shown to be the same compound by X-ray examination.

2.2. Analytical results

Qualitative analysis of a single crystal of $Yb(hyp)_3$ by a Jeol T300 scanning electron microscope using electron microprobe analysis, showed only the presence of the elements Yb and P. Elemental analyses for Yb and P were carried out, after dissolution of the crystals in dilute nitric acid, using a Perkin-Elmer Plasma 1000 inductively coupled plasma atomic emission spectrometer. H was determined by a Leco 900 CHN-analyser. Fluorolube mull IR spectra showed the compound to be anhydrous.

Anal. Calc. for $Yb(hyp)_3$: Yb, 47.02; P, 25.25; H, 1.64. Found: Yb, 49.0 ± 0.8; P, 23.2 ± 0.4; H, 1.61 ± 0.03.

2.3. Spectroscopic measurements

Infrared Nujol and fluorolube mull spectra (resolution 2 cm^{-1}) were recorded at 90 and 295 K over the range 400–4000 cm^{-1} using Bomem MB120 and Perkin-Elmer PE1600 spectrometers. Raman spectra were recorded at 295 K by a Spex 1403DM system using <20 mW of 514.5 nm argon ion radiation. Electronic absorption spectra in the mid- and near-IR regions (4000–13500 cm^{-1}) were recorded as previously described [8] by a Biorad FTS65A wide-range spectrometer equipped with PbSe and Si detectors, at temperatures down to 10 K, at the resolution 2 cm^{-1}. A Glann-Taylor polarizer was employed to select polarizations parallel and perpendicular to the *b* crystal axis. The crystal was oriented according to the locations of the faces determined by X-ray methods on a smaller crystal.

2.4. X-ray analyses

The details of the crystal parameters, data collection and structure refinement are given in Table 1. The structure was solved by the direct method and refined by full-matrix least-squares on F^2 using the Siemens SHELXTL-93 (PC Version) package of crystallographic software [9]. All non-hydrogen atoms were refined with anisotropic thermal parameters. A distance restraint, which refined to 1.468(5) Å, was applied to all P–H bonds with respect to the coordinates of the hydrogen atoms.

Table 1
Crystal data and structure refinement for $Yb(hyp)_3$

Formula	$Yb(H_2PO_2)_3$
Crystal habit	colourless needle
Crystal size (mm)	$0.03 \times 0.04 \times 0.40$
Formula weight	368.00
Temperature (K)	293(2)
Wavelength (Å)	0.71073
Crystal system	monoclinic
Space group	$C2/m$ (no. 12)
Unit cell dimensions	
a (Å)	14.281(3)
b (Å)	5.658(1)
c (Å)	12.006(2)
α (°)	90
β (°)	122.26(3)
γ (°)	90
Volume (Å^3)	820.4(3)
Z	4
Calculated density (Mg m^{-3})	2.980
Absorption coefficient (mm^{-1})	11.960
$F(000)$	676
Theta range for data collection (°)	2.86–42.50
Limiting indices	$0 \le h \le 27,\ -10 \le k \le 0,\ -22 \le l \le 19$
Reflections collected/unique	3237/3149 ($R_{int} = 0.0185$)
Completeness to $\theta = 42.50°$ (%)	99.7
Refinement method	Full-matrix least-squares on F^2
Data/restraints/parameters	3149/5/70
Goodness-of-fit on F^2	1.039
Final R indices ($I > 2\sigma(I)$)	$R_1 = 0.0350$, $wR_2 = 0.0943$
R indices (all data)	$R_1 = 0.0584$, $wR_2 = 0.1076$
Extinction coefficient	0.0072(4)
Max. and min. shift	0.003 and 0.000
Largest difference peak and hole (e Å^{-3})	1.609 and -2.544

3. Results

3.1. Crystal structure of $Yb(hyp)_3$

The atomic coordinates and thermal parameters are listed as supplementary data. Bond lengths and bond angles are given in Table 2.

The crystal structure of $Yb(hyp)_3$ contains two independent ytterbium ions and three independent hypophosphite anions. The Yb(1) and Yb(2) atoms occupy different special positions of site symmetry $2/m = C_{2h}$. All three $H_2PO_2^-$ groups are located in mirror planes (Fig. 1). However, two $H_2PO_2^-$ groups (those centred at P(1) and P(2) and designated as such for subsequent discussion) each have the PH_2 fragment lying in the crystallographic mirror plane (and hence the O–P–O bond angle is bisected by this plane),

Table 2
Bond lengths (Å) and angles (°) for $Yb(hyp)_3$

Yb(1)–O(3)	2.187(4)
Yb(1)–O(1)	2.206(3)
Yb(2)–O(2)	2.197(3)
Yb(2)–O(4)	2.198(4)
P(1)–O(1)	1.494(3)
P(2)–O(2)	1.493(3)
P(3)–O(3)	1.454(5)
P(3)–O(4)	1.464(4)
O(3)–Yb(1)–O(1)	90.63(13)
O(1)#1–Yb(1)–O(1) [a]	90.20(16)
O(2)–Yb(2)–O(2)#1	90.39(16)
O(2)–Yb(2)–O(4)	89.21(11)
O(1)#2–P(1)–O(1)	115.9(3)
P(1)–O(1)–Yb(1)	148.3(2)
O(2)–P(2)–O(2)#3	116.6(2)
P(2)–O(2)–Yb(2)	150.5(2)
O(3)–P(3)–O(4)	120.8(3)
P(3)–O(3)–Yb(1)	160.4(4)
P(3)–O(4)–Yb(2)	150.1(3)

[a] Symmetry transformations used to generate equivalent atoms: #1 $x, -y, z$; #2 $x, -y+1, z$; #3 $x, -y-1, z$.

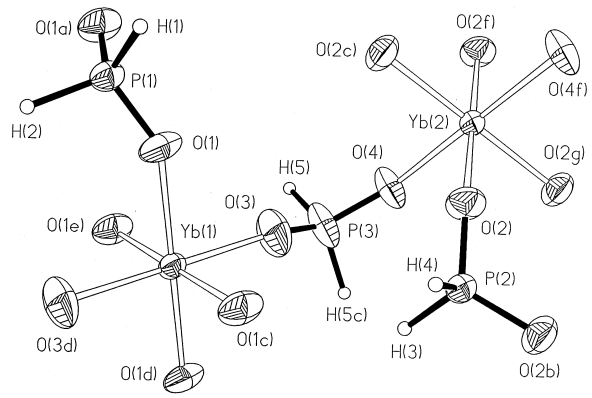


Fig. 1. Three independent hypophosphite groups and coordination environment about the ytterbium ions with atom labelling scheme. The non-hydrogen atoms are represented by thermal ellipsoids at the 50% probability level. Symmetry transformations: a $x, 1-y, z$; b $x, -1-y, z$; c $x, -y, z$; d $1-x, -y, -z$; e $1-x, y, -z$; f $1-x, -y, 1-z$; g $1-x, y, 1-z$.

whereas the third (designated as P(3)) has the PO_2 fragment lying in the crystallographic mirror plane. As seen from Fig. 2, the $H_2PO_2^-$ groups of type P(1) form double bridges between adjacent ytterbium atoms of type Yb(1) to form an infinite chain running parallel to the *b* axis. In an analogous manner, another chain is constructed from $H_2PO_2^-$ groups of type P(2) and ytterbium atoms of type Yb(2). These two kinds of chain are arranged alternately and cross-linked by $H_2PO_2^-$ groups of type P(3) to generate a corrugated layer as illustrated in Fig. 2. The crystal structure is composed of a stacking of such layers, whose mean planes correspond to the (200) family of planes, as shown in Fig. 3.

The coordination geometries of Yb(1) and Yb(2) are of distorted D_{4h} symmetry, each with two sets of Yb–O bond distances. The O–Yb–O angles are between 89.2 and 90.6°. These results are consistent with the study of Seddon et al. on $Dy(H_2PO_2)_3$ [6], but not with that of Aslanov et al. on $Er(H_2PO_2)_3$ [7]. From interpolation of the plot of Ln–O bond distance against ionic radius of Ln^{3+} (Ln = Dy, Yb), the mean Er–O bond distance is expected to be 2.22 Å, close to the average value 2.29 Å from [7]. However, the precision of measurement of individual Er–O bond distances in [7] is poor. The P(1)–O(1) and P(2)–O(2) bond distances in $Yb(hyp)_3$ are each about 0.4% shorter than the corresponding distances in $Dy(H_2PO_2)_3$, whereas the hypophosphite ion P(3) which bridges the non-equivalent Ln^{3+} ions has slightly longer ($<0.4\%$) P–O bond distances in $Yb(hyp)_3$.

The comparison of the mean Yb–O bond distance with those for other hypophosphite complexes of the six-coordinate group I cation Na^+ [10], group IIA cation Ca^{2+} [11] and group IIB cation Zn^{2+} [12] shows the trend of shorter M–O distances with decreasing ionic radius of M^{n+}. Each of these systems exhibits a range of P–O bond distances [10–

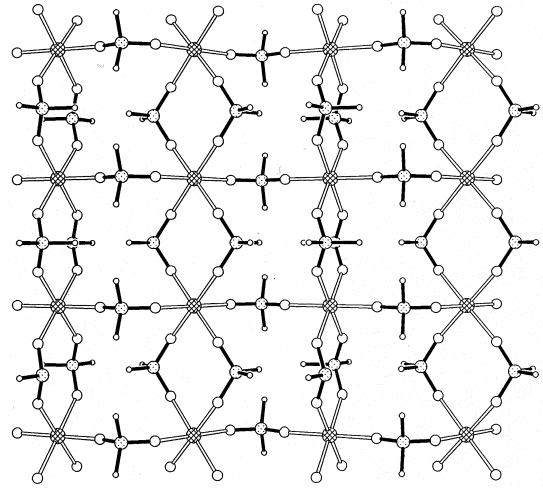


Fig. 2. A corrugated layer in the crystal structure of $Yb(H_2PO_2)_3$. The *b* axis is vertical, the *c* axis runs from left to right, and the mean plane of the layer is normal to the *a** axis. Starting from the left side of this figure, the structural motifs repeat in the following order: infinite chain built of Yb(1) and P(1), bridging P(3) groups, and infinite chain built of Yb(2) and P(2).

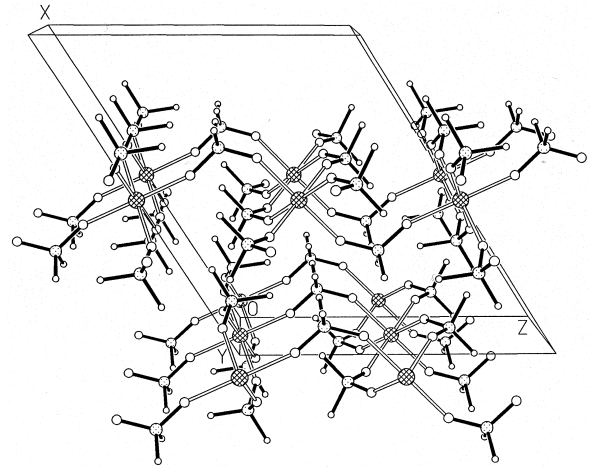


Fig. 3. Packing of adjacent corrugated layers in the crystal structure of $Yb(H_2PO_2)_3$. The origin of the unit cell lies in the lower left corner, with *a* pointing upward at a slant, *b* toward the reader, and *c* from left to right.

12], with values between 1.482–1.513 Å. The P(1)–O(1) and P(2)–O(2) distances in $Yb(hyp)_3$ fall within this range. However, the P(3)–(O) distances for the hypophosphite ion bridging the Yb(1) and Yb(2) chains are much shorter, in agreement with those reported for $Dy(H_2PO_2)_3$, and explicable by the longer O(hyp)–Ln distances in these cases. The Yb–O distances in $Yb(hyp)_3$ (ca. 2.2 Å) are much shorter than the Ln–O distances in the eight-coordinate earlier members of the series Ln = La, Pr (Ln–O between 2.4–2.6 Å).

Table 3
Unit cell group analysis of $H_2PO_2^-$ ions in $Yb(hyp)_3$. Irreducible representation of hypophosphite internal vibrational mode

Free ion mode, C_{2v}	Ion at C_s site symmetry	Ion in crystal, C_{2h} symmetry
P(1) and P(2)		
$(\nu_1,\nu_2,\nu_3,\nu_4)a_1 \rightarrow$	$a' \rightarrow$	$a_g + b_u$
$(\nu_5)a_2 \rightarrow$	$a'' \rightarrow$	$a_u + b_g$
$(\nu_6,\nu_7)b_1 \rightarrow$	$a' \rightarrow$	$a_g + b_u$
$(\nu_8,\nu_9)b_2 \rightarrow$	$a'' \rightarrow$	$a_u + b_g$
P(3)		
$(\nu_1,\nu_2,\nu_3,\nu_4)a_1 \rightarrow$	$a' \rightarrow$	$a_g + b_u$
$(\nu_5)a_2 \rightarrow$	$a'' \rightarrow$	$a_u + b_g$
$(\nu_6,\nu_7)b_1 \rightarrow$	$a'' \rightarrow$	$a_u + b_g$
$(\nu_8,\nu_9)b_2 \rightarrow$	$a' \rightarrow$	$a_g + b_u$

Table 4
Energies of bands in the room temperature Raman and IR spectra of $Yb(hyp)_3$

Wavenumber (cm^{-1})				Assignment [b]
IR		Raman		
		44	w [a]	rot. Or
		60	w	transl. YbO_6
		122	vw	δ(O–Yb–O)
		142	vw	rot. H_2PO_2
		176	m	δ(O–Yb–O)
		208	vw	δ(O–Yb–O)
254	mw			ν_{as}(Yb–O)
281	m	274	w	ν_{as}(Yb–O)
		300	w	ν_s(Yb–O)
454	m			
460	sh	464	m	PO_2 scissor ($\nu_4 a_1$)
484	m	482	w	
804	m			
814	m			PH_2 rock ($\nu_7 b_1$)
821	m	824	w	
(925)		922	vw	PH_2 twist ($\nu_5 a_2$)
(931)		938	w	
1064	s	1072	vs	PO_2 sym. stretch ($\nu_3 a_1$)
1076	s	1078	m	PH_2 wag ($\nu_9 b_2$)
1091	s	1098	m	
1141	sh	1153	vs	PH_2 scissor ($\nu_2 a_1$)
1154	vs			PO_2 antisym. stretch ($\nu_8 b_2$)
2345	w	2298	vw	combination bands
2361	sh	2382	m	
2377	s			PH_2 antisym. stretch ($\nu_6 b_1$)
2387	s	2393	s	PH_2 sym. stretch ($\nu_1 a_1$)
2403	sh			
2415	sh	2418	vw	

[a] s strong; m medium; w weak; sh shoulder; v very.
[b] rot. rotational; transl. translational; ν_{as}/antisym. antisymmetric stretch; ν_s/sym. symmetric stretch; δ bending mode. The labelling of hypophosphite modes and the C_{2v} symmetry irreps. are from [14].

3.2. Vibrational spectra of $Yb(hyp)_3$

Deuteration studies [13–15], the use of polarized radiation [16,17] and normal coordinate analyses [14,15,18] have enabled firm assignments to be made for the nine normal modes of vibration of the hypophosphite ion. The presence of three non-equivalent hypophosphite ions in the Bravais cell, and the lowering of free hypophosphite ion symmetry from C_{2v} to the $m = C_s$ site symmetry, give rise to multiplicity of bands and changes in intensity in the IR and Raman spectra. The unit cell group (UCG) analyses for the hypophosphite anions, presented in Table 3, show that the vibrations of the ions P(1) and P(2) transform similarly, giving rise to one IR active and one Raman active UCG mode for each parent ion vibration. The a_1 and a_2 mode irreps of P(3) transform similarly to those of P(1) and P(2), but b_1 and b_2 mode irreps transform differently. Mixing of UCG modes of the same symmetry species may occur, and thus each parent ion mode may lead to the appearance of three IR and three Raman bands.

Under low resolution, the IR spectrum of $Yb(hyp)_3$ is similar to that given by Seddon et al. for type C anhydrous lanthanide hypophosphites [6]. However, more detail is resolved under higher resolution, and a general assignment of the room temperature IR bands, together with those in the Raman spectrum, is given in Table 4. Since no more than three IR and three Raman bands are observed for each hypophosphite mode, the results are consistent with the UCG analysis. However, the complexity of the spectrum, together with overlapping of bands, does not enable more detailed assignments to be made.

The IR spectra are more clearly resolved at lower temperatures, and patterns of three bands for each parent $H_2PO_2^-$ mode are more readily apparent. For example, Fig. 4 shows the P–H stretch region of the IR spectrum at 90 K. The lowest

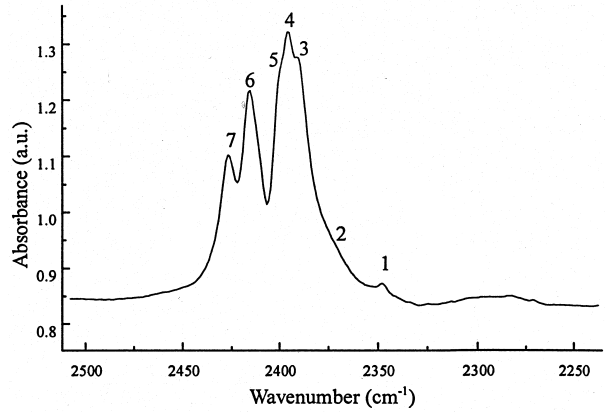


Fig. 4. 90 K Nujol mull IR absorption spectrum of $Yb(hyp)_3$ between 2250 and 2500 cm^{-1}.

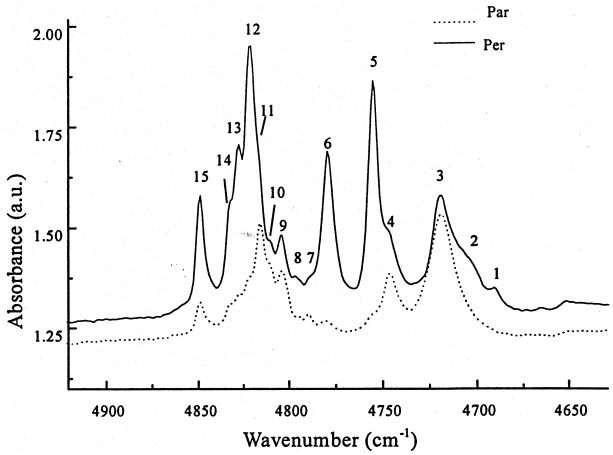


Fig. 5. 10 K mid-IR polarized absorption spectrum of a single crystal of $Yb(hyp)_3$ between 4600 and 4900 cm^{-1}. The polarization directions are parallel (par) and perpendicular (per) to the *b* crystal axis.

Table 5
Assignment of IR combination and overtone P–H stretching bands of $Yb(hyp)_3$ from the 10 K mid-IR spectrum [a]

Line, Fig. 5	Wavenumber (cm^{-1})	Assignment
1	4691	R2298 + IR2395 = 4693
2	4709	R2298 + IR2415 = 4713
3	4719	R2298 + IR2427 = 4725; R2298 + IR2415 = 4713
4	4747	R2398 + IR2348 = 4746
5	4755	R2380 + IR2373 = 4753
6	4780	R2390 + IR2390 = 4780; R2380 + IR2400 = 4780
7	4790	R2390 + IR2400 = 4790; R2380 + IR2409 = 4789
8	4796	R2380 + IR2415 = 4795; R2398 + IR2400 = 4798
9	4804	R2390 + IR2415 = 4805
10	4810	R2380 + IR2427 = 4807; R2412 + IR2400 = 4812
11	4817	R2426 + IR2390 = 4816; R2390 + IR2427 = 4817
12	4821	R2412 + IR2409 = 4821; R2426 + IR2395 = 4821
13	4828	R2426 + IR2400 = 4826; R2412 + IR2415 = 4827
14	4832	R2417 + IR2415 = 4832
15	4849	R2426 + IR2427 = 4853

[a] The energies (in cm^{-1}) of the fundamental modes are taken from the 90 K IR (2390, 2395, 2400, (2409?), 2415, 2427) and 80 K Raman (R) (2380, 2390, 2398, 2412, 2417, 2426) spectra. Alternative assignments are possible, but not presented, in many cases. As in other hypophosphite systems [2], Fermi-resonance enhanced combination bands are observed to low energy of the fundamental P–H stretching modes. These weak bands are at 2373 and 2348 cm^{-1} (IR) and 2298 cm^{-1} (R) at low temperatures.

energy bands (lines 1, 2: 2348, 2373 cm^{-1}) are assigned to Fermi-resonance enhanced combination bands, whereas the remaining bands (lines 3–7) between 2390 and 2427 cm^{-1} correspond to the UCG modes derived from ν_s(P–H) and ν_{as}(P–H). One exception to the three-band pattern in the IR spectrum is observed: four bands are clearly resolved in the ν_7 region. In this case, the lowest energy band (801 cm^{-1}) is again assigned to a Fermi-resonance, this time involving $\nu_4 + \nu_s$(Yb–O).

The first harmonic region of the P–H stretch was studied at 10 K using an oriented single crystal (Fig. 5), in order to confirm the assignments of the P–H stretch UCG modes. In all cases, the observed features can be assigned to the combination of one gerade and one ungerade UCG mode (Table 5). In addition, the polarization behaviour is in general agreement with the analysis given in Table 3, since combination/overtone modes of b_u (a_u) symmetry are expected in the perpendicular (parallel) spectrum. Whereas the transformation behaviour from the free ion to the UCG is the same for ν_1 ν_s(P–H) at all three of the hypophosphite sites, that of ν_6 ν_{as}(P–H) differs for site P(3), compared with P(1) and P(2). Thus, for example, the highest energy band (line 15), which must correspond to the overtone of the symmetric P–H stretching mode, is expected to be of $a_g + b_u = b_u$ symmetry. The overtone band $2\nu_6$ ν_{as}(P–H) (line 6) is also of b_u symmetry, being a combination of either $a_g + b_u$ or $a_u + b_g$ modes. However the combination bands $\nu_6 + \nu_1$ (lines 7–10) are of mixed polarization, since they may correspond to a_u and b_u symmetry. The temperature shifts from room temperature to 10 K are appreciable for bands in this region, being up to 50 cm^{-1} (for the $2\nu_1$ ν_s(P–H) band located at 4799 cm^{-1} at 295 K).

3.3. Electronic absorption spectrum of Yb(hyp)$_3$: pure electronic transitions

The electronic energy level scheme of the f^{13} ion Yb^{3+} is simple, consisting of two LSJ terms $^2F_{7/2}$ (ground state term) and $^2F_{5/2}$ separated by ca. 10000 cm^{-1}. The coordination

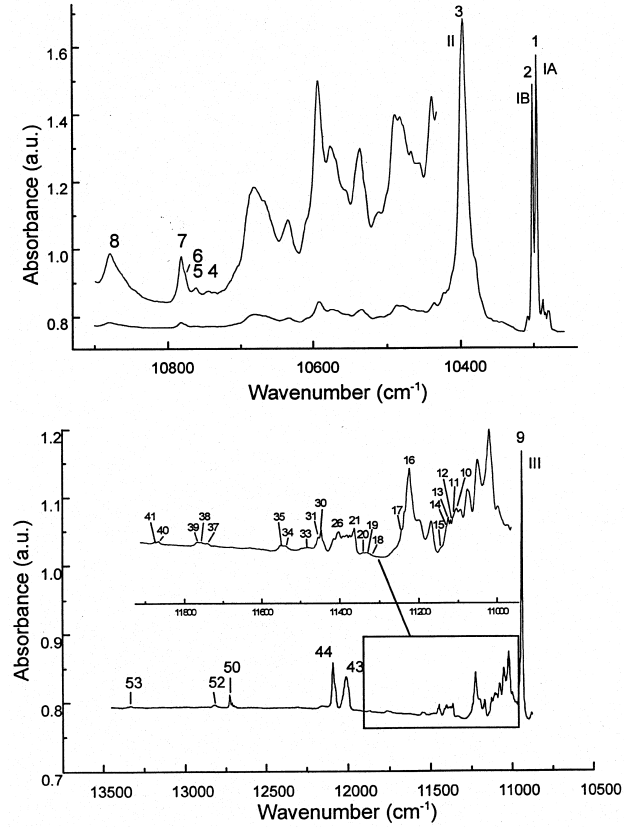


Fig. 6. 10 K single-crystal electronic absorption spectrum of $Yb(hyp)_3$ between 10250 and 13500 cm^{-1}.

Table 6
Assignment of hypophosphite mode bands in the electronic absorption spectrum of $Yb(hyp)_3$ at 10 K

Line, Fig. 6	Energy (cm^{-1})	Assignment of terminal electronic state with derived and IR vibrational energy [a]
1	10296s	IA
2	10302s	IB
3	10397vs	II
4	10745vw	IA, B + ν_4 447 (IR450)
5	10762w	IA, B + ν_4 464 (IR464; R464)
6	10777sh	IA + ν_4 481 (IR485; R482)
7	10783mw	IB + ν_4 481 (IR485; R482)
8	10880mw	II + ν_4 483 (IR485; R482)
9	10938ms	III
10	11105m	IA, IB + ν_7 806 (IR806; R800)
11	11114sh	IA + ν_7 818 (IR820; R810)
12	11120w	IB + ν_7 818 (IR820; R810)
13	11126mw	IA + ν_7 830 (IR830; R826)
14	11131sh	IB + ν_7 829 (IR830; R826)
15	11230sh	IA + ν_5 934 (IR934; R932)
16	11236w	IB + ν_5 934; IA + ν_5 940 (IR934, 943; R932, 940)
17	11244vw	IB + ν_5 942 (IR943; R940)
18	11325vw	II + ν_5 928 (IR928; R926)
19	11334vw	II + ν_5 937 (IR934; R940)
20	11343sh	II + ν_5 946 (IR943; R940)
21	11363mw	IA + ν_3 1067 (IR1065; R1071)
22	11369sh	IB + ν_3 1067 (IR1065; R1071)
23	11375w	IA + ν_3 1079 (IR1076, 1081; R1078)
24	11382w	IB + ν_3 1080 (IR1076, 1081; R1078)
25	11392sh	IA, B + ν_9 1093 (IR1093; R1098); III + ν_4 454 (IR450)
26	11403mw	III + ν_4 465 (IR464; R464)
27	11406sh	IA, B + ν_9 1103 (IR1100; R1098)
28	11416w	III + ν_4 478 (IR485; R482)
29	11441sh	IA, B + ν_2 1143 (IR1141; R1137?)
30	11447m	IA, B + ν_2 1148 (IR1149; R1144)
31	11454mw	IA, B + ν_8 1155 (IR1160; R1153)
32	11467b,vw	II + ν_3 1070 (IR1065, 1076; R1071)
33	11484b,vw	II + ν_9, ν_3 1087 (IR1086; R1078, 1098)
34	11498vw	II + ν_9 1101 (IR1100; R1098)
35	11538vw	II + ν_2 1141 (IR1141; R1144)
36	11551w	II + ν_8 1155 (IR1160; R1153)
37	11743vw	III + ν_7 805 (IR806; R800)
38	11757vw	III + ν_7 819 (IR820; R810)
39	11768vw	III + ν_7 830 (IR830; R826)
40	11867vw	III + ν_5 930 (IR928, 934; R926, 932)
41	11878vw	III + ν_5 941 (IR943; R940)
42	11993sh	III + ν_3 1055 (IR1065)
43	12010mw	III + ν_3 1072 (IR1076; R1071)
44	12073sh	III + ν_2 1135 (IR1141; R1137?)
45	12089mw	III + ν_2 1151 (IR1149; R1153)
46	12687vw	IA + ν_6 2392 (IR2390; R2390)
47	12693vw	IB + ν_6 2391 (IR2390; R2390)
48	12699vw	IB + ν_6 2404 (IR2400; R2398)
49	12710w	IA + ν_1 2415 (IR2415; R2417)
50	12721w	IA + ν_1 2423 (IR2427; R2426)
51	12726w	IB + ν_1 2424 (IR2427; R2426)
52	12818b,vw	II + ν_1 2421 (IR2427; R2417)
53	13331vw	III + ν_6 2393 (IR2395; R2390)
54	13337vw	III + ν_6 2399 (IR2400; R2398)
55	13356vw	III + ν_1 2418 (IR2415; R2417)
56	13367vw	III + ν_1 2429 (IR2427; R2426)

[a] The electronic ground state is the Kramers doublet corresponding to $\Gamma_6(O_h)$ in all cases.

Table 7
Electronic energy level schemes of Yb^{3+} in octahedral ($Cs_2NaYbCl_6$) and distorted octahedral ($Yb(hyp)_3$) symmetry environments at 10 K

SLJ term manifold	O_h irrep	Experimental energy (cm^{-1})	
		$Cs_2NaYbCl_6$ [19]	$Yb(hyp)_3$
$^2F_{7/2}$	Γ_6	0	0
	Γ_8	206	210, (331)
	Γ_7	572	
$^2F_{5/2}$	Γ_8	10248	site 1: 10296 (IA); site 2: 10302 (IB) (II) 10397
	Γ_7	10718	(III) 10938

geometry of this ion in $Yb(hyp)_3$ is that of a distorted octahedron, and the energy level scheme deduced in this study from the analysis of the 10 K single crystal absorption spectrum (Fig. 6, Table 6) is presented in Table 7. In octahedral symmetry, the transition to the lowest $^2F_{5/2}$ level, Γ_8, from the electronic ground state Γ_6, is magnetic dipole (and electric-quadrupole) allowed, whilst that to the further excited state, Γ_7, is electric-quadrupole allowed. For the two non-equivalent Yb^{3+} ions at C_{2h} sites in the unit cell of $Yb(hyp)_3$, there are several modifications, including the splitting of the Γ_8 Kramers quartet state into two Kramers doublets (these states are simply labelled I and II herein). In addition, the presence of two Yb^{3+} sites leads to a doubling of bands throughout the spectrum. This splitting is only resolved for the lowest energy transitions, to the Kramers doublets labelled IA, IB (split by 6 cm^{-1}). From the room temperature spectrum, hot bands are located at 175 cm^{-1} (and, less certainly, at 339 cm^{-1}) to high energy of the pure electronic transitions. At 120 K, these bands shift to 210 and 331 cm^{-1}, respectively, to high energy of the pure electronic transitions.

Owing to the orthogonal orientations of the Yb^{3+} ions at sites I and II, little additional information was available from polarized electronic absorption spectra. However, the transition to state III is relatively stronger in the polarization perpendicular, rather than parallel, to the *b* crystal axis. All of the pure electronic transitions in the absorption spectrum are electric-dipole forbidden since the Yb^{3+} ions are situated at centrosymmetric sites. The transition to the parent $\Gamma_7(O_h)$ state III acquires magnetic dipole intensity at the C_{2h} site. The total oscillator strength of the transitions IA, IB and II is 3.5×10^{-8}. This value may be compared with the calculated magnetic dipole oscillator strength of the parent ($^2F_{7/2}$) $\Gamma_6\rightarrow\Gamma_8$ ($^2F_{5/2}$) transition in octahedral $Cs_2NaYbCl_6$, 2.1×10^{-7}.

3.4. Electronic absorption spectrum of Yb(hyp)$_3$: vibronic structure

The remaining (vibronic) structure in the absorption spectrum is enabled by the electric dipole vibronic mechanism. By analogy with the spectra of octahedrally coordinated

Yb^{3+} in $Cs_2NaYbCl_6$, the most prominent bands are expected to involve one quantum of the YbO_6 odd-parity moiety modes. These vibrations are near (in cm^{-1}) 257 (ν_3), 108 (ν_4) and 86 (ν_6) for the $YbCl_6^{3-}$ anion [20].The vibronic structure built upon IA, IB is overlapped by the intense transition to II, but a clearer comparison is available for the sideband of the transition to III. Prominent bands are located at 83, 113, 137, 233 and 261–289 cm^{-1} above the zero phonon lines which are assigned to the C_{2h} components of t_{2u}, t_{1u} and t_{1u} (O_h) modes respectively. The features between 261–289 cm^{-1} clearly correspond to ν_{as}(Yb–O) modes, and are located at similar energy in the IR spectrum (Table 4).

Many other weaker features are apparent in Fig. 6, and these correspond to two-centre vibronic transitions involving Yb^{3+} and the hypophosphite ions. The conventional theory for the interpretation of two-centre vibronic transitions has been given by Stavola et al. (for example [21–23]), with comparisons and further discussion by Dexpert-Ghys and Auzel [24]. Following the latter authors, the electric dipole strength for the qth polarized component of the transition in which the Yb^{3+} ion (A) undergoes an intraconfigurational $4f^1$ transition, $A_1 \rightarrow A_2$, and one quantum of vibration is simultaneously excited at the hypophosphite centre (B: i.e. $B_1 \rightarrow B_2$), is:

$$P^q_{A_1B_1,A_2B_2} = |\langle A_1B_1|M^q_A + M^q_B|A_2B_2\rangle|^2 \quad (1)$$

where M_A and M_B operate over the coordinates of A and B respectively. Dropping the superscript q in the following, assuming that A_1 and B_1 refer to ground states with reference energy zero, and denoting intermediate states by the subscript u, the matrix element in Eq. (1) is expanded, with rounded kets denoting zeroth-order states [2]:

$$\langle A_1B_1|M_A+M_B|A_2B_2\rangle = (A_1B_1|M_A+M_B|A_2B_2) \quad (2a)$$

$$-\sum_{u\neq 1}(A_u|M_A|A_2)(A_1B_1|H_{AB}|A_uB_2)\times(E_{A_u}+E_{B_2})^{-1} \quad (2b)$$

$$-\sum_{u\neq 2}(B_u|M_B|B_2)(A_1B_1|H_{AB}|A_2B_u)\times(E_{A_2}+E_{B_u})^{-1} \quad (2c)$$

$$-\sum_{u\neq 2}(A_1|M_A|A_u)(A_uB_1|H_{AB}|A_2B_2)\times(E_{A_2}+E_{B_2}-E_{A_u})^{-1} \quad (2d)$$

$$-\sum_{u\neq 1}(B_1|M_B|B_u)(A_1B_u|H_{AB}|A_2B_2)\times(E_{A_2}+E_{B_2}-E_{B_u})^{-1} \quad (2e)$$

The first term (Eq. (2a)) is non-zero in the presence of odd crystal field terms (but zero in the present case for Yb^{3+} at the C_{2h} site) but was omitted by Stavola and Dexter [22]. Following several assumptions, such as the neglect of Eqs. (2c) and (2e), and of interference effects when squaring matrix elements, and the restriction of H_{AB} to dipole–dipole coupling interactions; and approximations such as the averaging over polarization directions and over LSJ-multiplet states of A, a simple expression for the dipole strength of the cooperative absorption $A_1B_1 \rightarrow A_2B_2$ was derived [22]:

$$P_{A_1B_1,A_2B_2} = (10e^4/3\kappa^2R^6)(2J+1)^{-1} \times \Xi^2(1,2)|(B_1|D_B|B_2)|^2|(A_1|U^{(2)}|A_2)|^2 \quad (3)$$

where the symbols are defined in [22], and it is sufficient for our purposes to note that D_B is the electric dipole operator, so that the squared matrix element involving this operator is proportional to the intensity of the relevant IR bands.

The vibronic bands involving two-centre transitions are assigned in detail in Table 6, and the following conclusions can be drawn.

(i) The two-centre vibronic structure can be assigned in terms of the UCG modes observed in the IR spectrum, with no more than three UCG modes being observed for each parent hypophosphite ion mode. In most cases, since the gerade–ungerade UCG splittings are small, the assignments could equally apply to Raman modes, except for several vibronic bands where the corresponding Raman features are not clearly observed.

(ii) The two-centre vibronic structure is stronger on IA, IB than on II. However, some of the structure based on III is the most intense. The relative intensities of the vibronic bands thus do not parallel the relative intensities of the zero phonon lines. This shows the importance of Ln^{3+}–hyp interaction mechanisms other than dipole–dipole interaction. In particular, both of the transitions of Yb^{3+} in octahedral symmetry, $(^2F_{7/2})\Gamma_6 \rightarrow \Gamma_8$, Γ_7, are electric-quadrupole allowed, so that the quadrupole–dipole terms in Eqs. (2c) and (2e) are important, and may not be neglected in this case.

(iii) The relative intensities within groups of UCG modes do not parallel those observed in the IR or Raman spectra; furthermore, the relative intensities of structure involving different vibrational modes do not parallel those observed in the IR or Raman spectra.

(iv) The comparison of the relative intensities of P–O and P–H modes in the vibronic sidebands does not provide clear conclusions. The PH_2 rocking and twisting modes are generally weak, but the P–H stretching modes are clearly observed. The PO_2 symmetric stretch is generally prominent, together with another higher energy band which has been assigned to the PH_2 scissor. If this assignment is correct, then the PO_2 antisymmetric stretch, which is the strongest IR band, is only observed weakly in the vibronic sidebands. However, the mixing of the vibrational modes between 1050–1170 cm^{-1} is appreciable so that assignment to single parent ion modes may not be meaningful. Since the Yb–O and O–P bonds are adjacent, mixing of the symmetry coordinates of the lower energy $H_2PO_2^-$ modes (notably ν_4) with the YbO_6 moiety modes may be appreciable, leading to vibronic intensity via the one-phonon mechanism [20,25].

The consequence of the importance of Eqs. (2c) and (2e), which involve the (virtual) excited states of the ligand, is that *gerade* vibrations are involved. These processes are distinguished from that of Eq. (2a), in which totally symmetric Franck–Condon replicas appear in an electric dipole transition enabled at a non-centrosymmetric site. The gerade–ungerade classification does not apply to the *parent* hypophosphite modes, but the strongest features in the P–O and P–H stretching regions of the vibronic sidebands appear to be parent ion symmetric rather than antisymmetric modes.

4. Summary and conclusions

$Yb(hyp)_3$ differs from that of the earlier members of the lanthanide series $Ln(hyp)_3$ (Ln = La, Pr, Nd) in that the coordination number of Ln^{3+} is six and not eight. The structure consists of a stacking of corrugated layers, each comprising a planar rectangular grid of Yb^{3+} ions that are doubly bridged by hypophosphite ions in the *b* direction and singly bridged in the *c* direction. The $Er(hyp)_3$ structure reported in [7] is not entirely incorrect, but the bond lengths and angles are of low precision. The unit cell dimensions also require confirmation. Our $Yb(hyp)_3$ structure is isostructural with the $Dy(hyp)_3$ structure reported in [6], but the Ln–O bonds are significantly shorter (by about 0.03 Å) for Ln = Yb, and the coordination octahedra are more regular.

The vibrational spectra have been rationalized using unit cell group theory. The low temperature electronic absorption spectra show that two independent Yb^{3+} ions are situated at centrosymmetric sites in the unit cell of $Yb(hyp)_3$. Furthermore, rich two-centre vibronic structure is observed at up to 2430 cm^{-1} above the zero phonon line energies. As far as we are aware, this is the first conclusive report of the observation of the same vibrational unit cell group modes in the electronic and vibronic spectra. We have simulated the relative intensities of the two-centre vibronic bands under a model which employs Eqs. (2b) and (2d), and the agreement is poor. Some of the reasons have been highlighted: the Yb^{3+}–hyp interaction terms of the type quadrupole–dipole are important, and mixing of YbO_6 internal modes with the lower energy hypophosphite modes occurs. We are presently investigating a quantitative description of the results.

Supplementary data

Further details of the crystal structure determination can be ordered from Fachinformationszentrum Karlsruhe, 76344, Eggenstein-Leopoldshafen, under the depository number CSD-410976.

Acknowledgements

We thank Professor Liu Yu-long for recording the Raman spectra, Otto Chan Ying-tai for technical assistance, and the HK UGC for financial assistance under CERG RG CityU 1067/99P and CUHK 303/96P.

References

[1] P.A. Tanner, J. Shamir, P. Starostin, J. Mol. Struct. 326 (1994) 267.
[2] P.A. Tanner, M.D. Faucher, T.C.W. Mak, Inorg. Chem. 38 (1999) 6008.
[3] V.M. Ionov, L.A. Aslanov, V.B. Rybakov, M.A. Porai-Koshits, Kristallografiya 18 (1973) 403 (in Russian).
[4] V.M. Ionov, L.A. Aslanov, M.A. Porai-Koshits, V.B. Rybakov, Kristallografiya 18 (1973) 405 (in Russian).
[5] J.A. Seddon, A.R.W. Jackson, R.A. Kresinski, A.W.G. Platt, Polyhedron 15 (1996) 1899.
[6] J.A. Seddon, A.R.W. Jackson, R.A. Kresinski, A.W.G. Platt, J. Chem. Soc., Dalton Trans. 13 (1999) 2183.
[7] L.A. Aslanov, V.M. Ionov, M.A. Porai-Koshits, V.G. Lebedev, B.N. Kulikovskii, O.N. Gilyarov, T.L. Novoderezhkina, Izv. Akad. Nauk. SSSR, Neorg. Mater. 11 (1975) 117.
[8] P.A. Tanner, J. Krishnan, Appl. Spectrosc. 47 (1993) 1522.
[9] G.M. Sheldrick, SHELXL-93, Program for the refinement of crystal structures, University of Göttingen, Germany, 1993.
[10] M. Catti, Acta Crystallogr., Sect. B 35 (1979) 1041.
[11] T. Matsuzaki, Y. Iitaka, Acta Crystallogr., Sect. B 25 (1969) 1933.
[12] P.A. Tanner, Y.-L. Liu, T.C.W. Mak, Polyhedron 16 (1997) 495.
[13] M. Abenoza, V. Tabacik, J. Mol. Struct. 26 (1975) 95.
[14] R.W. Lovejoy, E.L. Wagner, J. Phys. Chem. 68 (1964) 544.
[15] J.S. Ziomek, J.R. Ferraro, D.F. Peppard, J. Mol. Spectrosc. 8 (1962) 212.
[16] M. Tsuboi, J. Am. Chem. Soc. 79 (1957) 1351.
[17] M. Abenoza, P. Hillaire, M. Cadène, C.R. Acad. Sci. Paris B271 (1970) 346.
[18] L.S. Mayants, E.I. Matrasov, Izv. Akad. Nauk SSSR, Neorg. Mater. 1 (1965) 499.
[19] P.A. Tanner, V.V.R.K. Kumar, C.K. Jayasankar, M.F. Reid, J. Alloys Comp. 215 (1994) 349.
[20] R. Acevedo, P.A. Tanner, T. Meruane, V. Poblete, Phys. Rev. B 54 (1996) 3976.
[21] M. Stavola, J. Lumin. 31–32 (1984) 45.
[22] M. Stavola, D.L. Dexter, Phys. Rev. B 20 (1979) 1867.
[23] M. Stavola, L. Isganitis, M.G. Sceats, J. Chem. Phys. 74 (1981) 4228.
[24] J. Dexpert-Ghys, F. Auzel, J. Chem. Phys. 80 (1984) 4009.
[25] T.R. Faulkner, F.S. Richardson, Mol. Phys. 35 (1978) 1141.

PERGAMON

www.elsevier.nl/locate/poly

Polyhedron 19 (2000) 871–876

POLYHEDRON

Host–guest interactions of the cluster [*triangulo*-Hg_3(μ-dppm)$_3$]$^{4+}$ (dppm = bis(diphenylphosphino)methane) with halides and pseudohalides

Birgit Scheffter [a], Walter Schuh [a], Karl-Hans Ongania [b], Holger Kopacka [a], Richard Malleier [a], Klaus Wurst [a], Paul Peringer [a,*]

[a] *Institut für Allgemeine, Anorganische und Theoretische Chemie der Universität Innsbruck, Innrain 52a, A-6020 Innsbruck, Austria*
[b] *Institut für Organische Chemie der Universität Innsbruck, Innrain 52a, A-6020 Innsbruck, Austria*

Received 29 November 1999; accepted 14 February 2000

Abstract

The complexes [*triangulo*-Hg_3(μ-dppm)$_3X_n$]$^{(4-n)+}$ (X = Cl, Br and I, n = 1, 2) are formed in a small extent upon addition of halides to the cationic subvalent cluster [*triangulo*-Hg_3(μ-dppm)$_3$]$^{4+}$, whereas $SeCN^-$ and CN^- cause quantitative fragmentation. The cluster [*triangulo*-Hg_3(μ-dppm)$_3$(SCN)$_2$]$^{2+}$ is produced either by the reaction of [*triangulo*-Hg_3(μ-dppm)$_3$]$^{4+}$ with thiocyanate or via reduction of a mixture of Hg(SCN)$_2$, [Hg(Me_2SO)$_6$](O_3SCF_3)$_2$ and 3 mequiv. of dppm with elemental mercury. The X-ray structure of [Hg_3(μ-dppm)$_3$(SCN)$_2$](O_3SCF_3)$_2$ shows a Hg_3 triangle (Hg–Hg distances 286.60(14), 279.32(12) and 281.2(2) pm) spanned by three dppm ligands. The thiocyanate ions are positioned nearly parallel to the Hg_3 plane in the two cavities formed by the Hg_3 group at the bottom and the phenyl groups of the dppm ligands as the walls (Hg1–S1 277.5(6) and Hg3–S2 278.4(6) pm). Phosphorus-31 solution NMR indicates a rapid rotation of the SCN^- ligands about the Hg_3 triangle within the cavity. ©2000 Elsevier Science Ltd All rights reserved.

Keywords: Mercury; Clusters; Thiocyanate; Host–guest chemistry

1. Introduction

The subvalent mercury cluster $[Hg_2]^{2+}$ tends to disproportionate into elemental Hg and Hg^{2+} in the presence of strong Lewis bases. The driving force for this disproportionation has been suggested to be the population of antibonding orbitals by ligand donated electrons. The subvalent cyclic $[Hg_3]^{4+}$ cluster with the oxidation number of +4/3 accommodates strong Lewis bases as is demonstrated by the existence of the phosphine complex [*triangulo*-Hg_3(μ-dppm)$_3$]$^{4+}$ with six phosphorus donor atoms [1]. This cluster has been reported with the weakly coordinating anions SO_4^{2-}, SiF_6^{2-}, PF_6^-, $O_3SCF_3^-$ or $O_3SCH_3^-$ [1,2]. The [Hg_3(μ-dppm)$_3$]$^{4+}$ clusters are bifunctional recognition hosts and two anions of all these clusters are found inside the two cavities formed by the 12 phenyl groups of the dppm ligands and the Hg_3 triangle [2]. We were interested in the stability of [*triangulo*-Hg_3(μ-dppm)$_3$]$^{4+}$ towards stronger Lewis bases and report in this paper on the reactions with halides and pseudohalides. The feasibility of the coordination of additional strong donors was nurtured by the existence of [*triangulo*-Hg_3(μ-dmpm)$_4$]$^{4+}$ (dmpm = bis(dimetylphosphino)methane) in which eight strong donor atoms are coordinated to the $[Hg_3]^{4+}$ system [3]. Chloride coordinated to a $[Hg_3]^{4+}$ system is present in the mineral terlinguaite, an insoluble coordination polymer [4].

Halide capped M_3(μ-dppm)$_3$ complexes are quite common and the presence of the halides has been reported to organize M_3(μ-dppm)$_3$ systems [5,6].

2. Results and discussion

2.1. Reaction of [triangulo-Hg_3(μ-dppm)$_3$]$^{4+}$ with halides

Halide adducts [*triangulo*-Hg_3(μ-dppm)$_3$X]$^{3+}$ or [*triangulo*-Hg_3(μ-dppm)$_3X_2$]$^{2+}$ (X = Cl, Br, I) are formed in a small extent in addition to Hg(II)–dppm–halide complexes and elemental mercury upon addition of tetraalkylammonium halides to [*triangulo*-Hg_3(μ-dppm)$_3$]$^{4+}$, or upon reaction of HgX_2, [Hg(Me_2SO)$_6$](O_3SCF_3)$_2$ and 3 mequiv. of dppm

* Corresponding author.Tel.: +43-512-507-5112; fax: +43-512-507-2934; e-mail: paul.peringer@uibk.ac.at

0277-5387/00/$ - see front matter ©2000 Elsevier Science Ltd All rights reserved.
PII S0277-5387(00)00335-1

with elemental mercury. This is indicated by ^{31}P solution NMR spectroscopy showing two signals attributable to the complexes containing one or two halide ions, respectively, in a shift region at higher frequencies compared with Hg(II)–dppm–halide complexes. The concentrations were too low to observe ^{199}Hg NMR spectra or ^{31}P NMR signals of isotopomers containing ^{199}Hg nuclei. All attempts to isolate the halide adducts in the solid state produced dinuclear mercury(II) complexes of the type $[Hg_2(\mu\text{-dppm})_2(\mu\text{-X})X_2]^+$. The crystal structure of $[Hg_2(\mu\text{-dppm})_2(\mu\text{-Br})Br_2](O_3SCF_3)$ is shown in Fig. 1 and is closely related to the corresponding chloride which was previously obtained by the reaction of $Pd(dppm)_2Cl_2$ with elemental mercury [7].

The low equilibrium concentrations of the halide adducts $[triangulo\text{-}Hg_3(\mu\text{-dppm})_3X]^{3+}$ and $[triangulo\text{-}Hg_3(\mu\text{-dppm})_3X_2]^{2+}$ are probably controlled by the rates of decomposition and formation of the $[Hg_3]^{4+}$ system as indicated in Scheme 1: intermediate displacements of dppm-phosphorus atoms by halide ions might produce species with monodentate dppm ligands. The stability of the $[Hg_3]^{4+}$ system in solution seems to be tied to the presence of at least three bridging dppm or related ligands. All attempts to stabilize the cluster by monodentate phosphines or mixtures of dppm and monodentate phosphines failed and hence the intermediates containing monodentate dppm are likely to fragmentate into Hg(II) complexes and elemental mercury.

2.2. Reaction of [triangulo-$Hg_3(\mu$-dppm)$_3$]$^{4+}$ with thiocyanate

2.2.1. Synthesis and NMR spectroscopy

Treatment of $[triangulo\text{-}Hg_3(\mu\text{-dppm})_3](O_3SCF_3)_4$ with 2 mequiv. of KSCN gives $[triangulo\text{-}Hg_3(\mu\text{-dppm})_3(SCN)_2](O_3SCF_3)_2$ (Eq. (1)), which was isolated as pale yellow crystals with good yield.

$$[Hg_3(\mu\text{-dppm})_3]^{4+} + 2SCN^- \rightleftharpoons [Hg_3(\mu\text{-dppm})_3(SCN)_2]^{2+} \quad (1)$$

This cluster is also formed via reduction of a mixture of $Hg(SCN)_2$, $[Hg(Me_2SO)_6](O_3SCF_3)_2$ and 3 mequiv. of dppm with elemental mercury according to Eq. (2).

$$[Hg(Me_2SO)_6](O_3SCF_3)_2 + Hg(SCN)_2 + 3dppm + Hg \rightleftharpoons [Hg_3(\mu\text{-dppm})_3(SCN)_2](O_3SCF_3)_2 + 6Me_2SO \quad (2)$$

The coordination of the SCN^- ligands according to Eq. (1) is associated with a decrease in the ^{31}P chemical shift of ca. 10 ppm. Phosphorus-31 NMR spectroscopy shows the equivalence of all dppm phosphorus atoms in solution, demonstrating that, in contrast to the solid state structure (see below), the SCN^- ligands are not coordinated to individual Hg atoms on the NMR timescale, but are fluxional and undergo rapid intramolecular or intermolecular exchange between Hg atoms.

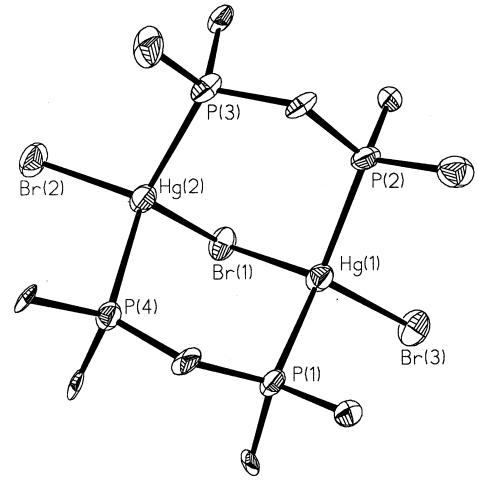
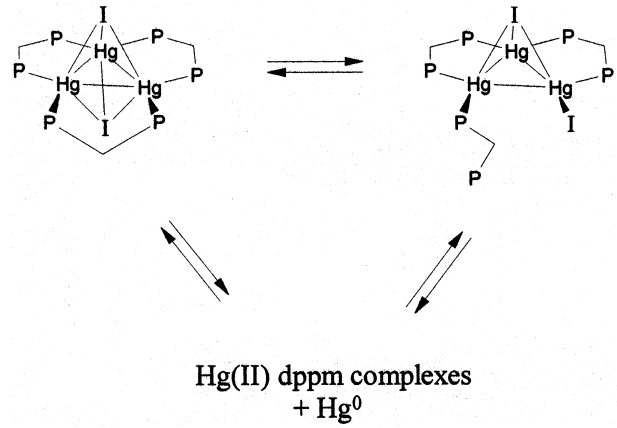


Fig. 1. Structure of $[Hg_2(\mu\text{-dppm})_2(\mu\text{-Br})Br_2]^+$. Selected interatomic distances (pm) and angles (°): Hg(1)–Br(1) 271.5(2), Hg(1)–Br(3) 260.2(2), Hg(2)–Br(1) 273.8(2), Hg(2)–Br(2) 259.1(2), Hg–P 247.6(4)–249.9(4), P(1)–Hg(1)–P(2) 122.48(12), P(1)–Hg(1)–Br(3) 107.85(10), P(2)–Hg(1)–Br(3) 108.45(10), P(1)–Hg(1)–Br(1) 109.66(9), P(2)–Hg(1)–Br(1) 105.29(10), Br(3)–Hg(1)–Br(1) 101.04(5), P(3)–Hg(2)–P(4) 124.49(12), P(3)–Hg(2)–Br(2) 110.05(10), P(4)–Hg(2)–Br(2) 107.31(9), P(3)–Hg(2)–Br(1) 107.97(10), P(4)–Hg(2)–Br(1) 104.15(10), Br(2)–Hg(2)–Br(1) 100.03(5), Hg(1)–Br(1)–Hg(2) 81.94(4).



Scheme 1.

The species containing one SCN^- ligand is present in solution in an equilibrium with $[Hg_3(\mu\text{-dppm})_3(SCN)_2]^{2+}$ and $[Hg_3(\mu\text{-dppm})_3]^{4+}$ according to Eq. (3): a low temperature (233 K) ^{31}P NMR spectrum of a solution of SCN^- and $[triangulo\text{-}Hg_3(\mu\text{-dppm})_3]^{4+}$ in the ratio of 1/1 consists of three signals at 54.0, 49.5 and 44.2 ppm, which are attributed to the species without, with one and with two SCN^- ligands.

$$2[Hg_3(\mu\text{-dppm})_3(SCN)]^{3+} \rightleftharpoons [Hg_3(\mu\text{-dppm})_3(SCN)_2]^{2+} + [Hg_3(\mu\text{-dppm})_3]^{4+} \quad (3)$$

The existence of only one ^{31}P NMR signal per species

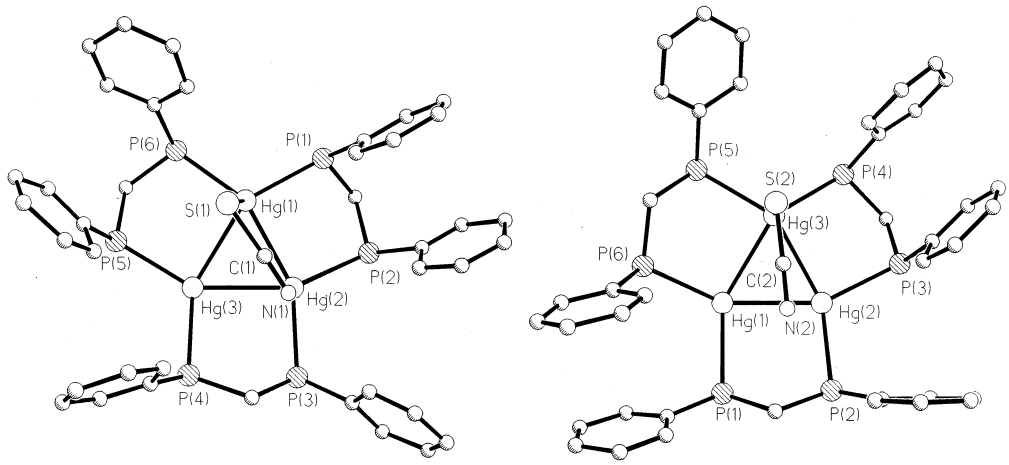


Fig. 2. Structure of $[Hg_3(\mu\text{-dppm})_3(SCN)_2]^{2+}$. Two projections show the position of the two SCN^- ligands within the cavities formed by the Hg_3 group at the bottom and the phenyl groups of the dppm ligands as the walls.

shows again the equivalence of the P atoms, but in this case an intermolecular exchange can be ruled out and the fluxionality must be caused by a rapid rotation of the SCN^- ligand about the Hg_3 triangle. At ambient temperature one broad signal indicates intermolecular SCN^- exchange between the species involved in the equilibrium Eq. (3). The species with one SCN^- ligand could not be isolated in the solid state.

2.2.2. Crystallography

The solid state structure of [*triangulo*-$Hg_3(\mu\text{-dppm})_3(SCN)_2](O_3SCF_3)_2$ has been determined by X-ray diffraction. Fig. 2 shows the structure of the cluster cation. Selected distances and angles are presented in Table 1. The $O_3SCF_3^-$ counterions have no contacts to the cation within the van der Waals estimates. The three Hg atoms form a triangle, each side of which is spanned by a bridging dppm ligand to form a roughly planar $[Hg_3P_6]$ core. Two essentially linear SCN^- ligands are located inside the two cavities formed by the Hg_3 group at the bottom and the phenyl groups of the dppm ligands as the walls.

The Hg–Hg distances are 286.60(14), 279.32(12) and 281.2(2) pm resulting in a mean of 282.4 compared with a range of 271.7(2)–286.49(13) pm for the [*triangulo*-$Hg_3(\mu\text{-dppm})_3]^{4+}$ cluster with the anions SO_4^{2-}, SiF_6^{2-}, PF_6^-, $O_3SCF_3^-$ or $O_3SCH_3^-$ [1,2], 270.3 pm for the mineral terlinguaite, $Hg_4Cl_2O_2$ [4], and 266.2–269.6 pm for $Hg_9As_4O_{16}$ [8], which both possess Hg_3 moieties. The Hg–Hg distances in $[Hg\text{–}Hg]^{2+}$ complexes centre around 250 pm [9]; the clusters $[Hg_n]^{2+}$ ($n=3$, 4) and $[Hg_{3-\delta}]^+$ involve values of 255–270 pm [10–19]. In crystalline elemental mercury each atom has six nearest neighbours at 299 pm. Whereas the distances between Hg1–Hg2 and Hg2–Hg3 in [*triangulo*-$Hg_3(\mu\text{-dppm})_3(SCN)_2](O_3SCF_3)_2$ are close together, the bond between Hg2 and Hg3, i.e. the mercury atoms coordinated by the SCN^- ligands, is distinctly longer. This is in keeping with [*triangulo*-$Hg_3(\mu\text{-dmpm})_4](O_3SCF_3)_4$, in which one edge of the Hg_3 triangle is doubly bridged by dmpm ligands and is significantly longer (295.53(14) pm) compared with the other two singly bridged edges [3]. In contrast, the M–M distances in [*triangulo*-$M_3(\mu_3\text{-CO})(\mu\text{-dppm})_3]^{2+}$ (M = Pd, Pt) are virtually unchanged upon addition of ligands. This indicates that an additional ligand binds to [*triangulo*-$M_3(\mu_3\text{-CO})(\mu\text{-dppm})_3]^{2+}$ using empty $6p_z$ orbitals of the metal atoms rather than empty σ* orbitals of the cluster [20].

The two SCN^- ligands are coordinated to different Hg atoms via the sulfur atoms. The distances between Hg and S of the SCN^- ligands are 277.5(6) and 278.4(6) pm, indicating a rather weak interaction when compared with other Hg–SCN complexes (236–273 pm) present in the Cambridge Crystallographic Data Base. For example, Hg–S distances of 256.6 and 257.4 pm have been reported for $Hg(PPh_3)_2(SCN)_2$ [21]. The coordination geometry of the SCN^- ligands is sketched in Fig. 3, showing the SCN^- groups to be nearly parallel to the Hg_3 plane. The orientation of the nitrogen atoms relative to the Hg_3 triangle is depicted in Fig. 2: the nitrogen atom N1 points to Hg2, i.e. the sole Hg atom which is not coordinated by sulfur donor atoms of the SCN^- ligands. The Hg2–N1 contact distance is 291 pm compared to the van der Waals sum of 296 or 319 pm when

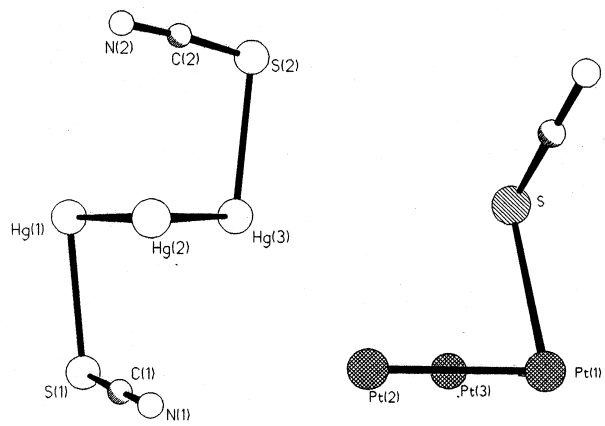


Fig. 3. The different coordination geometries of the SCN^- ligands relative to the M_3 triangles in $[Hg_3(\mu\text{-dppm})_3(SCN)_2]^{2+}$ and for the related cluster $[Pt_3(\mu_3\text{-CO})(SCN)(\mu\text{-dppm})_3]^+$. The dppm ligands and CO are omitted for clarity.

Table 1
Selected interatomic distances (pm) and angles (°) of $[Hg_3(\mu\text{-dppm})_3(SCN)_2]^{2+}$

Hg(1)–P(6)	253.0(6)
Hg(1)–P(1)	255.3(6)
Hg(1)–S(1)	277.5(6)
Hg(1)–Hg(2)	279.32(12)
Hg(1)–Hg(3)	286.60(14)
Hg(2)–P(3)	251.5(6)
Hg(2)–P(2)	252.5(7)
Hg(2)–Hg(3)	281.2(2)
Hg(3)–P(5)	251.9(7)
Hg(3)–P(4)	255.5(6)
Hg(3)–S(2)	278.4(6)
S(1)–C(1)	167(2)
S(2)–C(2)	159(3)
N(1)–C(1)	113(2)
N(2)–C(2)	117(3)
P(6)–Hg(1)–P(1)	110.6(2)
P(6)–Hg(1)–S(1)	99.9(2)
P(1)–Hg(1)–S(1)	110.0(2)
P(6)–Hg(1)–Hg(2)	148.80(13)
P(1)–Hg(1)–Hg(2)	89.67(12)
S(1)–Hg(1)–Hg(2)	94.71(12)
P(6)–Hg(1)–Hg(3)	94.03(13)
P(1)–Hg(1)–Hg(3)	147.12(12)
S(1)–Hg(1)–Hg(3)	85.71(13)
Hg(2)–Hg(1)–Hg(3)	59.58(4)
P(3)–Hg(2)–P(2)	112.1(2)
P(3)–Hg(2)–Hg(1)	152.4(2)
P(2)–Hg(2)–Hg(1)	95.47(12)
P(3)–Hg(2)–Hg(3)	92.4(2)
P(2)–Hg(2)–Hg(3)	151.24(13)
Hg(1)–Hg(2)–Hg(3)	61.50(4)
P(5)–Hg(3)–P(4)	117.2(2)
P(5)–Hg(3)–S(2)	86.7(2)
P(4)–Hg(3)–S(2)	110.5(2)
P(5)–Hg(3)–Hg(2)	148.65(14)
P(4)–Hg(3)–Hg(2)	91.5(2)
S(2)–Hg(3)–Hg(2)	95.3(2)
P(5)–Hg(3)–Hg(1)	89.73(14)
P(4)–Hg(3)–Hg(1)	142.3(2)
S(2)–Hg(3)–Hg(1)	96.17(13)
Hg(2)–Hg(3)–Hg(1)	58.92(3)
C(1)–S(1)–Hg(1)	87.9(8)
C(2)–S(2)–Hg(3)	92.4(9)
N(1)–C(1)–S(1)	179(2)
N(2)–C(2)–S(2)	177(2)

using a Hg radius of 150 or 173 pm [22]. N2 is located in between Hg1 and Hg3 and has Hg–N distances of 360 and 329 pm.

The Hg1–S1–C1 angle is 87.9(8)° which is somewhat smaller than Hg3–S2–C2 of 92.4(9)°, both showing values different from the Hg–S–C angle of ca. 100° found in most other Hg–SCN complexes in the Cambridge Crystallographic Data Base.

An essentially different coordination geometry of the SCN^- ligand relative to the M_3 triangle was observed for the related cluster $[Pt_3(\mu_3\text{-CO})(SCN)(\mu\text{-dppm})_3]^+$ which is also depicted in Fig. 3 [23]. This may be rationalized by the smaller size of the cavity caused by the smaller M–M and M–P distances for M = Pt compared with Hg: the tunnel spanned by the dppm phenyl groups in $[Pt_3(\mu_3\text{-CO})(SCN)(\mu\text{-dppm})_3]^+$ seems to be too small to allow a similar coordination geometry of SCN^- as in $[Hg_3(\mu\text{-dppm})_3(SCN)_2]^{2+}$.

The C–S bond lengths in [*triangulo*-$Hg_3(\mu\text{-dppm})_3(SCN)_2]^{2+}$ (159(3) and 167(2) pm) are in the range of non-coordinating SCN^- anions (160–170 pm).

The P atoms lie approximately in the plane defined by the Hg atoms. The Hg-Hg-P-C-P rings adopt envelope conformations with the methylene carbon at the flap. Two methylene groups lie above the Hg_3 plane and one below, causing four equatorial plus two axial and two equatorial plus four axial phenyl groups respectively positioned above the opposite faces of the Hg_3 triangle. The Hg–P distances do not show any peculiarities.

2.2.3. Mass spectrometry

FAB MS has been successfully applied for the characterization of the non-volatile, high molecular weight [*triangulo*-$M_3(\mu\text{-dppm})_3$] type clusters, e.g. [*triangulo*-$Ni_3(\mu_3\text{-L})(\mu_3\text{-I})(\mu\text{-dppm})_3]^{n+}$, {[*triangulo*-$Ni_3(\mu_3\text{-I})(\mu\text{-dppm})_3]_2(\mu_3,\mu_3,\eta^1,\eta^{1\prime}\text{-CN-R-NC})\}^{2+}$ [24] and [*triangulo*-$Hg_3(\mu\text{-dmpm})_4]^{4+}$ [3].

The FAB mass spectrum of [*triangulo*-$Hg_3(\mu\text{-dppm})_3(SCN)_2](O_3SCF_3)_2$ showed a methanol solvate of the molecular ion at *m/z* 2200.1 with an isotopic distribution which agrees with the calculated envelope, and the formation of dppm at *m/z* 384 as base peak. The fragmentation patterns are dominated by multiple loss of anions, dppm or Hg. Fragments containing three Hg atoms are $Hg_3(dppm)_3(SCN)(O_3SCF_3)_2$, $Hg_3(dppm)_3(SCN)_2(O_3SCF_3)$, $Hg_3(dppm)_3(O_3SCF_3)_2$ and $Hg_3(dppm)_2(O_3SCF_3)_2$.

Interestingly, electrospray mass spectrometry turned out not to be suitable although it is a softer technique than FAB.

2.3. Reaction of [triangulo-$Hg_3(\mu\text{-dppm})_3]^{4+}$ with selenocyanate and cyanide

Treatment of [*triangulo*-$Hg_3(\mu\text{-dppm})_3]^{4+}$ with KSeCN results in a complete degradation of the subvalent Hg cluster and the mercury(II) complex $[Hg(dppmSe)_2]^{2+}$ [25] is identified as the main product. This is thought to be the result of a selenium transfer from selenocyanate to dppm producing dppm-selenides which do not stabilize the $[Hg_3]^{4+}$ cluster. Not surprisingly, cyanide also causes an immediate and complete redox disproportionation of the [*triangulo*-$Hg_3(\mu\text{-dppm})_3]^{4+}$ cluster.

3. Experimental

3.1. Instrumentation

The ^{31}P NMR spectra were recorded on a Bruker AC 200 spectrometer at 81.015 MHz and are referenced against external 85% H_3PO_4. Mass spectra were recorded on a Finnigan

MAT 95 instrument with the fast atom bombardment technique. Microanalyses were obtained from the Mikroanalytisches Laboratorium, Institut für Physikalische Chemie, Universität Wien.

3.2. Crystallography

Crystal data and details of structure solution and refinement are summarized in Table 2. For [*triangulo*-$Hg_3(\mu\text{-dppm})_3(SCN)_2](O_3SCF_3)_2\cdot 4CH_3OH$ only Hg, P, S, N and the O and F atoms of one trifluoromethanesulfonate anion were refined anisotropically owing to the poor crystal quality. The other trifluoromethanesulfonate anion is disordered over two positions (S3A, F1–3A, C3A, O1–3A and S3B, F1–3B, C3B, O1–3B) with an occupancy of 2/1. Two methanol molecules are disordered over two positions (C91, O91A–B and C92, O92A–B) with occupancies of 1/1 respectively, and one methanol molecule over three positions (C93A–C, O93A–C) with an occupancy of 1/1/1. One phenyl group of one dppm ligand is disordered over two positions (C41, C42–46A, C41, C42–46B) with an occupancy of 1/1.

3.3. Syntheses

The cluster [*triangulo*-$Hg_3(\mu\text{-dppm})_3](O_3SCF_3)_4$ and $[Hg(Me_2SO)_6](O_3SCF_3)_2$ were prepared as described previously [1,26].

3.3.1. Synthesis of [triangulo-$Hg_3(\mu$-dppm$)_3(SCN)_2$]-$(O_3SCF_3)_2$

A solution of KSCN (9.7 mg, 0.1 mmol) in 0.4 ml of CH_3OH is added in 50 μl steps to a stirred solution of [*triangulo*-$Hg_3(\mu\text{-dppm})_3](O_3SCF_3)_4$ (117.6 mg, 0.05 mmol) in 0.5 ml of CH_3OH. First, the colour changes from a pale to a more intense yellow, then the product precipitates as a pale yellow powder, which is dissolved by dropwise addition of CH_2Cl_2 and crystallized at −19°C as yellow prisms. Yield 65.4 mg (60%); m.p. 139–142°C (dec.). ^{31}P NMR (CH_2Cl_2/CH_3OH, 298 K): 44.8 ppm. *Anal*. Found: C, 44.07;

Table 2
Crystal data of $[Hg_3(\mu\text{-dppm})_3(SCN)_2](O_3SCF_3)_2$ and $[Hg_2(\mu\text{-dppm})_2(\mu\text{-Br})Br_2](O_3SCF_3)$

	$[Hg_3(\mu\text{-dppm})_3(SCN)_2](O_3SCF_3)_2\cdot 4CH_3OH$ [a]	$[Hg_2(\mu\text{-dppm})_2(\mu\text{-Br})Br_2](O_3SCF_3)\cdot CH_3OH\cdot 3H_2O$ [a]
Molecular formula	$C_{79}H_{66}F_6Hg_3N_2O_6P_6S_4\cdot 4CH_3OH$	$C_{51}H_{44}Br_3F_3Hg_2O_3P_4S\cdot CH_3OH\cdot 3H_2O$
Formula weight	2297.34	1558.71
Crystal system	triclinic	triclinic
Space group	$P\bar{1}$	$P\bar{1}$
Unit cell dimensions		
a (pm)	1313.8(3)	1251.7(2)
b (pm)	1725.6(3)	1384.5(2)
c (pm)	2149.2(4)	1791.0(2)
α (°)	104.99	72.09
β (°)	107.54	72.77
γ (°)	94.46	79.97
Volume (nm^3)	4.423(2)	2.8090(7)
Z	2	2
Density (calc.) ($Mg\ m^{-3}$)	1.725	1.843
Absorption coefficient (mm^{-1})	5.518	7.792
F(000)	2244	1484
Colour, habit	pale yellow prism	colourless prism
Crystal size (mm)	0.4×0.2×0.2	0.4×0.3×0.2
θ Range for data collection (°)	2.67–21.26	2.54–21.49
Index ranges	$-1\le h\le 10,\ -16\le k\le 16,\ -20\le l\le 20$	$-9\le h\le 10,\ -13\le k\le 13,\ -18\le l\le 18$
Reflections collected	9918	6722
Independent reflections	7596 ($R_{int}=0.0522$)	5630 ($R_{int}=0.0395$)
Reflections with $I>2\sigma(I)$	4987	4446
Data/restraints/parameters	6501/5/644	5630/0/624
Goodness-of-fit on F^2	1.023	0.935
Final *R* indices ($I>2\sigma(I)$)	$R_1=0.0587$, $wR_2=0.1171$	$R_1=0.0486$, $wR_2=0.1168$
R indices (all data)	$R_1=0.1093$, $wR_2=0.1403$	$R_1=0.0680$, $wR_2=0.1306$
Largest difference peak and hole ($e\ nm^{-3}$)	976 and −988	2064 and −1995
Weighting scheme	calc. $w=1/[\sigma^2(F_o^2)+(0.0469P)^2+69.8713P]$ where $P=(F_o^2+2F_c^2)/3$	calc. $w=1/[\sigma^2(F_o^2)+(0.0901P)^2+29.9324P]$ where $P=(F_o^2+2F_c^2)/3$

[a] Details of structure determination and refinement which are common to both structures. Temperature, 213(2) K; radiation, Mo Kα (λ = 71.073 pm); absorption correction, ψ-scan; refinement method, full-matrix least-squares on F^2; diffractometer, Siemens P4; monochromator, highly oriented graphite crystal; scan type, ω; scan speed, variable (6.0–35.0° min^{-1} in ω); scan range (ω), 20.6°; standard reflections, 3 measured every 97 reflections; system used, SHELXS-86 [27] and SHELXL-93 [28]; solution, direct methods; hydrogen atoms, calculated, with isotropic displacement parameters 1.2 times higher than U_{eq} of the carbon atoms.

H, 2.89; N, 1.27. Calc. for $C_{79}H_{66}F_6Hg_3N_2O_6P_6S_4$: C, 43.74; H, 3.07; N, 1.29%.

3.3.2. Formation of [triangulo-$Hg_3(\mu$-dppm$)_3X_n]^{(4-n)+}$ (X = Cl, Br and I; n = 1, 2)

A mixture of HgX_2 (0.05 mmol, 0.0136 g $HgCl_2$, 0.0180 g $HgBr_2$, 0.0227 g HgI_2), $[Hg(Me_2SO)_6](O_3SCF_3)_2$ (0.15 mmol, 0.1451 g), dppm (0.3 mmol, 0.1153 g) and elemental mercury (0.05 ml) in CH_2Cl_2 is stirred for 12 h. ^{31}P NMR (CH_2Cl_2): [*triangulo*-$Hg_3(\mu$-dppm$)_3X]^{3+}$ X = Cl δ 49.7, X = Br δ 48.2, X = I δ 45.7; [*triangulo*-$Hg_3(\mu$-dppm$)_3X_2]^{2+}$ X = Cl δ 41.8, X = Br δ 39.3, X = I δ 33.1 ppm.

Alternatively, the complexes were obtained upon addition of a solution of NBu_4X in MeOH to $[Hg_3(\mu$-dppm$)_3](O_3SCF_3)_4$ dissolved in CH_2Cl_2/MeOH.

3.3.3. Synthesis of [$Hg_2(\mu$-dppm$)_2(\mu$-Br$)Br_2](O_3SCF_3)\cdot MeOH\cdot 3H_2O$

A solution of $[Hg_3(\mu$-dppm$)_3](O_3SCF_3)_4$ (0.05 mmol, 0.1176 g) in a mixture of CH_2Cl_2 (0.5 ml) and MeOH (0.25 ml) is treated with NBu_4Br (0.2 mmol, 0.0645 g) in MeOH (0.6 ml) and stirred for 30 min. The volatiles are removed in vacuo and the residue is dissolved in CH_2Cl_2 (0.5 ml). After addition of MeOH (0.25 ml), the solution is left for 5 days. Colourless platelets of the product formed and were suitable for X-ray crystallographic investigation. *Anal*. Found: C, 38.36; H, 2.91. Calc. for $C_{51}H_{44}Br_3F_3Hg_2O_3P_4S\cdot MeOH\cdot 3H_2O$: C, 37.97; H, 3.31%.

Supplementary data

Details of the crystal structure investigation, atomic coordinates, thermal parameters, complete bond distances and angles have been deposited with the Cambridge Crystallographic Data Centre, 12 Union Road, Cambridge CB2 1EZ, UK (fax: +44-1223-336033; e-mail: deposit@ccdc.cam.ac.uk) as supplementary material publication no. CCDC 137168 and CCDC 137169.

Acknowledgements

Financial support from the Fonds zur Förderung der wissenschaftlichen Forschung, Project P 11842-PHY is gratefully acknowledged.

References

[1] B. Hämmerle, E.P. Müller, D.L. Wilkinson, G. Müller, P. Peringer, J. Chem. Soc., Chem. Commun. (1989) 1527.
[2] A. Mühlecker-Knoepfler, B. Scheffter, H. Kopacka, K. Wurst, P. Peringer, J. Chem. Soc., Dalton Trans. (1999) 2525.
[3] A. Mühlecker-Knoepfler, E. Ellmerer-Müller, R. Konrat, K.H. Ongania, K. Wurst, P. Peringer, J. Chem. Soc., Dalton Trans. (1997) 1607.
[4] K. Brodersen, G. Göbel, G. Liehr, Z. Anorg. Allg. Chem. 575 (1989) 145.
[5] J.K. Bera, M. Nethadij, A.G. Samuelson, Inorg. Chem. 38 (1999) 218 and Refs. therein.
[6] A.A.M. Aly, D. Neugebauer, O. Orama, U. Schubert, H. Schmidbaur, Angew. Chem., Int. Ed. Engl. 90 (1978) 125.
[7] P.D. Harvey, K.T. Aye, K. Hierso, E. Isabel, I. Lognot, Y. Mugnier, F.D. Rochon, Inorg. Chem. 33 (1994) 5981.
[8] A.L. Wessels, W. Jeitschko, M.H. Möller, Z. Naturforsch., Teil B 52 (1997) 469.
[9] K. Brodersen, H.U. Hummel, in: G. Wilkinson (Ed.), Comprehensive Coordination Chemistry, vol. 5, Pergamon, Oxford, 1987, p. 1049.
[10] R.J. Gillespie, P.K. Ummat, J. Chem. Soc., Chem. Commun. (1971) 1168.
[11] R.D. Ellison, H.A. Levy, K.W. Fung, Inorg. Chem. 11 (1972) 833.
[12] B.D. Cutforth, C.G. Davies, P.A.W. Dean, R.J. Gillespie, P.R. Ireland, K. Ummat, Inorg. Chem. 12 (1973) 1343.
[13] B.D. Cutforth, R.J. Gillespie, P.R. Ireland, J. Chem. Soc., Chem. Commun. (1973) 723.
[14] B.D. Cutforth, R.J. Gillespie, P.R. Ireland, J.F. Sawyer, P.K. Ummat, Inorg. Chem. 22 (1983) 1344.
[15] I.D. Brown, R.J. Gillespie, K.R. Morgan, J.F. Sawyer, K.J. Schmidt, Z. Tun, P.K. Ummat, J.E. Vekris, Inorg. Chem. 26 (1987) 689.
[16] I.D. Brown, B.D. Cutforth, C.G. Davies, R.J. Gillespie, P.R. Ireland, J.E. Vekris, Can. J. Chem. 52 (1974) 791.
[17] Z. Tun, I.D. Brown, Acta Crystallogr., Sect. B 38 (1982) 2321.
[18] Z. Tun, I.D. Brown, P.K. Ummat, Acta Crystallogr., Sect. C 40 (1984) 1301.
[19] I.D. Brown, R.J. Gillespie, K.R. Morgan, Z. Tun, P.K. Ummat, Inorg. Chem. 23 (1984) 4506.
[20] R.J. Puddephatt, L. Manojlovic-Muir, K.W. Muir, Polyhedron 9 (1990) 2767.
[21] R.C. Makhija, A.L. Beauchamp, R. Rivest, J. Chem. Soc., Dalton Trans. (1973) 2447.
[22] A.J. Canty, G.B. Deacon, Inorg. Chim. Acta 45 (1980) L225.
[23] G. Ferguson, B.R. Lloyd, L. Manojlovic-Muir, K.W. Muir, R.J. Puddephatt, Inorg. Chem. 25 (1986) 4190.
[24] D.A. Morgenstern, C.C. Bonham, A.P. Rothwell, K.V. Wood, C.P. Kubiak, Polyhedron 14 (1995) 1129.
[25] A.M. Bond, R. Colton, J. Ebner, Inorg. Chem. 27 (1988) 1697.
[26] P. Peringer, Inorg. Nucl. Chem. 42 (1980) 1501.
[27] G.M. Sheldrick, SHELXS-86, program for crystal structure solutions, Göttingen, Germany, 1990.
[28] G.M. Sheldrick, SHELXL-93, program for refinement of crystal structures, Göttingen, Germany, 1993.

PERGAMON

www.elsevier.nl/locate/poly

Polyhedron 19 (2000) 879–890

POLYHEDRON

Regioselectivity of metallacycle formation via intramolecular CH activation

Kenneth M. Doxsee *, Jerrick J.J. Juliette

Department of Chemistry, University of Oregon, Eugene, OR 97403, USA

Received 6 July 1999; accepted 26 January 2000

Abstract

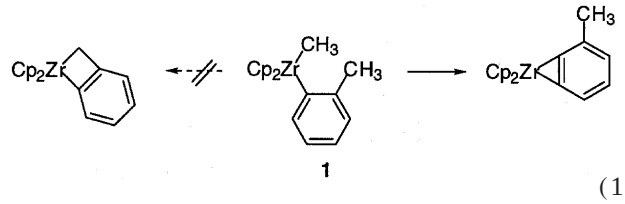
Carbometalation of alkynes by dimethyltitanocene affords vinyl complexes which serve as intermediates for the formation of titanacyclic products through subsequent hydrogen abstraction/methane elimination. Although multiple sites for hydrogen abstraction are present in the intermediate vinyl complexes, the hydrogen abstraction step is in most cases highly regioselective, leading to the formation of either titanacyclobutenes (via γ-H abstraction) or titanacyclopropanes (via β-H abstraction). Rotational isomerization, restricted in the case of larger vinyl group substituents, provides a simple and consistent explanation for the observed regioselectivities, and this effect is sufficiently pronounced to lead to preferential γ-aliphatic CH activation even in the presence of γ-aromatic hydrogens. The titanacyclopropanes may be alternatively formulated as allene complexes of titanocene. An independently prepared trimethylphosphine-ligated analog of 3-methyl-1,2-butadiene, representing the first titanocene allene complex to be reported, undergoes reductive coupling reactions with excess 3-methyl-1,2-butadiene and with alkynes. ©2000 Elsevier Science Ltd All rights reserved.

Keywords: C–H activation; Intramolecular bonds; Titanium; Metallacycles; Allenes; Carbometalation

1. Introduction

Reactions involving the insertion of transition metals into carbon–hydrogen bonds continue to receive considerable attention, at least in part given their potential for the activation of hydrocarbons toward catalytic functionalization [1]. Numerous examples of both intermolecular and intramolecular CH bond activation have been reported, including the well known α- and β-hydride elimination processes [2,3] and related cyclometalation reactions of heteroatom-containing ligands [4–6]. Longer-range intramolecular CH activation reactions have also been documented. Thus, orthometalation reactions of arylphosphine [4–7] and arylsilane [8] complexes represent γ-elimination processes, and thermolysis of a Ta(V) aryloxide complex is reported to proceed via sequential *ε*-elimination processes [9,10]. For recent examples of δ- and *ε*-activation processes in aniline, benzylamine and phenethylamine complexes of palladium, see [11,12]. These longer-range activation reactions, however, remain uncommon in comparison with the seemingly ubiquitous α- and β-hydride elimination processes.

A sufficient body of information regarding intramolecular CH-activation reactions has been amassed to allow some generalizations to be drawn. Aromatic CH bonds appear to be more reactive toward such processes than aliphatic CH bonds, despite the higher bond strength of the aromatic CH bond. Thus, for example, (*o*-tolyl)(methyl)zirconocene (**1**) undergoes aromatic β-CH bond activation to produce an aryne complex rather than the isomeric benzometallacyclobutene which would be formed through activation of a benzylic γ-CH bond (Eq. (1)) [13]. Dibenzylhafnocene



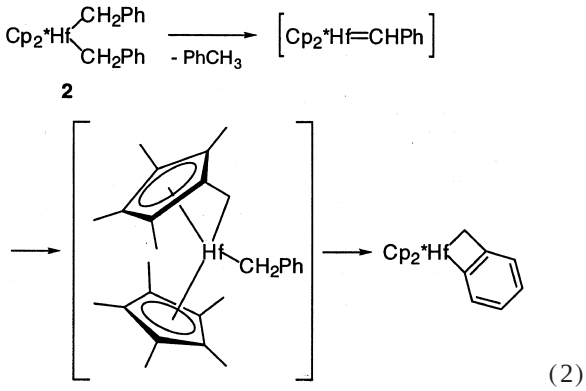
1

(1)

complex **2** undergoes kinetic α-elimination, while the resulting 'tucked in' benzyl complex then reacts through activation of an aromatic γ-CH bond, forming a benzohafnacyclobutene (Eq. (2)) [14]. Similarly, Petasis and Bzowej have noted apparent α-elimination reactions of dibenzyltitanocene and related derivatives [15,16].

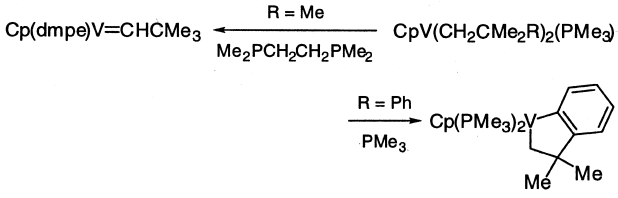
* Corresponding author. Tel.: +1-541-346-4628; fax: +1-541-346-2874; e-mail: doxsee@oregon.uoregon.edu

0277-5387/00/$ - see front matter ©2000 Elsevier Science Ltd All rights reserved.
PII S0277-5387(00)00325-9



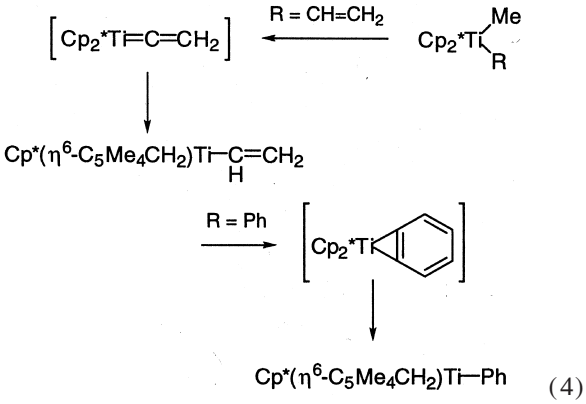
(2)

Teuben and co-workers have reported selective α-, β-, and δ-hydrogen elimination reactions of paramagnetic vanadium(III) dialkyls [17] (e.g., Eq. (3)) and several α- and



(3)

β-hydrogen elimination reactions of permethyltitanocene alkyls [18] (Eq. (4)). However, information is scarce



(4)

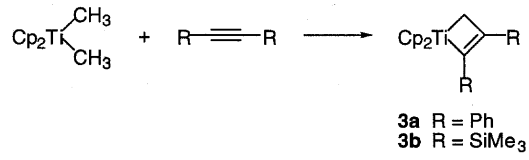
regarding the regiochemical preferences of intramolecular CH activation processes in which there is a less defined chemical difference between two (or more) potentially reactive sites, with the selective γ-elimination reactions of neopentyl platinum complexes providing perhaps the best known examples [19,20]. Interestingly, whereas the neopentyl platinum complexes undergo selective γ-elimination, tetraneopentyltitanium has recently been shown to undergo selective α-elimination [21].

In the course of our studies of the carbometalation reactions of dimethyltitanocene [22], which contrast with an early account reporting no thermal reaction between dimethyltitanocene and alkynes [23], we were afforded the opportunity to examine the intramolecular competition between two alternative sites for allylic CH activation, one representing a β-activation process and the other a γ-activation process [24]. Herein we present further studies of these competing allylic CH activation processes as well as an unusual example wherein allylic γ-CH activation is strongly favored over aromatic γ-CH activation.

2. Results and discussion

2.1. Selective γ-activation processes

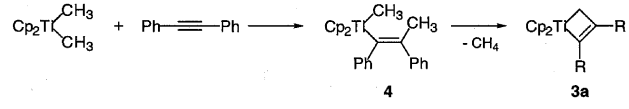
Diphenylacetylene and bis(trimethylsilyl)acetylene react cleanly with dimethyltitanocene in dry, deoxygenated benzene at moderate temperatures (65–80°C, 14–30 h) to produce the corresponding titanacyclobutenes (**3a**, R = Ph; **3b**, R = $SiMe_3$) in high yield (Eq. (5)) [22,25]. Although these



(5)

metallacycles may also be prepared through the addition of the alkynes to $Cp_2TiCH_2 \cdot Al(CH_3)_2Cl$ (Tebbe's reagent) [26], removal of the aluminum-containing byproducts can be problematic, reducing isolated yields of pure metallacycles. In contrast, the dimethyltitanocene route allows isolation of pure metallacycles in near-quantitative yield after a simple recrystallization while also avoiding the requirement for use of the highly air- and moisture-sensitive Tebbe's reagent. (In marked contrast, dimethyltitanocene may be isolated through standard bench top techniques, requiring no exclusion of air or moisture.)

Shorter reaction times in the diphenylacetylene reaction lead to formation of carbometalation product **4**, together with a small amount of the titanacyclobutene (Eq. (6)). Complex



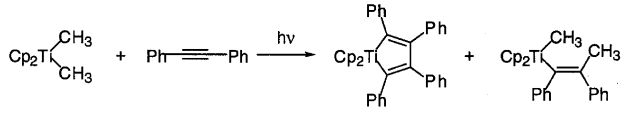
(6)

4, which may be isolated as a pure solid by crystallization at −20°C, serves as a precursor to titanacyclobutene **3a**, with thermolysis at ca. 80°C resulting in clean conversion to the metallacycle.

The allylic methyl group resonance appears at 1.48 ppm in the ^1H NMR spectrum of **4**, while the Ti–CH_3 group appears at −0.42 ppm. Similar upfield shifts are seen for other methyltitanocene complexes and may be attributed to an agostic interaction with a vacant titanium wedge plane orbital [27,28]. In the ^{13}C NMR spectrum of **4**, the allylic methyl resonance appears at 25.7 ppm and the Ti–CH_3 group at 50.3 ppm. High resolution mass spectral and elemental analytical data provide final confirmation of the proposed structure.

Both the carbometalation reaction and the subsequent methane elimination process are noteworthy. Carbometalation reactions of group 4 metallocene alkyl complexes are often sluggish, with formation of cationic alkyls typically used to accelerate the reactions [29,30]. Insertion reactions of dimethyltitanocene have scarcely been examined, although CO_2 and SO_2 insertions have been reported [31,32], and NO insertion reactions of dimethylzirconocene have also been noted [33]. The carbometalation of diphenylacetylene by dimethyltitanocene to form **4** is quite rapid. The reasons for the facility of this reaction are not clear, but may be rooted in the propensity of methyltitanocene derivatives to undergo Ti–CH_3 bond homolysis [34], with addition of CH_3• to the alkyne, followed by addition of the resulting vinyl radical to titanium providing a convenient pathway to the observed product.

Vinyl complex **4** was previously reported as the minor byproduct in the photochemical reaction between dimethyltitanocene and diphenylacetylene, the major product of which was a titanacyclopentadiene formed through the reductive coupling of 2 equiv. of the alkyne by transiently generated titanocene (Eq. (7)) [35–37]. Formation of **4** in this reaction



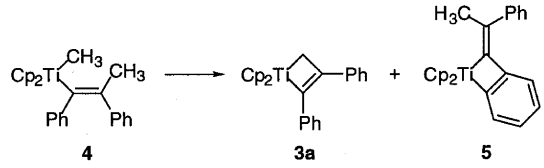
(7)

perhaps provides circumstantial support for the radical pathway for its formation, given the likelihood of generation of methyl radicals under photolytic conditions, although direct thermal insertion via σ-bond metathesis [38] is not ruled out.

Given the generally preferred reactivity of aromatic CH bonds relative to aliphatic CH bonds, the formation of the titanacyclobutene from **4** is intriguing, especially since preferential activation of the γ-aliphatic position occurs in the presence of a γ-aromatic CH bond. This may point toward a radical mechanism for the CH activation process, with initial Ti–CH_3 bond homolysis followed by preferential abstraction of an allylic hydrogen by the resulting methyl radical and subsequent collapse to the metallacyclobutene.

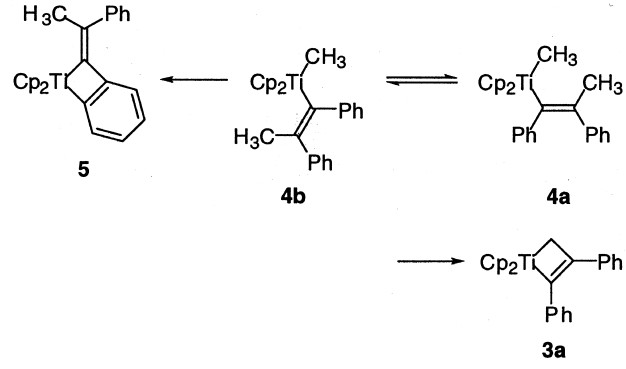
Formation of the titanacyclobutene could conceivably be initiated by the thermal extrusion of diphenylacetylene from **4**, regenerating dimethyltitanocene. Thermal decomposition of dimethyltitanocene can serve to generate $Cp_2Ti{=}CH_2$ [39,40], although this decomposition reaction is appreciably more complex than that of the permethyltitanocene analog [41], and this methylidene complex, based on the known chemistry of Tebbe's reagent and of titanacyclobutanes [26,42], would be expected to react with diphenylacetylene to form the titanacyclobutene. In order to address this possibility, vinyl complex **4** was thermolyzed at 90°C in the presence of an excess of bis(4-chlorophenyl)acetylene. Complex **4** is cleanly converted to diphenyltitanacyclobutene **3a**, providing support for the γ-CH activation process, although the alternate mechanism cannot be unequivocally ruled out by this result, given the possibility of slow exchange of bis(4-chlorophenyl)acetylene into the coordination sphere of the metal center. Further information regarding these mechanistic possibilities is provided in the discussion of the reactions of 2-butyne and 3-hexyne with dimethyltitanocene (vide infra).

Higher reaction temperatures in the thermolysis of **4** do lead to the formation of the isomeric titanacyclobutene (**5**) resulting from the less favorable aromatic CH activation step, although this metallacycle is formed in only low yield (up to ca. 25% at 110°C), with the allylic activation product still the major product of the reaction (Eq. (8)).



(8)

Given the anticipated steric preference of the vinyl group to lie in the wedge plane, two rotamers of **4** might be anticipated, one (**4a**) placing the γ-methyl group in close proximity to the departing Ti–CH_3 group and the other (**4b**) placing the aromatic γ-CH in this position (Eq. (9)). With

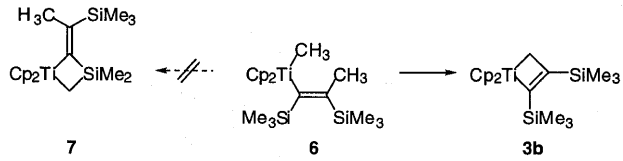


(9)

either concerted methane elimination or with Ti–CH_3 bond homolysis followed by hydrogen abstraction, rotamer **4a** would be expected to lead to formation of the titanacyclobutene (**3a**) and rotamer **4b** to the benzotitanacyclobutene (**5**). Restricted rotation of vinyl groups in permethyltitanocene chloride derivatives has been previously noted [43]. Although steric effects can be less pronounced in simple titanocenes than in the permethyl analogs, they are nonetheless often profound. For example, steric effects play an extreme role in the nitrile and aldehyde insertion reactions of titanacylobutenes [44,45]. It seems likely that the initial carbometalation step in the reaction of dimethyltitanocene with diphenylacetylene affords a single rotamer (**4a**), presenting a γ-H poised for abstraction and leading to the diphenyltitanacyclobutene. Thermolysis at higher temperatures facilitates rotational equilibration of **4a** with **4b**, leading to the formation of observable quantities of benzotitanacyclobutene **5**. Consistent with this hypothesis is the recent report of γ-elimination from (*Z*)-CpNi(CPh=CPh–CH_3), which deliv-

ers the γ-hydrogen close to the nickel center, but not from the (*E*) isomer, which maintains a longer distance between the nickel center and the γ-hydrogens [46].

The reaction between dimethyltitanocene and bis(trimethylsilyl)acetylene (Eq. (5), R = $SiMe_3$) affords no spectrally observable intermediates, even when carried out at comparatively low temperature (35°C), but presumably proceeds via an initial carbometalation step, affording vinyl complex **6** (Eq. (10)). An allylic CH activation process



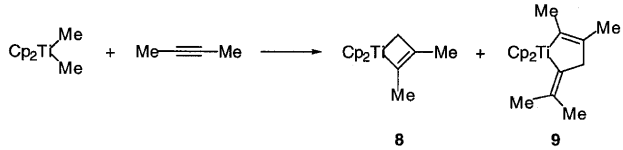
7 **6** **3b**

(10)

analogous to that seen for the diphenyl analog would then close up the titanacyclobutene ring. Again, a high degree of regiocontrol is apparent in this CH activation process. The isomeric metallacycle (**7**) which would result from activation of a silyl methyl group (Eq. (10)) is not observed, even though such reactivity of a silyl methyl group is well precedented for the later transition metals [47–49] and has been reported for a bis(trimethylsilyl)amide complex of titanocene as well [50]. As in the case of the diphenyl derivative, this is consistent with initial formation of a single reactive rotamer of the intermediate vinyl complex which displays significant steric inhibition of bond rotation. In contrast to the diphenyl case, in which formation of the anticipated isomeric titanacycle (**5**) is observed at higher reaction temperatures, rotation of the vinyl group in the bis(trimethylsilyl) derivative (**6**) is sufficiently hindered to preclude formation of detectable quantities of the silatitanacyclobutane (**7**) even at the highest temperatures examined (ca. 120°C, in toluene-d_8 in a sealed NMR tube).

2.2. Competitive β- and γ-activation processes

2-Butyne is partially polymerized in the presence of dimethyltitanocene at 65°C, and use of only 1 equiv. of this alkyne thus leads to rather intractable mixtures of organic and organometallic products as well as unreacted dimethyltitanocene. Use of two or more equivalents of 2-butyne, however, leads to much cleaner reaction chemistry. Unexpectedly, the dominant product (> 90%) of this reaction is not the titanacyclobutene (**8**), but rather a new metallacyclic complex (**9**) incorporating 2 equiv. of 2-butyne (Eq. (11)).



8 **9**

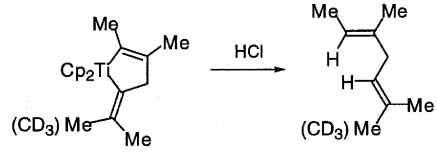
(11)

The new complex is easily purified through recrystallization from hexanes at −30°C. ^1H and ^{13}C NMR spectra provide unambiguous proof of the structure of complex **9**, and mass spectral and elemental analytical data are also supportive of this structure. Particularly revealing are two ^{13}C resonances in the downfield region of 180–195 ppm, highly characteristic of vinylic carbons attached to titanium [51].

In order to provide additional information about the formation of **9**, the reaction of 2-butyne with $Cp_2Ti(CD_3)_2$ was examined. The ^1H and ^{13}C NMR spectra of **9**-d_3 are virtually identical to those of **9**, with the exception of the loss of the highest field ^1H methyl resonance (0.8 ppm) and lowest field ^{13}C methyl resonance (24.8 ppm). (Loss of ^{13}C signal intensity for CD_3 groups due to spin–spin splitting is well known [52–54].) These chemical shifts unambiguously define the labeled methyl group as the isopropylidene methyl *cis* to the titanocene fragment [55]. An agostic interaction between this methyl group and the empty titanium wedge plane orbital seems likely, with the opposing shifts of the ^1H and ^{13}C resonances consistent with other reports of such agostic interactions [27,28].

In addition to allowing for the assignment of the outlying NMR resonances to this *cis*-methyl group, the deuterium labeling study also provides compelling information regarding the mechanism of formation of **9**. Thermal elimination of methane from dimethyltitanocene, generating $Cp_2Ti{=}CH_2$, may be virtually unequivocally ruled out as a mechanistic step, since neither a CD_2 group nor a CD_2H group, which might potentially be formed from a CD_2-containing intermediate, is found in **9**-d_3.

Given the mechanistic significance of the formation of **9**, its structure was further verified through protonolysis and analysis of the resulting diene **10** (Eq. (12)). (*E*)-2,5-di-



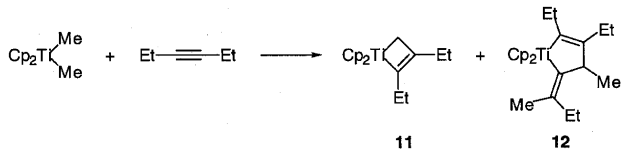
9 **10**

(12)

methylhepta-2,5-diene is formed with no loss of stereochemistry, being obtained as the sole volatile component of the protonolysis reaction (as demonstrated by gas chromatographic and NMR spectral analysis). Although two methyl resonances are degenerate in the ^1H NMR spectrum, all nine carbons in **10** are unambiguously resolved in the ^{13}C NMR spectrum. As in the ^{13}C NMR spectrum of its titanacyclic precursor, one of the methyl resonances is rather downfield (25.9 ppm) from the others. In this case, simple correlation tables point to the assignment of this resonance to the (*E*)-methyl of the isopropylidene group, shifted to lower field than the (*Z*)-methyl group due to the γ effect [56,57]. Protonolysis of the deuterated titanacycle, **9**-d_3, affords diene **10**-d_3, displaying ^1H and ^{13}C NMR spectral properties completely consistent with the location of the CD_3 group anticipated from the proposed structure of its titanacyclic precursor.

Dimethyltitanocene displays analogous reactivity toward 3-hexyne, but the titanacyclobutene is formed in appreciably

higher yield in this reaction than in that of 2-butyne. Again, methane is formed as a byproduct and two metallacyclic complexes, one incorporating a second equivalent of 3-hexyne, are obtained (Eq. (13)).



(13)

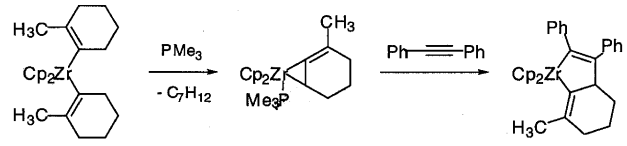
The most characteristic ^{1}H NMR spectral features of titanacyclopentene **12** are a methine quartet at 2.83 ppm coupled to a methyl doublet (1.16 ppm, $^3J_{HH} = 6$ Hz), a high-field methyl singlet (0.65 ppm), and two cyclopentadienyl resonances, clearly indicating the lack of a plane of symmetry in the complex. The ^{13}C NMR spectrum of **12** displays similar features to that of 2-butyne-derived complex **9**, most notably two downfield singlets (192.6, 193.0 ppm) for the sp^2-carbons attached to the titanium center, with the other vinyl carbons appearing near 132 ppm; assignment of resonances was facilitated by use of the DEPT (distortionless enhancement by polarization transfer) technique [58]. The methine carbon appears as a doublet ($^1J_{CH} = 125$ Hz) at 41.6 ppm.

Formation of both titanacyclobutenes and titanacyclopentenes in the reaction of dimethyltitanocene with alkynes is conveniently rationalized by initial alkyne carbometalation, followed by competitive allylic γ-CH activation, affording the titanacyclobutene, and β-CH activation, affording a titanacyclopropane (Scheme 1). Rotamer isomerization, affording access to elimination from the β-allylic position, is more facile in these cases than in the more hindered phenyl and trimethylsilyl derivatives. The product of this β-activation becomes dominant in the case of the 2-butyne reaction, while the increased steric bulk of the 3-hexyne derived intermediate allows for appreciable formation of the γ-activation product. Whereas the titanacyclobutenes are comparatively unreactive toward alkynes, the titanacyclopropanes undergo facile alkyne insertion, with steric issues directing the incoming alkyne to the observed insertion site rather than to the more crowded site, which would form unobserved isomer **13** (Scheme 1).

2.3. Metallacyclopropane (allene complex) intermediates

The titanacyclopropane intermediate may be represented in an alternative resonance form as an allene complex of titanocene [59,60]. Significantly, an intermediate is observed by NMR spectroscopy in both the 2-butyne and 3-hexyne reactions which displays a cyclopentadienyl ^{1}H resonance at ca. 4.7 ppm, a chemical shift similar to that displayed by isolable titanocene(II) derivatives, including $Cp_2Ti(PMe_3)_2$ (4.51 ppm) [61] and $Cp_2Ti(CO)_2$ (4.58 ppm) [62], and a cyclopentadienyl ^{13}C resonance at 98 ppm ($^1J_{CH} = 168$ Hz), in range with that reported for $Cp_2Ti(PMe_3)_2$ (91.2 ppm). Observation of these NMR resonances is consistent with intermediate formation of a titanocene(II) complex. While this observation does not unequivocally point to the allene complex as the observed intermediate, given the possibility of generation of other titanocene(II) species under the reaction conditions, the close resemblance of these spectral features to those of an independently prepared allene complex (vide infra) is noteworthy.

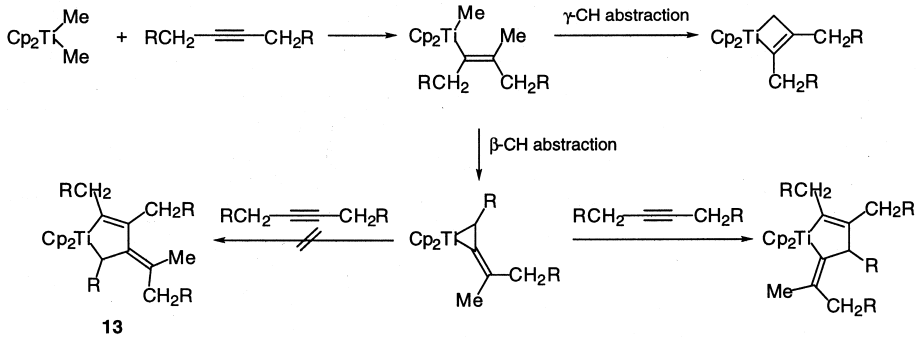
While this work was in progress, Jones and co-workers reported related chemistry in the zirconocene series [63]. Thermolysis of bis(methylcyclohexenyl)zirconocene in the presence of trimethylphosphine affords a 1,2-cyclohexadiene complex of zirconocene through a β-activation process (Eq. (14)). No evidence was reported for the formation of the



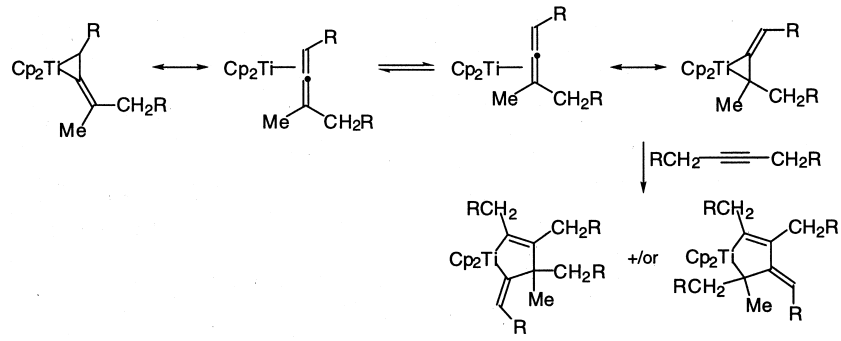
(14)

isomeric zirconacyclobutene which would arise from competitive γ-activation. The allene complex reacts with unsaturated substrates (e.g. diphenylacetylene) to afford zirconacyclic complexes analogous to **9** and **12**.

Given the likelihood of the intermediacy of allene complexes in the reactions of dimethyltitanocene with 2-butyne and 3-hexyne, the possibility of additional isomeric products is raised by the ability of allene complexes to undergo coordination isomerization [64] (for discussions of related issues for ketene complexes see Ref. [65]), as suggested in Scheme 2. In each case, however, the isomeric allene complex would



Scheme 1.

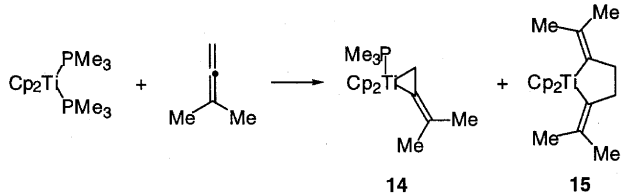


Scheme 2.

be expected to be sterically destabilized due to additional interactions between the cyclopentadienyl rings and the allene substituents.

The possibility that titanacyclopentene **9** arises from a follow-up reaction of titanacyclobutene **8** was ruled out by examining the reactivity of independently prepared dimethyltitanacyclobutene [26,66,67] toward 2-butyne. No spectral evidence was obtained for the formation of **9**, and the only noticeable reaction after 24 h at 70°C was the partial decomposition of the titanacyclobutene. The appearance of broad peaks in the allyl region of the ^{1}H NMR spectrum is suggestive of the polymerization of 2-butyne by the titanacyclobutene, supportive of earlier proposals regarding the possible intermediacy of metallacyclobutenes in certain catalytic alkyne polymerization mechanisms [68].

In order to establish more firmly the titanacyclopropane (allene complex) intermediate, the reaction between $Cp_2Ti(PMe_3)_2$ and 3-methyl-1,2-butadiene was examined. Two metallocene products are obtained, the allene complex **14** and titanacyclopentane **15**, incorporating 2 equiv. of the allene (Eq. (15)).



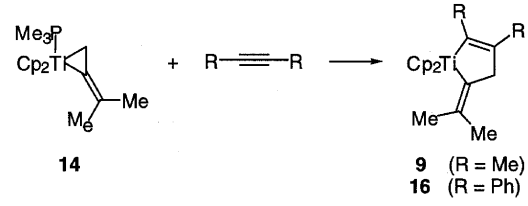
14 **15**

(15)

When the reaction is carried out in the presence of an excess of trimethylphosphine, complex **14**, apparently representing the first example of a titanocene allene complex (the first and, prior to our report, only preparation of a group 4 allene complex was that by Jones and co-workers [63]), is obtained cleanly and may be isolated in analytically pure form by simple evaporation of solvent and excess phosphine at ca. −5°C. In contrast to vinyl complex **4** and metallacycles **9** and **12**, for which NMR analysis suggests an agostic interaction between a proximal methyl group and the titanocene center, the methyl ^{1}H (2.02 and 2.41 ppm) and ^{13}C (24.2 and 29.7 ppm) resonances of complex **14** appear at rather typical chemical shifts. Clearly, the trimethylphosphine ligand in **14** overrides the weaker agostic interaction present in **4**, **9**, and **12**.

Attempted isolation of **14** through removal of solvent at higher temperature (25°C instead of −5°C) results in its partial conversion to the metallacyclopentane **15**. Treatment of $Cp_2Ti(PMe_3)_2$ with 2 equiv. of 3-methyl-1,2-butadiene permits the preparation of **15** in pure form. An agostic interaction between the methyl groups *cis* to the titanium center appears likely given the appearance of one methyl resonance in the ^{1}H NMR spectrum of **15** at appreciably higher field (0.75 ppm) than the other (1.48 ppm). Reductive coupling of allenes by zirconocene(II) has been noted previously [69,70], and a simple titanium(II) complex, $(iPrO)_2Ti$(1-propene), has very recently been reported to effect analogous allene coupling [71]. Allenes have also recently been incorporated successfully as reactants in the Pauson–Khand reaction [72]; although mechanistically unrelated, also noteworthy is the reductive coupling of allenes and alkynes mediated by hydrozirconation [73].

Importantly, allene complex **14** reacts readily with 2-butyne (1 h at 65°C) to form titanacyclopentene **9** (R = CH_3) (Eq. (16)), providing circumstantial evidence for the intermediacy of an allene complex in the reaction between 2-butyne and dimethyltitanocene. Diphenylacetylene also couples efficiently with allene complex **14** to form titanacyclopentene **16** (R = Ph) (Eq. (16)), suggesting potential synthetic applications in the form of cross couplings of unsaturated substrates [71].



14 **9** (R = Me) **16** (R = Ph)

(16)

2.4. Reaction kinetics

Kinetic analysis of the 2-butyne and 3-hexyne reactions is complicated by non-linearity at longer reaction times, at least in part due to the thermal decomposition of the titanacyclobutenes, but nonetheless qualitatively reveals some significant features of the reactions. First order consumption of dimethyltitanocene is observed at all temperatures examined

(ranging from 41 to 120°C). Interestingly, the rate of disappearance of dimethyltitanocene is significantly greater in the 2-butyne reaction than in the 3-hexyne reaction (a five-fold difference at 63°C), providing further circumstantial evidence against rate-determining formation of $Cp_2Ti{=}CH_2$ as a mechanistic step.

In contrast with the reaction of 2-butyne with dimethyltitanocene, which affords low yields of titanacyclobutene **8** together with titanacyclopentene **9** (Eq. (11)), the reaction with $Cp_2Ti(CD_3)_2$ affords only the titanacyclopentene at all temperatures examined. This suggests a substantial kinetic isotope effect, slowing the γ-CH(D) activation process, consistent with rate-determining CH(D) activation. A firm number for the isotope effect cannot be obtained due to the complete disappearance of the titanacyclobutene product in the $Cp_2Ti(CD_3)_2$ reaction. However, given the assumption that formation of $>2\%$ of the titanacyclobutene product would be detectable by ^{1}H NMR and ignoring any secondary isotope effects, a lower limit of $k_{\gamma\text{-H}}/k_{\gamma\text{-D}} = 3.2$ may be calculated. Interestingly, Janssens et al. have recently noted a similar dramatic change in reaction pathway for neopentyl groups on Pt(111) surfaces, with exclusive α-elimination seen for the protio derivative and exclusive γ-elimination for the α,α-d_2 derivative [74].

Formation of the titanacyclopentene product in the 2-butyne reaction was studied over a 50°C temperature range. An Eyring plot provides values for $\Delta H^{\ddagger} = 12.9$ kcal mol^{-1} and $\Delta S^{\ddagger} = -28$ eu, with the relatively large and negative entropy of activation consistent with a fairly ordered transition state. This could point toward a concerted methane elimination, requiring the proper alignment of Ti–CH_3 and β-H groups, but may also arise from rapid Ti–CH_3 bond homolysis, followed by rate-determining β-hydride abstraction.

The 3-hexyne reaction affords a unique opportunity to examine the competition between β- and γ-CH activation, since products arising from both processes are obtained at all reaction temperatures studied. An Eyring analysis of the product ratio as a function of temperature allows determination of $\Delta\Delta H^{\ddagger}_{\beta/\gamma} = 9.6$ kcal mol^{-1} and $\Delta\Delta S^{\ddagger}_{\beta/\gamma} = -8$ eu. The positive $\Delta\Delta H^{\ddagger}_{\beta/\gamma}$ is consistent with the formation of a more highly strained titanacyclopropane via β-hydride activation versus a less strained titanacyclobutene via γ-hydride activation. The small but negative $\Delta\Delta S^{\ddagger}_{\beta/\gamma}$ is in accord with a more organized transition state to bring the ethyl group bearing the β-hydrogen into proper alignment for elimination than is required to align the sterically less demanding methyl group bearing the γ-hydrogen.

3. Summary and conclusions

Alkynes undergo carbometalation by dimethyltitanocene, affording vinyl complexes which serve as intermediates for the formation of titanacyclic products through the elimination of methane. Rotational isomerization, restricted in the case of larger substituents, provides a simple and consistent explanation for the observed regioselectivity in the subsequent hydrogen abstraction/methane elimination step. Intermediates bearing vinyl groups able to undergo rotation favor formation of titanacyclopropanes through a β-activation process, while those unable to undergo rotation undergo a γ-activation process, leading to titanacyclobutenes. This selectivity is observed both for intermediate vinyl complexes presenting chemically very similar β- and γ-hydrogens (the 2-butyne and 3-hexyne reactions) and for those in which the competing sites for hydrogen abstraction are inequivalent (the diphenylacetylene and bis(trimethylsilyl)acetylene reactions) and appears to override the frequently observed preference for aromatic over aliphatic CH abstraction. Alternative formation of titanacyclobutenes through thermal decomposition of dimethyltitanocene, affording $Cp_2Ti{=}CH_2$, appears inconsistent with labeling and kinetic studies at moderate reaction temperatures, although it may appear as a competitive side reaction at very high temperatures.

The titanacyclopropanes may be alternatively formulated as allene complexes of titanocene. An independently prepared trimethylphosphine-ligated analog of 3-methyl-1,2-butadiene, representing the first titanocene allene complex to be reported, undergoes reductive coupling reactions with excess 3-methyl-1,2-butadiene and with alkynes.

4. Experimental

4.1. General

After purification and drying, all solids and solvents were stored under nitrogen in a Vacuum Atmospheres glove box equipped with a Dri-Train MO 40-1 inert gas purifier unit, RGF-1 regeneration flow unit, Pedatrol pressure control unit, DK-3E Dri-Kool refrigeration unit and Dri-Cold freezer. Unless otherwise noted, all operations were carried out under an atmosphere of argon and nitrogen, purified by passage first through activated BASF catalyst, then through activated molecular sieves.

4.2. Materials

Titanocene dichloride was purchased from Boulder Scientific and used without purification. Diphenylacetylene, bis(trimethylsilyl)acetylene, 3-hexyne, MeLi (1.4 M in diethyl ether), and CD_3Li (1.5 M in diethyl ether) were used as received from Aldrich. 2-Butyne was obtained from Farchan and used as received. Benzene-d_6 was purchased from MSD and distilled under a pre-purified nitrogen atmosphere from Na/K alloy and benzophenone. Toluene, benzene, THF and diethyl ether were distilled from Na/K alloy and benzophenone under a pre-purified nitrogen atmosphere. Alkanes (pentane and hexane) were washed with concentrated H_2SO_4, then with aqueous $NaHCO_3$, dried over calcium hydride, and distilled from Na/K alloy and benzophenone under a pre-purified nitrogen atmosphere. Trimethylphos-

phine (Aldrich) was stored in the glove box freezer and used without purification. Bis(trimethylphosphine)titanocene was prepared as described [61].

4.3. Instrumentation

Nuclear magnetic resonance (NMR) spectra of all samples were obtained on a GE QE-300 (300.152 MHz, ^{1}H; 75.481 MHz, ^{13}C). The following notation is used in reporting NMR data: (1) chemical shifts are reported in parts per million (ppm); (2) multiplicity of signal where s = singlet, d = doublet, t = triplet, m = multiplet, br = broad, dt = doublet of triplets, br s = broad singlet, etc; (3) coupling constants are reported in Hertz (Hz). Chemical shifts are referenced to residual solvent signals in benzene-d_6 (δ 7.150, ^{1}H; δ 128.00, ^{13}C), chloroform-d (δ 7.26, ^{1}H; δ 77.0, ^{13}C) and toluene-d_8 (δ 2.09, ^{1}H; δ 21.4, ^{13}C). Gas chromatographic analyses were performed on a Shimadzu GC-9A with He as the carrier gas with a flow rate of 50 ml min^{-1}, using an FID detector and an injection port temperature of 225°C. Mass spectroscopy was performed at the University of Oregon Mass Spectrometry Facility.

4.4. Preparation of dimethyltitanocene [39,40]

A Schlenk flask was charged with titanocene dichloride (5.0 g, 20.1 mmol) and diethyl ether. To the red suspension, cooled to −40°C, was added dropwise 32.0 ml of a 1.4 M solution of MeLi in diethyl ether (44.8 mmol, 2.23 equiv.). The mixture was stirred for 80 min while slowly warming to ca. 0°C, affording an orange solution. After cooling to −40°C, 40 ml of water was cautiously added. The organic phase was washed with water (2×25 ml) and brine (1×25 ml) and dried over $MgSO_4$. Removal of the solvent on a rotary evaporator afforded the crude product as an orange solid (3.9 g, 95%). Recrystallization from ca. 15 ml of pentane at −30°C afforded crystalline product (3.5 g, 85%). ^{1}H NMR (C_6D_6): δ 0.05 (s, 6H, CH_3), 5.68 (s, 10H, Cp). ^{13}C NMR: δ 45.9 (q, $^1J_{CH}$ = 124 Hz, CH_3), 113.2 (dm, $^1J_{CH}$ = 173 Hz, Cp). Dimethyltitanocene-d_6 was prepared analogously, using MeLi-d_3 in place of MeLi.

4.5. Reaction of dimethyltitanocene with diphenylacetylene: formation of vinyl intermediate **4**

To a Schlenk flask containing a solution of Cp_2TiMe_2 (1.00 g, 4.80 mmol) in toluene (25 ml) was added diphenylacetylene (1.71 g, 9.59 mmol, 2 equiv.). The flask was wrapped in aluminum foil to exclude light and heated at 72°C for 5 h. The solution underwent a color change from orange to deep-red. The solvent was then removed in vacuo, affording a brownish solid. This solid was mixed with 10 ml of hexanes and cooled at −20°C for 2 days, resulting in the precipitation of vinyl complex **4**, which was isolated as a reddish-brown solid by filtration (400 mg, 22%). (This product appears identical to the minor product obtained by Rausch and coworkers in the photochemical reaction between dimethyltitanocene and diphenylacetylene [35–37].) ^{1}H NMR (C_6D_6): δ −0.42 (s, 3H, Ti–CH_3), 1.45 (s, 3H, CH_3), 5.84 (s, 10H, Cp), 6.72 (d, 2H, $^3J_{HH}$ = 7.5 Hz, ArH), 6.82–6.87 (m, 4H, ArH), 6.91–7.01 (m, 4H, ArH). ^{13}C{^{1}H} NMR (C_6D_6): δ 25.7 (CH_3), 50.3 (Ti–CH_3), 112.5 (Cp), 123.7 (Ar), 123.9 (Ar), 124.9 (Ar), 127.3 (Ar), 127.5 (Ar), 128.3 (Ar), 135.5 (Ti–C=*C*), 146.4 (Ar), 147.2 (Ar), 189.6 (Ti–*C*=C). ^{13}C NMR (C_6D_6): δ 25.7 (q, $^1J_{CH}$ = 125 Hz, CH_3), 50.3 (q, $^1J_{CH}$ = 126 Hz, Ti–CH_3), 112.5 (d, $^1J_{CH}$ = 174 Hz, Cp), 123.7 (d, $^1J_{CH}$ = 160 Hz, Ar), 123.9 (m, Ar), 124.9 (d, $^1J_{CH}$ = 163 Hz, Ar), 127.3 (d, $^1J_{CH}$ = 161 Hz, Ar), 127.5 (d, $^1J_{CH}$ = 158 Hz, Ar), 128.3 (d, $^1J_{CH}$ = 161 Hz, Ar), 135.5 (s, Ti–C=*C*), 146.4 (s, Ar), 147.2 (s, Ar), 189.6 (s, Ti–*C*=C). HRMS. Calc. for $C_{26}H_{26}Ti$: 386.1514. Found: 386.1508. *Anal*. Calc. for $C_{26}H_{26}Ti$: C, 80.82; H, 6.78. Found: C, 80.67; H, 6.86%.

4.6. Thermolysis of **4**

Thermolysis of solutions of vinyl complex **4** in benzene-d_6 or toluene-d_8 at 70°C for 3 days resulted in the formation of methane (^{1}H NMR (C_6D_6): δ 0.15) and clean conversion to deep-red solutions of the titanacyclobutene (**3a**). Removal of solvent in vacuo afforded the titanacyclobutene in quantitative yield, with spectral properties identical to those previously reported [26,66,67]. ^{1}H NMR (C_6D_6): δ 3.45 (s, 2H, CH_2), 5.67 (s, 10H, Cp), 6.91–7.14 (m, 8H, ArH), 7.31–7.33 (d, 2H, ArH). ^{13}C{^{1}H} NMR (C_6D_6): δ 73.4 (CH_2), 100.6 (Ti–C=*C*), 112.4 (Cp), 124.5 (Ar), 125.9 (Ar), 126.2 (Ar), 129.5 (Ar), 129.6 (Ar), 138.7 (Ar), 147.6 (Ar), 210.9 (Ti–*C*=C).

Prolonged thermolysis of vinyl complex **4** at higher temperatures (28 h at 80–85°C) leads to the formation of a new product in up to a ca. 1:4 ratio to the titanacyclobutene. Although this complex has not been isolated in pure form, its ^{1}H NMR spectrum is consistent with the benzotitanacyclobutene **5**. ^{1}H NMR (C_6D_6): δ 0.70 (s, 3H, CH_3), 5.57 (s, 10H, Cp), 6.8–7.2 (m, ArH). Control experiments indicate that complex **5** is not formed via thermolysis of the titanacyclobutene.

4.7. Direct preparation of titanacyclobutene **3a** from dimethyltitanocene

Titanacyclobutene **3a** may also be prepared without isolation of the intermediate vinyl complex. Thus, Cp_2TiMe_2 (0.998 mg, 4.79 mmol) reacted with 0.902 g of diphenylacetylene (5.06 mmol, 1.06 equiv.) in 10 ml of toluene to afford, after heating for 16 h at 65–68°C and removal of solvent in vacuo, a dark-purple solid (1.815 g, 98%) composed of titanacyclobutene **3a** (ca. 80%) and vinyl complex **4** (ca. 20%). This material was redissolved in 10 ml of toluene and heated for 12–14 h at 80–85°C. Removal of solvent in vacuo quantitatively afforded the crude metallacycle. Crystallization of the crude product twice from hexanes afforded

the pure titanacyclobutene as a nicely crystalline, purple solid (60%).

4.8. Preparation of bis(trimethylsilyl)titanacyclobutene (**3b**) [26,66,67,75,76]

To a solution of 1.05 g of Cp_2TiMe_2 (5.0 mmol) in 30 ml of toluene in a 100 ml Schlenk flask was added 0.83 g of bis(trimethylsilyl)acetylene (1 equiv.). The flask was wrapped in aluminum foil and heated in an oil bath at 80°C for 14 h, at which point ^{1}H NMR analysis of an aliquot showed clean conversion to the titanacyclobutene. Solvent was removed in vacuo, yielding the product in a satisfactory state of purity as an oil in quantitative yield. Crystallization from hexanes at −30°C afforded a dark-red solid (1.46 g, 80%). ^{1}H NMR (C_6D_6): δ 0.21 (s, 9H, $Si(CH_3)_3$), 0.32 (s, 9H, $Si(CH_3)_3$), 4.67 (s, 2H, CH_2), 5.22 (s, 10H, Cp). $^{13}C\{^1H\}$ NMR (C_6D_6): δ 1.49 (CH_3), 2.80 (CH_3), 107.6 (Cp), 108.8 (CH_2).

4.9. Preparation of titanacyclopentene **9**

A side-arm round bottom flask was charged with 50 ml of dry toluene and 1.38 g of dimethyltitanocene (6.62 mmol). To this solution was added 2-butyne (1.04 ml, 717 mg, 2 equiv.). The flask was wrapped in foil and heated in an oil bath at 70°C for 12 h. ^{1}H NMR analysis of the reaction mixture at this point revealed conversion to a mixture of titanacyclopentene **9** and titanacyclobutene **8**, which displays identical spectral properties to those of an authentic sample [26,66,67,75,76]. The solvent was removed in vacuo and the residue was extracted with 25 ml of hexanes. The resulting solution was cooled to −30°C, then filtered. The pure product was isolated in ca. 35% yield by evaporation of the filtrand in vacuo. ^{1}H NMR (C_6D_6): δ 0.82 (s, 3H, CH_3), 1.17 (s, 3H, CH_3), 1.39 (s, 3H, CH_3), 1.52 (s, 3H, CH_3), 2.57 (br s, 2H, CH_2), 5.94 (s, 10H, Cp). $^{13}C\{^1H\}$ NMR (C_6D_6): δ 18.4 (CH_3), 20.4 (CH_3), 20.9 (CH_3), 24.8 (CH_3), 42.0 (CH_2), 113.8 (Cp), 119.6 (Ti–C=*C*), 125.1 (Ti–C=*C*), 185.6 (Ti–*C*=C), 188.1 (Ti–*C*=C). ^{13}C NMR (C_6D_6): δ 18.4 (q, $^1J_{CH}$ = 124 Hz, CH_3), 20.4 (q of t, $^1J_{CH}$ = 124 Hz, $^3J_{CH}$ = 4 Hz, CH_3), 20.9 (q, $^1J_{CH}$ = 124 Hz, CH_3), 24.8 (q of q, $^1J_{CH}$ = 123 Hz, $^3J_{CH}$ = 6 Hz, CH_3), 42.0 (t of q, $^1J_{CH}$ = 121 Hz, $^3J_{CH}$ = 4 Hz, CH_2), 113.8 (m, Cp), 119.6 (hextet, $^3J_{CH}$ = 6.5 Hz, Ti–C=*C*), 125.1 (heptet, $^3J_{CH}$ = 5.8 Hz, Ti–C=*C*), 185.6 (s, Ti–*C*=C), 188.1 (s, Ti–*C*=C). MS: *m/z* = 300 (M^+, 24%), 232 (M–C_5H_8, 14%), 218 (28%), 192 (17%), 178 (Cp_2Ti, 100%), 152 (26%), 128 (18%), 113 (CpTi, 76%). HRMS. Calc. for $C_{19}H_{24}Ti$: 300.1357. Found: 300.1370. *Anal*. Calc. for $C_{19}H_{24}Ti$: C, 75.99; H, 8.06. Found: C, 75.83; H, 8.12%.

4.10. Preparation of titanacyclopentene **9**-d_3

This complex was prepared analogously, using 400 mg of $Cp_2Ti(CD_3)_2$ (1.88 mmol) and 0.292 ml of 2-butyne (2 equiv.) and heating at 70°C for 24 h, then stirring at room temperature for an additional 12 h. ^{1}H NMR (C_6D_6): δ 1.17 (s, 3H, CH_3), 1.36 (s, 3H, CH_3), 1.49 (s, 3H, CH_3), 2.54 (br s, 2H, CH_2), 5.94 (s, 10H, Cp). $^{13}C\{^1H\}$ NMR (C_6D_6): δ 18.4 (CH_3), 20.3 (CH_3), 20.9 (CH_3), 42.0 (CH_2), 113.8 (Cp), 119.7 (Ti–C=*C*), 125.0 (Ti–C=*C*), 185.5 (Ti–*C*=C), 188.0 (Ti–*C*=C). *Anal*. Calc. for $C_{19}H_{24}Ti$: C, 75.99; H, 8.06. Found: C, 75.88; H, 8.17%.

4.11. Protonolysis of titanacyclopentene **9**

A side-arm round bottom flask was charged with titanacycle **9** (500 mg, 2.77 mmol) and 0.75 ml of C_6D_6. Excess dry HCl gas was gently introduced to the solution over the course of 5 min, then the volatile portion of the reaction mixture was isolated by vacuum transfer. Gas chromatographic analysis on a 30 m × 0.25 mm Carbowax column, 50–210°C at 10°C min^{-1}, revealed only a single component (retention time 5.2 min) in addition to the solvent. (*E*)-2,5-dimethylhepta-2,5-diene: ^{1}H NMR (C_6D_6): δ 1.54 (s, 3H, CH_3), 1.56 (s, 6H, 2 × CH_3), 1.66 (s, 3H, CH_3), 2.71 (d, 2H, J = 7.2 Hz, CH_2), 5.23–5.33 (m, 2H, 2 × =CH). $^{13}C\{^1H\}$ NMR (C_6D_6): δ 13.5 (CH_3), 15.9 (CH_3), 17.6 (CH_3), 25.8 (CH_3), 38.6 (CH_2), 118.5 (=CH), 123.3 (=CH), 132.2 (=*C*(CH_3)$_2$), 135.3 (=*C*(CH_3)CH_2). ^{13}C NMR (C_6D_6): δ 13.5 (q of d, $^1J_{CH}$ = 126 Hz, $^3J_{CH}$ = 4.5 Hz, CH_3), 15.9 (q, $^1J_{CH}$ = 125 Hz, $^3J_{CH}$ ~ 4 Hz, CH_3), 17.6 (m, $^1J_{CH}$ = 125 Hz, $^3J_{CH}$ ~ 4 Hz, CH_3), 25.8 (m, $^1J_{CH}$ = 125 Hz, $^3J_{CH}$ ~ 3.7 Hz, CH_3), 38.6 (t, $^1J_{CH}$ = 124 Hz, CH_2), 118.5 (m, $^1J_{CH}$ = 152 Hz, $^3J_{CH}$ ~ 6 Hz, =CH), 123.3 (m, $^1J_{CH}$ = 151 Hz, $^3J_{CH}$ ~ 5 Hz, =CH), 132.2 (heptet, $^3J_{CH}$ ~ 6 Hz, =*C*(CH_3)$_2$), 135.3 (s, =*C*(CH_3)CH_2). MS (70 eV): *m/z* = 97 (M–C_2H_3, 7%), 79 (10%), 69 (12%), 67 (15%), 65 (10%), 63 (10%), 56 (C_4H_8, 31%), 55 (23%), 54 (C_4H_6, 43%), 53 (18%), 51 (29%), 50 (19%), 44 (18%), 43 (65%), 42 (22%), 41 (C_3H_5, 100%), 40 (11%).

4.12. Protonolysis of titanacyclopentene **9**-d_3

Treatment of **9**-d_3 with excess dry HCl, as above, afforded the corresponding diene, (*E,E*)-1,1,1-d_3-2,5-dimethylhepta-2,5-diene, as the sole volatile product. ^{1}H NMR (C_6D_6): δ 1.54 (s, 3H, CH_3), 1.56 (s, 6H, 2 × CH_3), 2.70 (d, 2H, J = 7.5 Hz, CH_2), 5.25 (t, 1H, J = 7.5 Hz, =C*H*–CH_2), 5.28–5.34 (m, 1H, =CH). $^{13}C\{^1H\}$ NMR (C_6D_6): δ 13.5 (CH_3), 15.9 (CH_3), 17.6 (CH_3), 24.7 (m, $^1J_{CD}$ ~ 18 Hz, CD_3), 38.6 (CH_2), 118.5 (=CH), 123.3 (=CH), 132.1 (=*C*(CH_3)$_2$), 135.3 (=*C*(CH_3)CH_2). MS (70 eV): *m/z* = 127 (M^+, 5%), 109 (M–CD_3, 6%), 100 (M–C_2H_3, 7%), 95 (11%), 79 (11%), 73 (25%), 69 (14%), 67 (22%), 65 (12%), 63 (12%), 60 (10%), 59 (27%), 58 (16%), 57 (30%), 56 (C_4H_8, 57%), 55 (46%), 54 (C_4H_6, 56%), 53 (46%), 51 (46%), 50 (46%), 47 (43%), 46 (46%), 45 (46%), 44 (46%), 43 (94%), 42 (59%), 41 (C_3H_5, 100%), 40 (33%).

4.13. Reaction of dimethyltitanocene with 3-hexyne

An NMR tube was charged with 0.5 ml of C_6D_6, 42 mg of dimethyltitanocene (0.2 mmol), and 23 μl of 3-hexyne (1 equiv.). The tube was wrapped in foil and heated in an oil bath at 60°C for 12 h, with periodic ^{1}H NMR monitoring of the progress of the reaction. Upon complete consumption of the dimethyltitanocene, a 58:42 mixture (based on integration of the cyclopentadienyl resonances) of titanacyclopentene **12** and titanacyclobutene **11** was obtained. The titanacyclobutene displays spectral properties identical to those reported previously [51]. Titanacyclobutene **11**: ^{1}H NMR (C_6D_6): δ 0.92 (t, 3H, $^3J_{HH}$ = 7.5 Hz, CH_3), 1.04 (t, 3H, $^3J_{HH}$ = 7.5 Hz, CH_3), 1.95 (q, 2H, $^3J_{HH}$ = 7.5 Hz, CH_2), 2.53 (q, 2H, $^3J_{HH}$ = 7.5 Hz, CH_2), 3.30 (s, 2H, Ti–CH_2), 5.53 (s, 10H, Cp). ^{13}C{^{1}H} NMR (C_6D_6): δ 12.4 (CH_3), 15.8 (CH_3), 22.4 (CH_2), 29.3 (CH_2), 77.6 (Ti–CH_2), 92.5 (Ti–C=*C*), 110.0 (Cp), 221.0 (Ti–*C*=C). ^{13}C NMR (C_6D_6): δ 12.4 (q, $^1J_{CH}$ = 126 Hz, CH_3), 15.8 (q, $^1J_{CH}$ = 125 Hz, CH_3), 22.4 (t, $^1J_{CH}$ = 127 Hz, CH_2), 29.3 (t, $^1J_{CH}$ = 124 Hz, CH_2), 77.6 (t, Ti–CH_2), 92.5 (s, Ti–C=*C*), 110.0 (dm, $^1J_{CH}$ = 172 Hz, Cp), 221.0 (s, Ti–*C*=C). Titanacyclopentene **12**: ^{1}H NMR (C_6D_6): δ 0.65 (s, 3H, CH_3), 1.16 (d, 3H, $^3J_{HH}$ = 6 Hz, C*H*$_3$–CH), 2.83 (q, 1H, $^3J_{HH}$ = 6 Hz, CH_3–C*H*), 5.96 (s, 5H, Cp), 6.05 (s, 5H, Cp). (The remaining aliphatic resonances appear as a set of complex multiplets, partially obscured by the resonances of the titanacyclobutene, between 0.8–2.6 ppm.) ^{13}C{^{1}H} NMR (C_6D_6): δ 12.8 (CH_3), 13.2 (CH_3), 14.8 (CH_3), 21.1 (CH_3), 22.3 (CH_3), 22.9 (CH_2), 27.1 (CH_2), 27.6 (CH_2), 41.6 (*C*H–CH_3), 113.4 (Cp), 114.7 (Cp), 131.3 (Ti–C=*C*), 132.7 (Ti–C=*C*), 192.6 (Ti–*C*=C), 193.0 (Ti–*C*=C). ^{13}C NMR (C_6D_6): δ 12.8 (q, $^1J_{CH}$ ~ 127 Hz, CH_3), 13.2 (q, $^1J_{CH}$ ~ 123 Hz, CH_3), 14.8 (q, $^1J_{CH}$ ~ 120 Hz, CH_3), 21.1 (q, $^1J_{CH}$ ~ 123 Hz, CH_3), 22.3 (q, $^1J_{CH}$ ~ 126 Hz, CH_3), 22.9 (CH_2), 27.1 (CH_2), 27.6 (CH_2), 41.6 (d, $^1J_{CH}$ ~ 122 Hz, *C*H–CH_3), 113.4 (dm, $^1J_{CH}$ = 173 Hz, Cp), 114.7 (dm, $^1J_{CH}$ = 173 Hz, Cp), 131.3 (Ti–C=*C*), 132.7 (Ti–C=*C*), 192.6 (Ti–*C*=C), 193.0 (Ti–*C*=C). (Resonances for which no multiplicity information is provided were of insufficient intensity to permit such a determination.)

*4.14. Protonolysis of titanacyclopentene **12***

Treatment of **12** with excess dry HCl, as above, afforded the corresponding diene, (*Z*,*E*)-6-ethyl-3,5-dimethyl-3,6-nonadiene. ^{1}H NMR (C_6D_6): δ 0.87–0.99 (m, 9H, C*H*$_3$–CH_2), 1.18–1.29 (m, 3H, C*H*$_3$–CH), 1.39 (m, 1H, C*H*–CH_3), 1.65 (d, 2H, *J* = 0.6 Hz, CH_3–C=), 1.90–1.97 (m, 6H, C*H*$_2$CH$_3$), 4.81 (d, 1H, *J* = 5.1 Hz, =C*H*–CH(CH_3)), 5.15 (t, 1H, *J* = 7.2 Hz, =C*H*–CH_2CH_3).

*4.15. Preparation of (trimethylphosphine)(3-methyl-1,2-butadiene)titanocene (**14**)*

To a stirred solution of 100 mg of $Cp_2Ti(PMe_3)_2$ (0.303 mmol) in 2 ml of C_6D_6 was added 100 μl of trimethylphosphine and 30 μl of 3-methyl-1,2-butadiene (1 equiv.). The mixture was stirred at room temperature for 1 h, then frozen in a −5°C bath. Volatiles were removed from the frozen sample in vacuo, yielding **14** in analytically pure form as a greenish-brown solid (0.079 g, 81%), m.p. 120°C. ^{1}H NMR (C_6D_6): δ 0.29 (br s, 2H, CH_2), 0.83 (br s, 9H, PMe_3), 2.02 (s, 3H, CH_3), 2.41 (s, 3H, CH_3), 4.82 (s, 10H, Cp). ^{13}C{^{1}H} NMR (C_6D_6): δ 7.2 (PMe_3), 24.2 (CH_3), 29.7 (CH_3), 99.6 (Cp), 113.7 (Ti–CH_2), 118.5 (=*C*(CH_3)$_2$), 172.0 (Ti–*C*=C(CH_3)$_2$). ^{13}C NMR (C_6D_6): δ 7.2 (m, J_{app} = 150 Hz, PMe_3), 24.2 (q, $^1J_{CH}$ = 123 Hz, CH_3), 29.7 (q, $^1J_{CH}$ = 127 Hz, CH_3), 99.6 (d, $^1J_{CH}$ = 174 Hz, Cp), 113.7 (m, J_{app} = 3 Hz, Ti–CH_2), 118.5 (s, =*C*(CH_3)$_2$), 172.0 (s, Ti–*C*=C(CH_3)$_2$). *Anal*. Calc. for $C_{18}H_{27}PTi$: C, 67.08; H, 8.44; P, 9.61. Found: C, 67.12; H, 8.33; P, 9.50%.

4.16. Reaction of (trimethylphosphine)(3-methyl-1,2-butadiene)titanocene with 2-butyne

To a solution of 20 mg of allene complex **14** (0.062 mmol) in 0.5 ml of C_6D_6 in an NMR tube was added 9.5 μl of 2-butyne (2 equiv.). The tube was sealed, then heated at 65°C for 1.5 h, at which time spectral analysis revealed complete conversion of **14** to titanacyclopentene **9** (ca. 97%) and a trace of the product of reductive coupling of two equivalents of the allene (**15**, vide infra).

4.17. Reaction of (trimethylphosphine)(3-methyl-1,2-butadiene)titanocene with diphenylacetylene

Treatment of allene complex **14** with 1 equiv. of diphenylacetylene as described above afforded a ca. 9:1 mixture of titanacyclopentene **16** (R = Ph) and reductive coupling product **15** (vide infra). ^{1}H NMR (C_6D_6): δ 0.8 (s, 3H, CH_3), 1.52 (s, 3H, CH_3), 3.16 (s, 2H, CH_2), 6.02 (s, 10H, Cp), 6.8–7.4 (m, 10H, Ph).

4.18. Reductive coupling of 3-methyl-1,2-butadiene by $Cp_2Ti(PMe_3)_2$

To a solution of 250 mg of $Cp_2Ti(PMe_3)_2$ (0.758 mmol) in 8 ml of diethyl ether was added 100 μl of trimethylphosphine and 148 μl of 3-methyl-1,2-butadiene (2 equiv.). The mixture was kept at room temperature, with periodic monitoring of aliquots by ^{1}H NMR. After the reaction appeared complete (ca. 24 h), removal of all volatiles in vacuo afforded an orange solid. This crude product was extracted into pentane and the resulting solution was filtered to remove insoluble residues and evaporated, affording the titanacyclopentane **15** as a bright-orange solid (186 mg, 78%). ^{1}H NMR (C_6D_6): δ 0.75 (s, 6H, CH_3), 1.48 (s, 6H, 2×CH_3), 2.23 (s, 4H, CH_2), 6.05 (s, 10H, Cp). ^{13}C{^{1}H} NMR (C_6D_6): δ 21.4 (CH_3), 25.9 (CH_3), 31.3 (CH_2), 114.2 (Cp), 124.5 (Ti–C=*C*), 186.7 (Ti–*C*=C). MS (70 eV): *m/z* = 314 (M^+), 312, 310, 296, 272, 243, 192, 178 (Cp_2Ti), 113 (CpTi). HRMS. Calc. for $C_{20}H_{26}Ti$: 314.1514. Found:

314.1529. *Anal*. Calc. for $C_{20}H_{26}Ti$: C, 76.42; H, 8.34. Found: C, 76.34; H, 8.41%.

4.19. Kinetic studies

Reaction mixtures comprised 0.288 mM Cp_2TiMe_2 in C_6D_6, 2–10 equiv. of the alkyne, and 10 mol% of ferrocene as an internal standard were sealed under dry nitrogen in 5 mm NMR tubes. Reactions at $>70°C$ were carried out directly in the NMR probe ($\pm 0.5°C$), while reactions at lower temperatures were carried out in thermostatted oil baths, with the tubes wrapped in aluminum foil to preclude possible photochemical reactions. Reaction progress was monitored using the cyclopentadienyl resonances of the products, which were all clearly resolved.

Acknowledgements

This work was supported in part by the National Institutes of Health and in part by the National Science Foundation. J.J.J.J. was the recipient of a fellowship from the US Department of Education Graduate Assistance in Areas of National Need Program. Experimental assistance by Kenneth Zientara and Cynthia Ferguson is gratefully acknowledged.

References

[1] J.A. Davies, P.L. Watson, A. Greenberg, J.F. Liebman, Selective Hydrocarbon Activation, Principles and Progress, VCH, New York, 1990.
[2] T.J. Marks, R.D. Ernst, in: G. Wilkinson, F.G.A. Stone, E.W. Abel (Eds.), Comprehensive Organometallic Chemistry, Pergamon, Oxford, 1982, Ch. 21.
[3] M. Bothill, P.D. Gavens, J.W. Kelland, J. McMeeking, in: G. Wilkinson, F.G.A. Stone, E.W. Abel (Eds.), Comprehensive Organometallic Chemistry, Pergamon, Oxford, 1982, Ch. 22.3.
[4] M.I. Bruce, Angew. Chem., Int. Ed. Engl. 16 (1977) 73.
[5] E.C. Constable, Polyhedron 3 (1984) 1037.
[6] C. Hinderling, D.A. Plattner, P. Chen, Angew. Chem., Int. Ed. Engl. 36 (1997) 243.
[7] M.A. Bennett, T. Dirnberger, D.C.R. Hockless, E. Wenger, A.C. Willis, J. Chem. Soc., Dalton Trans. (1998) 271.
[8] M. Aizenberg, D. Milstein, Organometallics 15 (1996) 3317.
[9] I.P. Rothwell, Acc. Chem. Res. 21 (1988) 153.
[10] J.S. Vilardo, M.A. Lockwood, L.G. Hanson, J.R. Clark, B.C. Parkin, P.E. Fanwick, I.P. Rothwell, J. Chem. Soc., Dalton Trans. (1997) 3353.
[11] J. Albert, J. Granell, A. Luque, J. Minguez, R. Moragas, M. Fontbardia, X. Solans, J. Organomet. Chem. 522 (1996) 87.
[12] J. Vicento, I. Saurallamas, M.G. Palin, P.G. Jones, M.C.R. Dearellano, Organometallics 16 (1997) 826.
[13] S.L. Buchwald, R.B. Nielson, Chem. Rev. 88 (1988) 1047.
[14] J.W. Bulls, W.P. Schaefer, M. Serfas, J.E. Bercaw, Organometallics 6 (1987) 1219.
[15] N.A. Petasis, E.I. Bzowej, J. Org. Chem. 57 (1992) 1327.
[16] N.A. Petasis, E.I. Bzowej, Tetrahedron Lett. 34 (1993) 943.
[17] B. Hessen, J.-K.F. Buijink, A. Meetsma, J.H. Teuben, G. Helgesson, M. Håkansson, S. Jagner, A.L. Spek, Organometallics 12 (1993) 2268.
[18] G.A. Luinstra, J.H. Teuben, Organometallics 11 (1992) 1793.
[19] P. Foley, R. DiCosimo, G.M. Whitesides, J. Am. Chem. Soc. 102 (1980) 6713.
[20] S.S. Moore, R. DiCosimo, A.F. Sowinski, G.M. Whitesides, J. Am. Chem. Soc. 103 (1981) 948.
[21] J. Cheon, L.H. Dubois, G.S. Girolami, J. Am. Chem. Soc. 119 (1997) 6814.
[22] K.M. Doxsee, J.J.J. Juliette, J.K.M. Mouser, K. Zientara, Organometallics 12 (1993) 4682.
[23] H. Masai, K. Sonogashira, N. Hagihara, Bull. Chem. Soc. Jpn. 41 (1968) 750.
[24] K.M. Doxsee, J.J.J. Juliette, G. Nieckarz, K. Zientara, J. Am. Chem. Soc. 116 (1994) 2147.
[25] N.A. Petasis, D.-K. Fu, Organometallics 12 (1993) 3776.
[26] F.N. Tebbe, R.L. Harlow, J. Am. Chem. Soc. 102 (1980) 6149.
[27] M. Brookhart, M.L.H. Green, J. Organomet. Chem. 250 (1983) 395.
[28] M.L.H. Green, L.-L. Wong, J. Chem. Soc., Chem. Commun. (1984) 1442 and Refs. therein.
[29] J.J.W. Eshuis, Y.Y. Tan, A. Meetsma, J.H. Teuben, Organometallics 11 (1992) 362.
[30] A. Bertuleit, C. Fritze, G. Erker, R. Frohlich, Organometallics 16 (1997) 2891 and Refs. therein.
[31] R.F. Johnston, J.C. Cooper, Organometallics 6 (1987) 2448.
[32] P.C. Wailes, H. Weigold, A.P. Bell, J. Organomet. Chem. 33 (1971) 181.
[33] P.C. Wailes, H. Weigold, A.P. Bell, J. Organomet. Chem. 34 (1972) 155.
[34] P.W.N.M. VanLeeuwen, H. Van der Heijden, C.G.C.F. Roobeek, J.H.G. Frijns, J. Organomet. Chem. 209 (1981) 169.
[35] W.H. Boon, M.D. Rausch, J. Chem. Soc., Chem. Commun. (1977) 397.
[36] W.H. Boon, M.D. Rausch, H. Alt, J. Organomet. Chem. 141 (1977) 299.
[37] H. Alt, M.D. Rausch, J. Am. Chem. Soc. 96 (1974) 5936.
[38] N.M. Kablaoui, S.L. Buchwald, J. Am. Chem. Soc. 118 (1996) 3182.
[39] T.S. Piper, G. Wilkinson, J. Inorg. Nucl. Chem. 3 (1956) 104.
[40] K. Clauss, H. Bestian, Liebigs Ann. Chem. 654 (1962) 8.
[41] C. McDade, J.C. Green, J.E. Bercaw, Organometallics 1 (1982) 1629.
[42] J.B. Lee, G.J. Gajda, W.P. Schaefer, T.R. Howard, T. Ikariya, D.A. Straus, R.H. Grubbs, J. Am. Chem. Soc. 103 (1981) 7358.
[43] G.A. Luinstra, J. Vogelzang, J.H. Teuben, Organometallics 11 (1992) 2273.
[44] K.M. Doxsee, J.K.M. Mouser, Organometallics 9 (1990) 3012.
[45] K.M. Doxsee, J.K.M. Mouser, Tetrahedron Lett. 32 (1991) 1687.
[46] A. Pietrzykowski, S. Pasynkiewicz, P. Buchalski, Coll. Czech. Chem. Commun. 62 (1997) 318.
[47] B.C. Ankianiec, V. Christou, D.T. Hardy, Sk.K. Thomson, G.B. Young, J. Am. Chem. Soc. 116 (1994) 9963.
[48] T. Behling, G.S. Girolami, G. Wilkinson, R.G. Somerville, M.B. Hursthouse, J. Chem. Soc., Dalton Trans. (1984) 877.
[49] R.A. Andersen, R.A. Jones, G. Wilkinson, J. Chem. Soc., Dalton Trans. (1978) 446.
[50] C.R. Bennett, D.C. Bradley, J. Chem. Soc., Chem. Commun. (1974) 29.
[51] J.K.M. Mouser, Ph.D. Dissertation, University of Southern California, Los Angeles, CA, 1991.
[52] H.J. Reich, M. Jautelat, M.T. Messe, J.J. Weigert, J.D. Roberts, J. Am. Chem. Soc. 91 (1969) 7445.
[53] N.S. Bhacca, D.D. Giannini, W.S. Jankowski, M.E. Wolff, J. Am. Chem. Soc. 95 (1973) 8421.
[54] H. Eggert, C. Djerassi, J. Org. Chem. 38 (1973) 3788.
[55] E. Breitmaier, W. Voelter, Carbon-13 NMR Spectroscopy, VCH, New York, 3rd edn., 1987.
[56] G.C. Levy, R.L. Lichter, G.L. Nelson, Carbon-13 Nuclear Magnetic Resonance Spectroscopy, Wiley Interscience, New York, 2nd edn., 1980.
[57] J.B. Stothers, Q. Rev. Chem. Soc. 19 (1965) 144.

[58] D.M. Doddrell, D.T. Pegg, M.R. Bedall, J. Magn. Reson. 48 (1982) 323.
[59] M.J.S. Dewar, Bull. Soc. Chim. Fr. 18 (1951) C71.
[60] J. Chatt, L.A. Duncanson, J. Chem. Soc. (1953) 2939.
[61] L.B. Kool, M.D. Rausch, H.G. Alt, M. Herberhold, U. Thewalt, B. Wolf, Angew. Chem., Int. Ed. Engl. 24 (1985) 394.
[62] D.J. Sikora, D.W. Macomber, M.D. Rausch, Adv. Organomet. Chem. 25 (1986) 317.
[63] J. Yin, K.A. Abboud, W.M. Jones, J. Am. Chem. Soc. 115 (1993) 3810.
[64] D.J. Pasto, N. Huang, C.W. Eigenbrot, J. Am. Chem. Soc. 107 (1985) 3160.
[65] H. Hoberg, J. Korff, J. Organomet. Chem. 152 (1978) 255 and Refs. therein.
[66] F.N. Tebbe, G.W. Parshall, D.W. Ovenall, J. Am. Chem. Soc. 101 (1979) 5074.
[67] F.N. Tebbe, G.W. Parshall, G.S. Reddy, J. Am. Chem. Soc. 100 (1978) 3611.
[68] C.-C. Han, T. Katz, J. Organometallics 4 (1985) 2186.
[69] D.M. Duggan, Inorg. Chem. 20 (1981) 1164.
[70] J.R. Schmidt, D.M. Duggan, Inorg. Chem. 20 (1981) 318.
[71] D. Hideura, H. Urabe, F. Sato, Chem. Commun. (1998) 271.
[72] M. Ahmar, O. Chabanis, J. Gauthier, B. Cazes, Tetrahedron Lett. 38 (1997) 5277.
[73] K. Suzuki, T. Imai, S. Yamanoi, M. Chino, T. Matsumoto, Angew. Chem., Int. Ed. Engl. 36 (1997) 2469.
[74] T.V.W. Janssens, G.L. Jin, F. Zaera, J. Am. Chem. Soc. 119 (1997) 1169.
[75] J.D. Meinhart, B.D. Santarsiero, R.H. Grubbs, J. Am. Chem. Soc. 108 (1986) 3319.
[76] T.L. Howard, J.B. Lee, R.H. Grubbs, J. Am. Chem. Soc. 102 (1980) 6876.

PERGAMON

www.elsevier.nl/locate/poly

Polyhedron 19 (2000) 891–898

POLYHEDRON

Molecular structure, characterization and magnetic properties of novel mixed-valence copper(I,II) α,β-unsaturated carboxylate complexes with triphenylphosphine and methanol ligands

Yao-Yu Wang [a,*], Qian Shi [a], Qi-Zhen Shi [a], Yi-Ci Gao [b], Xun Hou [c]

[a] *Department of Chemistry, Northwest University, Xian 710069, People's Republic of China*

[b] *Department of Chemistry, Lanzhou University, Lanzhou 730000, People's Republic of China*

[c] *Xian Institute of Optics and Precision Mechanics, Chinese Academy of Sciences, Xian 710069, People's Republic of China*

Received 13 October 1999; accepted 1 February 2000

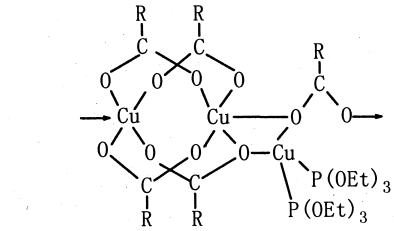
Abstract

Two new mixed-valence tetranuclear copper(I,II) α,β-unsaturated carboxylate complexes $Cu^{I}_{2}Cu^{II}_{2}A_{6}(PPh_3)_4(CH_3OH)_2$ (**1**, $A = CH_2{=}CH{-}COO^-$; **2**, $A = CH_2{=}C(CH_3){-}COO^-$) have been synthesized by partial reduction of $Cu_2A_4(H_2O)_2$ by triphenylphosphine in methanol solution, and characterized by elemental analyses, IR, ESR, electronic reflectance spectroscopies as well as magnetic susceptibility measurements. In complex **2** two copper(II) atoms in a molecule are linked by four carboxylate groups forming a dimeric unit $Cu^{II}_{2}A_4$, and each copper(II) atom coordinates with a copper(I) moiety through a μ_2-O,O′ carboxylate group. The electronic reflectance spectra in the solid state suggest a square pyramidal coordination environment around the copper(II) atoms. Bond valence calculations further confirm the presence of the mixed-valence system and the oxidation state of the copper atoms. Room temperature X-band ESR spectra of powdered samples and variable-temperature magnetic susceptibility studies indicate the presence of strong antiferromagnetic exchange interactions between two copper(II) atoms, with $2J = -310\ cm^{-1}$ for complex **1** and $2J = -288\ cm^{-1}$ for complex **2**. The formation mechanism of the title complexes and the structural interconversion among related mixed-valence copper(I,II) carboxylate complexes are also discussed.
©2000 Elsevier Science Ltd All rights reserved.

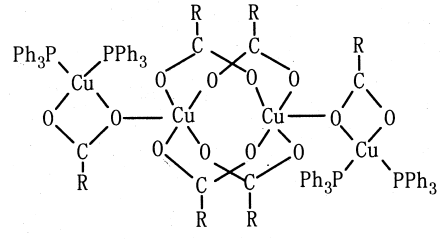
Keywords: Copper(I,II) complexes; α,β-Unsaturated carboxylates; Triphenylphosphine; Magnetic properties; Crystal structures

1. Introduction

Electron transfer between copper(I) and copper(II) remains a subject of intense interest [1–4]. Copper(I) and copper(II) polymers play an important role in copper-catalyzed substrate oxygenation in biochemical processes [5–8]. The crystal structure of mixed-valence copper(I,II) complexes has received a great deal of attention for what they may reveal about structural changes accompanying oxidation and reduction of copper in metalloenzymes [9]. Indeed, only a few structurally characterized mixed-valence copper(I,II) complexes containing carboxylate and phosphine ligands have been reported. Specifically, Beddoes et al. [10] and Connor et al. [11] characterized a one-dimensional chain of repeating $Cu^{II}_{2}Cu^{I}$ units (A) by partial reduction of copper(II) with triethylphosphine, and a tetrameric complex with triphenylphosphine (B) was synthesized and character-



A



B

* Corresponding author. Tel.: +86-29-830 3097; fax: +86-29-837 3398; e-mail: wyaoyu@nwu.edu.cn

0277-5387/00/$ - see front matter ©2000 Elsevier Science Ltd All rights reserved.
PII S0277-5387(00)00327-2

ized by Valigura et al. [12,13], as depicted in structural formulas, A and B.

Two mixed-valence copper(I,II) complexes, $Cu^{I}_{2}Cu^{II}_{2}(CH_2{=}CH{-}COO)_6(PPh_3)_4(CH_3OH)_2$ (**1**) and $Cu^{I}_{2}Cu^{II}_{2}[CH_2{=}C(CH_3){-}COO]_6(PPh_3)_4(CH_3OH)_2$ (**2**) synthesized here were characterized by elemental analyses, IR, ESR, electronic reflectance spectroscopies as well as magnetic susceptibility measurements. The crystal structure of complex **2** was determined by X-ray diffraction, and the oxidation states of the copper atoms have also been calculated with bond valence theory.

Both complexes **1** and **2** have a tetranuclear structure, in which two Cu(II) atoms are linked by four μ_2-O,O′ α-methacrylate groups forming a cage structural unit. It is interesting that the solvent molecule MeOH coordinates with the Cu(I) atom and completes its tetrahedral coordination environment along with two triphenylphosphine molecules and a μ-O,O′ α-methacrylate group. The Cu(I) moiety is linked with the Cu(II) atom through a μ-O,O′ α-methacrylate group. The formation mechanism of complexes **1** and **2** and the structural interconversion among the three related structures (A, B and the complex reported here) are discussed in this paper.

2. Experimental

2.1. Syntheses

All chemicals were purchased commercially and used as received. $Cu_2(CH_2{=}CH{-}COO)_4(H_2O)_2$ and $Cu_2[CH_2{=}C(CH_3){-}COO]_4(H_2O)_2$ were prepared as previously reported [14].

$Cu^{I}_{2}Cu^{II}_{2}(CH_2{=}CH{-}COO)_6(PPh_3)_4(CH_3OH)_2$ (**1**): a methanol solution (10 ml) of PPh_3 (2.68 g, 10.0 mmol) was added to a solution of $Cu_2(CH_2{=}CH{-}COO)_4(H_2O)_2$ (1.00 g, 2.24 mmol) in methanol (30 ml). The mixture was boiled for 2 h and filtered under warm conditions in a nitrogen atmosphere. Upon standing at room temperature for several days in vacuo, pale-green crystals were obtained. *Anal*. Calc. for $C_{92}H_{86}Cu_4P_4O_{14}$: C, 61.60; H, 4.83; Cu, 14.17. Found: C, 61.40; H, 4.92; Cu, 14.33%.

$Cu^{I}_{2}Cu^{II}_{2}[CH_2{=}C(CH_3){-}COO]_6(PPh_3)_4(CH_3OH)_2$ (**2**): this was prepared according to the same procedure as for complex **1**, using $Cu_2[CH_2{=}C(CH_3){-}COO]_4(H_2O)_2$ (1.13 g, 2.24 mmol) instead of $Cu_2(CH_2{=}CH{-}COO)_4(H_2O)_2$. *Anal*. Calc. for $C_{98}H_{98}Cu_4O_{14}P_4$: C, 62.60; H, 5.22; Cu, 13.53. Found: C, 62.73; H, 5.35; Cu, 13.45%.

2.2. Crystallography

A pale-green crystal of complex **2** with approximate dimensions 0.28×0.22×0.20 mm was mounted on a Siemens P4 diffractometer, using graphite-monochromated Mo Kα radiation ($\lambda = 0.71073$ Å). The data were collected with the ω–2θ scan technique ($2.03 \le \theta \le 23.99°$) by the XSCANS program. A total of 6163 reflections were collected (5874 independent reflections, $R_{int} = 0.0395$). Lp corrections and absorption correction were applied (transmission factors: 0.8071 and 0.7105). The structure was solved by direct methods and refined with full-matrix least-squares technique. The hydrogen atoms were generated in idealized positions. All calculations were performed on a IBM 486/PC using the Siemens SHELXTL-PC program. A summary of the crystallographic data collection is presented in Table 1.

2.3. Physical measurements

Elemental analyses were determined with a Perkin-Elmer model 240C automatic instrument. IR spectra were recorded on KBr pellets with a Nicolet 170SX FT-IR spectrometer. Electronic reflectance spectra were recorded on a Perkin-Elmer 40P spectrophotometer. ESR spectra were recorded on powder samples at X-band frequency of about 9.77 GHz with a Bruker ER200-D-SRC10/12 automatic spectrometer. Variable-temperature (77–300 K) magnetic susceptibility measurements were carried out on a CAHN-2000 Faraday balance with $Ni(en)_3S_2O_3$ as a standard at 5 T magnetic field. The diamagnetic corrections were evaluated from Pascal's constants [15]. The effective magnetic moments were calculated from the expression:

$$\mu_{eff} = 2.83\sqrt{\chi^{Cu}_{M}T} \quad (1)$$

Table 1
Summary of crystallographic data for $Cu^{I}_{2}Cu^{II}_{2}[CH_2{=}C(CH_3){-}COO]_6(PPh_3)_4(CH_3OH)_2$ (**2**)

Formula	$C_{98}H_{98}Cu_4O_{14}P_4$
Formula weight	1877.80
T (K)	293.2
Crystal system	Triclinic
Space group	$P\bar{1}$
Crystal size (mm)	0.28×0.22×0.20
a (Å)	13.567(2)
b (Å)	13.946(3)
c (Å)	14.569(3)
α (°)	66.068(14)
β (°)	84.234(14)
γ (°)	69.975(13)
V (Å^3)	2365.0(8)
Scan limit (°)	$2.03 \le \theta \le 23.99$
Limiting indices	$0 \le h \le 13$, $-13 \le k \le 13$, $-15 \le l \le 16$
Reflections collected	6163
Independent reflections	5874
ρ_{calc} (g cm^{-3})	1.317
Z	1
μ (mm^{-1})	1.015
$F(000)$	974
Radiation	Mo Kα ($\lambda = 0.71073$ Å)
R indices (all data)	$R_1 = 0.0992$, $wR_2 = 0.1460$
Final R indices ($I > 2\sigma(I)$) [a]	$R_1 = 0.0536$, $wR_2 = 0.1113$

[a] $R = \sum||F_o| - |F_c||/\sum|F_o|$; $wR = [\sum w(F_o^2 - F_c^2)^2/\sum w\sum F_o^4]^{1/2}$; $w = 1/\sigma^2(F_o^2)$.

3. Results and discussion

3.1. IR spectra

The IR spectra show strong bands corresponding to $\nu_{as}(COO)$ and $\nu_s(COO)$ at 1575 and 1430 cm^{-1} for complex **1**, and 1579 and 1421 cm^{-1} for complex **2**. The $\Delta\nu$ values of the two complexes are 145 and 158 cm^{-1}, respectively, which are close to the corresponding values of CH_2=CH–COONa (134 cm^{-1}) and CH_2=C(CH_3)–COONa (150 cm^{-1}), indicating that the α,β-unsaturated carboxylate group behaves as a bridging bidentate ligand between two Cu atoms [16,17], and complex **1** is likely to have a structure similar to that of complex **2**.

3.2. Crystal structure of $Cu^I_2Cu^{II}_2[CH_2=C(CH_3)–COO]_6(PPh_3)_4(CH_3OH)_2$ (2)

The selected bond lengths and angles for complex **2** are listed in Table 2. The ORTEP drawing of complex **2** is shown in Fig. 1. The molecule is centrosymmetric, with its pair of Cu(II) atoms bridged by four α-methacrylate groups forming a dimeric cage structural unit $Cu^{II}_2[CH_2=C(CH_3)–COO]_4$, which is connected at each end by a $Cu^I[CH_2=C(CH_3)–$

Table 2
Selected bond lengths (Å) and angles (°) of $Cu_4[CH_2=C(CH_3)–COO]_6(PPh_3)_4(CH_3OH)_2$ (**2**)

Cu(1)–O(1)	2.052(2)	Cu(1)–O(7)	2.176(2)	Cu(1)–P(1)	2.2396(13)
Cu(1)–P(2)	2.2280(13)	Cu(2)–O(3)	1.943(3)	Cu(2)–O(5)	1.962(2)
Cu(2)–O(4A) [a]	1.967(3)	Cu(2)–O(6)	1.980(2)	Cu(2)–O(2)	2.130(2)
Cu(2)–Cu(2A)	2.6465(10)	P(1)–C(1)	1.821(2)	P(1)–C(7)	1.821(2)
P(1)–C(13)	1.822(2)	P(2)–C(25)	1.813(2)	P(2)–C(19)	1.814(2)
P(2)–C(31)	1.819(2)	O(1)–C(37)	1.264(3)	O(2)–C(37)	1.221(3)
O(3)–C(41)	1.271(4)	O(4)–C(41)	1.236(4)	O(5)–C(45)	1.258(3)
O(6)–C(45A)	1.247(4)	O(7)–C(49)	1.352(5)		
O(1)–Cu(1)–O(7)	93.56(8)	O(1)–Cu(1)–P(2)	109.69(8)		
O(7)–Cu(1)–P(2)	111.40(8)	O(1)–Cu(1)–P(1)	105.71(8)		
O(7)–Cu(1)–P(1)	106.10(8)	P(2)–Cu(1)–P(1)	125.57(4)		
O(3)–Cu(2)–O(5)	90.29(12)	O(3)–Cu(2)–O(4A)	167.33(9)		
O(5)–Cu(2)–O(4A)	90.04(11)	O(3)–Cu(2)–O(6)	88.09(12)		
O(5)–Cu(2)–O(6)	166.71(8)	O(4A)–Cu(2)–O(6)	88.68(11)		
O(3)–Cu(2)–O(2)	102.87(9)	O(5)–Cu(2)–O(2)	97.82(9)		
O(4A)–Cu(2)–O(2)	89.64(9)	O(6)–Cu(2)–O(2)	95.40(9)		
O(3)–Cu(2)–Cu(2A)	85.93(6)	O(5)–Cu(2)–Cu(2A)	80.91(6)		
O(4A)–Cu(2)–Cu(2A)	81.62(6)	O(6)–Cu(2)–Cu(2A)	85.82(6)		
O(2)–Cu(2)–Cu(2A)	171.15(8)				

[a] Symmetry code A: $-x+1, -y-1, -z+1$.

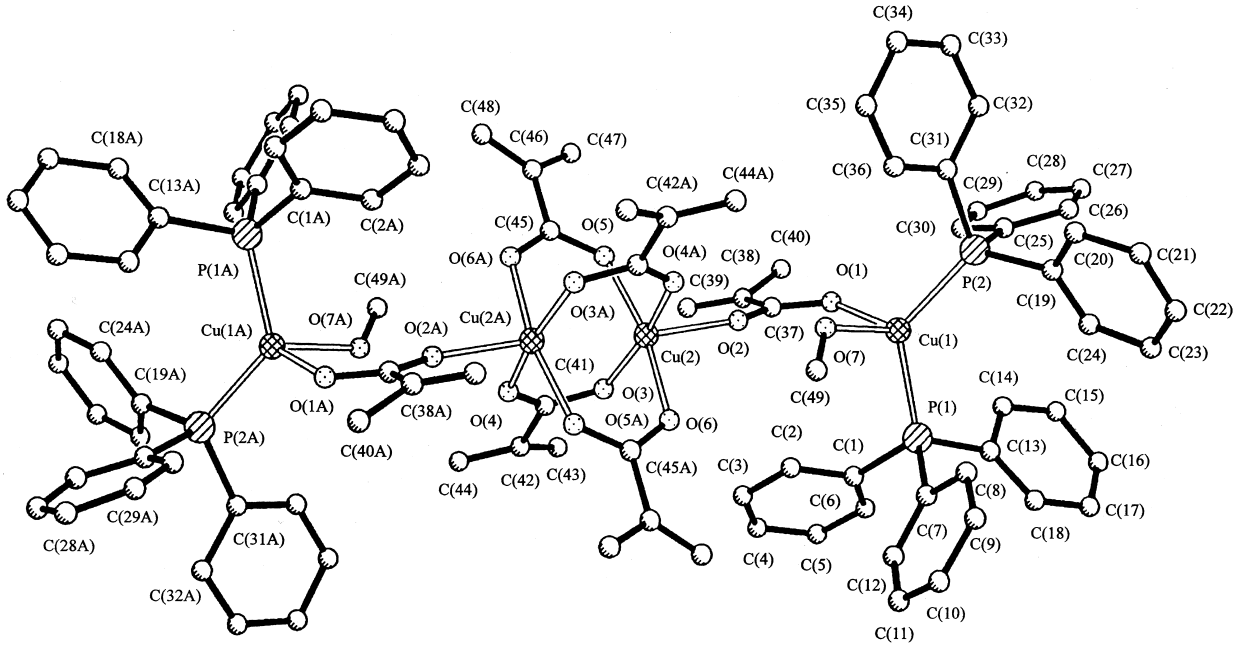


Fig. 1. ORTEP drawing of $Cu^I_2Cu^{II}_2[CH_2=C(CH_3)–COO]_6(PPh_3)_4(CH_3OH)_2$ (**2**).

COO](PPh$_3$)$_2$(CH$_3$OH) unit via an axial μ-O,O′ α-methacrylate group to form a tetranuclear structure.

The configuration of each Cu(II) atom is a square pyramid, in which the basal plane (average deviation: 0.0069 Å, plane 1) is composed of O(3), O(4A), O(5) and O(6) from four μ_2-O,O′ α-methacrylate groups of the $Cu^{II}_2[CH_2{=}C(CH_3){-}COO]_4$ unit. The Cu(II) atom is displaced from the basal plane towards the apical oxygen atom O(2) by 0.2204 Å, which is slightly larger than the corresponding value of 0.211 Å in $Cu^{I}_2Cu^{II}_2(CH_3{-}COO)_6(PPh_3)_4$ [12] owing to the influence of carboxylate and apical ligands. The average distance Cu(2)–O in the dimeric unit is 1.963 Å, shorter than the apical Cu(2)–O(2) distance of 2.130(2) Å. The O(2)–Cu(2)–O(basal) angles are in the range 89.64(9)–102.87(9)° with average value 96.44°. The atoms O(2), Cu(2) and Cu(2A) are not co-linear, with O(2)–Cu(2)–Cu(2A) = 171.15(8)°, which is slightly smaller in comparison with the values for dimeric copper(II) complexes such as 175.82° in $Cu_2(CH_2{=}CH{-}COO)_4(H_2O)_2$ [18], 178.69° in $Cu_2[CH_2{=}C(CH)_3{-}COO]_4(benzimH)_2$ [19] and 176.4° in $Cu_2(CH_2{=}CH{-}COO)_4(urea)_2$ [14]. The Cu(2)···Cu(2A) separation of 2.6465(10) Å is close to that in the dimer $Cu_2(CH_3{-}COO)_4(H_2O)_2$ (2.64 Å) [17,20], indicating the presence of strong interactions between two Cu(II) atoms, which is confirmed by the magnetic susceptibility studies. The Cu(II)···Cu(II) separation reported here is close to that in the complex $Cu^{I}_2Cu^{II}_2(CH_3{-}COO)_6(PPh_3)_4$ (2.642 Å) [12], but somewhat longer than that in the polymeric complex $[Cu^{I}Cu^{II}_2(CH_3{-}COO)_5\{P(OEt)_3\}_2]$ (2.56 Å) [10].

The Cu(I) atom in the $Cu^{I}[CH_2{=}C(CH_3){-}COO](PPh_3)_2(CH_3OH)$ moiety has a tetrahedral coordination environment, being surrounded by O(1) from a μ-O,O′ α-methacrylate group, O(7) of a methanol molecule and P(1), P(2) from two triphenylphosphine ligands. The angles O(1)–Cu(1)–O(7), O(1)–Cu(1)–P(1), O(1)–Cu(1)–P(2), O(7)–Cu(1)–P(2), O(7)–Cu(1)–P(1) and P(1)–Cu(1)–P(2) are 93.56(8), 105.71(8), 109.69(8), 111.40(8), 106.10(8) and 125.57(4)°, respectively. The bond distances Cu(1)–P(1) and Cu(1)–P(2) are 2.2396(13) and 2.2280(13) Å, respectively, close to the corresponding values in $[Cu^{I}Cu^{II}_2(CH_3{-}COO)_5\{P(OEt)_3\}_2]$ (2.21 and 2.22 Å) [10] and in $Cu^{I}_2Cu^{II}_2(CH_3{-}COO)_6(PPh_3)_4$ (2.249 and 2.225 Å) [12]. The distances Cu(1)–O(1) and Cu(1)–O(7) are 2.052(2) and 2.176(2) Å, longer than the corresponding values of Cu(2)–O(basal) and Cu(2)–O(apical), suggesting that the oxidation state is +2 for Cu(2) and Cu(2A), as well as +1 for Cu(1) and Cu(1A).

Table 3
Bond valence sums [a] for the Cu atoms in complex **2**

	R_i (Å)	S_i	ΣS_M
Cu(1)			1.05
Cu(1)–O(1)	2.052	0.26	
Cu(1)–O(7)	2.176	0.18	
Cu(1)–P(1)	2.2396	0.30	
Cu(1)–P(2)	2.2280	0.31	
Cu(2)			2.15
Cu(2)–O(2)	2.130	0.30	
Cu(2)–O(3)	1.943	0.49	
Cu(2)–O(4A)	1.967	0.46	
Cu(2)–O(5)	1.962	0.46	
Cu(2)–O(6)	1.980	0.44	

[a] Valence sums are calculated with the formula $S_i = \exp[(R_0 - R_i)/B]$ where S_i is the bond valence of bond '*i*', R_0 is a constant dependent on the bonded elements, R_i is the bond length of bond '*i*', $B = 0.37$. ΣS_M is the bond valence sum for the metal. R_0[Cu(II)–O] = 1.679, R_0[Cu(I)–O] = 1.55, and R_0[Cu(I)–P] = 1.79.

Atoms Cu(2), O(5), C(45), O(6A) and Cu(2A) lie on one plane (average deviation: 0.0132 Å, plane 2), and Cu(2), O(3), C(41), O(4) and Cu(2A) on another plane (average deviation: 0.00174 Å, plane 3). Plane 2 and plane 3 are nearly orthogonal with a dihedral angle of 90.8°.

3.3. Bond valence calculation

Bond valence calculations [21,22] were employed to quantify the charge distribution around each copper atom, and the results are summarized in Table 3. The calculated bond valence sum is 1.04 for Cu(1) and Cu(1A), and 2.14 for Cu(2) and Cu(2A).

3.4. Electronic reflectance spectra

The solid state spectra of **1** and **2** recorded in the range 200–1100 nm exhibit three absorptions, and the data are listed in Table 4. The intense reflectance bands (band III) at higher frequencies are assigned to the intraligand transitions [23,24] in the complexes. The absorptions at 26316 cm^{-1} for complex **1** and 27174 cm^{-1} for complex **2** are assigned as carboxylate-to-copper charge-transfer bands (LMCT) [25,26]. The visible reflectance spectra also contain bands at 13514 with a shoulder at 9765 cm^{-1} for complex **1** and 14286 with

Table 4
Electronic reflectance spectral data of the complexes

Complex	ν_{max} (cm^{-1})		
	Band I	Band II	Band III
$Cu^{I}_2Cu^{II}_2(CH_2{=}CH{-}COO)_6(PPh_3)_4(CH_3OH)_2$ (**1**)	13514, 9765	26316	47620, 37879
$Cu^{I}_2Cu^{II}_2[CH_2{=}C(CH_3){-}COO]_6(PPh_3)_4(CH_3OH)_2$ (**2**)	14286, 9687	27174	44643, 36765

a shoulder at 9687 cm^{-1} for complex **2**, which are characteristic of the Cu(II) $d_{xz}, d_{yz} \rightarrow d_{x^2-y^2}$ ($^2B_1 \rightarrow {}^2E$) transition in a tetragonal ligand field [27,28]. The shoulders are characteristic of a bridging system with antiferromagnetic interactions [29,30]. The electronic reflectance spectra show that both complexes **1** and **2** contain a binuclear cage structural unit, in which the coordination environment of the Cu(II) atom is a distorted square pyramid.

3.5. ESR spectra

The X-band ESR spectra obtained for the powdered samples of the complexes at room temperature are shown in Fig. 2. The spectra show absorptions at low and high fields H_{z1} and H_{z2} with asymmetrical absorptions H_{xy2}, where $H_{z1}=214$, $H_{z2}=6237$ and $H_{xy2}=4934$ Gs for complex **1**, $H_{z1}=224$, $H_{z2}=6171$ and $H_{xy2}=4934$ Gs for complex **2**. The H_{xy1} absorptions of the two complexes are missing because $|D| > h\nu$ at the X-band frequency used. The spectra can be interpreted using a spin Hamiltonian for axial symmetry,

$$\boldsymbol{H}=g_{\parallel}\beta\boldsymbol{H}_z\hat{\boldsymbol{S}}_z+g_{\perp}(\beta\boldsymbol{H}_x\hat{\boldsymbol{S}}_x+\boldsymbol{H}_y\hat{\boldsymbol{S}}_y)+\boldsymbol{D}(\hat{\boldsymbol{S}}_z^2+2/3)$$

where $S=1$ for the thermally accessible triplet state, and the other symbols have their usual meanings. The calculated ESR parameters are $g_{\parallel}=2.318$, $g_{\perp}=1.998$, $g_{av}=2.105$ and $D=0.3488\ cm^{-1}$ for complex **1**, and $g_{\parallel}=2.348$, $g_{\perp}=2.008$, $g_{av}=2.121$ and $D=0.3399\ cm^{-1}$ for complex **2**, where $g_{av}=(1/3)(g_{\parallel}+2g_{\perp})$. The values are comparable to those found in dimeric copper(II) α,β-unsaturated carboxylates [29,30], indicating the presence of the dimeric unit in the complexes.

3.6. Magnetic susceptibility

Magnetic susceptibilities in the temperature range 77–300 K were determined by the Faraday method and the corrected molar magnetic susceptibility data (χ_M) and effective magnetic moments (μ_{eff}) are listed in Table 5. The fact that χ_M or μ_{eff} decreases gradually with lowering of the temperature reveals the presence of antiferromagnetic coupling interactions through an effective O–C–O (bridging carboxylate) exchange pathway [31,32] for both complexes. The data were fitted to the Bleaney–Bowers equation, Eq. (2), allowing for the presence of paramagnetic impurity [33], where P is the mole fraction of the non-coupled copper(II) impurity, g_i is the average g factor for the impurity, and the other symbols have their usual meanings.

$$\chi_M=\frac{2Ng^2\beta^2}{3kT}\left[1+\frac{1}{3}\exp\left(\frac{-2J}{kT}\right)\right]^{-1}(1-P)+\frac{2Ng_i^2\beta^2}{4kT}P \quad (2)$$

The g values are obtained from the ESR spectra. The experimental and theoretical curves of χ_M of the two complexes

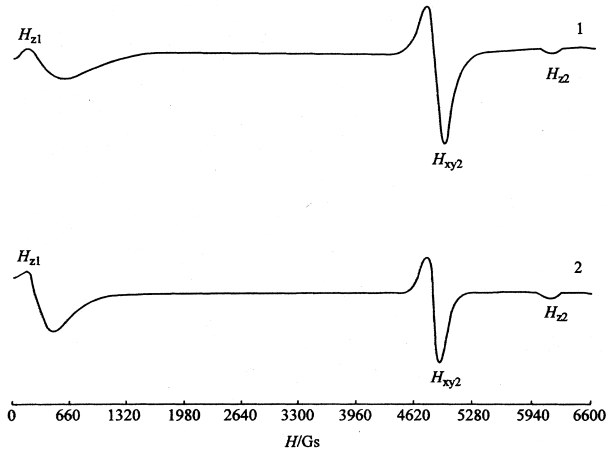


Fig. 2. Solid-state ESR spectra of $Cu_2^ICu_2^{II}(CH_2{=}CH{-}COO)_6(PPh_3)_4(CH_3OH)_2$ (**1**) and $Cu_2^ICu_2^{II}[CH_2{=}C(CH_3){-}COO]_6(PPh_3)_4(CH_3OH)_2$ (**2**).

are shown in Fig. 3, and the estimated parameters $2J$, g_i and P are listed in Table 6.

The energy of the singlet–triplet separation $2J$ values are $-310\ cm^{-1}$ for complex **1** and $-288\ cm^{-1}$ for complex **2**. The effective magnetic moments at room temperature are 1.34 BM for complex **1** and 1.41 BM for complex **2**, which are lower than that of an unpaired single electron (1.73 BM), indicating that strong antiferromagnetic exchange interactions exist between two Cu(II) atoms. The antiferromagnetic interaction in complex **2** is slightly weaker than that of complex **1** in terms of the $2J$ values. The $2J$ values obtained here are comparable with $2J=-270\ cm^{-1}$ for $Cu_2^ICu_2^{II}(CH_3{-}COO)_6(PPh_3)_4$ [12] and $2J=-248\ cm^{-1}$ for $[Cu^ICu_2^{II}(CH_3{-}COO)_5\{P(OEt)_3\}_2]$ [10].

3.7. Formation and structural interconversion

In the study of the chain type complex $[Cu^ICu_2^{II}(CH_3{-}COO)_5\{P(OR)_3\}_2]$ (structure A), Beddoes et al. [10] found that the NMR spectra in alcohol solution showed the presence of two types of acetate methyl proton resonance in the ratio of 3:2. This was explained in terms of a structure which contains three *syn–syn* acetate ligands bridging two copper(II) atoms and two unidentate acetate ligands linking each copper(II) with a four-coordinate copper(I). It was also proposed that the terminal copper(I) atom is coordinated by one or more alcohol solvent molecules, but it has not been demonstrated experimentally. In this work, it is notable that methanol solvent molecules coordinate with Cu(I) in the solid-state complex with structure D (Scheme 1). The formation and structural interconversion among three mixed-valence copper(I,II) carboxylate complexes with phosphine ligands D, E and G is suggested as shown in Scheme 1.

In alcohol solution, phosphine molecules partially reduce the dimer $Cu_2^{II}(R{-}COO)_4(H_2O)_2$ (A) and also act as ligands coordinating with Cu(I) of structure B [10]. The solvent molecules further disrupt the dimeric structure B forming a mononuclear Cu(I) moiety with tetrahedral configuration as

Table 5
Magnetic data

T (K)	$\chi_M \times 10^6$ (cm^3 mol^{-1})	μ_{eff} (BM)	T (K)	$\chi_M \times 10^6$ (cm^3 mol^{-1})	μ_{eff} (BM)
Complex **1**					
80	240	0.28	230	1465	1.16
85	291	0.31	234	1475	1.18
94	381	0.38	239	1484	1.19
104	479	0.45	244	1492	1.21
114	611	0.53	249	1496	1.22
124	720	0.60	254	1501	1.24
134	845	0.67	259	1503	1.25
144	972	0.75	264	1505	1.26
154	1015	0.79	269	1507	1.27
164	1132	0.86	274	1508	1.29
174	1245	0.93	279	1508	1.30
184	1290	0.97	284	1507	1.31
194	1345	1.02	289	1507	1.32
204	1392	1.07	294	1506	1.33
214	1415	1.10	299	1506	1.34
224	1455	1.14			
Complex **2**					
79	226	0.27	166	1348	0.95
86	301	0.32	173	1398	0.98
89	351	0.35	180	1447	1.02
92	395	0.38	188	1496	1.06
97	440	0.41	196	1542	1.10
100	493	0.44	204	1580	1.14
104	570	0.49	212	1596	1.16
109	652	0.53	220	1611	1.19
114	736	0.58	228	1632	1.22
120	798	0.62	238	1637	1.25
126	902	0.68	248	1642	1.28
132	1005	0.73	259	1651	1.31
138	1051	0.76	272	1650	1.34
145	1143	0.82	285	1650	1.37
152	1221	0.86	293	1649	1.39
159	1281	0.90	300	1649	1.41

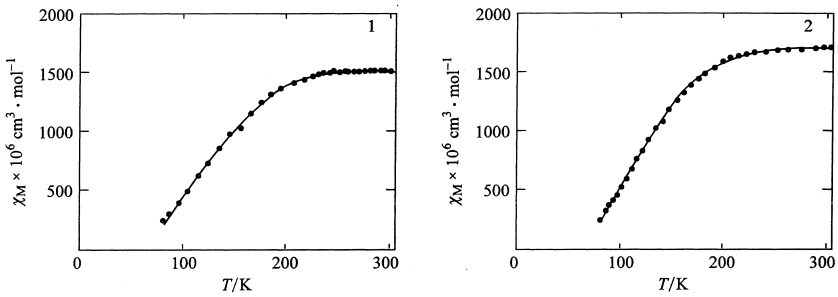
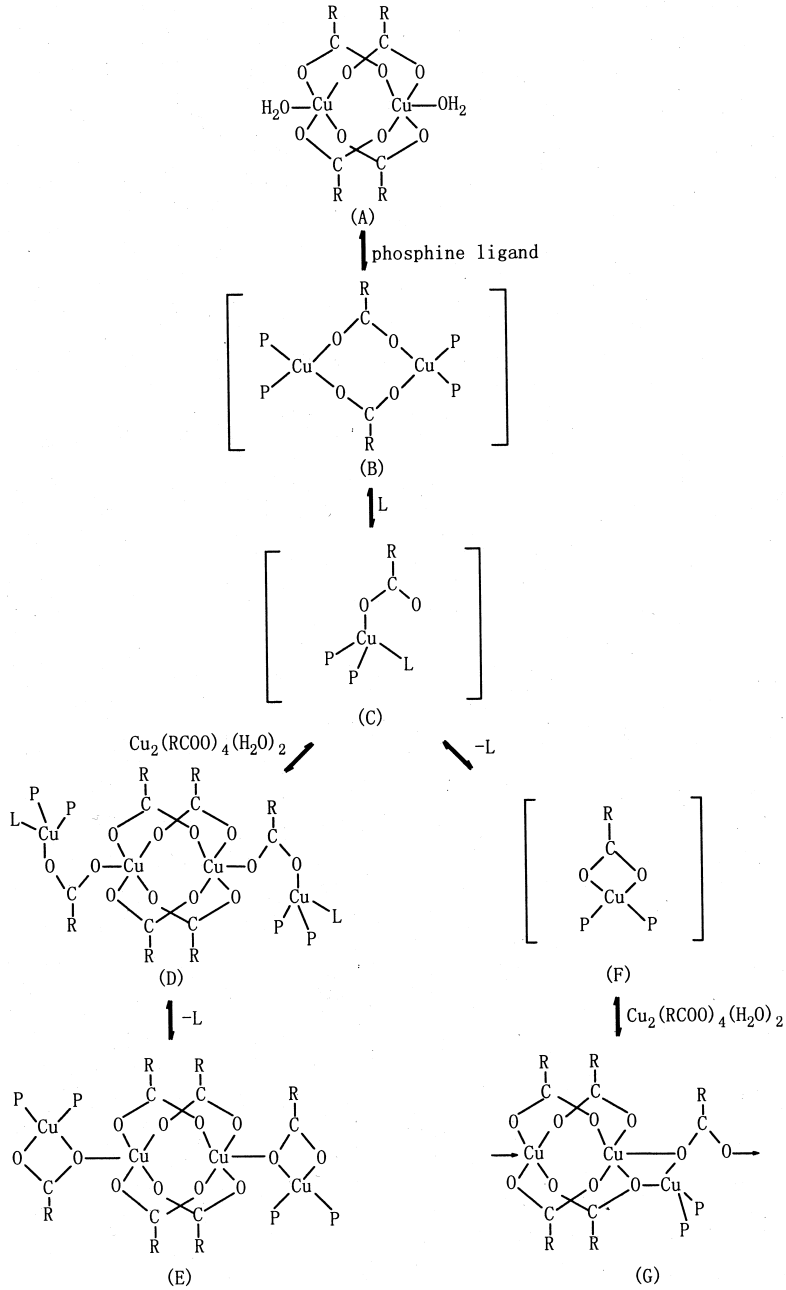


Fig. 3. Variation of magnetic susceptibilities with temperature of $Cu_2^ICu_2^{II}(CH_2{=}CH{-}COO)_6(PPh_3)_4(CH_3OH)_2$ (**1**) and $Cu_2^ICu_2^{II}[CH_2{=}C(CH_3){-}COO]_6(PPh_3)_4(CH_3OH)_2$ (**2**): (· · ·) experimental data, (—) calculated curve.

Table 6
Estimated parameters

Complex	$2J$ (cm^{-1})	g_i	$P \times 10^2$	R [a]
$Cu_2^ICu_2^{II}(CH_2{=}CH{-}COO)_6(PPh_3)_4(CH_3OH)_2$ (**1**)	−310	2.214	0.80	6.18×10^{-5}
$Cu_2^ICu_2^{II}[CH_2{=}C(CH_3){-}COO]_6(PPh_3)_4(CH_3OH)_2$ (**2**)	−288	2.232	0.049	1.97×10^{-4}

[a] $R = \sum_{i=1}^{m} (\chi_i^{calc} - \chi_i^{exp})^2 / \sum_{i=1}^{m} (\chi_i^{exp})^2$.



Scheme 1. Formation and structural interconversion of complexes (P = phosphine ligand; L = solvent).

in structure C [34]. Subsequent reaction then follows two alternative routes. In the first one, when a pair of Cu(I) moieties (C) substitute for two terminal aqua of structure A, the mixed-valence complex D is produced, the same as that synthesized in this work. In a reversible step, the loss of solvate molecules L from structure D results in another mixed-valence complex of structure E, which is similar to that reported by Valigura et al. [12,13]. In the second route, the coordination mode of the carboxylate group changes from monodentate to bidentate along with the loss of solvate molecule L from C, giving rise to structure F [10]. The Cu(I) moiety (F) substitutes for a terminal aqua of A, along with breakage of one Cu(I)–O(carboxyl) bond and linkage of Cu(I) to an O atom of a μ-O,O′ bridging carboxylate ligand, forming a mixed-valence chain complex with structure G similar to $[Cu^{I}Cu^{II}_{2}(CH_3–COO)_5\{P(OR)_3\}_2]$ [10].

Supplementary data

Additional material containing non-hydrogen and hydrogen atomic coordinates, thermal parameters, and the remaining bond lengths and angles are available from the Cambridge Crystallographic Data Centre, 12 Union Road, Cambridge CB2 1EZ, UK (fax: +44-1223-336033; e-mail: deposit@ccdc.cam.ac.uk) on request, quoting the deposition number 114065.

Acknowledgements

This work was supported by the National Natural Science Foundation of China (Grant 29831010) and the Foundation of the State Key Laboratory of Coordination Chemistry of Nanjing University.

References

[1] R.C. Long, D.N. Hendrickson, J. Am. Chem. Soc. 105 (1983) 1513.
[2] N.S. Hush, Coord. Chem. Rev. 54 (1985) 135.
[3] C. Harding, V. Mckee, J. Nelson, J. Am. Chem. Soc. 113 (1991) 9864.
[4] M.E. Barr, P.H. Smith, W.E. Antholine, B. Spencer, J. Chem. Soc., Chem. Commun. (1993) 1649.
[5] M. Mahroof Tahir, K.D. Karlin, J. Am. Chem. Soc. 114 (1992) 7599.
[6] K.D. Karlin, Y. Gultneh, Prog. Inorg. Chem. 35 (1987) 219.
[7] E.I. Solomon, M.J. Baldwin, M. Lowery, Chem. Rev. 92 (1992) 521.
[8] D.J. Darensbourg, M.W. Holtcamp, B. Khandelwal, K.K. Klausmeyer, J.H. Reibenspies, Inorg. Chem. 33 (1994) 2036.
[9] R.B. King, Encyclopedia of Inorganic Chemistry, Wiley, New York, 1994, p. 829.
[10] R.L. Beddoes, J.A. Connor, D. Dubowski, A.C. Jones, O.S. Mills, R. Price, J. Chem. Soc., Dalton Trans. (1981) 2119.
[11] J.A. Connor, A.C. Jones, R. Price, J. Chem. Soc., Chem. Commun. (1980) 137.
[12] D. Valigura, M. Koman, E. Durcanska, G. Ondrejovic, J. Mrozinski, J. Chem. Soc., Dalton Trans. (1986) 2339.
[13] M. Koman, D. Valigura, E. Durcanska, G. Ondrejovic, J. Chem. Soc., Chem. Commun. (1984) 381.
[14] Y.-Y. Wang, Q. Shi, Q.-Z. Shi, Y.-C. Gao, Z.-Y. Zhou, Chinese Sci. Bull. 43 (1998) 2512.
[15] A. Earnshaw, Introduction to Magnetochemistry, Academic Press, London, 1968.
[16] A.S. Dhindsa, Ph.D. Thesis, Punjabi University, Patiala, India, 1983.
[17] X.-M. Chen, X.-L. Feng, X.-L. Yu, T.C.W. Mak, Inorg. Chim. Acta 266 (1997) 121.
[18] Y.-Y. Wang, Q. Shi, Q.-Z. Shi, Y.-C. Gao, Chin. Acta Chim. Sinica 57 (1999) 541.
[19] Y.-Y. Wang, Q. Shi, Q.-Z. Shi, Y.-C. Gao, Z.-Y. Zhou, Sci. China (B) 42 (1999) 363.
[20] A.K. Gregson, R.L. Martin, S. Mitra, Proc. R. Soc. London, Ser. A 320 (1971) 473.
[21] I.D. Brown, D. Altermatt, Acta Crystallogr., Sect. B 41 (1985) 244.
[22] H.H. Thorp, Inorg. Chem. 31 (1992) 1585.
[23] H.P. Berends, D.W. Stephan, Inorg. Chem. 26 (1987) 749.
[24] E.I. Solomon, M.J. Baldwin, M.D. Lowery, Chem. Rev. (Washington, DC) 92 (1992) 521.
[25] R.C. Holz, J.M. Brink, F.T. Gobena, C.J. O'Connor, Inorg. Chem. 33 (1994) 6086.
[26] R.C. Holz, J.M. Bradshaw, B. Bennett, Inorg. Chem. 37 (1998) 1219.
[27] A.W. Addison, T.N. Rao, J. Reedijk, J.V. Rijn, G.C. Verschoor, J. Chem. Soc., Dalton Trans. (1984) 1349.
[28] M. Duggen, N. Ray, B.J. Hathaway, G. Tomlinson, P. Brint, K. Pelin, J. Chem. Soc., Dalton Trans. (1980) 1342.
[29] M. Melnik, M. Koman, L. Macašková, T. Glowiak, G. Gomek, J. Mrozinsky, J. Coord. Chem. 43 (1998) 159.
[30] M. Melnik, Coord. Chem. Rev. 36 (1981) 287.
[31] R.L. Beddoes, J.A. Connor, D. Dubowski, A.C. Jones, O.S. Mills, R. Price, J. Chem. Soc., Dalton Trans. (1979) 781.
[32] M. Kato, Y. Muto, Coord. Chem. Rev. 92 (1988) 45.
[33] A.P. Ginsberg, Inorg. Chim. Acta Rev. 5 (1971) 45.
[34] J.A. Connor, A.C. Jones, J. Chem. Soc., Chem. Commun. (1980) 137.

PERGAMON

www.elsevier.nl/locate/poly

Polyhedron 19 (2000) 899–906

POLYHEDRON

Metal–heterocyclic thione interactions. 12. Heterocyclic 2-thiolates of platinum(II) and palladium(II): the crystal structures of first examples of *cis*-[M(η^1-*S*-pyridine-2-thiolato)$_2$(L-L)] {M = Pt, Pd, L-L = 1,2-bis(diphenylphosphino)ethane; M = Pt, L-L = 1,2-bis(diphenylphosphino)ethene} complexes

Tarlok S. Lobana [a,*], Renu Verma [a], Geeta Hundal [a], Alfonso Castineiras [b]

[a] *Department of Chemistry, Guru Nanak Dev University, Amritsar-143 005, India*

[b] *Departamento de Quimica Inorganica, Universidade de Santiago de Compostela, 15706-Santiago, Spain*

Received 24 August 1999; accepted 4 February 2000

Abstract

A series of platinum(II) complexes of stoichiometry *cis*-[Pt(η^1-*S*-$C_5H_4NS)_2$(L-L)] were obtained from the reactions of platinum tetrachloride with pyridine-2-thione (C_5H_5NS) in the presence of Et_3N base in an ethanol–benzene mixture followed by the addition of bis(tertiary phosphines), viz. {Ph_2P–X–PPh_2}, or phosphine chalcogenides {Ph_2P–CH_2–P(E)Ph_2} {X(L-L) = $(CH_2)_2$(dppe) (**1**), CH=CH(dppen) (**2**), $(CH_2)_3$(dppp) (**3**), $(CH_2)_4$(dppb) (**4**), E = S, dppmPS (**5**), E = Se, dppmPSe (**6**)}. Palladium(II) complexes, viz. [Pd(η^1-*S*-$C_5H_4NS)_2$(L-L)] {L-L = dppm (X = CH_2) (**7**), dppe (**8**), dppp (**9**), dppmPS (**10**), dppmPSe (**11**)}, were prepared by reacting [$PdCl_2$(diphosphines)] suspended in ethanol with C_5H_5NS in the presence of aqueous NaOH. All these compounds have been characterised with the help of analytical data [IR, far-IR, NMR (^1H, ^{13}C, ^{31}P) spectroscopy] and X-ray crystallography (for compounds **1**, **2** and **8**). The geometry about each metal centre is distorted square planar with *trans* bond angles of: compound **1**, P–Pt–S, 170.31(11), 173.18(10)°; compound **2**, P–Pt–S, 168.97(5), 171.43(5)°; compound **8**, P–Pd–S, 170.78(8), 171.83(8)°. The bite angles P(1)–M–P(2) and angles *trans* to bite angles, S(1)–M–S(2), are, respectively: compound **1**, 85.68(11), 82.69(11)°; compound **2**, 86.65(5), 84.01(6)°; compound **8**, 85.19(8), 83.90(7)°. The dppe complexes (**1** and **8**) are isomorphous, monoclinic with space group *C*2/*c*, whereas the dppen complex is triclinic.These compounds represent the first examples of an interesting series of *cis*-platinum(II) and -palladium(II) derivatives of pyridine-2-thione containing chelating diphosphines and pendant pyridyl groups. ©2000 Elsevier Science Ltd All rights reserved.

Keywords: Bisphosphines; Heterocyclic thiones; Palladium(II) complexes; Platinum(II) complexes; Pyridyl

1. Introduction

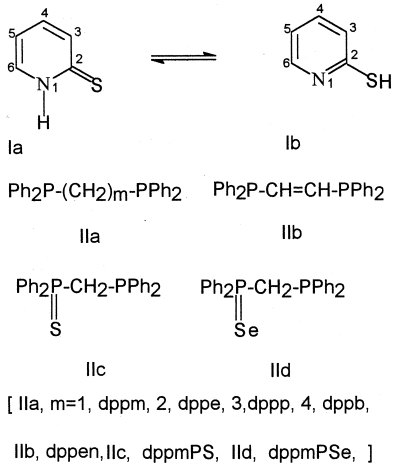
The interaction of heterocyclic thiones with metals has been the subject of several investigations as these ligands contain chemically active groups [–N(H)–C(=S)– ↔ –N=C(–SH)–] and are useful model compounds for sulfur-containing analogues of purine and pyrimidine bases. Heterocylic 2-thiones bind to a metal in several ways, leading to the formation of monomeric or polymeric complexes [1–4]. For example, the simplest prototype of heterocylic 2-thiones, i.e. pyridine-2-thione (hereafter C_5H_5NS, I), has several ways of binding, notably terminal S-bonding and S-bridging (in neutral form), whereas in anionic form the modes are terminal S-bonding, S-bridging, N,S-chelating, N,S-bridging, N,S-chelation-cum-S-bridging, N,S-bridging-cum-S-bridging [1–32].

The interactions of heavy metals such as platinum, gold with N,S-donor atoms have been recognised for their anticarcinogenic properties with the potential to develop metal-based drugs [1–4,33–36]. These drugs probably exert their therapeutic action via interaction with DNA [33,34]. Recently, some papers involving platinum(II or IV) and gold(I) complexes with tertiary phosphines as co-ligands have been published [37–42]. Using pyridine-2-thione (C_5H_5NS), only a few compounds of platinum(II) and

* Corresponding author. Tel.: +91-183-257604; fax: +91-183-258820; e-mail: tarlok@angelfire.com

0277-5387/00/$ - see front matter ©2000 Elsevier Science Ltd All rights reserved.
PII S0277-5387(00)00329-6

palladium(II) with tertiary phosphines (R_3P) have been reported: namely, monomeric $[Pt(\eta^2\text{-}N,S\text{-}C_5H_4NS)(PPh_3)_2]PF_6$ [43], *trans*-$[Pt(\eta^1\text{-}S\text{-}C_5H_4NS)_2(PPh_3)_2]$ [21], $[PdCl(\eta^2\text{-}N,S\text{-}C_5H_4NS)(PPh_3)]$ [44] and dimeric $[PdCl(\eta^2\text{-}N,S\text{-}C_5H_4NS)(PMe_3)]_2$ [45]. There is no report of these metals containing bis-tertiary phosphines and pyridine-2-thione (C_5H_5NS). Among the metals under discussion, *trans*-$[Pt(\eta^1\text{-}S\text{-}C_5H_4NS)_2(PPh_3)_2]$ [21] was the first compound reported, by Lobana et al. [21], containing a pendant pyridyl group in the *trans* position. In this paper, we report first examples of platinum(II) and palladium(II) complexes containing chelating bisphosphines(II) and pendant pyridyl groups in the *cis* position; these compounds may act as potential precursors for polymeric complexes [46].



2. Experimental

2.1. General materials

Platinum tetrachloride was procured from M/s Central Drug House Pvt. (Bombay). *cis*-1,2-Bis(diphenylphosphino)ethene ($Ph_2PCH{=}CHPPh_2$, dppen), bis(diphenylphosphino)methane ($Ph_2PCH_2PPh_2$, dppm) and bis(diphenylphosphino)propane $\{Ph_2P(CH_2)_3PPh_2$, dppp$\}$ were procured from Aldrich. 1,2-Bis(diphenylphosphino)ethane $\{Ph_2P(CH_2)_2PPh_2$, dppe$\}$ and 1,4-bis(diphenylphosphino)-butane $\{Ph_2P(CH_2)_4PPh_2$, dppb$\}$ were prepared by lithiation of PPh_3 in dry tetrahydrofuran followed by reaction with 1,2-dichloroethane or 1,4-dihalobutane as reported earlier [15]. 2-Hydroxypyridine was procured from M/s Sisco Laboratories (Bombay), and pyridine-2-thione was then prepared from it by treatment with P_4S_5 at 140–145°C, as reported earlier [5]. The monosulfide (or selenide) of dppm was prepared by reacting dppm with sulfur powder (or selenium metal) in 1:1 ratio in dry benzene [6]. The starting materials, $PdCl_2$(L-L), were prepared by reacting $PdCl_2$ solutions in CH_3CN with suitable bisphosphines [7].

2.2. Platinum complexes

2.2.1. *cis*-$[Pt(\eta^1\text{-}S\text{-}C_5H_4NS)_2(dppe)]$ (1)

To a solution of C_5H_5NS (0.07 g, 0.60 mmol) in 20 ml of benzene containing 2 ml of Et_3N base was added dropwise a solution of $PtCl_4$ (0.100 g, 0.30 mmol) in 20 ml of dry ethanol under magnetic stirring, followed by the addition of solid dppm (0.120 g, 0.30 mmol) when a clear solution formed, and was stirred overnight (24 h). The white salt of $Et_3NH^+Cl^-$ formed was separated by filtration and slow evaporation of the filtrate gave a light yellow complex. Yield, 80%; m.p., 219–220°C. *Anal*. Found: C, 52.8; H, 3.90; N, 3.24. Required for $C_{36}H_{32}N_2S_2P_2Pt$: C, 53.1; H, 3.93; N, 3.44%. IR (KBr, cm^{-1}): 1550s, 1445s, 1415s, 1120s (νC–S), 1095sh (νP–C), 1110s, 820s, 720s, 698vs, 540s, 405w (νPt–P), 360w (νPt–S). NMR ($CDCl_3$, δ ppm, *J*, Hz): ^{1}H, 8.47d (J_5, 4.8, H^6), 7.13m (H^3), 6.86m (H^4), 6.41m (H^5), 2.27sb ($-CH_2-$), 7.65m (Ph–P); ^{13}C, 166.3, 159.0 (C^2), 149.6, 147.8 (C^6), 137.4, 133.5 (C^4), 127.4, 121.1 (C^5), 119.7, 116.8 (C^3), 29.7 ($-CH_2$), 131.2 (*i*-C), 133.5 (*o*-C), 128.6 (*m*-C and *p*-C); ^{31}P, 45.5 ($J_{P\text{-}Pt}$, 2968.2 Hz). Coordination shift, $\Delta\delta$P 58.2 ppm. The crystals for X-ray study were grown from a benzene–ethanol mixture (1:1, v/v). Compounds **2–5** were prepared similarly.

2.2.2. *cis*-$[Pt(\eta^1\text{-}S\text{-}C_5H_4NS)_2(dppen)]$ (2)

Yield, 80%; m.p., 218–220°C. *Anal*. Found: C, 53.3; H, 3.62; N, 3.70. Required for $C_{36}H_{30}N_2S_2P_2Pt$: C, 53.3; H, 3.69; N, 3.45%. IR (KBr, cm^{-1}): 1580s, 1560s, 1435s, 1405s, 1195s, 1130s (νC–S), 1110s, 1095sh (νP–C), 1025w, 750s, 725s, 700vs, 560s, 540s, 415w (νPt–P), 350w (νPt–S). NMR ($CDCl_3$, δ ppm, *J*, Hz): ^{1}H, 8.48d (J_5, 4.6, H^6), 7.12m (H^3), 6.94m (H^4), 6.53m (H^5), 7.56m (Ph–P), 2.01sb (–CH=CH–); ^{13}C, 165.8 (C^2), 147.3 (C^6), 133.9 (C^4), 127.6 (C^5), 117.0 (C^3), 145.4 (–CH=CH–), 132.4 (*i*-C), 133.3 ($J_{C\text{-}P}$, 10.4, *o*-C), 126.8 (*m*-C), 131.3 (*p*-C); ^{31}P, 53.5 ($J_{P\text{-}Pt}$, 2958.5 Hz), 53.9 ($J_{P\text{-}Pt}$, 2969.4 Hz). Coordination shift, $\Delta\delta$P 77.1 ppm. The crystals for X-ray study were grown from benzene–ethanol mixture (1:1, v/v).

2.2.3. *cis*-$[Pt(\eta^1\text{-}S\text{-}C_5H_4NS)_2(dppp)]$ (3)

Yield, 75%; m.p., 224–226°C. *Anal*. Found: C, 53.2; H, 3.90; N, 3.20. Required for $C_{37}H_{34}N_2S_2P_2Pt$: C, 53.7; H, 4.11; N, 3.40%. IR (KBr, cm^{-1}): 1430s, 1170s, 1120s (νC–S), 1100m (νP–C), 690s (νPh), 675s, 625m, 560m. NMR ($CDCl_3$, δ ppm, *J*, Hz): ^{1}H, 8.48d (J_5, 4.8, H^6), 7.69t ($J_{3,5}$, 7.7, H^4), 7.45d (J_4, 7.0, H^3), 7.12t ($J_{4,6}$, 3.9, H^5), 1.42t ($-CH_2-$), 7.4–7.7m (Ph–P); ^{13}C, 158.9 (C^2), 149.5 (C^6), 137.3 (C^4), 121.1 (C^5), 119.7 (C^3), 29.3 ($-CH_2-$), 133.6 (*i*-C), 131.7 (*o*-C), 128.5 (*m*-C), 130.7 (*p*-C).

2.2.4. *cis*-$[Pt(\eta^1\text{-}S\text{-}C_5H_4NS)_2(dppb)]$ (4)

Yield, 78%; m.p., 230–232°C. *Anal*. Found: C, 54.7; H, 4.06; N, 3.73. Required for $C_{38}H_{36}N_2S_2P_2Pt$: C, 54.22; H, 4.28; N, 3.33%. IR (KBr, cm^{-1}): 1555m, 1440s, 1420m, 1175s, 1115m (νC–S), 1100sh (νP–C), 1030w, 1000m,

840m, 740s, 690s, 560s, 510s, 415w (νPt–P), 340w (νPt–S). NMR ($CDCl_3$, δ ppm, *J*, Hz): ^{1}H, 8.47d (J_5, 4.2, H^6), 7.69t ($J_{3,5}$, 5.7, H^4), 7.46d (J_4, 7.2, H^3), 7.11t ($J_{4,6}$, 4.0, H^5), 1.41t (–CH_2–), 7.63m (Ph–P); ^{13}C, –, 149.6 (C^6), 137.4 (C^4), 121.1 (C^5), 119.8 (C^3), 29.7 (–CH_2–), 131.8 (*i*-C), 130.7 (*o*-C), 128.4 (*m*-C and *p*-C).

*2.2.5. cis-[Pt(η^1-S-$C_5H_4NS)_2$(dppmPS)] (**5**)*

Yield, 75%; m.p., 128–130°C. *Anal*. Found: C, 50.28; H, 3.80; N, 3.50. Required for $C_{35}H_{30}N_2S_3P_2Pt$: C, 50.48; H, 3.60; N, 3.36%. IR (KBr, cm^{-1}): 1472m, 1435s, 1420s, 1115sh (νC–S), 1090s (νP–C), 730s, 680m, 610sh, 500m, 610w (νP–S), 405w (νPt–P), 355w (νPt–S). NMR ($CDCl_3$, δ ppm, *J*, Hz): ^{1}H, 8.47d (J_5, 4.8, H^6), 7.36m (H^4), 7.62d (J_4, 4.2, H^3), 7.1m (H^5), 3.11q (–CH_2–), 7.56m (Ph–P); ^{13}C, 159.0 (C^2), 149.4 (C^6), 137.3 (C^4), 121.0 (C^5), 119.7 (C^3), 29.5 (–CH_2–), 131.5 (*i*-C), 130.7 (*o*-C), 128.2 (*m*-C and *p*-C).

*2.2.6. cis-[Pt(η^1-S-$C_5H_4NS)_2$(dppmPSe)] (**6**)*

Yield, 78%; m.p., 146–149°C. *Anal*. Found: C, 47.4; H, 3.30; N, 3.50. Required for $C_{35}H_{30}N_2S_2P_2SePt$: C, 47.8; H, 3.41; N, 3.19%. IR (KBr, cm^{-1}): 1560s, 1470m, 1430s, 1115w (νC–S), 1090s (νP–C), 1030m, 860w, 735m, 680m, 500sb, 490s (νP–Se), 405w (νPt–P), 355w (νPt–S). NMR ($CDCl_3$, δ ppm, *J*, Hz): ^{1}H, 8.47d (J_5, 4.0, H^6), –, 7.60d (J_4, 2.0, H^3,), 7.10m (H^5), 3.06q (–CH_2–), 7.57m (Ph–P); ^{13}C, –, 149.5 (C^6), 137.3 (C^4), 121.0 (C^5), 119.7 (C^3), 29.6 (–CH_2–), 132.4 (*i*-C), 131.6 (*o*-C), 128.2 (*m*-C), 130.5 (*p*-C).

2.3. Palladium complexes

*2.3.1. cis-[Pd(η^1-S-$C_5H_4NS)_2$(dppm)] (**7**)*

To the solution of C_5H_5NS (0.040 g, 0.17 mmol) in 15 ml of water containing 0.3 mmol of NaOH was added a suspension of [$PdCl_2$(dppm)] (0.098 g, 0.17 mmol) in 25 ml of ethanol. The reaction mixture was heated for 15 min, and the clear solution formed was left to evaporate at room temperature. The product was recrystallised from chloroform and dried in vacuo. Yield, 78%; m.p., 117–120°C. *Anal*. Found: C, 59.2; H, 3.90; N, 3.80. Required for $C_{35}H_{30}N_2S_2P_2Pd$: C, 59.0; H, 4.21; N, 3.93%. IR (KBr, cm^{-1}): 1570s, 1430s, 1410w, 1132sh, 1120s (νC–S), 1095s (νP–C), 895m, 740s, 690s, 610w, 520s, 460w, 410w (νPd–P), 360m (νPd–S). NMR ($CDCl_3$, δ ppm, *J*, Hz): ^{1}H, 8.52d (J_5, 6.6, H^6), –, 6.98d (J_4, 5.6, H^3), –, 2.07t (–CH_2–), 7.6m (Ph–P); ^{13}C, 165.5 (C^2), 147.5 (C^6), 131.8 (C^4), 128.4 (C^5), 117.0 (C^3), 29.7 (–CH_2–), 133.8 (*i*-C), 132.5 (*o*-C), 128.5 (*m*-C), 130.8 (*p*-C). Complexes **8**–**11** were prepared similarly.

*2.3.2. cis-[Pd(η^1-S-$C_5H_4NS)_2$(dppe] (**8**)*

Yield, 80%; m.p., 188–190°C. *Anal*. Found: C, 60.0; H, 4.40; N, 4.10. Required for $C_{36}H_{32}N_2S_2P_2Pd$: C, 59.7; H, 4.41; N, 3.86%. IR (KBr, cm^{-1}): 1565s, 1540m, 1445s, 1415s, 1120m (νC–S), 1105s (νP–C), 1050w, 810s, 740m, 690s (νPh) 535s, 490m, 440m, 400w (νPd–P), 350m (νPd–S). NMR ($CDCl_3$, δ ppm, *J*, Hz): ^{1}H, 7.83m (H^6), 6.79td ($J_{3,5}$, 7.55, J_6, 1.8, H^4), 7.07d (J_4, 8.0, H^3), 6.44t ($J_{4,6}$, 6.1, H^5), 2.32t (–CH_2–), 7.32–7.79m (Ph–P); ^{13}C, 168.5 (C^2), 147.4 (C^6), 133.2 (C^4), 127.1 (C^5), 116.0 (C^3), 28.6 (–CH_2), 129.6 (*i*-C), 133.6 (*o*-C), 128.4 (*m*-C), 131.0 (*p*-C). The crystals for X-ray study were grown from ethanol.

*2.3.3. cis-[Pd(η^1-S-$C_5H_4NS)_2$(dppp)] (**9**)*

Yield, 72%; m.p., 128–130°C. *Anal*. Found: C, 58.9; H, 4.90; N, 3.40. Required for $C_{37}H_{34}N_2S_2P_2Pd$: C, 60.1; H, 4.60; N, 3.70%. IR (KBr, cm^{-1}): 1570s, 1440s, 1410w, 1180w, 1125m (νC–S), 1105m (νP–C), 830w, 750m, 725w, 700s, 545s, 510s, 420w (νPd–P), 390w, 365w (νPd–S). NMR ($CDCl_3$, δ ppm, *J*, Hz): ^{1}H, 8.40d (J_5, 8.0, H^6), –, 6.92d (J_4, 7.0, H^3), 6.65t ($J_{4,6}$ 6.4, H^5), 2.40t (–CH_2–), 7.5m (Ph–P); ^{13}C, 172.9 (C^2), 146.5 (C^6), 136.2 (C^4), 126.7 (C^5), 117.0 (C^3), 29.0 (–CH_2–), 132.9 (*i*-C), 133.5 (*o*-C), 128.5 (*m*-C), 130.7 (*p*-C).

*2.3.4. cis-[Pd(η^1-S-$C_5H_4NS)_2$(dppmPS)] (**10**)*

Yield, 70%; m.p., 150–152°C. *Anal*. Found: C, 56.1; H, 3.90; N, 3.70. Required for $C_{35}H_{30}N_2S_3P_2Pd$: C, 56.6; H, 4.04; N, 3.77%. IR (KBr, cm^{-1}): 1570w, 1475w, 1430s, 1185w, 1115s (νC–S), 1095m (νP–C), 995m, 780w, 735s, 680s, 610w (νP–S) 550m, 510s, 425sh (νPd–P). NMR ($CDCl_3$, δ ppm, *J*, Hz): ^{1}H, 8.54d (J_5, 5.6, H^6), –, 7.18d (J_4, 5.0, H^3), 6.73t ($J_{4,6}$, 7.0, H^5), 3.1q (–CH_2–), 7.6m (Ph–P); ^{13}C, –, 146.5 (C^6), 137.2 (C^4), 122.0 (C^5), 116.5 (C^3), 29.7 (–CH_2–), 133.7(*i*-C), 131.9 (*o*-C), 128.5 (*m*-C), 130.8 (*p*-C).

*2.3.5. cis-[Pd(η^1-S-$C_5H_4NS)_2$(dppmPSe)] (**11**)*

Yield, 70%; m.p., 170–172°C. *Anal*. Found: C, 53.4; H, 3.60; N, 3.70. Required for $C_{35}H_{30}N_2S_2P_2SePd$: C, 53.2; H, 3.80; N, 3.55%. IR (KBr, cm^{-1}): 1570m, 1490m, 1440s, 1410m, 1190, 1120m (νC–S), 1085sh (νP–C), 1030w, 1000w, 775sh, 740s, 700s, 490s (νP–Se), 425sh (νPd–P), 360w (νPd–S). NMR ($CDCl_3$, δ ppm): ^{13}C, 167.5 (C^2), 147.1 (C^6), 136.4 (C^4), 121.8 (C^5), 116.5 (C^3), 29.7 (–CH_2–), 133.7 (*i*-C), 132.4 (*o*-C), 128.4 (*m*-C), 130.7 (*p*-C).

2.4. Elemental analyses and spectroscopic techniques

C, H and N determinations were performed by the microanalytical laboratory of the Regional Sophisticated Instrumentation Centre (RSIC) of Panjab University, Chandigarh. Infrared (IR) spectra were recorded as KBr pellets in the range 4000–200 cm^{-1} on a Philips Analytical SP3-300 spectrophotometer. ^{1}H NMR spectra were recorded on a Bruker AC-200 spectrometer operating at a frequency of 200 MHz. $CDCl_3$ was used as a solvent with TMS (tetramethylsilane) as the internal reference. ^{13}C NMR spectra were recorded on a Bruker AC-200 spectrometer operating at a frequency of 50 MHz using $CDCl_3$ as solvent and TMS as the internal

Table 1
Summary of crystal data for compounds **1**, **2** and **8**

	1	**2**	**8**
Empirical formula	$C_{36}H_{32}N_2P_2PtS_2$	$C_{36}H_{30}N_2P_2PtS_2$	$C_{36}H_{32}N_2P_2PdS_2$
MW	813.79	811.77	725.10
T (K)	293(2)	293(2)	293(2)
λ (Å)	0.71073	0.71073	0.71073
Crystal system	monoclinic	triclinic	monoclinic
Space group	$C2/c$	$P\bar{1}$	$C2/c$
a (Å)	37.028(7)	8.862(2)	37.049(10)
b (Å)	8.827(2)	12.462(3)	8.8224(17)
c (Å)	23.698(5)	16.323(3)	23.722(7)
V (Å^3)	6545(2)	1635.3(6)	6559(3)
α (°)	90	92.35(3)	90
β (°)	122.33(3)	103.63(3)	122.227(19)
γ (°)	90	109.68(3)	90
Z	8	2	8
D_c (g cm^{-3})	1.652	1.649	1.468
μ (Mo Kα) (mm^{-1})	4.542	4.544	0.819
Scan type	ω–2θ	ω–2θ	ω–2θ
2θ Range (°)	2.60–44.98	3.50–45.02	4.06–52.40
h, k, l ranges	0, 39; 0, 9; −25, 21	0, 9; −13, 21; −17, 17	−38, 46; 0, 10; −29, 0
No. reflections collected	4351	4580	6742
No. unique reflections, R_{int}	4274, 0.0372	4245, 0.0440	6570, 0.0418
Maximum and minimum transmission	0.721 and 0.545	0.97661 and 0.58438	0.968 and 0.937
No. reflections with $I > 2\sigma(I)$, parameters	3920, 388	4138, 388	6570, 388
F(000)	3216	800	2960
Final R indices			
R_1 [a], wR_2	0.0421, 0.0960	0.0259, 0.0594	0.0547, 0.0732
R indices (all data), R_1 [b], wR_2	0.0741, 0.1401	0.0324, 0.0621	0.3040, 0.1056
S [c] on F^2	0.978	1.038	0.906
Peak and hole (e Å^{-3})	0.706 and −0.999	0.411 and −0.524	0.653 and −1.433

[a] $R_1 = \Sigma||F_o| - |F_c||/\Sigma|F_o||$.
[b] $R_1 = [\Sigma w(F_o^2 - F_c^2)^2/\Sigma w(F_o^2)^2]^{1/2}$.
[c] $S = [\Sigma w(F_o^2 - F_c^2)^2/(n-p)]^{1/2}$, where n is total number of reflections measured, p is number of parameters.

reference. ^{31}P NMR spectra were recorded on a Bruker ACP-300 spectrometer operating at a frequency of 121.4 MHz with 85% phosphoric acid as the external reference (δP 32.5 ppm).

2.5. Crystal structure determinations

The suitable light yellow prismatic crystals of compounds **1**, **2** and **8** were mounted on glass fibres and used for data collection. Cell constants and orientation matrix for data collection were obtained by least-squares refinement of the diffraction data from 25 reflections in the θ range of 8–20° for compounds **1** and **2** with XSCANS (Siemens Analytical X-Ray Instruments) and $7.567 < \theta < 11.889$° for compound **8**. No detectable decompositon of the crystals occurred during data collection. For compounds **1** and **2**, data were collected on a Siemens P4 diffractometer and for compound **8** on an Enraf-Nonius Mach 3 automatic diffractometer [47]. The data were collected using Mo Kα radiation ($\lambda = 0.71073$ Å) and ω–2θ scan technique, and corrected for Lorentz and polarisation effects [48]. A semi-empirical absorption correction (psi scan) was made [49]. The structure was solved by direct methods and refined by a full-matrix least-squares method based on F^2. All non-hydrogen atoms were refined anisotropically. Hydrogen atoms were fixed geometrically and were not refined for compounds **1** and **2**, but were refined for compound **8** using a riding model. Atomic scattering factors were used from International Tables for Crystallography [50]. Data reduction, structure solution, refinement and molecular graphics were performed using SHELXTL-PC [51–54]. A summary of the crystal data, experimental details and refinement results are listed in Table 1.

3. Results and discussion

3.1. Synthesis and IR spectroscopy

In a recent study, it was found that reaction of N,S-bridged dimeric $Pt(C_5H_4NS)_2$ {obtained from $PtCl_2$ with $Na^+C_5H_4NS^-$} in CH_3CN with PPh_3 formed *trans*-[$Pt(\eta^1$-*S*-$C_5H_4NS)_2(PPh_3)_2$] with pendant pyridyl groups in the *trans* position [21]. The *cis*-[$Pt(\eta^1$-*S*-$C_5H_4NS)_2$(L-L)] compounds [L-L = dppe, dppen, etc. (**1**–**6**)] were obtained by the reactions of $PtCl_4$ (soluble in ethanol, unlike $PtCl_2$) with neutral C_5H_5NS in benzene in the presence of Et_3N,

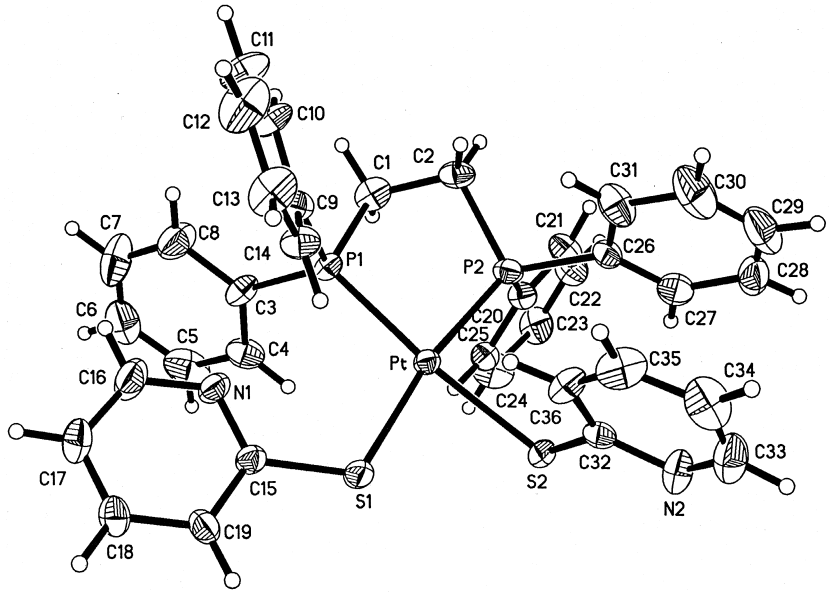


Fig. 1. Structure of monomeric *cis*-[Pt(η^1-*S*-$C_5H_4NS)_2$(dppe)] (**1**) showing the numbering scheme.

followed by addition of diphosphines or phosphine chalcogenides. Palladium(II) complexes were prepared by reacting $PdCl_2$ (diphosphines) with C_5H_5NS in the presence of aqueous NaOH.

The IR spectra of the complexes show various characteristic peaks of $C_5H_4NS^-$, diphosphines (see Section 2). The neutral C_5H_5NS shows ν(N–H) at 3162 cm^{-1}, and its absence in the complexes shows deprotonation of the pyridine-2-thione ligand (also confirmed by NMR data, see below). The coordination to Pt^{II}/Pd^{II} via S-donor atom is shown by the characteristic low-energy shift of ν(C–S) in the region 1110–1130 cm^{-1} occurring as a weak to strong peak. The ν(P=S) and ν(P=Se) peaks also undergo low-energy shifts, confirming coordination via P,S/P,Se-donor atoms of dppmPS and dppmPSe. Other tentative assignments due to ν(M–P) and ν(M–S) in the regions 400–420 cm^{-1} and 350–380 cm^{-1}, respectively, have been made.

3.2. Crystal and molecular structures

The atomic numbering schemes of *cis*-[Pt(η^1-*S*-$C_5H_4NS)_2$(dppe)] (**1**), *cis*-[Pt(η^1-*S*-$C_5H_4NS)_2$(dppen)] (**2**) and *cis*-[Pd(η^1-*S*-$C_5H_4NS)_2$(dppe)] (**8**) are shown in Figs. 1–3, respectively; the packing arrangements for compounds **1** and **2** are shown in Figs. 4 and 5, respectively. The basic monomer unit of compound **1** shows weak intermolecular interaction (4.036 Å) via phenyl groups of two different Ph_2P moieties (Fig. 4). However, no such interaction was visible in compound **2** (Fig. 5), as the closest distance between phenyl groups of two different molecules was 4.672 Å. In compound **1**, intramolecular interaction (3.663 Å) is observed between a pyridyl and a phenyl group of the same molecule (Fig. 4).

In complexes **1** and **2**, two P atoms of diphosphines and two S atoms of $C_5H_4NS^-$ groups coordinate to the Pt atom

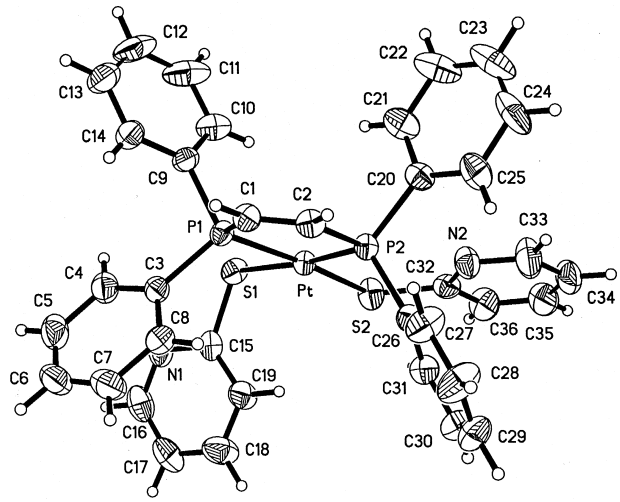


Fig. 2. Structure of monomeric *cis*-[Pt(η^1-*S*-$C_5H_4NS)_2$(dppen)] (**2**) showing the numbering scheme.

and the geometry about Pt centres is distorted square planar with *trans* P–Pt–S angles of 173.18(10), 170.31(11)° for compound **1** and 171.43(5), 168.97(5)° for compound **2** (Table 2). There is a small difference in the bite angles of both diphosphines [P(1)–Pt–P(2), 85.68° for compound **1** and 86.65(5)° for compound **2**] as well as in angles *trans* to these bite angles [S(1)–Pt–S(2), 82.69(11) and 84.01(6)° for compounds **1** and **2**, respectively]. Of the *cis* angles about Pt, only one is obtuse [P–Pt–S, 103.99(11)° for compound **1** and 104.38(5)° for compound **2**]; all the others are acute (Table 2). Significantly, an analogous complex, *trans*-[Pt(η^1-*S*-$C_5H_4NS)_2(PPh_3)_2$] (**A**) containing *trans* pendant pyridyl groups [21], showed *trans* bond angles (P–Pt–P* and S–Pt–S*) of exactly 180° and two acute (85.24°) and two obtuse (94.76°) angles about Pt. In a related diphosphine dimeric Pt complex [39], [(dppm)Pt(μ_2-*N*,*S*-TT)$_2$Pt-(dppm)] {**B**, dppm = $Ph_2PCH_2PPh_2$, H_2TT = 8-thiotheo-

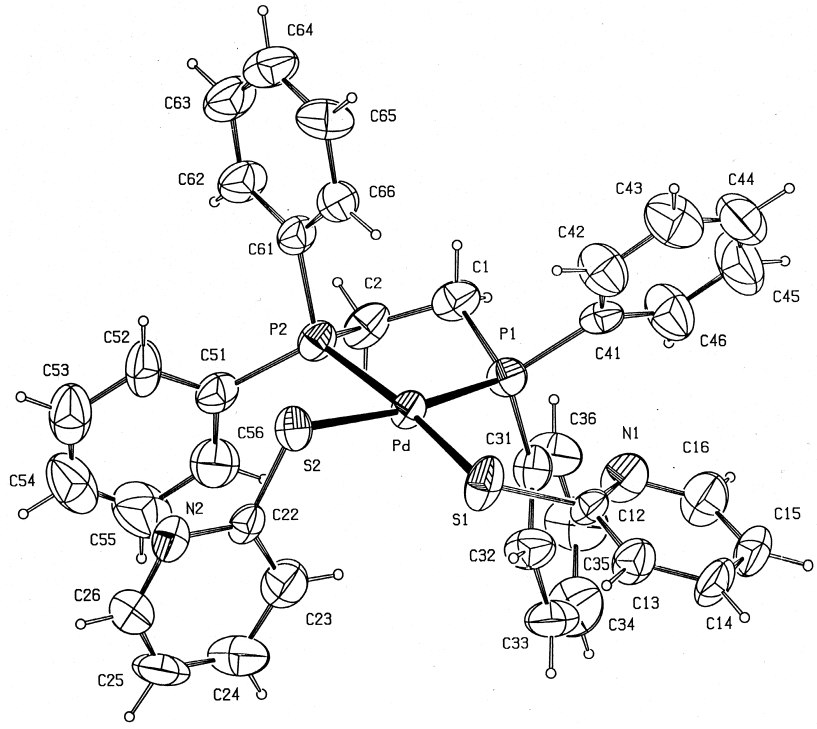


Fig. 3. Structure of monomeric *cis*-[Pd(η^1-*S*-$C_5H_4NS)_2$(dppe)] (**8**) showing the numbering scheme.

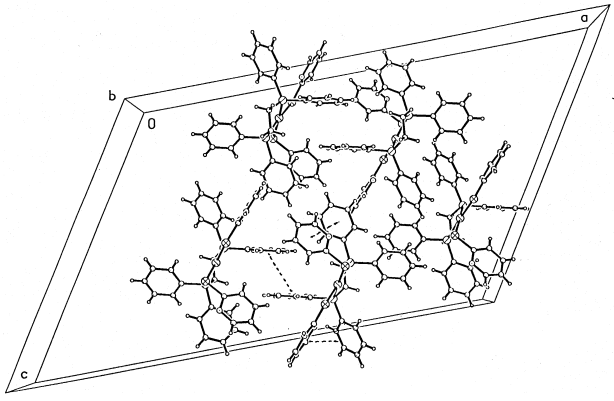


Fig. 4. Molecular packing arrangement of *cis*-[Pt(η^1-*S*-$C_5H_4NS)_2$(dppe)] (**1**).

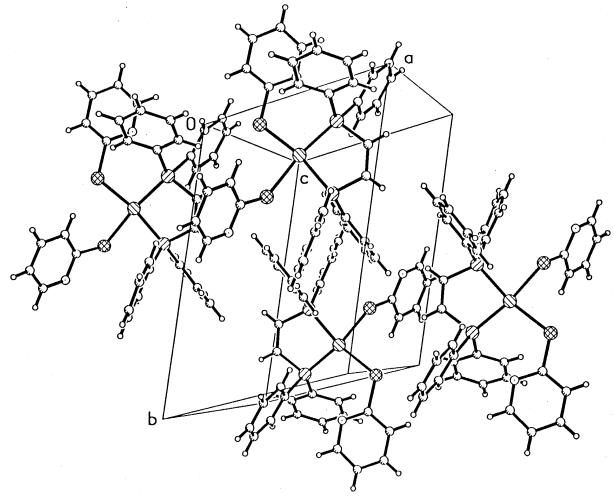


Fig. 5. Molecular packing arrangement of *cis*-[Pt(η^1-*S*-$C_5H_4NS)_2$(dppen)] (**2**).

phylline-N,S}, the diphosphine bite angle (P–Pt–P) was 73.35(12)° and *trans* P–Pt–S and P–Pt–N bond angles were 168.91(11) and 171.80(3)°, respectively; other *cis* angles about Pt were obtuse.

The Pt–P and Pt–S distances are similar in all four cases under discussion (Pt–P (Å): for compound **1**, 2.270(3), 2.256(3); compound **2**, 2.241(2), 2.268(1); compound **A**, 2.315 [21]; compound **B**, 2.270(3), 2.235(3) [6]. Pt–S (Å): compound **1**, 2.327(3), 2.389(3); compound **2**, 2.370(1), 2.332(2); compound **A**, 2.343(2) [21]; compound **B**, 2.356(3) [39]). There are small differences in P–C_{Ph} and P–$C_{alkane/alkene}$ bond lengths in compounds **1** and **2**. The S(1)–C(15) and S(2)–C(32) bond distances are slightly longer in compounds **1**, **2** and **B** compared with that in **A** (average: compound **1**, 1.7645(11); compound **2**, 1.753(6); compound **A**, 1.739(6); compound **B**, 1.751(12) Å). In compounds **1** and **2**, the bite angles of S(1)–C(15)–N(1) and S(2)–C(32)–N(2) are different: compound **1**, 119.8(1), 114.7(9)°; compound **2**, 113.4(5), 120.1(4)°, respectively. However, these bite angles (113–120°) are characteristic of an S-bonded monodentate $C_5H_4NS^-$ moiety [21,55]. Other characteristic bond angles, Pt–S(1)–C(15) and Pt–S(2)–C(32), are also different in the two cases: compound **1**, 116.9(4), 106.1(4)°; compound **2**, 109.1(2), 115.8(2)°.

Complexes **1** and **8** are isomorphous and their bond angles and distances are similar. Considering different planes for the complexes, the plane in compound **1** defined by the atoms $S^1S^2P^1P^2Pt$ makes an angle of 89.68° with the plane defined

Table 2
Selected bond lengths (Å) and bond angles (°) for **1**, **2** and **8** [a]

cis-[Pt(η^1-*S*-$C_5H_4NS)_2$(dppe)] (**1**)			
Pt–P(1)	2.270(3)	P(1)–Pt–P(2)	85.68(11)
Pt–P(2)	2.256(3)	P(1)–Pt–S(1)	103.99(11)
Pt–S(1)	2.327(3)	P(1)–Pt–S(2)	173.18(10)
Pt–S(2)	2.389(3)	P(2)–Pt–S(2)	87.67(11)
S(1)–C(15)	1.753(11)	P(2)–Pt–S(1)	170.31(11)
S(2)–C(32)	1.774(12)	S(1)–Pt–S(2)	82.69(11)
P(1)–C(1)	1.803(12)	Pt–S(1)–C(15)	116.9(4)
P(1)–C(3)	1.801(12)	Pt–S(2)–C(32)	106.1(14)
P(2)–C(2)	1.823(12)	S(1)–C(15)–N(1)	119.8(8)
P(2)–C(20)	1.823(11)	S(32)–C(32)–N(2)	114.7(9)
cis-[Pt(η^1-*S*-$C_5H_4NS)_2$(dppen)] (**2**)			
Pt–P(1)	2.241(2)	P(1)–Pt–P(2)	86.65(5)
Pt–P(2)	2.2678(14)	P(1)–Pt–S(1)	84.95(5)
Pt–S(1)	2.3701(14)	P(1)–Pt–S(2)	168.97(5)
Pt–S(2)	2.332(2)	P(2)–Pt–S(2)	104.38(5)
S(1)–C(15)	1.761(6)	P(2)–Pt–S(1)	171.43(5)
S(2)–C(32)	1.744(6)	S(1)–Pt–S(2)	84.01(6)
P(1)–C(1)	1.791(5)	Pt–S(1)–C(15)	109.1(2)
P(1)–C(3)	1.806(6)	Pt–S(2)–C(32)	115.8(2)
P(2)–C(2)	1.822(5)	S(1)–C(15)–N(1)	113.4(5)
P(2)–C(20)	1.821(6)	S(32)–C(32)–N(2)	120.1(4)
cis-[Pd(η^1-*S*-$C_5H_4NS)_2$(dppe)] (**8**)			
Pd–P(1)	2.297(2)	P(1)–Pd–P(2)	85.19(8)
Pd–P(2)	2.263(2	P(1)–Pd–S(1)	104.02(8)
Pd–S(1)	2.333(2)	P(1)–Pd–S(2)	171.83(8)
Pd–S(2)	2.382(2)	P(2)–Pd–S(2)	86.89(8)
S(1)–C(12)	1.744(7)	P(2)–Pd–S(1)	170.78(8)
S(2)–C(22)	1.757(8)	S(1)–Pd–S(2)	83.90(7)
P(1)–C(1)	1.838(6)	Pd–S(1)–C(12)	116.9(3)
P(1)–C(31)	1.819(7)	Pd–S(2)–C(22)	104.7(3)
P(2)–C(2)	1.839(7)	S(1)–C(12)–N(1)	120.4(6)
P(2)–C(51)	1.803(8)	S(2)–C(22)–N(2)	114.7(6)

[a] Symmetry transformations were used to generate equivalent atoms.

by the atoms $C^{32–36}$, N^2, and the angle is 5.98° with the second pyridyl group defined by atoms $C^{15–19}$, N^1. The corresponding angles are 12.19° for compound **3** and 74.94° for complex **2**. The orientation of pyridyl groups in compound **8** is similar to that of complex **2**, the corresponding angles being 7.36 and 84.10°. A further significant observation is the small angle of 13.07° between the planes defined by $C^{32–36}$, N^2 and $C^{26–31}$ for compound **1**; this explains the closest contact between a pyridyl group and a phenyl group as described earlier. It shows π-interactions between the two rings. In summary, the change in alkane moiety connecting Ph_2P groups from $–CH_2–CH_2–$ to –CH=CH– affects the orientation of the planes of Ph and py groups, in addition to inducing variations in bond distances and angles as discussed above.

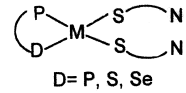
3.3. NMR spectroscopy

The observed ^1H and ^{13}C NMR resonances for all the complexes are given in Section 2. Deprotonation of C_5H_5NS in the complexes is evident from the absence of an NH proton signal (δ_{N-H}, 13.4 ppm (b) for free C_5H_5NS) and it shows platinum(II)–$C_5H_4NS^-$ bonding in complexes via S- or N,S-donor atoms [18–20]. The diagnostic H(6) proton signal of a pyridyl group in the vicinity of N atoms generally undergoes a shift to the low field in the complexes relative to neutral C_5H_5NS; other proton signals H(3), H(4) and H(5), all move upfield in the complexes. This behaviour of $C_5H_4NS^-$ is similar to that in *trans*-[Pt(η^1-*S*-$C_5H_4NS)_2(PPh_3)_2$] [21] and shows increased aromaticity of pyridyl groups in the complexes [55]. The $–(CH_2)_n–$, –CH=CH– and $C_6H_5–$ protons of diphosphine ligands show small low-field shifts.

The ^{13}C NMR spectra provide more convincing information about the uni- or bi-dentate behaviour of the $C_5H_4NS^-$ moiety [15–21,56]. The C(2) carbon signal of the pyridyl group moves upfield in the complexes (relative to free C_5H_5NS) and is characteristic of an S-bonded unidentate $C_5H_4NS^-$ moiety as a N,S-chelating moiety shows a low-field shift in the C(2) signal. Further C(3) and C(6) signals move downfield, while C(4) and C(5) signals move upfield, the latter carbon showing more pronounced shifts [15–21,56]. Finally, the $–CH_2–$ signals of diphosphine ligands show significant low-field shifts. The *ipso*-carbon of the $C_6H_5–$ group of free ligands moves upfield in all the complexes. The *meta*- and *para*-carbon signals either appear as separate or overlap; however, the *ortho*-carbon signal is almost unaffected. The –CH=CH– carbon signal of dppen appears as a triplet at δ 146.6t (J_{C-P}, 7.5 Hz) which shifts to a higher field at δ 145.4 ppm as an unresolved singlet in compound **2**. Thus NMR shows that, in all the complexes, pyridine-2-thiolate is coordinating to metals via an S-donor atom with pendant pyridyl groups in *cis* positions.

The ^{31}P NMR spectrum of compound **2** shows two ^{31}P NMR signals with corresponding pairs of satellites due to coupling from ^{195}Pt ($I = 1/2$), whereas compound **1** shows one ^{31}P signal with a pair of satellites. The presence of two sets of ^{31}P signals could be due to the non-equivalent pyridyl groups facing P atoms and this non-equivalence is probably not resolved in the dppe complex (**1**). While the J_{P-Pt} constants are similar in magnitude in the two cases (compound **1**, 2968.2 Hz; compound **2**, 2958.5, 2969.4 Hz), the coordination shifts ($\Delta\delta P$) are different (compound **1**, 58.2 ppm; compound **2**, 77.1 ppm). Thus, dppen is coordinating more strongly to the Pt centre than dppe is. The difference is attributed to the unsaturation in the –CH=CH– moiety of dppen, which could favour increased charge delocalisation in the Pt–dppen moiety.

In conclusion, *cis*-[M(η^1-*S*-$C_5H_4NS)_2$(diphosphines)]-(III) represent an interesting series of first examples with the potential to act as precursors to develop further polymetallic chemistry.



D= P, S, Se
III

Supplementary data

Supplementary data are available from the CCDC, 12 Union Road, Cambridge CB2 1EZ, UK (fax: +44-1223-

336033; e-mail: deposit@ccdc.cam.ac.uk) on request, quoting the deposition numbers 133755 for compound **1**, 133754 for compound **2**, 133351 for compound **8**.

Acknowledgements

Financial assistance from the University Grants Commission, Delhi [Project No. F. 12-47/93 (SR-I)] is gratefully acknowledged.

References

[1] E.S. Raper, Coord. Chem. Rev. 61 (1985) 115.
[2] E.S. Raper, Coord. Chem. Rev. 153 (1996) 199.
[3] E.S. Raper, Coord. Chem. Rev. 129 (1994) 91.
[4] E.S. Raper, Coord. Chem. Rev. 165 (1997) 475.
[5] D.C. Povey, G.W. Smith, T.S. Lobana, P.K. Bhatia, J. Crystallogr. Spectrosc. Res. 21 (1991) 9.
[6] T.S. Lobana, Prog. Inorg. Chem. 37 (1989) 495.
[7] W.L. Steffen, G.J. Palenik, Inorg. Chem. 15 (1976) 2432.
[8] T.S. Lobana, P.K. Bhatia, Indian J. Chem., Sect. A 30 (1991) 877.
[9] T.S. Lobana, P.K. Bhatia, Indian J. Chem., Sect. A 29 (1990) 1225.
[10] T.S. Lobana, P.K. Bhatia, E.R.T. Tiekink, J. Chem. Soc., Dalton Trans. (1989) 749.
[11] T.S. Lobana, P.K. Bhatia, J. Chem. Soc., Dalton Trans. (1992) 1407.
[12] T.S. Lobana, S. Paul, Transition Met. Chem. 21 (1996) 300.
[13] E.R.T. Tiekink, T.S. Lobana, R. Singh, J. Crystallogr. Spectrosc. Res. 21 (1991) 205.
[14] E. Horn, T.S. Lobana, R. Singh, E.R.T. Tiekink, Z. Kristallogr. 205 (1993) 291.
[15] T.S. Lobana, R. Singh, Polyhedron 14 (1995) 907.
[16] T.S. Lobana, R. Verma, R. Singh, A. Castineiras, Transition Met. Chem. 23 (1998) 25.
[17] T.S. Lobana, R. Verma, Indian J. Chem., Sect. A 38 (1999) 592.
[18] T.S. Lobana, S. Paul, A. Castineiras, Polyhedron 16 (1997) 4023.
[19] T.S. Lobana, S. Paul, A. Castineiras, J. Chem. Soc., Dalton Trans. (1999) 1819.
[20] T.S. Lobana, S. Paul, G. Hundal, S. Obrai, Transition Met. Chem. 24 (1999) 202.
[21] T.S. Lobana, R. Verma, A. Castineiras, Polyhedron 17 (1998) 3753.
[22] T.S. Lobana, P.K. Bhatia, J. Sci. Ind. Res. 48 (1989) 394.
[23] A.J. Deeming, K.I. Hardcastle, M.N. Meah, P.A. Bates, H.M. Dawes, M.B. Hursthouse, J. Chem. Soc., Dalton Trans. (1988) 227.
[24] P. Karagiannidis, P. Aslanidis, D.P. Kessissoglou, B. Krebs, M. Dartmann, Inorg. Chim. Acta 156 (1989) 47.
[25] P. Aslanidis, S.K. Hadjikakou, P. Karagiannidis, B. Kojic-Prodic, M. Luic, Polyhedron 13 (1994) 3119.
[26] P. Mura, B.G. Olby, S.D. Robinson, J. Chem. Soc., Dalton Trans. (1985) 2101.
[27] S.G. Rosenfield, H.P. Berends, L. Gelmini, D.W. Stephan, P.K. Mascharak, Inorg. Chem. 26 (1987) 2792.
[28] N. Zhang, S.R. Wilson, P.A. Shapley, Organometallics 7 (1988) 1126.
[29] L.A. Oro, M.A. Ciriano, F. Viguri, A. Tiripicchio-Camellini, F.J. Lahoz, Nouv. J. Chim. 10 (1986) 75.
[30] A.J. Deeming, M.N. Meah, P.A. Bates, M.B. Hursthouse, J. Chem. Soc., Dalton Trans. (1988) 235.
[31] A.J. Deeming, M. Karim, P.A. Bates, M.B. Hursthouse, Polyhedron 7 (1988) 1401.
[32] K. Umakoshi, I. Kinoshita, Y. Fukui-Yasuba, K. Matsumoto, S. Ooi, H. Nakai, M. Shiro, J. Chem. Soc., Dalton Trans. (1989) 815.
[33] J. Reedijk, Inorg. Chim. Acta 198–200 (1992) 873.
[34] M.J. Bloemink, J. Reedijk, in: H. Sigel, A. Sigel (Eds.), Metal Ions in Biological Systems, vol. 32, Marcel Dekker, New York, 1996, p. 641.
[35] S.S.G.E. van Boom, J. Reedijk, J. Chem. Soc., Chem. Commun. (1993) 1397.
[36] K.J. Barnham, M.I. Djuran, P. del Socorro Murdoch, P.J. Sadler, J. Chem. Soc., Chem. Commun. (1994) 721.
[37] L.J. McCaffrey, W. Henderson, B.K. Nicholson, J.E. Mackay, M.B. Dinger, J. Chem. Soc., Dalton Trans. (1997) 2577.
[38] L.T. McCaffrey, W. Henderson, B.K. Nicholson, Polyhedron 17 (1998) 221.
[39] E. Colacio, R. Cuesta, M. Ghazi, M. Angeles Huertas, J.M. Moreno, A. Navarrete, Inorg. Chem. 36 (1997) 1652.
[40] J.-M. Teuben, S.S.G.E. van Boom, J. Reedijk, J. Chem. Soc., Dalton. Trans. (1997) 3979.
[41] E.G. Talman, W. Bruning, J. Reedijk, A.L. Spek, N. Veldman, Inorg. Chem. 36 (1997) 854.
[42] G. Stucco, F. Gattuso, A.A. Isaab, C.F. Shaw III, Inorg. Chim. Acta 209 (1993) 129.
[43] S. Wang, R.J. Staples, J.P. Fackler Jr, Acta Crystallogr. Sect. C 50 (1994) 889.
[44] Y. Nakatsu, Y. Nakamura, K. Matsumoto, S. Ooi, Inorg. Chim. Acta 196 (1992) 81.
[45] J.H. Yamamoto, W. Yoshida, C.M. Jensen, Inorg. Chem. 30 (1991) 1353.
[46] J.A. Whiteford, C.V. Lu, P.J. Stang, J. Am. Chem. Soc. 119 (1997) 2524.
[47] B.V. Nonius, CAD-Express Software, Version 5.1/1.2, Enraf-Nonius, Delft, The Netherlands, 1994.
[48] M. Kretschmai, GENHKL program for the reduction of CAD4 diffractometer data. University of Tübingen, Germany, 1997.
[49] A.C.T. North, D.C. Phillips, F.S. Mathews, Acta Crystallogr. Sect. A 24 (1968) 351.
[50] International Tables for X-Ray Crystallography, Vol. C, Kluwer, Dordrecht, The Netherlands, 1995.
[51] G.M. Sheldrick, SHELXTL-PC, Release 5.03, Siemens Analytical X-Ray Instruments Inc., Madison, WI, 1995.
[52] G.M. Sheldrick, Acta Crystallogr. Sect. A 46 (1990) 467.
[53] G.M. Sheldrick, SHELXL-97, Program for the Refinement of Crystal Structure, University of Göttingen, Germany, 1997.
[54] A.L. Spek, Acta Crystallogr. Sect. A 46 (1990) C34.
[55] S. Wang, J.P. Fackler Jr., Inorg. Chem. 28 (1989) 2615.
[56] P.D. Cookson, E.R.T. Tiekink, J. Chem. Soc., Dalton Trans. (1993) 259.

PERGAMON

www.elsevier.nl/locate/poly

Polyhedron 19 (2000) 907–911

POLYHEDRON

Molybdenum(VI) equilibria at high perchloric acid concentration

J.J. Cruywagen *, J.B.B. Heyns

Department of Chemistry, University of Stellenbosch, Stellenbosch 7600, South Africa

Received 15 November 1999; accepted 7 February 2000

Abstract

Equilibria involving the protonation and dimerization of $MoO_2(OH)(H_2O)_3^+$ at high perchloric acid concentration have been investigated. A value for the protonation constant has been determined, $\log K = -2.23 \pm 0.09$. Values for the enthalpy and entropy changes for the reaction are $\Delta H = -21.4 \pm 1.8$ kJ mol^{-1} and $\Delta S = -90 \pm 6$ J mol^{-1} K^{-1} in 6.29 M $HClO_4$. For the dimerization reaction the values pertaining to 3.0 M Na(H)ClO_4 are $\Delta H = -30 \pm 5$ kJ mol^{-1} and $\Delta S = -63 \pm 10$ J mol^{-1} K^{-1} as determined by enthalpimetric titrations. Thermodynamic quantities for the conversion of $[MoO_4]^{2-}$ to the various mono- and dinuclear cationic species are reported. ©2000 Elsevier Science Ltd All rights reserved.

Keywords: Equilibrium constants; Molybenum(VI) cations; Thermodynamic quantities

1. Introduction

The successive protonation equilibria of $[MoO_4]^{2-}$ up to the formation of the cationic species, $MoO_2(OH)(H_2O)_3^+$, are well characterized, and equilibrium constants have been determined for different ionic media by various authors [1–9]. The total molybdate concentration must be lower than 10^{-4} M (mol dm^{-3}) for the species to be predominantly mononuclear in aqueous solution. A perchloric acid concentration of at least 1 M is required to have about 90% of molybdate protonated to $MoO_2(OH)(H_2O)_3^+$ [3]. There are indications that further protonation to a doubly charged cation occurs at higher acid concentration (>3 M) but the reaction has not been investigated in detail [3–5]. At high acid concentration, characterization of the equilibrium at constant ionic medium is problematic, whereas the tendency of molybdenum(VI) to form dinuclear cations [10–16] even at very low concentration must also be taken into account.

In this paper we report the results of a spectrophotometric study of these reactions in perchloric acid medium up to a concentration of 8 M. By introducing the hydrogen ion activity a quite satisfactory description of the equilibria can be obtained under these extreme conditions. The equilibrium constants can therefore be used to calculate relative concentrations of the species. It is shown to what extent dimerization is promoted by an increase in perchloric acid concentration at a given molybdate concentration.

The protonation of $MoO_2(OH)(H_2O)_3^+$ has been found to be an exothermic reaction. Thermodynamic quantities for the formation of the dimeric species have also been determined.

2. Experimental

Analytical grade chemicals (Merck, p.a.) were used and solutions were prepared with water purified with a Millipore Milli-Q system. A sodium molybdate stock solution of known concentration was prepared by weighing out an appropriate amount of $Na_2MoO_4 \cdot 2H_2O$. A stock solution of sodium perchlorate was prepared from recrystallized $NaClO_4$. These solutions were standardized by evaporating known volumes to dryness and heating at 160°C to constant weight. Perchloric acid was standardized indirectly against potassium hydrogen phthalate by titration with sodium hydroxide.

A GBC 920 UV–Vis double-beam spectrophotometer equipped with a Peltier thermocell was used for the absorption measurements. The temperature was kept constant at 25°C. Absorption spectra of molybdate(VI) solutions at two different concentrations (2.5×10^{-5} and 2.5×10^{-3} M) were recorded in the range 211–301 nm at intervals of 2 nm. Quartz cuvettes of path length 1.00 and 0.20 cm were used for measurements at the low and high concentrations, respectively. In each case a series of solutions (and corresponding blank solutions) were prepared of varying perchloric acid concentration in the range 0.40–8.0 M.

* Corresponding author. Tel.: +27-21-808 3332; fax: +27-21-808 3849; e-mail: jjc@maties.sun.ac.za

0277-5387/00/$ - see front matter ©2000 Elsevier Science Ltd All rights reserved.
PII S0277-5387(00)00331-4

An isothermal calorimeter, Tronac Model 1250, was used for the enthalpy measurements. Perchloric acid solutions (20.0 or 25.0 cm^3) of four different concentrations (0.50, 1.00, 2.00 and 3.00 M) were titrated with either 0.05 or 0.50 M sodium molybdate solution from a precision microburette (2.50 cm^3). The total heat measured for the titrations with 0.05 and 0.50 M molybdate was about 4.5 and 45 J, respectively. Some of the titrations were done in duplicate. All solutions were made 3.0 M with respect to perchlorate ions by addition of the appropriate amount of $NaClO_4$. Blank titrations of 3.0 M sodium perchlorate into solutions of perchloric acid and sodium perchlorate were done to correct for the heat of dilution (endothermic). This heat varied from $\sim$0.15 to 0.12 kJ mol^{-1} for $NaClO_4$ added to 3.0 M $HClO_4$, but was negligible in the case of 0.50 M $HClO_4$.

3. Results and discussion

3.1. Mononuclear species

The equilibria involved can be represented as follows:

$$MoO_3(H_2O)_3 + H^+ \leftrightharpoons MoO_2(OH)(H_2O)_3^+ \quad (1)$$

$$MoO_2(OH)(H_2O)_3^+ + H^+ \leftrightharpoons MoO_2(H_2O)_4^{2+} \quad (2)$$

There is little to choose between the alternative formulations for the uncharged mononuclear molybdic acid, i.e. $MoO_3(H_2O)_3$ and $MoO_2(OH)_2(H_2O)_2$. Slight preference is given to the former as discussed in a previous paper [17].

Although the focus is on the characterization of reaction (2), overlap of the equilibria necessitates the inclusion of reaction (1) in the description of the system. In the range of acid concentrations investigated, the maximum percentage concentration of $MoO_3(H_2O)_3$ is about 20%. To prevent the formation of dimeric cations the measurements had to be carried out at a very low molybdenum concentration (2.5×10^{-5} M). At this concentration the absorption in the UV is just high enough to yield results of sufficient accuracy for quantitative treatment. The change in absorption with change in perchloric acid concentration is shown in Fig. 1.

At varying ionic strength the protonation constants must be expressed in terms of the activities of the species; for example, for reaction (2) the constant is given by:

$$K_2 = \frac{[MoO_2(H_2O)_4^{2+}]y_2}{[MoO_2(OH)(H_2O)_3^+]y_1 a_{H^+}} \quad (3)$$

where y_2 and y_1 are the molar activity coefficients of the doubly and singly charged ions respectively and a_{H^+} is the molar activity of the hydrogen ion.

The activity of the hydrogen ion in perchloric acid is known [18,19] and can be substituted for the hydrogen ion concentration in the calculations. A reasonable approximation at high acid concentration is to assume that the activity coefficients of the molybdenum species vary roughly in the same manner, i.e. y_2/y_1 remains approximately constant. A value

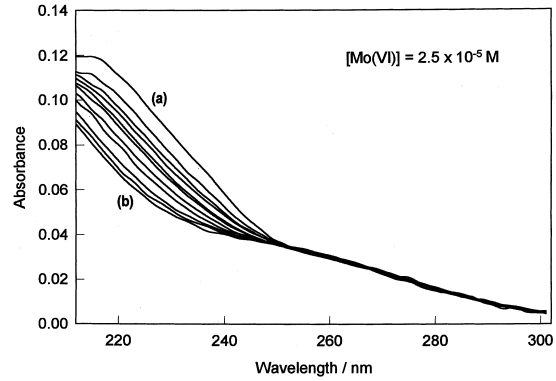


Fig. 1. Change in absorption spectra with change in perchloric acid concentration from 0.408 (a) to 8.15 M (b) of a 2.5×10^{-5} M molybdenum(VI) solution measured in a 1.00-cm cuvette.

for the protonation constant can therefore be determined from the change in the absorption with change in perchloric acid concentration.

By following this procedure and using the program EQUISPEC [20] to treat absorption data in the wavelength range 217–241 nm, where the greatest change in absorption occurs on protonation, a satisfactory fit between calculated and experimental points was obtained. The spectrum of the uncharged molybdic acid is known from previous work [3] so that the molar absorptivities at the wavelengths in question could be supplied to the program. The values calculated for the overall protonation constants were $\log \beta_1 = 0.95 \pm 0.01$ and $\log \beta_2 = -1.18 \pm 0.09$, where $\beta_1 = K_1$ and $\beta_2 = K_1K_2$.

The value for $\log \beta_1$ can be compared with the values 0.90 and 1.06 previously determined in 1.0 and 3.0 M Na(H)ClO_4 medium, respectively [3]. The calculated absorption spectra of the species are shown in Fig. 2. The spectrum of the singly charged cation agrees well with that previously reported, showing that the methodology followed provides an acceptable description of the behaviour of mononuclear molybdate at high acid concentration. From the distribution of the species with variation of perchloric acid concentration shown in Fig. 3 it is seen that a perchloric acid concentration higher than 6 M is required to obtain more than 50% protonation to the doubly charged cation.

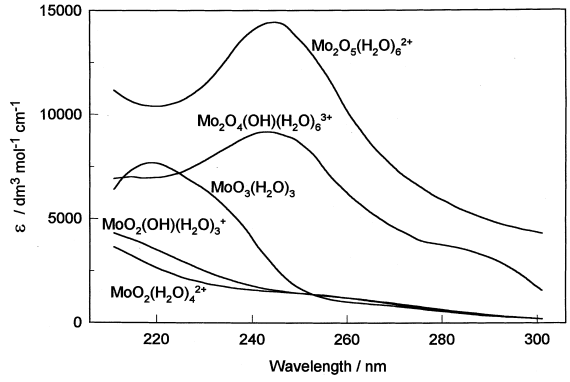


Fig. 2. Calculated absorption spectra of the various mono- and dinuclear species of molybdenum(VI).

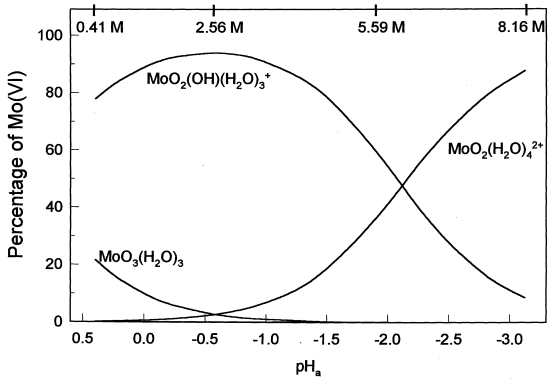


Fig. 3. Distribution of species as a function of pH_a ($-\log a_{H^+}$). The perchloric acid concentration corresponding to pH_a is shown on the upper axis.

The values $\log \beta_1 = -1.16$ and $\log \beta_2 = -3.98$ for the above reactions have been reported, by way of example, in the discussion of a program capable of calculating thermodynamic constants by correcting for variations in activity coefficients applying either Debye–Hückel, specific interaction or the modified Bromley theory [21]. However, as no information about the experimental conditions or the distribution of the species was given, a comparison with the results of the present work is not possible.

The enthalpy change for the protonation of $MoO_2(OH)(H_2O)_3^+$ has been determined from the variation in the equilibrium constant with temperature following a procedure analogous to that previously described [3]. The constant at a particular temperature can be calculated using Eq. (4):

$$K' = \frac{(\varepsilon_1 - \varepsilon)}{(\varepsilon - \varepsilon_2)[H^+]} \quad (4)$$

where ε_1, ε_2 and ε are the molar absorption coefficients of $MoO_2(OH)(H_2O)_3^+$, $MoO_2(H_2O)_4^{2+}$ and the sample solution, respectively. At the hydrogen ion concentration chosen for the measurements (6.29 M), the ratio of the concentration of the two cations is about 1 and $(\varepsilon_1 - \varepsilon)/(\varepsilon - \varepsilon_2) \sim 1$, which is the most suitable for the determination of the constant. Any shift in the equilibrium position due to a change in the temperature will result in the largest possible change in ε, while uncertainties in the values of $(\varepsilon_1 - \varepsilon)$ and $(\varepsilon - \varepsilon_2)$ will have the least effect on the calculated values of K'. This constant represents a concentration quotient and should also be regarded as a conditional protonation constant valid only for this particular medium, i.e. 6.29 M $HClO_4$. Perchloric acid is completely ionized up to about 6 M [22].

Assuming ΔH remains constant over the temperature range 16–36°C, the protonation constant is related to the enthalpy and entropy changes by the equation:

$$\log K' = \frac{(\Delta S - \Delta H/T)}{2.303R} \quad (5)$$

The average values of $\log K'$, calculated from absorbance measurements at the four wavelengths 217, 219, 221 and 223 nm plotted against $1/T$ are shown in Fig. 4. From the slope and intercept of the best straight line, obtained by a least-squares fit, the following values were calculated: $\Delta H = -21.4 \pm 1.8$ kJ mol^{-1}, $\Delta S = -90 \pm 6$ J mol^{-1} K^{-1}.

When compared with the small positive enthalpy change (6.0 kJ mol^{-1}) for the protonation of $MoO_3(H_2O)_3$ in 3.0 M $NaClO_4$ [3], the quite favourable enthalpy change for the protonation of $MoO_2(OH)(H_2O)_3^+$ appears to reflect the unusual medium in which the latter reaction occurs. However, ΔH values reported for the protonation of the ions $Hg(OH)^+$, $Fe(OH)^{2+}$ and $Cd(OH)^+$ (-30.1, -46 and -54.8 kJ mol^{-1}, respectively) are also favourable [23]. By considering the enthalpy involved in the formation of a water molecule (-54 kJ mol^{-1}) the trend has been explained in terms of a decrease in the metal–oxygen bond strengths in the order Hg > Fe > Cd. According to this reasoning, a favourable enthalpy change for the protonation of $MoO_2(OH)(H_2O)_3^+$ is to be expected compared with that of the protonation of $MoO_3(H_2O)_3$, where a double-bonded oxygen must accept the proton.

3.2. Equilibria involving dimeric cations

Depending on both the molybdenum and acid concentration the following three dimeric cations, $Mo_2O_5(OH)(H_2O)_5^+$, $Mo_2O_5(H_2O)_6^{2+}$ and $Mo_2O_4(OH)(H_2O)_6^{3+}$, have been found to exist in solution [10–13]. The formulations are based on a structure with a single oxo-bridge formed by elimination of one water molecule during dimerization. The presence of four terminal oxygens and a single bridging oxygen has been indicated by Raman spectroscopy [15] and an analysis of XANES (X-ray absorption near edge structure) and EXAFS (extended X-ray absorption fine structure) measurements [24]; an angle of $\sim 125°$ was suggested for the Mo–O–Mo bridge. Equilibrium constants for these cations have been determined in 3.0 M $Na(H)ClO_4$ medium and a satisfactory description of the system has been obtained despite the considerable changes in ionic medium necessitated by the high acid concentration [13].

The presence of these dimeric cations is indicated by a strong absorption band at ~ 246 nm. The increase in concentration of dimers with increase in perchloric acid concentration is seen from the experimental spectra of a series of

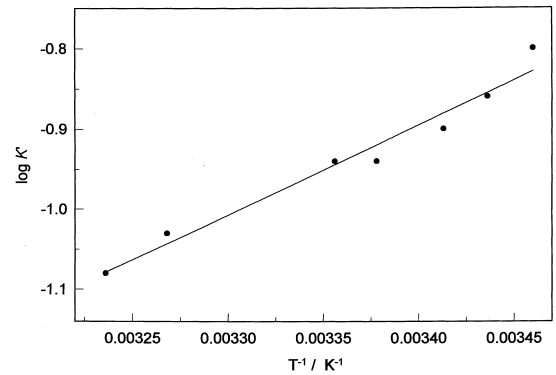


Fig. 4. Log K' as a function of the reciprocal of the Kelvin temperature.

molybdate solutions (2.5×10^{-3} M) measured in the concentration range 0.8–7.7 M (Fig. 5). Initially, there is a decrease in absorption at wavelengths lower than ~240 nm due to the formation of the monomeric cation, while a peak typical of dimeric cations develops at ~246 nm. These spectra (up to 6.29 M $HClO_4$) were used to obtain a rough estimate of the relative concentrations of the various monomers and dimers at high perchloric acid concentrations. Under these conditions, the singly charged dimer would be practically absent and only the following two equilibria have to be considered in addition to those involving the monomers:

$$2MoO_2(OH)(H_2O)_3^{+} \overset{K_D}{\leftrightarrow} Mo_2O_5(H_2O)_6^{2+} + H_2O) \quad (6)$$

$$2MoO_2(OH)(H_2O)_3^{+} + H^{+} \overset{K_{DI}}{\leftrightarrow} Mo_2O_4(OH)(H_2O)_6^{3+} + H_2O \quad (7)$$

Applying the same assumptions regarding the variation in activity coefficients as in the case of the mononuclear species and introducing the activity of the hydrogen ion as well as that of water [25], the spectrophotometric data (211–301 nm) were treated with the program EQUISPEC. To account for the presence of the mononuclear species their now-known absorption spectra and equilibrium constants were supplied to the program. In view of the approximations, the extraction of too many unknown parameters from the data would not be justified. The previously determined spectrum of $Mo_2O_5(H_2O)_6^{2+}$ [13] was therefore supplied to the program while the spectrum of the triply charged dimer was regarded as unknown to allow a comparison with the previous results. A quite reasonable fit (cf. error limits) of calculated to experimental absorption values was obtained, in particular at wavelengths in the region of the absorption band of the dimers. The shape of the spectrum obtained for the $Mo_2O_4(OH)(H_2O)_6^{3+}$ species (Fig. 2) agrees with that previously calculated from data pertaining to 3.0 M $Na(H)ClO_4$ medium [13] but lies higher. The difference most likely reflects the imperfections of the assumptions regarding the variation in activity coefficients of the species which in this case would have a greater effect than in the case of the protonation reactions described in the previous section, because the concentration of the mononuclear cation is now squared in the equilibrium expression. The values obtained for the two dimerization constants (3σ error limits), $\log K_D = 1.83\pm0.03$ and $\log K_{D1} = 1.14\pm0.21$ were used together with $\log \beta_1$ and $\log \beta_2$ to calculate the relative concentrations of the species in the perchloric acid concentration range 0.6–6.3 M (Fig. 6). The distribution curves, although approximate, illustrate the importance of the dimeric cations at high acid concentration even at this rather low molybdenum(VI) concentration (2.5×10^{-3} M).

3.3. Thermodynamic quantities for the dimerization reaction

The heat involved in the dimerization reaction was investigated by titrating a molybdate solution at constant ionic

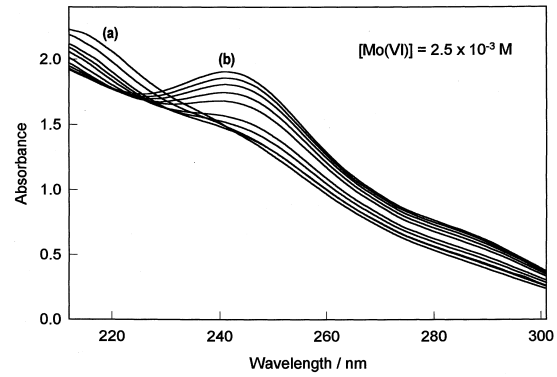


Fig. 5. Change in absorption spectra with change in perchloric acid concentration from 0.815 M (a) to 7.66 M (b) of a 2.5×10^{-3} M molybdenum(VI) solution measured in a 0.2-cm cuvette.

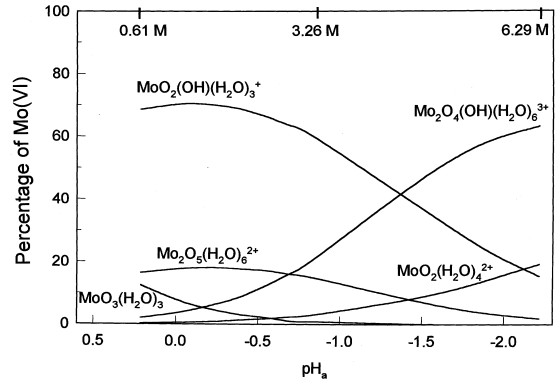


Fig. 6. Distribution of species as a function of pH_a ($-\log a_{H^+}$). The perchloric acid concentration corresponding to pH_a is shown on the upper axis.

medium (3.0 M $Na(H)ClO_4$) into perchloric acid at four different concentrations (0.50, 1.00, 2.00 and 3.00 M). Under these conditions, the formation of the two monomers $MoO_3(H_2O)_3$ and $MoO_2(OH)(H_2O)_3^{+}$ as well as that of the three dimeric cations contribute to the measured heat.

In principle the molar enthalpy change, ΔH_{pq}, of a particular species can be calculated from the measured heat, Q, by solving a set of linear equations of the form:

$$Q = \Sigma m_{pq} \cdot \Delta H_{pq}$$

where m_{pq} is the number of moles of a particular species and ΔH_{pq} the molar enthalpy change for its formation from $[MoO_4]^{2-}$ at 25°C in ionic medium 3.0 M $Na(H)ClO_4$. The subscripts p and q identify the species in terms of the stoichiometric coefficients of molybdate and hydrogen ions in the formation reaction.

The data were treated with the program SIRKO [26] using literature values for the formation constants of the various species [3,6,7,13]. The results are summarized in Table 1. The error limits given are estimated and are greater than those calculated by the program. The maximum concentration of $MoO_3(H_2O)_3$ is rather small (<10%) under the most favourable conditions and also changes very little during the titration. For this reason as well as some correlation with the concentration of $Mo_2O_5(OH)(H_2O)_5^{+}$, the enthalpy change for $MoO_3(H_2O)_3$ could not be calculated from the data. A

Table 1
Values for the thermodynamic quantities of molybdenum(VI) species formed from $[MoO_4]^{2-}$ in 3.0 M $Na(H)ClO_4$ medium

	Log K	ΔH (kJ mol^{-1})	ΔS (J mol^{-1} K^{-1})
$MoO_3(H_2O)_3$	7.75	$[-38\pm5]$ [a]	
$MoO_2(OH)(H_2O)_3^+$	8.81	-33.5 ± 1.0	56 ± 2
$Mo_2O_5(OH)(H_2O)_5^+$	18.93	-95 ± 5	44 ± 3
$Mo_2O_5(H_2O)_6^{2+}$	19.60	-97 ± 3	50 ± 3
$Mo_2O_4(OH)(H_2O)_6^{3+}$	18.98	-69 ± 5	132 ± 10
Dimerization (Eq. (6))	1.99	-30 ± 5	-63 ± 10

[a] See text.

fixed value (-38 ± 5 kJ mol^{-1}) based on the enthalpy change now obtained for the monomeric cation and its enthalpy change for ionization (-6.0 ± 1.2 kJ mol^{-1}) previously determined for this ionic medium [3] was supplied to the program after some preliminary runs. The best fit changed very little as long as the fixed value was kept within the limits given above, while the values for the other parameters remained well within the error limits given in Table 1. The fixed value(s) also seems very reasonable when compared with the enthalpy change determined spectrophotometrically for ionic medium 0.1 M NaCl, from the variation in the protonation constant with temperature (-29 ± 3 kJ mol^{-1}) [17].

From the results it can be seen that the dimerization reaction (6) is enthalpy-driven (-30 kJ mol^{-1}) coupled with an unfavourable entropy change; the favourable enthalpy change emanates mainly from the formation of a free water molecule and the unfavourable entropy change from the restriction placed on the system. Values have been reported at three different temperatures for a conditional dimerization constant pertaining to 0.50 M $HClO_4$ in 1.0 M $LiClO_4$ medium [16]. From these values one can estimate an enthalpy change of -23 ± 4 kJ mol^{-1}, which would be consistent with the present results.

In view of the discussion above (Section 3.1), the substantially more unfavourable enthalpy change for the protonation of the doubly charged dimer, $Mo_2O_5(H_2O)_6^{2+}$ (28 kJ mol^{-1}), compared with that of the singly charged dimer, $Mo_2O_5(OH)(H_2O)_5^+$ (-2 kJ mol^{-1}), is to be expected since protonation of any one of the double-bonded oxygen atoms of $Mo_2O_5(H_2O)_6^{2+}$ would be more difficult than protonation of the hydroxyl group of $Mo_2O_5(OH)(H_2O)_5^+$.

Acknowledgements

Financial support by the University of Stellenbosch and the National Research Foundation is gratefully acknowledged.

References

[1] J.J. Cruywagen, Adv. Inorg. Chem. 49 (2000) 127.
[2] J.J. Cruywagen, E.F.C.H. Rohwer, Inorg. Chem. 14 (1975) 3136.
[3] J.J. Cruywagen, J.B.B. Heyns, E.F.C.H. Rohwer, J. Inorg. Nucl. Chem. 38 (1976) 2033 and Refs. therein.
[4] S. Himeno, M. Hasegawa, Inorg. Chim. Acta 73 (1983) 255.
[5] K. Yokoi, N. Matsubayashi, T. Miyanaga, I. Watanaba, S. Ikeda, Polyhedron 12 (1993) 911.
[6] L. Pettersson, I. Anderson, L.O. Öhman, Acta Chem. Scand., Ser. A 39 (1985) 53.
[7] L. Pettersson, I. Anderson, L.O. Öhman, Inorg. Chem. 25 (1986) 4726.
[8] K.H. Tytko, G. Baethe, J.J. Cruywagen, Inorg. Chem. 24 (1985) 3132.
[9] P.L. Brown, M.E. Shying, R.N. Sylva, J. Chem. Soc., Dalton Trans. (1987) 2149.
[10] L. Krumenacker, Bull. Soc. Chim. (1971) 362.
[11] L. Krumenacker, Bull. Soc. Chim. (1971) 2820.
[12] J.F. Ojo, R.S. Taylor, A.G. Sykes, J. Chem. Soc., Dalton Trans. (1975) 500.
[13] J.J. Cruywagen, J.B.B. Heyns, E.F.C.H. Rohwer, J. Inorg. Nucl. Chem. 40 (1978) 53.
[14] S. Himeno, Y. Ueda, M. Hasegawa, Inorg. Chim. Acta 70 (1983) 53.
[15] S. Himeno, M. Hasegawa, Inorg. Chim. Acta 83 (1984) L5.
[16] J.D. Lydon, L.M. Schwane, R.C. Thompson, Inorg. Chem. 26 (1987) 2606.
[17] J.J. Cruywagen, J.B.B. Heyns, J. Chem. Educ. 66 (1989) 861.
[18] R.A. Robinson, R.H. Stokes, Electrolyte Solutions, 2nd edn., Butterworth, London, 1959.
[19] M. Gazith, Report No. I.A.-1004, Israel Atomic Energy Commission, Accession No. 11048, 1964.
[20] R.M. Dyson, S. Kaderli, G.A. Lawrance, M. Maeder, A.D. Zuberbühler, Anal. Chim. Acta 353 (1997) 381.
[21] R. Cazallas, M.J. Citores, N. Etxebarria, L.A. Fernandez, J.M. Madariaga, Talanta 41 (1994) 1673.
[22] J.W. Akitt, A.K. Covington, J.G. Freeman, T.H. Lilley, Trans. Faraday Soc. 65 (1969) 2701.
[23] R. Arnek, Ark. Kemi 32 (1970) 55.
[24] K. Yokoi, N. Matsubayashi, T. Miyanaga, I. Watanaba, K. Murata, S. Ikeda, Chem. Lett. (1987) 1453.
[25] C.J. O'Connor, J. Chem. Educ. 46 (1969) 686.
[26] V.I. Vetrogon, N.G. Lukyanenko, M.-J. Schwing-Weill, F. Arnaud-Neu, Talanta 41 (1994) 2105.

PERGAMON

www.elsevier.nl/locate/poly

Polyhedron 19 (2000) 913–923

POLYHEDRON

Palladium(II), platinum(II), and platinum(IV) complexes containing *trans*-1,2-bis(diphenylphosphino)ethene or *cis*,*trans*,*cis*-1,2,3,4-tetrakis(diphenylphosphino)cyclobutane: complete X-ray structural characterization of binuclear compounds

Werner Oberhauser [a], Thomas Stampfl [a], Christian Bachmann [a], Rainer Haid [a], Christoph Langes [a], Holger Kopacka [a], Karl-Hans Ongania [b], Peter Brüggeller [a,*]

[a] *Institut für Allgemeine, Anorganische und Theoretische Chemie, Universität Innsbruck, Innrain 52a, 6020 Innsbruck, Austria*

[b] *Institut für Organische Chemie, Universität Innsbruck, Innrain 52a, 6020 Innsbruck, Austria*

Received 8 December 1999; accepted 11 February 2000

Abstract

Several novel binuclear Pd^{II}, Pt^{II}, and Pt^{IV} complexes of *trans*-1,2-bis(diphenylphosphino)ethene (*trans*-dppen) or *cis*,*trans*,*cis*-1,2,3,4-tetrakis(diphenylphosphino)cyclobutane (dppcb) have been prepared and characterized by X-ray diffraction methods, $^{195}Pt\{^1H\}$ and $^{31}P\{^1H\}$ NMR spectroscopy, FAB mass spectrometry, IR spectroscopy, elemental analyses and melting points. The X-ray structure and NMR parameters of $[Pt_2I_4(trans\text{-dppen})_2]$ (**1**) confirm that homobimetallic complexes of the type $[M_2L_4(trans\text{-dppen})_2]$ ($M = Ni, Pd, Pt$; $L = Cl^-, I^-, CN^-$) contain two square planar coordination units joined by two *trans*-dppen bridges in the solid as well as in the solution state. An analogous structure type is retained in the Pt^{IV} compound $[Pt_2Cl_8(trans\text{-dppen})_2]$ (**2**). In contrast to the corresponding Pt^{II} complex of the new tetradentate phosphine dppcb, the X-ray structure of $[Pd_2Cl_4(dppcb)]$ (**3**) reveals only one conformation. This can be explained by the longer Pd–P bonds compared with the Pt–P bonds and the weaker square planar stabilization energy in **3**. In **3** dppcb acts as a binuclear tetraligate single-bridging ligand combining two square planar coordination centres. The reaction of $Pd(CN)_2$ with dppcb leads to $[Pd_2(CN)_4(dppcb)]$ (**4**). The removal of the coordinated chlorides in **3** by $AgBF_4$ followed by subsequent treatment with $NaNO_2$ produces $[Pd_2(NO_2)_4(dppcb)]$ (**5**). In an analogous reaction with 1,10-phenanthroline (phen) or 2,2′-bipyridine (bipy), $[Pd_2(dppcb)(phen)_2](BF_4)_4$ (**6**) and $[Pd_2(dppcb)(bipy)_2](BF_4)_4$ (**7**) are formed. The complexes **4**–**7** show structure types corresponding to the X-ray structure of **3**. The same is true for the treatment of **3** with $PMePh_2$ or PMe_2Ph, where $[Pd_2(dppcb)(PMePh_2)_4](BF_4)_2Cl_2$ (**8**) and $[Pd_2(dppcb)(PMe_2Ph)_4](BF_4)_4$ (**9**) are obtained. However, the X-ray structure of **8** reveals that the chlorides are coordinated in the solid state, and the crystal structure consists of *trans*-$[Pd_2Cl_2(dppcb)(PMePh_2)_2](BF_4)_2$ (**10**). The flexibility and stereochemical demands of dppcb in the compounds **3**–**10** and related species are discussed in view of the possible application of Pd^{II} complexes containing bidentate tertiary phosphine ligands as catalysts for the alternating copolymerization of ethene and carbon monoxide. In this respect dppcb can be regarded as a combination of two bidentate phosphines, where the cyclobutane ring corresponds to a relatively rigid ligand backbone. This produces strain in the five-membered rings of **3**–**10** which is released by 'envelope'-folding in the X-ray structures of **3** and **10**. ©2000 Elsevier Science Ltd All rights reserved.

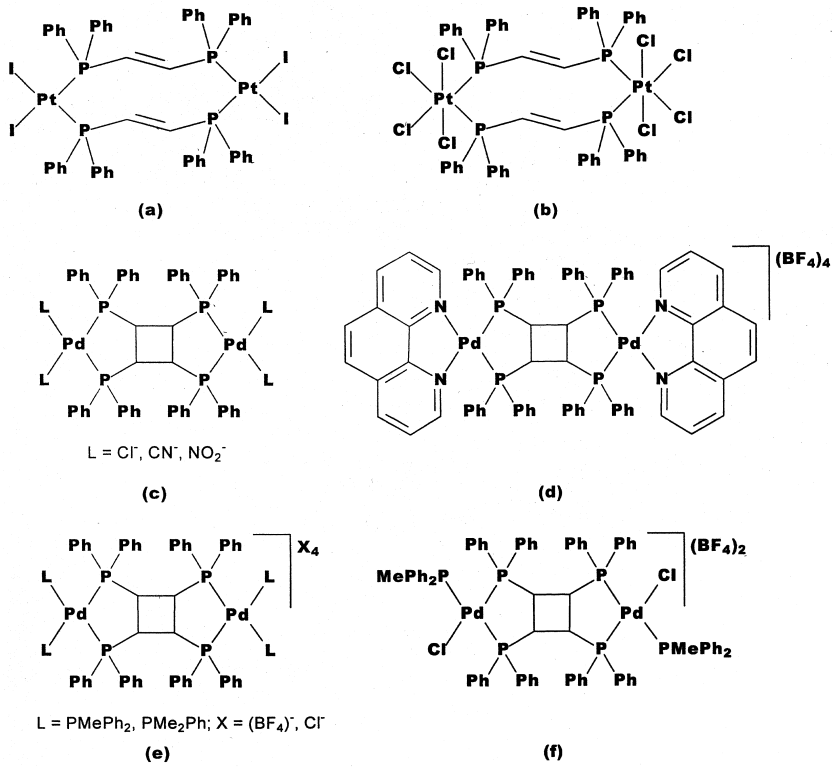
Keywords: Crystal structures; Palladium complexes; Platinum complexes; Diphosphine complexes; Tetraphosphine complexes; Bimetallic complexes

1. Introduction

Trans-1,2-bis(diphenylphosphino)ethene (*trans*-dppen) is a diphosphine-like 1,2-bis(diphenylphosphino)acetylene (dppa), in which the rigidity of the unsaturated carbon backbone forces two phosphorus atoms to remain too far apart for them both to bond to a single metal atom [1–3]. Furthermore, *trans*-dppen bridges preclude the possibility of a bridging halogen atom between the metal centres in bimetallic species, where the number of *trans*-dppen bridges varies from one to four [4–6]. In this work the structure of homobimetallic complexes of the type $[M_2L_4(trans\text{-dppen})_2]$ ($M = Ni, Pd, Pt$; $L = Cl^-, I^-, CN^-$) [7,8] is confirmed by the X-ray structure of the novel compound $[Pt_2I_4(trans\text{-dppen})_2]$ (**1**) corresponding to structure type (a) in Scheme 1. The NMR

* Corresponding author. Tel.: +43-512-507-5115; +43-512-507-2934; e-mail: peter.brueggeller@uibk.ac.at

0277-5387/00/$ - see front matter ©2000 Elsevier Science Ltd All rights reserved.
PII S0277-5387(00)00332-6



Scheme 1. Structure types observed in compounds **1**–**10**. Structure (a) occurs in $[Pt_2I_4(trans\text{-dppen})_2]$ (**1**), structure (b) in $[Pt_2Cl_8(trans\text{-dppen})_2]$ (**2**), structure (c) in $[Pd_2L_4(dppcb)]$ ($L=Cl^-$ (**3**), $L=CN^-$ (**4**), $L=NO_2^-$ (**5**)), structure (d) in $[Pd_2(dppcb)(phen)_2](BF_4)_4$ (**6**) and analogous to it in $[Pd_2(dppcb)(bipy)_2](BF_4)_4$ (**7**), structure (e) in $[Pd_2(dppcb)(PMePh_2)_4](BF_4)_2Cl_2$ (**8**) and $[Pd_2(dppcb)(PMe_2Ph)_4](BF_4)_4$ (**9**), and structure (f) in *trans*-$[Pd_2Cl_2(dppcb)(PMePh_2)_2](BF_4)_2$ (**10**).

parameters of **1** indicate that the same structure is retained in solution. The Pt^{IV} complex $[Pt_2Cl_8(trans\text{-dppen})_2]$ (**2**) shows the analogous structure type (b) in Scheme 1.

Only recently, *trans*-dppen together with Pt^{II} as a template have been used to produce the new tetradentate phosphine *cis,trans,cis*-1,2,3,4-tetrakis(diphenylphosphino)cyclobutane (dppcb) [7]. Comparable to the tetratertiary phosphine 2,3-bis[(diphenylphosphino)methyl]-1,4-bis(diphenylphosphino)butane, dppcb coordinates in a bis(bidentate) manner to two metals and favours homobimetallic complexes [9]. However, the rigidity of the cyclobutane ring in dppcb prevents the coordination of all four phosphorus atoms to one metal. Pd^{II} complexes containing bidentate tertiary phosphine ligands show high catalyst activity and yield for alternating CO/ethene copolymerization and opened the way for efficient synthesis of polyketone [10], where dppcb can be regarded as a combination of two bidentate phosphines. Since also Pd^{II} complexes of nitrogen-containing bidentate ligands are very active precatalysts in the copolymerization of styrene with carbon monoxide, an investigation of the structural possibilities of bimetallic Pd^{II} complexes with dppcb is interesting [11]. Therefore, the novel compounds $[Pd_2L_4(dppcb)]$ ($L=Cl^-$ (**3**), CN^- (**4**), NO_2^- (**5**)), $[Pd_2(dppcb)(phen)_2](BF_4)_4$ (**6**) and $[Pd_2(dppcb)(bipy)_2](BF_4)_4$ (**7**), where phen and bipy are 1,10-phenanthroline and 2,2′-bipyridine, respectively, have been prepared. They belong to structure types (c) and (d) in Scheme 1, where **7** is analogous to **6**, and have been confirmed by the X-ray structure of **3**.

Furthermore, in order to extend the type of potentially catalytic active compound for oligomerization and polymerization of olefins, Pd^{II} complexes of the type $[PdCl(diphosphine)(monophosphine)]^+$ have been synthesized [12]. The corresponding new complexes containing dppcb $[Pd_2(dppcb)(PMePh_2)_4](BF_4)_2Cl_2$ (**8**), $[Pd_2(dppcb)(PMe_2Ph)_4](BF_4)_4$ (**9**), and *trans*-$[Pd_2Cl_2(dppcb)(PMePh_2)_2](BF_4)_2$ (**10**) show structure types (e) and (f) in Scheme 1. Upon crystallization of **8**, the chloride anions coordinate to Pd^{II} and **10** is formed. **10** is fully characterized by an X-ray structure analysis.

2. Experimental

2.1. Reagents and chemicals

Reagent grade chemicals were used as received unless stated otherwise. *Trans*-1,2-bis(diphenylphosphino)ethene (*trans*-dppen) was purchased from Aldrich. $PMePh_2$ and PMe_2Ph were obtained from Strem. All other reagents and solvents were received from Fluka. Solvents used for NMR measurements and crystallization purposes were of purissimum grade quality. $PdCl_2$ and $Na_2PtCl_4\cdot 4H_2O$ were also obtained from Fluka.

2.2. Instrumentation

Fourier-mode $^{195}Pt\{^1H\}$ and $^{31}P\{^1H\}$ NMR spectra were obtained using Bruker AC-200 and DPX-300 spectrometers (internal deuterium lock) and were recorded at 43.02 (64.50) and 80.96 (121.44) MHz, respectively. Positive chemical shifts are downfield from the standards, where 1.0 M Na_2PtCl_6 and 85% H_3PO_4 were used as standards, respectively.

2.3. Syntheses of Pd^{II}, Pt^{II}, and Pt^{IV} complexes

A Schlenk apparatus and oxygen-free, dry Ar were used in the syntheses of all complexes. Solvents were degassed by several freeze–pump–thaw cycles prior to use. All reactions were carried out at room temperature unless stated otherwise. [Pt_2Cl_4(*trans*-dppen)$_2$] and dppcb were prepared as described earlier [7].

2.3.1. [Pt_2I_4(*trans*-dppen)$_2$] (**1**)

[Pt_2Cl_4(*trans*-dppen)$_2$] (0.075 mmol, 0.100 g) was dissolved in CH_2Cl_2/DMF (v/v = 2:1, 5 cm^3) and LiI (0.30 mmol, 0.040 g) was added with vigorous stirring and prevention of light. The reaction mixture was stirred at 45°C for 48 h. Then the solvent was completely removed, the yellow residue was filtered off in H_2O, washed with H_2O and dried in vacuo. An ochre-yellow powder was recrystallized from CH_2Cl_2/Et_2O. Yield 0.100 g (79%); m.p. > 310°C. *Anal*. Found: C, 36.8; H, 2.7. Calc. for $C_{52}H_{44}I_4P_4Pt_2$: C, 36.9; H, 2.6%. A sample for X-ray diffraction with the composition $C_{52}H_{44}I_4P_4Pt_2 \cdot 0.75$DMF was crystallized from $CHCl_3$/DMF with prevention of light.

2.3.2. [Pt_2Cl_8(*trans*-dppen)$_2$] (**2**)

Chlorine was bubbled through a solution of [Pt_2Cl_4(*trans*-dppen)$_2$] (0.075 mmol, 0.100 g) in DMF (10 cm^3) for 10 min with prevention of light. The volume of the solvent was reduced and a yellow precipitate formed. Then Et_2O was added, the precipitate was filtered off and dried in vacuo. A yellow powder was recrystallized from DMF. Yield 0.079 g (72%); m.p. 192–194°C. *Anal*. Found: C, 42.4; H, 3.1. Calc. for $C_{52}H_{44}Cl_8P_4Pt_2$: C, 42.6; H, 3.0%.

2.3.3. [Pd_2Cl_4(dppcb)] (**3**)

$PdCl_2$ (0.50 mmol, 0.089 g) was suspended in DMF (7 cm^3). Then dppcb (0.25 mmol, 0.198 g) was added with vigorous stirring. The reaction mixture was stirred at 55°C for 6 h and a white precipitate formed. The solvent was completely removed, the white residue was filtered off in CH_2Cl_2, washed with CH_2Cl_2 and dried in vacuo. A white powder was recrystallized from DMF. Yield 0.328 g (91%); m.p. > 320°C. *Anal*. Found: C, 53.2; H, 5.1; N, 3.8. Calc. for $C_{52}H_{44}Cl_4P_4Pd_2 \cdot 4$DMF: C, 53.4; H, 5.0; N, 3.9%. A sample for X-ray diffraction with the composition $C_{52}H_{44}Cl_4P_4Pd_2 \cdot 4$DMF was crystallized from DMF.

2.3.4. [$Pd_2(CN)_4$(dppcb)] (**4**)

Compound **4** was prepared in an analogous manner to **3**, where $Pd(CN)_2$ (0.50 mmol, 0.079 g) was used. A white powder was recrystallized from DMF. Yield 0.227 g (82%); m.p. 304°C. IR (KBr, cm^{-1}) CN: 2135 ν. *Anal*. Found: C, 60.4; H, 4.2; N, 4.8. Calc. for $C_{56}H_{44}N_4P_4Pd_2$: C, 60.6; H, 4.0; N, 5.0%.

2.3.5. [$Pd_2(NO_2)_4$(dppcb)] (**5**)

Compound **3** (0.060 mmol, 0.069 g) was suspended in DMF (6 cm^3). Then $AgBF_4$ (0.24 mmol, 0.047 g) was added with stirring. The reaction mixture was stirred for 2 h, the formed AgCl was filtered off and the solvent completely removed. The residue was dissolved in CH_2Cl_2/DMF (v/v = 10:1, 5 cm^3) and $NaNO_2$ (0.24 mmol, 0.017 g) was added slowly with vigorous stirring. After 5 h the solvent was completely removed, the yellowish residue was filtered off in H_2O, washed with H_2O and dried in vacuo. A yellowish powder was recrystallized from DMF. Yield 0.060 g (84%); m.p. 270–272°C dec. IR (KBr, cm^{-1}) NO_2: 1370 ν_a, 1318 ν_s, 814 δ. *Anal*. Found: C, 52.4; H, 3.7; N, 4.5. Calc. for $C_{52}H_{44}N_4O_8P_4Pd_2$: C, 52.5; H, 3.7; N, 4.7%.

2.3.6. [Pd_2(dppcb)(phen)$_2$](BF_4)$_4$ (**6**)

Compound **3** (0.060 mmol, 0.069 g) was suspended in DMF (6 cm^3). Then $AgBF_4$ (0.24 mmol, 0.047 g) was added with stirring. The reaction mixture was stirred for 2 h, the formed AgCl was filtered off and the solvent completely removed. The residue was dissolved in CH_2Cl_2 (5 cm^3) and 1,10-phenanthroline · H_2O (0.12 mmol, 0.024 g) was added slowly with vigorous stirring. A white precipitate immediately formed. After 5 h the precipitate was filtered off, washed with CH_2Cl_2 and dried in vacuo. A white powder was recrystallized from DMF. Yield 0.084 g (82%); m.p. > 320°C. *Anal*. Found: C, 53.3; H, 3.8; N, 3.2. Calc. for $C_{76}H_{60}B_4F_{16}N_4P_4Pd_2$: C, 53.3; H, 3.5; N, 3.3%.

2.3.7. [Pd_2(dppcb)(bipy)$_2$](BF_4)$_4$ (**7**)

Compound **7** was prepared in an analogous manner to **6**, where 2,2′-bipyridine (0.12 mmol, 0.019 g) was used. A white powder was recrystallized from DMF. Yield 0.062 g (62%); m.p. > 320°C. *Anal*. Found: C, 51.7; H, 3.7; N, 3.3. Calc. for $C_{72}H_{60}B_4F_{16}N_4P_4Pd_2$: C, 51.9; H, 3.6; N, 3.4%.

2.3.8. [Pd_2(dppcb)($PMePh_2$)$_4$](BF_4)$_2Cl_2$ (**8**) and trans-[Pd_2Cl_2(dppcb)($PMePh_2$)$_2$](BF_4)$_2$ (**10**)

Compound **3** (0.090 mmol, 0.104 g) was suspended in CH_2Cl_2/DMF (v/v = 7:1, 10 cm^3). Then $AgBF_4$ (0.18 mmol, 0.035 g) was added with stirring. The reaction mixture was stirred for 8 h, the formed AgCl was filtered off and the solvent completely removed. The residue was dissolved in CH_2Cl_2 (8 cm^3) and $PMePh_2$ (0.36 mmol, 0.072 g) was added via a syringe with vigorous stirring. The solution was stirred for 5 h. The ^{31}P ^1H NMR parameters of this solution correspond to **8**. The solvent was completely removed, the yellow residue was filtered off in EtOH, washed with EtOH

and dried in vacuo. A yellow powder was recrystallized from CH_2Cl_2. Yield 0.120 g (73%); m.p. 220–221°C. FAB mass spectrum: *m/z* 1528.3 $[Pd_2Cl(dppcb)(PMePh_2)_2](BF_4)^+$, 1127.9 $[Pd_2Cl(dppcb)](BF_4)^+$. *Anal.* Found: C, 52.6; H, 4.2. Calc. for $C_{78}H_{70}B_2Cl_2F_8P_6Pd_2 \cdot 2CH_2Cl_2$ corresponding to **10**$\cdot 2CH_2Cl_2$: C, 52.8; H, 4.1%. A sample for X-ray diffraction with the composition $C_{78}H_{70}B_2Cl_2F_8P_6Pd_2 \cdot 2CH_2Cl_2$ was crystallized from CH_2Cl_2.

*2.3.9. $[Pd_2(dppcb)(PMe_2Ph)_4](BF_4)_4$ (**9**)*

Compound **3** (0.060 mmol, 0.069 g) was suspended in DMF (6 cm^3). Then $AgBF_4$ (0.24 mmol, 0.047 g) was added with stirring. The reaction mixture was stirred for 2 h, the formed AgCl was filtered off and the solvent completely removed. The residue was dissolved in CH_2Cl_2/DMF (v/v = 5:1, 5 cm^3) and PMe_2Ph (0.24 mmol, 0.033 g) was added via a syringe with vigorous stirring. After 10 min a yellowish precipitate slowly formed. The slurry was stirred for 5 h. The solvent was completely removed, the yellow residue was filtered off in CH_2Cl_2, washed with CH_2Cl_2 and dried in vacuo. A yellow powder was recrystallized from DMF. Yield 0.053 g (46%); m.p. 208–210°C. FAB mass spectrum: *m/z* 1818.6 $[Pd_2(dppcb)(PMe_2Ph)_4](BF_4)_3^+$, 1593.7 $[Pd_2(dppcb)(PMe_2Ph)_3](BF_4)_2^+$. *Anal.* Found: C, 52.8; H, 4.8. Calc. for $C_{84}H_{88}B_4F_{16}P_8Pd_2$: C, 53.0; H, 4.7%.

2.4. X-ray data collection, structure determination and refinement

Details of the crystal and data collection are summarized in Table 1. The empirical absorption corrections were based on ψ-scans of nine reflections, respectively ($\chi = 78$–$102°$, 360° scans in 10° steps in ψ) [13]. All structure determination calculations were carried out using SHELXTL NT 5.10 including SHELXS-97 [14] and SHELXL-97 [15]. Final refinement on F^2 was carried out with anisotropic thermal parameters for all non-hydrogen atoms. The hydrogen atoms were included using a riding model with isotropic *U* values depending on U_{eq} of the adjacent carbon atoms.

3. Results

*3.1. Crystal structure of $[Pt_2I_4(trans\text{-}dppen)_2]$ (**1**)*

In order to characterize definitely $[Pt_2I_4(trans\text{-}dppen)_2]$ (**1**), its solid state structure was determined by X-ray crystallography. It is a further novel example showing that homobimetallic complexes of *trans*-dppen with d^8 metals are of the type $[M_2L_4(trans\text{-}dppen)_2]$ (M = Ni, Pd, Pt; L = Cl^-, I^-, CN^-) [7,8] corresponding to structure type (a) in Scheme 1. The crystal structure of **1** contains one discrete $[Pt_2I_4(trans\text{-}dppen)_2]$ molecule and a DMF molecule with a site occupation factor of 0.75 per asymmetric unit. Views of **1** are given in Fig. 1; Table 2 contains selected bond distances and bond angles of **1**.

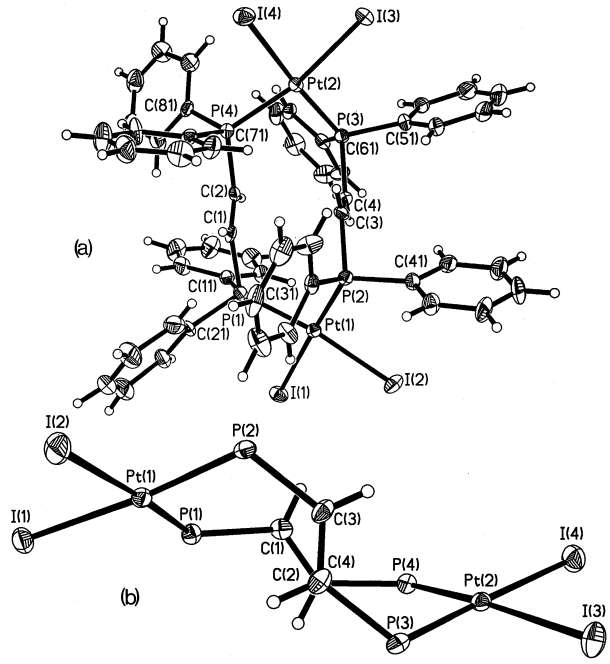


Fig. 1. (a) View of $[Pt_2I_4(trans\text{-}dppen)_2]$ (**1**), showing the atom labelling scheme; (b) C(2)···C(4) projection of $[Pt_2I_4(trans\text{-}dppen)_2]$ (**1**). Phenyl rings omitted for clarity.

The square planar coordinations in **1** are distorted, where the deviations from least-squares planes through the two coordination units are very different: Pt(1) −0.056, I(1) 0.032, I(2) −0.007, P(1) −0.007, P(2) 0.037 Å; Pt(2) −0.070, I(3) 0.109, I(4) −0.082, P(3) −0.079, P(4) 0.121 Å. This is in contrast to $[Pt_2Cl_4(trans\text{-}dppen)_2]$ (**11**) showing a largest deviation of only 0.059 Å for Pt(2) [7]. The difference can be explained by the stronger *trans* influence of I^- versus Cl^- [16,17], producing a longer mean Pt–P bond length of 2.273(5) Å in **1** than of 2.248(3) Å in **11**. Like in the case of other polyphosphines [18], the steric demands of two bridging *trans*-dppen ligands in a *cis* position (see Fig. 1(a)) lead to a 'steric pressure', which is opposed by the electronic demands of Pt(II). The weaker Pt–P bonds in **1** compared with **11** allow a release of the steric strain by larger deviations from ideal square planar coordinations in **1** than in **11**.

Owing to these differences, the angle between the coordination planes of 43.1° in **1** is larger than the corresponding parameter of 39.7° in **11**. This produces a significantly smaller Pt···Pt separation of 6.757(1) Å in **1** compared with 6.800(1) Å in **11**. The P–Pt–P angles of 96.15(11) and 96.65(10)° in **1** are significantly larger than the P–Pt–P angles of 94.77(14) and 95.08(14)° in **11**. This is a further consequence of the weaker Pt–P bonds in **1** than in **11**. This opening of the P–Pt–P angles in **1** leads to longer C(1)···C(3) and C(2)···C(4) distances of 3.093 and 3.076 Å, respectively, compared with the corresponding values of 2.837 and 2.858 Å in **11**. The C(2)···C(4) projection angle between the aliphatic double bonds (Fig. 1(b)) of 37.3° in **1** is very similar to the corresponding value of 37.6° in

Table 1
Crystallographic data for $[Pt_2I_4(trans\text{-dppen})_2]$ (**1**), $[Pd_2Cl_4(dppcb)]$ (**3**), and *trans*-$[Pd_2Cl_2(dppcb)(PMePh_2)_2](BF_4)_2$ (**10**)

	1	**3**	**10**
Empirical formula	$C_{52}H_{44}I_4P_4Pt_2 \cdot 0.75DMF$	$C_{52}H_{44}Cl_4P_4Pd_2 \cdot 4DMF$	$[C_{78}H_{70}Cl_2P_6Pd_2](BF_4)_2 \cdot 2CH_2Cl_2$
Colour	yellow–orange	colourless	colourless
Habit	prismatic	prismatic	irregular
Crystal size (mm)	0.4×0.1×0.1	0.35×0.3×0.1	1.2×0.4×0.2
a (Å)	11.701(2)	14.002(3)	13.484(2)
b (Å)	14.632(3)	13.921(3)	12.592(2)
c (Å)	18.962(4)	16.943(3)	24.452(5)
α (°)	91.53(3)		
β (°)	107.13(3)	105.72(3)	103.80(1)
γ (°)	111.57(3)		
V (Å^3)	2851.7(10)	3179.0(11)	4031.9(12)
Diffractometer	Siemens P4 (Mo Kα radiation)		
Crystal system	triclinic	monoclinic	monoclinic
Space group	$P\bar{1}$	$P2_1/n$	$P2_1/c$
Z	2	2	2
Scan type	ω	ω	ω
No. reflections collected	16142	8527	11222
No. independent reflections	13932	7052	9288
No. observed reflections ($I>3\sigma(I)$)	5210	3106	5579
R_{int}	0.024	0.021	0.029
Completeness (%)	83.7 (θ=1.98–30.00°)	96.6 (θ=2.10–27.49°)	91.0 (θ=2.02–28.50°)
Index ranges	$-1\le h\le 14$, $-20\le k\le 19$, $-26\le l\le 25$	$-1\le h\le 18$, $-1\le k\le 18$, $-21\le l\le 21$	$-1\le h\le 18$, $-1\le k\le 16$, $-31\le l\le 32$
No. parameters	604	374	470
GOF on F^2	0.99	1.02	1.03
Final R indices (observed data)			
R_1 [a]	0.0418	0.0387	0.0428
wR_2 [b]	0.1132	0.1202	0.1149
Largest difference peak (e Å^{-3})	1.45	0.69	1.03
Transmission	0.602–1.000	0.630–0.971	0.650–1.000
T (K)	213	173	213

[a] $R_1=(\sum||F_o|-|F_c||)/\sum|F_o|$.
[b] $wR_2=[(\sum w(F_o^2-F_c^2)^2)/\sum w(F_c^2)^2]^{1/2}$ with weight $=1/[\sigma^2(F_o^2)+(xP)^2+yP]$; $x=0.0414$, $y=0$ for **1**; $x=0.0497$, $y=3.50$ for **3**; $x=0.0564$, $y=10.25$ for **10**; $P=(F_o^2+2F_c^2)/3$.

$[Pd_2Cl_4(trans\text{-dppen})_2]$ [7], but different from the value of 34.8° in **11**. Comparable differences in the orientations of diphosphine-bridges have been observed in the X-ray structures of a series of dimers containing dppa [1–3]. All Pt–I bond lengths in **1** (see Table 2) are located within the typical range also found in $[Pt_2I_4(dppa)_2]$ [2]. Owing to the large P–Pt–P angles in **1**, the I–Pt–I angles of 87.62(5) and 85.81(4)° are significantly reduced to values below 90°, where the same effect is present in $[Pt_2I_4(dppa)_2]$. The X-ray structure of **1** reveals that replacement of Cl^- in **11** by I^- in **1** leads to a fine tuning of the actual structure also with respect to the orientations of the aliphatic double bonds. Since the intramolecular [2+2] photocycloaddition of these double bonds in **11** produces the new tetradentate phosphine dppcb [7], the observed fine tuning is important for the development of further Pt(II) templates, which will be used for the production of other new ligands.

3.2. Crystal structure of $[Pd_2Cl_4(dppcb)]$ (3)

The two conformations of $[Pt_2Cl_4(dppcb)]$ (**12**) seen in its X-ray structure [7] reveal the amount by which this molecular structure varies in the solution phase as the local solvent field varies with time, if we assume as a first approximation that the forces on the molecule in solution are of the same order as those in the solid [19]. Since this flexibility could influence the catalytic properties of homobimetallic complexes of dppcb, the solid state structure of **3** was also determined by X-ray crystallography. It confirms that compounds of the type $[Pd_2L_4(dppcb)]$, where L is Cl^-, CN^- or NO_2^- (**3–5**), $[Pd_2(dppcb)(phen)_2](BF_4)_4$ (**6**), and $[Pd_2(dppcb)(bipy)_2](BF_4)_4$ (**7**) correspond to structure types (c) and (d) in Scheme 1. The crystal structure of **3** consists of two discrete $[Pd_2Cl_4(dppcb)]$ molecules and eight molecules of DMF per unit cell. $[Pd_2Cl_4(dppcb)]$ is located on a centre of symmetry. Views of **3** are given in Fig. 2; Table 3 contains selected bond distances and bond angles of **3**.

As in the case of **12**, owing to crystallographic constraints produced by the centre of symmetry, the cyclobutane ring is completely planar in **3**. The mean C–C bond length of 1.557(4) Å in **3** is, within statistical significance, identical with the same parameter of 1.548(7) Å in **12** and within the usual range of 1.545–1.607 Å [20,21]. The 'envelope'-fold-

Table 2
Selected bond lengths (Å) and angles (°) for $[Pt_2I_4(trans\text{-dppen})_2]$ (**1**)

Pt(1)–P(1)	2.282(3)
Pt(1)–P(2)	2.262(3)
Pt(1)–I(1)	2.6649(13)
Pt(1)–I(2)	2.6355(13)
Pt(2)–P(3)	2.280(3)
Pt(2)–P(4)	2.267(3)
Pt(2)–I(3)	2.6253(13)
Pt(2)–I(4)	2.6450(11)
P(1)–C(11)	1.800(12)
P(1)–C(21)	1.814(10)
P(1)–C(1)	1.826(11)
P(2)–C(31)	1.811(11)
P(2)–C(41)	1.828(11)
P(2)–C(3)	1.804(10)
P(3)–C(51)	1.833(11)
P(3)–C(61)	1.813(11)
P(3)–C(4)	1.834(10)
P(4)–C(71)	1.837(11)
P(4)–C(81)	1.835(12)
P(4)–C(2)	1.826(10)
C(1)–C(2)	1.341(13)
C(3)–C(4)	1.289(14)
P(1)–Pt(1)–P(2)	96.15(11)
P(2)–Pt(1)–I(2)	90.37(8)
P(1)–Pt(1)–I(2)	172.98(7)
P(2)–Pt(1)–I(1)	175.30(7)
P(1)–Pt(1)–I(1)	85.68(8)
I(1)–Pt(1)–I(2)	87.62(5)
P(3)–Pt(2)–P(4)	96.65(10)
P(4)–Pt(2)–I(3)	168.63(7)
P(3)–Pt(2)–I(3)	90.64(8)
P(4)–Pt(2)–I(4)	86.97(8)
P(3)–Pt(2)–I(4)	176.37(7)
I(3)–Pt(2)–I(4)	85.81(4)
C(11)–P(1)–C(21)	106.4(6)
C(11)–P(1)–C(1)	100.3(5)
C(21)–P(1)–C(1)	101.2(5)
C(11)–P(1)–Pt(1)	115.1(4)
C(21)–P(1)–Pt(1)	114.0(4)
C(1)–P(1)–Pt(1)	118.0(3)
C(3)–P(2)–C(31)	106.0(6)
C(3)–P(2)–C(41)	100.1(5)
C(31)–P(2)–C(41)	103.7(5)
C(3)–P(2)–Pt(1)	115.2(4)
C(31)–P(2)–Pt(1)	109.8(4)
C(41)–P(2)–Pt(1)	120.6(4)
C(51)–P(3)–C(61)	102.6(6)
C(61)–P(3)–C(4)	104.9(5)
C(51)–P(3)–C(4)	100.6(5)
C(61)–P(3)–Pt(2)	114.6(4)
C(51)–P(3)–Pt(2)	117.7(4)
C(4)–P(3)–Pt(2)	114.6(4)
C(2)–P(4)–C(81)	100.3(5)
C(2)–P(4)–C(71)	103.1(5)
C(71)–P(4)–C(81)	107.2(5)
C(2)–P(4)–Pt(2)	116.7(3)
C(81)–P(4)–Pt(2)	111.1(4)
C(71)–P(4)–Pt(2)	116.8(4)
C(2)–C(1)–P(1)	120.2(8)
C(1)–C(2)–P(4)	124.4(9)
C(4)–C(3)–P(2)	124.7(10)
C(3)–C(4)–P(3)	124.9(9)

ing of 163.1° for the five-membered rings in **3** (see Fig. 2(b)) is in between the corresponding values of 153.1 and 168.3° for conformations A and B of **12**, respectively. This is reflected in the Pd(1)···Pd(1A) separation of 7.246(1) Å in **3** compared with the Pt···Pt separations of 6.952(1) and 7.327(1) Å in A and B. The same is true for the P(1)–Pd(1)–P(2) angle of 86.40(4)°, which is also in between the P–Pt–P chelate angles of 85.19(11)° in A and 89.11(10)° in B. Thus it seems likely that the effects leading to the two conformations in **12** are balanced in the solid state structure of **3**. The occurrence of two conformations in **12** has been explained by a subtle energetic balance between the preference of dppcb to release the strain of the five-membered rings by a larger 'envelope'-folding in A and the preference of Pt(II) for an ideal square planar environment in B [7]. However, the mean Pd–P bond length of 2.2372(8) Å in **3** is significantly larger than the mean Pt–P bond length of 2.222(2) Å in **12**. This reduces the strain of the five-membered rings in **3**. Furthermore, the square planar stabilization energy is smaller in **3** than in **12** [22]. Both differences lead to the occurrence of only one balanced conformation in **3**. This different flexibility in homobimetallic complexes of dppcb could be important for their catalytic application.

As a consequence of the reduced square planar stabilization energy in **3**, the Pd(1) atom deviates 0.082 Å from a least-squares plane through Cl(1), Cl(2), P(1), and P(2) (see Fig. 2(b)). Comparable large deviations of the Pd atoms in square planar complexes of tetradentate phosphines are well

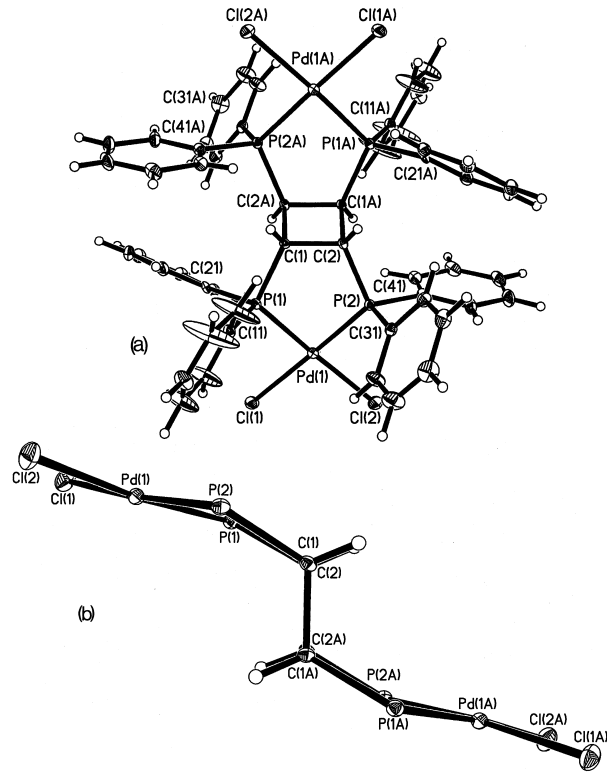


Fig. 2. (a) View of $[Pd_2Cl_4(dppcb)]$ (**3**), showing the atom labelling scheme; (b) view of $[Pd_2Cl_4(dppcb)]$ (**3**) with the cyclobutane plane perpendicular to the projection plane. Phenyl rings omitted for clarity.

Table 3
Selected bond lengths (Å) and angles (°) for $[Pd_2Cl_4(dppcb)]$ (**3**)

Pd(1)–P(1)	2.2402(12)
Pd(1)–P(2)	2.2341(12)
Pd(1)–Cl(1)	2.3638(12)
Pd(1)–Cl(2)	2.3702(13)
P(1)–C(11)	1.815(5)
P(1)–C(21)	1.813(4)
P(1)–C(1)	1.860(4)
P(2)–C(31)	1.829(5)
P(2)–C(41)	1.811(5)
P(2)–C(2)	1.854(4)
C(1)–C(2)	1.558(5)
C(1)–C(2) [a]	1.556(5)
P(1)–Pd(1)–P(2)	86.40(4)
P(1)–Pd(1)–Cl(1)	90.68(5)
P(2)–Pd(1)–Cl(1)	75.29(5)
P(1)–Pd(1)–Cl(2)	173.69(5)
P(2)–Pd(1)–Cl(2)	88.90(5)
Cl(1)–Pd(1)–Cl(2)	93.74(5)
C(11)–P(1)–C(21)	107.4(2)
C(21)–P(1)–C(1)	104.54(19)
C(11)–P(1)–C(1)	105.4(2)
C(21)–P(1)–Pd(1)	117.46(16)
C(11)–P(1)–Pd(1)	111.01(15)
C(1)–P(1)–Pd(1)	110.22(13)
C(31)–P(2)–C(41)	107.3(2)
C(41)–P(2)–C(2)	108.2(2)
C(31)–P(2)–C(2)	102.0(2)
C(41)–P(2)–Pd(1)	116.26(16)
C(31)–P(2)–Pd(1)	111.36(15)
C(2)–P(2)–Pd(1)	110.71(13)
C(2)[a]–C(1)–C(2)	90.4(3)
C(2)[a]–C(1)–P(1)	115.7(3)
C(2)–C(1)–P(1)	114.4(3)
C(1)[a]–C(2)–C(1)	89.6(3)
C(1)[a]–C(2)–P(2)	118.7(3)
C(1)–C(2)–P(2)	113.4(3)

[a] Symmetry transformations used to generate equivalent atoms: $-x+2, -y, -z$.

known and seem to be typical for Pd(II) [9,23]. The Pd–P bond lengths of 2.2402(12) and 2.2341(12) Å in **3** are in the typical range reported previously [9,24] for square planar Pd(II) complexes containing also chelating phosphines *trans* to chlorides. The chelate angle of 86.40(4)° in **3** is comparable to the corresponding parameters of 85.82(3)° in $[Pd(CN)_2$(*cis*-dppen)] [8] and 85.4(1)° in $[Pd(SCN)_2$-(*cis*-dppen)] [25], where *cis*-dppen is *cis*-1,2-bis-(diphenylphosphino)ethene. However, in contrast to **3** and analogous to **12**, $[PdCl_2$(dppe)] shows two conformations with chelate angles of 85.82(7) and 88.3(1)°, where dppe is 1,2-bis(diphenylphosphino)ethane [24,26]. Comparable to $[PdI_2$(*cis*-dppen)]·I_2 [27], in **3** the general impression is that despite the relatively rigid ligand backbone there is little strain in the molecule. The shorter M–P distances in the Pt species **12** are consistent with the stronger Pt–P bonding relative to Pd in **3** [28] and with the 'relativistic or Lanthanide contraction' [8].

3.3. Investigation of *1*–*9* in the solution state

The $^{195}Pt\{^1H\}$ and $^{31}P\{^1H\}$ NMR parameters of compounds **1**–**9** are summarized in Table 4. The NMR data for **1** are consistent with structure (a) in Scheme 1 showing four equivalent phosphorus atoms. This means that the two different diphosphine bridges indicated in the X-ray structure of **1** (see Fig. 1) are equalized in solution at room temperature. The ^1J(Pt,P) value of 3330 Hz in **1** is reduced compared with the analogous parameter of 3550 Hz in **11** in agreement with the stronger *trans* influence of I^- versus Cl^- [16,17] and with the difference of the mean Pt–P bond lengths (see above). The simultaneous presence of this ^1J(Pt,P) value in **1** typical for *trans* iodide and of ^4J(Pt,P) of 41 Hz confirms that complexes of the type $[M_2L_4$(*trans*-dppen)$_2]$ (M = Ni, Pd, Pt; L = Cl^-, I^-, CN^-) [7,8] are also binuclear in solution.

The clean preparation of the Pt(IV) complex **2** by halogenation of the corresponding Pt(II) species **11** indicates that no drastic structural change occurs [29]. This is confirmed by the NMR data for **2**, which are consistent with structure (b) in Scheme 1 also showing four equivalent phosphorus atoms. The δ(Pt) value of −3156 in **2** is comparable with the corresponding parameter of −3226 in the analogous complex $[Pt_2Cl_8(dppa)_2]$ [2]. The same is true for the ^1J(Pt,P) value of 2093 Hz in **2** located in the typical range for a phosphine *trans* to chloride in a Pt(IV) compound [2,16,17]. This is in agreement with *cis* diphosphine bridges, where as in the case of **1** the simultaneous presence of this ^1J(Pt,P) value in **2** typical for *trans* chloride and of ^4J(Pt,P) of 34 Hz confirms the binuclear structure of **2** in solution.

The single $^{31}P\{^1H\}$ NMR resonances for **3**–**7** indicate four equivalent phosphorus atoms in all these compounds, which is consistent with structures (c) and (d) in Scheme 1. The δ(P) downfield shifts of **3**–**7** compared with **1** and **2** show the typical five-ring contribution for chelating dppcb [7,30]. Thus the solution structure of **3** appears to be the same as its solid state structure. In **4** the presence of the cyanides is clearly indicated in the IR spectrum by the C≡N stretching frequency at 2135 cm^{-1}. It is normally found for $[Pd(CN)_2$(monophosphine)$_2]$ complexes that the *cis* isomer is thermodynamically more stable than the *trans* [31], leading to higher C≡N stretching vibrations for cyanides

Table 4
$^{195}Pt\{^1H\}$ and $^{31}P\{^1H\}$ NMR data for **1**–**9** [a]

Compound	δ(Pt)	δ(P)	^1J(Pt,P)	^4J(Pt,P)	^2J(P,P)$_{trans}$
1		1.9	3330	41	
2	−3156t	−6.8	2093	34	
3		78.0			
4		63.2			
5		58.8			
6		85.0			
7		81.0			
8		83.6d			309
		8.4d			309
9		74.0d			307
		10.0d			307

[a] *J* values in Hz. d, doublet; t, triplet. Spectra were run at 298 K. The following solvents were used: CH_2Cl_2 (**1**, **2**, **8**) and DMF (**3**–**7**, **9**).

trans to phosphines [8,32,33] than for cyanides *trans* to cyanides [34]. The stretching value in **4** is in agreement with *cis*-dicyanides. In the case of **5** the direct replacement of the chlorides of **3** by nitrites is not possible, though this transformation has been shown to occur via associative *cis* attack on chloride by nitrite [35]. For **5** the removal of the chlorides from **3** by precipitating AgCl with $AgBF_4$ was necessary for the completion of the reaction with nitrite. The δ(P) value of 77.4 for a DMF solution of the resulting cationic intermediate is consistent with $[Pd_2(dppcb)(DMF)_4](BF_4)_4$, which is analogous to the corresponding Pt(II) complex [7]. The IR spectrum of **5** shows $\nu_a(NO_2)$, $\nu_s(NO_2)$, and δ(ONO) at 1370, 1318, and 814 cm^{-1}, respectively, clearly indicating N-bonded NO_2^- leading to a unidentate nitro complex [36]. This is confirmed by the comparable vibrations in $[PtCl(NO_2)(cis\text{-dppen})]$ [32], where the unidentate N-bonded coordination of NO_2^- has been proven by an X-ray structure analysis [37]. Also for **6** and **7** the removal of the chlorides from **3** by the above procedure was necessary for the completion of the reaction with phen or bipy. The single $^{31}P\{^1H\}$ NMR signals for **6** and **7**, respectively, are consistent with structure (d) in Scheme 1 shown for the phen complex, which is confirmed by the analogous structure found in the corresponding Pt(II) compounds [7]. These complexes are further examples of the tendency for multiple five-ring formation [38].

The reaction of **3** with monophosphines strongly depends on the number of chlorides removed as AgCl. The removal of two chlorides and subsequent treatment with $PMePh_2$ leads to **8**. The $^{31}P\{^1H\}$ NMR data for **8** are in agreement with structure (e) in Scheme 1. The signal with δ(P) of 83.6 is attributed to chelating dppcb showing the typical downfield five-ring contribution [7,30] and the signal with δ(P) of 8.4 to coordinated $PMePh_2$. The $^2J(P,P)_{trans}$ value of 309 Hz is located within the typical range [8,16,23]. However, after isolation of **8** the FAB mass spectrum indicates a strong peak at *m/z* of 1528.3 consistent with $[Pd_2Cl(dppcb)(PMePh_2)_2](BF_4)^+$ and its elemental analysis is in agreement with the loss of two coordinated $PMePh_2$ groups. Since the removal of all chlorides from **3** and subsequent treatment with $PMePh_2$ led to no pure product, the solid state structure of **10** has been clarified by an X-ray structure analysis (see below). In the case of PMe_2Ph the complete replacement of the chlorides in **3** by this monophosphine leading to **9** has been successful. The $^{31}P\{^1H\}$ NMR data for **9** are consistent with structure (e) in Scheme 1. The downfield shifted signal with δ(P) of 74.0 is again attributed to chelating dppcb [7,30] and the signal with δ(P) of -10.0 to coordinated PMe_2Ph. The $^2J(P,P)_{trans}$ value of 307 Hz is nearly identical with the corresponding parameter in **8** and is also located within the typical range [8,16,23]. After isolation of **9** the FAB mass spectrum and elemental analysis are in full agreement with its formulation as $[Pd_2(dppcb)(PMe_2Ph)_4](BF_4)_4$.

The ^1H NMR resonances (CH_2Cl_2-d^2) for the aromatic protons in **1**–**9** occur at 6.5–8.2. In **1** and **2** the ^1H NMR signals of the ethene bridges are obscured by these aromatic resonances. For **3**–**9** broad ^1H NMR signals of the cyclobutane protons are observed at 4.2–4.6. In **8** and **9** the methyl group resonances of coordinated $PMePh_2$ and PMe_2Ph, respectively, occur at 2.1. For **3**–**9** the integrated intensities are in agreement with the proposed structures.

3.4. Crystal structure of trans-$[Pd_2Cl_2(dppcb)(PMePh_2)_2](BF_4)_2$ (10)

In order to characterize definitely the product obtained after isolation of **8**, its solid state structure was determined by an X-ray structure analysis. It shows that this product consists of *trans*-$[Pd_2Cl_2(dppcb)(PMePh_2)_2](BF_4)_2$ (**10**) corresponding to structure type (f) in Scheme 1. The crystal structure of **10** consists of two discrete *trans*-$[Pd_2Cl_2(dppcb)(PMePh_2)_2]^{2+}$ cations, four $(BF_4)^-$ anions, and four molecules of CH_2Cl_2 per unit cell. *Trans*-$[Pd_2Cl_2(dppcb)(PMePh_2)_2]^{2+}$ is located on a centre of symmetry. Views of the cation of **10** are given in Fig. 3; Table 5 contains selected bond distances and bond angles of **10**.

As in the cases of **3** and **12**, owing to crystallographic constraints produced by the centre of symmetry, the cyclobutane ring is completely planar in **10**. The mean C–C bond length of 1.556(3) Å in **10** is, within statistical significance, identical with the same parameters in **3** and **12** (see above)

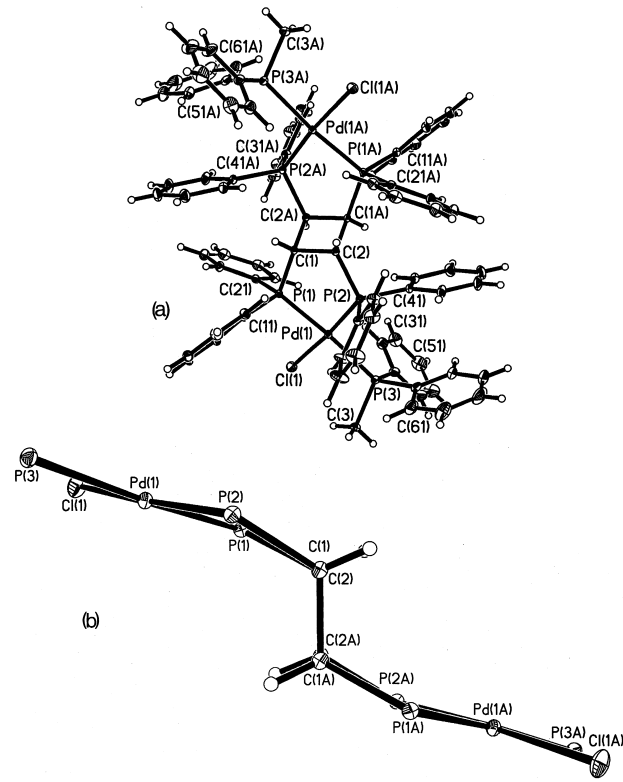


Fig. 3. (a) View of the cation of *trans*-$[Pd_2Cl_2(dppcb)(PMePh_2)_2](BF_4)_2$ (**10**), showing the atom labelling scheme; (b) view of the cation of *trans*-$[Pd_2Cl_2(dppcb)(PMePh_2)_2](BF_4)_2$ (**10**) with the cyclobutane plane perpendicular to the projection plane. Phenyl rings and methyl groups omitted for clarity.

Table 5
Selected bond lengths (Å) and angles (°) for *trans*-[Pd_2Cl_2(dppcb)($PMePh_2$)$_2$](BF_4)$_2$ (**10**)

Pd(1)–P(1)	2.2978(8)
Pd(1)–P(2)	2.2589(8)
Pd(1)–P(3)	2.3753(9)
Pd(1)–Cl(1)	2.3476(8)
P(1)–C(11)	1.810(3)
P(1)–C(21)	1.807(3)
P(1)–C(1)	1.855(3)
P(2)–C(31)	1.815(3)
P(2)–C(41)	1.821(3)
P(2)–C(2)	1.869(3)
P(3)–C(51)	1.813(4)
P(3)–C(61)	1.818(4)
P(3)–C(3)	1.820(3)
C(1)–C(2)	1.559(4)
C(1)–C(2) [a]	1.552(4)
P(1)–Pd(1)–P(2)	85.94(3)
P(1)–Pd(1)–Cl(1)	88.33(3)
P(2)–Pd(1)–Cl(1)	173.76(3)
P(1)–Pd(1)–P(3)	175.22(3)
P(2)–Pd(1)–P(3)	97.77(3)
Cl(1)–Pd(1)–P(3)	87.82(3)
C(11)–P(1)–C(21)	107.07(14)
C(11)–P(1)–C(1)	105.66(14)
C(21)–P(1)–C(1)	106.61(13)
C(11)–P(1)–Pd(1)	108.53(10)
C(21)–P(1)–Pd(1)	117.58(11)
C(1)–P(1)–Pd(1)	110.71(9)
C(31)–P(2)–C(41)	109.63(15)
C(31)–P(2)–C(2)	102.23(14)
C(41)–P(2)–C(2)	106.48(13)
C(31)–P(2)–Pd(1)	112.32(11)
C(41)–P(2)–Pd(1)	114.45(11)
C(2)–P(2)–Pd(1)	110.89(9)
C(51)–P(3)–C(61)	105.92(18)
C(51)–P(3)–C(3)	104.49(18)
C(61)–P(3)–C(3)	102.41(18)
C(51)–P(3)–Pd(1)	110.36(12)
C(61)–P(3)–Pd(1)	121.40(12)
C(3)–P(3)–Pd(1)	110.77(12)
C(2)[a]–C(1)–C(2)	89.5(2)
C(2)[a]–C(1)–P(1)	115.4(2)
C(2)–C(1)–P(1)	114.59(19)
C(1)[a]–C(2)–C(1)	90.5(2)
C(1)[a]–C(2)–P(2)	119.0(2)
C(1)–C(2)–P(2)	114.42(19)

[a] Symmetry transformations used to generate equivalent atoms: $-x+1, -y, -z$.

and also within the usual range [20,21]. However, the smaller 'envelope'-folding of 165.7° for the five-membered rings in **10** (see Fig. 3(b)) compared with the same parameter of 163.1° in **3**, already indicates strain in **10**. Though this produces a significantly larger Pd(1)···Pd(1A) separation of 7.378(1) Å in **10** than of 7.246(1) Å in **3**, the alignment of the phenyl rings containing C(61), C(41), and C(21A) in **10** (see Fig. 3(a)) is necessary to overcome unfavourable repulsive interactions. This stacking of aromatic rings has been observed in complexes of nucleobases also mediated by Pd(II) [39]. The *cis* isomer of **10** is destabilized by these interactions, since one side of the molecule becomes too crowded. A comparable preference of the *trans* isomer has been found for *trans*-[$PdCl(\mu\text{-}PPh_2)(PPh_2H)]_2$ [40]. Also the significantly smaller P(1)–Pd(1)–P(2) chelate angle of 85.94(3)° in **10** compared with 86.40(4)° in **3** is indicative of strain, presumably due to the 'steric pressure' [18] produced by the alignment of the phenyl rings.

The Pd(1)–P(1) bond length of 2.2978(8) Å is significantly larger than the Pd(1)–P(2) bond length of 2.2589(8) Å in **10**, in agreement with the stronger *trans* influence of a phosphine versus chloride [28,41,42]. This difference of Pd–P bond lengths is comparable with the corresponding parameters of 2.284(1) and 2.244(1) Å in [$PdCl(Ph_2PNPPh_2)(PEt_3)$] [12]. The same is true for the Pd–monophosphine bond lengths of 2.3753(9) Å in **10** and 2.366(1) Å in [$PdCl(Ph_2PNPPh_2)(PEt_3)$]. Like in **3** and typical for Pd(II) [9,23], the Pd(1) atom deviates 0.056 Å from a least-squares plane through Cl(1), P(1), P(2), and P(3) (see Fig. 3(b)). There is considerable steric blocking on one side of each coordination unit by the cyclobutane ring and the phenyl groups in **10** (see Fig. 3(a)). This causes an incoming fifth ligand to attach on the other side of the square plane leading to a square pyramidal coordination [43]. Together with the observed steric crowding in **10** leading to the alignment of the phenyl rings, this could initiate the loss of two $PMePh_2$ groups from **8** producing **10**.

When the crystals of **10** are redissolved in CH_2Cl_2/DMF (v/v = 1:1), the $^{31}P\{^1H\}$ NMR spectrum shows three different resonances consistent with the solid state structure of **10**. The single resonance at 81.1, showing the typical downfield five-ring contribution, is attributed to the phopshorus of dppcb *trans* to chloride. Furthermore, two doublets occur at 82.5 (dppcb) and 12.2 ($PMePh_2$), where $^2J(P,P)_{trans}$ is 430 Hz. However, several other signals are also observed in this spectrum indicating that **10** is not stable in solution.

4. Discussion

As already mentioned, some of the new complexes presented in this paper are potentially catalytic active compounds for the alternating CO/ethene copolymerization [10]. In this respect the rigidity of the cyclobutane backbone in homobimetallic complexes of dppcb with Pd(II) together with the orientations of the phenyl rings could influence the activity of these catalysts. Indeed preliminary experiments show that dppcb has beneficial effects on the copolymerization rate [44]. Obviously, like the tripodal the dppcb polyphosphine-control element is so effective that the combined bulk of the ligand–metal assembly and substrate operates to exclude alternatives so that one reaction path is specifically favoured [45]. However, the nature of the metal centre must be finely tuned, depending on the type of reaction involved.

In the case of Rh(I) the binuclear tetraligate single-bridging coordination of dppcb [46] leads to 'mechanical coupling' [47], where preliminary X-ray results show that steric interactions of the phenyl rings comparable with **10** produce

different coordination sites. For the tetradentate phosphine 1,2,4,5-tetrakis(diphenylphosphino)benzene, which is comparable with dppcb, any intramolecular electron transfer in the excited states of its dimetallic complexes also containing Pd(II) relies less on the presence of a low-lying, empty σ* orbital in the ligand than on superexchange or tunnelling interactions [48]. Homobimetallic complexes of dppcb with Ru(II) also show these interactions, since preliminary experiments indicate that their photochemical behaviour is completely different from analogous compounds containing diphosphines.

Since $[Pd(CH_3CN)_4](BF_4)_2$ has been found to catalyse the polymerization of acetylenes and olefins [49], the complex $[Pd_2(dppcb)(DMF)_4](BF_4)_4$ presented above could show comparable catalytic properties. Furthermore, Pd(II) complexes of $PhP(CH_2CH_2PPh_2)_2$ catalyse the electrochemical reduction of CO_2 to CO [18,50]. In this paper it is shown that compounds of the type $[Pd_2(dppcb)(monophosphine)_4]^{4+}$ are possible. Therefore, also $[Pd(dppcb)_2]^{2+}$ could be prepared. Similar to the chelating bis(phosphine) 3,5-bis[(diphenylphosphino)methyl]pyridine, which forms a trinuclear Pd complex, a metalloligand like $[Pd(dppcb)_2]^{2+}$ offers a straightforward approach for the generation of oligonuclear and multinuclear complexes [51]. Further work on this is in progress.

Supplementary data

Details on the structure determinations, atomic fractional coordinates and other relevant data are obtainable from the Cambridge Crystallographic Data Centre, 12 Union Road, Cambridge CB2 1EZ, UK on request (fax: +44-1223-336033; e-mail: deposit@ccdc.cam.ac.uk). The crystal structures of $[Pt_2I_4(trans\text{-}dppen)_2]$ (**1**), $[Pd_2Cl_4(dppcb)]$ (**3**), and *trans*-$[Pd_2Cl_2(dppcb)(PMePh_2)_2](BF_4)_2$ (**10**) have been allocated the deposition numbers CCDC 137542, CCDC 137543, and CCDC 137544, respectively.

Acknowledgements

We thank the Fonds zur Förderung der wissenschaftlichen Forschung, Austria, for financial support.

References

[1] H.C. Clark, G. Ferguson, P.N. Kapoor, M. Parvez, Inorg. Chem. 24 (1985) 3924.
[2] W. Oberhauser, C. Bachmann, T. Stampfl, P. Brüggeller, Inorg. Chim. Acta 256 (1997) 223.
[3] G. Hogarth, T. Norman, Polyhedron 15 (1996) 2859.
[4] J.M. Vila, M. Gayoso, M.T. Pereira, J.M. Ortigueira, A. Fernandez, N.A. Bailey, H. Adams, Polyhedron 12 (1993) 171.
[5] J.M. Vila, M. Gayoso, A. Fernandez, N.A. Bailey, H. Adams, J. Organomet. Chem. 448 (1993) 233.
[6] R.B. King, P.N. Kapoor, Inorg. Chem. 11 (1972) 1524.
[7] W. Oberhauser, C. Bachmann, T. Stampfl, R. Haid, C. Langes, H. Kopacka, A. Rieder, P. Brüggeller, Inorg. Chim. Acta 290 (1999) 167.
[8] W. Oberhauser, C. Bachmann, T. Stampfl, R. Haid, C. Langes, A. Rieder, P. Brüggeller, Polyhedron 17 (1998) 3211.
[9] M.R. Mason, C.M. Duff, L.L. Miller, R.A. Jacobson, J.G. Verkade, Inorg. Chem. 31 (1992) 2746.
[10] E. Drent, P.H.M. Budzelaar, Chem. Rev. 96 (1996) 663.
[11] M. Formica, C. Carfagna, G. Gatti, A. Musco, 33rd Int. Conf. on Coordination Chemistry, Florence, Italy, August 30–September 4, 1998, Book of Abstracts, p. 470.
[12] M. Gómez, G. Muller, J. Sales, X. Solans, J. Chem. Soc., Dalton Trans. (1993) 221.
[13] A.C.T. North, D.C. Phillips, F.S. Mathews, Acta Crystallogr., Sect. A 24 (1968) 351.
[14] G.M. Sheldrick, Acta Crystallogr., Sect. A 46 (1990) 467.
[15] G.M. Sheldrick, SHELXL-97, a computer program for crystal structure determination, University of Göttingen, Germany, 1997.
[16] P.S. Pregosin, R.W. Kunz, in: P. Diehl, E. Fluck, R. Kosfeld (Eds.), NMR Basic Principles and Progress, vol. 16, Springer, Berlin, 1979, p. 16
[17] E.G. Hope, W. Levason, N.A. Powell, Inorg. Chim. Acta 115 (1986) 187.
[18] H.A. Mayer, W.C. Kaska, Chem. Rev. 94 (1994) 1239.
[19] A. Martin, A.G. Orpen, J. Am. Chem. Soc. 118 (1996) 1464.
[20] H.-L. Ji, J.H. Nelson, A. DeCian, J. Fischer, C. Li, C. Wang, B. McCarty, Y. Aoki, J.W. Kenny III, L. Solvjic, E.B. Milosavljevic, J. Organomet. Chem. 529 (1997) 395.
[21] R. Gilardi, C. George, J.L. Flippen-Anderson, Acta Crystallogr., Sect. C 48 (1992) 1680.
[22] J.A. Rahn, D.J. O'Donnell, A.R. Palmer, J.H. Nelson, Inorg. Chem. 28 (1989) 2631.
[23] W. Oberhauser, C. Bachmann, P. Brüggeller, Polyhedron 14 (1995) 787.
[24] W.L. Steffen, G.L. Palenik, Inorg. Chem. 15 (1976) 2432.
[25] A.J. Paviglianiti, D.J. Minn, W.C. Fultz, J.L. Burmeister, Inorg. Chim. Acta 159 (1989) 65.
[26] S. Singh, N.K. Jha, P. Narula, T.P. Singh, Acta Crystallogr., Sect. C 51 (1995) 593.
[27] L.R. Gray, D.J. Gulliver, W. Levason, M. Webster, Inorg. Chem. 22 (1983) 2362.
[28] S.E. Saum, S.A. Laneman, G.G. Stanley, Inorg. Chem. 29 (1990) 5065.
[29] F.P. Fanizzi, G. Natile, M. Lanfranchi, A. Tiripicchio, F. Laschi, P. Zanello, Inorg. Chem. 35 (1996) 3173.
[30] P.E. Garrou, Chem. Rev. 81 (1981) 229.
[31] B. Bendiksen, W.C. Riley, M.W. Babich, J.H. Nelson, R.A. Jacobson, Inorg. Chim. Acta 57 (1982) 29.
[32] W. Oberhauser, C. Bachmann, P. Brüggeller, Inorg. Chim. Acta 238 (1995) 35.
[33] P. Brüggeller, Z. Naturforsch., Teil B 41 (1986) 1561.
[34] A.L. Balch, B.J. Davis, E.Y. Fung, M.M. Olmstead, Inorg. Chim. Acta 212 (1993) 149.
[35] P. Ghosh, A. Chakravorty, Inorg. Chem. 36 (1997) 64.
[36] K. Nakamoto, Infrared and Raman Spectra of Inorganic and Coordination Compounds, Wiley, New York, 5th edn., 1997, Part B, p. 49.
[37] C. Bachmann, C. Langes, T. Stampfl, R. Haid, H. Kopacka, K.-H. Ongania, P. Brüggeller, to be published.
[38] A. Castiñeiras, E. Bermejo, D.X. West, L.J. Ackerman, J. Valdés-Martínez, S. Hernández-Ortega, Polyhedron 18 (1999) 1463.
[39] M. Mizutani, I. Kubo, K. Jitsukawa, H. Masuda, H. Einaga, Inorg. Chem. 38 (1999) 420.
[40] R. Giannandrea, P. Mastrorilli, C.F. Nobile, Inorg. Chim. Acta 284 (1999) 116.
[41] S.E. Saum, G.G. Stanley, Polyhedron 6 (1987) 1803.

[42] K.D. Tau, D.W. Meek, Inorg. Chem. 18 (1979) 3574.
[43] G. Dyer, J. Roscoe, Inorg. Chem. 35 (1996) 4098.
[44] C. Bianchini, H.M. Lee, A. Meli, W. Oberhauser, F. Vizza, P. Brüggeller, R. Haid, C. Langes, to be published.
[45] C. Bianchini, A. Meli, M. Peruzzini, F. Vizza, F. Zanobini, Coord. Chem. Rev. 120 (1992) 193.
[46] F.A. Cotton, B. Hong, Prog. Inorg. Chem. 40 (1992) 179.
[47] D.G. McCollum, G.P.A. Yap, A.L. Rheingold, B. Bosnich, J. Am. Chem. Soc. 118 (1996) 1365.
[48] P.-W. Wang, M.A. Fox, Inorg. Chem. 34 (1995) 36.
[49] A. Sen, T.-W. Lai, Organometallics 1 (1982) 415.
[50] D.L. DuBois, A. Miedaner, J. Am. Chem. Soc. 109 (1987) 113.
[51] A. Weisman, M. Gozin, H.-B. Kraatz, D. Milstein, Inorg. Chem. 35 (1996) 1792.

PERGAMON

www.elsevier.nl/locate/poly

Polyhedron 19 (2000) 925–929

POLYHEDRON

Syntheses and structures of two complexes with incomplete cuboidal $Mo_3Te_4^{4+}$ and $Mo_3(\mu_3\text{-}S)Te_3^{4+}$ cluster cores

Xiang Lin, Hua-Yang Chen, Li-Sheng Chi, Can-Zhong Lu, Hong-Hui Zhuang *

State Key Laboratory of Structural Chemistry, Fujian Institute of Research on the Structure of Matter, Chinese Academy of Sciences, Fuzhou, Fujian 350002, People's Republic of China

Received 16 November 1999; accepted 14 February 2000

Abstract

The reaction of tributylphosphine, benzoic acid and $Mo_3Te_7(S_2P(OPr^i)_2)_3I$ produced a new compound with triangular cluster skeleton $Mo_3Te_4^{4+}$, $Mo_3Te_4[S_2P(OPr^i)_2]_3(\mu\text{-}PhCO_2)PBu_3$ (**1**). An unexpected compound including an $Mo_3Te_3S^{4+}$ skeleton, $Mo_3(\mu_3\text{-}S)Te_3[S_2P(OPr^i)_2]_3(\mu\text{-}PhNH_2CO_2)PBu_3$ (**2**), was obtained using aminobenzoic acid instead of benzoic acid. X-ray crystallographic analysis revealed that these complexes belong to the $Mo_3E_4^{4+}$ (E = S, Se, Te) incomplete cuboidal cluster family and are dimeric through the Te···Te interaction. ^1H and ^{31}P NMR and IR spectroscopic data were also used to characterize these compounds. ©2000 Elsevier Science Ltd All rights reserved.

Keywords: Cluster compounds; Molybdenum complexes; Tellurium-rich compounds; De-tellurium reaction; Crystal structures

1. Introduction

Intensive studies have been carried out on molybdenum/tungsten chalcogenide clusters since 1985 [1–5]. Compared with sulfides and selenides, the chemistry of tellurido complexes of molybdenum and tungsten is much less developed because many traditional reagents applicable to Mo/W–S/Se systems are not simply transferable to the Mo/W–Te system, and limited progress has been made in the exploration of effective reagents or starting materials [6]. Until recently, only a few such Mo/W–Te clusters, including the triangular cluster complex $Cs_{4.5}[Mo_3Te_7(CN)_6]I_{2.5}\cdot 3H_2O$ [7] with an $Mo_3(\mu_3\text{-}Te)(\mu\text{-}Te_2)_3^{4+}$ core, the tetrahedral clusters $K_7[Mo_4Te_4(CN)_{12}]\cdot H_2O$ and $K_6[W_4Te_4(CN)_{12}]\cdot 5H_2O$ containing the $M_4(\mu_3\text{-}Te)_4^{n+}$ ($n = 5, 6$) cuboidal core [8–10], and the octahedral cluster $[Na(Py)_6]^+[W_6Te_8(Py)_6]^-\cdot Py$ and $W_6Te_8(PiP)_6\cdot 6PiP$ with a W_6Te_8 core [11], have been reported. However, the absence of the Mo_3Te_4 type cluster, of which the sulfide and selenide analogues have been well studied, has drawn our attention to conversion of the Mo_3Te_7 cluster core to Mo_3Te_4. In comparison with those compounds containing Mo_3Te_7, Mo_4Te_4 or W_6Te_8 cores, the compound with an Mo_3Te_4 core has higher reactivity since it possesses a vacant subsite and three μ-Te ligands, making it potentially a good precursor for other tellurido cluster compounds.

A convenient route to the $M_3(\mu_3\text{-}E)(\mu\text{-}E)_3^{4+}$ (M = Mo, W; E = S, Se) cluster by reaction of $M_3(\mu_3\text{-}E)(\mu\text{-}E_2)_3^{4+}$ cluster compounds with phosphine or cyanide has been reported [12–15]. Saito and co-workers considered that the $Mo_3Te_7^{4+}$ fragment has an extraordinary stability in aqueous cyanide or in CH_3OH with PEt_3 [7]. However, our experiments showed that the $Mo_3Te_7^{4+}$ cluster core is stable in CH_2Cl_2 with PPh_3, and the reaction of $Mo_3Te_7[S_2P(OPr^i)_2]_3I$ with tributylphosphine leads to transformation of the $Mo_3Te_7^{4+}$ core to the $Mo_3Te_4^{4+}$ core. Another very interesting result in our experiments is that aromatic acids might have different effects on the transformation of the $Mo_3Te_7^{4+}$ cluster core to produce a Te-capping or S-capping triangular cluster core, which has never been observed in previous studies in this field. Herein we report the syntheses and molecular structures of two cluster compounds containing $Mo_3Te_4^{4+}$ and $Mo_3(\mu_3\text{-}S)Te_3^{4+}$ cores.

2. Experimental

All manipulations were carried out under dinitrogen atmosphere using standard Schlenk techniques. The solvents were degassed prior to use. Other materials were reagent-grade purity and used without further purification. The ^{31}P NMR

* Corresponding author. Tel.: +86-591-3711368; fax: +86-591-3714946; e-mail: zhh@ms.fjirsm.ac.cn

0277-5387/00/$ - see front matter ©2000 Elsevier Science Ltd All rights reserved.
PII S0277-5387(00)00334-X

Table 1
Crystallographic data for $Mo_3Te_4[S_2P(OPr^i)_2]_3(\mu\text{-}PhCO_2)PBu_3$ and $Mo_3(\mu_3\text{-}S)Te_3[S_2P(OPr^i)_2]_3(\mu\text{-}PhNH_2CO_2)PBu_3$

Formula	$Mo_3Te_4S_6P_4O_8C_{37}H_{74}$	$Mo_3Te_3S_7P_4O_8C_{37}NH_{75}$
FW	1762.42	1680.9
Space group	$C2/c$	$P\bar{1}$
a (Å)	29.8261(3)	15.9465(2)
b (Å)	16.4363(3)	16.0576(1)
c (Å)	26.6482(6)	16.3111(3)
α (°)	90	103.508(1)
β (°)	96.218(1)	115.859(1)
γ (°)	90	100.141(1)
V (Å^3)	12986.9(6)	3465.19(8)
Z	8	2
D_{calc} (g cm^{-3})	1.803	1.611
μ (mm^{-1})	2.664	2.112
R_1, wR_2 (%) [a]	7.95, 17.24	8.66, 20.24
Weighting scheme [b]	$w^{-1}=\sigma^2(F_o^2)+(0.0858P)^2+82.0874P$	$w^{-1}=\sigma^2(F_o^2)+(0.1149P)^2$

[a] $wR_2=\sqrt{\sum w(F_o^2-F_c^2)^2/\sum w(F_o^2)^2}$.
[b] $P=(F_o^2+2F_c^2)/3$.

spectra were obtained on a Varian Unity-500 spectrometer in CH_2Cl_2 solutions with 80% H_3PO_4 as external standard in a $^{31}P\{^1H\}$ mode. UV–Vis spectra were recorded on a Varian Cary-2390 spectrophotometer in CH_2Cl_2 solutions. IR spectra were recorded on a Nicolet Magna 750 FT-IR spectrophotometer using KBr pellets (4000–500 cm^{-1}) and CsI pellets (600–120 cm^{-1}). Element analyses were carried out by the Elemental Analysis Laboratory in our institute.

Preparation of $Mo_3Te_4S_6P_4O_8C_{37}H_{74}$ (**1**): 0.195 g (0.1 mmol) $Mo_3Te_7(S_2P(OPr^i)_2)_3I$, which was prepared according to the literature [16], 0.018 g (0.15 mmol) benzoic acid and 0.3 ml tributylphosphine were heated in 30 ml mixed-solvent of CH_2Cl_2–C_2H_5OH at 40°C for 3 h. The black crystals were isolated after the solution was allowed to stand for 4 days (0.072 g, yield 41%). *Anal*. Calc. for $Mo_3Te_4[S_2P(OPr^i)_2]_3(\mu\text{-}PhCO_2)PBu_3$: C, 25.23; H, 4.23. Found: C, 25.05; H, 4.29%. IR (KBr pellet, cm^{-1}): ν 1600, 1510 (CO), 716, 677 (C_6H_5). UV–Vis (CH_2Cl_2, nm): λ 370, 620. ^{31}P NMR (200 MHz, CH_2Cl_2, H_3PO_4): δ 111.7, 85.2, 22.3.

The preparation procedure of $Mo_3Te_3S_7P_4O_8C_{37}NH_{75}$ (**2**) was the same as for complex **1** except that 2-aminobenzoic acid was used instead of benzoic acid (0.053 g, yield 32%). *Anal*. Calc. for $Mo_3(\mu_3\text{-}S)Te_3[S_2P(OPr^i)_2]_3(\mu\text{-}PhNH_2CO_2)PBu_3$: C, 26.44; H, 4.5; N, 0.83. Found: C, 26.62; H, 4.91; N, 0.88%. IR (KBr pellet, cm^{-1}): ν 1614, 1498 (CO), 3361 (NH_2), 667 (C_6H_5), 414 (Mo–(μ_3-S)). UV–Vis (CH_2Cl_2, nm): λ 337, 580. ^{31}P NMR (200 MHz, CH_2Cl_2, H_3PO_4): δ 106.0, 85.6, 17.8.

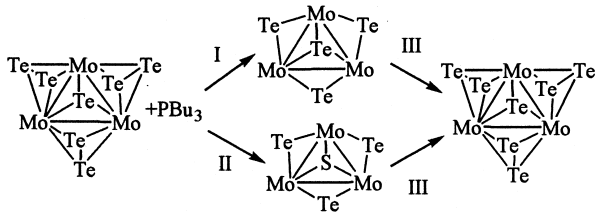
2.1. X-ray crystallography

The crystal data of complexes **1** and **2** were collected on a Siemens SMART CCD area detector diffractometer using graphite-monochromated Mo Kα radiation ($\lambda=0.71073$ Å) at 293 K, and empirical absorption correction by SADABS [17] was applied to the intensity data. Structure solution and refinement were performed on a SGI INDY workstation using the SHELXTL-5 program package [18]. The crystallographic data and refinement parameters are listed in Table 1.

3. Discussion

3.1. Synthesis

The preparation of complex **1**, $Mo_3Te_4[S_2P(OPr^i)_2]_3(\mu\text{-}PhCO_2)PBu_3$, using the abstraction of tellurium from an $Mo_3Te_7^{4+}$ cluster core to generate $Mo_3Te_4^{4+}$, is very similar to the preparation of the sulfide and selenide analogues, in which the bridging ligand is benzoic acid. This reaction can be completed at ambient temperature within a few hours. The preparation of complex **2**, $Mo_3(\mu_3\text{-}S)Te_3[S_2P(OPr^i)_2]_3(\mu\text{-}PhNH_2CO_2)PBu_3$, is similar to that of **1**, except that 2-aminobenzoic acid was employed instead of benzoic acid, and the capping tellurium atom of the cluster core was substituted by sulfur in complex **2**, which might originate from the decomposition of the DTP (dialkyldithiophosphinate) ligand. It seems plausible that there is 'competition' between sulfur and tellurium to occupy the cap site in solution, and the nature of the bridging ligand might affect the structure of the final product. We found that the formation of the $Mo_3Te_3S^{4+}$ skeleton was not an incidental event since we could repeat this experiment very well. Furthermore, by using 4-aminobenzoic acid instead of 2-aminobenzoic acid, a similar product can be obtained, in which the position of 2-aminobenzoic acid was replaced by 4-aminobenzoic acid but the cluster core was still $Mo_3Te_3S^{4+}$ [19]. These compounds are mildly air sensitive, and when their solutions were exposed in air for several days, a tellurium mirror at the bottom of the receptacles was found along with some dark-brown crystals, which proved to be $Mo_3Te_7[S_2P(OPr^i)_2]_3I$ by IR spectra and X-ray diffraction experiments. The reaction scheme can be represented as shown in Scheme 1.



Scheme 1.

3.2. Structure

The structures of cluster molecules **1** and **2** are shown in Fig. 1, and selected bond distances and angles are listed in Tables 2 and 3, respectively.

In complex **1**, the three molybdenum atoms define an approximate isosceles triangle with Mo–Mo distances of 2.940(2), 2.970(2) and 2.832(2) Å, respectively, of which the shortest side is bridged by a $PhCO_2^-$ ligand. The average Mo–Mo distance of 2.914 Å is slightly longer than the value of 2.891 Å in $Cs_{4.5}[Mo_3Te_7(CN)_6]I_{2.5}\cdot 3H_2O$ [7] and 2.889 Å in $Mo_3Te_7[S_2P(OPr^i)_2]_3I$ [16]. One μ_3-Te atom and three μ-Te atoms are located above and below the Mo_3 plane, respectively, to form an incomplete cuboidal cluster skeleton. The Mo–(μ-Te) distances range from 2.597(2) to 2.649(2) Å. The average Mo–(μ_3-Te) distance of 2.650 Å is comparable to those found in $Mo_3Te_{10}I_{10}$ (2.661 Å) [20], $[Mo_3Te_7(CN)_6]^{3-}$ (2.696 Å) and $[Mo_4Te_4(CN)_{12}]^{7-}$ (2.676 Å) [8–10]. In addition to the $PhCO_2^-$ ligand that bridges two Mo atoms and one PBu_3 molecule coordinated to the third Mo atom, there is a terminal $S_2P(OPr^i)_2^-$ ligand chelating to each Mo atom. As a result, each Mo atom has a distorted octahedral coordination geometry. The Mo–P distance of 2.615(5) Å is comparable to those of other complexes containing the Mo_3S_4 cluster core and PPh_3 ligand [21,22].

In comparison, the structure of complex **2** is similar to that of complex **1** with the (μ_3-Te) and bridging $PhCO_2^-$ ligand replaced by the (μ_3-S) and 2-aminobenzoic acid group. The average Mo–Mo distance of **2** is slightly shorter (ca. 0.01–

Table 2
Selected interatomic distances (Å) and angles (°) in $Mo_3Te_4[S_2P(OPr^i)_2]_3(\mu\text{-}PhCO_2)PBu_3$ (**1**)

Mo(1)–Te(2)	2.606(2)	Mo(2)–Te(1)	2.608(2)
Mo(1)–Te(1)	2.612(2)	Mo(2)–Te(4)	2.637(2)
Mo(1)–P(4)	2.615(5)	Mo(2)–Te(3)	2.639(2)
Mo(1)–S(1)	2.630(5)	Mo(2)–Mo(3)	2.831(2)
Mo(1)–S(2)	2.636(5)	Mo(3)–O(8)	2.207(10)
Mo(1)–Te(4)	2.663(2)	Mo(3)–S(6)	2.529(5)
Mo(1)–Mo(3)	2.946(2)	Mo(3)–S(5)	2.577(5)
Mo(1)–Mo(2)	2.972(2)	Mo(3)–Te(2)	2.597(2)
Mo(2)–O(7)	2.216(11)	Mo(3)–Te(4)	2.648(2)
Mo(2)–S(3)	2.540(5)	Mo(3)–Te(3)	2.649(2)
Mo(2)–S(4)	2.576(5)	Te(3)–Te(3)#1 [a]	3.103(2)
Te(2)–Mo(1)–P(4)	81.26(13)	S(4)–Mo(2)–Te(4)	155.66(13)
Te(2)–Mo(1)–Te(1)	100.68(6)	Te(1)–Mo(2)–Te(4)	108.42(6)
P(4)–Mo(1)–Te(1)	82.91(14)	O(7)–Mo(2)–Te(3)	84.9(3)
Te(2)–Mo(1)–S(1)	91.68(12)	S(3)–Mo(2)–Te(3)	157.22(13)
P(4)–Mo(1)–S(1)	84.3(2)	S(4)–Mo(2)–Te(3)	81.76(13)
Te(1)–Mo(1)–S(1)	160.58(14)	Te(1)–Mo(2)–Te(3)	91.25(6)
Te(2)–Mo(1)–S(2)	161.03(14)	Te(4)–Mo(2)–Te(3)	115.25(7)
P(4)–Mo(1)–S(2)	83.8(2)	O(8)–Mo(3)–S(6)	83.7(3)
Te(1)–Mo(1)–S(2)	88.99(13)	O(8)–Mo(3)–S(5)	82.8(3)
S(1)–Mo(1)–S(2)	75.2(2)	S(6)–Mo(3)–S(5)	77.0(2)
Te(2)–Mo(1)–Te(4)	108.98(7)	O(8)–Mo(3)–Te(2)	168.0(3)
P(4)–Mo(1)–Te(4)	163.17(14)	S(6)–Mo(3)–Te(2)	98.17(13)
Te(1)–Mo(1)–Te(4)	107.41(6)	S(5)–Mo(3)–Te(2)	86.11(13)
S(1)–Mo(1)–Te(4)	82.17(13)	O(8)–Mo(3)–Te(4)	82.2(3)
S(2)–Mo(1)–Te(4)	83.13(14)	S(6)–Mo(3)–Te(4)	81.93(14)
O(7)–Mo(2)–S(3)	82.7(3)	S(5)–Mo(3)–Te(4)	155.27(14)
O(7)–Mo(2)–S(4)	83.5(3)	Te(2)–Mo(3)–Te(4)	109.73(7)
S(3)–Mo(2)–S(4)	77.9(2)	O(8)–Mo(3)–Te(3)	84.0(3)
O(7)–Mo(2)–Te(1)	170.6(3)	S(6)–Mo(3)–Te(3)	157.8(2)
S(3)–Mo(2)–Te(1)	97.94(13)	S(5)–Mo(3)–Te(3)	83.23(14)
S(4)–Mo(2)–Te(1)	87.41(13)	Te(2)–Mo(3)–Te(3)	90.28(6)
O(7)–Mo(2)–Te(4)	81.0(3)	Te(4)–Mo(3)–Te(3)	114.53(7)
S(3)–Mo(2)–Te(4)	81.58(12)		

[a] Symmetry transformations used to generate equivalent atoms: #1: $-x-1/2$, $-y-1/2$, $-z+1$.

Table 3
Selected interatomic distances (Å) and and angles (°) in $Mo_3(\mu_3\text{-}S)Te_3[S_2P(OPr^i)_2]_3(\mu\text{-}PhNH_2CO_2)PBu_3$ (**2**)

Mo(1)–S(7)	2.384(4)	Mo(2)–S(4)	2.623(5)
Mo(1)–Te(2)	2.633(2)	Mo(2)–Te(1)	2.647(2)
Mo(1)–Te(1)	2.646(2)	Mo(2)–Te(3)	2.687(2)
Mo(1)–S(2)	2.657(5)	Mo(2)–Mo(3)	2.822(2)
Mo(1)–S(1)	2.659(5)	Mo(3)–O(7)	2.232(10)
Mo(1)–P(4)	2.675(5)	Mo(3)–S(7)	2.364(4)
Mo(1)–Mo(3)	2.900(2)	Mo(3)–S(6)	2.562(4)
Mo(1)–Mo(2)	2.921(2)	Mo(3)–S(5)	2.641(5)
Mo(2)–O(8)	2.261(11)	Mo(3)–Te(2)	2.644(2)
Mo(2)–S(7)	2.358(4)	Mo(3)–Te(3)	2.679(2)
Mo(2)–S(3)	2.571(4)	Te(3)–Te(3)#1 [a]	3.140(2)
S(7)–Mo(1)–Te(2)	107.57(12)	S(3)–Mo(2)–Te(1)	97.77(12)
S(7)–Mo(1)–Te(1)	106.38(11)	S(4)–Mo(2)–Te(1)	88.24(12)
Te(2)–Mo(1)–Te(1)	97.71(6)	O(8)–Mo(2)–Te(3)	83.5(3)
S(7)–Mo(1)–S(2)	83.5(2)	S(7)–Mo(2)–Te(3)	111.31(11)
Te(2)–Mo(1)–S(2)	162.87(13)	S(3)–Mo(2)–Te(3)	159.37(12)
Te(1)–Mo(1)–S(2)	91.41(12)	S(4)–Mo(2)–Te(3)	84.77(11)
S(7)–Mo(1)–S(1)	82.4(2)	Te(1)–Mo(2)–Te(3)	91.56(5)
Te(2)–Mo(1)–S(1)	93.10(12)	O(7)–Mo(3)–S(7)	82.7(3)
Te(1)–Mo(1)–S(1)	163.15(13)	O(7)–Mo(3)–S(6)	84.5(3)
S(2)–Mo(1)–S(1)	75.1(2)	S(7)–Mo(3)–S(6)	83.9(2)
S(7)–Mo(1)–P(4)	164.1(2)	O(7)–Mo(3)–S(5)	81.5(3)
Te(2)–Mo(1)–P(4)	82.12(14)	S(7)–Mo(3)–S(5)	156.8(2)
Te(1)–Mo(1)–P(4)	84.1(2)	S(6)–Mo(3)–S(5)	77.7(2)
S(2)–Mo(1)–P(4)	84.4(2)	O(7)–Mo(3)–Te(2)	169.5(3)
S(1)–Mo(1)–P(4)	84.6(2)	S(7)–Mo(3)–Te(2)	107.82(11)
O(8)–Mo(2)–S(7)	82.9(3)	S(6)–Mo(3)–Te(2)	97.08(12)
O(8)–Mo(2)–S(3)	84.3(3)	S(5)–Mo(3)–Te(2)	88.58(11)
S(7)–Mo(2)–S(3)	83.5(2)	O(7)–Mo(3)–Te(3)	84.9(3)
O(8)–Mo(2)–S(4)	82.6(3)	S(7)–Mo(3)–Te(3)	111.38(11)
S(7)–Mo(2)–S(4)	156.9(2)	S(6)–Mo(3)–Te(3)	160.06(13)
S(3)–Mo(2)–S(4)	77.2(2)	S(5)–Mo(3)–Te(3)	84.12(11)
O(8)–Mo(2)–Te(1)	169.9(3)	Te(2)–Mo(3)–Te(3)	90.45(5)
S(7)–Mo(2)–Te(1)	107.11(11)		

[a] Symmetry transformations used to generate equivalent atoms: #1: $-x+1$, $-y+1$, $-z+1$.

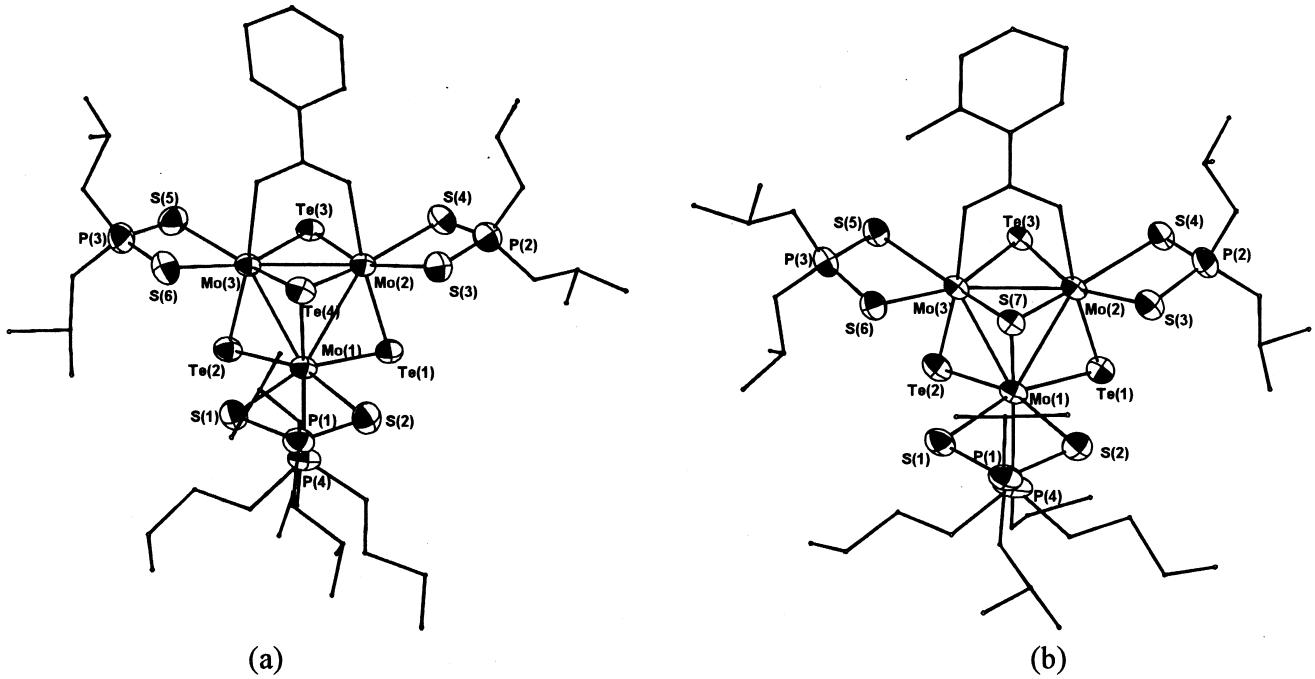


Fig. 1. Molecular drawings of (a) $Mo_3Te_4[S_2P(OPr^i)_2]_3(\mu\text{-}PhCO_2)PBu_3$ (**1**) and (b) $Mo_3(\mu_3\text{-}S)Te_3[S_2P(OPr^i)_2]_3(\mu\text{-}PhNH_2CO_2)PBu_3$ (**2**). The labels for carbon and oxygen atoms have been omitted for clarity.

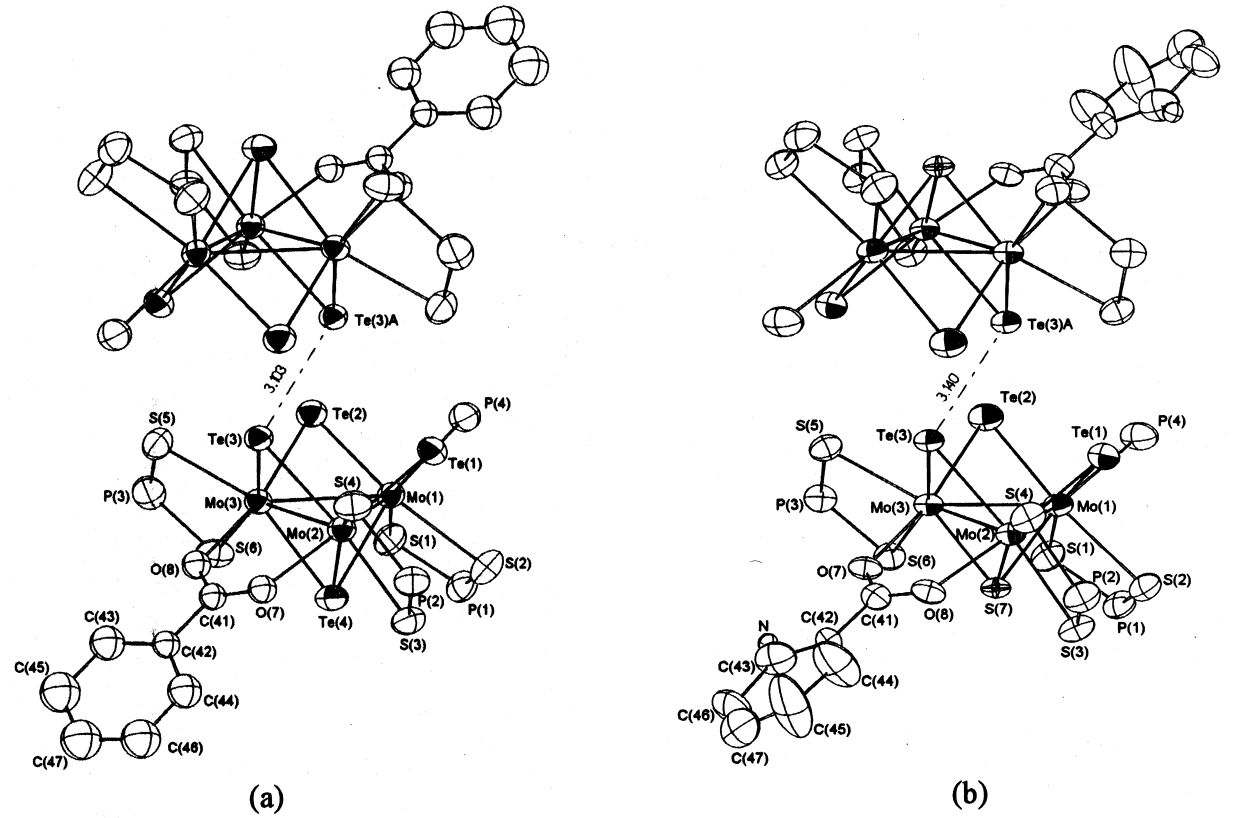


Fig. 2. ORTEP drawings of (a) $Mo_3Te_4[S_2P(OPr^i)_2]_3(\mu\text{-}PhCO_2)PBu_3$ (**1**) and (b) $Mo_3(\mu_3\text{-}S)Te_3[S_2P(OPr^i)_2]_3(\mu\text{-}PhNH_2CO_2)PBu_3$ (**2**) dimers showing the atom labelling scheme at 30% probability of thermal ellipsoids. The butyl and isopropoxy groups have been omitted for clarity.

0.05 Å) than that of **1** because the capping sulfur atom has a smaller covalent radius than tellurium. On the other hand, the Mo–(μ-Te) and the Mo–P distances are significantly elongated (ca. 0.02–0.03 Å for Mo–Te and 0.06 Å for Mo–P).

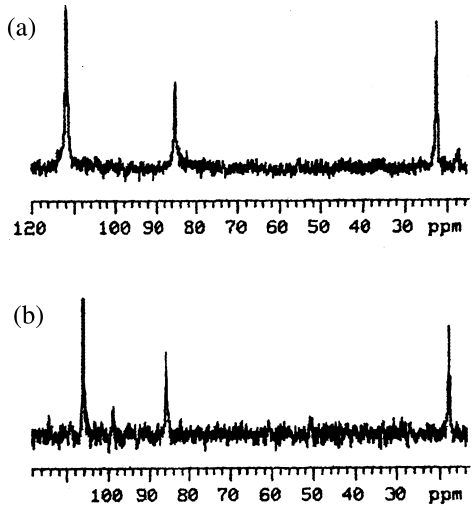


Fig. 3. ^{31}P spectra of (a) $Mo_3Te_4[S_2P(OPr^i)_2]_3(\mu\text{-}PhCO_2)PBu_3$ (**1**) and (b) $Mo_3(\mu_3\text{-}S)Te_3[S_2P(OPr^i)_2]_3(\mu\text{-}PhNH_2CO_2)PBu_3$ (**2**).

It is interesting that there is a short contact between Te(3) and Te(3A) of an adjacent molecule in both complexes (3.103(2) Å in **1** and 3.140(2) Å in **2**), leading to the formation of a dimer (Fig. 2). Consequently, the distances of Te(3) and Mo are elongated (ca. 0.03–0.05 Å) and the coordination environment of Te(3) is somewhat like that of the μ_3-Te (the distances Te(3)–Mo are comparable with Te(4)–Mo). EHMO calculation also attested that there is a weak bond between two Te(3) atoms [1] [23]. Although there are some examples of longer Te···Te interactions in existing tellurium-rich tellurides [24,25] (e.g. 3.07–3.17 Å in $LnTe_n$ ($n > 1.75$), 3.16 Å in $NaTe_3$), to our knowledge no example of dimerization of two triangular $Mo_3E_4^{4+}$ (E = S, Se) clusters through bonding interaction has been found, although the weaker dimerization through Se···Se interaction (3.415 Å) was reported in the $[M_3Se_4(CN)_9]^{5-}$ (M = Mo, W) [14] anion before.

The ^{31}P NMR spectra of complexes **1** and **2** are shown in Fig. 3. The chemical shift of P_1 of the DTP ligand is at 85.2 ppm for complex **1** (85.6 ppm for complex **2**). The peak at 111.8 ppm for complex **1** (106.0 ppm for complex **2**) with twice integration can be assigned to P_2 and P_3 of the DTP ligands, which coordinate symmetrically to Mo_2 and Mo_3, and the chemical shift of PBu_3 is at 22.3 ppm for complex **1** (17.8 ppm for complex **2**). Compared to their counterparts, δ_{P1} has no significant shift and δ_{P2}, δ_{P3} and δ_{PBu3} for complex **2** have shifted to high field. The substitution of capping-Te (in complex **1**) by capping-S (in complex **2**) in the cluster core should be mainly responsible for these shifts.

[1] Molecular orbital reduced overlap populations (MP) between Te(3) and Te(3A) are 0.052 for complex **1** and 0.027 for complex **2**. The EHMO calculations are based on the position of the atoms obtained from the X-ray structure analysis. Standard atomic parameters of the program were used. When we used a different atomic orbital parameter for tellurium (5s: −20.5, 2.57; 5p: −12.9, 2.16) [26], the MP between Te(3) and Te(3A) was 0.193 for complex **1** and 0.168 for complex **2**.

Supplementary data

Crystallographic data have been deposited with the Cambridge Crystallographic Data Centre, 12 Union Road, Cambridge, CB2 1EZ, UK (fax: +44-1223-336033; e-mail: deposit@ccdc.cam.ac.uk) and are available on request quoting the deposition numbers 135939 and 135940.

Acknowledgements

This research was supported by the National Natural Science Foundation of China and the State Key Laboratory of Structural Chemistry, Fujian Institute of Research on the Structure of Matter, Chinese Academy of Sciences.

References

[1] T. Saito, in: M.H. Chisholm (Ed.), Early Transition Metal Clusters with π-Donor Ligands, VCH, New York, 1995, p. 63.
[2] L.C. Roff, J.W. Kolis, Chem. Rev. 93 (1993) 1037.
[3] F. Basolo, Coord. Chem. Rev. 125 (1993) 13.
[4] M.G. Kanatzidis, S-P. Huang, Chem. Rev. 130 (1994) 509.
[5] I. Dance, K. Fisher, Prog. Inorg. Chem. 41 (1994) 637.
[6] D.R. Gardner, J.C. Fettinger, B.W. Eichhorn, Angew. Chem., Int. Ed. Engl. 33 (1994) 1859 and Refs. therein.
[7] V.P. Fedin, H. Imoto, T. Saito, W. McFarlane, A.G. Sykes, Inorg. Chem. 34 (1995) 5097.
[8] V.P. Fedin, I.V. Kalinina, A.V. Virovets, N.V. Podberezskaya, A.G. Sykes, J. Chem. Soc., Chem. Commun. (1998) 237.
[9] V.P. Fedin, I.V. Kalinina, D.G. Samsonenko, Y.V. Mironov, M.N. Sokolov, S.V. Tkachev, A.V. Virovets, N.V. Podberezskaya, M.R.J. Elsegood, W. Clegg, A.G. Sykes, Inorg. Chem. 38 (1999) 1956.
[10] R. Hernández-Molina, A. Geoffrey Sykes, J. Chem. Soc., Dalton Trans. (1999) 1337.
[11] X. Xie, R.E. McCarley, Inorg. Chem. 35 (1996) 2713.
[12] A Muller, U. Reinsch, Angew. Chem., Int. Ed. Engl. 19 (1980) 72.
[13] V.P. Fedin, M.N. Sokolov, Y.V. Minronov, V.A. Kolesov, S.V. Tkachev, V. Ye. Fedorov, Inorg. Chim. Acta 167 (1990) 39.
[14] V.P. Fedin, G.J. Lamprecht, T. Kohzuma, W. Clegg, M.J. Elsegood, A.G. Sykes, J. Chem. Soc., Dalton Trans. (1997) 1747.
[15] M. Nasredlin, G. Henkal, G. Kampmanm, B. Kvebs, G.J. Lamprecht, C.A. Routledge, A.G. Sykes, J. Chem. Soc., Dalton Trans. (1993) 737.
[16] X. Lin, H.Y. Cheng, L.S. Chi, H.H. Zhuang, Polyhedron 18 (1999) 217.
[17] G.M. Sheldrick, SADABS, Absorption Correction Program, University of Göttingen, Germany, 1996.
[18] Siemens, SHELXTL™ Version 5 Reference Manual, Siemens Energy & Automation Inc., Madison, WI, 1994.
[19] X. Lin et al., unpublished results, CCDC code 135941, 1999.
[20] V.P. Fedin, H. Imoto, T. Saito, J. Chem. Soc., Chem. Commun. (1995) 1559.
[21] J.Q. Huang, S.F. Lu, Y.H. Lin, J.L. Huang, J.X. Lu, Acta Chim. Sinica (1986) 301.
[22] F.A. Cotton, P.A. Kibala, M. Matusz, C.S. McCaleb, B.W. Sandor, Inorg. Chem. 28 (1989) 2623.
[23] C. Mealli, D.M. Proserpio, C.A.C.A.O., PC Version 4.0, J. Chem. Educ. 67 (1990) 399.
[24] P. Bottcher, Angew. Chem., Int. Ed. Engl. 27 (1988) 759.
[25] M.G. Kanatzidis, Angew. Chem., Int. Ed. Engl. 34 (1995) 2109.
[26] X Xie, R.E. McCarley, Inorg. Chem. 36 (1997) 4665.

PERGAMON

www.elsevier.nl/locate/poly

Polyhedron 19 (2000) 931–936

POLYHEDRON

Synthesis, structure and properties of mononuclear oxovanadium(V) alkoxides incorporating chelated ethane-1,2-diol and propane-1,3-diol

Kajal Krishna Rajak, Sujit Mondal, Sankar Prasad Rath *

Department of Inorganic Chemistry, Indian Association for the Cultivation of Science, Calcutta 700 032, India

Received 16 July 1999; accepted 17 February 2000

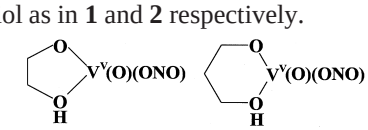
Abstract

Dark coloured complexes of type VO(L)(Heg) and VO(L)(Hpd) have been synthesized in excellent yields by reacting bis(acetylacetonato)oxovanadium(IV) with H_2L in the presence of excess ethane-1,2-diol (H_2eg) and propane-1,3-diol (H_2pd), respectively in acetone. Here L^{2-} are the deprotonated forms of N-(1-hydroxyethyl)naphthaldimine (H_2L^1) and N-(1-hydroxy-2-methylpropyl)-naphthaldimine (H_2L^2). Heg^- and Hpd^- form five- and six-membered V(O,O) chelate rings, respectively. The crystal structure of $VO(L^2)(Heg)$ is reported. The ONO-coordinating tridentate $[L^2]^{2-}$ spans meridionally and consists of two planar segments mutually rotated along a C–N bond. The Heg^- ligand forms a non-planar chelate ring in which the dimethylene bridge is in *gauche* conformation. The five V–O lengths are unequal, the shortest being V–O(oxo) and the longest is V–O(alcoholic) which is subjected to the *trans* influence of the oxo oxygen atom. In the crystal lattice, the $VO(L^2)(Heg)$ molecule forms an infinite chain helical pattern via intermolecular O···O hydrogen bonding. Methylene ^1H resonances are systematically shifted to lower field compared to those of free H_2eg and H_2pd, the shift of the CH_2OV resonances being particularly large. The complex multiplet ^1H structure in $CDCl_3$ is a good indication of the rigidity of the chelate ring in solution. ^{51}V chemical shifts are found to be diagnostic of the alcohol–alkoxide chelate ring size, the shift of VO(L)(Heg) being ~25 ppm downfield from that of VO(L)(Hpd). Low V(V)/V(IV) reduction potentials (ca. −0.30 V versus SCE) are indicative of the considerable VO^{3+} stabilization due to two alkoxide coordination. ©2000 Elsevier Science Ltd All rights reserved.

Keywords: Oxovanadium(V) alkoxides; Mononuclear chelation; Crystal structures; Hydrogen bonded helical structures

1. Introduction

The discovery of vanadium as a cofactor in bromoperoxidase [1] and nitrogenases [2] has attracted the current attention to the reactivity and coordination chemistry of oxovanadium(V) alkoxides [3–7]. Organic vanadates have been of recent interest to inorganic and organic chemists as well as biochemists, spectroscopists and material scientists with respect to structure and reactivity [8,9]. It has been known for a long time that, like phosphorus, vanadium forms esters with alcohols in their pentavalent state [10–12]. This analogy between phosphate and vanadate is of far reaching consequence and biological processes can be modified or adjusted via the addition of vanadate which naturally influences phosphate related phenomena. A more classical and developing field of application of vanadium alkoxide and related compounds is their use as a catalyst in polymerization [13–15], as selective redox reagents [16,17] and as mimics in studies of phosphorylation [18–20], haloperoxidation [21–23] and insulin action [24,25]. The present work concerns the formation of vanadate esters incorporating ethane-1,2-diol and propane-1,3-diol. Oxovanadium(V) esters incorporating dihydroxy alcohols are in most cases polymeric [26–33]; few mononuclear species are known [34,35]. This has motivated us to search for rational ways of making mononuclear esters chelated by diols. Herein we describe the synthesis, structure and solution properties of a series of oxovanadium(V) complexes incorporating ethane-1,2-diol and propane-1,3-diol as in **1** and **2** respectively.



1 **2**

The solid and solution structures of the complexes, as well as their properties, were probed using X-ray diffraction, spectroscopic and electrochemical methods. ^{51}V chemical shifts

* Corresponding author. Tel.: +91-33-473-4971; fax: +91-33-473-2805; e-mail: sankarrath@hotmail.com

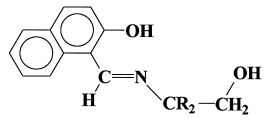
0277-5387/00/$ - see front matter ©2000 Elsevier Science Ltd All rights reserved.
PII S0277-5387(00)00336-3

have been found to be diagnostic of the alcohol–alkoxide chelate ring size.

2. Results and discussion

2.1. Synthesis and characterization

In the present work, two tridentate diacidic Schiff bases H_2L^1–H_2L^2 (**3**) (written generally as H_2L) have been used as coligand so as to block three coordination positions, leaving just two positions for possible diol chelation in a six-coordinated situation.



3

The coligand Schiff bases were prepared by condensing 2-hydroxynaphthaldehyde with amino alcohols such as ethanol amine and 2-amino-2-methyl-1-propanol respectively in ethanol. The stoichiometric reaction of bis(acetylacetonato)oxovanadium(IV) with H_2L in acetone in air in the presence of excess ethane-1,2-diol (H_2eg) or propane-1,3-diol (H_2pd) afforded the dark coloured complex VO(L)(Heg) or VO(L)(Hpd) in excellent yields. The oxygen in air is believed to be the oxidant ($V^{IV}O \rightarrow V^{V}O$). Excess diol was used in the above synthesis to ensure the formation of mononuclear esters.

All the complexes are diamagnetic, suggesting vanadium is in the +5 oxidation state. The V=O stretch occurs as a sharp strong peak in the range 975–985 cm^{-1} consistent with hexacoordination [36–39]. The hydrogen bonded OH stretch occurs as a broad peak near 3450 cm^{-1}. In solution the complexes display an intense band near 375 cm^{-1} associated with a relatively weak band near 480 cm^{-1}; these are believed to be of O(alkoxide) → V LMCT origin [23,40,41]. The complexes show a quasireversible one-electron cyclic voltammetric response near −0.30 V versus SCE. The oxovanadium(V) state is thus strongly stabilized by alkoxide coordination and this facilitates spontaneous $V^{IV}O/V^{V}O$ oxidation by aerial oxygen in the synthesis. Detailed characterization data are listed in Section 3.

2.2. Crystal structure

The structure of VO(L^2)(Heg) was determined; it crystallizes in the space group $P2_1$. The asymmetric unit consists of two metrically similar but crystallographically distinct molecules. In Fig. 1 only molecule 1 is shown. The numberings of the corresponding atoms in molecules 1 and 2 are respectively n and $n+50$, e.g. V(1)–O(5) and V(51)–O(55). Selected bond distances and angles are listed in Table 1.

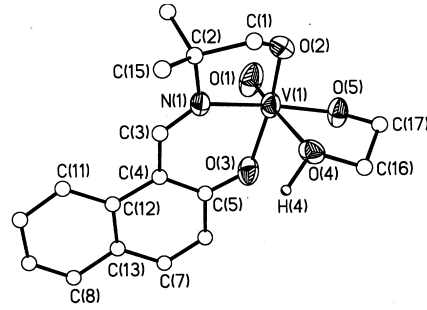


Fig. 1. Perspective view and atom labelling scheme for molecule 1 in VO(L^2)(Heg) showing the crucial hydrogen atom only.

Table 1
Selected bond lengths (Å) and angles (°) for VO(L^2)(Heg)

Molecule 1		Molecule 2	
V(1)–O(1)	1.586(7)	V(51)–O(51)	1.576(7)
V(1)–O(2)	1.818(8)	V(51)–O(52)	1.813(8)
V(1)–O(3)	1.892(7)	V(51)–O(53)	1.892(7)
V(1)–O(4)	2.357(6)	V(51)–O(54)	2.352(7)
V(1)–O(5)	1.838(6)	V(51)–O(55)	1.839(6)
V(1)–N(1)	2.099(7)	V(51)–N(51)	2.105(7)
O(1)–V(1)–O(2)	101.4(5)	O(51)–V(51)–O(52)	101.1(5)
O(1)–V(1)–O(3)	98.2(4)	O(51)–V(51)–O(53)	97.9(4)
O(1)–V(1)–O(4)	173.2(3)	O(51)–V(51)–O(54)	173.4(3)
O(1)–V(1)–O(5)	98.5(3)	O(51)–V(51)–O(55)	98.9(3)
O(2)–V(1)–O(3)	153.9(3)	O(52)–V(51)–O(53)	154.4(4)
O(2)–V(1)–O(4)	82.2(3)	O(52)–V(51)–O(54)	82.1(3)
O(2)–V(1)–O(5)	95.6(3)	O(52)–V(51)–O(55)	95.7(3)
O(3)–V(1)–O(4)	80.2(2)	O(53)–V(51)–O(54)	80.8(3)
O(3)–V(1)–O(5)	98.4(3)	O(53)–V(51)–O(55)	98.1(3)
O(4)–V(1)–O(5)	75.3(2)	O(54)–V(51)–O(55)	75.0(2)
O(1)–V(1)–N(1)	99.1(3)	O(51)–V(51)–N(51)	99.0(3)
O(2)–V(1)–N(1)	78.2(3)	O(52)–V(51)–N(51)	78.1(3)
O(3)–V(1)–N(1)	81.9(3)	O(53)–V(51)–N(51)	82.1(3)
O(4)–V(1)–N(1)	87.2(2)	O(54)–V(51)–N(51)	87.2(2)
O(5)–V(1)–N(1)	162.1(3)	O(55)–V(51)–N(51)	161.9(3)

The VO_5N coordination sphere is distorted octahedral, the metal atom is displaced by 0.31 Å (molecule 1) and 0.30 Å (molecule 2) towards the oxo oxygen away from the equatorial plane (mean deviation 0.006 Å) defined by O(2), O(3), O(5), N(1) (molecule 1) and O(52), O(53), O(55) and N(51) (molecule 2). The $[L^2]^{2-}$ is meridionally disposed and consists (excluding the methyl groups) of two planar segments mutually rotated around an N–C bond. The segments are $OC_{10}H_6CHN$ (plane A, mean deviation < 0.07 Å) and CCH_2O (plane B), the dihedral angle being ~50°. The metal atom does not lie on either plane and is displaced respectively by 0.43 and 0.16 Å (for molecule 1) and by 0.42 and 0.15 Å (for molecule 2). The Heg^- ligand forms a non-planar five-membered chelate ring in which the dimethylene bridges are in *gauche* configuration.

The five V–O bond lengths are unequal; the shortest distance is the bond to the oxo oxygen and the longest is that to the glycolic hydroxyl oxygen. The latter is subjected to the *trans* influence of the oxo oxygen. It is logical that the weaker alcoholic oxygen donor rather than the stronger alkoxidic

donor lies *trans* to the oxo oxygen. The V–O bond lengths follow the order V–O(oxo) < V–O(alkoxide) < V–O-(phenoxide) < V–O(alcoholic). The V–O(alkoxide) length in the V(L^2) fragment is shorter than the corresponding length in the V(Heg) fragment. The variation in V–O-(alkoxide) bond is presumably due to the *trans* influence of the azomethine nitrogen, in which the alkoxide oxygen of Heg^- is placed *trans* to it. The other bond distances are as usual.

The most striking feature of the crystal structure of the complex is the helical structure formed by intermolecular O···O hydrogen bonding between the alcoholic oxygen of one molecule with the alkoxide oxygen of Heg^- of the adjacent molecule. The relevant hydrogen bonding distances are O(4)···O(55) 2.625(11), and O(54)···O(5) 2.634(11) Å. The infinite helical chain pattern is shown in Fig. 2.

Despite our best efforts, we have been unable to grow single crystals of the VO(L)(Hpd) complexes suitable for X-ray diffraction studies. However, structure determination of complexes in which $[L]^{2-}$ is substituted by O,N,O-coordinating diionized tridentate ligands are known [34,35]. Our results are indicative of a similar structure.

2.3. ^1H and ^{51}V NMR

All spectral data were recorded in $CDCl_3$. Signals were assigned on the basis of intensity, spin–spin coupling patterns and chemical shift values. In VO(L)(Heg) complexes all the methylene protons, either from L^{2-} or from Heg^-, are inequivalent in the solid state. In solution the inequivalency is clearly resolved in the case of the methylene protons of the alkoxide carbon atoms; the inequivalency is relatively large for the ligand L (Fig. 3) compared with Heg^-. VO(L)(Hpd) complexes behave similarly; here the inequivalency of the alkoxidic methylene protons in the Hpd^- fragment is not well resolved (Fig. 4).

The methylene ^1H resonances of chelated Heg^- and Hpd^- are systematically shifted to lower fields compared to those of the free H_2eg and H_2pd, the shift of the –CH_2OV resonances being particularly large. The alkoxidic CH proton of the diol ligand occurs as an isolated ^1H signal shifted downfield by 1–1.5 ppm from the alcoholic CH proton. Thus ^1H NMR can be used for easy identification of the hydrolysis of bound Heg^- and Hpd^- to the corresponding free diols in solution. The VO(L)(Hpd) complexes are much more prone to hydrolysis than VO(L)(Heg) if the solvent is slightly wet. Thus the five-membered chelate ring **1** has superior hydrolytic stability compared to the six-membered chelate **2**. The documented failure [31–33] in producing vanadate esters having propane-1,3-diol chelation in aqueous media is thus understandable. Solution experiments were done in dry solvents to prevent possible hydrolysis. The complex multiplet ^1H structure is a good indication of chelate ring rigidity in solution [34,35]. The alcoholic OH signals occur as a broad signal near 4.9 ppm which 'disappears' on shaking with D_2O.

Complexes display a sharp and single ^{51}V resonance in $CDCl_3$. For a given L ligand, VO(L)(Hpd) complexes, having a six-membered chelate ring **2**, display a signal ~25 ppm upfield from that of VO(L)(Heg) incorporating a five-membered chelate ring **1**. ^{51}V chemical shifts are thus diagnostic of the V(O,O) chelate ring size. This trend is found to

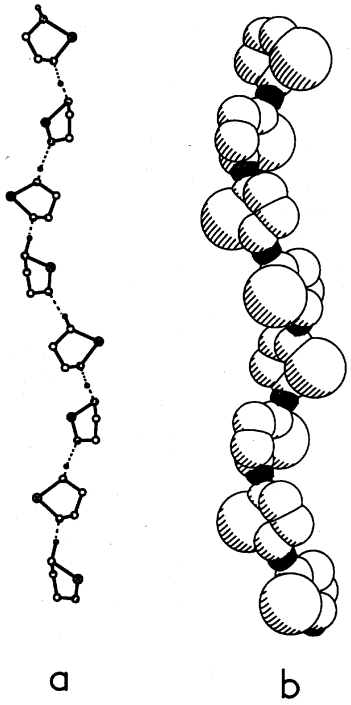


Fig. 2. (a) Perspective view and (b) space filling model of VO(L^2)(Heg) in the lattice showing the helical network formed via intermolecular O···O hydrogen bonds (for clarity only the V(Heg) fragment is shown).

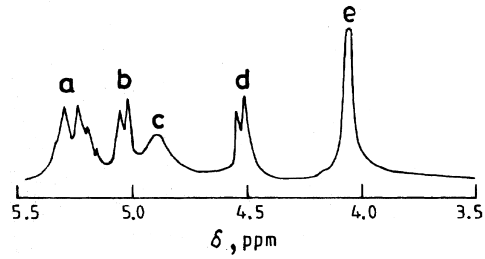


Fig. 3. Proton NMR spectrum (300 MHz, 3.5–5.5 δ) of VO(L^2)(Heg) in $CDCl_3$. Resonances *a* (for CH_2OV), *c* (for CH_2(O*H*)V) and *e* (for CH_2(OH)V) correspond to chelated Heg^- while *b* and *d* (for CH_2OV) correspond to L^2.

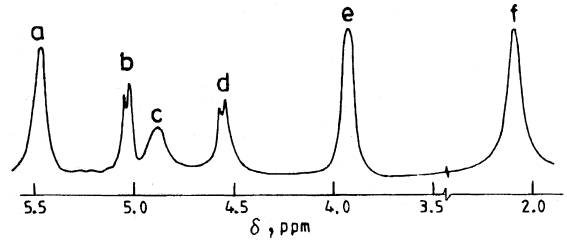


Fig. 4. Proton NMR spectrum (300 MHz) of VO(L^2)(Hpd) in $CDCl_3$ (only a selected portion is shown). Resonances *a* (for CH_2OV), *c* (for CH_2(O*H*)V), *e* (for CH_2(OH)V) and *f* (for C$H_2$$CH_2$OV) correspond to chelated Hpd^- while *b* and *d* (for CH_2OV) correspond to L^2.

be generally applicable, as observed in other cases [34,35]. Chemical shift values are listed in Section 3.

3. Experimental

3.1. Materials

Bis(acetylacetonato) oxovanadium(IV) [42] and tetraethylammonium perchlorate [43] were prepared by reported procedures. $CDCl_3$ was obtained from Sigma Chemicals. All other chemicals and solvents were of analytical grade and used as received.

3.2. Physical measurements

Proton NMR spectra were recorded on a Bruker FT 300 MHz spectrometer, IR spectra on a Perkin-Elmer 783 spectrophotometer and electronic spectra on a Hitachi 330 spectrophotometer. ^{51}V NMR spectra were drawn on a Varian spectrometer (78.8 MHz) at 25°C, externally referenced to $VOCl_3$. Electrochemical measurements were performed on a PAR model 370-4 system as described previously [44]. All potentials reported in this work are referenced to a saturated calomel electrode (SCE) and are uncorrected for junction contribution. A Perkin-Elmer elemental analyser was used to collect microanalytical data (C, H and N). For ^1H NMR, the proton numbering scheme used for the ligand L is as in Fig. 1.

3.3. Synthesis of the complexes

The VO(L)(Heg) complexes were prepared using a general procedure. Details are given below for a representative case of $VO(L^2)$(Heg). The VO(L)(Hpd) complexes were similarly prepared; here ethane-1,2-diol is replaced by propane-1,3-diol in the synthetic procedure.

$VO(L^2)$(Heg). To an acetone solution (20 cm^3) of $VO(acac)_2$ (0.10 g, 0.38 mmol) and H_2L^2 (0.92 g, 0.38 mmol) was added excess ethane-1,2-diol (1 cm^3, 17.88 mmol). The mixture was warmed on a water bath for 15 min and left to evaporate at room temperature in air. The dark coloured crystalline solid that deposited was filtered off, washed thoroughly with water and dried over P_4O_{10} in vacuo. Yield: 0.12 g (87%). *Anal.* Found: C, 55.21; H, 5.50; N, 3.72. Calc. for $C_{17}H_{20}NO_5V$: C, 55.28; H, 5.42; N, 3.79%. IR (KBr, ν_{max} (cm^{-1})): 978 (V=O); 1615 (C=N); 3420 (br, OH). UV–Vis (CH_2Cl_2, λ_{max} (nm) (ε (dm^3 mol^{-1} cm^{-1}))): 475 (1900), 375 (5580). VO^{3+}–VO^{2+} couple ($E_{1/2}$ (V) (ΔE_P (mV))): −0.31 (130). ^1H NMR ($CDCl_3$, δ): 5.03 (d, J=9.0, $H_A(1)$); 4.59 (d, J=8.6, $H_B(1)$); 9.32 (s, H(3)); 8.08 (d, J=8.44, H(6)); 7.22 (d, J=9.0, H(7)); 7.98 (d, J=8.4, H(8)); 7.42 (t, J=7.5, H(9)); 7.61 (t, J=7.5, H(10)); 7.81 (d, J=7.8, H(11)); 5.25 (m, CH_2OV); 4.89 (br, $CH_2O(H)V$); 4.06 (m, CH_2O(H)V); 1.76, 1.25 (s, CMe_2). ^{51}V ($CDCl_3$, δ): −531.

$VO(L^1)$(Heg). Yield: 0.11 g (83%). *Anal.* Found: C, 52.84; H, 4.64; N, 4.15. Calc. for $C_{15}H_{16}NO_5V$: C, 52.78; H, 4.70; N, 4.10%. IR (KBr, ν_{max} (cm^{-1})): 975 (V=O); 1620 (C=N); 3410 (br, OH). UV–Vis (CH_2Cl_2, λ_{max} (nm) (ε (dm^3 mol^{-1} cm^{-1}))): 480 (1860), 377 (5500). VO^{3+}–VO^{2+} couple ($E_{1/2}$ (V) (ΔE_P (mV))): −0.30 (120). ^1H NMR ($CDCl_3$, δ): 4.79 (m, $H_A(1)$); 4.21 (m, $H_B(1)$); 5.30 (m, $H_A(2)$); 4.72 (m, $H_B(2)$); 9.40 (s, H(3)); 8.35 (d, J=7.4, H(6)); 7.14 (d, J=9.0, H(7)); 7.98 (d, J=9.0, H(8)); 7.44 (t, J=6.9, H(9)); 7.61 (t, J=7.2, H(10)); 7.80 (d, J=8.1, H(11)); 5.15 (m, CH_2OV); 4.81 (br, $CH_2O(H)V$); 4.04 (m, CH_2O(H)V). ^{51}V ($CDCl_3$, δ): −541.

$VO(L^1)$(Hpd). Yield: 0.10 g (78%). *Anal.* Found: C, 54.16; H, 5.12; N, 3.88. Calc. for $C_{16}H_{18}NO_5V$: C, 54.08; H, 5.07; N, 3.94%. IR (KBr, ν_{max} (cm^{-1})): 985 (V=O); 1635 (C=N); 3420 (br, OH). UV–Vis (CH_2Cl_2, λ_{max} (nm) (ε (dm^3 mol^{-1} cm^{-1}))): 480 (1340), 372 (7015). VO^{3+}–VO^{2+} couple ($E_{1/2}$ (V) (ΔE_P (mV))): −0.33 (120). ^1H NMR ($CDCl_3$, δ): 4.91 (m, $H_A(1)$); 4.53 (m, $H_B(1)$); 5.00 (m, $H_A(2)$); 4.76 (m, $H_B(2)$); 9.36 (s, H(3)); 8.34 (d, J=8.4, H(6)); 7.14 (d, J=9.0, H(7)); 7.87 (d, J=8.4, H(8)); 7.43 (t, J=6.9, H(9)); 7.61 (t, J=7.8, H(10)); 7.79 (d, J=7.8, H(11)); 5.46 (m, CH_2OV); 4.86 (m, $CH_2O(H)V$); 4.16 (m, CH_2O(H)V); 2.04 (m, CH_2-CH_2OV). ^{51}V ($CDCl_3$, δ): −565.

$VO(L^2)$(Hpd). Yield: 0.12 g (81%). *Anal.* Found: C, 56.51; H, 5.80; N, 3.60. Calc. for $C_{18}H_{22}NO_5V$: C, 56.40; H, 5.74; N, 3.65%. IR (KBr, ν_{max} (cm^{-1})): 982 (V=O); 1610 (C=N); 3450 (br, OH). UV–Vis (CH_2Cl_2, λ_{max} (nm) (ε (dm^3 mol^{-1} cm^{-1}))): 478 (1415), 369 (7090). VO^{3+}–VO^{2+} couple ($E_{1/2}$ (V) (ΔE_P (mV))): −0.29 (125). ^1H NMR ($CDCl_3$, δ): 5.01 (d, J=9.3, $H_A(1)$); 4.56 (d, J=8.6, $H_B(1)$); 9.35 (s, H(3)); 8.06 (d, J=8.1, H(6)); 7.24(d, J=8.4, H(7)); 7.99 (d, J=9.0, H(8)); 7.44 (t, J=7.2, H(9)); 7.62 (t, J=7.2, H(10)); 7.80 (d, J=5.2, H(11)); 5.48 (m, CH_2OV); 4.95 (br, $CH_2O(H)V$); 3.93 (m, CH_2O(H)V); 1.78, 1.38 (s, CMe_2); 2.10 (m, CH_2CH_2OV). ^{51}V ($CDCl_3$, δ): −555.

3.4. X-ray crystallography

Black coloured crystals of $V^VO(L^2)$(Heg) (0.3×0.4×0.3 mm) were grown by slow evaporation of the reaction mixture in acetone. Cell parameters were determined by least-squares fitting of 30 machine centred reflections (2θ, 15–30°). The crystal system was confirmed to be monoclinic by suitable checking of the Laue symmetry. Data were collected by the ω-scan technique in the 2θ range 3–48° on a Siemens R3m/V four-circle diffractometer with graphite-monochromated Mo Kα radiation (λ=0.71 073 Å). Two check reflections measured after every 98 reflections showed no intensity reduction. All data were corrected for Lorentz polarisation effects and empirical absorption corrections were done on the basis of azimuthal scan of six reflections [45].

Table 2
Crystallographic data for $VO(L^2)(Heg)$

Formula	$C_{17}H_{20}NO_5V$
M	369.28
Crystal system	monoclinic
a (Å)	9.714(8)
b (Å)	18.217(9)
c (Å)	9.720(8)
β (°)	90.04(6)
U (Å^3)	1720(2)
Space group	$P2_1$
Z	4
D_c (Mg m^{-3})	1.426
T (K)	295
μ(Mo Mα) (mm^{-1})	0.602
F(000)	768
R_1 [a], wR_2 [b] ($I>2\sigma(I)$)	0.0606, 0.1303
S [c]	1.027
No. of parameters	333
Maximum, minimum $\Delta\rho$ (e Å^{-3})	0.446, −0.273

[a] $R_1=\Sigma||F_o|-|F_c||/\Sigma|F_o|$.
[b] $wR_2=[\Sigma\{w(F_o^2-F_c^2)^2\}/\Sigma\{w(F_o^2)^2\}]^{1/2}$;
$w^{-1}=\sigma^2(F_o^2)+(ap)^2+bp$, where $p=(F_o^2+2F_c^2)/3$ and a (0.0516) and b (2.5196) are constants adjusted by the program.
[c] $S=[\Sigma\{w(F_o^2-F_c^2)^2\}/(n-p)]^{1/2}$ where n is the number of data and p the number of parameters.

All calculations for data reduction, structure solution and refinement were done using the programs of SHEXTL, version 5.03 [46]. The structure was solved by direct methods and was refined by full-matrix least-squares on F^2. Total collected reflections were 3400 of which 3153 were unique and 2366 satisfying $I>2.0\sigma(I)$ were used for structure solution. The available observed data did not permit anisotropic refinement of all atoms. All non-hydrogen atoms except C4–C13 (molecule 1) and C54–C63 (molecule 2) were made anisotropic. The remaining atoms were refined isotropically. The crucial alcoholic hydrogen along with a few other hydrogens were directly located in difference Fourier maps. The remaining hydrogen atoms were included in calculated positions (Riding model). Significant crystal data are listed in Table 2.

4. Conclusions

Mononuclear chelation of ethane-1,2-diol and propane-1,3-diol to oxovanadium(V), as in **1** and **2**, has been achieved in the form of VO(L)(Heg) and VO(L)(Hpd), respectively. Here ethane-1,2-diol forms a five-membered alcohol–alkoxide chelate whereas propane-1,3-diol forms a six-membered chelate. The ligand L^{2-} binds in tridentate meridional fashion to the metal. In the crystal lattice of $VO(L^2)(Heg)$, the molecules form an infinite chain helical structure through intermolecular O···O hydrogen bonding. The complex multiplet ^{1}H structures are good indication of the preservation of chelate ring rigidity in solution. The vanadium(V) oxidation state is strongly stabilized (low V(V)/V(IV) potentials) by two alkoxide coordination. ^{51}V chemical shifts are found to be diagnostic of chelate ring size. For a given L, the VO(L)(Heg) resonates ~25 ppm down field from VO(L)(Hpd).

Supplementary data

Supplementary data are available from the Cambridge Crystallographic Data Centre, 12 Union Road, Cambridge CB2 1EZ, UK (fax: +44-1223-336033; e-mail: deposit@ccdc.cam.ac.uk) on request, quoting the deposition number 130243.

Acknowledgements

The authors thank Professor A. Chakravorty for providing facilities and useful suggestions. Financial support received from the Department of Science and Technology, New Delhi and Council of Scientific and Industrial Research, New Delhi, is acknowledged.

References

[1] H. Vilter, Phytochemistry 23 (1983) 1387.
[2] R.L. Robson, R.R. Eady, T.H. Richardson, R.W. Miller, M. Hawkins, J.R. Postgate, Nature (London) 322 (1986) 388.
[3] R. Fulwood, H. Schmidt, D. Rehder, J. Chem. Soc., Chem. Commun. (1995) 1443.
[4] J.Y. Kempf, B. Maigret, D.C. Crans, Inorg. Chem. 35 (1996) 6485.
[5] F. Jiang, O.P. Anderson, S.M. Miller, J. Chen, M. Mahroof-Tahir, D.C. Crans, Inorg. Chem. 37 (1998) 5439.
[6] A.S. Tracey, M.J. Gresser, Inorg. Chem. 27 (1988) 2695.
[7] Q. Chen, J. Zubieta, Coord. Chem. Rev. 114 (1992) 107.
[8] N.D. Chasteen (Ed.), Vanadium in Biological Systems, Kluwer, Boston, MA, 1990.
[9] D. Rehder, Angew. Chem., Int. Ed. Engl. 30 (1991) 148.
[10] W. Prandtl, L.Z. Hess, Z. Anorg. Chem. 82 (1913) 103.
[11] A.J. Blair, D.A. Pantony, G.J. Minkoff, J. Inorg. Nucl. Chem. 5 (1958) 316.
[12] F. Cartan, C.N. Caughlan, J. Phys. Chem. 64 (1960) 1756.
[13] S. Jiao, D. Su, D. Yu, L. Hu, Chin. J. Polym. Sci. 6 (1988) 135.
[14] E. Tsuchida, K. Yamamoto, M. Jikei, H. Nishide, Macromolecules 22 (1989) 4313.
[15] S.M. Aliwi, J. Photochem. Photobiol. A: Chem. 44 (1988) 179.
[16] T. Hirao, M. Mori, Y. Ohshiro, J. Org. Chem. 55 (1990) 358.
[17] T. Hirao, T. Fujii, T. Tanaka, Y. Ohshiro, J. Chem. Soc., Perkin Trans. 1 (1994) 3.
[18] R.N. Lindquist, J.L. Lynn Jr., G.E. Lienhard, J. Am. Chem. Soc. 95 (1973) 8762.
[19] D.C. Crans, C.M. Simonc, J.S. Blanchard, J. Am. Chem. Soc. 114 (1992) 4926.
[20] A.F. Nour-Eldeen, M.M. Craig, M.J. Gresser, J. Biol. Chem. 260 (1986) 6836.
[21] M.J. Clague, N.L. Keder, A. Butler, Inorg. Chem. 32 (1993) 4754.
[22] C.J. Carrano, M. Mohan, S.M. Holmes, R. de la Rosa, A. Butler, J.M. Charnock, C.D. Garner, Inorg. Chem. 33 (1994) 646.
[23] J.M. Arber, E. de Boer, C.D. Garner, S.S. Hasnain, R. Wever, Biochemistry 28 (1989) 7968.

[24] B.I. Posner, R. Faure, J.W. Burgess, A.P. Bevan, D. Lachance, G. Zhang-Sun, I.G. Fantus, J.B. Ng, D.A. Hall, B. Soo Lum, A. Shaver, J. Biol. Chem. 269 (1994) 4596.
[25] P.J. Stankiewicz, A.S. Tracey, D.C. Crans, in: H. Sigel, A. Sigel (Eds.), Metal Ions in Biological Systems, Marcel Dekker, New York, 1995, p. 287.
[26] W. Priebsch, D. Rehder, Inorg. Chem. 29 (1990) 3013.
[27] D.C. Crans, R.A. Felty, O.P. Anderson, M.M. Miller, Inorg. Chem. 32 (1993) 247.
[28] D.C. Crans, R.A. Felty, H. Chen, H. Eckert, N. Das, Inorg. Chem. 33 (1994) 2427.
[29] W.J. Ray Jr., D.C. Crans, J. Zheng, J.W. Burgner II, H. Deng, M. Mahroof-Thair, J. Am. Chem. Soc. 117 (1995) 6015.
[30] M.J. Gresser, A.S. Tracey, J. Am. Chem. Soc. 108 (1986) 1935.
[31] D.C. Crans, R.W. Marshman, M.S. Gottlieb, O.P. Anderson, M.M. Miller, Inorg. Chem. 31 (1992) 4939.
[32] A.S. Tracey, M.J. Gresser, Inorg. Chem. 27 (1988) 1269.
[33] A.S. Tracey, M.J. Gresser, Can. J. Chem. 66 (1988) 2570.
[34] S. Mondal, S.P. Rath, K.K. Rajak, A. Chakravorty, Inorg. Chem. 37 (1998) 1713.
[35] S.P. Rath, K.K. Rajak, S. Mondal, A. Chakravorty, J. Chem. Soc., Dalton Trans. (1998) 2097.
[36] C.J. Carrano, J.A. Bonadies, J. Am. Chem. Soc. 108 (1986) 4088.
[37] S. Holmes, C.J. Carrano, Inorg. Chem. 30 (1991) 1231.
[38] M. Mohan, S.M. Holmes, R.J. Butcher, J.P. Jasinski, C.J. Carrano, Inorg. Chem. 31 (1992) 2029.
[39] S. Ooi, M. Nishizawa, K. Matasuto, H. Kuroya, K. Saito, Bull. Chem. Soc. Jpn. 52 (1979) 452.
[40] M.J. Clague, N.L. Keder, A. Butler, Inorg. Chem. 32 (1993) 4754.
[41] C.J. Carrano, M. Mohan, S.H. Holmes, R. de la Rosa, A. Butler, J.M. Charnock, C.D. Garner, Inorg. Chem. 33 (1994) 646.
[42] R.A. Rowe, M.M. Jones, Inorg. Synth. 5 (1957) 113.
[43] D.T. Sawyer, J.L. Roberts Jr., Experimental Electrochemistry for Chemists, Wiley, New York, 1974, p. 212.
[44] G.K. Lahiri, S. Bhattacharya, B.K. Ghosh, A. Chakravorty, Inorg. Chem. 26 (1987) 4324.
[45] A.C.T. North, D.C. Phillips, F.S. Mathews, Acta Crystallogr., Sect. A 24 (1968) 351.
[46] G.M. Sheldrick, SHELXTL, version 5.03, Siemens Analytical Instruments Inc., Madison, WI, 1994.

PERGAMON

www.elsevier.nl/locate/poly

Polyhedron 19 (2000) 937–948

POLYHEDRON

Five-membered [C,N] and [N,O] metallocyclic complexes of palladium(II) with monoalkyl [α-(4-benzeneazoanilino)-*N*-benzyl]phosphonates: synthesis, characterization and antitumour activity

Ljerka Tušek-Božić [a,*], Marijana Komac [a], Manda Ćurić [a], Antonin Lyčka [b], Martina D'Alpaos [c], Vito Scarcia [d], Ariella Furlani [d]

[a] *Department of Physical Chemistry, Ruđer Bošković Institute, Bijenička c. 54, 10000 Zagreb, Croatia*
[b] *Research Institute for Organic Syntheses, 532 18 Pardubice-Rybitvi, Czech Republic*
[c] *Servizio di Spettrometria di Massa, Area di Ricerca del CNR, Corso Stati Uniti 4, 35100 Padua, Italy*
[d] *Dipartimento di Scienze Biomediche, Universitá degli Studi di Trieste, Via L. Giorgieri 7, 34127 Trieste, Italy*

Received 29 November 1999; accepted 21 February 2000

Abstract

The synthesis, spectroscopic and biological properties of the novel palladium(II) complexes with monoethyl (HL1) and monobutyl (HL2) esters of [α-(4-benzeneazoanilino)-*N*-benzyl]phosphonic acid, have been prepared and studied. These potential polydentate ligands form two types of metallocyclic compounds, those with [C,N] and [N,O] five-membered chelate rings. The former are cyclopalladated chloro-bridged binuclear complexes, $[PdL(\mu\text{-}Cl)]_2$, in which the deprotonated ligand undergoes palladation at the azo nitrogen and the *ortho*-carbon, while the latter mononuclear complexes, PdL_2, contain the organophosphorus ligand bonded through the aniline nitrogen and the deprotonated phosphonic acid oxygen. The complexes were identified and characterized by elemental analysis, magnetic and conductance measurements as well as by IR, ^1H, ^{13}C and ^{31}P nuclear magnetic resonance and ESI-mass spectroscopic studies. The in vitro antitumour activity of all the complexes was evaluated against the human KB cell line as a preliminary screening for their biological activity. The coordination behaviour of monoalkyl benzeneazophosphonates as well as the spectral and biological properties of their complexes were compared with the results reported for the corresponding dialkyl phosphonates and their palladium(II) complexes. ©2000 Elsevier Science Ltd All rights reserved.

Keywords: Palladium(II) complexes; Metallocycles; Aminophosphate complexes; Spectroscopy; Antitumour activity

1. Introduction

Organopalladium chemistry is one of the most extensive and varied areas of transition metal chemistry. Special attention has been paid to metallocyclic complexes with nitrogen donor ligands, such as various alkyl and aryl substituted amines and imines, azo, hydrazo and heterocyclic compounds. The chelate ring generally possesses three to seven members, with the five-membered ring being most favoured. These compounds are used successfully in organic synthesis [1–3], homogeneous catalysis [4], asymmetric synthesis [5], photochemistry [6] and optical resolution [7,8], and are rather promising as liquid crystals [9,10] and potential biologically active materials [11–13]. Complexes with O-bonding ligands are less abundant because palladium as a soft metal has a strong preference for N-donor ligands. Monodentate ligands of this type readily undergo substitution reactions [14–16], however, the chelate effect is important in favouring the final stability of a complex and there is a well developed chemistry for chelating ligands that combine a soft and a hard donor centre. There are known cyclometallated complexes in which the ligand is bonded through the carbon, nitrogen and oxygen atoms [17,18]. Derivatives of aminocarboxylic and aminophosphonic acids as [N,O] chelate ligands are of particular interest owing to their relevance to the natural systems and promising biological activity [19–22].

Our systematic investigation has been directed to the synthesis and characterization of new biological active palladium(II) complexes with dialkyl and monoalkyl esters of phosphonic acids derived from quinoline [14–16,21–23] and aniline [13,24,25]. It was found that most of these complexes

* Corresponding author. Tel.: +385-1-4680097; fax: +385-1-4680245; e-mail: tusek@rudjer.irb.hr

0277-5387/00/$ - see front matter ©2000 Elsevier Science Ltd All rights reserved.
PII S0277-5387(00)00339-9

displayed a certain in vitro antitumour activity against human and animal tumour cell lines. The greatest activity was found for complexes of dialkyl esters of [α-(4-benzeneazoanilino)-*N*-benzyl]phosphonic acid [13]. These ligands with several donor atoms serving as potential sites for metal coordination, i.e. the anilino and azo nitrogen as well as the phosphoryl oxygen, form two types of palladium(II) halide complexes: adducts and cyclometallated derivatives. The former are square planar with *trans*-bonded ligands through the azo nitrogen, while in the latter the deprotonated ligand undergoes palladation at the azo nitrogen and the *ortho*-carbon forming the binuclear organopalladium complexes. The anilino and phosphoryl groups are not involved in metal coordination and are free to be involved in hydrogen bonding, which is known to have some importance in metal–DNA approaching and binding interactions [26]. In the present paper we describe the synthesis as well as spectroscopic analyses and biological properties of new palladium(II) complexes of monoethyl (HL1) and monobutyl (HL2) esters of [α-(4-benzeneazoanilino)-*N*-benzyl]phosphonic acid. In the course of these investigations, the results obtained are compared with those obtained for palladium complexes of the corresponding dialkyl benzeneazophosphonates [13], and are discussed with respect to their structure–stability and structure–activity relationships. Differences in their complex-forming behaviour mainly arise from the presence of the phosphonic acid group in monoester derivatives, which enables these ligands to coordinate to the palladium ion in either their molecular or anionic form.

2. Results and discussion

2.1. Synthesis and properties

Investigations of the chelating behaviour of monoalkyl [α-(4-benzeneazoanilino)-*N*-benzyl]phosphonates (HL1 and HL2) towards the palladium(II) ion have shown that these ligands act in a bidentate manner forming two types of metallocyclic complexes, those with [C,N] and [N,O] five-membered chelate rings (Fig. 1). The reaction of HL1 and HL2 with $PdCl_4^{2-}$ (molar ratio M:L = 1:1) in methanol affords cyclopalladated binuclear complexes with metal–metal chloro bridge, $[PdL(\mu\text{-}Cl)]_2$ (**1** and **3**), in which the deprotonated ligand undergoes palladation at the azo nitrogen and the *ortho*-carbon. In basic media the phosphonate acid group is deprotonated and, thus, the reaction of sodium salts of monoalkyl phosphonates (NaL1 and NaL2) with $PdCl_4^{2-}$ in water (M:L = 1:2) gives [N,O] chelate complexes, PdL_2 (**2** and **4**), with coordinated ligand through the aniline nitrogen and the phosphonic acid oxygen. It should be noted that in an unsymmetrically substituted azobenzene derivative, orthopalladation can occur in either benzene ring with the possibility of obtaining an isomeric mixture, but in general it has been noticed that the palladium–carbon σ-bond is formed preferentially with the benzene ring having an electron-donating group [27,28]. Our results presented here, as well as those obtained for the cyclopalladated complexes of the corresponding dialkyl phosphonates [13], are in accordance with this assumption. In both cases the palladation occurred in the anilinobenzyl-substituted aromatic ring. It may be presumed that the simplified mechanism of cyclopalladation includes the initial coordination of azo nitrogen to metal ion followed by electrophilic substitution at the *ortho*-carbon atom. It is worth noting that in the case of dialkyl phosphonates, the complexes with monodentate azo N-bonded ligands could easily be isolated, while all efforts to prepare dihalide adducts of the monoester ligands were unsuccessful.

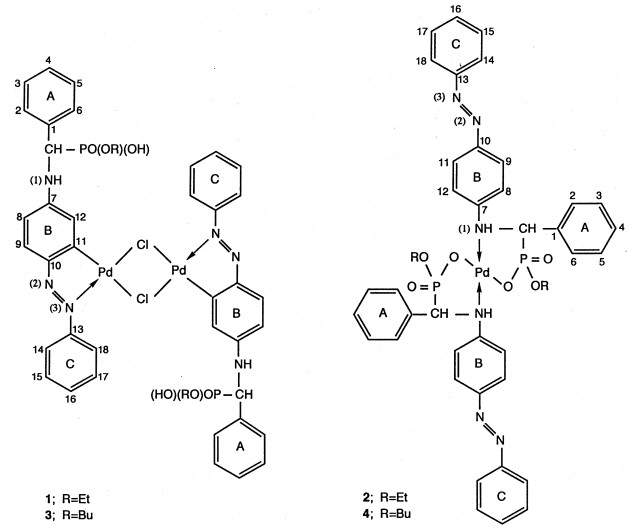


Fig. 1. Proposed chemical structures and numbering scheme of palladium complexes with monoalkyl [α-(4-benzeneazoanilino)-*N*-benzyl]phosphonates (HL1 and HL2).

The prepared complexes are red powder like or microcrystalline compounds, stable in the solid state under normal laboratory conditions. Their diamagnetic behaviour suggests square-planar stereochemistry around the palladium(II) ion. The molar conductance values (below 15 S cm^2 mol^{-1} in DMF) correspond to those of non-electrolytes. The complexes are insoluble in water, slightly soluble or soluble in common organic solvents, and very soluble in DMF and DMSO. In general, the binuclear complexes are more soluble than the mononuclear complexes, as are complexes of butyl ester with respect to complexes of its ethyl analogue. Because of the insolubility of the prepared complexes in suitable solvents, or because of their instability, we could not grow crystals for X-ray analysis. The structure of the complexes, as well as their stability and mode of decomposition, were deduced mainly from their IR, multinuclear magnetic resonance and mass spectroscopic studies. A detailed spectroscopic analysis of the free organophosphorus ligands has also been described.

2.2. Infrared spectra

There are great differences in the IR spectra of the two types of complexes, supporting different metal–ligand inter-

actions in these compounds. Significant differences may be noticed between 1600 and 1530 cm^{-1} where the NH deformation modes along with the benzene ring stretching vibrations are found. A very strong band at 1576 cm^{-1} with a shoulder at 1555 cm^{-1} is characteristic for the cyclopalladated complexes **1** and **3** with an aryl carbon–metal σ bond, while the chelate complexes **2** and **4** in this frequency region are characterized by two very intense bands near 1600 and 1585 cm^{-1}. There are marked differences also between 1250 and 950 cm^{-1} where absorption bands appear associated with the acidic monoalkyl phosphonate group PO(OR)(OH) [29,30]. In the cyclopalladated complexes two bands at 1237 and 1198 cm^{-1} could be ascribed to the P=O stretching absorption, while the PO–H stretching vibration is superimposed on the PO–C stretching, giving broad and complex bands between 1030 and 950 cm^{-1}.

In the spectra of the mononuclear complexes **2** and **4** there is no evidence of the bands associated with P–O–H vibrations, since in these complexes the phosphonate ligands act in the anionic form. This is confirmed by the presence of the $\nu(PO_2^-)$ absorptions as medium or strong bands between 1230 and 1200 cm^{-1} for the antisymmetric and between 1070 and 1025 cm^{-1} for the symmetric mode of this vibration. In the latter frequency range the ν(PO–C) absorption is superimposed upon that of the symmetric PO_2^- vibration [31,32].

The chloro-bridged cyclopalladated complexes **1** and **3** in the far-IR region show two Pd–Cl stretching bands. The higher-frequency band at 307 cm^{-1} is attributed to the vibration of the Pd–Cl bond *trans* to the nitrogen atom, while the lower-frequency band at 255 cm^{-1} is ascribed to the vibration of the Pd–Cl bond *trans* to the σ-bonded carbon. This is a consequence of a greater *trans* influence of a σ-bonded carbon compared to that of a nitrogen atom [33].

2.3. Mass spectra

Electrospray ionization mass spectrometry (ESI-MS) is a soft ionization technique which has recently been widely used in the structural analysis of non-volatile and thermally labile species such as large biomolecules [34,35] and various coordination metal compounds, especially polynuclear complexes [36,37]. This method allows pre-existing ions in solution to be very gently transferred to the gas phase with minimal fragmentation, followed by conventional mass spectrometry. The ESI mass spectrometric investigation of monoalkyl anilinobenzylphosphonates and their palladium(II) complexes has shown that their mass fragmentation pattern is much less extensive than that obtained for the corresponding dialkyl phosphonates and their palladium complexes studied under fast atom bombardment (FAB) conditions [24,25]. In the ESI negative-ion mass spectra of the free non-coordinated organophosphorus ligands, the deprotonated molecular ion was observed as the base and the only intense peak, since the phosphonic acid group could easily be deprotonated to give an anion. In the corresponding spectra obtained in the positive-ion mode, the ligand fragmentation is more pronounced and the most abundant fragment ion is formed by cleavage of the C–P bond and complete loss of the phosphonate ester group. The abundance of the protonated molecular ion is only about 5% as is shown in Fig. 2 for HL2, as an example of the common decomposition pattern for both alkyl monoesters in positive/negative ESI mass spectra. All palladium complexes have been investigated by spectrometric measurements carried out under positive/negative-ion ESI conditions with different cone voltages, using methanol as the solvent and the mobile phase. The negative-ion mass spectra give more relevant structural information than the spectra obtained in the positive-ion mode. The molecular ion as well as the fragment ions containing palladium are identified by the presence of the characteristic clusters of isotopic peaks covering about 10 *m/z* units, due to the presence of the numerous palladium isotopes. The fragmentation pathway depends mainly on the type of complex and the major structurally informative fragments in negative-ion mass spectra are summarized in Table 1. The first point to be noted is that all complexes exhibit the deprotonated molecular ion and its relative abundance is about 3% for the cyclopalladated binuclear complexes **1** and **3** and about 1% for the mononuclear palladium complexes **2** and **4**. There are great differences in mass spectroscopic behaviour between these two types of complexes.

The fragmentation pathways of the cyclopalladated complexes, including possible structures of Pd-containing ions, proposed on the basis of the accurate mass measurements and isotopic cluster analysis are reported in Scheme 1 and Fig. 3(a). The loss of $Cl^{\bullet}$ produces the fragment ion which corresponds to binuclear monobridged species. In this respect it

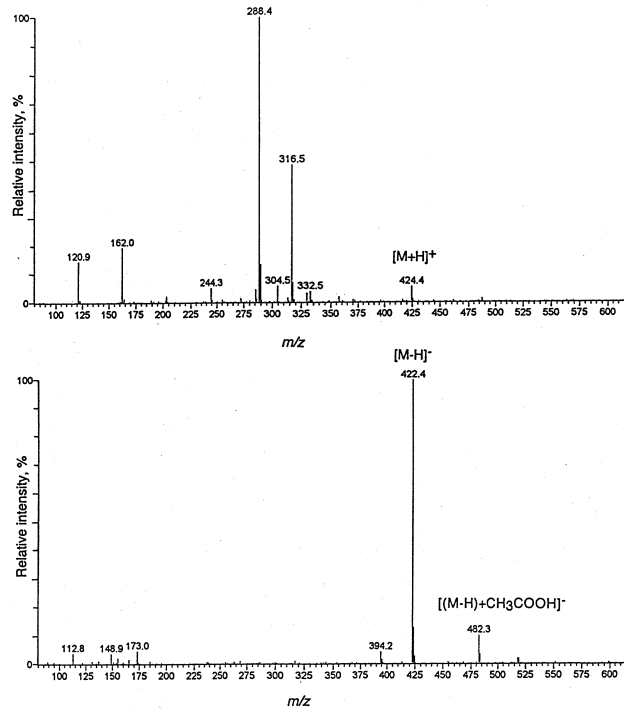


Fig. 2. Positive-ion and negative-ion ESI mass spectra of HL2 in a mixture of acetonitrile and water (50:50) with 0.1% acetic acid at a cone voltage of 50 V.

Table 1
Major ion fragments in negative-ion mass spectra of Pd(II) complexes [a]

Ionic species [b]	*m/z* (relative intensity %) [c]			
	1	**2**	**3**	**4**
$[(M–2H)+Na]^-$	1091 (7)		1147 (4)	
$[M–H]^-$	1069 (3)	893 (1)	1125 (3)	949 (0.9)
$[(M–2H)–Cl+Na]^{-\bullet}$	1056 (3.5)		1112 (3.5)	
$[(M–H)–Cl]^{-\bullet}$	1034 (9)		1090 (11)	
$[(M–H)–Cl–HCl]^{-\bullet}$	998 (11)		1054 (5)	
$[(HL)_2–2H+Na]^-$		811 (1)		867 (0.9)
$[(HL)_2–H]^-$		789 (0.4)		845 (0.5)
$[PdLCl_2+Me]^-$	585 (5)		613 (5)	
$[PdLCl_2]^-$	570 (12)		598 (17)	
$[(PdLCl)–2H+Na]^-$	556 (15)		584 (15)	
$[(PdLCl)–H+Me]^-$	549 (8)		577 (10)	
$[(PdLCl)–H]^-$	534 (100)		562 (100)	
$[(PdL)–H+MeOH]^{-\bullet}$	531 [d]	531 (0.8)	559 [d]	559 (1)
$[(PdL)–H]^{-\bullet}$	499 (14)	499 (0.7)	527 (10)	527 (0.3)
$[L+MeOH]^-$	426 (6)	426 (0.6)	454 (3)	454 (0.6)
$[L+Me]^-$	409 (29)	409 (0.7)	437 (11)	
$[L]^-$	394 (63)	394 (100)	422 (79)	422 (100)

[a] In methanol, cone voltage 50 V.
[b] L = L1, L2.
[c] Ion masses referenced to isotopes ^{106}Pd and ^{35}Cl.
[d] Partly overlapped with $[(PdLCl)–H]^-$ ion.

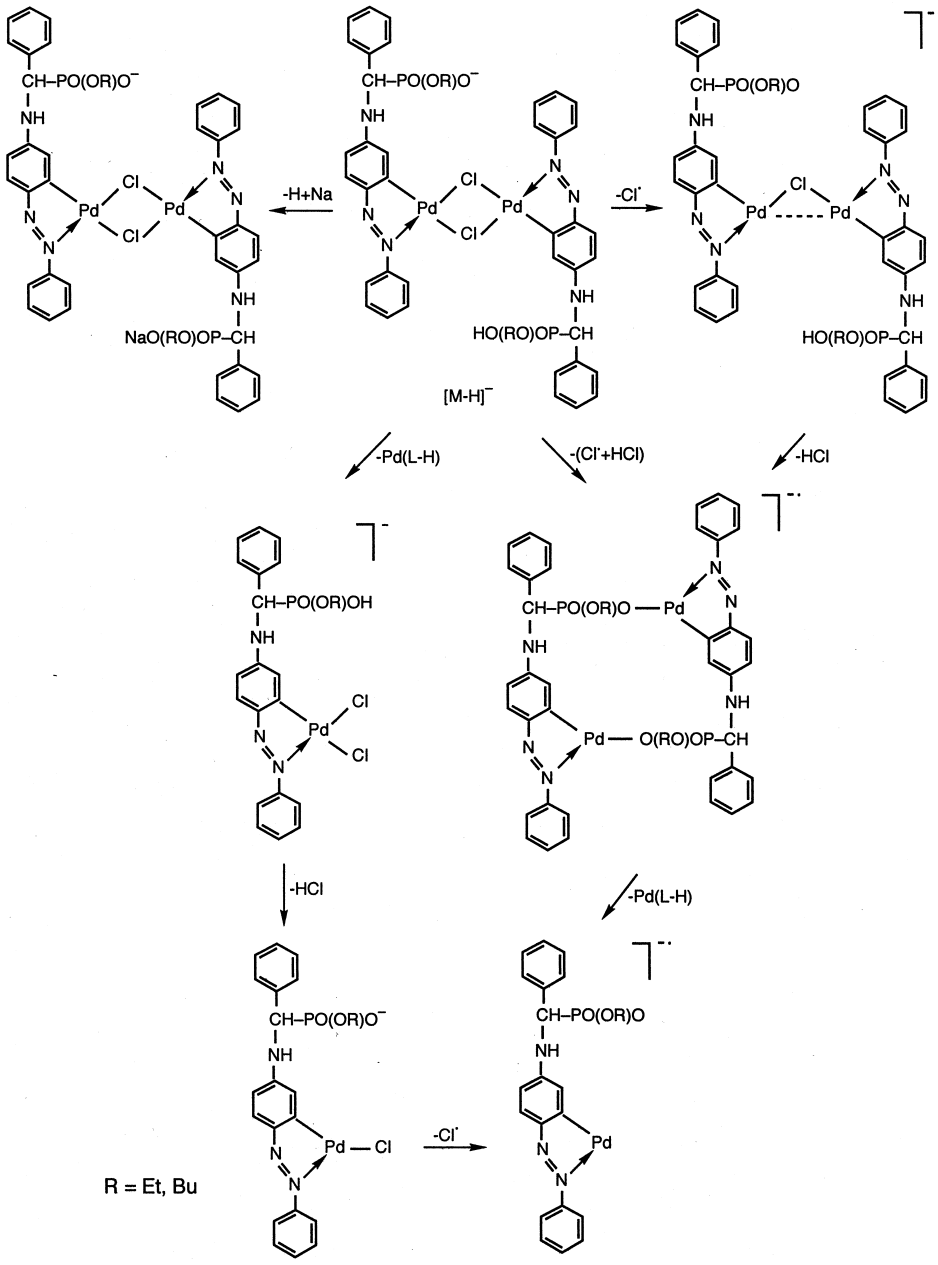
could be pointed out that some monohalide-bridged binuclear palladium complexes have been isolated and characterized [38,39]. The further loss of hydrogen chloride involves structural rearrangement of the species giving a dinuclear complex in which are two cyclopalladated moieties bonded through the deprotonated phosphonic acid groups. The loss of one palladium and one ligand molecule from the parent complex ion leads to a deprotonated dichloro monopalladated complex $[PdLCl_2]^-$, which by the sequential losses of HCl and $Cl^\bullet$ leads finally to the orthometallated species $[(PdLCl)–H]^-$ and $[(PdL)–H]^{-\bullet}$, respectively. The former mono-chloropalladium fragment ion is the base peak in the spectra of these complexes. The high stability of such metallated systems is in agreement with the reported high stability of palladium(II) five-membered cyclometallated systems having nitrogen donor ligands [24,40,41]. Of the organic fragments, the most intense peak (60–80%) corresponds to the deprotonated ligand molecule.

Investigations of decomposition properties of the mononuclear complexes **2** and **4** indicate much less stability of these compounds with respect to the binuclear cyclopalladated complexes. The predominant pathway for their fragmentation is complete dissociation of the phosphonate ligand molecules (Fig. 3(b)). The deprotonated ligand ion is the major and the only intense fragment ion in the spectra of these complexes. The relative abundance of all other fragment ions is very small amounting up to 1%. The most abundant palladium containing fragment ions are the parent molecular ion $[(PdL_2)–H]^-$, and the ion containing only one [N,O] bonded organophosphorus ligand. Dimerization of the free organophosphorus ligand gives rise to $[(HL)_2–H]^-$ ions at *m/z* 798 and 845, respectively. The sodium adducts are also present.

It is worth noting that the spectra of complexes show some ions based on addition of methanol as solvent molecules as well as addition of the sodium ion either to the parent complex or to the ligand molecules or their fragments; this is in agreement with the ESI mass results obtained for various complex compounds [37,42]. Some of the most abundant adduct ions are given in Table 1.

2.4. NMR spectra

^{1}H, ^{13}C and ^{31}P NMR data of free ligands HL1 and HL2, sodium salt NaL2 and both types of palladium complexes derived from the butyl ester (complexes **3** and **4**), obtained in $CDCl_3$ solution, are summarized in Tables 2 and 3, and presented in Figs. 4–7. The numbering scheme is shown in Fig. 1. Complexes of ethyl ester are not sufficiently soluble for spectral analysis. The results obtained are compared and discussed with those reported for dialkyl [α-(4-benzeneazoanilino)-*N*-benzyl]phosphonates and their palladium complexes [13,43]. The broadening of H/C aromatic absorptions in the free monoesters with respect to those observed in the corresponding diesters could be connected with their dimeric structure in chloroform solution [30]. The most pronounced broadening could be observed for protons H-9,11 and H-15,17, as shown in Figs. 4 and 5(a). The slight upfield shift (up to 0.25 ppm) of most of the aromatic protons with respect to those in diesters could be attributed to mutual interligand shielding between two hydrogen bonded monoester molecules lying parallel to one another. The ligand



Scheme 1. ESI negative-ion fragmentation pathway for complexes **1** and **3**.

association is ascribed to the strong intermolecular hydrogen bonding between the phosphonic acid groups, which is confirmed by the presence of a very broad absorption of the acidic OH resonance around 10 ppm. In the case of sodium salt (Fig. 5(c)) the signal broadening of the aromatic protons is not visible, as well as in the spectra of monoesters in DMSO solution (Fig. 5(b)), in which there is no ligand association. The assignment of all aromatic H/C resonances was confirmed unambiguously by two-dimensional homonuclear and heteronuclear NMR experiments. As examples, Fig. 4 shows a ^{1}H–^{1}H COSY spectrum of HL1 and Fig. 6 shows a part of the long-range ^{1}H–^{13}C HMBC spectrum of sodium salt NaL2. In addition, the signal assignment of the carbons C(1)–C(6) was supported with the long-range phosphorus–carbon couplings.

The spectra of both types of complexes are rather complex, caused either by the removal of the degeneracy of resonances due to metal coordination (complex **3**) or by the presence of more isomeric forms (complex **4**). The most pronounced chemical shift changes with respect to the uncomplexed ligand could be noticed for the atoms involved in metal binding and those in the vicinity of the ligation site. In the binuclear complex **3**, with palladation at the azo nitrogen and the *ortho*-carbon, there are significant differences in the B-phenyl and C-phenyl rings of the ligand molecule. The proton NMR spectrum shows a great broadening of all signals and an extensive overlapping of the aromatic resonances (Fig. 5(c)) due to the dimeric nature of this complex. The non-equivalence of the aromatic protons H(8) and H(12) and their upfield shifts of 0.41 and 0.19 ppm, respectively, supports

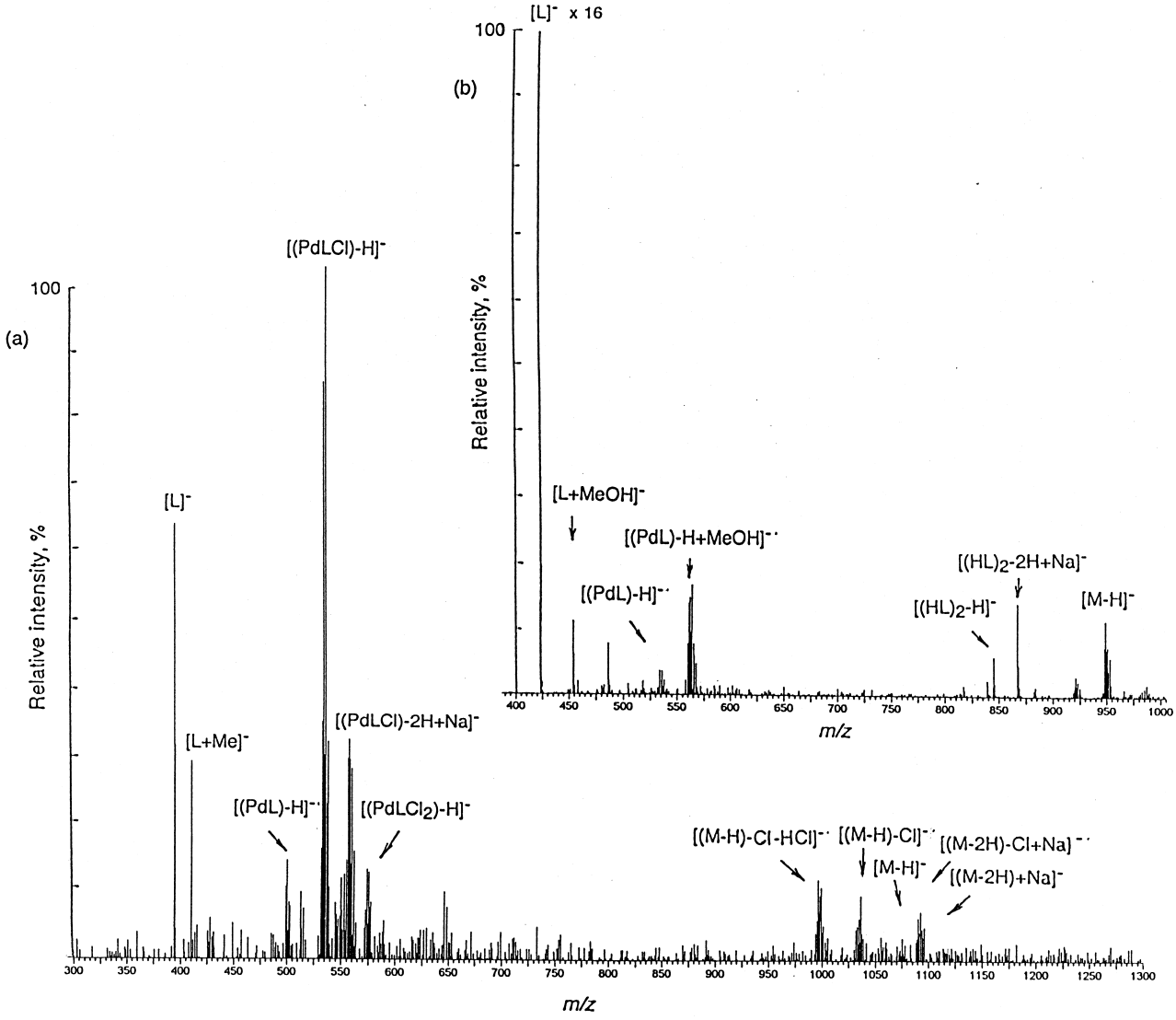


Fig. 3. Negative-ion ESI mass spectra of complexes **1** (a) and **4** (b) in methanol at a cone voltage of 50 V.

the metallation at C-11 of the B-phenyl ring. The shielding of these protons is caused by the flow of electron density from the d orbital of the palladium atom into this aromatic ring. Resonances of the other aromatic protons could not be clearly resolved owing to complex overlap of signals between 7.20 and 7.80 ppm. The ^{31}P NMR spectrum of this complex shows a broad signal at 21.88 ppm (Fig. 7(a)). The ^{13}C NMR spectrum of this complex gives much more spectral information. Comparing with the spectrum of the free ligand, the most important changes appear in resonances related to carbons C-7-C-12, as an identification of changes in the electron density of this aromatic ring due to *ortho*-metallation. For this reason none of these carbons are still equivalent. The palladium-bound C(11) is greatly shifted downfield by 31.66 ppm, C(9) and C(12) are shifted to a lesser extent by 5.87 and 2.93 ppm, respectively, while an upfield shift of 7.07 ppm for the C(8) atom, *para* to the Pd atom, clearly indicates the existence of some metal-to-ligand π-back-bonding. As expected, the overall spectral pattern of complex **3** is very similar to that of the cyclopalladated complex of dibutyl benzeneazophosphonate owing to the same palladium–ligand bonding [43].

The spectra of mononuclear complex **4** show a great complexity arising from the existence of more isomeric species in dynamic equilibrium with different magnetic environment. This can be interpreted by the presence of a new chiral centre on the nitrogen atom due to its coordination to palladium, in addition to that at the adjacent PCH asymmetric carbon and phosphorus atoms, as well as by the restricted rotation around the C–N linkage. As a consequence, the proton NMR spectrum of this complex shows a great broadening of all proton resonances (Fig. 5(d)), while its ^{13}C NMR spectrum is characterized by extensive signal splitting and multiple overlap of signals, which prevent signal assignments for almost all aromatic proton and carbon atoms. The existence of more isomeric species is visible in the ^{31}P NMR spectrum of this complex. There are few signals in the range 5–25 ppm as was shown in Fig. 7(b). The two most intense signals are at 14.46

Table 2
^{1}H NMR data [a]

	HL1	HL2 [b]	NaL2	**3**	**4**
H-2,6	7.54 d J(HH) = 7.5	7.54 d (7.56) J(HH) = 7.6 (7.0)	7.37 d J(HH) = 7.0	[c]	[c]
H-3,5	7.35 t J(HH) = 7.3	7.35 t (7.36) J(HH) = 7.3 (7.2)	7.21 t J(HH) = 7.0	[c]	[c]
H-4	7.29 t J(HH) = 7.4	7.29 t [d] (7.32) J(HH) = 7.4 (7.1)	7.17 t J(HH) = 7.6	[c]	[c]
H-8,12	6.75 d J(HH) = 8.8	6.72 d (6.76) J(HH) = 8.2 (8.8)	6.66 d J(HH) = 8.4	6.53, 6.31 br s [e]	6.62 br s
H-9,11	7.73 br s	7.72 br s (7.81 d) J(HH) = (8.7)	7.69 d J(HH) = 8.6	[c]	[c]
H-14,18	7.61 d J(HH) = 7.1	7.63 d (7.85) J(HH) = 6.5 (7.6)	7.78 d J(HH) = 7.5	[c]	[c]
H-15,17	7.21 br m [f]	7.22 br m [f] (7.47 d) J(HH) = (7.3)	7.43 t J(HH) = 7.5	[c]	[c]
H-16	7.31 t [g] J(HH) = 7.3	7.31 t [g] (7.39) J(HH) = 7.4	7.36 t [h] J(HH) = 7.2	[c]	[c]
PCH	4.97 d ^2J(PC) = 22.8	4.95 d (4.92) ^2J(PC) = 22.9 (23.9)	4.46 dd ^2J(PC) = 23.2 J(NH) = 6.4	4.91 br s	4.80 br d ^2J(PC) = 23.8
NH	7.18 [i]	7.20 [i] (5.83)	6.22 br s	6.09 br s	[j]
OH	9.80 [k]	10.40 [k]	3.28 br s [l]	[j]	
OCH_2	3.99, 3.82 m [m]	3.94, 3.76 m [m] (3.64; 3.91; 4.12) [o]	3.58, 3.53 m [n]	3.90, 3.65 br s [n]	3.70 br m [n]
$OCH_2CH_2CH_2CH_3$		1.52 m [p] (1.42; 1.63) [o]	1.36 m [p]	1.46 br s	1.40 br s
$OCH_2CH_2CH_2CH_3$		1.31 m [r] (1.23; 1.38) [o]	1.12 m [r]	1.25 br s	1.15 br s
CH_3	1.21 t J(HH) = 7.1	0.85 t (0.84; 0.90) [o] J(HH) = 7.3 (7.3)	0.72 t J(HH) = 7.2	0.83 br s	0.75 br s

[a] Spectra recorded in $CDCl_3$ (δ in ppm, coupling constants in Hz). Multiplicities: s, singlet; d, doublet; dd, doublet of doublet; t, triplet; m, multiplet; br, broad signal.
[b] Data for dibutyl [α-(4-benzeneazoanilino]-*N*-benzyl]phosphonate from Ref. [43] are given in parentheses for comparison.
[c] Resonance not resolved owing to extensive broadening and overlapping of signals between 6.8–8.0 ppm.
[d] Partly overlapped with H16.
[e] No equivalent protons. The first value is related to H-8 and the second to H-12.
[f] Overlapped with NH. Value obtained from a ^{1}H–^{1}H COSY experiment.
[g] Partly overlapped with H-4. Value obtained from a ^{1}H–^{1}H COSY experiment.
[h] Value obtained from a ^{1}H–^{13}C HMBC experiment. Signal partly overlapped with H-2,6.
[i] Overlapped with H-15,17. Tentative value obtained from a ^{1}H–^{13}C HMBC experiment.
[j] Resonance overlapped with aromatic protons.
[k] Very broad signal due to strong hydrogen bonding.
[l] OH resonance from H_2O.
[m] Centres of two multiplets. Separate resonances for two geminal protons.
[n] Centres of two multiplets. Resonances for two geminal protons are partly overlapped.
[o] Values in parentheses related to protons of two diastereotopic butyl groups of dibutyl ester.
[p] Appears as quintet with J(HH) ~ 7.2 Hz.
[r] Appears as sextet with J(HH) ~ 7.4 Hz.

and 18.90 ppm. The fact that the ^{31}P NMR chemical shifts of the complex do not differ much from that observed for the free ligand and its sodium salt at 18.59 and 19.19 ppm, respectively, supports the conclusion that coordination of phosphonate to metal ion is predominantly ionic and scarcely affects the electron density of the phosphonate phosphorus [44].

The NMR spectral studies have shown that complexes retain their integrity in chloroform solution, but decompose in DMSO. This solvent with strong complexing ability initiates dissociation of the complex moiety by displacing the organophosphorus ligand. As could be expected, the decomposition process is much more pronounced in the [N,O] chelate complexes.

In conclusion, the results obtained by NMR studies are in agreement with those of mass spectrometry, indicating that the five-membered [C,N] chelate ring in the binuclear chloro-bridged complexes is much more stable than the five-membered [N,O] ring in the mononuclear chelate complexes. This behaviour is in accordance with the assumption that the chelate ring where the cyclopalladation is assisted by the coordination of a nitrogen atom has a remarkable stability.

Table 3
^{13}C NMR data [a]

	HL1	HL2 [b]	NaL2	**3**
C-1	136.30	136.42 (135.50)	138.52	135.15
			^{2}J(PC) = 3.5	
C-2,6	127.89	128.00 (127.79)	127.47	127.82
	^{3}J(PC) = 4.9	^{3}J(PC) = 5.0 (5.5)	^{3}J(PC) = 4.1	
C-3,5	128.49	128.57 (128.54)	128.44	128.69
	^{4}J(PC) = 2.3	^{4}J(PC) = 2.3 (2.4)	^{4}J(PC) = 2.3	
C-4	127.69	127.76 (127.95)	127.27	128.15
	^{5}J(PC) = 2.9	^{5}J(PC) = 2.7 (3.1)	^{5}J(PC) = 3.4	
C-7	147.60	148.43 (149.08)	150.12	147.90
			^{3}J(PC) = 14.0	
C-8	114.55	114.57 (113.31)	113.86	107.50
C-12	114.55	114.57 (113.31)	113.86	117.50
C-9	124.20	124.04 (124.79)	124.90	129.91
C-11	124.20	124.04 (124.79)	124.90	155.70
C-10	141.42	141.59 (145.19)	145.21	144.50
C-13	154.28	153.74 (152.88)	152.97	150.28
C-14,18	120.48	120.68 (122.16)	122.30	123.62
C-15,17	128.86	128.96 (128.77)	128.90	128.05
C-16	129.45	129.55 (129.52)	129.66	129.01
PCH	56.86	56.92 (55.99)	56.82	56.10
	^{1}J(PC) = 146.2	^{1}J(PC) = 146.2	^{1}J(PC) = 139.3	^{1}J(PC) = 147.1
OCH_2	62.87	66.64 (66.99; 67.10) [c]	66.47	67.46
	^{2}J(POC) = 7.1	^{2}J(POC) = 7.3 (7.1)	^{2}J(POC) = 6.0	
CH_3	16.42	13.60 (13.39; 13.43) [c]	13.77	13.56
	^{3}J(POCC) = 6.2			
$OCH_2CH_2CH_2CH_3$		32.61 (32.19; 32.40) [c]	32.73	32.31
		^{3}J(POCC) = 6.2 (5.5)	^{3}J(POCC) = 6.9	
$OCH_2CH_2CH_2CH_3$		18.69 (18.37; 18.52) [c]	18.74	18.50

[a] Spectra recorded in $CDCl_3$ (δ in ppm, coupling constants in Hz).
[b] Data for dibutyl [α-(4-benzeneazoanilino]-*N*-benzyl]phosphonate from Ref. [43] are given in parentheses for comparison.
[c] Values of dibutyl ester are related to two diastereotopic butyl groups.

Furthermore, it is known that palladium as a soft metal prefers nitrogen bonding over that of oxygen and therefore the coordination of oxygen is more easily displaced. On the other hand, it is worth noting that our recently reported investigations of the coordination of monoethyl 2-quinolylmethylphosphonate to the palladium(II) ion have shown that this monophosphonate ligand forms a very stable PdL_2 complex with a six-membered [N,O] chelate ring via the quinoline nitrogen and the phosphonic acid oxygen [14], in spite of the general belief that the six-membered ring is less favoured. The differences observed in stability between the six-membered [N,O] ring in the quinoline complex and a five-membered ring in the benzeneazoanilino phosphonate complex could be ascribed on one side to the relatively low basicity of the benzalaniline nitrogen compared with that of the quinoline nitrogen, caused by participation of its electron pair in resonance with the adjacent azobenzene π-system, and, on the other side, to the influence of steric factors. The benzeneazoaniline ligands are more bulky than the quinoline derivative. The geometric and steric requirements of the ligand containing two or more donor atoms are very important in determining the number of donor atoms that will coordinate, the final geometry, and the stability of the metallic species.

2.5. In vitro antitumour activity

The antitumour activity of the complexes was determined in vitro on the KB cell line derived from a human oral epidermoid carcinoma as a preliminary screening for their biological activity. The results obtained have shown that the concentration of the complex required to inhibit tumour cell growth by 50% was higher than 10^{-5} mol l^{-1}. There are no significant differences in response between complexes of ethyl and butyl esters, nor between the two types of complexes in spite of their differential structural properties and most probably different DNA binding and nicking ability. When comparing results of the in vitro assays related to the cyclopalladated complexes **1** and **3** with those obtained for the corresponding palladated azobenzene complexes of dialkyl phosphonates [13], it could be seen that diester complexes show about ten times higher activity ($< 5 \times 10^{-6}$ mol l^{-1}) than the monoester complexes which may be ascribed to their greater lipophilicity and solubility. In this regard it is worth noting that similar effects were observed for the antitumour activity of palladium(II) complexes with diethyl and monoethyl esters of quinolylmethylphosphonic acids [15,16,21]. The lipophilicity of the complexes increases with increasing bulkiness from monoester to diester derivatives

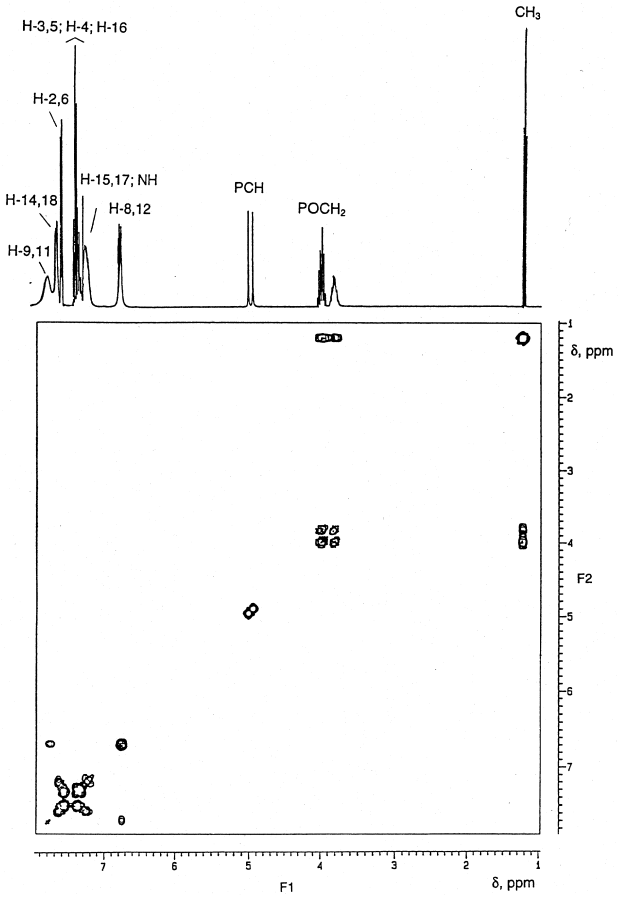


Fig. 4. ^1H–^1H COSY spectrum of HL1 in $CDCl_3$.

and may facilitate transport across the cellular membrane [45,46].

3. Experimental

3.1. Materials

Monoethyl and dibutyl [α-(4-benzeneazoanilino)-*N*-benzyl]phosphonates (HL1 and HL2) and their sodium salts (NaL1 and NaL2), prepared as previously described [47], were purified by recrystallization from absolute ethanol prior to use. All other reagents and solvents were analytical grade products and were used without purification.

3.2. Preparation of complexes

3.2.1. $[Pd(L1)Cl]_2$ (1)

The reaction of HL1 (0.205 g, 0.52 mmol) and $Na_2[PdCl_4]$ (0.160 g, 0.54 mmol) in methanol (10 ml) at room temperature gave after stirring for 5 days a precipitate, which was separated, washed with cold methanol, and dried under vacuum. The dried complex was dissolved in hot chloroform (5 ml), and after filtering to remove some black decomposition products, the solution was evaporated to dryness yielding a dark red glassy solid which was stored overnight under vacuum. Yield 0.156 g (56%). *Anal.* Found: C, 47.13; H, 4.17; N, 8.09; Pd, 19.11. Calc. for $C_{42}H_{42}N_6O_6Pd_2P_2Cl_2$: C, 47.03; H, 3.95; N, 7.84; Pd, 19.84%. IR: ν(C=C), δ(N–H), 1576vs, 1554sh; ν(P=O), 1237w, 1198w-m; ν(PO–C), ν(P–OH), 1031s, 997m; ν(Pd–Cl), 307w, 255vw.

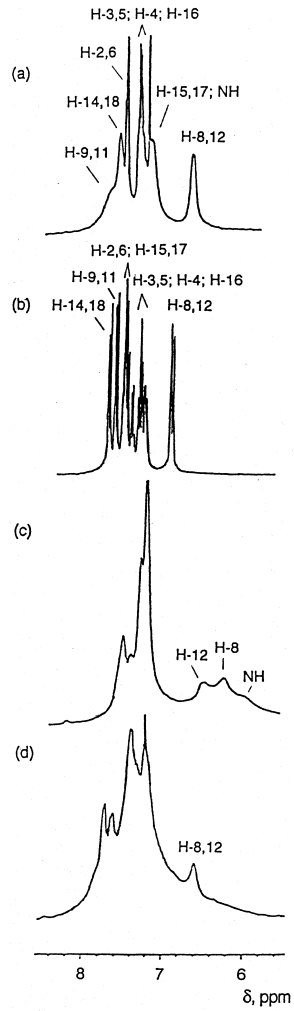


Fig. 5. Aromatic part of ^1H NMR spectra: (a) HL2 in $CDCL_3$, (b) HL2 in DMSO-d_6, (c) **3** in $CDCl_3$ and (d) **4** in $CDCl_3$.

3.2.2. $Pd(L1)_2$ (2)

A concentrated aqueous solution of $K_2[PdCl_4]$ (0.081 g, 0.25 mmol) was added dropwise to a stirred solution of NaL1 (0.203 g, 0.49 mmol) in water (10 ml). The reaction mixture was stirred continuously for 3 h at room temperature. The red precipitate formed was filtered off, washed with cold water and dried under vacuum over P_2O_5 for 24 h. Yield 0.214 g (52%). *Anal.* Found: C, 56.41; H, 4.97; N, 9.37; Pd, 12.41. Calc. for $C_{42}H_{42}N_6O_6PdP_2$: C, 56.35; H, 4.73; N, 9.40; Pd, 11.89%. IR: ν(C=C), δ(N–H), 1601vs, 1583vs; $\nu_{as}(PO_2^-)$, 1224m, 1207m; $\nu_{sym}(PO_2^-)$, ν(PO–C), 1070m, 1046s.

3.2.3. $[Pd(L2)Cl]_2$ (3)

This complex was prepared in a similar manner as complex **1** by stirring the reaction mixture of HL2 (0.204 g, 0.48

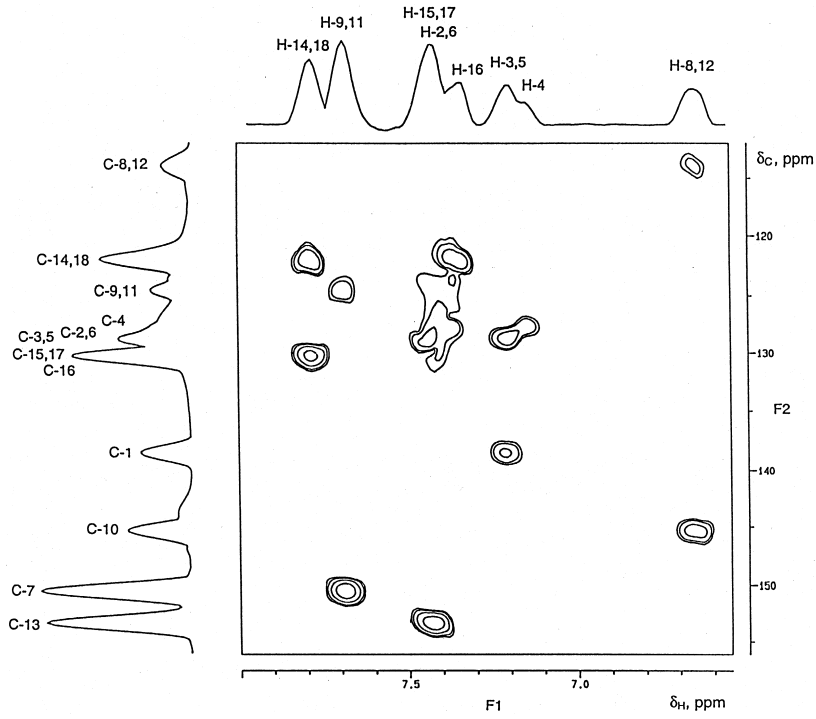


Fig. 6. Aromatic part of the long-range ^{1}H–^{13}C HMBC spectrum of NaL2.

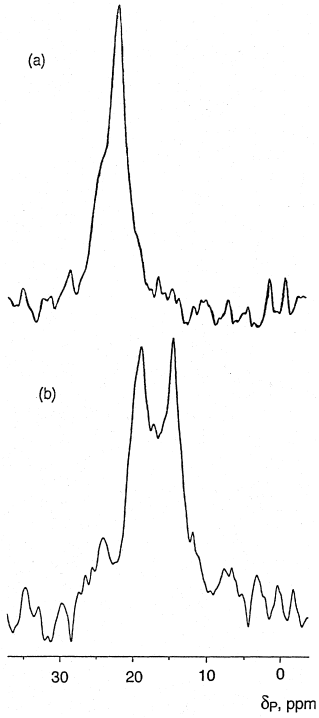


Fig. 7. ^{31}P NMR spectra of complexes **3** (a) and **4** (b).

mmol) and $Na_2[PdCl_4]$ (0.145 g, 0.49 mmol) in methanol (5 ml) for 3 days. Yield 0.114 g (42%). *Anal.* Found: C, 48.65; H, 4.49; N, 7.17; Pd, 18.87. Calc. for $C_{46}H_{50}N_6O_6Pd_2P_2Cl_2$: C, 48.95; H, 4.47; N, 7.45; Pd, 18.86%. IR: ν(C=C), δ(N–H), 1576vs, 1555sh; ν(P=O), 1235w, 1198m; ν(PO–C), ν(P–OH), 1023m-s, 997m-s; ν(Pd–Cl), 306w, 255vw.

*3.2.4. Pd(L2)$_2$ (**4**)*

This complex was prepared by almost the same procedure as complex **2** by reaction of sodium salt of L2 (0.206 g, 0.46 mmol) and $K_2[PdCl_4]$ (0.081 g, 0.25 mmol) in water (5 ml). Yield 0.175 g (80%). *Anal.* Found: C, 57.96; H, 5.39; N, 8.96; Pd, 11.40. Calc. for $C_{46}H_{50}N_6O_6PdP_2$: C, 58.08; H, 5.30; N, 8.84; Pd, 11.19%. IR: ν(C=C), δ(N–H), 1598vs, 1589vs; $\nu_{as}(PO_2^-)$, 1205s br; $\nu_{sym}(PO_2^-)$, ν(PO–C), 1063s, 1025s.

3.3. Physical measurements and analyses

Melting points were determined on a hot stage microscope and are uncorrected. Infrared spectra were recorded on a Perkin Elmer 580 B spectrophotometer using KBr (4000–250 cm^{-1}) and polyethylene (400–200 cm^{-1}) pellets.

The electrospray mass spectrometric measurements were performed on a Navigator (Finnigan, San Jose, CA) instrument equipped with ESI ion source. The ligands were recorded in positive and negative ion modes using methanol or a mixture of acetonitrile and water (50:50) with 0.1% acetic acid as the solvent and the mobile phase. Complexes were recorded in methanol in both modes. The sample solution (10 μl of 10^{-5} mol l^{-1}) was introduced into the ion source, at a flow rate of 0.3 ml min^{-1}, using a Rheodyne external loop injector coupled to a Thermo Separation (San Jose, CA) spectra series HPLC pump. The measurements were performed using nitrogen as nebulizing gas, and using different cone voltages (30, 50 and 120 V). Expected natural abundance isotope clusters patterns for various ion clusters were calculated with the Isotopic Distribution Program

(IDS) contained in the FTMS 7.01 application program of the NICOS operating system using polynomial expansion based on natural abundances of the Pd and Cl isotopes.

The ^{1}H and ^{13}C one- and two-dimensional NMR spectra were performed with Varian broadband Gemini 300 and Bruker AMX 360 spectrometers, operating at 75.46 and 90.56 MHz for the ^{13}C resonance, respectively. Spectra were recorded in $CDCl_3$ or DMSO-d_6 containing $SiMe_4$ as an internal standard. Digital resolution in ^{1}H NMR spectra was 0.25 Hz, while in ^{13}C NMR it was 0.60 Hz per point. The narrower spectral regions of special interest were measured also with a smaller spectral width and greater digital resolution (down to 0.2 Hz). The following techniques were used: proton-noise decoupling, attached proton test (APT), ^{1}H–^{1}H COSY, NOESY and ^{1}H–^{13}C COSY, long-range ^{1}H–^{1}H COSY, HMQC and HMBC. The ^{1}H–^{1}H COSY spectra were obtained in the magnitude mode, while NOESY spectra were obtained in the phase-sensitive mode. All two-dimensional experiments were performed by standard pulse sequences, using Gemini Data System software Version 6.3 Revision A (for VXR-4000) and Bruker microprograms of UXNMR software Version 940501.3 [48]. For proton decoupling Waltz-16 modulation was used. ^{31}P NMR spectra were measured at 145.79 MHz on a Bruker AMX 360 spectrometer in $CDCl_3$ with external 85% H_3PO_4 in a coaxial capillary.

Conductance measurements were carried out at room temperature using a CD 7A Tacussel conductance bridge for 10^{-3} mol l^{-1} solutions in DMF. Magnetic susceptibilities in the solid state were measured at room temperature by the standard Gouy method using a Cahn-Ventron RM-2 balance and $CuSO_4 \cdot 5H_2O$ as the susceptibility standard. Elemental analyses were performed in the Ruđer Bošković Institute.

3.4. In vitro antitumour assays

Antitumour activity was assayed with the human epidermoid KB cell line [49] according to previously described methods [21,22,50]. The cells were maintained in Eagle's minimum essential medium (MEM) supplemented with glutamine, non-essential amino acids (1%) and newborn calf serum (10%). The cell population doubling time was ca. 24 h. For the cytostatic assay a cell culture in the exponential growth phase was used. The compounds were dissolved immediately before use in sterile DMSO, and these solutions were diluted with the growth medium to the desired concentrations. The final DMSO concentration in the culture medium, 0.5%, showed no cytostatic effect in preliminary tests. At least five concentrations of each compound were used and each agent was assayed on at least three separate occasions. The incubation time was 72 h. The cell growth was determined by the sulforhodamine B (SRB) method [51]. The cytostatic activity was evaluated from the inhibition of cell growth in the treated cultures with respect to the controls. The significance of the results was evaluated by use of classical Student's t test ($p < 0.01$). The activity was expressed as the concentration of the complex at which tumour cell growth showed 50% inhibition (IC_{50}), and was calculated by linear regression analysis [52]. The activity threshold was set at 10^{-5} mol l^{-1}, since this appears to be a fairly realistic cutoff point for most compounds [53].

Acknowledgements

Financial support granted by the Ministry of Science, Technology and Informatics of the Republic of Croatia (grant No. 009806-07) is gratefully acknowledged. The authors would like to thank Mr Ž. Marinić and B. Metelko (Ruđer Bošković Institute) for some of the NMR spectra. A.L. thanks the Grant Agency of the Czech Republic (grant No. 104-99-0835) for financial support.

References

[1] A.D. Ryabov, Synthesis (1985) 233.
[2] M. Pfeffer, Pure Appl. Chem. 64 (1992) 335.
[3] W.A. Herrmann, C. Brossmer, K. Ofele, C.P. Reisinger, T. Priermeier, M. Beller, H. Fischer, Angew. Chem., Int. Ed. Engl. 34 (1995) 1844.
[4] A. Bose, C.H. Saha, J. Mol. Catal. 49 (1989) 271.
[5] V.I. Sokolov, Pure Appl. Chem. 55 (1983) 1837.
[6] R. Schwartz, G. Gliemann, J. Jolliet, A. von Zalevsky, Inorg. Chem. 28 (1989) 742.
[7] R.J. Doyle, G. Salem, A.C. Willis, J. Chem. Soc., Dalton Trans. (1995) 1867.
[8] J. Albert, J. Granell, G. Muller, D. Sainz, M.F. Bardia, X. Solans, Tetrahedron Asymm. 6 (1995) 325.
[9] A.M.G. Godquin, P.M. Maitlis, Angew. Chem., Int. Ed. Engl. 30 (1991) 375 and Refs. therein.
[10] M. Ghedini, F. Neve, D. Pucci, Eur. J. Inorg. Chem. (1998) 501.
[11] J.D. Higgins, J. Inorg. Biochem. 49 (1993) 149.
[12] C. Navarro-Ranninger, J. Lopez-Solera, J.M. Perez, J.M. Massanger, C. Alonso, Appl. Organomet. Chem. 7 (1993) 57.
[13] M. Ćurić, Lj. Tušek-Božić, D. Vikić-Topić, V. Scarcia, A. Furlani, J. Balzarini, E. De Clercq, J. Inorg. Biochem. 63 (1996) 125.
[14] Lj. Tušek-Božić, M. D'Alpaos, Polyhedron 17 (1998) 1481.
[15] Lj. Tušek-Božić, A. Furlani, V. Scarcia, E. De Clercq, J. Balzarini, J. Inorg. Biochem. 72 (1998) 201.
[16] Lj. Tušek-Božić, R. Trojko, Thermochim. Acta 339 (1999) 41.
[17] S. Tollari, G. Palmisano, F. Demartin, M. Grassi, S. Magnaghi, S. Cenini, J. Organomet. Chem. 488 (1995) 79.
[18] J.M. Vila, T. Pereira, J.M. Ortigueira, M. Lopez Torez, A. Castineiras, D. Lata, J.J. Fernandez, A. Fernandez, J. Organomet. Chem. 556 (1998) 21.
[19] L. Blaha, I. Lukeš, J. Rohovec, P. Hermann, J. Chem. Soc., Dalton Trans. (1997) 2621.
[20] T.G. Appleton, Coord. Chem. Rev. 166 (1997) 313.
[21] Lj. Tušek-Božić, I. Matijašić, G. Bocelli, G. Calestani, A. Furlani, V. Scarcia, A. Papaioannou, J. Chem. Soc., Dalton Trans. (1991) 195.
[22] Lj. Tušek-Božić, I. Matijašić, G. Bocelli, P. Sgarabotto, A. Furlani, V. Scarcia, A. Papaioannou, Inorg. Chim. Acta 185 (1991) 229.
[23] Lj. Tušek-Božić, R. Trojko, Thermochim. Acta 189 (1991) 175.
[24] Lj. Tušek-Božić, M. Ćurić, P. Traldi, Inorg. Chim. Acta 254 (1997) 49.
[25] M. Ćurić, Lj. Tušek-Božić, P. Traldi, Polyhedron 7 (1998) 531.
[26] J. Reedijk, A.M.J. Fichtinger-Schepman, A.T. von Oasteron, P. von de Putte, Struct. Bonding (Berlin) (1987) 67.
[27] M.I. Bruce, B.L. Goodall, F.G. Stone, J. Chem. Soc., Dalton Trans. (1978) 687.

[28] P.J. Steel, G.B. Caygill, J. Organomet. Chem. 327 (1987) 101.
[29] L.C. Thomas, Interpretation of Infrared Spectra of Organophosphorus Compounds, Heyden and Son, London, 1974.
[30] Lj. Tušek, V. Jagodić, Croat. Chem. Acta 49 (1977) 829.
[31] S.A. Katcyuba, N.I. Monakhova, L.Kh. Ashrafullina, R.R. Shagidulin, J. Mol. Struct. 269 (1992) 1.
[32] V. Jagodić, Lj. Tušek, Croat. Chem. Acta 44 (1972) 445.
[33] K. Nakamoto, Infrared and Raman Spectra of Inorganic and Coordination Compounds, Wiley-Interscience, New York, 4th edn., 1987.
[34] R.D. Smith, J.A. Loo, C.G. Edwards, C.J. Barinaga, H.D. Udseth, Anal. Chem. 62 (1990) 882.
[35] J.B. Fenn, M. Mann, C.K. Meng, S.F. Wong, C.M. Whitehouse, Mass Spectrom. Rev. 9 (1990) 747 and Refs. therein.
[36] R. Colton, A. D'Agostino, J.C. Traeger, Mass Spectrom. Rev. 14 (1995) 79.
[37] M. Bomchio, G. Licini, G. Modena, S. Moro, O. Bortolini, P. Traldi, W.A. Nugent, Chem. Commun. (1997) 869.
[38] D.M. Grove, G. van Koten, H.J.C. Ubbels, A.L. Spek, J. Am. Chem. Soc. 104 (1982) 4285.
[39] J. Terheijden, G. van Koten, D.M. Grove, K. Vrieze, J. Chem. Soc., Dalton Trans. (1987) 1359.
[40] I. Omae, in: Organometallic Intramolecular-Coordination Compounds, Elsevier, Amsterdam/New York, 1986 and Refs. therein.
[41] G.R. Newkome, W.E. Puckett, V.K. Gupta, G.E. Kiefer, Chem. Rev. 86 (1986) 451.
[42] W. Henderson, B.K. Nicholson, L.J. McCaffrey, Polyhedron 17 (1998) 4291.
[43] Lj. Tušek-Božić, M. Ćurić, D. Vikić-Topić, A. Lyčka, Collect. Czech. Chem. Commun. 62 (1997) 1888.
[44] K. Sawada, T. Miyagawa, T. Sakaguchi, K. Doi, J. Chem. Soc., Dalton Trans. (1993) 3777.
[45] J.P. Souchard, T.T.B. Ha, S. Cros, N.P. Johnson, J. Med. Chem. 34 (1991) 863.
[46] J. Reedijk, Chem. Commun. (1996) 801.
[47] V. Jagodić, L. Tušek, J. Org. Chem. 37 (1972) 222.
[48] W. Hull, in: W.R. Croasmun, R.M.K. Carlson (Eds.), Two-Dimensional NMR Spectroscopy. Application for Chemists and Biochemists, VCH, New York, 2nd edn., 1994, Ch. 2, p. 67.
[49] H. Eagle, Proc. Soc. Exptl. Biol. Med. 89 (1955) 362.
[50] C. Rossi, V. Ambrogi, G. Grandolini, V. Scarcia, A. Furlani, J. Pharm. Sci. 75 (1986) 784.
[51] P. Skehan, R. Storeng, D. Scudiero, A. Monks, J. McMahon, D. Vistica, J.T. Warren, H. Bokesch, S. Kenney, M.R. Boyd, J. Natl. Cancer Inst. 82 (1990) 1107.
[52] R.J. Tallarida, R.B. Murray, Manual of Pharmacological Calculations with Computer Programs, Springer, New York, 1987.
[53] P. Hakala, J.M. Rustum, in: V.T. De Vita Jr., H. Bussch (Eds.), Method in Cancer Research, vol. XVI, Academic Press, New York, 1979, p. 247.

PERGAMON

www.elsevier.nl/locate/poly

Polyhedron 19 (2000) 949–958

POLYHEDRON

Synthesis, reactivity and magnetochemical studies on copper(II) complexes derived from *N*-salicylidenearoylhydrazines. X-ray structure of [mononitrato*OO*(−1)(*N*-salicylidenatobenzoylhydrazine)-*ONO*(−1)]copper(II) monohydrate

M.F. Iskander [a,*], T.E. Khalil [a], R. Werner [b], W. Haase [b], I. Svoboda [c], H. Fuess [c]

[a] *Chemistry Department, Faculty of Science, Alexandria University, P.O. Box 426, Ibrahimia, Alexandria 21321, Egypt*

[b] *Institut für physikalische Chemie, AG Kondensierte Materie, Fachbereich Chemie, Technische Universität Darmstadt, Petersenstrasse 20, D-64287 Darmstadt, Germany*

[c] *Institut für Strukturforschung, Fachbereich Materialwissenschaft, Petersenstrasse 24, D-64287 Darmstadt, Germany*

Received 22 November 1999; accepted 21 February 2000

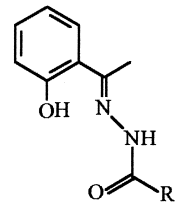
Abstract

A series of new mononuclear and binuclear copper(II) complexes derived from *N*-salicylidenearoylhydrazines (H_2L) of the types $K_2[\{Cu(L)(OH)\}_2]\cdot nH_2O$, $[Cu(HL)Cl\cdot H_2O]\cdot nH_2O$, $[\{Cu(HL)Cl\}_2]$, $[Cu(HL)NO_2]\cdot H_2O$, $[\{Cu(HL)\}_2]\cdot 2NO_3$, $[\{Cu(HL)H_2O\}_2]\cdot 2NO_3\cdot nH_2O$ and $[Cu(HL)NCS]\cdot H_2O$ have been prepared and characterized. The X-ray crystal and molecular structure of $[Cu(HSBzh)NO_3]\cdot H_2O$, where HSBzh refers to the mononegative *N*-salicylidenebenzoylhydrazine anion, has been determined. The complex is monomeric with the copper(II) adopting a (4+1) distorted square pyramidal coordination, with the ONO aroylhydrazone tridentate anion and an oxygen atom of the unsymmetric bidentate nitrate ion occupying the basal plane. The fifth coordination site is occupied by the other oxygen of the nitrate ion. The magnetic susceptibilities of both mononuclear and binuclear complexes were measured within the temperature range 4.2–298 K. All binuclear copper(II) complexes show strong antiferromagnetic interactions, and the singlet–triplet separation ($-2J$) recorded for μ-dihydroxy bridged complexes $K_2[\{Cu(L)OH\}_2]\cdot nH_2O$ are within the range 172–276 cm^{-1}, while ($-2J$) for binuclear complexes $[\{Cu(HL)Cl\}_2]$, $[\{Cu(HL)\}_2]\cdot 2NO_3$ and $[\{Cu(HL)H_2O\}_2]\cdot 2NO_3\cdot nH_2O$ are respectively within the range 400–460, ca. 340 and ca. 390 cm^{-1}. There are no appreciable exchange interactions between copper(II) ions in the monomeric complexes $[Cu(HL)Cl\cdot H_2O]\cdot nH_2O$, $[Cu(HL)NO_2]\cdot H_2O$ and $[Cu(HL)NCS]\cdot H_2O$. The IR spectra of the prepared complexes are also discussed.
©2000 Elsevier Science Ltd All rights reserved.

Keywords: *N*-salicylidenearoylhydrazines; Copper(II) complexes; X-ray crystal structures; Molecular structures; Magnetic properties; Infrared spectra

1. Introduction

N-salicylideneacylhydrazines (**1**) (H_2L) can act either as neutral, mononegative or dinegative ONO tridentate ligands [1–20]. A large number of monomeric and dimeric copper(II) complexes have been prepared and characterized [1–20]. Most recent studies have been directed towards structural studies and a number of X-ray crystal and molecular structures have been reported [16–20]. Less attention, however, has been directed towards magnetochemical studies [13–18]. In this paper we report the synthesis and characterization of some new mononuclear and dinuclear copper(II) complexes with *N*-salicylidenearoylhydrazines.



(1)

The single X-ray structure of the monomeric $[Cu(HBzh)NO_3]\cdot H_2O$ has been determined and the magnetic measurements recorded for the prepared complexes will be discussed. Hereafter, *N*-salicylidenebenzoylhydrazine

* Corresponding author. Tel.: +20-3-5423323; fax: +20-3-4911794; e-mail: iskandar@alexcomm.net

0277-5387/00/$ - see front matter ©2000 Elsevier Science Ltd All rights reserved.
PII S0277-5387(00)00340-5

and the corresponding *p*-methyl-, *p*-methoxy- and *p*-chlorobenzoylhydrazine are abbreviated as H_2SBzh, H_2S*p*-CH_3Bzh, H_2S*p*-CH_3Obzh and H_2S*p*-ClBzh, respectively.

2. Results and discussion

2.1. Synthesis and stoichiometry

In methanol, the reaction of copper(II) acetate with *N*-salicylidenearoylhydrazines (H_2L) (**1**, R = C_6H_5, *p*-$CH_3C_6H_4$, *p*-$CH_3OC_6H_4$ and *p*-ClC_6H_4) afforded the binuclear neutral copper(II) complexes [{Cu(L)}$_2$] (**2**, R = C_6H_5, *p*-$CH_3C_6H_4$, *p*-$CH_3OC_6H_4$ and *p*-ClC_6H_4). These binuclear copper(II) complexes were insoluble in water, alcohols, halogenated aliphatic hydrocarbons and aromatic hydrocarbons but soluble in DMSO or DMF. The dissolution of these binuclear complexes proceeded with the rupture of Cu–O–Cu bridges giving the solvated monomeric species [Cu(L)S] or [Cu(L)S_2] where S refers to the solvent molecule [12]. A similar behaviour was previously reported and recrystallization of the anhydrous dimeric copper(II) complexes with the dinegative anion of 5-chloro-2-hydroxo acetophenone salicylhydrazide from DMF gave the corresponding DMF adduct of the formula [Cu(L)DMF] where L refers to the dinegative hydrazone anion [16,17]. Neutral monodentate nitrogen Lewis bases such as diethylamine [$(Et)_2$NH] can also affect the rupture of the Cu–O–Cu bridges in **2** and eventually gave the corresponding monomeric ternary complex [Cu(L)HNEt_2] (**3**, R = C_6H_5).

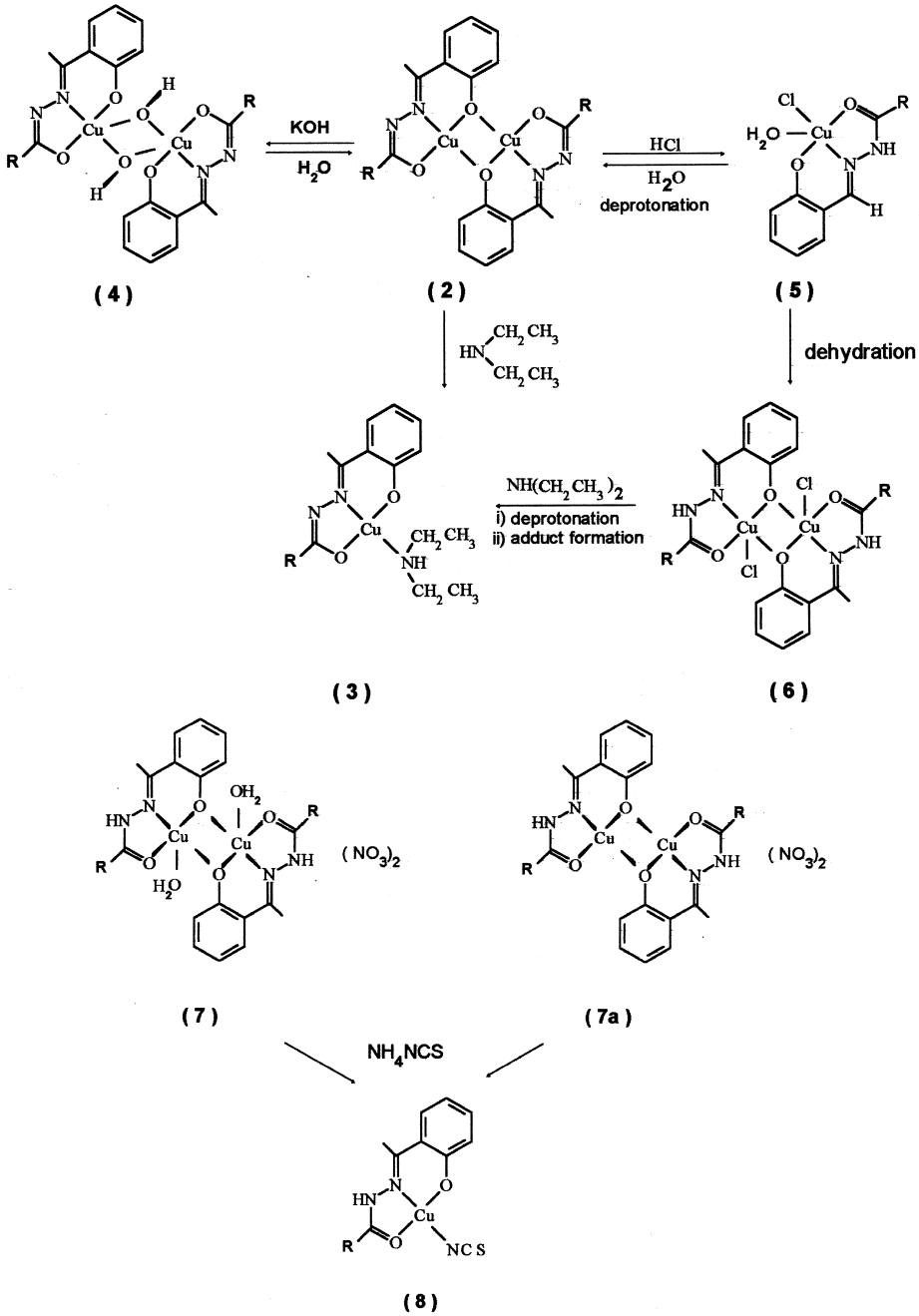
The reaction of the neutral dimeric copper(II) complexes [{Cu(L)}$_2$] (**2**, R = C_6H_5, *p*-$CH_3C_6H_4$ and *p*-$CH_3OC_6H_4$) with a large excess of KOH in dry methanol afforded the corresponding μ-hydroxo bridged copper(II) complexes of general formula K_2[{Cu(L)(OH)}$_2$] (**4**, R = C_6H_5, *p*-$CH_3C_6H_4$ and *p*-$CH_3OC_6H_4$). The isolated hydroxo complexes are soluble in methanol, ethanol and acetonitrile. In water, these complexes are readily hydrolysed giving the parent neutral dimer (**2**). The isolated hydroxo complexes together with elemental analysis are given in Table 1.

On the other hand, treatment of a suspension of [{Cu(L)}$_2$] (**2**, R = C_6H_5, *p*-$CH_3C_6H_4$, *p*-$CH_3OC_6H_4$ and *p*-ClC_6H_4) in absolute ethanol with an equivalent amount of aqueous hydrogen chloride afforded the hydrated monochloro complex [Cu(HL)Cl·H_2O]·*n*H_2O (**5**, R = C_6H_5, *p*-$CH_3C_6H_4$, *p*-$CH_3OC_6H_4$ and *p*-ClC_6H_4) (HL refers to the mononegative *N*-salicylidenearoylhydrazine anion). These

Table 1
Elemental analyses of copper(II) complexes derived from *N*-salicylidenearoylhydrazines

Complex		Found (calculated) (%)			
R	*n*	C	H	N	Cu
K_2[{Cu(L)OH}$_2$]·*n*H_2O (**4**)					
C_6H_5	2	44.55 (44.73)	3.07 (3.49)	7.20 (7.45)	16.73 (16.90)
p-$CH_3C_6H_4$	2	46.17 (46.20)	3.84 (3.88)	7.00 (7.18)	16.52 (16.30)
p-$CH_3OC_6H_4$	1	45.06 (45.39)	3.60 (3.55)	6.86 (7.06)	16.25 (16.01)
[Cu(HL)Cl·H_2O]·*n*H_2O (**5**)					
C_6H_5		47.16 (47.20)	3.59 (3.68)	7.83 (7.86)	17.57 (17.84)
p-$CH_3C_6H_4$		48.08 (48.65)	3.50 (4.08)	7.48 (7.57)	17.00 (17.16)
p-$CH_3OC_6H_4$	1	44.01 (44.56)	3.69 (4.24)	6.81 (6.93)	15.87 (15.72)
p-ClC_6H_4	1	40.46 (41.14)	2.75 (3.45)	7.07 (6.85)	15.41 (15.55)
[{Cu(HL)Cl}$_2$] (**5**)					
C_6H_5		49.57 (49.71)	3.18 (3.28)	8.43 (8.28)	18.53 (18.79)
p-$CH_3C_6H_4$		51.08 (51.14)	3.71 (3.72)	8.25 (7.95)	17.87 (18.04)
[Cu(HL)(NO_3)]·*n*H_2O					
C_6H_5	1	43.15 (43.93)	3.24 (3.42)	10.91 (10.98)	16.72 (16.60)
[{Cu(HL)}$_2$]·2NO_3 (**7**)					
C_6H_5		46.14 (46.09)	2.94 (3.04)	11.50 (11.52)	17.50 (17.42)
p-$CH_3OC_6H_4$		45.61 (45.63)	3.24 (3.32)	10.75 (10.64)	16.24 (16.09)
[{Cu(HL)(H_2O)}$_2$]·2NO_3·*n*H_2O (**7a**)					
p-$CH_3C_6H_4$	1	44.88 (44.39)	3.43 (3.97)	10.72 (10.35)	15.40 (15.66)
CH_3		33.62 (33.70)	3.55 (3.46)	12.73 (13.10)	20.02 (19.81)
[Cu(HL)(NCS)]·*n*H_2O (**8**)					
C_6H_5	1	47.23 (47.55)	3.33 (3.46)	11.09 (11.09)	16.41 (16.77)
p-$CH_3C_6H_4$		50.95 (51.95)	3.44 (3.50)	11.19 (11.21)	17.01 (16.95)
p-$CH_3OC_6H_4$		48.92 (49.16)	3.32 (3.35)	10.94 (10.75)	16.41 (16.26)
p-ClC_6H_4	2	41.52 (41.77)	3.04 (3.27)	9.35 (9.74)	14.42 (14.73)

complexes were also prepared in situ from the reaction of salicylaldehyde with the corresponding aroylhydrazine (1:1 molar ratio) in the presence of copper(II) chloride in ethanol or methanol. However, direct reaction of *N*-salicylidenearoylhydrazine (**1**, R = C_6H_5 and *p*-$CH_3C_6H_4$) with 1 equiv. of copper(II) chloride in absolute ethanol afforded the anhydrous brown chloro complexes $[Cu(HL)Cl]_2$ (**6**, R = C_6H_5 and *p*-$CH_3C_6H_4$). This reaction usually gave salicylaldehyde azine ($HOC_6H_4CH{=}N{-}N{=}CHC_6H_4OH$) as a side reaction product. Meanwhile, the direct reaction of *p*-methoxy- and *p*-chlorobenzoylhydrazones (**1**, R = *p*-$CH_3OC_6H_4$ and *p*-ClC_6H_4) with copper(II) chloride in ethanol or methanol gave the hydrated copper(II) complexes $[Cu(HL)Cl\cdot H_2O]$ (**5**, R = *p*-$CH_3OC_6H_4$ and *p*-ClC_6H_4) and attempts to prepare the corresponding anhydrous binuclear complexes were unsuccessful. Similar to the reaction of *N*-salicylidenearoylhydrazines with copper(II) chloride, the reaction of copper(II) nitrate gave either monomeric and/or dimeric nitrate complexes. The reaction of **1** (R = *p*-$CH_3C_6H_4$) with copper(II) nitrate trihydrate in boiling absolute ethanol afforded the hydrated binuclear complex $[\{Cu(HSp\text{-}CH_3Bzh)H_2O\}_2](NO_3)_2\cdot H_2O$ (**7**, R = *p*-$CH_3C_6H_4$), while the reaction with **1** (R = C_6H_5, *p*-$CH_3OC_6H_4$) gave the corresponding anhydrous complexes $[\{Cu(HSBzh)\}_2]\cdot 2NO_3$ and $[\{Cu(HSp\text{-}CH_3OBzh)_2]\cdot 2NO_3$ (**7a**, R = C_6H_5 and *p*-$CH_3OC_6H_4$), respectively. However, the in situ preparation, using benzoylhydrazine, gave the monomeric complex $[Cu(HSBzh)(NO_3)]\cdot H_2O$. The prepared mononuclear and binuclear copper(II) chloride and nitrate complexes together with elemental analysis are included in Table 1.



The reaction of either mononuclear or binuclear copper(II) chloride and nitrate complexes with an equivalent amount of NH_4SCN in methanol afforded the corresponding thiocyanato complexes $[Cu(HL)SCN]\cdot nH_2O$ (**8**, R = C_6H_5, *p*-$CH_3C_6H_4$, *p*-$OCH_3C_6H_4$) and *p*-ClC_6H_4), implying the ease of displacement of either Cl^- or NO_3^- by the thiocyanate ion. However, in the presence of large excess of NH_4SCN, the reaction proceeded by the reduction of copper(II) and copper(I) thiocyanate $[CuSCN]_2$ was precipitated. On the other hand, the reaction of thiocyanate with either μ-hydroxo bridged complexes (**5**) or the neutral binuclear copper(II) complexes $[\{Cu(L)\}_2]$ (**2**) failed to give the corresponding thiocyanato complexes, suggesting that the SCN^- cannot affect the rupture of Cu–O–Cu bridges in these complexes. The isolated thiocyanato complexes $[Cu(HL)SCN]\cdot nH_2O$ together with elemental analysis are also given in Table 1.

2.2. X-ray crystal structure of [mononitratoOO′(−1)(N-salicylidenebenzoylhydrazinato)ONO′(−1)]copper(II) monohydrate complex [Cu(HSBzh)(NO$_3$)]·H$_2$O

The crystal data and structure refinement for $[Cu(HSBzh)(NO_3)]\cdot H_2O$ are collected in Table 2. The molecular structure together with the numbering scheme used are shown in Fig. 1. Some selected bond distances and bond angles are listed in Table 3. In $[Cu(HBzh)(NO_3)]\cdot H_2O$, the *N*-salicylidenebenzoylhydrazinato anion behaves as a mononegative tridentate ligand and is coordinated to the Cu(II) via the deprotonated phenolic oxygen O(1), azomethine nitrogen N(1) and the ketoamide oxygen O(2). The Cu–O(1) (1.881 Å), Cu–N(1) (1.913 Å) and Cu–O(2) (1.97 Å) bond distances are within the range reported for other copper(II) complexes derived from *N*-salicylideneacylhydrazines [10,11,18–21]. The fourth coordinate site of the basal plane is occupied by the oxygen atom O(3) of the

Table 2
Crystal data and structure refinement for $[Cu(HSBzh)NO_3]\cdot H_2O$

Empirical formula	$C_{14}H_{13}CuN_3O_6$
Formula weight	382.84
Temperature (K)	300(2)
Wavelength (Å)	0.71093
Crystal system	orthorhombic
Space group	$P2_12_12_1$
Unit cell dimensions	
a (Å)	5.331(2)
b (Å)	16.231(2)
c (Å)	17.185(3)
α (°)	90
β (°)	90
γ (°)	90
Volume (Å^3)	1487.0(6)
Z	4
Density (calculated) (Mg m^{-3})	1.710
Absorption coefficient (mm^{-1})	1.435
F(000)	80
Crystal size (mm)	0.88×0.15×0.13
Theta range for data collection (°)	1.73–25.98
Index ranges	$-6\le h\le 6,\ -1\le k\le 19,\ -1\le l\le 21$
Reflections collected	3543
Independent reflections	2908 (R_{int} = 0.0291)
Refinement method	full-matrix least-squares on F^2
Data/restraints/parameters	2908/0/250
Goodness-of-fit on F^2	1.068
Final *R* indices ($I>2\sigma(I)$)	R_1 = 0.0418, wR_2 = 0.1093
R indices (all data)	R_1 = 0.0596, wR_2 = 0.1194
Absolute structure parameter	0.02(2)
Largest difference peak, hole (e Å^{-3})	0.639, −0.942

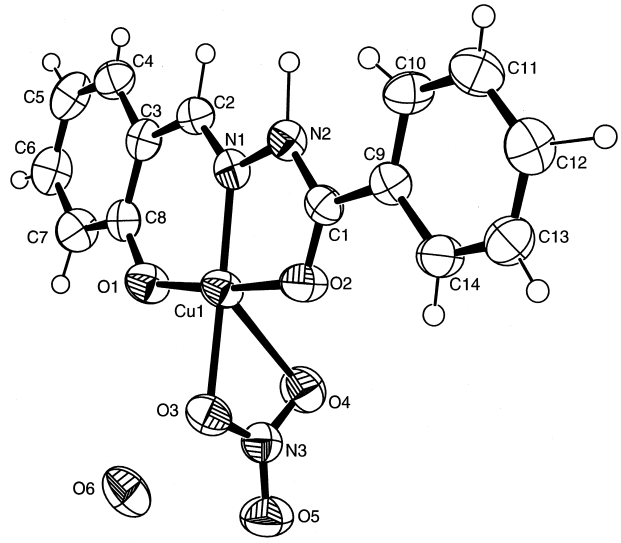


Fig. 1. ORTEP drawing of $[Cu(HSBzh)NO_3]\cdot H_2O$.

Table 3
Selected bond lengths (Å) and bond angles (°) for $[Cu(HSBzh)(NO_3)]\cdot H_2O$

Copper(II) polyhedron			
O(1)–Cu(1)	1.881(3)	O(1)–Cu(1)–N(1)	92.99(14)
O(2)–Cu(1)	1.947(3)	O(1)–Cu(1)–O(2)	174.31(13)
N(1)–Cu(1)	1.913(3)	O(1)–Cu(1)–O(3)	91.71(14)
O(3)–Cu(1)	1.993(3)	O(2)–Cu(1)–O(3)	93.64(13)
O(4)–Cu(1)	2.480(3)	O(4)–Cu(1)–O(3)	55.50(13)
		N(1)–Cu(1)–O(2)	81.49(13)
		N(1)–Cu(1)–O(3)	172.33(14)
Tridentate ligand			
C(1)–O(2)	1.252(5)	C(1)–N(2)–N(1)	113.9(3)
C(1)–N(2)	1.336(5)	C(1)–O(2)–Cu(1)	113.1(3)
C(1)–C(9)	1.488(6)	C(1)–N(2)–H(2N)	133.3(3)
C(2)–N(1)	1.283(5)	C(2)–N(1)–N(2)	119.1(3)
C(3)–C(8)	1.427(6)	C(2)–N(1)–Cu(1)	128.9(3)
C(8)–O(1)	1.305(6)	C(8)–O(1)–Cu(1)	127.8(3)
N(1)–N(2)	1.383(5)	N(1)–C(2)–C(3)	122.9(4)
N(2)–H(2N)	1.20(4)	N(1)–N(2)–H(2N)	113(2)
		N(2)–N(1)–Cu(1)	112.0(2)
		N(2)–C(1)–C(9)	119.5(4)
		O(1)–C(8)–C(3)	124.3(4)
		O(2)–C(1)–N(2)	119.5(4)
		O(2)–C(1)–C(9)	120.9(4)
Nitrate ligand			
N(3)–O(3)	1.288(5)	O(4)–N(3)–O(3)	115.3(4)
N(3)–O(4)	1.231(5)	O(5)–N(3)–O(3)	119.9(4)
N(3)–O(5)	1.208(5)	O(5)–N(3)–O(4)	124.8(4)
		N(3)–O(3)–Cu(1)	105.4(3)

nitrate group. The Cu(II) lies in the ligand plane and shows a slight deviation of 0.037 Å from the least square plane. The nitrate ion in this complex behaves as a bidentate ligand, and the fifth coordinate site is weakly bonded with the O(4) of the nitrate group. This bidentate nitrate is characterized by one short Cu–O(3) (1.993 Å) distance and a second much longer Cu–O(4) (2.480 Å) with a difference of 0.487 Å which falls within the range reported for the unsymmetrically coordinated bidentate nitrate group [22–25]. The small O(3)–Cu–O(4) angle (55.5°) is also in agreement with the bidentate nature of the nitrate ion in this complex.

The coordination polyhedron around the copper(II) is better described as (4+1) distorted square pyramidal as evident from the tetragonality parameter of Addison et al. [26], $\tau=(\beta-\alpha)/60=0.033$, where α and β are the N(1)–Cu–O(3) (172.33°) and O(2)–Cu–O(1) (174.31°) angles, respectively. The uncoordinated water molecule O(6) is involved in strong hydrogen bonding with the N(2) hydrogen atom (O(6)···H(2)N) $(1-x, -0.5+y, 1.5-z)$ (1.55 Å).

2.3. Magnetic measurements

At room temperature, the binuclear copper(II) complexes $[\{Cu(L)\}_2]$ (**2**, R = C_6H_5, *p*-$CH_3C_6H_4$, *p*-$CH_3OC_6H_4$ and *p*-ClC_6H_4) show subnormal magnetic moments (1.2–1.6 μ_B) and their electronic spectra agree with a square planar configuration [1–3,27]. The magnetic susceptibility measurements within the temperature range 97–297 K showed strong antiferromagnetic interactions. The exchange coupling constant ($-2J$) of these neutral dimeric complexes were found to vary from 594 to 680 cm^{-1} [27] in agreement with the formation of dimeric copper(II) complexes with Cu–O–Cu bridges [28]. Recent X-ray studies on binuclear copper(II) complexes with *N*-salicylideneacylhydrazines show that dimerization takes place via the phenolic oxygen rather than the deprotonated enolic oxygen [18–21].

The newly prepared di-μ-hydroxo-bridged binuclear copper(II) complexes $K_2[\{Cu(L)OH)\}_2]$ (**4**, R = C_6H_5, *p*-$CH_3C_6H_4$ and *p*-$OCH_3C_6H_4$) also show subnormal magnetic moments (1.50–1.65 μ_B) at room temperature. The variation of χ_M and μ_{eff}, recorded for $K_2[\{Cu(Sp\text{-}CH_3Bzh)OH\}_2]$ (**4**, R = *p*-$CH_3C_6H_4$), as a function of temperature (4.2–298 K) is shown in Fig. 2. The remarkable decrease in μ_{eff} (per copper atom) from 1.5 μ_B at 290 K to about 0.4 μ_B at 4.5 K suggests strong antiferromagnetic exchange interaction. Similar behaviour was also observed for the other di-μ-hydroxo-bridged copper(II) complexes (**4**, R = C_6H_5, and *p*-$CH_3OC_6H_4$). The experimental data were fitted to the modified Bleaney–Bowers equation Eq. (1),

$$\chi_M=(1-X_p)\frac{2N_L g^2\mu_\beta^2}{kT}\frac{\exp(2J/kT)}{1+3\exp(2J/kT)} + X_p\frac{2NLg^2\mu_\beta^2}{3k(T-\theta)}S(S+1)+2N_\alpha \quad (1)$$

where 2*J* is the singlet–triplet splitting or exchange integral,

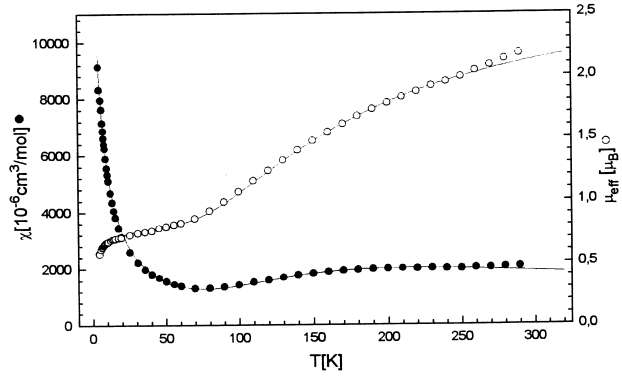


Fig. 2. Magnetic susceptibilities χ (●) and magnetic moments (o) vs. temperature for $K_2[\{Cu(Sp\text{-}CH_3Bzh)OH\}_2]\cdot 2H_2O$. Solid lines represent the best least squares fit to Eq. (1), with $J=-138$, $g=2.10$ and $X_p=4.1\%$.

X_p represents the fraction of a possible magnetically dilute copper(II) impurity ($S=1/2$), N_α is the temperature independent paramagnetism (60×10^{-6} cm^3 mol^{-1} per copper(II) ion) and the other symbols have their usual meaning and a non-linear regression analysis was carried out with *J*, *g*, and X_p as floating parameters. The obtained best fit parameters for the di-μ-hydroxo-bridged copper(II) complexes (**4**, R = C_6H_5, *p*-$CH_3C_6H_4$ and *p*-$CH_3OC_6H_4$) are listed in Table 4. The recorded $-2J$ values are within the range reported for other bis-μ-hydroxy bridged dicopper complexes with nearly planar Cu_2O_2 [28–33] and a binuclear structure (**4**) can be proposed for these complexes.

For di-μ-hydroxo dicopper(II) complexes with almost planar Cu_2O_2, the 2*J* values were found to decrease linearly with increasing either Cu–O–Cu angle φ (°) or Cu···Cu separation r_{Cu-Cu} (Å), and least square regression analyses of the available data gave [28]:

$$2J=-77.6\varphi+7555\ cm^{-1}\ (R=-0.95) \quad (2)$$

$$2J=-46.0r_{Cu\cdots Cu}+13389\ cm^{-1}\ (R=-0.95) \quad (3)$$

Substitution of the 2*J* values, recorded for **4** (R = C_6H_5, *p*-$CH_3C_6H_4$ and *p*-$OCH_3C_6H_4$), in Eq. (2) gave 99.6, 100.9 and 100.7° for the values of Cu–O–Cu angles, respectively. While 2.948, 2.971 and 2.967 Å are, respectively, the values calculated from Eq. (3) for the Cu···Cu separation.

The green hydrated chloro complexes $[Cu(HL)Cl\cdot H_2O]\cdot nH_2O$ (**5**, R = C_6H_5, *p*-$CH_3C_6H_4$, *p*-$CH_3OC_6H_4$, and *p*-ClC_6H_4) show normal magnetic moments (1.80–1.84 μ_B), Table 4, and the temperature dependent magnetic susceptibilities measured for these hydrated complexes, assuming Curie–Weiss behaviour, suggest a very weak antiferromagnetic coupling with θ values in the range of ca. −1.5 K. These mononuclear chloro complexes may adopt a square pyramidal coordination, the four in-plane donor atoms are provided by the tridentate ONO hydrazone and an oxygen from a coordinated water while the axial site is occupied by the chloride ion. A similar structure has been reported for $[Cu(HSAch)Cl\cdot H_2O]\cdot H_2O$, where HSAc refers to the mononegative *N*-salicylideneacetylhydrazine anion (**1**, R = CH_3) [21]. On the other hand, the brown anhydrous

Table 4
The magnetic parameters recorded for the prepared copper(II) complexes derived from *N*-salicylidenearoylhydrazones

Complex		μ_{eff} (μ_B) (298 K)	θ (K)	$-2J$ (cm^{-1})	g	X_p (%)
R	n					
$[\{Cu(L)(OH)\}_2]\cdot nH_2O$ (**4**)						
C_6H_5	2	1.65		171	2.05	6.75
p-$CH_3C_6H_4$	2	1.54		276	2.12	4.20
p-$CH_3OC_6H_4$	1	1.52		261	2.10	4.10
$[Cu(HL)Cl.H_2O]\cdot nH_2O$ (**5**)						
C_6H_5		1.80	−16.8			
p-$CH_3C_6H_4$		1.83	−15.4			
p-$CH_3OC_6H_4$	1	1.83	−17.2			
p-ClC_6H_4	1	1.84	−16.7			
$[\{Cu(HL)Cl\}_2]$ (**6**)						
C_6H_5		1.12		452	2.20	1.56
p-$CH_3C_6H_4$		1.21		406	2.19	1.80
$[Cu(HL)(NO_3)]\cdot nH_2O$						
C_6H_5	1	1.85	−8.5			
$[\{Cu(HL)(H_2O)\}_2](NO_3)_2$ (**7a**)						
C_6H_5		1.30		390	2.21	1.70
$[\{Cu(HL)(H_2O)\}_2](NO_3)_2\cdot nH_2O$ (**7**)						
CH_3		1.30		340	2.20	0.50
p-$CH_3C_6H_4$	1	1.45		338	2.21	1.60
$[Cu(HL)NCS]\cdot nH_2O$ (**8**)						
C_6H_5	1	1.87	1.35			
p-$CH_3C_6H_4$		1.89	1.75			
p-$CH_3OC_6H_4$		1.89	3.15			

chloro complexes $[\{Cu(HL)Cl\}_2]$ show, at room temperature, low lying magnetic moments within the range 1.12–1.21 μ_B. A plot of χ_M and μ_{eff}, measured for $[\{Cu(HSp\text{-}CH_3Bzh)Cl\}_2]$, as a function of temperature, Fig. 3, suggests strong antiferromagnetc interaction. Fitting the data to the Bleaney–Bowers equation gives $J=-203$ cm^{-1}, $g=2.19$, and $X_p=0.0179$. These values are comparable with those previously reported for $[\{Cu(HSBzh)Cl\}_2]$ (**6**, $R=C_6H_5$) [18]. The obtained $-2J$ values, Table 4, are within the range reported for bis-μ-aryloxo bridged dicopper complexes [18,28]. The copper(II) in these complexes has a distorted (4+1) tetragonal pyramidal coordination where the apical site is occupied by a chloride ion. Dimerization is achieved by sharing of phenoxy oxygen from each ligand through two copper atoms [18].

Similar to the chloro complexes $[\{Cu(HL)Cl\}_2]$ (**6**, $R=C_6H_5$, p-$CH_3C_6H_4$), the isolated binuclear nitrate complexes $[\{Cu(HSBzh)\}_2]\cdot 2NO_3$, $[\{Cu(HSp\text{-}CH_3Bzh)\cdot H_2O\}_2]\cdot H_2O\cdot 2NO_3$ and $[\{Cu(HSp\text{-}CH_3OBzh)\}_2]\cdot 2NO_3$ show subnormal magnetic moments (1.30–1.45 μ_B) at room temperature. A plot of the magnetic susceptibility data measured for $[\{Cu(HSBzh)_2\}]\cdot 2NO_3$ as a function of temperature (5–298 K), Fig. 4, indicates strong antiferromagnetic exchange coupling. Similar behaviour was also observed for both $[\{Cu(HSp\text{-}CH_3Bzh)\cdot H_2O\}_2]\cdot H_2O\cdot 2NO_3$ and

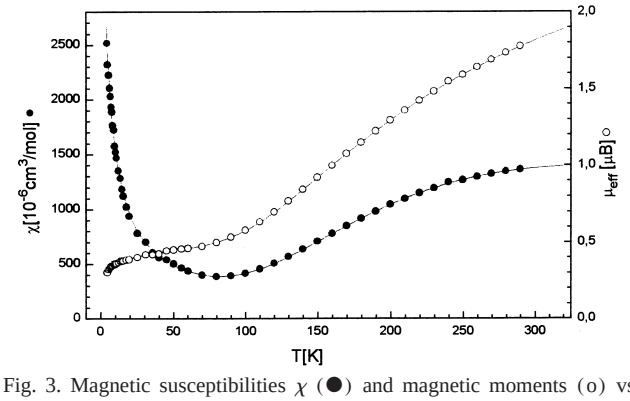


Fig. 3. Magnetic susceptibilities χ (●) and magnetic moments (o) vs. temperature for $[\{Cu(HSp\text{-}CH_3Bzh)Cl\}_2]$. Solid lines represent the best least squares fit to Eq. (1), with $J=-203$, $g=2.19$ and $X_p=1.8\%$.

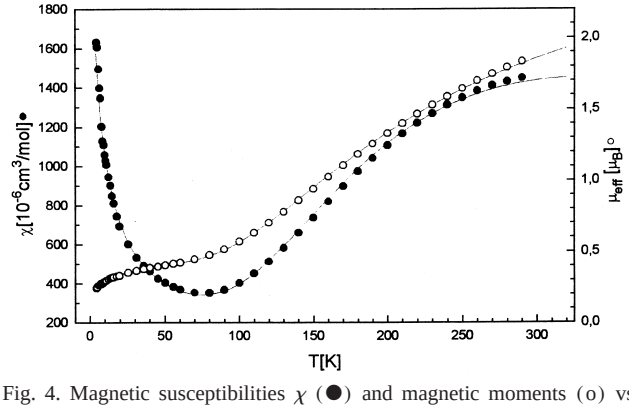


Fig. 4. Magnetic susceptibilities χ (●) and magnetic moments (o) vs. temperature for $[\{Cu(Sp\text{-}Bzh)\}_2]\cdot 2NO_3$. Solid lines represent the best least squares fit to Eq. (1), with $J=-195$, $g=2.21$ and $X_p=1.7\%$.

$[\{Cu(HSp\text{-}OCH_3Bzh)\}_2]\cdot 2NO_3$. The best fit parameters (J, g and X_p) obtained by fitting the variable temperature magnetic susceptibility data to the Bleaney–Bowers equation are listed in Table 4. The obtained $-2J$ values (338–390 cm^{-1}) suggest strong antiferromagnetic exchange interaction via bridged phenoxy oxygens [28]. Recently, the preparation and X-ray crystal and molecular structure of the analogous dinuclear complex $[\{Cu(HSAc)H_2O\}_2]\cdot 2NO_3$ have been reported [20]. This complex is a centrosymmetric (planar) dimer, the monomeric units being bridged through the phenoxy oxygen. The copper atom has a square-pyramidal geometry with the basal donor atoms coming from the ONO mononegative tridentate ligand and the symmetry related phenolate oxygen, while the fifth coordination site is occupied by water oxygen. The nitrate ions are not coordinated and act as counter ions [20]. Unfortunately, no variable-temperature magnetic data have been reported for this complex. In the present work, the room temperature magnetic moment of the dinuclear complex $[\{Cu(HSAc)H_2O\}_2]\cdot 2NO_3$ was found to be 1.29 μ_B which is more or less similar to the value reported previously by Chan et al. (1.28 μ_B) [20]. Fitting the variable temperature susceptibility data recorded for $[\{Cu(HSAc)H_2O\}_2]\cdot 2NO_3$ to a modified Bleaney–Bowers equation gives $J=-340$ cm^{-1}, $g=2.20$ and $X_p=2.2\%$. The obtained ($-2J$) is comparable to that reported for $[\{Cu(HSp\text{-}CH_3Bzh)\cdot H_2O\}_2]\cdot H_2O\cdot 2NO_3$ and a similar dimeric structure (**7**, $R=p\text{-}CH_3C_6H_4$) can be proposed for this complex, where the copper(II) is weakly bound to the oxygen of the coordinated water molecule. The anhydrous dimeric $[\{Cu(HSBzh)_2\}\cdot 2NO_3$ and $[\{Cu(HSp\text{-}OCH_3Bzh)\}_2]\cdot 2NO_3$ complexes, on the other hand, show relatively higher $-2J$ values (ca. 392 cm^{-1}) implying stronger antiferromagnetic exchange interaction between the two copper(II) centres. It seems that coordination of a water molecule in **7a** ($R=p\text{-}CH_3C_6H_4$) results in a slight distortion from planarity and decreases the strength of antiferromagnetic interactions relative to the more planar anhydrous dimers.

The thiocyanate complexes $[Cu(HL)SCN]\cdot nH_2O$, Table 1, have room temperature magnetic moments in excess of 1.8 μ_B, Table 4, suggesting that the paramagnetic centres are quite shielded by the diamagnetic matrix, and if the copper centres are spin coupled, exchange is likely to be weak. The magnetic moments of these complexes are more or less constant (ca. 1.87 μ_B) within the temperature range (35–300 K), but decrease below 35 K and drop to ca. 1.74 μ_B at 10 K, suggesting weak antiferromagnetic interactions. Assuming Curie–Weiss behaviour, plots of inverse magnetic susceptibility for **8** ($R=C_6H_5$, $p\text{-}CH_3C_6H_4$ and $p\text{-}ClC_6H_4$) versus temperature gave Curie–Weiss constants $\theta=-1.35$, -1.75 and -3.20, respectively. This magnetic behaviour can rule out the possible formation of a binuclear structure with phenoxy bridges similar to that reported for the corresponding chloride or nitrate complexes and a monomeric structure (**8**) can be proposed for these thiocyanate complexes. However, dimeric or polymeric structures with bridged thiocyanate cannot be ruled out, since no magnetic interactions between the copper(II) centres was observed in polymeric $[Cu(bheg)NCS]\cdot H_2O$ (where Hbheg is *N,N* bis(2-hydroxyethylglycine)) [34]. The actual structure of these isothiocyanate complexes must remain in doubt until complete X-ray molecular structures are available.

2.4. Infrared spectra

The IR spectra of *N*-salicylidenearoylhydrazines, Table 5, show a series of bands at ca. 3200, 1670, 1600 and 1340 cm^{-1}, respectively due to ν(N–H), ν(C=O) (amide I), ν(C=N), δ(N–H) (amide II), and ν(C–N) (amide III). The spectra of the corresponding binuclear complexes $[\{Cu(L)\}_2]$ (**2**) and $K[\{Cu(L)(OH)\}_2]\cdot nH_2O$ (**4**) lack any absorption which can be attributed to ν(N–H), ν(C=O) or δ(N–H), but show an intense absorption due to ν(C=N–N=C) as well as the amide III band, implying the deprotonation of the enolimine tautomer of the hydrazone ligand [1,2,35,36]. However, the spectra of the mononuclear complexes of the types $[Cu(HL)Cl\cdot H_2O]\cdot nH_2O$ (**5**), $[Cu(HSBzH)NO_2]\cdot H_2O$, and $[Cu(HL)NCS]\cdot nH_2O$ (**8**) as well as the binuclear complexes $[\{Cu(HL)Cl\}_2]$ (**6**), $[\{Cu(HL)H_2O\}_2](NO_3)_2\cdot nH_2O$ (**7**) $[\{Cu(HL)\}_2](NO_3)_2$ (**7a**), Table 5, show a series of bands at ca. 3180, 1615, 1600, 1540 and 1320 cm^{-1} due to ν(N–H), ν(C=O), ν(C=N), δ(N–H) and ν(C–N), respectively. The presence of ν(N–H), ν(C=O) and δ(N–H) in the IR spectra of these complexes indicate that the hydrazone molecule reacts in the ketoamine form. Moreover, the stoichiometry of these complexes as well as the pronounced shift in both ν(C=O) and ν(C=N) to lower frequencies relative to those of corresponding uncoordinated hydrazones suggest that these aroylhydrazones act as mononegative ONO tridentate ligands [1,2,35,36]. The IR spectrum of the mononuclear complex $[Cu(HSBzH)NO_2]\cdot H_2O$, Fig. 1, displays three bands at 1510, 1290 and 1000 cm^{-1}, respectively due to the ν(N=O), $\nu_{asym}(NO_2)$ and $\nu_{sym}(NO_2)$, in agreement with the unsymmetric bidentate nature of the coordinated nitrate. The spectra of the binuclear nitrate complexes $[\{Cu(HL)H_2O\}_2](NO_3)_2\cdot nH_2O$ (**7**) and $[\{Cu(HL)\}_2](NO_3)_2$ (**7a**), on the other hand, show an intense band at ca. 1380 cm^{-1} characteristic of ionic nitrate [22,37]. The spectra of the thiocyanate complexes **8** show an intense band at 2085 cm^{-1} indicating that the thiocyanate group acts as monodentate ligand, most probably through the nitrogen atom [37].

3. Experimental

3.1. Preparation of aroylhydrazines and N-salicylidene-aroylhydrazines

Aroylhydrazines were prepared, as previously described [38], by the hydrazinolysis of aromatic carboxylic methyl esters in methanol. The corresponding *N*-salicylidene aroyl-

Table 5
Selected IR spectral bands (cm^{-1}) for *N*-salicylidenearoylhydrazines and their corresponding copper(II) complexes

Compound		ν(N–H)	ν(C=O) (amide I)	ν(C=N), ν(C=C)	δ(N–H)	
R	*n*				(amide II)	(amide III)
$[H_2L]$ (**1**)						
C_6H_5		3250 m	I675 s	1635 s	1540 s	1355 m
p-$CH_3C_6H_4$		3200 m	1675 s	1640 s, 1620 s	1540 s	1362 m
p-$CH_3OC_6H_4$		3200 m	1670 sh	1636 s, 1604 s	1555 s	1355 s
p-ClC_6H_4		3205 m	1646 s	1620 s	1560 s	1365 s
$[\{Cu(L)\}_2\}]$ (**2**)						
C_6H_5				1618 s, 1594 s		1340 s
p-$CH_3C_6H_4$				1619 s, 1595 s		1342 m
p-$CH_3OC_6H_4$				1618 s, 1597 s		1342 s
p-ClC_6H_4				1619 s, 1593 s		1342 s
$K_2[\{Cu(L)OH\}_2]\cdot nH_2O$ (**4**)						
C_6H_5	2			1612s		1340 s
p-$CH_3C_6H_4$	2			1612s		1340 m
p-$CH_3OC_6H_4$	1			1615s		1343 m
p-ClC_6H_4				1614s		1338 s
$[Cu(HL)Cl.H_2O]\cdot nH_2O$ (**5**)						
C_6H_5		3120 m	1620 s	1600 s, 1590 sh	1545 m	1340 s
p-$CH_3C_6H_4$		3195 m	1618 s	1605 s	1535 s	1335 m
p-$CH_3OC_6H_4$	1	3200 m	1620 s	1605 s, 1590 s	1555 s	1330 m
p-ClC_6H_4	1			1590 s	1540 s	1318 m
$[\{Cu(HL)Cl\}_2]$ (**6**)						
C_6H_5		3125 m	1615 s	1595 s	1550 s	1344 m, 1312 m
p-$CH_3C_6H_4$		3130 m	1618 s	1590 s	1543 s	1326 m, 1308 m
$[Cu(HL)NO_3]\cdot nH_2O$						
C_6H_5	1	3195m	1622s	1603 s	1545 m	1335 m
$[\{Cu(HL)\}_2](NO_3)_2$ (**7a**)						
C_6H_5		3180 m	1618 s	1595 s	1545 m	1300m
p-$CH_3OC_6H_4$		3170 m	1620 s	1597 s	1540 m	1305m
$[\{Cu(HL)\cdot H_2O\}_2](NO_3)_2\cdot nH_2O$ (**7**)						
p-$CH_3C_6H_4$	1	3170 m	1620 s	1602 s, 1570	1545 m	1330 m
$[Cu(HL)(NCS)]\cdot nH_2O$ (**8**)						
C_6H_5	1	3146 m	1620 s	1605 s, 1590 s	1544 s	1327 m
p-$CH_3C_6H_4$		3195 m	1620 s	1605 s	1538 s	1335 m
p-$CH_3OC_6H_4$		3210	1623 s	1605 s	1540 m	1335 s

hydrazines were prepared by the condensation of salicylaldehyde with aroylhydrazines in methanol [38–40] (H_2SBzh, m.p. = 182°C; H_2S*p*-MeBzh, m.p. = 195°C; H_2S*p*-MeOBzh, m.p. = 173°C; H_2S*p*-ClBzh, m.p. = 208°C).

3.2. Preparation of copper(II) complexes of N-salicylidenearoylhydrazines

3.2.1. Preparation of [{Cu(L)}$_2$] (**2**, R = C_6H_5, *p*-$CH_3C_6H_4$, *p*-$CH_3OC_6H_4$ and *p*-ClC_6H_4)

To a solution of *N*-salicylidenearoylhydrazine (H_2L) (**1**, R = C_6H_5, *p*-$CH_3C_6H_4$, *p*-$CH_3OC_6H_4$ and *p*-ClC_6H_4) (0.01 mol) in dry methanol (30 cm^3), an equivalent amount of $Cu(CH_3COO)_2\cdot 2H_2O$ (0.012 mol) in dry methanol (50 cm^3) was added dropwise with constant stirring. During addition a green precipitate started to appear and after complete addition of copper acetate, the reaction mixture was refluxed, with constant stirring, for ca. 30 min. On cooling the formed green complex, $[Cu(L)]_2$, was filtered, washed with hot methanol and then dried in vacuo.

3.2.2. Preparation of $K_2[\{Cu(L)OH\}_2]\cdot nH_2O$ (**4**, R = C_6H_5, *p*-$CH_3C_6H_4$ and *p*-$OCH_3C_6H_4$)

To a suspension of [{Cu(L)}$_2$] complex (**2**, R = C_6H_5, *p*-$CH_3C_6H_4$ and *p*-$OCH_3C_6H_4$) (0.01 mol) in hot absolute ethanol (50 cm^3), an excess amount of KOH (0.025 mol) was added and the reaction mixture was refluxed until complete dissolution of [{Cu(L)}$_2$] complex. The resulting solution was filtered and then evaporated to half its volume. On cooling the formed green complex $K_2[\{Cu(L)OH\}_2]\cdot nH_2O$, Table 1, was isolated and then dried over $CaCl_2$.

3.2.3. Preparation of [Cu(HL)Cl]·nH_2O (**5**, R = C_6H_5, *p*-$CH_3C_6H_4$, *p*-$OCH_3C_6H_4$ and *p*-ClC_6H_4)

A solution of $CuCl_2\cdot 2H_2O$ (0.01 mol) in ethanol (20 cm^3) was added to a solution of salicylaldehyde (0.01 mol) in

ethanol (50 cm^3). The reaction mixture was heated for a few minutes and then an equivalent amount of aroylhydrazine (0.01 mol) was added dropwise with constant stirring. The resulting mixture was then refluxed for ca. 15 min and the isolated green complex $[Cu(HL)Cl \cdot H_2O] \cdot nH_2O$ (**5**, R = C_6H_5, *p*-$CH_3C_6H_4$, *p*-$CH_3OC_6H_4$ and *p*-ClC_6H_4) which was separated on cooling, was filtered, washed with ethanol then dried in vacuo.

*3.2.4. Preparation of $[\{Cu(HL)Cl\}_2] \cdot nH_2O$ (**6**, R = C_6H_5 and p-$CH_3C_6H_4$)*

To a solution of *N*-salicylidenearoylhydrazine (H_2L) (**1**, R = C_6H_5 or *p*-$CH_3C_6H_4$) (0.01 mol) in absolute ethanol (30 cm^3), an equivalent amount of $CuCl_2 \cdot 2H_2O$ (0.01 mol) in hot absolute ethanol (20 cm^3) was added dropwise with constant stirring, then refluxed for 1 h. On cooling the precipitated copper(II) complex (2.34, R = C_6H_5 or *p*-CH_3-C_6H_4) was filtered, washed with absolute ethanol and then dried in vacuo.

3.2.5. Preparation of $[Cu(HSBz)NO_3] \cdot H_2O$

A solution of $CuNO_3 \cdot 6H_2O$ (0.01 mol) in ethanol (20 cm^3) was added to a solution of salicylaldehyde (0.01 mol) in ethanol (50 cm^3). The reaction mixture was heated for a few minutes and then an equivalent amount of aroylhydrazine (0.01 mol) was added dropwise with constant stirring. The resulting mixture was refluxed for ca. 1 h. On cooling, the separated copper(II) complex $[Cu(HL)NO_3] \cdot H_2O$ was filtered, washed with ethanol and then dried in vacuo.

*3.2.6. Preparation of $[\{Cu(HL)NO_3\}_2] \cdot nH_2O$ (**7**, R = C_6H_5, p-$CH_3C_6H_4$, and p-$CH_3OC_6H_4$)*

To a solution of *N*-salicylidenearoylhydrazine H_2L (**1**, R = C_6H_5, *p*-$CH_3C_6H_4$ and *p*-$CH_3OC_6H_4$) (0.01 mol) in absolute ethanol (30 cm^3), an equivalent amount of $Cu(NO_3)_2 \cdot 6H_2O$ (0.015 mol) in absolute ethanol (50 cm^3) was added dropwise with constant stirring. The brownish-green nitrate complex, $[Cu(HL)NO_3]_2 \cdot nH_2O$, which was formed, was filtered off, washed with ethanol and then dried in vacuo.

*3.2.7. Preparation of $[Cu(HL)SCN] \cdot nH_2O$ (**8**, R = C_6H_5, p-$CH_3C_6H_4$, p-$CH_3OC_6H_4$ and p-ClC_6H_4)*

To a suspension of either copper chloride or copper nitrate copper(II) complexes (0.01 mol) in methanol (30 cm^3), the equivalent amount of NH_4SCN (0.015 mol) as a solid or in methanol (10 cm^3) was added dropwise and the reaction mixture was stirred at room temperature or refluxed for ca. 2 h. The green precipitate, which was formed, was isolated and washed with methanol, then dried in vacuo.

3.3. Physical measurements

The IR spectra were recorded on a Perkin-Elmer 1430 data system spectrophotometer and/or Perkin-Elmer FT IR spectrometer (PARAGON 100 PC). Calibration of frequency reading was made with polystyrene film. Solid samples were examined as KBr discs. Magnetic susceptibilities of powdered dried samples were recorded on a Faraday-type magnetometer using a sensitive computer controlled D-200 Cahn RG microbalance in the temperature range 4.2–298 K. The magnetic field applied was ~1.5 T. Details of the apparatus have been described elsewhere [41,42]. Experimental susceptibility data were corrected for the underlying diamagnetism. The elemental analyses (C, H and N) were performed at the microanalytical laboratory, Faculty of Science, Alexandria University and/or at the Darmstadt Technical University, Germany. The copper(II) content of the prepared complexes was determined volumetrically by titration with EDTA using PAN as indicator and/or by atomic absorption technique.

3.4. X-ray crystal and molecular structure

Suitable crystals were sealed in a fine focus glass capillary tube and mounted on a Nonius CAD-4 [43] diffractometer. Intensity data were collected at room temperature in the ω–θ scan mode, using graphite monochromatized Mo Kα radiation. Lattice constants were determined by full-matrix least-squares refinement. The solution of the crystal structures was carried out by using both SHELXS-86 [44] and SHELXL-93 [45] programs. The SHELXL-93 program was also used for structure refinement and for the evaluation of data. The Steo-REDU4 [46] and StoeX-RED [46] programs were used for computing data reductions. The graphics plotting of the molecular and crystal structures was carried out using the PLUTON-93 [47] program as well as ORTEP [48] method. The form factors for Cu(0) were taken from the international tables [49] and those for the other atoms are included as saved values in used programs.

Supplementary data

Atomic coordinates, equivalent isotropic displacement parameters, hydrogen coordinates, isotropic displacement parameters, anisotropic displacement parameters and complete lists of bond distances and bond angles have been deposited with the Cambridge Crystallographic Data Centre, 12 Union Road, Cambridge CB2 1EZ, UK (fax: +44-1223-336033; e-mail: deposit@ccdc.cam.ac.uk) and are available on request quoting no. CCDC 136950.

References

[1] M.F. Iskander, A.M. El-Aggaan, L.S. Refaat, L. El-Sayed, Inorg. Chim. Acta 14 (1975) 167.
[2] M.F. Iskander, L. El-Sayed, S. Saddeck, M.A. Abuo-Taleb, Transition Met. Chem. 5 (1980) 168.
[3] S.S. Biradat, B.R. Havinale, Inorg. Chim. Acta 17 (1976) 157.
[4] D.K. Rastogi, S.K. Dua, V.B. Rana, S.K. Sahni, J. Inorg. Nucl. Chem. 40 (1978) 1323.

[5] D.K. Rastogi, S.K. Sahni, V.B. Rana, S.K. Dua, J. Coord. Chem. 8 (1978) 97.
[6] D.K. Rastogi, S.K. Sahni, V.B. Rana, S.K. Dua, Transition Met. Chem. 3 (1978) 56.
[7] D.K. Rastogi, S.K. Sahni, V.B. Rana, S.K. Dua, J. Inorg. Nucl. Chem. 41 (1979) 21.
[8] D.K. Rastogi, S.K. Dua, S.K. Sahni, J. Inorg. Nucl. Chem. 42 (1980) 323.
[9] S.K. Dua, D.K. Rastogi, S.K. Sahni, J. Inorg. Nucl. Chem. 42 (1980) 1711.
[10] A.A. Aruffo, T.B. Murphy, D.K. Johnson, N.J. Rose, V. Schomaker, Inorg. Chim. Acta 67 (1982) L25.
[11] A.A. Aruffo, T.B. Murphy, D.K. Johnson, N.J. Rose, V. Schomaker, Acta Crystallogr., Sect. C 40 (1984) 1164.
[12] J. Jezierska, A. Jezierski, B.J. Tezebiatowska, A. Ozarowski, Inorg. Chim. Acta 68 (1983) 7.
[13] M. Mohan, N.S Gupta, A. Kumar, M. Kumar, Inorg. Chim. Acta 135 (1987) 167.
[14] M. Mohan, A. Kumar, M. Kumar, N.K. Jha, Inorg. Chim. Acta 136 (1987) 65.
[15] M. Mohan, N.S. Gupta, M.P. Gupta, A. Kumar, M. Kumar, N.K. Jha, Inorg. Chim. Acta 152 (1988) 25.
[16] M.S. Palacios, J.M. Dance, Inorg. Chim. Acta 7 (1988) 543.
[17] J.M. Dance, M.T. Do P. Gambardella, R.H. De A. Santos, E. Medina, F.G. Manrique, M.S. Palacios, Inorg. Chim. Acta 162 (1989) 239.
[18] W. Haase, K. Griesar, M.F. Iskander, Y. Galyametdinov, Mol. Mater. 3 (1993) 115.
[19] E.W. Ainscough, A.M. Brodie, J.D. Ranford, J.M. Waters, Inorg. Chim. Acta 236 (1995) 83.
[20] S.C. Chan, L.L. Koh, P.H. Leung, J.D. Ranford, K.Y. Sim, Inorg. Chim. Acta 236 (1995) 101.
[21] E.W. Ainscough, A.M. Brodie, A.J. Dobbs, J.D. Ranford, J.M. Waters, Inorg. Chim. Acta 267 (1998) 27.
[22] E.E. Addison, M. Logan, S.C. Wallwork, C.D. Gardner, Q. Rev. Chem. Soc. 25 (1971) 289.
[23] M.E. Hossain, M.N. Alam, J. Begum, M.A. Ali, M. Nazimuddin, F.S. Smith, R.C. Hynes, Inorg. Chim. Acta 249 (1996) 207.
[24] M.E. Hossain, M.N. Alam, M. Nazimuddin, F.S. Smith, R.C. Hynes, Polyhedron 15 (1996) 973.
[25] W.L. Driessen, R.A.G. De Graaff, F.J. Parlevliet, J. Reedijk, R.M. Devos, Inorg. Chim. Acta 216 (1994) 43.
[26] A.W. Addison, T.N. Rao, J. Reedijk, J. Van Rijn, G.C. Verschoor, J. Chem. Soc., Dalton Trans. (1984) 1349.
[27] A. Saymal, K.S. Kale, Indian J. Chem. 16A (1978) 46.
[28] M. Melnik, Coord. Chem. Rev. 42 (1982) 259.
[29] D.Y. Jeter, D.L. Lewis, J.C. Hempel, D.J. Hodgson, W.E. Hatfield, Inorg. Chem. 11 (1972) 1958.
[30] D.L. Lewis, W.E. Hatfield, D.J. Hodgson, Inorg. Chem. 11 (1972) 2216.
[31] D.L. Lewis, K.T. McGregor, W.E. Hatfield, D.J. Hodgson, Inorg. Chem. 13 (1974) 1013.
[32] V.H. Crawford, H.W. Richardson, J.R. Wasson, D.J. Hodgson, W.E. Hatfield, Inorg. Chem. 15 (1976) 2107.
[33] M.F. Charlot, S. Jeannin, O. Khan, J.L. Abul, J.M. Frere, Inorg. Chem. 18 (1979) 1675.
[34] H. Yamaguchi, Y. Inomata, T. Takeuchi, Inorg. Chim. Acta 172 (1990) 105.
[35] C. Colonna, A. Cosse-Barbi, R. Ben Abdelmoumene, J.P. Doucet, Bull. Soc. Chim. Belg. 102 (1993) 411.
[36] C. Colonna, J.P. Doucet, A. Cosse-Barbi, Transition Met. Chem. 20 (1995) 338.
[37] K. Nakamoto, Infrared Spectra of Inorganic and Coordination Compounds, Wiley, New York, 4th edn., 1986.
[38] G. Struve, J. Prak. Chem 50 (1894) 295.
[39] P. Grammaticakis, Bull. Chim. Soc. (France) (1950) 690.
[40] J.T. Edward, M. Gauthier, F.L. Chubb, P. Ponka, J. Chem. Eng. Data 33 (1988) 538.
[41] L. Merz, W. Haase, J. Chem. Soc., Dalton Trans. (1980) 875.
[42] S. Gehring, P. Fleischhauer, H. Paulus, W. Haase, Inorg. Chem. 23 (1993) 54.
[43] Nonius Diffractometer Control Software, release 5.1, Nonius GmbH, Solingen, Germany, 1993.
[44] G.M. Sheldrick, SHELXS-86, Program for the solution of crystal structure determination, University of Göttingen, Germany, 1986 and 1990.
[45] G.M. Shelrick, SHELEX-93, program for crystal structure determination, University of Göttingen, Germany, 1993.
[46] Stoe-REDU 4, Data reductions program, Version 6.2c., Stoe & Cie GmbH, Darmstadt, 1987, and StoeX-RED, data reductions program, Steo & Cie GmbH, Darmstadt, 1996.
[47] A.L. Speck, Pluton-93 program for the display and analysis of crystal and molecular structures, Utrecht University, The Netherlands, 1993.
[48] R.W. Jothan, S.F.A. Kettle, Inorg. Chim. Acta 4 (1970) 145.
[49] J.A. Ibers, W.C. Hamilton, International Tables for X-ray Crystallography, vol. IV, Kynoch Press, Birmingham, 1973.

PERGAMON

www.elsevier.nl/locate/poly

Polyhedron 19 (2000) 959–963

POLYHEDRON

Selective hydrolysis of the unactivated peptide bond in *N*-acetylated L-histidylglycine catalyzed by various palladium(II) complexes: dependence of the hydrolysis rate on the steric bulk of the catalyst

Miloš I. Djuran *, Snežana U. Milinković

Department of Chemistry, Faculty of Science, University of Kragujevac, R. Domanovića 12, P.O. Box 60, 34000 Kragujevac, Yugoslavia

Received 10 December 1999; accepted 24 February 2000

Abstract

Hydrolytic reactions between various palladium(II) complexes of the type *cis*-$[Pd(L)(H_2O)_2]^{2+}$ in which L is a chelating diamine (ethylenediamine, en; 1,2-propylenediamine, 1,2-pn; *N*-methylethylenediamine, Meen; isobutylenediamine, ibn and *N*,*N*,*N*′,*N*′-tetramethylethylenediamine, Me_4en) or *S*,*N*-coordinated amino acid (*S*-methyl L-cysteine, MeS-L-HCys and L-methionine, L-HMet) and *N*-acetylated L-histidylglycine (MeCO-His-Gly), were studied by ^{1}H NMR spectroscopy. The reactions were carried out in the pH range 2.0–2.5 and at 60°C. In all these reactions, a palladium(II) complex bound to a histidine residue effects the regioselective cleavage of the amide bond involving the carboxylic group of histidine. We found that the rate of hydrolysis decreases as the steric bulk of the palladium(II) complex increases (en > 1,2-pn > Meen > MeS-L-HCys > ibn > L-HMet > Me_4en). The observed rates of hydrolytic reaction are discussed in terms of steric hindrance of the chelating diamine or sulfur-containing amino acid on the palladium(II) complexes. This study is an important step in the development of new palladium(II) complexes as artificial metallopeptidases. ©2000 Elsevier Science Ltd All rights reserved.

Keywords: Palladium(II) complexes; Catalysts; Peptides; Hydrolysis

1. Introduction

Many biological processes involve hydrolysis of peptides and proteins, but relatively little is known about the mechanism of this reaction. The extreme inertness of the amide bond makes this reaction interesting from a chemical point of view. Several proteolytic enzymes are used for cleavage [1], but application of enzymes is limited by their rather narrow requirements for temperature and pH.

Transition-metal complexes hold promise as new reagents for protein cleavage by various mechanisms. Several cobalt(III) complexes coordinate to peptides and facilitate hydrolysis, but they cleave only the *N*-terminal amino acid [2]. However, practical applications usually require cleavage of internal amide bonds. Studies with some iron-EDTA complexes that are covalently attached to amino acid side chains revealed some mechanistic features of these hydrolytic reactions, but they did not result in practical methods for analytical biochemistry [3–12]. Although in some cases the cleavage was fast, the synthetic work involved in the attachment and the additional chemicals required for cleavage limit the applicability of this method. Recently, Kostić and coworkers have shown that platinum(II) [13] and palladium(II) [14–21] aqua complexes can be promising reagents for the hydrolytic cleavage of peptides and proteins. These complexes bind to the heteroatom in the side chain of methionine [13–17] or histidine [18–21] and promote cleavage of the amide bond involving the carboxylic group of this anchoring amino acid. Palladium(II) complexes, as cleavage agents, differ from the well known complexes of other transition metals because their attachment to substrates is achieved simply by mixing, the hydrolysis reactions have half-lives as short as 15 min, and the complexes are easily removed from the cleaved substrates.

The consistent regioselectivity in the cleavage of methionine or histidine containing peptides promoted by palladium(II) aqua complexes and the mechanism of this hydrolytic reaction are not completely understood yet. A better knowledge of the coordination chemistry of histidine-containing peptides with palladium(II) complexes is necessary for understanding the regioselectivity of peptide and protein cleavage promoted by such complexes. This paper reports a ^{1}H NMR investigation of the hydrolysis reac-

* Corresponding author. Tel.: +381-34-335-039; fax: +381-34-335-040; e-mail: djuran@uis0.uis.kg.ac.yu or djuran@knez.uis.kg.ac.yu

0277-5387/00/$ - see front matter ©2000 Elsevier Science Ltd All rights reserved.
PII S0277-5387(00)00342-9

tion of a model histidine-containing peptide, *N*-acetylated L-histidylglycine, catalyzed by a series of palladium(II) complex cations of the type *cis*-$[Pd(L)(H_2O)_2]^{2+}$ in which L is a chelating diamine ligand, which differ in the number of methyl groups at the nitrogen or carbon atom, or *S,N*-coordinated amino acid. The observed rates of reaction are explained in terms of steric hindrance of the chelating ligand on the palladium(II) complexes.

2. Experimental

2.1. Materials

Distilled water was demineralized and purified to a resistance greater than 10 MΩ cm. The compounds D_2O, DNO_3, NaOD, and $K_2[PdCl_4]$ were obtained from Aldrich Chemical Co. All common chemicals were of reagent grade. Dipeptide L-histidylglycine, amino acids, *S*-methyl-L-cysteine and L-methionine and all diamines were obtained from Sigma Chemical Co. The terminal amino group in His-Gly was acetylated by standard methods [14].

2.2. Synthesis of palladium(II) complexes

The palladium(II) complexes of the type *cis*-$[Pd(L)Cl_2]$ (L is ethylenediamine, en; *N*-methylethylenediamine, Meen; 1,2-propylenediamine, 1,2-pn; *S*-methyl L-cysteine, MeS-L-HCys; L-methionine, L-HMet; *N,N,N′,N′*-tetramethylethylenediamine, Me_4en; isobutylenediamine, ibn) were synthesized according to the procedures published in the literature [22–24]. K_2PdCl_4 was dissolved in water and mixed with an equimolar amount of diamine or amino acid. The pH of the solution was adjusted to ca. 3 by addition of 1 M HCl and the mixture was stirred at 80°C for 2 h. All complexes were crystallized from water at room temperature. The pure complexes were obtained by recrystallization from a small amount of water and cooling. The experimental results of the elemental analysis for C, H and N parameters for all palladium(II) complexes are in accordance with theoretical values calculated for *cis*-$[Pd(L)Cl_2]$ complexes. The chloro complexes were converted into the corresponding diaqua complexes by treatment with 2 equiv. of $AgNO_3$ at pH 2.0 according to a published method [25]. In each case, the solid AgCl was removed by filtration in the dark, and fresh stock solution of the aqua complex was used in further experiments.

2.3. Reactions of peptide with palladium(II) complexes

Reactions of MeCO-His-Gly with palladium(II) complexes were followed by ^{1}H NMR spectroscopy. Equimolar amounts of the palladium(II) complex and the peptide were mixed in an NMR tube. The final solution was 10 mM in each reactant. The pH was varied in the range 2.0–2.5. All reactions were carried out at 60°C.

2.4. pH Measurements

All pH measurements were made at 298 K. The pH meter (Iskra MA 5704) was calibrated with Fischer certified buffer solutions of pH 4.00 and 7.00. The results were not corrected for the deuterium isotope effect. Proton NMR spectra of D_2O solutions containing TSP (3-trimethylsilylpropane-1-sulfonate) as internal reference were recorded with Varian Gemini 200 spectrometer.

3. Results and discussion

In the present study hydrolytic reactions between various complexes of the type *cis*-$[Pd(L)(H_2O)_2]^{2+}$ (L is ethylenediamine, en; 1,2-propylenediamine, 1,2-pn; *N*-methylethylenediamine, Meen; *S*-methyl L-cysteine, MeS-L-HCys; isobutylenediamine, ibn; L-methionine, L-HMet; *N,N,N′,N′*-tetramethylethylenediamine, Me_4en) and *N*-acetylated L-histidylglycine, MeCO-His-Gly, were studied by ^{1}H NMR spectroscopy. The palladium(II) complexes are as shown in Fig. 1. The different chelate ligands (L) in these complexes are inert to substitution and are expected to remain bound to the palladium(II) atom during the reactions with the amino acids and peptides. The course of the hydrolytic reaction at pH 2.0 is shown in Scheme 1. As was shown in previous studies [18–20,26], acidic solutions are needed to suppress the formation of hydroxo-bridged oligomeric palladium(II) complexes, which are catalytically inactive.

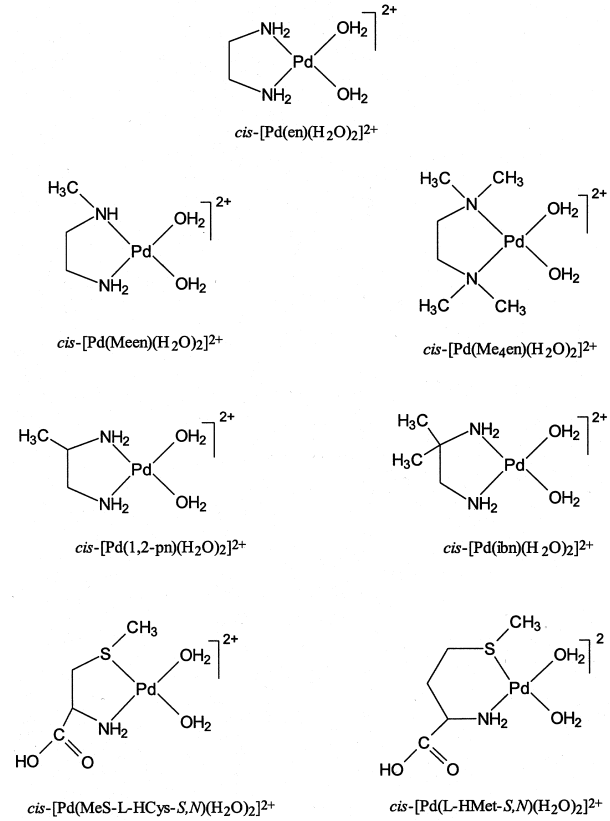
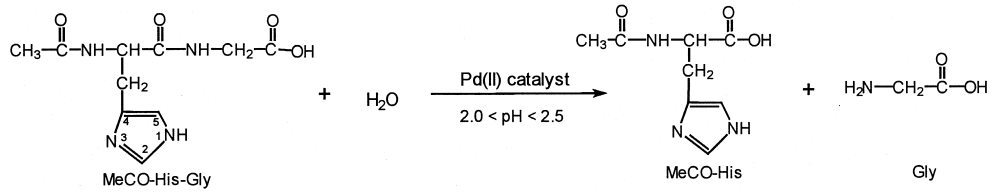


Fig. 1. Palladium(II) complexes used in the reaction with MeCO-His-Gly.



Scheme 1.

3.1. Binding of the catalysts to the substrate

The previous study with dipeptide MeCO-Gly-His and *cis*-$[Pd(en)(H_2O)_2]^{2+}$ showed that at pH < 3 five palladium(II)-peptide products formed [18–20]. These complexes were distinguished on the basis of the chemical shifts of the two imidazole protons, H-2 and H-5. The two major complexes are linkage isomers of each other with unidentate coordination of palladium(II) via the N-3 or N-1 atom to the imidazole ring. The three minor complexes contain more than one palladium(II) atom per dipeptide or involve more than one donor atom in the dipeptide. The experiments with MeCO-His-Gly selectively methylated at the N-1 or N-3 atom of imidazole and *cis*-$[Pd(en)(H_2O)_2]^{2+}$ showed that only the palladium(II) complex with monodentate coordination to the N-3 atom of imidazole can effect the cleavage of the amide bond involving the carboxylic group of histidine (Fig. 2); none of the four other modes of coordination is effective [19]. The cleavage of the amide bond is regioselective and the reaction is completed in less than 72 h. Also, the experiments with different histidine-containing peptides and different palladium(II) complexes showed that only unidentate coordination of the peptide via the N-3 atom of the imidazole to the Pd(II) ion effects hydrolytic cleavage of the amide bond. This was explained through the fact that this coordination mode permits the necessary close approach of the palladium(II) ion and of its aqua ligand to the scissile peptide bond [18,20].

When an equimolar amount of *cis*-$[Pd(L)(H_2O)_2]^{2+}$, where L is Meen, Me_4en, or 1,2-pn, was incubated with MeCO-His-Gly at 60°C and 2.0 < pH < 2.5, five NMR-detectable complexes formed. The complexes were distinguished on the basis of the chemical shifts of imidazole protons. These complexes are identical with those for the reaction of this peptide with *cis*-$[Pd(en)(H_2O)_2]^{2+}$ [18–20]. In the reaction between *cis*-$[Pd(ibn)(H_2O)_2]^{2+}$ and MeCO-His-Gly at 2.0 < pH < 2.5, only four complexes formed. The complex with bidentate coordination of peptide via the N-3 atom of the imidazole ring and deprotonated peptide nitrogen atom was not detected in solution even after the reaction mixture stayed for 5 days at 60°C. This is in accordance with the fact that two methyl groups on the ibn ligand cause steric crowding on palladium(II) and do not allow its interaction with the peptide nitrogen atom. Mixing of *cis*-$[Pd(L)(H_2O)_2]^{2+}$, where L is MeS-L-HCys or L-HMet, with an equimolar amount of MeCO-His-Gly under the same experimental conditions resulted in a spontaneous formation of three NMR-detectable complexes. In the two complexes peptide is a unidentate ligand coordinated via the N-3 or N-1 atom of the imidazole ring to palladium(II). In the third palladium(II)-peptide complex bidentate coordination of the peptide occurs via the N-3 atom of imidazole and the deprotonated peptide nitrogen atom of the terminal amino group of histidine.

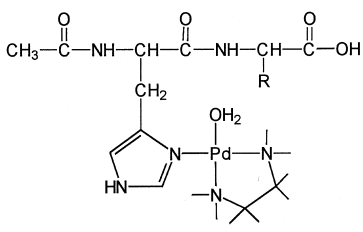


Fig. 2. Catalytically active form of the palladium(II)-peptide complex.

3.2. Regioselective cleavage of the peptide

The reactions between palladium(II) complexes of the type *cis*-$[Pd(L)(H_2O)_2]^{2+}$ and MeCO-His-Gly were carried out at 60°C and at 2.0 < pH < 2.5. The obtained results compared with those for *cis*-$[Pd(en)(H_2O)_2]^{2+}$ [18–20]. In all these reactions only the cleavage of the amide bond involving the carboxylic group of histidine was observed; see Scheme 1. In the reaction between the palladium(II) complex and MeCO-His-Gly, the ^{1}H NMR resonance at δ 3.96 ppm in the peptide decreased, while that at $\delta \sim 3.80$ ppm for free glycine increased. Upon addition of glycine to the reaction mixture its resonance is enhanced. The concentrations of the peptide and the hydrolysis products were determined from the known initial concentration of MeCO-His-Gly and from integrated resonance of the free glycine. Some of the liberated glycine reacts with the catalyst to form a small amount of the bis(bidentate) complex *cis*-$[Pd(L)(Gly\text{-}N,O)]^+$, easily detected by ^{1}H NMR spectroscopy by the resonance at δ 3.52 ppm. Indeed, the same complex is formed upon mixing of equimolar amounts of *cis*-$[Pd(L)(H_2O)_2]^{2+}$ and glycine.

3.3. Steric effects of the catalyst

The seven Pd(II) complexes in Fig. 1 differ in the chelate ligand. The palladium(II) complexes *cis*-$[Pd(Meen)(H_2O)_2]^{2+}$, *cis*-$[Pd(Me_4en)(H_2O)_2]^{2+}$, *cis*-$[Pd(1,2\text{-}pn)(H_2O)_2]^{2+}$ and *cis*-$[Pd(ibn)(H_2O)_2]^{2+}$ in relation to *cis*-$[Pd(en)(H_2O)_2]^{2+}$ have a bidentate ligand with different numbers of methyl groups at the nitrogen or carbon atom. These methyl groups contribute to the steric bulk of the palladium(II) complex. From Fig. 3 it can be concluded that the

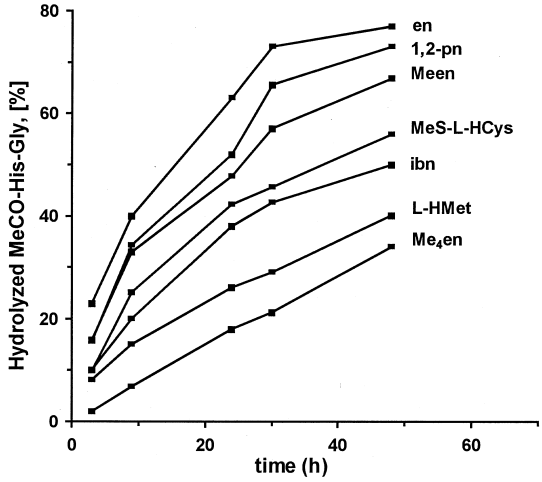


Fig. 3. Time dependence of hydrolytic reaction of MeCO-His-Gly with different palladium(II) complexes at $2.0 < pH < 2.5$ and at 60°C.

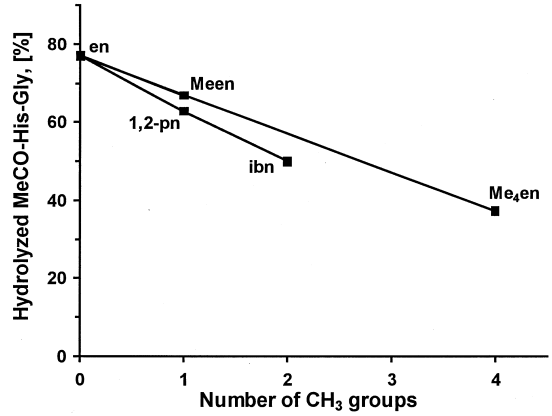
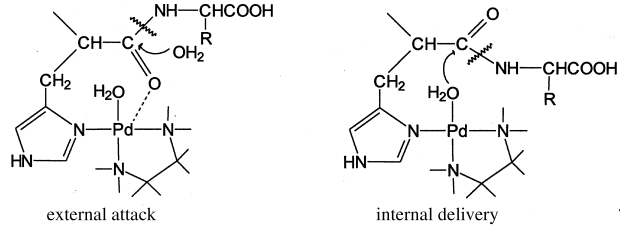


Fig. 4. Dependence of the hydrolysis rate on the steric bulk of the palladium(II). The reactions were carried out for 48 h at $2.0 < pH < 2.5$ and at 60°C.



Scheme 2.

rate of hydrolysis decreases as the steric bulk of the palladium(II) complex increases (en > 1,2-pn > Meen > MeS-L-HCys > ibn > L-HMet > Me_4en). The reaction between *cis*-$[Pd(en)(H_2O)_2]^{2+}$ and MeCO-His-Gly after 48 h at 60°C is almost two times faster in comparison with *cis*-$[Pd(Me_4en)(H_2O)_2]^{2+}$, or one and a half times faster in relation to *cis*-$[Pd(ibn)(H_2O)_2]^{2+}$. On comparing the ligand 1,2-pn with Meen, or Me_4en with ibn, we found that the former are more sterically demanding because the methyl groups bound directly to the nitrogen atoms are closer to the metal center, hindering the approach of a nucleophile. It is very illustrative to compare the rate of reactivity of MeCO-His-Gly with en, 1,2-pn and ibn, or this peptide with en, Meen and Me_4en palladium(II) complexes, see Fig. 4. It is obvious that increasing the number of methyl groups at the nitrogen or carbon atom of the chelate ligand decreases the amount of hydrolyzed His-Gly peptide bond. For comparison, parallel work has been done with MeCO-His-Gly and *cis*-[Pd(MeS-L-HCys-*S,N*)$(H_2O)_2]^{2+}$ and *cis*-[Pd(L-HMet-*S,N*)-$(H_2O)_2]^{2+}$. These two complexes differ in the ring size of the chelate ligand. The MeS-L-HCys-palladium(II) complex with five-membered chelate ring is more reactive than L-HMet-palladium(II) with six-membered ring in the square-planar plane. This inhibition of the hydrolytic reaction can be attributed to the steric bulk of the palladium(II) complex. A similar trend to our results has emerged in a previous study of *cis*-$[Pd(en)(H_2O)_2]^{2+}$ and MeCO-His-X peptides containing different C-terminal amino acids (X is Gly, Ala, Ser, Thr, Leu, Phe, Tyr) [18]. It was found that the rate constant of the hydrolytic reaction decreases smoothly as the volume of the leaving amino acid increases.

Summing up together our results with different palladium(II) complexes and previous results with different peptides [18], we can say that inhibition of the hydrolytic reaction can be attributed to the steric bulk of the palladium(II) complex as well as to the steric bulk of the leaving amino acid. These findings can be explained in terms of two possible limiting mechanisms for hydrolytic cleavage of the peptide bond promoted by palladium(II) [18–20], see Scheme 2. In the mechanism involving external attack by water, the palladium(II) atom, as a Lewis acid, polarizes the carbonyl group in the scissile peptide bond. In the mechanism involving internal attack by water, the palladium(II) atom delivers an aqua ligand to the scissile bond. As can be seen, both mechanisms require a close approach of the pendant catalyst to the adjacent peptide bond, and in both cases the steric bulk of the leaving amino acid as well as palladium(II) complex hinder this crucial interaction.

Acknowledgements

This work was funded in part by the Ministry of Science and Technology of the Republic of Serbia (grant 02E35) and by the Ministry of Science and Progress in Technology of the FR Yugoslavia (grant OSI-048/1-93). We are grateful to Professor Nenad M. Kostić (Department of Chemistry, Iowa State University, Ames, IA, USA) and his coworkers for providing K_2PdCl_4 and the peptides. We thank also B. Mojsilović for assistance with recording the ^{1}H NMR spectra.

References

[1] L.R. Croft, Handbook of Protein Sequence Analysis, Wiley, Chichester, 2nd edn., 1980.
[2] J. Suh, Acc. Chem. Res. 25 (1992) 273 and Refs. therein.
[3] T.M. Rana, C.F. Meares, Proc. Natl. Acad. Sci. USA 88 (1991) 10578.
[4] T.M. Rana, C.F. Meares, J. Am. Chem. Soc. 113 (1991) 1859.

[5] T.M. Rana, C.F. Meares, J. Am. Chem. Soc. 112 (1990) 2457.
[6] M.R. Ermácora, J.M. Delfino, B. Cuenoud, A. Schepartz, R.O. Fox, Proc. Natl. Acad. Sci. USA 89 (1992) 6383.
[7] I.E. Platis, M.R. Ermácora, R.O. Fox, Biochemistry 32 (1993) 12761.
[8] A. Schepartz, B. Cuenoud, J. Am. Chem. Soc. 112 (1990) 3247.
[9] D. Hoyer, H. Cho, P.G. Schultz, J. Am. Chem. Soc. 112 (1990) 3249.
[10] N. Ettner, W. Hillen, G.A. Ellestad, J. Am. Chem. Soc. 115 (1993) 2546.
[11] J.B. Ghaim, D.P. Greiner, C.F. Meares, R.B. Gennis, Biochemistry 34 (1995) 11311.
[12] M.R. Ermácora, D.W. Ledman, R.O. Fox, Nat. Struct. Biol. 3 (1996) 59.
[13] I.E. Burgeson, N.M. Kostić, Inorg. Chem. 30 (1991) 4299.
[14] L. Zhu, N.M. Kostić, Inorg. Chem. 31 (1992) 3994.
[15] L. Zhu, N.M. Kostić, J. Am. Chem. Soc. 115 (1993) 4566.
[16] L. Zhu, N.M. Kostić, Inorg. Chim. Acta 217 (1994) 21.
[17] E.N. Korneeva, M.V. Ovchinnikov, N.M. Kostić, Inorg. Chim. Acta 243 (1996) 9.
[18] T.N. Parac, N.M. Kostić, J. Am. Chem. Soc. 118 (1996) 51.
[19] T.N. Parac, N.M. Kostić, J. Am. Chem. Soc. 118 (1996) 5946.
[20] S.U. Milinković, T.N. Parac, M.I. Djuran, N.M. Kostić, J. Chem. Soc., Dalton Trans. (1997) 2771.
[21] X. Chen, L. Zhu, H. Yan, X. You, N.M. Kostić, J. Chem. Soc., Dalton Trans. (1996) 2653.
[22] H. Hohmann, R. van Eldik, Inorg. Chim. Acta 174 (1990) 87.
[23] A. Caubet, V. Moreno, E. Molins, C. Miravitlles, J. Inorg. Biochem. 48 (1992) 135.
[24] R.C. Warren, J.F. McConnell, N.C. Stephenson, Acta Crystallogr., Sect. B 26 (1970) 1402.
[25] G. Mehal, R. van Eldik, Inorg. Chem. 24 (1985) 4165.
[26] A.F.M. Siebert, Ph.D. Dissertation, University of Bochum, Germany, 1995, p. 166.

PERGAMON

www.elsevier.nl/locate/poly

Polyhedron 19 (2000) 965–969

POLYHEDRON

Heteronuclear multiple-quantum correlation ^{15}N–^{1}H, cross-polarized magic angle spinning ^{13}C, ^{15}N nuclear magnetic resonance and infrared spectroscopic studies of 1,2,4-triazolo-[1,5α]-pyrimidine and its Zn(II) halide and thiocyanate complexes

E. Szłyk [a,*], A. Grodzicki [a], L. Pazderski [a], E. Bednarek [b], B. Kamieński [c]

[a] *Department of Chemistry, Nicholas Copernicus University, Gagarina 7, Toruń, Poland*

[b] *Drug Institute, Chełmska 30/34, Warsaw, Poland*

[c] *Institute of Organic Chemistry, Kasprzaka 44/52, Warsaw, Poland*

Received 13 August 1999; accepted 25 February 2000

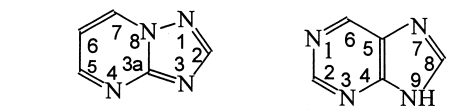
Abstract

1,2,4-Triazolo-[1,5α]-pyrimidine (tp) was studied by gradient heteronuclear multiple-quantum correlation ^{15}N–^{1}H NMR and by cross-polarized magic angle spinning ^{13}C, ^{15}N NMR. The ^{15}N signals were unambiguously assigned. The assignments of some IR absorption bands were proposed by comparison to purine and adenine spectra. The obtained results were used for the investigation of $Zn(tp)_2X_2$-type complexes (X = Cl, Br, I, NCS), suggesting a pseudo-tetrahedral configuration around the Zn(II) ion with unidentately N(3) bonded heterocycles and halides or thiocyanates (N bonded) in terminal positions. A slight shielding effect on the N(3) nucleus upon the formation of Zn(II)–N coordination bonding was observed. ©2000 Elsevier Science Ltd All rights reserved.

Keywords: Zn(II) complexes; 1,2,4-Triazolo-[1,5α]-pyrimidine; ^{15}N NMR; HETCOR; CPMAS

1. Introduction

1,2,4-Triazolo-[1,5α]-pyrimidine (tp) is a heterocycle isomeric compound with purine, its fused ring system differing from the purine skeleton in having the pyrimidine nitrogen atom in a bridge-head position (Fig. 1).



1,2,4-triazolo-[1,5α]-pyrimidine (tp) purine

Fig. 1. Tp and purine.

Tp has been the subject of many studies and its physical and chemical properties [1–3] as well as ^{1}H, ^{13}C and ^{15}N NMR spectra [4–13] have been examined. The latter spectrum was widely discussed but there was no agreement on ^{15}N assignments [9–13]. Some authors found four ^{15}N signals at analogous chemical shifts (in DMSO-d_6), but proposed different sequences for them (upfield): N(4) < N(1) < N(8) < N(3) [9], N(4) < N(1) < N(3) < N(8) [10,13], and N(1) < N(4) < N(3) < N(8) [11,12]. This problem becomes very important when ^{15}N NMR spectroscopy is used to determine the metallation sites in diamagnetic complexes. Recently, we have measured natural abundance ^{15}N NMR spectra of the following 5,7-disubstituted tp derivatives: 5,7-dimethyl-1,2,4-triazolo-[1,5α]-pyrimidine (dmtp), 5,7-diphenyl-1,2,4-triazolo-[1,5α]-pyrimidine (dptp), 5,7-di-*tert*-butyl-1,2,4-triazolo-[1,5α]-pyrimidine (dbtp) and 5,7-ditrifluoromethyl-1,2,4-triazolo-[1,5α]-pyrimidine (dftp) [14]. We have suggested, using selective decoupling techniques, the order N(1) < N(4) < N(3) < N(8) for the former three heterocycles and N(4) < N(1) < N(3) < N(8) for the latter heterocycle [14]. The lack of agreement on the ^{15}N assignment for tp has prompted us to record its ^{15}N–^{1}H NMR gradient heteronuclear multiple-quantum coherence (GHMQC) spectrum. Studies of ^{15}N–^{1}H spin–spin couplings have allowed us to make an unambiguous assignment of all the signals, settling the controversy in the literature. In order to complete the NMR spectral data for tp we have also measured its ^{13}C and ^{15}N NMR spectra in the solid state, by cross-polarized magic angle spinning

* Corresponding author. Tel.: +48-56-611-4304; fax: +48-56-654-2477; e-mail: eszlyk@chem.uni.torun.pl

0277-5387/00/$ - see front matter ©2000 Elsevier Science Ltd All rights reserved.
PII S0277-5387(00)00344-2

(CPMAS); to the best of our knowledge this is the first report for 1,2,4-triazolo-[1,5α]-pyrimidines.

The mass [15], electronic [16] and rotational [17] spectra of tp have already been described. However, there is only one report on the vibrational spectrum of 5- and 7-oxo analogues of tp (concerning CO stretching modes) [16] and the discussion of the two characteristic bands in the spectrum of dmtp [18]. In this paper we describe the IR spectrum of tp, based on a comparison with the purine and adenine spectra, and propose another assignment.

The new interpretation of the ^{15}N NMR and IR spectra of tp was used for structural determination of its Zn(II) halide and thiocyanate complexes of general formula $Zn(tp)_2X_2$ (X = Cl, Br, I, NCS). In addition to the known coordination compounds with other 1,2,4-triazolo-[1,5α]-pyrimidines (ZnL_2X_2, where L = dmtp, dptp, dbtp, X = Cl, Br, I, NCS) [18–22], there is only one report on $Zn(tp)_2Br_2 \cdot 0.5H_2O$ [23], where tp was N(3) bonded.

2. Experimental

2.1. Materials

Tp was purchased from Aldrich, whereas $ZnCl_2$, $ZnBr_2$, ZnI_2 of 98% purity were from POCh (Poland). $Zn(SCN)_2$ was obtained by reaction of HSCN in situ with $ZnCO_3$ [24].

2.2. Methods

^1H, ^{13}C and ^{15}N NMR spectra were recorded on a Varian GEMINI 200 XL spectrometer operating at 199.992, 50.293 and 20.270 MHz, respectively. Heteronuclear correlation (HETCOR) ^{15}N–^1H NMR spectra were detected on a Bruker DRX 500 spectrometer, using GHMQC with gradient selection, the frequency being 50.66 MHz for ^{15}N and 499.80 MHz for ^1H. The solvent was DMSO-d_6, the concentration of samples was 0.01 M for ^1H or ^{13}C and 0.1 M for ^{15}N spectroscopy, and the temperature was 295 K. The reference standard was TMS (internal) for ^1H or ^{13}C and CH_3NO_2 (external) for ^{15}N spectroscopy. The solid-state ^{13}C and ^{15}N NMR spectra were measured with the same type of spectrometer in 4 mm probeheads by CPMAS, two techniques being used: a standard technique (all C or N detected) and a short CP contact technique (protonated atoms only). The reference standard was glycine, the chemical shifts being recalculated to TMS for ^{13}C ($\delta(CH_2$ in glycine$) = +43.3$ ppm) or to nitromethane for ^{15}N ($\delta(NH_2$ in glycine$) = -347.6$ ppm). IR spectra were measured on a Perkin-Elmer spectrum 2000 FT-IR spectrometer, using KBr (400–4000 cm^{-1}) and polyethylene discs (100–400 cm^{-1}). The amounts of C, H, N in the complexes were determined by elemental semi-microanalysis, whereas that of Zn was determined by titration with EDTA (after mineralization).

2.3. Synthesis

Complexes of ZnX_2 (X = Cl, Br, I, SCN) with tp were prepared by a general procedure as follows: 5 mmol of ZnX_2 and 10 mmol of tp were dissolved in water, mixed and stirred at 90°C for 1 h. The obtained precipitate was filtered, washed with ethanol and dried in air (yield 50–75%). The elemental analyses were as follows. Calc. for $Zn(tp)_2Cl_2$, $ZnC_{10}H_8N_8Cl_2$: Zn, 17.4; C, 31.9; H, 2.1; N, 29.8. Found: Zn, 17.4; C, 32.0; H, 2.0; N, 30.1%. Calc. for $Zn(tp)_2Br_2$, $ZnC_{10}H_8N_8Br_2$: Zn, 14.0; C, 25.8; H, 1.7; N, 24.1. Found: Zn, 13.9; C, 26.0; H, 1.6; N, 23.9%. Calc. for $Zn(tp)_2I_2$, $ZnC_{10}H_8N_8I_2$: Zn, 11.7; C, 21.5; H, 1.4; N, 20.0. Found: Zn, 11.4; C, 21.7; H, 1.5; N, 20.2%. Calc. for $Zn(tp)_2(NCS)_2$, $ZnC_{12}H_8N_{10}S_2$: Zn, 15.5; C, 34.2; H, 1.9; N, 33.2. Found: Zn, 15.5; C, 34.4; H, 1.7; N, 33.1%.

3. Results and discussion

3.1. NMR spectra of tp

In the ^{15}N NMR one-dimensional spectrum of tp we have found four resonances with the following values of ^{15}N chemical shifts and ^{15}N–^1H spin–spin coupling constants (in DMSO-d_6): −102.3 ppm (doublet, $^2J_{N-H}$ 11.5 Hz), −105.2 ppm (doublet, $^2J_{N-H}$ 15.7 Hz), −149.6 ppm (doublet, $^2J_{N-H}$ 12.9 Hz), −153.6 ppm (doublet, $^2J_{N-H}$ 5.5 Hz). These results correspond well to the published data [9–13], however, they do not allow us to distinguish between N(1) and N(4) signals. The reason is that both are coupled to one proton (H(2) or H(5)) with $^2J_{NH}$ values being of the same magnitude. N(3) and N(8) resonances may be assigned properly because the value of $^2J_{NH}$ for N(3)–H(2) spin–spin interaction must be higher than that for N(8)–H(7). It is well known that ^{15}N–^1H coupling constants for pyridine-type nitrogens (possessing lone-pair electrons like N(3)) are larger than those for the pyrrole nitrogens (like N(8)) [25].

The assignment of ^{15}N signals became clear after the HETCOR ^{15}N–^1H NMR spectrum of tp was recorded by the GHMQC method (Fig. 2).

The N(4) and N(1) resonances can be easily distinguished as the former nucleus is coupled with H(5) and H(6), whereas the latter is coupled with H(2). Also, N(3) and N(8) have different coupling patterns, the former being coupled with H(2) and the latter with either H(2) or H(6) (coupling with H(7) was not registered in this experiment). These results finally prove that the order of ^{15}N signals in the tp spectrum is N(4) < N(1) < N(3) < N(8), as proposed earlier [10,13]. This sequence is consistent with the results of theoretical calculations of the absolute shielding constants, which are −40.2 for N(4), −20.3 for N(1), +22.2 for N(3) and +30.1 for N(8); the above-mentioned values were obtained by the gauge invariant atomic orbitals—coupled Hartree–Fock (GIAO-CHF) method [26].

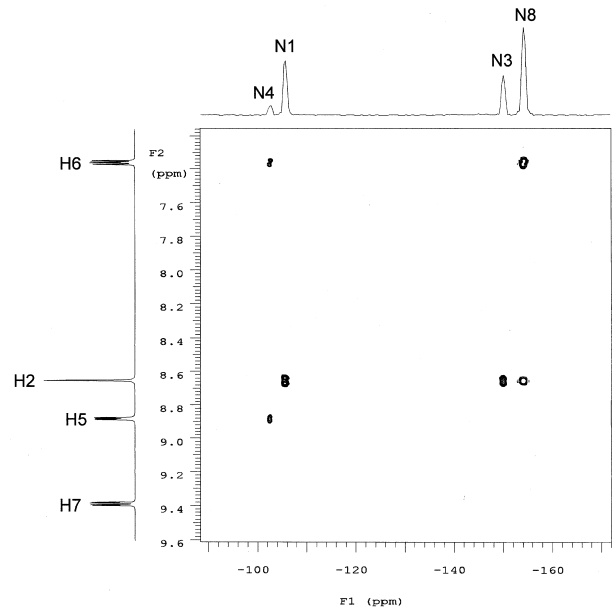


Fig. 2. ^{15}N–^{1}H HETCOR spectrum of tp.

N(8) is the only pyrrole-type nitrogen atom in the tp molecule and therefore it is more shielded than the others that are pyridine-type, which is a general rule for azoloazines [27]. However, the signal of N(3) is also detected at relatively high magnetic field compared to those of N(1) or N(4) (the difference in δ being about 45 ppm); this is probably associated with especially high electron density on this nitrogen. Earlier quantum-mechanical studies, performed by Salas et al., using the MNDO method, allowed evaluation of the electron density at N(3), N(1) and N(4) atoms as -0.240, -0.177, -0.171, respectively [28]. This fact also explains why N(3) is the preferred site in the processes of protonation and N-alkylation [5,12].

The ^{13}C CPMAS spectrum of tp exhibited signals from five carbons (including four protonated). They have been detected as follows: C(2)/C(5) 156.7/154.7, C(3a) 154.1, C(7) 138.7, C(6) 109.9 ppm. It is difficult to distinguish the C(2) and C(5) resonances, as both derive from CH carbons and have similar δ values. The signals of C(3a), C(6) and C(7) can be easily assigned because C(3a) is the only unprotonated carbon atom, whereas C(6) and C(7) have very characteristic chemical shifts, close to those reported for DMSO-d_6 solutions [8]. In the ^{15}N CPMAS spectrum of tp the two broad signals have been observed at -107.2 and -154.7 ppm. Their δ values indicate, by analogy with the measurements in DMSO-d_6, that they derive from the pairs N(1)/N(4) and N(3)/N(8). However, the coincidence of their chemical shifts does not allow us to separate them.

3.2. NMR spectra of Zn(II) complexes with tp

^{1}H and ^{13}C NMR spectra of the discussed Zn(II) complexes are nearly identical with those of tp and the observed deviations are within the limits of experimental error. This behaviour is quite different from that observed for Pd(II) chloride complexes with tp and its derivatives, where significant downfield shifts of ^{1}H resonances (maximum 0.6 ppm) and variable coordination shifts of ^{13}C signals (maximum 3.6 ppm) have been noticed [29].

The order of ^{15}N NMR resonances in the spectra of all Zn(II) complexes is the same as for tp and the chemical shifts of N(1), N(4) and N(8) are nearly identical. However, the signal of N(3) is slightly shifted upfield, 0.4–1 ppm, indicating that this atom is the coordination site (Table 1).

Similar coordination shifts of N(3) resonances (0.5–2 ppm) were observed for Zn(II) complexes with dmtp, dptp and dbtp [22]. The preference for complexation via N(3) is analogous to that via N(9) in adenine; hence, tp can be treated as a structural analogue of purine bases. It is also in accordance with the calculated highest electron density at N(3). However, in Zn(II) complexes with other N-donors possessing a similar coordination pattern, the measured shifts were usually more significant than in the case of 1,2,4-triazolo-[1,5α]-pyrimidines. For aqueous solutions of $Zn(NO_3)_2$ with imidazole or 1-methylimidazole they were in the range 10–60 ppm [30,31], whereas for adenosine complexes the shifts were between 2 and 9 ppm [32–34]. The increased shielding of the coordinated nitrogen atom is probably the result of its lone-pair electrons being engaged in Zn–N bonding. This effect seems to be analogous to that caused by protonation, N-oxidation or Pt(II) complexation of pyridine-type nitrogens in azine ring systems [25,35]. However, in the discussed Zn(II) complexes the magnitude of upfield shift is much smaller than that observed for tpH^+ (78 ppm) [12] or for $Pd(tp)_2Cl_2$ (88 ppm) [29].

Table 1
^{15}N–^{1}H HETCOR data for tp and its Zn(II) halide and thiocyanate complexes (δ coordination shifts, $\Delta\delta^{coord} = \delta^{complex} - \delta^{ligand}$, in parentheses)

Compound	N(4)	N(1)	N(3)	N(8)
tp [a]	−102.3	−105.2	−149.6	−153.6
Tp	−102.6	−105.6	−150.1	−154.2
$Zn(tp)_2Cl_2$	−102.7 (−0.1)	−105.6 (0)	−151.1 (−1.0)	−154.3 (−0.1)
$Zn(tp)_2Br_2$	−102.8 (−0.2)	−105.6 (0)	−151.1 (−1.0)	−154.2 (0)
$Zn(tp)_2I_2$	−102.7 (−0.1)	−105.7 (−0.1)	−151.1 (−1.0)	−154.3 (−0.1)
$Zn(tp)_2(NCS)_2$	−102.6 (−0.1)	−105.6 (0)	−150.5 (−0.4)	−154.1 (+0.1)

[a] ^{15}N NMR one-dimensional measurements.

3.3. Infrared spectrum of tp

In the literature there are no IR data on tp. Some authors have described the two characteristic absorption bands (at 1634 and 1544 cm^{-1}) in the dmtp spectrum, suggesting they are derived from the stretching vibrations of the pyrimidine and imidazole ring, respectively [18]. Recently, we have observed analogous bands in the IR spectra of dptp (at 1612 and 1543 cm^{-1}) and dbtp (at 1615 and 1530 cm^{-1}) [22]. However, the spectrum of tp reveals three bands in this region (1621, 1534 and 1515 cm^{-1}). Their assignment can be based on the known and assigned spectra of purine and adenine [36–43]. The origin of the others, observed in the range 100–1500 cm^{-1}, can be proved only by studies of the ^{2}H and ^{15}N analogues of tp, supported by Raman spectroscopy and quantum-mechanical calculations.

In the purine molecule the two characteristic bands at 1618 and 1570 cm^{-1} were assigned as the vibrations of the whole purine skeleton and of the pyrimidine ring, respectively, whereas those at 1464 and 1429 cm^{-1} were assigned as the imidazole ring modes [40]. By analogy, one can suggest that in the tp spectrum the band at 1621 cm^{-1} is the triazolopyrimidine mode (ν_{tp}), whereas the two bands at 1533 and 1515 cm^{-1} are the pyrimidine ring modes (split into ν_{py1} and ν_{py2}). Consequently, one can assume that in the dmtp spectrum the absorption bands at 1637 and 1550 cm^{-1} derive from ν_{tp} and ν_{py} vibrations, respectively; this assignment differs from that previously published [18].

3.4. Infrared spectra of Zn(II) complexes with tp

The coordination of Zn(II) ions by tp molecules results in a shift of either the ν_{tp} or ν_{py} bands, most frequently towards higher frequencies, as well as in the appearance of some new bands in the far-IR region (Table 2).

An analogous increase in energy of the skeletal vibrations has already been observed for Pd(II) chloride complexes with 1,2,4-triazolo-[1,5α]-pyrimidines [29]. It may be caused by the fact that after coordination the C=N and C=C bonds in the tp ring reveal a more pronounced double-bond character, due to the π-electron localization [44]. The band shift is more profound for ν_{py1} or ν_{py2} modes than for the ν_{tp} mode, as already observed for the Zn(II) complexes with dmtp, dptp and dbtp [22]. Although the average change in ν_{tp} and ν_{py} vibration energy does not exceed 10 cm^{-1}, this tendency is evident. Hence, one can suggest that these absorption bands are taken as an indication for the complexation of 1,2,4-triazolo-[1,5α]-pyrimidines. A similar behaviour was also described for their complexes with Co(II) [21], Ru(III) [45] and Cu(II) [46].

The presence of four bands in the far-IR region suggests a monomeric structure of all the complexes and pseudo-tetrahedral configuration around the Zn(II) atom; local symmetry C_{2v} results in two Zn–Cl and two Zn–N stretching vibrations. This geometry is consistent with that found or suggested for other Zn(II) complexes with 1,2,4-triazolo-[1,5α]-pyrimidines, the frequencies of Zn–X and Zn–N stretching vibrations being in a similar range [18–23]. Analogous results were obtained for pseudo-tetrahedral Zn(II) halide and thiocyanate complexes with pyridine–$Zn(py)_2X_2$ [47,48], imidazole–$Zn(imH)_2X_2$ [49], purine–$Zn(puH)Cl_2$ [50], adenine–$Zn(adH)Cl_2$, $Zn(adH)_2Cl_2$ [51] and adenosine–$Zn(ado)_2Cl_2$, $Zn(ado)_nCl_2 \cdot xH_2O$ ($n = 1,2,3$, $x > 1$) [33,34,51].

In the spectrum of $Zn(tp)_2(NCS)_2$ the stretching vibrations of C–N and C–S are observed at 2085 cm^{-1} (strong) and 840 cm^{-1} (weak), respectively. These values are similar to those reported for Zn(II) complexes with dmtp, dptp and dbtp [20,22], being typical for thiocyanate groups terminally bonded via the nitrogen atom [52]. The deformation S–C–N vibration, expected in the range 460–480 cm^{-1} [52], is not observed, probably owing to overlapping by the tp bands at 461 and 468 cm^{-1}.

4. Conclusions

HETCOR ^{15}N–^{1}H NMR studies of tp have been the basis of an unambiguous assignment of ^{15}N signals in the tp spectrum, which settles the controversy in the literature. The observed sequence of signals is N(4) < N(1) < N(3) < N(8) (upfield). These data are completed with the results of ^{13}C and ^{15}N CPMAS measurements in the solid state. The comparison of the IR spectrum of tp with those of purine and adenine allows us to propose the assignment of the two most characteristic absorption bands for 1,2,4-triazolo-[1,5α]-pyrimidines.

Zn(II) halide and thiocyanate complexes with tp have a monomeric structure with terminally bonded halogen atoms or NCS groups (via N). The geometry around the Zn(II) ion

Table 2
The ν_{tp}, ν_{py}, Zn–Cl and Zn–N absorption bands in the IR spectra of Zn(II) halide and thiocyanate complexes with tp (ν coordination shifts, $\Delta\nu^{coord} = \nu^{complex} - \nu^{ligand}$, in parentheses)

Complex	ν_{tp} (cm^{-1})	ν_{py} (cm^{-1})	ν(Zn–X) (cm^{-1})	ν(Zn–N) (cm^{-1})
$Zn(tp)_2Cl_2$	1621 (0)	1527 (+12); 1540 (+6)	300; 276	226; 198
$Zn(tp)_2Br_2$	1617 (−4)	1521 (+6); 1537 (+3)	273; [a]	[a]; [a]
$Zn(tp)_2I_2$	1622 (+1)	1526 (+11); 1534 (0)	200; 161	228; 205
$Zn(tp)_2(NCS)_2$	1623 (+2)	1528 (+13); 1541 (+7)	310; 274	218; 206

[a] Bands overlapped in the range 180–240 cm^{-1}.

is pseudo-tetrahedral. The tp molecule behaves as a unidentate ligand and coordinates by its N(3) atom. This nitrogen is slightly shielded owing to the formation of Zn–N coordination bonding, which is expressed by a small upfield shift (0.4–1 ppm) of the respective ^{15}N NMR signal. The observed complexation mode may be regarded as representative for 1,2,4-triazolo-[1,5α]-pyrimidines and analogous to coordination via N(9) in purine bases.

References

[1] G. Fischer, Z. Chem. 30 (1990) 305.
[2] G. Fischer, Adv. Het. Chem. 57 (1993) 81.
[3] E.S.H. Elashry, N. Rashed, Adv. Het. Chem. 72 (1999) 127.
[4] Y. Makisumi, H. Watanabe, K. Tori, Chem. Pharm. Bull. 12 (1964) 204.
[5] W.W. Paudler, L.S. Helmick, J. Het. Chem. 5 (1968) 691.
[6] E. Kleinpeter, R. Borsdorf, G. Fischer, H.J. Hofmann, J. Prakt. Chem. 314 (1972) 515.
[7] T. La Noce, A.M. Giuliani, Tetrahedron 34 (1978) 2927.
[8] R.J. Pugmire, J.C. Smith, D.M. Grant, B. Stanovnik, M. Tisler, B. Vercek, J. Het. Chem. 24 (1987) 805.
[9] W.W. Paudler, R.M. Sheets, B. Goodson, Org. Magn. Reson. 18 (1982) 87.
[10] M. Kuenstlinger, E. Breitmeier, Synthesis 1 (1983) 44.
[11] L. Stefaniak, M. Witanowski, U. Mahmoud, J.D. Roberts, G.A. Webb, J. Cryst. Spectrosc. Res. 19 (1989) 159.
[12] J.W. Wiench, L. Stefaniak, G.A. Webb, Magn. Reson. Chem. 32 (1994) 373.
[13] E. Kleinpeter, S. Thomas, G. Fischer, J. Mol. Struct. 355 (1995) 273.
[14] A. Grodzicki, E. Szłyk, L. Pazderski, A. Golinski, J.G. Haasnoot, Magn. Reson. Chem. 34 (1996) 725.
[15] Y. Tamura, J.H. Kin, M. Ikeda, J. Het. Chem. 12 (1975) 107.
[16] A.H. Beckett, R.G.W. Spickett, S.H.B. Wright, Tetrahedron 24 (1968) 2839.
[17] B. Velino, E. Cane, L. Gagliardi, A. Trombetti, W. Caminati, J. Mol. Spectrosc. 161 (1993) 136.
[18] J.M. Salas, M.A. Romero, A. Rahmani, R. Faure, G. Alvarez de Cienfuegos, E.R.T. Tiekink, J. Inorg. Biochem. 64 (1996) 259.
[19] J.M. Salas, M.A. Romero, A. Rahmani, R. Faure, Acta Crystallogr., Sect. C 50 (4) (1994) 510.
[20] J. Dillen, A. Lenstra, J.G. Haasnoot, J. Reedijk, Polyhedron 2 (1983) 195.
[21] E. Szłyk, A. Wojtczak, M. Jaskólski, M. Gilski, J.G. Haasnoot, J. Reedijk, Inorg. Chim. Acta 260 (1997) 145.
[22] A. Grodzicki, E. Szłyk, L. Pazderski, J. Sitkowski, Polish J. Chem. 72 (1998) 55.
[23] S.B. Sanni, J.M.M. Smits, P.T. Beurskens, J.G. Haasnoot, J. Schild, A.T.H. Lenstra, J. Cryst. Spectrosc. Res. 16 (1986) 823.
[24] A. Grodzicki, Polish J. Chem. 50 (1976) 33.
[25] M. Witanowski, L. Stefaniak, G.A. Webb, Annual Reports on NMR Spectroscopy, vol. 18, 1986, pp. 71, 78, 193.
[26] J.W. Wiench, Ph.D. Thesis, Warsaw, 1997, p. 38.
[27] M. Witanowski, L. Stefaniak, G.A. Webb, Annual Reports on NMR Spectroscopy, vol. 25, 1993, pp. 56–58.
[28] J.M. Salas, C. Enrique, M.A. Romero, K. Takagi, K. Aoki, Y. Miyashita, I.H. Sun, Polyhedron 11 (1992) 2903.
[29] E. Szłyk, A. Grodzicki, L. Pazderski, A. Wojtczak, G. Wrzeszcz, J. Sitkowski, B. Kamieński, J. Chem. Soc., Dalton Trans., in press.
[30] M. Alei, L.O. Morgan, W.E. Wageman, Inorg. Chem. 17 (1978) 2288.
[31] M. Alei, L.O. Morgan, W.E. Wageman, Inorg. Chem. 20 (1981) 940.
[32] W. Buchanan, J.B Stothers, Can. J. Chem. 60 (1982) 787.
[33] E. Szłyk, I. Łakomska, Polyhedron 11 (1992) 3147.
[34] E. Szłyk, Polish J. Chem. 68 (1994) 1209.
[35] J. Mason, Chem. Rev. 81 (1981) 205.
[36] E.D. Radchenko, A.M. Plokhotnichenko, G.G. Sheina, Yu. Blagoi, Biofizika 29 (1984) 553.
[37] S.G. Stepanian, G.G. Sheina, E.D. Radchenko, Yu. Blagoi, J. Mol. Struct. 131 (1985) 333.
[38] G.G. Sheina, S.G. Stepanian, E.D. Radchenko, Yu. Blagoi, J. Mol. Struct. 158 (1985) 275.
[39] M.J. Nowak, L. Łapiński, J.S. Kwiatkowski, J. Leszczyński, Spectrochim. Acta, Part A 47 (1991) 87.
[40] M. Majoube, M. Henry, G. Vergoten, J. Raman Spectrosc. 25 (1994) 233.
[41] M.J. Nowak, H. Rostkowska, L. Łapiński, J.S. Kwiatkowski, J. Leszczyński, Spectrochim. Acta, Part A 50 (1994) 1081.
[42] M.J. Nowak, H. Rostkowska, L. Łapiński, J.S. Kwiatkowski, J. Leszczyński, J. Phys. Chem. 98 (1994) 2813.
[43] L. Houben, K. Schoone, J. Smets, L. Adamowicz, G. Maes, J. Mol. Struct. 410–411 (1994) 397.
[44] M. Quiros, J.M. Salas, M.P. Sanchez, A.L. Beauchamp, X. Solans, Inorg. Chim. Acta 204 (1993) 213.
[45] A.H. Velders, L. Pazderski, F. Ugozzoli, M. Biagini-Cingi, A.M. Manotti-Lanfredi, J.G. Haasnoot, J. Reedijk, Inorg. Chim. Acta 273 (1998) 259.
[46] A. Grodzicki, E. Szłyk, A. Wojtczak, G. Wrzeszcz, L. Pazderski, T. Muziol, Polyhedron 18 (1999) 519.
[47] Y. Saito, M. Cordes, K. Nakamoto, Spectrochim. Acta, Part A 28 (1972) 1459.
[48] R.J.H. Clark, C.S. Williams, Spectrochim. Acta 22 (1966) 1081.
[49] B. Cornilsen, K. Nakamoto, J. Inorg. Nucl. Chem. 36 (1974) 2467.
[50] A.N. Speca, Ch.M. Mikulski, F.I. Iaconianni, L.L. Pytlewski, N.M. Karayannis, Inorg. Chim. Acta 46 (1980) 235.
[51] T. Beringhelli, M. Freni, F. Morazzoni, P. Romiti, R. Servida, Spectrochim. Acta, Part A 37 (1981) 763.
[52] K. Nakamoto, Infrared and Raman Spectra of Inorganic and Coordination Compounds, Wiley, New York, 1970, pp. 270–274.

PERGAMON

www.elsevier.nl/locate/poly

Polyhedron 19 (2000) 971–974

POLYHEDRON

Inductive effect of methyl groups on acidopentaaminecobalt(III) complexes

Fabián Benzo [a], Lothar Beyer* [1,b], Fernando Bozoglián [a], Karl-Heinz Hallmeier [b], Beatriz Sienra* [2,a]

[a] *Universidad de la República, Cátedra de Química Inorgánica, C.C. 1157, Montevideo, Uruguay*
[b] *University of Leipzig, Department of Inorganic Chemistry, Johannisallee 29, D-04103 Leipzig, Germany*

Received 22 November 1999; accepted 28 February 2000

Abstract

Electron spectroscopy for chemical analysis (ESCA) was performed for $[Co(NH_3)_5Cl](ClO_4)_2$, *trans*-$[Co(NH_3)_4(NH_2CH_3)Cl](ClO_4)_2$, $[Co(NH_2CH_3)_5Cl](ClO_4)_2$ and *trans*-$[Co(NH_3)_4(NH_2CH_3)(OSO_3)](ClO_4)$ complexes. Comparison of the results for the complexes $[Co(NH_3)_5Cl](ClO_4)_2$ and *trans*-$[Co(NH_3)_4(NH_2CH_3)Cl](ClO_4)_2$ shows clearly the electronic influence (+I effect) of the methylamine group on the cobalt and through this on the chlorine atom in *trans* position. Comparison of $[Co(NH_2CH_3)_5Cl](ClO_4)_2$ with *trans*-$[Co(NH_3)_4(NH_2CH_3)Cl](ClO_4)_2$ shows that methylation of the four *cis*-NH_3 ligands does not produce a proportional decrease in the binding energy of the cobalt atom, while the electron density of the chloro ligand is not affected. For the complex *trans*-$[Co(NH_3)_4(NH_2CH_3)(OSO_3)](ClO_4)$ the +I effect is almost completely compensated by the presence of the sulfato group in *trans* position. Acid dissociation constants are also reported for $[Co(NH_3)_5(OH_2)]^{3+}$ and *trans*-$[Co(NH_3)_4(NH_2CH_3)(OH_2)]^{3+}$ ions. The implications of these results for the mechanism of the acid and base hydrolysis reactions of acidopentaaminecobalt(III) complexes are discussed. The preparation of the *trans*-$[Co(NH_3)_4(NH_2CH_3)(OSO_3)](ClO_4)$ complex through the *trans*-$[Co(NH_3)_4(NH_2CH_3)(SO_3)]^+$ precursor is also described. ©2000 All rights reserved.

Keywords: Acidopentaaminecobalt(III) complexes; ESCA studies; ESI+ mass spectra; Acid dissociation constants

1. Introduction

Substitution reactions of octahedral cobalt(III) acidoammine complexes have been subjected to extensive and detailed investigation over recent decades [1,2]. Acid hydrolysis (or aquation) reactions of cobalt(III) complexes appear to be dissociative interchange processes, I_d, i.e. bond breaking substantially precedes bond making [3–9]. For base hydrolysis, a conjugate-base mechanism seems well defined (Eqs. (1)–(3)), although there is still some controversy on whether the process is entirely dissociative, Dcb, or whether it is partially concerted, I_dcb [10–21].

$$[Co(NH_3)_5X]^{n+} + OH^- \overset{K_a/K_w}{\rightleftarrows} [Co(NH_3)_4(NH_2)X]^{(n-1)+} + H_2O \quad (1)$$

$$[Co(NH_3)_4(NH_2)X]^{(n-1)+} \overset{k}{\rightarrow} [Co(NH_3)_4(NH_2)]^{2+} + X^{(3-n)-} \quad (2)$$

$$[Co(NH_3)_4(NH_2)]^{2+} + H_2O \overset{\text{fast}}{\rightarrow} [Co(NH_3)_5(OH)]^{2+} \quad (3)$$

Comparative studies on pentaammine and pentakis(methylamine) complexes [19,22] have been used to support these classifications. The increase in the rate for both reactions when the five ammine ligands in $[Co(NH_3)_5X]^{n+}$ are replaced by bulkier methylamine ligands is consistent with steric relief in a dissociated activated state. For example, the rate constant for aquation of $[Co(NH_2CH_3)_5Cl]^{2+}$ is 23 times that of $[Co(NH_3)_5Cl]^{2+}$, while for base hydrolysis the acceleration factor is 7.5×10^3. For *trans*-$[Co(NH_3)_4(NH_2CH_3)X]^{n+}$ ions there is only a modest rate enhancement of both aquation and base hydrolysis, when one NH_3 is substituted by a NH_2CH_3 ligand (*trans* position). Among other factors which may account for these variations

[1] *Corresponding author. Tel.: +49-341-9736161; fax: +49-341-9736199; e-mail: beyinorg@organik.chemie.uni-leipzig.de
[2] *Corresponding author. Tel.: +598-2-9249739; fax: +598-2-9241906.

0277-5387/00/$ - see front matter ©2000 All rights reserved.
PII S0277-5387(00)00346-6

in rate, we investigated the inductive effect of the methyl substituent, making use of ESCA on $[Co(NH_3)_5Cl](ClO_4)_2$, *trans*-$[Co(NH_3)_4(NH_2CH_3)Cl](ClO_4)_2$, $[Co(NH_2CH_3)_5Cl](ClO_4)_2$ and *trans*-$[Co(NH_3)_4(NH_2CH_3)(OSO_3)](ClO_4)$.

In the base hydrolysis reactions, if a conjugate base mechanism (Eqs. (1)–(3)) is operating, part of this acceleration could be due to an increased acidity of the N protons. Swaddle determined that $[Co(NH_2CH_3)_5(OH_2)]^{3+}$ was 6.3 times more acidic than $[Co(NH_3)_5(OH_2)]^{3+}$ [23], but the acidity of *trans*-$[Co(NH_3)_4(NH_2CH_3)(OH_2)]^{3+}$ has not yet been measured; therefore it was pertinent to accomplish this study.

2. Experimental

2.1. Preparation of compounds

$[Co(NH_3)_5Cl](ClO_4)_2$, $[Co(NH_3)_5OH_2](ClO_4)_3$, *trans*-$[Co(NH_3)_4(NH_2CH_3)Cl](ClO_4)_2$, *trans*-$[Co(NH_3)_4(NH_2CH_3)OH_2](ClO_4)_3$ and $[Co(NH_2CH_3)_5Cl](ClO_4)_2$ complexes were prepared as described in the literature [15,24,25].

trans-$[Co(NH_3)_4(NH_2CH_3)OSO_3]ClO_4$. The complex *trans*-$[Co(NH_3)_4(NH_2CH_3)(SO_3)]Cl$ [15] was dissolved (7.0 mmol) in H_2SO_4 (98%, 15 ml) saturated with Li_2SO_4 at room temperature. The resultant pink solution was poured carefully into cold methanol (0.4 l) to precipitate the *trans*-$[Co(NH_3)_4(NH_2CH_3)(OSO_3)]HSO_4\cdot H_2O$ complex. This was collected and washed with methanol and ether. Yield 68%. Chemical characterization of the compound included elemental analysis (Calc. for $CoH_{20}N_5S_2O_9C$: C, 3.25; H, 5.42; N, 18.97; S, 17.34; Co, 16.0. Found: C, 3.37; H, 5.34; N, 18.79; S, 17.61; Co, 16.0%), electronic ($\varepsilon_{357} = 55.1\ M^{-1}\ cm^{-1}$; $\varepsilon_{520} = 65.4\ M^{-1}\ cm^{-1}$), IR ($\nu_1 = 972\ cm^{-1}$, $\nu_2 = 441\ cm^{-1}$, $\nu_3 = 1036$–1100 and 1122–$1143\ cm^{-1}$, $\nu_4 = 597$ and $626\ cm^{-1}$). The electron spray ionization (ESI^+) spectrum clearly shows the presence of $[Co(NH_3)_4(NH_2CH_3)(OSO_3)]^+$ (signal at 254 Da). The other three significant signals at 237, 220 and 203 Da correspond to consecutive loss of three NH_3 groups. For the IR measurements, the *trans*-$[Co(NH_3)_4(NH_2CH_3)(OSO_3)]HSO_4\cdot H_2O$ complex was transformed to the bromide salt by dissolution in water and precipitation with concentrated HBr. The ESI^+ and ESCA spectra were performed on the perchlorate salt by treatment with concentrated $HClO_4$. The ESI spectra were recorded on a LC-MS Platform 1 spectrometer. The ^1H NMR spectrum (in D_6-DMSO) shows a single methyl signal (δ 1.74 ppm versus tetramethylsilane), corresponding to a methyl group *trans* to SO_4^{2-}. The salt was shown to be free of *trans*-$[Co(NH_3)_4(NH_2CH_3)(OH_2)]^{3+}$ by chromatography on Dowex 50W-X8 (Na^+ form) using 0.4 M $NaClO_4$ as eluant.

2.2. ESCA studies

The samples were studied with a VG Escalab 200iXL X-ray photoelectron spectrometer, using Al Kα radiation. The pressure during the measurements in the analyzer chamber was less than 10^{-8} mbar. The energy scale of the spectra was adjusted using the C_{1s} peak (285.0 eV) as reference. The values of the binding energies for C_{1s}, N_{1s}, $Co_{2p3/2}$, $Cl_{2p3/2}$, O_{1s} and $S_{2p3/2}$ were measured by multiplex scans.

2.3. Acid dissociation constants of aquo complexes

Potentiometric titrations of *trans*-$[Co(NH_3)_4(NH_2CH_3)(OH_2)]^{3+}$ and $[Co(NH_3)_5(OH_2)]^{3+}$ (complex concentrations between 0.987 and 2.981 mM) were carried out in the thermostated cell (25.0°C) of a Metrohm 713 Dosimat pH meter, using a glass and an Ag/AgCl (reference) electrode. Solutions made from the solid perchlorates (in the titration cell) in 20.00 ml, $NaClO_4$ 0.15 M and 2.00 ml, HCl 0.1003 M were titrated with NaOH 0.1005 M. During the course of the titrations presaturated argon (free of CO_2) was bubbled. The data were analyzed using SUPERQUAD program.

3. Results and discussion

The aquation and base hydrolysis for *trans*-$[Co(NH_3)_4(NH_2CH_3)X]^{n+}$ ions are four to eight times faster than for $[Co(NH_3)_5X]^{n+}$ complexes, while the acceleration for $[Co(NH_2CH_3)_5X]^{n+}$ ions is much more pronounced: i.e. rate increases of 30 and 10^3 for aquation and base hydrolysis respectively (when X = Cl) are observed. In the closely analogous ions studied here, the main factors which may account for the variation in rate are: (i) steric effects (steric acceleration), (ii) variations in the acidity of the protons of the amine ligands (only for the base hydrolysis reaction) and (iii) inductive effect of the methyl substituents.

The steric crowding of the $[Co(NH_2CH_3)_5Cl]^{2+}$ complex has been demonstrated by X-ray diffraction [25], while for the *trans*-$[Co(NH_3)_4(NH_2CH_3)Cl]^{2+}$ ion this effect is less important [26]. For example, the average Cl–Co–N(*cis*) bond angle is reduced from 89.4° in the $[Co(NH_3)_5Cl]^{2+}$ ion to 88.5° in the $[Co(NH_2CH_3)_5Cl]^{2+}$ complex, while it is 89.0° in *trans*-$[Co(NH_3)_4(NH_2CH_3)Cl]^{2+}$.

For base hydrolysis, the derivated rate law for the mechanism depicted in Eqs. (1)–(3) in Section 1 is:

$$\text{Rate} = kK_a/K_w[\text{complex}][OH^-]$$

provided K_a/K_w is small. Therefore, variations in the acidity of the protons of the coordinated amines (K_a) may produce variations in rate. The measurements of K_a for the coordinated amines is precluded in water by the low dissociation constants ($pK_a > 15$). Instead, the pK_a of the aquo complexes has been measured (Table 1). $[Co(NH_2CH_3)_5OH_2]^{3+}$ is 6.3 times more acidic than $[Co(NH_3)_5OH_2]^{3+}$ [23], but this still leaves an acceleration factor of 10^3 to be attributed to Eq. (2). On the other hand, the pK_a values of the latter complex and *trans*-$[Co(NH_3)_4(NH_2CH_3)OH_2]^{3+}$ are the same. In consequence, if N-proton and O-proton acidity trends are

Table 1
Acid dissociation constants of some acidopentaaminecobalt(III) complexes in aqueous solution

Complex	T (°C)	pK_a
$[Co(NH_3)_5(OH_2)](ClO_4)_3$	25.0	6.09 ± 0.01 [a]
	22.0	6.08 [b]
	1.9	6.53 [b]
trans-$[Co(NH_3)_4(NH_2CH_3)(OH_2)](ClO_4)_3$	25.0	6.090 ± 0.008 [a]
$[Co(NH_2CH_3)_5(OH_2)](ClO_4)_3$	1.9	5.73 [b]

[a] This work. $I = 0.15$ M ($NaClO_4$).
[b] Ref. [23]. $I = 0.047$ M ($NaClO_4$).

similar, this factor (K_a) cannot account for the observed accelerations.

It is also possible for the amine substituent to influence the release of X by donating negative charge to cobalt, i.e. an inductive assistance of the bond breaking step may be operating. The magnitude of this effect might be gauged from the data listed in Table 2.

The comparison of results for the complexes $[Co(NH_3)_5Cl](ClO_4)_2$ and *trans*-$[Co(NH_3)_4(NH_2CH_3)Cl](ClO_4)_2$ shows clearly the electronic influence (+I effect) of the methylamine group upon the cobalt and through this upon the chlorine atom in *trans* position, as the $Co_{2p3/2}$ and $Cl_{2p3/2}$ binding energies decrease 0.5 and 0.6 eV respectively; while the *cis*-NH_3 ligands are not affected (the experimental error is 0.1 eV).

For complex $[Co(NH_2CH_3)_5Cl](ClO_4)_2$ the $Co_{2p3/2}$ binding energy decreases to 781.6 eV (0.4 eV lower than for *trans*-$[Co(NH_3)_4(NH_2CH_3)Cl](ClO_4)_2$). Thus, methylation of the four *cis* ligands does not produces a proportional decrease in the binding energy of $Co_{2p3/2}$. Furthermore the $Cl_{2p3/2}$ binding energies for *trans*-$[Co(NH_3)_4(NH_2CH_3)Cl](ClO_4)_2$ and $[Co(NH_2CH_3)_5Cl](ClO_4)_2$ are the same, i.e. only the CH_3 group located in the ligand in *trans* position affects the electron density of the chloro atom.

We have recently been involved in the fine tuning of the spontaneous substitution reactions of neutral leaving ligands, L, on $[Co(NH_3)_5L]^{3+}$, $[Co(NH_2CH_3)_5L]^{3+}$ and *cis/trans*-$[Co(NH_3)_4(NH_2CH_3)L]^{3+}$ complexes [27]; our results indicated that the position and number of the more electron donating NH_2CH_3 ligands play a dramatic role in the dissociativeness of the processes. For example, the activation volumes for the aquation reaction of $[Co(NH_3)_5DMF]^{3+}$, *cis*-$[Co(NH_3)_4(NH_2CH_3)DMF]^{3+}$ and *trans*-$[Co(NH_3)_4(NH_2CH_3)DMF]^{3+}$ (where DMF is dimethylformamide) were +2.0, +4.0 and +14.0 $cm^3\ mol^{-1}$, respectively, i.e. the presence of a *cis*-methylamine ligand (instead of NH_3) only slightly increases the dissociativeness of the reaction while a *trans*-methylamine ligand produces a dramatic increase. Accordingly, the supposition has been advanced that the σ donor capability of the methylamine is more important when it is located in the *trans* position, i.e. the *cis*-methylamine ligand (instead of NH_3) increases the electron density on the cobalt centre to a lesser degree. These suppositions are now supported by the present results.

trans-$[Co(NH_3)_4(NH_2CH_3)OSO_3]ClO_4$ was also investigated in order to measure the effect produced by an increased negative charge on the X ligand. Results in Table 2 indicate that the inductive effect of the *trans*-methyl group upon the cobalt atom is almost completely compensated by the presence of the sulfato ligand, i.e. the $Co_{2p3/2}$ binding energy is the same (within experimental error) of that of $[Co(NH_3)_5Cl](ClO_4)_2$.

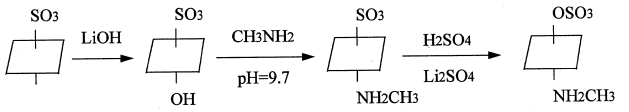
In summary, (i) data in Table 2 clearly support the electronic inductive effect of the CH_3 substituent on the *trans* Co–Cl bond and such an effect can explain the modest acceleration observed in the rate of aquation and base hydrolysis reactions of *trans*-$[Co(NH_3)_4(NH_2CH_3)X]^{n+}$ complexes; (ii) further methylation of the four *cis*-NH_3 ligands does not produce a proportional effect. In consequence, the inductive effect of the methyl groups is a minor component of the large acceleration observed for the aquation and base hydrolysis of the pentakis(methylamine) complexes. The major contribution is the reduction of the steric strain in the transition state.

Although complexes of the type *trans*-$[Co(NH_3)_4(NH_2CH_3)L]^{n+}$ have been prepared previously with uninegative (L = Cl, Br, ONO_2, NO_2, ONO) [15,28,29], and neutral (L = OH_2, $(CH_3)_2SO$, $(CH_3)_2NCHO$) [30] substituents, no *trans*-$[Co(NH_3)_4(NH_2CH_3)L]^{+}$ ion suitable for our purpose has yet been prepared. We chose to prepare such a complex with L = OSO_3^{2-}. The only *trans*-substituted pentaamminesulfato complex obtained so far was *trans*-

Table 2
Binding energies E_b (eV) and half-width of the components (in parentheses) of the photoelectron spectra and rate constants for the spontaneous (k_{aq}) and base-catalysed (k_{OH}) hydrolysis of some acidopentaaminecobalt(III) complexes [a]

Complex	N_{1s}	$Co_{2p3/2}$	$Cl_{2p3/2}$	$S_{2p3/2}$	$10^6 k_{aq}$ (s^{-1})	k_{OH} ($s^{-1}\ M^{-1}$)
$[Co(NH_3)_5Cl](ClO_4)_2$	400.5 (1.6)	782.5 (2.5)	198.8 (1.6)		1.72 [b]	0.24 [b]
trans-$[Co(NH_3)_4(NH_2CH_3)Cl](ClO_4)_2$	400.4 (1.5)	782.0 (2.4)	198.2 (1.6)		8.89 [c]	4.8 [c]
$[Co(NH_2CH_3)_5Cl](ClO_4)_2$	400.1 (1.6)	781.6 (2.0)	198.3 (1.5)		39.6 [b]	800 [b]
trans-$[Co(NH_3)_4(NH_2CH_3)OSO_3]ClO_4$	400.2 (2.0)	782.4 (3.0)		168.8 (1.8)	4.15 [d]	0.58 [d]

[a] Only the principal peaks are listed.
[b] Ref. [7].
[c] Ref. [21].
[d] Ref. [32].



Scheme 1. Realization of the complex cation *trans*-$[Co(NH_3)_4(NH_2CH_3)(OSO_3)]^+$.

$[Co(NH_3)_4(^{15}NH_3)(OSO_3)]^+$, which was prepared from *trans*-$[Co(NH_3)_4(NH_2CH_3)(OSO_2CF_3)]^{2+}$ and concentrated H_2SO_4, but this reaction produces 27% of *cis* isomer [18]. The present method of preparation of *trans*-$[Co(NH_3)_4(NH_2CH_3)(OSO_3)]^+$ follows that of the chloro complex as described earlier [10] and as modified by Balt et al. [31] (Scheme 1).

It produces an isomeric pure compound, as shown by the ^1H NMR data since the spectrum shows a single methyl signal (δ 1.74 ppm versus tetramethylsilane), corresponding to a methyl group *trans* to SO_4^{2-} [15,30].

Acknowledgements

We thank Dr H. Fraundorf, Department of Analytical Chemistry of the University of Leipzig, for recording of the ESI spectrum.

References

[1] R.G. Wilkins, Kinetics and Mechanism of Reactions of Transition Metal Complexes, VCH, 1991.
[2] M.L. Tobe, J. Burgess, Inorganic Reaction Mechanisms, Longman, 1999.
[3] D.A. Buckingham, B.M. Foxman, A.M. Sargeson, Inorg. Chem. 9 (1970) 1790.
[4] G.A. Lawrence, K. Schneider, R. van Eldik, Inorg. Chem. 23 (1984) 3922.
[5] N.J. Curtis, G.A. Lawrence, Inorg. Chem. 25 (1986) 1033.
[6] N.J. Curtis, G.A. Lawrence, P.A. Lay, A.M. Sargeson, Inorg. Chem. 25 (1986) 484.
[7] P.A. Lay, Inorg. Chem. 26 (1987) 2144.
[8] N.J. Curtis, G.A. Lawrence, R. van Eldik, Inorg. Chem. 28 (1989) 329.
[9] R.B. Jordan, Inorg. Chem. 35 (1996) 3725.
[10] D.A. Buckingham, I.I. Olsen, A.M. Sargeson, J. Am. Chem. Soc. 89 (1967) 5129.
[11] F.R. Nordmeyer, Inorg. Chem. 8 (1969) 2781.
[12] D.A. Buckingham, I.I. Creaser, A.M. Sargeson, Inorg. Chem. 9 (1970) 655.
[13] N.E. Dixon, W.G. Jackson, W. Marty, A.M. Sargeson, Inorg. Chem. 21 (1982) 688.
[14] W.G. Jackson, C.N. Hookey, M.L. Randall, P. Comba, A.M. Sargeson, Inorg. Chem. 23 (1984) 2473.
[15] S. Balt, H.J. Gamelkoorn, C.R. Píriz Mac-Coll, W.E. Rankema, Transition Met. Chem. 9 (1984) 224.
[16] F.P. Rotzinger, Inorg. Chem. 27 (1988) 768.
[17] F.P. Rotzinger, Inorg. Chem. 27 (1988) 772.
[18] N.E. Brasch, D.A. Buckingham, C.R. Clark, K.S. Finnie, Inorg. Chem. 28 (1989) 4567.
[19] Y. Kitamura, G. Lawrence, R. van Eldik, Inorg. Chem. 28 (1989) 333.
[20] F.P. Rotzinger, Inorg. Chem. 30 (1991) 2763.
[21] F. Benzo, A.L. Capparelli, D.O. Mártire, A. Massaferro, M. Queirolo, B. Sienra, Polyhedron 15 (1915) 1996.
[22] G. González, B. Moullet, M. Martínez, A.E. Merbach, Inorg. Chem. 33 (1994) 2330.
[23] T.W. Swaddle, Can. J. Chem. 55 (1977) 3166.
[24] M.J. Sisley, Th.W. Swaddle, Inorg. Chem. 20 (1981) 2799.
[25] B.M. Foxman, Inorg. Chem. 17 (1932) 1978.
[26] F. Benzo, B. Sienra, O.R. Piro, J. Chem. Crystallogr. 28 (1998) 69.
[27] F. Benzo, P.V. Bernhardt, G. González, M. Martínez, B. Sienra, J. Chem. Soc., Dalton Trans., in press.
[28] B. Sienra, A. Massaferro, C.R. Píriz Mac-Coll, Z. Anorg. Allg. Chem. 590 (1990) 222.
[29] A. Massaferro, M. Queirolo, B. Sienra, An. Quím. 88 (1992) 230.
[30] B. Sienra, A. Massaferro, Polyhedron 17 (1991) 2075.
[31] S. Balt, H.J. Gameldoorn, W.E. Renkema, J. Chem. Soc., Dalton Trans. 2415 (1983).
[32] F. Benzo, A.L. Caparelli, D.O. Mártire, B. Sienra, Inorg. React. Mechanims, in press.

PERGAMON

www.elsevier.nl/locate/poly

Polyhedron 19 (2000) 975–981

POLYHEDRON

Synthesis and characterization of piperidine platinum(II) complexes with dicarboxylates: crystal and molecular structure of *cis*-[Pt(piperidine)$_2$Cl$_2$]·H$_2$O

S. Rounaq Ali Khan [a], Ilse Guzman-Jimenez [b], Kenton H. Whitmire [b], Abdul R. Khokhar [a,*]

[a] *Department of Clinical Investigation, Box 52, The University of Texas M.D. Anderson Cancer Center, 1515 Holcombe Boulevard, Houston, TX 77030, USA*

[b] *Department of Chemistry, MS 60, Rice University, 6100 Main Street, Houston, TX 77005, USA*

Received 4 September 1999; accepted 15 February 2000

Abstract

A series of new platinum complexes of the type *cis*-[Pt(PIP)$_2$X] (where PIP = piperidine and X = dichloro, sulfato, oxalato, malonato, methylmalonato, dimethylmalonato, tartronato, 1,1-cyclopropyldicarboxylato (CPDCA) or 1,1-cyclobutyldicarboxylato (CBDCA) ligand) were synthesized and characterized by elemental analysis, IR, and ^{195}Pt nuclear magnetic resonance spectroscopy. The crystal structure of *cis*-[Pt(PIP)$_2$Cl$_2$]·H$_2$O was determined by X-ray crystallography. In this complex platinum has slightly distorted square planar geometry with two adjacent corners being occupied by two nitrogen atoms of piperidine, whereas the remaining two adjacent corners are occupied by two chloride atoms. An intricate network of intermolecular hydrogen bonding holds the crystal lattice together. In these complexes, piperidine acts as non-leaving ligand, whereas the dicarboxylic acids act as leaving groups. ©2000 Elsevier Science Ltd All rights reserved.

Keywords: Platinum(II) complexes; Piperidine; Synthesis; Crystal structures

1. Introduction

Platinum complexes are now amongst the most widely used drugs for the treatment of cancers [1,2]. Among them, cisplatin is one of the most effective antitumor agents used to treat various types of human cancers [3,4]. Although it is effective against bladder tumors, testicular tumors, ovarian carcinomas and tumors of the head and neck [5–7], its clinical effectiveness has been limited by significant undesirable side effects such as dose-dependent nephrotoxicity, ototoxicity, neurotoxicity, nausea, vomiting and myelosuppression [8–10]. To overcome these limitations, efforts were directed to develop new platinum-based anticancer drugs with improved clinical effectiveness, broader spectrum of activity and reduced toxicity. Thus, much effort has been devoted to develop second-generation antitumor platinum complexes with greater activity and less toxicity [11,12]. This can be done by altering the pharmacokinetics of cisplatin by replacing the labile chloro ligands with other leaving groups and extending the stable amine ligands to a series of either cyclic or acyclic amines. As a result, the second-generation platinum drug carboplatin came into clinical use [13,14]. Like cisplatin, however, the clinical effectiveness of carboplatin is limited by undesirable side effects like nephrotoxicity, emesis and myelosuppression [15].

In recent years there has been an intense interest in developing third-generation platinum-based anticancer drugs with a broader spectrum of activity, improved clinical effectiveness, lack of cross-resistance to cisplatin and enhanced water solubility [16,17]. In the third-generation platinum complexes, the goal was the creation of an agent that overcomes resistance to cisplatin and carboplatin. As a result, several third-generation platinum complexes having 1,2-DACH as the stable amine ligand such as oxaliplatin [18], JM216 [19], LNDDP [20], and lobaplatin [21] are currently in clinical trials.

We have been developing several complexes of cisplatin analogs with 1,2-DACH and *cis*-1,4-DACH as stable amine ligands, some of which have shown promising antitumor activity [22–26]. In our continuous efforts to design and synthesize new antitumor agents, we report the synthesis and characterization of a series of platinum complexes containing piperidine as non-leaving ligand and dicarboxylate as leaving

* Corresponding author. Tel.: +1-713-792-2837; fax: +1-713-792-6759; e-mail: akhokhar@mdanderson.org

0277-5387/00/$ - see front matter ©2000 Elsevier Science Ltd All rights reserved.
PII S0277-5387(00)00348-X

groups. Each complex has been characterized by elemental analysis, IR and ^{195}Pt nuclear magnetic resonance (NMR) spectroscopy. We also report the X-ray crystal structure of *cis*-$[Pt(PIP)_2Cl_2]\cdot H_2O$.

2. Experimental

2.1. Chemicals

K_2PtCl_4 was purchased from Johnson Matthey, Seabrook, NH. Silver nitrate was obtained from Fisher Scientific Co., Houston, TX. Piperidine, silver sulfate, oxalic acid, malonic acid, methylmalonic acid, dimethylmalonic acid, tartronic acid, 1,1-cyclopropanedicarboxylic acid (CPDCA) and 1,1-cyclobutanedicarboxylic acid (CBDCA) were obtained from Aldrich Chemical Co., Milwaukee, WI. All chemicals obtained from commercial sources were used as supplied.

2.2. Physical measurements

Elemental analysis of the complexes was performed by Robertson Laboratory Inc., Madison, NJ. Infrared (IR) spectra in the range of 600–4000 cm^{-1} were recorded in KBr pellets and far-IR spectra in the range of 150–600 cm^{-1} were recorded in polyethylene pellets on a Perkin-Elmer 2000 spectrophotometer. ^{195}Pt NMR spectra were recorded using a Bruker 200/AF spectrometer with a 10 mm tunable probe. The ^{195}Pt spectra were recorded at 43.055 MHz and the shifts were measured relative to an external standard of 2.2 M Na_2PtCl_6 in D_2O at 0.00 ppm.

2.3. Preparation of sodium salts

Oxalic acid (0.900 g, 10 mmol) was dissolved in 100 ml of ethanol and to this a solution of NaOH (0.400 g, 20 mmol) in 20 ml of water was added. The reaction mixture was stirred for 30 min and evaporated to dryness under reduced pressure at room temperature. A colorless sticky material formed. It was dissolved in 20 ml of methanol and evaporated to dryness. To the evaporated material 10 ml of ether was added. This was evaporated to dryness, collected, and dried under vacuum.

The sodium salts of malonic acid, methylmalonic acid, dimethylmalonic acid, tartronic acid, 1,1-cyclopropyldicarboxylic acid and 1,1-cyclobutyldicarboxylic acid were prepared in a manner similar to that mentioned above.

2.4. Preparation of cis-$[Pt(PIP)_2Cl_2]\cdot H_2O$ (**1**)

K_2PtCl_4 (20.76 g, 50 mmol) was dissolved in 250 ml of deionized water and filtered. KI (83.0 g, 0.5 mol) in 100 ml of water was added to it and the reaction mixture was stirred for 10 min. Then, PIP (8.5 g, 100 mmol) was added dropwise to the reaction mixture while stirring, to obtain a yellow precipitate, *cis*-$[Pt(PIP)_2I_2]$. The stirring was continued for a further 30 min and the precipitate was then collected by filtration. This compound was dissolved in dimethylformamide and filtered. To the filtrate excess cold water was added to obtain a bright yellow precipitate, *cis*-$[Pt(PIP)_2I_2]$, which was washed with water, ethanol and acetone and dried in vacuum. *cis*-$[Pt(PIP)_2I_2]$ (12.38 g, 20 mmol) was suspended in 250 ml of an aqueous solution of silver nitrate ($AgNO_3$) (6.72 g, 39.8 mmol). The reaction mixture was stirred for 24 h at room temperature in the dark. The AgI precipitate was filtered off and a solution of NaCl was added dropwise to the filtrate with constant stirring until a yellow precipitate of *cis*-$[Pt(PIP)_2Cl_2]$ formed. The precipitate was filtered and recrystallized from dimethylformamide. The yellow crystals obtained were washed with water, acetone and dried under vacuum. These crystals were used for X-ray crystallography.

2.5. cis-$[Pt(PIP)_2(OSO_3)H_2O]$ (**2**)

To a suspension of *cis*-$[Pt(PIP)_2Cl_2]$ (2.18 g, 5 mmol) in 100 ml of deionized water, an aqueous solution of Ag_2SO_4 (1.49 g, 4.8 mmol) was added. The reaction mixture was then stirred continuously in the dark for 24 h at room temperature. The yellow precipitate of AgCl was filtered off and the filtrate was evaporated to dryness under reduced pressure at 35°C. The pale yellow solid was then dried in vacuum.

2.6. $[Pt(PIP)_2(oxalato)]\cdot H_2O$ (**3**)

cis-$[Pt(PIP)_2(OSO_3)H_2O]$ (0.958 g, 2.0 mmol) was dissolved in 100 ml of water, and an aqueous solution of sodium oxalate (0.270 g, 2.0 mmol) prepared in situ was added. The reaction mixture was then stirred continuously for 24 h at room temperature. The off-white precipitate obtained was filtered and recrystallized from hot water. A white crystalline product finally obtained was isolated by filtration and then dried in vacuum.

2.7. $[Pt(PIP)_2(malonato)]\cdot H_2O$ (**4**)

cis-$[Pt(PIP)_2(OSO_3)H_2O]$ (0.958 g, 2.0 mmol) was dissolved in 100 ml of water, an aqueous solution of sodium malonate (0.300 g, 2.0 mmol) prepared in situ was added. The reaction mixture was then stirred continuously for 24 h at room temperature. A clear solution was formed; it was filtered and evaporated to 10 ml under reduced pressure and kept at room temperature for slow evaporation. The white crystalline compound obtained was isolated by filtration and then dried in vacuum.

2.8. $[Pt(PIP)_2(methylmalonato)]$ (**5**)

cis-$[Pt(PIP)_2(OSO_3)H_2O]$ (0.958 g, 2.0 mmol) was dissolved in 100 ml of water, and an aqueous solution of sodium methylmalonate (0.85 g, 2.00 mmol) prepared in situ was added. The reaction mixture was continuously stirred for

24 h at room temperature. The clear solution obtained was filtered and evaporated to 10 ml under reduced pressure and kept aside in the refrigerator so the compound could precipitate. This precipitate was isolated by filtration and then dried in vacuum.

2.9. [Pt(PIP)$_2$(dimethylmalonato)] (6)

This complex was prepared by a method similar to that for complex **4**, by using sodium dimethylmalonate.

2.10. [Pt(PIP)$_2$(tartronato)]·H$_2$O (7)

This complex was prepared by a method similar to that for complex **5**, by using sodium tartronate.

2.11. [Pt(PIP)$_2$(CPDCA)]·2H$_2$O (8)

This complex was prepared by a method similar to that for complex **4**, by using sodium 1,1-cyclopropyldicarboxylate.

2.12. [Pt(PIP)$_2$(CBDCA)]·H$_2$O (9)

This complex was prepared by a method similar to that for complex **5**, by using sodium 1,1-cyclobutyldicarboxylate.

2.13. Crystallographic measurements

The crystal was encapsulated in a thin shell of epoxy cement and mounted on the tip of a glass fiber. Data were collected with a Bruker AXS automated CCD diffractometer using the Bruker AXS package and using Mo Kα radiation ($\lambda = 0.71069$ Å). The structure was solved by direct methods. All non-hydrogen atoms were refined with anisotropic displacement parameters, and hydrogen atoms were calculated in ideal positions (riding model). Refinement of F^2 was for ALL reflections. The weighted R-factor (R_w) and all goodness of fit (S) values were based on F^2, while conventional R-factors (R) were based on F, with F set to zero for negative F^2. The threshold expression of $F^2 > 2\sigma(F^2)$ was used only for calculating R-factor(gt) etc. and was not relevant to the choice of reflections for refinement. R-factors based on F^2 were statistically about twice as large as those based on F, and R-factors based on all of the data were even larger (Table 1). All software used is contained in the SHELXTL 5.10 [27] program library.

Table 1
Crystal data and structure refinement for *cis*-[Pt(PIP)$_2$Cl$_2$]·H$_2$O

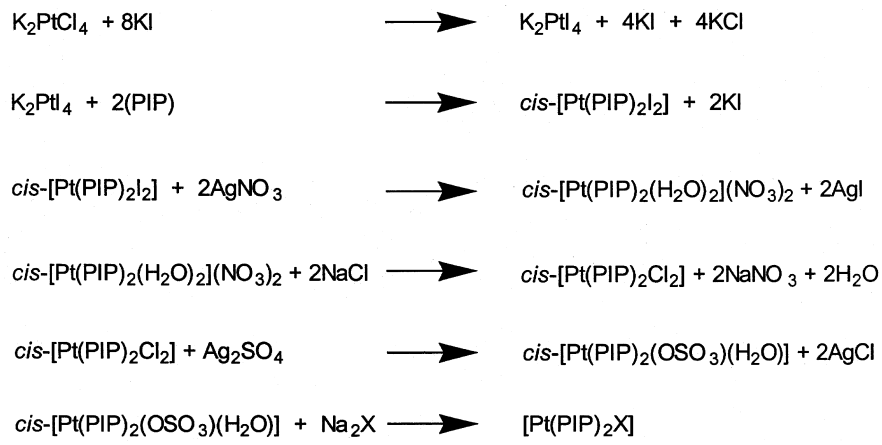
Empirical formula	$C_{10}H_{24}Cl_2N_2OPt$
Formula weight	454.30
Temperature (K)	293(2)
Wavelength (Å)	0.71073
Crystal system	tetragonal
Space group	*I*42*d*
Unit cell dimensions	
a (Å)	16.858(2)
b (Å)	16.858(2)
c (Å)	10.246(2)
Volume (Å^3)	2911.9(8)
Z	8
Density (calculated) (Mg m^{-3})	2.073
Absorption coefficient (mm)	9.989
F(000)	1744
Crystal size (mm)	0.304×0.352×0.352
θ Range for data collection (°)	2.33–23.29
Limiting indices	$-18 \le h \le 16$, $-18 \le k \le 7$, $-10 \le l \le 9$
Reflections collected	2991
Independent reflections	1031 ($R_{int} = 0.0361$)
Absorption correction	none
Refinement method	full-matrix least-squares on F^2
Data/restraints/parameters	1031/3/78
Goodness-of-fit on F^2	1.094
Final R indices ($I > 2\sigma(I)$) [a]	$R_1 = 0.0244$, $wR_2 = 0.0644$
R indices (all data) [a]	$R_1 = 0.0251$, $wR_2 = 0.0648$
Absolute structure parameter	−0.032(19)
Largest difference peak and hole (e Å^{-3})	0.853 and −1.001

[a] $R_1 = \sum||F_o| - |F_c||/\sum|F_o|$. $R_w = [\sum w(F_o^2 - F_c^2)^2]/\sum[w(F_o^2)^2]^{1/2}$. $w = [\sigma^2(F_o^2) + (aP)^2 + bP]^{-1}$. $P = (F_o^2 + 2F_c^2)/3$.

3. Results and discussion

3.1. Synthesis of platinum complexes

The steps involved in the synthesis of platinum complexes are shown in Scheme 1. K_2PtCl_4 was reacted with an excess



Scheme 1.

of KI to give K_2PtI_4 in solution. K_2PtI_4 was then reacted with 2 equiv. of piperidine to precipitate *cis*-$[Pt(PIP)_2I_2]$ (PIP = piperidine). The reaction of *cis*-$[Pt(PIP)_2I_2]$ with $AgNO_3$ led to the formation of *cis*-$[Pt(PIP)_2(H_2O)_2](NO_3)_2$, which was further converted to the corresponding dichloride *cis*-$[Pt(PIP)_2Cl_2]$ by treating it with an excess of NaCl. *cis*-$[Pt(PIP)_2(OSO_3)(H_2O)]$ was prepared by the reaction of *cis*-$[Pt(PIP)_2Cl_2]$ with Ag_2SO_4. Complexes of the type *cis*-$[Pt(PIP)_2X]$ (X = oxalato, malonato, methylmalonato, dimethylmalonato, tartronato, CPDCA or CBDCA ligand) were obtained by the reaction of *cis*-$[Pt(PIP)_2(SO_4)(H_2O)]$ with the sodium salt of the corresponding dicarboxylic acid.

3.2. Characterization of Pt complexes

The complexes were characterized by elemental analysis and IR and ^{195}Pt NMR spectroscopy. The composition of each complex as determined by elemental analysis showed good agreement between the theoretical and actual values. The analytical results are summarized in Table 2. The results of characterization by IR and ^{195}Pt NMR spectroscopy are shown in Table 3.

The IR spectra (Table 3) in general showed a broad absorption between 3153 and 3193 cm^{-1}, due to the N–H stretching frequency of coordinated amino group of piperidine. The carbonyl regions for the dicarboxylate complexes show patterns characteristic of carboxylate ligands bound to the platinum metal ion. The carboxyl groups in complexes **3–9** displayed a signal in the region 1570–1675 cm^{-1} corresponding to the $\nu_a(COO^-)$ band, while the $\nu_s(COO^-)$ band normally appears in the range of 1370–1410 cm^{-1}. Complex **2** showed two intense bands at around 620 and 1120 cm^{-1} indicating the presence of an SO_4 group in these complexes. The Pt–N stretching vibrations in all the complexes were observed in the region 475–580 cm^{-1}, whereas Pt–Cl stretching vibration for complex **1** was observed at 315 cm^{-1}, respectively.

The ^{195}Pt NMR spectra (Table 3) further confirmed the structures of the platinum complexes. Complex **1** showed a signal at −2282 ppm, which is characteristic of the square planar platinum(II) complexes in which the two adjacent corners are occupied by two amino nitrogen and the other two positions by two chlorides. Complex **2** showed a signal at −1805 ppm. The ^{195}Pt NMR spectra of complexes **3–9** showed singlets in the range of −1895 to −1978 ppm. Such

Table 2
Elemental analysis of platinum(II) complexes

Complex	Complex name	Observed (calculated)			Yield (%)
		C (%)	H (%)	N (%)	
1	*cis*-$[Pt(PIP)_2Cl_2]\cdot H_2O$	26.47 (26.43)	5.36 (5.28)	6.02 (6.16)	75
2	*cis*-$[Pt(PIP)_2(OSO_3)(H_2O)]$	25.13 (25.05)	5.03 (5.01)	5.72 (5.84)	80
3	$[Pt(PIP)_2(oxalato)]\cdot H_2O$	30.84 (30.57)	5.01 (5.09)	6.04 (5.94)	58
4	$[Pt(PIP)_2(malonato)]\cdot H_2O$	32.25 (32.16)	5.19 (5.36)	5.82 (5.77)	50
5	$[Pt(PIP)_2(methylmalonato)]$	34.79 (34.92)	5.38 (5.40)	5.76 (5.82)	55
6	$[Pt(PIP)_2(dimethylmalonato)]$	36.31 (36.36)	5.42 (5.65)	5.58 (5.65)	55
7	$[Pt(PIP)_2(tartronato)]\cdot H_2O$	31.03 (31.11)	5.16 (5.18)	5.56 (5.58)	50
8	$[Pt(PIP)_2(CPDCA)]\cdot 2H_2O$	34.01 (34.02)	5.83 (5.67)	5.36 (5.29)	55
9	$[Pt(PIP)_2(CBDCA)]\cdot H_2O$	36.50 (36.57)	5.40 (5.33)	5.25 (5.33)	55

Table 3
IR and ^{195}Pt NMR data for platinum(II) complexes

Complex	IR (cm^{-1})					^{195}Pt NMR (ppm)
	νN–H	νC=O	νC–O	νPt–N	νPt–O	
1	3188			520	315 (Pt–Cl)	−2282 [a]
2	3168			505	442	−1805 [b]
3	3193	1670	1407	515	445	−1978 [a]
4	3163	1655	1400	475	448	−1966 [b]
5	3189	1660	1390	580	446	−1971 [b]
6	3153	1660	1400	510	405	−1900 [b]
7	3187	1675	1410	536	440	−1955 [a]
8	3185	1570	1400	560	460	−1895 [b]
9	3191	1650	1370	560	470	−1953 [c]

[a] Recorded in DMF.
[b] Recorded in water.
[c] Recorded in methanol.

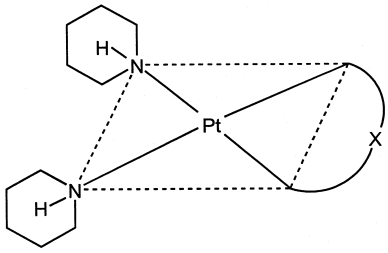


Fig. 1. Structure of *cis*-[Pt(PIP)$_2$X]. X = dichloro, sulfato, oxalato, malonato, methylmalonato, dimethylmalonato, tartronato, CPDCA and CBDCA in complexes **1**–**9**, respectively.

chemical shifts are characteristic for the square planar platinum(II) complexes having two nitrogen and two oxygen atoms as donor ligands (Fig. 1) [28].

3.3. Crystal structure

Fig. 2 shows a perspective view of the crystal structure of *cis*-[Pt(PIP)$_2$Cl$_2$]·H$_2$O (complex **1**) along with its atom labeling. Bond lengths and bond angles are given in Table 4. Significant hydrogen bond distances and angles are given in Table 5. As the data show, the platinum atom shows the usually square-planar coordination, with the two adjacent corners of the platinum plane occupied by two nitrogen of two piperidine molecules, whereas the remaining two *cis* positions are used to bind to two chloride ions. Both the piperidine rings are in chair configuration.

The coordination around the platinum atom in this complex has slightly distorted square-planar geometry. The distortion is indicated by the N(11)–Pt–Cl(1A) (178.9(2)°) and N(11A)–Pt–Cl(1) (178.9(2)°) angles, which depart from 180°. In addition, although the angle N(11)–Pt–Cl(1A) is 178.9(2)°, there is significant difference between the value of the N(11)–Pt–Cl(1) angle, 91.49(19)°, and that of the N(11)–Pt–N(11A) angle, 88.0(4)°.

The average Pt–Cl bond length of 2.315(2) Å is consistent with those found in structurally related complexes, such as

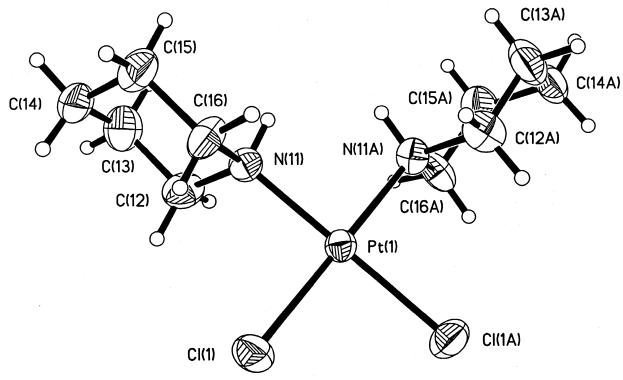


Fig. 2. ORTEP representation of the structure of a molecule of *cis*-[Pt(PIP)$_2$Cl$_2$]·H$_2$O with atom numbering scheme. The thermal ellipsoids are 50% equiprobability envelopes, with hydrogens as spheres of arbitrary diameter.

Table 4
Bond lengths (Å) and angles (°) with e.s.d.s in parentheses for *cis*-[Pt(PIP)$_2$Cl$_2$]·H$_2$O

Pt(1)–N(11)	2.050(6)
Pt(1)–N(11A)	2.050(6)
Pt(1)–Cl(1A)	2.315(2)
Pt(1)–Cl(1)	2.315(2)
N(11)–C(16)	1.474(10)
N(11)–C(12)	1.503(12)
C(12)–C(13)	1.502(14)
C(13)–C(14)	1.494(15)
C(14)–C(15)	1.532(13)
C(15)–C(16)	1.529(11)
N(11)–Pt(1)–N(11A)	88.0(4)
N(11)–Pt(1)–Cl(1A)	178.9(2)
N(11A)–Pt(1)–Cl(1A)	91.49(19)
N(11)–Pt(1)–Cl(1)	91.49(19)
N(11A)–Pt(1)–Cl(1)	178.9(2)
Cl(1A)–Pt(1)–Cl(1)	89.04(11)
C(16)–N(11)–C(12)	111.2(6)
C(16)–N(11)–Pt(1)	114.0(5)
C(12)–N(11)–Pt(1)	113.9(5)
C(13)–C(12)–N(11)	111.4(8)
C(14)–C(13)–C(12)	111.9(8)
C(13)–C(14)–C(15)	108.9(7)
C(16)–C(15)–C(14)	111.0(8)
N(11)–C(16)–C(15)	112.3(7)

Table 5
Significant hydrogen bond distances (Å) and angles (°) for *cis*-[Pt(PIP)$_2$Cl$_2$]·H$_2$O

O(1)···Cl(1)	3.302
O(1)···Cl(1B)	3.302
O(1)···N(11)	2.999
O(1)···N(11D)	2.999
Cl(1)···O(1)···Cl(1B)	107.5
Cl(1B)···O(1)···N(11D)	129.0
Cl(1)···O(1)···N(11E)	114.3
N(11D)···O(1)···N(11E)	56.7

cis-[Pt(py)$_2$Cl$_2$] (2.296(5) Å) [29], *cis*-[Pt(pyrazole)$_2$-Cl$_2$] (2.28(3) Å) [30], *cis*-[Pt(ethyleneimine)$_2$Cl$_2$] (2.30(2) Å) [31], *cis*-[Pt(cyclohexylamine)$_2$Cl$_2$] (2.32(4) Å) [32], and *cis*-[Pt(NH$_3$)(C$_6$H$_{11}$NH$_2$)Cl$_2$] (2.30(3) Å) [33]. The average Pt–N bond length of 2.05(6) Å is comparable with the Pt–N(sp^2) average value of (2.023(12) Å) derived for *cis*-PtL$_2$Cl$_2$ compounds [34]. The average Pt–N bond distance observed in this complex is also in agreement with the other structurally related complexes, such as *cis*-[Pt(py)$_2$Cl$_2$] (2.02(1) Å) [29], *cis*-[Pt(cyclohexylamine)$_2$Cl$_2$] (2.06(1) Å) [32] and *cis*-[Pt(NH$_3$)(C$_6$H$_{11}$NH$_2$)Cl$_2$] (2.04(10) Å) [33]. The N–Pt–N and Cl–Pt–Cl bond angles are contracted and are observed as 88.0 and 89.04°, respectively, which are compensated by the expansion of N–Pt–Cl bond angles to 91.49°.

Fig. 3 shows a view of the packing diagram including hydrogen bonds to the water molecule indicated by dashed

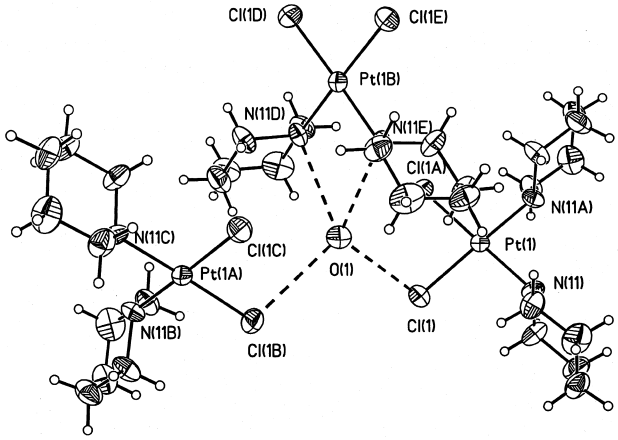


Fig. 3. A view of the packing diagram with hydrogen bonds to the water molecule indicated by dashed lines.

lines. There is an intricate network of intermolecular hydrogen bonding that holds the crystal lattice together. The interesting geometric features in the hydrogen bonding are that there are three molecules surrounding a water molecule. All the three independent molecules have virtually identical configuration. The nitrogen atoms N(11D) and N(11E) of one molecule and chloride atoms Cl(1) and Cl(1B) of the other two molecules are hydrogen bonded to the water molecule O(1). This molecular packing is clearly affected by the intermolecular hydrogen bonding occurring between O(1)···Cl(1) 3.302 Å, O(1)···Cl(1B) 3.302 Å, O(1)···N(11) 2.999 Å and O(1)···N(11D) 2.999 Å. These distances are somewhat longer compared with the known N–H···O hydrogen bond distances [35]. The angles due to hydrogen bonding are observed as Cl(1B)···O(1)···Cl(1) 107.5°, Cl(1B)···O(1)···N(11D) 129.0°, Cl(1)···O(1)···N(11E) 114.3° and N···O(1)···N 56.7°, respectively.

In summary, we have synthesized and characterized a series of new cisplatin analogs containing piperidine as nonleaving ligands and oxalato, malonato, methylmalonato, dimethylmalonato, tartronato, CPDCA, and CBDCA as leaving groups. The X-ray crystal structure of *cis*-[$Pt(PIP)_2Cl_2$]·H_2O was determined by X-ray crystallography.

Supplementary data

Full lists of bond lengths and bond angles, atomic coordinates and equivalent isotropic displacement parameters, anisotropic displacement parameters, hydrogen coordinates and isotropic displacement parameters, and observed and calculated structure factors have been deposited at the Cambridge Crystallographic Data Centre (CCDC). Supplementary material are available from the CCDC, 12 Union Road, Cambridge CB2 1EZ, UK (fax: +44-1223-336033; e-mail: deposit@ccdc.cam.ac.uk) on request, quoting the deposition number CCDC 140100. Any request to the CCDC for this material should quote the full literature citation.

Acknowledgements

This work was supported by DHP Grant No.148 to ARK from the American Cancer Society. KHW acknowledges Robert A. Welch Foundation for its generous support.

References

[1] H.M. Pinto, J.H. Schornagel (Eds.), Platinum and Other Metal Coordination Compounds in Cancer Chemotherapy 2, Plenum, New York, 1996.
[2] B. Lippert (Ed.), Cisplatin in Chemistry and Biochemistry of a Leading Anticancer Drug, Wiley-VCH, Weinheim, 1999.
[3] P.J. Loehrer, L. Einhorn, Ann. Intern. Med. 100 (1984) 704.
[4] W.B. Pratt, R.W. Ruddon, W.D. Ensminger, J. Maybaum, in: The Anti Cancer Drugs, Oxford University Press, New York, 1994, p. 133.
[5] K.M. Comess, S.J. Lippard, in: S. Neidle, M. Waring (Eds.), Molecular Aspects of Anticancer Drug–DNA Interactions, vol. 1, MacMillan, London, 1993, p. 134.
[6] J.B. Vermorken, H.M. Pinedos, Neth. J. Med. 25 (1982) 270.
[7] S.K. Carter, in: M.P. Hacker, E.B. Douple, I.H. Krakoff (Eds.), Platinum Coordination Complexes in Cancer Chemotherapy, Martinus Nijhoff, Boston, MA, 1984, p. 359.
[8] I.H. Krakoff, in: M. Nicolini (Ed.), Platinum and Other Metal Coordination Compounds in Cancer Chemotherapy, Martinus Nijhoff, Boston, MA, 1988, p. 351.
[9] L.R. Kelland, S.J. Clarke, M.J. Mckeage, Advances in Platinum Cancer Chemotherapy, Platinum Met. Rev. 36 (1992) 178.
[10] P.J. Loehrer, L.H. Einhorn, Ann. Intern. Med. 100 (1984) 704.
[11] L.R. Kelland, Platinum complexes, in: B.A. Teicher (Ed.), Cancer Therapeutics, Human Press, New York, 1997, p. 93.
[12] P. Pil, S.J. Lippard, Cisplatin and related drugs, in: J.R. Bertino (Ed.), Encyclopedia of Cancer, Academic Press, New York, 1997, p. 392.
[13] A.H. Calvert, S.J. Harland, D.R. Newell, Z.H. Siddik, K.R. Harrap, Cancer Treat. Rev. 12 (1985) 51.
[14] B.W. Booth, W.C. Weis, A.H. Korzun, W.C. Wood, R.W. Carey, L.P. Panasci, Cancer Treat. Rep. 69 (1985) 919.
[15] M.J. Peckham, A. Horwich, M. Barda, A. Drury, W.F. Hendry, Cancer Treat. Rev. Suppl. A 12 (1991) 101.
[16] M.P. Hacker, A.R. Khokhar, D.B. Brown, J. McCormack, I.H. Krakoff, Cancer Res. 45 (1985) 4748.
[17] A. Pasini, F. Zunimo, Angew. Chem. 99 (7) (1987) 632.
[18] J.M. Extra, M. Espie, F. Calvo, C. Ferme, L. Mignot, M. Marty, Cancer Chemother. Pharmacol. 25 (1990) 299.
[19] I. Judson, M. McKeage, J. Hanwell, C. Berry, P. Mistry, F. Raymond, G. Poon, B. Murrer, K. Harrap, Platinum and Other Metal Coordination Complexes in Cancer Chemotherapy: The Clinical Development of the Oral Platinum Anticancer Agent JM216, H.M. Press, New York, 1996, p. 83.
[20] R. Perez-Soler, G. Lopez-Berestein, J. Lautersztain, S. Al-Baker, K. Francis, D. Macias-Kiger, M.N. Raber, A.R. Khokhar, Cancer Res. 50 (1990) 4252.
[21] K. Mross, F. Meyberg, H.H. Fiebig, U. Hiebeir, P. Aulenbacher, D.K. Hossfeld, Onkologie 15 (1992) 139.
[22] A.R. Khokhar, S. Al-Baker, T. Brown, R. Perez-Soler, J. Med. Chem. 34 (1991) 325.
[23] A.R. Khokhar, S. Al-Baker, R. Perez-Soler, Anticancer Drugs 3 (1992) 95.
[24] Q. Xu, A.R. Khokhar, J. Inorg. Biochem. 48 (1992) 217.
[25] S. Shamsuddin, I. Takahashi, Z.H. Siddik, A.R. Khokhar, J. Inorg. Biochem. 61 (1996) 291.
[26] S. Shamsuddin, C.C. Santillan, J.L. Stark, K.H. Whitmire, Z.H. Siddik, A.R. Khokhar, J. Inorg. Biochem. 71 (1998) 29.
[27] G.M. Sheldrick, Bruker AXS, Madison, WI, 1997.

[28] S. Al-Baker, R. Perez-Soler, A.R. Khokhar, J. Coord. Chem. 29 (1993) 1.
[29] P. Colamarino, P.L. Orioli, J. Chem. Soc., Dalton Trans. (1975) 1656.
[30] M.A. Cinellu, S. Stoccoro, G. Minghetti, A.N. Bandini, G. Banditelli, B. Bovio, J. Organomet. Chem. 372 (1989) 311.
[31] J.C. Barnes, J. Iball, T.J.R. Weakley, Acta Crystallogr., Sect. B 31 (1975) 1435.
[32] C.J.L. Lock, R.A. Speranzini, M. Zvagulis, Acta Crystallogr., Sect. B 36 (1980) 1789.
[33] E.G. Talman, W. Bruning, J. Reedijk, A.L. Spek, N. Veldman, Inorg. Chem. 36 (1997) 854.
[34] G.P. Palenik, T.J. Giordano, J. Chem. Soc., Dalton Trans. (1987) 1175.
[35] A.F. Wells, Structural Inorganic Chemistry, Clarendon Press, Oxford, 5th edn., 1984, p. 357.

PERGAMON

www.elsevier.nl/locate/poly

Polyhedron 19 (2000) 983–989

POLYHEDRON

Synthesis and characterization of platinum(II) complexes with 3-methylpiperidine: crystal and molecular structure of [Pt(3-methylpiperidine)$_2$(malonato)]·H_2O

S. Rounaq Ali Khan [a], Ilse Guzman-Jimenez [b], Kenton H. Whitmire [b], Abdul R. Khokhar [a,*]

[a] *Department of Clinical Investigation, Box 52, The University of Texas M.D. Anderson Cancer Center, 1515 Holcombe Boulevard, Houston, TX 77030, USA*

[b] *Department of Chemistry, MS 60, Rice University, 6100 Main Street, Houston, TX 77005, USA*

Received 11 November 1999; accepted 15 February 2000

Abstract

A series of new platinum complexes of the type [Pt(3-mepip)$_2$X] (where 3-mepip = 3-methylpiperidine, and X = dichloro, sulfato, oxalato, malonato, methylmalonato, dimethylmalonato, tartronato, 1,1-cyclopropanedicarboxylato (CPDCA) or 1,1-cyclobutanedicarboxylato (CBDCA) ligand) were synthesized and characterized by elemental analysis, IR spectroscopy and ^{195}Pt nuclear magnetic resonance spectroscopy. The crystal structure of [Pt(3-mepip)$_2$(malonato)]·0.79H_2O was determined by single crystal X-ray diffraction. In this complex platinum has slightly distorted square planar geometry with two adjacent corners being occupied by two nitrogens of 3-methylpiperidine, whereas the remaining two adjacent corners are occupied by two oxygen atoms of the malonato group. An intricate network of intermolecular hydrogen bonds holds the crystal lattice together. In the other complexes, 3-mepip acts as non-leaving ligands, whereas the carboxylato ligands act as leaving groups. ©2000 Elsevier Science Ltd All rights reserved.

Keywords: Platinum complexes; 3-methylpiperidine; Dicarboxylates; Synthesis; Crystal structures

1. Introduction

Cisplatin is one of the most active and effectively used antitumor agents in the treatment of various types of human cancers today [1,2], especially because of its activity against testicular, ovarian, head and neck, cervical and bladder cancers [3–5]. However, the use of cisplatin has been restricted principally because of its severe dose toxicities such as nephrotoxicity, ototoxicity, neurotoxicity, nausea, vomiting and myelosuppression [6–8]. This limitation has stimulated the synthesis and evaluation of new platinum agents with reduced toxicity and better antitumor activity [9–12]. Therefore, researchers in many laboratories around the world are actively engaged in synthesizing and studying cisplatin and its analogs, hoping to discover a better antitumor drug, with less toxicity and better activity. Consequently new platinum drugs with equal or greater antitumor activity but less toxicity have been developed by modifying the pharmacokinectics of cisplatin by replacing the labile chloro ligands with other leaving groups and extending the stable amine ligands to a series of cyclic or acyclic amines. Efforts over the past two decades have resulted in clinical trials of several platinum drugs. As a result, the second-generation platinum drug carboplatin came into clinical use [13,14]. Like cisplatin, however the clinical effectiveness of carboplatin is limited by acquired drug resistance.

In recent years, there has been an intense interest in developing third-generation platinum-based anticancer drugs with a broader spectrum of activity, improved clinical effectiveness, lack of cross-resistance to cisplatin and carboplatin [15,16]. Thus, several platinum complexes that have 1,2-diaminocyclohexane (1,2-DACH) as a carrier ligand and that retain activity against cisplatin-resistant tumors have also been developed. A number of platinum drugs such as oxaliplatin [17], JM216 [18] and LNDDP [19], which have 1,2-DACH as a carrier ligand and chloride or carboxylate as leaving groups, are now in clinical trials.

We have reported several complexes of cisplatin analogs with various isomers of 1,2-DACH as a stable amine ligand, some of which have shown promising antitumor activity [20–24]. We have also carried out work with *cis*-1,4-DACH (1,4-diaminocyclohexane) as a carrier amine group, which has

* Corresponding author. Tel. +1-713-792-2837; fax: +1-713-792-6759; e-mail: akhokhar@mdanderson.org

0277-5387/00/$ - see front matter ©2000 Elsevier Science Ltd All rights reserved.
PII S0277-5387(00)00351-X

shown promising antitumor activity [25,26]. The compounds with *cis*-1,4-DACH as the carrier ligand are presently under investigation. In our continuous efforts to design new anticancer platinum drugs, we have synthesized a series of new platinum(II) complexes using 3-methylpiperidine as the carrier ligand and carboxylato ligands as leaving groups. Each complex has been characterized by elemental analysis, IR spectroscopy, and ^{195}Pt nuclear magnetic resonance (NMR) spectroscopy. The crystal structure of [Pt(3-mepip)$_2$(malonato)]·0.79H_2O was determined by single crystal X-ray diffraction.

2. Experimental

2.1. Chemicals

K_2PtCl_4 was purchased from Johnson Matthey, Seabrook, NH. Silver nitrate was obtained from Fisher Scientific Co., Houston, TX. 3-Methylpiperidine (3-mepip), silver sulfate, oxalic acid, malonic acid, methylmalonic acid, dimethylmalonic acid, tartronic acid, 1,1-cyclopropanedicarboxylic acid (CPDCA) and 1,1-cyclobutanedicarboxylic acid (CBDCA) were obtained from Aldrich Chemical Co., Milwaukee, WI. All chemicals obtained from commercial sources were used as supplied.

2.2. Physical measurements

Elemental analyses of the complexes were performed by Robertson Laboratory Inc., Madison, NJ. Infrared spectra in the range of 600–4000 cm^{-1} were recorded on KBr pellets, and far-IR spectra in the range of 150–600 cm^{-1} were recorded on polyethylene pellets on a Perkin-Elmer 2000 spectrophotometer. ^{195}Pt NMR spectra were recorded using a Bruker 200/AF spectrometer with a 10 mm tunable probe. The ^{195}Pt spectra were recorded at 43.055 MHz, and the shifts were measured relative to an external standard of 2.2 M Na_2PtCl_6 in D_2O at 0.00 ppm.

2.3. Preparation of cis-[Pt(3-mepip)$_2$Cl$_2$] (*1*)

K_2PtCl_4 (20.76 g, 50 mmol) was dissolved in 250 ml of deionized water and filtered. Then KI (83.0 g, 0.5 mol) in 100 ml of water was added to it and the reaction mixture was stirred for 10 min. To this solution, 3-methylpiperidine (9.9 g, 100 mmol) was added slowly, while stirring, to give a yellow precipitate, *cis*-[Pt(3-mepip)$_2$I$_2$], and the precipitate was collected by filtration. This compound was dissolved in dimethylformamide and filtered. To the filtrate excess cold water was added to give a bright yellow precipitate, *cis*-[Pt(3-mepip)$_2$I$_2$], which was washed with water, ethanol, acetone and ether and dried in vacuum. *cis*-[Pt(3-mepip)$_2$I$_2$] (12.94 g, 20 mmol) was suspended in 250 ml of aqueous solution of silver nitrate (6.72 g, 39.8 mmol). The reaction mixture was stirred for 24 h at room temperature in the absence of light. The AgI precipitate was filtered off, and a solution of NaCl was added dropwise to the filtrate with constant stirring until a yellow precipitate of *cis*-[Pt(3-mepip)$_2$Cl$_2$] formed. The precipitate was filtered and recrystallized from dimethylformamide. The yellow crystals obtained were washed with water and acetone and dried under vacuum.

2.4. cis-[Pt(3-mepip)$_2$(OSO$_3$)H_2O] (*2*)

To a suspension of *cis*-[Pt(3-mepip)$_2$Cl$_2$] (2.32 g, 5 mmol) in 100 ml of deionized water, an aqueous solution of Ag_2SO_4 (1.49 g, 4.8 mmol) was added. The reaction mixture was then continuously stirred in the dark for 24 h at room temperature. The AgCl precipitate was filtered off, and the filtrate was evaporated to dryness under reduced pressure at 35°C. The pale yellow solid obtained was then dried in vacuum.

2.5. [Pt(3-mepip)$_2$(oxalato)]·H_2O (*3*)

cis-[Pt(3-mepip)$_2$(OSO$_3$)H_2O] (1.01 g, 2.0 mmol) was dissolved in 100 ml of water, and an aqueous solution of sodium oxalate (0.270 g, 2.0 mmol) prepared in situ was added to it. The reaction mixture was then continuously stirred for 24 h at room temperature. The off-white precipitate obtained was filtered and recrystallized from methanol. The white crystalline product finally obtained was isolated by filtration and then dried in vacuum.

2.6. [Pt(3-mepip)$_2$(tartronato)] (*4*), [Pt(3-mepip)$_2$-(CBDCA)] (*5*)

Complexes **4** and **5** were prepared by a method similar to that used for complex **3**, with corresponding sodium salts of tartronic acid and 1,1-cyclobutanedicarboxylic acid (CBDCA), respectively.

2.7. [Pt(3-mepip)$_2$(malonato)]·0.79H_2O (*6*)

cis-[Pt(3-mepip)$_2$(OSO$_3$)H_2O] (1.01 g, 2.0 mmol) was dissolved in 100 ml of water, and an aqueous solution of sodium malonate (0.300 g, 2.0 mmol) prepared in situ was added to it. The reaction mixture was then continuously stirred for 24 h at room temperature. A clear solution obtained was filtered and evaporated to 10 ml under reduced pressure and kept at room temperature for slow evaporation. The white crystalline compound obtained was then isolated by filtration and then dried in vacuum.

The compound (100 mg) was then dissolved in 100 ml of methanol, after which the volume of the solution was reduced to 10 ml and kept aside for slow evaporation at room temperature. Within 3–4 days white crystals of [Pt(3-mepip)$_2$(malonato)]·0.79H_2O were separated from the solution, and were used for X-ray crystallography.

Table 1
Crystallographic data and structure refinement parameters for [Pt(3-methylpiperidine)$_2$(malonato)]·0.79H$_2$O

Empirical formula	$C_{15}H_{29.58}N_2O_{4.79}Pt$
Formula weight	509.72
Temperature (K)	298 K
Wavelength (Å)	0.71073
Crystal system	monoclinic
Space group	$C2/c$
Unit cell dimensions	
a (Å)	24.588(5)
b (Å)	15.137(3)
c (Å)	11.459(2)
α (°)	90.00
β (°)	111.07(3)
γ (°)	90.00
Volume (Å^3)	3979.9(14)
Z	8
Density (calculated) (Mg m^{-3})	1.701
Absorption coefficient	7.073
F(000) (mm^{-1})	1999
Crystal size (mm)	0.45×0.25×0.15
θ Range for data collection (°)	2.24–27.49
Index ranges	$0 \le h \le 26$, $0 \le k \le 19$, $-14 \le l \le 13$
Reflections collected	2899
Independent reflections	2798 (R_{int} = 0.0204)
Absorption correction	semi-empirical from ψ-scans
Max. and min. transmission	1.0000 and 0.6872
Refinement method	full-matrix least-squares on F^2
Data/restraints/parameters	2798/0/207
Goodness-of-fit on F^2	1.037
Final R indices ($I > 2\sigma(I)$) [a]	R_1 = 0.0355, wR_2 = 0.0933
R indices (all data) [a]	R_1 = 0.0719, wR_2 = 0.1069
Largest difference peak and hole (e Å^{-3})	1.665 and −0.636

[a] $R_1 = \sum||F_o| - |F_c||/\sum|F_o|$. $R_w = [\sum w(F_o^2 - F_c^2)^2]/\sum[w(F_o^2)^2]^{1/2}$. $w = [\sigma^2(F_o^2) + (aP)^2 + bP]^{-1}$. $P = (F_o^2 + 2F_c^2)/3$.

2.8. [Pt(3-mepip)$_2$(methylmalonato)] (7), [Pt(3-mepip)$_2$-(dimethylmalonato)] (8), [Pt(3-mepip)$_2$(CPDCA)] (9)

Complexes **7**, **8** and **9** were prepared by a method similar to that used for complex **6**, with corresponding sodium salts of methylmalonic acid, dimethylmalonic acid, or 1,1-cyclopropanedicarboxylic acid (CPDCA) respectively, except that the compounds were recrystallized from acetone.

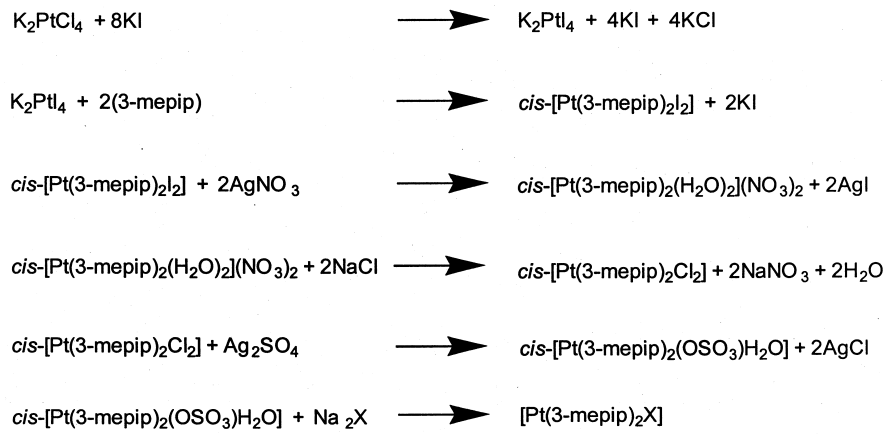
2.9. Crystallographic measurements

The crystal was encapsulated in a thin shell of epoxy cement and mounted on the tip of a glass fiber. Data were collected with a Rigaku AFC5-S automated four-circle diffractometer using the TEXSAN 5.0 software package [27] and were corrected for Lorentz/polarization effects and absorption (ψ-scans). Data collection and refinement parameters are summarized in Table 1. Scattering factors were taken from the literature [28]. The structure was solved using the direct methods routine of SHELXTL-PLUS software package (PC version) [29]. Refinement of F^2 for all reflections, except those with very negative F^2 values, was performed with a personal computer loaded with SHELXL-93 software [30]. Weighted R factors (R_W) and all goodness of fit (S) values were based on F^2, while conventional R factors (R) were based on F with F set to zero for negative F^2. The observed criterion of F^2 was used only for calculating R factors observed and was not relevant to the choice of reflections for refinement. R factors based on F^2 were statistically about twice as large as those based on F, and R factors based on all of the data were even larger. The weighing factor $w = [\sigma^2(F_o^2) + (xP)^2 + yP]^{-1}$, where $P = (F_o^2 + 2F_c^2)/3$, was refined for x and y. H-atom positions were refined using a riding model. The water molecules were refined to partial occupancy.

3. Results and discussion

3.1. Synthesis of platinum complexes

The steps involved in the synthesis of platinum complexes are shown in Scheme 1. *cis*-[Pt(3-mepip)$_2$Cl$_2$] (3-mepip = 3-methylpiperidine) was prepared according to Dhara's method [31]. This method was adopted because it is rapid, easy, and gives much higher yield compared to when K_2PtCl_4 is treated directly with 3-methylpiperidine. Reaction of K_2PtCl_4 with an excess of KI produced K_2PtI_4 in solution. K_2PtI_4 was then reacted with 2 equiv. of 3-methylpiperidine to precipitate *cis*-[Pt(3-mepip)$_2$I$_2$]. The reaction of *cis*-



Scheme 1.

[Pt(3-mepip)$_2$I$_2$] with $AgNO_3$ led to the formation of *cis*-[Pt(3-mepip)$_2$(H$_2$O)](NO$_3$)$_2$, which was further converted to *cis*-[Pt(3-mepip)$_2$Cl$_2$] with the treatment of excess NaCl. *cis*-[Pt(3-mepip)$_2$Cl$_2$] was then treated with Ag_2SO_4 to form *cis*-[Pt(3-mepip)$_2$(OSO$_3$)H$_2$O]. Complexes of the type [Pt(3-mepip)$_2$X] (X = oxalato, malonato, methylmalonato, dimethylmalonato, tartronato, CPDCA or CBDCA ligand) were obtained by the reaction of *cis*-[Pt(3-mepip)$_2$-(OSO$_3$)H$_2$O] with the sodium salts of the corresponding dicarboxylic acid. These complexes are soluble in water.

3.2. Characterization of Pt complexes

The complexes were characterized by elemental analysis, IR and ^{195}Pt NMR spectroscopy. The composition of each complex as determined by elemental analysis showed good agreement between the theoretical and actual values. The analytical results are summarized in Table 2. The results of characterization by IR and ^{195}Pt NMR spectroscopy are shown in Table 3. The IR spectra in general showed a broad absorption between 3155 and 3187 cm^{-1}, due to the coordinated NH group of 3-methylpiperidine. The carbonyl regions for the dicarboxylate complexes displayed patterns characteristic of carboxylate ligands bound to the platinum metal ion. The carboxyl group in complexes **3**–**9** displayed a signal in the region 1620–1695 cm^{-1} corresponding to the $\nu_a(COO^-)$ band, while the $\nu_s(COO^-)$ band normally appears in the range of 1350–1450 cm^{-1} [32]. Complex **2** showed two intense bands at around 620 and 1120 cm^{-1}, indicating the presence of an SO_4 group in this complex [25]. The Pt–N stretching vibrations in all the complexes were observed in the range of 505–560 cm^{-1}, whereas the Pt–O stretching vibrations in complexes **2**–**9** were observed in the range of 420–470 cm^{-1}, respectively [33]. The Pt–Cl stretching vibration for complex **1** was observed at 315 cm^{-1}.

The ^{195}Pt NMR spectra further confirmed the structures of these complexes. Complex **1** showed a signal at −2275 ppm, which is characteristic of the square planar platinum(II) complexes where the two adjacent corners are occupied by two amino nitrogens and the other two positions by two chlorides. Two peaks were observed at −1758 and −1799 ppm in the spectrum of complex **2** [25]. The ^{195}Pt NMR spectra of complexes **3**–**9** showed singlets in the range of −1880 to −1970 ppm (Fig. 1). Such chemical shifts are characteristic for the square planar platinum(II) complexes having two

Table 2
Elemental analysis of platinum(II) complexes

Complex	Complex name	Observed (calculated)			Yield (%)
		C (%)	H (%)	N (%)	
1	*cis*-[Pt(3-mepip)$_2$Cl$_2$]	31.14 (31.03)	5.71 (5.60)	6.27 (6.03)	75
2	*cis*-[Pt(3-mepip)$_2$(OSO$_3$)H$_2$O]	28.19 (28.40)	5.59 (5.52)	5.55 (5.52)	80
3	[Pt(3-mepip)$_2$(oxalato)]·H$_2$O	33.57 (33.53)	5.56 (5.58)	5.45 (5.58)	60
4	[Pt(3-mepip)$_2$(tartronato)]	34.98 (35.08)	5.53 (5.45)	5.43 (5.45)	45
5	[Pt(3-mepip)$_2$(CBDCA)]	40.08 (40.22)	6.07 (5.95)	5.13 (5.21)	55
6	[Pt(3-mepip)$_2$(malonato)]·0.79H$_2$O	35.17 (35.31)	5.89 (5.80)	5.38 (5.49)	50
7	[Pt(3-mepip)$_2$(methylmalonato)]	37.21 (37.57)	5.81 (5.87)	5.38 (5.47)	35
8	[Pt(3-mepip)$_2$(dimethylmalonato)]	38.94 (39.00)	6.02 (6.11)	5.11 (5.35)	40
9	[Pt(3-mepip)$_2$(CPDCA)]	39.22 (39.15)	5.79 (5.75)	5.25 (5.37)	50

Table 3
IR and ^{195}Pt NMR data for platinum(II) complexes

Complex	IR (cm^{-1})					^{195}Pt NMR (ppm)
	νN–H	νC=O	νC–O	νPt–N	νPt–O	
1	3172			540	315 (Pt–Cl)	−2275 [a]
2	3166			505	420	−1758 [b], −1799
3	3180	1695	1390	557	440	−1965 [c]
4	3155	1670	1405	510	446	−1958 [a]
5	3176	1620	1400	560	460	−1943 [c]
6	3157	1650	1380	540	440	−1951 [c]
7	3186	1650	1380	525	447	−1970 [b]
8	3187	1640	1400	503	450	−1890 [b]
9	3169	1645	1370	560	470	−1880 [c]

[a] Recorded in DMF.
[b] Recorded in water.
[c] Recorded in methanol.

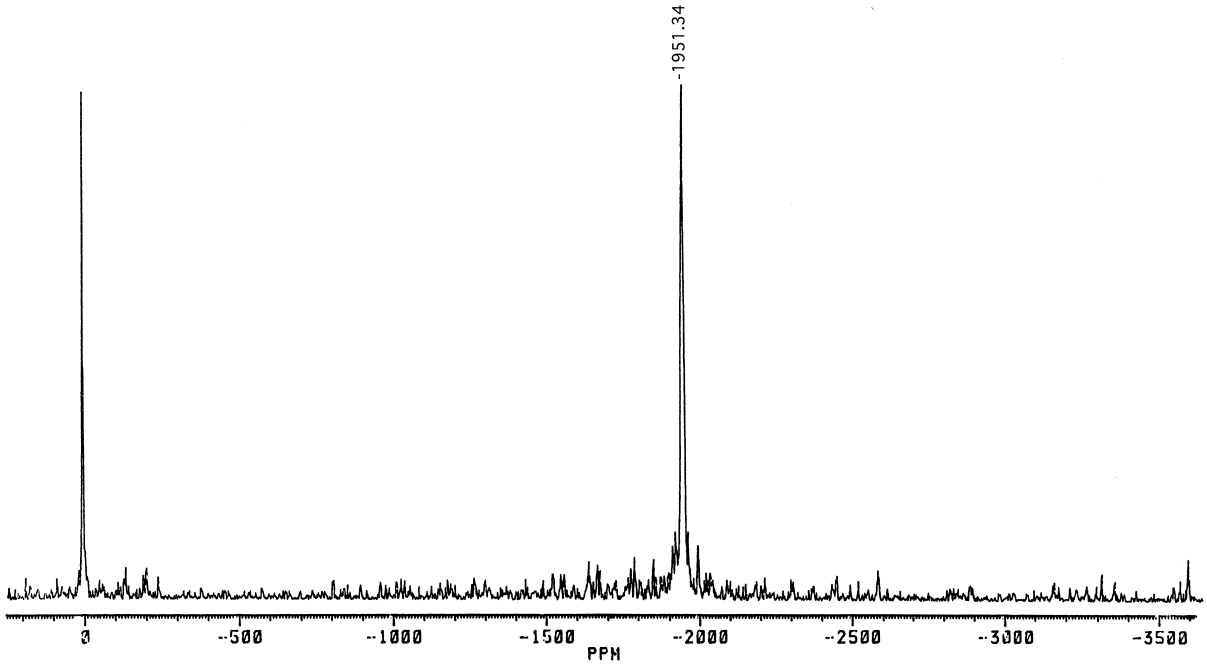


Fig. 1. The ^{195}Pt NMR spectrum of [Pt(3-methylpiperidine)$_2$(malonato)]·0.79H$_2$O recorded in methanol.

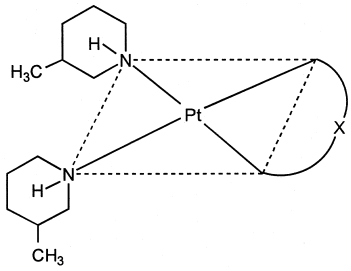


Fig. 2. Structure of [Pt(3-mepip)$_2$X]. X = dichloro, sulfato, oxalato, malonato, methylmalonato, dimethylmalonato, tartronato, CPDCA and CBDCA in complexes **1**–**9**, respectively.

nitrogen and two oxygen atoms as donor ligands [34] (Fig. 2).

3.3. Crystal structure of [Pt(3-mepip)$_2$(malonato)]·0.79H$_2$O

The crystal structure and atomic numbering scheme of [Pt(3-mepip)$_2$(malonato)]·0.79H$_2$O are shown in Fig. 3. Selected bond lengths and bond angles are given in Table 4. Atomic coordinates and equivalent isotropic displacement parameters are given in Table 5. As the data show, the coordination around the platinum atom in this complex has slightly distorted square planar geometry. The distortion appears to be caused by limitation in the bite distances of the chelating ligand. The two adjacent corners of the platinum planes are occupied by two nitrogens of 3-methylpiperidine, whereas the remaining two *cis* positions are used to bind to two oxygen atoms of the malonato group. All the average Pt–N and Pt–O bond lengths are in the range normally observed for other platinum(II) complexes. The average Pt–N bond length of 2.04 Å is consistent with those found in other platinum compounds. For example, this length is 2.038 Å in [Pt(*trans-dl*-1,2-diaminocyclohexane)(*N*-methyliminodiacetato)] [35], 2.04 Å in [Pt(1*R*,2*R*-diaminocyclohexane)-(malonato)], 2.05 Å in [Pt(1*R*,2*R*-diaminocyclohexane)-(oxalato)] [36] and 2.01 Å in [Pt(*cis*-diamine)(1,1-cyclobutanedicarboxylato)] [37]. The average Pt–O bond length of 2.018 Å is also consistent with the average Pt–O bond lengths observed in [Pt(1,4-diaminocyclohexane)-(malonato)] (2.02 Å) [38], [Pt(*trans*-1,2-diaminocyclohexane)bis(acetato)] (2.01 Å) and [Pt(*cis*-diamine)-(1,1-cyclobutanedicarboxylato)] (2.029 Å) [39]. Malonato forms a six-membered chelating ring with the platinum atom. The O–Pt–O bond angle of 91.2° within the chelating ring is normal compared with the other platinum(II) carboxylato complexes for which the angles were close to 90°, for example

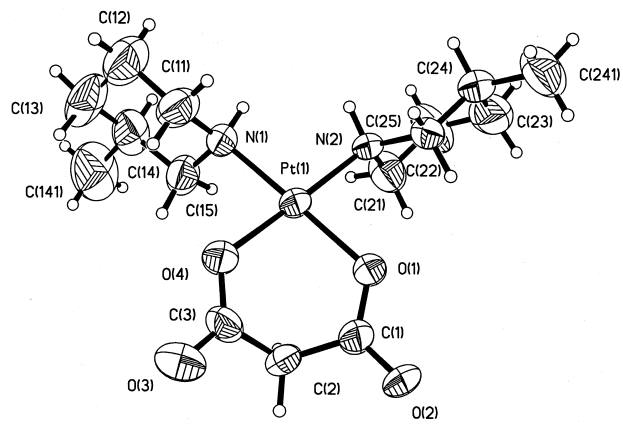


Fig. 3. ORTEP representation of the structure of the [Pt(3-methylpiperidine)$_2$(malonato)]·0.79H$_2$O molecule with atom numbering scheme. The thermal ellipsoids are 50% equiprobability envelopes, with hydrogens as spheres of arbitrary diameter.

Table 4
Selected bond lengths (Å) and bond angles (°) for [Pt(3-methylpiperidine)$_2$(malonato)]·0.79H$_2$O

Pt(1)–O(4)	2.014(7)
Pt(1)–O(1)	2.023(7)
Pt(1)–N(1)	2.038(8)
Pt(1)–N(2)	2.042(8)
O(4)–Pt(1)–O(1)	91.2(3)
O(4)–Pt(1)–N(1)	87.4(3)
O(1)–Pt(1)–N(1)	178.4(3)
O(4)–Pt(1)–N(2)	175.2(3)
O(1)–Pt(1)–N(2)	88.7(3)
N(1)–Pt(1)–N(2)	92.8(3)
C(1)–O(1)–Pt(1)	121.3(6)
C(3)–O(4)–Pt(1)	122.1(7)
C(11)–N(1)–Pt(1)	114.2(7)
C(15)–N(1)–Pt(1)	109.7(6)
C(21)–N(2)–Pt(1)	114.4(7)
C(25)–N(2)–Pt(1)	112.2(6)

Table 5
Atomic coordinates ($\times 10^4$) and equivalent isotropic displacement parameters (Å$^2 \times 10^3$) for [Pt(3-methylpiperidine)$_2$(malonato)]·0.79H$_2$O

Atom	*x*	*y*	*z*	U_{eq} [a]
Pt(1)	0.21112(2)	0.04331(2)	0.26183(4)	0.0467(2)
O(1)	0.2413(3)	−0.0797(5)	0.2518(8)	0.059(2)
C(1)	0.2063(5)	−0.1484(7)	0.2241(12)	0.058(3)
O(2)	0.2244(4)	−0.2233(4)	0.2216(8)	0.070(2)
C(2)	0.1415(5)	−0.1301(7)	0.1876(12)	0.065(3)
O(3)	0.0948(4)	−0.1164(6)	0.3364(10)	0.092(3)
C(3)	0.1270(5)	−0.0810(8)	0.2885(13)	0.061(3)
O(4)	0.1490(3)	−0.0052(5)	0.3203(8)	0.064(2)
N(1)	0.1785(4)	0.1657(6)	0.2714(9)	0.055(2)
C(11)	0.1761(6)	0.1877(8)	0.3938(12)	0.073(4)
C(12)	0.1534(7)	0.2784(10)	0.400(2)	0.101(5)
C(13)	0.0940(8)	0.2876(9)	0.303(2)	0.101(6)
C(14)	0.0940(6)	0.2689(8)	0.1706(14)	0.082(4)
C(141)	0.0327(7)	0.2721(12)	0.069(2)	0.139(7)
C(15)	0.1208(5)	0.1763(8)	0.1691(12)	0.067(3)
N(2)	0.2786(3)	0.0929(5)	0.2178(8)	0.045(2)
C(21)	0.2694(5)	0.0897(10)	0.0832(11)	0.074(4)
C(22)	0.3191(5)	0.1340(12)	0.0563(13)	0.096(5)
C(23)	0.3767(6)	0.0950(11)	0.1326(14)	0.094(5)
C(24)	0.3861(5)	0.0958(8)	0.2702(12)	0.063(3)
C(241)	0.4440(6)	0.0488(10)	0.357(2)	0.116(6)
C(25)	0.3351(4)	0.0522(7)	0.2933(11)	0.054(3)
O(100)	0.0339(10)	−0.0265(14)	−0.090(2)	0.099(7)
O(200)	0.0000	0.2399(12)	−0.2500	0.076(5)

[a] U_{eq} is defined as one third of the trace of the orthogonalized U_{ij} tensor.

90.3° in [Pt(1,2-diaminocyclohexane)(malonato)] [36] and 90.0° in [Pt(*cis*-1,4-diaminocyclohexane)(malonato)] [38]. N–Pt–O bond angles are contracted, which is compensated by the expansion of N–Pt–N and O–Pt–O bond angles. The N–Pt–N and the average O–Pt–O bond angles are observed as 92.8 and 88.0°, respectively. Both piperidine rings are in chair configuration.

Fig. 4 shows a stereoscopic view of the molecular packing in which the molecules in this crystal are held together by a system of hydrogen bonding. This molecular packing is clearly affected by the intramolecular hydrogen bonds occuring between N(2) of 3-methylpiperidine and O(1) of malonato, and also with N(1) of 3-methylpiperidine and O(2) of malonato, N(2)–H···O(1) 2.842 Å, N(1)–H···O(2) 2.897 Å, N(2)–H···O(2) 2.874 Å. These distances compare with known N–H···O hydrogen bond distances [40]. The lattice water molecules appear to interact with themselves and with the oxygen atoms of the malonato ligand at somewhat longer distances: O(100)–H···O(3) 2.921 Å, O(100)–H···O(4) 3.373 Å, O(200)–H···O(3) 2.873 Å, O(100)–H···O(100) 3.191 and 3.434 Å.

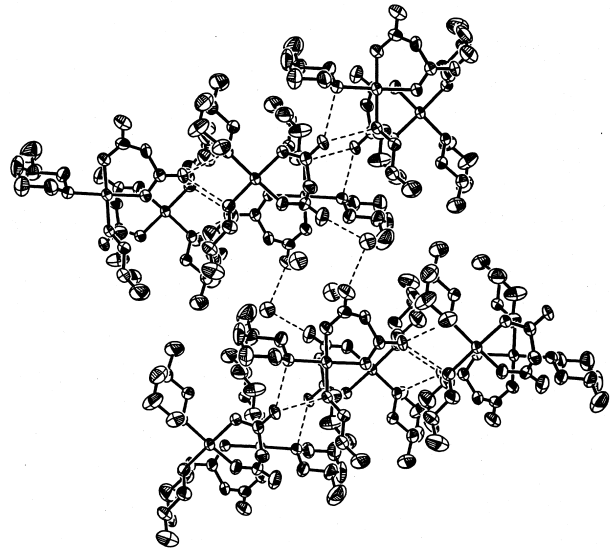


Fig. 4. A stereoscopic view of the molecular packing. Hydrogen bonds are indicated by dashed lines.

In summary, we have synthesized and characterized a series of new cisplatin analogs containing 3-methylpiperidine as non-leaving ligands and oxalato, malonato, methylmalonato, dimethylmalonato, tartronato, CPDCA, and CBDCA as leaving groups. The X-ray crystal structure of [Pt(3-mepip)$_2$(malonato)]·0.79H$_2$O was determined by X-ray crystallography. Since these complexes are highly water soluble, biological studies may reveal good antitumor activity; these are in progress and will be published in a separate paper.

Supplementary data

Full lists of bond lengths and bond angles, anisotropic displacement parameters, hydrogen coordinates and isotropic displacement parameters, and observed and calculated structure factors have been deposited at the Cambridge Crystallographic Data Centre (CCDC). Supplementary material is available from the CCDC, 12 Union Road, Cambridge CB2 1EZ, UK (fax: +44-1223-336033; e-mail: deposit@ccdc.cam.ac.uk) on request, quoting the deposition number 136035. Any request to the CCDC for this material should quote the full literature citation.

Acknowledgements

This work was supported by DHP grant no. 148 to Abdul R. Khokhar from the American Cancer Society. Kenton H. Whitmire acknowledges the support of the Robert A. Welch Foundation.

References

[1] P.J. Loehrer, L. Einhorn, Ann. Intern. Med. 100 (1984) 704.
[2] W.B. Pratt, R.W. Ruddon, W.D. Ensminger, J. Maybaum, in: The Anti Cancer Drugs, Oxford University Press, New York, 1994, p. 133.
[3] I.H. Krakoff, Cancer Treat. Rep. 63 (1979) 1523.
[4] J.B. Vermorken, H.M. Pinedos, Neth. J. Med. 25 (1982) 270.
[5] S.K. Carter, in: M.P. Hacker, E.B. Douple, I.H. Krakoff (Eds.), Platinum Coordination Complexes in Cancer Chemotherapy, Martinus Nijhoff, Boston, MA, 1984, p. 359.
[6] I.H. Krakoff, in: M. Nicolini (Ed.), Platinum and Other Metal Coordination Compounds in Cancer Chemotherapy, Martinus Nijhoff, Boston, MA, 1988, p. 351.
[7] P.L. Loehrer, S.D. Williams Sr., L.H. Einhorn, J. Natl. Cancer Inst. 80 (1980) 1373.
[8] P.J. Loehrer, L.H. Einhorn, Ann. Intern. Med. 100 (1984) 704.
[9] M.J. Cleare, P.C. Hydes, D.R. Hepburn, B.W. Melerbi, in: A.V. Prestayko, S.T. Crooke, S.K. Carter (Eds.), Cisplatin, Current Status and New Developments, Academic Press, New York, 1980, p. 149.
[10] T.A. Connors, M.J. Cleare, K.R. Harrap, Cancer Treat. Rep. 63 (1979) 1499.
[11] K.R. Harrap, in: F.M. Muggia (Ed.), Cancer Chemotherapy, vol. 1, Martinus Nijhoff, Boston, MA, 1983, p. 171.
[12] P.C. Hydes, in: M.P. Hacker, E.B. Douple, I.H. Krakoff (Eds.), Platinum Coordination Complexes in Cancer Chemotherapy, Martinus Nijhoff, Boston, MA, 1984, p. 216.
[13] A.H. Calvert, S.J. Harland, D.R. Newell, Z.H. Siddik, K.R. Harrap, Cancer Treat. Rev. (Suppl. A) 12 (1985) 51.
[14] B.W. Booth, W.C. Weis, A.H. Korzun, W.C. Wood, R.W. Carey, L.P. Panasci, Cancer Treat. Rep. 69 (1985) 919.
[15] M.P. Hacker, A.R. Khokhar, D.B. Brown, J. McCormack, I.H. Krakoff, Cancer Res. 45 (1985) 4748.
[16] A. Pasini, F. Zunimo, Angew Chem. 99 (7) (1987) 632.
[17] J.M. Extra, M. Espie, F. Calvo, C. Ferme, L. Mignot, M. Marty, Cancer Chemother. Pharmacol. 25 (1990) 299.
[18] I. Judson, M. McKeage, J. Hanwell, C. Berry, P. Mistry, F. Raymond, G. Poon, B. Murrer, K. Harrap, in: Platinum and Other Metal Coordination Complexes in Cancer Chemotherapy: The Clinical Development of the Oral Platinum Anticancer Agent JM216, H.M. Press, New York, 1996, p. 83.
[19] R. Perez-Soler, G. Lopez-Berestein, J. Lautersztain, S. Al-Baker, K. Francis, D. Macias-Kiger, M.N. Raber, A.R. Khokhar, Cancer Res. 50 (1990) 4252.
[20] A.R. Khokhar, S. Al-Baker, T. Brown, R. Perez-Soler, J. Med. Chem. 34 (1991) 325.
[21] A.R. Khokhar, S. Al-Baker, R. Perez-Soler, Anticancer Drugs 3 (1992) 95.
[22] Q. Xu, A.R. Khokhar, J. Inorg. Biochem. 48 (1992) 217.
[23] A.R. Khokhar, S. Al-Baker, S. Shamsuddin, Z.H. Siddik, J. Med Chem. 40 (1997) 112.
[24] S. Shamsuddin, S. Al-Baker, Z.H. Siddik, A.R. Khokhar, Inorg. Chim. Acta 241 (1996) 101.
[25] S. Shamsuddin, I. Takahashi, Z.H. Siddik, A.R. Khokhar, J. Inorg. Biochem. 61 (1996) 291.
[26] S. Shamsuddin, C.C. Santillan, J.L. Stark, K.H. Whitmire, Z.H. Siddik, A.R. Khokhar, J. Inorg. Biochem. 71 (1998) 29.
[27] TEXSAN, Single Crystal Analysis Software, Version 5.0, Molecular Structure Corporation, The Woodlands, TX, 1989.
[28] The scattering factors are part of the SHELX-93 package and can be found in the International Tables for X-ray Crystallography, vol. C, Kluwer, Dordrecht, The Netherlands, 1992, Tables 4.2.6.8 and 6.1.1.4.
[29] SHELXTL-PLUS PC, Version 4.2, Siemens Crystallographic Research Systems, Madison, WI, 1990.
[30] G.M. Sheldrick, SHELXL-93, University of Göttingen, Germany, 1993.
[31] S.C. Dhara, Ind. J. Chem. 8 (1970) 193.
[32] K. Nakamato, in: Infrared and Raman Spectra of Inorganic and Coordination Compounds, Wiley, New York, 1986, 4th edn., p. 383.
[33] M.S. Ali, K.H. Whitmire, T. Toyomasu, Z.H. Siddik, A.R. Khokhar, J. Inorg. Biochem., in press.
[34] S. Al-Baker, R. Perez-Soler, A.R. Khokhar, J. Coord. Chem. 29 (1993) 1.
[35] A.R. Khokhar, Q. Xu, S. Al-Baker, Inorg. Chim. Acta 194 (1992) 243.
[36] M.A. Bruke, R. Bau, M. Noji, K. Inagaki, Y. Kidani, Inorg. Chim. Acta 92 (1984) 279.
[37] S. Neidle, I.S. Ismail, P.J. Sadler, J. Inorg. Biochem. 13 (1980) 205.
[38] J.D. Hoeschele, H.D.H. Showalter, A.J. Kraker, W.L. Elliott, B.J. Robert, J.W. Kampf, J. Med. Chem. 37 (1994) 2630.
[39] F.D. Rochon, R. Melanson, J.P. Meacquet, F.B. Gariepy, A.L. Beauchamp, Inorg. Chim. Acta 17 (1995) 108.
[40] A.F. Wells, Structural Inorganic Chemistry, Clarendon Press, Oxford, 5th edn., 1984, p. 357.

PERGAMON

www.elsevier.nl/locate/poly

Polyhedron 19 (2000) 991–1004

POLYHEDRON

Coordination behaviour of sulfanilamide derivatives. Crystal structures of [Hg(sulfamethoxypyridazinato)$_2$], [Cd(sulfadimidinato)$_2$(H$_2$O)]·2H$_2$O and [Zn(sulfamethoxazolato)$_2$-(pyridine)$_2$(H$_2$O)$_2$]

Angel García-Raso [a,*], Juan J. Fiol [a], Santiago Rigo [a], Antonio López-López [a], Elies Molins [b], Enrique Espinosa [b], Elisa Borrás [c], Gloria Alzuet [c], Joaquín Borrás [c], Alfonso Castiñeiras [d]

[a] *Departament de Química, Universitat de les Illes Balears, 07071 Palma de Mallorca, Spain*
[b] *Institut de Ciència de Materials de Barcelona-CSIC, Campus Universitari de Bellaterra, 08193 Cerdanyola, Spain*
[c] *Departamento de Química Inorgánica, Universidad de Valencia, 46100 Burjassot (Valencia), Spain*
[d] *Departamento de Química Inorgánica, Universidad de Santiago de Compostela, 15703 Santiago de Compostela, Spain*

Received 4 January 2000; accepted 3 March 2000

Abstract

Hg(II), Cd(II) and Zn(II) complexes with the ligands sulfadimethoxine, sulfamethoxypyridazine, sulfadiazine, sulfamerazine, sulfadimidine and sulfamethoxazole have been prepared and characterised by spectral data. ^{1}H and ^{13}C NMR have been used to interpret the structural characteristics of the complexes in solution. The X-ray crystal structures of [Hg(sulfamethoxypyridazinato)$_2$] (**2a**), [Cd(sulfadimidinato)$_2$(H$_2$O)]·2H$_2$O (**4b**) and [Zn(sulfamethoxazolato)$_2$(py)$_2$(H$_2$O)$_2$] (**6d**) have been determined. In complex **2a** the Hg(II) ion lies on an inversion centre and exhibits linear coordination by two sulfonamidic nitrogen atoms [Hg–N(1) = 2.071(4) Å] of the two deprotonated sulfamethoxypyridazinato ligands. The polymeric Cd(II) complex (**4b**) exhibits a high distorted-octahedral geometry, involving the sulfonamidic nitrogen [Cd–N(1) = 2.328(6); Cd–N(1′) = 2.326(6) Å] and the heterocyclic N(3)/N(2′) [Cd–N(3) = 2.307(6) Å; Cd–N(2′) = 2.426(6) Å] of two bidentate sulfadimidine ligands, the terminal amino N(4′b) [Cd–N(4′b) = 2.379(7) Å] of a third sulfadimidine which is bonded to an adjacent Cd(II), and the O(3) atom of a coordinated water molecule [Cd–O(3) = 2.334(6) Å]. In complex **6d** the geometry around the Zn(II) ion can be described as a slightly distorted compressed octahedron. Two pyridine [Zn–N(16) = 2.1841(17) Å] and two isoxazole N atoms [Zn–N(2) = 2.1736(15) Å] are located in the equatorial plane and two oxygen atoms of two water molecules [Zn–O(4) = 2.0984(14) Å] are placed in the apical positions. IR and NMR spectral studies suggest a similar behaviour of the Cd(II) and Zn(II) complexes, both in solid state and solution, and different to the corresponding Hg(II) complexes. Thus ^{1}H and ^{13}C NMR spectra, in DMSO-d_6, of Cd(II) and Zn(II) compounds show coordination mainly through the heterocyclic nitrogen while the corresponding Hg(II) derivatives seem to be coordinated through the sulfonamidic nitrogen. ©2000 Elsevier Science Ltd All rights reserved.

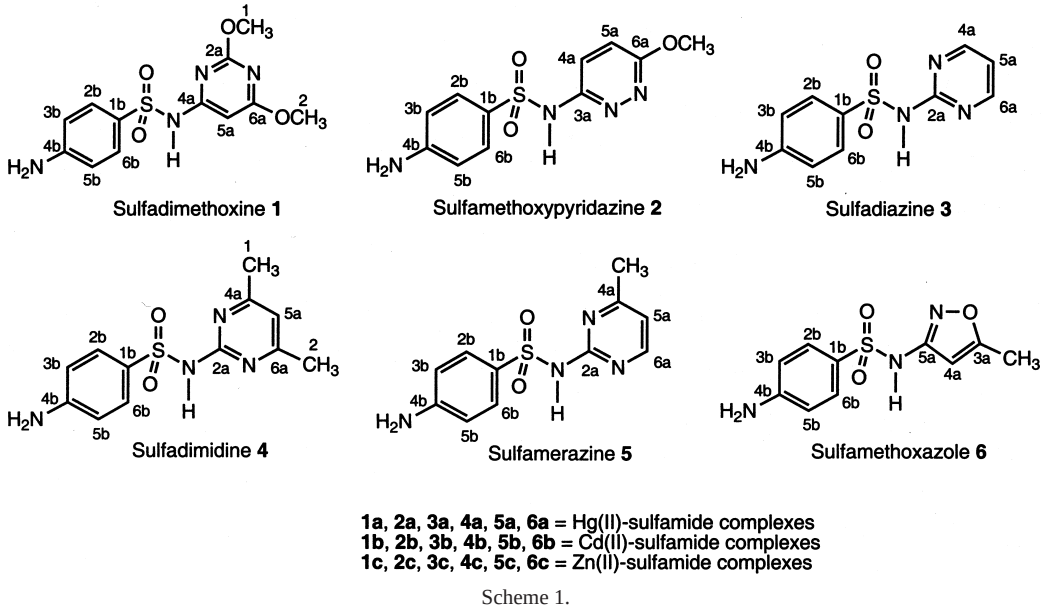
Keywords: Cadmium complexes; Mercury complexes; Sulfamides; X-ray structure; Zinc complexes

1. Introduction

The synthesis of metal sulfanilamide compounds has received much attention due to the fact that sulfanilamides were the first effective chemotherapeutic agents to be employed for the prevention and cure of bacterial infections in humans (see Scheme 1). Although sulfamides present bacteriostatic activity [1–3] related to the inhibition of the bacterial enzyme DHPS (dihydropteroate synthetase) which catalyses the incorporation of *p*-aminobenzoic acid into the precursor of folic acid, 2-amino-4-hydroxy-6-hydroxymethyl dihydropteridine pyrophosphate (see Scheme 2) [4–7], the pharmacological activity of these types of molecules is often enhanced by complexation with metal ions [8,9]. Thus, rapid healing of skin disorders has been promoted by silver–sulfadiazine complex [10,11] in human topical burn therapy, and zinc–sulfadiazine complex [12,13] in the prevention of bacterial infection in burned animals, where the effectiveness of burn treatment seems to depend not only on the presence

* Corresponding author. Tel.: +34-971-173263; fax: +34-971-173426; e-mail: dquagr0@clust.uib.es

0277-5387/00/$ - see front matter ©2000 Elsevier Science Ltd All rights reserved.
PII S0277-5387(00)00355-7



Scheme 1.

of a metal ion [slow release of the Ag(I) or Zn(II)], but also crucially on the nature of the material to which the metal ion is bound [12].

Morevoer, although interesting structural results have been described in the literature (sulfadiazine: Ag(I) [10,11,14], Zn(II) [12,13], Cu(II) [15] and Hg(II) [16]; sulfathiazole: Zn(II) [9], Cu(II) [17–20]; sulfadimetoxine: Co(II) [21]; sulfacetamide: Cu(II) [22]), no general studies related to the manner with which metal–sulfonamide interactions occur have been described. For this reason, in the present paper, we report on the synthesis and spectroscopic characterisation of the Zn(II), Cd(II) and Hg(II) complexes with six sulfonamides [sulfadimethoxine (**1**), sulfamethoxypyridazine (**2**), sulfadiazine (**3**), sulfadimidine (sulfamethazine) (**4**), sulfamerazine (**5**) and sulfamethoxazole (**6**)] and the X-ray structure determination of [Hg(sulfamethoxypyridazinato)$_2$] (**2a**), [Cd(sulfadimidinato)$_2$(H$_2$O)]·2H$_2$O (**4b**) and [Zn(sulfamethoxazolato)$_2$(py)$_2$(H$_2$O)$_2$] (**6d**) in order to show the general manner with which interactions between d^{10} metal ions and these ligands take place.

2. Experimental

2.1. Analysis and physical measurements

Satisfactory C, H, N and S analyses were obtained for all compounds and carried out using a Carlo-Erba Model 1106 microanalyser. The IR spectra in the solid state (KBr pellets) were recorded on a PE 683 spectrometer with a PE 1600 IR data station and on a Perkin-Elmer 843; electronic spectra were recorded on PE 552 and Shimadzu UV 2101PC spectrophotometers. 1D and 2D ^{1}H and ^{13}C NMR spectra were carried out on a Bruker AMX 300. Proton and carbon chemical shifts in DMSO-d_6 were referenced to DMSO-d_6 (^{1}H NMR, $\delta_{(DMSO)} = 2.60$ ppm; ^{13}C NMR, $\delta_{(DMSO)} = 43.5$ ppm). Solid state CP/MAS ^{13}C spectrum was recorded on a Varian Unity 300 spectrometer. Unequivocal C–H assignment was performed by 2D NMR experiments [HMQC [23] and HMBC [24]] or by comparison with spectra of related products. The 2D spectra were processed using commercial Bruker software and experimental characteristics are presented below.

2.1.1. ^{1}H-detected heteronuclear multiple quantum coherence spectroscopy (HMQC)

The one-bond ^{1}H–^{13}C shift correlation spectra resulted from a 502×2048 data matrix size with 48 scans (preceded by 16 dummy scans) per t_1 value. Predelay was 1.0 s, and a 10.3-μs 90° ^{13}C pulse width was used. A sine bell squared filter was used prior to Fourier transformation in the t_2 and t_1 dimensions.

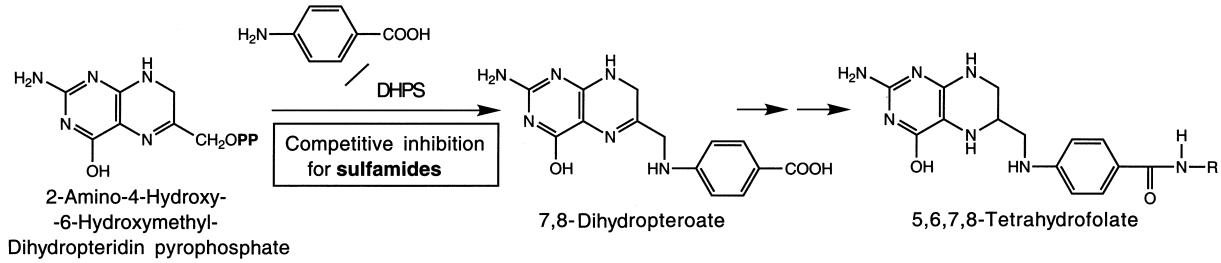
2.1.2. ^{1}H-detected multiple-bond heteronuclear multiple quantum coherence spectroscopy (HMBC)

The multiple-bond ^{1}H–^{13}C shift correlation spectra resulted from a 246×2048 matrix data size with 128 scans (preceded by 8 or 16 dummy scans) per t_1 value. Predelay was 1.0 s, and a 10.3-μs 90° ^{13}C pulse width were used. The delay between the first and the second 90° ^{13}C pulses was 75 ms. A sine bell squared filter was used prior to Fourier transformation in the t_2 and t_1 dimensions.

Sulfamides were used as received from Roig Farma. Zn(II), Cd(II) and Hg(II) acetates were supplied by Aldrich and used without purification.

2.2. Crystallographic studies

X-ray data from compounds **2a** and **4b** were collected on an Enraf-Nonius CAD4 diffractometer with Mo Kα radiation (0.71069 Å). The cell parameters and space group were determined from a least-square refinement of 25 reflections



Scheme 2.

randomly searched. Data collection employed an ω–2θ scan technique. Three reflections were measured every hour as intensity controls; an intensity decay of 1.5% (**2a**) and 7.7% (**4b**) was observed and corrected. The MOLEN [25] package was used for applying Lorentz polarization correction and ψ-scan empirical absorption corrections. The structures were solved by direct methods using the SHELXS 86 program [26] and refined by least-squares using the SHELXL 93 program [27]. Hydrogen atoms were placed in calculated positions, except for those corresponding to water molecules (for **4b**), which were located in Fourier-difference maps, and refined with an isotropic thermal factor constrained to 1.2 times U_{eq} of their bonded atom [1.5 (**2a**) or 1.3 (**4b**) times in the case of methyl groups].

X-ray data from compound **6d** were collected on an Enraf-Nonius CAD4 automatic diffractometer [28] with Cu Kα radiation ($\lambda = 1.54184$ Å). Cell constants and an orientation matrix for data collection were obtained by least-squares refinement of the diffraction data from 25 reflections. Data collection employed an ω-scan technique and were corrected for Lorentz and polarisation effects [29]. A semi-empirical absorption correction (Ψ scan) was made [30]. The structure was solved by direct methods [26] which revealed the position of all non-hydrogen atoms and refined on F^2 by a full-matrix least-squares procedure using anisotropic displacement parameters [31]. The hydrogen atoms were located from difference maps and refined isotropically. Atomic scattering factors were from International Tables for X-Ray Crystallography [32]. Molecular graphics were from ZORTEP [33].

Details of the data collection and processing are summarised in Table 1.

2.3. Preparation of Hg(II)–sulfamidato complexes

2.3.1. General procedure

Hg(II) acetate (1 mmol) in methanol (20 ml) was added dropwise to a stirred solution of the corresponding sulfamide (2 mmol) in methanol (20 ml). A white precipitate begins to form and the reaction is stirred during 18 h at room temperature. The precipitate is filtered off and air dried. Crystallisation in different mixtures of NH_4OH–H_2O or DMSO–MeOH yields white crystals.

2.3.2. Hg(sulfadimethoxynato)$_2$ (**1a**)

White solid (87% yield). Found: C, 35.00; H, 3.09; N, 13.52; S, 7.89. Calc. for $C_{24}H_{26}N_8S_2O_8Hg$: C, 35.18; H, 3.17; N, 13.68; S, 7.82%. Selected IR data (cm^{-1}): 911m, 946w, 962vw, 984w, 1009m, 1090s, 1113s, 1141vs, 1211vs, 1294s, 1362vs, 1419s, 1575vs, 1635s, 3244m, 3367s, 3454m. UV (DMSO): λ 274 nm (ε 4.5×10^4 dm^3 mol^{-1} cm^{-1}). Λ_M/Ω^{-1} cm^2 mol^{-1} (10^{-3} mol dm^{-3} in DMSO, 25°C) = 0.7. ^{1}H NMR (DMSO-d_6): δ 7.59d [2H, H(2b)/H(6b), J = 8.2 Hz], 6.57d [2H, H(3b)/H(5b), J = 8.2 Hz], 5.83s [1H, H(5a)], 5.80bs (2H, NH_2), 3.84s [3H, $OCH_3(1)$], 3.79s [3H, $OCH_3(2)$]. ^{13}C NMR (DMSO-d_6): δ 176.2 [C(6a)], 168.0 [C(2a)], 165.8 [C(4a)], 157.2 [C(4b)], 133.7 [C(2b)/C(6b)], 128.3 [C(1b)], 116.8 [C(3b)/C(5b)], 88.6 [C(5a)], 58.8 [$OCH_3(1)$], 58.0 [$OCH_3(2)$].

2.3.3. Hg(sulfamethoxypyridazinato)$_2$ (**2a**)

White solid (94% yield). White crystals in NH_4OH–H_2O (1:1). Found: C, 34.71; H, 2.88; N, 14.70; S, 8.33. Calc. for $C_{22}H_{22}N_8S_2O_6Hg$: C, 34.80; H, 2.90; N, 14.76; S, 8.44%. Selected IR data (cm^{-1}): 952s, 1016s, 1041m, 1091s, 1125m, 1153s, 1272vs, 1318m, 1351w, 1402vs, 1460s, 1503m, 1548w, 1602s, 3209m, 3363m. UV (DMSO): λ 273 nm (ε 3.5×10^4 dm^3 mol^{-1} cm^{-1}). Λ_M/Ω^{-1} cm^2 mol^{-1} (10^{-3} mol dm^{-3} in DMSO, 25°C) = 3.3. ^{1}H NMR (DMSO-d_6): δ 7.82d [2H, H(2b)/H(6b), J = 8.6 Hz], 7.62d [1H, H(4a), J = 9.6 Hz], 7.31d [1H, H(5a), J = 9.6 Hz], 6.68d [2H, H(3b)/H(5b), J = 8.6 Hz], 6.06bs (2H, NH_2), 4.01s (3H, OCH_3). ^{13}C NMR (DMSO-d_6): δ 165.8 [C(6a)], 158.0 [C(3a)], 156.7 [C(4b)], 133.1 [C(2b)/C(6b)], 129.9 [C(1b)], 125.5 [C(4a)], 124.4 [C(5a)], 116.7 [C(3b)/C(5b)], 58.3 (OCH_3).

2.3.4. Hg(sulfadiazinato)$_2$·2DMSO (**3a**)

Previously described [16].

2.3.5. Hg(sulfadimidinato)$_2$ (**4a**)

White solid (83% yield). Found: C, 37.91; H, 3.43; N, 14.78; S, 8.48. Calc. for $C_{24}H_{26}N_8S_2O_4Hg$: C, 38.16; H, 3.45; N, 14.84; S, 8.48%. Selected IR data (cm^{-1}): 892m, 956vw, 992m, 1086m, 1150vs, 1302s, 1343m, 1371s, 1395sh, 1434m(br), 1503m, 1555m(br), 1597s, 1629m, 3348m. UV (DMSO): λ 275 nm (ε 5.2×10^4 dm^3 mol^{-1} cm^{-1}). Λ_M/Ω^{-1} cm^2 mol^{-1} (10^{-3} mol dm^{-3} in DMSO, 25°C) = 0.3. ^{1}H NMR (DMSO-d_6): δ 7.88bd [2H, H(2b)/H(6b)], 6.66d

Table 1
Crystal data and structure refinements for complexes **2a**, **4b** and **6d**

	Hg(sulfamet)$_2$ (**2a**)	Cd(sulfadimid)$_2\cdot 3H_2O$ (**4b**)	Zn(sulfamoxaz)$_2$(py)$_2$(H$_2$O)$_2$ (**6d**)
Empirical formula	$C_{22}H_{22}HgN_8O_6S_2$	$C_{24}H_{32}CdN_8O_7S_2$	$C_{30}H_{38}N_8O_{10}S_2Zn$
Crystal size (mm)	0.18×0.20×0.55	0.14×0.17×0.28	0.30×0.15×0.10
Crystal system	monoclinic	monoclinic	triclinic
Space group	$C2/c$	$P2_1/a$	$P\bar{1}$
Unit cell dimensions			
a (Å)	22.424(4)	13.357(2)	9.0174(4)
b (Å)	10.642(1)	15.046(1)	9.8677(4)
c (Å)	11.222(2)	15.369(2)	10.4481(4)
α (°)			83.996(4)
β (°)	113.11(2)	97.60(1)	78.004(4)
γ (°)			86.455(3)
Volume (Å^3)	2463.1(7)	3061.6(6)	903.55(6)
Z	4	4	1
Formula weight	759.19	721.10	800.17
Density (calc.) (Mg m^{-3})	2.047	1.564	1.471
Absorption coefficient (mm^{-1})	6.477	0.905	2.587
$F(000)$	1480	1472	416
θ Range (°)	2.65–26.23	2.33–30.41	4.35–74.31
Index ranges	$-27\le h\le 23,\ -13\le k\le 0,\ 0\le l\le 13$	$0\le h\le 19,\ 0\le k\le 21,\ -21\le l\le 21$	$0\le h\le 11,\ -12\le k\le 12,\ -12\le l\le 13$
Reflections collected	2763	9623	3925
Independent reflections	2368 [$R_{int}=0.0255$]	9258 [$R_{int}=0.1088$]	3680 [$R_{int}=0.0111$]
Data/restraints/parameters	2368/0/179	9258/0/401	3680/0/309
Maximum, minimum transmission	0.999, 0.421	0.998, 0.823	0.981, 0.823
Final R indices [$I>2\sigma(I)$]	$R_1=0.0301$, $wR_2=0.0877$	$R_1=0.1125$, $wR_2=0.3007$	$R_1=0.0309$, $wR_2=0.0839$
R indices (all data)	$R_1=0.0398$, $wR_2=0.0921$	$R_1=0.2020$, $wR_2=0.3354$	$R_1=0.0365$, $wR_2=0.0875$
Goodness-of-fit on F^2	1.101	1.175	1.042
Largest difference peak, hole (e Å^{-3})	1.244, −1.114	2.081, −1.372	0.301, −0.351

[2H, H(3b)/H(5b), J=8.5 Hz], 6.85s [1H, H(5a)], 5.97bs (2H, NH_2), 2.37s (6H, CH_3). ^{13}C NMR (DMSO-d_6): δ 171.6 [C(4a)/C(6a)], 163.3 [C(2a)], 156.5 [C(4b)], 134.7 [C(2b)/C(6b)], 130.0 [C(1b)], 116.8 [C(5a)], 115.8 [C(3b)/C(5b)], 27.2 (CH_3).

2.3.6. Hg(sulfamerazinato)$_2\cdot 1.5H_2O$ (**5a**)

White solid (75% yield). Found: C, 35.05; H, 3.19; N, 14.62; S, 8.35. Calc. for $C_{22}H_{22}N_8S_2O_4Hg\cdot 1.5(H_2O)$: C, 35.03; H, 3.31; N, 14.86; S, 8.49%. Selected IR data (cm^{-1}): 917m, 944w, 975w, 1093s, 1143s, 1289s, 1312m, 1373s, 1391s, 1431m, 1457m, 1505m, 1557s, 1579vs, 1600s, 1638m, 3354s, 3450m. UV (DMSO): λ 272 nm (ε 4.9×10^4 dm^3 mol^{-1} cm^{-1}). Λ_M/Ω^{-1} cm^2 mol^{-1} (10^{-3} mol dm^{-3} in DMSO, 25°C) = 0.7. ^{1}H NMR (DMSO-d_6): δ 8.41d [1H, H(6a), J=4.8 Hz], 7.87d [2H, H(2b)/H(6b), J=8.6 Hz], 6.96d [1H, H(5a), J=4.7 Hz], 6.66d [2H, H(3b)/H(5b), J=8.6 Hz], 5.98bs (2H, NH_2), 2.42s (3H, CH_3). ^{13}C NMR (DMSO-d_6): δ 172.1 [C(4a)], 163.6 [C(2a)], 160.9 [C(6a)], 156.6 [C(4b)], 134.5 [C(2b)/C(6b)], 130.1 [C(1b)], 116.0 [C(3b)/C5b)], 117.7 [C(5a)], 27.4 (CH_3).

2.3.7. Hg(sulfamethoxazolato)$_2$ and Hg(sulfamethoxazolato)$_2\cdot 1.5$DMSO (**6a**)

White solid (89% yield). Found: C, 33.93; H, 2.84; N, 11.75; S, 9.08. Calc. for $C_{20}H_{20}S_2O_6Hg$: C, 34.06; H, 2.84; N, 11.92; S, 9.05%. White crystals in DMSO–MeOH. Found: C, 33.80; H, 3.54; N, 9.99; S, 13.67. Calc. for $C_{20}H_{20}S_2O_6Hg\cdot 1.5$DMSO: C, 33.59; H, 3.53; N, 10.22; S, 13.63%. Selected IR data (cm^{-1}): 903m, 952s, 1012m, 1061m, 1091s, 1136vs, 1288m(br), 1266s, 1296s, 1378w, 1416s, 1432s, 1472vs, 1504s, 1598s, 1613s, 1630s, 3378s, 3474m. UV (DMSO): λ 274 nm (ε 4.5×10^4 dm^3 mol^{-1} cm^{-1}). Λ_M/Ω^{-1} cm^2 mol^{-1} (10^{-3} mol dm^{-3} in DMSO, 25°C) = 0.6. ^{1}H NMR (DMSO-d_6): δ 7.76d [2H, H(2b)/H(6b), J=8.5 Hz], 6.69d [2H, H(3b)/H(5b), J=8.5 Hz], 6.13 s[1H, H(4a)], 6.11bs (2H, NH_2), 2.38s (3H, CH_3). ^{13}C NMR (DMSO-d_6): δ 174.7 [C(3a)], 165.9 [C(5a)], 157.0 [C(4b)], 133.4 [C(2b)/C(6b)], 129.2 [C(1b)], 116.7 [C(3b)/C(5b)], 99.4 [C(4a)], 16.4 (CH_3).

2.4. Preparation of Cd(II) and Zn(II)–sulfamidato complexes

2.4.1. General procedure

Cd(II) or Zn(II) acetate (1 mmol) in distilled water (20 ml) was added dropwise to a stirred solution of sodium sulfamidato (2 mmol) in distilled water (20 ml). A white precipitate begins to form and the reaction is stirred during 18 h at room temperature. The precipitate is filtered off and air dried. Crystallisation in different mixtures of NH_4OH–H_2O or DMSO–MeOH yields white crystals.

*2.4.2. Cd(sulfadimethoxynato)$_2$·1/2(NH_3)·H_2O and Cd(sulfadimethoxynato)$_2$·DMSO (**1b**)*

White solid (83% yield). White crystals in NH_4OH–H_2O (1:1). Found: C, 37.92; H, 3.84; N, 15.57; S, 8.37. Calc. for $C_{24}H_{26}N_8S_2O_8Cd \cdot 1/2(NH_3) \cdot H_2O$: C, 38.05; H, 3.89; N, 15.72; S, 8.46%. White crystals in DMSO–MeOH. Found: C, 38.41; H, 3.95; N, 13.72; S, 11.87. Calc. for $C_{24}H_{26}N_8S_2O_8Cd \cdot DMSO$: C, 38.59; H, 3.96; N, 13.85; S, 11.87%. Selected IR data (cm^{-1}): 881s, 932w, 961w, 989w, 1086s, 1145s, 1180m, 1215s, 1263s, 1363s, 1369s, 1396m, 1425s, 1461m, 1489m, 1558s, 1585vs, 1602vs, 2953m, 3337m(br), 3491m(br). UV (DMSO): λ 274 nm (ε 8.6×10^4 dm^3 mol^{-1} cm^{-1}). Λ_M/Ω^{-1} cm^2 mol^{-1} (10^{-3} mol dm^{-3} in DMSO, 25°C) = 10.2. ^{1}H NMR (DMSO-d_6): δ 7.59d [2H, H(2b)/H(6b), J = 8.2 Hz], 6.57d [2H, H(3b)/H(5b), J = 8.2 Hz], 5.83s [1H, H(5a)], 5.80bs (2H, NH_2), 3.84s [3H, OCH_3(1)], 3.79s [3H, OCH_3(2)]). ^{13}C NMR (DMSO-d_6): δ 175.7 [C(6a)], 169.6 [C(2a)], 167.6 [C(4a)], 155.6 [C(4b)], 132.6 [C(2b)/C(6b)], 132.3 [C(1b)], 116.4 [C(3b)/C(5b)], 87.7 [C(5a)], 58.3 [OCH_3(1)], 57.6 [OCH_3(2)].

*2.4.3. Zn(sulfadimethoxinato)$_2$·3/4(NH_3)·3/4(H_2O) (**1c**)*

White solid (90% yield). White crystals in NH_4OH–H_2O (1:9). Found: C, 40.45; H, 3.98; N, 17.35; S, 8.91. Calc. for $C_{24}H_{26}N_8S_2O_8Zn \cdot 3/4(NH_3) \cdot 3/4(H_2O)$: C, 40.58; H, 4.19; N, 17.26; S, 9.02%. IR (cm^{-1}): 883s, 996m, 1008sh, 1058s,s 1069w, 1144s, 1181m, 1213s, 1275s, 1362s, 1369s, 1394m, 1431m, 1461w, 1488m, 1599vs, 2953m, 3168m, 3259m, 3373m(br), 3472m(br). UV (DMSO): λ 275 nm (ε 4.6×10^4 dm^3 mol^{-1} cm^{-1}). Λ_M/Ω^{-1} cm^2 mol^{-1} (10^{-3} mol dm^{-3} in DMSO, 25°C) = 11.0. ^{1}H NMR (DMSO-d_6): δ 7.58d [2H, H(2b)/H(6b), J = 8.4 Hz], 6.59d [2H, H(3b)/H(5b), J = 8.6 Hz], 5.86s [H, H(5a)], 5.77bs (2H, NH_2), 3.81s [3H, OCH_3(1)], 3.73s [3H, OCH_3(2)]. ^{13}C NMR (DMSO-d_6): δ 175.4 [C(6a)], 170.1 [C(2a)], 167.6 [C(4a)], 155.7 [C(4b)], 132.8 [C(2b)/C(6b)], 132.8 [C(1b)], 116.5 [C(3b)/C(5b)], 88.4 [C(5a)], 58.2 [OCH_3(1)], 57.6 [OCH_3(2)].

*2.4.4. Cd(sulfamethoxypyridazinato)$_2$·2(H_2O) (**2b**)*

White solid (90% yield). Found: C, 37.34; H, 3.50; N, 15.71; S, 8.55. Calc. for $C_{22}H_{22}N_8S_2O_6Cd \cdot 2(H_2O)$: C, 37.37; H, 3.68; N, 15.85; S, 9.06%. Selected IR data (cm^{-1}): 836s, 971s, 1016s, 1047m, 1087s, 1138s, 1182m, 1254s, 1299s, 1367m, 1422vs, 1469s, 1503m, 1540m, 1601s, 1637m, 3264m, 3364s. UV (DMSO): λ 270 nm (ε 3.5×10^4 dm^3 mol^{-1} cm^{-1}). Λ_M/Ω^{-1} cm^2 mol^{-1} (10^{-3} mol dm^{-3} in DMSO, 25°C) = 5.1. ^{1}H NMR (DMSO-d_6): δ 7.65 d[2H, H(2b)/H(6b), J = 8.4 Hz], 7.42 d [1H, H(4a), J = 9.6 Hz], 7.16 d [1H, H(5a), J = 9.6 Hz], 6.55 d [2H, H(3b)/H(5b), J = 8.4 Hz], 5.72 bs (2H, NH_2), 3.95 s (3H, OCH_3). ^{13}C NMR (DMSO-d_6): δ 164.1 [C(6a)], 162.3 [C(3a)], 155.4 [C(4b)], 133.9 [C(1b)], 132.6 [C(2b)/C(6b)], 125.8 [C(4a)], 124.9 [C(5a)], 116.7 [C(3b)/C(5b)], 58.1 (OCH_3).

*2.4.5. Zn(sulfamethoxypyridazinato)$_2$·2.5(H_2O) (**2c**)*

White solid (55% yield). Found: C, 39.41; H, 3.90; N, 16.61; S, 9.84. Calc. for $C_{22}H_{22}N_8S_2O_6Zn \cdot 2.5(H_2O)$: C, 39.49; H, 4.04; N, 16.76; S, 9.57%. Selected IR data (cm^{-1}): 750m, 840m, 945m, 1015s, 1091s, 1133s, 1185m, 1293s, 1417vs, 1469vs, 1503m, 1599s, 1629m, 3240m(br), 3368m, 3446m(br). UV (DMSO): λ 271 nm (ε 3.5×10^4 dm^3 mol^{-1} cm^{-1}). Λ_M/Ω^{-1} cm^2 mol^{-1} (10^{-3} mol dm^{-3} in DMSO, 25°C) = 5.5. ^{1}H NMR (DMSO-d_6): δ 7.51d [2H, H(2b)/H(6b), J = 8.4 Hz], 7.49d [1H, H(4a), J = 9.7 Hz], 7.11d [1H, H(5a), J = 9.7 Hz], 6.51d [2H, H(3b)/H(5b), J = 8.4 Hz], 5.67bs (2H, NH_2), 3.90s (3H, OCH_3). ^{13}C NMR (DMSO-d_6): δ 163.0 [C(6a)], 162.1 [C(3a)], 155.2 [C(4b)], 134.3 [C(1b)], 132.2 [C(2b)/C(6b)], 127.6 [C(4a)], 124.6 [C(5a)], 116.5 [C(3b)/C(5b)], 58.0 (OCH_3).

*2.4.6. Cd(sulfadiazinato)$_2$·2(NH_3) (**3b**)*

White solid (80% yield). White crystals in NH_4OH–H_2O (1:1). Found: C, 37.29; H, 3.66; N, 21.56; S, 9.79. Calc. for $C_{20}H_{18}N_8S_2O_4Cd \cdot 2(NH_3)$: C, 37.24; H, 3.72; N, 21.72; S, 9.93%. Selected IR data (cm^{-1}): 725m, 785m, 806s, 846s, 964s, 980s, 1008s, 1090s, 1108m, 1262s, 1277s, 1352m, 1413vs, 1442s, 1501m, 1554s, 1584s, 1598s, 3154m, 3244m, 3315s, 3460m(br). UV (DMSO): λ 271 nm (ε 4.5×10^4 dm^3 mol^{-1} cm^{-1}). Λ_M/Ω^{-1} cm^2 mol^{-1} (10^{-3} mol dm^{-3} in DMSO, 25°C) = 5.1. ^{1}H NMR (DMSO-d_6): δ 8.37d [2H, H(6a), J = 4.9 Hz], 7.64d [2H, H(2b)/H(6b), J = 8.6 Hz], 6.77t [1H, H(5a)], 6.53d [2H, H(3b)/H(5b), J = 8.6 Hz], 5.64s (2H, NH_2). ^{13}C NMR (DMSO-d_6): δ 166.3 [C(2a)], 162.2 [C(4a)/C(6a)], 155.0 [C(4b)], 134.1 [C(1b)], 132.9 [C(2b)/C(6b)], 116.0 [C(3b)/C5b)], 115.1 [C(5a)].

*2.4.7. Zn(sulfadiazinato)$_2$·2(NH_3) (**3c**)*

Only small quantities of the complex have been obtained using the experimental procedure previously described [12] or the general procedure described in the present paper. Under these conditions, a mixture of neutral sulfadiazine and $Zn(OH)_2$ is present [14].

Improved results have been obtained by means of the following procedure. Zn(II) nitrate (1 mmol) in NH_4OH–H_2O (1:9) (20 ml) is added dropwise to a stirred solution of sulfadiazine (2 mmol) in NH_4OH–H_2O (1:9) (20 ml). The resulting solution is heated (60°C) until a white precipitate begins to form; the solution is then filtered and crystals are obtained after cooling (24–48 h). The crystalline complex is filtered off and air dried (65% yield). Selected IR data (cm^{-1}): 836m, 978m, 994m, 1014m, 1024m, 1082s, 1102s, 1124s, 1141s, 1182m, 1230s, 1269s, 1282m, 1296m, 1363m, 1418vs, 1426vs, 1453vs, 1502m, 1554s, 1597s, 1635m, 3226m, 3340s, 3459m. ^{1}H NMR (DMSO-d_6): δ 8.30d [2H, H(6a), J = 4.5 Hz], 7.65d [2H, H(2b)/H(6b), J = 8.2 Hz], 6.73t [1H, H(5a)], 6.56d [2H, H(3b)/H(5b), J = 8.4 Hz], 5.68s (2H, NH_2). ^{13}C NMR (DMSO-d_6): δ 166.1 [C(2a)], 161.9 [C(4a)/C(6a)], 155.0 [C(4b)], 134.1 [C(1b)],

133.1 [C(2b)/C(6b)], 116.0 [C(3b)/C5b)], 115.0 [C(5a)].

*2.4.8. [Cd(sulfadimidinato)$_2$(H$_2$O)]·2H$_2$O (**4b**)*

White solid (80% yield). White crystals in NH_4OH–H_2O (3:9). Found: C, 40.09; H, 4.49; N, 15.48; S, 8.67. Calc. for $C_{24}H_{26}N_8S_2O_4Cd\cdot 3H_2O$: C, 39.98; H, 4.44; N, 15.55; S, 8.88%. Selected IR data (cm^{-1}): 885s, 982m, 1082s, 1128vs, 1144s, 1184m, 1248s, 1347m, 1380vs, 1398m, 1434s, 1499m, 1564m, 1586s, 1601s, 1641m, 3160m, 3288m, 3371m, 3465m, 3545m. UV (DMSO): λ 273 nm (ε 6.7×10^4 dm^3 mol^{-1} cm^{-1}). Λ_M/Ω^{-1} cm^2 mol^{-1} (10^{-3} mol dm^{-3} in DMSO, 25°C) = 3.5. ^{1}H NMR (DMSO-d_6): δ 7.67bd [2H, H(2b)/H(6b)], 6.51bd [2H, H(3b)/H(5b)], 6.49s [1H, H(5a)], 5.62bs (2H, NH_2), 2.18s (6H, CH_3). ^{13}C NMR (DMSO-d_6): δ 171.2 [C(4a)/C(6a)], 166.1 [C(2a)], 154.9 [C(4b)], 134.2 [C(1b)], 133.5 [C(2b)/C(6b)], 115.6 [C(3b)/C5b)], 114.0 [C(5a)], 27.0 (CH_3).

*2.4.9. Zn(sulfadimidinato)$_2$·1.75(NH$_3$)·0.25(H$_2$O) (**4c**)*

White solid (71% yield). White crystals in NH_4OH–H_2O (1:9). Found: C, 43.87; H, 4.84; N, 20.90; S, 9.40. Calc. for $C_{24}H_{26}N_8S_2O_4Zn\cdot 1.75(NH_3)\cdot 0.25(H_2O)$: C, 44.06, H, 4.86; N, 20.88; S, 9.79%. Selected IR data (cm^{-1}): 886s, 984m, 1014m, 1058m, 1082s, 1128vs, 1144s, 1186m, 1274s, 1304w, 1349m, 1380s, 1400m, 1436s, 1501m, 1650m, 1588s, 1602s, 1644m, 3158m, 3281m(br), 3368m, 3456m, 3550m UV (DMSO): λ 273 nm (ε 2.1×10^4 dm^3 mol^{-1} cm^{-1}). Λ_M/Ω^{-1} cm^2 mol^{-1} (10^{-3} mol dm^{-3} in DMSO, 25°C) = 2.7. ^{1}H NMR (DMSO-d_6): δ 7.68d [2H, H(2b)/H(6b), J = 7.9 Hz], 6.53d [2H, H(3b)/H(5b), J = 7.6 Hz], 6.46s [1H, H(5a)], 5.62bs (2H, NH_2), 2.18s (6H, CH_3). ^{13}C NMR (DMSO-d_6): δ 170.9 [C(4a)/C(6a)], 165.9 [C(2a)], 155.0 [C(4b)], 133.6 [C(1b)], 133.6 [C(2b)/C(6b)], 115.7 [C(3b)/C5b)], 114.3 [C(5a)], 26.8 (CH_3).

*2.4.10. Cd(sulfamerazinato)$_2$·2H$_2$O (**5b**)*

White solid (83% yield). Found: C, 39.05; H, 3.67; N, 16.40; S, 9.26. Calc. for $C_{22}H_{22}N_8S_2O_4Cd\cdot 2H_2O$: C, 39.14; H, 3.85; N, 16.60; S, 9.48%. Selected IR data (cm^{-1}): 867m, 906m, 978m, 1086m, 1104m, 1113m, 1138s, 1253s, 1328m, 1391s, 1414s, 1436s, 1460m, 1498m, 1558m, 1566m, 1581s, 1597s, 3161m, 3257m, 3292m, 3360m, 3496m, 3553m. UV (DMSO): λ 271 nm (ε 4.8×10^4 dm^3 mol^{-1} cm^{-1}). Λ_M/Ω^{-1} cm^2 mol^{-1} (10^{-3} mol dm^{-3} in DMSO, 25°C) = 3.3. ^{1}H NMR (DMSO-d_6): δ 8.21bd [1H, H(6a)], 7.64d [2H, H(2b)/H(6b)], 6.63d [1H, H(5a)], 6.51bd [2H, H(3b)/H(5b)], 5.62bs (2H, NH_2), 2.18s (3H, CH_3). ^{13}C NMR (DMSO-d_6): δ 171.6 [C(4a)], 166.2 [C(2a)], 161.9 [C(6a)], 154.9 [C(4b)], 134.1 [C(1b)], 133.1 [C(2b)/C(6b)], 115.8 [C(3b)/C5b)], 114.7 [C(5a)], 26.9 (CH_3).

*2.4.11. Zn(sulfamerazinato)$_2$·2H$_2$O (**5c**)*

White solid (84% yield). Found: C, 41.76; H, 4.11; N, 17.46; S, 10.29. Calc. for $C_{22}H_{22}N_8S_2O_4Zn\cdot 2H_2O$: C, 42.07; H, 4.14; N, 17.85; S, 10.20%. Selected IR data (cm^{-1}): 865m, 980m, 981m, 1014m, 1087s, 1104m, 1113m, 1138s, 1252s, 1327m, 1398s, 1419vs, 1433s, 1462s, 1499m, 1566s, 1582s, 1598vs, 1624m, 3156m, 3247m, 3286m, 3366m, 3491m, 3554m. UV (DMSO): λ 272 nm (ε 5.0×10^4 dm^3 mol^{-1} cm^{-1}). Λ_M/Ω^{-1} cm^2 mol^{-1} (10^{-3} mol dm^{-3} in DMSO, 25°C) = 3.2. ^{1}H NMR (DMSO-d_6): δ 8.13s [1H, H(6a)], 7.67d [2H, H(2b)/H(6b), J = 8.2 Hz], 6.60s [1H, H(5a)], 6.54d [2H, H(3b)/H(5b), J = 8.2 Hz], 5.62bs (2H, NH_2), 2.19s (3H, CH_3). ^{13}C NMR (DMSO-d_6): δ 172.3 [C(4a)], 165.8 [C(2a)], 160.9 [C(6a)], 155.2 [C(4b)], 134.2 [C(1b)], 133.5 [C(2b)/C(6b)], 116.0 [C(3b)/C5b)], 114.8 [C(5a)], 27.3 (CH_3).

*2.4.12. Cd(sulfamethoxazolato)$_2$·2(H$_2$O) (**6b**)*

White solid (89% yield). Found: C, 37.11; H, 3.69; N, 12.80; S, 9.78. Calc. for $C_{20}H_{20}S_2O_6Cd\cdot 2(H_2O)$: C, 36.78; H, 3.67; N, 12.87; S, 9.80%. Selected IR data (cm^{-1}): 792m, 835s, 930s, 942s, 1090s, 1111vs, 1174s, 1216s, 1222s, 1264m, 1302m, 1320m, 1377w, 1418s, 1445m, 1477vs, 1506m, 1604m, 1628s, 3379m, 3431m, 3476m. UV (DMSO): λ 267 nm (ε 3.4×10^4 dm^3 mol^{-1} cm^{-1}). Λ_M/Ω^{-1} cm^2 mol^{-1} (10^{-3} mol dm^{-3} in DMSO, 25°C) = 12.4. ^{1}H NMR (DMSO-d_6): δ 7.58d [2H, H(2b)/H(6b), J = 8.6 Hz], 6.58d [2H, H(3b)/H(5b), J = 8.6 Hz], 5.89s [1H, H(4a)], 5.71bs (2H, NH_2), 2.26s (3H, CH_3). ^{13}C NMR (DMSO-d_6): δ 172.7 [C(3a)], 168.4 [C(5a)], 155.8 [C(4b)], 133.2 [C(1b)], 133.2 [C(2b)/C(6b)], 117.0 [C(3b)/C(5b)], 100.7 [C(4a)], 16.5 (CH_3).

*2.4.13. Zn(sulfamethoxazolato)$_2$·2(H$_2$O) (**6c**)*

White solid (79% yield). Found: C, 39.52; H, 3.96; N, 13.72; S, 10.52. Calc. for $C_{20}H_{20}S_2O_6Zn\cdot 2(H_2O)$: C, 39.64; H, 3.96; N, 13.87; S, 10.57%. Selected IR data (cm^{-1}): 818s, 838s, 884sh, 920s, 951s, 1010m, 1055m, 1086s, 1131vs, 1261s, 1274s, 1305m, 1323m, 1426s, 1476s, 1504m, 1577m, 1601s, 1636s, 1661m, 3071m, 3225s, 3365s, 3496s. UV (DMSO): λ 267 nm (ε 3.3×10^4 dm^3 mol^{-1} cm^{-1}). Λ_M/Ω^{-1} cm^2 mol^{-1} (10^{-3} mol dm^{-3} in DMSO, 25°C) = 10.2. ^{1}H NMR (DMSO-d_6): δ 7.60d [2H, H(2b)/H(6b), J = 8.6 Hz], 6.58d [2H, H(3b)/H(5b), J = 8.6 Hz], 5.97s [1H, H(4a)], 5.78s (2H, NH_2), 2.28s (3H, CH_3). ^{13}C NMR (DMSO-d_6): δ 172.8 [C(3a)], 167.3 [C(5a)], 156.2 [C(4b)], 133.2 [C(1b)], 132.2 [C(2b)/C(6b)], 116.9 [C(3b)/C(5b)], 100.9 [C(4a)], 16.4 (CH_3).

*2.4.14. Zn(sulfamethoxazolato)$_2$(py)$_2$(H$_2$O)$_2$ (**6d**)*

A solution of $ZnCl_2$ containing 10 mmol in 50 ml H_2O–py (3:1) was added to a solution of sulfamethoxazole (5 mmol in 50 ml H_2O–py, 1:1) with continuous stirring. Immediately, a white solid was obtained. The precipitate was isolated by filtration and the filtrate was left to stand at room temperature. From the filtrate colourless prismatic crystals suitable for X-ray measurement appeared after a month. Selected IR data (cm^{-1}): 670s, 700s, 750m, 800–820m, 840m, 900m, 930s, 1000m, 1040s, 1060m, 1080s, 1130vs, 1220s, 1250s, 1270s, 1315m, 1410s, 1440s, 1460s, 1500s, 1590s, 1600s, 1630s,

3350s, 3480s. UV (solid): 258 nm. UV (DMSO): λ 273 nm (ε 4.5×10^4 dm^3 mol^{-1} cm^{-1}). Λ_M/Ω^{-1} cm^2 mol^{-1} (10^{-3} mol dm^{-3} in DMSO at 25°C) = 10.0. ^{1}H NMR (DMSO-d_6): δ 8.69dt [2H, H(o-) py, J = 4.2 and 1.7 Hz], 7.96tt [1H, H(p-) py, J = 7.7 and 1.7 Hz], 7.57m [4H, H(2b)/H(6b) + H(m-) py], 6.61d [2H, H(3b)/H(5b), J = 8.6 Hz], 6.05s [1H, H(4a)], 5.87s (2H, NH_2), 2.30s (3H, CH_3). ^{13}C NMR (DMSO-d_6): δ 172.4 [C(3a)], 167.5 [C(5a)], 155.9 [C(4b)], 153.2 [C(o-) py], 142.1 [C(p-) py], 132.7 [C(2b)/C(6b)], 132.1 [C(1b)], 128.7 [C(m-) py], 116.5 [C(3b)/C(5b)], 100.6 [C(4a)], 16.2 (CH_3). Solid ^{13}C NMR (ppm) tentative assignment: 168.2 [(C(3a)], 163.0 [C(5a)], 150.3 [C(4b) and C(o-) py], 140.1 [C(p-) py], 131.1 [C(1b)], 127.0 and 123.1 [C(2b) or C(6b) + C(m-) py and C(6b) or C(2b)], 115.3 and 111.0 [C(5b) and C(3b)], 99.3 [C(4a)], 12.0 (CH_3).

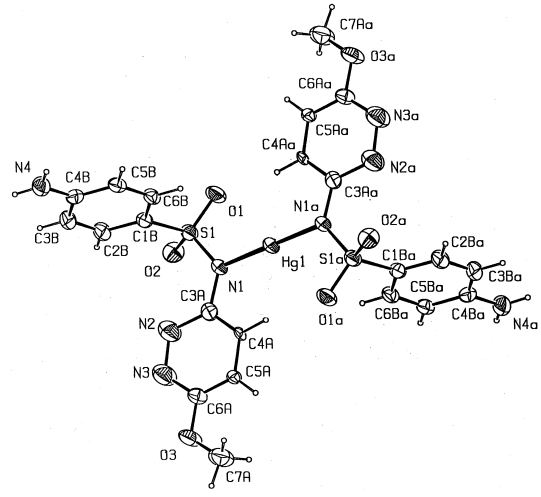


Fig. 1. ORTEP plot of [Hg(sulfamethoxypyridazinato)$_2$] (**2a**).

3. Results and discussion

3.1. Crystal structures

3.1.1. [Hg(sulfamethoxypyridazinato)$_2$] (*2a*)

The molecular structure of complex **2a** and the atom numbering scheme are shown in Fig. 1. The two sulfamethoxypyridazinato ligands are bound to the mercury atom via the sulfonamidic nitrogen N(1) in a linear arrangement. The Hg atom is at the centre of symmetry of the unit complex. The Hg–N bond distance [Hg–N(1) = 2.071(4) Å] (Table 2) is similar to previously reported distances in other Hg–N systems [16]. The bond lengths and angles of the benzene ring, the distances C(4b)–N(4b) = 1.392(7) Å, S(1)–N(1) = 1.625(4) Å, N(1)–C(3a) = 1.403(7) Å and the angle S(1)–N(1)–C(3a) conform well to those found in the free ligand. Sensitive changes in bonds and angles of the heterocyclic ring are observed by comparison with those of the free sulfamethoxypyridazine, as a consequence of a new restructuring of the ring charge. The trigonal arrangement around the sulfonamidic nitrogen is similar to those observed in the free ligand and the Hg–sulfadiazine complex [16]. The *gauche* conformation between the two rings regarding the S(1)–N(sulfonamidic) bond, the torsion angle [C(1b)–S(1)–N(sulfonamidic)–C(3a) = 74.59°] and the dihedral [O(1)–S(1)–N(sulfonamidic)–metal = 20.13°] are quite different to those observed in the Hg–sulfadiazine complex (dihedral 5.80°). The monomeric units are held through weak intermolecular hydrogen bonds between the SO_2 group and the NH_2 of an adjacent unit [N(4b)–H···OSO = 3.04°].

3.1.2. [Cd(sulfadimidinato)$_2$(H_2O)]·2H_2O (*4b*)

The molecular structure of compound **4b** and the atom numbering scheme are shown in Fig. 2. The Cd(II) ion in complex exhibits a high distorted-octahedral geometry, being coordinated to the sulfonamidic N(1) [Cd–N(1) = 2.328(6) Å; Cd–N(1′) = 2.326(6) Å] and the heterocyclic N(3)/N(2′) [Cd–N(3) = 2.307(6) Å; Cd–N(2′) = 2.426(6) Å] of two bidentate sulfadimidine ligands generating two four-membered rings. The terminal amino N(4′b) [Cd–N(4′b) = 2.379(7) Å] of a third sulfadimidine, which is bonded to an adjacent Cd(II), and the O(3) [Cd–O(3) = 2.334(6) Å] atom of a water molecule complete the coordination sphere. Although both ligands are bound in a bidentate form to the metal, only one sulfadimidine presents two equivalent Cd–N distances. The N(4)–C(4b) and N(4′)–C(4b′) distances are 1.393(11) and 1.413(9) Å, respectively, greater than the corresponding distances in the free ligand [N(4)–C(4b) = 1.384(6) Å], which is consistent with the coordination of the terminal amino group to the adjacent Cd(II). The bond lengths and angles of the benzene ring conform well to those found in the free sulfadimidine [34], whereas distances S(1)–N(1) = 1.609(7) Å, S(1′)–N(1′) = 1.578(7) Å, N(2)–C(3a) = 1.338(10) Å and N(2′)–C(3a′) = 1.348(9) Å are shorter in the Cd(II) complex. In this case the trigonal arrangement around the sulfonamidic nitrogen is similar to those observed in the Zn(II) and Cu(II)–sulfadiazine complexes [16]. The *gauche* conformation between the two rings regarding the S(1)–N(sulfonamidic) bond, with a torsion angle of [C(1b)–S(1)–N(sulfonamidic)–C(3a) = 65.51°] is similar to that of the Ag–sulfadiazine complex [10,11,14]. The packing of the complex units is governed by long chains formed by the bridging sulfadimidine ligands which are bound to Cd(1) via N(1)/N(3) and Cd(2) via NH_2 [N(4′b)–Cd = 2.379(7) Å]. Stacking interactions are present in the crystal structure involving benzene and heterocyclic rings (3.6 Å). In the complex units there are intramolecular hydrogen bonds between the NH_2 group and SO_2 of different ligands, and between SO_2 and coordinated H_2O molecules.

3.1.3. [Zn(sulfamethoxazolato)$_2$(py)$_2$(H_2O)$_2$] (*6d*)

The structure consists of centrosymmetric units of Zn(sulfamethoxazolato)$_2$·(py)$_2$(H_2O)$_2$ (Fig. 3). The geometry around the Zn(II) ion, placed at a crystallographic symmetry centre, can be described as a slightly distorted

Table 2
Selected bond lengths (Å) and angles (°) for complexes **2a**, **4b** and **6d**

Hg(sulfamethoxypyridazinato)$_2$ (**2a**)			
Hg(1)–N(1)	2.071(4)	Hg(1)–N(1) [a]	2.071(4)
N(1) [a]–Hg(1)–N(1)	180.0(3)		
C(3A)–N(1)–Hg(1)	114.4(3)	S(1)–N(1)–Hg(1)	120.8(2)
Cd(sulfadimidinato)$_2$ (**4b**)			
Cd(1)–N(3)	2.307(6)	Cd(1)–N(4′) [b]	2.379(7)
Cd(1)–N(1′)	2.326(6)	Cd(1)–N(2′)	2.426(6)
Cd(1)–N(1)	2.328(6)	Cd(1)–O(3)	2.334(6)
N(4′)–Cd(1) [c]	2.379(7)		
N(3)–Cd(1)–N(1′)	115.1(2)	N(1)–Cd(1)–N(2′)	120.7(2)
N(3)–Cd(1)–O(3)	97.6(2)	N(1)–Cd(1)–O(3)	95.7(2)
N(1′)–Cd(1)–O(3)	86.5(2)	N(3)–Cd(1)–N(2′)	96.6(2)
N(3)–Cd(1)–N(1)	56.7(2)	N(2′)–Cd(1)–N(1′)	56.4(2)
O(3)–Cd(1)–N(2′)	142.8(2)	N(1′)–Cd(1)–N(1)	171.7(2)
N(3)–Cd(1)–N(4′) [b]	144.1(2)	N(4′) [b]–Cd(1)–N(2′)	91.5(2)
N(1′)–Cd(1)–N(4′) [b]	98.5(2)	N(1)–Cd(1)–N(4′) [b]	89.3(2)
O(3)–Cd(1)–N(4′) [b]	96.7(3)		
C(3A)–N(1)–Cd(1)	96.1(5)	C(3A′)–N(1′)–Cd(1)	97.2(4)
S(1)–N(1)–Cd(1)	140.9(4)	S(1′)–N(1′)–Cd(1)	136.1(4)
C(3A)–N(3)–Cd(1)	98.5(5)	C(3A′)–N(2′)–Cd(1)	93.7(4)
C(6A)–N(3)–Cd(1)	144.5(6)	C(4A′)–N(2′)–Cd(1)	147.6(5)
C(4B′)–N(4′)–Cd(1) [c]	114.3(4)		
Zn(sulfamethoxazolato)$_2$(pyridine)$_2$(H_2O)$_2$ (**6d**)			
Zn–O(4)	2.0984(14)	Zn–O(4) [d]	2.0984(14)
Zn–N(2)	2.1736(15)	Zn–N(2) [d]	2.1736(15)
Zn–N(16)	2.1841(17)	Zn–N(16) [d]	2.1841(17)
N(16) [d]–Zn–N(16)	180.0	N(2)–Zn–N(2) [d]	180.0
N(2) [d]–Zn–N(16) [d]	92.50(6)	N(2)–Zn–N(16)	92.50(6)
N(2) [d]–Zn–N(16)	87.50(6)	N(2)–Zn–N(16) [d]	87.50(6)
O(4) [d]–Zn–N(2)	90.98(6)	O(4)–Zn–N(2) [d]	90.98(6)
O(4) [d]–Zn–N(2) [d]	89.02(6)	O(4)–Zn–N(2)	89.02(6)
O(4) [d]–Zn–N(16) [d]	92.35(7)	O(4)–Zn–N(16)	92.35(7)
O(4) [d]–Zn–N(16)	87.65(7)	O(4)–Zn–N(16) [d]	87.65(7)
O(4) [d]–Zn–O(4)	180.0		
C(5A)–N(2)–Zn	133.61(12)	C(11)–N(16)–Zn	121.84(15)
O(3)–N(2)–Zn	119.24(10)	C(15)–N(16)–Zn	120.74(16)

[a] Symmetry transformations used to generate equivalent atoms: $-x+1/2, -y+1/2, -z$.
[b] Symmetry transformations used to generate equivalent atoms: $-x+1/2, y+1/2, -z$.
[c] Symmetry transformations used to generate equivalent atoms: $-x+1/2, y-1/2, -z$.
[d] Symmetry transformations used to generate equivalent atoms: $-x+1, -y, -z+1$.

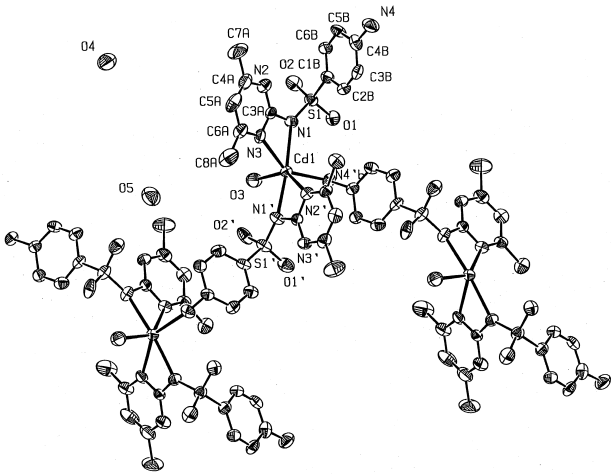


Fig. 2. ORTEP plot of [Cd(sulfadimidinato)$_2$(H_2O)·2H_2O (**4b**). All hydrogen atoms have been omitted for clarity.

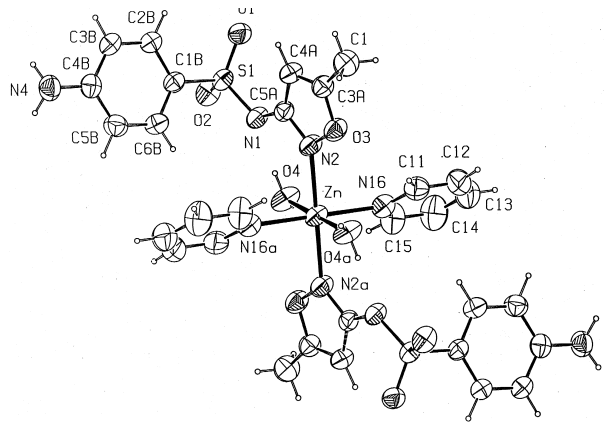


Fig. 3. ORTEP plot of [Zn(sulfamethoxazolato)$_2$(pyridine)$_2$(H_2O)$_2$] (**6d**).

compressed octahedron. The equatorial plane is formed by two pyridine N atoms [N(16) and N(16A)] and two isoxazole N atoms [N(2) and N(2A)] from two sulfamethoxazolate anions. Two oxygen atoms of two water molecules are placed in the apical positions. The equatorial M–N distances [2.1841(17) and 2.1736(15) Å] are almost equal and markedly longer than the axial M–OW ones [2.0984(14) Å]. The coordination angles around the metal, which range from 87.50(6) to 92.50(6)°, do not deviate significantly from a regular octahedron.

It should be noted that the coordination behaviour of the sulfamethoxazolate anion contrasts with that exhibited by the related sulfathiazolate in the Zn(sulfathiazolato)$_2 \cdot H_2O$ compound [18] in spite of the structural similarity between both sulfonamides. The sulfamethoxazolate acts as monodentate through the $N_{isoxazole}$, whereas the sulfathiazolate anion behaves as a bridge linking two metal ions through the $N_{thiazole}$ and N_{amino}.

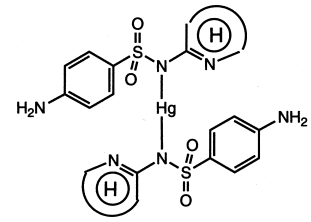
When comparing the bond lengths of the sulfamethoxazolate anion with those of the free sulfamethoxazole [35] a remarkable similarity of all bond distances is found. The most significant changes are: a small shortening of the N(1)–C(5A) distance [from 1.393(4) to 1.370(2) Å], a slight lengthening of the C(1B)–S(1) bond distance [from 1.734(3) to 1.7650(18) Å] and a marked shortening of the S(1)–N(1) length [from 1.645(3) to 1.5675(15) Å]. It must be noted that the S(1)–N(1) bond distance is very close to those of the S=N double bond (1.494–1.580 Å) [36]. Since these distances are comparable to the corresponding ones in the sulfamethoxazole sodium salt [36] and the sulfonamido group does not interact with the metal ion, these changes are ascribed to the deprotonation of this moiety. Moreover, the C(4B)–N(4) bond distance is longer than the corresponding one in the free sulfamethoxazole [1.394(3) Å in the complex, 1.358(5) Å in the ligand]. The lack of interaction of the amino N atom of the sulfamethoxazole with Zn(II) leads us to propose that this lengthening is determined by the intermolecular hydrogen bonds involving the amino group [N(4)–H···OW and N(4)···H–OW = 2.09 and 2.20 Å, respectively, N(4)–H···OSO = 2.20 Å]. The crystal structure is stabilised by an extensive network of intra- and intermolecular hydrogen bonds involving the water molecules, the sulfonamido N and O atoms and the terminal amino group. To be noticed the strong intramolecular interaction between a coordinated water molecule and the sulfonamido N(1) atom [N(1)···H–O(4) = 1.92 Å]. As found in metal complexes with other sulfonamides [18], the coordination through the heteroaromatic N atom does not significantly modify the bond lengths and bond angles of the ring. The isoxazole ring is planar and perpendicular to the benzene ring (angle between planes, 78.28°).

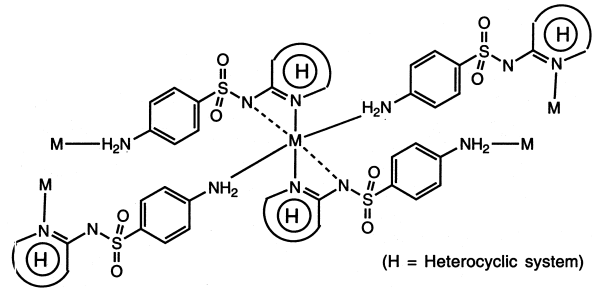
3.2. Infrared spectra

The infrared spectra of the complexes in the far-IR region to 200 cm^{-1} were compared with those of the free ligands. Similar modifications are observed in Zn(II)/Cd(II) complexes which are different to those in Hg(II) complexes. The bands that appear near 3500 and 3400 cm^{-1} due to $\nu_{asym}(NH_2)$ and $\nu_{sym}(NH_2)$ vibrations of the NH_2 group [16] are modified with respect to those of the free respective ligands. In general, these vibration modes appear at higher and lower wavenumbers, compared with those of the free ligand. When the amino N atom does not interact with the metal ion (this excludes the **4b** complex) these modifications are consequently due to the hydrogen bonds involving the amino group. The frequency ν(N–H) of the sulfonamido group, which in the free ligands is found at about 3125 cm^{-1}, is not present in the spectra of the complexes, confirming the deprotonation of the $–SO_2NH–$ moiety. Moreover, for the **6d** complex, in agreement with the coordination of the ligand through the isoxazole N atom, deduced from the crystal structure, the characteristic ring vibration is shifted from 1460 cm^{-1} in the free ligand to 1410 cm^{-1} in the complex. The strong band at (1370–1330 cm^{-1}) related to $\nu_{asym}(SO_2–N)$ [9,16,18] in each free ligand is also changed in frequency or split in the same way in Zn(II) and Cd(II) compounds and differently in Hg(II) derivatives. The 920–975 cm^{-1} band in the ligand is assigned to ν(S–N) [9,16] and changed to higher frequencies in all cases as a consequence of coordination to the metal. This shift to higher frequencies is in accordance with the shortening of the S–N bond lengths, which have been observed in the crystal structures of compounds **2a**, **4b** and **6d**. In complex **6d**, the bands at 1600, 1460, 1440, 1220, 760 and 700 cm^{-1} are assigned to vibrations of the pyridine rings [37,38].

3.3. NMR spectra

^1H and ^{13}C NMR of the complexes **1**–**6** are presented in Tables 3–14.





oligomeric or polymeric M(sulfamidato)$_2$ [M=Cd(II) or Zn(II)]

Proposed structures of M(sulfamidato)$_2$ in DMSO solution

Scheme 3.

Table 3
^{1}H NMR shift assignments of sulfadimethoxine (sulfadime-H, **1**) and its Hg (**1a**), Cd (**1b**) and Zn (**1c**) complexes in DMSO-d_6 [a]

Assignment	^{1}H (**1**)	^{1}H (**1a**)	$\Delta\delta$ (H) [b]	^{1}H (**1b**)	$\Delta\delta$ (H) [b]	^{1}H (**1c**)	$\Delta\delta$ (H) [b]
N(4a)–H	11.23						
C(5a)–H	6.03	5.94	**−0.09**	5.83	**−0.20**	5.86	**−0.17**
C(2b)–H	7.65	7.85	**+0.20**	7.59	−0.06	7.58	−0.07
C(3b)–H	6.69	6.72	+0.03	6.57	**−0.12**	6.59	**−0.10**
OCH_3(1)	3.89	3.95	+0.06	3.84	−0.05	3.81	−0.07
OCH_3(2)	3.88	3.89	+0.01	3.79	**−0.09**	3.73	**−0.15**
NH_2	6.21	6.18	−0.03	5.80	**−0.41**	5.77	**−0.44**

[a] Relative to TMS with DMSO-d_6 peak as reference (^{1}H, 2.60 ppm; ^{13}C, 43.5 ppm).
[b] $\Delta\delta = \delta_{(\text{sulfamide complex})} - \delta_{(\text{sulfamide})}$.

Table 4
^{13}C NMR shift assignments of sulfadimethoxine (sulfadime-H, **1**) and its Hg (**1a**), Cd (**1b**) and Zn (**1c**) complexes in DMSO-d_6 [a]

Assignment	^{13}C (**1**)	^{13}C (**1a**)	$\Delta\delta$ (C) [b]	^{13}C (**1b**)	$\Delta\delta$ (C) [b]	^{13}C (**1c**)	$\Delta\delta$ (C) [b]
C(2a)	168.4	168.0	−0.4	169.6	**+1.2**	170.1	**+1.7**
C(4a)	164.2	165.8	**+1.6**	167.6	**+3.4**	167.6	**+3.4**
C(5a)	88.3	88.6	+0.3	87.7	−0.6	88.4	+0.1
C(6a)	175.6	176.2	−0.4	175.7	+0.1	175.4	−0.2
C(1b)	128.2	128.3	+0.1	132.3	**+4.1**	132.8	**+4.6**
C(2b)/C(6b)	133.4	133.7	+0.3	132.6	−0.8	132.8	−0.6
C(3b)/C(5b)	116.5	116.8	+0.3	116.4	−0.1	116.5	+0.0
C(4b)	157.4	157.2	−0.2	155.6	**−1.8**	155.7	**−1.7**
OCH_3(1)	58.4	58.8	+0.4	58.3	−0.1	58.2	−0.2
OCH_3(2)	57.7	58.0	+0.3	57.6	−0.1	57.6	−0.1

[a] Relative to TMS with DMSO-d_6 peak as reference (^{1}H, 2.60 ppm; ^{13}C, 43.5 ppm).
[b] $\Delta\delta = \delta_{(\text{sulfamide complex})} - \delta_{(\text{sulfamide})}$.

Table 5
^{1}H NMR shift assignments of sulfamethoxypyridazine (sulfamet-H, **2**) and its Hg (**2a**), Cd (**2b**) and Zn (**2c**) complexes in DMSO-d_6 [a]

Assignment	^{1}H (**2**)	^{1}H (**2a**)	$\Delta\delta$ (H) [b]	^{1}H (**2b**)	$\Delta\delta$ (H) [b]	^{1}H (**2c**)	$\Delta\delta$ (H) [b]
N(3a)–H	11.8 (br)						
C(4a)–H	7.66	7.62	−0.04	7.42	**−0.24**	7.49	**−0.17**
C(5a)–H	7.35	7.31	−0.04	7.16	**−0.19**	7.11	**−0.24**
C(2b)–H	7.56	7.82	**+0.26**	7.65	+0.09	7.51	−0.05
C(3b)–H	6.65	6.68	+0.03	6.55	**−0.10**	6.51	**−0.14**
NH_2	6.03	6.06	+0.03	5.72	**−0.31**	5.67	**−0.36**
OCH_3	3.96	4.01	+0.05	3.95	−0.01	3.90	−0.06

[a] Relative to TMS with DMSO-d_6 peak as reference (^{1}H, 2.60 ppm; ^{13}C, 43.5 ppm).
[b] $\Delta\delta = \delta_{(\text{sulfamide complex})} - \delta_{(\text{sulfamide})}$.

All Hg(sulfamidato)$_2$ complexes (**1a–6a**) present a similar NMR pattern with two equivalent sulfamide groups. Thus, upon complexation, a downfield shift (+1.0 to +4.0 ppm) is observed for the carbon directly bonded to the sulfonamidic nitrogen [C(4a) for complex **1a**, C(3a) for complex **2a**, C(2a) for complexes **3a–5a** and C(5a) for complex **6a**]. Moreover, the downfield shift for H(2b)/H(6b) resonance (+0.14 to +0.26 ppm) could be related to the proximity of the Hg(II) which can be explained by a direct interaction, as in solid state, between the metallic ion and the sulfonamidic nitrogen (Scheme 3).

Cd(II) (**1b–6b**) and Zn(II) (**1c–6c**) complexes also show similar NMR patterns with two equivalent sulfamide groups. In these cases, important downfield shifts, higher than in the corresponding Hg(II) compounds, of the carbons directly bonded to the sulfonamidic moiety [C(4a) for complex **1a**, C(3a) for complex **2a**, C(2a) for complexes **3a–5a** and C(5a) for complex **6a** (+3.4 to +6.4 ppm) and C(1b) (+3.1 to 5.1 ppm)] together with different $\Delta\delta$ (H or C) of the resonances presented in the heterocyclic ring suggest a main metal–heterocyclic nitrogen interaction. However, secondary interaction with the sulfonamidic nitrogen cannot be completely discarded. On the other hand, the upfield shifts of the NH_2 (−0.31 to −0.47 ppm), H(3b)/H(5b) (−0.10 to −0.15 ppm) and C(4b) (−1.3 to −2.2 ppm) indicate that NH_2–metal(II) binding is also present, yielding equivalent

Table 6
^{13}C NMR shift assignments of sulfamethoxypyridazine (sulfamet-H, **2**) and its Hg (**2a**), Cd (**2b**) and Zn (**2c**) complexes in DMSO-d_6 [a]

Assignment	^{13}C (**2**)	^{13}C (**2a**)	Δδ (C) [b]	^{13}C (**2b**)	Δδ (C) [b]	^{13}C (**2c**)	Δδ (C) [b]
C(3a)	156.3	158.0	**+1.3**	162.3	**+6.0**	162.1	**+5.8**
C(4a)	128.8	125.5	**−3.3**	125.8	**−3.0**	127.6	**−1.2**
C(5a)	126.8	124.4	**−2.4**	124.9	**−1.9**	124.6	**−1.9**
C(6a)	163.9	165.8	**+1.9**	164.1	+0.2	163.0	−0.9
C(1b)	130.8	129.9	**−0.9**	133.9	**+3.1**	134.3	**+3.5**
C(2b)/C(6b)	132.7	133.1	+0.4	132.6	−0.1	132.2	−0.5
C(3b)/C(5b)	116.8	116.7	−0.1	116.7	−0.1	116.5	−0.3
C(4b)	156.7	156.7	+0.0	155.4	**−1.3**	155.2	**−1.5**
OCH_3	58.5	58.3	−0.2	58.1	−0.4	58.0	0.5

[a] Relative to TMS with DMSO-d_6 peak as reference (^{1}H, 2.60 ppm; ^{13}C, 43.5 ppm).
[b] $\Delta\delta = \delta_{(\text{sulfamide complex})} - \delta_{(\text{sulfamide})}$.

Table 7
^{1}H NMR shift assignments of sulfadiazine (sulfadia-H, **3**) and its Hg (**3a**), Cd (**3b**) and Zn (**3c**) complexes in DMSO-d_6 [a]

Assignment	^{1}H (**3**)	^{1}H (**3a**)	Δδ (H) [b]	^{1}H (**3b**) [c]	Δδ (H) [b]	^{1}H (**3c**) [c]	Δδ (H) [b]
N(2a)–H	11.35						
C(4a)–H	8.57	8.59	+0.02	8.37	**−0.19**	8.30	**−0.27**
C(5a)–H	7.11	7.08	−0.03	6.77	**−0.34**	6.73[c]	**−0.38**
C(2b)–H	7.70	7.87	**+0.17**	7.64	−0.06	7.64	−0.06
C(3b)–H	6.65	6.67	+0.02	6.53	**−0.12**	6.55	**−0.10**
NH_2	6.11	6.01	**−0.10**	5.64	**−0.47**	5.68	**−0.43**

[a] Relative to TMS with DMSO-d_6 peak as reference (^{1}H, 2.60 ppm; ^{13}C, 43.5 ppm).
[b] $\Delta\delta = \delta_{(\text{sulfamide complex})} - \delta_{(\text{sulfamide})}$.
[c] Spectrum presents broad peaks.

Table 8
^{13}C NMR shift assignments of sulfadiazine (sulfadia-H, **3**) and its Hg (**3a**), Cd (**3b**) and Zn (**3c**) complexes in DMSO-d_6 [a]

Assignment	^{13}C (**3**)	^{13}C (**3a**)	Δδ (C) [b]	^{13}C (**3b**)	Δδ (C) [b]	^{13}C (**3c**)	Δδ (C)
C(2a)	161.2	163.7	**+2.5**	166.3	**+5.1**	166.1	**+4.9**
C(4a)/C(6a)	162.2	162.4	+0.2	162.2	+0.0	161.9	−0.3
C(5a)	119.5	118.4	**−1.1**	115.1	**−4.4**	115.0	**−4.5**
C(1b)	128.8	129.8	**+1.0**	134.1	**+5.3**	134.1	**+5.3**
C(2b)/C(6b)	133.8	134.3	+0.5	132.9	−0.9	133.1	−0.7
C(3b)/C(5b)	116.1	116.0	+0.1	116.0	−0.1	116.0	−0.1
C(4b)	157.0	156.6	−0.4	155.0	**−2.0**	155.0	**−2.0**

[a] Relative to TMS with DMSO-d_6 peak as reference (^{1}H, 2.60 ppm; ^{13}C, 43.5 ppm).
[b] $\Delta\delta = \delta_{(\text{sulfamide complex})} - \delta_{(\text{sulfamide})}$.

Table 9
^{1}H NMR shift assignments of sulfadimidine (sulfadim-H, **4**) and its Hg (**4a**), Cd (**4b**) and Zn (**4c**) complexes in DMSO-d_6 [a]

Assignment	^{1}H (**4**)	^{1}H (**4a**)	Δδ(H) [b]	^{1}H (**4b**) [c]	Δδ (H) [b]	^{1}H (**4c**) [c]	Δδ (H) [b]
N(2a)–H	11.15 (br)						
C(5a)–H	6.84	6.85	+0.01	6.49 [d]	**−0.35**	6.46	**−0.38**
C(2b)–H	7.74	7.88	**+0.14**	7.67	−0.07	7.68	−0.06
C(3b)–H	6.65	6.66	+0.01	6.51	**−0.14**	6.53	**−0.12**
NH_2	6.06	5.97	**−0.09**	5.61	**−0.45**	5. 62	**−0.44**
CH_3	2.34	2.37	+0.03	2.18	**−0.16**	2.18	**−0.16**

[a] Relative to TMS with DMSO-d_6 peak as reference (^{1}H, 2.60 ppm; ^{13}C, 43.5 ppm).
[b] $\Delta\delta = \delta_{(\text{sulfamide complex})} - \delta_{(\text{sulfamide})}$.
[c] Spectrum presents broad peaks.
[d] Estimated.

Table 10
^{13}C NMR shift assignments of sulfadimidine (sulfadim-H, **4**) and its Hg (**4a**), Cd (**4b**) and Zn (**4c**) complexes in DMSO-d_6 [a]

Assignment	^{13}C (**4**)	^{13}C (**4a**)	$\Delta\delta$ (C) [b]	^{13}C (**4b**)	$\Delta\delta$ (C) [b]	^{13}C (**4c**)	$\Delta\delta$ (C) [b]
C(2a)	160.7	163.3	**+2.6**	166.1	**+5.4**	165.9	**+5.2**
C(4a)/C(6a)	171.3	171.6	+0.3	171.2	−0.1	170.9	−0.4
C(5a)	117.7	116.8	**−0.9**	114.0	**−3.7**	114.3	**−3.4**
C(1b)	129.0	130.0	**+1.0**	134.2	**+5.2**	133.6	**+4.6**
C(2b)/C(6b)	134.3	134.7	+0.3	133.5	−0.7	133.6	−0.7
C(3b)/C(5b)	115.9	115.8	−0.1	115.6	−0.3	115.7	−0.2
C(4b)	156.9	156.5	−0.4	154.9	**−2.0**	155.0	**−1.9**
CH_3	27.1	27.2	+0.1	27.0	−0.1	26.8	−0.3

[a] Relative to TMS with DMSO-d_6 peak as reference (^1H, 2.60 ppm; ^{13}C, 43.5 ppm).
[b] $\Delta\delta = \delta_{(\text{sulfamide complex})} - \delta_{(\text{sulfamide})}$.

Table 11
^1H NMR shift assignments of sulfamerazine (sulfamer-H, **5**) and its Hg (**5a**), Cd (**5b**) and Zn (**5c**) complexes in DMSO-d_6 [a]

Assignment	^1H (**5**)	^1H (**5a**)	$\Delta\delta$ (H) [b]	^1H (**5b**) [c]	$\Delta\delta$ (H) [b]	^1H (**5c**) [c]	$\Delta\delta$ (H) [b]
N(2a)–H	11.22 (br)						
C(5a)–H	6.98	6.96	−0.02	6.63	**−0.35**	6.60	**−0.38**
C(6a)–H	8.40	8.41	+0.01	8.21	**−0.19**	8.13	**−0.27**
C(2b)–H	7.72	7.87	**+0.15**	7.64	−0.08	7.67	−0.05
C(3b)–H	6.66	6.66	+0.00	6.51	**−0.15**	6.54	**−0.12**
NH_2	6.09	5.98	**−0.11**	5.62	**−0.47**	5.62	**−0.47**
CH_3	2.41	2.42	+0.01	2.18	**−0.23**	2.19	**−0.22**

[a] Relative to TMS with DMSO-d_6 peak as reference (^1H, 2.60 ppm; ^{13}C, 43.5 ppm).
[b] $\Delta\delta = \delta_{(\text{sulfamide complex})} - \delta_{(\text{sulfamide})}$.
[c] Spectrum presents broad peaks.

Table 12
^{13}C NMR shift assignments of sulfamerazine (sulfamer-H, **5**) and its Hg (**5a**), Cd (**5b**) and Zn (**5c**) complexes in DMSO-d_6 [a]

Assignment	^{13}C (**5**)	^{13}C (**5a**)	$\Delta\delta$ (C) [b]	^{13}C (**5b**)	$\Delta\delta$ (C) [b]	^{13}C (**5c**)	$\Delta\delta$ (C) [b]
C(2a)	161.0	163.6	**+2.6**	166.2	**+5.2**	165.8	**+4.8**
C(4a)	172.1	172.1	+0.0	171.6	−0.5	172.3	+0.2
C(5a)	118.9	117.7	**−1.2**	114.7	**−4.2**	114.8	**−4.1**
C(6a)	161.7	162.0	+0.3	161.9	+0.2	160.9	−0.8
C(1b)	129.0	130.1	**+1.1**	134.1	**+5.1**	134.2	**+5.2**
C(2b)/C(6b)	134.2	134.5	+0.3	133.1	**−1.1**	133.5	−0.7
C(3b)/C(5b)	116.1	116.0	−0.1	115.8	−0.3	116.0	−0.1
C(4b)	157.1	156.6	−0.5	154.9	**−2.2**	155.2	**−1.9**
CH_3	27.4	27.4	+0.0	26.9	−0.5	27.3	−0.1

[a] Relative to TMS with DMSO-d_6 peak as reference (^1H, 2.60 ppm; ^{13}C, 43.5 ppm).
[b] $\Delta\delta = \delta_{(\text{sulfamide complex})} - \delta_{(\text{sulfamide})}$.

Table 13
^1H NMR shift assignments of sulfamethoxazole (sulfamoxaz-H, **6**) and its Hg (**6a**), Cd (**6b**) and Zn (**6c**) complexes, and [Zn(sulfamethoxazolato)$_2$(py)$_2$(H_2O)$_2$] (**6d**) in DMSO-d_6 [a]

Assignment	^1H (**6**)	^1H (**6a**)	$\Delta\delta$ (H) [b]	^1H (**6b**)	$\Delta\delta$ (H) [b]	^1H (**6c**)	$\Delta\delta$ (H) [b]	^1H (**6d**)	$\Delta\delta$ (H) [b]
N(2a)–H	11.04								
C(4a)–H	6.18	6.13	−0.05	5.89	**−0.29**	5.97	**−0.21**	6.05	**−0.13**
C(2b)–H	7.58	7.76	**+0.18**	7.58	+0.00	7.60	+0.02	7.57(m)	−0.01
C(3b)–H	6.67	6.69	+0.02	6.58	**−0.09**	6.58	**−0.09**	6.60	−0.07
NH_2	6.18	6.11	−0.07	5.71	**−0.47**	5.78	**−0.40**	5.87	**−0.31**
CH_3	2.38	2.38	+0.00	2.26	**−0.12**	2.28	**−0.10**	2.30	−0.08

[a] Relative to TMS with DMSO-d_6 peak as reference (^1H, 2.60 ppm; ^{13}C, 43.5 ppm).
[b] $\Delta\delta = \delta_{(\text{sulfamide complex})} - \delta_{(\text{sulfamide})}$.

Table 14
^{13}C NMR shift assignments of sulfamethoxazole (sulfamoxaz-H, **6**) and its Hg (**6a**), Cd (**6b**) and Zn (**6c**) complexes and [Zn(sulfamethoxazolato)$_2$(py)$_2$(H_2O) (**6d**) in DMSO-d_6 [a]

Assignment	^{13}C (**6**)	^{13}C (**6a**)	$\Delta\delta$ (C) [b]	^{13}C (**6b**)	$\Delta\delta$ (C) [b]	$1^{13}C$ (**6c**)	$\Delta\delta$ (C) [b]	^{13}C (**6d**)	$\Delta\delta$ (C) [b]
C(3a)	174.0	174.7	+0.3	172.7	**−1.3**	172.8	**−1.2**	172.4	**−1.6**
C(4a)	99.4	99.4	+0.0	100.7	**+1.3**	100.9	**+1.5**	100.6	**+1.2**
C(5a)	162.0	165.9	**+3.9**	168.4	**+6.4**	167.3	**+5.3**	167.5	**+5.5**
C(1b)	128.2	129.2	**+1.0**	133.2	**+5.0**	133.2	**+5.0**	132.1	**+3.9**
C(2b)/C(6b)	132.9	133.4	+0.5	133.2	+0.3	132.2	−0.7	132.9	+0.0
C(3b)/C(5b)	116.7	116.7	+0.0	117.0	+0.3	116.9	+0.2	116.5	−0.2
C(4b)	157.4	157.0	−0.4	155.8	**−1.6**	156.2	**−1.2**	155.9	**−1.5**
CH_3	16.1	16.4	+0.3	16.5	+0.4	16.4	+0.3	16.2	+0.1

[a] Relative to TMS with DMSO-d_6 peak as reference (^1H, 2.60 ppm; ^{13}C, 43.5 ppm).
[b] $\Delta\delta = \delta_{(\text{sulfamide complex})} - \delta_{(\text{sulfamide})}$.

structures to the previously described polymeric Zn(sulfothiazolato)$_2$ [9] (Scheme 3). Similar results are obtained for compound **6d**. Moreover, the solid ^{13}C NMR spectrum shows the non-equivalence of the aromatic carbons of the bencenic moiety as can be observed in the crystal structure (Fig. 3).

The Λ_M (10^{-3} mol dm^{-3}) values in DMSO at 25°C imply the presence of non-electrolyte type species for all the complexes described in this work [39].

4. Conclusion

Spectral and X-ray data of the complexes show a general pathway for the interaction between the six sulfamides studied and the d^{10} metal ions. Thus, Cd(II) and Zn(II) compounds present coordination mainly through heterocyclic nitrogen whereas the corresponding Hg(II) derivatives seem to be coordinated through sulfonamidic nitrogen (Scheme 3).

Supplementary data

Supplementary data are available from the Cambridge Crystallographic Data Centre, 12 Union Road, Cambridge CB2 1EZ, UK (fax: +44-1223-336033; e-mail: deposit@ccdc.cam.ac.uk) on request, quoting the deposition numbers: 137958 (**2a**), 137959 (**4b**) and 137960 (**6d**).

Acknowledgements

This work was supported financially by the Vicerrectorat d'Investigació de la Universitat de les Illes Balears (UIB). A.G.-R. and J.J.F. are grateful for financial support from Spanish CICYT (PB-98-0123), and E.B., G.A. and J.B. acknowledge financial support from the Spanish CICYT (PM97-0105-C02-01). The authors thank Dr G. Martorell (Serveis Científico-Tècnics. Universitat de les Illes Balears) for the 2D NMR experiments and F. Estevan (University of Valencia, Spain) for recording the solid ^{13}C NMR spectrum.

References

[1] T. Nogrady, Medicinal Chemistry, Oxford University Press, Oxford, 2nd edn., 1988.
[2] R.B. Silverman, The Organic Chemistry of Drug Design and Drug Action, Academic Press, New York, 1992.
[3] C.J. Coulson, Molecular Mechanisms of Drug Action, Taylor and Francis, London, 2nd edn., 1994, p. 30.
[4] G.M. Brown, Adv. Biochem. 35 (1971) 35.
[5] G.H. Miller, P.H. Doukas, J.K. Seydal, J. Med. Chem. 15 (1972) 700.
[6] P. Narula, M. Haridas, T.P. Singh, Indian J. Phys., Sect. A 61 (1987) 132.
[7] Catálogo de Especialidades Farmacológicas, Consejo General de Colegios Oficiales de Farmaceúticos, Spain, 1997.
[8] A. Bult, H. Sigel, Metal Ions in Biological Systems, vol. 16, Marcel Dekker, New York, 1983, p. 261.
[9] J. Casanova, G. Alzuet, S. Ferrer, J. Borrás, S. García-Granda, E. Perez-Carreño, J. Inorg. Biochem. 51 (1993) 689 and Refs. therein.
[10] N.C. Baezinger, A.W. Strauss, Inorg. Chem. 15 (1976) 1807.
[11] D.S. Cook, M.F. Turner, J. Chem. Soc., Perkin Trans. 2 (1975) 1021.
[12] N.C. Baezinger, S.L. Modak, C.L. Fox Jr., Acta Crystallogr., Sect. C 39 (1983) 1620.
[13] C.J. Brown, D.S. Cook, L. Sengier, Acta Crystallogr., Sect. C 41 (1985) 718.
[14] A. Bult, N. Hulsing, J.N. Weyland, J. Pharm. Pharmacol. 33 (1981) 171.
[15] C.J. Brown, D.S. Cook, L. Sengier, Acta Crystallogr., Sect. C 43 (1987) 2332.
[16] A. García-Raso, J.J. Fiol, G. Martorell, A. López-Zafra, M. Quirós, Polyhedron 16 (1997) 613.
[17] J. Casanova, G. Alzuet, J. Borrás, J.M. Amigó, T. Debaerdemaeker, Z. Kristallogr. 209 (1994) 271.
[18] J. Casanova, G. Alzuet, J. Borrás, J. Timoneda, S. García-Granda, I. Cándano-González, J. Inorg. Biochem. 56 (1994) 65.
[19] J. Casanova, G. Alzuet, J. Borrás, O. Carugo, J. Chem. Soc., Dalton Trans. (1996) 2239.
[20] J. Casanova, G. Alzuet, J. Latorre, J. Borrás, Inorg. Chem. 36 (1997) 2052.
[21] Y.A. Simonov, M.D. Mazus, I.A. Popa, V.N. Shafranskii, T.I. Malinovskii, Zh. Strukt. Khim. 31 (1990) 77.
[22] F. Blasco, R. Ortiz, L. Perelló, J. Borrás, J. Amigó, T. Debaerdemaeker, J. Inorg. Biochem. 53 (1994) 117.
[23] A. Bax, S. Subramanian, J. Magn. Reson. 67 (1986) 565.

[24] A. Bax, M.F. Summers, J. Am. Chem. Soc. 108 (1986) 2093.
[25] C.K. Fair, MOLEN. An Interactive Intelligent System for Crystal Structure Analysis, Enraf-Nonius, Delft, 1990.
[26] G.M. Sheldrick, Acta Crystallogr., Sect. A 46 (1990) 467.
[27] G.M. Sheldrick, SHELXL 93, Program for Crystal Structure Refinement, University of Göttingen, Germany, 1993.
[28] Enraf-Nonius, CAD4-Express Software, Version 5.1, Enraf-Nonius, Delft, The Netherlands, 1995.
[29] A.L. Spek, HELENA. A Program for Data Reduction of CAD4 Data, University of Utrecht, The Netherlands, 1997.
[30] A.L. Spek, PLATON, A Multipurpose Crystallographic Tool, University of Utrecht, The Netherlands, 1997.
[31] G.M. Sheldrick, SHELXL 97, Program for the Refinement of Crystal Structures, University of Göttingen, Germany, 1997.
[32] International Tables for X-ray Crystallography, Vol. C, Kluwer, Dordrecht, The Netherlands.
[33] L. Zsolnai, ZORTEP, A Program for the Presentation of Thermal Ellipsoids, University of Heidelberg, Germany, 1997.
[34] R.K. Tiwari, M. Haridas, T.P. Singh, Acta Crystallogr., Sect. C 40 (1984) 655.
[35] L. Maury, J. Rambaud, B. Pauvert, Y. Lasserre, G. Berge, M. Audran, Can. J. Chem. 63 (1985) 3012.
[36] H. Nakai, M. Takasuka, M. Shiro, J. Chem. Soc., Perkin Trans 2 (1984) 1459.
[37] M. Cressey, E.D. McKenzie, S. Yates, J. Chem. Soc., Sect. A (1977) 2677.
[38] D.L. Arora, L. Kenti, S.P. Gupta, S.K. Sahni, Polyhedron 5 (1986) 1499.
[39] W.J. Geary, Coord. Chem. Rev. 7 (1971) 81.

PERGAMON

www.elsevier.nl/locate/poly

Polyhedron 19 (2000) 1005–1013

POLYHEDRON

Synthesis, X-ray crystal structure and spectroscopic, magnetic and EPR studies of copper(II) dimers with methoxy-di-(2-pyridyl)methoxide as bridging ligand

José M. Seco [a], Miguel Quirós [b], María J. González Garmendia [a,*]

[a] *Grupo de Química Inorgánica, Facultad de Ciencias Químicas, Universidad del País Vasco, UPV/EHU, Apartado 1072, E-20080 San Sebastián, Spain*
[b] *Departamento de Química Inorgánica, Facultad de Ciencias, E-10871 Granada, Spain*

Received 20 October 1999; accepted 3 March 2000

Abstract

The binuclear complexes $[\{Cu(bipy)\}_2\{\mu\text{-}[(NC_5H_4)_2C(OMe)O]\}_2]X_2\cdot 1/2H_2O$, $X^- = PF_6^-$ (**1**) or ClO_4^- (**2**) and $[\{Cu(phen)\}_2\text{-}\{\mu\text{-}[(NC_5H_4)_2C(OMe)O]\}_2]X_2\cdot 2[(NC_5H_4)_2CO]$, $X^- = PF_6^-$ (**3**) or ClO_4^- (**4**) have been synthesized by the reaction of $[\{Cu(NN)\}_2\text{-}(\mu\text{-}OH)_2]X_2\cdot nH_2O$ and di-2-pyridylketone in methanol. The compounds were characterized by conductance measurements and IR and electronic spectroscopies. The X-ray crystal structure of compounds **1**, **3** and **4** show the presence of two $[(NC_5H_4)_2C(OMe)O^-]$ uninegative tridentate N,O,N-donor $\eta^1{:}\eta^2{:}\eta^1{:}\mu_2$ ligands per dimer. The coordination sphere of Cu(II) is a very distorted octahedron. All four compounds are ferromagnetic, with a superexchange parameter $2J = 10.0$, 10.1, 16.7 and 15.8 cm^{-1} for compound **1**, **2**, **3** and **4**, respectively. Zero field splitting parameters (*D*, *E*) and *g* values have been calculated from the spin triplet state signals positions in the EPR spectra. ©2000 Elsevier Science Ltd All rights reserved.

Keywords: Crystal structures; Cu dimers; Di-(2-pyridyl)ketone; Ferromagnetic dimers; Magnetic properties; Spin triplet

1. Introduction

The magnetic aspects of dinuclear Cu(II) complexes, $[\{Cu(NN)\}_2(\mu\text{-}OH)_2]X_2$ with NN = bidentate nitrogen ligand, have been intensively studied since the magnetostructural correlations described by Hatfield and co-workers [1] for planar dimers of Cu(II) with the Cu_2O_2 group. More recently, these correlations have been extended and theoretically justified by Ruiz et al. [2,3].

In previous papers we described the interaction between the ligand PhNHpy and the dimers $[\{Cu(NN)(\mu\text{-}OH)\}_2]\text{-}X_2\cdot nH_2O$, where NN = 2,2′-bipyridine (bipy) or 1,10-phenanthroline (phen), and $X^- = PF_6^-$ [4] or ClO_4^- [5]. The corresponding magnetostructural correlations were established for the resulting dinuclear complexes.

Di-(2-pyridyl)ketone is a molecule that can exhibit different modes of coordination. As bidentate ligand may present a N,O-coordination giving a five-membered chelate ring or a N,N-coordination forming a six-membered ring [6–8]. Frequently the coordinated di-(2-pyridyl)ketone undergoes nucleophilic addition of water or an alcohol at the carbonylic carbon atom to form the diol or the corresponding hemiacetal, $(NC_5H_4)_2C(OR)(OH)$, which, deprotonated, acts as a mononegative, tridentate N,O,N-donor ligand. The three donor atoms may be coordinated to one metal atom [9–11] or to two metal atoms, bridging them, with a $\eta^1{:}\eta^2{:}\eta^1$ coordination [12–15]. In a dicubane type compound of Cu(II) the monoanion N,O$^-$,N presents a $\eta^1{:}\eta^3{:}\eta^1$ coordination between three copper atoms [16].

In this paper we describe the interaction between di-(2-pyridyl)ketone and $[\{Cu(NN)(\mu\text{-}OH)\}_2]X_2\cdot nH_2O$, where NN = 2,2′-bipyridine (bipy) or 1,10-phenanthroline (phen) and $X^- = PF_6^-$ or ClO_4^- in methanol. In all four cases the group $[(NC_5H_4)_2C(OMe)O^-]$ is formed and adopts a $\eta^1{:}\eta^2{:}\eta^1$ coordination between two copper atoms. Crystal structure and magnetic and EPR results are also decribed.

2. Experimental

2.1. Synthesis

$[\{Cu(NN)\}_2(\mu\text{-}OH)_2]X_2\cdot xH_2O$ where NN = 2,2′-bipyridyl (bipy) or 1,10-phenanthroline (phen) and

* Corresponding author. Tel.: +34-943-018208; fax: +34-943-212236; e-mail: qppgogam@sq.ehu.es

0277-5387/00/$ - see front matter ©2000 Elsevier Science Ltd All rights reserved.
PII S0277-5387(00)00356-9

$X^- = PF_6^-$ or ClO_4^- were prepared according to Harris et al. [17].

2.1.1. [{Cu(bipy)}$_2${μ-[(NC$_5$H$_4$)$_2$C(OMe)O]}$_2$]X$_2$·1/2H$_2$O, X$^-$ = PF$_6^-$ (1) and ClO$_4^-$ (2)

A solution of di-2-pyridylketone (1 mmol) in methanol (5 ml) was added to a suspension of [{Cu(bipy)}$_2$(μ-OH)$_2$]X$_2$·nH$_2$O (0.25 mmol) in hot methanol (50 ml). By the addition the solid was dissolved and a blue solution was formed. The volume was reduced, by boiling, to 10 ml. It was cooled and filtered. By slow evaporation of the solvent green crystals were formed.

Compound **1**. Yield: 58%. Dec. 124°C. Found: Cu, 10.7; C, 45.5; H, 3.3; N, 9.6. Calc. for $Cu_2C_{44}F_{12}H_{39}N_8O_{4.5}P_2$: Cu, 10.9; C, 45.2; H, 3.4; N, 9.6%. Compound **2**. Yield: 47%. Dec.: 134°C. Found: Cu, 11.8; C, 49.3; H, 3.3; N, 10.7. Calc. for $Cu_2C_{44}Cl_2H_{39}N_8O_{12.5}$: Cu, 11.8; C, 49.0; H, 3.7; N, 10.4%.

2.1.2. [{Cu(phen)}$_2${μ-[(NC$_5$H$_4$)$_2$C(OMe)O]}$_2$]X$_2$·2[(NC$_5$H$_4$)$_2$CO], X$^-$ = PF$_6^-$ (3) and ClO$_4^-$ (4)

The same procedure as for the above compounds, using 1.5 mmol of di-2-pyridylketone per 0.25 mmol of [{Cu(phen)}$_2$(μ-OH)$_2$]X$_2$·nH$_2$O, was employed.

Compound **3**. Yield: 37%. Dec. 127°C. Found: Cu, 8.2; C, 53.2; H, 3.3; N, 10.6. Calc. for $Cu_2C_{70}F_{12}H_{54}N_{12}O_6P_2$: Cu, 8.1; C, 53.3; H, 3.5; N, 10.7%. Compound **4**. Yield: 37%. Dec.: 136°C. Found: Cu, 8.4; C, 56.5; H, 3.4; N, 11.0. Calc. for $Cu_2C_{70}Cl_2H_{54}N_{12}O_{14}$: Cu, 8.6; C, 56.6; H, 3.7; N, 11.3%.

In all four cases, when the reaction solution volume was reduced below 10 ml, blue crystals of monomers [Cu(NN)$_3$]X$_2$ were obtained. Compounds **1**, **2**, **3** and **4** are soluble in acetonitrile, methanol, ethanol, acetone, dimethylformamide, nitromethane, nitrobenzene, dimethyl sulfoxide and dichloromethane. All solutions are blue, except that of nitrobenzene, which is green.

2.2. Physical measurements

C, H and N were analysed on a Perkin-Elmer 240C elemental analyser. Copper was measured with an atomic absorption spectrophotometer (Perkin-Elmer 2380), λ = 324.8 nm. Melting points were measured on an Electrothermal 9300. Conductivity measurements were made using a Metrhom E518 conductometer. IR spectra were recorded on a Nicolet FT-IR 510 spectrometer in the range 4000–400 cm^{-1} using KBr pellets and on a Nicolet 740 in the 650–50 cm^{-1} range using nujol on a polyethylene film. Electronic spectra were recorded on a Shimadzu UV-265 FW spectrophotometer.

Magnetic measurements were carried out in the 292–4.3 K range with a magnetometer (Manics DSM8) equipped with an He continuous flow cryostat and Drusch EAF 16UE electromagnet; the magnetic field was approximately 1.5 T. The EPR spectra were recorded on a Bruker ESP 300 spectrometer with a Bruker ER 035 M gaussmeter, Oxford ITC4 cryostat and HP 5325B frequency counter.

2.3. Crystal structure determination

The X-ray diffraction data were collected, at 293 K, with a STOE STADI-4 diffractometer for compound **1**, and with a Siemens P4 diffractometer for compounds **3** and **4**, with graphite-monochromated Mo Kα radiation (λ = 0.71069 Å), operating in the $2\theta/\omega$ scanning mode. The unit cell parameters were determinated from 25 reflections for compounds **1** and **3** and from 38 reflections for compound **4**. During data collection, three standard reflections were measured every 60, 90 and 97 min, showing a decay of 6.3, 0 and 3.66%, respectively. Data were corrected for Lorentz and polarization effects. Absorption corrections with the ψ scan method were applied for compounds **1** and **3**. The crystallographic data, conditions used for the data collection and some refinement data are listed in Table 1.

The structures were solved by direct methods and refined by full-matrix least-squares on F^2, using, for each compound, the weighting scheme indicated in Table 1. Scattering factors were taken from International Tables for Crystallography [18]. For compound **1**, copper, phosphorus and non-disordered fluorine atoms have been refined anisotropically, all others isotropically. Three of the four PF_6^- groups have been disordered into two positions, restraints having been applied to some of the P–F and F–F distances in order to obtain reasonable geometries. A similar procedure was applied for the perchlorate group in compound **4**. Hydrogen atoms were introduced in their ideal positions. The program package SHELXTL-V5 [19] was used for structure solution and refinement and for drawings.

3. Results and discussion

3.1. Electrical conductivity

The molar conductivity values in acetonitrile (Table 2) correspond to a 2:1 electrolyte [20], according to the dimeric character of the cations. The application of the Onsager equation [21] confirms the dimeric character of the cations. Table 2 shows found and calculated values for the slope of the plot of ($\Lambda_o - \Lambda_e$) versus $\sqrt{c_e}$. The concordance between calculated and observed values is clear.

3.2. IR spectra

The more significant bands are considered as those due to the Cu–O and C=O bonds and to the counterions PF_6^- and ClO_4^-. The stretching ν(O–H) band, at 3600 cm^{-1}, is not observed because of the removal of the OH bridge (Table 3).

The ν_{as}(Cu–O) band shifts to higher frequency compared with the original dimers. For complexes **3** and **4**, the ν(C=O)

Tuesday May 02 11:56 AM

Table 1
Crystallographic and refinement data for [{Cu(bipy}$_2${μ-[(NC$_5$H$_4$)$_2$C(OMe)O]}$_2$](PF$_6$)$_2$·1/2H2O(**1**), [{Cu(phen)}$_2$ {μ-[(NC$_5$H$_4$)$_2$C(OMe)O]}$_2$](PF$_6$)$_2$·2[(NC$_5$N$_4$)$_2$CO] (**3**) and [{Cu(phen}$_2$-{μ-[(NC$_5$H$_4$)$_2$C(OMe)O]}$_2$(ClO$_4$)$_2$·2[(NC$_5$N$_4$)$_2$CO] (**4**)

	Compound **1**	Compound **3**	Compound **4**
Crystal habit	prismatic	prismatic	prismatic
Crystal size (mm)	0.40×0.35×0.35	0.5×0.4×0.4	0.45×0.35×0.35
Chemical formula	[(Cubipy)$_2${μ-[py$_2$C(OMe)O]}$_2$](PF$_6$)$_2$·1/2H$_2$O	[(Cuphen)$_2${μ-[py$_2$C(OMe)O]}$_2$](PF$_6$)$_2$·2(py$_2$CO)	[(Cuphen)$_2${μ-[py$_2$C(OMe)O]}$_2$](ClO$_4$)$_2$·2(py$_2$CO)
Formula weight	1168.85	1576.27	1485.23
Crystal system	monoclinic	monoclinic	monoclinic
Space group	$P2_1/c$	$C2/c$	$C2/c$
a (Å)	25.197(2)	23.6841(15)	23.522(3)
b (Å)	14.495(2)	13.5757(0)	13.6089(10)
c (Å)	29.659(3)	23.0080(15)	22.327(2)
β (°)	115.550(10)	112.845(5)	112.478(6)
Unit cell volume, V (Å^3)	9773.1(18)	6817.4(8)	6604.0(10)
Number of formula units, Z	8	4	4
Calculated density (g cm^{-3})	1.589	1.536	1.494
F(000)	4728	3208	3048
Absorption coefficient, μ (mm^{-1})	1.034	0.767	0.802
θ Range for data collection (°)	1.52–20.01	1.77–29.98	1.77–25.00
Index ranges	(−21, −13, −21) to (24, 0, 28)	(−1, −1, −31) to (28, 19, 30)	(−1, −1, −26) to (26, 16, 24)
Collected reflections	9092	8113	6743
Independent reflections	9092	6640 (R_{int}=0.0169)	5721 (R_{int}=0.0274))
Observed reflections, $I>2\sigma(I)$	5668	5272	4721
Absorption correction	semi-empirical from ψ scans	semi-empirical from ψ scans	none
Maximum and minimum transmission	0.6991 and 0.5426	0.7469 and 0.6404	
Weighting scheme	$w^{-1}=\sigma^2F_o^2+(0.085P)^2+140P$; $P=(F_o^2+2F_c^2)/3$	$w^{-1}=\sigma^2F_o^2+(0.07P)^2+18P$; $P=(F_o^2+2F_c^2)/3$	$w^{-1}=\sigma^2F_o^2+(0.08P)^2+16P$; $P=(F_o^2+2F_c^2)/3$
Data/restraints/parameters	9059/76/735	6637/0/470	5720/18/448
Goodness-of-fit on F^2	1.052	1.038	1.057
Final R indices [$I>2\sigma(I)$]	R_1=0.1003; wR_2=0.2180	R_1=0.0510; wR_2=0.1344	R_1=0.0496; wR_2=0.1402
R indices (all data)	R_1=0.1543; wR_2=0.2734	R_1=0.0669; wR_2=0.1483	R_1=0.0616; wR_2=0.1521
Largest difference peak and hole (e Å^{-3})	0.768 and −0.481	0.912 and −0.487	0.896 and −0.661

StyleTag -- Journal: **POLY** (*Polyhedron*) Article: **3430**

Table 2
Electrical conductivity results [a]

Compound	c_M (mol l^{-1})	Λ_M (Ω^{-1} cm^2 mol^{-1})	A_{found}	A_{calc} [b]
1	5.12×10^{-4}	276	681	674
2	5.25×10^{-4}	269	620	657
3	5.45×10^{-4}	290	791	674
4	5.98×10^{-4}	294	658	665

[a] A is the slope of the plot of $(\Lambda_o-\Lambda_e)$ versus $(c_e)^{1/2}$, where Λ_e is equivalent conductivity, Λ_o is limit equivalent conductivity and c_e is equivalent concentration.
[b] Calculated for the ionization: $[\{Cu(NN)\}_2\{\mu\text{-}[(NC_5H_4)_2C(OMe)\text{-}O]\}_2]X_2 \rightarrow [\{Cu(NN)\}_2\{\mu\text{-}[(NC_5H_4)_2C(OMe)O]\}_2]^{2+} + 2X^-$.

band of the non-coordinated ligand molecule is observed at the free ligand frequency, 1675 cm^{-1} [11]. For the initial dimers the ClO_4^- ν_3 band is observed as a broad band, with shoulders, characteristic of the coordinated ClO_4^-. In $[\{Cu(bipy)\}_2(\mu\text{-}OH)_2](ClO_4)_2\cdot H_2O$, two oxygen atoms of perchlorate groups are in the axial positions of the two copper atoms of the dimer, at 2.797 Å [22]. In compounds **2** and **4** the ClO_4^- ν_3 band is narrowed and the shoulders are not observed, as a consequence of the non-coordination [23].

3.3. Electronic spectra

The electronic spectra of the solutions in acetonitrile exhibit, besides the different ligands bands, the d–d band of Cu(II) at 640 nm ($\varepsilon_{max}=198$ l cm^{-1} mol^{-1}) for compound **1**, at 641 nm ($\varepsilon_{max}=197$ l cm^{-1} mol^{-1}) for compound **2**, at 671 nm ($\varepsilon_{max}=170$ l cm^{-1} mol^{-1}) for compound **3** and at 682 nm ($\varepsilon_{max}=146$ l cm^{-1} mol^{-1}) for compound **4**. In all cases a shoulder assigned to charge transfer transition is observed at 310–295 nm. In the diffuse reflectance spectra the d–d band is very broad.

3.4. Structural analysis

3.4.1. *[(Cubipy)$_2$\{μ-[py$_2$C(OCH$_3$)O]\}$_2$](PF$_6$)$_2$·1/2H$_2$O* (**1**)

Compound **1** consists of $[(Cubipy)_2\{\mu\text{-}[py_2C(OCH_3)\text{-}O]\}_2]^{2+}$ divalent cationic dimers and $(PF_6)^-$ anions. Two

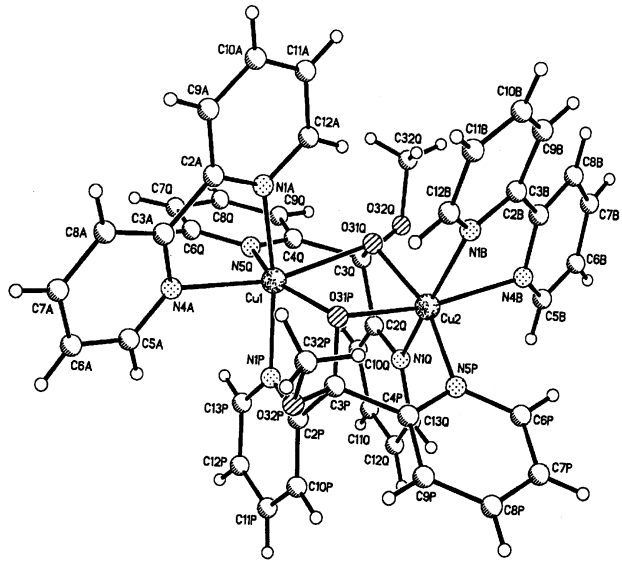


Fig. 1. Structure of the dimer Cu1–Cu2 in compound **1**.

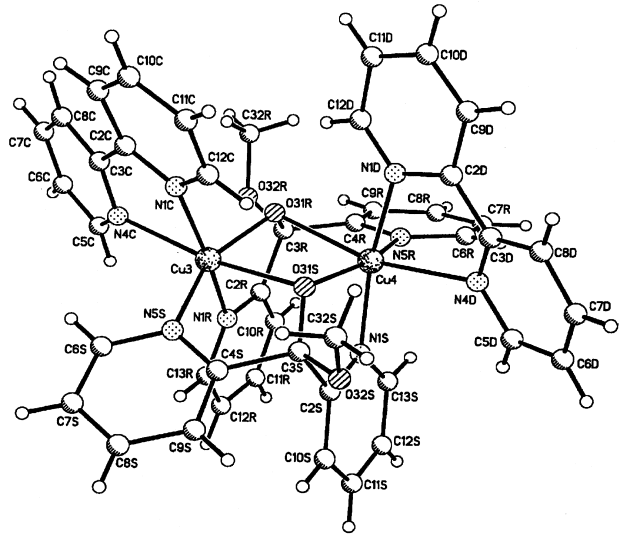


Fig. 2. Structure of the dimer Cu3–Cu4 in compound **1**.

chemically identical but crystallographically unequivalent dimeric units (Cu1–Cu2) (Fig. 1) and (Cu3–Cu4) (Fig. 2) are present in the asymmetric unit. Each dimer has approximately local C_2 symmetry, the corresponding twofold axis being roughly perpendicular to the average Cu_2O_2 plane.

Table 3
IR absorptions (cm^{-1})

Compound	PF_6^- $\nu_3(F_1)$	PF_6^- $\nu_4(F_{1u})$	ClO_4^- $\nu_3(F_2)$	ClO_4^- $\nu_4(F_2)$	ν(Cu−O)	ν(C=O)
$[\{Cu(bipy)\}_2(\mu\text{-}OH)_2](PF_6)_2\cdot2H_2O$	830	560			490	
$[\{Cu(bipy)\}_2(\mu\text{-}OH)_2](ClO_4)_2\cdot H_2O$			1100	623	490	
$[\{Cu(phen)\}_2(\mu\text{-}OH)_2](PF_6)_2\cdot2H_2O$	839	556			486	
$[\{Cu(phen)\}_2(\mu\text{-}OH)_2](ClO_4)_2\cdot H_2O$			1100	622	490	
$[\{Cu(bipy)\}_2\{\mu\text{-}[(py)_2C(OMe)O]\}_2](PF_6)_2\cdot1/2H_2O$ (**1**)	840	558			511	
$[\{Cu(bipy)\}_2\{\mu\text{-}[(py)_2C(OMe)O]\}_2](ClO_4)_2\cdot1/2H_2O$ (**2**)			1100	623	505	
$[\{Cu(phen)\}_2\{\mu\text{-}[(py)_2C(OMe)O]\}_2](PF_6)_2\cdot2[(py)_2CO]$ (**3**)	842	557			516	1667
$[\{Cu(phen)\}_2\{\mu\text{-}[(py)_2C(OMe)O]\}_2](ClO_4)_2\cdot2[(py)_2CO]$ (**4**)			1100	623	518	1674

Table 4
Selected interatomic distances (Å) and bond angles (°) for Cu1–Cu2 and Cu3–Cu4 dimers in compound **1**

Cu1–Cu2 dimer		Cu3–Cu4 dimer	
Cu(1)–Cu(2)	3.147(3)	Cu(3)–Cu(4)	3.145(3)
Cu(1)–N(1P)	2.042(12)	Cu(3)–N(1R)	2.059(12)
Cu(1)–O(31P)	1.934(09)	Cu(3)–O(31R)	1.923(10)
Cu(1)–N(5Q)	2.025(11)	Cu(3)–N(5S)	2.004(12)
Cu(1)–O(31Q)	2.429(10)	Cu(3)–O(31S)	2.405(09)
Cu(1)–N(1A)	2.057(13)	Cu(3)–N(1C)	2.026(13)
Cu(1)–N(4A)	2.298(12)	Cu(3)–N(4C)	2.300(13)
O(31P)–O(31Q)	2.898(14)	O(31R)–O(31S)	2.950(14)
Cu(2)–N(1Q)	2.037(12)	Cu(4)–N(1S)	2.035(12)
Cu(2)–O(31Q)	1.921(10)	Cu(4)–O(31S)	1.926(09)
Cu(2)–N(5P)	1.999(12)	Cu(4)–N(5R)	1.989(12)
Cu(2)–O(31P)	2.338(09)	Cu(4)–O(31R)	2.402(10)
Cu(2)–N(1B)	2.085(12)	Cu(4)–N(1D)	2.096(13)
Cu(2)–N(4B)	2.318(13)	Cu(4)–N(4D)	2.306(13)
O(31Q)–C(3Q)	1.36(2)	O(31S)–C(3S)	1.321(15)
O(32Q)–C(3Q)	1.46(2)	O(32S)–C(3S)	1.44(2)
O(31P)–C(3P)	1.38(2)	O(31R)–C(3R)	1.36(2)
O(32P)–C(3P)	1.42(2)	O(32R)–C(3R)	1.42(2)
O(32P)–C(32P)	1.42(2)	O(32S)–C(32S)	1.41(2)
O(32Q)–C(32Q)	1.43(2)	O(32R)–C(32R)	1.42(2)
N(1P)–Cu(1)–O(31P)	80.7(4)	N(1R)–Cu(3)–O(31R)	80.8(5)
N(1P)–Cu(1)–N(5Q)	96.9(5)	N(1R)–Cu(3)–N(5S)	93.7(5)
N(1P)–Cu(1)–O(31Q)	104.2(4)	N(1R)–Cu(3)–O(31S)	100.8(4)
N(1P)–Cu(1)–N(1A)	164.5(5)	N(1R)–Cu(3)–N(1C)	167.8(5)
N(1P)–Cu(1)–N(4A)	90.4(5)	N(1R)–Cu(3)–N(4C)	93.1(5)
O(31P)–Cu(1)–N(5Q)	153.4(4)	O(31R)–Cu(3)–N(5S)	156.0(5)
O(31P)–Cu(1)–O(31Q)	82.4(4)	O(31R)–Cu(3)–O(31S)	85.2(4)
O(31P)–Cu(1)–N(1A)	94.0(4)	O(31R)–Cu(3)–N(1C)	96.1(5)
O(31P)–Cu(1)–N(4A)	101.8(4)	O(31R)–Cu(3)–N(4C)	95.1(4)
N(5Q)–Cu(1)–O(31Q)	72.5(4)	N(5S)–Cu(3)–O(31S)	72.9(4)
N(5Q)–Cu(1)–N(1A)	94.3(5)	N(5S)–Cu(3)–N(1C)	93.7(5)
N(5Q)–Cu(1)–N(4A)	104.7(5)	N(5S)–Cu(3)–N(4C)	108.5(5)
N(1A)–Cu(1)–O(31Q)	89.4(4)	N(1C)–Cu(3)–O(31S)	90.6(4)
N(4A)–Cu(1)–O(31Q)	165.3(4)	N(4C)–Cu(3)–O(31S)	165.9(4)
N(1A)–Cu(1)–N(4A)	76.4(5)	N(1C)–Cu(3)–N(4C)	75.3(5)
N(1Q)–Cu(2)–O(31Q)	81.2(5)	N(1S)–Cu(4)–O(31S)	80.7(4)
N(1Q)–Cu(2)–N(5P)	94.9(5)	N(1S)–Cu(4)–N(5R)	94.4(5)
N(1Q)–Cu(2)–O(31P)	105.2(4)	N(1S)–Cu(4)–O(31R)	104.7(4)
N(1Q)–Cu(2)–N(1B)	162.8(5)	N(1S)–Cu(4)–N(1D)	163.4(5)
N(1Q)–Cu(2)–N(4B)	92.0(5)	N(1S)–Cu(4)–N(4D)	90.8(5)
O(31Q)–Cu(2)–N(5P)	159.7(5)	O(31S)–Cu(4)–N(5R)	157.3(5)
O(31Q)–Cu(2)–O(31P)	85.1(4)	O(31S)–Cu(4)–O(31R)	85.2(4)
O(31Q)–Cu(2)–N(1B)	90.9(4)	O(31S)–Cu(4)–N(1D)	92.2(5)
O(31Q)–Cu(2)–N(4B)	96.7(4)	O(31S)–Cu(4)–N(4D)	98.6(4)
N(5P)–Cu(2)–O(31P)	76.6(4)	N(5R)–Cu(4)–O(31R)	74.5(4)
N(5P)–Cu(2)–N(1B)	97.6(5)	N(5R)–Cu(4)–N(1D)	97.6(5)
N(5P)–Cu(2)–N(4B)	103.4(5)	N(5R)–Cu(4)–N(4D)	103.6(5)
N(1B)–Cu(2)–O(31P)	89.2(4)	N(1D)–Cu(4)–O(31R)	89.6(4)
N(4B)–Cu(2)–O(31P)	162.8(4)	N(4D)–Cu(4)–O(31R)	164.5(4)
N(1B)–Cu(2)–N(4B)	73.7(5)	N(1D)–Cu(4)–N(4D)	75.3(5)
Cu(1)–O(31Q)–Cu(2)	91.9(4)	Cu(3)–O(31S)–Cu(4)	92.5(4)
Cu(1)–O(31P)–Cu(2)	94.4(4)	Cu(3)–O(31R)–Cu(4)	92.6(4)
O(31P)–C(3P)–C(4P)	108.9(12)	O(31S)–C(3S)–C(4S)	109.4(11)
O(31P)–C(3P)–C(2P)	109.6(11)	O(31S)–C(3S)–C(2S)	112.7(12)
O(31P)–C(3P)–O(32P)	112.7(11)	O(31S)–C(3S)–O(32S)	116.0(12)
O(32P)–C(3P)–C(2P)	104.1(11)	O(32S)–C(3S)–C(2S)	101.5(11)
C(2P)–C(3P)–C(4P)	111.1(12)	C(2S)–C(3S)–C(4S)	109.2(12)
O(32P)–C(3P)–C(4P)	110.5(12)	O(32S)–C(3S)–C(4S)	107.7(11)
O(31Q)–C(3Q)–C(4Q)	107.5(12)	O(31R)–C(3R)–C(4R)	109.0(13)
O(32Q)–C(3Q)–C(4Q)	108.2(11)	O(32R)–C(3R)–C(4R)	107.4(12)
O(31Q)–C(3Q)–C(2Q)	113.7(12)	O(31R)–C(3R)–C(2R)	111.4(13)
O(32Q)–C(3Q)–C(2Q)	102.5(11)	O(32R)–C(3R)–C(2R)	103.6(12)
O(31Q)–C(3Q)–O(32Q)	114.4(12)	O(31R)–C(3R)–O(32R)	113.5(12)
C(2Q)–C(3Q)–C(4Q)	110.4(12)	C(2R)–C(3R)–C(4R)	111.8(13)

Selected interatomic distances and bond angles of the two crystallographically unequivalent dimeric units are collected in Table 4. Each of these dimers comprises two copper atoms bridged by two anions $py_2C(OCH_3)O^-$, where $py_2C(OCH_3)OH$ represents the methanolic hemiacetal of di(2-pyridyl)ketone. Each of the nitrogen atoms of this anion is bonded to one copper atom whereas the oxygen atom of the deprotonated hydroxyl group is simultaneously linked to both metal atoms, one of the corresponding Cu–O distances being much longer than the other. The coordination sphere of each copper atom is completed by a bipyridyl chelating molecule, with one Cu–N distance significantly longer than the other (see Table 4).

The geometry around each copper atom is distorted octahedral, with the longest Cu–O and Cu–N distances *trans* to each other: Cu(1)–O(31Q) and Cu(1)N(4A); Cu(2)–O(31P) and Cu(2)–N(4B); Cu(3)–O(31S) and Cu(3)–N(4C); Cu(4)–O(31R) and Cu(4)–N(4D). In the equatorial plane, the nitrogen and oxygen atoms of one $py_2C(OCH_3)O^-$ anion are placed *trans* of, respectively, the closest N atom of bipyridyl and the N atom of the other $py_2C(OCH_3)O^-$ anion. The Cu_2O_2 group is more symmetric in the Cu(3)–Cu(4) dimer than in the Cu(1)–Cu(2) dimer. The average angle Cu–O–Cu is 93.15° for Cu(1)–Cu(2) and 92.55° for Cu(3)–Cu(4). The average value of angle τ, formed by the O–O direction and the C(3)–O(3) bond, is 48.5° for Cu(1)–Cu(2) and 49.8° for Cu(3)–Cu(4). The angle γ (Fig. 3), indicating non-planarity of the Cu_2O_2 group, is 12.85° for Cu(1)–Cu(2) and 11.15° for Cu(3)–Cu(4).

Because of the addition of methanol to the py_2CO molecule, the central carbon of $py_2C(OCH_3)O^-$ is sp^3 (see angles on C(3P), C(3Q), C(3S) and C(3R) in Table 4) and this anion is no longer plane. Its two pyridine rings form an angle of 73.6–81.1° between them. The conformation around the C(3)–OCH_3 bond is with the methyl group *gauche* to the oxygen atom linked to the copper atoms, the torsion angle C(32)–O(32)–C(3)–O(31) ranging from 42.7 to 45.1°. The bond distances C(3)–O(31) and C(3)–O(32) correspond to the simple bond C–O length, being shorter than the distance with the oxygen atom of the methoxy group.

The asymmetric unit is completed by two half-occupancy water molecules and four PF_6^- anions, three of which have been found to be disordered into two positions.

3.4.2. [(Cuphen)$_2${μ-[py$_2$C(OCH$_3$)O]}$_2$](PF$_6$)$_2$·2[py$_2$CO] (3) and [(Cuphen)$_2${μ-[py$_2$C(OCH$_3$)O]}$_2$](ClO$_4$)$_2$·2[py$_2$CO] (4)

Compounds **3** and **4** consist of $[(Cuphen)_2\{\mu\text{-}[py_2C(OCH_3)O]\}_2]^{2+}$ divalent cationic dimers, $2PF_6^-$ or $2ClO_4^-$ anions and two free molecules of py_2CO per dimer. All dimers are crystallographically equivalent. A crystallographic twofold axis relates the two halves of the cation. The coordination mode and the conformation of the $py_2COCH_3O^-$ ligand is similar to that found in compound **1**. The asymmetric unit is formed by half a dimer, an anion

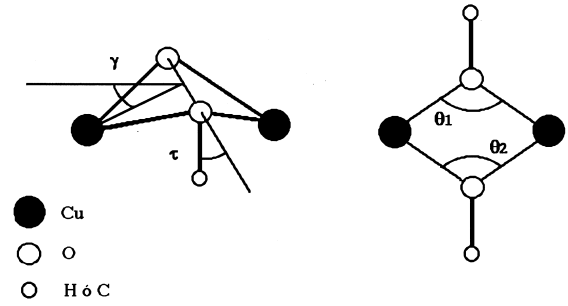


Fig. 3. θ, τ and γ angles in Cu_2O_2 group.

and a free ligand molecule (Fig. 4). Fig. 5 represents the structure of the complete dimer.

The more significant interatomic distances and angles are summarized in Table 5. As in compound **1**, each dimer comprises two copper atoms bridged by two anions

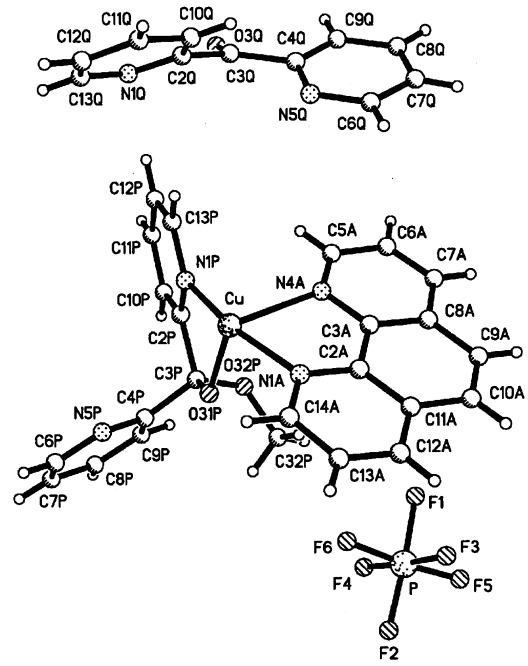


Fig. 4. Asymmetric unit of compound **3**.

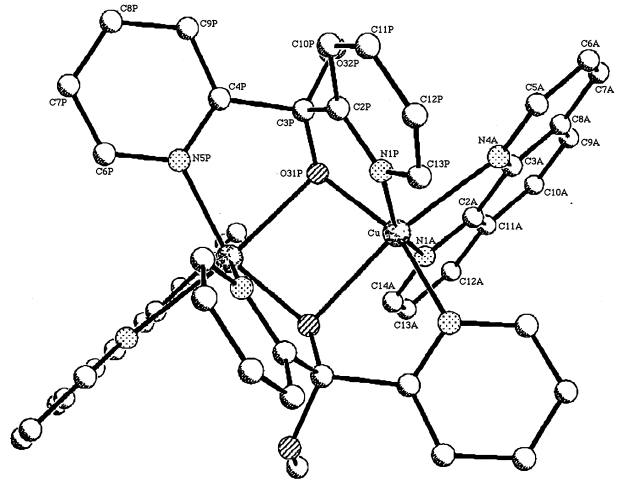


Fig. 5. Complete dimer in compound **3** or **4**.

Table 5
Selected interatomic distances (Å) and bond angles (°) for compounds **3** and **4** [a]

	Compound **3**	Compound **4**
Cu–O(31P)	1.923(2)	1.921(2)
Cu–N(5P′)	2.016(3)	2.015(3)
Cu–N(1P)	2.059(3)	2.068(3)
Cu–N(1A)	2.073(3)	2.084(3)
Cu–O(31P′)	2.359(2)	2.338(2)
Cu–N(4A)	2.375(3)	2.374(3)
Cu–Cu′	3.1046(6)	3.0901(7)
O(31P)–O(31P′)	2.861(3)	2.841(4)
O(31P)–C(3P)	1.353(4)	1.355(4)
C(3P)–O(32P)	1.433(3)	1.432(4)
O(32P)–C(32P)	1.419(4)	1.426(5)
C(2Q)–C(3Q)	1.503(5)	1.504(6)
C(3Q)–O(3Q)	1.216(5)	1.217(5)
C(3Q)–C(4Q)	1.508(6)	1.497(6)
O(31P)–Cu–N(1P)	80.88(10)	80.65(10)
N(5P′)–Cu–N(1P)	98.20(11)	98.54(11)
O(31P)–Cu–N(1A)	93.60(10)	92.63(11)
N(5P′)–Cu–N(1A)	94.02(11)	94.77(12)
N(1P)–Cu–N(1A)	160.37(10)	160.01(11)
O(31P)–Cu–O(31P′)	83.18(8)	83.07(9)
N(5P′)–Cu–O(31P′)	75.73(9)	75.92(10)
N(1P)–Cu–O(31P′)	108.66(9)	109.07(10)
N(1A)–Cu–O(31P′)	89.18(9)	89.57(10)
O(31P)–Cu–N(4A)	101.91(10)	101.83(11)
N(5P′)–Cu–N(4A)	100.56(11)	100.61(12)
N(1P)–Cu–N(4A)	87.43(10)	87.82(11)
N(1A)–Cu–N(4A)	75.23(10)	75.08(11)
O(31P′)–Cu–N(4A)	163.79(9)	163.04(10)
Cu–O(31P)–Cu′	92.39(8)	92.53(9)
O(31P)–C(3P)–O(32P)	113.8(2)	113.8(3)
O(31P)–C(3P)–C(2P)	111.6(3)	111.6(3)
O(32P)–C(3P)–C(2P)	103.3(2)	103.5(3)
O(31P)–C(3P)–C(4P)	109.7(2)	109.5(3)
O(32P)–C(3P)–C(4P)	109.0(3)	109.1(3)
C(2P)–C(3P)–C(4P)	109.2(2)	109.2(3)
O(3Q)–C(3Q)–C(2Q)	120.3(4)	120.4(4)
O(3Q)–C(3Q)–C(4Q))	119.4(4)	118.7(4)
C(2Q)–C(3Q)–C(4Q)	120.3(3)	120.8(4)

[a] Symmetry transformation used to generate equivalent atoms: $-x$, y, $-z+1/2$.

$py_2C(OCH_3)O^-$, coordinated as N,O,N-donor, $\eta^1{:}\eta^2{:}\eta^1{:}\mu_2$ ligand. Each of the nitrogen atoms of this anion is bonded to one copper atom, whereas the oxygen atom of the deprotonated hydroxyl group is simultaneously linked to both metal atoms, one of the corresponding Cu–O distances being much longer [Cu–O(31P′)] than the other [Cu–O(31P)]. The coordination sphere of each copper atom is completed by a phenanthroline chelating molecule, with one Cu–N distance significantly longer [Cu–N(4A)] than the other [Cu–N(1A)].

The Cu–O(31P)–Cu′ angles are very similar to those of compound **1**. The values of τ and γ (Fig. 3) are 43.6° and 15.4° for compound **3** and 42.8° and 15.3° for compound **4**, respectively. The non-coordinated interstitial py_2CO molecules are not planar, the angle formed by the two planar py groups being 46.6(3)° and 43.5(4)° for compounds **3** and **4**, respectively. The C(3Q)–O(3Q) bond distances agree with the double bond character, whereas C(2Q)–C(3Q), C(3Q)–C(4Q), O(31P)–C(3P), C(3P)–O(32P) and O(32P)–C(32P) bond distances correspond basically to simple bond lengths.

3.5. Magnetic results

Magnetic susceptibilities have been measured in the 4.3–292 K temperature range. The variation of the corrected molar magnetic susceptibility per Cu(II) atom, χ_M, and $\chi_M T$ versus temperature is similar for the four complexes and characteristic of a ferromagnetic intradimeric interaction. The corresponding plots for compound **3** are shown in Fig. 6. The $\chi_M T$ value is aproximately constant (0.450 $cm^3\,K\,mol^{-1}$; $\mu = 1.90$ μ_B) in the range 290–60 K. Below this temperature $\chi_M T$ increases until 0.569 cm^3 K mol^{-1} ($\mu = 2.14$ μ_B) at 4.7 K. The μ values at room and low temperature for compounds **1**–**4** are collected in Table 6.

The susceptibility data were fitted to the Bleaney–Bowers equation modified by the inclusion of the fraction of monomeric impurity [24]:

$$\chi_M = [C e^x (1-\rho)/(1+3e^x)] + C\rho/4 + N\alpha$$

where $C = Ng^2\beta^2/kT$, $x = 2J/kT$, ρ is the fraction of monomeric impurity, $N\alpha = 60\times10^{-6}$ cm^3 mol^{-1}. EPR g values were applied. The results of the best fit, shown as the solid line in Fig. 6, are collected in Table 6.

The correlation deduced by Hatfield and co-workers [1] between $2J$ and θ (bridging angle Cu–O–Cu) for di-μ-hydroxo planar copper dimers [$2J$ (cm^{-1}) $= -74.53\theta + 7270$] gives the 97.5° value as the limit between ferro- ($\theta < 97.5°$) and antiferromagnetic ($\theta > 97.5°$) character.

Ruiz et al. [2,3] studied the effect of other structural parameters for copper dimers with hydroxo and alkoxo bridges. These are, besides θ, the angle τ, formed between the O–O direction and the bond between the bridging oxygen atom and the hydrogen (carbon) atom, and the non-planarity of the Cu_2O_2 group, measured by γ (Fig. 3). High τ values are associated with lower values of θ and correspond to $2J$ more positive (ferromagnetism). For $\theta < 97.5°$ and $\tau > 40°$ a fer-

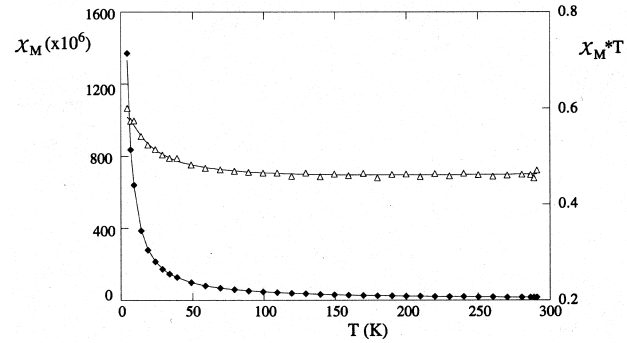


Fig. 6. Plot of of χ_M (♦) and $\chi_M T$ (△) vs. T for [{Cu(phen)}$_2${μ-[$(NC_5H_4)_2C(OMe)O$]}$_2$]$(PF_6)_2\cdot 2[(NC_5H_4)_2CO]$ (**3**).

Table 6
Magnetic results and significant structural data for compounds **1**–**4**

	1	**2**	**3**	**4**
μ (μ_B)	1.94 (290 K)	1.93 (292 K)	1.94 (291 K)	1.941 (291 K)
μ (μ_B)	2.14 (4.7 K)	2.13 (4.4 K)	2.19 (4.4 K)	2.18 (4.3 K)
g (from EPR)	2.135	2.140	2.151	2.144
$2J$ (cm^{-1})	10.0	10.1	16.7	15.8
$\rho\times10^2$ (%)	1.3	0.8	0.7	0.3
R [a]	6.80×10^{-5}	9.97×10^{-4}	1.41×10^{-5}	1.27×10^{-4}
θ (°)	92.8		92.4	92.5
τ (°)	49.1		43.6	42.8
γ (°)	12.0		15.4	15.3

[a] $R=\Sigma[(\chi_{Mi}T_i)_{exp}-(\chi_{Mi}T_i)_{calc}]^2/\Sigma[(\chi_{Mi}T_i)_{exp}]^2$.

romagnetic effect is to be expected. The non-planarity of the Cu_2O_2 group (γ) reduces the antiferromagnetic character and enhances the influence of τ.

For compounds **1**, **3** and **4**, $\theta<97.5°$ and $\tau>40°$. For compound **2** a structure similar to compound **1** may be assumed. These structural data may justify the ferromagnetic behaviour with $2J=10.0$, 10.1, 16.7 and 15.8 cm^{-1} for compounds **1**, **2**, **3** and **4**, respectively. The τ angle for the phen complexes (**3** and **4**) is lower than for the bipy complex (**1**). This fact should correspond to a more strong ferromagnetic interaction ($2J$ higher) in compounds **1** and **2** than in compounds **3** and **4**, but, at the same time, the γ angle (non-planarity of Cu_2O_2) is lower in compound **1** than in compounds **3** and **4**. According to Ruiz et al. the non-planarity of the Cu_2O_2 group enhances the ferromagnetic influence of τ, so the increase of the ferromagnetic effect in the phen complexes may be due to the stronger deviation of the planarity in the Cu_2O_2 group. All these results confirm the relation between the structural factors of the Cu_2O_2 group and the magnetic intradimer interaction.

3.6. EPR spectra

EPR spectra in the Q band at 100 K for powder samples have been recorded. In all cases the typical spectrum of the triplet state ($S=1$) for the ferromagnetic coupling in the dimer is observed. Furthermore, the six allowed $\Delta M=\pm1$ transitions, the forbidden $\Delta M=\pm2$ ($M=+1$ to $M=-1$) transition is resolved. The mononuclear impurity signal appears in the g_x zone. In Fig. 7 the spectra of compound **3** is shown.

The spectra were interpreted according to the Wasserman, Snyder and Yager equations [25,26], based on the hamiltonian: $H=gHS\beta+D[S_z^2-2/3]+E[S_x^2-S_y^2]$, with $D\neq0$ and $E\neq0$:

$$H_{x1}=(g_e/g_x)[(H_o-D'+E')(H_o+2E')]^{1/2}$$

$$H_{x2}=(g_e/g_x)[(H_o+D'-E')(H_o-2E')]^{1/2}$$

$$H_{y1}=(g_e/g_y)[(H_o-D'-E')(H_o-2E')]^{1/2}$$

$$H_{y2}=(g_e/g_y)[(H_o+D'+E')(H_o+2E')]^{1/2}$$

$$H_{z1}=(g_e/g_z)[(H_o-D')^2-E'^2]^{1/2}$$

$$H_{z2}=(g_e/g_z)[(H_o+D')^2-E'^2]^{1/2}$$

$$H_{min}=(g_e/g_{min})[(H_o^2/4)-(D'^2/3)+E'^2]^{1/2}$$

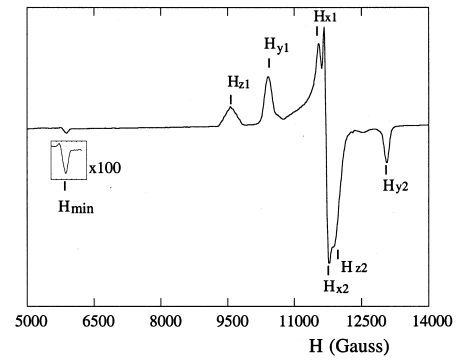


Fig. 7. EPR Q band spectra of powdered $[\{Cu(phen)\}_2\{\mu\text{-}[(NC_5H_4)_2C(OMe)O]\}_2](PF_6)_2\cdot2[(NC_5H_4)_2CO]$ (**3**), at 100 K.

Table 7
EPR results from Q band powder spectra at 100 K for compounds **1**–**4**

	1	**2**	**3**	**4**
$h\nu$ (cm^{-1})	1.129	1.135	1.131	1.135
H_{min} (G)	5740	5797	5797	5797
H_{z1} (G)	9634	9610	9562	9610
H_{y1} (G)	10409	10256	10407	10563
H_{x1} (G)	11634	11683	11536	11536
H_{x2} (G)	11634	11683	11969	11646
H_{z2} (G)	11945	12049	11864	
H_{y2} (G)	12819	12900	13056	13017
g_x	2.075	2.075	2.087	2.093
g_y	2.082	2.099	2.071	2.061
g_z	2.249	2.247	2.294	2.278
$g_{av}=1/3(g_x+g_y+g_z)$	2.135	2.140	2.151	2.144
$\lvert D\rvert$ (cm^{-1})	0.117	0.129	0.135	0.123
$\lvert E\rvert$ (cm^{-1})	0.039	0.043	0.040	0.035

$D' = D/g_e\beta$

$E' = E/g_e\beta$

The signal assignment, g values and the zero field splitting parameters resulting from the Wasserman et al. equations application are collected in Table 7.

For compounds **1** and **2**, $D = 3E$ and $H_{x1} = H_{x2}$. In compound **4**, H_{z2} and H_{x2} are not differentiated.

Supplementary data

Further structural data can be obtained on request from the Cambridge Crystallographic Data Centre, 12 Union Road, Cambridge CB2 1EZ, UK (fax: +44-1223-336033; e-mail: deposit@ccdc.cam.ac.uk). Deposition codes: 132658 for compound **1**, 132659 for compound **3** and 132660 for compound **4**.

Acknowledgements

This work was supported by the Diputación Foral de Gipuzkoa and the Universidad del País Vasco, UPV/EHU (Grant UPV 221.215-EA 077/96).

References

[1] V.H. Crawford, H.W. Richardson, J.R. Wasson, D.J. Hodgson, W.E. Hatfield, Inorg. Chem. 15 (1976) 2107.
[2] E. Ruiz, P. Alemany, S. Alvarez, J. Cano, Inorg. Chem. 36 (1997) 3683.
[3] E. Ruiz, P. Alemany, S. Alvarez, J. Cano, J. Am. Chem. Soc. 119 (1997) 1297.
[4] J.M. Seco, U. Amador, M.J. González Garmendia, Polyhedron 18 (1999) 3605.
[5] J.M. Seco, U. Amador, M.J. González Garmendia, Inorg. Chim. Acta 303 (2000) 257.
[6] M.F. El-Shazly, Inorg. Chim. Acta 26 (1978) 173.
[7] R.E. Dessy, J.C. Charkoudian, A. Rheingold, J. Am. Chem. Soc. 94 (1972) 738.
[8] V. Rattanaphani, W.R. McWhinnie, Inorg. Chim. Acta 9 (1974) 239.
[9] T.I.A. Gerber, H.J. Kemp, J. Du Preez, G. Bandoli, J. Coord. Chem. 28 (1993) 329.
[10] S.O. Sommerer, J.D. Baker, W.P. Jensen, A. Hamza, R.A. Jacobson, Inorg. Chim. Acta 210 (1993) 173.
[11] G. Bandoli, A. Dolmella, T.I.A. Gerber, J.G.H. du Preez, H.J. Kemp, Inorg. Chim. Acta 217 (1994) 141.
[12] A.C. Deveson, S.L. Heath, C.J. Harding, A.K. Powell, J. Chem. Soc., Dalton Trans. (1996) 3173.
[13] A.N. Papadopoulos, V. Tangoulis, C.P. Raptopoulou, A. Terzis, D.P. Kessissoglou, Inorg. Chem. 35 (1996) 559.
[14] V. Tangoulis, C.P. Raptopoulou, S. Paschalidou, A.E. Tsohos, E.G. Bakalbassis, A. Terzis, S.P. Perlepes, E.G. Bakalbassis, Inorg. Chem. 36 (1997) 5270.
[15] S.R. Breeze, S. Wang, J.E. Greedan, N.P. Raju, Inorg. Chem. 35 (1996) 6944.
[16] V. Tangoulis, S. Paschalidou, E.G. Bakalbassis, S.P. Perlepes, C.P. Raptopoulou, A. Terzis, Chem. Commun. (1996) 1297.
[17] C.M. Harris, E. Sinn, W.R. Walker, P.R. Woollians, Aust. J. Chem. 21 (1968) 631.
[18] International Tables for Crystallography, Vol. C, Kluwer, Dordrecht, 1992.
[19] G.M. Sheldrick, SHELXTL Version 5 for PC, Siemens Analytical X-ray Instruments, Inc, Madison, WI, 1994.
[20] W.J. Geary, Coord. Chem. Rev. 7 (1971) 81.
[21] R.K. Boggess, D.A. Zatko, J. Chem. Ed. 52 (1975) 649.
[22] M. Toofan, A. Boushehri, Mazhar-UI-Haque, J. Chem. Soc., Dalton Trans. (1976) 217.
[23] K. Nakamoto, Infrared and Raman Spectra of Inorganic and Coordination Compounds, 4th edn., Wiley-Interscience, New York, 1986.
[24] M. Nakashima, M. Mikuriya, Y. Muto, Bull. Chem. Soc. Jpn. 58 (1985) 968.
[25] E. Wasserman, L.C. Snyder, W.A. Yager, J. Chem. Phys. 41 (1964) 1763.
[26] A. Bencini, D. Gatteschi, EPR of Exchange Coupled Systems, Springer, 1990.

PERGAMON

www.elsevier.nl/locate/poly

Polyhedron 19 (2000) 1015–1020

POLYHEDRON

Cis–trans isomerism in nickel(II)–diamine nitrite: synthesis and single crystal structure of an unusual *cis*-dinitronickel(II) complex, $[NiL_2(NO_2)_2]$ (L = 1,2-diamino-2-methylpropane)

Inamur Rahaman Laskar [a], Ashutosh Ghosh [b], Golam Mostafa [c], Debasis Das [a], Arunendu Mondal [a], Nirmalendu Ray Chaudhuri [a,*]

[a] *Department of Inorganic Chemistry, Indian Association for the Cultivation of Science, Calcutta-700 032, India*
[b] *Department of Chemistry, University College of Science and Technology, 92 A.P.C. Road, Calcutta-700 009, India*
[c] *Krishnath College, Berhampur 742 109, India*

Received 7 September 1999; accepted 10 March 2000

Abstract

The complexes $[NiL_3](NO_2)_2 \cdot 2H_2O$ (violet, **1**) and *cis*-$[NiL_2(NO_2)_2] \cdot 0.5H_2O$ (pink, **1b**) (L = 1,2-diamino-2-methylpropane) have been synthesized from solution. The X-ray single crystal structure analysis of compound **1b** has been carried out, but the presence of a water molecule cannot be detected. Upon heating, complex **1b** undergoes dehydration followed by an endothermic phase transition to produce *trans*-$[NiL_2(NO_2)_2]$ (**1d**). The violet species (**1**) also undergoes dehydration upon heating with deamination resulting (**1d**). ©2000 Elsevier Science Ltd All rights reserved.

Keywords: *Cis–trans* isomerism; Crystal structures; 1,2-Diamino-2-methylpropane; Nickel(II) nitrite

1. Introduction

It is well known that the coordination mode of the nitrite ion, an ambidentate ligand, is influenced by the steric nature of neighbouring ligands [1–6]. This is best compared in the series of complexes of general formula Ni(diamine)$_2$-$(NO_2)_2$, formed mostly by N-substituted ethane-1,2-diamine, and it is apparent that there is a general trend for the nitrite to coordinate via nitrogen when little inter-ligand steric crowding is expected, but via oxygen when the ligands carry bulky substituents [1,7,8]. In all the cases, however, it is found that *trans*-octahedral geometry is preferred for the monodentate mode of coordination of the nitrite ion. On the contrary, reports regarding the influence of C-substituted ethane-1,2-diamine in which the substituted groups are somewhat apart from the donor nitrogen atom is scanty, although it has been found that they have considerable influence on the geometry around nickel(II) with several other counter-anions [9,10]. We report here the syntheses and characterization of $[NiL_3](NO_2)_2 \cdot 2H_2O$, *cis*- and *trans*-$[NiL_2(NO_2)_2]$ (L = 1,2-diamino-2-methylpropane) and the single crystal structure analysis of *cis*-$[NiL_2(NO_2)_2]$.

2. Experimental

2.1. Materials

1,2-Diamino-2-methylpropane (L) was purchased from Aldrich Chemical Company and used as received. Potassium hexanitronickelate(II) monohydrate was prepared using a standard method [11].

2.2. Physical measurements

Elemental analyses (carbon, hydrogen and nitrogen) were performed using a Perkin-Elmer 240C elemental analyser; nickel(II) content was estimated gravimetrically [12]. IR spectrum (4000–400 cm^{-1}) was taken at 27°C using a Perkin-Elmer IR 783 where KBr was used as medium. Electronic spectrum (1400–200 nm) was obtained at 27°C using an Hitachi UV–Vis–near-IR model U-3410 where Nujol was used as a medium as well as a reference. The magnetic susceptibility was measured at 27°C using an EG and G PAR

* Corresponding author. Tel.: +91-33-4734971; fax: +91-33-4732805; e-mail: icnrc@mahendra.iacs.res.in

0277-5387/00/$ - see front matter ©2000 Elsevier Science Ltd All rights reserved.
PII S0277-5387(00)00365-X

155 vibrating sample magnetometer, where [$HgCo(SCN)_4$] was used as a reference material; diamagnetic corrections were made using Pascal's constants.

2.3. Synthesis of the complexes

[NiL_3]$(NO_2)_2 \cdot 2H_2O$ (**1**) was synthesized by adding the diamine (3 mmol) in ethanol (5 cm^3) to an ethanolic suspension (10 cm^3) of potassium hexanitronickelate(II) monohydrate (1 mmol). The resulting deep-blue solution was kept in a $CaCl_2$ desiccator. After a few days, violet crystals separated out; these were filtered off, washed with ethanol and dried in the open air. Yield, 80%. Found: C, 31.8; H, 8.9; N, 24.8; Ni, 13.0%. $\mu_{eff} = 2.95\mu_M$. λ_{max} (Nujol) = 815, 525 nm. Calc. for $C_{12}H_{40}N_8O_6Ni$: C, 31.9; H, 8.9; N, 24.9; Ni, 13.0%.

cis-[$NiL_2(NO_2)_2$]$\cdot 0.5H_2O$[a] (**1b**) was synthesized in a similar way as (**1**) except that the amount of diamine (2 mmol) was different. After a few days, pink crystals separated out; these were filtered off, washed with ethanol and dried in a $CaCl_2$ desiccator. [When the compound is dried in air, a water molecule is found to be present, but on drying in a $CaCl_2$ desiccator the compound becomes *cis*-[$NiL_2(NO_2)_2$], (**1c**)]. Yield, 82%. Found: C, 29.2; H, 7.2; N, 25.7; Ni, 17.9%. $\mu_{eff} = 2.96\mu_M$. λ_{max} (Nujol) = 1148 and 718 nm. Calc. for $C_8H_{24}N_6O_4Ni$: C, 29.4; H, 7.3; N, 25.7; Ni, 18.0%.

trans-[$NiL_2(NO_2)_2$] (**1d**) was prepared pyrolytically in the solid state from compound **1** as well as from compound (**1b**). Found: C, 29.2; H, 7.3; N, 25.6; Ni, 18.0%. $\mu_{eff} = 2.99\mu_M$. λ_{max} (Nujol) = 1312, 1155 and 666 nm. Calc. for $C_8H_{24}N_6O_4Ni$: C, 29.4; H, 7.3; N, 25.7; Ni, 18.0%.

2.4. X-ray data collection and structure determination

A suitable single crystal of the title complex was mounted on a CAD4 Enraf-Nonius diffractometer. The unit cell parameters and crystal orientation matrix were determined by least-squares refinements of 25 accurately centred reflections. Intensity data were collected in the ω–2θ scan mode using graphite monochromated Mo Kα radiation. The crystal and instrument stabilities were monitored with a set of three standard reflections measured at a regular interval; in all cases no significant variations were found. The intensity data were corrected for Lorentz and polarization effects [13], and spherical absorption corrections were made. The systematic

Table 1
Crystal data and structure refinement for compounds **1c** and **1d**

	1c	**1d**
Empirical formula	$C_8H_{24}N_6NiO_4$	$C_8H_{24}N_6NiO_4$
Formula weight	327.04	327.04
Temperature (K)	293(2)	293(2)
Wavelength (Å)	0.71069	1.5406
Crystal system	monoclinic	monoclinic
Space group	*C*2	*C*2
a (Å)	11.506(10)	13.912(8)
b (Å)	6.636(3)	8.666(8)
c (Å)	20.227(10)	13.576(7)
β (°)°	101.24(7)	109.7(6)
V (Å^3)	1514.8(17)	1540.5(9)
Z	4	
D_{calc} (Mg m^{-3})	1.434	
Absorption coefficient (mm^{-1})	1.300	
F(000)	696	
Crystal size (mm)	0.36×0.32×0.29	powder
θ Range for data collection (°)	2.05–24.97	
Index ranges	$0 \le h \le 13$; $0 \le k \le 7$; $-24 \le l \le 23$	
Reflections collected	1454	
Independent reflections	1454 [$R_{int} = 0.0000$]	
Reflections observed ($>2\sigma$)	1248	
Refinement method	full-matrix least-squares on F^2	
Data/restraints/parameters	1454/0/171	
Goodness-of-fit on F^2	1.064	
Final *R* indices [$I>2\sigma(I)$], *S* [a]	R_1 [b] = 0.0647, wR_2 [c] = 0.1658	
R indices (all data)	$R_1 = 0.0784$, $wR_2 = 0.1745$	
Δ (σ)	0.010	
Absolute structure parameter	−0.01(7)	
Largest difference peak and hole (e Å^{-3})	1.059 and −1.214	

[a] $S = [\sum\{w(F_o^2 - F_c^2)^2\}/(N-P)]^{1/2}$ where *N* is the number of data and *P* is the total number of parameters refined.
[b] $R_1 = \sum(^0F_o - F_c^0)/\sum F_o$.
[c] $wR_2 = [\sum\{w(F_o^2 - F_c^2)^2\}/\sum\{w(F_o^2)^2\}]^{1/2}$.

absences show the space groups *C*2, *C* or *C*2/*m*. Of the three possible space groups *C*2 was confirmed by a successful structure refinement. A three-dimensional Patterson synthesis using SHELX-86 [14] showed the positions of the nickel(II) atoms at two special positions of (0, 0, 0) and (1/2, 0, 1/2). The remaining N, C and O atoms were located from the successive Fourier and difference Fourier syntheses. Full-matrix least-squares refinements on F^2 were carried out using SHELXL-93 [15] with anisotropic displacement parameters for all non-hydrogen atoms. Hydrogen atoms were constrained to ride on the respective carbon or nitrogen atoms (C–H, 0.97 Å; N–H, 0.900 Å) with an isotropic displacement parameter equal to 1.2 times the equivalent isotropic displacement parameter of the parent atom. Complex neutral atom scattering factors [16] were used throughout. All calculations were carried out using SHELXS-86, SHELXL-93, PARST [17] and ZORTEP [18] programs. Crystal data are summarized in Table 1. Selected bond lengths and bond angles are listed in Table 2.

Table 2
Selected bond lengths (Å) and bond angles (°) of compound **1c**

NiA–N(2A)	2.082(7)
NiA–N(2A) [a]	2.082(7)
NiA–N(3A) [a]	2.133(10)
NiA–N(3A)	2.133(10)
NiA–N(1A)	2.153(11)
NiA–N(1A) [a]	2.153(11)
NiB–N(2B) [b]	2.070(8)
NiB–N(2B)	2.070(8)
NiB–N(1B) [b]	2.124(11)
NiB–N(1B)	2.124(11)
NiB–N(3B) [b]	2.147(10)
NiB–N(3B)	2.147(10)
N(2A)–NiA–N(2A) [a]	177.3(7)
N(2A)–NiA–N(3A) [a]	92.6(4)
N(2A) [a]–NiA–N(3A) [a]	89.4(4)
N(2A)–NiA–N(3A)	89.4(4)
N(2A) [a]–NiA–N(3A)	92.6(4)
N(3A) [a]–NiA–N(3A)	83.0(5)
N(2A)–NiA–N(1A)	80.1(4)
N(2A) [a]–NiA–N(1A)	98.1(4)
N(3A) [a]–NiA–N(1A)	169.9(4)
N(3A)–NiA–N(1A)	90.0(3)
N(2A)–NiA–N(1A) [a]	98.1(4)
N(2A) [a]–NiA–N(1A) [a]	80.1(4)
N(3A) [a]–NiA–N(1A) [a]	90.0(3)
N(3A)–NiA–N(1A) [a]	169.9(4)
N(1A)–NiA–N(1A) [a]	97.8(6)
N(2B) [b]–NiB–N(2B)	179.3(7)
N(2B) [b]–NiB–N(1B) [b]	81.0(4)
N(2B)–NiB–N(1B) [b]	98.5(4)
N(2B) [b]–NiB–N(1B)	98.5(4)
N(2B)–NiB–N(1B)	81.0(4)
N(1B) [b]–NiB–N(1B)	99.8(7)
N(2B) [b]–NiB–N(3B) [b]	88.3(4)
N(2B)–NiB–N(3B) [b]	92.3(4)
N(1B) [b]–NiB–N(3B) [b]	89.4(4)
N(1B)–NiB–N(3B) [b]	169.3(5)
N(2B) [b]–NiB–N(3B)	92.3(4)
N(2B)–NiB–N(3B)	88.3(4)
N(1B) [b]–NiB–N(3B)	169.3(5)
N(1B)–NiB–N(3B)	89.4(4)
N(3B) [b]–NiB–N(3B)	82.0(5)

[a] Symmetry transformations used to generate equivalent atoms: $-x, y, -z$.
[b] Symmetry transformations used to generate equivalent atoms: $x+1, y, z+1$.

3. Results and discussion

The composition of the complexes $NiL_3(NO_2)_2\cdot 2H_2O$ (**1**) and $NiL_2(NO_2)_2\cdot 0.5H_2O$ (**1b**) has been confirmed by elemental analyses. Both compounds **1** and **1b** possess octahedral geometry as is evident from their magnetic and electronic spectral data. In complex **1**, the IR bands due to ν_{as}, ν_s and δ of the nitrite group appear at 1329, 1264 and 827 cm^{-1}, respectively, suggesting non-coordination of the anion [19,20]. However, in compound **1b**, the above bands are observed at 1338, 1315 and 810 cm^{-1}, respectively. Shifting of both ν_{as} and ν_s to higher frequencies compared with the free nitrite ion indicates that the nitrite ion is coordinated via the N atom [7,8]. It is interesting to note that no band corresponding to a water molecule is observed in the IR spectrum of (**1b**). The X-ray single crystal analysis of compound **1b** (it also becomes dehydrated during data collection; the dehydrated species is numbered as **1c**) shows that the diamine is chelated and its IR bands for the diamines are very similar to those of complex **1**, suggesting that the diamines are also chelated in compound **1**. Electronic spectrum in the near-IR region of compound **1b** shows no splitting in the d–d band (1148 nm), indicating *cis* configuration [21,22] (Fig. 1).

Upon heating, complex **1** loses two molecules of water and transforms to compound **1a**, which on further heating yields $NiL_2(NO_2)_2$ (**1d**). On the other hand, *cis*-$NiL_2(NO_2)_2\cdot 0.5H_2O$ (**1b**) upon heating becomes dehydrated, as is evident from thermal gravimetric–differential thermal analysis (TG–

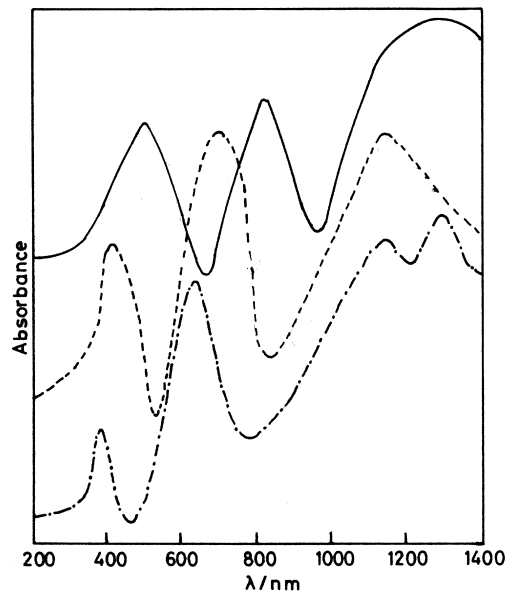


Fig. 1. Electronic spectra (Nujol) of (from top to bottom): $[NiL_3](NO_2)_2\cdot 2H_2O$ (**1**); *cis*-$[NiL_2(NO_2)_2]\cdot 0.5H_2O$ (**1b**); *trans*-$[NiL_2(NO_2)_2]$ (**1d**).

DTA) (Fig. 2), and then undergoes an irreversible endothermic phase transition ($\Delta H = 4.98$ kJ mol^{-1}) without showing any mass loss or visual colour change. The weight loss observed in the TGA curves for compounds **1** and **1b** [Found: 7.8 and 2.6%; Calc.: 8.0 and 2.7%, for compounds **1** and **1b**, respectively] corresponds to 2 and 0.5 moles of water, respectively. The species obtained from compounds **1** (after deaquation followed by deamination) and **1b** (after phase transition) are the same as they have identical X-ray diffraction powder pattern, IR and electronic spectra. The thermal reactions are summarized in Scheme 1.

Species **1d** is metastable and reverts slowly to compound **1b** as is evident from the X-ray powder diffraction pattern. It is found that the peaks characteristic of compound **1b** can be detected only after about 24 h of the isolation of compound **1d**. Gradually these peaks become dominant in the pattern and after about 10 days all the characteristic peaks of compound **1d** vanish completely. Thus it may be inferred that the metastable species **1d** remains pure for 24 h (without a detectable amount of compound **1b**) and completely transforms to compound **1b** in 10 days.

A ZORTEP view of compound **1c**, with atom numbering scheme, is shown in Fig. 3. With the metal atoms (NiA and NiB) lying at two special positions (0, 0, 0; 1/2, 0, 1/2), the crystallographic asymmetric units consist of two symmetrically independent half molecules. The coordination polyhedron of the metal atoms is best described as distorted octahedron. The angle N3A–Ni–N3A [83.0(5)° for A; 82.0(5)° for B] shows that the monodentate ligand moieties (NO_2) are coordinated in *cis* form. The angles N(amine)–Ni–N(amine) in *cis* arrangements are also close to 90°. The Ni–N bond distances are consistent with the corresponding values of other analogous octahedrally coordinated nickel(II)–amine complexes [23–27].

Relative humidity has a very interesting effect on the structure of compound **1b**. IR and crystal structure analysis of compound **1b** do not indicate the existence of a water molecule, but TG–DTA study indicates the presence of half a molecule of water per molecule of the complex. To study this effect we have used closed vessels of constant humidity (ca. 90 and 60%) [28]. At 90% humidity, complex **1b** does not lose any water molecule, but at 60% humidity and also in a $CaCl_2$ desiccator water is lost readily from compound **1b**, as is evident from the corresponding TG–DTA curves. The temperature of dehydration of compound **1b** (see below) or disappearance of a water molecule on keeping it in a desiccator suggests that the water molecule is too loosely bound. Both the hydrated and the dehydrated species upon heating show a phase transition at 103–143°C. Therefore, the presence of a water molecule in compound **1b** does not influence the phase-transition profile, which indicates that the water molecule does not alter the lattice of compound **1b**. This would have been impossible unless there exists a straight molecular sieve in the structure. This prompted us to calculate the void space in the unit cell of compound **1b** by using the program PLATON99 [29]. The calculated void space is 84 Å^3, which is sufficient to accommodate two molecules of water. It seems that the experimental conditions for IR-spectral run and X-ray data collection were not favourable for adherence of the loosely bound water molecule. The packing diagram in Fig. 4 shows channels that act as a water filter (H-bondings are shown by dashed lines). These filter-like channels contain water molecules (see below) which are lost on slight heating or low humidity (< 60%).

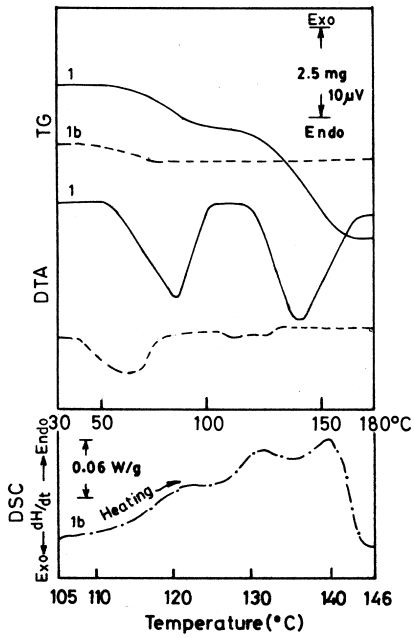
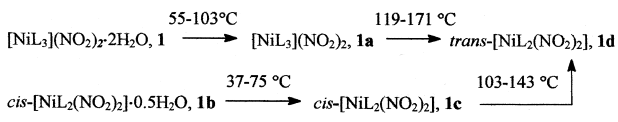


Fig. 2. Above: TG-DTA curves of $[NiL_3](NO_2)_2 \cdot 2H_2O$ (**1**) (sample mass, 12.7 mg) and *cis*-$[NiL_2(NO_2)_2] \cdot 0.5H_2O$ (**1b**) (sample mass, 12.38 mg). Below: DSC curve of $[NiL_2(NO_2)_2] \cdot 0.5H_2O$ (**1b**) (sample mass, 9.2 mg).



Scheme 1.

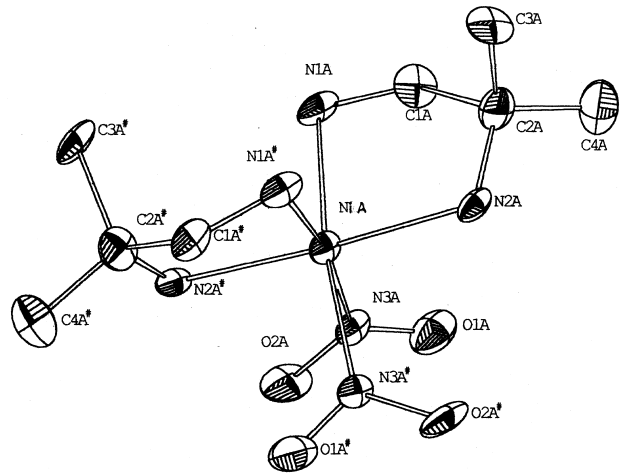


Fig. 3. ORTEP diagram of *cis*-$[NiL_2(NO_2)_2]$ (**1c**) (L = 1,2-diamino-2-methylpropane). Ellipsoids are drawn at 50% probability.

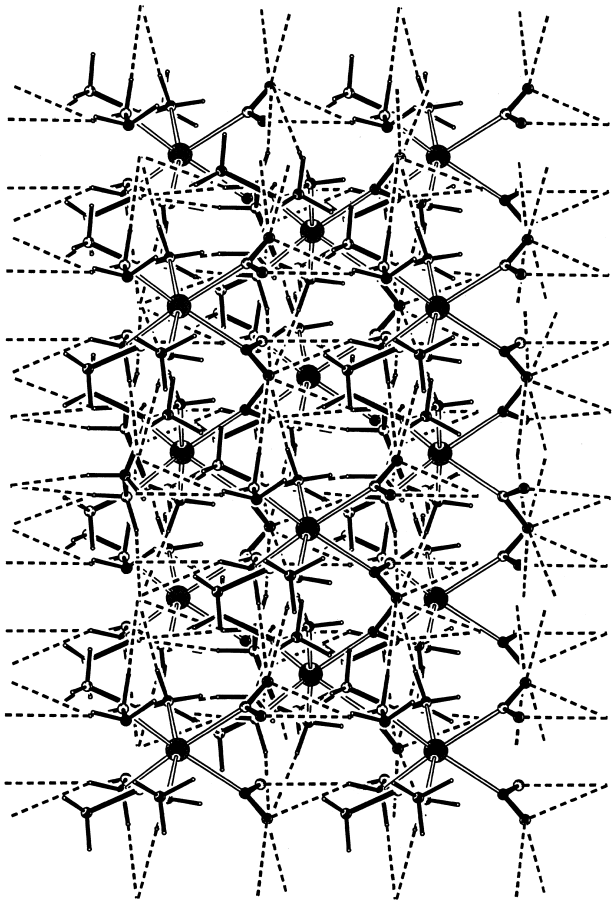


Fig. 4. Crystal packing diagram of *cis*-[$NiL_2(NO_2)_2$] (**1c**) (L = 1,2-diamino-2-methylpropane) showing the void space and H-bonds (- - - -) in the crystal structure.

Several attempts were made to obtain single crystals of compound **1d**, but they revert on crystallization. As a result we examined compound **1d** by X-ray powder diffraction data. Accurate θ_{hkl} spacings (°) were obtained from the powder pattern recorded. The initial cell parameters have been determined from powder diffraction data using the program TREOR [30], and accurate lattice parameters were obtained by least-squares refinements. The results are summarized in Tables 1 and 3. Powder diffraction studies show that the unit cell volume of compound **1d** is 25.7 Å^3 larger than that of compound **1c**. The magnetic susceptibility and the electronic spectral data of compound **1d** in the solid state correspond to octahedral nickel(II). The IR bands of the nitrite group in compound **1d** at 1375, 1324 and 812 cm^{-1} correspond to ν_{as}, ν_s and δ, respectively, suggesting the coordination of nitrite ion via N atom [6,7]. X-ray single crystal structure analysis reveals that the diamine is chelated in compound **1c**. Complex **1d** possesses very similar IR bands of the diamines to those of **1c**, suggesting that the diamines are also chelated in **1d**. The appearance of two bands (1312 and 1155 nm) at the near-IR [31] region in the electronic spectrum suggests that compound **1d** is a *trans*-dinitro octahedral species.

Table 3
X-ray powder diffraction data for compound **1d**

h	k	l	$2\theta_{obs}$	$2\theta_{calc}$
0	1	0	10.209	10.199
1	0	1	11.184	11.183
0	0	2	13.867	13.851
1	1	1	15.143	15.157
−2	0	2	15.691	15.759
2	1	0	16.969	16.960
−2	1	2	18.805	18.807
−2	0	3	20.654	20.665
3	1	0	22.771	22.794
−2	2	1	24.319	24.297
−2	0	4	26.563	26.573
−4	1	2	28.046	28.027
−3	2	2	29.034	29.051
2	2	2	30.559	30.588
4	1	1	32.125	32.113
1	3	1	32.952	32.986
3	0	3	33.995	33.991
−3	2	4	35.322	35.341
4	1	2	36.267	36.292
−2	2	5	39.188	39.165
−4	3	1	40.606	40.629

Table 4
H-bonding list for compound **1c**

D–H···A	D–H	H···A	D···A	∠D–H···A
N2A–H6A···O1A [a]	0.90	2.514	3.014(13)	115.6(9)
N1A–H1A···O2A [b]	0.90	2.188	3.023(14)	154.1(1)
N1A–H2A···O1A [c]	0.90	2.518	3.241(14)	137.8(1)
N2A–H5A···O2A [d]	0.90	2.340	3.200(11)	159.8(8)
N1A–H2A···O2A [c]	0.90	2.557	3.309(14)	141.5(1)
N1A–H2A···N3A [c]	0.90	2.795	3.638(15)	156.5(1)
N2B–H6B···O2B [d]	0.90	2.351	3.208(13)	159.8(8)
N1B–H1B···O1B [c]	0.90	2.553	3.287(16)	139.2(1)
N2B–H5B···O1B [a]	0.90	2.460	2.976(14)	116.9(9)
N1B–H1B···N3B [c]	0.90	2.808	3.658(15)	158.2(1)
N1B–H1B···O2B [c]	0.90	2.552	3.317(16)	143.2(1)
N1B–H2B···O2B [e]	0.90	2.189	3.021(13)	153.4(1)

[a] Symmetry codes: x, y, z.
[b] Symmetry codes: $-x+1/2, y+1/2, -z$.
[c] Symmetry codes: $x, y+1, z$.
[d] Symmetry codes: $x-1/2, y+1/2, z$.
[e] Symmetry codes: $-x+1/2+1, y+1/2, -z+1$.

The mechanism of phase transition may be explained as follows. In the *cis* species, N–H···O bonds would be expected to hinder the bond rotation of NO_2 groups and ligand moieties. These H-bonds (Table 4) are weakened upon onset of hindered rotation due to heating and thereby the *cis* molecule isomerizes to a *trans* molecule. Since X-ray diffraction studies indicate that the unit cell volume of compound **1d** is larger than that of compound **1c**, we may predict that the H-bonds and van der Waals interactions are weaker in compound **1d** than those of the *cis* species and thereby compound **1d** reverts slowly to compound **1c**.

Supplementary data

Supplementary data are available from the Cambridge Crystallographic Data Centre, 12 Union Road, Cambridge CB2 1EZ, UK (fax: +44-1223-336033; e-mail: deposit@ccdc.cam.ac.uk) on request, quoting deposition number 132800.

Acknowledgements

We thank the Director, CSMCRI, Bhavnagar-364 002, India, for use of the X-ray diffractometer, and the Council of Scientific and Industrial Research (grant to N.R.C.), New Delhi, India, for financial support.

References

[1] M.A. Hitchman, G.L. Rowbottom, Coord. Chem. Rev. 42 (1982) 55.
[2] D.M.L. Goodgame, M.A. Hitchman, Inorg. Chem. 3 (1964) 1389.
[3] D.M.L. Goodgame, M.A. Hitchman, Inorg. Chem. 4 (1965) 721.
[4] D.M.L. Goodgame, M.A. Hitchman, Inorg. Chem. 5 (1966) 1303.
[5] R. v. Eminger, S. Fallab, M. Zehnder, M. Dohler, Helv. Chim. Acta 75 (1992) 1245.
[6] T. Makino, S. Yano, S. Yoshikawa, Inorg. Chem. 18 (1979) 1048.
[7] A.J. Finney, M.A. Hitchman, C.L. Raston, G.L. Rowbottom, A.H. White, Aust. J. Chem. 34 (1981) 2047.
[8] D. Das, I.R. Laskar, A. Ghosh, A. Mondal, K. Okamoto, N. Ray Chaudhuri, J. Chem. Soc., Dalton Trans. (1998) 3987.
[9] Y. Ihara, T. Kamishima, R. Tsuchiya, Thermochim. Acta 67 (1983) 23.
[10] R. Roy, A. Ghosh, N. Ray Chaudhuri, Transition Met. Chem. 14 (1989) 443.
[11] R.W. Green, B. Bell, Aust. J. Chem. 26 (1973) 1663.
[12] A.I. Vogel, A Text Book of Quantitative Inorganic Analysis, 4th edn., Longman, New York, 1978.
[13] A.C.T. North, D.C. Philips, F.S. Mathews, Acta, Crystallogr., Sect. A 24 (1968) 351.
[14] G.M. Sheldrick, SHELXS 86. Program for the Solution of Crystal Structure, University of Göttingen, Germany, 1985.
[15] G.M. Sheldrick, SHELXL 93. Program for the Solution of Crystal Structure, University of Göttingen, Germany, 1993.
[16] International Tables for Crystallography, vol. C, 1992, Tables 4.2.6.8 and 6.1.1.4.
[17] M. Nardelli, Comput. Chem. 7 (1983) 1995.
[18] ZORTEP. A Program for the Presentation of Thermal Ellipsoids, University of Heidelberg, Germany, 1994.
[19] L. El-Sayed, R.O. Ragsdale, Inorg. Chem. 6 (1967) 1640.
[20] K. Nakamoto, J. Fujita, H. Murata, J. Am. Chem. Soc. 80 (1958) 4817.
[21] I.R. Laskar, D. Das, N. Ray Chaudhuri, G. Mostafa, A.J. Welch, Polyhedron 17 (1998) 1363.
[22] D. Das, N. Ray Chaudhuri, N.P. Nayak, A.K. Mukherjee, A. Ghosh, Polyhedron 16 (1997) 2361.
[23] A.K. Mukherjee, M. Mukherjee, S. Ray, A. Ghosh, N. Ray Chaudhuri, J. Chem. Soc., Dalton Trans. (1990) 2347.
[24] C. Pariya, A. Ghosh, M. Mukherjee, A.K. Mukherjee, N. Ray Chaudhuri, J. Chem. Soc., Dalton Trans. (1995) 337.
[25] C. Pariya, A. Ghosh, N. Ray Chaudhuri, S. Ghosh, M. Mukherjee, A.K. Mukherjee, Polyhedron 15 (1996) 1643.
[26] R. Vicente, A. Escuer, J. Ribas, X. Solans, J. Chem. Soc., Dalton Trans. (1994) 259.
[27] A.J. Blake, J.P. Danks, S. Parsons, M. Schröder, Acta Crystallogr., Sect. C 53 (1997) 411.
[28] The Merck Index, 1976, MISC 71 Merck, Rahway, NJ.
[29] A.L. Spek, PLATON, Molecular Geometry Program, University of Utrecht, The Netherlands, 1999.
[30] P.-E. Werner, L. Eriksson, M. Westdahl, J. Appl. Crystallogr. 18 (1985) 367.
[31] A.B.P. Lever, Inorganic Electronic Spectroscopy, 2nd edn., Elsevier, Amsterdam, 1984, p. 507.

PERGAMON

www.elsevier.nl/locate/poly

Polyhedron 19 (2000) 1021–1027

POLYHEDRON

Cyanamidonitrate–nickel(II) and –cobalt(II) complexes of imidazole ligands: X-ray crystallography and spectroscopic investigation

Mária Hvastijová [a,*], Jiří Kohout [a], Jozef Kožíšek [a], Lothar Jäger [b], Jesús García Díaz [a]

[a] *Department of Inorganic Chemistry, Slovak University of Technology, 812 37 Bratislava, Slovakia*
[b] *Fachbereich Chemie, Martin-Luther-Universität Halle-Wittenberg, D-06099 Halle/Saale, Germany*

Received 3 January 2000; accepted 16 March 2000

Abstract

New cyanamidonitrate complexes with imidazole (iz) and its methyl derivatives (meiz) of the type $[M(NO_2NCN)_2L_4]$ (with M = Ni, L = iz, 1-, 2-, 4-meiz; M = Co, L = iz, 1-, 4-meiz) and $[CoL_4](NO_2NCN)_2$ (with L = iz, 2-meiz) have been prepared and characterized by spectroscopic methods. The crystal structures of $[Ni(NO_2NCN)_2(1\text{-meiz})_4]$ and $[Co(NO_2NCN)_2(iz)_4]$ have been determined by X-ray crystallography. The metal(II) environment is practically octahedral, composed of four tertiary nitrogens from imidazole ligands and two nitrile nitrogens from cyanamidonitrate groups. According to the spectral results, similar molecular structures can be assumed for all remaining $[M(NO_2NCN)_2L_4]$ compounds. On the other hand, compounds $[CoL_4](NO_2NCN)_2$ consist of tetrahedral complex cations $[CoL_4]^{2+}$ which are electrostatically attracted with NO_2NCN^-. An isomeric pair, $[Co(NO_2NCN)_2(iz)_4]$ and $[Co(iz)_4](NO_2NCN)_2$, of octahedral and tetrahedral structure, respectively, were characterized. ©2000 Elsevier Science Ltd All rights reserved.

Keywords: Cobalt(II); Cyanamidonitrate; Electronic spectra; Imidazole ligands; IR spectra; Nickel(II); X-ray crystallography

1. Introduction

Previously, particular attention was paid to the investigation of coordination compounds with anionic ligands of non-linear pseudohalide type because of their interesting structure and physical properties [1–3]. The non-linear pseudohalide anion, cyanamidonitrate NO_2NCN^-, has until now only been sporadically studied [4–7]. In previous papers [8,9] we described new cyanamidonitrate–copper(II) complexes of the type $[Cu(NO_2NCN)_2L_4]$, where L = imidazole (iz), 1-, 2- or 4-methylimidazole (meiz), as well as $[Cu(NO_2NCN)_2(iz)_2]$. Whereas the L_4 compounds consist of molecular units in which the central Cu^{II} atoms are pseudo-octahedrally coordinated by N(meiz) and N(nitrile) atoms, in the iz_2 compound cyanamidonitrates act as bridges using N(nitrile) and O atoms as donors. However, considering the presence of four potential donor atoms, cyanamidonitrate as ligand has a variety of coordination possibilities, depending on the type of the central atom, especially with respect to its hardness [4].

We have therefore studied the coordination behaviour of cyanamidonitrate in the presence of the same neutral ligands of imidazole type, but with nickel(II) and cobalt(II) as central atoms. We have prepared nine new cyanamidonitrate compounds of Ni^{II} and Co^{II} with imidazole and its methyl derivatives and investigated them by means of infrared (IR) and electronic spectroscopy; in the case of $[Ni(NO_2NCN)_2(1\text{-meiz})_4]$ and $[Co(NO_2NCN)_2(iz)_4]$ the crystal structures were solved.

2. Experimental

2.1. Materials

The following chemicals were purchased: $Ni(NO_3)_2\cdot 6H_2O$ p.a., $Co(NO_3)_2\cdot 6H_2O$ p.a. (Chemapol, Czech Republic), imidazole, 1-methylimidazole, 2-methylimidazole, 4-methylimidazole (Merck). Potassium cyanamidonitrate (KNO_2NCN) was prepared from *N*-methyl-*N*-nitroso-*N′*-nitroguanidine according to the procedure described by Harris [10].

2.2. Preparation of the compounds

2.2.1. $[Ni(NO_2NCN)_2(iz)_4]$

Solutions of 1.25 mmol of $Ni(NO_3)_2\cdot 6H_2O$ in 3 cm^3 of water and of 2.5 mmol of KNO_2NCN in 8 cm^3 of water were

* Corresponding author. Tel.: +421-7-5932 5189; fax: +421-7-5249 3198; e-mail: hvastijo@chelin.chtf.stuba.sk

0277-5387/00/$ - see front matter ©2000 Elsevier Science Ltd All rights reserved.
PII S0277-5387(00)00367-3

Table 1
Analytical and other data for the compounds

Compound	Colour	Decomposition temperature (°C)	C (%) (calc.)	H (%) (calc.)	N (%) (calc.)	M (%) (calc.)
$[Ni(NO_2NCN)_2(iz)_4]$	light violet	190	33.30 (33.43)	3.05 (3.20)	38.60 (38.98)	11.56 (11.67)
$[Ni(NO_2NCN)_2(1\text{-meiz})_4]$	violet	200	38.43 (38.66)	4.30 (4.33)	35.01 (35.07)	10.53 (10.50)
$[Ni(NO_2NCN)_2(2\text{-meiz})_4]$	blue	220	38.31 (38.66)	4.34 (4.33)	34.87 (35.07)	10.58 (10.50)
$[Ni(NO_2NCN)_2(4\text{-meiz})_4]$	light violet	215	38.61 (38.66)	4.27 (4.33)	34.77 (35.07)	10.48 (10.50)
$[Co(NO_2NCN)_2(iz)_4]$	pink	115	33.33 (33.41)	3.15 (3.20)	38.91 (38.96)	11.60 (11.71)
$[Co(iz)_4](NO_2NCN)_2$	violet	155	33.16 (33.41)	3.35 (3.20)	38.57 (38.96)	11.42 (11.71)
$[Co(NO_2NCN)_2(1\text{-meiz})_4]$	orange	145	38.66 (38.65)	4.26 (4.32)	34.87 (35.06)	10.72 (10.53)
$[Co(2\text{-meiz})_4](NO_2NCN)_2$	violet	160	38.92 (38.65)	4.24 (4.32)	34.58 (35.06)	10.68 (10.53)
$[Co(NO_2NCN)_2(4\text{-meiz})_4]$	pink	170	38.51 (38.65)	4.35 (4.32)	35.04 (35.06)	10.42 (10.53)

mixed and poured into a solution of 5.0 mmol of iz in 8 cm^3 of methanol. From the solution a microcrystalline product was obtained which was filtered off, washed with diethyl ether and dried over KOH. Yield, 72%.

2.2.2. $[Ni(NO_2NCN)_2(1\text{-meiz})_4]$

Solutions of 1.25 mmol of $Ni(NO_3)_2 \cdot 6H_2O$ in 3 cm^3 of water and of 2.5 mmol of KNO_2NCN in 5 cm^3 of water were mixed and poured into a solution of 5.0 mmol of 1-meiz in 10 cm^3 of methanol. From the light-green solution crystals were isolated and treated as before. Yield, 58%.

2.2.3. $[Ni(NO_2NCN)_2L_4]$ (L = 2-meiz, 4-meiz)

Solutions of 1.25 mmol of $Ni(NO_3)_2 \cdot 6H_2O$ in 3 cm^3 of water and of 2.5 mmol of KNO_2NCN in 6 cm^3 of water were mixed and poured into a solution of 5 mmol of ligand L in 10 cm^3 of methanol. The formed turbid green solutions were filtered; the next day, crystals were isolated and treated as before. Yield, 55% (2-meiz), 64% (4-meiz).

2.2.4. $[Co(NO_2NCN)_2(iz)_4]$, $[Co(iz)_4](NO_2NCN)_2$

Solutions of 2.5 mmol of $Co(NO_3)_2 \cdot 6H_2O$ in 3 cm^3 of water and of 5.0 mmol of KNO_2NCN in 10 cm^3 of water were mixed and poured into a solution of 10 mmol of iz in 3 cm^3 of methanol. Next day, from the red–violet solution, crystals of $[Co(NO_2NCN)_2(iz)_4]$ formed on the side of the beaker and a microcrystalline suspension of $[Co(iz)_4](NO_2NCN)_2$ precipitated on the bottom. Yield, 50% $[Co(NO_2NCN)_2(iz)_4]$, 30% $[Co(iz)_4](NO_2NCN)_2$.

2.2.5. $[Co(NO_2NCN)_2L_4]$ (L = 1-meiz, 2-meiz, 4-meiz)

Solutions of 2.5 mmol of $Co(NO_3)_2 \cdot 6H_2O$ in 3 cm^3 of water and of 5.0 mmol of KNO_2NCN in 10 cm^3 of water were mixed and poured into a solution of 10 mmol of ligand L in 3 cm^3 of methanol. From the formed solutions of pink–red (1-meiz) or violet (2-meiz, 4-meiz) colour, compounds in crystalline or microcrystalline state were obtained and treated as before. Yield, 72% (1-meiz), 80% (2-meiz), 74% (4-meiz).

2.3. Analyses

Metal was determined chelatometrically after decomposition of the compounds by action of H_2SO_4 and $K_2S_2O_8$. The elemental analyses were carried out using a Carlo-Erba C, H, N analyser. The analytical data are listed in Table 1.

2.4. X-ray structure analysis and refinement

A summary of the crystal data and their collection for $[Ni(NO_2NCN)_2(1\text{-meiz})_4]$ (**1**) and $[Co(NO_2NCN)_2(iz)_4]$ (**2**) is given in Table 2. The final unit-cell parameters were obtained by least-squares on $2\sin\theta/\lambda$ values for 23 reflections with $2\theta = 6.6$–$18.4°$ for compound **1** and 34 reflections with $2\theta = 40.2$–$44.3°$ for compound **2**. The intensities of three standard reflections, measured every 2 h, showed only small random variations. The data reduction and empirical absorption correction were performed according to North et al. [11] for compound **1** and using Stoe-REDU4 [12] for compound **2**.

Both crystal structures were solved by the Patterson method and subsequent Fourier synthesis using SHELXS-86 [13]. Refinement was made by full-matrix least-squares SHELXL-93 software [14] to an $R(F)$ value of 0.0494 and 0.0334 for compounds **1** and **2**, respectively. Non-hydrogen atoms were treated anisotropically, and hydrogen atom positions were located from difference maps and constrained: imidazole C–H = 0.93 Å, N–H = 0.86 Å; CH_3 C–H = 0.96 Å with $U(H) = 1.2U_{eq}$ (C or N).

2.5. Physical measurements

The IR spectra were recorded, using a Philips Analytical PU 9800 FTIR spectrometer, in KBr disks (4000–400 cm^{-1}) and in Nujol mulls (500–200 cm^{-1}). The electronic spectra (0.4–2.8 μm^{-1}) were obtained from solid state samples on a Perkin-Elmer Lambda 19 apparatus. Thermal decompositions were performed on a MOM derivatograph (100 mg samples; heating rate, 6°C min^{-1}).

Table 2
Crystallographic data for $[Ni(NO_2NCN)_2(1\text{-meiz})_4]$ (**1**) and $[Co(NO_2NCN)_2(iz)_4]$ (**2**)

Compound	$[Ni(NO_2NCN)_2(1\text{-meiz})_4]$ (**1**)	$[Co(NO_2NCN)_2(iz)_4]$ (**2**)
Formula	$C_{18}H_{24}N_{14}O_4Ni$	$C_{14}H_{16}N_{14}O_4Co$
Formula weight	559.22	503.37
Crystal system	monoclinic	monoclinic
Space group	$C2/c$ (no. 15)	$P2_1/n$ (no. 14)
a (Å)	16.629(7)	9.880(1)
b (Å)	11.538(5)	12.774(4)
c (Å)	15.938(5)	17.966(2)
α (°)	90.0	90.0
β (°)	123.37(2)	97.51(1)
γ (°)	90.0	90.0
V (Å^3)	2554(2)	2248.0(7)
Z	4	4
D_{calc} (g cm^{-3})	1.454	1.487
Crystal size (mm)	0.15×0.35×0.65	0.12×0.24×0.46
Instrument	Syntex $P2_1$	Stoe Stadi-4
μ (Mo Kα) (mm^{-1})	0.814	0.760
Temperature (K)	293(2)	293(2)
θ Range (°)	2.27–27.57	1.96–25.99
Scan mode	$\omega/2\theta$	$\omega/2\theta$
Crystal decay	negligible	negligible
Reflections collected	2947	6119
Unique reflections	2857	4406
Reflections observed	1876	3050
Corrections applied	PL and ψ-scan absorption correction	PL and ψ-scan absorption correction
Minimum/maximum transmission	0.629/748	0.957/0.998
Residuals: R (F^2)	0.0494	0.0334
wR (F^2)	0.1406	0.0815
Goodness-of-fit	1.025	1.063
Parameters refined	169	301
Weighting scheme: $P=[\max(F_o^2, 0)+F_c^2]/3$	$1/\sigma^2(F_o^2)+(0.0830P)^2+0.805P$	$1/\sigma^2(F_o^2)+(0.0389P)^2+0.877P$
Residual density (e Å^{-3})	−0.32/0.55	−0.18/0.23

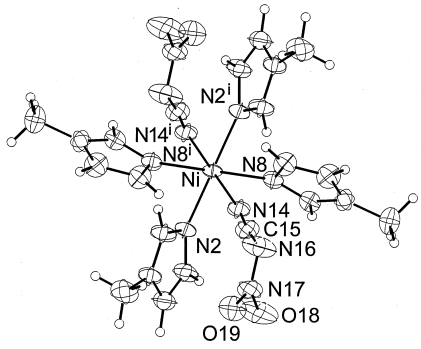


Fig. 1. ORTEP drawing of $[Ni(NO_2NCN)_2(1\text{-meiz})_4]$ (**1**) with thermal displacement ellipsoids [24] given at 30% probability. The symmetry codes used are the same as in Table 3. (i) = a.

3. Results and discussion

3.1. Description of the structures of $[Ni(NO_2NCN)_2(1\text{-meiz})_4]$ (1) and $[Co(NO_2NCN)_2(iz)_4]$ (2)

The crystal structure of compound **1** consists of discrete $[Ni(NO_2NCN)_2(1\text{-meiz})_4]$ molecules (Fig. 1). The central Ni^{II} atom is found in a crystallographic special position and appears to be octahedrally coordinated by six nitrogen donor atoms. In the equatorial plane there are four nitrogens from methylimidazole molecules, while in the axial positions there are two nitrile nitrogens from cyanamidonitrate anions. Differences in bond lengths in the equatorial plane and axial positions are within the standard deviations [Ni1–N2 = 2.093(3) Å, Ni1–N8 = 2.093(2) Å, Ni1–N14 = 2.100(3) Å] (Table 3).

The crystal structure of compound **2** (Fig. 2) is also formed by discrete $[Co(NO_2NCN)_2(iz)_4]$ molecules. There are two symmetrically independent molecules in the unit cell, each with the metal atom lying on a centre of symmetry. The orientation of two molecules expressed by the angle between two symmetrically independent cyanamidonitrate ligands is 140.4(1)°.

In both molecules, the central Co^{II} atom is pseudo-octahedrally coordinated by six nitrogen donor atoms [Co1–N1 = 2.141(2) Å, Co1–N3 = 2.130(2) Å, Co1–N5 = 2.167(2) Å for the first molecule and Co2–N8 = 2.143(2) Å, Co2–N10 = 2.121(2) Å, Co2–N12 = 2.164(2) Å for the second one] (Table 4).

In both crystal structures there is a system of hydrogen bonds and interatomic interactions. However, the correlation between the decomposition temperatures and strength of interatomic interactions is not very obvious (Tables 1, 3 and 4).

Table 3
Selected bond lengths (Å) and angles (°) (e.s.d.s in parentheses) for $[Ni(NO_2NCN)_2(1\text{-meiz})_4]$ (**1**)

Ni1–N2	2.093(3)	N2–Ni1–N8	90.1(1)	
Ni1–N2 [a]	2.093(3)	N2–Ni1–N2 [a]	180	
Ni1–N8	2.093(2)	N2–Ni1–N14	90.8(1)	
Ni1–N14	2.100(3)	N8–Ni1–N14	90.5(1)	
N14–C15	1.107(4)	Ni1–N14–C15	171.1(3)	
C15–N16	1.377(5)	N14–C15–N16	168.3(4)	
N16–N17	1.286(5)	C15–N16–N17	108.5(5)	
N17–O18	1.200(4)			
N17–O19	1.238(4)			
D–H···A	D–H	H···A	D···A	D–H···A
C5–H5···O18 [b]	0.930(5)	2.445(7)	3.295(6)	152.0(6)
C5–H5···O18 [c]	0.930(5)	2.474(8)	3.057(9)	120.8(4)
C9–H9···N14	0.930(5)	2.565(4)	3.058(4)	113.6(4)
C3–H3···N14 [d]	0.930(5)	2.586(6)	3.065(5)	112.5(4)
C11–H11···O19 [e]	0.930(5)	2.640(4)	3.382(4)	137.3(5)
C13–H13A···O18 [c]	0.960(5)	2.668(8)	3.304(8)	124.2(5)
C6–H6···N14	0.930(5)	2.684(4)	3.131(4)	110.3(4)
C12–H12···N14 [d]	0.930(5)	2.696(4)	3.122(4)	108.8(4)

[a] Symmetry codes: $-x, -y, -z$.
[b] Symmetry codes: $-x, -1-y, -z$.
[c] Symmetry codes: $1/2-x, -1/2-y, -z$.
[d] Symmetry codes: $-x, -y, -z$.
[e] Symmetry codes: $1/2-x, 1/2+y, 1/2-z$.

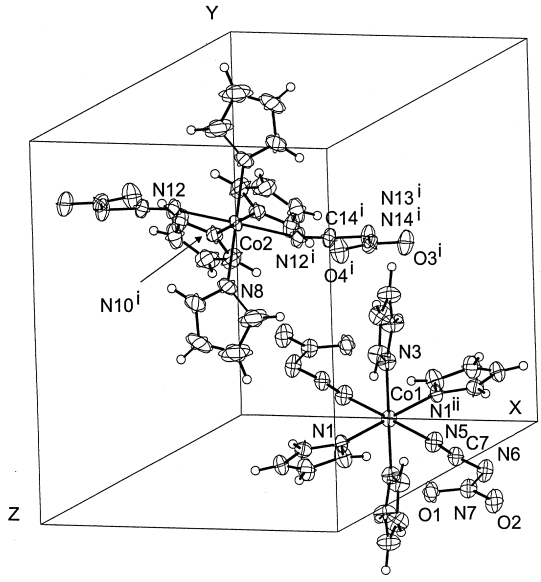


Fig. 2. Symmetrically independent part of unit cell for crystal structure of $[Co(NO_2NCN)_2(iz)_4]$ (**2**) with thermal displacement ellipsoids [24] given at 30% probability. The symmetry codes used are the same as in Table 4. (i) = a; (ii) = b.

3.2. Infrared spectra

The vibration characteristics of the cyanamidonitrate anions in the studied compounds were determined by comparison of the recorded spectra with those of KNO_2NCN [4,15], as well as of the free imidazole and its derivatives [15–17]. Relevant data together with those for KNO_2NCN are listed in Table 5.

Table 4
Selected bond lengths (Å) and angles (°) (e.s.d.s in parentheses) for $[Co(NO_2NCN)_2(iz)_4]$ (**2**)

Co1–N1	2.141(2)	Co2–N8	2.143(2)	
Co1–N1 [a]	2.141(2)	Co2–N8 [b]	2.143(2)	
Co1–N3	2.130(2)	Co2–N10	2.121(2)	
Co1–N5	2.167(2)	Co2–N12	2.164(2)	
N5–C7	1.144(3)	N12–C14	1.140(3)	
C7–N6	1.329(3)	C14–N13	1.335(3)	
N6–N7	1.338(3)	N13–N14	1.332(3)	
N7–O1	1.229(2)	N14–O3	1.247(3)	
N7–O2	1.246(2)	N14–O4	1.225(3)	
N1–Co1–N3	91.7(1)	Co1–N5–C7	174.9(2)	
N1–Co1–N5	88.7(1)	N5–C7–N6	172.6(3)	
N3–Co1–N5	91.7(1)	Co2–N12–C14	166.1(2)	
N8–Co2–N10	90.6(1)	N12–C14–N13	171.4(3)	
N8–Co2–N12	89.8(1)			
D–H···A	D–H	H···A	D···A	D–H···A
C9–H9···O3 [c]	0.930(4)	2.021(4)	3.808(4)	151.7(4)
C11–H11···O3 [d]	0.930(4)	2.068(3)	2.904(3)	164.0(4)
N2–H2···O2 [e]	0.860(4)	2.131(3)	2.940(3)	156.6(3)
N4–H4···O2 [f]	0.860(4)	2.252(3)	2.957(3)	139.2(3)
N4–H4···O1 [f]	0.860(4)	2.466(3)	3.236(3)	149.5(3)
N2–H2···N6 [g]	0.860(4)	2.473(3)	3.230(3)	147.3(3)
C4–H4···O4 [h]	0.930(4)	2.567(3)	3.362(3)	143.7(3)
C8–H8···N12	0.930(4)	2.659(4)	3.162(4)	114.7(3)
N11–H11···N13 [d]	0.860(4)	2.669(3)	3.329(3)	134.5(3)

[a] Symmetry codes used: $-1-x, -y, -z$.
[b] Symmetry codes used: $-x, 1-y, -z$.
[c] Symmetry codes used: $-1/2-x, y-1/2, 1/2-z$.
[d] Symmetry codes used: $1+x, y, z$.
[e] Symmetry codes used: $x-1, y, z$.
[f] Symmetry codes used: $3/2-x, 1/2+y, 1/2-z$.
[g] Symmetry codes used: $-x, 1-y, -z$.
[h] Symmetry codes used: $-x, -y, -z$.

The $\nu_{asym}(NCN)$ frequency value should reflect the bonding mode of NO_2NCN^-. In the case of the bond through nitrile nitrogen, a shift of these frequencies to higher values might be expected. However, inspection of the $\nu_{asym}(NCN)$ values for the compounds under study indicates shifts not only to higher but also to lower values. The latter shifts appear just for those compounds for which coordination of the NO_2NCN group through nitrile nitrogen was proved by X-ray crystallography. The shift of the $\nu_{asym}(NCN)$ to lower frequencies was also observed in the case of $[Co(iz)_4](NO_2NCN)_2$ and $[Co(2\text{-meiz})_4](NO_2NCN)_2$ in which the non-linear pseudohalide anions are not coordinated (see Section 3.3) and can interact with cations through hydrogen bondings only. In the 2-meiz compound this band is also expressively splitted, which can hardly be explained by the bonding state of the pseudohalide. Thus, it can be stated that in the present series of compounds the $\nu_{asym}(NCN)$ frequency values are not conclusive for assessing the bonding mode of the cyanamidonitrate anion.

The $\nu_{sym}(NCN)$ frequency values are almost always very near to the values for the potassium salt so that they are not distinctly influenced by the bonding mode of the pseudohal-

Table 5
Characteristic IR data (cm^{-1}) for compounds

Compound	$\nu_{asym}(NCN)$	$\nu_{asym}(NO_2)$	$\nu_{sym}(NO_2)$	$\nu_{sym}(NCN)$	ν(N–N)	$\delta(NO_2)$	ν(M–L)
KNO_2NCN	2196 vs	1440 s	1288 vs	1161 m	976 w	771 m	
$[Ni(NO_2NCN)_2(iz)_4]$	2227 s	1480 s	1282 vs	1170 m	960 mw	[a]	288 ms, 263 vs
$[Ni(NO_2NCN)_2(1\text{-meiz})_4]$	2180 vs	1464 vs	1257 vs	1170 ms	[a]	775 m b, 750 m [b]	279 m, 265 m, 250 m, 225 m
$[Ni(NO_2NCN)_2(2\text{-meiz})_4]$	2199 vs	[a]	1275 vs [c]	[a]	[a]	[a]	286 m [d], 236 w [d]
$[Ni(NO_2NCN)_2(4\text{-meiz})_4]$	2190 vs	[a]	[a]	1172 m	[a]	775 m [b], 763 m [b]	274 m, 256 ms, 237 ms
$[Co(NO_2NCN)_2(iz)_4]$	2189 vs	1462 s [b], 1431 sh [b]	1289 vs	1158 m	968 ms	778 sh, 775 m	244 ms
$[Co(iz)_4](NO_2NCN)_2$	2228 vs, 2187 vs	1433 m	1285 s	1171 ms	974 mw	[a]	430 m, 343 mw, 270 sh, 243 s
$[Co(NO_2NCN)_2(1\text{-meiz})_4]$	2199 vs	1464 vs	1265 vs	1169 ms	941 ms	771 m	275 sh, 231 ms
$[Co(2\text{-meiz})_4](NO_2NCN)_2$	2182 vs	[a]	1300 vs [c]	1167 w [b], 1149 sh [b]	[a]	[a]	536 m, 486 vw, 425 s, 316 ms
$[Co(NO_2NCN)_2(4\text{-meiz})_4]$	2208 vs	[a]	[a]	1167 ms	[a]	775 m [b], 763 m [b]	263 ms [b], 250 ms [b]

[a] Cannot be distinguished from the other ligand vibrations.
[b] One of these bands may belong to the imidazole ligand vibrations.
[c] Maximum shows a weak splitting; an average frequency is given.
[d] The band can involve an admixture of an imidazole ligand band.

ide anion. The assignment of the remaining pseudohalide vibrations is difficult because the relevant region contains many bands belonging to the imidazole ligands [15–17] and careful checking is necessary. According to the obtained values it is clear that the $\nu_{asym}(NO_2)$ and $\nu_{sym}(NO_2)$ vibrations are mostly shifted to higher and lower frequencies, respectively, in comparison with KNO_2NCN, as observed previously [8]. In the case of $[Co(iz)_4](NO_2NCN)_2$ and $[Co(2\text{-meiz})_4](NO_2NCN)_2$, these shifts, in agreement with the ionic bonding, were not observed.

In the far-IR region (up to 200 cm^{-1}) two to four bands between $\approx$540 and 225 cm^{-1} were observed, which can be assigned to the M–N stretching vibrations. In $[Ni(NO_2NCN)_2(1\text{-meiz})_4]$ the skeleton $NiN_4'N_2''$ is present, which with respect to the unequivalency of the N′ and N″ donors shows in fact a D_{4h} symmetry. Therefore, five skeletal stretching modes can be expected, two of which are infrared active: E_u as ν(Ni–N′) and A_{2u} as ν(Ni–N″). The site symmetry in the crystal lattice splits the E_u mode into two components, so that three ν(Ni–N) values are reasonable, but four values were observed (Table 5). For elucidation of this fact, interaction of the stretching modes of the same symmetry, belonging to the structure units in equivalent sites of the unit cell (correlation field effects), must be taken into account. For $[Co(NO_2NCN)_2(iz)_4]$ surprisingly only one ν(Co–N) value was ascertained, but the relevant band is broad and can comprise several closely lying components.

In the case of compounds $[Co(iz)_4](NO_2NCN)_2$ and $[Co(2\text{-meiz})_4](NO_2NCN)_2$ bands appear in a broad frequency region from $\approx$535 cm^{-1} to lower energies. The number and position of these bands agree well with a distorted tetrahedral (C_{2v}) arrangement about the central Co^{II} atom [18,19], which is in agreement with the observed electronic d–d spectra (see below).

3.3. Solid-state electronic spectra

The electronic spectra (Table 6) of the nickel(II) compounds exhibit three spin-allowed d–d absorptions whose positions are typical for octahedral configurations [20]. From the similarity of these spectral features it can be concluded that the molecular structure of all other compounds is analogous to that of $[Ni(NO_2NCN)_2(1\text{-meiz})_4]$, which was proved crystallographically (Fig. 1). The observed d–d absorptions in increasing energy order are assigned to the transitions $^3T_{2g} \leftarrow {}^3A_{2g}$, $^3T_{1g}(F) \leftarrow {}^3A_{2g}$ and $^3T_{1g}(P) \leftarrow {}^3A_{2g}$; the last transition appears only as a broad flat shoulder. The *Dq* values for these compounds are very near to 1050 cm^{-1}, indicating a small difference between the influence of different imidazole ligands. The β values are also very similar and show an appreciable amount of covalency [21].

The ligand field spectra of $[Co(NO_2NCN)_2L_4]$ are indicative of octahedral configuration [20] and, therefore, the crystallographically solved molecular structure of $[Co(NO_2NCN)_2(iz)_4]$ (Fig. 2) can be attributed to the other spectroscopically similar compounds. The low- and

Table 6
Electronic spectral data for the compounds

Compound	ν_{max} (μm^{-1}) [a]	Dq (cm^{-1})	B (cm^{-1})	β
$[Ni(NO_2NCN)_2(iz)_4]$	1.08 (1.19) (1.26) 1.79 (2.7–2.85)	1080	836	0.81
$[Ni(NO_2NCN)_2(1\text{-meiz})_4]$	1.03 (1.18) (1.36) 1.75 (2.65–2.75)	1030	842	0.82
$[Ni(NO_2NCN)_2(2\text{-meiz})_4]$	1.02 (1.19) (1.34) 1.70 (2.66)	1020	823	0.80
$[Ni(NO_2NCN)_2(4\text{-meiz})_4]$	1.06 (1.19) (1.36) 1.78 (2.75)	1060	843	0.82
$[Co(NO_2NCN)_2(iz)_4]$	1.03 (1.17–1.24 sh) (1.62–1.74) (1.89) (1.99) 2.06 (2.5–2.63)	1150	768	0.79
$[Co(iz)_4](NO_2NCN)_2$	(0.81) 0.96 (1.72) 1.76 (1.88) (2.57)	574	666	0.69
$[Co(NO_2NCN)_2(1\text{-meiz})_4]$	1.02 (1.21) 1.55 (1.88) (1.95) 2.07 2.35	1140	781	0.81
$[Co\ (2\text{-meiz})_4]\ (NO_2NCN)_2$	0.89 1.70 (1.76) (1.85) (2.24) (2.47)	530	672	0.69
$[Co(NO_2NCN)_2(4\text{-meiz})_4]$	1.05 (1.20) (1.55) (1.69) (1.77) (1.89) (1.96) 2.065 2.4	1170	758	0.78

[a] The data in parentheses relate to shoulders, whose positions are only approximately determined.

high-energy absorption bands can be assigned to the $^4T_{2g} \leftarrow {}^4T_{1g}(F)$ and $^4T_{1g}(P) \leftarrow {}^4T_{1g}(F)$ transitions, respectively. The electronically forbidden transition $^4A_{2g} \leftarrow {}^4T_{1g}(F)$ probably corresponds to the shoulders between 1.95 and 1.99 μm^{-1}, as the values of the ratio $E(^4A_{2g} \leftarrow {}^4T_{1g})/E(^4T_{2g} \leftarrow {}^4T_{1g})$ are very near to 1.9 [20]. Other absorptions in the visible region appearing as shoulders can be related to spin-forbidden transitions into some doublet states, spin-orbit coupling or other effects. The Dq values are visibly higher than for the Ni^{II} complexes, which is in agreement with the positions of the respective metals in the spectrochemical series of central atoms [21], and their changes are again relatively small. The very close β values are a little lower than for Ni^{II} complexes.

On the other hand, the ligand field spectra of $[Co(iz)_4](NO_2NCN)_2$ and $[Co(2\text{-meiz})_4](NO_2NCN)_2$ are considerably shifted to the lower energies compared with the foregoing group, and this spectral behaviour is diagnostic of tetrahedral coordination of the central Co^{II} atom. Therefore, it can be concluded that this central atom is tetrahedrally coordinated by four nitrogen atoms from the imidazole-type ligands and these complex cations are electrostatically attracted to the cyanamidonitrate anions. The visible and near-IR bands can be assigned to the $^4T_1(P) \leftarrow {}^4A_2$ and $^4T_1(F) \leftarrow {}^4A_2$ transitions, respectively [20]. The ligand field parameters Dq and β are considerably lower than for the octahedral compounds, as may be expected.

The near-IR bands of the foregoing compounds are very broad and, in the case of $[Co(iz)_4](NO_2NCN)_2$, a low-energy shoulder appears. This fact reveals that the tetrahedral stereochemistry around the cobalt(II) is considerably distorted and very likely has a C_{2v} symmetry [20,22,23] in which the tetrahedral $^4T_1(F)$ state is split into three orbital levels. The particular absorptions on the low-wavenumber sides of the visible bands can be related to the low-symmetry splitting of the tetrahedral $^4T_1(P)$ state.

4. Conclusions

Two different kinds of the cyanamidonitrate compounds of the type $[M(NO_2NCN)_2L_4]$ and $[CoL_4](NO_2NCN)_2$ were isolated. In the complexes of the first type, cyanamidonitrate is coordinated to the central M^{II} atom, whereas in the second type this group forms ionic bonds.

In comparison with other non-linear pseudohalide ligands, cyanamidonitrate exhibits only slight bridging ability in spite of its rich coordination possibilities.

The coordination of this pseudohalide through the nitrile nitrogen is surprisingly not significantly manifested on the $\nu_{asym}(NCN)$ frequency values and only $\nu_{asym}(NO_2)$ and $\nu_{sym}(NO_2)$ frequencies are more regularly influenced.

The coordination polyhedra of the $[M(NO_2NCN)_2L_4]$ compounds are relatively very regular, especially in the Ni^{II} compounds, in spite of the presence of chemically different nitrogen atoms in the coordination sphere. This unequivalency is, however, revealed by the ν(M–N) frequencies in the far-IR spectra.

While with iz an isomeric pair, viz. $[Co(NO_2NCN)_2(iz)_4]$ and $[Co(iz)_4](NO_2NCN)_2$, was obtained, 2-meiz gives with Co^{II} only the compound $[Co(2\text{-meiz})_4](NO_2NCN)_2$. This effect can be connected with steric hindrance of 2-meiz ligand, having better binding possibility in distorted tetrahedral configuration.

Supplementary data

Tables of hydrogen atom parameters, anisotropic thermal parameters, complete lists of bond lengths and angles, as well as measured and calculated structure factors for the structures of compounds **1** and **2** have been deposited with the Cambridge Crystallographic Data Centre, 12 Union Road, Cambridge CB2 1EZ, UK (fax: +44-1223-336033; e-mail: deposit@ccdc.cam.ac.uk).

References

[1] J. Kohout, L. Jäger, M. Hvastijová, J. Kožíšek, J. Coord. Chem. (in press).
[2] S.R. Batten, B.F. Hoskins, B. Moubaraki, K.S. Murray, R. Robson, J. Chem. Soc., Dalton Trans. (1999) 2977.
[3] S.R. Batten, P. Jensen, C.J. Kepert, M. Kurmoo, B. Moubaraki, K.S. Murray, D.J. Price, J. Chem. Soc., Dalton Trans. (1999) 2987.

[4] L. Jäger, C. Tretner, H. Hartung, M. Biedermann, Z. Anorg. Allg. Chem. 623 (1997) 1299.
[5] L. Jäger, C. Tretner, M. Biedermann, H. Hartung, J. Organomet. Chem. 530 (1996) 13.
[6] L. Jäger, C. Tretner, H. Hartung, M. Biedermann, C. Wagner, Z. Anorg. Allg. Chem. 624 (1998) 1558.
[7] L. Jäger, C. Tretner, H. Hartung, M. Biedermann, Chem. Ber. 130 (1997) 1007.
[8] J. Kohout, M. Hvastijová, J. Kožíšek, J.G. Diáz, M. Valko, L. Jäger, Inorg. Chim. Acta 287 (1999) 186.
[9] J. Kožíšek, J.G. Diáz, M. Hvastijová, L. Jäger, Acta Crystallogr., Sect. C 53 (1997) 703.
[10] S.R. Harris, J. Am. Chem. Soc. 80 (1958) 2302.
[11] A.C.T. North, D.C. Philips, F.S. Mathews, Acta Crystallogr., Sect. A 24 (1968) 351.
[12] REDU 4, Stoe Four-Circle Data Reduction Program, Version 7.08, Stoe & Cie, Darmstadt, Germany, 1993.
[13] G.M. Sheldrick, Acta Crystallogr., Sect. A 46 (1990) 467.
[14] G.M. Sheldrick, Program for the Refinement of the Crystal Structures, University of Göttingen, Germany, 1993.
[15] L. Jäger, M. Hvastijová, unpublished results.
[16] M. de N.D. Cordes, J.L. Walter, Spectrochim. Acta, Part A 24 (1968) 237.
[17] C. Perchard, A. Novak, Spectrochim. Acta, Part A 23 (1967) 1953.
[18] R.J.H. Clark, C.S. Williams, Inorg. Chem. 4 (1965) 350.
[19] R.J.H. Clark, C.S. Williams, Spectrochim. Acta 22 (1966) 1081.
[20] A.B.P. Lever, Inorganic Electronic Spectroscopy, 2nd edn., Elsevier, Amsterdam, 1984.
[21] C.K. Jörgensen, Absorption Spectra and Chemical Bonding in Complex, Pergamon, Oxford, 1962.
[22] A.A.G. Tomlinson, C. Bellitto, O. Piovesana, C. Furlani, J. Chem. Soc., Dalton Trans. (1972) 350.
[23] J.M. Land, J.A. Stubbs, J.T. Wrobleski, Inorg. Chem. 16 (1977) 1955.
[24] K. Brandenburg, Diamond. Visual Information System for Crystal Structures, Bonn, Germany, 1998.

PERGAMON

www.elsevier.nl/locate/poly

Polyhedron 19 (2000) 1031–1036

POLYHEDRON

Synthesis of layered dendritic carbosilanes

Chungkyun Kim, Soon Kyu Choi, Bohyun Kim *

Department of Chemistry, Dong-A University, Pusan 604-714, South Korea

Received 14 December 1999; accepted 21 February 2000

Abstract

Layered dendritic carbosilanes containing triple bonds on the peripheral layer, double bonds in the $(n-1)$th inner shell, and single bonds in the $(n-2)$th inner shell were prepared. The synthetic pathways used iterative hydrosilation, alkenylation, and alkynylation. The fourth generation G4-E96PA is composed of two generations of propylene layers (G1 and G2) and one ethenyl layer in the inner shell (G3), and 96 ethynyl groups on the periphery (G4). The dendrimers are characterized by NMR, MALDI-TOF mass spectrometry, UV, IR, SEC and elemental analysis. ©2000 Elsevier Science Ltd All rights reserved.

Keywords: Dendrimers; Carbosilanes; Platinum catalysts; Hydrosilation

1. Introduction

Dendrimers that are prepared via an iterative synthetic pathway on a central multifunctional core have recently received considerable attention [1–5]. One of the intriguing possibilities in this field is the synthesis of a spherical molecule without defects. To date, highly branched dendrimers with silicon-containing molecules have been prepared by many researchers who used the beautiful construction of molecular architecture [6–9]. We have observed a few methods for the preparation of carbosilane dendrimers possessing double and triple bonds [10–17]. A number of dendrimers containing two different rests between the progressing units and the last generation have been prepared, mostly focused on modification of peripheral dendritic properties [18–20]. However, very little is known about the synthetic approach to two and more layered dendritic macromolecules, which are composed of different generating layers in the outer and inner shells.

Platinum metal in activated carbon as a hydrosilation catalyst is very useful for the synthetic purpose, because the hydrosilation of all double and triple bonded dendrimers with chlorosilane ($HSiMe_nCl_{3-n}$) does not form side products and brings about quantitative yields. We wish to report the synthetic method and characterization of layered dendrimers with 96 phenylethynyl groups on the outermost dendritic surface.

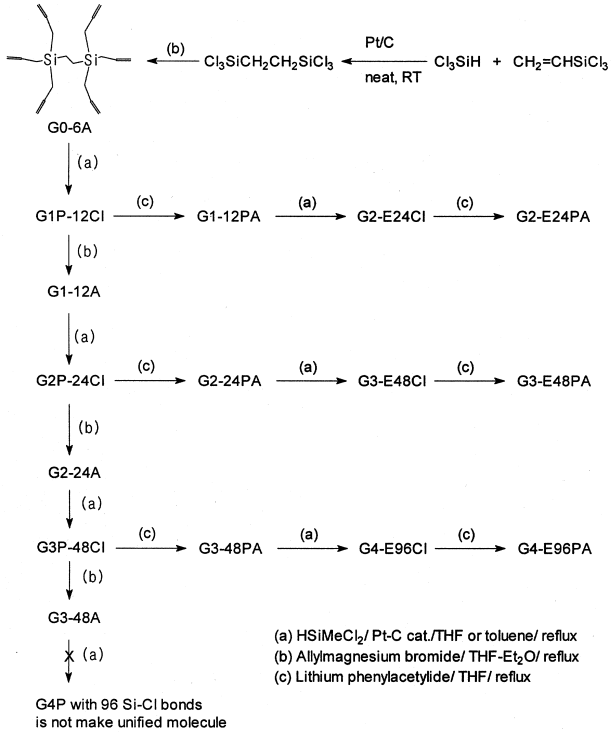
* Corresponding author. Tel.: +82-51-200-7247; fax: +82-51-200-7259; e-mail: ckkim@mail.donga.ac.kr

2. Results and discussion

The synthesis of carbosilane dendrimers with two different generating layers is based on two reaction mechanisms: hydrosilation [21] of double and triple bonds with chlorosilane ($HSiMe_nCl_{3-n}$) and alkenylation as well as alkynylation of dendrimers containing Si–Cl bonds (Scheme 1). The preparation of allyl groups containing low generations G*n*-*m*A ($n=0$–2; $m=6$, 12, and 24) was achieved by the use of iterative alkenylation with allylmagnesium bromide and hydrosilation with dichloromethylsilane based on 1,2-bis(triallylsilyl)ethane as the core [16,17]. The core molecule has six allylic branches that can be prepared by the reaction of 1,2-bis(trichlorosilyl)ethane with 6 equiv. allylmagnesium bromide. The G0-6A (core) with dichloromethylsilane under a platinum catalyst quantitatively provided G1P-12Cl. The yields of all allyl group-containing G*n*-*m*A type dendrimers were almost quantitative [16,17]. However, the hydrosilation of G3-48A with dichloromethylsilane did not produce the unified fourth generation G4-96Cl.

The reaction of G1P-12Cl with lithium phenylacetylide provided G1-12PA with 12 phenylethynyl groups on the periphery. G1-12PA has two different layers, which are composed of six propylene groups in the core and 12 ethynyl groups on the first generation layer. Using the same iterative synthetic method, G2-24PA and G3-48PA (Scheme 2) were synthesized in good yields (Table 1). The platinum catalyzed hydrosilation of triple bonds in dendritic molecules (G*n*-*m*PA) with dichloromethylsilane produced the chlorinated dendrimer G*n*-E2*m*Cl comprising propylene groups on the

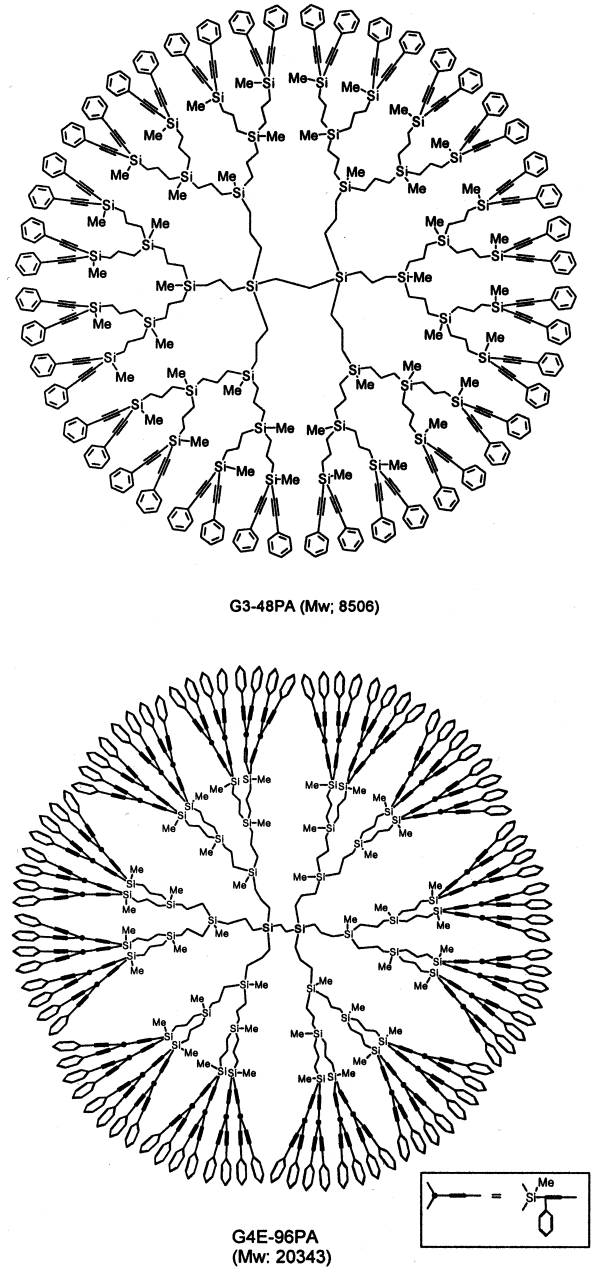
0277-5387/00/$ - see front matter ©2000 Elsevier Science Ltd All rights reserved.
PII S0277-5387(00)00338-7



Scheme 1. Schematic view of the synthetic route for G*n*-*m*A, G*n*P-*m*Cl, G*n*-*m*PA, G*n*-E*m*Cl, and G*n*-E*m*PA.

$(n-2)$th layer, ethenyl groups on the $(n-1)$th layer, and Si–Cl groups on the outermost periphery. For example, hydrosilation of the G1-12PA molecule with dichloromethylsilane under a platinum catalyst provided G2-E24Cl containing propylene groups in the core, ethenyl groups on the first generation layer, and 24 Si–Cl bonds on the periphery. The reaction of G2-E24Cl with lithium phenylacetylide provided G2-E24PA with 24 phenylethynyl groups on the periphery. The inner shell of G2-E24PA consisted of six propylene groups in the core and 12 ethenyl groups on the first generation layer. The platinum catalyzed hydrosilation process for triple bonded dendritic molecules with chlorosilane revealed a very high yield. Side products such as α-adducts of the hydrosilation reaction were not observed using this reaction procedure. By repetition of the hydrosilation of G*n*-*m*PA ($n=1$–3; $m=12$, 24 and 48) with dichloromethylsilane under a platinum catalyst and alkynylation with lithium phenylacetylide under reflux conditions, ethynyl group-containing dendrimers were prepared up to the fourth generation with good yields (Scheme 2 and Table 1). The formation of G5P by application of the same reaction mechanism was not possible in a uniformly ordered structure.

The identification and determination of the degree of reaction of dendritic branches are very important. In many cases, NMR spectroscopy is used for this purpose. For example, information on the transition from G2P-24Cl to G2-24A can be obtained from analysis of the ^{1}H NMR spectrum. The transition of methyl signals from G2P-24Cl at 0.77 ppm to G2-24PA at 0.43 ppm was observed. Also, the transition of methyl groups of the old generation (G*n*P-*m*Cl) to the new



Scheme 2. Planar views of G3-48PA and G4-E96PA.

generation (G*n*-*m*A) is very clearly observed by NMR spectroscopy. The transition from G2-24PA to G3-E48Cl and from G3-E48Cl to G3-E48PA was observed as the same pattern. Furthermore, the ^{13}C NMR spectroscopic attachments of the hydrosilation procedure revealed the transition from triple bond signals at 90.09 and 106.37 ppm to double bonds at 147.90 and 157.94 ppm. This evidence was observed in all dendritic transitions such as G*n*-*m*Cl to G*n*-*m*PA and G*n*-*m*PA to G*n*-E*m*Cl.

Using UV spectrometry, we observed a very interesting result. That is, the increasing number of triple bonds in G*n*-*m*PA and G*n*E-*m*PA generations ($n=2$–4; $m=24$, 48 and 96) was in direct proportion to the molar absorption (Table 1 and Fig. 1). In most cases the number of triple bonds in the

Table 1
Reaction conditions

Product (M_w)	Reaction conditions	Yield [a] (g, mmol, %)
G0P-6Cl (297)	$Cl_3SiCH{=}CH_2$ (14.3 g, 88.60 mmol) + Cl_3SiH (21.26 g, 157.74 mmol), without solvent, Pt/C 0.10 g, RT, overnight [b]	26 (87.56, 99)
G0-6A (330)	G0P-6Cl (8.13 g, 27.38 mmol) + $CH_2{=}CHCH_2MgBr$ (222 mmol), THF and Et_2O, reflux 3 h [b]	7.80 (23.59, 86)
G1P-12Cl (1020)	G0-6A (2.03 g, 6.14 mmol) + $HSiMeCl_2$ (8.87 g, 77.1 mmol), THF, reflux 2 h, Pt/C 0.10 g [b]	6.27 (6.14, 99)
G1-12PA (1809)	G1P-12Cl (2.30 g, 2.25 mmol) + LiC≡CPh (35 mmol), THF, reflux 3 h [b]	2.18 (1.21, 54)
G2-E24Cl (3189)	G1-12PA (2.14 g, 1.18 mmol) + $HSiMeCl_2$ (4.12 g, 35.18 mmol), Pt/C 0.06 g, toluene, reflux 3 h [b]	3.43 (1.08, 91)
G2-E24PA (4765)	G2-E24Cl (1.17 g, 0.54 mmol) + LiC≡CPh (16 mmol), THF, reflux 3 h	1.52 (0.32, 60)
G1-12A (1086)	G1P-12Cl (14.00 g, 13.21 mmol) + $CH_2{=}CHCH_2MgBr$ (190 mmol), THF and Et_2O, reflux 3 h [b]	12.57 (11.57, 84)
G2P-24Cl (2466)	G1-12A (2.03 g, 6.14 mmol) + $HSiMeCl_2$ (8.87 g, 77.1 mmol), THF, reflux 2 h, Pt/C 0.10 g [b]	3.74 (1.52, 99)
G2-24PA (4044)	G2P-24Cl (3.70 g, 1.52 mmol) + LiC≡CPh (36 mmol), THF, reflux 3 h [b]	4.26 (1.05, 82)
G3-E48Cl (6805)	G2-24PA (1.94 g, 0.48 mmol) + $HSiMeCl_2$ (3.74 g, 32.51 mmol), Pt/C 0.07 g, toluene, reflux 5 h	3.17 (0.47, 98)
G3-E48PA (9958)	G3-E48Cl (3.17 g, 0.47 mmol) + LiC≡CPh (30 mmol), THF, reflux 3 h	3.19 (0.31, 65)
G2-24A (2603)	G2P-24Cl (16.60 g, 6.77 mmol) + $CH_2{=}CHCH_2MgBr$ (200 mmol), THF and Et_2O, reflux 3 h	12.00 (4.61, 68)
G3P-48Cl (5364)	G2-24A (3.43 g, 1.32 mmol) + $HSiMeCl_2$ (10.00 g, 86.9 mmol), THF, reflux 2 h, Pt/C 0.10 g	6.80 (1.27, 96)
G3-48PA (8516)	G3P-48Cl (4.83 g, 0.90 mmol) + LiC≡CPh (52 mmol), THF, reflux 4 h [b]	3.22 (0.38, 42)
G4-E96Cl (14038)	G3-48PA (1.36 g, 0.16 mmol) + $HSiMeCl_2$ (2.14 g, 18.60 mmol), Pt/C 0.08 g, toluene, reflux 24 h	1.88 (0.13, 84)
G4-E96PA (20343)	G4-E96Cl (1.70 g, 0.12 mmol) + LiC≡CPh (14 mmol), THF, reflux 4 h	1.43 (0.07, 59)

[a] Obtained yields.
[b] Synthetic methods and characterizations, see also [16,17].

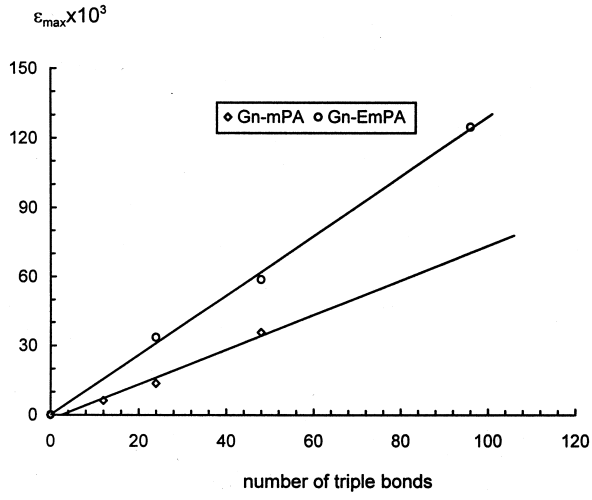


Fig. 1. Graphical view of UV data.

prepared dendrimers was in direct proportion to the maximal value of absorption at maximal wave number. The G*n*-E*m*PA type dendrimers showed higher molar absorptions than G*n*-*m*PA, because the former have more chromophores such as phenylethenyl groups in the inner shell (Fig. 1).

MALDI-TOF mass spectroscopy is a useful direct method for determination of the molecular weight of macromolecules. However, high mass molecules are difficult to characterize. The MALDI-TOF mass spectrum of G1-12PA showed one signal as the *m/z* value of the main signal at 1876 amu referring to $M^+ + 63$ (M + K and Na ion). G2-24PA showed one main signal at 4063 amu which refers to the M + Na ion. The MALDI-TOF mass spectrum of G3-48PA showed the M + K ion peak. However, the G2-E24PA and G3-E48PA spectra show the M^+ peak (Table 2), whereas the higher molecular weight G4-E96PA (20343 amu) was not observed in any spectrum from MALDI-TOF mass spectroscopy.

The polydispersity value (M_w/M_n) analyzed using SEC for the dendrimers G2-24PA to G4-E96PA shows that the prepared dendrimers have a very narrow range of molecular weight. As expected, the calculated molecular weights of the dendrimers were in inverse proportion to the retention time. The plot of the calculated molecular weights of G1-12PA to G4-E96PA versus retention time was a straight line (Table 2, Fig. 2). This suggests that the prepared dendrimers have regularly increased molecular weight. The characterization

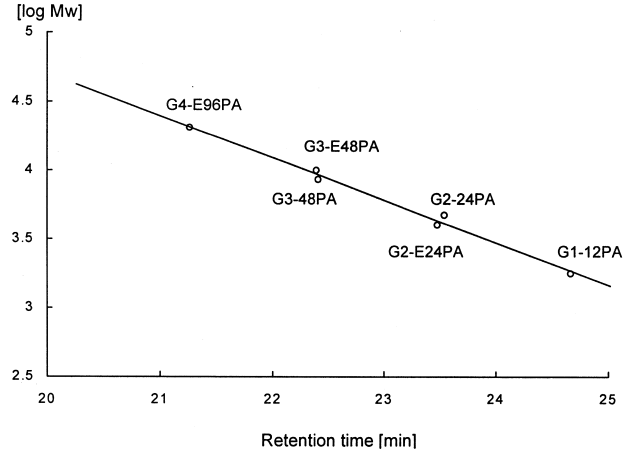


Fig. 2. Graphical view of GPC data.

Table 2
MALDI-TOF mass, GPC and UV data for dendritic carbosilanes

Compound	MALDI mass found/calc.	GPC Rt. (min) (M_n/M_w)	UV λ_{max} ($\varepsilon_{max}\times10^3$)
G0-6A	330/330 (by GC-MS)		
G1-12A	—/1086		
G2-24A	—/2603		
G3-48A	5693/5634 $(M+K+Na)^+$		
G1-12PA	1876/1809 $(M+K+Na)^+$	24.66 (1.06)	283 (6.2)
G2-24PA	4063/4044 $(M+Na)^+$	23.40 (1.14)	283 (13.6)
G3-48PA	8546/8506 $(M+K)^+$	22.41 (1.30)	283 (35.7)
G2-E24PA	4775/4765 $(M)^+$	23.53 (1.16)	285 (33.6)
G3-E48PA	9959/9958 $(M)^+$	22.39 (1.31)	285 (58.9)
G4-E96PA	— [a]/20343	21.56 (1.60)	285 (124.3)

[a] M^+ was not observed.

of the prepared dendrimers by the use of NMR, MALDI-TOF mass spectroscopy, UV, EA, and SEC methods is well justified for our experimental purpose.

3. Experimental

All reactions were carried out under a dried N_2 atmosphere. Ether and THF were dried by sodium-benzophenone ketyl, while solvents such as toluene were dried and distilled from sodium metal. The NMR spectra were recorded on a Bruker AC-200 spectrometer. The UV spectra were measured by an HP 8452A diode array UV–Vis spectrophotometer. DSC was measured with a Setram DSC-92 at a heating range of 10°C min^{-1} in aluminum crucibles. The Pusan and Taejon Branches of the Korean Basic Science Institute (KBSI) performed elemental analysis and the MALDI-TOF mass spectroscopy (KRATOS KOMPACKT MALDI-TOF 2). The following abbreviations are used in the experiments: G*n*-*m*A refers to dendritic silanes with allyl groups; G*n*P-*m*Cl refers to dendrimers with dichloromethylsilyl groups on the periphery and propylene groups in the inner shell; G*n*-*m*PA refers to dendrimers with phenylethynyl groups on the periphery and propylene groups in the inner shell; G*n*-E*m*Cl refers to dichloromethylsilyl groups on the periphery, and ethenyl groups in the $(n-1)$th layer, and propylene groups in the $(n-2)$th layer; G*n*-E*m*PA refers to phenylethynyl groups on the periphery and ethenyl groups in the $(n-1)$th layer and propylene groups in the $(n-2)$th layer. A description of the experimental methods has appeared in the literature [10–13,16,17], but the following may serve as examples. The reaction conditions are recorded in Table 1.

3.1. General procedure for GnP-mCl type dendrimers: G0P-6Cl

A mixture of 14.30 g (88.60 mmol) of $Cl_3SiCH{=}CH_2$, 21.26 g (157.74 mmol) of $HSiMeCl_2$, and 0.10 g of a hydrosilation catalyst (10% Pt content on activated carbon) was stirred for 12 h at room temperature. The platinum catalyst was filtered off with pentane. The volatile components were removed under reduced pressure, leaving 26 g (87.56 mmol, 99%) of G0P-6Cl as a colorless crystal. The G0P-6Cl was recrystallized in pentane [16,17].

3.2. General procedure for Gn-mA type dendrimers: G0-6A

222 mmol of allylmagnesium bromide in 200 ml ether was slowly added to 8.13 g (27.38 mmol) of G0P-6Cl in 50 ml THF. After the addition, the reaction mixture was refluxed for 3 h. After the reaction was completed, salt was filtered off and washed with pentane. The volatile components were removed under reduced pressure, leaving a colorless liquid. All compounds formed were chromatographed on silica gel with chloroform. The product G0-6A was obtained as colorless oil. Yield 7.80 g (23.59 mmol, 86%) [16,17].

3.3. General procedure for Gn-mPA type dendrimers: G1-12PA

35 mmol of lithium phenylacetylide in 35 ml THF was slowly added to 2.30 g (2.25 mmol) of G1P-12Cl in 25 ml THF. After the addition, the reaction mixture was refluxed for 3 h. After the reaction was completed, salt was filtered off and washed with toluene. The volatile components were removed under reduced pressure, leaving a yellow solid. All compounds formed were chromatographed on silica gel with toluene. The product G1-12PA was obtained as yellow oil to solid. Yield 2.18 g (1.21 mmol, 54%). *Anal*. Calc. for $C_{122}H_{118}Si_8$: C, 81.00; H, 6.57. Found: C, 81.18; H, 6.51%. FT-IR (KBr, cm^{-1}): 1584 (w, $\nu_{C=C\ aromatic}$), 2165 (s, $\nu_{C\equiv C}$), 3068 (w, $\nu_{C-H\ aromatic}$). T_g (°C): 143.65. ^1H NMR (ppm, $CDCl_3$): δ 0.40 (s, 18H, MeSi(G1)), 0.48 (s, 4H, CH_2(G0)), 0.62–0.81 (m, 12H, CH_2(G0)), 0.81–1.09 (m, 12H, CH_2(G0)), 1.48–1.80 (m, 12H, CH_2(G0)), 7.18–7.68 (m, 60H, Ph). ^{13}C NMR (ppm, $CDCl_3$): δ −1.19 (MeSi(G1)), 4.82 (CH_2(G0)), 16.05 (CH_2(G0)), 18.30 (CH_2(G0)), 20.69 (CH_2(G0)), 90.03 (SiC≡), 106.26 (≡CPh), 122.66 (C_{-q}), 128.12 (C_{-o}), 128.68 (C_{-p}), 132.02 (C_{-m}).

3.4. General procedure for Gn-EmCl type dendrimers: G2-E24Cl

A mixture of 2.14 g (1.18 mmol) of G1-12PA, 4.12 g (35.18 mmol) of $HSiMeCl_2$, and 0.06 g of a hydrosilation catalyst (10% Pt content on activated carbon) was refluxed for 3 h. The platinum catalyst was filtered off with toluene. The volatile components were removed under reduced pressure, leaving 3.43 g (1.08 mmol, 91%) of G2-E24Cl as a yellow crystal. ^{1}H NMR (ppm, $CDCl_3$): δ −0.46 (s, 18H, MeSi(G1)), 0.30 (m, 24H, CH_2(G0)), 0.48 (s, 4H, CH_2(G0)), 0.74 (s, 36H, MeSi(G2P)), 1.07 (m, 12H, CH_2(G0)), 6.53 (s, 12H, CH=(G1)), 6.90–7.53 (m, 60H, Ph). ^{13}C NMR (ppm, $CDCl_3$): δ −2.99 (MeSi(G1)), 4.54 (MeSi(G2P)), 5.18 (CH_2(G0)), 16.61 (CH_2(G0)), 18.33 (CH_2(G0)), 20.42 (CH_2 (G0)), 127.51 (C_{-m}), 128.16 (C_{-p}), 128.19 (C_{-o}), 140.44 (C_{-q}), 148.84 (CH=), 157.16 (=CPh).

3.5. General procedure for Gn-EmPA type dendrimers: G2-E24PA

16 mmol of lithium phenylacetylide in 16 ml THF was slowly added to 1.71 g (0.54 mmol) of G2-E24Cl in 25 ml THF. After the addition was finished, the reaction mixture was refluxed for 3 h. After the reaction was completed, the salt was filtered off and washed with toluene. The volatile components were removed under reduced pressure, leaving a yellow solid. All compounds formed were chromatographed on silica gel with toluene. The product, G2-E24PA, was obtained as yellow oil to solid. Yield 1.52 g (0.32 mmol, 60%). *Anal*. Calc. for $C_{326}H_{286}Si_{20}$: C, 82.16; H, 6.05. Found: C, 81.71; H, 6.06%. FT-IR (KBr, cm^{-1}): 1594 (w, $\nu_{C=C}$), 2158 (s, $\nu_{C\equiv C}$), 2914 (w, $\nu_{C-H\ aliphatic}$), 3055 (w, $\nu_{C-H\ aromatic}$). T_g (°C): 137.83. ^{1}H NMR (ppm, $CDCl_3$): δ −0.48 (s, 18H, MeSi(G1)), 0.20 (s, 24H, CH_2(G0)), 0.29 (m, 4H, CH_2(G0)), 0.43 (s, 36H, MeSi(G2)), 0.99 (m, 12H, CH_2(G0)), 6.68 (s, 12H, CH=(G1)), 6.78–7.75 (m, 180H, Ph). ^{13}C NMR (ppm, $CDCl_3$): δ −2.90 (MeSi(G1)), −0.85 (MeSi(G2)), 4.98 (CH_2(G0)), 16.89 (CH_2(G0)), 18.30 (CH_2(G0)), 20.53 (CH_2(G0)), 89.18 (SiC≡), 107.58 (≡CPh), 122.62 (C_{-q}), 126.45 (C_{-p}(G1)), 127.69 (C_{-m}(G1)), 128.08 (C_{-o}(G1)), 128.20 (C_{-o}), 128.87 (C_{-p}), 132.05 (C_{-m}), 143.22 (C_{-q}(G1)), 148.02 (CH=(G1)), 157.86 (=CPh(G1)).

3.6. G3-E48Cl

^{1}H NMR (ppm, $CDCl_3$): δ −0.46 (s, 36H, MeSi(G2)), −0.15 (s, 18H, MeSi(G1)), 0.29 (m, 48H, CH_2(G1)), 0.47 (s, 4H, CH_2(G0)), 0.51 (m, 24H, CH_2(G0)), 0.72 (s, 72H, MeSi (G3P)), 1.06 (m, 24H, CH_2(G1)), 1.26 (m, 12H, CH_2(G0)), 6.52 (s, 24H, CH=(G2)), 6.83–7.57 (m, 120H, Ph). ^{13}C NMR (ppm, $CDCl_3$): δ −5.07 (MeSi(G1)), −2.92 (MeSi(G2)), 4.54 (MeSi(G3P)), 5.07 (CH_2(G0)), 18.29 (CH_2(G1)), 18.41 (CH_2(G1)), 18.62 (CH_2(G0)), 19.26 (CH_2(G0)), 20.07 (CH_2(G1)), 127.49 (C_{-p}), 128.15 (C_{-m}), 128.17 (C_{-o}), 140.42 (C_{-q}), 148.84 (CH=), 157.09 (=CPh).

3.7. G3-E48PA

Anal. Calc. for $C_{674}H_{622}Si_{44}$: C, 81.29; H, 6.30. Found: C, 80.48; H, 6.11%. FT-IR (KBr, cm^{-1}): 1595 (w, $\nu_{C=C}$), 2157 (s, $\nu_{C\equiv C}$), 2912 (w, $\nu_{C-H\ aliphatic}$), 3057 (w, $\nu_{C-H\ aromatic}$). T_g (°C): 138.17. ^{1}H NMR (ppm, $CDCl_3$): δ −0.48 (s, 36H, MeSi(G2)), −0.29 (s, 18H, MeSi(G1)), 0.27 (m, 72H, CH_2(G1–G0)), 0.28 (m, 4H, CH_2(G0)), 0.40 (s, 72H, MeSi(G3)), 1.04 (m, 36H, CH_2 (G1–G0)), 6.67 (s, 24H, CH=(G2)), 6.89–7.57 (m, 360H, Ph). ^{13}C NMR (ppm, $CDCl_3$): δ −5.38 (MeSi(G1)), −2.81 (MeSi(G2)), −0.88 (MeSi(G3)), 5.36 (CH_2(G0)), 18.28 (CH_2(G1)), 18.39 (CH_2(G1)), 18.56 (CH_2(G0)), 19.46 (CH_2(G0)), 20.32 (CH_2(G1)), 89.18 (SiC≡), 107.58 (≡CPh), 122.58 (C_{-q}), 126.47 (C_{-p}(G2)), 127.69 (C_{-m}(G2)), 128.07 (C_{-o}(G2)), 128.18 (C_{-o}), 128.86 (C_{-p}), 132.02 (C_{-m}), 143.19 (C_{-q}(G2)), 147.90 (CH=(G2)), 157.94 (=CPh(G2)).

3.8. G4-E96Cl

^{1}H NMR (ppm, $CDCl_3$): δ −0.46 (s, 72H, MeSi(G3)), −0.15 (s, 36H, MeSi(G2)), −0.08 (s, 18H, MeSi(G1)), 0.29 (m, 96H, CH_2(G2)), 0.47 (s, 4H, CH_2(G0)), 0.50 (m, 72H, CH_2(G1–G0)), 0.71 (s, 144H, MeSi(G4P)), 1.09 (m, 48H, CH_2(G2)), 1.26 (m, 36H, CH_2 (G1–G0)), 6.52 (s, 48H, CH=(G3)), 6.81–7.63 (m, 240H, Ph). ^{13}C NMR (ppm, $CDCl_3$): δ −5.11 (MeSi(G1)), −5.02 (MeSi(G2)), −2.91 (MeSi(G3)), 4.55 (MeSi(G4P)), 5.34 (CH_2(G0)), 18.32 (CH_2(G2)), 18.37 (CH_2(G2)), 18.47 (CH_2(G1–G0)), 19.11 (CH_2(G1–G0)), 20.08 (CH_2(G2)), 127.49 (C_{-p}), 128.14 (C_{-m}), 128.17 (C_{-o}), 140.41 (C_{-q}), 148.85 (CH=), 157.09 (=CPh).

3.9. G4-E96PA

Anal. Calc. for $C_{1370}H_{1294}Si_{92}$: C, 80.89; H, 6.41. Found: C, 78.70; H, 6.41%. FT-IR (KBr, cm^{-1}): 1594 (w, $\nu_{C=C}$), 2158 (s, $\nu_{C\equiv C}$), 2912 (w, $\nu_{C-H\ aliphatic}$), 3056 (w, $\nu_{C-H\ aromatic}$). T_g (°C): 142.86. ^{1}H NMR (ppm, $CDCl_3$): δ −0.48 (s, 72H, MeSi(G3)), −0.29 (s, 36H, MeSi(G2)), −0.18 (s, 18H, MeSi(G1)), 0.20 (m, 168H, CH_2(G2–G0)), 0.27 (m, 4H, CH_2(G0)), 0.40 (s, 144H, MeSi(G4)), 1.04 (m, 84H, CH_2(G2–G0)), 6.67 (s, 48H, CH=(G3)), 6.86–7.96 (m, 720H, Ph). ^{13}C NMR (ppm, $CDCl_3$): δ −5.33 (MeSi(G2–G1)), −2.79 (MeSi(G3)), −0.88 (MeSi(G4)), 5.34 (CH_2(G0)), 18.37 (CH_2(G2)), 18.47 (CH_2(G2)), 18.52 (CH_2(G1–G0)), 19.26 (CH_2(G1–G0)), 20.30 (CH_2(G2)), 89.19 (SiC≡), 107.60 (≡CPh), 122.58 (C_{-q}), 126.48 (C_{-p}(G3)), 127.68 (C_{-m} (G3)), 128.05 (C_{-o} (G3)), 128.19 (C_{-o}), 128.87 (C_{-p}), 132.02

(C_{-m}), 143.21 (C_{-q} (G3)), 147.89 (CH=(G3)), 157.98 (=CPh (G3)).

Acknowledgements

This study was supported by the Korean Science and Engineering Foundation (Grant No. 995-0300-009-2).

References

[1] J. Issberner, R. Moore, F. Vögtle, Angew. Chem., Int. Ed. Engl. 33 (1994) 2413.
[2] M.K. Lothian-Tomalia, D.M. Hedstrand, D.A. Tomalia, A.B. Padias, H.K. Hall Jr., Tetrahedron 53 (1997) 15495.
[3] M. Fischer, F. Vögtle, Angew. Chem., Int. Ed. Engl. 38 (1999) 884.
[4] T.K. Lindhorst, Nachr. Chem. Tech. Lab. 44 (1996) 1073.
[5] M. Kawa, J.M. Fréchet, J. Chem. Mater. 10 (1998) 286.
[6] J.-P. Majoral, A.-M. Caminade, Chem. Rev. 99 (1999) 845.
[7] A. Sekiguchi, M. Nanjo, C. Kabuto, H. Sakurai, J. Am. Chem. Soc. 117 (1995) 4195.
[8] C.M. Casado, I. Cuadrado, M. Morán, B. Alonso, F. Lobeto, J. Losada, Organometallics 14 (1995) 2618.
[9] K. Lorenz, R. Mülhaut, H. Frey, U. Rapp, F.J. Mayer-Posner, Macromolecules 28 (1995) 6657.
[10] C. Kim, E. Park, E. Kang, Bull. Korean Chem. Soc. 17 (1996) 419.
[11] C. Kim, K. An, J. Organomet. Chem. 547 (1997) 55.
[12] C. Kim, K. An, Bull. Korean Chem. Soc. 18 (1997) 164.
[13] C. Kim, A. Kwon, Synthesis (1998) 155.
[14] C. Kim, M. Kim, J. Organomet. Chem. 563 (1998) 43.
[15] C. Kim, I. Jung, Inorg. Chem. Commun. 1 (1998) 427.
[16] C. Kim, E. Park, E. Kang, Bull. Korean Chem. Soc. 17 (1996) 592.
[17] C. Kim, I. Jung, J. Organomet. Chem. 588 (1999) 9.
[18] D. Seyferth, T. Kugita, A.L. Rheingold, G.P.A. Yab, Organometallics 14 (1995) 5362.
[19] K. Lorenz, H. Frey, B. Stühn, R. Mülhaut, Macromolecules 30 (1997) 6860.
[20] M.S. Wendland, S.C. Zimmerman, J. Am. Chem. Soc. 12 (1999) 1389.
[21] G.L. Larson, Advances in Silicon Chemistry, vol. 1, JAI Press, London, 1991, pp. 327–382.

PERGAMON

www.elsevier.nl/locate/poly

Polyhedron 19 (2000) 1037–1041

POLYHEDRON

Heterometallic lithium niobium complexes: synthesis and molecular structures of $LiNbO(O\text{-}2,6\text{-}PhMe_2)_4 \cdot 3THF$ and $[LiNbCl_3(O\text{-}2,6\text{-}PhMe_2)_2 \cdot 2THF]_2$

Seung Kju Park [a], Sang Man Koo [a,*], Yong Eun Lee [b]

[a] *Department of Industrial Chemistry and CPRC, College of Engineering, Hanyang University, Seoul 133-791, South Korea*
[b] *Highway Research Center, Korea Highway Corporation, Kyungki-do 461-380, South Korea*

Received 13 October 1999; accepted 24 February 2000

Abstract

The methathesis reactions between $NbCl_5$ and lithium-2,6-dimethylphenoxide, LiO-2,6-$PhMe_2$, afford $LiNbO(O\text{-}2,6\text{-}PhMe_2)_4 \cdot 3THF$ (**1**) and $[LiNbCl_3(O\text{-}2,6\text{-}PhMe_2)_2 \cdot 2THF]_2$ (**2**). The complexes **1** and **2** were characterized by X-ray single crystal diffraction analyses, elemental analyses, and FT-IR, ^1H and ^{13}C NMR spectroscopy. Complex **1** exists as a monomeric binuclear lithium niobium complex which has a terminal oxo ligand, and complex **2** exists as a dimeric tetranuclear lithium niobium complex where metal atoms are linearly connected by μ_2-chloride linkages, respectively. Lithium metal is coordinated by THF molecules as a counter ion. ©2000 Elsevier Science Ltd All rights reserved.

Keywords: Heterometallic aryloxides; Lithium niobate; Monomeric compounds; Niobium; Percursors

1. Introduction

Transition metal alkoxides are not only important starting materials for studying organometallic chemistry but are also extremely attractive precursors for the preparation of metal oxides. In particular, heterometallic alkoxides are potential single-source precursors for the fabrication of bimetallic (or multimetallic) oxides owing to the significant advantages they offer to the composition control of final ceramic materials and simplification of processes [1–10]. With the development of processes such as sol-gel and metal-organic chemical vapor deposition (MOCVD), demand for molecularly defined precursors has been increased [1–10]. Therefore, there has been many studies on the preparation of heterometallic alkoxides in recent years.

In particular, lithium niobium alkoxides are in an area of intense current interest owing to their utility as precursors for electro-optic materials [11–23]. However, the chemistry of lithium niobium alkoxides remains relatively unexplored. Since the first report of the syntheses of lithium niobium(V) alkoxides, $[LiNb(OR)_6]_X$ (R = Me, Et, ^{i}Pr, ^{t}Bu) [15], a few complexes have been synthesized and characterized: $[LiNb(OEt)_6]_X$ of helical structure [16] and $[LiNbO(OEt)_4 \cdot EtOH]_2$ [1,11,17] as intermediate in a hydrolysis reaction to $[LiNb(OEt)_6]_X$. More recently, $[LiNb(OR)_6]_2$ ($R = CH_2CMe_3$, CH_2SiMe_3), dimeric molecular precursors, have been prepared and characterized [18].

Our motivation for exploring lithium niobium alkoxides concerns the development of improved molecular single-source precursors for lithium niobate, $LiNbO_3$. To obtain molecular lithium niobium complexes without any intermolecular bonds or bridging units, we have introduced bulky aryl groups containing methyl side chains [24]. Syntheses and structural characterizations of niobium(V) aryl compounds such as homoleptic niobium aryloxides, $Nb(O\text{-}2,6\text{-}PhMe_2)_5$, $[Nb(O\text{-}4\text{-}PhMe)_5]_2$, and $[Nb(O\text{-}3,5\text{-}PhMe)_5]_2$, niobium oxo aryloxides, $NbO(O\text{-}2,6\text{-}PhMe_2)_3$ and $NbO(O\text{-}2,6\text{-}Ph^tBu_2)_3$, and niobium chloro aryloxides, $NbCl(MTP)_2$ ($MTP = 2,2'\text{-}CH_2(O\text{-}2,4\text{-}C_6H_2{}^tBu_2)_2$), $[Nb(O\text{-}2,6\text{-}Ph^iPr_2)_2Cl_3]_2$, and $Nb(O\text{-}2,6\text{-}PhMe_2)_2Cl_3 \cdot THF$ (THF = tetrahydrofuran) have been reported [25–29]. However, lithium niobium aryloxides, oxo aryloxides, or chloro aryloxides have not been synthesized yet. This study reports the syntheses and structural characterizations of the first examples of a monomeric lithium niobium(V) oxo aryloxide, $LiNbO(O\text{-}2,6\text{-}PhMe_2)_4 \cdot 3THF$ (**1**), and a dimeric lithium niobium(IV) chloro aryloxide, $[LiNbCl_3(O\text{-}2,6\text{-}PhMe_2)_2 \cdot 2THF]_2$ (**2**).

* Corresponding author. Tel.: +82-2-2290-0527; fax: 82-2-2281-4800; e-mail: sangman@email.hanyang.ac.kr

0277-5387/00/$ - see front matter ©2000 Elsevier Science Ltd All rights reserved.
PII S0277-5387(00)00341-7

2. Experimental

All reactions and manipulations were carried out under dry inert gas using standard Schlenk line techniques. Solvents were dried and purified by distillation from sodium benzophenone ketyl under nitrogen. Niobium chloride, lithium, and 2,6-dimethylphenol were used as received from Strem Chemicals and Aldrich Chemical Co. Lithium-2,6-dimethylphenoxide was prepared from 2,6-dimethylphenol and metallic lithium in diethyl ether. IR spectra were obtained as KBr pellet technique on a Nicolet Magna-IR 760 spectrometer. NMR spectra were registered on a Varian Gemini 300 spectrometer. Analytical data were obtained with a Thermoquest EA-1110 CHNS analyzer.

2.1. Synthesis of $LiNbO(O\text{-}2,6\text{-}PhMe_2)_4\cdot 3THF$ (1)

A solution of $NbCl_5$ (2 g, 7.4 mmol) in THF (50 ml) was added dropwise to a solution of 4 equiv. $LiO\text{-}2,6\text{-}PhMe_2$ (3.8 g, 29.7 mmol) in THF (50 ml). The resultant mixture was stirred at ambient temperature for 24 h. After removal of THF solvent, diethyl ether (150 ml) was added, and the mixture was filtered to eliminate LiCl. After concentration to half volume, THF (50 ml) was added and the solution was layered with *n*-hexane. Complex **1** was obtained as yellow crystals with 72% (4.35 g) yield. *Anal*. Found: C, 64.74; H, 7.67. Calc. for $C_{44}H_{60}O_8LiNb$: C, 64.70; H, 7.40%. FT-IR (cm^{-1}): 3010w, 2976m, 2880m, 1594w, 1467s, 1426s, 1372w, 1273vs, 1225vs, 1088m, 1048m, 918m, 880s, 754s, 737m, 713s, 566m, 546m. ^1H NMR ($CDCl_3$, 25°C, ppm): 6.94–6.51 (m, 12H, $OC_6H_3Me_2$); 3.66 (t, 12H, OCH_2CH_2); 2.15 (s, 24H, $OC_6H_3Me_2$); 1.76 (quintet, 12H, OCH_2CH_2). $^{13}C\{^1H\}$ NMR ($CDCl_3$, 25°C, ppm): 160.5, 128.5, 127.8, 127.2, 123.5, 121.1, 119.6, 118.9 ($OC_6H_5Me_2$); 68.2 (OCH_2CH_2); 25.4 (OCH_2CH_2); 17.0, 16.2 ($OC_6H_5Me_2$).

2.2. Synthesis of $[LiNbCl_3(O\text{-}2,6\text{-}PhMe_2)_2\cdot 2THF]_2$ (2)

A solution of 4 equiv. $LiO\text{-}2,6\text{-}PhMe_2$ (3.8 g, 29.7 mmol) in THF (50 ml) was added dropwise to $NbCl_5$ (2 g, 7.4 mmol). After a similar procedure to the preparation of complex **1**, complex **2** was obtained as dark brown crystals in a small amount. Satisfactory C and H analyses were obtained for complex **2**. FT-IR (cm^{-1}): 3010w, 2976m, 2881m, 1587w, 1467s, 1420m, 1379w, 1266s, 1208vs, 1092m, 1044m, 891s, 767m, 730s, 571m. ^1H NMR (CD_3OD, 25°C, ppm): 6.89–6.61 (m, 12H, $OC_6H_3Me_2$); 3.73 (t, 16H, OCH_2CH_2); 2.19 (s, 24H, $OC_6H_3Me_2$); 1.87 (quintet, 16H, OCH_2CH_2). $^{13}C\{^1H\}$ NMR (CD_3OD, 25°C, ppm): 129.3, 125.5, 120.7 ($OC_6H_5Me_2$); 68.8 (OCH_2CH_2); 26.5 (OCH_2CH_2); 16.6 ($OC_6H_5Me_2$).

2.3. Crystallography of $LiNbO(O\text{-}2,6\text{-}PhMe_2)_4\cdot 3THF$ and of $[LiNbCl_3(O\text{-}2,6\text{-}PhMe_2)_2\cdot 2THF]_2$

Single crystals suitable for X-ray diffraction studies were grown from THF and *n*-hexane for complexes **1** and **2**. A suitable crystal of each compound was mounted inside a glass capillary under nitrogen atmosphere and sealed with a flame. Diffraction data were collected on a Bruker P4 four circle instrument, with graphite-monochromated Mo Kα radiation ($\lambda = 0.71073$ Å). The unit cell parameters and basic information about data collection and structure refinement are given in Table 1. The structures were solved by direct methods with SHELXS-86 and refined against F^2 on all data by full-matrix least-squares with SHELXL-93. All non-hydrogen atoms were refined anisotropically. Hydrogen atoms

Table 1
Crystal data for $LiNbO(O\text{-}2,6\text{-}PhMe_2)_4\cdot 3THF$ and $[LiNbCl_3(O\text{-}2,6\text{-}PhMe_2)_2\cdot 2THF]_2$

Formula	$C_{44}H_{60}O_8LiNb$	$C_{48}H_{68}O_8Cl_6Li_2Nb_2$
FW	816.77	1184.4
Crystal system	monoclinic	monoclinic
Space group	$P2_1/n$	$P2_1/n$
a (Å)	13.226(1)	11.953(1)
b (Å)	20.709(2)	17.383(2)
c (Å)	16.559(2)	13.724(1)
β (°)	90.54(1)	95.94(1)
V (Å^3)	4535.3(8)	2836.2(5)
Z	4	2
Density ρ_{calc} (g cm^{-3})	1.196	1.388
Linear absorption coefficient μ (mm^{-1})	0.312	0.732
Temperature of measurement (K)	293(2)	293(2)
Scan type	θ–2θ	θ–2θ
Data collection range (°)	$1.83 \le \theta \le 22.52$	$1.90 \le \theta \le 22.51$
Octants collected	−14.0; −22.0; −17.17	0.12; −18.0; −14.14
$F(000)$	1728	1220
No. of data collected	6149	3895
No. of unique data collected	5877	3690
R_{int}	0.1737	0.0334
$R_1 = \Sigma \lvert\lvert F_o\rvert - \lvert F_c\rvert\rvert / \Sigma \lvert F_o\rvert$	0.0673(0.0889)	0.0369(0.0501)
$wR_2 = [\Sigma w(F_o^2 - F_c^2)^2 / \Sigma wF_o^4]^{1/2}$ for data with $I > 2\sigma(I)$	0.2030(0.2418)	0.0916(0.1036)
GOF $= [\Sigma w(F_o^2 - F_c^2)^2 / \Sigma(n-p)]^{1/2}$	1.028	1.011
Min./max. residual electron density (e Å^{-3})	−0.707/0.575	−0.377/0.364
No. of variables	547	332

were included at geometrically calculated positions and refined using a riding model.

3. Results and discussion

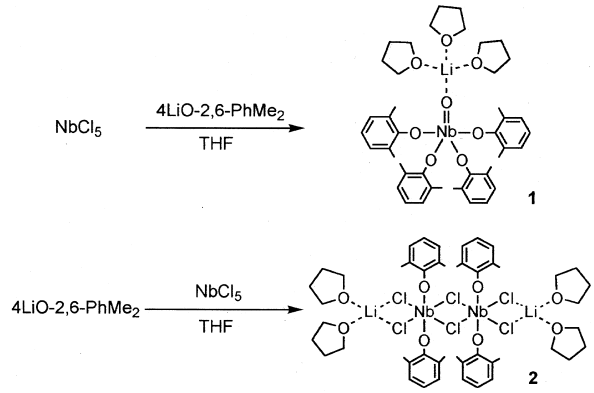
3.1. Synthesis and characterization

The methathesis reactions of niobium chloride, $NbCl_5$, with lithium-2,6-dimethylphenoxide, LiO-2,6-$PhMe_2$, were investigated in THF at room temperature. Complexes of formula $LiNbO(O\text{-}2,6\text{-}PhMe_2)_4 \cdot 3THF$ (**1**) and $[LiNbCl_3(O\text{-}2,6\text{-}PhMe_2)_2 \cdot 2THF]_2$ (**2**) were obtained (Scheme 1). Complex **1** was prepared by adding a THF solution of $NbCl_5$ to a THF solution of 4 equiv. LiO-2,6-$PhMe_2$ with 72% yield. Complex **1** was formed irrespective of the ligand-to-metal molar ratio, *R*, used (from 4 to 6) and was obtained in the same yield for each ratio. The formation of a terminal oxo ligand in situ may result from the abstraction of the oxygen atom from THF by $NbCl_5$ at the initial stage of the reaction [14,23,29,30]. However, the direct reaction between $NbOCl_3 \cdot 2CH_3CN$ and 4 equiv. LiO-2,6-$PhMe_2$ did not seem to be a useful route to complex **1**. On the other hand, the addition of a THF solution of 4 equiv. LiO-2,6-$PhMe_2$ to $NbCl_5$ led to the formation of complex **2**. The reaction of $NbCl_5$ with Li-2,6-$OPhMe_2$ in 1:2–1:6 molar ratio was carried out. An amount of complex **2** was obtained with the formation of a niobium chloro-aryloxide, $NbCl_x(OR)_{5-x}$, as the major product. The maximum yield of complex **2** was $>10\%$ at $R=4$. Complexes **1** and **2** were characterized by spectroscopic and analytical techniques.

The FT-IR spectra exhibit stretching modes from ν(C–O–C) of the coordinated THF molecules at 1048 (m) and 880 (s) cm^{-1} for complex **1** and at 1044 (m) and 891 (s) cm^{-1} for complex **2** and a sharp band at 918 (m) cm^{-1} for complex **1** from ν(Nb=O) which is shifted to lower frequencies compared to ν(Nb=O), 962 cm^{-1} of the $[NbOCl_4(THF)]^-$ anion [31]. The bands at 566 (m) and 546 (m) cm^{-1} in complex **1** and at 571 (m) cm^{-1} in complex **2** are assigned to ν(Nb–O) vibrations from aryloxo ligands [32]. In the ^1H and $^{13}C\{^1H\}$ NMR spectra of complex **2** in CD_3OD, the resonance signals corresponding to only one type of 2,6-dimethylphenoxy ligand and coordinated THF molecules are observed at room temperature, while those of complex **1** in $CDCl_3$ show two types of peaks for 2,6-dimethylphenoxy ligands. The presence of two types of signals suggests magnetically non-equivalent surroundings for 2,6-dimethylphenoxy ligands.

3.2. Molecular structures of $LiNbO(O\text{-}2,6\text{-}PhMe_2)_4 \cdot 3THF$ and of $[LiNbCl_3(O\text{-}2,6\text{-}PhMe_2)_2 \cdot 2THF]_2$

To establish the solid state structures, X-ray single crystal diffraction analyses of complexes **1** and **2** were used. The ORTEP diagrams of complexes **1** and **2** are presented in Figs. 1 and 2, respectively.



Scheme 1. Syntheses of lithium niobium oxo-aryloxides and chloro-aryloxides.

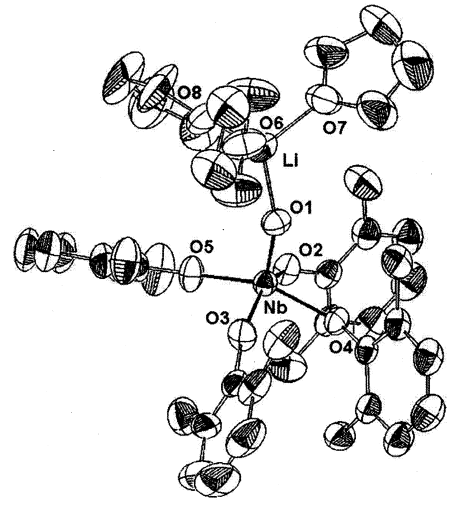


Fig. 1. ORTEP diagram of complex **1** in the solid state. The hydrogen atoms are omitted for clarity.

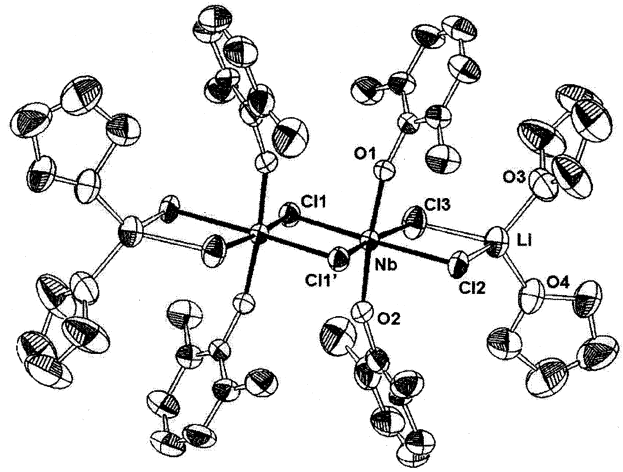


Fig. 2. ORTEP diagram of complex **2** in the solid state. The hydrogen atoms are omitted for clarity.

Complex **1** exists as a monomeric binuclear complex (Fig. 1). Selected bond lengths and angles are given in Table 2. The structure of complex **1** can be described as $[NbO(O\text{-}2,6\text{-}PhMe_2)_4]^-$ capped by an Li^+ cation which is solvated with three THF molecules. The molecular structure of com-

Table 2
Selected bond lengths (Å) and angles (°) for $LiNbO(O\text{-}2,6\text{-}PhMe_2)_4 \cdot 3THF$

Nb–O1	1.730(5)	Li–O1	1.88(2)
Nb–O2	1.948(4)	Li–O6	1.95(2)
Nb–O3	1.940(5)	Li–O7	1.96(2)
Nb–O4	1.985(4)	Li–O8	1.90(2)
Nb–O5	1.922(5)		
O1–Nb–O2	106.8(2)	O1–Li–O6	109.3(8)
O1–Nb–O3	103.2(2)	O1–Li–O7	112.5(8)
O1–Nb–O4	103.1(2)	O1–Li–O8	112.1(9)
O1–Nb–O5	101.5(2)	O6–Li–O7	106.3(9)
O2–Nb–O4	82.8(2)	O6–Li–O8	110.8(8)
O2–Nb–O5	87.3(2)	O7–Li–O8	105.6(8)
O3–Nb–O4	86.6(2)	C1–O2–Nb	144.6(4)
O3–Nb–O5	90.7(2)	C9–O3–Nb	158.0(6)
O2–Nb–O3	149.7(2)	C17–O4–Nb	138.7(4)
O4–Nb–O5	155.2(2)	C25–O5–Nb	169.9(5)
Nb–O1–Li	154.0(6)		

plex **1** includes niobium square pyramid and lithium tetrahedron units sharing a corner corresponding to the oxo ligand (Li–O1=Nb 154.0(6)°). The niobium is five-coordinated by a terminal oxo ligand in an axial position and four 2,6-dimethylphenoxy ligands in the basal plane of the square pyramid. The lithium is four-coordinated by three oxygen atoms of THF molecules and the terminal oxo ligand in the $[NbO(O\text{-}2,6\text{-}PhMe_2)_4]^-$ unit. The steric hindrance of the 2,6-dimethylphenoxy ligands stabilizes a low coordination number, with a terminal Nb=O bond [12,13,23].

The square pyramidal geometry around the niobium metal is severely distorted (O–Nb=O angles ranging from 101.5(2) to 106.8(2)°, *cis* O–Nb–O angles ranging from 82.8(2) to 90.7(2)°, and *trans* O–Nb–O angles ranging from 149.7(2) to 155.2(2)°), while the lithium tetrahedron is quite regular (O–Li–O angles ranging from 105.6(8) to 112.5(8)°). The average Nb–O bond length of 1.949 Å is significantly longer than those in analogous compounds such as $[LiNb(OEt)_6]_X$ (1.88 Å) [16], $[LiNb(OCH_2SiMe_3)_6]_2$ (1.893 Å) [18], and $Nb(O\text{-}2,6\text{-}PhMe_2)_5$ (1.899 Å) [25]. This is probably due to the formation of a double bond between niobium and the terminal oxygen in axial position, which results in the elongation of Nb–O bonds in *trans* positions. Interestingly, the four 2,6-dimethylphenoxy ligands in complex **1** are not identical. The bond distance Nb–O5 (1.922(5) Å) is shorter than those of the other Nb–O bonds in complex **1**. It can be assumed that the partial π interaction between the d orbital of niobium and p orbital of oxygen in Nb–O5 might cause the strong bond. The nearly linear Nb–O5–C25 angle (169.9(5)°) supports this assumption. In addition, the Nb=O1 bond length (1.730(5) Å) is longer than those in the following complexes: 1.710 Å in $[NbO(SPh)_4]^-$ [33], 1.699 Å in $NbO(N(SiMe_3)_2)_3$ [30], and 1.67–1.71 Å in six-coordinated oxo niobium complexes [34]. This probably results from the interaction between the terminal oxo ligand and lithium ion that makes the Nb=O bond relatively weaker.

Complex **2** exists as a dimeric tetranuclear complex (Fig. 2). Selected bond lengths and angles are given in Table 3. The center of the dimeric molecule is located on the crystallographic inversion center. The molecular structure of complex **2** can be described as niobium octahedra and lithium tetrahedra which are linearly connected by μ_2-chloride linkages along the Li–Nb–Nb–Li axis. The niobium is six-coordinated by four μ_2-chloride ligands and two 2,6-dimethylphenoxy ligands in *trans* positions. The lithium is four-coordinated by two μ_2-chloride ligands and two oxygen atoms of THF molecules.

The coordination environments of niobium and lithium are quite distorted (*cis* X–Nb–X (X = O or Cl) angles ranging from 83.62(4) to 104.01(3)° and X–Li–X angles ranging from 90.3(3) to 117.8(5)°). The average Nb–O bond length, 1.888 Å, is similar to those in previously known compounds but shorter than those in complex **1** by 0.06 Å [16,18,25]. The decrease in Nb–O bond length of complex **2** can be explained by the absence of an Nb=O bond. The average Nb–μ_2-Cl bond length, 2.484 Å, is significantly longer than those in chloride derivatives of niobium, probably as a consequence of interaction between the bridging chloride ligand and the lithium counter ion [14,27–29,31,34–36].

Complex **1** is the first monomeric lithium niobium(V) oxo aryloxide and complex **2** is also the first dimeric lithium niobium(IV) chloro aryloxide. Complex **1** is expected to act as a potential precursor for the fabrication of $LiNbO_3$ owing to its solubility in a variety of organic solvents and reduced sensitivity to hydrolytic processes [2]. In addition, complex **2** is an invaluable intermediate to interpret the formation of heterometallic alkoxides in organometallic chemistry. Further study will verify more detailed reaction mechanisms and reactivities of complexes **1** and **2**. In a preliminary study,

Table 3
Selected bond lengths (Å) and angles (°) for $[LiNbCl_3(O\text{-}2,6\text{-}PhMe_2)_2 \cdot 2THF]_2$

Nb–O1	1.887(3)	Nb–Nb′	3.0360(8)
Nb–O2	1.888(3)	Nb′–Cl1	2.4690(12)
Nb–Cl1	2.4626(11)	Li–Cl2	2.364(10)
Nb–Cl1′	2.4690(12)	Li–Cl3	2.358(10)
Nb–Cl2	2.5095(12)	Li–O3	1.905(11)
Nb–Cl3	2.5117(13)	Li–O4	1.896(11)
O1–Nb–Cl1	93.19(9)		
O1–Nb–Cl1′	89.65(9)		
O1–Nb–Cl2	87.91(9)	Nb–Cl1–Nb′	75.99(3)
O1–Nb–Cl3	88.74(9)	Nb–Cl2–Li	92.9(2)
O2–Nb–Cl1	92.55(10)	Nb–Cl3–Li	93.0(3)
O2–Nb–Cl1′	90.96(10)	Cl2–Li–Cl3	90.3(3)
O2–Nb–Cl2	86.05(10)	O3–Li–Cl2	108.5(5)
O2–Nb–Cl3	89.73(10)	O3–Li–Cl3	117.8(5)
Cl1–Nb–Cl1′	104.01(3)	O4–Li–Cl2	117.5(5)
Cl1–Nb–Cl3	84.77(4)	O4–Li–Cl3	113.1(5)
Cl2–Nb–Cl1′	87.63(4)	O3–Li–O4	108.9(5)
Cl2–Nb–Cl3	83.62(4)	C1–O1–Nb	163.4(3)
O1–Nb–O2	173.90(12)	C9–O2–Nb	157.1(3)
Cl1–Nb–Cl2	168.31(4)		
Cl3–Nb–Cl1′	171.15(4)		

complex **1** yields pure $LiNbO_3$ powder after heat treatment at 600°C in air. We are continuing the investigation into the application of complex **1** as a molecular precursor for fabrication of $LiNbO_3$.

Supplementary data

Supplementary data are available from the Cambridge Crystallographic Data Centre, 12 Union Road, Cambridge CB2 1EZ, UK (fax: +44-223-336033; e-mail: deposit@ccdc.cam.ac.uk) on request, quoting the deposition numbers CCDC 130855 for structure **1** and 136586 for structure **2**.

Acknowledgements

This work has been generously supported by grants from the Korea Science and Engineering Foundation (KOSEF-97K3-0603-02-05-3) through the Ceramic Processing Research Center at Hanyang University.

References

[1] W.A. Herrmann, N.W. Huber, O. Runte, Angew. Chem., Int. Ed. Engl. 34 (1995) 2187.
[2] R.C. Mehrotra, A. Singh, Chem. Soc. Rev. (1996) 1.
[3] K.G. Caulton, L.G. Hubert-Pfalzgraf, Chem. Rev. 90 (1990) 969.
[4] D.C. Bradley, Chem. Rev. 89 (1989) 1317.
[5] C.D. Chandler, C. Roger, M.J. Hampden-Smith, Chem. Rev. 93 (1993) 1205.
[6] D. Segal, J. Mater. Chem. 7 (1997) 1297.
[7] D.C. Bradley, Polyhedron 13 (1994) 1111.
[8] L.G. Hubert-Pfalzgraf, Polyhedron 13 (1994) 1181.
[9] U. Schubert, J. Chem. Soc., Dalton Trans. (1996) 3343.
[10] T.J. Boyle, R.W. Schwartz, Comments Inorg. Chem. 16 (1994) 243.
[11] E.P. Turevskaya, N.Y. Turova, A.V. Korolev, A.I. Yanovsky, Y.T. Struchkov, Polyhedron 14 (1995) 1531.
[12] R. Papiernik, L.G. Hubert-Pfalzgraf, J.C. Daran, Y. Jeannin, J. Chem. Soc., Chem. Commun. (1990) 695.
[13] S. Boulmaâz, R. Papiernik, L.G. Hubert-Pfalzgraf, B. Septe, J. Vaissermann, J. Mater. Chem. 7 (1997) 2053.
[14] P. Sobota, J. Utko, S. Szafert, Inorg. Chem. 36 (1997) 2227.
[15] R.C. Mehrotra, M.M. Agrawal, P.N. Kapoor, J. Chem. Soc. A (1968) 2673.
[16] D.J. Eichorst, D.A. Payne, S.R. Wilson, K.E. Howard, Inorg. Chem. 29 (1990) 1458.
[17] A.I. Yanovsky, E.P. Turevskaya, N.Y. Turova, Y.T. Struchkov, Sov. J. Coord. Chem. 11 (1985) 63.
[18] S.C. Goel, J.A. Hollingsworth, A.M. Beatty, K.D. Robinson, W.E. Buhro, Polyhedron 17 (1998) 781.
[19] H.J. Gais, J. Vollhardt, J. Am. Chem. Soc. 110 (1988) 978.
[20] M. Dreiss, H. Pritzkow, S. Martin, S. Rell, D. Fenske, G. Baum, Angew. Chem., Int. Ed. Engl. 35 (1996) 986.
[21] K.W. Henderson, R.E. Mulvey, F.D.M. Reinhard, W. Clegg, L. Horsburgh, J. Am. Chem. Soc. 116 (1994) 10777.
[22] M.J. Hampden-Smith, D.S. Williams, A.L. Rheingold, Inorg. Chem. 29 (1990) 4076.
[23] S.K. Park, S.M. Koo, Bull. Korean Chem. Soc. 20 (1999) 1115.
[24] V.W. Day, T.A. Eberspacher, W.G. Klemperer, S. Liang, Chem. Mater. 7 (1995) 1607.
[25] T.W. Coffindaffer, B.D. Steffy, I.P. Rothwell, K. Folting, J.C. Huffman, W.E. Streib, J. Am. Chem. Soc. 111 (1989) 4742.
[26] T.P. Kee, V.C. Gibson, Polyhedron 11 (1992) 587.
[27] L. Higham, M. Thornton-Pett, M. Bochmann, Polyhedron 17 (1998) 3047.
[28] J.R. Clark, A.L. Pulvirenti, P.E. Fanwick, M. Sigalas, O. Eisenstein, I.P. Rothwell, Inorg. Chem. 36 (1997) 3623.
[29] N. Kanehisa, Y. Kai, N. Kasai, H. Yasuda, Y. Nakayama, K. Takei, A. Nakamura, Chem. Lett. (1990) 2167.
[30] L.G. Hubert-Pfalzgraf, M. Tsunoda, G. Le Borgne, J. Chem. Soc., Dalton Trans. (1988) 533.
[31] H.C. Aspinall, M.M. Roberts, S.J. Lippard, Inorg. Chem. 23 (1984) 1782.
[32] K.C. Malhotra, U.K. Banerjee, S.C. Chaudhry, J. Indian Chem. Soc. 7L (1980) 868.
[33] J.W. Park, H.J. Hah, S.M. Koo, Bull. Korean Chem. Soc. 18 (1997) 685.
[34] V.C. Gibson, T.P. Kee, R.M. Sorrell, A.P. Bashall, M. McPartlin, Polyhedron 7 (1988) 2221.
[35] D.A. Brown, M.G.H. Wallbridge, W.S. Li, M. McPartlin, I.J. Scowen, Inorg. Chim. Acta 227 (1994) 99.
[36] F.A. Cotton, M.P. Diebold, W.J. Roth, Inorg. Chem. 24 (1985) 3509.

PERGAMON

www.elsevier.nl/locate/poly

Polyhedron 19 (2000) 1043–1048

POLYHEDRON

Phosphato complexes of beryllium(II): a ^{31}P and ^{9}Be nuclear magnetic resonance study

Liberato Ciavatta [a], Mauro Iuliano [b], Raffaella Porto [c], Paolo Innocenti [d], Alberto Vacca [e,*]

[a] *Dipartimento di Chimica dell'Università 'Federico II', Via Mezzocannone 4, I-80134 Naples, Italy*
[b] *Dipartimento di Scienze Ambientali della II Università di Napoli, Via Vivaldi, I-81100 Caserta, Italy*
[c] *Dipartimento di Chimica, Università della Calabria, Arcavacata di Rende, I-87030 Cosenza, Italy*
[d] *Istituto per lo Studio della Stereochimica ed Energetica dei Composti di Coordinazione, CNR, Via J. Nardi 39, I-50132 Florence, Italy*
[e] *Dipartimento di Chimica dell'Università di Firenze, Via Maragliano 77, I-50144 Florence, Italy*

Received 13 January 2000; accepted 25 February 2000

Abstract

^{31}P and ^{9}Be NMR spectra of mixtures of beryllium(II) and phosphoric acid have been interpreted to support the speciation previously proposed on the basis of potentiometric measurements. Nine ^{31}P lines were observed at ≈0.4, −3.67, −4.51, −5.57, −6.5, −7.08, −8.81, −9.3 and −11.0 ppm relative to 85% phosphoric acid as external standard. The signal in the range 0.36–0.56 was assigned to rapidly exchanging H_3PO_4, $H_2PO_4^-$ with a further contribution from $Be_3O(H_2PO_4)_6^{2-}$. The peaks at −3.67 and −4.51 ppm were ascribed to isomers of $Be(H_2PO_4)_2$. The species $Be(H_2PO_4)^+$ also gives a signal centred at −4.51 ppm. The peak at −6.5 ppm was assigned to $Be_3(OH)_3(H_2PO_4)_3$. The peaks at −5.58, −8.81 and −9.3 ppm are tentatively assigned to isomers of the complex $Be_2(OH)(H_2PO_4)^{2+}$. Signals observed at −7.08 and −11.0 ppm could not be assigned to any of the complexes proposed by potentiometry. The ^{9}Be NMR data are also consistent with the model previously proposed. ©2000 Elsevier Science Ltd All rights reserved.

Keywords: Beryllium; Phosphato complexes; Solution equilibria; ^{31}P NMR spectroscopy; ^{9}Be NMR spectroscopy; Speciation

1. Introduction

Complexes of beryllium(II) with phosphato ligands have been investigated previously [1] by potentiometry (25°C, 3 mol dm^{-3} $(Na)ClO_4$) using a glass electrode in the $-\log[H^+]$ range 1–4. The stoichiometry of the complexes formed is defined by Eq. (1).

$$pBe^{2+} + rH_3PO_4 \rightleftarrows Be_pH_{-q}(H_3PO_4)_r^{2p-q} + qH^+ \qquad (1)$$

On the basis of the analysis of the potentiometric data by SUPERQUAD [2] the most important species were identified as follows: $BeH_{-1}(H_3PO_4)^+$ $(111)^+$, $BeH_{-2}(H_3PO_4)_2$ (122), $Be_2H_{-2}(H_3PO_4)^{2+}$ $(221)^{2+}$, $Be_3H_{-6}(H_3PO_4)$ (361), $Be_3H_{-6}(H_3PO_4)_3$ (363) and $Be_3H_{-8}(H_3PO_4)_6^{2-}$ $(386)^{2-}$ [3]. These species constitute the 'potentiometric model' of the equilibrium system. Formation constants are given in Table 1. The present work was undertaken in order to obtain evidence to support the 'potentiometric model', especially since the model determination relies on the emf data having very high precision. We have assigned species to signals in both ^{31}P and ^{9}Be NMR spectra. Relative peak areas were compared with predictions from the 'potentiometric model'; the satisfactory agreement may be taken as an indirect but convincing demonstration of the correctness of the model proposed.

2. Notation

Reagents: Be^{2+}, H_2O and H_3PO_4.
Equilibria: $pBe^{2+} + rH_3PO_4 \rightleftarrows Be_pH_{-q}(H_3PO_4)_r^{2p-q} + qH^+, \beta_{pqr}$
$(pqr)^{2p-q} = Be_pH_{-q}(H_3PO_4)_r^{2p-q}$.
C_M = total concentration (mol dm^{-3}) of beryllium.
C_P = total concentration (mol dm^{-3}) of phosphate.
P_{pqr} = fraction of phosphorus in the species $(pqr)^{2p-q}$ $= r[Be_pH_{-q}(H_3PO_4)_r^{2p-q}]/C_P = r\beta_{pqr}[Be^{2+}]^p[H^+]^{-q}[H_3PO_4]^{r-1}/(1+\sum r\beta_{pqr}[Be^{2+}]^p[H^+]^{-q}[H_3PO_4]^{r-1})$.
B_{pqr} = fraction of beryllium in the complex $(pqr)^{2p-q}$ $= p[Be_pH_{-q}(H_3PO_4)_r^{2p-q}]/C_M = p\beta_{pqr}[Be^{2+}]^{p-1}[H^+]^{-q}[H_3PO_4]^r/(1+\sum p\beta_{pqr}[Be^{2+}]^{p-1}[H^+]^{-q}[H_3PO_4]^r)$.

* Corresponding author. Tel.: +39-55-321-6333; fax: +39-55-354845; e-mail: vacsab@chim1.unifi.it

0277-5387/00/$ - see front matter ©2000 Elsevier Science Ltd All rights reserved.
PII S0277-5387(00)00345-4

Table 1
Equilibrium constants ($\log \beta_{pqr}(\sigma)$, at $T = 25$°C and $I = 3.0$ mol dm^{-3} (Na)ClO_4) and composition of solutions used

$\log \beta_{011}$	$\log \beta_{002}$	$\log \beta_{012}$	$\log \beta_{111}$	$\log \beta_{122}$	$\log \beta_{221}$	$\log \beta_{361}$	$\log \beta_{363}$	$\log \beta_{386}$
$-1.89(1)$ [a]	$0.00(2)$ [a]	$-1.44(5)$ [a]	$-0.02(3)$ [b]	$0.60(1)$ [b]	$-0.45(1)$ [b]	$-12.12(3)$ [b]	$-2.06(2)$ [b]	$1.58(3)$ [b]

Solution	C_M	C_P	$-\log[H^+]$	B_{100}	Principal $P_{pqr}(pqr)$ values
1	0.010	0.100	1.49	0.08	0.51(001), 0.20(011), 0.14(122)
2	0.010	0.010	2.45	0.50	0.32(011), 0.24(122), 0.13(111), 0.11(363)
3	0.030	0.015	1.49	0.76	0.32(001), 0.26(122), 0.23(111), 0.13(011)
4	0.030	0.015	1.98	0.64	0.29(122), 0.22(111), 0.15(011), 0.14(221), 0.12(001), 0.05(363)
5	0.030	0.015	2.10	0.61	0.26(122), 0.21(111), 0.17(221), 0.14(011), 0.10(363)
6	0.030	0.030	1.75	0.50	0.38(122), 0.18(001), 0.16(111), 0.13(011)
7	0.030	0.030	1.97	0.44	0.34(122), 0.15(386), 0.14(111), 0.14(011), 0.11(001), 0.05(363)
8	0.030	0.060	1.70	0.24	0.36(122), 0.21(001), 0.20(386), 0.13(011)
9	0.032	0.064	1.92	0.17	0.36(386), 0.29(122), 0.13(001), 0.13(011)
10	0.030	0.090	1.69	0.09	0.29(122), 0.25(001), 0.24(386), 0.16(011)
11	0.100	0.010	1.00	0.94	0.40(001), 0.35(111), 0.11(221)
12	0.107	0.010	1.89	0.85	0.62(221), 0.24(111)
13	0.100	0.020	2.01	0.71	0.54(221), 0.21(111), 0.10(363)
14	0.100	0.050	1.49	60.61	0.35(122), 0.24(111), 0.16(221), 0.12(001), 0.03(363)

[a] Ref. [6].
[b] Ref. [1].

δ_{pqr} = chemical shift (ppm) of the $(pqr)^{2p-q}$ species.
I_A, I_B, … fractional peak areas: I_A is area of peak A divided by the sum of the areas of all the peaks in the spectrum.

3. Experimental

3.1. Chemicals and analysis

Reagents were prepared and analyzed as described elsewhere [1]. The solutions were made up to constant ionic strength, 3 mol dm^{-3}, with $NaClO_4$. The $-\log[H^+]$ values of the solutions investigated ranged between 1.0 and 2.5.

3.2. NMR measurements

$^{31}P\{^1H\}$ and $^9Be\{^1H\}$ NMR spectra were recorded at 81.02 and 28.18 MHz, respectively, using a Bruker AC 200 spectrometer. The probe temperature was 23 ± 1°C. Field-frequency stabilization was established by means of a capillary tube filled with D_2O inserted coaxially in the NMR tube. All ^{31}P chemical shifts are reported in ppm toward higher frequency with respect to external 85% H_3PO_4. No corrections were made for differences in bulk susceptibilities. Since the predominant species in 85% aqueous phosphoric acid is, according to Wertz and Cook [4], the dimer $(H_3PO_4)_2$, the chemical shifts refer to this species. The ^9Be chemical shifts are relative to external 0.1 mol dm^{-3} aqueous $BeSO_4$ [5].

3.3. Spectra and composition of the solutions used

The ^{31}P spectra are shown in Fig. 1 and the ^9Be spectra in Fig. 2. The composition of the solutions is given in Table 1. The resonances were assigned by measuring the peak integrals and comparing them with the P_{pqr} and B_{pqr} values predicted according to the 'potentiometric model'. Since the concentration of the complex $Be_3H_{-6}(H_3PO_4)$ (361) is expected to be negligible in the solutions examined here, no

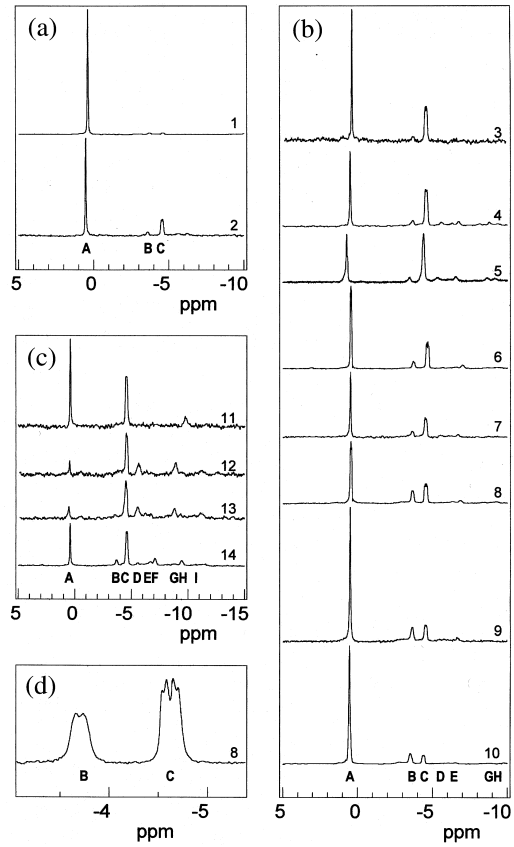


Fig. 1. ^{31}P NMR spectra at 23°C of solutions 1–14 (Table 1). (a) $C_M = 0.01$ mol dm^{-3}, (b) $C_M = 0.03$ mol dm^{-3}, (c) $C_M = 0.1$ mol dm^{-3}, (d) part of spectrum 8 expanded. Letters refer to assignments in Table 2.

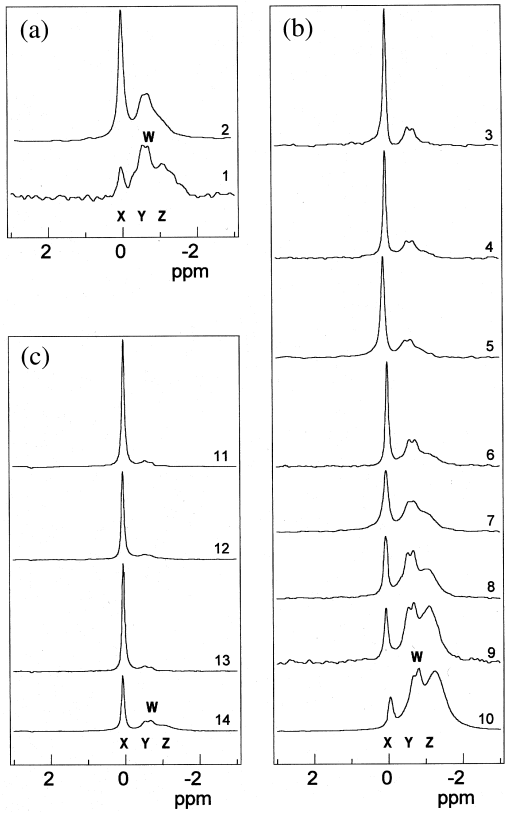


Fig. 2. ^{9}Be NMR spectra at 23°C of solutions 1–14 (Table 1). (a, b, c) as in Fig. 1. Letters refer to assignments in Table 5.

attempt has been made to assign an NMR signal to this species.

4. Results

4.1. ^{31}P NMR spectra

The chemical shifts of the observed signals are given in Table 2.

Peak A. The position of this peak shows a $[H^+]$-dependence which is reasonably explained in terms of a proton transfer reaction which is fast on the 81 MHz time-scale. The chemical shift, δ_A, can be expressed as in Eq. (2), where the summations are taken over all species which contribute to the peak.

$$\delta_A = \Sigma(\delta_{pqr} P_{pqr} / \Sigma P_{pqr}) \quad (2)$$

In the preliminary analysis of the data, the resonance was assigned to the species H_3PO_4 and $H_2PO_4^-$. For solutions 3, 4, 5, 11, 12, 13 and 14, peak integrals agreed within 10% with the sum $P_{001} + P_{011}$. For these solutions, the plot of δ_A versus $P_{011}/(P_{001} + P_{011})$ could be fitted with a straight line as expected in the presence of H_3PO_4 and $H_2PO_4^-$ only. However, for solutions 1, 2, 6, 7, 8, 9 and 10 the integrated intensity of peak A differs significantly from $P_{001} + P_{011}$ and the chemical shifts deviate markedly from the linear behaviour of the δ_A versus $P_{011}/(P_{001} + P_{011})$ of the first group of solutions. A detailed inspection of the 'potentiometric model' reveals the presence of the $(386)^{2-}$ complex in solutions of the second group, whilst no peak ascribable to this species can be found in the corresponding spectra. Peak A is therefore likely to be due to the three species H_3PO_4, $H_2PO_4^-$ and $Be_3H_{-8}(H_3PO_4)_6^{2-}$. This hypothesis was validated in two ways. Firstly, the comparison of peak integrals for all solutions with $P_{001} + P_{011} + P_{386}$ indicated satisfactory agreement within 6%. Secondly, δ_A, was expressed as in Eq. (3) and the most probable δ_{pqr} were calculated by processing the data by standard least-squares procedures.

$$\delta_A = (\delta_{001} P_{001} + \delta_{011} P_{011} + \delta_{386} P_{386}) / (P_{001} + P_{011} + P_{386}) \quad (3)$$

The calculations gave $\sigma(\delta_A) = 0.032$ and the best fit parameters (3σ) shown in Eq. (4).

$$\delta_{001} = 0.3_1 \pm 0.1,\ \delta_{011} = 0.69 \pm 0.06,\ \delta_{386} = 0.4_9 \pm 0.1 \quad (4)$$

Peak B, at -3.67 ppm, is ascribed to the (122) species, whereas peak C, at -4.56 ppm, has contributions from both $(111)^+$ and (122), except in solutions 11, 12 and 13; in these cases the concentration of (122) is small and the signal is generated by the $(111)^+$ species alone. In solutions 2 and 10 the ratio P_{111}/P_{122} is less than 0.1 but the corresponding spectra show both B and C with a ratio I_C/I_B greater than unity. The sum of peak areas agrees within 9% with $P_{111} + P_{122}$. The two peaks due to the (122) complex may be ascribed either to the two non-equivalent phosphorus atoms in the molecule or to isomers. Since $I_B/P_{122} = 0.30 \pm 0.15$, the explanation in terms of isomers is more likely. Fig. 1(d) illustrates the quartet nature of peaks B and C, due to coupling with the ^{9}Be nucleus ($I = 3/2$). The $^{2}J_{Be-P}$ coupling constant was estimated to be 5 ± 1 Hz. An analogous pattern of quartets has also been observed in the ^{19}F NMR spectra of fluoro complexes of beryllium [7]: in that case the fact that the fluorine atoms are bonded to the beryllium results in a much larger coupling constant, $^{1}J_{Be-F} = 34$–42 Hz.

Peaks D, G and H, which are observed as broad lines at ca. -5.57, -8.81 and -9.3 ppm, are strictly connected with each other. The appearance or disappearance of one of them is mirrored by the others. These three resonances are tenta-

Table 2
Peaks in ^{31}P NMR spectra

Peak	δ (ppm)	Assignment
A	0.36–0.56	H_3PO_4, $H_2PO_4^-$ and $Be_3H_{-8}(H_3PO_4)_6^{2-}$
B	-3.67 ± 0.04	$Be(H_2PO_4)_2$
C	-4.51 ± 0.03	$BeH_2PO_4^+$ and $Be(H_2PO_4)_2$
D	-5.57 ± 0.03	$Be_2H_{-2}(H_3PO_4)^{2+}$
E	-6.5 ± 0.2	$Be_3H_{-6}(H_3PO_4)_3$
F	-7.08	not assigned
G	-8.81 ± 0.09	$Be_2H_{-2}(H_3PO_4)^{2+}$
H	-9.3 ± 0.2	$Be_2H_{-2}(H_3PO_4)^{2+}$
I	-11.0 ± 0.2	not assigned

tively ascribed to the polynuclear complex $Be_2H_{-2}(H_3PO_4)^{2+}$; a comparison of peak areas with calculated P_{221} values is given in Table 3. The agreement can be considered acceptable in relation to the noise on the calculated peak integrals.

Peak E is observed in the spectra of solutions 2, 3, 4, 7, 13 and 14. Comparison of signal intensities with P_{pqr} values, shown in Table 4, suggests that it should be assigned to $Be_3H_{-6}(H_3PO_4)_3$.

Peaks F and I are only observed as weak signals in the spectra of solutions 13 and 14. The composition of these solutions is outside the composition range investigated by potentiometry. These peaks probably derive from species which are present in negligible amounts in the solutions studied by potentiometry, so no assignment has been attempted.

4.2. ^{9}Be NMR spectra

The spectra are characterized by signals either very close together or actually overlapping each other. The width at half height of the band at ≈ 0 ppm was estimated to be between 3 and 5 Hz. Chemical shifts observed in the ^{9}Be NMR spectra are listed in Table 5.

Peak X was assigned to the free $Be^{2+}(aq)$ ion on the basis of close agreement (within 3%) of the integrated intensity with B_{100} values calculated from the model. For the other peaks, overlap is too great to allow a quantitative evaluation of integrated intensity; the assignments of these peaks were made by searching for strong signals in spectra derived from solutions where a complex predominates. In this respect the most informative spectra are those obtained from solutions 1, 9, 10, 12 and 13; corresponding fractional concentration values are shown in Table 6.

In the spectrum of solution 2, peaks were found at -0.55, -0.69, -1.12 ppm with a shoulder at ≈ -0.35 ppm. We ascribe the resonances at -0.55 and -0.69 ppm to isomers of (122), and that at -1.12 ppm to $(386)^{2-}$ (see below). The shoulder might be assigned to $(111)^+$, but this could not be confirmed as there is no solution in which $(111)^+$ is predominant.

In solutions 12 and 13 the most intense peaks are at -0.55 and -0.69 ppm with a shoulder at about -1.1 ppm. Under these conditions we expect signals originating from $(221)^{2+}$ to be the most intense. In accordance with the findings of the preceding section we conclude that the shifts arise from isomers of the polynuclear complex $Be_2H_{-2}(H_3PO_4)^{2+}$.

In the spectra of solutions 9 and 10, three intense peaks are observed while two complexes are present in comparable amount. The shifts at -0.55, -0.69 ppm have been assigned to (122) and therefore that at -1.12 ppm is very likely to be due to $(386)^{2-}$.

As neither of the species $(111)^+$ and (363) are predicted to be predominant in any of the solutions studied, we have not attempted an assignment.

Table 3
Comparison of the fraction of phosphorus in the species $(221)^{2+}$, $Be_2H_{-2}(H_3PO_4)^{2+}$, (P_{221} in Table 1) with the total area of NMR peaks D, G, and H

Solution	P_{221}	Peak integrals			Total peak area
		D	G	H	
4	0.14	0.05	0.04	0.02	0.11
5	0.17	0.08	0.06	0.06	0.20
11	0.11	noise	noise	0.09	0.09
12	0.62	0.17	0.24	0.07	0.48
13	0.54	0.19	0.22	0.09	0.50
14	0.16	0.04	0.04	0.07	0.15

Table 4
Comparison of the fraction of phosphorus in the species (363), $Be_3H_{-6}(H_3PO_4)_3^{2+}$, ($P_{363}$ in Table 1) with the area of NMR peak E

Solution	P_{363}	Peak area of E
2	0.11	0.04
4	0.05	0.06
5	0.10	0.09
7	0.05	0.05
13	0.09	0.06
14	0.03	0.05

Table 5
Shifts in the ^{9}Be NMR spectra

Peak	δ (ppm)	Assignment
X	$+0.02 \pm 0.03$	Be^{2+}
Y	-0.55 ± 0.03	$Be(H_2PO_4)_2$, $Be_2H_{-2}(H_3PO_4)^{2+}$
W	-0.69 ± 0.01	$Be(H_2PO_4)_2$, $Be_2H_{-2}(H_3PO_4)^{2+}$
Z	-1.12 ± 0.02	$Be_3H_{-8}(H_3PO_4)_6^{2-}$, $Be_2H_{-2}(H_3PO_4)^{2+}$

Table 6
Composition of solutions (in terms of fraction of total beryllium in the main complex species present at equilibrium) used to assign the peaks Y, W and Z

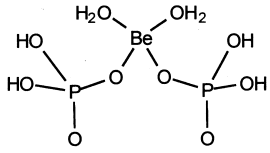
Solution	B_{111}	B_{122}	B_{221}	B_{386}
1	0.12	0.73	≈ 0	0.07
9	0.12	0.29	0.04	0.36
10	0.10	0.43	0.01	0.36
12	0.02	≈ 0	0.12	≈ 0
13	0.04	0.01	0.22	≈ 0

5. Discussion

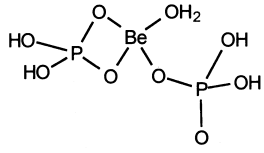
Information deduced from ^{31}P and ^{9}Be NMR spectrometry corroborates the 'potentiometric model'. The most convincing evidence comes from the agreement, within experimental

error, of the free metal and ligand concentrations calculated from the model with corresponding peak intensities.

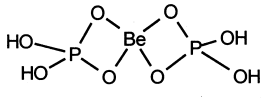
Though the sensitivity and resolution of the ^{31}P and ^{9}Be NMR spectra are not, at present, high enough to permit an independent equilibrium analysis to be performed on the NMR data, spectrometry is superior when it comes to establishing the presence of isomers. Isomerism may occur in phosphato complexes because the phosphate ligand may be either monodentate or bidentate. Thus, if $Be(H_2PO_4)_2$ is in fact a mixture of at least two isomers, as the NMR data suggest, structures (I) to (IV) are all possibilities.



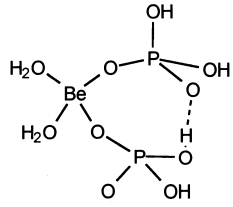
(I)



(II)



(III)

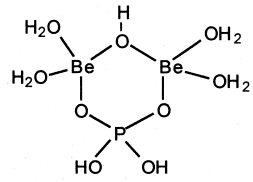


(IV)

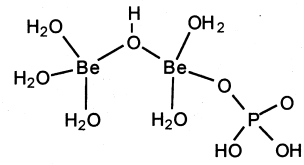
In order to explain the appearance of two bands it has to be postulated that the ^{31}P nuclei belonging to phosphate groups in different isomers give rise to signals which are nearly 1 ppm apart. We believe that forms (III) and (IV) are the most probable. Support for this idea is provided by the fact that the stepwise equilibrium constant for $Be^{2+} + Be(H_2PO_4)_2 \rightleftarrows 2BeH_2PO_4^+$ has a value of 0.3 which is much lower than 4, the value expected purely on the basis of statistical considerations. The extra stabilization of $Be(H_2PO_4)_2$ with respect to $BeH_2PO_4^+$ can be explained by the formation of the chelate rings present in (III) and (IV). Evidence for the existence of this kind of four-membered chelate ring and its stability is provided by the work of Bruno et al. [8] on beryllium carbonato complexes. In that paper the authors also refer to an X-ray crystal structure determination which they had performed on the complex $[Be_3(OH)_3(C_5H_4NCO_2)_3]\cdot H_2O$, in which the three pyridine-2-carboxylato ligands appear to act as bidentate ligands in relation to the beryllium in the same way as they propose for the carbonate. Unfortunately this work has not, to the best of our knowledge, been published.

The isomers of stoichiometry $Be_2H_{-2}(H_3PO_4)^{2+}$ may be postulated as being derivatives of $Be_2(OH)^{3+}$, the second most important species in beryllium hydrolysis [9]. The ligand is $H_2PO_4^-$ and it may be bridging bidentate, (V), monodentate, (VI), or chelating bidentate, (VII).

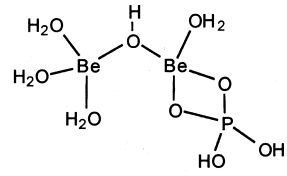
The stucture of the (363) species can reasonably be assumed to derive from the trimer, $Be_3(OH)_3^{3+}$, which is the major product of beryllium hydrolysis. The stoichiometry



(V)



(VI)



(VII)

then demands that the ligands be formulated as $H_2PO_4^-$ and the complex as $Be_3(OH)_3(H_2PO_4)_3$.

It is more difficult to assign a tentative structure to the other trinuclear species, of stoichiometry $Be_3H_{-8}(H_3PO_4)_6^{2-}$. The formula $Be_3O(H_2PO_4)_6^{2-}$ was proposed [1] for this complex and the structure proposed contains both bridging and terminal phosphate groups. The slow exchange of beryllium nuclei, as indicated by the ^{9}Be spectra, would be consistent with a structure in which there is a Be_3O core which is inert on the NMR time-scale. The ^{31}P spectra are not so easy to explain. A contribution from this species to resonance A in the ^{31}P spectra is required in order to make a quantitative assignment of peak areas and chemical shifts. However, the observation of a single line is difficult to reconcile with the structure previously proposed for this species. A single line implies that the phosphorus nuclei are either all chemically equivalent or exchanging rapidly. Equivalence is possible if all the phosphato ligands are monodentate, but this seems unlikely. If rapid exchange is present then a mechanism must be operating which does not operate in the case of the 221 complex. Another possibility is that some phosphato ligands (perhaps the monodentate ones) are in slow exchange with each other, so giving a line broadening which has made the line appear to be absent.

Acknowledgements

The authors thank the EU (HCM program ''Metals and Environmental Problems'' 1995–1998, Grant ERBCHRHX-CT94-0632) and the Ministero dell'Ambiente (Italy, Contract PR/1/C) for financial support.

References

[1] L. Ciavatta, M. Iuliano, R. Porto, Ann. Chim. (Rome) 87 (1997) 375.
[2] P. Gans, A. Sabatini, A.Vacca, J. Chem. Soc., Dalton Trans. (1985) 1195.
[3] There is an ambiguous relationship between the stoichiometry defined by *pqr* and the molecular formula. A positive *q* value may indicate either that water molecules have lost protons, with the formation of

and hydroxo complex or an oxo complex, or that a phosphoric acid molecule has lost a proton with the formation of a complex with $H_2PO_4^-$ as ligand.

[4] D.L. Wertz, G.A. Cook, J. Sol. Chem. 14 (1985) 41.

[5] L. Alderighi, P. Gans, S. Midollini, A. Vacca, in: A.G. Sykes (Ed.), Advances in Inorganic Chemistry, Academic Press, New York, in press.

[6] L. Ciavatta, M. Iuliano, Ann. Chim. (Rome) 86 (1996) 1.

[7] R. Anttila, I. Grenthe, J. Glaser, J. Bruno, B. Lagerman, Acta Chem. Scand. 45 (1991) 523.

[8] J. Bruno, I. Grenthe, M. Muñoz, J. Chem. Soc., Dalton Trans. (1987) 2445.

[9] C.F. Baes, R.E. Mesmer, The Hydrolysis of Cations, Wiley, New York, 1976.

PERGAMON

www.elsevier.nl/locate/poly

Polyhedron 19 (2000) 1049–1055

POLYHEDRON

Synthesis, characterization, and electrocatalytic oxidation of benzyl alcohol by a pair of geometric isomers of $[Ru(trpy)(4,4'\text{-}Me_2dppi)(OH_2)]^{2+}$ where 4,4′-dppi is 3,6-di-(4-methylpyrid-2-yl)pyridazine

Vincent J. Catalano* [1, a], Ryan A. Heck [a], Anna Öhman [b], Michael G. Hill* [2,b]

[a] *Department of Chemistry, University of Nevada, Reno, NV 89557, USA*

[b] *Department of Chemistry, Occidental College, Los Angeles, CA 90041, USA*

Received 26 July 1999; accepted 15 February 2000

Abstract

The geometric isomers, *in*-$[Ru(trpy)(4,4'\text{-}Me_2dppi)Cl]^+$ (**1a**), *in*-$[Ru(trpy)(4,4'\text{-}Me_2dppi)OH_2]^{2+}$ (**1b**), and *in*-$[Ru(trpy)(4,4'\text{-}Me_2dppi)(NCCH_3)]^{2+}$ (**1c**), *out*-$[Ru(trpy)(4,4'\text{-}Me_2dppi)Cl]^+$ (**2a**), *out*-$[Ru(trpy)(4,4'\text{-}Me_2dppi)OH_2]^{2+}$ (**2b**), and *out*-$[Ru(trpy)(4,4'\text{-}Me_2dppi)(NCCH_3)]^{2+}$ (**2c**), where trpy is 2,2′,2″-terpyridine and 4,4′-Me_2dppi is 3,6-di-(4-methylpyrid-2-yl)pyridazine, were synthesized and characterized by UV–Vis and ^{1}H NMR spectroscopy. The *in* and *out* notation refers to the orientation of the non-imine group which is directed towards the center of the complexes in the *in* complexes and away from the center in the *out* complexes. Compounds **1a** and **2c** were additionally characterized by X-ray crystallography. Reaction of **1a** or **2a** with aqueous silver ion produces the corresponding aqua complexes, **1b** and **2b**, which after dissolution in acetonitrile produces the analogous acetonitrile complexes, **1c** and **2c**. The redox properties of **1a**, **1b**, **2a**, and **2b** were examined using cyclic voltammetry. In acetonitrile, compounds **1a** and **2a** display reversible $1e^-$ waves assigned to the Ru(III)/Ru(II) couple, while in aqueous solutions **1b** and **2b** show pH-dependent $2e^-$ waves corresponding to the formation of Ru(IV)=O complexes. Second-order rate constants, k_{cat}, for oxidation of benzyl alcohol derivatives by the Ru(IV)=O complex **2b** were determined electrochemically. Complex **1b** severely passivated the working electrode upon oxidation, and reliable catalytic rate constants could not be measured. This passivation may be related to self oxidation of the Me_2dppi ligand by the electrochemically generated Ru(IV)=O complex. ©2000 Elsevier Science Ltd All rights reserved.

Keywords: Ruthenium; Polypyridine; Terpyridine; Electrocatalytic oxidation; Alcohol oxidation; Isomerization

1. Introduction

High-valent ruthenium oxo complexes catalyze a variety of small-molecule oxidations [1–4]. Recently, we studied the electrocatalytic oxidation of benzyl alcohol by $[Ru(trpy)(R_2dppi)(O)]^{2+}$ (where R_2dppi is a 6,6′-disubstituted dipyridopyridazine, with R = H, CH_3, or Cl) [5]. Interestingly, the catalytic rates correlated with the steric hindrance about the metal center, but not the thermodynamic driving force for oxidation. These observations are consistent with a mechanism in which the rate-determining step involves pre-association of the substrate with the catalyst, rather than electron transfer [6–10]. During the course of this study, we found that of the two possible geometric isomers of $Ru(trpy)(R_2dppi)(L)^{n+}$ (shown below as *in* and *out*), only one could be effectively isolated. Here, using a 4,4′-disubstituted dppi ligand, we report the synthesis of both isomers, and describe their structural and catalytic properties.

2. Experimental

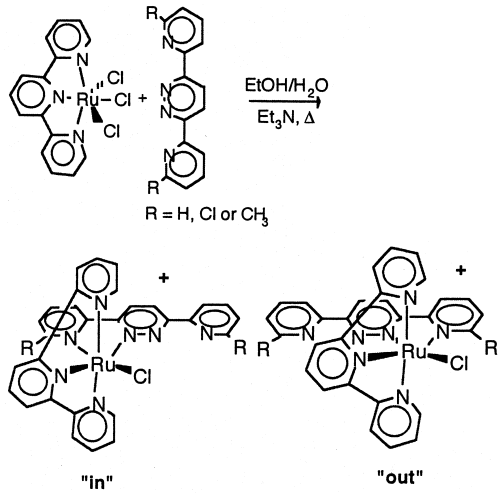
2.1. Materials

$RuCl_3 \cdot H_2O$ was obtained from Strem Chemical. All other chemicals were obtained from Acros and used without additional purification.

[1] *Corresponding author. Tel.: +1-775-784-6041; fax: +1-775-784-6804; e-mail: vjc@unr.edu

[2] *Corresponding author.

0277-5387/00/$ - see front matter ©2000 Elsevier Science Ltd All rights reserved.
PII S0277-5387(00)00347-8



2.2. Instrumentation and measurements

^{1}H NMR spectra were recorded on either a Varian Unity Plus 500 MHz spectrometer or General Electric QE-300 spectrometer, and all spectra were referenced to TMS as an internal standard. UV–Vis spectra were recorded using a Perkin-Elmer Lamda 11 spectrophotometer.

2.3. Electrochemistry

All electrochemical experiments were performed with a Bioanalytical Systems (BAS) model CV50-W electrochemical analyzer. Cyclic voltammetry (CV) and chronocoulometry (CC) were performed at 20 ± 3°C with a normal three-electrode configuration consisting of a highly polished glassy-carbon working electrode and an AgCl/Ag reference electrode containing 1.0 M KCl. The working compartment of the electrochemical cell was separated from the reference compartment by a modified Luggin capillary. All three compartments contained a 0.1 M solution of supporting electrolyte.

Acetonitrile (Burdick and Jackson) was distilled from P_2O_5 prior to use. Tetrabutylammonium hexafluorophosphate, $TBAPF_6$ (Southwest Analytical), was used as received. Acetonitrile electrolyte solutions were prepared and stored over 80-200 mesh activated alumina (Fisher Scientific Co.) and activated 4 Å molecular sieves. Potentials are reported versus AgCl/Ag and are not corrected for the junction potential. In acetonitrile, the ferrocenium/ferrocene couple has an $E^{o\prime}$ of 0.49 V, with $E_{pa} - E_{pc} = 87$ mV; the corresponding aqueous-solution potential is 0.11 V. Digital simulations were performed using the commercial Digisim 2.1 software package from BAS [11].

2.4. Preparations

$Ru(trpy)Cl_3$ [12] and trpy [13] were synthesized according to literature procedures. 4,4′-Me_2dppi was prepared analogously to the previously described dipyridopyridine ligands from 4-methyl-2-cyanopyridine [14].

2.4.1. In-[Ru(trpy)(4,4′-Me_2dppi)Cl](PF_6) (**1a**) and out-[Ru(trpy)(4,4′-Me_2dppi)Cl](PF_6) (**2a**)

0.157 g (0.60 mmol) 4,4′-Me_2dppi and 0.283 g $Ru(trpy)Cl_3$ (0.64 mmol) were refluxed for 3 h with 0.033 g LiCl and 16 drops of *N*-ethyl morpholine. The resulting solution was filtered hot through celite, and the solvent was removed in vacuo. The residue was dissolved in 40 ml of methanol, and 0.417 g NH_4PF_6 was added. The resulting solid was collected. The remaining solution was reduced to dryness on a rotary evaporator. The solid was then re-dissolved in acetone, and 30 ml of isopropanol was added. The acetone was slowly removed using a rotary evaporator until a precipitate was formed. The resulting solid was collected and chromatographed on activated alumina using a solution of 20% CH_3CN and 80% CH_2Cl_2. The first fraction was recrystallized from acetone and diethyl ether to give 0.198 g **2a** (42.6%) and 0.082 g **1a** (17.6%). The remaining bands on the column were $[Ru(tpy)_2]^{2+}$ and other side products; no attempt was made to isolate or purify them. **2a** ^{1}H NMR (Me_2CO-d_6): δ 10.19 (1H, d, ^3J(HH) = 5.5 Hz), 8.83 (2H, d, ^3J(HH) = 8.5 Hz), 8.80 (1H, s), 8.73 (1H, d, ^3J(HH) = 9.0 Hz), 8.60 (2H, d, ^3J(HH) = 8.0 Hz), 8.46 (1H, d, ^3J(HH) = 4.5 Hz), 8.42 (1H, t, ^3J(HH) = 8.0 Hz), 8.34 (1H, d, ^3J(HH) = 8.5 Hz), 8.07 (1H, d, ^3J(HH) = 5.5 Hz), 7.99 (2H, td, ^3J(HH) = 8 Hz, ^4J(HH) = 1.5 Hz), 7.90 (2H, d, ^3J(HH) = 5.5 Hz), 7.41 (2H, td, ^3J(HH) = 5.5 Hz, ^4J(HH) = 1.5 Hz), 7.30 (2H, m), 2.45 (3H, s), 2.43 (3H, s); UV–Vis [λ_{max} (nm) (ε_{max} (dm^3 mol^{-1} cm^{-1}))]: (CH_2Cl_2) 315 (5.2×10^4), 324 (3.3×10^4), 363 (5.4×10^3), 439 (6.1×10^3), 490 (8.5×10^3), 526 (1.1×10^4). **1a** ^{1}H NMR (Me_2CO-d_6): δ 9.12 (1H, d, ^3J(HH) = 9.0 Hz), 8.98 (1H, d, ^3J(HH) = 9.0 Hz), 8.87 (1H, d, ^3J(HH) = 0.5), 8.76 (2H, d, ^3J(HH) = 8.0 Hz), 8.73 (1H, d, ^3J(HH) = 5.0 Hz), 8.62 (3H, m), 8.24 (1H, t, ^3J(HH) = 8.0 Hz), 7.98 (4H, m), 7.56 (1H, d, ^3J(HH) = 5.5 Hz), 7.46 (1H, dd, ^3J(HH) = 5.5 Hz, ^4J(HH) = 0.5 Hz), 7.34 (2H, td, ^3J(HH) = 7.0 Hz, ^4J(HH) = 1.5 Hz), 7.08 (1H, dd, ^3J(HH) = 6.0 Hz, ^4J(HH) = 1.0 Hz), 2.45 (3H, s), 2.43 (3H, s); UV–Vis [λ_{max} (nm) (ε_{max} (dm^3 mol^{-1} cm^{-1}))]: (CH_2Cl_2) 318 (4.8×10^4), 384 (6.2×10^3), 410 (5.8×10^3), 455 (5.8×10^3), 479 (7.8×10^3), 521 (1.0×10^4).

2.4.2. Out-[Ru(trpy)(4,4′-Me_2dppi)H_2O](ClO_4)$_2$ (**2b**)

0.120 g of **2a** was refluxed for 3 h with 0.127 g $AgClO_4$ in 40 ml of a 3:1 acetone:water solution. The solution was cooled in an ice bath, filtered through celite, and the acetone removed in vacuo. A bright orange–red solid precipitated from solution to give 0.091 g of **2b**. ^{1}H NMR (Me_2CO-d_6/D_2O): δ 9.55 (1H, d, ^3J(HH) = 5.5 Hz), 8.80 (2H, d, ^3J(HH) = 8.0 Hz), 8.74 (1H, s), 8.67 (1H, d, ^3J(HH) = 9.0 Hz), 8.57 (2H, d, ^3J(HH) = 8.0 Hz), 8.47 (1H, t, ^3J(HH) = 8.0 Hz), 8.39 (1H, d, ^3J(HH) = 5.0 Hz), 8.21 (1H, d, ^3J(HH) = 8.5 Hz), 8.07 (1H, dd, ^3J(HH) = 6.0 Hz,

^4J(HH) = 1.0 Hz), 8.02 (2H, td, ^3J(HH) = 8.0 Hz, ^4J(HH) = 1.5 Hz), 7.93 (2H, d, ^3J(HH) = 5.5 Hz), 7.42 (2H, td, ^3J(HH) = 5.5 Hz, ^4J(HH) = 1.0 Hz), 7.28 (1H, dd, ^3J(HH) = 5.0 Hz, ^4J(HH) = 1.0 Hz), 7.16 (1H, s), 2.81 (3H, s), 2.35 (3H, s); UV–Vis [λ_{max} (nm) (ε_{max} (dm^3 mol^{-1} cm^{-1}))] (H_2O) 308 (4.3×10^4), 329 (1.9×10^4), 425 (5.7×10^3), 491 (8.0×10^3), 585 (1.5×10^3).

2.4.3. In-[Ru(trpy)(4,4′-Me$_2$dppi)H$_2$O](PF$_6$)$_2$ (**1b**)

0.091 g of **1a** (0.12 mmol) was gently heated for three hours with 0.221 g (0.63 mmol) of $TlPF_6$ in a 1:1 acetone: water solution. The solution was then cooled in an ice bath, filtered, and the solvent removed in vacuo. The crude product was dissolved in acetone and precipitated with diethyl ether to give 0.087 g of **1b** (82.1%). ^{1}H NMR (Me_2CO-d_6/D_2O): δ 8.91 (1H, d, ^3J(HH) = 9.5 Hz), 8.69 (1H, d, ^3J(HH) = 9.0 Hz), 8.58 (1H, d, ^3J(HH) = 8.5 Hz), 8.54 (2H, d, ^3J(HH) = 11.0 Hz), 8.43 (2H, m), 8.31 (1H, s), 8.23 (1H, t, ^3J(HH) = 8.0 Hz), 7.90 (1H, t, ^3J(HH) = 7.5 Hz), 7.74 (2H, d, ^3J(HH) = 5.5 Hz), 7.44 (2H, d, ^3J(HH) = 6.0 Hz), 7.27 (2H, d, ^3J(HH) = 6.0 Hz), 7.23 (2H, t, ^3J(HH) = 6.0 Hz), 6.89 (1H, d, ^3J(HH) = 5.5 Hz), 2.39 (3H, s), 2.28 (3H, s); UV–Vis [λ_{max} (nm) (ε_{max} (dm^3 mol^{-1} cm^{-1}))]: (H_2O) 272 (3.0×10^4), 279 (2.9×10^4), 307 (4.7×10^4), 331 (1.5×10^4), 394 (4.0×10^3), 449 (8.6×10^3), 480 (1.0×10^4), 542 (2.4×10^3).

2.5. X-ray data collection and processing

Crystals of **1a** and **2c** were grown by slow diffusion of diethyl ether through a thin layer of methanol into an acetonitrile solution of the complex. Suitable crystals of **1a** were coated with light hydrocarbon oil, mounted on a glass fiber and placed in the −100°C nitrogen cold stream of a Siemens P4 diffractometer. A crystal of **2c** was coated in epoxy cement, and the data were collected at room temperature.

Compound **1a** yielded 6293 reflections of which 4869 (R_{int} = 0.0473) were unique in the range $1.99 < \theta < 22.50°$. Over the range $1.84 < \theta < 22.50°$ **2c** yielded 4957 (R_{int} = 0.0445) independent reflections from a total of 6370 reflections. No absorption correction was applied to **1a** while a semi-empirical model derived from psi-scans was applied to **2c**.

The data were corrected for Lorentz and polarization effects. Crystal data are given in Table 1. Scattering factors and corrections for anomalous dispersion were taken from a standard source [15].

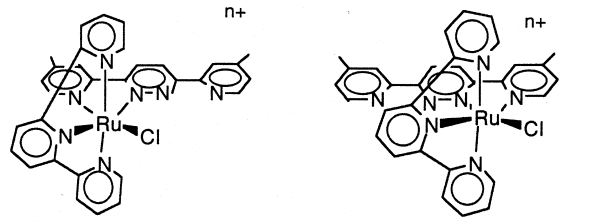
Calculations were performed using the Siemens SHELXTL PLUS (version 5.03) system of programs, refining on F^2. The structures were solved by direct methods. The structure of **2c** contains two BF_4^- anions one of which is disordered over eight positions. The structure also contains a one-half occupancy isopropanol molecule and a one-quarter occupancy water molecule. The structure of **1a** contains two PF_6^- anions one of which is positionally disordered. The structure also contains an acetone molecule and a one-half occupancy water molecule. Hydrogen atom positions were calculated using a riding model with a C–H distance fixed at 0.96 Å and a thermal parameter 1.2 times the host carbon atom. The largest peak in the final difference map corresponded to 1.07 e$^-$ Å^{-3} and was located 1.246 Å from B(2) in **2c**. In **1a** the largest unassigned peak corresponded to 0.67 e$^-$ Å^{-3} and was located 0.710 Å from F(1A).

Table 1
Crystal data for **1a** and **2c**

	1a	**2c**
Formula	$C_{34}H_{31}ClF_6N_7O_{2.5}PRu$	$C_{34.5}H_{25}B_2F_8N_8O_{0.75}Ru$
FW	859.15	838.32
a (Å)	8.8190(10)	12.878(4)
b (Å)	27.152(2)	12.565(3)
c (Å)	15.596(2)	23.537(2)
β (°)	95.26(3)	94.74(2)
V (Å^3)	3718.8(7)	3796(2)
Space group	*P*2(1)/*n*	*P*(2)1/*n*
Z	4	4
D_{calc} (g cm^{-3})	1.535	1.467
Crystal size (mm)	0.06×0.40×0.06	0.24×0.72×0.24
Radiation λ (Å)	0.71073	0.71073
Temperature (°C)	25	−100
Transmission factors	0.77–0.72	0.79–0.74
μ(Mo Kα) (mm^{-1})	0.609	0.491
R_1 [a], wR_2 [b] ($I > 2\sigma(I)$)	0.0690, 0.1553	0.0601, 0.1428

[a] $R_1 = \sum||F_o| - |F_c||/\sum|F_o|$.
[b] $wR_2 = [\sum[w(F_o^2 - F_c^2)^2]/\sum[w(F_o^2)^2]^{0.5}$.

3. Results and discussion



in *out*

1a (X = Cl, n=1) **2a**
1b (X = OH_2, n=2) **2b**
1c (X = $NCCH_3$, n=2) **2c**
1d (X = O, n=2) **2d**

3.1. Syntheses

As we have noted previously, the initial reaction of R_2dppi with Ru(tpy)Cl_3 produced two isomers of [Ru(trpy)-(R_2dppi)Cl]$^+$. The major product, the *out* isomer, has the chloride ligand directed away from the center of the R_2dppi ligand, while the *in* isomer has the chloride atom pointed toward the center of the R_2dppi ligand. While both the *in* and *out* isomers were characterized crystallographically for the H_2dppi ligand, the *in* could not be isolated in appreciable quantities. In addition, the *in* complex was never detected in

the 6,6′-Me_2dppi and Cl_2dppi complexes. However, simply changing the positions of the methyl groups on the dppi ligands from the 6,6′-positions to the 4,4′-positions afforded both the *in* and *out* isomers of $[Ru(trpy)(4,4'\text{-}Me_2\text{-}dppi)Cl]^+$, isolated in a 1:4 ratio. The initial reaction mixture is first passed through a column of activated alumina to remove the $[Ru(trpy)_2]^{2+}$ impurity. The two isomers can then be separated by slow recrystallization from acetone/diethyl ether. Once in hand, the chloride species are converted in good yield to the analogous aqua complexes (**1b** and **2b**) using Ag(I) or Tl(I) ion in refluxing acetone/water. The labile aqua ligands are easily replaced by donor solvents (e.g. acetonitrile to produce **1c** and **2c**.) Ru(IV)=O complexes (**1d** and **2d**) are generated in situ electrochemically [5].

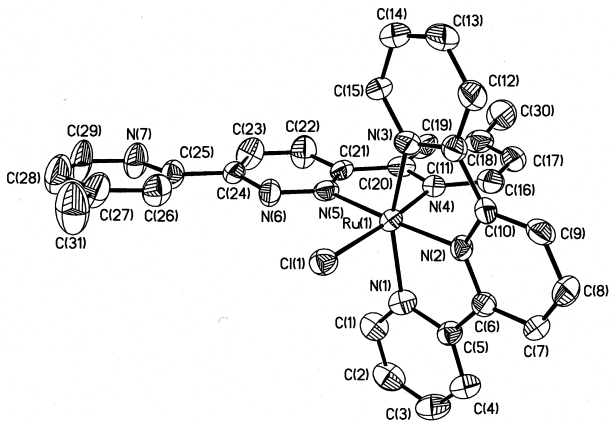


Fig. 1. Thermal ellipsoid (40% probability) drawing of *in*-$[Ru(trpy)(4,4'\text{-}Me_2dppi)Cl]^+$ (**1a**) with numbering scheme.

Table 2
Selected bond distances (Å) and angles (°) for **1a** and **2c**

	1a	2c
Ru(1)–N(1)	2.070(8)	2.080(6)
Ru(1)–N(2)	1.962(7)	1.973(6)
Ru(1)–N(3)	2.066(8)	2.074(6)
Ru(1)–N(4)	2.032(8)	2.087(6)
Ru(1)–N(5)	2.031(7)	2.009(6)
Ru(1)–N(8)		2.052(7)
Ru(1)–Cl(1)	2.413(3)	
N(1)–Ru(1)–N(2)	79.6(3)	79.6(2)
N(1)–Ru(1)–N(3)	158.9(3)	159.0(2)
N(3)–Ru(1)–N(3)	79.3(3)	79.5(3)
N(2)–Ru(1)–N(4)	99.2(3)	170.6(2)
N(2)–Ru(1)–N(5)	78.5(3)	78.5(2)
N(8)–Ru(1)–N(1)		90.5(2)
N(8)–Ru(1)–N(2)		93.9(3)
N(8)–Ru(1)–N(3)		89.2(3)
N(8)–Ru(1)–N(4)		95.5(3)
N(8)–Ru(1)–N(5)		173.5(3)
Cl(1)–Ru(1)–N(1)	90.3(2)	
Cl(1)–Ru(1)–N(2)	88.1(2)	
Cl(1)–Ru(1)–N(3)	90.2(2)	
Cl(1)–Ru(1)–N(4)	172.7(2)	
Cl(1)–Ru(1)–N(5)	94.2(2)	
Cl(1)–Ru(1)–N(1)	90.3(2)	
N(6)–C(24)–C(25)–N(7)	173.5(3)	177.5(3)

3.2. Structure analyses

*3.2.1. Structure of in-[Ru(trpy)(4,4′-Me_2dppi)Cl](PF_6)·($(CH_3)_2CO$·0.5H_2O (**1a**)*

The asymmetric unit of **1a** consists of the cation, a disordered PF_6^- anion, an acetone molecule, and a half-occupancy water molecule. A view of the cation is presented in Fig. 1, and selected bond distances and angles are given in Table 2. Consistent with the *in* geometry the chloride linkage is directed towards the center of the 4,4′-Me_2dppi ligand. The uncoordinated pyridine group is rotated away from the metal centers and is nearly coplanar with the pyridazine ring with a dihedral angle of only 4.1° and the N(6)–C(24)–C(25)–N(7) torsion angle of 173.5(3)°. As expected, placement of the methyl groups in the 4 and 4′ positions significantly reduces the steric congestion about the metal center as compared to the previously studied 6,6′-Me_2dppi complexes. The Ru(1)–Cl(1) separation is normal at 2.413(3) Å as are the remaining Ru–N separations. The Ru(1)–N(2) separation at 1.962(7) Å is slightly contracted, consistent with meridionally coordinated terpyridine. The contraction of the central pyridine is a result of the constrained bite angle of this ligand. As a result the *trans* spanning N(1)–Ru(1)–N(3) bond angle at 158.9(3)° is less than the ideal 180°. The terpyridine ligand is canted away from the 4,4′-Me_2dppi ligand with an N(2)–Ru(1)–N(4) angle of 99.2(3)°. Conversely, the *cis* angles, Cl(1)–Ru(1)–N(2) and Cl(1)–Ru(1)–N(5), at 88.1(2) and 94.2(2)°, are closer to the ideal *cis* angle of 90°.

*3.2.2. Structure of out-[Ru(trpy)(4,4′-Me_2dppi)($NCCH_3$)](BF_4)$_2$·0.5$(CH_3)_2CHOH$·0.25H_2O (**2c**)*

The asymmetric unit of **2c** contains the cation, two BF_4^- anions one-half of an isopropanol molecule and one-quarter of a water molecule. There are no unusual contacts between these moieties. Crystal data are reported in Table 1, and selected bond distances and angles are given in Table 2. A view of the cation is presented in Fig. 2. The structure reveals a Ru center in a distorted octahedral environment. The coordinated acetonitrile ligand is directed away from the 4,4′-

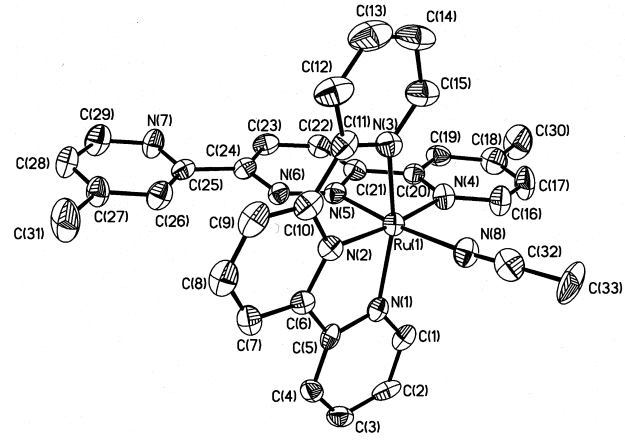


Fig. 2. Perspective view (40% probability ellipsoids) of the cation of *out*-$[Ru(trpy)(4,4'\text{-}Me_2dppi)(NCCH_3)](PF_6)_2$ (**2c**) with numbering scheme.

Me_2dppi ligand consistent with the *out* geometry. Like **1a**, the terpyridine group coordinates in a meridional fashion with a similar contraction of the Ru(1)–N(2) bond to 1.973(6) Å. The remaining Ru(1)–N separations fall within expected ranges. The angles around the acetonitrile group are slightly expanded with N(2)–Ru(1)–N(8) and N(4)–Ru(1)–N(8) opening to 93.9(3) and 95.5(3)°, respectively. Allowing for this expansion the N(2)–Ru(1)–N(5) angle contracts to 78.5(2)°. All other bond distances and angles fall within normal ranges.

3.3. ^{1}H NMR spectroscopy

The ^{1}H NMR spectra of the complexes support the proposed geometries. The spectra of the *out* isomers exhibit a downfield resonance due to the interaction of the 4,4′-dppi proton (on C(16) from Fig. 2) and the chloride, aqua or acetonitrile ligands. This diagnostic signal permitted all the resonances to be assigned unambiguously using NOE and COSY experiments. The spectral assignments for **2a** and **2b** are shown in Table 3. The *in* isomers lack this interaction since the chloride and aqua groups are directed towards the interior of the 4,4′-Me_2dppi ligand and are not in close contact with any protons.

3.4. Isomerization

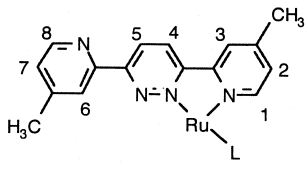
As expected for d^6 low spin complexes, **1a** and **2a** are substitutionally inert; however, once the chloride ligand is replaced by an aqua group, **1b** is prone to isomerization. Upon photolysis by visible light or reflux in methanol or acetone/water, solutions of *in*-[Ru(trpy)(4,4′-Me_2dppi)$(OH_2)]^{2+}$ readily and completely isomerize to *out*-[Ru(trpy)(4,4′-Me_2dppi)$(OH_2)]^{2+}$, but the reverse reaction was never detected, indicating that the *out* complexes are the thermodynamic products while the *in* products are the kinetic products. The mechanism for photo-isomerization likely involves excitation into a low-lying ligand-field transition [16,17]. Dissociation of the internal Ru–dppi bonds and rotation about the remaining Ru–dppi bond would interconvert the *in* isomer to the *out*, and this process could be affected thermally or photochemically. However, given that under identical conditions the chloro analogs are inert yet the relatively labile aqua species isomerize, the solvent may also play a role. Protecting the *in*-[Ru(trpy)(4,4′-Me_2dppi)$(OH_2)]^{2+}$ solutions from room light and operating at or below room temperature are enough to prevent isomerization.

3.5. Electronic absorption spectra

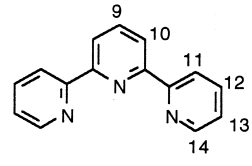
As tabulated in Table 4 compounds **1a** and **2a** both exhibited broad unsymmetrical bands in the visible region due to MLCT processes. The spectra also possess intense π to π* transitions in the UV region attributable to the polypyridine ligands. The λ_{max} for the MLCT transitions were 490 and 526 nm for **2a** and 479 and 521 nm for **1a**. For comparison, the λ_{max} for the analogous complex [Ru(trpy)(6,6′-Me_2dppi)Cl]$^+$, at 499 and 522 nm, are very similar to both **2a** and **1a**, a good indication of the similarity of the electronic nature of the complexes.

Table 3
^{1}H NMR chemical shifts of [Ru(trpy)(4,4′-Me_2dppi)(L)]$^{n+}$ complexes

4,4'-Me_2dppi protons



trpy protons



L	1	2	3	4	5	6	7	8	9	10	11	12	13	14
Cl (**2a**) [a]	10.19	8.07	8.80	8.73	8.34	7.30	7.30	8.46	8.42	8.83	8.60	8.00	7.41	7.90
H_2O (**2b**) [b]	9.55	8.07	8.74	8.67	8.21	7.16	7.28	8.39	8.47	8.80	8.57	8.02	7.42	7.93

[a] In d^6 acetone.
[b] In d_6 acetone/D_2O (5:1 v/v), chemical shifts relative to Me_4Si.

Table 4
Electrochemical half-wave potentials and spectroscopic data for [Ru(trpy)(R_2dppi)Cl]$^+$

Compound	Ru(III/II) [a]	Ligand reductions	MLCT λ_{max} (nm) (ε (M^{-1} cm^{-1})) [b]
in-[Ru(trpy)(4,4′-Me_2dppi)Cl]$^+$ (**1a**)	0.865	−1.21, −1.54, −1.86	479 (7800), 521 (10000)
out-[Ru(trpy)(4,4′-Me_2dppi)Cl]$^+$ (**2a**)	0.881	−1.20, −1.53, −1.59	490 (8500), 526 (11000)

[a] Obtained in CH_3CN.
[b] Obtained in CH_2Cl_2.

Table 5
Electrochemical and spectroscopic data for compounds **1b** and **2b**

Compound	Ru(IV/II) [a] (V)	k_{cat} [b] ($M^{-1} s^{-1}$)	pK_a	MLCT λ_{max} (nm) (ε ($M^{-1} cm^{-1}$)) [c]
in-[Ru(trpy)(4,4′-Me_2dppi)OH_2]$^{2+}$ (**1b**)	0.4	~9		480 (10000)
out-[Ru(trpy)(4,4′-Me_2dppi)OH_2]$^{2+}$ (**2b**)	0.440	20(1)	9.8	491 (8000)

[a] Obtained at pH 11 in aqueous phosphate buffer vs. SCE.
[b] Second-order rate constant obtained from analytical data as described in text.
[c] Obtained in pH 4 phosphate buffer.

The aqua complexes have similar spectra (Table 5). The low energy MLCT processes for **2b** shift to 491 nm and to 480 nm for **1b**. As with the previously studied aqua compounds, the MLCT shifts to higher energy upon substitution of the anionic chloride ligand for the neutral aqua ligand; deprotonation of the aqua ligands shifts the transitions to lower energy [18].

3.6. Electrochemistry

The cyclic voltammograms of **1a** and **2a** in acetonitrile both exhibit reversible one-electron oxidations (0.865 and 0.881 V versus Ag/AgCl, respectively). The complexes also displayed three ligand reductions. The oxidations are less anodic than that of the 6,6′-Me_2dppi complexes which had a Ru(III/II) couple at 0.98 V. The electronic nature of the ligands should be very similar, and the difference in oxidation potentials is likely a result of the different steric environments created by the two ligands. In fact, comparing the chloro complex of the 4,4′-Me_2dppi isomer (**2a**) to the unsubstituted H_2dppi complex shows that **2a** is easier to oxidize by 89 mV, fitting the expected trend now that the steric environment has been rendered more equal. In pH 11 phosphate buffer, **2b** displays a reversible two-electron oxidation at 0.44 V. **1b**, however, exhibits an oxidation wave but is accompanied by passivation of the electrode.

3.7. Electrocatalysis

The catalytic activity of **2b** towards a variety of substituted benzyl alcohol derivatives (1-phenylethanol, 1-phenyl-1-propanol and 2-methyl-1-phenyl-1-propanol) was studied to gain insight into the effects of sterics on the catalytic rate. The racemic alcohols were synthesized by a lithium aluminum hydride reduction on the corresponding commercially available ketone. These reactions proceeded cleanly, and the products required no additional purification.

The catalytic oxidation of these alcohols by *out*-[Ru(trpy)(4,4′-Me_2dppi)OH_2]$^{2+}$ was then studied in pH 11.2/phosphate buffer, with 50% t-butanol added to improve the solubility of the benzyl alcohols. Mixed solvent systems have been used by other groups for similar experiments with no adverse effects [19,20]. The addition of the t-butanol did not significantly affect the rate of catalysis of benzyl alcohol. All of the substrates were much more soluble in the modified buffer solution and yielded sigmoidally shaped voltammograms (characteristic of electrocatalysis) over the scan rate range 1 to 5 mV s^{-1}.

Data for these complexes are presented in Fig. 3. A nearly linear decrease in catalytic rate was observed as the number of carbon atoms around the alcohol group increased. The unhindered benzyl alcohol derivative has a rate constant of 19.8 $M^{-1} s^{-1}$ while the most hindered benzyl alcohol bearing the isopropyl substituent has a rate constant of only 2.7 $M^{-1} s^{-1}$. Clearly, sterics play an important factor in the catalytic mechanism since the driving force for the substrates is nearly the same. The rate constants of benzyl alcohol oxidation for the 4,4′-dppi complex can also be compared to the 6,6′-Me_2dppi isomer, which had a rate constant of 9 $M^{-1} s^{-1}$. The addition of a methyl group on the 6 and 6′ positions of the ligand retards the rate nearly identically to adding a methyl group to the substrate.

The electrocatalytic oxidation of benzyl alcohol by *in*-[Ru(trpy)(4,4′-Me_2dppi)OH_2]$^{2+}$ was also studied. This compound gave somewhat irreproducible results at a glassy carbon electrode owing to passivation upon oxidation: as much of 95% of the current is lost between the anodic and cathodic waves. Modification of the working electrode to include amide groups on the surface proved successful in reducing, but not eliminating, this passivation. With this modified electrode reversible Ru(IV/II) couples were observed and a catalytic rate constant of ~9 $M^{-1} s^{-1}$ was measured for the oxidation of benzyl alcohol. This value is nearly half

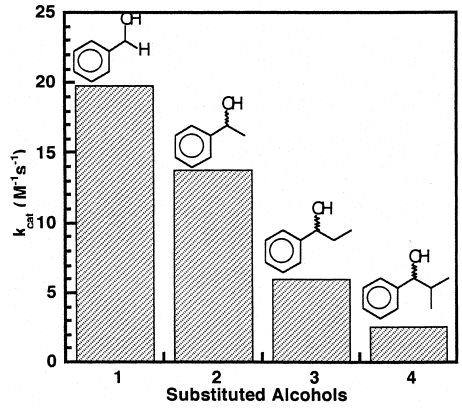


Fig. 3. Bar graph of the catalytic rate constant for the electrocatalytic oxidation of substituted benzyl alcohol derivatives by *out*-[Ru(trpy)(4,4′-Me_2dppi)OH_2]$^{2+}$.

of the corresponding *out* complex measured under identical conditions.

The smaller catalytic rate constant for the *in* versus the *out* complex and the irreversible electrochemistry on unmodified electrodes can be attributed to a variety of factors. One of these may be directly related to the previously mentioned instability of the *in* complex observed during the ligand substitution reactions. It is conceivable that an electrochemically induced *in* to *out* isomerization is possible; however, no evidence of the *out* complex was observed. A more likely explanation may be the catabolic oxidation of the 4,4′-Me_2dppi ligand and subsequent degradation of the compound. As seen in Fig. 1, the *in* complex directs what is to be the active oxo moiety towards the uncoordinated nitrogen on the pyridazine group, and intramolecular oxidation could occur upon Ru(IV)=O generation. The small rate constant measured may be more of a reflection of this process and not related to benzyl alcohol oxidation.

Supplementary data

Crystallographic data (excluding structure factors) for the structures reported in this paper have been deposited with the Cambridge Crystallographic Data Centre as supplementary publication nos. CCDC 132661 and 132662. Copies can be obtained free of charge on application to CCDC, 12 Union Road, Cambridge CB2 1EZ, UK (fax: +44-1223-336033; e-mail: deposit@ccdc.cam.ac.uk).

Acknowledgements

Acknowledgment is made to the National Science Foundation (CHE-9624281) (VJC), to the Camille and Henry Dreyfus Foundation (Faculty Start-up Grant to MGH) for their support of this research.

References

[1] R.H. Holm, Chem. Rev. 87 (1987) 1401.
[2] T.J. Meyer, J. Electrochem. Soc. 131 (1984) 221C.
[3] J.M. Madurro, G. Chiericato Jr., W.F. De Giovani, J.R. Romero, Tetrahedron Lett. 29 (1988) 765.
[4] M.S. Thompson, W.F. De Giovani, B.A. Moyer, T.J. Meyer, J. Org. Chem. 49 (1984) 4972.
[5] V.J. Catalano, R.A. Heck, C.E. Immoos, A. Ohman, M.G. Hill, Inorg. Chem. 37 (1998) 2150.
[6] M.S. Thompson, T.J. Meyer, J. Am. Chem. Soc. 104 (1982) 4106.
[7] A.B.P. Lever, Inorg. Chem. 29 (1990) 1271.
[8] A. Gerli, J. Reedijk, M.T. Lakin, A.L. Spek, Inorg. Chem. 34 (1995) 1836.
[9] L. Roecker, T.J. Meyer, J. Am. Chem. Soc. 109 (1987) 746.
[10] C.-M. Che, W.-T. Tang, W.-O. Lee, K.-Y. Wong, T.-C. Lau, J. Chem. Soc., Dalton Trans. (1992) 1551.
[11] M. Rudolph, D.P. Reddy, S.W. Feldberg, Anal. Chem. 66 (1994) 589A.
[12] B.P. Sullivan, J.M. Calvert, T.J. Meyer, Inorg. Chem. 19 (1980) 1404.
[13] D.L. Jameson, L.E. Guise, Tetrahedron Lett. 32 (1991) 1999.
[14] H.E. Baumgarten, Org. Synth. Coll. V (1973) 269.
[15] International Tables for X-ray Crystallography, vol. 4, Kynoch Press, Birmingham, 1974.
[16] B. Durham, S.R. Wilson, D.J. Hodgson, T.J. Meyer, J. Am. Chem. Soc. 102 (1980) 600.
[17] B.P. Sullivan, J.M. Calvert, T.J. Meyer, Inorg. Chem. 19 (1980) 1404.
[18] K.J. Takeuchi, M.S. Thompson, D.W. Pipes, T.J. Meyer, Inorg. Chem. 23 (1984) 1845.
[19] L. Roecker, T.J. Meyer, J. Am. Chem. Soc. 109 (1987) 746.
[20] J.M. Madurro, G. Chiericato Jr., W.F. De Giovani, J.R. Romero, Tetrahedron Lett. 29 (1988) 765.

PERGAMON

www.elsevier.nl/locate/poly

Polyhedron 19 (2000) 1057–1062

POLYHEDRON

Platinum(IV) tetraphenylporphyrin dibromide complexes: synthesis, characterization, and electrochemistry

L.M. Mink [a,*1], J.W. Voce [a], J.E. Ingersoll [a], V.T. Nguyen [a], R.K. Boggess [b,*2], H. Washburn [b], D.I. Grove [b]

[a] *Chemistry Department, California State University, San Bernardino, CA 92407-2397, USA*
[b] *Department of Chemistry and Physics, Radford University, Radford, VA 24142-6949, USA*

Received 6 December 1999; accepted 15 February 2000

Abstract

Platinum(IV) porphyrins of the type $[Pt^{IV}(p\text{-}X)_4TPP]Br_2$ where $(p\text{-}X)_4TPP$ is a *para*-substituted tetraphenylporphyrin have been synthesized by direct oxidation of their Pt(II) precursors with Br_2. Both the Pt(II) and Pt(IV) complexes have been characterized by visible and ^1H NMR spectroscopy and their electrochemical properties. In both the oxidation and reduction processes, a substituent effect is evident, and the reduction of $Pt^{IV} \rightarrow Pt^{II}$ is identified. The oxidation and reduction potentials of the $[Pt^{IV}(p\text{-}X)_4TPP]Br_2$ complexes are compared to those of the $[Pt^{II}(p\text{-}X)_4TPP]$ precursors and $[Pt^{IV}(p\text{-}X)_4TPP]Cl_2$ analogs. Addition of I_2 or I^- to Pt(II) porphyrins does not result in oxidative-addition to form Pt(IV) porphyrins. Instead, the addition of I^- to $[Pt^{IV}(p\text{-}X)_4TPP]Br_2$ results in the reduction of the platinum to form the corresponding $[Pt^{II}(p\text{-}X)_4TPP)]$. ©2000 Elsevier Science Ltd All rights reserved.

Keywords: Platinum(II); Platinum(IV); Bromide; Porphyrins; Electrochemistry; Voltammetry

1. Introduction

An extensive amount of research has focused on metalloporphyrins owing to the critical roles they play in electron transfer, photosynthesis, and oxygen transfer processes [1]. Their reactivity is found to be dependent upon the central metal, the substituents on the porphyrin ring, and the axially coordinated ligands. Platinum porphyrins have been investigated as oxygen sensing probes [2–6], photosensitizers [7–9], potential antitumor agents [10], and molecular conductors [11,12]. Most of the recent studies have focused on Pt(II) porphyrins. Pt(IV) porphyrins of the type $[Pt^{IV}(p\text{-}X)_4TPP]Br_2$, where X = CN, H, CH_3, and OCH_3, have been synthesized from the corresponding $[Pt^{II}(p\text{-}X)_4TPP]$ precursors through direct oxidative-addition of $Br_{2(l)}$. Stable $[Pt^{IV}(p\text{-}X)_4TPP]Br_2$ complexes are formed with axial Br^- ligands that generate large Δ splitting values in the Pt(IV) (5d, $t_{2g}^6e_g^0$) through σ donation [13]. Considerable attention has recently been devoted to the development of platinum(IV) dichloride complexes as pro-drug antitumor agents [14–18], whereas relatively few reports have involved the study of platinum(IV) dibromide compounds [19–21]. The compounds in this paper are prepared in a fashion similar to $[Pt^{IV}(p\text{-}X)_4TPP]Cl_2$ complexes previously reported [22]. The chemical and electrochemical reactivity of Pt(II) and Pt(IV) tetraphenylporphyrins with the halogens chlorine, bromine, and iodine is discussed in this research.

2. Experimental

2.1. General

^1H NMR spectra were recorded at 270.167 MHz with a JEOL ECLIPSE spectrometer (reference δ 7.24, $CHCl_3$). UV–Vis spectra were obtained with a Beckman DU-7500 diode array instrument using quartz cells with a path length of 1.0 cm. Cyclic voltammetry was carried out by the conventional three-electrode method in CH_2Cl_2 (distilled from CaH_2) with Bu_4NPF_6 (0.10 M) as a supporting electrolyte. Electrochemical measurements were made with either a PAR 174A electrochemical analyzer or an Amel model 551 potentiostat and a model 567 function generator. The concentration of the complex was usually between $(0.5\text{–}1.0) \times 10^{-3}$ M. Ferrocene was used as an internal standard. All potentials are

[1] *Corresponding author. Tel. +1-909-880-5478; fax: +1-909-880-7066; e-mail: lmink@csusb.edu
[2] *Corresponding author.

0277-5387/00/$ - see front matter ©2000 Elsevier Science Ltd All rights reserved.
PII S0277-5387(00)00349-1

referenced to the $E_{\frac{1}{2}}$ ($E_{\frac{1}{2}} = \frac{1}{2}(E_{pa} + E_{pc})$) for the $(C_5H_5)_2Fe/(C_5H_5)_2Fe^+$ couple; $E_{\frac{1}{2}}$ for ferrocene was typically $+0.48 \pm 0.02$ V versus the Ag|AgCl|NaCl(saturated) BAS reference electrode, near the 0.45 V reported for the ferrocene couple versus an SCE reference electrode [23].

Reagent grade chemicals and solvents were purchased from Aldrich Chemical Company, Fisher Scientific, and Spectrum. Platinum(II) chloride was obtained from Alfa Aesar, chlorine, from Matheson Gas Products, and bromine from Janssen Chimica. Chromatographic grade aluminum oxide, activated neutral, standard grade 150 mesh, 58 Å and silica gel (Merck grade 9385, 230-400, mesh 60 Å) were purchased from Aldrich Chemical Company. Elemental analyses were performed by Desert Analytics, Tucson, AZ.

2.2. Synthesis of $[Pt^{IV}(p\text{-}X)_4TPP]Br_2$ (X = CN, H, OCH_3, CH_3)

The synthesis of the $[Pt^{II}(p\text{-}X)_4TPP]$ complexes has been previously reported [22]. The $[Pt^{IV}(p\text{-}X)_4TPP]Br_2$ complexes were synthesized through direct addition of Br_2 to the corresponding $[Pt^{II}(p\text{-}X)_4TPP]$ complexes. A $Br_{2(l)}/CHCl_3$ solution was prepared by the addition of 12 drops of $Br_{2(l)}$ to 10 cm^3 of $CHCl_3$, and 50 drops of the mixture were added slowly to $[Pt^{II}(p\text{-}X)_4TPP]$ (0.022 mmol) dissolved in 20 cm^3 of $CHCl_3$ at 0°C. The reaction was monitored by UV–Vis spectroscopy and judged complete in 2 h by the gradual decrease of the Soret band near 403 nm associated with $[Pt^{II}(p\text{-}X)_4TPP]$ and the appearance of the Soret band near 421 nm associated with $[Pt^{IV}(p\text{-}X)_4TPP]Br_2$. The solution was concentrated to 5 cm^3 by rotary evaporation, and an equal volume of cold methanol precipitated the $[Pt^{IV}(p\text{-}X)_4TPP]Br_2$ crystalline solid. The complex was dissolved in a minimum amount of toluene and loaded onto a 3 cm × 18 cm silica gel column. Non-reacted $[Pt^{II}(p\text{-}X)_4TPP]$ was eluted as a light orange band with toluene. $[Pt^{IV}(p\text{-}X)_4TPP]Br_2$ was collected upon elution with 2% trifluoroacetic acetic acid (TFA) in chloroform and appeared as a dark red–purple band. Concentration of the TFA/chloroform solution to 25 cm^3 and addition of an equal volume of cold methanol precipitated the red–purple $[Pt^{IV}(p\text{-}X)_4TPP]Br_2$ crystalline solid. $[Pt^{IV}(p\text{-}X)_4TPP]Br_2$ was collected by filtration and then washed with cold methanol and water. $[Pt^{IV}(p\text{-}CN)_4TPP]Br_2$ was not purified by column chromatography owing to limited solubility. Final yields were in the range of 75%. Elemental analyses gave the following results. Calc. for $[Pt(p\text{-}H)_4TPP]Br_2$ ($C_{44}H_{28}PtN_4Br_2$): C, 54.62; H, 2.92; N, 5.79; Br, 16.52. Found: C, 53.95; H, 2.81; N, 5.57; Br, 16.09%. Calc. for $[Pt(p\text{-}OCH_3)_4TPP]Br_2$ ($C_{48}H_{36}PtN_4O_4Br_2$): C, 53.00; H, 3.34; N, 5.15; Br, 14.69. Found: C, 52.64; H, 3.01; N, 4.89; Br, 14.60%.

3. Results and discussion

As reported for the $[Pt^{IV}(p\text{-}X)_4TPP]Cl_2$ complexes, the UV–Vis spectra of the $[Pt^{IV}(p\text{-}X)_4TPP]Br_2$ complexes are dominated by the Soret, α, and β bands near 420, 573, and 536 nm, respectively (Table 1). These bands exhibit 20–25 nm bathochromic shifts (to longer wavelengths) with respect to the precursor $[Pt^{II}(p\text{-}X)_4TPP]$ complexes and are similar in absorption values to their $[Pt^{IV}(p\text{-}X)_4TPP]Cl_2$ analogs [22]. A slight bathochromic shift of ~4 nm is detected for the Soret band for the $[Pt^{IV}(p\text{-}X)_4TPP]Br_2$ complexes compared to their chloride counterparts. Thus, there is a substantial effect on the electronic spectra of the complexes as a result of the $Pt^{II} \rightarrow Pt^{IV}$ oxidation but little effect due to variance in the halogens at the axial positions. The bathochromic shifts resulting from $Pt^{II} \rightarrow Pt^{IV}$ have been interpreted as being indicative of a decrease in metal d to porphyrin π*-bonding [24]. As was observed for $[Pt^{II}(p\text{-}X)_4TPP]$ and $[Pt^{IV}(p\text{-}X)_4TPP]Cl_2$, the Soret, α, and β bands of the $[Pt^{IV}(p\text{-}X)_4TPP]Br_2$ complexes do not display any pronounced substituent effect.

In the ^1H NMR spectra, a distinct decrease in shielding of all proton resonances is evident upon oxidation of $[Pt^{II}(p\text{-}X)_4TPP]$ to $[Pt^{IV}(p\text{-}X)_4TPP]Br_2$ (Fig. 1), and a similar trend was observed for the analogous $[Pt^{IV}(p\text{-}X)_4TPP]Cl_2$ complexes [22]. In comparing the ^1H NMR of the $[Pt^{IV}(p\text{-}X)_4TPP]Br_2$ to the $[Pt^{IV}(p\text{-}X)_4TPP]Cl_2$ complexes, the bromide complexes display a slight upfield chemical shift of all ^1H NMR resonances (~0.02 ppm). The upfield chemical shift may be indicative of increased electron density about the platinum center for the dibromide complexes. Increased electron density about the platinum center would allow for increased platinum–porphyrin π*-backbonding resulting in increased shielding of the porphyrin proton resonances. This would be anticipated as Pt(IV) forms a weaker bond with the bromide than with the chloride ion [25], and this feature is evident in the electrochemical results. As was the case for the $[Pt^{IV}(p\text{-}X)_4TPP]Cl_2$ complexes, the J_{Pt-H} pyrrole coupling decreases from ca. 11 Hz for Pt(II) to ca. 8 Hz for Pt(IV) owing to the relative decrease in platinum 6s character (Table 2).

A porphyrin ring generally shows three or four well defined, quasireversible sites of redox activity. The LUMO of the porphyrin ring is considered to be the e_g (π*) orbital and the HOMO either an a_{2u} (π) or a_{1u} (π) orbital. In earlier

Table 1
Spectral data for $[Pt^{II}(p\text{-}X)_4TPP]$ and $[Pt^{IV}(p\text{-}X)_4TPP]Br_2$ complexes [a]

	Soret band	β band	α band
$Pt^{II}(p\text{-}CN)_4TPP$	403	511	541
$[Pt^{IV}(p\text{-}CN)_4TPP]Br_2$	427	538	573
$[Pt^{II}(TPP)]$	402	510	540
$[Pt^{IV}(TPP)]Br_2$	426	535	[b]
$[Pt^{II}(p\text{-}CH_3O)_4TPP]$	407	512	539
$[Pt^{IV}(p\text{-}CH_3O)_4TPP]Br_2$	430	537	573
$[Pt^{II}(p\text{-}CH_3)_4TPP]$	405	511	539
$[Pt^{IV}(p\text{-}CH_3)_4TPP]Br_2$	427	535	[b]

[a] Wavelengths in nanometers.
[b] Not observed.

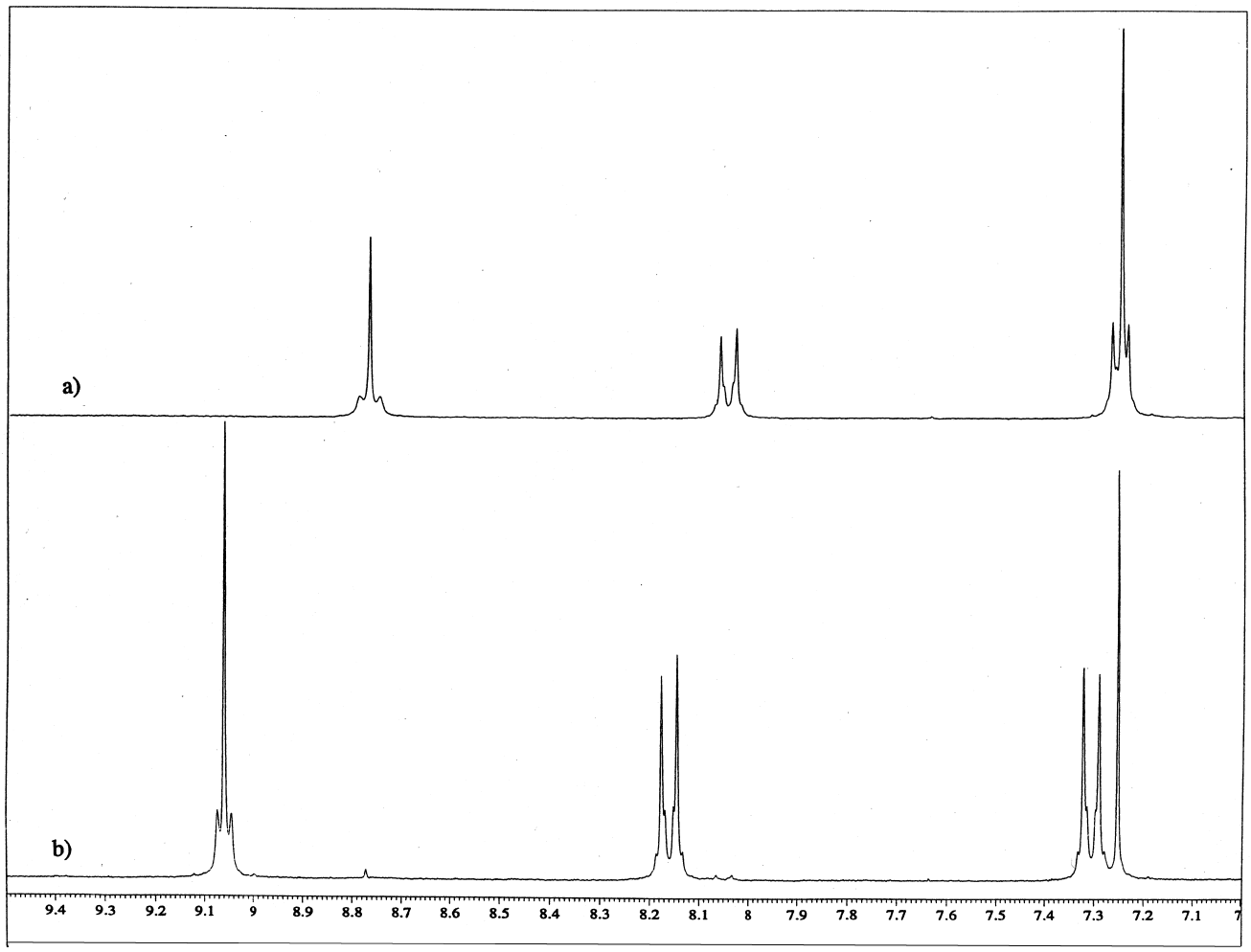


Fig. 1. NMR spectra of the aromatic region (270 MHz, reference δ 7.24, $CHCl_3$): (a) $[Pt^{II}(p\text{-}CH_3O)_4TPP]$, (b) $[Pt^{IV}(p\text{-}CH_3O)_4TPP]Br_2$.

Table 2
^{1}H NMR chemical shifts and coupling constants [a]

	H-pyr	H-*ortho*	H-*meta*	H-*para*	
$Pt^{II}(p\text{-}CN)_4TPP$	8.68 ($J_{Pt-H}=11$)	8.26	8.07		
$[Pt^{IV}(p\text{-}CN)_4TPP]Br_2$ [b]	9.10 ($J_{Pt-H}=8$)	8.38	8.21		
$[Pt^{II}(TPP)]$	8.76 ($J_{Pt-H}=12$)	8.15	7.74	7.75	
$[Pt^{IV}(TPP)]Br_2$	9.03 ($J_{Pt-H}=8$)	8.25	7.78	7.79	
$[Pt^{II}(p\text{-}CH_3O)_4TPP]$	8.78 ($J_{Pt-H}=10$)	8.05	7.26		($-OCH_3=4.13$)
$[Pt^{IV}(p\text{-}CH_3O)_4TPP]Br_2$	9.05 ($J_{Pt-H}=8$)	8.16	7.30		($-OCH_3=4.10$)
$[Pt^{II}(p\text{-}CH_3)_4TPP]$	8.76 ($J_{Pt-H}=11$)	8.03	7.53		($-CH_3=2.69$)
$[Pt^{IV}(p\text{-}CH_3)_4TPP]Br_2$	9.030 ($J_{Pt-H}=8$)	8.12	7.57		($-CH_3=2.70$)

[a] Chemical shifts in ppm, coupling constants in Hz.
[b] NMR in acetonitrile solvent.

work, we were able to observe the four redox waves for $H_2(TPP)$, but the oxidation at the most positive potential was distorted and did not display good redox characteristics [22]. Substitution of the *para* protons by –CN to give $H_2(p\text{-}CN)_4TPP$ provides a ligand that does exhibit all four well defined sites of redox activity (Table 3). The substituent effect observed in other $H_2(p\text{-}X)_4TPP$ ligands is evident for $H_2(p\text{-}CN)_4TPP$ as the first oxidation is shifted by $+0.23$ V and the first reduction by $+0.16$ V relative to $H_2(TPP)$. These are substantially larger changes than observed in other $H_2(p\text{-}X)_4TPP$ ligands as, for example, the first oxidation of $H_2(p\text{-}Cl)_4TPP$ relative to $H_2(TPP)$ is only $+0.09$ V.

In several instances, the electrochemistry of the $[Pt^{II}(p\text{-}X)_4TPP]$ complexes also shows four sites of redox activity attributable to the porphyrin ring, and the substituent effect is observed in the complexes as well as the free ligands. Reaction of the $[Pt^{II}(p\text{-}X)_4TPP]$ complexes with Cl_2 produced the $[Pt^{IV}(p\text{-}X)_4TPP]Cl_2$ complexes. The four sites of

Table 3
Electrochemical data for the $[Pt^{IV}(p\text{-}X)_4TPP]Br_2$ complexes

$H_2(TPP)$ [a]	+1.01	+0.55(85)		−1.67(70)	−2.00(80)
$H_2(p\text{-}CN)_4TPP$ [a]	+1.02(93)	+0.78(88)		−1.51(105)	−1.83(110)
$[Pt^{II}(p\text{-}CN)_4TPP]$ [a]		+0.91(80)		−1.64(70)	−2.04(90)
$[Pt^{IV}(p\text{-}CN)_4TPP]Br_2$ [b]		+1.14(80)	*−0.50*	−2.04(90)	
$[Pt^{IV}(TPP)]Br_2$ [a]		+0.89(100)	*−0.75*	−1.84(100)	
$[Pt^{IV}(p\text{-}CH_3)_4TPP]Br_2$ [a]		+0.85(90)	*−0.80*	−1.87(80)	
$[Pt^{IV}(p\text{-}CH_3O)_4TPP]Br_2$ [a]		+0.76(95)	*−0.81*	−1.86(95)	

[a] Electrochemistry performed in CH_2Cl_2. Scan rates were 200 mV s^{-1}. Potentials (mV) are referenced to the ferrocene/ferrocinium redox couple. Numbers in parentheses are ΔE_p (mV) and the numbers in italics are the $Pt^{IV} \rightarrow Pt^{II}$(V) reductions.
[b] Electrochemistry performed in CH_3CN.

redox activity remain, and a fifth irreversible reduction attributable to $Pt^{IV} \rightarrow Pt^{II}$ that showed a substantial substituent effect was observed. With the preparation of the corresponding $[Pt^{IV}(p\text{-}X)_4TPP]Br_2$ and $[Pt^{IV}(p\text{-}X)_4TPP]Cl_2$ complexes, the effect of the axial ligand as well as the substituents on the porphyrin ring can be studied. As was found for the $[Pt^{IV}(p\text{-}X)_4TPP]Cl_2$ complexes, only the first oxidation and first reduction waves of the ligand were always well defined. Replacement of the two axial Cl^- ligands on the $[Pt^{IV}(p\text{-}X)_4TPP]Cl_2$ complexes with Br^- caused only a slight negative shift (<0.05 V) in both of these waves. However, a substantial positive shift (between 0.19 and 0.31 V) in the $[Pt^{IV}(p\text{-}X)_4TPP]Br_2$ complexes relative to the $[Pt^{IV}(p\text{-}X)_4TPP]Cl_2$ complexes is observed for the irreversible $Pt^{IV} \rightarrow Pt^{II}$ reduction (Table 3). Thus, the axial ligands, which are directly coordinated to the Pt(IV), have a pronounced effect on that reduction, and the effect is in the direction expected as Cl^- should form the stronger bond to Pt(IV), making $[Pt^{IV}(p\text{-}X)_4TPP]Cl_2$ more difficult to reduce [25]. The reduction process for both the Cl^- and Br^- complexes can be described by:

$$[Pt^{IV}(p\text{-}X)_4TPP]X_2 + 2e^- \rightarrow [Pt^{II}(p\text{-}X)_4TPP] + 2X^- \quad (1)$$

To illustrate, for the $[Pt^{IV}TPP]Br_2$ complex, if the potential scan is initiated at 0.00 V in the anodic direction (Fig. 2, scan A), the first porphyrin oxidation and, upon reversal of the potential scan the subsequent reduction, is observed at +0.89 V. The $Pt^{IV} \rightarrow Pt^{II}$ reduction is then observed at −0.75 V, followed by the reduction, and upon reversal of the potential scan, the subsequent oxidation of the porphyrin ring at −1.84 V. When the scan is initiated at 0.00 V in the cathodic direction (Fig. 2, scan B), the $Pt^{IV} \rightarrow Pt^{II}$ reduction and first reduction and subsequent oxidation of the porphyrin ring are again observed. However, a new irreversible oxidation at +0.25 V appears as do some small impurities associated with the porphyrin oxidation–reduction at +0.89 V. If scan A is repeated but allowed to go through two cycles (Fig. 2, scan C), the first cycle is identical to scan A but the second cycle has the oxidation at +0.25 V and the small impurities associated with the +0.89 V peak. When scan A is repeated and allowed to go through the $Pt^{IV} \rightarrow Pt^{II}$ reduction, but not the ring reduction and subsequent oxidation at −1.84 V (Fig. 2, scan D), the oxidation at +0.25 V, and impurities on the porphyrin peak are present. The cyclic voltammograms clearly indicate that the oxidation at +0.25 V and the small impurities on the +0.89 V oxidation and reduction are associated with the reduction of the Pt^{IV} and can be described by the overall process:

$$[Pt^{IV}(TPP)]Br_2 + 2e^- \rightarrow [Pt^{II}(TPP)] + 2Br^- \quad (2)$$

Either simultaneously or in a subsequent step, once the Pt(IV) is reduced, the Br^- becomes non-coordinating and is irreversibly oxidized at +0.25 V. The small peaks associated with the porphyrin ring at +0.89 V are due to the small quantity of $[Pt^{II}(TPP)]$ formed near the electrode surface. Cyclic voltammetry of the $[Pt^{IV}(p\text{-}CH_3O)_4TPP]Br_2$ complex gave similar results. Proof that the +0.25 V peak was due to Br^- was obtained when a cyclic voltammogram of tetra(*n*-butyl)ammonium bromide gave the same peak.

An attempt was made to determine whether a six-coordinate Pt(II) species might at least temporarily result from the reduction above. If reaction (2) is a two-step process:

$$[Pt^{IV}(TPP)]Br_2 + 2e^- \rightarrow [Pt^{II}(TPP)]Br_2 \quad (3)$$

$$[Pt^{II}(TPP)]Br_2 \rightarrow [Pt^{II}(TPP)] + 2Br^- \quad (4)$$

the addition of a large excess of Br^- may retard reaction (4) and reaction (3) may become partially reversible. The sup-

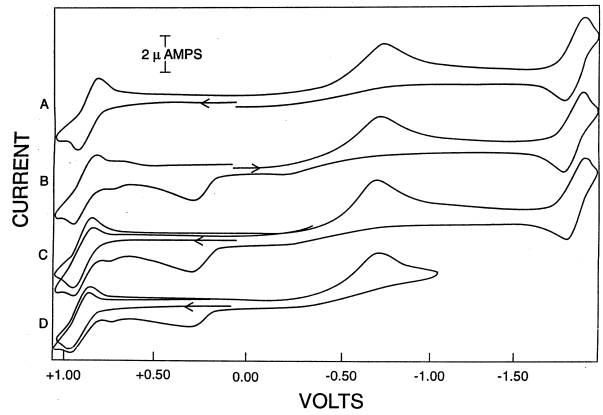


Fig. 2. Cyclic voltammograms for $[Pt^{IV}(TPP)]Br_2$ in CH_2Cl_2 at a scan rate of 100 mV s^{-1}; scan A initiated at 0.0 V in an anodic direction; scan B initiated at 0.0 V in a cathodic direction; scan C initiated at 0.0 V in an anodic direction, multiple cycles; scan D initiated at 0.0 V in an anodic direction, reversed after the Pt(IV) to Pt(II) reduction.

porting electrolyte tetra(*n*-butyl)ammonium hexafluorophosphate was replaced with tetra(*n*-butyl)ammonium bromide so that the [Br^-] was 0.10 M. The electrochemical results at scan rates to 500 mV s^{-1} were identical to the previous results and failed to reveal any evidence of a reversible nature to the $Pt^{IV} \rightarrow Pt^{II}$ reduction.

For the [Pt^{IV}(*p*-X)$_4$TPP]Br_2 complexes, the data of Table 3 illustrate that the first oxidation and the first reduction of the porphyrins do exhibit a substituent effect similar to that found for the [Pt^{IV}(*p*-X)$_4$TPP]Cl_2 complexes. The electron-donating CH_3O– and CH_3– groups shift the first oxidation and the first reduction to a more negative potential, and the electron-withdrawing –CN group shifts them toward a more positive potential. As has been observed with other Pt(II) systems, the addition of I_2 or I^- in the presence of the oxidizing agent hydrogen peroxide, H_2O_2, to Pt(II) porphyrins does not result in oxidative-addition generating Pt(IV) porphyrins [26–29]. The addition of I^- to [Pt^{IV}(*p*-X)$_4$TPP]Br_2 results in reduction of the platinum to form the corresponding Pt(II) porphyrins, [Pt^{II}(*p*-X)$_4$(TPP)]. However, addition of iodide to [Pt^{IV}(*p*-X)$_4$TPP]Cl_2 does not result in platinum reduction. This reduction process of Pt(IV) complexes by iodide has previously been observed and is believed to proceed through iodide–halide bond formation prior to the reduction in which the halogen acts as a bridging ligand [30–33]. The fact that iodide effectively reduces [Pt^{IV}(*p*-X)$_4$TPP]Br_2 and not [Pt^{IV}(*p*-X)$_4$TPP]Cl_2 is attributed to the more positive reduction potentials (by ca. 0.2 V) of the bromide species compared to their chloride counterparts. The enhanced ease of reduction of Pt(IV) bromide complexes compared to analogous Pt(IV) chloride complexes has previously been attributed to a weaker Pt(IV)–Br bond, and bromide being a good bridging ligand during the reduction process [25,28,29,34–38].

4. Conclusions

[Pt^{IV}(*p*-X)$_4$TPP]Br_2 complexes are readily accessible through direct oxidative-addition of Br_2 to [Pt^{II}(*p*-X)$_4$TPP]. The [Pt^{II}(*p*-X)$_4$TPP] porphyrins are non-reactive toward I_2 or iodide in the presence of an oxidizing agent. Iodide effectively reduces the [Pt^{IV}(*p*-X)$_4$TPP]Br_2 complexes whereas the [Pt^{IV}(*p*-X)$_4$TPP]Cl_2 complexes are unaffected. Replacement of axial Cl^- ligands on the Pt(IV) by Br^- has little effect on the electrochemistry of the complex other than to move the reduction of the Pt(IV) to considerably more positive potentials. The reduction results in the loss of the axial ligands and is described by:

$$[Pt^{IV}(p\text{-X})_4TPP]Br_2 + 2e^- \rightarrow [Pt^{II}(p\text{-X})_4TPP] + 2Br^-$$

Cyclic sweep voltammetry of the Pt(IV) complex shows the appearance of the corresponding Pt(II) complex. Use of a large excess of Br^- failed to make this reduction reversible.

Acknowledgements

Partial support for this work was provided by the National Science Foundation's Division of Undergraduate Education through grant DUE 9452076 for the purchase of the nuclear magnetic resonance spectrometer and by a Cottrell College Science Award of Research Corporation (LM). The authors thank Alfa Aesar, a Johnson Matthey Company, for their metal loan program, and CSUSB Associated Students, Inc. RKB wishes to acknowledge support by a Cottrell College Science Award by Research Corporation and the National Science Foundation (TFI-802595) for funds to purchase the electrochemical equipment.

References

[1] D. Dolphin (Ed.), The Porphyrins, vols. I–VII, Academic Press, New York, 1978.
[2] S.-K. Lee, I. Okura, Anal. Commun. 34 (1997) 185.
[3] S.-K. Lee, I. Okura, Anal. Chim. Acta 342 (1997) 181.
[4] A. Mills, A. Lepre, Anal. Chem. 69 (1997) 4653.
[5] D.B. Papkovsky, A.N. Ovchinnikov, G.V. Ponomarev, T. Korpela, Anal. Lett. 30 (1997) 699.
[6] D.B. Papkovsky, G.V. Ponomarev, O.S. Wolfbeis, Spectrochim. Acta A 52 (1996) 1629.
[7] R.R. de Haas, R.P.M. van Gijlswijk, E.B. van der Tol, J.M.A.A. Zijlmans, T. Bakker-Schut, J. Bonnet, N.P. Verwoerd, H.J. Tanke, J. Histochem. Cytochem. 45 (9) (1997) 1279.
[8] H. Kunkely, A. Vogler, Inorg. Chim. Acta 254 (1997) 417.
[9] J.A. Mercer-Smith, D.G. Whitten, J. Am. Chem. Soc. 100 (1978) 2620.
[10] H. Brunner, K.M. Schellerer, B. Treittinger, Inorg. Chim. Acta 264 (1997) 67.
[11] A. Ferri, G. Polzonetti, S. Licoccia, R. Paolesse, D. Favretto, P. Traldi, M.V. Russo, J. Chem. Soc., Dalton Trans. 23 (1998) 4063.
[12] H. Yuan, L. Thomas, L.K. Woo., Inorg. Chem. 35 (1996) 2808.
[13] D.J. Gulliver, W. Levason, K.G. Smith, J. Chem. Soc., Dalton Trans. 11 (1981) 2153.
[14] N.A. Kratochwil, A.I. Ivanov, M. Patriarca, J.A. Parkinson, A.M. Gouldsworthy, P.S. Murdoch, P.J. Sadler, J. Am. Chem. Soc. 121 (1999) 8193.
[15] S. Shamsuddin, C.C. Santillan, J.L. Stark, K.H. Whitmire, Z.H. Siddik, A.R. Khokar, J. Inorg. Biochem. 71 (1998) 29.
[16] K.M. Kim, Y.S. Sohn, Inorg. Chem. 37 (1998) 6109.
[17] H. Junicke, C. Bruhn, D. Ströh, R. Kluge, D. Steinborn, Inorg. Chem. 37 (1998) 4603.
[18] D. Lebwohl, R. Canetta, Eur. J. Cancer 34 (1998) 1522.
[19] J. Forniés, M.A. Gomez-Saso, A. Martín, F. Martínez, B. Menjon, J. Navarrete, Organometallics 16 (1997) 6024.
[20] R. Jones, P.F. Kelly, D.J. Williams, J.D. Woolins, J. Chem. Soc., Dalton Trans. 6 (1988) 1569.
[21] R.J.H. Clark, V.B. Croud, J. Chem. Soc., Dalton Trans. 1 (1988) 73.
[22] L.M. Mink, M.L. Neitzel, L.M. Bellomy, R.E. Falvo, R.K. Boggess, B.T. Trainum, P. Yeaman, Polyhedron 16 (1997) 2809.
[23] A.M. Stolzenberg, M.T. Stershic, J. Am. Chem. Soc. 110 (1988) 6391.
[24] J.W. Buchler, K.L. Lay, H. Stoppa, Z. Naturforsch., Teil b 35 (1980) 433.
[25] A.J. Poë, M.S. Vaidya, J. Chem. Soc. (1961) 1023.
[26] E.G. Hope, W. Levason, N.A. Powell, Inorg. Chim. Acta 115 (1986) 187.
[27] A. Peloso, R. Ettorre, G. Dolcetti, Inorg. Chim. Acta 1 (1967) 307.
[28] A. Peloso, Coord. Chem. Rev. 10 (1973) 123.

[29] A. Peloso, R. Ettorre, J. Chem. Soc. A (1968) 2253.
[30] W.K. Wilmarth, Y.T. Fanchiang, J.E. Byrd, Coord. Chem. Rev. 51 (1983) 141.
[31] C.E. Skinner, M.M. Jones, J. Am. Chem. Soc. 91 (1969) 4405.
[32] A.J. Poë, D.H. Vaughan, J. Am. Chem. Soc. 92 (1970) 7537.
[33] L.I. Elding, L. Gustafson, Inorg. Chim. Acta 19 (1976) 165.
[34] A.J. Poë, D.H. Vaughan, Inorg. Chim. Acta 2 (1968) 159.
[35] M.M. Jones, K.A. Morgan, J. Inorg. Nucl. Chem. 34 (1972) 259.
[36] K.A. Morgan, M.M. Jones, J. Inorg. Nucl. Chem. 34 (1972) 275.
[37] T. Shi, J. Berglund, L.I. Elding, Inorg. Chem. 35 (1996) 3498.
[38] T. Shi, J. Berglund, L.I. Elding, J. Chem. Soc., Dalton Trans. (1997) 2073.

PERGAMON

www.elsevier.nl/locate/poly

Polyhedron 19 (2000) 1063–1066

POLYHEDRON

Reactivity of $Mo(PMe_3)_5H_2$ towards catecholborane: synthesis and structure of $Mo(PMe_3)_4(\eta^2\text{-}H_2BCat)H$

Tony Hascall, Brian M. Bridgewater, Gerard Parkin *

Department of Chemistry, Columbia University, New York, NY 10027, USA

Received 4 October 1999; accepted 15 February 2000

Abstract

$Mo(PMe_3)_5H_2$ reacts with catecholborane (CatBH) to give $Mo(PMe_3)_4(\eta^2\text{-}H_2BCat)H$. Structural characterization by X-ray diffraction suggests that the complex is best represented as a borohydride complex, as opposed to a boryl-hydride derivative $Mo(PMe_3)_4(BCat)H_3$.
©2000 Elsevier Science Ltd All rights reserved.

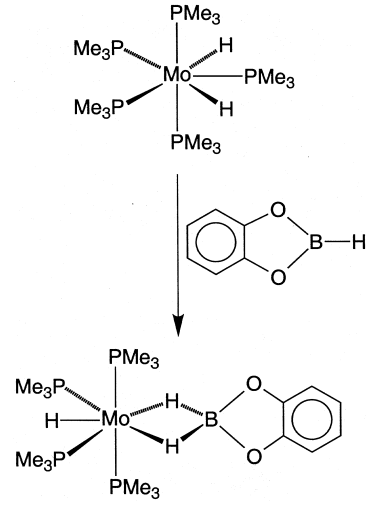
Keywords: Catecholborane; Reactivity

1. Introduction

Transition metal complexes, e.g. $(Ph_3P)_3RhCl$, have been used extensively as catalysts for promoting hydroboration reactions employing catecholborane (CatBH = $(C_6H_4O_2)$-BH) as a reagent [1]. A key step in the mechanism of the hydroboration reaction has been proposed to involve oxidative addition of the borane B–H bond to the transition metal center [1,2]; indeed, a variety of boryl-hydride complexes have been isolated which supports such a notion [3]. We have recently described the oxidative addition of a variety of X–H bonds (e.g. X = H [4], C [5], O [5], Hal [6]) to electron-rich molybdenum and tungsten complexes of the types $M(PMe_3)_6$, $M(PMe_3)_4(\eta^2\text{-}CH_2PMe_2)H$ and $M(PMe_3)_5H_2$. For this reason, we were interested in extending these studies by investigating the reactivity of borane derivatives towards the above complexes. In this paper, we report the reaction of $Mo(PMe_3)_5H_2$ towards CatBH.

2. Results and discussion

The dihydride $Mo(PMe_3)_5H_2$ reacts rapidly with CatBH in benzene solution to yield the red borohydride complex $Mo(PMe_3)_4(\eta^2\text{-}H_2BCat)H$ (Scheme 1). Characterization of $Mo(PMe_3)_4(\eta^2\text{-}H_2BCat)H$ as a dihydrocatecholborate derivative is based on a structure determination by single crystal X-ray diffraction (Fig. 1), which allowed the hydrogen atoms attached to both Mo and B to be located and refined. Viewing the $[\eta^2\text{-}H_2BCat]$ ligand as occupying a single coordination site, the structure of $Mo(PMe_3)_4(\eta^2\text{-}H_2BCat)H$ may be considered to be based on a distorted octahedron, with *trans* $[\eta^2\text{-}H_2BCat]$ and hydride ligands. Such a geometry is akin to that of the tetrahydroborate derivative, $Mo(PMe_3)_4(\eta^2\text{-}H_2BH_2)H$, which was obtained by the reaction of $MoCl_3(PMe_3)_3$ with $NaBH_4$ [7]. It should, however, be noted that, in contrast to $\eta^2\text{-}BH_4$ complexes [8], structurally characterized $\eta^2\text{-}H_2BCat$ derivatives are rare [9–11]. For comparison purposes, selected average bond



Scheme 1.

* Corresponding author. Tel.: +1-212-854-8247; fax: +1-212-932-1289; e-mail: parkin@chem.columbia.edu

0277-5387/00/$ - see front matter ©2000 Elsevier Science Ltd All rights reserved.
PII S0277-5387(00)00350-8

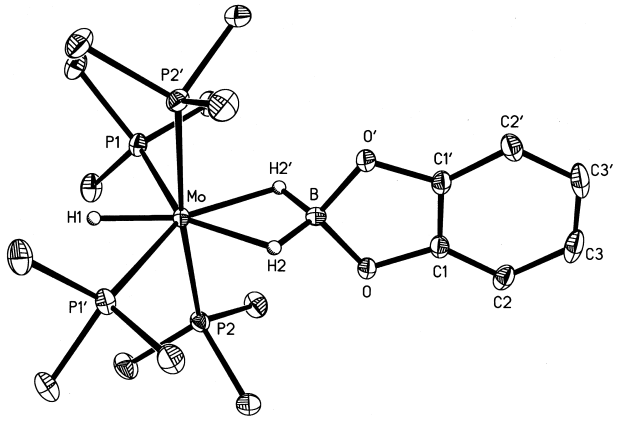


Fig. 1. Molecular structure of $Mo(PMe_3)_4(\eta^2\text{-}H_2Cat)H$.

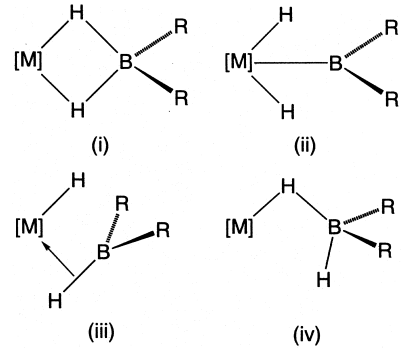


Fig. 2. Isomers of the $[MH_2BR_2]$ moiety: (i) η^2-borohydride, $\{[M](\eta^2\text{-}H_2BR_2)\}$, (ii) boryl-hydride, $\{[M](BR_2)H_2\}$, (iii) borane-hydride, $\{[M](\eta^2\text{-}H\text{–}BR_2)H\}$, and (iv) η^1-borohydride, $\{[M](\eta^1\text{-}HBHR_2)\}$.

lengths and angles for $Mo(PMe_3)_4(\eta^2\text{-}H_2BCat)H$ and $Mo(PMe_3)_4(\eta^2\text{-}H_2BH_2)H$ are summarized in Table 1. The isolation of $Mo(PMe_3)_4(\eta^2\text{-}H_2BCat)H$ is of interest since it demonstrates that the $[Mo(PMe_3)_4H_2]$ moiety does not preferentially oxidatively add the B–H bond to yield isomeric $Mo(PMe_3)_4(BCat)H_3$. Such reactivity is in contrast to the oxidative additions that have been observed upon reaction of other H–X bonds (e.g. X = H, F, Cl, Br) with low valent molybdenum phosphine compounds giving $Mo(PMe_3)_4\text{-}H_2X_2$ [4,12]b.

Although only one structurally characterized complex identified as a catecholborate derivative is listed in the Cambridge Structural Database [9], related isomers are known, since moieties of composition $[MH_2BR_2]$ may exist, in principle, with at least four different isomeric structures (Fig. 2) [2,3,11,13]. These structures may be classified as (i) η^2-borohydride, $\{[M](\eta^2\text{-}H_2BR_2)\}$, (ii) boryl-dihydride, $\{[M](BR_2)H_2\}$, (iii) borane-hydride, $\{[M](\eta^2\text{-}H\text{–}BR_2)\text{-}H\}$, and (iv) η^1-borohydride, $\{[M](\eta^1\text{-}HBHR_2)\}$; the first three isomers exhibit identical electron counts at the metal center, whereas the last isomer possesses two electrons fewer. An issue that arises in the discussion of compounds with $[MH_2BR_2]$ moieties is the extent to which the complex may be best represented by one of the four formalisms described above. With respect to catecholborane derivatives, i.e. $[MH_2BCat]$, only η^2-borohydride, $\{[M](\eta^2\text{-}H_2BR_2)\}$, and boryl-dihydride, $\{[M](BR_2)H_2\}$, forms have been discussed in the literature [14]. The relationship between $\{[M](\eta^2\text{-}H_2BR_2)\}$ and $\{[M](BR_2)H_2\}$ bears an analogy to the metal-olefin/metallacyclopropane issue of bonding, and the factors that influence the extent to which each of these forms best represents a particular complex are subtle. For example, Cp_2NbH_3 reacts with CatBH to give *endo*-$Cp_2Nb(BCat)H_2$, whereas 9-borabicyclononane yields a structure with predominantly η^2-borohydride character $Cp_2Nb[\eta^2\text{-}H_2B(C_8H_{14})]$ [13]. Smith has also demonstrated that related catecholate tantalum complexes exist as boryl-dihydrides, namely *exo*- and *endo*-$Cp_2Ta(BCat)H_2$ [15], and *endo*-$Cp^*_2Ta[B(O_2C_6H_3Bu^t)]H_2$ [11], but, in contrast, the pentamethylcyclopentadienyl niobium complex has been suggested to be an η^2-borohydride derivative $Cp^*_2Nb[\eta^2\text{-}H_2BCat]$ [11]. In view of the frequent uncertainty associated with locating hydrogen atom positions by X-ray diffraction, the M···B separation has been used as an indicator of boryl-dihydride versus η^2-borohydride character. For comparison, selected metrical data for boryl-dihydride and η^2-borohydride complexes are listed in Table 2, from which it can be seen that the former complexes are identified by marginally shorter M···B distances. Thus, the Nb···B distance in $Cp^*_2Nb[\eta^2\text{-}H_2B(O_2C_6H_3Bu^t)]$ (2.348(4) Å) is longer than in the cyclopentadienyl boryl-dihydride derivative $Cp_2Nb(BCat)H_2$ (2.292(5) Å) [13], and is effectively

Table 1
Comparison of the structures of $Mo(PMe_3)_4(\eta^2\text{-}H_2BCat)H$ and $Mo(PMe_3)_4(\eta^2\text{-}H_2BH_2)H$

	$Mo(PMe_3)_4(\eta^2\text{-}H_2BCat)H$	$Mo(PMe_3)_4(\eta^2\text{-}H_2BH_2)H$
d(Mo–H_{term}) (Å)	1.5(2)	1.63
d((Mo–H_{brid}) (Å)	1.90(3)	1.96
d(Mo–P_{trans}) (Å)	2.4321(7)	2.435(2)
d(Mo–P_{cis}) (Å)	2.4175(7)	2.381(2)
d(B–H_{brid}) (Å)	1.13(3)	1.12
d(Mo···B) (Å)	2.363(5)	2.468(12)
d(B–O) (Å)	1.462(3)	
P_{trans}–Mo–P_{trans} (°)	173.24(5)	168.4(1)
P_{trans}–Mo–P_{cis} (°)	90.97(3), 91.89(3)	92.93(2)
P_{cis}–Mo–P_{cis} (°)	129.91(4)	118.6(1)

Table 2
M···B, M···H and B···H distances associated with $[MH_2BH_2]$ moieties

	d(M···B) (Å)	d(M···H) (Å)	d(B···H) (Å)	Reference
$[M(\eta^2\text{-}H_2BR_2)]$				
$Mo(PMe_3)_4(\eta^2\text{-}H_2BCat)H$	2.363(5)	1.90(3)	1.13(3)	this work
$Mo(PMe_3)_4(\eta^2\text{-}H_2BH_2)H$	2.468(12)	1.96	1.12	[7]
$[Mo(CO)_4(\eta^2\text{-}H_2BH_2)][PPN]$	2.413(20)	2.04(8), 1.99(9)	1.14(9), 1.26(11)	[23]
$Cp^*_2Nb[\eta^2\text{-}H_2B(O_2C_6H_3Bu^t)]H$	2.348(4)	1.86(4), 1.63(4)	1.36(4), 1.46(4)	[11]
$Cp_2Nb[\eta^2\text{-}H_2B(C_8H_{14})]H$	2.40(1)	1.86(4), 1.80(4)	1.38(7), 1.39(6)	[13]
$Cp^*_2Nb(\eta^2\text{-}H_2BH_2)$	2.35(1)	1.88(7), 1.79(8)	1.17(7), 1.16(8)	[11]
$[MH_2(BR_2)]$				
endo-$Cp_2Nb(BCat)H_2$	2.292(5)	1.62(4), 1.58(5)	1.69(4), 1.62(5)	[13]
exo-$Cp_2Ta(BCat)H_2$	2.295(11)	1.76(12), 1.78(10)	$1.45(10)_{cent}$	[15]
endo-$Cp_2Ta(BCat)H_2$	2.263(6)	1.64(6), 1.54(5)	2.11(6), 1.75(6)	[15]

identical to that in $Cp^*_2Nb(\eta^2\text{-}H_2BH_2)$ (2.35(1) Å) [11]. In this regard, the Mo···B separation in $Mo(PMe_3)_4(\eta^2\text{-}H_2BCat)H$ (2.363(5) Å) is shorter than the corresponding value in $Mo(PMe_3)_4(\eta^2\text{-}H_2BH_2)H$ (2.468(12) Å) [7], thereby suggesting the possibility that it is closer to a boryl-dihydride representation than is $Mo(PMe_3)_4(\eta^2\text{-}H_2BH_2)H$. However, the locations of the hydrogen atoms are strongly suggestive of the η^2-borohydride formalism; for example, the Mo–H bond lengths involved in the Mo–H–B bridges (1.91(3) Å) are long, and the B–H bonds are short (1.13(3) Å), by comparison to the related values for the other complexes listed in Table 2. Comparison of the Mo···B separation in $Mo(PMe_3)_4(\eta^2\text{-}H_2BCat)H$ with that of a bona fide single Mo–B single bond would provide decisive evidence supporting the proposed η^2-borohydride formalism, but unfortunately the Cambridge Structural Database [10] lists no structures with single Mo–B bonds in which boron is three coordinate. Nevertheless, a Mo–B single bond may be estimated to be ca. 2.19 Å on the basis that Mo and W have very similar covalent radii [16] and that the W–B bond length in $Cp_2W(BCat)H$ is 2.190(7) Å [13,17]. Thus, the Mo···B separation in $Mo(PMe_3)_4(\eta^2\text{-}H_2BCat)H$ (2.363(5) Å) is substantially longer than would be expected for a boryl-hydride representation. Finally, further evidence counter to the boryl-hydride representation $Mo(PMe_3)_4(BCat)H_3$ is the molecular geometry, which is very different to the dodecahedral geometries observed for eight-coordinate $M(PMe_3)_4X_4$ derivatives [18].

3. Experimental

3.1. General considerations

All manipulations were performed using a combination of glovebox, high-vacuum or Schlenk techniques [19]. Solvents were purified and degassed by standard procedures. Commercially available reagents were not further purified. $Mo(PMe_3)_5H_2$ was prepared by the literature method [20].

3.2. Synthesis of $Mo(PMe_3)_4(\eta^2\text{-}H_2BCat)H$

A solution of $Mo(PMe_3)_5H_2$ (0.43 g, 0.90 mmol) in benzene (5 ml) was treated with a solution of catecholborane (0.22 g, 1.83 mmol) in benzene (2 ml), thereby resulting in the immediate formation of a red precipitate. The mixture was filtered and the solid was washed with benzene (5 ml) and dried in vacuo. Yield of $Mo(PMe_3)_4(\eta^2\text{-}H_2BCat)H$: 0.41 g (87%). IR data (KBr, cm^{-1}): 2963 (w), 2905 (w), 1818 (br, w) (ν_{Mo-H}), 1584 (m), 1475 (s), 1423 (m), 1366 (w), 1276 (m), 1233 (s), 1094 (w), 1059 (m), 1007 (m), 986 (m), 937 (vs), 848 (m), 749 (m), 701 (m), 647 (m), 483 (w).

3.3. X-ray structure determination

Crystallographic data for $Mo(PMe_3)_4(\eta^2\text{-}H_2BCat)H$ were collected on a Bruker P4 diffractometer equipped with a SMART CCD detector. The structure was solved using direct methods and standard difference map techniques, and was refined by full-matrix least-squares procedures using SHELXTL [21]. Hydrogen atoms on carbon were included in calculated positions. Systematic absences were consistent with *Aba*2 (no. 41) or *Acam* (no. 64), of which a successful solution was obtained in the non-centrosymmetric alternative *Aba*2 (no. 41). The correct choice of space group was confirmed by PLATON [22]. Crystal data, data collection and refinement parameters for all structures are summarized in Table 3.

4. Summary

In conclusion, the dihydride $Mo(PMe_3)_5H_2$ reacts with CatBH to give $Mo(PMe_3)_4(\eta^2\text{-}H_2BCat)H$. Previous studies have indicated that catecholborate derivatives may often be better described as boryl-hydrides, but structural characterization by X-ray diffraction, which located the positions of the hydrogen atoms attached to boron, indicates that the complex is best represented as a borohydride complex.

Table 3
Crystal, intensity collection and refinement data for $Mo(PMe_3)_4(\eta^2\text{-}H_2BCat)H$

Lattice	orthorhombic
Formula	$C_{18}H_{43}BMoO_2P_4$
Formula weight	522.15
Space group	*Aba*2 (no. 41)
a (Å)	13.4269(10)
b (Å)	16.3327(11)
c (Å)	11.9576(9)
α (°)	90
β (°)	90
γ (°)	90
V (Å^3)	2622.3(3)
Z	4
Temperature (K)	223
Radiation, λ (Å)	0.71073
ρ_{calc} (g cm^{-3})	1.323
μ (Mo Kα) (mm^{-1})	0.754
θ_{max} (°)	28.26
No. data	2859
No. parameters	133
R_1	0.0262
wR_2	0.0557
GOF	1.025

Supplementary data

Atomic coordinates for $Mo(PMe_3)_4(\eta^2\text{-}H_2BCat)H$ (CCDC No. 135054) have been deposited with the Cambridge Crystallographic Data Centre, 12 Union Road, Cambridge CB2 1EZ, UK (fax: +44-1223-336033; e-mail: deposit@ccdc.cam.ac.uk).

Acknowledgements

We thank the US Department of Energy, Office of Basic Energy Sciences (DE-FG02-93ER14339) for support of this research.

References

[1] See for example: K. Burgess, M.J. Ohlmeyer, Chem. Rev. 91 (1991) 1179.
[2] H. Wadepohl, Angew. Chem., Int. Ed. Engl. 36 (1997) 2441.
[3] See for example: (a) H. Braunschweig, Angew. Chem., Int. Ed. Engl. 37 (1998) 1787. (b) M.R. Smith III, Prog. Inorg. Chem. 48 (1999) 505. (c) G.J. Irvine, M.J.G. Lesley, T.B. Marder, N.C. Norman, C.R. Rice, E.G. Robins, W.R. Roper, G.R. Whittell, L.J. Wright, Chem. Rev. 98 (1998) 2685.
[4] (a) D. Rabinovich, G. Parkin, J. Am. Chem. Soc. 115 (1993) 353. (b) T. Hascall, D. Rabinovich, V.J. Murphy, M.D. Beachy, R.A. Friesner, G. Parkin, J. Am. Chem. Soc. 121 (1999) 11402.
[5] (a) D. Rabinovich, R. Zelman, G. Parkin, J. Am. Chem. Soc. 112 (1990) 9632. (b) D. Rabinovich, R. Zelman, G. Parkin, J. Am. Chem. Soc. 114 (1992) 4611. (c) T. Hascall, V.J. Murphy, G. Parkin, Organometallics 15 (1996) 3910. (d) V.J. Murphy, G. Parkin, J. Am. Chem. Soc. 117 (1995) 3522.
[6] V.J. Murphy, D. Rabinovich, T. Hascall, W.T. Klooster, T.F. Koetzle, G. Parkin, J. Am. Chem. Soc. 120 (1998) 4372.
[7] J.L. Atwood, W.E. Hunter, E. Carmona-Guzman, G. Wilkinson, J. Chem. Soc., Dalton Trans. (1980) 467.
[8] See for example: (a) T.J. Marks, J.R. Kolb, Chem. Rev. 77 (1977) 263. (b) J.D. Kennedy, Prog. Inorg. Chem. 32 (1983) 519. (c) M. Ephritikhine, Chem. Rev. 97 (1997) 2193. (d) R.W. Parry, G. Kodama, Coord. Chem. Rev. 128 (1993) 245. (e) Z.T. Xu, Z.Y. Lin, Coord. Chem. Rev. 156 (1996) 139.
[9] For example, only one such derivative, namely $Cp^*_2Nb[\eta^2\text{-}H_2B(O_2C_6H_3Bu^t)]$, is listed in the Cambridge Structural Database (Version 5.17). See [10,11].
[10] F.H. Allen, O. Kennard, 3D Search and Research Using the Cambridge Structural Database, Chem. Des. Automation News 8 (1) (1993) 1.
[11] D.R. Lantero, D.L. Ward, M.R. SmithIII, J. Am. Chem. Soc. 119 (1997) 9699.
[12] (a) M. Brookhart, K. Cox, F.G.N. Cloke, J.C. Green, M.L.H. Green, P.M. Hare, J. Bashkin, A.E. Derome, P.D. Grebenik, J. Chem. Soc., Dalton Trans. (1985) 423. (b) F.G.N. Cloke, K.P. Cox, M.L.H. Green, J. Bashkin, K. Prout, J. Chem. Soc., Chem. Commun. (1982) 393.
[13] J.F. Hartwig, S.R. De Gala, J. Am. Chem. Soc. 116 (1994) 3661.
[14] In addition to η^2-borohydride and boryl-dihydride derivatives, η^2-catecholborane complexes are also known, e.g. $Cp_2Ti(\eta^2\text{-}HBCat)_2$ and $Cp_2Ti(\eta^2\text{-}HBCat)(PMe_3)$ have been structurally characterized [a,c]. However, since these complexes do not have an additional metal hydride ligand, they do not correspond to isomer (iii) of Fig. 2. (a) J.F. Hartwig, C.N. Muhoro, X. He, O. Eisenstein, R. Bosque, J. Am. Chem. Soc. 118 (1996) 10936. (b) C.N. Muhoro, J.E. Hartwig, Angew. Chem., Int. Ed. Engl. 36 (1997) 1510. (c) C.N. Muhoro, X. He, J.F. Hartwig, J. Am. Chem. Soc. 121 (1999) 5033.
[15] D.R. Lantero, D.H. Motry, D.L. Ward, M.R. Smith, J. Am. Chem. Soc. 116 (1994) 10811.
[16] For example, the single bond metallic radii for Mo and W are 1.296 and 1.304 Å, respectively. See L. Pauling, The Nature of The Chemical Bond, Cornell University Press, Ithaca, NY, 3rd edn., 1960, p. 256.
[17] J.F. Hartwig, X. He, Organometallics 15 (1996) 5350.
[18] See, for example, Ref. [6] and Refs. therein.
[19] (a) J.P. McNally, V.S. Leong, N.J. Cooper, in: A.L. Wayda, M.Y. Darensbourg (Eds.), Experimental Organometallic Chemistry, American Chemical Society, Washington, DC, 1987, ch. 2, pp. 6–23. (b) B.J. Burger, J.E. Bercaw, in: A.L. Wayda, M.Y. Darensbourg (Eds.), Experimental Organometallic Chemistry, American Chemical Society, Washington, DC, 1987, ch. 4, pp. 79–98. (c) D.F. Shriver, M.A. Drezdzon, The Manipulation of Air-Sensitive Compounds, Wiley-Interscience, New York, 2nd edn., 1986.
[20] D. Lyons, G. Wilkinson, M. Thornton-Pett, M.B. Hursthouse, J. Chem. Soc., Dalton Trans. (1984) 695.
[21] G.M. Sheldrick, SHELXTL, an integrated system for solving, refining and displaying crystal structures from diffraction data, University of Göttingen, Germany, 1981.
[22] A.L. Spek, Acta Crystallogr., Sect. A 46 (1990) C34.
[23] S.W. Kirtley, M.A. Andrews, R. Bau, G.W. Grynkewich, T.J. Marks, D.L. Tipton, B.R. Whittesley, J. Am. Chem. Soc. 99 (1977) 7154.

PERGAMON

www.elsevier.nl/locate/poly

Polyhedron 19 (2000) 1067–1071

POLYHEDRON

X-ray structure of the zinc complex of the central metal chelation site of the antitumour drug streptonigrin

Georgina V. Long, Margaret M. Harding *, Peter Turner

School of Chemistry, University of Sydney, Sydney, NSW 2006, Australia

Received 15 December 1999; accepted 2 March 2000

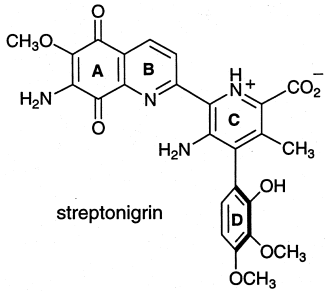
Abstract

The X-ray structure of the 1:1 complex between zinc(II) triflate and 3-amino-6,6′-bis(methoxycarbonyl)-2,2′-bipyridine is reported. This ligand contains the central chelation site present in the DNA-binding antitumour antibiotic streptonigrin. The complex is distorted octahedral involving the 2,2′-bipyridyl site and the carbonyl groups at the 6,6′-positions as well as two axial water molecules. The structure confirms that formation of similar complexes with streptonigrin is possible. ©2000 Elsevier Science Ltd All rights reserved.

Keywords: Streptonigrin; 2,2′-Bipyridyl; 6,6′-Dicarboxy-2,2′-bipyridyl; Antitumour; Zinc

1. Introduction

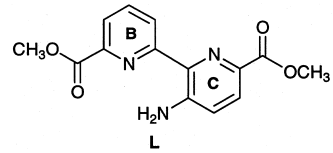
Streptonigrin is an aminoquinone antitumour antibiotic that is active against a range of human cancers [1–5]. A number of transition metal ions interact with the drug and have been shown to be involved in DNA strand cleavage either by direct complexation with streptonigrin or reduced streptonigrin and/or catalysing the production of hydroxyl radical close to DNA [6–19]. The exact role of the metal ions in the mechanism of action, however, is not fully understood.



streptonigrin

Streptonigrin contains many potential metal binding sites including the picolinic acid system, the 2,2′-bipyridyl system, the aminoquinone system, the 2-(3′-amino-2′-pyridyl)-quinoline system and the amino and phenolic groups on rings C and D. UV titrations have been used to establish the stoichiometries of a number of metal complexes with streptonigrin [6,7,10–15,19]. Independent NMR studies of the zinc(II) complex have shown that the structures and stabilities of the complexes are solvent dependent and that under biologically relevant conditions the 1:1 bipyridyl complex is present [20]. However, there are no X-ray crystal structures of any metal complexes of streptonigrin and the exact binding site(s) and coordination geometry of the metal centre in metal complexes of streptonigrin, which would be useful in the design of potential metal complexes for drug testing [5], are unknown.

In an effort to fully characterise the structures of the metal complexes of streptonigrin, we have reported studies on a number of model ligands that contain the key metal binding site in the drug [21–23], i.e., a 3-amino-2,2′-bipyridyl group flanked by carbonyls at the 6,6′-positions. These solution studies established the importance of the flanking carbonyls in stabilising the bipyridyl complexes [21–23] but no information about the coordination geometry at the metal centre could be obtained. We now report successful determination of the solid state structure of the zinc(II) complex of ligand **L**:



L

which contains the key metal binding site present in streptonigrin. This structure confirms our proposed solution structure [23] and provides important additional information

* Corresponding author. Tel.: +61-2-9351-2745; fax: +61-2-9351-3329; e-mail: harding@chem.usyd.edu.au

0277-5387/00/$ - see front matter ©2000 Elsevier Science Ltd All rights reserved.
PII S0277-5387(00)00352-1

about the coordination sphere and coordinated ligands at the metal binding site and a molecular level structure that may be used as the basis for modelling of metal complexes of streptonigrin.

2. Results and discussion

The 1:1 zinc(II) complex of ligand **L**, complex **1**, was prepared from an acetonitrile solution of the ligand and zinc(II) triflate. In the presence of 1 equiv. of zinc(II) both the 2:1 (ligand:metal) complex and 1:1 (ligand:metal) complexes are formed [23]. Hence, excess zinc(II) was added to the solution containing this mixture of complexes and, after a period of weeks, crystals of complex **1** suitable for X-ray diffraction were obtained. Fig. 1 shows an ORTEP depiction of the structure of the complex obtained from a single-crystal X-ray diffraction analysis, and structural details are summarised in Tables 1–3. The solid state structure agrees well with solution data, in which we have previously shown [23] that the flanking carbonyls are mobile and dynamic on the NMR time scale.

The metal ion coordination is distorted octahedral, with the bipyridyl N(1), N(2) atoms and the ester carbonyl O(3) and O(4) atoms defining the equatorial coordination plane (Fig. 1). The zinc to bipyridyl nitrogen distances are unre-

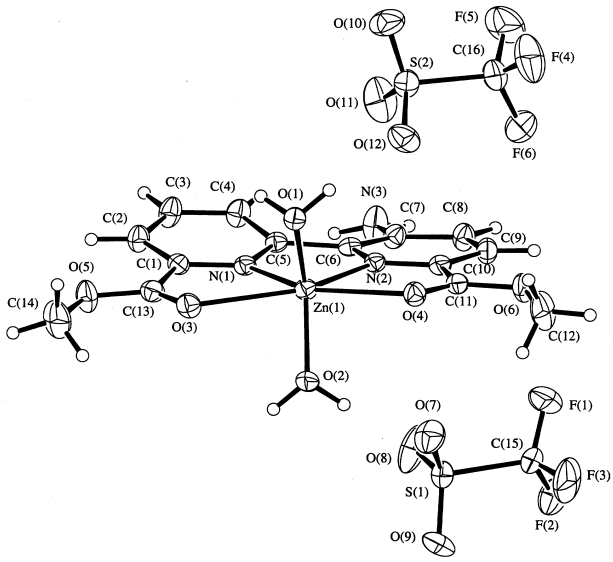


Fig. 1. An ORTEP depiction and numbering scheme for complex **1**, with atomic displacement ellipsoids shown at the 25% level.

Table 1
Crystallographic data for **1**

Formula	$C_{16}H_{17}F_6N_3O_{12}S_2Zn$
Formula weight	686.81
Crystal colour, habit	pale yellow, prism
Crystal size (mm)	0.30×0.25×0.22
Crystal system	monoclinic
Space group	$P2_1/n$ (no. 14)
Lattice type	primitive
No. of reflections used for unit cell determination (2θ range (°))	25 (19.2–24.2)
a (Å)	13.059(2)
b (Å)	12.213(2)
c (Å)	16.842(4)
β (°)	109.74(2)
V (Å^3)	2528.2(9)
Z	4
d_{calc} (g/cm^3)	1.804
μ(Mo Kα) (cm^{-1})	12.46
λ (Mo Kα) (Å)	0.71069
Residuals [a]: R; R_w	0.043; 0.043
Max./min. extrema (e/Å^3)	0.48/−0.33

[a] $R=\Sigma(|F_o|-|F_c|)/\Sigma|F_o|$; $R_w=(\Sigma w(|F_o|-|F_c|)^2/\Sigma w|F_o|^2)^{1/2}$; $w=1/\sigma^2(F_o)$.

Table 2
Selected bond lengths (Å) and bond angles (°) for complex **1**

Zn(1)–O(1)	1.981(4)
Zn(1)–O(2)	1.946(4)
Zn(1)–O(3)	2.437(3)
Zn(1)–O(4)	2.377(3)
Zn(1)–N(1)	2.098(4)
Zn(1)–N(2)	2.101(4)
O(1)–H(1Oa)	0.898(5)
O(1)–H(1Ob)	0.898(5)
O(2)–H(2Oa)	0.899(5)
O(2)–H(2Ob)	0.899(5)
N(3)–C(7)	1.349(7)
N(3)–H(3Na)	0.901(5)
N(3)–H(3Nb)	0.900(5)
O(1)–Zn(1)–O(2)	120.9(2)
O(1)–Zn(1)–O(3)	79.5(1)
O(1)–Zn(1)–O(4)	81.8(1)
O(1)–Zn(1)–N(1)	107.3(1)
O(1)–Zn(1)–N(2)	111.4(1)
O(2)–Zn(1)–O(3)	79.2(1)
O(2)–Zn(1)–O(4)	80.2(1)
O(2)–Zn(1)–N(1)	116.7(2)
O(2)–Zn(1)–N(2)	115.7(2)
O(3)–Zn(1)–O(4)	139.4(1)
O(3)–Zn(1)–N(1)	71.6(1)
O(3)–Zn(1)–N(2)	147.7(1)
O(4)–Zn(1)–N(1)	148.8(1)
O(4)–Zn(1)–N(2)	72.9(1)
N(1)–Zn(1)–N(2)	76.1(1)
H(1Oa)–O(1)–H(1Ob)	107(5)
H(2Oa)–O(2)–H(2Ob)	103(5)
H(3Na)–N(3)–H(3Nb)	114(5)

Table 3
Hydrogen bond geoemetry details for complex **1**

A	H	B	A…B	A–H…B
O(1)	H(1Oa)	O(8′) [a]	2.699(5)	163(6)
O(1)	H(1Ob)	O(12)	2.717(5)	174(5)
O(2)	H(2Oa)	O(7)	2.778(6)	168(6)
O(2)	H(2Ob)	O(10′) [b]	2.753(6)	177(6)
N(3)	H(3Nb)	O(11*) [c]	2.934(7)	130(7)

[a] Generated from O(8) with $1/2-x, 1/2+y, 1/2-z$.
[b] Generated from O(10) with $1/2-x, y-1/2, 1/2-z$.
[c] Generated from O(11) with $-x, -y, -z$.

markable at 2.098(4) and 2.101(4) Å for N(1) and N(2), respectively, as are the (pseudo) axial zinc to water bond lengths of 1.981(4) and 1.946(4) Å for O(1) and O(2) respectively. The zinc to carbonyl oxygen distances, however, are relatively long at 2.437(3) and 2.377(3) Å for O(3) and O(4) respectively. The metal to carbonyl bond lengths are of course constrained by the in-plane rigidity of the equatorial coordination framework. The N(1), N(2), O(3) and O(4) atoms are co-planar, with the least-squares plane deviations ranging from −0.0164(3) to 0.0333(4) Å. The Zn distance from the equatorial coordination least-squares plane is just 0.0301(4) Å. The O(1) to O(2) line forms an angle of 3.38(7)° with the equatorial coordination least-squares plane normal.

The metal coordination geometry may also be regarded as augmented tetrahedral in which the N(1), N(2), O(1) and O(2) atoms define a distorted tetrahedral coordination geometry that is augmented by the relatively long carbonyl oxygen to zinc bonds. The N(1)–Zn(1)–N(2) bond angle is 76.1(1)° and the O(1)–Zn(1)–O(2) angle is 120.9(2)°. The Zn(1) to O(1) and Zn(1) to O(2) bond lines form angles of 25.96(7) and 33.10(7)°, respectively, with the equatorial coordination least-squares plane normal.

The least-squares planes of the pyridyl residues form an angle of 13.6(1)°, and this equatorial ligand distortion is probably a response to the close contact between the amino N(3) and the pyridyl C(4). The distance between N(3) and C(4), at 3.034(6) Å, is less than the sum of their respective van der Waals radii. As Fig. 2 suggests, there is hydrogen bonding between the amine residue and a nearby triflate counter-ion and between the aqua ligands and neighbouring counterions (Table 2).

As far as we are aware, there are no other examples of a 1:1 metal complex of a 6,6′-dicarbonylsubstituted-2,2′-bipyridyl in which both the carbonyls and the bipyridine are coordinated to the metal centre, in the CCDC database, which could be used to model potential metal complexes of streptonigrin. There are a number of related 1:1 complexes including tetrahedral nickel(II) [24] and cobalt(II) complexes [25,26], and an octahedral ruthenium(II) complex formed with a 6,6-dialkylsubstituted 2,2′-bipyridine [27]. A palladium(II) 6,6′-disubstituted 2,2′-bipyridine complex has also been reported [28]; the strong square planar stereochemical preference of palladium(II) results in drastic deviation of the overall planar geometry, with the metal at a 40° angle to the plane of the bipyridine rings.

Complex **1** was prepared as a model for metal complexes of streptonigrin. The zinc(II) complex is of particular interest as it has been proposed that a ternary Zn–streptonigrin–DNA complex is formed under certain conditions [12], although studies with oligonucleotides are consistent with an electrostatic interaction with the phosphate backbone and N7 of sterically accessible guanines [29]. While complex **1** confirms that formation of the related complex **3** with streptonigrin is feasible (Fig. 3), some structural differences are noted. Firstly, streptonigrin contains a carboxylic acid in ring C, which leads to formation of the zwitterion in solution [30] and this is an important mechanism that contributes to aqueous solubility of the drug. In ligand **L**, the acid functional group was masked as a methyl ester to allow isolation and purification of the ligand. Hence, in vivo, formation of a complex in which the carboxylate oxygen (rather than the carbonyl) coordinates to the metal cannot be ruled out, and formation of complex **2** has been proposed [2–4] (Fig. 3). Secondly, the carbonyl group on ring A in streptonigrin is not freely rotating as in ligand **L** but is held in a fixed orientation by the quinone ring. The O(3)–C(13)–C(1)–N(1)

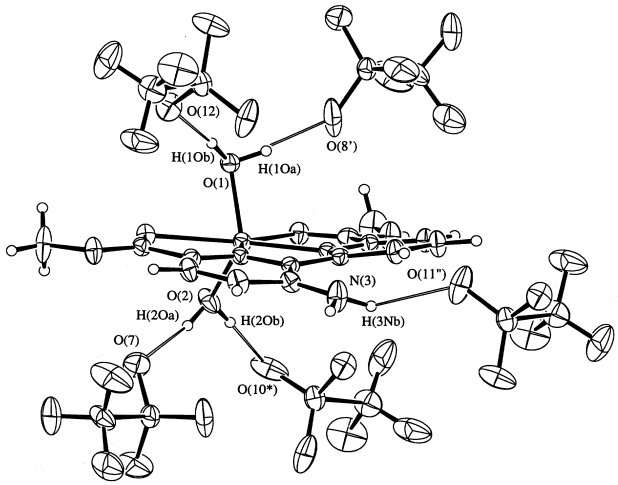


Fig. 2. An ORTEP depiction of the hydrogen bonding for complex **1**, in which O(8′) is generated from O(8) with $1/2-x, 1/2+y, 1/2-z$, O(10′) is generated from O(10) with $1/2-x, y-1/2, 1/2-z$ and O(11*) is generated from O(11) with $-x, -y, -z$.

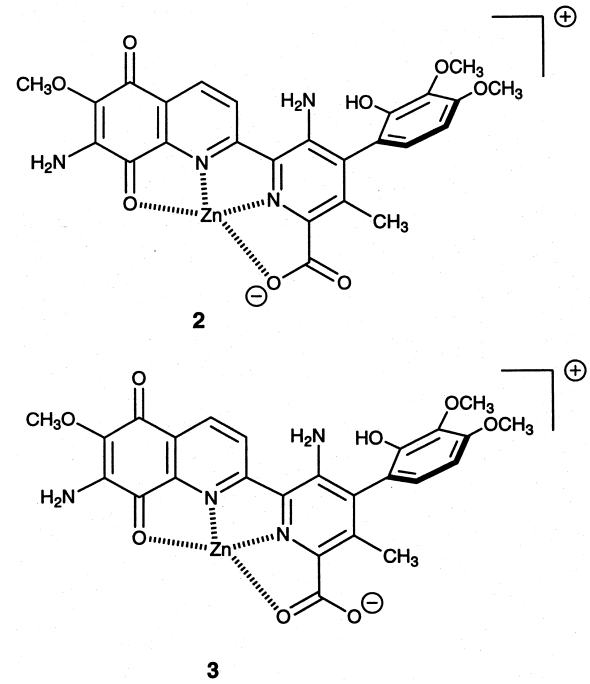


Fig. 3. Proposed complexes between streptonigrin and zinc(II) involving either the carbonyl **3** or carboxylate **2** oxygens of the acid functional group; coordination of additional water or solvent ligands to zinc(II) possible.

torsion angle is 7.6(7)° in complex **1** and these atoms are essentially coplanar, with least-squares plane deviations ranging from 0.010(3) to 0.038(5) Å. Thus, the structure of complex **1** establishes that the fixed carbonyl group of streptonigrin is unlikely to hinder formation of a streptonigrin metal complex with a similar geometry to that observed in **1**. Streptonigrin has the additional flexibility of carbonyl oxygen or oxyanion coordination, and oxyanion coordination may support the coordination of harder Lewis acids than zinc. The preparation of related metal complexes of ligand **L** and of streptonigrin are currently under investigation.

3. Experimental

3.1. Sample preparation

A mixture of the 2:1 and 1:1 zinc(II) complexes of 3-amino-6,6′-bis(methoxycarbonyl)-2,2′-bipyridine in acetonitrile was prepared as previously described [23]. Excess zinc(II) triflate (2 equiv.) was added to this solution. Crystals of the 1:1 complex **1** suitable for X-ray diffraction were grown by diffusion of benzene into the acetonitrile solution over a period of weeks.

3.2. X-ray crystallography

A very pale yellow (almost colourless) prismatic crystal having approximate dimensions of $0.30\times0.25\times0.22$ mm was attached to a thin glass fibre, and mounted on an Enraf-Nonius CAD4 diffractometer employing graphite monochromated Mo Kα radiation. Primitive monoclinic cell constants were obtained from a least-squares refinement using the setting angles of 25 reflections in the range $19.24<2\theta<24.18°$. Diffraction data were collected at a temperature of 21 ± 1°C using ω:1/3θ scans to a maximum 2θ value of 49.9°. The intensities of three representative reflections, measured every 60 min, decreased by 2.0% and a linear correction factor was accordingly applied to the data. An analytical absorption correction was applied and the data were also corrected for Lorentz and polarisation effects.

All calculations were undertaken with the teXsan [31] crystallographic software package. Neutral atom scattering factors were taken from Cromer and Waber [32]. Anomalous dispersion effects were included in F_{calc} [33] and the values for $\Delta f'$ and $\Delta f''$ were those of Creagh and McAuley [34]. The values for the mass attenuation coefficients were those of Creagh and Hubbell [35]. The structure was solved in the space group $P2_1/n$ (no. 14) by direct methods (SIR92: [36]) and expanded using Fourier techniques (DIRDIF94: [37]). Non-hydrogen atoms were modelled with anisotropic thermal parameters. The water and amine hydrogens were located and refined with distance restraints and the rest of the hydrogens were included at calculated positions with group thermal parameters (residual density was used to place the methyl hydrogens). An ORTEP projection of the molecule with 25% thermal ellipsoids is provided in Fig. 1 [38].

4. Supplementary data

Supplementary data are available from the CCDC, 12 Union Road, Cambridge CB2 1EZ, UK (fax: +44-1223-336033; e-mail: deposit@ccdc.cam.ac.uk) on request, quoting the deposition number 136086.

Acknowledgements

Financial support from the Sydney University Cancer Research Fund and the Australian Research Council is gratefully acknowledged. An Australian Postgraduate Research Award and a Sydney University Henry Bertie and Mabel Gritton Supplementary Postgraduate Scholarship (G.V.L.) are acknowledged.

References

[1] R.B. Livingston, S.K. Carter, Single Agents in Cancer Chemotherapy, IFI/Plenum, New York, 1970, p. 389.
[2] J. Hadju, E.C. Armstrong, J. Am. Chem. Soc. 103 (1981) 232.
[3] J. Hadju, Met. Ions Biol. Syst. 19 (1985) 53.
[4] H.S. Soedjak, B.L Bales, J. Hajdu, Basic Life Sci. 49 (1988) 203.
[5] G.V. Long, M.M. Harding, Curr. Med. Chem. 4 (1997) 385.
[6] A. Moustatih, A. Garnier-Suillerot, J. Med. Chem. 32 (1989) 1426.
[7] M.L. Fiallo, A. Garnier-Suillerot, Inorg. Chem. 29 (1989) 893.
[8] Y. Sugiura, J. Kuahara, T. Suzuki, Biochim. Biophys. Acta 782 (1984) 254.
[9] B.K. Sinha, Chem.-Biol. Interact. 36 (1981) 179.
[10] J.R. White, Biochem. Biophys. Res. Commun. 77 (1977) 387.
[11] J.R. White, H.N. Yeowell, Biochem. Biophys. Res. Commun. 106 (1982) 407.
[12] K.V. Rao, J. Pharm. Sci. 68 (1979) 853.
[13] R. Cone, S.K. Hasan, J.W. Lown, A.R. Morgan, Can. J. Biochem. 54 (1976) 219.
[14] J.W. Lown, S. Sim, Can. J. Biochem. 54 (1976) 446.
[15] J.W. Lown, S.K. Sim, Can. J. Chem. 54 (1976) 2563.
[16] N.R. Bachur, S.L. Gordon, M.V. Gee, Cancer Res. 38 (1978) 1745.
[17] N.R. Bachur, S.L. Gordon, M.V. Gee, H. Kon, Proc. Natl. Acad. Sci. 76 (1979) 954.
[18] J.M. Gutteridge, Biochem. Pharmacol. 33 (1984) 3059.
[19] X. Wei, L.-J. Ming, J. Chem. Soc., Dalton Trans. (1998) 2793.
[20] G.V. Long, M.M. Harding, J. Chem. Soc., Dalton Trans. (1996) 549.
[21] G.V. Long, M.M. Harding, P. Turner, T.W. Hambley, J. Chem. Soc., Dalton Trans. (1995) 3905.
[22] G.V. Long, S.E. Boyd, M.M. Harding, I.E. Buys, T.W. Hambley, J. Chem. Soc., Dalton Trans. (1993) 3175.
[23] G.V. Long, M.M. Harding, M.C.L. Xie, I.E. Buys, T.W. Hambley, J. Chem. Soc., Dalton Trans. (1995) 951.
[24] D.W. Evans, G.R. Newkome, F. Fronczek, Acta Crystallogr., Sect. C 46 (1990) 490.
[25] G.L. Baker, Acta Crystallogr., Sect. C 44 (1988) 1668.
[26] C. Bolm, M. Zhender, D. Bur, Angew. Chem., Int. Ed. Engl. 29 (1990) 205.
[27] P. Homanen, Organometallics 15 (1996) 4081.
[28] G.R. Newkome, F.R. Fronczek, V.K. Gupta, W.E. Puckett, D.C. Pantaleo, G.E. Kiefer, J. Am. Chem. Soc. 104 (1982) 1782.

[29] G.V. Long, M.M. Harding, J. Fan, W.A. Denny, Anti-Cancer Drug Des. 12 (1997) 453.
[30] M.M. Harding, G.V. Long, C.L. Brown, J. Med. Chem. 36 (1993) 3056.
[31] teXsan, Crystal Structure Analysis Package, Molecular Structure Corporation, 1985 and 1992.
[32] D.T. Cromer, J.T. Waber, International Tables for X-ray Crystallography, vol. 4, Kynoch Press, Birmingham, UK, 1974.
[33] J.A. Ibers, W.C. Hamilton, Acta Crystallogr. 17 (1964) 781.
[34] D.C. Creagh, W.J. McAuley, in: A.J.C. Wilson (Ed.), International Tables for Crystallography, vol. C, Kluwer, Boston, 1992, Table 4.2.6.8, p. 219.
[35] D.C. Creagh, J.H. Hubbell, in: A.J.C. Wilson (Ed.), International Tables for Crystallography, vol C, Kluwer, Boston, 1992, Table 4.2.4.3, p. 200.
[36] A. Altomare, M. Cascarano, C. Giacovazzo, A.J. Guagliardi, Appl. Cryst. 26 (1993) 343.
[37] P.T. Beurskens, G. Admiraal, G. Beurskens, W.P. Bosman, R. de Gelder, R. Israel, J.M.M. Smits, The DIRDIF-94 Program System, Technical Report of the Crystallography Laboratory, University of Nijmegen, Netherlands, 1994.
[38] C.K. Johnson, ORTEPII. Report ORNL-5138, Oak Ridge National Laboratory, Oak Ridge, TN, 1976.

PERGAMON

www.elsevier.nl/locate/poly

Polyhedron 19 (2000) 1073–1080

POLYHEDRON

Dithiolate complexes of ruthenium and osmium: X-ray structures of $[Ru_2(CO)_6(\mu\text{-}SCH_2CH_2S)]$ and $[\{(\mu\text{-}H)M_3(CO)_{10}\}_2(\mu\text{-}SCH_2CH_2CH_2S)]$ (M = Ru, Os)

Khandakar M. Hanif [a], Shariff E. Kabir [a], M. Abdul Mottalib [a], Michael B. Hursthouse [1,b], K.M. Abdul Malik [b,*], Edward Rosenberg [c]

[a] *Department of Chemistry, Jahangirnagar University, Savar, Dhaka-1342, Bangladesh*
[b] *Department of Chemistry, Cardiff University, P.O. Box 912, Park Place, Cardiff CF10 3TB, UK*
[c] *Department of Chemistry, The University of Montana, Missoula, MT 59812, USA*

Received 31 January 2000; accepted 21 February 2000

Abstract

A comparison between the reactivity of $[Ru_3(CO)_{12}]$ and $[Os_3(CO)_{10}(MeCN)_2]$ with 1,2-ethanedithiol ($HSCH_2CH_2SH$) and 1,3-propanedithiol ($HSCH_2CH_2CH_2SH$) is reported. The reaction of $[Ru_3(CO)_{12}]$ with 1,2-ethanedithiol at 68°C afforded $[Ru_2(CO)_6(\mu\text{-}SCH_2CH_2S)]$ (**1**) in 40% yield, whereas the reaction with 1,3-propanedithiol yielded $[\{(\mu\text{-}H)Ru_3(CO)_{10}\}_2(\mu\text{-}SCH_2CH_2CH_2S)]$ (**2**) and $[Ru_2(CO)_6(\mu\text{-}SCH_2CH_2CH_2S)]$ (**3**) in 30 and 19% yields respectively. Treatment of $[Os_3(CO)_{10}(MeCN)_2]$ with 1,2-ethanedithiol gave $[(\mu\text{-}H)Os_3(CO)_{10}(\mu\text{-}SCH_2CH_2SH)]$ (**4**) in 60% yield and with 1,3-propanedithiol it afforded $[\{(\mu\text{-}H)Os_3(CO)_{10}\}_2(\mu\text{-}SCH_2CH_2CH_2S)]$ (**5**) in 30% yield. Compounds **1** and **3** both react with equimolar amounts of PPh_3 at room temperature to give the monosubstituted products $[Ru_2(CO)_5(\mu\text{-}SCH_2CH_2S)(PPh_3)]$ (**6**) and $[Ru_2(CO)_5(\mu\text{-}SCH_2CH_2S)(PPh_3)]$ (**7**) respectively. When heated to 68°C, compound **2** transformed into **3**. The compounds have been characterized by spectroscopic studies, and in the case of **1**, **2** and **5** by X-ray crystallography. ©2000 Elsevier Science Ltd All rights reserved.

Keywords: Dithiolate complexes; Ruthenium; Osmium; X-ray structures

1. Introduction

The use of alkanedithiolates to stabilize transition metal cluster compounds by serving as chelating or bridging ligands and preventing cluster fragmentation during the course of catalytic reactions has received considerable attention [1–21]. The reactivity of polythiocycloalkanes towards metal carbonyl clusters is also of interest. It has been shown that some reactions proceed with retention of the cluster structure, while in other cases fragmentation into a dinuclear species as well as ring opening of the ligand takes place. For example, the reaction of $[Ru_3(CO)_{12}]$ with 1,2,5,6-tetrathiacyclooctane at 40°C gave a mixture of products from which the dinuclear and trinuclear complexes $[Ru_2(CO)_6(\mu\text{-}SCH_2CH_2S)]$, *anti*-$[Ru_3(CO)_7(\mu\text{-}SCH_2CH_2S)_2]$ and *syn*-$[Ru_3(CO)_7(\mu\text{-}SCH_2CH_2S)_2]$ containing the 1,2-ethanedithiolate ligand were isolated [22]. On the other hand, reactions of $[Ru_3(CO)_{12}]$ with 1,3-dithiacyclohexane, 1,3,5-trithiacyclohexane and 1,4,7-trithiacyclononane, yielded the respective complexes $[(\mu\text{-}H)Ru_3(CO)_9(\mu_3\text{-}\eta^3\text{-}1,3\text{-dithiacyclohexane})]$, $[Ru_3(CO)_9(\mu\text{-}\eta^3\text{-}1,3,5\text{-trithiacyclohexane})]$ and $[Ru_3(CO)_9(\mu\text{-}\eta^3\text{-}1,4,7\text{-trithiaheptane})]$ involving entirely different coordination modes of the ligands [23]. Recently, we have investigated the reactions of various dithiols with unsaturated triosmium clusters $[(\mu\text{-}H)Os_3(CO)_8\{Ph_2PCH_2P(Ph)C_6H_4\}]$ and $[(\mu\text{-}H)Os_3(CO)_9\{C_9H_5(R)N\}]$ (R = H or Me) [24,25] and saturated triruthenium clusters $[Ru_3(CO)_{10}(\mu\text{-dppm})]$ and $[Ru_3(CO)_{10}(\mu\text{-dppe})]$ [26], and observed several bonding modes of the dithiolate ligand depending on the cluster and the dithiol used. In the present work we report on the reactions of $[Ru_3(CO)_{12}]$ and $[Os_3(CO)_{10}(MeCN)_2]$ with 1,2-ethanedithiol and 1,3-propanedithiol and also the substitution reactions of the resulting diruthenium complexes with triphenylphosphine.

* Corresponding author. Tel.: +44-29-2087 4950; fax: +44-29-2087 4030; e-mail: malikka@cardiff.ac.uk

[1] Present address: Department of Chemistry, University of Southampton, Highfield, Southampton SO17 1BJ, UK.

0277-5387/00/$ - see front matter ©2000 Elsevier Science Ltd All rights reserved.
PII S0277-5387(00)00353-3

2. Results and discussion

Treatment of $[Ru_3(CO)_{12}]$ with 2 equiv. of 1,2-ethanedithiol afforded $[Ru_2(CO)_6(\mu\text{-}SCH_2CH_2S)]$ (**1**) (Scheme 1) in 40% yield. This compound was previously reported from the thermal degradation of $[Ru_3(CO)_7(\mu\text{-}CO)_2(1,1,1\text{-}\eta^3\text{-}9S3)]$ (9S3 = 1,4,7-trithiacyclononane) at 68°C in 16% yield [27] as well as from the reaction of $[Ru_3(CO)_{12}]$ with 1,2,5,6-tetrathiacyclooctane at 40°C in 26% yield [22], and characterized on the basis of spectroscopic data only. We undertook an X-ray structure determination of **1** to confirm the coordination mode of the ethanedithiolate ligand.

The X-ray structure of **1** is shown in Fig. 1, and selected bond distances and angles are presented in Table 1. The molecule is based on two ruthenium atoms, each containing three linear terminal carbonyl groups and mutually bridged by both the sulfur atoms of the ethanedithiolate ligand. The molecule possesses a non-crystallographic *mm* symmetry with the $[Ru_2(CO)_6]$ unit adopting the classic 'sawhorse' arrangement. The Ru–Ru bond at 2.6790(8) Å is significantly shorter than that (2.854 Å) in the parent compound $[Ru_3(CO)_{12}]$ [28], but close to the metal–metal distance (2.710(1) Å) in the osmium analog $[Os_2(CO)_6(\mu\text{-}SCH_2CH_2S)]$ which has been reported from the pyrolysis of $[Os_3(CO)_{11}(SCH_2CH_2SCH_2CH_2)]$ as well as from the direct reaction of $[Os_3(CO)_{12}]$ with 1,4-dithiacyclohexane [29]. The ethanedithiolate ligand serves as a bidentate bridging ligand across the metal–metal bond and donates six electrons to make **1** a 34-electron valence saturated bimetallic compound, with each metal atom achieving the expected 18-electron configuration. The Ru–S–Ru bridges are symmetrical with distances Ru(1)/Ru(2)–S(1) = 2.375(2)/2.374(2) and Ru(1)/Ru(2)–S(2) = 2.370(2)/2.370(2) Å. These values are comparable to those found in *syn*-$[Ru_3(CO)_7(\mu\text{-}SCH_2CH_2S)_2]$ (2.365 Å, average) [22] and $[Os_2(CO)_6(\mu\text{-}SCH_2CH_2S)]$ (2.392 Å, average) [29]. The Ru–S–Ru angles are highly acute with the values 68.69(5) and 68.84(4)° at S(1) and S(2) respectively.

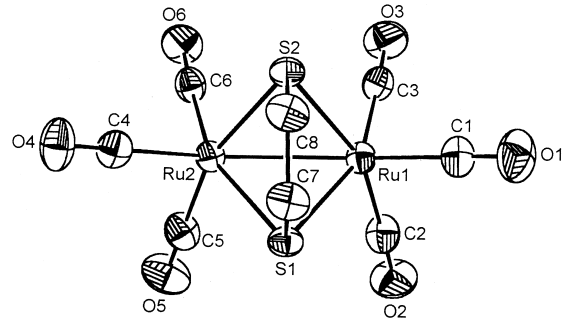
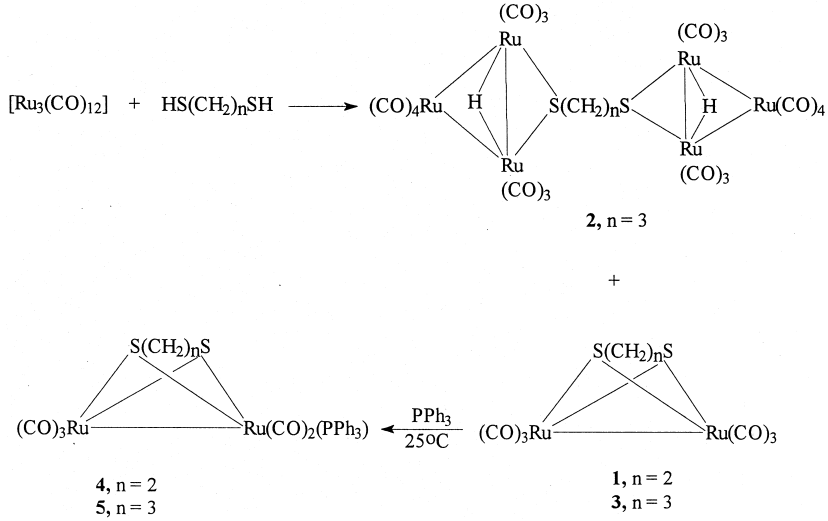


Fig. 1. Solid state structure of $[Ru_2(CO)_6(\mu\text{-}SCH_2CH_2S)]$ (**1**) showing the atom labeling scheme. Hydrogen atoms are omitted for clarity. Thermal ellipsoids are drawn at 40% probability level.

Table 1
Selected bond lengths (Å) and angles (°) for **1**

Ru(1)–Ru(2)	2.6790(8)	Ru(1)–S(1)	2.375(2)
Ru(1)–S(2)	2.370(2)	Ru(2)–S(1)	2.374(2)
Ru(2)–S(2)	2.370(2)	S(1)–C(7)	1.818(6)
S(2)–C(8)	1.825(6)		
C(3)–Ru(1)–C(2)	92.9(3)	C(3)–Ru(1)–C(1)	99.7(3)
C(2)–Ru(1)–C(1)	97.3(3)	C(3)–Ru(1)–S(2)	90.3(2)
C(2)–Ru(1)–S(2)	159.3(2)	C(1)–Ru(1)–S(2)	102.3(2)
C(3)–Ru(1)–S(1)	155.9(2)	C(2)–Ru(1)–S(1)	91.4(2)
C(1)–Ru(1)–S(1)	103.3(2)	S(2)–Ru(1)–S(1)	77.81(6)
C(6)–Ru(2)–C(5)	90.2(3)	C(6)–Ru(2)–C(4)	98.7(3)
C(5)–Ru(2)–C(4)	98.5(3)	C(6)–Ru(2)–S(2)	92.6(2)
C(5)–Ru(2)–S(2)	160.9(2)	C(4)–Ru(2)–S(2)	99.7(2)
C(6)–Ru(2)–S(1)	157.0(2)	C(5)–Ru(2)–S(1)	92.4(2)
C(4)–Ru(2)–S(1)	103.5(2)	S(2)–Ru(2)–S(1)	77.84(5)
Ru(2)–S(1)–Ru(1)	68.69(5)	Ru(2)–S(2)–Ru(1)	68.84(4)

The reaction of $[Ru_3(CO)_{12}]$ with 1,3-propanedithiol yielded the trimetallic and dimetallic compounds $[\{(\mu\text{-}H)(Ru_3(CO)_{10}\}_2(\mu\text{-}SCH_2CH_2CH_2S)]$ (**2**) and $[Ru_2(CO)_6(\mu\text{-}SCH_2CH_2CH_2S)]$ (**3**) (Scheme 1) in 30 and 19% yields respectively. Compound **2** has been characterized by elemental analysis, IR, ^1H and ^{13}C NMR spectroscopic data and by an X-ray study.



Scheme 1.

The structure of **2** is shown in Fig. 2, and selected bond distances and angles are presented in Table 2. An interesting feature of **2** is the presence of two $\{(\mu\text{-H})Ru_3(CO)_{10}\}$ moieties linked by a propanedithiolate ligand. The overall structure of **2** is very similar to that of the methanedithiolate osmium analog $[\{(\mu\text{-H})Os_3(CO)_{10}\}_2(\mu\text{-}\eta^2\text{-}SCH_2S)]$ obtained from the reaction of $[(\mu\text{-H})_2Os_3(CO)_{10}]$ with CS_2 [30,31]. Each $\{(\mu\text{-H})Ru_3(CO)_{10}\}$ unit in **2** consists of an approximately equilateral traingle of three ruthenium atoms with Ru–Ru distances lying in a narrow range 2.8212(8)–2.8429(9) Å. These values are very similar to the Ru–Ru distances found in $[(\mu\text{-H})Ru_3(CO)_{10}(\mu\text{-}SCH_2COOH)]$ (2.827(5)–2.839(4) Å) [32]. The positions of the hydride ligands were obtained from difference maps and they are found to bridge the same edge of each triangle as the sulfur atom. Large angles for the *cis* carbonyl groups (e.g. Ru(3)–Ru(1)–C(2)/C(3) = 111.1(2)/115.4(2), Ru(1)–Ru(3)–C(8)/C(9) = 113.1(2)/116.6(2), Ru(6)–Ru(4)–C(11)/C(13) = 113.9(2)/114.0(2), Ru(4)–Ru(6)–C(18)/C(19) = 113.5(2)/116.1(2)°) are consistent with the location of the bridging hydrides along the Ru(1)–(Ru(3) and Ru(4)–Ru(6) edges in the two Ru_3 triangles. The sulfur bridges are symmetrical with distances Ru(1)/Ru(3)–S(1) = 2.386(2)/2.391(2) and Ru(4)/Ru(6)–S(2) = 2.388(2)/2.379(2) Å. These values are comparable with the Ru–S distances found in **1** and also in *anti*-$[(\mu\text{-H})Ru_3(CO)_7(\mu\text{-}\eta^2\text{-}SCH_2CH_2S)_2]$ (2.376(2)–2.384(2) Å) [22]. The $Ru_2S(1)$ and $Ru_2S(2)$ planes are inclined from the corresponding Ru_3 planes by 77.93(4) and 76.25(4)° respectively. The C–S bond distances of S(1)–C(21) = 1.839(6) and S(2)–C(23) = 1.824(6) Å are very similar to the C–S single bond distances 1.80–1.82 Å observed in several thioalkanes [33–36].

The IR, ^1H and ^{13}C NMR spectra of **2** are consistent with the proposed formulation and X-ray structure. The ^1H NMR spectrum of **2** contains a triplet at δ 2.25, a quartet at δ 2.05 and a singlet at δ −15.41 with relative intensities 2:1:1. The triplet and quartet are due to the six methylene protons in a slightly different environment, whilst the singlet is attributed to the two bridging hydrides in identical stereochemical environment. The ^{13}C NMR spectrum exhibits two resonances at

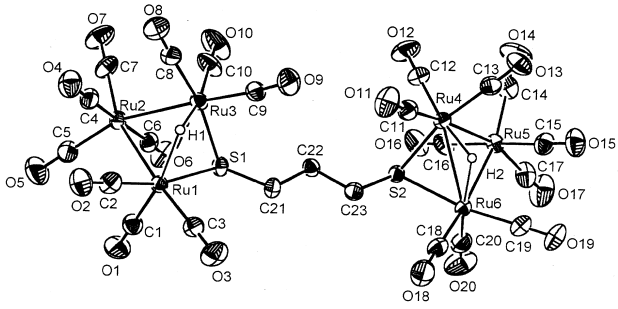


Fig. 2. Solid state structure of $[\{(\mu\text{-H})Ru_3(CO)_{10}\}_2(\mu\text{-}SCH_2CH_2CH_2S)]$ (**2**) showing the atom labeling scheme. Hydrogen atoms other than the bridging hydrides are omitted for clarity. Thermal ellipsoids are drawn at 40% probability level.

Table 2
Bond lengths (Å) and angles (°) for **2**

Ru(1)–Ru(3)	2.8212(8)	Ru(1)–Ru(2)	2.8338(7)
Ru(2)–Ru(3)	2.8429(9)	Ru(1)–S(1)	2.386(2)
Ru(3)–S(1)	2.391(2)	Ru(4)–S(2)	2.388(2)
Ru(4)–Ru(5)	2.8162(8)	Ru(4)–Ru(6)	2.8344(9)
Ru(5)–Ru(6)	2.8414(8)	Ru(6)–S(2)	2.379(2)
S(1)–C(21)	1.839(6)	S(2)–C(23)	1.824(6)
C(2)–Ru(1)–C(1)	95.5(3)	C(2)–Ru(1)–C(3)	94.4(3)
C(1)–Ru(1)–C(3)	96.3(3)	C(2)–Ru(1)–S(1)	165.0(2)
C(1)–Ru(1)–S(1)	96.5(2)	C(3)–Ru(1)–S(1)	93.2(2)
C(2)–Ru(1)–Ru(3)	111.1(2)	C(1)–Ru(1)–Ru(3)	135.6(2)
C(3)–Ru(1)–Ru(3)	115.4(2)	S(1)–Ru(1)–Ru(3)	53.88(4)
C(2)–Ru(1)–Ru(2)	90.3(2)	C(1)–Ru(1)–Ru(2)	85.7(2)
C(3)–Ru(1)–Ru(2)	174.7(2)	S(1)–Ru(1)–Ru(2)	81.68(4)
Ru(3)–Ru(1)–Ru(2)	60.36(2)	C(5)–Ru(2)–C(4)	92.2(3)
C(5)–Ru(2)–C(7)	100.0(3)	C(4)–Ru(2)–C(7)	92.4(3)
C(5)–Ru(2)–C(6)	90.5(3)	C(4)–Ru(2)–C(6)	175.7(3)
C(7)–Ru(2)–C(6)	90.4(3)	C(5)–Ru(2)–Ru(1)	98.4(2)
C(4)–Ru(2)–Ru(1)	86.8(2)	C(7)–Ru(2)–Ru(1)	161.6(2)
C(6)–Ru(2)–Ru(1)	89.5(2)	C(5)–Ru(2)–Ru(3)	157.9(2)
C(4)–Ru(2)–Ru(3)	85.3(2)	C(7)–Ru(2)–Ru(3)	102.0(2)
C(6)–Ru(2)–Ru(3)	91.0(2)	Ru(1)–Ru(2)–Ru(3)	59.60(2)
C(10)–Ru(3)–C(8)	94.3(4)	C(10)–Ru(3)–C(9)	97.3(3)
C(8)–Ru(3)–C(9)	90.0(3)	C(10)–Ru(3)–S(1)	95.9(3)
C(8)–Ru(3)–S(1)	166.8(2)	C(9)–Ru(3)–S(1)	97.0(2)
C(10)–Ru(3)–Ru(1)	135.0(3)	C(8)–Ru(3)–Ru(1)	113.1(2)
C(9)–Ru(3)–Ru(1)	116.6(2)	S(1)–Ru(3)–Ru(1)	53.72(4)
C(10)–Ru(3)–Ru(2)	85.8(2)	C(8)–Ru(3)–Ru(2)	91.0(2)
C(9)–Ru(3)–Ru(2)	176.6(2)	S(1)–Ru(3)–Ru(2)	81.41(4)
Ru(1)–Ru(3)–Ru(2)	60.04(2)	C(12)–Ru(4)–C(13)	92.9(3)
C(12)–Ru(4)–C(11)	97.4(3)	C(13)–Ru(4)–C(11)	94.9(3)
C(12)–Ru(4)–S(2)	93.5(2)	C(13)–Ru(4)–S(2)	165.7(2)
C(11)–Ru(4)–S(2)	97.0(2)	C(12)–Ru(4)–Ru(5)	89.5(2)
C(13)–Ru(4)–Ru(5)	84.7(2)	C(11)–Ru(4)–Ru(5)	173.1(2)
S(2)–Ru(4)–Ru(5)	82.59(4)	C(12)–Ru(4)–Ru(6)	135.4(2)
C(13)–Ru(4)–Ru(6)	114.0(2)	C(11)–Ru(4)–Ru(6)	113.9(2)
S(2)–Ru(4)–Ru(6)	53.38(4)	Ru(5)–Ru(4)–Ru(6)	60.38(2)
C(14)–Ru(5)–C(15)	91.1(3)	C(14)–Ru(5)–C(17)	101.6(3)
C(15)–Ru(5)–C(17)	91.7(3)	C(14)–Ru(5)–C(16)	92.2(3)
C(15)–Ru(5)–C(16)	174.5(3)	C(17)–Ru(5)–C(16)	91.9(3)
C(14)–Ru(5)–Ru(4)	95.5(2)	C(15)–Ru(5)–Ru(4)	88.4(2)
C(17)–Ru(5)–Ru(4)	162.9(3)	C(16)–Ru(5)–Ru(4)	87.0(2)
C(14)–Ru(5)–Ru(6)	155.1(2)	C(15)–Ru(5)–Ru(6)	83.5(2)
C(17)–Ru(5)–Ru(6)	102.9(3)	C(16)–Ru(5)–Ru(6)	91.7(2)
Ru(4)–Ru(5)–Ru(6)	60.13(2)	C(20)–Ru(6)–C(19)	93.5(3)
C(20)–Ru(6)–C(18)	98.6(4)	C(19)–Ru(6)–C(18)	91.8(3)
C(20)–Ru(6)–S(2)	94.3(2)	C(19)–Ru(6)–S(2)	169.7(2)
C(18)–Ru(6)–S(2)	93.7(2)	C(20)–Ru(6)–Ru(4)	134.2(2)
C(19)–Ru(6)–Ru(4)	116.1(2)	C(18)–Ru(6)–Ru(4)	113.5(2)
S(2)–Ru(6)–Ru(4)	53.67(4)	C(20)–Ru(6)–Ru(5)	87.3(3)
C(19)–Ru(6)–Ru(5)	91.5(2)	C(18)–Ru(6)–Ru(5)	173.0(2)
S(2)–Ru(6)–Ru(5)	82.19(4)	Ru(4)–Ru(6)–Ru(5)	59.50(2)
C(21)–S(1)–Ru(1)	109.4(2)	C(21)–S(1)–Ru(3)	110.0(2)
Ru(1)–S(1)–Ru(3)	72.40(5)	C(23)–S(2)–Ru(6)	109.7(2)
C(23)–S(2)–Ru(4)	111.1(2)	Ru(6)–S(2)–Ru(4)	72.95(5)
C(22)–C(21)–S(1)	110.3(4)	C(21)–C(22)–C(23)	110.4(5)
C(22)–C(23)–S(2)	110.2(4)		

δ 52.5 and 35.7 due to the carbon atoms of the dithiolate ligand as well as signals at δ 204.1, 202.6, 198.1, 192.8, 191.5 and 185.5 due to the carbonyl carbons. The ν(CO) stretching frequencies are similar to those of $[\{(\mu\text{-H})(Os_3(CO)_{10}\}_2(\mu\text{-}SCH_2S)]$ [30,31].

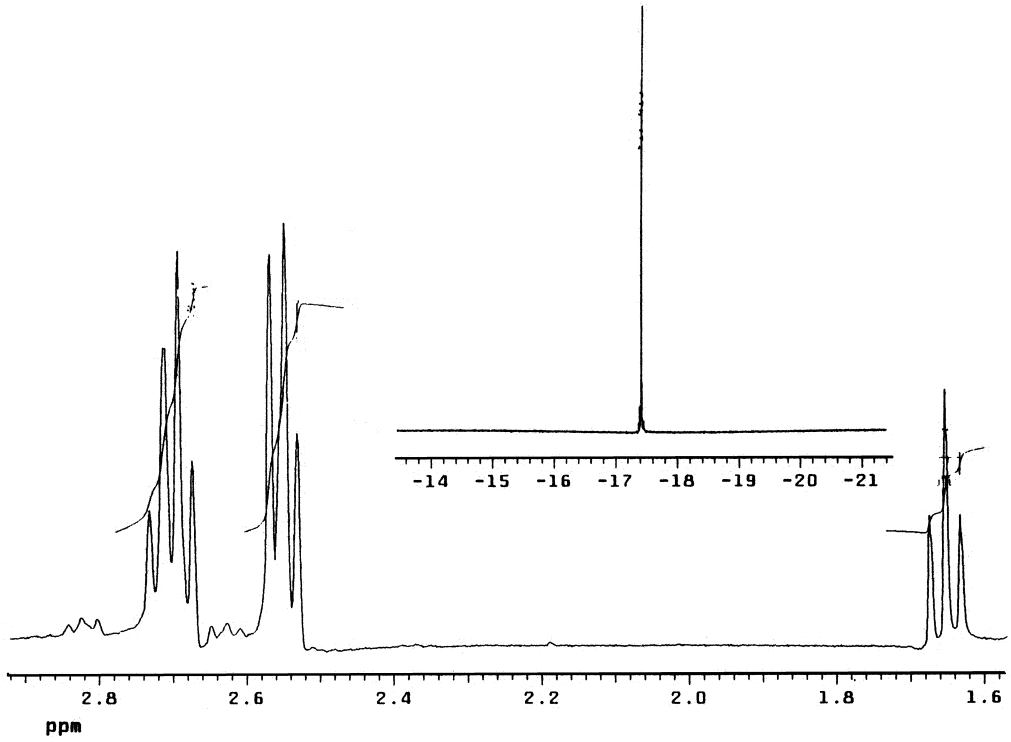
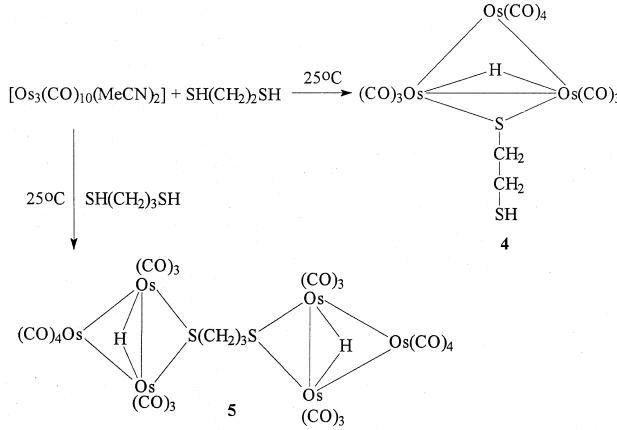


Fig. 3. ^{1}H NMR spectrum of [(μ-H)$Os_3(CO)_{10}$(μ-SCH_2CH_2SH)] (**4**) in $CDCl_3$.

The complex **3** has been characterized by elemental analysis, IR, ^{1}H NMR and mass spectroscopic data. The IR spectrum of **3** is very similar to that of **1** indicating that they are structurally similar. The ^{1}H NMR spectrum shows multiplets at δ 2.19 and 1.89 in a relative intensity of 2:1. The mass spectrum shows the molecular ion peak at *m/z* 478 as expected and the stepwise loss of six carbonyl groups is also observed. The structure of this complex is thus proposed as in Scheme 1.

The reaction of 1,2-ethanedithiol with [$Os_3(CO)_{10}$-$(MeCN)_2$] afforded [(μ-H)$Os_3(CO)_{10}$(μ-SCH_2CH_2SH)] (**4**) in 60% yield. The compound has been characterized by elemental analysis, IR, ^{1}H NMR and mass spectroscopic data. The IR spectrum of **4** in the carbonyl stretching region is very similar to that of [(μ-H)$Os_3(CO)_{10}$(μ-SR)] [37,38], suggesting that they have very similar structures. The ^{1}H NMR and mass spectra indicated the formation of a decacarbonyl compound by oxidative addition of one S–H bond while the other S–H bond remains free. The mass spectrum shows the molecular ion peak at *m/z* 950 with sequential loss of ten carbonyl ligands. The ^{1}H NMR spectrum (Fig. 3) contains four signals at δ 2.70 (dt, 2H, J = 8.0 Hz), 2.55 (t, 2H, J = 8.0 Hz), 1.65 (t, 1H, J = 8.0 Hz) and −17.42 (s, 1H). The S–H proton is observed at δ 1.65 as a triplet with J = 8.0 Hz presumably due to coupling with the adjacent methylene protons. The triplet at δ 2.55 is due to the methylene protons attached to the coordinated sulfur atom while the doublet of a triplet (deceptively appearing as a quartet) at δ 2.70 is assigned to the methylene protons adjacent to the sulfur atom of the free S–H group. The other possible structure with activation of both the S–H bonds can easily be ruled out, because such activation would result in a singlet resonance for methylene protons of the dithiolate ligand. Thus the spectroscopic data are consistent with the proposed structure for **4** (Scheme 2).

In contrast, 1,3-propanedithiol reacts with [$Os_3(CO)_{10}$-$(MeCN)_2$] at room temperature to give [{(μ-H)-$Os_3(CO)_{10}$}$_2$(μ-$SCH_2CH_2CH_2S$)] (**5**). This compound was previously structurally characterized by Lewis and coworkers [39], but no spectroscopic data were reported. We have now characterized it by both spectroscopic data and X-ray crystallography. The IR spectrum of **5** is different from that of the methanedithiolate dicluster [{(μ-H)$Os_3(CO)_{10}$}$_2$(μ-SCH_2S)] but is very similar to that of the propanedithiolate ruthenium analog **2** and the monocluster **4**. The ^{1}H NMR spectrum of **5** shows a pattern similar to



Scheme 2.

2 and contains a triplet at δ 2.44 for four equivalent methylene protons of the 1,3-propanedithiolate ligand, a quintet at δ 1.99 for the other two methylene protons and a high field singlet at δ −17.42 for the two equivalent bridging hydride ligands (one from each cluster). Compound **5** is found to be isostructural with **2**, in which two $\{(\mu\text{-H})Os_3(CO)_{10}\}$ groupings are bridged by the $SCH_2CH_2CH_2S$ ligand and each sulfur bridges two osmium atoms in separate Os_3 cluster units (Fig. 4). The molecular geometry parameters in **5** (Table 3) are comparable with the corresponding values in **2** and also with those obtained from the earlier study [39]. The Os–Os, Os–S and S–C distances (2.8441(10)–2.8652(10), 2.401(4)–2.414(4), 1.82(2)–1.83(2) Å) in **5** are virtually identical with the respective reported values (2.840(3)–2.860(3), 2.397(5)–2.424(5), 1.83(3)–1.85(4) Å) [39].

We have recently [26] found that substitution reaction of the iron-dithiolate compound $[Fe_2(CO)_6(\mu\text{-}SCH_2CH_2CH_2S]$ with tertiary phosphines gives $[Fe_2(CO)_5(\mu\text{-}SCH_2CH_2CH_2S)(PR_3)]$. Keeping this in mind we investigated the CO substitution reaction of **1** and **3** with PPh_3 and observed that an easy reaction occurs yielding the monosubstituted compounds $[Ru_2(CO)_5(\mu\text{-}SCH_2CH_2CH_2S)(PPh_3)]$ (**6**) and $[Ru_2(CO)_5(\mu\text{-}SCH_2CH_2CH_2S)(PPh_3)]$ (**7**). Suitable single crystals could not be grown for **6** and **7** for X-ray analysis; however, they are proposed to be structurally similar to $[Fe_2(CO)_5(\mu\text{-}SCH_2CH_2CH_2S)(PR_3)]$ on the basis of elemental analysis, IR, ^1H and $^{31}P\{^1H\}$ NMR and mass spectroscopic data. The mass spectra of **6** and **7** contain the molecular ion peaks at *m/z* 698 and 712 respectively with successive loss of five CO groups. The ^{31}P NMR spectra of **6** and **7** consist of a single resonance and do not show any significant change on varying the recording temperature. This suggests that **6** and **7** exist as single isomers. As expected, in addition to the signals for the phenyl protons of triphenylphosphine, the ^1H NMR spectra contain resonances due to dithiolate ligands. The IR spectra of **6** and **7** are very similar to that reported for $[Fe_2(CO)_5(\mu\text{-}SCH_2CH_2CH_2S)(PR_3)]$ in which the triphenylphosphine is coordinated at an axial site of one of the metal atoms [26]. When heated to reflux in hexane compound **2** was transformed into **3** by cluster degradation.

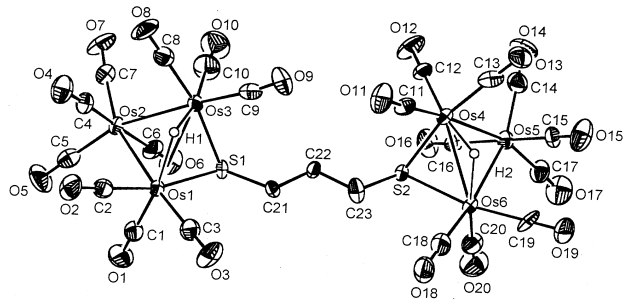


Fig. 4. Solid state structure of $[\{(\mu\text{-H})Os_3(CO)_{10}\}_2(\mu\text{-}SCH_2CH_2CH_2S)]$ (**5**) showing the atom labeling scheme. Hydrogen atoms other than the bridging hydrides are omitted for clarity. Thermal ellipsoids are drawn at 40% probability level.

Table 3
Selected bond lengths (Å) and angles (°) for **5**

Os(1)–Os(3)	2.8445(10)	Os(1)–Os(2)	2.8577(10)
Os(2)–Os(3)	2.8652(10)	Os(1)–S(1)	2.405(4)
Os(3)–S(1)	2.412(5)	Os(4)–Os(5)	2.8441(10)
Os(4)–Os(6)	2.8594(10)	Os(5)–Os(6)	2.8643(11)
Os(4)–S(2)	2.414(4)	Os(6)–S(2)	2.401(4)
S(1)–C(21)	1.82(2)	S(2)–C(23)	1.83(2)
C(1)–Os(1)–C(2)	93.4(8)	C(1)–Os(1)–C(3)	94.7(8)
C(2)–Os(1)–C(3)	94.5(7)	C(1)–Os(1)–S(1)	97.9(6)
C(2)–Os(1)–S(1)	165.9(6)	C(3)–Os(1)–S(1)	93.0(5)
C(1)–Os(1)–Os(3)	137.4(6)	C(2)–Os(1)–Os(3)	112.0(6)
C(3)–Os(1)–Os(3)	115.6(6)	S(1)–Os(1)–Os(3)	53.93(11)
C(1)–Os(1)–Os(2)	87.1(6)	C(2)–Os(1)–Os(2)	90.4(5)
C(3)–Os(1)–Os(2)	174.6(5)	S(1)–Os(1)–Os(2)	81.73(10)
Os(3)–Os(1)–Os(2)	60.33(2)	C(5)–Os(2)–C(4)	93.4(8)
C(5)–Os(2)–C(7)	99.2(8)	C(4)–Os(2)–C(7)	91.6(8)
C(5)–Os(2)–C(6)	90.1(8)	C(4)–Os(2)–C(6)	174.8(7)
C(7)–Os(2)–C(6)	91.6(7)	C(5)–Os(2)–Os(1)	98.7(6)
C(4)–Os(2)–Os(1)	87.0(5)	C(7)–Os(2)–Os(1)	162.1(6)
C(6)–Os(2)–Os(1)	88.7(5)	C(5)–Os(2)–Os(3)	158.2(6)
C(4)–Os(2)–Os(3)	83.8(5)	C(7)–Os(2)–Os(3)	102.5(6)
C(6)–Os(2)–Os(3)	91.5(6)	Os(1)–Os(2)–Os(3)	59.61(2)
C(10)–Os(3)–C(8)	92.3(9)	C(10)–Os(3)–C(9)	98.9(9)
C(8)–Os(3)–C(9)	90.3(7)	C(10)–Os(3)–S(1)	96.8(8)
C(8)–Os(3)–S(1)	168.1(6)	C(9)–Os(3)–S(1)	95.9(5)
C(10)–Os(3)–Os(1)	134.6(8)	C(8)–Os(3)–Os(1)	114.5(5)
C(9)–Os(3)–Os(1)	116.0(5)	S(1)–Os(3)–Os(1)	53.70(10)
C(10)–Os(3)–Os(2)	84.3(8)	C(8)–Os(3)–Os(2)	91.8(5)
C(9)–Os(3)–Os(2)	176.1(5)	S(1)–Os(3)–Os(2)	81.45(10)
Os(1)–Os(3)–Os(2)	60.07(2)	C(13)–Os(4)–C(12)	90.3(8)
C(13)–Os(4)–C(11)	96.1(8)	C(12)–Os(4)–C(11)	95.9(8)
C(13)–Os(4)–S(2)	166.4(6)	C(12)–Os(4)–S(2)	95.5(6)
C(11)–Os(4)–S(2)	95.6(6)	C(13)–Os(4)–Os(5)	85.3(6)
C(12)–Os(4)–Os(5)	90.7(6)	C(11)–Os(4)–Os(5)	173.2(5)
S(2)–Os(4)–Os(5)	82.33(10)	C(13)–Os(4)–Os(6)	115.1(6)
C(12)–Os(4)–Os(6)	137.5(6)	C(11)–Os(4)–Os(6)	113.3(5)
S(2)–Os(4)–Os(6)	53.35(10)	Os(5)–Os(4)–Os(6)	60.29(3)
C(17)–Os(5)–C(15)	92.3(8)	C(17)–Os(5)–C(14)	102.6(9)
C(15)–Os(5)–C(14)	89.6(8)	C(17)–Os(5)–C(16)	92.8(8)
C(15)–Os(5)–C(16)	173.9(8)	C(14)–Os(5)–C(16)	92.6(8)
C(17)–Os(5)–Os(4)	162.9(6)	C(15)–Os(5)–Os(4)	88.2(5)
C(14)–Os(5)–Os(4)	94.5(6)	C(16)–Os(5)–Os(4)	85.9(5)
C(17)–Os(5)–Os(6)	102.9(6)	C(15)–Os(5)–Os(6)	84.5(5)
C(14)–Os(5)–Os(6)	154.1(6)	C(16)–Os(5)–Os(6)	91.1(5)
Os(4)–Os(5)–Os(6)	60.12(3)	C(20)–Os(6)–C(19)	93.4(8)
C(20)–Os(6)–C(18)	97.5(9)	C(19)–Os(6)–C(18)	92.6(8)
C(20)–Os(6)–S(2)	95.3(6)	C(19)–Os(6)–S(2)	169.0(6)
C(18)–Os(6)–S(2)	92.9(6)	C(20)–Os(6)–Os(4)	136.7(6)
C(19)–Os(6)–Os(4)	115.3(6)	C(18)–Os(6)–Os(4)	111.9(6)
S(2)–Os(6)–Os(4)	53.78(11)	C(20)–Os(6)–Os(5)	89.8(6)
C(19)–Os(6)–Os(5)	91.3(6)	C(18)–Os(6)–Os(5)	171.5(6)
S(2)–Os(6)–Os(5)	82.13(10)	Os(4)–Os(6)–Os(5)	59.59(2)
C(21)–S(1)–Os(1)	109.6(5)	C(21)–S(1)–Os(3)	110.2(6)
Os(1)–S(1)–Os(3)	72.37(12)	C(23)–S(2)–Os(6)	109.0(6)
C(23)–S(2)–Os(4)	109.9(6)	Os(6)–S(2)–Os(4)	72.87(12)
C(22)–C(21)–S(1)	112.5(11)	C(21)–C(22)–C(23)	112.9(13)
C(22)–C(23)–S(2)	109.2(11)		

This work shows that the methylene chain length of the ditholate ligands as well as the metal atoms of the clusters have an important effect on product formation when reacted with trimetallic compounds. Longer methylene chain lengths favor dimer formation whilst a short chain length results in

the formation of bidentate chelate as well as monodentate thiolate bridge.

3. Experimental

All the reactions were routinely carried out under a pre-purified nitrogen atmosphere. Reagent grade solvents were freshly distilled from appropriate drying agents. Infrared spectra were recorded on a Schimadzu FTIR 8101 spectrophotometer. NMR spectra were recorded on a Varian Unity Plus 400 spectrometer. $[Ru_3(CO)_{12}]$ was purchased from Strem Chemicals Inc. and used without further purification. $[Os_3(CO)_{10}(MeCN)_2]$ was prepared according to the known procedure [40].

3.1. Reaction of $[Ru_3(CO)_{12}]$ with 1,2-ethanedithiol

A THF solution (80 ml) of $[Ru_2(CO)_{12}]$ (0.200g, 0.312 mmol) and 1,2-ethanedithiol (0.059 g, 0.626 mmol) was refluxed for 1 h. The solvent was removed under reduced pressure and the residue chromatographed by TLC on silica gel. Elution with hexane/CH_2Cl_2 (9:1, v/v) gave two bands. The major band afforded the known compound $[Ru_2(CO)_6(\mu\text{-}SCH_2CH_2S)]$ (0.050 g, 40%) as pale yellow crystals after recrystallization from hexane/CH_2Cl_2 at −20°C. IR (ν(CO), hexane): 2085m, 2056vs, 2018vs, 2004s, 1995m, 1968w cm^{-1}. ^1H NMR ($CDCl_3$): δ 2.37 (s). ^{13}C {^1H} NMR ($CDCl_3$): carbonyl region, 196.2 (4C), 188.6 (2C), hydrocarbon region, 36.1 (2C). MS (*m/z*): 464, M^+, 436 $[M-CO]^+$, 408 $[M-2CO]^+$, 380 $[M-3CO]^+$, 352 $[M-4CO]^+$, 324 $[M-5CO]^+$, 296 $[M-6CO]^+$. *Anal*. Calc. for $C_8H_4O_6Ru_2S_2$: C, 20.78; H, 0.87. Found: C, 20.95; H, 0.95%.

3.2. Reaction of $[Ru_3(CO)_{12}]$ with 1,3-propanedithiol

To a THF solution (100 ml) of $[Ru_3(CO)_{12}]$ (0.400 g, 0.625 mmol) was added 1,3-propanedithiol (0.135 g, 1.25 mmol) and the reaction mixture was refluxed for 1 h. The solvent and excess thiol were removed in vacuo and the residue was chromatographed by TLC on silica gel. Elution with hexane/CH_2Cl_2 (9:1, v/v) developed two bands. The faster moving band afforded $[\{(\mu\text{-}H)Ru_3(CO)_{10}\}_2(\mu\text{-}SCH_2CH_2CH_2S)]$ (**2**) (0.120 g, 30%) as orange crystals after recrystallization from hexane/CH_2Cl_2 at −20°C. Analytical and spectral data for **2**: (IR ν(CO), hexane): 2105m, 2067vs, 2057s, 2027vs, 2010w, 1998w cm^{-1}. ^1H NMR ($CDCl_3$): δ 2.25 (t, 4H, J=7.6 Hz), 2.05 (q, 2H, J=7.6 Hz), −15.41 (s, 2H). $^{13}C\{^1H\}$ NMR ($CDCl_3$): carbonyl region, δ 204.1 (2C), 202.6 (2C), 198.1 (4C), 192.8 (4C), 191.5 (4C), 184.5 (4C), hydrocarbon region, δ 55.1 (2C), 35.7 (1C). *Anal*. Calc. for $C_{23}H_8O_{20}Ru_6S_2$: C, 21.67; H, 0.63. Found: C, 21.82; H, 0.75%. The second band gave $[Ru_2(CO)_6(\mu\text{-}SCH_2CH_2CH_2S)]$ (**3**) (0.056 g, 19%) as pale yellow crystals after recrystallization from hexane/CH_2Cl_2 at −20°C. Analytical and spectral data for **3**: IR (ν(CO), hexane): 2086s, 2055vs, 2018vs, 2004s, 1994s, 1966w cm^{-1}. ^1H NMR ($CDCl_3$): δ 2.19 (s, 4H), 1.89 (s, 2H). MS (*m/z*): 478, M^+, 450 $[M-CO]^+$, 422 $[M-2CO]^+$, 394 $[M-3CO]^+$, 366 $[M-4CO]^+$, 338 $[M-5CO]^+$, 310 $[M-6CO]^+$. *Anal*. Calc. for $C_9H_6O_6Ru_2S_2$: C, 22.69; H,1.27. Found: C, 22.78; H, 1.43%.

3.3. Thermolysis of **2**

A THF solution (30 ml) of **2** (0.120 g, 0.094 mmol) was refluxed for 1.5 h. The solvent was removed under reduced pressure and the residue was chromatographed by TLC on silica gel. Elution with hexane/CH_2Cl_2 (9:1, v/v) afforded **3** (0.012 g, 34%) as pale yellow crystals.

3.4. Reaction of $[Os_3(CO)_{10}(MeCN)_2]$ with 1,2-ethanedithiol

To a dichloromethane solution (15 ml) of $[Os_3(CO)_{10}(MeCN)_2]$ (0.194 g, 0.208 mmol) was added 1,2-ethanedithiol (0.039 g, 0.414 mmol) and the reaction mixture was stirred at room temperature for 5 h. The solvent was removed by rotary evaporation and the residue was chromatographed by TLC on silica gel. Elution with hexane/CH_2Cl_2 (4:1, v/v) gave two bands. The faster moving major band gave $[(\mu\text{-}H)Os_3(CO)_{10}(\mu\text{-}SCH_2CH_2SH)]$ (**4**) as yellow crystals (0.117 g, 60%) from hexane/CH_2Cl_2 at 20°C and the second band gave too small an amount of a compound for complete characterization. Spectral and analytical data for **4**: IR (ν(CO) hexane): 2110m, 2069vs, 2060s, 2026vs, 2021m, 2001s, 1992m, 1986w cm^{-1}. ^1H NMR ($CDCl_3$): δ 2.70 (q, 2H, J=8.4 Hz), 2.55 (t, 2H, J=8.4 Hz), 1.65 (t, 1H, J=8.4 Hz), −17.41 (s, 1H). *Anal*. Calc. for $C_{12}H_6O_{10}Os_3S_2$: C, 15.25; H, 0.64. Found: C, 15.42; H, 0.78%. MS (*m/z*): 950 (M^+), 922 $[M-CO]^+$, 894 $[M-2CO]^+$, 866 $[M-3CO]^+$, 838 $[M-4CO]^+$, 810 $[M-5CO]^+$, 782 $[M-6CO]^+$, 754 $[M-7CO]^+$, 726 $[M-8CO]^+$, 698 $[M-9CO]^+$, 670 $[M-10CO]^+$.

3.5. Reaction of $[Os_3(CO)_{10}(MeCN)_2]$ with 1,3-propanedithiol

1,3-Propanedithiol (0.046 g, 0.428 mmol) was added to a dichloromethane solution (15 ml) of $[Os_3(CO)_{10}(MeCN)_2]$ (0.200 g, 0.214 mmol) in CH_2Cl_2 (15 ml) and the reaction mixture was stirred at room temperature for 3 h. The solvent was removed under reduced pressure and the residue was chromatographed by TCL on silica gel. Elution with hexane/CH_2Cl_2 (4:1, v/v) gave one major band which afforded $[\{\mu\text{-}H)Os_3(CO)_{10}\}_2(\mu\text{-}SCH_2CH_2CH_2S)]$ (**5**) (0.056 g, 30%) as yellow crystals from hexane/CH_2Cl_2 at −20°C. Analytical and spectral data for **5**: IR (ν(CO), hexane): 2110w, 2070s, 2060m, 2027s, 2022m, 2000m, 1991m cm^{-1}. ^1H NMR ($CDCl_3$): δ 2.44 (t, 4H, J=7.4 Hz), 1.91 (q, 2H, J=7.4 Hz), −17.42 (s, 2H). *Anal*. Calc. for

$C_{23}H_8O_{20}Os_6S_2$: C, 15.26; H, 0.44. Found: C, 15.49; H, 0.58%.

3.6. Reaction of *1* with PPh_3

A mixture of **1** (0.050 g, 0.108 mmol) and triphenylphosphine (0.028 g, 0.107 mmol) in hexane (35 ml) was stirred at room temperature for 1 h. The color of the solution changed from yellow to orange. The solvent was rotary evaporated and the residue was chromatographed by TLC on silica gel. Elution with hexane/CH_2Cl_2 gave a single band which afforded $[Ru_2(CO)_5(\mu\text{-}SCH_2CH_2S)(PPh_3)]$ (**6**) (0.041 g, 55%) as orange crystals after recrystallization from hexane/CH_2Cl_2 at −20°C. Analytical and spectral data for **6**: IR (ν(CO), CH_2Cl_2): 2060vs, 2004vs, 2024vw 1985w cm^{-1}. ^1H NMR ($CDCl_3$): δ 7.53–7.38 (m, 15H), 1.83 (m, 2H), 1.14 (m, 2H). $^{31}P\{^1H\}$ NMR ($CDCl_3$): δ 41.6 (s). MS (*m/z*): 698, M^+, 670 $[M-CO]^+$, 642 $[M-2CO)]^+$, 614 $[M-3CO]^+$, 586 $[M-4CO]^+$, 558 $[M-5CO]^+$. *Anal.* Calc. for $C_{25}H_{19}O_5PRu_2S_2$: C, 43.10; H, 2.75. Found: C, 43.32; H, 2.92%.

3.7. Reaction of *3* with PPh_3

A similar reaction to that above of **3** (0.030 g, 0.063 mmol) and PPh_3 (0.017 g, 0.065 mmol) in hexane (30 ml) followed by similar workup and chromatographic separation yielded $[Ru_2(CO)_5(\mu\text{-}SCH_2CH_2CH_2S)(PPh_3)]$ (**7**) (0.020 g, 44%) as orange crystals from hexane/CH_2Cl_2 at −20°C. Analytical and spectral data for **7**: IR (ν(CO), CH_2Cl_2): 2060vs, 2004vs, 1985m, 1946m cm^{-1}. ^1H NMR ($CDCl_3$): δ 7.67–7.42 (m, 15H), 1.81 (m, 2H), 1.37 (m, 2H), 0.98 (m, 2H). $^{31}P\{^1H\}$ NMR ($CDCl_3$): 42.1 (s). MS (*m/z*): 712, M^+, 684 $[M-CO]^+$, 656 $[M-2CO]^+$, 628 $[M-3CO]^+$, 600 $[M-4CO]^+$, 572 $[M-5CO]^+$. *Anal.* Calc. for $C_{26}H_{21}O_5PRu_2S_2$: C, 43.94; H, 2.98. Found: C, 44.18; H, 3.15%.

3.8. X-ray crystallography

Crystallographic data for **1** and **5** were recorded on a Delft Instruments FAST TV area detector and those for **2** were measured on a Turbo CAD4 diffractometer using monochromatized Mo Kα radiation ($\lambda = 0.71069$ Å) [41]. All data sets were corrected for absorption using DIFABS [42]. The structures were solved by direct methods (SHELXS-86) [43], developed via difference syntheses, and refined on F^2 by full-matrix least-squares (SHELXL-96) [44] using all unique data with intensities greater than zero. In all cases the non-hydrogen atoms were anisotropic. The bridging hydrides (H(1) and H(2)) in **2** were located from difference maps but not refined; all other hydrogen atoms were included in calculated positions (riding model). Compound **5** is isostructural with **2**, and so the refinement was carried out starting from the atomic coordinates for **2**. The crystallographic data are summarized in Table 4.

Table 4
Crystal data and details of data collection and structure refinement for **1**, **2** and **5** [a]

	Compound **1**	Compound **2**	Compound **5**
Chemical formula	$C_8H_4O_6Ru_2S_2$	$C_{23}H_8O_{20}Ru_6S_2$	$C_{23}H_8O_{20}Os_6S_2$
Formula weight	362.31	1274.83	1809.61
Crystal system	monoclinic	monoclinic	monoclinic
a (Å)	8.695(2)	14.748(3)	14.7855(11)
b (Å)	16.128(3)	14.088(2)	14.072(3)
c (Å)	9.957(2)	17.893(4)	17.867(2)
β (°)	98.22(2)	91.94(2)	91.981(12)
V (Å^{-3})	1381.9(5)	3715.5(12)	3715.4(9)
Space group	$P2_1/n$ (no. 14)	$P2_1/c$ (no. 14)	$P2_1/c$ (no. 14)
Z	4	4	4
Crystal size (mm)	0.12×0.10×0.08	0.45×0.20×0.06	0.20×0.16×0.12
Shape	prism	plate	prism
Colour	yellow	yellow	yellow
θ Range for data collection (°)	2.42–24.95	1.38–25.26	1.84–25.07
Reflections collected	5386	7246	14862
Unique reflections	2039	6704	5550
R_{int}	0.0491	0.0082	0.0549
Data/parameters in the refinement	2039/163	6704/460	5550/461
Goodness-of-fit on F^2	0.904	1.065	0.923
Final *R* [b] indices	$R_1 = 0.0726$ (0.0324) [c]	$R_1 = 0.0536$ (0.0393) [c]	$R_1 = 0.0702$ (0.0417) [c]
	$wR_2 = 0.0744$ (0.0726) [c]	$wR_2 = 0.1342$ (0.1188) [c]	$wR_2 = 0.0939$ (0.0884) [c]

[a] All measurements were done at 293(2) K.
[b] $R_1 = \sum(F_o - F_c)/\sum(F_o)$; $wR_2 = [\sum\{w(F_o^2 - F_c^2)^2\}/\sum\{w(F_o^2)\}^2]^{1/2}$.
[c] R_1 and wR_2 values for all unique data; those calculated for data with $I > 2\sigma(I)$ are given in parentheses.

Supplementary data

Full details of data collection and structure refinements are deposited with the Cambridge Crystallographic Data Centre, 2 Union Road, Cambridge CB2 1EZ, UK (fax: +44-1223-336033; e-mail: deposit@ccdc.cam.ac.uk), CCDC reference numbers 139585 (**1**), 139586 (**2**) 139587 (**5**).

Acknowledgements

The support of this research by the Bangladesh University Grants Commission is gratefully acknowledged. MBH and KMAM acknowledge the EPSRC support of the national X-ray Crystallography Service. ER acknowledges the National Science Foundation (CHE 9625367) for support of this research.

References

[1] H. Kawaguchi, K. Tatsumi, J. Am. Chem. Soc. 117 (1995) 3885.
[2] K. Tatsumi, H. Kawaguchi, I. Matsubara, A. Nakamura, K. Miki, N. Kasi, Inorg. Chem. 32 (1993) 2534.
[3] K.A. York, K. Folting, G. Christou, J. Chem. Soc., Chem. Commun. (1993) 1563.
[4] J.L. Martin, J. Takats, Can. J. Chem. 67 (1989) 1914.
[5] J.K. Money, J.C. Huffman, G. Christou, Inorg. Chem. 27 (1988) 507.
[6] J.R. Nicholson, J.C. Huffman, D.M. Ho, G. Christou, Inorg. Chem. 26 (1987) 3030.
[7] J.K. Money, K. Folting, J.C. Huffman, D. Collision, J. Temperley, F.E. Mabbs, G. Christou, Inorg. Chem. 25 (1986) 4583.
[8] R.N. Mukherjee, C.P. Rao, J.R. Dorfman, R.H. Holm, Inorg. Chem. 25 (1979) 2979.
[9] B.S. Snyder, C.P. Rao, R.H. Holm, Aust. J. Chem. 39 (1986) 963.
[10] B. Kang, M. Hong, T. Wen, H. Liu, J. Lu, J. Cluster Sci. 6 (1995) 379.
[11] D. Sellman, M. Wille, F. Knoch, Inorg. Chem. 32 (1993) 2534.
[12] F. Jiang, Z. Huang, D. Wu, B. Kang, M. Hong, H. Liu, Inorg. Chem. 32 (1993) 4971.
[13] J.A. Kowacs, R.H. Holm, Inorg. Chem. 26 (1978) 702.
[14] F. Jiang, X. Xie, M. Hong, B. Kang, R. Cao, H. Liu, J. Chem. Soc., Dalton Trans. (1993) 1447.
[15] A. Elduque, L.A. Oro, M.T. Pinillos, A. Tiripicchio, F. Ugozzoli, J. Chem. Soc., Dalton Trans. (1994) 385.
[16] P.M. Boorman, G.K.W. Freeman, M. Parvez, Polyhedron 11 (1992) 765.
[17] G. Henkel, B. Krebs, P. Betz, K. Saatkamp, Angew. Chem., Int. Ed. Engl. 27 (1988) 1326.
[18] T.C. Hsiesh, T. Nicholson, J. Zubieta, Inorg. Chem. 27 (1988) 241.
[19] J.K. Money, J.C. Huffman, G. Christou, J. Am. Chem. Soc. 109 (1987) 2210.
[20] M. Mckenna, L.L. Wright, D.J. Tanner, R.D. Haltiwanger, M. Rakowski DuBois, J. Am. Chem. Soc. 105 (1993) 5329.
[21] J. Birnbaum, G. Godziela, M. Maciejewski, T.L. Tonker, R.C. Haltiwanger, M. Rakowski DuBois, Organometallics 9 (1990) 394.
[22] R.D. Adams, J.H. Yamamoto, J. Cluster Sci. 7 (1996) 643.
[23] S. Rossi, K. Kallinen, J. Ruvsiainen, T.T. Pakkanen, T.A. Pakkanen, J. Organomet. Chem. 440 (1992) 367.
[24] M.A. Mottalib, Ph.D. Dissertation, Jaghangirnagar University, Savar, Dhaka, 1999.
[25] T.A. Siddique, M.Sc. Dissertation, Jahangirnagar University, Savar, Dhaka, 1998.
[26] S.E. Kabir, K.M.A. Malik, unpublished work.
[27] R.D. Adams, J.H. Yamamoto, Organometallics 14 (1995) 3704.
[28] M.R. Churchill, F.J. Hollander, J.P. Hutchinson, Inorg. Chem. 16 (1977) 2655.
[29] R.D. Adams, L. Chen, J.H. Yamamoto, Inorg. Chim. Acta 229 (1995) 47.
[30] R.D. Adams, N.M. Golembeski, J. Am. Chem. Soc. 101 (1979) 1306.
[31] R.D. Adams, N.M. Golembeski, S.P. Selegue, J. Am. Chem. Soc. 103 (1981) 546.
[32] J.Y. Jeannin, G. Lavigne, Inorg. Chem. 17 (1978) 2103.
[33] G.W. Frank, P.J. Degen, Acta Crystallogr., Sect. B 29 (1973) 1815.
[34] G. Vallee, V. Buselti, M. Mammi, G. Carazzolo, Acta Crystallogr., Sect. B 25 (1969) 1432.
[35] G. Vallee, V. Buselti, M. Mammi, G. Carazzolo, Acta Crystallogr., Sect. B 25 (1969) 1631.
[36] J.E. Fleming, H. Lynton, Can. J. Chem. 45 (1967) 353.
[37] V.F. Allen, R. Mason, P.B. Hitchcock, J. Organomet. Chem. 140 (1977) 297.
[38] J.T. Hung, S. Kumaresan, L. Lin, Y.S. Wen, L.K. Liu, K.L. Lu, J.R. Hwu, Organometallics 15 (1996) 5605.
[39] H.D. Holden, B.F.G. Johnson, J. Lewis, P.R. Raithby, G. Uden, Acta Crystallogr., Sect. C 39 (1983) 1205.
[40] J.N. Nicholls, M.D. Vargas, Inorg. Synth. 28 (1989) 232.
[41] J.A. Darr, S.R. Drake, M.B. Hursthouse, K.M.A. Malik, Inorg. Chem. 32 (1993) 5704.
[42] N.P.C. Walker, D. Stuart, Acta Crystallogr., Sect. A 39 (1983) 158 adapted for FAST geometry by A.I. Karaulov, University of Wales, 1991.
[43] G.M. Sheldrick, Acta Crystallogr., Sect. A 46 (1990) 467.
[44] G.M. Sheldrick, SHELXL-96 program for crystal structure refinement, University of Göttingen, Germany, 1996.

PERGAMON

www.elsevier.nl/locate/poly

Polyhedron 19 (2000) 1081–1084

POLYHEDRON

Metallation of 2-methyl-2-thiazoline at a triosmium cluster: X-ray structure of $[(\mu\text{-H})Os_3(CO)_{10}(\mu\text{-}\eta^2\text{-}CH_2\overline{C{=}NCH_2CH_2S})]$

Kazi A. Azam [a], Rahima Dilshad [a], Shariff E. Kabir [a], M. Abdul Mottalib [a], Michael B. Hursthouse [1,b], K.M. Abdul Malik [b,*]

[a] *Department of Chemistry, Jahangirnagar University, Savar, Dhaka-1342, Bangladesh*
[b] *Department of Chemistry, Cardiff University, P.O. Box 912, Park Place, Cardiff CF10 3TB, UK*

Received 28 January 2000; accepted 3 March 2000

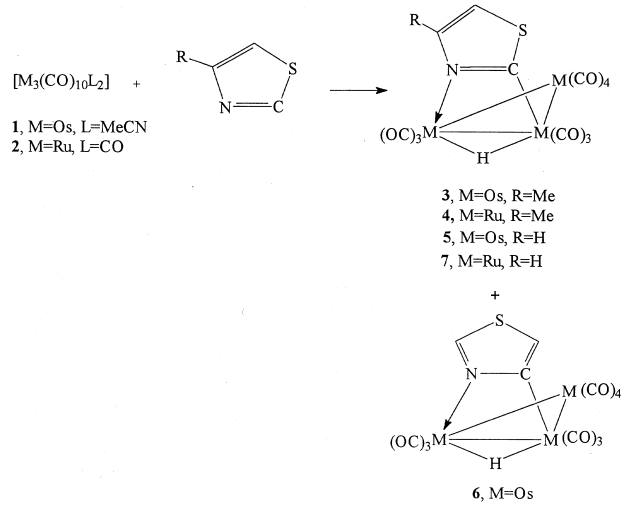
Abstract

The reaction of $[Os_3(CO)_{10}(MeCN)_2]$ with 2-methyl-2-thiazoline at ambient temperature results in the C–H activation of the methyl substituent of the heterocyclic ligand and this gives the new compound $[(\mu\text{-H})Os_3(CO)_{10}(\mu\text{-}\eta^2\text{-}CH_2\overline{C{=}NCH_2CH_2S}]$ (**8**) in 55% yield. Compound **8** undergoes decarbonylation and a further C–H bond activation by thermolysis at 98°C or by treatment with trimethylamine-*N*-oxide to give the dihydrido cluster $[(\mu\text{-H})_2Os_3(CO)_9(\mu\text{-}\eta^2\text{-}CH\overline{C{=}NCH_2CH_2S}]$ (**9**) in 45% yield. Both complexes have been characterized by elemental analyses, IR and ^{1}H NMR spectroscopy, together with X-ray crystallography for **8**. ©2000 Elsevier Science Ltd All rights reserved.

Keywords: Osmium; X-ray structures; Metallation

1. Introduction

The study of the reactivity of N and S containing heterocycles with trimetallic clusters of osmium and ruthenium continues to be the subject of considerable interest; this is due to their relevance to modelling the industrially important hydrodenitrogenation (HDN) and hydrodesulfurization (HDS) processes [1–7]. We have recently reported the thiazolide clusters $[(\mu\text{-H})M_3(CO)_{10}(\mu\text{-}2,3\text{-}\eta^2\text{-}\overline{C{=}NCMe{=}CHS})]$ (**3**, M = Os; **4**, M = Ru; Scheme 1), with metallation exclusively at the 2-position, from the reactions of $[M_3(CO)_{10}L_2]$ (**1**, M = Os, L = MeCN; **2**, M = Ru, L = CO) with 4-methyl thiazole [1]. We also found that the reaction of $[Os_3(CO)_{10}(MeCN)_2]$ with thiazole results in metallation at the 4- and 2-positions, leading to the isomeric compounds $[(\mu\text{-H})Os_3(CO)_{10}(\mu\text{-}2,3\text{-}\eta^2\text{-}\overline{C{=}NCH{=}CHS})]$ (**5**) and $[(\mu\text{-H})Os_3(CO)_{10}(\mu\text{-}3,4\text{-}\eta^2\text{-}H\overline{C{=}NC{=}CHS})]$ (**6**) [2]. In contrast, when reacted with $[Ru_3(CO)_{12}]$, thiazole preferentially metallates at the 2-position yielding $[(\mu\text{-H})Ru_3(CO)_{10}(\mu\text{-}2,3\text{-}\eta^2\text{-}\overline{C{=}NCH{=}CHS})]$ (**7**) [3].



Scheme 1.

Pyridine and 2-substituted pyridines react with triosmium and triruthenium clusters by orthometallation to give $[(\mu\text{-H})M_3(CO)_{10}(\mu\text{-L})]$ (L = C_5H_4N, 2-MeC_5H_3N, 3-MeC_5H_3N, 2-Et-C_5H_3N) [8–17]. In comparison to the extensive orthometallation chemistry of five- and six-membered heterocyclic rings, examples of the activation of their substituent groups are comparatively rare. An example of the ethenyl group C–H bond activation rather than those at the hetero-

* Corresponding author. Tel.: +44-29-2087 4950; fax: +44-29-2087 4030; e-mail: malikka@cardiff.ac.uk

[1] Present address: Department of Chemistry, University of Southampton, Highfield, Southampton SO17 1BJ, UK.

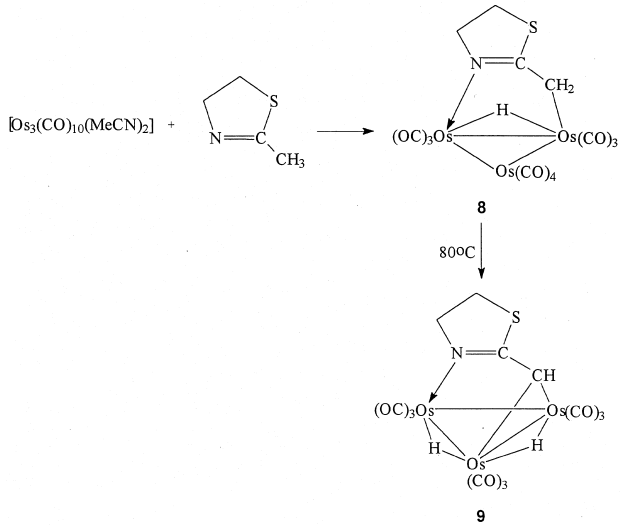
0277-5387/00/$ - see front matter ©2000 Elsevier Science Ltd All rights reserved.
PII S0277-5387(00)00354-5

cyclic ring has been observed when $[Os_3(CO)_{10}(MeCN)_2]$ was reacted with 2-ethenyl pyridine leading to the formation of the open triosmium cluster $[HOs_3(CO)_{10}(NC_5H_4\text{-}C{=}CH)]$ [18]. As part of our interest in the reactivity of N and S containing heterocycles with trimetallic clusters we have investigated the reaction of $[Os_3(CO)_{10}(MeCN)_2]$ with 2-methyl-2-thiazoline and report herein a rare example of the C–H activation of the substituent group of the ligand at ambient temperature.

2. Results and discussion

The lightly stabilized cluster $[Os_3(CO)_{10}(MeCN)_2]$ readily reacts with 2-methyl-2-thiazoline at room temperature to give the novel cluster $[(\mu\text{-}H)Os_3(CO)_{10}(\mu\text{-}\eta^2\text{-}CH_2\overline{C{=}NCH_2CH_2S}]$ (**8**) in 55% yield (Scheme 2). The compound **8** has been characterized by microanalysis, IR and ^{1}H NMR spectroscopy as well as X-ray crystallography. The ^{1}H NMR spectrum of **8** shows four multiplets at δ 3.24, 3.37, 3.89 and 4.18 for the ring protons, which remain intact, and two coupled doublets at δ 1.81 and 2.40 for the 2-CH_2 group along with a high field singlet at δ −14.20 each integrating for one hydrogen. The coupling of 20.0 Hz between these protons and their chemical shifts imply a coordinated CH_2 group and metallation at the substituent group. The spectroscopic data indicated the activation of the C–H bond of the methyl substituent of the heterocycle and subsequent coordination of the carbon to the metal. The exact nature of the bonding of the organic ligand to the cluster was obtained by a single crystal structure determination for **8**.

The structure of a single molecule of **8** is shown in Fig. 1, and selected bond lengths and angles are given in Table 1. The molecule consists of a triangular cluster of osmium atoms with three distinct metal–metal bonds (Os(1)–Os(2) = 2.9047(8), Os(1)–Os(3) = 2.8858(8) and Os(2)–Os(3) = 2.9414(10) Å). The Os(2)–Os(3) edge which is bridged simultaneously by the hydride and the heterocyclic ligand is significantly longer than the two unbridged edges.



Scheme 2.

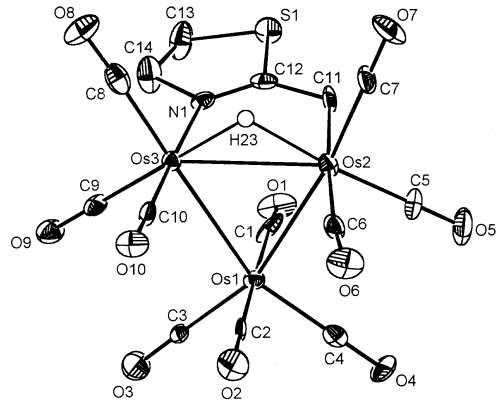


Fig. 1. X-ray structure of **8**, showing the atom labelling scheme. The ring hydrogens are omitted for clarity. Thermal ellipsoids are drawn at 40% probability level.

Table 1
Selected bond lengths (Å) and angles (°) for **8**

Os(1)–Os(2)	2.9047(8)	Os(1)–Os(3)	2.8858(8)
Os(2)–Os(3)	2.9414(10)	Os(2)–C(11)	2.190(11)
Os(3)–N(1)	2.165(9)	Os–C(CO)	1.923 [a]
Os(2)–H(23)	1.77 [b]	Os(3)–H(23)	1.72 [b]
S(1)–C(12)	1.747(11)	S(1)–C(13)	1.778(11)
N(1)–C(12)	1.284(14)	N(1)–C(14)	1.484(12)
C(11)–C(12)	1.477(13)	C(13)–C(14)	1.48(2)
C–O	1.138 [a]		
C(3)–Os(1)–C(4)	103.7(4)	C(3)–Os(1)–C(1)	94.4(5)
C(4)–Os(1)–C(1)	90.4(4)	C(3)–Os(1)–C(2)	89.4(4)
C(4)–Os(1)–C(2)	90.4(4)	C(1)–Os(1)–C(2)	175.7(5)
C(5)–Os(2)–C(7)	100.4(5)	C(5)–Os(2)–C(6)	92.3(4)
C(7)–Os(2)–C(6)	92.5(4)	C(5)–Os(2)–C(11)	84.7(4)
C(7)–Os(2)–C(11)	86.1(4)	C(6)–Os(2)–C(11)	176.3(4)
C(11)–Os(2)–Os(1)	93.8(3)	C(7)–Os(2)–Os(3)	113.2(3)
C(11)–Os(2)–Os(3)	84.2(3)	C(8)–Os(3)–C(10)	90.7(4)
C(8)–Os(3)–C(9)	96.1(4)	C(10)–Os(3)–C(9)	90.6(4)
C(8)–Os(3)–N(1)	88.8(4)	C(10)–Os(3)–N(1)	176.2(4)
C(9)–Os(3)–N(1)	93.2(4)	N(1)–Os(3)–Os(1)	91.5(2)
C(8)–Os(3)–Os(2)	118.9(3)	N(1)–Os(3)–Os(2)	82.9(2)
C(12)–S(1)–C(13)	91.7(6)	C(12)–N(1)–C(14)	113.2(10)
C(12)–N(1)–Os(3)	126.9(7)	C(14)–N(1)–Os(3)	119.6(7)
C(12)–C(11)–Os(2)	120.1(7)	N(1)–C(12)–C(11)	125.6(10)
N(1)–C(12)–S(1)	115.6(8)	C(11)–C(12)–S(1)	118.9(8)
C(14)–C(13)–S(1)	107.6(8)	C(13)–C(14)–N(1)	110.9(9)
Os(2)–H(23)–Os(3)	115 [b]	Os–C–O	176.5 [a]

[a] Average value.
[b] Approximate value.

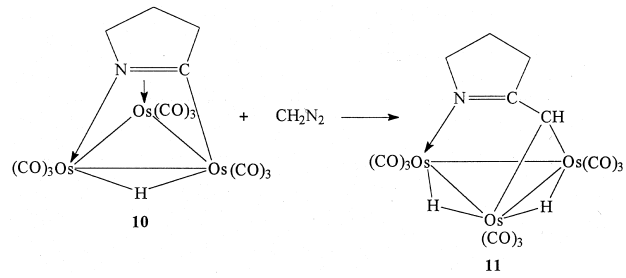
Similar lengthening of the doubly bridged Os–Os edges was also observed in $[(\mu\text{-}H)Os_3(CO)_{10}\{\mu\text{-}2,3\text{-}\eta^2\text{-}\overline{C{=}NC(Me){=}CHS}\}]$ (2.9340(8) versus 2.8590(7), 2.8849(8) Å), $[(\mu\text{-}H)Os_3(CO)_9\{\mu\text{-}2,3\text{-}\eta^2\text{-}\overline{C{=}NC(Me){=}CHS}\}(PPh_3)]$ (2.9674(9) versus 2.8619(13), 2.8779(9) Å) and $[(\mu\text{-}H)Os_3(CO)_8\{\mu\text{-}2,3\text{-}\eta^2\text{-}\overline{C{=}NC(Me){=}CHS}\}(PPh_3)_2]$ (2.9528(6) versus 2.8795(6), 2.9050(6) Å) [1]. The bridging hydride is located close to the plane of the Os_3 triangle, while the heterocyclic ligand is nearly perpendicular to it. The metal atoms Os(3) and Os(2) each contain three linear terminal carbonyl ligands while Os(1) is bonded to four. A notable feature of this structure is that a C–H activation of the methyl

group of 2-methyl-2-thiazoline occurs during the reaction. The organic ligand is η^2-coordinated to the longest Os(2)–Os(3) edge through a metal–carbon σ bond from C(11) to Os(2) and a two-electron donor bond from N(1) to Os(3). The Os(2)–C(11) bond length of 2.190(11) Å and Os(3)–N(1) bond length of 2.165(9) Å are comparable to those of the related compounds $[(\mu\text{-H})_2Ru_3(CO)_9(\mu_3\text{-}\eta^2\text{-}CH(Me)C{=}NCH_2CH_3)\}]$ and $[(\mu\text{-H})_2Os_3(CO)_9(\mu_3\text{-}\eta^2\text{-}CHC{=}NCH_2CH_2CH_2)]$ [19]. The C(12)–N(1) bond length of 1.284(14) Å is typical of carbon nitrogen double bonds in the related triosmium and triruthenium complexes [20–22], while the C(14)–N(1) bond length of 1.484(12) Å is close to that expected for a C–N single bond (1.47 Å) [23]. The S–C distances (1.747(11)–1.778(11), average 1.763 Å) are only slightly smaller than the value expected for a S–C single bond (1.81 Å) [23]. The Os–C(CO) distances (1.897(11)–1.954(12), average 1.923 Å) and the Os–C–O angles (171.3(10)–179.6(9), average 176.54°) are comparable to the corresponding values in triosmium decarbonyl compounds containing a 3, 3, 4 carbonyl ligand distribution and in which the heterocyclic ligand and the hydride bridge the same Os–Os edge [1,2,20,22].

Thermolysis of **8** in refluxing heptane at 98°C gives the dihydrido cluster $[(\mu\text{-H})_2Os_3(CO)_9(\mu_3\text{-}\eta^2\text{-}CHC{=}NCH_2CH_2S)]$ (**9**) in 45% yield (Scheme 1). The compound has been characterized on the basis of elemental analysis, IR and ^{1}H NMR spectroscopic data. A direct analog of **9** was obtained from the reaction of the μ_3-imidoyl compound $[(\mu\text{-H})Os_3(CO)_9(\mu_3\text{-}\eta^2\text{-}C{=}NCH_2CH_2CH_2)]$ (**10**) with diazomethane (Scheme 3) [19]. The ν(CO) frequencies of **9** are very similar to those of **11**, indicating that they have very similar distribution of the carbonyl ligands.

The aliphatic region of the ^{1}H NMR spectrum of **9** contains a doublet at δ 4.24 (J = 1.2 Hz) and three multiplets at δ 3.74, 3.47 and 3.17 in a relative intensity ratio of 1:1:1:2. The hydride region shows a doublet at δ −14.48 (J = 1.6 Hz) and a doublet of doublets at δ −14.61 (J = 1.6 and 1.2 Hz) in a relative intensity of 1:1. The doublet at δ 4.24 is due to the methyne proton and it exhibits coupling to one of the hydrides which appears as a doublet of doublets at δ −14.61. Irradiation of the methyne proton results in a collapse of the hydride doublet of doublets at δ −14.61 to a doublet. The hydride chemical shifts, their multiplicity and the long-range coupling between the methyne proton and one of the hydrides are almost identical with those reported for **11** (δ −14.30 (d, J = 1.7 Hz), −14.56 (dd, J = 1.7 and 0.8 Hz)) whose structure was established by X-ray diffraction studies [19]. The analytical data and spectroscopic features of **9** are thus in agreement with the proposed structure.

In order to examine whether the double bond of the heterocyclic ligand in **8** would exhibit the ability to coordinate to the rare metal atom yielding a μ_3-imidoyl type compound, the compound was treated with Me_3NO. Contrary to expectation, we observed a preferred reaction that involved a further C–H activation of the coordinated methylidyne ligand accompanied by a CO loss.



Scheme 3.

In conclusion, we have demonstrated herein an unusual C–H activation of the methyl substituent of 2-methyl-2-thiazoline at a triosmium centre to give $[(\mu\text{-H})Os_3(CO)_{10}(\mu\text{-}\eta^2\text{-}CH_2C{=}NCH_2CH_2S)]$ (**8**) which undergoes a further C–H activation to afford $[(\mu\text{-H})_2Os_3(CO)_9(\mu\text{-}\eta^2\text{-}CHC{=}NCH_2CH_2S)]$ (**9**). Decarbonylation of **8** using Me_3NO also gives **9** instead of the expected μ_3-imidoyl type product, indicating that C–H activation is more amenable than coordination of the double bond of the heterocycle to the rear metal atom.

3. Experimental

All reactions were carried out under a dry and oxygen-free atmosphere of N_2 by using standard Schlenk techniques. Reagent grade solvents were freshly distilled from the appropriate drying agents. ^{1}H NMR spectra were recorded on a Varian Unity Plus 400 MHz spectrometer. Infrared spectra were recorded on a FTIR 8101 spectrophotometer. The cluster $[Os_3(CO)_{10}(MeCN)_2]$ was prepared according to the known procedure [24].

3.1. Reaction of $[Os_3(CO)_{10}(MeCN)_2]$ with 2-methyl-2-thiazoline

To a dichloromethane solution (40 cm^3) of $[Os_3(CO)_{10}(MeCN)_2]$ (0.188 g, 0.201 mmol) was added 2-methyl-2-thiazoline (0.102 g, 1.0 mmol) and the reaction mixture was stirred at room temperature for 20 h. The solvent was removed in vacuo and the residue was chromatographed by TLC on silica gel. Elution with hexane/CH_2Cl_2 (7:3, v/v) gave one major band which afforded $[(\mu\text{-H})Os_3(CO)_{10}(\mu\text{-}\eta^2\text{-}CH_2C{=}NCH_2CH_2S)]$ (**8**) (0.105 g, 55%) as yellow crystals after recrystallization from hexane/CH_2Cl_2 at −20°C. *Anal.* Found: C, 17.82; H, 0.89; N, 1.59. $C_{14}H_7NO_{10}Os_3S$ requires: C, 17.66; H, 0.74; N, 1.47%. IR (ν(CO), hexane): 2103 m, 2061 vs, 2050 vs, 2022 vs, 2002 m, 1996 m, 1990 m, 1973 w cm^{-1}. ^{1}H NMR ($CDCl_3$): δ 1.81 (d, 1H, J = 20.0 Hz), 2.40 (d, 1H, J = 20.0 Hz), 3.24 (m, 1H), 3.37 (m, 1H), 3.89 (m, 1H), 4.18 (m, 1H), −14.24 (s, 1H).

3.2. Thermolysis of $[(\mu\text{-H})Os_3(CO)_{10}(\mu\text{-}\eta^2\text{-}CH_2C{=}NCH_2CH_2S)]$ (8)

A solution of **8** (0.070 g, 0.073 mmol) in heptane (20 cm^3) was heated to reflux for 22 h. The solvent was removed under reduced pressure and the residue was chromatographed by TLC on silica gel. Elution with hexane/CH_2Cl_2 (7:3,

v/v) developed three bands. The fast moving band gave $[Os_3(CO)_{12}]$ (0.008 g, 12%). The second band gave a too small amount (~0.002 g) for complete characterization. The third band gave $[(\mu\text{-H})_2Os_3(CO)_9(\mu\text{-}\eta^2\text{-}CHC{=}NCH_2CH_2S)]$ (**9**) (0.030 g, 45%) as yellow crystals after recrystallization from hexane/CH_2Cl_2 at −20°C. *Anal*. Found: C, 17.10; H, 0.82; N, 1.62. $C_{13}H_7NO_9Os_3$ requires: C, 16.90; H, 0.76; N, 1.51%. IR (ν(CO), CH_2Cl_2): 2103 s, 2076 vs, 2049 vs, 2019 vs, 2002 s, 1993 m, 1976 m cm^{-1}. ^1H NMR ($CDCl_3$): δ 3.21 (m, 2H), 3.47 (m, 1H), 3.74 (m, 1H), 4.24 (d, 1H, J = 1.2 Hz), −14.48 (d, 1H, J = 1.6 Hz), −14.61 (dd, 1H, J = 1.6, 1.2 Hz).

3.3. Reaction of **8** with Me_3NO

To a dichloromethane solution (20 cm^3) of **8** (0.070 g, 0.073 mmol) was added dropwise a CH_2Cl_2 solution (5 cm^3) of Me_3NO (0.011 g, 0.146 mmol) over a period of 15 min. The reaction mixture was stirred at room temperature for 20 h. A similar work-up to that above followed by a similar chromatographic separation of the residue gave **9** (0.024 g, 35%).

3.4. X-ray crystallography

Crystal data for **8**: $C_{14}H_7NO_{10}Os_3S$, M = 951.87, monoclinic, $C2/c$, a = 28.526(6), b = 7.758(2), c = 17.506(4) Å, β = 90.08(3)°, U = 3873(2) Å^3, Z = 8, D_c = 3.265 g cm^{-3}, μ(Mo Kα) = 197.98 cm^{-1}, λ = 0.71073 Å, T = 150 K, crystal size 0.22 × 0.15 × 0.12 mm.

Intensity data were recorded on a FAST area detector diffractometer [25], the structure solved by direct methods (SHELXS-86) [26], and refined on F^2 by full-matrix least-squares (SHELXL-96) [27] using all 2903 unique data and 262 parameters to final wR_2 = 0.0645 (on F^2, all data) and R_1 = 0.0286 (on F, 2484 data with $F_o^2 > 2\sigma(F_o^2)$). The bridging hydride was located from a difference map but not refined.

Supplementary data

Supplementary data are available from the Cambridge Crystallographic Data Centre, 12 Union Road, Cambridge CB2 1EZ, UK (fax: +44-1223-336033; e-mail: deposit@ccdc.cam.ac.uk), CCDC ref. no. 139497.

Acknowledgements

We gratefully acknowledge the Jahangirnagar University for support of this research. We thank Professor Edward Rosenberg for help in obtaining the 400 MHz ^1H NMR spectra at the University of Montana, USA. MBH and KMAM acknowledge the EPSRC support of the national X-Ray Crystallography Service.

References

[1] K.A. Azam, R. Dilshad, S.E. Kabir, K. Khatoon, L. Nessa, M.M. Rahman, E. Rosenberg, M.B. Hursthouse, K.M.A. Malik, A.J. Deeming, J. Chem. Soc., Dalton Trans. (1996) 1731.
[2] K.A. Azam, M.B. Hursthouse, S. Hossain, S.E. Kabir, K.M.A. Malik, M.M. Rahman, E. Rosenberg, J. Organomet. Chem. 559 (1998) 81.
[3] K.A. Azam, M.B. Hursthouse, S.E. Kabir, K.M.A. Malik, M. Tesmer, H. Vahrenkamp, Inorg. Chem. Commun. 1 (1998) 402.
[4] A.J. Deeming, K.I. Hardcastle, M. Karim, Inorg. Chem. 31 (1992) 371.
[5] Y.K. Au, K.K. Cheung, W.T. Wong, Inorg. Chim. Acta 228 (1995) 267.
[6] A.M. Brodie, H.D. Holden, J. Lewis, M.J. Taylor, J. Chem. Soc., Dalton Trans. (1986) 633.
[7] Y.K. Au, K.K. Cheung, W.T. Wong, J. Chem. Soc., Dalton Trans. (1995) 267.
[8] E.C. Constable, Polyhedron 3 (1984) 1037.
[9] M.I. Bruce, M.P. Cifuentes, M.G. Humphrey, Polyhedron 10 (1991) 277.
[10] K. Burgess, B.F.G. Johnson, J. Lewis, J. Organomet. Chem. 233 (1982) C55.
[11] C.C. Yin, A.J. Deeming, J. Chem. Soc., Dalton Trans. (1975) 2091.
[12] B.F.G. Johnson, J. Lewis, D.A. Pippard, J. Chem. Soc., Dalton Trans. (1982) 407.
[13] A.J. Deeming, R. Peters, M.B. Hursthouse, J.D. Backer-Dirks, J. Chem. Soc., Dalton Trans. (1982) 1205.
[14] G.A. Foulds, B.F.G. Johnson, J. Lewis, J. Organomet. Chem. 294 (1985) 123.
[15] M.I. Bruce, M.G. Humphrey, M.R. Snow, E.R.T. Tiekink, R.C. Wallis, J. Organomet. Chem. 314 (1986) 311.
[16] A. Eisenstadt, C.M. Giandomenico, M.F. Frederick, R.M. Laine, Organometallics 4 (1985) 2033.
[17] K.A. Azam, A.R. Das, M.B. Hursthouse, S.E. Kabir, K.M.A. Malik, J. Chem. Crystallogr. 28 (1998) 283.
[18] K. Burgess, H.D. Holden, B.F.G. Johnson, J. Lewis, M.B. Hursthouse, N.P.C. Walker, A.J. Deeming, P.J. Manning, R. Peters, J. Chem. Soc., Dalton Trans. (1985) 85.
[19] M. Day, W. Freeman, K.I. Hardcastle, M. Isomaki, S.E. Kabir, T. McPhillips, E. Rosenberg, L.G. Scott, E. Wolf, Organometallics 11 (1992) 3376.
[20] E. Rosenberg, S.E. Kabir, M. Day, K.I. Hardcastle, M. Irving, J. Cluster Sci. 5 (1994) 481.
[21] S.E. Kabir, M. Day, M. Irving, T. McPhillips, H. Minassian, E. Rosenberg, K.I. Hardcastle, Organometallics 10 (1991) 3997.
[22] E. Rosenberg, S.E. Kabir, K.I. Hardcastle, M. Day, E. Wolf, Organometallics 9 (1990) 2214.
[23] R.J. Gillespie, I. Hargittai, The VSEPR Model of Molecular Chemistry, Allyn and Bacon, Boston, MA, 1991, p. 18.
[24] B.F.G. Johnson, J. Lewis, D.A. Pippard, J. Chem. Soc., Dalton Trans. (1981) 407.
[25] J.A. Darr, S.R. Drake, M.B. Hursthouse, K.M.A. Malik, Inorg. Chem. 32 (1993) 5704.
[26] G.M. Sheldrick, Acta Crystallogr., Sect. A 46 (1990) 467.
[27] G.M. Sheldrick, SHELXL-96, Program for crystal structure refinement, University of Göttingen, Germany, 1996.

PERGAMON

www.elsevier.nl/locate/poly

Polyhedron 19 (2000) 1085–1096

POLYHEDRON

Study of solution equilibria between iron(III) ion and ciprofloxacin in pure nitrate ionic medium and micellar medium

Predrag Djurdjević [a,*], Milena Jelikić Stankov [b], Jadranka Odović [b]

[a] *Faculty of Science, Institute of Chemistry, P.O. Box 60, 34000 Kragujevac, Yugoslavia*
[b] *Faculty of Pharmacy, V. Stepe 450, 11000 Belgrade, Yugoslavia*

Received 4 November 1999; accepted 8 March 2000

Abstract

Prototropic equilibria (protonation, hydrolytic and complexation) in iron(III) ion + ciprofloxacin (Hcipx) solutions were studied in 0.1 and 0.5 mol dm^{-3} (Na)NO_3 ionic media in the absence and in the presence of ionic surfactants: sodium dodecyl sulfate (SDS) or cetyltrimethylammonium bromide (CTAB). Experiments were carried out at 298 ± 0.2 K using glass electrode potentiometric and UV–Vis spectrophotometric measurements. The concentration of SDS in Fe^{III}–ciprofloxacin solutions was 10 mmol dm^{-3} while that of CTAB was 8 mmol dm^{-3}. The hydrolysis of the iron(III) ion was studied separately within the concentration range of iron 1–5 mmol dm^{-3} and pH 1.6–3.0. Non-linear least-squares treatment of the data indicates that in both ionic media studied the main hydrolytic products were $Fe(OH)_2^{+}$ and $Fe_2(OH)_2^{4+}$. The effect of the concentration of the nitrate ion on the stability constants of these complexes is much more pronounced than the effect of the addition of either SDS or CTAB. The successive protonation constants of ciprofloxacin anion, $cipx^{-}$, relating to the formation of Hcipx and H_2cipx^{+} species, were influenced to a significant extent by the presence of SDS and, to a considerably lesser extent, by the presence of CTAB in both studied concentrations of NO_3^{-} ionic media. The complexation between iron(III) and ciprofloxacin was studied in the concentration range of iron(III) 0.15–0.58 mmol dm^{-3}, with ligand to metal concentration ratios ranging from 3:1 to 10:1 in the pH interval 2.0–6.0. The experimental data obtained could be explained by the formation of mononuclear complexes: $Fe(cipx)_2^{+}$, $Fe(cipx)^{2+}$ and Fe(OH)cipx. In the presence of either SDS or CTAB the same complexes were formed; however, much higher formation constants were obtained with SDS, while the effect of CTAB was sluggish. The structure and mechanism of formation of iron(III)–ciprofloxacin complexes in pure ionic and in micellar media are discussed. ©2000 Elsevier Science Ltd All rights reserved.

Keywords: Ciprofloxacin; Iron(III); Solution equilibria; Surfactants

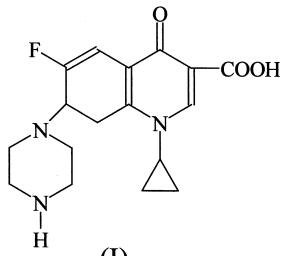
1. Introduction

Ciprofloxacin (1-cyclopropyl-6-fluoro-1,4-dihydro-4-oxo-7-(1-piperazinyl)quinolone-3-carboxylic acid), H(cipx), belongs to the class of fluorinated 4-quinolone antibiotics that find use in the treatment of urinary and respiratory infections. It exhibits strong activity against Gram-negative and some Gram-positive bacteria, although many anaerobic strains are resistant. The mechanism of its action is based on inhibition of bacterial DNA gyrase, thereby interfering with normal cell replication [1–3].

Clinical investigations have shown that concomitant intake of ciprofloxacin and iron-containing drugs (anti-anaemia or multivitamin preparations) results in reduced maximum serum concentration accompanied by the decrease in AUC (area under the concentration versus time curve), leading to decreased bioavailability of the drug, down to 30% [4–6]. The explanation for this interaction, bearing in mind the previous findings concerning some other quinolone–metal ions systems [7], is probably chelation between Fe^{3+} and the 3-carboxyl and 4-oxo functional groups of ciprofloxacin. From the formula of ciprofloxacin (I) it can be seen that it may exist in solution in diprotonated (H_2cipx^{+}), monoprotonated (Hcipx), zwitterionic ($Hcipx^{\pm}$) and anionic ($cipx^{-}$) forms. The vicinity of carbonyl and carboxyl groups makes the ciprofloxacin molecule a suitable ligand for binding hard base ions (Al^{3+}, Fe^{3+}, etc.). This property is important, not only in studying the pharmacological behaviour of ciprofloxacin in patients on parallel therapy with iron-containing drugs, but also for quantitative determination of ciprofloxacin in pharmaceutical formulations and in bio fluids (serum, saliva, urine, etc.).

* Corresponding author. Tel.: +381-34-335039; fax: +381-34-335040; e-mail: preza@ptt.yu

0277-5387/00/$ - see front matter ©2000 Elsevier Science Ltd All rights reserved.
PII S0277-5387(00)00357-0



(I)

Few literature data on solution equilibria between iron(III) ion and ciprofloxacin are available. Sultan and Suliman [8,9] reported the formation of $Fe(cipx)_2$ and Fe(cipx) complexes in sulfuric acid medium. The formation constant of Fe(cipx) complex was determined spectrophotometrically ($\log K = 7.76$). Lee et al. [10] characterized the formation of Fe(cipx) complex by Bjerrum ($\log K = 6.43$) and Scatchard methods ($\log K = 5.54$), while Turel et al. [11] reported the formation of $Fe(Hcipx)_3$ complex in 0.2 mol dm^{-3} KCl ionic medium ($\log \beta = 46.94$). Fratini and Schapoval [12] studied the formation of iron(III)–ciprofloxacin complexes in 1% HNO_3 medium and concluded that only Fe(cipx) complex is formed. Inspection of available literature data indicates that uncertainty exists concerning the species expected to be present in solution, particularly with regard to bis and tris complexes. There have been no reports of ternary Fe–OH–cipx or polynuclear complexes. The values of formation constants quoted for Fe(cipx) show large discrepancies, more than would be expected when account is taken of the effect of ionic medium on the formation constant concerned.

Various influences on iron(III)–ciprofloxacin solution equilibria (ionic strength, simultaneous presence of other complex-forming ligands, presence of surface-active substances) have not been studied. Of particular interest is the effect of surface-active substances on equilibria in iron(III)–ciprofloxacin solutions since in the body (gastrointestinal tract and gut, lungs, blood, etc.) various surfactants are normally present and can influence the complexation between iron(III) and ciprofloxacin. Thus, to mimic their function, in the present study, the detergents sodium dodecyl sulfate (SDS) and cetyltrimethylammonium bromide (CTAB) were used. Surfactants would have the effect of solubilizing both the quinolone and its chelate complex with iron, excluding water molecules from the complexation reaction sphere and preventing the binding of quinolone and iron(III) ion to serum proteins.

It is clear that complete equilibrium studies for the iron(III)–ciprofloxacin system are needed. Therefore, the primary aim of the present paper was to provide reliable data concerning speciation in iron(III) + ciprofloxacin + SDS (or CTAB) solutions, so that they could be used in modelling studies of the iron-based anti-anaemia drugs or multivitamin formulations, and ciprofloxacin interactions in vivo.

In the present paper, the equilibria between the iron(III) ion and ciprofloxacin in the absence and in the presence of SDS (or CTAB) were studied by potentiometry and spectrophotometry in a wide concentration range of iron to ciprofloxacin. The protonation equilibria of ciprofloxacin anion as well as the hydrolysis of iron were investigated in separate experiments.

2. Experimental

2.1. Reagents and analysis

The stock solution of iron(III) nitrate was prepared by dissolving doubly recrystallized $Fe(NO_3)_3 \cdot 6H_2O$ (p.a., Merck) in twice–distilled water. The appropriate amount of HNO_3 was added to avoid initial hydrolysis of Fe^{3+}. The iron content (0.4835 mol dm^{-3}) was determined gravimetrically by precipitation with ammonia. The concentration of the free acid (2.500 mol dm^{-3}) was determined potentiometrically using the Gran plot. The constancy of the total proton concentration with time was considered as a criterion for the absence of initial iron(III) hydrolysis and was periodically checked by titration against standard NaOH before each series of measurements.

Ciprofloxacin hydrochloride, pale yellow crystalline powder ($M_r = 385.8$) was from Bayer (Leverkusen, Germany). Standardization was performed by potentiometric titration against standard NaOH. Sodium dodecyl sulfate ($M_r = 288.4$) and cetyltrimethylammonium bromide ($M_r = 364.5$) were products of Merck (Germany). The concentrations of SDS (10.0 mmol dm^{-3}) and CTAB (8.0 mmol dm^{-3}) were higher than their critical micellar concentrations (8.2 and 0.7 mmol dm^{-3}, respectively). The sodium hydroxide solution was prepared from concentrated volumetric solutions (p.a., Merck) by diluting with freshly boiled doubly distilled water, cooled under constant flow of purified nitrogen. The alkali concentration was checked by titration against potassium hydrogen phthalate. The nitric acid solution was made from HNO_3 (Suprapure, Merck) and standardized against tris(hydroxymethyl)aminomethane. The solution of sodium nitrate was prepared from $NaNO_3$ (p.a., Merck) by dissolving the recrystallized salt in twice-deionized water. The concentration was determined by evaporation of a known volume of solution to dryness at 573 K and weighing the residue.

2.2. Equipment

Potentiometric measurements were carried out using an automatic titrator Titrilab Model 90 (Radiometer, Copenhagen) consisting of a TIM 900 titrator and ABU 901 autoburette. The titration vessel was fitted with a combined electrode (Radiometer GK 2401 B). The resolution of measurements was ± 0.1 mV or ± 0.001 pH units. A constant temperature was maintained with a VEB Prufgerate Model E3E circulating ultrathermostat. Spectrophotometric measurements were made with Beckman Model DU 60 UV–Vis double-beam spectrophotometer. Quartz cells (matching pair) with 1-cm

pathlength were used; the reference cell was filled with 0.1 or 0.5 mol dm^{-3} $NaNO_3$ solution in protonation measurements or, in complexation measurements, with a solution containing all components except iron. The pH of test solutions was measured with a glass/calomel combined electrode couple which was calibrated as hydrogen ion concentration probe according to the procedure described by Marsicano et al. [13]. Infrared (IR) spectra were taken on an IR spectrophotometer (Perkin-Elmer Model 983).

2.3. Procedure

All titrations were performed in a double-mantled, thermostated glass vessel closed with a Teflon cork. A constant temperature of 298.0 ± 0.2 K was maintained by circulating the thermostated water through the jacket. Purified and oxygen-free nitrogen gas was bubbled through the solution to provide an inert atmosphere and stirring. Additional stirring of the solution was achieved with a magnetic stirrer.

The electrochemical cell used for potentiometric measurements can be represented as RE/TS/GE, where TS is test solution and RE and GE denote reference and glass electrode, respectively. The general composition of the test solution in hydrolytic studies was M Fe^{3+}, H H^+, X SDS or CTAB, 0.1 or 0.5 mol dm^{-3} NO_3^-, where M, H and X denote total molar concentrations of corresponding species. The composition of the test solution in complexation studies was M Fe^{3+}, H H^+, X SDS, L cipx, 0.1 or 0.5 mol dm^{-3} NO_3^-, where L denotes total molar concentration of ciprofloxacin.

The potential of the glass electrode is given by the expression:

$$E = E_0 + Q \log h + E_j$$

where h is the concentration of free proton, E_0 is a constant which includes the standard potential of the glass electrode, Q is the slope of the glass electrode response and E_j is a liquid junction potential whose contribution to E was found to be negligible. E_0 was determined both before and during each titration of the test solution, according to a previously described procedure [13]. When the difference between two E_0 values was higher than 1.0 mV, the titration was rejected.

To reduce the concentration of the hydrogen ion, the alkali was added stepwise from an autoburette in small aliquots (0.005–0.01 ml). The potential was monitored after each addition of the titrant. The titration protocol was chosen in such a way that complexation reactions could proceed in the conditions as close to the true equilibrium as possible. To achieve this the potential readings were taken every 2 min until steady values to ± 0.1 mV min^{-1} were obtained. At some points titration was stopped and solution was left with no further addition of base for the next 2–3 h, with continuous monitoring of the potential. The titration was resumed only if the potential did not change more than ± 0.2 mV. No back-titrations were performed. Instead, agreement between duplicate titrations (better than 1%) served as criterion for the reversibility of the reaction.

2.4. Data treatment

Three kinds of equilibria should be considered in the present study: (a) protonation of ciprofloxacin anion (ciprofloxacinate), (b) hydrolysis of iron(III) ion and (c) general three-component equilibria:

$$p\mathrm{Fe}^{3+} + q\mathrm{H}^+ + r(\mathrm{cipx}^-) \rightleftharpoons [\mathrm{Fe}_p\mathrm{H}_q(\mathrm{cipx})_r]^{(3p+q-r)+}; \quad \beta_{p,q,r}$$

which includes the case $q = 0$, i.e. the formation of pure binary complexes of Fe^{3+}. Negative values of q denote hydroxo complexes. The equilibrium constant, $\beta_{p,q,r}$, represents the overall stability constant of the formed (p,q,r) complex. The overall protonation constants of ciprofloxacinate and stability constants of the hydrolytic complexes of iron(III) ion were determined in separate experiments. Thus, in evaluation of three-component equilibria (c), the binary models (a) and (b) were considered as known.

The mathematical analysis of the experimental data was performed with the aid of the general least-squares program Superquad [14]. In Superquad calculations the identity and stability of complexes that gave the best fit to the experimental data were determined by minimizing the error-squares sum of the potentials, U:

$$U = \sum w_i (E_{\mathrm{obs}} - E_{\mathrm{calc}})^2$$

where w_i represents a statistical weight assigned to each point of titration curve, E_{obs} and E_{calc} refer to the measured potential of the cell and the calculated one assuming the specific model and trial constants, respectively. The best model was chosen using the following criteria. (a) The lowest value of U. (b) Standard deviation in calculated stability constants less than 0.15 log units. (c) Standard deviations in potential residuals, defined as:

$$s = \frac{ewe^T}{N-k}$$

where e is a vector in potential residuals $(E_{\mathrm{obs}} - E_{\mathrm{calc}})$, w is a weighting matrix, N is the number of observations and k is the number of refinable parameters, with standard deviation in volume readings 0.0005 cm^3 and standard deviation in potential readings 0.1 mV, should be less than 3.0. (d) Goodness-of-fit statistics, χ^2 (Pearson's test) at 95% confidence level, with 6 degrees of freedom, less than 12.6. (e) Reasonably random scatter of potential residuals without any significant systematic trends. Along with Superquad the program Best [15] was also used in calculations.

The spectrophotometric data were evaluated with the aid of the program Squad [16]. In Squad calculations, the composition, stability and molar absorptivities, $\varepsilon_{p,q,r}$, of the complexes were determined by minimizing the sum, S, defined as:

$$S = \sum (A_{\mathrm{obs}} - A_{\mathrm{calc}})^2$$

where A_{obs} and A_{calc} refer to measured absorbance and that calculated according to the following equation:

$$A_{\mathrm{calc}} = \sum \beta_{p,q,r} [\mathrm{Fe}]^p [\mathrm{H}]^q [\mathrm{cipx}]^r \varepsilon_{p,q,r}$$

For Squad calculations the spectra were digitized at 3-nm intervals. Acceptance criteria for each particular model were: (a) S lower than 1.0×10^{-2}; (b) standard deviation of the fit of the spectrum (SD) less than 1.0×10^{-2}; (c) standard deviation in calculated stability constants less than 0.08 log units. All the calculations were performed on an IBM PC Pentium II 450 compatible computer.

2.5. Preparation of the complex

The iron(III)–ciprofloxacin complex was synthesized by mixing equimolar quantities (5 mmol) of sodium salt of ciprofloxacin acid and iron(III)–nitrate, which was dissolved in 10 ml of 0.1 mol dm^{-3} HNO_3. The total volume was brought up to 25 ml with doubly-distilled water. The pH of solution was then adjusted to 2.6 by the addition of an appropriate amount of solid $NaHCO_3$. The original volume was reduced to one-half by slow evaporation and was afterwards stored in a desiccator containing methanol. The complex, which crystallized after 3 days, was washed with water and methanol and dried in vacuo. Elemental analysis gave 12.14% for Fe (calc. for $Fe(cipx)(NO_3)_2\cdot2.5H_2O$, 12.5%). The nitrate content, found spectrophotometrically using diphenylamine, was 27.5% (calc. for $Fe(cipx)(NO_3)_2\cdot2.5H_2O$, 27.7%).

3. Results and discussion

In order to study speciation in the three-component system Fe^{3+}–H^+ (or OH^-)–ciprofloxacin, it is necessary first to characterize the binary equilibria, i.e. hydrolysis of iron(III) ion and protonation of ciprofloxacin anion, under exactly the same experimental conditions as for the complexation study.

3.1. Hydrolysis of iron(III) ion

Although the hydrolysis of iron has been the subject of extensive studies for almost a century, controversy still exists regarding the identity and stability of the species formed in solution. Various factors, such as the method of preparation of the solution, the degree of hydrolysis (defined as the molar ratio $m=[OH]/[Fe]$), pH range, temperature, concentration of reactants, nature and concentration of supporting ionic medium, type and rate of base addition, ageing time, have a great influence on the composition and stability of the hydrolytic complexes formed in solution of Fe^{3+}. This subject has been reviewed by, among others, Sylva [17], Baes and Mesmer [18], Flynn [19] and Blesa and Matijevic [20]. The consensus is that, at lower values of m (≤1) and low concentrations of iron (<5 mmol dm^{-3}) in the pH range 1.0–3.0, the main hydrolytic products of iron are $Fe(OH)^{2+}$, $Fe(OH)_2{}^+$ and $Fe_2(OH)_2{}^{4+}$. At very low iron concentrations (μM), Martin [21] assumed the formation of mononuclear hydrolytic complexes only, $Fe(OH)_n$ ($n=1$–3). At higher iron concentrations and $m<2$, the red cationic polymer with an OH^-:Fe ratio of 2.25–2.9 is probably the principal constituent of highly hydrolysed iron(III) solutions [19].

The data on iron hydrolysis in nitrate medium are controversial. Some authors [20,22,23] did not find the formation of any soluble hydrolytic complexes, whereas others [24–27] characterized some soluble species together with hydrolytic polymers of unknown composition. In view of these conflicting results it has been necessary to determine the composition and stability of the main iron hydrolytic species, under the same experimental conditions as for the iron–ciprofloxacin complexation study.

The experimental data obtained in the 0.1 and 0.5 mol dm^{-3} $NaNO_3$ medium at 298 K are summarized in Table 1. In the ionic media used the iron(III) hydrolyses between pH 1.6 and ca. 3.0, depending on its concentration. The maximum value of average hydroxide number, Z_{Fe}, defined as $Z_{Fe}=(h-H)/M$, before precipitation occurred was ca. 0.45. The data show that, for each concentration of the iron studied, a separate formation curve, $Z_{Fe}=Z(-\log h)$ was obtained. This indicates the formation of polynuclear hydrolytic complexes. The pH region in which hydrolysis occurs depends on the total concentration of iron. Thus, as the concentration of the iron(III) ion increases, the beginning of hydrolysis shifts towards lower pH values, while at the same time the degree of hydrolysis decreases. Possible complexation of iron(III) ion with nitrate ion from the ionic medium should appear as a constant effect because of relatively high concentration of the medium; therefore, it should not affect the number of hydroxide ions bound to iron. Although the titrations were performed in a wide pH range, for the purpose of calculations some reduction of the number of titration points was necessary. Points at low pH values, where hydrolysis is negligible, and at pH values higher than ~2.7, where solutions become turbid and colloid formation may take place, were excluded from calculations.

Reacting with water molecules, the iron(III) ion forms one or more hydrolytic complexes of the general composition $Fe_p(OH)_q{}^{(3p-q)+}$, further abbreviated as (p,q), whose overall formation constants, $\beta_{p,q}$, can be defined as:

$$\beta_{p,q}=C_{p,q}m^{-p}h^q$$

where $C_{p,q}$ denotes the equilibrium concentration of the (p,q) complex and m is the free concentration of Fe^{3+}. In the above reaction, the nitrate ions and water molecules were omitted from the coordination sphere.

First, each titration curve was processed separately using the program Best. On the basis of hydrolytic curves, $Z_{Fe}=Z(-\log h)$, the pH interval chosen was 1.6–2.7. Complexes from the initial set comprising (1, −1), (1, −2), (1, −3), (1, −4), (2, −1), (2, −2), (2, −3), (2, −4), (2, −6), (3, −3,), (3, −4), (3,−6), (6, −12), (6, −15), (6, −18), (8, −12) and (13, −32) were introduced one at a time until the minimum value of σ_{fit} [15] was obtained.

Table 1
Summary of potentiometric measurements of iron(III) ion hydrolysis [a]

Run no.	M	H	SDS	CTAB	pH range	Z_{max}
0.5 mol dm^{-3} $NaNO_3$ ionic medium						
1	0.967	6.811			2.167–2.561	0.414
2	2.418	14.865			1.827–2.396	0.236
3	4.835	24.848			1.604–2.348	0.190
4	0.967	5.490	10.0		2.160–2.644	0.462
5	2.514	14.313	10.0		1.854–2.429	0.240
6	5.028	28.536	10.0		1.559–2.303	0.193
7	0.967	5.287		8.0	2.277–2.766	0.302
8	2.514	14.360		8.0	1.843–2.390	0.253
9	5.028	26.909		8.0	1.571–2.124	0.206
0.1 mol dm^{-3} $NaNO_3$ ionic medium						
10	0.967	5.703			2.245–2.941	0.496
11	2.514	14.745			1.833–2.507	0.299
12	5.028	23.980			1.624–2.457	0.267
13	0.967	5.533	10.0		2.238–3.012	0.523
14	2.514	14.358	10.0		1.843–2.514	0.463
15	5.028	24.200	10.0		1.610–2.450	0.388
16	0.967	5.553		8.0	2.255–2.929	0.406
17	2.514	14.330		8.0	1.845–2.512	0.347
18	5.028	24.815		8.0	1.610–2.445	0.326

[a] M, H, SDS and CTAB denote analytical concentrations of iron(III), hydrogen ion, sodium dodecyl sulfate and cetyltrimethylammonium bromide in mmol dm^{-3}, respectively. Z_{max} is the maximal value of average hydroxide number of iron.

During the calculations all the titration parameters (M_0, H_0) were kept constant while pH values in repeated cycles of calculations were adjusted until the best possible value of σ_{fit} was obtained. The accepted set of complexes was $(1, -2)$, $(2, -2)$ and $(2, -4)$. Then all the titration curves were processed together, this time using the program Superquad. In Superquad calculations the E_0 values were allowed to float while all analytical parameters were held constant. All the complexes found in Best calculations were accepted with small differences in stability constants. Stepwise introduction of other complexes (higher polymers) from the initial set lead either in their rejection or in a much worse set of statistical parameters determining goodness of fit. No higher polymers were accepted, neither was the tridecamer. However, since residuals showed a systematic trend at the beginning and at the end of the pH interval chosen, the number of points used in the calculation was reduced, so that only the points from pH 1.7 to 2.6 ($Z_{max} \leq 0.25$) were included in the calculations. Repeated calculations ended with the rejection of the $(2, -4)$ complex. At the same time, the stability constant of the dimer $(2, -2)$ was lower, with a much better standard deviation. Other complexes remained practically unchanged. Generally, the fit was improved in terms of better scatter of residuals and lower value of *s*. The next iteration was forced with manual introduction of the binary monomer, $Fe(OH)^{2+}$. It was, however, rejected from all the models tested and consequently it was excluded from the final speciation scheme. The final results of the calculations are given in Table 2. It is seen that our results are in good agreement with available literature data. In contrast to other authors, we

Table 2
Results of non-linear least-squares analysis of protonation of ciprofloxacin and hydrolysis of iron(III) ion data [a]

Species	S	S + SDS	S + CTAB	S′	S′ + SDS	S′ + CTAB
Potentiometry						
Hcipx	9.07(5)	9.45(3)	9.13(1)	8.98(1)	9.14(1)	
H_2cipx	16.20(2)	18.28(5)	16.06(2)	15.46(3)	17.53(3)	
$Fe(OH)_2$	−6.14(9)	−6.08(9)	−6.13(4)	−6.38(4)	−6.31(5)	−6.32(8)
$Fe_2(OH)_2$	−2.79(3)	−2.70(3)	−2.80(3)	−3.17(3)	−3.10(3)	−3.12(4)
Spectrophotometry						
Hcipx	9.04(2)	9.65(1)	9.20(6)			
H_2cipx	16.23(8)	18.26(9)	16.03(6)			
$Fe(OH)_2$	−6.40(9)					
$Fe_2(OH)_2$	−2.79(3)					

[a] Protonation constants are defined as $\beta_n = [H_n cipx]/[H^+]^n[cipx]$ $(n = 1, 2)$; stability constants of hydrolytic complexes are given as $\beta_{p,q} = [Fe_p(OH)_q][H^+]^q/[Fe]^p$. Logarithms of constants are given together with standard deviations in parentheses. S, 0.1 mol dm^{-3} $NaNO_3$; S′, 0.5 mol dm^{-3} $NaNO_3$.

failed to identify the monohydroxo complex $Fe(OH)^{2+}$, probably because of its rapid further hydrolysis and polymerization.

The set of statistics obtained ($\chi^2 \leq 13.5$, $s \leq 2.3$), as well as scatter of residuals, indicates a good fit of the data. The distribution of the species over the pH range 1.0–3.0 using the program Species [28] indicates that the dimer $Fe_2(OH)_2^{4+}$ dominates over the pH range 1.7–3.0. The diol, $Fe(OH)_2^{+}$ begins to form at pH 2.0 and its concentration rapidly rises upon increasing the pH. Beyond pH 2.8, probably, the concentration of higher hydrolytic polymers sharply increases; they are the precursors of the polymer(s), which eventually precipitate(s) from the solution. Formation of either soluble or amorphous $Fe(OH)_3$ was not detected under our experimental conditions.

In addition to potentiometric measurements, the spectrophotometric measurements were also made to improve the reliability of the hydrolysis model. Spectral measurements were made on solutions in which the concentration of the iron was constant (9.67 mmol dm^{-3}) while the pH was varied between 1.357 and 2.297 (ten solutions). The spectra were taken in the 350–550 nm wavelength interval. The pH of solutions was adjusted by the addition of HNO_3 or NaOH (as appropriate). All test solutions were left to stand for 1 month before measurements were made. The pH of solutions was recorded daily. The stable readings (within ± 0.01 pH unit) were obtained after 1 week and remained stable during the next 2–3 days. Final spectra were recorded after 2 weeks. Part of the spectra obtained is shown in Fig. 1.

The spectral data were evaluated with the aid of the Squad program. In calculations the extinction coefficient of aqua iron(III) ion was set to zero in the chosen wavelength interval. The results of the calculation are given in Table 2. The calculated statistical parameters ($S = 1.5 \times 10^{-2}$, SD = 5×10^{-3}) indicate fairly good fit of the data. The results obtained are in agreement with the potentiometric ones, thus confirming the existence of (1, −2) and (2, −2) hydrolytic complexes with a high level of certainty.

Inspection of both potentiometric and spectrophotometric data reveals a pronounced effect of the concentration of the ionic medium on the stability constants of the iron(III) hydrolytic complexes ($\Delta\log\beta_{1,-1} = -0.24$ and $\Delta\log\beta_{2,-2} = -0.38$). The effect is considerably larger on the (2, −2) complex due to its higher charge. This is in agreement with the general Debye–Hückel–Onsager theory of the influence of the ionic medium on stability constants. In the case of hydrolytic complexes of iron, the additional influence arises from the lowered activity of water in more concentrated medium (0.5 mol dm^{-3} NO_3^-).

3.1.1. The effect of SDS or CTAB on the hydrolysis of iron(III) aqua ion

The experimental data obtained under the same medium and temperature conditions in the presence of SDS or CTAB are summarized in Table 1.

Under the experimental conditions chosen the iron ion hydrolyses between pH 1.5 and 2.9, depending on its concentration. The maximum value reached for the average hydroxide number, Z_{Fe}, was ca. 0.5. The data show that, for each concentration of iron studied, separate titration curves, $Z_{Fe} = Z(-\log h)$ were obtained. This indicates the formation of polynuclear complexes. It can be seen that in the presence of the surfactant the extent of hydrolysis is lowered while, at the same time, the beginning of hydrolysis is slightly shifted toward lower pH values for approximately 0.1 pH units.

The calculations indicate that the hydrolytic curves can be fitted with the same set of complexes as in the case of absence of surfactants. In Best calculations the obtained values of σ_{fit} were in the range 0.0015–0.002, thus indicating good fit of the data. Final values of the stability constants were obtained

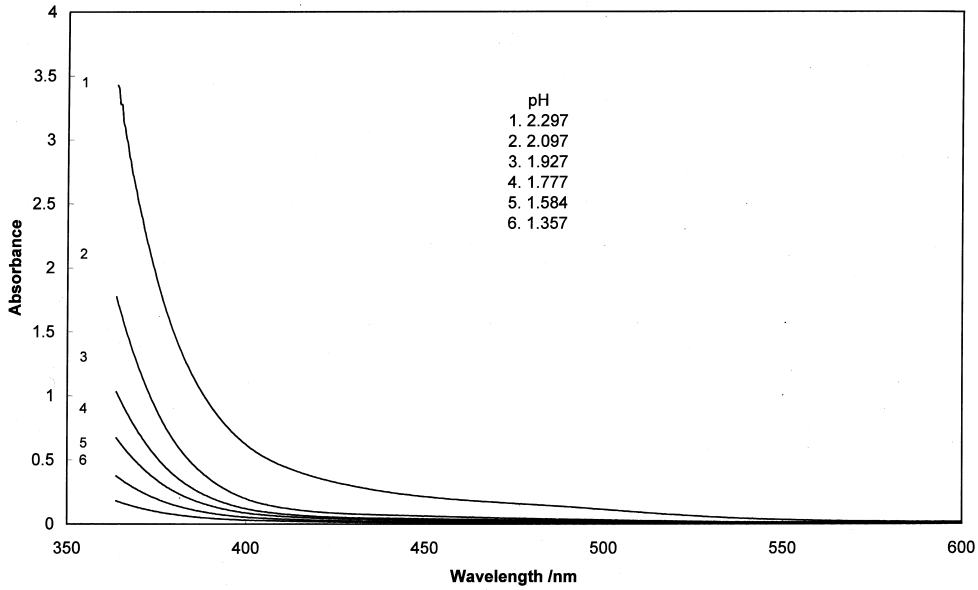


Fig. 1. Spectra of hydrolysed solutions of iron(III) ion. $C_{Fe} = 9.67$ mmol dm^{-3}.

with Superquad. The results of calculations are given in Table 2. The calculated statistical parameters of the fit satisfy all the acceptance criteria, thus confirming the existence of (1, −2) and (2, −2) hydrolytic complexes, in the presence of surfactants, with high probability. Generally, the effect of surfactants on the stability constants of iron(III) hydrolytic complexes in both concentration of the ionic medium is negligible. Probably it is due to very strong hydrolytic tendency of iron(III) ion and its high affinity towards oxygen donor from water. Thus, the change of local concentration of water caused by surfactants is insufficient to affect the hydrolysis.

3.2. Protonation of ciprofloxacin anion

Protonation constants, β_n, of ciprofloxacin anion, defined according to equilibrium:

$$n\mathrm{H}^+ + \mathrm{cipx}^- \rightleftharpoons \mathrm{H}_n\mathrm{cipx} \quad (n=1, 2)$$

were determined by glass electrode potentiometric titrations in 0.1 and 0.5 mol dm^{-3} $NaNO_3$ medium at 298 K. Three titrations were carried out with 0.5, 0.9 and 2.0 mmol dm^{-3} total ciprofloxacin concentrations, in the pH range 4.0–10.2. The experimental data were treated using the Superquad program. In total, 290 points were included in calculations. Spectrophotometric measurements were made on solutions in which the concentration of ciprofloxacin was the same (0.05 mmol dm^{-3}) while the pH values were varied between 4.0 and 9.4 (22 solutions were used). The spectra were taken in the 220–450 nm wavelength interval. Part of the obtained spectra is shown in Fig. 2. The spectra (Fig. 2a) show a high-intensity peak located at 270 nm and a broad lower energy band with two poorly resolved peaks at 320 and 340 nm. Isosbestic points exist at 345 nm and (very poorly defined) at 312 nm. For the purpose of Squad calculations the obtained spectra were digitized at every 3 nm. The calculated values of protonation constants are given in Table 2. Agreement between potentiometrically and spectrophotometrically obtained values was better than 1%.

3.2.1. Protonation of the ciprofloxacinate ion in the presence of surfactants

Protonation constants, β_n, of ciprofloxacin anion, in the presence of SDS or CTAB were determined under the same experimental conditions as in their absence. The concentration of surfactants used was 10.0 mmol dm^{-3} of SDS and 8.0 mmol dm^{-3} of CTAB, while the concentration range of ciprofloxacin was 0.5–2.0 mmol dm^{-3}. The experimental data were treated with the aid of Magec and Superquad programs. In total 180 points were included in the calculations. The results are given in Table 2. As can be seen from Table 2, protonation constants of the ciprofloxacin anion are considerably higher in the presence of SDS than in the pure ionic medium. The second protonation constant was particularly affected. It seems that the addition of SDS suppresses the dissociation of ciprofloxacin (3-carboxyl group). An explanation can be given on the basis of structural characteristics

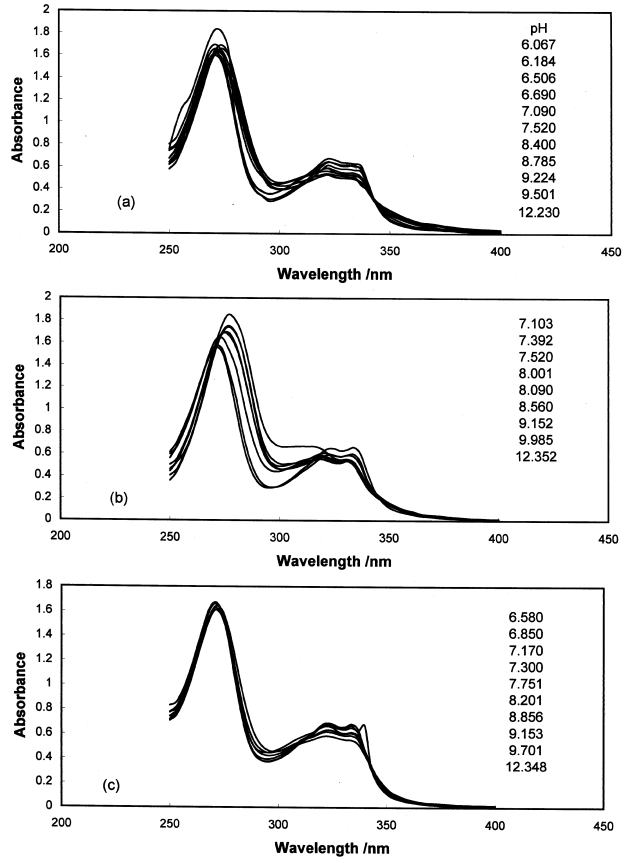


Fig. 2. Spectra of 0.05 mmol dm^{-3} solutions of ciprofloxacin. (a) No addition of surfactants, (b) +10.0 mmol dm^{-3} SDS, (c) +8.0 mmol dm^{-3} CTAB. The pH values run from top to bottom, relating to the peak at 270 nm.

of ciprofloxacin. It contains two highly polar groups (4-carbonyl and 3-carboxyl). In addition, the positively charged tertiary piperazinyl nitrogen in the ciprofloxacin cation constitutes another polar site in the molecule. These groups cause an electrostatic attraction with the SDS molecule, thus expelling water molecules around the cation and hence impeding proton transfer from cation to bulk water. Splitting off the first proton (from the 3-carboxyl group) is hindered because the hydrogen bond between the carboxyl proton and the 4-carbonyl oxygen is stabilized in the presence of SDS. On the other hand, the ciprofloxacin cation, H_2cipx^+, is additionally stabilized by electrostatic interactions with the negatively charged OSO_3^- group from SDS. CTAB exhibits a much lower effect on protonation constants due to its inefficient surrounding of the carboxylate group.

The spectrophotometric measurements in the presence of 10 mmol dm^{-3} SDS or 8 mmol dm^{-3} CTAB were made under the same experimental conditions as in their absence. Part of the spectra is shown in Fig. 2. It can be seen from Fig. 2b that the maximum of the higher energy band is shifted by approximately 10 nm towards the red, while the lower-energy band shows a blue shift with two peaks located at 315 and 320 nm, in comparison with the spectra obtained in the absence of SDS. CTAB (Fig. 2c) causes only a small red

shift of the lower-energy band. Since both low- and higher-energy bands arise from $n \rightarrow \pi^*$ and $\pi \rightarrow \pi^*$ transitions in the quinolone nucleus, the observed shifts could be explained by taking into account the change of solvation of the ciprofloxacin molecule in the presence of SDS, due to its solvatophobic effect. Both electronic transitions are very sensitive to variation of solvation and this explains the change in their energies in the absence and in the presence of SDS. The evaluation of the spectral data was done with the aid of the Squad program. The results are given in Table 2. They are in satisfactory agreement with the potentiometric results.

3.3. The iron(III)–ciprofloxacin system

3.3.1. Potentiometric measurements

The experimental data obtained by e.m.f. measurements in 0.1 and 0.5 mol dm^{-3} $NaNO_3$ medium at 298 K are summarized in Table 3. In the pH range studied (2.0–6.0) the maximum apparent ligand number reached Z_c, which is defined as:

$$Z_c = \frac{C_{cipx} - \frac{[cipx^-] - [H^+] + [OH^-]}{Z_H}}{C_{Fe}}$$

where C_X denotes analytical concentration of the corresponding species, and Z_H is the proton number of ciprofloxacin. The highest concentration ratio of ciprofloxacin to Fe^{III} was 10:1. Beyond pH $\sim$5.8, solutions became turbid and drifting potential readings were obtained. No higher concentration ratios of ciprofloxacin to Fe^{III} were used because they would seriously change the constancy of the medium and, in addition, the buffering effect of ciprofloxacin would hinder the reliable potentiometric measurements.

Analysis of the formation curves, plotted as the dependence of average ligand number, Z_c, on $-\log[cipx]$, indicates the formation of mononuclear complexes only. From the maximal Z_c (ca. 1.8) values attained it can be seen that either the complex $Fe(cipx)_2$ or some mixed complexes may be important.

The equilibria in the cipx + Fe^{3+} system can be represented in a general form:

$$p(Fe^{3+}) + q(H^+) + r(cipx^-) \rightleftharpoons Fe_pH_q(cipx)_r$$

The stability constants of various (p,q,r) species formed in the above reaction can be defined as:

$$\beta_{p,q,r} = C_{p,q,r} m^{-p} h^{-q} a^{-r}$$

where $C_{p,q,r}$ denotes the equilibrium concentration of the complex, and m, h and a denote free concentrations of iron(III), proton and ciprofloxacin, respectively. Negative values of q represent hydroxo complexes. To determine the composition and stability constants of the species formed, the titration data were analysed using the programs Best and Superquad. The following complexes were selected to find the model which best fit the experimental data: (1, 0, 1), (1, 0, 2), (1, 1, 1), (1, 2, 1), (1, 1, 2), (1, −1, 1), (1, −2, 1), (1, −3, 1), (1, −1, 2), (1, −2, 2) and (1, −2, 3). More than 20 models were tested. During the calculations analytical parameters (M_0, H_0 and L_0) were held constant while E_0 values were allowed to float. The hydrolytic complexes and

Table 3
Summary of potentiometric data on complexation equilibria in iron(III) + ciprofloxacin solutions [a]

Run no.	M	H	L	SDS	CTAB	pH range	Z_{max}
0.5 mol dm^{-3} $NaNO_3$ ionic medium							
1	0.145	6.254	0.446			2.208–4.306	1.855
2	0.290	2.308	0.902			2.630–4.540	1.876
3	0.580	4.463	1.804			2.350–3.960	1.248
4	0.145	6.699	0.746			2.172–4.093	1.750
5	0.290	2.216	1.503			2.653–5.896	1.781
6	0.145	7.020	1.503			2.154–4.967	1.428
7	0.290	2.303	0.898			2.638–4.808	1.800
8	0.580	4.453	1.804	10.0		2.354–5.238	1.743
9	0.145	7.111	0.746	10.0		2.164–5.870	1.414
10	0.290	2.300	1.503	10.0		2.643–5.143	1.765
0.1 mol dm^{-3} $NaNO_3$ ionic medium							
11	0.290	2.521	0.902			2.609–4.740	1.347
12	0.484	3.801	1.508			2.423–4.450	1.011
13	0.580	4.680	1.809			2.336–4.490	1.075
14	0.290	2.521	0.902	10.0		2.600–4.630	1.397
15	0.484	3.734	1.508	10.0		2.430–4.760	0.927
16	0.580	4.718	1.809	10.0		2.330–4.660	1.112
17	0.290	2.415	0.902		8.0	2.633–4.527	1.111
18	0.484	3.681	1.508		8.0	2.436–4.501	0.895
19	0.580	4.781	1.809		8.0	2.330–4.490	1.135

[a] M, H, L, SDS and CTAB denote analytical concentrations of iron(III), hydrogen ion, ciprofloxacin, sodium dodecyl sulfate and cetyltrimethylammonium bromide in mmol dm^{-3}, respectively. Z_{max} is maximal value of average ligand number.

protonated species of ciprofloxacinate were not refined during the calculations. First, each titration curve was treated separately using the program Best. Complexes were added in the model one at a time until the lowest value of σ_{fit} was achieved (usually less than 0.003). These complexes were then used as the starting model for the Superquad calculations. The following complexes were included: (1, 0, 1), (1, 0, 2), (1, −1, 1). Then the data belonging to all titration curves, referred to one particular ciprofloxacin to iron concentration ratio, were treated together. The refined values of E_0 served as the additional criterion for model selection. If they differed from experimental values by more than 0.5 mV, the model was considered as inadequate. The results of calculations indicate that the main species in iron–ciprofloxacin solutions are the binary complexes $Fe(cipx)_2$ and Fe(cipx) as well as the mixed hydroxy complex Fe(OH)cipx. Calculated values of the stability constants are presented in Table 4. From the data presented in Tables 2 and 4 one may calculate the formation constant, K, of the Fe(cipx) complex taking Hcipx as the component instead of cipx. The obtained value, $\log K = \log \beta_{1,0,1} - \log \beta_{0,1,1} = 15.91 - 9.07 = 6.84$ is in a reasonably good agreement with literature data [9,10].

The distribution of various complexes in solution is shown in Fig. 3. As seen from the distribution diagram, the complex Fe(cipx) reaches its maximum concentration at pH ~2.5. Beyond this value it begin to hydrolyse, forming the mixed hydroxy complex Fe(OH)cipx. The concentration of the mixed complex increases upon further increasing the pH and reaches the maximum at pH ~4.3. Bis complex $Fe(cipx)_2$ starts to form at pH ~3.0 with a steep rise in concentration with increasing pH. The main complex between pH 2.0 and 3.0 is Fe(cipx) and, therefore, the colorimetric determination of ciprofloxacin using Fe^{III} as colouring agent should be carried out in this pH interval.

Table 4
Results of non-linear least-squares analysis of the data on complexation equilibria in iron(III)–ciprofloxacin solutions [a]

Species	S	S + SDS	S + CTAB	S′	S′ + SDS
Potentiometry					
$Fe(cipx)^{2+}$	15.91(7)	17.91(2)	15.89(2)	15.20(9)	17.25(9)
$Fe(cipx)_2^{+}$	26.55(8)	29.99(2)	26.25(9)	26.45(5)	29.15(2)
Fe(OH)cipx	11.76(9)	13.31(4)	11.19(3)	10.25(6)	12.22(1)
Spectrophotometry					
$Fe(cipx)^{2+}$	15.28(1)	17.14(4)	15.81(5)		
Fe(OH)cipx	11.87(3)	13.82(5)	11.04(2)		

[a] Stability constants of complexes are defined as $\beta_{p,q,r} = [Fe_pH_q(cipx)_r]/[Fe]^p[H^+]^q[cipx]^r$. Logarithms of stability constants are given together with standard deviations in parentheses. S, 0.1 mol dm^{-3} $NaNO_3$; S′, 0.5 mol dm^{-3} $NaNO_3$; SDS, 10 mmol dm^{-3} sodium dodecyl sulfate; CTAB, 8.0 mmol dm^{-3} cetyltrimethylammonium bromide.

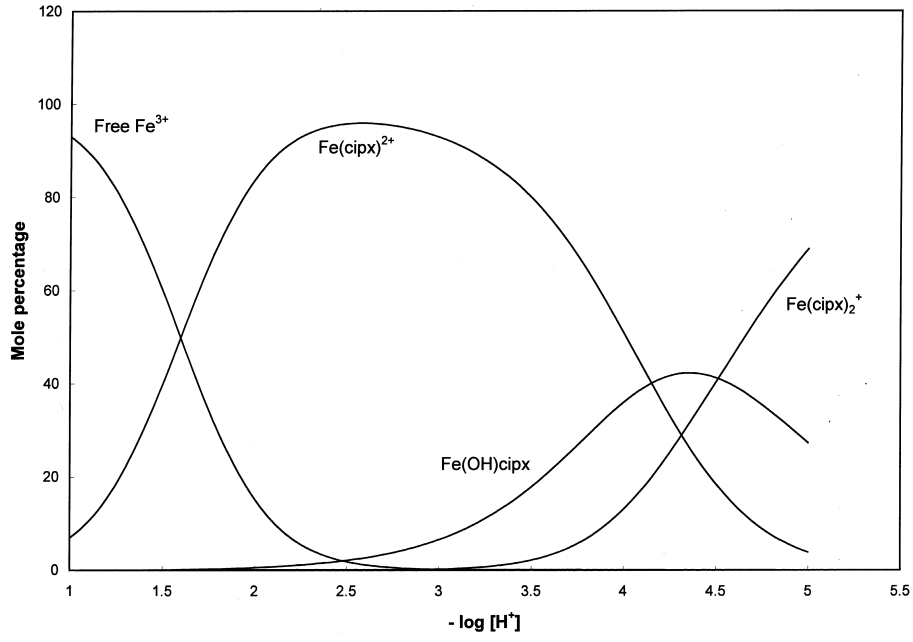


Fig. 3. The distribution of the complexes formed in iron(III) + ciprofloxacin solutions in 0.1 mol dm^{-3} $NaNO_3$ medium, at 298 K. $C_{Fe} = 1.0$ mmol dm^{-3}, $C_{cipx} = 3.0$ mmol dm^{-3}.

Bearing in mind the pH range in which the complex Fe(cipx) is formed, one may suppose that its formation proceeds according to reaction:

$$Fe(OH)_2^+ + H_2cipx^+ \rightleftharpoons Fe(cipx)^{2+} + 2H_2O$$

The isoelectric point of ciprofloxacin is at pH between 7.73 and 8.10 (depending on the ionic strength) so that, at pH values lower than 5.0, most ciprofloxacin exists in the cationic form. The reactive species of iron at pH 2.0–3.0 is the dihydroxo complex $Fe(OH)_2^{2+}$, so the above reaction would be more probable than that in which aqua-iron ion reacts with neutral ciprofloxacin:

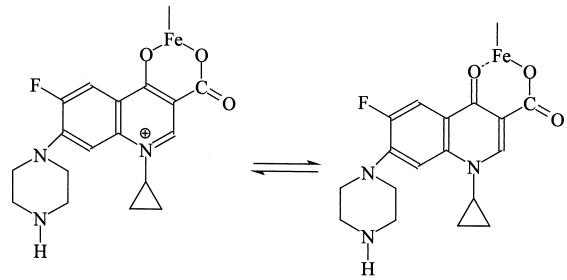
$$Fe^{3+} + Hcipx \rightleftharpoons Fe(cipx)^{2+} + H^+$$

The second molecule of ciprofloxacin may be directly bound to Fe(cipx), or it may react with the mixed hydrolytic complex to produce the bis complex:

$$Fe(OH)cipx + Hcipx \rightleftharpoons Fe(cipx)_2 + H_2O$$

It seems, judging by Fig. 3, that both reactions may take place simultaneously.

In the Fe(cipx) complex, 3-carboxyl and 4-carbonyl groups are involved in coordination owing to high affinity of iron toward oxygen. The IR spectrum of ciprofloxacin at 3600–3000 cm^{-1} shows two bands, one sharp at 3250 cm^{-1} belonging to OH group and a second at 3380 cm^{-1} characteristic of N–H vibration. In the 1800–1600 cm^{-1} wavenumber region, three bands are dominant: at 1710 cm^{-1} belonging to carboxyl group, 1625 cm^{-1} belonging to ketone carbonyl (involved in hydrogen bonding) and at 1610 cm^{-1} belonging to double-bond vibration. In the 3600–3000 cm^{-1} region the complex shows only one broad band, which covers the region and is indicative of the presence of a strong hydrogen bond. In the carbonyl region two bands are seen. The third band, at 1625 cm^{-1}, disappears, indicating that keto oxygen is involved in coordination. Thus, the binding sites for iron, in the ciprofloxacin molecule, involve keto and carbonyl oxygens. Two structural isomers are possible and we believe that an equilibrium between two forms exists. The equilibrium is, however, shifted to the right because of higher resonance stability of the structure in which the double carbonyl bond is not broken (see Scheme 1).



Scheme 1.

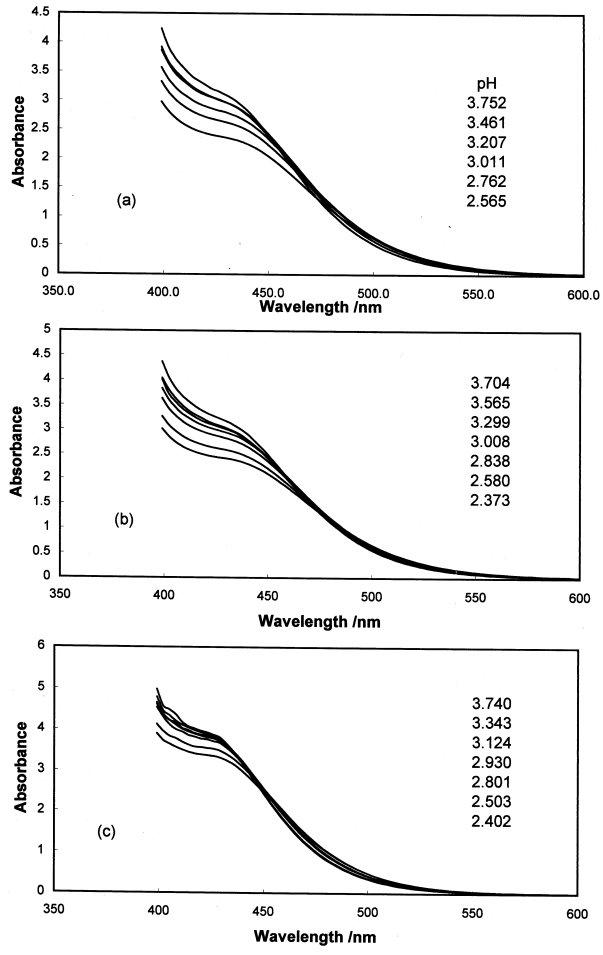


Fig. 4. Spectra of iron(III) + ciprofloxacin solutions. $C_{Fe} = 5.8 \times 10^{-4}$ mol dm^{-3}, $C_{cipx} = 1.5 \times 10^{-3}$ mol dm^{-3}. (a) No addition of surfactants, (b) + 8.0 mmol dm^{-3} CTAB, (c) + 10.0 mmol dm^{-3} SDS. The pH values run from top to bottom.

3.3.2. Spectrophotometric measurements

Spectral measurements were made on solutions in which the concentration of iron and ciprofloxacin were constant ($C_{Fe} = 5.80 \times 10^{-4}$ mol dm^{-3}, $C_{cipx} = 1.5 \times 10^{-3}$ mol dm^{-3}) while pH was varied between 2.0 and 4.0 (16 solutions). The pH of each test solution was checked daily, during 1 week. The stable values, within 0.01 pH and 0.004 absorbance units, were attained after 1 h and remained stable during a couple of days. Solutions with pH values higher than 4.5 required a longer time for equilibration, approximately 1 day. Spectra of the test solutions were recorded in the 350–600 nm wavelength interval. The experimentally obtained spectra are shown in Fig. 4. The spectra were not corrected for ciprofloxacin absorption. The spectra exhibit a high-intensity band between 360 and 390 nm. The plateau exists between 400 and 440 nm. The spectra are pH-dependent, so, upon increasing the pH, the absorbancy of the high-energy band and plateau increases.

The spectral data were evaluated with the aid of the Squad program. In calculations, the extinction coefficients of ciprofloxacinate ion, H(cipx) and H_2(cipx) were known from spectral measurements of ciprofloxacinate protonation and were fixed, while those of iron(III)–aqua ion were set to zero. To make the potentiometric and spectrophotometric measurements self-consistent, the calculations were carried

out in the following way. First, all the complexes found in appropriate potentiometric titrations were included in Squad calculations and their stability constants were fixed while the extinction coefficients were allowed to float. The Squad multiple regression option was used for these calculations. If negative values for extinction coefficients were obtained, the stability constants of the complexes were varied too, one at a time. Second, the complexes were added or excluded from the initial model also, one at a time. When the best possible fit was achieved (lowest *S* and SD values) the non-negative non-linear least-squares option of Squad was used in a final calculation cycle. With the obtained set of complexes and their stability constants, Superquad calculations of potentiometric titrations were repeated and statistical parameters of the fit re-determined. This cycling was repeated until the best possible agreement between potentiometric and spectrophotometric models was achieved. Results of the calculation are shown in Table 4. These results are in good agreement with potentiometric ones (Table 4).

3.3.3. The effect of surfactants on the complexation equilibria in the iron(III)–ciprofloxacin system

The experimental data obtained by e.m.f. measurements in 0.1 and 0.5 mol dm^{-3} $NaNO_3$ medium at 298 K are summarized in Table 3. In the pH range studied (3.0–5.0), the maximum apparent ligand number reached was ca. 1.7. The highest concentration ratio of ciprofloxacin to Fe^{III} was 5:1. Beyond pH 5.0, solutions became turbid and drifting potential readings were obtained. In the Fe^{III} + cipx system, with the addition of SDS, formation curves are shifted towards much higher pH values in comparison with those in the absence of SDS. This indicates higher stability of the complexes formed. The results of the mathematical analysis of titration data are presented in Table 4. It can be seen that the stability of all formed complexes is significantly increased in the presence of SDS while the effect of CTAB is very moderate. The distribution diagram (Fig. 5) of the complexes indicates that the pH interval in which the complex Fe(cipx) dominates is wider while at the same time its concentration is higher relative to the hydroxy complex Fe(OH)cipx. This is an obvious advantage for the determination of ciprofloxacin.

Higher stability of the Fe(cipx) complex in the presence of SDS may be explained on the basis of its structural characteristics.

As seen from the diagram (Scheme 2), one may suppose that the SDS chain is turned with its polar head towards the positively charged iron core. In this way, the planar structure of six-membered ring involving iron is enhanced. Hydrogen bond between oxygen from sulfonyl group of SDS and hydrogens from coordinated water makes the FeO_3 core stable and the long hydrocarbon chain surrounding this core hinders hydration of iron, thus preventing its hydrolysis.

Spectral measurements were made in the presence of SDS in the same way as in its absence. However, the pH region was restricted in such a way that formation of the Fe(cipx) complex would be dominant. The obtained spectra are shown in Fig. 4. It can be observed that, in the presence of SDS, the plateau is shorter and slightly shifted toward the blue. Results of Squad calculations of the spectra are presented in Table 4. The calculated stability constants are in satisfactorily good agreement with potentiometric data.

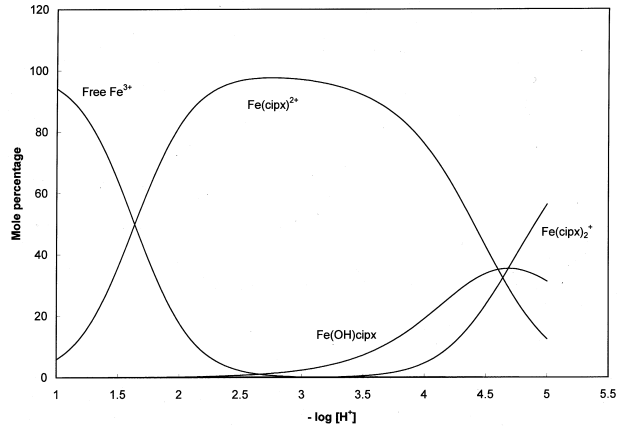
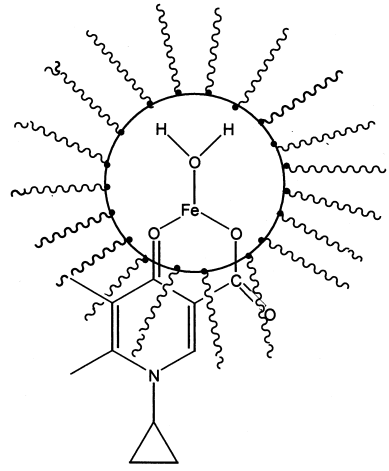


Fig. 5. The distribution of the complexes formed in iron(III) + ciprofloxacin + 10.0 mmol dm^{-3} SDS. $C_{Fe} = 1.0$ mmol dm^{-3}, $C_{cipx} = 3.0$ mmol dm^{-3}.



Scheme 2.

Consideration of the results obtained in the present work leads to the conclusion that the optimal conditions for consecutive simple complex formation in the iron(III) + ciprofloxacin system comprise relatively wide concentration ratios of ciprofloxacin to iron, ranging from 1:1 to 10:1 in the pH interval 2.0–5.0. Under these conditions, the maximum ligand number attained is 2 and, since ciprofloxacin acts as bidentate ligand, two other coordination sites are filled with water molecules.

References

[1] Ciprofloxacin. Proceedings of a Workshop held at the 14th International Congress of Chemotherapy, Kyoto, Japan, 23–28 June 1985, Sieber and McIntyre IncHong Kong, 1985.
[2] A. Aughot, H.C. Neu, Ciprofloxacin, Clinical Monograph, ADIS Press, Manchester, 1988.

[3] Ciproxin, Bayer Health Care EP, Leverkusen, Germany, 1986.
[4] R.E. Folk, D.P. Healy, J.V. Sahai, L. Drwal, E. Pracht, Antimicrob. Agents Chemother. 11 (1841) 1989.
[5] M. Kara, B.B. Hasinoff, D.W. McKay, N.R.C. Campbell, Br. J. Clin. Pharmacol. 31 (1991) 275.
[6] H. Lode, Rev. Infect. Dis. 10 (1988) 5132.
[7] K.M. Deppermann, H. Lode, Drugs 45 (Suppl. 3) (1993) 65.
[8] S.M. Sultan, E.O.F. Suliman, Analyst 117 (1992) 1523.
[9] E.O.F. Suliman, S.M. Sultan, Talanta 43 (1996) 559.
[10] D.S. Lee, H.J. Han, K. Kim, W.B. Park, J.K. Cho, J.H. Kim, J. Pharm. Biomed. Anal. 12 (1994) 157.
[11] I. Turel, N. Bukovec, E. Farkas, Polyhedron 15 (1996) 269.
[12] L. Fratini, E.E.S. Schapoval, Int. J. Pharm. 127 (1996) 279.
[13] F. Marsicano, C. Monberg, B.C. Marticingh, K. Murray, P.M. May, D.R. Williams, J. Coord. Chem. 16 (1988) 321.
[14] P. Gans, A. Sabatini, A. Vacca, J. Chem. Soc., Dalton Trans. (1985) 1195.
[15] A.E. Martell, R.J. Motekaitis, Determination and Use of Stability Constants, VCH, Weinheim, 1988.
[16] D.J. Leggett, Computational Methods for the Determination of Formation Constants, Plenum, New York, 1985, p. 159.
[17] R.N. Sylva, Pure Appl. Chem. 22 (1972) 115.
[18] C.F. Baes, R.E. Mesmer Jr., The Hydrolysis of Cations, Wiley, New York, 1976.
[19] C.M. Flynn, Chem. Rev. 84 (1984) 31.
[20] M.A. Blesa, E. Matijevic, Adv. Colloid Interface Sci. 29 (1989) 173.
[21] R.B. Martin, J. Inorg. Biochem. 44 (1991) 141.
[22] P.R. Danesi, R. Chiarizia, G. Scibona, R. Ricardi, Inorg. Chem. 12 (1973) 2089.
[23] G.N. Gontscharov, A.A. Efimov, A.V. Kalyamin, S.B. Tomilov, Zh. Obshch. Khim. 48 (1978) 2398.
[24] G.H. Khoe, P.L. Brown, R.N. Sylva, R.G. Robins, J. Chem. Soc., Dalton Trans. (1986) 1901.
[25] G.H. Khoe, R.G. Robins, J. Chem. Soc., Dalton Trans. (1988) 2015.
[26] V.N. Zabrodskii, N.E. Prokshin, V.V. Toropova, Zh. Neorg. Khim. 35 (1990) 1428.
[27] P. Djurdjevic, Transition Metal Chem. 15 (1990) 345.
[28] L.D. Pettit, University of Leeds, personal communication, 1988.

PERGAMON

www.elsevier.nl/locate/poly

Polyhedron 19 (2000) 1097–1103

POLYHEDRON

γ-Halogenated iridium(III) acetylacetonates

V.G. Isakova, I.A. Baidina, N.B. Morozova *, I.K. Igumenov

Institute of Inorganic Chemistry, Novosibirsk, Russia

Received 20 October 1999; accepted 3 February 2000

Abstract

γ-Halogenated iridium(III) acetylacetonates of the general formula $Ir(acacX)_n(acac)_{3-n}$ (where acacX is CH_3–CO–CX–CO–CH_3, acac is CH_3–CO–CH–CO–CH_3, $n = 1,2,3$, X = F, Cl, Br, I) have been synthesized, purified and characterized. Spectroscopic and thermogravimetric studies have been carried out, as well as study of the relative volatility and thermal stability of the complexes. For a series of compounds, X-ray diffraction studies have been conducted and crystallographic characteristics have been obtained. The structures of $Ir(acac)_3$, $Ir(acacCl)_3$, $Ir(acacBr)_3$, and $Ir(acacI)_3$ complexes have been determined. ©2000 Elsevier Science Ltd All rights reserved.

Keywords: Iridium; Acetylacetonates; Halogenation

1. Introduction

One of the main questions considered in works dealing with volatile β-diketonate complexes of platinum metals is the dependence of the properties of these compounds on the structure of the chelating ligand [1,2]. The volatile β-diketonates of trivalent metals forming a sequence by consequent substitution of methyl groups in the initial acetylacetonate ligand by $–CF_3$ and $–C(CH_3)_3$ groups have now been studied in detail. The synthesis of γ-halogenated acetylacetonates of inert metals has also been described. The synthesis is based on their characteristic reaction, i.e. electrophilic substitution of methine hydrogen atoms in the acetylacetonate ring, and does not require much effort. Compounds of this type with a wide range of γ-substituents (X = Cl, Br, I, NO_2, SCN, etc.) and different numbers of substituted ligands have been obtained by Collman and coworkers and others for Co(III), Cr(III), Rh(III), and Fe(III) [3–9]. In the sequence of iridium trichelates, the complexes containing substituents in the α-position are the best studied [10–14]. Compounds of iridium containing substituents in the γ-position of the acetylacetonate ligand (like $Ir(CH_3–CO–CX–CO–CH_3)_3$ where X is a substituent) are not well known. The absence of any interest in γ-substituted iridium(III) acetylacetonates is likely to be connected with the generally accepted opinion concerning the poor volatility of these chelates. According to the limited known data, any substitution of γ-hydrogen atoms in metal acetylacetonates causes a decrease in thermal stability [16]. However, one can assume that the thermal stability of iridium γ-substituted acetylacetonates could be relatively high, similar to the higher thermal stability of the initial $Ir(acac)_3$ in comparison with the corresponding complexes of other metals [10,11,13]. In addition, the volatility of $Ir(acac)_3$ is higher than that of $Rh(acac)_3$. This means that in the sequence of Co(III)–Rh(III)–Ir(III) acetylacetonates [10], the monotonic decrease in volatility is disturbed, although this decrease is observed for the corresponding fluorinated β-diketonates, as well as for the β-diketonates of light metals. It should also be noted that, unlike acetylacetonates of trivalent metals that are well studied from the point of view of crystal chemistry [15], structural data on γ-substituted tris-complexes are absent from the literature. Taking this into account, we believe it would be interesting to study the thermal properties and determine the crystal structures of γ-substituted iridium(III) acetylacetonates.

In the present work we have synthesized for the first time γ-halogenated iridium(III) acetylacetonates described by the general formula $Ir(acacX)_n(acac)_{3-n}$, where acacX = CH_3–CO–CX–CO–CH_3, acac = CH_3–CO–CH–CO–CH_3, $n = 1,2,3$, X = F, Cl, Br, I. These complexes were studied by IR and Raman spectroscopy, thermogravimetry and differential thermal analysis; structural data for individual compounds were obtained.

* Corresponding author. Tel.: +738-32-344-556; fax: +738-32-344-489; e-mail: mor@che.nsk.su

0277-5387/00/$ - see front matter ©2000 Elsevier Science Ltd All rights reserved.
PII S0277-5387(00)00358-2

2. Experimental

2.1. The synthesis of γ-halogenated iridium(III) acetylacetonates

γ-Chlorinated iridium(III) acetylacetonates were obtained by the following procedure. 250 mg of powdered $Ir(acac)_3$ were wetted with 5 ml of hydrochloric acid (1:1), then 5 ml of 30% hydrogen peroxide were added under weak heating (60°C) and mixing. After 10–15 min the precipitate became green. 5–10 min later the precipitate was separated by filtering or the mixture was dissolved in benzene, and the organic phase was separated from the inorganic phase.

γ-Bromine and iodine-substituted iridium(III) acetylacetonates were synthesized in a similar way using a 25% solution of HBr and HI.

γ-Fluorinated iridium(III) acetylacetonates were obtained by dissolving $Ir(acac)_3$ (200 mg) and XeF_2 (150 mg) in acetonitrile (a minimum amount). Then the solutions were mixed together and kept at room temperature for about 4 h. Then water was added (5 ml) in order to decompose the excess of XeF_2. The γ-fluorinated acetylacetonates formed were extracted with benzene.

The products obtained during the synthesis were isolated by chromatography on a column filled with Al_2O_3. A mixture of hexane with benzene was used as an eluent, the initial proportion being 3:1; during elution, the proportion was changed to 1:1 and then 1:3. For fluorinated compounds, the benzene concentration was increased further to pure benzene.

In all cases, the chromatograms exhibit four regions. The complexes $Ir(acacX)_3$ are the first to be eluted. The second region is represented by doubly substituted acetylacetonates and the third region contains monosubstituted iridium(III) acetylacetonates. The fourth region is small, as a rule; it is eluted with benzene and contains $Ir(acac)_3$. The elemental analysis of obtained compounds is presented in Table 1.

2.2. Devices and equipment

IR spectra were recorded with a Specord 75-IR spectrometer and Fourier spectrometer Bruker IFS-113 (200–700 cm^{-1}) in KBr tablets. Raman spectra were recorded with a DFS-24 apparatus with excitation wavelengths of the lines of He–Ne ($\lambda = 6328$ Å) and Ar ($\lambda = 4880$ Å) lasers. Thermal curves were recorded with a Q-1000 type derivatograph in He flow in open ceramic crucibles. The mass of weighed portions was 200 mg. Helium was fed into the working chamber of the derivatograph at a constant rate which was 120 ml min^{-1}. The temperature was measured at an accuracy of ± 10°C. The heating rate was 5°C min^{-1}.

2.3. X-ray diffraction patterns: crystal structure determination

For the X-ray diffraction study, crystals of $Ir(acacBr)_3$ and $Ir(acacI)_3$ were grown from solutions of the complexes in acetone. The $Ir(acacCl)_3$ crystals were grown by sublimation in a vacuum gradient furnace at a pressure of 5×10^{-2} Torr and hot zone temperature of 160°C. The crystals of $Ir(acac)_3$ were grown from acetone solution and by sublimation (vacuum gradient furnace, pressure 5×10^{-2} Torr, hot zone temperature 150°C). The crystals were orange or yellow plates. They are fairly stable in air.

A complete X-ray diffraction investigation was carried out for the complexes $Ir(acac)_3$, $Ir(acacCl)_3$, and $Ir(acacI)_3$. For $Ir(acacF)(acac)_2$, because of the poor quality of the crystals, only the elementary cell parameters were determined.

The elementary cell parameters were determined more precisely and a set of experimental intensities was obtained for the purpose of deciphering the structures with the help of a CAD-4 diffractometer (Mo Kα radiation, graphite monochromator, $\omega/2\theta$ scanning). The structures were calculated according to a standard heavy atom procedure and corrected within the anisotropic approximation; for $Ir(acacCl)_3$ the structure was corrected in anisotropic–isotropic approximation.

Table 1
Elemental analysis of the compounds

Compound	Yield (%)	Calculated (%)			Found (%)		
		C	H	Hal	C	H	Hal
$Ir(acacCl)_3$	46	30.4	3.0	18.0	31.1	3.6	17.8
$Ir(acacCl)_2(acac)$	25	32.3	3.4	12.7	33.0	3.5	12.4
$Ir(acacCl)(acac)_2$	14	34.4	3.8	6.8	35.0	3.9	6.8
$Ir(acacBr)_3$	55	24.8	2.5	33.1	25.3	2.5	32.6
$Ir(acacBr)_2(acac)$	10	27.8	2.9	24.7	27.3	2.8	25.0
$Ir(acacBr)(acac)_2$	16	31.7	3.5	14.1	32.6	3.9	14.3
$Ir(acacI)_3$	20	20.8	2.1	43.9	20.7	2.5	42.8
$Ir(acacI)_2(acac)$	31	24.3	2.6	34.3	25.0	2.8	34.8
$Ir(acacI)(acac)_2$	44	29.3	3.3	20.7	30.1	3.4	21.4
$Ir(acacF)_3$	<2	33.1	3.3	10.5	29.7	3.4	9.8
$Ir(acacF)_2(acac)$	18	34.3	3.6	7.2	34.1	3.4	6.5
$Ir(acacF)(acac)_2$	30	35.5	3.9	3.7	30.1	3.4	21.4

The major crystallographic characteristics of the studied compounds are presented in Table 2.

3. Results and discussion

3.1. Synthesis

The synthesis of γ-halogenated iridium(III) acetylacetonates made use of the characteristic features of the chemical behaviour of iridium tris-acetylacetonate, mainly its inertness towards abstraction of the coordinated ligands. Even when boiled in concentrated solutions of hydrogen halides $Ir(acac)_3$ remains practically unchanged. The addition of hydrogen peroxide helps to dissolve the chelate, but under soft conditions we observe halogenation of the methine groups in acetylacetonate ligands without any noticeable transformation of $Ir(acac)_3$ into soluble forms. We succeeded in selecting the conditions under which $Ir(acac)_3$ is transformed practically quantitatively into γ-substituted acetylacetonates (X = Cl, Br, I), although quantitative formation of the $Ir(acacX)_3$ form seems impossible in this case because mono- and disubstituted iridium(III) acetylacetonates are likely to be formed together with the first species. Attempts to increase the synthesis temperature or the time of synthesis led to oxidation of the central ion and to the formation of soluble iridium(IV) complexes.

We did not observe fluorination of $Ir(acac)_3$ in the mixture of hydrofluoric acid and hydrogen peroxide. This confirms the electrophilic character of interaction in the systems $Ir(acac)_3$–HX–H_2O_2 which is characteristic of the acetylacetonates of inert metals [5]. Halogenation can occur with the help of free haloids evolved at the first stage of the process.

Iridium acetylacetonate was fluorinated using XeF_2. It should be noted that $Ir(acacF)(acac)_2$ was the prevailing component of the mixture, and the yield of γ-fluorinated iridium acetylacetonates was not high (owing to the preferable formation of oxidized forms of the complexes).

3.2. IR and Raman spectra

The frequencies of vibrations in the IR and Raman spectra of trisubstituted iridium(III) acetylacetonates are shown in Table 3.

The following features can be mentioned as characterizing the effect of γ-hydrogen atom substitution in the ligands by halogens: (1) in the spectra of trisubstituted acetylacetonates, the absence of the vibrations $\sigma(CH\gamma)$ at 774–792 cm^{-1} (IR), and $\sigma(CCH\gamma)$ at 1200 cm^{-1} (IR, Raman), and the very low intensity of $\nu(C–H\gamma)$ valent vibrations; (2) the appearance of additional lines corresponding to $\sigma(CCX)$ at 380–420 cm^{-1} (Raman), $\sigma(CX)$ at 455–507 cm^{-1} (Raman) and $\nu(C–X)$ at 1030–1048 cm^{-1}. The vibrations $\nu(C–X)$ are mixed with $\sigma(CH_3)$ since they are within the region of CH_3 deformations. In transfer from $Ir(acac)_3$ to mono-, di- and trisubstituted γ-halogenated acetylacetonates, the vibrational spectra exhibit a corresponding decrease in relative intensity of vibrational bands with participation of the C–X bond without any essential frequency shift accompanying the change of haloid atom.

3.3. Volatility and thermal stability

γ-Halogenated iridium(III) acetylacetonates sublime at reduced pressure (10^{-2} Torr) and a temperature of about 150°C, except for $Ir(acacBr)_3$ which decomposes under these conditions.

Differential thermal analysis was used to compare the volatility and thermal stability of the chelates under investigation. Thermogravimetric curves obtained during heating the

Table 2
Crystallographic characteristics of the chelates

Compound	*a* *b* *c* (Å)	*α* *β* *γ* (°)	*V* Space group *Z*	V_{mol} D_{cal}	F_{ave} *R*
$Ir(acac)_3$ (**I**)	13.900(2)		1693.3	423.3	2841
	16.440(3)		$P2_1/b$	1.92	0.044
	7.494(2)	98.63(2)	4		
$Ir(acacF)(acac)_2$	8.21		1772	443	
	13.00			1.9	
	16.6		4		
$Ir(acacCl)_3$ (**II**)	7.999(2)	107.52(1)	1909.1	477.3	4302
	15.156(2)	90.57(2)	$P\bar{1}$	2.06	0.08
	9.990(2)	95.81(2)	4		
$Ir(acacBr)_3$ (**III**)	12.794(2)		1937.6	484.4	1748
	15.753(3)	105.76(2)	$P2_1/n$	2.49	0.048
	9.990(2)		4		
$Ir(acacI)_3$ (**IV**)	12.855(2)		2059.8	515	2817
	10.136(2)	104.6(2)	$P2_1/n$	2.80	0.032
	16.338(3)		4		

Table 3
IR and Raman spectroscopy of γ-halogenated iridium(III) acetylacetonates

$Ir(acac)_3$		$Ir(acacF)_3$	$Ir(acacCl)_3$		$Ir(acacBr)_3$		$Ir(acacI)_3$		Attribution
Raman	IR	Raman	Raman	IR	Raman	IR	Raman	IR	
283w [a]	316w		310w	330w	294w	329w	283w	328w	σ(cycle) + $\sigma(CCH_3)$
325m [b]		319m	334m		331m		328s [c]		σ(CCX)
		381w			418m		385s		
439w	430m			460m		456m		450w	ν(MO) +
473m	462m	474m	469m		476m	468m	471m	465m	ν(CC) +
482s		486m	470m	482s	483m		479s		σ(cycle)
			507w		461w		455m		σ(CX)
562m	650s	562w	558w	640m	556w	637w	550m	634w	σ(cycle)
	657s			663s		667s	639w	668s	$\sigma(CCH_3)$
	665s	664w	667m	675s	673w				
	702w			712w	680w	680s	674m		ν(MO) +
707w		710w	730w		726w		676m		ν(CC) +
713w		741s	735s		732s			682s	σ(cycle)
							732s	735w	
	774s								σ(CHγ)
	777s								
	792s								
934m	930m	939m	941m	922s	938m	925s	929m	923s	ν(CC) + ν(CO)
	938m						958m		+ σ(cycle)
	1018m	1010m	993w	983s	1016w	975s		963s	
1013w		1034w	1005w	1015w		1015w	1018s	1017m	$\sigma(CH_3)$ +
			1044s	1035s	1018s	1024s	1030m	1030m	ν(CX)
			1048s		1037w				
	1195m	1151m							ν(CF)
1207w	1270s								σ(CCHγ)
	1280m	1281m	1290s	1280m	1287m	1274w	1270m	1262w	ν(CC) +
									σ(cycle) +
									ν(CX)
	1363w	1368w	1363m	1345s	1357m	1338s		1337s	ν(CH) +
1370m			1387m	1358s	1379m	1357m	1369m		σ(cycle)
	1380s			1382m		1365m		1357m	
						1375m		1373m	
1406w	1420w	1424w	1416w	1418w	1408w	1415m	1405w	1417m	$\sigma(CH_3)$
	1440w			1450m	1410w	1450m		1445m	ν(CO) + ν(CC)
1518w	1544s		1457w	1545s	1452w	1530s		1522s	+ $\sigma(CH_3)$
1552w	1543s		1550w		1533w		1518w		
1576w	1558w	1584w	1563w		1548w		1531w		

[a] Weak.
[b] Medium.
[c] Strong.

complexes in He flow are shown in Figs. 1 and 2. A 100% mass loss during heating of the corresponding samples to 250°C (Fig. 1) is evidence of the high sublimation ability of practically all the chelates containing F and Cl substituents in the γ-position. Aside from these complexes, only $Ir(acacI)_3$ sublimates without decomposition under the mentioned conditions (Fig. 1, curve 2). Analysis of the sublimation curves (Figs. 1 and 2) and the 50% mass loss temperatures of the compounds under consideration (Table 4) suggest that there is an insignificant difference in their volatility, although both the configuration and the nature of the substituent have a definite effect on the changes of this characteristic. For the set of Cl-substituted complexes as an example, we can see that the highest volatility is exhibited by the monosubstituted compounds and the poorest volatility by disubstituted complexes. A similar order of volatility change is observed for the sublimation of other compounds in the temperature gradient furnace. The complexes $Ir(acacCl)(acac)_2$, $Ir(acacF)(acac)_2$ and $Ir(acacI)_3$ are close in volatility. This means that $Ir(acacI)_3$ is to be more volatile than $Ir(acacCl)_3$ which is connected (as we show below) with the structural features of the complexes $Ir(acacCl)_3$ and $Ir(acacI)_3$. Superimposing sublimation and decomposition processes for other chelates (Fig. 2) and an insignificant difference in temperature intervals within the whole sequence of compounds under investigation do not allow us to outline in general the dependence of the volatility on the number and type of haloid substituents. However, there

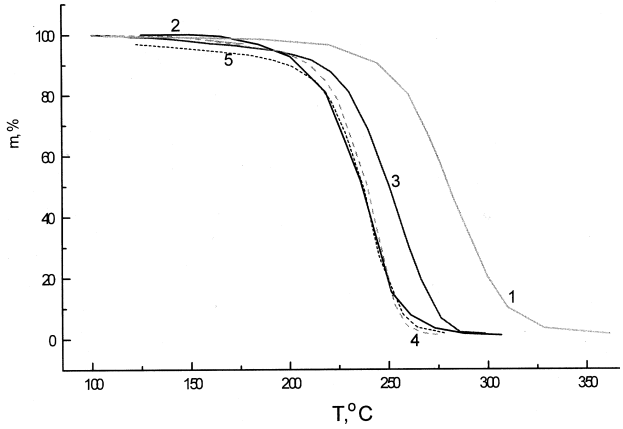


Fig. 1. Thermogravimetric curves of mass loss for $Ir(acac)_3$ (1), $Ir(acacI)_3$ (2), $Ir(acacCl)_3$ (3), $Ir(acacF)(acac)_2$ (4), $Ir(acacCl)(acac)_2$ (5).

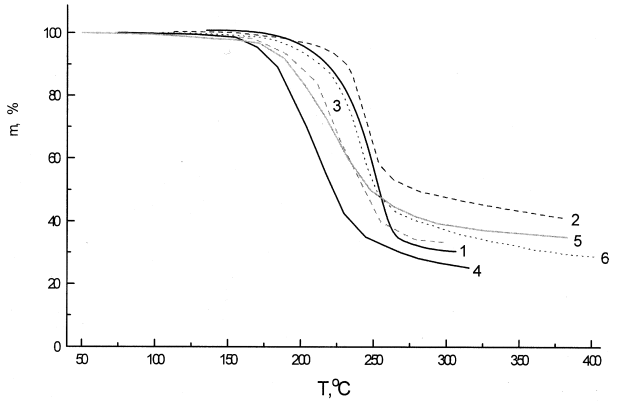


Fig. 2. Thermogravimetric curves of mass loss for $Ir(acacCl)_2(acac)$ (1), $Ir(acacI)_2(acac)$ (2), $Ir(acacI)(acac)_2$ (3), $Ir(acac)_3$ (4), $Ir(acacBr)(acac)_2$ (5), $Ir(acacBr)_3$ (6).

is no doubt that the volatility of γ-halogenated iridium(III) acetylacetonates increases, compared with the initial iridium(III) tris-acetylacetonate. The sublimation curve of the latter lies in the region of higher temperatures (Fig. 1, curve 1).

As far as thermostability is concerned, it decreases with respect to $Ir(acac)_3$ for the whole row of γ-halogenated iridium(III) acetylacetonates studied in the present work. Table 4 shows the decomposition points determined using the DTA curves. For the compounds that sublime completely under the above conditions, the temperatures were estimated under the same conditions but using tightly closed crucibles.

$Ir(acacBr)_3$ turned out to possess the poorest thermal stability, like the corresponding compounds of Co(III), Cr(III) and Rh(III) described in [3–5]. It decomposes at ~200°C. $Ir(acacI)_3$ exhibits the highest thermal stability among the I- and Br-substituted complexes. The thermal behaviour of Cl- and F-substituted iridium(III) acetylacetonates (except $Ir(acacF)_3$ which has not been investigated) resembles the behaviour of metal(III) tris-trifluoracetylacetonates. As a rule, the latter are less thermally stable in the condensed state than the corresponding acetylacetonates but possess higher volatility [12,13]. In the row of γ-halogenated iridium(III) acetylacetonates Cl- and F-substituted chelates possess the highest thermal stability.

3.4. Description of the structure

In the $Ir(acacCl)_3$ structure, two independent crystallographic iridium complexes are present. Figs. 3–6 show the packing of the complexes **I**, **II**, **III** and **IV** in the crystals.

In all the complexes, the central Ir atom has a slightly distorted octahedral coordination by six oxygen atoms belonging to three β-diketonate ligands.

The mean values of bond length Ir–O for the complexes **I**, **II**, **III** and **IV** are 2.02, 2.00, 1.99 and 2.00 Å, respectively, and the mean O–Ir–O chelate angles are 94.5, 93.7, 93.9 and 92.9°. This means that the bond lengths Ir–O and valent angles O–Ir–O in γ-halogenated iridium(III) acetylacetonates decrease, compared with $Ir(acac)_3$.

Bond lengths and valent angles of the chelate β-diketonate ligands are close to each other and agree with the literature data [15]. The mean distances Cγ–Hal in **II**, **III** and **IV** are 1.77, 1.93 and 2.12 Å, respectively. The mean angles C–Cγ–C with the methine carbon atom at the vertex are 128° with

Table 4
Thermal properties of γ-substituted iridium(III) acetylacetonates

Compound	Melting temperature (°C) (Kefler table)	Decomposition temperature (°C) (DTA, closed crucible)	*T*(50%) (°C) (DTA, open crucible)
$Ir(acac)_3$	268–270	350	310
$Ir(acacCl)(acac)_2$	253–255	280	240
$Ir(acacCl)_2(acac)$	258–259	275	265
$Ir(acacCl)_3$	278–279	290	250
$Ir(acacBr)(acac)_2$	235–236	240	
$Ir(acacBr)_2(acac)$	242–243	250	
$Ir(acacBr)_3$	dec. 200	200	
$Ir(acacI)(acac)_2$	247–248	255	
$Ir(acacI)_2(acac)$	238–240	245	
$Ir(acacI)_3$	257–260	270	245
$Ir(acacF)(acac)_2$	276–278	285	240
$Ir(acacF)_2(acac)$	265–266	275	250
$Ir(acacF)_3$		280	

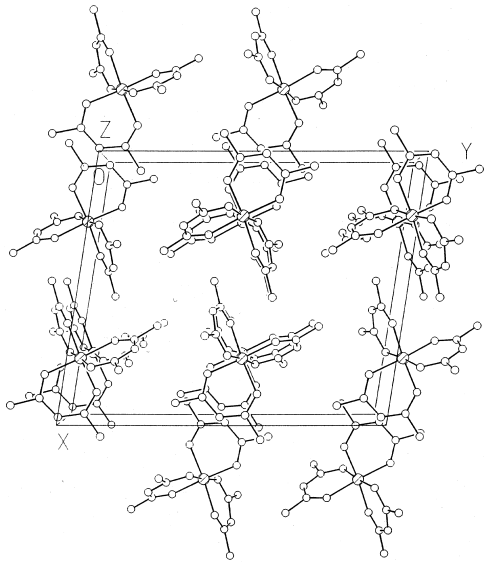


Fig. 3. Packing of $Ir(acac)_3$ complex in the crystal.

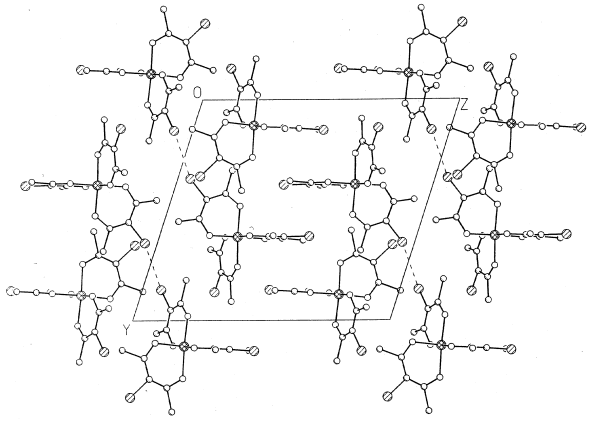


Fig. 4. Packing of $Ir(acacCl)_3$ complex in the crystal.

an accuracy of 1° in all the compounds. Chelate metal cycles in the complexes are not planar. The mean values of inflection angles of metal cycles along the O···O lines are 3° for pure iridium(III) acetylacetonate, and 4.2, 2.3, 3.2° for **II**, **III** and **IV**, respectively. In the crystals of the studied compounds, the complexes are connected by van der Waals interactions. Every iridium complex in the structures is surrounded by ten nearest neighbouring complexes. The distances between Ir atoms Ir···Ir can be estimated as >7.49 Å for **I**, 7.98–10.08 Å for **II**, and >8.10 Å for **III** and **IV**. It should be noted that compound II exhibits the shortest intermolecular contact Cl_2–Cl_4, this length being 3.26 Å. The crystal independent complexes Ir(I) and Ir(II) are connected with each other owing to this interaction in dimers. If we limit the estimate to 10 Å, intermolecular coordination numbers (ICN) of the studied structures are equal to 10.

4. Conclusions

Thus, we have synthesized and identified iridium(III) acetylacetonates and γ-halogenated Br-, I- and F-containing

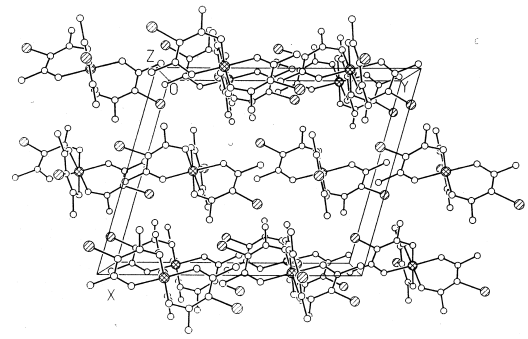


Fig. 5. Packing of $Ir(acacBr)_3$ complex in the crystal.

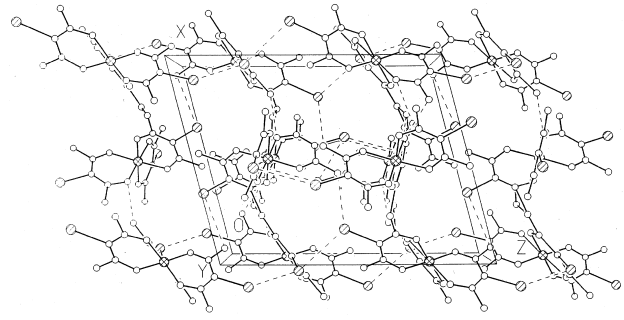


Fig. 6. Packing of $Ir(acacI)_3$ complex in the crystal.

compounds. We have investigated their spectroscopic and thermogravimetric properties. Crystal structures have been determined for a series of complexes. Monosubstituted complexes have been shown to be the most volatile and disubstituted complexes to be less volatile. The volatility of γ-halogenated iridium(III) acetylacetonates has been found to increase in comparison with the initial iridium(III) tris-acetylacetonate. The comparison with iridium(III) acetylacetonate has shown that the introduction of substituents into the γ-position does not have any substantial effect on crystallographic characteristics, except for the $Ir(acacCl)_3$ complex which is a dimer and because of this its volatility is lower than the volatility of the $Ir(acacI)_3$ complex (the complex $Ir(acacBr)_3$ decomposes during heating).

Supplementary data

Supplementary data are available from the Cambridge Crystallographic Data Centre, 12 Union Road, Cambridge CB2 1EZ, UK (fax: +44-1223-336033; e-mail: deposit@ccdc.cam.ac.uk) on request, quoting the deposition numbers 136097–136100.

Acknowledgements

The study has been financially supported by the Russian Foundation for Fundamental Investigations (Grant N 95-03-08703) and by the US Civilian Research and Development Foundation (CRDF, Grants N RE1-355 and RC1-512).

References

[1] K.C. Joshi, V.N. Pathak, Coord. Chem. Rev. 22 (1977) 37.
[2] J.P. Fackler, Prog. Inorg. Chem. 7 (1966) 362.
[3] J.P. Collman, R.A. Moss, H. Maltz, C.C. Heindel, J. Am. Chem. Soc. 83 (1961) 531.
[4] J.P. Collman, R.A. Moss, S.D. Goldby, W.S. Trahanovsky, Chem. Ind. 39 (1960) 1213.
[5] J.P. Collman, R.P. Blair, R.L. Marshall, L. Slade, Inorg. Chem. 2 (1963) 576.
[6] P.R. Singh, R. Sahai, Aust. J. Chem. 22 (1969) 1169.
[7] R.J. Balahura, A.J. Johnston, Inorg. Chem. 22 (1983) 3309.
[8] T.J. Cardwell, T.H. Lorman, Inorg. Chim. Acta 120 (1986) 5.
[9] S.C. Mahapatra, D.V.R. Rao, Indian J. Chem. A17 (1979) 522.
[10] V.G. Isakova, I.K. Igumenov, S.V. Zemskov, Koord. Khim. 11 (1985) 1377 (in Russian).
[11] V.G. Isakova, P.P. Semyannikov, V.M. Grankin, I.K. Igumenov, Koord. Khim. 14 (1988) 57 (in Russian).
[12] I.K. Igumenov, Yu.V. Chumachenko, V.G. Isakova, S.V. Zemskov, Zh. Fiz. Khim. 53 (1979) 1612 (in Russian).
[13] S.V. Zemskov, I.K. Igumenov, Yu.V. Chumachenko, V.G. Isakova, V.E. Durasov, Abstracts XIII All-Union Meet. on the Chemistry of Complex Compounds, Moscow, 1978, p. 159 (in Russian).
[14] M.A. Bennett, T.R.B. Mitchel, Inorg. Chem. 15 (1976) 2936.
[15] L.M. Shkol'nikova, M.A. Poray-Koshits, Itogi Nauki Tekh. Ser. Kristallokhim. 16 (1982) 117 (in Russian).
[16] S.J. Bett, G. Fletcher, J.L. Garnett, Radiat. Phys. Chem. 28 (1986) 207.

PERGAMON

www.elsevier.nl/locate/poly

Polyhedron 19 (2000) 1105–1110

POLYHEDRON

Weaker magnetic interactions of oxalato-copper(II) binuclear compounds: synthesis, spectroscopy, crystal structure and magnetism

Lei Zhang [a], Wei-Ming Bu [b], Shi-Ping Yan [a,*], Zong-Hui Jiang [a], Dai-Zheng Liao [a], Geng-Lin Wang [a]

[a] *Department of Chemistry, Nankai University, Tianjin 300071, China*
[b] *Laboratory of Supramolecular Spectroscopy, Jilin University, Changchun 130023, China*

Received 4 January 2000; accepted 8 March 2000

Abstract

Two binuclear copper(II) compounds, $Cu_2(tacn)_2(\mu\text{-ox})(ClO_4)_2$ (**I**) and $[Cu_2(bdpm)_2(H_2O)_2(\mu\text{-ox})](ClO_4)_2\cdot H_2O$ (**II**), where tacn = 1,4,7-triazacyclononane, ox = oxalate dianion, bdpm = bis(3,5-dimethylpyrazol-1-yl)methane, have been synthesized and characterized by X-ray diffraction. Each copper atom of compound **I** has a 4 + 1 + 1 elongated pseudo-octahedral environment; the copper atoms have distorted square pyramidal geometry in compound **II**. The magnetic susceptibilities (300–4 K) indicated that the binuclear copper(II) cores were antiferromagnetically coupled ($2J = -41$ cm^{-1} for compound **I**, $2J = -102$ cm^{-1} for compound **II**). The weakness of the interactions for both compounds is discussed on the basis of the structural features. ©2000 Elsevier Science Ltd All rights reserved.

Keywords: Crystal structures; Binuclear copper compounds; Magnetism; Oxalato-bridged compounds

1. Introduction

In the past decades, there has been many studies on the synthesis and magnetic coupling of metal atoms with polyatomic bridging ligands [1,2]. The oxalate dianion ($C_2O_4^{2-}$) is well known to function as a bridge ligand, and its bi-, tri-, tetranuclear, 1D, 2D and 3D network compounds have been prepared and characterized [3–22], of which some ferromagnetic interaction compounds between metal centres, particularly ferromagnets or ferrimagnets with T_c in the range of 0–50 K, have been obtained [12,13,23,24].

The simple binuclear copper(II) compounds involving a single symmetric, in-plane oxalate ion binding through two oxygen atoms to each of two metal centres have played a crucial role in the field of theoretical magnetic analysis [25–27]. Kahn and co-workers have described a theory to predict that the magnetic interactions in oxalato-bridged bicopper(II) compounds are responsible for the orientation of the magnetic orbital, sensitive to the geometry of copper. When the magnetic orbital of each copper(II) is placed on the ox plane, the absolute J value becomes the largest, resulting from the strong overlap of the magnetic orbital and the b_{2u} or b_{1g} (ox) orbital, which favours the antiferromagnetic interaction. Otherwise, the interaction becomes weak. The theory has been applied to rationalize the magnetic interactions observed for oxalate-bridged copper(II) compounds.

μ-Oxalato-dicopper(II) compounds of varying structural complexity through pronounced Jahn–Teller distortion are known. Great difficulties are faced to establish the correlation between the magnitude of the magnetic coupling and the structural factor. To address this issue, two compounds, $Cu_2(tacn)_2(\mu\text{-ox})(ClO_4)_2$ (**I**) and $[Cu_2(bdpm)_2(H_2O)_2(\mu\text{-ox})](ClO_4)_2\cdot H_2O$ (**II**) (tacn = 1,4,7-triazacyclononane, ox = oxalate dianion, bdpm = bis(3,5-dimethylpyrazol-1-yl)methane), have been prepared and characterized. Striking results have found that the structure of compound **I** possesses pseudo-octahedral coordination geometry, different from the earlier suggestion by Chaudhuri and Oder [28], and weaker antiferromagnetic interactions were observed for the two compounds. The results of the study on magneto-structural correlation for both compounds are presented and discussed in this context. The crystal structure of compound **I** has been briefly described in a preliminary communication [29].

* Corresponding author. Tel.: +86-22-23509957; fax: +86-22-23502458; e-mail: lzhang@nankai.edu.cn

0277-5387/00/$ - see front matter ©2000 Elsevier Science Ltd All rights reserved.
PII S0277-5387(00)00359-4

2. Experimental

2.1. Materials and methods

1,4,7-Triazacyclononane (tacn) and bis(3,5-dimethylpyrazol-1-yl)methane (bdpm) were prepared as described in Refs. [30,31]. All other chemicals were of reagent grade and used as received.

Analyses for C, H and N were obtained using a Model 240 Perkin-Elmer analyser at the Institute of Elemental Organic Chemistry, Nankai University. The IR spectra were recorded on an FTIR-1600 spectrophotometer in KBr discs. X-band powder EPR spectra were recorded on a Bruker ER 220 D-SRC ESR spectrometer. Variable-temperature magnetic susceptibilities were measured on a Model CF-1 vibrating sample magnetometer. Diamagnetic corrections were made with Pascal's constants for all the constituent atoms and the magnetic moments were calculated using the equation $\mu_{eff} = 2.828(\chi_M T)^{1/2}$.

2.2. Synthesis of the compounds

2.2.1. $Cu_2(tacn)_2(\mu\text{-}ox)(ClO_4)_2$ (*I*)

The blue compound was prepared according to Refs. [28,29]. The crude product was recrystallized from methanol twice. In the final stage, refrigeration allowed slow formation of crystals suitable for X-ray diffraction studied. The compound analysed satisfactorily for $Cu_2(tacn)_2(\mu\text{-}ox)(ClO_4)_2$. Yield, 43%. *Anal*. Calc. for $C_{14}H_{30}Cl_2Cu_2N_6O_{12}$: C, 25.0; H, 4.5; N, 12.5. Found: C, 24.8; H, 4.7; N, 12.2%.

2.2.2. $[Cu_2(bdpm)_2(H_2O)_2(\mu\text{-}ox)](ClO_4)_2 \cdot H_2O$ (*II*)

The preparation of compound **II** was similar to that for compound **I** with the exception that ligand, bdpm, was used in place of tacn. The compound crystallized as dark blue. Yield: 75%. *Anal*. Calc. for $C_{24}H_{38}Cl_2Cu_2N_8O_{15}$: C, 32.9; H, 4.4; N, 12.8. Found: C, 33.2; H, 4.7; N, 12.5%.

Caution! Although the perchlorate salts described in this work do not appear to be sensitive to shock, these materials, like all perchlorate salts, should only be prepared in small quantities and treated with caution.

2.3. X-ray crystallography

Crystals of dimensions $0.10 \times 0.16 \times 0.18$ mm for compound **I** and $0.08 \times 0.32 \times 0.38$ mm for compound **II** were mounted on a Siemens P4 diffractometer with graphite-monochromatized Mo Kα radiation ($\lambda = 0.71073$ Å) and used for data collection. Diffraction data were collected using ω–2θ scans at room temperature (293 K) over the range $1.8 \le \theta \le 25.0°$ for both compounds. The data for both compounds were processed using the Siemens SHELXTL crystallographic package (Version 5) [32]. Data were corrected for Lorentz polarization effects and semi-empirical absorption. The crystal data, data collection and refinement details are summarized in Table 1.

Table 1
Crystal data and details of structural determination of $Cu_2(tacn)_2(\mu\text{-}ox)(ClO_4)_2$ (**I**) and $[Cu_2(bdpm)_2(H_2O)_2(\mu\text{-}ox)](ClO_4)_2 \cdot H_2O$ (**II**)

	I	**II**
Empirical formula	$C_{14}H_{30}Cl_2Cu_2N_6O_{12}$	$C_{24}H_{38}Cl_2Cu_2N_8O_{15}$
Crystal size (mm)	$0.10 \times 0.16 \times 0.18$	$0.08 \times 0.32 \times 0.38$
Crystal system	triclinic	triclinic
Space group	$P\bar{1}$	$P\bar{1}$
a (Å)	10.0306(6)	8.2919(9)
b (Å)	10.8335(6)	10.6672(11)
c (Å)	11.5471(9)	11.4647(13)
α (°)	96.693(5)	99.421(7)
β (°)	97.441(6)	103.706(13)
γ (°)	97.714(6)	99.315(10)
V (Å^3)	1221.40(14)	950.4(2)
Z	2	1
ρ_{calc} (g cm^{-3})	1.828	1.563
$F(000)$	688	450
μ (Mo Kα) (mm^{-1})	2.031	1.336
θ Range	$1.8 < \theta < 25.0$	$1.8 < \theta < 25.0$
Limiting indices	$-1 \le h \le 9$, $-12 \le k \le 12$, $-13 \le l \le 13$	$-1 \le h \le 9$, $-12 \le k \le 12$, $-13 \le l \le 13$
Total reflections	4825	4044
Independent reflections	4041 [$R_{int} = 0.0338$]	3298 [$R_{int} = 0.0513$]
Data/restraints/parameters	4040/0/325	3146/0/210
Refinement method	full-matrix least-squares on F^2	full-matrix least-squares on F^2
Weighting scheme	$w^{-1} = [\sigma^2(F_o^2) + (0.0606P)^2 + 0.5275P]$, $P = (F_o^2 + 2F_c^2)/3$	$w^{-1} = [\sigma^2(F_o^2) + (0.0280P)^2]$, $P = (F_o^2 + 2F_c^2)/3$
Final R indices ($I > 2\sigma(I)$)	0.0443, 0.0509	0.0535, 0.0687
R indices (all data)	0.0482, 0.0588	0.0620, 0.0792
Goodness-of-fit on F^2	1.130	1.001
Largest difference and hole (e Å^{-3})	0.566, −0.872	0.830, −1.036

Both structures were solved by direct methods and in each case all non-hydrogen atoms were located from Fourier difference syntheses. Refinements were carried out with anisotropic thermal parameters for all non-hydrogen atoms and isotropic thermal parameters for all hydrogen atoms were fixed with ideal positions by full-matrix least-squares on F^2.

3. Results and discussion

3.1. Characterization of the compounds

The IR spectra for both compounds display the characteristic bands of the oxalate bridging ligand $\nu_{asym\ (C–O)}$ at 1650s, $\nu_{sym\ (C–O)}$ at 1356m and $\delta_{(O–C–O)}$ at 804m cm^{-1}, where s and m refer to strong and medium, respectively. This indicated that the oxalate ion is present as a bridging quadridentate ligand. For compound **I**, a sharp band at 3150 cm^{-1} was observed, indicative of the presence of N–H stretching vibrations. The ClO_4^- group vibration near 1100 cm^{-1} splitting into three sharp bands at 1142s, 1110s and 1086s cm^{-1}, and the presence of an intense band at 930 cm^{-1}, indicate coordinated perchlorate ions [33]. It can be seen that the IR spectra for compound **II** exhibit a broad band near 3400m cm^{-1}, indicative of the presence of H_2O. However, a broad band at 1100 cm^{-1}, typical for non-coordinated perchlorate ions, was present [34].

3.2. Molecular structure of $Cu_2(\mu\text{-}ox)(tacn)_2(ClO_4)_2$ (*I*)

The structure of compound **I** is made up of neutral oxalato-bridged copper(II) units, is shown in Fig. 1 with numbering scheme. Selected bond distances and angles with their estimated standard deviations are listed in Table 2.

The compound has two copper metal centres bridged by a planar bis(didentate) oxalate ligand. The geometry around each copper(II) ion is considered as an elongated octahedral environment with two nitrogen atoms of tacn and two oxygen atoms of oxalate bridge in the equatorial plane CuN2O2, and the third nitrogen atom of tacn occupying the apical position. The axial Cu–N bond distances (2.218 and 2.223 Å) are longer than those (1.996–2.014 Å) in the basal plane, as has been observed earlier [3–22]. The shortest Cu–O (perchlorate) distances are 2.770 Å (Cu1–O7) and 2.747 Å (Cu2–O9), and thus weak coordination of perchlorates to Cu(II) ions is apparent. The Cu(1) and Cu(2) atoms lie 0.043 Å and 0.049 Å from the basal planes towards the apical nitrogen. The four equatorial atoms around Cu atoms are planar. The Cu(1)–Cu(2) distance is 5.176 Å, approximately equal to the data observed (5.144–5.154 Å) [3–8]. C–O distances are in the range (1.253–1.260 Å), very close to the values found previously [3–8].

3.3. Molecular structure of $[Cu_2(bdpm)_2(H_2O)_2(\mu\text{-}ox)](ClO_4)_2\cdot H_2O$ (*II*)

The structure is made up of water molecules of crystallization, uncoordinated perchlorate anions and binuclear

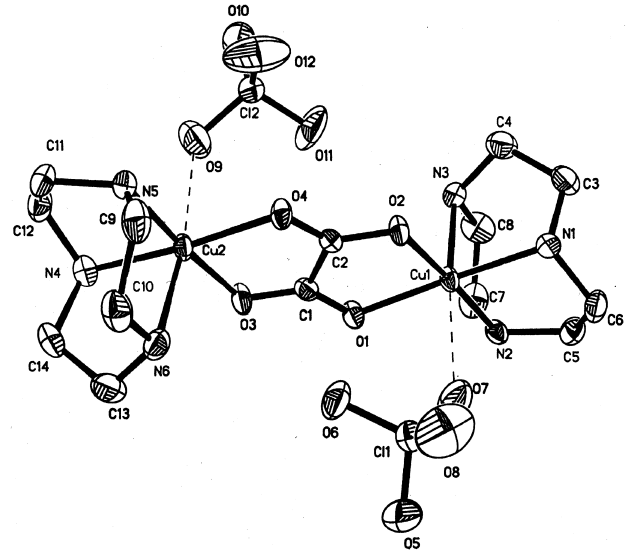


Fig. 1. ORTEP drawing (30% of thermal ellipsoid probability) of $Cu_2(tacn)_2(\mu\text{-ox})(ClO_4)_2$ (**I**) with atom-labelling scheme.

Table 2
Selected bond lengths (Å) and angles (°) for $Cu_2(tacn)_2(\mu\text{-ox})(ClO_4)_2$ (**I**)

Cu(1)–O(2)	1.974(4)	Cu(1)–N(2)	1.996(4)
Cu(1)–N(1)	2.001(4)	Cu(1)–O(1)	2.021(4)
Cu(1)–N(3)	2.218(5)	Cu(1)–O(7)	2.770(7)
Cu(2)–O(3)	2.000(4)	Cu(2)–O(4)	1.977(4)
Cu(2)–N(4)	2.014(5)	Cu(2)–N(5)	2.004(5)
Cu(2)–N(6)	2.223(5)	Cu(2)–O(9)	2.747(8)
O(1)–C(1)	1.257(6)	O(2)–C(2)	1.255(6)
O(3)–C(1)	1.260(6)	O(4)–C(2)	1.253(6)
C(1)–C(2)	1.528(7)		
O(2)–Cu(1)–N(2)	176.0(2)	O(2)–Cu(1)–N(1)	94.9(2)
N(2)–Cu(1)–N(1)	85.5(2)	O(2)–Cu(1)–O(1)	84.29(14)
N(2)–Cu(1)–O(1)	95.1(2)	N(1)–Cu(1)–O(1)	177.7(2)
O(2)–Cu(1)–N(3)	100.0(2)	N(2)–Cu(1)–N(3)	84.1(2)
N(1)–Cu(1)–N(3)	84.4(2)	O(1)–Cu(1)–N(3)	97.8(2)
O(4)–Cu(2)–O(3)	85.0(2)	O(4)–Cu(2)–N(5)	92.2(2)
O(3)–Cu(2)–N(5)	176.2(2)	O(4)–Cu(2)–N(4)	175.1(2)
O(3)–Cu(2)–N(4)	97.2(2)	N(5)–Cu(2)–N(4)	85.4(2)
O(4)–Cu(2)–N(6)	99.8(2)	O(3)–Cu(2)–N(6)	99.7(2)
N(5)–Cu(2)–N(6)	83.4(2)	N(4)–Cu(2)–N(6)	84.1(2)
C(1)–O(1)–Cu(1)	109.7(3)	C(2)–O(2)–Cu(1)	111.2(3)
C(1)–O(3)–Cu(2)	109.5(3)	C(2)–O(4)–Cu(2)	110.5(3)
O(1)–C(1)–O(3)	125.3(5)	O(1)–C(1)–C(2)	117.3(5)
O(3)–C(1)–C(2)	117.5(5)	O(4)–C(2)–O(2)	125.2(5)
O(4)–C(2)–C(1)	117.5(5)	O(2)–C(2)–C(1)	117.3(5)
C(3)–N(1)–Cu(1)	110.8(3)	C(6)–N(1)–Cu(1)	104.7(3)
C(7)–N(2)–Cu(1)	106.0(4)	C(5)–N(2)–Cu(1)	110.2(3)
C(8)–N(3)–Cu(1)	105.2(4)	C(4)–N(3)–Cu(1)	101.0(4)
C(14)–N(4)–Cu(2)	110.6(4)	C(12)–N(4)–Cu(2)	103.3(4)
C(9)–N(5)–Cu(2)	105.3(4)	C(11)–N(5)–Cu(2)	110.0(4)
C(10)–N(6)–Cu(2)	106.0(4)	C(13)–N(6)–Cu(2)	100.3(4)

$[Cu_2(bdpm)_2(H_2O)_2(\mu\text{-ox})]^{2+}$ having a symmetry centre at the midpoint of the C(1) and C(1′) bond ($-x+1$, $-y+1$, $-z+1$) of the oxalate bridge. The molecular structure with the atom-labelling scheme is shown in Fig. 2. Selected bond distances and angles involving non-hydrogen atoms are listed Table 3.

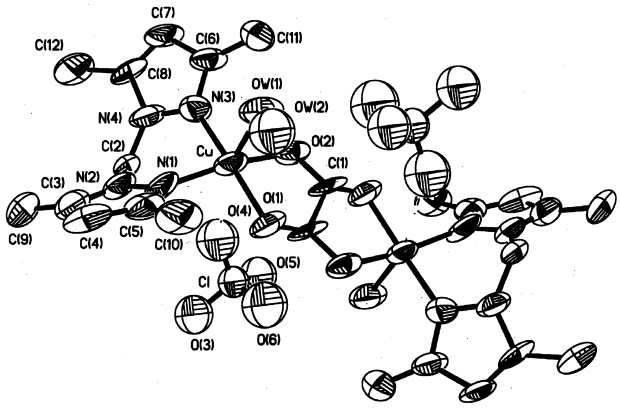


Fig. 2. ORTEP drawing (30% of thermal ellipsoid probability) of $[Cu_2(bdpm)_2(H_2O)_2(\mu\text{-ox})](ClO_4)_2\cdot H_2O$ (**II**) with atom-labelling scheme.

Table 3
Selected bond lengths (Å) and angles (°) for $[Cu_2(bdpm)_2(H_2O)_2(\mu\text{-ox})](ClO_4)_2\cdot H_2O$ (**II**)

Cu–N(1)	2.010(8)	N(1)–C(5)	1.333(6)
Cu–O(1)	1.957(8)	N(1)–N(2)	1.345(7)
Cu–N(3)	1.986(8)	N(2)–C(2)	1.386(8)
Cu–O(2)	2.002(9)	N(2)–C(3)	1.437(7)
Cu–OW1	2.244(9)	N(3)–N(4)	1.352(8)
O(1)–C(1)[a]	1.213(7)	N(3)–C(6)	1.356(9)
O(2)–C(1)	1.275(8)	N(4)–C(8)	1.372(9)
C(1)–C(1)[a]	1.583(9)	N(4)–C(2)	1.464(7)
N(1)–Cu–O(1)	92.7(5)	N(3)–Cu–O(2)	90.4(5)
N(1)–Cu–O(2)	166.3(5)	N(3)–Cu–O(1)	170.0(6)
N(1)–Cu–N(3)	90.3(5)	O(1)–Cu–O(2)	84.5(4)
N(1)–Cu–OW1	100.9(6)	N(3)–Cu–OW1	98.1(4)
O(1)–Cu–OW1	90.7(4)	O(2)–Cu–OW1	92.5(5)
C(1)[a]–O(1)–Cu	112.7(8)	C(1)–O(2)–Cu	111.2(8)
O(1)[a]–C(1)–O(2)	128.3(7)	O(2)–C(1)–C(1)[a]	113.7(9)
O(1)[a]–C(1)–C(1)[a]	117.8(9)	N(2)–N(1)–Cu	119.1(8)
N(4)–N(3)–Cu	119.7(8)		

[a] Symmetry transformations used to generate equivalent atoms: $-x+1$, $-y+1$, $-z+1$.

The copper coordination geometry is distorted square pyramidal with two nitrogen atoms from bdpm and two oxygen atoms from the oxalato bridging ligand in the basal plane, and the other oxygen atom from water molecular in the axial position. The Cu–Cu separation within the binuclear unit is 5.194 Å, very similar to the value for compound **I**. As far as the Cu–O distances are concerned, the average Cu–O (oxalate) (1.979 Å) is very close to the value for compound **I** (1.992 Å), much shorter than the Cu(1)–OW(water) distance (2.244 Å). The Cu–O (perchlorate) distances are 3.129 Å, much longer than those for compound **I**. The oxalate anion is almost planar, and the copper(II) ions are 0.3293 Å out of the plane towards the axial position. The bdpm ligands are in a six-membered boat coordination in compound **II**. C–O distances (1.213 and 1.275 Å) in the oxalate ion are apparently unequal, and the smaller of these values [C(1)[a]–O(1), [a] $-x+1$, $-y+1$, $-z+1$] is the shortest one found in the literatures for related species [3–22], very close to those found in oxalic acid bihydrate (1.207 and 1.281 Å, respectively) [35]. The perchlorate anions contribute to the packing by forming hydrogen bonds with coordinated and uncoordinated water molecules.

3.4. EPR spectra and magnetic properties

X-band EPR spectra of polycrystalline samples for both compounds at 110 K are similar, and close to the report earlier [28]. The $g_{\parallel}$ values (2.16 and 2.14 for compounds **I** and **II**, respectively), which are higher than $g_{\perp}$ (2.08 and 2.10 for compounds **I** and **II**, respectively) are indicative of a $d_{x^2-y^2}$ ground state.

In the 300–4 K temperature range investigated, the molar magnetic susceptibility for compound **I** increases, reaching a maximum at 35 K, and decreases, reaching a minimum at 7 K, then increases with temperature (see Fig. 3a). The magnetic moments decrease in the temperature range 7–300 K, and reach a constant about 0.36 μ_B below 7 K (Fig. 3b), indicating the presence of intramolecular antiferromagnetic interaction. A similar curve was obtained for compound **II** (Fig. 4). The single-triplet energy gap ($2J$) was deduced from least-squares fit of the experimental data to the temperature for isotropic exchange in copper(II) dimer [36] according to the Bleaney–Bowers equation modified accord-

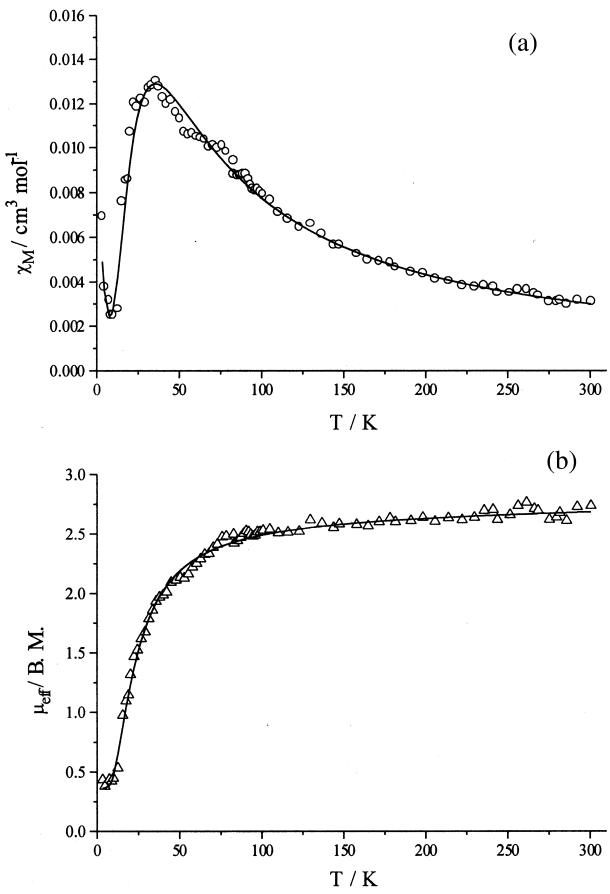


Fig. 3. Plots of χ_M (a) and μ_{eff} (b) of $Cu_2(tacn)_2(\mu\text{-ox})(ClO_4)_2$ (**I**) vs. *T*. Solid lines represent the best theoretical fit.

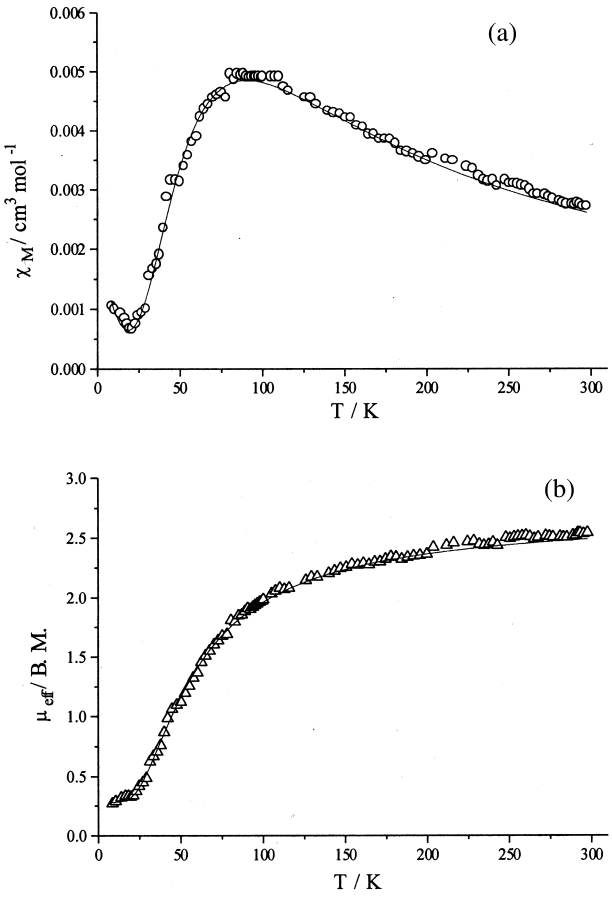


Fig. 4. Plots of χ_M (a) and μ_{eff} (b) of $[Cu_2(bdpm)_2(H_2O)_2(\mu\text{-ox})](ClO_4)_2\cdot H_2O$ (**II**) vs. *T*. Solid lines represent the best theoretical fit.

ing to Kahn and co-workers to take into account some paramagnetic impurity [37]:

$$\chi_M = \frac{2Ng^2\beta^2}{KT}\left[3+\exp\left(\frac{-2J}{KT}\right)\right]^{-1}(1-\rho)+\frac{Ng^2\beta^2}{2KT}\rho+2N\alpha$$

The symbols have their usual meanings, and ρ is the percentage non-coupled impurity. $N\alpha$ is the temperature-independent paramagnetism. The best fits, shown as the solid line in Figs. 3 and 4, afforded the parameter values $2J=-41$ cm^{-1}, $g=2.14$, $\rho=0.009$ with an agreement factor of $R=4.1\times10^{-5}$ for compound **I** and $2J=-102$ cm^{-1}, $g=2.16$, $\rho=0.01$, $R=4.4\times10^{-6}$ for compound **II** (R is defined as $\Sigma[(\chi_M)_{obs}-(\chi_M)_{calc}]^2/\Sigma(\chi_M)_{obs}^2$).

For compound **I**, the value of the singlet-triplet gap ($2J=-41$ cm^{-1}) is much weaker than those ($2J=-260$ to -300 cm^{-1}) for the compounds with non-centrosymmetric cores [38,39]. Significant weakness of the magnetic interaction can be understood according to $J_{AF}=-2S(\Delta^2-\delta^2)$ for the non-centrosymmetric dimer, Δ being the energy separation between the two single occupied molecular orbitals in the triplet state built from the magnetic orbitals, δ being the energy separation between the magnetic orbitals. With the lowering of symmetry, the δ value increases, leading to a corresponding decrease of the antiferromagnetic interaction. However, the magneto-structural correlation is still an open question and has not been quantified thoroughly. For compound **II**, the weaker antiferromagnetic interaction ($2J=-102$ cm^{-1}) is unexpected and significantly smaller than for compounds with centrosymmetric cores ($2J=-400$ to -300 cm^{-1}) [3–8]. It can be satisfactorily interpreted based on the structural data. When one looks at the structure of compound **II**, the height of the copper atom above the basal plane (0.3239 Å) is the longest in all compounds that are in a boat conformation. Furthermore, the C–O bond distances of the oxalate dianion are different (1.275 Å versus 1.213 Å), which indicates that the geometries around copper ions have somewhat deviated from square pyramid towards trigonal bipyramid. Thus the magnetic exchange interaction was reduced.

In the light of the results summarized in Table 4, three points deserve special comments on the week magnetic coupling in the μ-oxalato-bridged-dicopper(II) compounds:

Table 4
Selected structural and magnetic parameters for the oxalato-bridged dimers

Compound	h_{Cu} [a] (Å)	d_{Cu-Cu} [b] (Å)	d_{C-C} [c] (Å)	$2J$ (cm^{-1})	Reference
$[Cu_2(tmen)_2(H_2O)_2(C_2O_4)](ClO_4)_2\cdot 1.25H_2O$	0.147	5.147	1.56	−385	[40]
	0.182				
$[Cu_2(phen)_2(C_2O_4)(NO_3)_2]$	0.271	5.158	1.533	−330	[41]
$[Cu_2(bromazepam)_2(C_2O_4)](PF_6)_{1.5}(ClO_4)_{0.5}\cdot 1.5H_2O$	0.191		1.507	−347	[42]
$[Cu_2(mepirizole)_2(H_2O)_2(C_2O_4)](PF_6)_2\cdot$mepirizole$\cdot 3H_2O$	0.24	5.175	1.51	−201	[43]
$[Cu_2(mpym)_2(H_2O)_2(NO_3)_2(C_2O_4)]\cdot 2H_2O$	0.122	5.217	1.504	−142	[39]
	0.065				
$[Cu_2(tacn)_2(C_2O_4)(ClO_4)_2]$	0.043	5.176	1.528	−41	this work
	0.049				
$[Cu_2(bdpm)_2(H_2O)_2(C_2O_4)](ClO_4)_2\cdot H_2O$	0.3293	5.194	1.583	−102	this work
$[Cu_2(tmen)_2(2\text{-MeIm})_2(C_2O_4)](PF_6)_2$	0.184	5.434	1.562	−14	[40]
	0.084				
$[(dien)Cu(C_2O_4)Cu(H_2O)_2(tmen)](ClO_4)_2$		5.399	1.53	−76	[40]

[a] The height of the copper atom above the basal plane.
[b] The distance between the intramolecular copper atoms.
[c] The C–C bond length in the oxalate bridge.

1. The bending magnitude of the basal plane of the $C_2O_4^{2-}$ bridge is sensitive to the magnetic coupling interaction. The bonding significantly reduces antiferromagnetic interaction.
2. The difference in coordination environments of copper(II) ions is able to weaken the antiferromagnetic interactions, especially in the systems in which one of the oxalate oxygen atoms is in the basal plane and the other is apical.
3. The height of metal atoms above the basal plane is significant, which permits antiferromagnetic interaction; i.e. the height reduces the overlap of both magnetic orbitals through the σ-orbital of the oxalate: the higher the distance, the weaker the interaction observed. It should be noted that the cooperative effect of all three factors is very significant to weaken the magnetic interaction in the oxalato-bridged binuclear copper(II) system.

In conclusion, the exchange interaction between the transition metal ions propagated through the oxalate bridge is strongly dependent on the geometry around the metal ions and the bridging mode of the oxalate anion. The geometry of the metal ion exerts a marked influence on the magnetic exchange interaction. Further work is necessary to study the magneto-structural correlation in the $[Cu(\mu\text{-ox})Cu]^{2+}$ system.

Supplementary data

Supplementary crystallographic data are available from the Cambridge Crystallographic Data Centre, 12 Union Road, Cambridge CB2 1EZ, UK (fax: +44-1223-336033; e-mail: deposit@ccdc.cam.ac.uk) on request, quoting the deposition numbers 138285 and 138286. Least-squares plane equations, deviations of atoms (Å) and dihedral angles between planes (°) and listings of data resulting from the magnetic susceptibility measurements for compounds **I** and **II** are available from the corresponding author.

Acknowledgements

This work was supported by the National Natural Science Foundation of China and Foundation of the Coordination Chemistry State Key Laboratory of Nanjing University, Nanjing, China.

References

[1] R.D. Willett, D. Gatteschi, O. Kahn, Magneto-Structural Correlations in Exchange-Coupled Systems, Nato ASI Series C 140, D. Reidel, Dordrecht, the Netherlands, 1985.
[2] D. Gatteschi, O. Kahn, J.S. Miller, F. Palacio, Magnetic Molecular Materials, Kluwer, Dordrecht, 1991.
[3] A. Gleizes, M. Julve, M. Verdagner, J.A. Real, J. Fus, X. Selans, J. Chem. Soc., Dalton Trans. (1992) 3209.
[4] T. Sanada, T. Suzuki, T. Yoshida, S. Kaizaki, Inorg. Chem. 37 (1998) 4712.
[5] J. Glerup, P.A. Goodson, D.J. Hodgson, K. Michelsen, Inorg. Chem. 34 (1995) 6255.
[6] M. Julve, J. Faus, M. Verdaguer, X. Gleizer, J. Am. Chem. Soc. 106 (1984) 8306.
[7] M. Feist, S. Troyanov, E. Kemnitz, Inorg. Chem. 35 (1996) 3067.
[8] M. Ohba, H. Tamaki, N. Matsumoto, H. Okawa, Inorg. Chem. 32 (1993) 5385.
[9] M. Andruh, R. Melanson, C.V. Stager, F.D. Rochon, Inorg. Chim. Acta 251 (1996) 309.
[10] N. Stanica, C.V. Stager, M. Cimpoesu, M. Andruh, Polyhedron 17 (1998) 1787.
[11] F.D. Rochon, R. Melanson, M. Andruh, Inorg. Chem. 35 (1996) 6086.
[12] H. Oshio, U. Nagashima, Inorg. Chem. 31 (1992) 3295.
[13] J. Suárez-Varela, J.M. Domingue-Vera, E. Colacio, J.C. Avila-Rosón, M.A. Hidealgo, D. Martín-Ramos, J. Chem. Soc., Dalton Trans. (1995) 2143.
[14] S. Decurtins, H.W. Schmalle, R. Pellaux, P. Schneuwly, H. Hauser, Inorg. Chem. 35 (1996) 1451.
[15] G. De Munno, R. Ruiz, F. Lloret, J. Faus, R. Sessoli, M. Julve, Inorg. Chem. 34 (1995) 408.
[16] G. De Munno, M. Julve, F. Nicolo, F. Lloret, R. Ruiz, E. Sinn, Angew. Chem., Int. Ed. Engl. 32 (1993) 613.
[17] F. Bérézovsky, A.A. Hajem, S. Triki, J. Pala, P. Molinié, Inorg. Chim. Acta 284 (1999) 8.
[18] M. Carmen-Munoz, M. Julve, F. Lloret, J. Faus, M. Andrun, J. Chem. Soc., Dalton Trans. (1998) 3125.
[19] J. Larionova, B. Mombelli, J. Sanchiz, O. Kahn, Inorg. Chem. 37 (1998) 679.
[20] S. Decurtins, H.W. Schmalle, P. Schneuwly, H.R. Oswald, Inorg. Chem. 32 (1993) 1888.
[21] S. Decurtins, H.W. Schmalle, P. Schneuwly, J. Ensling, P. Gütlich, J. Am. Chem. Soc. 116 (1994) 9521.
[22] S. Decurtins, H.W. Schmalle, R. Pellaux, P. Fischer, A. Houser, Mol. Cryst. Liq. Cryst. 305 (1997) 227.
[23] A. Bhattacharjee, S. Iijima, F. Miztani, J. Magn. Magn. Mater. 153 (1996) 235.
[24] C. Mathoniere, C.J. Nattall, S.G. Carling, P. Day, Inorg. Chem. 35 (1996) 1201.
[25] O. Kahn, Angew. Chem., Int. Ed. Engl. 24 (1985) 839.
[26] S. Alvarez, M. Julve, M. Verdaguer, Inorg. Chem. 29 (1990) 4500.
[27] J. Cano, P. Alemany, S. Alvarez, M. Verolaguer, E. Ruiz, Chem. Eur. J. 4 (1998) 476.
[28] P. Chaudhuri, K. Oder, J. Chem. Soc., Dalton Trans. (1990) 1597.
[29] L. Zhang, H.L. Yan, S.P. Yan, Z.H. Jiang, D.Z. Liao, G.L. Wang, Polish J. Chem. 73 (1999) 391.
[30] R. Yang, L.J. Zompa, Inorg. Chem. 15 (1976) 1499.
[31] S. Julia, P. Sala, J.M.D. Mazo, M. Sancho, C. Ochoq, J. Elguero, J.P. Fayet, M.C. Vertut, J. Heterocycl. Chem. 19 (1982) 1141.
[32] G.M. Sheldrick, SHELXTL, Version 5, Siemens Analytical X-ray System, Inc., Madison, WI, 1995.
[33] R.T. Conley, Infrared Spectroscopy, Allynand, Boston, MA, 1966.
[34] W. Radecka-Paryzek, Inorg. Chim. Acta 34 (1979) 5.
[35] S. Shibata, M. Kimura, Bull. Chem. Soc. Jpn. 27 (1954) 485.
[36] B. Bleaney, K.D. Bowers, Proc. R. Soc. London, Ser. A 214 (1952) 451.
[37] Y. Journaux, J. Sletten, O. Kahn, Inorg. Chem. 24 (1985) 4063.
[38] T.R. Felthouse, E.J. Laskowski, D.N. Hendrickson, Inorg. Chem. 16 (1977) 1077.
[39] L. Soto, J. Garcia, E. Escriva, M. Beneto, F. Dahan, J.P. Tuchagues, J.P. Legros, J. Chem. Soc., Dalton Trans. (1991) 2619.
[40] M. Julve, M. Verdagner, A. Gleizes, M. Philoche-Levisalles, O. Kahn, Inorg. Chem. 23 (1984) 3808.
[41] A. Bencini, A.C. Fabretti, C. Zanchini, P. Zannini, Inorg. Chem. 26 (1987) 1445.
[42] J.A. Real, J. Borrás, X. Solans, M. Font-Altaba, Transition Met. Chem. 12 (1987) 254.
[43] L. Soto, J. Garcia, E. Escriva, J.-P. Legros, J.-P. Tuchagues, F. Dahan, A. Fuertes, Inorg. Chem. 28 (1989) 3378.

PERGAMON

www.elsevier.nl/locate/poly

Polyhedron 19 (2000) 1111–1116

POLYHEDRON

Bidentate phosphinophenol ligand: synthesis and characterization of oxo and phenylimido rhenium(V) complexes of 2-diisopropylphosphinophenol

Frédérique Loiseau [a], Yolande Lucchese [a], Michèle Dartiguenave [a,*], Yvon Coulais [b]

[a] *Laboratoire de Chimie Inorganique, Université Paul Sabatier, 118 route de Narbonne, 31062 Toulouse, France*

[b] *Laboratoire Traceurs et Traitement de l'Image, Hôpital Purpan, Université Paul Sabatier, Place du Dr Baylac, 31059 Toulouse, France*

Received 20 January 2000; accepted 8 March 2000

Abstract

Six-coordinate, monosubstituted and disubstituted phosphinophenol complexes $ReYX_2(PPh_3)(P\sim O)$ and $ReYX(P\sim O)_2$ (Y = O, NPh; X = Cl, Br, I) were obtained by reacting 2-diisopropylphosphinophenol (P ~ OH) with $ReOX_3(PPh_3)_2$ and $Re(NPh)X_3(PPh_3)_2$ in toluene. A mixture of the monosubstituted and disubstituted complexes $ReYX_2(PPh_3)(P\sim O)$ and $ReYX(P\sim O)_2$ was precipitated when the reactions were performed with a 2:1 ligand to metal ratio. Excess ligand (4 equiv.) was needed to obtain quantitatively the disubstituted complexes. ^1H and $^{31}P\{^1H\}$ NMR show that all monosubstituted and disubstituted complexes exist as single isomers with a *trans*-P,P 'twisted' octahedral geometry, the site *trans* to the multiple bond being filled by the oxygen donor of one P ~ O ligand. The compounds were also characterized by microanalysis, IR and mass spectrometry. ©2000 Elsevier Science Ltd All rights reserved.

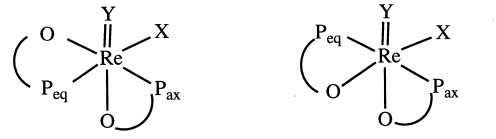
Keywords: Phosphinophenols; Rhenium

1. Introduction

Because of their chemical and structural diversity and their good coordinative properties, functionalized phosphines have attracted considerable attention in strategies aimed at developing new chelates for metallic radioisotopes to develop imaging (technetium) and therapeutic (rhenium) agents in nuclear medicine.

In the recent past, studies have been conducted on the reaction of $ReOCl_3(PPh_3)_2$, $Re(NPh)Cl_3(PPh_3)_2$ and $[TcO_4]^-$ with various diphenylphosphines functionalized with nucleophilic substituents such as $Ph_2P–Z–CO_2H$ (Z = CH_2, $CH_2–CH_2$, *o*-C_6H_4) [1,2], $Ph_2PCH{=}CPh(OH)$ [3], $Ph_2PC_6H_4OH$ [4–8], $Ph_2PCH_2C_6H_4OH$ [9] and $Ph_2PC_6H_4OSiMe_3$ [10], i.e. bidentate ligands with soft phosphorus(III) donor and hard carboxo, hydroxo or phenoxo groups. Although several configurations are possible for octahedral complexes bearing three different ligands, most of the previously reported oxo and imido complexes adopt the *cis*-P_{eq},P_{ax} 'twisted' octahedral arrangement A with an O=Re–O linkage (Scheme 1), while the *trans*-P_{eq},P_{ax} arrangement B with a PhN=Re–O linkage was observed for Re-imido species. Thus these ligands favour the formation of a single isomer, which is essential for radiopharmaceutical applications.

In contrast to the relatively abundant literature on the reactions of $Ph_2PC_6H_4OH$ ligands on rhenium precursors [4–8], to our knowledge the reactivity of dialkylphosphinophenols has not yet been investigated. This may be due in part to the increased reductive character of the alkylphosphines which are known to stabilize Re(III) complexes. In order to determine the influence of an alkyl substituent on the phosphinophenol reactivity, we have studied the reaction of 2-(diisopropylphosphino)phenol (P ~ OH) on $ReOX_3$-



A (cis-P,P « twisted ») **B** (trans-P,P « twisted »)

Scheme 1.

* Corresponding author. Tel.: +33-561-556 121; fax: +33-561-556 118; e-mail: dartigue@iris.ups-tlse.fr

0277-5387/00/$ - see front matter ©2000 Elsevier Science Ltd All rights reserved.
PII S0277-5387(00)00360-0

$(PPh_3)_2$ and $Re(NPh)X_3(PPh_3)_2$ (X = Cl, Br, I) by comparison with $Ph_2P\sim OH$. Isopropyl substituents increase the steric hindrance of the phosphine (cone angle of 137° for $^iPr_2P\sim OH$ compared to 127° for $Ph_2P\sim OH$) [11] and its basicity ($pKa(PPh_3) = 2.73$; $pKa(P^iPr_3) = 9.30$)) [12]. We observe the formation of Re(V) complexes without reduction of the metal centre whose structures are controlled by the steric hindrance of the ligand.

2. Experimental

2.1. Reagents and physical measurements

All reactions were carried out in a nitrogen atmosphere using standard Schlenk techniques. Ether and toluene were dried over sodium benzophenone ketyl and distilled prior to use. Ethanol and acetonitrile were distilled on molecular sieves (3 Å). $ReOX_3(PPh_3)_2$ [13,14], $Re(NPh)X_3(PPh_3)_2$ [15], and 2-diisopropylphosphinophenol [16] were prepared by literature methods.

Infrared spectra (4000–200 cm^{-1}) were recorded as CsI pellets on a Bruker Vector 22 spectrometer. ^1H, $^{13}C\{^1H\}$ and $^{31}P\{^1H\}$ NMR spectra were recorded at room temperature in CD_2Cl_2, $CDCl_3$ or C_6D_6 on Bruker ARX 400 and AMX 300 WB spectrometers, using $SiMe_4$ as internal reference (^1H, ^{13}C) and H_3PO_4 (82%/D_2O) as external reference (^{31}P). All chemical shifts are reported in ppm. Desorption chemical ionization using NH_3 (DCI/NH_3) was recorded on a NERMAG R 1010 mass spectrometer. Elemental analyses were run at the Laboratoire de Chimie de Coordination du CNRS, Toulouse, France.

2.2. Synthetic work

$ReOCl_2(PPh_3)(P\sim O)$ (**1**) and $ReOCl(P\sim O)_2$ (**2**). The two complexes were obtained from the reaction of $P\sim OH$ (0.373 g, 1.77 mmol) and $ReOCl_3(PPh_3)_2$ (0.739 g, 0.89 mmol) in refluxing toluene under N_2 for 35 h. Concentration of the solution in vacuo produced a green solid. Work-up with diethyl ether and cooling of the solution gave a mixture of **1** and **2**. Purification by column chromatography using silica as support gave **1** with chloroform and **2** with diethyl ether as eluents. Recrystallization from diethyl ether at −20°C gave **1** (yield 10%) and **2** (yield 43%) as green crystals.

1. *Anal*. Calc. for $C_{30}H_{33}Cl_2O_2P_2Re$: C, 48.39; H, 4.47. Found: C, 47.82; H, 4.78%. IR (CsI): 970 cm^{-1}, ν(Re=O). MS (DCI/NH_3): *m/z* 745 $[M+H]^+$, 709 $[M-HCl+H]^+$. $^{31}P\{^1H\}$ NMR (C_6D_6, 161.98 Hz, ppm): 7.1; 24.7 (dd, $^2J_{PP} = 262$ Hz). ^1H NMR (C_6D_6, 400.14 MHz, ppm): 1.36 (dd, 6H, CH_3, $^3J_{HH} = 7$ Hz, $^3J_{HP} = 15$ Hz); 1.50 (dd, 6H, CH_3, $^3J_{HH} = 7$ Hz, $^3J_{HP} = 17$ Hz); 3.33 (d of septets, 2H, CH, $^3J_{HH} = 7$ Hz, $^2J_{HP} = 2$ Hz); 6.22 (dd, 1H, Ph, $^3J_{HH} = 7$ Hz, $^4J_{HP} = 4$ Hz); 6.56 (dd, 1H, Ph, $^3J_{HH} = 7$ Hz); 6.93 (dd, 2H, Ph, $^3J_{HH} = 7$ Hz); 7.03 (m, 9H, Ph); 8.04 (ddd, 6H, Ph, $^3J_{HH} = 8$ Hz, $^4J_{HH} = 1$ Hz, $^3J_{HP} = 11$ Hz).

2. *Anal*. Calc. for $C_{24}H_{36}ClO_3P_2Re$: C, 43.93; H, 5.53; Cl, 5.40; P, 9.44; Re, 28.38. Found: C, 48.85; H, 5.56; Cl, 6.55; P, 9.19; Re, 26.13%. IR (CsI): 962 cm^{-1}, ν(Re=O). MS (DCI/NH_3): *m/z* 621 $[M-HCl+H]^+$. $^{31}P\{^1H\}$ NMR ($CDCl_3$, 161.98 MHz, ppm): 34.0; 41.6 (dd, $^2J_{PP} = 213$ Hz). ^1H NMR ($CDCl_3$, 400.14 MHz, ppm): 1.4 (dd, 12H, CH_3, $^3J_{HH} = 7$ Hz, $^3J_{HP} = 17$ Hz); 1.7 (dd, 12H, CH_3, $^3J_{HH} = 7$ Hz, $^3J_{HP} = 17$ Hz); 2.8 (d of septets, 1H, CH, $^3J_{HH} = 7$ Hz, $^2J_{HP} = 1$ Hz); 3.0 (d of septets, 2H, CH, $^3J_{HH} = 7$ Hz, $^2J_{HP} = 1$ Hz); 3.4 (d of septets, 1H, CH, $^3J_{HH} = 7$ Hz, $^2J_{HP} = 1$ Hz); 6.3–7.5 (m, 8H, Ph).

$ReOBr_2(PPh_3)(P\sim O)$ (**3**) and $ReOBr(P\sim O)_2$ (**4**). The same method was used as for **1** and **2**, starting from 0.380 g (1.8 mmol) of $P\sim OH$ and 0.873 g (0.9 mmol) of $ReOBr_3(PPh_3)_2$, stirred in 30 ml of refluxing toluene under N_2 for 46 h.

3. Green solid, yield 9%. *Anal*. Calc. for $C_{30}H_{33}Br_2O_2P_2Re$: C, 43.23; H, 3.99. Found: C, 44.27; H, 3.58%. IR (CsI): 969 cm^{-1}, ν(Re=O). MS (DCI/NH_3): *m/z* 835 $[M+H]^+$, 755 $[M-HBr+H]^+$. $^{31}P\{^1H\}$ NMR ($CDCl_3$, 161.98 MHz, ppm): 8.0; 26.1 (dd, $^2J_{PP} = 260$ Hz). ^1H NMR ($CDCl_3$, 400.14 MHz, ppm): 1.55 (dd, 6H, CH_3, $^3J_{HH} = 7$ Hz, $^3J_{HP} = 16$ Hz); 1.64 (dd, 6H, CH_3, $^3J_{HH} = 7$ Hz, $^3J_{HP} = 16$ Hz); 3.62 (d of septets, 2H, CH, $^3J_{HH} = 7$ Hz, $^2J_{HP} = 2$ Hz); 5.9–7.8 (m, 19H, Ph). $\Lambda(CH_3CN)$: 30.3 Ω^{-1} cm^2 M^{-1} (molecular).

4. Green solid, yield 50%. *Anal*. Calc. for $C_{24}H_{36}BrO_3P_2Re$: C, 41.15; H, 5.18. Found: C, 41.40; H, 4.92%. IR (CsI): 964 cm^{-1}, ν(Re=O). MS (DCI/NH_3): *m/z* 701 $[M+H]^+$, 621 $[M-HBr+H]^+$. $^{31}P\{^1H\}$ NMR ($CDCl_3$, 161.98 MHz, ppm): 34.1, 41.7 (dd, $^2J_{PP} = 212$ Hz). ^1H NMR ($CDCl_3$, 400.14 MHz, ppm): 1.1–1.7 (dd, 24H, CH_3, $^3J_{HH} = 7$ Hz, $^3J_{HP} = 16$ Hz); 2.8–3.1 (m, 4H, CH); 6.3–7.5 (m, 8H, Ph). $\Lambda(CH_3CN)$: 15.1 Ω^{-1} cm^2 M^{-1} (molecular).

$ReOI_2(PPh_3)(P\sim O)$ (**5**) and $ReOI(P\sim O)_2$ (**6**). The same method was used as for **1** and **2**, starting from the reaction of 0.45 g (2.14 mmol) of $P\sim OH$ and 1.185 g (1.07 mol) of $ReOI_3(PPh_3)_2$ in refluxing toluene under N_2 for 46 h. Concentration of the solution gave an oily solid. Work-up with diethyl ether and cooling the solution gave a mixture of **5** (yield 27%) and **6** (yield 9%) as a dark brown solid, which was filtered off and dried in vacuo. Purification by column chromatography as for the Cl and Br analogues gave **5** and **6** as pure compounds.

5. Brown solid, yield 27%. *Anal*. Calc. for $C_{30}H_{33}I_2O_2P_2Re$: C, 38.85; H, 3.59; I, 27.36. Found: C, 38.07; H, 3.28; I, 26.94%. ^{31}P NMR ($CDCl_3$, 161.98 MHz, ppm): 6.9; 17.4 (dd, $^2J_{PP} = 257$ Hz). MS (DCI/NH_3): *m/z* 929 $[M+H]^+$.

6. Brown solid, yield 9%. *Anal*. Calc. for $C_{24}H_{36}IO_3P_2Re$: C, 38.56; H, 4.85; I, 16.97. Found: C, 38.17; H, 4.60; I, 16.12%. $^{31}P\{^1H\}$ NMR ($CDCl_3$, 161.98 MHz, ppm): 33.1;

42.4 (dd, $^2J_{PP}$ = 210 Hz). MS (DCI/NH_3): *m/z* 749 $[M+H]^+$.

Re(NPh)Cl_2(PPh_3)(P∼O) (**7**) and Re(NPh)Cl(P∼O)$_2$ (**8**). The same method was used as for **1** and **2**, starting from the reaction of P∼OH (0.47 g, 2.24 mmol) and Re(NPh)Cl_3(PPh_3)$_2$ (1.02 g, 1.12 mmol) in refluxing toluene (40 ml) under N_2 for 37 h.

7. Beige solid, yield 45%. *Anal*. Calc. for $C_{36}H_{38}Cl_2NOP_2Re$: C, 52.75; H, 4.67; N, 1.71. Found: C, 51.91; H, 4.73; N, 1.78%. $^{31}P\{^1H\}$ NMR (CD_2Cl_2, 161.98 MHz, ppm): −5.2; 27.7 (dd, $^2J_{PP}$ = 260 Hz). MS (DCI/NH_3): *m/z* 820 $[M+H]^+$.

8. Beige solid, yield 10%. *Anal*. Calc. for $C_{30}H_{41}ClNO_2P_2Re$: C, 49.27; H, 5.65; N, 1.92. Found: C, 48.95; H, 5.90; N, 1.72%. $^{31}P\{^1H\}$ NMR (CD_2Cl_2, 161.98 MHz, ppm): 30.7; 33.3 (dd, $^2J_{PP}$ = 224 Hz). MS (DCI/NH_3): *m/z* 732 $[M+H]^+$.

Re(NPh)Br_2(PPh_3)(P∼O) (**9**) and Re(NPh)Br(P∼O)$_2$ (**10**). The same method was used as for **7** and **8**, starting from 0.55 g (2.6 mmol) of P∼OH and 1.362 g (1.3 mmol) of Re(NPh)Br_3(PPh_3)$_2$ in 35 ml of toluene. **9** yield 56%, and **10** yield 14%.

9. *Anal*. Calc. for $C_{36}H_{38}Cl_2NOP_2Re$: C, 47.59; H, 4.22; N, 1.54. Found: C, 46.95; H, 4.08; N, 1.42%. MS (DCI/NH_3): *m/z* 910 $[M+H]^+$. $^{31}P\{^1H\}$ NMR (C_6D_6, 161.98 MHz, ppm): −6.3; 24.1 (dd, $^2J_{PP}$ = 246 Hz).

10 was obtained in 30% yield by refluxing a mixture of 0.355 g (1.7 mmol) of P∼OH and 0.44 g (0.42 mmol) of Re(NPh)Br_3(PPh_3)$_2$ in 20 ml of toluene for 46 h. Concentration of the solution gave a brown precipitate, which was recrystallized from diethyl ether (20 ml). Cooling the solution at −20°C gave **10** as a brown solid which was filtered off, washed with diethyl ether and dried in vacuo. *Anal*. Calc. for $C_{30}H_{41}BrNO_2P_2Re$: C, 46.45; H, 5.33; N, 1.81. Found: C, 46.50; H, 4.77; N, 1.64%. IR (CsI): 1026 cm^{-1}, ν(Re=O). MS (DCI/NH_3): *m/z* 776 $[M+H]^+$. $^{31}P\{^1H\}$ NMR (C_6D_6, 161.98 MHz, ppm): 30.8; 33.1 (dd, $^2J_{PP}$ = 222 Hz). ^1H NMR (C_6D_6, 400.14 MHz, ppm): 0.7–1.6 (dd, 24H, CH_3, $^3J_{HH}$ = 7 Hz, $^3J_{HP}$ = 15 Hz); 2.5–3.4 (d of septets, 4H, CH, $^3J_{HH}$ = 7 Hz, $^2J_{HP}$ = 1 Hz); 6.6–7.8 (m, 13H, Ph).

Re(NPh)I_2(PPh_3)(P∼O) (**11**) and Re(NPh)I(P∼O)$_2$ (**12**). The complexes were synthesized as for **9** and **10**, with Re(NPh)I_3(PPh_3)$_2$ (1.237 g, 1.05 mmol) and P∼OH (0.44 g, 2.09 mmol) in toluene (35 ml) for 47 h. Work-up with ether and purification by column chromatography with $CHCl_3$ and ether as eluents and recrystallization from diethyl ether at −20°C gave **11** (yield 54%) and **12** (yield 13%) as brown microcrystalline compounds.

11. *Anal*. Calc. for $C_{36}H_{38}I_2NOP_2Re$: C, 43.12; H, 3.82; N, 1.40; I, 25.31. Found: C, 41.80; H, 3.75; N, 1.35; I, 25.05%. MS (DCI/NH_3): *m/z* 1004 $[M+H]^+$. $^{31}P\{^1H\}$ NMR ($CDCl_3$, 161.98 MHz, ppm): −6.3; 24.1 (dd, $^2J_{PP}$ = 246 Hz).

12. *Anal*. Calc. for $C_{30}H_{41}INO_2P_2Re$: C, 43.80; H, 5.02; N, 1.70; I, 15.43. Found: C, 41.92; H, 4.93; N, 1.65; I, 15.28%. MS (DCI/NH_3): *m/z* 824 $[M+H]^+$; 696 $[M-HI+H]^+$. $^{31}P\{^1H\}$ NMR ($CDCl_3$, 161.98 MHz, ppm): 31.8; 33.3 (dd, $^2J_{PP}$ = 217 Hz).

3. Results and discussion

3.1. Synthesis

$^iPr_2PC_6H_4OH$ (P∼OH) reacts readily, in refluxing toluene, on ReOX_3(PPh_3)$_2$ and Re(NPh)X_3(PPh_3)$_2$ but the reactions are sensitive to the ligand:metal ratio and care must be taken to use carefully dried and degassed solvents to prevent phosphine oxidation.

A 4:1 ligand to metal ratio gives quantitatively the disubstituted ReYX(P∼O)$_2$ complexes (Y = O, NPh; X = Cl, Br, I). However, when the reaction is performed in a stoichiometric ratio (L:M = 2:1), a mixture of monosubstituted and disubstituted ReYX_2(PPh_3)(P∼O) and ReYX(P∼O)$_2$ complexes is obtained; the ratio ReYX(P∼O)$_2$/ReYX_2(PPh_3)(P∼O) decreases as the size of the halide increases. Such a mixture of complexes was not observed with diphenylphosphinophenol whose reactions were stoichiometric, indicating that the basicity of the phosphine is not the main factor governing the reaction.

In an effort to follow the reaction, to detect intermediate compounds and to confirm that chelation of the phosphine ligand occurs with the concomitant release of both PPh_3 and Cl, we monitored the reaction of P∼OH with ReOCl_3(PPh_3)$_2$ by ^{31}P NMR (Fig. 1). The spectrum after 5 h reveals the presence of all of the expected species. Besides free PPh_3 (singlet at −4 ppm), the major species is ReOCl_2(PPh_3)(P∼O) (**1**) (pair of doublets at 7 and 25 ppm, $^2J_{PP}$ = 262 Hz), followed by ReOCl(P∼O)$_2$ (**2**) (pair of doublets at 34 and 42 ppm, $^2J_{PP}$ = 213 Hz) (vide infra). A third pair of doublets at 20.5 and 31 ppm ($^2J_{PP}$ = 220 Hz) could be assigned to the *trans*-P,P-*trans*-O,O complex ReOCl_2(P∼OH)(P∼O) containing a unidentate P∼OH ligand. The remaining signals, a pair of unresolved peaks at 21.2 and 23.2 ppm and a singlet at 27.2 ppm, which disappear quickly, could correspond to the thermodynamically unstable *cis*-P,P ReOCl(P∼O)$_2$ and the *trans*-P,P ReOCl_3(P∼OH)$_2$ species, respectively. After an extra 10 h under reflux, the spectrum shows free PPh_3, ReOCl_2(PPh_3)(P∼O) (**1**), ReOCl(P∼O)$_2$ (**2**) and ReOCl_2(P∼OH)(P∼O). 20 h later, the spectrum has become remarkably simple: besides free PPh_3, only ReOCl_2(PPh_3)(P∼O) (minor component) and ReOCl(P∼O)$_2$ (major component) are observed. Thus, ReOCl(P∼O)$_2$ is the thermodynamic product, since no further changes occur as heating is continued. Interestingly, under the same experimental conditions, using $Ph_2PC_6H_4OH$ as ligand produced quantitatively ReOCl(P∼O)$_2$.

The corresponding bromo and iodo complexes give the same final products when the reaction is run under identical conditions, starting from ReOBr_3(PPh_3)$_2$ and ReOI_3(PPh_3)$_2$, respectively. ReOBr_2(PPh_3)(P∼O) (**3**) and ReOBr(P∼O)$_2$ (**4**) form in roughly equal amounts, whereas

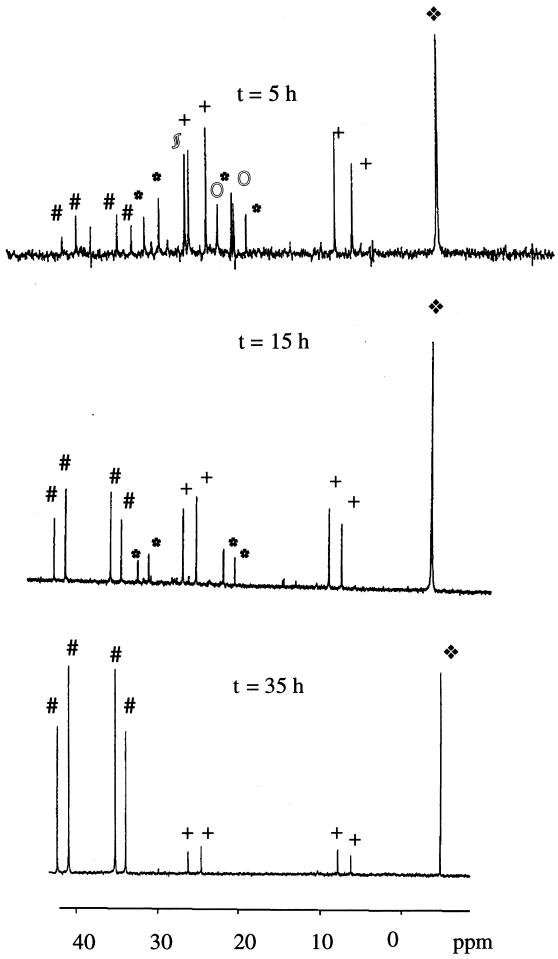


Fig. 1. Monitoring by $^{31}P\{^{1}H\}$ NMR of the reaction of P∼OH on $ReOCl_3(PPh_3)_2$ (2:1 ratio) in refluxing toluene. Spectra at $t = 5$ h (top) (Bruker AMX 300WB), 15 h (middle) and 35 h (bottom) (Bruker ARX 400). (♦) free PPh_3; +, *trans*-P,P $ReOCl_2(PPh_3)(P{\sim}O)$ (**1**); (#) *trans*-P,P $ReOCl(P{\sim}O)_2$ (**2**); (*), *trans*-P,P $ReOCl_2(P{\sim}OH)(P{\sim}O)$; (○) *cis*-P,P $ReOCl(P{\sim}O)_2$; (Ⓢ), *trans*-P,P $ReOCl_3(P{\sim}OH)_2$).

$ReOI_2(PPh_3)(P{\sim}O)$ (**5**) is predominant over $ReOI(P{\sim}O)_2$ (**6**) (∼4:1 ratio). This can be ascribed to the increasing size of the halogen.

The reaction of P∼OH with $Re(NPh)X_3(PPh_3)_2$ follows a similar pattern: a 2:1 ratio leads to a mixture of the monosubstituted and disubstituted species, whereas a 4:1 ratio is needed to obtain $Re(NPh)X(P{\sim}O)_2$.

In all cases, the monosubstituted and disubstituted complexes are successfully separated by column chromatography on silica, using $CHCl_3$ as eluent in one case and ether in the other, and recrystallized from ether.

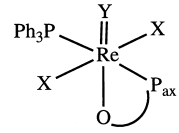
3.2. Characterization of the compounds

3.2.1. Rhenium(V) oxo complexes

Mass spectrometry confirms the mononuclear formulation based on elemental analysis: the DCI/NH_3 spectra all exhibit the $[M+H]^+$ parent peak. In several cases, $[M-HX+H]^+$ peaks due to halide loss are also observed, suggesting that the bidentate P∼O ligand is more tightly bound than the monodentate halide. Besides the main ligand vibrations, all complexes exhibit a Re=O stretching band in the 953–970 cm^{-1} range, typical of multiply bonded Re=O complexes [17].

Table 1
$^{31}P\{^{1}H\}$ NMR data

Complex	Solvent	δ (ppm)		J_{PP} (Hz)
$ReOCl_2(PPh_3)(P{\sim}O)$ (**1**)	C_6D_6	7.1, 24.7	dd	262
$ReOCl(P{\sim}O)_2$ (**2**)	$CDCl_3$	34.0, 41.6	dd	213
$ReOBr_2(PPh_3)(P{\sim}O)$ (**3**)	$CDCl_3$	8.0, 26.1	dd	260
$ReOBr(P{\sim}O)_2$ (**4**)	$CDCl_3$	34.1, 41.7	dd	212
$ReOI_2(PPh_3)(P{\sim}O)$ (**5**)	$CDCl_3$	6.9, 17.4	dd	257
$ReOI(P{\sim}O)_2$ (**6**)	$CDCl_3$	33.1, 42.4	dd	210
$Re(NPh)Cl_2(PPh_3)(P{\sim}O)$ (**7**)	CD_2Cl_2	−5.2, 27.7	dd	260
$Re(NPh)Cl(P{\sim}O)_2$ (**8**)	CD_2Cl_2	30.7, 33.3	dd	224
$Re(NPh)Br_2(PPh_3)(P{\sim}O)$ (**9**)	C_6D_6	−5.8, 26.3	dd	254
$Re(NPh)Br(P{\sim}O)_2$ (**10**)	C_6D_6	30.8, 33.1	dd	222
$Re(NPh)I_2(PPh_3)(P{\sim}O)$ (**11**)	$CDCl_3$	−6.3, 24.1	dd	246
$Re(NPh)I(P{\sim}O)_2$ (**12**)	$CDCl_3$	31.8, 33.3	dd	217



Scheme 2.

The ^{31}P NMR spectrum (in C_6D_6) of $ReOCl_2(PPh_3)(P{\sim}O)$ (**1**) consists of two doublets centred at 24.7 and 7.1 ppm, respectively, with a coupling constant of 262 Hz typical of a *trans*-P,P arrangement. In the structure proposed (Scheme 2), the very stable *trans*-[O=Re–O–] core is assumed to be retained. The downfield signal corresponds to the ring P_{ax} atom as confirmed by the exchange of PPh_3 with pyridine. When pyridine is added to a C_6D_6 solution of **1** in an NMR tube, the AB signal of **1** disappears within 2 h and the *trans*-P,P coupling is lost: new singlets appear at −4 ppm for free PPh_3 and at 19 ppm for a new pyridine complex. Thus, the doublet at 7.1 ppm for **1** corresponds to the labile PPh_3 ligand, which is stereoselectively substituted by pyridine. The upfield shift from 24.7 to 19 ppm experienced by the ring P atom is consistent with the substitution of PPh_3 by pyridine, a stronger σ donor and weaker π acceptor. The stereochemistry of **1** is confirmed by the ^{1}H NMR spectrum. The two pairs of CH_3 groups appear as doublets of doublets at 1.36 ppm ($^3J_{HH} = 7$ Hz, $^3J_{HP} = 15$ Hz) and 1.50 ppm ($^3J_{HH} = 7$ Hz, $^3J_{HP} = 17$ Hz) respectively, shifted slightly from the free ligand value. The two methine protons give a doublet of septets at 3.33 ppm ($^3J_{HH} = 7$ Hz, $^2J_{HP} = 2$ Hz). A

similar multiplet is present at 2.14 ppm ($^3J_{HH}=7$ Hz, $^2J_{HP}=2$ Hz) in the free ligand indicating that the signal has moved downfield on coordination, but that the magnetic equivalence of the two protons is not affected by the bonding to rhenium. This is consistent with the isomer containing the *trans*-[O=Re–O] core, since the other isomers would contain non-equivalent isopropyl groups and, as a consequence, probably give split methine signals. The aromatic protons give rise to five multiplets in the 6.2–8.0 ppm range.

The ^{31}P NMR spectrum of $ReOCl(P\sim O)_2$ (**2**) consists of a pair of doublets (AB spin system) with signals centred at 34.0 and 41.6 ppm, and a $^2J_{PP}$ value of 213 Hz, consistent with two equivalent P atoms occupying *trans* positions in a 'twisted' octahedron (B, Scheme 1). The structure is different to that obtained for diphenylphosphinophenol complexes where the ^{31}P NMR showed two non-equivalent P atoms occupying *cis* positions in a 'twisted' octahedron (A, Scheme 1), as observed in the crystal structure of $ReOCl(Ph_2P\sim O)_2$ [8]. The *trans*-P,P structure is consistent with the ^{1}H NMR data which show the inequivalence of all the protons of the two ligands. The two methyl signals of each ligand, corresponding to 12H, are observed as doublets of doublets centred at 1.4 and 1.7 ppm, respectively, with $^3J_{HP}=17$ Hz and $^3J_{HH}=7$ Hz shifted slightly downfield from the values of 0.9 and 1.1 ppm found in the free ligand. Doublets of septets at 2.8 (1H), 3.0 (2H) and 3.4 (1H) ppm, with coupling constants $^2J_{HP}=1$ Hz and $^3J_{HH}=7$ Hz, are due to the four non-equivalent methine hydrogens that have moved downfield upon coordination, but they are not individually affected by the low symmetry of the complex. Eight multiplets between 6.3 and 7.5 ppm originate from the aromatic protons.

3.2.2. Rhenium(V) imido complexes

The phenylimido complexes **7**–**12** are stable in the solid state and in organic solvents where they are soluble (DMSO, DMF, CH_2Cl_2, $CHCl_3$, THF). The formula proposed is based on microanalyses and mass spectra (DCI/NH_3), in which the parent $[M+H]^+$ peaks and $[M-HX+H]^+$ peaks corresponding to halide loss are observed. The Re=NPh stretch of phenylimido-Re(V) complexes, difficult to detect in the IR because of overlapping ligand vibrations, is only clearly identified at 1025 cm^{-1} for **9**, in agreement with the literature [17].

The trends observed above for the oxo systems apply to the imido complexes as well. The ^{31}P NMR spectra of the $Re(NPh)X(P\sim O)_2$ complexes (X=Cl, (**8**); X=Br, (**10**); X=I, (**12**)) in $CDCl_3$ all contain doublets at ~31 and ~33 ppm with J_{PP} coupling constants of ~220 Hz, consistent with *trans*-P,P 'twisted' octahedral species. The $Re(NPh)X_2(PPh_3)(P\sim O)$ compounds **7**, **9** and **11** also adopt a *trans*-P,P structure, since their ^{31}P NMR spectra show doublets around −6 and 26 ppm ($^2J_{PP}$ of 246–260 Hz). By analogy with $ReOCl_2(PPh_3)(P\sim O)$, the peak at ~26 ppm is assigned to the P~O ligand on the basis of PPh_3 exchange. When pyridine is added to a solution of $Re(NPh)Br_2(PPh_3)(P\sim O)$, the doublets at −6 and 26 ppm are replaced by two singlets, one at −4 ppm for free PPh_3 and the other at 22 ppm for the new pyridine complex.

4. Concluding remarks

All Re(V) complexes prepared in this study contain phosphinophenolato ligands in the bidentate anionic $P\sim O^-$ form, with one phenolato oxygen atom *trans* to the multiple bond. It has been shown previously that the disubstituted $ReOX(Ph_2P\sim O)_2$ complexes with a *cis*-P,P 'twisted' octahedral structure were the only products isolated when 2 equiv. of $Ph_2P\sim OH$ were reacted on $ReOCl_3(PPh_3)_2$ in refluxing toluene. However, under the same conditions, $^iPr_2P\sim OH$ leads to monosubstituted $ReOX_2(PPh_3)(P\sim O)$ complexes, along with $ReOX(P\sim O)_2$. Therefore chelation of one P~OH ligand takes place easily but binding the second ligand is more difficult, observations that suggest that although P~OH is a stronger σ donor, its reactivity is hampered by its greater steric demand. The fact that the *trans*-P,P 'twisted' octahedral structure is favoured for all $ReOX(P\sim O)_2$ complexes indicates that the electronic effect is not the factor determining the stereochemistry of the complexes and, as a consequence, that the steric effect is important. The reaction of the phenylimido precursor with P~OH does not follow the same trends as the oxo precursor since both ligands give *trans*-P,P isomers. A possible explanation is that the imido phenyl group increases steric hindrance as a whole even for $Ph_2P\sim OH$.

Thus, the thermodynamic stability and the structural variety of the Re(V) complexes with P~O ligands, together with their presence as a single isomer, suggest that it is worth pursuing the development of these molecules as candidates for eventual applications as radiopharmaceuticals.

Acknowledgements

This work was supported by The Ministère Français de l'Enseignement Supérieur, de la Recherche et de la Technologie and the Centre National de la Recherche Scientifique (MD) which are gratefully acknowledged.

References

[1] F. Refosco, G. Bandoli, E. Deutsch, A. Duatti, U. Mazzi, A. Moresco, M. Nicolini, F. Tisato, in: M. Nicolini, G. Bandoli, U. Mazzi (Eds.), Technetium and Rhenium in Chemistry and Nuclear Medecine, SGEditorali, Padua, 3rd edn., 1990, p. 221.
[2] F. Refosco, F. Tisato, G. Bandoli, E. Deutsch, J. Chem. Soc., Dalton Trans. (1993) 2901.
[3] F. Connac, Y. Lucchese, M. Dartiguenave, A.L. Beauchamp, Inorg. Chem. 36 (1997) 256.
[4] H. Luo, I. Setyawati, S.J. Rettig, C. Orvig, Inorg. Chem. 34 (1995) 2287.
[5] C. Bolzati, F. Tisato, F. Refosco, G. Bandoli, A. Dolmella, Inorg. Chem. 35 (1996) 6221.

[6] C. Bolzati, F. Tisato, F. Refosco, G. Bandoli, Inorg. Chim. Acta 247 (1996) 125.
[7] C. Bolzati, F. Refosco, F. Tisato, G. Bandoli, A. Dolmella, Inorg. Chim. Acta 201 (1992) 7.
[8] F. Loiseau, Y. Lucchese, M. Dartiguenave, F. Bélanger-Gariépy, A.L. Beauchamp, Acta Crystallogr., Sect. C 52 (1996) 1996.
[9] F. Connac, Y. Lucchese, M. Gressier, M. Dartiguenave, A.L. Beauchamp, Inorg. Chim. Acta 304 (2000) 52.
[10] R.G. Carvell, R.W. Hilts, H. Luo, R. McDonald, Inorg. Chem. 38 (1999) 897.
[11] C.A. Tolman, W.C. Seidel, L.W. Gosser, J. Am. Chem. Soc. 96 (1974) 53.
[12] S.J. Moore, L.G. Marzilli, Inorg. Chem. 37 (1998) 5329.
[13] N. Johnson, C.J.L. Lock, G. Wilkinson, Inorg. Synth. 9 (1967) 145.
[14] J. Chatt, G.A. Rowe, J. Chem. Soc. (1962) 4019.
[15] G. La Monica, S. Cenini, Inorg. Chim. Acta 29 (1978) 183.
[16] J. Heinicke, R. Kadyrov, M.K. Kindermann, M. Koesling, P.G. Jones, Chem. Ber. 129 (1996) 1547.
[17] W.A. Nugent, J.M. Meyer, Metal–Ligand Multiple Bonds,Wiley Interscience, New York, 1988.
[18] P.E. Garrou, Chem. Rev. 81 (1981) 229.

PERGAMON

www.elsevier.nl/locate/poly

Polyhedron 19 (2000) 1117–1121

POLYHEDRON

Microporous networks co-assembled by both rigid and flexible building blocks

Jian-Min Li [a,*], Yu-Gen Zhang [b], Jing-Hua Chen [a], Lei Rui [b], Quan-Ming Wang [c], Xin-Tao Wu [c]

[a] *Department of Chemical Physics, University of Science and Technology of China, Hefei, Anhui 230026, People's Republic of China*
[b] *Department of Chemistry, University of Science and Technology of China, Hefei, Anhui 230026, People's Republic of China*
[c] *State Key Laboratory of Structural Chemistry, Fujian Institute of Research of Structure of Matter, Chinese Academy of Science, Fuzhou, Fujian 350002, People's Republic of China*

Received 10 January 2000; accepted 8 March 2000

Abstract

The porous networks of $[Cu_2(malonato)_2(bipy)(H_2O)_2]\cdot H_2O$ (**I**) and $[Cd(malonato)(py)(H_2O)]$ (**II**) were co-assembled by rigid 4,4′-bipyridine or pyridine and the flexible malonate ion. In the network of compound **I**, 4,4′-bipy acts as a bone, separating and supporting the flexible malonate–Cu units to form a nearly strain-free square framework and a chiral square cavity in the solid state. In compound **II**, the rigid pyridine rings sustain the network by saturating the coordination sphere of Cd(II) ion to avoid a high coordination number and self-inclusion, and to prevent the two-dimensional network from forming a non-porous phase. ©2000 Elsevier Science Ltd All rights reserved.

Keywords: Rigid and flexible ligands; Self-assembly; Supramolecules; X-ray structure

1. Introduction

It is becoming increasingly clear that transition metal-based self-assembly processes can lead to functional supramolecular frameworks that exhibit potential applications as electrical conductors [1] and molecular magnets [2,3] and in inclusion chemistry [4,5], molecular recognition [6,7] and catalysis [8,9]. Previous strategies of designing open frameworks mostly focused on using rigid rod-like or tritopic ligands (e.g. cyanide, bi- or tri-pyridyl, *p*-quinone, pyrazine, trimesic acid) as spacer ligands [8–12]. Nearly all the spacer ligands used have one or several aromatic rings as the basic components [13–15]. Although this rigidity and aromatic component can assist in the design of network, it frequently limits their ability to accommodate ionic and non-ionic guest species and limits the variety of framework compositions and topologies [16]. In contrast, the assembly of inorganic polymers by flexible ligands always resulted in the formation of non-porous phases [17–20]. The exploitation of spacers with conformational freedom is expected to play important roles in self-assembly via coordination, in which the flexible components of such linkers in a coordination polymer usually lead to interpretation and self-inclusion, reflecting both the properties of the rigid aromatic ring and flexible connector [21–24]. Combining both rigid bone and flexible tissue in one system is the basic character existing throughout nature [25–28]. To investigate the parameters contributing to the assembly of materials from different molecular building blocks, we recently aimed at constructing porous polymers by co-assembling both rigid (4,4′-bipyridine or pyridine) and flexible (malonate anion) ligands with transition metal ions. Here, we report the syntheses and structural characters of two complexes $[Cu_2(malonato)_2(bipy)(H_2O)_2]\cdot H_2O$ (**I**) and $[Cd(malonato)(py)(H_2O)]$ (**II**), bearing both flexible and rigid ligands. The structure of complex **I** has been partly communicated [29].

2. Results and discussion

2.1. Structure of $[Cu_2(malonato)_2(bipy)(H_2O)_2]\cdot H_2O$ (*I*)

Complex **I** was synthesized by the reaction of $Cu(C_3H_2O_4)\cdot 2H_2O$ and 4,4′-bipyridine in H_2O–EtOH at ambient temperature. X-ray analysis reveals that the malonate ion and 4,4′-bipyridine co-assembled with Cu(II) ion in compound **I** to form a two-dimensional square network possessing two kind of squares (Fig. 1). A small planar square was constructed with Cu(II) ions and malonate ions at each

* Corresponding author. Tel.: +86-551-3601113; fax: +86-551-363176; e-mail: zhangyg@ustc.edu.cn

0277-5387/00/$ - see front matter ©2000 Elsevier Science Ltd All rights reserved.
PII S0277-5387(00)00361-2

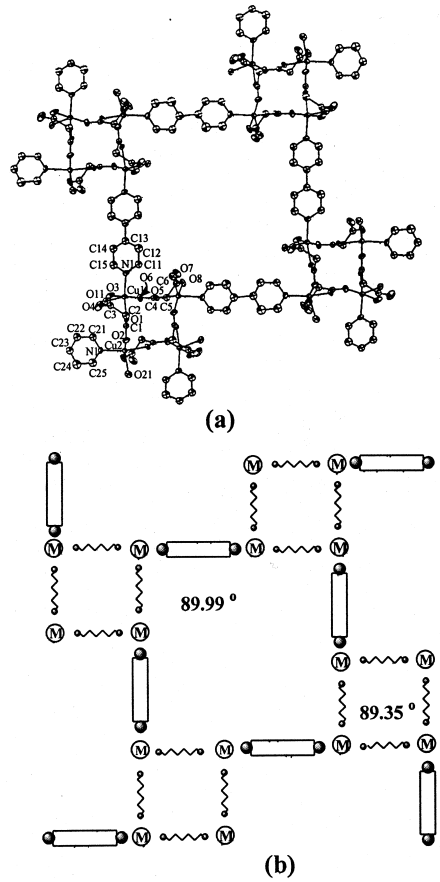


Fig. 1. (a) ORTEP diagram of compound **I** with labelling scheme. (b) Schematic representation of the rigid–flexible strain-free structure.

corner and side, respectively. Each Cu(II) is also bridged by one 4,4′-bipy, thus forming a large square with each edge shared by one malonate group and one 4,4′-bpy ligand. The coordination geometry about each Cu(II) is slightly distorted square pyramidal with three oxygen atoms from two different malonate ions and one nitrogen atom of 4,4′-bpy positioned in the basal plane and one water molecule occupying the apex position. The bond lengths observed in compound **I** are comparable to those found in similar structures (see Table 2) [30–35]. It is interesting that all the planar squares are distorted only to a very small extent, although the malonate ion is a typical flexible ligand. The square planar angles are 89.89(1) and 89.99(1)° in the large square and 89.25(3) and 89.35(3)° in the small one, very close to the ideal square planar. To the best of our knowledge, the square net motif in compound **I** is closest to the ideal square planar among similar 4,4′-bipy bridged networks. In the infinite network, the square planar angles are reported as ranging from 82.0 to 88.4° [8,9,15,36–41]. The ideal squares are only observed in zero-dimensional molecular cycles, for the right bond angles (90°) rule out the formation of other cyclic oligomers which must have significant ring strain [11,42]. Here, the rigid character of 4,4′-bpy is well preserved in this network and showed the co-effect of both rigid and flexible building blocks. Flexible malonate ions adopt a bridging position which enhances the stability of the two-dimensional network, adjusts the structural distortion and makes the network essentially strain-free, corresponding to the high-order square network. Rigid 4,4′-bpy functions as a bone linked by flexible tissue (small squares) to sustain and dominate the general formation of the network. The size of the squares of compound **I** have dimensions of $15.776(3) \times 15.786(2)$ Å and $4.644(2) \times 4.649(2)$ Å (Fig. 1). The two-dimensional networks are stacked parallel but in a staggered manner on each other along the *z*-axis, with an interplanar separation of 3.785 Å and angle of 45°. The packing of the two-dimensional polymers reveals that the small malonate rings in one layer fit exactly into the large rings in the next, almost as if the two rings are acting as templates for each other. The very short interplanar distance means that the networks are self-clathrated with the small squares of one layer fitting into the large squares of adjacent layers.

Complex **I** crystallizes in the chiral space group $P2_12_12_1$. It has crystallographically imposed C_2 symmetry with a half-cycle of the molecule in the asymmetric unit. Complex **I** is therefore a chiral infinite net array in the solid state. Therefore, no chiral auxiliary ligands are required [43–45]. Each edge of the small square, i.e. each pair of Cu2, has a helical structure. The overall structure of the small square in compound **I** could therefore be described as a cyclic helicate. The chirality of the small squares is succeeded by the large square of compound **I**, and forms large square cavities bearing chiral surroundings.

2.2. Structure of [Cd(malonato)(py)(H_2O)] (*II*)

Complex **II** was synthesized by the reaction of $(CdSO_4)_3 \cdot 7H_2O$, malonic acid and pyridine in aqueous solution. X-ray analysis reveals that complex **II** possesses a two-dimensional sheet structure (Fig. 2). Each Cd(II) atom is in an octahedral surrounding which is chelated by one malonate ion (forming a six-membered boat-type ring) and bound to carboxyl oxygen atoms of two adjacent six-membered boat-type rings. The apex positions are occupied by water and

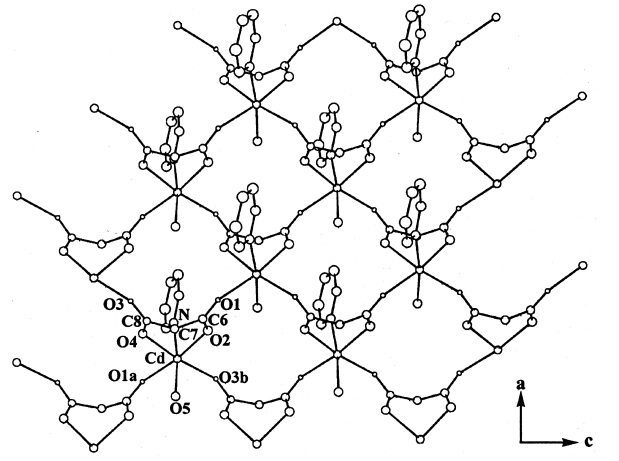


Fig. 2. Perspective view of the *ac* plane of the infinite two-dimensional layer sheet structure of compound **II**.

pyridine ligands, respectively. Every four adjacent Cd(II) atoms form a 16-membered large ring (Cd4O8C4) with size 5.71×5.58 Å. The four equatorial oxygen atoms are nearly coplanar with the Cd(II) atom and this coordination plane makes a 45° dihedral angle with the extended net plane (*ac* plane). Each equatorial coordination plane is perpendicular to four adjacent planes of bridged Cd octahedra. The N(pyridine)–Cd–O(H_2O) linkage is slightly bent (173.5(4)°) and nearly perpendicular to the equatorial coordination plane. The pyridine groups are alternatively located above and below the net plane. The malonate ion acts as a tetradentate ligand (chelate, bridge, bridge) in compound **II**. All boat-type six-membered malonato-Cd rings are arranged in one direction that lead to anisotropy of this network. Parallel layers stack along the *b*-axis and the interlayer distance is 9.105 Å (Fig. 3).

All malonate ligands in compound **II** act in the chelating mode to form a boat-type six-membered conformation and act as bridges to link adjacent metal ions, like the woof in the woven coordination polymer to form the two-dimensional network. Here, the rigid pyridine rings play an important role in sustaining this network by preventing it from intralayer shrinking, interlayer condensing, and by saturating the coordination space of Cd(II) ion to avoid a high coordination number and self-inclusion [25,30–35].

The flexibility of the malonate ion has been widely verified by X-ray structures of a series of malonate complexes [25–28,30–35,46–48]. It is also known that self-assembly of the malonate ion with metal ion always results in formation of a non-porous framework. Here, it is demonstrated that porous frameworks can be co-assembled by the flexible malonate ion accompanied by a rigid ligand. It is a new strategy for designing and constructing novel supramolecular topologies. The relation between the rigid building block and the flexible one is very important in designing frameworks with desirable topologies and architectures. In complex **I**, the rigid building block and the flexible one are co-assembled in the same layer. They are mutually linked, mutually sustained and adjusted to form a strain-free framework. The rigid and flexible blocks are separated by each other in the network of compound **I** and this is one key factor in the formation of chiral polyporous framework of compound **I**. By the bridging and chelating properties of flexible ligand malonate dianion, a chiral two-dimensional network with chiral large cavities is constructed (**I**). In complex **II**, the rigid ligand is pyridine, a terminal monodentate ligand. In contrast to compound **I**, the pyridine block is unable to separate the malonate–Cd units. But it is the rigid pyridine block that prevents the condensation of malonate–Cd network and separates the network layers. It is shown that the rigid template tends to lower the dimensionality and regularize a flexible system, whereas a flexible template decreases the structure strain in a rigid system. The co-assembly of both rigid and flexible ligands should be a very exciting strategy for the design of new materials having well-defined functions.

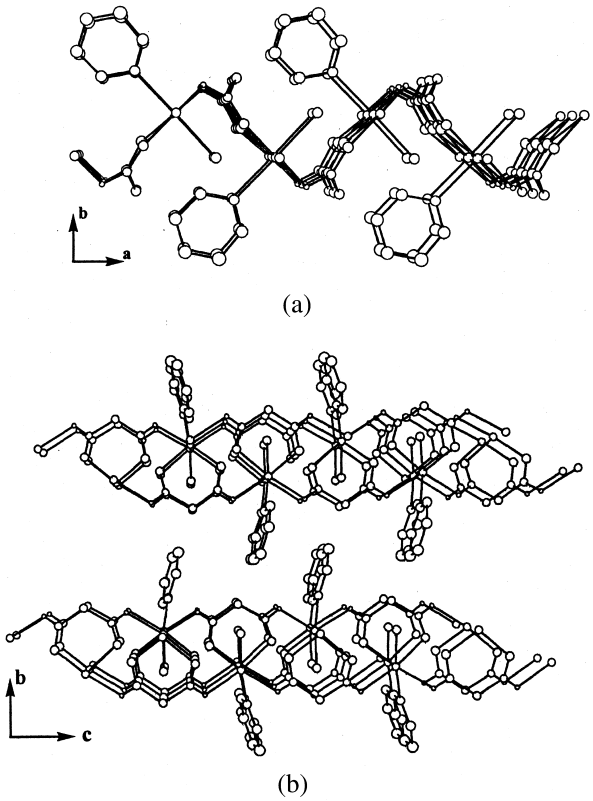


Fig. 3. (a) View of the layer structure of compound **II** projected onto the *ab* plane. (b) Packing of layers of compound **II** projected onto the *bc* plane.

3. Experimental

3.1. Materials and methods

All starting materials were purchased from Aldrich or other sources and used without further purification. Elemental analyses were carried out by the Structure Research Laboratory, University of Science and Technology of China.

3.2. Preparation of $Cu(C_3H_2O_4)\cdot 2H_2O$

To a mixture of copper(II) carbonate (2.0 mmol) and hot water (20 ml), malonic acid (1.9 mmol) was added and a dark blue solution was obtained. This was filtered and condensed to 5 ml and a large amount of crystals were obtained. *Anal*. Calc. for $CuC_3H_6O_6$: C, 17.70; H, 3.47. Found: C, 17.14; H, 3.59%.

3.3. Preparation of $[Cu_2(malonato)_2(bipy)(H_2O)_2]\cdot H_2O$ (*I*)

To an aqueous solution (30 ml) of $Cu(C_3H_2O_4)\cdot 2H_2O$ (1.0 mmol) an ethanol solution (10 ml) of 4,4′-bpy (0.5 mmol) was added. The initially formed very small amount of fine precipitate was filtered off, and the clear filtrate was allowed to stand for several days at ambient temperature to give deep-blue crystals. Yields in excess of 90% were

Table 1
Crystal data and structure refinement for compounds **I** and **II**

	I	**II**
Empirical formula	$C_{16}H_{18}Cu_2N_2O_{11}$	$C_8H_9CdNO_5$
Formula weight	543.42	311.57
Temperature (K)	293(2)	293(2)
Wavelength (Å)	0.71073	0.71073
Crystal system	orthorhombic	monoclinic
Space group	$P2_12_12_1$	$P2_1/c$
Unit cell dimensions		
a (Å)	16.348(3)	7.4411(4)
b (Å)	16.364(5)	18.2101(10)
c (Å)	7.570(1)	7.8112(4)
β (°)		91.4890(10)
Volume (Å^3)	2025.2(8)	1058.09(10)
Z	4	4
D_{calc} (g cm^{-3})	1.780	1.984
Absorption coefficient (mm^{-1})	2.170	1.057
F(000)	1104	618
Reflections collected	2075	5109
Independent reflections	2075	5109
Absorption correction	empirical	none
Maximum and minimum transmission	1.00 and 0.70	
Refinement method	full-matrix least-squares on F^2	full-matrix least-squares
Data/restraints/parameters	1579/0/199	1829/0/131
Goodness-of-fit on F^2	1.69	1.157
Final R indices [$I>2\sigma(I)$]	$R_1=0.055$, $wR_2=0.079$	$R_1=0.0859$, $wR_2=0.2413$
Largest difference peak and hole (e Å^{-3})	0.87 and −0.33	2.614 and −2.143

obtained. *Anal*. Calc. for compound **I**: C, 36.43; H, 3.44; N, 5.31. Found: C, 36.50; H, 3.21; N, 5.09%.

3.4. Preparation of [Cd(py)(malonate)] (II)

To an aqueous solution of $(CdSO_4)_3\cdot 7H_2O$ (0.333 mmol) was added pyridine (1 mmol) and malonic acid (1 mmol) with stirring. The pH was adjusted to 6 using dilute NaOH solution. Diffraction-quality crystals had grown after several days. Yield (291 mg, 92%). *Anal*. Calc. for compound **II**: C, 30.77; H, 2.88; N, 4.49. Found: C, 30.87; H, 2.91; N, 4.50%.

3.5. Crystal structure determinations

Data were measured on a Rigaku AFC5R diffractometer for complex **I** and an Enraf-Nonius CAD4 diffractometer for complex **II** with graphite-monochromated Mo Kα radiation at 293 K. Cell constants and orientation matrix for data collection were obtained from least-squares refinement, using the setting angles of 20 reflections in the range $8<\theta<27.5°$ for compound **I** and $2.24<\theta<24.93°$ for compound **II**, measured by the computer-controlled diagonal-slit method of centering. Scattering factors were taken from Cromer and Waber [49]. The ω–2θ scan mode with a maximum 2θ value of 50.0° was used to collect intensity data. The data were corrected for Lorentz polarization effects. The structure was solved by direct methods (SHELXS-86) and refined by full-matrix least-squares calculation (SHELXL-93). The non-hydrogen atoms were refined anisotropically. Hydrogen atoms were included, but their positions were not refined. All calculations were performed on an INDY workstation using a Mo1EN/PC [50]. Details of crystal data, collection and refinement of the two complexes are listed in Table 1. The selected bond distances and angles of compounds **I** and **II** are presented in Tables 2 and 3.

Table 2
Selected bond lengths (Å) and angles (°) for compound **I**

Cu1–O1	1.996(7)	Cu1–O3	1.93(1)
Cu1–O6	1.98(1)	Cu1–O11	2.20(1)
Cu1–N1	2.06(1)	Cu2–O2	1.97(1)
Cu2–O5 [a]	1.972(7)	Cu2–O8 [a]	1.93(1)
Cu2–O21	2.191(9)	Cu2–N2	2.06(2)
O1–Cu1–O3	89.6(4)	O1–Cu1–O6	89.3(4)
O1–Cu1–O11	91.4(3)	O1–Cu1–N1	166.2(4)
O3–Cu1–O6	174.9(4)	O3–Cu1–O11	93.2(4)
O3–Cu1–N1	87.1(4)	O6–Cu1–O11	91.7(4)
O6–Cu1–N1	92.8(4)	O11–Cu1–N1	102.1(4)
O2–Cu2–O5 [a]	89.5(4)	O2–Cu2–O8 [a]	174.1(4)
O2–Cu2–O21	92.5(3)	O2–Cu2–N2	167.1(5)
O5 [a]–Cu2–O8 [a]	89.8(4)	O5 [a]–Cu2–O21	92.4(3)
O5 [a]–Cu2–N2	167.1(5)	O8 [a]–Cu2–O21	93.3(4)
O8 [a]–Cu2–N2	87.8(4)	O21–Cu2–N2	100.4(4)

[a] $1-x, -y, z$.

Table 3
Selected bond lengths (Å) and angles (°) for compound **II**

Cd–O(3) [a]	2.301(11)	Cd–O(1) [b]	2.302(11)
Cd–O(4)	2.307(11)	Cd–O(2)	2.332(10)
Cd–N	2.334(13)	Cd–O(5)	2.357(11)
O(1)–C(6)	1.26(2)	O(1)–Cd [c]	2.302(11)
O(2)–C(6)	1.23(2)	O(3)–C(8)	1.23(2)
O(3)–Cd [d]	2.301(11)	O(4)–C(8)	1.28(2)
O(3) [a]–Cd–O(1) [b]	97.9(4)	O(3) [a]–Cd–O(4)	171.6(4)
O(1) [b]–Cd–O(4)	90.1(4)	O(3) [a]–Cd–O(2)	91.1(4)
O(1) [b]–Cd–O(2)	171.0(4)	O(4)–Cd–O(2)	80.9(4)
O(3) [a]–Cd–N	86.7(4)	O(1) [b]–Cd–N	93.0(4)
O(4)–Cd–N	90.3(4)	O(2)–Cd–N	87.1(4)
O(3) [a]–Cd–O(5)	89.2(4)	O(1) [b]–Cd–O(5)	92.5(4)
O(4)–Cd–O(5)	93.0(4)	O(2)–Cd–O(5)	87.9(4)
N–Cd–O(5)	173.5(4)		

[a] Symmetry transformations used to generate equivalent atoms: $x+1/2, -y+3/2, z-1/2$.
[b] Symmetry transformations used to generate equivalent atoms: $x-1/2, -y+3/2, z-1/2$.
[c] Symmetry transformations used to generate equivalent atoms: $x+1/2, -y+3/2, z+1/2$.
[d] Symmetry transformations used to generate equivalent atoms: $x-1/2, -y+3/2, z+1/2$.

Supplementary data

Supplementary data are available from the Cambridge Crystallographic Data Centre, 12 Union Road, Cambridge CB2 1EZ, UK (fax: +44-1223-336033; e-mail: deposit@ccdc.cam.ac.uk) on request, quoting the deposition numbers CCDC 182464 for compound **I** and CCDC 105841 for compound **II**.

Acknowledgements

Financial support was provided by NSFC Grant No. 29871027, State Key Laboratory of Structural Chemistry, Chinese Ministry of Education.

References

[1] O. Ermer, Adv. Mater. 3 (1991) 608.
[2] J.C. Nelson, J.G. Saven, J.S. Moore, P.G. Wolynes, Science 277 (1997) 1793.
[3] J.A. Real, E. Andres, M.C. Munoz, M. Julve, T. Granier, A. Bousseksou, F. Varret, Science 268 (1995) 265.
[4] T.L. Hennigar, D.C. MacQuarrie, P. Losier, R.D. Rogers, M.J. Zaworotko, Angew. Chem., Int. Ed. Engl. 36 (1997) 972.
[5] P.J. Stang, N.E. Persky, J. Manna, J. Am. Chem. Soc. 119 (1997) 4777.
[6] B.F. Hoskin, R. Robson, J. Am. Chem. Soc. 112 (1990) 1546.
[7] P. Losier, M.J. Zawarotko, Angew. Chem., Int. Ed. Engl. 35 (1996) 2779.
[8] M. Fujita, Y.J. Kwon, S. Washizu, K. Ogura, J. Am. Chem. Soc. 116 (1994) 1151.
[9] K.N. Power, T.L. Hennigar, M.J. Zaworotko, Chem. Commun. (1998) 595.
[10] S.S.-Y. Chui, S.M.-F. Lo, J.P.H. Charmant, A.G. Orpen, I.D. Williams, Science 283 (1999) 1148.
[11] P.J. Stang, B. Olenyuk, Acc. Chem. Res. 30 (1997) 502.
[12] D. Philp, J.F. Stoddart, Angew. Chem., Int. Ed. Engl. 35 (1996) 1154.
[13] O.M. Yaghi, H. Li, C. Davis, D. Richardson, T.L. Groy, Acc. Chem. Res. 31 (1998) 474.
[14] S. Kitagawa, M. Kondo, Bull. Chem. Soc. Jpn. 71 (1998) 1739.
[15] Y. Zhang, J. Li, W. Deng, M. Nishiura, T. Imamoto, Chem. Lett. (1999) 195.
[16] C.A. Hunter, Angew. Chem., Int. Ed. Engl. 34 (1995) 1079.
[17] S.R. Batten, R. Robson, Angew. Chem., Int. Ed. Engl. 37 (1998) 1461.
[18] C. Piguet, G. Bernardinelli, G. Hopfgartner, Chem. Rev. 97 (1997) 2005.
[19] D.S. Lawrence, T. Jiang, M. Levett, Chem. Rev. 95 (1995) 2229.
[20] A.E. Rowan, R.J.M. Nolte, Angew. Chem., Int. Ed. Engl. 37 (1998) 63.
[21] Y. Zhang, M. Nishiura, J. Li, W. Deng, T. Imamoto, Inorg. Chem. 38 (1999) 825.
[22] O.-S. Jung, S.H. Park, D.C. Kim, K.M. Kim, Inorg. Chem. 37 (1998) 610.
[23] M. Fujita, S. Nagao, M. Iida, K. Ogata, K. Ogura, J. Am. Chem. Soc. 115 (1993) 1574.
[24] R.V. Stone, D.I. Yoon, R.M. Calhoun, J.T. Hupp, J. Am. Chem. Soc. 117 (1995) 11813.
[25] D.E. Ingber, J. Cell Sci. 104 (1993) 613.
[26] N. Wang, J.P. Butler, D.E. Ingber, Science 260 (1993) 1124.
[27] C.S. Chen, M. Mrksich, S. Huang, G.M. Whitesides, D.E. Ingber, Science 276 (1997) 1425.
[28] D.E. Ingber, Annu. Rev. Physiol. 59 (1997) 575.
[29] J. Li, H. Zeng, J. Chen, Q. Wang, X. Wu, Chem. Commun. (1997) 1213.
[30] Y. Zhang, J. Li, J. Chen, W. Deng, M. Nishiura, T. Imamoto, X. Wu, Q. Wang (in preparation).
[31] I. Muro, F.A. Mautner, M. Insausti, L. Lezama, M.I. Arriortua, T. Rojo, Inorg. Chem. 37 (1998) 3243.
[32] E. Suresh, M.M. Bhadbhade, Acta Crystallogr., Sect. C 53 (1997) 193.
[33] A. Tosik, L. Sieron, M. Bukowska-Strzyzewska, Acta Crystallogr., Sect. C 51 (1995) 1987.
[34] D. Chattopadhyay, S.K. Chattopadhyay, P.R. Lowe, J. Chem. Soc., Dalton Trans. (1993) 913.
[35] W.L. Kwik, K.P. Ang, H.S.O. Chan, J. Chem. Soc., Dalton Trans. (1986) 2519.
[36] F. Lloret, G.D. Munno, M. Julve, J. Cano, R. Ruiz, A. Caneschi, Angew. Chem., Int. Ed. Engl. 37 (1998) 135.
[37] L.R. MacGillivray, R.H. Groeneman, J.L. Atwood, J. Am. Chem. Soc. 120 (1998) 2676.
[38] M. Kondo, T. Yoshitomi, K. Seki, H. Matsuzaka, S. Kitagawa, Angew. Chem., Int. Ed. Engl. 36 (1997) 1725.
[39] S.D. Huang, R. Xiong, Polyhedron 16 (1997) 3929.
[40] S. Subramanian, M.J. Zaworotko, Angew. Chem., Int. Ed. Engl. 34 (1995) 2127.
[41] J. Lu, T. Paliwada, S.C. Lim, C. Yu, T. Niu, A.J. Jacobson, Inorg. Chem. 36 (1997) 923.
[42] M. Fujita, J. Yazaki, K. Ogura, J. Am. Chem. Soc. 12 (1990) 5645.
[43] B. Olenyuk, J.A. Whiteford, P.J. Stang, J. Am. Chem. Soc. 118 (1996) 8211.
[44] P.J. Stang, B. Olenyuk, D.C. Muddiman, R.D. Smith, Organometallics 16 (1997) 3094.
[45] Y. Zhang, S. Wang, G.D. Enright, S.R. Breeze, J. Am. Chem. Soc. 120 (1998) 9398.
[46] K.H. Chung, E. Hong, Y. Do, C.H. Moon, J. Chem. Soc., Chem. Commun. (1995) 2333.
[47] K.H. Chung, E. Hong, Y. Do, C.H. Moon, J. Chem. Soc., Dalton Trans. (1996) 3363.
[48] M.L. Post, J. Trotter, J. Chem. Soc., Dalton Trans. (1974) 674, 1922.
[49] D.T. Cromer, J.T. Waber, International Tables for X-ray Crystallography, IV, 1974, The Kynoch Press, Birmingham, Table 2.2B.
[50] MOLEN, An Interactive Structure Solution Procedure, Enraf-Nonius, Delft, 1990.

PERGAMON

www.elsevier.nl/locate/poly

Polyhedron 19 (2000) 1123–1131

POLYHEDRON

An electron spin resonance study of coordination modes in the copper(II)–histamine and copper(II)–L-histidine systems in fluid aqueous solution

Terézia Szabó-Plánka [a,*], Antal Rockenbauer [b], László Korecz [b], Dorottya Nagy [a]

[a] *Department of Physical Chemistry, University of Szeged, P.O. Box 105, H-6701 Szeged, Hungary*

[b] *Chemical Research Center, Institute of Chemistry, Hungarian Academy of Sciences, H-1525 Budapest, Hungary*

Received 20 January 2000; accepted 10 March 2000

Abstract

Copper(II)–histamine and copper(II)–L-histidine equilibrium systems were studied in fluid aqueous solution by ESR spectroscopy. Eighty-seven spectra taken in a circulating system at various ligand-to-metal concentration ratios and pH were analysed. The experimental curves were decomposed to one to four component spectra which were built up from the hyperfine lines of ^{63}Cu and ^{65}Cu, and a maximum of four non-equivalent ^{14}N nuclei. The isotropic ESR parameters (*g*-factors, hyperfine coupling constants and relaxation parameters) and the relative concentrations of the different species were optimized. New, pH-potentiometrically non-identified species were also considered in the equilibrium models. In the copper(II)–histamine system the complex $[CuLH_{-2}]$ was added to the species $[CuLH]^{3+}$, $[CuL]^{2+}$, $[CuLH_{-1}]^{+}$, $[Cu_2L_2H_{-2}]$, $[CuL_2H]^{3+}$ and $[CuL_2]^{2+}$. In the copper(II)–L-histidine system, in addition to the complexes $[CuLH]^{2+}$, $[CuL]^{+}$, $[CuLH_{-1}]$, $[Cu_2L_2H_{-2}]$, $[CuL_2H_2]^{2+}$, $[CuL_2H]^{+}$ and $[CuL_2]$, the new species $[CuLH_2]^{3+}$ and $[CuLH_{-2}]^{-}$ were found. The relative concentrations obtained from the ESR spectra are in good accordance with the concentrations calculated from the literature pH-potentiometric formation constants. The two ligands in their 'LH' states are bound differently: the histamine by the imidazole, and the L-histidine through the amino and the carboxylate groups in equatorial positions (complexes $[CuLH]$, $[CuL_2H]$ and $[CuL_2H_2]$). For the $[CuL]$, $[CuL_2H]$ and $[CuL_2]$ complexes of both histamine and L-histidine, the first 'L' ligand is coordinated equatorially by the amino and imidazole nitrogens. The second 'L' ligand in the $[CuL_2]$ complexes is either bound in the former way, or its imidazole group occupies an axial site. The carboxylate group of L-histidine is coordinated to the metal ion in each complex, in either an equatorial or an axial position. The deprotonation of the $[CuL]$ complex takes place from the imidazole ring, which is followed by the proton loss of the equatorial water molecule in the highly alkaline region. ©2000 Elsevier Science Ltd All rights reserved.

Keywords: Electron spin resonance; Copper(II) complexes; Coordination modes; Histamine; L-Histidine; Isomerism

1. Introduction

The complex bis(L-histidinato)copper(II) of biological importance is a good example for the difficulties and controversy encountered in the investigation of coordination modes in solution. Histamine-like equatorial binding through the amino and imidazole nitrogen atoms of both ligands was suggested by CD [1], Raman [2] and electronic [3] spectral studies, and on the basis of 13-C and 1-H NMR relaxation evidence [4]. At the same time, other NMR [5] and visible spectral [6] data were interpreted by the histamine-like equatorial coordination of the first ligand, but the glycine-like equatorial binding of the second ligand by the amino nitrogen and carboxylate oxygen atoms. Other works showed the co-existence of both structures. Goodman et al. [7] analysed the superhyperfine (shf) structure in the high-field ^{63}Cu line of the second-derivative fluid-phase ESR spectrum. They obtained 50% relative concentration for both species. The same isomeric equilibrium was supported by CD and visible spectral evidence [8]. Valensin et al. found 24% 4N and 76% 3N isomers by 13-C and 1-H NMR relaxation measurements [9]. Pasenkiewicz-Gierula et al. [10] obtained 80% isomer of bis(histamine)-like coordination and 20% complex of mixed (histamine- and glycine-like) binding mode by ESR studies; they described the liquid-phase spectrum as that of fast-tumbling molecules of axial symmetry, fitting the anisotropic ESR parameters and the rotation correlation time.

Recently, we have developed a new computer program [11] for the decomposition of multicomponent liquid-phase

* Corresponding author. Tel.: +36-62-544-612; fax: +36-62-544-652; e-mail: szabot@chem.u-szeged.hu

0277-5387/00/$ - see front matter ©2000 Elsevier Science Ltd All rights reserved.
PII S0277-5387(00)00364-8

ESR spectra, which has been successfully applied to obtain the isotropic ESR parameters and the relative concentrations of the major and minor complexes in the copper(II)–glycylglycine [12] and copper(II)–L-serine [13] systems. For the bis complexes, equilibria of various coordination modes have been found.

In the present paper we report the results of an ESR study of the copper(II)–histamine and copper(II)–L-histidine systems. The aim of our work was to identify all complexes which form in fluid aqueous solution, including the possible isomers of the complex bis(L-histidinato)copper(II), and to characterize the modes of coordination for these species on the basis of their ESR parameters. We also scrutinized the real nature of 'histamine-like' coordination, since structural identification of the histidine complexes is generally based on comparison with the analogous histamine complexes. Furthermore, comparison of the corresponding histamine and histidine complexes may clarify the role of the carboxyl group in the coordination.

2. Experimental

2.1. Reagents and solutions

Reagents of analytical grade from Reanal (Hungary) were used without further purification. The neutral ligand histamine is denoted by L, while the zwitterionic L-histidine is symbolized by HL. The copper(II) concentration of the solutions was 5 mmol dm^{-3}. It seemed reasonable to make solutions in which the various species are predominant or form in as high a concentration as possible, so that we obtain the most reliable parameter values. At the same time, solutions with comparable concentrations of the species were also needed, mainly to verify the concentration distribution, although an important condition was that at most four complexes be present in a solution, since the EPR program allows decomposition of one to four component spectra. Accordingly, the ligand-to-metal concentration ratios were 1:1 and 20:1 in the case of histamine, and 1:1, 2:1, 4:1 and 20:1 for the copper(II)–L-histidine system. The optimum pH values were chosen according to the species distribution curves, which were calculated by the PSEQUAD program [14] from literature formation constants [15–20]. The pH was adjusted with HCl, then NaOH to an accuracy of 0.01 pH unit using a RADELKIS OP208/1 pH meter equipped with a RADIOMETER GK2401C combined glass electrode. The electrode was calibrated with IUPAC standard buffers from RADIOMETER.

2.2. ESR measurements

A stock solution of 20 cm^3 volume was titrated under argon atmosphere. The sample was mixed by bubbling the gas through the solution. A MASTERFLEX CL peristaltic pump ensured the circulation (14 cm^3 min^{-1}) of the solution through the capillary tube in the cavity. The ESR spectra were taken after 3 min circulation at the chosen pH at room temperature (291 K) on an upgraded JEOL JES-FE3X spectrometer with 100 kHz field modulation, using a manganese(II)-doped MgO powder for the calibration of g-measurements. A Lake Shore model 647 magnet power supply and a Stanford model SR830 DSP lock-in amplifier were applied. The field was measured by a temperature-stabilized Hall probe with an accuracy of 10^{-5} T. The spectrometer was controlled by a Pentium 100 computer. The spectrum of the capillary tube filled with distilled water was recorded together with the Mn(II)-doped MgO under the same conditions. This curve was subtracted from the spectra of the solutions.

2.3. Evaluation of spectra

The copper(II) chloride, used to make the stock solution, was a natural mixture of isotopes, therefore the spectrum of each species was calculated as the superposition of spectra containing ^{63}Cu and ^{65}Cu according to their natural abundances. The different widths of copper hyperfine lines were taken into consideration by fitting the relaxation parameters [21,22] α, β, γ, where $\sigma_{MI} = \alpha + \beta M_I + \gamma M_I^2$. The parameter g_0, the hyperfine (hf) coupling constant A_0, the nitrogen superhyperfine coupling constants a_{N0}, the above relaxation parameters, and the relative concentration of each species were varied, until the sum of the squares of differences between the calculated and measured intensities (SSQD) reached its minimum. The spectral fit is characterized by the average square deviation SQD (i.e. SSQD divided by the number of spectral points, 2000). The concentration of each species was related to the overall concentration of ESR-active species.

In the first step we evaluated those spectra which are dominated by one complex; this resulted in the ESR parameters of the major species. Next we proceeded to spectra in which the previously neglected minor complexes gain importance. Then parameters of new species were optimized, while those of known complexes were fixed. Iteration proceeded by analysing again the first spectra in which the minor components with fixed parameter sets were considered too. This procedure only allows the use of a reasonable number of adjusted parameters (no more than 20) in each consecutive step. The sensitivity of spectral fit to the various parameters was monitored by the values CNF (CNF is defined as the variation of the respective parameter that increases the SQD by the value of the square noise of the spectrum). They give the criterion for a given spectrum which parameter set(s) should be fixed (at the averages obtained from other spectra). The CNF values for the parameters of the species in low concentrations (below 10%) are large. In the computation of the average values and the standard deviations of the parameters, only the data of those spectra were considered in which the respective parameter set was optimized.

The Fermi term K was derived from two adjusted parameters: the isotropic hf coupling constant A_0 and g_0 as $K=A_0+P(g_0-g_e)$, where $P=0.036$ cm^{-1} is the dipole coefficient of the copper(II) ion and $g_e=2.0023$ is the free electron g-factor [23,24].

3. Results and discussion

3.1. Spectral fitting

The rate of interconversion between the different species is considered to be slow on the ESR time-scale, since the experimental curves could be well described as sums of individual spectra. A Lorentzian lineshape gave a satisfactory fit in all cases. Fig. 1 illustrates that the ESR spectra after the elimination of the 'glass' signal allow an excellent spectral fit. Typically, the average deviation of the calculated and measured intensities was 1.2–1.5 times as much as the noise.

3.2. Distribution of copper(II) amongst different species

Besides the good spectral fit, we rigorously insisted on another criterion, when verifying the equilibrium model for a system. A large number of spectra were analysed, and we accepted the set of species forming under the chosen conditions only if the ESR parameters of the different complexes did not show a systematic change with either the pH or the ligand concentration.

For the copper(II)–histamine system, in acidic and neutral solutions, the formation of the complexes $[CuLH]^{3+}$, $[CuL]^{2+}$, $[CuL_2H]^{3+}$ and $[CuL_2]^{2+}$ is generally accepted on the basis of pH-metric studies [15,16,25]. In equimolar solution above pH ~ 6 a deprotonated species, the complex $[Cu_2L_2H_{-2}]^{2+}$, was also shown [15,16], together with the monomer $[CuLH_{-1}]^{+}$ [16,25]. The corresponding concentration distribution curves are shown in Fig. 2. Our ESR results are in accordance with the above model (Fig. 2). The only difference is that the complex $[CuLH]^{3+}$ was formed in higher concentration than was expected on the basis of pH-metric data. Therefore, instead of the literature value of 12.88 [15], we used 13.2 as an estimate for the formation constant ($\log \beta_{111}$) of the species $[CuLH]^{3+}$ during the calculation of the distribution curves. Then the relative concentrations of the various species, obtained from the ESR spectra, agreed well with the calculated concentrations (Fig. 2). In equimolar solution over pH ~ 6, a considerable decrease in the ESR intensity was accompanied with the formation of the complex $[Cu_2L_2H_{-2}]^{2+}$. This fact confirms that the dinuclear complex is ESR inactive. The distributrion curve (Fig. 2) shows that some $[CuL_2]^{2+}$ complex is also present in addition to the dimer. The question is whether the complex $[CuLH_{-1}]^{+}$ forms [25,16], or not [15]. The spectra in the slightly alkaline pH region could not be described only with the parameters of the complex $[CuL_2]^{2+}$; they were of a mixed character. Their very low intensity, however, made the exact

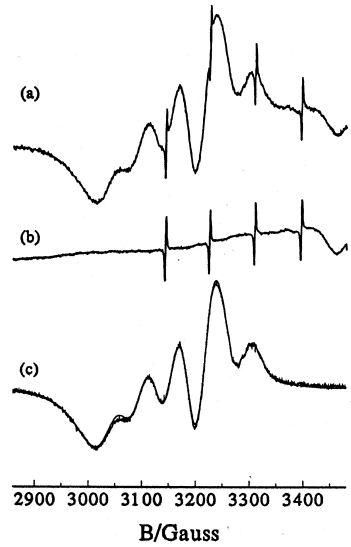


Fig. 1. The ESR spectra taken in equimolar solution of copper(II) and L-histidine at pH 4.42. (a) Spectrum together with the marker lines of Mn(II), (b) curve for the capillary filled with distilled water together with the marker lines, taken after titration, (c) corrected experimental spectrum (noisy curve) and the curve calculated as the superposition of spectra for the species Cu^{2+}, $[CuLH]^{2+}$, $[CuL]^{+}$ and $[CuL_2H]^{+}$.

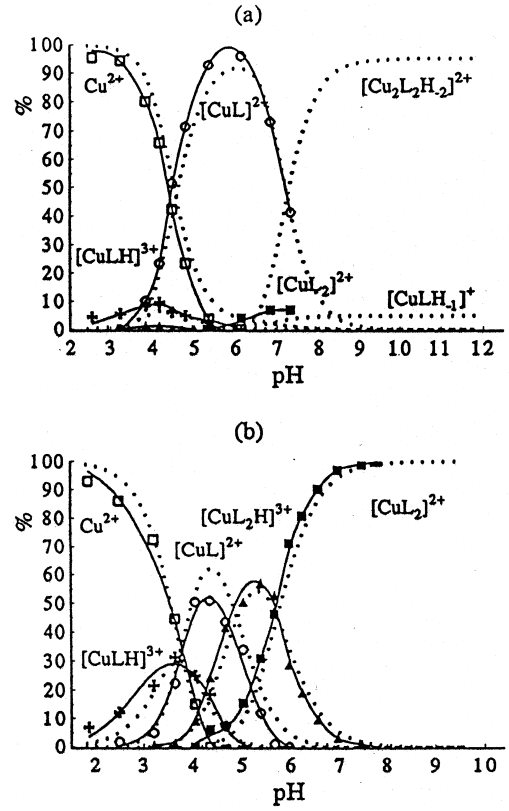


Fig. 2. Species distribution curves for the copper(II)–histamine system: (a) in equimolar solution, and (b) at a ligand-to-metal concentration ratio 20:1. The copper(II) concentration is 5 mM. Dotted lines show the concentrations of the complexes $Cu_pL_qH_r$, which were calculated from literature formation constants β_{pqr}: $\log \beta_{011}=9.81$, $\log \beta_{012}=15.84$, $\log \beta_{111}=12.88$, $\log \beta_{110}=9.56$, $\log \beta_{121}=21.82$, $\log \beta_{120}=16.06$ [15], $\log \beta_{11-1}=1.2$, and $\log \beta_{22-2}=7.0$ [16]; symbols connected by a solid line show relative concentrations from the ESR spectra.

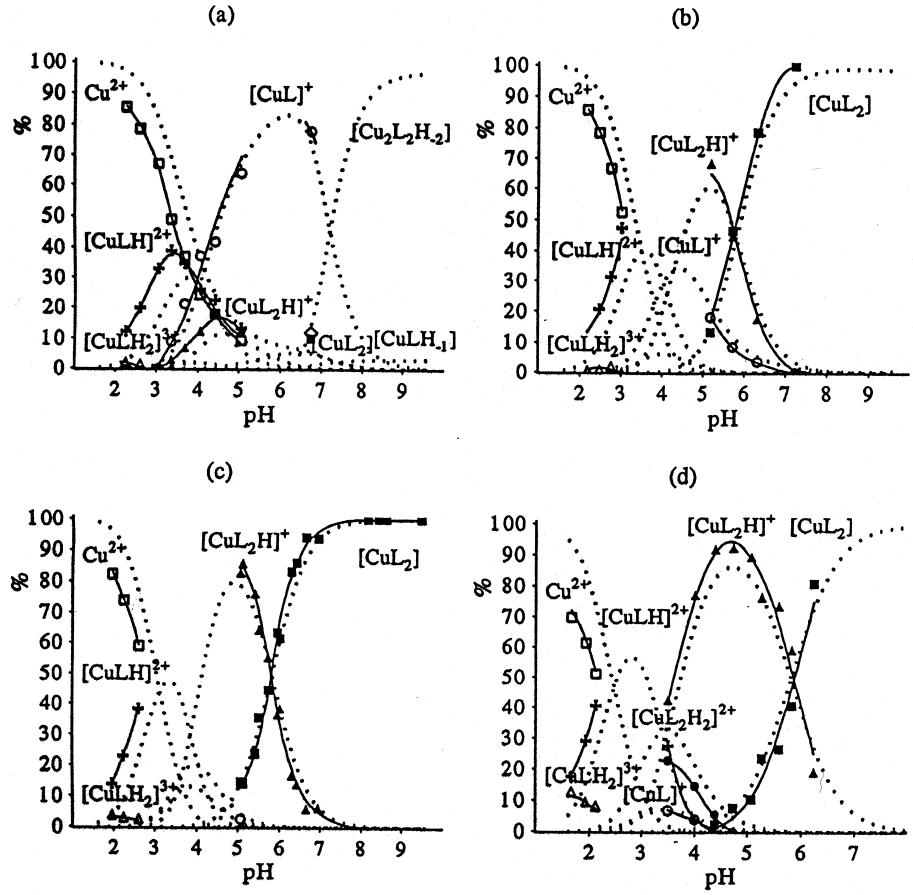


Fig. 3. Species distribution curves for the copper(II)–L-histidine system: (a) in equimolar solution; (b) at a ligand-to-metal concentration ratio 2:1; (c) at a ligand-to-metal concentration ratio 4:1; (d) at a ligand-to-metal concentration ratio 20:1. The copper(II) concentration is 5 mM. Dotted lines show the concentrations of the complexes $Cu_pL_qH_r$, which were calculated from literature formation constants β_{pqr}: $\log \beta_{011} = 9.06$, $\log \beta_{012} = 15.08$, $\log \beta_{013} = 16.62$, $\log \beta_{111} = 14.14$, $\log \beta_{110} = 10.15$, $\log \beta_{122} = 27.27$, $\log \beta_{121} = 23.83$, $\log \beta_{120} = 18.03$ [17], $\log \beta_{11-1} = 2.47$ [18,19], and $\log \beta_{22-2} = 8.0$ [20]; symbols connected by a solid line show relative concentrations from the ESR spectra.

evaluation impossible. The presence of a few per cent of the monomer $[CuLH_{-1}]^+$ really seems likely. Over pH ~ 11, a slow increase in intensity was observed in parallel with the formation of a new deprotonated ESR-active species, the complex $[CuLH_{-2}]$.

The pH-potentiometric measurements for the copper(II)–L-histidine system were interpreted in terms of the formation of the complexes $[CuLH]^{2+}$, $[CuL]^+$, $[Cu_2L_2H_{-2}]$, $[CuL_2H_2]^{2+}$ $[CuL_2H]^+$ and $[CuL_2]$ [17–20], and in equimolar alkaline solutions the presence of the complex $[CuLH_{-1}]$ was also assumed [18,19,25]. Our ESR results support the formation of all these species. In addition, we found two other complexes. In acidic solutions the ESR parameters of the aqua complex differed from those obtained in the absence of the ligand. The difference depended on the pH, and varied also with the ligand concentration. These facts suggested the coordination of the protonated amino acid $[LH_2]^+$ to the metal ion too. Completing the equilibrium model with the $[CuLH_2]^{3+}$ complex, the above anomalies ceased. As compared to the copper(II)–histamine system, another difference was that in equimolar alkaline solutions the deprotonated mono complex $[CuLH_{-1}]$ formed in a significantly higher concentration with the L-histidine ligand: we found in this region an intensity decrease of less extent than with the copper(II)–histamine system. From the amplitude ratio of the high-field copper peak to the manganese lines of the external standard in the cases of $[CuLH_{-1}]$ and $[CuL]^+$, we estimated the relative concentration of the $[CuLH_{-1}]$ complex to be about 20%, if the small linewidth change was also considered. This concentration corresponds to a formation constant of the complex larger than 1.5 [25], and closer to the other pH-metric $\log \beta_{11-1}$ of 2.47 [18,19]. Therefore we used this latter value for calculation of the concentration distribution (Fig. 3). With the above modifications in the strongly acidic and alkaline pH regions, the agreement between our relative concentrations and the pH-metric concentrations is good (Fig. 3). The relatively high concentration of the $[CuLH_{-1}]$ complex allowed us to obtain its ESR parameters, and to follow the deprotonation process leading to the formation of the $[CuLH_{-2}]^-$ complex over pH ~ 11. It should be noted that the interconversion of the deprotonated mono complexes proved to be reversible: their parameters obtained from the spectra taken during the 'ordinary' titration were in good agreement with the data gained

from the spectra recorded during the 'backward' titration of a strongly alkaline solution with HCl. That is, the copper(II)-catalysed oxidation of the ligand [25] could be neglected in argon atmosphere during the relatively short period of measuring the ESR spectra.

At excess of both ligands, in slightly acidic solution the species $[CuL_2H]$ is formed in high concentration (Figs. 2 and 3). Its ESR spectrum could be described well as a one-component curve with a 3N shf pattern, suggesting one kind of coordination in this complex.

The species $[CuL_2]$ is predominant at ligand excess in slightly alkaline media. In the case of the L-histidine complex an isomeric equilibrium was pointed out [7–10]. Our results also support the presence of different structures in this species: a much better agreement of the calculated and measured intensities could be achieved if the experimental curves were calculated as sums of two component spectra. The spectrum of lower g_0 and A_0 (spectrum 1) gave the major, while that of higher g_0 and A_0 (spectrum 2) the minor contribution to the overall curve. The SQD values were reduced by 45–50% as compared to those for the one-component model. The equilibrium was supposed to occur between the histamine-like equatorial binding of both ligands (4N coordination) and the mixed (glycine and histamine) type equatorial ligation (3N coordination) [7–10]. The question is, whether spectrum 1 is to be assigned to the 4N and spectrum 2 to the 3N molecules ('4N + 3N' model) or vice versa ('3N + 4N' model). Unfortunately, the analysis of the shf structure alone did not offer unambiguous proof for or against these models, since a spectral fit of the same quality could be obtained for them. Moreover, the '4N + 4N' model, which corresponds to a possible geometric isomerism of bis(histamine) coordination, could not be distinguished from the former models. The differences in SQD between the various models for the same spectra were 1–4%. It was striking, however, that spectrum 1 could be described well in all cases by a shf pattern of four equivalent nitrogen nuclei (models '4N + 3N' and '4N + 4N'), and spectrum 2 by the 3N pattern ('4N + 3N' model). At the same time, the assumption of a 4N splitting for the spectrum 2 (models '3N + 4N' and '4N + 4N') resulted in unreasonably low shf coupling constants (average value 8–9 G) compared to the other complexes in this system (Table 1) and to complexes of similar ligands [26]. It was only the '4N + 3N' model which resulted in reasonable shf coupling constants for both isomers. Further evidence against the '4N + 4N' model is that the CD curves indicated unambiguously the presence of the glycine-like bonded L-histidine in this complex [8]. At the same time, two additional facts support the '4N + 3N' model: (1) the 4N coordination represents a stronger ligand field which is likely to reduce g_0, compared to the 3N species (see details in Section 3.3); (2) the CD curves are highly dominated by the ligands of histamine-like binding [8], thus a higher concentration is expected for the 4N isomer. Accordingly, for the $[CuL_2]$ complex we assigned the 4N shf pattern to the major component spectrum of lower g_0 and A_0, while the 3N shf splitting was assigned to the minor component curve of higher g_0 and A_0. This model resulted in a good spectral fit also for the other spectra; the parameters and the weights of the component spectra did not depend on either the pH or the ligand concentration.

Our interpretation regarding the spectra and the coordination modes of the above complex differs in some points from that of Goodman et al. [7]. According to our data, the centres of the high-field ^{63}Cu peaks are at 3302 and 3309 G for the 3N and the 4N isomers, respectively, while this line lies at 3315 G for the $[CuL_2H]^+$ complex (at 9.5 GHz used in Ref. [7]). The same difference of 7 G in the line positions of the isomers was found in Ref. [7], however, owing to lack of accurate g_0 and A_0 Goodman et al. assigned the line at higher field to the 3N isomer, presumably because it is closer to the corresponding line of the $[CuL_2H]^+$ complex with three equatorial nitrogens (as can be seen in Fig. 5 of Ref. [7]).

The $[CuL_2]^{2+}$ complex of histamine is similar to the corresponding L-histidine complex in every respect. Its ESR spectra also indicate an isomeric equilibrium: the SQD values for the two-component models were lower by 20–25% than for the one-component description of the experimental spectra. The analysis of the superhyperfine structure led to the same conclusions, and we assigned the component spectra to the isomers in the same way as for the histidine complex. The only difference is that here the concentrations of the isomers are nearly equal.

3.3. ESR parameters and the structure of complexes

The conclusions with respect to the structure of the complexes were based upon the following statements.

A stronger ligand field in the equatorial plane tends to decrease g, and this leads to a larger value of A in the case of effective D_{4h} symmetry [23]. An increase in the ligand field is reflected in a blue shift of the visible absorption band; this effect is the largest for the amino nitrogen, intermediate for the imidazole nitrogen, smaller for the carboxylate oxygen of our ligands, and smallest for the hydroxide and water oxygen atoms [3]. More covalent metal–ligand bonds (that is, higher extent of electron delocalization from the $d_{x^2-y^2}$, d_{xy}, d_{xz} and d_{yz} orbitals to the ligands) promote the decrease in g and the parallel increase in A through reduction of the spin–orbit coupling constant too [27,28]. Stronger axial bonds, in turn, cause a moderate red shift of the d–d band [3], an increase in g and decrease in A [23].

The value of g_0 is slightly sensitive, while A_0 is highly sensitive to the geometric distortions. When a significant decrease in g_0 is accompanied with only a small increase or even a decrease in A_0, this change is a diagnostic sign of a rhombic distortion which induces a 3d–4s orbital mixing, reducing the Fermi term and hence A_0 [24].

In the case of the D_{4h} symmetry, the increase of the Fermi term indicates a less covalent in-plane σ-bond, except for those complexes in which the latter bond is highly ionic (then an opposite tendency was observed) [24].

Table 1
Average ESR parameters [a] of the copper(II) complexes of histamine and L-histidine

Ligand	Histamine							L-Histidine						
complex [b]	g_0	A_0 (G) [c]	a_{N0} (G)	α (G)	β (G)	γ (G)	%	g_0	A_0 (G) [c]	a_{N0} (G)	α (G)	β (G)	γ (G)	%
Cu	2.1974(6)	34.1(2)		51(2)	−1.6(4)	0.7(2)		2.1974(3)	33.9(6)		49(2)	−1.6(2)	0.9(4)	
[$CuLH_2$]								2.1893(8)	36.6(11)		48(2)	−5.9(6)	0.1(1)	
[CuLH]	2.175(2)	34.6(5)	10	48(3)	−7(1)	0.6(1)		2.1539(3)	56.9(3)	8.4(2)	30.5(9)	−8.9(5)	2.3(6)	
[CuL]	2.1436(4)	63.4(4)	12.7(9)	28(2)	−7.0(3)	0.7(1)		2.1461(6)	59.6(3)	12.3(8)	30.2(8)	−8.4(6)	1.6(4)	
			11.4(6)							11.6(2)				
[$CuLH_{-1}$]								2.1187(3)	66.0(3)	13.6(3)	25.5(6)	−9.6(9)	3.3(5)	
										12.2(2)				
[$CuLH_{-2}$]	2.1159(2)	78.0(3)	11.4(4)	24(2)	−6.6(2)	1.9(2)		2.1185(3)	76.4(2)	11.5(4)	22.2(8)	−8.8(9)	2.2(2)	
			11.2(5)							11.1(11)				
[CuL_2H_2]								2.1230(9)	64(1)	8.0(5)	24.0(7)	−12(1)	2.9(1)	
										8.0(5)				
[CuL_2H]	2.1316(2)	62.4(2)	14.0(2)	26(1)	−13.3(3)	2.2(3)		2.1186(2)	72.3(3)	12.2(4)	23.6(8)	−12.8(5)	2.8(1)	
			14.0(2)							10.6(3)				
			10.3(2)							10.2(2)				
[CuL_2]	2.1151(4)	74.4(3)	14.4(2)	19.4(7)	−6.4(3)	1.2(1)	53(2)	2.1223(3)	67.2(4)	12.4(3)	14.8(3)	−8.2(3)	3.4(3)	30(1)
3N isomer														
			10.3(4)							8.9(2)				
			10.3(4)							8.9(2)				
4N isomer	2.1006(5)	69.9(5)	12.2(3)	28.2(6)	−9.6(5)	0.01	47(2)	2.1141(6)	63.4(4)	11.3(2)	27.5(6)	−9.4(5)	0.05(5)	70(1)
			12.2(3)							11.3(2)				
			11.9(4)							11.3(2)				
			11.9(4)							11.3(2)				

[a] The uncertainties of the last digits are given in parentheses.
[b] Charges are omitted.
[c] Refers to ^{63}Cu.

Tuesday May 23 10:06 AM

StyleTag -- Journal: **POLY** (*Polyhedron*) Article: **3437**

The isotropic shf coupling constant a_{N0} is a direct measure of the unpaired spin density at the nitrogen nuclei [23]: both the stronger covalent character of the Cu–N in-plane σ-bonds (an enhanced electron delocalization from the $d_{x^2-y^2}$ orbital to the nitrogen atoms) and the larger s-character of the nitrogen hybrid orbitals in the ligand tend to increase it. This was also shown by systematic ENDOR studies [26]. With our ligands, at a similar covalency of the above metal–ligand bond, a larger shf coupling constant is expected for the imidazole, while a smaller constant is expected for the amino nitrogen donors.

For the $[CuLH_2]^{3+}$ complex of L-histidine both the amino and imidazole nitrogens are protonated, and it is only the carboxylate group that can bind to the copper(II). As compared to the aqua complex, the change of a water oxygen by a carboxylate oxygen atom induces only a slightly stronger ligand field, and hence a slight decrease in g_0, increase in A_0 and small changes in the relaxation parameters are expected. The parameters are in good accordance with the expectations (Table 1).

For the $[CuLH]^{3+}$ complex of histamine only a monodentate coordination of the ligand is possible, either by the imidazole or by the amino nitrogen. The ligation of the former is more probable, in accordance with its lower basicity (the p*K* for its protonation is ~6.2, while for the amino group it is ~9.9 [15]). The ESR parameters confirm this mode of coordination, reflecting a quite small increase in the ligand field, as compared to the aqua complex (Table 1). On the contrary, for the $[CuLH]^{2+}$ complex of L-histidine a considerable decrease in g_0 and increase in A_0, and relaxation parameters corresponding to a resolved hf structure (Table 1 and Fig. 4) reflect on a much stronger ligand field which can be attributed to a glycine-like equatorial coordination by the amino nitrogen and carboxylate oxygen atoms. This was also suggested by former Raman [2] and CD [8] studies.

The ESR parameters of the $[CuL]^{2+}$ and $[CuL]^{+}$ complexes of histamine and L-histidine, respectively, are closely identical (Table 1), suggesting a similar equatorial coordination, most likely by the amino and the imidazole nitrogen atoms. The considerable blue shift of the d–d absorption band [29], accompanied with the formation of these species, and the 2N shf pattern of the ESR spectra support this binding mode. The g_0 for the L-histidine complex is somewhat larger, while the A_0 is smaller than the corresponding data for the histamine complex, probably as a consequence of the axial binding of the carboxylate group in the former species. The tridentate coordination of L-histidine in this complex is confirmed also by CD spectroscopic evidence [8].

The deprotonation of the above species resulted in the formation of two new species: an ESR-inactive dimer, in which the monomer units are supposed to be connected by two hydroxide ions [16,18,19,25], and the corresponding monomer, which was shown by pH-potentiometry [18,19,25] and ESR spectroscopy (see above). Compared to the $[CuL]^{+}$ complex, in the $[CuLH_{-1}]$ monomer the deprotonation causes considerable changes in the parameters,

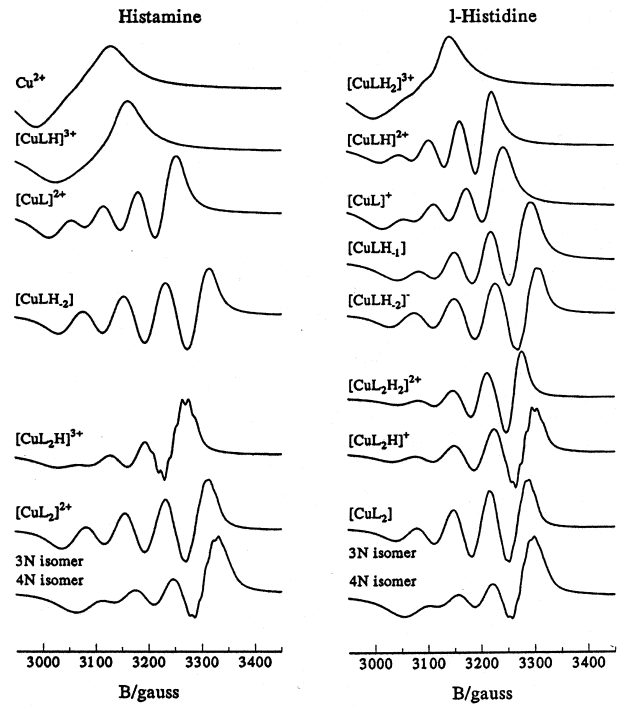


Fig. 4. Spectra of the various species in the copper(II)–histamine and copper(II)–L-histidine systems calculated from the average ESR parameters for ^{63}Cu at 9.4 GHz.

in particular, the decrease of g_0 is significant (Table 1), which indicates a much stronger ligand field. The substitution of an equatorial water molecule by a hydroxide ion modifies the ligand field only to a small extent [3], so it is more probable that the proton loss of the pirrolic nitrogen takes place in this species. The Fermi term decreases from 0.0111 to 0.0107 cm^{-1} upon the deprotonation, supporting the enhanced overall covalent character of the in-plane σ-bond [24].

The deprotonation process over pH ~ 11 is not accompanied with a change in g_0, which indicates that overall ligand field strength is not altered significantly, suggesting the proton loss of the equatorial water molecule in this step. The changes in the coupling constants, however, seem to reflect on alterations of the covalent character of various metal–ligand bonds. For the histidine complex the Fermi term has increased to 0.0117 cm^{-1}, and the decrease in the shf coupling constants is significant (Table 1), which shows a less covalent in-plane σ-bond compared to the $[CuLH_{-1}]$ complex. This is not accompanied with an increase in g_0 at all, suggesting an enhanced covalent character for the π-bonds which counterbalance the effect of the less covalent in-plane σ-bond. For the histidine complex g_0 is slightly larger, while A_0 is smaller then the corresponding data for the histamine complex, indicating the axial binding of the carboxylate group again. The coordination modes of the mono complexes are illustrated in Fig. 5.

The pH-potentiometric formation constants suggest a maximum concentration of about 30% for the $[CuL_2H_2]^{2+}$ complex of L-histidine even at a twenty-fold ligand excess, moreover, there are always three or more other species in a

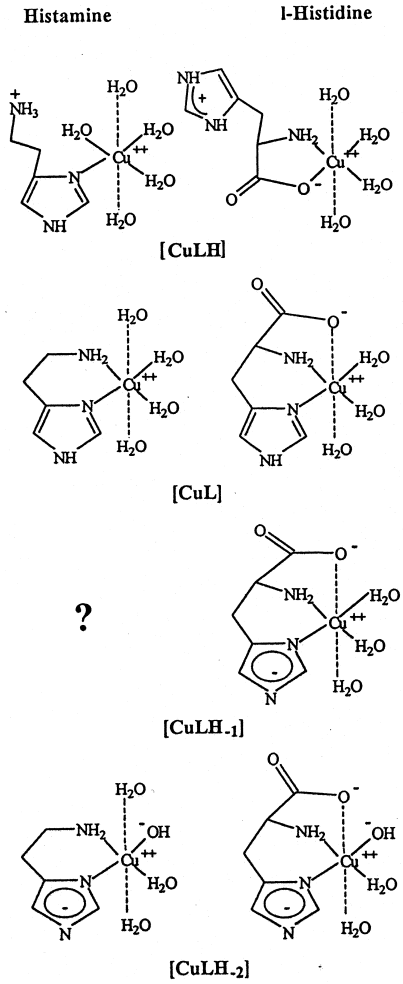


Fig. 5. Coordination modes in the mono-complexes of histamine and L-histidine (charges in formulas are omitted).

solution where this complex is formed (Fig. 3). Therefore we could obtain only limited structural information for this species. The 'bis(glycinate)' equatorial coordination through the amino nitrogen and the carboxylate oxygen atoms is most probable, while the imidazole rings remain in a protonated state. For amino acid complexes of similar coordination, *cis* and *trans* isomers were detected by ESR spectroscopy [7,13]. However, for the above reasons, we could describe the spectrum of the $[CuL_2H_2]^{2+}$ complex of L-histidine as a curve of only one species, even if two isomers were present. The parameters (Table 1) are close to the data for the analogous L-serine complex, obtained with a similar approximation [13].

The ESR parameters for the $[CuL_2H]^{3+}$ complex of histamine and the $[CuL_2H]^{+}$ complex of L-histidine are rather different, suggesting differences in the equatorial coordination, although for both spectra the three-nitrogen shf pattern proves that all three non-protonated nitrogen atoms occupy equatorial positions. The latter fact indicates that the 'L' ligand is bound equatorially through the amino and the imidazole nitrogen atoms, similarly to the [CuL] complexes. The comparison of the ESR parameters of the $[CuL_2H]$ complexes to those of the [CuL] species suggests that the 'LH' ligands bind to the [CuL] moiety differently, as in the [CuLH] complexes. In the histamine complex the ligation is monodentate, presumably through the imidazole nitrogen which alters the ligand field to a small extent, inducing only small changes in parameters (Table 1). This may be the most probable explanation for the large g_0 and small A_0 values. Two larger and one smaller shf coupling constants also support the equatorial binding of two imidazole and one amino nitrogens (Table 1). (It is worth noting that the higher a_{N0} values gained by the analysis of ESR spectra, which are assigned to the imidazole nitrogen atoms, are in good agreement with the nitrogen coupling constants for various imidazole complexes, obtained by ENDOR measurements [26].) On the contrary, for the $[CuL_2H]^{+}$ complex of L-histidine a considerable decrease in g_0 and increase in A_0 are accompanied with the coordination of the 'LH' ligand to the $[CuL]^{+}$ species, indicating a much stronger ligand field: the simultaneous equatorial bonding of the amino nitrogen and carboxylate oxygen atoms, while the 'second' imidazole nitrogen seems to remain in a protonated form. Two smaller and one larger nitrogen coupling constants support the equatorial coordination of two amino and one imidazole nitrogen atoms for the L-histidine complex too (Table 1). The CD spectra of the L-histidine complex were interpreted also in terms of the above mode of equatorial coordination [8] and the axial binding of the carboxylate group of the 'L' ligand. The proposed structures for the bis complexes are illustrated in Fig. 6.

For the 3N isomer of the $[CuL_2]$ complexes, one of the four nitrogen donors is bound in axial position. The question

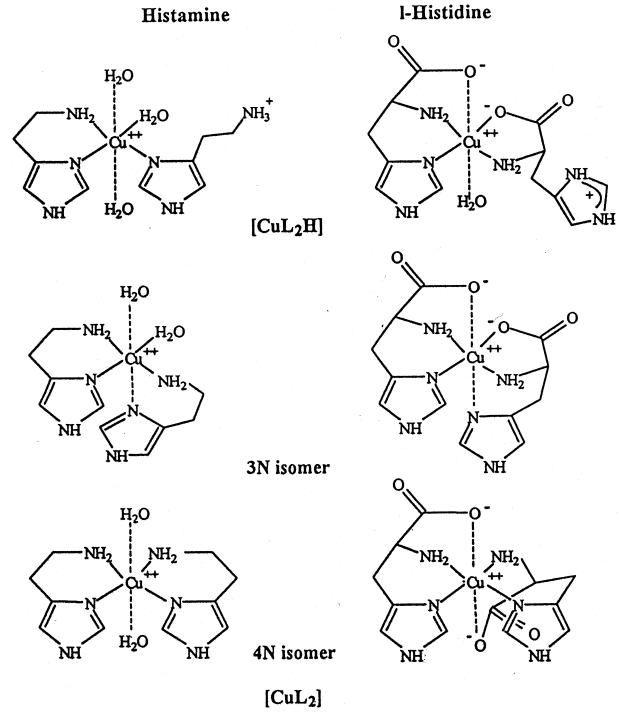


Fig. 6. Coordination modes in the bis-complexes of histamine and L-histidine (charges in formulas are omitted).

is whether an amino or an imidazole nitrogen occupies this site. For both ligands the relatively small g_0 and large A_0 of this species correspond to the equatorial coordination of one imidazole and two amino nitrogen atoms, thus the axial binding of an imidazole nitrogen is probable. The equatorial coordination of one imidazole and two amino nitrogen atoms is supported by one larger and two smaller a_{N0} coupling constants in both cases (Table 1).

The lower g_0 values for the 4N isomers of the $[CuL_2]$ complexes are in accordance with the stronger ligand fields as compared to the 3N isomers (see above); the copper hf coupling constants, however, are unexpectedly small (Table 1). We interpret this by a rhombic distortion which suggests a lower symmetry arrangement of the equatorial donor atoms, i.e. the nitrogens of the same type are in *cis* positions (Fig. 6). For such a coordination the carboxylate groups of the L-histidine ligands are on opposite sides of the equatorial plane, thus both of them can bind axially. This may be, at least in part, a probable explanation for the differences in the g_0 and A_0 values of the corresponding complexes of histamine and L-histidine (Table 1).

4. Conclusions

The good reproducibility of the ESR spectra recorded in a circulating system made it possible to take advantage of all opportunities offered by the EPR program. The decomposition of a large number of spectra has resulted in a consistent description of the copper(II)–histamine and copper(II)–L-histidine equilibrium systems. The pH-metric equilibrium model was completed by the carboxylate-coordinated complex in the strongly acidic region with the L-histidine ligand, and in equimolar alkaline solutions two deprotonated mono complexes were found for both ligands. We pointed out isomeric equilibria at excess histamine and L-histidine in nearly neutral solutions.

The nitrogen coupling constants were in good accordance with the literature ENDOR data. The accurate parameter values determined for all species gave an opportunity to study both the equatorial and the axial coordination, to decide which nitrogen donors are bound in different positions.

The main difference between histamine and L-histidine is the binding mode of the 'LH' ligand which has one of the nitrogen donors protonated. In the case of histamine a monodentate ligation occurs through the imidazole nitrogen atom, while the more basic amino group is protonated. For the L-histidine ligand a bidentate coordination takes place by the amino and the carboxylate groups; here the imidazole ring remains protonated.

For both histamine and histidine, in all complexes, which have one or two ligand(s) free from dissociable protons, the first 'L' ligand is coordinated equatorially by the amino and the imidazole nitrogens. The glycine-like equatorial coordination of the second L-histidine occurs in the minor isomer of the $[CuL_2]$ complex, while the major isomer has all nitrogens in equatorial positions with the *cis* arrangements of the nitrogens of the same kind. For the $[CuL_2]^{2+}$ complex of histamine the second amino nitrogen is bound equatorially, while the second imidazole group occupies an equatorial or an axial site with approximately equal probability.

The carboxylate group of histidine, when displaced from the equatorial positions, occupies an axial site.

Acknowledgements

We thank the Hungarian Scientific Research Fund OTKA I/3. 3067 and OTKA T-015 841 for financial support. We are indebted to Professor István Nagypál for helpful discussions.

References

[1] E.W. Wilson Jr., M.H. Kasperian, R.B. Martin, J. Am. Chem. Soc. 92 (1970) 5365.
[2] M. Itabashi, K. Itoh, Bull. Chem. Soc. Jpn. 53 (1980) 3131.
[3] H. Siegel, R.B. Martin, Chem. Rev. 82 (1982) 385.
[4] B. Henry, J.-C. Boubel, J.-J. Delpuech, Inorg. Chem. 25 (1986) 623.
[5] T.P.A. Kruck, B. Sarkar, Can. J. Chem. 51 (1973) 3563.
[6] P. Cocetta, S. Deiana, L. Erre, G. Micera, P. Piu, J. Coord. Chem. 12 (1983) 213.
[7] B.A. Goodman, D.B. McPhail, H.K.J. Powell, J. Chem. Soc., Dalton Trans. (1981) 822.
[8] L. Casella, M. Gullotti, J. Inorg. Biochem. 18 (1983) 19.
[9] G. Valensin, R. Basosi, W.E. Antholine, E. Gaggelli, J. Inorg. Biochem. 23 (1985) 125.
[10] M. Pasenkiewicz-Gierula, W. Froncisz, R. Basosi, W.E. Antholine, J.S. Hyde, Inorg. Chem. 26 (1987) 801.
[11] A. Rockenbauer, L. Korecz, Appl. Magn. Reson. 10 (1996) 29.
[12] T. Szabó-Plánka, A. Rockenbauer, L. Korecz, Magn. Reson. Chem. 37 (1999) 484.
[13] T. Szabó-Plánka, A. Rockenbauer, L. Korecz, Polyhedron 18 (1999) 1969.
[14] L. Zékány, I. Nagypál, G. Peintler, PSEQUAD for Chemical Equilibria, Technical Software Distributors, Baltimore, MD, 1991.
[15] S. Sjöberg, Pure Appl. Chem. 69 (1997) 1549.
[16] I. Sóvágó, A. Gergely, Inorg. Chim. Acta 20 (1976) 27.
[17] M. Remelli, C. Munerato, E. Pulidori, J. Chem. Soc., Dalton Trans. (1994) 2049.
[18] L. Pettit, Pure Appl. Chem. 56 (1984) 247.
[19] L. Pettit, J. Swash, J. Chem. Soc., Dalton Trans. (1976) 588.
[20] I. Sóvágó, T. Kiss, A. Gergely, J. Chem. Soc., Dalton Trans. (1978) 964.
[21] D. Kivelson, J. Chem. Phys. 27 (1957) 1087.
[22] A. Rockenbauer, P. Simon, J. Magn. Reson. 18 (1975) 320.
[23] B.A. Goodman, D.B. Raynor, Adv. Inorg. Chem. Radiochem. 13 (1970) 135.
[24] A. Rockenbauer, J. Magn. Reson. 35 (1979) 429.
[25] I. Sóvágó, T. Kiss, A. Gergely, Magy. Kém. Foly. 84 (1978) 130.
[26] M. Iwaizumi, T. Kudo, S. Kita, Inorg. Chem. 25 (1986) 1546.
[27] A.H. Maki, B.R. McGarvey, J. Chem. Phys. 29 (1958) 31.
[28] A.H. Maki, B.R. McGarvey, J. Chem. Phys. 29 (1958) 35.
[29] T. Szabó-Plánka, A. Rockenbauer, M. Györ, F. Gaizer, J. Coord. Chem. 17 (1988) 69.

PERGAMON

www.elsevier.nl/locate/poly

Polyhedron 19 (2000) 1133–1138

POLYHEDRON

cis-Dioxomolybdenum(VI) complexes with tridentate and tetradentate Schiff base ligands. Preparation, structures and inhibition of aerial oxidation of aldehydes

Janne Liimatainen, Ari Lehtonen, Reijo Sillanpää *

Department of Chemistry, University of Turku, FIN-20014 Turku, Finland

Received 4 January 2000; accepted 16 March 2000

Abstract

The synthesis and characterisation of four monomeric *cis*-dioxomolybdenum(VI) complexes involving Schiff base ligands is described. Ligands were obtained by condensation of salicylaldehyde with substituted aminoethanols. $[MoO_2(acac)_2]$ reacted with the prepared ligands forming six-coordinated *cis*-dioxoMo(VI) complexes. X-ray diffraction studies confirmed that ligands act in a tridentate manner and the sixth coordination site around Mo(VI) is occupied by methanol used as solvent. The complexes act as inhibitors in the oxidation of aldehydes by oxygen. ©2000 Elsevier Science Ltd All rights reserved.

Keywords: Molybdenum complexes; Aerial oxidation of aldehydes

1. Introduction

As molybdenum is widely available to biological systems, the coordination chemistry of Mo(VI) has aroused considerable interest in view of its biochemical significance [1,2]. For example, dioxomolybdenum(VI) complexes are studied as models for oxidised forms of molybdoenzymes, e.g. aldehyde oxidase and sulfite oxidase which are supposed to contain *cis*-MoX_2 units (X = O, S) coordinated to sulfur, nitrogen and oxygen donor atoms of the protein structure [3,4]. The present view of these enzymes indicates that the formal oxidation state of molybdenum cycles between 4+ and 6+ in reactions with substrate and oxidant. The two-electron oxygen atom transfer seems to be the relevant mechanism in understanding chemical role of enzymatic reactions.

A large number of important chemical reactions are catalysed by molybdenum(VI) compounds. Several industrial processes such as ammoxidation of propene to acrylonitrile [5], olefin epoxidation [6] and olefin metathesis [7] reactions are carried out over molybdenum catalysts. Molybdenum alkoxides are also used to isomerise allylic alcohols [8].

Complexes that contain a terminally bonded oxo group dominate the high oxidation states of molybdenum. Alkoxide and phenoxide ligands are widely used ancillary groups in combination with multiply bonded oxo ligands [9]. In our previous investigations, we have studied the coordination chemistry of monomeric dioxomolybdenum complexes with simple chelating alcohols, $[MoO_2(met)_2]$, $[MoO_2(pyr)_2]$ and $[MoO_2(Hbicy)(pyr)]$ (Hmet = 2-methoxyethanol, Hpyr = tetrahydropyrane-2-methanol, H_2bicy = 1,1′-bicyclohexane-1,1′-diol) [10]. Schiff bases derived from salicylaldehyde and aminoalcohols bearing both alcoholic and phenolic hydroxyl groups and also one neutral nitrogen donor (CH=N imino group) can be used as multidentate ligands in molybdenum chemistry [11–13]. In this paper we discuss the syntheses of monomeric dioxomolybdenum(VI) complexes with tridentate or tetradentate Schiff base ligands and their role in the oxidation of benzaldehyde and butanal. Two of the ligands are optically active. Crystal structures of four new complexes are also described.

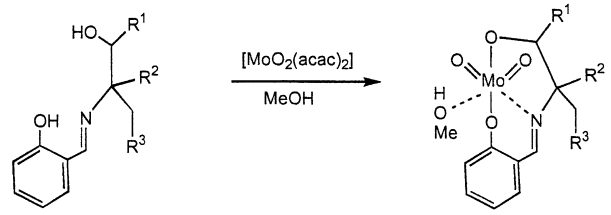
2. Results and discussion

2.1. Synthesis

In order to prepare dioxomolybdenum(VI) complexes having vacant coordination sites and/or labile ligands, we studied reactions of $[MoO_2(acac)_2]$ with Schiff base ligands

* Corresponding author. Tel.: +358-2-3336731; fax: +358-2-3336700; e-mail: sillanpa@utu.fi

0277-5387/00/$ - see front matter ©2000 Elsevier Science Ltd All rights reserved.
PII S0277-5387(00)00368-5



R^1	R^2	R^3	
H	Me	H	H_2L^1
H	H	Me	H_2L^2
H	Me	OH	H_3L^3
Ph	H	OH	H_3L^4

Scheme 1.

having nitrogen donor atom and two or three potential ionisable hydroxyl groups (Scheme 1). Molybdenum starting material and ligand precursors were dissolved in dry methanol in 1:1 molar ratio and the reaction mixtures were stirred at room temperature for several days. The reaction temperature proved to be vital for product composition. Syntheses carried out at higher temperatures increased the amount of side products, probably including the formation of dinuclear oxo-bridged Mo(V) species [14,15]. Compounds crystallised out from the reaction mixtures in moderate to high yields upon cooling. All compounds formed crystals, which were faint pale yellow. On acing they become more yellow and greenish in colour. The crystals are stable if stored under dry air in the dark. Spectral characterisation and X-ray crystal structure determinations showed that in spite of the variations in ligand structure, the reactions always yielded isostructural mononuclear distorted octahedral complexes of *cis*-dioxomolybdenum(VI), where the ligand is bonded to Mo(VI) in a tridentate meridional coordination mode.

2.2. Spectra

The ^{1}H NMR spectra of the ligands showed a chemical shift of about 14 ppm characteristic for aromatic OH group [16]. The ^{1}H NMR spectra of the complexes are indicative of binding of the ligands through a phenoxo, alkoxo and imine group, leaving any additional CH_2OH groups unbound. They also showed a bound CH_2O^- group in the CH_2 region. The resonances were assigned based on the splitting of resonance signal and spin coupling constants. Spectra of **3** and **4** are also consistent with an unbound CH_2OH group. The chemical shifts of imine carbon protons were about 8.3 ppm for free ligand precursors [17] and coordination of nitrogen shifted the resonance signals about 0.5 ppm downfield. The ^{1}H spectra of the complexes also showed a doublet (3.2 ppm, CH_3) and quartet (4.1 ppm, OH) of coordinated methanol. The IR spectra of the complexes show two strong absorption bands at 890–900 and 920–930 cm^{-1}, which are due to asymmetric and symmetric Mo=O stretches, respectively. Coordination of the imine centre through nitrogen is seen in the ν(C=N) (at 1626–1640 cm^{-1}), which is slightly lower than in uncoordinated bases. Both the ^{1}H NMR and IR spectra are in good agreement with those reported for comparable *cis*-MoO_2^{2+} complexes [11,12].

2.3. Structures of complexes

The molecular structures of complexes **1**–**4** are shown in Figs. 1–4, respectively, with the relevant bond distances and angles collected in Table 1. The coordination geometry around the Mo^{VI} cation is quite similar in all studied complexes. The Schiff base ligand is bonded to the *cis*-Mo(VI)O_2^{2+} ion in an *xy*-plane through a phenoxide and an alkoxide oxygen donor and an imine nitrogen atom, which is *trans* to an oxo group. A methanol molecule completes the distorted octahedral coordination sphere and is *trans* to another oxo group. In all compounds **1**–**4**, the O=Mo=O angles (105.9(2)–106.6(2)°) and the Mo=O distances (1.694(3)–1.721(3) Å) are typical for *cis*-dioxomolyb-

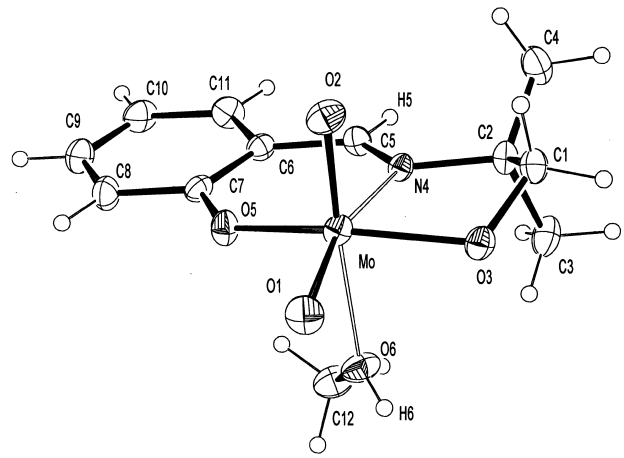


Fig. 1. ORTEP plot of **1** showing the labelling system of heavy atoms. Displacement ellipsoids are plotted at 30% probability level.

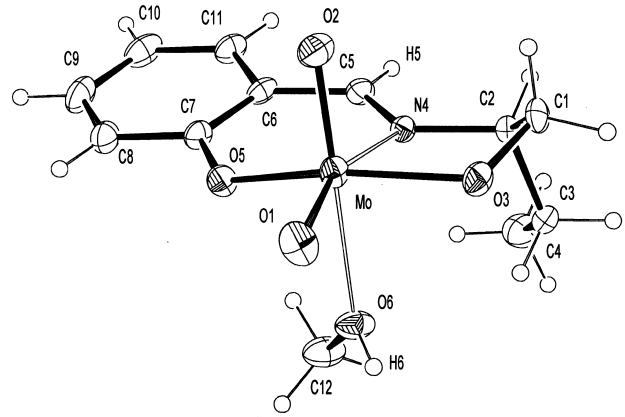


Fig. 2. ORTEP plot of **2** showing the labelling system of heavy atoms. Displacement ellipsoids are plotted at 30% probability level.

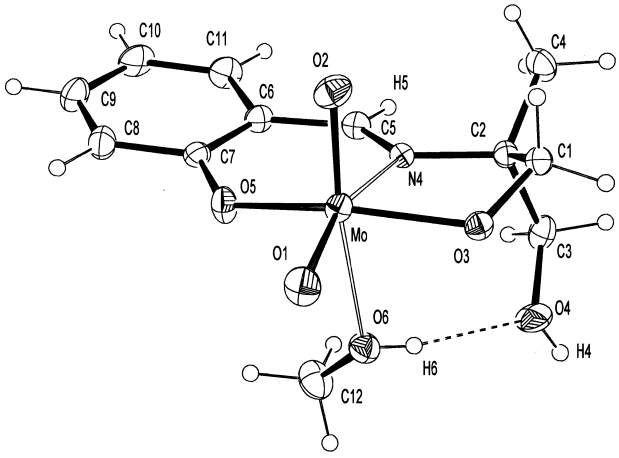


Fig. 3. ORTEP plot of **3** showing the labelling system of heavy atoms. Displacement ellipsoids are plotted at 30% probability level.

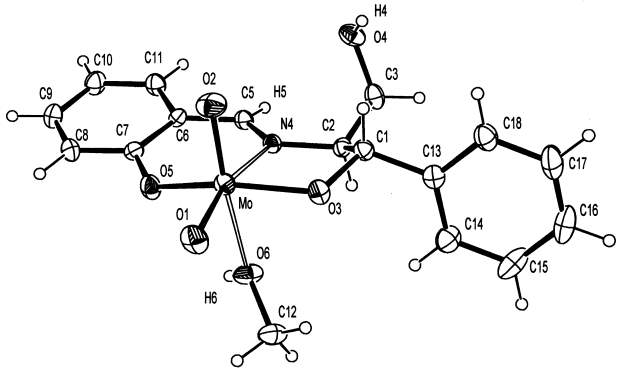


Fig. 4. ORTEP plot of **4** showing the labelling system of heavy atoms Displacement ellipsoids are plotted at 30% probability level.

Table 1
Selected bond lengths (Å) and angles (°) for compounds **1**–**4**

	1	**2**	**3**	**4**
Mo–O(1)	1.703(2)	1.714(5)	1.709(2)	1.721(3)
Mo–O(2)	1.699(2)	1.699(4)	1.702(2)	1.694(3)
Mo–O(3)	1.952(2)	1.951(4)	1.938(2)	1.920(3)
Mo–N(4)	2.291(2)	2.274(5)	2.296(3)	2.282(3)
Mo–O(5)	1.951(2)	1.962(4)	1.946(2)	1.964(3)
Mo–O(6)	2.385(2)	2.378(4)	2.376(2)	2.325(3)
O(1)–Mo–O(2)	105.9(1)	106.2(2)	106.2(1)	106.64(15)
O(1)–Mo–N(4)	160.8(1)	161.3(2)	161.1(1)	162.95(13)
O(1)–Mo–O(5)	101.4(1)	103.3(2)	100.5(1)	99.2(1)
O(2)–Mo–N(4)	92.5(1)	91.3(2)	92.0(1)	90.2(1)
O(2)–Mo–O(5)	99.3(1)	95.7(2)	98.9(1)	97.5(2)
O(2)–Mo–O(6)	172.0(1)	169.1(2)	168.7(1)	165.8(14)
O(3)–Mo–N(4)	74.56(8)	74.8(2)	74.26(8)	75.2(1)
O(3)–Mo–O(5)	150.7(1)	152.2(2)	151.1(1)	150.5(1)
N(4)–Mo–O(5)	80.75(8)	80.9(2)	81.4(1)	80.7(1)
C(1)–O(3)–Mo	115.3(2)	117.9(3)	118.6(2)	121.6(2)
C(7)–O(5)–Mo	138.8(2)	134.0(4)	135.0(2)	133.9(2)

denum(VI) complexes [18,19]. The imine nitrogen and methanol oxygen atoms, which are *trans* to the terminal oxo-groups, bond to Mo(VI) ions with distances of 2.274(5)–2.296(3) Å for nitrogen and 2.325(3)–2.385(2) Å for oxygen, respectively. The Mo–OR distances vary from 1.920(3) to 1.952(2) Å for the alkoxide and from 1.946(2) to 1.964(3) Å for the phenoxide, respectively, these being typical values for these types of bonds in hexa-coordinated dioxomolybdenum(VI) complexes [10,19]. On the whole the structures of compounds **1**–**4** are very similar to those of dioxomolybdenum(VI) complexes with other Schiff base ligands reported by Rao et al. [12]. Complexes **2** and **4** crystallise in an asymmetric space group $P2_12_12_1$ and form an asymmetric coordination site for methanol. In **3** and **4** there is an uncoordinated OH group, which in the case of **3** forms an intramolecular H-bond with the coordinated methanol. This kind of intramolecular H-bond can direct the orientation of incoming alcohols in the reactions, which occur at this coordination site.

2.4. Oxidation of aldehydes

Dioxomolybdenum complexes, e.g. $[MoO_2(cysS\text{-}OR)_2]$ (cysS-OR = S-deprotonated L-cysteinate alkyl ester) and $[MoO_2L]$ (L = pyridine-2,6-bis(1′,1′-diphenylethanethiolate)) are known to catalyse air oxidation of organic substrates [20,21]. On the other hand, molybdenum complexes with salicylaldehyde based ligands, $[MoO_2(SAP)]$ or $[MoO_2(SSP)]$ (SAP = 2-(salicylideneamino)phenolate, SSP = 2-(salicylideneamino)benzenethiolate) do not react with Ph_3P in DMF at 60°C [22,23]. It is also suggested that those complexes are not thermodynamically capable of carrying out substrate oxidation [24]. We tested the ability of our compounds to carry out aerial oxidation of aldehydes by mixing complexes **1**–**4** with aromatic (benzaldehyde) and aliphatic (butanal) aldehydes and exposing them to dry air. Reaction mixtures under continuous air flow were kept at room temperature and the progress of the reaction was followed by HPLC or spectroscopic methods. To our surprise, these complexes did not facilitate the oxidation reaction, but they seem to inhibit it. Addition of the molybdenum complex to the acetonitrile solution of benzaldehyde prevented entirely the formation of benzoic acid. When these compounds were added to neat butanal, the oxidation reaction occurred, but it was clearly slower than in pure aldehyde. The inhibition is probably due to the fact that Mo complexes react with the radicals formed in the oxidation reaction [25]. For example, Cu complexes with phenoxyl radicals can form aldehydes and hydrogen peroxide from alcohols and oxygen but do not oxidise aldehydes to carboxylic acids, although Ni complexes can oxidise aldehydes [26,27].

2.5. Conclusion

Monomeric, octahedral complexes of *cis*-MoO_2^{2+} can be prepared by the reaction of $[MoO_2(acac)_2]$ with salicylaldehyde-based ligand precursors bearing one phenolic –OH group and one or two CH_2OH moieties. The reaction must be carried out at room temperature in order to obtain high yields and nearly colourless products. These complexes

inhibit oxidation reactions of aldehydes to carboxylic acids. In the case of aromatic aldehyde, inhibition was total and no oxidation was detected. The oxidation of aliphatic aldehydes was much slower if a small amount of the prepared complexes was present in the reaction medium.

3. Experimental

$[MoO_2(acac)_2]$ was prepared by a known method [28]. Schiff bases were synthesised by condensing salicylaldehyde with aminoalcohols in refluxing ethanol and were characterised by NMR spectroscopy and elemental analyses. Benzaldehyde and butanal were distilled before use. Other chemicals were of commercial origin and were used without subsequent purification. HPLC analyses were performed by Spectra-Physics model 3500 equipment with an LKB Bromma 2158 UVICORD SD UV-detector using H_2O–MeOH (1:1) as an eluent. IR spectra were recorded on a Mattson Galaxy FTIR spectrometer. ^{1}H NMR spectra were recorded in $(CD_3)_2SO$ using a JEOL GSX-400 spectrometer and referenced to $SiMe_4$ as internal standard. Elemental analyses were performed by a Perkin-Elmer series II analyser.

3.1. Preparation of $[MoO_2L^1(MeOH)]$ (1)

To the solution of $[MoO_2(acac)_2]$ (406 mg, 1.25 mmol) in MeOH (25 ml) was added 255 mg (1.32 mmol) of H_2L^1 and the reaction mixture was stirred at room temperature for 70 h. Supernatant liquid was decanted and concentrated to 5 ml. Compound **1** crystallised as pale yellow crystals when kept overnight at −15°C (86 mg, 20%). *Anal*. Found: C, 41.30; H, 4.85; N, 3.90. Calc.: C, 41.05; H, 4.90; N, 4.00%. NMR: δ_H 8.6 (s, 1H, imine), 7.7–6.8 (m, aromatic), 4.2 (s, CH_2O^-), 1.35 (s, 6H, CH_3), 4.1 (m, 1H, CH_3OH) and 3.2 (d, 3H, CH_3OH). IR: 1626vs, 1599s, 1557m, 1452vs, 1289s, 1235m, 1215m, 1192m, 1163m, 1145m, 1125s, 1032vs, 995m, 980m, 926vs (br), 897vs (br), 829s, 791s, 754vs, 637m, 627s, 540s (br), 517m, 478w, 446m.

3.2. Preparation of $[MoO_2L^2(MeOH)]$ (2)

$[MoO_2(acac)_2]$ (460 mg, 1.41 mmol) was dissolved in 35 ml of MeOH and 277 mg (1.44 mmol) of H_2L^2 were added. The reaction mixture was stirred at room temperature for 140 h and then filtered. The filtrate was kept at −15°C for 11 days to obtain complex **2** as pale yellow crystals in 45% yield (222 mg). *Anal*. Found: C, 41.10; H, 4.85; N, 3.95. Calc.: C, 41.05; H, 4.90; N, 4.00%. NMR: δ_H 8.7 (s, 1H, imine), 7.7–6.8 (m, aromatic), 4.4 (m, 2H, CH_2O^-), 3.9 (m, 1H, CH), 1.8 (m, 2H, CH_2), 0.9 (s, 3H, CH_3), 4.1 (m, 1H, CH_3OH) and 3.2 (d, 3H, CH_3OH). IR: 1636s, 1597s, 1559s, 1452vs, 1319w, 1289s, 1246m, 1229m, 1213m, 1152m, 1134w, 1117m, 1099m, 1074m, 1026vs, 1013vs, 980m, 955m, 930s, 909vs (br), 853s, 810s, 760vs, 733s, 710m, 644w, 633m, 619s, 544vs, 521m, 507m, 463m, 446s.

3.3. Preparation of $[MoO_2HL^3(MeOH)]$ (3)

H_3L^3 (200 mg, 0.96 mmol) was dissolved in MeOH (20 ml) and 300 mg (0.92 mmol) of solid $[MoO_2(acac)_2]$ was added. The reaction mixture was stirred for 71 h at room temperature and then decanted. The solution was then concentrated to 10 ml and it was kept at 5°C for 8 days to obtain complex **3** as pale yellow crystals in 70% yield (235 mg). *Anal*. Found: C, 37.80; H, 4.35; N, 3.90. Calc.: C, 39.25; H, 4.65; N, 3.80%. NMR: δ_H 8.5 (s, 1H, imine), 7.7–6.8 (m, aromatic), 5.1 (m, 1H, CH_2OH), 3.5–3.4 (m, 2H, CH_2O^-), 4.6 (d, 1H, CH_2OH), 4.0 (d, 1H, CH_2OH), 1.3 (s, 3H, CH_3), 4.1 (m, 1H, CH_3OH) and 3.2 (d, 3H, CH_3OH). IR: 1626s, 1595m, 1555m, 1454vs, 1329s, 1294vs, 1219m, 1192m, 1165w, 1144m, 1119m, 1055s, 1030s, 988s, 926vs, 889vs (br), 822s, 791m, 750vs, 731s, 627s, 571s, 544s, 465m, 449m.

3.4. Preparation of $[MoO_2HL^4(MeOH)]$ (4)

To H_3L^4 solution (545 mg, 2.01 mmol) in MeOH (30 ml) was added $[MoO_2(acac)_2]$ (652 mg, 2.00 mmol) as a solid and the reaction mixture was stirred at room temperature for 24 h. The mixture was filtrated and filtrate was concentrated until some crystals had formed. The solution was kept at −15°C overnight to yield complex **4** as clear, slightly greenish yellow crystals (609 mg, 71%). Crystals for X-ray analysis were grown from methanol. *Anal*. Found: C, 47.20; H, 4.50; N, 3.25. Calc.: C, 47.55; H, 4.45; N, 3.25%. NMR: δ_H 8.75 (s, 1H, imine), 7.7–6.9 (m, aromatic), 4.0–3.8 (m, 2H, CH_2OH), 5.23 (d, CHO^-), 5.16 (m, 1H, CH_2OH), 3.6 (m, 1H, CH), 4.1 (m, 1H, CH_3OH) and 3.2 (d, 3H, CH_3OH). ^{13}C NMR: δ 163 (imine), 161–119 (aromatic), 85 (bound CHO^-), 75 (CH_2OH), 59 (CH) and 49 (CH_3OH). IR: 1640s, 1603m, 1561m, 1452vs, 1339w, 1289s, 1250s, 1219s, 1155m, 1130m, 1094m, 1072m, 1030vs, 990m, 930vs, 901vs, 882vs (br), 824s, 777s, 758s, 723s, 708s, 669s, 629s, 604s, 548w, 536m, 519s, 503s, 473m, 442m.

3.5. Oxidation of benzaldehyde

15 mg samples of benzaldehyde were added to the acetonitrile (2.0 ml) solutions of studied molybdenum complexes **1**–**4** (ca. 1 mg). Reaction mixtures were stored in open vessels in dry air at room temperature for 20 h and then analysed by HPLC. However, no benzoic acid could be seen in reaction mixtures.

3.6. Oxidation of butanal

In each experiment, a sample (ca. 5 mg) of molybdenum compound was dissolved in 1 g of butanal and dry air was bubbled (2–5 $cm^3\ min^{-1}$) into the mixture at room temper-

Table 2
Crystal data and experimental details for **1**–**4**

	1	**2**	**3**	**4**
Formula	$C_{12}H_{17}MoNO_5$	$C_{12}H_{17}MoNO_5$	$C_{12}H_{17}MoNO_6$	$C_{17}H_{19}MoNO_6$
Crystal size (mm)	0.32×0.22×0.16	0.22×0.18×0.16	0.26×0.24×0.22	0.38×0.32×0.22
Crystal system	monoclinic	orthorhombic	orthorhombic	orthorhombic
Space group	$C2/c$	$P2_12_12_1$	$Pbca$	$P2_12_12_1$
Z	8	4	8	4
a (Å)	27.356(6)	7.5266(17)	14.045(4)	13.356(2)
b (Å)	7.0407(8)	24.9202(13)	28.892(2)	18.971(3)
c (Å)	14.233(2)	7.2855(16)	6.923(3)	6.9372(17)
β (°)	96.220(16)	90	90	90
U (Å^3)	2725.2(8)	1366.5(4)	2809.3(13)	1757.7(6)
Observed reflections	2404	1425	2480	1786
Parameters	180	180	193	246
R_1 [a]	0.037 (0.025)	0.037 (0.031)	0.042 (0.027)	0.027 (0.021)
wR_2 [a]	0.061 (0.056)	0.077 (0.075)	0.072 (0.066)	0.050 (0.048)

[a] Values in parentheses for reflections with $I>2.0\sigma(I)$. $R_1=\sum||F_o|-|F_c||/\sum|F_o|$, $wR_2=\{\sum[w(F_o^2-F_c^2)^2]/\sum[w(F_o^2)^2]\}^{1/2}$ and $w=1/[\sigma^2(F_o^2)+(aP)^2+bP)]$, where $P=(2F_c^2+F_o^2)/3$.

ature. Reaction mixtures were analysed by IR spectroscopy after 1, 2 and 3 h, and in the case of compound **4** also by ^{1}H NMR. All reactions showed some formation of butyric acid, but the oxidation reaction was clearly fastest in the reference reaction, which was carried out without any Mo complex.

3.7. Crystal structure determinations

Crystal data for compounds **1**–**4**, along with other experimental details, are summarised in Table 2. Single-crystal data collections were performed at ambient temperature on a Rigaku AFC5S diffractometer using graphite-monochromatized Mo Kα radiation ($\lambda=0.71069$ Å). The unit cell parameters were determined by least-squares refinement of 25 carefully centred reflections. Data reduction and subsequent calculations were performed with teXsan for Windows [29]. The data was corrected for Lorentz and polarisation effects and for absorption (PSI-scans [30]). The structures were solved by direct methods using the SIR92 program [31] and full-matrix least-squares refinements on F^2 were performed using the SHELXL-97 program [32]. Non-hydrogen atoms were refined with anisotropic displacement parameters and the hydrogen atoms were included in the calculations at the fixed distances from their host atoms. Figures were drawn with Ortep-3 for Windows [33].

Supplementary data

Crystallographic data have been deposited with the Cambridge Crystallographic Data Centre, 12 Union Road, Cambridge, CB2 1EZ, UK (fax: +44-1223-336033; e-mail: deposit@ccdc.cam.ac.uk) and are available on request quoting the deposition numbers CCDC 138185–138188 for **1**–**4**, respectively.

Acknowledgements

We thank the Academy of Finland for financial support (to A.L).

References

[1] D. Collison, C.D. Garner, J.A. Joule, Chem. Soc. Rev. (1996) 25.
[2] R. Hille, Chem. Rev. 96 (1996) 2757.
[3] G.C. Tucci, J.P. Donahue, R.H. Holm, Inorg. Chem. 37 (1998) 1602.
[4] B.E. Schultz, S.F. Gheller, M.C. Muetterties, M.J. Scott, R.H. Holm, J. Am. Chem. Soc. 115 (1993) 2714.
[5] R.K. Grasselli, Catal. Today 49 (1999) 141.
[6] R.J. Cross, P.D. Newman, R.D. Peacock, D. Stirling, J. Mol. Catal. 144 (1999) 273.
[7] K.J. Ivin, J.C. Mol, Olefin Metathesis and Metathesis Polymerization, Academic Press, London, 1997.
[8] J. Belgacem, J. Kress, J.A. Osborn, J. Am. Chem. Soc. 114 (1992) 1501.
[9] W.A. Nugent, J.M. Mayer, Metal–Ligand Multiple Bonds, Wiley-Interscience, New York, 1988.
[10] A. Lehtonen, R. Sillanpää, Acta Chem. Scand. 53 (1999) 1078.
[11] Y.-L. Zhai, X.-X. Xu, X. Wang, Polyhedron 11 (1992) 415.
[12] C.P. Rao, A. Sreedhara, P.V. Rao, M.B. Verghese, K. Rissanen, E. Kolehmainen, N.K. Lokanath, M.A. Sridhar, J.S. Prasad, J. Chem. Soc., Dalton Trans. (1998) 2383.
[13] J. Topich, J.T. Lyon, Polyhedron 3 (1984) 55.
[14] M. Gullotti, A. Pasini, G.M. Zanderighi, J. Chem. Soc., Dalton Trans. (1981) 902.
[15] H. Arzoumanian, New J. Chem. 20 (1996) 699.
[16] R.H. Holm, Chem. Rev. 87 (1987) 1401.
[17] J.H. Cameron, J.A. McEwan, Inorg. Chim. Acta 211 (1993) 111.
[18] K. Yamanouchi, S. Yamada, Inorg. Chim. Acta 9 (1974) 161.
[19] M.H. Chisholm, K. Folting, J.C. Huffman, C.C. Kirkpatric, Inorg. Chem. 23 (1984) 1021.
[20] N. Ueyama, N. Yoshinaga, A. Nakamura, J. Chem. Soc., Dalton Trans. (1990) 387.
[21] J.M. Berg, R.H. Holm, J. Am. Chem. Soc. 107 (1985) 925.
[22] J. Topich, J.T. Lyon, Polyhedron 3 (1984) 61.
[23] J. Topich, J.T. Lyon, Inorg. Chem. 23 (1984) 3202.

[24] R.H. Holm, J.M. Berg, Acc. Chem. Res. 19 (1986) 363.
[25] C. Chatgilialoglu, D. Crich, M. Komatsu, I. Ryu, Chem. Rev. 99 (1999) 1991.
[26] P. Chaudhuri, M. Hess, J. Müller, K. Hildenbrand, E. Bill, T. Weyhermüller, K. Wieghardt, J. Am. Chem. Soc. 121 (1999) 9599.
[27] I. Klement, H. Lütjens, P. Knochel, Angew. Chem., Int. Ed. Engl. 36 (1997) 1454.
[28] G.J.-J. Chen, J.W. McDonald, W.E. Newton, Inorg. Chem. 15 (1976) 2612.
[29] teXsan for Windows, Structure Analysis Software, Molecular Structure Corporation, TX, 1997.
[30] A.C.T. North, D.C. Phillips, F.S. Mathews, Acta Crystallogr., Sect. A 24 (1968) 467.
[31] A. Altomare, G. Cascarano, C. Giacovazzo, A. Gualiardi, M.C. Burla, G. Polidori, M. Camalli, J. Appl. Crystallogr. 27 (1994) 435.
[32] G.M. Sheldrick, SHELXL-97, Program for crystal structure refinement, University of Göttingen, Germany, 1997.
[33] L.J. Farrugia, J. Appl. Crystallogr. 30 (1997) 565.

PERGAMON

www.elsevier.nl/locate/poly

Polyhedron 19 (2000) 1139–1143

POLYHEDRON

The synthesis and structural characterization of $[Et_4N]_2[Ti(SPh)_6]$ and trimeric $[Ti_3O(SPh)_3Cl_4(CH_3CN)_5]\cdot CH_3CN\cdot(C_2H_5)_2O$ complexes

Jun Tae Kim, Jung Woo Park, Sang Man Koo *

Department of Industrial Chemistry and Ceramic Processing Research Center, College of Engineering, Hanyang University, Seoul 133-791, South Korea

Received 5 January 2000; accepted 20 March 2000

Abstract

The reaction of $TiCl_4$ with 6 equiv. of NaSPh in the presence of organic cations such as Et_4N^+ or PPh_4^+ proceeds to yield a novel homoleptic arylthiolate Ti(IV) complex, $[Ti(SPh)_6]^{2-}$. The Et_4N salt of $[Ti(SPh)_6]^{2-}$ has been structurally determined. The coordination geometry around the metal ion is a regular octahedron in which the central titanium ion is located on the crystallographic inversion center. The infrared (IR) spectrum of compound **I** exhibits the characteristic Ti–S bond stretching vibrations of thiophenolate ligands at 480 and 430 cm^{-1}, and the ^1H NMR spectrum in CD_3CN displays characteristic Et_4N^+ resonance peaks and six thiophenolate resonance peaks which are consistent with the solid state structure. The reaction of $TiCl_4$ with 3 or 4 equiv. of NaSPh in CH_3CN yields the unexpected mixture of dark purple $[TiCl_3(CH_3CN)_3]$ and dark red $[Ti_3O(SPh)_3Cl_4(CH_3CN)_5]\cdot CH_3CN\cdot(C_2H_5)_2O$ (**II**) complexes. Complex **II** has been structurally determined by single X-ray crystallography. The IR spectrum of complex **II** exhibits a μ_3–O stretching vibration at 600 cm^{-1} and Ti–S vibrations of the thiophenolate ligand at 481 and 429 cm^{-1}. ©2000 Elsevier Science Ltd All rights reserved.

Keywords: Oxo ligands; Thiolates; Titanium; Trimers

1. Introduction

There has been an enormous study of the transition metal complexes with aliphatic or aromatic thiolate ligands, because they exhibit a variety of structural types with various nuclearities [1–9], and certain complexes can be used as precursors for corresponding transition metal sulfide complexes [10–15]. Among the transition metal thiolate complexes, mononuclear species with homoleptic thiolate ligands are fundamental types that can be used to derive cluster and cage types of molecules or corresponding thiometalates. Such early transition metal complexes with homoleptic thiolate ligands have been reported extensively in the last few years. For example, $M(SPh)_6^{n-}$ ($n=1$, 2; M = Nb, Ta) [16], $M(SPh)_4^{2-}$ (M = Mn, Fe, Co, Ni) [17,18] and $M(S_2C_2H_4)_3^-$ (M = Nb, Ta) [19], $M(S_2C_2H_4)_3^{n-}$ ($n=1$, 2; M = Ti, Co, Cr) [20,21] have been synthesized and fully characterized. In contrast to the other groups, the types and structural pattern of group IV metal thiolate complexes have not been fully studied. Recently, Tatsumi et al. reported $Zr(^tBuS)_5^-$ and $Zr(^tBuS)_6^{2-}$ complexes [22].

Reports on titanium complexes with thiolate ligands are limited to a few complexes, including Ti(S-2,4,6-$^iPr_3C_6H_2)_4^-$, Ti(S-2,4,6-$^tBu_3C_6H_2)_4^-$ [23] and dithiolate complexes of titanium [20,21]. Recently. Giolando et al. reported on the synthesis and structural characterization of dimeric $Ti_2(SMe)_9^-$, trimeric $Ti_3(SMe)_{12}$ complexes which were obtained from the reaction of $Ti(NR_2)_4$ with RSH (R = Me, Et) [24].

We are interested in obtaining Ti(IV) homoleptic monodentate thiolate complexes, potential starting materials for corresponding thiotitanates. Here, we report the synthesis and structural characterization of the homoleptic arylthiolate titanium complex $[Ti(SPh)_6]^{2-}$ (**I**) and the trimeric $[Ti_3O(SPh)_3Cl_4(CH_3CN)_5]\cdot CH_3CN\cdot(C_2H_5)_2O$ (**II**).

2. Experimental

All manipulations were performed using standard Schlenk line techniques under dinitrogen atmosphere. Diethyl ether was distilled after being refluxed with sodium–benzophenone. Acetonitrile was distilled after being refluxed over CaH_2 before use. $TiCl_4$, Et_4NBr and PPh_4Cl were purchased from Aldrich and used as received. Sodium thiophenolate

* Corresponding author. Tel.: +82-2-2290 0527; fax: +82-2-2281 4800; e-mail: sangman@email.hanyang.ac.kr

0277-5387/00/$ - see front matter ©2000 Elsevier Science Ltd All rights reserved.
PII S0277-5387(00)00374-0

(NaSPh) was prepared from the reaction of sodium and thiophenol in diethyl ether.

2.1. $[Et_4N]_2[Ti(SPh)_6]$ (**I**)

A 250-ml Schlenk flask was charged with 2.26 g (17.23 mmol) of NaSPh, 1.10 g (5.30 mmol) of Et_4NBr and a stirring bar. To this mixture was added 50 ml of CH_3CN via a cannula with stirring at ambient temperature and 0.29 ml (2.65 mmol) of $TiCl_4$ was injected using a syringe. The color of the solution turned to dark red immediately. After 2 h, the solution was filtered through a fine porosity fritted funnel; to the dark red filtrate, 50 ml of diethyl ether was added and the resulting solution was left to stand at ambient temperature. Finally, dark red crystalline materials were obtained in 80% yield. Calc. for $TiS_6N_2C_{52}H_{70}$: C, 64.83; H, 7.27; N, 2.92; S, 19.97. Found: C, 64.91; H, 7.34; N, 3.01; S, 21.52%. FT-IR (cm^{-1}): ν(Ti–SPh); 480, 430. ^1H NMR in acetonitrile-d_3: δ (CH_3 in Et_4N^+); 1.18 (t, 24H), δ (CH_2 in Et_4N^+); 3.21 (q, 16H), δ (C_6H_5 in SPh ligand); 6.97–7.42 (m, 30H). The Ph_4P^+ salt was also obtained by a similar synthetic procedure in 80% yield. Calc. for $TiS_6P_2C_{84}H_{70}$: C, 73.05; H, 5.07. Found: C, 73.23; H, 5.12%. IR (KBr disc) (cm^{-1}): ν(Ti–SPh), 480 and 420.

2.2. $[Ti_3O(SPh)_3Cl_4(CH_3CN)_5]\cdot CH_3CN\cdot(C_2H_5)_2O$ (**II**)

2.2.1. Method A

A 250-ml Schlenk flask was charged with 1.39 g (10.60 mmol) of NaSPh and a stirring bar. To this flask 30 ml of CH_3CN was added via a cannula with stirring at ambient temperature, and 0.29 ml (2.65 mmol) of $TiCl_4$ was injected using a syringe. The color of the solution turned to dark red. After 2 h, the solution was filtered through a fine porosity fritted funnel. To the red filtrate 100 ml of diethyl ether was added and the resulting solution was stood at ambient temperature. Dark purple crystals and dark red crystals were isolated and dried under vacuum. Finally, a 1:1 mixture of dark purple crystals of $TiCl_3(CH_3CN)_3$ and dark red crystals of $[Ti_3O(SPh)_3Cl_4(CH_3CN)_5]\cdot CH_3CN\cdot(C_2H_5)_2O$ were obtained (see below). The total yield was approximately 70% (based on Ti). ^1H NMR in DMF-d_7: δ (CH_2 in CH_3CN in ligand and free CH_3CN); 1.95 (br, 27H), δ (CH_3 in Et_2O); 3.382 (q, 4H), δ (CH_3 in Et_2O); 1.068 (t, 6H), δ (C_6H_5 in SPh ligand); 7.126–7.277 (m, 15H).

2.2.2. Method B

$TiCl_4$, 0.18 ml (1.68 mmol), was injected using a syringe into a 250-ml Schlenk flask containing 20 ml of CH_3CN. To this solution 0.01 ml (0.56 mmol) of H_2O diluted in 10 ml of CH_3CN was added and the solution was stirred at ambient temperature for 10 min. The solution was transferred via a cannula to a 250-ml schlenk flask charged with 0.88 g (6.72 mmol) of NaSPh and 20 ml of CH_3CN. After 2 h, the solution was filtered through a fine porosity fritted funnel; then to the red filtrate 100 ml of diethyl ether was added and the resulting solution was stood at ambient temperature. Finally, a dark red powder of $[Ti_3O(SPh)_3Cl_4(CH_3CN)_5]\cdot CH_3CN\cdot(C_2H_5)_2O$ was obtained in 74% yield.

Calc. for $Ti_3S_3O_2N_6Cl_4C_{34}H_{43}$: C, 43.03; H, 4.53; N, 8.85; S, 10.14. Found: C, 43.24; H, 4.24; N, 8.76; S, 12.01%. FT-IR (cm^{-1}): ν(Ti–O), 600.5; ν(CH_3CN), 2310.3, 2280; ν(Ti–SPh), 481, 429. ^1H NMR in DMF-d_7: δ (CH_3 in CH_3CN ligand and free CH_3CN); 1.92–1.97 (m, 18H), δ (CH_2 in Et_2O); 3.28 (q, 4H), δ (CH_3 in Et_2O); 1.06 (t, 6H), δ (C_6H_5 in SPh ligand); 7.252–7.285 (m, 15H).

2.3. X-ray crystallography

Single X-ray diffraction data for both crystals are presented in Table 1. Diffraction data were collected at ambient temperature on a Bruker P4 four circle diffractometer using Mo Kα radiation. Intensity data were collected by using a θ–2θ step scan technique and for all data sets the condition of the crystal was monitored by measuring 2 standard reflections. The solutions of both structures were carried out by a combination of heavy atom Patterson techniques, direct methods and Fourier techniques. The refinement of the structures by full-matrix least-squares methods was based on 2640 unique reflections ($2\theta = 45°$, $I > 2\sigma$) for compound **I**, and 4361 unique reflections ($2\theta = 22.5°$, $I > 2\sigma$) for compound **II**. Anisotropic temperature factors were used for all non-hydrogen atoms in compounds **I** and **II**, except solvent molecules packed in the lattice for compound **II**. At the current stage of refinement on 312 parameters for compound **I** and 459 parameters for compound **II** with all atoms present in the asymmetric units, $R = 0.0383$, $Rw = 0.0989$ for compound **I** and $R = 0.0715$, $Rw = 0.1982$ for compound **II**.

Table 1
Crystallographic data for $[Et_4N]_2[Ti(SPh)_6]$ (**I**) and $[Ti_3O(SPh)_3Cl_4(CH_3CN)_5]\cdot CH_3CN\cdot(C_2H_5)_2O$ (**II**)

	I	**II**
Formula	$TiS_6N_2C_{52}H_{70}$	$Ti_3S_3O_2N_6Cl_4C_{34}H_{43}$
FW	963.36	948.96
Crystal system	triclinic	monoclinic
Space group	$P\bar{1}$ (no. 2)	$P2_1/c$ (no. 14)
a (Å)	11.113(2)	13.139(1)
b (Å)	11.414(2)	8.653(1)
c (Å)	13.075(2)	38.544(3)
α (°)	112.89(1)	
β (°)	92.29(1)	90.94(1)
γ (°)	118.77(1)	
Z	2	4
V (Å^3)	1285.2(4)	4381.5(7)
T (°C)	20	20
λ (Å^3)	0.71073	0.71073
ρ_{calc} (g cm^{-3})	1.245	1.439
μ (cm^{-1})	4.46	9.58
R [a]	0.0383	0.0715
Rw [b]	0.0989	0.1982

[a] $R = \Sigma||F_o| - |F_c||/\Sigma|F_o|$.
[b] $Rw = [\Sigma w(|F_o| - |F_c|)^2/\Sigma w(|F_o|^2)]^{1/2}$, where $w = 1/\sigma^2(|F_o|)$.

2.4. Other physical measurements

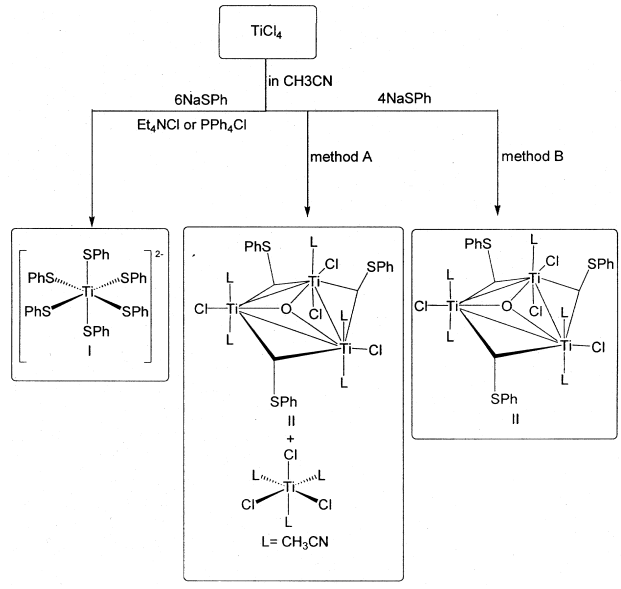
^{1}H NMR spectra (300 MHz) were obtained with a Varian Gemini 300 spectrometer. IR spectra were measured with a Nicolet Magna IR-760 spectrophotometer. C, H and N analyses were obtained with a Thermoquest EA-1110 CHNS analyzer.

3. Results and discussion

3.1. Synthesis and spectroscopic results

The reactions between titanium tetrachloride and sodium thiophenolate were investigated in CH_3CN at room temperature with different stoichiometries. The Et_4N^+ salts of compound **I** could be obtained from the reaction of $TiCl_4$ with 6 equiv. of NaSPh in CH_3CN solution in the presence of Et_4NBr. Upon the addition of solvent, the solution of the reaction mixture immediately turned to a deep red color, and was stirred for 2 h at ambient temperature under N_2 atmosphere. The solution was then filtered and dark red crystals of Et_4N^+ 'salts' were isolated with 80% yield by the slow diffusion of diethyl ether into the filtrate solution. The Ph_4P^+ 'salts' were also obtained in 70% yield using a similar method. The red crystals of compound **I** were very sensitive to air and moisture and even decomposed in a dry N_2 glove box within several days. The reaction of $TiCl_4$ with 4 equiv. of NaSPh in CH_3CN at ambient temperature produced a 1:1 mixture (as evidenced by ^{1}H NMR spectroscopy) of dark purple $[TiCl_3(CH_3CN)_3]$ and dark red $[Ti_3O(SPh)_3Cl_4(CH_3CN)_5]\cdot CH_3CN\cdot(C_2H_5)_2O$ complexes. Both complexes were identified by single crystal X-ray analysis.

The synthesis of compound **I** was accomplished by the simple ligand exchange reaction of chloride by thiophenolate group (Scheme 1). The precipitation of NaCl facilitated the completion of the reaction. This method afforded a simple and convenient route to obtain the monomeric titanium thiolate complex in high yield. When the reaction stoichiometry of 1:4 ($Ti:PhS^-$) was used to obtain the cluster type Ti–thiolate complex, the hydrolyzed complex **II** was inadvertently produced. In this reaction, titanium was reduced to +3 oxidation state with the concomitant oxidation of PhS^- to 1/2PhSSPh. This kind of reduction mechanism was reported earlier in the synthesis of $[Ph_4P]_2[Nb(SPh)_6]$ [16]. The oxygen in complex **II** presumably came from a trace of water in the CH_3CN solution. In fact, complex **II** could be obtained in excellent yield (74%) when the stoichiometric amount of water (3:1 molar ratio with $TiCl_4$ and H_2O) was added to the reaction medium. A similar reaction was reported by Müller's group [26] in which the reaction system $3TiCl_4$:$6S(SiMe_3)_2$:$3/2O_2$ led to a $[Ti_3O(S_2)_6Cl_6]^{2-}$ complex in which the oxygen atom came from the inert gas containing small amounts of O_2. Further study will verify a more detailed reaction mechanism.



Scheme 1.

The IR spectrum of $[Et_4N]_2[Ti(SPh)_6]$ exhibited the characteristic thiophenolate ligand Ti–S bond stretching vibrations at 480 and 430 cm^{-1}, which is typical of most metal thiolate complexes. The ^{1}H NMR spectrum in CD_3CN displayed the characteristic Et_4N^+ resonance peaks and six thiophenolate resonance peaks, which is consistent with the solid state structure. In the IR spectra the μ_3–O stretching vibration in the $[Ti_3O(SPh)_3Cl_4(CH_3CN)_5]\cdot CH_3CN\cdot(C_2H_5)_2O$ (**II**) complex was observed at 600 cm^{-1}, and doublet peaks at 2310 and 2280 cm^{-1} were assigned to the C≡N vibrations in the CH_3CN ligand. Also the Ti–S vibrations in the thiophenolate ligand were observed at 481 and 429 cm^{-1}. The ^{1}H NMR spectrum in DMF-d_7 displayed the characteristic CH_2 (δ 3.382) and CH_3 (δ 1.608) resonance peaks from one diethyl ether molecule and three thiophenolate resonance peaks (δ 7.126–7.277). In the ^{1}H NMR spectra of the product, which was prepared by method A, a broad single resonance peak at δ 1.95 due to five coordinated CH_3CN, free CH_3CN molecule in complex **II** and coordinated CH_3CN in $TiCl_3(CH_3CN)_3$ were observed. The integral ratio of those peaks compared to the thiophenolate ligands suggested that $TiCl_3(CH_3CN)_3$ and complex **II** existed as a 1:1 mixture. However, the ^{1}H NMR spectra for the product prepared by method B suggested that only complex **II** was produced by this method.

3.2. X-ray structures

The structures of compounds **I** and **II** were determined; the ORTEP diagrams of the anion in complex **I** and complex **II** are shown in Figs. 1 and 2.

The selected bond distances and angles of anion in complex **I** are presented and compared with those of the $[Ti(S_2C_2H_4)_3]^{2-}$ anion [21] in Table 2. The coordination geometry around the metal ion is a regular octahedron in which the central titanium ion is located on the crystallo-

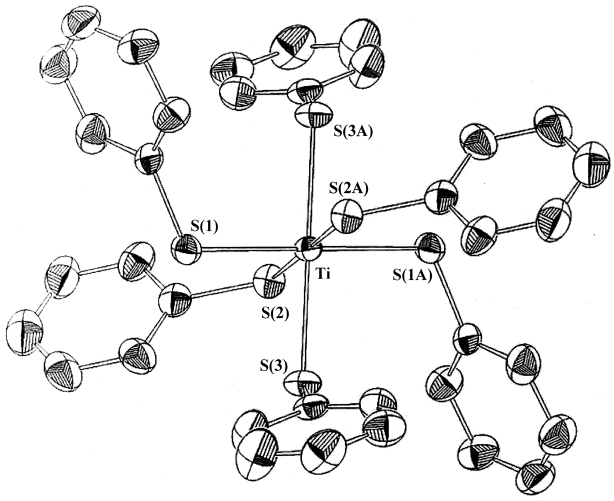


Fig. 1. Structure and labeling of the anion **I** in the $[Et_4N]_2[Ti(SPh)_6]$ complex. Thermal ellipsoids as drawn by ORTEP represent the 40% probability surfaces. Symmetry-generated atoms have the suffix 'A'.

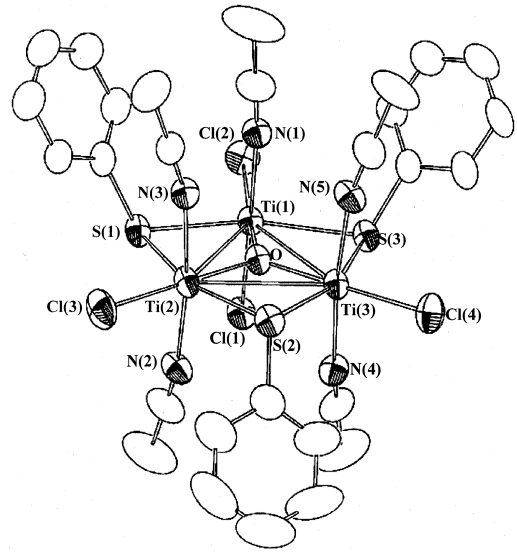


Fig. 2. Structure and labeling of complex **II**. Thermal ellipsoids as drawn by ORTEP represent the 40% probability surfaces.

Table 2
Selected bond lengths (Å) and angles (°) for anion in complex **I** and $[Ti(edt)_3]^{2-}$

	I	$[Ti(edt)_3]^{2-}$ [a]
M–S(1)	2.4240(8) [b]	range 2.419(2)–2.438(2)
M–S(2)	2.4283(9)	mean 2.428
M–S(3)	2.4434(8)	
S–C	1.777(3)	range 1.789(7)–1.820(7)
	1.765(3)	mean 1.81
	1.767(3)	
S–M–S (neighbored)	84.05(3) [b]	range 82.8(1)–89.1(1)
	95.51(3)	
	84.44(3)	

[a] From [21].
[b] The numbers in parentheses represent the individual standard deviations.

graphic inversion center. The titanium–sulfur distances range from 2.424 to 2.443 Å, which are typical for metal–sulfur bonds in transition metal thiolate complexes. The slightly longer Ti–S distance (mean 2.432 Å) than that of $[Ti(S_2C_2H_4)_3]^{2-}$ (mean 2.428 Å) is mainly due to the chelating effect of dithiolate ligands in the $[Ti(S_2C_2H_4)_3]^{2-}$ complex. The S–M–S angles are 84.05, 84.44 and 95.51°, respectively.

The selected bond distances and angles of complex **II** are presented in Table 3. In complex **II**, the oxygen atom bridges three Ti atoms with μ_3-mode and all four atoms exist nearly in the plane. The distance of Ti–O (1.922 Å) is comparable to that of $(CpTi)_6(\mu_3\text{-}S)_4(\mu_3\text{-}O)_4$ (1.97 Å) [25]. The bond angles of Ti–O–Ti (119.87°) and the three nearly identical distances of three Ti–O bonds suggest that the oxygen atom

Table 3
Selected bond lengths (Å) and angles (°) for complex **II**

Ti(1)–O	1.934(7) [a]	Ti(1)–Cl(1)	2.369(3)
Ti(2)–O	1.914(6)	Ti(1)–Cl(2)	2.396(3)
Ti(3)–O	1.917(7)	Ti(2)–Cl(3)	2.323(3)
Ti(1)–S(1)	2.574(3)	Ti(3)–Cl(4)	2.333(3)
Ti(1)–S(3)	2.576(3)	Ti(1)–Ti(3)	3.323(2)
Ti(2)–S(2)	2.560(3)	Ti(1)–Ti(2)	3.332(2)
Ti(2)–S(1)	2.585(3)	Ti(2)–Ti(3)	3.322(2)
Ti(3)–S(2)	2.553(3)	Ti–N (mean)	2.166
Ti(3)–S(3)	2.571(3)		
O–Ti–N(mean)	90.68	Ti–Ti–Ti (mean)	59.99
O–Ti(1)–Cl(1)	97.8(2) [a]	$Ti–O_b–Ti$ (mean)	119.87
O–Ti(1)–Cl(2)	170.6(2)	N(1)–Ti(1)–S(1), S(3)	90.0(2), 92.1(2)
O–Ti(2)–Cl(3)	179.0(2)	N(2)–Ti(2)–S(1), S(2)	84.6(3), 96.6(3)
O–Ti(3)–Cl(4)	177.0(2)	N(3)–Ti(2)–S(1), S(2)	90.2(3), 90.2(3)
N(1)–Ti(1)–Cl(1)	176.0(3)	N(4)–Ti(3)–S(2), S(3)	97.2(3), 83.2(3)
N(1)–Ti(1)–Cl(2)	84.7(2)	N(5)–Ti(3)–S(2), S(3)	90.6(2), 90.1(3)
N(3)–Ti(2)–Cl(3)	87.8(3)	Cl(1)–Ti(1)–S(1), S(3)	89.24(10), 90.03(10)
N(2)–Ti(2)–Cl(3)	88.1(3)	Cl(2)–Ti(1)–S(1), S(3)	100.30(12), 100.37(11)
N(4)–Ti(3)–Cl(4)	90.0(3)	Cl(3)–Ti(2)–S(1), S(2)	101.17(13), 99.97(13)
N(5)–Ti(3)–Cl(4)	87.0(3)	Cl(4)–Ti(3)–S(2), S(3)	98.40(12), 102.03(12)
$Ti–S_b–Ti$(mean)	80.64	Cl(1)–Ti(1)–Cl(2)	91.57(11)

[a] The numbers in parentheses represent the individual standard deviations.

is located at the center of triangular geometry formed by three titanium atoms. Each titanium is contained within a pseudo-octahedral geometry in which two sulfur atoms, a chloride atom and an oxygen atom form the equatorial plane. All CH_3CN ligands are located in the axial position (O–Ti–N 90.68°) and all Cl ligands are located in the equatorial position (O–Ti–Cl 175.5°), except Cl(1) which is in the axial position (O–Ti(1)–Cl(1) 97.8°). The Ti–Ti distances in complex **II**, which range from 3.322 to 3.332 Å, are slightly longer than those in $[Ti_3O(S_2)_6Cl_6]^{2-}$ (3.14–3.18 Å) [26].

The reactivity characteristics of the anion in complex **I** and its conversion to titanium sulfide complexes as a precursor are currently under investigation in our laboratory.

Supplementary data

The full crystallographic data are available from the Cambridge Crystallographic Data Center, 12 Union Road, Cambridge CB2 IEZ, UK (fax: +44-1223-336033; e-mail: deposit@ccdc.cam.ac.uk) on request, quoting the deposition numbers 136711 (**I**) and 136712 (**II**).

Acknowledgements

The support of this work by a grant from the Korean Ministry of Education (BSRI-98-3415) is gratefully acknowledged. The authors also acknowledge support from the Research Institute of Industrial Science (99-06-08) at Hanyang University.

References

[1] N. Govindaswamy, J. Moy, M. Millar, M.A. Koch, Inorg. Chem. 31 (1992) 1992.
[2] J.R. Nicholson, G. Christou, J.C. Huffman, K. Folting, Polyhedron 6 (1987) 863.
[3] T. Costa, J.R. Dorfman, K.S. Hagen, R.H. Holm, Inorg. Chem. 22 (1983) 4091.
[4] D. Coucouvanis, R.K. Lester, M.G. Kanatszidis, D.P. Kessissoglou, J. Am. Chem. Soc. 107 (1985) 8279.
[5] I.W. Boyd, I.G. Dance, K.S. Murray, A.G. Wedd, Aust. J. Chem. 31 (1978) 279.
[6] A. Silver, M. Millar, J. Chem. Soc., Chem. Commun. (1992) 948.
[7] P.C. Leverd, M. Lance, M. Nierlich, J. Vigner, M. Ephritikhine, J. Chem. Soc., Dalton Trans. (1994) 3563.
[8] A. Müller, G. Henkel, Chem. Commun. (1996) 1005.
[9] K. Otsuka, M. Kamata, K. Hirotsu, T. Higuchi, J. Am. Chem. Soc. 103 (1981) 3011.
[10] K.S. Hagen, R.H. Holm, J. Am. Chem. Soc. 104 (1982) 5496.
[11] G. Henkel, W. Tremel, B. Krebs, Angew. Chem., Int. Ed. Engl. 22 (1983) 319.
[12] W. Gaete, J. Ros, X. Solans, M. Font-Altaba, J.L. Briansó, Inorg. Chem. 23 (1984) 39.
[13] S.A. Koch, L.E. Maelia, M.J. Millar, J. Am. Chem. Soc. 105 (1983) 5944.
[14] M.R. Snow, J.A. Ibers, Inorg. Chem. 12 (1973) 249.
[15] G. Christou, J.C. Huffman, J. Chem. Soc., Chem. Commun. (1983) 558.
[16] S.M. Koo, R. Begero, A. Salifoglou, D. Coucouvanis, Inorg. Chem. 29 (1990) 4844.
[17] D. Coucouvanis, C.N. Murphy, E. Simhon, P. Stremple, M. Draganjac, Inorg. Synth. 21 (1982) 23.
[18] D. Coucouvanis, D. Swenson, N.C. Baenziger, C. Murphy, D.G. Holah, N. Sfarnas, A. Simopoulos, A. Kostikas, J. Am. Chem. Soc. 103 (1981) 3350.
[19] K. Tatsumi, Y. Sekiguchi, A. Nakamura, R.E. Cramer, J.J. Rupp, Angew. Chem., Int. Ed. Engl. 25 (1986) 86.
[20] C.P. Rao, J.R. Dorfman, R.H. Holm, Inorg. Chem. 25 (1986) 428.
[21] J.R. Dorfman, C.P. Rao, R.H. Holm, Inorg. Chem. 24 (1985) 453.
[22] H. Kawaguchi, K. Tatsumi, R.E. Cramer, Inorg. Chem. 35 (1996) 4391.
[23] G.A. Sigel, P.P. Power, Inorg. Chem. 26 (1987) 2819.
[24] W. Stüer, K. Kirschbaum, D.M. Giolando, Angew. Chem. 106 (1994) 2028.
[25] A.V. Firth, D.W. Stephan, Inorg. Chem. 36 (1997) 1206.
[26] U. Müller, V. Krug, Angew. Chem., Int. Ed. Engl. 27 (1988) 293.

PERGAMON

www.elsevier.nl/locate/poly

Polyhedron 19 (2000) 1145–1154

POLYHEDRON

Interactions in binary and ternary systems including Cu(II), uridine, uridine 5′-monophosphate or diamine

Lechoslaw Lomozik *, Renata Jastrzab, Anna Gasowska

Faculty of Chemistry, A. Mickiewicz University, 60-780 Poznan, Poland

Received 31 January 2000; accepted 20 March 2000

Abstract

Results of equilibrium and spectral studies have shown that, in the systems of uridine (Urd) or uridine 5′-monophosphate (UMP) with the diamines (PA) ethylenediamine, 1,3-diaminopropane or putrescine, molecular complexes of the type $(Urd)H_x(PA)$ and $(UMP)H_x(PA)$ are formed. Overall stability constants of the adducts and equilibrium constants of their formation have been determined. The tendency towards complex formation increases with growing length of the PA. The pH range of adduct formation is found to coincide with that in which the PA is protonated, whereas Urd or its monophosphate is deprotonated. The NH_3^+ groups from PA and N(3) atoms and phosphate groups from the nucleosides have been identified as the centres of non-covalent interactions. Overall stability constants of the Cu(II) complexes with Urd and UMP have been determined. It was found that, in the $Cu(Urd)^+$ and $Cu(Urd)(OH)_x$ complexes, the reaction of metallation mainly involves N(3) atoms from the pyrimidine bases. Results of the spectral and equilibrium studies of the Cu/UMP system indicate coordination involving the N(3) atom and the phosphate groups from UMP, whereas in the complexes $Cu(UMP)(OH)_x$, appearing at high pH, the involvement of the N(3) atom has been excluded and the main sites of metallation are oxygen atoms from carbonyl groups, besides those from hydroxyl groups. The mode of coordination of Cu(II) complexes with Urd or UMP, including diamines, was also determined.
©2000 Elsevier Science Ltd All rights reserved.

Keywords: Copper(II); Diamines; Uridine; Uridine 5′-monophosphate

1. Introduction

It has been established beyond doubt that the interactions of metal ions with nucleic acids and their fragments determine the character of many chemical processes occurring in living organisms, in particular in the processes of genetic information transfer [1–3]. One of the basic problems so far unresolved is the coordination of metal ions in complexes with nucleosides and nucleotides as well as the character of the interactions of this group of bioligands with polyamines (PA) occurring in living cells. The donor atoms N(1) or N(7) are the potential sites of coordination of purine nucleosides, and N(3) in the systems with pyrimidine bases [4–6].

An additional effective coordination site in nucleotides are the donor oxygen atoms from phosphate groups. Determination of the structure of the complexes in solutions is indispensable for the understanding of the anti-tumour effect of platinum complexes. The participation of metals in the processes of replication and transcription of nucleic acids is essential. The metal ion interactions with the bioligands discussed induce changes in their conformations [7,8]. The scope and character of the changes correspond to the mode of coordination and stabilities of the complexes formed with either metal ions or PA. In general, the hard metals from the main groups enter into coordination with donor oxygen ions, whereas the soft transition group metals prefer coordination with nitrogen atoms [1,2,9]. The complexing abilities of the nucleosides change in the order: Guo > Ado ≥ Cyd > Urd ≥ Thd [10–12]. With respect to affinity with metal ions, uridine (Urd) and uridine 5′-monophosphate (UMP) are the least reactive fragments of the nucleic acids. Analysis of the hitherto published works on this subject indicates considerable differences in estimations of the thermodynamic stability of the complexes formed of Cu(II) with this nucleoside (e.g. $\log \beta_{110} = 2.77$ [13], $\log \beta_{110} = 4.57$ [14]), or leads to much controversy on the mode of coordination, which according to some authors involves only the oxygen atoms from the nucleotide [15] and according to others the nitrogen atoms

* Corresponding author. Tel.: +48-61-869 9181; fax: +48-61-8658 8008; e-mail: lomozik@main.amu.edu.pl

0277-5387/00/$ - see front matter ©2000 Elsevier Science Ltd All rights reserved.
PII S0277-5387(00)00375-2

as well [13,16]. These ambiguities prompted us to study the systems mentioned above as one of the steps towards elucidating the character of interactions in the complexes.

This paper presents results of the equilibrium and spectral studies of the interactions of uridine (Urd) and uridine 5′-monophosphate (UMP) with diamines (PA) in metal-free systems as well as of studies of the complexation reactions in binary and ternary systems of these bioligands with Cu(II).

2. Experimental

Uridine (Urd) and uridine 5′-monophosphate (disodium salt), purchased from Fluka, and uridine 5′-monophosphate (UMP) and putrescine hydrochloride (Put·2HCl), from Sigma, were used without further purification. All diamines (PA) were used in the form of hydrochlorides. The dihydrochlorides of ethylenediamine (en) or 1,3-diaminopropane (tn) were obtained by mixing one chemical equivalent of the amine suspended in methanol, with two chemical equivalents of a water–methanol solution of HCl. The salts precipitated were dried over P_4O_{10}. The results of the elemental analysis were in agreement with theoretically calculated values ($\pm 0.5\%$). Copper(II) nitrate (from POCh, Poland) was purified by recrystallisation from water. The concentration of copper ions was determined by the complexometric method [17]. Potentiometric titration was performed on a Titrino 702 Metrohm equipped with an autoburette with a previously calibrated [18] glass electrode 6.233.100 Metrohm. All potentiometric titrations were made at 20 ± 1°C at a constant ionic strength of 0.1 M (KNO_3) in an atmosphere of neutral gas (helium) at metal:ligand ratios between 1:2.5 and 1:5; $C_{Cu} = 0.0003$ M, for Urd and UMP $C = 0.0008$–0.0017 M. The titrant was 0.15229 M CO_2-free NaOH. For the calculation of stability constants with the SUPERQUAD program [19], fragments of the titration curves up to pH of about 7 in the binary systems with Urd and about 7.5 in the binary systems with UMP were used (in the conditions of the potentiometric measurements at higher pH values a precipitate started to appear). Moreover, for the calculations we have also used some of the curves for the binary systems with Urd and UMP, for which the precipitate was found to dissolve (at pH of about 9) while the total amount of the metal remained in the solution. In the metal-free systems, the concentration of both ligands was the same and equal to 0.01 M. In the ternary systems, as in the binary systems with metal ions, the concentration of copper(II) was $C_{Cu} = 0.0003$ M, while the concentration of both ligands was $C_L = 0.0003$ or 0.0008 M. Distributions for particular systems and simulated titration curves were calculated using the HALTAFALL program [20]. Measurements of ^{13}C, ^{31}P, ^{15}N NMR and IR were performed in D_2O, and the pD of the solution was adjusted by NaOD and DCl, taking into account that $pD = pH + 0.40$ [21]. The concentration of the ligands used for NMR measurements was 0.05–0.1 M (1 M for ^{15}N NMR) at the M:L molar ratio of 1:70. NMR spectra were recorded on Gemini 300 Varian and Unity 300 Varian instruments using dioxane as an internal standard for ^{13}C NMR spectra, nitromethane for ^{15}N NMR, and orthophosphoric acid for ^{31}P NMR spectra. The ligand concentration for IR was 0.3–0.5 M; the M:L ratio of concentrations varied from 1:1 to 1:5. The IR spectra were recorded on an IFS 113v Bruker spectrometer, in the cells KRS-5. Samples for UV–Vis studies were prepared in H_2O at the M:L ratio 1:1 and at a Cu(II) concentration of 0.05 M. The spectra were recorded on a UV 160 Shimadzu spectrometer using a 1-cm cell. EPR studies were carried out at 77 K, using glass capillary tubes for water:glycol (3:1); the concentration of Cu(II) was 0.005 M, and the M:L ratio was 1:1. The spectra were recorded on an SE/X 2547 Radiopan instrument.

3. Results and discussion

3.1. Urd, UMP/PA metal-free systems

The protonation constants of Urd and UMP are given in Table 1 and are consistent with literature data [14,15,22,23]. For UMP only two constants of protonation have been determined from computer analysis of the titration data: $\log K_1 = 9.50$ and $\log K_2 = 5.63$. The fully protonated UMP occurs only in very acidic medium, so accurate determination of the third protonation constant by the potentiometric method is impossible; however, a value approximated from literature data is $\log K_3 \approx 0.7 \pm 0.3$ [24].

Non-covalent interactions of Urd or UMP with PA in metal-free systems lead to a change in the acid–base character of the bioligands [25,26]. Because the formation of molecular complexes in the systems studied is accompanied by release of protons, the processes could be observed by the potentiometric method:

$$H_x(\text{Nuc}) + H_y(\text{PA}) \rightleftharpoons (\text{Nuc})H_{(x+y-n)}(\text{PA}) + nH^+$$

Table 1 presents the stoichiometry of complexes and overall stability constants of the adducts. In the systems Urd/en and Urd/tn, molecular complexes are not formed. In the systems with Put, the complexes form in the pH range in which the amine is protonated, while molecules or fragments of the nucleic acids are at least partly deprotonated. These results support the earlier proposed model [25–27] with ion–dipole interactions. Fig. 1 presents distribution curves of molecular complexes in the Urd/Put and UMP/Put systems.

The complexes of Urd with Put start forming from about pH 8, and at pH 10 about 40% of the components occur as adducts. The acidity range in which Urd forms molecular complexes with PA is markedly shifted towards higher pH (protonation constant for Urd is 9.2) than the corresponding ranges in which the complexes with adenosine (Ado) or cytidine (Cyd) are formed (protonation constants, log *K*, of 3.9 and 4.5, respectively). The process of H^+ release from Ado and Cyd occurs at lower pH and adducts form from pH about 3 [26,27]. Moreover, the pH range of molecular com-

Table 1
Overall stability constants of Cu(II) binary complexes and equilibrium constants of adduct formations for Urd, UMP and PA systems

System	Equilibrium	log β	log K_e
Urd	$Urd^- + H^+ \rightleftharpoons HUrd$	9.22(2)	
Urd/en	–		
Urd/tn	–		
Urd/Put	$HPut^+ + Urd^- \rightleftharpoons UrdHPut$	13.00(1)	2.17
	$H_2Put^{2+} + Urd^- \rightleftharpoons UrdH_2Put^+$	21.70(7)	1.19
Urd/Cu(II)	$Cu^{2+} + UrdH \rightleftharpoons CuUrdH^{2+}$	11.55(4)	2.33
	$Cu^{2+} + Urd^- \rightleftharpoons CuUrd^+$	4.32(2)	
	$2Cu^{2+} + 2Urd^- \rightleftharpoons Cu_2Urd_2^{2+}$	12.86(3)	
	$Cu^{2+} + Urd^- + H_2O \rightleftharpoons CuUrd(OH) + H^+$	−3.72(3)	
	$Cu^{2+} + Urd^- + 2H_2O \rightleftharpoons CuUrd(OH)_2^- + 2H^+$	−12.96(3)	
	$Cu^{2+} + Urd^- + 3H_2O \rightleftharpoons CuUrd(OH)_3^{2-} + 3H^+$	−23.78(3)	
UMP	$H^+ + UMP^{3-} \rightleftharpoons HUMP^{2-}$	9.50(2)	
	$2H^+ + UMP^{3-} \rightleftharpoons H_2UMP^-$	15.13(1)	
UMP/en	$Hen^+ + HUMP^{2-} \rightleftharpoons UMPH_2en^-$	22.29(1)	2.64
	$H_2en^{2+} + HUMP^{2-} \rightleftharpoons UMPH_3en$	29.94(1)	2.99
UMP/tn	$Htn^+ + HUMP^{2-} \rightleftharpoons UMPH_2tn^-$	23.01(1)	2.81
	$H_2tn^{2+} + HUMP^{2-} \rightleftharpoons UMPH_3tn$	32.31(1)	3.17
	$H_2tn^{2+} + H_2UMP^- \rightleftharpoons UMPH_4tn^+$	38.48(1)	3.71
UMP/Put	$HPut^+ + HUMP^{2-} \rightleftharpoons UMPH_2Put^-$	22.85(4)	2.52
	$H_2Put^{2+} + HUMP^{2-} \rightleftharpoons UMPH_3Put$	32.33(3)	2.32
	$H_2Put^{2+} + H_2UMP^- \rightleftharpoons UMPH_4Put^+$	38.21(6)	2.57
UMP/Cu(II)	$Cu^{2+} + UMP^{3-} \rightleftharpoons CuUMP^-$	6.03(6)	
	$Cu^{2+} + UMP^{3-} + H_2O \rightleftharpoons CuUMP(OH)^{2-} + H^+$	−2.82(3)	
	$Cu^{2+} + UMP^{3-} + 2H_2O \rightleftharpoons CuUMP(OH)_2^{3-} + 2H^+$	−13.02(2)	
	$Cu^{2+} + UMP^{3-} + 3H_2O \rightleftharpoons CuUMP(OH)_3^{4-} + 3H^+$	−23.64(6)	
en	$H^+ + en \rightleftharpoons Hen^+$	10.15(2) [a]	
	$2H^+ + en \rightleftharpoons H_2en^{2+}$	17.45(2) [a]	
tn	$H^+ + tn \rightleftharpoons Htn^+$	10.70(2) [a]	
	$2H^+ + tn \rightleftharpoons H_2tn^{2+}$	19.64(2) [a]	
Put	$H^+ + Put \rightleftharpoons HPut^+$	9.35(2) [a]	
	$2H^+ + Put \rightleftharpoons H_2Put^{2+}$	16.35(2) [a]	

[a] Ref. [26].

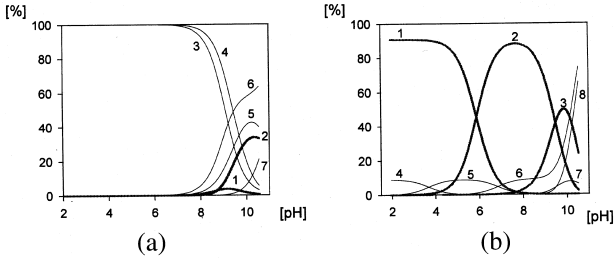
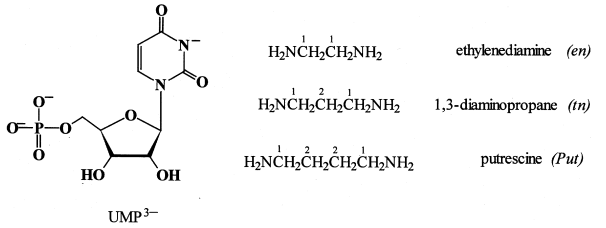


Fig. 1. Distribution diagrams for the systems. (a) Urd/Put: 1, (Urd)-H_2(Put)$^+$; 2, (Urd)H(Put); 3, H(Urd); 4, H_2(Put)$^{2+}$; 5, H(Put)$^+$; 6, Urd$^-$; 7, Put; $C_{Urd} = C_{Put} = 0.01$ M. (b) UMP/Put: 1, (UMP)H_4(Put)$^+$; 2, (UMP)H_3(Put); 3, (UMP)H_2(Put)$^-$; 4, H_2(Put)$^{2+}$; 5, H(Put)$^+$; 6, Put; 7, H(UMP)$^{2-}$; 8, UMP^{3-}; $C_{UMP} = C_{Put} = 0.01$ M.

plex formation in the system Urd/Put is significantly shifted with respect to that in the system UMP/Put (Fig. 1) (the deprotonation of the nucleoside takes place only at high pH). High basicity of the N(3) atom implies a considerable decrease in the equilibrium constant of (Urd)H_2(Put)$^+$ adduct formation with respect to that of (Urd)H(Put) formation. The equilibrium constants (K_e) for the formation of the adducts calculated from the overall stability constants and the protonation constants ($\log K_e = \log \beta_{(Urd)Hx(Put)} - \log \beta_{HxPut}$) are 2.17 and 1.19 for $x = 1$ and 2, respectively, (Table 1). This decrease can be explained by partial neutralization of the nucleoside donor nitrogen atoms by the proton cloud (which is possible because the protonation constants of bioligands are similar), which weakens the electrostatic interaction with a protonated molecule of Put.

Analysis of the results of equilibrium studies indicates that apart from the charge, also the ligand structure has a significant influence on the interactions. The results obtained for the systems of Urd and UMP, supported by those obtained for the systems with Ado and Cyd as well as adenosine and cytidine monophosphates [25–28] suggest that increasing chain length of amine usually leads to a greater tendency for adduct formation. The interactions of ethylenediamine or 1,3-diaminopropane with Urd are not detectable. However, such complexes form in the systems with Put, which corresponds to the different character of this biogenic amine occurring in living organisms.

The character of bioligand interactions in metal-free systems was confirmed by the results of ^{13}C NMR studies. The NMR signals were assigned to particular atoms on the basis



Scheme 1.

of literature data [29–33]. The numbering of the carbon atoms in uridine monophosphate and polyamines is shown in Scheme 1.

At pH from about 9 to 10, i.e. in the range of occurrence of $(Urd)H_2(Put)^+$ and (Urd)H(Put) molecular complexes the changes in the ^{13}C NMR spectra indicate that the interaction centers are the nitrogen N(3) atoms of the pyrimidine rings from uridine.

At pH 10 the chemical shifts of C(2) and C(4) atoms of Urd are 1.52 and 2.03 ppm, respectively, much higher than for C(5) and C(6) atoms and also much higher compared to the changes in the pH range at which no adducts are formed (Fig. 1(a), Table 2). The pattern of signal shifts for Put indicates that such centres in PA are the protonated $–NH_2$ groups (Table 2).

A similar agreement between the results of the potentiometric studies and the results of ^{13}C and ^{31}P NMR investigation was also found for the systems with UMP (Table 2). Formation of the $(UMP)H_3(en)$ adduct occurring in the pH range from 4 to about 8 (at pH ~6, about 65% of components occur in the form of molecular complex) involves interaction of PA and a negatively charged phosphate group (evidenced by the chemical shift of the ^{31}P NMR signal which is about 0.18 ppm, and small shifts of the ^{13}C NMR signals of the carbon atoms of ribose) (Table 2). The shifts of ^{13}C NMR signals of ribose carbon atoms are considerably higher in the range of the $(UMP)H_3(en)$ domination (i.e. at pH 6), when compared to the range in which the $(UMP)H_2(en)^-$ complex occurs, i.e. pH 6–10.5 (at pH 9, about 55% of the total amount of bioligands is bound in the adducts). With increasing pH, the change in the ^{13}P signal decreases, while that of the carbon atoms in the vicinity of N(3), i.e. C(2) and C(4) from UMP, increases (Table 2). Moreover, the shift of the ^{31}P NMR signal from the phosphate group is small at about pH 10, which means that in the molecular complex $(UMP)H_2(en)^-$ the ligands interact mainly through the N(3) atom and the protonated amine groups of the PA. A similar type of interaction with no involvement of the phosphate group has been observed for the AMP/Spm system [33].

In the system of UMP and tn in which, according to the potentiometric studies, three adducts are formed, significant chemical shifts of the signals in the ^{31}P NMR spectrum were observed at pH corresponding to the dominance of the form $(UMP)H_4(tn)^+$, i.e. in the pH range below 6 (where 85% of the components is in the form of the adduct). In this range of acidity, also the shifts of the signals attributed to ribose carbon atoms were observed (there is no change in the signal positions from C(2) and C(4) atoms), which confirms that only the phosphate group is involved in formation of this adduct. At higher pH where the adduct $(UMP)H_3(tn)$ dominates (Fig. 2), in the ^{13}C NMR spectrum the signals assigned to the carbon atoms of ribose, as well as to C(2) and C(4) of the base, are shifted.

Moreover, a change of the ^{31}P NMR spectrum is observed (Table 2). This change points to the possibility of interactions through the phosphate group and the nitrogen atom N(3). The $(UMP)H_3(tn)$ species is an intermediary form between

Table 2
Differences between ^{13}C NMR chemical shifts for the ligands in the Urd/Put and UMP/PA systems in relation to the single ligands

System	pD	Uridine 5′-monophosphate										Polyamine	
		C(2)	C(4)	C(5)	C(6)	C(1′)	C(2′)	C(3′)	C(4′)	C(5′)	P(α)	C(1)	C(2)
Urd/Put	6.0	0.023	0.067	0.047	0.107	0.054	0.051	0.013	0.079	0.058		0.003	0.032
	8.0	0.115	0.077	0.051	0.088	0.070	0.073	0.022	0.062	0.095		0.032	0.015
	9.5	1.518	2.033	0.152	0.197	0.106	0.061	0.396	0.015	0.091		0.364	0.106
	10.0	0.182	0.318	0.061	0.046	0.203	0.045	0.030	0.091	0.061		0.948	0.266
UMP/en	2.0	0.000	0.020	0.013	0.006	0.027	0.013	0.007	0.021	0.000	–	0.042	
	4.0	0.020	0.047	0.040	0.040	0.013	0.013	0.054	0.054	0.014	0.122	0.072	
	6.0	0.027	0.000	0.060	0.000	0.120	0.047	0.014	0.094	0.080	0.183	0.186	
	8.0	0.040	0.080	0.027	0.013	0.033	0.026	0.007	0.040	0.006	0.129	0.303	
	10.0	0.075	0.086	0.000	0.014	0.002	0.020	0.020	0.006	0.014	0.015	0.301	
UMP/tn	4.0	0.013	0.027	0.000	0.014	0.013	0.006	0.013	0.014	0.006	0.153	0.007	0.034
	6.0	0.087	0.100	0.066	0.320	0.146	0.227	0.100	0.521	0.608	0.145	0.086	0.017
	8.0	0.261	0.334	0.053	0.007	0.080	0.053	0.034	0.093	0.060	0.091	0.233	0.085
	10.0	3.925	5.348	0.254	0.781	0.067	0.033	0.033	0.327	0.060	0.030	0.616	2.990
UMP/Put	4.0	0.074	0.113	0.002	0.013	0.027	0.017	0.003	0.004	0.031	0.115	0.057	0.045
	6.0	0.108	0.122	0.059	0.010	0.139	0.053	0.026	0.135	0.095	0.443	0.014	0.072
	8.0	0.237	0.343	0.019	0.105	0.237	0.079	0.111	0.225	0.080	0.007	0.048	0.004
	10.0	0.480	0.629	0.020	0.046	0.212	0.039	0.148	0.167	0.120	0.046	0.887	0.205

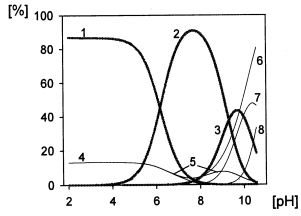


Fig. 2. Distribution diagrams for the UMP/tn system: 1, $(UMP)H_4(tn)^+$; 2, $(UMP)H_3(tn)$; 3, $(UMP)H_2(tn)^-$; 4, $H_2(UMP)^-$; 5, $H_2(tn)^{2+}$; 6, UMP^{3-}; 7, $H(tn)^+$; 8, tn; $C_{UMP} = C_{tn} = 0.01$ M.

the compound with interactions mainly through the phosphate group, as discussed above ($(UMP)H_4(tn)^+$ complex), and the molecular complex $(UMP)H_2(tn)^-$ formed at high pH, where the main reaction center is the N(3) atom of the nucleotide. At pH about 10 (40% of the substances occur as diprotonated adduct) only the shifts of the ^{13}C NMR signals due to C(2) and C(4) atoms by 3.92 and 5.35 ppm, respectively, were observed, while the signal in the ^{31}P NMR spectrum was practically unchanged (a shift by only 0.03 ppm).

The shift of the ^{31}P NMR signal (e.g. 0.44 ppm at pH 6) for the UMP/Put system in acidic medium — i.e. in the pH range of the adduct $(UMP)H_4(Put)^+$ occurrence (pH ~4–6) (Fig. 1(b)) — indicates the involvement of the phosphate group in formation of this molecular complex. In the same pH range, ^{13}C NMR spectra also reveal a change in the signal assigned to ribose carbon atom C(5′) (0.1 ppm), which confirms the above conclusion. With increasing pH (in the range of pH from 6.5 to ca. 10.5), the shift of C(2) and C(4) signals increases, which means that in these conditions in which both adducts [i.e. $(UMP)H_3(Put)$ and $(UMP)H_2(Put)^-$] are formed, the ligands interact mainly through the N(3) atom from the pyrimidine base (the ^{31}P NMR signals shift only by 0.01 and 0.05 ppm) and the protonated amine groups of PA. At pH 8 and pH 10, 85% and 50% of the total amount of components, respectively, is bound in the adducts (Fig. 1(b)).

3.2. Cu(II)/Urd or UMP binary systems

Results of the computer analysis of the potentiometric titration data for the systems Cu(II)/Urd and Cu(II)/UMP are shown in Table 1. The protonated complex of Urd and Cu(II) forms in solution already at low pH values (Fig. 3(a)). This complex species has been described previously [14,22]. The binuclear complex of type M_2L_2 starts to form at pH 6 and at higher pH disappears and practically the total amount of metal ions is bound in the hydroxo complexes formed.

The value of the $Cu(UMP)^-$ complex stability constant is significantly higher than that of the $Cu(Urd)^+$ species, suggesting a different mode of coordination (Table 1). The $Cu(UMP)^-$ complex starts forming from about pH 5.5 (Fig. 3(b)). In the basic medium, the hydroxo compounds dominate and from pH 9 they bind practically all the copper ions available.

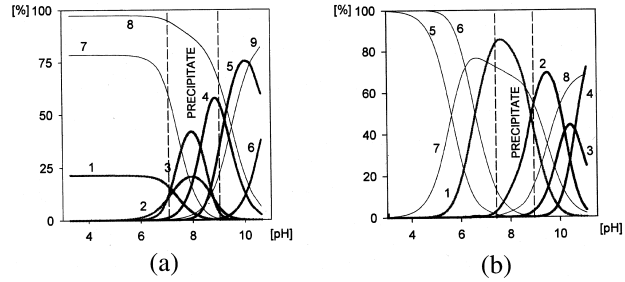


Fig. 3. Distribution diagrams for the systems: (a) Urd/Cu(II): 1, $Cu(Urd)H^{2+}$; 2, $Cu(Urd)^+$; 3, $(Cu)_2(Urd)_2^{2+}$; 4, $Cu(Urd)(OH)$; 5, $Cu(Urd)(OH)_2^-$; 6, $Cu(Urd)(OH)_3^{2-}$; 7, Cu^{2+}; 8, H(Urd); 9, Urd^-; $C_{Cu} = 0.0003$ M, $C_{Urd} = 0.0008$–0.0017M. (b) UMP/Cu(II): 1, $Cu(UMP)^-$; 2, $Cu(UMP)(OH)^{2-}$; 3, $Cu(UMP)(OH)_2^{3-}$; 4, $Cu(UMP)(OH)_3^{4-}$; 5, $H_2(UMP)^-$; 6, Cu^{2+}; 7, $H(UMP)^{2-}$; 8, UMP^{3-}; $C_{Cu} = 0.0003$ M, $C_{UMP} = 0.0008$–0.0017 M.

The mode of coordination of the complexes was determined on the basis of the equilibrium studies and spectral analysis. The λ_{max} of 713 nm for the $Cu(Urd)^+$ complex at pH 6.5 points to the monofunctional coordination of N1 type, which agrees with the results of the earlier studies of the systems with Ado and Cyd [27,34]. As follows from the results of the EPR study, an increase in the number of coordinated donor atoms is accompanied by a decrease in the value of $g_{||}$ and an increase in $A_{||}$, which has been observed for the chromophores $Cu–N_x$ ($x = 1$–6) and $Cu–N_xO_y$ ($x = 0$–4, $y = 0$–4) [35,36]. The values of $g_{||} = 2.3333$ and $A_{||} = 164$ at pH ~6.1 for the $Cu(Urd)^+$ complex indicate the coordination through a single nitrogen atom (Table 3, Fig. 4(b)). On the other hand, an increase in the $g_{||}$ value with decreasing pH (in the range in which only the $CuHUrd^{2+}$ complex

Table 3
EPR data for Urd/Cu(II) and UMP/Cu(II) complexes

System	Ph	$g_{\|\|}$	$A_{\|\|}$	Coordination
Urd/Cu(II)	5.9	2.4042	132	Cu(II) aqua
	6.1	2.3333	164	1N
	7.0	–	–	dimer
	10.5	2.2246	200	1N2O
UMP/Cu(II)	5.4	2.4103	137	Cu(II) aqua
	7.5–8.5			precipitate
	9.0–10.5	2.2389	200	3O–4O

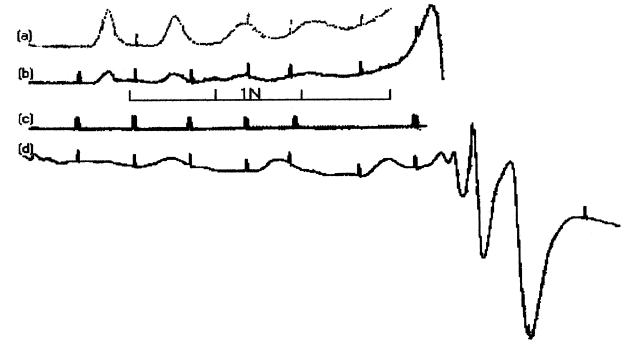


Fig. 4. The pH dependence of low-temperature (77 K) EPR spectra of Cu(II)/Urd complexes: (a) pH 4.0; (b) pH 6.0; (c) pH 7.0; (d) pH 10.0.

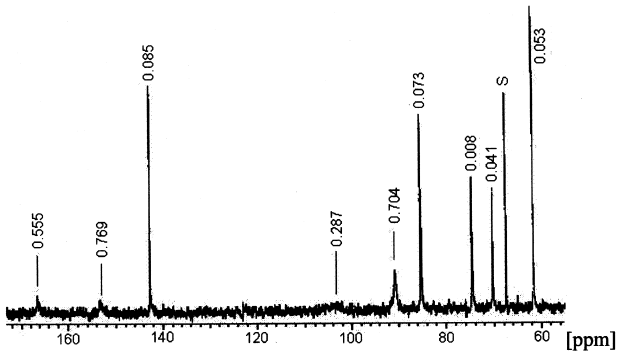


Fig. 5. ^{13}C NMR spectra of the Cu(II)/Urd system at pD = 6, C_{Urd} = 0.1 M, C_{Cu} = 0.0013 M, with changes in the signal position relative to those in the spectrum of a metal-free system at the same pD. The greatest changes are for C(2) 0.555 ppm and C(4) 0.769 ppm, and also for C(1′) 0.704 ppm.

occurs) indicates a weakening of the Cu–N interaction in the protonated complex.

The results of the EPR study also confirm the presence of the dimer $Cu_2(Urd)_2^{2+}$. A disappearance of the signal is observed at about pH 7 (Fig. 4(c)), due to spin coupling in the binuclear complex.

The changes in NMR signals were analysed taking into account the limitations of this method following from the presence of paramagnetic ions in the systems studied. In order to minimize the NMR signal broadening, the spectra were recorded for very low concentrations of the metal. As observed for analogous systems [13,15,16,18,19], significant changes of the shifts were found to occur only in the pH ranges of complex formation (the ranges have been determined from potentiometric studies). Fig. 5 presents an example of the ^{13}C NMR spectrum obtained by the method of decoupling of the complex of Cu(II) with Urd. This technique was also used to determine the coordination mode in similar systems with paramagnetic species [30,31,37]. The conclusions on the sites of coordination following from NMR studies have been verified by the UV–Vis and EPR results as well as comparative analysis of the equilibrium study data. Good correlation between results of independent methods makes it possible to make reliable inference about the coordination mode.

In the system Cu/Urd, at pH ~6, at which the $Cu(Urd)^+$ and $Cu_2(Urd)_2^{2+}$ forms exist, the ^{13}C NMR spectrum shows the shift of the C(2), C(4) and C(5) signals by 0.77, 0.56 and 0.29 ppm, respectively, which indicates coordination through the N(3) atom of the nucleoside (Table 4). At pH 4 (i.e. in conditions at which only the $CuHUrd^{2+}$ complex is formed) the shifts are much lower (changes for C(2) and C(4) atoms are only 0.018 and 0.008 ppm, respectively).

In the whole pH range considered, the positions of the IR stretching vibration bands assigned to the carbonyl groups (1652 and 1692 cm^{-1} for C(2)=O and C(4)=O, respectively) are not changed in the spectra of the system Cu(II)/Urd relative to their positions in the spectra of metal-free Urd, which testifies to the lack of interactions of these groups of the bioligand with metal ions. On the other hand, the observed changes in the positions of the β N(3)–H band (at 1524 cm^{-1}) support the above conclusion of coordination through N(3) atoms in both complexes. The IR bands were assigned on the basis of literature data [38,43,44].

At pH of about 10–11 (i.e. in the range of occurrence of $Cu(Urd)(OH)_x$ complexes), the position of the UV–Vis band indicates a coordination with the contribution of the nitrogen atom from Urd and oxygen atoms from OH^- groups. In order to draw more reliable conclusions on the mode of coordination in the complex studied, a series of absorption measurements was performed for the systems Cu(II)/acetylacetone and Cu(II)/acetylacetone/NH_3 (also with possible N_xO_y type of chromophore). In the pH range of the Cu(acac) complex domination (i.e. for the coordination of O2 type), λ_{max} = ~680 nm, while, in the range of domination of the $Cu(acac)_2$ complex (O4 chromophore), λ_{max} = 630 nm. In the ternary system Cu/acac/NH_3, at Cu:acac ratio 1:1, the band of λ_{max} = 663 nm was recorded irrespective of ammonia concentration, which indicates a coordination with the O2N1 chromophore. In spite of different types of ligands, the position of the band corresponding to $Cu(Urd)(OH)_x$ species (λ_{max} = 660 nm), suggests the interaction of copper ions with the N(3) atom of the nucleoside and oxygen atoms from hydroxyl groups. The suggested involvement of N(3) is confirmed by the shifts of ^{13}C NMR signals from the atoms C(2) and C(4) located in the neighborhood of the donor atom, 0.18 and 0.42 ppm, respectively (Table 4). The above conclusion is also confirmed by supplementary ^{15}N NMR study. The shifts of the signal attributed to N(3) atom is

Table 4
Differences between ^{13}C NMR chemical shifts for the ligands in the Urd/Cu and UMP/Cu systems in relation to metal-free systems

System	pD	Urd or UMP									
		C(2)	C(4)	C(5)	C(6)	C(1′)	C(2′)	C(3′)	C(4′)	C(5′)	P(α)
Urd/Cu(II)	4.0	0.018	0.008	0.021	0.002	0.000	0.004	0.002	0.005	0.011	
	6.0	0.769	0.555	0.287	0.085	0.704	0.041	0.008	0.073	0.053	
	7.0	0.403	0.656	0.528	0.046	0.327	0.042	0.077	0.046	0.008	
	10.7	0.182	0.425	0.045	0.060	0.045	0.000	0.046	0.015	0.030	
UMP/Cu(II)	4.2	0.062	0.006	0.090	0.043	0.004	0.032	0.073	0.043	0.031	–
	7.0	0.676	1.183	–	0.000	0.809	0.091	0.026	0.064	0.140	4.183
	10.0	0.243	0.060	0.046	0.061	0.121	0.015	0.000	0.060	0.015	0.038

0.123 ppm (the shift of the signal from N(1) atom is only 0.001 ppm). The ^{15}N NMR signal positions were assigned on the basis of literature data [39,40]. The involvement of oxygen atoms from carbonyl groups should be excluded on the basis of IR study in which no signal shifts were observed for the complex relative to the band positions for a free ligand.

In the ^{13}C NMR spectra of the systems of Cu(II) with UMP at pH ~7, the range at which the Cu(UMP)$^-$ complex dominates, the greatest changes in the chemical shift were found for the signals of C(2) and C(4) atoms, 0.68 and 1.18 ppm, respectively (Table 4). These shifts suggest the coordination through the oxygen atoms of the carbonyl groups or the nitrogen atom of the base. The question was solved by IR study. No shifts of the IR bands corresponding to the carbonyl groups (C(2)=O and C(4)=O) were observed, which excludes the involvement of the oxygen atoms from these groups in the Cu(UMP)$^-$ complex. As already mentioned, the value of the stability constant for Cu(UMP)$^-$, significantly higher than that of Cu(Urd)$^+$, suggests the involvement of an additional coordination site in the complex with the nucleotide. The change in the ^{13}C NMR signal ascribed to C(5′) at pH 7 is 0.14 ppm, and the chemical shifts of the phosphorus signal in the ^{31}P NMR spectrum, 4.18 ppm (Table 4), indicate that this additional site of interaction in Cu(UMP)$^-$ are the phosphate groups of the nucleotide. In conclusion, the above results point to coordination of N1O1 type.

The mode of coordination of Cu(UMP)(OH)$_x$ complexes (formed at pH above 9 in the condition when precipitate dissolves) was found to be substantially different from that of the Cu(UMP)$^-$ complex. At pH ~10 no shifts in the position of ^{31}P NMR signals were observed, which excludes the involvement of the phosphate group in the interactions (Table 4). On the other hand, analysis of the changes in IR band positions for Cu(UMP)(OH)$_x$ species indicates that only the oxygen atom from the C(2)=O group from the nucleotide is involved in the coordination. The stretching band at 1692 cm^{-1} is shifted, whereas that corresponding to C(4)=O at 1652 cm^{-1} remains unchanged (Fig. 6).

Moreover, the ^{13}C NMR signal from the C(2) atom is shifted by 0.24 ppm, while the signal attributed to C(4) is shifted by only 0.06 ppm (Table 4). The fact that Cu(II) interacts with the oxygen atom C(2)=O and does not interact with N(3) is confirmed by additional ^{15}N NMR study. The shifts of the signals attributed to N(3) and N(1) (unavailable for coordination) are practically the same (0.7 ppm). Moreover, the position of the absorption band at pH >9 (λ_{max}=674 nm) as well as the EPR parameters (Table 3) support the above conclusion concerning the coordination of metal ions only through the oxygen atoms from UMP and those from hydroxyl groups, in the absence of interactions with nitrogen atoms.

3.3. Cu(II)/Urd/PA ternary systems

Table 5 presents the stability constants of complexes formed in ternary systems comprising Cu(II) ions, nucleosides and the PA studied. The change in the size of the ring in the mixed-ligand complex related to the increasing length of the PA is manifested as a decrease in the thermodynamic stability of the coordination complexes.

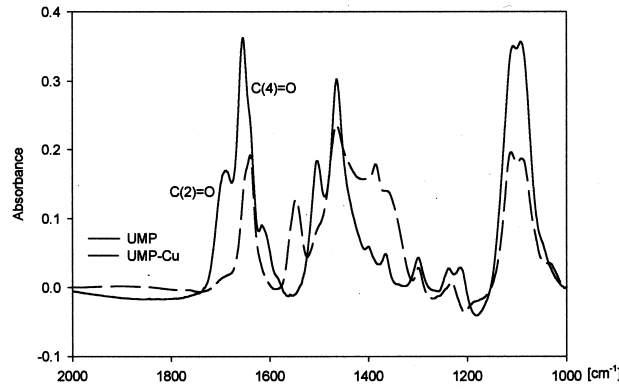


Fig. 6. The changes in IR spectra for the Cu(II)/UMP system in relation to free UMP at pH above 10.0.

The most stable compound, Cu(Urd)(en)$^+$, starts forming from pH of about 4.5, while the compounds with tn and Put form from pH of about 6.5 and 8, respectively (Fig. 7). The concentration of the Cu(Urd)(Put)$^+$ species is relatively low, which is consistent with a tendency of Put to assume a monofunctional coordination and to form protonated complexes [41,42].

Analysis of the chemical shifts of ^{13}C NMR signals indicate that the coordination site in Urd is the N(3) atom in all studied ternary systems. For example, the shifts of the signals corresponding to C(2) and C(4) atoms from the Urd molecule in the system Cu/Urd/en, at pH 6.5, are 0.202 and 0.235 ppm, respectively. The analogous shifts for the system Cu/Urd/tn are 1.115 and 0.930 ppm (pH 9), and for the system Cu/Urd/Put they are 0.829 and 1.204 ppm at pH 8. The above conclusions are in good agreement with the results of EPR and UV–Vis studies (Table 6).

The equilibrium constants of formation of the complexes Cu(PA)$^{2+}$ + Urd$^-$ ⇋ Cu(Urd)(PA)$^+$, calculated from the stability constant values of binary and mixed-ligand complexes ($\log K_e = \log \beta_{Cu(Urd)(PA)} - \log \beta_{Cu(PA)}$), are 6.65, 5.32 and 2.90 for the complexes Cu(Urd)(en)$^+$, Cu(Urd)tn$^+$ and Cu(Urd)(Put)$^+$, respectively. Taking into consideration the fact that the mode of Urd interaction (as discussed above) is the same in all studied systems, a significantly lower log K_e value for the Cu(Urd)(Put)$^+$ complex formation suggests monofunctional coordination of PA. In turn, the equilibrium constants of formation of the complexes Cu(Urd)(PA)$_2^+$ ($\log K_e = \log \beta_{Cu(Urd)(PA)2} - \log \beta_{Cu(PA)}$) (PA=en or tn), equal to 8.3 and 7.1, suggest difunctional interaction of the second molecule of en and tn. Although the overlapping of the domination range makes it difficult to identify the coordination mode of some species, in certain complexes, e.g. Cu(Urd)(en)$_2^+$, the N5-type of coordination was determined ($g_{||}$=2.218, $A_{||}$=179). The position of the band with λ_{max}=648 nm in the electronic spectrum also suggests this type of chromophore (probably formation

Table 5
Overall stability constants of Cu(II) ternary complexes for Urd, UMP and PA systems

Complex	Equilibrium	log β
$Cu(Urd)(en)^{+}$	$Cu^{2+}+Urd^{-}+en \rightleftharpoons Cu(Urd)(en)^{+}$	17.43(6)
$Cu(Urd)(en)_2^{+}$	$Cu^{2+}+Urd^{-}+2en \rightleftharpoons Cu(Urd)(en)_2^{+}$	25.71(9)
$Cu(Urd)(en)_2(OH)$	$Cu^{2+}+Urd^{-}+2en+H_2O \rightleftharpoons Cu(Urd)(en)_2(OH)+H^{+}$	15.54(10)
$Cu(Urd)H_2(en)_3^{3+}$	$Cu^{2+}+Urd^{-}+3en+2H^{+} \rightleftharpoons Cu(Urd)H_2(en)_3^{3+}$	47.60(5)
$Cu(Urd)(tn)^{+}$	$Cu^{2+}+Urd^{-}+tn \rightleftharpoons Cu(Urd)(tn)^{+}$	15.00(8)
$Cu(Urd)(tn)_2^{+}$	$Cu^{2+}+Urd^{-}+2tn \rightleftharpoons Cu(Urd)(tn)_2^{+}$	22.10(7)
$Cu(Urd)H(tn)_2^{2+}$	$Cu^{2+}+Urd^{-}+2tn+H^{+} \rightleftharpoons Cu(Urd)H(tn)_2^{2+}$	30.50(6)
$Cu(Urd)H_2(tn)_2^{3+}$	$Cu^{2+}+Urd^{-}+2tn+2H^{+} \rightleftharpoons Cu(Urd)H_2(tn)_2^{3+}$	38.12(8)
$Cu(Urd)(tn)_2(OH)$	$Cu^{2+}+Urd^{-}+2tn+H_2O \rightleftharpoons Cu(Urd)(tn)_2(OH)+H^{+}$	12.92(8)
$Cu(Urd)(tn)_2(OH)_2^{-}$	$Cu^{2+}+Urd^{-}+2tn+2H_2O \rightleftharpoons Cu(Urd)(tn)_2(OH)_2^{-}+2H^{+}$	2.23(12)
$Cu(Urd)(Put)^{+}$	$Cu^{2+}+Urd^{-}+Put \rightleftharpoons Cu(Urd)(Put)^{+}$	11.52(10)
$Cu(Urd)H(Put)^{2+}$	$Cu^{2+}+Urd^{-}+Put+H^{+} \rightleftharpoons Cu(Urd)H(Put)^{2+}$	20.52(7)
$Cu(Urd)(Put)(OH)^{-}$	$Cu^{2+}+Urd^{-}+Put+H_2O \rightleftharpoons Cu(Urd)(Put)(OH)+H^{+}$	2.88(6)
$Cu(UMP)(en)^{-}$	$Cu^{2+}+UMP^{3-}+en \rightleftharpoons Cu(UMP)(en)^{-}$	19.63(5)
$Cu(UMP)H_2(en)^{+}$	$Cu^{2+}+UMP^{3-}+en+2H^{+} \rightleftharpoons Cu(UMP)H_2(en)^{+}$	31.96(3)
$Cu(UMP)(en)(OH)^{2-}$	$Cu^{2+}+UMP^{3-}+en+H_2O \rightleftharpoons Cu(UMP)(en)(OH)^{2-}$	9.23(9)
$Cu(UMP)(tn)^{-}$	$Cu^{2+}+UMP^{3-}+tn \rightleftharpoons Cu(UMP)(tn)^{-}$	15.42(4)
$Cu(UMP)H(tn)$	$Cu^{2+}+UMP^{3-}+tn+H^{+} \rightleftharpoons Cu(UMP)H(tn)$	23.27(5)
$Cu(UMP)H_2(tn)^{+}$	$Cu^{2+}+UMP^{3-}+tn+2H^{+} \rightleftharpoons Cu(UMP)H_2(tn)^{+}$	30.09(3)
$Cu(UMP)H(Put)$	$Cu^{2+}+UMP^{3-}+Put+H^{+} \rightleftharpoons Cu(UMP)H(Put)$	22.30(10)
$Cu(en)^{2+}$	$Cu^{2+}+en \rightleftharpoons Cu(en)^{2+}$	10.78(8) [a]
$Cu(en)_2^{2+}$	$Cu^{2+}+2en \rightleftharpoons Cu(en)_2^{2+}$	19.88(10) [a]
$Cu(tn)^{2+}$	$Cu^{2+}+tn \rightleftharpoons Cu(tn)^{2+}$	9.68(12) [a]
$Cu(tn)_2^{2+}$	$Cu^{2+}+2tn \rightleftharpoons Cu(tn)_2^{2+}$	16.79(26) [a]
$Cu(tn)_3^{2+}$	$Cu^{2+}+3tn \rightleftharpoons Cu(tn)_3^{2+}$	21.66(32) [a]
$CuH(tn)^{3+}$	$Cu^{2+}+tn+H^{+} \rightleftharpoons CuH(tn)^{3+}$	15.78(14) [a]
$Cu(Put)^{2+}$	$Cu^{2+}+Put \rightleftharpoons Cu(Put)^{2+}$	8.62(13) [b]
$Cu(Put)_2^{2+}$	$Cu^{2+}+2Put \rightleftharpoons Cu(Put)_2^{2+}$	13.40(18) [b]
$Cu(Put)_2(OH)^{+}$	$Cu^{2+}+2Put+H_2O \rightleftharpoons Cu(Put)_2(OH)^{+}+H^{+}$	0.065(6) [b]
$CuH(Put)^{3+}$	$Cu^{2+}+Put+H^{+} \rightleftharpoons CuH(Put)^{3+}$	15.83(17) [b]

[a] Ref. [26].
[b] Refs. [26,42].

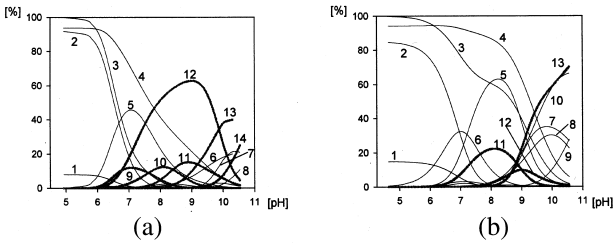


Fig. 7. Distribution diagrams for the systems. (a) Cu/Urd/tn: 1, $CuH(Urd)^{2+}$; 2, Cu^{2+}; 3, $H_2(tn)^{2+}$; 4, H(Urd); 5, $Cu(tn)^{2+}$; 6, Urd^{-}; 7, $Cu(Urd)(OH)_2^{-}$; 8, $Cu(Urd)(OH)_3^{2-}$; 9, $Cu(Urd)H_2(tn)_2^{-}$; 10, $Cu(Urd)H(tn)_2^{2+}$; 11, $Cu(Urd)(tn)_2^{+}$; 12, $Cu(Urd)(tn)^{+}$; 13, $Cu(Urd)(tn)_2(OH)$; 14, $Cu(Urd)(tn)_2(OH)_2^{-}$; $C_{Cu}=0.0003$ M, $C_{Urd}=C_{tn}=0.0008$ M. (b) Cu/Urd/Put: 1, $CuH(Urd)^{2+}$; 2, Cu^{2+}; 3, $H_2(Put)^{2+}$; 4, H(Urd); 5, $Cu(Put)^{2+}$; 6, $CuH(Put)^{3+}$; 7, $Cu(Put)_2^{2+}$; 8, $H(Put)^{+}$; 9, Put; 10, Urd^{-}; 11, $Cu(Urd)H(Put)^{2+}$; 12, $Cu(Urd)(Put)^{+}$; 13, Cu(Urd)(Put)(OH); $C_{Cu}=0.0003$ M, $C_{Urd}=C_{Put}=0.0008$ M.

of a square pyramidal complex occurs), as can be inferred from analysis of the spectra of analogous systems [35]. The change in $g_{||}$, and in particular in $A_{||}$ value, at pH 10.5, thus in the area of domination of the $Cu(Urd)(en)_2(OH)$ hydroxo complex, testifies to the presence of the N5O1 chromophore. Similarly, analysis of the electronic spectrum of Cu/Urd/tn indicates N3 or N3O1 coordination in $Cu(Urd)(tn)^{+}$ and $Cu(Urd)(tn)(OH)_x$, respectively. A particularly important result is the confirmation of the monofunctional coordination of Put in $Cu(Urd)H(Put)^{2+}$, for which the values of $g_{||}=2.263$, $A_{||}=158$ and $\lambda_{max}=649$ (Table 6) indicate N2 coordination.

3.4. Cu(II)/UMP/PA ternary systems

Protonated complexes in the system Cu/UMP/Put start forming from about pH 5.5 (Fig. 8). The shortest of the diamines, en, practically does not form compounds of this kind, while the medium-length one, tn, forms both heteroligand complexes of the MLL′ type and protonated species. The stability constants of the complexes forming in the system Cu/UMP/diamine are given in Table 5.

The formation of $Cu(UMP)(en)^{-}$ from pH of about 5.5 is accompanied by a shift of the ^{31}P NMR signal (at pH 8 by about 0.1 ppm). Moreover, in the ^{13}C NMR spectrum, the positions of the peaks corresponding to the C(2) and C(4) atoms are shifted (0.127 and 0.075 ppm, respectively, at pH ~8), which suggests that besides a coordination involving

Table 6
EPR data for PA/Urd and UMP/Cu(II) complexes

Complexes	PH	EPR		UV–Vis (λ_{max})	Coordination
		$g_{\|\|}$	$A_{\|\|}$		
$Cu(Urd)H_2(en)_3^{3+}$	6.5	2.212	185	550	5–6N
$Cu(Urd)(en)_2^{+}$	9	2.218	179	648	5N
$Cu(Urd)(en)_2(OH)$	10.5	2.218	198	600	5NO
$Cu(Urd)(tn)^{+}$	9	2.234	188	601	3N
$Cu(Urd)(tn)_2(OH)_x$	10.5	2.235	196	602	3NO
$Cu(Urd)H(Put)^{2+}$	8	2.263	158	649	2N
Cu(Urd)(Put)(OH)	10	2.230	195	630	3N
$Cu(UMP)(en)^{-}$	6	2.219	198	629	3NO
$Cu(UMP)(tn)^{-}$	8.5	2.232	189	592	3NO
Cu(UMP)H(Put)	8	2.265	161	611	2NO

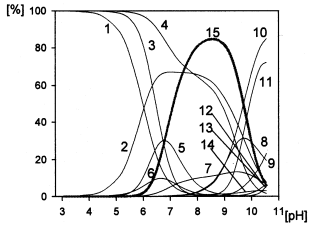


Fig. 8. Distribution diagrams for the Cu/UMP/Put system: 1, $H_2(UMP)^{-}$; 2, $H(UMP)^{2-}$; 3, Cu^{2+}; 4, $H_2(Put)^{2+}$; 5, $Cu(UMP)^{-}$; 6, $CuHPut^{3+}$; 7, $Cu(Put)^{2+}$; 8, $H(Put)^{+}$; 9, Put; 10, UMP^{3-}; 11, $Cu(Put)_2^{2+}$; 12, $Cu(UMP)(OH)_2^{3-}$; 13, $Cu(UMP)(OH)_3^{4-}$; 14, $Cu(UMP)(OH)^{2-}$; 15, Cu(UMP)H(Put); $C_{Cu} = 0.0003$ M, $C_{UMP} = C_{Put} = 0.0008$ M.

the phosphate group also the N(3) atom of the nucleotide is involved in coordination. The values of the EPR parameters (at pH 6, $g_{||} = 2.219$, $A_{||} = 198$) confirm the presence of the N3O1 chromophore (both nitrogen atoms from the PA), which is also confirmed by the position of the visible band with $\lambda_{max} = 629$ nm.

For the systems with tn, the EPR parameters (Table 6) and the significant shifts of NMR signals assigned to the phosphorus atom and C(2) and C(4) atoms indicate N3O coordination involving both the phosphate groups, the N(3) atom from the pyrimidine ring and the PA donor atoms. This mode of coordination is also implied by the position of the electron band with $\lambda_{max} = 592$ nm (pH 8.5).

According to the parameters of the EPR and visible spectra, the heteroligand complex Cu(UMP)H(Put) has a coordination mode type N2O ($g_{||} = 2.217$, $A_{||} = 196$, $\lambda_{max} = 565$, at pH 8). Taking into account the values of the chemical shifts of NMR signals of phosphorus and carbon atoms from the pyrimidine ring (in the complex Cu(UMP)H(Put) the shifts for phosphorus and C(2) and C(4) atoms are 0.672, 0.542 and 0.899 ppm, respectively, at pH 8), it is reasonable to assume a coordination involving the phosphate group of the nucleotide, N(3) atom from the pyrimidine ring and one donor atom from the amine.

As follows from the above discussion, the presence of PA changes the coordination character of UMP. In the Cu/UMP binary system, at high pH, the N(3) atom from pyrimidine ring and a phosphate group do not take part in complexation. On the other hand, in the Cu/UMP/Put system, these groups are involved in coordination, similar to the systems with en and tn.

Acknowledgements

This work was supported by the Grant No. T09A 092 12 of the Polish State Committee for Scientific Research.

References

[1] R.B. Martin, Metal ions binding to nucleoside and nucleotides, in: A.V. Xavier (Ed.), Frontiers in Bioinorganic Chemistry, VCH, Weinheim, 1986.
[2] L.G. Marzilli, Metal complex of nucleic acid derivatives and nucleotides: Binding sites and structures, in: G.L. Eichhorn, L.G. Marzilli (Eds.), Metal Ions in Genetic Information Transfer, Elsevier/North-Holland, Amsterdam, 1981, p. 47.
[3] H. Sigel, Complexes of metal ions with various nucleic acids components, in: G. Berthon (Ed.), Handbook of Metal–Ligand Interactions in Biological Fluids, Marcel Dekker, New York, 1995, p. 451.
[4] K.C. Tewari, J. Lee, N.C. Li, Trans. Faraday Soc. 66 (1970) 2069.
[5] R.B. Martin, Acc. Chem. Res. 18 (1985) 32.
[6] B. De Castro, J. Pereira, P. Gameiro, J.L. Lima, J. Inorg. Biochem. 45 (1992) 53.
[7] P. Kopf-Maier, H. Kopf, Chem. Rev. 87 (1987) 1137.
[8] S.E. Sherman, S.J. Lippard, Chem. Rev. 87 (1987) 1153.
[9] H. Sigel, Eur. J. Biochem. 65 (1987) 165.
[10] G.L. Eichhorn, Complex of nucleosides and nucleotides, in: G.L. Eichhorn (Ed.), Inorganic Biochemistry, Elsevier, Amsterdam, 1973, p. 1193.
[11] M. Fiskin, M. Beer, Biochemistry 4 (1965) 1289.
[12] C. Ropars, R. Viovy, J. Biol. Chem. 230 (1958) 797.
[13] H. Sigel, S.S. Massoud, Inorg. Chem. 27 (1988) 1447.
[14] E. Casassas, A. Izquierdo-Ridorsa, R. Tauler, J. Inorg. Biochem. 39 (1990) 327.
[15] E. Casassas, A. Izquierdo-Ridorsa, R. Tauler, J. Inorg. Biochem. 56 (1994) 187.
[16] T. Nawrot-Jankowska, H. Kozlowski, I. Sovago, J. Inorg. Biochem. 53 (1994) 49.
[17] L. Lomozik, Monatsh. Chem. 115 (1984) 261.
[18] M.H. Irving, M.G. Miles, L.D. Pettit, Anal. Chim. Acta 38 (1967) 475.

[19] P. Gans, A. Sabatini, A. Vacca, J. Chem. Soc., Dalton Trans. (1985) 1195.
[20] N. Ingri, W. Kakolowicz, L.G. Sillen, B. Warqvist, Talanta 14 (1967) 1261.
[21] P.K. Glasoe, F.A. Long, J. Phys. Chem. 64 (1960) 188.
[22] T. Kowalik-Jankowska, H. Kozlowski, I. Sovago, B. Nawrot, E. Sochacka, A. Malkiewicz, J. Inorg. Biochem. 53 (1994) 49.
[23] N. Ogasawara, Y. Inoue, J. Am. Chem. Soc. 27 (1976) 7048.
[24] S.S. Massoud, H. Sigel, Inorg. Chem. 27 (1988) 1447.
[25] L. Lomozik, A. Gasowska, J. Inorg. Biochem. 62 (1996) 103.
[26] L. Lomozik, A. Gasowska, L. Bolewski, J. Chem. Soc., Perkin Trans. 2 (1997) 1161.
[27] L. Lomozik, A. Gasowska, J. Inorg. Biochem. 63 (1996) 191.
[28] L. Lomozik, A. Gasowska (in press).
[29] C.J. Pouchert, J. Behnke, The Aldrich Library of ^{13}C and ^{1}H FT NMR Spectra, Vol. 3, Aldrich Chemical Company, 1993, pp. 371, 394.
[30] G. Kotowicz, O. Suzuki, Biochemistry 12 (1973) 3434.
[31] N. Berger, G. Eichhorn, Biochemistry 10 (1971) 1857.
[32] G. Kotowicz, Can. J. Chem. 52 (1974) 924.
[33] S. Bunce, E.S. Kong, Biophys. Chem. 8 (1978) 357.
[34] A. Gasowska, L. Lomozik, Monatsh. Chem. 126 (1995) 13.
[35] L. Lomozik, L. Bolewski, R. Dworczak, J. Coord. Chem. 41 (1997) 261.
[36] R. Barbucci, M.J.M. Campbell, Inorg. Chim. Acta 16 (1976) 113.
[37] U. Weser, G.J. Strobel, H. Rupp, W. Voelter, Eur. J. Biochem. 50 (1974) 91.
[38] M. Mathlouthi, M.A. Seuvere, J. Koenig, Carbohydr. Res. 122 (1983) 31.
[39] E. Sletten, J. Sletten, N.A. Froystein, Acta Chem. Scand., Part A 42 (1988) 413.
[40] S. Steinkopf, Q. Liv, N.A. Froystein, Acta Chem. Scand. 46 (1992) 446.
[41] A. Wojciechowska, L. Bolewski, L. Lomozik, Monatsh. Chem. 122 (1991) 131.
[42] L. Lomozik, A. Gasowska, Monatsh. Chem. 124 (1993) 109.
[43] P. Carmona, M. Molina, R. Escobar, J. Mol. Struct. 243 (1991) 297.
[44] I.R. Gould, M.A. Vincent, I.H. Hiller, J. Chem. Soc., Perkin Trans. 2 (1992) 69.

PERGAMON

www.elsevier.nl/locate/poly

Polyhedron 19 (2000) 1155–1161

POLYHEDRON

Effect of metal size on coordination geometry of *N*,*N*′,*N*″-tris(2-pyridylmethyl)-*cis*,*cis*-1,3,5-triaminocyclohexane: synthesis and structure of $[M^{II}L](ClO_4)_2$ (M = Zn, Cd and Hg)

G. Park [a], N. Ye [a], R.D. Rogers [b], M.W. Brechbiel [c], R.P. Planalp [a,*]

[a] *Department of Chemistry, University of New Hampshire, Durham, NH 03824, USA*
[b] *Department of Chemistry, The University of Alabama, Tuscaloosa, AL 35487, USA*
[c] *The Chemistry Section, Radiation Oncology Branch, National Institutes of Health, Bethesda, MD 20892, USA*

Received 17 January 2000; accepted 14 March 2000

Abstract

The hexadentate ligand *N*,*N*′,*N*″-tris(2-pyridylmethyl)-*cis*,*cis*-1,3,5-triaminocyclohexane (tachpyr) forms stable metal complexes from the salts $M(ClO_4)_2 \cdot 6H_2O$ (M = Zn^{2+} and Cd^{2+}) and $Hg(ClO_4)_2$ in methanol or ethanol. The complexes $[Zn(tachpyr)](ClO_4)_2 \cdot CH_3OH$ (**1**·CH_3OH), $[Cd(tachpyr)](ClO_4)_2$ (**2**) and $[Hg(tachpyr)](ClO_4)_2$ (**3**) have been isolated, and their solid state structures have been determined and analyzed. The coordination sphere changes from octahedral to trigonal-prismatic geometry with increasing metal radius. The trigonal twist angles (α) are 43.7(2)° in compound **1**·CH_3OH, range between 11.0(4)° and 21.7(2)° in compound **2** and range between 3.1(3)° and 5.5(2)° in compound **3**. To accommodate larger metal ions there is also a slight outward expansion of the triaminocyclohexane nitrogens, which leads to a reduction in the average cyclohexyl ring C–C–C–C torsion angles (β) with concomitant flattening of the ring. The torsion angles (β) in **1**·CH_3OH are 52.3(6)° and 52.4(6)°, range between 46.1(9)° and 52.7(9)° in compound **2** and range between 45.1(6)° and 52.9(7)° in compound **3**. ©2000 Elsevier Science Ltd All rights reserved.

Keywords: Cd(II); Hg(II); tachpyr; Torsion angles; Twist angles; Zn(II)

1. Introduction

Ligands that are preorganized or predisposed to bind metal ions form particularly thermodynamically or kinetically stable complexes [1–4]. We previously reported an efficient synthesis of a novel hexadentate ligand, *N*,*N*′,*N*″-tris(2-pyridylmethyl)-*cis*,*cis*-1,3,5-triaminocyclohexane (referred to as tachpyr; Fig. 1) [5], based on *cis*,*cis*-1,3,5-triaminocyclohexane (tach) which is a versatile face-capping N_3 ligand and can form complexes with a large number of first-row transition metal ions with varied charges and sizes [6–10]. In studying the complexation properties of the tachpyr ligand, we reported the preparation and structure of the first metal complexes of this chelator, $[Ga(tachpyr)](NO_3)_3$ and $[In(tachpyr)](NO_3)_3$ [10]. The tachpyr ligand readily makes metal complexes by a ring flip from an open all-equatorial conformation to a closed all-axial conformation (Fig. 1), encapsulating metal ions ranging in size from Ga^{3+} (six-coordinate ionic radius of 0.76 Å) through many first-row transition elements [11] to In^{3+} (radius 0.94 Å) in alcoholic or aqueous media. Study of the interaction of Fe(II) and Fe(III) with tachpyr, which affords mono and diimino Fe(II) complexes by oxidative dehydrogenation of one or two of the aminomethylene group(s) of tachpyr in the presence of oxygen, has also been reported [12].

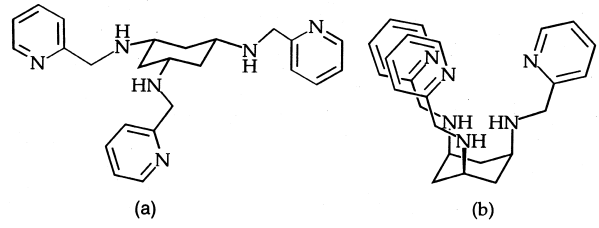


Fig. 1. Structures of tachpyr: open (a) and closed (b) conformation.

Since the group IIB metal ions (Zn^{2+}, Cd^{2+} and Hg^{2+}) do not have an electronic preference for either an octahedral or a trigonal prismatic coordination geometry, their tachpyr complexes may reveal effects of metal radius and ligand conformational preferences on geometry. Herein we report the preparation, characterization and structures of these complexes.

* Corresponding author. Tel.: +1-603-8622471; fax: +1-603-8624278; e-mail: roy.planalp@unh.edu

0277-5387/00/$ - see front matter ©2000 Elsevier Science Ltd All rights reserved.
PII S0277-5387(00)00380-6

2. Experimental

Caution! Although we have not encountered any problems, it should be noted that perchlorate salts are potentially explosive and should be handled with care.

2.1. Materials and methods

Diethyl ether was distilled from Na/K. Anhydrous grade MeOH and CH_3CN and the salts $Zn(ClO_4)_2\cdot 6H_2O$, $Cd(ClO_4)_2\cdot 6H_2O$ and $Hg(ClO_4)_2$ were obtained from Aldrich. Anhydrous grade EtOH was obtained from Pharmco. Tachpyr was prepared as previously reported [5].

Proton NMR spectra were obtained at 360 MHz with a Bruker AM360 instrument. Chemical shifts are reported in ppm on the δ scale relative to TMS (DMSO-d_6 or CH_3CN-d_3 solutions). Proton chemical shifts are annotated as follows: ppm (multiplicity or spin system, coupling constant if measurable, integral, assignment). Fast atom bombardment (FAB-MS) mass spectra were obtained on an Extrel 4000. Elemental analyses were performed by Atlantic Microlabs (Atlanta, GA).

2.1.1. Preparation of zinc(II) tachpyr diperchlorate methanol solvate (*1*·CH_3OH)

To a colorless solution of $Zn(ClO_4)_2\cdot 6H_2O$ (0.0906 g, 2.43×10^{-4} mol) in anhydrous EtOH (3 ml) was added a yellow solution of tachpyr (0.0986 g, 2.45×10^{-4} mol) in anhydrous MeOH (3 ml), affording a pale yellow precipitate. After standing for 2 h, the pale yellow precipitate was isolated by decanting the supernatant and washed with Et_2O and MeOH. The product was dried under reduced pressure, affording 22.0% yield (0.0370 g, 5.28×10^{-5} mol) as a white solid. *Anal*. Calc. for $C_{24}H_{30}Cl_2N_6O_8Zn\cdot CH_3OH$: C, 42.97; H, 4.90; N, 12.03. Found: C, 42.91; H, 4.67; N, 12.19%. ^{1}H NMR (360 MHz, DMSO-d_6, 25°C): δ 8.11, 7.81, 7.63, 7.50 (t, d, d, t, 4H, $^3J=7.8$ and 5.7 Hz, $^4J=1.3$ Hz, C_5H_4N); 4.71 (dd, *A*XY, 1H, $^3J=8.5$ and 8.4 Hz, N*H*–CH_2-py); 4.14 (m (two dd), A*XY*, 2H, NH–C*H*$_2$–py); 3.26 (br s, *A*MM′XX′, 1H, cyclohexyl methine H′s); 2.34 (br d, A*MM*′XX′, 1H, equatorial cyclohexylmethylene H diastereotopic), 1.90 (br d, AMM′*XX*′, 1H, axial cyclohexylmethylene H′s, diastereotopic). MS (FAB/glycerol): 465 (M−2ClO_4^-).

2.1.2. Preparation of cadmium(II) tachpyr diperchlorate (*2*)

To a colorless solution of $Cd(ClO_4)_2\cdot 6H_2O$ (0.088 g, 2.1×10^{-4} mol) in anhydrous EtOH (8 ml) was added a yellow solution of tachpyr (0.084 g, 2.1×10^{-4} mol) in anhydrous MeOH (8 ml) affording a brown suspension immediately. After standing for 2 h, feather-shaped crystals precipitated. The product was isolated by decanting the supernatant, washing the residue with Et_2O and then drying under reduced pressure, affording a white solid in 51% yield (76.3 mg, 1.07×10^{-4} mol). *Anal*. Calc. for $C_{24}H_{30}CdCl_2N_6O_8$: C, 40.37; H, 4.24; N, 11.77. Found: C, 40.12; H, 4.22; N, 11.48%. ^{1}H NMR (360 MHz, CH_3CN-d_3, 25°C): δ 8.80, 7.99, 7.55, 7.49 (d, t, t, d, 4H, $^3J=7.8$ and 5.5 Hz, C_5H_4N); 4.21 (dd, *A*MX, 1H, $^2J=15.8$ Hz, $^3J=15.8$ Hz, NH–C*H*$_2$–py, diastereotopic), 4.01 (dd, A*M*X, 1H, $^2J=15.8$ Hz, $^3J=5.5$ Hz, NH–C*H*$_2$–py, diastereotopic); 3.55 (br d (dd), AM*X*, 1H, $^3J=15.8$ and 5.5 Hz, N*H*–CH_2–py); 3.46 (br s, *A*MM′XX′, 1H, cyclohexylmethine H); 2.28 (br d, A*MM*′XX′, 1H, equatorial cyclohexylmethylene H′s), 2.02 (br d, AMM′*XX*′, 1H, axial cyclohexylmethylene H′s, diastereotopic). MS (FAB/glycerol): 614 (M−ClO_4^-).

2.1.3. Preparation of mercury(II) tachpyr diperchlorate (*3*)

To a solution of $Hg(ClO_4)_2$ (0.038 g, 9.4×10^{-5} mol) prepared by sonication (5 min) in anhydrous EtOH (4 ml) was added a yellow solution of tachpyr (0.038 g, 9.4×10^{-5} mol) in anhydrous EtOH (2 ml), affording a yellowish-white precipitate. The yellowish-white precipitate was isolated by decanting the supernatant. The residue was washed with Et_2O (4 ml) and dried under reduced pressure, giving a pale yellow solid. The crude product was dissolved in CH_3CN (5 ml), and Et_2O was diffused into it, forming a mixture of yellow precipitate and white crystals. The white crystals were isolated manually and re-dissolved in CH_3CN (5 ml). Et_2O was diffused into a CH_3CN solution of the crude product, forming prisms which were isolated by decanting the supernatant and dried under reduced pressure, affording a 52% yield (39.1 mg, 4.87×10^{-5} mol). *Anal*. Calc. for $C_{24}H_{30}Cl_2HgN_6O_8$: C, 35.94; H, 3.77; N, 10.48. Found: C, 36.24; H, 3.72; N, 10.39%. ^{1}H NMR (360 MHz, DMSO-d_6, 25°C): δ 9.13, 8.06, 7.68 (d, t, m (2H), 4H, $^3J=7.9$ and 5.7 Hz, C_5H_4N); 4.91 (br d (dd), *A*MX, 1H, $^3J=13.7$ and 3.5 Hz, N*H*–CH_2–py); 4.35 (dd, A*M*X, 1H, $^2J=13.9$ Hz, $^3J=13.7$ Hz, NH–C*H*$_2$–py); 3.94 (dd, AM*X*, 1H, $^2J=13.9$ Hz, $^3J=3.5$ Hz, N*H*–CH_2–py); 3.44 (brs, *A*MM′XX′, 1H, cyclohexylmethine H); 2.44 (br d, A*MM*′XX′, 1H, equatorial cyclohexylmethylene H′s), 1.94 (br d, AMM′*XX*′, 1H, axial cyclohexylmethylene H′s, diastereotopic). MS (FAB/glycerol): 603 (M−2ClO_4^-).

2.2. X-ray data collection, structure solution and refinement for compounds *1*·CH_3OH, *2* and *3*

Single crystals suitable for X-ray crystallography of compounds **1**·CH_3OH, **2** and **3** were grown by diethyl ether diffusion into the acetonitrile solution of the corresponding metal complexes. Transparent single crystals were mounted on fibers and transferred to the goniometer. The crystals were cooled to −100°C during data collection by using a stream of cold nitrogen gas. Data collection was made on a Siemens SMART diffractometer with a CCD area detector, using graphite monochromated Mo Kα radiation. SHELXTL, version 5, software was used for solutions and refinement [13]. Absorption correction was carried out using the program SADABS [14]. The model was refined by full-matrix least-squares on F^2. A summary of data collection parameters is given in Table 1.

Table 1
Crystal data and structure refinement for [Zn(tachpyr)]$(ClO_4)_2\cdot CH_3OH$ (**1**$\cdot CH_3OH$), [Cd(tachpyr)]$(ClO_4)_2$ (**2**) and [Hg(tachpyr)]$(ClO_4)_2$ (**3**)

	1$\cdot CH_3OH$	**2**	**3**
Color/shape	colorless/fragment	colorless/fragment	colorless/parallelepiped
Empirical formula	$C_{25}H_{34}Cl_2N_6O_9Zn$	$C_{24}H_{30}CdCl_2N_6O_8$	$C_{24}H_{30}Cl_2HgN_6O_8$
Formula weight	698.85	713.84	802.03
Temperature (K)	173(2)	173(2)	173(2)
Wavelength (Å)	0.71073	0.71073	0.71073
Crystal system	cubic	monoclinic	monoclinic
Space group	$P2_13$	$P2_1/c$	$P2_1/c$
Unit cell dimensions			
a (Å)	14.3088(1)	13.3620(3)	13.3481(4)
b (Å)		13.9104(3)	14.0714(2)
c (Å)		15.4736(3)	15.4171(4)
β (°)		108.611(1)	109.043(1)
Volume (Å^3)	2929.61(4)	2725.69(10)	2737.27(12)
Z	4	4	4
Density (calc.) (Mg m^{-3})	1.584	1.740	1.946
Absorption coefficient (mm^{-1})	1.083	1.058	5.879
$F(000)$	1448	1448	1576
Crystal size (mm)	0.35×0.50×0.70	0.35×0.40×0.40	0.20×0.25×0.30
θ Range for data collection (°)	1.84–21.67	1.61–27.85	1.61–27.82
Index ranges	$-12\le h\le 18$, $-18\le k\le 16$, $-18\le l\le 18$	$-17\le h\le 15$, $0\le k\le 17$, $0\le l\le 20$	$-17\le h\le 16$, $-15\le k\le 18$, $-20\le l\le 19$
No. reflections collected	18785	6332	17006
No. independent reflections (R_{int})	2329 (0.1145)	6332 (0.0000)	6324 (0.0231)
Absorption correction	SADABS [a]	SADABS [a]	SADABS [a]
Absolute structure parameters	0.03(2)		
Extinction coefficient	0.0004(4)	0.0004(2)	0.00064(10)
Data/restraints/parameters	2326/0/138	6329/0/447	6319/0/379
Goodness-of-fit on F^2	1.183	1.389	1.014
Weighting scheme [b]	0.0256, 2.1225	0.0000, 9.3373	0.0398, 10.3997
Final R indices [$I>2\sigma(I)$]			
R_1	0.0660	0.0645	0.0345
wR_2	0.0898	0.1157	0.0816
R indices (all data)			
R_1	0.1084	0.0699	0.0469
wR_2	0.1054	0.1178	0.0883
Largest difference peak and hole (e Å^{-3})	0.291 and −0.475	0.914 and −0.893	2.417 and −1.421

[a] SADABS [14].
[b] SHELX-93 weight parameters.

The structures were solved by direct methods. The cyclohexyl group and three nitrogens bonded to it in compound **2** were found to be disordered and resolved into two orientations with N1–C6 at 60% occupancy and N1′–C6′ at 40% occupancy. The two orientations differ in a twist of the chair conformation of the cyclohexyl ring. High thermal motion was also observed for anions, as is often found for perchlorate ions. Disorder models were not resolvable for these molecules. Although there is some evidence in the structure of compound **3** for the disorder observed for compound **2**, the slight elongation of thermal ellipsoids for N2, N3 and some of the cyclohexyl carbon atoms could not be resolved into a reasonable disorder model. The slight elongation of thermal ellipsoids could affect quantitative parameters, although the overall structure is clear. For the three structures, the geometrically constrained hydrogen atoms were placed in calculated positions and allowed to ride on the bonded atom with $B=1.2U_{eq}(C)$. Refinement of non-hydrogen atoms (except for C5′ in compound **2**, which could not be refined anisotropically) was carried out with anisotropic temperature factors. Selected bond lengths and angles of compounds **1**$\cdot CH_3OH$, **2** and **3** are presented in Table 2.

3. Results and discussion

3.1. Synthesis and solution behavior

The complexes [Zn(tachpyr)]$(ClO_4)_2\cdot CH_3OH$ (**1**$\cdot CH_3OH$), [Cd(tachpyr)]$(ClO_4)_2$ (**2**) and [Hg(tachpyr)]$(ClO_4)_2$ (**3**) were prepared by the reactions of the respective metal ion perchlorate salts $M(ClO_4)_2\cdot 6H_2O$ [M=Zn(II) and Cd(II)] or $M(ClO_4)_2$ [M=Hg(II)] and the ligand (1:1) in a mixture of methanol and ethanol. Colorless crystals of compounds **2** and **3** were obtained with reasonable yield

Table 2
Selected bond distances (Å) and bond angles (°) in [Zn(tachpyr)](ClO$_4$)$_2$·CH$_3$OH (**1**·CH$_3$OH), [Cd(tachpyr)](ClO$_4$)$_2$ (**2**) and [Hg(tachpyr)](ClO$_4$)$_2$ (**3**)

*[Zn(tachpyr)](ClO$_4$)$_2$·CH$_3$OH (**1**)*					
Zn–N(1), Zn–N(1) [a], Zn–N(1) [b]	2.160(3)	N(1)–Zn–N(2)	79.01(14)	C(4)–N(2)–Zn	114.9(3)
Zn–N(2), Zn–N(2) [a], Zn–N(2) [b]	2.165(4)	N(1)–Zn–N(1) [a]	90.21(14)	C(8)–N(2)–Zn	126.9(3)
N(1)–C(1)	1.486(5)	N(1)–Zn–N(2) [b]	166.24(14)		
N(1)–C(3)	1.475(5)	N(2)–Zn–N(2) [a]	93.97(14)		
N(2)–C(8)	1.354(5)	C(1)–N(1)–C(3)	113.9(4)		
N(2)–C(4)	1.337(6)	C(1)–N(1)–Zn	113.9(3)		
*[Cd(tachpyr)](ClO$_4$)$_2$ (**2**), disorder model 1*					
Cd–N(3)	2.302(6)	N(4)–C(8)	1.346(10)	N(4)–Cd–N(2)	111.1(2)
Cd–N(5)	2.352(4)	N(4)–C(12)	1.350(6)	C(1)–N(1)–Cd	118.2(4)
Cd–N(6)	2.359(4)	N(1)–Cd–N(4)	71.2(2)	C(1)–N(1)–C7	114.3(6)
Cd–N(4)	2.361(4)	N(2)–Cd–N(5)	71.0(2)	C(8)–N(4)–Cd	114.0(3)
Cd–N(2)	2.388(6)	N(3)–Cd–N(6)	73.0(2)	C(12)–N(4)–Cd	125.7(3)
Cd–N(1)	2.400(5)	N(1)–Cd–N(2)	80.2(2)		
N(1)–C(7)	1.453(8)	N(1)–Cd–N(5)	141.9(2)		
N(1)–C(7)	1.453(8)	N(4)–Cd–N(6)	98.20(14)		
*Additional parameters of compound **2** derived from disorder model 2*					
Cd–N(1′)	2.332(13)	N(1′)–CdN(4)	70.4(3)	N(4)–Cd–N(2′)	138.3(3)
Cd–N(2′)	2.347(9)	N(2′)–Cd–N(5)	71.9(2)	C(1′)–N(1′)–Cd	116.0(9)
Cd–N(3′)	2.422(9)	N(3′)–Cd–N(6)	71.6(2)	C(1′)–N(1′)–C7	119.6(11)
N(1′)–C(7)	1.28(2)	N(1′)–Cd–N(2′)	81.7(5)		
N(1)–C(1′)	1.55(2)	N(1′)–Cd–N(5)	120.8(6)		
*[Hg(tachpyr)](ClO$_4$)$_2$ (**3**)*					
Hg–N(6)	2.334(4)	N(4)–C(12)	1.361(7)	N(4)–Hg–N(2)	127.9(3)
Hg–N(2)	2.335(6)	N(4)–C(8)	1.339(6)	C(1)–N(1)–Hg	115.6(3)
Hg–N(4)	2.377(4)	N(1)–Hg–N(4)	70.43(14)	C(1)–N(1)–C(7)	114.5(4)
Hg–N(1)	2.438(4)	N(2)–Hg–N(5)	69.4(2)	C(8)–N(4)–Hg	114.8(3)
Hg–N(5)	2.461(4)	N(3)–Hg–N(6)	71.0(2)	C(8)–N(4)–C(12)	118.6(4)
Hg–N(3)	2.487(6)	N(1)–Hg–N(2)	88.3(2)		
N(1)–C(7)	1.449(7)	N(1)–Hg–N(5)	134.05(14)		
N(1)–C(1)	1.502(7)	N(4)–Hg–N(6)	105.5(2)		

[a] Symmetry transformations used to generate equivalent atoms: $z-1/2, -x-3/2, -y-1$.
[b] Symmetry transformations used to generate equivalent atoms: $-y-3/2, -z-1, x+1/2$.

(>50%); however, the yield of colorless crystalline compound **1**·CH$_3$OH was poor (<25%).

The formation of complexes and the rigidity of coordination spheres of compounds **1**, **2** and **3** were investigated by proton NMR studies of Zn(II) and Hg(II) (DMSO-d_6 solvent) and Cd(II) (CH$_3$CN-d_3 solvent) complexes. The formation of metal complexes was easily confirmed by changes in the chemical shift and splitting patterns of the cyclohexyl protons relative to free tachpyr (Fig. 1a). The three 2-pyridylmethyl arms of tachpyr are assumed to coordinate M(II) in either the Λ or Δ configuration [15]. Proton NMR studies indicated that this configuration is static on the NMR time scale at room temperature, as shown by the chemically inequivalent methylene protons, (cyclohexylamine)NH–CH_2–pyridyl, which form an AMX (or AXY) spin system (H$_A$ is the amine hydrogen on tach).

3.2. Structural studies

X-ray structures of compounds **1**·CH$_3$OH), **2** and **3** are depicted in Figs. 2–4, respectively. Crystals of compounds **1**·CH$_3$OH, **2** and **3** consist of the di-cations $[LZn]^{2+}$, $[LCd]^{2+}$ and $[LHg]^{2+}$, respectively, and perchlorate anions. The Zn(II) complex (**1**·CH$_3$OH) crystallizes in the cubic space group $P2_13$, whereas the Cd(II) complex (**2**) and the Hg(II) complex (**3**) are essentially isostructural and

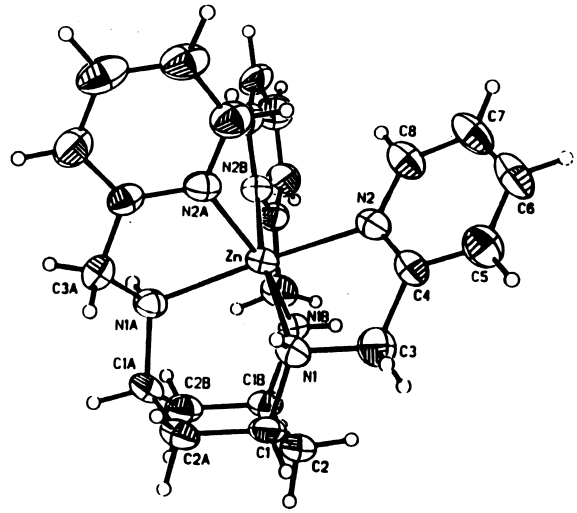


Fig. 2. Molecular structure of the metal complex cation of [Zn(tachpyr)](ClO$_4$)$_2$·CH$_3$OH (**1**·CH$_3$OH).

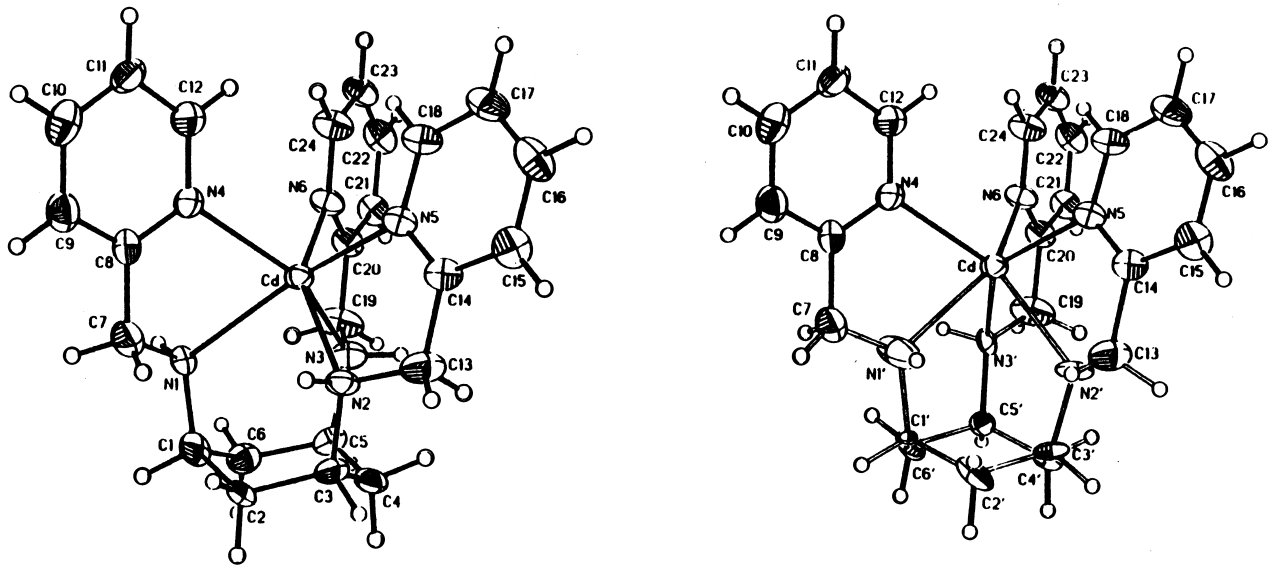


Fig. 3. Molecular structure of the metal complex cation of $[Cd(tachpyr)](ClO_4)_2$ (**2**) showing two disordered molecules with N1–C6 at 60% occupancy (left) and N1′–C6′ at 40% occupancy (right).

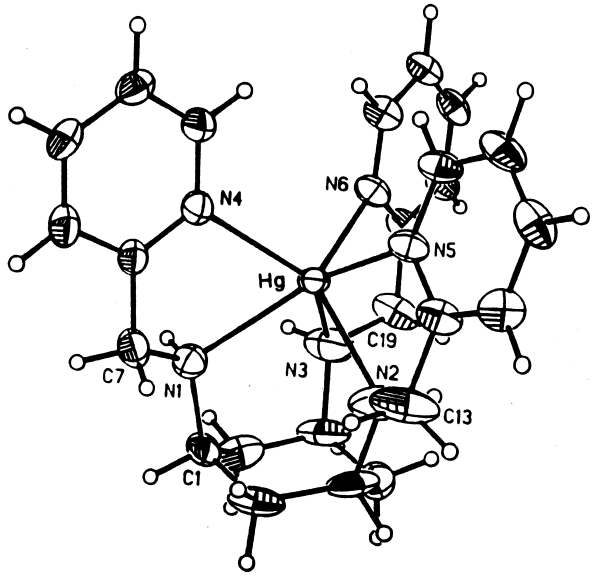


Fig. 4. Molecular structure of the metal complex cation of $[Hg(tachpyr)](ClO_4)_2$ (**3**).

crystallize in the monoclinic space group $P2_1/c$. Interestingly, the disorder obvious in the structure of the Cd(II) complex is not resolvable for the Hg(II) complex.

Tachpyr provides six nitrogens which can coordinate to metal ions, including group IIB [Zn(II), Cd(II) and Hg(II)]. Since these metal ions do not have an electronic preference for either an octahedral or a trigonal-prismatic configuration, the structures of their tachpyr complexes should reflect the conformational preference of tachpyr and non-bonded repulsions between donor groups. The coordination sphere of MN_6 in compound $\mathbf{1}\cdot CH_3OH$ is best described as a distorted octahedron, whereas that of compound **2** is classified as an intermediate between octahedral and trigonal-prismatic and that of compound **3** is close to trigonal-prismatic. The average twist angle (α) (Fig. 5) of compound **1** is 43.7(2)°, while those of compound **2** (disorder models 1 and 2) are 20.8(4) and 11.4(9)°, and that of compound **3** is 5(1)°. Without a major perturbation caused by the metal ion, the tachpyr ligand seems to have a ligand conformation preference for an octahedral geometry.

As the six-coordinate ionic radius increases from Zn^{2+} (0.88 Å) to Cd^{2+} (1.09 Å) and then to Hg^{2+} (1.16 Å) [16,17], the 2-pyridylmethyl arms straighten out to accommodate the longer metal–nitrogen bonds, two nitrogens on the same pendant arms come closer to being eclipsed, and the coordination geometry of the metal complexes approaches trigonal-prismatic. Similar trends have been observed in tricationic tachpyr complexes of Ga^{3+} (0.76 Å) and In^{3+} (0.93 Å) [10] and in di-cationic tachpyr complexes of Ni^{2+} (0.83 Å) and Mn^{2+} (high-spin, 0.97 Å) [11]. These structural features have also been reported in the complexes of *N*,*N*′,*N*′-tris(2-pyridylmethyl)-1,4,7-triazacyclononane [18,19].

The bond lengths M–N are larger for compounds **2** and **3** than for $\mathbf{1}\cdot CH_3OH$ (Table 3), reflecting the difference in six-coordinate ionic radii from Zn^{2+} in $\mathbf{1}\cdot CH_3OH$ to Cd^{2+} and Hg^{2+} in compounds **2** and **3**, respectively. The bond lengths of Zn–N (tach amine) and Zn–N (pyridyl) in $\mathbf{1}\cdot CH_3OH$ are 2.160(3) and 2.165(4) Å, which compare well with those

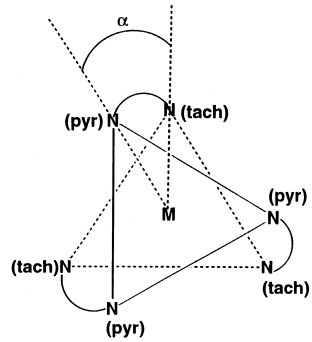


Fig. 5. The twist angle defined for the coordination sphere of $M(tachpyr)^{2+}$.

Table 3
Comparison of structural parameters in [Zn(tachpyr)]$(ClO_4)_2 \cdot CH_3OH$ (**1**·CH_3OH), [Cd(tachpyr)]$(ClO_4)_2$ (**2**) and [Hg(tachpyr)]$(ClO_4)_2$ (**3**)

Parameters	**1**·CH3OH	**2**		**3**
		Disorder model 1	Disorder model 2	
M–N bond distances (Å)				
M–N (tach amine)	2.160(3)	2.302(6)–2.400(5)	2.332(13)–2.422(9)	2.335(6)–2.487(6)
M–N (pyridyl)	2.165(4)	2.352(4)–2.361(4)	2.352(4)–2.361(4)	2.334(4)–2.461(4)
Twist angle α (°)	43.7(2)	19.6(2)–21.7(2) av. 20.8(4)	11.0(4)–12.0(8) av. 11.4(9)	3.1(3), 5.0(3), 5.5(2) av. 5(1)
C–C–C–C torsion angles of cyclohexyl framework (°)	52.3(6), 52.4(6) av. 52.35(3)	46.1(9)–52.7(9) av. 49(2)	49(1)–52(1) av. 49(4)	45.1(6)–52.9(7) av. 49(2)

of other ZnN_6 complexes. Typical Zn–N distances in zinc hexamine complexes are 2.143(5) Å (Zn–N (amine)) and 2.215(5) Å (Zn–N (pyridyl)) in $[Zn(ampy)_3]^{2+}$ (ampy = (2-pyridylmethyl)amine) [20] and an average Zn–N distance of 2.23 Å in $[LZn]^{2+}$ (L = 1,4,7-tris(*o*-aminobenzyl)-1,4,7-triazacyclononane) [21].

There are small differences in M–N bond lengths between compounds **2** and **3** (Table 3). The bond lengths of M–N in compound **3** are slightly longer than those in compound **2**, consistent with a difference in the six-coordinate ionic radii of Hg^{2+} and Cd^{2+} of 0.07 Å. The bond lengths of Cd–N in compound **2** and Hg–N in compound **3** are typical of metal hexamine complexes. The bond lengths of Cd–N (tach amine) in compound **2** range between 2.302(6) and 2.422(6) Å (average 2.36(2) Å), and those of Hg–N (tach amine) in compound **3** range between 2.335(6) and 2.487(6) Å (average 2.420(9) Å). The bond lengths of Cd–N (pyridyl) in compound **2** range between 2.352(4) and 2.361(4) Å (average 2.357(7) Å), and those of Hg–N (pyridyl) in compound **3** range between 2.334(4) and 2.461(4) Å (average 2.391(7) Å). These bond lengths of Cd–N and Hg–N compare well with those of other CdN_6 and HgN_6 polyhedra reported in the literature. Typical Cd–N distances in cadmium hexamine complexes are 2.34(2)–2.42(2) Å (Cd–N in $[Cd(en)_3]^{2+}$ (en = ethylenediamine) [22]) and 2.338(3) Å (Cd–N (amine)) and 2.343(4)–2.370(4) Å (Cd–N (pyridyl)) in $[Cd(bispicam)_2]^{2+}$ (bispicam = bis(2-pyridylmethyl)amine) [23]. Typical Hg–N distances in HgN_6 complexes are 2.350(4)–2.404(4) Å (Hg–N (amine)) and 2.352(4)–2.557(5) Å (Hg–N (pyridyl)) in $[Hg(bispicam)_2]^{2+}$ [24] and an average Hg–N distance of 2.43 Å in $[LHg]^{2+}$ (L = 1,4,7-tris(*o*-aminobenzyl)-1,4,7-triazacyclononane) [21].

Another effect of metal ion radius on the structures of the tachpyr metal complexes is a distortion of the cyclohexyl ring, as manifested in the C–C–C–C torsion angles (β) (Table 3). The torsion angles (β) in compound **1**·CH_3OH range between 52.3(6) and 52.4(6)° (average 52.35(3)°); in compound **2** they range between 46.1(9) and 52.7(9)° (average 49(2)°), and in compound **3** they range between 45.1(6) and 52.9(7)° (average 49(2)°). As the metal ion radius increases, increased distortion of the cyclohexane framework by the expansion of the cyclohexyl nitrogens away from the axial positions is effected to accommodate the metal. There is no significant difference in the distortion of the C–C–C–C torsion angles (β) between compounds **2** and **3**, which is consistent with the six-coordinate ionic radii of compounds **2** and **3**, which are similar.

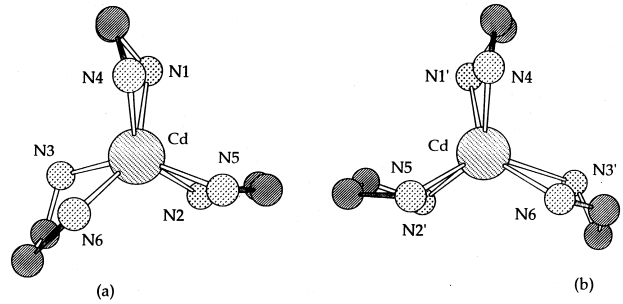


Fig. 6. Isomers of [Cdtachpyr]$(ClO_4)_2$: (a) $\Delta(\lambda\lambda\lambda)$ (isomer 1, 60%); (b) $\Lambda(\delta\delta\delta)$ (isomer 2, 40%).

The disorder in compound **2** indicates the presence of two different stereoisomers formed by two different twist directions (clockwise and counter-clockwise) of the twist of pendant arms. The counter-clockwise twist of the pendant arms forms a $\Delta(\lambda\lambda\lambda)$ isomer, and a clockwise twist of the pendant arms generates a $\Lambda(\delta\delta\delta)$ isomer. The $\Delta(\lambda\lambda\lambda)$ and $\Lambda(\delta\delta\delta)$ isomers are not enantiomers of each other (Fig. 6) since the $\Lambda(\delta\delta\delta)$ isomer has a lesser twist (average angle 11.4(9)°) and thus is closer to a trigonal-prismatic geometry than the $\Delta(\lambda\lambda\lambda)$ isomer (average angle 20.8(4)°). As expected, the presence of two different stereoisomers was not detected in the investigation by proton NMR at room temperature.

The structure of compound **3** can be defined as a $\Lambda(\delta\delta\delta)$ isomer, which is the most stable isomer among the four diastereomers ($\delta\delta\delta$, $\delta\delta\lambda$, $\delta\lambda\lambda$ and $\lambda\lambda\lambda$) due to a combination of steric and entropic factors [15]. Repulsive effects between puckered rings favor a $\Lambda(\delta\delta\delta)$ isomer; however, the entropy consideration that $\delta\delta\lambda$ and $\delta\lambda\lambda$ isomers are three times as probable as the $\delta\delta\delta$ and $\lambda\lambda\lambda$ isomers also plays a role [15].

4. Conclusions

Group IIB metal complexes with the ligand *N*,*N*′,*N*″-tris(2-pyridylmethyl)-*cis*,*cis*-1,3,5-triaminocyclohexane (tachpyr)

exhibit effects of metal radius on coordination geometry and ligand conformation. The tachpyr ligand forms a nearly octahedral complex with Zn(II), while it forms a complex intermediate between octahedral and trigonal-prismatic with Cd(II) and a slightly distorted trigonal-prismatic complex with Hg(II). Studies of the complexation chemistry of tachpyr and a variety of pendant-arm derivatives of tachpyr with first-row transition metal ions are in progress.

Supplementary data

Supplementary data are available from the Cambridge Crystallographic Data Centre, 12 Union Road, Cambridge CB2 1EZ, UK (fax: +44-1223-336033; e-mail: deposit@ccdc.cam.ac.uk) on request, quoting deposition number CCDC 138897 for $[Zn(tachpyr)](ClO_4)_2 \cdot CH_3OH$ (**1**$\cdot CH_3OH$), CCDC 138898 for $[Cd(tachpyr)](ClO_4)_2$ (**2**) and CCDC 138899 for $[Hg(tachpyr)](ClO_4)_2$ (**3**).

Acknowledgements

R.P. thanks the NIH for financial support of his sabbatical leave.

References

[1] D.H. Busch, Chem. Rev. 93 (1993) 847.
[2] R.D. Hancock, A.E. Martell, Chem. Rev. (1989) 1875.
[3] Z. Hou, T.D.P. Stack, C.J. Sunderland, K.N. Raymond, Inorg. Chim. Acta 263 (1997) 341.
[4] S. de Angelis, A. Batsanov, T.J. Norman, D. Parker, K. Senanayake, J. Vepsalainen, J. Chem. Soc., Chem. Commun. (1995) 2361.
[5] T. Bowen, R.P. Planalp, M.W. Brechbiel, Bioorg. Med. Chem. Lett. 6 (1996) 807.
[6] R.A.D. Wentworth, J.J. Felten, J. Am. Chem. Soc. 90 (1968) 621.
[7] R.A.D. Wentworth, Inorg. Chem. 7 (1968) 1030.
[8] U. Brand, H. Vahrenkamp, Inorg. Chim. Acta 198–200 (1992) 663.
[9] J.E. Bollinger, J.T. Mague, D.M. Roundhill, Inorg. Chem. 33 (1994) 1241.
[10] K.A. Hilfiker, R.D. Rogers, M.W. Brechbiel, R.P. Planalp, Inorg. Chem. 36 (1997) 4600.
[11] R.P. Planalp, G. Park, R.D. Rogers, M.W. Brechbiel, 218th ACS National Meeting, August 1999, INOR 516.
[12] G. Park, F.H. Lu, N. Ye, M.W. Brechbiel, S.V. Torti, F.M. Torti, R.P. Planalp, J. Biol. Inorg. Chem. 3 (1998) 449.
[13] G.M. Sheldrick, SHELXTL, version 5.05, Siemens Analytical X-Ray Instruments Inc., 1996.
[14] G.M. Sheldrick, Program for Semiempirical Absorption Correction of Area Detector Data, 1996.
[15] F.A. Cotton, G. Wilkinson, Advanced Inorganic Chemistry, 6th edn., Wiley, New York, 1999, p. 33.
[16] R.D. Shannon, C.T. Prewitt, Acta Crystallogr., Sect. B 25 (1969) 925.
[17] R.D. Shannon, Acta Crystallogr., Sect. A 32 (1976) 751.
[18] M.J. van der Merwe, J.C.A. Boeyens, R.D. Hancock, Inorg. Chem. 22 (1983) 3489.
[19] M.J. van der Merwe, J.C.A. Boeyens, R.D. Hancock, Inorg. Chem. 24 (1985) 1208.
[20] M. Mikami-Kido, Y. Saito, Acta Crystallogr., Sect. B 38 (1982) 452.
[21] O. Schlager, K. Wieghardt, H. Grondey, A. Rufinska, B. Nuber, Inorg. Chem. 34 (1995) 6440.
[22] C. Mahadevan, M. Seshasayee, S. Sastry, C. Subrahmanyam, Z. Kristallogr. 171 (1985) 173.
[23] J. Glerup, P.A. Goodson, D.J. Hodgson, K. Michelsen, K.M. Nielsen, H. Weihe, Inorg. Chem. 31 (1992) 4611.
[24] D.C. Bebout, A.E. DeLanoy, D.E. Ehmann, M.E. Kastner, D.A. Parrish, R.J. Butcher, Inorg. Chem. 37 (1998) 2952.

PERGAMON

www.elsevier.nl/locate/poly

Polyhedron 19 (2000) 1163–1166

POLYHEDRON

Modification of the solid state structures of dithiadiazolyl radicals: crystal structure of *p*-iodophenyl-1,2,3,5-dithiadiazolyl

Neil Bricklebank [a,*], Stephen Hargreaves [a], Sharon E. Spey [b]

[a] *Division of Chemistry and Materials Research Institute, Sheffield Hallam University, City Campus, Sheffield S1 1WB, UK*
[b] *Department of Chemistry, University of Sheffield, Western Bank, Sheffield S3 7HF, UK*

Received 4 January 2000; accepted 27 March 2000

Abstract

The solid state structure of the 1,2,3,5-dithiadiazolyl *p*-IC_6H_4CNSSN (**3**) is described. The molecules associate in dimer pairs, across an inversion centre, in an unusual *trans*-cofacial manner. The separation between the heterocyclic rings is 3.121 Å. The intradimer sulfur contacts (3.696 Å) are larger than those observed in dithiadiazolyls that associate in the more usual *cis*-cofacial manner. Individual *p*-IC_6H_4CNSSN molecules are linked into zigzag chains through weak I···S interactions (3.82 Å); each half of a [*p*-$IC_6H_4CNSSN]_2$ dimer is a member of separate chains that run in opposite directions. ©2000 Elsevier Science Ltd All rights reserved.

Keywords: Dithiadiazolyl radicals

1. Introduction

In recent years, 1,2,3,5-dithiadiazolyl (DTDA) radicals have been studied as building blocks for the design and synthesis of molecular magnets [1–5] and conductors [6–9]. The steric and electronic effects of the substituent R can be used to modify the molecular structure and hence the physical behaviour of the radical. In the solid state the majority of DTDA radicals associate as spin-paired dimers through the formation of out-of-plane intermolecular S···S interactions (Fig. 1) with a typical intermolecular separation in the range 3.0–3.2 Å. Crystal engineering of DTDAs has focused on obtaining materials in which the radicals are aligned into infinite chains or stacked in columns; one of the principal tools used to achieve this has been to use nitrile groups as structure-influencing supramolecular synthons [1,2,8,9]. The idea behind this strategy stemmed from the structure of *p*-iodobenzonitrile [10] and the cyanogen halides [11], which associate as ribbon-like chains through weak X···CN interactions. Similarly, cyano-functionalised DTDAs (e.g. compounds **1** and **2**) also associate as chains through CN···S interactions [1,2,8].

Halogen atoms can also have a marked effect on the molecular packing, although only fluorinated systems have received extensive study [1–4,12,13]. Partial fluorination of the aryl group can lead to the disruption of the dimerisation process; for example, [2,3-$F_2C_6H_3CNSSN]_2$ associates as an unusual twisted dimer [12], whereas 2,5-$F_2C_6H_3CNSSN$ assembles in uniform stacks with an unusually long interannular spacing [3.544(3) Å] [12]. Total fluorination results in more dramatic changes; both *p*-NCC_6F_4CNSSN (**2**) [1–3] and *p*-BrC_6F_4CNSSN [4] do not associate as dimers and consequently are paramagnetic at room temperature. The latter compound associates in columns, whereas the combination of fluorine atoms and a nitrile group in compound **2** leads to a compound that assembles with a chain-like structure [1,2]. Upon cooling to below 36 K, one polymorph of compound **2** undergoes a transition to a weakly ferromagnetic state [3]. This is the highest ferromagnetic ordering temperature reported to date for a non-metallic molecular magnet.

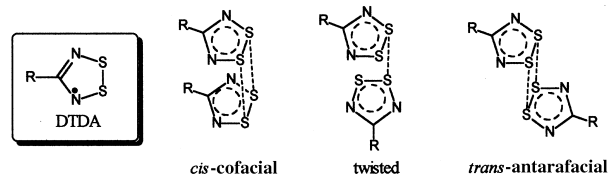


Fig. 1. Modes of dimerisation for DTDA radicals.

We are currently investigating the effect of the heavier halogen atoms on the supramolecular structures of dithiadiazolyl radicals. As part of this work, we decided to make *p*-iodophenyl-DTDA (**3**). In particular, we were keen to determine the structure-influencing properties of the iodine

* Corresponding author. Tel.: +44-114-225 4931; fax: +44-114-225 3066; e-mail: n.bricklebank@shu.ac.uk

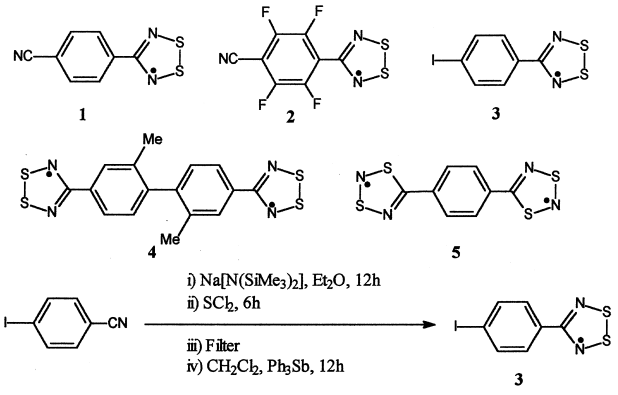
0277-5387/00/$ - see front matter ©2000 Elsevier Science Ltd All rights reserved.
PII S0277-5387(00)00384-3

atom and to see whether it would also promote the assembly of the molecules into chains, as is observed for *p*-iodobenzonitrile and cyano-functionalised DTDAs (**1** and **2**).

2. Results and discussion

Compound **3** was prepared from *p*-iodobenzonitrile using a slightly modified version of the proven metal amidine route (Scheme 1). We have found that sodium bis(trimethylsilyl)amide gives slightly higher yields with iodo-, bromo- and chloro-substituted aromatic nitriles than lithium bis(trimethylsilyl)amide, which is usually employed in dithiadiazolyl synthesis [14]. Crystals suitable for X-ray diffraction were grown by vacuum sublimation as described in Section 4. The asymmetric unit of compound **3** (Fig. 2) contains one molecule of unexceptional geometry. The bond lengths and angles of the heterocycle (Table 1) are similar to those of other members of this class [14]. Within each molecule the aryl and dithiadiazolyl rings are essentially coplanar with a slight twist angle between the dithiadiazole ring [root mean square (r.m.s.) $\Delta = 0.0077$ Å] and the aryl ring [r.m.s. $\Delta = 0.0089$ Å] of 8°. However, compared with other DTDAs, the mode of association in compound **3** is unusual. Two *p*-IC_6H_4CNSSN molecules associate in a *trans*-cofacial manner across an inversion centre (Fig. 3). The only other example of a DTDA radical adopting this mode of association is the 2,2′dimethylbiphenylene radical (**4**), which was reported very recently [5]. The distance between the heterocycles within dimers of compound **3** (measured from the mid-point of the rings) is 3.121 Å. This is significantly shorter than that in compound **4** (3.24 Å) and is similar to those observed in DTDAs that associate in the *cis*-cofacial or *trans*-antarafacial modes. However, the intradimer sulfur contacts in compound **3** [d(S1···S2A) and d(S2···S1A) = 3.696 Å] are long when compared with the equivalent distance in DTDAs that associate in a *cis*-cofacial or *trans*-antarafacial manner (typically 3.0–3.2 Å) and are similar to those in compound **4** [3.68(2) Å]. Each dimer pair also has two sets of intradimer sulfur–nitrogen interactions [d(S1···N2A), d(S1A···N2) = 3.116 Å] and [d(S2···N1A), d(S2A···N1) = 3.152 Å]. The asymmetry in these interactions results from a further interaction between one of the sulfurs with the iodine atom of an adjacent molecule (see below).

As noted by Oakley and co-workers [5], the *trans*-cofacial mode of dimerisation adopted by compounds **3** and **4** lies close to the transition state for the proposed photochemical isomerisation of 1,3,2,4- to 1,2,3,5-DTDAs (Scheme 2)



Scheme 1.

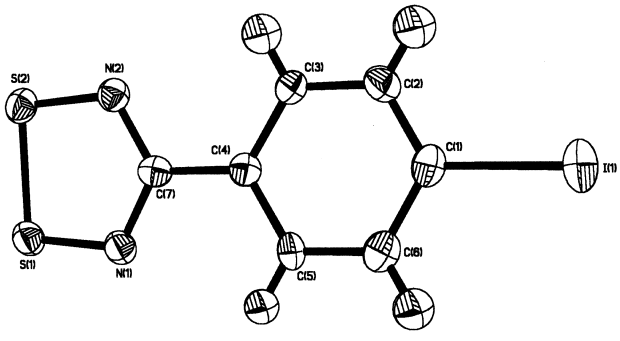


Fig. 2. ORTEP plot of asymmetric unit of compound **3** showing atom labelling scheme.

Table 1
Bond lengths (Å) and angles (°) in compound **3**

I1–C1	2.094(6)	C1–C2	1.371(7)
S1–S2	2.098(2)	C1–C6	1.388(8)
S1–N1	1.635(5)	C2–C3	1.376(8)
S2–N2	1.629(5)	C3–C4	1.398(8)
N1–C7	1.337(7)	C4–C5	1.410(7)
N2–C7	1.347(6)	C5–C6	1.365(7)
C7–C4	1.464(7)		
N1–S1–S2	94.45(18)	C3–C4–C5	117.3(5)
N2–S2–S1	94.26(17)	C3–C4–C7	121.3(5)
C7–N1–S1	114.6(4)	C5–C4–C7	121.4(5)
C7–N2–S2	114.8(4)	C6–C5–C4	121.5(5)
C2–C1–C6	120.9(5)	C5–C6–C1	119.2 (5)
C2–C1–I1	120.6(4)	N1–C7–N2	121.9(5)
C6–C1–I1	118.4(4)	N1–C7–C4	119.4(5)
C1–C2–C3	119.7(5)	N2–C7–C4	118.7(5)
C2–C3–C4	121.2(5)		

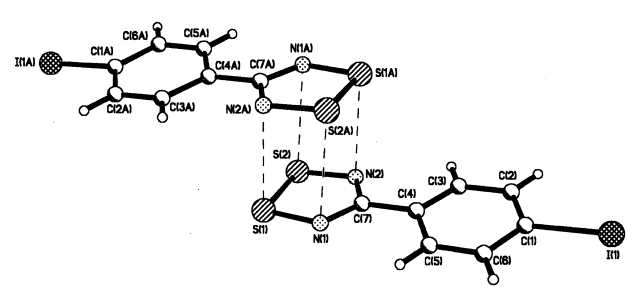
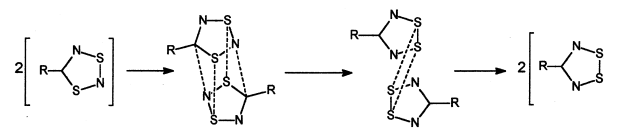


Fig. 3. Dimerisation in compound **3** illustrating the *trans*-cofacial mode of association.



Scheme 2.

[14]. Indeed, the molecular structures of compounds **3** and **4** show many similarities with that of 5,5′-(1,4-phenylene)bis(1,3,2,4-dithiadiazolyl) (**5**), which contains short S···S (3.214 Å) and S···N (3.346 Å) interactions between parallel CN_2S_2 rings [15].

Individual *p*-IC_6H_4CNSSN molecules in compound **3** are linked in a chain-like motif through a weak interaction between the iodine atom and one of the sulfurs of an adjacent molecule [d(I1···S2) = 3.82 Å]. The I···S distance is significantly longer than a conventional S–I bond [16] but is within bonding contact when compared with the sum of the van der Waal's radii of iodine and sulfur (which lies in the range 3.4–4.1 Å, depending on the orientation of the contact vector relative to the bonds) [17]. The distance between the iodine atom and the other sulfur atom of the disulfide bond [d(I1···S1) = 4.068 Å] is long and lies at the limit of the van der Waal's radius for a I···S contact, indicative of a very weak interaction. Each half of a [*p*-$IC_6H_4CNSSN]_2$ dimer is a member of separate chains that run in opposite directions. Adjacent molecules within the molecular chains occupy orthogonal positions such that the chains have a 'zigzag' alignment (Fig. 4). Analogous Cl···S interactions are seen in the structure of [*p*-$ClC_6H_4CNSSN]_2$, although in this derivative the molecules dimerise in a *cis*-cofacial manner [18]. The zigzag arrangement of the molecules in compound **3** contrasts with DTDAs **1** and **2** and the parent *p*-iodobenzonitrile, all of which form linear chains.

In addition, it is well known that compounds containing carbon–iodine bonds can undergo metal-catalysed coupling reactions, with carbon–carbon bond formation. Thus, it is possible that compound **3** could be utilised in similar reactions, providing a new synthetic route to biphenylbis(dithiadiazolyl) derivatives.

3. Conclusions

From the results reported here we see that the iodine atom has a marked effect on the supramolecular structure of compound **3**. As anticipated, the iodine substituent promotes the assembly of the molecules into chains by interacting with the sulfur atom of an adjacent molecule. The *trans*-cofacial mode of dimerisation observed in compound **3** is unusual, and we speculate that the molecules dimerise in this way to alleviate steric hindrance between two iodine atoms that would occur if the molecules associated in a *cis*-cofacial manner. However, it is less obvious why the *trans*-antarafacial or twisted geometries are disfavoured in this instance.

4. Experimental

All reactions and manipulations were carried out under an atmosphere of dry nitrogen using standard double-manifold and glove box techniques. Solvents were dried, distilled and degassed prior to use. *p*-Iodobenzoyl chloride (Aldrich), sodium bis(trimethylsilyl)amide (Aldrich), triphenylantimony (Aldrich), phosphorus pentoxide (Fisher) and sulfur dichloride (Fluka) were all obtained commercially and used as received.

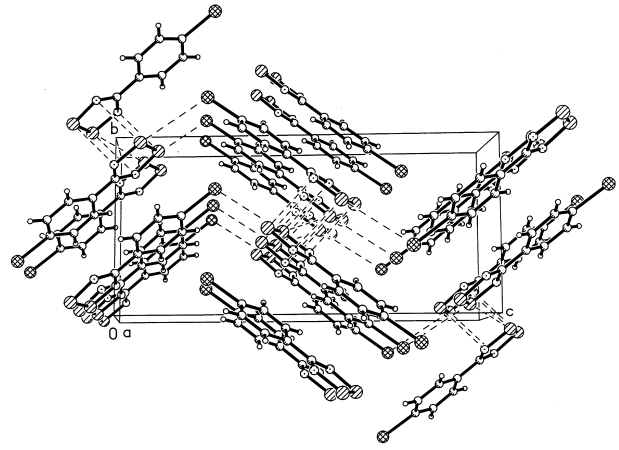


Fig. 4. Molecular packing of compound **3** parallel to crystallographic *a*-axis.

4.1. p-Iodobenzonitrile

Finely powdered *p*-iodobenzoyl chloride (5.32 g, 0.02 mol) was slowly added to ice-cold 0.880 ammonia solution (20 ml). The mixture was then stirred for 2 h and allowed to warm to room temperature. The resulting precipitate, *p*-iodobenzamide, was filtered, washed with water and dried. The *p*-iodobenzamide was then transferred to a 250-cm^3 round-bottom flask fitted with a side-arm and stopcock, together with a cold finger. An excess of phosphorus pentoxide was added to the flask and the reactants were thoroughly mixed. The flask was then heated in vacuo (130°C). Under these conditions the *p*-iodobenzonitrile product sublimes directly from the reaction mixture onto the cold finger as white needles. The *p*-iodobenzonitrile is then recovered and purified by a further vacuum sublimation (2.68 g, 59% yield; m.p. 124–126°C, lit. 124–125°C) [9]. ν_{max} (cm^{-1}): 2225 (C≡N), 1578, 1475, 1390, 1054, 1010, 894, 541. δ_H (250 MHz; $CDCl_3$; Me_4Si): 7.85 (2H, d, J 8.3 Hz) 7.37 (2H, d, J 8.3 Hz). δ_c (250 MHz; $CDCl_3$; Me_4Si): 138.86, 133.53, 118.57, 112.09, 100.68. m/e 228.9 (m^+), 102.0, 75.0.

4.2. 4-Iodophenyl-1,2,3,5-dithiadiazolyl

Sodium bis(trimethylsilyl amide) (1.673 g, 0.01 mol) and *p*-iodobenzonitrile (2.29 g, 0.01 mol) were stirred together in diethyl ether (50 cm^3) at room temperature for 18 h. Sulfur dichloride (1.3 cm^3, 0.02 mol) was slowly added, with cooling in an ice-bath, to produce an immediate orange precipitate which was stirred for 12 h, filtered off, washed with diethyl ether (3×10 cm^3) and pumped to dryness. The crude product was then reduced in situ by adding dichloromethane (50 cm^3) and triphenylantimony (0.176 g, 0.0005 mol). After 12 h, the dichloromethane was removed in vacuo. The residue was placed in a gradient sublimer (25–120°C, 10^{-3} torr). Under

these conditions, the product forms as deep red–black blocks (0.56 g, 18% yield; m.p. 172.5°C). Found: C, 27.13; H, 1.32; N, 9.05. $C_7H_4IN_2S_2$ requires: C, 27.37; H, 1.31; N, 9.12%. ν_{max} (cm^{-1}): *m/e* 307.1 (m^+), 261.1, 229.1, 180.0, 134.1, 102.1, 77.9.

4.3. Crystal data

$C_7H_4IN_2S_2$ (M = 307.14) crystallises as deep red blocks; crystal dimensions 0.20 × 0.10 × 0.10 mm. Monoclinic, $a = 5.7193(7)$, $b = 8.6096(11)$, $c = 18.320(2)$ Å, $\beta = 97.054(2)°$, $U = 895.26(19)$ $Å^3$, $Z = 4$, $D_c = 2.279$ Mg m^{-3}, space group $P2_1/n$ (a non-standard setting of $P2_1/c$, C_{2h}^5, No. 14), Mo Kα radiation ($\bar{\lambda} = 0.71073$ Å), μ(Mo Kα) = 3.984 mm^{-1}, $F(000) = 580$. Data collected were measured on a Bruker Smart CCD area detector with Oxford Cryosystems low-temperature system. Cell parameters were refined from the setting angles of 111 reflections (θ range 2.24–28.31°). Reflections were measured from a hemisphere of data collected of frames each covering 0.3 degrees in omega. Of the 5746 reflections measured, all of which were corrected for Lorentz and polarisation effects and for absorption by semi-empirical methods based on symmetry-equivalent and repeated reflections (minimum and maximum transmission coefficients of 0.5030 and 0.6914), 1474 independent reflections exceeded the significance level $|F|/\sigma(|F|) > 4.0$. The structure was solved by direct methods and refined by full-matrix least-squares methods on F^2. Hydrogen atoms were placed geometrically and refined with a riding model and with U_{iso} constrained to be 1.2 times U_{eq} of the carrier atom. Refinement converged at a final $R = 0.0478$ ($wR_2 = 0.1125$, for all 2139 data, 109 parameters, mean and maximum δ/σ 0.000, 0.000) with allowance for the thermal anisotropy of all non-hydrogen atoms. Minimum and maximum final electron density was −1.464 and 1.772 e $Å^{-3}$. A weighting scheme $w = 1/[\sigma^2(F_o^2) + (0.0587P)^2 + 0.00P]$, where $P = (F_o^2 + 2F_c^2)/3$ was used in the latter stages of refinement. Complex scattering factors were taken from the program package SHELXTL [19] as implemented on a Viglen Pentium computer.

Supplementary data

Supplementary data are available from the CCDC, 12 Union Road, Cambridge CB2 1EZ, UK (fax: +44-1223-336033; e-mail: deposit@ccdc.cam.ac.uk) on request, quoting the deposition number 137/938.

Acknowledgements

We would like to thank Sheffield Hallam University for a studentship (S.H.), the Royal Society for an equipment grant (N.B.) and the Royal Society of Chemistry Research Fund and the Nuffield Foundation for financial support (N.B.).

References

[1] A.J. Banister, N. Bricklebank, W. Clegg, M.R.J. Elsegood, C.I. Gregory, I. Lavender, J.M. Rawson, B.K. Tanner, J. Chem. Soc., Chem. Commun. (1995) 679.
[2] A.J. Banister, N. Bricklebank, I. Lavender, J.M. Rawson, C.I. Gregory, B.K. Tanner, W. Clegg, M.R.J. Elsegood, F. Palacio, Angew. Chem., Int. Ed. Engl. 35 (1996) 2533.
[3] F. Palacio, G. Antorrena, M. Castro, R. Burriel, J.M. Rawson, J.N.B. Smith, N. Bricklebank, J. Novoa, C. Ritter, Phys. Rev. Lett. 79 (1997) 2336.
[4] G. Antorrena, J.E. Davies, M. Hartley, F. Palacio, J.M. Rawson, J.N.B. Smith, A. Steiner, Chem. Commun. (1999) 1393.
[5] T.M. Barclay, A.W. Cordes, N.A. George, R.C. Haddon, M.E. Itkis. R.T. Oakley, Chem. Commun. (1999) 2269.
[6] A.W. Cordes, R.C. Haddon, R.T. Oakley, Adv. Mater. 6 (1994) 798.
[7] C.D. Bryan, A.W. Cordes, R.M. Fleming, N.A. George, S.H. Glarum, R.C. Haddon, R.T. Oakley, T.T.M. Palstra, A.S. Perel, L.F. Schneemeyer, J.V. Waszczak, Nature 365 (1993) 821.
[8] A.W. Cordes, R.C. Haddon, R.G. Hicks, R.T. Oakley, T.T.M. Palstra, Inorg. Chem. 31 (1992) 1802.
[9] A.W. Cordes, C.M. Chamchoumis, R.G. Hicks, R.T. Oakley, K.M. Young, R.C. Haddon, Can. J. Chem. 70 (1992) 919.
[10] E.O. Schlemper, D. Britton, Acta Crystallogr. 18 (1965) 419.
[11] R.B. Heiart, G.B. Carpenter, Acta Crystallogr. 9 (1956) 60.
[12] A.J. Banister, A.S. Batsanov, O.G. Dawe, P.L. Herbertson, J.A.K. Howard, S. Lynn, I. May, J.N.B. Smith, J.M. Rawson, T.E. Rogers, B.K. Tanner, G. Antorrena, F. Palacio, J. Chem. Soc., Dalton Trans. (1997) 2539.
[13] A.M.T. Bell, J.N.B. Smith, J.P. Attfield, J.M. Rawson, K. Shankland, W.I.F. David, New J. Chem. (1999) 565.
[14] A.J. Banister, I. Lavender, J.M. Rawson, Adv. Heterocyl. Chem. 62 (1995) 137.
[15] A.J. Banister, J.M. Rawson, W. Clegg, S.L. Birkby, J. Chem. Soc., Dalton Trans. (1991) 1099.
[16] N. Bricklebank, P.J. Skabara, D.E. Hibbs, M. Hursthouse, K.M.A. Malik, J. Chem. Soc., Dalton Trans. (1999) 3007.
[17] S.C. Nyburg, C.H. Faerman, Acta Crytsallogr., Sect. B 41 (1985) 274.
[18] R.T. Boere, K.H. Moock, M. Parvez, Z. Anorg. Allg. Chem. 620 (1994) 1589.
[19] SHELXTL, An integrated system for solving and refining crystal structures from diffraction data (revision 5.1), Brucker AXS Ltd.

PERGAMON

www.elsevier.nl/locate/poly

Polyhedron 19 (2000) 1167–1172

POLYHEDRON

Synthesis and characterization of a novel macrocyclic ligand containing catechol donor groups and its oxovanadium(IV) complex

Tingli Ma [1]*, Takahiko Kojima, Yoshihisa Matsuda [2]*

Department of Chemistry and Physics of Condensed Matter, Graduate School of Sciences, Kyushu University, Hakozaki, Fukuoka, 812-8581, Japan

Received 14 December 1999; accepted 27 March 2000

Abstract

A novel macrocyclic ligand containing catechol moieties, 9,10,21,22-tetrahydroxy-7,12,19,24-tetraoxo-2,3,4,5:8,9,10,11:14,15,16,17:20,21,22,23-tetrabenzena-1,6,13,18-tetraazacyclotetracosane ($\mathbf{H_4L}$), was designed and synthesized. For comparison, an acyclic ligand, 1,4-bis(2,3-dihydroxybenzammido)benzene ($\mathbf{H_4L^a}$), was also synthesized. Their oxovanadium(IV) complexes K(ppn)[VO(L)] and K_2[VO(L^a)] were prepared and characterized by IR, UV–Vis and ESR spectroscopies. The ESR spectra of the complexes measured at 77 K in diethyl sulfoxide–ethanol revealed unusual rhombic characteristics of the complexes, suggesting the coordination geometry of the complexes was distorted square-pyramidal. Based on these data, the complex is proposed to possess a bowl-like structure capped by the VO^{2+} moiety with a hydrophobic cavity. ©2000 Elsevier Science Ltd All rights reserved.

Keywords: Catechols; Macrocyclic ligands; Oxovanadium complexes; ESR parameters; Distorted square-pyramid; Hydrophobic cavities

1. Introduction

Macrocyclic ligands have been recognized as a strong framework to construct attractive compounds in terms of their structures and functionality. Their versatile utility has been proven in molecular and ion recognition [1], catalysis, and bioinorganic chemistry to mimic the structure and function of metalloproteins [2,3]. For these macrocyclic ligands, coordination to metal ion(s) is made through amine or imine nitrogens, ether oxygens and so on. Besides these electrostatically neutral ligands, highly charged macrocyclic ligands also show intriguing properties; for example, deprotonated tetraamide ligands having a charge of −4 prepared by Collins et al. have been shown to stabilize high-valent metal ions such as Ni(III) [4], Mn(V) [5–8], Fe(IV) [9–12] and so on. On the other hand, for highly and negatively charged macrocyclic ligands other than those mentioned above, the research groups of Vögtle [13,14], Martell [15,16], and Raymond [17–20] have reported catechol-containing macrocycles in which such catechol moieties are linked tightly together with amide bonds. They have utilized these ligands to encapsulate the Fe(III) ion based on the well-known strong interaction between Fe(III) and catechols.

Furthermore, Raymond and co-workers have explored the perspective of the coordination chemistry of catechol-based multidentate ligands, including vanadium ions. They prepared a number of oxovanadium(IV) complexes with their ligands; however, no report has appeared concerning catechol-containing macrocycles in which such catechol moieties are connected by aromatic amines. The use of an aromatic amine as a spacer connected by amide bonds in a vanadyl coordination sphere will allow us to access a new bowl-like hydrophobic cavity capped with vanadyl unit as a template, which is reminiscent of a calixarene due to the distortion around the amide moiety (Chart 1).

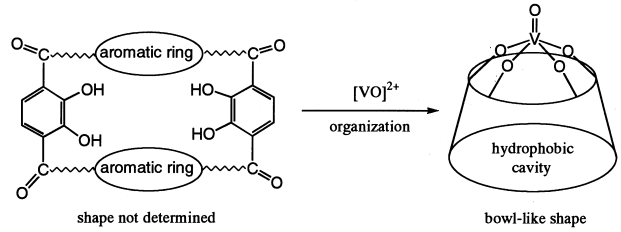


Chart 1

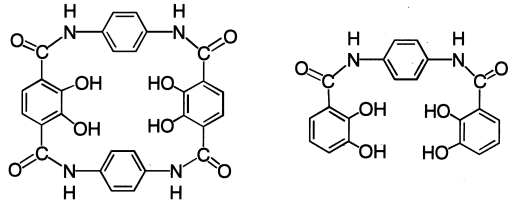
In order to construct such a vanadyl complex having hydrophobic cavity, we designed and synthesized a macrocyclic ligand ($\mathbf{H_4L}$) containing two catechol donor groups bridged by *p*-phenylenediamine (Chart 2(a)) and its oxovana-

[1] * Corresponding author. Tel.: +81-942-81-3640; fax: +81-942-81-3690; e-mail: ma@kniri.go.jp. Present address: Kyushu National Industrial Research Institute 807-1, Shuku, Tosu, Saga, 841-0052, Japan.

[2] * Corresponding author. Tel./fax: +81-92-642-2570; e-mail: matsuscc@mbox.nc.kyushu-u.ac.jp

0277-5387/00/$ - see front matter ©2000 Elsevier Science Ltd All rights reserved.
PII S0277-5387(00)00387-9

dium(IV) complex. In addition, we prepared an acyclic analog containing two catechols and one bridging *p*-phenylenediamine (Chart 2(b)) and its vanadyl complex as comparison.



(a) (b)

Chart 2

2. Materials and methods

2,3-Dimethoxyterephthalic acid bis(2-mercaptothiazolide) (**1**) was prepared by the method described in the literature [21]. 3-(2,3-Dimethoxybenzoyl)-1,3-thiozolidine-2-thione (**4**) was synthesized in accordance with a published procedure [22]. Vanadyl acetylacetonate ($VO(acac)_2$), was recrystallized from acetone. All solvents were dried by standard methods before use. All reactions were performed in an inert atmosphere in a glove box.

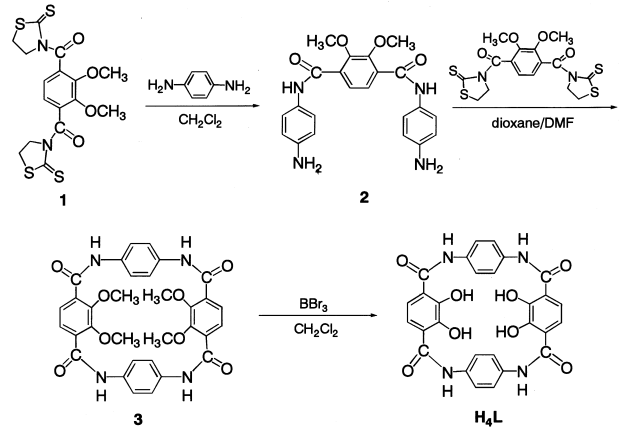
^{1}H NMR spectra were measured at 295 K on JEOL GX 400 MHz and EX 270 MHz spectrometers at 400 and 270 MHz, respectively. The chemical shifts were determined in ppm relative to TMS as an internal reference. IR spectra (4000–400 cm^{-1}) were recorded on a Shimadzu FT-IR-8600 spectrometer by the KBr method. UV–Vis absorption spectra were measured on a JASCO Ubest-50 spectrophotometer. Electron spin resonance (ESR) spectra were obtained on a JEOL JES-FE3X spectrometer at 300 or 77 K. C, H, and N analyses were carried out at the Service Center of the Elemental Analysis of Organic Compounds, Kyushu University.

2.1. Preparation of the ligands and the complexes

2.1.1. Synthesis of the macrocyclic ligand (*H_4L*) (Scheme 1)

*2.1.1.1. 2,3-Dimethoxy-1,4-[bis(4-amino-phenylene-diamide)] benzene (**2**).* To a solution of *p*-phenylenediamine (1.72 g, 15.90 mmol) in 300 ml of CH_2Cl_2, **1** (2.27 g, 5.30 mmol) was added and the solution was stirred at ambient temperature for 2.5 days. The solvent was removed to obtain crude **2** as orange oil. The crude product was dissolved in THF and precipitated by addition of diethyl ether. The resulting solid was filtered and washed three times with CH_2Cl_2 to remove unreacted starting materials. A yellow crystal of **2** was obtained by recrystallization from DMF/ether (1.50 g, 61%, based on **1**).

^{1}H NMR (DMSO-d_6): δ 9.90 (s, 2H, NH), 7.35 (dd, J=8.6, 3.6 Hz, 2H, ArH(amine)), 7.33 (s, 2H, ArH(cat)), 6.53 (dd, J=8.6, 3.6 Hz, 2H, ArH(amine)), 5.10 (bs, 4H, NH_2), 3.87 (s, 6H, OCH_3). (+)FAB-MS: m/z 406 $[M]^+$, 407 $[M+H]^+$. *Anal.* Calc. for $C_{22}H_{22}N_4O_4$: C, 65.02; H, 5.46; N, 13.79. Found: C, 64.82; H, 5.35; N, 13.50%.



Scheme 1.

*2.1.1.2. 9,10,21,22-Tetramethoxy-7,12,19,24-tetraoxo-2,3,4,5:8,9,10,11:14,15,16,17:20,21,22,23-tetrabenzena-1,6,13,18-tetraazacyclotetracosane (**3**).* To a solution of **2** (0.50 g, 1.23 mmol) in 500 ml of distilled dioxane and 100 ml of DMF, equimolar **1** and 1 ml of Et_3N were added at room temperature. The mixture was refluxed for 3 days. Filtration gave brown solids, which were washed with CH_2Cl_2 and hot THF. The brown powder was dissolved in DMF and insoluble material was filtered off. The yellow powder was obtained by repeated reprecipitation with DMF/ether. Recrystallization from DMSO gave **3** as yellow microcrystals (0.53 g, 36%).

^{1}H NMR (DMSO-d_6): δ 10.36 (bs, 4H, NH), 7.73 (bs, 8H, ArH(amine)), 7.39 (bs, 4H, ArH(cat)), 3.90 (bs, 12H, OCH_3). ^{1}H NMR (DMF-d_7): δ 10.40 (s, 4H, NH), 7.91 (s, 8H, ArH(amine)), 7.55 (s, 4H, ArHcat), 4.03 (s, 12H, OCH_3). (+)FAB-MS: m/z 597 $[M+H]^+$. *Anal.* Calc. for $C_{32}H_{28}N_4O_8$: C, 64.42; H, 4.70; N, 9.40. Found: C, 63.98; H, 4.49; N, 9.66%.

2.1.1.3. 9,10,21,22-Tetrahydroxy-7,12,19,24-tetraoxo-2,3,4,5:8,9,10,11:14,15,16,17:20,21,22,23-tetrabenzena-1,6,13,18-tetraazacyclotetracosane (H_4L*).* To a degassed solution of **3** (0.50 g, 0.84 mmol) in 80 ml of CH_2Cl_2 was added 5.60 ml of BBr_3 via a syringe at 0°C. The yellow suspension formed was stirred for 5 days at ambient temperature. After slow addition of distilled H_2O at 0°C, the mixture was brought to the boil. Brown precipitate was filtered from the hot aqueous suspension. The solid was successively washed with H_2O and MeOH, and was recrystallized from DMSO/2-propanol to yield **H_4L** as yellow microcrystals (0.39 g, 86%).

^{1}H NMR (DMSO-d_6): δ 12.00 (bs, 4H, OH), 10.60 (bs, 4H, NH), 7.75 (bs, 8H, ArH(amine)), 7.50 (bs, 4H, ArH(cat)). IR (KBr, cm^{-1}): 3550(m), 1655(w), 1560(w), 1516(s), 1437(m), 1408(m), 1331(bs), 1290(sh, w), 1231(s), 1142(m), 1030(w), 929(m),

831(s), 737(w), 650(w), 509(s), 412(m). UV–Vis (DMSO): λ_{max} = 338 nm. *Anal*. Calc. for $C_{28}H_{20}N_4O_8$: C, 62.22; H, 3.73; N, 10.37. Found: C, 61.93; H, 3.95; N, 10.10%.

2.1.2. Synthesis of the acyclic ligand ***H_4L^a*** *(Scheme 2)*

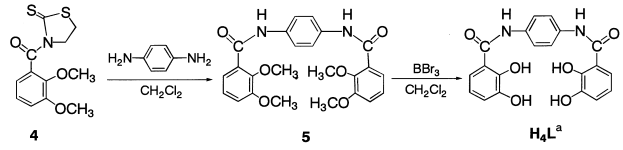
*2.1.2.1. N,N′-Bis(2,3-dimethoxybenzoyl)-1,4-phenylene-diamine (**5**).* To a solution of *p*-phenylenediamine (1.04 g, 9.60 mmol) dissolved in 50 ml of CH_2Cl_2 was added a solution of 3-(2,3-dimethoxybenzoyl)-1,3-thiazolidine-2-thione (**4**), (5.45 g, 19.20 mmol) in 200 ml of CH_2Cl_2 and the mixture was refluxed for 3 days. The reaction mixture was cooled and washed with 2×100 ml of 0.10 M NaOH, and then with 100 ml of brine, and dried over anhydrous $MgSO_4$. CH_2Cl_2 was removed by a rotary evaporator to give yellow oil. This oil was chromatographed on a silica column eluted with $CHCl_3$/MeOH (95/5) to afford a white powder of **5**. Recrystallization from $CHCl_3$/hexane gave colorless needles (84%).

^{1}H NMR ($CDCl_3$): δ 10.02 (s, 2H, NH), 7.78 (dd, *J* = 7.8, 1.5 Hz, 2H, ArH), 7.69 (s, 4H, ArH), 7.20 (dd, *J* = 8.1, 7.8 Hz, 2H, ArH), 7.09 (dd, *J* = 8.1, 1.5 Hz, 2H, ArH), 3.99 (s, 6H, OCH_3), 3.92 (s, 6H, OCH_3). EI-Mass: *m*/*e* 436 [M]. *Anal*. Calc. for $C_{24}H_{24}N_2O_6$: C, 66.06; H, 5.51; N, 6.42. Found: C, 65.79; H, 5.56; N, 6.34%.

*2.1.2.2. N,N′-Bis(2,3-dihydroxybenzoyl)1,4-phenylene-diamine (**H_4L^a**).* The ligand **H_4L^a** was prepared by a similar procedure to that of **H_4L** (96%). ^{1}H NMR (DMSO-d_6): δ 11.77 (bs, 2H, OH), 10.37 (s, 2H, NH), 9.39 (bs, 2H, OH), 7.70 (s, 4H, ArHamine), 7.47 (dd, *J* = 8.1, 1.3 Hz, 2H, ArHcat), 6.98 (dd, *J* = 7.8, 1.3 Hz, 2H, ArHcat), 6.78 (dd, *J* = 8.1, 7.8 Hz, 2H, ArHcat). IR (KBr, cm^{-1}): 3480(m), 1647(m), 1596(w), 1560(s), 1454(s), 1408(m), 1329(s), 1275(s), 1281(w), 1175(s), 858(w), 750(s), 831(s), 738(m), 577(m), 521(w), 444(m). UV–Vis (DMSO): λ_{max} = 338 nm. (+)FAB-MS: *m*/*e* 381 $[M+H]^+$. *Anal*. Calc. for $C_{20}H_{16}N_2O_6 \cdot EtOH$: C, 61.96; H, 5.16; N, 6.57. Found: C, 61.93; H, 5.22; N, 6.53%.

2.1.3. Syntheses of the oxovanadium complexes

2.1.3.1. K(ppn)[VO(L)]. An ethanolic solution of KOH (4.20 ml, 0.40 M, 1.60 mmol) was added to a solution of **H_4L** (0.23 g, 0.42 mmol) in 20 ml of degassed EtOH. After stirring for 15 min at ambient temperature, $VO(acac)_2$ (0.11 g, 0.42 mmol) in EtOH was added. The mixture was refluxed for 18 h to give a green suspension. The solid material was filtered, washed with water and EtOH (3×50 ml), and then dried in vacuo to give a deep green powder of $K_2[VO(L)]$ (0.20 g, 60%). One of the K^+ cations was substituted for the ppn^+ cation by the following procedure, where ppn^+ stands for the bis(triphenylphosphoranylidene) ammonium ion: $K_2[VO(L)]$ (0.20 g, 0.29 mmol) was suspended in 150 ml of DMSO and (ppn)Cl (0.44 g, 0.58 mmol) was added. The mixture was stirred for 12 h at 85°C. After solid material was filtered off, the filtrate was evaporated under vacuum, and the solid residue obtained was recrystallized from DMF/ether to give green microcrystals.



Scheme 2.

IR (KBr, cm^{-1}): 1650(w), 1514(s), 1439(m), 1406(w), 1325(s), 1261(w), 1115(s), 1032(m), 949(m), 804(s), 723(s), 692(s), 548(m), 534(s), 502(m). UV–Vis (DMF): 334 nm, 464 nm. (+)FAB-MS: *m*/*e* 538 $[ppn]^+$, (−)TOF-MS 642 $[KVOL]^-$. *Anal*. Calc. for $C_{64}H_{46}N_5O_9VP_2K \cdot DMF \cdot H_2O$: C, 63.26; H, 4.36; N, 6.61; V, 4.00. Found: C, 62.69; H, 4.65; N, 6.40; V, 4.32%.

2.1.3.2. $K_2[VO(L)^a]$. The ligand **H_4L^a** (0.50 g, 1.30 mmol) was added to 0.50 M KOH (10.50 ml, 5.20 mmol) in EtOH and the nitrogen gas was bubbled through the solution. A solution of $VO(acac)_2$ (0.35 g, 1.30 mmol) in 200 ml of EtOH was added dropwise into the basic ligand solution. This mixture was stirred for 20 h at room temperature and the solvent was removed under reduced pressure. The resulting green solid was dissolved in 5 ml of MeOH and the solution was loaded onto a Sephadex LH-20 column eluted with MeOH. The green band was collected and the solvent was removed by evaporation. The resulted green solid was dissolved into MeOH and vapor diffusion of Et_2O gave 0.22 g (31%) of $K_2[VO(L^a)]$ as blue–green powder.

IR (KBr, cm^{-1}) 1655(s), 1589(m), 1516(s), 1439(s), 1408(w), 1344(s), 1258(s), 1228(s), 1169(w), 1061(w), 953(m), 847(w), 799(w), 764(m), 677(m), 580(w), 505(m), 419(m). UV–Vis (EtOH): 293 nm, 573 nm, 660 nm. (−)FAB-MS: *m*/*e* 482 $[M-K^+]^-$. *Anal*. Calc. for $C_{20}H_{12}O_7N_2VK_2 \cdot CH_3OH$: C, 45.57; H, 2.91; N, 5.07; V, 9.38. Found: C, 45.86; H, 2.62; N, 5.30; V, 9.59%.

3. Results and discussion

3.1. Syntheses of the ligands and the complexes

To prepare the macrocyclic ligand, first, we attempted the direct cyclization of 2,3-dimethoxyterephthaloyl chloride and *p*-phenylenediamine under high dilution conditions in the presence of triethylamine. The yield of macrocycle **3** was only 3%, accompanied by the formation of a larger size macrocyclic compound [23]. By a stepwise method, modifying the procedures described by Raymond and co-workers [21], **3** was obtained in 11% total yield [23]. Our stepwise synthetic strategy is depicted in Scheme 1; the total yield was improved up to 49%. The purification in each step also became simple because of the lack of troublesome formation

of oligomers or by-products. Removing the methyl group with BBr_3 affords the ligand **H_4L** which is stable both as solid and in solution, but air-sensitive in alkaline solution. The solubility of **3** and **H_4L** toward chloroform at room temperature is significantly low. In strong polar organic solvents, such as DMSO and DMF, they are relatively soluble.

The acyclic biscatecholamide ligand **H_4L^a** was synthesized according to Scheme 2 [24]. Although the total yield (87%) of this synthetic method is slightly lower than that by a procedure recently published [25], in which 2,3-dimethoxybenzoyl chloride is used as a starting material, the handling described in Scheme 2 is easy due to the stability and robustness of the starting material.

Two oxovanadium complexes were prepared anaerobically by the ligand substitution reaction of $VO(acac)_2$ under basic conditions. The composition of these vanadyl complexes was confirmed by elemental analysis and mass spectroscopy. The complexes were stable as solids, but were air-sensitive in solution. The solubility of the macrocyclic complex is low toward organic solvent. Efforts to obtain single crystals of these complexes for X-ray diffraction analysis have been unsuccessful so far despite numerous attempts with a variety of cations and solvent systems.

3.2. Characterization of the complexes

3.2.1. Infrared spectroscopy

IR spectral data of the complexes prepared are shown in Table 1. The V=O stretching frequencies for the complexes $[VO(L)]^{2-}$ and $[VO(L^a)]^{2-}$ were observed at 949 and 953 cm^{-1}, respectively. They are lower frequencies compared to those of reported oxovanadium complexes (1100–960 cm^{-1}) [26]. The relatively low frequency indicates that the V=O bond is weakened by strong σ and π electron donation of catechol moieties to the antibonding orbital of the V=O group. A similar decrease in V=O stretching frequency has been reported for $K_2[VO(cat)_2]$ (970 cm^{-1}) [27] and $K_2[VO(bencam)]$ (955 cm^{-1}) (bencam: 1,3-bis[2-(2,3-dihydroxybenzamido)ethyl]benzene) [22], respectively. Other infrared bands associated with the anions, $[VO(L)]^{2-}$ and $[VO(L^a)]^{2-}$, were those due to ν(C–O) of the catechol moieties at 1261 and 1258 cm^{-1}, and ν(V–O) of the vanadium–catechol bonds at 503 and 505 cm^{-1}, respectively [28].

3.2.2. Electronic absorption spectra

The UV–Vis spectra of $[VO(L)]^{2-}$ and $[VO(L^a)]^{2-}$ are displayed in Fig. 1, and the numerical data are shown in Table 1. For oxovanadium(IV) complexes, three d–d bands corresponding to the $b_2(d_{xy}) \rightarrow e(d_{xz},d_{yz})$, $b_2(d_{xy}) \rightarrow b_1(d_{x^2-y^2})$, and $b_2(d_{xy}) \rightarrow a_1(d_{z^2})$ transitions are expected for a square-pyramidal structure [28]. The electronic spectrum of $[VO(L^a)]^{2-}$ measured in EtOH exhibited d–d bands assignable to those transitions at 660 and 573 nm, respectively, as shown in Fig. 1 (bottom, a). For comparison, $[VO(cat)_2]^{2-}$ and $[VO(bencam)]$ have been reported to exhibit the corresponding bands at 656 and 540 nm in NaOH aqueous solution, and 650 and 528 nm(sh) in MeOH, respectively, suggesting idealized C_{4v} symmetry at the metal center in each complex [22, 27]. In contrast to these complexes, the spectrum of the macrocyclic complex $[VO(L)]^{2-}$ shows considerable difference in the UV–Vis spectrum. An intense band at 334 nm and a d–d band of VO^{2+} at 464 nm as a shoulder were observed as shown in Fig. 1 (top, b). The intense band (334 nm) is assigned to a π–π^* transition of the aromatic ring of the ligand. However, no band was observed in the range from 650 to 500 nm; it is considered that a blue shift in the $b_2 \rightarrow b_1$ transition was caused by strong equatorial σ-donors [29]. An electron-rich environment

Table 1
Summary of spectral data for the oxovanadium complexes and related complexes

Complex	UV–Vis		IR	Ref.
	λ (nm)	Solvent	$\nu_{V=O}$ (cm^{-1})	
$[VO(L)]^{2-}$	334 464	DMF	949	this work
$[VO(L^a)]^{2-}$	573 660	EtOH	953	this work
$[VO(cat)_2]^{2-}$	540 656	KOH/H_2O	970 950(sh)	[27]
$[VO(becam)]^{2-}$	528 650	MeOH	955	[22]

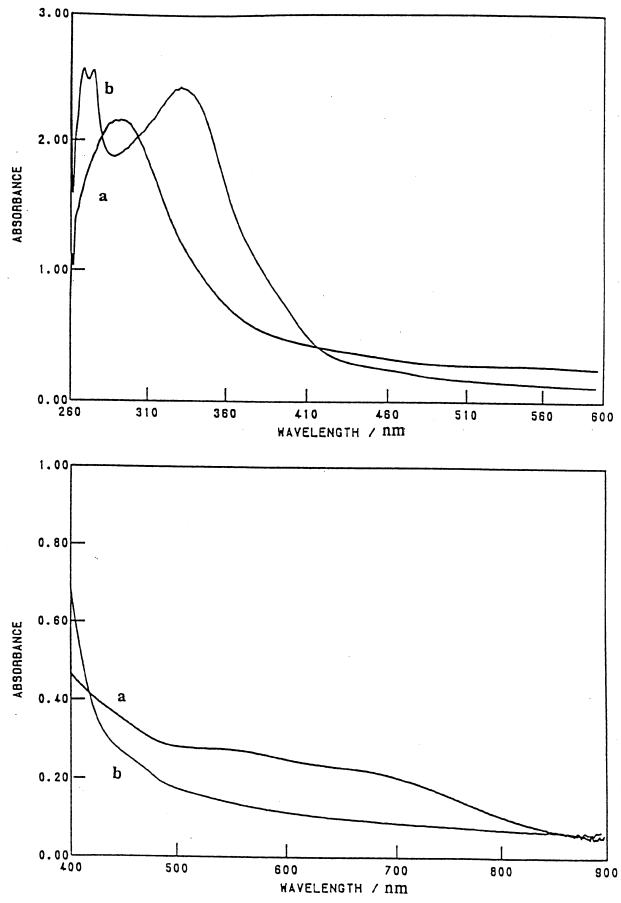


Fig. 1. UV–Vis absorption spectra of (a) $[VO(L^a)]^{2-}$ in EtOH solution and (b) $[VO(L)]^{2-}$ in DMF solution at ambient temperature (top: 260–600 nm; bottom: 400–900 nm).

about the vanadium center provided by equatorial dicatecholate ligands is further evidence for elevating the energy of the b_1 orbital. The extinction coefficient could not be determined because of the low solubility of the complexes.

3.2.3. ESR spectroscopy

At ambient temperature, intense ESR signals were observed for the complexes prepared in this work. The spectrum of $[VO(L)]^{2-}$ measured in a mixture of DMF/CH_2Cl_2 (80:20) is shown in Fig. 2. This spectrum displays the typical eight-line pattern of the d^1 vanadium(IV) center due to hyperfine splitting by the ^{51}V nucleus ($I=7/2$) as expected. The signals are centered at $g=1.973$, with an isotopic hyperfine splitting constant of 81×10^{-4} cm^{-1}.

For $[VO(L)]^{2-}$ and $[VO(L^a)]^{2-}$, the ESR spectra were measured at 77 K in the frozen solution of DMSO/EtOH (80:20) and $MeOH/CH_2Cl_2$ (80:20), respectively. The spectra are shown in Figs. 3 and 4. The g and A values obtained by simulation are given in Table 2 together with the related complexes. The parameters for $[VO(L)]^{2-}$ were determined to be $g_x=1.979$ ($A_x=53\times10^{-4}$ cm^{-1}), $g_y=1.983$ ($A_y=48\times10^{-4}$ cm^{-1}), and $g_z=1.950$ ($A_z=158\times10^{-4}$ cm^{-1}), as for $[VO(L^a)]^{2-}$, $g_x=1.984$ ($A_x=53\times10^{-4}$ cm^{-1}), $g_y=1.987$ ($A_y=50\times10^{-4}$ cm^{-1}), and $g_z=1.954$ ($A_z=155\times10^{-4}$ cm^{-1}). These values exhibit $g_z<g_x, g_y$ and $A_z>A_x, A_y$ and are lying in the expected range for catecholato oxovanadium complexes. The ESR spectra of vanadium(IV) can be classified into two groups, that is, those with a $d_{x^2-y^2}$ ground state displaying $g_z<g_x$, $g_y<2$ and $A_z>A_x, A_y$, and those with a d_{z^2} ground state $g_x, g_y<g_z\cong2$ and $A_z\ll A_x, A_y$. The former parameters are associated with square-pyramidal geometry and the latter parameters are attributable to a geometry distorted octahedral to trigonal prism [29,30]. Based on this claim, these values observed for $[VO(L)]^{2-}$ and $[VO(L^a)]^{2-}$ indicated that these complexes have a square-pyramidal geometry. Moreover, rhombic features ($g_x\neq g_y\neq g_z$, $A_x\neq A_y\neq A_z$) were observed in the ESR spectra of both $[VO(L)]^{2-}$ and $[VO(L^a)]^{2-}$. Such a rhombicity has not been observed for other catecholato complexes reported thus far.

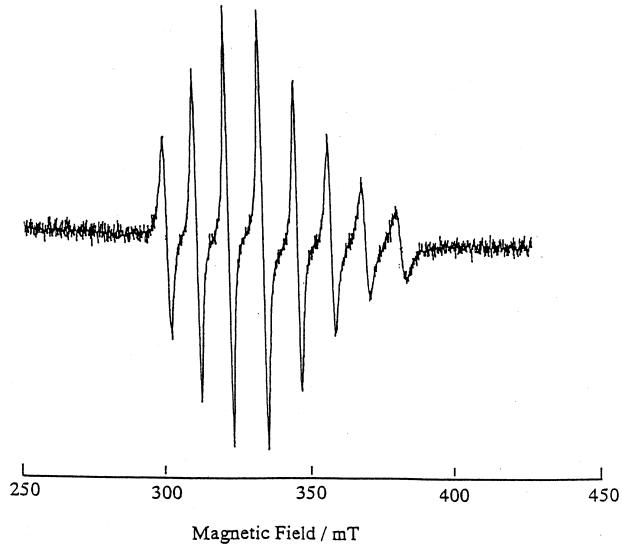


Fig. 2. ESR spectrum of $[VO(L)]^{2-}$ in DMF/CH_2Cl_2 (80/20) solution at ambient temperature.

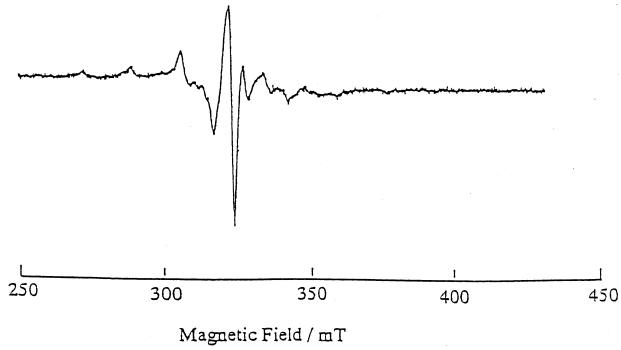


Fig. 3. ESR spectrum of $[VO(L)]^{2-}$ in DMSO/EtOH (80/20) solution at 77 K.

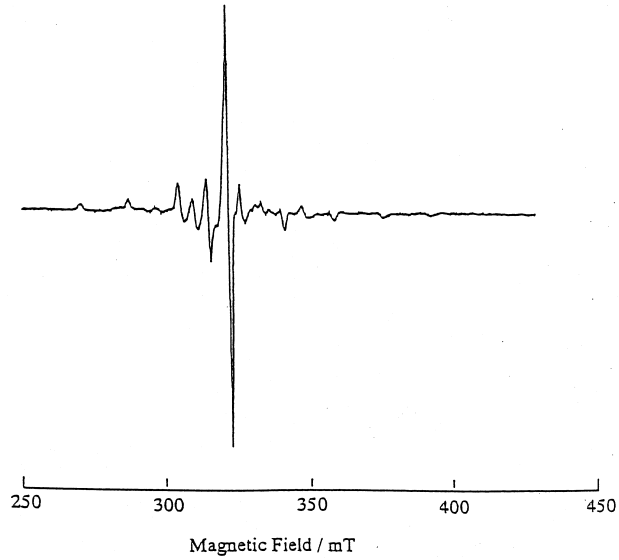


Fig. 4. ESR spectrum of $[VO(L^a)]^{2-}$ in $MeOH/CH_2Cl_2$ (80/20) solution at 77 K.

In general, the rhombicity in the equatorial components is observed for the complexes of mixed donor atoms in equatorial planes, such as [VO(salen)] (salen: N,N′-ethylenebis(salicylideneiminate)) and [VO(busaln)] (busaln: butylsalicylideneiminate) [31]. In spite of the fact that four donors in the equatorial plane of complexes in this study are all oxygen atoms, the unique rhombic nature was observed. It can be explained by the fact that the basal plane formed by four oxygen atoms in the complexes is apparently rectangular, rather than square as observed in $[VO(cat)_2]^{2-}$ and [VO(bencam)]. Moreover, the spectrum of the macrocyclic complex shows a relatively stronger rhombic property than that of $[VO(L^a)]^{2-}$. This suggests that distortion from a square in the basal plane for $[VO(L)]^{2-}$ becomes clearer than that for $[VO(L^a)]^{2-}$.

According to the results mentioned above, it can be presumed that the coordination geometry around the vana-

Table 2
ESR parameters of oxovanadium complexes [a]

Complex	g_z	g_x	g_y	A_z	A_x	A_y	Solvent	Ref.
				A (10^{-4} cm^{-1})				
$[VOL]^{2-}$	1.950	1.979	1.983	158	53	48	DMSO/EtOH (80/20)	this work
$[VOL]^{2-}$ [a]	1.954	1.984	1.987	155	53	50	MeOH/CH_2Cl_2 (80/20)	this work
$[VO(cat)_2]^{2-}$	1.950	1.981	1.981	154	50	50	H_2O	[27]
$[VO(becam)]^{2-}$	1.953	1.982	1.982	154	52	52	MeOH	[22]
$[VO(salen)]^{2-}$	1.955	1.986	1.989	166	56	55	MeCN	[31]
$[VO(busaln)_2]^{2-}$	1.951	1.983	1.987	167	58	56	C_6H_6	[31]

[a] g_z, g_x, g_y, A_z, A_x, A_y (absolute values) in frozen solution.

dium(IV) ions in $[VO(L)]^{2-}$ and $[VO(L^a)]^{2-}$ is distorted square-pyramidal.

4. Conclusions

We have synthesized a novel macrocyclic ligand containing two catechol moieties linked by two aromatic amines, *p*-phenylenediamine, and its oxovanadium(IV) complex. The complex showed rhombic distortion in square-pyramidal structure and its rhombicity was larger than those of catechol-bound oxovanadium(IV) complexes reported so far, and than the complex with an acyclic analog. This rhombic distortion around the vanadium is assumed to result in a bowl-like structure of the ligand which is organized by the vanadium coordination. Such a structural motif is reminiscent of calixarenes for molecular recognition chemistry. Thus, the formation of $[VO(L)]^{2-}$ described here can be considered as a metal-templated formation of a hydrophobic receptor [32].

References

[1] J.-M. Lehn, Supramolecular Chemistry: Concepts and Perspectives, VCH, Weinheim, 1995.
[2] W. Nam, R. Ho, J.S. Valentine, J. Am. Chem. 113 (1991) 7052.
[3] D.E. Fenton, Chem. Soc. Rev. 28 (1999) 159.
[4] T.J. Collins, T.R. Nichols, E. Uffelman, J. Am. Chem. Soc. 113 (1991) 4708.
[5] C.G. Miller, S.W. Gordon-Wylie, C.P. Horwitz, S.A. Strazisar, D.K. Peraino, G.R. Clark, S.T. Weintraub, T.J. Collins, J. Am. Chem. Soc. 120 (1998) 11540.
[6] J.M. Workman, R.D. Powell, A.D. Procyk, T.J. Collins, D.F. Bocian, Inorg. Chem. 31 (1992) 1550.
[7] T.J. Collins, R.D. Powell, C. Slebodnick, E.S. Uffelman, J. Am. Chem. Soc. 112 (1990) 899.
[8] T.J. Collins, S.W. Gordon-Wylie, J. Am. Chem. Soc. 111 (1989) 4511.
[9] M.J. Bartos, S.W. Gordon-Wylie, B.G. Fox, L.J. Wright, S.T. Weintraub, K.E. Kauffmann, E. Münck, K.L. Kosta, E.S. Uffelman, C.E.F. Rickard, K.R. Noon, T.J. Collins, Coord. Chem. Rev. 174 (1998) 361.
[10] T.J. Collins, Acc. Chem. Res. 27 (1994) 279.
[11] T.J. Collins, B.G. Fox, Z.G. Hu, K.L. Kosta, E. Münck, C.E.F. Rickard, L.J. Wright, J. Am. Chem. Soc. 114 (1992) 8724.
[12] T.J. Collins, K.L. Kosta, E. Münck, E.S. Uffelman, J. Am. Chem. Soc. 112 (1990) 5637.
[13] W. Kiggen, F. Vögtle, Angew. Chem., Int. Ed. Engl. 23 (1984) 714.
[14] W. Kiggen, F. Vögtle, S. Franken, H. Puff, Tetrahedron 42 (1986) 1859.
[15] Y. Sun, A.E. Martell, R.J. Motekaitis, Inorg. Chem. 24 (1985) 4343.
[16] Y. Sun, A.E. Martell, R.J. Motekaitis, Inorg. Chem. 25 (1986) 4780.
[17] J.R. Steven, Y.N. Chiu, K.N. Raymond, J. Am. Chem. Soc. 107 (1985) 4094.
[18] J.R. Steven, C.W. Lee, Y.N. Chiu, K.N. Raymond, Inorg. Chem. 26 (1987) 1622.
[19] K.N. Raymond, Coord. Chem. Rev. 105 (1990) 135.
[20] T.B. Karpishin, T.D.P. Stack, K.N. Raymond, J. Am. Chem. Soc. 115 (1993) 6115.
[21] T.B. Karpishin, T.D.P. Stack, K.N. Raymond, J. Am. Chem. Soc. 115 (1993) 182.
[22] T.M. Dewey, J.D. Bois, K.N. Raymond, Inorg. Chem. 32 (1993) 1729.
[23] T. Ma, Doctor Thesis, Kyushu University, Japan, 1999, p. 34.
[24] T. Ma, Y. Matsuda, The 35th Symposium on ESR, Fukuoka, Japan, 1997, p. 153.
[25] M. Meyer, B. Kersting, R.E. Powers, K.N. Raymond, Inorg. Chem. 36 (1997) 5179.
[26] J. Selbin, Chem. Rev. 65 (1965) 163.
[27] S.R. Cooper, Y.B. Koh, K.N. Raymond, J. Am. Chem. Soc. 104 (1982) 5092.
[28] P.A. Wicklund, D.G. Brown, Inorg. Chem. 15 (1976) 396.
[29] A.S. Borovik, T.M. Dewey, K.N. Raymond, Inorg. Chem. 32 (1993) 413.
[30] M. Branca, G. Micera, A. Dessi, D. Sanna, K.N. Raymond, Inorg. Chem. 29 (1990) 1588.
[31] J. Jezierski, J.B. Raynor, J. Chem. Soc., Dalton Trans. (1981) 1.
[32] A. Caselli, E. Solari, R. Scopelliti, C. Floriani, J. Am. Chem. Soc. 121 (1999) 8296.

PERGAMON

www.elsevier.nl/locate/poly

Polyhedron 19 (2000) 1175–1179

POLYHEDRON

Synthesis, crystal structure, thermal and magnetic properties of $[Mn(H_2O)_6][Cu(pdta)]\cdot 2H_2O$ (pdta = 1,3-propylenediamine-*N*,*N*,*N*′*N*′-tetraacetate)

Margarita Hernández-Padilla [a], Erasmo Chinea [a], Sixto Domínguez [a], Alfredo Mederos [a,*1], M. Carmen Muñoz [b], Francesc Lloret [c,*2]

[a] *Departamento de Química Inorgánica, Universidad de La Laguna, Tenerife, Canary Islands, Spain*
[b] *Departamento de Física Aplicada, Universidad Politécnica de València, Camino de Vera s/n, 46071 València, Spain*
[c] *Departament de Química Inorgànica, Facultat de Química de la Universitat de València, Dr. Moliner 50, 46100 Burjassot, València, Spain*

Received 3 October 1999; accepted 9 March 2000

Abstract

On mixing concentrated aqueous solutions of pdta, Cu(II) and Mn(II) in the ratio 1:1:1 at pH 4.5, single crystals of the complex $[Mn(H_2O)_6][Cu(pdta)]\cdot 2H_2O$ (**1**) (pdta = 1,3-propylenediamine-*N*,*N*,*N*′*N*′-tetraacetate) were obtained. X-ray structural analysis revealed that in the anion $[Cu(pdta)]^{2-}$ the coordination polyhedron around the Cu(II) ion can be described as a tetragonaly distorted CuN_2O_4 octahedron, whereas the cation $[Mn(H_2O)_6]^{2+}$ can be described as a very regular MnO_6 octahedron. Thermogravimetric analysis shows that at 110°C compound **1** loses its eight water molecules yielding the anhydrous compound [MnCu(pdta)] (**2**). Variable-temperature magnetic susceptibility measurements indicate that no magnetic interactions are present in **1** while weak antiferromagnetic interactions occur in **2**.
©2000 Elsevier Science Ltd All rights reserved.

Keywords: 1,3-propylenediaminetetraacetate; Cu(II) complexes; Mn(II) complexes; Crystal structures; Thermal properties; Magnetic properties

1. Introduction

A great deal of attention has been devoted to diamino-polycarboxylato complexes [1–5] and especially to the edta family (edta = ethylenediamine-*N*,*N*,*N*′,*N*′-tetraacetate) [6]. The complexes formulated as $M'M(edta)(H_2O)_4\cdot 2H_2O$ (M and M′ are divalent first-row transition metal ions) belong to a series of ferrimagnetic systems in which both the 1-d character and the cationic ordering are well stabilized [7–9]. The structure may be roughly described as infinite zig-zag chains involving alternating metal ions. One of them (M′) is surrounded by four water molecules and two oxygen atoms, belonging to bridging carboxylate groups, while the other (M) exhibits hexacoordination through the edta ligand. In the heterometallic complexes (M ≠ M′), a clear preference of the cations to be coordinated into either the 'hydrated' or 'chelated' form has been confirmed by a study comparing their visible spectra with those of homometallic complexes [10], as well as potentiometric measurements [11,12]. These studies show unambiguously that the Mn(II) ion will be in the 'hydrated' position when sufficient Cu(II) ion is present to occupy the 'chelated' position. Thus $MnCu(edta)\cdot 6H_2O$ is formed by infinite zig-zag chains built up with alternating 'hydrated' and 'chelated' octahedra bridged by carboxylate groups [13]: $-Mn(H_2O)O_2-Cu(edta)-Mn(H_2O)O_2-Cu(edta)-$... Owing to the selective occupation of both sites, distinct spin sublattices are expected to result in so-called ferrimagnetic 1-d behaviour [14,15]. Similar structural and magnetic behaviour has been observed in other edta-like metal complexes [16,17]. On the other hand, by conducting the synthesis under conditions of high temperature and pressure, three-dimensional crystalline polymers have been obtained [18–20]. In these, the removal of some water molecules from the parent hexahydrates results in an intercrossing of the chains through carboxylate bridges, with the consequent increase in dimensionality of the system. This strategy has also been used in the oxamido systems such as $MnCu(obbz)\cdot 5H_2O$ [21–23] and $MnCu(obze)\cdot 6H_2O$ [24,25]. Partial dehydration yields the three-dimensional

[1] *Corresponding author.
[2] *Corresponding author. Tel.: +34-96-386-4856; fax: +34-96-386-4322; e-mail: francisco.lloret@uv.es

0277-5387/00/$ - see front matter ©2000 Elsevier Science Ltd All rights reserved.
PII S0277-5387(00)00362-4

compounds MnCu(obbz)·H_2O and MnCu(obze)·$2H_2O$ which order ferromagnetically at 14 and 5 K, respectively.

In this work, we present the synthesis and structural determination of the complex [Mn(H_2O)$_6$][Cu(pdta)]·$2H_2O$ (**1**), (pdta = 1,3-propylenediamine-*N*,*N*,*N*′,*N*′-tetraacetate). Study of the thermal and magnetic properties, including those of the dehydrated compound [MnCu(pdta)] (**2**), is also reported.

2. Experimental

2.1. Preparation of the complexes [Mn(H_2O)$_6$][Cu(pdta)]·$2H_2O$ (**1**) and [MnCu(pdta)] (**2**)

H_4pdta (1,3-propylenediamine-*N*,*N*,*N*′,*N*′-tetraacetic acid) was synthesized as previously reported [26]. A concentrated aqueous solution of H_4pdta (pH was fixed at 4.5 with NaOH solution) was mixed with a concentrated aqueous solution of Cu(NO_3)$_2$·$3H_2O$ and Mn(NO_3)$_2$·$4H_2O$ with a ratio H_4pdta:Cu(II):Mn(II) = 1:1:1. Finally, the pH of the mixed solution was also fixed at 4.5. Addition of ethanol to the solution resulted in the precipitation of a blue polycrystalline dust. The precipitate was filtered off and washed several times with ethanol. Blue crystals suitable for X-ray crystallography were grown by liquid–liquid diffusion [27,28] using water as solvent and ethanol as precipitant.

Compound **1** loses its eight water molecules when heated at $120 < T < 170$°C, yielding the dehydrated compound **2**. Thermogravimetrical analysis revealed a loss of weight of 26% that closely corresponds to 8 mol of water per molecular unit. Afterwards, the weight remained constant. This loss of water also became clear from the disappearance of the bands characteristic of water in the IR spectra. Elemental analyses were performed on a Carlo Erba 1106 automatic analyser. Copper and manganese were determined by atomic absorption. Found: C, 23.09; H, 5.17; N, 4.76; Cu, 10.94; Mn, 9.65. Calc. for $C_{11}H_{30}N_2O_{16}CuMn$ (**1**): C, 23.39; H, 5.35; N, 4.96; Cu, 11.25; Mn, 9.73%.

2.2. Instrumentation

The IR spectrum was taken on a Perkin-Elmer 1750 FTIR spectrophotometer as KBr pellets in the 4000–300 cm^{-1} region. Magnetic susceptibility measurements were carried out with a fully automated AZTEC DSM5 pendulum-type susceptometer equipped with a TBT continuous-flow cryostat and a Brüker BE15 electromagnet, operating at 1 T. The apparatus was calibrated with mercury tetrakis(thiocyanato)cobaltate(II). The corrections for the diamagnetism of compounds **1** and **2** were estimated from Pascal constants as -280×10^{-6} (**1**) and -210×10^{-6} (**2**) $cm^3\ mol^{-1}$ and were substracted from the experimental molar susceptibility to obtain the paramagnetic molar susceptibilities. Thermal analyses were performed by using a Setaram B70 thermobalance. The samples were heated at 1°C min^{-1} either under N_2 flow or air atmosphere.

2.3. Diffraction data

A prismatic blue crystal of complex **1** of approximate dimensions $0.1\times0.1\times0.1$ mm was used for data collection at 293 K. Diffraction data were taken with an Enraf-Nonius CAD-4 diffractometer using graphite-monochromated Mo Kα radiation. The cell parameters were determined from least-squares refinements of 25 well centred reflections in the range $12 < \theta < 20°$. A total of 2677 independent reflections were collected (in the range $2 < 2\theta < 64°$). Three reference reflections monitored throughout data collection showed no significant sign of crystal deterioration. The usual corrections for Lorentz and polarisation effects were carried out, but no absorption corrections.

The crystal was orthorhombic, space group *Pnna*, $a = 11.893(9)$, $b = 13.337(6)$, $c = 13.790(6)$ Å, $V = 2187(2)$ Å^3 (by least-squares refinement from 25 automatically centred reflections in the range $12 < \theta < 20°$), $M_r = 564.85$, $Z = 4$, $D_c = 1.72$ g cm^{-3}, $F(000) = 1168$. Mo Kα radiation, $\lambda = 0.71069$ Å, μ(Mo Kα) = 16.28 cm^{-1}.

The structure was solved by direct methods using SHELXS86 [29], and refined by least-squares methods using SHELXL93 [30]. All non-hydrogen atoms were refined anisotropically. The hydrogen atoms were located from a difference synthesis and refined with an overall isotropic thermal parameter. The refinement converged to $R_1 = 0.0383$ and $wR_2 = 0.1729$. Molecular plots were produced using SCHAKAL [31].

Crystal data are given in Table 1, while important bond lengths and angles are listed in Table 2.

3. Results and discussion

3.1. X-ray structure

The structure of **1** consists of [Cu(pdta)]$^{2-}$ and [Mn(H_2O)$_6$]$^{2+}$ complex units and water molecules of crystallization linked by electrostatic forces and an extensive hydrogen bond network. A perspective view is given in Fig. 1 along with the numbering scheme adopted.

In the molecule [Mn(H_2O)$_6$][Cu(pdta)]·$2H_2O$, pdta is a hexadentate ligand, the donor atoms being O(1) and O(3) and N(1). The coordination polyhedron around the Cu ion can be described as a tetragonally distorted CuN_2O_4 octahedron: two O(1) (two different carboxylates) and two N(1) atoms form the equatorial plane and two O(3) atoms of another two carboxylates fill the axial sites. The two O(1) and two N(1) atoms lie approximately in a plane. The maximum deviation from the plane is 0.135(2) Å (O(1)).

The coordination polyhedron around the Mn(II) ion can be described as a very regular MnO_6 octahedron (d(Mn–O) between 2.16 and 2.19 Å). The pdta ligand prefers to form a

Table 1
Crystal data and structure refinement for **1**

Empirical formula	$C_{11}H_{30}CuMnN_2O_{16}$
Formula weight	564.84
Temperature (K)	293(2)
Wavelength (Å)	0.71069
Crystal system	orthorhombic
Space group	*Pnna*
Unit cell dimensions	
a (Å)	11.893(9)
b (Å)	13.337(6)
c (Å)	13.790(6)
α (°)	90
β (°)	90
γ (°)	90
Volume (Å^3)	2187(2)
Z	4
Density (calculated) (Mg m^{-3})	1.715
Absorption coefficient (mm^{-1})	1.628
$F(000)$	1168
Crystal size (mm)	0.1×0.1×0.1
θ Range for data collection (°)	2.12–31.95
Index ranges	$0 \le h \le 16$, $0 \le k \le 19$, $0 \le l \le 20$
Independent reflections	2677
Refinement method	full-matrix least-squares on F^2
Data, restraints, parameters	2614, 0, 169
Goodness-of-fit on F^2	1.475
Final R indices ($I > 2\sigma(I)$)	$R_1 = 0.0383$, $wR_2 = 0.1729$
R indices (all data)	$R_1 = 0.0533$, $wR_2 = 0.1790$
Extinction coefficient	0.004(2)
Largest difference peak and hole (e Å^{-3})	0.475 and −0.728

Table 2
Selected bond lengths (Å) and angles (°) for **1**

Cu(1)–N(1)	2.049(2)
Cu(1)–O(1)	1.973(2)
Cu(1)–O(3)	2.285(3)
Mn(1)–O(5)	2.169(2)
Mn(1)–O(6)	2.156(3)
Mn(1)–O(7)	2.185(2)
N(1)–C(1)	1.485(4)
N(1)–C(3) [a]	1.496(4)
N(1)–C(5)	1.491(4)
O(1)–C(2)	1.278(3)
O(2)–C(2)	1.239(3)
O(3)–C(4)	1.250(3)
O(4)–C(4)	1.248(4)
C(2)–C(1)	1.507(4)
C(3)–C(4)	1.520(4)
C(5)–C(6)	1.521(4)
O(1)–Cu(1)–N(1)	84.10(10)
O(1)–Cu(1)–O(3)	92.13(9)
N(1)–Cu(1)–O(3)	93.85(10)
O(6)–Mn(1)–O(5)	91.93(11)
O(6)–Mn(1)–O(7)	89.13(10)
O(5)–Mn(1)–O(7)	89.12(10)

[a] Symmetry transformation used to generate equivalent atoms: $-x+3/2, y, -z+3/2$.

chelate complex with Cu(II) as indicated by its stability constants in aqueous solution [32] (25°C, $I = 0.1$): $[Cu(pdta)]^{2-}$, $\log K = 18.80$; $[Mn(pdta)]^{2-}$, $\log K = 10.06$.

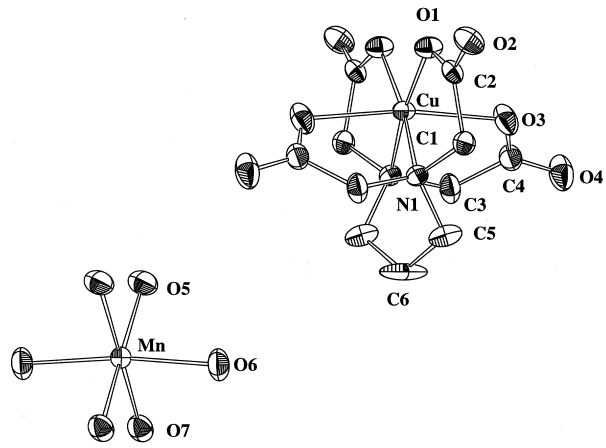


Fig. 1. Perspective view of complex **1** with the atom-numbering scheme. Hydrogen atoms have been omitted for simplicity.

There are two crystallographically independent glycine rings: one is in the plane of the six-membered chelate rings and forms part of a girdle about the copper atom; the other lies in a plane nearly perpendicular to the plane of the octahedron. The former glycine ring (Cu, N(1), C(1), C(2), O(1)) is nearly planar and O(2) deviates by about 0.243(4) Å from the least-squares plane, while the latter ring (Cu, N(1), C(3), C(4), O(3)) shows significant departure from planarity and O(4) is 0.383(5) Å out of the plane of the chelate ring. The six-membered chelate ring adopts a twisted-boat form: the atoms N(1) and C(5′) are 0.525(3) and 0.618(4) Å out of the plane defined by Cu, C(5), C(6) and N(1′). The other two non-coordinated water molecules in **1** are linked to the pdta ligand and coordinated waters by hydrogen bonds.

A similar distorted CuN_2O_4 octahedron is found in the complexes $K_2[Cu(edta)]$ [33] and $Ca[Cu(edta)]$ [34,35]. In $H_2[Cu(edta)]\cdot H_2O$ [36], the edta ligand is pentadentate and in the complex $[Co(edta)]^-$ the coordination octahedral of the Co(III) is more regular, as expected [37].

3.2. Thermogravimetric study

The thermogravimetric curve of complex **1** is shown in Fig. 2. It can be seen how the weight loss starts at ca. 40°C and stops at 110°C, a plateau being observed between this temperature and 170°C. At this stage, the weight loss is ca. 26%, a value which corresponds to eight water molecules per molecular unit. The lack of the characteristic stretching vibrations of water in the IR spectrum of this dehydrated phase supports its formulation as [MnCu(pdta)] (**2**).

The proximity of the carboxylate groups could account for the easy loss of the coordinated water molecules. The carboxylate-assisted water loss is a well known phenomenon [18–25,38]. In this sense, the water-oxygens of the coordination sphere of the manganese(II) ion would be substituted by the carboxylate-oxygen atoms. That is, the complex

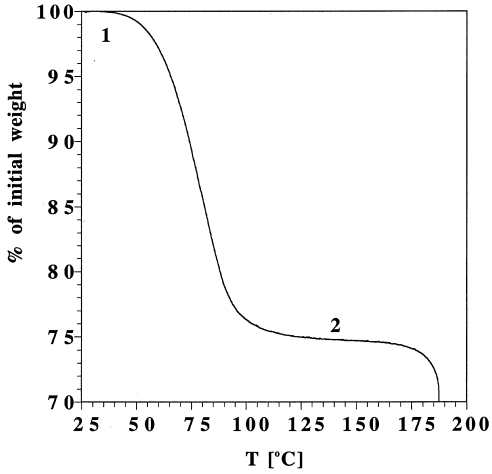


Fig. 2. Thermogravimetric curve of **1**.

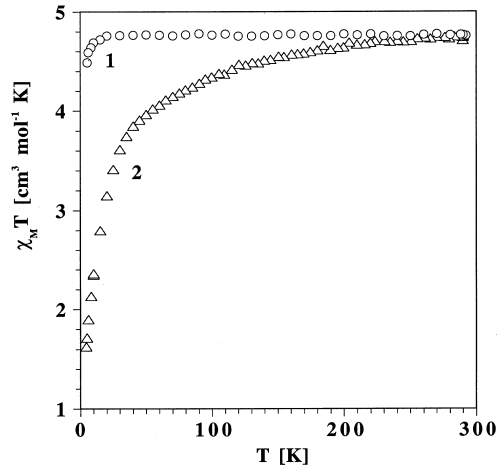


Fig. 3. Thermal dependence of the $\chi_M T$ product for **1** and **2**.

$Cu(pdta)^{2-}$ would act as a ligand towards the manganese(II) ion through its free carboxylate-oxygens in the dehydration process. A two- or three-dimensional solid would result from the polymerization of the metal ions through carboxylato bridging.

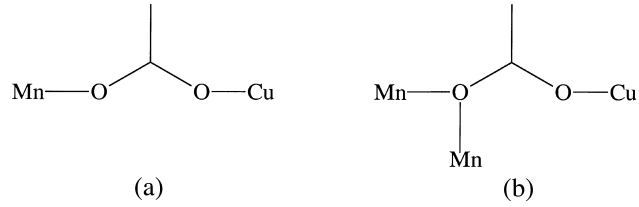
3.3. Magnetic properties

The thermal dependence of the $\chi_M T$ product (χ_M being the molar magnetic susceptibility) for **1** and its dehydrated species **2** is depicted in Fig. 3. The $\chi_M T$ value for **1** is practically constant and equal to 4.77 cm^3 mol^{-1} K from room temperature until 10 K, as expected for a pair of non-interacting Mn(II)–Cu(II). Then, it decreases smoothly at lower temperatures most likely due to a small zero field splitting of the $^6A_1$ ground state of the complex $[Mn(H_2O)_6]^{2+}$. In fact, this magnetic behaviour is matched satisfactorily through the axial $S=5/2$ zfs Hamiltonian

$$\boldsymbol{H}=D[\boldsymbol{S}_z^2-\tfrac{1}{3}S(S+1)+g\beta\boldsymbol{H}\boldsymbol{S}]$$

with $g(Mn)=1.99$ and $D=|0.4|$ cm^{-1} and keeping constant $g(Cu)=2.05$. Consequently, it is suggested that no magnetic coupling is present in complex **1**. In contrast to that, the magnetic curve of compound **2** exhibits a continuous decrease from room temperature, attaining a value of 1.6 cm^3 mol^{-1} K at 4.3 K, revealing that an antiferromagnetic coupling occurs.

During the dehydration process, the crystals of **1** crack and consequently, the crystal structure of **2** could not be determined. However, some structural information can be inferred from the magnetic study. If the polymerization process involves the formation of the carboxylate-bridging Mn(II) and Cu(II) shown in Scheme 1(a), as the only magnetic pathway, we would deal with a bimetallic system with alternating local $S=1/2$ (Cu(II)) and $S=5/2$ (Mn(II)) spins which would exhibit a ferrimagnetic-like behaviour: the $\chi_M T$ curve would present a minimum and a further increase at lower temperatures; the value of $\chi_M T$ at the minimum is predicted to be greater than 3 cm^3 mol^{-1} K, the value corresponding to an antiferromagnetically coupled Cu(II)–Mn(II) pair. Given that the magnetic properties of **2** do not agree with this description, other structural elements such as that indicated in Scheme 1(b) have to be involved. The occurrence of the antiferromagnetic interactions between Mn(II) ions bridged by a single carboxylate-oxygen atom (Scheme 1(b)) would cancel the magnetic moment of the Mn(II)–Mn(II) pair in agreement with the magnetic curve of **2**.



Scheme 1.

Additional support for this conclusion comes from the fact that the four free carboxylate-oxygens of the $Cu(pdta)^{2-}$ are not enough to keep the six-coordination of Mn(II) (the situation where Scheme 1(a) would be the only structural unit present) and thus sharing of some of these oxygen atoms would be required as shown in Scheme 1(b).

Supplementary data

Tables of atomic coordinates and equivalent isotropic displacement parameters, complete bond lengths and angles, least-squares mean planes, anisotropic displacement parameters, thermal parameters and observed and calculated structure factors (4 pages) are available from the Cambridge Crystallographic Data Centre, 12 Union Road, Cambridge, CB2 1EZ, UK (fax: +44-1223-336033; e-mail: deposit@ccdc.cam.ac.uk) on request, the deposit number being 133983.

Acknowledgements

This work was partially supported by the CICYT (Spain) through Projects PB97-1397 (Valencia) and APC94-0031 (La Laguna). Instrumental and computing facilities of the

Servicio de Espectroscopía y Centro de Cálculo de la Universitat de València are gratefully acknowledged.

References

[1] S. Dominguez, A. Mederos, P. Gili, A. Rancel, A.E. Rivero, F. Brito, F. Lloret, X. Solans, C. Ruiz-Pérez, M.L. Rodríguez, I. Brito, Inorg. Chim. Acta 225 (1997) 367.
[2] M.W. Brechbiel, O.A. Gansow, C.G. Pippin, R.D. Rogers, R.P. Planalp, Inorg. Chem. 35 (1996) 6343.
[3] J.D. Zukowski, D.L. Perry, E.J. Valente, S. Lott, Inorg. Chem. 34 (1995) 6409.
[4] D.J. Radanovic, S.R. Trifonovic, M.S. Cvijovic, C. Maricondi, B.E. Douglas, Inorg. Chim. Acta 196 (1992) 161.
[5] H. Ogino, M. Shimoi, Y. Saito, Inorg. Chem. 28 (1989) 3596.
[6] E. Coronado, in: D. Gatteschi, O. Kahn, J.S. Miller, F. Palacio (Eds.), Magnetic Molecular Materials, NATO ASI Series, vol. E198, Kluwer, 1991, pp. 267–280.
[7] J.J. Borrás-Almenar, E. Coronado, D. Gatteschi, C. Zanchini, Inorg. Chem. 31 (1992) 294.
[8] E. Coronado, M. Drillon, P.R. Nugteren, L.J. De Jongh, D. Beltrán, R. Georges, J. Am. Chem. Soc. 111 (1989) 3874.
[9] E. Coronado, M. Drillon, A. Fuertes, D. Beltrán, A. Mosset, J. Galy, J. Am. Chem. Soc. 108 (1986) 900.
[10] E. Escrivá, A. Fuertes, D. Beltrán, Transition Met. Chem. 9 (1984) 184.
[11] R.M. Smith, A.E. Martell, in: Critical Stability Constants, vol. 6, Second Supplement, Plenum, New York, 1989, p. 108.
[12] A.E. Martell, R.M. Smith, in: Critical Stability Constants, vol. 1, Aminoacids, Plenum, New York, 1974.
[13] J.J. Borrás-Almenar, E. Coronado, D. Gatteschi, C. Zanchini, Inorg. Chim. Acta 207 (1993) 105.
[14] F. Lloret, R. Ruiz, B. Cervera, I. Castro, M. Julve, J. Faus, J.A. Real, F. Sapiña, Y. Journaux, J.C. Colin, M. Verdaguer, J. Chem. Soc., Chem. Commun. (1994) 2615.
[15] M. Drillon, E. Coronado, D. Beltrán, J. Curely, R. Georges, P.R. Nugteren, L.J. De Jongh, J.L. Genicon, J. Magn. Magn. Mater. 54–57 (1986) 1507.
[16] A. Fuertes, C. Miratvilles, E. Escrivá, E. Coronado, D. Beltrán, L. Padel, J. Chem. Soc., Dalton Trans. (19890 863.
[17] J.J. Borrás-Almenar, E. Coronado, C.J. Gómez-García, L. Ouahab, Angew. Chem., Int. Ed. Engl. 32 (1993) 561.
[18] P. Gómez-Borrero, G.B. Jameson, N. Casañ-Pastor, E. Coronado, D. Beltrán, Inorg. Chem. 25 (1986) 3171.
[19] F. Sapiña, E. Coronado, P. Gómez-Borrero, D. Beltán, R. Burriel, R.L. Carlin, J. Appl. Phys. 67 (1990) 6003.
[20] F. Sapiña, E. Coronado, D. Beltán, R. Burriel, J. Am. Chem. Soc. 113 (1991) 7940.
[21] F. Lloret, M. Julve, R. Ruiz, Y. Journaux, K. Nakatani, O. Kahn, J. Sletten, Inorg. Chem. 32 (1993) 27.
[22] N. Nakatani, Y. Carriat, Y. Journaux, O. Kahn, F. Lloret, J.P. Renard, Y. Pei, J. Sletten, M. Verdaguer, J. Am. Chem. Soc. 111 (1989) 5739.
[23] F. Lloret, K. Nakatani, Y. Journaux, O. Kahn, Y. Pei, J.P. Renard, J. Chem. Soc., Chem. Commun. (1988) 642.
[24] Y. Journaux, P. van Koningsbruggen, F. Lloret, K. Nakatani, Y. Pei, O. Kahn, J.P. Renard, J. Phys. (Paris) 49 (1988) C851.
[25] Y. Pei, O. Kahn, K. Nakatani, E. Kodjovi, C. Mathoniere, J. Sletten, J. Am. Chem. Soc. 113 (1991) 6558.
[26] G. Schwarzenbach, H. Ackermann, Helv. Chim. Acta 31 (1948) 1209.
[27] C. Orvig, J. Chem. Educ. 62 (1985) 84.
[28] P. Jones, Chem. Br. 17 (1981) 222.
[29] G.M. Sheldrick, Acta Crystallogr., Sect. A 46 (1990) 467.
[30] G.M. Sheldrick, SHELXL-93, University of Göttingen, Germany, 1993.
[31] K. Keller, SCHAKAL, program for the graphic representation of molecular and crystallographic models, University of Freiburg, Germany, 1987.
[32] V. Novak, M. Suicekova, E. Drovakova, I. Valaskova, J. Mayer, Chem. Zvest. 35 (1981) 481.
[33] M.A. Porai-Kohits, N.V. Novozhilova, T.N. Polynova, T.V. Filippova, L.I. Martinenko, Kristallografiya 18 (1973) 171.
[34] Y.N. Nestorova, M.A. Porai-Kohits, V.A. Logrinenko, Zh. Struck. Khim. 24 (1979) 2273.
[35] Y.N. Nestorova, M.A. Porai-Kohits, V.A. Logrinenko, Zh. Neorg. Khim. 21 (1980) 2273.
[36] F.S. Stephens, J. Chem. Soc. (A) (1969) 1723.
[37] R. Nagao, F. Marumo, Y. Saito, Acta Crystallogr., Sect. B 28 (1972) 1852.
[38] J. Cano, G. De Munno, J.L. Sanz, R. Ruiz, J. Faus, F. Lloret, M. Julve, A. Caneschi, J. Chem. Soc., Dalton Trans. (1997) 1915.

PERGAMON

www.elsevier.nl/locate/poly

Polyhedron 19 (2000) 1181–1191

POLYHEDRON

Synthesis, characterization and magnetochemical studies of some imidazole and imidazolate copper(II) ternary complexes derived from *N*-salicylidenearoylhydrazines. X-ray crystal and molecular structures of [(*N*-salicylidene-*p*-chlorobenzoylhydrazine)*ONO*(−2)imidazole]-copper(II) monohydrate and dimeric [(*N*-salicylidene-*p*-methylbenzoyl-hydrazine)*ONO*(−2)imidazole]copper(II) hemihydrate

M.F. Iskander [a,*], T.E. Khalil [a], R. Werner [b], W. Haase [b], I. Svoboda [c], H. Fuess [c]

[a] *Chemistry Department, Faculty of Science, Alexandria University, P.O. Box 426, Ibrahimia, Alexandria 21321, Egypt*

[b] *Institut für physikalische Chemie, AG Kondensierte Materie, Fachbereich Chemie, Technische Universität Darmstadt, Petersenstrasse 20, D-64287 Darmstadt, Germany*

[c] *Strukturforschung, Fachbereich Materialwissenschaft, Petersenstrasse 24, D-64287 Darmstadt, Germany*

Received 10 December 1999; accepted 16 March 2000

Abstract

The reactions of imidazole (Him) with *N*-salicylidenearoylhydrazine copper(II) complexes have been studied and a number of ternary copper(II) complexes, $[Cu(L)Him]\cdot nH_2O$, $[Cu(HL)X\cdot Him]\cdot nH_2O$ and $[\{Cu(L)\}_2Im]\cdot nH_2O$, have been prepared and characterized (HL and L refer, respectively, to mono- and dinegative *N*-salicylidenearoylhydrazine anions and X is a mononegative monodentate ligand). The X-ray crystal and molecular structure of [(*N*-salicylidene-*p*-chlorobenzoylhydrazine)imidazole]copper(II) monohydrate, $[Cu(Sp\text{-}ClBzh)Him]\cdot H_2O$, and [(*N*-salicylidene-*p*-methylbenzoylhydrazine)imidazole]copper(II) hemihydrate, $[Cu(Sp\text{-}CH_3Bzh)Him]\cdot 1/2H_2O$, were measured. The *p*-chloro complex $[Cu(Sp\text{-}ClBzh)Him]\cdot H_2O$ is monomeric with the Cu(II) in a distorted square planar environment and is coordinated to the tridentate hydrazone via phenoxy oxygen, azomethine nitrogen and enolimide oxygen, the fourth coordination site is occupied by the imidazole nitrogen. The *p*-methyl complex $[Cu(Sp\text{-}CH_3Bzh)Him]\cdot 1/2H_2O$ was found to be a centrosymmetric dimer, the monomeric unit being bridged through the phenoxy oxygen. The Cu(II) is in a square pyramidal environment and is bounded in the equatorial plane with the enolimide oxygen, azomethine nitrogen and phenoxy oxygen of the hydrazone ligand while the fourth site is occupied by the symmetry related phenoxy oxygen of the other unit; the axial fifth coordination site is occupied by the imidazole nitrogen. The magnetic susceptibility measurements at different temperatures (5–298 K) have been recorded and are discussed. The binuclear imidazolate complexes show antiferromagnetic exchange coupling interactions, the measured $-J$ values are within the range 17.0–20.0 cm^{-1}, while the imidazole complexes do not show any appreciable exchange interactions. ©2000 Elsevier Science Ltd All rights reserved.

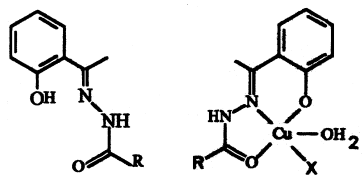
Keywords: *N*-salicylidenearoylhydrazine copper(II) complexes; Copper(II) imidazole ternary complexes; Copper(II) imidazolate ternary complexes; X-ray crystal structures; Molecular structures; Magnetic properties; Infrared spectra

1. Introduction

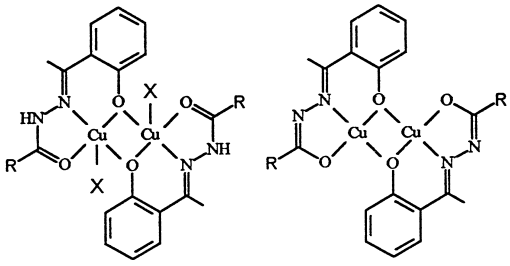
N-salicylideneacylhydrazines (**1**) (hereafter abbreviated as H_2L) and their corresponding copper(II) complexes have been reported to show a wide spectrum of biological activities [1–7]. For better understanding of their mode of action within biological systems, the coordination chemistry of this class of acylhydrazones as well as the molecular structure of a number of copper(II) complexes have been extensively studied [8–12]. *N*-salicylideneacylhydrazines can act as either mononegative or dinegative ONO tridentate ligands, forming with copper(II) salts either monomeric (**2**) or dimeric copper(II) complexes (**3** and **4**). The tendency for dimerization via phenoxy oxygens is to achieve the most favourable coordination number four or five of the central copper(II).

* Corresponding author. Tel.: +203-5423323; fax: +203-4911794; e-mail: iskandar@alexcomm.net

0277-5387/00/$ - see front matter ©2000 Elsevier Science Ltd All rights reserved.
PII S0277-5387(00)00366-1

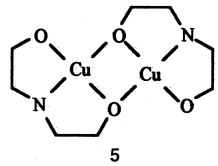


1 2

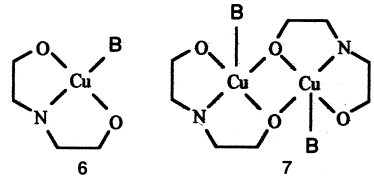


3 4

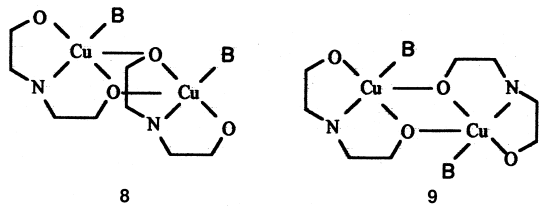
A large number of dimeric copper(II) complexes with other ONO tridentate Schiff base dianions have also been prepared and their magnetic properties have been investigated [11–20]. The reactivity of dimeric copper(II) complexes of ONO tridentate Schiff base anions (**5**) towards monodentate neutral Lewis bases continues to attract considerable attention [21–26]. The reactions of dimeric copper(II) complexes of type **5** with different Lewis bases, B, have been studied and they were found to give either monomeric square planar monobase adducts (**6**), with the rupture of Cu–O bridges, or five-coordinate (usually square pyramidal) dimeric bis adducts. Two types of dimeric adduct (**7** and **8**) have been characterized. In **7** the Lewis base donor atom occupies the apical site and is perpendicular to the square planar $CuNO_3$ plane, while in **8** the Lewis base donor atom is in the basal plane and the fifth coordination site is occupied by the two bridged oxygens. Furthermore, the two Lewis bases may attain either *cis* (**8**) or *trans* configuration (**9**) depending on the nature of the donor atom of B as well as the steric requirements of the ONO tridentate ligands [26].



5



6 7



8 9

As ternary adduct formation may play an important role in the in vivo activity of *N*-salicylidenearoylhydrazine copper(II) complexes through binding with biological ligands containing an imidazole ring, this paper is devoted to study of the reactivity of some copper(II) complexes of the types $[Cu(HL)X\cdot H_2O]$ (**2**), $[\{Cu(HL)X\}_2]$ (**3**) and $[\{Cu(L)\}_2]$ (**4**) towards imidazole (Him), aiming to prepare a series of new imidazole and imidazolate copper(II) ternary complexes. The spectral and magnetic properties of the isolated ternary complexes have been examined and the X-ray crystal and molecular structures of $[Cu(Sp\text{-}ClBzh)Him]\cdot H_2O$ and $[\{Cu(Sp\text{-}CH_3Bzh)Him\}_2]\cdot H_2O$ have been determined. This may enable better understanding of the mode of interaction between these *N*-salicylideneacylhydrazine copper(II) complexes with biological ligands in vivo. Hereafter, *N*-salicylidenebenzoylhydrazine and the corresponding *p*-methyl-, *p*-methoxy- and *p*-chlorobenzoylhydrazines are abbreviated respectively as H_2SBzh, $H_2Sp\text{-}CH_3Bzh$, $H_2Sp\text{-}CH_3OBzh$ and $H_2Sp\text{-}ClBzh$.

2. Results and discussion

2.1. Synthesis

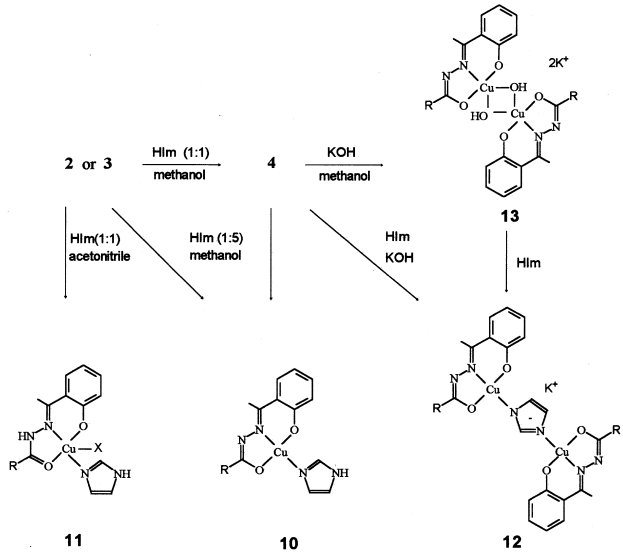
In methanol, the reaction of hydrated mononuclear copper(II) complexes $[Cu(HL)X\cdot H_2O]$ (**2**, $R=C_6H_5$, *p*-$CH_3C_6H_4$, *p*-$CH_3OC_6H_4$ and *p*-ClC_6H_4; $X=Cl$) and $[Cu(HSBzh)NO_3]\cdot H_2O$ as well as the anhydrous binuclear complexes $[\{Cu(HL)X\}_2]$ (**3**, $R=C_6H_5$ and *p*-$CH_3C_6H_4$; $X=Cl$) and $[\{Cu(HL)\}_2]\cdot 2NO_3$ [27] with 1 equiv. of imidazole resulted in the deprotonation of the hydrazone residue and afforded the neutral dimeric copper(II) complexes $[\{Cu(L)\}_2]$ (**4**, $R=C_6H_5$, *p*-$CH_3C_6H_4$, *p*-$CH_3OC_6H_4$ and *p*-ClC_6H_4). However, in the presence of a large excess of imidazole (4.0–5.0 equiv.) the reaction proceeded with the formation of the corresponding ternary imidazole adducts $[Cu(L)Him]$ (**10**, $R=C_6H_5$, *p*-$CH_3C_6H_4$, *p*-$CH_3OC_6H_4$ and *p*-ClC_6H_4). These adducts were also obtained from the reaction of the neutral dimeric copper(II) complexes $[\{Cu(L)\}_2]$ (**4**, $R=C_6H_5$, *p*-$CH_3C_6H_4$, *p*-$CH_3OC_6H_4$ and *p*-ClC_6H_4) with large excess of imidazole in methanol. In principle the imidazole adducts $[Cu(L)Him]$ may be either monomeric square planar (type **6**) or may dimerize to form the dimeric bis adduct of the type **7**, **8** or **9**.

In acetonitrile, the reaction of the monomeric copper(II) complexes $[Cu(HL)Cl\cdot H_2O]$ (**2**, $R=C_6H_5$, *p*-$CH_3C_6H_4$, *p*-$CH_3OC_6H_4$ and *p*-ClC_6H_4) with 1 equiv. imidazole or dimeric $[\{Cu(HL)Cl\}_2]$ (**3**, $R=C_6H_5$, *p*-$CH_3C_6H_4$) complexes with 2 equiv. of imidazole gave the chloro imidazole complexes of the stoichiometric composition $[Cu(HL)(Cl)Him]$ (**11**, $R=C_6H_5$, *p*-$CH_3C_6H_4$, *p*-$CH_3OC_6H_4$ and *p*-ClC_6H_4). Similarly, the reaction of imidazole with either $[Cu(HSBzh)NO_3]\cdot H_2O$ or $[\{Cu(HSBzh)\}_2]\cdot 2NO_3$, in acetonitrile, also gave the corresponding copper(II) nitrate adducts $[Cu(HSBzh)NO_3\cdot Him)]$ (**11**, $R=C_6H_5$;

Table 1
Elemental analyses of imidazole and imidazolate copper(II) complexes derived from *N*-salicylidenearoylhydrazine

Compound	Found (calc.) (%)				μ_{eff}/μ_B (298 K)
	Cu	C	H	N	
1-Imidazole complexes					
(i) [Cu(L)Him]					
[Cu(SBzh)Him]	17.20 (17.18)	54.92 (55.21)	3.91 (3.82)	16.15 (15.15)	1.79
[Cu(Sp-CH_3Bzh)Him]$_2\cdot H_2O$	16.60 (16.17)	54.94 (40.05)	4.32 (4.36)	14.28 (14.26)	1.88
[Cu(Sp-CH_3Obzh)Him]	16.19 (15.89)	53.56 (54.06)	4.05 (4.03)	14.22 (14.01)	1.86
[Cu(Sp-ClBzh)Him]$\cdot H_2O$	15.75 (15.05)	48.63 (48.35)	3.46 (3.58)	13.46 (13.27)	1.80
(ii) [Cu(HL)X·Him]					
[Cu(HSBzh)Cl·Him]	15.79 (15.64)	50.14 (50.25)	3.66 (3.72)	13.51 (13.79)	1.87
[Cu(HSp-CH_3Bzh)Cl·Him]	15.30 (15.12)	51.05 (51.43)	4.01 (4.08)	13.33 (13.33)	1.89
[Cu(HSp-CH_3OBzh)Cl·Him]	14.50 (14.56)	49.48 (49.55)	3.87 (3.93)	12.76 (12.84)	1.88
[Cu(HSp-ClBzh)Cl·Him]	14.50 (14.42)	46.24 (46.32)	3.04 (3.20)	12.52 (12.71)	1.89
[Cu(HSBzh)NO_3·Him]	14.62 (14.68)	47.18 (47.17)	3.26 (3.49)	16.13 (16.18)	1.88
[Cu(HSBzh)SCN·Him]	14.38 (14.81)	50.00 (50.40)	3.40 (3.52)	16.28 (16.33)	1.98
[Cu(HSp-CH_3OBzh)SCN·Him]	13.52 (13.84)	49.57 (49.72)	3.65 (3.73)	14.66 (15.26)	1.87
2-Imidazolate complexes					
K[{Cu(HL)}$_2$Im]					
K[{Cu(SBzh)}$_2$Im]	17.54 (17.91)	53.50 (52.46)	3.90 (3.27)	10.28 (11.48)	1.85
K[{Cu(Sp-CH_3Bzh)}$_2$Im]$\cdot 2H_2O$	16.20 (16.42)	51.69 (51.22)	4.08 (4.04)	10.58 (10.86)	1.82
K[{Cu(Sp-CH_3OBzh)}$_2$Im]$\cdot 2H_2O$	15.60 (15.77)	48.61 (49.19)	3.65 (3.88)	10.16 (10.43)	1.84

X = NO_3). The thiocyanate imidazole complexes [Cu(HL)-SCN·Him] (**11**, R = C_6H_5 and *p*-$CH_3OC_6H_4$; X = SCN) were similarly prepared.



In the presence of KOH, the reaction of the dimeric copper(II) complexes [{Cu(L)}$_2$] (**4**, R = C_6H_5, *p*-$CH_3C_6H_4$, *p*-$CH_3OC_6H_4$ and *p*-ClC_6H_4) with imidazole using 1:1 molar ratio in methanol proceeded by the deprotonation of imidazole, giving finally the corresponding imidazolate bridged copper(II) complexes K[LCu·Im·CuL] (**12**, R = C_6H_5, *p*-$CH_3C_6H_4$ and *p*-$CH_3OC_6H_4$). These complexes can also be obtained by the reaction of the di-μ-hydroxo copper(II) complexes K[{Cu(L)OH}$_2$]$\cdot n H_2O$ (**13**, R = C_6H_5, *p*-$CH_3C_6H_4$ and *p*-$CH_3OC_6H_4$) [27] with imidazole using 1:1 molar ratio in methanol or by the reaction of the hydroxo derivative (**13**) with the copper(II) imidazole adduct [Cu(L)Him] (**10**, R = C_6H_5, *p*-$CH_3C_6H_4$, *p*-$CH_3OC_6H_4$ or *p*-ClC_6H_4). In this reaction the coordinated hydroxide can act as a proton acceptor, and can affect the deprotonation of the imidazole ring, and the two copper(II) centres are bridged by the imidazolate anion. The analytical data for all the isolated imidazole and imidazolate copper(II) complexes are given in Table 1.

2.2. Infrared spectra

The IR spectra of the ternary imidazole complexes [Cu(L)Him] (**10**, R = C_6H_5, *p*-$CH_3C_6H_4$, *p*-$OCH_3C_6H_4$ and *p*-ClC_6H_4), Table 2, show an intense band in the 3114–3130 cm^{-1} region due to ν(N–H) of the coordinated imidazole besides a series of bands at ca. 3050, 2995, 2930 and 2850 cm^{-1} which can be attributed to ν(C–H) as well as ν(C–H) + ν(N–H) coupled vibrations. The spectra lack absorptions due to both amide I (ν(C=O)) and amide II (δ(N–H) + ν(C–N)) bands, confirming the deprotonation of the enolimide hydrazone tautomer. The spectra, however, show strong absorption at ca. 1625 cm^{-1} due to the ν(–N=C–C=N–) of the deprotonated hydrazone ligand. The spectra also show the amide III band (ν(C–O)) at ca. 1340 cm^{-1}. The spectra of the chloro, nitrato and thiocyanato imidazole complexes [Cu(HL)X·Him] (**11**, R = C_6H_5, *p*-$CH_3C_6H_4$, *p*-$CH_3OC_6H_4$ and *p*-ClC_6H_4; X = Cl, NO_3 and SC*N*), Table 2, show the imidazole ν(*N*–H) as well as the aroylhydrazone ν(*N*–H) at ca. 3200 and 3100 cm^{-1}, respectively. The ν(C–H) patterns in the spectra of these complexes are more or less similar to that recorded for [Cu(L)Him] (**10**). The spectra also show the coordinated ν(C=O), amide I, band within the range 1630–1615 cm^{-1} while the ν(N=C) + ν(C=C) band appears at 1615–1590 cm^{-1}. In addition, the spectra are char-

Table 2
Significant bands in the IR spectra of imidazole and imidazolate copper(II) complexes

Complex	ν(N–H)	ν(N–H) + ν(C–H)	ν(C=O) Amide I	ν(C=N) + ν(C=C)	Amide II	δ(N–H) Imidazole	Amide III
1-imidazole complexes							
(i) [Cu(L)Him]·nH$_2$O							
[Cu(SBzh)Him]	3123 m	3030 m, 2926 m, 2824 m		1615 s, 1608 s		1445 m	1330 m, 1294 m
[Cu(Sp-CH$_3$Bzh)Him]$_2$·H$_2$O	3130 m	3049 m, 2922m, 2894 m		1618 s, 1607 s		1439 m	1330 m, 1295 m
[Cu(Sp-CH$_3$Obzh)Him]	3114 m	3050 m, 2993 m, 2929 m, 2858 m,		1610 s, 1605 s		1453 m	1330 m, 1300 m
[Cu(Sp-ClBzh)Him]·H$_2$O	3129 m	3056 m, 2961 m, 2929 m, 2847 m		1607 s, 1585 s		1445 m	1325 m, 1308 m
(ii) [Cu(HL)Him·X]							
[Cu(HSBzh)Cl·Him]	3125 s, 3185 sh	3046 m, 2947 m, 2831 m	1616 s	1607 s	1553 s	1435 m	1350 m, 1307 m
[Cu(HSp-CH$_3$Bzh)Cl·Him]	3112 s, 3190 sh	3050 m, 2948 m, 2838 s	1620 s	1608 s	1544 s	1440 m	1330 m, 1306 s
[Cu(HSp-CH$_3$OBzh)Cl·Him]	3129 s, 3195 sh	3050 m, 2944 m, 2872 m, 2837 s	1628 s	1607 s	1544 s	1435 m	1350 m, 1327 s
[Cu(HSp-ClBzh)Cl·Him]	3116 s, 3185 sh	3049 m, 2945 m, 2819 m	1619 s	1607 s	1543 s	1435 m	1353 m, 1324 m
[Cu(HSBzh)(NO$_3$)Him]	3152 s, 3190 sh	3055 m, 2952 m, 2883 m	1622 s	1602 s	1547 s		1339 s
[Cu(HSBzh)(SCN)Him]	3144 m	3058 m, 2920 m, 2852 m	1628 s	1608 s	1550 s	1506 s	1362 s
[Cu(HSp-OCH$_3$Bzh)(SCN)Him]	3120 m	3060 m, 3005 m, 2923 m, 2834 m	1622 s	1602 s	1542 s	1502 s	1339 s
2-Imidazolate complexes							
K[{Cu(SBzh)}$_2$Im]				1609 s			1382 s, 1334 s
K[{Cu(Sp-CH$_3$Bzh)}$_2$Im]·2H$_2$O				1608 s			1383 s, 1333 s
K[{Cu(Sp-OCH$_3$Bzh)}$_2$Im]·2H$_2$O				1611 s			1385 s, 1329 s

acterized by a very intense band at 1550 cm^{-1} which can be attributed to δ(*N*–H) of the aroylhydrazone ligand. The amide III ν(C–O) band of [Cu(HL)X·Him] (**11**) complexes appear at higher frequencies (1307–1350 cm^{-1}) compared to those recorded for the [Cu(L)Him] (**10**) complexes. This may be due to the higher delocalization in the aroylhydrazone residue of the [Cu(L)Him)] complexes which in its turn decreases the C–N double bond character relative to that in [Cu(HL)X·Him].

The spectra of the nitrate complex [Cu(HSBzh)-NO$_3$·Him] (**11**, R = C$_6$H$_5$) show a split band at 1500 cm^{-1} due to ν(N=O) besides two bands at 1350 and 1065 cm^{-1} due to ν_{asy}(NO$_2$) and ν_{sy}(NO$_2$), respectively. The frequency difference $\Delta\nu = [\nu(N{=}O) - \nu_{asy}(NO_2)] = 150$ cm^{-1} is in agreement with the unidentate coordination mode of the nitrate anion [28–30]. The thiocyanate ν(NCS) in the spectra of [Cu(HL)SCN·Him] (**11**, R = C$_6$H$_5$ and *p*-CH$_3$OC$_6$H$_4$; X = SCN) appear as one intense band at ca. 2075 cm^{-1} indicating a unidentate mode of coordination, most probably through the nitrogen atom [29]. The spectra of the bridged imidazolate copper(II) complexes K[CuL·Im·CuL] (**12**, R = C$_6$H$_5$, *p*-CH$_3$C$_6$H$_4$ and *p*-CH$_3$OC$_6$H$_4$) lack absorption due to both aroylhydrazone and imidazole ν(N–H).

2.3. X-ray crystal and molecular structure of [Cu(Sp-ClBzh)-(Him)]·H$_2$O and [{Cu(Sp-CH$_3$Bzh)Him}$_2$]·H$_2$O

From all the prepared imidazole and imidazolate adducts, only the hydrated imidazole adducts [Cu(Sp-ClBzh)-Him]·H$_2$O and [{Cu(Sp-CH$_3$Bzh)Him}$_2$]·H$_2$O gave crystals suitable for X-ray diffraction studies. The crystal data and structure refinement parameters for these adducts are given in Table 3. The structure of [Cu(Sp-ClBzh)-Him]·H$_2$O together with the atom numbering scheme are shown in Fig. 1, and some selected bond distances and bond angles are given in Table 4. In this complex, the dinegative tridentate *N*-salicylidene-*p*-chlorobenzoylhydrazine is coordinated to Cu(II) through the deprotonated phenolic oxygen O(1), azomethine nitrogen N(1) and deprotonated enolimide oxygen O(2) forming respectively five- and six-membered chelate rings. The fourth coordination site is occupied by the imidazole nitrogen atom N(3). The copper(II) is in a distorted square planar arrangement and lies approximately in the ligand plane and shows a slight deviation of 0.099 Å from the best fit least-squares plane through the four donor atoms and Cu(II) atoms. The distortion from regular square planar is seen in the departure from 180° of the angles O(1)–Cu–O(2) (171.17°) and N(1)–Cu–N(3) (172.05°) and from 90° of the bite angles N(1)–Cu–O(2) (81.11°), N(1)–Cu–O(1) (93.57°), O(1)–Cu–N(3) (92.92°) and O(2)–Cu–N(3) (92.99°). This distortion may be imposed by the rigidity of the formed two chelate rings. The bond distances and angles recorded for the coordinated Schiff base in [Cu(Sp-ClBzh)Him]·H$_2$O as well as those involving the Cu(II) atom, Table 4, are more or less similar to those

Table 3
Crystal data and structure refinement for [Cu(Sp-ClBzh)(Him)]·H_2O and [{Cu(Sp-CH_3Bzh)(Him)}$_2$]·H_2O

	[Cu(Sp-ClBzh)(Him)]·H_2O	[Cu(Sp-CH_3Bzh)(Him)]·1/2H_2O
Empirical formula	$C_{17}H_{15}ClCuN_4O_3$	$C_{18}H_{17}CuN_4O_{2.5}$
Formula weight	422.35	392.93
Temperature (K)	300(2)	302(2)
Wavelength (Å)	0.71093	0.71093
Crystal system	monoclinic	monoclinic
Space group	$P2/c$	$C2/c$
Unit cell dimensions		
a (Å)	12.975(2)	25.861(9)
b (Å)	11.853(2)	10.057(10)
c (Å)	12.951(2)	17.977(6)
α (°)	90	90
β (°)	116.820(10)	132.26(2)
γ (°)	90	90
Volume (Å^3)	1777.5(5)	3460(2)
Z	4	8
Density (calculated) (Mg m^{-3})	1.578	1.508
Absorption coefficient (mm^{-1})	1.41	1.28
F(000)	860	1616
Crystal size (mm)	1.250×0.225×0.175	1.0×0.2×0.175
θ Range for data collection (°)	1.72–25.98	2.13–25.49
Index ranges	$-15 \le h \le 15$, $-14 \le k \le 0$, $-15 \le l \le 15$	$-31 \le h \le 31$, $-12 \le k \le 0$, $-21 \le l \le 21$
Reflections collected	6942	6426
Independent reflections	3479 (R_{int} = 0.0204)	3218 (R_{int} = 0.0503)
Absorption correction	empirical ψ-scan	semi-empirical from ψ-scans
Max. and min. transmission	0.8117 and 0.6993	0.8341 and 0.7339
Refinement method	full-matrix least-squares on F^2	full-matrix least-squares on F^2
Data/restraints/parameters	3479/0/280	3217/0/235
Goodness-of-fit on F^2	0.924	1.067
Final R indices ($I > 2\sigma(I)$)	R_1 = 0.0365, wR_2 = 0.0918	R_1 = 0.0377, wR_2 = 0.0911
R indices (all data)	R_1 = 0.0574, wR_2 = 0.1104	R_1 = 0.0493, wR_2 = 0.0978
Largest difference peak and hole (e Å^{-3})	0.413 and −0.727	0.831 and −0.693

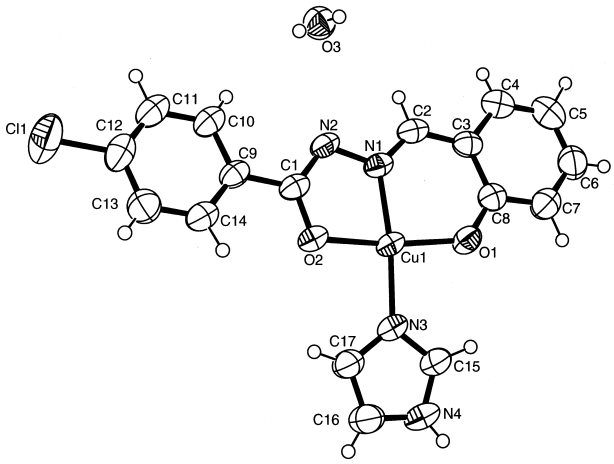


Fig. 1. X-ray structure of [Cu(Sp-ClBzh)Him]·H_2O.

reported for other *N*-salicylidenacylhydrazine copper(II) complexes [8–12]. The imidazole is planar and lies at an angle of 0.78° to the plane of best fit through the copper coordination sphere. The bond distance between the imidazole nitrogen N(3) and the copper(II) atom (1.953(2) Å) is comparable with other four coordinated copper(II) complexes containing imidazole molecule [22,23,31–34].

The crystal lattice is stabilized through the intermolecular hydrogen bonds between the two water hydrogens and the uncoordinated hydrazidic nitrogen of one molecule and the phenolic oxygen of the neighbouring molecule. The water oxygen, on the other hand, acts as a hydrogen bond acceptor forming a hydrogen bond with the N–H imidazole hydrogen from a third molecule as shown in Fig. 2. The intermolecular hydrogen bond distances and angles are listed in Table 5.

Different from [Cu(Sp-ClBzh)Him]·H_2O which exists in monomeric units where copper(II) is four coordinate and is situated in a square planar environment, the structure of [Cu(Sp-CH_3Bzh)Him]·1/2H_2O consists of dimeric units, Fig. 3, in which each Cu(II) atom is five-coordinated through the deprotonated phenolic oxygen O(1), azomethine nitrogen N(1) and deprotonated enolimide oxygen O(2) of the dinegative tridentate ligand. The phenolic oxygen O(1) of the salicylidene part of the tridentate ligand is bound in the basal plane of the Cu(II) coordination pyramid and acts as bridging atom forming the apex of an adjacent second pyramid. Accordingly, dimerization is achieved by sharing of the phenolic oxygen O(1) atom from each ligand through two copper atoms with intramolecular Cu–O(1) distance of 1.911 Å and intermolecular Cu–O1′ distance of 2.577 Å. The Cu–Cu separation is 3.257 Å and each copper atom lies approx-

Table 4
Selected bond lengths (Å) and angles (°) for [Cu(Sp-ClBzh)(Him)]·H_2O

Cu(II) polyhedron			
O(1)–Cu(1)	1.903(2)	O(1)–Cu(1)–N(1)	93.57(9)
O(2)–Cu(1)	1.934(2)	O(1)–Cu(1)–O(2)	171.17(8)
N(1)–Cu(1)	1.920(2)	N(1)–Cu(1)–O(2)	81.11(9)
N(3)–Cu(1)	1.953(2)	O(1)–Cu(1)–N(3)	92.92(9)
		N(1)–Cu(1)–N(3)	172.05(10)
		O(2)–Cu(1)–N(3)	92.99(9)
		C(2)–N(1)–Cu(1)	126.8(2)
		N(2)–N(1)–Cu(1)	114.7(2)
		C(8)–O(1)–Cu(1)	126.7(2)
		C(1)–O(2)–Cu(1)	110.9(2)
		C(15)–N(3)–Cu(1)	127.7(2)
		C(17)–N(3)–Cu(1)	127.0(2)
Tridentate ligand			
C(1)–O(2)	1.293(3)	O(2)–C(1)–N(2)	123.8(3)
C(1)–N(2)	1.311(4)	O(2)–C(1)–C(9)	117.9(3)
C(1)–C(9)	1.480(4)	N(2)–C(1)–C(9)	118.3(2)
C(2)–N(1)	1.284(4)	N(1)–C(2)–C(3)	125.0(3)
C(2)–C(3)	1.425(4)	C(4)–C(3)–C(2)	118.3(3)
C(3)–C(8)	1.425(4)	C(8)–C(3)–C(2)	123.4(3)
C(8)–O(1)	1.321(3)	O(1)–C(8)–C(7)	118.7(3)
N(1)–N(2)	1.395(3)	O(1)–C(8)–C(3)	123.8(3)
		C(1)–N(2)–N(1)	109.4(2)
		C(2)–N(1)–N(2)	118.5(2)
Imidazole ring			
C(15)–N(3)	1.317(3)	C(15)–N(3)–C(17)	105.4(3)
C(15)–N(4)	1.316(4)	C(15)–N(4)–C(16)	107.9(3)
C(16)–N(4)	1.346(5)	C(15)–N(4)–H(4N)	124.0(2)
C(17)–N(3)	1.370(4)	C(16)–N(4)–H(4N)	128.0(2)
C(16)–C(17)	1.341(4)	C(16)–C(17)–N(3)	108.8(3)
N(4)–H(4N)	0.87(4)	C(17)–C(16)–N(4)	106.8(3)
		N(3)–C(15)–N(4)	111.1(3)

imately in the ligand plane showing a slight deviation of 0.153 Å. The basal plane of the pyramid is completed with the N(3) atom from the imidazole molecule. The coordination polyhedron around the copper(II) is better described as a (4+1) distorted square pyramidal. This is in agreement with the value 0.15 of Addison et al.'s parameter τ [35] calculated from $\tau=(\beta-\alpha)/60$, where α is O(1)–Cu–O(2) (173.58°) and β is N(1)–Cu–N(3) (164.16°). The molecule is characterized by a two-fold axis perpendicular to the CuO1Cu′O1′ plane resulting in centrosymmetric dimers. In this dimeric structure, the imidazole molecules are in *trans* positions with respect to each other and perpendicular to the Cu_2O_2 plane with angles O(1)–Cu–N(3) and O(2)–Cu–N(3) of 91.78 and 94.18° respectively. The presence of two imidazole rings in a *trans* position may be attributed to the steric effect imposed by the crystal packing formed as a result of hydrogen bonds. Similar behaviour was reported for the urea adduct of *N*-salicylidene α-amino acidato copper(II) complex. The bond lengths and angles between Cu(II) and the donor atoms, Table 6, do not differ significantly from the values reported for other similar complexes [8–12].

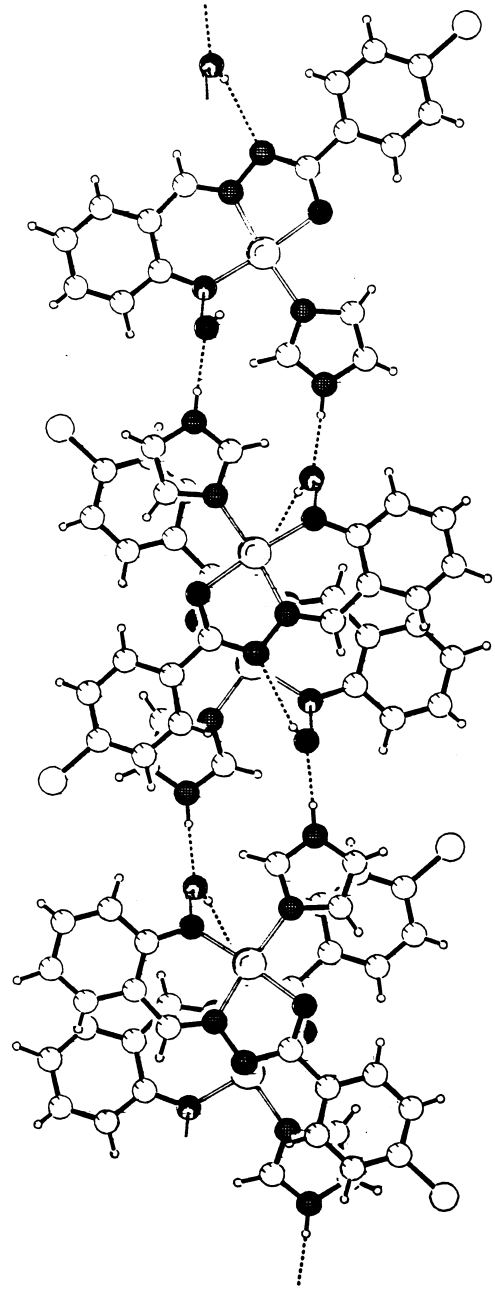


Fig. 2. Hydrogen bonds in [Cu(Sp-ClBzh)Him]·H_2O.

Table 5
Intermolecular hydrogen bond distances and angles in monomeric Cu[(Sp-ClC_6H_4Bzh)(Him)]·H_2O

X–H···Y	Symmetry transformation	X···Y (Å)	X–H (Å)	H···Y (Å)	X–H–Y (°)
O(3)–H···O(1)	$2-x, +y, 0.5-z$	2.779	0.81	1.988	175.9
O(3)–H···N(2)	$+x, y, +z$	2.889	0.56	2.355	176.6
N(4)–H···O(3)	$1+x, -y, 0.5+z$	2.704	0.87	1.842	177.4

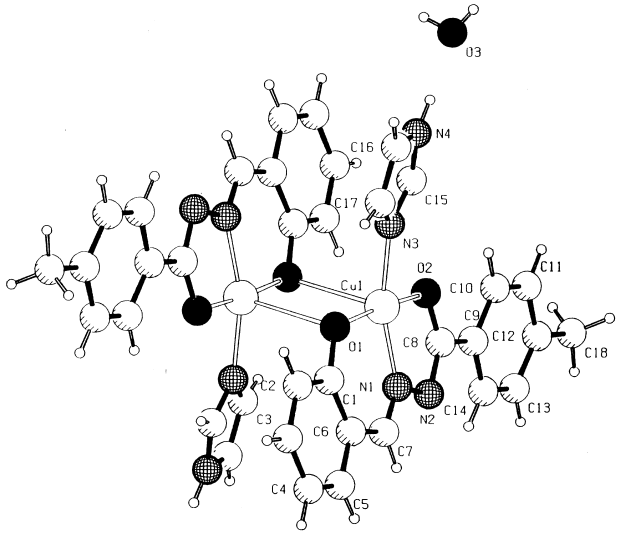


Fig. 3. X-ray structure of $[\{Cu(Sp\text{-}CH_3Bzh)Him\}_2]\cdot H_2O$.

Table 6
Selected bond lengths (Å) and angles (°) for $[\{Cu(Sp\text{-}CH_3Bzh)(Him)\}_2]\cdot H_2O$

Cu(II) polyhedron			
O(1)–Cu(1)	1.911(2)	O(1)–Cu(1)–N(1)	93.84(7)
O(2)–Cu(1)	1.944(2)	O(1)–Cu(1)–O(2)	173.58(7)
N(1)–Cu(1)	1.926(2)	N(1)–Cu(1)–O(2)	81.01(7)
N(3)–Cu(1)	1.973(2)	O(1)–Cu(1)–N(3)	91.78(7)
		N(1)–Cu(1)–N(3)	164.16(8)
		O(2)–Cu(1)–N(3)	94.18(7)
		C(1)–O(1)–Cu(1)	126.10(14)
		C(8)–O(2)–Cu(1)	110.69(14)
		C(7)–N(1)–Cu(1)	126.7(2)
		N(2)–N(1)–Cu(1)	114.87(14)
		C(15)–N(3)–Cu(1)	126.6(2)
		C(17)–N(3)–Cu(1)	127.5(2)
Tridentate ligand			
C(1)–O(1)	1.321(3)	O(1)–C(1)–C(2)	118.0(2)
C(1)–C(6)	1.420(3)	O(1)–C(1)–C(6)	124.4(2)
C(6)–C(7)	1.437(3)	C(5)–C(6)–C(7)	117.7(2)
C(7)–N(1)	1.287(3)	C(1)–C(6)–C(7)	123.5(2)
C(8)–O(2)	1.283(3)	N(1)–C(7)–C(6)	124.7(2)
C(8)–N(2)	1.323(3)	O(2)–C(8)–N(2)	124.1(2)
N(1)–N(2)	1.388(3)	O(2)–C(8)–C(9)	118.3(2)
		N(2)–C(8)–C(9)	117.5(2)
		C(14)–C(9)–C(8)	122.2(2)
		C(10)–C(9)–C(8)	119.8(2)
		C(7)–N(1)–N(2)	118.3(2)
		C(8)–N(2)–N(1)	109.2(2)
Imidazole ring			
C(15)–N(3)	1.310(3)	N(3)–C(17)–H(17)	125.36(14)
C(15)–N(4)	1.326(3)	C(15)–N(3)–C(17)	105.5(2)
C(16)–N(4)	1.360(4)	C(15)–N(4)–C(16)	107.5(2)
C(17)–N(3)	1.373(4)	C(16)–C(17)–N(3)	109.3(2)
C(16)–C(17)	1.340(4)	C(17)–C(16)–N(4)	106.4(3)
N(4)–H(4N)	0.86(4)	N(3)–C(15)–N(4)	111.3(2)
		N(3)–C(15)–H(15)	124.34(14)
		N(4)–C(15)–H(15)	124.34(14)

The hydrogen bonds, Table 7, mainly determine the crystal packing. The water molecule acts as hydrogen donor towards the two uncoordinated nitrogen atoms N(2) of two different dimers in the unit cell, while the oxygen atom acts as hydrogen acceptor and is linked to two different N(4)–H imidazole hydrogens of two other different dimers in the cell. The whole of the hydrogen bond system leads to an infinite three-dimensional array as shown in Fig. 4.

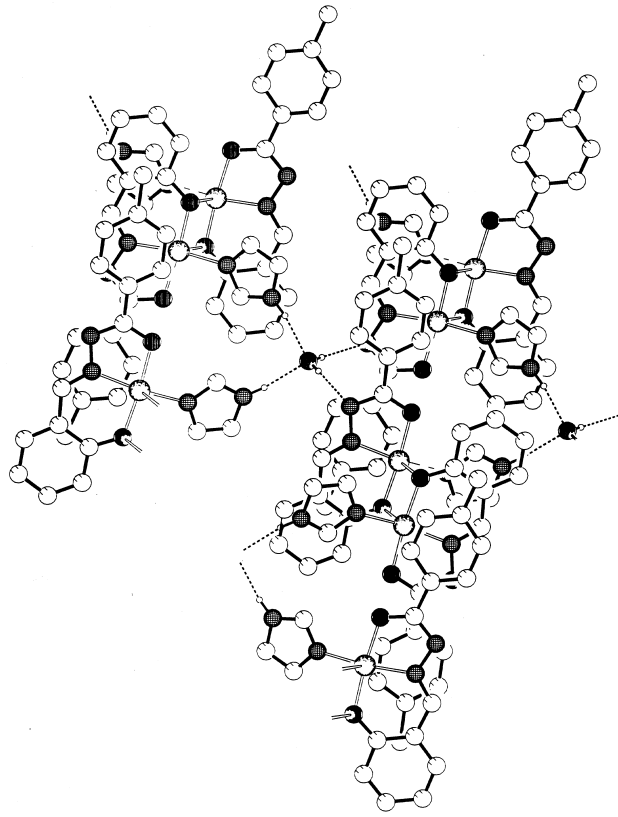


Fig. 4. Hydrogen bonds in $[\{Cu(Sp\text{-}CH_3Bzh)Him\}_2]\cdot H_2O$.

From the previous X-ray structure analyses, it is quite apparent that the reaction of imidazole with the dinuclear copper(II) complexes (**4**) may afford either monomeric ternary adducts as shown in $[Cu(Sp\text{-}ClBzh)Him]\cdot H_2O$, Fig. 1, or dimeric adducts as shown by $[\{Cu(Sp\text{-}CH_3Bzh)Him\}_2]\cdot H_2O$, Fig. 3, depending on the nature of the substituents on the tridentate *N*-salicylidenearoylhydrazine ligand. In such conjugated ligands, the electron-withdrawing substituents as in **4** ($R = p\text{-}ClC_6H_4$) result in a decrease of the negative charge on the phenoxy oxygen and the Cu–O bridges become more susceptible to bond rupture, eventually giving the monomeric square planar adduct $[Cu(SpClBzh)Him]\cdot H_2O$. On the other hand, the presence of electron-donating substituents in **4** ($R = p\text{-}CH_3C_6H_4$) increases the strength of the Cu–O bridges so they can withstand bond rupture, and in this case the reaction proceeds with the formation of a dinuclear ternary adduct.

2.4. Magnetic properties of imidazole and imidazolate ternary complexes

At room temperature, the ternary imidazole copper(II) adducts of the general formula $[Cu(L)Him]\cdot nH_2O$ and

Table 7
Intermolecular hydrogen bond distances and angles dimeric $[\{Cu(Sp\text{-}CH_3Bzh)(Him)\}_2]\cdot H_2O$

X–H···Y	Symmetry transformation	X···Y (Å)	X–H (Å)	H···Y (Å)	X–H–Y (°)
N(4)–H···O(3)	*x*, *y*, *z*	2.786	0.86	1.951	168.5
N(4)–H···O(3)	$1-x$, *y*, $0.5-z$	2.786	0.86	1.951	168.5
O(3)–H···N(2)	$1-x$, $-1+y$, $0.5+z$	2.837	0.76	2.095	176.3
O(3)–H···N(2)	*x*, $-1+y$, *z*	2.837	0.76	2.095	176.3

[Cu(HL)X·Him], Table 1, show normal magnetic moments (1.82–1.88 μ_B), within the range expected for magnetically diluted mononuclear copper(II) complexes. Different from other dimeric copper(II) complexes with dinegative tridentate *N*-salicylidene Schiff bases which show subnormal magnetic moments due to strong antiferromagnetic exchange coupling [18–21], the dimeric imidazole copper(II) complex $[\{Cu(Sp\text{-}CH_3Bzh)Him\}_2]\cdot H_2O$ shows normal magnetic behaviour ($\mu_{eff}=1.88$ μ_B). The variation of molar magnetic susceptibility over the temperature range 4.2–295 K, Fig. 5, reveals no substantial deviation from Curie's behaviour characteristic for magnetically isolated copper(II) centres. A plot of $1/\chi$ versus temperature gave $\theta=-0.80$ K indicating very weak antiferromagnetic intermolecular interaction. This magnetic behaviour can be attributed to the orientation of the di-μ-oxo bridge relative to the CuO_2N_2 plane. As shown in Fig. 3, the Cu–N(3) are approximately perpendicular to the Cu_2O_2 plane with the N(3)–Cu(1)–O(1) bond angle of 91.78°, and the di-μ-oxo bridge is placed in the *xz* plane. Accordingly the magnetic orbitals of the copper ions ($d_{x^2}-d_{y^2}$) which point towards the CuN_2O_2 plane are oriented parallelly with no possible significant overlap. This does not mean that there is no interaction between the two copper atoms. Actually, for this peculiar geometry ferromagnetic and antiferromagnetic contributions compensate each other and the singlet and triplet states arising from this possible interaction are accidentally degenerate [36]. The geometry of this dimer is an example of dimeric adducts of type **9** which differs from the fairly common four-coordinate square planar dimers (type **5**) or five-coordinate square pyramidal bis adducts of the type **7**, where the two oxo bridges are in the *xy* plane and accordingly show strong antiferromagnetic exchange coupling [18–21].

The ternary imidazolate copper(II) complexes K[LCu·Im·CuL] (**12**, R = C_6H_5, *p*-$CH_3C_6H_4$ and *p*-$CH_3OC_6H_4$), also show normal magnetic moments (1.82–1.88 μ_B) at room temperature. However, the variation of molar magnetic susceptibility χ_M measured for the imidazolate complexes (**12**, R = C_6H_5, *p*-$CH_3C_6H_4$ and *p*-$CH_3OC_6H_4$), within the temperature range 4.2–297 K suggests antiferromagnetic exchange coupling. A plot of χ_M versus *T* for K[(CuSBzh)$_2$Im] (**12**, R = C_6H_5), Fig. 6, shows a maximum around ca. 40 K. This behaviour is typical of antiferromagnetic coupled dinuclear imidazolate bridged copper(II) complexes [37–53]. Similar behaviour was also observed for the other imidazolate complexes (**12**, *p*-$CH_3C_6H_4$ and *p*-$CH_3OC_6H_4$). The variable temperature susceptibility data were fitted to the Bleany–Bowers equation [54]:

$$\chi_M=(1-X_p)\frac{2N_L g^2\mu_B^2}{kT}\frac{\exp(2J/kT)}{1+3\exp(2J/kT)}+X_p\frac{2N_L g^2\mu_B^2}{4kT}S(S+1)+2N_\alpha$$

$$\chi_M=(1-X_p)\frac{2N_L g^2\mu_B^2}{k(T-\theta)}\frac{\exp(2J/kT)}{1+3\exp(2J/kT)}+X_p\frac{2N_L g^2\mu_B^2}{4k(T-\theta)}S(S+1)+2N_\alpha$$

where N_α is the temperature independent paramagnetism, X_p is the fraction of monomeric impurity, and θ is a correction term for interdimer interactions [55,56] and the recorded *J*,

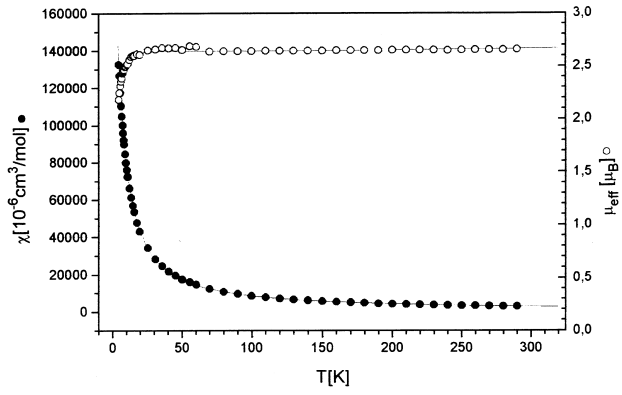


Fig. 5. Magnetic susceptibilities χ (●) and magnetic moments (○) vs. temperature for $[\{Cu(Sp\text{-}CH_3Bzh)Him\}_2]\cdot H_2O$.

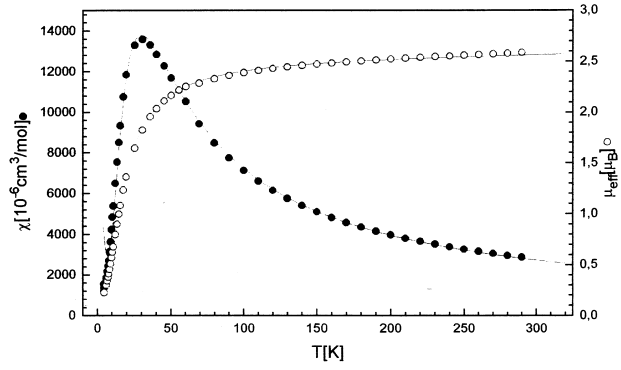


Fig. 6. Magnetic susceptibilities χ (●) and magnetic moments (○) vs. temperature for K[{Cu(SBzh)}$_2$Im]. Solid lines represent the best least-squares fit to Eq. (1), with $J=-17.2$, $g=2.11$, $\theta=-1.26$ and $X_p=2.0$.

g, θ and X_p values are listed in Table 8. The recorded J values are within the range (0 to -88 cm^{-1}) reported for other antiferromagnetic μ-imidazolate copper(II) complexes [39–53]. A comparison of the J values given in Table 8 with the values reported for other imidazolate complexes of known structures [53], reveals that the J values of the prepared imidazolate complexes (**12**, R = C_6H_5, *p*-$CH_3C_6H_4$ and *p*-$CH_3OC_6H_4$) are more or less similar to that reported for $[Cu_2(Gly\text{-}GlyO)_2Im]$, where Gly-GlyO refers to glycylglycinate(-2), suggesting an average value of ca. 158° for the $Cu–N_{im}–N_{im}$ angle. Unfortunately, the absence of a complete X-ray molecular structure for any of the prepared imidazolate complexes, due to the lack of suitable crystals, makes any further discussion of their magnetic properties irrelevant.

Table 8
The best fit magnetic parameters for $K[\{CuL\}_2Im]$ (**12**, R = C_6H_5, *p*-$CH_3C_6H_4$ and *p*-$OCH_3C_6H_4$) complexes

Complex	J (cm^{-1})	g	θ	X_p (%)
$K[\{CuSBzh\}_2Im]$	−17.2	2.11	−1.26	2.0
$K[\{CuSp\text{-}CH_3Bzh\}_2Im]\cdot 2H_2O$	−18.9	2.19	0.19	2.2
$K[\{CuSp\text{-}OCH_3Bzh\}_2Im]\cdot 2H_2O$	−19.7	2.11	0.00	2.6

3. Experimental

3.1. Materials used

Hydrazine hydrate (B.D.H.) (99%), ethylbenzoate (Aldrich), *p*-methyl ethylbenzoate (B.D.H.), *p*-methoxy ethylbenzoate (Aldrich), *p*-chloro ethylbenzoate (B.D.H.), salicylaldehyde (Prolabo) and imidazole were used without further purification. Dry methanol was purified according to the standard method; acetonitrile was dried over P_2O_5 and then distilled, while all the other solvents were used without further purification. Copper(II) nitrate trihydrate was prepared from cupric carbonate (B.D.H.) according to the standard method while copper(II) chloride dihydrate (Merck) and copper acetate monohydrate (B.D.H.) were reagent grade and used as received. The copper(II) complexes $[Cu(HL)X\cdot H_2O]\cdot nH_2O$ (**2**, R = C_6H_5, *p*-$CH_3C_6H_4$, *p*-$OCH_3C_6H_4$ and *p*-ClC_6H_4; X = Cl, NO_3 or SCN), $[\{Cu(HL)X\}_2]$ (**3**, R = C_6H_5; X = Cl), $[\{CuL\}_2]$, (**4**, R = C_6H_5, *p*-$CH_3C_6H_4$, *p*-$OCH_3C_6H_4$ and *p*-ClC_6H_4) and $[\{(CuL\cdot OH)\}_2]\cdot nH_2O$ were prepared as previously described [27].

3.2. Preparation of $[Cu(L)Him]\cdot nH_2O$ (**10**, $R = C_6H_5$, *p*-$CH_3C_6H_4$, *p*-$OCH_3C_6H_4$ and *p*-ClC_6H_4)

To a suspension of the $[\{Cu(L)\}_2]$ complex (**4**, R = C_6H_5, *p*-$CH_3C_6H_4$, *p*-$OCH_3C_6H_4$ or *p*-ClC_6H_4) (0.01 mol) in methanol (30 ml), a sufficient amount of solid imidazole (0.05 mol) was added and the reaction mixture was heated until complete dissolution of the $[\{Cu(L)\}_2]$ then heated under reflux for ca. 1 h during which the imidazole–copper complex $[Cu(L)Him]\cdot nH_2O$ was precipitated. The isolated complex was filtered, washed with diethyl ether and then dried in a vacuum.

3.3. Preparation of $[Cu(HL)Cl\cdot Him]$ (**11**, $R = C_6H_5$, *p*-$CH_3C_6H_4$, *p*-$OCH_3C_6H_4$ and *p*-ClC_6H_4; $X = Cl$)

To a suspension of $[\{Cu(HL)Cl\}_2]\cdot nH_2O$ (**3**, R = C_6H_5, *p*-$CH_3C_6H_4$, *p*-$OCH_3C_6H_4$ and *p*-ClC_6H_4 or *p*-$OCH_3C_6H_4$) (0.01 mol) in acetonitrile (30 ml), an equivalent amount of solid imidazole (0.02 mol) was added. The reaction mixture was stirred at room temperature for ca. 2 h during which the green $[Cu(HL)Cl\cdot Him]$ was formed. The formed complex was filtered, washed with warm acetonitrile then dried in a vacuum.

3.4. Preparation of $[Cu(HSBzh)NO_3\cdot Him]$ (**11**, $R = C_6H_5$; $X = NO_3$)

A solution of $[Cu(HSBzh)NO_3]\cdot H_2O$ [27] (0.01 mol) in acetonitrile (70 cm^3) was treated with an equivalent amount of imidazole (0.01 mol) and the reaction mixture was stirred at room temperature for 1 h during which a green precipitate was formed. The isolated product was filtered, washed with methanol and then dried in vacuum.

3.5. Preparation of $[Cu(HL)Him\cdot SCN]$ (**11**, $R = C_6H_5$ and *p*-$OCH_3C_6H_4$; $X = SCN$)

These complexes were prepared from $[Cu(HL)SCN]$ [27] using the same procedure described for the corresponding chloro complexes.

3.6. Preparation of $K[\{Cu(L)\}_2Im]$ (**12**, $R = C_6H_5$, *p*-$CH_3C_6H_4$, and *p*-$CH_3OC_6H_4$)

A suspension of $[\{CuL\}_2]$ (**4**, R = C_6H_5, *p*-$CH_3C_6H_4$ or *p*-$OCH_3C_6H_4$) (0.01 mol) in dry methanol (50 ml) was treated with a large excess of KOH (ca. 0.05 mol). The resulting mixture was heated under reflux for about 1 h then filtered. To the clear filtrate an equivalent amount of imidazole (0.01 mol) was added and the reaction mixture was further refluxed for ca. 1 h, then evaporated till dryness. The isolated crude product was recrystallized from an acetonitrile–toluene mixture.

3.7. Physical measurements

The IR spectra were recorded on a Perkin-Elmer 1430 Data system spectrophotometer and/or Perkin-Elmer FTIR spectrometer (PARAGON 100 PC). Frequency readings were calibrated with polystyrene film. Solid samples were examined as KBr discs. Magnetic susceptibilities of powdered dried samples were recorded on a Faraday-type magnetometer using a sensitive computer controlled D-200 Cahn RG

microbalance in the temperature range 4.2–298 K. The magnetic field applied was ~1.5 T. Details of the apparatus have been described elsewhere [57–58]. Experimental susceptibility data were corrected for the underlying diamagnetism.

3.8. X-ray crystal and molecular structure

Suitable crystals were sealed in a fine focus glass capillary tube and mounted on a Nonius CAD-4 [59] diffractometer. Intensity data were collected at room temperature in the ω–θ scan mode, using graphite-monochromatized Mo Kα radiation. Lattice constants were determined by full-matrix least-squares refinement. The solution of the crystal structures was carried out using both SHELXS-86 [60] and SHELXL-93 [61] programs. The SHELXL-93 program was also used for structure refinement and for the evaluation of data. The StoeREDU4 [62] and StoeX-RED [63] programs were used for computing data reductions. The graphics plotting of the molecular and crystal structures were carried out using the PLUTON-93 [64] program as well as the ORTEP [65] method. The form factors for Cu(0) were taken from the international tables [66] and those for the other atoms are included as saved values in used programs.

Supplementary data

Atomic coordinates, equivalent isotropic displacement parameters, hydrogen coordinates, isotropic displacement parameters, anisotropic displacement parameters and complete list of bond distances and bond angles of [Cu(Sp-ClBzh)(Him)·H_2O and [{Cu(Sp-CH_3Bzh)Him}$_2$]·H_2O have been deposited with the Cambridge Crystallographic Data Center as supplementary publication no. CCDC 137464 and 137465, respectively.

Acknowledgement

Thanks are due to BMBF/Forschungszentrum, Juelich, for supporting this bilateral project.

References

[1] H.A. Offe, W. Siefken, G. Domagk, Z. Naturforsch., Teil B 7 (1952) 449.
[2] J.R. Dimmock, G.B. Baker, W.G. Taylor, Can. J. Pharm. Sci. 7 (1972) 100.
[3] P. Ponka, J. Borova, J. Neuwirt, O. Fuchs, E. Necas, Biochim. Biophys. Acta 586 (1979) 278.
[4] C. Hershco, S. Avramovici-Grisaru, G. Link, L. Gelfand, S. Sarel, J. Lab. Clin. Med. 98 (1981) 99.
[5] D.K. Johnson, T.B. Murphy, N.J. Rose, W.H. Goodwin, L. Pickart, Inorg. Chim. Acta 67 (1982) 159.
[6] D.K. Johnson, M.J. Pippard, T.B. Murphy, N.J. Rose, J. Pharmacol. Exp. Ther. 221 (1982) 399.
[7] L. Pickart, W.H. Goodwin, W. Burgua, T.B. Murphy, D.K. Johnson, Biochem. Pharmacol. 32 (1983) 3868.
[8] A.A. Aruffo, T.B. Murphy, D.K. Johnson, N.J. Rose, V. Schomaker, Inorg. Chim. Acta 67 (1982) L25.
[9] A.A. Aruffo, T.B. Murphy, D.K. Johnson, N.J. Rose, V. Schomaker, Acta Crystallogr., Sect. C 40 (1984) 1169.
[10] E.W. Ainscough, A.M. Brodie, J.D. Ranford, J.M. Waters, Inorg. Chim. Acta 236 (1995) 83.
[11] S.C. Chan, L.L. Koh, P.-H. Leung, J.D. Ranford, K.Y. Sim, Inorg. Chim. Acta 236 (1995) 101.
[12] E.W. Ainscough, A.M. Brodie, A.J. Dobbs, J.D. Ranford, J.M. Waters, Inorg. Chim. Acta 267 (1998) 27.
[13] M.F. Iskander, A.M. El Aggan, L.S. Refaat, L. El Sayed, Inorg. Chim. Acta 14 (1975) 167.
[14] M.F. Iskander, L. El Sayed, A.F.M. Hefny, S.E. Zayan, J. Inorg. Nucl. Chem. 38 (1976) 2209.
[15] M.S. Palacios, J.M. Dance, Polyhedron 7 (1998) 543.
[16] J.M. Dance, M.T. Do, P. Gambardella, R.H. De, A. Santos, E. Medina, F.G. Manrique, M.S. Palacios, Inorg. Chim. Acta 162 (1989) 239.
[17] W. Haase, K. Grieser, M.F. Iskander, Y. Galyametdinov, Mol. Mater. 3 (1993) 115.
[18] M. Kato, H.B. Jonessen, J.C. Fanning, Chem. Rev. (1964) 99.
[19] E. Sinn, C.M. Harris, Coord. Chem. Rev. 4 (1969) 391.
[20] M. Melnik, Coord. Chem. Rev. 42 (1982) 259.
[21] M. Kato, Y. Muto, Coord. Chem. Rev. 92 (1988) 45.
[22] J. Sivy, V. Kettman, J. Kratsmar-Smogrovic, O. Svajlenova, C. Frieble, G. Plesch, Z. Anorg. Allg. Chem. 583 (1990) 55.
[23] G. Plesch, C. Friebel, O. Svajlenova, J. Kratsmar-Smogrovic, Polyhedron 10 (1991) 893.
[24] G. Plesch, C. Friebel, O. Svajlenova, J. Kratsmar-Smogrovic, Polyhedron 14 (1995) 1185.
[25] G. Plesch, C. Friebel, S.A. Warda, J. Sivy, O. Svajlenova, Transition Met. Chem. 22 (1997) 433.
[26] S.A. Warda, P. Dahlke, S. Wocadlo, W. Massa, C. Friebel, Inorg. Chim. Acta 268 (1998) 117.
[27] M.F. Iskander, T.E. Khalil, R. Werner, W. Haase, I. Svoboda, H. Fuess, Polyhedron 19 (2000) 949.
[28] E.E. Addision, M. Logan, S.C. Wallwork, C.D. Gardner, Q. Rev. Chem. Soc. 25 (1971) 289.
[29] K. Nakamoto, Infrared Spectra of Inorganic and Coordination Compounds, Wiley, New York, 4th edn., 1986.
[30] A. Sancho, B. Gimeno, J. Mario Amigo, L. Enrigue Ochando, T. Debaerdemaehen, J. Vicente Folgado, L. Sato, Inorg. Chim. Acta 248 (1996) 153.
[31] A.C. Bonamartini, S. Bruni, F. Cariati, L.P. Battaglia, G. Pelozi, Inorg. Chim. Acta 205 (1993) 99.
[32] H.K. Fun, B.Y.P.Z. Lu, C. Driane, Y. Tsan, X.Z. You, Transition Met. Chem. 21 (1996) 193.
[33] J.-P. Costes, F. Dahan, M.B. Fernandez Fernandez, M.I. Fernandez Garcia, A.M. Garacia Deibe, J. Sanmartin, Inorg. Chim. Acta 274 (1998) 73.
[34] L.L. Koh, J.O. Ranford, W.T. Robenson, J.O. Sevensson, A.L.C. Tan, D. Wu, Inorg. Chem. 35 (1996) 6466.
[35] A.W. Addison, T.N. Rao, J. Reedijk, J. Van Rijn, J.C. Verschoor, J. Chem. Soc., Dalton Trans. (1984) 1349.
[36] O. Kahn, Molecular Magnetism, VCH, New York, 1993, Ch. 8.
[37] M.S. Haddad, D.N. Hendrickson, Inorg. Chem. 17 (1978) 2622.
[38] M.S. Haddad, E.N. Duesler, D.N. Hendrickson, Inorg. Chem. 18 (1979) 141.
[39] K.G. Strothkamp, S.J. Lippard, Acc. Chem. Res. 10 (1982) 318.
[40] P.K. Coughlin, A.E. Martin, J.C. Dewan, E.I. Watanabe, J.E. Bulkowski, J.M. Lehn, S.J. Lippard, Inorg. Chem. 23 (1984) 1004.
[41] P.K. Coughlin, S.J. Lippard, Inorg. Chem. 23 (1984) 1446.
[42] P.K. Coughlin, S.J. Lippard, J. Am. Chem. Soc. 106 (1984) 2328.
[43] C. Benelli, R.K. Bunting, D. Gatteschi, C. Zanchini, Inorg. Chem. 23 (1984) 3074.

[44] A. Bencini, D. Gatteschi, C. Zanchini, J.G. Haasnoot, R. Prins, J. Reedijk, Inorg. Chem. 24 (1985) 2812.
[45] A. Bencini, C. Benelli, D. Gatteschi, C. Zanchini, Inorg. Chem. 25 (1986) 398.
[46] J.-P. Costes, J.-F. Serra, F. Dahan, J.-P. Laurent, Inorg. Chem. 25 (1986) 2790.
[47] J.-P. Costes, M.L.F. Garcia, Inorg. Chim. Acta 173 (1990) 247.
[48] J.-P. Costes, F. Dahan, J.-P. Laurent, Inorg. Chem. 30 (1991) 1887.
[49] M. Zongwan, C. Dong, T. Wenxia, Y. Kaibei, L. Li, Polyhedron 11 (1992) 191.
[50] M. Zongwan, F. Degang, H. Quinwei, T. Wenxia, Y. Kaibei, Polyhedron 12 (1993) 1465.
[51] M. Zong Wan, H. Qin-Wie, T. Wen-Xia, L. Shi-Xiaung, Ze-Min, H. Jin-Ling, Polyhedron 15 (1996) 321.
[52] E. Kimura, V. Kurogi, M. Shinoya, M. Shiro, Inorg. Chem. 30 (1991) 3454.
[53] S.M. Morehouse, Inorg. Chim. Acta 243 (1996) 327.
[54] B. Bleany, K.D. Bowers, Proc. R. Soc. London, Ser. A 214 (1952) 451.
[55] K.T. McGregor, J.A. Barnes, W.E. Hatfield, J. Am. Chem. Soc. 95 (1973) 7993.
[56] S. Sikorav, I. Bkouche-Waksman, O. Kahn, Inorg. Chem. 23 (1984) 490.
[57] L. Merz, W. Haase, J. Chem. Soc., Dalton Trans. (1980) 875.
[58] S. Gehring, P. Fleischhauer, H. Paulus, W. Haase, Inorg. Chem. 23 (1993) 54.
[59] Nonius Diffractometer Control Software, release 5.1, Nonius GmbH, Solingen, Germany, 1993.
[60] G.M. Sheldrick, SHELXS-86, program for the solution of crystal structure determination, University of Göttingen, Germany, 1986 and 1990.
[61] G.M. Sheldrick, SHELXL-93, program for crystal structure determination, University of Göttingen, Germany, 1993.
[62] Stoe-REDU4, data reductions program, version 6.2c., Stoe & Cie GmbH, Darmstadt, Germany, 1987.
[63] StoeX-RED, data reductions program, Steo & Cie GmbH, Darmstadt, Germany, 1996.
[64] A.L. Speck, PLUTON-93, program for the display and analysis of crystal and molecular structures, Utrecht University, The Netherlands, 1993.
[65] R.W. Jothan, S.F.A. Kettle, Inorg. Chim. Acta 4 (1970) 145.
[66] J.A. Ibers, W.C. Hamilton, International Tables for X-ray Crystallography, vol. 1V, Kynoch Press, Birmingham, 1973.

PERGAMON

www.elsevier.nl/locate/poly

Polyhedron 19 (2000) 1193–1203

POLYHEDRON

Axial ligand substitution and photoisomerization reactions in ruthenium(II) *trans* mixed-chelate complexes containing the ligands 1,2-phenylenebis(dimethylarsine) and 2,2′-bipyridine or 1,10-phenanthroline

Benjamin J. Coe [a,*], Christopher I. McDonald [a], Samantha M. Couchman [b], John C. Jeffery [b], Leigh H. Rees [b], Simon J. Coles [c], Thomas Gelbrich [c], Michael B. Hursthouse [c]

[a] *Department of Chemistry, University of Manchester, Oxford Road, Manchester M13 9PL, UK*
[b] *Department of Chemistry, University of Bristol, Cantock's Close, Bristol BS8 1TS, UK*
[c] *EPSRC X-ray Crystallography Service, Department of Chemistry, University of Southampton, Highfield, Southampton SO17 1BJ, UK*

Received 28 January 2000; accepted 25 February 2000

Abstract

The nitrosyl complex in *trans*-[RuCl(pdma)(bpy)(NO)][PF_6]$_2$ (pdma = 1,2-phenylenebis(dimethylarsine), bpy = 2,2′-bipyridine) reacts at room temperature with stoichiometric NaN_3, followed by an excess of a neutral ligand L_1 in 2-butanone under reflux, to afford high yields of the mono-substituted derivatives *trans*-[RuCl(pdma)(bpy)L_1]PF_6 (L_1 = pyridine (py) **1**, triphenylphosphine (PPh_3) **2**, *N*-methylimidazole (mim) **3**, acetonitrile (MeCN) **4**, dimethylsulfoxide (dmso) **5** or pyrazine (pyz) **6**). The related compound *trans*-[RuCl(pdma)(phen)(NO)][PF_6]$_2$ (phen = 1,10-phenanthroline) reacts similarly to yield *trans*-[RuCl(pdma)(phen)L_1]PF_6 (L_1 = py **8**, PPh_3 **9**, mim **10** or pyz **11**). The pyrazine complexes in **6** and **11** react with MeI at room temperature in acetone to afford *trans*-[RuCl(pdma)(L–L)(mpyz$^+$)][PF_6]$_2$ (mpyz$^+$ = *N*-methylpyrazinium, L–L = bpy **7** or phen **12**, respectively). **3** reacts with an excess of a neutral ligand L_2 in the presence of stoichiometric $AgCF_3CO_2$ in water/acetone under reflux to afford high yields of the di-substituted derivatives *trans*-[Ru(pdma)(bpy)mim(L_2)][PF_6]$_2$ (L_2 = mim **13**, py **14** or MeCN **15**) and **2** reacts similarly with $AgCF_3CO_2$ in water/MeCN to give *trans*-[RuCl(pdma)(bpy)PPh_3(MeCN)][PF_6]$_2$ (**16**). The complexes in **1**–**16** exhibit intense $d_\pi(Ru^{II}) \rightarrow \pi^*(L–L)$ and $d_\pi(Ru^{II}) \rightarrow \pi^*(L_1/L_2)$ (L_1/L_2 = py, pyz or mpyz$^+$) metal-to-ligand charge-transfer absorption bands in the near-UV–visible region and are mildly photosensitive in solution. Solar irradiation leads to isomerization; for example **3** is converted into *cis*-[RuCl(pdma)(bpy)mim]PF_6 (**17**) over a period of ca. 100 h exposure to diffuse sunlight in acetone. Single crystal X-ray structures have been determined for **1**, **2**·DMF, **3**, **12**·3MeCN, **14**·DMF and **17**. ©2000 Elsevier Science Ltd All rights reserved.

Keywords: Photoisomerization; Ruthenium

1. Introduction

It has recently become apparent that ruthenium(II) complexes of N-heterocyclic chelating ligands such as 2,2′-bipyridine (bpy), 1,10-phenanthroline (phen) or 2,2′:6′,2″-terpyridine have potential for applications as components of photoactive molecular-level devices [1,2]. Of particular current interest is the discovery that relatives of the prototypical complex $[Ru^{II}(bpy)_3]^{2+}$ can act as efficient sensitizers when covalently attached to the surfaces of semiconducting nanocrystalline metal oxide electrodes in photovoltaic cells [3,4]. The utility of organotransition metal complexes in these and related devices rests upon the fact that photon absorption by metal-to-ligand charge-transfer (MLCT) chromophores can induce sequential, intramolecular electron or energy-transfer processes. The design of potentially useful MLCT-based molecular devices requires optimization of both electronic and stereochemical properties, and a particular emphasis on structurally well defined systems has emerged recently [5–7]. With functionalized octahedral MLCT chromophores, a *trans* disposition of attached donor/acceptor ('quencher') units is likely to be advantageous in order to achieve phenomena such as long-lived charge-separation. One approach to the preparation of such assemblies involves controlled ligand substitutions at *trans* octahedral metal centres.

Although 'chromophore-quencher' complexes based on *trans*-$\{Ru^{II}(bpy)_2\}^{2+}$ centres have been prepared [8], these undergo extremely facile photoinitiated ligand dissociation

* Corresponding author. Tel.: +44-161-275-4601; fax: +44-161-275-4598; e-mail: b.coe@man.ac.uk

0277-5387/00/$ - see front matter ©2000 Elsevier Science Ltd All rights reserved.
PII S0277-5387(00)00369-7

and isomerization reactions. In attempts to identify alternative systems suitable for the preparation of stable *trans* MLCT chromophoric assemblies, we have chosen to explore the derivative chemistry of ruthenium(II) complexes of the chelating ligand 1,2-phenylenebis(dimethylarsine) (pdma). The precursor *trans*-$[Ru^{II}Cl(pdma)_2(NO)]^{2+}$ [9] readily undergoes nitrosyl substitution reactions to afford mono- and dinuclear derivatives containing the non-chromophoric *trans*-$\{Ru^{II}Cl(pdma)_2\}^+$ core [10,11], but subsequent chloride substitutions are remarkably difficult [10]. We have recently reported the mixed-chelates *trans*-$[Ru^{II}Cl(pdma)(L–L)(NO)]^{2+}$ (L–L = bpy or phen) [12], which were designed to act as versatile synthetic precursors to functionalized *trans* assemblies via stepwise axial ligand substitutions. The reactivity of these complexes and the photostability of the resulting products are the subjects of the present report.

2. Experimental

2.1. Materials and procedures

The compound $RuCl_3 \cdot 2H_2O$ was supplied by Johnson Matthey plc and pdma was obtained from Dr P.G. Edwards, University of Wales College of Cardiff. The salts *trans*-$[RuCl(pdma)(L–L)(NO)][PF_6]_2$ (L–L = bpy or phen) were prepared according to published procedures [12]. All other reagents were obtained commercially and used as supplied. All reactions were conducted under an argon atmosphere. Products were dried overnight at room temperature in a vacuum desiccator ($CaSO_4$) prior to characterization.

2.2. Instrumentation

^{1}H NMR spectra were recorded on a Varian Gemini 200 spectrometer and all shifts are referenced to $SiMe_4$. The complex fine splitting of the pyridine or 2,2′-bipyridine proton resonances is ignored and the signals are reported as simple doublets or triplets. Elemental analyses were performed by the Microanalytical Laboratory, University of Manchester. Infrared spectra were obtained as KBr discs with an ATI Mattson Genesis Series FTIR instrument. FAB mass spectra were recorded using a Kratos Concept spectrometer with a 6–8 keV Xe atom beam and 3-nitrobenzyl alcohol as matrix.

Cyclic voltammetric measurements were carried out using an EG&G PAR model 173 potentiostat/galvanostat with a model 175 universal programmer. A single-compartment cell was used with the saturated calomel reference electrode (SCE) separated by a salt bridge from the platinum-bead working electrode and platinum-wire auxiliary electrode. Acetonitrile (HPLC grade) was used as received and tetra-*n*-butylammonium hexafluorophosphate, twice recrystallized from ethanol and dried in vacuo, was used as supporting electrolyte. Solutions containing ca. 10^{-3} mol dm^{-3} analyte (0.1 mol dm^{-3} electrolyte) were deaerated by purging with N_2. All $E_{1/2}$ values were calculated from $(E_{pa}+E_{pc})/2$ at a scan rate of 200 mV s^{-1}.

2.3. Preparations

2.3.1. *trans*-[RuCl(pdma)(bpy)py]PF_6 (1)

A solution of *trans*-$[RuCl(pdma)(bpy)(NO)][PF_6]_2$ (50 mg, 0.056 mmol) and NaN_3 (3.7 mg, 0.057 mmol) in pyridine (10 cm^3) was stirred at room temperature for 2 h, then heated at reflux for 1 h. Addition of aqueous NH_4PF_6 yielded a deep red precipitate which was filtered off, washed with water and dried. Yield: 39 mg, 87%. *Anal*. Found: C, 37.4; H, 3.65; N, 5.10. Calc. for $C_{25}H_{29}As_2ClF_6N_3PRu$: C, 37.4; H, 3.65; N, 5.25%. ^{1}H NMR (200 MHz, CD_3CN): δ 9.27 (2H, d, J = 5.8 Hz, $H^{6,6'}$), 8.55 (2H, d, J = 8.0 Hz, $H^{3,3'}$), 8.17 (2H, t, $H^{4,4'}$), 8.05 (2H, m, C_6H_2), 7.82 (2H, t, $H^{5,5'}$), 7.73–7.65 (5H, m, $pyH^{2,4,6}$ and C_6H_2), 6.93 (2H, t, $pyH^{3,5}$), 1.78 (6H, s, 2AsMe), 1.62 (6H, s, 2AsMe). *m/z*: 658 ($[M-PF_6^-]^+$) and 579 ($[M-PF_6^- - py]^+$).

2.3.2. *trans*-[RuCl(pdma)(bpy)PPh_3]PF_6 (2)

A solution of *trans*-$[RuCl(pdma)(bpy)(NO)][PF_6]_2$ (51 mg, 0.057 mmol) and NaN_3 (3.7 mg, 0.057 mmol) in acetone (5 cm^3) was stirred at room temperature for 2 h. A solution of PPh_3 (594 mg, 2.27 mmol) in 2-butanone (10 cm^3) was added, the acetone was removed in vacuo, and the solution was heated at reflux for a further 2 h. The solvent was reduced to a small volume in vacuo and diethyl ether was added to give a golden-coloured precipitate which was filtered off, washed with diethyl ether, and dried. The product was purified by reprecipitation from acetonitrile/diethyl ether to afford a yellow solid. Yield: 45 mg, 80%. *Anal*. Found: C, 46.35; H, 3.80; N, 3.20; P, 6.05. Calc. for $C_{38}H_{39}As_2ClF_6N_2P_2Ru$: C, 46.3; H, 4.00; N, 2.85; P, 6.30%. ^{1}H NMR (200 MHz, CD_3CN): δ 8.34 (2H, d, J = 8.2 Hz, $H^{6,6'}$), 8.24 (2H, d, J = 5.2 Hz, $H^{3,3'}$), 8.07–7.98 (4H, m, $H^{4,4'}$ and C_6H_2), 7.77 (2H, m, C_6H_2), 7.32–7.23 (5H, m, $H^{5,5'}$ and $3PhH^4$), 7.13–7.04 (6H, m, $3PhH^{3,5}$), 6.93 (6H, m, $3PhH^{2,6}$), 1.74 (6H, s, 2AsMe), 1.54 (6H, s, 2AsMe). *m/z*: 841 ($[M-PF_6^-]^+$) and 578 ($[M-PF_6^- - PPh_3]^+$). A reaction was also carried out using the above method, but instead of heating at reflux after the addition of PPh_3, the solution was stirred at room temperature for 93 h. This afforded 26 mg of **2** (46%, pure by ^{1}H NMR).

2.3.3. *trans*-[RuCl(pdma)(bpy)mim]PF_6 (3)

A solution of *trans*-$[RuCl(pdma)(bpy)(NO)][PF_6]_2$ (50 mg, 0.056 mmol) and NaN_3 (3.7 mg, 0.057 mmol) in acetone (5 cm^3) was stirred at room temperature for 2 h. *N*-Methylimidazole (mim, 5 cm^3) was added, the acetone was removed in vacuo, and the solution was heated at ca. 100°C for 1 h. After cooling to room temperature, addition of aqueous NH_4PF_6 and water afforded a red precipitate which was filtered off, washed with water and dried. Reprecipitation from acetone/diethyl ether gave a deep red solid. Yield: 42 mg, 94%. *Anal*. Found: C, 36.2; H, 3.75; N, 7.05. Calc. for

$C_{24}H_{30}As_2ClF_6N_4PRu$: C, 35.75; H, 3.75; N, 6.95%. ^{1}H NMR (200 MHz, CD_3COCD_3): δ 9.53 (2H, d, J = 5.2 Hz, $H^{6,6'}$), 8.72 (2H, d, J = 8.0 Hz, $H^{3,3'}$), 8.21 (2H, t, $H^{4,4'}$), 8.12 (2H, m, C_6H_2), 7.76 (2H, t, $H^{5,5'}$), 7.67 (2H, m, C_6H_2), 7.31 (1H, s, $C_3H_3N_2$), 6.95 (1H, s, $C_3H_3N_2$), 6.36 (1H, s, $C_3H_3N_2$), 3.54 (3H, s, Me), 1.83 (6H, s, 2AsMe), 1.72 (6H, s, 2AsMe). *m/z*: 660 ($[M-PF_6^-]^+$) and 577 ($[M-PF_6^- - mim]^+$).

2.3.4. trans-[RuCl(pdma)(bpy)(MeCN)]PF_6 (4)

This was prepared in a similar manner to **1** by using acetonitrile in place of pyridine. The reaction was cooled to room temperature, and the solvent removed in vacuo. The resulting yellow/orange oil was dissolved in acetone (3 cm^3), and addition of aqueous NH_4PF_6 afforded an orange precipitate which was filtered off, washed with water and dried. Reprecipitation from acetone/diethyl ether yielded an orange solid. Yield: 36 mg, 82%. *Anal*. Found: C, 35.8; H, 4.00; N, 5.00. Calc. for $C_{22}H_{27}As_2ClF_6N_3PRu \cdot 0.5C_3H_6O$: C, 35.55; H, 3.80; N, 5.30%. ^{1}H NMR (200 MHz, CD_3COCD_3): δ 9.50 (2H, d, J = 5.9 Hz, $H^{6,6'}$), 8.73 (2H, d, J = 7.4 Hz, $H^{3,3'}$), 8.27 (2H, t, $H^{4,4'}$), 8.14 (2H, m, C_6H_2), 7.83 (2H, t, $H^{5,5'}$), 7.69 (2H, m, C_6H_2), 2.28 (3H, s, Me), 1.67 (12H, s, 4AsMe). ν(C≡N) 2267 w cm^{-1}. *m/z*: 620 ($[M-PF_6^-]^+$) and 578 ($[M-PF_6^- - MeCN]^+$).

2.3.5. trans-[RuCl(pdma)(bpy)dmso]PF_6 (5)

This was prepared and purified in an identical manner to **3**, but using dmso in place of mim, to afford a yellow solid. Yield: 33 mg, 74%. *Anal*. Found: C, 32.7; H, 3.90; N, 3.40; S, 3.40. Calc. for $C_{22}H_{30}As_2ClF_6N_2OPRuS$: C, 32.95; H, 3.75; N, 3.50; S, 4.00%. ^{1}H NMR (200 MHz, CD_3COCD_3): δ 9.55 (2H, d, J = 4.8 Hz, $H^{6,6'}$), 8.72 (2H, d, J = 7.4 Hz, $H^{3,3'}$), 8.34 (2H, t, $H^{4,4'}$), 8.09 (2H, m, C_6H_2), 7.90 (2H, t, $H^{5,5'}$), 7.69 (2H, m, C_6H_2), 2.96 (6H, s, 2Me), 1.93 (12H, s, 4AsMe). ν(S=O) 1085 m cm^{-1}. *m/z*: 657 ($[M-PF_6^-]^+$) and 579 ($[M-PF_6^- - dmso]^+$).

2.3.6. trans-[RuCl(pdma)(bpy)pyz]PF_6 (6)

This was prepared in an identical manner to **2**, but using pyrazine (181 mg, 2.26 mmol) in place of PPh_3. Reprecipitation from acetone/diethyl ether afforded a red solid. Yield: 37 mg, 78%. *Anal*. Found: C, 36.7; H, 3.50; N, 7.05. Calc. for $C_{24}H_{28}As_2ClF_6N_4PRu \cdot 0.5C_3H_6O$: C, 36.75; H, 3.75; N, 6.75%. ^{1}H NMR (200 MHz, CD_3CN): δ 9.18 (2H, d, J = 5.6 Hz, $H^{6,6'}$), 8.57 (2H, d, J = 8.0 Hz, $H^{3,3'}$), 8.20 (2H, t, $H^{4,4'}$), 8.05 (2H, m, C_6H_2), 7.99 (2H, d, J = 4.6 Hz, pyz), 7.86 (2H, d, J = 4.6 Hz, pyz), 7.73–7.66 (4H, m, $H^{5,5'}$ and C_6H_2), 1.77 (6H, s, 2AsMe), 1.66 (6H, s, 2AsMe). *m/z*: 659 ($[M-PF_6^-]^+$) and 579 ($[M-PF_6^- - pyz]^+$).

2.3.7. trans-[RuCl(pdma)(bpy)($mpyz^+$)][PF_6]$_2$ (7)

A solution of **6** (50 mg, 0.062 mmol) in DMF (1.5 cm^3) and MeI (0.5 cm^3) was stirred at room temperature for 24 h. The excess MeI was removed in vacuo, and addition of aqueous NH_4PF_6 afforded a purple precipitate which was filtered off and washed with water. The crude product was dissolved in acetone and the solution was filtered to remove an insoluble tan residue. Addition of diethyl ether to the filtrate gave a purple precipitate which was filtered off and washed with diethyl ether. Repeated recrystallization from acetonitrile/diethyl ether yielded the purple product. Yield: 11 mg, 18%. *Anal*. Found: C, 32.0; H, 3.55; N, 5.95. Calc. for $C_{25}H_{31}As_2ClF_{12}N_4P_2Ru \cdot 0.5C_2H_3N$: C, 31.7; H, 3.35; N, 6.40%. ^{1}H NMR (200 MHz, CD_3COCD_3): δ 9.22 (2H, d, J = 4.8 Hz, $H^{6,6'}$), 8.99 (2H, d, J = 5.3 Hz, $mpyz^+$), 8.89 (2H, d, J = 8.2 Hz, $H^{3,3'}$), 8.40 (2H, t, $H^{4,4'}$), 8.21 (4H, m, C_6H_2 and $mpyz^+$), 7.85 (2H, t, $H^{5,5'}$), 7.77 (2H, m, C_6H_2), 3.98 (3H, s, Me), 1.90 (6H, s, 2AsMe), 1.88 (6H, s, 2AsMe). *m/z*: 819 ($[M-PF_6^-]^+$) and 579 ($[M-2PF_6^- - mpyz]^+$).

2.3.8. trans-[RuCl(pdma)(phen)py]PF_6 (8)

This was prepared and purified in an identical manner to **1** by using *trans*-[RuCl(pdma)(phen)(NO)][PF_6]$_2$ (100 mg, 0.108 mmol) in place of *trans*-[RuCl(pdma)(bpy)(NO)][PF_6]$_2$. A red solid was obtained. Yield: 80 mg, 89%. *Anal*. Found: C, 39.3; H, 3.70; N, 5.05. Calc. for $C_{27}H_{29}As_2ClF_6N_3PRu$: C, 39.2; H, 3.55; N, 5.10%. ^{1}H NMR (200 MHz, CD_3CN): δ 9.66 (2H, d, J = 5.2 Hz, $H^{2,9}$), 8.72 (2H, d, J = 8.2 Hz, $H^{4,7}$), 8.24 (2H, s, $H^{5,6}$), 8.11–8.01 (4H, m, $H^{3,8}$ and C_6H_2), 7.86 (2H, d, J = 6.4 Hz, $pyH^{2,6}$), 7.72 (2H, m, C_6H_2), 7.49 (1H, t, pyH^4), 6.84 (2H, t, $pyH^{3,5}$), 1.87 (6H, s, 2AsMe), 1.69 (6H, s, 2AsMe). *m/z*: 682 ($[M-PF_6^-]^+$) and 603 ($[M-PF_6^- - py]^+$).

2.3.9. trans-[RuCl(pdma)(phen)PPh_3]PF_6 (9)

This was prepared and purified in an identical manner to **2** by using *trans*-[RuCl(pdma)(phen)(NO)][PF_6]$_2$ (100 mg, 0.108 mmol) in place of *trans*-[RuCl(pdma)(bpy)(NO)][PF_6]$_2$. A yellow solid was obtained. Yield: 88 mg, 80%. *Anal*. Found: C, 47.2; H, 3.95; N, 3.00; P, 6.00. Calc. for $C_{40}H_{39}As_2ClF_6N_2P_2Ru$: C, 47.55; H, 3.90; N, 2.75; P, 6.15%. ^{1}H NMR (200 MHz, CD_3COCD_3): δ 9.09 (2H, d, J = 4.6 Hz, $H^{2,9}$), 8.75 (2H, d, J = 7.2 Hz, $H^{4,7}$), 8.27 (2H, s, $H^{5,6}$), 8.23 (2H, m, C_6H_2), 7.82 (4H, m, $H^{3,8}$ and C_6H_2), 7.31 (3H, t, $3PhH^4$), 7.08 (6H, t, $3PhH^{3,5}$), 6.75 (6H, t, $3PhH^{2,6}$), 1.94 (6H, s, 2AsMe), 1.70 (6H, s, 2AsMe). *m/z*: 864 ($[M-PF_6^-]^+$) and 602 ($[M-PF_6^- - PPh_3]^+$).

2.3.10. trans-[RuCl(pdma)(phen)mim]PF_6 (10)

This was prepared and purified in an identical manner to **3** by using *trans*-[RuCl(pdma)(phen)(NO)][PF_6]$_2$ (200 mg, 0.217 mmol) in place of *trans*-[RuCl(pdma)(bpy)(NO)][PF_6]$_2$. A red solid was obtained. Yield: 158 mg, 82%. *Anal*. Found: C, 38.85; H, 4.20; N, 6.35. Calc. for $C_{26}H_{30}As_2ClF_6N_4PRu \cdot C_3H_6O$: C, 39.25; H, 4.10; N, 6.30%. ^{1}H NMR (200 MHz, CD_3COCD_3): δ 9.94 (2H, d, J = 5.0 Hz, $H^{2,9}$), 8.81 (2H, d, J = 8.2 Hz, $H^{4,7}$), 8.32 (2H, s, $H^{5,6}$), 8.14 (4H, m, $H^{3,8}$ and C_6H_2), 7.70 (2H, m, C_6H_2), 7.22 (1H, s, $C_3H_3N_2$), 6.85 (1H, s, $C_3H_3N_2$), 6.33 (1H, s, $C_3H_3N_2$), 3.42 (3H, s, Me), 1.92 (6H, s, 2AsMe), 1.81 (6H, s,

2AsMe). *m/z*: 684 ([M−PF_6^-]$^+$) and 603 ([M−PF_6^-−mim]$^+$).

*2.3.11. trans-[RuCl(pdma)(phen)pyz]PF_6 (**11**)*

This was prepared and purified in an identical manner to **6** by using *trans*-[RuCl(pdma)(phen)(NO)][PF_6]$_2$ (100 mg, 0.108 mmol) in place of *trans*-[RuCl(pdma)-(bpy)(NO)][PF_6]$_2$. A red solid was obtained. Yield: 80 mg, 89%. *Anal*. Found: C, 37.75; H, 3.60; N, 6.50. Calc. for $C_{26}H_{28}As_2ClF_6N_4PRu$: C, 37.7; H, 3.40; N, 6.75%. ^{1}H NMR (200 MHz, CD_3CN): δ 9.68 (2H, d, J=4.4 Hz, $H^{2,9}$), 8.76 (2H, d, J=6.0 Hz, $H^{4,7}$), 8.26 (2H, s, $H^{5,6}$), 8.13–8.02 (4H, m, $H^{3,8}$ and C_6H_2), 7.89 (4H, m, pyz), 7.73 (2H, m, C_6H_2), 1.86 (6H, s, 2AsMe), 1.73 (6H, s, 2AsMe). *m/z*: 683 ([M−PF_6^-]$^+$) and 603 ([M−PF_6^-−pyz]$^+$).

*2.3.12. trans-[RuCl(pdma)(phen)(mpyz$^+$)][PF_6]$_2$ (**12**)*

This was prepared and purified in an identical manner to **7**, but using **11** (50 mg, 0.061 mmol) in place of **6**. A deep purple solid was obtained. Yield: 29 mg, 48%. *Anal*. Found: C, 32.8; H, 3.05; N, 5.50. Calc. for $C_{27}H_{31}As_2ClF_{12}N_4P_2Ru$: C, 32.85; H, 3.15; N, 5.65%. ^{1}H NMR (200 MHz, CD_3COCD_3): δ 9.66 (2H, d, J=5.2 Hz, $H^{2,9}$), 8.99 (4H, m, $H^{4,7}$ and mpyz$^+$), 8.44 (2H, s, $H^{5,6}$), 8.27–8.12 (6H, m, $H^{3,8}$, C_6H_2 and mpyz$^+$), 7.79 (2H, m, C_6H_2) 3.93 (3H, s, Me), 1.99 (6H, s, 2AsMe), 1.97 (6H, s, 2AsMe). *m/z*: 843 ([M−PF_6^-]$^+$), 698 ([M−2PF_6^-]$^+$) and 602 ([M−2PF_6^-−mpyz$^+$]$^+$).

*2.3.13. trans-[Ru(pdma)(bpy)(mim)$_2$][PF_6]$_2$ (**13**)*

A solution of **3** (50 mg, 0.062 mmol), $AgCF_3CO_2$ (13.8 mg, 0.062 mmol) and mim (0.2 cm^3) in acetone (5 cm^3) was heated at reflux for 75 min. Water (5 cm^3) was added, and reflux was continued for a further 3 h. The reaction mixture was then filtered through celite to remove AgCl, and addition of aqueous NH_4PF_6 and water yielded an orange precipitate, which was filtered off, washed with water, and dried. Reprecipitation from acetone/diethyl ether afforded an orange solid. Yield: 50 mg, 81%. *Anal*. Found: C, 34.0; H, 3.45; N, 8.50. Calc. for $C_{28}H_{36}As_2F_{12}N_6P_2Ru$: C, 33.7; H, 3.65; N, 8.45%. ^{1}H NMR (200 MHz, CD_3COCD_3): δ 9.61 (2H, d, J=4.8 Hz, $H^{6,6'}$), 8.78 (2H, d, J=8.0 Hz, $H^{3,3'}$), 8.36 (2H, t, $H^{4,4'}$), 8.25 (2H, m, C_6H_2), 7.91 (2H, t, $H^{5,5'}$), 7.78 (2H, m, C_6H_2), 7.22 (2H, s, 2$C_3H_3N_2$), 6.96 (2H, s, 2$C_3H_3N_2$), 6.25 (2H, s, 2$C_3H_3N_2$), 3.49 (6H, s, 2Me), 1.80 (12H, s, 4AsMe). *m/z*: 852 ([M−PF_6^-]$^+$), 707 ([M−2PF_6^-]$^+$), 624 ([M−2PF_6^-–mim]$^+$) and 543 ([M−2PF_6^-−2mim]$^+$).

*2.3.14. trans-[Ru(pdma)(bpy)(mim)py][PF_6]$_2$ (**14**)*

This was prepared and purified in an identical fashion to **13** but using pyridine (0.4 cm^3) in place of mim. A yellow/orange solid was obtained. Yield: 43 mg, 66%. *Anal*. Found: C, 36.5; H, 3.65; N, 6.65. Calc. for $C_{29}H_{35}As_2F_{12}N_5P_2Ru\cdot C_3H_6O$: C, 36.5; H, 3.95; N, 6.65%. ^{1}H NMR (200 MHz, CD_3COCD_3): δ 9.69 (2H, d, J=4.6 Hz, $H^{6,6'}$), 8.76 (2H, d, J=8.0 Hz, $H^{3,3'}$), 8.35 (2H, t, $H^{4,4'}$), 8.29–8.24 (4H, m, $pyH^{2,6}$ and C_6H_2), 7.96 (2H, t, $H^{5,5'}$), 7.82–7.76 (3H, m, pyH^4 and C_6H_2), 7.22–7.12 (3H, m, $pyH^{3,5}$ and $C_3H_3N_2$), 6.97 (1H, s, $C_3H_3N_2$), 6.15 (1H, s, $C_3H_3N_2$), 3.47 (3H, s, Me), 1.91 (6H, s, 2AsMe), 1.80 (6H, s, 2AsMe). *m/z*: 849 ([M−PF_6^-]$^+$), 703 ([M−2PF_6^-]$^+$), 624 ([M−2PF_6^-−py]$^+$) and 543 ([M−2PF_6^-−py–mim]$^+$).

*2.3.15. trans-[Ru(pdma)(bpy)(mim)MeCN][PF_6]$_2$ (**15**)*

This was prepared in an identical fashion to **13** but using acetonitrile (0.4 cm^3) in place of mim, with no reprecipitation of the crude product. An orange solid was obtained. Yield: 52 mg, 88%. *Anal*. Found: C, 32.7; H, 3.50; N, 7.70. Calc. for $C_{26}H_{33}As_2F_{12}N_5P_2Ru$: C, 32.65; H, 3.50; N, 7.30%. ^{1}H NMR (200 MHz, CD_3COCD_3): δ 9.46 (2H, d, J=5.4 Hz, $H^{6,6'}$), 8.87 (2H, d, J=8.0 Hz, $H^{3,3'}$), 8.45 (2H, t, $H^{4,4'}$), 8.26 (2H, m, C_6H_2), 7.93 (2H, t, $H^{5,5'}$), 7.79 (2H, m, C_6H_2), 7.20 (1H, s, $C_3H_3N_2$), 7.01 (1H, s, $C_3H_3N_2$), 6.20 (1H, s, $C_3H_3N_2$), 3.50 (3H, s, $C_3H_3N_2$–*Me*), 2.24 (3H, s, Me), 1.94 (6H, s, 2AsMe), 1.90 (6H, s, 2AsMe). *m/z*: 811 ([M−PF_6^-]$^+$), 666 ([M−2PF_6^-]$^+$), 625 ([M−2PF_6^-−MeCN]$^+$) and 544 ([M−2PF_6^-−MeCN−mim]$^+$).

*2.3.16. trans-[Ru(pdma)(bpy)(PPh_3)(MeCN)][PF_6]$_2$ (**16**)*

This was prepared and purified in an identical manner to **15** by using **2** (50 mg, 0.051 mmol) in place of **3**. A yellow solid was obtained. Yield: 37 mg, 64%. *Anal*. Found: C, 41.95; H, 3.75; N, 3.70; P, 7.85. Calc. for $C_{40}H_{42}As_2F_{12}N_3P_3Ru$: C, 42.25; H, 3.70; N, 3.70; P, 8.20%. ^{1}H NMR (200 MHz, CD_3COCD_3): δ 8.92 (2H, d, J=5.0 Hz, $H^{6,6'}$), 8.65 (2H, d, J=7.6 Hz, $H^{3,3'}$), 8.30 (4H, m, $H^{4,4'}$ and C_6H_2), 7.89 (2H, m, C_6H_2), 7.74 (2H, t, $H^{5,5'}$), 7.40 (3H, t, $3PhH^4$), 7.15 (6H, t, $3PhH^{3,5}$), 6.76 (6H, t, $3PhH^{2,6}$), 2.22 (3H, s, Me), 1.96 (6H, s, 2AsMe), 1.66 (6H, s, 2AsMe). *m/z*: 991 ([M−PF_6^-]$^+$), 845 ([M−2PF_6^-]$^+$), 583 ([M−2PF_6^-−PPh_3]$^+$) and 542 ([M−2PF_6^-−PPh_3−MeCN]$^+$).

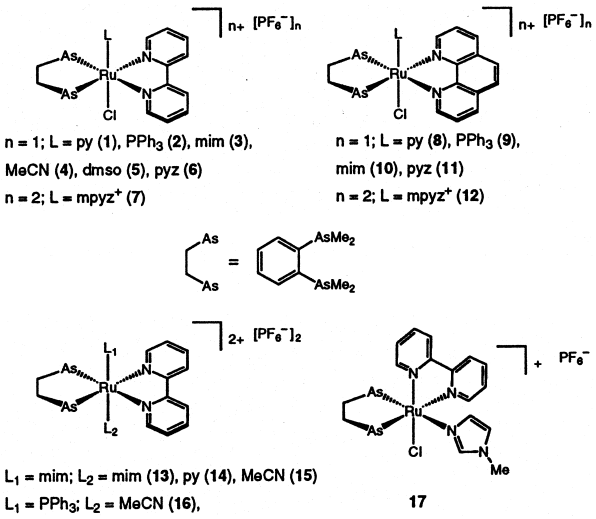
*2.3.17. cis-[RuCl(pdma)(bpy)mim]PF_6 (**17**)*

A solution of **3** (40 mg, 0.050 mmol) in acetone (20 cm^3) was exposed to sunlight for 100 h, during which time the isomerization was completed (as shown by ^{1}H NMR spectroscopy on a smaller sample in acetone-d_6). The addition of diethyl ether gave a precipitate which was filtered off, washed with diethyl ether and dried to afford a deep red solid. Yield: 31 mg, 78%. *Anal*. Found: C, 35.9; H, 4.00; N, 7.05. Calc. for $C_{24}H_{30}As_2ClF_6N_4PRu$: C, 35.75; H, 3.75; N, 6.95%. ^{1}H NMR (200 MHz, CD_3COCD_3): δ 9.96 (1H, d, J=6.0 Hz, bpy), 8.97 (1H, d, J=5.4 Hz, bpy), 8.56 (2H, t, bpy), 8.12 (1H, t, bpy), 8.10–7.99 (2H, m, C_6H_2), 7.93–7.80 (3H, m, bpy and $C_3H_3N_2$), 7.65–7.58 (2H, m, C_6H_2), 7.46 (1H, t, bpy), 7.09 (1H, s, $C_3H_3N_2$), 6.74 (1H, s, $C_3H_3N_2$), 3.71 (3H, s, $C_3H_3N_2$–*Me*), 1.92 (3H, s, AsMe), 1.56 (3H, s, AsMe), 1.48 (3H, s, AsMe), 0.74 (3H, s, AsMe). *m/z*: 661 ([M−PF_6^-]$^+$) and 579 ([M−PF_6^-−mim]$^+$).

2.4. X-ray crystallography

Crystals of **1**, **3**, **12**·3MeCN and **17** were grown by slow diffusion of diethyl ether vapour into acetonitrile solutions of the complex salts at 4°C. Those of **2**·DMF and **14**·DMF were obtained in similar manner, but using DMF solutions. The approximate dimensions (mm) of the crystals chosen for diffraction studies were as follows: **1** (0.15×0.15×0.10), **2**·DMF (0.40×0.10×0.10), **3** (0.40×0.20×0.05), **12**·3MeCN (0.15×0.15×0.05), **14**·DMF (0.30×0.20×0.05), **17** (0.10×0.10×0.05).

Data collection details are as follows: for **1**, **2**·DMF and **3** data were collected on a Siemens SMART CCD area-detector diffractometer. Empirical absorption corrections were applied by using multiple measurements of equivalent reflections, and the data were integrated by using SAINT [13]. For **12**·3MeCN, **14**·DMF and **17** data were collected on a Nonius Kappa CCD area-detector diffractometer controlled by the Collect software package [14]. The data were processed by Denzo [15] and corrected for absorption by using the empirical method employed in Sortav [16,17] from within the MAXUS suite of programs [18].



The structures of **1**, **2**·DMF and **3** were solved by direct methods and refined by full-matrix least-squares on all F_o^2 data using Siemens SHELXTL 5.03 [13]. The same approach was used for **12**·3MeCN, **14**·DMF and **17**, but using SHELXS-90 [19] and SHELXL-97 [20]. In all cases, all non-hydrogen atoms were refined anisotropically with hydrogen atoms included in idealized positions with thermal parameters riding on those of the parent atom. Static disorder is present in the PF_6^- anions of **1** and **17**, and in the axial ligands of **14**·DMF (50% occupancy by py and mim in both positions).

Representations of the complex cations in **1**, **2**·DMF, **3**, **12**·3MeCN, **14**·DMF and **17** are given in Figs. 1–6. Crystallographic data and refinement details are presented in Table 1, and selected bond distances and angles in Table 2.

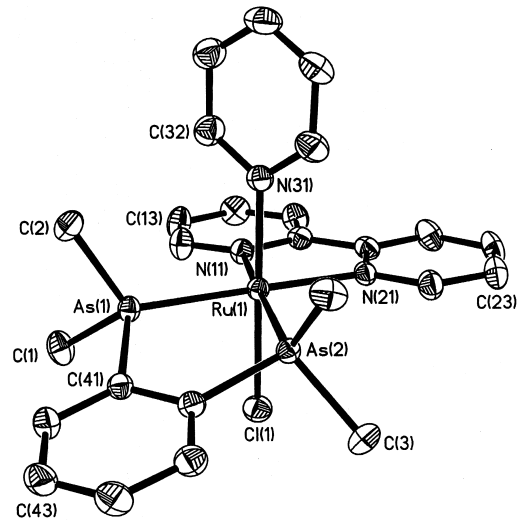


Fig. 1. Structural representation of the complex cation in the salt **1**, with hydrogen atoms omitted (50% probability ellipsoids).

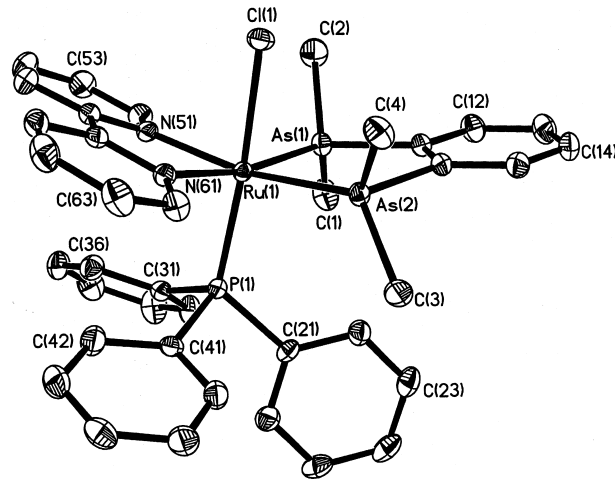


Fig. 2. Structural representation of the complex cation in the salt **2**·DMF, with hydrogen atoms omitted (50% probability ellipsoids).

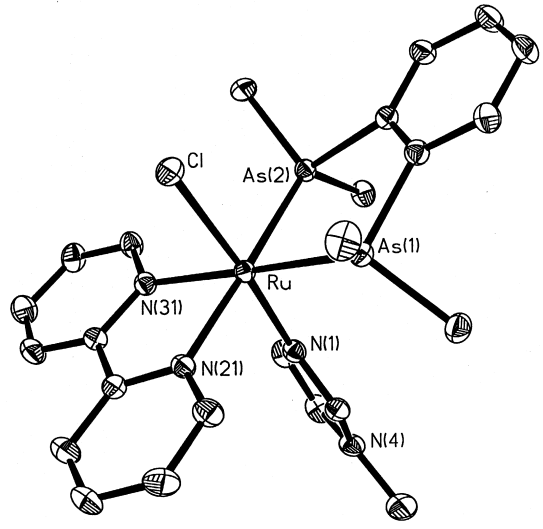


Fig. 3. Structural representation of the complex cation in the salt **3**, with hydrogen atoms omitted (50% probability ellipsoids).

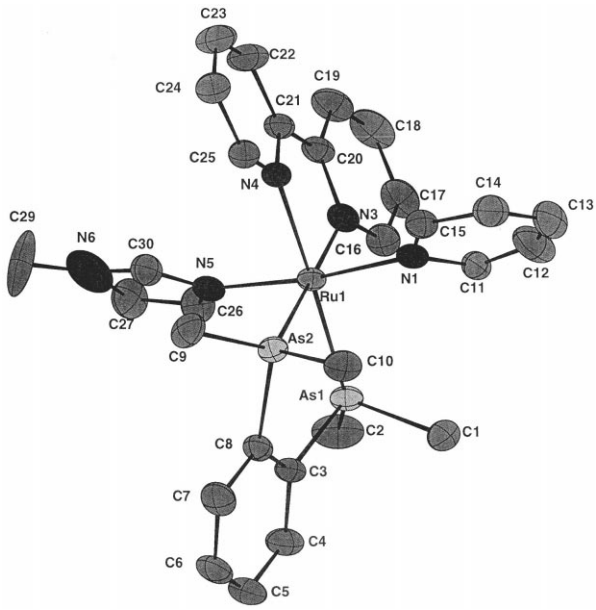


Fig. 4. Structural representation of the complex cation in the salt **12**·3MeCN, with disorder removed and hydrogen atoms omitted (50% probability ellipsoids).

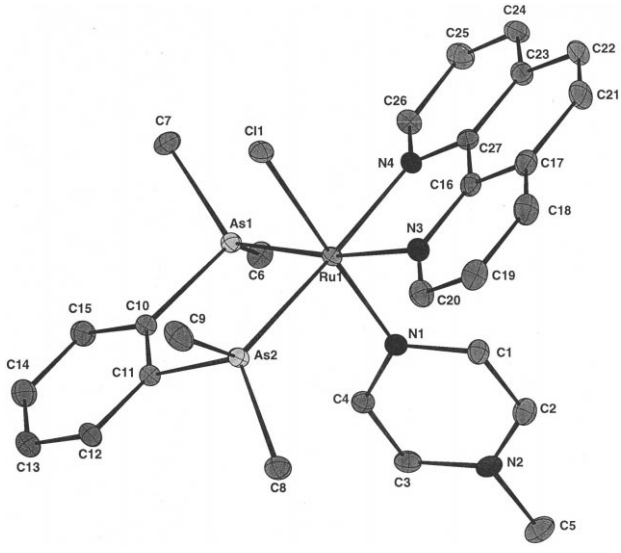


Fig. 5. Structural representation of the complex cation in the salt **14**·DMF, with hydrogen atoms omitted (50% probability ellipsoids).

3. Results and discussion

3.1. Synthesis and characterization

It is well established that sufficiently electrophilic, linearly coordinated nitrosyl ligands react with nucleophiles [21,22], and the reaction with azide ion is a versatile means to convert ruthenium(II) nitrosyls into substituted derivatives via dinitrogen or solvento intermediates [10,11,23–25]. The ν(NO) values in *trans*-[$Ru^{II}Cl(pdma)(L–L)(NO)][PF_6]_2$, 1878 cm^{-1} (L–L = bpy) and 1874 cm^{-1} (L–L = phen) [12], are indicative of relatively electron-deficient nitrosyl ligands [21,22], and these complexes hence react readily with stoi-

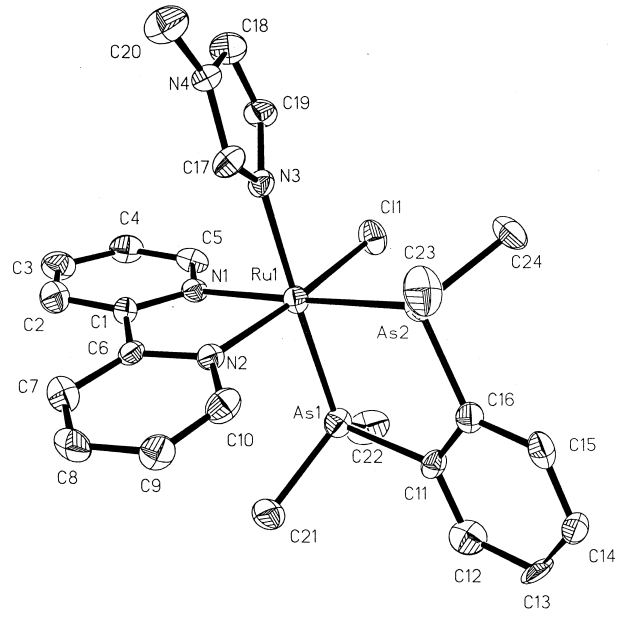


Fig. 6. Structural representation of the complex cation in the salt **17**, with hydrogen atoms omitted (50% probability ellipsoids).

chiometric azide at room temperature in acetone. The resulting intermediates, most likely *trans*-[$Ru^{II}Cl(pdma)(L–L)N_2]^+$, react with a range of neutral ligands to give clean substitution of the position formerly occupied by NO^+. These reactions take place only slowly at room temperature, but occur much more rapidly upon heating at ca. 80°C in 2-butanone.

Unlike the related complexes *trans*-[$Ru^{II}Cl(pdma)_2L]^+$ (L = py, mim, etc.) [10], the pdma/L–L *trans* mixed-chelates react with neutral ligands in the presence of $AgCF_3CO_2$ to substitute the chloride ligands, although heating is required to give reasonably efficient reactions. For example, **15** was also isolated from a reaction at room temperature, but in a yield of only 14%. The efficacy of these substitution reactions depends to varying degrees upon the nature of the starting complex and the incoming ligand. The best results were obtained with salt **3**, from which the derivatives **13**–**15** were prepared. The presence of the *trans* geometry in the salts **1**–**16** is confirmed by the ^{1}H NMR spectra which each show a single AA′BB′ pattern for the pdma ligand, either one or two singlets for the AsMe groups and four signals for bpy or phen.

3.2. Photoisomerization reactions

Previous studies have shown that *trans*-{$Ru^{II}(L–L)_2\}^{2+}$ (L–L = bpy or phen) complexes readily photoisomerize to their more stable *cis* isomers [8,26]. By contrast, when L–L = pdma, no evidence for photoinstability has been found [10]. Given these observations, it is perhaps unsurprising that the new *trans*-{Ru(pdma)(L–L)$\}^{2+}$ (L–L = bpy or phen) complexes show an intermediate degree of photostability. ^{1}H NMR experiments in d_6-acetone show that salts **1**–**16** undergo complete isomerization to their *cis* forms, with partial decomposition in some cases, following exposure to

Table 1
Crystallographic data and refinement details for the complex salts **1**, **2**·DMF, **3**, **12**·3MeCN, **14**·DMF and **17**

	1	**2**·DMF	**3**	**12**·3MeCN	**14**·DMF	**17**
Formula	$C_{25}H_{29}As_2ClF_6N_3PRu$	$C_{41}H_{46}As_2ClF_6N_3OP_2Ru$	$C_{24}H_{30}As_2ClF_6N_4PRu$	$C_{33}H_{40}As_2ClF_{12}N_7P_2Ru$	$C_{32}H_{42}As_2F_{12}N_6OP_2Ru$	$C_{24}H_{30}As_2ClF_6N_4PRu$
FW	802.84	1059.11	805.85	1111.02	1067.57	805.85
Crystal system	monoclinic	monoclinic	monoclinic	triclinic	triclinic	orthorhombic
Space group	$P2_1/c$	$P2_1/n$	$P2_1/c$	$P\bar{1}$	$P\bar{1}$	$Pbca$
a (Å)	10.4102(12)	14.686(2)	10.560(3)	11.707(2)	11.837(2)	8.9694(4)
b (Å)	15.609(3)	10.4026(9)	15.673(2)	12.217(2)	13.049(3)	16.5043(9)
c (Å)	17.438(2)	28.806(4)	17.413(4)	16.562(3)	15.315(3)	39.139(2)
α (°)				72.40(3)	83.81(3)	
β (°)	95.828(9)	103.878(7)	96.25(2)	80.24(3)	71.56(3)	
γ (°)				73.40(3)	67.15(3)	
U (Å^3)	2818.8(6)	4272.1(8)	2865.0(10)	2154.8(6)	2067.7(7)	5793.9(5)
Z	4	4	4	2	2	8
D_c (Mg m^{-3})	1.892	1.647	1.868	1.712	1.718	1.848
Temperature (K)	173(2)	173(2)	173(2)	150(2)	293(2)	150(2)
λ (Å)	0.710 73 (Mo Kα)	0.710 73 (Mo Kα)	0.710 73 (Mo Kα)	0.710 73 (Mo Kα)	0.710 73 (Mo Kα)	0.710 73 (Mo Kα)
$F(000)$	1584	2128	1592	1104	1066	3184
μ (mm^{-1})	3.099	2.105	3.051	2.110	2.135	3.017
Scan type	$\varphi+\omega$	$\varphi+\omega$	$\varphi+\omega$	$\varphi+\omega$	$\varphi+\omega$	$\varphi+\omega$
θ Range (°)	1.76–27.49	1.46–27.47	1.75–27.49	1.82–26.39	1.69–26.00	2.47–25.25
h, k, l ranges	±13, ±20, ±22	±19, ±13, ±37	−13/11, −20/16, ±22	±14, ±15, ±20	±14, ±16, ±19	±10, ±19, −40/46
Reflections collected	28629	42781	18047	44788	44404	35774
Unique reflections (R_{int})	6469 (0.0415)	9784 (0.0351)	6559 (0.0410)	8820 (0.0576)	8109 (0.0453)	5183 (0.1204)
Data/restraints/parameters	6468/221/410	9784/0/520	6559/0/352	8820/0/558	8089/72/532	5183/22/401
Final R indices ($I>2\sigma(I)$) [a,b]	$R_1=0.0298$, $wR_2=0.0629$	$R_1=0.0293$, $wR_2=0.0649$	$R_1=0.0321$, $wR_2=0.0663$	$R_1=0.0307$, $wR_2=0.0995$	$R_1=0.0471$, $wR_2=0.1612$	$R_1=0.0480$, $wR_2=0.0843$
Final R indices (all data)	$R_1=0.0473$, $wR_2=0.0697$	$R_1=0.0418$, $wR_2=0.0687$	$R_1=0.0577$, $wR_2=0.0746$	$R_1=0.0357$, $wR_2=0.1058$	$R_1=0.0542$, $wR_2=0.1693$	$R_1=0.1019$, $wR_2=0.0937$
Weighting factors (x, y) [b]	0.0335, 0.3513	0.0301, 2.0533	0.0364, 0	0.1000, 0	0.1000, 0	0.0411, 0
Goodness of fit, (S)	1.038	1.092	0.935	0.873	1.379	0.934
Peak and hole (e Å^{-3})	0.666, −0.720	1.118, −0.810	0.551, −0.694	1.067, −0.764	0.986, −0.979	1.126, −0.688

[a] Structures were refined on F_o^2 using all data; the values of R_1 are given for comparison with older refinements based on F_o with a typical threshold of $F_o>4\sigma(F_o)$.
[b] $wR_2=[\sum w(F_o^2-F_c^2)^2/\sum w(F_o^2)^2]^{1/2}$; $S=[\sum w(F_o^2-F_c^2)^2/(M-N)]^{1/2}$ where M is the number of reflections and N is the number of parameters; $w^{-1}=[\sigma^2(F_o^2)+(xP)^2+yP]$ and $P=[\max(F_o^2,0)+2F_c^2]/3$.

Table 2
Selected bond distances (Å) and angles (°) for the complex salts **1**, **2**·DMF, **3**, **12**·3MeCN, **14**·DMF and **17**

1			
Ru(1)–N(31)	2.088(3)	Ru(1)–As(1)	2.4117(6)
Ru(1)–N(21)	2.103(3)	Ru(1)–As(2)	2.4186(5)
Ru(1)–N(11)	2.108(3)	Ru(1)–Cl(1)	2.4254(10)
N(31)–Ru(1)–N(21)	87.36(11)	N(11)–Ru(1)–As(2)	173.18(8)
N(31)–Ru(1)–N(11)	87.90(11)	As(1)–Ru(1)–As(2)	82.123(13)
N(21)–Ru(1)–N(11)	77.88(11)	N(31)–Ru(1)–Cl(1)	175.06(8)
N(31)–Ru(1)–As(1)	93.63(8)	N(21)–Ru(1)–Cl(1)	90.49(8)
N(21)–Ru(1)–As(1)	178.74(8)	N(11)–Ru(1)–Cl(1)	87.30(8)
N(11)–Ru(1)–As(1)	101.38(8)	As(1)–Ru(1)–Cl(1)	88.45(2)
N(31)–Ru(1)–As(2)	97.77(8)	As(2)–Ru(1)–Cl(1)	86.95(3)
N(21)–Ru(1)–As(2)	98.51(7)		
2·DMF			
Ru(1)–N(61)	2.093(2)	Ru(1)–As(1)	2.4160(4)
Ru(1)–N(51)	2.101(2)	Ru(1)–As(2)	2.4278(4)
Ru(1)–P(1)	2.2947(7)	Ru(1)–Cl(1)	2.4629(7)
N(61)–Ru(1)–N(51)	78.23(8)	P(1)–Ru(1)–As(2)	98.55(2)
N(61)–Ru(1)–P(1)	92.26(6)	As(1)–Ru(1)–As(2)	84.727(12)
N(51)–Ru(1)–P(1)	93.60(6)	N(61)–Ru(1)–Cl(1)	84.45(6)
N(61)–Ru(1)–As(1)	168.98(6)	N(51)–Ru(1)–Cl(1)	83.41(6)
N(51)–Ru(1)–As(1)	97.76(6)	P(1)–Ru(1)–Cl(1)	175.93(2)
P(1)–Ru(1)–As(1)	98.27(2)	As(1)–Ru(1)–Cl(1)	84.90(2)
N(61)–Ru(1)–As(2)	96.97(6)	As(2)–Ru(1)–Cl(1)	84.24(2)
N(51)–Ru(1)–As(2)	167.13(6)		
3			
Ru–N(1)	2.087(3)	Ru(1)–As(1)	2.4081(7)
Ru–N(21)	2.107(3)	Ru(1)–As(2)	2.4028(5)
Ru–N(31)	2.107(3)	Ru(1)–Cl	2.4494(11)
N(1)–Ru–N(21)	87.36(11)	N(21)–Ru–Cl	90.41(8)
N(1)–Ru–N(31)	87.32(11)	N(31)–Ru–As(1)	174.64(8)
N(1)–Ru–As(1)	96.99(8)	N(31)–Ru–As(2)	100.84(8)
N(1)–Ru–As(2)	93.20(7)	N(31)–Ru–Cl	88.43(8)
N(1)–Ru–Cl	175.55(8)	As(1)–Ru–Cl	87.18(3)
N(21)–Ru–N(31)	77.47(11)	As(1)–Ru–As(2)	82.16(2)
N(21)–Ru–As(1)	99.48(8)	As(2)–Ru–Cl	88.91(3)
N(21)–Ru–As(2)	178.20(8)		
12·3MeCN			
Ru(1)–N(1)	2.019(2)	Ru(1)–As(1)	2.4067(9)
Ru(1)–N(3)	2.120(2)	Ru(1)–As(2)	2.4182(7)
Ru(1)–N(4)	2.118(2)	Ru(1)–Cl(1)	2.4146(10)
N(1)–Ru(1)–N(4)	92.49(8)	N(1)–Ru(1)–N(3)	92.28(8)
N(4)–Ru(1)–N(3)	78.39(9)	N(1)–Ru(1)–As(1)	94.82(6)
N(4)–Ru(1)–As(1)	96.84(6)	N(3)–Ru(1)–As(1)	171.62(6)
N(1)–Ru(1)–Cl(1)	176.24(6)	N(4)–Ru(1)–Cl(1)	87.56(6)
N(3)–Ru(1)–Cl(1)	84.04(6)	As(1)–Ru(1)–Cl(1)	88.90(3)
N(1)–Ru(1)–As(2)	90.59(6)	N(4)–Ru(1)–As(2)	176.81(5)
N(3)–Ru(1)–As(2)	100.64(6)	As(1)–Ru(1)–As(2)	83.74(3)
Cl(1)–Ru(1)–As(2)	89.31(3)		
14·DMF			
Ru(1)–N(3)	2.11(2)	Ru(1)–N(1)	2.10(2)
Ru(1)–N(4)	2.11(2)	Ru(1)–N(5)	2.12(2)
Ru(1)–As(1)	2.439(3)	Ru(1)–As(2)	2.447(3)
N(3)–Ru(1)–N(1)	88.1(8)	N(3)–Ru(1)–N(4)	77.7(8)
N(1)–Ru(1)–N(4)	89.2(8)	N(3)–Ru(1)–N(5)	87.0(8)
N(1)–Ru(1)–N(5)	173.0(7)	N(4)–Ru(1)–N(5)	84.8(8)
N(3)–Ru(1)–As(1)	99.8(6)	N(1)–Ru(1)–As(1)	94.5(5)
N(4)–Ru(1)–As(1)	175.5(5)	N(5)–Ru(1)–As(1)	91.3(6)
N(3)–Ru(1)–As(2)	179.3(6)	N(1)–Ru(1)–As(2)	92.4(5)
N(4)–Ru(1)–As(2)	101.9(6)	N(5)–Ru(1)–As(2)	92.5(5)
As(1)–Ru(1)–As(2)	80.61(9)		
17			
Ru(1)–N(1)	2.101(4)	Ru(1)–N(2)	2.056(4)
Ru(1)–N(3)	2.122(4)	Ru(1)–As(1)	2.3686(7)
Ru(1)–As(2)	2.3836(7)	Ru(1)–Cl(1)	2.4377(14)
N(1)–Ru(1)–N(2)	78.46(18)	N(1)–Ru(1)–N(3)	85.04(16)
N(2)–Ru(1)–N(3)	89.36(16)	N(1)–Ru(1)–As(1)	97.58(11)
N(2)–Ru(1)–As(1)	91.04(12)	N(3)–Ru(1)–As(1)	177.37(12)
N(1)–Ru(1)–As(2)	177.06(12)	N(2)–Ru(1)–As(2)	100.13(12)
N(3)–Ru(1)–As(2)	92.38(12)	As(1)–Ru(1)–As(2)	85.00(2)
N(1)–Ru(1)–Cl(1)	92.83(13)	N(2)–Ru(1)–Cl(1)	171.26(13)
N(3)–Ru(1)–Cl(1)	90.69(12)	As(1)–Ru(1)–Cl(1)	89.31(4)
As(2)–Ru(1)–Cl(1)	88.60(4)		

diffuse sunlight for ca. 100 h. The isomerized samples show no reversion to their *trans* forms after extended periods in the dark. The ^{1}H NMR spectra of the *cis* isomers are characterized by increased numbers of signals due to reduced symmetry, together with shifts of as much as 1 ppm for some of the resonances. In particular, the lowest field bpy/phen doublets are shifted downfield and some of the AsMe signals shift upfield, upon *trans* → *cis* isomerization. In the case of the two forms of $[Ru^{II}Cl(pdma)(bpy)mim]PF_6$ (**3** and **17**), the isomerization was further confirmed by X-ray structural studies (see later).

3.3. UV–visible studies

Electronic absorption spectra for all of the new complex salts were recorded in acetonitrile and results are presented in Table 3. All show relatively intense, broad $d_\pi(Ru^{II}) \rightarrow \pi^*$(bpy/phen) MLCT bands [27,28] in the region 360–460 nm. For the series *trans*-$[Ru^{II}Cl(pdma)(bpy)L_1][PF_6]_n$ ($n = 1$ or 2, **1**–**5** and **7**), the MLCT energy decreases as the overall electron donor strength of L_1 increases, in the order L_1 = dmso < $PPh_3 \approx mpyz^+$ < MeCN < py < mim. This ordering reflects a steady destabilization of the Ru-based HOMO. Similar trends are observed for the phen complexes in **8**–**10** and **12** and for the *trans*-$[Ru(pdma)(bpy)mim(L_2)][PF_6]_2$ series **13**–**15**. The disubstituted derivatives **13**–**15** all have higher MLCT energies than their parent complex in **3** because mim, py and MeCN are less basic than chloride. For the same reasons, substitution of the chloride ligand in **2** by MeCN to give **16** produces a blue shift of ca. 0.25 eV.

The complexes containing py or pyz co-ligands also show $d_\pi(Ru^{II}) \rightarrow \pi^*$(py/pyz) MLCT bands which in many cases overlap with the $d_\pi(Ru^{II}) \rightarrow \pi^*$(bpy/phen) absorptions. In the complexes in **7** and **12**, $d_\pi(Ru^{II}) \rightarrow \pi^*(mpyz^+)$ bands are observed at especially low energy owing to the strongly π-accepting nature of the $mpyz^+$ ligand. The spectra of the

isomeric pair of complexes in **3** and **17** are somewhat different, with the $d_\pi(Ru^{II}) \rightarrow \pi^*(bpy)$ band maximum occurring at higher energy by ca. 0.19 eV in the *cis* isomer. Besides their MLCT bands, all of the complexes also show one or more intense UV absorptions due to intraligand $\pi \rightarrow \pi^*$ excitations.

3.4. Electrochemical studies

All of the new complex salts were studied by cyclic voltammetry in acetonitrile and results are presented in Table 3. All exhibit reversible or quasi-reversible $Ru^{III/II}$ oxidation waves, together with ligand-based reduction processes which

Table 3
Electrochemical and UV–vis data for complex salts in acetonitrile

Complex salt	$E_{1/2}$ (V vs. SCE) (ΔE_p (mV)) [a]		λ_{max} (nm)	Assignment
	$Ru^{III/II}$	Ligand waves	(ε ($dm^3\ mol^{-1}\ cm^{-1}$)) [b]	
1 *trans*-[RuCl(pdma)(bpy)py]PF_6	0.88 (60)	−1.49 (70)	440sh (4100)	$d\pi \rightarrow \pi^*$(bpy)
			342 (7600)	$d\pi \rightarrow \pi^*$(py)
			296 (21800)	$\pi \rightarrow \pi^*$
			246 (14800)	$\pi \rightarrow \pi^*$
2 *trans*-[RuCl(pdma)(bpy)PPh_3]PF_6	1.29 (60)	−1.30 (170)	398 (4400)	$d\pi \rightarrow \pi^*$(bpy)
			298 (17600)	$\pi \rightarrow \pi^*$
3 *trans*-[RuCl(pdma)(bpy)mim]PF_6	0.68 (70)	−1.54 (90)	458 (3900)	$d\pi \rightarrow \pi^*$(bpy)
			344 (4700)	$\pi \rightarrow \pi^*$
			296 (19400)	$\pi \rightarrow \pi^*$
			248 (12100)	$\pi \rightarrow \pi^*$
4 *trans*-[RuCl(pdma)(bpy)(MeCN)]PF_6	0.96 (60)	−1.53 (70)	430 (4000)	$d\pi \rightarrow \pi^*$(bpy)
			292 (20600)	$\pi \rightarrow \pi^*$
			244 (12400)	$\pi \rightarrow \pi^*$
5 *trans*-[RuCl(pdma)(bpy)dmso]PF_6	1.47 [c]	−1.38 (70)	378 (3900)	$d\pi \rightarrow \pi^*$(bpy)
			292 (14900)	$\pi \rightarrow \pi^*$
			246 (11000)	$\pi \rightarrow \pi^*$
6 *trans*-[RuCl(pdma)(bpy)pyz]PF_6	1.04 (70)		430 (10000)	$d\pi \rightarrow \pi^*$(pyz/bpy)
			294 (25200)	$\pi \rightarrow \pi^*$
			248 (20800)	$\pi \rightarrow \pi^*$
7 *trans*-[RuCl(pdma)(bpy)($mpyz^+$)][PF_6]$_2$	1.29 (90)	−0.48 (80)	572 (20200)	$d\pi \rightarrow \pi^*(mpyz^+)$
		−1.52 [d]	402 (5400)	$d\pi \rightarrow \pi^*$(bpy)
		−1.72 [d]	288 (22900)	$\pi \rightarrow \pi^*$
8 *trans*-[RuCl(pdma)(phen)py]PF_6	0.88 (80)	−1.48 (110)	438 (7400)	$d\pi \rightarrow \pi^*$(phen)
			266 (45200)	$\pi \rightarrow \pi^*$
9 *trans*-[RuCl(pdma)(phen)PPh_3]PF_6	1.28 (80)	−1.24 (60)	398 (4900)	$d\pi \rightarrow \pi^*$(phen)
			268 (35500)	$\pi \rightarrow \pi^*$
10 *trans*-[RuCl(pdma)(phen)mim]PF_6	0.67 (80)	−1.55 (100)	448 (9200)	$d\pi \rightarrow \pi^*$(phen)
			268 (33000)	$\pi \rightarrow \pi^*$
11 *trans*-[RuCl(pdma)(phen)pyz]PF_6	1.02 (90)	−1.42 (130)	410 (6700)	$d\pi \rightarrow \pi^*$(pyz/phen)
			268 (33600)	$\pi \rightarrow \pi^*$
12 *trans*-[RuCl(pdma)(phen)($mpyz^+$)][PF_6]$_2$	1.30 (110)	−0.44 (70)	572 (16900)	$d\pi \rightarrow \pi^*(mpyz^+)$
		−1.37 (170)	394 (5200)	$d\pi \rightarrow \pi^*$(phen)
			268 (36000)	$\pi \rightarrow \pi^*$
13 *trans*-[Ru(pdma)(bpy)$(mim)_2$][PF_6]$_2$	1.06 (110)	−1.36 (80)	412 (3700)	$d\pi \rightarrow \pi^*$(bpy)
			292 (20400)	$\pi \rightarrow \pi^*$
			246 (12400)	$\pi \rightarrow \pi^*$
14 *trans*-[Ru(pdma)(bpy)(mim)py][PF_6]$_2$	1.25 (140)	−1.32 (80)	398 (4400)	$d\pi \rightarrow \pi^*$(bpy)
			288 (20600)	$\pi \rightarrow \pi^*$
			244 (14500)	$\pi \rightarrow \pi^*$
15 *trans*-[Ru(pdma)(bpy)mim(MeCN)][PF_6]$_2$	1.28 (150)	−1.39 (70)	390 (6100)	$d\pi \rightarrow \pi^*$(bpy)
			288 (20700)	$\pi \rightarrow \pi^*$
			246 (14200)	$\pi \rightarrow \pi^*$
16 *trans*-[Ru(pdma)(bpy)PPh_3(MeCN)][PF_6]$_2$	1.82 (120)	−1.23 (50)	364 (6000)	$d\pi \rightarrow \pi^*$(bpy)
			288 (15900)	$\pi \rightarrow \pi^*$
17 *cis*-[RuCl(pdma)(bpy)mim]PF_6	0.67 (80)	−1.56 (80)	428 (6200)	$d\pi \rightarrow \pi^*$(bpy)
			320sh (7700)	$\pi \rightarrow \pi^*$
			290 (24600)	$\pi \rightarrow \pi^*$

[a] Measured in solutions ca. 10^{-3} mol dm^{-3} in analyte and 0.1 mol dm^{-3} in $NBu^n_4PF_6$ at a platinum-bead working electrode with a scan rate of 200 mV s^{-1}. Ferrocene internal reference $E_{1/2} = 0.41$ V, $\Delta E_p = 90$ mV.
[b] Solutions (5–7) $\times 10^{-5}$ mol dm^{-3}.
[c] E_{pa} for an irreversible oxidation process.
[d] E_{pc} for an irreversible reduction process.

range from reversible to irreversible. Within the series *trans*-$[Ru^{II}Cl(pdma)(bpy)L_1][PF_6]_n$ ($n = 1$ or 2, **1**–**7**) the $Ru^{III/II}$ $E_{1/2}$ values become more positive as the overall electron donor strength of L_1 decreases, in the order $L_1 = mim > py > MeCN > pyz > mpyz^+ \approx PPh_3 > dmso$. As expected, this trend parallels that observed in the $d_\pi(Ru^{II}) \rightarrow \pi^*(bpy)$ MLCT data (see earlier). The $Ru^{III/II}$ $E_{1/2}$ values of the phen complexes in **8**–**12** are essentially identical to those of their bpy counterparts, and the same dependence upon L_1 is evident. Similarly, in the disubstituted complex salts *trans*-$[Ru^{II}(pdma)(bpy)mim(L_2)][PF_6]_2$ (**13**–**15**) the $Ru^{III/II}$ $E_{1/2}$ values shift to more positive potentials as the electron donor strength of L_2 decreases in the order $mim > py > MeCN$. The complex in **16** has an especially anodic $Ru^{III/II}$ $E_{1/2}$ due to the combined π-electron-withdrawing abilities of the MeCN and PPh_3 ligands. The cyclic voltammograms of **3** and **17** are essentially identical, showing that isomerization does not affect the redox properties of these complexes.

3.5. Structural studies

Single-crystal X-ray structures were determined for **1**, **2**·DMF, **3**, **12**·3MeCN, **14**·DMF and **17**. Representations of the complex cations are shown in Figs. 1–6. The complexes in **1**, **2**·DMF and **3** show the expected *trans* arrangement of the pdma and bpy ligands. In **2**·DMF, the steric bulk of the PPh_3 causes the pdma and bpy ligands to bend slightly towards the chloride, giving an average E–Ru–Cl (E = As or N) bond angle of 84.25(9)°. The corresponding average bond angles in **1** and **3** are 88.3(1) and 88.7(1)°, respectively, showing very little distortion of the octahedral coordination geometries. The Ru–Cl bond distances increase in the order **1** < **3** < **2**·DMF, with a difference of ca. 0.04 Å between **1** and **2**·DMF. This trend reveals the structural *trans*-effect (STE) order with respect to *trans* chloride of $py < mim < PPh_3$.

The structure of **14**·DMF confirms that the *trans* geometry of **3** is maintained upon substitution of the chloride with a pyridine ligand, and the *trans* structure is also found in **12**·3MeCN. In the latter salt, the Ru–N($mpyz^+$) distance (2.019(2) Å) is ca. 0.1 Å shorter than the average Ru–N(phen) distance, owing to a greater degree of π-back donation to the $mpyz^+$ ligand. The complex in $[Ru^{II}(NH_3)_5(mpyz^+)]I_3$ exhibits a still shorter Ru–N($mpyz^+$) distance (1.95(1) Å) [29], indicating that the presence of the strongly basic ammine ligands gives rise to more extensive $Ru^{II} \rightarrow mpyz^+$ back-bonding than is found in **12**·3MeCN.

The structure of **17** confirms that the isomerization of **3** has taken place, with the chloride ligand now *trans* to a bpy N atom. The cation in **17** is chiral and only one absolute configuration at Ru is found in the crystal. The Ru–Cl bond distance in **17** is ca. 0.01 Å shorter than that in **3**, showing that mim has a slightly larger STE than bpy with respect to chloride. Also, the Ru–N(bpy) bond distances are 2.056(4) Å (*trans* to chloride) and 2.101(4) Å (*trans* to pdma), showing that the pdma ligand exerts a rather greater STE on bpy than does chloride. The Ru–As bond distances of 2.3836(7) Å (*trans* to bpy) and 2.3686(7) Å (*trans* to mim) indicate that the STE of bpy on pdma is slightly larger than that of mim.

4. Conclusion

Stepwise substitutions of the axial nitrosyl and chloride ligands are readily achieved in the mixed-chelates *trans*-$[Ru^{II}Cl(pdma)(L–L)(NO)][PF_6]_2$ (L–L = bpy or phen). However, the resulting products are mildly photosensitive in solution and isomerize irreversibly to their *cis* forms. The preparation of chromophore-quencher complexes based on *trans*-$\{Ru^{II}(pdma)(L–L)\}^{2+}$ centres is therefore unlikely to be a worthwhile objective.

Supplementary data

Supplementary data (fractional atomic coordinates, anisotropic thermal parameters, and full listings of bond lengths and angles) are available from the Cambridge Crystallographic Data Centre, 12 Union Road, Cambridge CB2 1EZ, UK (fax: +44-1223-336033; e-mail: deposit@ccdc.cam.ac.uk) on request, quoting the deposition numbers CCDC 139504 (**1**), CCDC 139505 (**2**·DMF), CCDC 139506 (**3**), CCDC 139507 (**12**·3MeCN), CCDC 139508 (**14**·DMF) and CCDC 139509 (**17**).

Acknowledgements

Thanks are due to the Nuffield Foundation for financial support and to the EPSRC for provision of a studentship (CIM). We are grateful to Johnson Matthey plc for a generous loan of ruthenium trichloride.

References

[1] T.J. Meyer, Acc. Chem. Res. 22 (1989) 163.
[2] V. Balzani, F. Scandola, Supramolecular Photochemistry, Ellis Horwood, Chichester, 1991.
[3] B. O'Regan, M. Grätzel, Nature 353 (1991) 737.
[4] K. Kalyanasundaram, M. Grätzel, Coord. Chem. Rev. 177 (1998) 347.
[5] V. Grosshenny, A. Harriman, M. Hissler, R. Ziessel, Platinum Metals Rev. 40 (1996) 26, 72.
[6] F.R. Keene, Coord. Chem. Rev. 166 (1997) 121.
[7] J.-P. Collin, P. Gaviña, V. Heitz, J.-P. Sauvage, Eur. J. Inorg. Chem. 1 (1998) 1.
[8] B.J. Coe, D.A. Friesen, D.W. Thompson, T.J. Meyer, Inorg. Chem. 35 (1996) 4575.
[9] P.G. Douglas, R.D. Feltham, H.G. Metzger, J. Am. Chem. Soc. 93 (1971) 84.
[10] B.J. Coe, M. Chery, R.L. Beddoes, H. Hope, P.S. White, J. Chem. Soc., Dalton Trans. (1996) 3917.

[11] B.J. Coe, S. Hayat, R.L. Beddoes, M. Helliwell, J.C. Jeffery, S.R. Batten, P.S. White, J. Chem. Soc., Dalton Trans. (1997) 591.
[12] B.J. Coe, C.I. McDonald, R.L. Beddoes, Polyhedron 17 (1998) 1997.
[13] SHELXTL 5.03 program system, Siemens Analytical X-Ray Instruments, Madison, WI, 1995.
[14] R. Hooft, Collect, Data collection software, Nonius BV, Delft, The Netherlands, 1998.
[15] Z. Otwinowski, W. Minor, Methods Enzymol. 276 (1997) 307.
[16] R.H. Blessing, Acta Crystallogr., Sect. A 51 (1995) 33.
[17] R.H. Blessing, J. Appl. Crystallogr. 30 (1997) 421.
[18] S. Mackay, C.J. Gilmore, C. Edwards, M. Tremayne, N. Stewart, K. Shankland, MAXUS, a computer program for the solution and refinement of crystal structures from diffraction data, University of Glasgow, UK, Nonius BV, Delft, The Netherlands and MacScience Co. Ltd., Yokohama, Japan, 1998.
[19] G.M. Sheldrick, Acta Crystallogr., Sect. A 46 (1990) 467.
[20] G.M. Sheldrick, SHELXL 97, Program for crystal structure refinement, University of Göttingen, Germany, 1997.
[21] F. Bottomley, Acc. Chem. Res. 11 (1978) 158.
[22] J.A. McCleverty, Chem. Rev. 79 (1979) 53.
[23] S.A. Adeyemi, E.C. Johnson, F.J. Miller, T.J. Meyer, Inorg. Chem. 12 (1973) 2371.
[24] C.A. Bignozzi, S. Roffia, C. Chiorboli, J. Davila, M.T. Indelli, F. Scandola, Inorg. Chem. 28 (1989) 4350.
[25] B.J. Coe, T.J. Meyer, P.S. White, Inorg. Chem. 34 (1995) 593.
[26] P. Bonneson, J.L. Walsh, W.T. Pennington, A.W. Cordes, B. Durham, Inorg. Chem. 22 (1983) 1761.
[27] P. Ford, F.P. De Rudd, R. Gaunder, H. Taube, J. Am. Chem. Soc. 90 (1968) 1187.
[28] C.R. Johnson, R.E. Shepherd, Inorg. Chem. 22 (1983) 2439.
[29] J.F. Wishart, A. Bino, H. Taube, Inorg. Chem. 25 (1986) 3318.

PERGAMON

www.elsevier.nl/locate/poly

Polyhedron 19 (2000) 1205–1211

POLYHEDRON

Synthesis and fungitoxic activity of manganese(II) complexes of fumaric acid: X-ray crystal structures of $[Mn(fum)(bipy)(H_2O)]$ and $[Mn(Phen)_2(H_2O)_2](fum)\cdot 4H_2O$ ($fumH_2$ = fumaric acid; bipy = 2,2′-bipyridine; phen = 1,10-phenanthroline)

Michael Devereux [a,*], Malachy McCann [b], Vanessa Leon [a], Majella Geraghty [b], Vickie McKee [c], Jan Wikaira [d]

[a] *Dublin Institute of Technology, Cathal Brugha Street, Dublin, Ireland*
[b] *Chemistry Department, The National University of Ireland Maynooth, Maynooth, Co. Kildare, Ireland*
[c] *School of Chemistry, The Queen's University, Belfast BT9 5AG, UK*
[d] *Chemistry Department, University of Canterbury, Private Bag 4800, Christchurch, New Zealand*

Received 14 December 1999; accepted 20 March 2000

Abstract

The reaction of fumaric acid with $Mn(CH_3COO)_2\cdot 4H_2O$ gives the polymeric complex $\{Mn(fum)\}_n$ (**1**). Complex **1** reacts with 2,2′-bipyridine in ethanol to yield $[Mn(fum)(bipy)(H_2O)]_n$ (**2**). Reaction of **1** with 2 equiv. of 1,10-phenanthroline produces $[Mn_2(fum)_2(phen)_{2.5}]\cdot 3H_2O$ (**3**) and $[Mn(phen)_2(H_2O)_2](fum)\cdot 4H_2O$ (**4**). The molecular structures of **2** and **4** were determined by X-ray crystallography. In **2** the fumarate anions link the manganese ions so that each is seven coordinate, being bonded to a bidentate bipyridine, two bidentate carboxylates and one H_2O molecule. In **4** the asymmetric unit contains a $[Mn(phen)_2(H_2O)_2]^{2+}$ cation, half of each of two independent fumarate anions and four lattice H_2O molecules. The cations and anions are interconnected by water molecules hydrogen bonded to both coordinated water molecules and fumarate oxygens. The fumarate complexes, the metal free ligands and a number of simple manganese salts were each tested for their ability to inhibit the growth of *Candida albicans*. Only the 'metal free' 1,10-phenanthroline and its fumarate complexes exhibit fungitoxic activity ©2000 Elsevier Science Ltd All rights reserved.

Keywords: Manganese(II) complexes; Fumaric acid; Crystal structures; Fungitoxic activity

1. Introduction

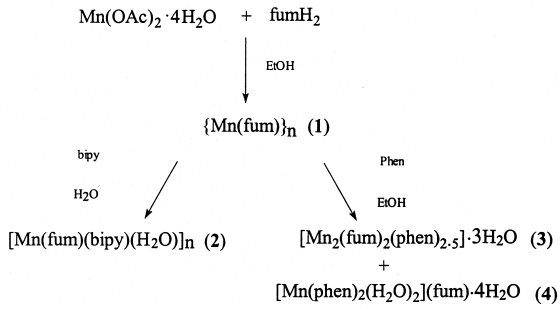
The yeast *Candida albicans* is a commensal of the human body and is considered to be an important fungal pathogen. Opportunistic infection can lead to the development of vaginal candidosis (thrush), a condition from which over 75% of women suffer at some stage in their lifetime. Systemic candidosis is often fatal in immunocompromised patients [1–4]. The state-of-the-art drugs currently used to treat *Candida* infections are often ineffective because of problems with resistance or toxicity and subsequently the search for novel anti-fungal agents has gathered momentum [5]. A number of publications has appeared in the literature highlighting the fungicidal activity of novel transition metal complexes, see for example Ref. [6]. Recently, we have shown that a range of cobalt carboxylate complexes inhibit the growth of *Candida albicans* [7]. Whereas metal complexes of aliphatic monocarboxylic acids have been extensively studied, relatively few papers describing the structures of their diacid equivalents have been published [8]. Rarer still are reports documenting the structures of complexes of unsaturated aliphatic diacids. We have previously described the synthesis, X-ray crystal structures and catalytic activity of a number of manganese(II) complexes containing saturated aliphatic α,ω-dicarboxylic acid ligands [9–13]. Herein we report the synthesis and structural characterisation of two new manganese(II) complexes of fumaric acid. In addition the in vitro anti-*Candida* activities of the compounds are discussed.

2. Results and discussion

Synthetic routes to complexes **1**–**4** are shown in Scheme 1. $\{Mn(fum)\}_n$ (**1**) was prepared in high yield by reacting

* Corresponding author. Tel.: +353-1-402 4486; fax: +353-1-402 4499; e-mail: michael.devereux@dit.ie

0277-5387/00/$ - see front matter ©2000 Elsevier Science Ltd All rights reserved.
PII S0277-5387(00)00372-7



Scheme 1.

manganese(II) acetate tetrahydrate with fumaric acid. Reaction of **1** with excess 2,2′-bipyridine gave $[Mn(fum)(bipy)(H_2O)]_n$ (**2**). When an ethanolic suspension of complex **1** was reacted with 1,10-phenanthroline in a 1:2 molar ratio $[Mn_2(fum)_2(phen)_{2.5}]\cdot 3H_2O$ (**3**) was obtained in high yield. The filtrate from this reaction, when left standing, produced yellow crystals of $[Mn(phen)_2(H_2O)_2](fum)\cdot 4H_2O$ (**4**).

The X-ray structure of **2** is shown in Fig. 1 and selected bond lengths and angles for the complex are given in Tables 1 and 2, respectively. The structure consists of zig-zag polymeric chains running approximately parallel to the *b* axis and in which the monomer is the asymmetric unit $[Mn(fum)(bipy)(H_2O)]$. The *trans*-fumarate anions link the manganese ions so that each is seven coordinate, being bonded to a bidentate bipyridine, two bidentate carboxylates and one H_2O molecule (Fig. 1). The geometry at the manganese ions is quite irregular, the four Mn–O(carboxylate) distances are quite different from each other (Table 1), with that to O(21) being particularly long (2.388(1) Å); unexpectedly, the shortest bond is to the coordinated water molecule (Mn–O1w 2.174(1) Å).

The polymeric chains themselves are linked into sheets in the *ab* plane by hydrogen bonding (Fig. 2) involving coordinated H_2O on one chain and two of the fumarate oxygen atoms on a neighbouring chain (Table 2).

Finally, the two-dimensional sheets are linked by weak π–π stacking of bipyridine groups in adjacent sheets (Fig. 2) (interplanar stacking distance, ~3.8 Å). This long π–π distance may be enforced by the steric constraints of the relatively rigid fumarate dianion.

The X-ray structure of **4** is shown in Fig. 3 and selected bond lengths and angles are listed in Tables 3 and 4, respectively. The asymmetric unit contains a $[Mn(phen)_2(H_2O)_2]^{2+}$ cation, half of each of two independent fumarate anions and four lattice H_2O molecules. The manganese is six coordinate in a *cis*-conformation. One of the fumarate anions (containing O21 and O22) is hydrogen bonded in a 'bidentate' way to both the coordinated water molecules (O1w and O2w). Since this fumarate lies on a centre of symmetry, it acts as a hydrogen-bonded bridge between two neighbouring cations. The second fumarate anion is linked to the cation via a single hydrogen bond (to O2w); this anion also lies on a centre of symmetry, bridging two cations. The lattice therefore contains polymeric, hydrogen-bonded chains of alternating cations and anions.

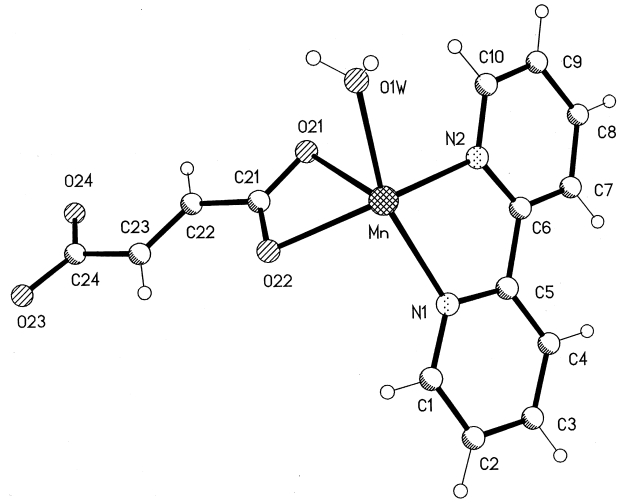


Fig. 1. The asymmetric unit of $[Mn(fum)(bipy)(H_2O)]_n$ (**2**).

Table 1
Selected bond lengths (Å) and angles (°) for complex **2**

Mn–O(1W)	2.1737(14)
Mn–O(22)	2.2473(12)
Mn–N(2)	2.2720(15)
Mn–N(1)	2.2923(15)
Mn–O(24)	2.3036(11)
Mn–O(23)	2.3297(12)
Mn–O(21)	2.3877(13)
O(1W)–Mn–O(22)	105.25(5)
O(1W)–Mn–N(2)	94.16(5)
O(22)–Mn–N(2)	128.96(5)
O(1W)–Mn–N(1)	162.40(5)
O(22)–Mn–N(1)	92.07(5)
N(2)–Mn–N(1)	71.98(5)
O(1W)–Mn–O(24)	96.78(5)
O(22)–Mn–O(24)	83.04(4)
N(2)–Mn–O(24)	141.55(4)
N(1)–Mn–O(24)	88.25(5)
O(1W)–Mn–O(23)	81.90(5)
O(22)–Mn–O(23)	139.94(4)
N(2)–Mn–O(23)	88.61(4)
N(1)–Mn–O(23)	86.86(5)
O(24)–Mn–O(23)	56.90(4)
O(1W)–Mn–O(21)	79.67(5)
N(2)–Mn–O(21)	82.47(4)
N(1)–Mn–O(21)	108.30(5)
O(24)–Mn–O(21)	135.75(4)
O(23)–Mn–O(21)	158.84(5)
O(22)–Mn–O(21)	56.41(4)

The four uncoordinated lattice water molecules show extensive hydrogen bonding, to the anion oxygen atoms, the coordinated water and other lattice water molecules (Fig. 4). This results in a complicated hydrogen-bonded network that extends throughout the lattice. The cations and anions are

Table 2
Hydrogen bond lengths (Å) and angles (°) for complex **2** [a]

D–H···A	*d*(D–H)	*d*(H···A)	*d*(D···A)	∠(DHA)
O(1W)–H(1WA)···O(22)#1	0.81(2)	1.97(2)	2.7241(17)	155(2)
O(1W)–H(1WB)···O(24)#2	0.83(2)	1.94(2)	2.7057(17)	153(2)

[a] Symmetry transformations used to generate equivalent atoms: #1 $x+1/2, y, -z+1/2$, #2 $-x+1/2, y+1/2, z$.

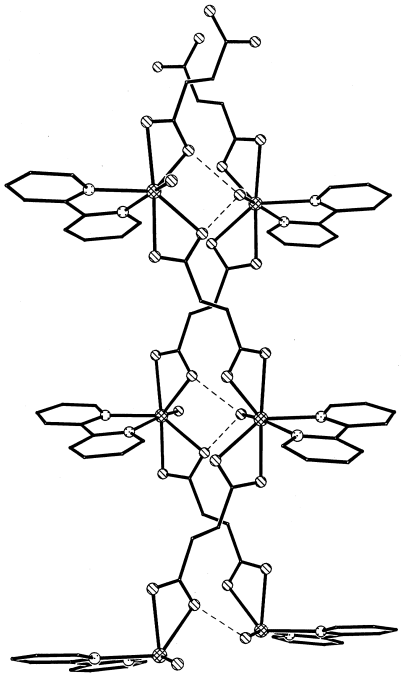


Fig. 2. The polymeric chains in $[Mn(fum)(bipy)(H_2O)]_n$ (**2**).

interconnected by water molecules hydrogen bonded to both coordinated water molecules and fumarate oxygens.

The IR spectrum of **1** contains prominent $\nu_{OCOasym}$ and ν_{OCOsym} stretching bands around 1575 and 1387 cm^{-1}, respectively. The relatively large value of Δ_{OCO} ($\nu_{OCOasym} - \nu_{OCOsym}$) calculated for the complex (188 cm^{-1}) is close to the value expected for a unidentate coordination mode of the carboxylate moiety [14]. Its relative insolubility in most common solvents suggests that it may have a polymeric structure. Indeed, we have found in previous studies that the saturated aliphatic dicarboxylic acids usually give polymeric complexes when reacted with manganese(II) acetate [9–13]. Complex **1** is sparingly soluble in ethanol and its molar conductivity ($\Lambda_M = 0.43$ S cm^2 mol^{-1}) suggests that it is a non-electrolyte in this solvent. The Δ_{OCO} value for complex **2** (114 cm^{-1}) is as expected for a chelating coordination mode of the carboxylate moieties [14]. The molar conductivity value for an aqueous solution of complex **2** ($\Lambda_M = 163$ S cm^2 mol^{-1}) suggests that it forms a 1:1 electrolyte in water and dissociates to give the cationic $[Mn(bipy)]^{2+}$ and the anionic fum^{2-} species, respectively. Complex **3** was isolated as a powder which was only sparingly soluble in methanol and chloroform. The value of Δ_{OCO}

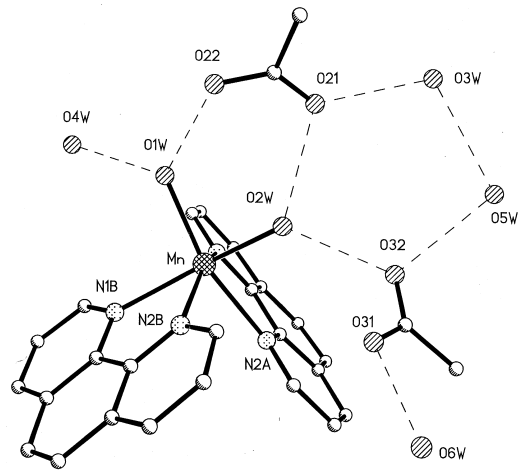


Fig. 3. The asymmetric unit of $[Mn(Phen)_2(H_2O)_2](fum)\cdot 4H_2O$ (**4**).

Table 3
Selected bond lengths (Å) and angles (°) for complex **4**

Mn–O(2W)	2.1297(10)
Mn–O(1W)	2.1433(10)
Mn–N(2B)	2.2690(12)
Mn–N(1A)	2.2728(11)
Mn–N(1B)	2.2965(11)
Mn–N(2A)	2.3157(12)
O(2W)–Mn–O(1W)	84.77(4)
O(2W)–Mn–N(2B)	89.32(4)
O(1W)–Mn–N(2B)	108.83(4)
O(2W)–Mn–N(1A)	109.66(4)
O(1W)–Mn–N(1A)	92.98(4)
N(2B)–Mn–N(1A)	152.52(4)
O(2W)–Mn–N(1B)	161.69(4)
O(1W)–Mn–N(1B)	95.47(4)
N(2B)–Mn–N(1B)	73.22(4)
N(1A)–Mn–N(1B)	88.63(4)
O(2W)–Mn–N(2A)	87.96(4)
O(1W)–Mn–N(2A)	161.05(4)
N(2B)–Mn–N(2A)	88.51(4)
N(1A)–Mn–N(2A)	73.04(4)
N(1B)–Mn–N(2A)	96.89(4)

($\nu_{OCOasym} - \nu_{OCOsym}$) calculated for the complex (182 cm^{-1}) is similar to that for complex **1**, suggesting that the carboxylate functions may be coordinated to the manganese centres in a similar mode. The molar conductivity value of **3** ($\Lambda_M = 1.52$ S cm^2 mol^{-1}) suggests that it does not dissociate in methanol. Although the fumarate ligand is uncoordinated in complex **4** the relatively high Δ_{OCO} value (215 cm^{-1})

Table 4
Hydrogen bond lengths (Å) and angles (°) for complex **4** [a]

D–H···A	*d*(D–H)	*d*(H···A)	*d*(D···A)	∠(DHA)
O(1W)–H(1WA)···O(22)	0.88	1.87	2.7372(14)	169.9
O(1W)–H(1WB)···O(4W)	0.85	1.87	2.6980(14)	164.4
O(2W)–H(2WA)···O(21)	0.91	1.79	2.6987(14)	175.7
O(2W)–H(2WB)···O(32)	0.88	1.73	2.6184(13)	177.2
O(3W)–H(3WA)···O(21)	0.86	1.96	2.8072(14)	167.5
O(3W)–H(3WB)···O(5W)	0.91	1.92	2.8295(17)	172.8
O(4W)–H(4WA)···O(6W)#1	0.84	1.91	2.7393(16)	170.3
O(4W)–H(4WB)···O(22)#2	0.88	1.86	2.7433(15)	174.0
O(5W)–H(5WA)···O(32)	0.85	1.99	2.8248(15)	167.7
O(5W)–H(5WB)···O(3W)#3	0.77	2.15	2.9089(17)	167.9
O(6W)–H(6WA)···O(3W)#4	0.91	1.93	2.8339(17)	172.2
O(6W)–H(6WB)···O(31)	0.91	1.87	2.7758(16)	177.3

[a] Symmetry transformations used to generate equivalent atoms: #1 $x-1, y-1, z$, #2 $-x+1, -y, -z+1$, #3 $-x+1, -y+1, -z$, #4 $x+1, y, z$.

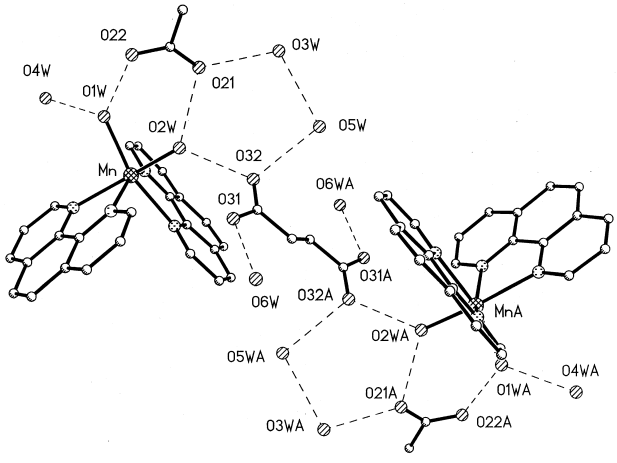


Fig. 4. The structure of $[Mn(Phen)_2(H_2O)_2](fum)\cdot 4H_2O$ (**4**) with hydrogen-bonding interactions.

possibly results from the extensive hydrogen bonding that exists between the carboxylate oxygens and both the coordinated and uncoordinated water molecules within the crystal. The room temperature magnetic moments of powdered samples of complexes **1**, **2**, **3** and **4** (5.65, 5.89, 5.99 and 5.76 BM respectively) were in the range expected for manganese complexes where there is no significant exchange interaction between metal centres [15].

The fumarate complexes, the metal-free ligands and a number of simple manganese salts were each tested for their ability to inhibit the growth of *Candida albicans* (Table 5). Fumaric acid exhibits negligible fungitoxic activity. The simple manganese(II) salts are essentially inactive also. The fumarate complex **1** does not show fungistatic activity at all against the *Candida*. Both the uncoordinated 2,2′-bipyridine and its fumarate derivative (complex **2**) are also ineffective against the pathogen. However, the phenanthroline complexes **3** and **4** both exhibit discrete anti-*Candida* activity causing 69 and 67% inhibition of cell growth respectively. Significantly the 'metal free' 1,10-phenanthroline itself shows the greatest activity causing 77% inhibition of cell growth. However, we believe that the so-called metal-free

Table 5
Anti-*Candida* activity [a]

Test compound	% Cell growth Isolate
Control	100
Fumaric acid	106 ± 8
1,10–phenanthroline	23 ± 2
2,2′–bipyridine	114 ± 6
$MnCl_2$	110 ± 5
$Mn(NO_3)_2$	133 ± 7
$Mn(OAc)_2$	117 ± 10
$Mn(SO_4)$	98 ± 9
[Mn(fum)] (**1**)	98 ± 10
$[Mn(fum)(bipy)(H_2O)]_n$ (**2**)	115 ± 6
[Mn(fum)(phen)] (**3**)	31 ± 2
$[Mn(phen)_2(H_2O)_2](fum)\cdot 4H_2O$ (**4**)	33 ± 2

[a] The compounds were tested at concentrations of 10 μg cm^{-3} of aqueous RPMI medium. Complexes **1**–**4** were insoluble in water and were used as suspensions. Yeast cells were grown for 24 h at 37°C. Results are presented as % cell growth and the effectiveness of the compounds is compared to the growth of the control (no compound added).

1,10-phenanthroline is probably coordinating to metal ions (other than the manganese) that are present in trace amounts in the growth medium and that it is these resulting metal–phenanthroline complexes that are responsible for the high anti-*Candida* activity. Studies are currently underway in our laboratories to examine this theory.

In conclusion, it would appear that fumaric acid whether coordinated or uncoordinated to manganese does not possess any anti-*Candida* properties. Furthermore, the presence of the NN-donor 2,2′-bipyridine does not improve the activity of the complex. The 1,10-phenanthroline molecule is a potent anti-*Candida* agent and upon reaction with the manganese fumarate yields complexes with comparable fungitoxic activity.

3. Experimental

Chemicals were purchased from commercial sources and used without further purification. IR spectra were recorded

in the region 4000–400 cm^{-1} on a Nicolet-400 Impact spectrometer. Magnetic susceptibility measurements were made using a Johnson Matthey magnetic susceptibility balance. $[HgCo(SCN)_4]$ was used as a reference. Conductivity readings were obtained using a Ciba Corning model check-mate 90 conductivity meter. Satisfactory microanalytical data for the complexes were reported by the Microanalytical Laboratory, University College Cork, Ireland.

3.1. $\{Mn(fum)\}_n$ (1)

To a solution of $fumH_2$ (3.15 g, 27.14 mmol) in ethanol (100 cm^3) was added manganese(II) acetate (5.94 g, 24.44 mmol), and the reaction mixture was refluxed for 2 h. The product formed as a colourless solid. The reaction mixture was allowed to cool to room temperature and then the product was filtered. The material was washed with two portions of ethanol and then dried in air. Yield 3.72 g (90.06%). Complex **1** was sparingly soluble in warm EtOH and MeOH, and insoluble in distilled H_2O, acetone, ether and chloroform. *Anal*. Found: C, 28.20; H, 1.31. Calc.: C, 28.43; H, 1.19%. IR: 3449.25, 3086.57, 2361.19, 1575.37, 1467.91, 1387.31, 1199.25, 991.04, 809.70, 688.81, 594.78 cm^{-1}. $\mu_{eff} = 5.65$ BM. $\Lambda_M(EtOH) = 0.43$ S cm^2 mol^{-1}.

3.2. $[Mn(fum)(bipy)(H_2O)]_n$ (2)

Complex **1** (0.5 g, 2.96 mmol) and 2,2′-bipyridine (1.25 g, 8.00 mmol) were stirred in deionised water (100 cm^3) for 4 h to give a pale green solution. On standing for several days at room temperature the product formed as yellow crystals. The crystals were filtered off, washed with deionised water and ethanol and then air dried. Yield 0.77 g (84.05%). Complex **2** was sparingly soluble in warm distilled H_2O, and insoluble in EtOH, MeOH, acetone, ether and chloroform. *Anal*. Found: C, 48.75; H, 3.42; N, 8.14. Calc.: C, 48.99; H, 3.52; N, 8.16%. IR: 3415.67, 3106.7, 3079.85, 1689.55, 1608.86, 1588.81, 1555.22, 1494.21, 1474.63, 1441.04, 1387.31, 1320.15,1246.27, 1219.40, 1158.96, 1105.22, 1058.21, 1004.48, 977.61, 802.99, 762.69, 735.82, 682.09, 647.76, 628.36, 561.19, 486.53 cm^{-1}. $\mu_{eff} = 5.89$ BM. $\Lambda_M(H_2O) = 163$ S cm^2 mol^{-1}.

3.3. $[Mn_2(fum)_2(phen)_{2.5}]\cdot 3H_2O$ (3) and $[Mn(phen)_2(H_2O)_2](fum)\cdot 4H_2O$ (4)

Complex **1** (1.00 g, 5.92 mmol) and 1,10-phenanthroline (2.12 g, 10.69 mmol) were refluxed in ethanol (150 cm^3) for 2 h. Upon cooling to room temperature the resulting yellow suspension was filtered to give a yellow powder and a yellow filtrate. The yellow product (**3**) was washed with ethanol and then air dried. Yield 1.86 g (37.29%). Complex **3** was sparingly soluble in warm MeOH and chloroform, and insoluble in distilled H_2O, EtOH, acetone and ether. *Anal*. Found: C, 54.23; H, 3.31; N, 8.63. Calc.: C, 54.17; H, 3.59; N, 8.31%. IR: 3449.13, 1602.24, 1514.93, 1420.90, 1205.97, 1151.60, 1105.22, 991.04, 970.22, 843.28, 809.70, 775.40, 729.10, 675.37, 634.32 cm^{-1}. $\mu_{eff} = 5.76$ BM. $\Lambda_M(MeOH) = 1.52$ S cm^2 mol^{-1}.

Upon standing at room temperature for 7 months yellow crystals of complex **4** precipitated from the filtrate. The crystals were filtered, washed with acetone and then dried in air. Yield 0.27 g (0.07%). Complex **4** was sparingly soluble in warm MeOH and insoluble in distilled H_2O, EtOH, acetone, chloroform and ether. *Anal*. Found: C, 56.35; H, 4.02; N, 9.67. Calc.: C, 52.75; H; 4.74; N, 8.79%. IR: 3388.81, 1575.37, 1514.93, 1427.61, 1360.45, 1212.69, 1089.51, 850.00 cm^{-1}. $\mu_{eff} = 5.99$ BM. $\Lambda_M(MeOH) = 0$ S cm^2 mol^{-1}.

3.4. X-ray crystallography

Crystal data for $[Mn(fum)(bipy)(H_2O)]_n$ (**2**) and $[Mn(phen)_2(H_2O)_2](fum)\cdot 4H_2O$ (**4**) are summarised in Table 6. Data sets for both complexes were collected using a Siemens SMART CCD diffractometer and were corrected for Lorentz, polarisation and absorption effects. The structures were solved by direct methods [16] and refined by full-matrix least-squares on F^2 using all the data. All the non-hydrogen atoms were refined with anistropic atomic displacement, hydrogen atoms were inserted at calculated positions with their isotropic displacement parameters riding on U_{ij} of their carrier atoms (except for those on the water molecules which were located from difference Fourier maps and their positions either allowed to refine (for complex **2**) or were not further refined (for complex **4**)). The programmes used in the final structure refinement are contained in the SHELXL-97 package [17].

3.5. Anti-Candida susceptibility testing

Candida albicans isolate was obtained commercially from Oxid Culti-loops (ATCC 10231). The isolate was stored on Sabouraud dextrose agar (SDA) plates at 4°C.

Suspensions of the test complexes were prepared by grinding them to a fine powder (0.02 g) followed by addition to sterile distilled water (100 cm^3). This process yielded stock suspensions of 200 μg cm^{-3}. These suspensions were furthered diluted to 100 μg cm^{-3}.

RPMI-1640 broth medium (Sigma R 7755) was used for the anti-*Candida* susceptibility testing. The medium (1 dm^3) was supplemented with L-glutamine (0.3 g) and morpholinepropanesulfonic acid (MOPS) (34.6 g) and was then adjusted to pH 7.0 using sterile NaOH (0.2 M). The broth microdilution reference method was used, NCCLS publication M27-P [18]. Prior to testing, yeast cells were grown on Sabouraud dextrose agar (SDA) at 37°C for 24 h. Cell suspensions were prepared in sterile phosphate buffered saline (5 cm^3) to a density of 1 McFarland standard. A 1:100 dilution of these cell suspensions were made in RPMI-1640 medium so that the cell concentration of the final inoculum was 3.5×10^4–5.0×10^5 cells cm^{-3}. The prepared cell sus-

Table 6
Summary of crystal data, data collection, structure solution and refinement details for complexes **2** and **4**

	2	**4**
Complex	[Mn(fum)(bipy)(H_2O)]	[Mn(Phen)$_2$(H_2O)$_2$](fum)·4H_2O
Formula	$C_{14}H_{12}MnN_2O_5$	$C_{28}H_{30}MnN_4O_{10}$
Description	pale yellow block	pale yellow block
Crystal size (mm)	0.24×0.45×0.6	0.52×0.50×0.28
Temperature (K)	158(2)	164(2)
a (Å)	9.105(3)	10.6034(17)
b (Å)	15.057(4)	10.6499(17)
c (Å)	19.814(5)	13.565(2)
α (°)	90	96.122(2)
β (°)	90	94.658(3)
γ (°)	90	105.002(2)
U (Å^{-3})	2879(1)	1461(4)
F(000)	1400	662
Crystal system	orthorhombic	triclinic
Space group	*Pbca*	$P\bar{1}$
Z	8	2
Density calc. (Mg m^{-3})	1.584	1.448
μ (mm^{-1})	0.942	0.515
T_{max}, T_{min}	1.00, 0.829	1.00, 0.860
θ Range (°)	2.06–26.49	2.00–26.35
Index ranges	$-11 \le h \le 11$, $-19 \le k \le 12$, $-24 \le l \le 24$	$-11 \le h \le 13$, $-13 \le k \le 13$, $-8 \le l \le 16$
Reflections collected	34298	11962
Independent reflections	2943	5861
R_{int}	0.0342	0.0160
Data/restraints/parameters	2943/0/205	5861/0/389
Goodness of fit on F^2	1.054	1.043
R_1, wR_2 ($I > 2\sigma(I)$)	0.0277, 0.0751	0.0280, 0.0797
R_1, wR_2 (all data)	0.0351, 0.0767	0.0315, 0.0815

pension (900 μl) was dispensed into sterile test tubes and to this was added the test complex solutions (100 μl) to yield working solutions of the test complexes of concentration 10 μg cm^{-3}. The test tubes were then incubated in a shaking water bath for 24 h at 37°C with continuous shaking. Each complex was assessed in triplicate and three independent experiments were performed.

Supplementary data

Supplementary data for the three structures are available from the Cambridge Crystallographic Data Centre, 12 Union Road, Cambridge CB2 1EZ, UK (fax: +44-1223-336033; e-mail: deposit@ccdc.cam.ac.uk), on request quoting the deposition numbers CCDC 137687 and CCDC 137688, respectively.

Acknowledgements

M. Devereux acknowledges the late Noel O'Reilly (DIT) and Iris Swift (DIT) for technical assistance, and V. Leon acknowledges the SRD and Seed funding schemes (DIT/EU) for financial support.

References

[1] T.J. Walsh, J.W. Hiemenz, E. Anaissie, Infect. Dis. Clin. North Am. 29 (1996) 365.
[2] A.H. Groll, J. Infect. 33 (1996) 23.
[3] G.Y. Minamoto, A.S. Rosenberg, Med. Clin. North Am. 81 (1997) 381.
[4] A.H. Groll, A.J. De Lucca, T.J. Walsh, Trends Microbiol. 6 (1998) 117.
[5] A.L. Barry, S.D. Brown, Antimicrob. Agents Chemother. 40 (1996) 1948.
[6] M. Petric, F. Pohleven, I. Turel, P. Segedin, A. White, D. Williams, Polyhedron 17 (1998) 255.
[7] M. Geraghty, M. McCann, M. Devereux, F. Cronin, M. Curan, V. McKee, Metal Based Drugs 6 (1999) 41.
[8] R.C. Mehrotra, R. Bohra, Metal Carboxylates, Academic Press, London, 1983.
[9] M.T. Casey, M. McCann, M. Devereux, M. Curran, C. Cardin, M. Convery, V. Quillet, C. Harding, J. Chem Soc., Chem. Commun. (1994) 2643.
[10] M. McCann, M.T. Casey, M. Devereux, M. Curran, V. McKee, Polyhedron 16 (1997) 2741.
[11] M. McCann, M.T. Casey, M. Devereux, M. Curran, G. Ferguson, Polyhedron 16 (1997) 2547.
[12] S. McCann, M. Devereux, M. McCann, M.T. Casey, V. McKee, P. McMichael, J. McCrea, Polyhedron 16 (1997) 4247.
[13] M. Geraghty, M. McCann, M.T. Casey, M. Devereux, M. Curran, V. McKee, J. McCrea, Inorg. Chim. Acta 277 (1998) 257.

[14] K. Nakamoto, Infrared and Raman Spectra of Inorganic and Coordination Compounds, Wiley, New York, 3rd edn., 1978.
[15] F.A. Cotton, G.K. Wilkinson, Advanced Inorganic Chemistry, Wiley, New York, 5th edn., 1988, p. 702.
[16] J. Díez, M. Pilar Gamasa, J. Gimeo, A. Tiripicchio, M. Tiripicchio Camellini, J. Chem. Soc., Dalton Trans. (1987) 1275.
[17] G.M. Sheldrick, SHELXL-97, University of Göttingen, Germany, 1997.
[18] NCCLS (National Committee for Clinical Laboratory Standards), reference method for broth dilution antifungal susceptibility testing of yeasts, proposed standard, NCCLS publication M27-P, NCCLS, Villanova, PA, 1992.

PERGAMON

www.elsevier.nl/locate/poly

Polyhedron 19 (2000) 1213–1218

POLYHEDRON

Kinetics of oxidation of ascorbic acid by the $[Mn_3^{IV}(\mu\text{-}O)_4(bipy)_4(H_2O)_2]^{4+}$ ion (bipy = 2,2′-bipyridine)

Biswapriya Mondal [a], Anup K. Bhattacharya [a], Rupendranath Banerjee [a,*1], G.S. Bhrahma [b], A.C. Dash [b,*2]

[a] *Department of Chemistry, Jadavpur University, Calcutta 700 032, India*
[b] *Department of Chemistry, Utkal University, Vani Vihar, Orissa, India*

Received 14 September 1999; accepted 20 March 2000

Abstract

In the pH range 1.91–5.24, an aqueous solution of the complex $[Mn_3^{IV}(\mu\text{-}O)_4(bipy)_4(H_2O)_2]^{4+}$ (**1**) oxidises ascorbic acid quantitatively to dehydroascorbic acid and is itself reduced to Mn^{II}. In the presence of excess ascorbic acid, the reaction follows first-order kinetics. The first-order rate constant k_0 measured in the presence of excess ascorbic acid increases linearly with increasing concentration of the reductant but decreases as more and more 2,2′-bipyridine is added. k_0 also increases with $[H^+]$ but tends to saturate at higher $[H^+]$. The proposed rate-determining step involves simultaneous transfer of one electron and one proton from the ascorbate ion to $[Mn_3^{IV}(\mu\text{-}O)_4(bipy)_3(H_2O)_4]^{4+}$, an aquated form of **1**. Subsequent rapid reactions via a dinuclear $\{Mn_2O_2\}^{3+}$ intermediate lead to the final products. ©2000 Elsevier Science Ltd All rights reserved.

Keywords: Kinetics; Manganese(IV); Ascorbic acid; Electroprotic reactions

1. Introduction

In the recent past, kinetics of redox reactions of three dinuclear higher-valent manganese complexes have been determined to elucidate the reaction mechanism [1–8]; this is of interest because these complexes are related [9–11] to the oxygen evolving complex (OEC) in photosystem II [12–14]. However, we are not aware of any kinetic studies on manganese complexes with nuclearity greater than two.

The crystallographically characterised trimer $[Mn_3^{IV}(\mu\text{-}O)_4(bipy)_4(H_2O)_2]^{4+}$ (**1**) (Fig. 1) [15] has three important features which are known or assumed for the OEC: (a) oxo-bridged manganese ions in higher oxidation state, (b) two sets of Mn–Mn distances ~2.7 and ~3.3 Å [16], and (c) terminal aqua ligands bound to high-valent manganese [17,18]. Complex **1** is a useful catalyst in the oxidation of olefins and hydrocarbons by potassium peroxymonosulfate [19].

UV–Vis spectra of the complex in aqueous solution do not change within a few hours and illustrate the stable nature of the complex in water, in spite of the high-valency state of the three manganese ions. Measurement of the kinetics of its redox reactions may elucidate the mechanistic pathways for the reactions of the multinuclear complexes; hence this study.

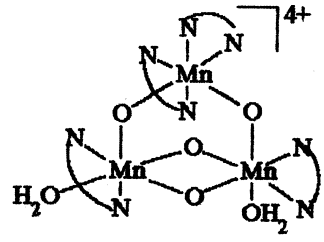


Fig. 1. Graphic drawing of the complex ion $[Mn_3^{IV}(\mu\text{-}O)_4(bipy)_4(H_2O)_2]^{4+}$; bipy is 2,2′-bipyridine.

The reducing agent ascorbic acid (H_2A) is of importance as a hydroxylase cofactor [20] and as an antioxidant [21]. Brown et al. utilised ascorbic acid as a source of reducing equivalent in a multicomponent system that promotes the photo-reduction of water [22]. Metal complexes generally oxidise ascorbic acid (H_2A) to dehydroascorbic acid (A) with a net transaction of two electrons, but this change is almost always accomplished in one-electron steps [23–25]. In one important exception, a ferriporphyrin dimer [25] oxidises ascorbic acid by a two-electron pathway, thus avoiding free-radical generation.

[1] *Corresponding author. Tel.: +91-33-555-1665; e-mail: dsther28@cd2.vsnl.net.in
[2] *Corresponding author.

0277-5387/00/$ - see front matter ©2000 Elsevier Science Ltd All rights reserved.
PII S0277-5387(00)00376-4

2. Experimental

L-Ascorbic acid (Aldrich) was used without further purification. Complex **1** $(ClO_4)_4 \cdot 5H_2O$ was prepared in small batches [15], by slow evaporation of a pH 1.9 (HNO_3) solution containing 50–100 mg of the dimer $[Mn_2^{III,IV}(\mu\text{-}O)_2(bipy)_4](ClO_4)_3 \cdot 2H_2O$ in a lot. The C, H, N analyses were found satisfactory for characterisation of the complex. Its spectral features agree with those reported earlier in the range 500–900 nm [15,26]. All other materials [4] and preparation [26] of the complex $[Mn_2^{III,IV}(\mu\text{-}O)_2(bipy)_4](ClO_4)_3 \cdot 2H_2O$ have been described earlier.

Kinetics was measured in the presence of excess ascorbic acid at 15.0°C, I 1.0 mol dm^{-3} ($NaNO_3$). The reactions were monitored by the loss in absorbance at 370 nm with a stopped-flow spectrophotometer (HITECH SF-51), interfaced to an Apple II GS personal computer for data acquisition and analyses of absorbance–time data for rate constants. The reaction mixtures contained excess c_{bipy} ($c_{bipy} = [Hbipy^+] + [bipy]$) and were thus lightly buffered. Solution pH were measured with an Orion 710A2 pH/ion meter and an Orion Ross combination (model 81-02) electrode. The $[H^+]$ values were evaluated as described earlier [27].

The reaction stoichiometry was determined in the presence of excess ascorbic acid under the kinetic conditions. After complete reaction, an excess of $Fe(NO_3)_3$ solution was added to oxidise the remaining ascorbate quantitatively. The Fe^{II} thus produced generated $[Fe(bipy)_3]^{2+}$ with excess bipy present in the reaction media and was measured spectrophotometrically at 522 nm ($\varepsilon_{max}^{522} = 8.5 \times 10^3$ dm^3 mol^{-1} cm^{-1}) [1].

Table 1
Stoichiometric measurements for the oxidation of ascorbic acid by the trinuclear Mn_3^{IV} complex; T 25°C; concentrations in mmol dm^{-3}

[Complex]	c_{asc}	pH	C_{bipy}	Δ[red]/Δ[ox] [a]
1.0	10	4.50	20	3.10
1.0	12	3.54	34	3.04
2.0	16	1.85	40	3.14
1.0	16	2.58	20	3.08
0.6	10	4.08	12	2.94
1.0	8	4.08	12	2.98

[a] Average 3.04 ± 0.10.

Table 2
Kinetic data [a] for the oxidation of ascorbic acid by the trinuclear Mn_3^{IV} complex

pH	c_{bipy} (mmol dm^{-3})	c_{asc} (mmol dm^{-3})	k_0 (s^{-1})
1.91	5.0	1.0	81.5 (81.7)
2.54			78.4 (80.6)
2.89			75.1 (78.9)
3.50			72.2 (71.3)
3.94			57.8 (60.8)
4.54			47.0 (45.9)
5.24			38.8 (37.0)
4.50	4.0		57.5 (58.1)
	5.1		46.5 (44.7)
	6.5		36.5 (35.8)
	8.0		30.1 (29.1)
	9.5		23.2 (24.5)
	12.0		18.5 (19.4)
	18.0		13.0 (12.9)
	34.0		6.5 (6.8)
	5.0	0.5	23.0 (23.2)
		1.0	47.5 (46.5)
		1.5	68.1 (69.7)
		2.0	95.1 (93.0)
		2.5	120.3 (116.3)
		3.0	136.3 (139.5)
		3.5	160.0 (162.8)
		4.0	189.1 (186.1)

[a] Average of 4–5 independent experiments, standard deviation 2–6%. [Complex] 0.10 mmol dm^{-3}; I 1.0 mol dm^{-3} ($NaNO_3$); T 15.0°C. Parenthetical values were calculated using Eq. (5).

3. Results and discussion

Measurement of unreacted ascorbic acid (Table 1) indicated a 3:1 stoichiometry according to Eq. (1).

$$[Mn_3^{IV}(\mu\text{-}O)_4(bipy)_4(H_2O)_2]^{4+} + 2H^+ + 3H_2A \rightarrow 3Mn^{II} + 4bipy + 6H_2O + 3A \quad (1)$$

The reaction followed excellent first-order kinetics at least up to 90% completion. The first-order rate constants k_0 (Table 2) increased with increasing concentration of ascorbic acid ($c_{asc} = [H_2A] + [HA^-]$) without any suggestion of rate saturation even for $c_{asc} = 40$[complex]; a plot of k_0 versus c_{asc} is a good straight line ($r = 0.992$) passing through the origin. k_0 decreased with increasing c_{bipy} but increased with increasing $[H^+]$ tending to saturate at higher $[H^+]$ (Fig. 2). However, k_0 decreased with increasing c_{bipy} and a plot of k_0 versus $1/c_{bipy}$ is a good straight line passing through the origin (Fig. 3, $r = 0.995$).

Ascorbic acid (H_2A, $pK_a = 4.03$ [28]) and ascorbate anion (HA^-, $pK_a' = 11.3$ [29]) coexist in the experimental pH

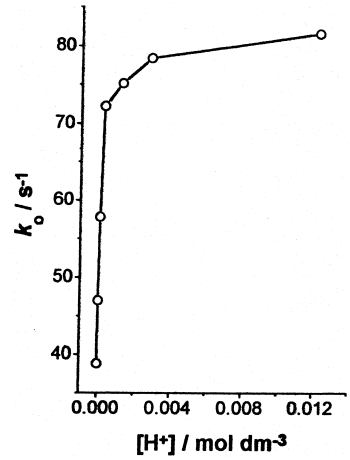


Fig. 2. Dependence of k_0 on $[H^+]$: [complex] 0.10 mmol dm^{-3}, c_{bipy} 5.0 mmol dm^{-3}, c_{asc} 1.0 mmol dm^{-3}, I 1.0 mol dm^{-3}, T 15.0°C.

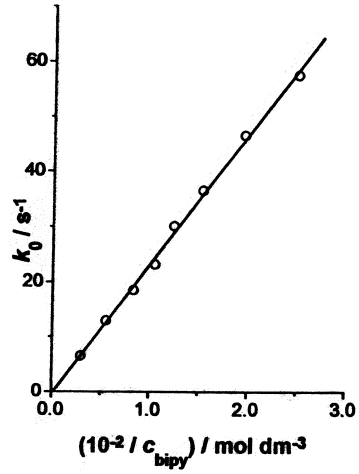


Fig. 3. Linear dependence of k_0 on $(c_{bipy})^{-1}$: [complex] 0.10 mmol dm^{-3}, c_{asc} 1.0 mmol dm^{-3}, pH 4.50, I 1.0 mol dm^{-3}, T 15.0°C.

range 1.91–5.24. The rate of oxidation of ascorbic acid generally decreases with increasing acidity, because H_2A is $\sim 10^4$ times less active [30] than HA^-. An increase in k_0 with $[H^+]$ in the present case, therefore, strongly suggests involvement of the trinuclear complex in a protic equilibrium, generating a kinetically more reactive form of the oxidising agent at lower pH. The equilibrium (2) seems to be a reasonable choice. It predicts increased rate with decreasing pH and also with decreasing c_{bipy}, provided **2** is kinetically much more active than **1**.

$$[\underset{\mathbf{1}}{Mn_3^{IV}(\mu\text{-}O)_4(bipy)_4(H_2O)_2}]^{4+} + H^+ + 2H_2O$$

$$\overset{K_H}{\rightleftharpoons} [\underset{\mathbf{2}}{Mn_3^{IV}(\mu\text{-}O)_4(bipy)_3(H_2O)_4}]^{4+} + Hbipy^+ \qquad (2)$$

$$[\underset{\mathbf{2}}{Mn_3^{IV}(\mu\text{-}O)_4(bipy)_3(H_2O)_4}]^{4+} + HA^- \overset{k}{\rightarrow} \text{product} \qquad (3)$$

However, the concentration of HA^-, the active reductant presumed in Eq. (3), is too low at lower pH and the consequent decrease in rate is not compensated fully by the increased concentration of **2**. The rate therefore tends to saturate.

The UV–Vis spectra of **1** change reversibly with a change in $[Hbipy^+]$ as brought about by a change in pH at a constant c_{bipy} (spectra 1–4 in Fig. 4). The spectra do not change if both pH and c_{bipy} are changed, keeping $[Hbipy^+]$ constant. For example, spectrum number 3 in Fig. 4, recorded at $[Hbipy^+] = 3.62$ mmol dm^{-3} (c_{bipy} 5.0 mmol dm^{-3}, pH 4.0), did not change when c_{bipy} and pH were both changed to 8.0 mmol dm^{-3} and 4.50, respectively, keeping $[Hbipy^+]$ fixed at 3.62 mmol dm^{-3}. The spectral changes thus lend support for the presumed equilibrium (Eq. (2)) but the changes are too small to be used in the evaluation of the equilibrium constant.

The absence of a clear isosbestic point in Fig. 4, as would be expected for a fully reversible process, may be a result of interference by an equilibrium other than Eq. (2). One pos-

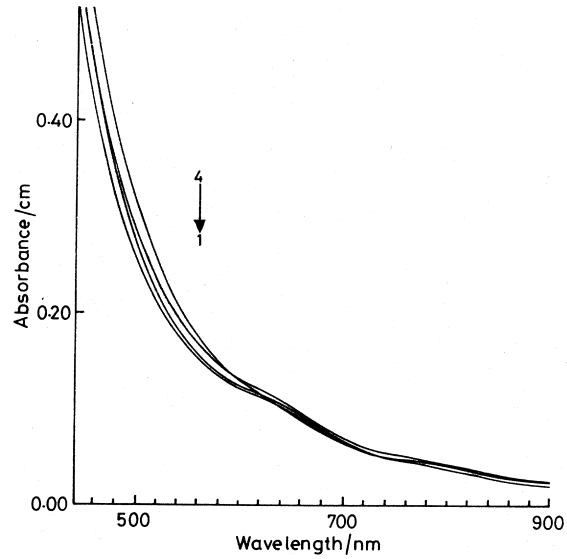


Fig. 4. Spectra of an aqueous solution of **1**: [complex] 0.20 mmol dm^{-3}, T 25.0°C, pH 3.0 (1), 3.5 (2), 4.0 (3), and 4.5 (4), c_{bipy} 5.0 mmol dm^{-3} for (1–4). Spectrum 3 does not change if pH and c_{bipy} are changed simultaneously to 4.5 and 8.0 mmol dm^{-3}, respectively, keeping $[Hbipy^+]$ constant at 3.62 mmol dm^{-3}. The observed spectral changes are reversible.

sibility is deprotonation of coordinated water at the higher pH, generating hydroxo aqua species. Such a deprotonated species may affect the spectra but not the kinetics since conjugate bases are in general kinetically less active oxidants than the parent aqua complexes. Moreover, in the pH-window of this study, the concentration of the hydroxo species is likely to be too low to be kinetically significant. It might be mentioned in this context that no hydroxo aqua form could be detected kinetically [5] for the complex ion $[Mn_2^{IV}(\mu\text{-}O)_2(\mu\text{-}O_2CMe)(bipy)_2(H_2O)_2]^{3+}$ up to pH 5.5.

The kinetic results of the present study suggest that the trinuclear complex is reduced only after the dissociation of one ligand molecule from the cluster. This means that the cluster containing four bipy molecules is not reduced or is reduced much more slowly. Similar situations were observed with some dinuclear manganese complexes. For example, $[Mn_2^{III,IV}(\mu\text{-}O)_2(L)_4]^{3+}$ (L = 1,10-phenanthroline or 2,2′-bipyridine) ions are reduced at a much slower rate than $[Mn_2^{III,IV}(\mu\text{-}O)_2(L)_3(H_2O)_2]^{3+}$. Similarly, the reduction of $[Mn_2^{IV}(\mu\text{-}O)_2(\mu\text{-}O_2CMe)(bipy)_2(H_2O)_2]^{4+}$ is much slower than the reduction of $[Mn_2^{IV,IV}(\mu\text{-}O)_2(\mu\text{-}O_2CMe)(bipy)(H_2O)_4]^{4+}$ [4,7]. In yet another report, it was concluded that the first step in the formation of **1** from $[Mn_2^{III,IV}(\mu\text{-}O)_2(bipy)_4]^{3+}$ is a rapid generation of an active intermediate, which in subsequent redox changes produces **1**. This proposed intermediate is the diaqua species $[Mn_2^{III,IV}(\mu\text{-}O)_2(bipy)_3(H_2O)_2]^{3+}$ [31]; the parent complex is inactive in the redox changes. Aqua complexes exhibit greater activity also in several redox reactions of mononuclear chelates [27,32] of high valent manganese. There may be four possible reasons for the higher reactivity: (i) replacement of a chelating ligand by the weaker donor H_2O makes the metal centre more open and more electron-defi-

cient, thus increasing its strength as an oxidant; (ii) there are more H_2O molecules in the aquated species, e.g. **2**, hence hydrogen bonding with H_2O may stabilise the oxidant–reductant precursor better in **2** than in **1**; (iii) the metal–OH_2 bonds can stretch more easily than the metal–bipy bonds; metal–OH_2 bonds are more numerous in **2**, which therefore has a lower Frank–Condon barrier during structural rearrangements subsequent to electron transfer; (iv) the reductant can approach **2** closer than the parent species **1**.

The effect of pH on the redox potential of **1** in aqueous ligand buffer has not yet been measured experimentally, but a cyclic voltammogram in phosphate buffer shows that **1** becomes a stronger oxidant as the pH is lowered [15], because the reduction involves simultaneous transfer of one electron and one proton. The authors of this work did not consider the possibility of ligand loss at lower pH and the question as to how the thermodynamic oxidising strength changes with aquation remains unanswered. Moreover, the tacit assumption that phosphate is just an innocent buffer may be incorrect [13].

One can derive Eq. (4) for the reaction sequence represented by Eqs. (2) and (3).

$$k_0 = \frac{kK_H[H^+][HA^-]}{[Hbipy^+]+K_H[H^+]} = \frac{kK_HK_a(K_1+[H^+])c_{asc}}{(K_a+[H^+])\{c_{bipy}+K_H(K_1+[H^+])\}} \quad (4)$$

Eq. (4) transforms to Eq. (5) provided the inequality Eq. (6) holds:

$$k_0(K_a+[H^+]) = kK_HK_ac_{asc}(K_1+[H^+])/(c_{bipy}) \quad (5)$$

$$c_{bipy} \gg [K_H(K_1+[H^+])] \quad (6)$$

Here K_a and K_1 are the proton dissociation constants of H_2A and $[Hbipy^+]$ respectively. Their literature values are $K_a = 9.33\times10^{-5}$ mol dm^{-3} at 15°C, I 1.0 mol dm^{-3} [28,33] and $K_1 = 3.8\times10^{-5}$ mol dm^{-3} at 25°C, I 1.0 mol dm^{-3} [34,35][3].

A plot of $k_0(K_a+[H^+])$ versus $(K_1+[H^+])/c_{bipy}$ at a fixed c_{asc} is an excellent straight line ($r = 0.999$) passing through the origin and supports the proposed sequence and associated kinetic assumptions. From the slope of the plot, the value for kK_H is $(4.52\pm0.25)\times10^6$ dm^3 mol^{-1} s^{-1}. Assuming the diffusion controlled limit of the rate constant to be 10^{10} dm^3 mol^{-1} s^{-1} for the reaction of **2** with HA^-, one can evaluate a lower limit for K_H of 4.5×10^{-4}. The inequality Eq. (6), under our experimental conditions, i.e. $[H^+] \geq 3.16\times10^{-4}$ mol dm^{-3} and $c_{bipy} \geq 5.0\times10^{-3}$ mol dm^{-3} imposes an upper limit of $K_H \leq 14$, i.e. $k \geq 3\times10^5$ dm^3 mol^{-1} s^{-1}.

[3] The value of K_1 shows weak dependences on temperature and ionic strength. For example, variation of T in the range 20–25°C and I in the range 0–0.33 mol dm^{-3} causes 17% variation in K_1 ($(3.7–4.46)\times10^{-5}$ dm^3 mol^{-1}) [35]. The effect of such changes is nominal on the kK_H value, which changes only 11% with a 20% change in the value of K_1.

K_H values are known for a few other multinuclear manganese complexes such as $[Mn_2^{III,IV}(\mu\text{-}O)_2(phen)_4]^{3+}$ (35 ± 10) [3], $[Mn_2^{III,IV}(\mu\text{-}O)_2(bipy)_4]^{3+}$ (139 ± 10) [36] and $[Mn_2^{IV}(\mu\text{-}O)_2(\mu\text{-}O_2CMe)(H_2O)_2(bipy)_2]^{4+}$ (26.3) [5]. The equilibrium affects insignificantly the spectral properties and kinetics for $[Mn_2^{IV}(\mu\text{-}O)_2(phen)_4]^{4+}$, $[Mn_3^{IV}(\mu\text{-}O)_4(phen)_4(H_2O)_2]^{4+}$, and $[Mn_4^{IV}(\mu\text{-}O)_6(bipy)_6]^{4+}$; K_H values for these complexes are therefore not known. The overall charge and nuclearity of the clusters and basicity of the ligands should control K_H but the individual effects appear difficult to assess.

The rate of oxidation of $S_2O_3^{2-}$ by the $[Mn_3^{IV}(\mu\text{-}O)_4(phen)_4(H_2O)_2]^{4+}$ ion (**1′**), the 1,10-phenanthroline analogue of **1**, exhibits a first-order dependence on $[H^+]$ but it is independent of c_{phen} [37]. Complex **1′** suffered no ligand loss in the experimental range pH ≥ 4 and the $[H^+]$-dependence arose from a rate determining, coupled one-electron one-proton transfer step. Such an electroprotic mechanism operates [1] in the reduction of the dinuclear complex $[Mn_2^{III,IV}(\mu\text{-}O)_2(bipy)_4]^{3+}$ by HA^- and in the advancement of the 'S-states' in Kok's cycle for photosystem II [38]. A similar electroprotic mechanism may be envisioned for chemical reduction of **2** by the ascorbate ion, which supplies both an electron and a proton (Eq. (7)).

$$[Mn_3^{IV}(\mu\text{-}O)_4(\underset{\mathbf{2}}{bipy})_3(H_2O)_4]^{4+} + HA^- \xrightarrow{k} [Mn_2^{IV}Mn^{III}(\mu\text{-}O)_3(\mu\text{-}OH)(bipy)_3(H_2O)_4]^{4+} + A^- \quad (7)$$

Reaction (7) is favoured strongly by the enhanced acidity of HA^- on oxidation (pK ca. −0.4 for HA^-) [39] and the enhanced basicity expected for **2** after reduction; it is known [1] that the base strength of the oxo groups in $[Mn_2^{III}(\mu\text{-}O)_2(bipy)_4]^{2+}$ is $\sim10^9$ times greater than that in $[Mn_2^{III,IV}(\mu\text{-}O)_2(bipy)_4]^{3+}$.

In connection with the question of intimate mechanism, a relevant question is why complex **2**, in spite of the presence of four coordinated water molecules, does not utilise an inner-sphere path for the electron transfer. Plausibly, the replacement of coordinated H_2O from the Mn^{IV} (d^3) centre is much slower than the electroprotic reaction. It is interesting to mention here that the known [18] rates of water-exchange by the manganese cluster of the S_3 state of photosystem II are much less than the lower limit of k in Eq. (7).

The overall reaction (3) must be a multistep process. The observed exponential profile along with the absence of any absorbance drop immediately after mixing indicate that the first act of electron transfer is rate-determining. Subsequent steps are rapid and therefore kinetically silent. In search of any such intermediate, we recorded the spectra of **1**, mixed with different amounts of ascorbic acid (Fig. 5) and thus noticed the generation of the binuclear complex $[Mn_2^{III,IV}(\mu\text{-}O)_2(bipy)_4]^{3+}$ (**3**) as an intermediate, which subsequently decayed in the presence of excess ascorbic acid. The spectrum

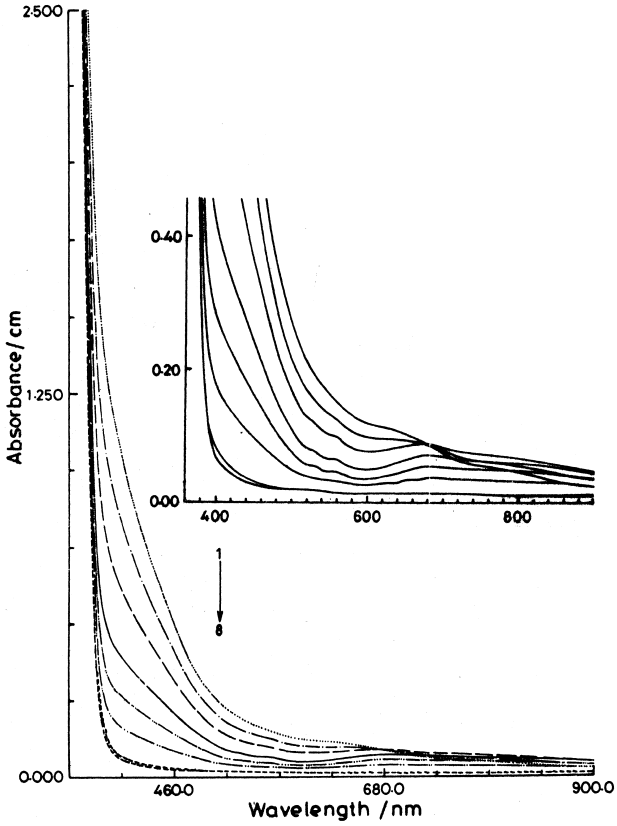


Fig. 5. Spectra of equilibrium mixtures of complex **1** (0.20 mmol dm^{-3}) with different concentrations (mmol dm^{-3}) of ascorbic acid in c_{bipy} 20.0 mmol dm^{-3}, pH 4.50. c_{asc} 0 (1), 0.10 (2), 0.15 (3), 0.30 (4), 0.40 (5), 0.50 (6), 0.60 (7), 0.80 (8).

3 in Fig. 5 recorded with $c_{asc}/[\mathbf{1}] = 0.75$ shows strong resemblance to that of the $Mn^{III}Mn^{IV}$ dimer **3** and manifests all the characteristic UV–Vis spectral features [26,40] for **3**, like a broad maximum at ~830 nm as a shoulder of a band at 684 nm and two other shoulders at 559 and 527 nm. The ratio of absorbance at 683, 559, and 527 nm (1:0.8:0.95) in this spectrum is almost the same (1:0.8:0.9) as that for **3**. The final absorbance (0.080) at 683 nm corresponds to near quantitative (103%) conversion of **1** to **3**, according to Eq. (8):

$$4[Mn_3^{IV}(\mu\text{-}O)_4(bipy)_4(H_2O)_2]^{4+} + 2H^+ + 8bipy + 3H_2A \rightarrow 6[Mn_2(\mu\text{-}O)_2(bipy)_4]^{3+} + 12H_2O + 3A \quad (8)$$

3

It is known [1] that excess ascorbic acid reduces **3** to Mn^{II} according to Eq. (8a)

$$2[Mn_2^{III,IV}(\mu\text{-}O_2)(bipy)_4]^{3+} + 3H_2A + 2H^+ \rightarrow 4Mn^{II} + 8bipy + 4H_2O + 3A \quad (8a)$$

Eqs. (8) and (8a) when properly combined [8 + 3 × (8a)] yield Eq. (1), the stoichiometric equation for quantitative reduction of **1** by excess H_2A.

A reaction, Eq. (9), analogous to Eq. (8) occurs when complex **1** is stored for 24 h in the ligand buffer [40]. We verified, however, that reaction (9) is very slow and does not interfere with the reduction of **1** by ascorbic acid:

$$2[Mn_3^{IV}(\mu\text{-}O)_4(bipy)_4(H_2O)_2]^{4+} + 4H^+ + 4bipy + 3R \rightarrow 3[Mn_2(\mu\text{-}O)_2(bipy)_4]^{3+} + 6H_2O + 3R^+ \quad (9)$$

In all probability, **3** is an intermediate for reaction (3). One observation needs to be addressed at this point. The known [1] first-order rate constant for the reduction of the $Mn^{III}Mn^{IV}$ dimer by HA^- is comparable to that measured by us for the trinuclear complex. One can thus expect a sequence of first-order consecutive reactions, not a simple first-order profile as observed. This apparent anomaly might have two reasonable sources: (i) the ascorbate radical generated during the reduction of Mn_3^{IV} species reduces the dinuclear species more rapidly than, and in addition to, HA^-; (ii) the $Mn^{III}Mn^{IV}$ dimer first produced is not **3**, it is rather a bis(bipyridine) species $[Mn_2^{III,IV}(\mu\text{-}O)_2(bipy)_2(H_2O)_4]^{3+}$, which changes to an equilibrium mixture of the corresponding tris(bipyridine) and tetrakis(bipyridine) complexes. The bis(bipyridine) and the tris(bipyridine) species are more aquated than **3** and hence kinetically more active and reduced rapidly, perhaps before they can transform to the kinetically less active tetrakis(bipyridine) complexes. It might be noted here that the structure of **1** also requires that an aquated form of **3** be produced on reduction of **1**. If, for example, the Mn^{IV} centre at the top of the structure **1** is removed by reduction, then $[Mn_2^{III,IV}(\mu\text{-}O)_2(bipy)_2(H_2O)_4]^{3+}$ should be generated. Such possibilities cannot be verified by the UV–Vis spectral studies mentioned above; complex **3** and its aqua derivatives have similar spectra [2,26], and inter conversions are likely to be rapid in the time-scale for spectral measurements.

This work presents a systematic study of redox kinetics of a trinuclear oxo-bridged Mn_3^{IV} species. It shows the importance of the binuclear $Mn^{III}Mn^{IV}$ species as intermediate in the redox reactions leading to the formation and collapse of higher-valent manganese clusters. The study also reiterates the importance of ligand dissociation equilibria in such chemical changes and upholds the possibility that multinuclear manganese complexes undergo proton coupled electron transfer, a process of proven importance [9] in photosystem II.

References

[1] M.C. Ghosh, J.W. Reed, R.N. Bose, E.S. Gould, Inorg. Chem. 33 (1994) 73.
[2] S. Chaudhuri, S. Mukhopadhyay, R. Banerjee, J. Chem. Soc., Dalton Trans. (1995) 621.
[3] S. Kundu, A.K. Bhattacharya, R. Banerjee, J. Chem. Soc., Dalton Trans. (1996) 3951.
[4] B. Mondal, S. Kundu, R. Banerjee, Polyhedron 16 (1997) 2199.
[5] A.K. Bhattacharya, A.B. Mondal, R. Banerjee, J. Chem. Soc., Dalton Trans. (1997) 2351.
[6] S. Chaudhuri, R. Banerjee, Polyhedron 16 (1997) 3493.
[7] R. Banerjee, B. Mondal, S. Kundu, J. Chem. Soc., Dalton Trans. (1997) 4341.
[8] A.B. Mondal, A.K. Bhattacharya, D. Maji, R. Banerjee, Polyhedron 17 (1998) 1693.

[9] J. Limberg, V.A. Szalai, G.W. Brudvig, J. Chem. Soc., Dalton Trans. (1999) 1353.
[10] U. Bossek, T. Weyhermuller, K. Wieghardt, B. Nuber, J. Weiss, J. Am. Chem. Soc. 112 (1990) 6387.
[11] M.W. Wemple, D.M. Adam, K. Folting, D.W. Hendrickson, G. Christou, J. Am. Chem. Soc. 117 (1995) 7275.
[12] C. Philouze, G. Blondin, J.J. Girerd, J. Geuilhem, C. Pascard, D. Lexa, J. Am. Chem. Soc. 116 (1994) 8557.
[13] M.-N.C. Dunand-Sauthier, A. Deronzier, X. Pradon, S. Menge, C. Philouze, J. Am. Chem. Soc. 119 (1997) 3173.
[14] M.K. Chan, W.H. Armstrong, J. Am. Chem. Soc. 113 (1991) 5055.
[15] J.E. Sarneski, H.H. Thorp, G.W. Brudvig, R.H. Crabtree, G.K. Shulte, J. Am. Chem. Soc. 112 (1990) 7255.
[16] G.N. George, R.C. Prince, S.P. Gramer, Science (1989) 243.
[17] W. Riittinger, G.C. Dismukes, Chem. Rev. 97 (1997) 1.
[18] W. Hiller, J. Messinger, T. Wydrzynski, Biochemistry 37 (1998) 16908.
[19] J.E. Sarneski, H.H. Thorp, G.W. Brudvig, R.H. Crabtree, J. Mol. Catal. 133A (1996) 13.
[20] E. Adams, L. Frank, Annu. Rev. Biochem. 49 (1980) 1030.
[21] E. Cadenas, Annu. Rev. Biochem. 58 (1989) 79.
[22] G.M. Brown, B.S. Brunschwig, C. Creutz, J.F. Endicott, N. Sutin, J. Am. Chem. Soc. 101 (1979) 1298.
[23] R.A. Rickman, R.L. Sorenson, K.O. Watkins, G. Davies, Inorg. Chem. 16 (1977) 1570.
[24] J.J. Jwo, A. Haim, J. Am. Chem. Soc. 98 (1976) 1172.
[25] F.L. Harris, D.L. Toppen, Inorg. Chem. 17 (1978) 74.
[26] S.R. Cooper, M. Calvin, J. Am. Chem. Soc. 99 (1977) 6623.
[27] S. Mukhopadhyay, R. Banerjee, J. Chem. Soc., Dalton Trans. (1993) 933.
[28] E. Pellizzetti, E. Mentasti, E. Pramauro, Inorg. Chem. 15 (1976) 2898.
[29] J. Xu, R.B. Jordon, Inorg. Chem. 29 (1990) 4180.
[30] D.H. Macartney, N. Sutin, Inorg. Chim. Acta 74 (1983) 221.
[31] R. Manchandra, G.W. Brudvig, R.H. Crabtree, New J. Chem. 18 (1994) 561.
[32] R. Banerjee, R. Das, A.K. Chakraburtty, J. Chem. Soc., Dalton Trans. (1990) 3277.
[33] E. Pellizzetti, E. Mentasti, E. Pramauro, Inorg. Chem. 17 (1978) 1181.
[34] G.F. Condike, A.E. Martell, J. Inorg. Nucl. Chem. 31 (1969) 2455.
[35] A.E. Martell (Ed.), Stability Constants of Metal Ion Complexes, The Chemical Society Special Publication No. 17, Table 783, 1964.
[36] B. Mondal, Ph.D.(Sc.) Thesis, Jadavpur University, 1999.
[37] D. Maji, R. Banerjee, unpublished work.
[38] B. Kok, B. Forbush, M. McGloin, Photochem. Photobiol. 11 (1970) 457.
[39] G.P. Laroff, R.W. Fessenden, R.H. Schuler, J. Am. Chem. Soc. 94 (1972) 9062.
[40] K.R. Reddy, M.V. Rajasekharan, N. Arulasamy, D.J. Hodgson, Inorg. Chem. 35 (1996) 2283.

PERGAMON

www.elsevier.nl/locate/poly

Polyhedron 19 (2000) 1219–1225

POLYHEDRON

Octanuclear oxomolybdenum(V) clusters with pyridine or alkyl-substituted pyridines: crystal structures of $[Mo_8O_{16}(OCH_3)_8L_4]$ (L = 3-methylpyridine, 3,5-lutidine)

Barbara Modec *, Jurij V. Brenčič, Ljubo Golič

Faculty of Chemistry and Chemical Technology, University of Ljubljana, Aškerčeva 5, 1000 Ljubljana, Slovenia

Received 16 December 1999; accepted 21 March 2000

Abstract

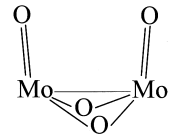
Simple synthetic routes for the preparation of octanuclear oxomolybdenum(V) clusters with stoichiometry $[Mo_8O_{16}(OCH_3)_8L_4]$ (L = 4-methylpyridine (4-MePy) (**a**), 4-ethylpyridine (4-EtPy) (**b**), 4-*tert*-butylpyridine (4-Bu^{t}Py) (**c**), pyridine (Py) (**d**), 3-methylpyridine (3-MePy) (**e**), 3,5-lutidine (3,5-Lut) (**f**)) are described. Crystal structures of **e** and **f** were investigated by X-ray diffraction. The puckered ring structure made up of eight molybdenum atoms linked together by pairs of methoxy groups and pairs of oxo groups was recognized in both. The solubility of the compounds in pyridines was employed for the substitution of coordinated pyridine for a different pyridine. The octanuclear clusters have been found to react in pyridines at elevated temperatures to oxomolybdenum(V,VI) clusters with the formula $[Mo_{10}O_{26}L_8]$. ©2000 Elsevier Science Ltd All rights reserved.

Keywords: Oxomolybdenum(V) compounds; Clusters; $Mo_2O_4^{2+}$ unit; Pyridine; Alkyl-substituted pyridines

1. Introduction

The title compounds belong to a group of oxomolybdenum(V) clusters built of $Mo_2O_4^{2+}$ units (Scheme 1). The $Mo_2O_4^{2+}$ moiety is frequently encountered in Mo(V) chemistry. Its geometry is virtually independent of other ligands. Molybdenum to bridging oxygen distances are 1.9–2.0 Å. The bent Mo(μ-O)$_2$Mo bridge enables a close approach of two molybdenum atoms. The short distance 2.5–2.7 Å is indicative of a single metal–metal bond which accounts for the diamagnetism of the $Mo_2O_4^{2+}$ compounds [1]. The substantial *trans* influence due to the strong bonding between molybdenum and the terminal oxygen (distances span the range 1.6–1.8 Å) leads to weakening of the bond between molybdenum and the *trans* positioned ligand or in the extreme case to a vacancy at this coordination site [2].

The linkage of dimers into larger aggregates is achieved via oxygen donor groups which can serve not only as terminal but also as μ, μ_3 or μ_4-bridging ligands, with the polyhedra sharing common corners, edges or faces [3]. The properties of clusters are essentially the properties of $Mo_2O_4^{2+}$ units. Although the literature abounds with data on the $Mo_2O_4^{2+}$ clusters which occur among the coordination compounds, alkoxides and even organometallic compounds, the overwhelming majority are anionic species [1]. A variety of structural types is exhibited among them. We limit the scope to compounds which bear resemblance to oxomolybdenum(V) clusters with pyridines. Linking two dimers in such a way that the octahedra share common edges leads to a stable tetranuclear framework $[Mo_4O_4(\mu\text{-}O)_2(\mu_3\text{-}O)_2(\mu\text{-}OR)_2]^{2+}$ ($OR^- = OCH_3^-$, $OC_2H_5^-$, O-*i*-Pr^-) to which peripheral ligands can be attached to, for example N-donor ligand pyridine in $[Mo_4O_8(O\text{-}i\text{-}Pr)_4Py_4]\cdot 2Py$ (O-*i*-Pr^- = $OC_3H_7^-$) [4].



Scheme 1. $Mo_2O_4^{2+}$ unit.

The structure of $[Mo_8O_{16}(OCH_3)_8(PMe_3)_4]$ [5] is analogous to structures of the octanuclear clusters described in this paper. Four $Mo_2O_4^{2+}$ units are joined together by pairs of methoxy bridges, forming a pattern of alternating short Mo–Mo distances, 2.557–2.578 Å, with longer Mo···Mo contacts, 3.441–3.474 Å. The ring is bent. The cluster was obtained from a methanol solution of *fac*-[Mo(CO)$_3$-

* Corresponding author. Tel.: +386-61-1760-581; fax: +386-61-1258-220; e-mail: barbara.modec@uni-lj.si

0277-5387/00/$ - see front matter ©2000 Elsevier Science Ltd All rights reserved.
PII S0277-5387(00)00377-6

$(PMe_3)_3]$ in the presence of oxygen and sunlight. Planar conformation of the ring was found in the anionic $[Mo_8O_{16}(OCH_3)_8(C_2O_4)]^{2-}$ [6] and $[Mo_8O_{16}(OC_2H_5)_8(C_2O_4)]^{2-}$ [7], both known as $(n\text{-}C_4H_9)_4N^+$ salts. The planarity is imposed by the oxalate anion which occupies the central cavity and is bonded to four molybdenum atoms. Another Mo_8 complex $[Mo_8O_{12}(OH)_6(OC_2H_5)_4Cl_6(HOC_2H_5)_4]$ [8] has a $Mo_8(\mu_3\text{-}O)_4(\mu\text{-}O)_8$ core encapsulated by terminal oxo, hydroxy, chloro and ethanol ligands. The structure of the central core is closely related to the structure of MoO_2.

Among the oxomolybdates(VI) different octanuclear cores were observed. Two tetranuclear units are either connected by two vertices as in $[Mo_8O_{20}(OCH_3)_4\{(OCH_2)_3CCH_3\}_2]^{2-}$ [9] or by two edges as in $[Mo_8O_{24}(OCH_3)_4]^{4-}$ [10]. The structure found in a Mo(V)/Mo(VI) compound, $((n\text{-}C_4H_9)_4N)_4[Mo_4O_8(OCH_3)_2(MoO_4)_2(HMoO_4)_2]\cdot CH_3OH\cdot H_2O$, may be viewed as a tetranuclear framework with four tetrahedral MoO_4^{2-} appended, two as terminal ligands and two as chelates [11]. A heterometallic mixed valence $[Mg_2Mo_8O_{22}(OCH_3)_6(HOCH_3)_4]^{2-}$ [12] has two tetranuclear units fused along two edges forming a central cavity which is occupied by two $\{Mg(OCH_3)_2\}$ moieties.

We observed before that in the reaction of $(PyH)_2[MoOCl_5]$ with a mixture of pyridine, methanol and acetonitrile $[Mo_8O_{16}(OCH_3)_8Py_4]$ is formed [13]. Although the compound was obtained in crystalline form, the yields were low and highly irreproducible.

Reactions of $(PyH)_2[MoOCl_5]$ with the mixture of methanol and pyridine or its alkyl substituted derivatives under varying conditions have led to oxomolybdenum(V) clusters with coordinated methoxide ions and pyridines, i.e. pentanuclear $[Mo_5O_{11}(OCH_3)_4Py_4]\cdot CH_3OH$ [14], tetranuclear $[Mo_4O_8(OCH_3)_2Cl_2Py_4]\cdot 2Py$ and $[Mo_4O_8(OCH_3)_4(4\text{-}MePy)_4]$, hexanuclear $[Mo_6O_{12}(OCH_3)_6Py_4]$, decanuclear $[Mo_{10}O_{26}Py_8]\cdot 7Py$ [15] and octanuclear $[Mo_8O_{16}(OCH_3)_8L_4]$ (L = 4-MePy, 4-EtPy, 4-Bu^{t}Py, Py, 3-MePy, 3,5-Lut) with $Mo_2O_4^{2+}$ building blocks as a common structural motif. The aim of our research was to define conditions which would lead solely to $[Mo_8O_{16}(OCH_3)_8L_4]$. Knowledge of the factors which influence the formation of octanuclear clusters may provide insight into the processes that eventually lead to their formation. To support our assumptions that octanuclear clusters can be used as precursors in the synthesis of high nuclearity clusters with chemical evidence, systematic investigation of their reactivity was undertaken.

2. Experimental

2.1. General comments

$(NH_4)_2[MoCl_5(H_2O)]$ [16] and $(PyH)_2[MoOCl_5]$ [17] were synthesized according to published procedures. Solvents were reagent grade and they were used without additional purification. They were obtained from the following sources: Merck (pyridine, 3,5-lutidine, methanol and nitromethane), Acros Organics (4-ethylpyridine and 4-*tert*-butylpyridine), BDH Chemicals (3-methylpyridine and 4-methylpyridine).

Infrared spectra of Nujol (4000–400 cm^{-1} range) and hexachlorobutadiene (4000–1200 cm^{-1} range) mulls between CsBr plates were measured on a Perkin-Elmer 1720 X Fourier transform IR spectrometer. Far IR spectra of Nujol mulls (700–100 cm^{-1} range) on a polyethylene foil were measured on a Perkin-Elmer 2000 Fourier transform IR spectrometer. Elemental analyses were obtained by a Perkin-Elmer 2400 CHN analyser at University of Ljubljana (Department of Organic Chemistry).

2.2. Syntheses

2.2.1. Synthesis of $[Mo_8O_{16}(OCH_3)_8(4\text{-}MePy)_4]$ (**a**)

10 mmol (3.27 g) of $(NH_4)_2[MoCl_5(H_2O)]$ was added to the mixture of 10 ml of 4-methylpyridine, 10 ml of nitromethane and 75 ml of methanol. The yellow–green mixture was refluxed (approximately 15 min) until it changed into a red colour. The orange microcrystalline product was filtered off. The yield was 750 mg (37%).

2.2.2. Synthesis of $[Mo_8O_{16}(OCH_3)_8L_4]$ (L = 4-MePy (**a**), 4-EtPy (**b**), 4-Bu^{t}Py (**c**), 3-MePy (**e**))

1 mmol (450 mg) of $(PyH)_2[MoOCl_5]$ was added to the mixture of 5 ml of ligand and 15 ml of methanol in the case of **b** and **c**. The solution was refluxed (approximately 15 min) until an orange compound started to precipitate out of the reaction mixture. The product was filtered off. The yields were 75 mg (35%) for **b** and 118 mg (52%) for **c**.

For **a**, slightly different amounts were used; 1.5 mmol (675 mg) of $(PyH)_2[MoOCl_5]$ was added to the mixture of 5 ml of 4-methylpyridine and 20 ml of methanol. The yield was 92 mg (30%).

Orange, rod-shaped ($0.05\times0.05\times0.40$ mm) single crystals of **e** were obtained in 10% yield from the mixture of 1 mmol (450 mg) of $(PyH)_2[MoOCl_5]$, 5 ml of 3-methylpyridine and 25 ml of methanol which was left at ambient conditions for 4 h.

2.2.3. Synthesis of $[Mo_8O_{16}(OCH_3)_8L_4]$ (L = 4-EtPy (**b**), Py (**d**), 3-MePy (**e**), 3,5-Lut (**f**))

0.152 mmol (250 mg) of $[Mo_8O_{16}(OCH_3)_8(4\text{-}MePy)_4]$ was added to 10 ml of the ligand. After 15 min of stirring the solution was filtered and methanol (100, 80, 150 and 65 ml in the case of **b**, **d**, **e** and **f**, respectively) was added to the red filtrate. Orange, rod-shaped crystals started to grow in the mixture. After a few hours the product was filtered off. The yields were 190 mg (74%) for **b**, 200 mg (83%) for **d**, 150 mg (60%) for **e** and 105 mg (40%) for **f**.

Suitable crystals for X-ray structural analysis of **f** ($0.06\times0.06\times0.40$ mm) were also obtained by a described procedure.

Note: the yield of $[Mo_8O_{16}(OCH_3)_8Py_4]$ is improved compared to the published procedure [13].

2.3. IR and elemental analysis data

2.3.1. $[Mo_8O_{16}(OCH_3)_8(4\text{-}MePy)_4]$ (**a**)

IR data (cm^{-1}): 3042(w), 2966(sh), 2926(m), 2820(w), 2815(w), 1623(s), 1505(w), 1440(m), 1425(m), 1232(m), 1214(m), 1169(w), 1154(w), 1072(m), 1069(m), 1032(s), 999(vs), 967(vs), 949(s), 874(w), 817(s), 764(s), 734(m), 722(m), 670(w), 579(vs), 550(m), 522(m), 500(vs), 411(m), 363(m), 336(m), 317(m), 281(m). *Anal*. Calc. for $C_{32}H_{52}Mo_8N_4O_{24}$: C, 23.37; H, 3.19; N, 3.41. Found: C, 23.09; H, 3.09; N, 3.49%.

2.3.2. $[Mo_8O_{16}(OCH_3)_8(4\text{-}EtPy)_4]$ (**b**)

IR data (cm^{-1}): 3048(w), 2973(m), 2931(m), 2878(w), 2823(m), 1622(vs), 1556(m), 1504(m), 1455(m), 1431(s), 1378(w), 1226(m), 1214(w), 1171(w), 1152(w), 1070(m), 1031(s), 1001(vs), 968(vs), 950(s), 871(w), 835(m), 795(w), 760(s), 736(m), 722(sh), 669(w), 576(vs), 503(s), 409(m), 367(m), 356(w), 337(w), 316(s), 283(m). *Anal*. Calc. for $C_{36}H_{60}Mo_8N_4O_{24}$: C, 25.43; H, 3.56; N, 3.29. Found: C, 25.67; H, 3.41; N, 3.18%.

2.3.3. $[Mo_8O_{16}(OCH_3)_8(4\text{-}Bu^tPy)_4]$ (**c**)

IR data (cm^{-1}): 3085(w), 3066(w), 2966(s), 2930(s), 2906(sh), 2867(m), 2824(m), 1620(vs), 1548(m), 1501(m), 1474(sh), 1461(m), 1423(s), 1398(w), 1368(m), 1302(w), 1275(m), 1248(w), 1230(m), 1204(w), 1171(w), 1153(w), 1072(s), 1031(s), 1001(vs), 970(vs), 950(vs), 865(w), 844(m), 834(s), 761(vs), 736(m), 669(w), 578(vs), 548(m), 505(vs), 410(m), 368(m), 338(m), 316(m), 283(m). *Anal*. Calc. for $C_{44}H_{76}Mo_8N_4O_{24}$: C, 29.16; H, 4.23; N, 3.09. Found: C, 29.07; H, 4.20; N, 3.16%.

2.3.4. $[Mo_8O_{16}(OCH_3)_8(Py)_4]$ (**d**)

IR data (cm^{-1}): 3071(w), 3058(w), 3045(w), 2924(m), 2822(m), 1607(m), 1486(w), 1450(m), 1375(w), 1242(w), 1220(s), 1163(m), 1072(s), 1046(s), 1015(vs), 987(s), 976(vs), 959(s), 762(s), 754(s), 731(m), 701(s), 652(w), 642(m), 574(vs), 517(sh), 503(vs), 440(m), 407(m), 366(m), 355(m), 333(sh), 315(m), 284(w). *Anal*. Calc. for $C_{28}H_{44}Mo_8N_4O_{24}$: C, 21.18; H, 2.79; N, 3.53. Found: C, 21.08; H, 2.47; N, 3.15%.

2.3.5. $[Mo_8O_{16}(OCH_3)_8(3\text{-}MePy)_4]$ (**e**)

IR data (cm^{-1}): 3076(w), 3030(w), 2960(w), 2928(m), 2875(w), 2823(w), 1612(m), 1582(m), 1484(m), 1452(m), 1431(m), 1386(w), 1250(w), 1231(w), 1194(w), 1177(w), 1152(w), 1132(w), 1112(m), 1067(m), 1001(vs), 968(vs), 943(s), 912(w), 822(w), 805(m), 756(s), 735(w), 713(w), 702(m), 669(w), 658(w), 629(w), 573(vs), 522(m), 488(s), 418(sh), 409(m), 365(m), 339(m), 317(m), 284(m). *Anal*. Calc. for $C_{32}H_{52}Mo_8N_4O_{24}$: C, 23.37; H, 3.19; N, 3.41. Found: C, 23.76; H, 2.96; N, 3.49%.

2.3.6. $[Mo_8O_{16}(OCH_3)_8(3,5\text{-}Lut)_4]$ (**f**)

IR data (cm^{-1}): 3015(w), 2958(w), 2927(m), 2824(m), 1601(m), 1452(m, br), 1381(m), 1251(w), 1185(w), 1168(w), 1156(s), 1041(m), 1004(vs), 968(vs), 950(vs), 939(s), 870(m), 771(s), 761(s), 735(s), 711(w), 701(s), 669(w), 575(vs), 540(m), 520(sh), 504(s), 477(w), 429(w), 409(w), 366(m), 356(m), 333(w), 316(m), 285(m). *Anal*. Calc. for $C_{36}H_{60}Mo_8N_4O_{24}$: C, 25.43; H, 3.56; N, 3.29. Found: C, 25.61; H, 3.34; N, 3.38%.

2.4. X-ray structural determination

Data were collected on an Enraf Nonius CAD-4 diffractometer with graphite-monochromated Mo Kα radiation ($\lambda=0.71069$ Å) at room temperature. Crystal data parameters are given in Table 1. For **e** a total of 3412 reflections were measured ($\theta_{max}=27.98°$; $0\le h\le24$, $-8\le k\le24$, $-9\le l\le9$) and reduced to a unique set of 1731 reflections ($R_{int}=0.062$); for **f** a total of 16062 reflections were measured ($\theta_{max}=24.96°$; $-21\le h\le21$, $-21\le k\le21$, $-8\le l\le7$) and reduced to a unique set of 2374 reflections ($R_{int}=0.11$). Cell parameters for **e** were determined from 50 reflections from the 6.03–14.4° θ range and for **f** from 50 reflections from the 6.0–11.8° θ range. Data collection followed routine procedures. All data were corrected for Lorentz and polarization effects. In neither case was absorption correction applied. Structures were solved by direct methods using SIR-92 [18]. All non-hydrogen atoms were refined using anisotropic thermal parameters. The program used was XTAL 3.4 [19]. The hydrogen atoms were inserted in calculated positions. The least-squares refinement on F for **e** converged at $R=0.024$ and $R_w=0.024$ for 154 least-squares parameters and 850 data ($F_o>3\sigma(F_o)$ (the weighting

Table 1
Crystallographic data for $[Mo_8O_{16}(OCH_3)_8L_4]$ (L = 3-MePy (**e**), 3,5-Lut (**f**))

	e	**f**
Formula	$C_{32}H_{52}Mo_8N_4O_{24}$	$C_{36}H_{60}Mo_8N_4O_{24}$
Formula weight	1644.3	1700.4
Space group	tetragonal, $I\bar{4}$ (no. 82)	tetragonal, $P4_2/n$ (no. 86)
a (Å)	18.914(1)	22.309(3)
c (Å)	7.458(6)	7.384(1)
V (Å^3)	2668.0(4)	3675(1)
Z	2	2
ρ_{calc} (g cm^{-3})	2.047	1.537
μ (cm^{-1})	18.5	13.46

scheme used was $w = W_F \times W_S$, where $W_F(F_o < 79) = (F_o/79)^2$, $W_F(F_o > 100) = (100/F_o)^{0.4}$ and $W_F(79 < F_o < 100) = 1$; $W_S(\sin\theta < 0.36) = (0.36/\sin\theta)^{0.80}$, $W_S(\sin\theta > 0.54) = (\sin\theta/0.54)^4$ and $W_S(0.36 < \sin\theta < 0.54) = 1$). The final difference synthesis maximum and minimum were $+0.491$ and -0.367 e Å^{-3}. The least-squares refinement for **f** converged at $R = 0.038$ and $R_w = 0.043$ for 163 least-squares parameters and 858 data ($F_o > 3\sigma(F_o)$) (the weighting scheme used was $w = W_F \times W_S$, where $W_F(F_o < 46) = (F_o/46)^{1.5}$, $W_F(F_o > 130) = (130/F_o)^{1.5}$ and $W_F(46 < F_o < 130) = 1$; $W_S(\sin\theta < 0.24) = (0.24/\sin\theta)^{2.2}$, $W_S(\sin\theta > 0.43) = (\sin\theta/0.43)^1$ and $W_S(0.24 < \sin\theta < 0.43) = 1$). The final difference synthesis maximum and minimum were $+0.576$ and -0.488 e Å^{-3}.

3. Results and discussion

3.1. Infrared spectra

Apart from the ligand absorptions the IR spectra of all $[Mo_8O_{16}(OCH_3)_8L_4]$ are similar; characteristic absorptions are given in Table 2. The complexity of the spectra in the 1630–400 cm^{-1} region due to the superposition of ligand absorptions with the $[Mo_8O_8(\mu\text{-}O)_8(\mu\text{-}OCH_3)_8]$ absorptions prevents the unambiguous assignment of bands. Bands around 2930 and 2820 cm^{-1} observed in the spectra of all compounds can be associated with the C–H stretching modes of the methoxy groups; the observed bands are comparable to the absorption at 2930 cm^{-1} in $((n\text{-}C_4H_9)_4N)_2[Mo_8O_{16}(OCH_3)_8(C_2O_4)]$ [6] and at 2820 cm^{-1} in $((n\text{-}C_4H_9)_4N)_2[V_8O_8(OCH_3)_{16}(C_2O_4)]$ [7]. The C–O stretching vibrations of the alkoxy groups usually absorb in the 1150–1000 cm^{-1} region [20]; a strong absorption around 1000 cm^{-1} found in the spectra of $[Mo_8O_{16}(OCH_3)_8L_4]$ can be tentatively assigned as C–O stretching vibration. Two bands around 970 and 950 cm^{-1} are assigned to the Mo=O$_t$ stretching vibrations, the appearance of two bands stems from a different chemical environment of two molybdenum atoms of the $Mo_2O_4^{2+}$ pair, one being in a square pyramidal and the other one in an octahedral environment. Strong bands at ~575 and ~500 cm^{-1} in the spectra of all $[Mo_8O_{16}(OCH_3)_8L_4]$ are attributed to the bridging methoxy groups [21]. The low frequency bands around 365, 335, 315 and 283 cm^{-1} are also typical for the $[Mo_8O_8(\mu\text{-}O)_8(\mu\text{-}OCH_3)_8]$ framework.

3.2. Description of structures

Structures of **e** and **f** are almost identical to the structures of $[Mo_8O_{16}(OCH_3)_8Py_4]$ [13] and $[Mo_8O_{16}(OCH_3)_8(PMe_3)_4]$ [5]. Comparison of bond lengths and angles in **d**, **e** and **f** with the appropriate bond lengths and angles in $[Mo_8O_{16}(OCH_3)_8(PMe_3)_4]$ shows that the ring geometry does not change with the coordination of pyridines instead of trimethylphosphine.

Relevant geometric parameters of **d**, **e** and **f** are presented in Table 3. The asymmetric unit in **e** is shown in Fig. 1. The asymmetric units are related by a crystallographic $\bar{4}$ axis in the centre of the molecule (Fig. 2), the overall molecular symmetry is thus S_4.

Eight molybdenum atoms, alternately bridged by two oxygen atoms or two methoxy groups, form a cyclic 'tiara' framework $[Mo_8O_8(\mu\text{-}O)_8(\mu\text{-}OCH_3)_8]$ [6]. Short Mo–Mo distances, 2.558(1) Å for **e** and 2.561(2) Å for **f**, alternate with longer distances, 3.433(1) Å for **e** and 3.433(2) Å for **f**. The deviation from planarity of the bridging unit $Mo_2(\mu\text{-}O)_2$ is shown by the fold angle which is 148.8(8)° in **e** and 148.4(3)° in **f**. One molybdenum atom (Mo2) of the $Mo_2O_4^{2+}$ pair is in a square pyramidal environment and the other one (Mo1) to which the pyridine ligand is bonded, is in a distorted octahedral environment as shown in Fig. 2. The dimensions of the $Mo_2O_2(\mu\text{-}O)_2$ unit in both are the same, within experimental error, as in other $Mo_2O_4^{2+}$ compounds. Alkyl-substituted pyridine coordinates to Mo1 at a distance of 2.26(1) Å in **e** and 2.29(1) Å in **f**. The values are comparable to those reported for $[Mo_4O_8(O\text{-}i\text{-}Pr)_4Py_4]\cdot 2Py$ (2.229(3)–2.269(3) Å) [4]. The aromatic ligands are oriented outward from the central cavity whose perimeter may be defined by the O3···O3^{i} (4.343(7) Å for **e** and 4.30(1) Å for **f**) and O3···O3^{ii} (5.062(7) Å for **e** and 5.02(1) Å for **f**) distances (symmetry codes for **e**: (i) $1-y, -1+x, 2-z$, (ii) $2-x, -y, z$; symmetry codes for **f**: (i) $y, -x+1/2, -z+1/2$, (ii) $-x+1/2, -y+1/2, z$). In both the rings are stacked one upon another along the *z*-axis, in **f** in such a way that parallel to the one-dimensional chain of molecules channels of void space are formed. The shortest intermolecular contact O4···C4^{iii} (3.35(1) Å (symmetry code: (iii) $3/2-x, 1/2-y, -1/2+z$) between bridging oxygen and aromatic

Table 2
Characteristic IR absorptions in $[Mo_8O_{16}(OCH_3)_8L_4]$ (cm^{-1})

L	
4-MePy (**a**)	2926(m), 2820(w), 999(vs), 967(vs), 949(s), 579(vs), 500(vs), 411(m), 363(m), 336(m), 317(m), 281(m)
4-EtPy (**b**)	2931(m), 2823(m), 1001(vs), 968(vs), 950(s), 576(vs), 503(s), 409(m), 367(m), 337(w), 316(s), 283(m)
4-Bu^{t}Py (**c**)	2930(s), 2824(m), 1001(vs), 970(vs), 950(vs), 578(vs), 505(vs), 410(m), 368(m), 338(m), 316(m), 283(m)
Py (**d**)	2924(m), 2822(m), 1015(vs), 976(vs), 959(s), 574(vs), 503(vs), 407(m), 366(m), 355(m), 333(sh), 315(m), 284(w)
3-MePy (**e**)	2928(m), 2823(w), 1001(vs), 968(vs), 943(s), 573(vs), 488(s), 409(m), 365(m), 339(m), 317(m), 284(m)
3,5-Lut (**f**)	2927(m), 2824(m), 1004(vs), 968(vs), 950(vs), 575(vs), 504(s), 409(w), 366(m), 333(w), 316(m), 285(m)

Table 3
Selected bond lengths (Å) and angles (°) in $[Mo_8O_{16}(OCH_3)_8L_4]$ (L = Py (**d**), 3-MePy (**e**) and 3,5-Lut (**f**)) [a]

	d [13]	**e**	**f**
Mo1–Mo2	2.570(1)	2.558(1)	2.561(2)
Mo1–O_t	1.682(4)	1.670(7)	1.68(1)
Mo1–N	2.255(5)	2.26(1)	2.29(1)
Mo1–O_b	1.916(4), 1.926(4)	1.918(7), 1.934(7)	1.91(1), 1.95(1)
Mo1–O(methoxy)	2.138(4), 2.220(4)	2.137(6), 2.204(7)	2.15(1), 2.21(1)
Mo2–O_t	1.664(4)	1.681(8)	1.68(1)
Mo2–O_b	1.929(4), 1.936(4)	1.918(7), 1.928(8)	1.91(1), 1.92(1)
Mo2–O(methoxy)	2.017(4), 2.040(4)	2.022(7), 2.056(7)	2.02(1), 2.05(1)
Mo1···Mo2	3.435(1)	3.433(1)	3.433(2)
O_b–Mo1–O_b	93.1(2)	92.6(3)	92.1(3)
O(methoxy)–Mo1–O(methoxy)	67.6(1)	67.9(3)	67.7(4)
O_b–Mo2–O_b	92.3(2)	92.8(3)	92.9(3)
O(methoxy)–Mo2–O(methoxy)	73.4(1)	73.0(3)	73.3(4)
Mo1–O_b–Mo2	83.6(2), 83.7(1)	83.2(2), 83.4(3)	83.1(4), 83.8(4)
Mo1–O(methoxy)–Mo2	108.2(2), 110.6(2)	108.6(3), 109.9(3)	108.5(4), 109.9(5)
Fold angle	150.1(2)	148.8(8)	148.4(3)

[a] Abbrevations used: O_t, terminal oxygen; O_b, bridging oxygen; O(methoxy), bridging methoxy group oxygen donor; fold angle, an angle between two $Mo(O_b)_2$ planes.

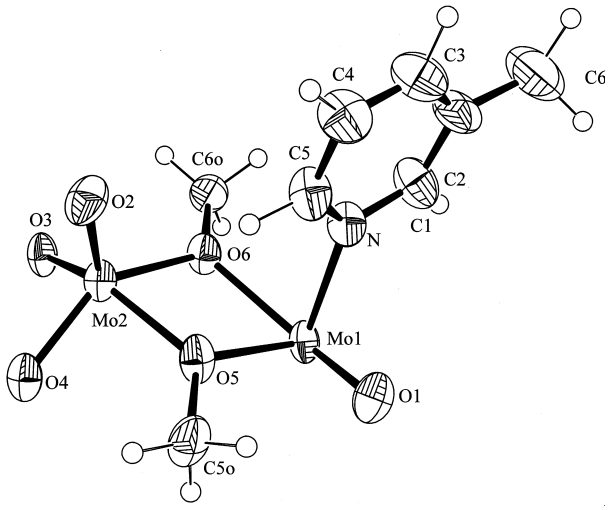


Fig. 1. An ORTEP III [24] picture of the asymmetric unit in **e**, drawn with 50% probability displacement ellipsoids and with H atoms shown as arbitrarily sized spheres.

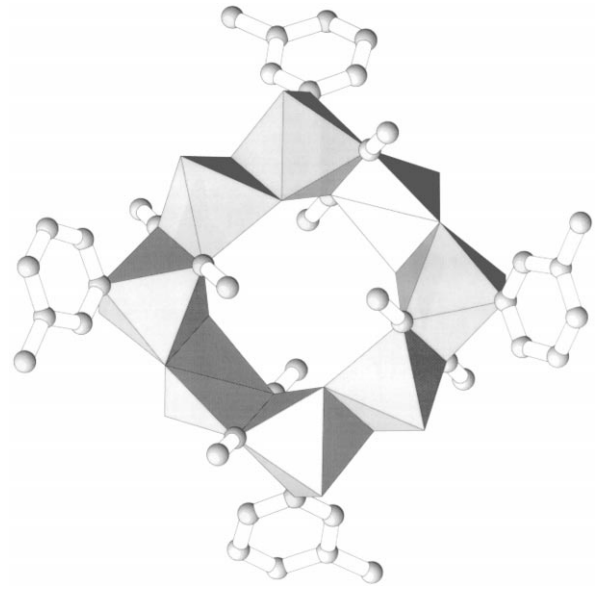


Fig. 2. The ATOMS [25] polyhedral representation of **e**.

carbon in **e** is longer than the sum of the van der Waals radii (3.22 Å) [22]. The shortest intermolecular contact O1···C6^{iv} (symmetry code: (iv) $x, y, 1+z$) between terminal oxygen and methyl carbon from 3,5-lutidine in **f** is 3.30(2) Å.

3.3. Reactivity

In the mixtures of $[MoOCl_5]^{2-}$, methanol and pyridine or its alkyl-substituted derivative, a rapid substitution of chloro ligands with methoxide ions takes place. The methoxide ions are formed in the protolytic reaction between pyridine and methanol. Owing to their high reactivity, the substituted derivatives of $[MoOCl_5]^{2-}$ react further to $Mo_2O_4^{2+}$; by subsequent linkage of dimers more stable clusters are formed. Attempts to isolate any of the substituted mononuclear or dinuclear species from what is probably a very complex mixture have failed so far. Reactive molybdenum(III) species, i.e. $[MoCl_5(H_2O)]^{2-}$, were also found to react with the mixture of methanol and pyridines in the presence of nitromethane to oxomolybdenum(V) clusters. Nitromethane might be playing a key role in the oxidation of molybdenum(III) to molybdenum(V), in its absence no oxidized species were detected [16].

In spite of the limited knowledge of the extent to which factors such as the molar ratios of the reactants, their concentration and temperature influence the reaction course, we have found that $[Mo_8O_{16}(OCH_3)_8L_4]$ is formed in the absence of water and when the ratio of methanol versus pyridine is in favour of methanol not only at room temperature but also at

boiling temperatures of the reaction mixtures. Among the oxomolybdenum clusters, $[Mo_4O_8(OCH_3)_2Cl_2Py_4]\cdot 2Py$, $[Mo_4O_8(OCH_3)_4(4\text{-MePy})_4]$, $[Mo_6O_{12}(OCH_3)_6Py_4]$ [15] and $[Mo_5O_{11}(OCH_3)_4Py_4]\cdot CH_3OH$ [14], which were also obtained from similar reaction systems, octanuclear compounds are the most reactive. In view of the apparent coordinative unsaturation of the pentacoordinated molybdenum, the ease of further reactions seems plausible. The diamagnetism is a property that the octanuclear compounds have in common with other oxomolybdenum(V) clusters with pyridines; in contrast to others they are sparingly soluble in methanol, nitromethane and pyridines. Solutions are not stable, slow decomposition takes place with time. The solubility in pyridines was employed for recrystallization and also for substitution of coordinated ligand for another ligand added in a huge excess.

$$[Mo_8O_{16}(OCH_3)_8L_4] + 4L' \rightarrow [Mo_8O_{16}(OCH_3)_8L'_4] + 4L \quad (1)$$

The recrystallized product or product with substituted ligand was precipitated from the solution by the addition of methanol. For example, 4-methylpyridine in $[Mo_8O_{16}(OCH_3)_8(4\text{-MePy})_4]$ was substituted for pyridine, 3-methylpyridine, 3,5-lutidine and 4-ethylpyridine, whereas with 4-*tert*-butylpyridine the substitution did not take place. The limiting factor of this reaction seems to be solubility.

Recrystallization of $[Mo_8O_{16}(OCH_3)_8(4\text{-MePy})_4]$ from 4-methylpyridine resulted in a partial decomposition of the starting material, namely the mixture of crystals of $[Mo_8O_{16}(OCH_3)_8(4\text{-MePy})_4]$ and $[Mo_4O_8(OCH_3)_4(4\text{-MePy})_4]$ [15] was obtained.

$$[Mo_8O_{16}(OCH_3)_8(4\text{-MePy})_4] + 4(4\text{-MePy}) \rightarrow 2[Mo_4O_8(OCH_3)_4(4\text{-MePy})_4] \quad (2)$$

We assume that the ring cleavage in solutions is followed by the aggregation of smaller fragments into stable and unsoluble clusters. It is reported in the literature that by reacting a mixed valence hexanuclear $[Mo_6O_{10}(O\text{-}i\text{-Pr})_{12}]$ with pyridine, $[Mo_4O_8(O\text{-}i\text{-Pr})_4Py_4]$ was obtained. It was shown by NMR studies that the chain of six metal centres linked together was cleaved into fragments with preserved Mo–Mo bonds and mononuclear molybdenum(VI) units [23].

Further evidence is also given by the reactions in pyridines at elevated temperatures where partial oxidation to Mo(VI) took place.

$$[Mo_8O_{16}(OCH_3)_8L_4] + L \rightarrow [Mo_{10}O_{26}L_8] \quad (3)$$

The oxidizing agent is probably oxygen. The mixed valence $[Mo_{10}O_{26}L_8]$ contains two molybdenum(VI) centres, the rest of the molybdenum atoms are part of $Mo_2O_4^{2+}$ units, as proved by X-ray crystallography [15]. Since no precaution was taken to eliminate traces of water inherent in pyridines the formation of μ_3-O ligands found in $[Mo_{10}O_{26}L_8]$ could have its origin in hydrolysis and not in C–O bond cleavage. We believe that $[Mo_{10}O_{26}L_8]$ is not the only product. By analogy, employing the same procedure only with a different pyridine, decanuclear clusters with substituted ligands were obtained.

$$[Mo_8O_{16}(OCH_3)_8L_4] + L' \rightarrow [Mo_{10}O_{26}L'_8] \quad (4)$$

4. Concluding remarks

From a seemingly simple reaction system of $[MoOCl_5]^{2-}$, methanol and pyridines, neutral oxomolybdenum(V) clusters of different nuclearity have been isolated. At present the processes giving rise to them remain obscure and are topics for future research.

Supplementary data

Tables of atomic coordinates, bond lengths, bond angles and thermal parameters are available from the Cambridge Crystallographic Data Centre, 12 Union Road, Cambridge CB2 1EZ, UK (fax: +44-1223-336033; e-mail: deposit@ccdc.cam.ac.uk). The CCDC reference numbers are 137764 for **e** and 137765 for **f**. Observed and calculated structure factors are available from the authors upon request.

Acknowledgements

Financial support of the Slovenian Ministry of Science and Technology is gratefully acknowledged (grant J1-1460-0103-99).

References

[1] H.K. Chae, W.G. Klemperer, T.A. Marquart, Coord. Chem. Rev. 128 (1993) 209.
[2] E.I. Stiefel, Prog. Inorg. Chem. 22 (1977) 1.
[3] M.I. Khan, J. Zubieta, Prog. Inorg. Chem. 43 (1995) 1.
[4] M.H. Chisholm, J.C. Huffman, C.C. Kirkpatrick, J. Leonelli, K. Folting, J. Am. Chem. Soc. 103 (1981) 6093.
[5] D.J. Darensbourg, R.L. Gray, T. Delord, Inorg. Chim. Acta 98 (1985) L39.
[6] Q. Chen, S. Liu, J. Zubieta, Angew. Chem., Int. Ed. Engl. 27 (1988) 1724.
[7] Q. Chen, S. Liu, J. Zubieta, Inorg. Chem. 28 (1989) 4433.
[8] A.J. Blake, A.J. Downs, C. Limberg, S. Parsons, J. Chem. Soc., Dalton Trans. (1995) 3263.
[9] L. Ma, S. Liu, J. Zubieta, J. Chem. Soc., Chem. Commun. (1989) 440.
[10] E.M. McCarron III, R.L. Harlow, J. Am. Chem. Soc. 105 (1983) 6179.
[11] S. Liu, J. Zubieta, Polyhedron 8 (1989) 537.
[12] M.Yu. Antipin, L.P. Didenko, L.M. Kachapina, A.E. Shilov, A.K. Shilova, Y.T. Struchkou, J. Chem. Soc., Chem. Commun. (1989) 1467.
[13] B. Modec, J.V. Brenčič, R. Rotar, L. Golič, K. Prout, Acta Crystallogr., Sect. C 54 (1998) 1573.

[14] B. Modec, J.V. Brenčič, I. Leban, Inorg. Chem. Commun. 1 (1998) 161.
[15] B. Modec, J.V. Brenčič, L. Golič, G. Giester, submitted to Inorg. Chim. Acta.
[16] J.V. Brenčič, L. Golič, I. Leban, R. Rotar, J. Sieler, Z. Anorg. Allg. Chem. 622 (1996) 2124.
[17] G.R. Hanson, A.A. Brunette, A.C. McDonell, K.S. Murray, A.G. Wedd, J. Am. Chem. Soc. 103 (1981) 1953.
[18] A. Altomare, G. Cascarano, C. Giacovazzo, A. Guagliardi, M.C. Burla, G. Polidori, M. Camalli, J. Appl. Crystallogr. 27 (1994) 435.
[19] S.R. Hall, G.S.D. King, J.M. Stewart, Xtal 3.4 User's Manual, University of Western Australia, Australia, 1995.
[20] G.-S. Kim, D. Huffman, C.W. DeKock, Inorg. Chem. 28 (1989) 1279.
[21] V.G. Kessler, A.V. Mironov, N.Ya. Turova, A.I. Yanovsky, Y.T. Struchkov, Polyhedron 12 (1993) 1573.
[22] B. Douglas, D. McDaniel, J. Alexander, Concepts and Models of Inorganic Chemistry, Wiley, New York, 1994.
[23] M.H. Chisholm, K. Folting, J.C. Huffman, C.C. Kirkpartick, Inorg. Chem. 23 (1984) 1021.
[24] M.N. Burnett, C.K. Johnson, ORTEP III, Oak Ridge thermal ellipsoid plot program for crystal structure illustrations, Oak Ridge National Laboratory Report ORNL-6895, 1996.
[25] ATOMS, Atomic Structure Display Software, Version 2.0, SHAPE SOFTWARE, Kingsport, TN, USA.

PERGAMON

www.elsevier.nl/locate/poly

Polyhedron 19 (2000) 1227–1232

POLYHEDRON

Chemistry of 2-(phenylazo)pyridine complexes of osmium: synthesis, characterization and reactivities

Anindya Das [a], Shie-Ming Peng [b], Samaresh Bhattacharya [a,*]

[a] *Department of Chemistry, Inorganic Chemistry Section, Jadavpur University, Calcutta 700032, India*
[b] *Department of Chemistry, National Taiwan University, Taipei, Taiwan, ROC*

Received 5 January 2000; accepted 24 February 2000

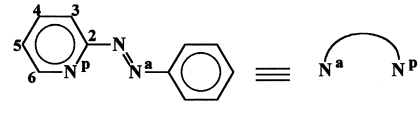
Abstract

Reaction of 2-(phenylazo)pyridine (pap) with $[Os(PPh_3)_3Br_2]$ afforded a mixed ligand complex of the type $[Os(PPh_3)_2(pap)Br_2]$. The structure of this complex was determined by X-ray crystallography. The PPh_3 ligands are *trans* and the bromides are in *cis* positions. The pap ligand is coordinated to osmium as a bidentate N,N-donor forming a five-membered chelate ring. The complex is diamagnetic (low-spin d^6, $S=0$) and in dichloromethane solution shows intense MLCT transitions in the visible region. The two bromides were replaced from the coordination sphere of $[Os(PPh_3)_2(pap)Br_2]$ under mild conditions by a series of anionic ligands L (where L = quinolin-8-olate (q), picolinate (pic), oxalate (Hox), 1-nitroso-2-naphtholate (nn) and acetyl acetonate (acac)) to afford complexes of the type $[Os(PPh_3)_2(pap)(L)]^+$, which were isolated and characterized as the perchlorate salt. The structure of the $[Os(PPh_3)_2(pap)(acac)]ClO_4$ complex was determined by X-ray crystallography. The PPh_3 ligands occupy *trans* positions and the acetylacetonate anion is coordinated to osmium as a bidentate O,O-donor forming a six-membered chelate ring. The $[Os(PPh_3)_2(pap)(L)]^+$ complexes are diamagnetic and show multiple MLCT transitions in the visible region. $[Os(PPh_3)_2(pap)Br_2]$ shows an osmium(II)–osmium(III) oxidation at 0.49 V versus SCE. The same oxidation is displayed by the $[Os(PPh_3)_2(pap)(L)]^+$ complexes within 0.69 to 0.96 V versus SCE. Two successive one-electron reductions of the coordinated pap ligand are also observed in all the complexes below −0.90 V versus SCE. ©2000 Elsevier Science Ltd All rights reserved.

Keywords: Osmium; Triphenylphosphine; 2-(Phenylazo)pyridine; Synthesis; Structures; Reactivities

1. Introduction

The chemistry of osmium has been receiving considerable attention [1–18], largely because of the variety of reactivities exhibited by its complexes. Most of these reactions require direct contact of the reactant with the metal center. As osmium is usually coordinatively saturated in its complexes, such direct links can only be established via dissociation of relatively weak metal–ligand bonds. Osmium complexes having potentially labile ligands are of particular importance in this regard. In the present work, which has emerged from our interest in the chemistry of osmium in different coordination environments [19–23], we have chosen an $OsBr_2$ moiety as the reactive fragment, because the Os–Br bonds are known to undergo dissociation under rather mild conditions [24,25]. To satisfy the remaining four coordination sites of osmium in this $OsBr_2$ moiety, two π-acid ligands, i.e. 2-(phenylazo)pyridine (pap, **1**) and triphenylphosphine (PPh_3), have



pap, 1

been utilized. 2-(Phenylazo)pyridine is well known for its strong π-acidity [26–28], by virtue of which it stabilizes the lower oxidation states of a metal. Triphenylphosphine also favors the lower oxidation states of a metal via dπ–dπ interaction. Coordination by these π-acid ligands has been planned in order to stabilize the bivalent state of osmium, which in turn is expected to favor dissociation of the Os–Br bonds. The targeted complex, $[Os(PPh_3)_2(pap)Br_2]$, has been synthesized and the reactivity of the $OsBr_2$ fragment towards displacement by a group of bidentate ligands (L) of different types has been studied. An account of the chemistry of $[Os(PPh_3)_2(pap)Br_2]$ and $[Os(PPh_3)_2(pap)(L)]^+$ complexes is reported here with special reference to synthesis, structure and redox properties.

* Corresponding author. Tel.: +91-33-483-8393; fax: +91-33-473-4266; e-mail: samaresh_b@hotmail.com

0277-5387/00/$ - see front matter ©2000 Elsevier Science Ltd All rights reserved.
PII S0277-5387(00)00378-8

2. Experimental

2.1. Materials

Osmium tetroxide was purchased from Arora Matthey, Calcutta, India and was converted into $[NH_4]_2[OsBr_6]$ by reduction with HBr [29]. $[Os(PPh_3)_3Br_2]$ was synthesized from $[NH_4]_2[OsBr_6]$ using a literature method [30]. Triphenylphosphine, acetylacetone (Hacac), oxalic acid (H_2ox) and 1-nitroso-2-naphthol (Hnn) were purchased from Loba Chemie, Mumbai, India. Picolinic acid (Hpic) and quinoline-8-ol (Hq) were purchased from E. Merck (India). 2-(Phenylazo) pyridine was prepared by following a literature procedure [31]. All other chemicals and solvents were reagent grade commercial materials and were used as received. Purification of acetonitrile and dichloromethane, and preparation of tetrabutylammonium perchlorate (TBAP) for electrochemical work were performed as reported in the literature [32,33].

2.2. Preparation of the complexes

2.2.1. $[Os(PPh_3)_2(pap)Br_2]$

To a mixture of $[Os(PPh_3)_3Br_2]$ (100 mg, 0.09 mmol) and 2-(phenylazo)pyridine (16 mg, 0.09 mmol), 2-methoxyethanol (30 cm^3) was added. The resulting mixture was refluxed for 2 h. A red crystalline precipitate started to separate during reflux. After cooling the solution to room temperature, the precipitate was collected by filtration, washed thoroughly with ethanol and dried in air. The yield was 52 mg (56%).

2.2.2. $[Os^{II}(PPh_3)_2(pap)(L)]ClO_4$ (L = pic, q, Hox, nn, acac) complexes

The $[Os^{II}(PPh_3)_2(pap)(L)]ClO_4$ (L = pic, q, Hox, nn, acac) complexes were synthesized using a general procedure. Yields varied in the range of 60–65%. Specific details are given for one complex.

$[Os(PPh_3)_2(pap)(acac)]ClO_4$. $[Os(PPh_3)_2(pap)Br_2]$ (100 mg, 0.10 mmol) was dissolved in dichloromethane (20 cm^3) and to this solution was added acetylacetone (10 mg, 0.10 mmol) followed by ethanol (30 cm^3) and triethylamine (10 mg, 0.10 mmol). The solution was boiled for a few minutes in air to remove dichloromethane as much as possible and then it was heated at reflux for 48 h. After being cooled to room temperature, a saturated aqueous solution of $NaClO_4$ (0.5 cm^3) was added to it. $[Os(PPh_3)_2(pap)(acac)]ClO_4$ precipitated as a red solid and was collected by filtration, washed with ice-cold water and dried in vacuo over P_4O_{10}. Purification of the product was done by thin layer chromatography on a silica-gel plate, using 1:1 benzene–acetonitrile as the eluant. A red band separated and was extracted with acetonitrile. On evaporation of the acetonitrile solution, $[Os(PPh_3)_2(pap)(acac)]ClO_4$ was obtained as a red microcrystalline solid. The yield was 64 mg (61%).

In the case of HL = Hq and Hnn, 2-methoxyethanol was used as solvent instead of ethanol and triethanolamine was used as base instead of triethylamine.

2.3. Physical measurements

Microanalyses (C, H, N) were performed using a Perkin-Elmer 240C elemental analyzer. Infrared spectra were obtained on a Perkin-Elmer 783 spectrometer with samples prepared as KBr pellets. Electronic spectra were recorded on a Shimadzu UV 1601 spectrophotometer. Magnetic susceptibilities were measured using a PAR 155 vibrating sample magnetometer fitted with a Walker Scientific L75FBAL magnet. ^1H NMR spectra were obtained on a Bruker AC-200 NMR spectrometer using TMS as the internal standard. Solution electrical conductivities were measured using a Philips PR 9500 bridge with a solute concentration of 10^{-3} M. Electrochemical measurements were made using a PAR model 273 potentiostat. A platinum disk or graphite working electrode, a platinum wire auxiliary electrode and an aqueous saturated calomel reference electrode (SCE) were used in a three-electrode configuration. A RE 0089 X-Y recorder was used to trace the voltammograms. Dinitrogen gas was purified by successively bubbling it through alkaline dithionite and concentrated sulfuric acid and all electrochemical measurements were performed under this dinitrogen atmosphere. All electrochemical data were collected at 298 K and are uncorrected for junction potentials.

2.4. Crystallography

Single crystals of $[Os(PPh_3)_2(pap)Br_2]$ were obtained directly from the synthetic reaction carried out in 2-methoxyethanol. Selected crystal data and data collection parameters are given in Table 1. Data were collected on a Siemens Smart CCD diffractometer using graphite-monochromated Mo Kα radiation ($\lambda = 0.71073$ Å) by frame using ω scans within the angular range $1.48° < \theta < 26.37°$. X-ray data reduction and structure solution and refinement were done using the SHELXTL package. The structure was solved by direct methods.

Single crystals of $[Os(PPh_3)_2(pap)(acac)]ClO_4$ were grown by slow diffusion of hexane into a dichloromethane solution of the complex. Selected crystal data and data collection parameters are given in Table 1. Data were collected on a Siemens Smart CCD diffractometer using graphite-monochromated Mo Kα radiation ($\lambda = 0.71073$ Å) by frame using ω scans within the angular range $1.57° < \theta < 26.37°$. X-ray data reduction and structure solution and refinement were done using the SHELXTL package. The structure was solved by direct methods.

Table 1
Crystallographic data for $[Os(PPh_3)_2(pap)Br_2]$ and $[Os(PPh_3)_2(pap)(acac)]ClO_4$

Formula	$C_{47}H_{39}Br_2N_3P_2Os$	$C_{52}H_{46}ClN_3O_6P_2Os$
FW	1057.77	1096.51
Space group	monoclinic, $P2_1/c$	monoclinic, $P2_1/n$
a (Å)	10.1561(2)	14.3739(1)
b (Å)	17.3501(2)	15.2881(1)
c (Å)	22.8526(3)	22.2380(1)
α (°)	90	90
β (°)	97.624(1)	99.894(1)
γ (°)	90	90
V (Å^3)	3991.24(11)	4814.11(5)
Z	4	4
ρ_{calc} (g cm^{-3})	1.760	1.513
λ (Å)	0.71073	0.71073
Crystal size (mm)	0.18×0.08×0.03	0.80×0.12×0.10
T (K)	295(2)	295(2)
μ (mm^{-1})	5.316	2.823
R_1 [a]	0.0503	0.0322
wR_2 [b]	0.0793	0.0664
GOF on F^2 [c]	1.078	1.093

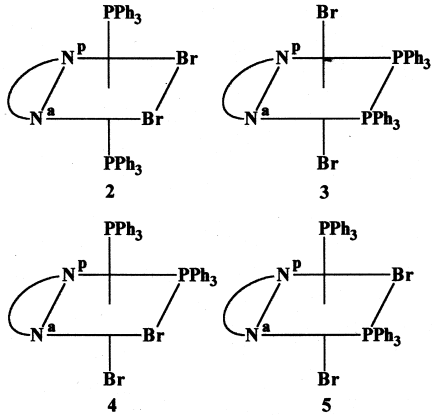
[a] $R_1 = \Sigma||F_o| - |F_c||/\Sigma|F_o|$.
[b] $wR_2 = [\Sigma[w(F_o^2 - F_c^2)^2]/\Sigma[w(F_o^2)^2]]^{1/2}$.
[c] GOF $= [\Sigma[w(F_o^2 - F_c^2)^2]/(M-N)]^{1/2}$, where M is the number of reflections and N is the number of parameters refined.

3. Results and discussion

3.1. Synthesis and characterization

3.1.1. $[Os(PPh_3)_2(pap)Br_2]$

Smooth displacement of one PPh_3 from $[Os(PPh_3)_3Br_2]$ by 2-(phenylazo)pyridine in refluxing 2-methoxyethanol affords the $[Os(PPh_3)_2(pap)Br_2]$ complex in decent yield. The composition of the complex was confirmed by its elemental (C, H, N) analytical data (Table 2). The complex is diamagnetic, which corresponds to the +2 oxidation state of osmium (low-spin d^6, $S=0$) in this complex. As 2-(phenylazo)pyridine is an unsymmetrical bidentate ligand, this $[Os(PPh_3)_2(pap)Br_2]$ complex may, in principle, exist in four geometrical isomeric forms (**2**–**5**). To find out



the actual stereochemistry of $[Os(PPh_3)_2(pap)Br_2]$, its structure was determined by X-ray crystallography. The

Table 2
Characterization data of the $[Os(PPh_3)_2(pap)Br_2]$ and $[Os(PPh_3)_2(pap)(L)]ClO_4$ complexes

Compound	Yield	Analytical data [a]			Electronic spectral data	Cyclic voltammetric data [c]
	(%)	C (%)	H (%)	N (%)	λ_{max} (nm) (ε (M^{-1} cm^{-1}))	$E_{1/2}$ (V vs. SCE) (ΔE_p (mV))
$[Os(PPh_3)_2(pap)]Br_2$ [d]	56	53.36 (53.36)	3.71 (3.69)	3.99 (3.97)	504 (4600), 408 [b] (7000), 340 [b] (4300), 252 [b] (12900), 228 (42200)	0.49 (80), −0.98 (100), −1.35 (100)
$[Os(PPh_3)_2(pap)(q)]ClO_4$ [e]	64	58.94 (58.92)	3.99 (3.95)	4.93 (4.91)	538 (5800), 337 [b] (10300), 250 [b] (34200), 219 (61500)	1.01 (80), −0.92 (110), −1.29 (110)
$[Os(PPh_3)_2(pap)(pic)]ClO_4$ [e]	60	56.87 (56.86)	3.86 (3.84)	5.03 (5.01)	480 (1700), 312 (6800), 260 [b] (10200), 220 (56900), 208 [b] (51500)	0.83 (80), −1.03 (120), −1.36 (120)
$[Os(PPh_3)_2(pap)(Hox)]ClO_4$ [e]	65	49.67 (49.66)	3.31 (3.29)	3.57 (3.55)	484 (4600), 328 (14800), 252 [b] (35000), 216 (59000)	0.69 (80), −1.12 (110), −1.53 (120)
$[Os(PPh_3)_2(pap)(nn)]ClO_4$ [e]	62	59.56 (59.54)	3.87 (3.85)	4.78 (4.79)	508 (5300), 335 [b] (11300), 223 (56900)	0.84 (70), −1.28 (130), −1.63 (140)
$[Os(PPh_3)_2(pap)(acac)]ClO_4$ [e]	61	56.96 (56.91)	4.21 (4.20)	3.85 (3.83)	602 [b] (500), 501 (5000), 319 [b] (15900), 260 [b] (26500), 227 [b] (4700), 216 (53900)	0.92 (70), −0.91 (100), −1.33 (110)

[a] Calculated values are in parentheses.
[b] Shoulder.
[c] Supporting electrolyte, TEAP; scan rate, 50 mV s^{-1}; $E_{1/2} = 0.5(E_{pa} + E_{pc})$, where E_{pa} and E_{pc} are anodic and cathodic peak potentials respectively; $\Delta E_p = E_{pa} - E_{pc}$.
[d] Solvent, dichloromethane.
[e] Solvent, acetonitrile.

structure is shown in Fig. 1 and selected bond parameters are listed in Table 3. The pap ligand is coordinated to osmium in the usual manner with a bite angle of 76.6(2)°. The two PPh_3 ligands are mutually *trans*, while the two bromides occupy mutually *cis* positions. The structure determination thus shows that $[Os(PPh_3)_2(pap)Br_2]$ has stereochemistry 2. The $N_2P_2Br_2$ coordination sphere around osmium is distorted from ideal octahedral geometry, as reflected in the bond parameters centering osmium. The Os–P and Os–Br bond distances are quite normal, as observed in other complexes containing these bonds [23,24]. While the Os–N1 length is also normal [24], the Os–N3 bond is noticeably short and the azo N2–N3 distance is longer than the uncoordinated azo distance [34,35]. The short Os–N3 distance and increase in N2–N3 bond order reflect the considerable π-interaction between osmium(II) and the azo function.

The ^1H NMR spectrum of $[Os(PPh_3)_2(pap)Br_2]$ was recorded in $CDCl_3$ solution. The spectrum is rather complex in nature owing to overlapping of signals and hence assignment of all the signals in this region to specific protons has not been possible. However, two doublets (1H each) observed at 8.22 and 7.87 ppm are assigned to the two pyridine-protons of pap at positions 6 and 3, respectively (see **1**). The other resonances appear within 6.7 to 7.5 ppm and intensity measurement of these signals corresponds to the remaining number (37) of protons present in the complex. The IR spectrum of $[Os(PPh_3)_2(pap)Br_2]$ shows many vibrations in the 1600–400 cm^{-1} region. Strong vibrations observed at 740, 690, and 522 cm^{-1} indicate the presence of the $Os(PPh_3)_2$ moiety [36]. A sharp and strong vibration at 1310 cm^{-1} is assigned to the $\nu_{N=N}$ stretch [37]. The $[Os(PPh_3)_2(pap)Br_2]$ complex is poorly soluble in solvents such as acetonitrile, acetone, ethanol, etc. and moderately soluble in solvents such as dichloromethane, chloroform, *N*,*N*-dimethylformamide, etc., producing intense red solution. The electronic spectrum of the complex has been recorded in dichloromethane solution. The complex shows intense absorptions in the visible and UV region (Table 2).

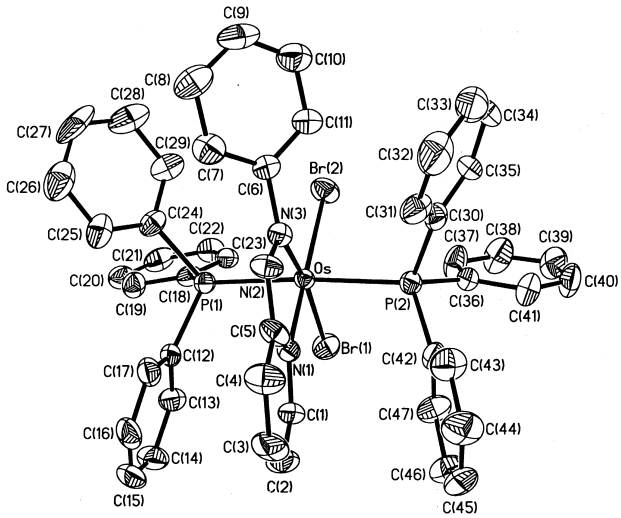


Fig. 1. Structure of $[Os(PPh_3)_2(pap)Br_2]$.

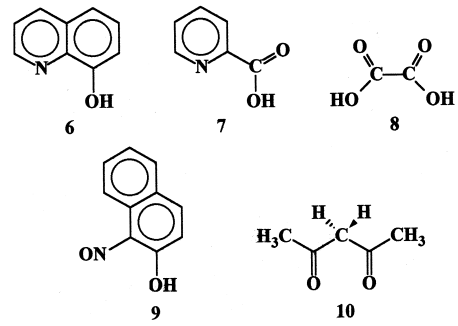
Table 3
Selected bond distances and bond angles for $Os(PPh_3)_2(pap)Br_2$ and $[Os(PPh_3)_2(pap)(acac)]ClO_4$

$[Os(PPh_3)_2(pap)Br_2]$		$[Os(PPh_3)_2(pap)(acac)]ClO_4$	
Os–P1	2.417(2)	Os–P1	2.4485(10)
Os–P2	2.430(2)	Os–P2	2.4740(9)
Os–N1	2.031(5)	Os–O1	2.082(2)
Os–N3	1.978(5)	Os–O2	2.096(2)
Os–Br1	2.5872(7)	Os–N1	2.033(3)
Os–Br2	2.5602(7)	Os–N3	1.977(3)
N2–N3	1.314(7)	O1–C13	1.297(5)
		O2–C15	1.280(4)
		N2–N3	1.329(4)
N1–Os–N3	76.6(2)	N3–Os–N1	76.29(12)
N1–Os–Br1	170.5(2)	N3–Os–O1	171.77(11)
N3–Os–Br2	175.05(14)	N1–Os–O2	175.89(10)
P1–Os–P2	175.10(6)	P1–Os–P2	172.77(3)
		O1–Os–O2	87.89(10)

The absoptions in the UV region are attributable to transitions within the ligand orbitals, whereas the absorptions in the visible region are probably due to allowed metal-to-ligand charge-transfer transitions.

3.1.2. $[Os(PPh_3)_2(pap)(L)]ClO_4$

One major objective of undertaking this present work has been to scrutinize the reactivity of the $OsBr_2$ fragment of $[Os(PPh_3)_2(pap)Br_2]$ towards displacement by ligands of different types. This was carried out by reacting $[Os(PPh_3)_2(pap)Br_2]$ with five selected acidic ligands, i.e. quinoline-8-ol (Hq, **6**), picolinic acid (Hpic, **7**), oxalic acid (H_2ox, **8**), 1-nitroso-2-naphthol (Hnn, **9**) and acetylacetone (Hacaac, **10**). The reactions proceed smoothly in



ethanol/2-methoxyethanol medium (a little dichloromethane was necessary initially to take $[Os(PPh_3)_2(pap)Br_2]$ into alcoholic medium) in the presence of a base to afford the expected complexes of the type $[Os(PPh_3)_2(pap)(L)]^+$ (L = q, pic, Hox, nn and acac). It is interesting to note here that during the reaction with oxalic acid, only one proton is lost and the monoanionic oxalate ion (Hox) coordinates to osmium. The complex cations were isolated as perchlorate salts in the solid state. Microanalytical data of these five complexes agree well with their compositions (Table 2). These complexes are diamagnetic which shows that the +2 state of osmium is retained in them. Several geometric iso-

mers are possible for these complexes. The structure of $[Os(PPh_3)_2(pap)(acac)]ClO_4$ was determined by X-ray crystallography. The structure is shown in Fig. 2 and selected bond distances and angles are presented in Table 3. The coordination sphere around osmium is $N_2O_2P_2$ which is slightly distorted octahedral in nature, as reflected in all the bond angles with osmium as the central atom. The acetylacetonate anion is coordinated to osmium as a O,O-donor with a bite angle of 87.89°. The two PPh_3 ligands are mutually *trans* as observed in the parent $[Os(PPh_3)_2(pap)Br_2]$ complex. Distances within the $Os(PPh_3)_2(pap)$ fragment are comparable to those observed in the $[Os(PPh_3)_2(pap)Br_2]$ complex [23]. The bond lengths in the Os(acac) fragment are also normal [21,38]. The other four $[Os(PPh_3)_2(pap)(L)]^+$ complexes have the same $Os(PPh_3)_2(pap)$ fragment and hence they are assumed to have similar structures with the PPh_3 ligands in mutually *trans* positions. Synthesis of the $[Os(PPh_3)_2(pap)(L)]^+$ complexes from $[Os(PPh_3)_2(pap)Br_2]$ is therefore stereoretentive.

^{1}H NMR spectra of the $[Os(PPh_3)_2(pap)(L)]ClO_4$ complexes, recorded in $CDCl_3$ solution, show many signals in the aromatic region and the spectra are complex in nature. In the $[Os(PPh_3)_2(pap)(acac)]ClO_4$ complex, two sharp methyl resonances are observed at 1.67 and 1.58 ppm due to the coordinated acac, and the central C–H proton signal of the same ligand appears at 5.09 ppm. Infrared spectra of the $[Os(PPh_3)_2(pap)(L)]ClO_4$ complexes are mostly similar to the spectrum of the parent $[Os(PPh_3)_2(pap)Br_2]$ complex. Some additional vibrations are observed in all the $[Os(PPh_3)_2(pap)(L)]ClO_4$ complexes, of which the two intense ones observed near 1100 and 625 cm^{-1} indicate the presence of perchlorate ion. The $\nu_{CO(carboxylate)}$ vibration is observed at 1700 cm^{-1} in the L = pic complex and at 1650 cm^{-1} in the L = Hox complex. In the L = nn complex the ν_{NO} vibration is observed at 1256 cm^{-1}. The $[Os(PPh_3)_2(pap)(L)]ClO_4$ complexes are soluble in acetonitrile solution, producing brown solutions. Conductivity measurements in acetonitrile solution show that all these complexes behave as 1:1 electrolytes (Λ_M = 145–160 Ω^{-1} cm^2 M^{-1}), as expected. Electronic spectra of the $[Os(PPh_3)_2(pap)(L)]ClO_4$ complexes, recorded in acetonitrile solution (Table 2), show several intense absorptions in the visible and UV region as before.

3.2. Cyclic voltammetric properties

Electrochemical properties of all the complexes were studied by cyclic voltammetry. Voltammetric data are given in Table 2 and selected voltammograms are shown in Fig. 3. Cyclic voltammetry on $[Os(PPh_3)_2(pap)Br_2]$ in dichloromethane solution shows a reversible oxidative response at 0.49 V (all potentials are referenced to SCE) and two quasi-reversible reductive responses at −1.03 and −1.40 V. The oxidation is assigned to osmium(II)–osmium(III) oxidation. The one-electron nature of this oxidation was established by comparing its current heights with those of standard ferrocene–ferrocenium couple under identical experiment. The reductions are assigned to reductions of the coordinated 2-(phenylazo)pyridine ligand. The 2-(phenylazo)pyridine ligand is known to accept successively two electrons in its lowest unoccupied molecular orbital which is largely azo in nature [39]. Both of these reductions are indeed observed in $[Os(PPh_3)_2(pap)Br_2]$. Cyclic voltammetry on the $[Os(PPh_3)_2(pap)(L)]^+$ complexes in acetonitrile solution also shows a reversible osmium(II)–osmium(III) oxidation and two reductions of the coordinated pap (Table 2, Fig. 3). The potential of the osmium(II)–osmium(III) oxidation varies significantly (0.69–1.01 V) as L is varied. Reductions of the coordinated pap are observed below −0.9 V.

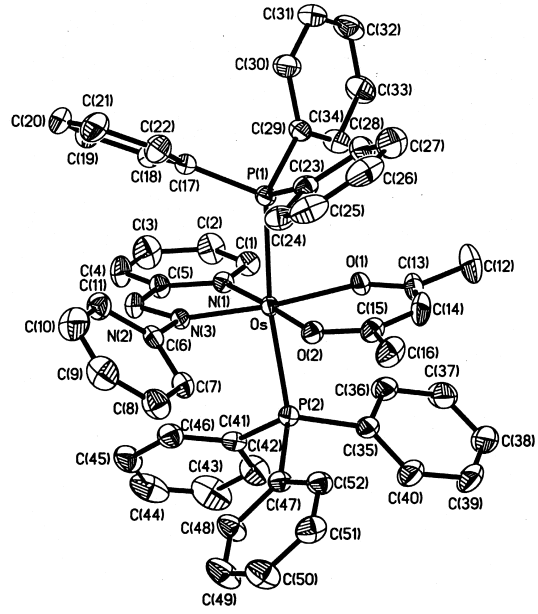


Fig. 2. Structure of $[Os(PPh_3)_2(pap)(acac)]ClO_4$.

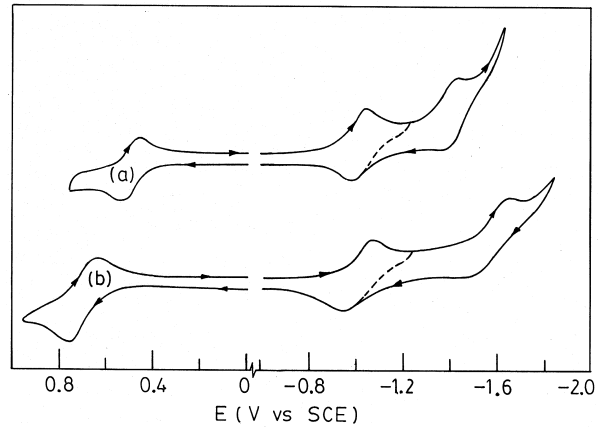


Fig. 3. Cyclic voltammograms of (a) $[Os(PPh_3)_2(pap)Br_2]$ in dichloromethane solution (0.1 M TBAP) and (b) $[Os(PPh_3)_2(pap)(Hox)]ClO_4$ in acetonitrile solution (0.1 M TBAP) at a scan rate of 50 mV s^{-1}.

4. Conclusion

The Os–Br bonds in the $[Os(PPh_3)_2(pap)Br_2]$ complex are found to be displaceable by bidentate chelating ligands

under relatively mild conditions. Hence this complex appears to be suitable as a building unit for the preparation of complexes of higher nuclearity and such possibilities are currently being explored.

Supplementary data

Supplementary data are available from the Cambridge Crystallographic Data Centre, 12 Union Road, Cambridge CB2 1EZ, UK (fax: +44-1223-336033; e-mail: deposit@cdc.cam.ac.uk), on request quoting the deposition numbers CCDC 137568 and CCDC 137569.

Acknowledgements

Financial assistance received from the Department of Science and Technology, New Delhi (Grant No. SP/S1/F33/98) is gratefully acknowledged. Thanks are also due to the Third World Academy of Sciences for financial support enabling the purchase of an electrochemical cell system.

References

[1] K.R. Seddon, Coord. Chem. Rev. 41 (1982) 159.
[2] D.S. Moore, Coord. Chem. Rev. 44 (1982) 127.
[3] D.J. Gulliver, W. Levason, Coord. Chem. Rev. 46 (1982) 1.
[4] E.A. Seddon, Coord. Chem. Rev. 67 (1985) 243.
[5] M.O. Albers, D.J. Robinson, E. Singleton, Coord. Chem. Rev. 79 (1987) 1.
[6] N.C. Thomas, Coord. Chem. Rev. 93 (1989) 225.
[7] D. Rong, H.G. Hong, Y.I. Kim, J.S. Krueger, J.E. Mayer, T.E. Mallouk, Coord. Chem. Rev. 97 (1990) 237.
[8] V.W.W. Yam, C.M. Che, Coord. Chem. Rev. 97 (1990) 93.
[9] R. Hage, Coord. Chem. Rev. 111 (1991) 161.
[10] J.P. Collin, S. Guillerez, J.P. Sauvage, F. Barigelletti, L. Flamigni, L.D. Cola, V. Balzani, Coord. Chem. Rev. 111 (1991) 291.
[11] L.D. Cola, F. Barigelletti, V. Balzani, P. Belser, A.V. Zelewsky, C. Seel, M. Frank, F. Vogtle, Coord. Chem. Rev. 111 (1991) 255.
[12] E.C. Constable, C.E. Housecroft, Coord. Chem. Rev. 124 (1993) 183.
[13] M.D. Ward, Coord. Chem. Rev. 127 (1993) 1.
[14] M. Furue, K. Maruyama, Y. Kanematsu, T. Kushida, M. Kamachi, Coord. Chem. Rev. 132 (1994) 201.
[15] F. Barigelletti, L. Flamigni, V. Balzani, J.P. Collin, J.P. Sauvage, A. Sour, E.C. Constable, A.M.W.C. Thompson, Coord. Chem. Rev. 132 (1994) 209.
[16] K. Kalyansundaram, S.M. Zakeeruddin, M.K. Nazeeruddin, Coord. Chem. Rev. 132 (1994) 259.
[17] M.G. Richmond, Coord. Chem. Rev. 141 (1995) 63.
[18] M.D. Ward, Coord. Chem. Rev. 146 (1995) 99.
[19] F. Basuli, S.M. Peng, S. Bhattacharya, Inorg. Chem. 36 (1997) 5645.
[20] F. Basuli, S.M. Peng, S. Bhattacharya, Polyhedron 17 (1998) 2191.
[21] F. Basuli, S.M. Peng, S. Bhattacharya, Polyhedron 18 (1998) 391.
[22] F. Basuli, M. Ruf, C.G. Pierpont, S. Bhattacharya, Inorg. Chem. 37 (1998) 6113.
[23] A. Das, F. Basuli, S.M. Peng, S. Bhattacharya, Polyhedron 18 (1999) 2729.
[24] B.K. Ghosh, A. Mukhopadhyay, S. Goswami, S. Ray, A. Chakravorty, Inorg. Chem. 23 (1984) 4633.
[25] E.M. Kober, J.V. Casper, B.P. Sullivan, T.J. Meyer, Inorg. Chem. 27 (1988) 4587.
[26] R.A. Krause, K. Krause, Inorg. Chem. 19 (1980) 2600.
[27] S. Goswami, A.R. Chakravarty, A. Chakravorty, Inorg. Chem. 20 (1981) 2246.
[28] R.A. Krause, K. Krause, Inorg. Chem. 21 (1982) 1714.
[29] F.P. Dwyer, J.W. Hogarth, Inorg. Synth. 5 (1957) 204.
[30] P.R. Hoffman, K.G. Caulton, J. Am. Chem. Soc. 97 (1975) 4221.
[31] N. Campbell, A.W. Henderson, D. Taylor, J. Chem. Soc. (1953) 1281.
[32] D.T. Sawyer, J.L. Roberts Jr., Experimental Electrochemistry for Chemists, Wiley, New York, 1974, pp. 167–215.
[33] M. Walter, L. Ramaley, Anal. Chem. 45 (1973) 165.
[34] A. Seal, S. Ray, Acta Crystallogr., Sect. C 40 (1984) 929.
[35] P. Majumdar, S.M. Peng, S. Goswami, J. Chem. Soc., Dalton Trans. (1998) 1569.
[36] S. Bhattacharya, C.G. Pierpont, Inorg. Chem. 30 (1991) 2906.
[37] B.K. Ghosh, S. Goswami, A. Chakravorty, Inorg. Chem. 22 (1983) 3358.
[38] K. Sui, S.M. Peng, S. Bhattacharya, Polyhedron 18 (1999) 631.
[39] S. Goswami, R.N. Mukherjee, A. Chakravorty, Inorg. Chem. 22 (1983) 2825.

PERGAMON

www.elsevier.nl/locate/poly

Polyhedron 19 (2000) 1233–1243

POLYHEDRON

Dinuclear ruthenium(II) and/or osmium(II) complexes of bipyridyl ligands bridged by rigid spacers: synthesis, characterization, electrochemical behavior and luminescence properties

Anvarhusen K. Bilakhiya, Beena Tyagi, Parimal Paul *

Discipline of Silicates and Catalysis, Central Salt and Marine Chemicals Research Institute, Bhavnagar 364 002, India

Received 18 November 1999; accepted 23 March 2000

Abstract

New bridging ligands, 1,4-bis[4-(4′-methyl)-2,2′-bipyridyl)imine]benzene (BL^1) and 4,4′-bis[4-(4′-methyl)-2,2′-bipyridyl)-imine]benzene (BL^2), and their dinuclear complexes of the type $[(bpy)_2Ru\text{-}BL\text{-}Ru(bpy)_2]^{4+}$, $[(bpy)_2Os\text{-}BL\text{-}Os(bpy)_2]^{4+}$ and $[(bpy)_2Ru\text{-}BL\text{-}Os(bpy)_2]^{4+}$ (where $BL = BL^1$ and BL^2) have been synthesized and characterized. Mononuclear model complexes $[(bpy)_2RuL^1]^{2+}$, $[(bpy)_2OsL^1]^{2+}$ and $[(bpy)_2RuL^2]^{2+}$, where L^1 = [4-(4′-methyl)-2,2′-bipyridyl)imine]-4-aminobenzene and L^2 = [4-(4′-methyl)-2,2′-bipyridyl)imine]-4-aminodiphenylene, have also been synthesized. Ligands and metal complexes were characterized on the basis of elemental analysis, FAB mass, IR and ^1H NMR data. All metal complexes exhibit characteristic MLCT absorption and luminescence bands in the visible region. Cyclic and square wave voltammograms of all complexes exhibit metal-based oxidations (M(II) → M(III)) in the potential ranges +1.20 to +1.23 V for Ru(II) and +0.75 to +0.82 V for Os(II). Ligand-based reductions occurred in the potential range −1.28 to −1.90 V. Mixed-valence species of the dinuclear complexes were generated by the addition of a standard solution of ammonium cerium(IV) nitrate. The excited state life-time of all complexes were measured in acetonitrile and also in a methanol–ethanol (4:1) mixture at room temperature. The homodinuclear complexes exhibit significantly long life-times, which are attributed to delocalization of excited electron on the conjugated bridging unit. In heterodinuclear complexes the Ru-based emission life-time decreased significantly; this quenching process takes place via energy transfer from Ru(II) to Os(II) center through spacers. The rate constants for energy transfer are calculated. ©2000 Elsevier Science Ltd All rights reserved.

Keywords: Electrochemical studies; Heterodinuclear complexes; Homodinuclear complexes; Luminescence properties; Osmium(II) complexes; Ruthenium(II) complexes; Syntheses

1. Introduction

In the past few years, there has been explosive growth in the field of supramolecular chemistry of ruthenium(II) and osmium(II) with polypyridyl ligands because of their rich electrochemical and excited-state properties which predict their utility in a variety of photoredox applications [1–9]. Such systems can be developed by covalent linking of prefabricated molecular components (building blocks) with spacers having bidentate donor sets [3,4]. A suitable choice of the building blocks and spacers, and an appropriate designing of the structure can, in fact, allow the occurrence of energy/electron transfer along the supramolecular array [3,4,9–14]. Bis(bipyridyl)ruthenium(II)/osmium(II) exhibit suitable redox and excited-state properties to play the role of building blocks for the construction of photoactive supramolecular systems [15]. However, the key component of the supramolecular systems is the bridging ligands; the size, shape and electronic nature of the bridge controls the interactions between the units, and thereby properties of the molecule as a whole. There are number of reports of homo- and heterodinuclear complexes using 2,2′-bipyridyl-based dinucleating spacers, the bidentate donor sites of which are bridged by various aliphatic/aromatic moieties of different size and shape [16–31].

We were interested to study long-range metal–metal interactions by using spacers, the bidentate chelating sites of which are bridged by rigid aromatic moieties of various lengths. To develop such systems we synthesized two new spacers in which two 4-methyl-2,2′-bipyridyl donor sites are bridged by –CH=N–C_6H_4–N=CH– (BL^1) and –CH=N–C_6H_4–C_6H_4–N=CH– (BL^2) moieties, which make complete

* Corresponding author. Tel.: +91-278-567760; fax: +91-278-566970; e-mail: salt@bhavnagar.com

0277-5387/00/$ - see front matter ©2000 Elsevier Science Ltd All rights reserved.
PII S0277-5387(00)00379-X

conjugations between the chromophores. Homo- and heterodinuclear complexes of Ru(II) and Os(II) have been synthesized by the reaction of BL^1/BL^2 with the building blocks *cis*-$[M(bpy)_2Cl_2]$ [M = Ru(II) and Os(II)]. Heterodinuclear complexes have been synthesized following a new route which excluded the possibility of the presence of homodinuclear complexes as impurity. We also synthesized mononuclear complexes of ligands having one 4-methyl-2,2′-bipyridyl donor site connected to the bridging unit and these have been used as model compounds to compare their properties to that of the corresponding dinuclear complexes. Herein, we report the synthesis, characterization, electrochemical and luminescence properties of these novel complexes.

2. Experimental

2.1. Materials

2,2′-Bipyridyl (bpy), 4,4′-dimethyl-2,2′-bipyridyl, ammonium hexachloroosmate(IV), ammonium hexafluorophosphate, ammonium tetrafluoroborate and ammonium cerium(IV) nitrate were purchased from Aldrich. *p*-Phenylenediamine and 4,4′-diphenylenediamine were purchased from S-D Fine Chemicals. Neutral alumina was obtained from National Chemicals Co. Hydrated ruthenium trichloride was purchased from Arora Matthey. 4′-Methyl-2,2′-bipyridyline-4-carbaldehyde [21], *cis*-$[Ru(bpy)_2Cl_2]\cdot 2H_2O$ [32] and *cis*-$[Os(bpy)_2Cl_2]\cdot 2H_2O$ [33] were prepared according to the literature methods.

2.2. Physical measurements

Elemental analysis (C, H, N) were performed on a model 2400 Perkin-Elmer elemental analyzer. FAB mass spectra were recorded on a JEOL SX 102/DA-6000 mass spectrometer using xenon (6 kV, 10 mA) as the FAB gas. The accelerating voltage was 10 kV and the spectra were recorded at room temperature. *m*-Nitrobenzyl alcohol was used as the matrix. Infrared (IR) spectra were recorded on a Perkin-Elmer spectrum GX FT-IR spectrophotometer as KBr pellets. ^{1}H NMR spectra were recorded on a model DPX 200 Bruker FT-NMR instrument. The UV–Vis spectra were recorded on a model 8452A Hewlett-Packard diode array spectrophotometer. NIR spectra were recorded on a model UV-3101PC UV–Vis–NIR (Shimadzu) spectrophotometer. Electrochemical experiments were performed with a model 273A EG&G Princeton Applied Research potentiostat. All experiments were conducted in an argon atmosphere with a glassy-carbon working electrode, SCE electrode as reference and 0.1 mol dm^{-3} $[NBu^n_4][BF_4]$ as supporting electrolyte. Luminescence spectra were recorded on a Perkin-Elmer LS-50B spectrofluorimeter in acetonitrile and in methanol–ethanol (4:1) solutions at room temperature.

Flash photolysis experiments were carried out with an Applied Photophysics SP-Quanta Ray GCR-2 (10) Nd–YAG laser using the third harmonic output of 355/532 nm with a pulse width of 8 ns. A DHS2 dichroic harmonic separator was used to separate the third harmonic from the second harmonic and the fundamental of the Nd–YAG laser. The output was directed towards the sample using prisms. The oscilloscope is optically triggered using the photodiode. The monitoring source was a 250 W pulsed xenon lamp which was focused on the sample, at right-angles to the incident laser beam, using lenses and an adjustable iris positioned in front of the sample holder. The beam emerging from the sample was focused on to a Czerny Turner monochromator using a pair of lenses. The monochromator was fitted with a stepper motor control in order to drive the monochromator to the desired wavelength. The detection was carried out using a Hamamatsu R-928 photomultiplier tube. The signals were captured using a Hewlett-Packard 54201A 100 MHz digital storage oscilloscope. The data were transferred to the computer and analyzed using a software developed in-house. Experiments were performed in acetonitrile/methanol–ethanol (4:1) solutions under argon atmosphere.

2.3. Synthesis of ligands

2.3.1. Preparation of 1,4-bis[4-(4′-methyl)-2,2′-bipyridyl)-imine]benzene (BL^1)

The compound 4′-methyl-2,2′-bipyridyline-4-carbaldehyde (mbca) (396 mg, 2 mmol) and *p*-phenylenediamine (108 mg, 1 mmol) were added to ethanol (25 cm^3) and the mixture was heated at reflux for 8 h. During reflux a yellow microcrystalline compound was separated from the solution. After isolation of this compound by filtration, the filtrate was kept at room temperature over night, during which another crop of the same compound separated from the solution. The combined product was washed with ethanol and diethyl ether and dried. Yield 82%. Found: C, 76.67; H, 5.28; N, 17.74. Calc. for $C_{30}H_{24}N_6$: C, 76.90; H, 5.16; N, 17.93%. IR (cm^{-1}): 1621 ($\nu_{C=N}$). ^{1}H NMR ($CDCl_3$): δ 2.48 (s, 6H), 7.20 (dd, 2H, J = 5.0, 1.0 Hz), 7.37 (s, 4H), 7.90 (dd, J = 5.3, 1.3 Hz), 8.31 (s, 2H), 8.60 (d, 2H, J = 5 Hz), 8.63 (s, 2H), 8.82 (d, 2H, J = 4.4 Hz), 8.83 (s, 2H).

2.3.2. Preparation of [4-(4′-methyl)-2,2′-bipyridyl)imine]-4-aminobenzene (L^1)

The compound 4′-methyl-2,2′-bipyridyline-4-carbaldehyde (198 mg, 1 mmol) was dissolved in ethanol (4 cm^3) at ~60°C and the hot solution was added dropwise to a hot (~60°C) ethanolic solution (4 cm^3) of *p*-phenylenediamine (130 mg, 1.2 mmol) and the mixture was kept at the same temperature for 0.5 h, during which shining yellow crystals were deposited. The compound was isolated by filtration and washed with ethanol and diethyl ether. Yield 70%. Found: C, 74.65; H, 5.42; N, 19.18. Calc. for $C_{18}H_{16}N_4$: C, 74.98; H, 5.59; N, 19.43%. IR (cm^{-1}): 3435, 3317, 3207 (ν_{NH_2}), 1631 ($\nu_{C=N}$). ^{1}H NMR ($CDCl_3$): δ 2.46 (s, 3H), 3.80 (s, 2H),

6.73 (d, 2H, $J=8.0$ Hz), 7.17 (d, 1H, $J=4.2$ Hz), 7.24 (d, 2H, $J=8.2$ Hz), 7.86 (d, 1H, $J=4.2$ Hz), 8.27 (s, 1H), 8.57 (d, 1H, $J=6.0$ Hz), 8.59 (s, 1H), 8.72 (s, 1H), 8.76 (d, 1H, $J=6.0$ Hz).

2.3.3. Preparation of 4,4′-bis[4-(4′-methyl)-2,2′-bipyridyl)-imine]diphenylene (BL^2)

This ligand was synthesized following the same procedure as described for BL^1. The only difference is that *p,p′*-diphenylenediamine was taken instead of *p*-phenylenediamine. Yield 76%. Found: C, 79.09; H, 5.15; N, 15.11. Calc. for $C_{36}H_{28}N_6$: C, 79.39; H, 5.18; N, 15.43%. IR (cm^{-1}): 1626 ($\nu_{C=N}$). ^1H NMR ($CDCl_3$): δ 2.48 (s, 6H), 7.20 (dd, 2H, $J=4.3, 1.3$ Hz), 7.39 (d, 4H, $J=8.4$ Hz), 7.72 (d, 4H, $J=8.4$ Hz), 7.92 (dd, 2H, $J=5.0, 1.5$ Hz), 8.29 (s, 2H), 8.60 (d, 2H, $J=4.8$ Hz), 8.75 (s, 2H), 8.81 (s, 2H), 8.83 (d, 2H, $J=5.2$ Hz).

2.3.4. Preparation of [4-(4′-methyl)-2,2′-bipyridyl)imine]-4′-aminodiphenylene (L^2)

This ligand was synthesized following the same procedure as described for L^1. The only difference is that *p,p′*-diphenylenediamine was taken instead of *p*-phenylenediamine. Yield 70%. Found: C, 78.60; H, 5.59; N, 15.21. Calc. for $C_{24}H_{20}N_4$: C, 79.09; H, 5.53; N, 15.37%. IR (cm^{-1}): 3414, 3340, 3231 (ν_{NH_2}), 1639 ($\nu_{C=N}$). ^1H NMR ($CDCl_3$): δ 2.47 (s, 3H), 3.77 (s, 2H), 6.78 (d, 2H, $J=8.4$ Hz), 7.21 (d, 1H, $J=4.2$ Hz), 7.34 (d, 2H, $J=8.4$ Hz), 7.46 (d, 2H, $J=8.4$ Hz), 7.61 (d, 2H, $J=8.4$ Hz), 7.90 (d, 1H, $J=4.2$ Hz), 8.29 (s, 1H), 8.58 (d, 1H, $J=6.0$ Hz), 8.63 (s, 1H), 8.79 (s, 1H), 8.81 (d, 1H, $J=6.0$ Hz).

2.4. Synthesis of metal complexes

*2.4.1. Preparation of $[(bpy)_2Ru(L^1)][PF_6]_2\cdot H_2O$ (**1**)*

A mixture of *cis*-$Ru(bpy)_2Cl_2\cdot 2H_2O$ (520 mg, 1 mmol) and L^1 (288 mg, 1 mmol) in ethanol–water (2:1, 45 cm^3) was refluxed for 10 h. The volume of the reaction mixture was reduced to about 20 cm^3 by rotary evaporation, then an aqueous solution (10 cm^3) of NH_4PF_6 (815 mg, 4 mmol) was added. The precipitate was filtered off and washed with water and diethyl ether. The compound was purified by column chromatography packed with neutral alumina, with acetonitrile–toluene (2:1) as eluent. The solvent was removed by rotary evaporation and the residue was redissolved in a minimum volume (10 cm^3) of acetonitrile and precipitated by the addition of diethyl ether. The precipitate was filtered off and vacuum dried. Yield 75%. Found: C, 45.02; H, 3.20; N, 10.92. Calc. for $C_{38}H_{34}F_{12}N_8OP_2Ru$: C, 45.20; H, 3.39; N, 11.09%. IR (cm^{-1}): 3409, 3221 (ν_{NH_2}), 1619 ($\nu_{C=N}$), 841 (PF_6^-). ^1H NMR (CD_3CN): δ 2.56 (s, 3H), 4.53 (s, 2H), 6.71 (d, 2H), 7.27 (m, 1H), 7.30 (d, 2H), 7.40 (m, 4H), 7.54 (d, 1H), 7.67–7.81 (m, 6H), 8.05 (t, 4H), 8.49 (d, 5H), 8.69 (s, 1H), 8.87 (s, 1H).

*2.4.2. Preparation of $[(bpy)_2Os(L^1)][PF_6]_2\cdot H_2O$ (**2**)*

cis-$Os(bpy)_2Cl_2\cdot 2H_2O$ (305 mg, 0.5 mmol) and L^1 (144 mg, 0.5 mmol) were refluxed in 2-methoxyethanol–water (4:1, 20 cm^3) for 8 h. The volume of the solution was reduced to dryness by rotary evaporation and the residue was dissolved in water (5 cm^3). The solution was filtered and to the filtrate an aqueous solution (5 cm^3) of NH_4PF_6 (408 mg, 2 mmol) was added. The precipitate thus obtained was isolated by filtration and washed with water and diethyl ether. The complex was purified following the same procedure as described for complex **1**. Yield 62%. Found: C, 41.28; H, 3.20; N, 10.06. Calc. for $C_{38}H_{34}F_{12}N_8OP_2Os$: C, 41.54; H, 3.12; N, 10.20%. IR (cm^{-1}): 3408, 3220 (ν_{NH_2}), 1618 ($\nu_{C=N}$), 843 (PF_6^-). ^1H NMR (CD_3CN): δ 2.65 (s, 3H), 4.44 (s, 2H), 6.70 (d, 2H), 7.09 (m, 2H), 7.27–7.33 (m, 4H), 7.42 (d, 2H), 7.52–7.59 (m, 6H), 7.78 (t, 4H), 8.45 (s, 1H), 8.47 (d, 4H), 8.68 (s, 1H), 8.83 (s, 1H).

*2.4.3. Preparation of $[(bpy)_2Os(mbca)][PF_6]_2\cdot H_2O$ (**3**)*

This complex was synthesized by the reaction of *cis*-$Os(bpy)_2Cl_2\cdot 2H_2O$ (305 mg, 0.5 mmol) and 4′-methyl-2,2′-bipyridyline-4-carbaldehyde (mbca) (100 mg, 0.5 mmol) in 2-methoxyethanol following the same procedure as described for compound **2**. Yield 80%. Found: C, 37.90; H, 2.63; N, 8.16. Calc. for $C_{32}H_{28}F_{12}N_6O_2P_2Os$: C, 38.10; H, 2.80; N, 8.33%. IR (cm^{-1}): 1704 ($\nu_{C=O}$), 841 (PF_6^-). ^1H NMR (CD_3CN): δ 2.67 (s, 3H), 7.28–7.35 (m, 5H), 7.57 (d, 1H), 7.60–7.71 (m, 5H), 7.87–7.95 (m, 5H), 8.49 (d, 5H), 8.79 (s, 1H), 10.11 (s, 1H).

*2.4.4. Preparation of $[(bpy)_2Ru\text{-}BL^1\text{-}Ru(bpy)_2][PF_6]_4\cdot 2H_2O$ (**4**)*

A mixture of *cis*-$Ru(bpy)_2Cl_2\cdot 2H_2O$ (260 mg, 0.5 mmol) and BL^1 (117 mg, 0.25 mmol) in ethanol–water (2:1, 30 cm^3) was refluxed for 16 h. The volume of the reaction mixture was reduced to about 10 cm^3 by rotary evaporation and filtered. To the filtrate an aqueous solution (5 cm^3) of NH_4PF_6 (408 mg, 2 mmol) was added. The orange precipitate thus obtained was filtered off and washed with water and diethyl ether. The compound was dissolved in a minimum volume of acetonitrile (10 cm^3) in a small beaker which was kept inside a bottle containing diethyl ether (50 cm^3). The bottle was closed and vapor diffusion was allowed for 48 h. The microcrystalline compound thus deposited was collected by filtration and the recrystallization procedure was repeated three times, which gave complex **4** in pure form. Yield 68%. Found: C, 43.76; H, 3.29; N, 10.07. Calc. for $C_{70}H_{60}F_{24}N_{14}O_2P_4Ru_2$: C, 43.98; H, 3.16; N, 10.26%. IR (cm^{-1}): 1620 ($\nu_{C=N}$), 842 (PF_6^-). ^1H NMR (CD_3CN): δ 2.57 (s, 6H), 7.28 (d, 2H), 7.37–7.44 (m, 8H), 7.49 (s, 4H), 7.72–7.89 (m, 12H), 8.06 (t, 8H), 8.51 (m, 12H), 8.77 (s, 2H), 8.94 (s, 2H).

*2.4.5. Preparation of $[(bpy)_2Os\text{-}BL^1\text{-}Os(bpy)_2][PF_6]_4\cdot H_2O$ (**5**)*

This complex was synthesized by the reaction of *cis*-$Os(bpy)_2Cl_2\cdot 2H_2O$ (305 mg, 0.5 mmol) and BL^1 (117 mg,

0.25 mmol) in ethanol–water (2:1, 30 cm^3) following the same procedure as described for compound **4**. Yield 60%. Found: C, 40.34; H, 2.93; N, 9.57. Calc. for $C_{70}H_{58}F_{24}N_{14}OP_4Os_2$: C, 40.59; H, 2.82; N, 9.47%. IR (cm^{-1}): 1620 ($\nu_{C=N}$), 843 (PF_6^-). ^1H NMR (CD_3CN): δ 2.65 (s, 6H), 7.20 (d, 2H), 7.28–7.36 (m, 8H), 7.48 (s, 4H), 7.61–7.71 (m, 12H), 7.87 (t, 8H), 8.48 (d, 10H), 8.68 (s, 2H), 8.75 (s, 2H), 8.90 (s, 2H).

2.4.6. Preparation of $[(bpy)_2Ru\text{-}BL^1\text{-}Os(bpy)_2][PF_6]_4\cdot H_2O$ (6)

A mixture of complexes **1** (252 mg, 0.25 mmol) and **3** (252 mg, 0.25 mmol) was dissolved in acetonitrile (15 cm^3); ethanol (50 cm^3) was added to the solution and heated at reflux for 8 h. The volume of the solution was reduced to about 20 cm^3 and an aqueous solution (10 cm^3) of NH_4PF_6 (815 mg, 4 mmol) was added. The precipitate was filtered off and washed with water and diethyl ether. The product was purified following the same procedure as described for compound **4**. Yield 60%. Found: C, 42.62; H, 2.92; N, 9.59. Calc. for $C_{70}H_{58}F_{24}N_{14}OP_4RuOs$: C, 42.41; H, 2.95; N, 9.89%. IR (cm^{-1}): 1620 ($\nu_{C=N}$), 843 (PF_6^-). ^1H NMR (CD_3CN): δ 2.56 (s, 3H), 2.65 (s, 3H), 7.27–7.43 (m, 10H), 7.48 (s, 4H), 7.67–7.86 (m, 12H), 8.05 (t, 8H), 8.34–8.52 (m, 12H), 8.76 (s, 1H), 8.79 (s, 1H), 8.91 (s, 1H), 8.96 (s, 1H).

2.4.7. Preparation of $[(bpy)_2Ru(L^2)][PF_6]_2\cdot H_2O$ (7)

This complex was prepared following the same procedure as described for compound **1**. Yield 78%. (Found: C, 48.38; H, 3.63; N, 10.21. Calc. for $C_{44}H_{38}F_{12}N_8OP_2Ru$: C, 48.67; H, 3.53; N, 10.32%. IR (cm^{-1}): 3411, 3220, (ν_{NH_2}), 1619 ($\nu_{C=N}$), 841 (PF_6^-). ^1H NMR (CD_3CN): δ 2.57 (s, 3H); 4.32 (s, 2H); 6.73 (d, 2H); 7.24 (d, 2H), 7.30–7.48 (m, 7H), 7.56 (d, 2H), 7.66–7.84 (m, 7H), 8.07 (t, 4H), 8.54 (d, 5H), 8.82 (s, 1H), 9.01 (s, 1H).

2.4.8. Preparation of $[(bpy)_2Ru\text{-}BL^2\text{-}Ru(bpy)_2][PF_6]_4\cdot 2H_2O$ (8)

This complex was synthesized by the reaction of *cis*-$Ru(bpy)_2Cl_2\cdot 2H_2O$ and BL^2 following the same procedure as described for compound **4**. The complex was purified by column chromatography packed with neutral alumina and eluted with acetonitrile–toluene (2:1). The solvent of the desired fraction was evaporated to dryness by rotary evaporation and the orange residue was redissolved in acetonitrile and precipitated by addition of diethyl ether. Yield 72%. Found: C, 45.56; H, 3.27; N, 9.74. Calc. for $C_{76}H_{64}F_{24}N_{14}O_2P_4Ru_2$: C, 45.93; H, 3.24; N, 9.87%. IR (cm^{-1}): 1618 ($\nu_{C=N}$), 841 (PF_6^-). ^1H NMR (CD_3CN): δ 2.56 (s, 6H), 7.22–7.41 (m, 14H), 7.53 (d, 2H), 7.62 (d, 2H), 7.73–7.87 (m, 12H), 7.95–8.07 (m, 8H), 8.34–8.51 (m, 12H), 8.80 (s, 2H), 8.95 (s, 2H).

2.4.9. Preparation of $[(bpy)_2Os\text{-}BL^2\text{-}Os(bpy)_2][PF_6]_4\cdot 2H_2O$ (9)

cis-$Os(bpy)_2Cl_2\cdot 2H_2O$ (305 mg, 0.5 mmol) and BL^2 (136 mg, 0.25 mmol) in 2-methoxyethanol–water (4:1, 20 cm^3) was heated under reflux for 12 h in an inert atmosphere. The volume of the solution was reduced to dryness under vacuum and the residue was dissolved in water (5 cm^3), filtered and to the filtrate aqueous NH_4PF_6 (408 mg, 2 mmol) was added. The precipitate thus formed was isolated by filtration and washed with water and diethyl ether. The compound was purified following the same procedure as described for compound **8**. Yield 60%. Found: C, 42.36; H, 3.08; N, 8.96. Calc. for $C_{76}H_{64}F_{24}N_{14}O_2P_4Os_2$: C, 42.15; H, 2.98; N, 9.05%. IR (cm^{-1}): 1618 ($\nu_{C=N}$), 841(PF_6^-). ^1H NMR (CD_3CN): δ 2.67 (s, 6H), 7.20–7.55 (m, 18H), 7.60–7.74 (m, 12H), 7.84–8.03 (m, 8H), 8.47–8.51 (m, 12H), 8.78 (s, 2H), 8.91 (s, 2H).

2.4.10. Preparation of $[(bpy)_2Ru\text{-}BL^2\text{-}Os(bpy)_2][PF_6]_4\cdot H_2O$ (10)

This complex was prepared by the reaction of compounds **7** and **3** following the same procedure as described for compound **6**. Purification of this complex was performed on an alumina column, similar to that described for compound **8**. Yield 68%. Found: C, 44.14; H, 3.09; N, 9.35. Calc. for $C_{76}H_{62}F_{24}N_{14}OP_4RuOs$: C, 44.34; H, 3.03; N, 9.53%. IR (cm^{-1}): 1618 ($\nu_{C=N}$), 841 (PF_6^-). ^1H NMR (CD_3CN): δ 2.58 (s, 3H), 2.67 (s, 3H), 7.20–7.55 (m, 18H), 7.64–7.75 (m, 8H), 7.81–7.85 (m, 8H), 8.03–8.11 (m, 4H), 8.28–8.51 (m, 12H), 8.79 (s, 1H), 8.81 (s, 1H), 8.92 (s, 1H), 8.97 (s, 1H).

2.5. Oxidation with Ce(IV)

Ru(II) complexes (1×10^{-5} M) were oxidized in 2:3 (v/v) acetonitrile–nitric acid (6%) solution by adding ammonium cerium(IV) nitrate (5×10^{-3} M) dissolved in HNO_3 (6%). The Os(II) complexes were oxidized in acetonitrile–water (5:1) solution following a similar procedure to that described for Ru(II). The oxidation was performed by monitoring the change in absorbance in the visible region.

3. Results and discussion

3.1. Synthesis of ligands

The ligands BL^1 and BL^2 were synthesized by the reaction of 4′-methyl-2,2′-bipyridyline-4-carbaldehyde with *p*-phenylenediamine/4,4′-diphenylenediamine (1:2 molar ratio) in refluxing ethanol. In both cases yellow crystalline compounds were obtained in pure form with excellent yield. For L^1 and L^2 the reaction between aldehyde and diamines (1:1 molar ratio) was conducted under mild conditions of 60°C for 0.5 h; at this temperature L^1 and L^2 were almost insoluble in ethanol and separated from the solution as shin-

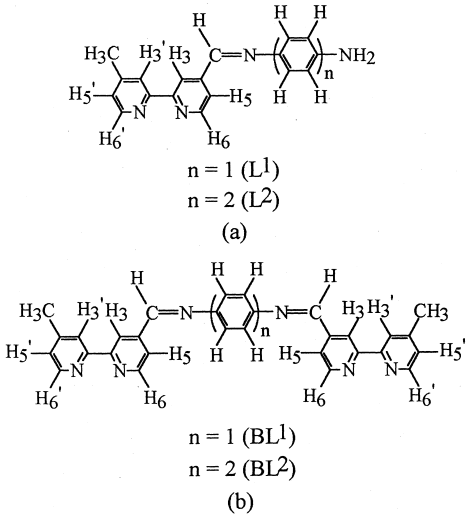


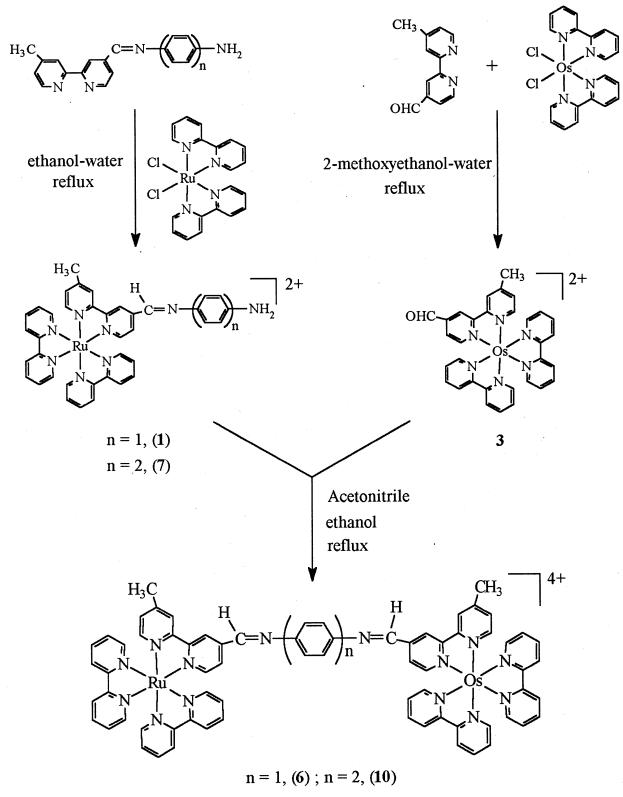
Fig. 1. Ligands used in the preparation of mononuclear (a) and binuclear (b) complexes.

ing yellow crystals. It may be noted that the experimental conditions for the synthesis of L^1 and L^2 is important; reverse sequence of addition of reactants, higher temperature and/or longer reaction time yielded significant amounts of bridging ligand (BL^1/BL^2), for which the separation from L^1/L^2 is difficult. All four ligands gave satisfactory elemental analysis. The ligands L^1, L^2, BL^1 and BL^2 are shown in Fig. 1.

3.2. Synthesis of metal complexes

The mononuclear and homodinuclear metal complexes were prepared by the reaction of the building blocks *cis*-$[M(bpy)_2Cl_2]\cdot 2H_2O$ [M = Ru(II), Os(II)] with appropriate ligand in refluxing ethanol–water or 2-methoxyethanol–water followed by the addition of NH_4PF_6. But we found difficulty for the synthesis of pure heterodinuclear complexes following the conventional route, which involves the preparation of mononuclear complexes, $[Ru(bpy)_2BL^1]^{2+}$/$[Ru(bpy)_2BL^2]^{2+}$, followed by the reaction of this mononuclear complex with *cis*-$[Os(bpy)_2Cl_2]\cdot 2H_2O$. We noticed that $[Ru(bpy)_2BL^1]^{2+}/[Ru(bpy)_2BL^2]^{2+}$, obtained by the reaction of *cis*-$[M(bpy)_2Cl_2]$ and BL^1/BL^2, were always contaminated with a small amount of the binuclear complex, separation of which was difficult. We synthesized heterodinuclear complexes following a different route, which is shown in Scheme 1. This procedure ruled out the possibility of contamination by the homodinuclear complex as impurity. Most of the complexes were purified by column chromatography using deactivated alumina (5% H_2O) as packing material and acetonitrile–toluene mixture as eluent. A few complexes were purified by repeated crystallization following the vapor diffusion method. The homo- and heterodinuclear complexes are shown in Fig. 2.

All complexes gave satisfactory C, H and N analysis. The FAB mass data of the dinuclear complexes are shown in Table 1. Elemental analysis and FAB mass data confirmed the composition of the complexes.



Scheme 1.

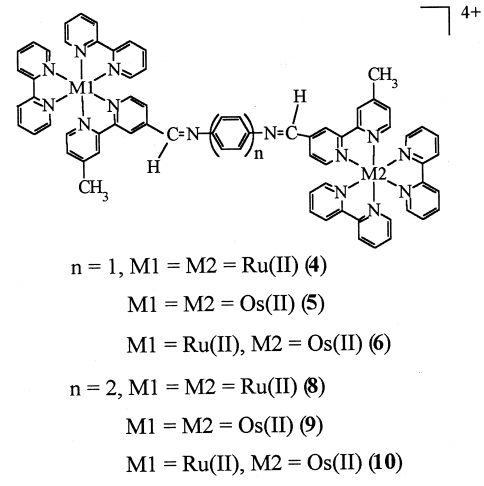


Fig. 2. Structural drawings of homo- and heterodinuclear complexes of Ru(II) and Os(II).

3.3. Infrared spectra

The IR spectra of the ligands L^1 and L^2 exhibit three peaks in the region 3207–3435 cm^{-1}, which are assigned to N–H stretchings of the NH_2 group [34]. The $\nu_{(C=N)}$ vibrational peak of all four ligands appeared in the range 1620–1640 cm^{-1} [34]. In the metal complexes the NH_2 and $\nu_{(C=N)}$ peaks appeared in the range 3220–3408 and 1618–1620 cm^{-1}, respectively. Complex **3** shows a strong band at 1704 cm^{-1}, which is assigned to $\nu_{(C=O)}$ [35]. All complexes show a strong band in the region 841–843 cm^{-1} due to PF_6^-.

Table 1
FAB mass data for ruthenium and osmium complexes

Complex	m/z [a]		
	$[M-PF_6]^+$	$[M-2PF_6]^{2+}$	$[M-3PF_6]^{3+}$
$[(bpy)_2RuL^1](PF_6)_2\cdot H_2O$ (**1**)	847 (846.8)	702 (701.8)	
$[(bpy)_2OsL^1](PF_6)_2\cdot H_2O$ (**2**)	940 (935.9)	791 (790.9)	
$[(bpy)_2Ru\text{-}BL^1\text{-}Ru(bpy)_2](PF_6)_4\cdot 2H_2O$ (**4**)	1732 (1730.3)	1586 (1585.3)	1442 (1440.4)
$[(bpy)_2Os\text{-}BL^1\text{-}Os(bpy)_2](PF_6)_4\cdot H_2O$ (**5**)	1909 (1908.6)	1764 (1763.6)	1619 (1618.7)
$[(bpy)_2Ru\text{-}BL^1\text{-}Os(bpy)_2](PF_6)_4\cdot 2H_2O$ (**6**)	1820 (1819.4)	1675 (1674.5)	
$[(bpy)_2RuL^2](PF_6)_2\cdot H_2O$ (**7**)	923 (922.8)	778 (777.9)	
$[(bpy)_2Ru\text{-}BL^2\text{-}Ru(bpy)_2](PF_6)_4\cdot 2H_2O$ (**8**)	1807 (1806.4)	1662 (1661.5)	1517 (1516.5)
$[(bpy)_2Os\text{-}BL^2\text{-}Os(bpy)_2](PF_6)_4\cdot 2H_2O$ (**9**)	1985 (1984.7)	1840 (1839.8)	1695 (1694.8)
$[(bpy)_2Ru\text{-}BL^2\text{-}Os(bpy)_2](PF_6)_4\cdot 2H_2O$ (**10**)	1896 (1895.6)	1751 (1750.6)	

[a] m/z observed for the largest isotropic peaks. Calculated values for m/z are given in parentheses.

3.4. ^1H NMR spectra

The ^1H NMR spectra of the ligands and their metal complexes were recorded in $CDCl_3/CD_3CN$ and the data are presented in Section 2. The CH_3 protons of all ligands appeared as a singlet in the region δ 2.46–2.48 [21]. The NH_2 of L^1 and L^2 appeared as a broad singlet at δ 3.80 and 3.77, respectively [34]. In all ligands the resonances for protons of the two pyridyl rings of the bipyridyl moieties are divided into two sets [21]. As CH_3 is an electron-donating group and –CH=N– is an electron-deficient center, the more shielded sets of resonances are due to the protons associated with pyridyl rings having CH_3 substituents. Therefore, the signals at δ 7.30 (dd), 8.60 (d) and 8.63 (s) of BL^1 are assigned to H_6', H_5' and H_3' (see Fig. 1 for numbering scheme), respectively. The other set of signals at δ 7.90 (dd), 8.82 (d) and 8.83 (s) are due to H_6, H_5 and H_3 protons, respectively. The assignment of these signals is made on the basis of multiplicity, coupling constants and other reported data in the literature [36]. The ligand BL^2 exhibits similar spectra except for two doublets at δ 7.39 (J = 8.4 Hz) and 7.72 (J = 8.4 Hz), which appeared for biphenyl moiety in place of a singlet at δ 7.34 for phenylene moiety of BL^1. The ^1H NMR data thus suggest that the two halves of the bridged ligands are magnetically identical in solution. The ligands L^1 and L^2 are unsymmetrical and, therefore, the phenyl moiety of L^1 appeared as two doublets at δ 6.73 (J = 8.0 Hz) and 7.24 (J = 8.2 Hz); the biphenylene moiety of L^2 showed four doublets at δ 6.78, 7.34, 7.46 and 7.61 (J = 8.4 Hz for all four doublets). The most shielded doublets can be assigned to the CH *ortho* to NH_2 (on the basis of ^1H NMR data of free diamines).

In the mononuclear and homodinuclear complexes the CH_3 protons exhibited a singlet, whereas in the dinuclear complexes it showed two singlets. The CH_3 attached to Ru(II) and Os(II) chromophores appeared in the ranges δ 2.56–2.58 and δ 2.65–2.67, respectively. The low-field shift of CH_3 resonances of all complexes compared to free ligands is due to ligand-to-metal σ donation, which resulted in deshielding of protons associated with pyridyl rings [37]. Complexes **1**, **2** and **7** show a broad singlet at δ 4.53, 4.44 and 4.32, respectively, which are assigned to NH_2. The CHO of compound **3** appeared as a singlet at δ 10.11.

In the aromatic region, a large number of peaks overlapped; exact assignment of peaks is therefore extremely difficult without performing other NMR techniques. Octahedral metal centers with bidentate ligands generally show stereoisomerism [38,39]; thus, in this case, there is a strong possibility of formation of stereoisomers. The resonance of CH_3 for different stereoisomers may show the same or very close (not resolved) chemical shifts, as they are in remote positions with respect to the metal centers. But the protons, which are close to the coordinated nitrogens, are expected to show different chemical shifts for different stereoisomers [39]. This isomerism, therefore, gives additional complication to the ^1H NMR, in particular the aromatic region. However, from the analysis of the spectra it appears that in all complexes H_3 protons appeared as doublets in the region δ 8.3–8.5, H_4 as doublets of doublets (dd) in the region δ 7.6–7.9; H_5 and some of the H_6 protons as multiplets (overlapped) in the region δ 7.2–7.4 (usual numbering of bpy is used). The phenylene protons of complexes **4**–**6** exhibit a singlet at δ 7.48. The biphenylene moiety of complexes **8**–**10** show two doublets in the region δ 7.5–7.7. In general, after coordination chemical shifts of most of the protons, viz. H_3, H_4 and H_5 of bpy and substituted bpy, of the ligands show slight down-field shift, as expected because of ligand-to-metal σ donation [37,39]. But H_6 shows significant up-field shift, which is definitely due to ring current effect. The facing of H_6 protons towards the ring current zone of the pyridyl ring of the neighboring ligands results in strong shielding effect on these protons [37,39,40].

3.5. UV–Vis spectra

The absorption spectra of all complexes were recorded in acetonitrile, and the data are summarized in Table 2. The spectra of complexes **4**–**6** are illustrated in Fig. 3. The low-energy absorption bands in the visible region (450–700) of all complexes are due to metal-to-ligand charge transfer

Table 2
UV–Vis spectral data for ruthenium and osmium complexes [a]

Complex	λ_{max}, nm (ε, $dm^3\ mol^{-1}\ cm^{-1}$)			
$[(bpy)_2RuL^1](PF_6)_2\cdot H_2O$ (**1**)		472 (2.4×10^4)	290 (6.6×10^4)	248 (3.2×10^4)
$[(bpy)_2OsL^1](PF_6)_2\cdot H_2O$ (**2**)	670 (6.1×10^3) [b]	496 (2.0×10^4)	292 (7.2×10^4)	246 (4.1×10^4)
$[(bpy)_2Ru\text{-}BL^1\text{-}Ru(bpy)_2](PF_6)_4\cdot 2H_2O$ (**4**)		478 (4.2×10^4)	288 (1.2×10^5)	246 (6.0×10^4)
$[(bpy)_2Os\text{-}BL^1\text{-}Os(bpy)_2](PF_6)_4\cdot H_2O$ (**5**)	665 (9.3×10^3)	498 (3.8×10^4)	292 (1.4×10^5)	248 (6.6×10^4)
$[(bpy)_2Ru\text{-}BL^1\text{-}Os(bpy)_2](PF_6)_4\cdot 2H_2O$ (**6**)	665 (4.5×10^3)	476 (3.9×10^4)	290 (1.3×10^5)	248 (6.1×10^4)
$[(bpy)_2RuL^2](PF_6)_2\cdot H_2O$ (**7**)		464 (1.7×10^4)	290 (5.8×10^4)	250 (2.6×10^4)
$[(bpy)_2Ru\text{-}BL^2\text{-}Ru(bpy)_2](PF_6)_4\cdot 2H_2O$ (**8**)		458 (3.6×10^4)	288 (1.5×10^5)	246 (6.0×10^4)
$[(bpy)_2Os\text{-}BL^2\text{-}Os(bpy)_2](PF_6)_4\cdot 2H_2O$ (**9**)	660 (8.7×10^3)	486 (3.2×10^4)	292 (1.4×10^5)	246 (6.4×10^4)
$[(bpy)_2Ru\text{-}BL^2\text{-}Os(bpy)_2](PF_6)_4\cdot 2H_2O$ (**10**)	660 (5.0×10^3)	458 (3.7×10^4)	290 (1.4×10^5)	246 (6.4×10^4)

[a] In acetonitrile solution at room temperature.
[b] Weak band/shoulder.

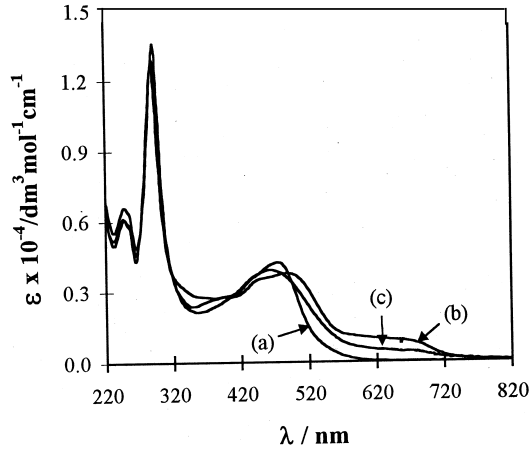


Fig. 3. Electronic absorption spectra of complexes **4** (a), **5** (b) and **6** (c), recorded in acetonitrile.

(MLCT) transitions ($d\pi\rightarrow\pi^*$) [9,21,26,29]. For Os(II) complexes the broad band in the 600–700 nm region is due to the spin forbidden MLCT transitions [9,29,36,41]. Each metal ion is coordinated to two bpy ligands and a substituted bpy moiety of the bridging ligand; therefore, two types of MLCT bands, $d\pi\rightarrow\pi^*$ (BL) and $d\pi\rightarrow\pi^*$ (bpy), are expected. These bands are closely spaced and overlapped. However, it is observed that the λ_{max} of the MLCT bands of the complexes containing BL^1 are significantly red shifted (10–20 nm) compared to that of the similar complexes containing BL^2. This observation is consistent with the fact that the MLCT bands move to the lower energy as the metal–metal separation decreases [42]. This behavior suggests that the acceptor orbital of the MLCT transition is located on the substituted bpy moieties belonging to the bridging ligand. The electrochemical studies also suggested that the first reduction is associated with the bridging ligand. Therefore, the lowest energy spin allowed MLCT bands can be assigned to $d\pi\rightarrow\pi^*$ (BL). The high-energy bands which appeared around 290 and 246 nm are ligand-centered charge transfer (CT) due to $\pi\rightarrow\pi^*$ transitions [9,21,29]. There are slight differences in the λ_{max} of MLCT bands [6 nm for Ru(II) and 2 nm for Os(II)] between dinuclear complexes and the corresponding mononuclear model complexes, indicating weak or no electronic interaction between the metal centers [29,30].

3.6. Electrochemistry

The square-wave and cyclic voltammograms of all new complexes were recorded in acetonitrile and the results are listed in Table 3. Cyclic voltammograms of complexes **9** and **10** are shown in Fig. 4. An analysis of the electrochemical data revealed that: (1) Ru(II) → Ru(III) oxidation occurred in the potential range +1.20 to +1.23 V; (2) Os(II) → Os(III) oxidation occurred in the potential range +0.75 to +0.82 V; (3) in the homodinuclear complexes two one-electron metal-centered oxidations take place at closely spaced (indistinguishable) potentials; (4) heterodinuclear complexes exhibit two one-electron oxidations at well-separated potentials; (5) Os(II) is easier to oxidize than Ru(II); (6) all reductions are ligand-based and occurred in the potential range −1.28 to −1.90 V.

Among three ligand-based reductions, the first two are one-electron processes and the third wave is a closely spaced two one-electron processes (based on current height). Similar reductions pattern have also been noted in many binuclear complexes [21,28,43]. Each metal-containing unit of these complexes can be viewed as a mixed-ligand complex as the coordination sites of the bridging ligands have properties different to those of bpy because of the presence of substituents at 4 and 4′ positions. The methyl group is electron donating; therefore, methyl-substituted bpy reduces at a more negative potential compared with bpy [16,44,45]. However, the bridging unit between the chromophores also influences the reduction potentials [29]. It has been observed that, if the bridging unit is a saturated aliphatic chain ($-CH_2-CH_2-$), it does not affect reduction potential significantly [4]. But an unsaturated bridging unit, in particular, with complete conjugation between two chromophores shifts the reduction peak significantly to a less negative potential even in the presence of methyl substituent in the bpy units [4,21]. It seems that, in the dinuclear complexes, the positive shift of the first reduction potential by conjugation effect of the bridging unit dominates over the negative shift due to the methyl substituent in

Table 3
Electrochemical data for ruthenium and osmium complexes [a]

Complex	$E_{1/2}$, V (ΔE_p, mV) [b]				
	Oxidation		Reduction		
	Ru	Os			
$[(bpy)_2RuL^1](PF_6)_2\cdot H_2O$ (**1**)	+1.23 (67)		−1.40 (67)	−1.56 (120)	−1.84 (120)
$[(bpy)_2OsL^1](PF_6)_2\cdot H_2O$ (**2**)		+0.82 (95)	−1.28 (70)	−1.46 (110)	−1.90 (120)
$[(bpy)_2Ru\text{-}BL^1\text{-}Ru(bpy)_2](PF_6)_4\cdot 2H_2O$ (**4**)	+1.22 (61) [c]		−1.38 (60)	−1.56 (112)	−1.81 (100) [c]
$[(bpy)_2Os\text{-}BL^1\text{-}Os(bpy)_2](PF_6)_4\cdot H_2O$ (**5**)		+0.76 (63) [c]	−1.30 (58)	−1.45 (130)	−1.81 (108) [c]
$[(bpy)_2Ru\text{-}BL^1\text{-}Os(bpy)_2](PF_6)_4\cdot 2H_2O$ (**6**)	+1.21 (61)	+0.75 (67)	−1.35 (60)	−1.51 (123)	−1.82 (135) [c]
$[(bpy)_2RuL^2](PF_6)_2\cdot H_2O$ (**7**)	+1.22 (65)		−1.40 (80)	−1.57 (100)	−1.82 (70)
$[(bpy)_2Ru\text{-}BL^2\text{-}Ru(bpy)_2](PF_6)_4\cdot 2H_2O$ (**8**)	+1.20 (75) [c]		−1.39 (100)	−1.57 (110)	−1.80 (60) [c]
$[(bpy)_2Os\text{-}BL^2\text{-}Os(bpy)_2](PF_6)_4\cdot 2H_2O$ (**9**)		+0.76 (90) [c]	−1.32 (80)	−1.52 (120)	−1.81 (110) [c]
$[(bpy)_2Ru\text{-}BL^2\text{-}Os(bpy)_2](PF_6)_4\cdot 2H_2O$ (**10**)	+1.20 (75)	+0.76 (66)	−1.34 (78)	−1.55 (110)	−1.79 (122) [c]

[a] In acetonitrile solution.
[b] Potential values versus SCE.
[c] Two-electron processes.

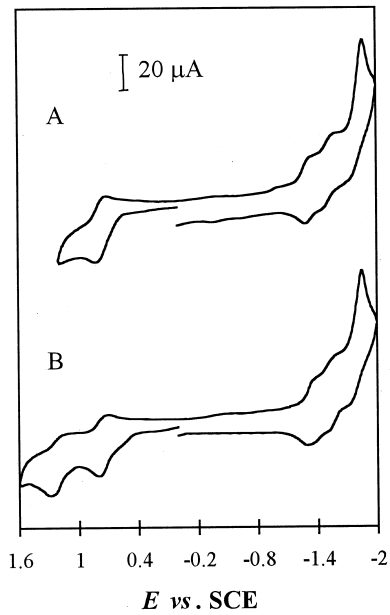


Fig. 4. Cyclic voltammograms of complexes **9** (A) and **10** (B), recorded in acetonitrile; scan rate 100 mV s^{-1}.

$$[(bpy)(bpy)Ru^{III}\text{-}BL\text{-}Os^{III}(bpy)(bpy)]^{6+}$$
$$+e \downarrow\uparrow -e$$
$$[(bpy)(bpy)Ru^{II}\text{-}BL\text{-}Os^{III}(bpy)(bpy)]^{5+}$$
$$+e \downarrow\uparrow -e$$
$$[(bpy)(bpy)Ru^{II}\text{-}BL\text{-}Os^{II}(bpy)(bpy)]^{4+}$$
$$-e \uparrow\downarrow +e$$
$$[(bpy)(bpy)Ru^{II}\text{-}BL^{-}\text{-}Os^{II}(bpy)(bpy)]^{3+}$$
$$-e \uparrow\downarrow +e$$
$$[(bpy)(bpy)Ru^{II}\text{-}BL^{2-}\text{-}Os^{II}(bpy)(bpy)]^{2+}$$
$$-2e \uparrow\downarrow +2e$$
$$[(bpy)(bpy^{-})Ru^{II}\text{-}BL^{2-}\text{-}Os^{II}(bpy)(bpy^{-})]$$
$$(BL = BL^1 \text{ and } BL^2)$$

Scheme 2.

the bpy moieties. Therefore, the first two one-electron reductions in the dinuclear complexes are assigned to the reduction of substituted bpy units of the bridging ligands, BL^1/BL^2. The third peak corresponding to two unresolved one-electron reductions is associated with bpy ligands. The sequential electron transfer processes in the heterodinuclear complexes are illustrated in Scheme 2. It may be noted that there are no significant differences between oxidation potentials of the dinuclear complexes and corresponding mononuclear model complexes containing L^1 and L^2 ligands. Ligand-based first reduction of dinuclear complexes, however, show slight anodic shift. These observations indicate a weak or no electronic interaction between the chromophores.

3.7. Mixed-valence properties

The mixed-valence species were generated by partial oxidation of dinuclear complexes by the addition of ammonium cerium(IV) nitrate dissolved in 6% HNO_3. The oxidation of Ru(II) was carried out in deoxygenated 2:3 (v/v) acetonitrile–nitric acid (6%) solution, whereas oxidation of Os(II) was performed in acetonitrile–water (5:1, v/v) solution under inert atmosphere. Addition of a standard Ce(IV) solution caused remarkable changes in the MLCT bands. For homodinuclear complexes the MLCT bands decreased linearly with increasing addition of oxidant. However, on exposing the solution to air the MLCT band starts increasing and within 10–15 min this band returns to its original position. This observation indicates that the oxidation and reduction processes are reversible and the complexes remain intact when metal ions are oxidized. For heterodinuclear complexes, addition of one equivalent of oxidant resulted in the disappearance of Os-based absorption, as expected because Os(II) oxidizes at a lower potential than Ru(II). For all mixed-valence species [Ru(II)–Ru(III) and Ru(II)–Os(III)] absorption spectra up to 1400 nm were recorded but no intervalence charge transfer bands with significant ε value were observed. Similar observations were also noted in homo- and heterobimetallic complexes containing bicyclo-

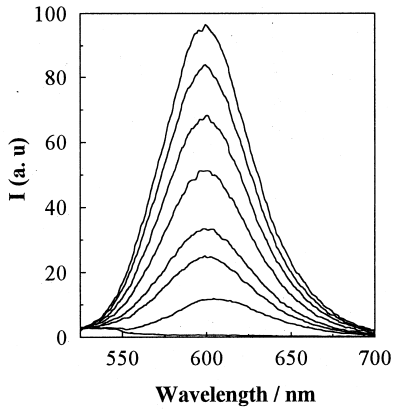


Fig. 5. Change in the emission spectra for an acetonitrile–nitric acid (6%) (2:3; v/v) solution of complex **8** upon addition of ammonium cerium(IV) nitrate.

octane as spacer [29]. But energy transfer took place in heterodinuclear complex of Ru(II) and Os(II) [29].

Oxidation of the dinuclear complexes caused a decrease in the luminescence intensity. In heterodinuclear complexes, addition of one equivalent of oxidant resulted in complete quenching of Os-based luminescence. For homodinuclear complexes, the intensity of luminescence decreased with increasing the amount of added oxidant, and completely disappeared when two equivalents were added, as shown in Fig. 5.

3.8. Luminescence

All of the Ru(II) and/or Os(II) complexes exhibit the characteristic MLCT emission band at room temperature in acetonitrile and in MeOH–EtOH (4:1) solutions. The luminescence data are summarized in Table 4. The band intensity in acetonitrile solution was significantly low compared with that in MeOH–EtOH mixture with equimolar solutions. In acetonitrile solution λ_{max} (em) shows a slight red shift [2–5 nm for Ru(II) and 6–10 nm for Os(II)] compared to that in MeOH–EtOH solution.

Emission life-times of all complexes were measured at room temperature in de-aerated acetonitrile and 4:1 (v/v) MeOH–EtOH solution; the data are presented in Table 4. Luminescence decay of compound **4** in acetonitrile is illustrated in Fig. 6. There is no significant difference in life-time in acetonitrile and MeOH–EtOH solutions. The life-times of mononuclear and homodinuclear complexes are significantly high compared with some other reported data for dinuclear complexes bridged by saturated organic moieties such as bicyclo-2,2,2-octane, adamantane and diadamantane [4,29–31]. But our values are comparable to those reported by Meyer's group [21] and Schmehl's group [26] for some dinuclear complexes with ethene and 1,4-ethynyl benzene as spacers, respectively. This long life-time can be attributed to delocalization of excited electron across the bridging units to a significant extent [21]. However, in the heterodinuclear complexes, the emission life-time of the Ru-based unit is significantly short. This could be due to the quenching of the Ru-based emission by Os-based unit via energy transfer. The rate constant for energy transfer from Ru-based unit to Os-based unit can be calculated from the equation [3,29]:

$$k_{en} = \frac{1}{\tau} - \frac{1}{\tau^0}$$

where τ and τ^0 are the luminescence life-times of the Ru-based component in the heterodinuclear complex $[(bpy)_2Ru\text{-}BL\text{-}Os(bpy)_2]^{4+}$, and in the homodinuclear model complex $[(bpy)_2Ru\text{-}BL\text{-}Ru(bpy)_2]^{4+}$, respectively. The rate constants for energy transfer thus calculated for the heterodinuclear complexes **6** and **10** are 5.9×10^6 and 3.2×10^6 s^{-1} in acetonitrile and 6.8×10^6 and 3.4×10^6 s^{-1} in MeOH–EtOH (4:1) mixture, respectively. The results indicate that BL^1 transfers electronic energy more efficiently than BL^2. This is obviously due to the short length of BL^1 compared to BL^2. Similar energy transfer processes have been reported for many Ru(II)–Os(II) dinuclear complexes with different type of spacers [29–31]. The rate constants are high ($>1\times10^8$ s^{-1}) when the M–M distance is short

Table 4
Luminescence data for ruthenium(II) and osmium(II) complexes

Complex	Ru				Os			
	Acetonitrile		MeOH–EtOH (4:1)		Acetonitrile		MeOH–EtOH (4:1)	
	λ_{max} (nm) [a]	τ (ns) [b]	λ_{max} (nm)	τ (ns)	λ_{max} (nm)	τ (ns)	λ_{max} (nm)	τ (ns)
$[(bpy)_2RuL^1](PF_6)_2\cdot H_2O$ (**1**)	615	1122	610	817				
$[(bpy)_2OsL^1](PF_6)_2\cdot H_2O$ (**2**)					720	43	712	45
$[(bpy)_2Ru\text{-}BL^1\text{-}Ru(bpy)_2](PF_6)_4\cdot 2H_2O$ (**4**)	615	1032	611	807				
$[(bpy)_2Os\text{-}BL^1\text{-}Os(bpy)_2](PF_6)_4\cdot H_2O$ (**5**)					720	48	710	46
$[(bpy)_2Ru\text{-}BL^1\text{-}Os(bpy)_2](PF_6)_4\cdot 2H_2O$ (**6**)	614	145	612	124	722	62	715	54
$[(bpy)_2RuL^2](PF_6)_2\cdot H_2O$ (**7**)	615	982	611	947				
$[(bpy)_2Ru\text{-}BL^2\text{-}Ru(bpy)_2](PF_6)_4\cdot 2H_2O$ (**8**)	615	878	612	846				
$[(bpy)_2Os\text{-}BL^2\text{-}Os(bpy)_2](PF_6)_4\cdot 2H_2O$ (**9**)					722	57	715	40
$[(bpy)_2Ru\text{-}BL^2\text{-}Os(bpy)_2](PF_6)_4\cdot 2H_2O$ (**10**)	615	232	612	220	722	58	716	42

[a] Emission spectra were recorded in air-equilibrated solution.
[b] Emission life-times were recorded in de-aerated solution.

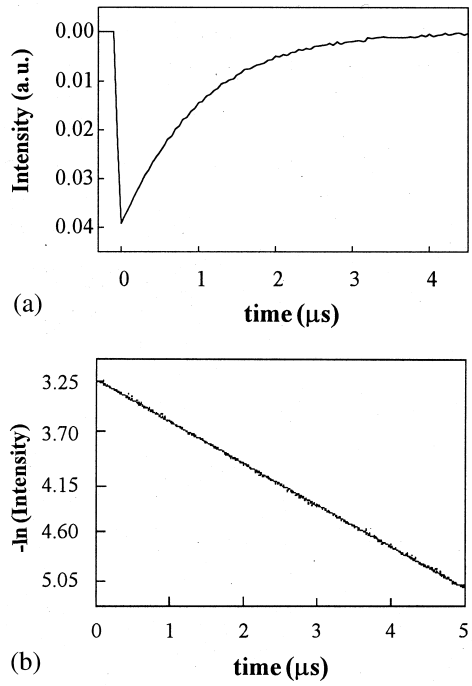


Fig. 6. (a) Emission decay at 615 nm for complex **8** in deoxygenated acetonitrile solution at room temperature; excitation wavelength 532 nm. (b) Plot for the calculation of rate constant and thereby life-time (correlation coefficient = −0.9996).

and the spacers provide complete conjugation between the metal centers [4]. Recently it has been reported that in dinuclear Ru(II)–Os(II) complexes with polyphenylene spacers energy transfer takes place even if the metal–metal separation is as great as around 40 Å [9]. It may be noted that even an interaction of a few reciprocal centimeters, which can not be noticed in spectroscopic and electrochemical experiments, is sufficient to cause fast intercomponent energy and electron transfer processes [10,29,30].

The transient absorption difference spectrum of complex **8** in deoxygenated acetonitrile solution is shown in Fig. 7. It was recorded following excitation at 532 nm and after 150 ns of the flash. This spectrum exhibits strong bleaching around 450 nm. This is due to bleach of the MLCT band, found in many other Ru(II) complexes [8,21,23]. It also shows a weak positive absorption band around 530 nm, which could be due to a $\pi_1^* \rightarrow \pi_2^*$ transition of a ligand localized excited state [22].

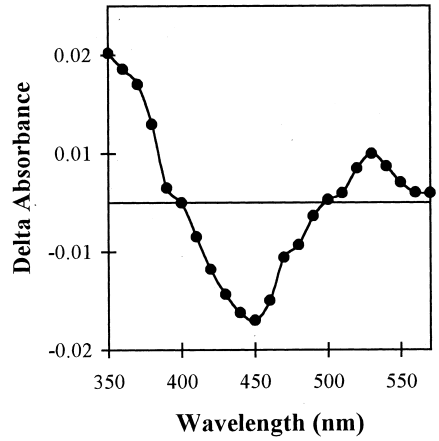


Fig. 7. Transient absorption spectra of complex **8**, recorded in deoxygenated acetonitrile solution following excitation at 532 nm and 150 ns after the flash.

4. Conclusions

Two novel bridging ligands made of two 4-methyl-2,2′-bipyridyl chelating units separated by rigid spacers having complete conjugations have been synthesized. Homo- and heterodinuclear complexes of these ligands have been prepared and characterized. For the synthesis of heterodinuclear complexes a new synthetic strategy has been employed which eliminated the possibility contamination by homodinuclear complex as impurity. Electrochemical studies and UV–Vis data of these complexes suggest a weak or no interaction between the metal centers. Mixed-valence species of the dinuclear complexes did not show intervalence charge transfer band. However, addition of oxidant gradually decreased luminescence intensity, and the band disappeared when two equivalents of oxidant were added. Laser flash photolysis experiments of the homodinuclear complexes show a long excited state life-time. It appears that the excited electron is delocalized on the bridging ligand. In heterodinuclear complexes, energy transfer takes place from the Ru-based unit to the Os-based unit and the rate constants indicate that BL^1 transfers energy more efficiently than BL^2.

Acknowledgements

We are grateful to the Department of Science and Technology (DST), Government of India, for the financial support. A.K.B. gratefully acknowledges CSIR for awarding a Senior Research Fellowship (SRF). Our sincere thanks to Professor P. Natarajan and Dr P. Ramamurthy for providing us with the facilities of the National Center for Ultrafast Processes (NCUFP) to perform laser flash photolysis experiments. Our thanks are due to RSIC (CDRI), Lucknow for providing FAB mass spectra. Our sincere thanks to Dr P.K. Ghosh and Dr R.V. Jasra for their keen interest and encouragement. We also thank Dr S. Muthusamy and Dr P. Subramanian for recording NMR spectra.

References

[1] V. Balzani, S. Campagna, G. Denti, A. Juris, S. Serroni, M. Venturi, Acc. Chem. Res. 31 (1998) 26.
[2] M. Venturi, S. Serroni, A. Juris, S. Campagna, V. Balzani, Top. Curr. Chem. 197 (1998) 193.
[3] L. De Cola, P. Belser, Coord. Chem. Rev. 177 (1998) 301.
[4] V. Balzani, A. Juris, M. Venturi, S. Campagna, S. Serroni, Chem. Rev. 96 (1996) 759.
[5] V. Balzani, L. De Cola, Supramolecular Chemistry, Kluwer, Dordrecht, 1992.

[6] D.N. Reinhoudt, Comprehensive Supramolecular Chemistry, Pergamon, New York, 1996.
[7] J.-M. Lehn, Supramolecular Chemistry VCH, Weinheim, 1995.
[8] A.I. Baba, J.R. Shaw, J.A. Simon, R.P. Thummel, R.H. Schmehl, Coord. Chem. Rev. 171 (1998) 43.
[9] B. Schlicke, P. Belser, L. De Cola, E. Sabbioni, V. Balzani, J. Am. Chem. Soc. 121 (1999) 4207.
[10] V. Balzani, F. Scandola, Supramolecular Photochemistry Horwood, Chichester, 1991.
[11] P.T. Gulyas, T.A. Smith, M.N. Paddon-Row, J. Chem. Soc., Dalton Trans. (1999) 1325.
[12] P. Belser, A. von Zelewsky, M. Frank, C. Seel, F. Vogtle, L. De Cola, F. Barigelletti, V. Balzani, J. Am. Chem. Soc. 115 (1993) 4076.
[13] G. Denti, S. Campagna, S. Serroni, M. Ceano, V. Balzani, J. Am. Chem. Soc. 114 (1992) 2944.
[14] A. Juris, V. Balzani, S. Campagna, G. Denti, S. Serroni, G. Frei, H.U. Gudel, Inorg. Chem. 33 (1994) 1491.
[15] A. Juris, V. Balzani, F. Barigelletti, S. Campagna, P. Belser, A. von Zelewsky, Coord. Chem. Rev. 84 (1988) 85.
[16] R. Sahai, D.A. Baucom, D.P. Rillema, Inorg. Chem. 25 (1986) 3843.
[17] M. Furue, T. Yoshidzumi, S. Kinoshita, T. Kushida, S. Nozakura, M. Kamachi, Bull. Chem. Soc. Jpn. 64 (1991) 1632.
[18] A. Macatangay, G.Y. Zheng, D.P. Rillema, D.C. Jackman, J.W. Merkert, Inorg. Chem. 35 (1996) 6823.
[19] M. Furue, K. Mruyama, Y. Kanematsu, T. Kushida, M. Kamachi, Coord. Chem. Rev. 132 (1994) 201.
[20] S.L. Larson, S.M. Hendrickson, S. Ferrere, D.L. Derr, C.M. Elliott, J. Am. Chem. Soc. 117 (1995) 5881.
[21] G.F. Strouse, J.R. Schoonover, R. Duesing, S. Boyde, W.E. Jones Jr., T.J. Meyer, Inorg. Chem. 34 (1995) 473.
[22] A.I. Baba, H.E. Ensley, R.H. Schmehl, Inorg. Chem. 34 (1995) 1198.
[23] V. Grosshenny, A. Harriman, F.M. Romero, R. Ziessel, J. Phys. Chem. 100 (1996) 17472.
[24] C.K. Ryu, R.H. Schmehl, J. Phys. Chem. 93 (1989) 7961.
[25] C.K. Ryu, R. Wang, R.H. Schmehl, S. Ferrere, M. Ludwikow, J.W. Merkert, C.E.L. Headford, C.M. Elliott, J. Am. Chem. Soc. 114 (1992) 430.
[26] J.R. Shaw, R.T. Webb, R.H. Schmehl, J. Am. Chem. Soc. 112 (1990) 1117.
[27] S.C. Rasmussen, D.W. Thompson, V. Singh, J.D. Petersen, Inorg. Chem. 35 (1996) 3449.
[28] Y. Wang, W.J. Perez, G.Y. Zheng, D.P. Rillema, C.L. Huber, Inorg. Chem. 37 (1998) 2227.
[29] L. De Cola, V. Balzani, F. Barigelletti, L. Flamigni, P. Belser, A. von Zelewsky, M. Frank, F. Vogtle, Inorg. Chem. 32 (1993) 5228.
[30] M. Frank, M. Nieger, F. Vogtle, P. Belser, A. von Zelewsky, L. De Cola, V. Balzani, F. Barigelletti, L. Flamigni, Inorg. Chim. Acta 242 (1996) 281.
[31] L. De Cola, Chimia 50 (1996) 214.
[32] B.P. Sullivan, D.J. Salmon, T.J. Meyer, Inorg. Chem. 17 (1978) 3334.
[33] E.M. Kober, J.V. Caspar, B.P. Sullivan, T.J. Meyer, Inorg. Chem. 27 (1988) 4587.
[34] P. Paul, K. Nag, Inorg. Chem. 26 (1987) 1586.
[35] P. Paul, B. Tyagi, M.M. Bhadbhade, E. Suresh, J. Chem. Soc., Dalton Trans. (1997) 2273.
[36] E.Z. Jandrasics, F.R. Keene, J. Chem. Soc., Dalton Trans. (1997) 153.
[37] P. Paul, B. Tyagi, A.K. Bilakhiya, M.M. Bhadbhade, E. Suresh, G. Ramachandraiah, Inorg. Chem. 37 (1998) 5733.
[38] F.R. Keene, Coord. Chem. Rev. 166 (1997) 121.
[39] P. Paul, B. Tyagi, A.K. Bilakhiya, P. Dastidar, E. Suresh, Inorg. Chem. 39 (2000) 14.
[40] R.P. Thummel, F. Lefoulon, J.D. Korp, Inorg. Chem. 26 (1987) 2370.
[41] V. Balzani, D.A. Bardwell, F. Barigelletti, R.L. Cleary, M. Guardigli, J.C. Jeffery, T. Sovrani, M.D. Ward, J. Chem. Soc., Dalton Trans. (1995) 3601.
[42] F. Barigelletti, L. Flamigni, V. Balzani, J.P. Collin, J.P. Sauvage, A. Sour, E.C. Constable, A.M.W.C. Thompson, J. Am. Chem. Soc. 116 (1994) 7692.
[43] E. Ishow, A. Gourdon, J.-P. Launay, C. Chiorboli, F. Scandola, Inorg. Chem. 38 (1999) 1504.
[44] D.P. Rillema, G. Allen, T.J. Meyer, D. Conrad, Inorg. Chem. 22 (1983) 1617.
[45] W.F. Wacholtz, R.A. Auerbach, R.H. Schmehl, Inorg. Chem. 25 (1986) 227.

PERGAMON

www.elsevier.nl/locate/poly

Polyhedron 19 (2000) 1245–1254

POLYHEDRON

Synthesis and crystal structures of five new rhenium acetamidate complexes

Robert W. McGaff [a], Nancy Carter Dopke [b], Randy K. Hayashi [b], Douglas R. Powell [b], Paul M. Treichel [b,*]

[a] *Department of Chemistry, University of Wisconsin-LaCrosse, La Crosse, WI, USA*
[b] *Department of Chemistry, University of Wisconsin-Madison, 1101 University Avenue, Madison, WI 53706, USA*

Received 7 December 1999; accepted 4 March 2000

Abstract

Syntheses are reported of five rhenium(III) cluster complexes with acetamidate ligands: $[(C_4H_9)_4N]_2[\{Re_2Cl_6(\mu\text{-}1,2\text{-}NHCOCH_3)\}_2]$ (**1**), $[(C_2H_5)_4N][Re_3Cl_8(\mu\text{-}1,2\text{-}NHCOCH_3)(\mu\text{-}2,3\text{-}NHCOCH_3)]\cdot 2.5(C_4H_{10}O)$ (**2**), $[(C_4H_9)_4N]_2[Re_3Cl_{10}(\mu\text{-}1,2\text{-}NHCOCH_3)]$ (**3**), $[(C_4H_9)_4N]_2[\{Re_3Cl_8(\mu\text{-}1,2\text{-}NHCOCH_3)(OH)\}_2]\cdot 1.7(C_4H_{10}O)$ (**4**), and $(C_4H_9)_4N[Re_3Cl_9(H_2O)(\mu\text{-}1,2\text{-}NHCOCH_3)]\cdot C_3H_6O$ (**5**). The acetamidate ligands in these complexes arise via reactions of acetonitrile–rhenium halide species (either dirhenium or trirhenium chloride clusters) and water. Coordination activates the nitrile to hydrolysis; proton loss and chelation of the acetamidate ligand with displacement of chloride ion leads to the products. Initial formation of a rhenium(III) acetonitrile complex can be assisted using a halide acceptor, Ag^+, to generate an open coordination site on the metal. The reaction with $K_4Mo_2Cl_8$ and Ag^+ ion in acetonitrile gives $Mo_2Cl_4(NCCH_3)_4$ (**6**). The use of MALDI mass spectrometry in support of synthetic efforts and as a characterization tool is described, and the molecular structures of **1**–**6** were established using X-ray crystallography. ©2000 Elsevier Science Ltd All rights reserved.

Keywords: Trirhenium(III) clusters; Rhenium clusters; Acetamidate; Dimolybdenum(II); MALDI; Mass spectroscopy

1. Introduction

Determinations of the structures of $Cs_3Re_3Cl_{12}$ [1], $(Re_3Cl_9)_x$ [2] and $K_2Re_2Cl_8\cdot 2H_2O$ [3] and the realization in the early 1960s [4] that a quadruple bond links the metal atoms in $[Re_2Cl_8]^{2-}$ were instrumental in bringing the metal cluster area to the attention of the chemical community. Since then, the chemistry of metal clusters has been intensively investigated. Rhenium cluster species, in particular, have been a subject of numerous studies [5].

Five new complexes of rhenium(III) that contain acetamidate ligands are described in this paper. The ligand in these compounds was formed by nucleophilic attack of water on a coordinated acetonitrile. We also describe synthesis and structural characterization of a molybdenum(II) acetonitrile complex and its failure to undergo a similar reaction.

The use of modern mass spectrometric techniques in this study is also noted. Most projects in the metal cluster area have relied on elemental analysis to determine the formulas of new species and single crystal X-ray diffraction studies to identify structures. Both have limitations: elemental analyses are often not definitive and it is frequently difficult to obtain diffraction quality crystals. In addition, neither technique typically provides the important rapid feedback of information on the progress of the reaction, the presence of intermediates, and the occurrence of secondary products, information that is usually very helpful in guiding a synthetic chemist during a synthetic procedure and often essential for developing mechanistic hypotheses to understand the chemistry involved.

We have been interested in the use of mass spectrometry in the analysis of metal cluster syntheses. Using modern ionization techniques, specifically MALDI (matrix assisted laser desorption/ionization) and ESI (electrospray ionization), it is now possible to obtain data on many compounds not previously amenable to mass spectrometric analysis. Both techniques are easy to use and can potentially provide rapid feedback on, for example, the identity and purity of a crude product from a reaction mixture. Obtaining mass spectra of some representative compounds to establish a database for reference is an important initial step to using these techniques. In this context, we reported on MALDI mass spectra of several rhenium halide clusters in a recent paper [6].

* Corresponding author. Tel.: +1-608-262-8828; fax: +-608-262-6143; e-mail: treichel@chem.wisc.edu

0277-5387/00/$ - see front matter ©2000 Elsevier Science Ltd All rights reserved.
PII S0277-5387(00)00382-X

In an initial stage of the investigations described in that paper, ESI spectra were obtained on a well characterized compound, $Cs_3Re_3Cl_{12}$. The procedure selected used acetonitrile as a solvent. These spectra indicated the presence of complexes containing one or two acetamidate ligands in solution. The results led to the investigation described here.

Several papers have appeared recently that describe work related to the results reported here. The first described $[(C_4H_9)_4N]_2[Re_2Cl_6(\mu\text{-}NHCOC_6H_5)]\cdot 0.5CH_2Cl_2$, a compound prepared from $[(C_4H_9)_4N]_2Re_2Cl_8$ and benzonitrile in ethanol [7]. From the same group came the report of a related study that produced the compound $[(C_4H_9)_4N]_2$-$[Re_2Cl_5(\mu\text{-}NHCOCH_3)(\mu\text{-}NC(OH)CH_3)]\cdot 3CH_2Cl_2$ in a similar reaction using acetonitrile. A dppm derivative of this species was also described [8]. Compound **1** reported here is yet a third species that originates from a reaction of this dinuclear precursor. Compound **1** is structurally different from the compounds reported earlier in that it is dimeric via chloride bridges. There are also differences in the synthetic methodology which bear further comment. Finally, a recent paper describing the formation of a tetrarhenium(III) cluster is also noted. Again, the formation of this ligand involved hydration of the acetonitrile being used as a solvent [9].

2. Experimental

2.1. Materials

Literature procedures were used to synthesize $Cs_3Re_3Cl_{12}$ [1] and $K_4Mo_2Cl_8\cdot 2H_2O$ [10]. Silver tetrafluoroborate (98%), $AgPF_6$ (98%), $[(C_4H_9)_4N]_2Re_2Cl_8$, $Re_2(CO)_{10}$, $[(C_4H_9)_4N]Cl\cdot H_2O$ (98%), and various solvents were obtained from commercial sources. In one case a sublimed sample of $(Re_3Cl_9)_x$ was used, but in most syntheses the commercial material (obtained from Pressure Chemical Co.) was used directly without further purification with no obvious problems being encountered. Tetraethylammonium chloride monohydrate (98%) was recrystallized from anhydrous ethanol/diethyl ether prior to use. Acetonitrile and dichloromethane were dried by refluxing over CaH_2 and acetone was dried by refluxing over $CaSO_4$. Tetrahydrofuran, diisopropyl ether, and diethyl ether were dried by refluxing over Na/benzophenone and distilled immediately prior to use. All manipulations were carried out under an atmosphere of dry nitrogen using standard Schlenk techniques.

2.2. X-ray crystallographic and spectroscopic measurements

Crystallographic data were collected on a Siemens P4 diffractometer using a CCD detector. Table 1 provides details on the six structural determinations carried out in this study. Electronic spectra were measured on a Cary 4Bio spectrophotometer. Proton NMR spectra were recorded on a Bruker AC 300 spectrometer operating at 300 MHz. Matrix assisted laser desorption/ionization (MALDI) mass spectra were recorded on a Bruker Reflex II mass spectrometer equipped with a N_2 laser operating with an accelerating voltage of -20 kV and a reflectron voltage of -21.2 kV. Spectra were obtained in the negative ion mode. In the positive mode, only peaks due to the cation were present; no rhenium species were detected. All spectra were obtained using a dithranol as the matrix and are the sum of 50 shots. Samples for MALDI analysis were dissolved in acetonitrile and then mixed with an acetonitrile solution of the matrix prior to deposition onto the target. Ion signals were assigned based on *m/z* values and the match of experimental and calculated isotopic patterns. In this regard, it is noted that the isotopes of rhenium (^{185}Re and ^{187}Re) and chlorine (^{35}Cl and ^{37}Cl) result in highly definitive patterns for rhenium chloride species. ESI spectra were obtained using a Micromass Autospec triple sector mass spectrometer equipped with a Mark II electrospray source. The accelerating and sampling cone voltage were 4000 V, the needle voltage 3948 V, and nitrogen was used as the nebulizer and bath gas. The solution of $Cs_3Re_3Cl_{12}$ in acetonitrile was sprayed at the rate of either 32 or 15 $\mu l\ m^{-1}$.

2.3. Synthesis of $[(C_4H_9)_4N]_2[\{Re_2Cl_6(\mu\text{-}1,2\text{-}NHCOCH_3)\}_2]$ (**1**)

A 50 ml flask equipped with a Teflon coated stir bar was charged with 28 mg (0.143 mmol) of $AgBF_4$ in 15 ml acetonitrile. Another 50 ml flask was charged with 82 mg (0.072 mmol) of $[(C_4H_9)_4N]_2Re_2Cl_8$, and 10 ml of acetonitrile. Deionized water (0.05 ml, 2.8 mmol) was added to the flask containing $[(C_4H_9)_4N]_2Re_2Cl_8$, then the $AgBF_4$ solution was added. A copious amount of precipitate (AgCl) formed immediately. The reaction mixture was stirred at room temperature for 12 h; then the volatile materials were removed under dynamic vacuum. The residue that remained was extracted with 8 ml of acetonitrile, giving a blue solution and lightly colored solid. The blue solution was filtered three times by means of filter-tipped cannulas, then concentrated to approximately 4 ml and filtered into a Schlenk tube. The solution was carefully layered with diethyl ether. On standing, dark blue prism-shaped crystals of $[(C_4H_9)_4N]_2$-$[\{Re_2Cl_6(\mu\text{-}1,2\text{-}NHCOCH_3)\}_2]$ (**1**) formed (21% yield of the purified product). Initial characterization and assessment of purity was based on a mass spectrum (see Section 3; discussion). The structure of this compound was determined by X-ray crystallography.

Using less than 2 equiv. of silver in this reaction (with otherwise similar conditions) resulted in diminished yields with starting material being recovered.

^1H NMR spectrum (CD_2Cl_2): singlet, 3.05 ppm, plus resonances arising from the tetrabutylammonium cation. Vis (CH_2Cl_2): 651 nm ($\varepsilon = 2780\ M^{-1}\ cm^{-1}$). MALDI MS: *m/z* = 643.6 (calc. 643.74), $[Re_2Cl_6(NHCOCH_3)]^-$; *m/z* = 605.7 (calc. 605.78), $[Re_2Cl_5(NHCOCH_3)]^-$.

Table 1
Structural parameters for **1**–**6**

Compound	**1**	**2**	**3**
Chemical formula	$C_{36}H_{80}Cl_{12}N_4O_2Re_4$	$C_{42.9}H_{97.25}Cl_{16}N_4O_4Re_3$	$C_{36}H_{76}Cl_{10}N_3O_{4.5}Re_3$
Formula weight	1771.24	2445.30	1456.08
Space group	$P2_1/c$	$P\bar{1}$	$P\bar{1}$
a (Å)	10.8601(2)	12.4852(2)	12.4415(2)
b (Å)	16.0264(2)	13.1671(2)	13.3242(2)
c (Å)	16.7615(3)	27.7160(4)	16.8294(2)
α (°)	90	82.210(2)	104.072(2)
β (°)	104.598(2)	84.326(2)	99.781(2)
γ (°)	90	62.475(2)	92.917(2)
V (Å^3)	2823.13(8)	3999.91(11)	2657.37(7)
Z	2	2	2
ρ_{calc} (g cm^{-3})	2.084	2.030	1.822
T (°C)	−140	−140	−140
λ (Å)	0.71073	0.71073	0.71073
μ (cm^{-1})	91.49	96.14	73.55
R (F_o) observed data	0.0248	0.0635	0.0499
R_w (F_o^2) all data	0.0570	0.1679	0.1255

Compound	**4**	**5**	**6**
Chemical formula	$C_{30}H_{69}Cl_8N_3O_{4.5}Re_3$	$C_{16}H_{18}Cl_9N_2O_4Re_3$	$C_8H_{12}Cl_4Mo_2N_4$
Formula weight	1386.08	1200.13	497.90
Space group	$P2_1/n$	$P2_1$	$Pca2_1$
a (Å)	12.0493(3)	10.1785(3)	16.0085(2)
b (Å)	23.1391(6)	32.5290(2)	8.2113(2)
c (Å)	17.2034(5)	10.7394(4)	136644(5)
α (°)	90	90	90
β (°)	90.784(2)	111.926(2)	90
γ (°)	90	90	90
V (Å^3)	4796.1(2)	3298.58(16)	1796.19(8)
Z	4	4	4
ρ_{calc} (g cm^{-3})	1.920	2.417	1.841
T (°C)	−140	−140	−120
λ (Å)	0.71073	0.71073	0.71073
μ (cm^{-1})	80.33	117.36	19.80
R (F_o) observed data	0.0331	0.0616	0.0463
R_w (F_o^2) all data	0.0797	0.1464	0.0977

*2.4. Synthesis of [$(C_2H_5)_4N$][Re_3Cl_8(μ-1,2-NHCOCH$_3$)(μ-2,3-NHCOCH$_3$)] · 2.5$C_4H_{10}O$ (**2**)*

A 100 ml flask was charged with 185 mg (0.211 mmol) of $(Re_3Cl_9)_x$ and 35 mg (0.211 mmol) of $[(C_2H_5)_4N]Cl \cdot H_2O$. The contents of the flask were dissolved in acetonitrile (50 ml), with immediate formation of Re_3Cl_9(acetonitrile)$_3$ as noted by the dark red color of the solution [11]. Deionized water (0.4 ml, 22 mmol) was added. A 16-gage needle, attached to a dry N_2 line, was introduced through a rubber septum in the sidearm of the flask. The top end of the condenser was connected to a bubbler containing a saturated aqueous solution of $AgNO_3$. The needle was positioned at the bottom of the flask and the solution was purged with N_2 with the exit gas passing through the $AgNO_3$ solution. When the solution was heated to reflux temperature a white precipitate (AgCl) was observed in the $AgNO_3$ bubbler, indicating evolution of HCl. Heating was continued for 2.5 h; at this point the solution was a dark purple color. The solution was concentrated to 10 ml, filtered, and diethyl ether was layered above the acetonitrile solution. Crystals that grew over the course of several days were collected and weighed. The calculated yield of $[(C_2H_5)_4N][Re_3Cl_8(\mu\text{-}1,2\text{-}NHCOCH_3)(\mu\text{-}2,3\text{-}NHCOCH_3)] \cdot 2.5C_4H_{10}O$ (**2**) was 51%. The identity of this sample was established by comparison of the negative ion MALDI mass spectra of this species and a sample with a different cation obtained by the non-systematic procedure described next.

^{1}H NMR spectrum (CD_3CN): 2.32 (s) ppm, plus resonances associated with the cation. UV–Vis (CD_3CN): 316 nm (ε = 4700 M^{-1} cm^{-1}), 325 nm (sh), 447 nm (sh) and 539 nm (ε = 700 M^{-1} cm^{-1}). MALDI MS: *m/z* = 958.7 (calc. 958.68), $[Re_3Cl_8(NHCOCH_3)_2]^-$; *m/z* = 923.8 (calc. 923.8), $[Re_3Cl_7(NHCOCH_3)_2]^-$.

2.5. Alternative synthesis: $[(C_4H_9)_4N][Re_3Cl_8(\mu\text{-}1,2\text{-}NHCOCH_3)(\mu\text{-}2,3\text{-}NHCOCH_3)]\cdot 2.5C_4H_{10}O$ (**2′**)

A 50 ml flask was charged with 99 mg (0.071 mmol) of $[(C_4H_9)_4N]_2[Re_3Cl_9S]$ [12], and 15 ml of acetonitrile. Some, but not all, of the material dissolved. A solution containing $[Re(CO)_3(CH_3CN)_3]PF_6$, prepared in situ from 29 mg (0.071 mmol) of $Re(CO)_5Br$, 10 mg (0.071 mmol) of $AgPF_6$, and 20 ml of acetonitrile [13], was then transferred into the flask by means of a filter-tipped cannula. The reaction mixture was stirred overnight at room temperature. The red–brown solution was filtered into a 100 ml flask. This solution was evaporated to dryness under dynamic vacuum. The residue was redissolved in acetone (5 ml), and approximately 2 ml of the acetone solution was filtered into a 12 mm O.D. tube and layered with diethyl ether. Dark red prism-shaped crystals of $[(C_4H_9)_4N][Re_3Cl_8(\mu\text{-}1,2\text{-}NHCOCH_3)(\mu\text{-}2,3\text{-}NHCOCH_3)]\cdot 2.5C_4H_{10}O$ (**2′**) grew over the course of several weeks. The isolated yield of **2′** was low. The compound was identified by X-ray diffraction.

2.6. Synthesis of $[(C_4H_9)_4N]_2[Re_3Cl_{10}(\mu\text{-}1,2\text{-}NHCOCH_3)]$ (**3**)

A 100 ml flask was charged with 81.0 mg (0.0586 mmol) of $Cs_3Re_3Cl_{12}$ and 50 mg (0.180 mmol) of $[(C_4H_9)_4N]Cl\cdot H_2O$. Acetonitrile (20 ml) was added and the contents of the flask were stirred for 10 min. Deionized water (0.10 ml, 5.5 mmol) was added and the contents of the flask were stirred vigorously for 90 min. A solution of $AgBF_4$ (34.2 mg, 0.176 mmol, in 15 ml acetonitrile) was then added dropwise via cannula over 30 min. The reaction mixture was stirred for 6 h at room temperature, yielding a purple solution and a light colored precipitate (AgCl). The solid was separated by filtration and discarded; the purple solution was concentrated to about 6 ml under vacuum. Approximately 1.5 ml of the concentrated solution was then filtered into a Schlenk tube. Diethyl ether was carefully layered above the acetonitrile solution. Dark purple prism-shaped crystals of $[(C_4H_9)_4N]_2[Re_3Cl_{10}(\mu\text{-}1,2\text{-}NHCOCH_3)]$ (**3**) formed on standing. Mass spectroscopic data and X-ray crystallography were used to characterize **3**.

^{1}H NMR spectrum (CD_3CN): singlet, 2.2 ppm, plus resonances arising from the tetrabutylammonium cation. UV–Vis (CH_2Cl_2): 524 nm ($\varepsilon = 620$ M^{-1} cm^{-1}). MALDI MS: $m/z = 935.6$ (calc. 935.60), $[Re_3Cl_9(NHCOCH_3)]^-$; $m/z = 900.7$ (calc. 900.7), $[Re_3Cl_8(NHCOCH_3)]^-$.

2.7. Alternative synthesis of **3**

Sublimed $(Re_3Cl_9)_x$ (0.0295 g, 0.034 mmol) was added to 20 ml of a 1.0 M solution of HCl in anhydrous diethyl ether (in which the rhenium complex partially dissolves). Solid $[(C_4H_9)_4N]Cl\cdot H_2O$ (0.0440 g, 0.16 mmol) was added; immediately, an oil separated from the solution. The solvent was decanted, and the oil was dissolved in methylene chloride. A solid product precipitated from this solution when diethyl ether was added. In one attempt to recrystallize this compound, the crude product was dissolved in a minimum amount of acetonitrile and the solution layered with diethyl ether. The crystalline product that formed was filtered and dried; analysis using mass spectroscopy (MALDI) identified the anion of this species. A single crystal diffraction study confirmed the identity of the product as **3**.

2.8. Preparation of $[(C_4H_9)_4N]_2[\{Re_3Cl_8(\mu\text{-}1,2\text{-}NHCOCH_3)(OH)\}_2]\cdot 1.7(C_4H_{10}O)$ (**4**)

A 100 ml flask was charged with 80.3 mg (0.058 mmol) of $Cs_3Re_3Cl_{12}$ and 50 mg (0.180 mmol) of $[(C_4H_9)_4N]Cl\cdot H_2O$. Acetonitrile (40 ml) was added and the contents of the flask were stirred for 20 min. Deionized water (0.20 ml, 11 mmol) was added and stirring was continued for an additional 80 min. Then a solution of $AgBF_4$ (46.4 mg, 0.238 mmol, in 45 ml acetonitrile) was added over 10 min. An additional 25 ml acetonitrile was used to rinse the flask that contained the $AgBF_4$ solution, and this was also added to the reaction mixture. The contents of the reaction flask were stirred overnight at room temperature, resulting in a purple solution and a copious amount of a light-colored precipitate (AgCl). The solution was filtered by means of a filter-tipped cannula into a 125 ml flask, then the solvent was removed under dynamic vacuum. The residue that remained was dissolved in 3 ml acetone. This solution was filtered into a Schlenk tube and carefully layered with diethyl ether. Dark red opaque plate-shaped crystals of $[(C_4H_9)_4N]_2[\{Re_3Cl_8(\mu\text{-}1,2\text{-}NHCOCH_3)(OH)\}_2]\cdot 1.7C_4H_{10}O$ (**4**) formed in the tube over several weeks. The compound was identified by X-ray diffraction. The isolated yield of compound **4** was low and additional data on this compound were not obtained. An aquo complex, $(C_4H_9)_4N[Re_3Cl_9(H_2O)(\mu\text{-}1,2\text{-}NHCOCH_3)]$ (**5**) is presumably an intermediate in the formation of **4**. In one instance, a very small amount of a crystalline sample of **5** was obtained and characterized by X-ray diffraction.

2.9. Preparation of $Mo_2Cl_4(NCCH_3)_4$ (**6**)

A 125 ml flask was charged with 77.8 mg (0.123 mmol) of $K_4Mo_2Cl_8\cdot 2H_2O$. Acetonitrile (45 ml) was added and the resulting slurry was stirred vigorously for 20 min. Deionized water (0.15 ml, 8.3 mmol) was added. A solution of $AgBF_4$ (0.97 mg, 0.493 mmol) in acetonitrile (30 ml) was added over 45 min, producing a blue solution and a light colored precipitate (AgCl). The reaction mixture was stirred overnight at room temperature, then the blue solution was separated from the precipitate by means of a filter-tipped cannula. Removal of solvent from the solution affords a 99% yield of a waxy solid, $Mo_2Cl_4(NCCH_3)_4$ (**6**).

To obtain crystalline samples of **6**, the blue solution obtained after filtration was concentrated to approximately 12 ml, and ca. 5 ml of this solution was filtered into a vapor

diffusion tube. The sidearm on the vapor diffusion tube was filled with diisopropyl ether. Dark blue plate-shaped crystals grew on the walls of the tube as diisopropyl ether diffused into the acetonitrile solution over several weeks. These crystals were identified by X-ray diffraction. This complex has been reported previously [14] but it had not been structurally characterized.

UV–Vis (CH_3CN): 602 nm, in accord with published data [14].

3. Results and discussion

Initial evidence that acetamidate complexes are formed in an acetonitrile solution of a rhenium(III) complex was obtained from a negative ion ESI spectra of $Cs_3Re_3Cl_{12}$ using acetonitrile as a solvent (Fig. 1). Seen in these spectra are peaks with *m/z* values at 924 and 959 corresponding to $[Re_3Cl_n(NHCOCH_3)_2]^-$ ($n=7$, 8) and at 901 and 936, corresponding to $[Re_3Cl_n(NHCOCH_3)]^-$ ($n=8$, 9). The first set of peaks became more prominent as the solution of $Cs_3Re_3Cl_{12}$ aged while peaks associated with the $[Re_3Cl_{12}]^{3-}$ cluster at 912, 878, and 843 (corresponding to $[Re_3Cl_n]^-$, $n=10$, 9, 8) [6] diminished and eventually disappeared from the spectrum. The acetamidate ligands in these species were presumably formed by nucleophilic attack of water (or OH^-) at a coordinated nitrile. Water had not been specifically added as a reagent but it was assumed to be present in the reaction system, either in the acetonitrile (although this solvent had been dried using standard procedures) or in the lattice of the rhenium compound. References to $Cs_3Re_3Cl_{12}$ do not mention the presence of water, but the synthesis of this species involves aqueous chemistry and traces of water would probably be overlooked in analysis of analytical and crystallographic data.

Hydration of coordinated nitriles has been studied using a variety of metals [7,15]. Typical procedures for these reactions utilize basic conditions to effect OH^- addition to the carbon of the nitrile, followed by protonation. The key mechanistic step is nucleophilic attack at the ligand, enhanced by coordination to a metal ion. Most studies involve monometallic complexes but, in one instance, catalysis of the hydration reaction using a dipalladium complex (giving acetamide) was observed [16]. Rhenium(III) nitrile complexes have been known for over 30 years [17]. Prior to the recent work cited above [7–9], however, nucleophilic attack by water at the nitrile ligand in a rhenium(III) complex was observed in one instance [18]. This reference is to an interesting reaction in which the final product is a complex with carboxylate rather than amidate ligands. The activation of nitriles to nucleophilic attack in rhenium(IV) compounds is noted, however; amines and alcohols add to the coordinated nitrile in $ReCl_4(NCR)_2$ ($R=CH_3$, C_6H_5) [17].

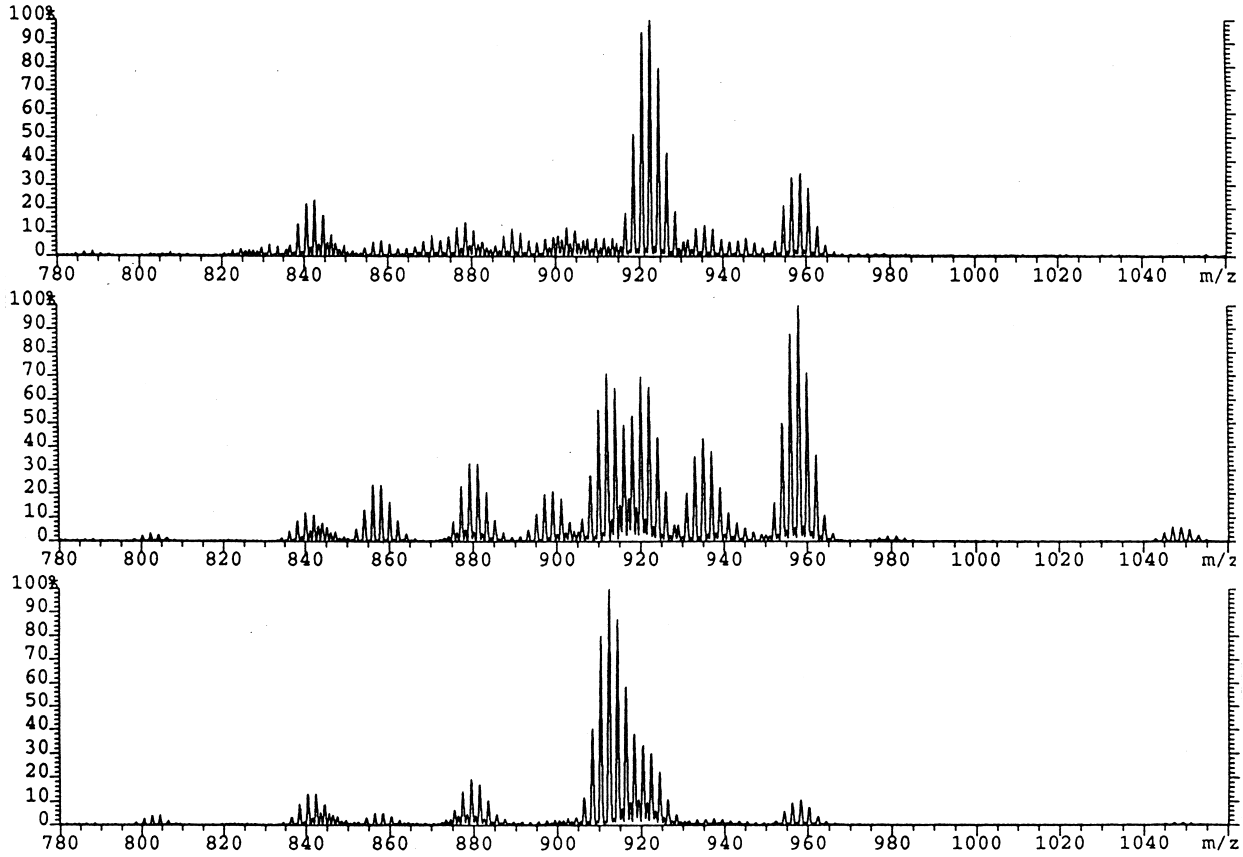


Fig. 1. ESI (electrospray) mass spectra of $Cs_3Re_3Cl_{12}$ using acetonitrile as a solvent at different times: bottom, immediately after preparing the solution; middle, after 1 day; top, after 10 days.

To prepare $[(C_4H_9)_4N]_2[\{Re_2Cl_6(\mu\text{-}1,2\text{-}NHCOCH_3)\}_2]$ (**1**) a procedure was selected that involved initial addition of 2 equiv. of Ag^+ to an acetonitrile solution of $[(C_4H_9)_4N]_2Re_2Cl_8$. The intent was to form in situ a nitrile complex, $Re_2Cl_6(NCCH_3)_2$, that would then be susceptible to further reaction with water. A halide acceptor was assumed to be needed since replacement of halide ion by acetonitrile is not itself a favorable reaction. There are numerous examples in the literature in which silver ion assists in reactions in which other ligands replace a coordinated halide ion with insoluble AgCl being formed [19]. The targeted intermediate, the nitrile complex, has not been reported before, but compounds with similar stoichiometry are known with other ligands, notably phosphines [5]. The reaction between $AgPF_6$ and $[(C_4H_9)_4N]_2Re_2Cl_8$ occurs readily as judged by the immediate precipitation of AgCl. Subsequently, work-up of the reaction mixture by standard techniques led to $[(C_4H_9)_4N]_2[\{Re_2Cl_6(\mu\text{-}1,2\text{-}HNCOCH_3)\}_2]$ (**1**) in 21% isolated yield. The overall reaction is represented in Eq. (1):

$$2[(C_4H_9)_4N]_2Re_2Cl_8 + 4Ag^+ + 2CH_3CN + 4H_2O \rightarrow 4AgCl(s) + 2H_3O^+ + 2(C_4H_9)_4N^+ + [(C_4H_9)_4N]_2[\{Re_2Cl_6(\mu\text{-}1,2\text{-}NHCOCH_3)\}_2] \quad (1)$$

The role of Ag^+ in this reaction is open to question. Silver ion was not a component of the reported reactions between $[(C_4H_9)_4N]_2Re_2Cl_8$ and benzonitrile [7] or acetonitrile [8] in ethanol. We have found that in the absence of ethanol, however, $[(C_4H_9)_4N]_2Re_2Cl_8$ and CH_3CN do not react appreciably over 3 days (room temperature). So, Ag^+ appears to be essential in this reaction if ethanol is not used as a solvent.

Further observations confirming the importance of Ag^+ are noted. An ESI spectrum of $[(C_4H_9)_4N]_2Re_2Cl_8$ run several hours after preparing a solution of this compound in acetonitrile contains peaks associated with the $[Re_2Cl_8]^{2-}$ ion only, indicating no reaction in this short time period. (In contrast, acetamidate complexes are noted in the ESI spectrum of $Cs_3Re_3Cl_{12}$ within an hour, vide supra.) Indirect evidence is provided in experiments with less than 2 equiv. of Ag^+. Over 1 day, these reactions produced a mixture of starting material and product, in a ratio suggesting that when Ag^+ had been expended the reaction did not proceed measurably further. Note in Eq. (1) that 2 equiv. of this reagent are needed for complete reaction, with 2 equiv. of AgCl precipitating.

The mechanism postulated [7] for the conversion of a nitrile to an acetamidate ligand appears logical: initial coordination of acetonitrile to a rhenium atom, addition of water to the nitrile carbon, hydrogen migration and deprotonation to yield a monodentate acetamidate ligand. Chelation through oxygen to the second metal atom with displacement of another chloride ion then gives the product.

The interesting aspect of this synthesis is that when acetonitrile is the solvent (and no ethanol is present) the reaction did not occur. Since activation of the nitrile requires its initial coordination to rhenium, it is attractive to conclude that such a complex must form if ethanol is used as a solvent.

Based on our results, it would appear that the formation of such an intermediate is not favored in acetonitrile. In the absence of ethanol and without Ag^+, a nitrile complex could form in two ways, and in both instances a solvent could presumably influence the process. Solvation could influence the direct replacement of a chloride ion by the nitrile. This kind of reaction is known for other ligands such as phosphines but not for nitriles. Second, the nitrile could coordinate to $[Re_2Cl_8]^{2-}$ in an axial position, that is, *trans* to the metal–metal bond. Complexes with the stoichiometry $[Re_2Cl_8(L)_2]^{2-}$ are known; for example, in some reported crystal structure studies on octahalodirhenium complexes water is present as an axial ligand [20]. In other cases axially coordinated water is not present, however, and it is reasonable to suppose that the interaction between axial ligand and metal is weak. Ethanol could affect the extent to which such a complex is formed.

In our early experiments water was not added as a reagent. Water presumably was present in the starting material or in the solvent. Hoping to intercept an intermediate nitrile complex, efforts were made to exclude water. Solvents were carefully dried and the rhenium starting material was heated in vacuum at about 100°C in an attempt to remove traces of water. In each instance, however, only the acetamidate-containing product **1** was obtained. The conclusion reached is that hydration must be both favorable and very rapid.

Structural characterization of **1** was achieved by a single crystal X-ray diffraction study. The structure of the anion of **1** is shown in Fig. 2. Two dirhenium moieties are linked via bridging chloride ions, The rhenium–rhenium bond distance in each half of the anionic species is short (2.229 Å), the bond distance being similar to values found in $[(C_4H_9)_4N]_2Re_2Cl_8$ (2.222 Å) [21] and in $[(C_4H_9)_4N]_2$-

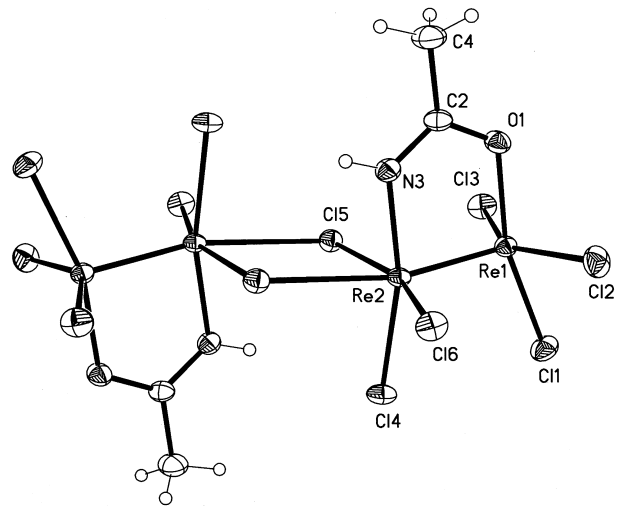


Fig. 2. Structure of the anion of $[(C_4H_9)_4N]_2[\{Re_2Cl_6(\mu\text{-}1,2\text{-}HNCOCH_3)\}_2]$ (**1**).

$[Re_2Cl_6(\mu\text{-}C_6H_5CONH)]\cdot 0.5CH_2Cl_2$ (2.2209 Å) [7], and representative of a quadruple bond [3,4].

The geometry of ligand substitution for each metal atom in the starting material is similarly retained; three chloride ligands and the oxygen or nitrogen of the acetamidate lie in a square planar arrangement about the metal. There is an eclipsed orientation of the ligands on the two rhenium atoms. Specific parameters (bond lengths and bond angles) are unexceptional.

A structure determination of **1** was done several times using good crystals from several different syntheses. In each case, an analysis assuming an ordered structure gave a better fit of data than a disordered model. The structure placed oxygen and nitrogen atoms in the dirhenium unit so that the two halves of the anion are linked through chloride bridges to rhenium atoms to which the nitrogen atoms of the coordinated acetamidate ligands are attached. Noted in passing is the structure of $[(C_4H_9)_4N]_2[Re_2Cl_6(\mu\text{-}C_6H_5CONH)]\cdot 0.5CH_2Cl_2$ in which oxygen and nitrogen atoms were also not disordered [7].

Related dirhenium species with bridging carboxylate ligands having the general formulas $Re_2(O_2CR)_4X_2$, $Re_2(O_2CR)_3X_3$, and $Re_2(O_2CR)_2X_4$ (where R is an organic group in a carboxylate ligand and X represents Cl, Br, or I) are known [5]. Dirhenium acetamidate complexes are formed by reactions of $Re_2(O_2CCH_3)_4Cl_2$ with amides at elevated temperatures [22,23]. Compounds with a 2-hydroxypyridinate ligand, structurally resembling amidate complexes, are also known [18,24].

Trirhenium complexes having acetamidate ligands were also prepared in this study. Here, the role of Ag^+ in the synthesis was less equivocal, and methods both with and without this halide acceptor are reported. Again, the synthetic strategy involves the formation of a nitrile complex as the key intermediate. In this context, the reaction occurring with $(Re_3Cl_9)_x$, acetonitrile, and water was straightforward. Polymeric $(Re_3Cl_9)_x$ dissolves readily in acetonitrile giving a deep red solution of $Re_3Cl_9(NCCH_3)_3$ [11]. On heating, the solution rapidly turns purple. Hydrogen chloride is produced in the reaction; this was detected by purging the reaction system with N_2 and passing the exit gases passed through a saturated aqueous solution of silver nitrate in which a white precipitate of AgCl is seen to form. The reaction is complete in 2.5 h; no further HCl evolution is detected. Addition of tetraethylammonium chloride and subsequent work-up gave a 51% yield of $(C_2H_5)_4N[Re_3Cl_8\text{-}\mu\text{-}1,2\text{-}(HNCOCH_3)\text{-}\mu\text{-}2,3\text{-}(HNCOCH_3)]$ (**2**) (Eq. (2)).

$$Re_3Cl_9(CH_3CN)_3 + 2H_2O + [(C_2H_5)_4N]Cl \rightarrow CH_3CN + 2HCl + (C_2H_5)_4N[Re_3Cl_8 \times (\mu\text{-}1,2\text{-}HNCOCH_3)(\mu\text{-}2,3\text{-}HNCOCH_3)] \quad (2)$$

The same anion was isolated (with a different cation) from a quite different reaction. The compound, $(C_4H_9)_4N[Re_3Cl_8(\mu\text{-}1,2\text{-}HNCOCH_3)(\mu\text{-}2,3\text{-}HNCOCH_3)]$ (**2′**), was formed in low yield in a reaction of $[(C_4H_9)_4N]_2[Re_3Cl_9S]$ [12] with $[Re(CO)_3(CH_3CN)_3]PF_6$. The abstraction of sulfide ion from $[(C_4H_9)_4N]_2[Re_3Cl_9S]$ by $[Re(CO)_3(CH_3CN)_3]^+$ is probably a key step in the process. The structure of **2′** was established by a single crystal X-ray diffraction study. The anion (Fig. 3) has two acetamidate ligands bridging axial positions on opposite sides of the plane defined by the $Re_3(\mu\text{-}Cl_3)$ fragment, resulting in one of the three rhenium atoms in the anion being coordinated by two acetamidate ligands at its two axial positions.

Compound **3**, $[(C_4H_9)_4N]_2[Re_3Cl_{10}(\mu\text{-}1,2\text{-}HNCOCH_3)]$, was obtained in a two step reaction. Here, $(Re_3Cl_9)_x$ was first allowed to react with a 1.0 M solution of anhydrous HCl in diethyl ether; then tetrabutylammonium chloride was added. The product obtained in this reaction is $[(C_4H_9)_4N]_4[\{Re_3Cl_{11}\}_2]$, the anion of which has two $[Re_3Cl_{11}]^{2-}$ subunits linked via chloride bridges [25]. When acetonitrile was used in a purification step, compound **3** formed. Water was presumably introduced into the reaction mixture when the tetraalkylammonium salt was added. It is reasonable to assume that the halide bridge is readily broken by acetonitrile yielding $[(C_4H_9)_4N]_2[Re_3Cl_{11}(NCCH_3)]$. At this point, hydrolysis and elimination of HCl leads to the observed product. Again, reaction with only a trace of water being present speaks to the facile character of the hydration step in this reaction.

The structure of the anion of **3** is shown in Fig. 4. The similarity to structures of other known trirhenium species is apparent [5]; the anion of **3** contains a triangle of rhenium atoms, linked by metal–metal bonds and bridging halide ligands. Each metal atom has, in addition, three terminal ligands. The acetamidate ligand bridges axial positions of two rhenium atoms and chloride ions occupy the remaining terminal positions.

Compound **3** was also obtained in a reaction that used Ag^+ to generate an open coordination site on rhenium. Silver tetrafluoroborate was added to $Cs_3Re_3Cl_{12}$ and acetonitrile, with AgCl precipitating immediately. The mechanism of forma-

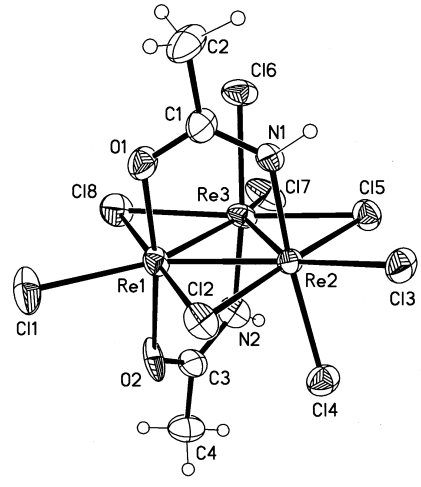


Fig. 3. Structure of the anion of $[(C_4H_9)_4N][Re_3Cl_8(\mu\text{-}1,2\text{-}HNCOCH_3)\text{-}(\mu\text{-}2,3\text{-}HNCOCH_3)]\cdot 2.5(C_4H_{10}O)$ (**2′**).

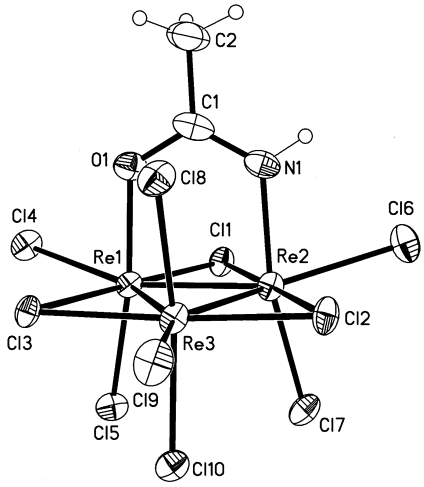


Fig. 4. Structure of the anion of $[(C_4H_9)_4N]_2[Re_3Cl_{10}(\mu\text{-}1,2\text{-}HNCOCH_3)]$ (**3**).

tion is presumably the same as was postulated for **1**: initial loss of chloride ion from the rhenium coordination sphere and coordination of acetonitrile followed by reaction with water, loss of H^+, and chelation gives the product.

An attempt to synthesize a trirhenium species containing two acetamidate ligands via a route involving chloride abstraction using Ag^+ ions was unsuccessful, however. The reaction of $[(C_4H_9)_4N]_3Re_3Cl_{12}$ with 4 equiv. of $AgBF_4$ produced a small amount of an acetamidate compound identified as $[(C_4H_9)_4N]_2[\{Re_3Cl_8(OH)(\mu\text{-}1,2\text{-}NHCOCH_3)\}_2]\cdot 1.7(C_4H_{10}O)$ (**4**). The anion of this species (Fig. 5) consists of two trirhenium fragments bridged through hydroxide ligands, each trirhenium fragment containing a single chelating acetamidate ligand. It is reasonable to suppose that **3** is initially formed in this system and that further reaction with additional Ag^+ resulted in coordination of water rather than acetonitrile, forming $(C_4H_9)_4N[Re_3Cl_9(H_2O)(\mu\text{-}1,2\text{-}NHCOCH_3)]\cdot C_3H_6O$ (**5**) (Fig. 6), a compound also isolated and structurally characterized in this study. Loss of H^+ followed by dimerization via bridging hydroxide ligand groups gives **4**.

Structural parameters for the trirhenium species mirror closely the parameters of known trirhenium complexes. In particular the Re–Re distances are representative, with dimensions appropriate for double bond character (**2**, 2.4650(8) and 2.4669(8) Å; **3**, 2.4702(5) and 2.5062(5) Å; **4**, 2.4437(3) and 2.4511(3) Å; **5**, 2.4489(13) and 2.4557(14) Å). Particularly, note the values for **4** that identify it as a rhenium(III) complex and confirm that this species contains bridging OH^- ligands and not bridging oxide ligands. Oxo and hydroxo ligands would otherwise not be readily differentiated in the structure determination.

An attempt to extend this study to molybdenum chemistry did not result in formation of an acetamidate complex. The reaction of $K_4Mo_2Cl_8$ with $AgPF_6$ in acetonitrile/water gave the blue crystalline species $Mo_2Cl_4(NCCH_3)_4$ (**6**) in good yield (Fig. 7). Although $[Re_2Cl_8]^{2-}$ and $[Mo_2Cl_8]^{4-}$ are isoelectronic species, molybdenum(II) here apparently does

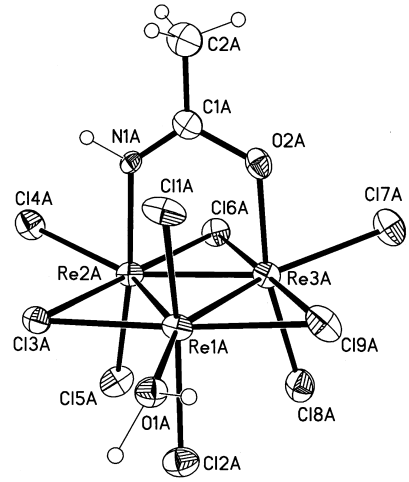


Fig. 6. Structure of the anion of $(C_4H_9)_4N[Re_3Cl_9(H_2O)(\mu\text{-}1,2\text{-}NHCOCH_3)]\cdot C_3H_6O$ (**5**).

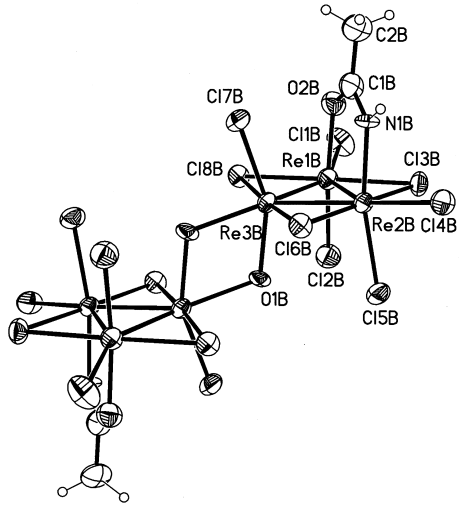


Fig. 5. Structure of the anion of $[(C_4H_9)_4N]_2[\{Re_3Cl_8(\mu\text{-}1,2\text{-}NHCOCH_3)(OH)\}_2]\cdot 1.7(C_4H_{10}O)$ (**4**).

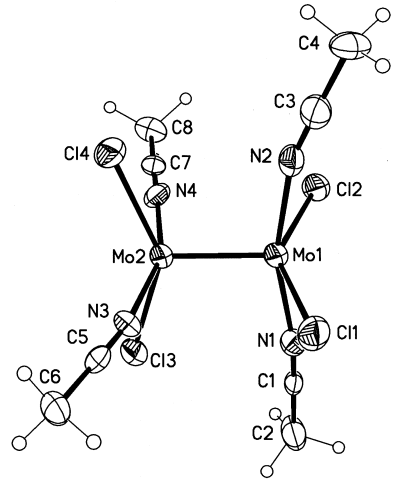


Fig. 7. Structure of $Mo_2Cl_4(NCCH_3)_4$ (**6**).

not activate the nitrile toward hydration. The factors that govern this must be subtle, however. Hydrolysis of a related complex, $[Mo_2(NCCH_3)_8]^{4+}$ to give $[Mo_2(NCCH_3)_6(\mu\text{-}NHCOCH_3)]^{3+}$ has recently been reported [26].

Compound **6** has been made previously but not structurally characterized [14]; however, a closely related compound, $Mo_2Cl_4(NCC_6H_5)_4$ has the same structure [27]. The structural motif in **6** has also been seen numerous times in the chemistry of quadruply bonded dimolybdenum complexes with the formula $Mo_2X_4L_4$, where L is a neutral donor ligand and X is a halogen [5,28].

In our earlier study on MALDI spectra of $Cs_3Re_3Cl_{12}$ and $[(C_4H_9)_4N]_2Re_2Cl_8$, two tentative conclusions were reached [6]. Mass spectra were useful in defining the nuclearity of the anion. Spectra obtained using this technique on these rhenium cluster species are fairly simple, containing only a few ion signals generated either by loss of a ligand group (Cl^-) or adduction of a matrix molecule, and in each case the nuclearity was retained. Second, loss of halide ions to create a detectable species with a -1 charge was a common occurrence. MALDI experiments typically detect ions with unitary charges. Ions that have higher charges are usually not detected, and a chemically logical means of reduction of the charge is seen to occur. For rhenium halide complexes, halide loss seems to be a common occurrence. In other systems, including some boron hydride anions when prepared as Na^+ salts [25], cation–anion aggregation is seen.

Proof of the effectiveness of MALDI in characterization must come, of course, in its use with unknown species. A broader goal of our research is to use MALDI spectra to predict the identity of new products. The match of MALDI data on **1**, **2**, and **3** with predicted spectra is preliminary evidence for the efficacy of this technique.

The MALDI spectrum of **2** (in which the anion has a single negative charge) contained only two sets of peaks, identified with the species $[Re_3Cl_8(HNCOCH_3)_2]^-$ ($[\mathbf{P}]^-$, $m/z=$ 958.7) and $[Re_3Cl_7(HNCOCH_3)_2]^-$ ($[\mathbf{P}-Cl]^-$ $m/z=$ 923.8), **P** here representing the parent anion. The spectrum obtained for **3** also matched predictions. In this instance, the compound contains a dinegative ion and, as in the previous study [6], loss of a chloride to give a -1 ion occurs. The spectrum for **3** contained peaks for the two ions $[Re_3Cl_9(HNCOCH_3)]^-$ ($[\mathbf{P}-Cl^-]^-$, $m/z=935.6$) and $[Re_3Cl_8(HNCOCH_3)]^-$ ($m/z=900.7$). The MALDI spectrum of compound **1** introduces a new, but not unexpected, dimension. In this compound, the dinegative ion is made up of two dinuclear fragments linked by chloride bridges, and the highest mass ion pattern corresponds to half of this whole unit, $[Re_2Cl_6(HNCOCH_3)]^-$ ($[\mathbf{P}/2]^-$, $m/z=643.7$). Presumably, the halide bridges also represent a weak link in this molecule, and cleavage of the $Re_2(\mu\text{-}Cl)_2$ unit of the compound is the most facile route to a monocharged species. Further examples are required to learn whether facile cleavage of a M–X–M bridge is a general result. Many cluster species aggregate in one dimension (chains) or in two dimensions (sheets), and it will be important to know whether these structural features can be established using MALDI.

ESI spectroscopy, although only used in one instance in this study, offer the possibility of more information. In results reported here, an intermediate (the mono-acetamido complex) as well as the eventual product (the bis-acetamido complex) was detected in a reaction mixture at early stages in the reaction. The ESI MS data provided evidence as to the progress of the reaction (which required more than 1 day and less than 10 days). MALDI requires removal of solvent to obtain a sample for analysis; in most instances use of this technique will be restricted to products. This allows MALDI to be used to determine whether a starting material and/or a desired product is present in a crude mixture. This simple analytical procedure, taking about 30 min to perform, will be of significant assistance in moving ahead in a synthetic project. Still, as noted, further examples and more data are needed to strengthen the case for the use of MALDI as a routine tool in characterization.

Supplementary data

Crystallographic data have been deposited with the Cambridge Crystallographic Data Centre, 12 Union Road, Cambridge, CB2 1EZ, UK (fax: +44-1223-336033; e-mail: deposit@ccdc.cam.ac.uk) and are available on request quoting the deposition numbers CCDC 140534 through CCDC 140539 (in order, structures **1**–**6**).

Acknowledgements

We are pleased to acknowledge the support for this work provided by the Research Corporation. Instrumentation (both mass spectrometers and the X-ray diffractometer) was obtained with partial support from NSF to the UW Department of Chemistry in the form of major instrumentation grants. We thank Kevin C. Moore (UW La Crosse) for assistance in rechecking reactions of $[(C_4H_9)_4N]_2[Re_2Cl_8]$.

References

[1] J.A. Bertrand, F.A. Cotton, W.A. Dollase, Inorg. Chem. 2 (1963) 1166.
[2] F.A. Cotton, J.T. Mague, Inorg. Chem. 3 (1964) 1402.
[3] F.A. Cotton, C.B. Harris, Inorg. Chem. 4 (1965) 130.
[4] F.A. Cotton, N.F. Curtis, C.B. Harris, B.F.G. Johnson, S.J. Lippard, J.T. Mague, W.R. Robinson, J.S. Wood, Science 145 (1964) 1305.
[5] F.A. Cotton, R.A. Walton, Multiple Bonds Between Metal Atoms, Clarendon Press, Oxford, 2nd edn., 1963. Chapter 1 provides an interesting review of the early work in this area.
[6] N.C. Dopke, P.M. Treichel, M.M. Vestling, Inorg. Chem. 37 (1998) 1272.
[7] C.B. Bauer, T.E. Concolino, J.L. Eglin, R.D. Rogers, R.J. Staples, J. Chem. Soc., Dalton Trans. (1998) 2813.
[8] T.E. Concolino, J.L. Eglin, R.J. Staples, Polyhedron 18 (1999) 915.

[9] Y.V. Mironov, Eur. J. Inorg. Chem. (1999) 997.
[10] J.V. Brencic, F.A. Cotton, Inorg. Chem. 8 (1969) 7.
[11] F.A. Cotton, R.A. Walton, Inorg. Chem. 5 (1966) 1802.
[12] R.W. McGaff, R.K. Hayashi, D.R. Powell, P.M. Treichel, Polyhedron 17 (1998) 4425.
[13] R.H. Reimann, F. Singleton, J. Organomet. Chem. 59 (1973) C24.
[14] J. San Filippo Jr., H.J. Sniadoch, R.L. Grayson, Inorg. Chem. 13 (1974) 2121.
[15] A.W. Parkins, Platinum Met. Rev. 40 (1996) 169.
[16] C.J. McKenzie, R. Robson, J. Chem. Soc., Chem. Commun. (1988) 112.
[17] G. Rouschias, G. Wilkinson, J. Chem. Soc. A (1968) 489.
[18] P.M. Treichel, P.J. Vincenti, Inorg. Chem. 24 (1985) 228.
[19] F.A. Cotton, W.T. Hall, Inorg. Chem. 16 (1977) 1867.
[20] F.A. Cotton, B.A. Frenz, B.R. Stults, T.R. Webb, J. Am. Chem. Soc. 98 (1976) 2768.
[21] F.A. Cotton, J. Lu, T. Ten, Polyhedron 13 (1994) 807.
[22] F.A. Cotton, J. Lu, Y. Huang, Inorg. Chem. 35 (1996) 1839.
[23] A.R. Cutler, R.A. Walton, Inorg. Chim. Acta 105 (1985) 219.
[24] A.R. Cutler, S.M.V. Esjornson, P.E. Fanwick, R.A. Walton, Inorg. Chem. 27 (1988) 287.
[25] N.C. Dopke, P.M. Treichel, unpublished results.
[26] F.A. Cotton, L.M. Daniels, S.C. Haefner, F.E. Kuhn, Inorg. Chim. Acta 287 (1999) 159.
[27] F.A. Cotton, R. Poli, J. Am. Chem. Soc. 110 (1988) 830.
[28] K.J. Moynihan, P.M. Boorman, J.M. Ball, V.D. Patel, K.A. Kerr, Acta Crystallogr., Sect. B 38 (1982) 2258.

PERGAMON

www.elsevier.nl/locate/poly

Polyhedron 19 (2000) 1255–1262

POLYHEDRON

Spectral and structural studies of metal complexes of isatin 3-hexamethyleneiminylthiosemicarbazone prepared electrochemically

Elena Labisbal [a], Antonio Sousa [a], Alfonso Castiñeiras [a], Jose A. García-Vázquez [a], Jaime Romero [a], Douglas X. West [b,*]

[a] *Departamento de Quimica Inorganica, Universidad de Santiago de Compostela, E-15706 Santiago de Compostela, Spain*
[b] *Department of Chemistry, Illinois State University, Normal, IL 61790-4160, USA*

Received 27 September 1999; accepted 14 March 2000

Abstract

Cobalt(II), nickel(II), copper(II), zinc(II), cadmium(II) and lead(II) complexes of isatin 3-hexamethyleneiminylthiosemicarbazone, $[M(Ishexim)_2]$, as well as a thallium(I) complex, [Tl(Ishexim)], have been prepared by electrochemical synthesis. The crystal structures of $[Zn(Ishexim)_2]$ and $[Pb(Ishexim)_2]$ have been solved, and the metal complexes have been characterized by their ^1H and ^{13}C NMR, IR, UV–Vis and mass spectra. Coordination of the Ishexim anions is via the imine nitrogen and thiolato sulfur atoms with evidence for weak interaction of the amide oxygen with the isatin portion of the ligand. ©2000 Elsevier Science Ltd All rights reserved.

Keywords: Thiosemicarbazone; Isatin; Crystal structures; Zinc; Lead; Hexamethyleneimine; Metal(II) complexes

1. Introduction

The 3-thiosemicarbazones of isatin have been of interest since 1-methylisatin-3-thiosemicarbazone was found to be active in the treatment of smallpox [1–3] some forty years ago. It has been suggested that thiosemicarbazone drugs may act to inhibit virus growth by binding to copper ions which are constituents of the virus [4]. Therefore, a study of metal complexes for a wide range of thiosemicarbazones has been pursued in numerous studies [5]. Although substitution at N4-position of the thiosemicarbazone moiety (Fig. 1) was found to reduce anti-smallpox activity of isatin thiosemicarbazones [6], two butyl groups attached at the N4-position provides a compound with demonstrated activity against ectromelia (a vaccina virus unaffected by Marboran™) and also against type 2 polio, which is an enterovirus and quite unrelated to the vaccina family [7].

Metal complexes of N4-2-pyridyl- [6], N4-phenyl- [8], N4-ethyl- [9] and N4-dimethylthiosemicarbazones derived from isatin [10] have been studied. More recently, a study of the spectroscopic properties of the copper(II) complexes of eight N4-substituted thiosemicarbazones of isatin was communicated [11]. In this latter communication the crystal structure of the isatin 3-hexamethyleneiminylthiosemicarbazone, HIshexim, was reported, but none of the copper(II) complexes produced crystals of a quality sufficient for structural studies. In this study we report a structural and spectroscopic study of metal complexes of HIshexim prepared by electrochemical oxidation of the various metals.

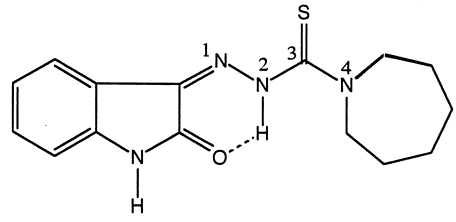


Fig. 1. Representation of HIshexim and numbering for the thiosemicarbazone moiety.

2. Experimental

HIshexim was prepared by reaction of equimolar amounts of 3-hexamethyleneiminylthiosemicarbazide, synthesized following the procedure developed by Holmberg and Psilanderhielm [12] and modified by Scovill [13], with isatin (Aldrich, 98%) at room temperature in absolute ethanol with a catalytic amount of conc. H_2SO_4. The product precipitated as a yellow powder in less than 1 h, and was collected by suction filtration and washed with cold absolute ethanol

* Corresponding author. Tel.: +1-309-438-7019; fax: +1-309-438-5538; e-mail: dxwest@ilstu.edu

0277-5387/00/$ - see front matter ©2000 Elsevier Science Ltd All rights reserved.
PII S0277-5387(00)00383-1

(yield, 76%). Complexes were prepared by electrochemical oxidation of the metals in a solution of HIshexim (0.056 g, 0.19 mmol) in CH_3CN (40 ml) containing 10 mg of tetramethylammonium perchlorate for 1 h at 5 mA and a potential of 10–20 V. A loss of 5.5 mg (Co), 5.5 mg (Ni), 6.1 mg (Zn), 10.5 mg (Cd), 11.8 mg (Cu), 38.1 mg (Tl) and 19.3 mg (Pb) from the anode resulted during the preparation of the complexes. The yields for the complexes and their percentage yield based on metal consumed were as follows: [Co(Ishexim)$_2$], 37 mg, 60%; [Ni(Ishexim)$_2$], 48 mg, 77%; [Cu(Ishexim)$_2$], 17 mg, 28%; [Zn(Ishexim)$_2$], 45 mg, 72%; [Cd(Ishexim)$_2$], 58 mg, 87%; [Tl(Ishexim)], 48 mg, 78%; [Pb(Ishexim)$_2$], 43 mg, 57%. During the reaction the solutions turned from yellow to the color of the various solids, which formed on slow evaporation of the solvent. The initial product, an amorphous dark brown solid, of the electrochemical oxidation of copper analyzes as [Cu(Ishexim)]. Found: C, 49.2; H, 4.7; N, 15.5. Calc.: C, 49.4; H, 4.7; N, 15.4%. This was not characterized further, but crystals formed on slow evaporation of the MeCN solvent analyze as [Cu(Ishexim)$_2$], Table 7.

Elemental analyses were performed with a Carlo Erba 1108 microanalyser. The magnetic susceptibilities were measured with a Digital Measurements system MSB-MKI calibrated with tetrakis(isothiocyanato)cobaltate(II) ion. ^{1}H and ^{13}C NMR spectra were recorded in deuterated $(CD_3)_2SO$ with a Brucker WM-300 spectrometer. Infrared spectra were recorded from 4000–400 cm^{-1} with a Mattson Instruments Cygnus 100 FTIR spectrometer using KBr pellets. UV–Vis spectra were recorded as Nujol mulls adhered to filter paper with a Cary 5E spectrophotometer. Electrospray mass spectral data were obtained with 5×10^{-4} M solutions (MeOH) by flow injection into a Hewlett-Packard 1100 series MSD. The carrier solvent was 50% MeOH in H_2O. Electrospray ionization conditions were as follows: nitrogen drying gas flow, 10.0 l min^{-1}; nebulizer pressure, 40 psig; drying gas temperature, 350°C; capillary voltage, 4 kV. The capillary exit voltage was varied from 0 to 150 V. The ESR spectrum of [Cu(Ishexim)$_2$] was acquired in 3 mm Pyrex tubes with a Brucker EMX spectrometer using a conventional insert Dewar at liquid nitrogen temperature.

Orange prismatic crystals of [Zn(Ishexim)$_2$] and [Pb(Ishexim)$_2$] were mounted on glass fibers and used for data collection on an Enraf-Nonius CAD4 automatic diffractometer. Cell constants and an orientation matrix for data collection were obtained by least-squares refinement of the diffraction data from 25 reflections in the range $21.25<\theta<45.11°$ for [Zn(Ishexim)$_2$] and $22.945<\theta<45.420°$ for [Pb(Ishexim)$_2$]. Data were collected using the ω-scan technique and corrected for Lorentz and polarization effects [14]. A semi-empirical absorption correction, Ψ-scan, was made for both crystals [15]. The structure was solved by direct methods [16] and subsequent difference Fourier maps, and refined on F^2 by a full-matrix least-squares procedure using anisotropic displacement factors [17]. All hydrogen atoms for [Zn(Ishexim)$_2$] were located from difference Fourier maps and refined isotropically and those for [Pb(Ishexim)$_2$] were located in their calculated positions (C–H 0.93–0.97 Å) and refined using a riding model. Atom scattering factors were taken from Ref. [18] and molecular graphics are from ZORTEP [19].

3. Results and discussion

3.1. Structural studies

The crystal data for [Zn(Ishexim)$_2$] and [Pb(Ishexim)$_2$] are shown in Table 1; Table 2 has selected bond distances and Table 3 selected bond angles. Perspective views of [Zn(Ishexim)$_2$] and [Pb(Ishexim)$_2$] are shown in Figs. 2 and 3, respectively. Both compounds are thermochromic; the change for [Pb(Ishexim)$_2$] is an irreversible change from orange to red at ca. 240°C and [Zn(Ishexim)$_2$] is reversible from yellow–orange to deep orange at ca. 100°C.

In [Zn(Ishexim)$_2$] the two Ishexim ligands are coordinated by the imine nitrogen and thiolato sulfur atoms of the thiosemicarbazonato moiety. Additional coordination is by the amide oxygen of the isatin moiety, O11, of one of the ligands, which has a longer bond distance, 2.452(3) Å, than the Zn–S bond distances. However, the oxygen, O21, of the second ligand is at a greater distance from the zinc center, 2.532(3) Å, and is not formally coordinated (i.e. this distance is longer than 1.3 times the sum of the covalent radii, $1.3\times\{1.20(Zn)+0.73(O)\}=2.509$ Å, and is not considered a bond by our X-ray program) as shown in Fig. 2. The geometrical parameter τ, i.e. $\tau=(\beta-\alpha)/60$, where α and β are N12–Zn–N23 and S1–Zn–O11 bond angles, respectively, has a value of 0.2. This suggests that [Zn(Ishexim)$_2$] has a square pyramidal geometry with a 20% distortion towards a trigonal bipyramid. The axial position can be considered to be occupied by S2 with O11, N12, S2 and N22 making up the basal plane. The angles involving S2 range from 122.20(10)° for S2–Zn–N12 to 81.77(9)° for S2–Zn–N22, the latter affected by the rigidity of the thiosemicarbazone moiety.

Intermolecular hydrogen bonding by the NH of the isatin moiety for each ligand (i.e. N11H and N21H in the two ligands) to the oxygens of the isatin moiety on two different molecules, O11A and O21B, yields a molecular chain. As would be expected, the hydrogen bonding distances and angles for N11H···O11A and N21H···O21B are quite similar (Table 4). The rms plane deviations for the two isatin moieties in [Zn(Ishexim)$_2$] are minimal (Table 5) and are at an angle of 101.3(5)° to each other. The thiosemicarbazone moieties, S1–C19–N14–N13–N13–C12 and S2–C29–N24–N23–N22–C22, have greater deviations; their rms plane deviations are 0.0304 and 0.0491 Å, and the two planes are at an angle of 79.65(20)°. The planar portion, N12–S2–N22, of the approximately trigonal bipyramidal arrangement of the donor atoms has a rms plane deviation of 0.0000 and the Zn atom is 0.3642(20) Å from this plane.

Table 1
Crystal data and structure refinement for metal complexes of isatin 3-hexamethyleneiminylthiosemicarbazone

Empirical formula	$C_{30}H_{34}N_8O_2S_2Zn$	$C_{30}H_{34}N_8O_2S_2Pb$
Color, habit	orange, prism	orange, prism
Formula weight	668.14	809.96
Temperature (K)	293(2)	293(2)
Crystal system	monoclinic	triclinic
Space group	$P2_1/c$ (no. 14)	$P\bar{1}$ (no. 2)
a (Å)	10.9343(16)	10.4123(8)
b (Å)	14.2567(11)	11.8842(14)
c (Å)	20.334(3)	12.7422(12)
α (°)	90(0)	89.892(9)
β (°)	92.887(11)	78.783(8)
γ (°)	90(0)	81.928(6)
Volume (Å^3)	3165.8(7)	1580.8(3)
Z	4	2
Density (Mg m^{-3})	1.402	1.757
Absorption coefficient (mm^{-1})	2.646	12.340
Crystal size (mm)	0.40×0.10×0.10	0.40×0.35×0.25
Diffractometer	Nonius CAD4	Nonius CAD4
Radiation (λ, Å)	Cu Kα (1.54184)	Cu Kα (1.54184)
θ Range for data collection (°)	3.79–76.00	3.54–75.92
Index ranges	$0 \le h \le 13,\ -17 \le k \le 0,\ -25 \le l \le 25$	$-13 \le h \le 0,\ -14 \le k \le 14,\ -16 \le l \le 15$
Reflections collected	6964	6727
Independent reflections	6615 (R_{int} = 0.0387)	6363 (R_{int} = 0.0504)
Absorption correction	semi-empirical	Ψ-scan
Max./min. transmission	0.978/0.928	0.986/0.738
Refinement method, F^2	full-matrix least-squares	full-matrix least-squares
Data/parameters	6165/525	6363/461
Goodness-of-fit on F^2	0.999	1.057
Final R indices ($I > 2\sigma(I)$)	R_1 = 0.0490, wR_2 = 0.1035	R_1 = 0.0442, wR_2 = 0.0767
R indices (all data)	R_1 = 0.1389, wR_2 = 0.1321	R_1 = 0.1768, wR_2 = 0.1000
Largest difference peak/hole (e Å^{-3})	0.361 and −0.347	0.338 and −0.506

Table 2
Selected bond distances (Å) for [Zn(Ishexim)$_2$] and [Pb(Ishexim)$_2$] [a]

	[Zn(Ishexim)$_2$]	[Pb(Ishexim)$_2$]
M–N12	2.074(3)	2.602(4)
M–N22	2.078(3)	2.654(4)
M–S1	2.3631(14)	2.6854(14)
M–S2	2.3618(14)	2.7273(14)
M–O11	2.452(3)	2.829(4)
M–O21	2.532(3)	2.834(4)
S1–C19	1.720(4)	1.727(5)
S2–C29	1.703(4)	1.726(5)
N12–C12	1.308(4)	1.308(6)
N22–C22	1.305(3)	1.300(6)
N12–N13	1.335(4)	1.338(6)
N22–N23	1.338(4)	1.346(5)
N13–C19	1.357(4)	1.360(6)
N23–C29	1.371(5)	1.354(7)
N14–C19	1.343(4)	1.340(6)
N24–C29	1.347(5)	1.343(7)
O11–C11	1.229(4)	1.231(6)
O21–C21	1.226(4)	1.211(7)

[a] Although M–O distances are shown, only O11 is coordinated in [Zn(Ishexim)$_2$] and neither oxygen in [Pb(Ishexim)$_2$].

For [Pb(Ishexim)$_2$] the two oxygens are at a greater distance from the Pb(II) center than either the nitrogen or sulfur donor atoms, suggesting that the oxygens are weakly interacting with the lead center as is indicated in Fig. 3. For [Pb(Ishexim)$_2$], τ = 0.04, suggesting a square pyramidal geometry with only a 4% distortion towards a trigonal bipyramid and the lone pair on the lead atom in the apical position. The geometry of the complex shows that the lone pair on the lead is stereochemically active, and the enormous deviation from the trigonal bipyramidal geometry can be explained as the result of the electrostatic repulsion of this electron pair. The N_2S_2 basal plane has S1–Pb–S2 and N12–Pb–N22 angles of 89.78(5) and 132.65(12)° and there is a deviation by as much as 0.5 Å from the plane of the four donor atoms. Another four coordinate lead-thiosemicarbazone complex [20], [Pb(Ac4M)OAc] (Ac4M = anion of 2-acetylpyridine N(4)-methylthiosemicarbazone), has Pb–N12 and Pb–S1 distances of 2.482(7) and 2.730(3) Å compared to averages of 2.628(4) and 2.7064(14) Å for [Pb(Ishexim)$_2$]. [Pb(Ac4M)OAc] is regarded as derived from a trigonal bipyramid with S1 occupying an axial position and N12 an equatorial position, which helps to account for the differences in bond distances. The N12–Pb–S1 chelate angle in [Pb(Ac4M)OAc] is 69.1(2)°, which is larger than 67.52(9) and 66.35(9)° found for N12–Pb–S1 and N22–Pb–S2 in [Pb(Ishexim)$_2$] consistent with the S1 of the former compound being in an axial position.

The metal–ligand bonds of [Pb(Ishexim)$_2$] are about 0.3 Å longer than the analogous bonds of [Zn(Ishexim)$_2$], as

Table 3
Selected bond angles (°) for [Zn(Ishexim)$_2$] and [Pb(Ishexim)$_2$] [a]

	[Zn(Ishexim)$_2$]	[Pb(Ishexim)$_2$]
N12–M–N22	145.35(12)	132.65(12)
N12–M–S2	122.20(10)	84.57(9)
N12–M–S1	81.63(9)	67.52(9)
N12–M–O11	75.38(11)	63.50(12)
N12–M–O21	77.62(10)	141.75(13)
N22–M–S2	81.77(9)	66.35(9)
N22–M–S1	120.31(9)	75.52(9)
N22–M–O11	79.27(11)	127.99(12)
N22–M–O21	74.44(10)	62.81(12)
S2–M–S1	102.01(6)	89.78(5)
S2–M–O11	92.45(8)	67.79(9)
S2–M–O21	155.69(7)	127.47(8)
S1–M–O11	156.87(7)	127.28(9)
S1–M–O21	94.35(8)	89.85(11)
O11–M–O21	78.44(10)	141.97(14)
C19–S1–M	95.23(14)	103.50(17)
C29–S2–M	95.05(14)	102.93(17)
C11–O11–M	103.5(3)	108.7(3)
C21–O21–M	101.7(2)	110.7(3)
C12–N12–M	118.6(2)	117.8(3)
C22–N22–M	119.1(2)	119.4(3
N13–N12–M	123.1(2)	124.4(3)
N23–N22–M	122.2(2)	124.4(3)
C12–N12–N13	118.2(3)	116.1(4)
N12–N13–C19	113.4(3)	113.7(4)
N13–C19–N14	114.3(3)	114.5(4)
N13–C19–S1	126.0(3)	126.8(4)
N14–C19–S1	119.6(3)	118.7(4)
C22–N22–N23	118.5(3)	116.2(4)
N22–N23–C29	113.3(3)	114.0(4)
N23–C29–N24	113.5(4)	114.2(5)
N23–C29–S2	126.1(3)	126.4(4)
N24–C29–S2	120.4(3)	119.4(4)
O11–C11–N11	127.5(4)	125.8(5)
O11–C11–C12	126.5(4)	127.4(5)
O21–C21–N21	126.6(4)	126.4(5)
O21–C21–C22	127.2(4)	128.4(5)

[a] Although angles for the oxygens with the metals are shown, only O11 is coordinated in [Zn(Ishexim)$_2$] and neither oxygen in [Pb(Ishexim)$_2$].

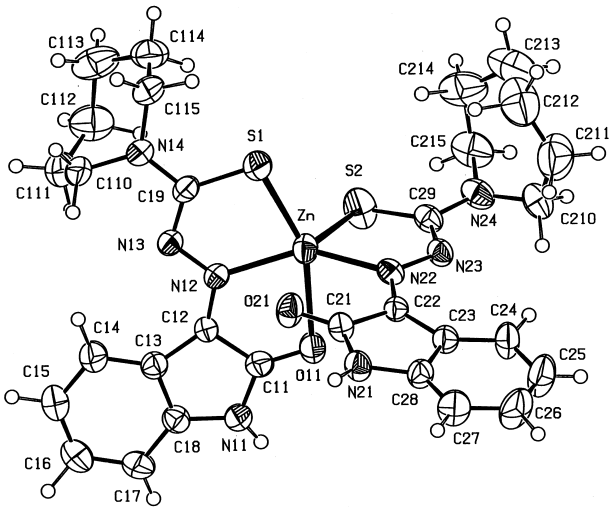


Fig. 2. Ortep diagram of [Zn(Ishexim)$_2$] at 50% probability.

would be expected based on the larger ionic radius of Pb, and the bond distances to nitrogen and to sulfur are not very different for [Pb(Ishexim)$_2$]. Differences in the bonding to the metal center between the two ligands of a complex are much greater for [Pb(Ishexim)$_2$] than for [Zn(Ishexim)$_2$]; the Pb–N and Pb–S bond distances differ by about 0.05 and 0.04 Å, respectively, but Zn–N and Zn–S by only 0.004 and 0.001 Å, respectively.

Intermolecular hydrogen bonding by the NH of the isatin moiety occurs for each ligand (i.e. N11H and N21H in the two ligands). N11H is bifurcated between an oxygen of the isatin moiety on another molecule, O11C, and a thiolato sulfur of the thiosemicarbazone of the second ligand in the same molecule, S2C. N21H hydrogen bonds to hydrazinic nitrogen of another molecule, N13D. The hydrogen bonding interactions are weaker for [Pb(Ishexim)$_2$] than for [Zn(Ishexim)$_2$], Table 4. The rms plane deviations for the two isatin moieties in [Pb(Ishexim)$_2$] are greater than for [Zn(Ishexim)$_2$], but the amide oxygen is included in the former, but not the latter (Table 5). The angle between the two isatin planes is 89.45(11)° for [Pb(Ishexim)$_2$] compared to 101.3(5)° for [Zn(Ishexim)$_2$]. The thiosemicarbazone moieties, S1–C19–N14–N13–N13–C12 and S2–C29–N24–N23–N22–C22, have rms plane deviations of 0.0292 and 0.0678 Å, and the two planes are at an angle of 116.68(52)°.

Table 6 shows a comparison of the bond distances and angles of HIshexim [11] with the average of the two ligands in [Zn(Ishexim)$_2$] and [Pb(Ishexim)$_2$]. Since formation of the monoanionic ligands causes C19–S1 to convert from a formal double bond to a single bond, changes in its bond distance would be expected to be greatest among the various ligand bonds. The change from 1.672(4) Å for HIshexim to 1.711(4) and 1.726(6) Å for [Zn(Ishexim)$_2$] and [Pb(Ishexim)$_2$], respectively, is not, however, to the bond distance usually associated with a C–S single bond. For example, [Pd(6MAchexim)Cl] and [Pt(6MAchexim)Cl], where 6MAchexim is the monoanion of 6-methyl-2-acetylpyridine 3-hexamethyleneiminylthiosemicarbazone, have C–S bond distances of 1.769(4) and 1.782(10) Å [21]. However, in both [Zn(Ishexim)$_2$] and [Pb(Ishexim)$_2$] there is not a significant change in the imine bond, C12–N12, even though N12 is coordinated in both complexes. Even the

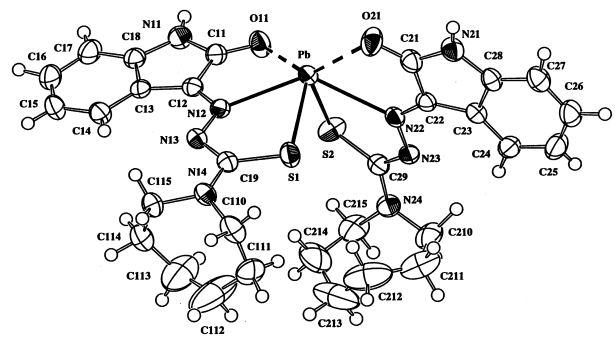


Fig. 3. Ortep diagram of [Pb(Ishexim)$_2$] at 50% probability.

Table 4
Hydrogen bonding (Å, °) for [Zn(Ishexim)$_2$] and [Pb(Ishexim)$_2$]

Compound	Donor	Acceptor [a]	D–H	H···A	D···A	∠D–H···A
[Zn(Ishexim)$_2$]	N11	O11A	0.81(4)	2.11(4)	2.887(5)	163(4)
	N21	O21B	0.85(4)	2.05(4)	2.887(4)	166(4)
[Pb(Ishexim)$_2$]	N11	O11C	0.86	2.44	2.968(6)	120.5
	N11	S2C	0.86	2.96	3.758(5)	155.8
	N21	N13D	0.71(9)	2.79(9)	3.329(7)	150(9)

[a] Symmetry transformation used to generate equivalent atoms: A, $-x+1$, $-y$, $-z$; B, $-x+2$, $-y$, $-z$; C, $-x+1$, $-y+1$, $-z+1$; D, $-x+1$, $-y+1$, $-z+2$.

Table 5
Root mean squared plane deviations (Å) and angles (°) between planes

[Zn(Ishexim)$_2$] [a]			[Pb(Ishexim)$_2$] [b]		
Plane	Rms deviation	∠ with previous plane	Plane	Rms deviation	∠ with previous plane
A	0.0077		F	0.0292	
B	0.0304	7.32(0.16)	G	0.0287	4.51(0.24)
C	0.0000	77.27(0.06)	H	0.0172	89.45(0.11)
D	0.0491	2.48(0.14)	I	0.0678	22.72(0.17)
E	0.0054	14.25(0.17)			

[a] Plane A C11–C12–C13–C14–C15–C16–C17–C18–N11; plane B S1–C19–N14–N13–N12–C12; plane C N12–S2–N22; plane D S2–C29–N24–N23–N22–C22; plane E C21–C22–C23–C24–C25–C26–C27–C28–N21.
[b] Plane F S1–C19–N14–N13–N12–C12; plane G O11–C11–N11–C12–C13–C14–C15–C16–C17–C18; plane H O21–C21–N21–C32–C33–C34–C35–C36–C37–C38; plane I S2–C29–N24–N23–N22–C22.

Table 6
A comparison of HIshexim bond distances (Å) and angles (°) with the average of the two ligands in [Zn(Ishexim)$_2$] and [Pb(Ishexim)$_2$]

	HIshexim	[Zn(Ishexim)$_2$]	[Pb(Ishexim)$_2$]
C12–N12	1.305(5)	1.306(4)	1.304(6)
N12–N13	1.362(6)	1.337(4)	1.342(6)
N13–C19	1.375(4)	1.364(5)	1.357(7)
C13–S1	1.672(4)	1.711(4)	1.726(6)
C19–N14	1.339(6)	1.345(5)	1.342(7)
C11–O11	1.236(7)	1.228(4)	1.221(7)
C12–N12–N13	115.4(4)	118.4(3)	116.2(4)
N12–N13–C19	119.8(4)	113.4(3)	113.8(4)
N13–C19–N14	114.6(4)	113.9(4)	114.4(5)
N13–C19–S1	121.5(4)	126.0(3)	126.6(4)
N14–C19–S1	123.9(3)	120.0(3)	119.0(4)
N11–C11–O11	127.7(4)	127.0(4)	126.1(5)
C12–C11–O11	126.3(4)	126.8(4)	127.9(5)

weakly interacting amide oxygens cause a greater change in C11–O11 in the complexes. However, the N12–N13–C19 bond angle is much smaller at about 113.6° for the complexes compared to 119.8(4)° for HIshexim, and C12–N12–N13 is also different in the complexes. Both N–C–S bonds undergo significant changes in the complexes, but C12–C11–O11 is not changed by more than three times the combination of the estimated standard deviations of the angles.

3.2. Spectral studies

The colors, partial elemental analyses and magnetic susceptibilities of the seven complexes formed electrochemically from HIshexm are listed in Table 7. All but [Tl(Ishexim)] have two ligands per metal center and the yellow and orange colors are in part due to the original color of the ligand, the formation of a conjugated thiosemicarbazone moiety on loss of N3H and L → M charge transfer bands.

The assignments for N11*H* and N13*H* in the ^{1}H NMR spectrum of HIshexim were previously reported as 11.258 and 13.504 ppm [11]. Assignments for the resonances that undergo change in the diamagnetic metal complexes formed from HIshexim are listed in Table 8. Loss of the N13H hydrogen on coordination results in the absence of a resonance above 13 ppm in the spectra of the metal complexes and N1*H* ranges from 10.673 ppm in [Tl(Ishexim)] to 11.018 ppm in [Cd(Ishexim)$_2$]. The difference between the ^{1}H NMR spectrum of HIshexim and its metal complexes involves the protons of the hexamethyleneiminyl ring. Listed in Table 7 are the hydrogens attached to the α-carbon atoms of the ring, which are different owing to restricted rotation about the C–N bond connecting the ring to the thioamide carbon. This bond distance is more consistent with a double bond than a single bond. In HIshexim the distance of this bond is 1.339(6) Å [11], and its distance in [Zn(Ishexim)$_2$] and [Pb(Ishexim)$_2$] averages 1.345(5) and 1.342(7) Å, respectively. In the complexes these resonances are downfield from their position in the spectrum of HIshexim. There are differences in the complexes between the hydrogens attached to the two β-carbons and γ-carbons, which is probably due to the different environment for the two ligands in a complex.

In the ^{13}C spectrum of isatin [22] the amide carbon, C11, is assigned at 159.4 ppm and the ketonic carbon, C12, at

Table 7
Colors, partial elemental analyses and magnetic susceptibilities of the metal complexes of HIshexim

Compound	Color	Found (calc.)			μ_{eff} (BM)
		C (%)	H (%)	N (%)	
[Co(Ishexim)$_2$]	brown	54.4 (54.4)	4.9 (5.1)	16.8 (16.9)	4.1
[Ni(Ishexim)$_2$]	dark brown	54.5 (54.5)	5.0 (5.1)	17.0 (16.9)	3.4
[Cu(Ishexim)$_2$]	dark brown	54.1 (54.1)	5.2 (5.1)	17.2 (16.8)	1.9
[Zn(Ishexim)$_2$]	yellow–orange	54.5 (53.9)	5.0 (5.1)	17.0 (16.8)	0
[Cd(Ishexim)$_2$]	yellow–orange	49.8 (50.3)	4.6 (4.7)	15.4 (15.6)	0
[Tl(Ishexim)]	orange	35.3 (35.6)	3.3 (3.3)	11.0 (11.0)	0
[Pb(Ishexim)$_2$]	orange	44.0 (44.4)	4.2 (4.2)	13.7 (13.8)	0

Table 8
^{1}H and ^{13}C NMR spectral assignments (ppm) for HIshexim and its metal complexes

Compound	N1*H*	C*H*$_2$ [a]	C*H*$_2$ [b]	*C*=S	*C*=N	*C*=O
HIshexim	11.258	4.073	3.814	178.5	134.8	162.9
[Zn(Ishexim)$_2$]	10.864	4.081	4.023	184.3	131.1	166.7
[Cd(Ishexim)$_2$]	11.018	4.129	4.090	184.2	130.4	167.4
[Tl(Ishexim)]	10.673	4.136	4.084	189.6	135.2	168.7
[Pb(Ishexim)$_2$]	10.856	4.118	3.917	185.6	129.4	168.1

[a] Furthest downfield signal for the hydrogens attached to an α-C of the hexamethyliminyl ring.
[b] Upfield signal for the hydrogens attached to an α-C of the hexamethyliminyl ring.

Table 9
Infrared and electronic spectra (cm^{-1}) for HIshexim and its metal complexes

Compound	ν(CO)	ν(CN)	ν(CS)	Intraligand	CT, d→d
Hishexim	1690s	1584m	868m	39970, 35780, 27820	
[Co(Ishexim)$_2$]	1665s	1569w	750m	38600, 34590	23340, 16810, 8300
[Ni(Ishexim)$_2$]	1665s	1567m	748m	37370, 34290	24830, 21710, 20520, 17520, 14540, 10910
[Cu(Ishexim)$_2$]	1700s	1543s	753m	38360, 34590, 27700	25020, 22310, 16640
[Zn(Ishexim)$_2$]	1682m	1570m	747m	39070, 37280, 33990	27280, 22320
[Cd(Ishexim)$_2$]	1667s	1565m	747m	38950, 37100, 34170	26680, 22310
[Tl(Ishexim)]	1680m	1540m	743m	[a]	
[Pb(Ishexim)$_2$]	1671m	1548m	745m	41770, 38950, 34980	25310, 20940

[a] Not recorded.

184.4 ppm. In the the eight isatin N(4)-substituted thiosemicarbazones [11], the ketonic (now azomethine) carbon signal is at significantly higher field (i.e. 131.5–134.8 ppm), the exact position being dependent on the nature of the substituent of the thiosemicarbazone moiety. Its resonance in the spectrum of HIshexim is 134.8 ppm and C11 is at 162.9 ppm and C19 at 178.5 ppm, Table 8. In the spectra of the complexes the thioamide and amide carbons, C19 and C11, respectively, are found downfield from their position in the spectrum of HIshexim, suggesting coordination by the thiolato sulfur and amide oxygen. In the spectra of the complexes the imine carbon, C12, is found upfield indicating coordination of the imine nitrogen. The lone exception is [Tl(Ishexim)] which shows C12 essentially unshifted, but has a significantly larger shift of C19 and a larger shift of C11. Like the ^{1}H NMR spectra the complexes have more peaks for the carbons of the hexamethyleneiminyl ring than does HIshexim.

The IR bands, Table 9, assigned to ν(CO), ν(CN) and ν(CS) generally undergo shifts from their positions in the spectrum of HIshexim to lower energy on coordination to the metal ions. These shifts indicate coordination of the amide oxygen, imine nitrogen and thiolato sulfur atoms for most of the complexes. In the spectrum of [Cu(Ishexim)$_2$], ν(CO) is found at higher energy than in the spectrum of HIshexim, suggesting that the oxygen is not strongly coordinated in this complex. The shifts in these bands for [Tl(Ishexim)], which are generally comparable to those of the remaining complexes with divalent metal ions, suggest that the thiolato sulfur atom may be bridging to adjacent Tl centers rather than the amide oxygen.

The UV–Vis spectra of HIshexim and the complexes are included in Table 9. The highest energy $\pi \rightarrow \pi^*$ band is at lower energy in the spectrum of [Zn(Ishexim)$_2$] and higher energy for [Pb(Ishexim)$_2$] compared to HIshexim. The $\pi \rightarrow \pi^*$ band at 35780 cm^{-1} in the spectrum of HIshexim is

Table 10
Positive ion mass spectral data for the metal complexes of HIshexim

Compound	Positive ion mass fragments (m/z values and relative intensities)
[Co(Ishexim)$_2$]	M+1 (662, 12 and 661, 31), M−301 (361, 6.5 and 360, 31, Ishexim [a])
[Ni(Ishexim)$_2$]	M−301 (360, 47, Ishexim)
[Cu(Ishexim)$_2$]	M+1 (667, 100), M−301 (364, 16, Ishexim), M−364 (303, 14, Ishexim, Cu)
[Zn(Ishexim)$_2$]	M+1 (667, 47), M−16 (651, 38, O), M−32 (635, 18, S), M−301 (366, 22, 365, 100, Ishexim), M−366 (301, 24, Ishexim, Zn)
[Cd(Ishexim)$_2$]	M−301 (413, 1.5, Ishexim)
[Tl(Ishexim)]	M+1 (507, 7), M−16 (491, 14, O), M−301 (205, 6, Ishexim)
[Pb(Ishexim)$_2$]	M+1 (811, 66), M−301 (509, 21, Ishexim), M−507 (303, 27, Ishexim, Pb)

[a] Species suggested to be lost.

at higher energy in the spectra of the complexes, suggesting it likely arises from one of the functional groups that is coordinating rather than the aromatic ring. In the spectrum of HIshexim the band at 27820 cm^{-1} is very broad and likely involves n→π* transitions for the C=O, C=N and C=S functions. The two lowest energy bands in the spectra of the complexes are assigned to L→M charge transfer transitions with the lowest energy band probably associated with the thiolato sulfur donor.

The positive ion mass spectra of the complexes, Table 10, show a cluster of ions with significant intensity centered at *m/z* for their molecular ions, $(M+1)^+$, with the exception of [Ni(Ishexim)$_2$] and [Cd(Ishexim)$_2$]. The other significant cluster of peaks in their spectra occurs at $(M-302)^+$, due to loss of an Ishexim ligand. The loss of this ligand appears to be a one-step process because there is little indication of its partial decompostion (i.e. ions between M−1 and M−302) except for [Zn(Ishexim)$_2$] which shows $(M-16)^+$ and $(M-32)^+$ fragments due to loss of oxygen and either sulfur or oxygens from both ligands. [Tl(Ishexim)] also shows a $(M-16)^+$ fragment. [Cu(Ishexim)$_2$], [Zn(Ishexim)$_2$] and [Pb(Ishexim)$_2$] all show a signficant peak at *m/z* 301, suggesting loss of the metal as well as one of the Ishexim ligands.

[Cd(Ishexim)$_2$], based on its various spectral properties, is expected to have a similar stereochemistry to that of [Zn(Ishexim)$_2$]. [Tl(Ishexim)] is probably four coordinate with the thiolato sulfur serving as the bridging donor atom based on its large downfield shift of *C*(S) in its ^{13}C NMR spectrum and the large decrease in energy of ν(CS) on coordination. The IR spectrum of [Cu(Ishexim)$_2$] shows that ν(CO) is shifted to higher energy compared to HIshexim, suggesting that the amide oxygens of the two ligands are not coordinated. Consistent with CuN_2S_2 coordination is the d→d composite band at 16640 cm^{-1} [23], and its EPR parameters of $g_\parallel = 2.190$, $g_\perp = 2.059$, $g_{av} = 2.103$ and $A_\parallel = 162$ G for the solid at liquid nitrogen temperature. The *g*-values are considerably higher than those of a CuN_2S_2 center such as [Cu(Buhexim)] (Buhexim = dianion of 2,3-butanedione bis{3-hexamethyleniminylthiosemicarbazone}), which has $g_\parallel = 2.104$, $g_\perp = 2.030$, $g_{av} = 2.055$. Therefore, the parameters for [Cu(Ishexim)$_2$] suggest that the carbonyl oxygens interact more strongly with the copper center at the lower temperature. Copper(II) complexes with N_2S_2 coordination generally have $g_\parallel = 2.145$ [24]. The resolution of the $g_\parallel$ feature is presumably due to the bulkiness of the ligand; at room temperature we are unable to assign $g_\parallel$.

For [Co(Ishexim)$_2$] assignment of the bands at 8300 and 16810 cm^{-1} to $^4T_{1g}(F) \rightarrow {}^4T_{2g}$ and $^4T_{1g}(F) \rightarrow {}^4T_{1g}(P)$, respectively, allows calculation [25] of $^4T_{1g}(F) \rightarrow {}^4A_{2g}$ as 17600 cm^{-1}, $B = 633$ cm^{-1}, $\beta = 0.65$ and $D_q = 930$ cm^{-1}, which are reasonable parameters for approximately octahedral $CoO_2N_2S_2$ coordination. In contrast, assignment of 10910 cm^{-1} to $^3A_{2g} \rightarrow {}^3T_{2g}$ and either 14540 or 17520 cm^{-1} as $^3A_{2g} \rightarrow {}^3T_{1g}(F)$ for [Ni(Ishexim)$_2$] does not give reasonable values for *B*, β and D_q for an octahedral $NiO_2N_2S_2$ center. This suggests, based on $\nu(CO) = 1665$ cm^{-1}, indicating oxygen coordination, and $\mu = 3.4$ BM, that [Ni(Ishexim)$_2$] is six coordinate and more tetragonally distorted than [Co(Ishexim)$_2$] [26,27].

Supplementary data

Crystallographic data for $C_{30}H_{34}N_8O_2S_2Zn$, [Zn(Isheixm)$_2$], CCDC 134850, and $C_{30}H_{34}N_8O_2S_2Pb$, [Pb(Isheixm)$_2$], CCDC 134851 have been deposited with the Cambridge Crystallographic Data Centre as supplementary publication no. CCDC-1003/m. Copies of available material can be obtained, free of charge, on application to CCDC, 12 Union Road, Cambridge CB2 1EZ, UK (fax: +44-1223-336033; e-mail: deposit@ccdc.cam.ac.uk).

Acknowledgements

EL thanks the Universidad de Santiago de Compostela for financial support to carry out research at Illinois State University.

References

[1] R.L. Thompson, S.A. Milton, J.E. Officer, G.H. Hitchings, J. Immunol. 70 (1953) 229.

[2] D.J. Bauer, Br. J. Exp. Path. 36 (1956) 105.
[3] D.J. Bauer, P.W. Sadler, Br. J. Pharmacol. 15 (1960) 101.
[4] C.L. Hoagland, S.M. Ward, L.E. Smadel, T.M. Rivers, J. Exptl. Med. 74 (1941) 69.
[5] D.X. West, S.B. Padhye, P.B. Sonawane, Structure Bonding 76 (1991) 1.
[6] G.M. Abu El Reash, M.A. Khattab, U.I. El-Ayaan, Synth. React. Inorg. Met.-Org. Chem. 22 (1992) 1417.
[7] P.W. Sadler, Ann. NY Acad. Sci. 130 (1965) 71.
[8] K.M. Ibrahim, A.A. El-Asmy, M.M. Bekheit, M.M. Mostafa, Synth. React. Inorg. Met.-Org. Chem. 15 (1985) 1247.
[9] K.M. Ibrahim, Synth. React. Inorg. Met.-Org. Chem. 23 (1993) 1351.
[10] R.N. Pathak, L.K. Mishra, J. Indian Chem. Soc. 65 (1988) 119.
[11] G.A. Bain, D.X. West, J. Krejci, J. Valdés-Martínez, S. Hernández-Ortega, R.A. Toscano, Polyhedron 16 (1997) 855.
[12] B. Holmberg, B. Psilanderhielm, J. Prakt. Chem. 82 (1910) 440.
[13] J.P. Scovill, Phosphorus Sulfur Silicon 60 (1991) 15.
[14] H. Kretschmar, GENHKL, program for the reduction of CAD4 diffractometer data, University of Tübingen, Germany, 1997.
[15] A.C.T. North, D.C. Phillips, F.S. Mathews, Acta Crystallogr., Sect. A 24 (1968) 351.
[16] G.M. Sheldrick, Acta Crystallogr., Sect. A 46 (1990) 467.
[17] G.M. Sheldrick, SHELX-97, program for the refinement of crystal structures, University of Göttingen, Germany, 1997.
[18] International Tables for X-ray Crystallography, vol. C, Kluwer, Dordrecht, 1995.
[19] L. Zsolnai, a program for the presentation of thermal elipsoids, University of Heidelberg, Germany, 1997.
[20] A. Castiñeiras, R. Domínguez, L. Bresolin, A.J. Bortoluzzi, R.A. Burrow, M. Hörner, Z. Naturforsch., Teil B 53 (1998) 81.
[21] K.I. Goldberg, J. Valdes-Martínez, G. Espinosa-Pérez, S. Hernández-Ortega, L.J. Ackerman, D.X. West, Polyhedron 18 (1999) 1177.
[22] M.S. Morales-Rios, P. Joseph-Nathan, Magn. Res. Chem. 29 (1991) 893.
[23] L. Casella, M. Gullotti, R. Vigano, Inorg. Chim. Acta 124 (1986) 121.
[24] D.X. West, J.S. Ives, G.A. Bain, A.E. Liberta, J. Valdés-Martínez, K.H. Ebert, S. Hernández-Ortega, Polyhedron 16 (1997) 855.
[25] A.B.P. Lever, J. Chem. Educ. 45 (1968) 711.
[26] M. Biddau, M. Massacesi, R. Pinna, G. Ponticelli, Transition Met. Chem. 3 (1978) 153.
[27] H.K. Soni, J.R. Shah, Synth. React. Inorg. Met-Org. Chem. 15 (1985) 1157 and Refs. cited therein.

PERGAMON

www.elsevier.nl/locate/poly

Polyhedron 19 (2000) 1263–1270

POLYHEDRON

Synthesis, spectral and electrochemical properties of 1-alkyl-2-(naphthyl-β-azo)imidazole complexes of platinum(II) and the reaction with pyridine bases. Single-crystal X-ray structure of dichloro-[1-ethyl-2-(naphthyl-β-azo)imidazole]platinum(II)

Sanjib Pal [a], Debasis Das [a], Pabitra Chattopadhyay [a], Chittaranjan Sinha [a,*], Kaliyamoorthy Panneerselvam [b], Tian-Huey Lu [b]

[a] *Department of Chemistry, The University of Burdwan, Burdwan 713104, India*

[b] *Department of Physics, National Tsing Hua University, Hsinchu 300, Taiwan, Republic of China*

Received 6 January 2000; accepted 27 March 2000

Abstract

1-Alkyl-2-(naphthyl-β-azo)imidazoles (β-NaiX, X = Me (**3a**), Et (**3b**), and CH_2Ph (**3c**)) have been synthesized and reacted with K_2PtCl_4 in boiling MeCN–water (1:1, v/v) and Pt(β-NaiX)Cl_2 (**4**) are isolated as orange–brown products. IR spectra support *cis*-$PtCl_2$ configuration and the structural configuration has been carried out by the X-ray diffraction study of Pt(β-NaiEt)Cl_2 (**4b**). The treatment of aqueous silver nitrate solution, followed by the addition of pyridine bases (Rpy) and $NaClO_4$ to an acetonitrile solution of Pt(β-NaiX)Cl_2 under boiling conditions has yielded [Pt(β-NaiX)$(Rpy)_2$]$(ClO_4)_2$ (**5–7**). The structure has been established by spectroscopic data (IR, UV–Vis, ^{1}H NMR). The redox properties of the complexes exhibit azo reductions. ©2000 Elsevier Science Ltd All rights reserved.

Keywords: Naphthylazoimidazoles; Platinum(II); PtN_4 coordination; Electrochemistry; X-ray structures

1. Introduction

The chemistry of the arylazoimidazoles (**1**) of palladium(II) was developed recently by our group [1–5]. The ligand is isoelectronic with α-diimine and the active function is the azoimine group (–N=N–C=N–), abbreviated as *N,N′* (N(imine) refers to *N* and N(azo) refers to *N′*). They form Pd(*N,N′*)Cl_2 complexes [1]. The reactivity of the Pd–Cl group is exhibited by the synthesis of mixed ligand complexes of dioxolene [2,3], dithiocarbamato and xanthate complexes [4]. Reactions of pyridine bases (Rpy) substitute the chelating ligand followed by isomerization to synthesize *trans*-Pd$(Rpy)_2Cl_2$ [5]. The parallel development for platinum(II) has remained unexplored and has prompted us to undertake the present work.

Platinum(II) chemistry of azoles, pyridines and bipyridines is of recent interest for their medicinal [6–8] and photochemical [9] activity. Research into platinum(II) compounds is mostly dedicated to synthesize new compound analogues of cisplatin [10–17]. The rich chemistry of azoimidazoles and the importance of platinum(II) chemistry have attracted our attention. In this work we use new ligands 2-(naphthyl-β-azo)imidazole (**2**) and 1-alkyl-2-(naphthyl-β-azo)imidazole (β-NaiX, **3**). Platinum(II) complexes, Pt(β-NaiX)Cl_2 (**4**), have been synthesized and characterized by spectroscopic techniques and, in one case, structural confirmation has been carried out by X-ray diffraction study. The reaction of Pt(β-NaiX)Cl_2 with pyridine bases (Rpy) has also been studied and the products [Pt(β-NaiX)-$(Rpy)_2$]$(ClO_4)_2$ are characterized by spectroscopic and cyclic voltammetric data.

2. Experimental

2.1. Materials

Imidazole (Loba-chemie Indo-Austranal Co., India), β-naphthylamine, pyridine (py), benzyl chloride ($PhCH_2Cl$), acetonitrile (Merck), 4-methylpyridine (4-Mepy), 4-(*N,N*-dimethyl)pyridine (4-NMe_2py) (Lancaster, UK) and

* Corresponding author. Tel.: +91-342-57683; fax: +91-342-64452; e-mail: bdnuvlib@giasclol.vsnl.net.in

0277-5387/00/$ - see front matter ©2000 Elsevier Science Ltd All rights reserved.
PII S0277-5387(00)00385-5

$H_2PtCl_6 \cdot xH_2O$ (Arrora Matthey, India) were reagent grade. K_2PtCl_4 was prepared by a published procedure [18]. All other solvents were used as previously described. CH_3I and EtI were prepared before use by a literature procedure [19].

2.2. Instrumentation

Instrumentation is described in Ref. [20].

2.3. Synthesis of ligands

2-(Naphthyl-β-azo)imidazole was prepared following the procedure as described for 2-(arylazo)imidazoles [1]. The details are given as follows: to an aqueous solution of imidazole (3.0 g, 0.044 mol) and Na_2CO_3 (7.0 g, 0.066 mol) at 0–5°C was added, dropwise with continuous stirring, a diazotized solution of β-naphthylammine (6.5 g, 0.045 mmol) (prepared by adding a $NaNO_2$ (3.2 g) solution into a 1 M HCl (50 cm^3) suspension of β-naphthylamine at 0–5°C and filtering). The temperature was controlled at ice cold conditions. The orange compound thus precipitated was filtered, washed with cold water and extracted with 2N HCl (15 $cm^3 \times 4$). The solution was neutralized with Na_2CO_3 and the pH regulated to 7. The precipitate was filtered, washed and dried. Yield: 8.4 g (86%).

2.4. Alkylation of 2-(naphthyl-β-azo)imidazole: synthesis of 1-methyl-2-(naphthyl-β-azo)imidazole (β-NaiMe)

To a dry THF solution (30 cm^3) of 2-(naphthyl-β-azo)imidazole (β-NaiH) (2.0 g, 9.05 mmol) NaH (50% paraffin) (0.8 g) was added in small portions and stirred at cold conditions for 1 h. Methyl iodide (1.3 g, 9.15 mmol) was added slowly for a period of 1 h and then refluxed over a steam bath for an additional 3 h. The solution was filtered, evaporated, extracted with $CHCl_3$ solution (3×15 cm^3), washed with 10% NaOH solution and finally with distilled water (3×20 cm^3). It was chromatographed over silica gel prepared in benzene and the desired compound was eluted by acetonitrile–benzene (1:11, v/v). Orange crystalline needles were separated on slow evaporation. Yield: 0.94 g (44%).

Other ligands were prepared by an identical procedure using ethyl iodide and benzyl chloride. Yields: 30–45%. Melting points of the compounds: β-NaiMe (**3a**), 176 ± 2°C; β-NaiEt (**3b**), 122 ± 1°C; β-NaiCH_2Ph (**3c**), 140 ± 2°C.

2.5. Preparation of dichloro[1-methyl-2-(naphthyl-β-azo)imidazole]platinum(II) (*4a*)

To a MeCN–water (1:1, v/v; 40 cm^3) solution of K_2PtCl_4 (0.85 g, 2.05 mmol) 1-methyl-2-(naphthyl-β-azo)imidazole (β-NaiMe) (0.4 g, 1.7 mmol) in the same solvent (5 cm^3) was added dropwise and the mixture was refluxed for 24 h. The brown precipitate which gradually appeared on slow evaporation of the solvent in air was recovered by filtration and washed with cold MeCN–water (1:1, v/v). The dried mass, dissolved in minimum CH_2Cl_2, was chromatographed over a silica gel column. The pure product was eluted as an orange–brown band by C_6H_6–MeCN (3:1, v/v) and evaporated in air. Yield: 0.62 g (73%).

Other complexes were prepared under identical conditions and the yield varied in the range 65–75%.

2.5.1. Preparation of bis(pyridine)[1-methyl-2-(naphthyl-β-azo)imidazole]platinum(II) perchlorate

Route A: A suspension of Pt(β-NaiMe)Cl_2 (0.2 g, 0.4 mmol) in 50 cm^3 MeCN and pyridine (0.065 g, 0.082 mmol) was refluxed continuously for 72 h. The solution colour changed from orange–brown to greenish–brown. The solution was filtered and the filtrate evaporated to half of its original volume. A saturated $NaClO_4$ solution (5 ml) was added into it and the precipitated brown mass filtered and dried. The product, dissolved in minimum CH_2Cl_2, was chromatographed over a silica gel column by a light green band (small amount). The solution was evaporated in air and the product was collected. Yield: 10%.

Route B: To a MeCN solution (20 cm^3) of Pt(β-NaiMe)Cl_2 (0.2 g, 0.4 mmol) was added an aqueous solution (5 cm^3) of $AgNO_3$ (0.06 g, 0.86 mmol); this was refluxed for 2 h and the precipitated AgCl filtered off through a G-4 crucible. To this filtrate an acetonitrile solution of pyridine (0.065 g, 0.82 mmol) was added dropwise, then refluxed over a steam bath for a further 4 h and slowly evaporated in air to half of its original volume. An aqueous saturated solution of $NaClO_4$ was added to this solution at cold conditions and the brown precipitate filtered, and washed with cold MeCN–water (1:1, v/v). The product was purified as before. Yield of the brown product: 56%.

Other products were prepared similarly with varying yields in the range 50–65%.

2.5.2. X-ray crystal structure and analysis

A crystal suitable for the X-ray diffraction study of dichloro[1-ethyl-2-(naphthyl-β-azo)imidazole]platinum(II) (Pt(β-NaiEt)Cl_2, **4b**) was grown by diffusion of hexane into CH_2Cl_2 solution at room temperature. The crystal size was $0.32 \times 0.29 \times 0.20$ mm^3. X-ray diffraction data (Table 1) were collected at 293(2) K with the Siemens SMART CCD using graphite-monochromatized Mo Kα radiation ($\lambda =$ 0.71073 Å). Unit cell parameters were determined from least-squares refinement of setting angles of 3254 reflections with 2θ in the range 10–31°. A summary of the crystallographic data and structure refinement parameters is given in Table 1. Of 8213 collected reflections 3652 unique reflections were recorded using the ω-scan technique. Data were corrected for Lorentz polarization effects and for linear decay. Semi-empirical absorption corrections based on ψ-scans were applied [21]. The structure was solved by heavy atom methods using SHELXS-97 [22] and successive difference Fourier syntheses. All non-hydrogen atoms were refined anisotropically. The hydrogen atoms were fixed geometrically and refined

Table 1
Summarized crystallographic data for Pt(β-NaiEt)Cl_2 (**4b**)

Crystal parameters	
Empirical formula	$C_{15}H_{14}Cl_2N_4Pt$
M	516.29
Crystal system	triclinic
Space group	$P\bar{1}$
a (Å)	7.3121(5)
b (Å)	10.0821(6)
c (Å)	12.3961(8)
α (°)	68.332(1)
β (°)	84.453(1)
γ (°)	74.383(1)
V (Å^3)	817.93(9)
λ (Å)	0.71073
ρ_{calcd} (Mg m^{-3})	2.096
Z	2
T (K)	293(2)
μ(Mo Kα) (mm^{-1})	8.904
Refined parameters	200
R [a] ($I>2\sigma(I)$)	0.0281
wR [b]	0.0547
GOF [c]	0.976

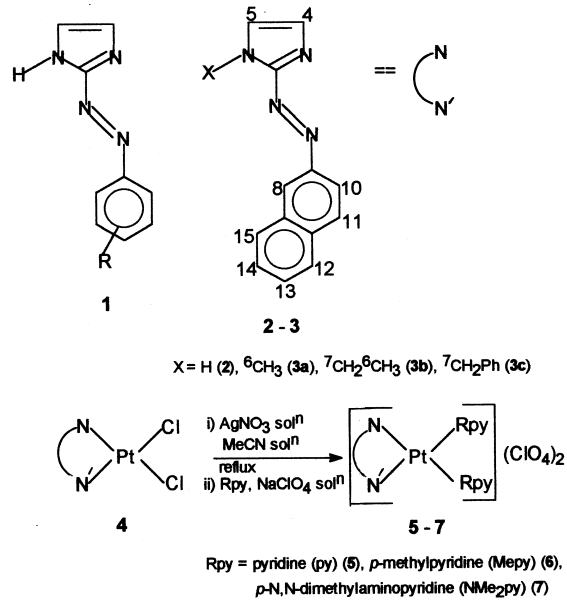
[a] $R=\Sigma|F_o-F_c|/\Sigma F_o$.
[b] $wR=[\Sigma w(F_o^2-F_c^2)/\Sigma wF_o^4]^{1/2}$; $w=1/[\sigma^2(F_o^2)+(0.0473P)^2+14.3394P]$, $P=(F_o^2+2F_c^2)/3$.
[c] GOF (goodness of fit) is defined as $[w(F_o-F_c)/(n_o-n_v)]^{1/2}$, where n_o and n_v denote the numbers of data and variables, respectively.

using the riding model. In the final difference Fourier map the residual maxima and minima were 0.831 and −0.794 e Å^{-3}. All calculations were carried out using SHELXL-97 [23].

3. Results and discussion

3.1. Synthesis

2-(Naphthyl-β-azo)imidazole (β-NaiH, **2**) is synthesized by coupling the β-naphthyldiazonium ion with imidazole at pH 7. 1-Alkyl-2-(naphthyl-β-azo)imidazoles (β-NaiX) are synthesized by the alkylation of β-NaiH with alkyl halide (MeI, EtI, $PhCH_2Cl$) in dry THF in the presence of NaH. The complexes are abbreviated as β-NaiX where X = Me (**3a**), Et (**3b**), and CH_2Ph (**3c**). The active function is the azoimine group, –N=N–C=N–, and is designated as an *N*,*N*′-chelator (N(imidazole) refers to *N* and N(azo) refers to *N*′). They react with K_2PtCl_4 under reflux in MeCN–water (1:1, v/v) for 24 h and the products Pt(*N*,*N*′)Cl_2 (**4**) have been purified by chromatography. The complexes are characterized by elemental analyses and IR, UV–Vis, ^{1}H NMR data. The structure has been confirmed by the X-ray structure of Pt(β-NaiEt)Cl_2 (**4b**).



3.2. Structural studies

A view of the molecule Pt(β-NaiEt)Cl_2 (**4b**) is shown in Fig. 1 and selected bond lengths and bond angles are listed in Table 2. The entire molecule is essentially planar with the exception of the ethyl group. The atomic arrangement Pt, N(1), N(3), Cl(1), Cl(2) forms a good square plane (deviation ~0.0004 Å). The chelate plane consisting of Pt, N(3), C(1), N(2), N(1) is planar (deviation with maximum of 0.003 Å) and the chelate bite angle N(1)–Pt(1)–N(3) is 77.4(2)°. Other angles around Pt are supported by square planar geometry (Table 2). The Pt–N(1) (N(1) refers to N(azo)) and Pt–N(3) (N(3) refers to N(imidazole)) dis-

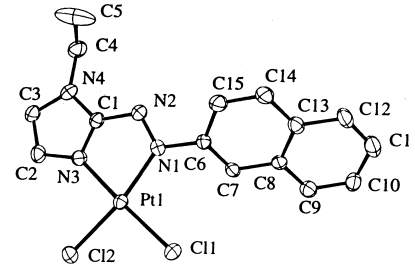


Fig. 1. Single-crystal X-ray structure of Pt(β-NaiEt)Cl_2 showing atom numbering scheme. For clarity, all hydrogen atoms have been omitted.

Table 2
Selected bond distances (Å) and angles (°) for Pt(β-NaiEt)Cl_2 along with their estimated standard deviations

Distances (Å)		Angles (°)	
Pt(1)–N(1)	2.039(4)	N(1)–Pt(1)–N(3)	77.4(2)
Pt(1)–N(3)	1.983(4)	Cl(1)–Pt(1)–Cl(2)	89.7(1)
Pt(1)–Cl(1)	2.290(1)	N(1)–Pt(1)–Cl(2)	170.3(1)
Pt(1)–Cl(2)	2.278(1)	N(1)–Pt(1)–Cl(1)	100.0(1)
N(1)–N(2)	1.280(5)	N(3)–Pt(1)–Cl(1)	177.4(1)
		N(3)–Pt(1)–Cl(2)	92.9(1)

tances are 2.039(4) and 1.983(4) Å respectively. The shortening of Pt–N(imidazole) accounts for the greater affinity of platinum to imidazole-N [24] than that of azo-N. Dichloro{2-(phenylazo)pyridine}platinum(II) also shows a longer Pt–N(py) (2.010 Å) bond than Pt–N(azo) (1.988 Å) [26]. Thus, imidazole-N has a special fascination to Pt(II) compared with other platinum metals and pyridine-N. This is the reverse of our earlier results for ruthenium(II) complexes [25]. The N(1)–N(2) distance is 1.280(5) Å and is comparable with the previously reported azo distances in metal-azo compounds [25,27]. Pt–Cl distances are supported by data from other platinum(II) complexes [28]. The naphthyl ring does not lie in a plane to the chelate ring; it makes an angle 43.88° with the metallated azoimine motif and suggests a stereochemically non-equivalent C–H function [25].

3.3. Spectral studies

The alkylation is supported by the elimination of a broad band at ca. 3400 cm^{-1} in β-NaiH. The ν(N=N) and endocyclic ν(C=N) appear at 1420 and 1580 cm^{-1}, respectively. In Pt(β-NaiX)Cl_2 (**4**), ν(N=N) is shifted to 1380–1390 cm^{-1} and is corroborated with N(azo) coordination [1]. The presence of two Pt–Cl stretches at 335–340 and 290–305 cm^{-1} is in agreement with the *cis*-$PtCl_2$ configuration [29].

The solution electronic spectra of β-NaiX (**3**) in CH_2Cl_2 exhibit intense absorptions at 390, 375 and 260 nm. In the complexes, the bands below 400 nm are discarded due to intraligand charge transitions. Multiple transitions are observed at around 608, 548, 475 and 415 nm (Table 3), which are different from aryl analogues [30]. The presence of a naphthyl ring may provide a large number of accessible energy states for transition in the metallated azo fragment [31].

The structures of the ligands and complexes are supported by ^{1}H NMR data. The signals are assigned on the basis of spin–spin interaction, and comparative integration between aliphatic and aromatic regions. β-NaiH exhibits a broad concentration-dependent resonance at 10.4 ppm corresponding to the N–H proton, which is eliminated on shaking with D_2O. Alkylated derivatives (β-NaiX) do not exhibit this resonance, which supports 1-alkylation. β-NaiMe (**3a**) shows δ(Me) at 4.07 ppm; β-NaiEt (**3b**) gives a triplet at 1.50 for $–CH_3$ and a quartet for $–CH_2–$ at 4.47 ppm; β-NaiCH_2Ph (**3c**) exhibits a sharp singlet at 5.73 ppm corresponding to methylene ($–CH_2–$) protons (Table 4). This is in agreement with our earlier observation [25]. The aromatic region shows a broad singlet at the most downfield position and is assigned to 8-H, and the downfield shifting is due to the closest position of the azo function [1]. The broadening may be due to the spin–spin interaction of 8- and 15-H. The next higher field doublet refers to 10-H. Other naphthyl protons (11- 15-H) appear as multiplets in the upfield position. Imidazole 4- and 5-H appear as separate doublets at 6.9–7.2 and 6.8–7.0 ppm, respectively.

In complexes Pt(β-NaiR)Cl_2 (**1**), imidazoles 4- and 5-H suffer maximum downfield shifting ($\Delta\delta$ = 0.2–0.4 ppm). This supports the platinaphilicity of the imidazole unit. This is corroborated by the shorter Pt–N(imidazole) (1.983 Å) compared to Ru–N(imidazole) (2.04 Å) bond length [25]. Metal ion coordination affects naphthyl protons in different ways. The characteristic features are 8- and 15-H shifts in the downward direction relative to the free ligand position of which 8-H suffers serious downfield movement ($\Delta\delta \cong 0.5$ ppm for 8-H and 0.05 ppm for 15-H). Other naphthyl protons move haphazardly and the spectral data are collected in Table 4. The marked difference in the signals of 8- and 10-H is due to their stereochemical orientation. The 8-H is assigned as stereochemically nearer to the metal centre than 10-H (*vide supra*) and may be the reason for downfield shifting. Another important difference of the spectra from the free ligand is the appearance of coupling with ^{195}Pt ($I = 1/2$, abundance 33.7%) for 4-H and 8-H. The coupling constant $^3J_{(Pt–H)}$ is 25–28 Hz for 4-H and 15–18 Hz for 8-H (Fig. 2).

3.4. Reaction with pyridines

The reaction of pyridine bases (Rpy) with the suspension of Pt(β-NaiX)Cl_2 in MeCN (route A) for a prolonged period (72 h) under reflux followed by the addition of saturated $NaClO_4$ solution has synthesized [Pt(β-NaiX)$(Rpy)_2$]$(ClO_4)_2$ in low yield (<10%). The reaction in $AgNO_3$(aq) solution (route B) followed by the addition of Rpy to Pt(β-NaiX)Cl_2 and $NaClO_4$ has yielded the same product [Pt(β-NaiX)$(Rpy)_2$]$(ClO_4)_2$ in high yield (<55%) within 6 h only. Both reactions have yielded very small amounts of unidentified green product. The conductance measurement (Λ_M = 160–180 Ω^{-1} cm^2 M^{-1}) suggests a 1:2 electrolytic nature of the complex in MeCN. Microanalytical data support the composition of the complex (Table 2). The reaction of Rpy with palladium(II) analogues under identical conditions ended with the release of chelating ligand and formation of *trans*-Pd$(Rpy)_2Cl_2$ [5].

Infrared spectra (KBr disc) exhibit a broad medium-intense band centred at 3445 cm^{-1} which is absent in the parent complex and refers to $\nu(H_2O)$ [32]. The complexes show three structured consecutive transmissions at 1120–1080 and two transmissions at 640–625. They correspond to $\nu(ClO_4)$ and support the significant coordination of ClO_4^- in the solid state [33]. The ν(N=N) appears at 1420–1425 cm^{-1} and is higher than that of the parent chloro complex. This shows a weaker azo coordination to platinum(II) in [Pt(β-Naix)$(Rpy)_2$]$(ClO_4)_2$ (**5**) than parent complexes (**4**).

The solution electronic spectra of these complexes differ markedly from Pt(β-NaiR)Cl_2 (**4**) (Table 2). Four transitions in the visible region of the parent complex are shifted to the longer wavelength region. The main transitions are observed at 800–810, 710–740, 440–480 nm along with a weak shoulder at 520–540 nm. The transitions below 400 nm are not considered. Thus, nucleophilic association decreases

Table 3
Microanalytical, UV–Vis and redox data

Compounds	Elemental analyses [a] (%)			UV–Vis spectral data [b]	Ligand reduction [c]
	C	H	N	λ_{max} (nm (10^3 ε, $dm^3\,mol^{-1}\,cm^{-1}$))	E° (V (ΔE_p [d], mV))
β-NaiMe (**3a**)	71.20 (71.19)	5.07 (5.08)	23.68 (23.73)	263(1.2), 376(2.2), 391(2.2)	−1.084(90), −1.335(140)
β-NaiEt (**3b**)	72.02 (72.00)	5.56 (5.60)	22.38 (22.40)	264(1.1), 378(2.2), 391(2.2)	−1.099(73), −1.314(160)
β-NaiCH_2Ph (**3c**)	76.88 (76.92)	5.10 (5.13)	14.99 (14.95)	269(1.2), 377(2.0), 392(1.9)	−1.08(80), −1.358(150)
Pt(β-NaiMe)Cl_2 (**4a**)	33.39 (33.46)	2.41 (2.39)	11.20 (11.15)	608(1.1), 549(1.8)[s], 475(1.8), 413(2.4)	−0.585(90), −0.873(125)
Pt(β-NaiEt)Cl_2 (**4b**)	31.17 (31.14)	2.30 (2.42)	9.73 (9.69)	609(0.8), 544(1.4), 472(1.7), 413(2.6)	−0.549(85), −0.805(110)
Pt(β-NaiCH_2Ph)Cl_2 (**4c**)	46.40 (46.50)	2.98 (3.10)	10.7 (10.85)	608(0.9), 547(1.5)[s], 478(1.3), 416(1.8)	−0.493(85), −0.734(130)
[Pt(β-NaiMe)$(py)_2$]$(ClO_4)_2\cdot H_2O$ (**5a**)	36.6 (36.54)	2.80 (2.79)	10.59 (10.66)	807(0.5), 725(0.3), 455(2.1)	0.017(64), −0.685(81), −1.12 [e]
[Pt(β-NaiEt)$(py)_2$]$(ClO_4)_2\cdot H_2O$ (**5b**)	37.5 (37.4)	3.0 (2.99)	10.48 (10.47)	805(0.5), 721(0.3), 456(3.2)	0.025(70), −0.574(73), −1.04 [e]
[Pt(β-NaiCH_2Ph)$(py)_2$]$(ClO_4)_2\cdot H_2O$ (**5c**)	41.70 (41.66)	2.62 (2.77)	9.88 (9.72)	808(0.6), 729(0.6), 440(2.3)	0.035(90), −0.518(78), −1.05 [e]
[Pt(β-NaiMe)(4-Mepy)$_2$]$(ClO_4)_2\cdot H_2O$ (**6a**)	38.4 (38.23)	3.10 (3.18)	10.25 (10.20)	807(0.5), 740(0.5), 480(1.8)	−0.008(70), −0.711(85), −1.26 [e]
[Pt(β-NaiEt)(4-Mepy)$_2$]$(ClO_4)_2\cdot H_2O$ (**6b**)	40.0 (39.03)	3.40 (3.37)	10.08 (10.12)	805(0.5), 731(0.7), 471(1.8)	0.004(82), −0.678(90), −1.20 [c,e]
[Pt(β-NaiCH_2Ph)(4-Mepy)$_2$]$(ClO_4)_2\cdot H_2O$ (**6c**)	43.50 (43.04)	3.40 (3.36)	9.35 (9.41)	805(0.5), 716(0.5), 477(2.1)	0.013(80), −0.639(75), −1.19 [e]
[Pt(β-NaiMe)(4-NMe_2py)$_2$]$(ClO_4)_2\cdot H_2O$ (**7a**)	38.60 (38.44)	3.40 (3.66)	12.75 (12.81)	810(0.4), 728(0.7), 480(2.6)	−0.118(70), −0.835(90), −1.33 [e]
[Pt(β-NaiEt)(4-NMe_2py)$_2$]$(ClO_4)_2\cdot H_2O$ (**7b**)	39.4 (39.18)	3.90 (3.83)	12.58 (12.61)	805(0.8), 723(0.8), 475(1.4)	−0.044(80), −0.764(95), −1.35 [e]
[Pt(β-NaiCH_2Ph)(4-NMe_2py)$_2$]$(ClO_4)_2\cdot H_2O$ (**7c**)	43.0 (42.94)	3.65 (3.58)	12.0 (11.79)	800(0.8), 713(0.8), 471(1.0)	−0.023(75), −0.7481(80), −1.30

[a] Calculated values are in parentheses.
[b] Solvent: MeCN.
[c] Solvent: CH_3CN, glassy carbon milli working electrode, SCE reference, $[NBu_4]\{ClO_4\}$ supporting electrolyte, 50 mV s^{-1} scan rate, potentials are in V vs. SCE.
[d] $\Delta E_p = 0.5(E_{pc} + E_{pa})$ where E_{pc} and E_{pa} are cathodic and anodic peak potentials.
[e] E_{pc}.

Table 4
^{1}H NMR spectral data [a]

Compound	δ (ppm (*J*, Hz))												
	4-H [b]	5-H [b]	8-H	10-H [d]	11-H [d]	12-H [d]	13,14-H [d]	15-H	16,16a-H	17,17a-H	6-CH_3	7-CH_2	R
β-NaiH (**2**)	7.55 [c]	7.55 [c]	8.75 [c]	8.22 [b] (8.0)	8.00	7.75	7.75	8.10 [d]					
3a	7.04 (7.4)	6.85 (7.4)	8.18 [c]	8.04	7.84 [d]	7.58	7.58	7.70 [d]			4.07 [e]		
3b	7.17 (7.0)	7.00 (7.0)	8.24 [c]	7.92	7.80	7.60	7.60	7.68 [d]			1.53 [g] (8.0)	4.47 [f] (10.0)	
3c	7.24 (7.0)	7.04 (7.0)	8.12 [c]	7.99	7.88	7.54	7.54	7.67 [d]				5.73 [h]	
4a	7.11 [j] (8.0)	7.21 (8.0)	8.68 [c,k]	7.92	7.87	7.67	7.67	7.78 [b] (8.0)			4.08 [e]		
4b	7.42 [j] (8.0)	7.29 (8.0)	8.69 [c,k]	7.89	7.86	7.62	7.62	7.73 [b] (9.0)			1.66 [g] (8.0)	4.54 [f] (12.0)	
4c	7.47 [j] (8.0)	(8.0)	7.20	8.63 [c,k]	7.93	7.82	7.68	7.68 (9.0)	7.77 [h]				5.56 [h]
5a	7.18 [j] (8.0)	6.96 (8.0)	8.21 [c,k]	7.88	7.82	7.59	7.59	7.70 [h] (8.0)	8.44 [b,l] (8.0)	8.00 [d]	4.35 [e]		
5b	7.22 [j] (7.0)	7.00 (7.0)	8.18 [c,k]	8.01	7.88	7.58	7.58	7.75 [b] (8.0)	8.40 [b,l] (8.0)	7.95 [d]	1.42 [g] (8.0)	4.40 [f] (11.0)	
5c	7.24 [j] (7.0)	7.03 (7.0)	8.24 [c,k]	7.96	7.89	7.67	7.67	7.80 [b] (8.0)	8.46 [b,l] (8.0)	8.01 [d]	5.60 [h]		
6a	7.16 [j] (8.0)	6.95 (8.0)	8.16 [c,k]	7.85	7.80	7.56	7.56	7.73 [b] (8.0)	8.31 [b,l] (8.0)	7.20 [b] (8.0)	4.27 [e]		2.11
6b	7.18 [j] (8.0)	6.98	8.10 [c,k]	7.82	7.77	7.54	7.54	7.58 [b] (8.0)	8.27 [b,l] (8.0)	7.14 [b] (8.0)	1.40 [g] (8.0)	4.31 [f] (10.0)	2.08
6c	7.20 [j] (7.0)	7.00	8.13 [c,k]	8.00	7.79	7.52	7.52	7.62 [b] (8.0)	8.29 [b,l] (8.0)	7.15 (8.0)		5.52 [h]	2.07
7a	7.02 [j] (7.0)	6.85 (7.0)	8.00 [c,k]	7.75 [d]	7.66	7.50	7.50	7.28 [b] (8.0)	7.98 [b,l] (8.0)	6.70 [b] (8.0)	4.15 [e]		2.17
7b	7.00 [j] (8.0)	6.81	7.93 [c,k]	7.71	7.62	7.44	7.44	7.22 [b] (8.0)	7.94 [b,l] (8.0)	6.64 [b] (8.0)	1.44 [g] (8.0)	4.53 [f] (10.0)	2.19
7c	7.03 [j] (8.0)	6.88	8.02 [c,k]	7.77	7.68	7.54	7.54	7.30 [b] (8.0)	8.00 [b,l] (8.0)	6.73 (8.0)		5.55 [h]	2.18

[a] In $CDCl_3$.
[b] Doublet.
[c] Broad.
[d] Multiplet.
[e] Singlet.
[f] N(1)–CH_2(quartet).
[g] (N(1)–CH_2) CH_3(triplet).
[h] –CH_2(Ph) singlet.
[i] Phenyl protons 7.30–7.50 ppm.
[j] $^{3}J_{Pt–H}$ = 25–28 Hz.
[k] $^{3}J_{Pt–H}$ = 15–18 Hz.
[l] $^{3}J_{Pt–H}$ = 20–24 Hz.

Monday Jun 19 11:57 AM

StyleTag -- Journal: **POLY** (*Polyhedron*) Article: **3456**

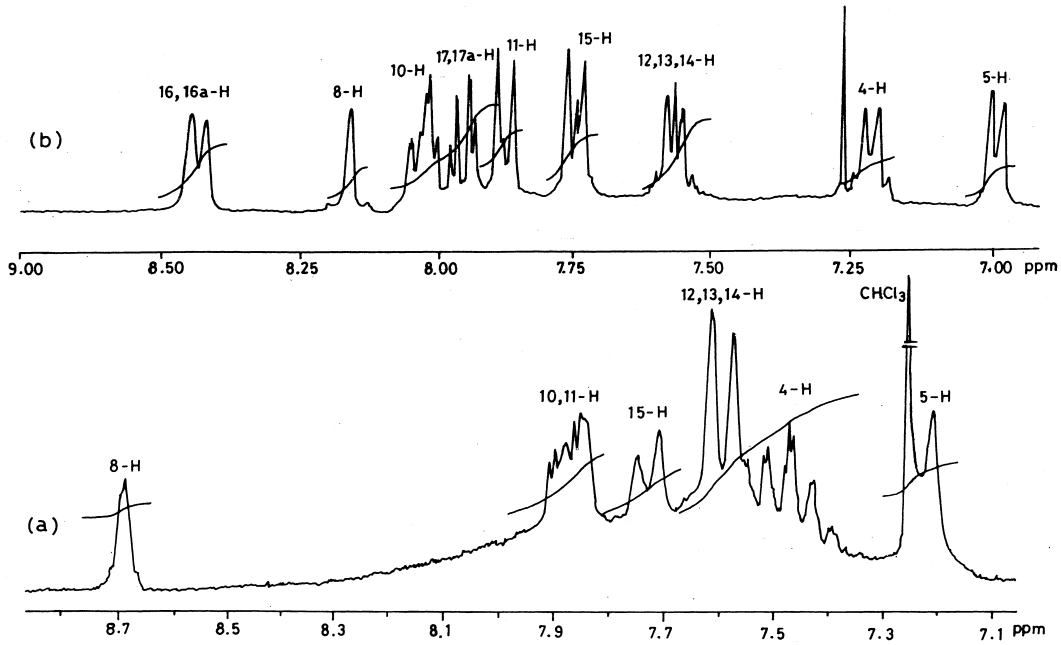


Fig. 2. ^{1}H NMR spectra of (a) Pt(β-NaiEt)Cl_2 (**4b**) and (b) [Pt(β-NaiEt)$(py)_2$]$(ClO_4)_2$ (**5b**) in $CDCl_3$ at 300 MHz.

the energy difference between the ground and excited states and may be the reason for longer wavelength transitions.

The structure and stereochemistry of [Pt(β-NaiX)$(Rpy)_2$]$(ClO_4)_2$ are established by ^{1}H NMR spectral data (Table 4) and on comparison with the spectra of the parent complexes. The distinguishable observation is the appearance of a doublet at the most downfield position, which significantly moves with the substituent in the pyridine ring. Thus, it is assigned to *ortho* H to pyridine-N (16,16a -H). The resonance corresponding to *meta*/*para* H to pyridine-N (17,17a -H) (18,18a -H) appears at the upfield side. This difference may be due to the coordination of Rpy to the platinum(II) centre. Upfield signals are assigned to the resonances of imidazole 4- and 5-H protons. Naphthyl protons appear as singlet (8-H), doublet (10-H) and others are multiplet. In general, naphthyl protons appear in the upfield position relative to the corresponding signals in the parent complex. Imidazole 4-H, naphthyl 8-H and *ortho* pyridine-H (16,16a -H) exhibit significant coupling with ^{195}Pt (Fig. 2) and support the coordination to platinum(II) [34].

3.5. Redox studies

Redox properties of the complexes were examined cyclic voltammetrically using a glassy carbon milli working electrode in MeCN in the presence of tetrabutylammonium perchlorate (n-NBu_4ClO_4) as supporting electrolyte. The potentials are expressed with reference to the saturated calomel electrode (SCE). Voltammetric data are set out in Table 3. The complexes exhibit two/three reductive responses negative to SCE. Pt(β-NaiX)Cl_2 show two consecutive reductions at less negative potentials than that of the free ligand (Table 3). The first reduction is more reversible than the second one, as evident from the peak-to-peak separation (ΔE_p). It is believed that the peaks correspond to the reduction of the organic ligand and the aof electrons are accommodated at the LUMO possibly characterized by the azoimine function. This conjecture is based on the report of our systematic studies on the ruthenium(II) and palladium(II) complexes [1–4,20,32] of the azoimine system. In pyridine derivatives, [Pt(β-NaiX)$(Rpy)_2]^{+2}$, the reduction potentials are shifted towards the more positive side. This is expected due to better stabilization of the LUMO in a PtN_4 environment where donor centres are sp^2-N. The first two couples are reversible to quasi-reversible, as expected ($\Delta E_p = 60$–90 mV), and the reduced species on further electron acceptance does not appear to be stable and, on scan reversal, no definite anodic response is observed. The last response may be localized on the pyridine derivative (Rpy) and is unstable.

4. Supplementary data

Supplementary data are available from the CCDC, 12 Union Road, Cambridge CB2 1EZ, UK; fax: +44-1223-336033; e-mail: deposit@ccdc.cam.ac.uk, on request. The deposition number is 137584.

Acknowledgements

Financial assistance from the Department of Science and Technology, New Delhi, is gratefully acknowledged. THL and KP thank the National Science Council, ROC, for support grants under NSC89-2112-M001-043 and NSC89-2811-M007-018.

References

[1] D. Das, M.K. Nayak, C. Sinha, Transition Met. Chem. 22 (1997) 172.
[2] D. Das, T.K. Misra, C. Sinha, Transition Met. Chem. 23 (1998) 233.
[3] D. Das, C. Sinha, Transition Met. Chem. 23 (1998) 517.
[4] D. Das, C. Sinha, Indian J. Chem. 37A (1998) 531.
[5] G. Rauth, C. Sinha, unpublished results.
[6] P. Banerjee, Coord. Chem. Rev. 19 (1999) 190.
[7] S.-W. Lai, M.C.-W. Chan, S.-M. Peng, C.-M. Che, Inorg. Chem. 38 (1999) 4046.
[8] B. Lippert, Coord. Chem. Rev. 18 (1999) 263.
[9] M.M. Muir, M.E. Cadiz, A. Baez, Inorg. Chim. Acta 151 (1988) 209.
[10] S.J. Brow, S.Ch. Chow, S.J. Lippard, in: R.B. King (Ed.), Encyclopedia of Inorganic Chemistry, Wiley, New York, 1994, pp. 3305–3315 and Refs. therein.
[11] S.J. Lippard, in: I. Bertini, H.B. Gray, S.J. Lippard, J.S. Valentine (Eds.), Bioinorganic Chemistry, University Science Books, Mill Valley, CA, 1994, p. 505.
[12] N. Farrell, Transition Metal Complexes as Drugs and Chemotherapeutic Agents, Kluwer, Dordrecht, The Netherlands, 1989.
[13] S.O. Ana, F.P. Intini, G. Natile, L.G. Marzilli, Inorg. Chem. 38 (1999) 2989.
[14] M. Mikola, K.D. Klika, A. Hakala, J. Arpalatti, Inorg. Chem. 38 (1999) 571.
[15] P.D. Beer, Acc. Chem. Res. 31 (1998) 71.
[16] Y.S. Yoo, Y.S. Sohn, Y.K. Do, J. Inorg. Biochem. 73 (1999) 187.
[17] A.H. Veldres, A.C.G. Hotze, J.G. Haasanoot, J. Reedijk, Inorg. Chem. 38 (1999) 2762.
[18] S.E. Livingstone, Synth. React. Inorg. Met.-Org. Chem. 1 (1971) 1.
[19] A.I. Vogel, A Text Book of Practical Organic Chemistry, 3rd ed., Longman, London, UK, 1959, p. 287.
[20] P.K. Santra, D. Das, T.K. Misra, C. Sinha, A.M.Z. Slawin, J.D. Woollins, Polyhedron 18 (1999) 1909.
[21] G.M. Sheldrick, SHELXL-Plus, Siemens, Analytical X-ray Instruments Inc., Madison, WI, 1990.
[22] G.M. Sheldrick, Acta Crystallogr., Sect. A 46 (1990) 467.
[23] G.M. Sheldrick, Program for Refinement of Crystal Structures, University of Göttingen, Germany, 1997.
[24] J. Arpalahti, P. Lehikoinen, Inorg. Chem. 29 (1990) 2564.
[25] T.K. Misra, D. Das, P. Ghosh, C.K. Pal, C. Sinha, Inorg. Chem. 37 (1998) 1672.
[26] G.K. Rauth, S. Pal, D. Das, C. Sinha, A.M.Z. Slawin, J.D. Woollins, Polyhedron, submitted.
[27] D. Das, Ph.D. Thesis, Burdwan University, India, 1988.
[28] S. Chattopadhyay, C. Sinha, P. Basu, A. Chakravorty, Organometallics 10 (1991) 1135.
[29] C.K. Pal, S. Chattopadhyay, C. Sinha, D. Bandyopadhyay, A. Chakravorty, Polyhedron 13 (1994) 999.
[30] S. Pal, C. Sinha, unpublished results.
[31] Y. Wakatsuki, H. Yamazaki, P.A. Grutsch, M. Santhanam, C. Kutal, J. Am. Chem. Soc. 107 (1985) 8153.
[32] T.K. Misra, C. Sinha, Transition Met. Chem. 24 (1999) 467.
[33] K. Nakamoto, Infrared and Raman Spectra of Inorganic and Coordination Compounds, 4th ed., Wiley, New York, 1986, p. 253.
[34] C. Sinha, Polyhedron 12 (1993) 2363.

PERGAMON

www.elsevier.nl/locate/poly

Polyhedron 19 (2000) 1271–1278

POLYHEDRON

Synthesis and reactivity of copper(I) phosphine–alkene complexes: X-ray crystal structure of $CuCl(Ph_2PCPh{=}CH_2)_2$

Simon J. Coles [a], Paul Faulds [b], Michael B. Hursthouse [a], David G. Kelly [b,*], Andrew J. Toner [b]

[a] *Department of Chemistry, University of Southampton, Highfield, Southampton, SO17 1BJ, UK*

[b] *Department of Chemistry and Materials, Manchester Metropolitan University, Chester Street, Manchester, M1 5GD, UK*

Received 15 October 1999; accepted 27 March 2000

Abstract

Copper(I) chloride complexes containing bifunctional phosphine/alkene ligands of the form $CuCl(Ph_2PCH{=}CH_2)_n$ ($n=1$, 3) and $CuCl(Ph_2PCPh{=}CH_2)_2$ have been synthesized, with the latter being characterized by single crystal X-ray diffraction. Complexes decompose rapidly on reaction with hydroborating agents $NaBH_4$ and $Na[B(OMe)_3H]$, although the thermally unstable $Cu(BH_4)(Ph_2PCPh{=}CH_2)_2$ may be observed by NMR spectroscopy. The complexes show considerable resistance to thermally initiated alkene polymerization, the only significant reactivity for diphenylvinylphosphine complexes being trace ligand dissociation and subsequent aerobic oxidation to $Ph_2P(O)CH{=}CH_2$. Similar dissociation/oxidation is not observed for $CuCl(Ph_2PCPh{=}CH_2)_2$. Lewis acid initiated polymerization, using $Et_2O\cdot BF_3$, results in the facile formation of copper(I) coordinated polymeric phosphine ligands for diphenylvinylphosphine complexes, but again no reactivity is induced in the more sterically hindered α-styrenyl analogue. ©2000 Elsevier Science Ltd All rights reserved.

Keywords: Phosphine; Alkene; Polymerization; Hydroboration; Copper(I) complexes

1. Introduction

The coordination chemistry of copper has been the subject of extensive research over several decades [1]. Despite such thorough activity, the structure and reactivity of copper complexes remains the focus of considerable research effort [2,3]; copper biochemistry and the stoichiometric use of organocopper reagents in synthesis are particularly significant [4,5]. The stabilization of copper(I) by tertiary phosphines forms some of the earliest studies of coordination chemistry [6,7]. Subsequent work has demonstrated a diversity of structure and stoichiometry derived from the absence of electronic factors in the d^{10} electronic configuration. Thus, whilst monophosphine complexes commonly adopt cubane or stepped tetrameric solid state structures [8,9], more sterically demanding phosphines can favour the formation of dimeric and even monomeric complexes [10,11]. The bridging halide ligands which occur in monophosphine complexes may be cleaved by the use of greater phosphine:copper(I) stoichiometries; once again the absence of ligand field control leads to the isolation of numerous products in which the copper salt, phosphine, reaction solvent and experimental conditions are all influential. The reactivity of copper chloride systems with triphenylphosphine is illustrative of this reagent and condition-based diversity. In addition to $[CuCl(PPh_3)]_4$ formed directly from CuCl or by the phosphine reduction of $CuCl_2\cdot 2H_2O$ [12], $CuCl(PPh_3)_2$ or $(Ph_3P)_2CuCl_2$-$Cu(PPh_3)/CuCl(PPh_3)_3$ may be isolated from 1:2 metal:ligand reactions in chloroform and thf, respectively [13,14]. $CuCl(PPh_3)_3$ can also be formed from 1:3 reactions in a variety of solvents or molten PPh_3 [14,15]. Whilst numerous tertiary phosphine complexes of copper(I) are reported, the present work focuses on structure and reactivity in the presence of ancillary alkene functionalities. Thus, as part of recent investigations of the phosphine/alkene complexes [16,17] we report the synthesis of diphenylvinyl- and diphenyl-α-styrenyl-phosphine complexes of copper(I), their potential for thermal and catalysed alkene polymerization, and reactivity towards hydroborating agents.

2. Results and discussion

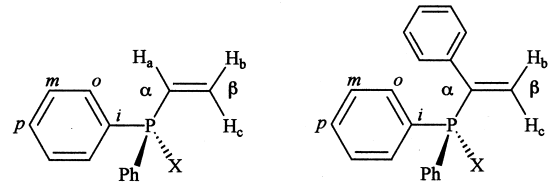
2.1. Synthesis of complexes

The reaction of copper(I) chloride with 1 equiv. of $Ph_2PCH{=}CH_2$ in CH_2Cl_2 affords the monophosphine com-

* Corresponding author. Tel.: +44-161-247-1425; fax: +44-161-247-6357; e-mail: d.g.kelly@mmu.ac.uk

0277-5387/00/$ - see front matter ©2000 Elsevier Science Ltd All rights reserved.
PII S0277-5387(00)00386-7

plex CuCl($Ph_2PCH{=}CH_2$) (**1**), Table 1. Whilst reports exist of bidentate diphenylvinylphosphine complexes of silver(I) [18], IR spectroscopic evidence is indicative of non-bonded alkene functions in **1**. Thus, although **1** has not been structurally characterized, analogy with known complexes suggests the formation of tetrameric solid state species [8]. ^{1}H NMR spectroscopy is in accord with the presence of pendant alkene moieties. However, whilst vinylic proton resonances occur at broadly similar chemical shifts and with similar couplings to those of free ligand and metal complexed systems [19], it is notable that the chemical shifts of the terminal vinyl protons H_b and H_c, Scheme 1, are less separated than in comparable systems. These resonances are in fact overlaid and lie at chemical shifts which are reversed relative to their normal field positions, Table 2. Whilst the assignment of these overlaid and coupled resonances is readily elucidated by ^{1}H 2D COSY NMR spectroscopy, Fig. 1, the origin of this anomalous behaviour is less clear. Since the overlying of H_b and H_c principally originates from the larger than normal downfield shift of H_c, it must be speculated that additional deshielding interactions occur through this moiety. However, as this effect is not reflected in additional ^{1}H NMR spectroscopic coupling or shifted $^{13}C\{^1H\}$ chemicals shifts for the associated β-carbon, Table 3, it must be considered as a minor effect.



X = CuCl **(1)**
X = $CuCl(Ph_2CH{=}CH_2)_2$ **(2)**
X = O **(4)**

X = $CuCl(Ph_2PCPh{=}CH_2)$ **(3)**
X = O **(5)**

Scheme 1. Atom numbering in **1**–**5**.

The reaction of CuCl and three molar equivalents of $Ph_2PCH{=}CH_2$ generates the tris-phosphine complex $CuCl(Ph_2PCH{=}CH_2)_3$ (**2**). ^{1}H, $^{13}C\{^1H\}$, $^{31}P\{^1H\}$ NMR spectroscopy confirms the conventional P-bound nature of the phosphine ligands which are spectroscopically equivalent in solution. $^1H/^{13}C\{^1H\}$ 2D COSY NMR spectroscopy, Fig. 2, confirms the assignment of $^{13}C\{^1H\}$ NMR resonances. **2** precipitates from solution as microcrystalline material cor-

Table 1
Physical and analytical data for complexes **1**–**4**

Complex	Colour	Melting point (°C)	ν(C=C) [a] (cm^{-1})	Elemental analysis [b]	
				C (%)	H (%)
$CuCl(Ph_2PCH{=}CH_2)$ (**1**)	white	146	1633	54.0 (54.2)	4.3 (4.1)
$CuCl(Ph_2PCH{=}CH_2)_3$ [c] (**2**)	white	88	1635	67.3 (66.6)	6.0 (6.3)
$CuCl(Ph_2PCPh{=}CH_2)_2$ (**3**)	white	145	1683	71.3 (71.1)	5.3 (5.0)
$Ph_2P(O)CH{=}CH_2$ (**4**)	white	104	1627	64.7 (64.5)	6.0 (5.7)

[a] IR, KBr DRIFT reflectance.
[b] Expected values in parentheses.
[c] **2**·0.5thf.

Table 2
^{1}H NMR ($CDCl_3$) spectroscopic data for complexes **1**–**5**

Complex	Position	Shift (δ)	Multiplicity	$^3J_{ab}$ (Hz)	$^3J_{ac}$ (Hz)	$^2J_{bc}$ (Hz)	$^nJ_{PH}$ (Hz)
$CuCl(Ph_2PCH{=}CH_2)$ (**1**)	Ph	7.34–7.56	m				
	H_a	6.49	ddd	11.4	12.5		18.0
	H_b	5.96	dd	11.4		0.0	40.7
	H_c	6.01	dd		12.5	0.0	26.0
$CuCl(Ph_2PCH{=}CH_2)_3$ (**2**)	Ph	7.14–7.52	m				
	H_a	6.33	ddd	11.7	17.8		20.3
	H_b	5.84	dd	11.7		0.0	34.4
	H_c	5.60	dd		17.8	0.0	17.8
$CuCl(Ph_2PCPh{=}CH_2)_2$ (**3**)	Ph	7.12–7.73	m				
	H_b	6.09	d			0.0	24.9
	H_c	5.32	d			0.0	11.7
$Ph_2P(O)CH{=}CH_2$ (**4**)	Ph	7.20–7.55	m				
	H_a	6.68	ddd	12.5	18.7		24.5
	H_b	6.31	ddd	12.5		1.8	41.0
	H_c	6.27	ddd		18.7	1.8	22.3
$Ph_2P(O)CPh{=}CH_2$ (**5**)	Ph	7.18–7.84	m				
	H_b	6.25	dd			1.1	40.3
	H_c	5.76	dd			1.1	19.4

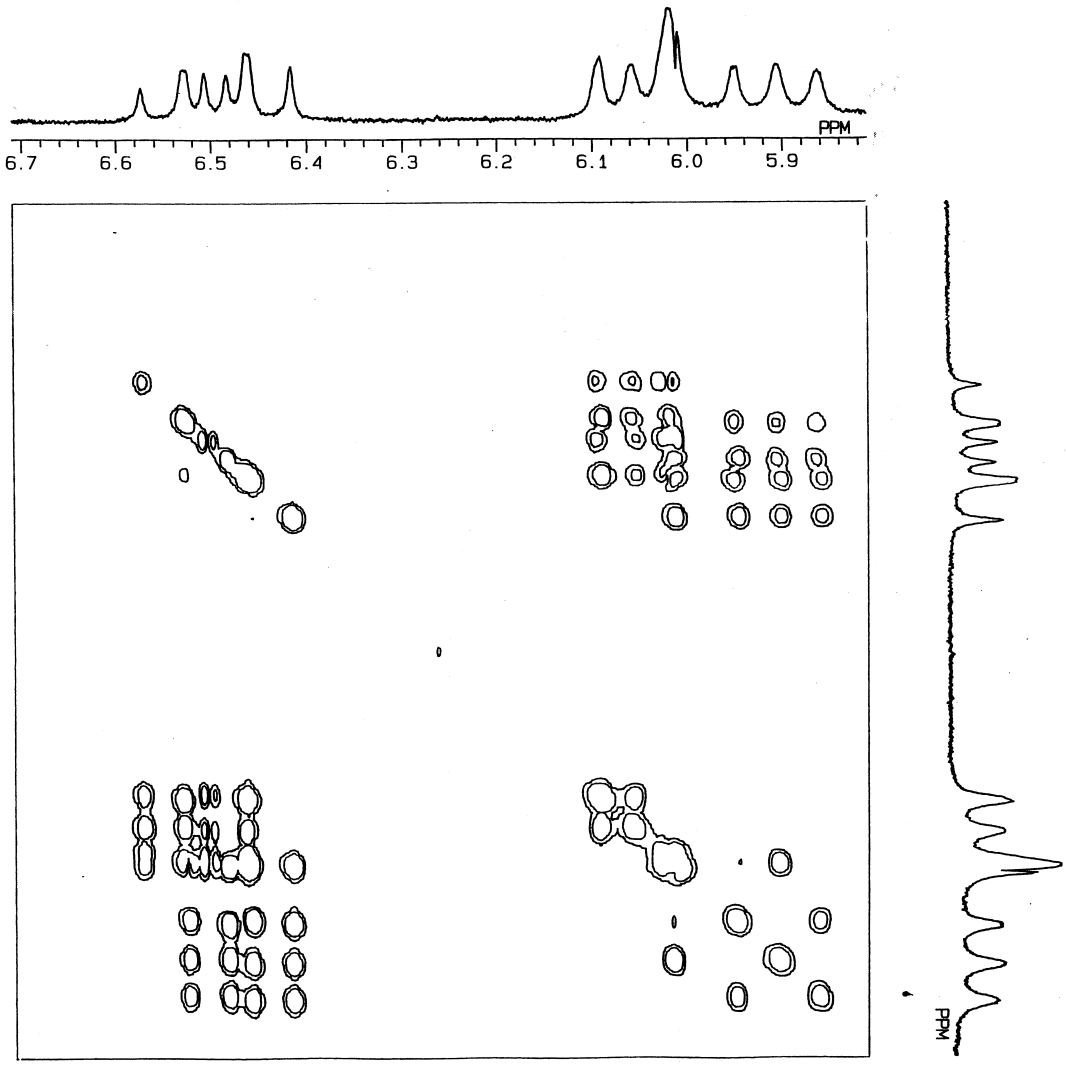


Fig. 1. ^{1}H 2D COSY NMR spectrum of $CuCl(Ph_2PCH{=}CH_2)$ (**1**) in $CDCl_3$ showing coupling of vinylic protons.

Table 3
$^{31}P\{^{1}H\}$ and $^{13}C\{^{1}H\}$ NMR spectroscopic data for complexes **1**–**5**

Complex	$^{31}P\{^{1}H\}$ [a] (δ)	$^{13}C\{^{1}H\}$ [b] (δ)						
		α	β		*i*	*o*	*m*	*p*
$CuCl(Ph_2PCH{=}CH_2)$ (**1**)	−5.6 [c]	132.29	131.70		133.24	128.96	133.62	130.29
	−8.6 [d]	(18.3)	(8.6)		(38.0)	(9.7)	(14.8)	(s)
$CuCl(Ph_2PCH{=}CH_2)_3$ (**2**)	−9.8 [c]	131.97	130.40		132.80	127.71	132.94	129.99
	−11.3 [d]	(20.7)	(8.5)		(27.3)	(8.5)	(13.5)	(s)
$CuCl(Ph_2PCPh{=}CH_2)_2$ (**3**)	0.0 [c]	139.98	132.04	PPh_2	130.76	128.57	134.38	130.08
	−1.2 [d]	(14.7)	(9.8)		(31.8)	(9.8)	(14.6)	(s)
				PC*Ph*	130.85	128.34	127.84	127.67
					(6.1)	(s)	(10.9)	(s)
$Ph_2P(O)CH{=}CH_2$ (**4**)	23.3 [c]	131.65	135.04		132.80	131.75	128.97	132.26
	18.7 [d]	(96.5)	(s)		(106.2)	(9.7)	(12.2)	(2.5)
$Ph_2P(O)CPh{=}CH_2$ (**5**)	19.4 [c]							
	16.0 [d]							

[a] $Ph_2PCH{=}CH_2$, $^{31}P\{^{1}H\}$, $CDCl_3$, $\delta = -11.4$; $Ph_2PCPh{=}CH_2$, $^{31}P\{^{1}H\}$, $CDCl_3$, $\delta = -6.8$.
[b] $^{n}J(CP)$ (Hz) in parentheses, $CDCl_3$.
[c] $CDCl_3$.
[d] C_7D_8.

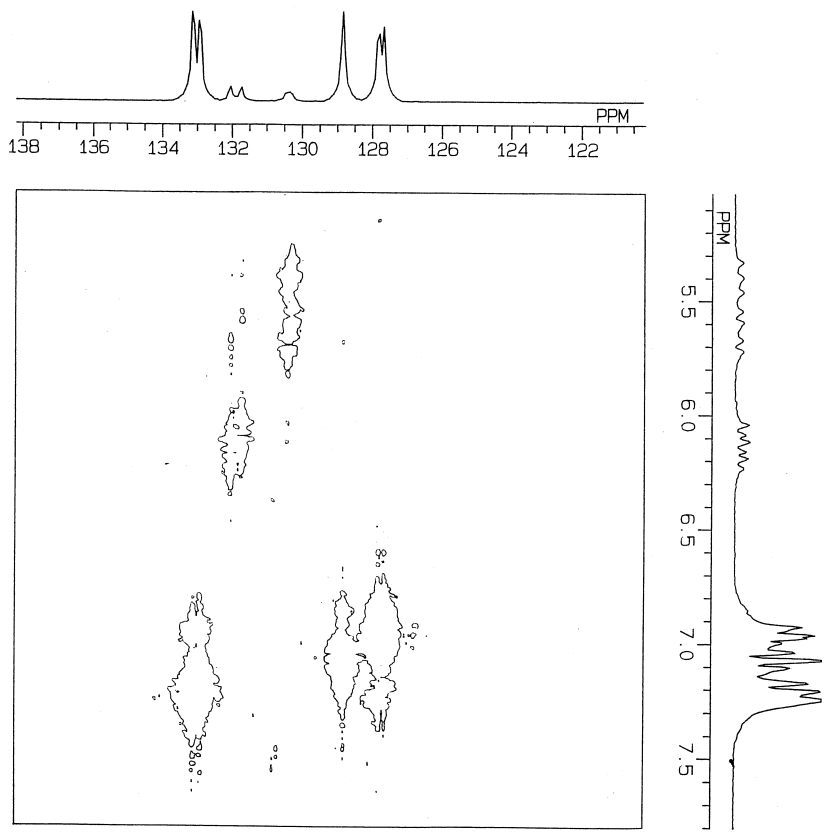


Fig. 2. $^{1}H/^{13}C\{^{1}H\}$ 2D COSY NMR spectrum of $CuCl(Ph_2PCH{=}CH_2)_3$ (**2**) in $CDCl_3$.

responding to the solvate **2**·0.5thf. Evidence for this formulation is provided by ^{1}H NMR spectroscopy which identifies non-bonded thf at $\delta = 1.82$ (t) and 3.70 (t) in $CDCl_3$, and thermogravimetric analysis which yields a mass loss of 4.5% (4.7%) in the temperature range 50–60°C.

In contrast to the formation of **2**, the reaction of CuCl and 3 equiv. of $Ph_2PCPh{=}CH_2$ results in the isolation of $CuCl(Ph_2PCPh{=}CH_2)_2$ (**3**) on recrystallization from CH_2Cl_2/Et_2O. The increased cone angle of the α-styrenyl ligand evidently favours bis-complex formation on steric grounds. Such changes in stoichiometry from reactant to product are not unusual, the facile modification of metal:ligand stoichiometry has been observed in other copper(I) phosphines, for example the shift from $Cu(NO_3)(PPh_3)_3$ to $Cu(NO_3)(PPh_3)_2$ on recrystallization [20]. Phenyl substitution in **3** relative to the vinyl complexes **1** and **2** results in a significant simplification of the ^{1}H NMR features associated with the alkene moiety, with protons centred at the β-carbon being reduced to phosphorus-coupled doublets, Table 2.

Since phosphine oxidation forms a facile deactivation pathway for both phosphine ligands and complexes at ambient or elevated temperatures [21,22], the phosphine oxides $Ph_2P(O)CH{=}CH_2$ (**4**) and $Ph_2P(O)CPh{=}CH_2$ (**5**) have been prepared by peroxydisulfate oxidation of the corresponding phosphines. Analytical and spectroscopic data again confirm the integrity of these products, Tables 1–3. Attempts to assign the $^{13}C\{^{1}H\}$ NMR resonances of **4** using proton-coupled ^{13}C NMR spectroscopy result in complex spectra as a consequence of extensive $^{2}J(CH)$ and $^{3}J(CH)$ coupling. $^{1}H/^{13}C\{^{1}H\}$ 2D COSY NMR spectroscopy provides in simpler route to such interpretation, Fig. 3, from which $^{13}C\{^{1}H\}$ and ^{13}C NMR resonances, as well as $^{n}J(CP)$ and $^{n}J(CH)$ couplings, can be assigned. The latter couplings are typical of phosphorus(V) interaction with aromatic and alkene sp^2 carbons.

2.2. Thermal and Lewis acid catalysed polymerization studies

The thermal effects of heating complexes **1**–**3** to 100°C in deuterated toluene have been followed using $^{31}P\{^{1}H\}$ NMR spectroscopy. In inert atmospheres no evidence for chemical change can be observed for **1**–**3** over 8 h. Under similar conditions in air, **1** and **2** show trace oxidation ($<5\%$) to free **4** ($^{31}P\{^{1}H\}$ C_7D_8 $\delta = 18.7$), although no loss of integrity is recorded for the more sterically hindered α-styrenyl complex **3**. Since vinyl and α-styrenyl substituted phosphine ligands are readily distinguish from their saturated or polymerized analogues in $^{31}P\{^{1}H\}$ NMR spectroscopy by the respective presence and absence of diamagnetic deshielding [16], it is evident that these complexes display no propensity for thermally initiated alkene polymerization.

Early reports have demonstrated that both free $Ph_2PCH{=}CH_2$ [23] and its silver(I) complexes [18] undergo Lewis acid catalysed alkene polymerization. Thus,

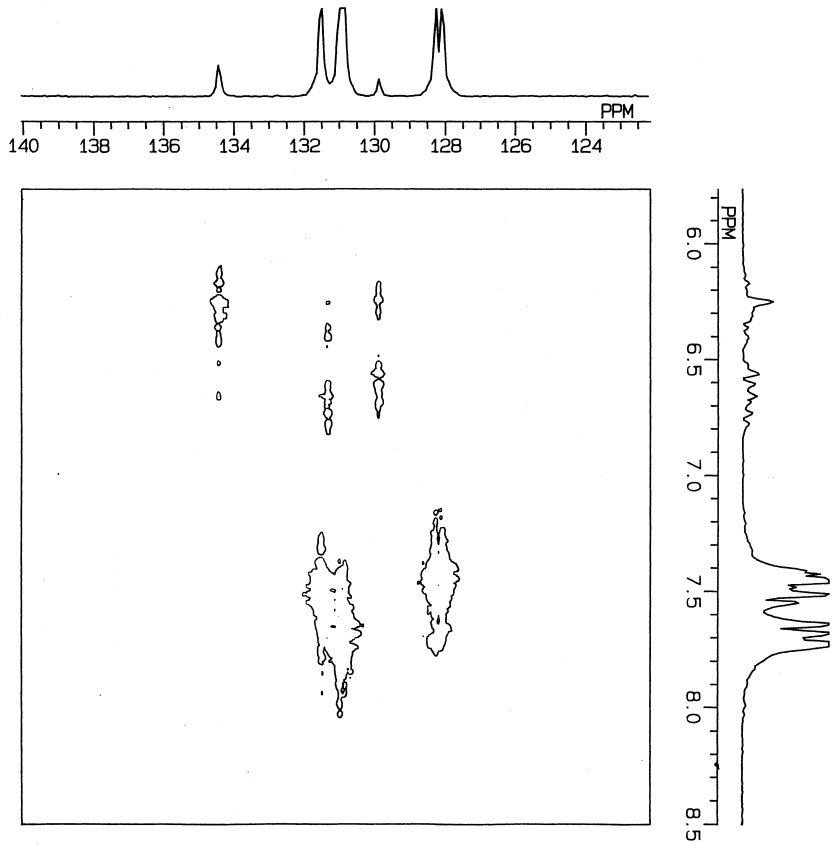


Fig. 3. $^{1}H/^{13}C\{^{1}H\}$ 2D COSY NMR spectrum of $Ph_2P(O)CH{=}CH_2$ (**4**) in $CDCl_3$.

$Et_2O \cdot BF_3$ catalysed polymerization studies have been performed in $CDCl_3$ and followed using NMR spectroscopy. The exposure of **1** to $Et_2O \cdot BF_3$ over ca. 1 h results in the precipitation of $[CuCl(Ph_2PCH–CH_2–)_n]$ (**6**) (C 54.0 (54.3); H 4.2 (4.2)) in ca. 80% yield. The corresponding reaction of **2** affords precipitates of variable hydrocarbon content consistent with concomitant ligand polymerization and dissociation. Since $[CuCl(Ph_2PCH–CH_2–)_n]$ (**6**) (and its corresponding product obtained from **2**) are insoluble in common NMR solvents, spectroscopic evidence to support polymerization is limited. No IR band corresponding to $\nu(C{=}C)$ can be located, however, such absorbances are often weak and difficult to assign even in authentic diphenylvinylphosphines. Thus interpretation is limited to elemental analysis consistent with the formation of **6**. Whilst it is obvious that **2** would provide identical elemental analysis, the considerable solubility of **2**, $Et_2O \cdot BF_3$ and the common decomposition product **4**, in $CDCl_3$ preclude the presence of these materials. The composition of the remaining reaction solution material is complex and dynamic. $^{31}P\{^{1}H\}$ NMR spectroscopy identifies five principal components, although their relative proportions vary with time and decrease overall relative to numerous other species. After 1 day a copper(I) phosphine complex ($\delta = -5.4$ and 2.5 ppm), the $[Ph_2PCH{=}CH_2 \cdot BF_3]$ adduct ($\delta = 1.7$ ppm) and additional products $\delta = 17.1$ ppm (dd $J = 62.5$ and 1187.6 Hz) and $\delta = 22.3$ ppm (dd $J = 58.9$ and 183.9 Hz) are all observed. The propensity for rapid phosphine exchange, plus the complex vinylic and ethylene resonances present in ^{1}H NMR spectra, make detailed interpretation impossible. However, further BF_3 reactivity beyond simple Lewis acid behaviour is certainly possible. Fluoride and tetrafluoroborate complexes of copper(I) phosphines are known [24], whilst the formation of BF_4^- complexes from the reaction of $Et_2O \cdot BF_3$ and $PdCl_2P_2$ complexes is well established [25].

$CuCl(Ph_2PCPh{=}CH_2)_2$ (**3**) is inert under the conditions which produce reactivity in **1** and **2**; **3** is recovered unchanged from exposure to $Et_2O \cdot BF_3$. In view of the ease with which styrene undergoes thermal and catalysed polymerization relative to ethene, the greater stability of **3** is notable. Since neither structural nor spectroscopic characterization of **3** suggests anomalous behaviour compared to **1**, **2** or $CuCl(PPh_3)_n$, it must be suggested that coordination to the relatively crowded $CuClP_2$ centre and the presence of the α-phenyl moiety are sufficient to inhibit reactivity.

2.3. Reactivity of copper complexes towards hydroborating agents

Although $Cu(BH_4)$ decomposes below ambient temperature, in the presence of tertiary phosphine and/or phenanthroline ligands, $NaBH_4$ reacts with copper(I) salts to form

stabilized complexes. The system is particularly sensitive to the nature of the phosphine employed with only triarylphosphines, PPh_2Me and various chelating phosphines containing PPh_2 fragments affording products with extended lifetimes at, or above, ambient temperature [26]. Since initial reports in this area, several strands of activity have been pursued, focusing on both structure and reactivity. Interest centres on the relationship between stoichiometry and tetrahydroborate bonding [27], and on the application of transition metal tetrahydroborates to regioselective reduction [28]. Substituted tetrahydroborates have allowed further modification of reduction reactivity, and have afforded the stable hexameric hydride $[CuH(PPh_3)]_6$ from the reaction of $Na[B(OMe)_3H]$ and $CuCl(PPh_3)$ [29], although the latter reaction is again critically dependent on the phosphine present.

Since the range of tertiary phosphines which stabilize copper(I) tetrahydroborates and hydrides is limited, it is inevitable that the isolation of $Ph_2PCH{=}CH_2$ and $Ph_2PCPh{=}CH_2$ complexes will be, at best, difficult. Indeed the reaction of **1**–**3** and $Na[B(OMe)_3H]$ at $-10°C$ proceeds through a transient red intermediate to afford metallic copper and free $Ph_2PCH{=}CH_2$ or $Ph_2PCPh{=}CH_2$; the coloration of the intermediate is consistent with that of $[CuH(PPh_3)]_6$. At lower temperatures reaction and decomposition progress more slowly, but there is no evidence for the formation of a kinetically stable hydride. **1** and **2** also form unstable products on reaction with $NaBH_4$, metallic copper and free $Ph_2PCH{=}CH_2$ being identified. Once again the reactivity of **3** contrasts with that of **1** and **2**. Reaction of **3** with a slight excess of finely ground $NaBH_4$ in $CDCl_3$ at $-10°C$ affords complete conversion to $Cu(BH_4)(Ph_2PCPh{=}CH_2)_2$ (**7**). The long-term instability of **7** has prevented elemental analysis; however, NMR is consistent with the formulation presented. ^1H NMR data are clearly indicative of a change of $Ph_2PCPh{=}CH_2$ environment with modifications in both chemical shift and $^3J(PH)$ couplings for H_b and H_c (^1H ($CDCl_3$) $\delta = 6.16$ (d, $^3J(PH) = 25.7$ Hz), 5.38 (d, $^3J(PH) = 12.6$ Hz)), and since there is no evidence for free phosphine, it is reasonable to assume the 1:2 copper:phosphine stoichiometry is maintained. The BH_4^- moiety is observed in ^1H and $^{11}B\{^1H\}$ NMR (^1H ($CDCl_3$) $\delta = 1.59$ (q, $^1J(^{11}BH) = 24.3$ Hz), $^{11}B\{^1H\}$ ($CDCl_3$) $\delta = -36.5$). $^{31}P\{^1H\}$ NMR spectroscopy is less informative owing to the facility of copper(I) complexes to undergo rapid ligand exchange, a feature which is typified by the observation of a single resonance for $Cu(BH_4)(PPh_2Me)_3$ and PPh_2Me mixtures [28]. In **7** a single new $^{31}P\{^1H\}$ NMR spectroscopic resonance is recorded at 1.0 ppm. Supporting evidence for the presence of coordinated BH_4^- is provided by solid state IR spectroscopy, from which bands at 2381 and 2011 cm^{-1} are identified. These are less separated than the terminal and bridging $\nu(Cu–H_t)$ and $\nu(Cu–H_b)$ bands of most pseudo-tetrahedral $Cu(\eta^2\text{-}BH_4)P_2$ systems, but are certainly indicative of BH_4^- coordination [30].

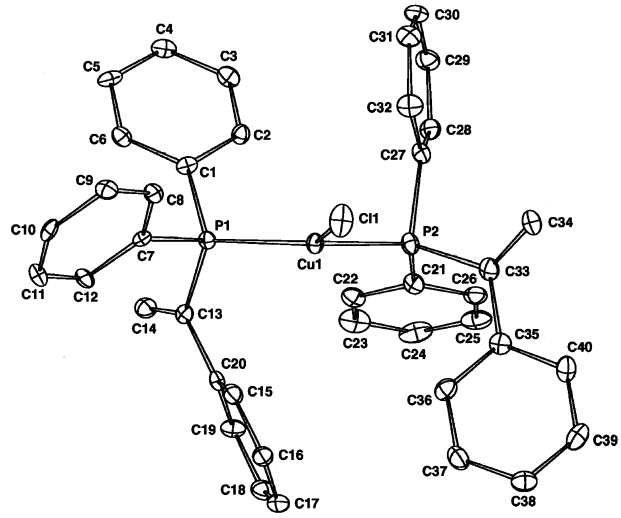


Fig. 4. Single crystal X-ray diffraction structure of $CuCl(Ph_2PCPh{=}CH_2)_2$ (**3**).

2.4. Single crystal X-ray diffraction characterization of $CuCl(Ph_2PCPh{=}CH_2)_2$ (3)

Whilst numerous copper(I) phosphine complexes have been crystallographically characterized, the majority of studies have focused on elucidating the relationship between complex structure and phosphine steric/electronic parameters in $[CuClP]_n$ complexes [1]. Structural determinations of $CuClP_2$ donor sets are less common; only $CuCl[P(o\text{-}tolyl)_3]_2$ [31] and two forms of solvated $CuCl(PPh_3)_2$ [9,14] have been reported. Thus, suitable crystals of **3**, formed by recrystallization from CH_2Cl_2/Et_2O, were studied by X-ray diffraction. Structural characterization, Fig. 4, indicates a three coordinate copper(I) structure with P-bound ligands and pendant styrene moieties. No local symmetry is observed at the metal centre; however, NMR spectroscopic evidence consistently demonstrates the equivalence of phosphine ligands in solution. Thus, in the absence of ligand field influences, solid state asymmetry is clearly dependent on steric and packing factors.

Bond lengths in **3** are broadly similar to those of $CuCl(PPh_3)_2$, Table 4. Bond angles indicate an almost planar arrangement around the copper centre. The steric repulsion of the phosphine ligands is demonstrated by the large P–Cu–P angle, with considerable asymmetry being apparent from the two P–Cu–Cl angles. Once again similar features have been observed in $CuCl(PPh_3)_2$, although the deviations from an idealized trigonal planar geometry are more pronounced in **3**.

3. Conclusions

Copper(I) forms complexes with diphenylvinyl- and diphenyl-α-styrenyl-phosphine in which phosphine ligands adopt P-bound coordination. Pendant alkene moieties are thermally stable, but vinyl functions polymerize in the pres-

Table 4
Selected bond lengths (Å) and angles (°) for $CuCl(Ph_2PCPh{=}CH_2)_2$ (**3**)

	$CuCl(Ph_2PCPh{=}CH_2)_2$ (**3**)	$CuCl(PPh_3)_2\cdot 0.5thf$ [a]	$CuCl(PPh_3)_2\cdot 0.5C_6H_6$ [b]
Cu–Cl	2.214(2)	2.214(1)	2.208(2)
Cu–P(1)	2.224(2)	2.2564(9)	2.260(2)
Cu–P(2)	2.242(2)	2.2676(9)	2.272(2)
C(13)–C(14)	1.319(7)		
C(33)–C(34)	1.344(8)		
Cl(1)–Cu–P(1)	120.95(6)	120.58(4)	120.74(6)
Cl(1)–Cu–P(2)	109.61(6)	113.86(4)	113.76(7)
P(1)–Cu–P(2)	127.93(6)	125.55(4)	125.48(7)

[a] Ref. [14].
[b] Ref. [9].

ence of boron trifluoride. Phenyl substitution of the α-carbon renders the alkene less susceptible to polymerization, but also affords a tetrahydroborate complex that is sufficiently stable to allow NMR characterization.

4. Experimental

4.1. Single crystal X-ray diffraction

Crystal data for $[CuCl(Ph_2PCPh{=}CH_2)_2]$ (**3**), $C_{40}H_{34}ClCuP_2$. Crystal dimensions $0.05\times0.05\times0.2$ mm. $M=675.60$, monoclinic, space group $P2_{1/C}$. $a=9.207(2)$, $b=9.894(2)$, $c=36.510(7)$ Å, $\beta=93.80(3)°$, $V=3318.5(12)$ Å^3, $Z=4$, $D_{calc}=1.352$ g cm^{-3}, $T=293(2)$ K, λ(Mo Kα) $=0.71073$ nm, μ(Mo Kα) $=0.863$ mm^{-1}; observed data 4748, unique no. of observed data 3115 ($I>2\sigma(I)$), $R=0.0566$, $wR=0.1352$. Max./min. final difference $+0.472/-0.390$ e Å^{-3}. Intensity data were recorded on a FAST TV area detector following previously described procedures [32]. The structure was solved by direct methods (SHELXS-86) and refined by full matrix least squares on F^2 (SHELX-92), with all non-hydrogen atoms being refined anisotropically. Hydrogen atoms were assigned fixed positions and thermal parameters defined by their respective carbon atoms.

4.2. Spectroscopy

All reactions were carried out under nitrogen using dry degassed solvents using previously described methods [33]. ^{1}H, ^{13}C{^{1}H}, ^{13}C and ^{31}P{^{1}H} NMR spectra were obtained at 270.05, 67.8 and 81.1 MHz, respectively, in $CDCl_3$ and/or C_7D_8, on a JEOL GSX-270 instrument. Standard acquisition parameters were used in each case, although 8–10 s pulse delays were found necessary to obtain reasonable ^{13}C{^{1}H} and ^{13}C NMR spectra. ^{1}H/^{13}C{^{1}H} 2D COSY NMR spectra were obtained using the pulse sequence ($\pi/2$, ^{1}H)–($t^1/_2$)–Δ_1–($\pi/2$, ^{1}H; $\pi/2$, ^{13}C)–Δ_2, where $\Delta_1={}^1/_2J$ and $\Delta_2={}^1/_4J$ and $J=120$ Hz [19].

4.3. Ligand synthesis

$Ph_2PCH{=}CH_2$ was prepared by the Grignard route from commercial $CH_2{=}CHMgBr$ and Ph_2PCl. $Ph_2PCPh{=}CH_2$ was similarly prepared using Grignard formed by the reaction of α-bromostyrene and magnesium turnings. Syntheses followed conventional procedures [34]. In each case the ^{1}H and ^{31}P{^{1}H} NMR data are comparable with literature values [35].

4.4. Complex synthesis

Two synthetic routes were utilized, i.e. the stoichiometric reaction of copper(I) chloride or the reduction of hydrated copper(II) chloride in the presence of excess phosphine. Whilst both routes are acceptable, the former is preferable in terms of yield and control of metal:ligand stoichiometry. Thus the following is typical; 2.00 g copper(I) chloride (2.02 mmol) is slurried in dry dichloromethane (45 cm^3). One equivalent of $Ph_2PCH{=}CH_2$ (ca. 4.5 g, 2.1 mmol) is added and the reactants stirred until the insoluble salt is consumed. The solution is then filtered and **1** precipitated by the addition of hexane. Separation of the resulting solid by filtration and drying in vacuo affords **1** in 95% yield.

4.5. Phosphine oxide synthesis

4.5.1. $Ph_2P(O)CH{=}CH_2$

$Ph_2PCH{=}CH_2$ (1.08 g; 5.1 mmol) was dissolved in CH_2Cl_2 (25 cm^3) and slurried with Oxone® for 1 day, after which the solution was filtered and concentrated to dryness affording $Ph_2P(O)CH{=}CH_2$ in quantitative yield. ^{1}H, ^{13}C{^{1}H} and ^{31}P{^{1}H} NMR: see Tables 2 and 3. IR (KBr): ν(O=P) 1174 cm^{-1}. MS (EI) $m/e=228$ (100%). $Ph_2P(O)CPh{=}CH_2$: The compound was similarly prepared and characterized by ^{1}H and ^{31}P{^{1}H} NMR spectroscopy (see Table 3). IR (KBr): ν(O=P) 1189 cm^{-1}. MS (EI) $m/e=305$ (100%).

4.6. Thermal polymerization studies

The following is typical: **1** (4.3 mg) was dissolved in dry degassed C_7D_8 (2.0 cm^3) and placed in a sealed 4.0 mm

NMR tube under nitrogen. The solution was heated to 100°C for periods of 1 h for up to 8 h. After each hour the tube was cooled to ambient temperature and the NMR spectrum recorded.

4.7. BF_3 initiated polymerization studies

An NMR sample of **1** (6.3 mg) was prepared in $CDCl_3$ as above and $Et_2O \cdot BF_3$ (10 μl) added under nitrogen. The NMR spectrum was obtained after 1 h, 1 day and 7 days at ambient temperature, precipitated material being removed by filtration and dried in vacuo. Additional $CDCl_3$ was added to the remaining solution to maintain constant volume.

4.8. Reactions with $NaBH_4$ and $NaB(OMe)_3H$

$NaBH_4$ (5.0 mg; 0.13 mmol) was placed in a dry 4.0 mm NMR tube under nitrogen and cooled to −10°C. A solution of **1** (23.3 mg; 0.11 mmol) was prepared in $CDCl_3$ (2.0 cm^3), precooled to −10°C and transferred to the NMR tube under nitrogen. NMR spectra were obtained after 1 h and 1 day.

Supplementary data

Crystallographic data for structural analysis have been deposited with the Cambridge Crystallographic Data Centre, CCDC No. 134113. Copies of this information may be obtained free of charge from The Director, CCDC, 12 Union Road, Cambridge CB2 1EZ, UK (fax: +44-1223-336033; e-mail: deposit@ccdc.cam.ac.uk or http://www.ccdc.cam.ac.uk).

Acknowledgements

Mr P. Warren is thanked for his help and advice in obtaining NMR data. PF and AT acknowledge the award of HEFC and MMU Faculty funded studentships.

References

[1] B.J. Hathaway, in: G. Wilkinson, R.D. Gillard, J.A. McCleverty (Eds.), Comprehensive Co-ordination Chemistry, vol. 4, Pergamon, Oxford, 1987, Ch. 53.
[2] P.D. Akivos, H.J. Katsikis, A. Koumoutsi, Coord. Chem. Rev. 167 (1997) 95.
[3] P. Power, in: Progress in Inorganic Chemistry, vol. 39, Wiley, New York, 1991, p. 75.
[4] G.H. Posner, An Introduction to Synthesis using Organocopper Reagents, Wiley, New York, 1980.
[5] K.D. Karlin, J. Zubieta, Copper Coordination Chemistry; Biochemical and Inorganic Perspectives, Adenine, New York, 1983.
[6] G. Mann, D. Purdie, A.F. Wells, J. Chem. Soc. (1936) 1503, 1826.
[7] A.F. Wells, Kristallogen 94 (1936) 447.
[8] C.A. McAuliffe, D.G. Kelly, in: J.J. Zuckerman, A.D. Norman (Eds.), Inorganic Reactions and Methods, vol. 8, VCH, New York, 1991, pp. 57–60.
[9] G.A. Bowmaker, J.C. Dyson, P.C. Healy, L.M. Engelhardt, C. Pakawatchi, A.H. White, J. Chem. Soc., Dalton Trans. (1987) 1089.
[10] M.R. Churchill, F.J. Rotella, Inorg. Chem. 18 (1979) 166.
[11] G.A. Bowmaker, J.D. Cotton, P.C. Healy, J.D. Kildea, S.B. Silong, B.W. Skelton, A.H. White, Inorg. Chem. 28 (1989) 1462.
[12] F.H. Jardine, L. Rute, A.G. Vohra, J. Chem. Soc. A (1970) 238.
[13] J.T. Gill, J.J. Mayerle, P.S. Welcker, D.F. Lewis, D.A. Ucko, D.J. Barton, D. Stowens, S.J. Lippard, Inorg. Chem. 15 (1976) 1155.
[14] T. Krauter, B. Neumuller, Polyhedron 15 (1996) 2851.
[15] G. Costa, E. Reisenhofer, L. Stefani, J. Inorg. Nucl. Chem. 27 (1965) 2581.
[16] S.J. Coles, P. Faulds, M.B. Hursthouse, D.G. Kelly, G.C. Ranger, N.M. Walker, J. Chem. Res. (1999) 418 (S), 1811 (M).
[17] S.J. Coles, P. Faulds, M.B. Hursthouse, D.G. Kelly, G.C. Ranger, A.J. Toner, N.M. Walker, J. Organomet. Chem. 586 (1999) 234.
[18] C. Wu, F.J. Welch, J. Org. Chem. 30 (1965) 1229.
[19] D.J. Rahn, M.S. Holt, M. O'Neil-Johnson, J.H. Nelson, Inorg. Chem. 27 (1988) 1317.
[20] F.H. Jardine, A.G. Vohra, F.J. Young, J. Inorg. Nucl. Chem. 33 (1971) 2941.
[21] S.M. Godfrey, D.G. Kelly, C.A. McAuliffe, R.G. Pritchard, J. Chem. Soc., Dalton Trans. (1993) 2053.
[22] J.D. Yoke, D.D. Schmidt, J. Am. Chem. Soc. 93 (1971) 637.
[23] D.M. Paisley, C.S. Marvel, J. Polym. Sci. 56 (1962) 533.
[24] D.J. Gulliver, W. Levason, M. Webster, Inorg. Chim. Acta 52 (1981) 153.
[25] C.E. Eaborn, N. Farrell, J.L. Murphy, A. Pidcock, J. Chem. Soc., Dalton Trans. (1976) 58.
[26] T.J. Marks, J.R. Kolb, Chem. Rev. 77 (1977) 263 and Refs. therein.
[27] I.D. Potter, B.D. James, Polyhedron 18 (1999) 1201.
[28] P.N. Davey, G.W. Fleet, P.J.C. Harding, J. Chem Res. (S) (1981) 336.
[29] M.R. Churchill, J.M. Wormald, J. Am. Chem. Soc. 93 (1971) 2063.
[30] F. Cariati, L. Naldini, Gazz. Chim. Ital. 95 (1965) 3.
[31] G.A. Bowmaker, L.M. Engelhardt, P.C. Healy, J.D. Kildea, R.I. Papasergio, A.H. White, Inorg. Chem. 26 (1987) 3533.
[32] J.A. Darr, S.R. Drake, M.B. Hursthouse, K.M.A. Malik, Inorg. Chem. 32 (1993) 5704.
[33] S.J. Coles, M.B. Hursthouse, D.G. Kelly, G.C. Ranger, A.J. Toner, N.M. Walker, J. Organomet. Chem. 580 (1999) 304.
[34] V.D. Biano, S. Doronzo, Inorg. Synth. 16 (1976) 155.
[35] L. Maier, in: L. Maier, G.M. Kosolapoff (Eds.), Organic Phosphorus Compounds, vol. 1, Wiley-Interscience, New York, 1972, Ch. 1 and Refs. therein.

PERGAMON

www.elsevier.nl/locate/poly

Polyhedron 19 (2000) 1279–1282

POLYHEDRON

Spectral and single crystal X-ray structural studies on disulfide complexes: reaction of bis(dialkyldithiocarbamato)M(II) with iodine and crystal structure determination of diiodo(bipiperidinethiuramdisulfide)M(II) (M = zinc, cadmium)

S. Thirumaran [a], K. Ramalingam [a,*], G. Bocelli [b], A. Cantoni [b]

[a] *Department of Chemistry, Annamalai University, Annamalai nagar 608 002, India*

[b] *Centro di Studio per la Structturistica Diffrattometrica del CNR, Viale delle Scienze, 43100 Parma, Italy*

Received 30 November 1999; accepted 28 March 2000

Abstract

Unique diiodo(bipiperidinethiuramdisulfide)zinc(II) (**1**) and diiodo(bipiperidinethiuramdisulfide)cadmium(II) (**2**) were prepared by the oxidation of the corresponding bis-dithiocarbamates with iodine and the crystal structures of the compounds are reported. Metal ions are situated at the centre of a tetrahedral arrangement of two sulfur atoms of the piperidine thiuramdisulfide and two iodide ions. Two sets of significantly different C–S distances clearly correspond to single- and double-bonded C–S distances. The disulfide S–S distance in [Zn(bipiptds)I_2] is long compared to the distance in [Cd(bipiptds)I_2]. The two C=S bonds of the disulfide in the present complexes are on the same side, as a requirement for coordination with metal ions. IR spectral studies are in keeping with the thioureide distances. ©2000 Elsevier Science Ltd All rights reserved.

Keywords: Disulfides; Thioureides; Dithiocarbamates; Tetrahedral coordination

1. Introduction

Dithioacid complexes of the ML_2 (M = Zn or Cd, LH = X-CS_2H or X_2PS_2H) type are coordinatively unsaturated; this leads to the formation of compounds of higher coordination number either by the addition of one or two molecules of a Lewis base or by polymerization of ML_2. Zinc dithiocarbamates and their adducts with primary and secondary amines have previously been prepared [1–3] and some of the complexes are very active accelerators for the vulcanization of rubber by sulfur [4] and the low temperature vulcanization of latex [5]. As a continuation of our efforts to understand the reactivity of dithiocarbamates [6–8], the reaction of I_2 with M(pipdtc)$_2$ (pipdtc$^-$ = $C_5H_{10}NCS_2^-$) (M = Zn, Cd) was carried out. Interesting four-coordinate [M(bipiptds)I_2] resulted. The chemistry and crystal structure of the [Zn(bipiptds)I_2] (**1**) and [Cd(bipiptds)I_2] (**2**) are reported.

* Corresponding author. Tel.: +91 413 202 834; fax: +91 414 422 265; e-mail: aulib@hotmail.com

2. Experimental

All the reagents and solvents employed were commercially available analytical grade materials used as supplied, without further purification. IR spectra were recorded on a JASCO IR-700 spectrophotometer (range 4000–400 cm^{-1}) as KBr pellets. Electronic spectra were recorded using a JASCO UVIDEC-650 spectrophotometer with chloroform as the solvent.

2.1. X-ray crystallography

Details of the crystal data, data collection and refinement parameters are summarized in Table 1. ORTEP plots of the molecules **1** and **2** are given in Figs. 1 and 2. Intensity data were collected on a Philips PW1100 diffractometer using graphite monochromated Mo Kα radiation (λ = 0.71069 Å). The intensity of a standard reflection measured for every 100 reflections showed no significant change. The absorption correction was performed with the DIFABS [9] program using the method of Walker and Stuart [10]. Structure was solved by direct methods using SIR92 [11] and was refined by

0277-5387/00/$ - see front matter ©2000 Elsevier Science Ltd All rights reserved.
PII S0277-5387(00)00388-0

Table 1
Crystal data, data collection, and refinement parameters for [Zn(bipiptds)I_2] and [Cd(bipiptds)I_2]

Empirical formula	$C_{12}H_{20}I_2N_2S_4Zn$	$C_{12}H_{20}CdI_2N_2S_4$
M	639.7	686.8
Crystal dimensions (mm)	0.170×0.23×0.26	0.31×0.25×0.27
Crystal system	monoclinic	monoclinic
Space group	*I*2/*a*	*I*2/*a*
a (Å)	15.082(2)	15.324(2)
b (Å)	8.735(3)	8.821(4)
c (Å)	15.939(3)	15.817(2)
α (°)	90	90
β (°)	104.01(2)	104.16(3)
γ (°)	90	90
U (Å^3)	2037.4	2073.1
Z	4	4
D_c (g cm^{-3})	2.0856	2.20
μ (cm^{-1})	43.78	43.82
F(000)	1223.85	1296
λ (Å)	Mo Kα (0.71069)	Mo Kα (0.71069)
	3–30	3–28
Speed (° sec^{-1})	0.05–0.16	0.05–0.16
Scan range (°)	4.8–17.9	4.8–17.8
Index ranges	$-20 \le h \le 20$, $0 \le k \le 9$, $0 \le l \le 4$	$-20 \le h \le 19$, $0 \le k \le 11$, $0 \le l \le 20$
Reflections collected	804	2496
Independent reflections	754	813
Observed reflections	726	779
Weighting scheme	$W = A/(\sigma^2F^2 + Bp^2)$	$W = A/[\sigma^2(F_o^2) + (Bp)^2]$
	$A = 0.5192$, $B = 0.002435$	$A = 1$, $B = 0.0633$
	$p = (\max(F_o^2) + 2F_c^2)/3$	$p = (\max(F_o^2) + 2F_c^2)/3$
No. parameters refined	136	137
Final *R*, *wR* (obs. data)	0.0334, 0.0344	0.0272, 0.1211
GOF	0.560	0.773

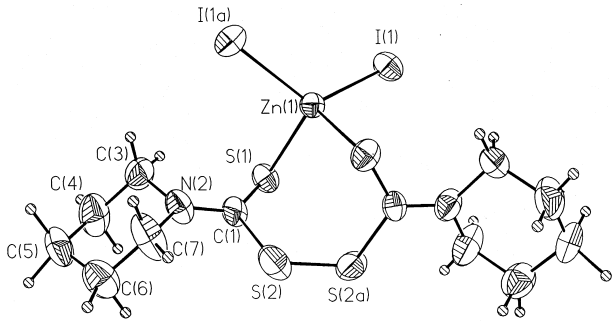


Fig. 1. ORTEP plot of [Zn(bipiptds)I_2].

SHELX 76 [12] and SHELX 93 [13]. All the non-hydrogen atoms were refined anisotropically.

2.2. IR and UV–Vis spectra

IR spectra were recorded on a JASCO IR-700 spectrophotometer (range 4000–400 cm^{-1}) as KBr pellets. UV–Vis spectra were recorded on a JASCO UVIDEC-650 with pure chloroform as the reference.

2.3. Preparation of the complexes

(a) Bis(piperidinedithiocarbamato)M(II) (M = Zn, Cd) complexes were prepared by the general methods reported earlier [8].

(b) Iodine (1 mmol) in chloroform (50 ml) was added dropwise to the solution containing M(pipdtc)$_2$ (1 mmol) in chloroform (20 ml) over a period of 2 h with continuous stirring. Light turbidity appeared in the solution after some time, which was removed by filtration. The filtrate was left undisturbed at room temperature. After 2 days pale yellow crystals separated from the solution. The crystals were filtered, washed with chloroform and then dried.

3. Results and discussion

3.1. Spectral studies

Both the zinc and cadmium complexes are of pale yellow colour. The electronic spectra contained only charge transfer bands in the 260–320 nm range for both complexes. IR spectra of both compounds showed weak disulfide bands around 480 cm^{-1}. The ν(C–S) bands appeared around 750 cm^{-1}. The thioureide band was observed around 1475 cm^{-1}.

3.2. Single-crystal X-ray studies

Unit cell constants and data collection parameters for the crystals are given in Table 1. Selected bond lengths and angles for the crystal structures **1** and **2** are given in Tables 2 and 3.

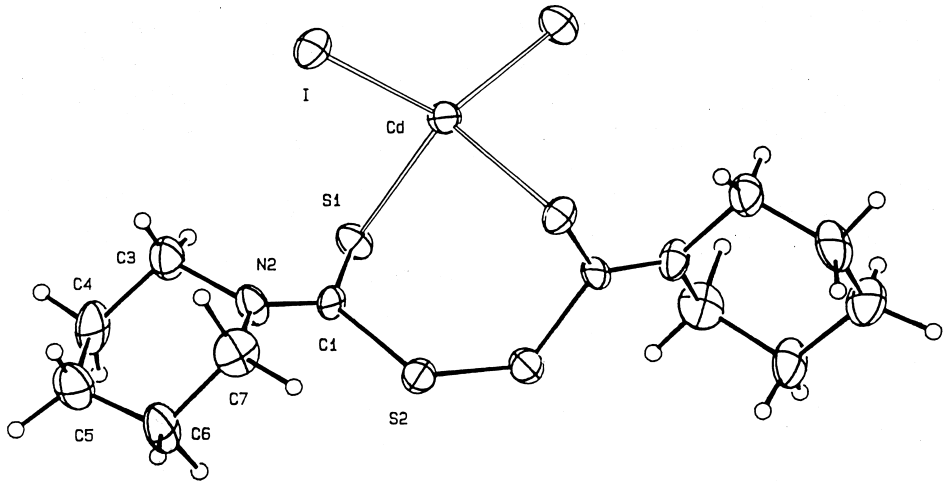


Fig. 2. ORTEP plot of [Cd(bipiptds)I_2].

Table 2
Bond distances (Å) and angles (°) for [Zn(bipiptds)I_2]

Zn1–I1	2.552(2)	N2–C3	1.469(20)
Zn1–S1	2.445(4)	N2–C7	1.494(30)
S1–C1	1.684(18)	C3–C4	1.522(24)
S2–C1	1.793(14)	C4–C5	1.504(34)
S2–S2A	2.251(6)	C5–C6	1.511(24)
C1–N2	1.314(18)	C6–C7	1.495(24)
S1–Zn1–I1A	105.7(1)	C1–N2–C7	123.9(13)
I1–Zn1–I1A	123.1(1)	C1–N2–C3	123.6(13)
I1–Zn1–S1	107.1(1)	C3–N2–C2	112.5(12)
Zn1–S1–C1	93.1(6)	N2–C3–C4	107.9(15)
C1–S2–S2A	121.7(5)	C3–C4–C5	112.8(18)
S1–C1–S2	121.9(7)	C4–C5–C6	111.0(13)
S2–C1–N2	113.2(10)	C5–C6–C7	111.5(16)
S1–C1–N2	124.9(11)	N2–C7–C6	110.7(18)

Table 3
Bond distances (Å) and angles (°) for [Cd(bipiptds)I_2]

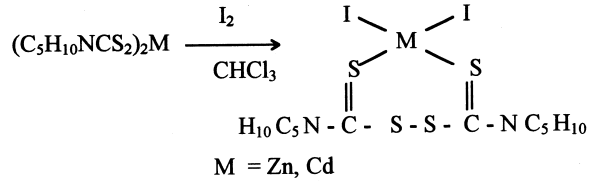
Cd–I1	2.699(1)	N2–C7	1.479(14)
Cd–S1	2.654(3)	C3–C4	1.493(20)
S1–C1	1.687(10)	C4–C5	1.527(21)
S2–C1	1.823(9)	C5–C6	1.511(20)
C1–N2	1.312(14)	C6–C7	1.547(19)
N2–C3	1.482(15)	S2–S2′	1.998(5)
I1–Cd–S1	103.1(1)	C3–N2–C7	112.8(9)
Cd–S1–C1	91.2(3)	N2–C3–C4	108.3(10)
S1–C1–S2	120.5(6)	C3–C4–C5	113.6(10)
S2–C1–N2	112.8(6)	C4–C5–C6	111.2(11)
S1–C1–N2	126.6(7)	C5–C6–C7	109.6(11)
C1–N2–C7	125.5(8)	N2–C7–C6	108.3(9)
C1–N2–C3	121.8(8)		

The unit cell contains eight and four molecules in **1** and **2** respectively. The thiuramdisulfide of piperidinedithiocarbamate and two iodide ions are involved in complex formation with the metal ions. Both the metal ions are in near tetrahedral environment. Two sets of significantly different C–S distances are observed (mean C–S distances: 1.684(18), 1.793(14); 1.687(10) and 1.823(9) Å) for the compounds **1** and **2**, respectively. These distances clearly correspond to single- and double-bonded C–S bonds in each. The two C=S bonds of the disulfides in the present complex are on the same side, as a requirement for coordination with metal.

The Zn–S and Cd–S distances are 2.445(4) and 2.654(3) Å, respectively, which are significantly longer compared to the distances observed in the dithiocarbamate complexes. The M–S interactions, therefore, are relatively weak in [M(bipiptds)I_2] compared to their parent dithiocarbamates. The Zn–I and Cd–I bond distances are 2.552(2) and 2.699(1) Å respectively in keeping with the ionic radii of the central ions. The I–Zn–S and I–Cd–S angles are 107.1(1) and 103.1(1)° respectively, which indicate the near tetrahedral environment around the metal ions.

The disulfide S–S distance in [Cd(bipiptds)I_2) is 1.998(5) Å which is close to the distances observed in free disulfides [14–16]. In the case of [Zn(bipiptds)I_2], the S–S distance is 2.251(6) Å which is longer than those observed in free disulfides. Very significant increase observed in the disulfide S–S bond distance in the present compound is due to the larger strain involved in forcing the two C=S bonds to assume a *cis* form in order to coordinate to the zinc ion. The C–N thioureide distances observed in [Zn(bipiptds)I_2] (1.314(18) Å) and [Cd(bipiptds)I_2] (1.312(14) Å) are similar to those observed in other dithiocarbamate complexes, which confirms the considerable double-bond character associated with the thioureide bonds. The IR spectroscopic data support the structural determinations because ν(C–N) bands occur at 1478 and 1474 cm^{-1} for [Zn(bipiptds)I_2] and [Cd(bipiptds)I_2], respectively, indicating the partial double-bond nature.

Coordination of iodide ions to M(II) ions takes place by a concomitant oxidation of the dithiocarbamate moiety into the corresponding disulfide as per the following reaction:



Supplementary data

Supplementary data are available from the CCDC, 12 Union Road, Cambridge CB2 1EZ, UK; fax: +44-1223-336033; e-mail: deposit@ccdc.cam.ac.uk, on request, quoting the deposition number(s) CCDC 136923 and CCDC 136924.

References

[1] K.A. Fraser, M.M. Harding, Acta Crystallogr. 22 (1967) 75.
[2] H.P. Klug, Acta Crystallogr., Sect. B 21 (1966) 536.
[3] M. Bonamico, G. Marzzone, A. Vaciago, L. Zambonelli, Acta Crystallogr. 19 (1965) 898.
[4] G.M.C. Higgins, B. Saville, J. Chem. Soc. (1963) 2812.
[5] L. Bateman (Ed.), The Chemistry and Physics of Rubber Like Substances, Maclaren, London, 1963, p. 532.
[6] V. Venkatachalam, K. Ramalingam, R. Akilan, K. Sivakumar, K. Chinnakali, Hoong-kun Fun, Polyhedron 15 (1996) 1289.
[7] S. Thirumaran, K. Ramalingam, G. Bocelli, A. Cantoni, Polyhedron, in press.
[8] V. Venkatachalam, K. Ramalingam, G. Bocelli, A. Cantoni, Inorg. Chim. Acta 257 (1997) 49.
[9] P. Gluzinski, Set of Programs for X-ray Structural Calculations, ICHO Polish Academy of Sciences, Warsaw, Poland, 1989.
[10] N. Walker, D. Stuart, Acta Crystallogr., Sect. A 39 (1983) 158.
[11] A. Altomare, M.C. Burla, M. Cumalli, G. Cascarano, C. Giacovazzo, A. Guagliardi, G. Polidori, J. Appl. Crystallogr. 27 (1994) 435.
[12] G.M. Sheldrick, SHELX76, Program for Crystal Structure Determination, University of Cambridge, UK, 1976.
[13] G.M. Sheldrick, SHELX93, Program for Crystal Refinement, University of Göttingen, Germany, 1993.
[14] I.L. Karle, J.A. Esstlin, K. Britis, Acta Crystallogr. 22 (1967) 273.
[15] G.C. Rout, M. Seshasayee, G. Aravamudan, Cryst. Struct. Commun. 11 (1982) 1389.
[16] V. Kumar, G. Aravamudan, M. Seshasayee, Acta Crystallogr., Sect. C 46 (1990) 674.

PERGAMON

www.elsevier.nl/locate/poly

Polyhedron 19 (2000) 1283–1291

POLYHEDRON

Studies on α-$C_3S_5^{2-}$ ($dmit^{2-}$) and its dinuclear Ni(II) complex: spectroscopic and structural characterization

Jonathan G. Breitzer, Thomas B. Rauchfuss *

School of Chemical Sciences and Frederick Seitz Materials Research Laboratory, University of Illinois, Urbana, IL 61801, USA

Received 22 November 1999; accepted 14 March 2000

Abstract

The optical properties of the $dmit^{2-}$ ion ($dmit^{2-}$ = 4,5-dimercapto-1,3-dithiol-2-thiolate) have been characterized under a range of conditions. The oxidatively sensitive anion is highly solvatochromic: λ_{max} = 504 (H_2O), 514 (MeOH), 568 (MeCN), and 632 nm (DMF). With a shift in absorption maximum of 4000 cm^{-1} (DMF versus H_2O), $dmit^{2-}$ is possibly the most solvatochromic species known. The dianion is monoprotonated by NH_4^+ and binds CS_2 to form a thioxanthate ($C_3S_5 \cdot CS_2^{2-}$). ^{13}C NMR measurements of ^{13}C-enriched $dmit^{2-}$ demonstrated that $C_3S_5 \cdot CS_2^{2-}$ exchanges with free CS_2 via an associative pathway involving binding of a second molecule of CS_2. Titration with acid showed that the M_2dmit (M = Na, Cs) dissolves to give the dianion in protic solvents, rather than $Hdmit^-$. The conversion of α-$C_3S_5^{2-}$ to its β-isomer ('Steimecke rearrangement') occurs very slowly with purified Na_2dmit, in contrast to the literature method. The salt $(NBu_4)_2[Ni(dmit)_2]$ is also highly solvatochromic but its behavior does not follow any simple pattern. Treatment of $(NBu_4)_2[Ni(dmit)_2]$ with 1/3 equiv. of $[Ni(NCMe)_6](BF_4)_2$ gave the dinuclear compound $(NBu_4)_2[Ni_2(dmit)_3]$, the first Ni–$dmit^{2-}$ complex with a Ni/$dmit^{2-}$ ratio that is not 1:2. The binuclear salt crystallizes as the CH_2Cl_2 solvate as dark purple prisms. The planar $Ni(dmit)_2^{2-}$ is bridged to Ni(dmit) via two sulfur atoms; the anion features a short Ni–Ni distance of 2.71 Å. ©2000 Elsevier Science Ltd All rights reserved.

Keywords: Dithiolene; Nickel; Dinuclear complexes; Acid–base; Solvatochromism; Carbon disulfide

1. Introduction

The inorganic heterocycle 4,5-dimercapto-1,3-dithiole-2-thione, with formula $C_3S_5^{2-}$ referred to here as $dmit^{2-}$, is the basis for a substantial amount of research. The anion is of interest primarily as a precursor to electronic and photonic materials. This extensive research has been facilitated considerably by the efficient synthesis of $dmit^{2-}$ by the alkali metal reduction of carbon disulfide [1–3]. In this preparation, a mixture of carbon disulfide and dimethylformamide is treated with sodium to give an equimolar mixture of the $dmit^{2-}$ and trithiocarbonate ions. Separation of the two anions is readily achieved by treating the mixture with an aqueous solution of Zn^{2+}, which selectively complexes to the $dmit^{2-}$ (Scheme 1).

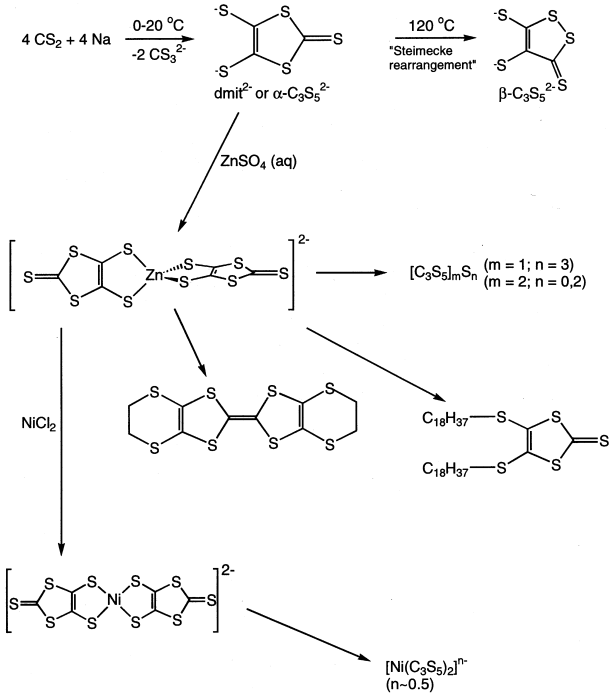
The chemistry of $dmit^{2-}$ can be roughly divided into three branches:

1. Organic derivatives, which are commonly related to the preparation of tetrathiafulvalenes [4], but have been extended to Langmuir–Blodgett films [5].
2. Binary carbon sulfides, illustrated by our recent synthesis of $[C_8S_8]_n$ [6,7].
3. Coordination compounds, illustrated by $[Ni(dmit)_2]^{2-}$ and organometallic derivatives, e.g. $Cp_2Ti(dmit)$ [8–10].

The third area, coordination complexes of $dmit^{2-}$, especially those of nickel, has recently been particularly active. Since 1990, over 200 publications have appeared on derivatives of $[Ni(dmit)_2]^{n-}$ ($0 < n < 2$). This explosion of interest is attributable to the discovery that certain salts of $[Ni(dmit)_2]^{n-}$ are metallic. A representative investigation in this area is the recent electrocrystallization of $[Ni(dmit)_2]^{0.3-}$ with Li(15-crown-5)$^+$ as the counterion. The resulting material was found to be both an electrical and a lithium-ion conductor; such materials are sought for cathode materials in lithium-ion batteries [11]. In addition to displaying metallic conductivity, eight $[M(dmit)_2]^{n-}$ salts (M = Ni, Pd) are superconductors; they are the only transition-metal coordination compounds that have been found to display this property [12]. These remarkable electrical properties are attributed to the sulfur-rich exterior of these complexes that results in relatively strong intra- and inter-stack interactions. Recent work has shown that $[Ni(dmit)_2]^{2-}$ exhibits a large third-order optical non linearity; hence appli-

* Corresponding author. Tel.: +1-217-333-7355; fax: +1-217-333-2685; e-mail: rauchfuz@uiuc.edu

0277-5387/00/$ - see front matter ©2000 Elsevier Science Ltd All rights reserved.
PII S0277-5387(00)00381-8



Scheme 1. Synthesis and reactions of $[Zn(dmit)_2]^{2-}$ and $[Ni(dmit)_2]^{2-}$.

cations of these materials can be envisioned in the area of photonics [13].

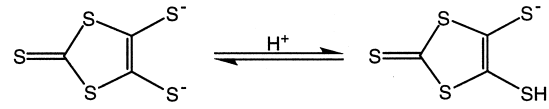
While the organic and coordination chemistries of $dmit^{2-}$ have been examined extensively [14], little attention has been paid to the properties of the dianion itself, as well as some fundamental aspects of its coordination chemistry. The UV–Vis spectrum of $dmit^{2-}$ has been reported previously [15,16], but it appears that both of these reported spectra are not of actual $dmit^{2-}$, but rather the product of air oxidation. A separate report will describe the redox properties of $dmit^{2-}$ and related thioanions [17].

In this paper, the spectroscopic properties of $dmit^{2-}$ are examined, and conclusions about the chemistry of this species are drawn from these properties. As indicated above, the $[Ni(dmit)_2]^{n-}$ system has been heavily examined for various oxidation states of nickel; this paper reports the first homoleptic Ni–dmit complex in which the dmit/Ni^{2+} ratio is other than 2:1 and illustrates a new bridging mode for the $dmit^{2-}$ ligand [18–22].

2. Results and discussion

2.1. Acid–base properties of $dmit^{2-}$

One of the surprising properties of $dmit^{2-}$ that has not been systematically investigated is its apparent solvatochromism (vide infra). Prior to investigating this property, we needed to determine whether the wide variety of absorption maxima exhibited by $dmit^{2-}$ in various solvents is due to actual solvatochromism or to protonation of $dmit^{2-}$ in protic solvents. DMF solutions of Na_2dmit and Cs_2dmit (the Cs salt crystallizes well and is less hygroscopic than the sodium salt [23]) are deep blue, having a λ_{max} at 632 nm ($\varepsilon = 5510\ M^{-1}\ cm^{-1}$). A DMF solution of Cs_2dmit turns red immediately on treatment with an excess of NH_4Br, with an absorption maximum (510 nm) close to that of a methanolic solution of Na_2dmit (514 nm), as shown in Fig. 1. We assign the red color in DMF to the monoprotonated species $dmitH^-$ (Eq. 1), rather than the diprotonated species, because H_2dmit, which is deep yellow in solution, decomposes, eliminating H_2S to form C_6S_8, an insoluble solid [25].



(1)

Based on the similarity of the optical properties of $dmitH^-$ in DMF and $dmit^{2-}$ in methanol, we originally concluded that $dmit^{2-}$ is so basic ($pK_a > 15$) that it actually exists as $dmitH^-$ in water and methanol. Subsequent investigations established, however, that $dmit^{2-}$ indeed exists as a dianion in water and methanol [24]. A solution of Cs_2dmit in oxygen-free water ($\lambda_{max} = 504$ nm) has similar spectroscopic properties to those of a methanolic solution of Na_2dmit. No color change was observed after treatment with a large excess of NaOH; this observation alone would mean that either $dmit^{2-}$ exists as such in water, or that $dmit^{2-}$ is extremely basic (i.e. $Hdmit^-$ is not deprotonated by NaOH).

To distinguish these possibilities, an aqueous Cs_2dmit solution was titrated (anaerobically) with HCl, monitoring by UV–Vis spectroscopy (Fig. 2). Isobestic behavior was observed at ≤ 1 equiv. of HCl; the solution was yellow and homogeneous at that point. Only upon addition of > 1 equiv. of HCl did a precipitate form; this precipate is either $H_2C_3S_5$ or its decomposition product C_6S_8 [25]. Based on the data from the titration of $dmit^{2-}$ with HCl, we conclude that $dmit^{2-}$ exists as the dianion in both protic (water, methanol) and aprotic solvents (DMF). The conclusion that $dmit^{2-}$ exists as the dianion in both protic and aprotic solvents means that the variation of color in different solvents is actually due

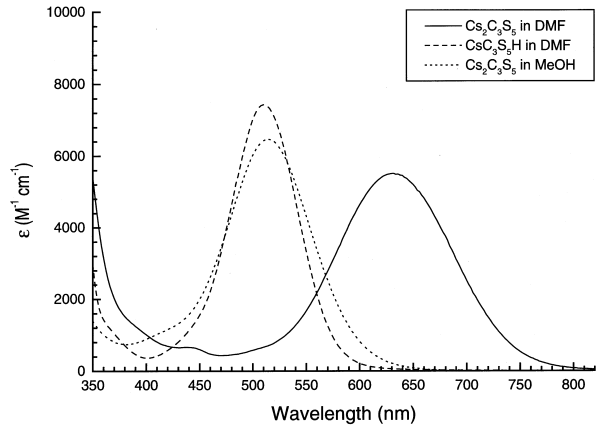


Fig. 1. Comparison of UV–Vis spectra of Na_2dmit in MeOH solution and NaHdmit in DMF solution, and UV–Vis spectrum of Na_2dmit in DMF solution.

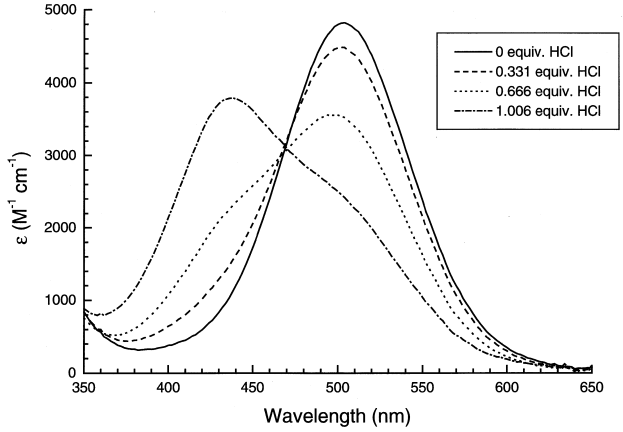


Fig. 2. UV–Vis spectra for the titration of aqueous Cs_2dmit with HCl.

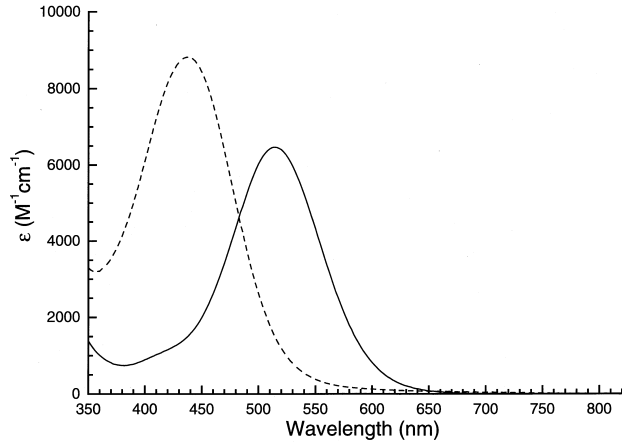


Fig. 3. UV–Vis spectra of Na_2dmit in MeOH solution before (solid) and after (dotted) oxidation with air.

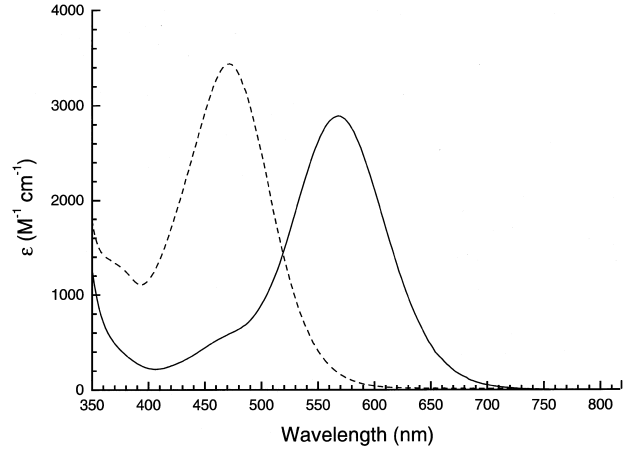


Fig. 4. UV–Vis spectra of Na_2dmit in MeCN solution before (solid) and after (dotted) oxidation with air.

to solvatochromism, and it is only coincidence that $dmitH^-$ in DMF and $dmit^{2-}$ in water/methanol have similar absorption maxima.

2.2. Optical properties of $dmit^{2-}$

The free anion, $dmit^{2-}$, can be made soluble in water and non-protic solvents, and is oxygen sensitive in all of them. The color of $dmit^{2-}$ in solution is dependent on the solvent, ranging from red in water and methanol to blue in DMF. The most convenient preparation of the free anion involves the addition of excess NaOMe to a methanolic suspension of the thioester, $C_3S_5[C(O)Ph]_2$ [26], giving Na_2dmit as a red solution (Eq. 2) ($\lambda_{max}=514$ mm, $\varepsilon=5710\ M^{-1}\ cm^{-1}$), having an absorption maximum at 514 nm.

$$C_3S_5[C(O)Ph]_2 + 2NaOMe \rightarrow Na_2C_3S_5 + 2MeOC(O)Ph \quad (2)$$

Fig. 3 shows the UV–Vis spectrum of Na_2dmit in methanol before and after exposure to air for a few seconds. The yellow coloration for $dmit^{2-}$ solutions ($\lambda_{max}=438$ nm) indicates oxidation. The red color of authentic Na_2dmit in methanol ($\lambda_{max}=514$ nm) has been described by Svenstrup, Matsubayashi and others [4,27], and these results were confirmed by us. The absorption maximum of Na_2dmit in ethanol has however been listed by Reuter and Gattow to be 412 nm [15], which may actually be this yellow oxidized species. Removing the solvent from a methanolic Na_2dmit solution and adding dry, oxygen-free acetonitrile results in a purple solution ($\lambda_{max}=568$ nm). As shown in Fig. 4, this solution also turns yellow within seconds on exposure to air ($\lambda_{max}=472$ nm). Singh and Singh [16] recently listed the absorption of Na_2dmit in acetonitrile to be 475 nm; again, based on the similarities of the listed absorption maxima, the compound they examined appears to have been an oxidized derivative of $dmit^{2-}$.

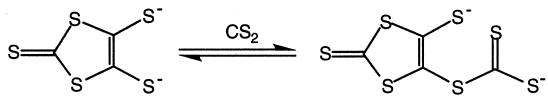
Because the energy of the absorption maximum increases with increasing solvent polarity, the effect is characterized as hypsochromism. The difference between the absorption maxima for $dmit^{2-}$ in water and in DMF corresponds to 4020 cm^{-1}; this response to solvent polarity is comparable to (or exceeds) the most solvatochromic compounds known. One such compound is a merocyanine dye [28] with a difference in absorbance maxima of 9500 cm^{-1}, but this is between toluene and water, which is a greater range of polarity than is available for $dmit^{2-}$ due to solubility constraints.

2.3. The $dmit^{2-}$–CS_2 system

In the most widely used synthetic route to $dmit^{2-}$, CS_2 is reduced with sodium metal in DMF solution. The $dmit^{2-}$ anion is not isolated directly; instead, it is usually coordinated to Zn^{2+} and isolated as the salt, $(R_4N)_2[Zn(C_3S_5)_2]$. Prior to the addition of zinc, however, the $dmit^{2-}$ solution is bright red. Such a solution should be anhydrous and highly basic, considering the presence of the Na_2CS_3 byproduct and the excess Na. It is therefore inconceivable that such a solution would contain a significant amount of the protonated species, $dmitH^-$. Another explanation is required to explain the red color of the reaction mixture, rather than the blue color ($\lambda_{max}=632$ nm) observed for M_2dmit in DMF (M = Na, Cs).

We initiated a series of experiments based on the hypothesis that the red coloration of the crude (but anhydrous) reaction solutions is due to adducts of CS_2 and $dmit^{2-}$. CS_2 is known to form adducts with a variety of nucleophiles, including thiolates [29–31], and CS_2 is usually used in a large excess in the synthesis of $dmit^{2-}$. Furthermore, the CS_2 adduct of β-$C_3S_5^{2-}$ (an isomer of $dmit^{2-}$, see Scheme 1) has been crystallographically characterized [32]. We found that the addition of CS_2 to a DMF solution of Cs_2dmit effected an immediate color change from blue to the red color of the synthesis solution ($\lambda_{max} = 490$ nm).

We further investigated the nature of the CS_2–$dmit^{2-}$ reaction through ^{13}C NMR studies using ^{13}C-enriched $dmit^{2-}$. Due to the high cost of $^{13}CS_2$, we first modified the synthesis of $dmit^{2-}$ so that it uses CS_2 more efficiently. Fig. 5 shows a ^{13}C NMR spectrum of a DMF-d_7 solution of ^{13}C-enriched $dmit^{2-}$. ^{13}C NMR resonances are observed at δ 209 and 144, which are assigned to the thiocarbonyl and the alkenyl centers, respectively. Upon treatment of this solution with an excess of unlabeled CS_2 (δ 193), a new species was formed, having signals at δ 214 (*C*=S) and broad signals at δ 172 and 122. The latter two peaks are assigned to the now-inequivalent alkenyl carbon centers of the CS_2 monoadduct of $dmit^{2-}$ (Eq. 3).



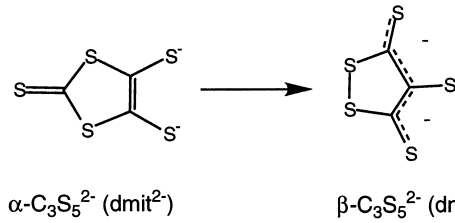
(3)

The broadness of these alkenyl peaks is attributed to an exchange of the trithiocarbonate and thiolate functions.

The excess CS_2 was then removed from the DMF solution by distillation under reduced pressure. The ^{13}C NMR spectrum of the resulting purplish solution shows the absence of free CS_2 and resonances corresponding to both $dmit^{2-}$ and $C_3S_5 \cdot CS_2^{2-}$.

2.4. Comments on the Steimecke rearrangement

It is well known that a mixture of sodium and carbon disulfide in DMF, when heated to 120°C, produces an isomer of $dmit^{2-}$, which we previously termed [25] β-$C_3S_5^{2-}$ (Eq. 4).



(4)

It was of interest to know whether this isomerization mechanism is intramolecular or whether other species are involved. UV–Vis spectroscopy would be suitable for monitoring this isomerization because of the different optical properties of the two isomers: the λ_{max} of $dmit^{2-}$ in DMF is 632 nm (blue color, as stated above), while the λ_{max} of β-$C_3S_5^{2-}$ in DMF is 530 nm (red color). A DMF solution of Na_2dmit remained unchanged after 24 h at 120°C, based on UV–Vis measurements. This initial experiment was conducted at a concentration (6×10^{-5} M) appropriate for UV–Vis spectroscopy. Recognizing the possibility that the rearrangement might be bimolecular, the experiment was repeated at a concentration (0.8 M) closer to that typically used in a reaction mixture [25]; however, the characteristic color change required approximately 15 days at 120°C. Evidently a catalyst, which we have not identified, is present in the reaction mixture when the Steimecke rearrangement is carried out.

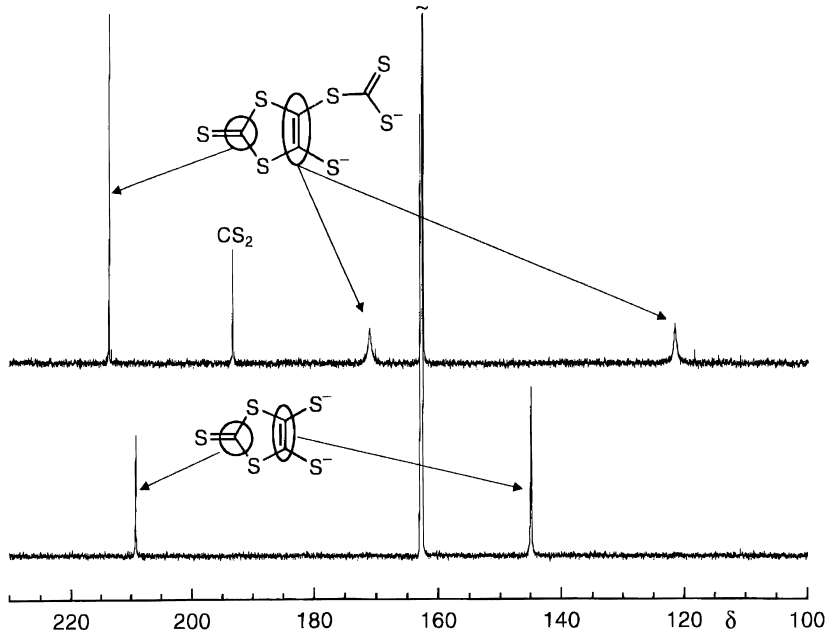


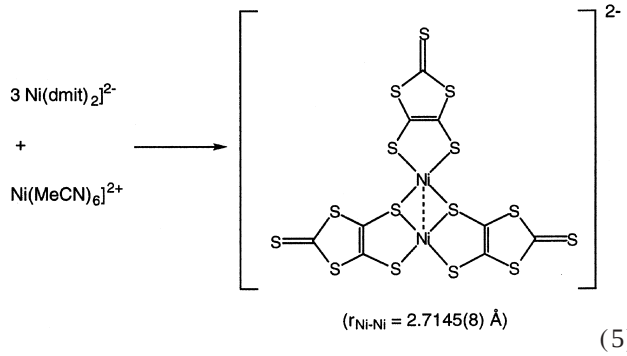
Fig. 5. 125 MHz ^{13}C NMR spectra (DMF-d_7) of Cs_2dmit (bottom), Cs_2dmit with excess CS_2 added (middle), and with most of the CS_2 removed (top).

2.5. Comments on the optical properties of $[Ni(dmit)_2]^{2-}$

We began this aspect of the work by examining the solution properties of $[Ni(dmit)_2]^{2-}$, the precursor to many conductive materials [33,34]. Spectrophotometric measurements show that $(NBu_4)_2[Ni(dmit)_2]$ is highly solvatochromic. The position of its absorption maximum does not, however, correlate with the $E_T(30)$ or the E_T^N solvent index of Reichardt and Harbusch-Goernert [35] of the solvent. THF ($E_T^N = 0.207$) solutions are blue, with a λ_{max} of 596 nm. DMF ($E_T^N = 0.386$) solutions are green, with a λ_{max} of 626 nm. This would seem to indicate that the compound is bathochromic; however, the trend reverses for acetonitrile (E_T^N index = 0.46, λ_{max} = 596 nm, blue solution) and methanol (E_T^N index = 0.762, λ_{max} = 554 nm, purple solution). There may be other factors affecting the absorption maximum besides solvatochromism, such as dimerization or ligation of a solvent.

2.6. Synthesis and structure of $[Ni_2(dmit)_3]^{2-}$

While the $[Ni(dmit)_x]^{n-}$ system has been investigated for many values of *n*, variations in *x*, the Ni/dmit ratio, have not been reported. Treatment of an acetonitrile solution of $(NBu_4)_2[Ni(dmit)_2]$ with 1/3 equiv. of $[Ni(MeCN)_6]^{2+}$ gave a red solution containing the salt $(NBu_4)_2[Ni_2(dmit)_3]$ (Eq. 5).



(5)

In contrast to $[Ni(dmit)_2]^{2-}$, solutions of the dinickel compound are sensitive to oxygen. This finding is somewhat counterintuitive because the negative charge is delocalized over a larger molecule. A major product of air oxidation of this compound was characterized crystallographically to be $(NBu_4)[Ni(dmit)_2]$, which is well known [36–38].

The structure of $(NBu_4)_2[Ni_2(dmit)_3]$ was established by single crystal X-ray diffraction (Fig. 6). The anion is binuclear with two bridging dmit ligands such that the complex has idealized C_s symmetry. Bond lengths and angles are listed in Table 1. The noteworthy feature is the Ni–Ni distance of 2.7145(8) Å. An example of a compound with an unsupported Ni–Ni bond is $[Ni(C_{10}H_{14}N_8)]_2$ [39], with a Ni–Ni bond distance of 2.788(2) Å. This establishes that the nickel–nickel distance observed in this work is close enough to be characterized as a bond. The ethanedithiolate derivative $[Ni_2(S_2C_2H_4)_3]^{2-}$ [40] has a wider average Ni–S–Ni angle

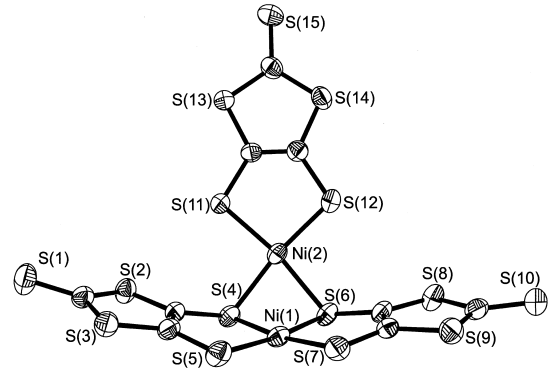
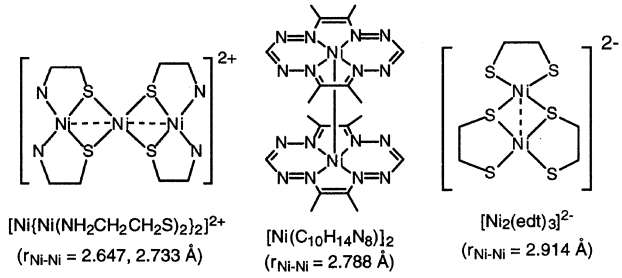


Fig. 6. The molecular structure of the anion, $[Ni_2(dmit)_3]^{2-}$, with thermal ellipsoids at the 50% probability level.

Table 1
Selected bond lengths (Å) and angles (°) for the anion in $(Bu_4N)_2[Ni_2(C_3S_5)_3]\cdot CH_2Cl_2$

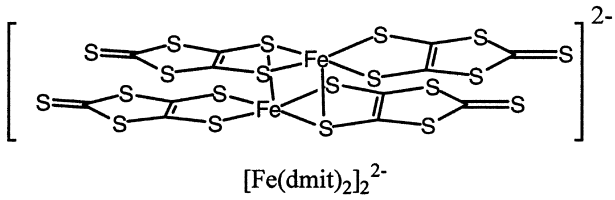
Ni(1)–Ni(2)	2.7145(8)	S(4)–C(4)	1.745(5)
Ni(1)–S(7)	2.1699(13)	S(11)–C(1)	1.734(5)
Ni(1)–S(4)	2.1696(13)	S(12)–C(2)	1.745(5)
Ni(1)–S(6)	2.1803(14)	C(4)–C(5)	1.349(6)
Ni(1)–S(5)	2.1839(14)	C(2)–C(1)	1.354(6)
Ni(2)–S(12)	2.1699(14)	C(7)–C(8)	1.353(6)
Ni(2)–S(11)	2.1794(13)		
Ni(2)–S(4)	2.2367(14)	Ni(1)–S(4)–Ni(2)	76.04(4)
Ni(2)–S(6)	2.2449(13)	Ni(1)–S(6)–Ni(2)	75.66(4)
S(6)–C(7)	1.747(5)	S(7)–Ni(1)–S(4)	171.96(6)
S(5)–C(5)	1.735(5)	S(6)–Ni(1)–S(5)	173.40(5)
S(7)–C(8)	1.730(5)	S(4)–Ni(1)–S(5)	94.29(5)
		S(4)–Ni(2)–S(6)	77.63(5)

(83.4°) than that observed here (75.8°) and a correspondingly longer Ni–Ni distance (2.914(1) Å).



Although not completely analogous in structure, an example of a short Ni–Ni bond distance bridged by a thiolate is the cation $[Ni\{Ni(NH_2CH_2CH_2S)_2\}_2]^{2+}$ [41]. Here, the two nickel–nickel distances are 2.733 and 2.647 Å, the range of these distances indicates the 'softness' of the Ni–Ni interaction. An explanation is required for an apparently attractive interaction involving a pair of filled $3d_{z^2}$ orbitals. Under lower symmetry, the $3d_{z^2}$ orbitals mix with empty $4p_z$ orbitals. This mixing lowers the energies of the $3d_{z^2}$ orbitals, resulting in a weak bonding interaction overall. The idealized symmetry environment around the nickel atoms in $[Ni_2(dmit)_3]^{2-}$ is C_s, which would also allow for mixing of the $3d_{z^2}$ and $4p_z$ orbitals on the nickel centers.

Although no compound has been structurally characterized in which $dmit^{2-}$ bridges two metal centers in an analogous fashion to $[Ni_2(dmit)_3]^{2-}$, there are other examples of bridging $dmit^{2-}$ ligands, such as in the $Cp^*_2Fe^+$ salt of $[Fe(dmit)_2]_2^{2-}$ [20].

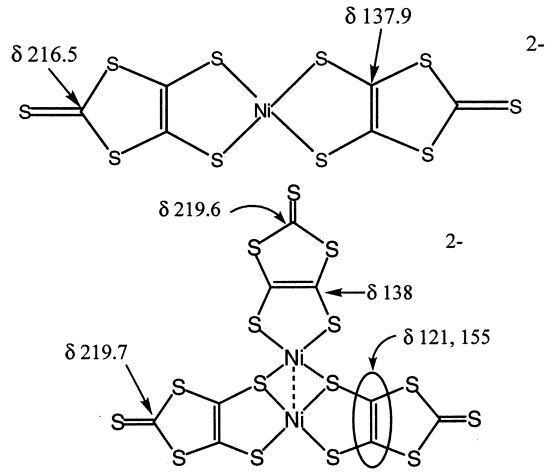


$[Fe(dmit)_2]_2^{2-}$

In this anionic dimer, the iron atoms are in a square pyramidal environment. Only one thiolate sulfur from the $dmit^{2-}$ ligand functions as a bridging ligand. The Fe–S bond lengths, both within and between $[Fe(dmit)_2]^-$ units, are all 2.24 ± 0.01 Å.

^{13}C NMR measurements were conducted on solutions of $[Ni_2(dmit)_3]^{2-}$ in order to establish its solution structure. Due to the lack of nOe effects and limited solubility, these measurements were carried out using a 10 mm sample tube and $dmit^{2-}$ that was ~16% ^{13}C. The ^{13}C NMR spectrum of $(NBu_4)_2[Ni(dmit)_2]$ features resonances at 216.5 and 137.9 [42].

On the basis of the crystallographic results, one would expect five resonances for $[Ni_2(dmit)_3]^{2-}$: three for the ethylenic carbon atoms and two for the thiocarbon atoms. The ^{13}C NMR spectrum is shown in Fig. 7. Due to the ^{13}C enrichment, ^{13}C–^{13}C coupling is evident as satellites around two of the peaks. The assignments for the peaks are as follows:



The peaks at δ 121 and 155 can be assigned to the alkenyl carbons in the $Ni(dmit)_2$ moiety because the satellites indicate coupling to a carbon in a different environment. The peak at δ 138 has no satellites, so it can be assigned to the other alkenyl carbons. The thione carbons are in such similar environments that their chemical shifts differ by only 0.1 ppm.

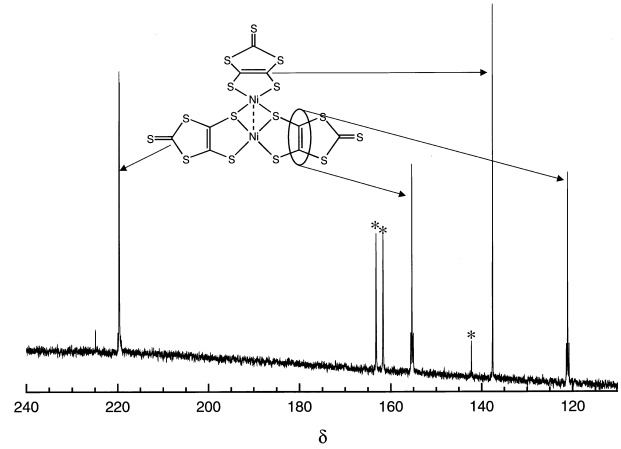
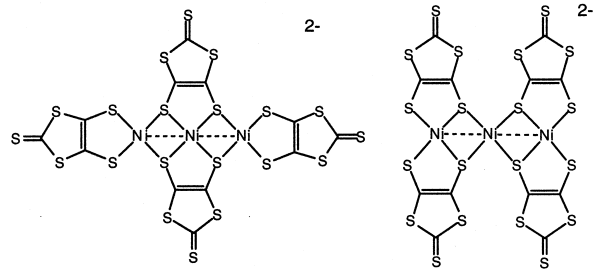


Fig. 7. 125 MHz ^{13}C NMR spectra (CD_2Cl_2) of $(Bu_4N)_2[Ni_2(dmit)_3]$. The peaks labeled with asterisks are assigned to a higher nuclearity impurity discussed in Section 2.7.

2.7. Higher oligomers of Ni–dmit^{2-}

Inspection of the ^{13}C NMR spectrum of $[Ni_2(dmit)_3]^{2-}$ reveals two additional peaks at δ 162 and 163. We attribute these to the alkenyl carbon atoms in a higher-nuclearity derivative of $Ni(dmit)_2^{2-}$. Two possible structures of this impurity are shown below.



A **B**

Both of these structures would have two types of ethylenic carbons. The ethanedithiolate analog of **B** is known [43]. However, **A** appears to be the more plausible in this case due to the lack of ^{13}C–^{13}C coupling in its NMR spectrum. The ^{13}C NMR spectrum of $(Bu_4N)_2[Ni_2(dmit)_3]$ in acetone-d_6 shows no evidence for this higher-nuclearity impurity.

Combining MeCN solutions of $Ni(dmit)_2^{2-}$ and $[Ni(MeCN)_6](BF_4)_2$ in a 1:1 ratio produced a greenish solid, which analyzed as $(Bu_4N)_2[Ni_{15}(dmit)_{16}]$. A similar study was carried out on the nickel complex of the β-$C_3S_5^{2-}$. Treatment of $(Bu_4N)_2[Ni(\beta\text{-}C_3S_5)_2]$ with $[Ni(MeCN)_6](BF_4)_2$ resulted only in an insoluble product; no intermediate products were detected. The black solid analyzed as NiC_3S_5, and preliminary electrical measurements on a pressed pellet of this solid showed it to be insulating.

3. Summary

The following are the principal conclusions of this study.

1. The $dmit^{2-}$ ion is strongly solvatochromic, having an absorption that shifts to higher energy with increasing

solvent polarity. Its color in solution ranges from red in water and methanol to blue in DMF.
2. Aqueous and alcoholic solutions of $dmit^{2-}$ indeed consist of the dianion, not the monoprotonated monoanion, $Hdmit^{-}$. The extreme solvatochromism combined with the oxygen sensitivity has been the source of previous confusion in this area.
3. CS_2 reversibly binds $dmit^{2-}$ to give the thioxanthate ($C_3S_5 \cdot CS_2^{2-}$). This adduct exchanges with free CS_2.
4. DMF solutions of pure $dmit^{2-}$ undergo the Steimecke rearrangement much more slowly than in the reaction mixture used for β-$C_3S_5^{2-}$ synthesis.
5. The well known anion $[Ni(dmit)_2]^{2-}$ reacts with a source of Ni^{2+} to form $[Ni_2(dmit)_3]^{2-}$, which features a short Ni–Ni distance ($\sim$2.71 Å).

4. Experimental

4.1. Materials and methods

$^{13}CS_2$ was obtained from Cambridge Isotopes (Cambridge, OH, USA). $[Ni(MeCN)_6](BF_4)_2$ was prepared from Ni metal and $NOBF_4$ [44]. The $C_3S_5(COPh)_2$ was prepared from the treatment of $(Bu_4N)_2[Zn(C_3S_5)_2]$ [2] with benzoyl chloride [1]. Unless otherwise noted, reactions and work-ups were conducted under nitrogen using degassed solvents. Electronic spectra were collected using an HP8452 diode-array spectrophotometer. A 1 cm path length cell was used.

4.2. Synthesis

4.2.1. Preparation of ^{13}C-enriched $(Bu_4N)_2[Zn(C_3S_5)_2]$

The usual methods for the preparation of $dmit^{2-}$ [2,45] were revised so as to make the most efficient use of $^{13}CS_2$, which is expensive. The $^{13}CS_2$ was diluted with five portions of isotopically normal CS_2. An alloy was prepared from potassium metal (0.94 g, 0.0233 mol) and sodium metal (0.515 g, 0.0224 mol), and was chilled to 0°C. Distilled DMF (10 ml) was added, followed by ^{13}C-enriched CS_2, prepared as above (2.41 ml, 0.0401 mol). The mixture took on a yellow color immediately, which progressed through orange to a deep red within 15 min. The reaction mixture was allowed to warm to room temperature over the course of 24 h, after which the mixture became a purplish-blue, porous semisolid. Residual alkali metal was oxidized with isopropanol (20 ml), followed by a few milliliters of ethanol. After 0.5 h, most of the alcohols were removed by evaporation. The purple DMF solution was treated with a solution of $ZnSO_4 \cdot 7H_2O$ (1.44 g, 5.01 mmol) in water (50 ml), chilled to 0°C, and treated with a solution of Bu_4NBr (3.24 g, 10.1 mmol) in water (50 ml). A fine red powder formed, which was collected. This was recrystallized by dissolution in $\sim$20 ml of acetone, diluting with a similar volume of methanol, and successively concentrating and diluting with methanol until red crystals formed, which were washed with ether. Yield: 2.32 g, 49% based on CS_2.

4.2.2. Preparation and characterization of $dmit^{2-}$

$Cs_2C_3S_5 \cdot 1.5H_2O$ was prepared from $C_3S_5(COPh)_2$ and $CsOH \cdot H_2O$ according to the method of Gasiorowski et al. [24]. The ^{13}C NMR spectrum was collected of a solution of the ^{13}C-enriched $Cs_2C_3S_5$ (0.06 g, 0.12 mmol in $\sim$0.8 ml of DMF-d_7). UV–Vis spectroscopic characterization was carried out by charging a sealed cuvette with a DMF solution (10 ml, 0.12 mM) of $Cs_2C_3S_5 \cdot 1.5H_2O$ in an inert atmosphere chamber. ^{13}C NMR (DMF-d_7): δ 209, 145. UV–Vis, λ_{max}, nm (ε, $M^{-1}\,cm^{-1}$): 628 (5500). The solution used for the UV–Vis measurement (4 ml, 1.2×10^{-4} M) was treated with 0.02 g (0.2 mmol) of NH_4Br, which did not fully dissolve. UV–Vis, λ_{max}, nm (ε, $M^{-1}\,cm^{-1}$): 510 (7430).

4.2.3. ^{13}C NMR monitoring of the $dmit^{2-} + CS_2$ reaction

The solution of 0.06 g (0.12 mmol) of ^{13}C-enriched Cs_2dmit used for the ^{13}C NMR spectroscopic characterization (see above) was treated with 0.08 ml of isotopically normal CS_2 (1.3 mmol), causing the color to turn from blue to orange–red immediately. ^{13}C NMR (DMF-d_7): δ 213, 193 (CS_2), 171 (br), 122 (br). Most of the CS_2 was then removed by subjecting the red solution briefly to a dynamic vacuum, causing the color to turn from orange–red to purple. ^{13}C NMR (DMF-d_7): δ 213, 171, 122. See Fig. 5.

4.2.4. $(Bu_4N)_2[Ni_2(C_3S_5)_3] \cdot CH_2Cl_2$

The ^{13}C-labeled nickel coordination compound, $(Bu_4N)_2[Ni(*C_3S_5)_2]$ (*C = 16% ^{13}C), was prepared from $(Bu_4N)_2[Zn(*C_3S_5)_2]$ according to literature procedures [1]. A solution of 0.1790 g (0.1910 mmol) of $(Bu_4N)_2[Ni(*C_3S_5)_2]$ in acetonitrile (20 ml) was treated with a solution of $[Ni(NCCH_3)_6](BF_4)_2$ (0.0321 g, 0.064 mmol) in CH_3CN (0.5 ml). Within seconds, the color of the solution changed from green to red. The MeCN was removed by evaporation, and the residue extracted into CH_2Cl_2 in $\sim$0.5 ml. Dilution with diethyl ether ($\sim$1 ml) produced dark purple crystals. Yield: 0.1454 g, 96%. *Anal*. Calc. for $C_{42}H_{74}N_2Cl_2Ni_2S_{15}$: C, 39.52; H, 5.84; N, 2.19. Found: C, 39.54; H, 6.03; N, 2.07%. ^{13}C NMR (CD_2Cl_2): δ 121 (s, 16% d, $J_{C-C} = 0.6$ Hz), 138 (s), 155 (s, 16% d, $J_{C-C} = 0.6$ Hz), 162 (s), 163 (s), 219.6 (s), 219.7 (s). ^{13}C NMR (acetone-d_6): δ 121 (s, 16% d, $J_{C-C} = 0.6$ Hz), 138 (s), 156 (s, 16% d, $J_{C-C} = 0.6$ Hz), 220 (s).

4.2.5. Titration of $Cs_2C_3S_5$ with HCl

$Cs_2C_3S_5$ (32.0 mg, 69.2 μmol) was dissolved in deionized, oxygen-free water (12.46 ml) to make a 5.56 mM 'stock' solution. This solution was treated with 1 equiv. of HCl in steps of 0.1 equiv. After each step, a UV–Vis spectrum was collected by diluting a small aliquot of the reaction mixture to about 0.06 mM in a 1 cm path length cuvette fitted with a valve to exclude air. In calculating the equivalents added, the

total amount of $Cs_2C_3S_5$ was adjusted for the aliquots used for the measurements.

4.2.6. Attempted Steimecke rearrangement of Na_2dmit

Sodium metal (0.0247 g, 1.07 mmol) was allowed to react with 8 ml of MeOH. To this solution was added the thioester $C_3S_5(COPh)_2$. This yellow slurry was allowed to react for 30 min at ambient temperature, then the methanol was removed by evaporation. The pink residue was washed with ether (4×15 ml) to remove the methyl benzoate byproduct. Anhydrous DMF (7.5 ml) was added to the residue, resulting in a blue solution of the $dmit^{2-}$ salt and solid NaOH. An aliquot (15 ml) of the solution was decanted from the NaOH and added to DMF (7.5 ml) in a 1 cm path length cell (conc. 5.9×10^{-5} M). No change, either in appearance or UV–Vis spectroscopic properties, was observed after 3.8 h at 100.5°C. 0.8 M solution of $Na_2{}^-$dmit ($\sim$1 ml), prepared in a similar manner, was then flame-sealed in a Pyrex tube and maintained at 12 °C. No color change was observed after 21 h. After 15 days, the color was deep brown.

4.2.7. Crystallographic analysis of $(Bu_4N)_2[Ni_2(C_3S_5)_3]\cdot CH_2Cl_2$

A CH_2Cl_2 solution of $(Bu_4N)_2[Ni_2(C_3S_5)_3]\cdot CH_2Cl_2$ was layered with diethyl ether. A black, prismatic crystal of approximate dimensions $0.14\times0.14\times0.18$ mm was selected for analysis and mounted on a glass fiber with Paratone-E (Exxon). Intensity data were collected at 198(2) K using a Siemens CCD area detector utilizing Mo Kα radiation ($\lambda=0.71073$ Å). The completeness of data collection in the range $2\theta=3.22$ to 56.56° was 96.5%. The data were corrected for absorption using the empirical method with maximum and minimum transmission factors of 0.9901 and 0.8546, respectively. The data merged to form a set of 14320 independent reflections with $R_{int}=0.0734$. The space group, $P2_1/n$ (no. 14), was selected on the basis of systematic conditions and was verified by subsequent refinement. The structure was solved by direct methods and refined by full-matrix least-squares methods on F^2. Hydrogen atom positions were calculated using a riding model. All non-hydrogen atoms were refined anisotropically. The SOF for one of the butyl groups was refined between two positions. The largest peak and hole in the difference map was 0.529 and -0.509 e Å^{-3}, respectively. Additional crystal data: $a=17.7947(5)$, $b=14.4605(4)$, $c=23.7863(6)$ Å; $\beta=102.38°$; $V=5978.9(3)$ Å^3; $Z=4$; $\rho(\text{calc})=1.418$ Mg m^{-3}; $\mu=1.274$ mm^{-1}; index ranges $-18\le h\le23$, $-19\le k\le19$, $-31\le l\le14$; number of data and parameters 14320 and 595, respectively; final R_1/wR_2 ($I>2\sigma(I)$) 0.0665/0.1032; GoF = 1.077.

Supplementary data

Supplementary data are available from the Cambridge Crystallographic Data Centre, 12 Union Road, Cambridge CB2 1EZ, UK (fax: +44-1223-336033; e-mail: deposit@ccdc.cam.ac.uk) on request, quoting the deposition number CCDC 133733.

Acknowledgements

This research was supported by the Department of Energy (DOE DEFG02-96ER45439).

References

[1] G. Steimecke, H.-J. Sieler, R. Kirmse, E. Hoyer, Phosphorus Sulfur 7 (1979) 49.
[2] L. Yu, D. Zhu, Phosphorus Sulfur Silicon 116 (1996) 225. C.S. Wang, A.S. Batsanov, M.R. Bryce, J.A.K. Howard, Synthesis (1998) 1615.
[3] G.S. Girolami, T.B. Rauchfuss, R.J. Angelici, Synthesis and Technique in Inorganic Chemistry, University Science Books, Sausalito, CA, 1999.
[4] N. Svenstrup, J. Becher, Synthesis (1995) 215.
[5] Y. Zhang, M.A. Firestone, T.B. Rauchfuss, P.W. Bohn, J. Phys. Chem. 100 (1996) 13804.
[6] J.-H. Chou, T.B. Rauchfuss, J. Am. Chem. Soc. 119 (1997) 4537.
[7] J.-H. Chou, T.B. Rauchfuss, Z. Naturforsch., Teil B 52 (1997) 1549.
[8] M. Fourmigué, Coord. Chem. Rev. 178–180 (1998) 823.
[9] A.E. Pullen, R.-M. Olk, Coord. Chem. Rev. 188 (1999) 211.
[10] X. Yang, T.B. Rauchfuss, S.R. Wilson, J. Am. Chem. Soc. 111 (1989) 3465.
[11] T. Nakamura, T. Akutagawa, K. Honda, A.E. Underhill, A.T. Coomber, R.H. Friend, Nature 394 (1998) 159.
[12] A.E. Pullen, R.-M. Olk, S. Zeltner, E. Hoyer, K.A. Abboud, J.R. Reynolds, Inorg. Chem. 36 (1997) 958.
[13] I. Malfant, N. Cordente, P.G. Lacroix, C. Lepetit, Chem. Mater. 10 (1998) 4079.
[14] R.-M. Olk, W. Dietzsch, J. Mattusch, J. Stach, C. Nieke, E. Hoyer, W. Meiler, W. Robien, Z. Anorg. Allg. Chem. 544 (1987) 199.
[15] U. Reuter, G. Gattow, Z. Anorg. Allg. Chem. 421 (1976) 143.
[16] J.D. Singh, H.B. Singh, Polyhedron 12 (1993) 2849.
[17] J.G. Breitzer, L.F. Szczepura, T.B. Rauchfuss, manuscript in preparation.
[18] G.-E. Matsubayashi, A. Yokazawa, J. Chem. Soc., Chem. Commun. (1991) 68.
[19] G. Matsubayashi, K. Natsuaki, M. Nakano, H. Tamura, R. Arakawa, Inorg. Chim. Acta 262 (1997) 103.
[20] S. Tanaka, G.-E. Matsubayashi, J. Chem. Soc., Dalton Trans. (1992) 2837.
[21] E. Cerrada, A. Laguna, M. Laguna, P.G. Jones, J. Chem. Soc., Dalton Trans. (1994) 1325.
[22] E. Cerrada, P.G. Jones, A. Laguna, M. Laguna, Inorg. Chem. 35 (1996) 2995. H. Tamura, S. Tanaka, G.-E. Matsubayashi, W. Mori, Inorg. Chim. Acta 232 (1995) 51.
[23] R. Gasiorowski, T. Jorgensen, J. Moller, T.K. Hansen, M. Pietraszkiewicz, J. Becher, Adv. Mater. 4 (1992) 568.
[24] S. Schmidt, F. Dietze, A. Jokuszies, S. Zeltner, R.-M. Olk, J. Reinhold, E. Hoyer, Sulfur Lett. 19 (1995) 119.
[25] C.P. Galloway, D.D. Doxsee, D. Fenske, T.B. Rauchfuss, S.R. Wilson, X. Yang, Inorg. Chem. 33 (1994) 4537.
[26] K.S. Varma, A. Bury, N.J. Harris, A.E. Underhill, Synthesis 9 (1987) 837.
[27] G.-E. Matsubayashi, K. Akiba, T. Tanaka, Inorg. Chem. 27 (1988) 4744.
[28] C. Reichardt, Chem. Rev. 94 (1994) 2319.
[29] D. Hoerner, G. Gattow, Z. Anorg. Allg. Chem. 442 (1978) 195.
[30] J. Shi, A. Linden, H. Heimgartner, Helv. Chim. Acta 77 (1994) 1903.

[31] G. Gattow, W. Behrendt, Carbon Sulfides and Their Inorganic and Complex Chemistry, vol. 2, Georg Thieme, Stuttgart, 1977.
[32] D. Lentz, S. Ruediger, K. Seppelt, J. Fluorine Chem. 84 (1997) 103.
[33] P. Cassoux, L. Valade, H. Kobayashi, A. Kobayashi, R.A. Clark, A.E. Underhill, Coord. Chem. Rev. 110 (1991) 115.
[34] R.-M. Olk, B. Olk, W. Dietzsch, R. Kirmse, E. Hoyer, Coord. Chem. Rev. 117 (1992) 99.
[35] C. Reichardt, E. Harbusch-Goernert, Liebigs Ann. Chem. (1983) 721.
[36] D. Mentzafos, A. Hountas, A. Terzis, Acta Crystallogr., Sect. C 44 (1988) 1550.
[37] O. Lindquist, L. Anderson, J. Sieler, G. Steimecke, E. Hoyer, Acta Chem. Scand., Ser. A 36 (1982) 855.
[38] L. Sjolin, J. Sieler, G. Steimecke, Eur. Cryst. Meet., 1977, p. 197.
[39] S.-M. Peng, V.L. Goedken, J. Am. Chem. Soc. 98 (1976) 8500.
[40] B.S. Snyder, C.P. Rao, R.H. Holm, Aust. J. Chem. 39 (1986) 963.
[41] C.H. Wei, L.F. Dahl, Inorg. Chem. 9 (1970) 1878.
[42] R.-M. Olk, W. Dietzsch, K. Koehler, R. Kirmse, J. Reinhold, E. Hoyer, Z. Anorg. Allg. Chem. 567 (1988) 131.
[43] J.R. Nicholson, G. Christou, J.C. Huffman, K. Folting, Polyhedron 6 (1987) 863.
[44] A. Sen, T.-W. Lai, R.R. Thomas, J. Organomet. Chem. 358 (1988) 567.
[45] G. Steimecke, H.-J. Sieler, R. Kirmse, W. Dietzsch, E. Hoyer, Phosphorus Sulfur 12 (1982) 237.

PERGAMON

www.elsevier.nl/locate/poly

Polyhedron 19 (1900) 1293

POLYHEDRON

Author Index of Volume 19/10

Banerjee, R., 1213
Bhattacharya, A.K., 1213
Bhattacharya, S., 1227
Bhrahma, G.S., 1213
Bilakhiya, A.K., 1233
Bocelli, G., 1279
Breitzer, J.G., 1283
Brenčič, J.V., 1219

Cantoni, A., 1279
Carter Dopke, N., 1245
Castiñeiras, A., 1255
Chattopadhyay, P., 1263
Chinea, E., 1175
Coe, B.J., 1193
Coles, S.J., 1193, 1271
Couchman, S.M., 1193

Das, A., 1227
Das, D., 1263
Dash, A.C., 1213
Devereux, M., 1205
Domínguez, S., 1175

Faulds, P., 1271
Fuess, H., 1181

García-Vázquez, J.A., 1255
Gelbrich, T., 1193
Geraghty, M., 1205
Golič, L., 1219

Haase, W., 1181
Hayashi, R.K., 1245
Hernández-Padilla, M., 1175
Hursthouse, M.B., 1193, 1271

Iskander, M.F., 1181

Jeffery, J.C., 1193

Kelly, D.G., 1271
Khalil, T.E., 1181

Labisbal, E., 1255
Leon, V., 1205
Lloret, F., 1175
Lu, T.-H., 1263

McCann, M., 1205
McDonald, C.I., 1193
McGaff, R.W., 1245
McKee, V., 1205
Mederos, A., 1175
Modec, B., 1219
Mondal, B., 1213
Muñoz, M.C., 1175

Pal, S., 1263
Panneerselvam, K., 1263
Paul, P., 1233
Peng, S.-M., 1227
Powell, D.R., 1245

Ramalingam, K., 1279
Rauchfuss, T.B., 1283
Rees, L.H., 1193
Romero, J., 1255

Sinha, C., 1263
Sousa, A., 1255
Svoboda, I., 1181

Thirumaran, S., 1279
Toner, A.J., 1271
Treichel, P.M., 1245
Tyagi, B., 1233

Werner, R., 1181
West, D.X., 1255
Wikaira, J., 1205

Elsevier Science Ltd.

PERGAMON

www.elsevier.nl/locate/poly

Polyhedron 19 (2000) 1295–1304

POLYHEDRON

Chemistry of aroylhydrazones II.☆ Enol-form coordination of 4,5-diazafluorene-9-one salicyloylhydrazone (H_2L) to transition metals and crystal structures of H_2L, $Mn(HL)_2(H_2O)_2$ and $Co(HL)_2(DMF)_2$

Wen Xiao [a,c], Zhong-Lin Lu [a,c], Xiu-Jian Wang [a], Cheng-Yong Su [a], Kai-Bei Yu [b], Han-Qin Liu [a], Bei-Sheng Kang [a,*]

[a] *School of Chemistry and Chemical Engineering, Zhongshan University, Guangzhou, Guangdong 510275, PR China*
[b] *Chengdu Institute of Organic Chemistry, Chinese Academy of Sciences, Chengdu, Sichuan 610041, PR China*
[c] *State Key Laboratory of Organometallic Chemistry, Shanghai Institute of Organic Chemistry, Chinese Academy of Sciences, Shanghai 200032, PR China*

Received 18 January 2000; accepted 28 March 2000

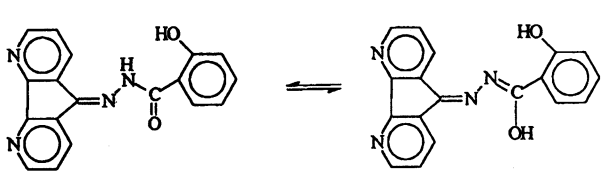
Abstract

Transition metal complexes $M(HL)_2 \cdot nH_2O$ (M(II) = Mn, $n = 2$ (**1**); Co, $n = 3$ (**2**); Ni, $n = 4$ (**3**); Cu, $n = 3$ (**4**); Zn, $n = 2$ (**5**); Pb, $n = 0$ (**6**)) of 4,5-diazafluorene-9-one salicyloylhydrazone (H_2L), have been prepared by the reaction of H_2L with the metal(II) acetates in EtOH–DMF. X-ray diffraction studies showed that the ligand in the solid state has a *pseudo*-helical structure in the keto-form. In complexes $Mn(HL)_2(H_2O)_2$ (**1**) and $Co(HL)_2(DMF)_2$ (**2a**), the ligand coordinates to the metal ion as a mononegative ion in the enol-form with the enolic oxygen and azomethine nitrogen atoms of the aroylhydrazone group forming a five-membered chelate ring, while the phenolic hydroxyl group and pyridyl-N atoms of the diazafluorene moiety are free. The metal atoms are in octahedral geometry with N_2O_4 from two ligands HL in the equatorial plane and the axial sites occupied by solvent molecules. The structures were also characterized by IR and ^1H NMR spectroscopy. © 2000 Elsevier Science Ltd. All rights reserved.

Keywords: Diazafluorenone aroylhydrazone; Transition metal aroylhydrazone complexes; Crystal structures; Enolization; ^1H NMR spectroscopy; IR

1. Introduction

Aroylhydrazones have attracted much attention from chemists in recent years because of their biological activities [1–3], strong tendency to chelate to transition metals [4,5], lanthanide metals [6,7], and main group metals [8,9], forming complexes with the aroylhydrazone acting as a neutral or mononegative bidentate ligand, or even as a dianionic ligand depending on the aroyl substituents and the reaction conditions [10,11]. Recently, a series of ruthenium complexes with ferrocenyl aroylhydrazones have been reported [12] in which the aroylhydrazone moiety behaves as a neutral ligand and chelates to the Ru ion in the keto-form via the carbonyl oxygen and azomethine nitrogen atoms. 4,5-Diazafluorene-9-one and its derivatives are also strong chelating agents [13,14] and have been used as ligands to form Ru complexes [15].



Keto-form Enol-form (1)

In order to further investigate the coordination mode of aroylhydrazone and to compare the coordination

☆ Part 1 of this series: Ref. [12].

* Corresponding author. Fax: +86-20-8411-0318.
E-mail address: ceslhq@zsu.edu.cn (B.-S. Kang).

0277-5387/00/$ - see front matter © 2000 Elsevier Science Ltd. All rights reserved.
PII: S0277-5387(00)00389-2

abilities of the diazafluorene moiety and of the hydrazone group toward transition metals, the condensed products 4,5-diazafluorene-9-one aroylhydrazones have been designed and synthesized. We have reported the crystal structure of the first such compound, 4,5-diazafluorene-9-one isonicotinylhydrazone, in 1996 [16]. Here we present a new ligand, 4,5-diazafluorene-9-one salicyloylhydrazone (H_2L) and six of its transition metal complexes, with the crystal structures of two of them described to identify the coordination mode of the ligand.

2. Experimental

2.1. Reagents

Metal(II) acetates and other analytical grade reagents were available commercially. Salicyloylhydrazine was prepared by the condensation of methyl salicylate with hydrazine hydrate in ethanol. 4,5-Diazafluorene-9-one was obtained by the method described in the literature [17].

2.2. Synthesis of 4,5-diazafluorene-9-one salicyloylhydrazone (H_2L)

The reaction mixture of 4,5-diazafluorene-9-one (1.82 g, 5.0 mmol) in ethanol (40 cm^3) and salicyloylhydrazone (1.52 g, 5.0 mmol) in warm ethanol (40 cm^3) was refluxed for 4 h and filtered. The yellow precipitate was collected, washed with cold ethanol, and dried in vacuo, m.p. 315°C. Analytical data and yield are listed in Table 1. Pale-yellow single crystals suitable for X-ray analysis were prepared by slow evaporation of a solution of the compound in EtOH–DMF in air.

2.3. Syntheses of complexes *1–6*

All complexes were prepared by a similar procedure: a solution containing hydrated $M(OAc)_2$ (0.25 mmol) (M = Mn, Co, Ni, Cu, Zn, and Pb) and the ligand $H_2L{\cdot}H_2O$ (0.17 g, 0.50 mmol) in 30 cm^3 of EtOH–DMF (2:1, v/v) was refluxed for 6 h. The precipitates thus produced were collected, washed several times with warm ethanol and dried in vacuo. The formula, formula weight, color, yield, and elemental analysis data are also listed in Table 1.

Dark red single crystals of complexes **1** and **2a** suitable for X-ray diffraction analyses were obtained by slow evaporation of a solution of **1** in DMF and by diffusion of Et_2O into a solution of **2** in DMF, respectively.

2.4. Physical measurements

Elemental analyses were performed on a Perkin–Elmer 240C analytical instrument. IR spectra were obtained on a Nicolet FTIR-170SX spectrophotometer in KBr pellets in the 4000–400 cm^{-1} region. ^1H NMR data were recorded on a Bruker Aspect AM500 spectrometer at 45°C in DMSO-d_6 with TMS as internal standard.

2.5. Crystal structure determination

Intensity data were collected on a Bruker SMART CCD for H_2L and **1**, and on a Siemens P4 diffractometer by the $\omega - 2\theta$ scan technique for **2a**, both with graphite monochromated Mo Kα radiation (λ = 0.71073 Å). Absorption corrections were applied. The crystal data, data collection and refinement parameters are summarized in Table 2.

Table 1
Some physical properties and elemental analysis data of the ligand H_2L and its complexes **1–6**

Code	Formula	Formula weight	Color	Yield (%)	*Anal.* Found (Calc.) (%)		
					C	H	N
H_2L	$C_{18}H_{12}N_4O_2{\cdot}H_2O$	334.33	Pale yellow	70	64.36 (64.66)	4.02 (4.22)	16.46 (16.76)
1	$Mn(HL)_2{\cdot}2H_2O$ ($C_{36}H_{26}N_8O_6Mn$)	721.59	red	65	59.71 (59.92)	3.45 (3.63)	15.40 (15.53)
2	$Co(HL)_2{\cdot}3H_2O$ ($C_{36}H_{28}N_8O_7Co$)	743.59	red	66	58.56 (58.15)	3.51 (3.80)	15.33 (15.07)
3	$Ni(HL)_2{\cdot}4H_2O$ ($C_{36}H_{30}N_8O_8Ni$)	761.37	red	85	56.77 (56.79)	3.53 (3.97)	14.48 (14.72)
4	$Cu(HL)_2{\cdot}3H_2O$ ($C_{36}H_{28}N_8O_7Cu$)	748.21	black	90	58.09 (57.79)	3.45 (3.77)	15.14 (14.98)
5	$Zn(HL)_2{\cdot}2H_2O$ ($C_{36}H_{26}N_8O_6Zn$)	732.04	yellow	75	59.23 (59.06)	3.16 (3.58)	15.02 (15.31)
6	$Pb(HL)_2$ ($C_{36}H_{22}N_8O_4Pb$)	837.82	yellow	89	51.48 (51.60)	2.55 (2.65)	13.28 (13.38)

Table 2
Crystallographic data and data collection parameters for H_2L, **1** and **1a**

	H_2L	**1**	**2a**
Formula	$C_{18}H_{12}N_4O_2$	$C_{36}H_{26}MnN_8O_6$	$C_{42}H_{36}CoN_{10}O_6$
M_r	316.32	721.59	835.74
Color and habit	yellow, block	dark red, prism	dark red, prism
Crystal size (mm)	$0.2\times0.2\times0.2$	$0.4\times0.2\times0.1$	$0.7\times0.2\times0.1$
Crystal system	orthorhombic	monoclinic	monoclinic
Space group	$P2_12_12_1$	$P2_1/c$	$P2_1/c$
a (Å)	4.8140(10)	8.737(2)	9.906(3)
b (Å)	15.412(2)	17.157(3)	20.723(4)
c (Å)	19.096(3)	10.509(2)	10.630(2)
α (°)	90	90	90
β (°)	90	99.75(3)	113.78(2)
γ (°)	90	90	90
V (Å^3)	1416.8(4)	1552.6(5)	1996.9(8)
Z	4	2	2
ρ (g cm^{-3})	1.483	1.544	1.390
μ (Mo Kα) (mm^{-1})	0.101	0.490	0.491
$F(000)$	656	742	866
2θ range (°)	4–54	4–47	4–50
Independent reflections	2993	2240	3515
Observed reflections [$I>2\sigma(I_o)$]	2024	1710	1984
R [a]	0.0373	0.0332	0.0423
wR [b]	0.0747	0.0846	0.0763
No. of variables	217	232	319
Goodness-of-fit	0.890	1.029	0.837
$\Delta(\rho)_{max,\ min}$ (e Å^{-3})	0.131, −0.131	0.248, −0.260	0.222, −0.220

[a] $R=\Sigma\big||F_o|-|F_c|\big|/\Sigma|F_o|$.
[b] $wR=[\Sigma\, w(|F_o^2|-|F_c^2|)^2/\Sigma\, w|F_o^2|^2]^{1/2}$; $w=1/[\sigma^2|F_o^2|+(xP)^2+0.0000P]$, where $P=[|F_o^2|+2|F_c^2|]/3$; $x=0.0380$ (H_2L); 0.0505 (**1**); 0.0344 (**2a**).

The coordinates of the metal atoms were determined by direct methods and the remaining non-hydrogen atoms were located from successive difference Fourier syntheses. The structures were refined by full-matrix least-squares method with anisotropic thermal parameters for all the non-hydrogen atoms. The positions of the hydrogen atoms were placed in idealized positions isotropically and used in structural factor calculations but not refined for the ligand and **1**, while those for **2a** were found from the difference Fourier map and refined isotropically except those in DMF, which were generated geometrically. All calculations were performed on IBM PC computer with the Siemens SHELXTL program package [18].

3. Results and discussion

3.1. Synthesis

The ligand 4,5-diazafluorene-9-one salicyloylhydrazone was prepared by condensation of 4,5-diazafluorene-9-one with salicyloylhydrazine in molar ratio 1:1 as shown in Eq. (1). It is insoluble in weakly polar or non-polar solvents such as ether, benzene and alkanes; soluble to some extent in moderately polar solvents such as methanol, ethanol and acetonitrile, and easily soluble in strongly polar solvents DMF and DMSO. When reacted with transition metal acetates in mixed solvents EtOH–DMF, the ligand enolizes and chelates to the metal ions forming complexes **1**–**6** (Eq. (2)). In contrast to ligands of the type salicylaldehyde benzoylhydrazone, where the hydroxyl group is attached to the same phenyl group as the $N_{azomethine}$ atom, this ligand is a bidentate rather than a tridentate chelator [10,11]. In ligand H_2L with the hydroxyl group substituted on the amide side of the aroylhydrazone, the hydroxy proton is less prone to dissociate in neutral or mildly acidic conditions. The result also shows that the coordinating activity of the aroylhydrazone moiety is stronger than the two pyridyl nitrogens in diazafluorene, so that the former chelates to the metal atom and the latter are free, obviously caused by increased electronegativity of an oxygen atom in the hydrazone moiety. The fact that the ligand 4,5-diazafluorene-9-one thiosemicarbazone coordinates to a transition metal via the N:S atoms [19], rather than the N:N atoms of the diazafluorene moiety, is also an effect of the more electron donating sulfur atom.

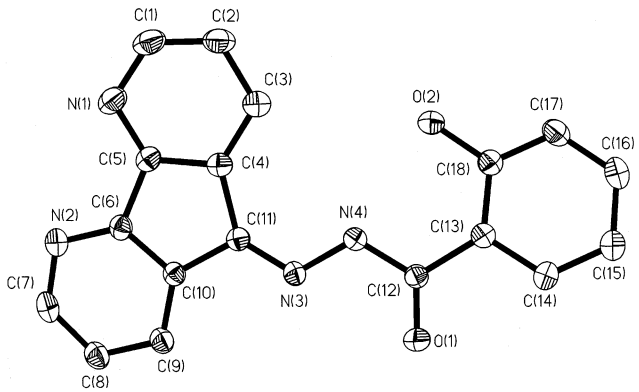


Fig. 1. Molecular structure of the ligand 4,5-diazafluorene-9-one salicyloylhydrazone (H_2L) with thermal ellipsoids at 30% probability level.

All the complexes dissolve only in DMF and DMSO. They are stable in the solid state and decompose above 320°C. Elemental analyses showed that they conform to the formula $M(HL)_2{\cdot}nH_2O$.

$$H_2L{\cdot}H_2O + M(OAc)_2{\cdot}nH_2O \rightarrow M(HL)_2{\cdot}nSol \quad (2)$$

Table 3
Selected atomic distances (Å) and bond angles (°) of H_2L

C(11)–N(3)	1.280(2)	C(12)–C(13)	1.491(3)
N(3)–N(4)	1.370(2)	C(4)–C(11)	1.491(3)
N(4)–C(12)	1.372(3)	C(10)–C(11)	1.470(3)
C(12)–O(1)	1.219(2)	C(18)–O(2)	1.368(3)
N(1)–C(1)	1.341(3)	N(2)–C(6)	1.339(3)
N(1)–C(5)	1.328(3)	N(2)–C(7)	1.346(3)
C(4)–C(11)–C(10)	105.78(17)	N(4)–C(12)–O(1)	121.85(19)
C(4)–C(11)–N(3)	134.00(18)	N(4)–C(12)–C(13)	116.77(18)
C(10)–C(11)–N(3)	120.19(17)	O(1)–C(12)–C(13)	121.4(2)
C(11)–N(3)–N(4)	118.70(16)	O(2)–C(18)–C(13)	119.09(18)
N(3)–N(4)–C(12)	118.52(16)	O(2)–C(18)–C(17)	120.71(19)

Table 4
Selected atomic distances (Å) and bond angles (°) for complex **1**

Mn(1)–O(1)	2.067(2)	N(4)–C(12)	1.333(3)
Mn(1)–N(3)	2.415(2)	C(12)–O(1)	1.265(3)
Mn(1)–O(1w)	2.209(2)	C(12)–C(13)	1.481(3)
C(5)–N(3)	1.295(3)	C(4)–C(5)	1.477(3)
N(3)–N(4)	1.388(3)	C(5)–C(6)	1.477(3)
N(1)–C(1)	1.342(3)	N(2)–C(9)	1.341(3)
N(1)–C(11)	1.331(3)	N(2)–C(10)	1.334(3)
O(2)–C(18)	1.356(3)		
O(1)–Mn(1)–N(3)	72.01(7)	O(1)–Mn(1)–O(1w)	91.79(7)
N(3)–Mn(1)–O(1w)	85.24(7)	Mn(1)–O(1)–C(12)	119.2(2)
Mn(1)–N(3)–N(4)	108.35(13)	N(3)–N(4)–C(12)	113.7(2)
C(4)–C(5)–N(3)	131.0(2)	C(6)–C(5)–N(3)	122.6(2)
C(4)–C(5)–C(6)	106.4(2)	C(5)–N(3)–N(4)	114.9(2)
N(4)–C(12)–C(13)	115.5(2)	N(4)–C(12)–O(1)	125.9(2)
O(2)–C(18)–C(13)	121.3(2)	O(1)–C(12)–C(13)	118.5(2)
O(2)–C(18)–C(17)	118.5(2)		

Table 5
Selected atomic distances (Å) and bond angles (°) for complex **2a**

Co–O(1)	2.025(2)	Co–N(2)	2.212(2)
Co–O(3)	2.090(2)	C(1)–N(2)	1.307(3)
N(2)–N(1)	1.388(3)	N(1)–C(12)	1.337(3)
C(12)–O(1)	1.263(3)	C(12)–C(13)	1.482(4)
C(1)–C(11)	1.475(4)	N(3)–C(5)	1.332(5)
C(1)–C(2)	1.479(4)	N(3)–C(6)	1.342(4)
N(4)–C(7)	1.330(4)	O(2)–C(14)	1.363(4)
N(4)–C(8)	1.341(5)		
O(1)–Co–N(2)	75.51(8)	Co–N(2)–N(1)	109.5(2)
N(2)–Co–O(3)	96.38(8)	Co–O(1)–C(12)	114.6(2)
O(1)–Co–O(3)	89.86(8)	C(1)–N(2)–N(1)	115.0(2)
C(2)–C(1)–C(11)	106.4(3)	N(2)–N(1)–C(12)	111.6(2)
C(2)–C(1)–N(2)	122.4(3)	N(1)–C(12)–C(13)	115.6(3)
N(2)–C(1)–C(11)	131.1(3)	N(1)–C(12)–O(1)	125.3(3)
O(2)–C(14)–C(13)	122.5(3)	O(1)–C(12)–C(13)	119.2(3)
O(2)–C(14)–C(15)	117.6(3)		

Complex	M	*n*Sol	Complex	M	*n*Sol
1	Mn	$2H_2O$	**4**	Cu	$3H_2O$
2	Co	$3H_2O$	**5**	Zn	$2H_2O$
2a	Co	2DMF	**6**	Pb	–
3	Ni	$4H_2O$			

3.2. Structures

The molecular structure of the ligand H_2L is shown in Fig. 1, while those of complexes **1** and **2a** are depicted in Figs. 3 and 5, respectively. The selected atomic distances and bond angles are listed in Tables 3–5. A comparison of relevant structural parameters is shown in Table 6. The ligand in the solid state exists in the keto-form (C=O distance 1.219(2) Å), as also identified by IR absorption (vide infra). The atoms $N_{azomethine}$–N_{amide}–C–O in the acylhydrazone moiety, both in the free ligand and in complexes **1** and **2a**, are arranged in a *syn*-position and situated nearly in a plane with the torsion angles $N_{azomethine}$–N_{amide} versus C–O_{amide} in range of 5–9° only. In addition to that, the sp^2 hybridization of the carbon atoms C(11) (C_{FLU}) in diazafluorene ring (FLU) and C(12) (C_{amide}) of the amide group affords the whole ligand molecule nearly planar with the two aromatic moieties FLU and the phenolic ring (PhOH) forming a dihedral angle of only 16°. Because of this *quasi*-coplanarity, the ligand molecule is asymmetric with one of the pyridyl ring (Py-I) of FLU situated in *syn*-position with the amide oxygen O(1) (O_{amide}), while the hydroxyl group of PhOH is oriented toward the other pyridyl group (Py-II). In addition, the proton of the hydroxyl group in PhOH forms intermolecular hydrogen bond with the nitrogen atom of Py-I of a neighboring molecule with

$N_{Py\text{-}I}\cdots OH$ distance of 2.808 Å. The difference between the two pyridyl rings Py-I and Py-II in a FLU group is also depicted by ^1H NMR studies which will be described below. The hydrogen donor and acceptor behavior of the ligand affords a one-dimensional *pseudo*-helical chain structure as depicted in Fig. 2. Similar structure has been reported for the chiral ligand methyl 2-pyridylmethylidenehydrazinecarbodithioate [20]. Otherwise, the structural data of the ligand are comparable to those of a similar compound [16].

Both **1** and **2a** are centrosymmetric neutral molecules of the composition $M(HL)_2(solvent)_2$, where M = Mn, solvent = H_2O for **1** and M = Co, solvent = DMF for **2a,** with the center of symmetry sitting on the metal ion. The metal atoms in both complexes are hexacoordinated by N_2O_4 in a distorted octahedral geometry with $N_{azomethine}$ and O_{amide} atoms from two enolic mononegative HL groups in the equatorial plane, forming restricted bite angles $N_{azomethine}$–M–O_{amide} of 72.01(7)° for **1** and 75.51(8)° for **2a**, while the O atoms from the solvent molecules occupy the axial sites.

Table 6
Comparison of significant structure parameters (Å or °) of the ligand H_2L and the complexes **1** and **2a**

Structural parameter (Å or °)	H_2L	**1**	**2a**
Aroylhydrazone region			
C_{amide}–O_{amide} [a]	1.219	1.265	1.263
C_{amide}–N_{amide}	1.372	1.333	1.337
C_{amide}–C_{Ph}	1.491	1.481	1.482
N_{amide}–$N_{azomethine}$	1.370	1.388	1.388
N_{amide}–C_{amide}–O_{amide}	121.85	125.9	125.3
N_{amide}–C_{amide}–C_{Ph}	116.77	115.5	115.6
O_{amide}–C_{amide}–C_{Ph}	121.4	118.5	119.2
Diazafluorene(FLU) region			
C_{FLU}–$N_{azomethine}$	1.280	1.295	1.307
C_{FLU}–$C_{Py\text{-}I}$	1.470	1.477	1.479
C_{FLU}–$C_{Py\text{–}II}$	1.491	1.477	1.475
$N_{azomethine}$–C_{FLU}–$C_{Py\text{-}I}$ [c]	120.2	122.6	122.4
$N_{azomethine}$–C_{FLU}–$C_{Py\text{-}II}$ [c]	134.0	131.0	131.1
$C_{Py\text{-}II}$–C_{FLU}–$C_{Py\text{-}I}$	105.8	106.4	106.4
C_{Ph}–O_H	1.368	1.356	1.363
M–O_{sol} [b]	–	2.209	2.090
$N_{azomethine}$–N_{amide}–C_{FLU}	118.52	113.7	111.6
Torsion angle			
$N_{azomethine}$–C_{FLU} vs. N_{amide}–C_{amide}	179.1	166.6	176.2
$N_{azomethine}$–N_{amide} vs. C_{amide}–O_{amide}	4.6	8.3	9.2

[a] The O_{amide} atom becomes enolic oxygen in the complexes, but is a carbonyl oxygen in the ligand.

[b] O_{sol} denotes the oxygen atom of the solvent attached to the metal, from H_2O in **1** and DMF in **2a**.

[c] The carbon atom in the pyridyl group in diazafluorene *cis* to the amide oxygen atom in the aroylhydrazone is represented by $C_{Py\text{-}I}$, while that *trans* to the amide oxygen is $C_{Py\text{-}II}$.

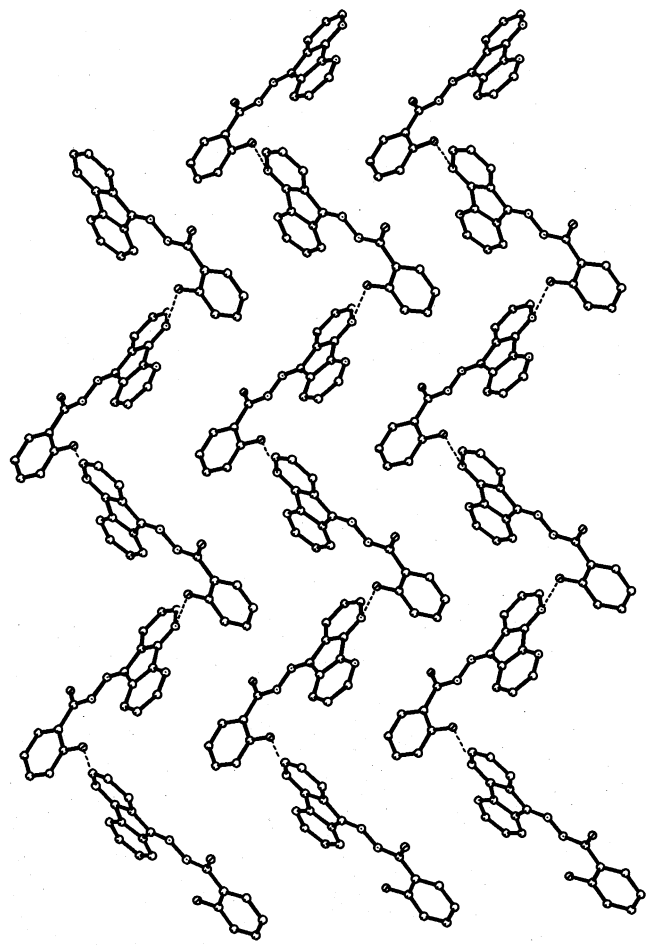


Fig. 2. *Pseudo*-helical structure of the ligand 4,5-diazafluorene-9-one salicyloylhydrazone (H_2L) showing the intermolecular hydrogen bond $N_{Py\text{-}I}\cdots HOPh$.

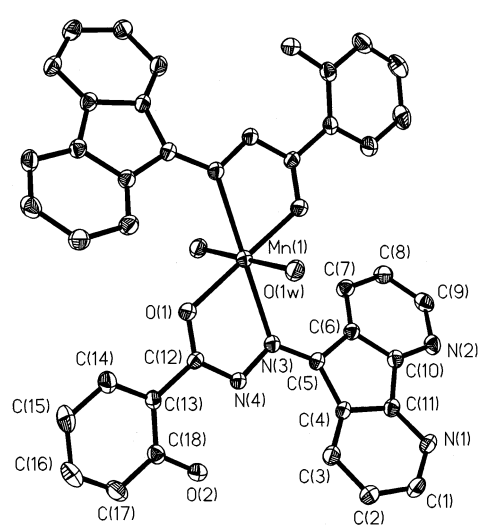


Fig. 3. Molecular structure of $Mn(HL)_2{\cdot}2H_2O$ (**1**) with thermal ellipsoids at 30% probability level.

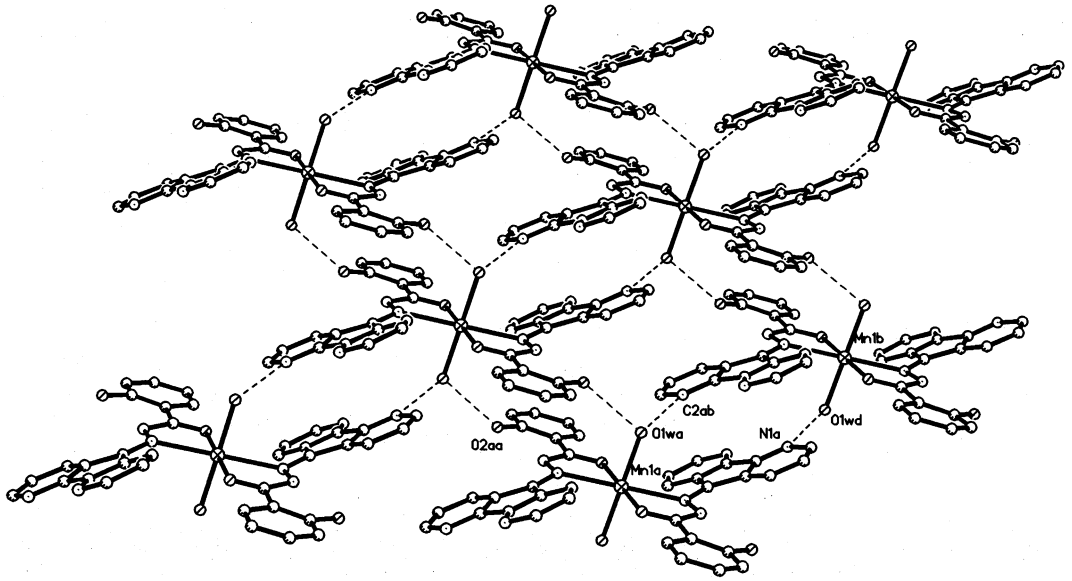


Fig. 4. Crystal packing of $Mn(HL)_2{\cdot}2H_2O$ (**1**) showing the layered structure formed by intermolecular hydrogen bonds $N_{Py\text{-}I}\cdots HOH$ (2.831 Å) and $HOH\cdots OHPh$ (2.805 Å).

The in-plane bond distances of **1** showed that the Mn–O_{amide} bond (2.067(2) Å) is somewhat shorter and the Mn–$N_{azomethine}$ bond (2.415(2) Å) is somewhat longer than those of other Mn(II) complexes in which the aroylhydrazone moiety is either in the enolic form [21] (2.190(5) and 2.280(5) Å, respectively) or in the ketonic form [22,23] (average 2.28 and 2.27–2.33 Å, respectively), where the Mn(II) ion is hepta-coordinated in pentagonal bipyrimidal geometry. As there is no similarly enolic coordinated cobalt complexes of aroylhydrazones in literature for comparison, we will look at a few of the ketonic complexes $[Co(H_2L^A)(H_2O)(MeOH)]^{2+}$ $[H_2L^A = 2,5\text{-}C_6H_3N(C(CH_3)NNHC(O)NH_2)_2]$, $[Co(H_2L^B)(H_2O)(NO_3)]^{+}$ $[H_2L^B = 2,5\text{-}C_6H_3N(C(CH_3)NNHC(O)Ph)_2]$, and $[Co(H_2L^C)(H_2O)_2]^{2+}$, $[H_2L^C = 2,5\text{-}C_6H_3N(C(CH_3)NNHC(O)(2\text{-}Py))_2]$, and found that the Co–$O_{amide}$ bond (2.025(2) Å) in **2a** is again shorter than the average value of that bond (2.227 Å) in these complexes, while the Co–$N_{azomethine}$ bond (2.212(2) Å) is slightly longer (average 2.195 Å) [24–26]. Therefore, the geometry of the central metal atom has much larger effect on the structural parameters than the actual coordination mode of the hydrazones.

The five-membered chelate rings $\overline{MNNCO}$ in the equatorial plane in both complexes are nearly planar with mean deviation from least-square planes of 0.0368 Å for **1** and 0.0860 Å for **2a**. They form dihedral angles of 32.7 and 30.1° for **1** and **2a**, respectively, with the FLU ring and 4.8 for **1** and 2.5° for **2a** with the PhOH ring, indicating that a certain degree of delocalization could occur throughout the molecule, which can be interpreted by the lengthening of bonds C_{FLU}–$N_{azomethine}$ and shortening of bond C–N_{amide}, as compared to the free ligand (see Table 6). The shortening of the latter is an evidence of enolization, as expected. The lengthening of the former is reasonable for coordination of the atom $N_{azomethine}$ to the metal atom with the formation of a chelate ring. Notably, the bond $N_{azomethine}$–N_{amide} also increases (by 0.02 Å) in the complexes, a further indication of delocalization over the whole ligand molecule, particularly within the chelate ring.

On close examination of the structural parameters in Table 6, it will be noticed that the C–O_{amide} bond of 1.265(3) Å (**1**) and 1.263(3) Å (**2a**) in the complexes with elongation of 0.04–0.05 Å, as compared to the free ligand, can not be considered long as would be

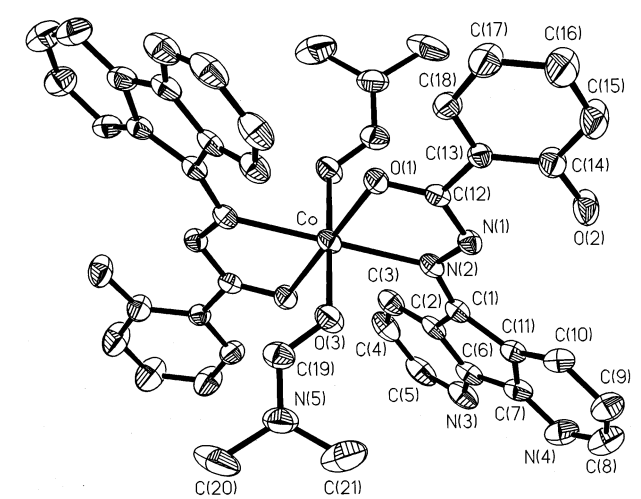


Fig. 5. Molecular structure of $Co(HL)_2{\cdot}2DMF$ (**2a**) with thermal ellipsoids at 30% probability level.

Table 7
Important IR data (cm^{-1}) of the ligand H_2L and its complexes **1**–**6**

Code	$\nu_{(HOH, NH)}$	$\nu_{(C=O)}$	$\nu_{(C=N)}$	$\delta_{(O-H)}$	$\nu_{(C-OH)}$ [a]	$\nu_{(C-O)}$	$\delta_{(C-H)}$ [b]
H_2L	3320br	1684vs	1604s	1404	1280m	–	751vs
1	3400br	–	1595vs	1398	1250m	1046vs	751vs
2	3400br	–	1588s	1398	1250m	1046vs	744vs
3	3420br	–	1588s	1405	1243m	1053vs	751s
4	3450br	–	1588s	1405	1243s	1053vs	751vs
5	3472br	–	1602s	1405	1236m	1068vs	744vs
6	–	–	1595s	1398	1250m	1053vs	751vs

[a] For the stretching absorption of the C–OH bond in the phenolic group.
[b] For the C–H out-of-plane bending absorption on the aromatic ring.

expected for enolization of the ligand. The evidence for the enolization should further be provided by the spectroscopic data, such as a disappearance of the carbonyl absorption in IR, which is indeed the case for the complexes **1**–**6** (Table 7), and should also be accompanied by the balance of electric charge in the molecules. Carbonyl distances of 1.24–1.25 Å have been reported for the keto-coordination of an aroylhydrazone [10], which are only 0.1–0.2 Å shorter than in **1** and **2a**. Therefore, the length of the C–O bond may not be a sufficient criterion for the identification of coordination modes; other effects such as coordination geometry of the central atom influence the bond distances even more significantly.

An interesting feature is observed in the five-membered central ring in FLU of the free ligand, the two C_{FLU}–C_{Py} bonds C(11)–C(10) and C(11)–C(4) are not equivalent: the former to $C_{Py\text{-}I}$ (*syn* to amide) is 0.02 Å shorter than the latter to $C_{Py\text{-}II}$ (*anti* to amide), which could have been caused by the asymmetry of the ligand. This difference disappears on coordination to the metal ions and the complexes lose chirality. Such a phenomenon is also reflected in the bond angles around the sp^2 hybridized C_{FLU}: the two outer angles $N_{azomethine}$–C_{FLU}–C_{Py} differ by 14° in the ligand, nearly twice as much in the complexes (8.5°). Such change of symmetry of the FLU ring could partially be induced by the co-planarity of the two aromatic moieties: it is larger in the ligand than in the complexes.

In both complexes, the planes of the diazafluorene moiety of two neighboring molecules are parallel to each other (dihedral angle 0°), with the center to center distance of 3.706 Å in **1** and 4.137 Å in **2a**, implying weak interactions, which stabilize the complexes. The molecules of **1**, as shown in Fig. 4, are further connected by intermolecular hydrogen bonds $N_{Py\text{-}II}\cdots OH_2$ (2.831 Å) with one molecule and $PhHO\cdots OH_2$ (2.805 Å) with another. Having two H_2O molecules in *trans*-positions and with a center of symmetry for the molecules of **1**, a total of eight hydrogen bonds exist in the complex. The resulting layered network is composed of four molecules forming two linked rings, one within the other, with the size of the inside cavity about 7.2 × 11.0 Å, composed of two HL ligands and two water molecules with four hydrogen bonds. The outer ring involves four Mn atoms, four HL ligands providing two PhOH and two FLU moieties, and four H_2O molecules.

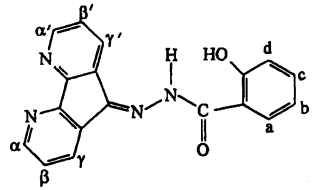
Complex **2a** with two molecules of DMF in the axial sites does not possess interactions other than the rather weak π···π stacking mentioned above, due to the absence of hydrogen bond donors.

3.3. IR spectroscopy

Infrared spectral studies showed that both the ligand and the complexes contained solvated water molecules as shown by the broad bands in region 3200–3500 cm^{-1}, where the NH stretching absorption of the ligand is also buried under. Notably, the carbonyl absorption at 1684 cm^{-1} in the ligand has disappeared in all the complexes. Instead, strong bands of the $C–O_{enol}$ absorptions appeared in range 1046–1068 cm^{-1} [27] (see Table 7): a convincing evidence for the enolization of the keto-form of the ligand to the enol-form when coordinated to transition metals in protic solvents. The moderately strong aromatic C–OH absorption (1280 cm^{-1}) of the phenolic group in the free ligand is still present in the complexes (1236–1250 cm^{-1}) [28], which is shifted to lower frequencies, indicating that the hydrogen bonding involving the hydroxyl group in the ligand might not be so effective in the complexes.

The coordination of the azomethine nitrogen atom to the metal ions was indicated by the displacement of $\nu_{(C=N)}$ from 1604 cm^{-1} in the ligand to 1588–1602 cm^{-1} in the complexes, which overlapped with the band ν(C=N–N=C). This result shows that the contribution of C=N stretching has been reduced as the nitrogen atom is involved in bond formation with the metal ion. The strong absorption at 1567 cm^{-1} in all the complexes for the C⋯N stretching vibration in the FLU ring [29] has not changed much, both in frequency

Table 8
^{1}H NMR data (δ/ppm, J/Hz) [a] for the ligand H_2L and complex **6** in DMSO-d_6 at 45°C



		Hα	$J_{\alpha\beta}$	Hβ	$J_{\beta\gamma}$	Hγ	Hα′	$J_{\alpha'\beta'}$	Hβ′	$J_{\beta'\gamma'}$	Hγ′	Ha	J_{ab}	Hb	J_{bc}	Hc	J_{cd}	Hd
H_2L	δ	8.803 (dd, 1H)		7.504 (m, 2H)		8.640 (dd, 1H)	8.737 (dd, 1H)		7.504 (m, 2H)		8.054 (dd, 1H)	8.258 (d, 1H)		7.055 (t, 1H)		7.578 (dd, 1H)		7.112 (d, 1H)
	^3J		5.0		7.5			5.0		7.5			6.5		5.0		8.0	
	^4J			1 [b]					1.5 [c]						<1.0 [d]			
6	δ	8.660 (d, 1H)		7.311 (m, 1H)		8.739 (d, 1H)	8.568 (d, 1H)		7.311 (m, 1H)		8.260 (d, 1H)	7.977 (d, 1H)		6.777 (t, 1H)		7.464 (dd, 1H)		6.854 (d, 1H)
	^3J		5.0		7.5			4.5		7.5			8.0		5.0		8.0	
	^4J			[e]					[e]						[e]			

[a] d:, doublet; dd, doublet of doublet; t, triplet; m, multiplet.
[b] Coupling constant $J_{\alpha\gamma}$.
[c] Coupling constant $J_{\alpha'\gamma'}$.
[d] Coupling constant J_{ac} or J_{bd}.
[e] Indistinguishable due to broadness of peaks.

and in intensity, from the free ligand (1565 cm^{-1}), implying the non-coordination of this fragment. All of this evidence indicates that the ligand coordinates to the metal center through the depronated enolic aroylhydrazone group while the FLU and the PhOH moieties are free. Interestingly, although these two moieties are two different aromatic groups with three and four adjacent protons, respectively, there appeared only one very strong and sharp C–H out-of-plane bending absorption in range 744–751 cm^{-1}, which is characteristic for the fluorene group, since this band is always resent in all compounds containing this moiety [29].

3.4. ^1H MNR spectroscopy

The relevant ^1H NMR spectral data of the ligand and complex **6** in DMSO-d_6 are listed in Table 8, together with the assignments and coupling constants. NMR spectra were not measured for the other complexes due either to the paramagnetic nature or to their low solubilities. The proton signals of H_N and H_{OH} of the free ligand appeared at 11.582 and 12.050 ppm, respectively (not listed in Table 8), indicating that the ketonic form exists not only in the solid state, but also in strongly polar non-protic solvent. The disappearance of the H_N signal in **6** shows that H_2L has deprotonated and coordinated to the metal ion in the enolic form. The chemical shifts of the phenolic proton (14.055 pm in **6**), and Hγ and Hγ′ have shifted to a lower field after complexation, while all the other signals shifted somewhat to a higher field due to the heavy atom effect of lead. The data showed clearly the asymmetry of the ligand with the two protons Hγ and Hγ′ nearest to the $N_{azomethine}$ have the largest difference. We have tentatively assigned protons on Py-I to the α-series and those on Py-II to the α′-series, a result caused probably by the *cis*-situated $N_{azomethine}$ atom [19].

4. Summary

This work showed that 4,5-diazafluorene-9-one salicyloylhydrazone adopts a *pseudo*-helical structure formed from intermolecular hydrogen bonding, which would be interesting if chiral complexes could be prepared from it. However, when reacted with transition metals, two of the ligand monoanions lie in the equatorial plane of the complexes with the two axial sites occupied by two solvent molecules, yielding centrosymmetric complexes. The weaker coordinating FLU moiety is not involved in complex formation, and the protic solvent H_2O molecules connect the molecules of **1** with intermolecular hydrogen bonds to form a layered network when accompanied by π···π interaction. With DMF as the axial ligand as in complex **2a**, no hydrogen bonding is possible so that only π···π stacking interaction exists in the complex. By proper selection of axial ligands, it should be possible to obtain low dimensional or 3D supramolecular compounds containing aroylhydrazones, which could have applications in biological systems. It should also be possible to obtain chiral coordination complexes by selection of aroylhydrazones to avoid the generation of molecular symmetry. Furthermore, these mononuclear complexes can still act as building blocks to construct polynuclear complexes by chelating on the diazafluorene side, which would be of interest for their potential multi-redox and long range energy transfer properties. Further work is in progress.

5. Supplementary material

Supplementary data are available from the CCDC, 12 Union Road, Cambridge CB2 1EZ, UK (fax: +44-1223-336033; e-mail: deposit@ccdc.cam.ac.uk or www: http://www.ccdc.cam.ac.uk) on request. The deposition numbers for 4,5-diazafluorene-9-one salicyloylhydrazone (H_2L), $Mn(HL)_2{\cdot}2H_2O$ (**1**), and $Co(HL)_2{\cdot}2DMF$ (**2a**) are 137883, 137885 and 137884, respectively.

Acknowledgements

Financial support from NNSF of China (grant No. 29973059), NSF of Guangdong Province are greatly appreciated.

References

[1] Ng.Ph. Buu-Hoi, Ng.D. Xuong, Ng.H. Ham, F. Binon, R. Roger, J. Chem. Soc. (1953) 1358.
[2] L.El. Sayed, M.F. Iskander, J. Inorg. Nucl. Chem. 33 (1971) 435.
[3] T.S. Ma, T.M. Tien, Antibiot. Chemother. 3 (1953) 491.
[4] B. Singh, A.K. Srivastav, P. Sahai, Synth. React. Inorg. Met. Org. Chem. 24 (1994) 631.
[5] Y.M. Liang, C.M. Liu, Y.X. Ma, Q.S. Li, Trans. Met. Chem. 23 (1998) 97.
[6] Y.X. Ma, Z.Q. Ma, G. Zhao, Y. Ma, M. Yan, Polyhedron 8 (1989) 2105.
[7] R.K. Agarwal, R.K. Sarin, R. Prasad, Pol. J. Chem. 67 (1993) 1947.
[8] M. Carcelli, C. Pelizzi, G. Pelizzi, P. Mazza, F. Zani, J. Organomet. Chem. 488 (1995) 55.
[9] Z.Y. Yang, R.D. Yang, K.B. Yu, Polyhedron 15 (1996) 3749.
[10] J.D. Ranford, J.J. Vittal, Y.M. Yang, Inorg. Chem. 37 (1998) 1226.
[11] E.W. Ainscough, A.M. Brodie, A.J. Dobbs, J.D. Ranford, J.M. Waters, Inorg. Chim. Acta 267 (1998) 27.
[12] Z.-L. Lu, W. Xiao, B.-S. Kang, C.-Y. Su, J. Liu, J. Mol. Struct. 523 (2000) 133.
[13] X.H. Shi, X.Z. You, C. Li, R.G. Xiong, K.B. Yu, Trans. Met. Chem. 20 (1995) 191.
[14] Z.L. Lu, C.Y. Duan, Y.P. Tian, X.Z. You, H.K Fun, B.C. Yip, E. Hovstreydt, Polyhedron 16 (1997) 187.

[15] Y.X. Wang, W. Perez, G.Y. Zheng, D.P. Rillema, Inorg. Chem. 37 (1998) 2051.
[16] Z.L. Lu, B.Z. Shan, C.Y. Duan, Y.P. Tian, X.Z. You, H.K. Fun, K. Sivakumar, Acta Crystallogr., Sect. C 52 (1996) 1720.
[17] L.J. Henderson, J.F.R. Fronczek, W.R. Cherry, J. Am. Chem. Soc. 106 (1984) 5876.
[18] (a) G.M. Sheldrick, shelxl-pc, Siemens Analytical X-ray Instruments, Inc., Madison, WI, 1990. (b) G.M. Sheldrick, in: D. Sayre (Ed.), Computational Crystallography, Oxford University, New York, 1982.
[19] Z.H. Liu, C.Y. Duan, J. Hu, X.Z. You, Inorg. Chem. 38 (1999) 1719.
[20] C.-Y. Su, X.-P. Yang, B.-S. Kang, K.-B. Yu, Y.-X. Tong, T.C.W. Mak, Bull. Chem. Soc. Jpn. 72 (1999) 2217.
[21] C. Pelizzi, G. Pelizzi, G. Predieri, S. Resola, J. Chem. Soc., Dalton Trans. (1982) 1349.
[22] C. Lorenzini, C. Pelozzi, G. Pelozzi, G. Predieri, J. Chem. Soc., Dalton Trans. (1983) 721.
[23] C. Pelizzi, G. Pelizzi, G. Predieri, F. Vitali, J. Chem. Soc., Dalton Trans. (1985) 2387.
[24] K. Andelkovic, I. Ivanvoic, B.V. Prelsnik, V.M. Leovac, D. Poleti, Polyhedron 15 (1996) 4361.
[25] T.J. Giordano, G.J. Palenik, R.C. Palenik, D.A. Sullivan, Inorg. Chem. 18 (1979) 2445.
[26] C. Pelizzi, G. Pelizzi, F. Vatali, Trans. Met. Chem. 11 (1986) 401.
[27] H.-Y. Zhang, F. Li, P.-K. Chen, D.-J. Che, D.-L. Chen, H.-Q. Zhang, Polyhedron 12 (1993) 165.
[28] R.A. Lal, M.L. Pal, S. Adhikari, Synth. React. Inorg. Met. Org. Chem. 26 (1996) 997.
[29] C.Y. Duan, L.G. Zhu, X.Z. You, Acta Chim. Sin. 50 (1992) 715.

PERGAMON

www.elsevier.nl/locate/poly

Polyhedron 19 (2000) 1305–1309

POLYHEDRON

Synthesis and physicochemical characterization of rhodium sulfosalicylate

Michael S. Nothenberg [a,*], Aparecido R. de Souza [b], Jivaldo do R. Matos [c]

[a] *Faculty of Pharmaceutical Sciences, University of São Paulo, PO Box 66083, 05315-970 Sao Paulo, Brazil*
[b] *Institute of Chemistry, Federal University of Goias, Goias, Brazil*
[c] *Institute of Chemistry, University of São Paulo, Sao Paulo, Brazil*

Received 22 July 1999; accepted 21 March 2000

Abstract

Rhodium sulfosalicylate, prepared from 5-sulfosalicylic acid, distinguishes itself from most rhodium carboxylates by its high solubility in water. Magnetic resonance, infrared, ultraviolet, and visible spectroscopic techniques were used for structure determination and the resulting spectra suggested that the molecule bears the characteristic binuclear structure (two rhodium atoms complexing four equatorial ligand molecules) described for other transition metal carboxylates. Titrimetry, with a standardized base solution, indicated the presence of four free sulfonic acid functions in the molecule. Thermo analytical procedures (TG/DTG and DSC) indicated a loss of six water molecules by the complex at temperatures below 200°C. The X-ray diffraction powder pattern for rhodium sulfosalicylate shows the end product of thermal decomposition as being metallic rhodium. © 2000 Elsevier Science Ltd. All rights reserved.

Keywords: Rhodium(II) complexes; Rhodium(II) carboxylates; Rhodium sulfosalicylate; Thermogravimetric analysis; Spectroscopic analysis; Anticancer drugs

1. Introduction

The study of antineoplastic properties of transition metal complexes prompted by Rosenberg's discovery of the antitumor activities of cisplatine [1] led to syntheses and antitumor evaluations of several metal complexes, including rhodium carboxylates [2]. Some authors attempted the modification of biological activities of these octahedral $Rh_2(Le_4)\cdot 2La$ complexes (Le stands for equatorial ligands while La represents axial ligands) by replacing the solvent molecules, usually occupying the two axial sites, with other species [3]. One reason for attempting these modifications was to reduce the toxicity exhibited by most rhodium carboxylates. As toxic effects seem to correlate with the lipophilic character of active complexes, several authors synthesized hydrophilic carboxylates, including citrate [4], ketogluconate, and glucuronate [5]. Souza et al. [6] evaluated the solubilizing effect of isonicotinic acid molecules as axial ligands in rhodium propionate. The reported tumor inhibitory activity of water-soluble rhodium complexes, citrate in particular, prompted the synthesis of rhodium sulfosalicylate. The complex was characterized by thermo analytical and spectroscopic methods. A volumetric technique indicated the presence of four free sulfonic acid moieties.

2. Material and methods

2.1. Synthesis

A mixture containing 0.2 mmol of rhodium propionate prepared previously [3] and 4 mmol of 5-sulfosalicylic acid (Merck) was heated for 30 min at about 120°C in a glass tube submerged in glycerin, with occasional stirring. The dark-green melt, generated by the fusion of the ligand, was cooled and transferred to a beaker with small portions of cold water. After 24 h, the solution was filtered on a sintered glass filter in order to isolate crystals of unreacted rhodium propi-

* Corresponding author.
E-mail address: msnothen@usp.br (M.S. Nothenberg).

0277-5387/00/$ - see front matter © 2000 Elsevier Science Ltd. All rights reserved.
PII: S0277-5387(00)00394-6

onate. Rhodium sulfosalicylate was further isolated from the parent carboxylate by repeated extraction of the aqueous solution with ethyl ether. Extractions were continued until the ether phase was colorless. The aqueous phase was evaporated on a steam bath, and the green solid rhodium sulfosalicylate was washed with acetone, filtered, and dried at 105°C for 3 h.

2.2. Instrumental analyses

Carbon and hydrogen content of the new carboxylate was determined by standard microanalytical procedures using a Perkin–Elmer PE2400CHN elemental analyzer. The sulfur content was established by the Schöniger combustion flask technique.

Thermoanalytical determinations — TG/DTG and DSC measurements — were performed on Shimadzu TGA50 and DSC50 instruments, respectively. TG/DTG curves were obtained from a 5 mg sample in a platinum crucible, under a current of air (flow rate 50 ml min^{-1}), and a heating rate of 10°C min^{-1}. DSC curves were obtained from 2 mg samples in aluminum crucibles, under nitrogen current (flow rate 50 ml min^{-1}), and a heating rate of 5°C min^{-1}.

Infrared spectra were recorded on a Bomen MB102 FTIR spectrophotometer from KBr pellets (2000–1200 cm^{-1}) and Nujol mulls (4000–200 cm^{-1}). UV–Vis spectra were obtained on a Hitachi U-3000 spectrophotometer, using 10^{-4} and 10^{-3} mol l^{-1} methanol solutions.

X-ray powder patterns were obtained on a Philips PW-1710 diffractometer from a product isolated at 360°C, using Cu Kα radiation ($\lambda = 1.541$ Å).

^{1}H and ^{13}C NMR spectra were generated for 5-sulfosalicylic acid and for rhodium sulfosalicylate on a Bruker Avance DPX300 300 MHz/52 mm spectrometer from deuterated water solutions stirred for 24 h and concentrated by evaporation.

The volumetric determination of the pK_a of rhodium sulfosalicylate was performed with 20 mg samples, dissolved in 10 ml of water. The solutions were titrated with drop wise addition of potassium hydroxide (2.83×10^{-3} mol l^{-1}). The titration curve — pH versus added base solution — was plotted from data generated using a portable Corning pH meter.

3. Results and discussion

Elemental analyses of rhodium sulfosalicylate afforded the following values: C, 29.30; H, 2.67; S, 10.30%. This is consistent with the molecular formula $C_{28}H_{20}O_{24}S_4Rh_2.6H_2O$, M_W 1182.60. The theoretical composition of hexahydrated rhodium sulfosalicylate is: C, 28.44; H, 2.73; S, 10.84%. The probable structure of the new complex is shown in Fig. 1. The yield was 75%.

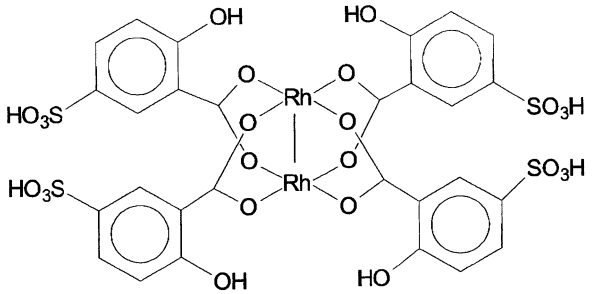


Fig. 1. Structure proposed for rhodium 5-sulfosalicylate.

3.1. Thermal analyses

TG/DTG procedures indicated that hexahydrated rhodium sulfosalicylate maintained structural integrity up to 40°C and suffered progressive dehydration above this temperature. The loss of six molecules of water was calculated from the endothermal with peak temperature at 57°C and $\Delta H = 81$ kJ mol^{-1}) that appears on the DSC curve (Fig. 2). A sample of the complex, previously dried at 200°C, was equally submitted to DSC. The resulting curve was similar to the one obtained from the hydrated complex, which suggests that the water molecules were quickly recovered from the atmosphere upon cooling. They are, presumably, essential to the stability of the complex.

The TG/DTG curve for rhodium sulfosalicylate indicated that the anhydrous complex starts decomposing at 200°C. The breakdown proceeds slowly during the

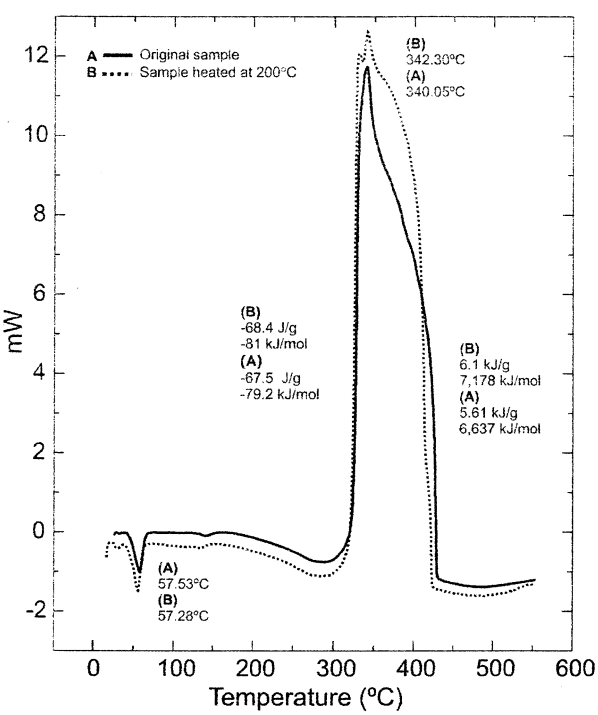


Fig. 2. DSC curves for heated and unheated samples of rhodium 5-sulfosalicylate.

dehydration, accelerating after 330°C. Stoichiometric calculations suggest that the final decomposition product, at about 360°C, is metallic rhodium. The chemical nature of the material was confirmed by X-ray powder diffratometry [7]. It is inferred that the decomposition of the anhydrous complex results in carbonization. The formation of elementary carbon and the metals cation reactive properties are factors that favor the reduction of rhodium to its metallic form, Rh^0. The thermal decomposition process of rhodium sulfosalicylate, peaking at 340°C, is highly exothermic ($\Delta H = -6637$ kJ mol^{-1}).

3.2. Infrared spectrophotometry

Some peak assignments are based on published spectra of sulfosalicylic acid [8–11] (Table 1) and are reliable. Bands associated with deformations in the plane of the OH group (δ_{OH}), stretching vibrations for C–O, and asymmetric stretching of the SO_3^- group occur at very close frequencies, between 1250 and 1140 cm^{-1}, and are difficult to assign accurately.

Bands assigned to O–H stretching vibrations of the hydrated sulfonyl group, between 2800 and 1650 cm^{-1}, approximately, are broad. That phenomenon may be related to the presence of small quantities of water, which promote the ionization of the sulfonyl groups, originating ionic species $-SO_3^- H_3O^+$.

Evidences for the coordination of 5-sulfosalicylic acid to rhodium through its carboxyl groups comes from the analysis of the C–O stretching modes in the acid and complex spectra. The band associated to the stretching vibration of the acids carboxyl group (ν_{COOH}), at 1432 cm^{-1}, unfolds, in the complexes' spectrum, into asymmetrical ($\nu_{asCOO} = 1588$ cm^{-1}) and symmetrical ($\nu_{sCOO} = 1440$ cm^{-1}) stretching vibrations. According to Deacon et al. [12,13], metallic carboxylates whose spectra display Δ values (ν_{asCOO}–ν_{sCOO}) higher than 200 cm^{-1} are monodentate. The value of $\Delta = 148$ cm^{-1} observed in the spectrum of rhodium sulfosalicylate suggests the occurrence of a bridged or chelated bidentate coordination.

Table 1
Proposed band assignments for the infrared spectra of 5-sulfosalicylic acid and rhodium 5-sulfosalicylate [a]

$Rh_2(SS)_4 \cdot 6H_2O$	$SSA \cdot xH_2O$	Assignments
1680vw		?
	1665w, 1652w, 1644w	a' fundamental, ν(CO), C–OH ring
1620s		a' fundamental, ν(CC), ν_{8a}, ring
	1604w, 1592w, 1582w	a' fundamental, ν(CC), ν_{8b}, ring
1588s		antisymmetry CO_2^- str. (a')
1560w		
1508*vw		
1478*m	1482*m	a' fundamental, ν(CC), ν_{19a}
1440*s		symmetry CO_2^- str. (a')
	1432*m	COOH group
	1351*m	a' fundamental, ν(CC), ν_{14}
1374*m		
1303m	1297m	a' fundamental, β(CH), ν_3
1254vs	1242m	a' fundamental, ν(CO), ν_{7a}
1220s	1197m	a' fundamental, δ(OH)
	1159vs	antisymmetry SO_3^- str. (a')
1156vs, 1124vs	1140vs, 1121vs	antisymmetry SO_3^- str. (a')
1086m	1084m	a' fundamental, β(CH), ν_{9a}
1026vs	1027vs	antisymmetry SO_3^- str. (a')
	967w	a'' fundamental, γ(CH), ν_{17a}
	930vw	
894vw	891vw	COOH group
	864vw	a'' fundamental, γ(CH), ν_{10a}
834w	838w	
818w		
792m	795vw	
	778w	
735sh		
678s	665m	a' fundamental, ν_1, ring
597s	584s	
548sh	541m	
473m	451w	
447vw	427w	
380vw	396m	
304vw	303w	

[a] *, bands observed on spectra obtained from KBr pellets; vs, very strong; s, strong; m, medium; w, weak; vw, very weak; SS, sulfosalicylate; SSA, sulfosalicylic acid.

3.3. UV–Visible spectroscopy

The spectra of rhodium sulfosalicylate in the ultraviolet and visible regions are similar to those of other rhodium carboxylates described in the literature [14]. Major absorption bands between 200 and 900 nm, and their respective absorptivity values, are listed in Table 2. Norman and Kolari [15] assigned the bands at 584 nm (band 1) and 434 nm (band 2), in the visible region, to the electron dipole allowed transitions $\pi^*_{(Rh-Rh)} \rightarrow \sigma^*_{(Rh-Rh)}$ ($2e_g \rightarrow 2a_u$, in D_{4h}), and $\pi^*_{(Rh-Rh)} \rightarrow \sigma^*_{(Rh-O)}$ ($2e_g \rightarrow 2b_{2u}$, in D_{4h}), respectively. Their assignments are based in a correspondence among calculated and experimental energy values, as well as in an observed influence of axial ligands on the energy levels of the bands. Dubicki and Martin [16] have also evaluated the relationship between ligands and carboxylate UV spectra. They stated that while band 1 is affected strongly by the nature of the axial ligands, band 2 is practically unaffected.

3.4. Magnetic resonance spectroscopy

Band assignment for ^1H and ^{13}C magnetic resonance spectra for 5-sulfosalicylic acid and rhodium sulfosalicylate in D_2O (Tables 3a and 3b) were accomplished with the aid of published data for sulfosalicylic acid

Table 2
Proposed band assignments for the UV–Vis spectrum of rhodium 5-sulfosalicylate

Band	λ_{max} (nm)	ε (M^{-1} cm^{-1})
1	584.00	250.85
2	434.00	214.37
3	304.00	23 211.03
4	259.20	29 785.48
5	231.00	70 976.04
6	214.40	192 212.59

[17,18]. Reference peaks were those of deuterated water, at 4.6 ppm (^{1}H NMR), and of methanol, at 49.9 ppm (^{13}C NMR).

3.5. pK determination

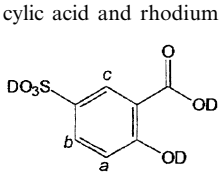
Titration of rhodium sulfosalicylate with potassium hydroxide is illustrated in Fig. 3. Application of the Boltzman correction to the experimental points generated the sigmoid curve. The pK_a value for rhodium sulfosalicylate (6.2) was found graphically as the inflection point of the curve.

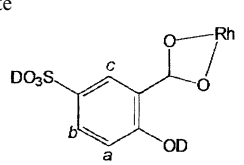
It should be noted that the experimental points in Fig. 3 tend to increase beyond the neutralization of the sulfonic groups. This can be attributed to the partial reaction with carboxylate functions, freed after a presumed progressive decomposition of the complex in alkaline media. The disintegration proposition is strengthened by the color change — from the typical green to yellow — which occurs at this stage.

From the volume of alkali solution consumed at the point of inflection of the curve, the stoichiometry of the reaction was determined to be:

$$R\text{–}(SO_3H)_4 + 4KOH \rightarrow R\text{–}(SO_3K)_4 + 4H_2O \quad (1)$$

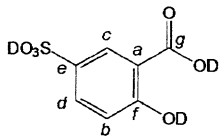
Table 3a
Proposed band assignments for the ^{1}H NMR spectra of 5-sulfosalicylic acid and rhodium 5-sulfosalicylate

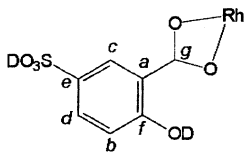




5-Sulfosalicylic acid		Rhodium 5-sulfosalicylate	
a	6.51	a	6.53
	6.54		6.57
b	7.36	b	7.38
	7.37		7.39
	7.39		7.41
	7.40		7.42
c	7.76	c	7.92
	7.77		7.93

Table 3b
Proposed band assignments for the ^{13}C NMR spectra of 5-sulfosalicylic acid and rhodium 5-sulfosalicylate





5-Sulfosalicylic acid		Rhodium 5-sulfosalicylate	
a	113.5	a	113.5
b	118.9	b	118.9
c	129.5	c	129.5
d	133.9	d	133.4
e	135.2	e	134.9
f	163.2	f	160.9
g	172.4	g	187.1
Ref. (MeOH)	49.9	Ref. (MeOH)	49.9

Calculations established that: (a) each ml of KOH 2.83×10^{-3} M solution contains 0.16 mg of alkali; (b) each ml of KOH 2.83×10^{-3} M solution reacts with 0.84 mg of rhodium sulfosalicylate; (c) the consumption of 20 ml of alkali solution during the neutralization of a 17.2 mg sample of rhodium sulfosalicylate allowed the recovery of 16.8 mg, equivalent at 97.7% of the theoretical mass.

4. Conclusions

Among its physico-chemical and structural characteristics, the rhodium sulfosalicylate molecule exhibits four stable solvated sulfonic acid groups. These confer ex-

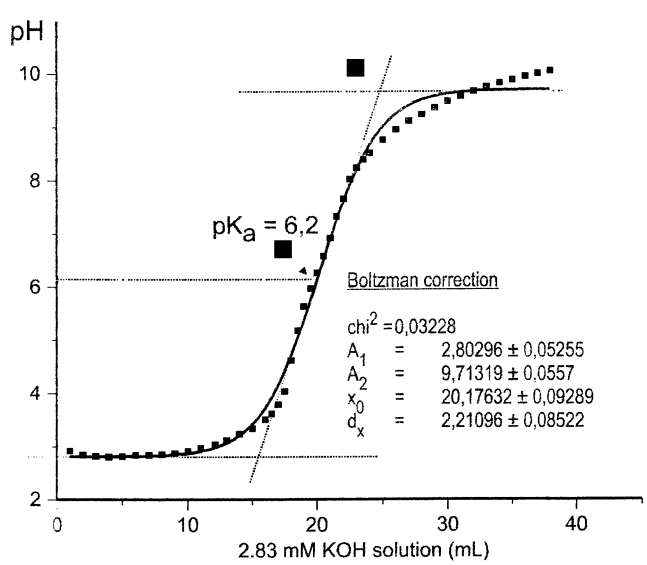


Fig. 3. Neutralization curve of rhodium 5-sulfosalicylate with a standardized KOH solution.

treme hydrofilicity to the complex, turning it into an interesting candidate for future biological activity evaluations, in the wake of the few previously studied water-soluble rhodium carboxylates.

Acknowledgements

The authors are grateful to Professor Dr Renato Najjar, from the Institute of Chemistry of the University of São Paulo, for supplying the rhodium chloride used in the preparation of rhodium sulfosalicylate.

References

[1] B. Rosenberg, L. Van Camp, T. Krigas, Nature 205 (1965) 698.
[2] J.L. Bear, A. Erck, L. Rainen, J. Whileyman, I.M. Chang, A.P. Kimball, Proc. Soc. Exp. Biol. Med. 145 (1974) 1278.
[3] M.S. Nothenberg, G.K.F. Takeda, R. Najjar, J. Inorg. Biochem. 42 (1991) 217.
[4] S. Zyngier, E. Kimura, R. Najjar, Braz. J. Med. Biol. 22 (1989) 397.
[5] E.S. Gil, M.I.A. Gonçalves, E.I. Ferreira, S.B. Zyngier, R. Najjar, Met. Based Drugs 6 (1999) 19.
[6] A.R. Souza, R. Najjar, S. Glikmanas, S.B. Zyngier, J. Inorg. Biochem. 64 (1996) 1.
[7] Powder Diffraction File of the Joint Committee on Powder Diffraction Data, International Center for Diffraction Data, Swarthmore, PA, 1990.
[8] J.H.S. Green, W. Kynaston, A.S. Lindsey, Spectrochim. Acta 17 (1961) 486.
[9] P.V. Khadikar, S.M. Ali, B. Heda, J. Therm. Anal. 30 (1985) 305.
[10] P.V. Khadikar, Thermochim. Acta 127 (1988) 37.
[11] Spectrum 23808, The Sadtler Standard Spectra, Midget ed., vol. 23, Philadelphia, PA, 1967.
[12] G.B. Deacon, R.J. Phillips, Coord. Chem. Rev. 33 (1980) 227.
[13] G.B. Deacon, F. Huber, R.J. Phillips, Inorg. Chim. Acta 104 (1985) 41.
[14] V.M. Miskowski, Inorg. Chem. 23 (1984) 1154.
[15] J.G. Norman Jr., H.J. Kolari, J. Am. Chem. Soc. 100 (1978) 791.
[16] L. Dubicki, R.L. Martin, Inorg. Chem. 9 (1970) 673.
[17] Spectrum 28c, in: C.J. Pouchert, J.R. Campbell (Eds.), The Aldrich Library of NMR Spectra, vol. X, Aldrich Chemical Co., Milwaukee, WI, 1974.
[18] Spectrum 3074c, Sadtler Standard Carbon-13 NMR Spectra, Sadtler Research Laboratories, Philadelphia, PA, 1977.

PERGAMON

www.elsevier.nl/locate/poly

Polyhedron 19 (2000) 1311–1316

POLYHEDRON

Thermal decomposition of oxovanadium(IV) complexes with *N*,*N*′-ethylenebis(amino acids)

Naohisa Yanagihara* [a,1], Yoshimune Yumoto [a], Keizo Arai [a], Kenji Kawabe [b], Yoshitane Kojima* [b,2]

[a] *Department of Materials Science and Engineering, Teikyo University, 1-1 Toyosatodai, Utsunomiya 320-8551, Japan*
[b] *Department of Chemistry, Graduate School of Science, Osaka City University, Sugimoto, Sumiyoshi-ku, Osaka 558-8585, Japan*

Received 7 December 1999; accepted 5 April 2000

Abstract

Six oxovanadium(IV) complexes with *N*,*N*′-ethylenebis(amino acid) of general formula, $[VO(XeX)(H_2O)]\cdot nH_2O$, where e and X represent ethylene group and (*S*)-α-amino acid, respectively; and X = G (Gly) **1**, (*S*)-A (Ala) **2**, (*S*)-V (Val) **3**·$2H_2O$, (*S*)-P (Pro) **4**, ^{m}G or G^{m} (Sar or *N*-methylglycine) **5**·H_2O and (*S*)-M (Met) **6**) were prepared. These complexes were characterized by means of TG, DTA, and XRD, and the thermal decomposition processes of these complexes up to 650°C were investigated. The thermal studies showed that the dehydration processes for **3** and **5** having water of crystallization were endothermic, whereas decompositions of all the complexes were exothermic. Calcinations of these complexes at 650°C resulted in the formation of vanadium(V) oxide V_2O_5. Choosing **1** as a leading example of the oxovanadium(IV) complexes, an over all reaction scheme for the thermal decomposition was proposed on the basis of IR and MS analyses of both the solid and the volatile decomposition products at different temperatures. © 2000 Elsevier Science Ltd. All rights reserved.

Keywords: Oxovanadium(IV) complexes; *N*,*N*′-Ethylenebis(amino acid); TG-DTA

1. Introduction

After the pioneering investigations revealing that both vanadium(IV) and (V) ions have an insulin-mimetic activity [1,2], much attention has been given to research concerning insulin-mimetic vanadium complexes. It is known that the vanadium ions, especially those of an oxidation state of +4 (i.e. vanadyl or oxovanadium) and +5 (vanadate), can adopt various coordination numbers and geometries [3], and to date a variety of vanadium complexes have been prepared [4]. However, since it has been pointed out that oxovanadium(IV) is less toxic than vanadate [5], it seems that a current strategy of investigation involving vanadium ions in the field of biochemistry and physiology is inclined to designing a new functional vanadium(IV) complex with a higher insulin-mimetic activity [6–9].

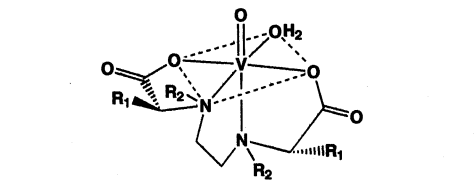
Recently, it has been reported that the complexes with a $VO(N_2O_2)$ coordination mode, such as oxovanadium(IV)–picolinate complexes with a metal-to-ligand ratio of 1:2, also exhibit insulin-mimetic effects [10]. So far we know, however, that the oxovanadium(IV) complexes with a tetradentate ligand in 1:1 molar ratio, in which the ligand especially has a structure type of *N*,*N*′-ethylenebis(amino acid) (XeX′: e = ethylene group, X and X′ = α-amino acid), have not been well recognized. It is a bright prospect to consider using α-C and/or *N*-substituent groups of XeX′, since they can lead the various characteristics of $VO(N_2O_2)$ type complexes. Furthermore, it is expected that the stability of the oxovanadium(IV) complex with mono-tetradentate will be much greater than that of the complex with a bis-bidentate ligand. Next, our efforts have been utilized to improve a new synthetic route to obtain these XeX′ ligands, and we were successful in both preparing and characterizing a variety of oxovanadium(IV)–(XeX′) complexes [11–14].

In the course of our fundamental studies on vanadium chemistry, it was discovered that little attention

[1] *Corresponding author. Tel.: +81-28-627-7204; fax: +81-28-627-7185; e-mail: yanagi@koala.mse.teikyo-u.ac.jp

[2] *Corresponding author. Tel.: +81-6-6605-2549; fax: +81-6-6605-3122; e-mail: kojima@sci.osaka-cu.ac.jp

0277-5387/00/$ - see front matter © 2000 Elsevier Science Ltd. All rights reserved.
PII: S0277-5387(00)00397-1



1 X = G (Gly), n = 0, $R_1 = R_2 = H$
2 X = (*S*)-A (Ala), n = 0, $R_1 = CH_3$, $R_2 = H$
3 X = (*S*)-V (Val), n = 2, $R_1 = CH(CH_3)_2$, $R_2 = H$
4 X = (*S*)-P (Pro), n = 0, $R_1 - R_2 = (CH_2)_3$
5 X = ^{m}G or G^{m} (Sar), n = 1, $R_1 = H$, $R_2 = CH_3$
6 X = (*S*)-M (Met), n = 0, $R_1 = (CH_2)_2SCH_3$, $R_2 = H$

Fig. 1. Schematic description of oxovanadium(IV) complexes with *N*,*N*′-ethylenebis(amino acids), [VO(XeX)(H_2O)].

has been paid to the thermal analyses of oxovanadium-(IV) complexes containing α-amino acid as ligands [15]. Some of the studies involving vanadium complexes are as follows. Thermal decomposition behavior of oxovanadium(IV) complexes with salicylic acid and nuclear-substituted salicylic acids was investigated [16,17]. Thermogravimetric studies on vanadium(IV) and (V) complexes with bidentate chelating ligands such as quinoline, pyrazole and dibenzoylmethane derivatives were carried out [18]. More recently, characterization and thermal analyses of oxovanadium(IV) complexes of the tetradentate Schiff bases [19] and the vanadium(II) oxalate [20] were reported.

In this paper, as a series of our continuing investigation in vanadium chemistry, we report on a thermal study performed on the oxovanadium(IV) complexes with *N*,*N*′-ethylenebis(amino acids).

2. Experimental

2.1. Preparation of oxovanadium(IV) complexes and physical measurements

All reagents and solvents were of analytical grade and used without purification. The oxovanadium(IV) complexes with *N*,*N*′-ethylenebis(amino acids) of a general formula [VO(XeX)(H_2O)]·$n$$H_2O$ (X = α-amino acid and; e = ethylene group and n = 0, 1 and 2), were prepared according to the previously reported method [11,12]. A schematic description of the six complexes is illustrated in Fig. 1, and the abbreviated formula used in this text are as follows: [VO(GeG)(H_2O)] (**1**), G = Gly (glycine); [VO(AeA)(H_2O)] (**2**), A = (*S*)-Ala (alanine); [VO(VeV)(H_2O)]·2H_2O (**3**), V = (*S*)-Val (valine); [VO(PeP)(H_2O)] (**4**), P = (*S*)-Pro (proline); [VO(^{m}GeG^{m})(H_2O)]·H_2O (**5**), ^{m}G or G^{m} = Sar (sarcosine or *N*-methylglycine); [VO(MeM)(H_2O)] (**6**), M = (*S*)-Met (methionine). All the complexes were purified by recrystallization from hot water, and were identified by elemental analysis and IR spectra. The analytical data, some physical data, and the IR data for these complexes are collected in Table 1.

2.2. Thermal analyses

TG and DTA curves were obtained by heating up to 650°C, using a Shimadzu DT-40. The heating rate was 5°C min^{-1} in a dynamic atmosphere of N_2. A small portion (ca. 15–20 mg) of the sample was used for the TG, and the highly sintered α-Al_2O_3 was the thermally inert reference material used for the DTA.

2.3. Analyses of solid and gaseous products obtained by the calcinations

Powder diffractograms of the calcination products were obtained by means of a Shimadzu XD-610 with a source of Cu Kα radiation. For identification purposes, diffraction patterns [(I/I_0) versus d spacing (Å)] of the products were matched with the relevant data on JCPDS cards. The IR spectra of the calcined products at various temperatures were prepared as KBr disks and recorded with the aid of a Shimadzu FT-IR 4300. Mass spectra (MS) of gas phase decomposition products were obtained with a JEOL AV505W in the electron-impact positive-ion mode.

Table 1
Analytical and physical data for the complexes

Complex	Abbreviation for complex	Yield (%)	M.p. (°C)	Elemental analysis (%) found (Calc.)			Infrared spectra data [a] (cm^{-1})		
				C	H	N	$\nu_{as}(CO_2)$	$\nu_{s}(CO_2)$	ν(V=O)
[VO(GeG)(H_2O)]	**1**	41	245–250(dec.)	27.79(27.81)	4.67(4.67)	10.82(10.81)	1674s 1622vs	1386m	956m
[VO(AeA)(H_2O)]	**2**	89	242–245(dec.)	33.21(33.46)	5.70 (5.62)	9.67(9.76)	1623vs	1387m	984m
[VO(VeV)(H_2O)]·2H_2O	**3**·2H_2O	34	177–184(dec.)	37.72(38.00)	7.48(7.44)	7.39(7.39)	1631vs 1575s	1417m 1388m	967m
[VO(PeP)(H_2O)]	**4**	52	267–269(dec.)	42.37(42.49)	5.99(5.94)	8.28 (8.26)	1625vs 1602sh	1403sh 1385s	980m
[VO(^{m}GeG^{m})(H_2O)]·H_2O	**5**·H_2O	33	181–185(dec.)	31.58(31.49)	5.88(5.94)	9.19(9.18)	1633vs 1605vs	1389sh 1373s	976m
[VO(MeM)(H_2O)]	**6**	67	215–223(dec.)	35.18(35.38)	6.04(5.94)	6.89(6.88)	1625sh 1599vs	1394m 1376m	976m

[a] vs = very strong; s = strong; m = medium; sh = shoulder.

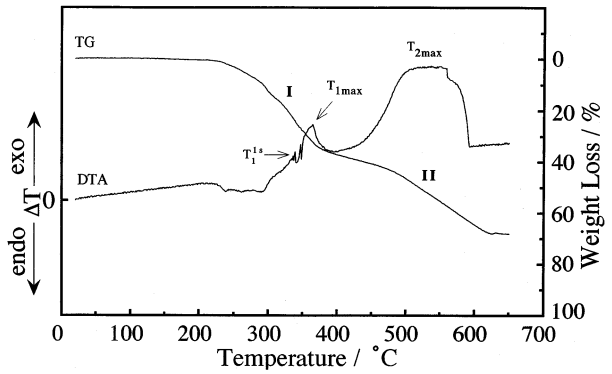


Fig. 2. TG and DTA curves for compound [VO(GeG)(H_2O)] (**1**).

3. Results and discussion

3.1. Dehydration and decomposition processes

Fig. 2 shows the simultaneous DTA and TG curves for [VO(GeG)(H_2O)] (**1**) as a typical example of the thermal analysis of oxovanadium(IV) complexes, and the DTA curves for all the complexes studied are presented in Fig. 3. For convenience, each weight loss (WL) step monitored on the TG curve is designated in Roman numerals, and the corresponding peak temperature on the DTA curve is denoted as T_{1max}, T_{2max}, and so on. In addition, the superscripts 's' and 'sh' in the peak temperature signify small peak and shoulder peak, respectively. The reaction temperatures along with the WL obtained from both TG and DTA curves are summarized in Table 2.

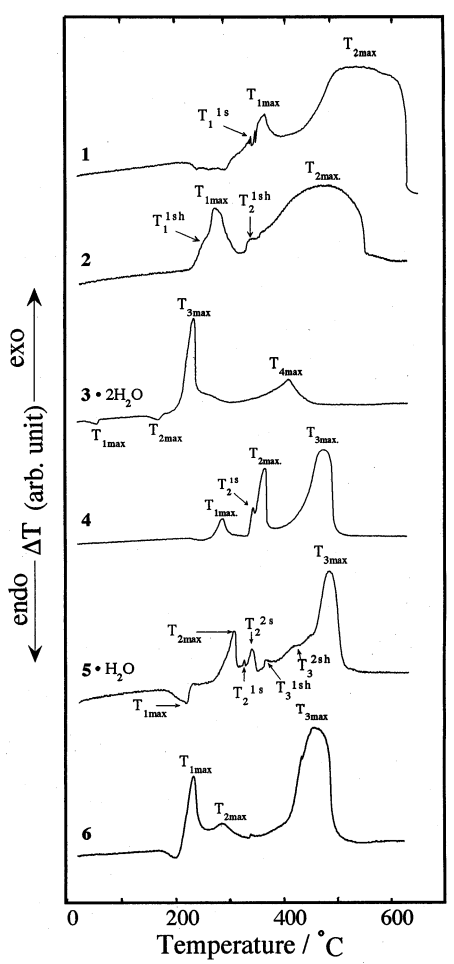


Fig. 3. DTA curves for oxovanadium(IV) complexes (see text for roman numerals).

TG studies revealed that the decomposition of the oxovanadium(IV) complexes could be classified into two categories, which depend on whether a water of crystallization exists or not (see Table 1 for each formula of the complexes). The decomposition of the complexes **3** and **5** occurred in two main stages. The first stage involved a stepwise dehydration to the anhydrous state, followed by the decomposition of the complexes to stable final products. On the other hand, complexes **1**, **2**, **4** and **6** showed only decomposition steps. Although the ambiguous endothermic peaks were shown just before the exothermic decomposition processes in each DTA curve for **1**, **4** and **6**, and since there were no well-defined weight losses in the corresponding TG curves, it has been considered that these ambiguous subtle changes in the DTA curves may not be classified as one of the peaks resulting from some endothermic processes.

As shown in Table 2, the observed WL values that were found in both the dehydration and decomposition processes are in good agreement with the calculated values. In conjunction with the TG curves, it is obvious that the endothermic peaks correspond to each dehydration step, and the exothermic peaks correspond to the decomposition (see Fig. 3). Complex **3** began to lose the first of the two water molecules of crystallization at 34°C, then the second hydrated water was lost at 168°C, which was just before the subsequent decomposition stage. Since complex **5** has one water molecule of crystallization, the corresponding endothermic peak was observed solely at 218°C. When the dehydration stages were completed for complexes 3 and **5**, as well as the rest of each complex, rather complicated peaks were observed in the decomposition temperature region around 230–540°C, which may explained the multiplicities by the postulate that the decomposition process also occurs step by step. For each of the complexes, after the complete decomposition, the TG curve tends to be a continuous horizontal plateau.

The crystallographic characterizations of the oxovanadium(IV) used in the present study were carried out previously, and the coordination geometry of each complex was revealed [12,14]. It is worth noting, however, that the thermal analyses for complexes **3** and **5** could also distinguish the different types of hydrated water molecules, and the observations were consistent with the X-ray crystallographic studies on the com-

Table 2
Thermal analysis data for oxovanadium(IV) complexes

Complex	Step number	Temperature (°C)		Weight loss observed (Calc.) (%)	Effect type
		Range	Peak		
1	I	221 ~ 392	$T_{1max} = 367$ $T_1^{1s} = 342$	36.8	exothermic
	II	403 ~ 633	$T_{2max} = 537$	67.2 (64.9 [b])	exothermic
2	I	230 ~ 313	$T_{1max} = 272$ $T_1^{1sh} = 253$	30.6	exothermic
	II	327 ~ 558	$T_{2max} = 480$ $T_2^{1sh} = 342$	71.6 (68.3 [b])	exothermic
3·2H_2O	I	34 ~ 64	$T_{1max} = 55$	8.7 (9.5 [a])	endothermic
	II	145 ~ 180	$T_{2max} = 168$	14.3 (14.2 [a])	endothermic
	III	193 ~ 297	$T_{3max} = 252$	58.8	exothermic
	IV	324 ~ 474	$T_{4max} = 410$	76.7 (76.0 [b])	exothermic
4	I	263 ~ 302	$T_{1max} = 287$	10.6	exothermic
	II	331 ~ 375	$T_{2max} = 367$ $T_2^{1s} = 347$	57.2	exothermic
	III	395 ~ 496	$T_{3max} = 475$	76.3 (73.6 [b])	exothermic
5·H_2O	I	178 ~ 227	$T_{1max} = 218$	8.5 (6.0 [a])	endothermic
	II	262 ~ 348	$T_{2max} = 304$ $T_2^{1s} = 322$ $T_2^{2s} = 337$	56.7	exothermic
	III	348 ~ 504	$T_{3max} = 481$ $T_3^{1sh} = 422$ $T_3^{2sh} = 448$	71.1 (70.2 [b])	exothermic
6	I	175 ~ 256	$T_{1max} = 233$	24.9	exothermic
	II	261 ~ 333	$T_{2max} = 286$	40.7	exothermic
	III	338 ~ 523	$T_{3max} = 456$	76.4 (77.7 [b])	exothermic

[a] Calculated as loss of hydrated H_2O.
[b] Calculated as V_2O_5.

plexes. Considering the fact that water of crystallization is just packed in the crystal lattice and is not bound to any other atom, upon heating the complex it should be easily liberated at a relatively low temperature region. In fact, for both the complexes **3** and **5**, the dehydration temperatures for the loss of such water molecules of crystallization were observed below 220°C, and in which such temperatures were lower than those of the corresponding decomposition temperatures. Consequently, it is reasonably concluded that the other type of hydrated water molecule, i.e. the coordinated water molecules, which are strongly bonded to the oxovanadium(IV) cation, are expected to be difficult to liberate and the loss of such water molecules could be involved in the decomposition stages. This assumption is supported by the observations that any of the complexes **1**, **2**, **4** and **6**, which have no water molecules of crystallization, have not shown any endothermic peaks.

In addition, for all the oxovanadium(IV) complexes studied here, an attempt to correlate the decomposition temperature with such the intermolecular distances as V–O (vanadyl oxygen), V–O (coordinated water oxygen) and V–O (carboxylate oxygen) was made. It is concluded, however, that no significant dependence was found between the thermal studies and the crystallographic characterization of the oxovanadium(IV) complexes.

*3.2. Characterization of thermal decomposition process for [VO(GeG)(H_2O)] (**1**)*

Since **1** has the simplest amino acid moiety in the ligand, and choosing this complex as a leading complex of [VO(XeX)(H_2O)], an effort was made to reveal an overall thermal decomposition process for the complexes prepared in this study. First, in order to identify the solid products remaining after the decomposition, the calcined products of **1** at 650°C in a dynamic atmosphere of N_2 were subjected to an XRD study. As seen in Table 3, it is clear that the observed XRD data matched the reference data (JCPDS 41-1426) very well, and it was found that the final decomposition product of **1** is to be V_2O_5. This conclusion is consistent with the results of the TG analysis (see Table 2); i.e. the theoretical value (35.1%) for the final residual weight of the decomposed sample, which is calculated based on the formula of V_2O_5, is in agreement with the experimental value (32.8%). Furthermore, the fact that the calcication product of **1** was V_2O_5 is the same result as previously reported on thermal studies involving oxovanadium(IV) complexes [16,18,19].

Table 3
A comparison of X-ray powder diffraction data of V_2O_5

h k l	Reference [a]		Observed		Δd (Å) [b]
	d (Å)	I/I_0	*d* (Å)	I/I_0	
2 0 0	5.768	33	5.756	29	−0.012
0 01	4.379	00	4.371	100	−0.008
1 0 1	4.090	27	4.088	29	−0.002
1 1 0	3.408	75	3.404	70	−0.004
3 0 1, 4 0 0	2.882	52	2.879	58	−0.003
0 1 1	2.764	23	2.763	27	−0.001
3 1 0	2.614	25	2.609	29	−0.005
0 0 2	2.186	11	2.186	16	0
4 1 1	1.994	10	1.992	13	−0.002
6 0 0	1.919	14	1.917	20	−0.002
3 0 2	1.900	8	1.898	11	−0.002
0 1 2	1.864	8	1.863	11	−0.001
0 2 0	1.782	16	1.781	20	−0.001
3 2 1, 4 2 0	1.516	8	1.515	13	−0.001
7 1 0	1.494	9	1.492	14	−0.002

[a] JCPDS 41-1426; for convenience, peaks with intensity less than 7% are omitted.
[b] $\Delta d = d_{obsd.} - d_{ref.}$

IR and MS analyses of the calcined solid- and gas-phase products of **1** were carried out, so as to characterize the overall thermal decomposition process. Fig. 4 exhibits the IR spectra taken over the frequency range of 4000–700 cm^{-1} of **1** and its calcined solid products

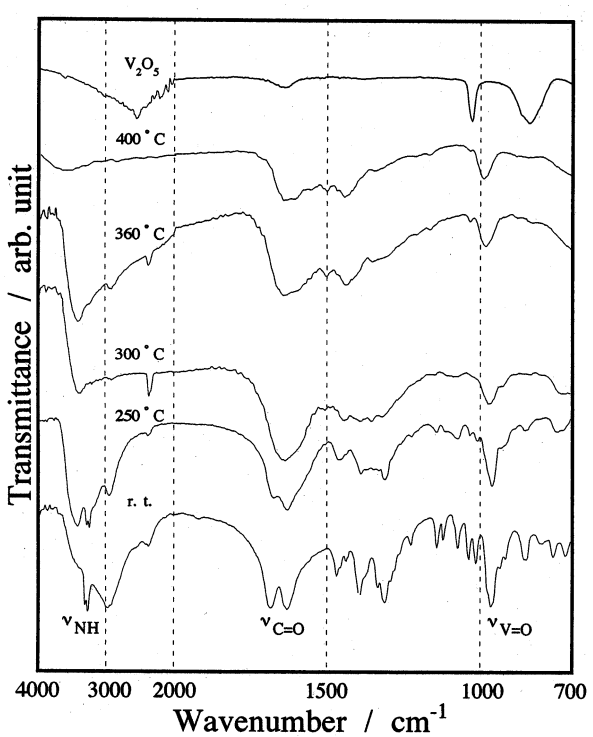


Fig. 4. IR spectra taken for [VO(GeG)(H_2O)] (**1**), its solid decomposition products obtained at the temperature indicated and V_2O_5 as the final decomposition product.

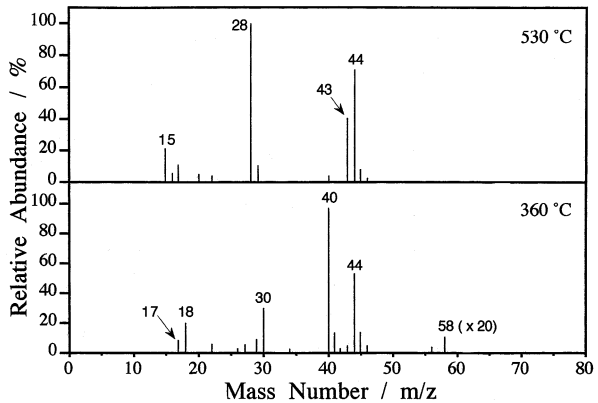
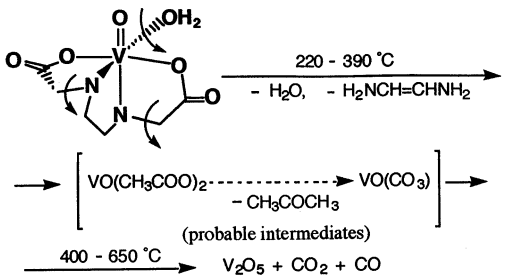


Fig. 5. MS spectra of the volatile products obtained in the pyrolysis of [VO(GeG)(H_2O)] (**1**) at the temperature indicated.

after heating to various temperatures for 10 min. As shown in these IR spectra, it is interesting to note that sharp absorptions at 3310 and 3280 cm^{-1}, which have been observed in the original complex and are due to ν(NH) vibrations [21], disappear around 300°C, and no peaks assignable to the ν(NH) are found in the IR spectrum at 400°C. On the other hand, strong and broad peaks at 1680 and 1630 cm^{-1} [ν(CO)] and a medium-strong absorption at 980 cm^{-1} [ν(VO)], which are observed at r.t., still remains clearly evident at 400°C. Moreover, the IR spectrum of V_2O_5, which was obtained as the final product, is not compatible with that taken at 400°C. Therefore, it is reasonably safe to conclude that a part of the ligand in the complex, especially the moiety containing the NH group, decomposes during the early stages of the pyrolysis, and that vanadium oxidation occurs in the last step in the range 400–650°C.

Support for the above IR results were furnished by MS analyses. Mass spectra of the volatile products obtained in the pyrolysis at 360°C, at which the first stage of the thermal decomposition of **1** occurred, show a molecular ion peak at m/z 58 as shown in Fig. 5. This peak can be considered a $NH_2CH{=}CHNH_2$ molecule, which might be generated as a result of the cleavage of the C_α–N bonds of the ligand. It is, therefore, reasonable to conclude that this base peak leads such fragment ions and molecular peaks as observed at m/z 44 ($CH_2{=}CHNH_3^+$), 40 ($CH_2C{=}N^+$), 30 ($CH_2{=}NH_2^+$), 18 (NH_4^+) and 17 (NH_3). In these fragment ions, the first iminium ion is known to be a very prominent fragment ion, which is commonly observed in the fragmentation of amino acid derivatives [22]. Moreover, it should be emphasized that the peak at m/z 18 in the same MS obviously includes the H_2O molecule.

On the other hand, the mass spectra of the volatiles evolved near the T_{2max} present peaks at m/z 44, 43 and 28 with relatively high intensities. The peaks at m/z 44 and 28 are easily recognized as molecular ion peaks of



Scheme 1.

CO_2 and CO, respectively. Those peaks at m/z 43 (CH_3CO^+) and 15 (CH_3^+) can be considered fragment ion peaks that subsequently arise from the molecular ion of acetone. Although the corresponding base peak was not found in the spectra, the above results make it possible to assume that the CH_3COCH_3 molecule was present in the gaseous product of the second decomposition stage around 530°C.

In summary, in conjunction with the above experimental results and our previous X-ray structural analysis of **1** [12,14], the probable pathway of the thermal decomposition can be rationalized as shown in Scheme 1.

Species such as oxovanadium(IV) acetate and oxovanadium(IV) carbonate were not detected directly in the present study. However, it has been elucidated that metal acetate complexes decompose thermally to corresponding oxides evolving CO_2 and CO, via formation of oxovanadium(IV) carbonate as an intermediate [23]. Therefore, as proposed in Scheme 1, the pathway for the thermal decomposition of **1** might be reasonably accepted. The oxidation of the vanadium from +IV to +V state is probably caused by intermolecular atomic rearrangements during fragmentation in the thermal decomposition.

Although attempts to characterize the other oxovanadium(IV) complexes were not made, their thermal decompositions may proceed in a similar manner as above, even though a part of the bis(amino acid) ligands is different from one another.

Acknowledgements

The authors are grateful to Mr Takahisa Nomura for his help in MS analyses and the Analytical Center, Graduate School of Science, Osaka City University for elemental analyses. This study was supported by a grant (No. 09554040) from the Ministry of Education, Science, Sport and Culture, Japan.

References

[1] Y. Shechter, S.J.D. Karlish, Nature 284 (1980) 556.
[2] G.R. Dubyak, A. Kleinzeller, J. Biol. Chem. 255 (1980) 5306.
[3] C.E. Holloway, M. Melnik, Rev. Inorg. Chem. 7 (1985) 75.
[4] K.H. Thompson, J.H. McNeill, C. Orvig, Chem. Rev. 99 (1999) 2561 and references cited therein.
[5] F.T.G. Hudson, Toxicology and Biological Significance, Elsevier, New York, 1964.
[6] H. Sakurai, A. Tsuji, in: J.O. Nriagu (Ed.), Vanadium in the Environment, Wiley, New York, 1998, pp. 297–315.
[7] B.A. Reul, S.S. Amin, J.P. Buchet, L.N. Ongemba, D.C. Crans, S.M. Brichard, Br. J. Pharmacol. 126 (1999) 467.
[8] J. Costa Pessoa, I. Cavaco, I. Correia, M.T. Duarte, R.D. Gillard, R.T. Henriques, F.J. Higes, C. Madeira, I. Tomaz, Inorg. Chim. Acta 293 (1999) 1.
[9] D. Rehder, Coord. Chem. Rev. 182 (1999) 297.
[10] H. Sakurai, K. Fujii, H. Watanabe, H. Tamura, Biochem. Biophys. Res. Commun. 214 (1995) 1095 and references cited therein.
[11] M. Watanabe, Y. Kojima, K. Kawabe, E. Hatamoto, E. Tsuru, H. Miyake, T. Yamashita, Synthesis (1996) 452.
[12] K. Kawabe, M. Tadokoro, Y. Kojima, Y. Fujisawa, H. Sakurai, Chem. Lett. (1998) 9.
[13] K. Kawabe, T. Suekuni, T. Inada, K. Yamato, M. Tadokoro, Y. Kojima, Y. Fujisawa, H. Sakurai, Chem. Lett. (1998) 1155.
[14] K. Kawabe, M. Tadokoro, A. Ichimura, Y. Kojima, T. Takino, H. Sakurai, J. Am. Chem. Soc. 121 (1999) 7937.
[15] B. Jezowska-Trzebiatowska, A. Antonów, H. Kozlowski, Bull. Acad. Pol. Sci., Ser. Sci. Chim. 22 (1974) 399.
[16] P.V. Khadikar, S.M. Ali, B. Heda, J. Therm. Anal. 30 (1985) 305.
[17] M.Y. Khauhawar, G.Q. Khaskheli, J. Chem. Soc. Pak. 13 (1991) 10.
[18] W. Bechmann, E. Uhlemann, W. Ludwig, Z. Anorg. Allg. Chem. 545 (1987) 235.
[19] M.Y. Khauhawar, A.G. Bhatti, J. Chromatogr. 558 (1991) 187.
[20] A.K. Davies, J.V. Gilligan, S.A. Jones, J. Therm. Anal. 46 (1996) 1567.
[21] K. Nakamoto, Infrared and Raman Spectra of Inorganic and Coordination Compounds, fifth ed., Wiley, New York, 1997.
[22] G.R. Waller, Biochemical Applications of Mass Spectrometry, Wiley, New York, 1972.
[23] G.A. Hussein, J. Thermal Anal. 42 (1994) 1091.

PERGAMON

www.elsevier.nl/locate/poly

Polyhedron 19 (2000) 1317–1328

POLYHEDRON

Characteristic mechanisms of the homogeneous and heterogeneous oxidation of aromatic amines with transition metal–oxalate complexes

A.B. Zaki [a], M.Y. El-Sheikh [a], J. Evans [b,*], S.A. El-Safty [a]

[a] *Department of Chemistry, Faculty of Science, Tanta University, Tanta, Egypt*
[b] *Department of Chemistry, Southampton University, Southampton SO17 1BJ, UK*

Received 31 January 2000; accepted 11 April 2000

Abstract

The oxidation–reduction reactions of aromatic amines {*o*-aminophenol (*o*-AP), *o*-phenylenediamine (*o*-PDA) and *p*-phenylenediamine (*p*-PDA)} with Co(III)–, Mn(III)–, and Cu(II)–oxalate complexes have been investigated in homogeneous and heterogeneous systems. The kinetics of the redox reaction of both systems have been studied spectrophotometrically. The redox products were identified and characterised by diffuse reflectance spectroscopy (DRS), and mass spectrometry. The redox reactions follow first-order kinetics with respect to each of the reactants and first order in [amines] in homogeneous and heterogeneous (supported complexes on Amberlite IRA 904 anion-exchange resin) phases, respectively. However, the specific oxidation rate of the amines is found to follow the order, *p*-PDA > *o*-AP > *o*-PDA. The effect of the oxalate anion on the reaction rate of both systems was examined. There is a significant difference in the behaviour of the oxidation of *o*-AP and *o*-, *p*-PDA with all the metal complexes in both systems. Moreover, the oxidation of *o*-AP and *o*-, *p*-PDA appears to follow the outer- and inner-sphere mechanistic classification, respectively. © 2000 Elsevier Science Ltd. All rights reserved.

Keywords: Aromatic amines; Amberlite anion-exchange resin; Oxalate anions; Metal–oxalate complexes; Oxidation; Homogeneous and heterogeneous

1. Introduction

The oxidation of aromatic amines in human erythrocytes is very useful for producing phenoxazine compounds via the intervention of human oxyhaemoglobin [1]. One of the main objectives has been the elucidation of the oxidation product of the aromatic amines, which has been shown to be a phenoxazine [2–4]. The phenoxazine, also known as questiomycin A, is related to the naturally occurring antibiotic actinomycin D [5,6] that is used clinically for the treatment of certain types of cancer [7].

The oxidation of *p*-PDA in an aqueous sulphuric acid medium by Mn(III) acetate has been examined [8]. The reaction followed second-order kinetics, first order with respect to [amines] and [Mn(III)]. The reaction shows a positive salt effect. In aqueous solution, the redox reaction between *p*-PDA and Ag(I) ions has also been envisaged [9–11]. An induction period was dependent on pH and the concentration of *p*-PDA, but not on the Ag(I) ion concentration. Furthermore, the effect of pH on the equilibrium in the *p*-PDA–ferricyanide redox system has been discussed [12–14]. The equilibria were established very rapidly at all pH values. Finally, the oxidation of *o*-aminophenol (*o*-AP) by O_2 to amino 3-*H*-phenoxazine-3-one (APX) can be catalysed by cobalt(II) salts, cobalt(II)–phthalocyanine derivatives and copper compounds [15–18]. Some tris-oxalato complexes are also known to be strong oxidising agents in aqueous solution [19]. The kinetics of reduction of tris-oxalato–cobaltate(III) by amines have been investigated [20,21] in aqueous acidic media. The specific rate constants and the corresponding activation parameters have been evaluated at constant ionic strength.

* Corresponding author. Tel.: +44-23-8059-3307; fax: +44-23-8059-3781.
E-mail address: je@soton.ac.uk (J. Evans).

0277-5387/00/$ - see front matter © 2000 Elsevier Science Ltd. All rights reserved.
PII: S0277-5387(00)00401-0

The oxidative condensation mechanism of amines involves a $6e^-$ oxidation coupling process [22,23]. It has been suggested that the reaction occurs via a sequence of three consecutive $2e^-$ oxidations, alternating with conjugate addition of the amine moiety to benzoquinoneimine type intermediates, followed by a tautomerisation step to afford a phenoxazine compound. A sequence for the inner- or outer-sphere mechanisms may be seen in Refs. [24,25].

We have carried out a systematic study of the kinetics and mechanism of such redox systems in heterogeneous (supported metal oxalate complexes on Amberlite IRA 904 anion-exchange resin) and homogeneous systems. A related study reported the kinetics and mechanism of the sorption of the same amines into Amberlite IRA 904 anion-exchange resin in chloride form [26]. An important result from that work is that the rate of diffusion into the particle is accelerated by the presence of supported metal oxalate complexes. Moreover, the overall redox reaction is controlled by a combination of intraparticle reaction and intraparticle diffusion. The latter can never be the sole rate-determining step.

2. Experimental

2.1. Materials

All the materials used in the present work such as amines {*o*-aminophenol (*o*-AP), *o*-phenylenediamine (*o*-PDA) and *p*-phenylenediamine (*p*-PDA)} and the Amberlite IRA-904 anion-exchange resin (spherical-shaped beads of quaternary ammonium styrene divinylbenzene copolymer) were supplied by the Sigma-Aldrich Company Ltd., UK. The stock solutions of the amines (0.01 M) were prepared in an ethanol–water mixture as follows: 10% for *o*-AP and 20% for both *o*- and *p*-PDA, and were diluted to obtain the suitable concentration of the amine. In all cases, the percentage of ethanol is not more than 2% in the amine solution during the redox reactions of all amines. The $K_3[Mn(C_2O_4)_3]$ (**I**), $K_3[Co(C_2O_4)_3]$ (**II**), and $K_2[Cu(C_2O_4)_2]$ (**III**) complexes were prepared by standard methods [27–30]. The UV–Vis absorption spectra of the 0.01 M solutions of complexes **I** and **II** in aqueous solution and complex **III** (in aqueous potassium oxalate) agreed with the literature [27–30].

2.2. Resin support with transition metal–oxalate complexes

The anion-exchange resin was immersed in doubly distilled water and the highly diluted solutions of the metal–oxalate complexes were added dropwise with continuous stirring in the dark until a slight excess of the complexes was detected by UV–Vis spectrophotometry. The resin was collected and washed by distilled water, and then it was air dried in the dark.

2.3. Apparatus

The spectrophotometric measurements were performed with a Shimadzu 2100S spectrophotometer equipped with a TCC-260 temperature controller, and a Perkin Elmer Lambda 19 UV–Vis/NIR spectrometer, equipped with temperature control. The mass spectrometric experiments were recorded on a Micromass Platform quadrupole mass analyser. APCI (atmospheric pressure chemical ionisation) spectra were recorded under operating conditions of: a capillary 3.5 kV, HV lens 0 kV, cone voltage 20 V, source temperature 150°C, probe temperature 450°C, ES eluent; 100% acetonitrile at 200 μl min^{-1}, nitrogen drying gas 250 l h^{-1} and APCI sheath gas 50 l h^{-1}. A Crison 501 pH meter was used and calibrated just before the measurements were recorded. Diffuse reflectance spectroscopy (DRS) measurements of the resins were recorded on the Perkin Elmer Lambda 19 UV–Vis/NIR spectrometer.

2.4. Kinetic measurements

The heterogeneous redox reaction between the amines (*o*-AP, *o*-PDA, and *p*-PDA) and a known amount of Amberlite IRA 904 supported with complexes **I**–**III** was carried out at four temperatures (range 25–45°C) $\pm$ 0.1°C in aqueous/trace ethanol solution. The reaction was performed using a thermostatted shaker, where the rate of shaking was constant for all reactions. After a set interval of time, the container was removed from the thermostat and the reaction was quenched quickly by suction. The homogeneous redox reaction was carried out in the spectrophotometer cell at controlled temperatures (25–50°C precision $\pm$ 0.1°C). The concentration of the oxidation product of the amines in homogeneous and heterogeneous systems was monitored spectrophotometrically at 435 nm for *o*-AP, 420 nm for *o*-PDA [15,24] and 510 nm for *p*-PDA [31], except with complex **II** where the reactions were monitored at 435 and 450 nm for *o*- and *p*-PDA, respectively [32].

3. Results and discussion

3.1. Analysis of the supported resin and oxidation products of the amines

DRS was utilised to observe the influence of the supported complexes and the oxidation reaction of the amines on the Amberlite IRA 904 anion-exchange resin (Fig. 1). The observed absorption bands at $\lambda = 604$ and

420 nm shown in Fig. 1(b) are attributed to the strong support of complex **II** on the resin after ion exchange [19,27]. Additionally, the absorption band at $\lambda = 604$ nm for complex **II** disappears and the band at $\lambda = 435$ nm becomes apparent (Fig. 1(b,c)). These results provide good evidence for the reduction of the metal ion in the redox system and strong adsorption of the oxidation product on the Amberlite resin after the redox reaction.

Mass spectrometry APCI was used for the molecular weight determination of the oxidation product of the redox reaction (Fig. 2). This showed that the oxidation product of *o*-AP, *p*-PDA and *o*-PDA exhibited a molecular ion consistent with the formation of dimers and a trimer as follows: $[M]^+ = 215$, 319 and 211 for the oxidation product of *o*-AP, *p*-PDA and *o*-PDA, respectively. These ions were consistent with the molecular formulae $[C_{12}H_{11}N_2O_2]^+$, $[C_{18}H_{19}N_6]^+$ and $[C_{12}H_{11}N_4]^+$. These ions are consistent with the protonated forms of the oxidation products of the amines, as shown in Schemes 1–3. These analyses are consistent with literature values [24,33], and are appropriate for the reaction of the complexes **I**–**III** with the amines to produce benzoquinoneimine and benzoquinonediimine compounds.

3.2. Schematic representations of the diverse reactions

The oxidative condensation process involves a $4e^-$ oxidation for *o*-AP to produce 2-aminophenoxazine-3-ol (APZ) (Scheme 1). However, the $6e^-$ oxidation is described for the oxidation of *o*-PDA and *p*-PDA to get 2,3-diaminophenazine (DAP) and 2,2′-diaminoazabenzene (AB), respectively (Schemes 2 and 3). Generally, the first $2e^-$ oxidation is a result of the reduction of the metal–oxalate complexes **I**–**III** [23,32]. This means that two equivalents of the metal complexes are initially reduced by one equivalent of the various amines. Since the benzoquinone imines react with another molecule of the amines to afford the dimeric or trimeric oxidation products, the reaction sequence of the expected oxidation products is shown in Schemes 1–3.

3.3. Kinetic parameters of the redox reactions

All the redox reactions between the amines (*o*-AP, *o*-PDA and *p*-PDA) and a known amount of the Amberlite IRA 904 supported complexes **I**–**III** obeyed first-order kinetics with respect to [amine]. The plot of

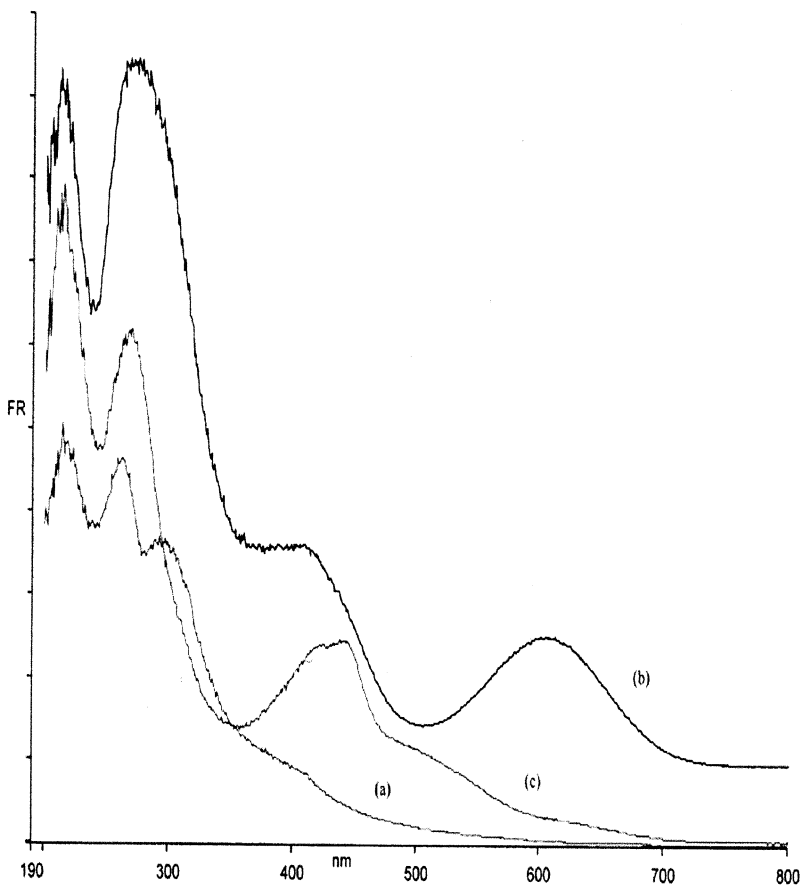


Fig. 1. Diffuse reflectance spectra of Amberlite IRA 904 anion-exchange resin (a) before supporting with complex, (b) after supporting with the Co(III)–oxalate complex, and (c) after the redox reaction with the amines used in this work at 25°C.

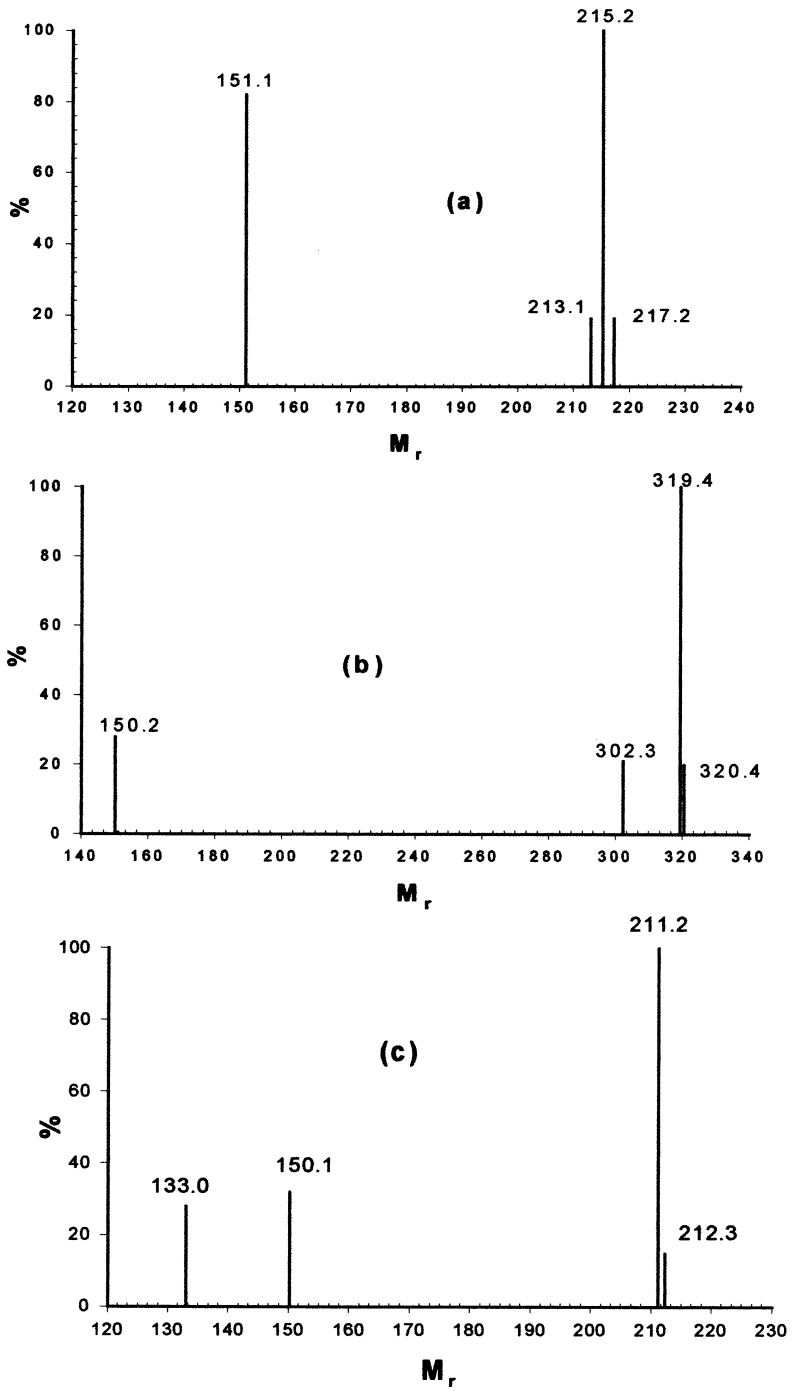
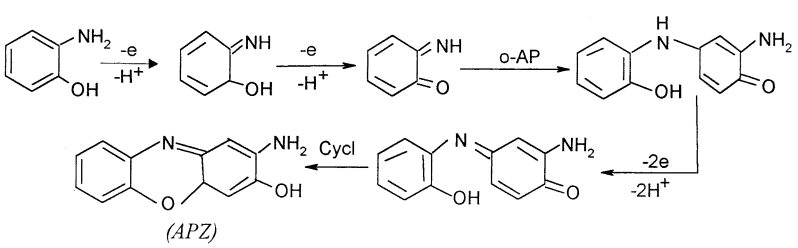
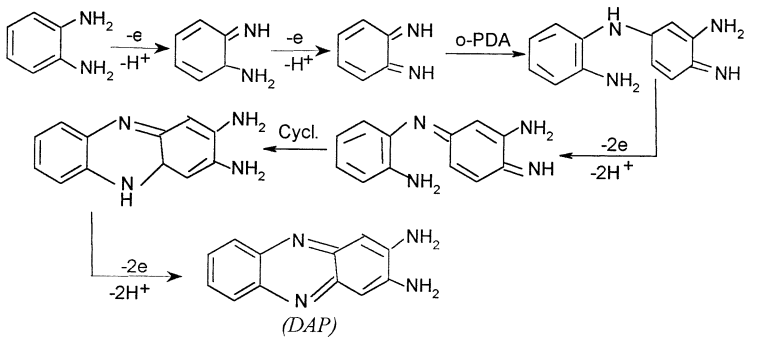


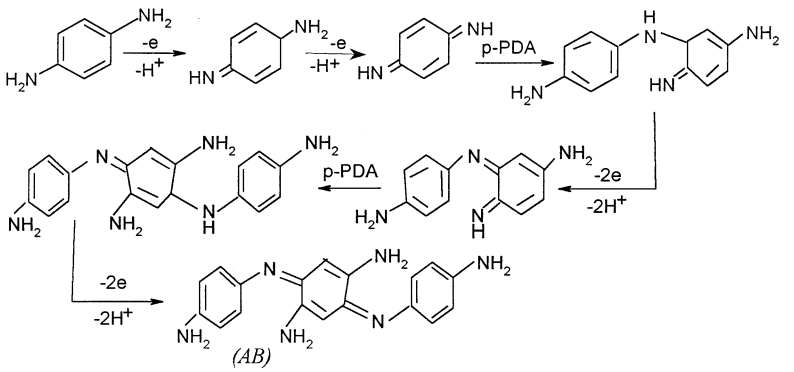
Fig. 2. Mass spectra of isolated oxidation reaction products of (a) *o*-AP, (b) *p*-PDA, and (c) *o*-PDA with metal–oxalate complexes at 25°C.



Scheme 1.



Scheme 2.



Scheme 3.

the logarithm of the $A_f/A_f - A_t$ versus time (Fig. 3) gives a straight line passing through the origin whose slope is equal to the observed rate constant (k_{obs}) according to the following equation [34]:

$$\ln(A_f/A_f - A_t) = k_{obs}wt$$

where A_f is the absorbance at infinite time, A_t is the absorbance at time t and w is the mass (g) of dry supported resin.

The true rate constants (k_t) per gram of dry resin (pgdr), which are independent of the amount of supported resin, were calculated and are summarised in Table 1.

The homogeneous redox reactions were performed under pseudo first-order conditions, with a large excess of the amine, except in the case of the reaction of complex **II** with *o*-AP and *o*-PDA where there was a large excess of the complex. In both cases, the reaction rate was determined by following the oxidation product of the amines at the characteristic absorption band as shown in Fig. 4. The rate equation in most cases can generally be written as follows:

$$\text{Rate} = k_{true}[\text{amine}]^m[\text{complex}]^n$$

The partial order with respect to [amine] and [complex] was obtained under pseudo first-order conditions. A plot of $\ln k_{obs}$ (k_o) against ln[amine] or ln[complex] gave a straight line whose slope and intercept are the order (m and n) of the [reactants] and k_{true} (k_t), respectively (Fig. 5(a,b)). The values of m and n were determined to be $1.0(\pm 0.1)$. Hence, the k_t values of this second-order reaction are listed in Table 2.

According to the data shown in Tables 1 and 2, the true rate constant of the homogeneous and heteroge-

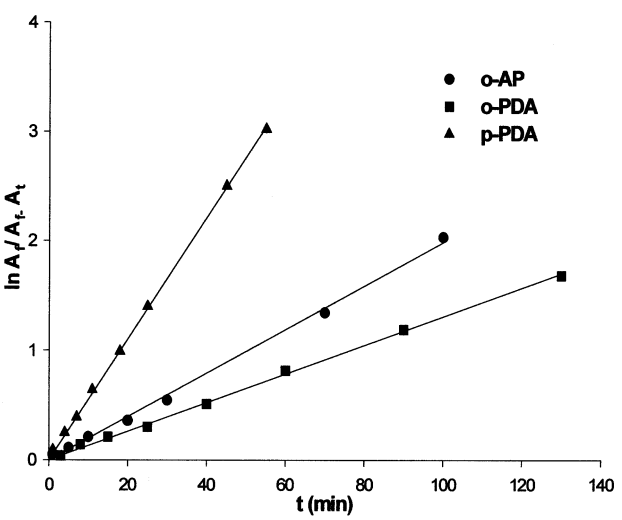


Fig. 3. Integrated first-order rate equation of the heterogeneous oxidation reaction between amines and the Cu(II)–oxalate complex supported on Amberlite IRA-904 anion-exchange resin at 35°C.

Table 1
Illustration of the rate constant k (pgdr) and the activation parameters of the redox reaction of amines [A] (7.35×10^{-4} M) using Amberlite IRA 904 anion-exchange resin supported with transition metal oxalate complexes

Complex	[A]	$k_t \times 10^4$ s^{-1} [a]					E (kJ mol^{-1})	$\Delta H^{\neq}$ (kJ mol^{-1})	$\Delta G^{\neq}$ (kJ mol^{-1})	$\Delta S^{\neq}$ (J mol^{-1} deg^{-1})
		25°C	30°C	35°C	40°C	45°C				
I	*o*-AP	11.91	15.30	20.73	32.25		51.0 (8)	48.46	90.87	−139 (3)
	o-PDA	7.81	9.486	11.23	14.88		39.0 (5)	36.26	92.81	−185 (2)
	p-PDA	14.71	19.99	31.88	57.34		70 (1)	67.91	89.92	−72 (4)
III	*o*-AP		6.143	8.45	11.33	16.41	52.0 (2)	49.37	94.03	−143.2 (7)
	o-PDA		3.154	4.005	5.903	9.407	59.0 (8)	56.37	95.73	−128 (3)
	p-PDA	9.05	12.53	16.09	22.23		47.0 (3)	44.50	91.99	−157.2 (8)
II	*o*-AP	10.58	14.06	18.72	27.71		46.0 (8)	43.25	91.55	−158 (2)
	o-PDA	5.28	6.93	9.19	14.78		52.2 (8)	49.67	92.90	−142 (3)
	p-PDA	14.00	18.40	23.20	31.07		40.4 (4)	37.80	91.05	−174 (2)

[a] Standard deviations were in the range $1–8 \times 10^{-2}$ for all rate constants.

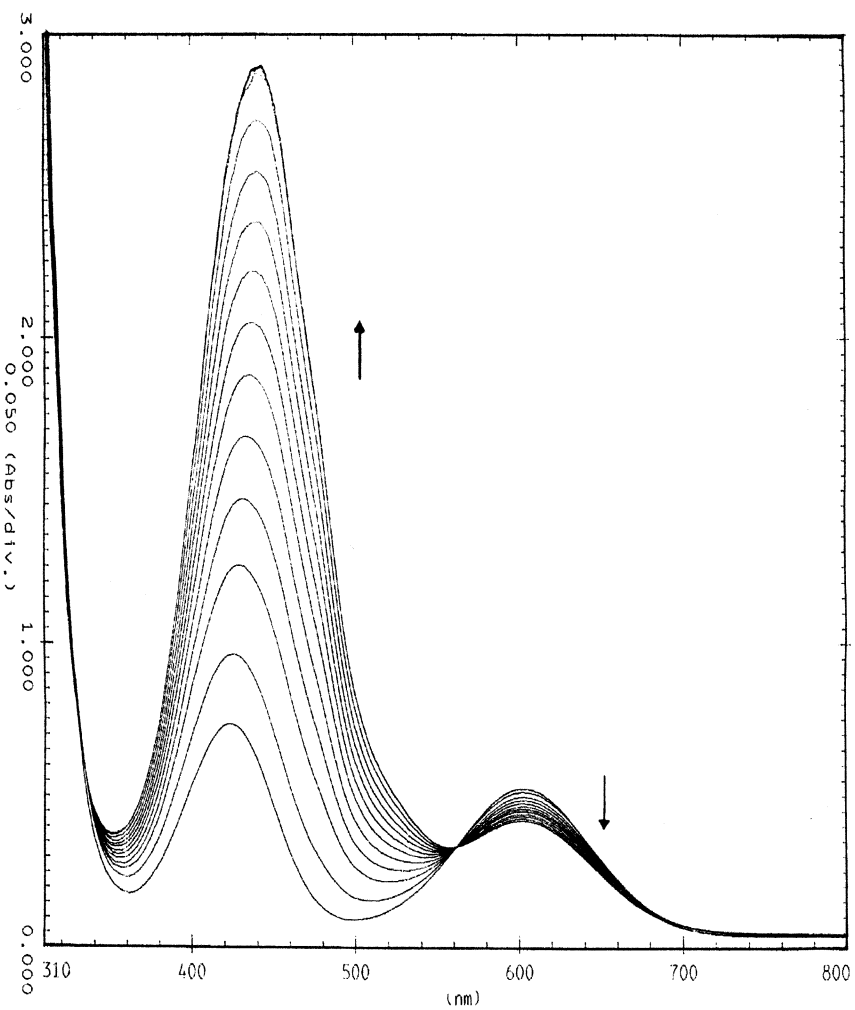


Fig. 4. Time sequence of the increase in the absorption band of the oxidation product of *o*-PDA for the homogeneous reaction with the Co(III)–oxalate complex in the reaction medium.

Table 2
Illustration of the true rate constant k_t and the activation parameters of the homogeneous redox reaction of amines [A] and transition metal oxalate complexes

Complex	[A]	$k_t \times 10^2$ l mol^{-1} s^{-1} [a]						E (kJ mol^{-1})	$\Delta H^{\neq}$ (kJ mol^{-1})	$\Delta G^{\neq}$ (kJ mol^{-1})	$\Delta S^{\neq}$ (J mol^{-1} deg^{-1})
		25°C	30°C	35°C	40°C	45°C	50°C				
I	*o*-AP	81.9	107.8	128.4	164.8			50.6 (2)	48.0	88.45	−133.0 (8)
	o-PDA	38.67	57.68	74.1	95.1			37.0 (4)	34.61	76.33	−154 (1)
	p-PDA	95.12	128.4	191.6	300.4			60.5 (5)	57.92	73.89	−52 (2)
III	*o*-AP	3.87	5.18	8.63	13.2			65.0 (6)	62.45	81.69	−63 (2)
	o-PDA			1.624	2.375	3.47	4.64	58.5 (4)	55.85	86.81	−98 (1)
	p-PDA			12.62	22.31	42.7	60.65	89.0 (1)	86.22	80.66	18.0 (4)
II	*o*-AP			1.984	3.508	5.23	7.81	71.4 (6)	68.80	85.95	−54 (2)
	o-PDA			0.463	0.783	1.17	1.74	71.0 (3)	68.46	89.89	−68 (1)
	p-PDA	5.502	8.804	13.26	20.80			73.2 (8)	70.50	83.42	−41 (3)

[a] Standard deviations were in the range $1–7 \times 10^{-2}$ for all rate constants.

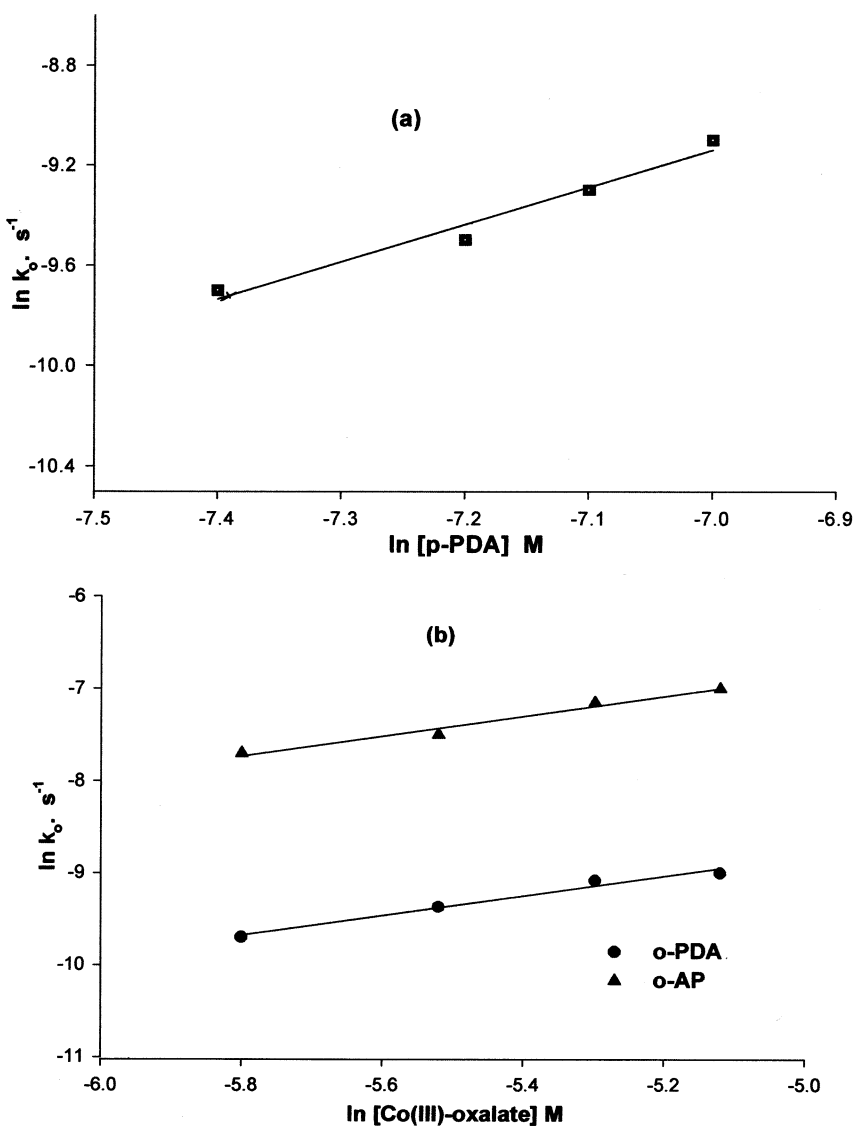


Fig. 5. Logarithmic plot of the relationship between the observed rate constant and (a) the [*p*-PDA] at constant of Co(III)–oxalate complex (7×10^{-5} M) and (b) the varied [Co(III)–oxalate] at constant amines concentration (2×10^{-4} M) at 40°C.

neous oxidation of amines has the following order pattern:

p-PDA > o-AP > o-PDA

which is attributed to the effects of the electron donating and electron density of the amine substituents. This is the same trend as observed with our previous work carried out on the oxidation of these amines by transition metal complexes incorporated with mesoporous silica materials [35].

Also, the oxidation activity of the metal–oxalate complexes increases in the following order:

III < II < I

The stability constant of the oxalate complexes decreases in the following sequence: **II** ≥ **I** ≫ **III** [28], but the reduction potential of Mn(III) → Mn(II) is larger than that of Co(III) → Co(II) in the reaction medium [36]. Hence, the reduction potential of the metal has more effect on the reactivity than the stability constant of these metal complexes.

3.4. Activation parameters of the redox reactions

The dependence of reaction rate of the redox reactions on the temperature is shown for one example of a heterogeneous reaction in Fig. 6.

The activation energy (E) was deduced from an Arrhenius plot, exemplified for a homogeneous case in Fig. 7. The other activation parameters $\Delta G^{\neq}$, $\Delta H^{\neq}$ and $\Delta S^{\neq}$ were calculated from Eyring's equation and are listed in Tables 1 and 2.

From these results, it can be seen that $\Delta S^{\neq}$ and E of amines for complexes **I**–**III** follow the same sequence as the rate constant of the reaction as follows: p-PDA > o-AP > o-PDA, except only in the cases of amine oxidation reaction with complexes **II** and **III** supported on the Amberlite resin, which show an inverse sequence. This may be due to the high negative $\Delta S^{\neq}$ value suggesting that the transition state is charged and rigid [37,38].

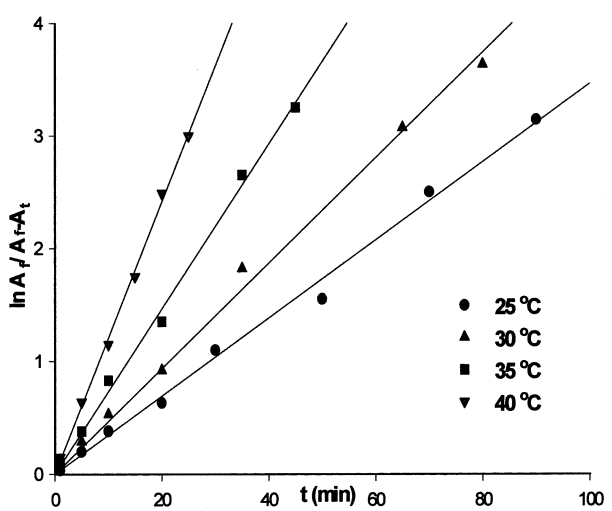


Fig. 6. Integrated first-order rate equation of the heterogeneous oxidation reaction between p-PDA (7.35×10^{-4} M) and the Mn(III)–oxalate complex supported on Amberlite IRA-904 (0.4 g) anion-exchange resin at different temperatures.

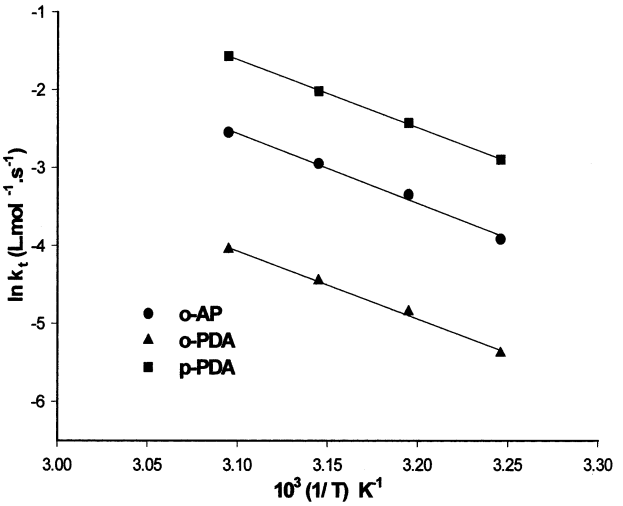


Fig. 7. Arrhenius plot of the redox reaction between amines and the Cu(II)–oxalate complex in solution.

On the other hand, the activation energy (E) of the redox reaction of the metal–oxalate complexes with amines (o-AP, o-PDA and p-PDA) increases in the following order with slight deviation in the case of the complex **I** in the heterogeneous system:

I < II < III

Hence the greater the reduction potential of the metal ion, the more facile is the metal–oxalate complexes to be reduced, and the smaller is the activation energy. Moreover, the value of $\Delta H^{\neq}$ of activation is in the range of chemical reaction control [39]. Also, this value shows that the electron transfer reaction steps may include the substitution reaction process [40]. The $\Delta G^{\neq}$ value is found to be in the range 74–95.7 kJ mol^{-1} (Tables 1 and 2), which is within the range of values for the oxidation of these amines by the iron(III)–oxalate complex $[Fe(C_2O_4)_3]^{3-}$ [41]. The above observations are consistent with the mechanisms of the redox reactions being the same in the homogeneous and heterogeneous systems.

3.5. Effect of oxalate ions on the redox reactions

The effect of added oxalate anion on the redox reaction rate has been studied in solution as well as in the heterogeneous system. This study was done after establishing an absence of any effect of oxalate anion concentration on the resin supported metal oxalate complexes by DRS measurements.

As shown in Fig. 8, an increase in the concentration of oxalate ion causes an inhibition in the reaction rate in the cases of o-PDA and p-PDA. The presence of the

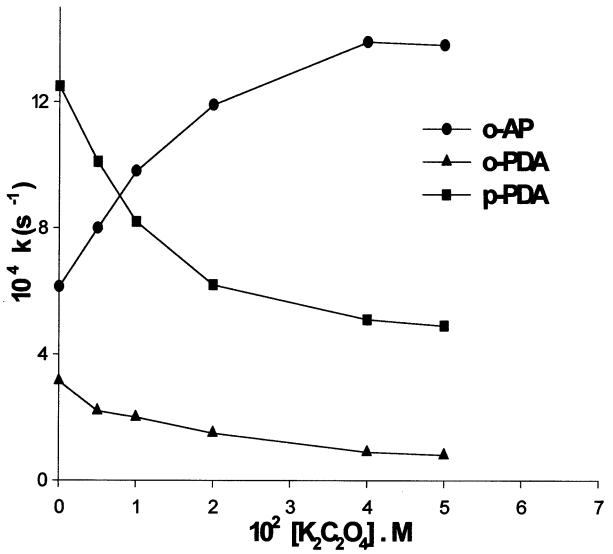


Fig. 8. Illustration of the effect of the oxalate ion concentration on the rate constant k (pgdr) for heterogeneous redox reaction between amines (7.35×10^{-4} M) and the Cu(II)–oxalate complex supported on Amberlite IRA 904 anion-exchange resin at 30°C.

oxalate ions in the reaction medium causes the reaction to shift towards the side of the reacting species. This causes the reacting species to be even more stable than the activated complexes and that renders the reaction less facile [42]. This result suggests the oxidation of *o*-PDA and *p*-PDA may follow a stepwise inner-sphere mechanism. On the contrary, in the case of redox reaction of *o*-AP with metal oxalate complexes, the rate of the reaction increases with increasing concentration of oxalate ions until at a particular concentration, the rate is constant. This means that the presence of oxalate ions in the reaction medium causes stabilisation of the activated complex and accelerates the reaction rate. The oxidation of *o*-AP by the metal oxalate complexes may follow the outer-sphere mechanism.

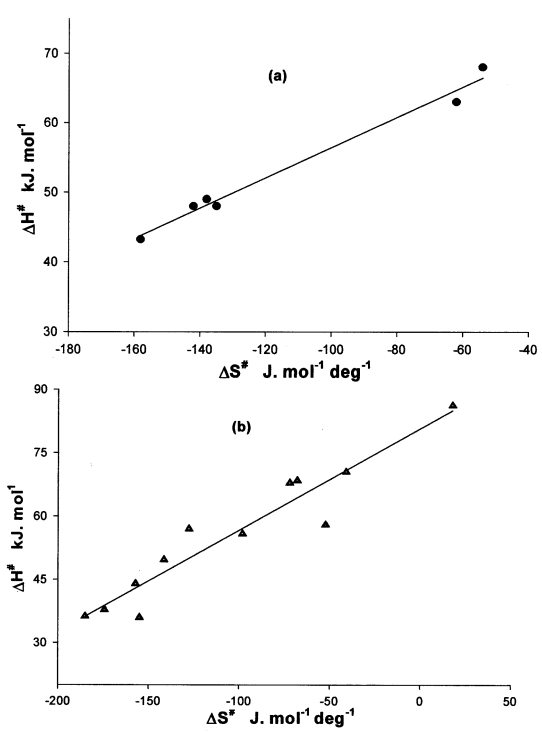


Fig. 9. Isokinetic relationship plot of heterogeneous and homogeneous redox reaction between metal–oxalate complexes and amines (a) *o*-AP and (b) *o*- and *p*-PDA used in this work.

3.6. Isokinetic relationship

These results suggest two different types of the oxidation reaction mechanisms. To confirm that, the isokinetic temperature (β) was tested by plotting a graph of $\Delta H^{\neq}$ versus $\Delta S^{\neq}$ (Fig. 9(a,b)) for the heterogeneous and homogeneous oxidation reactions of *o*-AP, *o*-PDA and *p*-PDA with metal oxalate complexes, which provide correlation coefficients of 0.95 and 0.90, respectively, on a linear relationship (Fig. 9(a,b)). It is evident that there is a significant difference in the redox reaction mechanism in the case of *o*-AP as opposed to those of *o*-PDA and *p*-PDA.

The value of the isokinetic temperature β was found to be 218 and 240 K, respectively. These values are below the mean experimental temperature, thereby suggesting that these are entropy-controlled reactions [43].

3.7. The reaction mechanism

In view of the experimental findings, it would seem appropriate to discuss the mechanism of the redox reaction. The *outer-sphere mechanism* of the redox reaction between *o*-AP and metal–oxalate complexes is proposed as follows in the following reaction scheme (Eqs. (1)–(8)) [44–46]. In all types of mechanism (L = 0 or $C_2O_4^{2-}$ in the cases of the second and third oxidation state of transition metal, respectively):

$$[ML(C_2O_4)_2]^{n-} + AP \underset{k_{-1}}{\overset{k_1}{\rightleftharpoons}} \{[ML(C_2O_4)_2]^{n-}\cdots AP\} \quad (1)$$

(formation of the encounter pair)

$$\{[ML(C_2O_4)_2]^{n-}\cdots AP\} \underset{k_{-2}}{\overset{k_2}{\rightleftharpoons}} \{[ML(C_2O_4)_2]\text{–}AP^{n-}\} \quad (2)$$

(restructuring of the encounter complex to set up the electron transfer)

$$\{[M\,L(C_2O_4)_2\,] - AP\}^{n-} \xrightarrow[slow]{k_3} [M\,L(C_2O_4)]^{(n-1)-} + HC_2O_4^{-} + AP^{\cdot} \xrightarrow[\text{Oxidation product}]{rapid\ \downarrow k_4} \quad (3)$$

$$dx/dt = k_3\{[ML(C_2O_4)_2]\text{–}AP\}^{n-} \quad (4)$$

Under pre-equilibrium conditions:

$$dx/dt = k_3K_1K_2[ML(C_2O_4)_2]^{n-}[AP] \quad (5)$$

where $K_1 = k_1/k_{-1}$ and $K_2 = k_2/k_{-2}$.

Applying the steady-state approximation for the intermediate:

$$\begin{aligned} &d\{[ML(C_2O_4)_2]\text{–}AP\}^{n-}/dt \\ &= k_2\{[ML(C_2O_4)_2]^{n-}\cdots AP\} \\ &\quad - k_{-2}\{[ML(C_2O_4)_2]\text{–}AP\}^{n-} \\ &\quad - k_3\{[ML(C_2O_4)_2]\text{–}AP\}^{n-} = 0 \end{aligned} \tag{6}$$

$$\text{i.e. } \{[ML(C_2O_4)_2]\text{–}AP\}^{n-} = \frac{k_2K_1[ML(C_2O_4)_2]^{n-}[AP]}{k_{-2}+k_3} \tag{7}$$

$$dx/dt = \frac{k_3k_2K_1[ML(C_2O_4)_2]^{n-}[AP]}{k_{-2}+k_3} \tag{8}$$

The *inner-sphere mechanism* of the redox reaction between *o*-PDA and *p*-PDA, and metal–oxalate complexes is also suggested as follows in the following reaction scheme (Eqs. (9)–(16)) [44,47,48]:

$$[ML(C_2O_4)_2]^{n-} + PDA \underset{k_{-1}}{\overset{k_1}{\rightleftharpoons}} \{[ML(C_2O_4)_2]^{n-}\cdots PDA\}$$

(formation of the encounter pair) (9)

$$\{[ML(C_2O_4)_2]^{n-}\cdots PDA\} \underset{k_{-2}}{\overset{k_2}{\rightleftharpoons}} [ML(C_2O_4)PDA]^{(n-1)-} + HC_2O_4^-$$

(formation of the inner-sphere complex) (10)

$$[M\,L(C_2O_4)\,PDA]^{(n-1)-} \xrightarrow[slow]{k_3} [M\,L(C_2O_4)]^{(n-1)-} + PDA \quad (rapid \downarrow k_4)$$

Oxidation product (11)

$$dx/dt = k_3[ML(C_2O_4)PDA]^{(n-1)-} \tag{12}$$

Applying a pre-equilibrium approximation:

$$dx/dt = k_3K_1K_2\frac{[ML(C_2O_4)_2]^{n-}[PDA]}{[HC_2O_4^-]} \tag{13}$$

where $K_1 = k_1/k_{-1}$ and $K_2 = k_2/k_{-2}$

Applying the steady state approximation for the intermediate:

$$\begin{aligned} &d[ML(C_2O_4)PDA]^{(n-1)-}/dt \\ &= k_2\{[ML(C_2O_4)_2]^{n-}\cdots PDA\} \\ &\quad - k_{-2}[ML(C_2O_4)PDA]^{(n-1)-}[HC_2O_4^-] \\ &\quad - k_3[ML(C_2O_4)PDA]^{(n-1)-} = 0 \end{aligned} \tag{14}$$

i.e. $[ML(C_2O_4)PDA]^{(n-2)-}$

$$= \frac{k_2K_1[ML(C_2O_4)_2]^{n-}[PDA]}{k_{-2}[HC_2O_4^-]+k_3} \tag{15}$$

$$dx/dt = \frac{k_3k_2K_1[ML(C_2O_4)_2]^{n-}[PDA]}{k_{-2}[HC_2O_4^-]+k_3} \tag{16}$$

From the two suggested mechanisms, the $[C_2O_4^{2-}]$ appearing in the denominator of the rate expression for the inner-sphere mechanism only, provides an explanation for a slight inverse dependence on $[C_2O_4^{2-}]$ in the oxidation of *o*-PDA and *p*-PDA. In each mechanism, the reaction rate is proportional to $[ML(C_2O_4)_2]^{n-}$ and [amine]. This means that the reaction follows second-order kinetics in the homogeneous system, and first-order for kinetics for $[MLC_2O_4)_2]^{n-}$ and [amine], and first-order kinetics for [amine] in the heterogeneous system.

From Eq. (16), we can derive the following relationship:

$$\frac{1}{k} = \frac{k_{-2}[HC_2O_4^-]}{k_3k_2K_1} + \frac{k_3}{k_2K_1} \tag{17}$$

By applying the relationship $1/k_{obs}$ versus [oxalate], a plot of Eq. (10) gives a good linear relationship in the case of the oxidation reaction of *o*-PDA and *p*-PDA, which provides correlation coefficients of 0.994 and 0.996, respectively. In contrast, a poor straight line with

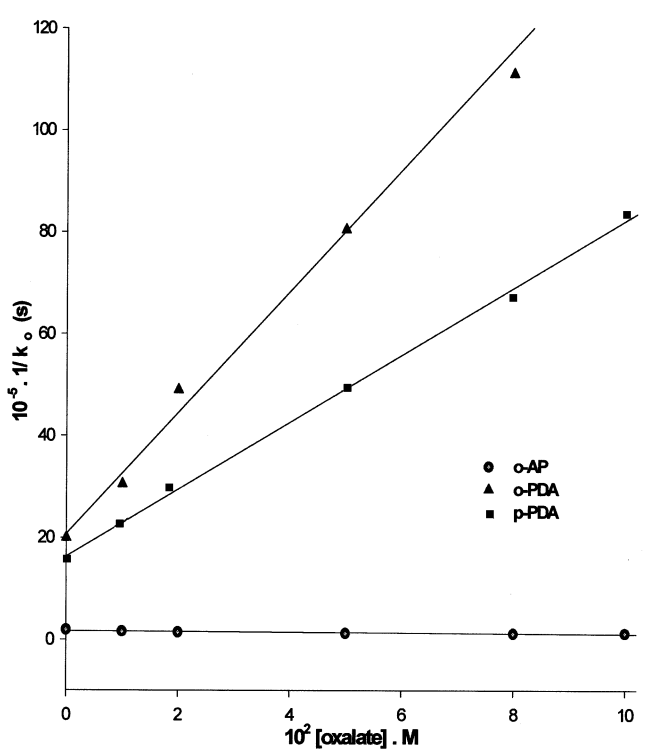
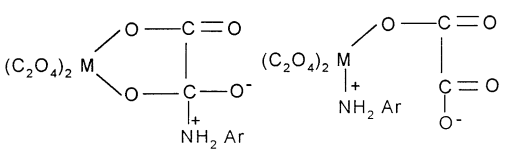


Fig. 10. Illustration of the relationship $1/k_{obs}$ vs. [oxalate] of the homogeneous redox reaction between the amines and the Co(III)–oxalate complex at 40°C.

a correlation coefficient of 0.75 and an inverse linear relationship was found in the oxidation of *o*-AP, as shown in Fig. 10. It is evident that the redox reaction mechanism in the oxidation of *o*-AP is different to those of *o*-PDA and *p*-PDA. The rate equation of the outer-sphere mechanism of *o*-AP oxidation is independent of [oxalate]. Thus, the effect of oxalate represents the medium effect on the oxidation reaction of *o*-AP in both redox systems. On contrary, the reaction rate of the oxidation of *o*-PDA and *p*-PDA was significantly affected with [oxalate] anion. This suggests that the inner-sphere mechanism is predominant to those amines oxidation reaction.

Generally, these tris-oxalato complexes may be considered to be kinetically inert, especially for the d^6 complex of Co(III), and thus be improbable candidates for an inner-sphere mechanism. However, it is known that $[Co(C_2O_4)_3]^{3-}$ does undergo racemisation, oxygen exchange and aquation under ambient conditions. Several possibilities exist for an inner-sphere complex which are consistent with discussion about these coordination sphere modifications [49,50]:



Only the last of these might release oxalate, and would obviously result in rate retardation by this anion. However, it is reported that the rate of oxygen exchange is also depressed by oxalate, and so the other alternatives may be valid [51].

4. Conclusion

It can be concluded that the kinetics and the activation parameters of the redox reaction are in good agreement with both the behaviour of the redox reactants in solution and the heterogeneous system. The effects of added anions on the redox reaction can be used to differentiate between the inner- and outer-sphere mechanisms that are ascertained as the detailed pathway for the electron transfer process in complex systems.

References

[1] A. Tomoda, J. Yamaguchi, H. Kojima, H. Amemiya, Y. Yoneyama, FEBS Lett. 196 (1986) 44.
[2] L.I. Simandi, Int. Rev. Phys. Chem. 8 (1989) 21.
[3] L.I. Simandi, T. Barna, S. Nemeth., J. Chem. Soc., Dalton Trans. (1996) 473.
[4] P.W. Iseminger, M. Gregory, J.R. Timothy, G. Caple, A.G. Sykes, J. Org. Chem. 62 (1997) 2643.
[5] U. Hollstien, Chem. Rev. 74 (1974) 625.
[6] E. Katz, H. Weissbach, J. Biol. Chem. 237 (1962) 882.
[7] E. Frei, Cancer Chemother. Rep. 58 (1974) 49.
[8] M.S. Ramachandran, T.S. Vivekanadam, N.R. Subbaratnam, N. Rajaram, Indian J. Chem. 22A (1983) 895.
[9] U. Nickel, N. Ruehl, B.M. Zhou, Z. Phys. Chem. 148 (1986) 33.
[10] M. Ignaczak, J. Dziegiec, Kinet. Katal. 30 (1989) 1026.
[11] M. Ignaczak, J. Dziegiec, L. Leszczynski, Pol. J. Chem. 64 (1990) 21.
[12] J.F. Corbett, J. Chem. Soc. B (1969) 207.
[13] Y. Mao, B. Zhou, X. Ren, Canguang Kexue Yu Kuang Huaxue 4 (1989) 50.
[14] K.C. Brown, J.F. Corbett, J. Chem. Soc., Perkin Trans. II (1979) 308.
[15] Z. Szeverenyi, E.R. Milaeva, L.I. Simandi, J. Mol. Catal. 67 (1991) 251.
[16] Z. Szeverenyi, E.R. Milaeva, L.I. Simandi, Stud. Surf. Catal. 99 (1991) 616.
[17] A. Tomoda, J. Yamayuchi, H. Amemiya, Y. Yoneyama, FEBS Lett. 34 (1993) 717.
[18] L.I. Simandi, T.M. Barna, L. Korecz, A. Rockenbauer, Tetrahedron Lett. 34 (1993) 717.
[19] K.V. Krishnamurty, G.M. Harris, Chem. Rev. 61 (1961) 213.
[20] A.K. Basak, D. Banerjea, J. Indian, Chem. Soc. 54 (1977) 1015.
[21] A.K. Basak, D. Banerjea, Indian J. Chem. 17A (1979) 250.
[22] C.E. Barry, P.G. Nayar, T.P. Begley, Biochem. 28 (1988) 6323.
[23] Y. Yano, M. Ikuta, Y. Amamiya, T. Nabeshima, Chem. Lett. (1991) 461.
[24] V.K. Krylov, M.V. Bavina, Y.N. Kukushkin, J. Appl. Chem. USSR 65 (1992) 1622.
[25] O. Josehine, J. Ehighaorkhuo, O. Folorunso, O. Olusegun, J. Chem. Soc., Dalton Trans. (1985) 1665.
[26] A.B. Zaki, M.Y. El-Sheikh, J. Evans, S.A. El-Safty, J. Colloid Interface Sci. 221 (2000) 56.
[27] D.N. Grindley, An Advanced Course in Practical Inorganic Chemistry, Butterworth, London, 1964.
[28] D.P. Graddom, J. Inorg. Nucl. Chem. 3 (1956) 308.
[29] G.H. Carttedge, W.P. Ericks, J. Am. Chem. Soc. 58 (1936) 2061.
[30] E.L. Wehry, Q. Rev. 21 (1967) 213.
[31] T. Perezuiz, C. Martinez, V. Tomas, F.J. Corrion, Intern. J. Environ. Anal. Chem. 53 (1993) 195.
[32] N. Takashi, H. Tadanori, Y. Masakazu, M. Hiroshi, S. Yasuhiko, Bull. Chem. Soc. Jpn. 48 (1975) 3709.
[33] Y. Zhu, J. Li, Z. Liu, G. Cheng, S. Dong, E. Wang, J. Mol. Catal, B: Enzym. 4 (1998) 33.
[34] C.W. Davies, G.G. Thomas, J. Chem. Soc. (1952) 1607.
[35] J. Evans, A.B. Zaki, M.Y. El-Sheikh, S.A. El-Safty, J. Phys. Chem. (submitted for publication).
[36] D.F. Shriver, P.W. Atkins, C.H. Langford, Inorganic Chemistry, Oxford University Press, London, 1990.
[37] R.G. Pearson, J. Chem. Phys. 20 (1952) 1478.
[38] R.D. Kushik, D.R. Joshi, S. Kumari, Asian J. Chem. 10 (1998) 573.
[39] F. Helfferich, Ion Exchange, McGraw-Hill, New York, 1962 (Chapter 11).
[40] B. Bänsch, P. Martinez, D. Uribe, J. Zuluaga, R. Van Eldik, Inorg. Chem. 30 (1991) 4555.
[41] A.A. Ismail, Activity of Iron(III)–Oxalate Complex Towards the Oxidation of some Organic Compounds, Tanta University, Egypt, 1996, p. 41.
[42] B. Bänsch, R. Van Eldik, Inorg. Chim. Acta 201 (1992) 75.
[43] K.L. Laidler, Chemical Kinetics, TMH Publishing, New Delhi, 1977, p. 90.
[44] B. Grossman, A. Haim, J. Am. Chem. Soc. 93 (1971) 6490.
[45] D.R. Rosseinsky, Chem. Rev. 72 (1972) 215.

[46] S.M. Hubig, R. Rathore, J.K. Kochi, J. Am. Chem. Soc. 121 (1999) 617.
[47] J.F. Endicott, K. Kumar, T. Ramasami, F.P. Rotzinger, Prog. Inorg. Chem. 30 (1983) 141.
[48] S. Fukuzumi, J.K. Kochi, Bull. Chem. Soc. Jpn. 56 (1983) 969.
[49] J.A. Broomhead, J. Chem. Soc. A (1971) 645.
[50] (a) C.A. Bunton, J.H. Carter, D.R. Lieweellyn. C. O'Connor, A.L. Odell, Y. Yih, J. Chem. Soc. (1964) 4615. (b) C.A. Bunton, J.H. Carter, D.R. Lieweellyn, A.L. Odell, Y. Yih, J. Chem. Soc. (1964) 4622. (c) D.R. Lieweellyn. C. O'Connor, A.L. Odell, Y. Yih, J. Chem. Soc. (1964) 6426.
[51] N. Serpone, D.G. Bickley, Prog. Inorg. Chem. 17 (1971) 391.

PERGAMON

www.elsevier.nl/locate/poly

Polyhedron 19 (2000) 1329–1332

POLYHEDRON

Preparation and solution behavior of diphosphinepalladium nitrite complexes

Jennifer A. Moser, Robert A. Stockland Jr., Gordon K. Anderson *

Department of Chemistry, University of Missouri - St. Louis, 8001 Natural Bridge Road, St. Louis, MI 63121, USA

Received 29 November 1999; accepted 3 April 2000

Abstract

Diphosphinepalladium nitrite complexes of the type $[Pd(NO_2)_2L_2]$ (L_2 = dppm, dppe, dppp) have been prepared by treatment of $[PdCl_2(CH_3CN)_2]$ with silver nitrite, followed by addition of the appropriate diphosphine. The nitrite complexes are fluxional in solution at 298 K, but on cooling to 220 K signals due to three species could be detected. These have been assigned to the N-bonded, the O-bonded, and the mixed coordination compounds. Treatment of $[PdCl_2(dppe)]$ with two equivalents of $TlPF_6$, followed by addition of $Na^{15}NO_2$, produced $[Pd(^{15}NO_2)_2(dppe)]$, whose ^{31}P NMR spectrum allowed identification of the three isomers. The analogous platinum complex $[Pt(NO_2)_2(dppe)]$ exists as a single isomer, which is static at 298 K, and a $^{15}NO_2$-labeling experiment indicated that it contains N-bonded nitrite ligands. © 2000 Elsevier Science Ltd. All rights reserved.

Keywords: Palladium; Platinum; Nitrite; Diphosphines; Isomerism; Fluxionality

1. Introduction

The phenomenon of linkage isomerism, which is exhibited by ambidentate ligands such as thiocyanate, nitrite, and dimethylsulfoxide, has been known for many years, and it is discussed in most inorganic textbooks. The thiocyanate ligand, for example, usually acts as an S-donor towards soft metal centers, but as a N-donor towards smaller, hard metals. Steric effects may also be important, particularly for the bulkier dimethylsulfoxide. Although one form is often considerably more thermodynamically stable than the other, rearrangement of the kinetic product into the thermodynamic one may be slow. Such is the case for the classic example of $[Co(NH_3)_5(NO_2)]Cl_2$ [1], where conversion of the nitrito to the corresponding nitro complex takes place over several days at ambient temperature. Nitrito to nitro isomerization of octahedral cobalt(III) complexes may be base-catalyzed [2], whereas the reverse process has been shown to be catalyzed by acid [3]. Isomerization may proceed in liquid ammonia [4] or even in the solid state [5,6]. Reversible nitro–nitrito linkage isomerization at a ruthenium center may be redox-induced [7–9]. For the chromium complex $[Cr(\eta^5\text{-}C_5H_5)(NO)_2(NO_2)]$, a mixture of linkage isomers was found, the nitrito form predominating, but exchange between the two forms was slow on the NMR timescale [10].

Palladium nitrite complexes, in particular, exhibit reactivity in a number of areas, including the oxidation of alkenes to ketones [11], in carboxylation reactions [12], and in oxygen transfer reactions [13]. Oxygen transfer reactions catalyzed by nickel nitrite complexes have been suggested to involve intermediate O-bonded nitrite ligands [14]. Interconversion between N- and O-bonded nitrites may be important in many of these reactions, but such rearrangements are typically slow, at least under ambient conditions.

We have prepared a series of palladium nitrite complexes of the type $[Pd(NO_2)_2L_2]$ (L_2 = dppm, dppe, dppp), which exhibit broad ^{31}P NMR resonances at ambient temperature. This behavior suggests that they are fluxional at this temperature and that the energy barrier between the different forms is quite low. We have employed variable temperature NMR spectroscopy, as well as ^{15}N-labeling experiments, in order to establish the nature of this behavior. The results of these studies will be presented here.

* Corresponding author. Tel.: +1-314-516-5437; fax: +1-314-516-5342.

E-mail address: ganderson@umsl.edu (G.K. Anderson).

0277-5387/00/$ - see front matter © 2000 Elsevier Science Ltd. All rights reserved.
PII: S0277-5387(00)00407-1

Table 1
$^{31}P\{^{1}H\}$ NMR parameters for $[Pd(NO_2)_2L_2]$, $[Pd(NO_2)(ONO)L_2]$ and $[Pd(ONO)_2L_2]$ [a]

L_2	$[Pd(NO_2)_2L_2]$	$[Pd(NO_2)(ONO)L_2]$		$[Pd(ONO)_2L_2]$	Isomer ratio
	δP	δP	^2J(P,P)	δP	
dppm	−43.5s	−45.6d −44.4d	90	−46.2 s	1.00:0.49:0.06
dppe	53.6s	54.4d 57.4d	19	59.3 s	1.00:0.60:0.05
dppp	1.5s	−0.3d 9.0d	44	not observed	1.00:0.31:<0.05

[a] Recorded for $CDCl_3$ solutions at 220 K. Coupling constants are in hertz.

2. Results and discussion

Treatment of $[PdCl_2(CH_3CN)_2]$ with excess silver nitrite in CH_3CN solution produced $[Pd(NO_2)_2(CH_3CN)_2]$, along with a precipitate of AgCl [15–18]. Following filtration, addition of one molar equivalent of the appropriate diphosphine gave a complex of the type $[Pd(NO_2)_2L_2]$ (L_2 = dppm, dppe, dppp). Each of these complexes contains two monodentate nitrite ligands, which are forced to adopt a *cis* configuration due to the presence of the chelate ring. In each case, when the ^1H NMR spectrum was recorded in $CDCl_3$ solution, the resonances expected for the diphosphine ligand were observed, but no resonances could be detected in the $^{31}P\{^1H\}$ NMR spectrum at ambient temperature. Upon cooling to 220 K, however, ^{31}P signals were observed in each case (Table 1). The $^{31}P\{^1H\}$ NMR spectrum of $[Pd(NO_2)_2(dppm)]$ at 220 K is shown in Fig. 1. It contains signals due to three species; two of these must contain equivalent P atoms and give rise to singlet resonances, whereas the third has non-equivalent P atoms and produces a pair of doublets (AB quartet). When the $^{31}P\{^1H\}$ NMR spectrum was recorded in CD_2Cl_2 solution at temperatures between 180 and 250 K, there was no discernible change in the relative concentrations of the three components. We propose that the three sets of resonances are due to the linkage isomers shown in Fig. 2.

Several palladium nitrite complexes containing monodentate phosphines have been prepared [19,20]. Using ^{15}N-labeling experiments, the nitrite ligand was shown to be coordinated through nitrogen in each case, but no fluxional behavior was reported. The complex *trans*-$[Pd(NO_2)_2(PMePh_2)_2]$ was prepared by treatment of $K_2[Pd(NO_2)_4]$ with $PMePh_2$ [21], and we have prepared this complex by an alternative route, namely, treatment of $[PdCl_2(PMePh_2)_2]$ with silver nitrite. We have found that *trans*-$[Pd(NO_2)_2(PMePh_2)_2]$ is not fluxional in solution, as shown by sharp resonances in its ^{31}P NMR spectrum over the temperature range 220–298 K. The diphosphinepalladium complex $[PdPh(NO_2)(dppe)]$ has been reported, but no ^{31}P NMR data were provided [11].

Treatment of the platinum complex $[PtCl_2(dppe)]$ with $AgNO_2$ resulted in the formation of the expected $[Pt(NO_2)_2(dppe)]$, which is static in solution. The reaction takes place in a stepwise fashion, with $[PtCl(NO_2)(dppe)]$ (δP 28.2 br d, ^1J(Pt,P) = 2923 Hz, ^2J(P,P) = 8 Hz; δP 37.8 d, ^1J(Pt,P) = 3707 Hz) being formed when one molar equivalent of $AgNO_2$ was added. Addition of a second equivalent of $AgNO_2$ resulted in complete conversion to $[Pt(NO_2)_2(dppe)]$ (δP 27.9, ^1J(Pt,P) = 3052 Hz).

In order to assign the linkage isomers, we carried out ^{15}N-labeling experiments. When up to ten equivalents of $Na^{15}NO_2$ was added to a CH_3CN solution of $[PtCl_2(dppe)]$, mixtures of $[PtCl(^{15}NO_2)(dppe)]$ and $[PtCl_2(dppe)]$ only were obtained. In order to ensure complete conversion to the bis(nitrite)platinum species, $[PtCl_2(dppe)]$ was first treated with $TlPF_6$ in acetone, followed by addition of two equivalents of $Na^{15}NO_2$.

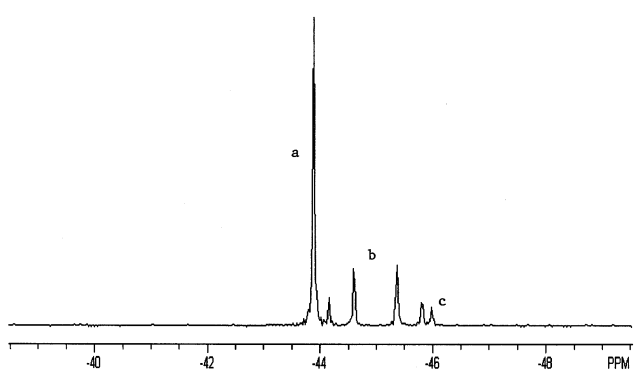


Fig. 1. $^{31}P\{^1H\}$ NMR spectrum of $[Pd(NO_2)_2(dppm)]$ (a), $[Pd(NO_2)(ONO)(dppm)]$ (b) and $[Pd(ONO)_2(dppm)]$ (c) recorded in $CDCl_3$ solution at 220 K.

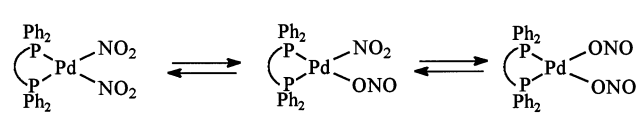


Fig. 2. Equilibria involving N- and O-bonded nitrite complexes.

This generated [Pt($^{15}NO_2$)$_2$(dppe)] quantitatively. Its ^{31}P NMR spectrum contained a central doublet at 27.9 ppm (^2J(P,N) = 65 Hz) and, consistently, the ^{15}N NMR spectrum exhibited a doublet at 464 ppm with a separation of 65 Hz. These data confirmed that the two nitrite ligands were coordinated to platinum through nitrogen. (The ^{31}P and ^{15}N NMR spectra should both exhibit AA′XX′ coupling patterns [22], but the magnitudes of most of the coupling constants were small and only the separation of the main doublet could be ascertained.)

The corresponding palladium complex [Pd($^{15}NO_2$)$_2$(dppe)] was prepared by the same method. Its ^{31}P NMR spectrum was again very broad at ambient temperature, but cooling to 220 K allowed identification of three species. The major species exhibited a broad doublet (actually part of an AA′XX′ system) centered at 54.5 ppm (^2J(P,N) = 56 Hz), indicating that the mode of coordination of the two nitrites was through nitrogen, namely, [Pd($^{15}NO_2$)$_2$(dppe)]. A second species exhibited a doublet of doublets at 58.5 ppm (^2J(P,P) = 16 Hz, ^2J(P,N) = 64 Hz) and a doublet at 55.1 ppm (^2J(P,P) = 16 Hz). This was consistent with [Pd($^{15}NO_2$)(O^{15}NO)(dppe)], the signal at δP 58.5 being due to the P atom lying *trans* to N. Only a trace of [Pd(O^{15}NO)$_2$(dppe)] was observed, which exhibited a single resonance at 59.3 ppm. Thus, the three linkage isomers could be identified at low temperature, but interconversion between the three was rapid at 298 K.

In each case, [Pd(NO_2)$_2$L$_2$] is the major species, with the dinitritopalladium complex being least favored. The dinitropalladium derivative is present in the greatest concentration for the bulkiest ligand dppp, perhaps unexpectedly because the –NO_2 group is more sterically demanding than the –ONO fragment, but the other two cases do not follow this trend. In contrast, the analogous thiocyanate complexes were isolated as [Pd(SCN)$_2$(dppm)], [Pd(SCN)(NCS)(dppe)] and [Pd(NCS)$_2$(dppp)], respectively [23]. Here it appears that the more sterically demanding –SCN ligands are favored with the less bulky diphosphine ligands. It should be noted, however, that this study was of solid state structures, and it does not necessarily follow that these are the more stable species in solution.

The difference in solution behavior between the monodentate phosphine complexes *trans*-[Pd(NO_2)$_2$L$_2$] (L = PPh_3, $PMePh_2$, PMe_2Ph, PEt_3) and those where L_2 = dppm, dppe or dppp may be attributed to the high *trans*-influence [24] of the phosphine ligand. When monodentate phosphines are employed, they adopt a mutually *trans* arrangement, causing the nitrite ligands to be *trans* to each other. In the diphosphine complexes, however, the nitrite ligands are forced to lie *trans* to tertiary phosphino groups. The greater *trans*-influence of the latter weakens the palladium–nitrite bond, thereby allowing isomerization between N- and O-bonded ligands more readily. The stronger Pt–N bonds in [Pt(NO_2)$_2$(dppe)] may preclude ligand rearrangement even though the nitrites lie *trans* to phosphino groups.

3. Summary

The results described above provide evidence that palladium nitrite complexes may exchange readily between N- and O-bonded forms when the nitrite group lies opposite a ligand with a high *trans*-influence [24]. This is in contrast to a number of platinum and palladium complexes that have been reported previously to be coordinated through nitrogen exclusively. Formation of oxygen-bound palladium nitrite complexes may be the first step in many palladium-catalyzed oxygen transfer reactions, and this study provides evidence that such species do exist and, indeed, may make up a significant proportion of the metal complex in solution, even at low temperatures.

4. Experimental

[$PdCl_2(CH_3CN)_2$] and [Pd(NO_2)$_2$(CH_3CN)$_2$] were prepared as described previously [11]. All reactions were carried out under an argon atmosphere and in the absence of light. $AgNO_2$ and Na$^{15}NO_2$ were purchased from Aldrich and Cambridge Isotope Laboratories, respectively, and used as received. NMR spectra were recorded on a Bruker ARX-500 spectrometer. ^{1}H chemical shifts were measured in ppm relative to the residual solvent signal, and ^{31}P and ^{15}N shifts were determined relative to external H_3PO_4 and $MeNO_2$, respectively, positive shifts representing deshielding. Elemental analyses were performed by Atlantic Microlab Inc., Norcross, GA. The ratios of isomers of [Pd(NO_2)$_2$L$_2$] were obtained by integration of the ^{31}P{^{1}H} NMR spectra (gated decoupled).

4.1. Preparation of [Pd(NO_2)$_2$(dppm)]

[$PdCl_2(CH_3CN)_2$] (0.10 g, 0.39 mmol) was dissolved in CH_3CN (30 ml) and $AgNO_2$ (0.18 g, 1.2 mmol) was added. The reaction mixture was allowed to stir for 12 h. The solution was filtered and dppm (0.15 g, 0.39 mmol) was added to the filtrate. The mixture was stirred for a further 5 min, then the solvents were removed. The residue was extracted with CH_2Cl_2 and filtered. The solvent was removed and the resulting solid was dried in vacuo to leave the product as a pale yellow solid (0.22 g, 99%). *Anal.* Calc. for $C_{25}H_{22}N_2O_4P_2Pd$: C, 51.52; H, 3.81. Found: C, 51.10; H, 3.92%. ^{1}H NMR ($CDCl_3$): δ 4.05 (t, ^2J(P,H) = 10.3 Hz, 2H, PCH_2); 7.4–7.75 (m, 20H, P(C_6H_5)$_2$).

[$Pd(NO_2)_2$(dppp)] was prepared analogously, and isolated as a colorless powder in 43% yield. *Anal.* Calc. for $C_{27}H_{26}N_2O_4P_2Pd$: C, 53.08; H, 4.30. Found: C, 52.99; H, 4.23%. ^{1}H NMR ($CDCl_3$): δ 2.1 (br, 2H, PCH_2CH_2); 2.4 (br, 4H, PCH_2); 7.4–7.7 (m, 20H, $P(C_6H_5)_2$).

4.2. Preparation of [$Pd(NO_2)_2$(dppe)]

[$PdCl_2(CH_3CN)_2$] (0.10 g, 0.39 mmol) was dissolved in CH_3CN (30 ml) and $AgNO_2$ (0.18 g, 1.2 mmol) was added. The reaction mixture was allowed to stir for 12 h. The solution was filtered, then dppe (0.15 g, 0.39 mmol) was added. A precipitate formed, which was collected by filtration. It was washed with CH_3CN and ether, then dried in vacuo to leave the product as a colorless powder (0.16 g, 71%). *Anal.* Calc. for $C_{26}H_{24}N_2O_4P_2Pd$: C, 52.31; H, 4.03. Found: C, 51.80; H, 4.06%. ^{1}H NMR ($CDCl_3$): δ 2.21–2.35 (m, 4H, PCH_2); 7.4–7.5 (m, 20H, $P(C_6H_5)_2$).

4.3. Preparation of [$Pt(NO_2)_2$(dppe)]

[$PtCl_2$(dppe)] (0.15 g, 0.23 mmol) was dissolved in CH_3CN (30 ml). $AgNO_2$ (0.14 g, 0.90 mmol) was added and the mixture was allowed to stir for 48 h. The solution was filtered and the solvent was removed. The resulting solid was extracted with CH_2Cl_2 and filtered. The solvent was removed again to leave the product as a colorless solid (0.12 g, 77%). *Anal.* Calc. for $C_{26}H_{24}N_2O_4P_2Pd$: C, 45.54; H, 3.50. Found: C, 45.47; H, 3.60%. ^{1}H NMR ($CDCl_3$): δ 2.20–2.50 (m, 4H, PCH_2); 7.5–7.8 (m, 20H, $P(C_6H_5)_2$).

4.4. Preparation of [$Pd(NO_2)_2(PMePh_2)_2$]

[$PdCl_2(PMePh_2)_2$] (0.10 g, 0.17 mmol) was dissolved in CH_2Cl_2 (30 ml), and $AgNO_2$ (0.080 g, 0.52 mmol) and methanol (2 ml) were added. The reaction mixture was allowed to stir for 24 h, the solvents were removed and the residue was extracted with CH_2Cl_2 and filtered. The solvent was removed again and the sample was dried in vacuo to leave the product as a colorless solid (0.086 g, 83%).

4.5. Preparation of $^{15}NO_2$-labeled complexes

In a typical experiment, [MCl_2L_2] (ca. 0.02 g) was dissolved in acetone. $TlPF_6$ (two molar equivalents) was added and the reaction was allowed to stir for 2 h. After this time, $Na^{15}NO_2$ (two molar equivalents) was added and the mixture was allowed to stir for a further 2 h. The acetone was removed, and the solid was extracted with CH_2Cl_2. The solvent was removed again and the product was dried in vacuo.

Acknowledgements

Thanks are expressed to the National Science Foundation (grant No. CHE-9508228) for support of this work, to Mallinckrodt Inc. for a graduate student fellowship (R.A.S.J.), to the donors of the Brunngraber Fellowship (J.A.M.), and to Dr Janet Braddock-Wilking for help with some of the NMR experiments. Thanks are also expressed to the US Department of Energy (grant No. DE-FG02-92CH10499) for funds to purchase the NMR spectrometer.

References

[1] W.M. Philips, S. Choi, J.A. Larabee, J. Chem. Educ. 67 (1990) 267.
[2] F. Bozoglian, M. Queirolo, B. Sienra, Polyhedron 17 (1998) 3551.
[3] W.G. Jackson, Inorg. Chem. 26 (1987) 3857.
[4] S. Balt, H.J.A.M. Kuipers, W.E. Renkema, J. Chem. Soc., Dalton Trans. (1983) 1739.
[5] E.V. Boldyreva, A.A. Sidel'nikov, N.Z. Lyakhov, Thermochim. Acta 92 (1985) 109.
[6] M. Kubota, S. Ohba, Acta Crystallogr., Sect. B: Struct. Sci. B48 (1992) 627.
[7] H. Nishimura, H. Nagao, F.S. Howell, M. Mukaida, H. Kakihana, Chem. Lett. (1990) 133.
[8] D. Ooyama, N. Nagao, H. Nagao, Y. Miura, A. Hasegawa, K. Ando, F.S. Howell, M. Mukaida, K. Tanaka, Inorg. Chem. 34 (1995) 6024.
[9] D. Ooyama, H. Nagao, N. Nagao, F.S. Howell, M. Mukaida, Chem. Lett. (1996) 759.
[10] J.L. Hubbard, C.R. Zoch, W.L. Elcesser, Inorg. Chem. 32 (1993) 3333.
[11] M.A. Andrews, K.P. Kelly, J. Am. Chem. Soc. 103 (1981) 2894.
[12] R. Ugo, A. Chiesa, J. Chem. Soc., Perkin Trans. (1987) 2625.
[13] C.J. Jones, J.A. McCleverty, A.S. Rothin, H. Adams, N.A. Bailey, J. Chem. Soc., Dalton Trans. (1986) 2055.
[14] J. Kriege-Simondsen, G. Elbaze, M. Dartiguenave, R.D. Feltham, Y. Dartiguenave, Inorg. Chem. 21 (1982) 230.
[15] R.J. Puddephatt, P.J. Thompson, J. Chem. Soc., Dalton Trans. (1976) 2091.
[16] J.A. Kaduk, J.A. Ibers, Inorg. Chem. 16 (1977) 3278.
[17] S.A. Bhaduri, I. Bratt, B.F.G. Johnson, A. Khair, J.A. Segal, R. Walters, C. Zurraco, J. Chem. Soc., Dalton Trans. (1981) 234.
[18] R.A. Middleton, G. Wilkinson, M.B. Hursthouse, N.P. Walker, J. Chem. Soc., Dalton Trans. (1982) 663.
[19] R.D. Feltham, J. Kriege, J. Am. Chem. Soc. 101 (1979) 5064.
[20] J. Kriege-Simondsen, R.D. Feltham, Inorg. Chim. Acta 71 (1983) 185.
[21] R.D. Feltham, G. Elbaze, R. Ortega, C. Eck, J. Dubrawski, Inorg. Chem. 24 (1985) 1503.
[22] F.A. Bovey, Nuclear Magnetic Resonance Spectroscopy, Academic, New York, 1969, pp. 87–127.
[23] G.J. Palenik, M. Mathew, W.L. Steffen, G. Beran, J. Am. Chem. Soc. 97 (1975) 1059.
[24] T.G. Appleton, H.C. Clark, L.E. Manzer, Coord. Chem. Rev. 10 (1973) 335.

PERGAMON

www.elsevier.nl/locate/poly

Polyhedron 19 (2000) 1333–1338

POLYHEDRON

Synthesis, structural characterisation and electronic behaviour of iron(II) and nickel(II) complexes of *N*,*N*-bis(2-pyridylmethyl)aniline

Alan Hazell [a], Christine J. McKenzie [b], Lars Preuss Nielsen [b,*]

[a] *Chemistry Institute, Aarhus University, DK-8000 Aarhus, Denmark*

[b] *Department of Chemistry, University of Southern Denmark, Odense Campus, Campusvej 55, DK-5230 Odense M, Denmark*

Received 2 February 2000; accepted 14 April 2000

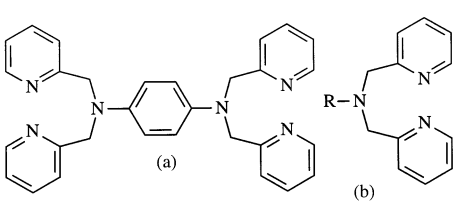
Abstract

Ni(II) and Fe(II) complexes of the new ligand *N*,*N*-bis(2-pyridylmethyl)aniline (phdpa) of the general formula $[M(phdpa)_2](ClO_4)_2$ have been prepared and characterised. $[Ni(phdpa)_2](ClO_4)_2 \cdot 0.5\ H_2O$ was characterised by X-ray crystallography. For comparison, the X-ray structure of $[Ni(medpa)_2](ClO_4)_2$ (where medpa is bis(2-pyridylmethyl)methylamine) has been determined. The ligand in both $[Ni(phdpa)_2](ClO_4)_2$ and $[Ni(medpa)_2](ClO_4)_2$ exhibit *cis–facial* geometry. © 2000 Elsevier Science Ltd. All rights reserved.

Keywords: Nickel(II); Iron(II); Crystal structures; Electronic spectra

1. Introduction

Our recent work with the redox-active bis-tridentate ligand, *N*,*N*,*N*′,*N*′-tetrakis(2-pyridylmethyl)benzene-1,4-diamine (tpbd) (Scheme 1(a)) has resulted in the isolation of a series of transition metal complexes of varied M:L ratio. Mononuclear complexes were obtained with zinc, $(tpbd)ZnCl_2$ [1], and ruthenium, $[(tpbd)Ru(tpbd)]^{2+}$ [1],dinuclear complexes with palladium, $[ClPd(tpbd)PdCl]^{2+}$ [1], and copper, $[(H_2O)_2Cu(tpbd)Cu(H_2O)_2]^{4+}$ [2], and proposed oligomeric/polymeric complexes with iron and nickel, $[M(tpbd)]_n^{2n+}$, M = Fe or Ni, and copper, $[(tpbd)Cu(\mu\text{-}L)_2Cu]_n^{2n+}$ or $[(tpbd)Cu(\mu\text{-}L)_2Cu]L^{2+}$, L = Cl or NO_3 [1]. Structural characterisation of these insoluble polymeric complexes has been hampered by the lack of success in growing crystals suitable for X-ray structural determination, and NMR studies have afforded only limited information. In order to assist in establishing the structures of these polymers we have prepared the Ni(II) and Fe(II) complexes of the new tridentate ligand *N*,*N*-bis(2-pyridylmethyl)aniline (phdpa) (Scheme 1(b)) in the expectation that these might act as monomeric structural models for the putative polymeric tpbd complexes. The tertiary nitrogen atoms of tpbd are expected to be weaker Lewis bases compared with the aliphatic nitrogens in the known related ligands, i.e. bis(2-pyridylmethyl)amine (dpa) and bis(2-pyridylmethyl)methylamine (medpa) (Scheme 1) due to the electron withdrawing effect of the phenylene group on the attached nitrogen atom's lone pair. Prediction of the coordination mode (*trans*/*cis fac* versus *mer*) of phdpa is complicated due to a number of parameters (i.e. σ-donor strength, π-acceptor strength, geometry of the ligand/metal, etc.) which are affected by substituting H or CH_3 by a phenyl group in the dpa derived ligands.



Scheme 1. Schematic representation of (a) tpbd and (b) dpa, R = H; medpa, R = Me; phdpa, R = ph.

* Corresponding author. Tel.: +45-6550-2529; fax: +45-6615-8780.

E-mail address: lpn@chem.sdu.dk (L.P. Nielsen).

0277-5387/00/$ - see front matter © 2000 Elsevier Science Ltd. All rights reserved.
PII: S0277-5387(00)00409-5

Structurally characterised bis-dpa complexes with Cu(II) [3], Fe(II) [4], Ni(II) [5], Mn(II) [6], Zn(II) [6] and Cd(II) [6] and bis-medpa with Fe(II) [7] exhibit *cis–facial* coordination, whereas, to the best of our knowledge, only one *mer* six-coordinated coordinated metal complex with dpa-derived ligands has been synthesised; a di-μ-oxo dimer of Cr(III) with two squarate molecules as monodentate ligands [8].

2. Experimental

2.1. Physical measurements

UV–Vis absorption spectra were recorded on a Shimadzu UV-3100 spectrophotometer. FAB mass spectrometry was carried out on a Kratos MS50TC instrument. NMR spectra were recorded on a Bruker AC 250. Elemental analyses were carried out by the Microanalytical Laboratory of the H.C. Ørsted Institute, Copenhagen.

2.2. Materials

All commercially available chemicals were used without any prior purification, apart from aniline, which was freshly distilled. *N*,*N*-Bis(2-pyridylmethyl)-methylamine (medpa) was used as medpa·3HClO$_4$ as described elsewhere [9], and [Ni(tpbd)]$_n$(ClO$_4$)$_{2n}$ and [Fe(tpbd)]$_n$Cl$_{2n}$ were prepared as previously reported [1].

2.3. *N*,*N*-Bis(2-pyridylmethyl)aniline, phdpa

A solution of 2-(chloromethyl)pyridine hydrochloride (6.00 g, 36.6 mmol) in water (3 ml) was neutralised by addition of NaOH (1.46 g, 36.6 mmol) in water (7 ml) at 0°C. Aniline (1.70 g, 18.3 mmol) was added to the vigorously stirred solution at 0°C over a period of 2 h, followed by methylene chloride (5 ml). Over 7 days NaOH (1.46 g, 36.6 mmol) in water (7 ml) was added in small portions and the pH was kept below 9. The reaction was stirred for another 7 days. The pH was adjusted to 8 with NaOH or HCl, and the phases were separated. The aqueous phase was extracted with CH_2Cl_2 (3 × 30 ml) and the combined organic extracts were washed with water (10 ml), dried over anhydrous sodium sulfate and evaporated to dryness. The crude product was purified by a Soxhlet apparatus using petrol (b.p. 60–80°C). Yield 2.4 g, 47.6% of pale yellow crystals. *Anal*. Found: C, 78.34; H, 6.33; N, 15.26. Calc. for $C_{18}H_{17}N_3$: C, 78.52; H, 6.22; N, 15.26%. FABMS, *m*/*z*: 276 (M^+, 100%). ^{1}H NMR ($CDCl_3$): $\delta = 4.83$ (s, 4H, CH_2), 6.72 (m, 3H, ph-$H^2 + H^4$), 7.17 (m, 4H, py-H^5 + ph-H^3), 7.24 (d, 4H, py-H^3, $J = 6.9$ Hz), 7.61 (dt, 4H, py-H^4, $J = 7.8$, 1.8), 8.59 (m, 2H, py-H^6). ^{13}C NMR ($CDCl_3$): $\delta = 57.56$ (CH_2), 112.85 (ph-C^2), 117.55 (ph-C^4), 121.14, 122.35 (py-C^3, py-C^5), 129.65 (ph-C^3), 137.17 (py-C^4), 148.61 (ph-C^1), 150.12 (py-C^6), 159.29 (py-C^2).

Caution! The following perchlorate compounds should be handled as potential explosives.

2.4. [(Bis(*N*,*N*-bis(2-pyridylmethyl)methylamine)nickel-(II)]diperchlorate, [Ni(medpa)$_2$](ClO$_4$)$_2$

Ni(ClO$_4$)$_2$·6H$_2$O (160 mg, 0.440 mmol) and medpa·3HClO$_4$ (453 mg, 0.880 mmol) were suspended in water (40 ml). 2 M NaOH was added dropwise until all material was dissolved. The purple solution was allowed to stand for 2 days before the product was isolated as purple crystals. Yield 157 mg, 52.2%. *Anal*. Found: C, 45.66; H, 4.10; N, 12.12. Calc. for $C_{26}H_{30}Cl_2N_6NiO_8$: C, 45.64; H, 4.42; N, 12.12%. UV–Vis (CH_3CN): λ/nm (ε/dm^3 mol^{-1} cm^{-1}): 259 (12 490), 556 (18), 815 sh, 936 (13). FABMS, *m*/*z*: 583 ([Ni(medpa)$_2$ClO$_4$]$^+$, 18%), 370 ([Ni(medpa)ClO$_4$]$^+$, 100), 271 ([Ni(medpa)]$^+$, 95).

2.5. [(Bis(*N*,*N*-bis(2-pyridylmethyl)aniline)nickel(II)]-diperchlorate, [Ni(phdpa)$_2$](ClO$_4$)$_2$

Ni(ClO$_4$)$_2$·6H$_2$O (33.2 mg, 0.091 mmol) in MeOH (1 ml) was added to phdpa (50 mg, 0.182 mmol). Precipitation began after a few minutes. The purple crystals were isolated by filtration. Yield 65.4 mg, 89%. *Anal*. Found: C, 52.43; H, 4.39; N, 10.03. Calc. for $C_{36}H_{34}Cl_2N_6NiO_8$: C, 52.33; H, 4.39; N, 10.17%. UV–Vis (CH_3CN): λ/nm (ε/dm^3 mol^{-1} cm^{-1}): 250 (15 400), 305 (2100), 573 (15), 824 sh, 941 (13). FABMS (*m*/*z*): 707 ([Ni(phdpa)$_2$ClO$_4$]$^+$, 7%), 432 ([Ni(phdpa)ClO$_4$]$^+$, 100). Crystals for X-ray structure determination were obtained by recrystallisation from MeOH/water.

2.6. [(Bis(*N*,*N*-bis(2-pyridylmethyl)aniline)iron(II)]-diperchlorate, [Fe(phdpa)$_2$](ClO$_4$)$_2$

This synthesis was carried out under an inert atmosphere. Fe(ClO$_4$)$_2$·6H$_2$O (33 mg, 0.091 mmol) in abs. ethanol (1.5 ml) was added to a solution of phdpa (50 mg, 0.182 mmol) in abs. ethanol (4 ml). Immediate precipitation of the pale yellow product, which was filtered under argon. Yield 56.4 mg, 73.7%. *Anal*. Found C 53.95; H 4.59; N 9.98. Calc. for $C_{36}H_{34}Cl_2FeN_6O_8$: C 53.68; H 4.25; N 10.43. UV–Vis (CH_3CN): λ/nm (ε/dm^3 mol^{-1} cm^{-1}): 248 (22 970), 300 sh, 1025 (br, 9). FABMS, *m*/*z*: 705 ([Fe(phdpa)$_2$ClO$_4$]$^+$, 2%), 605 ([Fe(phdpa)$_2$ − H]$^+$, 1), 430 ([Fe(phdpa)ClO$_4$]$^+$, 13).

Table 1
Crystal and experimental data for $[Ni(phdpa)_2](ClO_4)_2 \cdot 0.5H_2O$ (**1**) and $[Ni(medpa)_2](ClO_4)_2$ (**2**)

	1	**2**
Formula weight	819.36	684.20
Crystal system	monoclinic	orthorhombic
Space group	$P2_1/n$	$P2_12_12_1$
Unit cell dimensions		
a (Å)	20.5792(3)	9.5478(6)
b (Å)	19.2347(3)	17.448(1)
c (Å)	20.9911(1)	18.114(1)
α (°)	90.0	90.0
β (°)	115.794(1)	90.0
γ (°)	90.0	90.0
V (Å^3)	7481.1(1)	3017.6(3)
Z	8	4
$F(000)$	3400	1416
T (K)	298	296
Radiation	Mo Kα	Mo Kα
Wavelength, λ (Å)	0.71073	0.71073
Diffractometer	Siemens SMART	Siemens SMART
Linear absorption coefficient (cm^{-1})	0.722	0.878
Absorption correction	empirical	integration
D_{calc} (g cm^{-3})	1.455	1.506
Intensity data collection		
Crystal size (mm)	$0.425 \times 0.15 \times 0.13$	$0.54 \times 0.34 \times 0.26$
Index range (°)	$-27 \le h \le 24$, $-26 \le k \le 26$, $-27 \le l \le 26$	$-11 \le h \le 12$, $-22 \le k \le 22$, $-15 \le l \le 23$
θ Range (°)	1.5–27.5	1.6–28.3
Reflections collected	53 369	18 449
Independent reflections	18 983	3973
R_{int}	0.035	0.032
Reflections with $I > 3\sigma(I)$	11 289	3361
Structure refinement		
R	0.054	0.040
wR	0.079	0.041
Goodness-of-fit (S)	2.224	0.958
Data/restraints/parameters	11 289/92/950	3361/0/389
Largest difference peak and hole (e Å^{-3})	1.2(1) and −0.4(1)	0.7(1) and −0.8(1)

2.7. X-ray structural determination

The structures were determined at room temperature using graphite monochromatised radiation. Data were collected on a Siemens SMART diffractometer [10]. Crystal data and experimental parameters are presented in Table 1. The data were corrected for Lorentz-polarisation effects and for absorption [10]. The structures were solved by direct methods using SIR-97 [11] and refined by least-squares techniques using programs from the KRYSTAL [12] package. Atomic scattering factors were taken from elsewhere [13].

2.7.1. $[Ni(phdpa)_2](ClO_4)_2 \cdot H_2O$

The complex crystallises in the centrosymmetric monoclinic space group $P2_1/n$ with eight molecules in the unit cell. All non-hydrogen atoms were refined anisotropically, hydrogen atoms of the water molecule were located from a difference map and refined isotropically, hydrogen atoms of the ligands were kept fixed in calculated positions (C–H = 0.95 Å). The perchlorate ions containing Cl3 and Cl4 were both disordered and were each modelled as two ideal tetrahedra, occupation factors and a common Cl–O distance were refined. Anisotropic displacement factors for the disordered perchlorate ions were described by **T** and **L** tensors [14].

2.7.2. $[Ni(medpa)_2](ClO_4)_2$

The complex crystallises in the non-centrosymmetric monoclinic space group $P2_12_12_1$ with four molecules in the unit cell. All non-hydrogen atoms were refined anisotropically, while hydrogen atoms were placed in fixed calculated positions (C–H = 0.95 Å).

3. Results and discussion

3.1. Ligand synthesis

The ligand phdpa was prepared by nucleophilic substitution of 2-(chloromethyl)pyridine with aniline in a two-phase system (water/methylene chloride) and was isolated as an off-white crystalline product in acceptable yields. All Rdpa (R = H, Me or Ph) complexes were prepared by reaction of the ligand with the relevant metal perchlorate in 2:1 ratios. In the case of $[Ni(medpa)_2](ClO_4)_2$, the perchloric acid ligand salt medpa·3HClO$_4$ was neutralised with base after the addition of nickel perchlorate. A preparation of this complex, but no crystal structure has been reported earlier [15].

3.2. Nickel complexes

The X-ray structures of $[Ni(phdpa)_2](ClO_4)_2$ and $[Ni(medpa)_2](ClO_4)_2$, show a *cis–facial* arrangement of the ligands, which is the case in almost all octahedral complexes with bis(2-pyridylmethyl)amine derived ligands [3–7]. Both structures consist of $[Ni(Rdpa)_2]^{2+}$ cations, perchlorate anions and, for R = phenyl, water of crystallisation. The two almost identical cations in the asymmetric unit of $[Ni(phdpa)_2](ClO_4)_2$ have approximate two-fold symmetry as is shown in Fig. 1, coordination at the nickel atom is roughly octahedral, with two tridentate ligands coordinating in *cis–fac* configuration. Principal bond lengths and angles for $[Ni(Phdpa)_2](ClO_4)_2$, $[Ni(Medpa)_2](ClO_4)_2$ and, for comparison, $[Ni(dpa)_2](ClO_4)_2$ [5], are summarised in Table 2. The medpa structure consists of

$[Ni(medpa)_2]^{2+}$ cations and perchlorate anions. A view of the cation is shown in Fig. 2. Again the nickel atom is octahedrally coordinated with *cis–fac* configuration so that the cation has approximate two-fold symmetry.

The average $Ni–N_{amine}$ distances increases with the size of the alkyl substituent, 2.106(4), 2.196(3) and 2.278(1) Å for dpa, medpa and phdpa, respectively; however, there is no significant difference between the corresponding average $Ni–N_{py}$ distances, 2.083(3), 2.111(2) and 2.096(1) Å.

The electronic spectra for $[Ni(Rdpa)_2](ClO_4)_2$ and $[Ni(tpbd)]_n(ClO_4)_{2n}$ are shown in Fig. 3. Absorption maxima are listed in Table 3. The green colour of $[Ni(tpbd)]_n(ClO_4)_{2n}$, caused by the broad band below 450 nm, centred at 312 nm (sh), is believed to arise from transitions in the phenylene backbone. This feature is not as pronounced in the UV–Vis spectrum of the corresponding complex with the less conjugated ligand, phdpa. A shift towards higher energy is observed of the low energy field spin-allowed d–d* transition bands in the $[Ni[dpa)_2]^{2+}$ (797 and 877 (sh) nm) compared with the corresponding Ni(II) complexes with substituted dpa ligands (ca. 820 (sh) and ca. 930 nm). This is due to a stronger ligand field nature of dpa compared with medpa, phdpa and tpbd in nickel(II) complexes. There is little difference in the electronic spectra of the complexes of *N*-alkylated DPA. Thus very similar geometries are expected.

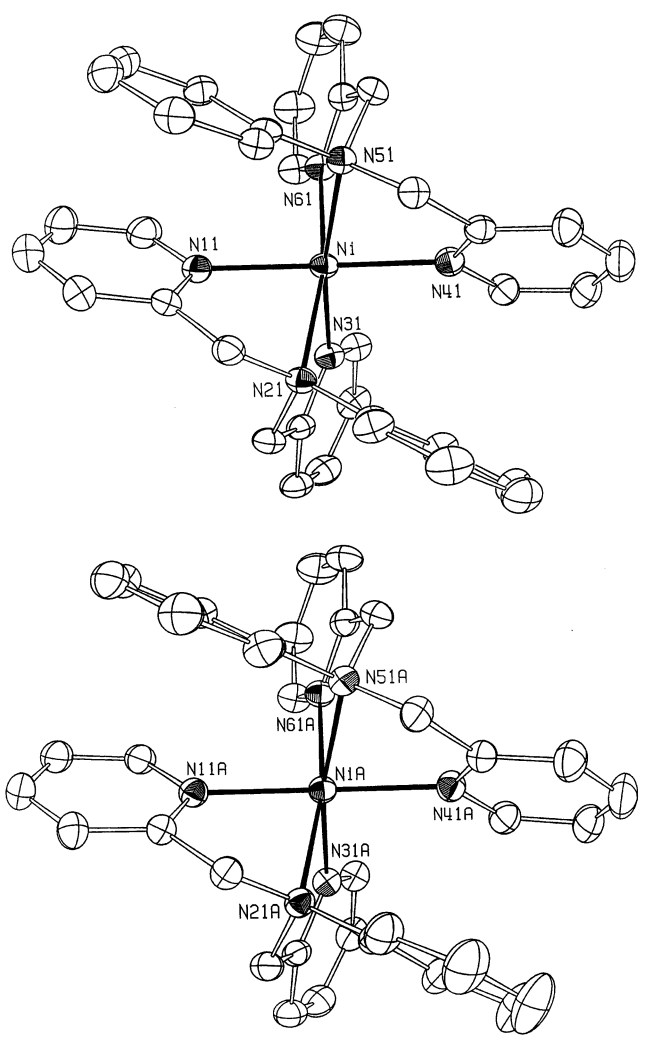


Fig. 1. ORTEP [17] drawing of the $[Ni(phdpa)_2]^{2+}$ cations. Ellipsoids are drawn at the 30% probability level. (a) Cation 1 and (b) cation 2.

Table 2
Selected bond distances (Å) and angles (°) for $[Ni(phdpa)_2](ClO_4)_2·H_2O$ (**1a** for molecule 1, **1b** for molecule 2), $[Ni(medpa)_2](ClO_4)_2$ (**2**) and $[Ni(dpa)_2](ClO_4)_2$ (**3**) [5]

	1a	**1b**	**2**	**3**
Ni–N11	2.108(3)	2.112(3)	2.141(4)	2.073(4)
Ni–N21	2.279(3)	2.260(3)	2.182(4)	2.106(4)
Ni–N31	2.091(3)	2.084(3)	2.083(4)	2.093(4)
Ni–N41	2.087(3)	2.107(3)	2.130(3)	2.073(4)
Ni–N51	2.281(3)	2.291(3)	2.210(4)	2.106(4)
Ni–N61	2.089(3)	2.088(3)	2.090(4)	2.093(4)
N11–Ni–N21	76.2(1)	76.1(1)	75.3(2)	89.9(2)
N11–Ni–N31	94.4(1)	94.9(1)	102.2(1)	103.7(1)
N11–Ni–N41	167.4(1)	166.8(1	156.9(2)	167.8(2)
N11–Ni–N51	94.8(1)	95.5(1)	90.9(1)	82.1(1)
N11–Ni–N61	92.6(1)	93.6(1)	92.8(2)	84.1(1)
N21–Ni–N31	79.5(1)	79.6(1)	79.5(1)	80.3(1)
N21–Ni–N41	96.6(1)	96.2(1)	90.8(1)	82.1(1)
N21–Ni–N51	101.6(1)	102.3(1)	108.8(1)	98.00(3)
N21–Ni–N61	168.8(1)	169.6(1)	165.4(1)	173.9(2)
N31–Ni–N41	94.3(1)	94.1(1)	93.1(1)	84.1(1)
N31–Ni–N51	170.7(1)	169.6(1)	166.1(1)	173.9(2)
N31–Ni–N61	101.0(1)	100.6(1)	95.2(1)	101.9(2)
N41–Ni–N51	76.5(1)	75.6(1)	76.0(1)	89.9(2)
N41–Ni–N61	94.6(1)	94.2(1)	103.1(1)	103.7(1)
N51–Ni–N61	79.8(1)	79.3(1)	79.2(1)	80.3(1)

3.3. Iron complexes

The pale yellow high-spin (HS) iron(II) complex, $[Fe(phdpa)_2](ClO_4)_2$, is relatively stable in air both as a solid and in solution. In the corresponding yellow medpa complex, $[Fe(medpa)_2]^{2+}$, HS behaviour was verified by magnetic susceptibility measurements [15]. In contrast the red dpa complex, $[Fe(dpa)_2]^{2+}$, is low-spin (LS) [15]. X-ray structures of $[Fe(dpa)](BF_4)_2$ [4] and $[Fe(medpa)_2](ClO_4)_2$ [7] reveal a *cis–facial* coordination geometry in both cases.

Electronic spectra of acetonitrile solutions of $[Fe(dpa)_2]^{2+}$, $[Fe(medpa)_2]^{2+}$, $[Fe(phdpa)_2]^{2+}$ and $[Fe(tpbd)]_n^{2n+}$ all have absorption maxima at 251–262 nm, due to ligand π–π* transitions. LS behaviour of $[Fe(dpa)_2]^{2+}$ is evident from the medium intensity d–d* transition band at 531 nm. Spectra of $[Fe(medpa)_2]^{2+}$, $[Fe(phdpa)_2]^{2+}$ and $[Fe(tpbd)]_n^{2n+}$ show medium intensity absorption bands in the area from 300 to 410 nm.

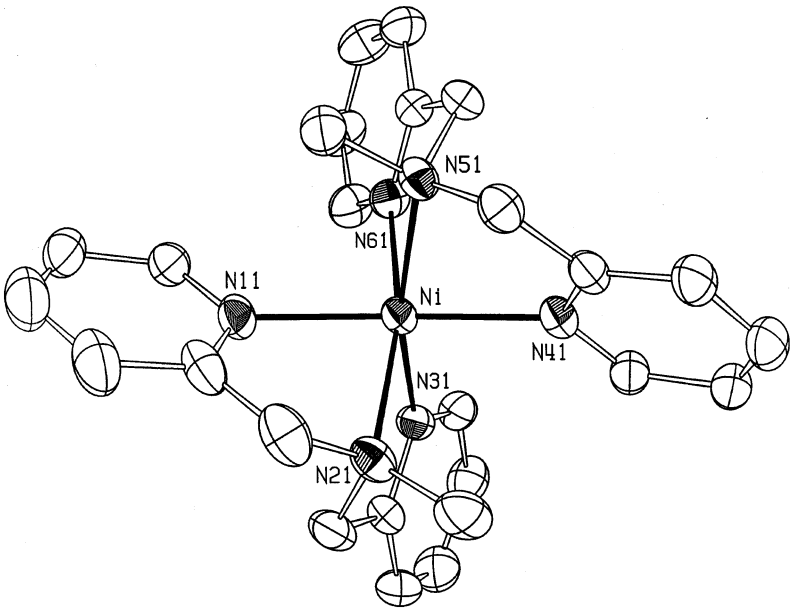


Fig. 2. ORTEP drawing of the $[Ni(medpa)_2]^{2+}$ cation. Ellipsoids are drawn at the 30% probability level.

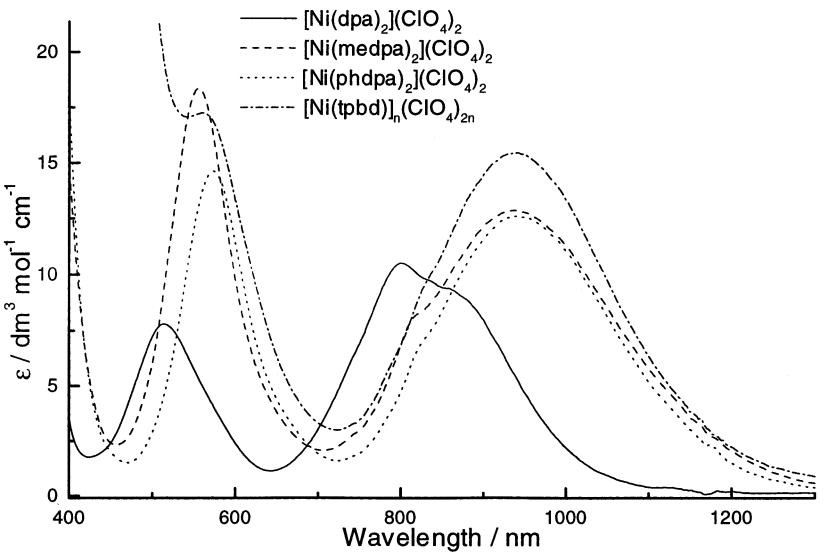


Fig. 3. UV–Vis spectra of the nickel complexes in CH_3CN solutions.

Such bands are generally believed to stem from MLCT from the iron(II) centre to pyridine ligands [16]. $[Fe(medpa)_2](ClO_4)_2$ and $[Fe(phdpa)_2](ClO_4)_2$ show comparable absorption characteristics in the area from 920 to 1075 nm. This further consolidates the strong field nature of dpa compared with the substituted analogues which was observed in the Ni(II) complexes. Due to the similarity of the spectra of $[Fe(phdpa)_2]^{2+}$ and $[Fe(tpbd)]_n^{2n+}$ with the spectrum of $[Fe(medpa)_2]^{2+}$ it is believed that the former two have analogous *cis–fac* geometries. Absorption maxima are listed in Table 3.

Table 3
UV–Vis absorption maxima for acetonitrile solutions of $[Ni(dpa)_2]^{2+}$, $[Ni(medpa)_2]^{2+}$, $[Ni(phdpa)_2]^{2+}$ and $[Ni(tpbd)]_n^{2n+}$

Complex	λ_{max} (ε/dm^3 mol^{-1} cm^{-1})
$[Ni(dpa)_2](ClO_4)_2$	514 (8), 801 (10), 859 sh
$[Ni(medpa)_2](ClO_4)_2$	556 (18), 815 sh, 936 (13)
$[Ni(phdpa)_2](ClO_4)_2$	573 (15), 824 sh, 941 (13)
$[Ni(tpbd)]_n(ClO_4)_{2n}$	561 (17), 827 sh, 937 (15)
$[Fe(dpa)_2](ClO_4)_2$	382 sh, 431 (8990)
$[Fe(medpa)_2](ClO_4)_2$	363 sh, 921 (8), 1024 sh
$[Fe(phdpa)_2](ClO_4)_2$	300 sh, 363 sh, 1025 (9) broad
$[Fe(tpbd)]_nCl_{2n}$	312 sh, 360 sh, 414 sh

4. Conclusions

Comparable ligand field properties are found in nickel(II) and iron(II) complexes of medpa, phdpa and tpbd in contrast to the much stronger donating ligand dpa.

The ligands are coordinated in a *cis–fac* fashion in $[Ni(phdpa)_2]^{2+}$ and $[Ni(medpa)_2]^{2+}$. UV–Vis results indicate similar coordination modes in phdpa and tpbd, suggesting a *cis–fac* binding of each end of tpbd in the polymeric $[Ni(tpbd)]_n^{2n+}$ and $[Fe(tpbd)]_n^{2n+}$.

5. Supplementary material

Crystallographic data have been deposited with the Cambridge Crystallographic Data Centre as CCDC No. 139600 for $[Ni(phdpa)_2](ClO_4)_2 \cdot 0.5H_2O$ and CCDC No. 139601 for $[Ni(medpa)_2](ClO_4)_2$. Copies of the data can be obtained, free of charge, on application from: The Director, CCDC, 12 Union Road, Cambridge, CB2 1EZ, UK (fax: +44-1223-336-033; e-mail: deposit@ccdc.cam.ac.uk or www: http://www.ccdc.cam.ac.uk).

Acknowledgements

A.H. is indebted to the Carlsberg Foundation for the diffractometer. This work was supported by grant No. 28808 to C.J.M. from the Danish Natural Science Research Council.

References

[1] A. Hazell, C.J. McKenzie, L.P. Nielsen, J. Chem. Soc., Dalton Trans. (1998) 1751.
[2] T. Buchen, A. Hazell, L. Jessen, C.J. McKenzie, L.P. Nielsen, J.Z. Pedersen, D. Schollmeyer, J. Chem. Soc., Dalton Trans. (1997) 2697.
[3] M. Palaniandavar, R.J. Butcher, A.W. Addison, Inorg. Chem. 35 (1996) 467.
[4] R. Butcher, A.W. Addison, Inorg. Chim. Acta 158 (1989) 211.
[5] M. Velusamy, M. Palaniandavar, K.R.J. Thomas, Polyhedron 17 (1998) 2179.
[6] J. Glerup, P.A. Goodson, D.J. Hodgson, K. Michelsen, K.M. Nielsen, H. Weihe, Inorg. Chem. 31 (1992) 4611.
[7] T. Buchen, D. Schollmeyer, personal communication.
[8] E. Bang, K. Michelsen, K.M. Nielsen, E. Pedersen, Acta Chem. Scand., Ser. A 43 (1989) 748.
[9] K.B. Jensen, C.J. McKenzie, O. Simonsen, H. Toftlund, A. Hazell, Inorg. Chim. Acta 257 (1997) 163.
[10] Siemens, SMART Area Detector Control and Integration Software, Siemens Analytical X-ray Institute Inc., Madison, WI, USA, 1995.
[11] G. Cascarano, A. Altomare, C. Giacovazzo, A. Guagliardi, A.G.G. Moliterni, D. Siliqi, M.C. Burla, G. Polidori, M. Camalli, Acta Crystallogr., Sect. A 52 (1996) C79.
[12] A. Hazell, KRYSTAL, An Integrated System of Crystallographic Programs, Aarhus University, Denmark, 1995.
[13] International Tables for X-ray Crystallography, vol. IV, Kynoch Press, Birmingham, UK, 1974 (present distributor: Kluwer, Dordrecht).
[14] G.S. Pawley, Adv. Struct. Res. Diffr. Methods 4 (1971) 1.
[15] S.M. Nelson, J. Rodgers, J. Chem. Soc. A (1968) 272.
[16] A. Diebold, K.S. Hagen, Inorg. Chem. 37 (1998) 215.
[17] M.N. Burnett, C.K. Johnson, ORTEP-III, Report ORNL-6895, Oak Ridge National Laboratory, TN, USA, 1996.

PERGAMON

www.elsevier.nl/locate/poly

Polyhedron 19 (2000) 1339–1346

POLYHEDRON

Formation of a mixed-valence Ru(IV)–Fe(II) binuclear complex via the reaction of $[Ru^{III}(edta)(H_2O)]^-$ and $[Fe^{III}(CN)_6]^{3-}$ in aqueous solution

Matthew S. Ward [a], Debabrata Chatterjee* [b,1], Rex E. Shepherd* [a,2]

[a] *Department of Chemistry, University of Pittsburgh, Pittsburgh, PA 15260, USA*
[b] *Chemistry Section, Central Mechanical Engineering Research Institute, Durgapur 713209, India*

Received 22 November 1999; accepted 25 April 2000

Abstract

The combination of $[Ru^{III}(edta)(H_2O)]^-$ ($edta^{4-}$ = ethylenediamine-*N*,*N*,*N*′*N*′-tetraacetate) and $[Fe^{III}(CN)_6]^{3-}$ in aqueous solution results in the rapid formation of $[Ru^{III}(edta)(NC)Fe^{III}(CN)_5]^{4-}$ (**1**), which has been isolated and characterized by physical methods. An aqueous solution of complex **1** shows two characteristic absorption maxima in the visible spectral region located at 420 and 620 nm. Examination of the same solution after 72 h shows that a spectral change has occurred, forming a species with a new band maximum at 870 nm. Spectral (IR, UV–Vis, ^1H and ^{13}C NMR spectra showing a paramagnetic complex, and time-dependent magnetic susceptibility data) provide evidence for the formation of a mixed-valence $[Ru^{IV}(edta)(NC)Fe^{II}(CN)_5]^{4-}$ complex **2** by the process, which causes the appearance of the 870 nm band. The results are compared with the known reactions between $[Ru^{III}(NH_3)_5(H_2O)]^{3+}$ and $[Fe(CN)_6]^{3-}$, which have been reported by Taube and co-workers (V.G. Poupopoulu, Z.W. Li, H. Taube, Inorg. Chim. Acta 225 (1994) 173) to sequentially form $\{[Ru^{III}(NH_3)_5(H_2O)]^{3+}, [Fe^{III}(CN)_6]^{3-}\}$ ion-pairs, converting to a (Ru^{III}–CN^- bridged-Fe^{III}) binuclear complex (an analogue of **1**, and upon intramolecular electron transfer, the (Ru^{IV}–CN^- bridged-Fe^{II}) binuclear complex (an analogue of **2**). The events reported for the conversion of **1** into **2** ensue without appreciable accumulation of ion pairs as both $[Ru^{III}(edta)(H_2O)]^-$ and $[Fe^{III}(CN)_6]^{3-}$ are anionic. Magnetic susceptibility data imply that both **1** and **2** are paramagnetic $S = 1$ ions. The d electron manifold filling is $d^2_{xy}d^2_{xz}d^1_{yz}$ in **1** and $d^2_{xy}d^1_{xz}d^1_{yz}$ in **2**, whereas a filling of $d^2_{xy}d^2_{xz}d^0_{yz}$ seems to account for the prior observations with the $[Ru^{IV}(NH_3)_5(NC)Fe^{II}(CN)_5]$ system studied by Taube and co-workers. © 2000 Elsevier Science Ltd. All rights reserved.

Keywords: Mixed-valence complexes; Ruthenium–edta complexes; Ferricyanide; Cyanobridged complexes; Intramolecular electron transfer

1. Introduction

The chemistry of binuclear complexes containing the $[Ru^{III}(NH_3)_5]$ moiety has been a topic of continued interest, especially in the context of the electron transfer process as the electron acceptor from metal centers that are bridged to it by small molecules [1–10]. Only a few studies have been carried toward the preparation and electron transfer studies with the related $[Ru^{III}(edta)]$ acceptor moiety in place of the more commonly studied $[Ru(NH_3)_5]$ analogues [11,12]. The suitability of such studies is prompted by the unusually high substitution lability of $[Ru^{III}(edta)(H_2O)]^-$, which renders this complex as a substitutionally labile and kinetically accessible Ru^{III} center, as noted by Creutz in former studies [13,14] and described in detail in a recent review [15].

Moreover, the Ru–edta complexes undergo easy intercoversion between low-spin Ru^{II}/Ru^{III} redox changes (d^6/d^5) without significant needs for structural changes that limit electron transfer steps. Less is known about the Ru^{III}/Ru^{IV} redox changes as the latter may occur only by including an oxo or hydroxy group at the solvent position on the Ru center in complexes such as $[Ru^{III}(edta)(H_2O)]^-$. However, rather facile Ru^{IV}/Ru^{II} conversions are obtained by the oxidation of alcohols by Ru^{IV}(polyaminopolycarboxylate) complexes — changes being sufficiently rapid to allow electrochemical detection of enhanced currents of the Ru^{IV}/Ru^{II} waves [16]. Thus, there is some indication that formation of Ru^{IV} species within polyaminopolycarboxylate

[1] *Corresponding author.
[2] *Corresponding author. Tel.: +1-412-624-8510; fax: +1-412-624-8611; e-mail: shepherd+@pitt.edu

0277-5387/00/$ - see front matter © 2000 Elsevier Science Ltd. All rights reserved.
PII: S0277-5387(00)00414-9

environments is sufficiently facile that the Ru^{IV} oxidation state might be readily obtained from a $[Ru^{III}(edta)]$ center as a stable product electronic state if the Ru^{III} site were bridged to an electron sink via an inner-sphere bridging ligand. The bridging ligand might also prevent hydrolysis reactions at the Ru center, which in forming an oxo group out of a solvent or hydroxy group could lead to non-bridged products, e.g. in displacement of the second metal site from the Ru^{IV} product species.

The chemistry of $[Ru^{III}(edta)(H_2O)]^-$ and derivative complexes has been a continuing area of study by Chatterjee et al. [17–21]. In particular, the cyano-bridged complexes, $[Ru^{III}(L)(NC)Fe^{II}(CN)_5]^{5-}$, L = $edta^{4-}$ and $hedta^{3-}$ (ethylenediamine-*N*,*N*,*N*′,*N*′-tetraacetate and *N*-hydroxyethylethylenediamine-*N*,*N*′,*N*′-triacetate) have been characterized previously in Chatterjee's laboratories [22,23]. The characterization of such cyano-bridged (III, II) ions of the general formulation $[Ru^{III}(edta)(NC)M(CN)_5]^{5-}$ for $M = Ru^{II}$, Os^{II} and Fe^{II} were recently described in studies by Olabe and co-workers [24]. Analogous pentaammine complexes of the formulation $[Ru^{III}(NH_3)_5(NC)Ru^{II}(CN)_5]^-$ have been characterized by Shepherd and co-workers [3b], Vogler and Kisslinger [33] and Ludi [34].

We have observed a slow spectral change that occurs for the related (III, III) ion, $[Ru^{III}(edta)(NC)Fe^{III}(CN)_5]^{4-}$ (**1**), that changes its visible spectral maxima from 420 and 620 nm to a new value of 870 nm over a period of more than 72 h. Since a related species, $[Ru^{III}(NH_3)_5(NC)Fe^{III}(CN)_5]$, has been reported to undergo intramolecular electron transfer forming a reputed $[Ru^{IV}(NH_3)_5(NC)Fe^{II}(CN)_5]$ complex [25], we examined the $[Ru^{III}(edta)(NC)Fe^{III}(CN)_5]^{4-}$ (**1**) complex by several physical methods to deduce if the related $[Ru^{IV}(edta)(NC)Fe^{II}(CN)_5]^{4-}$ (**2**) species is generated in the step producing the 870 nm transition.

2. Experimental

2.1. Reagents

K[Ru(edtaH)Cl] was prepared according to the published procedure [26]. In aqueous solution the $[Ru^{III}(edtaH)Cl]^-$ ion undergoes rapid aquation, forming the reactive $[Ru^{III}(edtaH)(H_2O)]$ complex, which is the dominant form in solution in the pH range 5.0–6.0 [27]. Synthesis and characterization of the binuclear complex $K_4[Ru^{III}(edta)(NC)Fe^{III}(CN)_5]$ (**1**) was carried out (in Durgapur) as described previously [22]. All reagents were of analytical grade. Double distilled water or deionized distilled water was used throughout the spectral and stopped-flow experiments. Concentrations are as reported in the main text and figures.

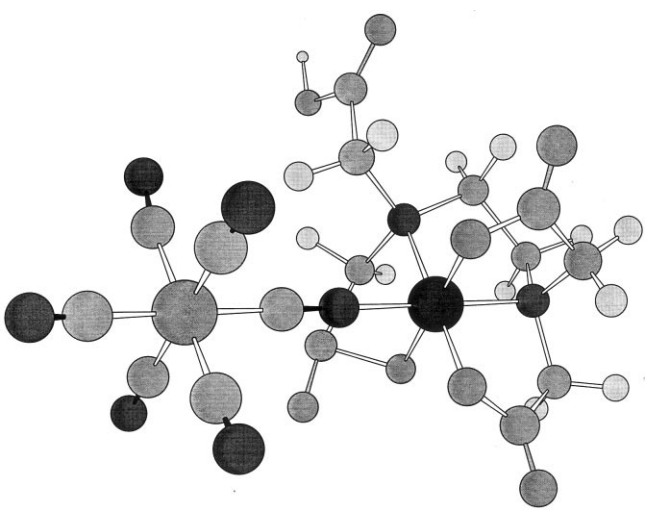
Samples for the NMR work and magnetic susceptibility studies were independently prepared (in Pittsburgh) by the following procedures. Complex **1** was prepared by dissolving 1.01×10^{-3} mol each of $K_3Fe(CN)_6$ (0.333 g) and $[Ru^{III}(edtaH)(H_2O)]\cdot 4H_2O$, prepared for a previous study [19], in 100.00 ml of distilled deionized water. The solution was swirled for nearly 5 min using magnetic stirring via a rice-sized stirring bar added to the volumetric flask. This sample was then stored, wrapped in aluminum foil and kept in a dark cabinet at room temperature for a period of 14 days to assure complete reaction in forming complex **2**. The solution was rotary evaporated to near dryness and then the sample was pumped in a vacuum desiccator to remove any remaining free water. A small amount of this product was redissolved in D_2O (Aldrich) to prepare the sample for ^1H and ^{13}C NMR studies. The ^1H NMR spectrum was taken immediately to avoid any problems with H/D exchange. The ^1H NMR resonances were absent due to paramagnetism of the product as discussed in the main text.

Samples of **1** for the magnetic susceptibility studies were first prepared at 9.712×10^{-3} M by combining 0.07995 g of $K_3Fe(CN)_6$ and 0.11686 g of $[Ru^{III}(edtaH)(H_2O)]\cdot 4H_2O$ in a 25.00 ml flask. Magnetic measurements were made and compared with a 9.716×10^{-3} M solution of $K_3Fe^{III}(CN)_6$ (0.07997 g in 25.00 ml). These two samples were left unprotected from air, but were stored in the dark. Measurements of the magnetic susceptibility varied non-systemmatically with time. This prompted a repeat experiment in samples protected from air by purging the deionized water with N_2, transferring the water by syringe techniques to a flask containing 0.05749 g of $K_3Fe^{III}(CN)_6$ and 0.08415 g of $[Ru^{III}(edtaH)(H_2O)]\cdot 4H_2O$ in a septum-sealed and prepurged 25.00 ml flask. Adding the purged water solvent produced a 6.984×10^{-3} M solution of **1**. This sample was transferred by syringe methods to a purged sample tube of the magnetic susceptibility device. A blank solution of 7.004×10^{-3} M $[Ru^{III}(edtaH)(H_2O)]\cdot 4H_2O$ was also prepared under N_2. The magnetic susceptibilities of both complexes of **1** and the $[Ru^{III}(edtaH)(H_2O)\cdot 4H_2O$ blank remained constant with time. All values of magnetic susceptibility were obtained in cgs units in accordance with the equations supplied in the Johnson–Matthey Susceptibility Balance Instruction Manual. The magnetic susceptibility of **1** was consistent with the anticipated $S = 1$ complex, and of $S = 1/2$ for the parent Ru^{III} complex.

2.2. Instrumentation

Microanalyses were carried out using a Carlo Erba elemental analyser. UV–Vis spectra were recorded with a GBC Cintra 10 spectrophotometer using quartz cells. Infrared spectra were recorded on a Carl Zesis Specord

M80 spectrophotometer. Cyclic voltammetric studies were performed in Durgapur using a Princeton Applied Research Model 174A electrochemical instrument. The working electrode was a glassy carbon probe with a standard calomel reference. All potentials are corrected to the NHE scale. NMR spectra were examined on Bruker 300 MHz NMRs in Pittsburgh using standard techniques. The spectra revealed that no detectable resonance for the edta portion of complexes **1** or **2** could be observed due to the local paramagnetism of the Ru^{III} center in **1** and the Ru^{IV} center in **2**, nor could a ^{13}C NMR signal be detected for the cyano carbons of the Fe^{II} center in complex **2** due to the Ru^{IV} paramagnetism and/or rapid electron transfer between metal centers, which delocalizes the paramagnetic properties of **2**. The paramagnetism as a function of time was recorded in solution using a Johnson–Matthey magnetic susceptibility balance. The N_2-protected sample gave constant readings of the magnetic susceptibility for over 72 h, the time period for which spectral conversion of **1** to **2** is noted by the changes in the UV–Vis spectra.



Scheme 1. Energy minimized structure via MM2 calculations for the [Ru(edta)NCFe(CN)$_5$] binuclear species **1**.

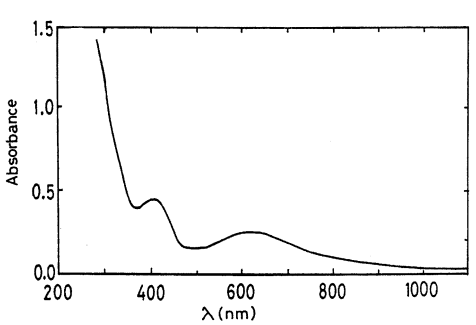


Fig. 1. UV–Vis spectrum of the Ru^{III}–Fe^{III} starting complex **1**; [complex **1**] = 2.45×10^{-4} M, room temperature, $\mu = 0.50$ (KCl); pH 5.5; 1.00 cm cell.

2.3. Kinetic studies

Fast kinetics experiments for the substitution reaction that forms **1** were performed with a Hi-Tech SF-51 stopped flow spectrophotometer interfaced to an Apple IIe data analysis system. Slow reactions were followed by conventional techniques using the GBC Cintra-10 spectrophotometer. Both instruments were thermostated to ± 0.1°C. Rate constant data represent the average of three runs that were reproducible to $\times 4\%$. Acetic acid–acetate buffers were used to maintain the desired pH in the kinetic experiments, whereas KCl was used to control the ionic strength. pH readings were made with a Digisun pH meter calibrated with standard buffers.

An energy minimized representation of the cyano-bridged [Ru(edta)NCFe(CN)$_5$] structural unit is shown in Scheme 1. The atom locations were obtained by energy minimization on the MM2 program using CHEM-PRO-3D software and assigning the metal centers to octahedral coordination with a linear cyano bridge. The system was minimized on the {Ru(III)–Fe(III)} binuclear complex.

3. Results and discussion

3.1. Formation of the Ru^{III}–Fe^{III} binuclear complex 1

Reaction of $[Ru^{III}(edta)(H_2O)]^-$ with $[Fe(CN)_6]^{3-}$ in aqueous solution results in the rapid formation of $[Ru^{III}(edta)(NC)Fe^{III}(CN)_5]^{4-}$ (**1**), which was isolated and characterized previously [22]. The absorption spectrum of **1** in aqueous solution has two bands as shown in Fig. 1. The band at 420 nm ($\varepsilon_{420} = 1600 \pm 40$ M^{-1} cm^{-1}) is characteristic of the ferricyanide moiety within complex **1** as $[Fe(CN)_6]^{3-}$ has the same band at 417 nm and $[Fe(CN)_5(H_2O)]^{2-}$ absorbs at 394 nm [28,29]. The band at 620 nm ($\varepsilon_{620} = 1020 \pm 30$ M^{-1} cm^{-1}) is assigned to a metal-to-metal charge transfer (MMCT) transition analgous to the same assignment for the pentaammine system, $[Ru^{III}(NH_3)_5(NC)Fe^{III}(CN)_5]$ (**3**), by Taube and co-workers, where the band appears at 540 nm ($\varepsilon_{540} = 900$ M^{-1} cm^{-1}) [25]. The observed shift from 540 nm for the $[Ru^{III}(NH_3)_5]$ environment to that of 620 nm for the $[Ru^{III}(edta)]$ environment is attributed to the stabilization of the higher Ru^{IV} state in the photo-oxidized electronic configuration by the anionic carboxylate donors of the $edta^{4-}$ ligand in **2** compared with lesser stabilization of Ru^{IV} by ammines alone in **3**.

The infrared spectrum of the Ru^{III}–Fe^{III} complex **1** exhibited bands at 2130 and 2090 cm^{-1} of the cyanide stretching region [30]. These are, respectively, assigned to the five terminal and one bridging cyano groups in **1**. The 2130 cm^{-1} stretch is virtually the same as for

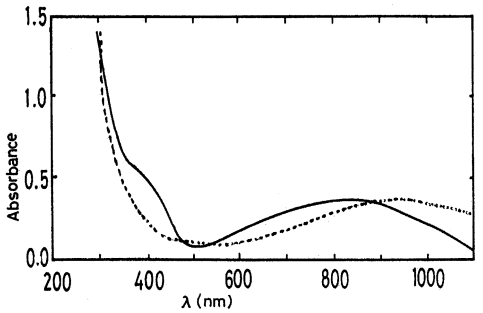


Fig. 2. UV–Vis spectrum of Ru^{IV}–Fe^{II} complex **2**; solid curve before ascorbate reduction, [complex **2**] = 1.25×10^{-4} M, room temperature, $\mu = 0.50$ (KCl), pH 5.5, 1.00 cm cell; dashed curve, Ru^{III}–Fe^{II} complex **5** formed via ascorbate reduction, [complex **5**] = 1.25×10^{-4} M after reduction with 2.0×10^{-3} M ascorbate at pH 5.5 and other conditions the same as before reduction.

$K_3[Fe^{III}(CN)_6]$ at 2135 and 2130 cm^{-1} [31]. A cyclic voltammogram on complex **1** exhibited two reversible waves at 0.06 V for the $Ru^{III/II}$ wave and 0.60 V for the $Fe^{III/II}$ wave versus NHE. The $Fe^{III/II}$ wave is more positive than the 0.36 V value for the $[Fe^{III/II}(CN)_6]^{3-/4-}$ couple due to the influence of the withdrawing effect of the coordinated, positive Ru^{III} center at potentials approaching the $Fe^{III/II}$ wave.

Thus, UV–Vis, IR and electrochemical data establish complex **1** as the Ru^{III}–Fe^{III} binuclear complex that retains the oxidation states of the $[Ru^{III}(edta)(H_2O)]^-$ and $[Fe^{III}(CN)_6]^{3-}$ reactants that form **1** in the substitution process that occurs immediately upon mixing. The energy-minimized structural drawing clearly shows that there is minimal steric interaction between the cyano ligands of the Fe center and the chelate functionalities of the $edta^{4-}$ ligand of the Ru center. All bonds and angles that were determined for the energy minimized structure were those common to M(edta) and $M'(CN)_6$ structural moieties, and hence, unexceptional, emphasizing the absence of steric strain between the metal centers in **1** and its redox isomer **2** (to be described later in the text).

The kinetic progress of the substitution process was followed directly by monitoring the appearance of the 640 nm band in stopped-flow experiments that combined these two reactants. The rate was observed to be first-order in each $[Ru^{III}(edta)(H_2O)]^-$ and $[Fe(CN)_6]^{3-}$ reactant. Rate measurements were made at pH 5.2 (acetate buffer) and $\mu = 0.50$ (KCl). The substitution reaction has a formation rate constant, k_{obs}, of 10 ± 2 M^{-1} s^{-1} at 25°C. This is 10-fold slower than the substitution of $[Fe^{II}(CN)_6]^{4-}$ on $[Ru^{III}(edta)(H_2O)]^-$ in forming the known Ru^{III}–Fe^{II} binuclear complex [22]. Therefore, the mechanism to generate **1** does not involve any outer-sphere electron transfer pathway that precedes the simple substitution step of Eq. (1).

$$Ru^{III}(edta)(H_2O)]^- + [Fe^{III}(CN)_6]^{3-} \xrightarrow{k_{obs}} [Ru^{III}(edta)(NC)Fe^{III}(CN)_5]^{4-}\ (\mathbf{1}) \quad (1)$$

The substitution of $[Fe(CN)_6]^{3-}$ on $[Ru^{III}(edta)(H_2O)]^-$ is strikingly more rapid than for the substitution process of $[Fe(CN)_6]^{3-}$ on $[Ru^{III}(NH_3)_5(H_2O)]^{3+}$ ($k = 5.9 \times 10^{-5}$ s^{-1} [25]). The former process obeys second-order kinetics for the formation of **1**, whereas the pentaammine complex **3** is produced by the slow first-order rearrangement of the ion-pair. Clearly, the difference in charge for the $[Ru^{III}(edta)(H_2O)]^-$ versus $[Ru^{III}(NH_3)_5(H_2O)]^{3+}$ reactants is a key factor in the different mechanisms of the formation of **1** and **3**, the latter using the strong ion-pair pathway that is imposed by the $(3+)(3-)$ attractions that are absent in forming **1** via two anions [25]. The rates of substitution on the Ru^{III} center in the labilized $[Ru^{III}(edta)(H_2O)]^-$ complex is rather rapid [15]. By contrast, the inherently slow substitution of $[Ru^{III}(NH_3)_5(H_2O)]^{3+}$ allows a sufficiently long time that all the Ru^{III} species will have formed ion pairs prior to any step that will produce **3**. Thus, only ion-paired species exist as available precursor species in forming **3**. But in forming **1**, the transition state species that proceed to produce **1** are those collisions of $[Fe(CN)_6]^{3-}$ with $[Ru^{III}(edta)(H_2O)]^-$ molecules that are in the act of dissociation of the coordinated water in I_a pathways [15] at the time of approach of the $[Fe^{III}(CN)_6]^{3-}$ ion. That is, no pool of ion-paired species act as the reactant species that forms **1**. Hence, second-order kinetics are followed, distinguishing this process that produces **1** from the pathway that forms **3**.

3.2. Formation of the Ru^{IV}–Fe^{II} binuclear complex 2

Taube and co-workers observed a slow change in complex **3**, converting **3** into a Ru^{IV}–Fe^{II} complex **4** [25]. We examined complex **1** as a function of time in order to seek evidence for a similar change in **1** transforming into another Ru^{IV}–Fe^{II} complex **2**. Indeed, over a 72 h period, the bands in the visible spectrum at 420 and 620 nm decreased with time, while concurrently, a new band appeared at 870 nm as shown in Fig. 2. The extinction coefficient at 870 nm for **2** is 3020 ± 30 M^{-1} cm^{-1}. Acetone was added to precipitate **2** as its K^+ salt after 6 days to assure completion of the reaction. The infrared spectrum of complex **2** showed new IR bands at 2120 and 2040 cm^{-1}. Note that these values differ from the Ru^{III}–Fe^{III} species **1** with stretches at 2130 and 2090 cm^{-1}, but also differ from the value of 2080 cm^{-1} reported for the Ru^{III}–Fe^{II} complex [22]. The band at 2040 cm^{-1} is virtually the same as reported for the F_{1u} modes of $K_4[Fe(CN)_6]$ [31]. This feature indicates an Fe^{II}-cyano chromophore is present in **2**.

Based upon the similarity of the infrared stretch of the product species to that of Fe^{II}–CN stretches, the appearance of a totally different near-IR band in the visible spectrum concomitant with the loss of features

assignable to the Ru^{III}–Fe^{III} species, and magnetic information to be described later, we assign the changes mentioned in the sample of **1** over the 72 h period as being those due to the formation of a Ru^{IV}–Fe^{II} complex **2** in analogous processes that convert the pentaammine Ru^{III}–Fe^{III} species **3** into the pentaammine Ru^{IV}–Fe^{II} complex **4**. The kinetics of the process was determined from the time dependence of the appearance of the 870 nm band, and by the decay of the 620 m band, both yielding the same rate. A rate constant of $k_{obs} = 2.0 \times 10^{-5}$ s^{-1} at 25°C, pH 5.5 and $\mu = 0.50$. The initial concentration of **1** was 2.0×10^{-4} M. The rate constant for this process is an order of magnitude faster than the 1.6×10^{-6} s^{-1} value reported by Taube and co-workers for the conversion of **3** into **4**. This difference is attributed to the greater reducing power of the Ru^{III} center in the $edta^{4-}$ environment compared with the pentaammine environment, and the stabilizing influence of the carboxylate donors toward the Ru^{IV} product species. Removal of an electron from the positively charged $[Ru^{III}(NH_3)_5]^{3+}$ center comes at a greater rearrangement cost than for the transfer of an electron away from the anionic $[Ru^{III}(edta)]^{-}$ site, resulting in the latter process having a lower kinetic barrier (and a faster intramolecular electron transfer rate).

3.3. Reduction of binuclear complexes *1* and *2* by ascorbic acid

Addition of ascorbic acid to an aqueous solution of the Ru^{IV}–Fe^{II} complex **2** produced an immediate reduction that resulted in the known mixed-valence $[Ru^{III}(edta)(NC)Fe^{II}(CN)_5]^{5-}$ complex **5** that has been characterized in previous studies [22]. The spectral changes occur with the appearance of a new band at 945 nm that is characteristic of **5**.

The rate of reduction of complexes **1** and **2** were studied in stopped-flow experiments under conditions where [ascorbate] $= 2.0 \times 10^{-3}$ M as a pseudo-first order excess reagent, pH 5.50, $\mu = 0.50$ and $T = 25.0$°C. The conditions were chosen to match those of van Eldik's study of the reduction of $[Fe^{III}(CN)_6]^{3-}$ by ascorbate [32] in order to make direct comparison with results from the ascorbate reduction of **1** and **2**. Under identical experimental conditions the reduction of $[Fe^{III}(CN)_6]^{3-}$ has a rate constant of 2.16 s^{-1} [32]. The reduction of the Ru^{III}–Fe^{III} complex **1** yielded a reduction rate constant of 1.95 ± 0.08 s^{-1} (kinetic data was reproducible to $\pm$ 4%) with the ascorbate reagent. This implies that the reduction of the Ru^{III}–Fe^{III} complex **1** is Fe^{III} centered in forming complex **5**.

Reduction of the Ru^{IV}–Fe^{II} complex **2** by ascorbate in forming complex **5** proved difficult to follow spectrophotometrically as the absorbance change in going from a maximum at 870 nm to a new species with its maximum at 945 nm was not large. The best fit among several kinetic traces yielded a value of 105 ± 10 s^{-1} (kinetic data was reproducible to no better than $\pm$ 10% in this system) for the ascorbate reduction of **2** to **5**. Recalling that the measured rate constant for the ascorbate/**1** reaction under the same conditions is only 1.95 s^{-1}, the ascorbate reduction clearly identifies the redox capability of complex **2** as a more potent oxidant than complex **1**. Also, given that the reduction of the Fe^{III} site of complex **1** occurs with a rate nearly identical to that of an isolated Fe^{III} center in $[Fe^{III}(CN)_6]^{3-}$, the reduction of **2** at an approximately 50 times faster rate by ascorbate must be occurring at the Ru center. Since the product is a Ru^{III} species, this implies that the oxidation state of the Ru site is higher than Ru^{III} in complex **2**. Therefore, one is forced to conclude that species **2** has the redox assignment of Ru^{IV}–Fe^{II} as has been the tacit nature of our prior discussion, which has been presented before full proof of the Ru^{IV} oxidation state within **2** has been given.

3.4. Magnetic susceptibility study on the *1* to *2* conversion process

A freshly prepared sample of complex **1** was prepared at 9.712×10^{-3} M by a 1:1 combination of $[Ru^{III}(edta)(H_2O)]^{-}$ and $[Fe^{III}(CN)_6]^{3-}$ reactants. This sample was allowed to react in the dark for 14 days to assure complete conversion to **2** before being concentrated by rotary evaporation and dessication to achieve a sample of **2** with low water content. This sample was redissolved in D_2O at ca. 0.020 M for the ^1H and ^{13}C NMR studies described later. Another preparation was studied at 6.984×10^{-3} M on freshly prepared **1** that was purged with N_2 as described in the Section 2 and transferred immediately to the sample tube of a Johnson–Matthey magnetic susceptibility balance. Since the manipulations were accomplished much slower than the time to form **1**, as shown by the stopped-flow experiments, it is clear that the sample in the susceptibility balance tube is **1** at the start of the magnetic studies.

Magnetic susceptibility data were obtained as a function of time with calibration of the instrument against $K_3[Fe^{III}(CN)_6]$ and the $[Ru^{III}(edtaH)(H_2O)]\cdot 4H_2O$ monomer complexes. Equal molar amounts of the two standards gave the same calculated net spin per complex of $S = 1/2$ ($n = 1$ unpaired electron for each standard complex).

In the experiments of Taube and co-workers on the pentaammine Ru^{III}–Fe^{III} complex **3**, which converts to the Ru^{IV}–Fe^{II} complex **4**, a decrease in the solution magnetic moment was initially observed, but a complete study of the magnetic changes was prevented by the precipitation of product **4** when the solubility was exceeded. Since our product species **2** is a 4− anion, the probability that precipitation would cause problems

was greatly lowered. Thus, we attempted to observe the slow electron transfer process that was detected by the change from 420 and 620 nm maxima of **1** to the new 870 nm maximum of **2** by means of changes in the magnetic susceptibility. This would occur if the change in spin states happens as in Eq. (2):

$$\{Ru^{III}\ (S=1/2);\ Fe^{III}\ (S=1/2)\}\ (\text{net}\ S=1) \rightarrow \{Ru^{IV}\ (S=0)\ \text{LS};\ Fe^{II}\ (S=0)\ \text{LS}\}\ (\text{net}\ S=0) \quad (2)$$

The study of the magnetic susceptibility as a function of time for over a period of 72 h on samples protected from exposure to O_2 from the air showed that no net spin change occurs on the same time frame that produces the changes in the visible electronic spectrum. Calibrated against the two standard complexes, equimolar amounts of the $K_3[Fe(CN)_6]$ and $[Ru^{III}(edtaH)(H_2O)]\cdot 4H_2O$ were allowed to react, first forming **1** via the substitution route. The magnetic susceptibility data when compared with the equimolar standards imply an effective net spin of $S=0.75$ ($n=1.5$) rather than the anticipated values of $S=1$ ($n=2$) for complex **1**. However, the net spin is definitely not zero for a diamagnetic complex.

The reduced number of available free spins that were determined in the experiment may arise from difficulties in making significant diamagnetic corrections for the ligand contributions for the paramagnetically dilute sample (6.98×10^{-3} M), or may arise from the existence of a spin-crossover equilibrium between $S=1$ and $S=0$ forms of **1** near room temperature. The later explanation is rejected as the exact same net spin amount in the sample was retained as the complex converted to the redox isomer **2**. It is nearly impossible to believe that the two redox isomers would both be spin-crossover complexes resting at exactly the same position in the spin equilibrium. Such an unbelievable coincidence would require a spin-crossover {Ru(III)–Fe(III)} system that exhibits an identical spin-crossover equilibrium at the Ru^{IV} center by itself in the {Ru(IV)–Fe(II)} redox isomer with the spin crossover equilibrium as modulated by the local $edta^{4-}$ environment around the Ru^{IV} site exactly mimicing the delocalization and through-space coupling in the original redox isomer **1**. A simpler explanation is surely correct.

Rather, the experimental difficulties of measuring the dilute paramagnetism contribution on a sample with a large diamagnetic correction to the measurable magnetic susceptibility is a much more logical explanation for an observed constant net spin effective value of $S=0.75$ ($n=1.5$) rather than the anticipated $S=1$ and $n=2$ ideal values. The important point for the measurement is that upon mixing and formation of **1** there remains a substantial paramagnetism that is closer in magnitude to that of a species of two unpaired electrons than to a species of zero unpaired electrons. The sample tube containing the components that form **1** is more paramagnetic than for the sample tube and N_2-purged solvent alone. Furthermore, as the changes in the electronic spectrum occur in forming the redox isomer **2**, there is no change in the samples paramagnetism. The number of unpaired electrons is conserved although an electronic rearrangement has occurred.

This is explained only if the Ru^{IV} species is generated as a high-spin complex, wherein the d^4 center has the filling of $d^2_{xy}d^1_{xz}d^1_{yz}$ (taking the unique axis along the Ru(NC)Fe bond as the z axis in the system). Thus, the electron transfer process must occur as in Eq. (3):

$$\{Ru^{III}\ (S=1/2);\ Fe^{III}\ (S=1/2)\}\ (\text{net}\ S=1) \rightarrow \{Ru^{IV}\ (S=1)\ \text{HS};\ Fe^{II}\ (S=0)\ \text{LS}\}\ (\text{net}\ S=1) \quad (3)$$

Supporting evidence for the paramagnetic nature of complex **2** was obtained indirectly in attempts to obtain the ^1H and ^{13}C NMR spectra of **2**. Neither of these spectra revealed suitable lines for the proton resonances of the edta portion of the ^1H NMR spectrum or for the CN^- carbons of the ^{13}C NMR spectrum. The conclusion from the ^1H NMR results is that paramagnetic broadening of the edta ligand resonances is present in complex **2**. This is consistent with the retention of a net spin of $S=1$ during the electron transfer process, as described in Eq. (3), but not as in Eq. (2). Thus, none of the glycinato or ethylenediamine backbone protons is sufficiently removed from the paramagnetic center to allow for its detection by the ^1H NMR method.

In a separate attempt to obtain the ^{13}C NMR spectrum of complex **2**, it was hoped that the ferrocyanide-like end of the binuclear complex **2** might offer enough electronic isolation that ^{13}C resonances would appear, similar to those of the $[Fe^{II}(CN)_6]^{4-}$ complex, but perhaps shifted by the charge and induction of the $[Ru^{IV}(edta)]$ portion of **2** that is linked by the cyano bridge. No ^{13}C NMR resonances for the cyano ligands were detected after overnight signal averaging. Thus, although the infrared data from the CN^- stretches in **2** support an $[Fe^{II}(CN)_5(CN)\ldots]$ chromophore, there is sufficient ground state electronic delocalization that the CN^- ligands sense the presence of a paramagnetic center nearby, which broadens the signal via relaxation processes. These relaxation processes prevent a ^{13}C resonance being detected for the $[Fe^{II}(CN)_5(CN)\ldots]$ portion of complex **2**. This means that there is sufficient resonance character (delocalization) in the ground state wave function, although predominantly $\Psi(Ru^{IV}\text{–}Fe^{II})$ in character, has a small component of $\Psi(Ru^{III}\text{–}Fe^{III})$ character that is sufficient to cause ^{13}C relaxation processes that prevent detection of the cyano ^{13}C resonances in species **2**.

4. Conclusions

Reaction of $[Ru^{III}(edta)(H_2O)]^-$ with $[Fe^{III}(CN)_6]^{3-}$ initially forms a binuclear complex **1** of net spin $S = 1$ as a $[Ru^{III}–Fe^{III}]$ entity that has ferricyano-like CN^- stretches, reduces with ascorbate with a rate virtually the same as an isolated ferricyanide chromophore to a known complex of electronic assignment $[Ru^{III}–Fe^{II}]$, species **5**, and has electronic transitions similar to ferricyanide at 420 nm. The initially formed complex **1** undergoes a slow intramolecular electron transfer reaction that makes a $[Ru^{IV}–Fe^{II}]$ complex **2**. The product species **2** exhibits infrared stretches similar to the ferrocyanide complex, and reduction with ascorbate occurs at a rate 50-fold faster than for an Fe^{III}–cyano centered reduction, implying the more potent Ru^{IV} center is the one reduced, again creating complex **5**, but by a different pathway.

Finally, the magnetic susceptibility data shows that the net spin state of $S = 1$ is conserved in the electron transfer process that converts **1** into complex **2**. The ^1H and ^{13}C NMR data on species **2** confirm the paramagnetism that is maintained without net change during the electron transfer process. This will be the outcome if the ligand field symmetry around the Ru site is lowered from pseudo octahedral in the parent $[Ru^{III}(edta)(H_2O)]^-$ complex by the addition of the $(NC)Fe^{III}(CN)_5$ chromophore. Upon electron transfer, the Ru^{IV} center will have the filling of $d^2_{xy}d^1_{xz}d^1_{yz}$ as long as the splitting between the d_{xz} and the d_{yz} orbitals is less than the pairing energy. In the case of the $[Ru^{IV}(edta)(NC)Fe^{II}(CN)_5]^{4-}$ complex, the differences among the carboxylate and en-backbone donors appears to be too small to force a large splitting that would have produced the low-spin $d^2_{xy}d^2_{xz}d^0_{yz}$ configuration. This would have been accompanied by the decrease in magnetic susceptibility, as the {Ru^{IV} ($S = 0$) LS; Fe^{II} ($S = 0$) LS} complex would be created. Interestingly, although the Taube group could not follow the entire electron transfer process due to precipitation problems, they have suggested that a decrease in net spin occurs in the reaction of the pentaammine system where $[Ru^{III}–Fe^{III}]$ **3** converts to the $[Ru^{IV}–Fe^{II}]$ complex **4** [25]. The ammine environment is a stronger ligand field that could cause a larger splitting among the $d_{xy}d_{xz}d_{yz}$ levels, as discussed above, but it is also possible that in forming the Ru^{IV} oxidation state in the pentaammine system, the $Ru^{IV}–NH_3$ bonding allows for dissociation of a proton forming the strongly π-donating coordinated amide group that stabilizes Ru^{IV} in the **4** system. This coordination of an amide to stabilize Ru^{IV}, as mentioned as a possibility by the authors in Ref. [25], although they could not examine the product complex in detail.

Amido coordination with its strong π donation would come with a large increase in ligand field splitting for complex **4** compared with only bond distance shortening via carboxylate ligands in complex **2**. Therefore, the slight differences that have been observed between the behavior of the Ru^{IV} moiety in the Taube complex **4** compared with our observations on the edta complex **2** are reasonably reconciled on the basis of different ligand field factors between the two systems.

Acknowledgements

D.C. expresses his gratitude to S.H. Singh, Director of the CMERI, for encouragement and support in the execution of these studies. R.E.S. thanks the Petroleum Research Fund administered by the American Chemical Society for support.

References

[1] (a) H. Fisher, G.M. Tom, H. Taube, J. Am. Chem. Soc. 98 (1976) 5512. (b) S.K. Zawacky, H. Taube, J. Am. Chem. Soc. 103 (1981) 3389. (c) C. Creutz, H. Taube, J. Am. Chem. Soc. 95 (1973) 1086.
[2] (a) C. Creutz, Prog. Inorg. Chem. 30 (1983) 1. (b) T.J. Meyer, Prog. Inorg. Chem. 30 (1983) 389. (c) G. McLendon, Coord. Chem. Rev. 68 (1985) 1. (d) K.R. Seddon, Coord. Chem. Rev. 41 (1982) 29. (e) D.E. Richardson, H. Taube, Coord. Chem. Rev. 60 (1984) 107. (f) K. Wong, P.N. Schatz, Prog. Inorg. Chem. 28 (1981) 370.
[3] (a) W.W. Henderson, R.E. Shepherd, Inorg. Chem. 24 (1985) 2398. (b) S. Siddiqui, W.W. Henderson, R.E. Shepherd, Inorg. Chem. 26 (1987) 3101.
[4] (a) D.E. Richardson, H. Taube, Inorg. Chem. 20 (1981) 1278. (b) C.A. Stein, H. Taube, J. Am. Chem. Soc. 103 (1981) 693. (b) C.A. Stein, N.A. Lewis, H. Taube, J. Am. Chem. Soc. 104 (1982) 2596. (d) J.E. Sutton, H. Taube, Inorg. Chem. 20 (1981) 3125.
[5] D.E. Richardson, H. Taube, J. Am. Chem. Soc. 105 (1983) 40.
[6] (a) N.S. Hush, Prog. Inorg. Chem. 8 (1967) 391. (b) N.S. Hush, Chem. Phys. 10 (1975) 361. (c) B. Mayoh, P. Day, Inorg. Chem. 13 (1974) 2273. (d) M.B. Robin, P. Day, Adv. Inorg. Radiochem. 10 (1967) 247.
[7] (a) C. Creutz, P. Kroger, T. Matsubara, T.L. Netzel, N. Sutin, J. Am. Chem. Soc. 101 (1979) 5442. (b) W. Kaim, V. Kashach, Inorg. Chem. 29 (1990) 4696. (c) S. Ernst, V. Kasahach, W. Kaim, Inorg. Chem. 27 (1988) 1146.
[8] (a) A. Haim, Adv. Chem. Ser. 253 (1997) 239. (b) A. Yeh, A. Haim, Comments Inorg. Chem. 4 (1985) 113. (c) U. Furholz, A. Haim, Inorg. Chem. 26 (1987) 3243. (d) A. Bureweiz, A. Haim, Inorg. Chem. 27 (1988) 1611. (e) M.J. Akhtar, A. Haim, Inorg. Chem. 27 (1988) 1608. (f) J.A. Olabe, A Haim, Inorg. Chem. 28 (1989) 3278.
[9] H.Y. Huang, W.J. Cheng, C.C. Yang, A. Yeh, Inorg. Chem. 30 (1991) 1862.
[10] A.E. Almarez, L.A. Gentil, L.M. Baraldo, J.A. Olabe, Inorg. Chem. 35 (1996) 7718.
[11] M.S. Ram, A. Haim, Inorg. Chem. 30 (1991) 1319.
[12] L.A.A. Oleveira, L.D. Cianne, A. Haim, Inorg. Chim. Acta 225 (1994) 129.
[13] T. Matsubara, C. Creutz, Inorg. Chem. 18 (1979) 1956.
[14] T. Matsubara, C. Creutz, J. Am. Chem. Soc. 100 (1978) 6255.
[15] D. Chatterjee, Coord. Chem. Rev. 113 (1998) 273.

[16] S. Zhang, L.A. Holl, R.E. Shepherd, Transition Met. Chem. (Lond.) 17 (1992) 390.
[17] D. Chatterjee, H.C. Bajaj, J. Chem. Soc., Dalton Trans. (1993) 1065.
[18] D. Chatterjee, J. Mol. Catal. 127 (1997) 57.
[19] D. Chatterjee, M.S. Ward, R.E. Shepherd, Inorg. Chim. Acta 285 (1999) 170.
[20] D. Chatterjee, H.C. Bajaj, A. Das, J. Chem. Soc., Dalton Trans. (1995) 2497.
[21] D. Chatterjee, J. Mol. Catal. 127 (1997) 57.
[22] D. Chatterjee, H.C. Bajaj, A. Das, Inorg. Chem. 32 (1993) 4049.
[23] D. Chatterjee, H.C. Bajaj, A. Das, Inorg. Chim. Acta 224 (1994) 189.
[24] P. Forlano, F.D. Cukiernik, O. Poizat, J.A. Olabe, J. Chem. Soc., Dalton Trans. (1997) 1595.
[25] V.G. Poulopoulu, Z.W. Li, H. Taube, Inorg. Chim. Acta 225 (1994) 173.
[26] A.A. Diamantis, J.V. Dubrawski, Inorg. Chem. 20 (1981) 1142.
[27] H.C. Bajaj, R. van Eldik, Inorg. Chem. 28 (1989) 1980.
[28] (a) C.S. Naiman, J. Chem. Phys. 35 (1961) 323. (b) R. Gale, J.A. McCaffery, J. Chem. Soc., Dalton Trans. (1973) 1344.
[29] (a) G. Emschwiller, C.K. Jorgensen, Chem. Phys. Lett. 5 (1970) 561. (b) J.H. Espenson, S.G. Wolenuk, Inorg. Chem. 11 (1972) 2034.
[30] N. Nakamoto, Infrared and Raman Spectra of Inorganic and Coordination Compounds, Wiley, New York, 1977, p. 259.
[31] W.P. Griffith, G.T. Turner, J. Chem. Soc. A (1970) 858.
[32] P. Martinez, J. Zuluaga, J. Kraft, R. van Eldik, Inorg. Chim. Acta 9 (1986) 146.
[33] A. Vogler, J. Kisslinger, J. Am. Chem. Soc. 104 (1982) 2311.
[34] A. Ludi, Chimia 26 (1972) 647.

PERGAMON

www.elsevier.nl/locate/poly

Polyhedron 19 (2000) 1347–1354

POLYHEDRON

Synthesis and characterisation of mixed-ligand platinum(II)–sulfoxide complexes, [PtCl(DMSO)(L)], for potential use as chemotherapeutic agents (HL = *N*,*N*-dialkyl-*N*′-(3-*R*-benzoyl)thiourea)

C. Sacht *, M.S. Datt

Department of Chemistry, Rhodes University, PO Box 94, Grahamstown 6140, South Africa

Received 7 February 2000; accepted 26 April 2000

Abstract

A novel series of mixed-ligand platinum(II) complexes of the type [PtCl(DMSO)(L)], where HL = *N*,*N*-diethyl-*N*′-(3-*R*-benzoyl)thiourea, *N*,*N*-di(2-hydroxyethyl)-*N*′-(3-*R*-benzoyl)thiourea or *N*-morpholino-*N*′-(3-*R*-benzoyl)thiourea (R = H, Cl, NO_2, CH_3O, CH_3), have been synthesised and characterised by elemental analysis, IR spectroscopy and ^1H and ^{195}Pt NMR spectroscopy. The spectroscopic data are consistent with the complexes containing an O, S chelated ligand and an S-bonded sulfoxide ligand which is in a *cis* arrangement to that of the sulfur donor atom of the chelated ligand. Trends in the NMR spectra can be correlated with the electronic effects of the substituents on the phenyl ring of the acylthiourea ligands. © 2000 Elsevier Science S.A. All rights reserved.

Keywords: Platinum(II); Sulfoxide; *N*,*N*-Dialkyl-*N*′-(3-*R*-benzoyl)thiourea; Acylthiourea; NMR; Chemotherapeutic agents

1. Introduction

The successful use of inorganic complexes as chemotherapeutic agents is best exemplified by cisplatin and its analogue carboplatin, which have been used clinically since 1971 and 1981, respectively [1]. Because of the beneficial clinical efficacy of cisplatin, the past 30 years have witnessed tremendous effort and progress in trying to understand the mechanism of action of this metal-based anticancer drug [1]. Moreover, the clinical success of cisplatin has sparked considerable interest and research in the search for improved metal-based drugs for the use as chemotherapeutic agents [1,2]. Several approaches have been taken over the past three decades and some of these include the synthesis of cisplatin analogues, variation of the metal ion as well as the preparation of platinum complexes that are not structurally analogous to cisplatin [1,2]. Recent reports in the literature have revealed that the latter approach has yielded some exciting and successful results and two of these complexes are currently undergoing Phase I clinical trials, such as ZD0473 (*cis*-amminedichloro(2-methylpyridine)platinum(II)) and BBR3464, a trinuclear 4+ charged platinum(II) complex, introduced by Farrell et al., the structure of which is best described as two *trans*-$[PtCl(NH_3)_2]^+$ units bridged by a non-covalent tetra-amine *trans*-$[Pt(NH_3)_2\{NH_2(CH_2)_6NH_2\}_2]^{2+}$ unit [1,2]. These results are encouraging and thus this approach continues to be a promising strategy in the design of metal-based drugs. This can be achieved by the variation of either the firmly bound non-leaving ligands or the labile leaving groups or both. The non-leaving ligands could influence both the target selection and reactivity of the metal ion. For instance, the ligands may determine whether the compound may enter a hydrophobic environment like membranes, approach charged biomolecules like DNA or fit into the ligand binding pocket of a particular protein. The leaving groups will be exchanged for more nucleophilic biomolecules and thereby infer a biological lesion. Or

* Corresponding author. Tel.: +27-46-603-8260; fax: +27-46-622-5109.

E-mail address: c.sacht@ru.ac.za (C. Sacht).

0277-5387/00/$ - see front matter © 2000 Elsevier Science S.A. All rights reserved.
PII: S0277-5387(00)00419-8

the metal complex may require an exchange of one or more of the labile ligands by water in order to become activated. These factors are also influenced by the non-leaving ligand.

In our laboratory we have focused on preparing a series platinum(II) complexes of the type [Pt(acylthioureato)Cl(RR′SO)], in which we have varied both the non-leaving ligands and the labile leaving groups attached to the platinum(II) centre [3]. We have used the acylthiourea ligand system, $R^1C(O)NHC(S)NR^2R^2$, as the R^1 and R^2 groups can be readily varied to give a wide range of ligand systems with different physical and chemical properties, which could be used to fine-tune the biological activity of the resultant complexes. We have reported recently the synthesis and characterisation of the following [Pt(acylthioureato)Cl(RR′SO)] complexes with the acylthiourea ligands: *N*,*N*-di(2-hydroxyethyl)-*N*′-benzoylthiourea, *N*,*N*-diethyl-*N*′-benzoylthiourea and *N*,*N*-adipoylbis(*N*′,*N*′-diethylthiourea) and the sulfoxides: dimethylsulfoxide (DMSO), methylphenylsulfoxide (MPSO), *R*-methyl(*p*-tolyl)-sulfoxide (*R*-MTSO) and *S*-methyl(*p*-tolyl)sulfoxide (*S*-MTSO) [3]. We have since extended this series by preparing [Pt(acylthioureato)Cl(DMSO)] complexes using *N*,*N*-diethyl-*N*′-(3-*R*-benzoyl)thiourea, *N*,*N*-di-(2-hydroxyethyl)-*N*′-(3-*R*-benzoyl)thiourea and *N*-morpholino-*N*′-(3-*R*-benzoyl)thiourea ligands, where R = H, Cl, NO_2, OCH_3 and CH_3. Variation of the amine attached to the thiocarbonyl functionality and substitutents on the phenyl ring could influence the lipophilicity/hydrophilicity and electronic properties of the complexes and thus also affect the lability of the leaving groups which could control the reactivity and biological activity of the complexes. To this end, we herein report the synthesis and full characterisation of this novel series of platinum(II) complexes.

2. Experimental

2.1. Materials and physical methods

The potassium tetrachloroplatinate (Johnson Matthey), DMSO (Merck), 3-substituted benzoyl chlorides (Aldrich), benzoyl chloride (SaArchem) were used as supplied. The diethyl amine, morpholine and acetone were dried and distilled before use. All other solvents were commercial grade and used as received. The known complexes *cis*-[$PtCl_2(DMSO)_2$] [4], [PtCl(DMSO)(*N*,*N*-diethyl-*N*′-benzoylthioureato)] and [PtCl(DMSO)(*N*,*N*-di(2-hydroxyethyl)-*N*′-benzoylthioureato)] [3] were prepared by literature procedures. The IR spectra were recorded as KBr disks on Perkin–Elmer FT IR spectrum 2000, between 4000 and 250 cm^{-1}. ^1H NMR (1D and 2D) spectra were recorded at 400.13 MHz on a Bruker 400AMX spectrometer at 30 ± 1°C. All samples were prepared using deuterated solvents purchased from Aldrich Chemical Company, and 5 mm NMR tubes were used throughout. Chemical shifts are reported in parts per million (ppm) relative to the central line of the solvent proton resonance of known shifts relative to TMS, and coupling constants are reported in hertz (Hz). ^{195}Pt NMR spectra were recorded at 86.02 MHz on a Bruker 400AMX spectrometer at 30 ± 1°C using 70–100 KHz spectral widths and 13 μs pulses with 1 s pulse delay. Between 2048 and 16 000 transients, with a line broadening factor of 10 Hz, gave good spectra. All ^{195}Pt shifts are quoted relative to external H_2PtCl_6 (500 mg in 1 ml 30% (v/v) D_2O/1 M HCl). Melting points were determined on a Reichert hot-stage microscope and are uncorrected. Differential scanning calorimetry (DSC) was performed on a Perkin–Elmer Delta series 7 instrument, under a nitrogen atmosphere. The temperature range for the DSC experiments was 50–250°C. Elemental analyses were carried out at the microanalytical unit at the University of Cape Town, South Africa. Thin-layer chromatography (TLC) was performed on silica sheets $60F_{254}$ (Merck, Darmstadt). Reverse phase TLC was performed on glass backed RP-$C18F_{254}S$ plates (Techware). Flash chromatography was performed on silica gel 60 (Merck, Darmstadt).

2.2. Preparation of ligands

The ligands were prepared according to the method of Douglass and Dains [5]. The synthesis of *N*,*N*-di(2-hydroxyethyl)-*N*′-benzoylthiourea (**L3a**) has been reported recently [6,7]. The preparation of *N*,*N*-diethyl-*N*′-(3-*R*-benzoyl)thioureas and *N*-morpholino-*N*′-(3-*R*-benzoyl)thioureas (**L1a**–**d**; **L2a**–**d**), where R = H, Cl, NO_2 and OCH_3, have also been described recently [8–10]. The analytical data and selected IR data for the new ligands are given below.

N,*N*-Di(2-hydroxyethyl)-*N*′-(3-nitrobenzoyl)thiourea, **L3c**: (70%), m.p. 138–141°C. *Anal.* required for $C_{12}H_{15}N_3O_5S$: C, 46.00; H, 4.82; N, 13.41; S, 10.23. Found: C, 46.23; H, 4.85; N, 13.48; S, 9.93%. IR (KBr pellet, cm^{-1}): *ν*(N–H) 3175 (vs, br), *ν*(C=O) 1697 (vs, sh).

N,*N*-Di(2-hydroxyethyl)-*N*′-(3-methoxybenzoyl)-thiourea, **L3d**: (77%), m.p. 103–106°C. *Anal.* required for $C_{13}H_{18}N_2O_4S$: C, 52.33; H, 6.08; N, 9.39; S, 10.74. Found: C, 53.11; H, 6.29; N, 9.42; S, 10.40%. IR (KBr pellet, cm^{-1}): *ν*(N–H) 3232 (vs, br), *ν*(C=O) 1688 (vs, sh).

N,*N*-Di(2-hydroxyethyl)-*N*′-(3-chlorobenzoyl)-thiourea, **L3b**: (69%), m.p. 132–134°C. *Anal.* required for $C_{12}H_{15}ClN_2O_3S$: C, 47.60; H, 4.99; N, 9.25; S, 10.59. Found: C, 47.72; H, 5.09; N, 9.33; S, 10.58%. IR (KBr pellet, cm^{-1}): *ν*(N–H) 3180 (s, br), *ν*(C=O) 1693 (vs, sh).

N,*N*-Di(2-hydroxyethyl)-*N*′-(3-methylbenzoyl)-thiourea, **L3e**: (75%), m.p. 136–138°C. *Anal.* required for $C_{13}H_{18}N_2O_3S$: C, 55.29; H, 6.42; N, 9.92; S, 11.35. Found: C, 56.12; H, 6.57; N, 9.48; S, 11.36%. IR (KBr pellet, cm^{-1}): ν(N–H) 3192 (s, br), ν(C=O) 1693 (vs, sh).

N-Morpholino-*N*′-(3-methylbenzoyl)thiourea, **L2e**: (72%), m.p. 141–142°C. *Anal.* required for $C_{13}H_{16}N_2O_2S$: C, 59.06; H, 6.10; N, 10.60; S, 12.13. Found: C, 59.12; H, 6.15; N, 10.58; S, 11.75%. IR (KBr pellet, cm^{-1}): ν(N–H) 3150 (m), ν(C=O) 1657 (vs, sh).

N,*N*-Diethyl-*N*′-(3-methylbenzoyl)thiourea, **L1e**: (55%), m.p. 96–97°C. *Anal.* required for $C_{13}H_{18}N_2OS$: C, 62.36; H, 7.25; N, 11.19; S, 12.81. Found: C, 62.37; H, 7.28; N, 11.21; S, 12.20%. IR (KBr pellet, cm^{-1}): ν(N–H) 3311 (s, sh), ν(C=O) 1646 (s, sh).

2.3. Preparation of platinum(II) sulfoxide complexes

The complexes were prepared according to the following general procedure.

A solution of *N*,*N*-dialkyl-*N*′-(3-*R*-benzoyl)thiourea (0.50 mmol) in 10 ml acetonitrile–7 ml ethanol was added dropwise to a stirred solution of *cis*-$[PtCl_2(DMSO)_2]$ (0.50 mmol) in 1.5 ml acetonitrile–2.5 ml dimethylsulfoxide. Sodium acetate (0.063 g, 0.77 mmol) in 1.5 ml water was then added. The solution was allowed to stir for 48 h. The yellow solution was concentrated to ca. 10 ml and water (40 ml) was added whereupon the solution became opaque. The opaque solution was placed in the fridge (4°C) overnight. The yellow precipitate was collected by filtration, washed with water, a little ethanol and dried in vacuo over silica gel. In some cases ,column chromatography is required in order to obtain the pure product.

3. Results and discussion

3.1. Ligand synthesis and characterisation

The ligands were prepared according to the method of Douglass and Dains [5] and were obtained in yields ranging from 55–77%. The synthesis involves the reaction of a 3-substituted benzoyl chloride with potassium thiocyanate in acetone followed by condensation of the 3-*R*-benzoylisothiocyanate with the appropriate secondary amine. The ligands were purified by recrystallisation from ethanol and characterised by elemental analysis, ^{1}H NMR and IR spectroscopy. The analytical and spectroscopic data are consistent with the proposed structures given in Fig. 1.

The assignments of the ^{1}H NMR spectra of the *N*,*N*-diethyl-*N*′-(3-*R*-benzoyl)thiourea, *N*,*N*-di(2-hydroxyethyl)-*N*′-benzoylthiourea and *N*-morpholino-*N*′-(3-*R*-benzoyl)-thiourea ligands were in general straightforward, except for the assignments of the H_4 and H_6 protons which were confirmed by 2D [^{1}H, ^{13}C] HMBC experiments. The chemical shift data are given in Table 1. The data for the ligands that have been reported already are included for comparison. The numbering scheme for the thioamide protons are as given in Tables 3–5.

A notable feature of the ^{1}H NMR spectra of the ligands is the observation of separate resonances for the methylene protons (H_α) attached to the nitrogen of the respective thioamides. The magnetic inequivalence of these methylene protons can be ascribed to the restricted rotation around the C–N bond between the thiocarbonyl and the amine nitrogen due to the partial double bond character of this bond.

The ^{1}H NMR spectra of the *N*,*N*-di(2-hydroxyethyl)-*N*′-(3-*R*-benzoyl)thiourea ligands in DMSO-d_6 show inequivalent proton resonances for the hydroxyl protons. The lower field signal is broad and unresolved, while the higher field signal is a well-resolved triplet. This inequivalence of the hydroxyl protons is due to the presence of an intramolecular hydrogen bond between one hydroxyl moiety and the amide N–H [6].

The proton resonances for the phenyl ring and N–H protons are significantly affected by the presence of electron-withdrawing and electron-releasing substituents on the benzoyl moiety. As shown in Table 1, on increasing the electron withdrawing ability of the *R*-group there is a downfield shift of the proton resonances, the most pronounced shifts being observed for the ligands **L1c**, **L2c** and **L3c** which contain the nitro substituent.

3.2. Synthesis of [PtCl(DMSO)(L)] complexes

The complexes were prepared according to the general method described by Eqs. (1) and (2), where HL represents an acylthiourea ligand. The structural formulae for the complexes are given in Fig. 1.

$$K_2PtCl_4 + 3DMSO \rightarrow cis\text{-}[PtCl_2(DMSO)_2] \quad (1)$$

$$cis\text{-}[PtCl_2(DMSO)_2] + HL \xrightarrow{Base} [PtCl(DMSO)(L)] + cis\text{-}[Pt(L)_2] \quad (2)$$

As indicated by Eq. (2), it was found, for ligands **L1a**–**e** and **L2a**–**e**, that in addition to the formation of the desired complex, [PtCl(DMSO)(L)], the corresponding neutral *cis*-$[Pt(L)_2]$ complex was also formed as a minor product. This was evident from both the TLC and the ^{1}H NMR spectra. Integration of the proton resonances indicated that the *cis*-$[Pt(L)_2]$ was present as the minor product (ca. 5–15%). The *cis*-$[Pt(L)_2]$ complexes have a higher mobility on silica gel (R_f ca. 0.8) compared to the [PtCl(DMSO)(L)] complexes (R_f 0.5–0.6) and consequently the complexes were readily separated using flash column chromatography. The

platinum complexes containing the *N*,*N*-di(2-hydroxyethyl)-*N*′-(3-*R*-benzoyl)thiourea ligands were isolated by filtration free of the *cis*-[Pt(L)$_2$] complex. This is most likely due to the *cis*-[Pt(L)$_2$] complex being more hydrophilic than the [PtCl(DMSO)(L)] complex.

The analytical data, ^{195}Pt NMR chemical shifts and relevant IR data for the [PtCl(DMSO)(L)] complexes are given in Table 2. The ^{1}H NMR data for all the platinum complexes are given in Tables 3–5.

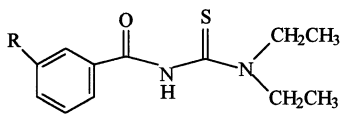
3.3. Characterisation of [PtCl(DMSO)(L)] complexes

3.3.1. Infrared spectra

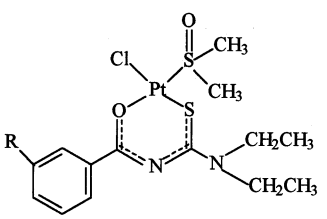
The IR spectra of the platinum(II) sulfoxide complexes are very similar. Notable features of the infrared spectra of the platinum complexes are the disappearance of the N–H stretching vibrations and shifts of the ν(C=O) peaks to higher frequencies upon complexation of the acylthiourea ligands. A shift to a higher frequency would also be expected for the C=S stretch vibration, but this vibration could not be assigned unambiguously. The strong IR band in the region of 1130–1150 cm^{-1} is assigned to the ν(SO) stretching frequency. The ν(SO) peak is shifted to a higher frequency upon complexation, relative to the uncoordinated dimethylsulfoxide, which is indicative of a sulfoxide bonded through the sulfur atom [4,11].

3.3.2. NMR spectra

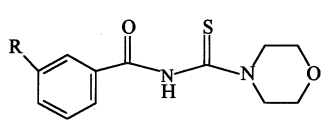
In accordance with the IR spectra, the N–H signal, observed for the ligands in the 8–11 ppm region, disappears upon complexation. A downfield shift is



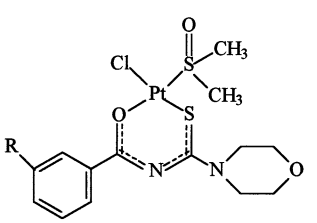
L1a: R = H
L1b: R = Cl
L1c: R = NO$_2$
L1d: R = OCH$_3$
L1e: R = CH$_3$



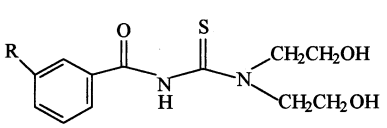
1a: R = H
1b: R = Cl
1c: R = NO$_2$
1d: R = OCH$_3$
1e: R = CH$_3$



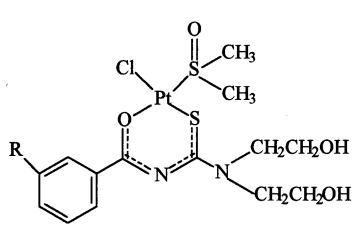
L2a: R = H
L2b: R = Cl
L2c: R = NO$_2$
L2d: R = OCH$_3$
L2e: R = CH$_3$



2a: R = H
2b: R = Cl
2c: R = NO$_2$
2d: R = OCH$_3$
2e: R = CH$_3$



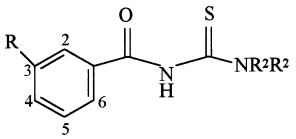
L3a: R = H
L3b: R = Cl
L3c: R = NO$_2$
L3d: R = OCH$_3$
L3e: R = CH$_3$



3a: R = H
3b: R = Cl
3c: R = NO$_2$
3d: R = OCH$_3$
3e: R = CH$_3$

Fig. 1. The structural formulae of the ligands and their corresponding platinum(II) sulfoxide complexes.

Table 1
^{1}H NMR data for the acylthiourea ligands



Ligand	R-group	δH_2	δH_3	δH_4	δH_5	δH_6	δH_α	δH_β	δH_γ	δH_R	δH_{NH}
L1a	H	7.823	7.461	7.563	7.461	7.823	4.018 3.606	1.322			8.238
L1b	Cl	7.816		7.539	7.410	7.692	4.016 3.594	1.222			8.165
L1c	NO_2	8.654		8.170	7.662	8.418	3.987 3.595	1.322			8.774
L1d	OCH_3	7.324		7.065	7.324	7.324	3.993 3.580	1.300		3.815	8.428
L1e	CH_3	7.639		7.355	7.355	7.608	4.026 3.605	1.328		2.403	8.176
L2a	H	7.832	7.488	7.594	7.488	7.832	4.230 3.663	3.838			8.410
L2b	Cl	7.828		7.565	7.431	7.696	4.228 3.644	3.835			8.361
L2c	NO_2	8.681		8.181	7.712	8.443	4.232 3.659	3.844			8.577
L2d	OCH_3	7.375		7.119	7.375	7.375	4.226 3.670	3.853		3.853	8.386
L2e	CH_3	7.642		7.395	7.363	7.610	4.226 3.656	3.837		2.413	8.380
L3a [a]	H [b]	7.85	7.50	7.59	7.50	7.85	3.97 3.73	3.75 3.69	5.60 4.85		10.86
L3b [a]	Cl	7.882		7.671	7.540	7.811	3.990 3.726	3.726	5.516 4.843		10.818
L3c [a]	NO_2	8.659		8.279	7.792	8.435	4.007 3.735	3.735	5.538 4.857		11.129
L3d [a]	OCH_3	7.438		7.162	7.438	7.438	3.985 3.742	3.742	5.624 4.840	3.814	10.829
L3e [a]	CH_3	7.685		7.413	7.382	7.650	3.981 3.742	3.742	5.621 4.840	2.368	10.813

[a] Spectra were recorded in DMSO-d_6.
[b] Ref. [6].

observed for the H_2 and H_6 aromatic protons and an upfield shift for the H_3, H_4 and H_5 proton resonances relative to that of the free ligand, with the exception of the H_4 proton resonances for complexes **1c**, **2c** and **3a**–**d** which undergo downfield shifts.

The ^{1}H NMR chemical shift for the methyl protons of the coordinated dimethylsulfoxide are shifted 1 ppm downfield relative to free dimethylsulfoxide, which is typical for sulfur bonded sulfoxides [3,4]. The assignment of the mode of coordination of the dimethylsulfoxide was further supported by the presence of platinum satellites due to vicinal coupling of the methyl protons of the dimethylsulfoxide with the platinum centre, ^{195}Pt (33.7%, $I = 1/2$). The $^3J(^{195}Pt–^1H)$ coupling constants were approximately 23 Hz, which is the same order of magnitude found for sulfur bonded sulfoxides [4]. The data are consistent with that reported for the [PtCl(L)(RR′SO)] complexes with *N*,*N*-dialkyl-*N*′-benzoylthiourea ligands, which were confirmed by the crystal structure of the [PtCl(*N*,*N*-diethyl-*N*′-benzoylthioureato)(MPSO)] complex [3]. The methylphenyl sulfoxide (MPSO) is sulfur bonded to the platinum and *cis* to the sulfur of the *N*,*N*-diethyl-*N*′-benzoylthiourea ligand. Variation of the electronic properties of the benzoyl moieties appears to have little affect on the ^{1}H NMR chemical shift position of the methyl protons of the coordinated sulfoxide.

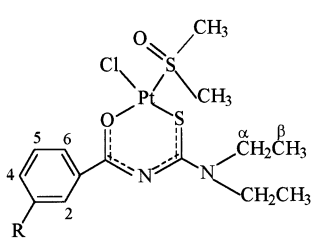
All the [Pt(acylthioureato)Cl(DMSO)] complexes show ^{195}Pt chemical shifts in the -3200 to -3300 ppm region. This chemical shift range is characteristic of complexes with the coordination sphere [PtSOSCl] [3]. The 3-substitution of the benzoyl moiety of these complexes results in a small but significant difference in the ^{195}Pt chemical shifts for the [Pt(acylthioureato)Cl(DMSO)] complexes, demonstrating the sensitivity of the ^{195}Pt nucleus to subtle electronic changes on

Table 2
Analytical and selected spectroscopic data for the platinum(II) sulfoxide complexes

Compound	R-group	M.p. (°C) [a]	Yield (%)	Analytical data (% C/H/N/S) [b]	ν(S=O) (cm^{-1})	^{195}Pt NMR (ppm)
1a	H	139–141	72	31.84; 3.93; 5.19; 11.69 (30.91; 3.89; 5.15; 11.79)	1139	−3256 −3229 [c]
1b	Cl	160–162	67	29.48; 3.51; 4.78; 11.07 (29.07; 3.48; 4.84; 11.08)	1144	−3250
1c	NO_2	187–190	60	28.56; 3.34; 6.88; 10.68 (28.55; 3.42; 7.14; 10.89)	1153	−3242
1d	OCH_3	138–140	80	31.52; 4.06; 4.93; 11.13 (31.38; 4.04; 4.88; 11.17)	1137	−3256
1e	CH_3	109–111	45	32.57; 4.20; 4.94; 11.18 (32.28; 4.15; 5.02; 11.49)	1137	−3257
2a	H	197–dec [a]	51	30.92; 3.54; 4.80; 10.82 (30.13; 3.43; 5.02; 11.49)	1147	−3231 [c]
2b	Cl	165–dec [a]	89	28.52; 3.04; 4.77; 11.13 (28.38; 3.06; 4.73; 10.82)	1148	−3224 [c]
2c	NO_2	208–dec [a]	94	28.39; 3.12; 6.87; 10.65 (27.88; 3.01; 6.97; 10.63)	1145	−3219 [c]
2d	OCH_3	189–dec [a]	49	31.00; 3.58; 4.74; 10.92 (30.64; 3.60; 4.76; 10.90)	1150	−3230 [c]
2e	CH_3	187–dec [a]	86	31.63; 3.65; 4.98; 11.28 (31.49; 3.70; 4.90; 11.21)	1147	−3232 [c]
3a	H	139–140	75	29.17; 3.66; 4.81; 11.05 (29.19; 3.67; 4.86; 11.13)	1146	−3229 [c]
3b	Cl	130–132	77	28.20; 3.34; 4.79; 10.41 (27.54; 3.30; 4.59; 10.50)	1138	−3223 [c]
3c	NO_2	152–154	68	27.44; 3.26; 6.84; 10.19 (27.08; 3.25; 6.77; 10.32)	1146	−3219 [c]
3d	OCH_3	145–147	69	30.14; 4.00; 4.87; 10.40 (29.73; 3.82; 4.62; 10.58)	1148	−3228 [c]
3e	CH_3	127–129	35	30.73; 3.86; 4.84; 10.79 (30.53; 3.93; 4.75; 10.87)	1149	−3231 [c]

[a] Melting points were determined by DSC.
[b] Calculated values are given in parentheses.
[c] Spectra recorded in DMSO-d_6.

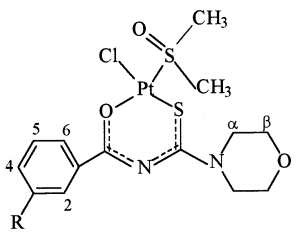
Table 3
^{1}H NMR data for *N*,*N*-diethyl-*N*′-(3-*R*-benzoyl)thiourea platinum(II) sulfoxide complexes [a]



R-group	δH_2	δH_3	δH_4	δH_5	δH_6	δH_α	δH_β	δH_{Sme}	δH_R
H	8.181	7.370	7.484	7.370	8.181	1.357 1.296	3.829	3.595	
Cl	8.116		7.455	7.312	8.070	1.361 1.301	3.825	3.598	
NO_2	8.968		8.336	7.580	8.522	1.362	3.843	3.608	
OCH_3	7.739		7.038	7.279	7.789	1.355 1.299	3.822	3.594	3.833
CH_3	7.911		7.238	7.192	7.911	1.276 1.212	3.749	3.596	2.313

[a] The spectra were recorded in $CDCl_3$ at 303 K.

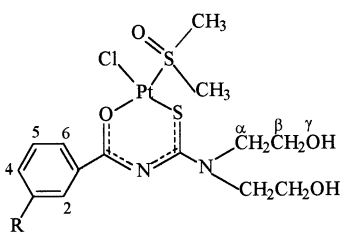
Table 4
^{1}H NMR data for *N*-morpholino-*N*′-(3-*R*-benzoyl)thiourea platinum(II) sulfoxide complexes [a]



R-group	δH_2	δH_3	δH_4	δH_5	δH_6	δH_α	δH_β	δH_{Sme}	δH_R
H	8.164	7.376	7.503	7.376	8.164	4.205 4.093	3.799	3.602	
Cl	8.089		7.472	7.318	8.056	4.183 4.096	3.809	3.604	
NO_2	8.917		8.352	7.587	8.507	4.228 4.118	3.833	3.614	
OCH_3	7.705		7.054	7.285	7.765	4.197 4.090	3.789	3.600	3.837
CH_3	7.959		7.313	7.254	7.959	4.200 4.092	3.803	3.601	2.384

[a] The spectra were recorded in $CDCl_3$ at 303 K.

Table 5
^{1}H NMR data for *N*,*N*-di(2-hydroxyethyl)-*N*′-(3-*R*-benzoyl)thiourea platinum(II) sulfoxide complexes [a]



R-group	δH_2	δH_3	δH_4	δH_5	δH_6	δH_α	δH_β	δH_γ	δH_R
H	8.069	7.441	7.602	7.441	8.069	4.008 3.921	3.772 3.696	5.052 4.936	
Cl	7.985		7.678	7.526	8.014	4.005 3.924	3.780 3.689	5.060 4.944	
NO_2	8.759		8.445	7.794	8.445	4.042 3.939	3.789 3.717	5.077 4.957	
OCH_3	7.594		7.176	7.397	7.651	3.993 3.913	3.785 3.709	5.052 4.932	3.792
CH_3	7.870		7.416	7.361	7.870	4.001 3.917	3.775 3.694	5.048 4.930	2.366

[a] The spectra were recorded in DMSO-d_6 at 303 K.

the benzoyl moiety [11]. The electron-withdrawing affect of the nitro- and chloro- substituents results in notable downfield shifts of the ^{195}Pt signal: NO_2 ($\Delta\delta$: 10–14 ppm) > Cl ($\Delta\delta$: 6–7 ppm) > $OCH_3 \approx H \approx CH_3$, which is consistent with the mesomeric/inductive effects expected for a 3-substituted benzoyl group and parallels the trend observed for the ^{1}H NMR data. No significant effect was observed with variation of the thioamide moiety.

The sensitivity of the ^{195}Pt NMR signal to changes in the benzoyl substituent indicates that these groups influence the electron density at the platinum centre and are therefore expected to have an influence on the substitution reaction kinetics of these complexes. Since the rate of substitution of the dimethylsulfoxide and chloride ligands is of utmost importance in gaining insight into the reactivity and mode of binding of these complexes to DNA detailed studies are underway cur-

rently to evaluate the substitution kinetics of these complexes. In the meanwhile, preliminary substitution reaction kinetic studies of [PtCl(DMSO)(*N*,*N*-diethyl-*N*′-(3-*R*-benzoyl)thioureato)] and the anionic nucleophile azide have revealed that the rate of substitution of the chloride leaving group is influenced by the electronic properties of the R group on the phenyl ring. The rate of substitution decreases in the order of $NO_2 > Cl > OCH_3 \approx H \approx CH_3$. These results are in agreement with the ^{195}Pt NMR results, which provide evidence that the electron-withdrawing substituents on the phenyl ring results in a decrease in the electron density at the Pt centre thereby making it more susceptible to nucleophilic attack. The substitution of the chloride-leaving group was established from the ^{1}H NMR spectrum of the complex. In the presence of the azide anion a significant upfield shift was observed for the protons of the coordinated DMSO and there was no significant appearance of free DMSO at 2.5 ppm.

It is also noteworthy to mention that preliminary in vitro cytotoxicity studies against a HeLa cell line have shown that both the benzoyl substituent and the thioamide moiety play an important role in determining whether the complexes exhibit any anticancer activity. The [PtCl(DMSO)(*N*,*N*-diethyl-*N*′-benzoylthioureato)], and [PtCl(DMSO)(*N*,*N*-di(2-hydroxyethyl)-*N*′-benzoylthioureato)] complexes did not exhibit any cytotoxic behaviour, whereas a notable concentration-dependent anti-proliferative effect was observed for the HeLa cell line treated with the [Pt(acylthioureato)Cl(DMSO)] complexes containing the *N*,*N*-diethyl-*N*′-(3-nitrobenzoyl)thiourea, *N*-morpholino-*N*′-(3-nitrobenzoyl)thiourea or *N*-morpholino-*N*′-(3-methoxybenzoyl)thiourea ligands [12]. These preliminary results are most encouraging in that they support our hypothesis that the acylthiourea ligand could play an important role in the biological activity of this series of complexes and can thus be used to fine-tune their anti-tumour behaviour. Detailed studies are thus currently underway to investigate the biological activity of this series of complexes and to try and establish a structure–activity relationship.

Acknowledgements

We wish to thank Rhodes University and the National Research Foundation for financial support, Johnson Matthey for the generous loan of K_2PtCl_4 and Kerry Horne for the synthesis of ligands **L1b** and **L1d**.

References

[1] B. Lippert (Ed.), Cisplatin: Chemistry and Biochemistry of a Leading Anticancer Drug, Wiley-VCH, Weinheim, 1999.
[2] E. Wong, C.M. Giandomenico, Chem. Rev. 99 (1999) 2451.
[3] C. Sacht, M.S. Datt, S. Otto, A. Roodt, J. Chem. Soc., Dalton Trans. (2000) 727.
[4] J.H. Price, A.N. Williamson, R.T. Schramm, B.B. Wayland, Inorg. Chem. 11 (1972) 1280.
[5] I.B. Douglass, F.B. Dains, J. Am. Chem. Soc. 56 (1934) 719.
[6] K.R. Koch, C. Sacht, S. Bourne, Inorg. Chim. Acta 232 (1995) 109.
[7] F. Dietze, S. Schmidt, E. Höyer, L. Beyer, Z. Anorg. Allg. Chem. 595 (1991) 35.
[8] A. Mohamadou, I. Déchamps-Olivier, J.-P. Barbier, Polyhedron 13 (1994) 1363.
[9] A. Mohamadou, I. Déchamps-Olivier, J.-P. Barbier, Polyhedron 13 (1994) 3277.
[10] I. Déchamps-Olivier, E. Guillon, A. Mohamadou, J.-P. Barbier, Polyhedron 20 (1996) 3617.
[11] P.S. Pregosin, Coord. Chem. Rev. 44 (1982) 247.
[12] C. Sacht, M.S. Datt, M. Lottering, J. Seegers, T.W. Hambley, L. Ellis, Presented in Part at the Eight International Symposium on Platinum and other Metal Coordination Compounds in Cancer Chemotherapy, Oxford, 1999.

PERGAMON

www.elsevier.nl/locate/poly

Polyhedron 19 (2000) 1355–1361

POLYHEDRON

Interaction between iron(II) tetrasulfophthalocyanine and the neurotransmitters, serotonin and dopamine

Joshua Oni, Tebello Nyokong *

Department of Chemistry, Rhodes University, Grahamstown 6140, South Africa

Received 4 February 2000; accepted 8 May 2000

Abstract

This work reports on the kinetics of interaction of iron(II) tetrasulfophthalocyanine, $[FeTSPc]^{4-}$, with dopamine (DA) and serotonin (5-HT). The interaction results in the coordination of dopamine and serotonin to $[FeTSPc]^{4-}$, followed by internal electron transfer and the formation of $[(DA^{+})Fe^{I}TSPc]^{4-}$ and $[(5\text{-}HT^{+})\ Fe^{I}TSPc]^{4-}$ complexes, respectively. The rate constants for the coordination of dopamine or serotonin to $[FeTSPc]^{4-}$ and the formation of the $Fe^{I}TSPc$ species were found to be $k_f = 6.8$ and 9.3 $dm^3\ mol^{-1}\ s^{-1}$, respectively. The equilibrium constants were 2.2×10^3 and 1.5×10^3 $dm^3\ mol^{-1}$, respectively, for the interaction of dopamine or serotonin to $[FeTSPc]^{4-}$. © 2000 Elsevier Science Ltd. All rights reserved.

Keywords: Iron; Phthalocyanine; Dopamine; Serotonin; Coordination

1. Introduction

There has been an extensive interest in developing methods for the analysis of neurotransmitters [1–6]. Both dopamine and serotonin are important neurotransmitters in the mammalian central nervous system [7]. Brightly coloured complexes are known to form when iron(III) interacts with dopamine and these are often used for qualitative analysis of dopamine [8,9]. Following coordination of dopamine to iron(III), internal electron transfer occurs with the formation of iron(II) and semiquinone [9]. Some members of the catecholamine family such as 6-hydroxydopamine react directly with iron(III) to form iron(II) and semiquinone via outer sphere electron transfer without first forming a complex with iron(III) [10]. This work examines the interaction of iron(II) tetrasulfophthalocyanine with dopamine (DA) and serotonin (5-HT) (Fig. 1). We examine the spectroscopic behaviour of iron phthalocyanine in the presence of dopamine and serotonin.

Metallophthalocyanine (MPc) complexes are well known catalysts for the oxidation or reduction of a wide variety of molecules [11]. The catalytic behaviour of MPc complexes is dependent on the nature of the central metal ion. MPc complexes that contain redox active central metals, such as CoPc and FePc, show better catalytic activity than those that exhibit ring based redox behaviour such as CuPc [11]. The catalytic activity of MPc complexes often involve electron transfer processes which in many cases are mediated by axial ligation (to the MPc complex) of the species to be catalysed [12–14]. Nickel(II) tetraaminophthalocyanine (NiTAPc) has been shown to exhibit electrocatalytic behaviour towards the oxidation of dopamine when adsorbed onto a glassy carbon electrode [2]. The electrocatalytic behaviour was attributed to an electron transfer from dopamine to the $Ni^{III}TAPc$ species.

Because of the role played by iron(III) in the analysis of dopamine, and the biological importance of studying the mechanism of the interaction of neurotransmitters with porphyrins and porphyrin-type molecules, such as phthalocyanines, we chose the water soluble iron(II) tetrasulfophthalocyanine ($[FeTSPc]^{4-}$) complex for the study of the interaction with dopamine and serotonin. $[Fe^{II}TSPc]^{4-}$ may be oxidised to $[Fe^{III}TSPc]^{4-}$ or reduced to $[Fe^{I}TSPc]^{4-}$ by electrochemical [15] and chemical means.

* Corresponding author. Tel.: +27-46-603-8260; fax: +27-46-622-5109.

E-mail address: t.nyokong@ru.ac.za (T. Nyokong).

0277-5387/00/$ - see front matter © 2000 Elsevier Science Ltd. All rights reserved.
PII: S0277-5387(00)00421-6

Axial ligand exchange reactions in MPc complexes are dissociative with the formation of a highly reactive five-coordinate intermediate [16,17] (Eqs. (1) and (2)):

$$(L)_2MPc \underset{k_{-1}}{\overset{k_1}{\rightleftharpoons}} (L)MPc + L \quad (1)$$

$$E + (L)MPc \underset{k_{-2}}{\overset{k_2}{\rightleftharpoons}} (L)(E)MPc \quad (2)$$

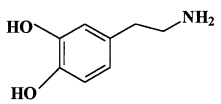
where L is the leaving ligand and E is the entering ligand.

Axial ligand coordination in MPc complexes may be accompanied by electron transfer between MPc complexes and the ligands. In this work, we use UV–Vis spectroscopy to monitor the interaction of $[FeTSPc]^{4-}$ with serotonin and dopamine.

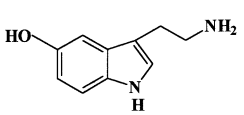
2. Experimental

2.1. Materials

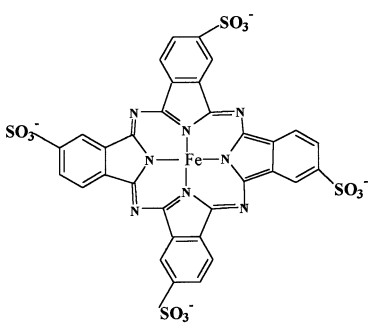
Dopamine (4-(2-aminoethyl)benzene-1,2-diol) hydrochloride and serotonin (5-hydroxytryptamine) creatinine sulfate monohydrate were purchased from Sigma. Sodium salts of the tetrasulfophthalocyanine complexes of iron(II), cobalt(II) and nickel(II) (Na_4[FeTSPc], Na_4[CoTSPc] and Na_4[NiTSPc]) were synthesised and purified according to established procedures [18]. The complexes were characterised by IR and UV–Vis spectroscopy and by elemental analysis. Solid complexes formed between $[FeTSPc]^{4-}$ and serotonin or dopamine were obtained following evaporation of water from an aqueous solution containing the respective species, following the change of colour from blue to green. The solid products were characterised by elemental analysis, IR, UV–Vis and NMR spectroscopies.



Dopamine



Serotonin



Iron(II) Tetrasulfophthalocyanine ($[FeTSPc]^{4-}$)

Fig. 1. Molecular structures of dopamine, serotonin and iron(II) tetrasulfophthalocyanine ($[FeTsPc]^{4-}$).

2.1.1. $[FeTSPc]^4$, dopamine complex

Anal. Calc. for $C_{40}H_{24}N_9S_4O_{19}ClNa_4Fe$ (including one H_2O of cystallisation): C, 38.55; H, 1.93; N, 10.12. Found: C, 38.46; H, 3.56; N, 10.31%. UV–Vis (H_2O) λ_{max} (log ε): 659 (3.77) nm. IR ν_{max}/cm^{-1} (KBr disks): 3420, 3054, 2763, 1714, 1622, 1364, 1189, 1024, 819, 754, 693, 636.

2.1.2. $[FeTSPc]^4$, serotonin complex

Anal. Calc. for $C_{46}H_{37}N_{13}S_5O_{24}Na_4Fe$ (including one H_2O of cystallisation): C, 37.73; H, 2.55; N, 13.27. Found: C, 37.79; H, 4.69; N, 15.29%. UV–Vis (H_2O) λ_{max} (log ε): 663 (3.58) nm. IR ν_{max}/cm^{-1} (KBr disks): 3367, 2930, 1707, 1637, 1545, 1456, 1414, 1344, 1102, 1028, 701, 601.

UV–Vis spectra was recorded with the Cary 500 UV–Vis/NIR spectrophotometer. Infrared spectra (KBr discs) were recorded with the Perkin–Elmer spectrum 2000 FTIR spectrophotometer. Nuclear magnetic resonance (^1H NMR) data in D_2O was recorded with the Bruker EMX 400 NMR spectrometer

2.2. Kinetics and equilibria

Kinetic and equilibrium studies were run at 20 ± 0.5°C and monitored with the Cary 500 UV–Vis NIR spectrophotometer. We monitored the appearance of the spectra due to the product formed following the addition of serotonin or dopamine to solutions of $[FeTSPc]^{4-}$ in water (unbuffered pH 6.3). Typically, a known volume of the aqueous solution of $[FeTSPc]^{4-}$ was added to a 1 cm path length spectrophotometric cell and deaerated using nitrogen. Then a known volume of aqueous solution of either serotonin or dopamine was added to the cell and the changes in absorbance monitored with time. For kinetic studies, concentrations of the $[FeTSPc]^{4-}$ were kept constant at 2.0×10^{-5} mol dm^{-3}, while dopamine concentrations were varied from 1.7×10^{-4} to 8.3×10^{-4} mol dm^{-3} and serotonin concentrations ranged from 6.7×10^{-5} to 4.7×10^{-4} mol dm^{-3}. The extinction coefficient of 4.8×10^4 mol^{-1} dm^3 cm^{-1} was used for the calculation of $[FeTSPc]^{4-}$ concentration. Since the concentrations of dopamine and serotonin were larger than that of $[FeTSPc]^{4-}$, pseudo-first order conditions were assumed for kinetic studies.

3. Results and discussion

3.1. Spectroscopic characterisation

Electronic absorption spectra of $[MTSPc]^{4-}$ complexes have been well studied [19,20] These complexes exist as dimers in equilibrium with the monomers in aqueous solutions, the spectra of $[MTSPc]^{4-}$ thus con-

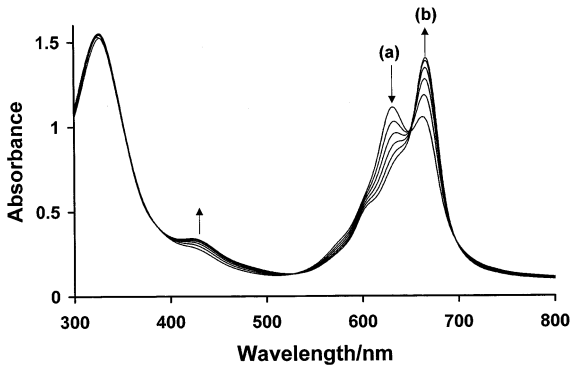


Fig. 2. Electronic absorption spectral changes observed on addition of dopamine to aqueous solutions of $[FeTSPc]^{4-}$. Spectra before (a) and spectra 5 min after (b) addition of 3.3×10^{-5} mol dm^{-3} dopamine.

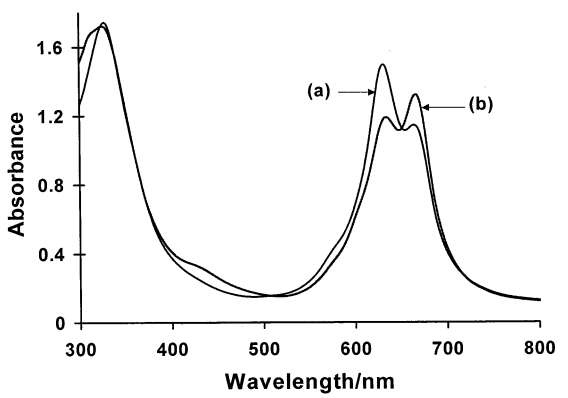


Fig. 3. Electronic absorption spectral changes observed on addition of serotonin to aqueous solutions of $[FeTSPc]^{4-}$. Spectra before (a) and spectra 1 min after (b) addition of 2.7×10^{-4} mol dm^{-3} serotonin.

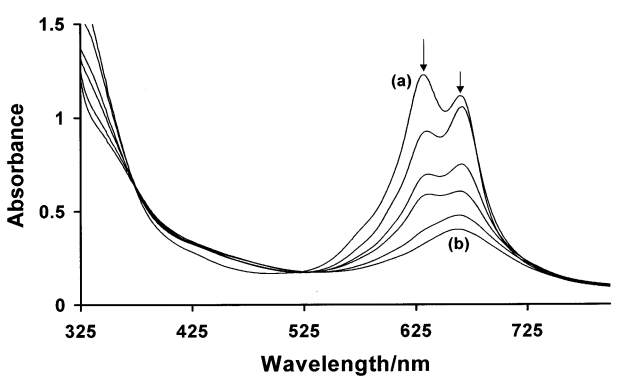


Fig. 4. Electronic absorption spectral changes observed following addition of serotonin to aqueous solutions of $[FeTSPc]^{4-}$. (a) Spectra after 1 min and (b) spectra after 20 min of addition of 2.7×10^{-4} mol dm^{-3} serotonin.

sist of two peaks in the Q band region. The high energy absorption band near 620 nm is associated with the dimeric species and the low energy band near 670 nm is due to the monomeric species [19]. For $[FeTSPc]^{4-}$ in water, the peak due to the monomeric species is observed at 665 nm and the dimeric peak at 633 nm. The Soret or B band peak is observed at 327 nm. Fig. 2 shows spectral changes observed on addition of dopamine to solutions of $[FeTSPc]^{4-}$ in water. The peak due to the monomeric species at 665 nm is enhanced greatly with a small shift in wavelength to 667 nm, whereas the peak due to the dimeric species at 633 nm disappeared. These changes were only observed at concentrations of DA less than 1×10^{-4} mol dm^{-3}. The increase in the monomeric peak occurred with clear isosbestic points at 651, 529 and 389 nm.

Equilibrium data were determined by standard spectroscopic techniques using Eq. (3):

$$\log[(A_{eq} - A_0)/(A_\infty - A_{eq})] = \log K + n\log[DA] \quad (3)$$

where A_{eq} is the equilibrium absorbance at 667 nm, A_0 is the absorbance at 665 nm before the addition of DA and A_∞, the absorbance after complete shifting of the equilibrium to the monomeric side, was determined from the final absorbance at 667 nm (Fig. 2). From the plot of $\log[(A_{eq} - A_0)/(A_\infty - A_{eq})]$ versus log[DA], an equilibrium constant of $K = 5.4 \pm 0.4 \times 10^5$ dm^3 mol^{-1} was determined for the shifting of the dimer–monomer equilibrium to the monomeric side.

Spectral changes observed on addition of serotonin to solutions of $[FeTSPc]^{4-}$ are shown in Fig. 3. Contrary to the observation above for dopamine, disappearance of the peak due to the dimeric species was not complete on addition of 5-HT to $[FeTSPc]^{4-}$, the peaks due to both the monomeric and dimeric species were observed regardless of the concentration of serotonin added. There was however, a reduction in the intensity of the peak due to the dimeric species and an increase in the monomeric peak on initial addition of serotonin to $[FeTSPc]^{4-}$. Also the increase in the intensity of the monomeric peak occurred without any measurable shift in the wavelength. The peak due to the monomeric species did not show an increase with time that was observed for DA (Fig. 2) regardless of the concentration of 5-HT added.

The enhancement in the peak due to the monomeric species on addition of either DA or 5-HT to $[FeTSPc]^{4-}$ shows that the dimer–monomer equilibrium for the $[FeTSPc]^{4-}$ species is shifted towards the monomeric side. The dimer–monomer equilibrium in $[MTSPc]^{4-}$ complexes can be affected by ionic strength [20] and by axial ligation [21,22]. The spectral changes observed with time, on addition of 5-HT to $[FeTSPc]^{4-}$ solutions are shown in Fig. 4.

The spectral changes in this case involved the decrease in both the dimeric and monomeric peaks and the formation of a broad peak at 663 nm. The new peak was formed with isosbestic points at 521 and 374 nm. Fig. 5 shows spectral changes observed on addition of DA concentrations larger than 1×10^{-4} mol dm^{-3}

to solutions of $[FeTSPc]^{4-}$. Under these conditions pseudo-first-order conditions apply and were assumed for kinetic studies below. Spectral changes in Fig. 5 consisted of the decrease in the intensity of the peak due to the monomeric species at 667 nm accompanied by a shift to 659 nm and no further decrease in intensity. These spectral changes occurred with isosbestic points at 545, 454 and 305 nm. The peak at 428 nm decreased in intensity and a new broad feature developed near 500 nm. The Soret band shifted to higher energies. Accompanying the spectral changes shown in Figs. 4 and 5 were changes in the colour of the solution from blue to green. The spectral and colour changes are similar to those observed on reduction of the $[Fe^{II}TSPc]^{4-}$ species to $[Fe^{I}TSPc]^{4-}$ using sodium borohydride. Thus the final spectra in Figs. 4 and 5 are due to the reduction of the central metal in $[Fe^{II}TSPc]^{4-}$ with the formation of the $Fe^{I}TSPc$ species, as a result of the electron transfer from DA or 5-HT. Ligation of species such as NO_2^- or cysteine to $[CoTSPc]^{4-}$ has been shown to be accompanied by oxidation of $[Co^{II}TSPc]^{4-}$ to the $[Co^{III}TSPc]^{4-}$ species [21,22]. Axial ligation, followed by electron transfer, has also been suggested for the interaction of the neurotransmitter, NO with iron porphyrins [23]. It has been shown before that coordination of DA to Fe^{III} results in the formation of an Fe^{III}(DA) complex involving the use of both oxygen atoms in DA [9]. This is followed by internal electron transfer forming Fe^{II} and a semiquinone, hence the dissociation of the complex [9]. We suggest in this work that axial ligation of DA or 5-HT to $[FeTSPc]^{4-}$ occurs prior to internal electron transfer resulting in the formation of $(DA^+)Fe^{I}TSPc$ and $(5\text{-}HT^+)Fe^{I}TSPc$ species, respectively. The one-electron oxidation product of DA is likely to be a semiquinone.

The fact that the final spectra following addition of DA or 5-HT to $[Fe^{II}TSPc]^{4-}$ is observed at different wavelengths shows that the final $Fe^{I}TSPc$ species formed are slightly different. This can be explained by differences in the complexes formed due to ligation of DA or 5-HT, with the formation of $[(DA^+)Fe^{I}TSPc]^{4-}$ and $[(5\text{-}HT^+)Fe^{I}TSPc]^{4-}$, respectively.

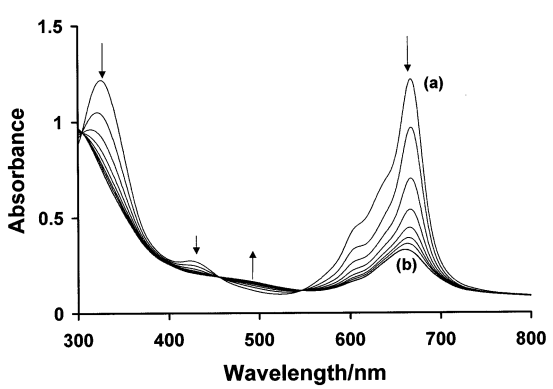


Fig. 5. Electronic absorption spectral changes observed following addition of large concentrations of dopamine to aqueous solutions of $[FeTSPc]^{4-}$. (a) Spectra after 2 min and (b) spectra after 20 min of addition of 3.3×10^{-4} mol dm^{-3} dopamine.

IR spectra of the solid complex formed following evaporating water from a solution containing $[FeTSPc]^{4-}$ and DA as explained in Section 2, showed a new peak at 819 cm^{-1} which could not be identified with either DA or $[FeTSPc]^{4-}$. Fe–O vibrations are observed in the 800–830 cm^{-1} region for oxoiron porphyrin complexes [24]. The vibration at 819 cm^{-1} is thus in the range for Fe–O vibrations, suggesting the presence of an Fe–O bond in the complex between $[FeTSPc]^{4-}$ and DA. Also a new vibration at 3419 cm^{-1} was observed for the complex between DA and $[FeTSPc]^{4-}$. This band is due to indole N–H vibrations and gives evidence of cyclisation in DA following its oxidation. Prominent vibrations due to DA at 1931 and 1500 cm^{-1} and between 800 and 1000 cm^{-1} disappeared on formation of a complex between $[FeTSPc]^{4-}$ and DA.

For the complex between $[FeTSPc]^{4-}$ and 5-HT, no new peaks were evident in the 800–830 cm^{-1} region where Fe–O vibrations are expected, this could be due to overlap with serotonin vibrations. The indole N–H vibration is observed at 3475 cm^{-1} for serotonin. Upon interaction between serotonin and $[FeTSPc]^{4-}$, this band disappeared and a sharp new band was observed at 2927 cm^{-1}.

^{1}H NMR spectra of MPc complexes is characterised by weak multiplets near 9.30 and 8.60 ppm due to the α and β protons of the phthalocyanine ring [25,26]. The ^{1}H NMR spectra of dopamine showed a multiplet at 6.95 ppm due to the aromatic protons of the ring, and two sets of triplets due to side chain protons at 3.30 and 2.90 ppm. The ^{1}H NMR spectra observed following interaction between $[FeTSPc]^{4-}$ and DA showed no changes in the 3.30 and 2.90 resonances of DA, but showed a small shift in the resonances of the aromatic protons (6.95–6.80 ppm). This shift is probably a result of changes in the electronic effects of the ring following cyclisation of DA. There was also an improvement in the resolution of the resonances due to the phthalocyanine ring following the interaction between DA and $[FeTSPc]^{4-}$. This could be due to improved solubility of the axially ligated $Fe^{I}TSPc$ species. For serotonin, the resonances for the protons of the fused aromatic rings were observed at different positions (6.85, 7.06, 7.25 and 7.38 ppm) due to their different environments. The side chain protons gave resonances at 3.29 and 4.19 ppm, while the protons due to the creatinine unit were observed at $\delta = 3.08$ ppm. Upon interaction between 5-HT and $[FeTSPc]^{4-}$, significant changes in the ^{1}H NMR spectra were observed. The spectra broadened and in general the resonances due to the protons

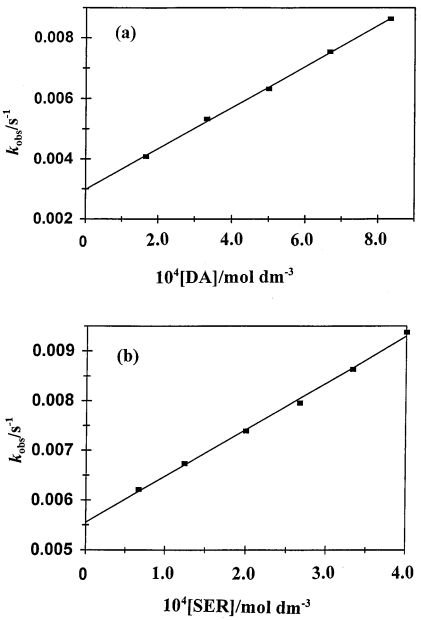


Fig. 6. Plots of the observed rate constants, k_{obs} (s^{-1}) versus concentration for the coordination of (a) dopamine and (b) serotonin to $[FeTSPc]^{4-}$.

of the fused rings shifted upfield, except for the resonance at 7.38 ppm which shifted downfield to 7.45 ppm. The resonances due to the side chain protons and due to creatinine unit remained unchanged. The shifting and broadening of the 5-HT resonances may be a result both of its coordination to $[FeTSPc]^{4-}$ and its oxidation.

3.2. Interactions between dopamine and serotonin with other MPc complexes

Addition of DA or 5-HT to solutions of $[CoTSPc]^{4-}$ or $[NiTSPc]^{4-}$ resulted in small changes in the spectra of $[MTSPc]^{4-}$ species. A small increase in the peak due to the monomer peak and a small decrease in the dimer peak were observed. There was no evidence for the formation of the reduced $[CoTSPc]^{4-}$ or $[NiTSPc]^{4-}$ species. The differences in the behaviour of $[NiTSPc]^{4-}$ in the presence of DA or 5-HT when compared to $[FeTSPc]^{4-}$ may be explained by the fact that for the $[NiTSPc]^{4-}$ complex, reduction or oxidation occurs at the phthalocyanine ring and not at the central metal [27]. Also NiPc complexes are square planar and do not favour axial ligation. For $[Co^{II}TSPc]^{4-}$ complexes, reduction occurs at the central metal forming $[Co^{I}TSPc]^{4-}$, and hence this complex would be expected to behave in a manner similar to $[FeTSPc]^{4-}$ on interaction with DA or 5-HT. However reduction of the $[Co^{II}TSPc]^{4-}$ to $[Co^{I}TSPc]^{4-}$ was not observed in the presence of DA or 5-HT.

3.3. Kinetic studies for the interaction of $[FeTSPc]^{4-}$ with DA or 5-HT

Kinetic data for the coordination of DA or 5-HT to $[FeTSPc]^{4-}$ were obtained by monitoring the formation of the peak due to $[(DA^{+})Fe^{I}TSPc]^{4-}$ or $[(5\text{-}HT^{+})\text{-}Fe^{I}TSPc]^{4-}$ complexes with Q bands at 659 and 663 nm, respectively, under conditions of Figs. 4 and 5. For DA coordination, the formation of the $[(DA^{+})\text{-}Fe^{I}TSPc]^{4-}$ species was monitored following the complete shift of the monomeric side, hence the starting spectra in Fig. 5 is that of the monomeric species, thus avoiding influences due to the dimeric species. For the coordination of serotonin, the presence of the dimeric species cannot be ruled out. For both complexes, plots of the logarithm of absorbance versus time were linear showing that the reaction was first order in $[FeTSPc]^{4-}$. The slopes of these plots gave the observed rate constant, k_{obs} and plots of k_{obs} versus the concentration of DA or 5-HT were linear (Fig. 6) showing that the coordination was first order in both DA and 5-HT. As discussed above, the axial ligand substitution reactions in MPc complexes are dissociative resulting in a highly reactive five-coordinate intermediate [16,17]. It is expected that the monomeric form of $[FeTSPc]^{4-}$ is coordinated to water molecules in aqueous solutions forming the $[(H_2O)_2FeTSPc]^{4-}$ species. The coordination of DA or 5-HT to $[(H_2O)_2FeTSPc]^{4-}$ may then be represented by Eqs. (4) and (5):

$$(H_2O_2)Fe^{II}TSPc \underset{k_{-1}}{\overset{k_1}{\rightleftharpoons}} (H_2O)Fe^{II}TSPc + H_2O \quad (4)$$

$$(H_2O)Fe^{II}TSPc + DA \underset{k_{-2}}{\overset{k_2}{\rightleftharpoons}} (H_2O)(DA^{+})Fe^{I}TSPc \quad (5)$$

The rate law for axial ligand exchange reactions in MPc complexes shown by reactions 4 and 5 is generally given by Eq. (6):

$$k_{obs} = k_f[DA] + k_r \quad (6)$$

where k_f, the rate constant for the forward reaction is given by $k_1k_2/(k_{-1}[H_2O])$ and k_r is the rate constant for the reverse reaction. Least-square analysis of the data presented in Fig. 6 gave $k_f = 6.8 \pm 0.2$ dm^3 mol^{-1} s^{-1} from the slope and $k_r = 3.0 \pm 0.1 \times 10^{-3}$ s^{-1} from the intercept, for the coordination of DA. For serotonin $k_f = 9.3 \pm 0.3$ dm^3 mol^{-1} s^{-1} and $k_r = 5.6 \pm 0.1 \times 10^{-3}$ s^{-1} were obtained. Using these values of rate constants, the value of the equilibrium constant for DA coordination to $[FeTSPc]^{4-}$ was estimated to be $K = 2.3 \times 10^3$ dm^3 mol^{-1} from the relationship, $K_1 = k_f/k_r$. For 5-HT, the equilibrium constant was determined to be $K = 1.7 \times 10^3$ dm^3 mol^{-1}. The values for the equilibrium and rate constants are in the range reported for axial ligand exchange reactions in FePc complexes [28].

Similar to the kinetic studies, for DA coordination, the equilibrium data was determined following com-

plete shifting of the equilibrium to the monomeric side, and the spectral changes for the decrease in the peak due to the monomeric species were followed. For the interaction between DA and $[FeTSPc]^{4-}$, the equilibrium for the formation of the $[(DA^{+})Fe^{I}TSPc]^{4-}$ was studied by monitoring the decrease in the peak due to the monomeric species at 667 nm (Fig. 5) using Eq. (3), where A_{eq} is the equilibrium absorbance at 667 nm and A_0 is the starting absorbance (at 667 nm) of the monomeric, $[FeTSPc]^{4-}$ species. A_{∞}, the absorbance after complete formation of the $[(DA^{+})Fe^{I}TSPc]^{4-}$ complex, was determined from the final absorbance at 659 nm. Fig. 7(a) shows the plot of $\log[(A_{eq}-A_0)/(A_{\infty}-A_{eq})]$ versus log[DA]. A linear plot with a slope near unity ($n=0.9\pm0.2$) was obtained, showing that only one mole of DA was coordinated to the $[FeTSPc]^{4-}$ species. The linearity of the plot confirms the coordination of DA to the $[FeTSPc]^{4-}$ complex. Least-square analysis gave an equilibrium constant of $K=2.2\pm0.1\times10^{3}$ dm^{3} mol^{-1}, in agreement within experimental error with the value calculated from the kinetic data above.

For the coordination of 5-HT to $[FeTSPc]^{4-}$, the equilibrium data was determined by using the spectra due to the formation of the reduced $[(5\text{-}HT^{+})\text{-}Fe^{I}TSPc]^{4-}$ species. Thus in this case, A_{eq} is the equilibrium absorbance at 665 nm, A_0 is the absorbance at 665 nm before addition of 5-HT and A_{∞}, the absorbance after complete formation of the $[(5\text{-}HT^{+})\text{-}Fe^{I}TSPc]^{4}$ complex, was determined from the final absorbance at 663 nm. The plot of $\log[(A_{eq}-A_0)/(A_{\infty}-A_{eq})]$ versus log[5-HT] is shown in Fig. 7(b), a linear plot with a slope $n=0.9\pm0.1$ was obtained and the value of K was determined to be $K=1.5\pm0.2\times10^{3}$ dm^{3} mol^{-3}, again in agreement with the value determined using k_f/k_r.

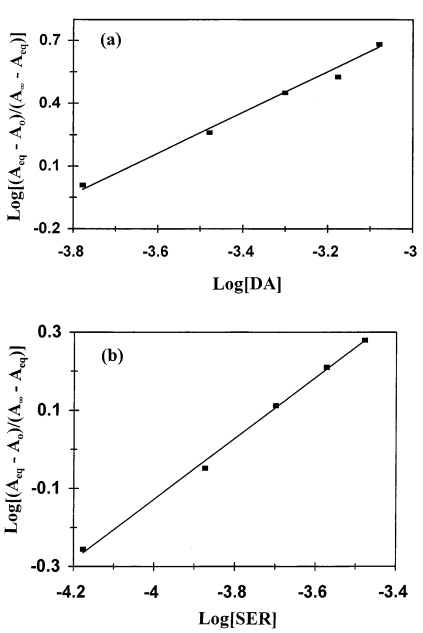


Fig. 7. Plot of $\log[(A_{eq}-A_0)/(A_{\infty}-A_{eq})]$ versus (a) log[dopamine] and (b) log[serotonin] for the coordination to $[FeTSPc]^{4-}$.

In conclusion, we have shown in this work that DA and 5-HT interact with $[FeTSPc]^{4-}$ resulting in the reduction of the latter to the $Fe^{I}TSPc$ species. There was spectroscopic evidence for the coordination of DA and 5-HT to the $[FeTSPc]^{4-}$ species. Studies on the interaction of DA and 5-HT with metallophthalocyanine and metalloporphyrin complexes are of importance since they may provide means for the analysis of these neurotransmitters.

Acknowledgements

This work was supported by Rhodes University and by the National Research Foundation of South Africa.

References

[1] K. Miyazaki, G. Matsumoto, M. Yamada, S. Yasui, H. Kanedo, Electrochim. Acta 44 (1999) 3809.
[2] T.F. Kang, G.L. Shen, R.Q. Yu, Anal. Chim. Acta 356 (1997) 245.
[3] Z. Gao, D. Yap, Y. Zhang, Anal. Sci. 14 (1998) 1059.
[4] E.L. Ciolkowski, K.M. Maness, P.S. Cahill, R. Wightman, D.H. Evans, B. Fosset, C. Amatore, Anal. Chem. 66 (1994) 3611.
[5] Y. Liju, G.F. Yang, P. Tuzhi, Y. Hangsheng, G. Cong, L. Guoging, Electroanalysis 11 (1999) 438.
[6] K.S.D. Burgess, J.W. Kable, J.B. Justice Jr., Electroanalysis 11 (1999) 337.
[7] G.I. Stevenson, R. Baker, Educ. Chem. (1996) 124.
[8] U. El-Uyaan, R.F. Jameson, W. Linert, J. Chem. Soc., Dalton Trans. (1998) 1315.
[9] U. El-Uyaan, E. Herlinger, R.F. Jameson, W. Linert, J. Chem. Soc., Dalton Trans. (1997) 2813.
[10] W. Linert, E. Herlinger, R.F. Jameson, E. Kienzyl, K. Jillinger, M.B.H. Youdin, Biochim. Biophys. Acta 1316 (1996) 160.
[11] J.H. Zagal, Coord. Chem. Rev. 119 (1992) 89.
[12] N. Nensala, A. Nzimande, T. Nyokong, J. Photochem. Photobiol. A: Chem. 98 (1996) 213.
[13] T. Nyokong, J. Chem. Soc., Chem. Commun. (1994) 1883.
[14] P.A. Bernstein, A.B.P. Lever, Inorg. Chem. 29 (1990) 608.
[15] S. Zecevic, B. Simic-Glavaski, E. Yeager, A.B.P. Lever, P.C. Minor, J. Electroanal. Chem. 196 (1985) 339.
[16] P. Ascenzi, M. Brunori, P. Pennesi, C. Ercolani, F. Monacelli, J. Chem. Soc., Dalton Trans. (1990) 105.
[17] T. Nyokong, J. Chem. Soc., Dalton Trans. (1993) 3601.
[18] J.H. Weber, D.H. Busch, Inorg. Chem. 4 (1965) 469.
[19] L.C. Gruen, R.J. Blagrove, Aust. J. Chem. 26 (1973) 319.
[20] E.W. Abel, J.M. Pratt, R. Whelan, J. Chem. Soc., Dalton Trans. (1976) 509.
[21] M. Sekota, T. Nyokong, Polyhedron 16 (1997) 3279.
[22] N. Chebotareva, T. Nyokong, J. Coord. Chem. 46 (1998) 433.

[23] N.A. Davies, M.T. Wilson, E. Slade, S.P. Fricker, B.A. Murrer, N.A. Powell, G.R. Henderson, Chem. Commun. (1997) 47.
[24] K.J. Paeng, D.H. Shin, I.R. Paeng, Inorg. Chem. 36 (1997) 2901.
[25] L.J. Boucher, P. Rivera, Inorg. Chem. 19 (1980) 1816.
[26] N. Kobel, M. Hanack, Inorg. Chem. 25 (1986) 103.
[27] A.B.P. Lever, E.R. Milaeva, G. Speier, in: C.C. Leznoff, A.B.P. Lever (Eds.), Phthalocyanines: Properties and Applications, vol. 3, VCH, New York, 1993.
[28] T. Nyokong, J. Chem. Soc., Dalton Trans. (1993) 3601.

PERGAMON

www.elsevier.nl/locate/poly

Polyhedron 19 (2000) 1363–1371

POLYHEDRON

Syntheses, molecular structures, and dynamic solution behavior of nitrido (oxo) molybdenum(VI) siloxides☆

Gyu-Shik Kim [a,*], Carroll W. DeKock [b,1]

[a] *Department of Science Education, Kangwon National University, Chunchon 200-701, South Korea*
[b] *Department of Chemistry, Oregon State University, Corvallis, OR 97331, USA*

Received 22 February 2000; accepted 9 May 2000

Abstract

Cocondensation reaction of MoO_3 with hexamethyldisilazane, followed by work-ups produced the nitrido molybdenum(VI) compounds, $[MoN(OSiMe_3)_3(NH_3)]_2$ (**1**), $[MoN(OSiMe_3)_3(py)]$ (**2**), and a very unusual μ_2-oxo-μ_2-nitrido tetranuclear molybdenum(VI) compound, $[Mo_2N_2O(OSiMe_3)_4(py)_2]_2{\cdot}2py$ (**3**). When **1** is reacted with excess methanol it results in another oxonitrido Mo(VI) compound, $Mo_4N_4O_2(OH)_8(H_2O)(MeOH)_3$ (**4**). The compounds were characterized by elemental analyses, FT-IR, ^1H and ^{13}C NMR, mass spectrometry, and by single-crystal X-ray diffraction for **1** and **3**. Compound **1** is dimeric in the solid state with two bridging siloxo groups; however, in toluene solution and at ambient temperature, the dimer readily dissociates into the monomer. The molecular geometry changes rapidly via a pseudorotation process as deduced from the variable temperature ^1H and ^{13}C NMR study. However, as the temperature is lowered, monomer↔dimer equilibrium is attained. The $\Delta G^{\neq}$ for the pseudorotation of **1** is 13.1 kcal mol^{-1} and $\Delta G^{\neq}$ for the monomer↔dimer association is 9.9 kcal mol^{-1}. Compound **2** is also fluxional, but remains monomeric in toluene solution down to 190 K. The $\Delta G^{\neq}$ for the pseudorotation of **2** is 12.2 kcal mol^{-1}. In contrast, **3** is tetranuclear in the solid state and is not fluxional in solution. Instead, it is slowly disproportionated to **2** and, presumably, an oxonitrido Mo(VI) pyridine adduct. © 2000 Elsevier Science Ltd. All rights reserved.

Keywords: Molybdenum; Nitrides; Alkoxides; Synthesis; X-ray structures; NMR fluxionality; Pseudorotation

1. Introduction

Numerous nitrido transition metal complexes accompanying various organic and/or inorganic ligands have been reported for the past several decades [1]. Nitride ion (N^{3-}), isoelectronic with the oxide ion (O^{2-}), is the strongest π bonding ligand and forms a unique class of compounds with interesting characteristics and properties [2]. Recently, research results on these compounds such as non-linear optical (NLO) and luminescence property [3], olefin metathesis catalysis [4], N-atom transfer reaction [5], and theoretical calculation [6] have emerged. However, until recently, little attention has been paid to the transition metal nitrido alkoxide and siloxide chemistry [7,9,18,19]. Quite recently Mo(N)(O-*t*-Bu)$_3$ together with the sterically bulky monomeric tris(alkylarylamido) Mo(III) complex was shown to accelerate the dinitrogen cleavage reaction [8]. There is an interesting analogy between cyclic and linear nitrido transition metal complexes, conjugated organic polyenes and cyclic aromatic compounds [9]. These research results warrant further synthetic effort and reactivity study of nitrido transition metal complexes.

We utilized cocondensation reactions to generate highly energetic coordinatively unsaturated molybdenum trioxide fragments that in turn reacted further with organosilanes. The cocondensation reactions, in many cases, generated hard-to-obtain and structurally interesting, and sometimes unique, compounds due to the intrinsic kinetic and energetic nature of the reaction [10]. For example, we were able to prepare a series of thermally unstable molybdenum oxoalkoxides and oxosiloxides through this synthetic route, the results are reported elsewhere [11].

☆ A partial preliminary account of this work was published in J. Chem. Soc., Chem. Commun. (1989) 1166–1168.

* Corresponding author. Tel.: +82-361-250-6737; fax: +82-361-251-7091.

E-mail address: gskim@cc.kangwon.ac.kr (G.-S. Kim).

[1] Emeritus Professor.

0277-5387/00/$ - see front matter © 2000 Elsevier Science Ltd. All rights reserved.
PII: S0277-5387(00)00423-X

In this paper, we wish to report the reaction, product characterization including two X-ray structures, and dynamic solution behavior of the products isolated from the MoO_3-hexamethyldisilazane cocondensation reaction. Until recently, although many transition metal nitrido complexes have been reported, only a handful of compounds have been subjected to solution studies. In this context, the solution NMR results described here may shed some light on the understanding of the energetics in the fundamental structural chemistry. In addition, we report an alternative high yield synthesis for **1** by using a conventional synthetic route.

2. Experimental

2.1. General considerations

All manipulations were performed either under an argon atmosphere using standard Schlenk techniques or in an argon-filled Vacuum Atmospheres® glovebox. Solvents were dried rigorously using appropriate literature procedures and stored over 4 Å molecular sieves just prior to use. Hexamethyldisilazane was purchased from Petrarch and used as received. MoO_3 (Matheson Coleman and Bell) was used without further purification. $MoO_3 \cdot 2H_2O$ was prepared as a crystalline yellow solid by the literature method [12]. IR spectra were obtained on a Mattson Sirius® 100 FT-IR or on a Nicolet 5XDB FT-IR with 2 cm^{-1} resolution. Nujol mull or KBr pellet with 3–5 wt.% sample loading was employed. Elemental analyses were performed by Galbraith Laboratories, Knoxville, TN, USA. NMR spectra were taken on a Bruker AM-400 spectrometer that was equipped with a temperature controller. Mass spectrometry was performed on a Finnigan 4000-23 spectrometer with a 4500 ion source by using pulsed-ion–positive-ion–negative-ion chemical ionization (PIPINICI) with methane as the secondary ion generator and by using 70–100 eV ionization potential. Mass data reported are based on ^{98}Mo for mononuclear species and on ^{96}Mo for dinuclear species. The cocondensation reaction was carried out using the equipment that has previously been described [13]. MoO_3 was sublimed from a resistively heated niobium tube with five to six holes punched in from the upper side. Cocondensation occurred over a period from 0.5 to 1.5 h. Yield based on MoO_3 condensed on the wall of the reactor was determined by taking the mass difference before and after the reaction.

2.2. Preparation of $[MoN(OSiMe_3)_3(NH_3)]_2$ (1): method 1 (from the cocondensation reaction)

MoO_3 (1.574 g, 10.94 mmol) was cocondensed at 77 K with $HN(SiMe_3)_2$ (48.6 g, 301 mmol). When the reactor was warmed to ambient temperature, the volatile was stripped off using dynamic vacuum at 10^{-3} Torr overnight. A yellow–green solid (2.558 g) was obtained. A 1.193 g portion of the solid was dissolved in 30 ml of hexane and filtered twice through a coarse glass frit to give a yellow–brown solution. The solution volume was reduced to 10 ml by a vacuum line in a Schlenk tube and placed in a freezer at 253 K. A colorless needle-shaped crystalline solid was formed overnight. Decanting the solution, followed by washing with cold hexane (5 ml) and vacuum drying at ambient temperature gave a colorless crystalline solid (0.180 g). Crystallization of the decanted solution gave another crop of the product (0.112 g). The total yield was 14.5% based on the cocondensed MoO_3. *Anal.* Calc. for $C_{18}H_{60}N_4O_6Si_6Mo_2$: C, 27.4; H, 7.66; N, 7.60; Mo, 24.3. Found: C, 27.4; H, 7.75; N, 7.05; Mo, 24.0%. ^1H NMR 400 MHz (in benzene-d_6, 293 K, referenced to the solvent protio peak at 7.15 ppm): δ 0.38 (s, 27H, Me_3SiO), 1.97 (s, br, 3H, NH_3). ^{13}C NMR 100.614 MHz (in benzene-d_6, 293 K, referenced to the solvent ^{13}C peak at 128.00 ppm): δ 2.17 (Me_3SiO). IR data (KBr): 3401 (m), 3350 (m), 3234 (m), 3156 (m), 2954 (s), 2899 (m), 2726 (vw), 2667 (vw), 2098 (vw), 2000 (vw), 1932 (vw), 1876 (vw), 1612 (m), 1434 (m), 1402 (m), 1384 (m), 1313 (m), 1249 (s), 1215 (m), 1049 (s), 942 (s), 867 (sh), 844 (vs), 815 (s), 750 (s), 713 (sh), 684 (m), 632 (m), 481 (s), 473 (s). Mass data (m/z [% intensity, assignment]): 308 [5, $MoO_2(OSiMe_3)_2^-$], 379 [100, $MoN(OSiMe_3)_3^-$].

2.3. Method 2 (solution preparation)

$MoO_3 \cdot 2H_2O$ (0.189 g) was placed in a 25 ml round-bottomed flask along with a Teflon-coated magnetic stir bar. To this solution was added 7.0 ml of $HN(SiMe_3)_2$ and the mixture was heated to 358 K while stirring. The yellow solid dissolved in 15 min to give a pale yellow homogeneous solution. Further heating resulted in color change from yellow to orange and then finally to red–brown. The solution was stirred for 5 h at this temperature. The volatile was pumped off using a dynamic vacuum line to give a colorless plate-shaped crystalline solid slightly contaminated with a red–brown thick oil (0.363 g). Pure compound may be obtained by crystallization from the hexane solution at 253 K. Yield 87%. IR, ^1H and ^{13}C NMR results confirmed that the product is identical to the one described above.

2.4. Preparation of deuterated ammonia adduct of 1

ND_3 gas was bubbled through a hexane solution of **1** in a Schlenk flask for 5 min. The flask was sealed and placed in a freezer at 253 K overnight. The colorless crystalline solid formed was isolated the same way as **1**.

IR data (KBr): 3136 (m, br), 2954 (m), 2901 (m), 2538 (w), 2491 (w), 2370 (w), 2318 (w), 1612 (w, br), 1434 (m), 1402 (m), 1313 (m), 1310 (w), 1250 (s), 1052 (s), 1019 (m), 939 (s), 846 (vs), 819 (sh), 751 (s), 684 (m), 631 (m).

2.5. Preparation of $MoN(OSiMe_3)_3(py)$ (2)

$[MoN(OSiMe_3)_3(NH_3)]_2$ (**1**) (0.419 g) was dissolved in 5 ml of pyridine to give a dark yellow solution. The volatile was pumped off under dynamic vacuum at ambient temperature to give a pale yellow solid (0.452 g). *Anal. Calc.* for $C_{14}H_{32}N_2O_3Si_3Mo$: C, 36.8; H, 7.07; N, 6.14; Mo, 21.0. Found: C, 36.0; H, 6.83; N, 5.79; Mo, 20.9%. ^{1}H NMR 400 MHz (in toluene-d_8, 297 K, referenced to the solvent protio peak at 2.09 ppm): δ 0.26 (s, 27H, Me_3SiO), 6.54 (m, 2H, py), 6.88 (m, 1H, py), 8.38 (m, 2H, py). ^{13}C NMR 100.614 MHz (in toluene-d_8, 297 K, referenced to the solvent ^{13}C peak at 20.40 ppm): δ 1.39, 124.41, 137.97, 150.61. IR data (KBr): 3143 (w, br), 2959 (s), 2898 (m), 2837 (w), 2788 (w), 1993 (vw), 1932 (vw), 1870 (vw), 1606 (m), 1446 (s), 1399 (m), 1384 (m), 1355 (w), 1320 (w), 1219 (w), 1185 (vw), 1150 (w), 1069 (m), 1057 (s), 1044 (m), 1015 (m), 963 (s), 904 (vs), 882 (vs), 872 (vs), 838 (vs), 749 (s), 700 (m), 685 (m), 638 (m), 630 (sh), 486 (m), 458 (m). Mass data (m/z [% intensity, assignment]): 379 [100, $MoN(OSiMe_3)_3^-$].

2.6. Preparation of $[Mo_2N_2O(OSiMe_3)_4(py)_2]_2{\cdot}2py$ (3)

To the brown hexane solution after compound **1** was isolated (vide supra) was added 2.0 ml of pyridine to give a brown precipitate. The brown precipitate was filtered off twice through a coarse glass frit. The resulting filtrate was placed in a freezer at 253 K. Many block crystals formed overnight were filtered, washed with cold hexane (5 ml) and dried in dynamic vacuum to give a yellow crystalline solid (0.162 g). The yield was 8.45% based on the cocondensed MoO_3. *Anal.* Calc. for $C_{54}H_{102}Mo_4N_{10}O_{10}Si_8$: C, 39.1; H, 6.19; N, 8.44; Mo, 23.1. Found: C, 38.5; H, 6.50; N, 7.95; Mo, 22.6%. ^{1}H NMR 400 MHz (in toluene-d_8, 297 K, referenced to the solvent protio peak at 2.09 ppm): δ 0.06 (s, 36H, Me_3SiO), 0.25 (s, 36H, Me_3SiO), 6.80 (m, 12H, py), 7.01 (m, 6H, py), 8.82 (m, 12H, py). ^{13}C NMR 100.614 MHz (in toluene-d_8, 297 K, referenced to the solvent ^{13}C peak at 20.40 ppm): δ 1.41 (Me_3SiO), 2.36 (Me_3SiO), 123.83 (py), 130.58 (py), 150.69 (py). IR data (KBr): 3146 (vw), 3111 (sh), 3089 (sh), 3074 (m), 3041 (vw), 3020 (vw), 2999 (vw), 2954 (m), 2896 (m), 2827 (vw), 2802 (vw), 2470 (vw), 2087 (vw), 1990 (vw), 1953 (vw), 1872 (w), 1629 (w), 1598 (s), 1580 (w), 1573 (w), 1482 (m), 1444 (s), 1401 (m), 1384 (m), 1353 (w), 1313 (w), 1246 (vs), 1215 9s), 1150 (m), 1072 (m), 1051 (m), 1036 (s), 1026 (m), 1005 (s), 911 (vs), 835 (vs), 751 (s), 697 (s), 659 (vs), 650 (vs), 630 (s), 622 (s), 459 (s), 451 (s), 434 (vs). Mass data (m/z [% intensity, assignment]): 308 [62, $MoO_2(OSiMe_3)_2^-$], 379 [100, $MoN(OSiMe_3)_3^-$], 453 [5, $Mo(OSiMe_3)_3(HNSiMe_3)^-$], 527 [1, $Mo(OSiMe_3)_3(HNSiMe_3)_2^-$], 612 [1, $Mo_2O_4(OSiMe_3)_4^-$], 685 [2, $Mo_2O_3(OSiMe_3)_5^-$], 754 [1, $Mo_2N_2(OSiMe_3)_6^-$].

2.7. Preparation of $[Mo_4N_4O_2(OH)_8(H_2O)(CH_3OH)_3]$ (4)

Compound **1** (0.185 g) was dissolved in 2.0 ml of toluene. Addition of dried methanol (0.50 ml) to this solution caused a white precipitate to form in a few minutes. The mixture was set aside for a day at ambient temperature. The volatile was thoroughly pumped off for 2 days under dynamic vacuum at 10^{-3} Torr to give a white powder (0.085 g, yield 100%). *Anal.* Calc. for $C_3H_{22}N_4O_{14}Mo_4$: C, 4.99; H, 3.07; N, 7.76; Mo, 53.2. Found: C, 4.24; H, 3.06; N, 7.35; Mo, 54.0%. ^{1}H NMR 400 MHz (in DMSO-d_6, 297 K, referenced to the solvent protio peak at 2.49 ppm): δ 2.29 (s, 3H, CH_3OH), 3.16 (s, 9H, CH_3OH), 5.70 (s, br, OH, H_2O). IR (Nujol mull): 3157 (vs, br), 2733 (sh), 2684 (sh), 1676 (w), 1616 (w), 1400 (s), 1304 (m), 1158 (w), 1018 (s), 886 (vs), 857 (s), 720 (vs), 673 (s), 534 (m), 467 (m), 454 (m).

2.8. Preparation of deuterated methanol adduct of 4

The same procedure as described above was used. Compound **1** (62.4 mg) when reacted with CD_3OD (0.20 ml) gave 31.9 mg of a white solid after drying under dynamic vacuum. Selected IR data (Nujol mull): 1020 (s), 721 (vs), 669 (s).

3. Results and discussion

3.1. Synthesis and characterization

Vaporization of molybdenum trioxide under high vacuum and its condensation with an excess coreactant at 77 K (liquid nitrogen temperature) is expected to generate matrix-isolated four-coordinate, pseudo-tetrahedral $(MoO_3)_x$ species, where $x = 1–5$ [15]. The most abundant species are known to be trimer or tetramer, depending on the experimental condition of mass spectral studies [15]. Upon warming the cocondensate, the highly energetic coordinatively unsaturated oxo molybdenum species react with organosilane to produce various species. One of the initially formed products could be a ligand coordinated species such as $MoO_3[HN(SiMe_3)_2]_x$, where $x = 1$ or 2. However, as the temperature increases, the trimethylsilyl groups can migrate to the more nucleophilic oxygen sites of MoO_3,

presumably due to the oxophilicity of the silyl group. Here, the bond energies for N–Si versus O–Si play an important role [16]. Previously, this kind of reaction was observed by Nugent et al. [17]. They rationalized this facile rearrangement due to the differences in N–Si and O–Si bond energies and the relief of steric repulsion in the congested bis(trimethylsilyl)amido group. However, Lam et al. reported that CrO_2Cl_2 reacted with HMDS produced $CrO_2[N(SiMe_3)_2]_2$, but MoO_2Cl_2 reacted with HMDS instead produced $Mo(NSiMe_3)_2(OSiMe_3)_2$ [18].

Hexamethyldisilazane, when reacted with MoO_3, is expected to generate, depending on the reaction condition, various metal-bound moieties, such as bis(trimethylsilyl)amido, trimethylsilylamido, trimethylsilylimido, ammonia, amido, imido, and nitrido groups. In particular, the nitride ion (N^{3-}), isoelectronic to oxide ion (O^{2-}), can function as a strong π bonding ligand showing structural diversity [1,2].

In our case, the most abundant isolable molecular product was the fully silylated nitrido compound, $[MoN(OSiMe_3)_3(NH_3)]_2$ (1) (Eq. (1)).

$$MoO_3 + HN(SiMe_3)_2 \rightarrow [MoN(OSiMe_3)_3(NH_3)]_2 + Mo_2N_2O(OSiMe_3)_4 \quad (1)$$

The coordinated ammonia is definitely from the degraded HMDS. The identity of ammonia in **1** was confirmed by several lines of evidence. First, the ^1H NMR spectrum of **1** in deuterated benzene showed a broad singlet at 1.80 ppm. Secondly, the ^{13}C NMR spectrum showed a single peak that is assigned to Me_3SiO and therefore the peak at 1.80 ppm in the ^1H NMR spectrum is from a non-carbon moiety. Thirdly, the IR spectrum of **1** showed four stretches at 3156, 3234, 3350, and 3401 cm^{-1}, of which two or three bands can be assigned to the N–H stretches of the coordinated NH_3[2].

To make positive identity, the deuterated ammonia adduct of **1** was prepared. In the IR spectrum of the ND_3-**1**, these peaks shifted to 2318, 2370, 2491, and 2538 cm^{-1}, while maintaining the identical peak pattern. The ν(H/D) ratio is $1.35 + 0.01$. (The differences in peak positions are 850 ± 13 cm^{-1}.) The most convincing evidence came from the X-ray crystallographic work in which all three hydrogen atoms were observed around the nitrogen atom (vide infra).

[2] K. Nakamoto, Infrared and Raman Spectra of Inorganic and Coordination Compounds, Wiley, New York, 1986, pp. 191–196. (b) As one of the referees pinpointed, there must be only two (A_1, E) stretching modes for the local C_{3v} symmetry and three modes at lower symmetry (C_1 or C_s) for the coordinated ammonia in **1**. We fully agree with the referee's opinion that the nitrido moiety of **1** can partially be hydrolyzed to give imido- or less likely amido-containing by-product(s). However, because the presence of the coordinated ammonia was definitely confirmed by the X-ray work, we did not further follow the reactivity and IR studies for **1**.

The pyridine adduct $MoN(OSiMe_3)_3(py)$ (**2**) was quantitatively prepared by replacing the coordinated ammonia with pyridine shown in Eq. (2).

$$[MoN(OSiMe_3)_3(NH_3)]_2 + py \ (xs) \rightarrow 2MoN(OSiMe_3)_3(py) + 2NH_3 \quad (2)$$

Recently this compound was prepared in 27% yield by reacting MoO_2Cl_2(dme) (dme = dimethoxyethane) with hexamethyldisilazane, followed by pyridine addition, and its X-ray structure was reported by Chiu et al. [19]. This compound showed only one type of Me_3SiO in the ambient temperature ^1H and ^{13}C NMR spectra.

Another product after isolation of **1** was the mixed oxo-bridged nitrido molybdenum siloxy species, i.e. $[Mo_2N_2O(OSiMe_3)_4]$. This four-coordinate oxo-bridged species is further stabilized by pyridine and was isolated as a crystalline material from the hexane solution. See Eqs. (1) and (3). Attempts to prepare this compound by reacting **1** with excess pyridine, as shown in Eq. (4), was unsuccessful, instead the pyridine adduct **2** was isolated (vide supra). Compounds **1** and **2** showed interesting fluxional behavior in toluene solution (vide infra).

$$2Mo_2N_2O(OSiMe_3)_4 + py \ (xs.) \rightarrow [Mo_2N_2O(OSiMe_3)_4(py)_2]_2 \quad (3)$$

$$2[MoN(OSiMe_3)_3(NH_3)]_2 + py \ (xs.) \not\rightarrow [Mo_2N_2O(OSiMe_3)_4(py)_2]_2 + 2(Me_3Si)_2O + 4NH_3 \quad (4)$$

The reaction of $Mo(N)(O\text{-}t\text{-}Bu)_3$ with less bulky alcohols produced alcoholysis products [7a]. To test the alcoholysis reaction for **1**, we performed the reaction with various alcohols. ^1H NMR tube reactions of **1** with ROH (R = H, Me, Et, *i*-Pr, *n*-Bu, *t*-Bu) in a hydrocarbon solvent showed quantitative generation of Me_3SiOR and white microcrystalline precipitates. The reaction rate seems to be inversely proportional to the bulkiness of the R group of ROH. For example, it took 38 h for the completion of the reaction with EtOH, but 1 week for the reaction with *t*-BuOH at ambient temperature. As observed, **1** reacted with excess methanol and produced a hydroxo oxonitrido compound, as shown in Eq. (5).

$$4[MoN(OSiMe_3)_3(NH_3)] + 15MeOH \rightarrow Mo_4N_4O_2(OH)_8(MeOH)_3(H_2O) + 12Me_3SiOMe + H_2O + 4NH_3 \quad (5)$$

The presence of a nitrido group in the product was deduced from the presence of a strong Mo≡N stretch at 1018 cm^{-1}. The two IR bands at 720 and 670 cm^{-1} might be due to the asymmetric and symmetric Mo–O–Mo stretches. The presence of the coordinated methanol and water was confirmed by ^1H NMR and elemental analysis. The IR spectrum of the deuterated

methanol adduct showed a similar spectral pattern, indicating the IR peak assignment for the oxonitrido Mo skeleton is correct (see Section 2).

Since the yield of **1** from the cocondensation reaction was merely 14.5%, we continued further to develop an alternative high yield synthesis. A high yield one-pot synthesis of **1** was achieved by reacting $[MoO_3]\cdot 2H_2O$ [12] with hexamethyldisilazane without employing additional solvent at 358 K (85°C, typically 60–80% yield, see Eq. (6)). Therefore, the preparation of the pyridine adduct **2** starting from this compound is a better synthetic protocol in terms of yield than the one (27%) described by Chiu et al. [19].

$$MoO_3\cdot 2H_2O + HN(SiMe_3)_2 \text{ (xs.)} \rightarrow [MoN(OSiMe_3)_3(NH_3)]_2] \quad (6)$$

3.2. IR spectroscopy

The characteristic trend of the Mo≡N IR stretches [2] of the title compounds is noteworthy. Compound **1** in the solid state showed a strong sharp peak at 1049 cm^{-1}, assignable to the Mo≡N stretch (ND_3-**1** showed the band at 1052 cm^{-1}). Compound **2** showed the band at 1057 cm^{-1} in the solid state (Chiu et al. reported the band at 1059 cm^{-1} in hexane solution [19]). Compound **3** showed the band at 1036 cm^{-1}. However, the deca (oxo/hydroxo) tetranitrido Mo complex **4** showed the band at 1018 cm^{-1} (1020 cm^{-1} for the deuterated methanol adduct). Compound **2** showed the highest stretching frequency and then **1**, **3**, and **4** followed in descending order. Clearly this trend reflects the relative Mo≡N bond strength. The Mo≡N bond in monomeric **2** is the strongest since there is no *trans* ligand competing with the Mo≡N triple bond, as observed in the X-ray structure [19]. Compound **1** is ranked second because only the datively bonded [20] bridging siloxy group (2.65 Å, vide infra), which is *trans* to the nitrido group, minimally competes with the Mo≡N bond. Then, because **3** and **4** possess bent Mo≡N→Mo bonds and also *trans* ligands, the Mo≡N stretches were even lower. Compound **4** is assumed to have more basic oxygen atoms (oxo and hydroxo groups) compared with **3**. Therefore, they compete more for π bonding with the Mo≡N bonds, thereby giving the lowest frequency value. The Mo≡N band positions in these closely related compounds are internally consistent and, consequently, show the subtle relative order of the bond strength.

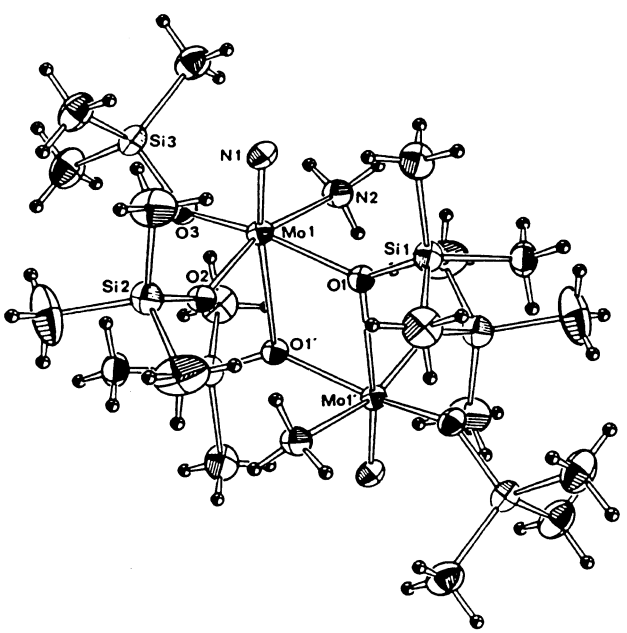


Fig. 1. ORTEP drawing of **1** showing 20% thermal ellipsoids for the non-hydrogen atoms. Selected bond distances (Å) and angles (°): Mo1–N1, 1.626(6); Mo1–O3, 1.920(5); Mo1–O2, 1.922(4); Mo1–O1, 1.981(4); Mo1–N2, 2.272(6); Mo1–O1′, 2.669(4).

3.3. Molecular structures

Transition metal nitrido complexes show various structural types [1,2]. There appeared monomeric complexes with coordination numbers ranging from 4 to 6 depending upon the bulkiness of the attached ligand [21]. The entities with coordination number five showed two possible structures, namely tetragonal pyramid (TP) and trigonal bypyramid (TBP). Di-, tri-, and tetranuclear complexes can possess either nitrido-bridged or ligand-bridged geometry with coordination number 5 or 6. Some complexes show a nitrido-bridged linear chain structure, examples are the five-coordinate nitrido alkoxides, $MN(OR)_3$ (where M = Mo, W; R = *i*-Pr, *t*-Bu) in solid state [7a–c].

When the hypothetical four-coordinate nitridoalkoxide is further supported by a coordinating ligand, either a monomeric five-coordinate structure or a dimeric six-coordinate structure is expected. The association mode is also either through nitrido- or ligand-bridges. A tetrameric rectangular nitrido structure is exclusively observed for the nitrido molybdenum halide complexes [22].

A brief description of structures [14] of the title complexes was published elsewhere [11c]. Herein, we only wish to describe the information that is relevant and necessary for the subsequent solution NMR discussion. Title complex **1**, shown in Fig. 1, is the first structurally characterized siloxo-bridged dinuclear nitrido molybdenum compound. (Chisholm et al. reported the *t*-$BuMe_2SiO$-bridged dinuclear tungsten compound, but no X-ray structure was reported [9].)

The molecule possesses crystallographically imposed C_i symmetry and is composed of two fragments of five-coordinate $Mo(N)(OSiMe_3)_3(NH_3)$ (TP structure). The nitrido group is situated at the apical position with a Mo–N distance of 1.626(6) Å. The Mo–O distance of

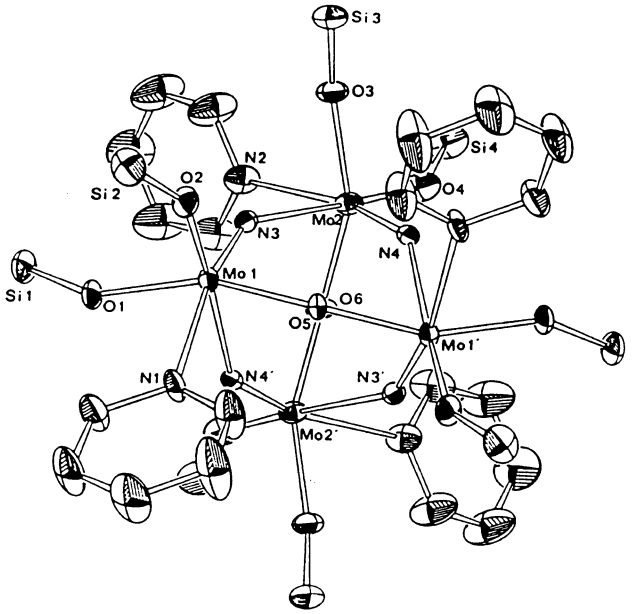


Fig. 2. ORTEP drawing of **3** showing 20% thermal ellipsoids. Hydrogen and methyl carbon atoms are omitted for clarity. Selected bond distances (Å) and angles (°): Mo1–N3, 1.680(7); Mo1–O5, 1.904(3); Mo1–O2, 1.915(6); Mo1–O1, 1.922(6); Mo1–N4′, 2.155(7); Mo2–N4, 1.685(7); Mo2–O6, 1.911(3); Mo2–O3, 1.914(6); Mo2–O4, 1.902(7); Mo2–N3, 2.157(7).

the terminal siloxy group *trans* to ammonia is 1.922(4) Å and the one *trans* to the bridging siloxy group is 1.920(5) Å. The bond distance of the bridging siloxy group is 1.981(4) Å, which is 0.06 Å longer than those of the terminal ones. This discrepancy clearly shows the bonding competition of the siloxo oxygen of the bridging siloxy moiety by the two Mo atoms.

The long Mo1–O1′ distance (2.669(4) Å) indicates a weak dative bond [20] exists in the dimer. This weak bond is easily broken in hydrocarbon solution even at ambient temperature, as evidenced by a sharp singlet from $OSiMe_3$ in the ^1H and ^{13}C NMR spectra (vide infra). This weak bond in the solid state results from the *trans* influence [23] exerted by the strongly π bonding Mo≡N group.

The molecule has a $Mo_2N_4(\mu_2\text{-}O)_2O_4$ core that was observed in the nitrosyl compound $Mo_2(NO)_2(O\text{-}i\text{-}Pr)_6(HNMe_2)_2$ [24]. A similar structure composed of an alkoxy bridge, but with TBP structure, was observed in the alkylidyne tungsten complex, $[W(\equiv CMe)(O\text{-}t\text{-}Bu)_3]_2$ [7b,c], and nitrosyl chromium alkoxide, $Cr_2(NO)_2(O\text{-}i\text{-}Pr)_6$ [25]. $Mo_2(NO)_2(OR)_6$, where R = *t*-Bu, *i*-Pr, Np, shows fluxionality in NMR spectroscopy with a 2:1 ratio of alkoxy groups at frozen-out temperature [26].

Although we were unable to grow X-ray quality crystals of **2**, recently Chiu et al. reported the X-ray structure [19]. The structure was shown to be monomeric and is in a distorted tetragonal pyramidal environment with an apical Mo≡N bond [19]. For this compound, we were able to confirm that monomeric nature persists in hydrocarbon solution by using the VT solution NMR study (vide infra).

An ORTEP drawing of **3** is given in Fig. 2. This is the first example, to our knowledge, of a transition metal cage compound supported both by μ_2-O and μ_2-N bridges [27].

The molecule possesses C_2 point group symmetry. The bridging N and O atoms are placed on the plane that contain two Mo atoms and the centeroid of the Mo_4 tetrahedron. This perfect Mo_4 tetrahedron clearly shows the bridging nature of N and O atoms in the molecule. The asymmetric bond distances of Mo–N of nitrido groups [1.69(1) and 2.15(1) Å] are similar to the values observed for the cyclic halide tetramers of $[MoNX_3(L)]_4$ [22]. In contrast to the asymmetric bond distances for Mo≡N, the molecule possesses two totally symmetric Mo–O [1.91(1) Å] bridges. In a mono oxo bridged imido Mo compound $Mo_2(=NH)_2(\mu\text{-}O)_2(Np)_6$ [28a], a Mo–O distance of 1.956(4) Å was reported. This bridging bond is slightly longer than ours because it is *trans* to the doubly bonded imino group. The Mo–N(py) bond distance (2.47 Å avg.) is quite long compared with those of other molybdenum compounds including **2** (2.287 Å, *cis* to Mo≡N bond [19]), which is again a consequence of *trans* influence [23] of the nitrido group. This molecule can be viewed as a paired entity of the five-coordinate oxo-bridged dinuclear fragments formed in a cross-wise manner exclusively through the bent Mo≡N → Mo bonds. For the stability of **3** in a hydrocarbon solution at ambient temperature, refer to Section 3.4.

3.4. Variable temperature NMR work

To understand the solution structures, a variable temperature NMR study of **1**–**3** was undertaken. Variable temperature ^{13}C NMR spectra of **1** in toluene-d_8 are shown in Fig. 3.

At 297 K, a sharp single resonance was observed in both ^1H and ^{13}C NMR spectra. (Proton NMR is not shown.) This is in contrast to the solid state dimeric structure as determined by single crystal diffraction work in which three types of trimethylsiloxy group are present. This can be understood by the fact that the weak dative bond between Mo and the bridging siloxo group (2.67 Å) is easily broken in solution (vide supra). Again the NMR observation does not fit with the tetragonal pyramidal structure (half of the solid state structure).

Only two situations are consistent with this NMR observation; the solution structure is either a frozen mononuclear trigonal bypramid (TBP) with three equatorial siloxy groups or a tetragonal pyramid (TP) structure rapidly interconverting through trigonal bypyramidal (TBP) intermediacy on the NMR time scale. It is

well known that the energy gap between TBP and tetragonal pyramidal (TP) structures is very narrow [6a]. Therefore, it is quite likely that the latter is a more plausible description. Lowering the solution temperature confirms this. At 273 K, the singlet becomes broad ($fwhh = 19$ Hz for the ^{1}H NMR) and, at 260 K, it splits into two peaks with an integral ratio of 1:2. The more sensitive ^{13}C NMR peak also becomes a doublet with 1:2 intensity ratio at 273 K. This indicates that the tetragonal pyramidal structure was frozen at this temperature and the TBP structure is slightly lower in energy than the tetragonal pyramidal one (see Scheme 1).

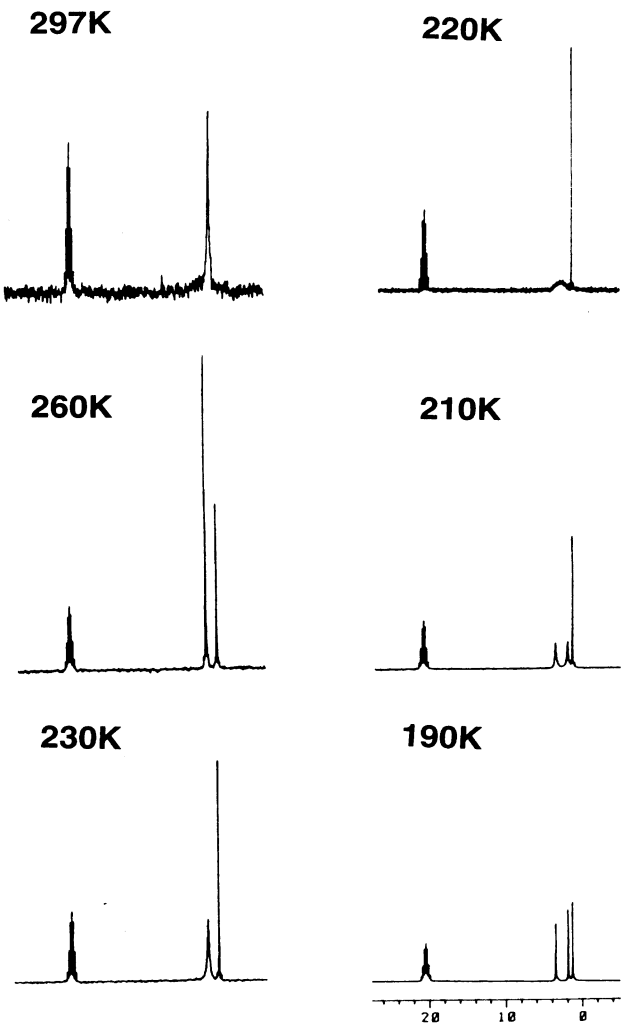
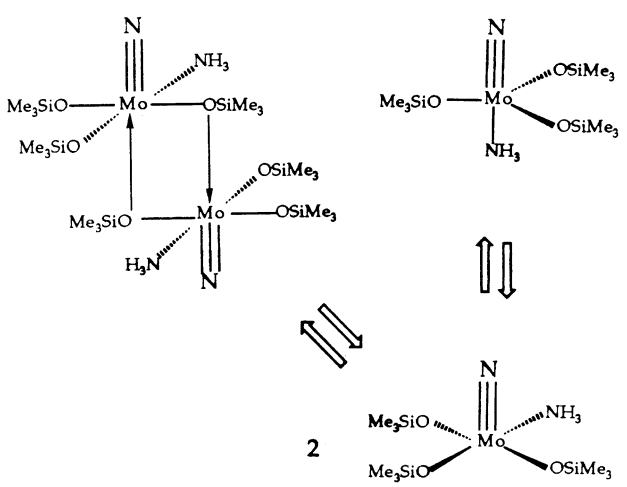


Fig. 3. Variable temperature ^{13}C NMR spectra of **1** in toluene-d_8. Asterisks denote methyl carbon of toluene solvent.



Scheme 1.

Calculation of rate constant for this well known pseudorotation process [28] using the equation [30], $k = 2.22\ \Delta\nu$, for these uncoupled exchanging carbons ($\Delta\nu = 140$ Hz) gave $k = 311\ s^{-1}$. By using the well established relationship between k and $\Delta G^{\neq}$ [29] (Eq. (7)),

$$\Delta G^{\neq} = 4.58 T_c[10.32 + \log(T_c/k)]\ \text{cal mol}^{-1} \quad (7)$$

where $T_c = 279$ K, $k = 311\ s^{-1}$, $\Delta G^{\neq} = 13.1$ kcal mol^{-1} was obtained. This value is about 10 kcal mol^{-1} higher than the theoretically calculated energy for the TBP↔TP interconversion (Berry pseudorotation) of transition metal-nitrido compounds [6a]. This discrepancy may be, albeit in part, due to the steric hindrance arising from site exchange of the bulky trimethylsiloxy groups.

Further cooling of the solution of **1** revealed the monomer↔dimer equilibrium. At around 215 K, the peak with intensity 2 coalesced and further lowering the temperature showed that two peaks with equal intensity appeared ($\Delta\nu = 160$ Hz in ^{13}C NMR) down to the limiting lowest temperature of the solvent, i.e. 190 K. Using the same equations, we can obtain the rate constant and activation free energy values for this rare monomer↔dimer equilibrium: $k = 355\ s^{-1}$ and $\Delta G^{\neq} = 9.9$ kcal mol^{-1}. This final NMR observation and the interpretation is totally consistent with the solid state molecular structure (vide supra) (see Scheme 1). Interestingly, the NMR spectra of **1** in CD_2Cl_2 showed that only two peaks with an integral ratio of 2:1 persist down to 190 K, the same behavior observed for **2** (vide infra). This is presumably due to the solvent effect.

Compound **2** was also subjected to a VT NMR study (in toluene-d_8) to compare its behavior with that of **1**. In a similar condition, the ^{1}H and ^{13}C NMR spectra showed a singlet as the temperature lowered and coalesced at around 253 K. Below this temperature two peaks with an intensity ratio of 1:2 grew up and the spectral pattern did not change down to the solvent limiting temperature of 190 K. The peak separation of 64 Hz in the ^{1}H NMR spectrum gave $k = 142\ s^{-1}$ and $\Delta G^{\neq} = 12.2$ kcal mol^{-1}. This value is somewhat lower than that of **1**. The reason that **2** did not form a dimer is quite obvious from the solid state X-ray structure [19]. In **2**, the coordinated pyridine molecule exerts bulkiness and the metal center is more crowded than **1**.

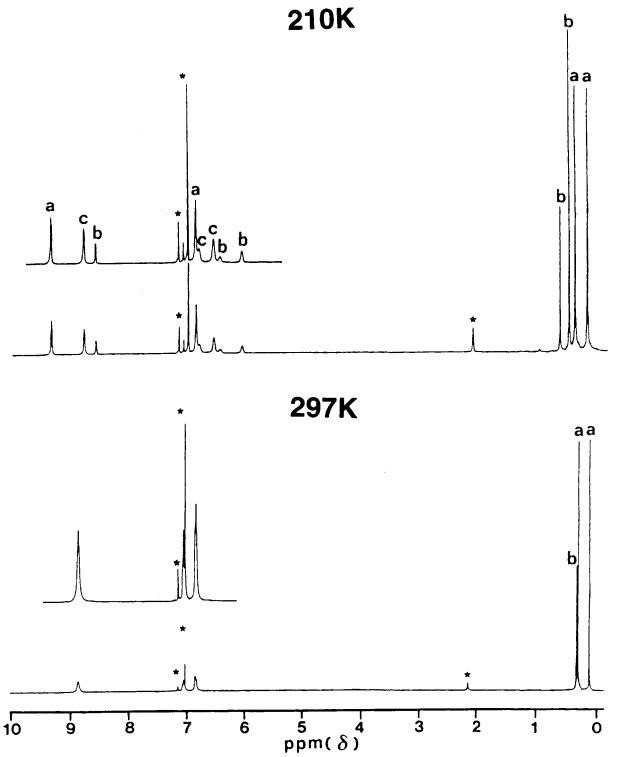


Fig. 4. Variable temperature ^{1}H NMR spectra of **3** in toluene-d_8. Asterisks denote protio peaks of toluene solvent.

Another interesting feature of the ^{1}H NMR pattern with regard to that of **1** is in the reversal of the peak intensity (2:1 for **1** and 1:2 for **2** from downfield side). This may be ascribed to the diamagnetic anisotropy exerted by the ring current effect of the coordinated pyridine compared the coordinated ammonia. The NMR spectral patterns of **1** and **2** are totally reversible in the temperature range.

The ^{1}H VT NMR spectra of tetranuclear oxonitrido complex **3** are shown in Fig. 4.

The spectrum at 297 K shows two peaks with equal intensity in the Me_3SiO region. However, with time, another peak in the downfield side grew up with concomitant intensity decreases in the two upper field peaks. Lowering the temperature made the downfield peak at 0.273 ppm coalesce and the peak split into two peaks with 1:2 intensity ratio. This behavior is exactly the same as observed for **2** (vide supra), therefore this species can be safely assigned to **2**.

The peak intensity and pattern of the remaining two peaks at 0.061 and 0.247 ppm with 1:1 intensity remained unaltered. These peaks can be assigned to **3** and are consistent with the solid state X-ray structure in which two types of siloxy groups present; one *trans* to bridging oxygen and the other *trans* to nitrido moiety (vide supra). The low temperature NMR spectra obtained with time confirmed these assignments. With the elapse of time, the two upfield equal intensity peaks were decreased with the concomitant intensity increases in the downfield 1:2 intensity peaks.

Even more interesting is the presence of three types of pyridine peaks that are frozen out in ^{1}H and ^{13}C NMR spectra [30]. Down to 270 K, only a single type of pyridine was observed, indicating fast exchange in the NMR time scale. However, below this temperature the pyridine resonance become broad and at around 230 K three types of pyridines have emerged. The far downfield resonance marked as (a) in Fig. 4 is assigned to **3**. The other two types are from the disproportionation reaction; the resonance marked (b) can be assigned to **2** and those marked (c) belong to a purely inorganic Mo (VI) cluster-pyridine adduct, which does not contain a siloxy group. This slow disproportionation reaction can be written as in Eq. (8).

$$3[Mo_2N_2O(OSiMe_3)_4(py)_2]_2\cdot 2py \rightarrow 8MoN(OSiMe_3)_3(py) + [Mo_2N_2O_3(py)_4]_2 + 2py \quad (8)$$

The assignments were easily made by comparison with the VT NMR spectra of authentic **2** and the time-dependent intensity behavior (increases and decreases) of the VT NMR spectra of **3**. This disproportionation is not due to hydrolysis because no hexamethyldisiloxane or trimethylsilanol, the expected hydrolysis products, were observed in the aged solution spectra. In addition, no precipitate was formed and no peak from trimethylsiloxy resonance was observed for the aged solution other than those from **2** and **3**.

It is interesting to note that trimethylsiloxy groups can easily migrate from one metal center to another even at ambient temperature. This implicates that **3** is thermally unstable. The addition of pyridine did not alter the reaction course and rate of this disproportionation reaction.

4. Conclusions

The cocondensation reaction of molybdenum trioxide with hexamethyldisilazane produced several structurally interesting nitrido (oxo) molybdenum (6+) siloxides of which some interesting complexes were isolated and characterized. These complexes show subtle differences in dynamical solution structures in hydrocarbon and render some insight into the energetics of the well known pseudorotation and the monomer↔dimer association processes.

5. Supplementary material

X-ray data are available from the Cambridge Crystallographic Data Centre, 12 Union Road, Cambridge,

CB2 1EZ, UK on request quoting the reference codes, KANNIW (for **1**) and KANNOC (for **3**).

Acknowledgements

We thank Mr Roger Konhert for the help in the VT NMR work and Mr Brian Arbogast for the mass spectral work.

References

[1] Reviews on transition metal nitrido complexes: (a) K. Dehnicke, J. Strähle, Angew. Chem., Int. Ed. Engl. 31 (1992) 955. (b) K. Dehnicke, J. Strähle, Angew. Chem., Int. Ed. Engl. 20 (1981) 413.

[2] W.A. Nugent, J.M. Mayer, Metal–Ligand Multiple Bonds, Wiley, New York, 1988.

[3] T.P. Pollagi, T.C. Stoner, R.F. Dallinger, T.M. Gilbert, M.D. Hopkins, J. Am. Chem. Soc. 113 (1991) 703–704.

[4] W.A. Herrmann, A.W. Stumpf, T. Priermeier, S. Bogdanovic, V. Dufaud, J.-M. Basset, Angew. Chem., Int. Ed. Engl. 35 (1996) 2803.

[5] M.J.A. Johnson, P.M. Lee, A.L. Odom, W.M. Davis, C.C. Cummins, Angew. Chem., Int. Ed. Engl. 36 (1997) 87.

[6] (a) R.A. Wheeler, M.-H. Whangbo, T. Hughbanks, R. Hoffmann, J.K. Burdett, T.A. Albright, J. Am. Chem. Soc. 108 (1986) 2222. (b) A. Neuhaus, A. Veldkamp, G. Frenking, Inorg. Chem. 33 (1994) 5278.

[7] For nitrido Mo/W alkoxide complexes, see (a) D.M.-T. Chan, M.H. Chisholm, K. Folting, J.C. Huffman, N.S. Marchant, Inorg. Chem. 25 (1986) 4170. (b) M.H. Chisholm, D.M. Hoffman, J.C. Huffman, Inorg. Chem. 22 (1983) 2903. (c) R.R. Schrock, M.L. Liestemann, L.G. Sturgeoff, J. Am. Chem. Soc. 104 (1982) 4291. (d) T.P. Pollagi, J. Manna, S.J. Geib, M.D. Hopkins, Inorg. Chim. Acta 243 (1996) 177.

[8] C.E. Laplaza, A.R. Johnson, C.C. Cummins, J. Am. Chem. Soc. 118 (1996) 709–710.

[9] M.H. Chisholm, K. Folting-Streib, D.B. Tiedtke, F. Lemoigno, O. Einstein, Angew. Chem., Int. Ed. Engl. 34 (1995) 110.

[10] (a) K.J. Klabunde, Chemistry of Free Atoms and Particles, Academic Press, New York, 1980. (b) J.R. Blackborrow, D. Young, Metal Vapor Synthesis in Organometallic Chemistry, Springer-Verlag, Berlin, 1979.

[11] (a) G.-S. Kim, D. Huffman, C.W. DeKock, Inorg. Chem. 28 (1989) 1279. (b) G.-S. Kim, D.A. Keszler, C.W. DeKock, Inorg. Chem. 30 (1991) 574. (c) G.-S. Kim, C.W. DeKock, J. Chem. Soc., Chem. Commun. (1989) 1166.

[12] G. Brauer (Ed.), Handbook of Preparative Inorganic Chemistry, vol. 2, second ed., Academic Press, New York, 1965, pp. 1412–1413.

[13] C.W. DeKock, S.R. Ely, T.E. Hopkins, M.A. Brault, Inorg. Chem. 17 (1978) 625.

[14] TEXAN, Texray Structure Analysis Package, Molecular Structure Corporation, 3200A Research Forest Drive, The Woodlands, TX 77381, USA.

[15] (a) J. Berkowitz, M.G. Inghram, W.A. Chupka, J. Chem. Phys. 26 (1957) 842. (b) E.K. Kazenas, D.M. Chizhikov, Y.V. Tsvetkov, Issled. Protsessov Met. Tsvet. Redk. Metal. (1969) 19. (b) D.M. Chizhikov (Ed.), Izd. Nauka, Moscow, USSR. (c) Y. Ikeda, H. Ito, T. Mizuno, K. Amioka, G. Matsumoto, High Temp. Sci. 16 (1983) 1.

[16] Bond energies are as follow; Me_3Si–OH, 128 kcal mol^{-1}; Me_3Si–NHMe 100 kcal mol^{-1}. See R. Walsh, Acc. Chem. Res. 14 (1981) 246.

[17] (a) W.A. Nugent, Inorg. Chem. 22 (1983) 965. (b) W.A. Nugent, R.L. Harlow, Inorg. Chem. 19 (1980) 777.

[18] (a) H.-W. Lam, G. Wilkinson, B. Hussin-Bates, B. Hursthoust, J. Chem. Soc., Dalton Trans. (1993) 1477. (b) W.A. Herrmann, M. Denk, F. Dyckhoff, J. Behm, Chem. Ber. 124 (1991) 2401.

[19] H.-T. Chiu, Y.-P. Chen, S.-H. Chuang, J.-S. Jen, G.-H. Lee, S.-M. Peng, J. Chem. Soc., Chem. Commun. (1996) 139.

[20] A. Haaland, Angew. Chem., Int. Ed. Engl. 28 (1989) 992.

[21] (a) A.L. Odom, C.C. Cummins, J. Am. Chem. Soc. 117 (1995) 6613. (b) A.L. Odom, C.C. Cummins, Polyhedron 17 (1998) 675. (c) Z. Gebeyehu, F. Weller, B. Neumueller, K. Dehnicke, Z. Anorg. Allg. Chem. 593 (1991) 99. (d) W.A. Herrmann, S. Bogdanovic, T. Priermeier, R. Poli, J.C. Fettinger, Angew. Chem., Int. Ed. Engl. 34 (1995) 112. (e) J.C. Kim, W.S. Rees Jr., V.L. Goedken, Inorg. Chem. 33 (1994) 3191. (f) For M≡N bond distance/bond strength relationship, see J.C.J. Bart, V. Ragani, Acta Crystallogr., Sect. B 36 (1980) 1351.

[22] (a) W. Kolitsch, K. Dehnicke, Z. Naturforsch., Teil B 25 (1970) 1080. (b) J. Strähle, U. Weiher, K. Dehnicke, Z. Naturforsch., Teil B 33 (1978) 1347. (c) U. Mueller, R. Kujanek, K. Dehnicke, Z. Anorg. Allg. Chem. 495 (1982) 127. (d) J. Strähle, Z. Anorg. Allg. Chem. 375 (1970) 238. (e) K. Dehnicke, J. Strähle, Z. Anorg. Allg. Chem. 339 (1965) 171.

[23] P.D. Lyne, D.M.P. Mingos, J. Chem. Soc., Dalton Trans. (1995) 1635.

[24] M.H. Chisholm, J.C. Huffman, R.L. Kelly, Inorg. Chem. 19 (1980) 2762.

[25] D.C. Bradley, C.W. Newing, M.H. Chisholm, R.L. Kelly, D.A. Haitko, D. Little, F.A. Cotton, P.E. Fanwick, Inorg. Chem. 19 (1980) 3010–3014.

[26] $Mo_2(NO)_2(OR)_6$,where R = *t*-Bu, *i*-Pr, Np, show fluxionality in NMR with a 2:1 ration of alkoxy groups at frozen-out temp. See M.H. Chisholm, F.A. Cotton, M.W. Extine, R.L. Kelly, J. Am. Chem. Soc. 100 (1978) 3354.

[27] Recently dinuclear imino (=NH) transition metal complexes with a bridging oxo ligand have appeared. (a) W.A. Herrmann, S. Bogdanovic, R. Poli, T. Priermeier, J. Am. Chem. Soc. 116 (1994) 4989. (b) J.C. Peters, A.R. Johnson, A.L. Odom, P.W. Wanandi, W.M. Davis, C.C. Cummins, J. Am. Chem. Soc. 118 (1996) 10175.

[28] (a) R.S. Berry, Rev. Mod. Phys. 32 (1960) 447. (b) R.S. Berry, J. Chem. Phys. 32 (1960) 933. Some examples of pseudorotation, see (c) M.H. Chisholm, J.A. Heppert, J.C. Huffman, C.D. Ontiveros, Organometallics 8 (1989) 976. (d) M.H. Chisholm, K. Folting, J.A. Heppert, D.M. Hoffman, J.C. Huffman, J. Am. Chem. Soc. 107 (1985) 1234.

[29] (a) J. Sandström, Dynamic NMR Spectroscopy, Academic Press, London, 1980, pp. 79–80 and 96–97. (b) J.I. Kaplan, G. Fraenkel, NMR of Chemically Exchanging Systems, Academic Press, New York, 1980. (c) For the influence of errors in the equation, see D. Kost, E.H. Carlson, M. Raban, J. Chem. Soc., Chem. Commun. (1971) 656.

[30] M.H. Chisholm, K. Folting, J.C. Huffman, I.P. Rothwell, J. Am. Chem. Soc. 104 (1982) 4389–4399.

PERGAMON

www.elsevier.nl/locate/poly

Polyhedron 19 (2000) 1373–1379

POLYHEDRON

Synthesis and spectroscopic characterisation of tritelluroether, triselenoether, and trithioether complexes of Cr(0), Mo(0) and W(0)

Andrew J. Barton, Julie Connolly, William Levason *, Arantza Mendia-Jalon, Simon D. Orchard, Gillian Reid

Department of Chemistry, University of Southampton, Highfield, Southampton SO17 1BJ, UK

Received 29 March 2000; accepted 5 May 2000

Abstract

The complexes *fac*-$[M(CO)_3L^3]$ (M = Mo or W, $L^3 = MeC(CH_2SMe)_3$, $MeC(CH_2SeMe)_3$ or $MeC(CH_2TeMe)_3$) have been prepared from $[M(CO)_3(MeCN)_3]$ and characterised by analysis, FAB mass spectrometry, IR, ^1H, $^{13}C\{^1H\}$, ^{77}Se, ^{125}Te and ^{95}Mo NMR spectroscopies. The complexes are prone to decomposition in solution into tetracarbonyls, and attempts to isolate $[Cr(CO)_3L^3]$ have been unsuccessful. The complexes *cis*-$[Cr(CO)_4\{\eta^2\text{-}MeC(CH_2SMe)_3\}]$, *cis*-$[Mo(CO)_4(\eta^2\text{-}MeC(CH_2SeMe)_3\}]$ and the robust $[M(CO)_4(S_3)]$ (M = Cr, Mo or W, S_3 = 1,4,7-trithiacyclononane or 1,4,7-trithiacyclodecane) have been similarly characterised. © 2000 Elsevier Science Ltd. All rights reserved.

Keywords: Selenoether; Telluroether; Sulfur macrocycles; Chromium; Molybdenum; Tungsten

1. Introduction

We have been exploring the chemistry of tridentate seleno- and telluro-ether ligands with a variety of metal centres including both homoleptic and halocomplexes with Pd(II), Pt(II), Rh(III) and Ir(III) [1,2], Ru(II) [3], Rh(I) and Ir(I)-olefin and diene complexes [4], and homoleptic Cu(I) and Ag(I) [2]. Carbonyl complexes have received less attention and reports are currently limited to our studies of *fac*-$[M(CO)_3(\text{tridentate})]^+$ (M = Mn or Re) [5]. Here we report studies of Group 6 carbonyl derivatives of $MeC(CH_2SeMe)_3$ (tse) and $MeC(CH_2TeMe)_3$ (tte) (Fig. 1) and we include corresponding studies with $MeC(CH_2SMe)_3$ (tth) and two S_3-donor macrocycles [9]aneS_3 (1,4,7-trithiacyclononane) and [10]aneS_3 (1,4,7-trithiacyclodecane) to permit comparisons between the Group 16 donors. These complexes are the first triselena- or tritellura-ligand complexes of these metal carbonyls, but several trithioether systems have been described in the literature. These include $[Mo(CO)_3([14]aneS_4)]$, $[Mo(CO)_3([16]aneS_4)]$, $[\{Mo(CO)_3\}_2([18]aneS_6)]$ and $[\{W(CO)_4\}_2([18]aneS_6)]$ in which the thioether is assigned as either tri- or bi-dentate [6,7]. Yoshida and co-workers [8] have reported the preparation of $[Mo(CO)_2(L)]$ (L = 3,3,7,7,11,11,15,15 - octamethyl - 1,5,9,13 - tetrathiacyclohexadecane) and the bis-dinitrogen derivative $[Mo(N_2)_2(L)]$ [9], both of which have been structurally characterised. $[Mo(CO)_3([9]aneS_3)]$ is well established and has been structurally characterised [10], showing *fac* tridentate ligation of the thioether, Mo–S = 2.504(6)–2.543(7) Å, Mo–C = 1.93(2)–1.97(2) Å. Indeed this species is involved in the template synthesis of [9]aneS_3 [11] and similar routes yield C-func-

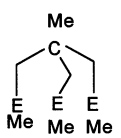


Fig. 1. Structure of ligands.

* Corresponding author. Tel.: +44-2380-593-792; fax: +44-2380-593-781.

E-mail address: wxl@soton.ac.uk (W. Levason).

0277-5387/00/$ - see front matter © 2000 Elsevier Science Ltd. All rights reserved.
PII: S0277-5387(00)00425-3

Table 1
$^{13}C\{^1H\}$ and ^{95}Mo NMR and IR spectroscopic data

Compound	$\delta^{13}C\{^1H\}$ (ppm) [a]	$\delta^{95}Mo$ [b]	$\delta^{77}Se/^{125}Te$ [a]	$\nu(CO)$ (cm^{-1}) [c]
fac-[$Mo(CO)_3$(tth)]	221.0 (CO), 44.3 (CH_2), 41.3 (C), 27.7 (MeS), 24.0 (Me)	−1138		1930, 1816
fac-[$W(CO)_3$(tth)]	215.0 ($^1J_{WC}$ = 178 Hz) (CO), 44.5 (CH_2), 41.5 (C), 29.6 (MeS), 24.2 (Me)			1923, 1807
fac-[$Mo(CO)_3$(tse)]	221.8 (CO), 40.7(C), 35.2(CH_2), 23.7 (Me), 17.5 (MeSe)	−1216	81	1927, 1816
fac-[$W(CO)_3$(tse)]	215.0 ($^1J_{WC}$ = 160 Hz) (CO), 40.6 (C), 36.5 (CH_2), 25.0 (Me), 19.5 (MeSe)		53	1921, 1809
fac-[$Mo(CO)_3$(tte)]	216.8 (CO), 34.4 (CH_2), 33.3 (C), 22.8 (Me), −9.1 (MeTe)	−1336	179	1930, 1820
fac-[$W(CO)_3$(tte)]	213.3 (CO), 35.0 (CH_2), 34.5 (C), 23.0 (Me), −7.0 (MeTe)		110	1921, 1821
fac-[$Cr(CO)_3$([9]aneS_3)]	232.0 (CO), 31.9 (CH_2) [e]			1905, 1810 sh, 1781 [d]
fac-[$Cr(CO)_3$([10]aneS_3)]	232.1 (1 CO), 228.5 (2 CO), 32.1 (4 CH_2), 28.4 (2 CH_2), 27.1 (1 CH_2) [e]			1910, 1807, 1790 sh [d]
fac-[$Mo(CO)_3$([9]aneS_3)]	222.0 (CO), 33.9 (CH_2) [e]	−1345		1910, 1819 sh, 1785 [d]
fac-[$Mo(CO)_3$([10]aneS_3)]	222.1 (1 CO), 219.9 (2 CO), 32.2 (4 CH_2), 29.9 (2 CH_2), 24.3 (1 CH_2) [e]	−1311		1913, 1811 sh, 1792 [d]
fac-[$W(CO)_3$([9]aneS_3)]	215.3 ($^1J_{WC}$ = 179 Hz) (CO), 31.8 (CH_2) [e]			1906, 1811, 1781 [d]
fac-[$W(CO)_3$([10]aneS_3)]	215.3 ($^1J_{WC}$ = 185 Hz) (CO), 212.6 ($^1J_{WC}$ = 179 Hz)(2 CO), 33.3 (4 CH_2), 30.0 (2 CH_2), 24.9 (CH_2) [e]			1901, 1808 sh, 1779 [d]
cis-[$Cr(CO)_4$(tth)]	226.2, 214.9 (CO), 49.0, 48.6 (CH_2), 40.3 (C), 29.0 (Me), 26.8, 18.0 (MeS) [b]			2016, 1902, 1810 sh, 1854
cis-[$Mo(CO)_4$(tse)]	217.3, 207.9 (CO), 40.7, 37.9 (CH_2), 29.9 (Me), 16.0, 7.5 (MeSe) [b]	−1296	31.4, 20.0 [b]	2021, 1909, 1890 sh, 1855

[a] Spectra were recorded at 240 K in CH_2Cl_2 solution unless indicated otherwise.
[b] At 300 K.
[c] CH_2Cl_2 CO region only; sh, shoulder.
[d] CsI discs.
[e] DMSO solution.

tionalised derivatives of [9]aneS_3 [12]. Other trithioether complexes have been reported [13–15]. The results of the present studies may also be compared with those from our previous work on [$M(CO)_4$(bidentate)] (bidentate = various dithio-, diseleno- and ditelluro-ethers) [16].

2. Results and discussion

2.1. Tripodal ligand complexes

Although Group 6 carbonyl complexes are often regarded as among the more stable low valent complexes, the *fac*-[$M(CO)_3L^3$] of $L^3 = MeC(CH_2SMe)_3$ (tth), $MeC(CH_2SeMe)_3$ (tse) and $MeC(CH_2TeMe)_3$ (tte) proved surprisingly difficult to isolate in the pure state, and prone to decomposition in solution, and as a result considerable care was necessary both in the syntheses and in obtaining reliable spectroscopic data. For M = Mo or W, the starting materials in each case were the nitrile complexes [$M(CO)_3(MeCN)_3$] [17] made in situ from the hexacarbonyls in MeCN, which were treated with the ligand tth. After stirring at room temperature overnight, the solvent was removed in vacuo, the complex extracted with dry CH_2Cl_2, filtered and the solvent removed. The resulting solid was washed with diethyl ether which extracts any tetracarbonyl complex present, leaving the [$M(CO)_3$(tth)] in moderate yield. The identity of the products as *fac*-tricarbonyls follows from the two $\nu(CO)$ stretches at ca. 1930 and 1810 cm^{-1} (Table 1) (theory $a_1 + e$), the FAB mass spectra which show parent ions with the correct isotope patterns, and microanalysis. The solids appear stable under nitrogen for several weeks, but the complexes are surprisingly unstable in solution. A freshly prepared $CDCl_3$ solution of [$Mo(CO)_3$(tth)] exhibits a simple ^1H NMR spectrum with singlets at δ 1.15 (MeC), 2.1 (MeS) and 2.45 (CH_2); however, on standing some brown solid precipitates and new resonances appear, some of which can be

associated with uncoordinated tth (δ 0.95, 2.0 and 2.5). The $^{13}C\{^1H\}$ NMR spectrum obtained from CH_2Cl_2–$CDCl_3$ solution at 300 K is also more complex than expected for $[Mo(CO)_3(tth)]$, and changes with time. The $^{13}C\{^1H\}$ NMR spectrum was also obtained at 240 K which slowed, but did not stop the decomposition. From a freshly prepared solution immediately cooled to 240 K, the major $^{13}C\{^1H\}$ resonances are attributable to $[Mo(CO)_3(tth)]$ and occur at δ 221.0 (CO), 44.3 (CH_2), 41.6 (C), 27.7 (MeS) and 24.0 (MeC). Much weaker features at δ 44.2 (CH_2), 18.0 (MeS), are associated with free tth, and other features at 216, 208 (CO), 44.1 and 18.5 (MeS) are attributed to the tetracarbonyl *cis*-$[Mo(CO)_4(\eta^2\text{-tth})]$, (the MeC and C resonances are not resolved from those in the tricarbonyl). After the solution had stood for some hours at room temperature, the $^{13}C\{^1H\}$ NMR resonances associated with the *fac*-tricarbonyl had greatly diminished and the free tth and the tetracarbonyl were the major species present. A ^{95}Mo NMR spectrum of freshly prepared $[Mo(CO)_3(tth)]$ solution at 300 K[1] had $\delta = -1138$, but this disappeared on standing, and a new resonance at -1283 grew in. The latter value is close to that observed [16] for $[Mo(CO)_4(MeSCH_2CH_2CH_2SMe)]$ (-1294), consistent with the generation of a tetracarbonyl complex. Confirmation came from an IR spectrum of the final solution used to record the $^{13}C\{^1H\}$ NMR spectrum, which showed ν(CO) at 2024, 1911, 1885(sh) and 1858 cm^{-1}, which may be compared with similar values 2023, 1910, 1895(sh), 1856 cm^{-1} in $[Mo(CO)_4(MeSCH_2CH_2CH_2SMe)]$ [16]. It is thus clear that whilst pure *fac*-$[Mo(CO)_3(tth)]$ can be isolated, it decomposes readily in solution into *cis*-$[Mo(CO)_4(\eta^2\text{-tth})]$, tth and an unidentified brown solid. The analogous *fac*-$[W(CO)_3(tth)]$ was isolated as a pale brown solid and thoroughly characterised (Table 1), and shows similar but slower decomposition to tth and a tetracarbonyl complex in CH_2Cl_2 solution. Pyramidal inversion at sulfur is fast on the NMR timescales in thioether complexes of Group 6 carbonyls [16,18] but exchange between the free and coordinated MeS groups in the tetracarbonyls is not observed in the NMR spectra.

The instability of the *fac*-tricarbonyl complex was greatest in the chromium–tth system. The reaction of $[Cr(CO)_3(MeCN)_3]$ in situ in MeCN with tth gave a yellow solution which contained *fac*-$[Cr(CO)_3(tth)]$, identified by ν(CO) modes at 1926, 1812 cm^{-1}. However repeated attempts to isolate a pure sample of the solid *fac* complex have been unsuccessful, either from this solution, or using pre-isolated $[Cr(CO)_3(MeCN)_3]$ in benzene [15]. Work up of such solutions gave some green solid, large amounts of yellow $[Cr(CO)_4(\eta^2\text{-tth})]$ which was isolated and is described below, and free tth. An alternative route via $[Cr(CO)_6]$, tth and $NaBH_4$ in ethanol [19], which was successful for the macrocyclic thioethers (below), gave only green decomposition products in this case. The instability of *fac*-$[Cr(CO)_3(tth)]$ is in keeping with the facile decomposition of the heavier analogues W < Mo (≪ Cr), but is surprising when compared with the recently isolated *fac*-$[Cr(CO)_3\{MeSi(CH_2SMe)_3\}]$ [15] which has been structurally characterised.

The $[M(CO)_3L^3]$ (M = Mo or W, L^3 = tse or tte) were isolated as pale brown (Mo) or brown (W) powders from reaction of the appropriate $[M(CO)_3(MeCN)_3]$ with the ligand in MeCN, any tetracarbonyl impurity being washed out with diethyl ether. The IR and NMR spectroscopic data are given in Table 1. *fac*-$[Cr(CO)_3(tse)]$ was made in solution from $[Cr(CO)_3(MeCN)_3]$ and identified in situ by ν(CO) bands at 1923, 1812 cm^{-1}, but as with the tth analogue we have not so far been able to isolate a pure solid sample due to its facile decomposition to the tetracarbonyl. The $[Mo(CO)_3(tse)_3]$ partially decomposes in CH_2Cl_2 solution at 300 K to *cis*-$[Mo(CO)_4(\eta^2\text{-tse})]$, tse (identified by a combination of ^1H, $^{13}C\{^1H\}$ NMR and IR spectroscopies) and an unidentified brown precipitate. Decomposition is very slow at 240 K and at this temperature the $^{13}C\{^1H\}$ NMR data (Table 1) and a single ^{77}Se resonance at δ 81 (free tse has δ = 23) are assignable to the *fac*-tricarbonyl. The *fac*-$[W(CO)_3(tse)]$ behaves similarly. The complexes of the tritelluroether *fac*-$[M(CO)_3(tte)]$ (M = Mo or W) are the most stable of the series, showing no decomposition in CH_2Cl_2 at 240 K during the several hours taken to record $^{13}C\{^1H\}$ NMR spectra. At ambient temperatures in CH_2Cl_2, some decomposition is evident after several hours with weak features in the NMR spectra attributable to tetracarbonyls and some dark precipitate, but in contrast to the other systems, the free ligand (tte) is not present in detectable amounts. It is also notable that only a single *fac*-tricarbonyl species is present in the telluroether complexes. Previous studies of $[M(CO)_4(bidentate)]$ (bidentate = dithio-, diseleno- or ditelluroether) [16] have shown that whilst pyramidal inversion at the Group 16 atom is fast at 300 K (on the NMR timescale) for dithioethers and for some diselenoethers, the barriers are much higher for tellurium inversion, and thus we would expect to see invertomers in the last case. For a *fac*-

[1] Previous studies [16,18] have shown that ^{95}Mo NMR resonances in related complexes broaden rapidly when the samples are cooled, probably due to the substantial quadrupole moment, and spectra are best obtained at ambient temperatures.

$[M(CO)_3\{MeC(CH_2TeMe)_3\}]$ complex two invertomers are expected with *sym* or *anti* methyl groups [5], but only a single form with one δ(Te) and one δ(^{13}C–TeMe) was found (the *sym* isomer). It would appear that only the *sym* invertomer (with a propeller-like arrangement of Me groups) is present in significant amounts in the tte, and probably the tse complexes. We note that in the $[M(CO)_3L^3]^+$ (M = Mn or Re) [5] and $[Ru(L^3)_2]^{2+}$ [3] the NMR spectra, and in several cases X-ray crystallographic data have identified only *sym* invertomers, and $[M(CO)_3\{MeSi(CH_2SMe)_3\}]$ are also *sym* in the solid state [15].

We have described detailed studies of $[M(CO)_4$(bidentate)] elsewhere [16], and the tetracarbonyl complexes formed by η^2-coordination of the tripodal ligands are not fundamentally different. For comparison we describe two examples, *cis*-$[Cr(CO)_4(\eta^2$-tth)] and *cis*-$[Mo(CO)_4(\eta^2$-tse)]. The chromium complex was isolated during attempts to prepare the tricarbonyl from $[Cr(CO)_3(MeCN)_3]$, and $[Mo(CO)_4$(tse)] from reaction of $[Mo(CO)_4((MeCN)_2]$ and tse. The spectroscopic data (Table 1) are, as expected, very similar to those of the corresponding *cis*-$[M(CO)_4\{MeE(CH_2)_3EMe\}]$ (M = Cr E = S, M = Mo E = Se) [16], which also contain six-membered chelate rings, with extra NMR features due to the free arm of the tripodal ligand. In contrast to the *fac*-$[M(CO)_3(L_3)]$ these tetracarbonyls appear stable both in the solid state and in solution.

2.2. S_3 macrocycles

In contrast to the tripodal complexes described above, the macrocyclic thioether complexes proved quite robust, although rather poorly soluble in most solvents. Reaction of $[Cr(CO)_6]$ with one molar equivalent of L (L = [9]aneS$_3$ or [10]aneS$_3$) in degassed EtOH solution at room temperature in the presence of an excess of $NaBH_4$, gave the *fac*-$[Cr(CO)_3L]$ in moderate yields as pale yellow solids (heating led to decomposition). This route is similar to that reported by Chatt and co-workers for the preparation of phosphine substituted complexes of Cr(0), Mo(0) and W(0) carbonyls [19]. Attempts to prepare $[Cr(CO)_3$([9]aneS$_3$)] or $[Cr(CO)_3$([10]aneS$_3$)] from a 1:1 mixture of $[Cr(CO)_6]$ and thioether in MeCN were not successful, yielding unreacted starting materials and green solutions from which no tractable product could be isolated. The literature route to $[Mo(CO)_3$([9]aneS$_3$)] is via the $[Mo(CO)_3(NCMe)_3]$ intermediate [9,10], and we have successfully repeated this reaction. However, we also found that this compound can be prepared from $[Mo(CO)_6]$ and [9]aneS$_3$ in refluxing EtOH solution containing $NaBH_4$. Reaction of $[Mo(CO)_6]$ with [10]aneS$_3$ in refluxing MeCN yields $[Mo(CO)_3$([10]aneS$_3$)] as a light brown solid. The preparation of the tungsten analogues was achieved by reaction of $[W(CO)_3(NCMe)_3]$ in MeCN in situ with [9]aneS$_3$ or [10]aneS$_3$ at room temperature (heating these solutions resulted in decomposition).

These Group 6 carbonyl compounds are poorly soluble in most organic solvents, although they show sufficient solubility in DMSO to enable spectroscopic characterisation, and in contrast to the complexes of the acyclic tripodal ligands, they show no tendency to decompose to tetracarbonyls. The FAB mass spectra show highest mass peaks with the correct isotopic distributions corresponding to $[M(CO)_3L]^+$, and other peaks arising from fragmentation via loss of CO are also observed. For *fac* compounds two CO stretching vibrations ($a_1 + e$) are predicted in the IR spectrum, although strictly the [10]aneS$_3$ complex does not have C_{3v} symmetry. Typically the complexes show two strong bands, although the low frequency band shows an additional shoulder. The data for our sample of $[Mo(CO)_3$([9]aneS$_3$)] are in accord with the literature (KBr: ν(CO) = 1915, 1783 cm^{-1}) [10,11].

$^{13}C\{^1H\}$ NMR spectra were recorded in DMSO solution and the data for the compounds are presented in Table 1. For the complexes of [9]aneS$_3$, a single resonance is seen in the CO region, and a single methylene carbon resonance occurs around + 30 ppm, confirming a symmetrically bound [9]aneS$_3$ ligand. For the complexes of [10]aneS$_3$, two CO resonances (1:2 ratio), and three methylene carbon resonances (4:2:1 ratio) are observed, as expected for tridentate coordination via the macrocycle. In the case of the tungsten complexes, satellites due to coupling to ^{183}W ($I = 1/2$, 14.3%) are also seen on each of the CO resonances, giving $^1J_{WC}$ approximately 180 Hz. This compares with 126 Hz in $[W(CO)_6]$ [20]. ^{95}Mo ($I = 5/2$, 15.7%) NMR spectra were also recorded for the Mo(0) compounds. These show single resonances at − 1345 and − 1311 ppm respectively for $[Mo(CO)_3$([9]aneS$_3$)] and $[Mo(CO)_3$([10]aneS$_3$)]. These shifts are ca. 500 ppm to high frequency of $[Mo(CO)_6]$ (δ(^{95}Mo) = − 1856) [21] indicating decreased electron density on Mo(0) in the thioether compounds. It is notable that in the $[Mo(CO)_3L_3]$ (L_3 = tth, tse or tte) the δ(^{95}Mo) shifts progressively to high frequency with *trans* donor Te < Se < S, consistent with increasing σ-donation as Group 16 is descended [5]. The two macrocyclic trithioether complexes are significantly more shielded that the tth complex.

3. Experimental

Physical measurements were made as described previously [16]. The $M(CO)_6$, [9]aneS$_3$ and [10]aneS$_3$ (Aldrich) were used as received. The ligands tth [22], tse [23], and tte [24] were made by literature methods.

3.1. *fac*-[Mo(CO)$_3$(tth)]

$Mo(CO)_6$ (0.2 g, 0.76 mmol) was refluxed in dry degassed MeCN (50 cm^3) under argon for 16 h. to give $[Mo(CO)_3(MeCN)_3]$. The ligand tth (0.17 g, 0.8 mmol) was added and the mixture stirred under argon for a further 16 h. An IR spectrum of the solution showed the absence of $[Mo(CO)_3(MeCN)_3]$. The solvent was removed in vacuo, and the resulting oil dissolved in CH_2Cl_2 (20 cm^3), and filtered through Celite. The solvent was removed in vacuo, and the solid washed with diethyl ether (20 cm^3) to remove any tetracarbonyl complex. The pale brown powder was rinsed with *n*-pentane (10 cm^3) and dried in vacuo (yield 0.15 g, 52%). *Anal*. Found: C, 34.1; H, 4.7. Calc. for $C_{11}H_{18}MoO_3S_3$: C, 33.8; H, 4.7%. FAB MS (3-NOBA matrix): found $m/z = 392$; calc. for $[^{98}Mo(CO)_3\{MeC(CH_2SMe)_3\}]^+$ $m/z = 392$. ^{1}H NMR (300 MHz, $CDCl_3$, 300 K): δ 1.15 (Me), 2.1 (MeS), 2.45 (CH_2).

3.2. *fac*-[Mo(CO)$_3$(tse)]

This was made analogously as a pale brown powder (yield 0.19 g, 47%). *Anal*. Found: C, 25.2; H, 3.3. Calc. for $C_{11}H_{18}MoO_3Se_3$: C, 24.9; H, 3.4%. FAB MS (3-NOBA matrix): found $m/z = 532$, 448; calc. for $[^{98}Mo(CO)_3\{MeC(CH_2^{80}SeMe)_3\}]^+$ $m/z = 536$, $[^{98}Mo\{MeC(CH_2^{80}SeMe)_3\}]^+$ $m/z = 452$. ^{1}H NMR (300 MHz, $CDCl_3$, 300 K): δ 1.3 (Me), 2.1 (MeSe), 2.7 (CH_2).

3.3. *fac*-[Mo(CO)$_3$(tte)]

This was made analogously as a pale brown powder (yield 0.23 g, 45%). *Anal*. Found: C, 20.0; H, 2.9. Calc. for $C_{11}H_{18}MoO_3Te_3$: C, 19.5; H, 2.7%. FAB MS (3-NOBA matrix): found $m/z = 678$, 594; calc. for $[^{98}Mo(CO)_3\{MeC(CH_2^{130}TeMe)_3\}]^+$ $m/z = 686$, $[^{98}Mo\{MeC(CH_2^{130}TeMe)_3\}]^+$ $m/z = 602$. ^{1}H NMR (300 MHz, $CDCl_3$, 300 K): δ 1.3 (Me), 2.1 (MeTe), 2.8 (CH_2).

3.4. *fac*-[W(CO)$_3$(tth)]

$W(CO)_6$ (0.2 g, 0.57 mmol) was refluxed in dry degassed MeCN (50 cm^3) under argon for 4 d to give $[W(CO)_3(MeCN)_3]$. The ligand tth (0.13 g, 0.6 mmol) was added and the mixture stirred for a further 16 h, at which time an IR spectrum showed the absence of $[W(CO)_3(MeCN)_3]$. The solvent was removed in vacuo, the residue dissolved in CH_2Cl_2 and the solution filtered through Celite. The solvent was again removed in vacuo, the pale brown solid washed with diethyl ether (10 cm^3) and *n*-pentane (20 cm^3) and dried in vacuo (yield 0.44 g, 52%). *Anal*. Found: C, 27.3; H, 4.0. Calc. for $C_{11}H_{18}O_3S_3W$: C, 27.6; H, 3.8%. FAB MS (3-NOBA matrix): found $m/z = 478$; calc. for $[^{184}W(CO)_3\{MeC(CH_2SMe)_3\}]^+$ $m/z = 478$. ^{1}H NMR (300 MHz, $CDCl_3$, 300 K): δ 1.1 (Me), 2.2 (MeS), 2.6 (CH_2).

3.5. *fac*-[W(CO)$_3$(tse)]

This was made analogously (yield 0.14 g, 39%). *Anal*. Found: C, 21.5; H, 3.1. Calc. for $C_{11}H_{18}O_3Se_3W$: C, 21.3; H, 2.9%. ^{1}H NMR (300 MHz, $CDCl_3$, 300 K): δ 1.3 (Me), 2.05 (MeSe), 2.8 (CH_2).

3.6. *fac*-[W(CO)$_3$(tte)]

This was made analogously (yield 0.24 g, 55%). *Anal*. Found: C, 17.3; H, 2.3. Calc. for $C_{11}H_{18}O_3Te_3W$: C, 17.3; H, 2.4%. ^{1}H NMR (300 MHz, $CDCl_3$, 300 K): δ 1.5 (Me), 2.0 (MeTe), 2.2 (CH_2).

3.7. *cis*-[Cr(CO)$_4$(η^2-tth)]

This was made from $[Cr(CO)_3(MeCN)_3]$ and tth in benzene, following the method used [15] for $[Cr(CO)_3\{MeSi(CH_2SMe)_3\}]$. The product was extracted in diethyl ether, the solvent removed and the yellow solid washed with *n*-pentane. *Anal*. Found: C, 38.5; H, 4.3. Calc. for $C_{12}H_{18}CrO_4S_3$: C, 39.1; H, 4.9%. ^{1}H NMR (300 MHz, $CDCl_3$, 300 K): δ 1.12 (Me), 2.2, 2.4 (MeS), 2.6, 2.7 (CH_2).

3.8. *cis*-[Mo(CO)$_4$(η^2-tse)]

$Mo(CO)_6$ (0.2 g, 0.76 mmol) was refluxed in dry degassed MeCN (50 cm^3) under argon for 8 h. to give $[Mo(CO)_4(MeCN)_2]$ (identified in situ by IR spectroscopy). The ligand tse (0.28 g, 0.8 mmol) was added and the mixture stirred for a further 16 h. The solvent was removed in vacuo and the resulting oil dissolved in CH_2Cl_2 (20 cm^3) and filtered through Celite. The solvent was removed in vacuo, the residue dissolved in diethyl ether (10 cm^3) and filtered. The solvent was again removed in vacuo, and the solid washed with *n*-pentane, and died in vacuo. *Anal*. Found: C, 25.3; H, 3.0. Calc. for $C_{12}H_{18}MoO_4Se_3$: C, 25.8; H, 3.2%. FAB MS (3-NOBA matrix): found $m/z = 560$, 532; calc. for $[^{98}Mo(CO)_4\{MeC(CH_2^{80}SeMe)_3\}]^+$ $m/z = 564$, $[^{98}Mo(CO)_3\{MeC(CH_2^{80}SeMe)_3\}]^+$ $m/z = 536$. ^{1}H NMR (300 MHz, $CDCl_3$, 300 K): δ 1.2 (Me), 2.1, 2.45 (MeSe), 2.7, 2.8 (CH_2).

3.9. *fac*-[Cr(CO)$_3$([9]aneS$_3$)]

To a degassed solution of [Cr(CO)$_6$] (0.049 g, 0.22 mmol) and NaBH$_4$ (0.038 g, 1.0 mmol) in dry EtOH (25 cm^3) was added [9]aneS$_3$ (0.040 g, 0.22 mmol). The resulting mixture was stirred at room temperature (r.t.) for ca. 24 h, during which time a yellow solution was produced. The reaction volume was reduced to ca. 15 cm^3 in vacuo to give a white solid and yellow solution. Following filtration, the filtrate was concentrated in vacuo and diethyl ether was added to give a yellow solid, which was filtered, washed with H$_2$O and dried in vacuo (yield 0.028 g, 40%). *Anal*. Found: C, 33.7; H, 4.7. Calc. for C$_9$H$_{12}$CrO$_3$S$_3$: C, 34.2; H, 3.8%. FAB MS (3-NOBA matrix): found $m/z = 316$, 232; calc. for [^{52}Cr(CO)$_3$([9]aneS$_3$)]$^+$ $m/z = 316$, [^{52}Cr([9]aneS$_3$)]$^+$ $m/z = 232$. ^{1}H NMR (300 MHz, d_6-DMSO, 300 K): δ 3.0–2.6 (br m CH$_2$).

3.10. *fac*-[Cr(CO)$_3$([10]aneS$_3$)]

Method as for [Cr(CO)$_3$([9]aneS$_3$)] above, but using [Cr(CO)$_6$] (0.023 g, 0.1 mmol), NaBH$_4$ (0.018 g, 0.46 mmol) and [10]aneS$_3$ (0.020 g, 0.1 mmol), giving a pale yellow precipitate, which was recrystallised from MeNO$_2$ (yield 0.020 g, 59%). *Anal*. Found: C, 33.1; H, 4.1. Calc. for C$_{10}$H$_{14}$CrO$_3$S$_3$·MeNO$_2$: C, 33.7; H, 4.3%. FAB MS (3-NOBA matrix): found $m/z = 330$, 274, 246; calc. for [^{52}Cr(CO)$_3$([10]aneS$_3$)]$^+$ $m/z = 330$, [^{52}Cr(CO)-([10]aneS$_3$)]$^+$ $m/z = 274$, [^{52}Cr([10]aneS$_3$)]$^+$ $m/z = 246$. ^{1}H NMR (300 MHz, d_6-DMSO, 300 K): δ 3.25–2.85, 2.50 (br, m, CH$_2$).

3.11. *fac*-[Mo(CO)$_3$([9]aneS$_3$)]

Method 1: [Mo(CO)$_6$] (0.059 g, 0.22 mmol) was added to a stirred solution of [9]aneS$_3$ (0.040 g, 0.22 mmol) in dry, degassed MeCN (25 cm^3). The solution was gently refluxed under N$_2$ for 6 h. After cooling the solution was concentrated in vacuo to ca. 3 cm^3. Subsequent addition of diethyl ether afforded a light yellow/brown precipitate that was filtered, washed with diethyl ether and dried in vacuo (yield 0.030 g, 38%).

Method 2: [Mo(CO)$_6$] (0.059 g, 0.22 mmol), [9]aneS$_3$ (0.040 g, 0.22 mmol) and NaBH$_4$ (0.025 g, 0.67 mmol) were heated to reflux for 5 h in dry, degassed EtOH (25 cm^3) under N$_2$. The yellow solution that formed was stirred at r.t. for a further 12 h. After concentrating the solution in vacuo, diethyl ether was added to afford a light yellow precipitate which was filtered, washed with H$_2$O and dried in vacuo (yield: 0.025 g, 31%). FAB MS (3-NOBA matrix): found $m/z = 363$; calc. for [^{98}Mo(CO)$_3$([9]aneS$_3$)]$^+$ $m/z = 362$. ^{1}H NMR (300 MHz, d_6-DMSO, 300 K): δ 3.1–2.8 (br m CH$_2$).

3.12. *fac*-[Mo(CO)$_3$([10]aneS$_3$)]

[Mo(CO)$_6$] (0.068 g, 0.26 mmol) was added to a stirred solution of [10]aneS$_3$ (0.050 g, 0.26 mmol) in dry, degassed MeCN (30 cm^3). The solution was gently refluxed under N$_2$ for 18 h. After cooling the solution was concentrated in vacuo to ca. 3 cm^3. Subsequent addition of diethyl ether afforded a light yellow precipitate that was filtered, washed with diethyl ether and dried in vacuo (yield 0.060 g, 62%). *Anal*. Found: C, 31.8, H, 3.4. Calc. for C$_{10}$H$_{14}$MoO$_3$S$_3$: C, 32.0; H, 3.7%. FAB MS (3-NOBA matrix): found $m/z = 376$; calc. for [^{98}Mo(CO)$_3$([10]aneS$_3$)]$^+$ $m/z = 376$. ^{1}H NMR (300 MHz, d_6-DMSO, 300 K): δ 3.1–2.6 (m, CH$_2$).

3.13. *fac*-[W(CO)$_3$([9]aneS$_3$)]

[W(CO)$_6$] (0.100 g, 0.28 mmol) was refluxed in dry MeCN (50 cm^3) under argon for 4 days to give *fac*-[W(CO)$_3$(MeCN)$_3$]. After cooling to r.t. [9]aneS$_3$ (0.051 g, 0.28 mmol) was added and the reaction mixture stirred under argon for 3 days during which time a pale brown solid was deposited. The solution was then concentrated in vacuo and diethyl ether was added to give a fawn solid that was filtered, washed with diethyl ether and dried in vacuo (yield 0.037 g, 26%). *Anal*. Found: C, 24.1; H, 2.4. Calc. for C$_9$H$_{12}$O$_3$S$_3$W: C, 24.1; H, 2.7%. FAB MS (3-NOBA matrix): found $m/z = 448$, 365; calc. for [^{184}W(CO)$_3$([9]aneS$_3$)]$^+$ $m/z = 448$, [^{184}W([9]aneS$_3$)]$^+$ $m/z = 364$. ^{1}H NMR (300 MHz, d_6-DMSO, 300 K): δ 2.9–2.5 (m, CH$_2$).

3.14. *fac*-[W(CO)$_3$([10]aneS$_3$)]

Method as for [W(CO)$_3$([9]aneS$_3$)] above, but using [W(CO)$_6$] (0.100 g, 0.28 mmol) and [10]aneS$_3$ (0.055 g, 0.28 mmol), giving a light brown precipitate which was recrystallised from CHCl$_3$ (yield 0.040 g, 30%). *Anal*. Found: C, 23.7; H, 2.3. Calc. for C$_{10}$H$_{14}$O$_3$S$_3$W·CHCl$_3$: C, 22.7; H, 2.6%. FAB MS (3-NOBA matrix): found $m/z = 461$; calc. for [^{184}W(CO)$_3$([10]aneS$_3$)]$^+$ $m/z = 462$. ^{1}H NMR (300 MHz, CDCl$_3$, 300 K): δ 3.20–2.85 (m, CH$_2$).

Acknowledgements

We thank the EPSRC for support. A.M.-J. thanks the Universidad de Burgos for study leave.

References

[1] E.G. Hope, W. Levason, S.G. Murray, G.L. Marshall., J. Chem. Soc., Dalton Trans. (1985) 2185.
[2] W. Levason, S.D. Orchard, G. Reid, Inorg. Chem., in press.

[3] W. Levason, S.D. Orchard, G. Reid, J. Chem. Soc., Chem. Commun. (1999) 1071.
[4] W. Levason, S.D. Orchard, G. Reid, J.M. Street, J. Chem. Soc. Dalton Trans., in press.
[5] (a) W. Levason, S.D. Orchard, G. Reid, J. Chem. Soc., Dalton Trans. (1999) 823. (b) J. Connolly, A.R.J. Genge, W. Levason, S.D. Orchard, S.J.A. Pope, G. Reid, J. Chem. Soc., Dalton Trans. (1999) 2343.
[6] D. Sevdic, M. Curic, Lj. Tusek-Bozic, Polyhedron 8 (1989) 505.
[7] P. Baker, M.C. Durrant, B. Goerdt, S.D. Harris, D.L. Hughes, R.L. Richards, J. Organomet. Chem. 469 (1994) C22.
[8] T. Yoshida, T. Adachi, T. Ueda, M. Watanabe, M. Kaminaka, T. Higuchi, Angew. Chem., Int. Ed. Engl. 26 (1987) 1171.
[9] T. Yoshida, T. Adachi, M. Kaminaka, T. Ueda, J. Am. Chem. Soc. 110 (1988) 4872.
[10] M.T. Ashby, D.L. Lichtenberger, Inorg. Chem. 24 (1985) 636.
[11] (a) D. Sellmann, L. Zapf, Angew. Chem., Int. Ed. Engl.23 (1984) 807. (b) D. Sellmann, L. Zapf, J. Organomet. Chem. 289 (1985) 57.
[12] R.J. Smith, S.N. Salek, M.J. Went, P.J. Blower, N.J. Barnard, J. Chem. Soc., Dalton Trans. (1994) 3165.
[13] O.P. Siclovan, R.J. Angelici, Inorg. Chem. 37 (1998) 432.
[14] G.J. Grant, J.P. Carpenter, W.N. Setzer, D.G. VanDerveer, Inorg. Chem. 28 (1989) 4128.
[15] H.W. Yim, L.M. Tran, E.D. Dobbin, D. Rabinovich, L.M. Liable-Sands, C.D. Incarvito, K.-C. Lam, A.L. Rheingold, Inorg. Chem. 38 (1999) 2211.
[16] A.J. Barton, W. Levason, G. Reid, J. Organomet. Chem. 579 (1999) 235.
[17] (a) D.P. Tate, W.R. Knipple, Inorg. Chem. 2 (1962) 433. (b) G.J. Kubas, Inorg. Synth. 27 (1990) 4.
[18] E.W. Abel, D.E. Budgen, I. Moss, K.G. Orrell, V. Sik, J. Organomet. Chem. 362 (1989) 105.
[19] J. Chatt, G.J. Leigh, N. Thankarajan, J. Organomet. Chem. 29 (1971) 105.
[20] B.E. Mann, B.F. Taylor, ^{13}C NMR Data for Organometallic Compounds, Academic, London, 1981.
[21] M. Minelli, J.H. Enemark, R.T.C. Brownlee, M.J. O'Connor, A.G. Wedd, Coord. Chem. Rev. 68 (1985) 169.
[22] R. Ali, S.J. Higgins, W. Levason, Inorg. Chim. Acta 84 (1984) 65.
[23] D.J. Gulliver, E.G. Hope, W. Levason, S.G. Murray, D.M. Potter, G.L. Marshall, J. Chem. Soc., Perkin Trans. II (1984) 429.
[24] E.G. Hope, T. Kemmitt, W. Levason, Organometallics 7 (1988) 78.

PERGAMON

www.elsevier.nl/locate/poly

Polyhedron 19 (2000) 1381–1394

POLYHEDRON

Raman spectroscopic characteristics of phthalocyanine and naphthalocyanine in sandwich-type (na)phthalocyaninato and porphyrinato rare earth complexes

Jianzhuang Jiang* [a,b,1], Llew Rintoul [a], Dennis P. Arnold* [a,2]

[a] *Centre for Instrumental and Developmental Chemistry, Queensland University of Technology, GPO Box 2434, Brisbane 4001, Australia*
[b] *Department of Chemistry, Shandong University, Jinan 250100, People's Republic of China*

Received 29 February 2000; accepted 4 May 2000

Abstract

The Raman spectroscopic data for a series of 50 phthalocyaninato and/or porphyrinato rare earth complexes including monomeric Tb[T(4-Cl)PP]acac, and sandwich-type $RE(Pc')_2$ [RE = Ce, Eu, Gd, Tb, Y; Pc′ = Pc, $Pc(OC_5H_{11})_8$, $Pc(OC_8H_{17})_8$, $Pc(C_7H_{15})_8$], $RE(Nc^*)_2$ [RE = La, Ce, Pr, Nd, Eu, Gd, Tb, Er, Y; Nc* = $Nc(^tBu)_4$, $Nc(SC_{12}H_{25})_8$], (Pc)RE(Pc*)RE(Pc*) [RE = Eu, Tb, Er; Pc* = $Pc(OC_5H_{11})_8$], (Pc)Eu(Pc*)Er(Pc*) [Pc* = $Pc(OC_8H_{17})_8$], Eu(Pc)(Pc*) [Pc* = $Pc(OC_5H_{11})_8$, $Pc(C_7H_{15})_8$], Eu(Por)(Pc′) [Por = TPP, TPyP, T(4-Cl)PP, T(4-OMe)PP, T(4-^{t}Bu)PP; Pc′ = Pc, $Pc(C_7H_{15})_8$], Eu(Por)(Nc) [Por = TPyP, T(4-Cl)PP], HEu(Por)(Pc), Ce(TPyP)(Pc), $RE_2(Por)_2(Pc)$ [RE = Ce, Eu; Por = TPP, TPyP, T(4-Cl)PP, T(4-^{t}Bu)PP], and $RE_2(Por)(Pc')_2$ [RE = Eu, Ce, Y; Por = TPP, TPyP, T(4-Cl)PP, T(4-OMe)PP, T(4-^{t}Bu)PP, OEP; Pc′ = Pc, $Pc(OC_8H_{17})_8$, $Pc(C_7H_{15})_8$], and (TPyP)RE(Pc*)RE′(Pc*) [RE ≠ RE′ = Eu, Y; Pc* = $Pc(C_7H_{15})_8$] have been collected in the solid state using a Raman microprobe and excitation at 632.8 nm (and in some cases, 780 nm). The Raman characteristics for unsubstituted and substituted (na)phthalocyaninato mono-radical anions $Pc'^{\bullet -}$ (Pc′ = Pc, Pc*), $Nc^{*\bullet -}$ and dianions Pc'^{2-} (Pc′ = Pc, Pc*) are thus comparatively described. The intense band at ca. 1500 cm^{-1} was confirmed to be the marker band for $Pc'^{\bullet -}$ and Pc'^{2-} anions. © 2000 Elsevier Science Ltd. All rights reserved.

Keywords: Phthalocyanines; Naphthalocyanines; Porphyrins; Raman; Sandwich complexes; Lanthanides

1. Introduction

Sandwich type phthalocyaninato double-deckers, in which the large conjugated π systems are held in close proximity by rare earth ions, have attracted great attention due to their application in organic materials science [1,2]. These sandwiches have recently been found to be good candidates for potential applications in the fields of molecular electronics, molecular optronics, and molecular iono-electronics [3–12]. As the bulk characteristics of a molecular material are largely related to the properties of individual molecules, various modifications have been made on these sandwiches with the aim of improving their performance as advanced materials. Thus there has been intense research into substituted bis(phthalocyaninato), bis(naphthalocyaninato), heteroleptic bis(phthalocyaninato), and mixed porphyrinato–phthalocyaninato metal complexes, especially since the beginning of the 1990s [13–23]. As fully summarised in our recent paper concerning the IR spectroscopic characteristics of sandwich porphyrinato and/or phthalocyaninato rare earth complexes [24], IR spectroscopy is a versatile technique for studying the intrinsic properties of the sandwiches [25–29]. For the bis(phthalocyaninato) complexes $M(Pc')_2$ (M = RE, Th, U, Zr, Hf, Bi, Sn; Pc′ = Pc, Pc*) [30–34] and porphyrinato–phthalocyaninato double-deckers M(Por)(Pc′) (Pc′ = Pc, Pc*; M = RE, Th, U, Zr, Hf) [35,36], the IR peak around 1310–1330 cm^{-1} has been confirmed to be the diagnostic band for the $Pc'^{\bullet -}$ and Pc'^{2-} anions

[1] *Corresponding author. Tel.: +61-7-3864-2482; fax: +61-7-3864-1804; e-mail: jzjiang@sdunetnms.sdu.edu.cn, j.jiang@qut.edu.au
[2] *Corresponding author. Tel.: +61-7-3864-2482; fax: +61-7-3864-1804; e-mail: d.arnold@qut.edu.au

0277-5387/00/$ - see front matter © 2000 Elsevier Science Ltd. All rights reserved.
PII: S0277-5387(00)00426-5

(for a list of abbreviations, see the Appendix). Raman spectroscopy is potentially another valuable tool for analysing the extent of charge (de)localisation in porphyrin or phthalocyanine π radicals. However, it has so far not been as extensively used for characterising the sandwich-type porphyrinato and/or phthalocyaninato metal complexes as the IR technique [37,38]. Since 1989, Aroca has described the resonance Raman spectra of lutetium and ytterbium bis(phthalocyaninato) compounds in thin solid films [39]. Meanwhile, Homborg and co-workers also reported the synthesis and structures of a series of bis(phthalocyaninato) rare earth complexes together with their vibrational (IR and Raman) spectroscopic characterisations [30,31,40–42]. In 1994, Tran-Thi et al. compared the FT-Raman spectra (excited at 1064 nm) for several sandwich phthalocyaninato and porphyrinato Gd and Ce compounds and proposed that the intense band at 1500 cm^{-1} is the marker band to estimate the hole (de)localisation within the Pc moiety [37]. We are currently developing novel synthetic methods for a series of sandwich porphyrinato and/or phthalocyaninato rare earth compounds and are investigating the ring–ring interaction between or among the macrocycles (porphyrinato and phthalocyaninato ligands) through electrochemical and spectroscopic methods [13,14,16–23,43–46]. In this paper we describe and compare the Raman spectroscopic characteristics for the (na)-phthalocyanine ligand in various examples of double- and triple-decker sandwich complexes containing phthalocyanine(s), naphthalocyanine(s) and porphyrins.

2. Experimental

The sandwich-type rare earth complexes were prepared according to the reported procedures [13–26,45,60]. Raman spectra were recorded with a Renishaw Raman Microprobe, equipped with a Spectra Physics model 127 He–Ne laser excitation source emitting at a wavelength of 632.8 nm and a Renishaw diode laser emitting at 780 nm, and a cooled charge-coupled device (CCD) camera. An Olympus BHZ-UHA microscope was attached and was fitted with three objective lenses (× 10, × 20, × 50). For these experiments, the × 10 objective was employed giving a spot size on the sample of about 5 μm. Laser power at the sample was ca. 0.08 mW. Sample preparation consisted simply of placing a very small amount of the solid on a clean stainless steel plate on the microscope stage. Spectra of excellent quality were generally obtained in ca. 3 min. Some porphyrin-containing samples suffered from strong fluorescence, as noted in the text.

3. Results and discussion

3.1. Raman characteristics of homoleptic double-deckers $RE(Pc)_2$, $RE(Pc^*)_2$, and heteroleptic double-deckers $RE(Pc)(Pc^*)$

Although sandwich phthalocyaninato metal compounds have not been as extensively studied by the Raman technique as by the IR method, both Aroca and Homborg have paid considerable attention to both the Raman and IR spectroscopic properties of bis(phthalocyaninato) rare earth complexes [30,31,39–42]. In their systematic work on the vibrational spectra and structures of thin films of metal bis(phthalocyaninato) complexes, Aroca noticed the difference between the Q-state excitation (676.4 nm) resonance Raman spectra of green $RE(Pc')_2$ and blue $HRE(Pc')_2$. The strong band around 680 cm^{-1} and a medium strong band around 740 cm^{-1} assigned to macrocycle (Pc) breathing and Pc ring modes, respectively, appear in the resonance Raman spectra of the green species [39,47–50]. For the lower symmetry blue species $HRE(Pc')_2$, an additional peak at about 730 cm^{-1} was observed between these two bands [39,47]. Closely similar characteristics have also been observed by Homborg in the resonance Raman spectra of $La(Pc)_2$ [51] and $[M^{III}(Pc)_2]^-$ (M = La, Ce, Bi, Y, In) [30,31]. By using the 647.1 nm laser line to excite the Raman spectra of a series of bis(phthalocyaninato) rare earth complexes, Homborg proposed that the Q band-enhanced resonance Raman spectra have almost the same signature for the Pc^{2-} and $Pc^{\bullet -}$ ligands. However, with excitation wavelengths further from resonance, in particular between 457 and 514 nm, three strong vibrational peaks were observed at about 1110, 1170 and 1595 cm^{-1} for all the radical anion-containing double-deckers $M^{III}(Pc)_2$ (M = La, Nd, Gd, Ho, Lu, Bi, Y, In) [30,31,51,52], and these were thus attributed to the typical $Pc^{\bullet -}$ marker bands. Further studies revealed that removing an electron from $M(Pc)_2$ (M = Y, In, Ho, Pr) to form $[M(Pc)_2]^+$ does not change the corresponding resonance Raman bands significantly [31,53,54]. Using instead a long wavelength laser line at 1064 nm (in near-resonance with the intramolecular charge transfer transition of the neutral species) to excite the Raman spectra of $M^{III}(Pc)_2$ (M = La···Lu except Ce, Pm; Y, In) [31,51] and $[M^{III}(Pc)_2]^+$ (M = La···Lu except Ce, Pm; Y, In) [31,53], Homborg found that the band assigned to the Pc skeletal mode vibration around 1515 cm^{-1} experiences a successive blue-shift from La to Lu. Moreover, in the resonance Raman spectra of both $M^{III}(Pc)_2$ and $[M^{III}(Pc)_2]^+$, the appearance of only one set of the $Pc^{\bullet -}$ bands in $M^{III}(Pc)_2$ (M = La···Lu except Ce, Pm; Y, In) [31,51,52] indicates strong ring–ring interaction and hole delocalisation over both the Pc chromophores on the time scale of Raman spectroscopy. Through detailed work on the

FT-Raman spectra (1064 nm excitation) for a series of phthalocyanine-containing sandwiches, Tran-Thi et al. found a significant upshift of a redox-sensitive Raman band at ca. 1500 cm^{-1} after oxidation of Pc^{2-}, the extent of which was used to judge the (de)localisation of the unpaired electron in the sandwiches [37]. According to his proposal that an upshift of over 15 cm^{-1} is the indication of the localisation of the hole in the Pc ring, the hole in both $Gd(Pc)_2$ and Gd(TPP)(Pc) is predominantly located on the Pc ligand. This conclusion for $Gd(Pc)_2$ is in contrast with that deduced from IR measurements [24] and that of Homborg also from Raman measurements [30,31,51–54].

The sandwich phthalocyaninato and/or porphyrinato rare earth double-deckers contain a large number of atoms and are expected to have many normal vibrational modes. For example, even the unsubstituted $RE(Pc)_2$ complex has 113 atoms and 333 normal modes. Assuming a C_{4v} point group, the Raman-active modes are $44A_1$, $42B_1$, $42B_2$, and $83E$, and IR-active modes include $44A_1$ and $83E$ vibrational fundamentals [39]. It has been clearly shown that despite the large number of IR-active modes, the experimental IR spectra of sandwich phthalocyaninato rare earth double-deckers $RE(Pc)_2$ are composed of a small number of fundamentals, including the following main IR absorption groups corresponding to characteristic vibrations of phthalocyanine molecules. The aromatic C–H wagging vibration around 730 cm^{-1}, the aromatic C–H bending vibration at 1115 cm^{-1}, and two isoindole stretching vibrations at 1320 and 1450 cm^{-1} are observed for these double-decker compounds [24]. According to their work for both IR and Raman vibrational properties of bis(phthalocyaninato) rare earth compounds, Aroca and co-workers pointed out that groups of characteristic phthalocyanine vibrations could be clearly distinguished in the IR and resonance Raman spectra [39]. Aromatic C–H vibrations are responsible for the IR and resonance Raman spectra of Pc molecules in the region of 1000–1300 cm^{-1}, which are correlated with phthalonitrile and indole frequencies, except for the pyrrole ring vibration band at about 1140 cm^{-1}. Vibrational frequencies in the range 1320–1650 cm^{-1} are derived from isoindole ring stretches and the aza group stretch, for which the pyrrole stretching vibrations at ca. 1330 and 1510 cm^{-1}, and *ortho*-disubstituted benzene stretchings at ca. 1560, 1590 and 1610 cm^{-1} can be distinguished by frequency and relative intensity. The spectral region from 1000 to 400 cm^{-1} has main contributions from the dihedral plane deformation involving the aromatic C–H groups (wagging and torsion vibration) which is normally seen in the IR spectra, and ring radial vibrations of the isoindole moieties and the macrocycle which show strong Raman signals. The assignment to different symmetry types was thus carried out according to the following principles. A vibration that gives signals in both IR and Raman but with stronger relative intensity in the Raman was assigned to the A_1 type. The reverse was assumed to be the case for E type. A number of new frequencies appearing in the Raman spectra are most likely related to A_2, B_1 and B_2 type in view of the Herzberg–Teller mechanism.

In our experiments, the 632.8 nm laser line, which is in close resonance with the Q absorption band of bis(phthalocyaninato) rare earth compounds (λ_{max}: ca. 670–690 nm), was used to excite the Raman spectra. The proposed partial assignment of observed values in the Raman spectra of homoleptic $RE(Pc')_2$ and heteroleptic RE(Pc)(Pc*) is given in Table 1. The results for the Raman shifts of $Eu(Pc)_2$ are comparable to those of Aroca and Homborg for a series of $RE(Pc)_2$ [30,31] when they used 676.4 and 647.1 nm excitation, respectively. As expected, neither the introduction of substituted groups onto the phthalocyanine ring nor the variation in sandwiched metal seems to induce significant changes in the resonance Raman spectra. For instance, the Raman spectra for both heteroleptic Eu(Pc)(Pc*) and homoleptic $Eu(Pc^*)_2$ [Pc* = $Pc(OC_5H_{11})_8$, $Pc(OC_8H_{17})_8$, $Pc(C_7H_{15})_8$] are similar to their analogue $Eu(Pc)_2$, while the resonance Raman spectrum for $Eu[Pc(C_7H_{15})_8]_2$ resembles closely that for $Y[Pc(C_7H_{15})_8]_2$. However, when tetravalent cerium is involved in double-decker phthalocyaninato compounds, significant band shifts and intensity changes, especially for the marker band of Pc ring at ca.1500 cm^{-1}, take place in the Raman spectrum of $Ce^{IV}(Pc')_2$ (Pc′ = Pc, Pc*) compared with those of $RE^{III}(Pc')_2$ (Pc′ = Pc, Pc*). It is worth noting that the band at ca. 1500 cm^{-1} for the phthalocyanine ring is attributed to a ν_3 porphyrin-like mode which contains nearly equal C=C (pyrrole) and C=N (aza group) character according to Tran-Thi [37]. Fig. 1 compares the Raman spectra of $Gd^{III}[Pc(OC_8H_{17})_8]_2$ and $Ce^{IV}[Pc(OC_8H_{17})_8]_2$. In the Raman spectrum of the latter, the ν_3 porphyrin-like mode of the phthalocyanine ring gives a band near 1500 cm^{-1} and the most intense band is located at 1174 cm^{-1}, which is assigned to an aromatic C–H bend. When the tetravalent cerium in the bis(phthalocyanine) compound is substituted with tervalent rare earth ions, dramatic changes occur in the Raman spectra. The former band with contributions from both C=C (pyrrole) and C=N (aza group) stretches, upshifts to 1515 cm^{-1}. These changes are considered to result from (i) the intrinsic difference between the monoanion radical $Pc^{\bullet-}$ in $RE^{III}(Pc')_2$ and dianion Pc^{2-} in $Ce^{IV}(Pc')_2$ and (ii) the different degree of resonance of the excitation laser line (632.8 nm) with the Q absorption of tervalent rare earth (Eu, Gd, Tb, Y) phthalocyaninato double-deckers (λ_{max}: ca. 670–690 nm) and tetravalent cerium bis(phthalocyaninato) complexes (λ_{max}: 649 nm) [13–15,20,23,44]. This result is in good

Table 1
Characteristic Raman bands of phthalocyanine for $RE(Pc)_2$, $RE(Pc^*)_2$, RE(Pc)(Pc*) [RE = Eu, Y; Pc* = $Pc(C_7H_{15})_8$, $Pc(OC_5H_{11})_8$, $Pc(OC_5H_{11})_8$], $Ce(Pc')_2$ [Pc′ = Pc, $Pc(OC_8H_{17})_8$] [a]

1	2	3	4	5	6	6′	7	8	9	10	Assignment
576 w	576 w	576 w	564 w	562 w	564 w	562 w	565 w		580 m	563 m	
	627 w		627 w	628 w	626 w	628 w				625 w	macrocycle breathing
679 m	681 m	681 m	684 s	684 s	684 s	684 s	688 m	686 m	678 s	681 s	macrocycle breathing
740 m	742 m	743 m	744 m	743 s	743 s	742 s	744 w	757 w	742 s	741 m	δ macrocycle
779 w	783 w	781 w	769 m	782 w	783 w	783 w	759 m		776 m	783 w	ν C–N (aza)
815 w	813 w	814 w	864 sh	868 w	868 w	868 w			822 m	866 m	
937 w	937 w								934 m	934 w	benzene breathing
1030 w	1031 m		1078 w	1080 w	1079 w	1067 w			1026 w	1026 w	δ C–H
1103 m	1104 m		1108 w			1109 w	1115 w	1114 w	1104 m	1107 w	δ C–H
1146 m	1140 m	1105 m	1134 m	1132 m	1135 m	1134 m	1136 m	1135 m	1142 m	1137 m	pyrrole breathing
1174 w	1174 w	1142 m	1175 m	1172 m	1172 m	1172 m			1192 m	1174 s	δ C–H
1216 m	1215 m	1176 w	1204 m	1204 w	1205 w	1205 w	1203 m	1205 m	1209 m	1201 m	δ C–H
		1218 m	1274 w	1273 m						1296 w	
1302 m	1301 m					1312 m			1303 m	1306 w	δ C–H
1331 m	1328 m	1303 m	1323 m	1321 m	1320 m				1332 sh		
1346 m	1343 m	1334 m	1340 sh	1349 sh	1339 sh	1338 w	1340 m	1338 m	1339 s	1346 w	ν C_α–C_β(pyrrole)
1362 w	1365 w	1345 m				1384 w					
1403 sh	1413 sh		1406 m	1406 m	1409 m	1404 m	1403 m	1398 m	1424 m	1407 s	ν C=N
1414 m							1409 w				
1449 w	1448 w		1443 w	1441 w	1441 w		1447 w		1450 m	1433 s	ν C=N
									1500 s	1500 s	ν C_β–C_β(pyrrole)
1515 s	1516 s	1520 s	1514 s	1515 s	1516 s	1512 s	1522 s	1515 s			ν C=N (aza)
	1536 w			1596 w			1613 w			1599 w	ν benzene

[a] $Eu(Pc)_2$ (**1**), Eu(Pc)[$Pc(OC_5H_{11})_8$] (**2**), Eu(Pc)[$Pc(C_7H_{15})_8$] (**3**), Eu[$Pc(OC_5H_{11})_8]_2$ (**4**), Gd[$Pc(OC_8H_{17})_8]_2$ (**5**), Tb[$Pc(OC_8H_{17})_8]_2$ (**6**), Eu[$Pc(OC_8H_{17})_8]_2$ (**6′**) (λ_{ex} = 780 nm), Y[$Pc(C_7H_{15})_8]_2$ (**7**), Eu[$Pc(C_7H_{15})_8]_2$ (**8**), $Ce(Pc)_2$ (**9**), Ce[$Pc(OC_8H_{17})_8]_2$ (**10**).

accordance with the conclusions of Aroca and Tran-Thi [37,55,56] and with the experimental data reported by Homborg [30,31,51,57–59]. When trying to use the Langmuir–Blodgett films of $RE(Pc')_2$ as tobacco smoke sensors, Aroca and co-workers found that the radical-containing green form $RE(Pc')_2$ was reduced after chemisorption of the tobacco side stream smoke to the blue form $[RE(Pc')_2]^-$, which showed a different pattern of relative intensities in the surface-enhanced Raman spectrum (612 nm excitation) compared to the original green sample [56]. Most significantly, the band at 1513 cm^{-1} for green $Pr[Pc(^tBu)_4]_2$ shifts to 1493 cm^{-1} for blue $\{Pr[Pc(^tBu)_4]_2\}^-$.

It is worth noting that the use of the 780 nm excitation laser line does not induce any significant change in the Raman spectra of $RE[Pc(OC_8H_{17})_8]_2$. The Raman spectrum of $Eu[Pc(OC_8H_{17})_8]_2$ (λ_{ex}: 780 nm) is just identical with that measured by means of the 632.8 nm laser line (Table 1). This result is consistent with those of Homborg on $RE(Pc)_2$ [30,31,51,52] and is probably due to the fact that neither laser line is in close resonance with the electronic absorption band of $RE[Pc(OC_8H_{17})_8]_2$. When Homborg used excitation wavelengths even farther removed from the Q absorption, namely between 457 and 514 nm, an intense band at ca. 1595 cm^{-1} for all the radical anion-containing double-deckers $M^{III}(Pc)_2$ (M = La, Nd, Gd, Ho, Lu, Bi, Y, In) [30,31,51,52] was also observed.

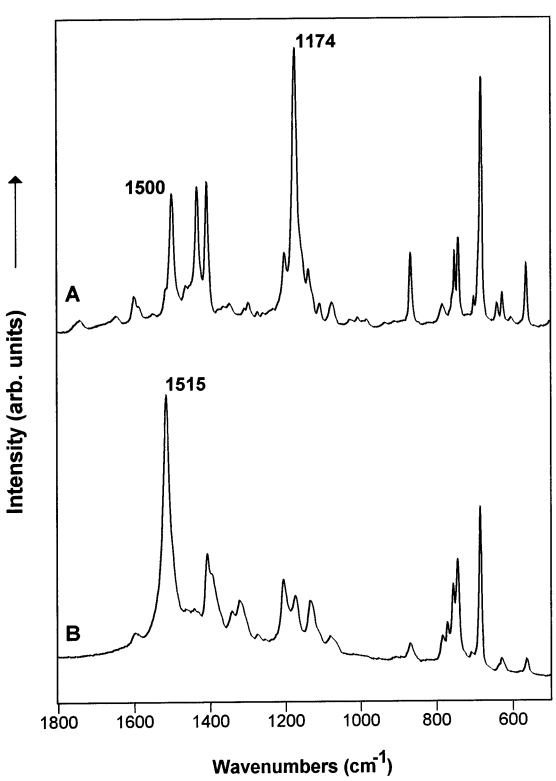


Fig. 1. Raman spectra of (A) $Ce^{IV}[Pc(OC_8H_{17})_8]_2$ and (B) $Gd^{III}[Pc(OC_8H_{17})_8]_2$.

Table 2
Characteristic Raman bands of phthalocyanine for (Pc)RE(Pc*)RE(Pc*) and (Pc)Eu(Pc*)Er(Pc*) [Pc* = $Pc(OC_5H_{11})_8$] [a]

11	12	13	14	Assignment
565 w	565 w	565 w	567 w	
577 w	577 w	579 w	577 m	
628 w	628 w	628 w	628 w	
633 w	633 w	633 w	638 w	
681 m	680 m	681 m	681 s	macrocycle breathing
728 w	728 w	728 w		
744 m	745 m	745 m	744 m	δ macrocycle
766 w	766 w	766 w	765 sh	ν C–N (aza)
781 w	781 w	781 w	777 w	
817 w	817 w	819 w	817 m	
867 m	867 m	869 m	869 w	
934 w	934 w	938 w	933 w	benzene breathing
984 w	984 w	984 w		
1006 w	1006 w	1006 w	1005 w	δ C–H
1028 w	1028 w	1029 w	1027 w	δ C–H
1079 w	1079 w	1079 w		
1106 w	1105 w	1105 w	1103 w	δ C–H
1124 sh	1124 sh	1124 sh	1124 w	δ C–H
1138 m	1138 m	1138 m	1136 m	pyrrole breathing
1177 m	1177 m	1176 m	1174 m	δ C–H
1201 m	1201 m	1197 m	1194 m	δ C–H
1302 m	1303 m	1304 m	1301 m	δ C–H
1337 m	1337 m	1337 m	1337 m	ν C_α–C_β(pyrrole)
1359 w	1361 w	1363 w	1361 w	
1402 m	1405 m	1410 m	1413 m	ν C=N
1446 m	1447 m	1448 m	1446 m	ν C=N
1498 s	1502 s	1505 s	1500 s	ν C_β–C_β(pyrrole)
1525 sh	1527 sh	1527 sh	1526 sh	ν C=N (aza)
1601 w	1601 w	1601 w	1598 w	ν benzene

[a] (Pc)Eu(Pc*)Eu(Pc*) (**11**), (Pc)Tb(Pc*)Tb(Pc*) (**12**), (Pc)Er(Pc*)Er(Pc*) (**13**), (Pc)Eu(Pc*)Er(Pc*) [Pc* = $Pc(OC_5H_{11})_8$] (**14**).

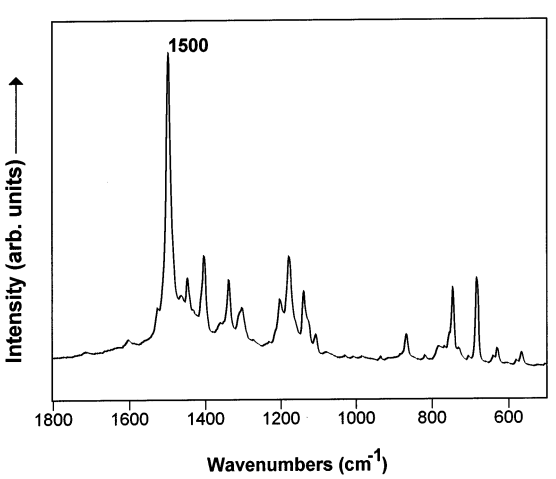


Fig. 2. Raman spectrum of (Pc)Eu[$Pc(OC_8H_{17})_8$]Eu[$Pc(OC_8H_{17})_8$].

3.2. Raman characteristics of homo-dinuclear triple-deckers (Pc)RE(Pc*)RE(Pc*) and hetero-dinuclear triple-deckers (Pc)Eu(Pc*)Er(Pc*)

Our Raman results for triple-decker (Pc)RE(Pc*)-RE(Pc*) (RE = Eu, Tb, Er) and (Pc)Eu(Pc*)Er(Pc*) [Pc* = $Pc(OC_8H_{17})_8$] are collected in Table 2 and assigned based on the partial assignment for the double-deckers $RE(Pc')_2$. Fig. 2 shows the Raman spectrum of triple-decker $Eu_2(Pc)(Pc^*)_2$ [Pc* = $Pc(OC_8H_{17})_8$], which is typical of this class. To a large degree, these spectra are quite similar to that of $Ce^{IV}[Pc(OC_8H_{17})_8]_2$ instead of to those of other tervalent rare earth bis(phthalocyaninato) compounds. The most intense band for all four of these triple-deckers is the one attributed to the ν_3 porphyrin-like mode which has contributions from C=C (pyrrole) and C=N (aza group) stretches around 1500 cm^{-1} as in $Ce^{IV}(Pc')_2$. This is due to the similar electronic structure of phthalocyanine rings in $RE_2^{III}(Pc^{2-})(Pc^{*2-})_2$ and $Ce^{IV}(Pc^{*2-})_2$ and the correspondingly similar electronic absorption properties for these two kinds of sandwiches. The most intense electronic absorptions in triple-deckers $RE_2^{III}(Pc^{2-})(Pc^{*2-})_2$ and double-deckers $Ce^{IV}(Pc^{*2-})_2$ are their Q bands around 639–643 and 649 nm, respectively, both of which are in close resonance with the excitation line (632.8 nm). This contrasts with the results for $RE^{III}(Pc')_2$ which have Q band maxima between 670 and 690 nm. The similarity of the Raman spectra of $RE_2^{III}(Pc^{2-})(Pc^{*2-})_2$ and $Ce^{IV}(Pc^{*2-})_2$ confirms that the existence of the monoanion radical $Pc^{\bullet-}$ in $RE^{III}(Pc')_2$ is responsible for the different Raman characteristics between the double-deckers $RE^{III}(Pc^*)_2$ and $Ce^{IV}(Pc^*)_2$ mentioned above. This conclusion is consistent with those derived from the IR measurements [24].

3.3. Raman characteristics of $RE(Nc^*)_2$ [Nc* = $Nc(^tBu)_4$, $Nc(SC_{12}H_{25})_8$]

In contrast to the situation of bis(phthalocyaninato) rare earth compounds, neither the synthesis nor the spectroscopic characterisation of bis(naphthalocyaninato) rare earth compounds has been extensively studied. Before our work on both the synthesis and the IR spectroscopic characterisation for the substituted $RE[Nc(^tBu)_4]_2$ [43,60], $Eu[Nc(SC_{12}H_{25})_8]_2$ [43], and RE(TPyP)(Nc′) [8], only the synthesis, electronic absorption, and electrochemical properties of unsubstituted naphthalocyanine-containing $Lu(Nc)_2$, Lu(Pc)-(Nc), and $Lu_2(Nc)_3$ had been described by L'Her, Simon and Ishikawa [61–67]. Recently L'Her and coworkers briefly described the IR spectroscopic results for $Lu(Nc)_2$ and Lu(Pc)(Nc) [62]. However, there has been no previous report on the Raman spectroscopic properties of sandwich naphthalocyaninato rare earth complexes.

By analogy to the Raman characteristics of sandwich phthalocyaninato rare earth compounds, the Raman characteristics of $RE(Nc^*)_2$ [Nc* = $Nc(^tBu)_4$,

$Nc(SC_{12}H_{25})_8]$ and $[Eu(Nc^*)_2]^+$ [$Nc^* = Nc(^tBu)_4$] were partially assigned and are summarised in Table 3. Fig. 3 shows the Raman spectrum of $Tb(Nc^*)_2$ [$Nc^* = Nc(^tBu)_4$]. Due to the similar electronic structure and electronic absorption properties among the whole series of naphthalocyaninato double-decker complexes, all these compounds show similar Raman characteristics. Moreover, the fact that the Raman spectrum of $Eu(Nc^*)_2$ is similar to that of $[Eu(Nc^*)_2]^+$ indicates that removing an electron from $Eu(Nc^*)_2$ does not change the corresponding Raman marker bands significantly. This is also comparable with the result of Homborg on the resonance Raman spectra of $RE(Pc)_2$ and $[RE(Pc)_2]^+$ [31,53]. Probably because the excitation laser line (632.8 nm) used in this experiment is far away from resonance with the most intense Q absorption band of $RE(Nc^*)_2$ (767–799 nm), the *ortho*-disubstituted benzene quadrant stretchings around 1590 cm^{-1} appear as the most intense band instead of those from pyrrole C=C group and C=N aza group stretchings at 1510 and 1520 cm^{-1}. This postulate is confirmed by exciting the Raman spectra with the 780 nm laser line, which is in resonance with the Q absorption band of naphthalocyaninato rare earth double-deckers. The Raman spectra of $Tb(Nc^*)_2$ [$Nc^* = Nc(^tBu)_4$] excited at the two wavelengths are compared in Fig. 3. With excitation by 780 nm light, the peak at ca. 1520 cm^{-1} becomes the most intense band in that region of the

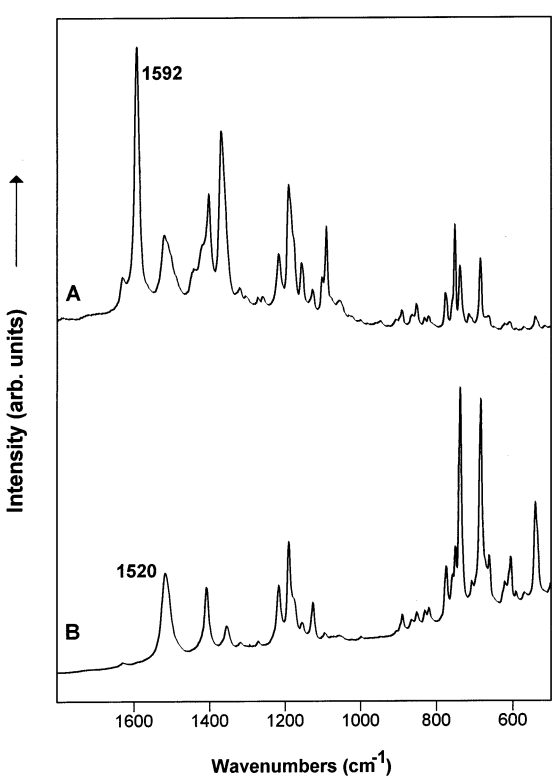


Fig. 3. Raman spectra of $Tb[Nc(^tBu)_4]_2$ with excitation at (A) 632.8 and (B) 780 nm.

resonance Raman spectra of $RE(Nc^*)_2$ [RE = Tb, Er; $Nc^* = Nc(^tBu)_4$] and no band around 1590 cm^{-1} attributed to the *ortho*-disubstituted benzene quadrant stretchings was observed. This result is consistent with the above-mentioned result for $RE(Pc^*)_2$ [RE = Eu, Nd; $Pc^* = Pc(OC_8H_{17})_8$] and those of Homborg on $RE(Pc)_2$ [30,31,51,52]. The other frequencies are assigned to the various vibrational fundamentals based on the work on phthalocyaninato double- and triple-deckers detailed above.

3.4. Raman characteristics of RE(Por)(Pc′) (Pc′ = Pc, Pc), HEu(TPyP)(Pc), and Eu(Por)(Nc)*

We begin this section by noting that for the purpose of comparison, the Raman spectrum of monomeric Tb[T(4-Cl)PP]acac excited at 632.8 nm was also recorded and the data are included in Table 4. The spectrum of this complex is comparable to the preresonance Raman spectrum of Zn(TPP) excited at 1064 nm reported by Tran-Thi et al. [37]. As also noted by Tran-Thi, the porphyrin ligand and the Pc ligand can be easily distinguished by both the frequencies of their respective characteristic Raman bands and their different intensity patterns. The band in the region near 1500 cm^{-1} for the Pc moiety played an important role in this respect. Furthermore, the Q_y absorption bands of phthalocyanines are generally at longer wavelengths and thus are in closer resonance to the 632.8 nm laser line than are those of porphyrins, so the phthalocyanine contributions appear to dominate the Raman spectra in the mixed Por–Pc′–RE sandwich compounds, as described below.

The characteristic Raman bands for RE(Por)(Pc′) (Pc′ = Pc, Pc*) (λ_{max}: 467–476 nm), HEu(TPyP)(Pc) (λ_{max}: 640 nm), and RE(Por)(Nc) (λ_{max}: 630 nm) are organised in Table 4. The characteristic Raman spectroscopic patterns of Ce(TPyP)(Pc) are similar to those of Ce(TPP)(Pc) reported by Tran-Thi [37] but with minor band-shifts and different relative intensities probably due to the different excitation wavelengths. The Raman marker band for Pc^{2-} appears as an intense band at 1493 cm^{-1}, which downshifts about 7 cm^{-1} compared with that in $Ce(Pc')_2$ but corresponds well with that in the triple-deckers $RE_2(Por)_2(Pc)$ and $RE_2(Por)(Pc')_2$ as will be discussed below. It is reasonable that the Raman spectrum of HEu(TPyP)(Pc) is very similar to that of Ce(TPyP)(Pc) due to their identical macrocycle oxidation level and hence electronic structure and electronic absorptions. When the protonated HEu(Por)(Pc) is oxidised to Eu(Por)(Pc′) (Pc′ = Pc, Pc*) which contains phthalocyanine monoanion radical $Pc^{\bullet -}$, the previously intense band at 1493 cm^{-1} for Pc^{2-} in Ce(TPyP)(Pc) and HEu(TPyP)(Pc) remains as a very weak band. Meanwhile, a relatively intense band appears in the region of 1513–1518 cm^{-1}. The

Table 3
Characteristic Raman bands of phthalocyanine for $RE(Nc^*)_2$ [RE = La, Pr, Nd, Eu, Gd, Tb, Er, Y; $Nc^* = Nc(^tBu)_4$, $Nc(SC_{12}H_{25})_8$] [a]

15	16	17	18	19	20	21	21′	22	23	23′	24	25	Assignment
571 w	539 w	538 w	538 w	538 w	564 w	538 w	539 m	539 w	538 w	540 m	552 w	536 w	
		612 w	608 w	608 w	613 w	606 w	604 w	607 w	607 w	604 w	565 w	570 w	
	666 w	666 w	665 w	663 w	640 w	662 w	660 w	661 sh	664 sh	660 w	580 w	665 w	macrocycle breathing
683 m	682 w	681 w	683 m	684 m	681 w	683 w	682 s	684 m	684 m	683 s	670 w	683 w	macrocycle breathing
	714 w	714 w	713 w	712 w	704 w	714 m	705 w	712 w	713 w	706 w	689 m	713 w	
	736 w	735 w	736 w	737 w	736 m	737 m	736 s	737 m	738 m	738 s	737 m	736 w	δ macrocycle
	751 m	749 m	751 m	751 m	756 m	751 m	749 sh	751 m	752 m	751 sh	751 w	751 m	ν C–N (aza)
	776 w	774 w	776 w	776 w	776 w	774 w	772 w	774 w	775 w	774 w	783 m	775 w	
	820 w	820 w	819 w	819 w		819 w	818 w	819 w	820 w	818 w		818 w	
	850 w	850 w	850 w	851 w	851 w	850 w	850 w	851 w	852 w	850 w	863 m	864 w	
	890 w	890 w	890 w	890 w	894 w	889 w	887 w	889 w	891 w	889 w	892 w	900 w	
1087 m	1089 m	1088 m	1089 m	1090 m	1093 m	1090 m	1093 w	1090 m	1090 m	1093 w	1089 m	1089 m	δ C–H
1124 w	1126 w	1124 w	1126 w	1126 w	1122 w	1125 w	1124 m	1125 w	1126 w	1125 m	1128 m	1126 w	δ C–H
1155 w	1156 m	1154 m	1155 m	1155 m	1147 m	1155 m	1153 w	1155 m	1155 m	1153 w		1155 w	pyrrole breathing
1185 m	1191 m	1189 m	1191 m	1189 m	1190 m	1189 m	1189 m	1188 m	1189 m	1189 m	1188 s	1186 m	δ C–H
1218 w	1218 m	1216 m	1217 m	1217 m	1216 m	1215 m	1215 m	1215 m	1215 m	1215 m	1212 m	1216 w	δ C–H
	1261 w	1258 w	1259 w	1258 w	1264 w	1258 w		1258 w	1258 w		1256 w	1257 w	
	1272 w	1272 w	1271 w	1271 w		1271 w	1269 w	1270 w	1271 w	1270 w		1271 w	
	1301 w	1301 w	1300 w		1304 w	1303 w		1303 w	1303 w		1299 m	1302 w	δ C–H
	1320 w	1318 w	1319 w	1319 w	1324 w	1319 w	1317 w	1318 w	1318 w	1317 w	1346 w	1321 w	
1368 m	1368 s	1367 s	1369 s	1369 s	1366 s	1368 s	1353 w	1369 s	1369 s	1355 w	1366 m	1368 s	ν C_α–C_β(pyrrole)
1401 w	1400 m	1399 m	1400 m	1401 m	1399 m	1401 m	1407 m	1402 m	1404 m	1409 m	1404 s	1400 m	ν C=N
	1416 sh	1416 sh	1418 sh	1418 sh		1418 sh		1418 sh	1420 sh			1419 w	ν C=N
	1442 sh	1442 sh	1441 sh	1444 sh	1460 w	1439 sh		1441 sh	1442 sh		1456 w		
1509 m	1504 m	1505 m	1502 m	1506 m	1515 s	1518 m	1516 s	1520 m	1523 m	1522 s	1509 s	1508 w	ν C_β–C_β(pyrrole)
1590 w	1591 s	1590 s	1591 s	1591 s	1593 s	1592 s		1592 s	1593 s		1583 s	1592 s	ν naphthalene
1628 w	1629 w	1628 w	1628 w	1628 w	1623 w	1628 w	1627 w	1628 w	1628 w	1628 w	1623 m	1627 w	

[a] $La(Nc^*)_2$ (**15**), $Ce(Nc^*)_2$ (**16**), $Pr(Nc^*)_2$ (**17**), $Nd(Nc^*)_2$ (**18**), $Eu(Nc^*)_2$ (**19**), $Gd(Nc^*)_2$ (**20**), $Tb(Nc^*)_2$ (**21**), $Y(Nc^*)_2$ (**22**), $Er(Nc^*)_2$ (**23**) [$Nc^* = Nc(^tBu)_4$], $Eu[Nc(SC_{12}H_{25})_8]_2$ (**24**), $[Eu(Nc^*)_2]^+$ (**25**), $Tb(Nc^*)_2$ (**21′**) ($\lambda_{ex} = 780$ nm), $Er(Nc^*)_2$ (**23′**) ($\lambda_{ex} = 780$ nm).

Table 4
Characteristic Raman bands of phthalocyanine for RE(Por)(Pc) [RE = Eu, Ce; Por = TPP, T(4-Cl)PP, TPyP], Eu(Por)[Pc(C_7H_{15})$_8$] [Por = TPP, TPyP, T(4-Cl)PP, T(4-^{t}Bu)PP], Eu(Por)(Nc) [Por = TPyP, T(4-Cl)PP], HEu(TPyP)(Pc), and Tb[T(4-Cl)PP]acac [a]

26	**27**	**28**	**29**	**30**	**31**	**32**	**33**	**34**	**35**	**36**	**37**	**35′**	Assignment
574 w	586 w	573 w	577 w	579 w	575 w		564 w	573 w	568 w			559 w	
623 w					622 w		625 w		610 w			611 w	
637 w					664 w			662 w		611 w		638 w	macrocycle breathing
680 s	678 m	676 m	675 m	680 m	689 w	688 m	689 m	690 w	680 w	679 m	686 w	680 s	macrocycle breathing
702 w						718 w	708 w	709 w	698 w		708 w		
720 w		734 sh	741 m	718 w	719 w	747 m	723 w	722 w	732 w	733 w	749 w	734 s	δ macrocycle
744 s	743 s	743 m		741 m	747 w	781 w	744 m	748	752 w	758 w		755 w	ν C–N (aza)
773 w	774 w	783 w	796 w	797 sh	796 w	795 w		760 w		781 w		797 w	
816 m	813 m	811 m	811 w	812 m	823 m	846 w	809 w	807 m		798 w	806 m	820 w	
836 w	865 w		865 w	867 w	843 w	868 w	847 w	846 w	840 w	844 w		844 w	
884 w	895 w	888 w	893 w	895 w	882 w	894 w	889 w	889 w				890 w	
938 w	939 w	937 w	933 w	937 w	937 w					957 w			
979 w	983 w	983 m	983 w	984 w	979 w	983 m	983 w	981 w	978 w	980 w		982 m	
1002 m	998 m	1002 w	1001 m	1000 m	1001 w	1000 m	1000 sh	1000 w		999 w	1005 s	998 m	δ C–H
	1074 w				1067 w					1062 w	1074 m	1075 w	δ C–H
1087 w	1091 w		1088 w	1085 w		1085 w	1084 w	1084 w	1089 m	1092 s		1088 w	
1105 w			1101 w	1105 w								1096 w	δ C–H
1119 w	1118 w	1113 w	1118 w	1117 w	1114 w	1115 w	1122 w	1115 w	1121 w	1123 m		1124 w	δ C–H
1140 m	1137 m		1137 w	1136 w	1136 w	1137 w	1136 m	1136 w	1147 w	1149 m		1147 w	pyrrole breathing
			1159 w	1175 w						1174 w	1176 w		δ C–H
1201 m	1198 w		1232 w		1211 s	1222 m	1208 s	1218 s	1216 w	1221 w	1235 m	1223 m	δ C–H
	1237 w		1254 m	1237 m		1234 sh	1226 w	1260 w			1262 w	1276 w	
1274 w	1278 m	1299 w	1297 w	1279 w	1281 w	1278 w	1277 w	1297 w					δ C–H
1303 w	1301 sh			1319 sh	1308 m	1315 w	1305 w	1315 m		1305 w		1312 w	
1331 m					1329 m			1328 w		1322 w		1334 sh	ν C_α–C_β(pyrrole)
1340 m	1340 s	1339 w	1339 s	1338 m		1339 m	1339 m				1342 s		
1349 sh	1356 m		1359 s	1356 m	1352 sh	1356 m	1352 sh	1352 w	1350 s	1357 s		1352 m	
1391 w	1399 w	1390 w	1382 m	1394 w	1391 m	1392 m	1389 w	1390 w	1395 m	1403 m	1409 w	1403 w	ν C–N
1423 w	1425 w		1425 w	1423 w	1413 w	1414 w	1412 w		1422 w	1425 m		1423 w	
1462 w	1447 w		1444 w	1442 w	1462 m	1439 w	1436 w	1436 w		1437 sh	1444 w	1469 w	ν C–N
1493 w	1494 s	1488 w	1493 s	1493 s	1497 sh	1493 s	1491 m	1491 w	1496 m	1505 m	1495 w	1499 m	ν C_β–C_β(pyrrole)
	1517 m			1514 sh	1518 sh	1513 m		1515 sh	1521 w				ν C=N (aza)
1537 m	1534 sh	1532 m	1547 s	1545 m	1537 s	1541 s	1534 s	1537 s		1533 m	1541 m	1528 m	
	1545 m		1590 w	1593 w	1594 w	1592 m		1592 w	1587 s	1596 s	1582 w	1596 w	ν benzene
						1611 sh						1621 w	

[a] Eu(TPP)(Pc) (**26**), Eu(TPyP)(Pc) (**27**), Eu[T(4-Cl)PP](Pc) (**28**), Ce(TPyP)(Pc) (**29**), HEu(TPyP)(Pc) (**30**), Eu(TPP)[Pc(C_7H_{15})$_8$] (**31**), Eu(TPyP)[Pc(C_7H_{15})$_8$] (**32**), Eu[T(4-^{t}Bu)PP][Pc(C_7H_{15})$_8$] (**33**), Eu[T(4-Cl)PP][Pc(C_7H_{15})$_8$] (**34**), Eu(TPyP)(Nc) (**35**), Eu[T(4-Cl)PP](Nc) (**36**), Tb[T(4-Cl)PPacac (**37**), Eu(TPyP)(Nc) (**35′**) (λ_{ex} = 780 nm).

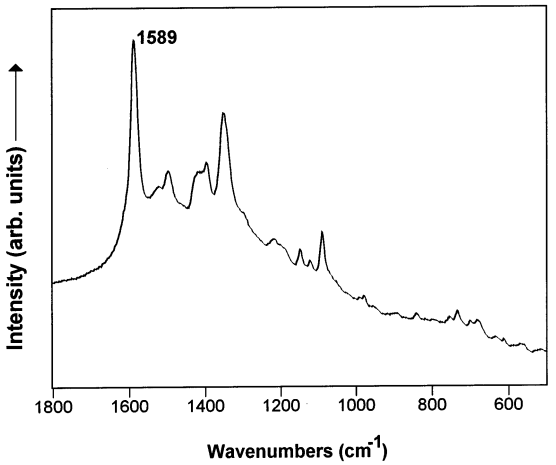


Fig. 4. Raman spectrum of Eu(TPyP)(Nc).

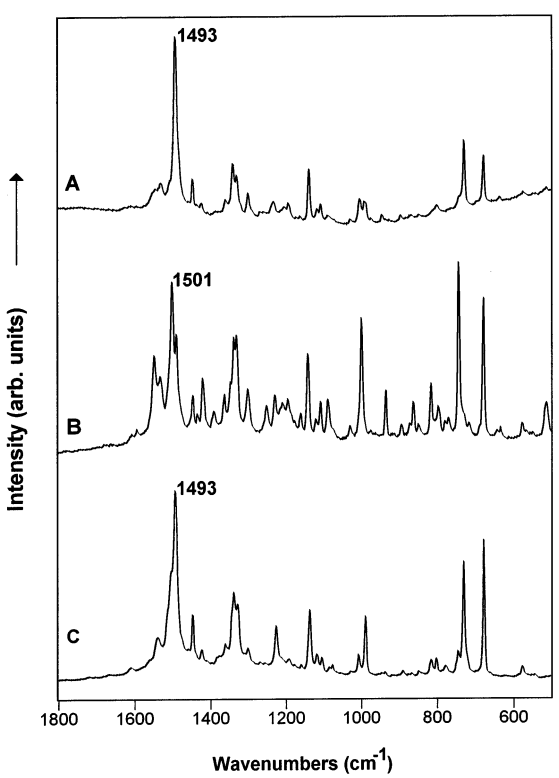


Fig. 5. Raman spectra of (A) (TPyP)Ce(Pc)Ce(TPyP), (B) (Pc)Ce(TPyP)Ce(Pc), and (C) [T(4-^{t}Bu)PP]Eu(Pc)Eu(Pc).

spectrum for Eu[T(4-Cl)PP](Pc) was of poor quality due to the strong fluorescence under the conditions of our Raman measurements.

The Raman spectrum of Eu(TPyP)(Nc) is exhibited in Fig. 4. The spectra for the compounds Eu(Por)(Nc) [Por = TPyP, T(4-Cl)PP] are obviously dominated by the contributions from the naphthalocyanine monoanion radical, $Nc^{\bullet -}$. Except for slight band-shifts and slightly different relative intensities, the Raman spectroscopic patterns of Eu(Por)(Nc) are virtually the same as those of $RE(Nc^*)_2$ [$Nc^* = Nc(^tBu)_4$].

As expected from the change in the Raman spectra of $RE(Nc^*)_2$ induced by the change of excitation source, similar changes took place in the Raman spectrum of Eu(TPyP)(Nc) when 780 nm light was applied. The peak at ca. 1528 cm^{-1} gains intensity and becomes the most intense band in the resonance Raman spectrum of Eu(TPyP)(Nc), while the most intense band at 1587 cm^{-1} under 632.8 nm excitation, attributed to the *ortho*-disubstituted benzene quadrant stretchings, loses most of its intensity and appears as a very weak band.

3.5. Raman characteristics of $RE_2(Por)_2(Pc)$, $RE_2(Por)_2(Pc^*)$, $RE_2(Por)(Pc)_2$, $RE_2(Por)(Pc^*)_2$, $(Por)RE(Pc^*)RE'(Pc^*)$

The Raman characteristic bands together with partial assignment according to the above-described conclusions for $RE_2(Por)_2(Pc)$ (λ_{max}: 600–610 nm), $RE_2(Por)(Pc)_2$ (λ_{max}: 615–620 nm), $RE_2(Por)(Pc^*)_2$, and $(Por)RE(Pc^*)RE'(Pc^*)$ (λ_{max}: 610–660 nm) are summarised in Table 5. Fig. 5 compares the Raman spectra of (TPyP)Ce(Pc)Ce(TPyP), (Pc)Ce(TPyP)Ce(Pc), and [T(4-^{t}Bu)PP]Eu(Pc)Eu(Pc). The similarity among these three clearly suggests that the spectra for all these kinds of triple-deckers are dominated by Pc^{2-} contributions. There is no obvious band that can be ascribed to the Por moiety. In both series of triple-deckers (Por)RE(Pc)RE(Por) and (Por)RE(Pc)RE(Pc), the ν_3 porphyrin-like mode (of the Pc moiety) shows a strong band at ca. 1493 cm^{-1}, while for (Pc)Ce(TPyP)Ce(Pc), this mode displays a strong band at 1501 cm^{-1} along with a shoulder at 1490 cm^{-1}. All these results are in good correspondence with those of Tran-Thi for solution-state FT-Raman spectra (1064 nm) of (TPP)RE(Pc′)RE(TPP) [RE = Ce, Gd, Pc′ = Pc, $Pc(OMe)_8$] and (Pc)Ce[T(4-OMe)PP]Ce(Pc), apart from a blue shift by an average of 3–4 cm^{-1}. It is interesting that the characteristic pattern of the Raman spectra for these three kinds of triple-deckers are so similar despite the widely differing excitation wavelength used in our experiments.

For the purpose of comparison, the Raman spectra of (TPP)Gd(Pc)Gd(TPP) and (TPP)Gd(Pc)Gd(Pc) with excitation at 780 nm were also recorded and the data are included in Table 5. It is reasonable that they are quite similar to those of their analogues excited with 632.8 and 1064 nm as described above.

As can be expected from the above results on phthalocyaninato rare earth double-deckers, the introduction of alkyl or alkoxyl substituents onto the periphery of phthalocyanine rings in triple-deckers (Por)RE(Pc)RE′(Pc) does not cause significant changes in the Raman spectra. Furthermore, the close similarity among the Raman spectra of (TPyP)Y(Pc*)Y(Pc*), (TPyP)Y(Pc*)Eu(Pc*), and (TPyP)Eu(Pc*)Y(Pc*) [$Pc^* = Pc(C_7H_{15})_8$] indicates that variation of rare earth

Table 5
Characteristic Raman bands of phthalocyanine for $RE_2(Por)_2(Pc)$ and $RE_2(Por)(Pc')_2$ [RE = Eu, Ce; Por = TPP, T(4-Cl)PP, T(4-OMe)PP, T(4-^{t}Bu)PP, OEP; Pc′ = Pc, $Pc(C_7H_{15})_8$] [a]

38	**39**	**40**	**41**	**42**	**43**	**44**	**45**	**46**	**47**	**48**	**49**	**50**	**51′**	**52′**	Assignment
543 w					547 w	561 w								549 w	
	576	575 w	576 w			582 w			569 w		572 w	573 w	573 w	577 m	
	637 w		638 w		635 w	634 w			635 w			635 w	622 w		
						669 w	658 w	658 w			658 w		660 w		macrocycle breathing
677 s	676 m	677 s	678 s	682 m	688 m	689 m	689 m	687 m	681 m	681 m	676 m	678 m	676 m	675 s	macrocycle breathing
	709 w		715 w		715 w	716 w	716 w	716 w		708 w			702 w		
730 s	730 m	730 s			730 m	730 w	730 m	730 m	727 s		730 s	729 m	727 m	729 w	
744 w			742 s	746 m	742 m	749 w	747 m	747 m		745 m	748 w	741 sh		741 s	δ macrocycle
776 w	779 w	780 w	769 w		776 w	776 w	775 w	776 w			782 w		762 w	766 w	ν C–N (aza)
					791 w	792 w	791 w	792 w							
801 w	802 sh	801 w	796 w		805 w	808 w	806 w	805 w	802 w	813 w	800 w	799 w	799 m	799 w	
814 w	811 w	815 w	815 m								812 w		826 m	816 m	
847 w	845 w	845 w	847 w		849 w	850 w	850 w	849 w				847 w	842 w		
			861 m		872 w	873 w	872 w				865 w	867 w			
889 w	883 w	888 w	893 w		895 m	896 w	895 m	895 w	884 w		889 w	895 w	882 w		
			934 m						929 w		946 w	944 w	945 w	932 m	
988 m	987 m	989 m			992 m	995 m	992 m	993 m	985 m	981 w	986 m	990 w	984 m	984 w	
1006 w	1004 m	1006 w	999 s		1006 m	1008 m	1006 m	1006 m	1006 m	1000 m	1005 m	1003 m	1001 m	1004 w	δ C–H
		1027 w	1029 w		1032 w	1032 w	1032 w		1033 w		1029 w		1030 w	1025 w	δ C–H
1076 w	1077 w	1076 w					1081 m		1063 w						
1084 w	1086 w	1087 w	1087 m		1082 m	1085 w		1084 m			1087 w	1088 w	1084 w		
1104 w	1104 w	1103 w	1107 m						1109 w		1106 w	1107 w	1107 w	1102 m	δ C–H
			1119 w		1117 w	1119 w	1119 w	1117 w		1120 w			1115 m	1115 w	δ C–H

Table 5 (*Continued*)

38	**39**	**40**	**41**	**42**	**43**	**44**	**45**	**46**	**47**	**48**	**49**	**50**	**51′**	**52′**	Assignment
1136 m	1137 m	1136 m	1140 m	1133 m	1135 m	1136 m	1136 m	1136 m	1141 m	1137 w	1135 m	1138 m	1136 m	1138 s	pyrrole breathing
1158 w			1160 w								1161 w	1161 w		1157 w	δ C–H
1177 w				1175 w	1177 w		1178 w	1177 w						1174 w	δ C–H
1190 w	1191 w	1190 w	1194 w	1203 w	1196 w		1194 w		1196 w		1191 w	1192 w	1194 w	1190 w	δ C–H
			1208 w		1213 w	1213 w								1208 m	δ C–H
1225 m	1227 m	1227 w	1228 w		1232 m	1229 m	1231 m	1232 m	1228 m	1230 m	1225 w	1232 w	1225 m		
	1260 w	1268 w	1250 w		1260 w	1258 w	1258 w	1258 w		1260 w			1265 w		
1268 w	1273 w				1273 m	1274 w	1272 m	1275 m		1280 w	1268 w	1268 w			
1300 w	1301 w	1300 w	1300 m						1302 w	1300 w	1301 w	1300 m	1301 w	1300 m	δ C–H
1328 m	1328 m	1326 sh	1331 s	1312 w	1325 w	1326 m	1326 w			1323 m	1330 m	1331 m	1327 m	1331 s	ν C_α–C_β(pyrrole)
1338 m		1336 m	1337 s		1333 w	1334 m		1333 m	1332 w	1339 w	1342 m	1340 m	1341 m		
	1342 m				1344 m	1349 m	1344 s	1346 m	1341 m	1355 m	1361 w	1359 w	1389 w		
1360 w	1358 w	1360 w	1363 w		1360 m	1361 m	1360 m	1361 m							
1422 w	1420 w	1426 w	1420 m	1406 m	1411 w	1415 w	1413 w	1410 w				1423 w		1418 w	ν C–N
1447 m	1446 w	1447 m	1446 w		1441 w	1444 w	1440 m	1444 m			1448 m	1447 m	1437 w	1445 m	ν C–N
					1460 w	1460 w	1463 w	1460 w	1488 w		1462 w				
1493 s	1492 s	1492 s	1490 s		1491 s	1494 s	1491 s	1493 s	1491 m	1491 s	1495 s	1493 s	1491 s	1494 s	ν C_β–C_β(pyrrole)
			1501 s	1500 s					1503 s	1519 w					
1538 w	1541 m	1540 m	1532 w	1542 w			1543 s		1538 m	1536 m	1541 m	1531 w	1539 m		ν C=N (aza)
	1564 w		1548 m		1545 m	1550 m		1550 s		1566 w	1548 m	1544 sh			
			1593 w		1593 w	1593 w	1595 w	1593 w		1590 w					ν benzene
1608 w	1609 w	1607 w	1607 w		1617 w	1616 w	1616 w	1616 w			1608 w	1608 w		1606 w	

[a] Eu_2[T(4-^{t}Bu)PP](Pc)$_2$ (**38**), Eu_2[T(4-Cl)PP](Pc)$_2$ (**39**), Eu_2[T(4-OMe)PP](Pc)$_2$ (**40**), (Pc)Ce(TPyP)Ce(Pc) (**41**), Eu_2(OEP)[Pc(OC_8H_{17})$_8$]$_2$ (**42**), Eu_2(TPyP)[Pc(C_7H_{15})$_8$]$_2$ (**43**), Y_2(TPyP)[Pc(C_7H_{15})$_8$]$_2$ (**44**), (TPyP)Eu[Pc(C_7H_{15})$_8$]Y[Pc(C_7H_{15})$_8$] (**45**), (TPyP)Y[Pc(C_7H_{15})$_8$]Eu[Pc(C_7H_{15})$_8$] (**46**), Eu_2(TPP)$_2$(Pc) (**47**), Eu_2[T(4-Cl)PP]$_2$(Pc) (**48**), Eu_2[T(4-^{t}Bu)PP]$_2$(Pc) (**49**), Ce_2(TPyP)$_2$(Pc) (**50**), Gd_2(TPP)$_2$(Pc) (**51′**) (λ_{ex} = 780 nm), Gd_2(TPP)(Pc)$_2$ (**52′**) (λ_{ex} = 780 nm).

metals in the triple-decker does not change significantly the electronic structure of phthalocyanine ligands in these triple-deckers. The strong fluorescence of (OEP)Eu[Pc(OC_8H_{17})$_8$]Eu[Pc(OC_8H_{17})$_8$] and the consequent poor quality of the Raman spectrum for this compound prevents us from further comparison of the effects of different porphyrin ligands on the Raman characteristics of phthalocyanine in the triple-deckers.

4. Conclusions

1. When the laser excitation is in close resonance with the Q band absorption of phthalocyanine-containing sandwich rare earths, the band at ca. 1500 cm^{-1} with contributions from both C=C (pyrrole) and C=N (aza group) stretches, is a good Raman marker band for the phthalocyanine dianion Pc'^{2-} (Pc′ = Pc, Pc*) in double-deckers $Ce^{IV}(Pc')_2$ [Pc′ = Pc, Pc(OC_8H_{17})$_8$] and triple-deckers (Pc)RE(Pc*)RE(Pc*) [Pc* = Pc(OC_8H_{17})$_8$]. In $Pc'^{\bullet -}$ radical anion-containing double-deckers $RE^{III}(Pc')_2$ (Pc′ = Pc, Pc(OC_5H_{11})$_8$, Pc(OC_8H_{17})$_8$, Pc(C_7H_{15})$_8$], this band blue-shifts to ca. 1515 cm^{-1}.
2. When the laser excitation is far away from resonance with the Q band absorption of double-decker naphthalocyaninato rare earth complexes, the strongly enhanced Raman band at ca. 1590 cm^{-1}, which is assigned to the benzene quadrant stretch of the Nc ring, is a typical feature of naphthalocyanine monoanion radical, $Nc^{*\bullet -}$, in RE(Nc*)$_2$ [Nc = Nc(^{t}Bu)$_4$, Nc($SC_{12}H_{25}$)$_8$].
3. The marker band of Pc^{2-} in double-deckers Ce^{IV}(TPyP)(Pc) and HEu(TPyP)(Pc), and triple-deckers (Por)RE(Pc)RE(Por), (Por)RE(Pc′)RE(Pc′) (Pc′ = Pc, Pc*) is located at ca. 1493 cm^{-1}, but is at 1501 cm^{-1} along with a shoulder at 1490 cm^{-1} for (Pc)Ce(TPyP)Ce(Pc). For $Pc'^{\bullet -}$ radical–anion in double-deckers RE^{III}(Por)(Pc′) (Pc′ = Pc, Pc*), the band appears at 1515 cm^{-1}.
4. In the Raman spectra of $RE^{III}(Pc')_2$ (Pc′ = Pc, Pc*), only the $Pc'^{\bullet -}$ π radical anion marker bands instead of those for both $Pc'^{\bullet -}$ and Pc'^{2-} are observed, which suggests that the hole in the double-decker phthalocyaninato rare earth compounds delocalises over both phthalocyanine rings on the Raman timescale. This result is in line with the conclusion deduced from the IR measurements [24] and also in good accordance with the fact that both $[Eu(Nc^*)_2]^+$ and Eu(Nc*)$_2$ [Nc* = Nc(^{t}Bu)$_4$] showed quite similar Raman marker bands in their Raman spectra as described above. For a wider assessment on the question of the nature of the (na)phthalocyanine ligands in the various sandwich complexes, and the physical techniques (EPR, X-ray crystallography, UV–Vis) applied to the problem, our review can be consulted [38].
5. The Raman microscope is a rapid and convenient experimental technique for recording the solid state Raman spectra of porphyrinato and (na)phthalocyaninato rare earth complexes.

Acknowledgements

The authors thank the National Natural Science Foundation of China (Grant No. 29701002, 29992590-4), the National Educational Ministry of China, the Science Committee of Shandong Province, Shandong University, and the Centre for Instrumental and Developmental Chemistry, Queensland University of Technology (Australia) for financial support. Thanks are also due to Professor Heiner Homborg for his kind informative discussions during the preparation of this manuscript.

Appendix A. List of abbreviations

H_2P	general phthalocyanine or porphyrin
$H_2(Pc')$	general phthalocyanine
H_2Pc	unsubstituted phthalocyanine
$H_2(Pc^*)$	substituted phthalocyanine
$H_2(Nc')$	general naphthalocyanine
H_2Nc	unsubstituted naphthalocyanine
$H_2(Nc^*)$	substituted naphthalocyanine
H_2[Pc(OC_5H_{11})$_8$]	2,3,9,10,16,17,23,24-octapentyloxyphthalocyanine
H_2[Pc(OC_8H_{17})$_8$]	2,3,9,10,16,17,23,24-octaoctyloxyphthalocyanine
H_2[Pc(C_7H_{15})$_8$]	2,3,9,10,16,17,23,24-octaheptylphthalocyanine
H_2[Nc(^{t}Bu)$_4$]	3(4),12(13),21(22),30(31)-tetra(*tert*-butyl)-2,3-naphthalocyanine
H_2[Nc($SC_{12}H_{25}$)$_8$]	3,4,12,13,21,22,30,31-octa(dodecylthio)-2,3-naphthalocyanine
$H_2(Por)$	general porphyrin
$H_2(OEP)$	2,3,7,8,12,13,17,18-octaethylporphyrin
$H_2(TPP)$	5,10,15,20-tetraphenylporphyrin
$H_2(TTP)$	5,10,15,20-tetra-*p*-tolylporphyrin
$H_2(TPyP)$	5,10,15,20-tetra(pyridyl)porphyrin
H_2[T(4-Cl)PP]	5,10,15,20-tetra(4-chloro)-phenylporphyrin
H_2[T(4-^{t}Bu)PP]	5,10,15,20-tetra(4-*tert*-butyl)-phenylporphyrin
H_2[T(4-OCH_3)PP]	5,10,15,20-tetra(4-methoxy)-phenylporphyrin

$H_2[T(4\text{-}OC_{12})PP]$	5,10,15,20-tetra(4-dodecyloxy)-phenylporphyrin
Hacac	acetylacetone
RE	rare earth

References

[1] I.S. Kirin, P.N. Moskalev, Yu.A. Makashev, Russ. J. Inorg. Chem. 10 (1965) 1065.
[2] I.S. Kirin, P.N. Moskalev, N.V. Ivannikova, Russ. J. Inorg. Chem. 12 (1967) 497.
[3] J.-J. Andre, K. Holczer, P. Petit, M.-T. Riou, C. Clarisse, R. Even, M. Fourmigue, J. Simon, Chem. Phys. Lett. 115 (1985) 463.
[4] D. Markovitsi, T.-H. Tran-Thi, R. Even, J. Simon, Chem. Phys. Lett. 137 (1987) 107.
[5] M. Mardru, G. Guillaud, M. Al Sadoun, M. Maitrot, C. Clarisse, M. Le Contellec, M.J.-J. Andre, J. Simon, Chem. Phys. Lett. 142 (1987) 103.
[6] P. Turek, P. Petit, J.-J. Andre, J. Simon, R. Even, B. Boudjema, G. Guillaud, M. Maitrot, J. Am. Chem. Soc. 109 (1987) 5119.
[7] J. Simon, F. Tournilhac, J.-J. Andre, J. Appl. Phys. 62 (1987) 3304.
[8] J. Jiang, D. Du, M.T.M. Choi, J. Xie, D.K.P. Ng, Chem. Lett. (1999) 261.
[9] M. Maitrot, G. Guillaud, B. Boudjema, J.-J. Andre, H. Strzelecka, J. Simon, R. Even, Chem. Phys. Lett. 133 (1987) 59.
[10] H.-H. Tran-Thi, D. Markovtsi, R. Even, J. Simon, Chem. Phys. Lett. 139 (1987) 207.
[11] Z. Belarbi, M. Maitrot, K. Ohta, J. Simon, J.-J. Andre, P. Petit, Chem. Phys. Lett. 143 (1988) 400.
[12] R. Madru, G. Guillaud, M. Al Sadoun, M. Maitrot, J.-J. Andre, J. Simon, R. Even, Chem. Phys. Lett. 145 (1988) 343.
[13] J. Jiang, R.C.W. Liu, T.C.W. Mak, T.D.W. Chan, D.K.P. Ng, Polyhedron 16 (1997) 515.
[14] J. Jiang, W. Liu, W.-F. Law, J. Lin, D.K.P. Ng, Inorg. Chim. Acta 268 (1998) 49.
[15] J. Jiang, J. Xie, D.K.P. Ng, Y. Yan, Mol. Cryst. Liq. Cryst. 337 (1999) 305.
[16] J. Jiang, T.C.W. Mak, D.K.P. Ng, Chem. Ber. 129 (1996) 933.
[17] D. Chabach, A. De Cian, J. Fischer, R. Weiss, M. El, M. Bibout, Angew. Chem., Int. Ed. Engl. 35 (1996) 898.
[18] J. Jiang, R.L.C. Lau, T.W.D. Chan, T.C.W. Mak, D.K.P. Ng, Inorg. Chim. Acta 255 (1997) 59.
[19] R.L.C. Lau, J. Jiang, D.K.P. Ng, T.W.D. Chan, J. Am. Soc. Mass Spectrosc. 8 (1997) 161.
[20] J. Jiang, W. Liu, W.-F. Law, D.K.P. Ng, Inorg. Chim. Acta 268 (1998) 141.
[21] D.K.P. Ng, J. Jiang, Chem. Soc. Rev. 26 (1997) 433.
[22] J. Jiang, M.T.M. Choi, W.-F. Law, J. Chen, D.K.P. Ng, Polyhedron 17 (1998) 3903.
[23] J. Jiang, J. Xie, M.T. M Choi, S. Sun, D.K.P. Ng, J. Porphyrins Phthalocyanines 3 (1999) 322.
[24] J. Jiang, D.P. Arnold, H. Yu, Polyhedron 18 (1999) 2129.
[25] I.S. Kirin, P.N. Moskalev, Yu.A. Makashev, Russ. J. Inorg. Chem. 12 (1967) 369.
[26] P.N. Moskalev, I.S. Kirin, Russ. J. Inorg. Chem. 15 (1970) 7.
[27] G.A. Corker, B. Grant, N.J. Clecak, J. Electrochem. Soc. 126 (1979) 1339.
[28] M. M'Sadak, J. Roncali, F. Garnier, J. Electroanal. Chem. 189 (1985) 99.
[29] C. Clarisse, M.T. Riou, Inorg. Chim. Acta 130 (1987) 139.
[30] G. Ostendorp, H. Homborg, Z. Anorg. Allg. Chem. 622 (1996) 873.
[31] G. Ostendorp, H. Homborg, Z. Anorg. Allg. Chem. 622 (1996) 1358.
[32] J. Jiang, unpublished results.
[33] J. Jiang, W. Liu, J. Lin, D.K.P. Ng, Huaxue Tongbao 7 (1997) 14.
[34] J. Janczak, Pol. J. Chem. 72 (1998) 1871.
[35] K.M. Kadish, G. Moninot, Y. Hu, D. Dubois, A. Ibnlfassi, J.-M. Barbe, R. Guilard, J. Am. Chem. Soc. 115 (1993) 8153.
[36] R. Guilard, J.-M. Barbe, A. Ibnlfassi, A. Zirneh, V.A. Adamian, K.M. Kadish, Inorg. Chem. 34 (1995) 1472.
[37] T.H. Tran-Thi, T.A. Mattioli, D. Chabach, A. De Cian, R. Weiss, J. Phys. Chem. 98 (1994) 8279.
[38] J. Jiang, K. Kasuga, D.P. Arnold, in: H.S. Nalwa (Ed.), Handbook of Advanced Electronic and Photonic Materials, Academic, New York, in press.
[39] R. Aroca, R.E. Clavijo, C.A. Jennings, G.A. Kovacs, J.M. Duff, R.O. Loutfy, Spectrochimica Acta 45A (1989) 957.
[40] M.S. Haghighi, A. Franken, H. Homborg, Z. Naturforsch., Teil b 49 (1994) 812.
[41] M.S. Haghighi, H. Homborg, Z. Anorg. Allg. Chem. 620 (1994) 1278.
[42] M.S. Haghighi, G. Peters, H. Homborg, Z. Anorg. Allg. Chem. 620 (1994) 1285.
[43] T. Nyokong, F. Furuya, N. Kobayashi, W. Liu, D. Du, J. Jiang, Inorg. Chem. 39 (2000) 128.
[44] W. Liu, J. Jiang, D. Du, D.P. Arnold, Aust. J. Chem. 53 (2000) 131.
[45] J. Jiang, W. Liu, N. Pan, D.P. Arnold, Inorg. Chim. Acta, in press.
[46] J. Jiang, unpublished results.
[47] D. Battisti, L. Tomilova, R. Aroca, Chem. Mater. 4 (1992) 1323.
[48] D. Battisti, R. Aroca, J. Am. Chem. Soc. 114 (1992) 1201.
[49] J. Souto, L. Tomilova, R. Aroca, J.A. DeSaja, Langmuir 8 (1992) 942.
[50] M.L. Rodriguez, R. Aroca, J.A. DeSaja, Chem. Mater. 5 (1993) 933.
[51] G. Ostendorp, H. Homborg, Z. Naturforsch., Teil b 50 (1995) 1200.
[52] G. Ostendorp, H. Homborg, Z. Anorg. Allg. Chem. 622 (1996) 1222.
[53] G. Ostendorp, H.W. Rotter, H. Homborg, Z. Anorg. Allg. Chem. 622 (1996) 235.
[54] M.S. Haghighi, M. Rath, H.W. Rotter, H. Homberg, Z. Anorg. Allg. Chem. 619 (1993) 1887.
[55] R.E. Clavijo, D. Battisti, R. Aroca, G.J. Kovacs, C.A. Jennings, Langmuir 8 (1992) 113.
[56] M.L.R. Mendez, Y. Khoussed, J. Souto, J. Sarabia, R. Aroca, J.A. de Saja, Sensors Actuators B 18–19 (1994) 89.
[57] M.S. Haghighi, H. Homborg, Z. Naturforsch., Teil b 46 (1991) 1641.
[58] M.S. Haghighi, C.L. Teske, H. Homborg, Z. Anorg. Allg. Chem. 608 (1992) 73.
[59] G. Ostendorp, S. Sievertsen, H. Homborg, Z. Anorg. Allg. Chem. 621 (1995) 451.
[60] J. Jiang, W. Liu, K.-W. Poon, D.P. Arnold, D.K.P. Ng, Eur. J. Inorg. Chem. (2000) 205.
[61] F. Guyon, A. Pondaven, P. Guenot, M. L'Her, Inorg. Chem. 33 (1994) 4787.

[62] F. Guyon, A. Pondaven, J.-M. Kerbaol, M. L'Her, Inorg. Chem. 37 (1998) 569.
[63] M. Bouvet, J. Simon, Chem. Phys. Lett. 172 (1990) 299.
[64] N. Ishikawa, O. Ohno, Y. Kaizu, Chem. Phys. Lett. 180 (1991) 51.
[65] N. Ishikawa, O. Ohno, Y. Kaizu, J. Phys. Chem 97 (1993) 1004.
[66] M. Bouvet, P. Bassoul, J. Simon, Mol. Cryst. Liq. Cryst. 252 (1994) 31.
[67] M. Passard, A. Pauly, J.P. Germain, C. Maleysson, Synth. Met. 80 (1996) 25.

PERGAMON

www.elsevier.nl/locate/poly

Polyhedron 19 (2000) 1395–1406

POLYHEDRON

Reactivity of the di-μ-hydroxo-complexes $[\{Pd(N–N)\}_2(\mu\text{-}OH)_2][ClO_4]_2$ (N–N = bis(pyrazol-1-yl)alkanes) towards protic electrophiles. Hydration of coordinated nitriles at a palladium(II) site

Gregorio Sánchez [a], Jose L. Serrano [b], M. Carmen Ramírez de Arellano [c], José Pérez [a], Gregorio López [a,*]

[a] *Departamento de Química Inorgánica, Universidad de Murcia, 30071 Murcia, Spain*

[b] *Departamento de Ingeniería Minera, Geológica y Cartográfica (Area de Química Inorgánica), Universidad Politécnica de Cartagena, 30203 Cartagena, Spain*

[c] *Departamento de Química Orgánica. Facultad de Farmacia, Universidad de Valencia, 46100 Valencia, Spain*

Received 18 February 2000; accepted 4 May 2000

Abstract

The hydroxo-complexes $[\{Pd(\mu\text{-}OH)(N–N)\}_2][ClO_4]_2$ (N–N = bpzm:bis(pyrazol-1-yl) methane: **a**-compounds, bpzm*:bis(3,5-dimethylpyrazol-1-yl)methane; **b**-compounds) react with a wide variety of weak protic electrophiles H(LL) in a 1:2 molar ratio to give the mononuclear cationic palladium(II) derivatives of general formula $[Pd(LL)(N–N)][ClO_4]$ [LL = 2-pyridine-methoxo (OCH_2-py) (**1a**,**b**); picolinate (pic) (**2a**,**b**); 8-hydroxiquinolinate (oxin) (**3a**,**b**)] or the dinuclear complexes $[\{Pd(N–N)\}_2(\mu\text{-ox})][ClO_4]_2$ [ox = oxalate: (**4a**,**b**)] and $[\{Pd(\mu\text{-}LL)(N–N)\}_2][ClO_4]_2$ [LL = pyrazolate (pz) (**5a**,**b**); *p*-thiocresolate (SC_6H_4Me-*p*) (**6a**,**b**); triazolate (tz) (**7b**); thiophenolate (SPh) (**8b**)] when reacting with oxalic acid, azoles or thiols in the same molar ratio. In a related reaction, deprotonation of secondary amines by the hydroxo-complexes in the presence of carbon disulfide leads to the corresponding dithiocarbamate complexes $[Pd(S_2CNR_2)(N–N)][ClO_4]$ [R = Me (**9a**,**b**), Et (**10a**,**b**) C_5H_{10} (**11a**,**b**)]. The hydroxo complexes also promote the nucleophilic addition of water to pyridine-2-carbonitrile and mononuclear complexes containing pyridine-2-carboxamidate ligands are formed (**12a**,**b**). The new compounds have been characterized by partial elemental analyses, conductance measurements and spectroscopic (IR, ^1H and ^{13}C NMR) methods. The crystal structures of compounds **6b** and **11a** have been determined by X-ray diffraction analysis. © 2000 Elsevier Science Ltd. All rights reserved.

Keywords: Palladium; Hydroxo complexes; Pyrazolylalkane complexes; Crystal structures

1. Introduction

The recent surge of interest in the chemistry of hydroxo complexes of the nickel group elements is undoubtedly related to their wide reactivity and potential relevance to catalysis [1]. The syntheses of the binuclear ionic complexes $[\{M(C_6F_5)_2(\mu\text{-}OH)\}_2]^{2-}$ (M = Ni, Pd, Pt) [2–4] and $[\{M(N–N)(\mu\text{-}OH)\}_2]^{2+}$ (M = Pd or Pt; N–N = bipy or phen [5]; M = Pd; N–N = α-diimine [6]; M = Pd; N–N = bpzm:bis(pyrazol-1-yl) methane, bpzm*:bis(3,5-dimethylpyrazol-1-yl)methane [7]) have been reported. Their use as precursors in synthetic work is based on the considerable nucleophilicity of the bridging OH groups, which is consistent with their high-field proton resonances. Thus, previous work demonstrated that di-μ-hydroxo complexes are useful precursors for the preparation of an interesting variety of complexes [7–16], by means of a simple acid–base reaction with protic electrophiles. We also realized that deprotonation of amines or alcohols by the hydroxo-complex in the presence of carbon disulfide leads to the formation of the corresponding dithiocarbamate or xanthate complexes, respectively [9,17]. Moreover, the reaction of the hydroxo-bridged

* Corresponding author. Tel.: +34-68-367-462; fax: +34-68-364-148.

E-mail address: gll@fcu.um.es (G. López).

0277-5387/00/$ - see front matter © 2000 Elsevier Science Ltd. All rights reserved.
PII: S0277-5387(00)00427-7

nickel complex with malononitrile leads to the formation of an unprecedented dicyanomethanide-bridged anionic complex [18].

On the other hand, although the chemistry of metal poly(pyrazol-1-yl)borato complexes has been studied extensively in recent years [19], comparable development of the isoelectronic, but neutral poly(pyrazol-1-yl)alkanes has received little attention [20]. Most of the published material concerns first-row transition metals [21] and some ruthenium(II) examples [22], while coordination to metals having the d^8 configuration is rare and it basically includes complexes of rhodium(I) [23] and some derivatives of dimethylgold(III) [24] and methyl or dimethylplatinum(II) [25] with tris(pyrazol-1-yl)alkanes. The interaction of the bis(pyrazol-1-yl)alkanes with palladium(II) is still largely unexplored [26], and only a few cationic allylic complexes have been reported [27]. In this sense, we have described recently the synthesis of the precursors $[Pd(N–N)(CH_3CN)_2][ClO_4]_2$ and $[Pd(N–N)(\mu\text{-}OH)]_2[ClO_4]_2$ (N–N = bpzm:bis(pyrazol-1-yl)methane, bpzm*:bis(3,5-dimethylpyrazol-1-yl)methane) [7].

Following our systematic study of the reactivity shown by hydroxo-complexes of the nickel group elements, we have now investigated the former complexes $[Pd(N–N)(\mu\text{-}OH)]_2[ClO_4]_2$ [7] in reactions towards a wide variety of protic electrophiles and related reactions like that against amines in the presence of carbon disulfide. The addition of water to pyridine-2-carbonitrile in the presence of the above hydroxo-palladium complexes has also been studied.

Table 1
Crystal data and summary of data collection and refinement for complexes **11a** and **6b**

	11a	**6b**·$(CH_3)_2CO·H_2O$
Crystal color	orange	orange
Crystal habit	tablet	plate
Crystal size (mm)	$0.44\times0.36\times0.18$	$0.64\times0.42\times0.06$
Chemical formula	$[C_{13}H_{18}N_5PdS_2][ClO_4]$	$[C_{39}H_{54}N_8O_2Pd_2S_2][ClO_4]_2·C_3H_6O·H_2O$
a (Å)	17.539(3)	10.838(2)
b (Å)	15.845(3)	12.951(2)
c (Å)	13.461(2)	17.816(3)
α (°)	90	82.504(10)
β (°)	90.283(12)	75.577(12)
γ (°)	90	80.614(10)
V (λ, Å^3)	3740.7(11)	2378.8 (6)
Radiation (Å)	Mo Kα (0.71073)	Mo Kα (0.71073)
Crystal system	monoclinic	triclinic
Space group	$P2_1/c$	$P\bar{1}$
Z	8	2
Diffractometer type	Siemens P4	Siemens P4
Data collection method	ω scans	ω scans
Temperature (K)	173(2)	173(29
Reflections collected	14|222	9051
Unique reflections	6567	8357
R_{int}	0.0415	0.1017
Reflections observed [$I>2\sigma(I)$]	4919	6585
2θ range, min–max (°)	6.1–50.0	6.1–50.0
Absorption correction	φ scans	φ scans
Max. transmission (%)	0.868	0.558
Min. transmission (%)	0.630	0.717
R_1 [a]	0.0594	0.0446
wR_2 [b]	0.1411	0.1134
Parameters	463	538
Form of refinement	F^2	F^2
Treatment of hydrogens	riding	riding

[a] $R_1=\sigma\||F_o|-|F|\|/\sigma|F_o|$ for reflections with $[I>2\sigma(I)]$.

[b] $wR_2=\{\sigma[w(F_o^2-F_c^2)^2]/\sigma[w(F_o^2)^2]\}^{0.5}$ for all reflections; $w^{-1}=\sigma^2(F^2)+(aP)^2+bP$, where $P=(2F_c^2+F_o^2)/3$ and a and b are constants set by the program.

2. Experimental

2.1. Materials and physical measurements

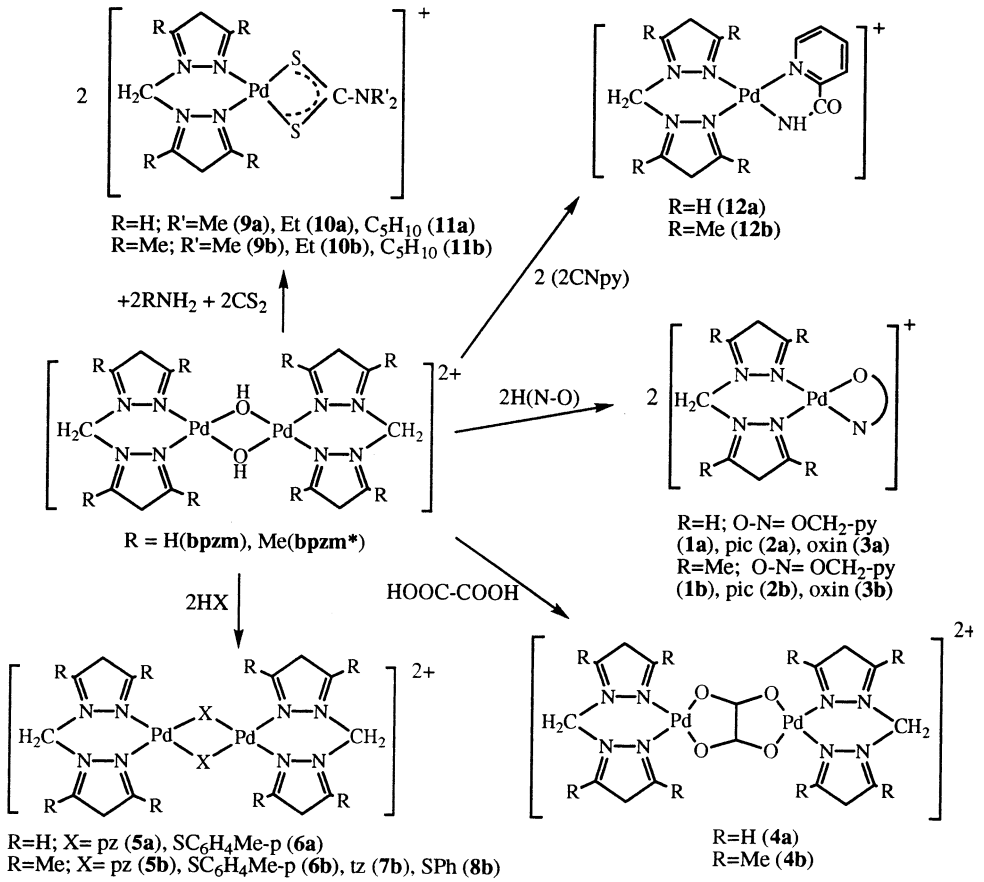
C, H, N and S analyses were carried out with a Carlo Erba model EA 1108 microanalyzer. IR spectra were recorded on a Perkin–Elmer 16PC FT IR spectrophotometer using Nujol mulls between polyethylene sheets. NMR data were recorded on a Bruker AC 200E or a Varian Unity 300 spectrometer. Decomposition points were determined on a Reichert microscope provided with heating plate. Conductance measurements were performed with a Crison 525 conductimeter (in acetone; $c=10^{-3}$ M). Mass spectrometric analyses were performed on a Fisons VG Autospec double-focusing spectrometer, operated in positive mode. Ions were produced by fast atom bombardment (FAB) with a beam of 25-Kev Cs atoms. The mass spectrometer was operated with an accelerating voltage of 8 kV and a resolution of at least 1000.

The bis(pyrazol-1-yl)alkane precursors $[Pd(N–N)(\mu\text{-}OH)]_2[ClO_4]_2$ were prepared by a procedure described elsewhere [7]. The protic ligands were obtained commercially and used without further purification and all the solvents were dried by standard methods before use.

2.2. Preparation of the complexes

2.2.1. Complexes *1a*–*6a*

The complexes were obtained by treating $[\{Pd(\mu\text{-}OH)(bpzm)\}_2][ClO_4]_2$ with the corresponding protic ligand (molar ratio 1:2; 1:1 in **4a**) in acetone according to the following general method. To an acetone (15 ml) suspension of $[\{Pd(\mu\text{-}OH)(bpzm)\}_2][ClO_4]_2$ (0.10 g, 0.13 mmol) was added the stoichiometric amount of ligand



Scheme 1.

(0.26 mmol, 0.13 mmol in **4a**). The solution was stirred at room temperature (r.t.) for 15 min, then concentrated under reduced pressure until ca. one fifth of the initial volume. Slow addition of diethyl ether caused the precipitation of the title complexes, which were filtered off, washed with ether and air-dried.

[Pd(O–CH_2-py)(bpzm)][ClO_4] (**1a**) was obtained in 66% yield. *Anal.* Calc. for $C_{13}H_{14}ClN_5O_5Pd$: C, 32.2; H, 3.1; N, 15.2. Found: C, 32.0; H, 3.3; N, 15.1%. M.p. (dec.) = 150°C. $\Lambda_M = 117\ \Omega^{-1}\ cm^2\ mol^{-1}$. IR ($cm^{-1}$): 1604 (C=N str).

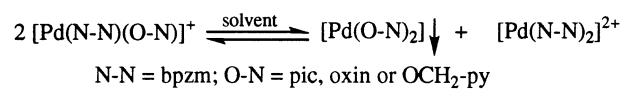
[Pd(pic)(bpzm)][ClO_4] (**2a**) was obtained in 69% yield. *Anal.* Calc. for $C_{13}H_{12}ClN_5O_6Pd$: C, 32.8; H, 2.5; N, 14.7. Found: C, 32.5; H, 2.3; N, 14.4%. M.p. (dec.) = 332°C. $\Lambda_M = 119\ \Omega^{-1}\ cm^2\ mol^{-1}$. IR ($cm^{-1}$): 1682 (C=O str), 1610 (C=N str).

[Pd(oxin)(bpzm)][ClO_4] (**3a**) was obtained in 69% yield. *Anal.* Calc. for $C_{16}H_{14}ClN_5O_5Pd$: C, 38.6; H, 2.8; N, 14.7. Found: C, 38.5; H, 2.5; N, 14.5%. M.p. (dec.) = 212°C. $\Lambda_M = 108\ \Omega^{-1}\ cm^2\ mol^{-1}$. IR ($cm^{-1}$): 1569 (C=N str).

[{Pd(bpzm}$_2$(μ-ox)][ClO_4]$_2$ (**4a**) was obtained in 70% yield. *Anal.* Calc. for $C_{16}H_{16}Cl_2N_8O_{12}Pd_2$: C, 24.1; H, 2.1; N, 14.1. Found: C, 24.2; H, 2.4; N, 14.3%. M.p. (dec.) = 240°C. IR (cm^{-1}): 1620 (C=O str). FAB MS (positive mode) *m*/*z*: 707 [Pd_2(bpzm)$_2$(ClO_4)$_2$]$^+$, 597 [Pd_2(bpzm)$_2$(ox)]$^+$, 404 [Pd(bpzm)$_2$]$^+$, 254 [Pd(bpzm)]$^+$.

[{Pd(μ-pz)(bpzm)}$_2$][ClO_4]$_2$ (**5a**) was obtained in 80% yield. *Anal.* Calc. for $C_{20}H_{22}Cl_2N_{12}O_8Pd_2$: C, 28.6; H, 2.6; N, 20.0. Found: C, 28.5; H, 2.5; N, 20.3%. M.p. (dec.) = 360°C. $\Lambda_M = 138\ \Omega^{-1}\ cm^2\ mol^{-1}$. IR ($cm^{-1}$): 1634 (C=N str). FAB MS (positive mode) *m*/*z*: 744 [Pd_2(pz)$_2$(bpzm)$_2$(ClO_4)]$^+$, 644 [Pd_2(pz)$_2$(bpzm)$_2$]$^+$, 595 [Pd_2(pz)$_2$(bpzm)(ClO_4)]$^+$, 496 [Pd_2(pz)$_2$(bpzm)]$^+$, 429 [Pd_2(pz)(bpzm)]$^+$.

[{Pd(μ-SC_6H_4Me-p)(bpzm)}$_2$][ClO_4]$_2$ (**6a**) was obtained in 71% yield. *Anal.* Calc. for $C_{28}H_{30}Cl_2N_8O_8S_2Pd_2$: C, 35.3; H, 3.1; N, 11.7; S, 6.7. Found: C, 35.0; H, 3.3; N, 11.6; S, 6.5.%. M.p. (dec) = 270°C. $\Lambda_M = 178\ \Omega^{-1}\ cm^2\ mol^{-1}$. IR ($cm^{-1}$): 500 (Pd–S). FAB MS (positive mode) *m*/*z*: 855 [Pd_2(SC_6H_4Me-p)$_2$(bpzm)$_2$(ClO_4)]$^+$, 756 [Pd_2(SC_6H_4Me-p)$_2$(bpzm)$_2$]$^+$, 707 [Pd_2(SC_6H_4Me-p)$_2$(bpzm)(ClO_4)]$^+$, 608 [Pd_2(SC_6H_4Me-p)(bpzm)]$^+$, 377 [Pd(SC_6H_4Me-p)(bpzm)]$^+$.



Scheme 2.

Table 2
^{1}H and ^{13}C NMR chemical shifts (δ) and coupling constants (Hz) for complexes **1a**–**12a** and **1b**–**12b**

Compound	^{1}H	$^{13}C\{^{1}H\}$
1a [a]	4.67 (s, 2H, –CH_2–OCH_2-py) 6.40 (m, 1H, $H^{4'}$) 6.68 (m, 1H, H^{4}) 7.02 (d, 1H, $H^{3'}$, $J_{3'4'} = 2.1$) 7.16 (m, 3H, CH_2 of bpzm + H^{3}–OCH_2-py) 7.61 (m, 1H, H^{5}–OCH_2-py) 7.93 (m, 1H, H^{4}–OCH_2-py) 8.18 (m, 3H, $H^{3,5}$ of bpzm + H^{6}–OCH_2-py) 8.36 (d, 1H, H^{5}, $J_{54} = 2.5$)	64.0 (CH_2 of bpzm) 78.0 (CH_2 of OCH_2-py) 108.4 ($C^{4'}$) 108.9 (C^{4}) 125.5 (C^{3} of OCH_2-py) 125.6 (C^{5} of OCH_2-py) 134.6 ($C^{5'}$) 136.2 (C^{5}) 140.1 ($C^{3'}$) 142.3 (C^{4} of OCH_2-py) 145.2 (C^{3}) 152.9 (C^{6} of OCH_2-py) 164.2 (C^{2} of OCH_2-py)
2a [a]	6.68 (m, 1H, $H^{4'}$) 6.85 (m, 1H, H^{4}) 7.34 (s, 2H, CH_2 of bpzm) 7.99 (m, 3H, $H^{3,3'}$ + H^{3} of pic) 8.44 (m, 5H, $H^{5,5'}$ + $H^{4,5,6}$ of pic)	63.0 (CH_2 of bpzm) 107.9 ($C^{4'}$) 108.9 (C^{4}) 127.7 (C^{3} of pic) 129.8 (C^{4} of pic) 135.0 ($C^{5'}$) 135.1 (C^{5}) 142.8 (C^{5} of pic) 144.5 ($C^{3'}$) 144.8 (C^{3}) 150.2 (C^{2} of pic) 151.0 (C^{6} of pic) 171.5 (CO of pic)
3a [a]	6.70 (m, 1H, $H^{4'}$) 6.83 (m, 1H, H^{4}) 7.04 (d, 1H, H^{7} of oxin, $J_{76} = 7.8$) 7.23 (d, 1H, H^{5} of oxin, $J_{56} = 7.8$) 7.32 (s, 2H, –CH_2 of bpzm) 7.53 (m, 2H, H^{6} of oxin) 7.70 (m, 1H, H^{3} of oxin) 8.08 (d, 1H, $H^{3'}$, $J_{3'4'} = 2.2$) 8.40 (m, 3H, H^{3}, $H^{5'}$ + H^{4} of oxin) 8.51 (d, 1H, H^{5}, $J_{54} = 2.8$) 8.64 (d, 1H, H^{2} of oxin, $J_{23} = 8.3$)	63.1 (CH_2 of bpzm) 108.2 ($C^{4'}$) 109.2 (C^{4}) 113.7 (C^{7} of oxin) 114.2 (C^{5} of oxin) 122.4 (C^{3} of oxin) 130.6 (C^{6} of oxin) 130.8 (C^{10} of oxin) 135.3 ($C^{5'}$) 136.2 (C^{5}) 140.6 (C^{4} of oxin) 142.8 ($C^{3'}$) 144.8 (C^{9} of oxin) 145.1 (C^{3}) 148.2 (C^{2} of oxin) 166.0 (C^{8} of oxin)
5a [b]	6.42 (m, 2H, H^{4} of pz) 6.65 (m, 4H, $H^{4,4'}$) 7.25 (s, 4H, CH_2 of bpzm) 7.53 (d, 4H, $H^{3,5}$ of pz, $J_{34} = 2.1$) 7.63 (d, 4H, $H^{3,3'}$, $J_{34} = 2.0$) 8.41 (d, 4H, $H^{5,5'}$, $J_{54} = 2.3$)	63.0 (–CH_2 of bpzm) 107.3 (C^{4} of pz) 108.3 ($C^{4,4'}$) 135.5 ($C^{5,5'}$) 141.7 ($C^{3,5}$ of pz) 144.9 ($C^{3,3'}$)
6a [a]	2.14 (s, 6H, Me-pthioc) 6.18 (m, 4H, $H^{4,4'}$) 6.59 (d, 4H, H^{2}-pthioc, $J_{23} = 7.7$) 6.75 (s, 4H, –CH_2 of bpzm) 7.03 (d, 4H, H^{3}-pthioc, $J_{32} = 7.7$) 7.45 (s, 4H, $H^{3,3'}$) 8.02 (s, 4H, $4H^{5,5'}$)	21.1 (Me-pthioc) 64.1 (–CH_2 of bpzm) 108.5 ($C^{4,4'}$) 128.8 (C^{1}-pthioc) 129.2 ($C^{2,6}$-pthioc) 129.6 ($C^{3,5}$-pthioc) 135.0 (C^{4}-pthioc) 135.4 ($C^{5,5'}$) 143.9 ($C^{3,3'}$)
9a [a]	3.45 (s, 6H, Me-dtc) 6.65 (m, 2H, $H^{4,4'}$)	38.9 (Me-dtc) 63.9 (–CH_2 of bpzm)

Table 2 (*Continued*)

Compound	^{1}H	^{13}C{^{1}H}
	7.07 (s, 2H, CH_2 of bpzm)	108.6 ($C^{4,4'}$)
	7.82 (d, 2H, $H^{3,3'}$, $J_{34} = 2.2$)	135.6 ($C^{5,5'}$)
	8.35 (d, 2H, $H^{5,5'}$, $J_{54} = 2.7$)	144.3 ($C^{3,3'}$)
10a [a]	1.36 (t, 6H, Me-dtc, $J = 7.2$)	12.3 (Me-dtc)
	3.88 (cd, 4H, –CH_2 of dtc, $J = 7.2$)	45.8 (–CH_2-dtc)
	6.65 (m, 2H, $H^{4,4'}$)	63.9 (CH_2 of bpzm)
	7.08 (s, 2H, –CH_2 of bpzm)	108.7 ($C^{4,4'}$)
	7.82 (d, 2H, $H^{3,3'}$, $J_{34} = 1.8$)	135.6 ($C^{5,5'}$)
	8.36 (d, 2H, $H^{5,5'}$, $J_{54} = 2.3$)	144.3 ($C^{3,3'}$)
11a [a]	1.80 (m, 6H, pip)	24.6 (C^4 of pip)
	3.95 (m, 4H, pip)	26.1 ($C^{3,5}$ of pip)
	6.65 (m, 2H, $H^{4',4}$)	49.8 ($C^{2,6}$ of pip)
	7.08 (s, 2H, –CH_2 of bpzm)	63.9 (–CH_2 of bpzm)
	7.81 (d, 2H, $H^{3,3'}$, $J_{34} = 1.8$)	108.7 ($C^{4,4'}$)
	8.36 (d, 2H, $H^{5,5'}$, $J_{54} = 2.5$)	135.6 ($C^{5,5'}$)
		144.3 ($C^{3,3'}$)
12a [b]	6.65 (m, 1H, $H^{4'}$)	62.9 (–CH_2 of bpzm)
	6.76 (m, 1H, H^4)	108.0 ($C^{4'}$)
	6.81 (s, 1H, NH–2AMD-py)	108.8 (C^4)
	7.10 (s, 2H, –CH_2 of bpzm)	125.6 (C^3–2AMD-py)
	7.86 (m, 2H, $H^{3,5}$–2AMD-py)	128.5 (C^5–2AMD-py)
	8.16 (d, 1H, $H^{3'}$, $J_{3'4'} = 2.2$)	135.3 ($5C^{5'}$)
	8.36 (m, 5H, $H^{3,5,5'} + H^{4,6}$–2AMD-py)	142.1 (C^4–2AMD-py)
		144.4 ($C^{3'}$)
		144.7 (C^3)
		149.2 (C^6–2AMD-py)
		153.6 (C^2–2AMD-py)
		171.7 (CO–2AMD-py)
1b [a]	2.36 (s, 3H, $Me^{3'}$)	10.8 ($Me^{5'}$)
	2.51 (s, 3H, $Me^{5'}$)	10.9 (Me^5)
	2.53 (s, 3H, Me^5)	12.6 ($Me^{3'}$)
	2.56 (s, 3H, Me^3)	14.1 (Me^3)
	4.65 (d, 1H, CH_2 of OCH_2-py, $J_{AB} = 18.0$)	58.7 (–CH_2 of bpzm*)
	5.40 (d, 1H, CH_2 of OCH_2-py, $J_{AB} = 18.0$)	77.6 (–CH_2 of OCH_2-py)
	6.11 (s, 1H, $H^{4'}$)	108.5 ($C^{4'}$)
	6.26 (s, 1H, H^4)	109.4 (C^4)
	6.74 (d, 1H, CH_2 of bpzm*, $J_{AB} = 15.4$)	125.5 (C^3–OCH_2-py)
	7.32 (d, 1H, CH_2 of bpzm*, $J_{AB} = 15.,4$)	128.2 (C^5–OCH_2-py)
	7.47 (m, 1H, H^4–OCH_2-py)	142.0 (C^4–OCH_2-py)
	7.61 (d, 1H, H^3–OCH_2-py, $J_{34} = 7.9$)	143.9 ($C^{5'}$)
	8.06 (m, 2H, $H^{5,6}$–OCH_2-py)	145.1 (C^5)
		150.3 (C^6–OCH_2-py)
		152.8 (C^2–OCH_2-py)
		154.1 ($C^{3'}$)
		154.7 (C^3)
2b [a]	2.43 (s, 3H, $Me^{3'}$)	10.7 ($Me^{5'}$)
	2.52 (s, 3H, $Me^{5'}$)	10.9 (Me^5)
	2.58 (s, 3H, Me^5)	12.5 ($Me^{3'}$)
	2.62 (s, 3H, Me^3)	14.2 (Me^3)
	6.19 (s, 1H, $H^{4'}$)	58.1 (–CH_2 of bpzm*)
	6.37 (s, 1H, H^4)	108.2 ($C^{4'}$)
	6.90 (d, 1H, CH_2 of bpzm*, $J_{AB} = 15.4$)	109.4 (C^4)
	7.49 (d, 1H, CH_2 of bpzm*, $J_{AB} = 15.4$)	127.4 (C^3 of pic)
	7.90 (m, 2H, $H^{3,5}$ of pic)	129.5 (C^5 of pic)
	8.24 (s, 1H, H^4 of pic)	142.5 (C^4 of pic)
	8.40 (m, 1H, H^6 of pic)	145.5 ($5C^{5'}$*)
		150.0 (C^3 of pic)
		153.0 ($C^{3'}$)
		153.2 (C^3)
		153.6 (C^6 of pic)
		171.5 (CO of pic)

Table 2 (*Continued*)

Compound	^{1}H	^{13}C{^{1}H}
3b [a]	2.51 (s, 3H, $Me^{3'}$) 2.57 (s, 3H, $Me^{5'}$) 2.59 (s, 3H, Me^{5}) 2.63 (s, 3H, Me^{3}) 6.19 (s, 1H, $H^{4'}$) 6.35 (s, 1H, H^{4}) 6.90 (d, 1H, CH_2 of bpzm*, $J_{AB} = 15.4$) 6.98 (d, 1H, H^7 of oxin, $J_{76} = 7.8$) 7.12 (d, 1H, H^5 of oxin, $J_{56} = 7.8$) 7.45 (m, 2H, CH_2 of bpzm* $+H^6$ of oxin) 7.67 (m, 1H, H^3 of oxin) 7.96 (m, 1H, H^4 of oxin) 8.50 (m, 1H, H^2 of oxin)	10.7 ($Me^{5'}$) 10.9 (Me^{5}) 12.5 ($Me^{3'}$) 14.4 (Me^{3}) 58.6 (–CH_2 of bpzm*) 108.1 ($C^{4'}$) 109.3 (C^{4}) 113.2 (C^7 of oxin) 113.8 (C^5 of oxin) 122.1 (C^3 of oxin) 130.5 (C^6 of oxin) 130.6 (C^{10} of oxin) 140.3 (C^4 of oxin) 143.7 ($C^{5'}$) 144.2 (C^9 of oxin) 145.0 (C^5) 148.7 (C^2 of oxin) 152.7 ($C^{3'}$) 153.1 (C^3) 167.3 (C^8 of oxin)
5b [b]	1.92 (s, 12H, $Me^{3,3'}$) 2.51 (s, 12H, $Me^{5,5'}$) 6.23 (s, 4H, $H^{4,4'}$) 6.29 (t, 2H, H^4 of pz, $J = 2.3$) 6.93 (d, 2H, CH_2 of bpzm*, $J_{AB} = 15.5$) 7.35 (d, 4H, $H^{3,5}$ of pz, $J = 2.3$) 7.60 (d, 2H, CH_2 of bpzm*, $^{J}{}_{AB} = 15.5$)	10.8 ($Me^{5,5'}$) 13.6 ($Me^{3,3'}$) 58.2 (CH_2 of bpzm*) 106.8 (C^4 of pz) 108.2 ($C^{4,4'}$) 142.6 ($C^{3,5}$ of pz) 144.3 ($C^{5,5'}$) 152.1 ($C^{3,3'}$)
6b [a]	2.11 (s, 12H, $Me^{3,3'}$) 2.42 (s, 12H, $Me^{5,5'}$) 2.83 (s, 6H, Me-pthioc) 5.77 (s, 4H, $H^{4,4'}$) 6.74 (d, 2H, CH_2 of bpzm*, $J_{AB} = 15.9$) 6.97 (d, 4H, $H^{3,5}$ of pthioc, $J = 8.3$) 7.84 (d, 2H, CH_2 of bpzm*, $J_{AB} = 15.9$) 8.02 (d, 4H, $H^{2,6}$ of pthioc, $J = 8.3$)	10.9 ($Me^{5,5'}$) 13.8 ($Me^{3,3'}$) 21.2 (Me–pthioc) 59.9 (CH_2 of bpzm*) 108.4 ($C^{4,4'}$) 127.6 ($C^4$of pthioc) 130.3 ($C^{3,5}$ of pthioc) 135.2 ($C^{2,6}$ of pthioc) 141.1 (C^1 of pthioc) 144.6 ($C^{5,5'}$) 152.6 ($C^{3,3'}$)
7b [b]	1.96 (s, 12H, $Me^{3,3'}$) 2.55 (s, 12H, $Me^{5,5'}$) 6.28 (s, 4H, $H^{4,4'}$) 7.00 (d, 2H, CH_2 of bpzm*, $J_{AB} = 15.5$) 7.58 (d, 2H, CH_2 of bpzm*, $J_{AB} = 15.5$) 8.09 (s, 4H, taz)	11.0 ($Me^{5,5'}$) 13.6 ($Me^{3,3'}$) 58.3 (CH_2 of bpzm*) 108.6 ($C^{4,4'}$) 144.7 ($C^{5,5'}$) 152.4 ($C^{3,3'}$) 153.6 ($C^{3,5}$ of taz)
8b [a]	2.16 (s, 12H, $Me^{3,3'}$) 2.43 (s, 12H, $Me^{5,5'}$) 5.79 (s, 4H, $H^{4,4'}$) 6.77 (d, 2H, CH_2 of bpzm*, $J_{AB} = 15.9$) 7.21 (m, 6H, $H^{3,4,5}$ of SPh) 7.83 (d, 2H, CH_2 of bpzm*, $J_{AB} = 15.9$) 8.23 (d, 4H, $H^{2,6}$ of SPh, $J = 7.1$)	10.8 ($Me^{5,5'}$) 13.9 ($Me^{3,3'}$) 59.9 (CH_2 of bpzm*) 108.4 ($C^{4,4'}$) 127.5 (C^4 of SPh) 130.8 ($C^{3,5}$ of SPh) 135.0 ($C^{2,6}$ of SPh) 141.0 (C^1 of SPh) 144.7 ($C^{5,5'}$) 152.6 ($C^{3,3'}$)
9b [a]	2.29 (s, 6H, $Me^{3,3'}$) 2.56 (s, 6H, $Me^{5,5'}$) 3.40 (s, 6H, Me-dtc)	11.1 ($Me^{5,5'}$) 14.4 ($Me^{3,3'}$) 38.8 (Me-dtc)

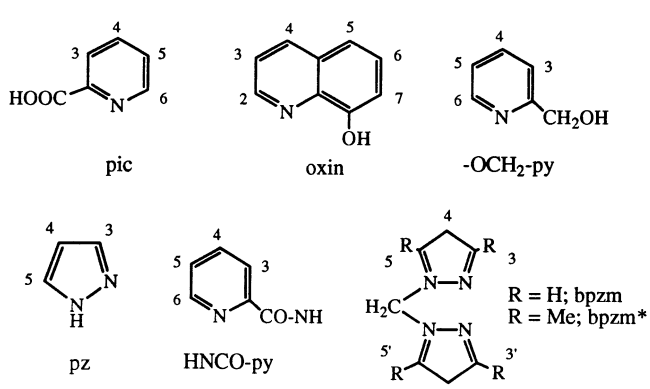
Table 2 (*Continued*)

Compound	^{1}H	^{13}C{^{1}H}
	6.19 (s, 2H, $H^{4,4'}$) 7.07 (s, 2H, CH_2 of bpzm*)	58.8 (CH_2 of bpzm*) 108.8 ($C^{4,4'}$) 144.5 ($C^{5,5'}$) 153.6 ($C^{3'3'}$)
10b [a]	1.33 (t, 6H, Me-dtc, $J = 7.2$) 2.31 (s, 6H, $Me^{3,3'}$) 2.56 (s, 6H, $Me^{5,5'}$) 3.82 (cd, 4H, CH_2 of dtc, $J = 7.2$) 6.19 (s, 2H, $H^{4,4'}$) 6.84 (s, 2H, CH_2 of bpzm*)	11.1 ($Me^{5,5'}$) 12.5 (Me-dtc) 14.4 ($Me^{3,3'}$) 45.6 (CH_2 of dtc) 58.8 (CH_2 of bpzm*) 108.8 ($C^{4,4'}$) 144.5 ($C^{5,5'}$) 153.8 ($C^{3,3'}$)
11b [a]	1.68 (m, 6H, pip) 2.31 (s, 6H, $Me^{3,3'}$) 2.56 (s, 6H, $Me^{5,5'}$) 3.90 (m, 4H, pip) 6.19 (s, 2H, $H^{4,4'}$) 6.85 (s, 2H, CH_2 of bpzm*)	11.1 ($Me^{5,5'}$) 14.4 ($Me^{3,3'}$) 24.7 (C^4 of pip) 26.2 ($C^{3,5}$ of pip) 49.5 ($C^{2,6}$ of pip) 58.8 (CH_2 of bpzm*) 108.8 ($C^{4,4'}$) 144.5 ($C^{5,5'}$) 153.8 ($C^{3,3'}$)
12b [a]	2.47 (s, 3H, $Me^{3'}$) 2.48 (s, 3H, $Me^{5'}$) 2.60 (s, 3H, Me^5) 2.61 (s, 3H, Me^3) 5.68 (s, 1H, NH–2AMD-py) 6.24 (s, 1H, $H^{4'}$) 6.33 (s, 1H, H^4) 6.90 (d, 1H, CH_2 of bpzm*, $J_{AB} = 15.5$) 7.49 (d, 1H, CH_2 of bpzm*, $J_{AB} = 15.5$) 7.80 (m, 1H, H^5–2AMD-py) 7.94 (d, 1H, H^3–AMD-py, $J_{34} = 7.8$) 8.36 (m, 2H, $H^{4,6}$–2AMD-py)	10.7 ($Me^{5'}$) 10.8 (Me^5) 13.6 ($Me^{3'}$) 14.1 (Me^3) 58.1 (CH_2 of bpzm*) 108.1 ($C^{4'}$) 108.8 (C^4) 125.5 (C^3–2AMD-py) 128.2 (C^5–2AMD-py) 142.0 (C^4–2AMD-py) 144.3 ($C^{5'}$) 144.4 (C^5) 150.1 (C^6–2AMD-py) 152.1 ($C^{3'}$) 153.3 (C^3) 153.6 (C^2–2AMD-py) 171.8 (CO–2AMD-py)

[a] In acetone.
[b] In DMSO.

2.2.2. Complexes ***1b–8b***

The complexes were obtained by treating [{Pd(μ-OH)(bpzm*)}$_2$][ClO$_4$]$_2$ with the corresponding protic ligand (molar ratio 1:2, 1:1 in **4b**) in acetone according to the following general method. To an acetone (15 ml) suspension of [{Pd(μ-OH)(bpzm*)}$_2$][ClO$_4$]$_2$ (0.10 g, 0.12 mmol) was added the stoichiometric amount of ligand (0.24 mmol, 0.12 mmol in **4b**). The solution was refluxed for 1 h, then concentrated under reduced pressure until ca. one fifth of the initial volume. Slow addition of diethyl ether caused the precipitation of the title complexes, which were filtered off, washed with ether and air-dried.



Scheme 3.

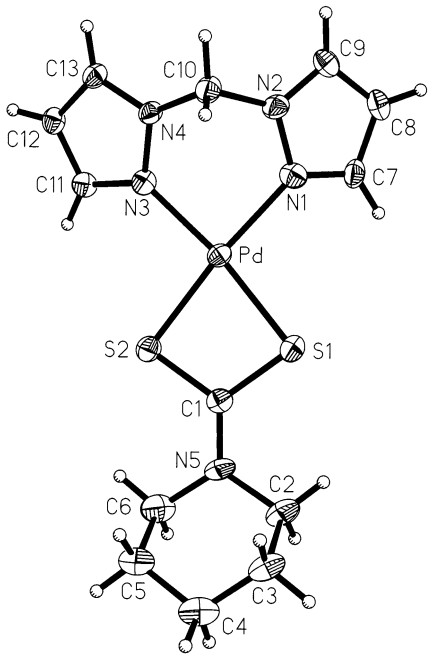


Fig. 1. Molecular structure of complex **11a**.

Table 3
Selected bond lengths (Å) and angles (°) for **11a** and **6b**

	Lengths (Å)		Angles (°)	
11a	Pd–N(3)	2.054(6)	N(3)–Pd–N(1)	89.2(3)
	Pd–N(1)	2.075(7)	N(3)–Pd–S(2)	95.9(2)
	Pd–S(2)	2.267(2)	N(1)–Pd–S(2)	173.5(2)
	Pd–S(1)	2.282(2)	N(3)–Pd–S(1)	171.9(2)
	S(1)–C(1)	1.735(8)	N(1)–Pd–S(1)	98.7(2)
	S(2)–C(1)	1.714(8)	S(2)–Pd–S(1)	76.31(7)
			C(1)–S(1)–Pd	86.7(3)
			C(1)–S(2)–Pd	87.7(3)
			S(2)–C(1)–S(1)	109.2(4)
6b	Pd(1)–N(3)	2.060(4)	N(3)–Pd(1)–N(1)	86.2(2)
	Pd(1)–N(1)	2.071(4)	N(3)–Pd(1)–S(1)	174.46(12)
	Pd(1)–S(1)	2.2884(14)	N(1)–Pd(1)–S(1)	98.12(13)
	Pd(1)–S(2)	2.2923(13)	N(3)–Pd(1)–S(2)	95.53(12)
	Pd(1)–Pd(2)	3.1421(7)	N(1)–Pd(1)–S(2)	177.01(12)
	Pd(2)–N(5)	2.055(4)	S(1)–Pd(1)–S(2)	80.04(5)
	Pd(2)–N(7)	2.061(4)	N(3)–Pd(1)–Pd(2)	127.66(12)
	Pd(2)–S(2)	2.2812(13)	N(1)–Pd(1)–Pd(2)	130.64(12)
	Pd(2)–S(1)	2.2947(14)	S(1)–Pd(1)–Pd(2)	46.80(3)
	S(1)–C(1)	1.791(5)	S(2)–Pd(1)–Pd(2)	46.46(3)
	S(2)–C(11)	1.787(5)	N(5)–Pd(2)–N(7)	85.3(2)
			N(5)–Pd(2)–S(2)	175.59(13)
			N(7)–Pd(2)–S(2)	95.73(12)
			N(5)–Pd(2)–S(1)	98.67(13)
			N(7)–Pd(2)–S(1)	175.57(12)
			S(2)–Pd(2)–S(1)	80.14(5)
			N(5)–Pd(2)–Pd(1)	129.68(12)
			N(7)–Pd(2)–Pd(1)	129.11(12)
			S(2)–Pd(2)–Pd(1)	46.75(3)
			S(1)–Pd(2)–Pd(1)	46.63(3)

[Pd(O-CH_2-py)(bpzm*)][ClO_4] (**1b**) was obtained in 81% yield. *Anal.* Calc. for $C_{17}H_{22}ClN_5O_5Pd$: C, 39.4; H, 4.2; N, 13.5. Found: C, 39.6; H, 4.3; N, 13.6%. M.p. (dec.) = 163°C. $\Lambda_M = 123\ \Omega^{-1}\ cm^2\ mol^{-1}$. IR ($cm^{-1}$): 1624 (C=N str).

[Pd(pic)(bpzm*)][ClO_4] (**2b**) was obtained in 69% yield. *Anal.* Calc. for $C_{17}H_{20}ClN_5O_6Pd$: C, 38.4; H, 3.7; N, 13.2. Found: C, 38.5; H, 3.8; N, 13.4%. M.p. (dec.) = 324°C. $\Lambda_M = 118\ \Omega^{-1}\ cm^2\ mol^{-1}$. IR ($cm^{-1}$): 1682 (C=O str), 1608 (C=N str).

[Pd(oxin)(bpzm*)][ClO_4] (**3b**) was obtained in 90% yield. *Anal.* Calc. for $C_{20}H_{24}ClN_5O_5Pd$: C. 44.8; H, 4.0; N, 12.6. Found: C, 44.7; H, 3.9; N, 12.5%. M.p. (dec.) = 224°C. $\Lambda_M = 113\ \Omega^{-1}\ cm^2\ mol^{-1}$. IR ($cm^{-1}$): 1578 (C=N str).

[{Pd(bpzm*}$_2$(μ-ox)][ClO_4]$_2$ (**4b**) was obtained in 65% yield. *Anal.* Calc. for $C_{24}H_{16}Cl_2N_8O_{12}Pd_2$: C, 31.7; H, 3.5; N, 12.3. Found: C, 31.6; H, 3.4; N, 12.3%. M.p. (dec.) = 265°C. IR (cm^{-1}): 1632 (C=O str). FAB MS (positive mode) m/z: 807 [Pd_2(bpzm*)$_2$(ox)(ClO_4)]$^+$, 708 [Pd_2(bpzm*)$_2$(ox)]$^+$, 310 [Pd(bpzm*)]$^+$.

[{Pd(μ-pz)(bpzm*)}$_2$][ClO_4]$_2$ (**5b**) was obtained in 81% yield. *Anal.* Calc. for $C_{28}H_{38}Cl_2N_{12}O_8Pd_2$: C, 35.3; H, 4.0; N, 17.6. Found: C, 35.5; H, 4.2; N, 17.4%. M.p. (dec.) = 348°C. $\Lambda_M = 140\ \Omega^{-1}\ cm^2\ mol^{-1}$. IR ($cm^{-1}$): 1630 (C=N str). FAB MS (positive mode) m/z: 856 [Pd_2(pz)$_2$(bpzm*)$_2$(ClO_4)]$^+$, 755 [Pd_2(pz)$_2$(bpzm*)$_2$]$^+$, 648 [Pd_2(pz)$_2$(bpzm*)(ClO_4)]$^+$, 552 [Pd_2(pz)$_2$(bpzm*)]$^+$, 485 [Pd_2(pz)(bpzm*)]$^+$.

[{Pd(μ-SC_6H_4Me-p)(bpzm*)}$_2$][ClO_4]$_2$ (**6b**) was obtained in 76% yield. *Anal.* Calc. for $C_{36}H_{46}Cl_2N_8O_8Pd_2S_2$: C, 40.6; H, 4.3; N, 10.5; S, 6.0. Found: C, 40.5; H, 4.3; N, 10.6; S, 5.9.%. M.p. (dec.) = 290°C. $\Lambda_M = 176\ \Omega^{-1}\ cm^2\ mol^{-1}$. IR ($cm^{-1}$): 500 (Pd–S). FAB MS (positive mode) m/z: 965 [Pd_2(SC_6H_4Me-p)$_2$(bpzm*)$_2$(ClO_4)]$^+$, 865 [Pd_2(SC_6H_4Me-p)$_2$(bpzm*)$_2$]$^+$, 662 [Pd_2(SC_6H_4Me-p)$_2$(bpzm*)]$^+$, 433 [Pd(SC_6H_4Me-p)(bpzm)]$^+$.

[{Pd(μ-tz)(bpzm*)}$_2$][ClO_4]$_2$ (**7b**) was obtained in 73% yield. *Anal.* Calc. for $C_{26}H_{36}Cl_2N_{14}O_8Pd_2$: C, 32.7; H, 3.7; N, 20.5. Found: C, 32.5; H, 3.8; N, 20.4%. M.p. (dec.) = 350°C. $\Lambda_M = 130\ \Omega^{-1}\ cm^2\ mol^{-1}$. IR ($cm^{-1}$): 1500 (C=N str). FAB MS (positive mode) m/z: 858 [Pd_2(tz)$_2$(bpzm*)$_2$(ClO_4)]$^+$, 757 [Pd_2(tz)$_2$(bpzm*)$_2$]$^+$, 651 [Pd_2(tz)$_2$(bpzm*)(ClO_4)]$^+$, 554 [Pd_2(tz)$_2$(bpzm*)]$^+$, 486 [Pd_2(tz)(bpzm*)]$^+$.

[{Pd(μ-SPh)(bpzm*)}$_2$][ClO_4]$_2$ (**8b**) was obtained in 69% yield. *Anal.* Calc. for $C_{34}H_{42}Cl_2N_8O_8Pd_2S_2$: C, 39.4; H, 4.1; N, 10.8; S, 6.2. Found: C, 39.5; H, 4.1; N, 10.9; S, 6.0.%. M.p. (dec.) = 275°C. $\Lambda_M = 170\ \Omega^{-1}\ cm^2\ mol^{-1}$. IR ($cm^{-1}$): 488 (Pd–S). FAB MS (positive mode) m/z: 937 [Pd_2(SPh)$_2$(bpzm*)$_2$(ClO_4)]$^+$, 840 [Pd_2(SPh)$_2$(bpzm*)$_2$]$^+$, 733 [Pd_2(SPh)$_2$(bpzm*)(ClO_4)]$^+$, 419 [Pd(SPh)(bpzm*)]$^+$.

*2.2.3. N,N-Dialkyldithiocarbamate complexes **9a–11a** and **9b–11b***

In separate experiments, to a suspension of the precursors [{Pd(μ-OH)(bpzm*)}$_2$][ClO_4]$_2$ (0.10 g, 0.12

mmol) or [{Pd(μ-OH)(bpzm)}$_2$][ClO$_4$]$_2$ (0.10 g, 0.13 mmol) in acetone (15 ml) was added the corresponding amine (1:2 molar ratio) and slight excess of carbon disulfide. The solution was refluxed for 1 h and then concentrated under reduced pressure until ca. one fifth of the initial volume. Slow addition of diethyl ether caused the precipitation of the orange complexes, which were filtered off, washed with ether and air-dried.

[Pd(S$_2$CNMe$_2$)(bpzm][ClO$_4$] (**9a**) was obtained in 64% yield. *Anal.* Calc. for $C_{10}H_{14}ClN_5O_4PdS_2$: C, 32.6; H, 3.8; N, 19.0; S, 17.4. Found: C, 32.5; H, 3.6; N, 19.2; S, 17.6%. M.p. (dec.) = 250°C. $\Lambda_M = 100\ \Omega^{-1}\ cm^2\ mol^{-1}$. IR (cm^{-1}): 1568 (C=N str), 966, (C–S str).

[Pd(S$_2$CNEt$_2$)(bpzm)][ClO$_4$] (**10a**) was obtained in 67% yield. *Anal.* Calc. for $C_{12}H_{18}ClN_5O_4PdS_2$: C, 36.4; H, 4.5; N, 17.7; S, 16.2. Found: C, 36.2; H, 4.3; N, 17.6; S, 15.9%. M.p. (dec.) = 255°C. $\Lambda_M = 115\ \Omega^{-1}\ cm^2\ mol^{-1}$. IR (cm^{-1}): 1546 (C=N str), 910, (C–S str).

[Pd(S$_2$CNC$_5$H$_{10}$)(bpzm)][ClO$_4$] (**11a**) was obtained in 70% yield. *Anal.* Calc. for $C_{13}H_{18}ClN_5O_4PdS_2$: C, 38.3; H, 4.4; N, 17.2; S, 15.7. Found: C, 38.1; H, 4.2; N, 17.3; S, 15.6%. M.p. (dec.) = 266°C. $\Lambda_M = 107\ \Omega^{-1}\ cm^2\ mol^{-1}$. IR (cm^{-1}): 1540 (C=N str), 1004, (C–S str).

[Pd(S$_2$CNMe$_2$)(bpzm*][ClO$_4$] (**9b**) was obtained in 66% yield. *Anal.* Calc. for $C_{14}H_{22}ClN_5O_4PdS_2$: C, 39.6; H, 5.6; N, 16.5; S, 15.1. Found: C, 39.4; H, 5.4; N, 16.4; S, 14.9%. M.p. (dec.) = 249°C. $\Lambda_M = 105\ \Omega^{-1}\ cm^2\ mol^{-1}$. IR (cm^{-1}): 1538 (C=N str), 968, (C–S str).

[Pd(S$_2$CNEt$_2$)(bpzm*)][ClO$_4$] (**10b**) was obtained in 68% yield. *Anal.* Calc. for $C_{16}H_{26}ClN_5O_4PdS_2$: C, 42.5; H, 5.7; N, 15.5; S, 14.2. Found: C, 42.4; H, 5.7; N, 15.3; S, 14.1%. M.p. (dec.) = 254°C. $\Lambda_M = 112\ \Omega^{-1}\ cm^2\ mol^{-1}$. IR (cm^{-1}): 1530 (C=N str), 988, (C–S str).

[Pd(S$_2$CNC$_5$H$_{10}$)(bpzm*)][ClO$_4$] (**11b**) was obtained in 70% yield. *Anal.* Calc. for $C_{17}H_{26}ClN_5O_4PdS_2$: C, 44.0; H, 5.6; N, 15.1; S, 13.8. Found: C, 44.2; H, 5.5; N, 14.9; S, 13.7%. M.p. (dec.) = 271°C. $\Lambda_M = 118\ \Omega^{-1}\ cm^2\ mol^{-1}$. IR (cm^{-1}): 1538 (C=N str), 1010, (C–S str).

2.2.4. Hydration of coordinated aminonitriles: complexes *12a* and *12b*

In separate experiments, to a suspension of the precursors [{Pd(μ-OH)(bpzm*)}$_2$][ClO$_4$]$_2$ (0.10 g, 0.12 mmol) and [{Pd(μ-OH)(bpzm)}$_2$][ClO$_4$]$_2$ (0.10 g, 0.13 mmol) in acetone–H$_2$O (15:1 ml) was added pyridine-2-carbonitrile in stoichiometric amount (1:2). The resultant clear solution was stirred at r.t. for 15 min and then concentrated under reduced pressure until ca. one fifth of the initial volume. Slow addition of diethyl ether caused the precipitation of the yellow complexes, which were filtered off, washed with ether and air-dried.

[Pd(HNCO-py)(bpzm)][ClO$_4$] (**12a**) was obtained in 90% yield. *Anal.* Calc. for $C_{13}H_{13}ClN_6O_5Pd$: C, 32.8; H, 2.7; N, 17.7. Found: C, 32.7; H, 2.7; N, 17.5%. M.p. (dec.) = 194°C. $\Lambda_M = 112\ \Omega^{-1}\ cm^2\ mol^{-1}$. IR (cm^{-1}): 3172 (N–H str), 1642 (C=O str).

[Pd(HNCO-py)(bpzm*)][ClO$_4$] (1**2b**) was obtained in 89% yield. *Anal.* Calc. for $C_{17}H_{21}ClN_6O_6Pd$: C, 38.4; H, 3.9; N, 15.8. Found: C, 38.5; H, 4.1; N, 15.7%. M.p. (dec.) = 284°C. $\Lambda_M = 120\ \Omega^{-1}\ cm^2\ mol^{-1}$. IR (cm^{-1}): 3204 (N–H str), 1650 (C=O str).

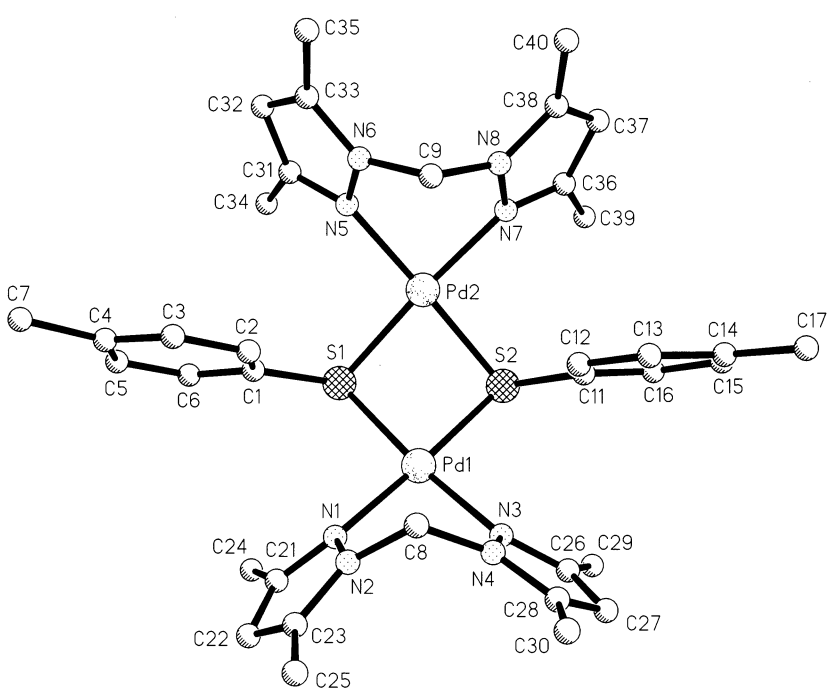


Fig. 2. Molecular structure of complex **6b**.

2.3. X-ray structural analysis of complexes $[Pd(S_2CNC_5H_{10})(bpzm)][ClO_4]$ (**11a**) and $[\{Pd(\mu\text{-}SC_6H_4Me\text{-}p)(bpzm^*)\}_2][ClO_4]_2$ (**6b**)

Crystals were mounted on glass fibers and transferred to the diffractometer (Siemens P4 with LT2 low-temperature attachment) as summarized in Table 1. The structure was solved by direct methods (**6b**·$(CH_3)_2CO\cdot H_2O$) or by the heavy atom method (**11a**) and refined anisotropically on F^2 (program SHELXL-93) [28]. For compound **6b**·$(CH_3)_2CO\cdot H_2O$ both perchlorate anions and the methyl groups of the acetone molecule are disordered over two positions. Hydrogen atoms for the water molecule were not found and the others included using a riding model. For compound **11b**, two independent molecules were found in the asymmetric unit with one of the perchlorate anions disordered over two sites.

3. Results and discussion

3.1. Reactivity of $[Pd(N–N)(\mu\text{-}OH)]_2[ClO_4]_2$ (N–N = bpzm and bpzm*)

The markedly basic character of complexes $[Pd(bpzm)(\mu\text{-}OH)]_2[ClO_4]_2$ and $[Pd(bpzm^*)(\mu\text{-}OH)]_2[ClO_4]_2$ is consistent with their chemical reactivity, exhibited towards a wide variety of protic acids H(LL) and summarized in Scheme 1. Its efficiency as precursors in coordination chemistry comes from their ability to yield the new complexes in one clean step, with the concomitant release of water.

Thus, the hydroxo-complexes react in acetone under mild to strong conditions with weak protic acids H(LL) to give mono- or binuclear species, depending on whether the deprotonated acid $(LL)^-$ is *exo*- or *endo*-bidentate. These reactions can be considered as an initial proton abstraction by the hydroxo-palladium complex, which provides $(LL)^-$ and the metal substrate subsequently, trapped by the anion to form the new complexes. In a similar way, the preparation of the dithiocarbamato-complexes (**9a**–**11a** and **9b**–**11b**) should involve a first step of amine deprotonation, followed by nucleophilic attack of R_2N^- to carbon disulfide present in the reaction medium to form the dithiocarbamate anion.

In previous work we pointed out marked differences in reactivity between the hydroxo-complexes studied [6,16], although it was always under the general pattern described above. Sometimes these differences can be explained on the basis of the distinct activation of the OH groups, and other reasonable explanations are provided by the relative lability of the backbone ligands (bpzm and bpzm* in this paper), easily displaced from the coordination sphere if a competitive insoluble product is forming, or when strong steric requirements of the incoming ligand are operating. In this sense, the unequal behavior showed by the hydroxo-complexes object of our study in this paper was not unexpected, and can be regarded as a consequence of the differences both steric and electronics between the ligands bpzm and bpzm*.

Thus, when $[Pd(bpzm)(\mu\text{-}OH)]_2^{2+}$ reacts in acetone with HO–N donor ligands in short time (15 min) under mild conditions, the new complexes **1a**–**3a** were obtained in good yield. If the same reactions are stirred for longer periods, dissociation of complexes occurs with the formation of insoluble species $[Pd(O–N)_2]$ and solutions containing the cationic complex with two bpzm units (Scheme 2).

This dissociation reactions are strongly dependent on the solvent employed, being faster when increasing its donor properties. On the other hand, reactions involving the bis(3,5-dimethylpyrazol-1-yl) methane (bpzm*) precursor and O–N-donor ligands did not present this behavior and the expected complexes were obtained normally, even requiring stronger conditions. In this case the presence of methyl groups in bpzm* may increase the donor capability of this ligands respect bpzm, as it can avoid the dissociation mechanism by solvent attack through the *z*-axis of the square-planar complexes.

The attemps to obtain the corresponding thiolate and azolate complexes from $[Pd(bpzm)(\mu\text{-}OH)]_2[ClO_4]_2$ and $[Pd(bpzm^*)(\mu\text{-}OH)]_2[ClO_4]_2$ revealed once more, differences in reactivity between them. Thus, reactions of the bpzm precursor with triazole and activated thiols yield insoluble species where the bpzm ligand was not detected, probably labilized from the coordination sphere as a consequence of the formation of polimeric compounds.

In contrast, the reactivity presented for both precursors against carbon disulfide and secondary amines was the same, yielding the corresponding dithiocarbamate complexes **9a**–**11a** and **9b**–**11b** as explained in Section 2.

3.2. Hydration of coordinated aminonitriles

The activation of nitriles with respect to attack by nucleophiles in the coordination sphere of metal ions has attracted considerable interest [29–31] and we have recently described the nucleophilic attack of OH^- and MeO^- on benzonitrile coordinated to Pt(II) [4]. We also reported the use of the hydroxo-complex $[\{Ni(C_6F_5)_2(\mu\text{-}OH)\}_2]^{2-}$ in the formation of complexes containing amidate ligands [32]. In acetone–H_2O, the precursors $[Pd(bpzm)(\mu\text{-}OH)]_2[ClO_4]_2$ and $[Pd(bpzm^*)(\mu\text{-}OH)]_2[ClO_4]_2$ react smoothly with pyridine-2-carbonitrile (CNpy) leading to the formation of the corresponding complexes with pyridine-2-carboxamidate ligand (compounds **12a** and **12b** in Scheme 1).

3.3. Characterization

The new compounds are air-stable, yellow–orange solids, and measurements of their molar conductivity in acetone solutions indicate that the complexes behave as 1:1 (**1**–**3** and **9**–**12**) or 1:2 (**4**–**8**) electrolytes [33], in accordance with the proposed formulae. The most significant IR absorption bands of the new complexes are collected in Section 2. The IR spectra of the complexes also show the characteristic bands of the ligands bpzm and bpzm* at ca. 1520, 770 and 640 cm^{-1} and 1556, 790 and 680 cm^{-1}, respectively, together with the bands attributed to the anion perchlorate at 1070 and 624 cm^{-1}.

The ^{1}H and ^{13}C NMR data are listed in Table 2 and Scheme 3 shows the labeled ligands. The ^{1}H spectra exhibit the expected resonances for the corresponding anionic ligands, together with the corresponding resonances of the pyrazolyl groups. As we reported in a previous paper [7], the two pyrazolyl groups were identical or spectroscopically different depending on the asymmetry of complexes, and one or two sets of pyrazolyl signals were respectively observed. Regarding to the methylene NMR-signals showed by the compounds, we found the expected patterns reported for bis(pyrazol-1-yl)methane ligands [7,22,26,27]. The assignment was made by comparison with our previous data and by means of different NMR experiments ($^{1}H-^{13}C$ heteronuclear correlations for ^{13}C assignment).

Further evidence for the dinuclearity of complexes **4a**–**6a** and **4b**–**8b** comes from the FAB mass spectrometry (see Section 2). Spectra of the new bridged compounds show a similar pattern of fragmentation which includes, as the most outstanding feature, the peaks corresponding to $[Pd_2(N–N)_2(L)_2(ClO_4)]^+$, $[Pd_2(N–N)_2(L)_2]^+$ and $[Pd_2(N–N)(L)_2(ClO_4)]^+$ (N–N = bpzm or bpzm*; L = pz, taz, SPh and SC_6H_4Me-p). This technique becomes an excellent tool to characterize the μ-oxalate compounds **4a** and **4b**, whose marked insolubility prevent their proper characterization by NMR spectroscopy. The abundances of the signals around the parent ion are consistent with the natural isotopic abundances. Additional peaks are observed, indicating further fragmentation and formation of some adducts with the matrix [34].

3.4. Crystal structures of complexes *11a* and *6b*

The crystal structure of **11a** consists of cationic mononuclear palladium complexes and perchlorate anions. Two molecules of the complex appear in the asymmetrical unit, as shown in Fig. 1. The planar coordination around palladium is slightly distorted. Bond distances and angles are similar to those found in other palladium(II) complexes with dithiocarbamate ligands [35], and a selection is presented in Table 3. The angle S(2)–Pd–S(1) is appreciably smaller than 90° (76.3°) as a consequence of geometrical restrictions of the chelate ring, and, as expected, the S–Pd–N angles are over 90° (95.9 and 98.7°) [36].

The dinuclearity of complex **6b** was unambiguously established by single-crystal X-ray diffraction. Selected geometrical features are given in Table 3. The structure consists of binuclear $[\{Pd(\mu\text{-}SC_6H_4Me\text{-}p)(bpzm^*)\}_2]^+$ cations (Fig. 2) joining ClO_4^- anions by electrostatic interactions and one molecule of crystallization of $(CH_3)_2CO$ and H_2O. The geometry about each palladium atom is approximately planar-square, with predictable narrowing of the S–Pd–S (80.04 and 80.14°) and N–Pd–N (86.2 and 85.3°) angles in both centers to accommodate the bridged structure, as usual in bridging arylthiolates [37].

On the other hand, it is well known that, depending on the units $M(\mu\text{-}SR)_2M$ being planar or bend and the relative positions of substituents, there are five possible geometrical isomers [38]. In our complex, the structure presents a bend $Pd(\mu\text{-}SC_6H_4Me\text{-}p)_2Pd$ unit with *syn–endo* geometry and a dihedral angle between $N_2Pd(1)S_2$ and $S_2Pd(2)N_2$ of 52.6°.

4. Supplementary data

Crystallographic data have been deposited with the CCDC, 12 Union Road, Cambridge, CB2 1EZ, UK (fax: +44-1223-336033; e-mail: deposit@ccdc.cam.ac.uk or www: http://www.ccdc.cam.ac.uk) and are available on request quoting the deposition Nos. CCDC 140465 and 140466.

Acknowledgements

We thank The Dirección General de Enseñanza Superior e Investigación Científica (project No. PB97-1036), Spain, for financial support. J.L. Serrano thanks Cajamurcia (Spain) for a postdoctoral grant.

References

[1] H.E. Bryndza, W. Tam, Chem. Rev. 88 (1988) 1163.
[2] G. López, G. García, G. Sánchez, J. García, J. Ruiz, J.A. Hermoso, A.Vegas, M. Martínez-Ripoll, Inorg. Chem. 31 (1992) 1518.
[3] G. López, J. Ruiz, G. García, C. Vicente, J. Casabó, E. Molins C. Miravitlles, Inorg. Chem. 30 (1991) 2607.
[4] G. López, J. Ruiz, G. García, C. Vicente, J.M. Martí, J.A. Hermoso, A. Vegas, M. Martínez-Ripoll, J. Chem. Soc., Dalton Trans. (1992) 53.
[5] S. Wimmer, P. Castan, F.L. Wimmer, N.P. Johnson, J. Chem. Soc., Dalton. Trans. (1989) 403.
[6] G. Sánchez, A. Sanmartin, J. García, G. López, Transition Met. Chem. 22 (1997) 545.

[7] G. Sánchez, J.L. Serrano, J. Pérez, M.C. Ramírez de Arellano, G. López, E. Molins, Inorg. Chim. Acta 295 (1999) 13.
[8] G. López, G. Sánchez, G. García, J. García, A. Martínez, J.A. Hermoso, M. Martínez-Ripoll, J. Organomet. Chem. 435 (1992) 193.
[9] G. López, J. Ruiz, G. García, C. Vicente, J.M. Martí, V. Rodríguez, J. Organomet. Chem. 436 (1992) 121.
[10] G. Sánchez, J.A. Muñoz, M.J. Vidal, G. García, G. López, J. Organomet. Chem. 463 (1993) 239.
[11] G. Sánchez, F. Ruiz, M.D. Santana, G. García, G. López, J.A. Hermoso, M. Martínez-Ripoll, J. Chem. Soc., Dalton Trans. (1994) 19.
[12] J. Ruiz, V. Rodríguez, G. López, P.A. Chaloner, P.B. Hitchcock, Organometallics 15 (1996) 1662.
[13] J. Ruiz, V. Rodríguez, C. Vicente, G. López, Transition Met. Chem. 22 (1997) 502.
[14] J. Ruiz, V. Rodríguez, G. López, P.A. Chaloner, P.B. Hitchcock, J. Chem. Soc., Dalton Trans. (1997) 4271.
[15] J. Ruiz, C. Vicente, V. Rodriguez, G. López, Polyhedron 17 (1998) 1503.
[16] G. Sánchez, J.L. Serrano, J. García, G. López, J. Pérez, E. Molins, Inorg. Chim. Acta 287 (1999, 37.
[17] G. López, G. Sánchez, G. García, J. García, A. Sanmartín, M.D. Santana, Polyhedron 10 (1991) 2821.
[18] G. López, G. Sánchez, G. García, J. Ruiz, J. García, M.A. Martínez-Ripoll, A. Vegas, J.A. Hermoso, Angew. Chem., Int. Ed. Engl. 30 (1991) 716.
[19] S. Trofimenko, Chem. Rev. 93 (1993) 943.
[20] (a) A. Llobet, D.J. Hodgson, T.J. Meyer, Inorg. Chem. 29 (1990) 3760. (b) A. Llobet, M.A. Curry, H.T. Evans, T.J. Meyer, Inorg. Chem. 28 (1989) 3131. (c) A. Llobet, P. Doplet, T.J. Meyer, Inorg. Chem. 27 (1988) 514.
[21] (a) F. Mani, Inorg. Chim. Acta 38 (1980) 97. (b) F. Mani, R. Morassi, Inorg. Chim. Acta 36 (1979) 63. (c) J. Verbiest, J.A.C. van Ooijen, J. Reedijk, J. Inorg. Nucl. Chem. 42 (1980) 971.
[22] (a) M. Fajardo, A. de la Hoz, E. Diez-Barra, F.A. Jalón, A. Otero, A. Rodríguez, J. Tejeda, D. Belleti, M. Lanfranchi, M.A. Pellinghelli, J. Chem. Soc., Dalton Trans. (1993) 1935. (b) F.A. Jalón, A. Otero, A. Rodríguez, J. Chem. Soc., Dalton Trans. (1995) 1629. (c) F.A. Jalón, A. Otero, A. Rodríguez, M. Pérez-Manrique, J. Organomet. Chem. 508 (1996) 69.
[23] P. Ballesteros, C. López, R.M. Claramunt, J.J. Jiménez, M. Cano, J.V. Heras, E. Pinilla, A. Monge, Organometallics 13 (1994) 289.
[24] A.J. Canty, N.J. Minchin, P.C. Healy, A.H. White, J. Chem. Soc., Dalton Trans. (1982) 1795.
[25] A.J. Canty, N.J. Minchin, N.J. Patrick, A.H. White, J. Chem. Soc., Dalton Trans. (1983) 1253.
[26] G. Minghetti, M.A. Cinellu, A.L. Bandini, G. Banditelli, F. Demartin, M. Manassaro, J. Organomet. Chem. 315 (1986) 387.
[27] F.A. Jalón, B.R. Manzano, A. Otero, M.C. Rodríguez-Pérez, J. Organomet. Chem. 494 (1995) 179.
[28] G.M. Sheldrik, SHELXL-93, Program for Crystal Structure Refinement University of Göttingen, Germany, 1993.
[29] M. Wada, T. Shimohigashi, Inorg. Chem. 15 (1976) 954.
[30] I.I. Creaser, J. Mac B. Harrowfield, F.R. Keene, A.M. Sargeson, J. Am. Chem. Soc. 103 (1981) 3559.
[31] R. McCrindle, G. Ferguson, G.J. Arsenault, A.J. McAlees, J. Chem. Soc., Chem. Commun. (1983) 571.
[32] G. Sánchez, F. Ruiz, M.C. Ramírez de Arellano, G. López, Helv. Chim. Acta 80 (1997) 2477.
[33] W.J. Geary, Coord. Chem. Rev. 7 (1971) 81.
[34] C. Fenselau, R.J. Cotter, Chem. Rev. 87 (1987) 501.
[35] D.L. Reger, D.G. Garza, L. Lebioda, Organometallics 1 (1991) 902.
[36] P.M. Bailey, S.T. Taylor, P.M. Maitlis, J. Am. Chem. Soc. 100 (1978) 4711.
[37] E.M. Padilla, J.A. Golen, P.N. Richmann, C.M. Jensen, Polyhedron 10 (1991) 1343.
[38] J.P. Fackler, W.J. Zegarski, J. Am. Chem. Soc. 95 (1973) 8566.

PERGAMON

www.elsevier.nl/locate/poly

Polyhedron 19 (2000) 1407–1414

POLYHEDRON

Oxomolybdenum coordination compounds with alkyl-substituted pyridines. Solvothermal syntheses and structural characterization of $[Mo_{10}O_{26}(3,5\text{-Lut})_8]\cdot 2(3,5\text{-Lut})$, $[Mo_{10}O_{26}(3\text{-MePy})_8]\cdot(3\text{-MePy})$, $[Mo_{10}O_{26}(3\text{-MePy})_8]$ and $[Mo_{12}O_{28}(OCH_3)_2Cl_2(3\text{-MePy})_8]$

Barbara Modec [a,*], Jurij V. Brenčič [a], Ljubo Golič [a], Lee M. Daniels [b]

[a] *Faculty of Chemistry and Chemical Technology, University of Ljubljana, Aškerčeva 5, SL-1000 Ljubljana, Slovenia*
[b] *Laboratory for Molecular Structure and Bonding, Texas A&M University, College Station, TX 77843, USA*

Received 25 February 2000; accepted 12 May 2000

Abstract

Reactions of $(PyH)_2[MoOCl_5]$ with methanol and 3,5-lutidine or 3-methylpyridine carried out under conditions of solvothermal synthesis at 130°C have resulted in two Mo(V, VI) clusters containing the same molybdenum oxide framework, $[Mo_{10}O_{26}(3,5\text{-Lut})_8]\cdot 2(3,5\text{-Lut})$ (3,5-Lut = 3,5-lutidine (C_7H_9N)) (**i**) and $[Mo_{10}O_{26}(3\text{-MePy})_8]\cdot(3\text{-MePy})$ (3-MePy = 3-methylpyridine (C_6H_7N)) (**ii**), and in a novel $[Mo_{12}O_{28}(OCH_3)_2Cl_2(3\text{-MePy})_8]$ (**iv**). $[Mo_{10}O_{26}(3\text{-MePy})_8]$ (**iii**) was also obtained by oxidizing $(NH_4)_2[MoCl_5(H_2O)]$ in a mixture of methanol, 3-methylpyridine and nitromethane. X-ray structural analyses revealed $Mo_2O_4^{2+}$ unit as a common structural motif in both cluster types. In **i**–**iii** ten molybdenum atoms are grouped into four Mo_2^{V} pairs with Mo–Mo bonds and two Mo(VI) sites. The oxomolybdenum core of **iv** is composed of six Mo_2^{V} pairs connected through oxo and methoxo bridges. © 2000 Elsevier Science Ltd. All rights reserved.

Keywords: Solvothermal synthesis; Crystal structures; Oxomolybdenum(V) coordination compounds; Mo(V, VI) compounds; Alkyl-substituted pyridines

1. Introduction

A decanuclear oxomolybdenum(V, VI) cluster with stoichiometry $[Mo_{10}O_{26}L_8]$ (L = 3,5-Lut, 3-MePy) and a new, dodecanuclear $[Mo_{12}O_{28}(OCH_3)_2Cl_2(3\text{-MePy})_8]$ are two more examples of the vast family of high-nuclearity oxoalkoxymolybdate complexes with oxygen, nitrogen and sulfur donor ligands that has emerged in the past two decades. The molecular building approach based on the assembly of preorganized templates combined with the technique of hydrothermal synthesis has led to polyoxometalates of very complex stoichiometries, some with finite oxometalate core structures, and some with infinite chains, sheets or lattice frameworks [1]. The organic components added to the reaction mixture have been found to play a key role in the design of novel oxide-based composite materials: with the appropriate selection of the organic template its structural information can be imprinted onto the inorganic framework [2]. $(NH_4)_7[NaMo_{16}(OH)_{12}O_{40}]\cdot 4H_2O$, a class of superclusters $[Na(H_2O)_3H_{13}Mo_{42}O_{109}\{(OCH_2)_3CR\}_7]^{9-}$ or $[MoO_3H_{14}Mo_{42}O_{109}\{(OCH_2)_3CR\}_7]^{9-}$ ($(OCH_2)_3$-CR = trisalkoxy group) [3,4] with $Mo_2O_4^{2+}$ as a common structural motif in all, $[\{Cu(pyrd)\}_4(\gamma\text{-}H_4Mo_8O_{26})]$ (pyrd = pyridazine) [5] and $[\{Cu_3(4,7\text{-phen})_3\}_2\{Mo_{14}O_{45}\}]$ (4,7-phen = 4,7-phenanthroline) [6] where the molybdate cluster is entrained within a scaffolding provided by the coordination cation polymer, are just a few examples. A curious feature of the latter is the presence of two distinct types of molybdenum cluster $[Mo_6O_{19}]^{2-}$ and $\beta\text{-}[Mo_8O_{26}]^{4-}$ which are linked through $[Cu_3(4,7\text{-phen})_3]^{3+}$ in a two-dimensional structure.

In the literature two molybdate(VI) pyridine compounds are reported. $(PyH)_4[Mo_8O_{26}Py_2]$, which is built of pyridinium cations and discrete $[Mo_8O_{26}Py_2]^{4-}$ an-

* Corresponding author. Tel.: +386-61-1760-581; fax: +386-61-1258-220.
E-mail address: barbara.modec@guest.arnes.si (B. Modec).

0277-5387/00/$ - see front matter © 2000 Elsevier Science Ltd. All rights reserved.
PII: S0277-5387(00)00430-7

ions, was the first isopolymolybdate(VI) containing a ligand other than oxygen [7]. The polymeric structure of $[MoO_3Py]$ is believed to consist of oxide layers separated by organic layers with nitrogen directly coordinated to molybdenum [8].

We found that $(PyH)_2[MoOCl_5]$ reacts with methanol and pyridines through a series of reactions, starting with the facile replacement of chloro ligands, followed by dimerization into $Mo_2O_4^{2+}$ moieties, which eventually link into larger, stable assemblies. The properties of the neutral oxomolybdenum(V) clusters are similar to those of $Mo_2O_4^{2+}$ units. The puckered $Mo(\mu_2\text{-}O)_2Mo$ ring, whose two molybdenum atoms are a short distance apart (2.5–2.7 Å), allows the formation of a localized single metal–metal bond which accounts for the experimentally-observed diamagnetism [9]. From the identity of the isolated clusters, i.e. $[Mo_4O_8(OCH_3)_2Cl_2Py_4]\cdot 2Py$ [10], $[Mo_5O_{11}(OCH_3)_4Py_4]\cdot CH_3OH$ [11], $[Mo_6O_{12}(OCH_3)_6Py_4]$ [10], $[Mo_8O_{16}(OCH_3)_8L_4]$ (L = pyridine, 3-methylpyridine, 4-methylpyridine, 4-ethylpyridine, 4-*tert*-butylpyridine, 3,5-lutidine) [12,13] and $[Mo_{10}O_{26}Py_8]\cdot 7Py$ [10], we could infer that the nuclearity of the clusters and the degree of substitution of chloro ligands are highly dependent on the reaction conditions. In order to obtain the 'final' product of the polymerization, some of the reaction systems were tested under the conditions of the solvothermal synthesis. Herein we report on two types of oxomolybdenum cluster obtained by employing this technique.

2. Experimental

2.1. General comments

$(NH_4)_2[MoCl_5(H_2O)]$ [14] and $(PyH)_2[MoOCl_5]$ [15] were synthesized according to published procedures. Solvents were reagent grade and they were used without additional purification. They were obtained from the following sources: Merck (3,5-lutidine, methanol and nitromethane) and BDH Chemicals (3-methylpyridine).

IR spectra of Nujol (4000–400 cm^{-1}) and hexachlorobutadiene (4000–1200 cm^{-1}) mulls between CsBr plates were measured on a Perkin–Elmer 1720 X FT-IR spectrometer. Far IR spectra of Nujol mulls (700–100 cm^{-1}) on a polyethylene foil were measured on a Perkin–Elmer 2000 FT-IR spectrometer.

2.2. Preparations

2.2.1. Preparation of $[Mo_{10}O_{26}(3,5\text{-}Lut)_8]\cdot 2(3,5\text{-}Lut)$ (i)

A 50 mg (0.11 mmol) sample of $(PyH)_2[MoOCl_5]$ was added to a mixture of 2 ml of methanol and 7 ml of 3,5-lutidine. The sealed glass tube was heated in an autoclave under autogenous pressure at 130°C for 146 h. Dark, red crystals were obtained in 30% yield (8 mg).

Anal. Calc. for $C_{56}H_{72}Mo_{10}N_8O_{26}$ (dried sample): C, 30.13; H, 3.25; N, 5.02. Found: C, 30.37; H, 3.27; N, 5.08%.

IR data (cm^{-1}): 1608(m), 1600(m), 1310(w), 1252(w), 1184(w), 1157(s), 1038(m), 974(m), 961(vs), 945(m), 922(w), 868(m), 796(m), 779(m), 757(vs), 740(vs), 720(vs), 702(vs), 649(w), 617(m), 537(sh), 516(m), 494(m), 413(w).

2.2.2. Preparation of $[Mo_{10}O_{26}(3\text{-}MePy)_8]\cdot(3\text{-}MePy)$ (ii)

A 428 mg (0.95 mmol) sample of $(PyH)_2[MoOCl_5]$ was added to a mixture of 5 ml of methanol and 15 ml of 3-methylpyridine. A total of 2 ml of water was added to the solution. The sealed glass tube was heated in an autoclave under autogenous pressure at 130°C for 104 h. Dark, almost black crystals were obtained in 9% yield (18 mg).

IR data (cm^{-1}): 1614(m), 1584(m), 1251(w), 1201(s), 1135(s), 1111(s), 1068(s), 1037(w), 957(vvs), 946(vvs), 935(m), 910(w), 825(w), 798(vs), 752(vvs), 741(vs), 726(m), 707(vs), 696(vs), 661(m), 618(vs), 534(sh), 520(sh), 502(s), 484(s), 453(m), 419(sh), 408(sh).

2.2.3. Preparation of $[Mo_{10}O_{26}(3\text{-}MePy)_8]$ (iii)

A 90 mg (0.273 mmol) sample of $(NH_4)_2[MoCl_5(H_2O)]$ was added to a mixture of 2.2 ml of 3-methylpyridine, 2.2 ml of nitromethane and 6.6 ml of methanol. After stirring for 30 min, 0.2 ml of water was added to the solution. The solution was left for 3 days under ambient conditions. Red, plate-shaped crystals were obtained in 24% yield (14 mg).

Anal. Calc. for $C_{48}H_{56}Mo_{10}N_8O_{26}$: C, 27.19; H, 2.66; N, 5.28. Found: C, 26.92; H, 2.48; N, 5.02%.

IR data (cm^{-1}): 1612(m), 1583(w), 1198(m), 1130(m), 1111(m), 1066(m), 1037(w), 958(vvs), 948(sh), 823(w), 796(vs), 753(vs), 741(vs), 725(sh), 706(vs), 661(m), 621(s), 519(sh), 500(s), 487(sh), 452(w).

2.2.4. Preparation of $[Mo_{12}O_{28}(OCH_3)_2Cl_2(3\text{-}MePy)_8]$ (iv)

A 428 mg (0.95 mmol) sample of $(PyH)_2[MoOCl_5]$ was added to a mixture of 5 ml of methanol and 15 ml of 3-methylpyridine. The sealed glass tube was heated in an autoclave under autogenous pressure at 130°C for 96 h. Black crystals were obtained in 28% yield (55 mg).

Anal. Calc. for $C_{50}H_{62}Cl_2Mo_{12}N_8O_{30}$: C, 24.24; H, 2.52; N, 4.52. Found: C, 24.53; H, 2.52; N, 4.46%.

IR data (cm^{-1}): 2811(w), 1612(m), 1582(m), 1200(m), 1133(m), 1113(m), 1065(s), 1047(s), 962(vvs), 938(vs), 826(w), 794(m), 761(vs), 747(s), 704(vs), 692(vs), 672(m), 661(m), 617(m), 543(w), 508(vs), 480(sh), 437(w), 419(m), 392(w), 366(w), 347(w), 332(w), 307(m), 290(sh), 269(m).

2.3. X-ray structural determination

Crystal data parameters are given in Table 1. Data for compound **i** were collected on a Nonius FAST area detector diffractometer. A total of 10 359 reflections were measured ($\theta_{max} = 22.76°$; $-13 \le h \le 13$, $-14 \le k \le 14$, $-15 \le l \le 15$) and reduced to a unique set of 5250 reflections ($R_{int} = 0.071$). The program used for data collection was MADNES [16]. The structure was solved by direct methods. The program used for structure solution and refinement was SHELXTL-96 [17]. All non-hydrogen atoms were refined using anisotropic thermal parameters. The least-squares refinement on F^2 for **i** converged at $R = 0.0599$ and $R_w = 0.1282$ for 523 parameters, 18 restraints and 4896 data ($I > 2\sigma(I)$) (the weighting scheme used was $w = 1/\{\sigma^2(F_o^2) + (0.03P)^2 + 35.0P\}$ where $P = (F_o^2 + 2F_c^2)/3$).

Data for compounds **ii**–**iv** were collected on an Enraf–Nonius CAD-4 diffractometer. For **ii** a total of 12 909 reflections were measured ($\theta_{max} = 24.99°$; $-14 \le h \le 0$, $-15 \le k \le 15$, $-26 \le l \le 26$) and reduced to a unique set of 6452 reflections ($R_{int} = 0.0379$); for **iii** a total of 17 768 reflections were measured ($\theta_{max} = 28.12°$; $-15 \le h \le 15$, $-17 \le k \le 0$, $-30 \le l \le 30$) and reduced to a unique set of 8489 reflections ($R_{int} = 0.072$); for **iv** a total of 23 729 reflections were measured ($\theta_{max} = 24.98°$; $-48 \le h \le 48$, $-48 \le k \le 48$, $-14 \le l \le 4$) and reduced to a unique set of 7124 reflections ($R_{int} = 0.092$). Cell parameters for **ii** were determined from 100 reflections in the 9.01–14.29° θ range, for **iii** from 50 reflections in the 8.15–13.1° θ range and for **iv** from 75 reflections in the 8.20–14.17° θ range. Data collection followed routine procedures. All data were corrected for Lorentz and polarization effects. No absorption corrections were applied. Structures were solved by direct methods using SIR-92 [18]. All non-hydrogen atoms were refined using anisotropic thermal parameters. The program used was XTAL 3.4 [19]. The hydrogen atoms were inserted in calculated positions. The least-squares refinement on F for **ii** converged at $R = 0.033$ and $R_w = 0.042$ for 451 parameters and 4529 data ($F_o > 3\sigma(F_o)$) (the weighting scheme used was $w = W_F W_S$, where $W_F(F_o < 32) = (F_o/32)^1$, $W_F(F_o > 76) = (76/F_o)^1$ and $W_F(32 < F_o < 76) = 1$, and $W_S(\sin\theta < 0.4) = (0.4/\sin\theta)^1$, $W_S(\sin\theta > 0.54) = (\sin\theta/0.54)^1$ and $W_S(0.4 < \sin\theta < 0.54) = 1$). The least-squares refinement for **iii** converged at $R = 0.088$ and $R_w = 0.089$ for 415 parameters and 3492 data ($F_o > 3\sigma(F_o)$) (the weighting scheme used was $w = W_F W_S$, where $W_F(F_o < 40) = (F_o/40)^1$, $W_F(F_o > 90) = (90/F_o)^1$ and $W_F(40 < F_o < 90) = 1$, and $W_S(\sin\theta < 0.33) = (0.33/\sin\theta)^{2.0}$, $W_S(\sin\theta > 0.43) = (\sin\theta/0.43)^3$ and $W_S(0.33 < \sin\theta < 0.43) = 1$). The least-squares refinement for **iv** converged at $R = 0.047$ and $R_w = 0.050$ for 460 parameters and 3744 data ($F_o > 3\sigma(F_o)$) (the weighting scheme used was $w = W_F W_S$, where $W_F(F_o < 146) = (F_o/146)^1$, $W_F(F_o > 268) = (268/F_o)^1$ and $W_F(146 < F_o < 268) = 1$, and $W_S(\sin\theta < 0.32) = (0.32/\sin\theta)^{3.0}$, $W_S(\sin\theta > 0.48) = (\sin\theta/0.48)^1$ and $W_S(0.32 < \sin\theta < 0.48) = 1$).

3. Results and discussion

3.1. Description of structures

3.1.1. Crystal structures of $[Mo_{10}O_{26}(3,5\text{-Lut})_8]\cdot 2(3,5\text{-Lut})$ (i), $[Mo_{10}O_{26}(3\text{-MePy})_8]\cdot(3\text{-MePy})$ (ii) and $[Mo_{10}O_{26}(3\text{-MePy})_8]$ (iii)

X-ray structural analyses have shown that compounds **i**–**iii** contain discrete neutral molecules com-

Table 1
Crystallographic data for compounds **i**–**iv**

	i	ii	iii	iv
Formula	$C_{70}H_{90}Mo_{10}N_{10}O_{26}$	$C_{54}H_{63}Mo_{10}N_9O_{26}$	$C_{48}H_{56}Mo_{10}N_8O_{26}$	$C_{50}H_{62}Cl_2Mo_{12}N_8O_{30}$
Formula weight	2446.9	2213.5	2120.4	2477.3
Space group	$P\bar{1}$ (no. 2)	$P2_1/n$ (no. 14)	$P2_1/c$ (no. 14)	$R\bar{3}$ (no. 148)
a (Å)	12.550(10)	12.1956(10)	11.925(3)	40.999(4)
b (Å)	13.323(6)	12.7373(10)	12.961(3)	40.999(4)
c (Å)	14.210(10)	22.5836(10)	23.404(7)	12.547(2)
α (°)	91.36(4)	90	90	90
β (°)	110.82(7)	92.791(10)	101.56(3)	90
γ (°)	108.15(6)	90	90	120
V (Å^3)	2086(2)	3504.0(4)	3544(2)	18 265(5)
Z	1	2	2	9
T (°C)	−60	20	20	20
λ (Å)	0.71073	0.71073	0.71073	0.71073
D_{calc} (g cm^{-3})	1.948	2.095	1.987	2.027
μ (cm^{-1})	15.3	18.1	18.0	19.3

Table 2
Selected bond distances (Å) for $[Mo_{10}O_{26}L_8]$ (L = 3,5-Lut (**i**), 3-MePy (**ii**, **iii**)) [a]

	i	ii	iii
Mo–Mo	2.568(2), 2.590(2)	2.5576(8), 2.6128(8)	2.575(3), 2.594(3)
Mo–N	2.206(9)–2.231(9)	2.213(6)–2.251(6)	2.223(16)–2.275(17)
Mo–O_t	1.671(7)–1.687(7)	1.678(5)–1.686(5)	1.609(15)–1.707(15)
Mo–O(μ_2)	1.830(7)–2.056(8)	1.812(4)–2.050(5)	1.790(15)–2.111(12)
Mo–O(μ_3)	1.950(7)–2.286(7)	1.946(4)–2.290(4)	1.948(12)–2.307(12)
Mo–O(μ_4)	1.970(7)	1.979(4)	2.011(14)
	1.982(7)	1.992(4)	2.017(12)
	2.309(7)	2.294(4)	2.253(12)
	2.613(8)	2.643(4)	2.600(11)
Mo(VI)–O_t	1.675(8)	1.684(5)	1.679(14)
Mo(VI)–O(μ_2)	1.830(7)	1.812(4)	1.790(15)
Mo(VI)–O(μ_2)	1.853(7)	1.857(5)	1.855(15)
Mo(VI)–O(μ_3)	1.986(7)	1.989(4)	1.954(14)
Mo(VI)–O(μ_3)	2.006(7)	1.995(4)	2.002(12)
Mo(VI)–O(μ_4)	2.613(8)	2.643(4)	2.600(11)

[a] O_t, terminal oxygen; O(μ_2), doubly bridging oxygen; O(μ_3), triply bridging oxygen; O(μ_4), quadruply bridging oxygen.

posed of a common oxomolybdenum framework. The same structure has been identified before for $[Mo_{10}O_{26}Py_8]\cdot 7Py$ [10]. Some of the principal dimensions of the $[Mo_{10}O_{10}(\mu_2\text{-}O)_8(\mu_3\text{-}O)_6(\mu_4\text{-}O)_2]$ core for compounds **i**–**iii** are given in Table 2. Geometric parameters for **i** are listed in Table 3. The structure of **i** is shown in Fig. 1. The centrosymmetric molecules contain eight Mo(V) atoms, two Mo(VI) atoms, 26 oxo groups and eight nitrogen donor ligands. The eight Mo(V) centers form four binuclear units with single Mo–Mo bonds, in which the average Mo–Mo distances are 2.579(2), 2.585(9) and 2.585(3) Å for **i**–**iii**, respectively. Two oxygen atoms adopt a μ_4-bridging mode. The coordination of O(μ_4) to one Mo(VI) and three Mo(V) sites is unsymmetrical. In **i**, for example, the distances to the Mo(V) centers are 1.970(7), 1.982(7) and 2.309(7) Å and the distance to Mo(VI) is 2.613(8) Å. The two hexavalent molybdenum atoms can be clearly distinguished from the Mo(V) centers which are part of the $Mo_2O_4^{2+}$ units. The distorted octahedral environment of each Mo(V) atom consists of five oxygen atoms and one nitrogen atom. The coordination environment of each Mo(VI) site is composed solely of oxygen atoms at distances ranging from 1.675(8) to 2.613(8) Å in **i**. One terminally bound oxo group, two doubly bridging, two triply bridging and a quadruply bridging oxo group constitute the highly distorted octahedral environment of Mo(VI). The weak interaction between Mo(VI) and O(μ_4), 2.613(8) Å in **i** manifests a strong *trans* influence of a terminally bound oxygen. The structure may be alternatively viewed (Fig. 2) as a parallel alignment of the Mo–Mo vectors of four $Mo_2O_4^{2+}$ units forming a fourfold pattern with the Mo=O groups of each dimer perpendicularly oriented towards its adjacent neighbors. The front and back face

Table 3
Bond distances (Å) and angles (°) for $[Mo_{10}O_{26}(3,5\text{-Lut})_8]\cdot 2(3,5\text{-Lut})$ (**i**)

Mo1–O1	1.684(7)	Mo3–O15	1.966(7)
Mo1–O13	1.912(8)	Mo3–O31	1.997(7)
Mo1–O15	1.950(7)	Mo3–N3	2.231(9)
Mo1–O16	2.031(7)	Mo3–O23	2.286(7)
Mo1–N1	2.220(9)	Mo4–O12	1.687(7)
Mo1–O14	2.309(7)	Mo4–O24	1.905(7)
Mo1–Mo3	2.568(2)	Mo4–O14	1.970(7)
Mo2–O21	1.682(7)	Mo4–O11	2.056(8)
Mo2–O24	1.946(7)	Mo4–N4	2.209(9)
Mo2–O14	1.982(7)	Mo4–O31[i]	2.218(7)
Mo2–O23	2.076(7)	Mo4–Mo5	2.999(3)
Mo2–N2	2.206(9)	Mo5–O10	1.675(8)
Mo2–O15[i]	2.235(7)	Mo5–O16	1.830(7)
Mo2–Mo4	2.590(2)	Mo5–O11	1.853(7)
Mo3–O32	1.671(7)	Mo5–O23[i]	1.986(7)
Mo3–O13	1.929(7)	Mo5–O31[i]	2.006(7)
O1–Mo1–O13	106.4(3)	O13–Mo3–N3	83.1(3)
O1–Mo1–O15	107.9(3)	O15–Mo3–N3	163.6(3)
O13–Mo1–O15	94.5(3)	O31–Mo3–N3	87.5(3)
O1–Mo1–O16	95.3(3)	O32–Mo3–O23	161.6(3)
O13–Mo1–O16	157.3(3)	O13–Mo3–O23	85.5(3)
O15–Mo1–O16	84.9(3)	O15–Mo3–O23	86.1(3)
O1–Mo1–N1	90.5(3)	O31–Mo3–O23	70.6(3)
O13–Mo1–N1	82.7(3)	N3–Mo3–O23	77.7(3)
O15–Mo1–N1	161.4(3)	O12–Mo4–O24	105.4(4)
O16–Mo1–N1	90.7(3)	O12–Mo4–O14	106.9(3)
O1–Mo1–O14	167.3(3)	O24–Mo4–O14	95.8(3)
O13–Mo1–O14	79.2(3)	O12–Mo4–O11	99.1(3)
O15–Mo1–O14	82.7(3)	O24–Mo4–O11	154.6(3)
O16–Mo1–O14	78.2(3)	O14–Mo4–O11	83.2(3)
N1–Mo1–O14	78.7(3)	O12–Mo4–N4	87.4(4)
O21–Mo2–O24	102.0(3)	O24–Mo4–N4	85.9(3)
O21–Mo2–O14	103.4(3)	O14–Mo4–N4	164.5(3)
O24–Mo2–O14	94.1(3)	O11–Mo4–N4	88.7(3)
O21–Mo2–O23	97.5(3)	O12–Mo4–O31[i]	163.3(3)
O24–Mo2–O23	157.9(3)	O24–Mo4–O31[i]	87.0(3)
O14–Mo2–O23	91.3(3)	O14–Mo4–O31[i]	82.4(3)
O21–Mo2–N2	86.0(3)	O11–Mo4–O31[i]	67.7(3)
O24–Mo2–N2	84.9(3)	N4–Mo4–O31[i]	82.3(3)
O14–Mo2–N2	170.5(3)	O10–Mo5–O16	105.6(4)
O23–Mo2–N2	86.2(3)	O10–Mo5–O11	104.9(4)
O21–Mo2–O15[i]	166.8(3)	O16–Mo5–O11	96.4(3)
O24–Mo2–O15[i]	77.6(3)	O10–Mo5–O23[i]	103.0(3)
O14–Mo2–O15[i]	89.8(3)	O16–Mo5–O23[i]	94.3(3)
O23–Mo2–O15[i]	81.0(3)	O11–Mo5–O23[i]	146.1(3)
N2–Mo2–O15[i]	80.8(3)	O10–Mo5–O31[i]	108.4(3)
O32–Mo3–O13	105.4(3)	O16–Mo5–O31[i]	146.0(3)
O32–Mo3–O15	107.6(3)	O11–Mo5–O31[i]	76.2(3)
O13–Mo3–O15	93.4(3)	O23–Mo5[i]–O31[i]	77.0(3)
O32–Mo3–O31	96.7(3)	Mo1–O13–Mo3	83.9(3)
O13–Mo3–O31	155.7(3)	Mo4–O14–Mo2	81.9(3)
O15–Mo3–O31	89.3(3)	Mo1–O15–Mo3	81.9(3)
O32–Mo3–N3	88.7(4)	Mo4–O24–Mo2	84.5(3)

[i] Symmetry code: $1-x, -y, -z$.

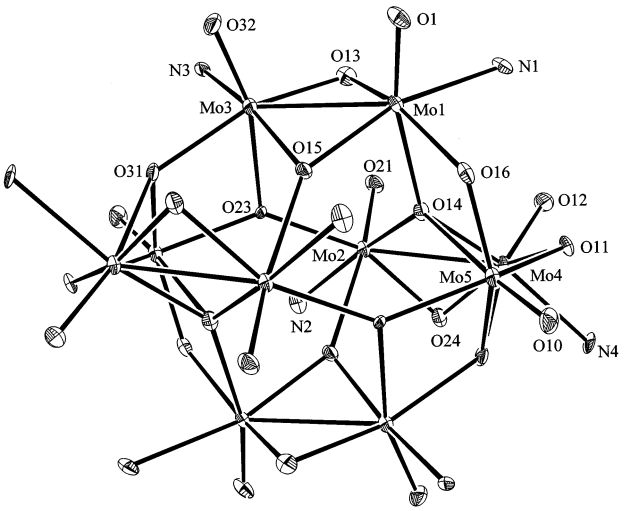


Fig. 1. ORTEP III [20] drawing of the $[Mo_{10}O_{26}(3,5\text{-Lut})_8]$ molecule in **i** with the atomic labeling scheme. Thermal ellipsoids are drawn at the 30% probability level. Carbon atoms are omitted for clarity.

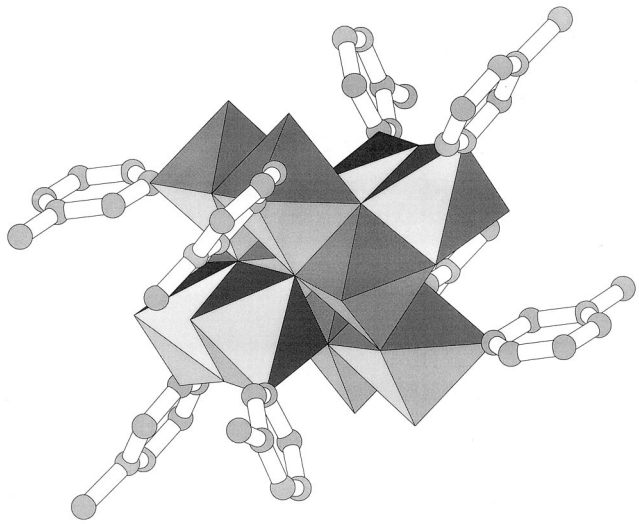


Fig. 3. ATOMS [21] polyhedral representation of the $[Mo_{10}O_{26}(3\text{-MePy})_8]$ molecule in **ii**.

of the geometric shape thus obtained are capped with two Mo(VI) moieties. Fig. 3 shows how the polyhedra are assembled together.

The structure of **i** also contains 3,5-lutidine molecules of crystallization. Compound **ii** contains a disordered solvent of crystallization. The shortest contact between two cluster molecules in **ii** is between a 3-methylpyridine carbon and a terminally bound oxygen, C24···O2^{ii} (symmetry code: (ii) $-x, 1-y, 1-z$) at a distance of 3.166(10) Å. The shortest contact in **iii** formed between C11 and O7^{ii} is 3.10(4) Å (symmetry code: (ii) $-x, 1-y, 1-z$).

The decanuclear anion found in $(NBu_4)_4[Mo_{10}O_{28}(SCH_2CH_2O)_2(HOCH_3)_2]\cdot 2CH_3OH$, which also features molybdenum in two oxidation states, has a different structure [22]. It consists of six Mo(VI) and four Mo(V) atoms which are part of two Mo_2^V units.

*3.1.2. Crystal structure of $[Mo_{12}O_{28}(OCH_3)_2Cl_2(3\text{-MePy})_8]$ (**iv**)*

The centrosymmetric cluster consists of a $[Mo_{12}O_{12}(\mu_2\text{-O})_4(\mu_3\text{-O})_{10}(\mu_4\text{-O})_2(\mu_2\text{-OCH}_3)_2]^{2+}$ framework to which are attached two chloro and eight 3-methylpyridine ligands. An extensive list of bond lengths and angles is given in Table 4, while values for different bonding modes of the ligands are listed in Table 5. An ORTEP III [20] picture of **iv** is given in Fig. 4. The 12 molybdenum atoms are arranged into six Mo_2^V pairs with Mo–Mo distances of 2.562(2), 2.590(2) and 2.682(2) Å. The oxygen atoms are of five distinct types. Twelve are terminal oxo groups with characteristic Mo–O distances in the range 1.643(9)–1.681(6) Å and two are methoxy oxygen donors adopting a doubly bridging mode with Mo–O distances 2.054(9) and 2.219(10) Å. Four oxygen atoms coordinate in a μ_2 fashion and ten in a μ_3 fashion. An unusual structural

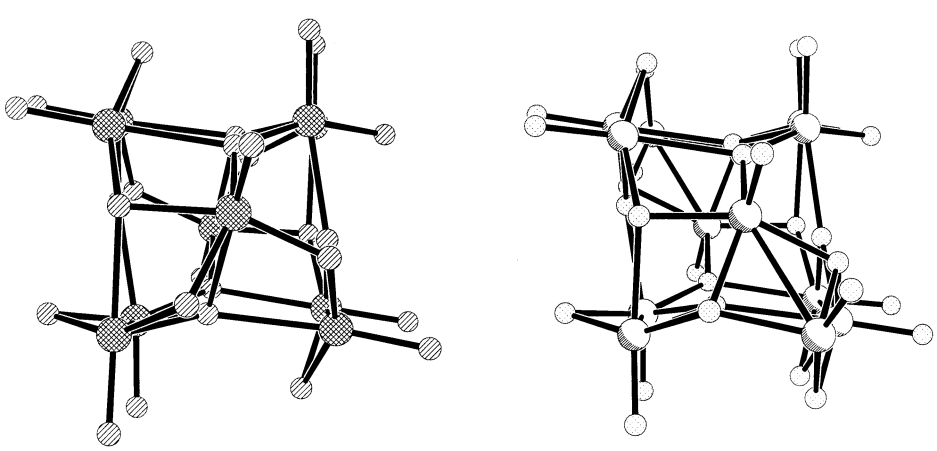


Fig. 2. Alternative view of cluster molecules in **i** (left) and **iv** (right). Carbon atoms are omitted.

Table 4
Bond distances (Å) and angles (°) for $[Mo_{12}O_{28}(OCH_3)_2Cl_2(3\text{-}MePy)_8]$ (**iv**)

Mo1–Mo2	2.5901(15)	Mo4–O4	1.681(6)
Mo1–O1	1.643(9)	Mo4–O9	1.969(7)
Mo1–O7	1.951(5)	Mo4–O10	1.951(8)
Mo1–O8	1.990(8)	Mo4–O11	2.058(8)
Mo1–O9	2.205(8)	Mo4–N4	2.237(11)
Mo1–O12	2.076(6)	Mo4–O12^{iii}	2.304(6)
Mo1–N1	2.251(11)	Mo5–Mo6	2.6819(18)
Mo2–O2	1.660(10)	Mo5–O5	1.673(9)
Mo2–O7	1.897(9)	Mo5–O12	1.975(8)
Mo2–O8	1.987(5)	Mo5–O13	1.971(6)
Mo2–O11	2.220(8)	Mo5–O8^{iii}	2.625(8)
Mo2–O14	2.127(9)	Mo5–O11^{iii}	1.954(7)
Mo2–N2	2.223(8)	Mo5–O14^{iii}	1.982(8)
Mo3–Mo4	2.5622(15)	Mo6–O6	1.653(12)
Mo3–O3	1.676(7)	Mo6–O13	2.056(8)
Mo3–O9	1.956(8)	Mo6–Cl	2.344(6)
Mo3–O10	1.924(9)	Mo6–O16	2.219(10)
Mo3–O13	2.071(8)	Mo6–N6	2.246(12)
Mo3–O16	2.054(9)	Mo6–O14^{iii}	1.962(8)
Mo3–O8^{iii}	2.405(6)		
O1–Mo1–O7	102.2(3)	Mo3–O10–Mo4	82.8(3)
O1–Mo1–O8	107.0(4)	Mo5–O13–Mo6	83.5(2)
O1–Mo1–O9	165.2(4)	Mo5^{iii}–O14–Mo6^{iii}	85.7(3)
O1–Mo1–O12	95.3(3)	O4–Mo4–O9	105.3(4)
O1–Mo1–N1	86.0(4)	O4–Mo4–O10	106.6(4)
O7–Mo1–O8	93.7(3)	O4–Mo4–O11	94.4(4)
O7–Mo1–O9	79.2(3)	O4–Mo4–N4	87.1(4)
O7–Mo1–O12	159.5(3)	O4–Mo4–O12^{iii}	161.7(4)
O7–Mo1–N1	81.9(3)	O9–Mo4–O10	93.8(3)
O8–Mo1–O9	87.5(3)	O9–Mo4–O11	89.0(3)
O8–Mo1–O12	91.1(3)	O9–Mo4–N4	167.3(3)
O8–Mo1–N1	167.0(3)	O9–Mo4–O12^{iii}	85.9(3)
O9–Mo1–O12	81.2(3)	O10–Mo4–O11	157.2(3)
O9–Mo1–N1	79.7(3)	O10–Mo4–N4	84.6(4)
O12–Mo1–N1	89.0(3)	O10–Mo4–O12^{iii}	86.6(3)
O2–Mo2–O7	107.2(5)	O11–Mo4–N4	87.7(4)
O2–Mo2–O8	108.2(3)	O11–Mo4–O12^{iii}	71.1(2)
O2–Mo2–O11	162.3(4)	N4–Mo4–O12^{iii}	81.4(3)
O2–Mo2–O14	96.4(5)	O5–Mo5–O12	103.2(4)
O2–Mo2–N2	89.7(4)	O5–Mo5–O13	108.5(4)
O7–Mo2–O8	95.5(3)	O5–Mo5–O8^{iii}	177.1(2)
O7–Mo2–O11	87.5(3)	O5–Mo5–O11^{iii}	107.5(3)
O7–Mo2–O14	155.3(4)	O5–Mo5–O14^{iii}	106.0(4)
O7–Mo2–N2	84.8(4)	O12–Mo5–O13	94.3(3)
O8–Mo2–O11	79.3(3)	O12–Mo5–O8^{iii}	78.4(3)
O8–Mo2–O14	83.9(3)	O12–Mo5–O11^{iii}	80.6(3)
O8–Mo2–N2	161.0(4)	O12–Mo5–O14^{iii}	147.0(4)
O11–Mo2–O14	68.0(3)	O13–Mo5–O8^{iii}	73.7(3)
O11–Mo2–N2	81.7(3)	O13–Mo5–O11^{iii}	143.9(3)
O14–Mo2–N2	88.0(4)	O13–Mo5–O14^{iii}	90.6(3)
O3–Mo3–O9	105.6(4)	O8^{iii}–Mo5–O11^{iii}	70.2(3)
O3–Mo3–O10	105.0(4)	O8^{iii}–Mo5–O14^{iii}	71.8(3)
O3–Mo3–O13	97.5(4)	O11^{iii}–Mo5–O14^{iii}	76.3(3)
O3–Mo3–O16	97.4(4)	O6–Mo6–O13	105.4(5)
O3–Mo3–O8^{iii}	172.6(4)	O6–Mo6–Cl	95.7(4)
O9–Mo3–O10	95.0(4)	O6–Mo6–O16	162.1(4)
O9–Mo3–O13	87.7(3)	O6–Mo6–N6	84.7(5)
O9–Mo3–O16	153.7(3)	O6–Mo6–O14^{iii}	106.2(4)
O9–Mo3–O8^{iii}	79.6(3)	O13–Mo6–Cl	158.8(3)
O10–Mo3–O13	155.7(2)	O13–Mo6–O16	73.4(3)
O10–Mo3–O16	91.1(4)	O13–Mo6–N6	88.9(4)
O10–Mo3–O8^{iii}	79.5(3)	O13–Mo6–O14^{iii}	88.7(3)
O13–Mo3–O16	76.6(4)	Cl–Mo6–O16	86.3(3)
O13–Mo3–O8^{iii}	77.2(3)	Cl–Mo6–N6	92.6(4)
O16–Mo3–O8^{iii}	76.4(3)	Cl–Mo6–O14^{iii}	85.8(3)
Mo1–O7–Mo2	84.6(3)	O16–Mo6–N6	77.5(5)
Mo1–O8–Mo2	81.3(2)	O16–Mo6–O14^{iii}	91.7(3)
Mo3–O9–Mo4	81.5(3)	N6–Mo6–O14^{iii}	169.1(5)

^{iii} Symmetry code: $1-x$, $1-y$, $1-z$.

feature is a quadruply bridging oxygen atom labeled O8, surrounded by four molybdenum atoms (Mo1, Mo2, Mo3 and Mo5) which lie at the vertices of a distorted tetrahedron. Among the Mo–O(μ_4) distances, 1.987(5), 1.990(8), 2.405(6) and 2.625(8) Å, the two longer bonds are formed as expected, i.e. *trans* to two terminal Mo=O groups. In view of these long Mo–O distances, the Mo sites are highly distorted octahedra that may be alternatively described as square pyramidal sites with weak axial interactions *trans* to the multiply bonded apical oxygen. Some molybdenum atoms have one, two or three terminally bound ligands. Although the structure of **iv** represents a hitherto unknown structural type, it bears some resemblance to $[Mo_{10}O_{26}L_8]$ (L = Py, 3,5-Lut (**i**), 3-MePy (**ii**, **iii**)). The analogy becomes obvious by noting that four of the six $Mo_2O_4^{2+}$ units are aligned with their Mo–Mo vectors parallel to each other, similar to the previously described $[Mo_{10}O_{26}L_8]$ cluster type with the front and rear faces in **iv** capped with two $Mo_2O_4^{2+}$ units (Fig. 2). A polyhedral representation of **iv** is given in Fig. 5.

The core of **iv** may be compared with the $Mo_{12}^{V}O_{40}$ core found in an organometallic cation, $[(C_5Me_5Rh)_8Mo_{13}O_{40}]^{2+}$ [23]. Six $Mo_2O_4^{2+}$ units, assembled together with a tetrahedral T_d symmetry, form a cage whose center accommodates a Mo(VI) site. In the analogous $(NH_4)_7[NaMo_{16}(OH)_{12}O_{40}]\cdot 4H_2O$ and $(Me_2NH_2)_6[H_2Mo_{16}(OH)_{12}O_{40}]$ complexes the central cavity hosts a sodium cation or two protons [3]. These anions may be rewritten as $[(Mo^{VI}O_3)_4Mo_{12}^{V}(OH)_{12}O_{28}]^{8-}$ where four faces of the $Mo_{12}^{V}O_{40}$ core are capped with four $Mo^{VI}O_3$ units.

3.2. IR spectra

In the IR spectra of the $[Mo_{10}O_{26}L_8]$ clusters (L = 3,5-Lut (**i**), 3-MePy (**ii**, **iii**)), a number of intense bands were observed in the region for stretching frequencies of terminal Mo=O groups. Not only do the molybdenyl groups in a centrosymmetric decanuclear cluster adopt five distinct coordination environments, they also differ in the oxidation state of molybdenum. The positions of the bands in the $[Mo_{10}O_{26}L_8]$ clusters also differ. Furthermore, the spectra of **ii** and **iii** are not the same, even though the main difference is the content of the solvent of crystallization. In the former, apart from two common absorption bands at ~ 957 and ~ 946 cm^{-1},

Table 5
Selected bond distances (Å) for $[Mo_{12}O_{28}(OCH_3)_2Cl_2(3\text{-}MePy)_8]$ (**iv**) [a]

Mo–Mo	2.562(2), 2.590(2), 2.682(2)
Mo–N	2.223(8)–2.251(11)
Mo–O_t	1.643(9)–1.681(6)
Mo–O(μ_2)	1.897(9)–1.951(5)
Mo–O(μ_3)	1.954(7)–2.304(6)
Mo–O(μ_4)	1.987(5)–2.625(8)
Mo–OCH_3(μ_2)	2.054(9), 2.219(10)
Mo–Cl	2.344(6)

[a] O_t, terminal oxygen; O(μ_2), doubly bridging oxygen; O(μ_3), triply bridging oxygen; O(μ_4), quadruply bridging oxygen; OCH_3(μ_2), doubly bridging methoxy group.

bands of medium intensity at 935 and 910 cm^{-1} have appeared.

The spectrum of $[Mo_{12}O_{28}(OCH_3)_2Cl_2(3\text{-}MePy)_8]$ (**iv**) displays absorption bands at 962 and 938 cm^{-1}, which are similar to absorptions at 961 and 942 cm^{-1} found in another oxomolybdenum(V) compound $[Mo_4O_8(OCH_3)_2Cl_2Py_4]\cdot 2Py$ [10]. A complex pattern of bands in the far-IR region prevents the unambiguous assignment of the Mo–Cl stretching vibration for **iv**. In $[Mo_4O_8(OCH_3)_2Cl_2Py_4]\cdot 2Py$ these were found at 351 and 320 cm^{-1} [10]. The absorption at 2811 cm^{-1} in **iv** can be ascribed to the C–H stretching vibration of the methoxy group. The observed band is comparable to the absorption at 2820 cm^{-1} in $[(n\text{-}C_4H_9)_4N]_2[V_8O_8(OCH_3)_{16}(C_2O_4)]$ [24].

3.3. Synthetic considerations

From previous studies of the reactions of $(PyH)_2[MoOCl_5]$ with methanol and pyridine or its alkyl-substituted analogues we have recognized a number of factors which have a determining influence over numerous processes taking place in solution which eventually lead to final products [10]. Traces of water have been found to change the reaction course, always leading to Mo(V, VI) clusters which no longer contain neither chloro ligands nor methoxide groups, i.e. $[Mo_{10}O_{26}L_8]$. The sensitivity towards water makes the reactions irreproducible and difficult to control. The domain of the solvothermal synthesis provides a more stable and reproducible environment for the reaction systems described. Exploiting the advantageous conditions offered by this technique, such as the reduced

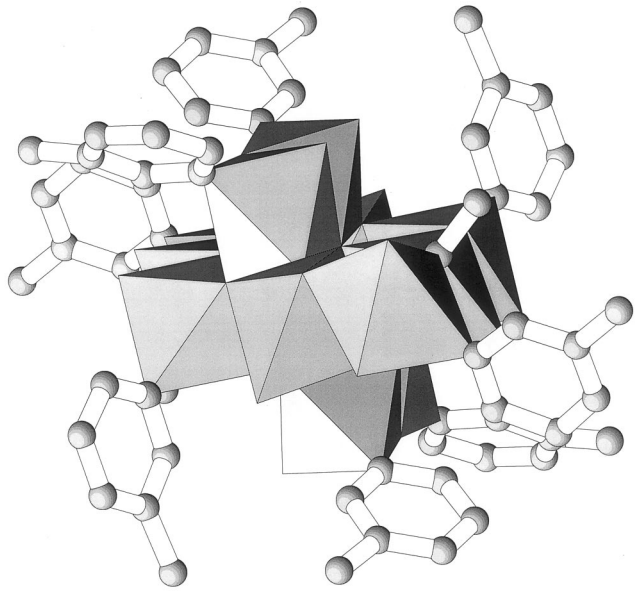


Fig. 5. ATOMS [21] polyhedral representation of $[Mo_{12}O_{28}(OCH_3)_2Cl_2(3\text{-}MePy)_8]$ (**iv**).

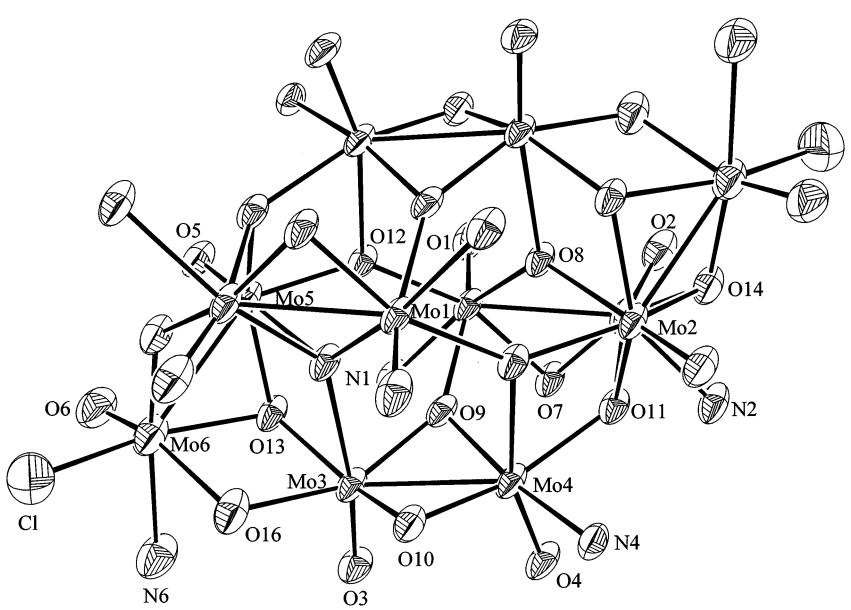


Fig. 4. ORTEP III [20] drawing of $[Mo_{12}O_{28}(OCH_3)_2Cl_2(3\text{-}MePy)_8]$ (**iv**) with the atomic naming scheme shown. Thermal ellipsoids are drawn at the 30% probability level. Carbon atoms are omitted for clarity.

viscosity of the solvent resulting in enhanced crystal growth [4], enabled new species to be prepared in the crystalline form, as shown by the isolation of $[Mo_{12}O_{28}(OCH_3)_2Cl_2(3\text{-}MePy)_8]$ (**iv**).

Note that the same structural types occur in different contexts, i.e. $[Mo_4O_8(OCH_3)_4(4\text{-}MePy)_4]$ [10], $[Mo_4O_8(O\text{-}i\text{-}Pr)_4Py_4]\cdot 2Py$ [25] and $((n\text{-}C_4H_9)_4N)_4[Mo_4O_8(OCH_3)_2(C_4O_4)_2(C_4O_4H)_2]\cdot CH_3OH$ [26], which all consist of the tetranuclear framework $[Mo_4O_4(\mu_2\text{-}O)_2(\mu_3\text{-}O)_2(\mu_2\text{-}OR)_2]^{2+}$ (OR = alkoxy group) made of two $Mo_2O_4^{2+}$ building blocks fused together. Also, in $[Mo_8O_{16}(OCH_3)_8(PMe_3)_4]$ [27] and $[Mo_8O_{16}(OCH_3)_8L_4]$ (L = pyridine or alkyl-substituted pyridine) [13], the linkage of four $Mo_2O_4^{2+}$ moieties through pairs of methoxy bridges results in a cyclic $[Mo_8O_8(\mu_2\text{-}O)_8(\mu_2\text{-}OCH_3)_8]$ array. Apart from the well-known stability of the $Mo_2O_4^{2+}$ dimer, the occurrence of some $Mo_2O_4^{2+}$ assemblies in diverse fields suggests their remarkable stability. A series of decanuclear clusters $[Mo_{10}O_{26}L_8]$ (L = Py, 3-MePy, 3,5-Lut) with a common $[Mo_{10}\text{-}O_{10}(\mu_2\text{-}O)_8(\mu_3\text{-}O)_6(\mu_4\text{-}O)_2]$ core, and $(NH_4)_7[NaMo_{16}(OH)_{12}O_{40}]\cdot 4H_2O$ and $(Me_2NH_2)_6[H_2Mo_{16}(OH)_{12}O_{40}]$, which both contain $[(Mo^{VI}O_3)_4Mo^{V}_{12}(OH)_{12}O_{28}]^{8-}$ [3], illustrate the same trend. Additionally both cluster types were obtained through both conventional and solvothermal synthesis, suggesting they can be formed under various conditions.

4. Supplementary material

Tables of atomic coordinates, bond lengths, bond angles and thermal parameters are available from the Cambridge Crystal Data Centre, quoting the CCDC reference numbers 140809, 140810, 140811 and 140812 for complexes **i**–**iv**, respectively. Observed and calculated structure factors are available from the authors upon request.

Acknowledgements

Financial support from the Slovenian Ministry of Science and Technology is gratefully acknowledged (grant J1-1460-0103-99).

References

[1] M.I. Khan, J. Zubieta, Prog. Inorg. Chem. 43 (1995) 1.
[2] P.J. Hagrman, D. Hagrman, J. Zubieta, Angew. Chem., Int. Ed. Engl 38 (1999) 2638.
[3] M.I. Khan, A. Müller, S. Dillinger, H. Bögge, Q. Chen, J. Zubieta, Angew. Chem., Int. Ed. Engl. 32 (1993) 1780.
[4] M.I. Khan, Q. Chen, J. Salta, C.J. O'Connor, J. Zubieta, Inorg. Chem. 35 (1996) 1880.
[5] D. Hagrman, C. Sangregorio, C.J. O'Connor, J. Zubieta, J. Chem. Soc., Dalton Trans. (1998) 3707.
[6] D. Hagrman, P.J. Zapf, J. Zubieta, Chem. Commun. (1998) 1283.
[7] E.M. McCarron III, J.F. Whitney, D.B. Chase, Inorg. Chem. 23 (1984) 3275.
[8] J.W. Johnson, A.J. Jacobson, S.M. Rich, J.F. Brody, J. Am. Chem. Soc. 103 (1981) 5246.
[9] H.K. Chae, W.G. Klemperer, T.A. Marquart, Coord. Chem. Rev. 128 (1993) 209.
[10] B. Modec, J.V. Brenčič, L. Golič, G. Giester, Inorg. Chim. Acta (submitted for publication).
[11] B. Modec, J.V. Brenčič, I. Leban, Inorg. Chem. Commun. 1 (1998) 161.
[12] B. Modec, J.V. Brenčič, R. Rotar, L. Golič, K. Prout, Acta Crystallogr., Sect. C 54 (1998) 1573.
[13] B. Modec, J.V. Bren(i(, L. Goli(, Polyhedron 19 (2000) 1219.
[14] J.V. Brenčič, L. Golič, I. Leban, R. Rotar, J. Sieler, Z. Anorg. Allg. Chem. 622 (1996) 2124.
[15] G.R. Hanson, A.A. Brunette, A.C. McDonell, K.S. Murray, A.G. Wedd, J. Am. Chem. Soc. 103 (1981) 1953.
[16] J.W. Pflugrath, A. Messerschmidt, MADNES-92, Munich Area Detector Systems, Delft Instruments, Delft, The Netherlands, 1992.
[17] G.M. Sheldrick, SHELXTL-96, Structure Determination Program, Version 5.0.5, Siemens Analytical X-ray Instruments Inc., Madison, WI, USA, 1996.
[18] A. Altomare, G. Cascarano, C. Giacovazzo, A. Guagliardi, M.C. Burla, G. Polidori, M. Camalli, J. Appl. Crystallogr. 27 (1994) 435.
[19] S.R. Hall, G.S.D. King, J.M. Stewart, XTAL 3.4 User's Manual, University of Western Australia, Australia, 1995.
[20] M.N. Burnett, C.K. Johnson, ORTEP III: Oak Ridge Thermal Ellipsoid Plot Program for Crystal Structure Illustrations, Oak Ridge National Laboratory Report ORNL-6895, 1996.
[21] ATOMS, Atomic Structure Display Software, Version 2.0, Shape Software, Kingsport, TN, USA.
[22] S. Liu, X. Sun, J. Zubieta, J. Am. Chem. Soc. 110 (1988) 3324.
[23] H.K. Chae, W.G. Klemperer, D.E. Paez Loyo, V.W. Day, T.A. Eberspacher, Inorg. Chem. 31 (1992) 3187.
[24] Q. Chen, S. Liu, J. Zubieta, Inorg. Chem. 28 (1989) 4433.
[25] M.H. Chisholm, J.C. Huffman, C.C. Kirkpatrick, J. Leonelli, K. Folting, J. Am. Chem. Soc. 103 (1981) 6093.
[26] Q. Chen, S. Liu, J. Zubieta, Inorg. Chim. Acta. 164 (1989) 115.
[27] D.J. Darensbourg, R.L. Gray, T. Delord, Inorg. Chim. Acta 98 (1985) L39.

PERGAMON

www.elsevier.nl/locate/poly

Polyhedron 19 (2000) 1415–1421

POLYHEDRON

Mixed ligand Co(II), Ni(II) and Cu(II) complexes containing terephthalato ligands. Crystal structures of diaqua(2,2′-dipyridylamine)(terephthalato)metal(II) trihydrates (metal = cobalt or nickel)

Jelena Rogan [a,*], Dejan Poleti [a], Ljiljana Karanović [b], Goran Bogdanović [c], Anne Spasojević-de Biré [d], Dragoslav M. Petrović [e]

[a] *Department of General and Inorganic Chemistry, Faculty of Technology and Metallurgy, PO Box 494, 11001 Belgrade, Yugoslavia*
[b] *Laboratory of Crystallography, Faculty of Mining and Geology, Djušina 7, 11000 Belgrade, Yugoslavia*
[c] *Laboratory 020/2, Institute of Nuclear Sciences 'Vinča', PO Box 522, 11001 Belgrade, Yugoslavia*
[d] *Laboratoire de Structures, Propriétés et Modélisation des Solides (SPMS), Unité Mixte du CNRS, Ecole Centrale Paris, Grande Voie des Vignes, F-92295 Châtenay-Malabry Cedex, France*
[e] *Institute of Physics, Faculty of Sciences, Trg D. Obradovića 4, 21000 Novi Sad, Yugoslavia*

Received 28 January 2000; accepted 15 May 2000

Abstract

A series of nine ternary Co(II), Ni(II) and Cu(II) complexes with some aromatic diamines and dianion of terephthalic acid (tpht) have been synthesized and characterized by elemental analysis, magnetic susceptibility measurements, IR and diffuse-reflectance spectroscopy. All compounds were obtained as microcrystalline solids, stable in air and insoluble in common solvents. Two of them, $[M(tpht)(dipya)(H_2O)_2]\cdot 3H_2O$ [M = Co(II), Ni(II); dipya = 2,2′-dipyridylamine], were obtained as single crystals and their crystal structures have been determined by X-ray structure analysis. Both structures consist of discrete $[M(tpht)(dipya)(H_2O)_2]^{2+}$ complex units with two H_2O molecules in the *trans* position. Three additional H_2O molecules together with coordinated H_2O and O atoms from COO groups make a three-dimensional network of hydrogen bonds. Terephthalato ligands are coordinated by only one COO group, which acts as a chelating ligand. Central metal ions are in a distorted octahedral environment. Based on the above-mentioned analysis and known crystal structures, the possible structures and geometry of the complexes are discussed. All Co(II) and Ni(II) complexes are pseudooctahedral and mononuclear, with only one of the tpht COO groups coordinated in a chelate mode. Cu(II) complexes have probably distorted octahedral geometry with bridging role of tpht ions and monodentate or strongly asymmetric coordination of COO groups. © 2000 Elsevier Science Ltd. All rights reserved.

Keywords: Transition metal complexes; Terephthalate ions; Aromatic diamines; Crystal structures; Spectral data

1. Introduction

Among anions of benzenedicarboxylic acids as possible polydentate and bridging ligands, phthalate (pht) or hydrogen phthalate ions are the most widely used in coordination chemistry (see for example [1–3] and references therein). On the contrary, very few complexes with isophthalate ion have been described so far [4,5].

Interest for terephthalato (tpht) complexes arose in 1985, when an unexpected strong antiferromagnetic interaction was found in $[Cu_2(\mu\text{-tpht})(bipy)_2(H_2O)_2](ClO_4)_2$, where bipy = 2,2′-bipyridine [6]. Very soon after, it was shown [7] that moderately strong magnetic interactions can exist, even if two Cu(II) magnetic centers are 11.3 Å away from each other. Most articles concerning ternary complexes with tpht ligands concentrated on Cu(II) complexes and their magnetic

* Corresponding author. Tel.: +381-11-337-0477; fax: +381-11-337-0847.
E-mail address: jmrogan@elab.tmf.bg.ac.yu (J. Rogan).

0277-5387/00/$ - see front matter © 2000 Elsevier Science Ltd. All rights reserved.
PII: S0277-5387(00)00435-6

properties, and on quantum-chemical studies of the relative orientation of magnetic orbitals which influences exchange interaction through the bridging ligand [6–13]. Nevertheless, several tpht complexes containing some other transition metals were also described [14,15].

Besides the Cu(tpht)·3H_2O itself [16], numerous tpht complexes were structurally characterized [5,7,8,10–14,17]. As a rule, the complexes are binuclear and bridging tpht ligands are coordinated in a bis-monodentate manner [7,8,12,13]. Moreover, bis-bidentate, [8,17] bridging, [14,16], as well as combined [11] modes of coordination are encountered. It seems that the number of polymeric complexes [10,11,14,16] is smaller than the number of binuclear complexes.

To the best of our knowledge, only a few systematic studies about transition metal complexes with tpht ions have been undertaken so far. In a paper by Bakalbassis et al. [9], five ternary Cu(II) complexes containing some polyamines are described. In addition, several ternary Co(II) and Ni(II) complexes with 1,10-phenanthroline, 2,2′-bipyridine and its derivatives, as diamine ligands, and tpht [18,19] or substituted tpht ions have been characterized [20].

In this study we report synthesis and characterization of nine ternary Co(II), Ni(II) and Cu(II) complexes containing dianion of terephthalic acid and 2,2′-dipyridylamine (dipya), 1,10-phenanthroline (phen) or 2,2′-bipyridine as aromatic diamine ligands.

2. Experimental

2.1. Preparation and characterization of the complexes

With the exception of aromatic diamines, which were of purum quality, the other reagents were of analytical grade and were used without further purification. All complexes were prepared in a similar way using the following procedure.

An aqueous solution of $M(NO_3)_2 \cdot xH_2O$ (M = Co, Ni and Cu, $x = 6$ or 3, $n = 5.0 \times 10^{-3}$ mol in 200 cm^3 of H_2O) and a solution of 5.0×10^{-3} mol diamine ligand in 20 cm^3 of EtOH were mixed firstly. Then a solution of Na_2tpht (5.0×10^{-3} mol in 75 cm^3 of H_2O) was added dropwise at room temperature for about 2 h under continuous magnetic stirring. The instantly formed microcrystalline precipitate was filtered off after standing overnight, washed several times with small portions of water, EtOH and Et_2O and dried at room temperature. Formulae of the complexes, together with their color, yield and analytical data are listed in Table 1. Further on in the text, the complexes will be denoted by the corresponding numbers in Table 1.

Elemental analysis was carried out by standard analytical micromethods. The metal content was determined by dry combustion of samples followed by heating at 800–1000°C and weighing of the residual metal oxide (as MO). Total content of water of crystallization was confirmed by thermal analysis performed on a Perkin–Elmer model TGS-2 thermobalance (heating rate: 10°C min^{-1}, sample mass: less than 10 mg,

Table 1
Colour, yield and analytical data of complexes [a]

No.	Complex	Color	Yield (%)	*Anal.* Found (Calc.) (%)				
				Metal	C	H	N	H_2O {*t*, °C} [b]
1	Co(tpht)(dipya)·5H_2O	pink	90.5	12.60 (12.17)	44.55 (44.66)	4.50 (4.74)	8.96 (8.68)	17.90 {108} (18.60)
2	Ni(tpht)(dipya)·5H_2O	light blue	92.8	11.81 (12.12)	44.18 (44.66)	5.11 (4.79)	9.02 (8.68)	18.32 {121} (18.61)
3	Cu(tpht)(dipya)·H_2O	green	92.3	15.50 (15.24)	52.04 (51.86)	3.55 (3.63)	10.17 (10.08)	4.22 {105} (4.32)
4	Co(tpht)(phen)·4H_2O	light orange	79.8	12.20 (12.40)	50.16 (50.54)	3.82 (4.24)	6.16 (5.89)	14.86 {145} (15.16)
5	Ni(tpht)(phen)·4H_2O	light blue	63.2	12.52 (12.35)	50.12 (50.56)	4.17 (4.24)	6.12 (5.90)	14.55 {152} (15.17)
6	Cu(tpht)(phen)·1.3H_2O	light blue	89.4	15.12 (14.73)	55.86 (55.70)	3.41 (3.41)	6.27 (6.50)	5.43 {169} (5.43)
7	Co(tpht)(bipy)·4H_2O	light orange	68.3	13.49 (13.06)	48.29 (47.91)	4.68 (4.47)	6.35 (6.21)	15.65 {150} (15.97)
8	Ni(tpht)(bipy)·4H_2O	light blue	86.5	12.99 (13.01)	48.20 (47.93)	4.16 (4.47)	6.36 (6.21)	15.98 {162} (15.98)
9	Cu(tpht)(bipy)·1.8H_2O	blue	99.5	15.50 (15.26)	52.02 (51.94)	4.04 (3.78)	6.41 (6.73)	7.84 {265} (7.79)

[a] Abbreviations: tpht, dianion of terephthalic acid; dipya, 2,2′-dipyridylamine; phen, 1,10-phenanthroline; bipy, 2,2′-bipyridine.
[b] Temperature for complete dehydration is given in large brackets.

furnace atmosphere: dry nitrogen with flow rate of 60 $cm^3\ min^{-1}$). Only complex **6** dehydrates in two steps, indicating clearly the presence of a loosely bound lattice H_2O (0.3 mol) and coordinated H_2O (1 mol) molecules. The dehydration of other complexes is very similar: they lose H_2O in a single step and it was not possible to distinguish between coordinated and lattice H_2O.

Magnetic susceptibility measurements were made at room temperature using an MSB-MK1 magnetic susceptibility balance (Sherwood Scientific Ltd., Cambridge, UK). The data were corrected for diamagnetic susceptibilities. Infrared spectra in the 4000–400 cm^{-1} range were recorded on a Bomem MB-100, Hartmann Braun FT IR spectrophotometer using KBr pellets. Diffuse-reflectance spectra were obtained on an SPM-2 quartz monochromator (Zeiss, Jena). Spectra were taken at room temperature in the interval 10.0–45.0 kK using MgO as the reference compound and the reflection cell of the R-45/0 type.

2.2. Structure determination of complexes *1* and *2*

Single crystals were prepared by slow diffusion of two, A and B, solutions through a glass filter. The solution A contained 5.0×10^{-4} mol of each $Co(NO_3)_2 \cdot 6H_2O$ [or $Ni(NO_3)_2 \cdot 6H_2O$] and dipya in a H_2O–EtOH mixture, whereas B was a solution of Na_2tpht ($c = 0.1$ mol dm^{-3}) in water. The first crystals appeared within a 1 h period, but the single crystals of a suitable size were filtered off after about 7 days.

Data were collected on an Enraf–Nonius CAD-4 diffractometer using Mo Kα radiation ($\lambda = 0.71069$ Å) and $\omega/2\theta$ scan in 2.10–26.97° θ range for Co and 2.11–27.97° θ range for the Ni complex. The intensities of the Ni complex were corrected for absorption by the integration method ($T_{min} = 0.826$, $T_{max} = 0.930$) [21]. The structures were solved by heavy atom and difference Fourier methods and refined on F^2 by full-matrix least-squares method. All H atoms were found in ΔF maps and refined isotropically. The procedures for unit cell determination and data collection, as well as details of structure solution and refinement, were similar to those described in a recent paper [22].

2.2.1. Complex *1*: $[Co(tpht)(dipya)(H_2O)_2] \cdot 3H_2O$

A red, cubic crystal of $0.29 \times 0.29 \times 0.28$ mm size was chosen for data collection. Crystal data: $C_{18}H_{23}CoN_3O_9$, $M_r = 484.32$, triclinic system, space group $P\bar{1}$, $a = 10.103(3)$, $b = 10.970(3)$, $c = 11.242(4)$ Å, $\alpha = 105.82(2)$, $\beta = 109.15(2)$, $\gamma = 107.55(2)°$, $V = 1022.3(6)$ Å^3, $Z = 2$. A total number of 4767 reflections was collected, which after averaging gave 4429 independent observations (3980 with $I > 2\sigma(I)$, $R_{int} = 0.0256$). Final agreement indices for 372 refined parameters were: $S = 1.054$, $wR(F^2) = 0.0873$, $w = 1/[\sigma^2(F_o^2) + (0.0565P)^2 + 0.1173P]$ with $P = (F_o^2 + 2F_c^2)/3$, for all data; $R = 0.0302$ for data with $I > 2\sigma(I)$.

2.2.2. Complex *2*: $[Ni(tpht)(dipya)(H_2O)_2] \cdot 3H_2O$

A light-blue, prismatic crystal of $0.35 \times 0.16 \times 0.08$ mm size was used for data collection. Crystal data: $C_{18}H_{23}N_3NiO_9$, $M_r = 484.10$, triclinic system, space group $P\bar{1}$, $a = 10.076(1)$, $b = 10.963(1)$, $c = 11.242(2)$ Å, $\alpha = 105.77(2)$, $\beta = 109.33(2)$, $\gamma = 107.66(1)°$, $V = 1016.4(2)$ Å^3, $Z = 2$. A total number of 5319 reflections was collected, which after averaging gave 4895 independent observations (3870 with $I > 2\sigma(I)$, $R_{int} = 0.0413$). Final agreement indices for 372 refined parameters were: $S = 1.008$, $wR(F^2) = 0.0980$, $w = 1/[\sigma^2(F_o^2) + (0.0585P)^2]$ with $P = (F_o^2 + 2F_c^2)/3$ for all data; $R = 0.0357$ for data with $I > 2\sigma(I)$.

3. Results and discussion

3.1. Synthesis and formulae of complexes

All complexes were obtained as microcrystalline products from diluted solutions containing diamine ligand, M(II) and tpht ions in a 1:1:1 molar ratio. The general formula (Table 1) is $M(tpht)(diamine) \cdot xH_2O$ (M = Co, Ni, Cu) with $x = 1$–5. In comparison with Co and Ni complexes, all Cu complexes contain a smaller number of water of crystallization. The compounds are insoluble in common polar and non-polar solvents and this fact suggests that some of them could be polymeric.

It should be pointed out that complexes **2**, **4**, **5**, and **8** have empirical formulae identical to the previously described phthalato complexes, while complexes **3**, **6** and **9** have very similar empirical formulae [2,23–25]. (There are no data about pht compounds analogous to complex **7**.) The only significant difference was found in complex **1**, which in Co–pht–dipya system has been reported [24] as anhydrous substance, i.e. it should be similar to **3** not to **2**. Therefore, it seems that formulae are mainly determined by bulkiness of the constituents present, not by the position of COO groups in dicarboxylato ligands. These observations also indicate that similarities in the geometry and coordination mode of the tpht ion could be expected (vide infra).

It is interesting to note that the use of different synthetic routes (and stoichiometry) results in binuclear complexes: $[Cu_2(\mu\text{-}tpht)(bipy)_2(H_2O)_2](ClO_4)_2$, [6] $[Ni_2(\mu\text{-}tpht)_2(bipy)_4](ClO_4)_2$ [17] and $[Co_2(\mu\text{-}tpht)L_4](ClO_4)_2$ with L = bipy, phen or Me_2bipy [19].

3.2. Crystal structures of complexes *1* and *2*

As follows from crystal data given in Section 2, these complexes are isostructural and only the Co complex will be described in detail. Selected bond distances and

Table 2
Selected bond distances (Å) and angles (°)

Complex **1**		Complex **2**		Complex **1**		Complex **2**	
In coordination polyhedron				*In COO groups*			
Co–N1	2.063(2)	Ni–N1	2.020(2)	O1–C17	1.265(2)	O1–C17	1.267(2)
Co–N2	2.067(2)	Ni–N2	2.024(2)	O2–C17	1.260(2)	O2–C17	1.263(2)
Co–O6	2.086(2)	Ni–O6	2.070(2)	O3–C18	1.253(2)	O3–C18	1.255(3)
Co–O5	2.104(1)	Ni–O5	2.070(2)	O4–C18	1.248(2)	O4–C18	1.241(3)
Co–O1	2.165(1)	Ni–O1	2.116(2)	C11–C17	1.497(3)	C11–C17	1.497(3)
Co–O2	2.186(1)	Ni–O2	2.156(2)	C14–C18	1.512(3)	C14–C18	1.512(3)
N1–Co–N2	90.17(6)	N1–Ni–N2	91.49(7)	O1–C17–O2	120.0(1)	O1–C17–O2	119.3(2)
N1–Co–O6	93.84(7)	N1–Ni–O6	93.31(8)	O2–C17–C11	120.3(1)	O2–C17–C11	120.7(2)
N2–Co–O6	93.44(6)	N2–Ni–O6	92.79(8)	O1–C17–C11	119.7(1)	O1–C17–C11	119.9(2)
N1–Co–O5	89.42(6)	N1–Ni–O5	89.63(7)	O3–C18–O4	124.5(2)	O3–C18–O4	124.4(2)
N2–Co–O5	91.36(6)	N2–Ni–O5	91.58(7)	O3–C18–C14	117.8(1)	O3–C18–C14	117.9(2)
N2–Co–O1	102.95(6)	N2–Ni–O1	102.24(6)	O4–C18–C14	117.6(2)	O4–C18–C14	117.7(2)
O6–Co–O1	85.44(7)	O6–Ni–O1	85.61(8)				
O5–Co–O1	90.29(6)	O5–Ni–O1	90.47(7)				
N1–Co–O2	106.54(6)	N1–Ni–O2	104.78(7)				
O6–Co–O2	86.78(6)	O6–Ni–O2	86.52(7)				
O5–Co–O2	87.68(6)	O5–Ni–O2	88.43(6)				
O1–Co–O2	60.35(5)	O1–Ni–O2	61.49(6)				

angles listed in Table 2 show that main differences are in coordination polyhedra where, for example, all Ni–ligand bond distances are shorter. The other bond distances and angles are very similar and in most cases agree within the 3σ range.

The structure (Fig. 1) consists of discrete [Co(tpht)(dipya)$(H_2O)_2$] complex units and three lattice H_2O molecules. The dipya acts as a usual chelating ligand, while the tpht ion is coordinated by only one of its COO groups which chelates the central metal atom. Thus, the compound belongs to the rare tpht complexes where only one of the COO groups is coordinated. Since in the other known example, Cu(tpht)·$3H_2O$, the COO group bridges two Cu(II) ions [16]. Compounds described here can be regarded as the new structural type of tpht complexes.

The analogy with pht-compounds continues and the complex is similar to [Ni(pht)(dipya)$(H_2O)_3$]·$2H_2O$, where only one of the (*ortho*) COO groups is coordinated, but in a monodentate manner [23].

Crystal packing is governed by a three-dimensional network of hydrogen bonds which are in the range of 2.723(4)–3.093(4) Å and with O–H···O angles between 151(6) and 178(4)°. The H_2O molecules act as double H bond donors, while O7 and O9 are also H bond acceptors. The amine N atom (N3) is a H bond donor too. All carboxylate O atoms are H bond acceptors (O3 and O4: 3 ×, O1 and O2: 1 ×). Such an extended system of H bonds increases the stability of crystal lattice and together with its non-electrolyte character can explain the high insolubility of the complexes.

All aromatic rings, as well as the equatorial plane are reasonably planar with deviation less than 5σ. The angle between two pyridine rings is 17.66(7)°. If one neglects the two axial H_2O molecules, the whole molecule does not deviate significantly from planarity. For example, dihedral angles between the benzene ring and the equatorial plane, as well as the plane of coordinated and uncoordinated COO group are 10.35(5), 7.1(2) and 161.8(2)°, respectively.

Co (or Ni) is in a distorted octahedral environment (Table 2). Chelating behavior of the C1O1O2 group causes the main distortion with the O1–Co–O2 angle of only 60.35(5)°. The coordination geometry is similar to that in [Ni_2(μ-tpht)$_2$(bipy)$_4$]$(ClO_4)_2$ [17] and in the previously mentioned [Ni(pht)(dipya)$(H_2O)_3$]·$2H_2O$ [23].

3.3. Spectral and magnetic properties

The reflectance spectra of Co and Ni complexes are in accordance with octahedral or pseudooctahedral geometry of the metal site. In both cases, three spin-allowed transitions [assigned as $^4T_{1g}(F)$ to $^4T_{2g}$ (ν_1),

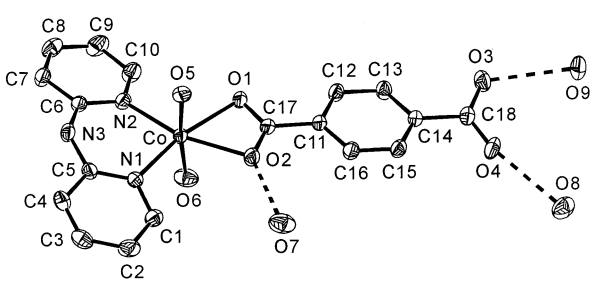


Fig. 1. Numbering of atoms and view of the [Co(tpht)(dipya)$(H_2O)_2$]·$3H_2O$ complex (40% probability displacement ellipsoids) [26]. Only part of H bonds (within an asymmetric unit) is shown as dashed lines.

Table 3
Magnetic moments and spectral data of complexes

No.	Complex	μ (BM)	λ_{max} (kK)	ν_{as}(COO) (cm^{-1})	ν_s(COO) (cm^{-1})	$\Delta\nu$ (cm^{-1})
1	Co(tpht)(dipya)·$5H_2O$	4.87	16.6; 21.9	1542	1381	161
2	Ni(tpht)(dipya)·$5H_2O$	3.06	10.8; 26.0	1545	1384	161
3	Cu(tpht)(dipya)·H_2O	1.96	13.4; 23.2	1574	1384	190
4	Co(tpht)(phen)·$4H_2O$	4.80	16.6; 22.4	1542	1376	166
5	Ni(tpht)(phen)·$4H_2O$	3.43	11.0; 25.6	1543	1377	166
6	Cu(tpht)(phen)·$1.3H_2O$	2.01	13.2	1575	1375	200
7	Co(tpht)(bipy)·$4H_2O$	4.81	16.8; 21.6	1544	1378	166
8	Ni(tpht)(bipy)·$4H_2O$	3.21	11.2; 26.5	1527	1362	165
9	Cu(tpht)(bipy)·$1.8H_2O$	1.90	14.0	1576	1370	206

$^4A_{2g}(F)$ (ν_2) and $^4T_{1g}(P)$ (ν_3) for Co(II), and $^3A_{2g}$ to $^3T_{2g}$, (ν_1), $^3T_{1g}(F)$ (ν_2) and $^3T_{1g}(P)$ (ν_3) for Ni(II) complexes] are expected [27]. The lowest energy transitions, ν_1, belong to the near-IR region and were outside the measurement limit of the instrument.

The highest energy transition $^4T_{1g}(F) \rightarrow {}^4T_{1g}(P)$, characteristic for octahedral Co(II) complexes, is presented in the 21.6–22.4 kK region (Table 3). The second (ν_2) band, corresponding to the forbidden two-electron transition, appeared as a shoulder in the 16.6–16.8 kK region. It was also possible to notice two more spin forbidden transitions (near 11.0 and 20.0 kK) originated in the ^2G state.

The two bands presented in the spectra of Ni(II) complexes lie in the ranges 10.8–11.2 kK (ν_2) and 25.6–26.5 kK (ν_3).

The spectra of all Cu(II) complexes show usual, broad and asymmetric bands in the 13.2–14.0 kK region (Table 3). In complex **3** there is a band at 23.2 kK, which is also observed in the other Cu(II)–dipya complexes [28] and probably belongs to the charge transfer. It is well known that electronic spectra of Cu(II) complexes are a poor indication for their geometry [29]. However, criteria established by Hathaway and Billing [30] suggest that Cu(II) ions are in an elongated tetragonal–octahedral or *cis*-distorted octahedral ligand field with D_{4h} or C_{2v} symmetry, respectively. This can be interpreted as the presence of the $CuN_2O_2O'_2$ chromophore originated from chelate coordination of two COO groups.

Although phen and bipy are planar with extended π-bonds system, while dipya does not belong to that type of ligand, no systematic shifts of transition maxima have been observed.

In addition to the d–d bands mentioned, the reflectance spectra of all complexes exhibit very broad and intensive maxima in the range 27.0–40.0 kK. By comparison with ligand spectra, these bands were identified as intraligand transitions.

As expected, all Co and Ni complexes are high-spin and μ_{eff} values (Table 3) are characteristic for (pseudo)octahedral complexes (Co, 4.7–5.2 BM; Ni, 2.9–3.4 BM [29]). This supports previous conclusions about the geometry of central atoms.

The usual magnetic moments of simple Cu(II) complexes lie between 1.75 and 2.20 BM [29] and the observed μ_{eff} values (Table 3) are also in this range. The μ_{eff} values are significantly greater than the spin-only value (1.73 BM), indicating the presence of intense orbital contribution.

No strong magnetic interactions were observed at room temperature in any case. At least for complexes **1** and **2** such behavior is not surprising, since the only possible interactions could be of a very weak, intermolecular type.

The presence of coordinated and/or lattice H_2O molecules caused the appearance of strong and broad ν(O–H) stretching bands centered at 3452–3267 cm^{-1}. In accordance with the different number of H_2O molecules, the shape and position of these bands were different. Characteristic vibrations of aromatic nucleus [ν(C=C), ν(C=N)] for bipy and phen complexes are near 1580 and 1445 cm^{-1}, bzw. 1590, 1503 and 1430 cm^{-1}, respectively, while ν(C–H) deformation vibrations are about 765 cm^{-1} (bipy) and 726 cm^{-1} (phen). Both facts confirm coordination of these ligands.

The IR spectra of dipya complexes exhibit very similar features. Strong absorption bands ν(NH) near 3200 cm^{-1}, overlapped with ν(O–H) stretching, were seen. Also ν(C=C) or ν(C=N) vibrations of aromatic nucleus, which are around 1600 cm^{-1} in uncoordinated ligand shift to about 1650 cm^{-1} and verify the coordination of dipya.

The most salient feature in the IR spectra was the existence of two very strong and broad bands in the 1580–1360 cm^{-1} region, attributed to the ν_{as}(COO) and ν_s(COO) stretching vibrations of the tpht ligand. Positions of these bands, together with their difference, $\Delta\nu$, are listed in Table 3.

Coordination modes of COO groups and their distinction by IR spectroscopy are well documented in many general textbooks [29,31]. Practically all predictions are based on an extensive study published by Deacon and Phillips [32]. The procedure requires comparison of $\Delta\nu$ data with the appropriate value ($\Delta\nu_i$) for

purely ionic salt. In this case, $\Delta\nu_i$ was found to be 170 cm^{-1} for K_2tpht [9].

It is evident (Table 3) that $\Delta\nu$ values for Co and Ni complexes are smaller than $\Delta\nu_i$. Such behavior is in accordance with the presence of chelating COO groups in **1** and **2** and can be extended to the rest of Co and Ni complexes. Very similar intensity and the shape of COO bands also support this conclusion. $\Delta\nu$ values for Cu complexes are greater than $\Delta\nu$ for the Co and Ni complexes, and significantly greater than $\Delta\nu_i$. At first sight, this can be interpreted as monodentate coordination of COO groups. However, the situation with Cu complexes is always complicated since O–Cu bonds have high covalent character and, due to plasticity of Cu(II) coordination sphere, chelating or bridging COO groups are always coordinated asymmetrically. Therefore, the presence of such COO groups can not be excluded [33].

Under the synthetic conditions used in this work, prepared Co(II) and Ni(II) complexes containing tpht ions are mononuclear and pseudooctahedral, with only one of the COO groups coordinated in a chelate mode. It is quite surprising to find that the tpht can form mononuclear complexes, because previous experience shows that bi- or polynuclear complexes are always formed. On the other hand, Cu(II) complexes probably have bridging tpht ions and monodentate or asymmetric chelate coordination of COO groups with distorted octahedral geometry. The complexes described are very similar to the analogous pht compounds [1–3] where, as a rule, Co(II) and Ni(II) complexes are also mononuclear, whereas binary and ternary Cu(II) complexes are polymeric.

4. Supplementary data

Supplementary crystallographic data are available from the Cambridge Crystallographic Data Centre, 12 Union Road, Cambridge CB2 1EZ, UK (fax: +44-1223-336033; e-mail: deposit@ccdc.cam.ac.uk or www: http://www.ccdc.cam.ac.uk) on request, quoting the deposition Nos. 136142 and 136141 for the structures of complexes **1** and **2**, respectively.

Acknowledgements

This work was supported by the Ministry for Science and Technology of the Republic Serbia.

References

[1] (a) S. Musumeci, E. Rizzarelli, S. Sammartano, A. Seminara, Z. Anorg. Allg. Chem. 433 (1964) 297. (b) M. Biagini Cingi, A.M. Manotti Lanfredi, A. Tiripicchio, M. Tiripicchio Camellini, Acta Crystallogr., Sect. B 34 (1978) 774. (c) M. Biagini Cingi, A.M. Manotti Lanfredi, A. Tiripicchio, M. Tiripicchio Camellini, Acta Crystallogr., Sect. B 35 (1979) 312. (d) S.L. Ma, D.Z. Liao, Z.H. Jiang, S.P. Yan, F.C. Xue, G.L. Wang, Synth. React. Inorg. Met. Org. Chem. 24 (1994) 137. (e) D. Poleti, Lj. Karanović, G. Bogdanović, A. Spasojević-de Biré, Acta Crystallogr., Sect. C 55 (1999) 2061.

[2] D. Poleti, L. Karanović, B.V. Prelesnik, Acta Crystallogr., Sect. C 46 (1990) 2465.

[3] D. Poleti, L. Karanović, B. Prelesnik, Acta Crystallogr., Sect. C 49 (1993) 1249.

[4] (a) E. Cardarelli, G.D. Ascenzo, A.D. Magri, A. Pupella, Termochim. Acta 33 (1979) 267. (b) S.K. Shakhatreh, E.G. Bakalbassis, C.A. Tsipis, J. Mrozinski, Z. Anorg. Allg. Chem. 547 (1989) 199. (c) Y.T. Li, D.Z. Liao, Z.H. Jiang, G.L. Wang, Synth. React. Inorg. Met. Org. Chem. 25 (1995) 319. (d) Y.T. Li, Z.H. Jiang, M.M. Miao, D.Z. Liao, S.P. Yan, G.L. Wang, Synth. React. Inorg. Met. Org. Chem. 24 (1994) 769.

[5] J. Cano, G. De Munno, J.L. Sanz, R. Ruiz, F. Lloret, J. Faus, M. Julve, An. Quim. 93 (1997) 174.

[6] E.G. Bakalbassis, C.A. Tsipis, J. Mrozinski, Inorg. Chem. 24 (1985) 4231.

[7] Ph. Chaudhuri, K. Oder, K. Wieghardt, S. Gehring, W. Haase, B. Nuber, J. Weiss, J. Am. Chem. Soc. 110 (1988) 3657.

[8] M. Verdaguer, J. Gouteron, S. Jeannin, Y. Jeannin, O. Kahn, Inorg. Chem. 23 (1984) 4291.

[9] E.G. Bakalbassis, J. Mrozinski, C.A. Tsipis, Inorg. Chem. 25 (1986) 3684.

[10] E.G. Bakalbassis, A.P. Bozopoulos, J. Mrozinski, P.J. Rentzeperis, C.A. Tsipis, Inorg. Chem. 27 (1988) 529.

[11] E. Bakalbassis, P. Bergerat, O. Kahn, S. Jeannin, Y. Jeannin, Y. Dromzee, M. Gullot, Inorg. Chem. 31 (1992) 625.

[12] E. Bakalbassis, C. Tsipis, A. Bozopoulos, W. Dreissig, H. Hartl, J. Mrozinski, Inorg. Chim. Acta. 186 (1991) 113.

[13] C.E. Xanthopoulos, M.P. Sigalas, G.A. Katsoulos, C.A. Tsipis, A. Terzis, M. Mentzafos, A. Hountas, Inorg. Chem. 32 (1993) 5433.

[14] J. Cano, G. De Munno, J. Sanz, R. Ruiz, F. Lioret, J. Faus, M. Julve, J. Chem. Soc., Dalton Trans. (1994) 3465.

[15] Y.T. Li, C.W. Yan, D.Z. Liao, Synth. React. Inorg. Met. Org. Chem. 29 (1999) 155.

[16] S. Cueto, V. Gramlich, W. Petter, F.S. Rys, P. Rys, Acta Crystallogr., Sect. C 47 (1991) 75.

[17] Zh.-L. Deng, J. Shi, Z.-H. Jiang, D.-Zh. Liao, Sh.-Ping Yan, G.-L. Wang, Polyhedron 11 (1992) 885.

[18] J.M. Shi, D.Z. Liao, Z.H. Jiang, G.L. Wang, Pol. J. Chem. 69 (1995) 346.

[19] Sh.L. Ma, D.Zh. Liao, Z.H. Jiang, Sh.P. Yan, F.Ch. Xue, G.L. Wang, Synth. React. Inorg. Met. Org. Chem. 23 (1993) 239.

[20] M.M. Miao, D.Z. Liao, Z.H. Jian, P. Cheng, J.M. Shi, G.L. Wang, Trans. Met. Chem. 22 (1997) 39.

[21] G.T. DeTita, J. Appl. Crystallogr. 18 (1985) 75.

[22] L. Karanović, D. Poleti, G. Bogdanović, A. Spasojević-deBiré, Acta Crystallogr., Sect. C 55 (1999) 911.

[23] D. Poleti, D.R. Stojaković, B.V. Prelesnik, L. Manojlović-Muir, Acta Crystallogr., Sect. C 46 (1990) 399.

[24] D. Poleti, D. Stojaković, Thermochim. Acta 205 (1992) 225.

[25] (a) B. Prelesnik, R. Herak, D. Stojaković, D. Poleti, Zeit. Kristallogr. 194 (1991) 41. (b) I. Krstanović, L. Karanović, D. Stojaković, Acta Crystallogr., Sect. C 41 (1985) 43.

[26] (a) M.N. Burnett, C.K. Johnson, ORTEP III, Oak Ridge Thermal Ellipsoid Plot Program for Crystal Structure Illustrations, Oak Ridge National Laboratory, Report ORNL-6895, 1996. (b) P. McArdle, J. Appl. Crystallogr. 28 (1995) 65.

[27] B.P. Lever, Inorganic Electronic Spectroscopy, second ed., Elsevier, Amsterdam, 1984, pp. 480–505 and 507–544.

[28] N.J. Ray, L. Hulett, R. Sheahan, B.J. Hathaway, J. Chem. Soc., Dalton Trans. (1981) 1463.
[29] F.A. Cotton, G. Wilkinson, Advanced Inorganic Chemistry, fifth ed., Intersience, New York, 1988, pp. 483–484, 729–732, 744–748 and 766–774.
[30] B.J. Hathaway, D.E. Billing, Coord. Chem. Rev. 5 (1970) 143.
[31] K. Nakamoto, Infrared and Raman Spectra of Inorganic and Coordination Compounds, Wiley, New York, 1978, pp. 59–62.
[32] G.B. Deacon, R.J. Phillips, Coord. Chem. Rev. 33 (1980) 227.
[33] D. Poleti, in preparation.

PERGAMON

www.elsevier.nl/locate/poly

Polyhedron 19 (2000) 1423–1428

POLYHEDRON

Magneto–structural studies of monohydroxo-bridged dicopper(II) complexes $M[Cu_2L_2(OH)]\cdot 2H_2O$ ($M = Na^+$ (**1**) and K^+ (**2**); H_2L = 2,6-bis[*N*-(phenyl)carbamoyl]pyridine). Effect of Cu–OH–Cu bridge angle on antiferromagnetic coupling

Apurba Kumar Patra, Manabendra Ray, Rabindranath Mukherjee *

Department of Chemistry, Indian Institute of Technology, Kanpur 208 016, India

Received 11 January 2000; accepted 3 April 2000

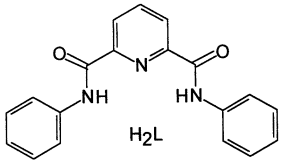
Abstract

Using a tridentate bis-amide ligand 2,6-bis[*N*-(phenyl)carbamoyl]pyridine (H_2L), in its deprotonated form, two new monohydroxo-bridged dicopper(II) complexes $M[Cu_2L_2(OH)]\cdot 2H_2O$ ($M = Na^+$ (**1**) and K^+ (**2**)) have been prepared and characterised by a number of methods, including X-ray crystallography. Each copper(II) ion is terminally coordinated by one pyridyl and two amide nitrogen donors. The two copper(II) centres are bridged by a hydroxo group, with each copper(II) centre assuming a distorted square planar geometry. The observation of short Cu–N_{py} and long Cu–N_{amide} bonds is caused by the steric requirement of the ligand. Interestingly, each cation Na^+/K^+ is coordinated to four different $[Cu_2L_2(OH)]^-$ units through the amide *O*-donors, in an uncommon distorted tetrahedral coordination environment. Temperature-dependent magnetic susceptibility measurements revealed that the compounds have $S = 0$ ground state with singlet–triplet energy separation, $2J = -334$ and -296 cm^{-1} for **1** and **2**, respectively. The larger Cu–OH–Cu bridge angle in **1** (131.1(6)°) causes better antiferromagnetic exchange coupling than that in **2** (125.7(6)°). © 2000 Elsevier Science Ltd. All rights reserved.

Keywords: Copper(II) complexes; Deprotonated pyridine-2,6-dicarboxamide ligands; Singly hydroxo-bridged; Crystal structures; Magnetism

1. Introduction

During the past few years we have been investigating the coordination chemistry of peptide ligands containing pyridine-2-carboxamide (bidentate [1,2] and tetradentate [3–6]) and pyridine-2,6-dicarboxamide (tridentate [7,8]) functionality, in their deprotonated form. We have demonstrated that sterically and/or electronically demanding pyridine amide ligands can dictate the geometry and coordination number of such complexes. For example, the rigid tridentate dianionic bis-amide ligand L(2-) (H_2L = 2,6-bis[(*N*-phenyl)carbamoyl]pyridine) imposes tetragonally compressed geometry (two unusually short M–N_{py} axial bonds compared to four equatorial M–N_{amide} bonds) around highly stabilised Fe(III) ($S = 1/2$) [7], Co(III) ($S = 0$) [7], Ni(II) ($S = 1$) [8] and Ni(IV) ($S = 0$) [8] centres in their bis-chelate complexes. The present work stems from our interest in studying the coordinative behaviour of L(2-) toward copper(II). Here we report the synthesis and X-ray structural characterisation of two monohydroxo-bridged copper(II) complexes, $M[Cu_2L_2(OH)]\cdot 2H_2O$ ($M = Na^+$ (**1**) and K^+ (**2**)). The synthetic reaction between $Cu(O_2CMe)_2\cdot H_2O$ and Na_2L afforded compound **1** whose structural analysis revealed that each Na^+ ion is coordinated by four amide *O*-donors, in an uncommon distorted tetrahedral arrangement. As a first step towards generalisation of the existence of such a structural feature we decided to investigate the synthetic reaction with K^+ salt of L(2-) as well. Temperature-dependent magnetic studies on solid samples of **1** and **2** give us a unique opportunity to pinpoint the structural effect on the magnetic properties of the copper(II) centres in these complexes.



* Corresponding author. Tel.: +91-512-597-437; fax: +91-512-597-436.

E-mail address: rnm@iitk.ac.in (R. Mukherjee).

0277-5387/00/$ - see front matter © 2000 Elsevier Science Ltd. All rights reserved.
PII: S0277-5387(00)00390-9

2. Experimental

2.1. Materials

All chemicals were obtained from commercial sources and used as received. Solvents were dried as reported previously [3,7,8]. The ligand 2,6-bis[*N*-(phenyl)carbamoyl]pyridine was prepared as before [7].

2.2. Synthesis of copper(II) complexes

2.2.1. $Na[Cu_2L_2(OH)]\cdot 2H_2O$ (1)

To a bluish green N_2-purged DMF solution (10 cm^3) of $Cu(O_2CMe)_2\cdot H_2O$ (0.25 g, 1.25 mmol) was added a light yellow DMF solution (10 cm^3) of H_2L (0.4 g, 1.25 mmol) treated with NaH (0.09 g, 3.75 mmol). The resulting moss green solution was stirred for 8 h at 298 K in air. The solvent was then distilled off under reduced pressure and the resulting solid was dissolved in EtOH. The green solution thus obtained was filtered and concentrated to a small volume. Addition of CH_3CO_2Et afforded moss green crystals of **1** (yield 0.25 g, ca. 48%). *Anal.* Found: C, 54.5; H, 3.6; N, 9.9. Calc. for $C_{38}H_{31}Cu_2N_6NaO_7$: C, 54.8; H, 3.8; N, 10.2%. IR (KBr disc, selected peaks): 3610 (sharp) and 3420 (broad) cm^{-1} [ν(OH)]. Conductivity (DMF, $\approx 10^{-3}$ mol dm^{-3} solution at 298 K): $\Lambda_M = 58\ \Omega^{-1}\ cm^2\ mol^{-1}$. Absorption spectra [$\lambda_{max}$/nm ($\varepsilon$, $dm^3\ mol^{-1}\ cm^{-1}$)]: (DMF solution) 305 (20 880) and 590 (490); (Nujol mull) 320 and 580. Slow diffusion of CH_3CO_2Et to the concentrated DMF solution of the product deposited shining block-like crystals suitable for structural studies.

2.2.2. $K[Cu_2L_2(OH)]\cdot 2H_2O$ (2)

A similar procedure as that for **1** was followed with H_2L (0.6 g, 1.89 mmol), KH (0.23 g, 5.67 mmol), and $Cu(O_2CMe)_2\cdot H_2O$ (0.38 g, 1.89 mmol). The product is well formed dark green crystals (yield 0.48 g, ca. 59%). *Anal.* Found: C, 54.9; H, 3.5; N, 10.0. Calc. for $C_{38}H_{31}Cu_2KN_6O_7$: C, 54.8; H, 3.8; N, 10.2%. IR (KBr disc, selected peaks): 3600 (sharp) and 3420 (broad) cm^{-1} [ν(OH)]. Conductivity (DMF, $\approx 10^{-3}$ mol dm^{-3} solution at 298 K): $\Lambda_M = 62\ \Omega^{-1}\ cm^2\ mol^{-1}$. Absorption spectra [$\lambda_{max}$/nm ($\varepsilon$, $dm^3\ mol^{-1}\ cm^{-1}$)]: (in DMF) 300 (16 950) and 603 (480); (Nujol mull) 330 and 600 (sh). X-ray quality crystals were obtained following the same procedure as that for **1**.

2.3. Measurements

Elemental analyses were obtained from the National Chemical Laboratory, Pune, India. Solution electrical conductivity measurements were carried out with an Elico (Hyderabad, India) Type CM-82 T conductivity bridge. Spectroscopic data were obtained by using the following instruments: infrared, Perkin–Elmer M-1320; electronic, Perkin–Elmer Lambda 2.

2.4. Magnetism

Variable-temperature solid-state magnetic susceptibility measurements were done by the Faraday technique using a locally-built magnetometer [6,7]. All measurements were made at a fixed main field strength of ≈ 10 kG. Susceptibilities were corrected for diamagnetic contribution [9].

2.5. Crystallography

Moss green block-shaped crystals of **1** and **2** were used for data collection (θ–2θ scan technique) using graphite-monochromated Mo Kα radiation (λ = 0.71073 Å) on an Enraf–Nonius CAD4-Mach diffractometer. Lattice parameters were obtained from least-squares analyses of 25 machine-centred reflections. Intensity data were corrected for Lorentz-polarisation effects; analytical absorption corrections were also applied. All calculations were performed using the XTAL 3.2 program package [10]. The structures were solved by direct methods and expanded by Fourier-difference syntheses. All refinements were performed by full-matrix least-squares on *F*. We could not locate hydrogen atoms of OH bridge and of two water molecules of crystallisation, to give any chemical significance. The positions of the hydrogen atoms were calculated assuming ideal geometries, but not refined. Except for O atoms, which were refined isotropically, all other atoms were refined with anisotropic thermal parameters. Pertinent crystallographic parameters are summarised in Table 1.

3. Results and discussion

3.1. Synthesis and properties

The reaction between $Cu(O_2CMe)_2\cdot H_2O$ and Na_2L in DMF at 298 K did not yield a bis-chelate complex $[Cu^{II}L_2]^{2-}$. However, all our attempts led only to the isolation of a dark green crystalline solid of composition $Na[Cu_2L_2(OH)]\cdot 2H_2O$ (**1**), irrespective of the mole ratio used (1:1 or 1:2). The product from a similar reaction with K_2L gave a dark green complex of composition $K[Cu_2L_2(OH)]\cdot 2H_2O$ (**2**). The absence of ν(N–H) in the IR spectra confirms that the ligand is coordinated in the deprotonated form. The absorptions observed at $\sim 3600\ cm^{-1}$ (sharp) and $\sim 3400\ cm^{-1}$ (broad) are due to ν(OH) vibrations, with the former one due to hydroxo bridge and the latter due to water of crystallisation. Identical IR spectra of **1** and **2** reveal that they are isostructural. Elemental analysis, IR, and

solution electrical conductivity data (expected range for a 1:1 electrolyte: 65–85 Ω^{-1} cm^2 mol^{-1} [11]) are in agreement with the above formulation for **1** and **2**. The electronic spectra, measured both in the solid state (dispersed in mineral oil mull) and in DMF solution are closely similar, implying that the stereochemistry of the copper(II) centre does not change on dissolution in DMF. In DMF **1** and **2** exhibit a crystal-field transition at $\sim$600 nm, with an additional LMCT transition at $\sim$300 nm of $OH^- \rightarrow$Cu(II) origin.

3.2. Description of molecular structure of $M[Cu_2L_2(OH)]\cdot 2H_2O$ ($M = Na^+$ (**1**) and K^+ (**2**))

Complexes **1** and **2** were found to be isostructural (cf. IR spectra). In the dimeric $[Cu_2L_2(OH)]^-$ unit of **1** and **2** (Fig. 1), each copper(II) ion is terminally coordinated by two amide nitrogens and one pyridyl nitrogen of L(2-). The dianionic ligand L(2-) adopts a *mer* configuration, as before [7,8]. The two copper atoms are bridged by an OH group with a Cu–OH–Cu angle of 131.1(6)° in **1** and 125.7(6)° in **2**. In both structures the CuN_3O planes are coplanar within experimental error. At each copper site, significant deviation of the bond angles involving the chelation by L(2-) is observed (Table 2). The coordination geometry about each copper is distorted square planar, with hydroxide oxygen *trans* to the pyridyl nitrogen. Due to the strong donor capacity of deprotonated amide N donors providing two negative charges on the equatorial plane, it is expected to have shorter Cu–N_{amide} bond lengths. In contrast, Cu–N_{py} bond lengths are considerably shorter

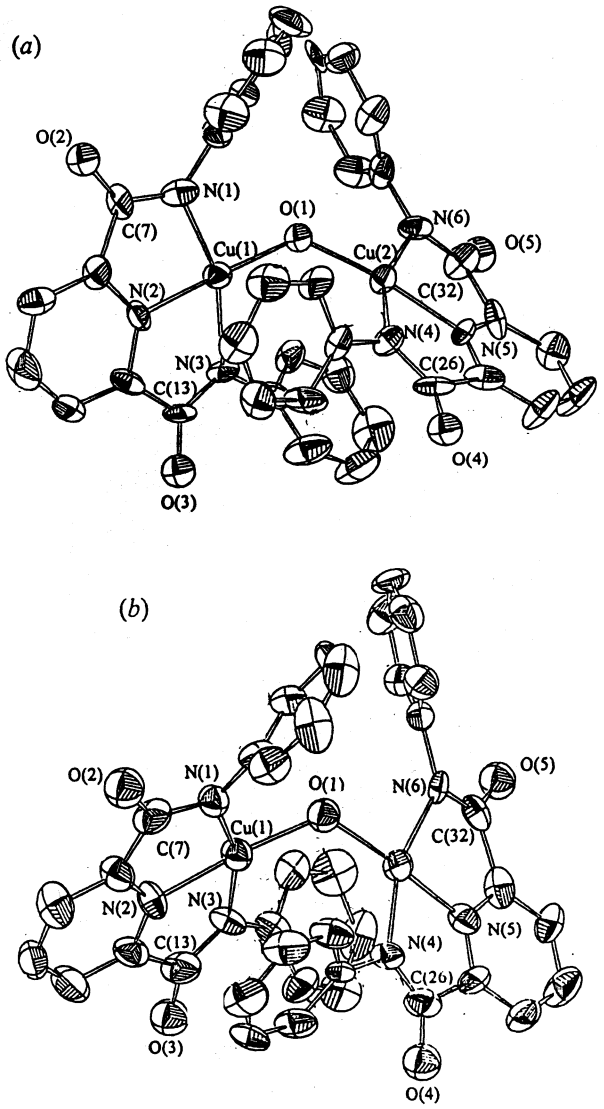


Fig. 1. Views of the structure of the dimeric anion $[Cu_2L_2(OH)]^-$ in the crystal of (a) $Na[Cu_2L_2(OH)]\cdot 2H_2O$ (**1**) and (b) $K[Cu_2L_2(OH)]\cdot 2H_2O$ (**2**).

Table 1
Data collection and structure refinement parameters for $Na[Cu_2(L)_2(OH)]\cdot 2H_2O$ (**1**) and $K[Cu_2(L)_2(OH)]\cdot 2H_2O$ (**2**)

	1	**2**
M	833.68	849.68
Crystal system	orthorhombic	orthorhombic
a (Å)	8.975(9)	8.491(2)
b (Å)	19.243(3)	19.915(4)
c (Å)	21.130(7)	22.077(8)
U (Å^3)	3649.28(4)	3733.18(2)
T (K)	293	293
Space group	$P2_12_12_1$ (no. 19)	$P2_12_12_1$ (no. 19)
Z	4	4
μ (Mo Kα) (mm^{-1})	1.24	1.31
Number of unique reflections	3620	2776
Number of observed data ($I>2\sigma(I)$)	2352	2088
R [a]	0.074	0.063
R' [b]	0.082	0.074

[a] $R = \Sigma(||F_o| - |F_c||)/\Sigma|F_o|$.
[b] $R' = [\Sigma w(|F_o| - |F_c|)^2/\Sigma w|F_o|^2]^{1/2}$.

($\sim$0.1 Å) than Cu–N_{amide} bond lengths (Table 2). We believe that the observed opposite behaviour is the result of steric predominance over electronic effects. A similar bonding situation was observed before [12–15]. To the best of our knowledge, only three unsupported monohydroxo-bridged copper(II) dimers with bidentate/tridentate terminal coordination are reported in the literature [16–18]. Within such complexes the geometry around copper(II) centres is invariably distorted octahedral, square-pyramidal or trigonal bipyramidal. Note that in the reported examples of monohydroxo-bridged copper(II) dimers with square planar coordination [19], the copper(II) centres are additionally bound to the tetradentate binucleating ligands. To the best of our knowledge, the structures of **1** and **2** represent the first

structurally characterised monohydroxo-bridged dicopper(II) complexes with terminal amide coordination.

Interestingly, in the crystal packing of **1** and **2** each Na^+or K^+ ion is bound through four amide *O* donors from four different $[Cu_2L_2(OH)]^-$ modules. Each $[Cu_2L_2(OH)]^-$ module is in turn surrounded by four Na^+/K^+ ions, giving rise to a 3D array of cation–anion interactions [20,21]. The network structure of compound **2** is displayed in Fig. 2. Interestingly, copper(II) and other metal complexes with deprotonated salicylamide ligands 1,2-(2-hydroxybenzamido)benzene and 1,2-(2-hydroxybenzamido)ethane act as multidentate ligands due to coordination by both amidate *N* and amide *O* donors [22,23]. In fact, they give rise to multi-dimensional structures, including coordination of K^+ counterions by amide *O* donors, as observed here. However, it should be noted that coordination of Na^+/K^+ ions solely by *O* donors as in **1** and **2** is novel. In fact, in **1** and **2** the sodium/potassium ions are forced to have an uncommon MO_4 distorted tetrahedral geometry due to hydrophobic pocket created by an ensemble of four dimeric anions. Sodium and potassium enolates of pinacolone [24] and cyclic aluminophosphonate [25], potassium hydrogen DL-methylsuccinate [26] and potassium hydrogen bis(homophthalate) [27] exhibit similar MO_4 coordination. The present structures represent, to the best of our knowledge, the first examples where each Na^+/K^+ ion is coordinated by only amide oxygen donors in a distorted tetrahedral coordination environment. Moreover, two water molecules present in **1** and **2** are involved in an intermolecular hydrogen bonding (O(1w)···O(2w) 3.029(9) Å for **1** and 3.297(8) Å for **2**) and they are not in contact distances with either cop-

Table 2
Selected bond lengths (Å) and angles (°) of $Na[Cu_2L_2(OH)]\cdot 2H_2O$ (**1**) and $K[Cu_2L_2(OH)]\cdot 2H_2O$ (**2**)

	1		**2**
Cu(1)–O(1)	1.899(1)	Cu(1)–O(1)	1.913(1)
Cu(1)–N(1)	2.021(1)	Cu(1)–N(1)	1.999(1)
Cu(1)–N(2)	1.909(1)	Cu(1)–N(2)	1.927(1)
Cu(1)–N(3)	2.026(1)	Cu(1)–N(3)	2.030(1)
Cu(2)–O(1)	1.876(1)	Cu(2)–O(1)	1.874(1)
Cu(2)–N(4)	2.044(1)	Cu(2)–N(4)	2.034(1)
Cu(2)–N(5)	1.929(1)	Cu(2)–N(5)	1.899(1)
Cu(2)–N(6)	2.004(1)	Cu(2)–N(6)	2.026(1)
Na–O(2)	2.335(1)	K–O(2)	2.674(1)
Na–O(3)	2.391(2)	K–O(3)	2.641(2)
Na–O(4)	2.263(2)	K–O(4)	2.563(1)
Na–O(5)	2.223(1)	K–O(5)	2.550(1)
Cu(1)–Cu(2)	3.437	Cu(1)–Cu(2)	3.370
O(1)–Cu(1)–N(1)	100.11(6)	O(1)–Cu(1)–N(1)	99.76(5)
O(1)–Cu(1)–N(2)	175.20(5)	O(1)–Cu(1)–N(2)	175.27(6)
O(1)–Cu(1)–N(3)	99.95(5)	O(1)–Cu(1)–N(3)	99.79(5)
N(1)–Cu(1)–N(2)	79.82(6)	N(1)–Cu(1)–N(2)	80.70(6)
N(1)–Cu(1)–N(3)	159.86(6)	N(1)–Cu(1)–N(3)	160.44(6)
N(2)–Cu(1)–N(3)	80.35(6)	N(2)–Cu(1)–N(3)	79.86(6)
O(1)–Cu(2)–N(4)	100.60(5)	O(1)–Cu(2)–N(4)	99.73(5)
O(1)–Cu(2)–N(5)	171.68(6)	O(1)–Cu(2)–N(5)	171.34(6)
O(1)–Cu(2)–N(6)	100.87(5)	O(1)–Cu(2)–N(6)	99.14(5)
N(4)–Cu(2)–N(5)	80.17(6)	N(4)–Cu(2)–N(5)	80.55(6)
N(4)–Cu(2)–N(6)	157.72(6)	N(4)–Cu(2)–N(6)	160.81(6)
N(5)–Cu(2)–N(6)	79.46(6)	N(5)–Cu(2)–N(6)	81.33(6)
O(2)–Na–O(3)	115.29(5)	O(2)–K–O(3)	122.03(5)
O(2)–Na–O(4)	122.10(6)	O(2)–K–O(4)	119.66(5)
O(2)–Na–O(5)	110.81(5)	O(2)–K–O(5)	123.07(4)
O(3)–Na–O(4)	86.11(5)	O(3)–K–O(4)	74.86(5)
O(3)–Na–O(5)	107.32(5)	O(3)–K–O(5)	100.98(4)
O(4)–Na–O(5)	112.30(6)	O(4)–K–O(5)	105.44(4)
Cu(1)–O(1)–Cu(2)	131.11(6)	Cu(1)–O(1)–Cu(2)	125.74(6)

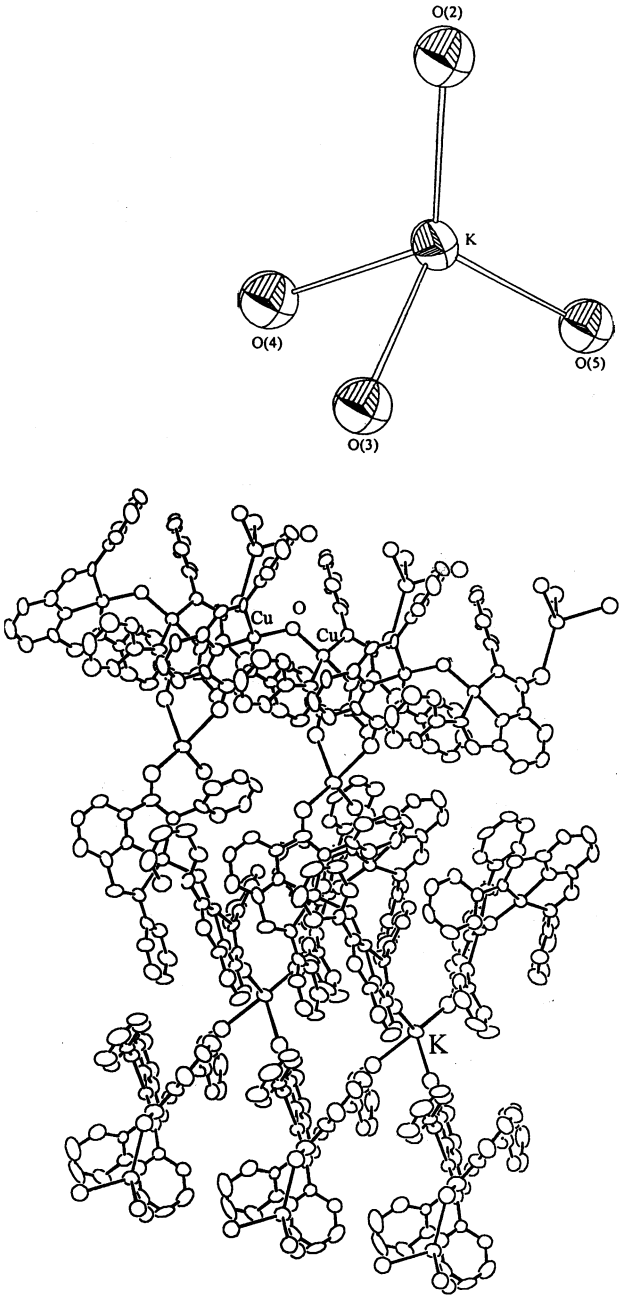


Fig. 2. The 3D network of cation–anion interactions in $K[Cu_2L_2(OH)]\cdot 2H_2O$ (**2**).

per(II) (for **1** Cu(1)–O(1w) 6.382, Cu(1)–O(2w) 6.612, Cu(2)–O(1w) 8.621 and Cu(2)–O(2w) 9.341 Å; for **2** Cu(1)–O(1w) 6.435, Cu(1)–O(2w) 7.162, Cu(2)–O(1w) 9.006 and Cu(2)–O(2w) 8.604 Å) or sodium/potassium ions (for **1** Na–O(1w) 5.560 and Na–O(2w) 5.720 Å; for **2** K–O(1w) 5.184 and K–O(2w) 6.995 Å). The structural data reveal that the water molecules are present in the lattice as separate entities.

Although in each ligand the two *N*-phenyl rings and the pyridine ring are planar, the two phenyl rings, however, make an angle of ~108 and ~108° to each other in **1** and ~113 and ~116° to each other in **2**. In **1** the two phenyl rings make angles of ~58 and ~134° at the Cu(1) site and ~57 and ~126° at the Cu(2) site, with the central pyridine ring. The corresponding angles for **2** are ~53 and ~132° at the Cu(1) site and ~52 and ~127° at the Cu(2) site. This explains the observation of distorted square planar stereochemistry at the copper(II) centre and associated bonding parameters. A close match between electronic and steric requirement of each L(2-) has restricted each copper(II) centre to have distorted square planar geometry and due to the presence of four surrounding $[Cu_2L_2(OH)]^-$ units every Na^+/K^+ ion has been forced to be coordinated by only four amide oxygen donors. We believe that the 3D network structure observed here is the outcome of mutual synergism between the cations and the anions.

3.3. Magnetism

The presence of a hydroxo bridge between two copper(II) centres is well known to lead to antiferromagnetic exchange between the metal centres [16–19] and the temperature-dependent (25–300 K) magnetic measurements on powdered samples of **1** and **2** were carried out accordingly. The magnetic behaviour (Fig. 3) is typical of strong antiferromagnetic coupling between pairs of copper(II) centres. The μ_{eff} per Cu (300 K) values are 1.30 and 1.35 μ_B for **1** and **2**, respectively. The experimentally observed χ_M values (per dimer) may be expressed (the Cu···Cu separations between interdimers: 7.88–15.90 Å for **1** and 8.03–15.99 Å for **2**) using the modified [28,29] Bleaney–Bowers expression (1),

$$\chi_M = 2N\beta^2g^2/3kT[1 + 1/3\exp(-2J/kT)]^{-1}(1-\rho) + (N\beta^2g^2/2kT)\rho + 2N_\alpha \quad (1)$$

which includes a very small corrective term, ρ, for non-coupled copper(II) impurity and N_α is the temperature-independent paramagnetism. The singlet–triplet energy gap is expressed in terms of $2J$ and other symbols have their usual meanings. Keeping N_α fixed at 60×10^{-6} cm^3 mol^{-1}, the J, g and ρ parameters were determined by minimising $R = \Sigma(\chi_m^{obs} - \chi_m^{calc})^2/\Sigma(\chi_m^{obs})^2$. Non-linear regression analyses [28,29] of the data using Eq. (1) gave good data fits: $J = -167$ cm^{-1}, $g = 2.039$, $\rho = 0.033$ and $R = 3.127 \times 10^{-8}$ for **1**; $J = -149$ cm^{-1}, $g = 2.034$, $\rho = 0.038$ and $R = 5.580 \times 10^{-8}$ for **2**.

The coordination geometry of copper(II) centres in **1** and **2** is almost square planar (cf. X-ray structures) and the bridging hydroxide group occupies an equatorial position. Hence in both cases the copper(II) ground state is $d_{x^2-y^2}$. For this type of geometry a stronger antiferromagnetic interaction is expected as the bridging angle approaches 180°, since the copper(II) $d_{x^2-y^2}$ orbitals are then more favourably positioned to overlap in a σ fashion with the bridging moiety [30]. The strong antiferromagnetic coupling observed in **1** and **2** must be due to the angle Cu–OH–Cu being towards linear (131.1(6)° for **1** and 125.7(6)° for **2**) and rather short Cu–O bond lengths (1.876(1) and 1.899(1) Å for **1**, and 1.874(1) and 1.913(1) Å for **2**); magnetic exchange interaction can take place effectively through the OH bridge. Compared with **2** the larger antiferromagnetic coupling in **1** must be associated with its larger Cu–OH–Cu bond angle, as they are otherwise identical. In fact, an increase in Cu–OH–Cu bridge angle by ~5° causes an increase in the extent of antiferromagnetic

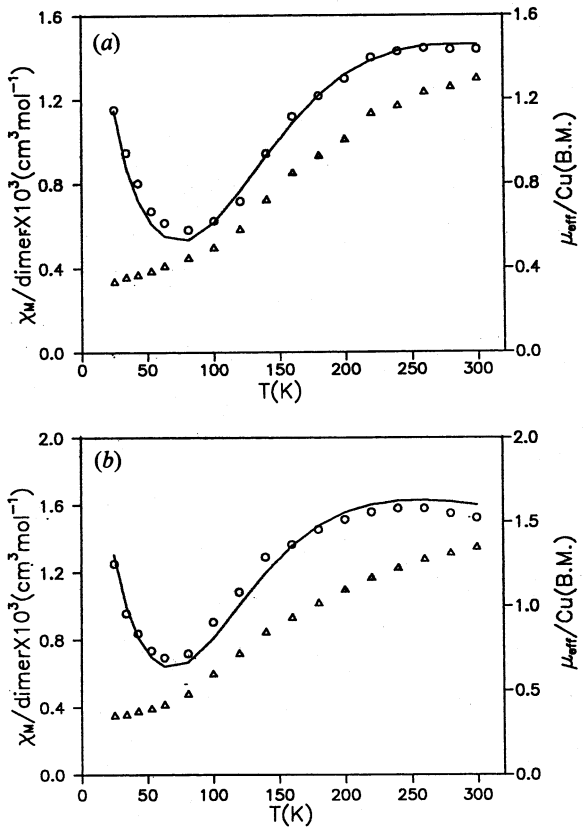


Fig. 3. Temperature dependence of the molar susceptibility (○) and of the magnetic moment (△) of solid (a) $Na[Cu_2L_2(OH)]\cdot 2H_2O$ (**1**) and (b) $K[Cu_2L_2(OH)]\cdot 2H_2O$ (**2**). The solid lines represent the result of the fitting calculation.

exchange coupling by $\sim 20\ cm^{-1}$. The *J* values obtained here are comparable to monohydroxo-bridged copper(II) complexes $[Cu_2(dien)_2(OH)(OClO_3)_3]$ (dien = diethylenetriamine) and $[Cu_2(dpm)_2L(OH)][ClO_4]_3 \cdot 2H_2O$ (dpm = di(2-pyridy)methane; L = 1,1,2,2-tetrakis(2-pyridyl)-ethylene) with the $d_{x^2-y^2}$ ground state [31,32]. It must be noted, however, that the former complex has a supported perchlorate bridge. In essence, the present investigation has given us a unique opportunity to compare the extent of antiferromagnetic magnetic exchange coupling as a function of Cu–OH–Cu bridge angle, brought about by crystal-packing effects.

4. Conclusion

Even though L(2-) imposes tetragonally compressed geometry around metal centre in bis-chelate complexes [7,8], in full agreement with our expectation $[Cu^{II}L_2]^{2-}$ was not formed; however, monohydroxo-bridged copper(II) dimers $M[Cu_2L_2(OH)] \cdot 2H_2O$ ($M = Na^+$ (**1**) and K^+ (**2**)) were isolated. The amide function in L(2-) not only interacts with the Cu(II) centre via the *N*-atom, but also binds to Na^+ or K^+ ion via the *O*-atom. The observation of distorted tetrahedral coordination of Na^+/K^+ is a bonus to the present structural analysis. As expected, the Cu(II) centres are strongly antiferromagnetically coupled and the extent of exchange coupling is dependent on the Cu–OH–Cu bridge angle.

5. Supplementary data

Full tables of bond lengths and angles, tables of non-hydrogen and hydrogen atomic coordinates, anisotropic thermal parameters for non-hydrogen atoms are available upon quoting the CCDC deposition numbers 138917 and 138918 for **1** and **2**, respectively. Copies of this information may be obtained free of charge from: The Director, CCDC, 12 Union Road, Cambridge, CB2 1EZ, UK (fax: +44-1223-336-033; e-mail: deposit@ccdc.cam.ac.uk or www: http://www.ccdc.cam.ac.uk).

Acknowledgements

This work was supported by grants from the Department of Science and Technology (DST) and the Council of Scientific and Industrial Research, Government of India. Financial assistance from the National X-ray Diffractometer Facility by the DST at this Department is gratefully acknowledged.

References

[1] M. Ray, R. Mukherjee, J.F. Richardson, M.S. Mashuta, R.M., Buchanan, J. Chem. Soc., Dalton Trans. (1994) 965.
[2] A.K. Patra, M. Ray, R. Mukherjee, J. Chem. Soc., Dalton Trans. (1999) 2461.
[3] M. Ray, S. Mukerjee, R. Mukherjee, J. Chem. Soc., Dalton Trans. (1990) 3635.
[4] M. Ray, R. Mukherjee, Polyhedron 11 (1992) 2929.
[5] M. Ray, R. Mukherjee, J.F. Richardson, R.M. Buchanan, J. Chem. Soc., Dalton Trans. (1993) 2451.
[6] A.K. Patra, R. Mukherjee, Polyhedron 18 (1999) 1317.
[7] M. Ray, D. Ghosh, Z. Shirin, R. Mukherjee, Inorg. Chem. 36 (1997) 3568.
[8] A.K. Patra, R. Mukherjee, Inorg. Chem. 18 (1999) 1388.
[9] C.J. O'Connor, Prog. Inorg. Chem. 29 (1982) 203.
[10] S.R. Hall, H.D. Flack, J.M. Stewart, XTAL 3.2 Reference Manual, Universities of Western Australia, Geneva, and Maryland, 1992.
[11] W.J. Geary, Coord. Chem. Rev. 7 (1971) 81.
[12] F.A. Chavez, M.M. Olmstead, P.K. Mascharak, Inorg. Chem. 25 (1996) 1410 and Refs. cited therein.
[13] T. Kawamoto, O. Prakash, R. Ostrander, A.L. Rheingold, A.S. Borovik, Inorg. Chem. 34 (1995) 4294.
[14] T. Kawamoto, B.S. Hammes, B. Haggerty, G.P.A. Yap, A.L. Rheingold, A.S. Borovik, J. Am. Chem. Soc. 118 (1996) 285.
[15] T. Kawamoto, B.S. Hammes, R. Ostrander, A.L. Rheingold, A.S. Borovik, Inorg. Chem. 37 (1998) 3424.
[16] M.S. Haddad, S.R. Wilson, D.J. Hodgson, D.N. Hendrickson, J. Am. Chem. Soc. 103 (1981) 384.
[17] J.F. Folgado, V. Coronado, D. Beltrán-Porter, T. Rojo, A. Fuertes, J. Chem. Soc., Dalton Trans. (1989) 237.
[18] M. Studer, A. Riesen, T.A. Kaden, Helv. Chim. Acta 72 (1989) 307.
[19] L.K. Thompson, T.C. Woon, D.B. Murphy, E.J. Gabe, F.L. Lee, L.Y. Page, Inorg. Chem. 24 (1985) 4719.
[20] A.J. Blake, I.A. Fallis, R.O. Gould, S. Parsons, S.A. Ross, M. Schröder, J. Chem. Soc., Chem. Commun. (1994) 2467.
[21] A.J. Blake, I.A. Fallis, R.O. Gould, S. Parsons, S.A. Ross, M. Schröder, J. Chem. Soc., Dalton Trans. (1996) 4379.
[22] Y. Sunatsuki, M. Nakamura, N. Matsumoto, F. Kai, Bull. Chem. Soc. Jpn. 70 (1997) 1851.
[23] Y. Sunatsuki, T. Matsuo, M. Nakamura, F. Kai, N. Matsumoto, J.-P. Tuchagues, Bull. Chem. Soc. Jpn. 71 (1998) 2611 and Refs. cited therein.
[24] P.G. Williard, G.B. Carpenter, J. Am. Chem. Soc. 108 (1986) 462.
[25] Y. Yang, J. Pinkas, M. Noltemeyer, H.W. Roesky, Inorg. Chem. 37 (1998) 6404.
[26] Y. Schouwstra, Acta Crystallogr., Sect. B 28 (1972) 2217.
[27] M.P. Gupta, D.S. Dubey, Acta Crystallogr., Sect. B 28 (1972) 2677.
[28] D. Ghosh, R. Mukherjee, Inorg. Chem. 37 (1998) 6597.
[29] R. Gupta, S. Mukherjee, R. Mukherjee, J. Chem. Soc., Dalton Trans. (1999) 4025.
[30] P.J. Hay, J.C. Thibeault, R. Hoffmann, J. Am. Chem. Soc. 97 (1975) 4884.
[31] I. Castro, J. Faus, M. Julve, F. Lloret, M. Verdaguer, O. Kahn, J. Chem. Soc., Dalton Trans.(1990) 2207.
[32] E. Spodine, J. Manzur, M.T. Garland, M. Kiwi, O. Peña, D. Grandjean, L. Toupet, J. Chem. Soc., Dalton Trans.(1990) 365.

PERGAMON

www.elsevier.nl/locate/poly

Polyhedron 19 (2000) 1429–1435

POLYHEDRON

Magnetic interactions in dicopper(II) complexes of a new endogenous alkoxo bridging ligand with exogenous pyrazolate, azide and acetate bridges. X-ray structure of $[Cu_2L(\mu\text{-}C_3H_3N_2)(OClO_3)(H_2O)](ClO_4)\cdot H_2O$ (HL = 1,3-bis[*N*-methyl-*N*-(2-pyridylethyl)amino]propan-2-ol)

Rajeev Gupta, Rajeev Hotchandani, Rabindranath Mukherjee *

Department of Chemistry, Indian Institute of Technology, Kanpur 208 016, India

Received 11 January 2000; accepted 3 April 2000

Abstract

Using a new dinucleating ligand, 1,3-bis[*N*-methyl-*N*-(2-pyridylethyl)amino]propan-2-ol (HL), in its deprotonated form, three new binuclear copper(II) complexes $[Cu_2(L)(\mu\text{-}X)(ClO_4)(H_2O)](ClO_4)\cdot H_2O$ ($X = C_3H_3N_2^-$ (prz), N_3^- and $MeCO_2^-$) have been synthesized. The crystal structure of pyrazolate (prz) compound was determined and revealed that the complex contains an endogenous bridging alkoxide ligand and an exogenous bridging prz ligand. A water molecule is coordinated to a copper(II) center and is hydrogen-bonded to the alkoxide O atom. A perchlorate ion is 'semi-coordinated' to another copper(II) center as a monodentate ligand and is hydrogen-bonded to a second water molecule. The coordination geometry around both copper centers resembles a distorted square pyramid. The magnetochemical characteristics of these compounds were determined by temperature-dependent magnetic studies, revealing their antiferromagnetic behavior [$-2J$ (in cm^{-1}) values: 550 ± 25 for prz, 360 ± 10 for azide and 100 ± 10 for acetate]. The ground state magnetic orbital involved in spin coupling is similar ($d_{x^2-y^2}$) in these complexes. Differences in the magnetic behavior have been rationalized in terms of the bridging ligand orbital complementary/countercomplementary concept. Spectroscopic properties of these complexes are also reported. © 2000 Elsevier Science Ltd. All rights reserved.

Keywords: Dinucleating alkoxide ligands; Copper(II) complexes; X-ray structures; Hetero-bridged complexes; Magnetism; Magneto-structural trends

1. Introduction

Continuing interest in the copper(II) complexes of binucleating ligands derives from their structural and magnetic properties [1–4] and their ability to model the active site in dicopper-containing proteins [5,6]. As part of our activity in the chemical modeling of tyrosinase, we investigated magnetic interactions in structurally characterized copper(II) dimers [7] involving (i) two dissimilar bridging ligands, a μ-phenoxo- and a μ-hydroxo- **1a** and (ii) a symmetrically dibridged species, a bis(μ-hydroxo)- **1b**. As the terminal coordination in **1a** and **1b** is invariant, we identified the effect of the Cu_2O_2 ring planarity on the trend of antiferromagnetic coupling. Very recently we have structurally characterized a bis(μ-phenoxo)dicopper(II) compound **2a** and from a systematic comparative studies between **2a** and **2b** the effect of Cu_2O_2 ring planarity caused by pyrazole ring methyl substituents on the extent of antiferromagnetic coupling has been identified [8].

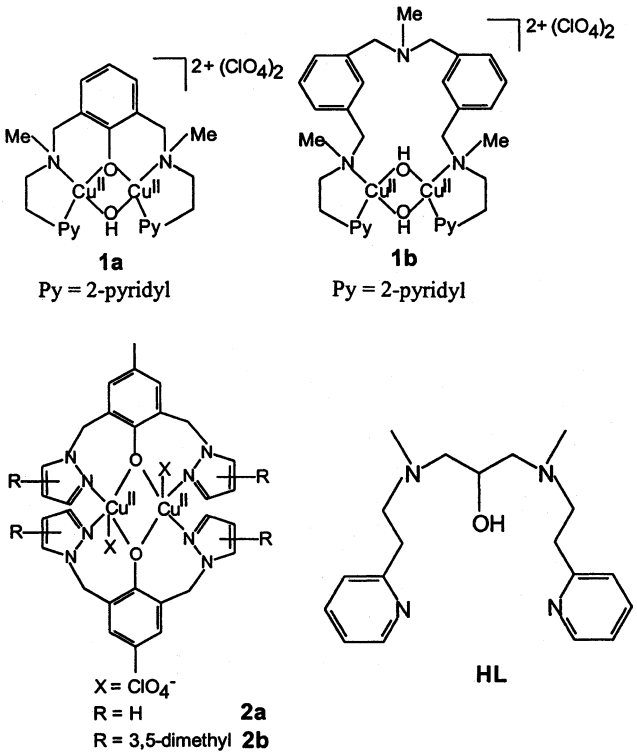
The present work stems from our interest in investigating the magnetic exchange interactions associated with an endogenous alkoxo-bridged dicopper(II) system, derived from a new tailor-made ligand with identical terminal coordination as that in **1a**/**1b**, with variable exogenous bridging ligands. Here we have synthesized

* Corresponding author. Tel.: +91-512-597437; fax: +91-512-597436.

E-mail address: rnm@iitk.ac.in (R. Mukherjee).

0277-5387/00/$ - see front matter © 2000 Elsevier Science Ltd. All rights reserved.
PII: S0277-5387(00)00391-0

and characterized a group of three dicopper(II) complexes of HL, in its deprotonated form, with additional exogenous bridging by pyrazolate (prz), azide or acetate. The prz complex has been subjected to X-ray structural analysis. Temperature-dependent magnetic properties and the observed magneto-structural trend have been presented. It is worth mentioning here that among reported [9–14] endogenous alkoxo-bridged copper(II) systems with ligands derived from 2-hydroxy-1,3-diaminopropane backbone having terminal N-coordination, a six-membered chelate ring forming dinucleating ligand as that considered here is rare [14].



2. Experimental

2.1. Materials

All chemicals were obtained from commercial sources and used as received. Solvents were dried as reported previously [8,15]. Copper(II) perchlorate hexahydrate was prepared as before [8].

2.2. Syntheses

2.2.1. 1,3-Bis[N-methyl-N-(2-pyridylethyl)amino]-propan-2-ol (HL)

A solution of 2-(2-methylaminoethyl)pyridine (1 g, 7.35 mmol) in MeOH (25 cm^3) was added slowly to a vigorously stirred solution of Et_3N (0.743 g, 7.35 mmol) in MeOH (12 cm^3) at $\sim$10°C. To the resulting mixture a solution of 1,3-dichloro-2-propanol (0.483 g, 3.75 mmol) in MeOH (25 cm^3) was added dropwise over a period of $\sim$15 min. The solution was then stirred at $\sim$10°C for 2.5 h. After stirring at room temperature (r.t.) for 2 days the solvent was removed at reduced pressure and the ligand was extracted with $CHCl_3$ (25 cm^3). The $CHCl_3$ layer was then washed with water and finally dried over anhydrous Na_2SO_4. After removal of Na_2SO_4 the solvent was removed to afford pale yellow oil (yield 0.110 g, 87%). ^1H NMR ($CDCl_3$): δ 2.4 (6H, s, CH_3), 2.9 (8H, s, CH_2CH_2), 3.15 (4H, s, CH_2), 3.9 (1H, quintet, 2-CH), 6.53–7.51 (6H, m, aromatic protons) and 8.56 (2H, d, pyridine 6-H protons).

2.2.2. $[Cu_2L(prz)(ClO_4)(H_2O)](ClO_4)\cdot H_2O$ (3a)

A solution of Et_3N (0.185 g, 1.83 mmol) in EtOH (3 cm^3) was added to a solution of HL (0.200 g, 0.61 mmol) in EtOH (4 cm^3). Solid pyrazole (0.40 g, 0.615 mmol) was added to this mixture. Addition of a solution of $Cu(ClO_4)_2\cdot 6H_2O$ (0.452 g, 1.22 mmol) in EtOH (3 cm^3) to the above magnetically stirred solution resulted in a blue solution. After 1 h of stirring the solution was kept in the air at r.t. for slow evaporation. The solid thus precipitated was filtered, washed with cold EtOH and dried under vacuum. The compound was recrystallized by slow vapor diffusion of diethyl ether to a MeCN solution (yield 0.220 g, 48%). Found: C, 35.2; H, 4.4; N, 11.0. Calc. for $C_{22}H_{34}N_6Cl_2O_{11}Cu_2$: C, 34.9; H, 4.5; N, 11.1%. IR (KBr disc, selected peaks): 3540, 3460 [ν(OH)]; 1110, 1090, 1060 and 625 cm^{-1} [$\nu(ClO_4)$]. Conductivity (MeCN, $\sim 10^{-3}$ mol dm^{-3} solution at 298 K): $\Lambda_M = 260\ \Omega^{-1}\ cm^2\ mol^{-1}$. Absorption spectrum [MeCN solution, λ_{max}/nm (ε/dm^3 mol^{-1} cm^{-1})]: 605 (450), 353 (3 420), 290 (sh) and 260 (15 450); (Nujol mull) 990 (sh), 620 (sh) and 360 (sh).

2.2.3. $[Cu_2L(N_3)(ClO_4)(H_2O)](ClO_4)\cdot H_2O$ (3b)

A similar procedure as that described for **3a** was followed with HL (0.202 g, 0.615 mmol), Et_3N (0.125 g, 1.23 mmol), NaN_3 (0.40 g, 0.615 mmol) and $Cu(ClO_4)_2\cdot 6H_2O$ (0.456 g, 1.23 mmol). The compound was recrystallized by slow diffusion of diethyl ether to a MeCN solution (yield 0.260 g, 58%). Found: C, 31.0; H, 4.2; N, 13.1. Calc. for $C_{19}H_{31}N_7Cl_2O_{11}Cu_2$: C, 31.1; H, 4.2; N, 13.2%. IR (KBr disc, selected peaks): 3480 [ν(OH)]; 2050 [$\nu(N_3)$]; 1140, 1120, 1080, 630 and 625 cm^{-1} [$\nu(ClO_4)$]. Conductivity (MeCN, $\sim 10^{-3}$ mol dm^{-3} solution at 298 K): $\Lambda_M = 225\ \Omega^{-1}\ cm^2\ mol^{-1}$. Absorption spectrum [MeCN solution, λ_{max}/nm (ε/dm^3 mol^{-1} cm^{-1})]: 609 (620), 420 (sh), 367 (3 950), 290 (sh) and 261 (14 350); (Nujol mull) 1 000 (sh), 620 and 420.

2.2.4. $[Cu_2L(O_2CMe)(ClO_4)(H_2O)](ClO_4)\cdot H_2O$ (3c)

This complex was prepared following a similar method to that for **3a** and **3b** using ligand HL (0.200 g, 0.610 mmol), Et_3N (0.185 g, 1.83 mmol), $NaO_2CMe\cdot 3H_2O$ (0.083 g, 0.610 mmol) and $Cu(ClO_4)_2\cdot 6H_2O$

(0.452 g, 1.22 mmol). The compound was recrystallized by layering of *n*-hexane to an acetone solution (yield 0.120 g, 44%). Found: C, 33.5; H, 4.4; N, 7.6. Calc. for $C_{21}H_{34}N_4Cl_2O_{13}Cu_2$: C, 33.6; H, 4.5; N, 7.5%. IR (KBr disc, selected peaks): 3440 [ν(OH)]; 1555 and 1440 [$\nu(MeCO_2)$]; 1150, 1120, 1080, 630 and 625 cm^{-1} [$\nu(ClO_4)$]. Conductivity (MeCN, $\sim 10^{-3}$ mol dm^{-3} solution at 298 K): $\Lambda_M = 255\ \Omega^{-1}\ cm^2\ mol^{-1}$. Absorption spectrum [MeCN solution, λ_{max}/nm (ε/$dm^3\ mol^{-1}\ cm^{-1}$)]: 656 (280), 360 (sh), 290 (sh) and 262 (16 150); (Nujol mull) 1000 (sh), 660 and 370 (sh).

CAUTION! Perchlorate and azide salts of metal complexes are potentially explosive and should be handled in small quantities with care.

2.3. Measurements

Elemental analyses were obtained from the Department of Inorganic Chemistry, Indian Association for the Cultivation of Science, Calcutta. Solution electrical conductivity measurements were carried out with an Elico (Hyderabad, India) Type CM-82 T conductivity bridge. Spectroscopic data were obtained by using the following instruments: infrared spectra, Perkin–Elmer M-1320; electronic spectra, Perkin–Elmer Lambda 2; ^{1}H NMR spectra, PMX-60 JEOL (60 MHz) spectrometer.

2.4. Magnetic studies

Variable-temperature solid-state magnetic susceptibility measurements were carried out using the Faraday technique with a locally built magnetometer [7,15]. All measurements were made at a fixed main field strength of ≈ 10 kG. Susceptibilities were corrected for diamagnetic contribution, by using literature tabulations [16].

2.5. Crystal structure determination and refinement

The blue rectangular plate-like single crystal ($0.2 \times 0.1 \times 0.05$ mm) of **3a** was mounted on a glass fiber and coated with epoxy resin. Intensity and lattice parameter measurements were made on an Enraf–Nonius CAD4-Mach diffractometer using graphite-monochromated Mo Kα radiation ($\lambda = 0.710\ 73$ Å). Unit cell parameters were determined by a least-squares fit of 25 reflections (2θ, 12.0–27.1°). Data were collected at 293 K using the θ–2θ scan technique to a maximum 2θ value of 45.0°. 6040 reflections measured out of which 2830 ($I > 3\sigma(I)$) were used in all calculations.

2.5.1. Crystal data

$C_{22}H_{34}Cl_2N_6O_{11}Cu_2$, $M = 756.5$, monoclinic, space group $P2_1/n$, $a = 8.548(2)$, $b = 13.599(2)$, $c = 25.883(2)$ Å, $\beta = 97.81(1)°$, $V = 2981(6)$ Å^3, $Z = 4$, $D_{calc} = 1.686$ g cm^{-3}, $\mu = 16.7\ cm^{-1}$, $F(000) = 1552$.

Intensity data were corrected for Lorentz-polarization effects. The structure was solved by direct methods and refined by full-matrix least-squares and Fourier techniques. The positions of the hydrogen atoms were calculated assuming ideal geometry, and their positions and thermal parameters were not refined. All other atoms were refined with anisotropic thermal parameters. The final cycle of refinement included 388 variable parameters. The refinement on F converged to a final $R = 0.059$, $R_w = 0.069$ and goodness-of-fit = 3.871, with the largest difference peak and hole 1.19 and -1.30 e Å^{-3}, respectively. The quantity minimized was $\Sigma w(|F_o| - |F_c|)^2$ with $w = 1$. All calculations are performed using the XTAL3.2 program package [17].

3. Results and discussion

3.1. Syntheses

The new dinucleating ligand HL was synthesized in high yield from the reaction between 1,3-dichloro-2-propanol and 2-(2-methylaminoethyl)pyridine in a 1:2 molar ratio, in cold (~ 10°C) MeOH in the presence of Et_3N. The dicopper(II) complexes were prepared by the stoichiometric reaction between $Cu(ClO_4)_2{\cdot}6H_2O$, HL and exogenous ligand (pyrazole + Et_3N)/NaN_3/$MeCO_2Na$, in a 2:1:1 molar ratio in an ethanolic medium. While the azide complex is a green solid the acetate and prz complexes are blue in color.

In the IR spectra for all three compounds, broad bands at $\sim 3500\ cm^{-1}$ are seen, associated with O–H stretch of water of crystallization or coordinated water or both. For the prz complex this band is split. A strong band at $\sim 1100\ cm^{-1}$ and a medium intensity band at $\sim 620\ cm^{-1}$ are characteristic of the presence of ionic perchlorate. However, for all three compounds, the $\nu_3(ClO_4)$ vibration at $\sim 1100\ cm^{-1}$ shows significant splitting, suggesting the presence of a low-symmetry perchlorate, possibly acting as a 'semi-coordinated' ligand [8]. The X-ray structure determination for the prz complex shows the presence of a coordinated perchlorate and a coordinated water molecule, in addition to the presence of a water molecule of crystallization (vide infra). The azide complex has an intense IR band at 2050 cm^{-1} assignable to $\nu_{asym}(N_3)$ vibration of μ-1,1-azido bridge [18]. For the acetate complex bands at 1555 and 1440 cm^{-1} are assignable to the ν_{asym}(OCO) and ν_{sym}(OCO) vibrations of the bridging acetate [15]. Barring the characteristic absorption region due to the exogenous ligand, the IR spectra of the present complexes are closely similar, revealing that they are isostructural. The solution electrical conductivity data in MeCN revealed their 1:2 electrolytic behavior (expected range for 1:2 electrolytes in MeCN: 220–300 $\Omega^{-1}\ cm^2\ mol^{-1}$ [19]), implying weak coordi-

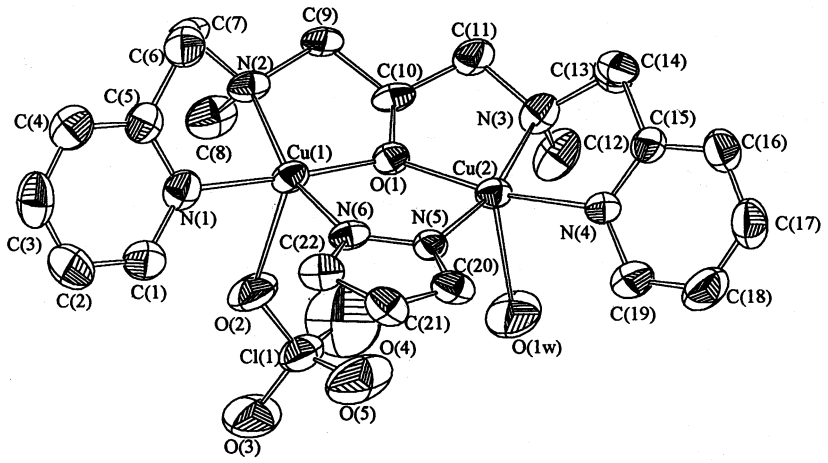


Fig. 1. Perspective view of the cation $[Cu_2(L)(prz)(OClO_3)(H_2O)]^+$ in complex **3a**. The thermal ellipsoids are at the 50% probability level. Hydrogen atoms are omitted.

nation of perchlorate ion in the sold state. Based on the above facts and microanalytical data, we propose the composition of these three new complexes as $[Cu_2L(X)(OClO_3)(H_2O)](ClO4)\cdot H_2O$ [$X = C_3H_3N_2^-$ (prz) (**3a**), N_3^- (**3b**), $MeCO_2^-$ (**3c**)], which was finally confirmed by the X-ray structural analysis of **3a**.

3.2. Description of the crystal structure of $[Cu_2L(\mu\text{-}prz)(OClO_3)(H_2O)]$–$(ClO_4)\cdot H_2O$

A perspective drawing of the complex together with the atom-labeling scheme is shown in Fig. 1. Table 1 contains pertinent bond distances and angles. The crystal structure of **3a** comprises $[Cu_2L(\mu\text{-}prz)(OClO_3)(H_2O)]^+$ cation, ClO_4^- anion and water of crystallization in the ratio of 1:1:1. The cation features each copper(II) center coordinated by one common alkoxide bridge, one pyridyl and one aliphatic nitrogen, besides from exogenous ligand coordination (prz, perchlorate and water) in an asymmetric manner. The geometry around each copper(II) is best described as square-pyramidal with a small trigonal-bipyramidal component (τ) of 0.24 for Cu(1) and 0.07 for Cu(2) [$\tau = (\beta - \alpha)/60$, with α and β being the two largest coordination angles). In a perfect square-pyramidal geometry τ equals 0, while it is 1 in a perfect trigonal-bipyramidal geometry [20]. The two copper centers, alkoxo O-atom and two prz nitrogen atoms are almost coplanar (the angle between the planes Cu(1)–O(1)–Cu(2) and Cu(1)–N(6)–N(5)–Cu(2) is 1.94°). The Cu(1) and Cu(2) atoms sit above the mean plane of three N-atoms and one alkoxide O-atom by 0.15 and 0.19 Å towards axial coordination, respectively. An additional water molecule is hydrogen-bonded to 'semi-coordinated' ClO_4^- and the coordinated H_2O molecule is hydrogen-bonded to the alkoxide O atom.

The Cu–N(amine) distances are longer than that observed for complexes **1a** and **1b**; however, the Cu–N(pyridyl) distances are comparable [7]. The Cu–N(prz) and the Cu···Cu distances both are on the higher end but Cu–O(alkoxide) distances are on the lower end of that reported for closely similar prz bridged compounds [12,13]. Interestingly, the Cu–OR–Cu bridge angle is on the higher end [12,13].

3.3. Absorption spectra

To gain insight into the coordination geometry of the present complexes, the absorption spectral behavior was investigated in MeCN solution as well as in the solid state (dispersed in mineral oil mull). In the solid state, a broad d–d transition is observed at 620 nm (for **3a** and **3b**) and at 656 nm (for **3c**), which is indicative of a square-based geometry around copper(II) [21]. A measurable red shift in the case of **3c** could be due to

Table 1
Selected bond lengths (Å) and angles (°) for $[Cu_2(L)(prz)(OClO_3)(H_2O)](ClO_4)\cdot H_2O$ (**3a**)

Cu(1)–Cu(2)	3.377(3)	Cu(2)–O(1)	1.916(6)
Cu(1)–O(1)	1.874(7)	Cu(2)–O(1w)	2.360(1)
Cu(1)–O(2)	2.552(2)	Cu(2)–N(3)	2.080(1)
Cu(1)–N(1)	1.972(9)	Cu(2)–N(4)	2.008(8)
Cu(1)–N(2)	2.062(9)	Cu(2)–N(5)	1.983(9)
Cu(1)–N(6)	1.959(8)		
Cu(1)–O(1)–Cu(2)	125.9(4)	O(1w)–Cu(2)–O(1)	102.0(3)
O(2)–Cu(1)–O(1)	94.9(3)	O(1w)–Cu(2)–N(3)	99.6(4)
O(2)–Cu(1)–N(1)	87.0(3)	O(1w)–Cu(2)–N(4)	88.3(4)
O(2)–Cu(1)–N(2)	96.3(3)	O(1w)–Cu(2)–N(5)	93.0(4)
O(2)–Cu(1)–N(6)	100.4(3)	O(1)–Cu(2)–N(3)	83.7(3)
O(1)–Cu(1)–N(1)	176.5(3)	O(1)–Cu(2)–N(4)	169.2(3)
O(1)–Cu(1)–N(2)	85.4(3)	O(1)–Cu(2)–N(5)	85.6(3)
O(1)–Cu(1)–N(6)	86.5(3)	N(3)–Cu(2)–N(4)	91.5(4)
N(1)–Cu(1)–N(2)	91.5(4)	N(3)–Cu(2)–N(5)	164.9(3)
N(1)–Cu(1)–N(6)	96.0(4)	N(4)–Cu(2)–N(5)	97.2(4)
N(2)–Cu(1)–N(6)	161.9(4)		

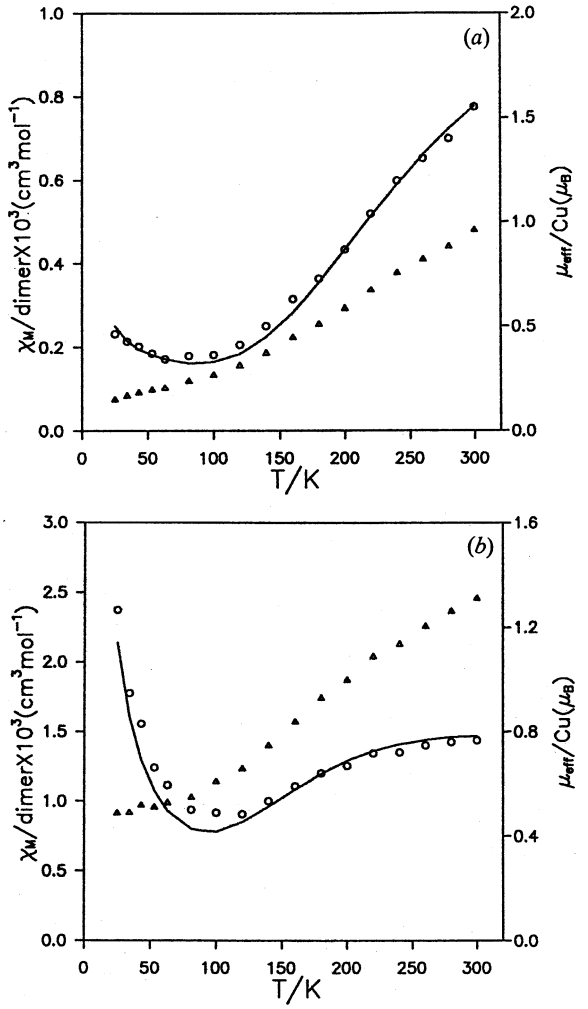


Fig. 2. Plots of χ_M (left scale) per dinuclear complex and μ_{eff}/Cu (right scale) vs. T for (a) $[Cu_2(L)(prz)(OClO_3)(H_2O)](ClO_4)\cdot H_2O$ (**3a**) and $[Cu_2(L)(N_3)(OClO_3)(H_2O)](ClO_4)\cdot H_2O$ (**3b**). The circles are susceptibility data and triangles are magnetic moment data; the line is the calculated fit based on the parameters given in the text.

the fact that the copper(II) centers are slightly more distorted toward trigonal-bipyramidal (cf. X-ray structure of **3a**). In going from solid state to solution the visible band position for **3a** and **3b** is ~10–15 nm blue shifted, due to the dissociation of the perchlorate ion (cf. conductivity data); thus giving rise to a square-planar geometry of the Cu(II) center. For **3c** no measurable shift in the position of this band was observed. Here dissociation of perchlorate ion must be associated with solvent coordination, retaining its five-coordinate square-based geometry. In solution compounds **3a**–**3c** show distinct features between 260–450 nm. The bands between 280 and 370 nm are assignable to LMCT transitions, based on their extinction coefficients. The characteristic band at 420 nm for **3b**, which does not change on dissolution in MeCN, is due to the $N_3^- \rightarrow$ Cu(II) CT transition [14]. For these complexes intraligand transitions are observed at ~260 nm.

3.4. Magnetism

The magnetic properties of the present complexes are clearly of interest owing to the presence of an invariant alkoxide bridge and variable exogenous bridge. Therefore, they were subjected to magnetic susceptibility measurements in the temperature range 25–300 K for **3a** and **3b** and in the range 34–300 K for **3c**. The μ_{eff}/Cu values (at 300 K) are 0.96, 1.31 and 1.73 μ_B for **3a**, **3b** and **3c**, respectively. Plots of molar susceptibility and effective magnetic moment versus temperature for **3a** and **3b** are illustrated in Fig. 2 and similar plots for **3c** are in Fig. 3. For **3a** a rise in susceptibility at high temperatures, with the Néel point clearly far above r.t., indicates the presence of very strong antiferromagnetic exchange coupling. The maximum in susceptibility at ca. 250 K for **3b** and at ca. 100 K for **3c** is indicative of medium-strength and comparatively weak intramolecular antiferromagnetic coupling in **3b** and **3c**, respectively. The observed magnetic susceptibility data were fitted to the modified Bleaney–Bowers [22] Eq. (1) by allowing for the presence of monomeric impurity [7,8], where ρ is the mole-fraction of

$$\chi_M = 2N\beta^2g^2/3kT[1 + 1/3\exp(-2J/kT)]^{-1}(1-\rho) + N\beta^2g^2\rho/2kT + 2N_\alpha \quad (1)$$

the non-coupled copper(II) impurity. In this expression, N, g, and k have their usual meaning; $2J$ is the energy difference between the singlet and triplet states; χ_M is the molar susceptibility per dimer. The values of g and temperature-independent paramagnetic susceptibility (N_α) were kept fixed at 2.10 [typical value for a tetragonal Cu(II)] and 60×10^{-6} cm^3 mol^{-1} during fitting procedure. The best-fit parameters of J and ρ using Eq.

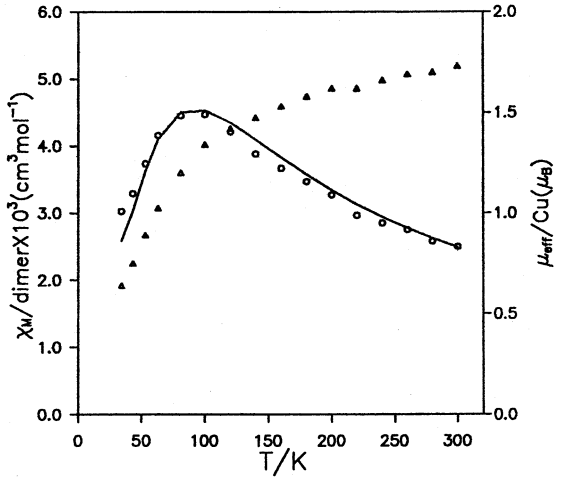


Fig. 3. Plot of χ_M (left scale) per dinuclear complex and μ_{eff}/Cu (right scale) vs. T for $[Cu_2(L)(O_2CMe)(OClO_3)(H_2O)](ClO_4)\cdot H_2O$ (**3c**). The circles are susceptibility data and triangles are magnetic moment data; the line is the calculated fit based on the parameters given in the text.

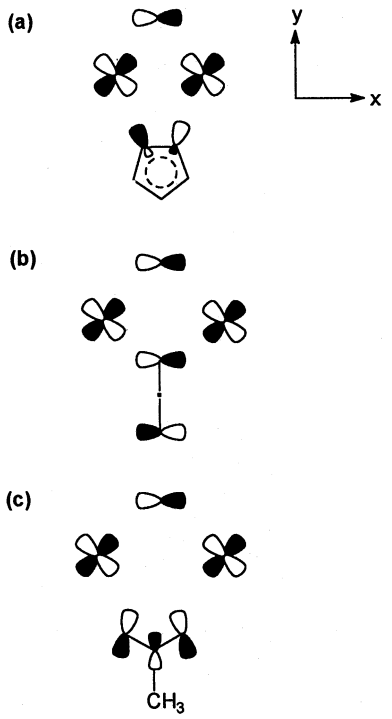


Fig. 4. Bridging ligand orbital interactions with $d_{x^2-y^2}$ orbitals of copper for various dibridged systems: (a) complementarity of alkoxide/prz, (b) countercomplementarity of alkoxide/1,1-azide and (c) countercomplementarity of alkoxide/acetate. Only the antisymmetric combination of copper magnetic orbitals is illustrated.

(1) were obtained by a nonlinear least-squares fitting procedure [7,8]. The quality of fit was estimated by the R index defined as $R = \Sigma(\chi_M^{expt} - \chi_M^{calc})^2/\Sigma(\chi_M^{expt})^2$. The following parameters were obtained: $J = -275$ cm^{-1}, $\rho = 0.0039$ and $R = 3.92 \times 10^{-9}$ for **3a**; $J = -183$ cm^{-1}, $\rho = 0.0610$ and $R = 2.66 \times 10^{-7}$ for **3b**; $J = -56$ cm^{-1}, $\rho = 0.0700$ and $R = 4.33 \times 10^{-7}$ for **3c**. Given the presence of a considerable amount of paramagnetic impurities (particularly in **3b** and **3c**) the calculated J values are far too accurate. Based on the data, we put a range of $-2J$ values as: 550 ± 25 cm^{-1} (**1**), 360 ± 10 cm^{-1} (**2**) and 100 ± 10 cm^{-1}. However, the analyses correspond to excellent agreement between observed and calculated magnetic data (Figs. 2 and 3). The strong antiferromagnetic coupling observed for the prz complex is due to (i) the planarity of the Cu(1)–O(1)–Cu(2)–N(5)–N(6) unit and (ii) an enhanced Cu–OR–Cu bridge angle of $\sim 126°$ (cf. X-ray structure). As before [10], we note that small changes in the coordination geometry at the copper(II) ions can bring about a profound effect on the extent of antiferromagnetic exchange coupling.

3.5. Magnetostructural correlations

Based on the X-ray structure of **3a** and closely similar spectral properties of **3a**–**3c** [cf. (i) IR spectra of **3a**–**3c**, (ii) identical d–d band position of **3a** and **3b** (the copper(II) centers in **3c** might have slightly more trigonal bipyramidal components, compared with **3a** and **3b**)] we could assume that the present complexes have predominantly square-based copper(II) centers. According to theoretical predictions made by Hoffmann and co-workers [23], strong antiferromagnetic interactions arise in any dimer when the energy separation between the highest d-like molecular orbitals, viz. symmetric (ϕ_s) and antisymmetric (ϕ_a) combinations of magnetic orbitals is large, irrespective of which combination of the orbitals is lower in energy. In the case of an alkoxide bridge [24–27] the intervening oxygen p_x orbital interacts with the ϕ_a orbital and exerts no effect on it (Fig. 4). Nishida and co-workers [24–27] and Reed and co-workers [11] have indicated that in a dicopper complex with two different bridging groups (endogenous alkoxide and exogenous X groups), the bridging groups act 'complementary' or 'countercomplementary' in inducing antiferromagnetic interaction depending on the symmetries of their HOMOs which interact with metal d-like orbitals. Based on the above considerations, we provide here a rationale of the observed magnetic behavior of **3a**–**3c** (Fig. 4).

For the prz complex **3a** both bridging ligands provide orbital interaction pathways that act in concert (bridging ligand orbital complementarity) to increase the energy of ϕ_a. For **3b** the energy of ϕ_a orbital is lowered, because the highest occupied orbital of an azide ion in the μ-1,1-mode does not have the correct symmetry (in the antibonding sense) to interact with ϕ_a orbital. For **3c** the acetate bridge has no net overlap with the ϕ_a orbitals; therefore, no net change in energy of ϕ_a is expected with this orbital combination. However, the energy of ϕ_s orbital is raised, because the highest occupied orbital of an acetate ion has the correct symmetry (in the antibonding sense) to interact with ϕ_s orbital (not shown in Fig. 4). Thus, effectively the gap between ϕ_a and ϕ_s decreases (countercomplementary) in **3b** and **3c**, thereby diminishing the antiferromagnetic interaction. Even though μ-1,1-N_3^- bridge exerts a ferromagnetic contribution [28], which in the present case does not entirely compensate the strong antiferromagnetic contribution due to the alkoxo-bridge. Similar situations have been encountered with phenolato-bridged dicopper(II) compounds [29,30]. The observed trend between **3b** and **3c** is comparable with that observed for a closely related system, albeit not structurally characterized, with terminal five-membered chelate ring [12]. However, here we observe a more pronounced antiferromagnetic pathway of exchange coupling. We note that the $2J$ values for phenoxo-/hydroxo complex **1a** and bis(hydroxo) complex **1b** are -440 and -258 cm^{-1}, respectively [7].

Some interesting general trends emerge from the present results. (i) Within the endogenous alkoxo

bridge, with variation in the exogenous bridging groups the order of the strength of the exchange interaction is **3a** > **3b** > **3c**. (ii) Within the endogenous alkoxo bridge, a six-membered chelate ring (an ethylpyridine compared to a methylpyridine [12]) gives a more negative J, a factor that is presumably due to increased terminal ligand flexibility. It should be noted however that the present ligand has N-methyl groups instead of NH groups present in the reported system [12]. This ligand flexibility probably provides a more favorable superexchange pathway.

4. Concluding remarks

Using a new dinucleating ligand with an endogenous alkoxo bridging unit, three dicopper(II) complexes have been synthesized with additional mono-anionic exogenous bridging ligand prz (structurally characterized), azide and acetate. Temperature-dependent magnetic susceptibility studies show that (i) there is antiferromagnetic exchange between pairs of copper(II) ions in each case resulting in $S = 0$ ground state; (ii) the magnitude of the antiferromagnetic exchange depends on the identity of the exogenous bridge (prz > azide > acetate). The concept of complementary versus countercomplementary effect has been used to explain the magnetic behavior of the complexes.

5. Supplementary material

Further details of the structure determination, including atomic coordinates, bond lengths and angles, thermal parameters of all non-hydrogen atoms for the structure is available on request as supplementary material from The Director, Cambridge Crystallographic Data Center, 12 Union Road, Cambridge CB2 1EZ, UK (fax: +44-1223-336-033; e-mail: deposit@ccdc.cam.ac.uk or www: http://www.ccdc.cam.ac.uk) (CCDC deposition number, 138906).

Acknowledgements

This work was supported by grants from the Council of Scientific & Industrial Research (CSIR) and Department of Science and Technology (DST), Government of India, New Delhi. R.G. gratefully acknowledges the award of a fellowship (SRF) by CSIR. The financial assistance of the National X-ray diffractometer facility by DST at this Department is gratefully acknowledged.

References

[1] V.H. Crawford, H.W. Richardson, H.R. Wasson, D.J. Hodgson, W.E. Hatfield, Inorg. Chem. 15 (1976) 2107.
[2] D.J. Hodgson, Inorg. Chem. 15 (1976) 3174.
[3] O. Kahn, Inorg. Chim. Acta 62 (1982) 3.
[4] M. Melník, Coord. Chem. Rev. 42 (1982) 259.
[5] E.I. Solomon, U.M. Sundaram, T.E. Machonkin, Chem. Rev. 96 (1996) 2563.
[6] F. Zippel, F. Ahlers, R. Werner, W. Haase, H.-F. Noltine, B. Krebs, Inorg. Chem. 35 (1996) 3409.
[7] D. Ghosh, R. Mukherjee, Inorg. Chem. 37 (1998) 6597, and references therein.
[8] R. Gupta, S. Mukherjee, R. Mukherjee, J. Chem. Soc., Dalton Trans. (1999) 4025, and references therein.
[9] V. McKee, J.V. Dagdigian, R. Bau, C.A. Reed, J. Am. Chem. Soc. 103 (1981) 7000.
[10] V. McKee, M. Zvagulis, J.V. Dagdigian, M.G. Patch, C.A. Reed, J. Am. Chem. Soc. 106 (1984) 4765.
[11] V. McKee, M. Zvagulis, C.A. Reed, Inorg.Chem. 24 (1985) 2914.
[12] W. Mazurek, B.J. Kennedy, K.S. Murray, M.J. O'Connor, J.R. Rodgers, M.R. Snow, A.G. Wedd, P.R. Zwack, Inorg. Chem. 24 (1985) 3258.
[13] H. Nie, S.M.J. Aubin, M.S. Mashuta, R.A. Portar, J.F. Richardson, D.N. Hendrickson, R.M. Buchanan, Inorg. Chem. 35 (1996) 3325.
[14] K.D. Karlin, I. Sanyal, A. Farooq, R.R. Jacobson, S.N. Shaikh, J. Jubieta, Inorg. Chim. Acta 174 (1990) 13.
[15] T.K. Lal, R. Mukherjee, Inorg. Chem. 37 (1998) 2373.
[16] C.J. O'Connor, Prog. Inorg. Chem. 29 (1982) 203.
[17] S.R. Hall, H.D. Flack, J.M. Stewart (Eds.), The XTAL 3.2 Reference Manual, Universities of Western Australia, Geneva, and Maryland, 1992.
[18] K.D. Karlin, B.I. Cohen, J.C. Hayes, A. Farooq, J. Zubieta, Inorg. Chem. 26 (1987) 147, and references therein.
[19] W.J. Geary, Coord. Chem. Rev. 7 (1971) 81.
[20] A.W. Addison, T.N. Rao, J. Reedijk, J. van Rijn, G.C. Verschoor, J. Chem. Soc., Dalton Trans. (1984) 1349.
[21] B.J. Hathaway, in: G. Wilkinson, R.D. Gillard, J.A. McCleverty (Eds.), Comprehensive Coordination Chemistry, vol. 5, Pergamon, Oxford, 1987, p. 533.
[22] B. Bleaney, K.D. Bowers, Proc. R. Soc. Lond. A 214 (1952) 451.
[23] P.J. Hay, J.C. Thibeault, R. Hoffmann, J. Am. Chem. Soc. 97 (1975) 4884.
[24] Y. Nishida, M. Takeuchi, K. Takahashi, S. Kida, Chem. Lett. (1985) 631.
[25] Y. Nishida, S. Kida, J. Chem. Soc., Dalton Trans., (1986) 2633.
[26] Y. Nishida and S. Kida, Inorg. Chem. 27 (1988) 447, and references therein.
[27] T. Kawata, M. Yamanaka, M. Ohba, Y. Nishida, M. Nagamatsu, T. Tokii, M. Kato, O.W. Steward, Bull. Chem. Soc. Jpn. 65 (1992) 2739.
[28] T. Mallah, O. Kahn, J. Gouteron, S. Jeannin, Y. Jeannin, C.J. O'Connor, Inorg. Chem. 26 (1987) 1375, and references therein.
[29] T.N. Sorrell, Tetrahedron 45 (1989) 3.
[30] K.D. Karlin, A. Farooq, J.C. Hayes, B.I. Cohen, T.M. Rowe, E. Sinn, J. Zubieta, Inorg. Chem. 26 (1987) 1271.

PERGAMON

www.elsevier.nl/locate/poly

Polyhedron 19 (2000) 1437–1446

POLYHEDRON

Photoredox reactions of oxomolybdenum(V) with phosphines

Ralph A. Isovitsch [1], Jerome G. May, Frank R. Fronczek, Andrew W. Maverick *

Department of Chemistry, Louisiana State University, Baton Rouge, LA 70803-1804, USA

Received 24 September 1999; accepted 21 March 2000

Abstract

The fluorescent molybdenum(V)–oxo complex $MoOCl_4(H_2O)^-$, and oxomolybdenum(V)–phosphine complexes derived from it, undergo thermal and photochemical reactions in acetonitrile with the series of phosphines PEt_3, PEt_2Ph, $PEtPh_2$, and PPh_3. PEt_3 reacts spontaneously to form several products: crystalline $(PPh_4)[Mo^{III}Cl_4(PEt_3)_2]$ and $(PPh_4)_2[Mo^{V}OCl_5]\cdot 2CH_2Cl_2$; and a maroon oil that contains $OPEt_3$, $Mo^{IV}OCl_2(PEt_3)_3$ and $Mo^{IV}Cl_4(PEt_3)_2$. The Mo(III) and $OPEt_3$ products show that oxygen atom transfer has occurred. PEt_2Ph and $PEtPh_2$ show no significant redox activity with oxomolybdenum(V) in the dark, but irradiation ($\lambda > 320$ nm, CH_3CN solution) leads to reduction of Mo(V) and production of the corresponding phosphine oxides. The molybdenum(III) product, *cis-mer*-$MoCl_3(OPEt_2Ph)_2(PEt_2Ph)$, was isolated from the PEt_2Ph experiment. PPh_3 is not oxidized under these conditions; instead, spectral evidence suggests that photoinduced ligand substitution occurs, producing $MoOCl_3(PPh_3)_2$. Selective irradiation of the longer-wavelength Mo(V) absorption bands leads to similar photoredox reactions, but much more slowly. X-ray analyses of two reaction products, $(PPh_4)_2[Mo^{V}OCl_5]\cdot 2CH_2Cl_2$ and *cis-mer*-$Mo^{III}Cl_3(OPEt_2Ph)_2(PEt_2Ph)$, are reported. © 2000 Elsevier Science Ltd. All rights reserved.

Keywords: Molybdenum–oxo complexes; Photochemistry; Photooxidation; Phosphines; Phosphine oxides; Crystal structures

1. Introduction

Complexes that contain a transition metal with a multiply bonded main-group element have been the subject of intense study [1]. The importance of such complexes is reflected in the large array of such reagents in organic chemistry: oxo derivatives of chromium(VI), $KMnO_4$, OsO_4, RuO_4 and others are known to transfer oxygen atoms to organic substrates. Metal–oxo complexes are also believed to be important in metalloenzymes that catalyze the transfer of an oxygen atom to or from a substrate [2]. Thermal oxygen-atom transfer has also been studied in a variety of inorganic systems [3,4].

The photophysics and photochemistry of metal complexes with multiply bonded main-group elements have received less attention. Most such studies have been based on early electronic-structure investigations of monooxo complexes of Mo(V), Cr(V), and V(IV) [5]. A variety of d^2 M≡N and MO_2 complexes have been studied more recently. For example, the rhenium(V)–nitrido cations $[ReN(R_2PCH_2CH_2PR_2)_2Cl]^+$ (R = Me, Et, Ph, cyclohexyl) phosphoresce in solution with lifetimes of 0.3–2 μs [6] and Che and co-workers have explored the photophysical properties of $[Os^{VI}N(2,3\text{-diamino-}2,3\text{-dimethylbutane})_2Cl]^{2+}$ and $[Os^{VI}N(NH_3)_4]^{3+}$ [7]. The dioxo species are exemplified by *trans*-$[ReO_2(py)_4]^+$, which shows a phosphorescence lifetime of 10 μs in CH_3CN at room temperature [8].

Photochemical experiments have also been carried out with these d^2 systems. The 'd–d' lowest-energy excited states also possess M → MN π* (or M → MO π*) character, making the N (or O) atom more basic. This principle has been demonstrated by excited-state protonations of the rhenium(V) nitrido [6] and dioxo [9] complexes, and by the sensitivity of the ReO_2^+ phosphorescence lifetimes to hydrophilic/hydrophobic environments [10]. Photoredox reactions have also been observed, beginning with the report that ReO_2^{+}* reduces methylviologen and other acceptors [11]. The resulting $Re^{VI}O_2^{2+}$ species, which can also be generated

* Corresponding author. Tel.: +1-225-388-4415; fax: +1-225-388-3458.

E-mail address: awm@chem.lsu.edu (A.W. Maverick).

[1] Present address: Division of Science and Mathematics, University of the Virgin Islands, St. Thomas, Virgin Islands 00802, USA.

0277-5387/00/$ - see front matter © 2000 Elsevier Science Ltd. All rights reserved.
PII: S0277-5387(00)00395-8

electrochemically, oxidizes organic substrates such as silanes and secondary alcohols. An analogous dioxorhenium(VI) complex has been isolated and its properties studied [12]. Finally, photochemical oxygen atom transfer reactions have been reported from two phosphorescent *trans*-dioxoosmium(VI) complexes to phosphines, sulfides, and alkenes [13].

We have focused on photoredox reactions of molybdenum. We first studied the two-electron photooxidation of $Mo(NCS)_6^{3-}$ to a molybdenum(V) oxo dimer, $(SCN)_3MoO(\mu\text{-}O)_2MoO(NCS)_3^{4-}$ [14]. We also showed that one of the simplest molybdenum(V) oxo complexes, $MoOCl_4(NCCH_3)^-$, shows d–d fluorescence in acetonitrile solution with a lifetime (110 ns) sufficient for reaction with one-electron oxidants and reductants [15]. In the present work we explore the photochemistry of oxomolybdenum(V) with the series of phosphines PEt_3, PEt_2Ph, $PEtPh_2$ and PPh_3 as oxygen atom acceptors, with the goal of achieving photochemical oxygen atom transfer. We find that PEt_3, PEt_2Ph and $PEtPh_2$ are oxidized to the corresponding phosphine oxide, with PEt_3 reacting spontaneously and PEt_2Ph and $PEtPh_2$ requiring irradiation. Molybdenum-containing reduction products were isolated in the reactions with PEt_3 and PEt_2Ph. The only photochemical activity observed with PPh_3 appears to be ligand substitution.

2. Experimental

2.1. Materials and procedures

All reactions and manipulations were performed using standard dry-box techniques. Anhydrous solvents were obtained from Aldrich Chemical Co. PEt_3, PEt_2Ph, and $PEtPh_2$ were obtained from Organometallics, Inc. The phosphines were free of phosphine oxides, as determined by GC–MS and ^{31}P NMR. $(PPh_4)[MoOCl_4(H_2O)]$ was prepared according to the literature procedure [16].

A Perkin–Elmer 1760X spectrometer was used to record FT-IR spectra; samples were thin films or KCl pellets. Electronic absorption spectra were recorded on an Aviv 14DS spectrophotometer. Fluorescence measurements utilized a Spex Fluorolog 2 model F112X instrument, with Hamamatsu R406 (S-1) PMT. ^{31}P NMR spectra were recorded on Bruker 250 and 300 MHz spectrometers operating at 101.2 and 121.4 MHz, respectively, with samples dissolved in CD_3CN; chemical shifts are reported in ppm referenced to 85% H_3PO_4.

2.2. Thermal reaction of $MoOCl_4(H_2O)^-$ with PEt_3

A green solution of $(PPh_4)[MoOCl_4(H_2O)]$ (0.31 g, 0.51 mmol) was prepared in 25 ml of CH_2Cl_2. To this was added 0.072 g (0.61 mmol) PEt_3, causing an immediate color change to maroon. The mixture was stirred for 1 h and then flooded with pentane. The resulting yellow suspension was left to stand overnight, and the greenish–yellow solid collected. The filtrate was evaporated to give a maroon oil, whose analysis is described in Section 3.

2.3. $(PPh_4)_2[MoOCl_5]\cdot 2CH_2Cl_2$

The greenish–yellow solid isolated from the $MoOCl_4(H_2O)^-/PEt_3$ reaction (see above) contained crystals suitable for X-ray analysis (see below). This compound is stable for extended periods in inert atmosphere, but in moist air, it shows green surface discoloration over a period of several weeks. *Anal.* Calc. for $C_{50}H_{44}Cl_9MoOP_2$: C, 52.78; H, 3.90; Cl, 28.04. Found: C, 54.05, 54.49; H, 4.60, 4.54; Cl, 27.91, 27.79%. Although the microanalytical data were poor for this compound, the X-ray (see below), UV–Vis (see Section 3), EPR (spectra for this material are similar to those for $(PPh_4)[MoOCl_4(H_2O)]$), and XANES analyses (see Section 6) all support the Mo(V) oxidation state assignment.

2.4. Irradiation of Mo(V)–phosphine mixtures

Solutions prepared from $(PPh_4)[MoOCl_4(H_2O)]$ (3.2 mM) and the desired phosphine (4 equiv.) in CH_3CN were irradiated in Pyrex vessels using a 150-W xenon arc lamp, with or without Corning colored-glass longpass filters. Reaction progress was monitored by removing aliquots at 1-day intervals for UV–Vis analysis. The reaction was judged complete when no further change was noted in the UV–Vis spectra. The solvent was then evaporated from the reaction mixture and the resulting residue analyzed. Control mixtures were prepared and analyzed identically, with the flasks tightly wrapped in aluminum foil to eliminate light.

2.5. ^{31}P NMR analysis of reaction products

After a thermal (dark) or photochemical reaction, the solvent was removed under vacuum, and the residue dissolved in CD_3CN for measurement of its ^{31}P NMR spectrum. In all cases, resonances were observed in these spectra for PPh_4^+ and unreacted phosphine. Phosphine oxides were identified as products in these mixtures, by comparison either with literature data ($OPEt_3$ [17]) or with samples prepared separately from the phosphines and NaOCl(aq) (chemical shifts for the reaction products sometimes differed from reference values by 1–2 ppm, and the resonances were typically broad; we attribute these effects to the presence of paramagnetic complexes, e.g. Mo(III) or Mo(V), in the solutions). In the photochemical experiments, the production of phosphine oxide was also confirmed by GC–MS analysis.

Table 1
Crystal data [a]

Compound	$(Ph_4P)_2[MoOCl_5]\cdot 2CH_2Cl_2$	*cis-mer*-$MoCl_3(OPEt_2Ph)_2(PEt_2Ph)$
Formula	$C_{50}H_{44}Cl_9MoOP_2$	$C_{30}H_{45}Cl_3MoO_2P_3$
F_w	1137.9	732.9
Space group	$P\bar{1}$	$P2_1/c$
Z	1	4
λ (Å)	0.71073	0.71073 (Mo Kα)
a (Å)	10.131(2)	16.225(2)
b (Å)	11.182(2)	11.8374(11)
c (Å)	12.407(2)	18.288(2)
α (°)	70.52(1)	
β (°)	79.49(1)	92.292(6)
γ (°)	80.93(1)	
V (Å^3)	1295.8(6)	3510(1)
D_{calc} (g cm^{-3})	1.458	1.387
μ (cm^{-1})	8.11	7.54
Relative transmission coefficient	0.902–1.000	0.7767–0.9992
Observed data [$I>1\sigma(I)$]	3650	3259
$R(F)$ [b] (observed data)	0.077	0.075
$R_w(F)$ [c]	0.057	0.047

[a] Estimated standard deviations in the least significant digits of the values are given in parentheses.
[b] $R=\Sigma\|\|F_o\|-\|F_c\|\|/\Sigma|F_o|$.
[c] $R_w=[\Sigma w(|F_o|-|F_c|)^2/\Sigma wF_o^2]^{0.5}$; $w=4F_o^2/[\sigma^2(I)+(0.02F_o^2)^2]$.

2.6. X-ray analyses

Diffraction data (see summary in Table 1) were collected on an Enraf–Nonius CAD4 diffractometer fitted with Mo Kα source and graphite monochromator, using the $\theta-2\theta$ scan method. Final unit cell constants were determined from the orientations of 25 centered high-angle reflections. The intensities were corrected for absorption using ψ scan data for five reflections. The MOLEN [18] set of programs was used for structure solution and refinement.

3. Results

3.1. Thermal reaction of $MoOCl_4(H_2O)^-$ with PEt_3

Addition of 1.2 equiv. of PEt_3 to $MoOCl_4(H_2O)^-$ dissolved in dichloromethane produced an immediate change in color from green to maroon, as illustrated by the electronic spectral changes in Fig. 1. Treatment of the reaction mixture with pentane produced three different substances: a greenish–yellow crystalline material, an orange crystalline material, and a maroon oil that is soluble in pentane and CH_2Cl_2 (similar changes occurred when the reaction was carried out with a larger excess of PEt_3, or when it was performed in CH_3CN solvent).

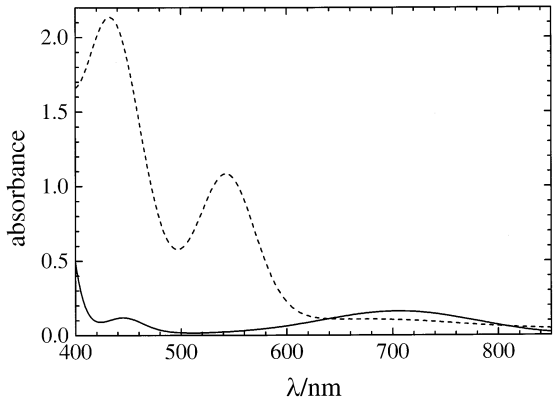


Fig. 1. Electronic absorption spectra illustrating the reaction of $MoOCl_4(H_2O)^-$ with PEt_3 in CH_2Cl_2. (—) $MoOCl_4(H_2O)^-$; (---) immediately after addition of PEt_3.

3.1.1. Greenish–yellow material

This was obtained in crystalline form by the above procedure; it was identified as $(PPh_4)_2[Mo^VOCl_5]\cdot 2CH_2Cl_2$ by X-ray analysis. An ORTEP [19] drawing of the $MoOCl_5^{2-}$ ion in this structure appears in Fig. 2; distances and angles in the anion are listed in Table 2. The unit-cell parameters closely match those of a number of other compounds (located by means of the Cambridge Crystallographic Database [20]; two isostructural examples are $(PPh_4)_2[W^VOCl_5]\cdot 2CH_2Cl_2$ and $(PPh_4)_2[Re^VOCl_5]\cdot 2CH_2Cl_2$ [21].

The $MoOCl_5^{2-}$ ion lies on a center of symmetry, with one position ('O1Cl3') half-occupied by Cl3 and the other half by O1. We were unable to resolve separate positions for Cl3 and O1. As a result, the refined Mo–O1Cl3 distance is shorter than the other Mo–Cl distances and longer than a typical Mo≡O distance (this is similar to the results obtained in previous studies of MoO/MoCl disorder [22]). The largest residual electron density, 1.39 e Å^{-3}, is 0.5 Å from the Mo position. This peak, the size of the Mo ellipsoid, and the orientation of its long axis nearly along the

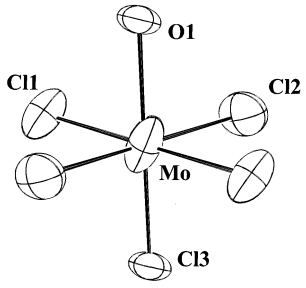


Fig. 2. ORTEP drawing of the $MoOCl_5^{2-}$ anion in $(Ph_4P)_2[MoOCl_5]\cdot 2CH_2Cl_2$, with ellipsoids at the 40% probability level. The O1 and Cl3 atoms are shown separately, but the two positions are superimposed by the crystallographically imposed inversion center; they are modeled as 50% Cl, 50% O ('O1Cl3'), with one set of coordinates and displacement parameters.

Table 2
Selected interatomic distances (Å)

$(Ph_4P)_2[MoOCl_5]\cdot 2CH_2Cl_2$			
Mo–Cl1	2.387(1)	Mo–Cl2	2.362(2)
Mo–Cl/O3	2.230(2)		
cis-mer-$MoCl_3(OPEt_2Ph)_2(PEt_2Ph)$			
Mo–Cl1	2.417(2)	Mo–P1	2.532(2)
Mo–Cl2	2.424(2)	Mo–O1	2.182(4)
Mo–Cl3	2.430(2)	Mo–O2	2.106(4)

Mo–O1Cl3 vector are evidence that the Mo atom in a single molecule is displaced slightly out of the equatorial Cl_4 plane, and actually occupies two different but unresolved positions as a result of the disorder (because this displacement is likely to occur in the direction of the O atom, it will tend to minimize the apparent difference between Mo≡O and Mo–Cl distances). There is evidence that the disorder in the structure may be more complex than our model describes: the B_{eq} value for the overlapped O1Cl3 atom, 4.32(5) $Å^2$, is somewhat smaller than those for Cl1 and Cl2 (6.55(4) and 5.56(4) $Å^2$, respectively), suggesting that the O atom is distributed into the Cl1 and Cl2 sites with some smaller populations. We attempted to refine this more complex disorder model, but we obtained no significant improvement in the fit to the data.

We considered alternative models for this structure that would not require disordered O and Cl ligands. For example, both the Mo(VI) complex *trans*-$MoO_2Cl_4^{2-}$ and the Mo(IV) complex $MoCl_6^{2-}$ are centrosymmetric, and isostructural $(Ph_4P)_2[MO_2Cl_4]\cdot 2CH_2Cl_2$ [23] and $(Ph_4P)_2[MCl_6]\cdot 2CH_2Cl_2$ compounds [24] have been reported. However, when we attempted to fit the X-ray data with Mo(VI) or Mo(IV) models, the results were unsatisfactory. When we refined the anion as Mo(VI) (i.e. *trans*-$MoO_2Cl_4^{2-}$, with a fully occupied O atom), B_{eq} for the O atom refined to a value near zero, R_w was worse (0.099), and two peaks of density 2 e $Å^{-3}$ (0.4 Å from the O position) were present in the resulting difference map. With a Mo(IV) model ($MoCl_6^{2-}$), on the other hand, one of the three crystallographically independent Mo–Cl distances was still unexpectedly short (Mo–Cl3 2.23 Å, vs. 2.38 Å for the other two), and the B_{eq} value for Cl3 was somewhat larger than those of Cl1 and Cl2. The R_w value for this model was also high (0.067).

Our characterization of this compound as containing Mo(V) is further supported by the similarity of its electronic (see below) [15,25–27] and ESR [28] and XANES [29] spectra (see Section 6) to those for other Mo(V) compounds. The IR spectrum of the solid shows a band at 946 cm^{-1}, providing additional support for the presence of the Mo–oxo unit (compare 985 and 950 cm^{-1} for the bipyridinium and triphenylphosphonium salts of $MoOCl_5^{2-}$, respectively [27,30], and 980 cm^{-1} for $(Ph_4P)[MoOCl_4(H_2O)]$ [31].

Therefore, X-ray analysis and spectroscopic data support the description of the greenish–yellow crystalline plates as $(PPh_4)_2[Mo^VOCl_5]\cdot 2CH_2Cl_2$.

In a previous crystal-structure study of K_2MoOCl_5, the geometry of the $MoOCl_5^{2-}$ anion was found to be similar to that described here [32]. Though the species that forms when molybdenum(V) dissolves in concentrated HCl(aq) is often described as $MoOCl_5^{2-}$, Boorman and co-workers [26] showed that the principal constituent of these solutions is $MoOCl_4(H_2O)^-$. To illustrate the difference between the two anions, we prepared a solution of $(PPh_4)_2[MoOCl_5]\cdot 2CH_2Cl_2$ in CH_2Cl_2; it was deep yellow in color, showing electronic absorption bands at 697 and 440 nm [33]. However, when this solution was shaken with conc. HCl(aq), its color changed immediately to green, and the absorption bands shifted to 715 and 441 nm. The latter values are very similar to those for solutions prepared directly from $(PPh_4)[MoOCl_4(H_2O)]$ in CH_2Cl_2 (716 and 447 nm).

3.1.2. Orange crystalline material

The orange product of the Mo(V)/PEt_3 reaction crystallized as needles along with the greenish–yellow plates of $(PPh_4)_2[MoOCl_5]\cdot 2CH_2Cl_2$. X-ray analysis of one of the orange needles identified it as the molybdenum(III) salt $(PPh_4)[MoCl_4(PEt_3)_2]$. The production of this molybdenum(III) compound shows that reduction of $MoOCl_4(H_2O)^-$ by PEt_3 has occurred. $(PPh_4)[MoCl_4(PEt_3)_2]$, and analogs with PEt_2Ph and $PEtPh_2$, have been made and studied in solution by ^1H NMR by Poli and Gordon [34] and the crystal structures of these derivatives have been reported by Cotton and Vidyasagar [35]. The unit-cell parameters and atomic coordinates we obtained for $(PPh_4)[MoCl_4(PEt_3)_2]$ are essentially identical to those of Cotton and Vidyasagar.

3.1.3. Maroon oil

The pentane-soluble maroon oil contains several species. The ^{31}P NMR spectrum of this material (recorded immediately after isolation to minimize decomposition; see Table 3) shows signals attributable to $OPEt_3$ and *cis-mer*-$MoOCl_2(PEt_3)_3$ (δ 9.4 ppm [d, $^2J_{P-P}$ 18 Hz], 17.2 ppm [t, 18 Hz]). The resonances assigned to the latter oxomolybdenum(IV) complex are very similar to those of $MoOCl_2(PEt_2Ph)_3$ [22,36,37]. Also, the formation of *cis-mer*-$MoOCl_2(PEt_3)_3$ in our experiment is indicated by an IR absorption in the reaction products at 963 cm^{-1} [ν(MoO)]; the analogous band in $MoOCl_2(PMe_3)_3$ occurs at 960 cm^{-1} [38] (another similar pattern was present at 10.5 [d, 20 Hz] and 38.9 ppm [t, 20 Hz], but its much lower intensity precluded identification). The most intense peak in the ^{31}P NMR

Table 3
Products observed in reaction of oxomolybdenum(V) with phosphines

Phosphine	Dark reaction			Irradiation		
	^{31}P NMR [a]	X-ray [b]	Electronic spectrum [c]	^{31}P NMR [a]	X-ray [b]	Electronic spectrum [c]
PEt_3	$OPEt_3$, *cis-mer*-$Mo^{IV}OCl_2(PEt_3)_3$	$Mo^{III}Cl_4(PEt_3)_2^-$, $Mo^{V}OCl_5^{2-}$	$Mo^{IV}Cl_4(PEt_3)_2$	not performed		
PEt_2Ph	$OPEt_2Ph$ (trace), *cis-mer*-$Mo^{IV}OCl_2(PEt_2Ph)_3$			$OPEt_2Ph$	*cis-mer*-$Mo^{III}Cl_3(OPEt_2Ph)_2(PEt_2Ph)$	
$PEtPh_2$		$Mo_2^{V}O_4Cl_4^{2-}$		$OPEtPh_2$		*fac*-$Mo^{V}OCl_3(PEtPh_2)_2$
PPh_3	no reaction					*fac*-$Mo^{V}OCl_3(PPh_3)_2$

[a] Identified by ^{31}P NMR spectroscopy; see Section 2 for details. Phosphine oxides were also identified by GC–MS analysis.
[b] Identified by X-ray crystallography.
[c] Identified by electronic absorption spectroscopy.

spectrum is attributable to $OPEt_3$; PEt_3 and *cis-mer*-$MoOCl_2(PEt_3)_3$ appear to be present in smaller amounts. We believe the maroon color of this oil is due to the molybdenum(IV) complex $MoCl_4(PEt_3)_2$, as outlined in Section 4 (see below).

Thus, Mo(V) exhibits redox activity with PEt_3, including oxygen atom transfer reactions. Since rapid redox reactions occur even without irradiation, we did not study the effects of light on this system.

3.2. Irradiation of Mo(V) with PEt_2Ph, $PEtPh_2$, and PPh_3

The other phosphines showed little or no reactivity with Mo(V) in the dark. Therefore, we explored their photochemical reactions in acetonitrile solution. In the following paragraphs, the starting material is referred to as oxomolybdenum(V) for simplicity. The Mo(V) source, $MoOCl_4(H_2O)^-$, is ordinarily converted to $MoOCl_4(NCCH_3)^-$ in acetonitrile solution [15], but further spectral changes (in both absorption and fluorescence; see below) on addition of phosphines suggest that at least some additional ligand substitution is occurring, possibly making $MoOCl_4(phosphine)^-$. Solid $MoOCl_4(phosphine)^-$ salts appear not to have been reported previously in the literature, and we were unable to isolate well-defined solids from these Mo(V)–phosphine mixtures.

3.2.1. PEt_2Ph

On addition of PEt_2Ph (4 equiv.) to oxomolybdenum(V) in acetonitrile, the solution changed from green to brown–green. The absorption maxima for the brown–green solution are at 674 and 446 nm. No fluorescence was observed from these Mo(V)–PEt_2Ph solutions. On irradiation, the color changed gradually to deep red–brown; see spectra in Fig. 3. After irradiation, one maximum was present at 405 nm with a shoulder at 475 nm. GC–MS analysis of the reaction mixture, after as little as 1 day of irradiation, showed that both PEt_2Ph ($m/e = 166$) and $OPEt_2Ph$ ($m/e = 182$) were present. At the end of the irradiation, the ^{31}P NMR spectrum showed intense peaks due to $OPEt_2Ph$ and unreacted PEt_2Ph. A reduced Mo product was also isolated, as follows.

Removal of solvent from the product mixture gave a brown–red oil, which dissolved readily in CH_2Cl_2. Treatment of this CH_2Cl_2 solution with pentane produced orange–yellow crystals, which were shown by X-ray analysis to be the unusual mixed-ligand molybdenum(III) complex *cis-mer*-$MoCl_3(OPEt_2Ph)_2(PEt_2Ph)$ (see data in Tables 1 and 2, and ORTEP plot in Fig. 4). This compound is similar to $MoI_3(PMe_2Ph)_2(OPMe_2Ph)$, which was also produced by reduction of a higher-valent molybdenum compound [39].

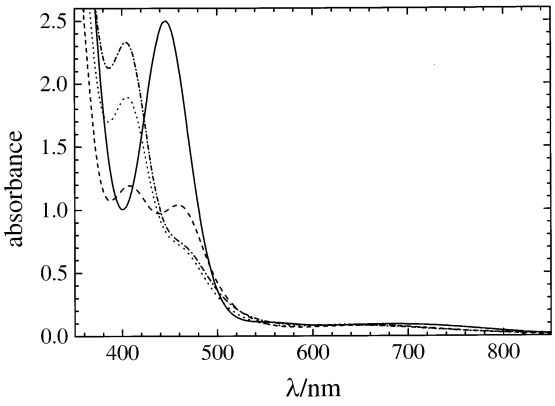


Fig. 3. Electronic absorption spectra illustrating the photochemical reaction of oxomolybdenum(V) with PEt_2Ph in CH_2Cl_2. Irradiation times: (—) initial spectrum, (---) 1 day, (···) 2 days, (-·-·-) 3 days.

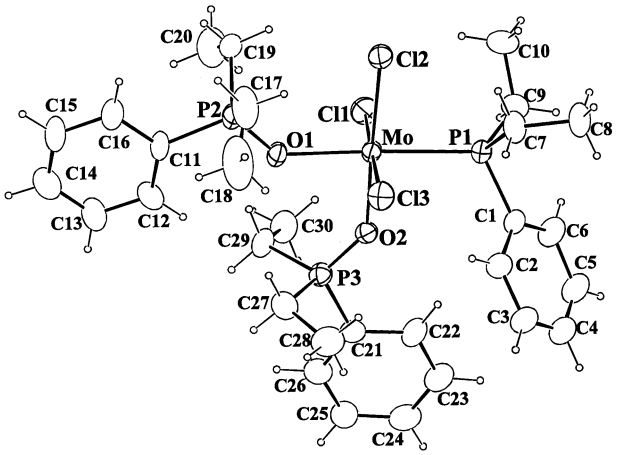


Fig. 4. ORTEP drawing of *cis-mer*-$MoCl_3(OPEt_2Ph)_2(PEt_2Ph)$, with ellipsoids at the 30% probability level.

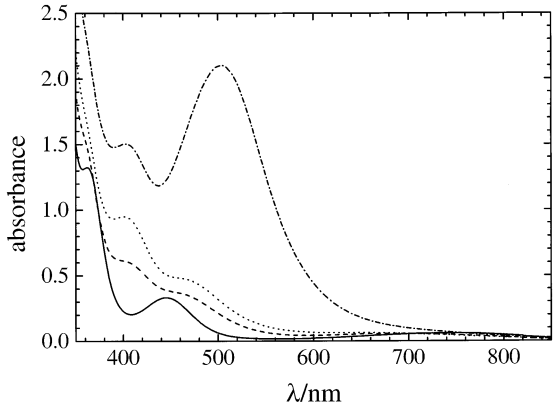


Fig. 5. Electronic absorption spectra illustrating the photochemical reaction of oxomolybdenum(V) with $PEtPh_2$ in CH_2Cl_2. Irradiation times: (—) initial spectrum, (---) 1 day, (···) 2 days, (-·-·-) 3 days.

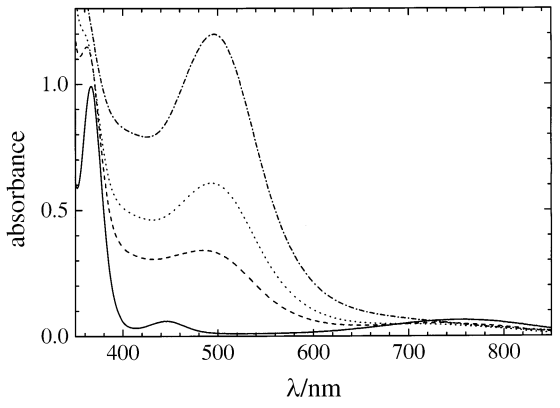


Fig. 6. Electronic absorption spectra illustrating the photochemical reaction of oxomolybdenum(V) with PPh_3 in CH_2Cl_2. Irradiation times: (—) initial spectrum, (---) 1 day, (···) 2 days, (-·-·-) 3 days.

Thus, irradiation of oxomolybdenum(V) with PEt_2Ph causes oxidation of PEt_2Ph and reduction of molybdenum, as judged by the production of $OPEt_2Ph$ and the Mo(III) product *cis-mer*-$MoCl_3(OPEt_2Ph)_2(PEt_2Ph)$.

3.2.2. $PEtPh_2$

Irradiation of oxomolybdenum(V) in CH_3CN with 4 equiv. of the less nucleophilic $PEtPh_2$ produced a change in color similar to that for irradiation with PEt_2Ph. The initial color of the Mo(V)–$PEtPh_2$ mixture was brown–green, with maxima at 446 and 741 nm. This solution was also fluorescent, with λ_{max} (ca. 930 nm) slightly blue-shifted relative to $MoOCl_4(NCCH_3)^-$, and it was also noticeably less intense. During 3 days of irradiation, the solution turned deep red–brown, with final absorption maxima at 403 and 503 nm (see spectra in Fig. 5). Evaporation of solvent from the irradiated solution left a brown–red oil. Both $PEtPh_2$ and $OPEtPh_2$ were present in this residue, as shown by GC–MS (*m*/*e* 214, 230) and ^{31}P NMR (see Table 3) analysis.

Reduced Mo species were expected to form along with the oxidation product $OPEtPh_2$. However, we were unable to isolate such species. Instead, the UV–Vis and IR spectra of the brown–red oil were similar to those of *fac*-$MoOCl_3$(dppe) [40]. No new ^{31}P NMR signals were observed.

Thus, irradiation of oxomolybdenum(V) with $PEtPh_2$ causes photooxidation to $OPEtPh_2$. The major electronic spectral changes are associated with formation of Mo(V) complexes, likely including $MoOCl_3(PEtPh_2)_2$; this indicates that ligand substitution is an important component of the photoinduced reactions.

3.2.3. PPh_3

Addition of PPh_3 to oxomolybdenum(V) produced green–brown solutions, with absorption maxima at 446 and 754 nm, and fluorescence λ_{max} 935 nm (the latter value slightly blue-shifted relative to $MoOCl_4(NCCH_3)^-$). Irradiation of these solutions produced a change in color similar to that noted in the irradiations with PEt_2Ph and $PEtPh_2$: after 3 days the solution had turned deep red–brown (see spectra in Fig. 6).

After removal of solvent, the residue was washed with benzene to remove excess PPh_3. A red–brown solid remained, which showed an absorption maximum of 472 nm in CH_3CN and ν(MoO) at 972 cm^{-1}. The similarity of these features to those for *fac*-$MoOCl_3$(dppe) [40] suggests that the major product in our reaction is *fac*-$MoOCl_3(PPh_3)_2$. Thus, we believe the principal photoreaction in the Mo^VO–PPh_3 system is ligand substitution. No redox products ($OPPh_3$ or isolable reduced molybdenum products) were observed in these irradiated mixtures.

3.3. Reactivity of Mo(V) with PEt_2Ph, $PEtPh_2$, and PPh_3 in the dark

To confirm that the reactions discussed above were indeed photochemical, identical solutions were placed

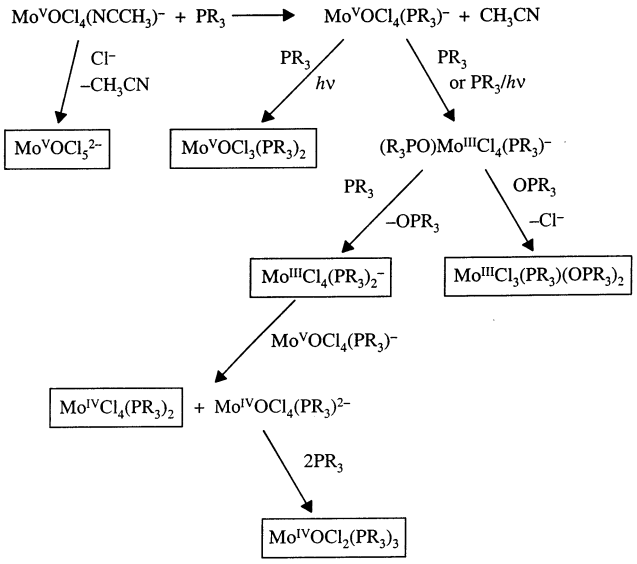
in the dark for 3–4 days and their spectra monitored. Only minor changes occurred, as follows.

3.3.1. PEt_2Ph

The electronic spectrum of the solution changed slightly (final λ_{max} 441 and 640 nm) after 3 days. ^{31}P NMR analysis of the products showed a small signal due to $OPEt_2Ph$ (also present were weak resonances at 20.2 (t) and 15.0 ppm (d), with a pattern similar to that mentioned above for *cis-mer*-$MoOCl_2(PEt_2Ph)_3$). The presence of some $OPEt_2Ph$ (integration ratio $OPEt_2Ph$:PEt_2Ph ca. 1:40) indicates a small amount of thermal oxidation over the course of the dark reaction. As a control experiment, we prepared a similar solution without Mo; this solution also produced a small amount of $OPEt_2Ph$ on standing in the dark. We believe both processes are likely due to traces of O_2 entering the flasks.

3.3.2. $PEtPh_2$

When a Mo(V)–$PEtPh_2$ mixture was allowed to stand for 3 days in the dark, there was essentially no change in its electronic absorption spectrum. Removal of solvent left a brown–green solid, which showed no resonances attributable to $OPEtPh_2$ in its ^{31}P NMR spectrum. Dissolution of this solid in a minimum of CH_2Cl_2, followed by flooding with pentane, gave a solution that slowly deposited a small quantity of orange crystals. These crystals were identified by X-ray analysis as the molybdenum(V) dimer $(PPh_4)_2$-$[Mo_2O_4Cl_4]\cdot CH_2Cl_2$ [41]. Thus, although some ligand substitution occurs in this system, we found no products (e.g. $OPEtPh_2$, or reduced Mo species) that suggested redox processes.



Scheme 1. Proposed routes for formation of molybdenum complexes in the oxomolybdenum(V)–phosphine reaction (phosphine, represented by PR_3, is PEt_3, PEt_2Ph, $PEtPh_2$, or PPh_3). Species in boxes have been identified by spectroscopic methods or by X-ray crystallography.

3.3.3. PPh_3

A dark experiment with Mo(V) and PPh_3 produced no detectable changes after 4 days. The electronic absorption maxima were unchanged. Removal of solvent gave a green solid; this material showed only PPh_4^+ and PPh_3 in its ^{31}P NMR spectrum.

4. Discussion

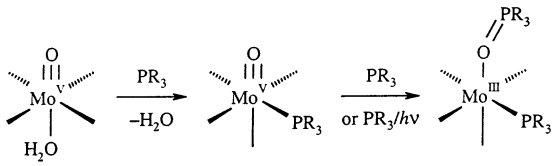
In this work, we attempted to exploit the attractive photophysical properties of $MoOCl_4(NCCH_3)^-$ for use in photochemical oxygen atom transfer. For example, photoreduction of a molybdenum(V)–oxo complex via O atom transfer would yield molybdenum(III). Since some Mo(III) complexes are already known to undergo photoinitiated two-electron oxidation to Mo(V) [14,42] our ultimate goal was to construct a Mo(III)–Mo(V) cycle for use in photochemical two-electron transformations of substrate molecules.

The products we have observed, and proposed routes for their formation, are shown in Scheme 1.

We began our studies with triethylphosphine, because it is the best electron donor in the series PEt_3, PEt_2Ph, $PEtPh_2$, PPh_3, and we expected it to be the most reactive (for example, in the reduction of $MoO_2(S_2CNEt_2)_2$ by this series of phosphines, PEt_3 gives the highest thermal oxygen atom transfer rate constant [43]). Treatment of $MoOCl_4(H_2O)^-$ with PEt_3 in CH_2Cl_2 leads to an immediate change in color from green to maroon. Similar color changes occur when the reaction is performed in CH_3CN, except that the maroon solution gradually turns yellow–orange. In either solvent, numerous products form: $Mo^{V}OCl_5^{2-}$, $Mo^{III}Cl_4(PEt_3)_2^-$, and $OPEt_3$ have been clearly identified, and two additional products appear to be $Mo^{IV}OCl_2(PEt_3)_3$ and $Mo^{IV}Cl_4(PEt_3)_2$ (identified by ^{31}P NMR and UV–Vis spectroscopy, respectively).

Several pieces of evidence argue in favor of the initial step, rapid substitution of phosphine *cis* to the oxo group: the previously documented rapid aquation of $MoOCl_5^{2-}$ (as discussed above) and solvation of $MoOCl_4(H_2O)^-$ in CH_3CN [15], and the initial spectral changes observed on mixing PEt_2Ph, $PEtPh_2$, or PPh_3 with Mo(V).

In the next step, we propose that a molecule of PR_3 reacts with the oxo group of the molybdenum(V)–oxo complex, producing coordinated phosphine oxide and reducing the Mo center to the trivalent state. These initial steps are illustrated in Scheme 2 (reaction of $Mo^{V}O$ with PR_3 is spontaneous for PEt_3, but requires irradiation for PEt_2Ph and $PEtPh_2$). The Mo(III)–OPR_3



Scheme 2. Possible initial steps in the reactions of oxomolybdenum(V) with phosphines.

complex is likely to react readily with an additional molecule of phosphine, releasing the phosphine oxide and giving $Mo^{III}Cl_4(PR_3)_2^-$ as the product.

The other Mo(V) and Mo(IV) products may form as follows. Comproportionation of a molecule of $Mo^{V}OCl_4(PEt_3)^-$ with $Mo^{III}Cl_4(PEt_3)_2^-$ would produce two molybdenum(IV) complexes: $MoOCl_4(PEt_3)^{2-}$ and $MoCl_4(PEt_3)_2$. Substitution of two PEt_3 ligands for Cl^- in $MoOCl_4(PEt_3)^{2-}$ would produce $MoOCl_2(PEt_3)_3$. The chloride ions released in this substitution would be free to react with $MoOCl_4(PEt_3)^-$ to produce $MoOCl_5^{2-}$.

The visually most striking feature of the $MoOCl_4(H_2O)^-/PEt_3$ reaction is the deep maroon color (λ_{max} 546 nm; see Fig. 1) produced almost immediately on mixing the reactants. We were unable to isolate the maroon material by evaporation of the solvent from the pentane solution: this procedure left a brown residue that gave a brown solution in CH_2Cl_2. The maroon color is unlikely to be due to *cis-mer*-$MoOCl_2(PEt_3)_3$, since such complexes are reported to be blue [22]. We believe a more likely explanation of the maroon color is the non-oxo Mo(IV) complex $MoCl_4(PEt_3)_2$. This would be closely related to the Mo(III) anion $MoCl_4(PEt_3)_2^-$ already observed in this system, and other *trans*-$MoCl_4(PR_3)_2$ complexes have been reported to be maroon [37,44], though no electronic absorption spectral data have been published.

Thus, PEt_3 reacts with Mo(V) to give the oxygen atom transfer products of Scheme 1, and other products. The rapid redox activity exhibited with PEt_3, even without irradiation, led us to explore the use of less basic phosphines as oxygen atom accepting substrates. Fewer products were observed in the reactions with other phosphines, but they are also consistent with Scheme 1.

Irradiation of Mo(V) with PEt_2Ph produces $OPEt_2Ph$ and the molybdenum(III) complex $MoCl_3(OPEt_2Ph)_2(PEt_2Ph)$. The formation of these products can be explained by referring to Scheme 1. Displacement of one chloride ligand in $Mo^{III}Cl_4(OPEt_2Ph)(PEt_2Ph)^-$ by $OPEt_2Ph$ would give $MoCl_3(OPEt_2Ph)_2(PEt_2Ph)$, one of the species we have isolated in crystalline form (this route would also yield the *cis-mer* isomer of the mixed phosphine–phosphine oxide complex, as observed in the X-ray structure).

Irradiation of Mo(V) with $PEtPh_2$ produces a change in color similar to that noted with PEt_2Ph. Spectroscopic evidence shows that $OPEtPh_2$ is produced, but the nature of the reduced molybdenum product(s) is unknown.

Irradiation of Mo(V) with PPh_3, the phosphine in the series that is most difficult to oxidize, does not appear to lead to redox reactions. Instead, we believe the major photoprocess is ligand substitution, to give $MoOCl_3(PPh_3)_2$.

The major electronic spectral changes during the irradiations with $PEtPh_2$ and PPh_3 consist of decreasing absorbance beyond 700 nm, increasing (but still weak) absorbance in the 650–700 nm region, and sharply increasing absorbance near 500 nm. The fact that these changes occur with PPh_3, which shows no photoinduced redox activity, suggests that they are due to another process, such as ligand substitution. We have been unable to isolate pure compounds from these irradiated solutions. However, the similarity of these spectral features to those of $MoOCl_3$(dppe) (λ_{max} 496 nm in CH_3CN) [40] suggests that a photoinduced ligand substitution process is important in these systems, with the major product being $MoOCl_3(PR_3)_2$. Because of the complexity and low overall efficiency of the photochemical reactions, and because the most prominent spectral changes appear to reflect photosubstitution rather than the more interesting photoredox reaction, we did not attempt to determine quantum yields for these processes.

Reaction of Mo(V) with PEt_2Ph in the dark also produced a small amount of $OPEt_2Ph$, as indicated by its ^{31}P NMR spectrum. However, the ratio of phosphine oxide to phosphine in the dark reaction is much smaller (by a factor of ca. 25) than in the photochemical reaction.

4.1. Longer-wavelength irradiation of Mo(V) with phosphines

For the photochemical experiments described above, we used Pyrex-filtered xenon-arc light. We also wished to ascertain whether these reactions proceeded via the lowest-energy $^2E(d_{xz}, d_{yz})$ excited state. Therefore, we repeated the Mo(V)/PEt_2Ph and Mo(V)/$PEtPh_2$ irradiations (those that showed definite photoredox activity) using the following Corning colored glass filters: 3–67 ($\lambda > 530$ nm transmitted), 0–51 ($\lambda > 390$ nm) and 0–52 ($\lambda > 360$ nm) [45]. The 3–67 filter allows irradiation in only the lowest-energy absorption band (ca. 750 nm; $^2B_2(d_{xy}) \rightarrow {}^2E(d_{xz}, d_{yz})$), and the other two filters allow irradiation in the first two bands (ca. 450 nm also; $^2B_2(d_{xy}) \rightarrow {}^2B_1(d_{x^2-y^2})$). The starting Mo(V) concentration was kept as high as possible (0.03–0.07 M) in these experiments, in order to maximize the absorbance of the solutions: typical initial absorbances near 450 and

750 nm were 0.5–1, so that 70–90% of the excitation light was absorbed. For example, the Mo(V)/PEt_2Ph mixture was irradiated for 6 days using the 3–67 filter. Although the electronic spectrum of the irradiated solution was almost unchanged, ^{31}P NMR analysis showed the production of a small amount of $OPEt_2Ph$ ($OPEt_2Ph$:PEt_2Ph ratio approximately four times as great as for the dark reaction). Also, irradiation of the Mo(V)/$PEtPh_2$ mixture using the 0–51 filter for 4 days produced slight changes in the electronic spectrum, similar to those observed after 1 day of irradiation in Fig. 5. Thus, these photochemical redox reactions occur, at least to some extent, from the lowest-energy fluorescent excited state. The photochemical reactivity appears to be greater on higher-energy irradiation, but this cannot be established quantitatively because of the difficulty of obtaining quantum yield data (see above).

5. Conclusions

We have examined the chemistry and photochemistry of oxomolybdenum(V) using the series of phosphines PEt_3, PEt_2Ph, $PEtPh_2$ and PPh_3 as potential oxygen atom acceptors. The reaction with PEt_3 occurs spontaneously, producing $[MoOCl_5]^{2-}$, $[MoCl_4(PEt_3)_2]^-$, and a multicomponent maroon oil that contains $OPEt_3$ and the molybdenum(IV) oxo complex $MoOCl_2(PEt_3)_3$. PEt_2Ph and $PEtPh_2$ require irradiation to react with Mo(V), producing the corresponding phosphine oxides and reduced Mo complexes, along with ligand-substitution products. Irradiation of oxomolybdenum(V) with PPh_3 leads only to ligand substitution. The order of reactivity we observe is consistent with the electronic properties of the phosphines: PEt_3 is most electron-rich at P and therefore the easiest to convert to its oxide, and PPh_3 is the most difficult to oxidize.

6. Supplementary material

XANES spectra for $(Ph_4P)_2[MoOCl_5]\cdot 2CH_2Cl_2$ and related compounds, and an ORTEP illustration of the Ph_4P^+ and CH_2Cl_2 portions of the $(Ph_4P)_2[MoOCl_5]\cdot 2CH_2Cl_2$ structure, are available from the authors. Crystallographic data (excluding structure factors) for the structures in this paper have been deposited with the Cambridge Crystallographic Data Centre as supplementary publication nos. CCDC-134165 ($(Ph_4P)_2[MoOCl_5]\cdot 2CH_2Cl_2$) and CCDC-134166 (*cis-mer*-$MoCl_3(OPEt_2Ph)_2(PEt_2Ph)$). Copies of the data can be obtained, free of charge, on application to: The Director, CCDC, 12 Union Road, Cambridge, CB2 1EZ, UK (fax: +44-1223-336-033; e-mail: deposit@ccdc.cam.ac.uk or www: http://www.ccdc.cam.ac.uk).

Acknowledgements

This work was supported in part by the Louisiana Educational Quality Support Fund (Grant LEQSF(1990-92)-RD-A-06 and, for improvements to the X-ray Crystallography Facility, Grant LEQSF(1996-97)-ENH-TR-10) administered by the Louisiana Board of Regents. We thank Drs Roland A. Tittsworth and Volker Saile (LSU Center for Advanced Microstructures and Devices), Dr Tammy Dugas for assistance with the XANES and ESR spectra, and Zuzanna T. Cygan for assistance with photochemical experiments.

References

[1] W.A. Nugent, J.M. Mayer, Metal–Ligand Multiple Bonds, Wiley, New York, 1988.
[2] (a) R.H. Holm, J.M. Berg, Acc. Chem. Res. 19 (1986) 363. (b) R.H. Holm, Chem. Rev. 87 (1987) 1401. (c) R.H. Holm, J.P. Donahue, Polyhedron 12 (1993) 571.
[3] J.A. Craig, R.H. Holm, J. Am. Chem. Soc. 111 (1989) 2111.
[4] D.E. Over, S.C. Critchlow, J.M. Mayer, Inorg. Chem. 31 (1992) 4643.
[5] (a) C.J. Ballhausen, H.B. Gray, Inorg. Chem. 1 (1962) 111. (b) H.B. Gray, C.R. Hare, Inorg. Chem. 1 (1962) 363. (c) C.R. Hare, I. Bernal, H.B. Gray, Inorg. Chem. 1 (1962) 831.
[6] (a) G.A. Neyhart, M. Bakir, J. Boaz, W.J. Vining, B.P. Sullivan, Coord. Chem. Rev. 111 (1991) 27. (b) G.A. Neyhart, K.J. Seward, J. Boaz, B.P. Sullivan, Inorg. Chem. 30 (1991) 4486.
[7] (a) C.-M. Che, Pure Appl. Chem. 67 (1995) 225. (b) C.-M. Che, K.-Y. Wong, H.-W. Lam, K.-F. Chin, Z.-Y. Zhou, T.C.W. Mak, J. Chem. Soc., Dalton Trans. (1993) 857.
[8] J.R. Winkler, H.B. Gray, Inorg. Chem. 24 (1985) 346.
[9] W. Liu, H.H. Thorp, Inorg. Chem. 33 (1994) 1026.
[10] H.H. Thorp, C.V. Kumar, N.J. Turro, H.B. Gray, J. Am. Chem. Soc. 111 (1989) 4364.
[11] H.H. Thorp, J. Van Houten, H.B. Gray, Inorg. Chem. 28 (1989) 889.
[12] J.C. Brewer, H.H. Thorp, K.M. Slagle, G.W. Brudvig, H.B. Gray, J. Am. Chem. Soc. 113 (1991) 3171.
[13] (a) V.W.-W. Yam, C.-M. Che, J. Chem. Soc., Dalton Trans. (1990) 3741. (b) V.W.-W. Yam, C.-M. Che, Coord. Chem. Rev. 97 (1990) 93.
[14] Q. Yao, A.W. Maverick, J. Am. Chem. Soc. 108 (1986) 5346.
[15] (a) A.K. Mohammed, A.W. Maverick, Inorg. Chem. 31 (1992) 4441. (b) A.W. Maverick, Q. Yao, A.K. Mohammed, L.J. Henderson Jr., Advan. Chem. Ser. 238 (1993) 131. (c) Salts of $MoOCl_4^-$ had previously been reported to fluoresce in the solid state: J.R. Winkler, Ph.D. Dissertation, California Institute of Technology, Pasadena, CA, 1983.
[16] M.D. Carducci, C. Brown, E.I. Solomon, J.H. Enemark, J. Am. Chem. Soc. 116 (1994) 11856.
[17] M.C.R. Symons, G. Eaton, J. Chem. Soc., Faraday Trans. 1 78 (1982) 3033.
[18] C.K. Fair, MOLEN: An Interactive Structure Solution Procedure, Enraf–Nonius, Delft, The Netherlands, 1990.
[19] C.K. Johnson, ORTEP-II: A Fortran Thermal-Ellipsoid Plot Program for Crystal-Structure Illustrations, Report ORNL-5138, National Technical Information Service, US Department of Commerce, Springfield, VA, 1976.

[20] F.H. Allen, O. Kennard, R. Taylor, Acc. Chem. Res. 16 (1983) 146.
[21] D. Fenske, K. Stahl, E. Hey, K. Dehnicke, Z. Naturforsch., Teil b 39 (1984) 850.
[22] (a) K. Yoon, G. Parkin, A.L. Rheingold, J. Am. Chem. Soc. 114 (1992) 2210. (b) K. Yoon, G. Parkin, A.L. Rheingold, J. Am. Chem. Soc. 113 (1991) 1437.
[23] P. Klingelhofer, U. Muller, Z. Anorg. Allg. Chem. 556 (1988) 70.
[24] $(PPh_4)_2Ru^{IV}Cl_6{\cdot}2CH_2Cl_2$, $(AsPh_4)_2Os^{IV}Cl_6{\cdot}2CH_2Cl_2$, and β-$(PPh_4)_2U^{IV}Cl_6{\cdot}2CH_2Cl_2$: E. Conradi, R. Boher, R. Weber, U. Muller, Z. Kristallogr. 181 (1987) 187.
[25] H.K. Saha, M.C. Halder, J. Inorg. Nucl. Chem. 33 (1971) 705.
[26] P.M. Boorman, C.D. Garner, F.E. Mabbs, J. Chem. Soc., Dalton Trans. (1975) 1299.
[27] H.K. Saha, M.C. Halder, J. Inorg. Nucl. Chem. 33 (1971) 3719.
[28] The ESR spectrum of powdered $(PPh_4)_2[Mo^{V}OCl_5]{\cdot}2CH_2Cl_2$, recorded at room temperature, is very similar to that previously reported for $MoOCl_4(H_2O)^-$ (see Ref. [26]).
[29] (a) S.P. Cramer, P.K. Eidem, M.T. Paffett, J.R. Winkler, Z. Dori, H.B. Gray, J. Am. Chem. Soc. 105 (1983) 799. (b) T.K. Sham, Acc. Chem. Res. 19 (1986) 99.
[30] R.G. Bhattacharyya, D.C. Bera, J. Indian Chem. Soc. 51 (1974) 988.
[31] D. Garner, L.H. Hill, F.E. Mabbs, D.L. McFadden, A.T. McPhail, J. Chem. Soc., Dalton Trans. (1977) 853.
[32] V.V. Tkachev, O.N. Krasochka, L.O. Atovmyan, J. Struct. Chem. USSR 17 (1976) 807. In this case, the $MoOCl_5^{2-}$ anion was not disordered, and showed Mo–O 1.61(1) Å, equatorial Mo–Cl 2.369(7)–2.397(7) Å, and *trans* axial Mo–Cl 2.587(6) Å.
[33] In addition to the two species already mentioned ($MoOCl_5^{2-}$ and $MoOCl_4(H_2O)^-$), the five-coordinate complex $MoOCl_4^-$ may also be important in the chemistry of Mo(V) in noncoordinating solvents (the equilibrium $MoOCl_5^{2-} \rightleftarrows MoOCl_4^- + Cl^-$ was originally studied by Boorman et al. [26]). Thus, for example, the CH_2Cl_2 solution prepared from $(PPh_4)_2[MoOCl_5]{\cdot}2CH_2Cl_2$ is spectroscopically similar to a solution of $(PPh_4)[MoOCl_4]$ (prepared by heating $(PPh_4)[MoOCl_4(H_2O)]$ under vacuum at ca. 80°C for 30 h) in CH_2Cl_2 (λ_{max} 691, 442 nm). Addition of $(PPh_4)Cl$ (to suppress dissociation of $MoOCl_5^{2-}$) or $SOCl_2$ (to react with traces of H_2O and therefore convert any $MoOCl_4(H_2O)^-$ present back to $MoOCl_4^-$/$MoOCl_5^{2-}$) to these Mo(V)/CH_2Cl_2 solutions caused blue shifts in the absorption band near 700 nm and substantial weakening in the band near 440 nm. For example, a solution of $(PPh_4)_2[MoOCl_5]{\cdot}2CH_2Cl_2$ in CH_2Cl_2, treated with added $SOCl_2$ (ca. 5% v/v) and $(Ph_4P)Cl$ (2 equiv., excess) has a much weaker yellow color; the absorption bands in the visible region are shifted to 686 and 447 nm, the latter band being much less intense than in the initially prepared solution. Thus, although CH_2Cl_2 solutions prepared from $(PPh_4)_2[MoOCl_5]{\cdot}2CH_2Cl_2$ are clearly different in spectroscopic properties from those of other well-recognized oxomolybdenum(V) species, these solutions may contain $MoOCl_4^-$ and small amounts of $MoOCl_4(H_2O)^-$ in addition to $MoOCl_5^{2-}$.
[34] R. Poli, J.C. Gordon, Inorg. Chem. 30 (1991) 4550.
[35] F.A. Cotton, K. Vidyasagar, Polyhedron 14 (1995) 3077.
[36] We prepared *cis-mer*-$MoOCl_2(PEt_2Ph)_3$ (by the method of Butcher and Chatt [37]) as part of our study of the phosphorescence of Mo(IV) oxo complexes (R.A. Isovitsch, A.S. Beadle, F.R. Fronczek, A.W. Maverick, Inorg. Chem. 37 (1998) 4258). The ^{31}P NMR spectrum of $MoOCl_2(PEt_2Ph)_3$ shows a triplet at 17.7 ppm ($^2J(P,P) = 19$ Hz) and a doublet at 11.8 ppm ($^2J(P,P) = 19$ Hz) which integrate in a ratio of 1:2.
[37] A.V. Butcher, J. Chatt, J. Chem. Soc., A (1970) 2652.
[38] E. Carmona, A. Galindo, L. Sanchez, A.J. Nelson, G. Wilkinson, Polyhedron 3 (1984) 347.
[39] F.A. Cotton, R. Poli, Inorg. Chem. 25 (1986) 3624.
[40] (a) A.V. Butcher, J. Chatt, J. Chem. Soc., A (1971) 2356. (b) R.A. Isovitsch, F.R. Fronczek, A.W. Maverick, Polyhedron 17 (1998) 1617.
[41] K.J. Moynihan, P.M. Boorman, J.M. Ball, V.D. Patel, K.A. Kerr, Acta Crystallogr., Sect. B 38 (1982) 2258.
[42] A.K. Mohammed, R.A. Isovitsch, A.W. Maverick, Inorg. Chem. 37 (1998) 2779.
[43] M.S. Reynolds, J.M. Berg, R.H. Holm, Inorg. Chem. 23 (1984) 3057.
[44] $MoCl_4(PMe_2Ph)_2$ is reported to be red, but again without electronic spectral data: J.R. Moss, B.L. Shaw, J. Chem. Soc., A (1970) 595.
[45] D.R. Lide (Ed.), Handbook of Chemistry and Physics, 73rd ed., CRC, Boca Raton, FL, 1992, pp. 10–311 and 10–317.

PERGAMON

www.elsevier.nl/locate/poly

Polyhedron 19 (2000) 1447–1453

POLYHEDRON

Molecular structure and spectroscopic characterization of cobalt and copper complexes with a hexadentate nitrogen ligand, 1,10-bis(2-pyridylmethyl)-1,4,7,10-tetraazadecane

Caroline Jubert, Aminou Mohamadou *, Emmanuel Guillon, Jean-Pierre Barbier

G.R.E.C.I., Université de Reims Champagne-Ardenne, B.P. 1039, F-51687 Reims Cedex 2, France

Received 28 January 2000; accepted 5 April 2000

Abstract

The syntheses of the cobalt(III) and copper(II) complexes with the hexadentate nitrogen ligand 1,10-bis(2-pyridylmethyl)-1,4,7,10-tetraazadecane (bpteta) are reported. NMR spectra and X-ray structure determination have shown that these octahedral complexes have a β-*cis* configuration with pyridine nitrogen atoms mutually *cis* and *trans* to amine nitrogen atoms. A large distortion due to the Jahn–Teller effect is observed in the case of the copper(II) compound. © 2000 Elsevier Science Ltd. All rights reserved.

Keywords: Copper(II); Cobalt(III); NMR spectroscopy; Pyridylmethyl-tetraazadecane

1. Introduction

Tetradentate N_4 or hexadentate N_6 ligands containing pyridylmethyl groups are able to form di- or tetranuclear complexes in which biologically interesting metallic ions are present at different oxidation states and are studied for their relevance as models for enzymes [1,2]. The hexadentate nitrogen ligand 1,10-bis(2-pyridylmethyl)-1,4,7,10-tetraazadecane was described for the first time by Arulsamy et al. [2], who obtained $ML(ClO_4)_2$ complexes ($M = Fe^{2+}$, Mn^{2+}, Ni^{2+}) and tetranuclear iron(III) compounds. The stability constants of the complexation of metallic ions (Cu^{2+}, Ni^{2+}, Co^{2+}, Zn^{2+}) with this ligand have been determined by Kim et al. [3,4]. Surprisingly, none of these authors has described either copper or cobalt coordination with this ligand. In this report, we examine the isomeric identification of diamagnetic octahedral cobalt(III) complexes using two-dimensional NMR spectroscopy, ESR spectra and electrochemical behavior for the copper(II) compound. Structural determinations have been carried out for both these complexes.

2. Experimental

2.1. Materials and methods

All the solvents were purified by conventional procedures [5] and distilled prior to use. All the reagents were commercially available (Aldrich) and used without further purification.

Elemental analyses (C, H and N) were carried out on a Perkin–Elmer 2400 C, H, N element analyzer in our university. The metal percentage was performed on an ICP AES Liberty Series II Varian apparatus. The UV–Vis spectra were recorded on a Perkin–Elmer Lambda 6 spectrophotometer. IR spectra were obtained using KBr sample pellets. Magnetic susceptibilities were determined at room temperature (r.t.) (20°C) using $Hg-Co(SCN)_4$ as a calibrant; diamagnetic susceptibility corrections were calculated from Pascal's constants [6].

All NMR spectra were recorded in D_2O at r.t. with a Bruker AC 250 or a Bruker DRX 500 spectrometer. Chemical shifts for ^1H and ^{13}C NMR spectra were referenced to residual solvent.

* Corresponding author: Tel.: +33-3-2691-3334; fax: +33-3-2691-3243.

E-mail address: aminou.mohamadou@univ-reims.fr (A. Mohamadou).

0277-5387/00/$ - see front matter © 2000 Elsevier Science Ltd. All rights reserved.
PII: S0277-5387(00)00398-3

The crystal data were collected at 173 K on a Kappa CCD diffractometer using graphite monochromated Mo Kα radiation ($\lambda = 0.71073$ Å). For both compounds, X-ray experimental data are given in Table 1.

Three standard reflections measured every hour during the entire data collection period showed no significant trend. The raw data were collected for Lorentz polarization and absorption factor (psi scans of seven reflections). The structure was solved by the heavy atom method. After refinement of the non-hydrogen atoms, difference-Fourier maps revealed maxima of residual electron density close to positions expected for hydrogen atoms. Hydrogen atoms were refined at calculated positions with a riding model in which the C–H vector was fixed at 0.95 Å with isotropic temperature factors. A final Fourier difference map revealed no significant maxima. All calculations were performed on a DEC Alpha 3000 computer using the Nonius OPENMOLEN package [7]. Neutral atom scattering factor coefficients and anomalous dispersion coefficients were taken from a standard source [8].

Table 1
X-ray experimental data

Formula	$C_{18}H_{30}Cl_3CoN_6O_9$	$C_{18}H_{28}Cl_2CuN_6O_8$
Molecular weight	639.77	590.91
Crystal system	monoclinic	monoclinic
Space group	$P2_{1/n}$	$P2_{1/c}$
a (Å)	8.0899(3)	12.5805(5)
b (Å)	15.1063(7)	12.2540(5)
c (Å)	20.8894(7)	16.3000(5)
b (°)	92.970(3)	105.928(2)
V (Å^3)	2549.4(3)	2416.4(3)
Z	4	4
Color	orange	blue
Crystal dimensions (mm)	$0.20 \times 0.20 \times 0.14$	$0.20 \times 0.14 \times 0.14$
D_{calc} (g cm^{-3})	1.67	1.62
$F000$	1320	1220
μ (mm^{-1})	1.048	1.181
Temperature (K)	173	173
Wavelength (Å)	0.71073	0.71073
Radiation	Mo Kα graphite monochromated	Mo Kα graphite monochromated
Diffractometer	Kappa CCD	Kappa CCD
Scan mode	phi scans	phi scans
hkl limits	0.10/0.19/−26.26	0.16/0.15/−21.20
Theta limits (°)	2.5/27.50	2.5/27.52
Number of data measured	17 889	16 998
Number of data with $I > 3\sigma(I)$	4277	4015
Weighting scheme	$4F_o^2/(\sigma^2(F_o)^2 + 0.0064F_o^4)$	$4F_o^2/(\sigma^2(F_o)^2 + 0.0064F_o^4)$
Number of variables	361	316
R	0.044	0.033
R_w	0.074	0.051
GOF	1.434	1.004
Largest peak in final difference (e Å^{-3})	1.287	0.356

The cyclic voltammetry experiments were carried out with a conventional three electrode cell using an EG&G PAR model 362 scanning potentiostat and a Kipp & Zonen BD91 X-Y recorder. A platinum disk (2 mm diameter) working electrode and a platinum wire auxiliary electrode were used. The reference was a saturated calomel electrode. Acetonitrile was purified using standard methods, while tetraethylammonium perchlorate was recrystallized from water before use. The copper(II) complex (10^{-3} mol l^{-1}) was dissolved in deoxygenated acetonitrile containing tetraethylammonium perchlorate (0.1 mol l^{-1}). All solutions were kept under nitrogen during electrochemical measurements.

The ESR spectra in acetonitrile were obtained in the X-band at 77 K and at r.t. with a Varian E109 spectrophotometer. The g values were measured relative to the strong pitch.

2.2. Syntheses

The ligand 1,10-bis(pyridylmethyl)-1,4,7,10-tetraazadecane tetrahydrochloride monohydrate was prepared according to the method described by Arulsamy et al. [2], which involved the condensation of pyridine-2-carboxaldehyde with triethylenetetramine and then the reduction of the obtained imine by sodium borohydride. The compound was identified by elemental analyses and ^{1}H NMR spectra.

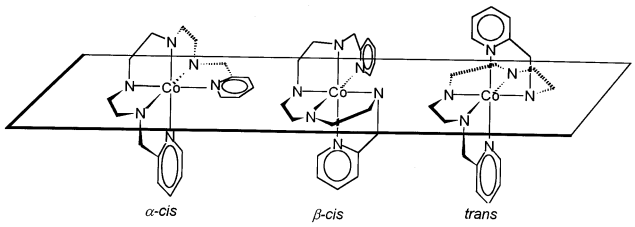
Caution! Perchlorate salts of metal complexes with organic ligands are potentially explosive and should be handled with care.

2.3. Cu(bpteta)(ClO$_4$)$_2$

The complex was synthesized in a similar manner as the manganese or nickel complexes described by Arulsamy et al. [2]. Yield: 71%; m.p. = 188°C. $C_{18}H_{28}Cl_2CuN_6O_8$ (590.91 g mol^{-1}): Calc. C, 36.59; H, 4.78; N, 14.22; Cu, 10.7. Found: C, 36.54; H, 4.30; N, 13.86; Cu, 10.4%. IR: $\nu(ClO_4^-) = 1086$ cm^{-1}. Magnetism: $\chi_M = 1630 \times 10^{-6}$ uem cgs, $\mu = 1.97$ BM. Electronic spectrum: $\lambda = 615$ nm, $\varepsilon = 107$ l mol^{-1} cm^{-1}.

2.4. Co(bpteta)(ClO$_4$)$_2$Cl·H$_2$O

Sodium acetate (4 mmol) was added to bpteta·4HCl·H$_2$O (1 mmol) in absolute ethanol. The mixture was stirred, brought to the boil (10 min), and filtered. 1 mmol of Co(ClO$_4$)$_2$·6H$_2$O was then added to the filtrate, the solution was stirred under air bubbling over 10 h in order to completely oxidize the Co(II) into Co(III). Yield 32%; m.p. = 212°C. $C_{18}H_{30}Cl_3CoN_6O_9$ (639.77 g mol^{-1}): Calc. C, 33.76; H, 4.69; N, 13.13; Co, 9.2. Found: C, 33.93; H, 4.41; N, 12.93; Co, 8.9%. IR: $\nu(ClO_4^-) = 1086$ cm^{-1}. Electronic spectrum: $\lambda = 464$



Scheme 1.

nm, $\varepsilon = 142$ l mol^{-1} cm^{-1}. The diamagnetism of the cobalt complex is indicative of a complete oxidation of cobalt(II) into cobalt(III).

3. Results and discussion

3.1. NMR spectra

The ^{1}H NMR spectrum of the ligand reveals four well-resolved signals for the pyridine moiety with typical values of coupling constants (see Table 2) [9], one multiplet for the equivalent methylen groups and a singlet for the two pyridyl moieties.

The 1D and 2D NMR spectra which have allowed the determination of the geometry of cobalt(III) complexes with tetradentate or pentadentate ligands containing nitrogen and/or sulfur donor atoms [10] have been used to determinate the configuration of the cobalt complex. Octahedral metal complexes containing a hexadentate N_6 ligand can exist in α-*cis*, β-*cis* or *trans* configurations which have one, two or three ethylen groups, respectively, in the same plane (Scheme 1).

Therefore the ^{1}H NMR spectrum of the cobalt compound must reveal several resonances for each proton. By combined use of COSY and decoupling methods, it is possible to assign all ^{1}H resonances for the both pyridine moieties. The decoupling experiments and the coupling constants are the key elements for the determination of the proton resonances. Any ambiguities are resolved via the COSY experiment (Fig. 1).

The complete ^{1}H assignment is extended to the ^{13}C resonances by reference to the ^{1}H-^{13}C HMBC and ^{1}H-^{13}C HMQC data. The ^{1}H NMR spectrum of the cobalt compound shows a slight deshielding for H^{1}, H^{2}, H^{3}, H^{4}, H^{13} and H^{14} pyridine protons compared with those of the ligand according to electronic density

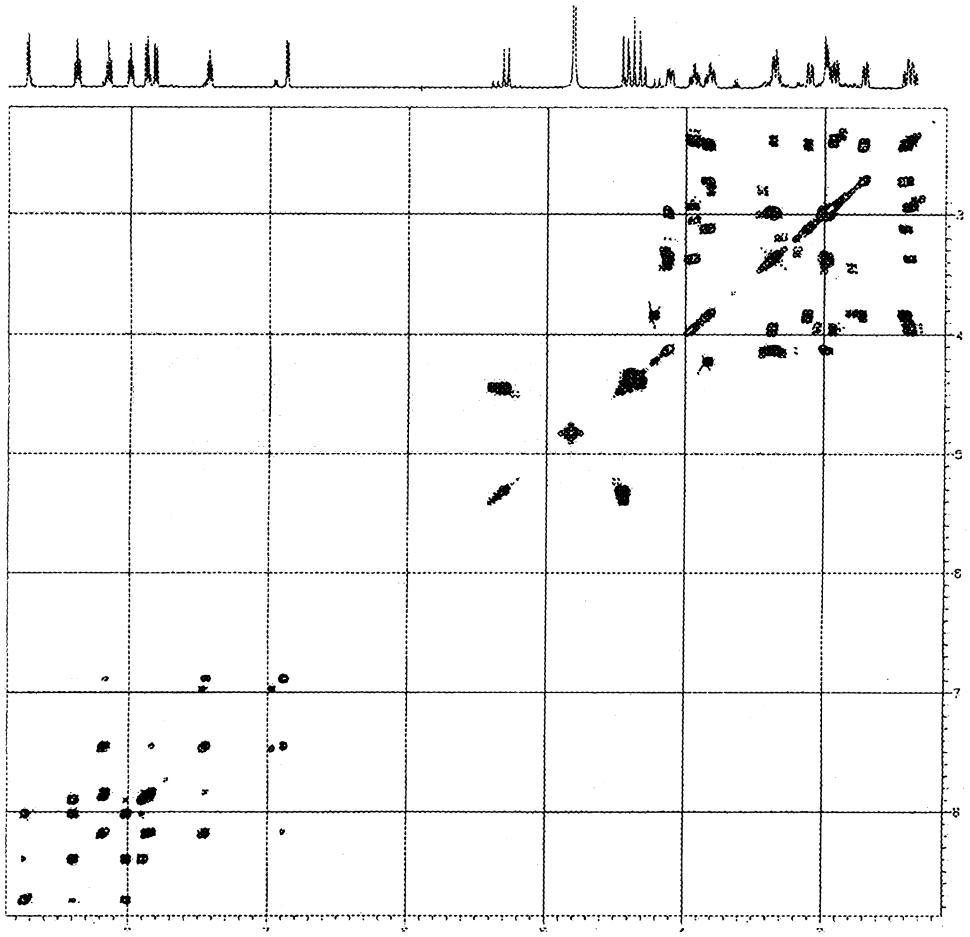
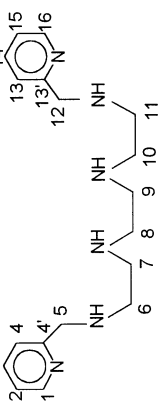


Fig. 1. COSY of $[Co(bpteta)](ClO_4)_2Cl$ in D_2O.

Table 2
^{1}H, ^{13}C NMR data [δ in ppm, J in Hz]



		H^1	H^2	H^3	H^4	$H^{4'}$	H^5	H^6	H^7	H^8	H^9	H^{10}	H^{11}	H^{12}	$H^{13'}$	H^{13}	H^{14}	H^{15}	H^{16}
Ligand	^{1}H	8.70 d, $J_{1,2}=5.0$	7.70 [a], br	8.15 [a], $J_{2,3}=7.8$, $J_{1,3}=1.6$	7.75 d, $J_{3,4}=7.9$		4.50 s	3.60 m	3.60 m	3.60 m	3.60 m	3.60 m	3.60 m	4.50 s		7.75 d, $J_{3,4}=7.9$	8.15 [a], $J_{2,3}=7.8$, $J_{1,3}=1.6$	7.70 [a], br	8.70 d, $J_{1,2}=5.0$
	^{13}C	149.0	128.2	145.2	128.5	151.7	52.7	47.0	46.0	46.1	46.1	46.0	47.0	52.7	151.7	128.5	145.2	128.2	149.0
CoL	^{1}H	8.74 d, $J_{1,2}=5.9$	8.01 t, $J_{2,3}=6.7$	8.39 [a], $J_{3,4}=7.8$, $J_{1,3}=0.9$	7.89 d, $J_{3,4}=7.9$		AB spin system, H_A: 5.34 d, H_B: 4.45 d, $J_{AB}=18.3$	3.80 [a], $^3J=14.3$, $^2J=4.7$, 3.11 m	2.72, dd, $^3J=14.3$, $^2J=4.7$, 2.38 m	4.12, dd br, $^3J=14.3$, $^2J=4.7$, 3.36 m	2.93 dd, $^3J=13.3$, $^2J=4.7$, 2.98 m	2.38 m, 2.98 m	3.95 [a], $^3J=14.3$, $^2J=4.8$, 3.36 m	AB spin system H_A: 4.40 d, H_B: 4.30 d, $J_{AB}=18.3$		7.83 d, $J_{3,4}=7.9$	8.17 [a], $J_{3,4}=7.8$, $J_{1,3}=1.0$	7.44 t, $J_{2,3}=6.8$	6.88 d, $J_{1,2}=5.9$
	^{13}C	151.6	128.1	142.9	124.8	163.8	60.4	59.6	49.5	49.8	53.2	52.7	54.2	61.9	163.3	123.8	142.2	127.0	150.1

[a] Split triplet.

decreasing due to the Co(III) metallic cation. On the other hand, shielding for the H^{15} signal (-0.26 ppm) which resonates at 7.44 ppm as a triplet and a very large shielding for H^{16} (-1.82 ppm) which resonates at 6.88 ppm as a doublet with the typical $J_{1,2}$ (5.9 Hz) coupling in the pyridine moiety are also observed. The presence of these two pyridine protons in the interatomic ring currents anisotropic contributions of the other pyridine induces this shielding. This effect for H^{15} and H^{16} involves a β-*cis* configuration which is the only one inducing this shielding for these two protons of the complex.

From this configuration we can assign all resonances from the ^{1}H-^{13}C HMQC and ^{1}H-^{13}C HMBC spectra. The singlet at 4.50 ppm in the ligand was replaced in the cobalt compound by two AB patterns at 4.45 and 5.34 ppm with a J(AB) of 18.3 Hz for H^5 and at 4.30 and 4.40 ppm with the same J(AB) of 18.3 Hz for H^{12}. These proton resonances are confirmed by the HMBC spectrum, which shows a correlation between H^5, H^{12} and $H^{4'}$, $H^{13'}$, respectively, and a very weak correlation between H^4 and H^{13}.

There is also a correlation between this ^{1}H resonance (H^5 and H^{12}) and two carbons at 59.6 and 54.2 ppm. This carbon must be part of the ethylenediamine chain, since the HMQC experiment correlates a proton resonance to these ^{13}C resonances at 3.11/3.80 ppm and 3.36/3.95 ppm which are assigned to H^6 and H^{11}. The non-equivalence of the two protons of each methylen group is due to the shielding effect of the neighboring five-membered ring (Co, N, $C^{4'}$, C^5, N for H^6 protons and Co, N, C^{12}, $C^{13'}$, N for H^{11} protons) anisotropic bond contributions. Finally, H^7, H^8, H^9 and H^{10} protons are assigned by a similar way using simultaneously 1D and 2D experiments. From which, weak but distinguishable, correlations are observed for the high field ^{1}H resonance in the HMBC spectrum which confirm the assignment of the three ethylenediamine protons.

From this study, we can deduce the β-*cis* configuration of the cobalt compound. Only the presence of protons in the interatomic ring current anisotropic contribution allows one to elucidate the configuration of the complex with this type of hexadentate ligand. Moreover, no splitting was observed for any proton or carbon signal indicating only one isomer.

This β-*cis* configuration was confirmed by X-ray analyses.

3.2. X-ray crystallography

Each structure consists of $[Mbpteta]^{n+}$ cations M = Co^{3+} or Cu^{2+} which are well separated from anions. Principal bond distances and angles are listed for the two complexes in Tables 3 and 4. A view of the cobalt and the copper cations is given in Figs. 2 and 3.

Table 3
Selected bond lengths (Å) and bond angles (°) for the cobalt complex

Co–N(1)	1.958(3)	Co–N(4)	1.950(3)
Co–N(2)	1.974(3)	Co–N(5)	1.985(2)
Co–N(3)	1.983(3)	Co–N(6)	1.968(3)
N(1)–Co–N(2)	84.0(1)	N(3)–Co–N(4)	84.9(1)
N(1)–Co–N(3)	94.3(1)	N(3)–Co–N(5)	172.1(1)
N(1)–Co–N(4)	176.3(1)	N(3)–Co–N(6)	96.3(1)
N(1)–Co–N(5)	93.6(1)	N(4)–Co–N(5)	87.1(1)
N(1)–Co–N(6)	92.3(1)	N(4)–Co–N(6)	91.4(1)
N(2)–Co–N(3)	86.4(1)	N(5)–Co–N(6)	83.6(1)
N(2)–Co–N(4)	92.3(1)		
N(2)–Co–N(5)	94.2(1)		
N(2)–Co–N(6)	175.6(1)		

Table 4
Selected bond lengths (Å) and bond angles (°) for the copper complex

Cu–N(1)	>2.506(2)	Cu–N(4)	2.057(2)
Cu–N(2)	2.057(2)	Cu–N(5)	>2.329(2)
Cu–N(3)	2.030(2)	Cu–N(6)	2.046(2)
N(1)–Cu–N(2)	76.06(8)	N(3)–Cu–N(4)	83.91(8)
N(1)–Cu–N(3)	89.92(8)	N(3)–Cu–N(6)	176.89(8)
N(1)–Cu–N(4)	99.37(8)	N(4)–Cu–N(6)	95.50(8)
N(1)–Cu–N(5)	171.26(8)	N(5)–Cu–N(2)	103.43(8)
N(1)–Cu–N(6)	93.18(8)	N(5)–Cu–N(3)	98.75(8)
N(2)–Cu–N(3)	84.87(8)	N(5)–Cu–N(4)	82.80(8)
N(2)–Cu–N(4)	197.90(8)	N(5)–Cu–N(6)	78.26(8)
N(2)–Cu–N(6)	95.95(8)		

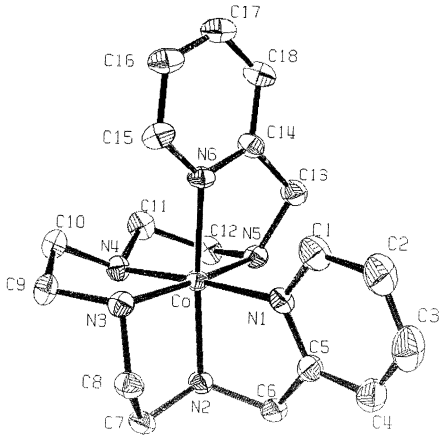


Fig. 2. View of the $[Co(bpteta)]^{3+}$.

The $[Cobpteta]^{3+}$ cation has a slightly distorted octahedral coordination geometry whereas the copper cation exhibits a strong distortion of the octahedral geometry with a large elongation along the *z* axis. The ligand encircles the metal atom through the six ligating nitrogen atoms. Though several isomers can be obtained with this hexadentate ligand, only those obtained with the first transition metal series (Fe(II) [2], Co(III), Ni(II) [2] or Cu(II)) have the pyridine nitrogen atom in the *cis* position.

The $[Cobpteta]^{3+}$ cation is very similar to those of iron(II) and nickel(II) described by Arulsamy et al. [2]; however the octahedral polyhedron around the cobalt is less distorted than those around the iron and nickel: the N–Co–N angles being nearer 90° for the *cis* nitrogen donor atom and 180° for the *trans* nitrogen donor atom. The cobalt–nitrogen bond lengths are practically the same for the ligating of pyridine and amine nitrogen atoms and are consistent with those found in the CoN_6 chromophore [11–13]. However all the metal–nitrogen bond lengths in the cobalt complex are shorter than those in the nickel or iron complexes, in agreement with the radius of Co(III). One perchlorate ion in the cobalt(III) compound is ordered and the Cl–O bond lengths and the O–Cl–O angles are consistent with those reported in the literature [2], but the latter is disordered.

The $[Cubpteta]^{2+}$ cation can be described as pseudo-octahedral with a $N_{pyridine}$–Cu–$N_{pyridine}$ angle of 93.2°. Four bond lengths are nearly equal in the distorted square with three Cu–N_{amine} and one Cu–$N_{pyridine}$ whereas a strong Jahn–Teller distortion is observed along the *z* axes with an increasing bond length of 0.45 Å for the Cu–$N_{pyridine}$ and of 0.30 Å for the Cu–N_{amine}.

3.3. Electrochemical measurements

The cyclic voltammogram of the free ligand presents a reduction peak at a strong negative potential ($E_{1/2} = -0.50$ V versus SCE). The copper complex voltammogram shows an oxidation peak at 0.50 V indicative of the presence of copper(III) in solution. As the separation of the anodic and the cathodic peaks potential ($\Delta E_p = E_{p_a} - E_{p_c}$) is around 0.13 V, the Cu(III)/Cu(II) redox system appears quasi-reversible ($E_{1/2} = 0.43$ V). Unfortunately, several attempts to prepare the solid Cu(III) complex have failed.

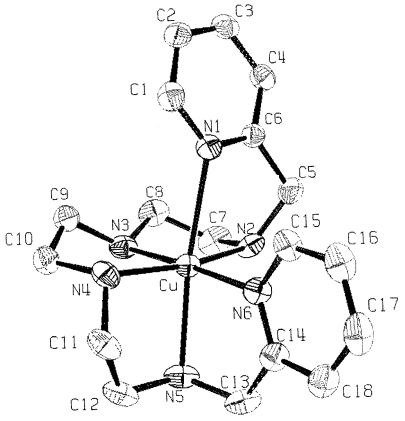
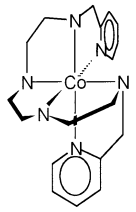


Fig. 3. View of the $[Cu(bpteta)]^{2+}$.

3.4. ESR spectra

The ESR spectrum of the copper complex dissolved in acetonitrile was recorded at r.t. (Fig. 4(a)): an isotropic ESR signal is obtained at $g_{iso} = 2.140$ with $A_{iso} = 71.10^{-4}$ cm^{-1}. The values of $g_{\parallel}$ (2.257), $A_{\parallel}$ (184.10^{-4} cm^{-1}), $g_{\perp}$ (2.081) and $A_{\perp}$ (14.10^{-4} cm^{-1}) are obtained from the spectrum recorded at 77 K (Fig. 4(b)). The values are typical of a strong tetragonally elongated octahedral copper (II) compound.

In conclusion, chromatography experiments and NMR spectroscopy indicate that only one isomer is obtained with the 1,10-bis(2-pyridylmethyl)-1,4,7,10-tetraazadecane.



β-cis

X-ray crystallography has shown that the geometry of these β-*cis* octahedral complexes is more and more

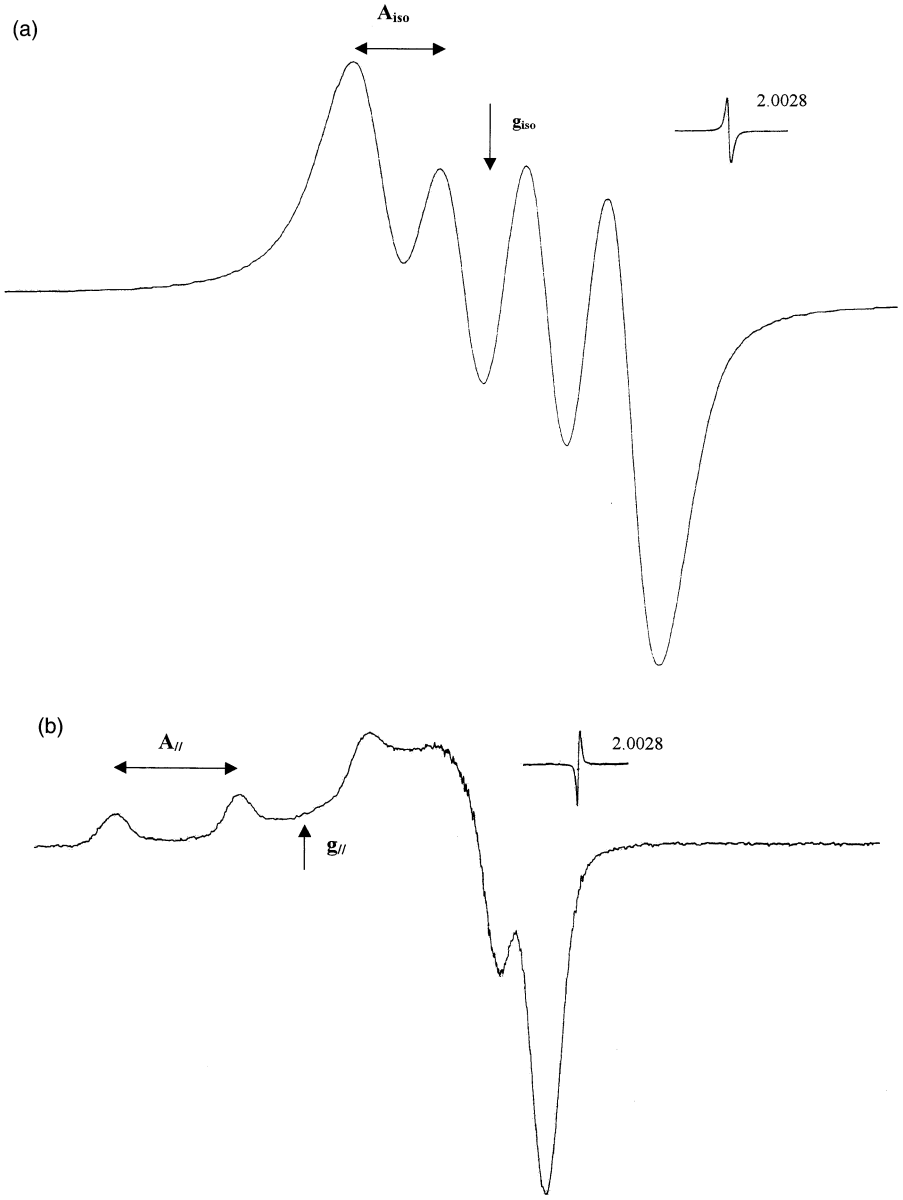


Fig. 4. ESR spectra of [Cu(bpteta)](ClO$_4$)$_2$.

distorted in the following order of the metal ion: Co(III), Fe(II), Ni(II), Cu(II).

4. Supplementary material

Crystallographic data (excluding structure factors) for the structures reported in this paper have been deposited at the Cambridge Crystallographic Data Centre as supplementary publication no. CCDC 135906 for the copper complex and no. CCDC 135907 for the cobalt compound. Copies of the data can be obtained free of charge on application to CCDC, 12 Union Road, Cambridge CB2 1EZ, UK (Fax: +44-1223-336-033; e-mail, deposit@ccdc.cam.ac.uk).

Acknowledgements

We thank Professor J.G. Fischer and Dr A. De Cian (Université Louis Pasteur, Strasbourg, France), for the single-crystal X-ray analyses.

References

[1] N. Arulsamy, J. Glerup, A. Hazell, D.J. Hodgson, C.J. McKenzie, H. Toftlund, Inorg. Chem. 33 (1994) 3023.
[2] N. Arulsamy, J. Glerup, D.J Hodgson, Inorg. Chem. 33 (1994) 3043.
[3] S.D. Kim, J.K. Kim, W.S. Jung, Bull. Korean Chem. Soc. 17 (1996) 80.
[4] S.D. Kim, J.K. Kim, W.S. Jung, Polyhedron 17 (1998) 1223.
[5] D. Perrin, W.L.F. Armarego, R.D. Perrin, Purification of Laboratory Chemicals, third ed., Pergamon, Oxford, 1988.
[6] A. Earnshaw, Introduction to Magnetochemistry, Academic Press, London, 1968, p. 5.
[7] OPENMOLEN, Interactive Structure Solutions, Nonius B.V., Delft, The Netherlands, 1997
[8] D.T. Cromer, J.T. Waber, International Tables for X-Ray Crystallography, vol. IV, Kynoch Press, Birmingham, 1974.
[9] S. Castellano, C. Sun, R. Kostelnik, J. Chem. Phys. 46 (1967) 327.
[10] R.M. McClure, K.W. Jung, J.H. Worrell, Coord. Chem. Rev. 174 (1998) 33.
[11] Y. Yoshikawa, K. Toriumi, T. Ito, H. Yamatera, Bull. Chem. Soc. Jpn. 55 (1982) 1422.
[12] P. Comba, Inorg. Chem. 28 (1989) 426.
[13] G.H. Searle, Bull. Chem. Soc. Jpn 62 (1989) 4021.

PERGAMON

www.elsevier.nl/locate/poly

Polyhedron 19 (2000) 1455–1459

POLYHEDRON

Synthesis of novel water-soluble heterocyclic phosphino amino acids with bulky aromatic substituents on phosphorus

Andrey A. Karasik [b,*1], Igor O. Georgiev [b], Oleg G. Sinyashin [b], Evamarie Hey-Hawkins [a,*2]

[a] *Institut für Anorganische Chemie der Universität Leipzig, Johannisallee 29, D-04103 Leipzig, Germany*
[b] *A.E. Arbuzov Institute of Organic and Physical Chemistry, Russian Academy of Sciences, Kazan Scientific Center, Arbuzov str. 8, 420088 Kazan, Russia*

Received 24 February 2000; accepted 7 April 2000

Abstract

One-step syntheses of a number of water-soluble sodium and potassium phosphino amino acid salts from primary arylphosphines (2,4,6-$R_3C_6H_2$)PH_2 (R = H, Me, Pr^i), formaldehyde and sodium or potassium glycinate, with unsubstituted and 2,4,6-trisubstituted aryl substituents on the phosphorus atom are reported. The structures of the disodium and dipotassium 1,3-di(carboxylatomethyl)-5-aryl-1,3,5-diazaphosphorinanes were established on the basis of IR and ^1H, ^{13}C and ^{31}P NMR data.
© 2000 Elsevier Science Ltd. All rights reserved.

Keywords: Water-soluble phosphines; Phosphino amino acid salts; Disodium or dipotassium 1,3-di(carboxylatomethyl)-5-aryl-1,3,5-diazaphosphorinanes

1. Introduction

The advantage of homogeneous over heterogeneous catalysis with respect to activity (relative to metal content), selectivity (particularly enantioselectivity), mildness of reaction conditions, freedom from diffusion problems, sensitivity towards catalyst poisons, variability of steric and electronic properties of the catalysts and mechanistic understanding of processes are well established [1]. However, the problem of separating the expensive catalysts from the products is often a major obstacle to industrial applications [1]. The main way of overcoming this problem is to 'heterogenize' a homogeneous catalyst by utilizing a liquid–liquid (usually water–organic solvent) biphasic system, in which solutions of the catalyst and of the substrate are separated by a phase barrier [2]. This approach generated intense interest in water-soluble ligands, especially phosphines [2–5].

Recently we described the synthesis of novel water-soluble [6,7] and chiral water-soluble [8] phosphines by the reaction of bis(hydroxymethyl)phenylphosphine, formaldehyde and *o*-aminobenzoic acid or the potassium salt of optically active phenylglycine, respectively. A number of their water-soluble complexes with transition metals were also reported [6,7]. It is of interest to vary the steric demand of the ligands, because the stereoselectivity of catalytic reactions is very sensitive to the nature of the ligands attached to the transition metal.

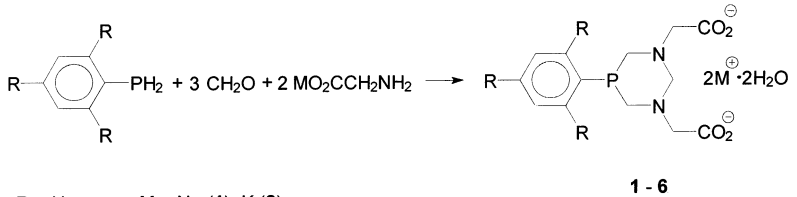
We now report the synthesis of water-soluble phosphino amino acids based on phenylphosphine ($PhPH_2$) and the bulky primary arylphosphines mesitylphosphine ($MesPH_2$) and 2,4,6-triisopropylphenylphosphine ($TippPH_2$) and alkali metal salts of glycine.

2. Results and discussion

To prepare the desired disodium or dipotassium 1,3-di(carboxylatomethyl) - 5 - aryl - 1,3,5 - diazaphosphorinanes we developed a new one-step synthesis directly from the primary phosphine, formaldehyde and amino acid salts (Eq. 1).

[1] *Corresponding author.
[2] *Corresponding author. Tel. +49-341-973-6151; fax: +49-341-973-9319; e-mail: hey@rz.uni-leipzig.de

0277-5387/00/$ - see front matter © 2000 Elsevier Science Ltd. All rights reserved.
PII: S0277-5387(00)00400-9

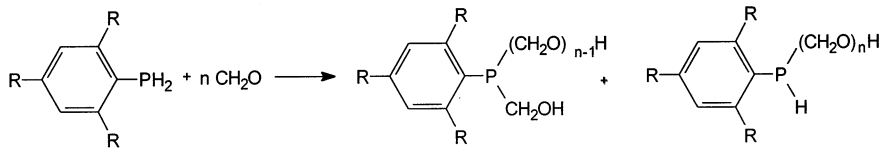


1 - 6

R = H, M = Na (**1**), K (**2**)
R = Me, M = Na (**3**), K (**4**)
R = Pr^i, M = Na (**5**), K (**6**)

(1)

This route allowed us to avoid handling air-sensitive hydroxymethylphosphines. This is especially important for bulky $MesPH_2$ and $TippPH_2$, because they react with two and even three molecules of formaldehyde to give mainly monosubstituted secondary phosphines (Eq. 2).



n = 2, 3	R = H	>95%	
n = 2	R = Me	28%	72%
n = 3	R = Pr^i	16%	84%

(2)

After heating the reaction mixtures of primary phosphine and formaldehyde to 120–130°C, the ^{31}P NMR signal of the primary phosphine disappeared, and the signal of the secondary phosphine appeared (R = Me: −79.6 ppm, $^1J(PH) = 221.9$ Hz; R = Pr^i: −89.1 ppm, $^1J(PH) = 214.5$ Hz) together with a minor signal (16–28%) for the tertiary bis(hydroxymethyl)arylphosphine (R = Me: −22.2 ppm; R = Pr^i: −27.5 ppm). The formation of hemiacetals from $P(CH_2OH)_3$ and formaldehyde has already been demonstrated [9]. In a second step, the secondary phosphines were reacted with sodium or potassium glycinate to yield the cyclic phosphines **1**–**6**, but the overall yields were noticeably lower than that of the one-step reaction.

Compounds **1**–**6** are white, air-stable microcrystalline powders. The IR spectra of **1**–**6** exhibit strong bands for the carboxylate group (1600 cm^{-1}), water of crystallization (3200–3400 cm^{-1}), and also absorption bands for the backbone vibrations of heterocylic bonds [10]. In the ^{31}P NMR spectrum, only one signal was found in the characteristic region of 1,3,5-diazaphosphorinanes [11] (Table 1). The chemical shifts of **1**–**6** are correlated with the donor ability of the aromatic substituents on the phosphorus atom, decreasing in the series R = H > Me > Pr^i. Elemental analysis data were also in agreement with the formation of the hydrated salts **1**–**6**.

The ^{13}C and ^1H NMR spectra are consistent with the heterocylic phosphine structure [8,11,12]. In the ^{13}C NMR spectrum, signals for the methylene groups of the P–CH_2–N, N–CH_2–N and N–CH_2–CO_2 fragments were observed (Table 2). The signal for the methylene carbon atom of the P–CH_2–N and N–CH_2–CO_2 fragments afforded the coupling constants $^1J(CP)$ and $^3J(CP)$.

It was shown previously that ^1H NMR data provide additional information on the conformational behavior of heterocyclic phosphines [11,12]. The ^1H NMR spectra of **1**–**6** are more complex than their ^{13}C and ^{31}P NMR spectra and that of the previously described 1,3,5-diazaphosphorinanes [11], due to overlap of the signals of the $(AB)_2(CD)X$ spin system of cyclic and exocyclic methylene groups. 2D COSY NMR spectra were used for the assignment of multiplets and to establish the order of spin–spin coupling.

In the ^1H NMR spectra, readily identified signals of the aryl substituents on the phosphorus atom and of the N–CH_2–N fragment are observed. The chemical shifts of the N–CH_2–N hydrogen atoms depend on the solvent. The chemical shift of the low-field doublet did not change, but that of the high-field signal moved to higher field ($\Delta\delta = -0.56$ ppm) on changing the solvent from water to methanol (see Section 3.3). This high-field signal was interpreted as a doublet of doublets with a four-bond coupling to phosphorus and could be

Table 1
^{31}P NMR data of phosphines **1**–**6**

Compound	δ (Methanol)	δ (Water)
1	−55.5	−62.1
2	−55.4	−61.0
3	−57.7	−66.0
4	−54.4	−66.1
5	−69.7	−77.1
6	−68.7	−77.1

Table 2
Selected ^{13}C NMR data of phosphines **1**–**6**

Compound	N–CH_2–CO_2^-			P–CH_2–N			N–CH_2–N		–CO_2^-
	δ	^1J(CH)	^3J(CP)	δ	^1J(CH)	^1J(CP)	δ	^1J(CH)	δ
1 [a]	51.05	141.1	10.1	60.54	136.8	6.4	75.98	143.3	178.75
2 [a]	50.95	137.7	10.7	60.55	133.2	6.2	76.03	147.3	178.55
3 [a]	51.45	139.3	9.0	59.69	133.1	10.6	75.58	146.7	178.87
4 [a]	51.45	142.6	9.1	59.67	132.1	11.8	75.62	143.1	178.90
5 [b]	52.87	139.6	8.1	62.41	134.4	9.4	77.61	159.0	178.02
6 [b]	52.85	139.9	8.2	62.87	141.3	9.2	77.92	159.0	177.94

[a] –D_2O.
[b] –CD_3OD.

assigned to the equatorial proton in a chair conformation according to the W rule [11].

The methylene protons of the N–CH_2–CO_2 fragments gave rise to two doublets (**1**–**5**) or the singlet (**6**) of an AB spin system. Raising the temperature from 25 to 98°C did not lead to the coalescence of these signals; this indicates that the AB spin system is due not to the non-fluxional behavior of corresponding six-membered ring substituents but to magnetically inequivalent N–CH_2–CO_2 protons.

The most interesting signals of P–CH_2–N protons with stereospecific geminal PH coupling constant represent $(AB)_2X$ spin systems (Table 3). Both H^A and H^B protons were registered as doublets of doublets, but their coupling constants ^2J(PH) were noticeably different. $^2J(PH^A)$ and $^2J(H^AH^B)$ were approximately equal ($\sim$13 Hz), but the $^2J(PH^B)$ values were smaller than 6.1 Hz, ranging from 4.0–4.5 (**1**, **2**) to 5.7–6.1 Hz (**3**–**6**). 1,3-Diaryl-5-phenyl-1,3,5-diazaphosphorinanes in organic solvents have similar ^1H NMR spectra [11]. Thus, the ^1H NMR data in water, methanol, and other organic solvents are similar. It was shown previously [11,12] by ^1H NMR spectroscopy, measurement of the dipole moment and X-ray analysis that 1,3-diaryl-5-phenyl-1,3,5-diazaphosphorinanes exist mainly in chair conformation with an equatorial phenyl group on the phosphorus atom. The stereospecific coupling constant $^2J(PH^B)$ increased with decreasing X–P–C–H (X = lone pair) torsion angle [11,12]. Hence, the increase in this coupling constant for **1**–**6** in comparison with 1,3-diaryl-5-phenyl-1,3,5-diazaphosphorinanes and from **1**, **2** to **3**–**6** can be explained by an increasing content of the conformer with an axial substituent on the phosphorus atom. NMR measurements at different magnetic fields (400 and 250 MHz), $^1H\{^{31}P\}$ NMR data and 2D COSY experiments confirmed the assignment of the coupling constants.

Changing from an organic solvent to water led to a decrease in the ^{31}P NMR chemical shifts by approximately 10 ppm (for methanol/water) and minor changes in the ^1H NMR spectra. Hence, the structure and fluxional behavior of these heterocyclic compounds do not dramatically change in water in comparison with common organic solvents.

The phosphines **5** and **6** form suspensions in water, and their water solubility does not exceed 0.01 M, in accordance with the hydrophobic properties of the bulky substituent on the phosphorus atom. The salts of 1,3-di(carboxylatomethyl)-5-phenyl(or mesityl)-1,3,5-diazaphosphorinanes **1**–**4** show high water solubility; 1 M solutions in water can be obtained, in the range practical for catalytic application.

3. Experimental

All experiments were carried out under purified dry argon. NMR spectra: Avance DRX 400 (Bruker), WM-250 (Bruker), standards: ^1H NMR (400 MHz, 250 MHz): C_6H_6, ^{13}C NMR (100.6 MHz): internal solvent, ^{31}P NMR (162 MHz): external 85% H_3PO_4. The IR spectra were recorded as KBr mulls on a Perkin–Elmer FT-IR spectrometer System 2000 in the range 350–4000 cm^{-1}. The melting points were determined in sealed capillaries and are uncorrected.

Table 3
Selected ^1H NMR data of phosphines **1**–**6**

Compound	P–CH_2–N δ (^2J(HH), ^2J(PH) Hz)	
	H^A	H^B
1 [a]	3.30 (13.4, 13.4)	3.17 (13.4, 4.5)
2 [a]	3.27 (13.2, 13.2)	3.19 (13.2, 4.0)
3 [a]	3.51 (12.7, 12.7)	3.58 (12.7, 5.7)
3 [b]	3.19–3.21 (m)	
4 [a]	3.35 (12.7, 12.7)	3.44 (12.7, 6.1)
5 [b]	3.11 (11.8, 11.8)	3.39 (11.8, 6.0)
6 [b]	3.14 (11.6, 11.6)	3.21 (11.6, 5.9)

[a] –D_2O.
[b] –CD_3OD.

3.1. Preparation of disodium 1,3-di(carboxylatomethyl)-5-phenyl-1,3,5-diazaphosphorinane dihydrate (**1**)

A solution of 0.98 g of sodium hydroxide (25 mmol) in 10 ml of dry methanol was added dropwise to a stirred mixture of 1.34 g (12 mmol) of phenylphosphine, 1.10 g (36 mmol) paraformaldehyde, 1.83 g (24 mmol) of glycine and 5 ml of dry methanol. The mixture became transparent and was noticeably warm. The resulting solution was kept at room temperature (r.t.) and stirred for 12 h and was then concentrated to about 3–4 ml. After 0.5–1 h, a fine white solid was collected on a thick glass filter, washed twice with 1:1 MeOH–Et_2O and then with Et_2O and dried in vacuum to give 3.83 g of **1**, yield 84%. M.p. > 250°C (with decomposition).

^{1}H NMR (400.1 MHz, D_2O): δ 7.51 (t, 2H, ^3J(HH) = 6.7 Hz, ^3J(PH) = 6.7 Hz, *o*-H, Ph), 7.31–7.36 (m, 3H, *m*-H, *p*-H of Ph), 4.72 (s, H_2O), 3.53 (d, 1H, ^2J(HH) = 11.4 Hz, N–CH_2–N), 3.41 (dd, 1H, ^2J(HH) = 11.4, ^4J(PH) = 1.5 Hz, N–CH_2–N), 3.30 (t, 2H, ^2J(HH) = 13.4, ^2J(PH) = 13.4 Hz, P–CH^A–N), 3.17 (dd, 2H, ^2J(HH) = 13.4, ^2J(PH) = 4.5 Hz, P–CH^B–N), 3.18 (d, 2H, ^2J(HH) = 16.2 Hz, N–CH_2–CO_2), 3.16 (d, 2H, ^2J(HH) = 16.2 Hz, N–CH_2–CO_2). ^{13}C NMR (100.6 MHz, D_2O): δ 178.75 (s, 2C, CO_2), 136.85 (d, 1C, ^1J(CP) = 12.4 Hz, *ipso*-C of Ph), 131.84 (ddd, 2C, ^1J(CH) = 160.9, ^2J(CP) = 15.2 Hz, ^2J(CH) = 7.1 Hz, *o*-C of Ph), 129.47 (dd, 2C, ^1J(CH) = 161.8, ^3J(CP) = 5.4 Hz, *m*-C of Ph), 129.31 (d, 1C, ^1J(CH) = 162.0 Hz, *p*-C of Ph), 75.98 (t, 1C, ^1J(CH) = 143.3 Hz, N–CH_2–N), 60.54 (td, 2C, ^1J(CH) = 136.8, ^1J(CP) = 6.4 Hz, P–CH_2–N), 51.05 (td, 2C, ^1J(CH) = 141.1, ^3J(CP) = 10.1 Hz, N–CH_2–CO_2). ^{31}P NMR (162 MHz): in MeOH: δ −55.5; in H_2O: δ −62.1. IR ($\tilde{\nu}$/cm^{-1}, KBr): 1594 (CO, Ph, H_2O), 3427 (H_2O). $C_{13}H_{19}N_2Na_2O_6P$ (376.27): Calc.: C, 41.49; H, 5.09; N, 7.44; P, 8.23. Found: C, 42.32; H, 4.91; N, 7.60; P, 8.40%.

3.2. Preparation of dipotassium 1,3-di(carboxylatomethyl)-5-phenyl-1,3,5-diazaphosphorinane dihydrate (**2**)

Phosphino amino acid salt **2** was synthesized by a procedure analogous to that of **1** with KOH instead of NaOH. Yield 62%. M.p. > 250°C (with decomposition).

The NMR data of **2** are similar to those of **1** (Tables 1–3). IR ($\tilde{\nu}$/cm^{-1}, KBr): 1607 (CO, Ph, H_2O), 3374 (H_2O). $C_{13}H_{19}K_2N_2O_6P$ (408.49): Calc.: C, 38.22; H, 4.69; N, 6.85; P, 7.58. Found: C, 38.92; H, 4.57; N, 6.98; P, 7.72%.

3.3. Preparation of disodium 1,3-di(carboxylatomethyl)-5-mesityl-1,3,5-diazaphosphorinane dihydrate (**3**)

(A) The phosphino amino acid salt **3** was synthesized by a procedure analogous to that for **1** with $MesPH_2$ instead of $PhPH_2$. Yield 72%.

(B) 0.26 g (8.8 mmol) of paraformaldehyde was reacted with 0.67 g (4.4 mmol) of mesitylphosphine with heating (125–130°C), and the mixture was diluted with 5 ml of dry methanol. To the stirred mixture of the hydroxyalkylphosphine, 0.13 g (4.4 mmol) of paraformaldehyde, 0.66 g (8.8 mmol) of glycine and 5 ml of dry methanol and a solution of 0.35 g (8.8 mmol) of sodium hydroxide in 5 ml of dry methanol was added dropwise. The reaction mixture became transparent and was noticeably warm. The resulting solution was kept at r.t. and stirred for 12 h and then was concentrated to about 3–4 ml. After 0.5–1 h the white fine solid was collected on a thick glass filter, washed twice with 1:1 MeOH–Et_2O and then with Et_2O and dried in vacuum to give 0.72 g of **3**, yield 39%. M.p. > 250°C (with decomposition).

^{1}H NMR (400.1 MHz, D_2O): δ 6.84 (s, 2H, *m*-H of Mes), 4.72 (s, H_2O), 3.67 (d, 1H, ^2J(HH) = 12.0 Hz, N–CH_2–N), 3.55 (dd, 1H, ^2J(HH) = 12.0, ^4J(PH) = 2.6 Hz, N–CH_2–N), 3.58 (dd, 2H, ^2J(HH) = 12.7, ^2J(PH) = 5.7 Hz, P–CH^B–N), 3.51 (t, 2H, ^2J(HH) = 12.7, ^2J(PH) = 12.7 Hz, P–CH^A–N), 3.43 (d, 2H, ^2J(HH) = 16.2 Hz, N–CH_2–CO_2), 3.28 (d, 2H, ^2J(HH) = 16.2 Hz, N–CH_2–CO_2), 2.39 (s, 6H, *o*-CH_3 of Mes), 2.15 (s, 3H, *p*-CH_3 of Mes). ^{1}H NMR (400.1 MHz, CD_3OD): δ 6.68 (s, 2H, *m*-H of Mes), 4.79 (s, H_2O), 3.67 (d, 1H, ^2J(HH) = 10.2 Hz, N–CH_2–N), 3.19–3.21 (m, 4H, P–CH_2–N), 3.12 (d, 2H, ^2J(HH) = 16.2 Hz, N–CH_2–CO_2), 3.04 (d, 2H, ^2J(HH) = 16.2 Hz, N–CH_2–CO_2), 2.89 (dd, 1H, ^2J(HH) = 10.2, ^4J(PH) = 4.2 Hz, N–CH_2–N), 2.40 (s, 6H, *o*-CH_3 of Mes), 2.08 (s, 3H, *p*-CH_3 of Mes). ^{13}C NMR (100.6 MHz, D_2O): δ 178.87 (s, 2C, CO_2), 143.42 (d, 2C, ^2J(CP) = 11.6 Hz, *o*-C of Mes), 140.00 (s, 1C, *p*-C of Mes), 130.57 (d, 2C, ^1J(CH) = 160.8 Hz, *m*-C of Mes), 128.77 (d, 1C, ^1J(CP) = 21.3 Hz, *ipso*-C of Mes), 75.58 (t, 1C, ^1J(CH) = 146.7 Hz, N–CH_2–N), 59.69 (td, 2C, ^1J(CH) = 133.1 Hz, ^1J(CP) = 10.6 Hz, P–CH_2–N), 51.45 (td, 2C, ^1J(CH) = 139.3, ^3J(CP) = 9.0 Hz, N–CH_2–CO_2), 23.31 (qd, 2C, ^1J(CH) = 115.9, ^3J(CP) = 14.0 Hz, *o*-CH_3 of Mes), 20.45 (q, 1C, ^1J(CH) = 127.3 Hz, *p*-CH_3 of Mes). ^{31}P NMR (162 MHz): in MeOH: δ −57.7; in H_2O: δ −66.0. IR ($\tilde{\nu}$/cm^{-1}, KBr): 1606 (CO, aryl, H_2O), 3407 (H_2O). $C_{16}H_{25}N_2Na_2O_6P$ (418.35): Calc.: C, 45.94; H, 6.02; N, 6.69; P, 7.40. Found: C, 46.1; H, 5.98; N, 6.66; P, 7.31%.

3.4. Preparation of dipotassium 1,3-di(carboxylatomethyl)-5-mesityl-1,3,5-diazaphosphorinane dihydrate (**4**)

(A) Compound **4** was synthesized by a procedure analogous to that for **3** (given in Section 3.3 (A)) with KOH instead of NaOH. Yield 63%.

(B) Compound **4** was synthesized by a procedure analogous to that for **3** (given in Section 3.3 (B)) with KOH instead of NaOH. Yield 45%.

M.p. > 250°C (with decomposition).

The NMR data of **4** are similar to those of **3** (Tables 1–3). IR ($\tilde{\nu}$/cm^{-1}, KBr): 1606 (CO, aryl, H_2O), 3382 (H_2O). $C_{16}H_{25}K_2N_2O_6P$ (450.57): Calc.: C, 42.65; H, 5.59; N, 6.21; P, 6.87. Found: C, 42.9; H, 5.9; N, 6.8; P, 6.6%.

*3.5. Preparation of disodium 1,3-di(carboxylatomethyl)-5-(2,4,6-triisopropylphenyl)-1,3,5-diazaphosphorinane dihydrate (**5**)*

The phosphino amino acid salt **5** was synthesized by a procedure analogous to that for **1** with $TippPH_2$ instead of $PhPH_2$. Yield 46%. M.p. > 250°C (with decomposition).

^{1}H NMR (400.1 MHz, CD_3OD): δ 7.51 (s, 2H, *m*-H of Tipp), 5.36 (s, H_2O), 4.10 (dsept, 2H, $^3J(HH) = 6.8$, $^2J(PH) = 6.8$ Hz, *o*-CH(CH$_3$)$_2$), 3.85 (d, 1H, $^2J(HH) = 10.0$ Hz, N–CH$_2$–N), 3.39 (dd, 2H, $^2J(HH) = 11.8$, $^2J(PH) = 6.0$ Hz, P–CH^B–N), 3.11 (dd, 2H, $^2J(HH) = 11.8$, $^2J(PH) = 11.8$ Hz, P–CH^A–N), 3.28 (d, 2H, $^2J(HH) = 16.2$ Hz, N–CH$_2$–CO$_2$), 3.21 (d, 2H, $^2J(HH) = 16.2$ Hz, N–CH$_2$–CO$_2$), 3.00 (dd, 1H, $^2J(HH) = 10.0$, $^4J(PH) = 4.0$ Hz, N–CH$_2$–N), 2.83 (sept, 1H, $^3J(HH) = 6.9$ Hz, *p*-CH(CH$_3$)$_2$) 1.71 (d, 12H, $^3J(HH) = 6.8$ Hz, *o*-CH(CH_3)$_2$), 1.68 (d, 6H, $^3J(HH) = 6.8$ Hz, *p*-CH(CH_3)$_2$). ^{13}C NMR (100.6 MHz, CD_3OD): δ 178.02 (s, 2C, CO_2), 157.16 (d, 2C, $^2J(CP) = 12.9$ Hz, *o*-C of Tipp), 152.1 (s, 1C, *p*-C of Tipp), 126.14 (d, 1C, $^1J(CP) = 25.9$ Hz, *ipso*-C of Tipp), 123.14 (d, 2C, $^1J(CH) = 152.8$ Hz, *m*-C of Tipp), 77.61 (t, 1C, $^1J(CH) = 159.0$ Hz, N–CH$_2$–N), 62.41 (td, 2C, $^1J(CH) = 134.4$, $^1J(CP) = 9.4$ Hz, P–CH$_2$–N), 52.87 (td, 2C, $^1J(CH) = 139.6$, $^3J(CP) = 8.1$ Hz, N–CH$_2$–CO$_2$), 35.50 (d, $^1J(CH) = 127.6$ Hz, *p*-*C*H(CH$_3$)$_2$), 32.91 (dd, $^1J(CH) = 127.0$, $^3J(CP) = 21.0$ Hz, *o*-*C*H(CH$_3$)$_2$), 25.37 (q, 4C, $^1J(CH) = 125.6$ Hz, *o*-CH(*C*H$_3$)$_2$), 24.20 (q, 2C, $^1J(CH) = 125.7$ Hz, *p*-CH(*C*H$_3$)$_2$). ^{31}P NMR (162 MHz): in MeOH: δ −69.7; in H_2O: δ −77.1. IR ($\tilde{\nu}$/cm^{-1}, KBr) 1598 (CO, aryl, H_2O), 3424 (H_2O). $C_{22}H_{37}N_2Na_2O_6P$ (502.51): Calc.: C, 52.58; H, 7.42; N, 5.57; P, 6.16. Found: C, 52.3; H, 7.76; N, 5.28; P, 5.83%.

*3.6. Preparation of dipotassium 1,3-di(carboxylatomethyl)-5-(2,4,6-triisopropylphenyl)-1,3,5-diazaphosphorinane dihydrate (**6**)*

The phosphino amino acid salt **6** was synthesized by a procedure analogous to that for **2** with $TippPH_2$ instead of $PhPH_2$. Yield 54%. M.p. > 250°C (with decomposition).

The NMR data of **6** are similar to those of **5** (Tables 1–3). IR ($\tilde{\nu}$/cm^{-1}, KBr): 1606 (CO, aryl, H_2O), 3382 (H_2O). $C_{22}H_{37}K_2N_2O_6P$ (534.73): Calc.: C, 49.42; H, 6.97; N, 5.24; P, 5.79. Found: C, 49.2; H, 7.04; N, 5.55; P, 4.90%.

Acknowledgements

A.A. Karasik thanks the Sächsisches Ministerium für Wissenschaft und Kunst (SMWK) for financial support (Az.: 4-7531.50-04-0361-99/16).

References

[1] B. Cornils, W.A. Herrmann, in: B. Cornils, W.A. Herrmann (Eds.), Applied Homogeneous Catalysis with Organometallic Compounds, VCH, Weinheim, 1996.
[2] B. Cornils, W.A. Herrmann, in: B. Cornils, W.A. Herrmann (Eds.), Aqueous-Phase Organometallic Catalysis. Applied Homogeneous Catalysis with Organometallic Compounds, Wiley-VCH, Weinheim, 1998.
[3] F. Joo, A. Katho, J. Mol. Catal. A 116 (1997) 3.
[4] L. Toth, I. Guo, B.E. Hanson, J. Mol. Catal. A 116 (1997) 217.
[5] D. Sinou, Bull. Soc. Chim. Fr. 3 (1987) 480.
[6] I.O. Georgiev, A.A. Karasik, F.F. Nigmadzyanov, G.N. Nikonov, Russ. J. Coord. Chem. 21 (1995) 222.
[7] I.O. Georgiev, A.A. Karasik, G.N. Nikonov, Phosphorus, Sulfur and Silicon 111 (1996) 133.
[8] A.A. Karasik, I.O. Georgiev, R.I. Vasiliev, O.G. Sinyashin, Mendeleev Commun. (1998) 140.
[9] P.A.T. Hoye, P.G. Pringle, M.B. Smith, K. Worboys, J. Chem. Soc., Dalton Trans. (1993) 269.
[10] R.Sh. Khadiullin, A.A. Karasik, A.Kh. Plyamovatyi, R.R. Shagidullin, J. Mol. Struct. 293 (1993) 85.
[11] B.A. Arbuzov, O.A. Erastov, G.N. Nikonov, T.A. Zyablikova, R.R. Arshinova, R.A. Kadyrov, Izv. Akad. Nauk SSSR, Ser. Khim. (1980) 1571.
[12] B.A. Arbuzov, O.A. Erastov, G.N. Nikonov, T.A. Zyablikova, D.S. Yufit, Yu.T. Struchkov, Izv. Akad. Nauk SSSR, Ser. Khim. (1981) 1539.

PERGAMON

www.elsevier.nl/locate/poly

Polyhedron 19 (2000) 1461–1464

POLYHEDRON

Magnetic properties of two 1D complexes with mixed bridging ligands

You Song, Dun-Ru Zhu, Kou-Ling Zhang, Yan Xu, Chun-Ying Duan, Xiao-Zeng You *

State Key Laboratory of Coordination Chemistry, Coordination Chemistry Institute, Center for Advanced Studies in Science and Technology of Microstructures, Nanjing University, Nanjing 210093, PR China

Received 15 December 1999; accepted 11 April 2000

Abstract

The crystal structure of a 1D chain complex, $[Cu(SCN)(deae)]_n$ (**1**) (Hdeae = *N*,*N*-diethylamino ethanol), with mixed bridges was determined. The structure is composed of a dimeric Cu(II) unit with two bridging μ^3-η^2-aminoethanolato ligands, while the units are bridged by end-to-end thiocyanato groups to form a 1D chain. The variable temperature magnetic susceptibility of **1** and $[Cu(SCN)(dmae)]_n$ (**2**) (Hdmae = *N*,*N*-dimethylamino ethanol) in the temperature 5–300 K have been interpreted in terms of simple dimer model approximation ($H = -2JS_A \cdot S_B$). The magnetic behaviors show that the aminoethanolato bridges mediate a moderately strong antiferromagnetic exchange interaction with the fitting values $g = 1.96(3)$, $J = -175(3)$ cm^{-1} for **1** and $g = 2.016(7)$, $J = -205.4(7)$ cm^{-1} for **2**, respectively. © 2000 Elsevier Science Ltd. All rights reserved.

Keywords: Alternating chain; Dimer complex; Crystal structure; Magnetic properties

1. Introduction

Low-dimensional magnetic compounds as important precursors of molecular magnets have attracted great interest in the past two decades [1]. The pseudohalide bridging ligands (NCO^-, NCS^-, N_3^-) have been utilized extensively in preparing extended structures, because they can bridge between paramagnetic centers with versatile binding modes to form a one-dimensional chain (1D) [2–4] or 2D [5] and 3D [6] network compounds. Many compounds with uniform bridging ligands have been reported [2,3], but those with more than one kind of bridging ligand [4] are studied rarely. Variation of the bridging groups has a great advantage in the modification of the magnetic coupling interactions.

N,*N*-Dialkylamino ethanol (Hdaae) is a kind of effective bridging ligand, which can bridge between paramagnetic centers to form cluster compounds with acetate [7] and 1D chain complexes with pseudohalide ligands [4c]. However, to our knowledge, detailed magnetic properties of the compounds with daae bridging ligands have not yet been reported. As an extension of our study on alternating chain systems, we report here, a new Cu(II)-containing 1D alternating chain complex, $[Cu(SCN)(deae)]_n$ (Hdeae = *N*,*N*-diethylamino ethanol) (**1**), with mixed di-μ_2-thiocyanato and di-μ_2-oxo bridging ligands, and the magneto-structural correlation of this kind of compound.

2. Experimental

2.1. Materials

All chemicals were commercial products of reagent grade and used without purification.

2.2. Preparation

2.2.1. $[Cu(SCN)(deae)]_n$ (1)

The synthesis procedure was lightly modified as described previously [4c]. To 10 ml of stirred ethanolic

* Corresponding author. Tel.: +86-25-359-2969; fax: +86-25-331-4502.

E-mail address: xyz@netra.nju.edu.cn (X.-Z. You).

0277-5387/00/$ - see front matter © 2000 Elsevier Science Ltd. All rights reserved.
PII: S0277-5387(00)00402-2

solution of $Cu(OAc)_2{\cdot}H_2O$ (0.10 g, 0.5 mmol) and $(C_2H_5)_2NCH_2CH_2OH$ (0.18 g, 1.5 mmol, 0.2 ml) was added KSCN (0.049 g, 0.5 mmol) at room temperature. The dark-green mixture was stirred continually for ca. 5 min, during which time the KSCN was dissolved completely, and then filtered rapidly. The dark-green polyhedral crystals were obtained by slow evaporation of the filtrate, yielding 86 mg, 72.3%. *Anal.* Found: C, 35.71; H, 6.01; N, 11.72. Calc. for $C_7H_{14}CuN_2OS$: C, 35.35; H, 5.93; N, 11.78%. IR: ν_{max} (cm^{-1}): 2800s (CH_3, CH_2), 2105vs (SCN^-). Electronic reflectance spectra ($BaSO_4$ pellet, nm): 500–1200 (broad d–d bond: $\lambda_{max} = 660$ nm).

2.2.2. [Cu(SCN)(dmae)]$_n$ (2)

This complex was prepared in a similar way to that of **1**, except for the use of Hdeae (1.5 mmol, 0.13 g, 0.15 ml) instead of Hdeae, yielding 82 mg, 77.2%. *Anal.* Found: C, 28.33; H, 4.78; N, 13.15. Calc. for $C_5H_{10}CuN_2OS$: C, 28.63; H, 4.80; N 13.35%. IR: ν_{max} (cm^{-1}): 2800s (CH_3, CH_2), 2100vs (SCN^-). Electronic reflectance spectra ($BaSO_4$ pellet, nm): 500–1140 (broad d–d bond: $\lambda_{max} = 680$ nm).

2.3. Physical measurements

CHN analysis was determined on a Perkin–Elmer 240C elemental analyzer. The infrared spectra were recorded on a Nicolet-170 SX FT-IR spectrometer with KBr discs in the 4000–400 cm^{-1}. Solid electronic reflectance spectra were obtained on a Hitachi U3400 spectrophotometer in 400–1500 nm. Magnetic susceptibility in the temperature range 5–300 K on microcrystalline samples was carried out with a Quantum Design MPMS SQUID system.

2.4. X-ray crystallography

$C_{14}H_{28}Cu_2N_4O_2S_2$, $M_r = 475.6$, monoclinic, space group $P2_1/n$, $a = 7.991(5)$, $b = 13.681(6)$, $c = 9.411(4)$ Å, $\beta = 100.15(5)°$, $V = 1012.7(9)$ Å^3, $Z = 2$ for **1**.

Suitable X-ray-quality crystals of **1** were obtained as described above. The diffraction experiments (crystal size $0.40 \times 0.30 \times 0.20$ mm) were carried out on a Siemens P4 four-circle diffractometer with monochromated Mo Kα ($\lambda = 0.71073$ Å) radiation using the $\theta - 2\theta$ ($2.66 \leq \theta \leq 25.00°$) scan mode with a variable scan speed 5–50° min^{-1} in ω. The data were corrected for Lorentz and polarization effects during data reduction using XSCANS [8].

The structures were solved by direct method and refined on F^2 by full-matrix least-squares methods using SHELXTL version 5.0 [9]. All the non-hydrogen atoms were refined anisotropically. All the hydrogen atoms were placed in calculated positions with assigned fixed isotropic thermal parameters at 1.2 times the equivalent isotropic U of the atoms to which they are attached (1.5 times for the O–H and methyl groups) and allowed to ride on their respective parent atoms. The contributions of these hydrogen atoms were included in the structure-factor calculations. All computations were carried out on a PC-586 computer using the SHELXTL-PC program package [9]. The final R_1 (wR_2) value was 0.0766 (0.1699) for 120 parameters and 1760 observed reflections [$I \geq 2\sigma(I)$]. The goodness-of-fit on F^2 is 1.143.

3. Results and discussion

3.1. Description of the structure [Cu(SCN)(deae)]$_n$ (1)

Each complex of this kind consists of an alternating chain in which two neighboring Cu(II) ions are bridged by two alkoxo oxygen atoms from two different aminoethanolate ligands, while the dimer units are linked by two end-to-end thiocyanato bridging ligands. Between the neutral chains, there are no any other linkages but the van der Waals forces. The geometry of a chain, in which the thiocyanates bridge between dimer units, with the copper coordination spheres is showed in Fig. 1. The structure of [Cu(SCN)(dmae)]$_n$ (**2**) is described as reported previously [4c]. For complex **1**, the geometry of a discrete dimer unit is illustrated in Fig. 2. Selected bond distances and angles relevant to the copper coordination spheres are listed in Table 1.

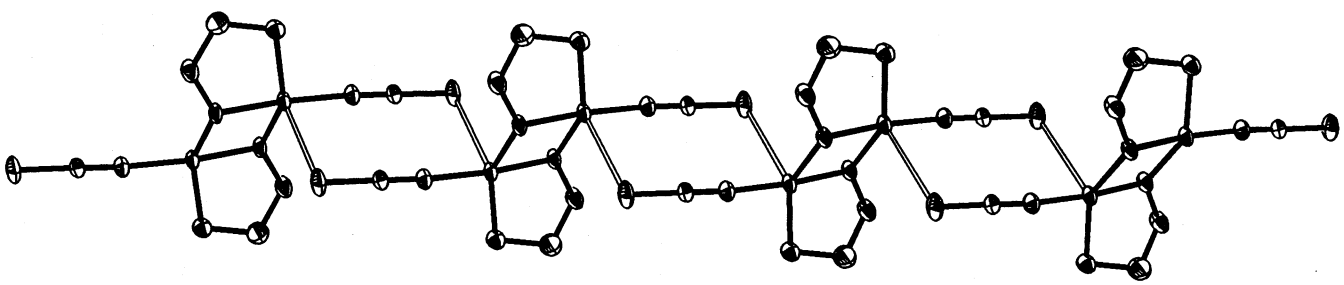


Fig. 1. View of the 1D chain with alternating thiocyanatoes and aminoethanolatoes bridging ligands. Displacement ellipsoids are drawn at the 30% probability level: methyl and ethyl groups have been omitted for clarity.

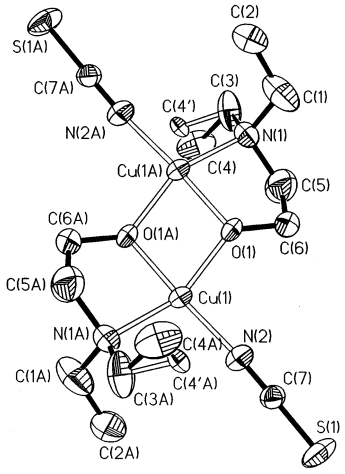


Fig. 2. View of the structure of $[Cu(SCN)(deae)]_2$ (**1**) with numbering scheme adopted. Ellipsoids are drawn at 50% probability: hydrogen atoms have been omitted for clarity.

Table 1
Selected bond lengths (Å) and angles (°) relevant to the copper coordination spheres and hydrogen bond distances (Å) of probability level [a]

Cu(1)–O(1A)	1.908(3)	Cu(1)–N(2)	1.927(4)
Cu(1)–O(1)	1.936(3)	Cu(1)–N(1A)	2.078(4)
Cu(1)···Cu(1A)	2.979(2)	Cu(1)···S(1B)	2.951(2)
O(1A)–Cu(1)–N(2)	175.1(1)	O(1A)–Cu(1)–O(1)	78.4(1)
N(2)–Cu(1)–O(1)	98.3(1)	O(1A)–Cu(1)–N(1A)	85.1(1)
N(2)–Cu(1)–N(1A)	99.6(2)	O(1)–Cu(1)–N(1A)	147.3(2)
S(1B)–Cu(1)–O(1)	94.1(1)	S(1B)–Cu(1)–O(1A)	87.1(1)
S(1B)–Cu(1)–N(2)	89.6(1)	S(1B)–Cu(1)–N(1A)	113.1(1)

[a] Methyl and ethyl groups have been omitted for clarity. Symmetry code A, $-x$, $-y+1$, $-z+1$; B, $-x+1$, $-y+1$, $-z+1$.

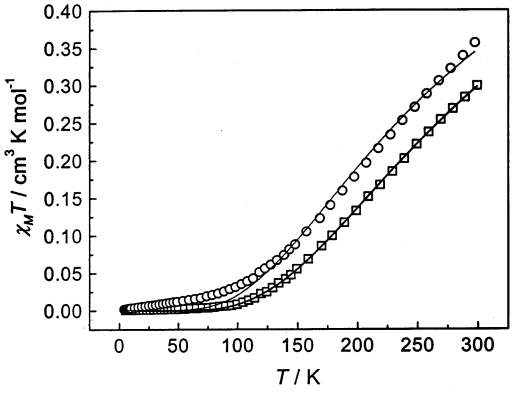


Fig. 3. Temperature dependence of the magnetic susceptibility on the form of the $\chi_M T$ versus T curve: (○) and (□) experimental points of **1** and **2**; (—) theoretical curve.

In the dimer unit, each copper(II) ion exhibits an extremely distorted square-pyramidal geometry with the mean deviations of 0.2565 Å from their basal plane. A nitrogen atom and two bridging oxygen atoms of two $deae^-$ ligands and a nitrogen atom of a bridging thiocyanato group coordinate to the copper(II) ion in the basal plane with metal-donor distances in the ranges of 1.908–2.078 Å, which are comparable with those of $[Cu(SCN)(C_4H_{10}NO)]_n$ [4c], $Cu_9(CHCl_2COO)_{10}(C_4H_{10}NO)_6(OH)_2$ and $Cu_4(CHCl_2COO)_4(C_4H_{10}NO)_4$ [7]. The other bridging thiocyanato group coordinates to the Cu(II) ion in the axial position via the S atom. Around the Cu(1) atom, the S(1B) (symmetry code B: $-x+1$, $-y+1$, $-z+1$) at the axial position is 2.950(2) Å away, which is comparable to very weak S–Cu(II) bond distances of 2.933(1)–3.174(2) Å reported previously [5a] and Cu(1) is displaced by 0.2134 Å from its basal plane, O(1)O(1A)N(2)N(1A). The Cu(II)···Cu(II) separation in the dimer unit is 2.979(2) Å, which is comparable to that of $[Cu(SCN)(C_4H_{10}NO)]_n$ [4c], but the shortest intrachain and interchain Cu(II)···Cu(II) distances are 5.792 and 7.526 Å, respectively. They are longer than those of $[Cu(SCN)(C_4H_{10}NO)]_n$ [4c] (5.375 and 4.987 Å) because the ethyl groups of $deae^-$ replace the methyl groups of $dmae^-$.

3.2. Magnetic properties

Variable-temperature magnetic susceptibility measurements of **1** and **2** performed on a crystalline sample from 300 to 5 K are shown in Fig. 3 in the form $\chi_M T$ versus T. The experimental data were corrected for inherent diamagnetism using Pascal's constants [10] and for temperature-independent paramagnetism (TIP).

In the whole temperature range, **1** and **2** show similar magnetic behavior. Two domains are clearly distinguished. At 299 K, the values of product $\chi_M T$ per two Cu(II) ions unit of $[Cu(SCN)(deae)]_2$ and $[Cu(SCN)(dmae)]_2$ are 0.36 and 0.30 cm^3 K mol^{-1}, respectively, which are less than the spin-only value of 0.75 cm^3 K mol^{-1}, indicating that a significant antiferromagnetic coupling contribution is involved. When the system cools down, the product $\chi_M T$ for **2** decreases quickly and reaches a critical point at about 100 K with $\chi_M T = 0.009$ cm^3 K mol^{-1}, but that of **1** decreases more smoothly than **2**, which suggest the presence of a strongly antiferromagnetic interaction. In the lower temperature domain $\chi_M T$ exhibits a plateau at 0.005 cm^3 K mol^{-1} for **1** and 0.001 cm^3 K mol^{-1} for **2**, indicative of an effective zero spin per unit in this temperature range.

The data can be interpreted in terms of a one-dimensional chain model with alternating coupling constants J_1 and J_2 and a simple dimer model with intermolecular coupling interaction in accordance with the structures of **1** and **2**. However, reasonable fitting results cannot be obtained using the former model ($H = -2J\,\Sigma[S_{2i}\cdot S_{2i-1} + \alpha S_{2i}\cdot S_{2i+1}]$ [11]. This could be attributed to the limitation of the chain model because it cannot be used to explain the behavior in the very low

temperature range [12]. For the latter model, two bridging thiocyanato groups linking adjacent Cu(II) ions in the axial position can not result in the effective magnetic exchange pathway between the dimer units because the single electron does not occupy in the d_{z^2} orbital. As well as, there is no any magnetic exchange pathways between chains besides the very weak van der Waals effect in **1** and **2**. Therefore, the intrachain Cu(II) ions by the extended bridging thiocyanato and interchain Cu(II) ions magnetic coupling interactions can be neglected and the magnetic behavior can be represented using the simple dimer model.

We assume that there is only one kind of exchange coupling (J), which exists only between the two Cu(II) ions bridged by two alkoxo oxygen atoms in the dimer units. The magnetic system can be interpreted by using the Heisenberg–Dirac–van Vleck $S_A = S_B = 1/2$ spin-coupled dimer model ($H = -2JS_A \cdot S_B$). The expression of magnetic susceptibility of **1** and **2** is

$$\chi_M = \frac{2Ng^2\beta^2}{kT} \times \frac{1}{3 + e^{-2J/kT}} \times (1-\rho) + \frac{Ng^2\beta^2}{2kT}\rho \qquad (1)$$

where N, g, β, k, ρ and T have their usual meanings. The least-squares fits to the magnetic susceptibility data to give the parameters: $g = 1.96(3)$, $J = -175(3)$ cm^{-1} and $R = 7.17 \times 10^{-5}$ ($R = \Sigma[(\chi_M T)_{calc} - (\chi_M T)_{obs}]^2 / \Sigma(\chi_M T)^2_{obs}$) for **1**, and $g = 2.016(7)$, $J = -205.4(7)$ cm^{-1} and $R = 2.46 \times 10^{-6}$ for **2**, respectively, fixing $\rho = 0$. The J values indicate the moderately strong antiferromagnetic exchange coupling within the copper(II) dimer units. The correction term $(1-\rho)$ attempts to take into account the paramagnetic impurities in copper(II)-containing compounds, but the fitting results give $g = 2.09(6)$, $J = -175(3)$ cm^{-1}, $\rho = 0.12(5)$ and $R = 6.67 \times 10^{-5}$ for **1**, and $g = 2.05(1)$, $J = -205.5(7)$ cm^{-1}, $\rho = 0.030(9)$ and $R = 2.08 \times 10^{-6}$ for **2**, respectively. As a matter of fact, the paramagnetic impurities often influence on the magnetic measurement for copper(II)-containing compounds, but it is suggested that the former fitting for **1** is identical to its magnetic properties rather than the latter with too large paramagnetic impurities.

Usually, in the square-pyramidal configuration of a central Cu(II) ion, the unpaired electron occupies the $d_{x^2-y^2}$ orbital. For example of the Cu(II) dimer unit of complex **1**, two alkoxo oxygen atoms [O(1) and O(1A)] of two different aminoethanolato ligands bridge between paramagnetic centers of Cu(1) and Cu(1A) in the equatorial plane involving the magnetic $d_{x^2-y^2}$ orbitals of two Cu(II) ions. The Cu(1)···Cu(1A) distance of 2.979(2) Å being comparable to that of the hydroxide-bridged systems (2.847–3.000 Å) [13] and the bridge angle falling in the antiferromagnetic realm would be expected for moderately strongly antiferromagnetic exchange between Cu(II) ions with non-orthogonal magnetic orbitals and two magnetically active oxygen bridges [13].

4. Supplementary material

Crystallographic data (including structure factors) for structures **1** and **2** reported in this paper have been deposited with the Cambridge Crystallographic Data Centre as supplementary publication nos. CCDC-137230 and CCDC-137231, respectively. Further details on the structure determinations can be obtained free of charge on application to CCDC, 12 Union Road, Cambridge CB2 1EZ, UK (fax: +44-1223-336 033; e-mail: deposit@ccdc.cam.ac.uk; or www: http://www.ccdc.cam.ac.uk). Structure factors are available upon request from author You Song.

Acknowledgements

This work was supported by a grant from the National Natural Science Foundation of China.

References

[1] C.-T. Chen, K.S. Suslick, Coord. Chem. Rev. 128 (1993) 293.
[2] (a) B.W. Dockum, W.M. Reiff, Inorg. Chem. 21 (1982) 2613. (b) R. Vicente, A. Escuer, J. Ribas, X. Solans, J. Chem. Soc., Dalton Trans. (1994) 259 and references therein. (c) A.K. Gregson, N.T. Moxon, Inorg. Chem. 21 (1982) 586.
[3] (a) G. De Munno, M.G. Lombardi, M. Julve, F. Lloret, J. Faus, Inorg. Chim. Acta 282 (1998) 82 and references therein. (b) J. Ribas, M. Monfort, C. Diaz, C. Bastos, X. Solans, Inorg. Chem. 33 (1994) 484. (c) R. Cortés, L. Lezama, J.L. Pizarro, M.I. Arriortua, X. Solans, T. Rojo, Angew. Chem., Int. Ed. Engl. 33 (1994) 2488 and references therein. (d) I. Bkouche-Waksman, M.-L. Boillot, O. Kahn, S. Sikorav, Inorg. Chem. 23 (1984) 4454. (e) A. Escuer, R. Vicente, J. Ribas, M.S. EI Fallah, X. Solans, M. Font-Bardía, Inorg. Chem. 32 (1993) 3727.
[4] (a) J.A. Real, R. Ruiz, J. Faus, F. Lloret, M. Julve, Y. Journaux, M. Philoche-Levisalles, C. Bois, J. Chem. Soc., Dalton Trans. (1994) 3769. (b) Z.N. Chen, H.X. Zhang, K.B. Yu, B.S. Kang, H. Cai, C.Y. Su, T.W. Wang, Z.L. Lu, Inorg. Chem. 37 (1998) 4775. (c) W. Haase, R. Mergehenn, W. Krell, Z. Naturforsch. 31b (1976) 85. (d) Z. Shen, J.L. Zuo, Z. Yu, Y. Zhong, J.F. Bai, C.M. Che, H.K. Fun, J.J. Vittal, X.Z. You, J. Chem. Soc., Dalton Trans. (1999) 3393.
[5] (a) M. Julve, M. Verdaguer, G. De Munno, J.A. Real, G. Bruno, Inorg. Chem. 32 (1993) 795 and references therein. (b) R. Cortés, L. Lezama, J.L. Pizarro, M.I. Arriortua, T. Rojo, Angew. Chem., Int. Ed. Engl. 35 (1996) 1810.
[6] F.A. Mautner, R. Cortés, L. Lezama, T. Rojo, Angew. Chem., Int. Ed. Engl. 35 (1996) 78.
[7] (a) U. Turpeinen, R. Hämäläinen, J. Reedjik, Inorg. Chim. Acta 134 (1987) 87. (b) U. Turpeinen, R. Hämäläinen, M. Ahlgrén, Acta Crystallogr., Sect. B 36 (1980) 927.
[8] Siemens, XSCANS (version 2.1), Siemens Analytical X-ray Instruments Inc., Madison, USA, 1994.
[9] Siemens, SHELXTL (version 5.0), Siemens Industrial Automation Inc., Analytical Instrumentation, USA, 1995.
[10] R.L. Carlin, Magneto Chemistry, Springer Verlag, New York, 1986.
[11] W.E. Hatfield, J. Appl. Phys. 52 (1981) 1985.
[12] R. Cortés, M. Drillon, X. Solans, L. Lezama, T. Rojo, Inorg. Chem. 36 (1997) 677.
[13] H. van Crawford, H.W. Richardson, J.R. Wasson, D.J. Hodgson, W.E. Hatfield, Inorg. Chem. 15 (1976) 2107.

PERGAMON

www.elsevier.nl/locate/poly

Polyhedron 19 (2000) 1465–1470

POLYHEDRON

Synthesis, spectral and crystal structures of two new copper(I) complexes of di-2-pyridyl ketone (DPK) containing uncoordinated N-protonated ligand; $[(DPK)H][CuX_2]$ (X = I and NCS)

Mohamed A.S. Goher [a,*], Najeeb A. Al-Salem [b], Thomas C.W. Mak [c]

[a] *Department of Chemistry, Faculty of Science, Alexandria University, PO Box 426, Ibrahimia, 21321 Alexandria, Egypt*
[b] *Department of Chemistry, Faculty of Science, Kuwait University, PO Box 5969, Safat 13060, Kuwait*
[c] *Department of Chemistry, Chinese University of Hong Kong, Shatin, Hong Kong*

Received 4 January 2000; accepted 11 April 2000

Abstract

Two new copper(I) complexes of di-2-pyridyl ketone (DPK); $[(DPK)H][CuI_2]$ (**1**) and $[(DPK)H][(Cu\{NCS)_2]$ (**2**) have been prepared and characterized by spectroscopic and crystallographic methods. Both complexes are colored and exhibit very broad and strong MLCT bands in the visible region. The IR spectra of these complexes are measured and discussed. The structure determination of complex **1** shows that it consists of discrete $[(DPK)H]^+$ cation contains N–H···N hydrogen bonds, and polymeric $[CuI_2]^-$ anion. In the anion, each copper atom is in a distorted tetrahedral environment with Cu–I bond lengths from 2.570(4) to 3.072(4) Å. The structure of complex **2**, which is similar to **1**, features uncoordinated N-protonated di-2-pyridyl ketone cations and corrugated layers of $[Cu(NCS)_2]_n$, in which the copper atom is in a distorted tetrahedral CuS_2N_2 chromophore; Cu–N bond lengths are 1.954(2) and 1.958(2) Å, and Cu–S distances are 2.4120(8) and 2.4501(7) Å. © 2000 Elsevier Science Ltd. All rights reserved.

Keywords: Copper(I) complexes; Di-2-pyridyl ketone; Crystal structures; Electronic and IR spectra

1. Introduction

Di-2-pyridyl ketone (DPK) has the ability to coordinate initially via one of the two modes, either through the two nitrogen atoms of the pyridine rings or through one nitrogen atom and the carbonyl group of the ligand. At present, evidence shows that in aqueous solution, the former mode is favored. The observed reaction is hydration of the carbonyl forming a diol group [1]. The metal promoted hydration of DPK has been of interest for some time since the ligand has the ability to undergo a reaction after initial coordination to a transition metal ion. Another interesting aspect of DPK can be found in reported solid state structures of metal–DPK (1:2) complexes [2–4]. These structures show that one of the oxygen atoms from the newly formed diol on the ligand also interacts with the metal atom, thereby making the ligand tridentate in character rather than bidentate. Recently, DPK has been used to produce different copper(II) clusters [5,6], e.g. $[Cu_4(DPK{\cdot}CH_3O)_4(CH_3O)_2](ClO_4)_2$ (DPK·CH_3OH = monomethylated diol of di-2-pyridyl ketone) [5] and $[Cu_8(DPK{\cdot}OH)_8(O_2CCH_3)_4](ClO_4)_4{\cdot}9H_2O$ (DPK·H_2O = the hydrated gem-diol form of di-2-pyridyl ketone) [6]. Also, it has been found [7] that copper(I)–PPh_3–DPK complexes are efficient photocatalysts for norbornadiene–quadricyclane conversion, which is important as a solar energy storage process [8,9].

Previously, we have shown that when a mixture of excess $Cu^{I}I$ or $Cu^{I}NCS$ and 2-benzoylpyridine (2-Bzpy) in an ethanol medium stands over ca. 2 weeks in contact with air, an intramolecular oxidative cyclization occurs with the formation of the ionic compounds [9-oxo-indolo[1,2-*a*]pyridinium]$^+[CuX_2]^-$ [10,11]. In the present study we have undertaken the reactions

* Corresponding author. Tel.: +2-3-492-2918; fax: +2-3-582-0844.
E-mail address: mohamed_goher@yahoo.com (M.A.S. Goher).

0277-5387/00/$ - see front matter © 2000 Elsevier Science Ltd. All rights reserved.
PII: S0277-5387(00)00403-4

between $Cu^{I}X$ dissolved in excess NaX or KX and DPK to investigate the coordination behavior of DPK when combined with a copper(I) ion and to compare the compounds resulted in this case with those of 2-Bzpy. Such reactions afforded solid complexes only for the iodide and thiocyanate salts, for which good quality crystals have been isolated. The results of these reactions along with the structural characterization of both complexes as elucidated by spectroscopic and crystallographic methods are reported in the present paper.

Table 1
Crystal data and structure refinement for complexes **1** and **2**

	1	**2**
Empirical formula	$C_{11}H_9CuI_2N_2O$	$C_{13}H_9CuN_4OS_2$
Formula weight	502.54	364.90
Temperature (K)	293(2)	293(2)
Wavelength (Å)	0.71073	0.71073
Crystal system	monoclinic	monoclinic
Space group	*Cc*	$P2_1/c$
Unit cell dimensions		
a (Å)	12.513(3)	5.711(1)
b (Å)	15.099(3)	25.283(8)
c (Å)	7.113(1)	10.068(1)
α (°)	90	90
β (°)	91.20(3)	98.51(3)
γ (°)	90	90
V (Å^3), *z*	1343.6(5), 4	1437.8(6), 4
D_{calc} (Mg m^{-3})	2.484	1.686
Absorption coefficient (mm^{-1})	6.205	1.811
F(000)	4928	736
Crystal size (mm)	$0.40\times0.30\times0.20$	$0.44\times0.12\times0.08$
θ Range for data collection (°)	2.11–25.00	2.20–28.30
Limiting indices	$0\le h\le14$, $0\le k\le17$, $-8\le l\le8$	$-7\le h\le7$, $-32\le k\le25$, $-12\le l\le13$
Reflections collected	1244	10 017
Independent reflections	1244 [$R_{int}=0.0000$]	3548 [$R_{int}=0.0333$]
Refinement method	full-matrix least-squares on F^2	full-matrix least-squares on F^2
Data/restraints/parameters	1243/2/155	3584/0/228
Goodness-of-fit on F^2	1.071	0.917
Final *R* indices [$I<2\sigma(I)$]	$R_1=0.0348$, $wR_2=0.0787$	$R_1=0.0367$, $wR_2=0.0749$
R indices (all data)	$R_1=0.0463$, $wR_2=0.1057$	$R_1=0.0679$, $wR_2=0.0833$
Extinction coefficient	0.0002(2)	0.0023(3)
Largest difference peak and hole (e Å^{-3})	1.046 and −1.112	0.562 and −0.738

2. Experimental

Di-2-pyridyl ketone was purchased from Aldrich and other chemicals are of analytical grade quality.

2.1. Preparation of complexes

2.1.1. [(DPK)H][CuI_2] complex **1**

An aqueous solution of $Cu(NO_3)_2\cdot3H_2O$ (2 mmol) was mixed with an aqueous solution of NaI in presence of L(+)-ascorbic acid. The precipitated CuI was washed several times with water and then dissolved by addition of a concentrated aqueous solution of NaI and filtered. To the filtrate, an ethanol solution of DPK (4 mmol) was added and the final mixture was allowed to stand in a cool place for ca. 1 week. The complex was deposited as black crystals suitable for X-ray diffraction. Yield 20%. *Anal*. Found: C, 26.2; H, 1.7; Cu, 12.8; I, 51.0, N, 5.6. Calc. for $C_{11}H_9CuI_2N_2O$; C, 26.3; H, 1.6; Cu, 12.6; I, 50.5; N, 5.6%. IR (KBr pellet, w = weak, m = medium, s = strong, v = very, cm^{-1}); 2749m, ν(N–H···N), 1685vs, ν(C=O), 1599s, 1577s, 1514s, 1453ms, 1436m, 1342m, 1328m, 1303m, 1270vs, 1255m, 1222s, 1161s, 1091ms, 1040m, 1009s, 947wm, 930m, 827ms, 786wm, 749vs, 663s, 633m, 611wm (pyridyl ring vibrations).

2.1.2. [(DPK)H][$(CuNCS)_2$] complex **2**

This complex was prepared according to the procedure given above in which $Cu^{I}NCS$ was dissolved in excess KNCS, filtered and mixed with an ethanol solution of DPK. The complex was separated as black long needle-like crystals upon allowing the final mixture to stand open in air over several days. Yield 70%. *Anal*. Found: C, 36.3; H, 1.8; Cu, 30.1; N, 13.4; S, 14.7. Calc. for $C_{13}H_8N_4OCu_2S_2$: C, 36.5; H, 1.9; Cu, 29.7; N, 13.1; S, 15.0%. IR (KBr pellet, cm^{-1}); 2100vs, ν(CN), 1672s, ν(C=O), 1589s, 1569s, 1504m, 1450m, 1431m, 1348(w), 1315(m), 1300(m), 1270(vs), 1246(ms), 1223(s), 1155(s), 1088(m), 1035m, 1005s, 963wm, 922m, 821ms, 765wm, 727wm, 653ms, 629wm (pyridyl ring vibrations).

2.2. Physical measurements

The experimental procedures and instruments used for different physical measurements are as described previously [12]

2.3. X-ray crystallography

Details of crystal parameters, data collection and structure refinement are given in Table 1. Raw intensities collected on a Rigaku AFC7R four-circle diffractometer at room temperature (293 K) were corrected for absorption using the DIFABS program [13]. Patterson superposition yields the positions of all non-hydro-

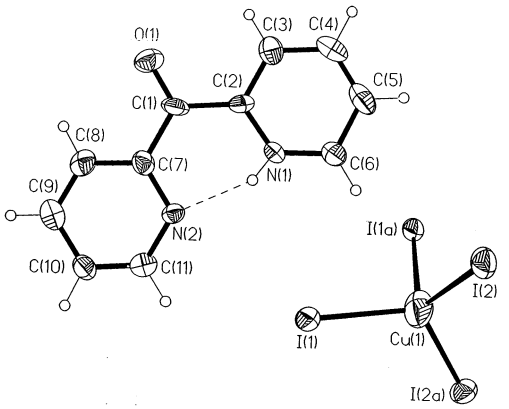


Fig. 1. The structure of the cation and coordination about Cu in the anion in $[(DPK)H]\cdot[CuI_2]$ (**1**) along with atom numbering scheme.

gen atoms, which were subjected to anisotropic refinement. All hydrogens are generated geometrically (C–H bonds fixed at 0.96 Å) but H(1) attached to N(1) in complex **1**, which was found on the difference Fourier map and allowed to ride on their respective parent atoms; they were assigned the same isotropic temperature factors ($U = 0.08$ Å^2) and included in the structure–factor calculations. Computations were performed using the SHELTXL/PC program package [14,15] on a PC 486 computer. Analytic expressions of atomic scattering factors were employed, and anomalous dispersion corrections were incorporated [16]. The residual maxima in the last difference map all lie in the neighborhood of the I atom.

3. Results and discussion

Two new copper(I) complexes have been isolated from the reactions between copper(I) iodide or copper(I) thiocayanate dissolved in excess of the respective potassium or sodium salt. Similar reactions in the case of chloride and bromide salts yielded no solid compounds, even upon allowing the mixtures to stand over several months. In case of the cyanide and azide salts, the mixture turned dark brown, from which a black material deposited on the walls of the container or black massive gelatinous material is formed, respectively. We could not obtain, however, defined solid compounds in both cases. Both complexes **1** and **2** are black, diamagnetic and sufficiently stable, over more than 1 year, against air oxidation when well dried. They are insoluble in water, methanol and ethanol, but slightly soluble in acetone with a change in color to pale green–yellow.

3.1. Structures

Fig. 1 illustrates the essential structural features of complex **1** which consists of a packing of $[(DPK)H]^+$ cations and polymeric $[CuI_2]^-$ anion; bond distances and bond angles are given in Table 2. DPK is thus protonated at the nitrogen atom N(1) giving rise to a hydrogen bond of the type N(1)–H···N(2) [N(1)–H(1) = 0.81(2), N(2)···H(1) = 1.95(1) Å], and hence a cation is formed. Di-2-pyridyl ketone, therefore, does not enter the coordination sphere of the copper atom, this represents a novelty in the chemistry of this class of polyfunctional molecules. The C(1)–O(1) bond length of 1.21(2) Å is significantly shorter than the corresponding distances in chromium or ruthenium complexes of hydrated DPK [average 1.392 Å] [1]. Thus the existence of a pyridyl ring in DPK instead of a phenyl ring in 2-benzoylpyridine, prevents the intramolecular oxidative cyclization of DPK, and instead a protonation occurs at a nitrogen atom with the formation of a hydrogen bond between the two pyridyl nitrogen atoms. In the polymeric CuI_2^- species, the copper and iodine atoms constitute columns of edge-

Table 2
Bond lengths (Å) and bond angles (°) for complex **1** [a]

(*i*) *Coordination geometry about Cu atom*			
I(1)–Cu(1)	2.645(4)	I(1)–Cu(1) # 1	3.074(5)
I(2)–Cu(1) # 1	2.569(3)	I(2)–Cu(1)	2.640(4)
I(2)–Cu(1)–I(1)	102.8(1)	I(1)–Cu(1)–I(1) # 2	107.8(1)
I(2)–Cu(1)–I(1) # 2	113.2(1)	I(2) # 2–Cu(1)–I(1)	120.7(1)
I(2) # 2–Cu(1)–I(2)	118.5(2)	I(2) # 2–Cu(1)–I(1) # 2	93.7(1)
Cu(1)–I(1)–Cu(1) # 1	76.81(9)	Cu(1) # 1–I(2)–Cu(1)	86.50(9)
(*ii*) *Di-2-pyridyl ketone*			
O(1)–C(1)	1.21(2)	N(1)–C(2)	1.34(2)
N(1)–C(6)	1.34(2)	N(2)–C(7)	1.34(2)
N(2)–C(11)	1.35(2)	C(1)–C(2)	1.49(2)
C(1)–C(7)	1.47(2)	C(2)–C(3)	1.39(2)
C(3)–C(4)	1.39(3)	C(4)–C(5)	1.33(3)
C(5)–C(6)	1.42(2)	C(7)–C(8)	1.39(2)
C(8)–C(9)	1.36(3)	C(9)–C(10)	1.41(3)
C(10)–C(11)	1.35(2)		
C(2)–N(1)–C(6)	126(1)	C(7)–N(2)–C(11)	119(1)
O(1)–C(1)–C(2)	118(1)	O(1)–C(1)–C(7)	120(2)
C(2)–C(1)–C(7)	122(1)	N(1)–C(2)–C(1)	122(1)
N(1)–C(2)–C(3)	117(1)	C(1)–C(2)–C(3)	121(1)
C(2)–C(3)–C(4)	120(2)	C(3)–C(4)–C(5)	120(2)
C(4)–C(5)–C(6)	121(2)	N(1)–C(6)–C(5)	116(2)
N(2)–C(7)–C(1)	119(1)	N(2)–C(7)–C(8)	121(1)
C(1)–C(7)–C(8)	120(2)	C(7)–C(8)–C(9)	120(2)
C(8)–C(9)–C(10)	118(2)	C(9)–C(10)–C(11)	120(1)
(*iii*) *Hydrogen bonding*			
N(1)–H(1)	0.81(2)	N(2)···H(1) 1.95(2)	
N(1)–H(1)···N(2)	149(1)		

[a] Similarity transformations: # 1 (x, $1-y$, $-0.5+z$); # 2 (x, $1-y$, $0.5+z$).

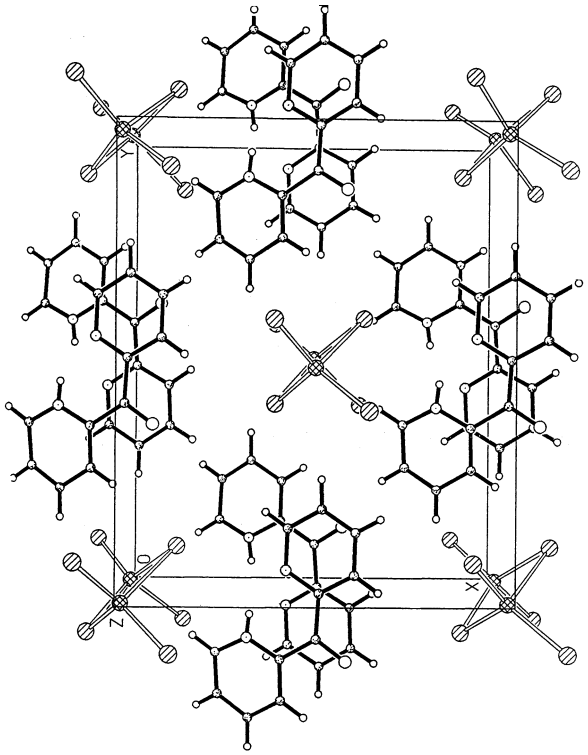


Fig. 2. A perspective view showing the packing of the cation and polymeric anion in [(DPK)H][CuI_2] (**1**) in the unit cell.

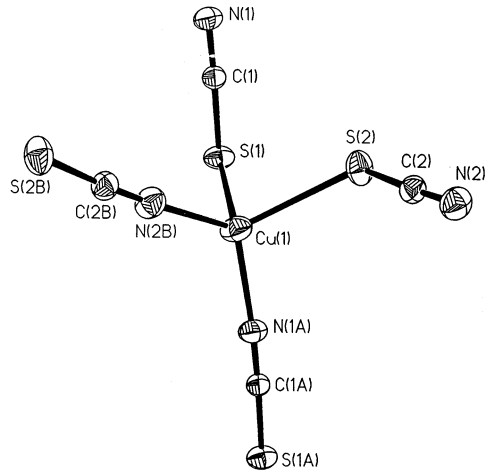


Fig. 3. The molecular structure of [(DPK)H][$Cu(NCS)_2$] (**2**) along with the atom numbering scheme.

sharing CuI_4 tetrahedra running parallel to the *b* axis (Fig. 2) with three Cu–I bond lengths of 2.618 Å (average) and a long Cu–I distance of 3.074(5) Å. These Cu–I distances (Table 2), however, are much longer than those reported [2.394(2) and 2.383(1) Å] in the previously described linear CuI_2-species [17], but closely corresponded to the distances observed in CuI complexes in which Cu is bound to two iodines in the dimeric Cu_2I_2 units, e.g. av. = 2.686 Å in [CuI(quinoline)$_2$]$_2$ [18], av = 2.655 Å in {CuI(3-Me-pyridine)$_2$]$_2$ [19]. Compared to complexes in which Cu links four iodine atoms, the Cu–I distances in the present CuI_2^- species are shorter than those (av. = 2.711 Å) in the complex $(Cu_4I_6)K_2$(15-crown-5) [20] and (av. = 2.72 Å) in $[Cu(NH_3)_4][CuI_2]_2$ [21]. The structure of the present CuI_2^- species is very similar to that found in the structure of [9-oxo-indolo[1,2-*a*]pyridinium]$^+$[CuI_2]$^-$, except that the four Cu–I bond lengths are comparable to each other [from 2.682 to 2.705 Å] and the angles I(1)–Cu(1)–I(2a) [114.6(1)°] and Cu(1)–I(2)–Cu(1a) [75.7(1)°] are much smaller [10] than in the present species (Table 2).

The principle structure features of complex **2** are illustrated in Fig. 3; bond distances and bond angles are given in Table 3. The structure consists of uncoordinated N-protonated di-2-pyridyl ketone cations and corrugated layers of $[(CuNCS)_2]_n$ at $y = 1/4$, along the *b*-axis of the unit cell (Fig. 4). Each copper atom in the layer attains an approximate tetrahedral CuS_2N_2 coordination. The Cu–N bond lengths of 1.954(2) and 1.958(2) Å, and the Cu–S distances of 2.4120(8) and 2,4501(7) Å fall within the range of those reported previously for related compounds [22,23]. The structure of this $[(CuNCS)_2]_n$ species differs from that of $[Cu(NCS)_2]_n^-$ species found in the structure of [(9-oxo-indolo[1,2-*a*]pyridinium]$^+$[$Cu(NCS)_2$]$^-$ [11]. In the later species, one independent thiocayanato group functions as a μ-N,S,S bridging tridentate ligand in which a sulfur atom links two different copper atoms and the nitrogen atom binds a third copper atom, giving rise to a puckered layer. The second thiocyanato group acts as a N-monodentate ligand.

3.2. IR spectra

The IR spectra of complexes **1** and **2** exhibit a broad band of medium intensity centered around 2749 cm^{-1} assignable to ν(N–H···N) [22]. The spectrum of free DPK does not contain such a band. The carbonyl stretching frequency which appears at 1682 cm^{-1} in the spectrum of free DPK is not influenced at all and appeared at 1685 cm^{-1} in the spectrum of **1**, suggesting that the C=O group does not participate in the bonding formation. In complex **2**, this frequency is shifted slightly to a lower frequency and appeared at 1678 cm^{-1}. This slight shift may be attributed to the packing of DPK molecules in the complex. It is well known that coordination via the lone pair of electrons of the nitrogen atom of the pyridine can shift the ring vibrations to higher frequencies [23]. The blue shifts of such bands, however, caused by complex formation by pyridine are smaller for transition metal atoms than for H^+ ion [24]. In accordnace with this, the bands due to the pyridyl rings in the range 1600–400 cm^{-1} experience large shifts in complexes **1** and **2** where a H^+ protonates one

nitrogen atom of the two pyridyl rings forming a hydrogen bond with the other, when compared with corresponding bands in free DPK. The IR spectrum of complex **2** shows a very strong and sharp band at 2100 cm^{-1}, associated with the ν(CN) of the thiocyanate group. This result is not consistent with the μ-N,S bridging mode determined by the X-ray structure analysis given above. This value, however, is not uncommon and has been observed for many other complexes containing this mode of bonded thiocayanate groups [25,26].

3.3. Electronic spectra

The electronic spectra of the solid complexes **1** and **2** mulled in Nujol (Fig. 5) exhibit very strong bands in the visible region, a very broad band covers the 350–600 nm range for **2** and at least two bands centered around 435 and 590 nm for **1**. These intense charge transfer bands may be due to XLCT (X = anion) transitions since the ligand is protonated and not coordinated in both complexes. These CT bands in both complexes, however, are significantly shifted to lower energies when compared with CT bands in corresponding complexes of 2-benzoylpyridine which appear in the range 330–480 nm [10,11]. This may be attributed to the presence of two pyridyl rings in DPK which would decrease the HOMO–LUMO gap when compared with 2-benzoylpyridine. The positions of these bands, however, are similar to those observed in the case of copper(I) complexes of pyrazine [27,28].

In CuIX ligand systems containing a ligand that permits CT transitions, or a copper–copper distance of less than 2.8 Å, emission spectra of different origins are observed usually [29–31]. Accordingly, complexes **1** and **2** are expected to demonstrate visible evidence of emission. However, neither **1** nor **2** display emission at room temperature. This result is similar to those re-

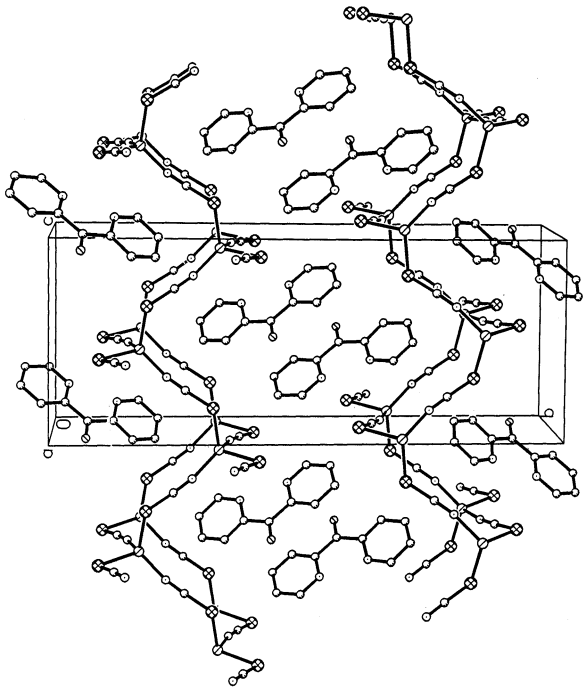


Fig. 4. A perspective view showing the packing of [(DPK)H]-[$Cu(NCS)_2$] (**2**) in the unit cell.

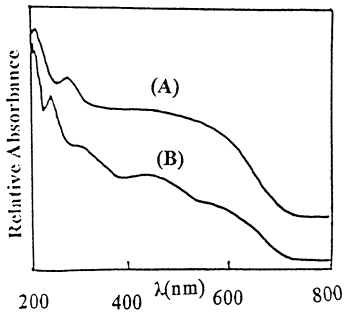


Fig. 5. The electronic spectra of solid complexes: (A) [(DPK)H]-[$Cu(NCS)_2$]; (B) [(DPK)H][CuI_2].

Table 3
Bond lengths (Å) and bond angles (°) for complex **2** [a]

Cu(1)–N(1) # 1	1.951	Cu(1)–N(2) # 2	1.963(1)
Cu(1)–S(1)	2.4121(6)	Cu(1)–S(2)	2.4495(5)
S(1)–C(1)	1.647(1)	S(2)–C(2)	1.650(1)
O(1)–C(3)	1.211(1)	N(1)–C(1)	1.150(1)
N(2)–C(2)	1.150(2)	N(3)–C(8)	1.331(2)
N(3)–C(4)	1.344(2)	N(4)–C(13)	1.336(2)
N(4)–C(9)	1.340(1)	C(3)–C(4)	1.496(2)
C(3)–C(9)	1.511(2)	C(4)–C(5)	1.380(2)
C(5)–C(6)	1.380(2)	C(6)–C(7)	1.367(2)
C(7)–C(8)	1.382(2)	C(4)–C97)	1.367(2)
C(10)–C(11)	1.387(2)	C(11)–C(12)	1.365(2)
C(12)–C(13)	1.364(2)		
N(1) # 1–Cu(1)–N(2) # 2	120.65(4)	N(1) # 1–Cu(1)–S(1)	108.02(4)
N(2) # 2–Cu(1)–S(1)	107.60(4)	N(1) # 1–Cu(1)–S(2)	109.46(3)
N(2) # 2–Cu(1)–S(1)	115.27(3)	S(1)–Cu(1)–S(2)	91.63(2)
C(1)–S(1)–Cu(1)	96.11(5)	C(2)–S(2)–Cu(1)	117.60(4)
C(8)–N(3)–C(4)	118.5(1)	C(13)–N(4)–C(9)	123.0(1)
N(1)–C(1)–S(1)	177.5(1)	N(2)–C(2)–S(2)	176.8(1)
O(1)–C(3)–C(4)	120.5(1)	O(1)–C(3)–C(9)	117.4(1)
C(4)–C(3)–C(9)	122.0(1)	N(3)–C(4)–C(5)	122.1(1)
N(3)–C(4)–C(3)	117.7(1)	C(5)–C(4)–C(3)	120.2(1)
C(4)–C(5)–C(6)	118.8(1)	C(7)–C(6)–C(5)	119.2(1)
C(6)–C(7)–C(8)	119.1(1)	N(3)–C(8)–C(7)	122.3(1)
N(4)–C(9)–C(10)	118.5(1)	N(4)–C(9)–C(3)	119.8(1)
C(10)–C(9)–C(3)	121.7(1)	C(9)–C(10)–C(11)	119.7(1)
C(12)–C(11)–C(10)	119.9(1)	C(13)–C(12)–C(11)	119.1(1)
N(4)–C(13)–C(11)	119.9(1)		

[a] Symmetry transformations used to generate equivalent atoms; # 1, $x+1$, y, z; # 2, x, $-y+3/2$, $z+1/2$.

ported for $Cu^{I}CN$ and $Cu^{I}NCS$ complexes of 2-benzoylpyridine [11] and $Cu^{I}I$–quinaldate complexes [32]. The non-emitting character of these complexes may be affected by the electron withdrawing carbonyl group which alters the energy levels of the aromatic ring to make excitation of greater energy or to make other radiationless mechanisms more efficient.

4. Supplementary data

Supplementary data are available from the CCDC, 12 Union Road, CB2 IEZ, UK (fax: +44-1223-336-033; e-mail: deposit@ccdc.cam.ac.uk or www.ccdc.cam.ac.uk) quoting the deposition numbers 121782 and 121742 for complexes **1** and **2**, respectively.

Acknowledgements

M.A.S.G. acknowledges the financial support of this work by the Kuwait University Research Administration (Project No. SC 097), and the Department of Chemistry Facility Projects (Analab). T.C.W.M. acknowledges the Hong Kong Research Grants Council Earmarked Grant Ref. no. 4022/98P.

References

[1] S. Sommerer, W.P. Jensen, R.A. Jacobson, Inorg. Chim. Acta 172 (1990) 3.
[2] G. Annibale, L. Canovese, L. Cattalini, G. Natile, M. Biagini-Cingi, A. Manotti-Lanfredi, A. Tiripecchio, J. Chem. Soc., Dalton Trans. (1981) 2280.
[3] P.K. Byers, A.J. Canty, L.M. Engelhardt, J.M. Patric, A.H. White, J. Chem. Soc., Dalton Trans. (1985) 981.
[4] S.L. Wang, J.W. Richardson, S.J. Briggs, R.A. Jacobson, W.P. Jensen, Inorg. Chim. Acta 111 (1986) 67.
[5] V. Tangoulis, C.P. Raptopoulou, S. Paschalidou, A.E. Tsohos, E.G. Bakalbassis, A. Terzis, S.P. Perelepes, Inorg. Chem. 36 (1997) 5270.
[6] V. Tangoulis, C.P. Raptopoulou, A. Terzis, S. Paschalidou, S.P. Perlepes, E.G. Bakalbassis, Inorg. Chem. 36 (1997) 3996.
[7] A. Basu, A.R. Saple, N.Y. Sapre, J. Chem. Soc., Dalton Trans. (1989) 1797.
[8] (a) D.J. Fite, W.M. Moore, K.W. Morse, J. Am. Chem. Soc. 107 (1985) 7077. (b) R.R. Hautala, J. Little, E. Sweet, Sol. Energy 19 (1977) 503. (c) G. Jones, T.E. Reinhardt, W.R. Bergmark, Sol. Energy 20 (1978) 241.
[9] (a) G. Jones, S. Chiang, P.T. Xnan, Photochemistry 10 (1978) 1. (b) S.W. Orchard, C. Kutal, Inorg. Chim. Acta 64 (1982) 195. (c) R.F. Sterling, C. Kutal, Inorg. Chem. 19 (1980) 1502. (d) N. Borsub, S. Chang, C. Kutal, Inorg. Chem. 21 (1982) 538.
[10] M.A.S. Goher, A.E.H. Abdou, B.S. Luo, T.C.W. Mak, J. Coord. Chem. 36 (1995) 71.
[11] M.A.S. Goher, R.J. Wang, T.C.W. Mak, J. Coord. Chem. 38 (1996) 151.
[12] M.A.S. Goher, T.C.W. Mak, Polyhedron 17 (1998) 3485.
[13] N. Walker, D. Stuart, Acta Crystallogr., Sect. A 39 (1983) 158.
[14] G.M. Sheldrick, in: G.M. Sheldrick, C. Kruger, R. Goddard (Eds.), Crystallographic Computing 3: Data Collection, Structure Determination, Proteins and Databases, Oxford University, New York, 1985, pp. 175–189.
[15] G.M. Sheldrick, SHELXTL-PC Manual, Siemens Analytical X-ray Instruments Inc., Madison, WI, 1990.
[16] International Tables for X-ray Crystallography, vol. IV, Kynoch, Birmingham, 1974, pp. 55, 99, 149 (now distributed by Kluwer Academic, Dordrecht).
[17] N.P. Rath, E.M. Holt, J. Chem. Soc., Chem. Commun. (1986) 311.
[18] N.P. Rath, E.M. Holt, J. Chem. Soc., Dalton Trans. (1986) 2303.
[19] N.P. Rath, J.L. Maxwell, E.M. Holt, J. Chem. Soc., Dalton Trans. (1986) 2449.
[20] N.P. Rath, E.M. Holt, J. Chem. Soc., Chem. Commun. (1985) 665.
[21] J.A. Baglio, H.A. Weaklime, F. Demallio, P.A. Vaughan, J. Inorg. Nucl. Chem. 35 (1970) 795.
[22] I. Nakagawa, T. Shimanouchi, Spectrochim. Acta 20 (1964) 429.
[23] K. Nakamoto, Infrared and Raman Spectra of Inorganic and Coordination Compounds, Wiley, New York, 1978.
[24] P.C.H. Mitchell, J. Inorg. Nucl. Chem. 21 (1961) 382.
[25] (a) J. Chatt, L.A. Duncanson, Nature 178 (1956) 997. (b) J. Chatt, F.A. Hart, P.G. Owston, Nature 181 (1958) 43.
[26] (a) P.G. Owston, J.M. Rowe, Acta Crystallogr. 13 (1960)253. (b) M.A.S. Goher, L.A. Al-Shatti, F.A. Mautner, Polyhedron 16 (1997) 889.
[27] J.M. Moreno, J. Suarez-Varela, E. Colacio, J.C. Avita-Roson, M.A. Hidalgo, D. Martin-Ramos, Can. J. Chem. 73 (1995) 1595.
[28] M.A.S. Goher, F.A. Mautner, Polyhedron MS. 99-208.
[29] (a) K.R. Kyle, P.C. Ford, J. Am. Chem. Soc. 111 (1989) 5005. (b) K.R. Kyle, W.E. Polke, P.C. Ford, Coord. Chem. Rev. 97 (1990) 35.
[30] (a) K.R. Kyle, C.K. Ryu, J.A. DiBenedetto, P.C. Ford, J. Am. Chem. Soc. 113 (1991) 2954. (b) N.P. Rath, E.M. Holt, K. Taminura, Inorg. Chem. 24 (1985) 3934. (c) C.K. Ryu, K.R. Kyle, P.C. Ford, Inorg. Chem. 30 (1991) 3982.
[31] M. Vitale, W.E. Palke, P.C. Ford, J. Phys. Chem. 96 (1992) 8329.
[32] J.A. Tompkins, J.L. Maxwell, E.M. Holt, Inorg. Chim. Acta 127 (1987) 1.

PERGAMON

www.elsevier.nl/locate/poly

Polyhedron 19 (2000) 1471–1478

POLYHEDRON

Hexanuclear complexes of molybdenum(V) containing $[Mo_6O_{12}(OCH_3)_4(acac)_3]^-$ anion

Marina Cindrić *, Gordana Pavlović, Višnja Vrdoljak, Boris Kamenar

Chemistry Department, Laboratory of General and Inorganic Chemistry, Faculty of Science, University of Zagreb, Ulica kralja Zvonimira 8, 10000 Zagreb, Croatia

Received 28 January 2000; accepted 13 April 2000

Abstract

The novel hexanuclear oxoclusters of the general formula $R[Mo_6O_{12}(OCH_3)_4(acac)_3]$ (**1**–**7**), where $R = CH_3NH_3$ (**1**), C_5H_5NH (**2**), $(CH_3)_2CHNH_3$ (**3**), $(CH_3)_3CNH_3$ (**4**), $C_5H_{11}NH$ (**5**), $(C_2H_5)_3NH$ (**6**), and $C_6H_5NC_{11}H_{13}O_2$ (**7**) have been obtained by the reactions of the binuclear oxomolybdenum(V) complex $[Mo_2O_3(acac)_4]$ (acac = acetylacetonate ion) with a variety of alkyl or aryl amines or corresponding alkyl or aryl ammonium chlorides in methanol. The formation of 3,5-diacyl-2,6-dimethyl-1-pheny-l-pyridinium cation in **7** is explained by the cyclization via Hantzsch condensation of acetylacetone, formaldehyde and aniline. The molecular structures of complexes **5**, **6** and **7** have been determined by a single-crystal X-ray diffraction study. In all salts the anion is of hexanuclear nature in which molybdenum atoms are bridged by oxo-oxygen and methoxo-oxygen atoms. Six Mo-octahedra are fused through edges, thus allowing the formation of localized metal–metal bonds between three pairs of molybdenum atoms. © 2000 Elsevier Science Ltd. All rights reserved.

Keywords: Molybdenum; Oxocluster complexes; Hantzsch synthesis; Crystal structures; Hexanuclear molybdenum(V) complexes

1. Introduction

Organic derivatives of isopolymolybdate anions have been extensively studied as models for the investigation of the interactions between organic molecules and catalytic metal oxide surfaces, as well as in the catalytic photo-oxidation of organic compounds [1–10]. The isopolymolybdate complexes containing alkoxo ligands are particularly known and investigated as models for selective hydrolysis of ethylene oxide to monoethylene glycol and for oxidation of primary and secondary alcohols [11–14]. However, whereas in all known cases high nuclearity molybdenum complexes usually contain either Mo(VI) ions or mixed valence Mo(VI)/Mo(V) clusters, the complexes of isopolymolybdates(V) containing more than four Mo(V) atoms with organic ligands are still relatively unknown [15]. The rare examples are $[Mo_6O_6Cl_6(\mu_3\text{-}O)_2(\mu\text{-}OC_2H_5)_6(\mu\text{-}Cl)_2]$ [16], $[(n\text{-}C_4H_9)_4N]_2[Mo_8O_{16}(OC_2H_5)_8(C_2O_4)]$ [17], $[Mo_8O_{16}(OCH_3)_8\{P(CH_3)_3\}_4]$ [18] and $[Mo_6O_{15}(PO_4)_4]^{12-}$ [19,20].

In continuation of our previous research on molybdenum(V) complexes, we have synthesized novel hexanuclear oxocluster salts with different cations: $R[Mo_6O_{12}(OCH_3)_4(acac)_3]$, where $R = CH_3NH_3$ (**1**), C_5H_5NH (**2**), $(CH_3)_2CHNH_3$ (**3**), $(CH_3)_3CNH_3$ (**4**), $C_5H_{11}NH$ (**5**), $(C_2H_5)_3NH$ (**6**), and $C_6H_5NC_{11}H_{13}O_2$ (**7**). They were prepared by the reactions of $[Mo_2O_3(acac)_4]$ with a variety of alkyl or aryl amines or corresponding alkyl or aryl ammonium chlorides in methanol.

The molecular structures of complexes **5**, **6** and **7** have been determined by a single-crystal X-ray diffraction study thus proving the hexanuclear nature of the anion in all prepared salts. The coordination octahedra within the hexanuclear anions are interconnected by sharing common edges, thus allowing the formation of localized metal–metal bonds between three pairs of molybdenum ions in such a way that they follow the alkoxide structural pattern found in the tetranuclear molybdenum(V) complexes $[Mo_4Cl_4O_6(O^nPr)_4(HO^nPr)_2]$ [21,22], $[Mo_4O_8(O^iPr)_4(py)_4]$ [23], $[Mo_4Cl_4O_8(OEt)_2(HOEt)_2]^{2-}$ [24] and $[Mo_4Cl_4O_6(OEt)_4(HOEt)_2]$ [25], as

* Corresponding author. Tel.: +385-1-4606653; fax: +385-1-4611191.

E-mail address: marina@chem.pmf.hr (M. Cindrić).

0277-5387/00/$ - see front matter © 2000 Elsevier Science Ltd. All rights reserved.
PII: S0277-5387(00)00405-8

well as in the tetranuclear β-diketonato complexes $[Mo_4O_6S_2(R'COCHCOCH_3)_2(OSCR'')_2]$ ($R' = -CH_3$ or $-C_6H_5$ and $R'' = -C_6H_5$, $-CH_3$, $-C(CH_3)_3$ or $-CH_2CH(CH_3)_2$) [26].

In preparing **7** by reacting $[Mo_2O_3(acac)_4]$ with aniline, we did not obtain anilinium but 3,5-diacyl-2,6-dimethyl-1-phenylpyridinium salt showing that the formation of the cation occurred via Hantzsch condensation [27,28] in which aniline, formaldehyde and acetylacetone form an intermediate, which on further oxidation produces a cyclic product.

2. Experimental

All chemicals were of reagent grade and used as purchased. Methanol was dehydrated on magnesium and distilled immediately before use. The starting acetylacetonato complex $[Mo_2O_3(acac)_4]$ was prepared as described in the literature [29,30]. C, H and N analyses were provided by the Analytical Services Laboratory of Institute Rudjer Bošković. Molybdenum was determined according to the method described in the literature [31]. Infrared spectra were recorded in KBr with an FT-IR 1600 Fourier transform spectrophotometer in the 4500–450 cm^{-1} region. Thermogravimetric (TG) analyses were measured on a Mettler TG 50 thermobalance using aluminum crucibles under oxygen atmosphere with a heating rate of 5°C min^{-1}. For all experiments the temperature ranged from 30 to 600°C. The results were developed by applying the GrafVare 2.1. program.

2.1. General procedures for the synthesis of complexes

Method A. $[Mo_2O_3(acac)_4]$ (0.25 g, 0.4 mmol) was suspended in dry methanol (25 ml) and appropriate amine (0.4 mmol) was added. The mixture was gently warmed for 1.5 h. An orange–red crystalline product was obtained from solution left at room temperature (r.t.) for 5–10 days. It was filtered off, washed with cold methanol and dried. Yields are based on $[Mo_2O_3(acac)_4]$.

Method B. $[Mo_2O_3(acac)_4]$ (0.25 g, 0.4 mmol) and appropriate organoammonium chloride (0.4 mmol) were suspended in dry methanol (25 ml). The mixture was gently warmed for 1 h. Within minutes the suspension cleared to an orange solution from which a small amount of pale orange solid precipitated. The by-product was collected by filtration, washed with cold methanol and dried. The filtrate was left at r.t. for 5–10 days. An orange–red crystalline product was filtered off, washed with cold methanol and dried. IR and elemental analyses showed that compounds (**1**–**7**) were identical to those prepared by method A.

2.1.1. Methylammonium μ_3-methoxo-tri-μ-methoxo-tri-μ_3-oxo-tri-μ-oxo-tris(acetylacetonato)hexaoxohexamolybdate(V), $(CH_3NH_3)[Mo_6O_{12}(OCH_3)_4(acac)_3]$ (1)

Yield: 0.05 g, 31.3% (method A, obtained from the reaction with CH_3NH_2), and 0.03 g, 18.8% (method B, obtained from the reaction with $CH_3NH_2{\cdot}HCl$). *Anal.* Calc. for $C_{20}H_{39}Mo_6NO_{22}$ ($M_r = 1221.162$): C, 19.67; H, 3.22; Mo, 47.14; N, 1.15. Found: C, 19.98; H, 3.68; Mo, 46.85; N, 1.55%. TG: 70.48% MoO_3 (Calc. 70.72%). IR data (KBr, cm^{-1}): 3212 (m), 2924 (m), 2815 (m), 1572 (s), 1512 (s), 1428 (m), 1361 (s), 1271 (m), 1048 (m), 960 (s), 740 (m), 704 (m), 669 (m), 546 (m), 484 (m).

2.1.2. Pyridinium μ_3-methoxo-tri-μ-methoxo-tri-μ_3-oxo-tri-μ-oxo-tris(acetylacetonato)hexaoxohexamolybdate(V) 2,5-diethyl-3,6-dimethyl-1,4-benzenedicarboxylic acid solvate (1/1), $(C_5H_5NH)[Mo_6O_{12}(OCH_3)_4(acac)_3]{\cdot}C_{12}H_{18}O_4$ (2)

When the product **1** was separated by filtration and the resulting filtrate left to stand for further 5 days new red crystals of **2** were obtained. Yield: 0.01 g, 5.1% (method A), and 0.01 g, 5.1% (method B). *Anal.* Calc. for $C_{36}H_{57}Mo_6NO_{26}$ ($M_r = 1495.466$): C, 28.91; H, 3.84; Mo, 38.49; N, 0.94. Found: C, 28.27; H, 4.02; Mo, 37.93; N, 1.58%. TG: 57.46% MoO_3 (Calc. 57.75%). IR data (KBr, cm^{-1}): 3421 (m), 2921 (m), 2819 (m), 1702 (s), 1573 (s), 1515 (s), 1429 (s), 1362 (s), 1272 (s), 1052 (s), 960 (s), 749 (m), 670 (s), 518 (m), 472 (s).

2.1.3. i-Propylammonium μ_3-methoxo-tri-μ-methoxo-tri-μ_3-oxo-tri-μ-oxo-tris(acetylacetonato)-hexaoxohexamolybdate(V), $[(CH_3)_2CHNH_3][Mo_6O_{12}(OCH_3)_4(acac)_3]$ (3)

Yield: 0.05 g, 30.5% (method A, obtained from the reaction with $(CH_3)_2CHNH_2$), and 0.02 g, 12.2% (method B, obtained from the reaction with $(CH_3)_2CHNH_2{\cdot}HCl$). *Anal.* Calc. for $C_{22}H_{43}Mo_6NO_{22}$ ($M_r = 1249.214$): C, 21.15; H, 3.47; Mo, 46.08; N, 1.12. Found: C, 20.98; H, 3.73; Mo, 46.32; N, 1.41%. TG: 69.48% MoO_3 (Calc. 69.13%). IR data (KBr, cm^{-1}): 3159 (m), 2931 (m), 2820 (m), 1512 (s), 1426 (m), 1356 (s), 1274 (m), 1049 (m), 964 (s), 741 (m), 704 (m), 668 (m), 546 (m), 486 (m).

2.1.4. t-Butylammonium μ_3-methoxo-tri-μ-methoxo-tri-μ_3-oxo-tri-μ-oxo-tris (acetylacetonato)hexaoxo-hexamolybdate(V) methanol solvate (1/1), $[(CH_3)_3CNH_3][Mo_6O_{12}(OCH_3)_4(acac)_3]{\cdot}CH_3OH$ (4)

Yield: 0.05 g, 29.5% (method A, obtained from the reaction with $(CH_3)_3CNH_2$), and 0.02 g, 11.8% (method B, from the reaction with $(CH_3)_3CNH_2{\cdot}HCl$). *Anal.* Calc. for $C_{24}H_{49}Mo_6NO_{23}$ ($M_r = 1295.28$): C, 22.25; H, 3.81; Mo, 44.44; N, 1.08. Found: C, 21.92; H, 4.48; Mo, 44.64; N, 1.23%. TG: 67.10% MoO_3 (Calc. 66.67%);

2.24% methanol (Calc. 2.47%) corresponding to one methanol per one complex molecule. IR data (KBr, cm^{-1}): 3146 (m), 2975 (m), 2924 (m), 2820 (m), 1572 (s), 1512 (s), 1425 (m), 1364 (s), 1271 (m), 1032 (m), 960 (s), 744 (m), 704 (m), 665 (m), 547 (m), 484 (m).

2.1.5. Piperidinium μ_3-methoxo-tri-μ-methoxo-tri-μ_3-oxo-tri-μ-oxo-tris(acetylacetonato)hexaoxohexamolybdate(V), $[C_5H_{12}N][Mo_6O_{12}(OCH_3)_4(acac)_3]$ (5)

Yield: 0.09 g, 53.9% (method A, from the reaction with $C_5H_{11}N$), and 0.04 g, 23.9% (method B, from the reaction with $C_5H_{11}N{\cdot}HCl$). *Anal.* Calc. for $C_{24}H_{45}Mo_6NO_{22}$ ($M_r = 1275.25$): C, 22.60; H, 3.56; Mo, 45.14; N, 1.10. Found: C, 22.32; H, 4.23; Mo, 45.54; N, 1.39%. TG: 67.98% MoO_3 (Calc. 67.72%). IR data (KBr, cm^{-1}): 2921 (m), 2820 (m), 1572 (s), 1514 (s), 1428 (m), 1360 (s), 1272 (m), 1051 (m), 963 (s), 746 (m), 671 (m), 547 (m), 474 (m).

2.1.6. Triethylammonium μ_3-methoxo-tri-μ-methoxo-tri-μ_3-oxo-tri-μ-oxo-tris(acetylacetonato)hexaoxohexamolybdate(V), $[(C_2H_5)_3NH][Mo_6O_{12}(OCH_3)_4(acac)_3]$ (6)

Yield: 0.05 g, 29.5% (method A, from the reaction with $(C_2H_5)_3N$), and 0.02 g, 11.8% (method B, from the reaction with $(C_2H_5)_3N{\cdot}HCl$ *Anal.* Calc. for $C_{25}H_{49}Mo_6NO_{22}$ ($M_r = 1291.29$): C, 23.25; H, 3.83; Mo, 44.58; N, 1.08. Found: C, 23.06; H, 4.23; Mo, 44.48; N, 1.03%. TG: 67.21% MoO_3 (Calc. 66.88%). IR data (KBr, cm^{-1}): 2923 (m), 2814 (m), 1580 (s), 1513 (s), 1474 (m), 1449 (m), 1425 (m), 1365 (s), 1269 (m), 1053 (s), 962 (s), 742 (m), 703 (m), 669 (m), 546 (m), 483 (m).

2.1.7. 3,5-Diacyl-2,6-dimethyl-1-phenylpyridinium μ_3-methoxo-tri-μ-methoxo-tri-μ_3-oxo-tri-μ-oxo-tris-(acetylacetonato)hexaoxohexamolybdate(V), $[C_{17}H_{18}NO_2][Mo_6O_{12}(OCH_3)_4(acac)_3]$ (7)

Yield: 0.03 g, 15.7%, (method A, from the reaction with $C_6H_5NH_2$; the product **7** was not obtained by method B). *Anal.* Calc. for $C_{36}H_{51}Mo_6NO_{24}$ ($M_r = 1457.42$): C, 29.67; H, 3.53; Mo, 39.50; N, 0.96. Found: C, 30.16; H, 4.21; Mo, 39.14; N, 1.15%. TG: 59.65% MoO_3 (Calc. 59.26%). IR data (KBr, cm^{-1}): 3073 (w), 2921 (m), 2821 (m), 1711 (m), 1686 (m), 1574 (s), 1516 (s), 1458 (m), 1429 (m), 1363 (s), 1272 (m), 1053 (s), 1026 (m), 970 (s), 959(s), 940 (m), 748 (m), 672 (m), 515 (m), 476 (m).

2.2. X-ray crystallography

A summary of crystallographic data is given in Table 1. Intensity data for all structures were corrected for Lorentz-polarization effects, but not for absorption. Accurate cell constants were determined by full-matrix least-squares refinement of the carefully centered and randomly selected reflections (35 reflections in the range $9.1 \leq \theta \leq 19.2°$ for **5**, 28 in the range $10.0 \leq \theta \leq 14.7°$ for **6** and 28 in the range $10.0 \leq \theta \leq 17.4°$ for **7**). Cell refinement, data collection procedure and Lp corrections were performed by STADI4 [32] and X-RED [33] programs.

The structure solution and refinement were performed through direct, Fourier and full-matrix least-squares methods performed by SHELXS-96 [34] and SHELXL-97 [35] for **6** and **7** and by NRCVAX program package [36] for **5**. Hydrogen atoms were generated by stereochemical constraints and refined by applying a riding model (C–H 0.95 Å and $U_{iso}(H) = 1.2\ U_{eq}(Csp^2$ or $Csp^3)$ in **5**; Csp^3–H 0.96 Å, Csp^2–H 0.93 Å and $U_{iso}(H) = 1.2\ U_{eq}$ (Csp^2) or 1.5 for Csp^3 in **6** and **7**).

The presence of a 'heavy' hexanuclear Mo core in the complex anion and the holes generated in the crystal structures by ions in order to accommodate small organic cations have been limiting factors in the refinement of organic cations. Therefore, due to possible positional disorder, the ring atoms of the piperidinium cation in **5** as well as C and N atoms of triethylammonium cation in **6** have not been properly resolved. In both structures they were refined isotropically. The H atom belonging to the nitrogen atom in **6** was found in different Fourier maps at the last stage of refinement at the N–H distance of 0.98 Å. Since it was not well defined, it was generated at an ideal geometrical position and allowed to ride on the parent N atom. In **7**, all non-H atoms were refined anisotropically. The molecular graphics have been performed by the PLATON98 program [37].

Fig. 1. shows an ORTEP drawing of the complex anion in the structure of triethylammonium derivative **6**.

Fig. 2 represents 3,5-diacyl-2,6-dimethyl-1-phenylpyridinium cation in the structure of $[C_{17}H_{18}NO_2]$-$[Mo_6O_{12}(OCH_3)_4(acac)_3]$ (**7**). The same atomic numbering scheme as that in Fig. 1 has been applied for the atoms in the anions of **5** and **7**.

3. Results and discussion

3.1. Synthesis and characterization of complexes

Complexes of general formula $R[Mo_6O_{12}(OCH_3)_4(acac)_3]$ (**1**–**7**) have been prepared by using $[Mo_2O_3(acac)_4]$ as starting reagent in the reaction with a variety of alkyl or aryl amines of cyclic, acyclic, primary, secondary and tertiary type: (i) CH_3NH_2; (ii) $(CH_3)_2CHNH_2$; (iii) $(CH_3)_3CNH_2$; (iv) $C_5H_{11}NH$; (v) $(C_2H_5)_3N$ and (vi) $C_6H_5NH_2$. The obtained complexes were characterized as novel oxocluster salts containing hexanuclear anions and different organoammonium cations.

However, while the reaction products with secondary and tertiary amines were of the expected nature, those

Table 1
General and crystal data and summary of intensity data collection and structure refinement [a,b]

Compound	**5**	**6**	**7**
Formula	$C_{24}H_{45}Mo_6NO_{22}$	$C_{25}H_{49}Mo_6NO_{22}$	$C_{36}H_{51}Mo_6NO_{24}$
M_r	1275.25	1291.29	1457.42
Crystal system and habit	monoclinic, prism	monoclinic, prism	triclinic, prism
Space group	$P2_1/n$	$C2/c$	$P\bar{1}$
Unit cell parameters			
a (Å)	16.025(9)	29.550(3)	12.140(3)
b (Å)	13.103(6)	13.0214(15)	12.764(3)
c (Å)	21.763(15)	22.926(3)	17.921(2)
α (°)			79.144(9)
β (°)	109.20(5)	101.503(16)	70.916(13)
γ (°)			72.033(17)
V (Å^3)	4316(4)	8644.3(17)	2484.5(9)
Z	4	8	2
D_c (g cm^{-3})	1.963	1.984	1.948
μ (mm^{-1})	1.72	1.76	1.55
$F(000)$	2496	5072	1436
2θ range for data collection (°)	4–54	4–54	4–54
h, k, l range	−20–19, 0–16, 0–27	−37–36, 0 –16, 0–29	−14–15, −16–16, 0–22
Scan type	ω	$\omega/2\theta$	$\omega/2\theta$
Number of measured reflections	9545	9530	11097
Number of independent reflections (R_{int})	9344(0.026)	9293(0.0704)	10745(0.2085)
Number of refined parameters	448	465	604
Number of observed reflections, $I \geq 2\sigma(I)$	5384	6655	5988
Refinement method	full-matrix least-squares on F	full-matrix least-squares on F^2	
R, wR [$I \geq 2\sigma(I)$]	0.053, 0.103	0.050, 0.120	0.078, 0.191
R, wR (all data)		0.080, 0.135	0.147, 0.235
Goodness of fit on F (for 5) or F^2 (for **6** and **7**), S	1.02	1.018	0.967
Max., min. electron density (e Å^{-3})	−1.06;1.31	−1.16; 1.32	−1.75; 2.75
Maximum Δ/σ	0.004	0.002	0.001

[a] Data in common: ambient temperature for data collection on Philips PW1100 automatic four-circle diffractometer.
[b] Radiation used: Mo Kα ($\lambda = 0.71073$ Å).

with primary amines were not. In the reaction of methylamine or methylammonium chloride with $[Mo_2O_3(acac)_4]$, two different salts of hexanuclear molybdenum(V) clusters were obtained: methylammonium salt **1** as a less soluble reaction product and compound **2** as the pyridinium salt, which cocrystalize together with terephthalic acid derivative. After **1** was separated and the resulting filtrate was left to stand for 5 days, the new red crystalline product was precipitated. The appearance of dicarboxylic acid was not expected but it may be explained by the condensation of a variety unidentified by-products present in the solution. In the analogous reactions with *i*-propylamine or *t*-butylamine (or *i*-propylammonium or *t*-butylammonium chloride), besides of **3** and **4**, the similar red crystalline products were also obtained but the resulting crystals were stable in solution only for 2–3 h. The obtained amounts however were insufficient for chemical analyses, and the crystals were of very small size, fragile and not suitable for X-ray data collections.

In the reaction of $[Mo_2O_3(acac)_4]$ with aniline, only one product was obtained and it was identified as

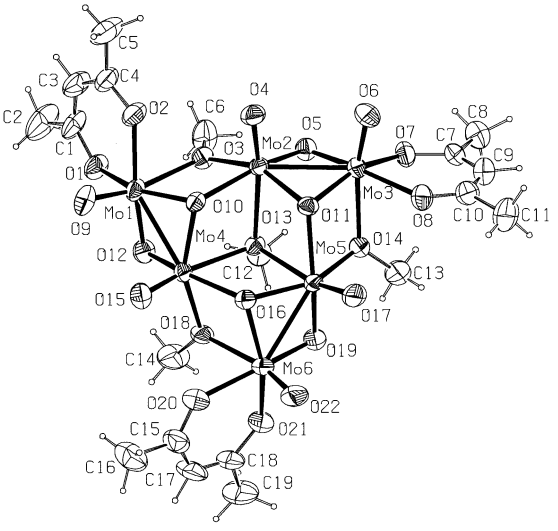


Fig. 1. The ORTEP drawing with crystallographic atom numbering scheme of the $[Mo_6O_{12}(OCH_3)_4(acac)_3]^-$ anion in the structure of $[(CH_3CH_2)_3NH][Mo_6O_{12}(OCH_3)_4(acac)_3]$ (**6**). Thermal ellipsoids represent 50% probability.

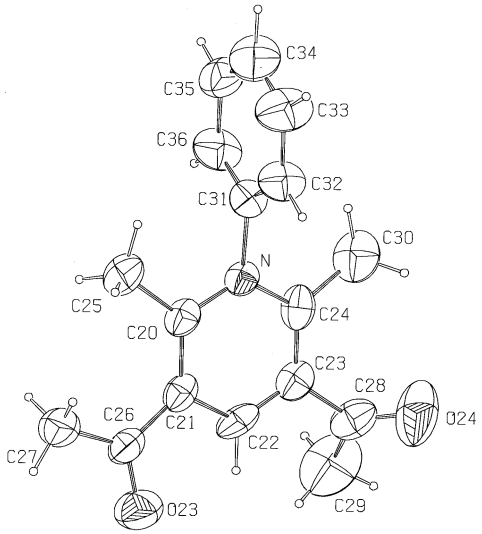


Fig. 2. The ORTEP drawing with crystallographic atom numbering scheme of 3,5-diacyl-2,6-dimethyl-1-phenylpyridinium cation in the structure of $[C_{17}H_{18}NO_2][Mo_6O_{12}(OCH_3)_4(acac)_3]$ (**7**). The thermal ellipsoids represent 50% probability.

$[C_{17}H_{18}NO_2][Mo_6O_{12}(OCH_3)_4(acac)_3]$ (**7**). The formation of such a pyridinium derivative (Fig. 2) may only be explained by the Hantzsch condensation of 2,4-pentandione with formaldehyde in the presence of amine, and it has already been observed and described in the literature [27,28]. It is reasonable to suppose that the intermediate formaldehyde was produced in situ from molybdenum catalyzed oxidation of methanol [11–14], while the β-diketone was the by-product of the same reaction. Further aromatization of a cyclic product, N-substituted dihydropyridine, is most probably the result of oxidation due to the presence of oxygen [38,39]. This mechanism was supported by further experiment: if the reaction was carried out in the atmosphere of dry nitrogen, the corresponding pyridinium salt was not obtained thus proving that such a catalytic cycle is indispensably dependent upon the presence of oxygen.

Additionally, it should be mentioned that such a product was obtained only if freshly distilled dry methanol was used in the reaction. Otherwise the traces of water inhibit the formation of formaldehyde due to the hydrolysis of methoxo groups. According to the elemental and spectroscopic analyses, the colourless solids obtained from the reaction carried out in aqueous methanol gave the corresponding ammonium octamolybdates with $[Mo_8O_{26}]^{4-}$ anions. The octamolybdate(VI) compounds have been identified chemically as well as by IR spectra and some of them by single-crystal X-ray structure analysis [40]. In addition, more species are present in solution but they do not precipitate together owing to their different solubility. All products from **1** to **7** were considerably unstable in methanol solution and their decomposition was accompanied by colour changes of their solutions, after 2 or 3 weeks, from bright orange to dark green and finally blue.

Complexes **1**–**7** were insoluble in almost all common organic solvents except their slight solubility in methanol, but they were extraordinarily soluble in water. However, in all cases the dissolution in water was accompanied by fast (1 or 2 min) oxidation of molybdenum(V) to molybdenum(VI) showing colour change from orange red to colourless.

The complexes were also characterized by IR spectroscopy. The single strong absorption found at about 960 cm^{-1} is characteristic of ν(Mo=O), while the bands at 740 and 705 cm^{-1} were assigned to the double and triple bridging oxo groups (MoOMo and Mo_3O), respectively. Also, the bands at about 665 and 545 cm^{-1} correspond to the vibrations of doubly and triply bridging methoxo groups ($Mo(OCH_3)Mo$ and Mo_3OCH_3), respectively. The remaining frequencies in the IR spectra were definitely due to the vibrations within the cation and ligands.

Samples of all complexes **1**–**7** showed similar thermographic behaviour. A weight loss between r.t. and 100°C observed only in the case of *t*-butyl salt **4** could be attributed to the loss of a solvated methanol molecule, while significant weight losses between 200–450°C observed for all samples are indicative of their decomposition. Thermal decompositions should proceed through complex intermediates finally resulting in the solid residues (in oxygen atmosphere) identified as MoO_3. The agreements between calculated and experimental mass losses are within experimental error, thus proving the formulation of each particular complex.

3.2. Structural studies

Compounds **5**, **6** and **7** have been structurally characterized by X-ray single-crystal diffractometry. The composition and structure of **2** was also confirmed by X-ray structural analysis, but owing to the poor quality of the obtained single crystal, the final refinement could not be performed (its unit cell parameters were determined as: $a = 22.813(3)$, $b = 13.045(1)$, $c = 31.957(5)$ Å, $\beta = 103.57(2)°$, $V = 9244.8(17)$ Å^3, monoclinic space group, $I2/a$, $Z = 8$). All of them contain different cations but the same hexameric cluster anion $[Mo_6O_{12}(OCH_3)_4(acac)_3]^-$. Such an anion contains six Mo(V) ions each coordinated by six oxygen atoms in the form of a distorted octahedron. These oxygens originate from different ligands: terminal-oxo oxygens, bridging and triply bridging oxo and methoxo groups or from acetylacetonato ligands. As can be seen from Fig. 1, its structure can be considered as a metal-oxide core surrounded by organic ligands.

Polynuclear Mo(V) oxo complexes containg more than four Mo(V) centres and with Mo(V) d-electrons

engaged in the formation of Mo(V)–Mo(V) single bonds are rare and can be regarded as high-nuclearity species [15]. The Mo(V) chloro–oxo complex $[Mo_6O_6Cl_6(\mu_3\text{-}O)_2(\mu\text{-}OC_2H_5)_6(\mu\text{-}Cl)_2]$ [16] with six Mo(V) centres is the only example known so far. The investigated hexametallic clusters with the unique Mo(V) oxo core moiety represent the first example of such types of high-nuclearity oxomolybdenum(V) clusters. Such a structural motif arranged as edge-sharing MoO_6 octahedra minimizes the distortion of each molybdenum coordination sphere as well as steric interactions between the ligands. The six Mo ions do not have the same coordination environment: three of them, Mo1, Mo3 and Mo6 are surrounded by one terminal oxygen, one bridging oxygen, one triply bridging oxygen, one methoxy bridging oxygen atom, and two oxygen atoms from bidentate acetylacetonate ligands, while the another three Mo atoms, Mo2, Mo4 and Mo5 are surrounded by one terminal oxygen, one bridging oxygen, two triply bridging oxygen, one methoxo bridging oxygen atom, and one triply bridging methoxo group (Fig. 1). Such metal centre aggregations enable three pairs of metal–metal bonding with Mo–Mo bond lengths in the range 2.593(2)–2.598(2) Å in **5**, 2.595(1)–2.608(1) Å in **6** and 2.597(2)–2.603(1) Å in **7**. The diamagnetic behaviour of our complexes is confirmed by these Mo–Mo single bonds (Table 2).

The coordination octahedra around all six molybdenum atoms are significantly distorted in all three structures. These distortions are most evident within the octahedra with an angle occupied by triply bridging μ_3-O oxygen atoms (Table 3).

The Mo–O bond distances are listed in Table 2. They depend upon the nature of the bridging role of any single oxygen atom and upon the *trans* influence of $Mo{=}O_t$ and $Mo{-}O_b$ bonds. The $Mo{=}O_t$ distances are within expected values ranging between 1.651(9) and 1.694(8) Å for all three structures. The Mo–O (doubly bridging) bond length values vary between 1.887(7) and 1.935(8) Å in **5**; 1.901(4) and 1.937(4) Å in **6** and 1.903(8) and 1.950(7) Å in **7**. The Mo–O (triply bridging) bond length values vary between 1.990(7) and 2.139(6) Å in **5**, 2.004(4) and 2.119(4) Å in **6** and 1.999(7) and 2.159(7) Å in **7**.

Three of four OCH_3 groups form a double bridge between two Mo atoms, while one methoxo-O atom acts as a triple bridge between three Mo atoms. The Mo–O bond length values in comparison to the doubly bridging methoxo-O atoms are considerably different and depend upon the position within particular Mo coordination ocahedra. Out of six, three bonds *trans* to $Mo{=}O_t$ are remarkably longer than the others (Table 2). The $Mo{-}O(OCH_3)$ (triply bridging) bond lengths be-

Table 2
The Mo–O bond lengths within the complex anion $[Mo_6O_{12}(OCH_3)_4(acac)_3]^-$ of **5**, **6** and **7** (Å)

Compound	Mo–Mo	Mo–O_t	Mo–Ob(μ_2)	Mo–Ob (μ_3)	Mo–OCH_3 (μ_2)	Mo–OCH_3(μ_3)	Mo–O (acac)
5	2.598(2)	1.685(8)	1.935(8)	2.002(7)	2.240(7)	2.260(6)	2.041(9)
	2.593(2)	1.670(7)	1.887(7)	2.139(6)	2.012(7)	2.268(6)	2.075(8)
	2.597(2)	1.672(8)	1.887(7)	2.015(7)	2.026(7)	2.276(6)	2.078(8)
		1.693(7)	1.925(8)	2.129(6)	2.226(7)		2.099(8)
		1.675(7)	1.922(7)	2.024(6)	2.227(7)		2.121(8)
		1.658(7)	1.932(7)	2.017(7)	2.021(6)		2.137(7)
				2.022(6)			
				1.990(7)			
				2.134(6)			
6	2.595(1)	1.679(5)	1.935(4)	2.018(4)	2.249(4)	2.270(4)	2.042(5)
	2.603(1)	1.683(4)	1.901(4)	2.004(4)	2.019(4)	2.291(4)	2.054(4)
	2.608(1)	1.671(4)	1.935(4)	2.130(4)	2.228(4)	2.312(4)	2.061(5)
		1.681(4)	1.921(4)	2.014(4)	2.038(4)		2.113(5)
		1.671(5)	1.920(4)	2.119(4)	2.010(4)		2.139(5)
		1.669(5)	1.937(5)	2.012(4)	2.240(4)		2.141(5)
				2.010(4)			
				2.008(4)			
				2.119(4)			
7	2.599(2)	1.651(9)	1.931(7)	2.020(7)	2.249(7)	2.277(7)	2.058(8)
	2.597(2)	1.693(8)	1.927(8)	2.122(7)	2.010(7)	2.315(7)	2.060(8)
	2.603(1)	1.686(9)	1.903(8)	2.012(7)	2.252(8)	2.309(8)	2.074(9)
		1.672(8)	1.946(8)	1.999(7)	2.022(7)		2.089(8)
		1.694(8)	1.932(7)	2.009(7)	2.028(7)		2.121(8)
		1.688(8)	1.950(7)	2.159(7)	2.241(8)		2.131(8)
				2.141(7)			
				2.006(7)			
				2.007(7)			

Table 3
Selected bond angles of complex anion $[Mo_6O_{12}(OCH_3)_4(acac)_3]^-$ in **5**, **6** and **7** (°)

Compound	O1–Mo1–O10 O2–Mo1–O12 O3–Mo1–O9	O3–Mo2–O11 O4–Mo2–O13 O5–Mo2–O10	O5–Mo3–O8 O6–Mo3–O14 O7–Mo3–O11	O10–Mo4–O18 O13–Mo4–O15 O12–Mo4–O16	O11–Mo5–O19 O13–Mo5–O17 O14–Mo5–O16	O18–Mo6–O22 O19–Mo6–O20 O16–Mo6–O21
5	157.6(3) 163.7(3) 164.8(4)	154.7(3) 163.8(3) 159.2(3)	164.9(3) 165.5(4) 158.1(3)	154.3(3) 163.2(3) 158.4(3)	156.6(3) 165.3(3) 153.9(3)	162.3(3) 163.4(3) 157.8(3)
6	157.4(2) 164.4(2) 166.1(2)	154.2(2) 164.2(2) 158.3(2)	165.3(2) 162.4(2) 158.1(2)	153.3(2) 165.5(2) 158.6(2)	156.0(2) 164.7(2) 152.9(2)	155.6(2) 164.6(2) 164.1(2)
7	157.9(3) 166.2(3) 164.6(3)	154.0(3) 164.7(3) 157.3(3)	164.9(3) 165.7(4) 156.1(3)	153.7(3) 164.7(4) 158.6(3)	158.1(3) 164.7(4) 153.3(3)	164.2(4) 164.9(3) 157.2(3)

tween O13 atom and Mo4, Mo5 and Mo6 atoms are among the longest ones varying in the range 2.260(6)–2.315(7) Å for all three structures. It seems that such a triply-bridging role for one methoxo-oxygen atom is the first example observed in the structural chemistry of Mo(V) complexes. However, as far as we know there are only two such examples in the chemistry of Mo(VI): (i) $[Mo_4O_{10}(OMe)_4(Me_2CNHO)_2]$ [41] with Mo–O(OCH_3) (triply bridging) bond lengths varying from 2.360(3) to 2.304(3) Å and (ii) $[NBu^n_4][Mo_4O_{10}(NO)(OMe)(Me_2CNO)_2]$ [42] with this bond ranging from 2.209(7) to 2.481(7) Å. Otherwise, oxo-oxygens as a triple bridge between three Mo atoms are frequently established in the structures of different polyoxomolybdates.

The Mo–O(acac) bond lengths are within the expected range of values. They exhibit a pattern of three shorter (2.041(9)–2.099(8) Å in **5**, 2.042(5)–2.061(5) Å in **6** and 2.058(8)–2.074(9) Å in **7**) and three longer (2.099(8)–2.137(7) Å in **5**, 2.113(5)–2.141(5) Å in **6** and 2.089(8)–2.131(8) Å in **7**) bond distances, again depending upon the position in the structure, i.e. either *cis* or *trans* to terminal or bridging oxo-oxygen atoms (Table 2).

In the structure of the triethylammonium derivative **6**, an intramolecular hydrogen bond is formed between the NH group of the cation and the terminal O4 atom of the anion [N–H 0.91 Å; H···O4 2.317 Å; ∠N–H···O4 150.9°; N···O 3.14(2) Å]. Also, the observed intra- and intermolecular hydrogen bonds of the type C–H···O seem to be additional stabilizing factors in all three crystal structures.

Acknowledgements

This research was supported by the Ministry of Science and Technology of the republic of Croatia (Grant No. 119407).

References

[1] M.T. Pope, Heteropoly and Isopoly Oxometalates, Springer-Verlag, New York, 1983.
[2] A. Ionnidis, E. Papaconstantinou, Inorg. Chem. 24 (1985) 439.
[3] R.F. Renneke, C.L. Hill, J. Am. Chem. Soc. 108 (1986) 3528.
[4] V.W. Day, W.G. Klemperer, Science 228 (1985) 533.
[5] S. Liu, S.N. Shaikh, J. Zubieta, Inorg. Chem. 26 (1987) 4303.
[6] S. Liu, S.N. Shaikh, J. Zubieta, Inorg. Chem. 27 (1988) 3064.
[7] S. Liu, L. Ma, D. McGowty, J. Zubieta, Polyhedron 9 (1990) 1541.
[8] T. Yamase, J. Chem. Soc., Dalton Trans. (1985) 2585.
[9] L. Ma, S. Liu, J. Zubieta, J. Chem. Soc., Chem. Commun. (1989) 440.
[10] J.R. Briggs, A.M. Harrison, J.H. Robson, Polyhedron 5 (1986) 281.
[11] E.M. McCarron III, R.L. Harlow, J. Am. Chem. Soc. 105 (1983) 6179.
[12] E.M. McCarron III, R.H. Staley, A.W. Sleight, Inorg. Chem. 23 (1984) 1043.
[13] E.M. McCarron III, A.W. Sleight, Polyhedron 5 (1986) 129.
[14] W.E. Farneth, F. Ohuchi, R.H. Staley, U. Chowdhry, A.W. Sleight, J. Phys. Chem. 89 (1985) 2493.
[15] H.K. Chae, W.G. Klemperer, T.A. Marquart, Coord. Chem. Rev. 128 (1993) 209.
[16] C. Limberg, S. Parsons, A.J. Downs, J. Chem. Soc., Chem. Commun. (1994) 497.
[17] Q. Chen, S. Liu, J. Zubieta, Inorg. Chem. 28 (1989) 4433.
[18] D.J. Darensbourg, R.L. Gray, T. Delord, Inorg. Chim. Acta 98 (1985) L39.
[19] R.C. Haushalter, F.W. Lai, Inorg. Chem. 28 (1989) 2904.
[20] R.C. Haushalter, F.W. Lai, Angew. Chem., Int. Ed. Engl. 28 (1989) 743.
[21] J.A. Beaver, M.G.B. Drew, J. Chem. Soc., Dalton Trans. (1973) 1376.
[22] S. Lincon, S.A. Koch, Inorg. Chem. 25 (1986) 1594.
[23] M.H. Chisholm, J.C. Huffman, C.C. Kirkpatrick, J. Leonelli, K. Folting, J. Am. Chem. Soc. 103 (1981) 6093.
[24] M. Ferrari Belicchi, G. Gasparri Fava, C. Pelizzi, J. Chem. Soc., Dalton Trans. (1983) 65.
[25] C. Limberg, A.J. Downs, A.J. Blake, S. Parsons, Inorg. Chem. 35 (1996) 4439.
[26] M. Cindrić, D. Matković-Ćalogović, V. Vrdoljak, B. Kamenar, Inorg. Chim. Acta 284 (1999) 223.
[27] U. Eisner, J. Kuthan, Chem. Rev. 72 (1972) 1.

[28] A. Sausiņš, G. Duburs, Heterocycles 27 (1988) 291.
[29] B. Kamenar, B. Korpar-Ćolig, M. Cindrić, D. Matković-Ćalogovic, M. Penavić, Bull. Chem. Technol. Maced. 16 (1977) 33.
[30] F.W. Moore, R.E. Rice, Inorg. Chem. 7 (1968) 2510.
[31] G.A. Parker, Analytical Chemistry of Molybdenum, Springer-Verlag, New York, 1983.
[32] Stoe and Cie, STADI4, Diffractometer Control Program for Windows, 1995, Darmstadt, Germany.
[33] Stoe and Cie, X-RED, Data Reduction Program for Windows, 1995, Darmstadt, Germany.
[34] G.M. Sheldrick, SHELXS-97, Program for the Automatic Solution of Crystal Structures, University of Göttingen, Germany.
[35] G.M. Sheldrick, SHELXL-97, Program for the Refinement of Crystal Structures, University of Göttingen, Germany, 1997.
[36] E.J. Gabe, Y. Le Page, J.-P. Charland, F.L. Lee, P.S. White, J. Appl. Crystallogr. 22 (1989) 384.
[37] A.L. Spek, PLATON98 for Windows, University of Utrecht, The Netherlands, 1998.
[38] N.R. Davis, R.A. Anwar, J. Am. Chem. Soc. 90 (1970) 3778.
[39] A.I. Meyers, S. Singh, Tetrahedron 25 (1969) 4161.
[40] H.-K. Fun, B.-C. Yip, J.-Y. Niu, X.-Z. You, Acta Crystallogr., Sect. C 52 (1996) 506.
[41] A. Proust, P. Gouzher, F. Robert, J. Chem. Soc., Dalton. Trans. (1994) 819.
[42] A. Proust, P. Gouzher, F. Robert, J. Chem. Soc., Dalton. Trans. (1994) 825.

PERGAMON

www.elsevier.nl/locate/poly

Polyhedron 19 (2000) 1479–1484

POLYHEDRON

Structural and spectroscopic characterisation of tris(2-benzimidazolylmethyl)amine coordination compounds of Zn(II), Cd(II) and Hg(II)

Elba Quiroz-Castro [a], Sylvain Bernès [a], Noráh Barba-Behrens [a,*], Rafael Tapia-Benavides [b], Rosalinda Contreras [c], Heinrich Nöth [d]

[a] *Facultad de Química, Universidad Nacional Autónoma de México, CU 04510, Mexico DF, Mexico*
[b] *Centro de Investigaciones Químicas, Universidad A. del Estado de Hidalgo, Carretera Pachuca-Tulancingo, Km. 45. U. Universitaria, Pachuca Hidalgo CP 42074, Mexico*
[c] *Departamento de Química, Centro de Investigación y Estudios Avanzados del IPN, Apdo. Postal 14-740, 07000 Mexico DF, Mexico*
[d] *Institute of Inorganic Chemistry, University of Munich, Butenandtstraße 5-13 (Haus D), D-81377 Munich, Germany*

Received 5 January 2000; accepted 3 April 2000

Abstract

Zinc(II), cadmium(II) and mercury(II) coordination compounds derived from tris(2-benzimidazolylmethyl)amine (ntb) were characterised by ^{1}H and ^{13}C NMR in solution, IR and X-ray single crystal diffraction for $[Zn(ntb)Cl]_2[ZnCl_4]\cdot 4EtOH$, $[Cd(ntb)(\mu_2\text{-}NO_3)]NO_3\cdot 2DMSO$ and $[Hg(ntb)Cl]_2[HgCl_4]\cdot 4EtOH$. The complexes derived from zinc(II), cadmium(II) and mercury(II) halides form $[M(ntb)X]^+$ cations, where the metal ions are pentacoordinated and have a distorted trigonal bipyramidal geometry, with tetrahedral anions $[MX_4]^{2-}$. In the $[Cd(ntb)(\mu_2\text{-}NO_3)]NO_3\cdot 2DMSO$ complex, by analogy with the Zn(II) and Hg(II) compounds, the NO_3^- could be considered as the fifth apical substituent in a distorted trigonal bipyramid geometry. In all complexes the ligand is coordinated to the metal through the imidazolic nitrogen atoms and has a weak coordination with the tertiary amine. The counter ion (halide or nitrate) remains bonded to the metal ion in solution and in the solid state as was evidenced by NMR and X-ray diffraction. The structures presented interactions between the coordinated counterion and the nearest C–H of the aromatic rings. All cations show an approximate *C*3 symmetry. The distortions found in the solid state were attributed to intermolecular hydrogen bonding and stacking between the benzimidazolic rings of neighbouring molecules. © 2000 Elsevier Science Ltd. All rights reserved.

Keywords: Zinc(II); Cadmium(II); Mercury(II); Tris(2-benzimidazolylmethyl)amine; X-ray diffraction structures; NMR data

1. Introduction

The coordination compounds of tripodal ligands have been widely investigated, since they may serve as models for the active site of metalloproteins [1–3]. Due to the great flexibility and polyfunctionality of the tripodal tris(2-benzimidazolylmethyl)amine ligand (**1**), the actual coordination geometry for the metal ions can not always be unambiguously assigned. Most of its reported complexes have been characterised by means of various spectroscopic techniques [4–8], but for some of them the structure has been completely characterised [9–19].

In this context we have been investigating coordination compounds of diamagnetic metal ions with ligand **1** in solid state, and when possible, by X-ray crystallography, as well as in solution by NMR, in order to get information on intra- and intermolecular interactions between the ligand and the metallic centers. Therefore, we have prepared compounds with the zinc(II) (**2**–**4**), cadmium(II) (**5**–**7**) and mercury(II) (**8**–**10**) chlorides, bromides and nitrates. These were characterised by spectroscopic techniques and by ^{1}H and ^{13}C NMR, and compounds **2**, **7** and **8** were also characterised by X-ray diffraction.

* Corresponding author. Tel.: +525-6-223-810.
E-mail address: norah@servidor.unam.mx (N. Barba-Behrens).

0277-5387/00/$ - see front matter © 2000 Elsevier Science Ltd. All rights reserved.
PII: S0277-5387(00)00406-X

2. Experimental

2.1. Materials

The metal salts (J.T. Baker) were used without further purification. Ligand **1** was prepared as previously described [20].

2.2. Synthesis of complexes: general procedure

All coordination compounds were synthesised following the same procedure, as described for compound **2**.

2.2.1. $[Zn(ntb)Cl]_2[ZnCl_4]\cdot 4EtOH$ (**2**)

Tris(2-benzimidazolylmethyl)amine (0.102 g, 0.25 mmol) was dissolved in 10 ml of hot ethanol and added to a solution of $ZnCl_2$ (0.034 g, 0.25 mmol) in 10 ml of ethanol. Crystals were obtained by slow evaporation of an ethanol solution. *Anal*. Calc. for $C_{48}H_{42}Cl_6N_{14}Zn_3$: C, 47.10; H, 3.43; N, 16.03. Found: C, 46.89; H, 3.36; N, 15.87%. The crystals suffered cracking within minutes when taking them out of the solution obviously by loss of crystal solvent. For this reason the elemental analysis of this compound was carried out on a powder sample and the following calculated composition does not include alcohol molecules. Colourless crystals (90 mg, 86%) were isolated 2 days later.

2.2.2. $[Zn(ntb)Br]_2[ZnBr_4]$ (**3**)

The resulting powder (101 mg, 81%) was filtered off, washed and dried in vacuo. *Anal*. Calc. for $C_{48}H_{42}Br_6N_{14}Zn_3$: C, 38.67; H, 2.82; N, 13.16. Found: C, 39.07; H, 3.26; N, 12.95%.

2.2.3. $[Zn(ntb)NO_3]NO_3\cdot 3H_2O$ (**4**)

A white powder (137 mg, 85%) was obtained. The solid was separated by filtration and dried in vacuo. *Anal*. Calc. for $C_{24}H_{21}N_9O_6Zn\cdot 3H_2O$: C, 44.40; H, 4.17; N, 19.31. Found: C, 44.27; H, 4.34; N, 18.71%.

2.2.4. $[Cd(ntb)Cl]_2[CdCl_4]$ (**5**)

The white precipitate (89 mg, 79%) was collected by filtration, washed with ethanol, and dried in vacuo. *Anal*. Calc. for $C_{48}H_{42}Cd_3Cl_6N_{14}$: C, 42.2; H, 3.08; N, 14.36. Found: C, 42.8; H, 3.96; N, 13.86%.

2.2.5. $[Cd(ntb)Br]_2[CdBr_4]$ (**6**)

The white powder (116 mg, 79.0%) was filtered off, washed and dried in vacuo. *Anal*. Calc. for $C_{48}H_{42}Br_6Cd_3N_{14}$: C, 35.33; H, 2.59; N, 12.02. Found: C, 35.22; H, 2.41; N, 12.09%.

2.2.6. $[Cd(ntb)(\mu_2\text{-}NO_3)]NO_3\cdot 2DMSO$ (**7**)

A white powder was obtained which was recrystallised from DMSO. The elemental analysis of this compound was carried out on a powder sample and the following calculated composition does not include DMSO molecules (104 mg, 65%). *Anal*. Calc. for $C_{24}H_{21}CdN_9O_6$: C, 44.94; H, 3.35; N, 19.51. Found: C, 44.63; H, 3.32; N, 19.49%.

2.2.7. $[Hg(ntb)Cl]_2[HgCl_4]\cdot 4EtOH$ (**8**)

Colourless crystals (97 mg, 48%) were isolated 3 days later. The elemental analysis of this compound does not include ethanol molecules. *Anal*. Calc. for $C_{48}H_{42}Cl_6Hg_3N_{14}$: C, 35.38; H, 2.60; N, 12.03. Found: C, 35.29; H, 2.65; N, 12.02%.

2.2.8. $[Hg(ntb)Br]_2[HgBr_4]$ (**9**)

Colourless crystals (97 mg, 48%) were isolated by filtration. *Anal*. Calc. for $C_{48}H_{42}Br_6Hg_3N_{14}$: C, 30.4; H, 2.23; N, 10.34. Found: C, 29.49; H, 1.76; N, 10.37%.

2.2.9. $[Hg(ntb)NO_3]NO_3$ (**10**)

A white precipitate (0.167 g, 91.0%) was filtered off, washed and dried in vacuo. *Anal*. Calc. for $C_{24}H_{21}HgN_9O_6$: C, 39.38; H, 2.89; N, 17.22. Found: C, 39.61; H, 2.99; N, 17.18%.

2.3. Physical measurements

IR spectra were recorded with a Nicolet FT-IR 740 spectrophotometer using KBr pellets in the 4000–400 cm^{-1} region. Elemental analyses were performed on a Fisons EA 1108 elemental analyser. ^1H and ^{13}C NMR data (67.80 MHz) were obtained in DMSO-d_6 on a Jeol GSX-270 spectrometer.

2.4. X-ray crystallographic study

Suitable single crystals of compounds **2**, **7** and **8** were mounted on a glass fibre in a small amount of perfluoroether oil. Data were collected at 193 K on a Siemens P4 diffractometer equipped with a Siemens CCD area detector, using 10 s exposure per frame in a hemisphere scan mode. Data reduction was performed with the program SAINT, and an empirical absorption correction was applied using SADABS. Pertinent crystal data and other crystallographic parameters are listed in Table 1. Computations were performed with the SHELX-97 [21] package on a personal computer.

3. Results and discussion

3.1. Spectroscopic characterisation

The IR spectrum of the free ligand **1** presents two bands associated to the ν(C=N) and ν(C–N) vibrations at 1536 and 1438 cm^{-1}, respectively; these bands shifted to ca. 1545 and ca. 1450 cm^{-1} in all complexes due to the coordination of the nitrogen atoms to the

Table 1
Summary of crystallographic data for **2**, **7** and **8**

Compound	**2**	**7**	**8**
Formula	$C_{48}H_{42}Cl_6N_{14}Zn_3{\cdot}4EtOH$	$C_{24}H_{21}CdN_9O_6{\cdot}2DMSO$	$C_{48}H_{42}Cl_6Hg_3N_{14}{\cdot}4EtOH$
Formula weight	1408.04	800.15	1813.70
Crystal dimensions (mm)	$0.3\times0.3\times0.3$	$0.31\times0.22\times0.15$	$0.4\times0.38\times0.1$
Crystal system	monoclinic	monoclinic	monoclinic
Space group	$C2/c$	$P2_1/c$	$C2/c$
a (Å)	23.1664(4)	14.7652(4)	23.6287(2)
b (Å)	16.9281(4)	13.6929(2)	17.0021(3)
c (Å)	16.1417(4)	16.8399(1)	16.171(1)
β (°)	95.161(1)	103.180(1)	94.413(1)
V (Å^3)	6304.5(2)	3314.99(1)	6477.4(1)
Z	4	4	4
D_{calc} (g cm^{-3})	1.483	1.603	1.860
μ (mm^{-1})	1.443	0.847	7.395
$F(000)$	2896	1632	3496
Temperature (K)	193	193	193
Reflections collected	18295	18507	18085
Independent reflections [R_{int} (%)]	6558 (8.74)	5797 (3.40)	5984 (4.86)
Reflections observed [$F_o>4\sigma(F_o)$]	3610	4700	4818
Goodness-of-fit	1.029	1.071	1.061
Final R_1 (observed data)	0.0704	0.0408	0.0531
Final wR_2 (all data)	0.1415	0.0959	0.1395

metal ions. For complexes **4**, **7** and **10** a strong absorption at 1384 cm^{-1} for the uncoordinated nitrate ion did not allow us to observe the vibrations associated with the coordinated nitrate [22].

In the ^{1}H NMR spectra of compounds **2**–**10** (Table 2), the imidazolic N–H tautomeric equilibrium present in the free ligand is absent, indicating that the imine group is coordinated to the metal ion. The fact that the band associated with the methylene groups shifts to higher frequencies indicates that the tertiary amine nitrogen atom is also bonded to the metal centre. Therefore, we can assume that the ligand is tetradentate. For each metal family, there is a chemical shift to higher frequencies of H_a depending on the nature of the anion, indicating that the anion remains linked to the metal and stays close to the H_a. The deshielding effect of these intramolecular interactions is stronger for Br followed by Cl and to a lesser extent for NO_3.

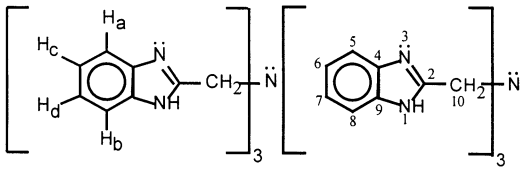
Tha ^{13}C NMR spectra of these compounds also show the effect of coordination of the ligand to the metal centre, i.e. the C4, C5 and C6 signals become different to those observed for C7, C8 and C9 (Table 2) e.g. in benzazole N–BH_3 adducts [23].

3.2. Solid state structures

From the studied compounds three of them crystallised **2**, **7** and **8** and their X-ray structures were obtained. This allowed us to compare the coordination behaviour of the ligand in the solid state with that in solution. $[Zn(ntb)Cl]_2[ZnCl_4]{\cdot}4EtOH$ (**2**) and $[Hg(ntb)Cl]_2[HgCl_4]{\cdot}4EtOH$ (**8**) are crystallographically isostructural and present similar structures (Fig. 1, Table 1). The ntb behaves as a tetradentate ligand where the three imidazolic nitrogen atoms are coordinated to the M(II) with M–N distances ranging from 2.009(4) to 2.067(4) Å for Zn and 2.217(6) to 2.294(7) Å for Hg (Table 3). The fourth position is occupied by a chloride atom with a normal M–Cl bond length (Zn–Cl, 2.280(1) Å; Hg–Cl, 2.415(2) Å). There is also an interaction of the tertiary N(1) of the amine to the metal ion (Zn(1)–N(1) = 2.549(4) Å), which is in the range of those reported for analogous zinc(II) ntb complexes, i.e. 2.518 Å [9] and 2.540 Å [18], where a bipyramidal geometry is proposed, while a longer bond distance (Zn(1)–N(1) 2.590 Å [10]) is observed for a tetrahedral structure. The bond length Hg(1)–N(1) = 2.810(6) Å is shorter than those reported for other Hg(II)–N bonds (2.87(2) and 2.84(2) Å [24]), which is an indication of the coordination of the quaternary nitrogen in this complex. The distorted geometry in the cations $[M(ntb)X]^+$ is reflected in the bond angles around the metal centres, which are more in agreement with a trigonal bipyramidal than with a distorted tetrahedral geometry [10,15,18] (see Table 3). The complexes contain isolated tetrahedral $[MX_4]^{2-}$ anions.

The structures are stabilised by intramolecular hydrogen bonds between the aromatic hydrogen atoms H7A, H17A and H27A of the benzimidazole groups and the M–Cl chloride (for Zn: H7A···Cl 2.729, H17A···Cl 2.735 and H27A···Cl 2.836; for Hg: H7B···Cl 3.043, H17A···Cl 2.927 and H27A···Cl 3.266 Å). These

Table 2
^{1}H and ^{13}C NMR data (ppm in DMSO-d_6) [a]



Compound	δH_a (m)	δH_b (m)	δH_c (m)	δH_d (m)	δCH_2 (s)	δNH (bs)		
[9]*^{1}H NMR*								
Ligand **1**	7.56	7.56	7.16	7.16	4.14	12.2		
$[Zn(ntb)Cl]_2[ZnCl_4]\cdot 4EtOH$ (**2**)	8.67	7.60	7.30	7.30	4.60	13.3		
$[Zn(ntb)Br]_2[ZnBr_4]$ (**3**)	8.82	7.60	7.34	7.34	4.56			
$[Zn(ntb)NO_3]NO_3\cdot 3H_2O$ (**4**)	7.78	7.63	7.36	7.36	4.67			
$[Cd(ntb)Cl]_2[CdCl_4]$ (**5**)	8.11	7.55	7.30	7.30	4.54	13.3		
$[Cd(ntb)Br]_2[CdBr_4]$ (**6**)	8.23	7.57	7.32	7.32	4.55	13.3		
$[Cd(ntb)(\mu_2\text{-}NO_3)]NO_3\cdot 2DMSO$ (**7**)	7.88	7.59	7.34	7.34	4.51	13.4		
$[Hg(ntb)Cl]_2[HgCl_4]\cdot 4EtOH$ (**8**)	8.08	7.62	7.32	7.32	4.48	13.4		
$[Hg(ntb)Br]_2[HgBr_4]$ (**9**)	8.08	7.62	7.32	7.32	4.48	13.4		
$[Hg(ntb)NO_3]NO_3$ (**10**)	7.85	7.62	7.35	7.35	4.55	13.6		
	C2	C4	C5	C6	C7	C8	C9	C10
[9]*^{13}C NMR*								
1	152.2	139.5	114.9	121.5	121.6	114.9	138.5	51.4
2	155.4	139.1	118.3	122.8	123.7	112.2	133.9	51.6
3	155.3	139.1	118.5	122.7	123.6	112.2	134.1	51.2
4	155.6	138.2	116.9	123.4	123.9	112.5	133.9	52.4
5	153.4	139.9	117.6	122.6	123.3	112.0	133.5	52.6
6	153.7	139.8	117.4	122.7	123.4	112.1	133.4	52.7
7	153.8	139.5	118.1	122.4	123.4	112.0	133.8	51.7
8	153.6	140.3	117.1	122.5	123.3	112.5	133.8	50.9
9	154.2	140.91	117.5	123.8	123.8	113.3	134.2	51.3
10	153.9	139.2	117.3	123.2	123.9	112.4	133.7	51.3

[a] m, multiplet; s, singlet; bs, broad singlet.

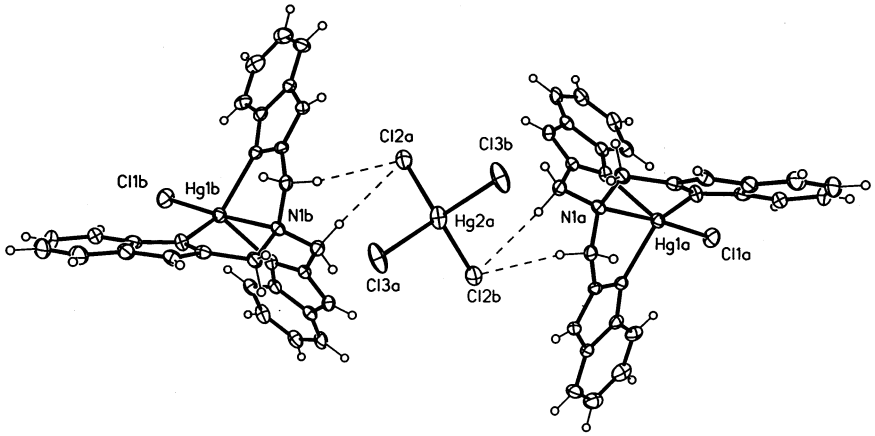


Fig. 1. View for $[Hg(ntb)Cl]_2$ $[HgCl_4]\cdot 4EtOH$ (**8**). Two equivalent cations are represented. Dotted lines denote short intermolecular contact. Solvent molecules are omitted for clarity.

interactions are responsible for the chemical shifts observed by NMR for H_a.

The ligand presents an almost non-crystallographic threefold axis in compounds **2** and **8**, as shown in Fig. 1. The lack of symmetry in the complexes is attributed to intermolecular stacking: the phenylene ring of one molecule is stacked with an imidazolic ring of a neighbouring molecule (Fig. 2). The distances between the centroids of five- and six-membered rings are 3.708 and 3.633 Å for Zn and Hg, respectively [25][1].

[1] The distance between the planes in graphite is 3.354 Å.

The crystal structure of $[Cd(ntb)(\mu_2\text{-}NO_3)]NO_3 \cdot 2DMSO$ (**7**) shows that the geometry around the metal ion does not fit with any regular geometry for hexacoordinated systems. An analogy of this cadmium compound with the zinc and mercury compounds could be proposed if the N8 of the nitrate is considered the fifth apical substituent in a distorted trigonal bipyramid geometry as shown in Fig. 3. The bond lengths and angles are listed in Table 3.

Table 3
Selected bond lengths (Å) and bond angles (°) for **2**, **7** and **8**

	2	**7**	**8**
M(1)–N(1)	2.549(4)	2.690(3)	2.810(6)
M(1)–N(2)	2.047(4)	2.294(3)	2.294(7)
M(1)–N(3)	2.009(4)	2.253(3)	2.217(6)
M(1)–N(4)	2.067(4)	2.228(3)	2.262(6)
M(1)–Cl(1)	2.28(2)		2.415(2)
N(1)–M(1)–Cl(1)	175.8(1)		171.5(1)
N(2)–M(1)–Cl(1)	105.1(1)		106.9(2)
N(3)–M(1)–Cl(1)	109.5(1)		119.7(2)
N(4)–M(1)–Cl(1)	103.8(1)		109.3(2)
N(2)–M(1)–N(1)	73.23(1)	69.5(1)	67.9(2)
N(3)–M(1)–N(1)	74.70(1)	68.7(1)	68.7(2)
N(4)–M(1)–N(1)	73.76(1)	69.9(1)	67.5(2)
N(3)–M(1)–N(2)	108.9(1)	106.4(1)	107.8(3)
N(4)–M(1)–N(2)	113.8(1)	104.0(1)	107.8(2)
N(4)–M(1)–N(3)	115.1(2)	114.2(1)	104.9(2)
M(1)–O(1)		2.391(3)	
M(1)–O(2)		2.446(3)	
N(1)–M(1)–O(1)		147.6(1)	
N(2)–M(1)–O(2)		94.7(1)	
N(3)–M(1)–O(1)		92.8(1)	
N(4)–M(1)–O(2)		90.9(1)	
N(1)–M(1)–O(2)		150.2(1)	
N(4)–M(1)–O(1)		142.2(1)	
N(2)–M(1)–O(1)		92.2(1)	
N(3)–M(1)–O(2)		141.1(1)	
O(1)–M(1)–O(2)		53.4(1)	

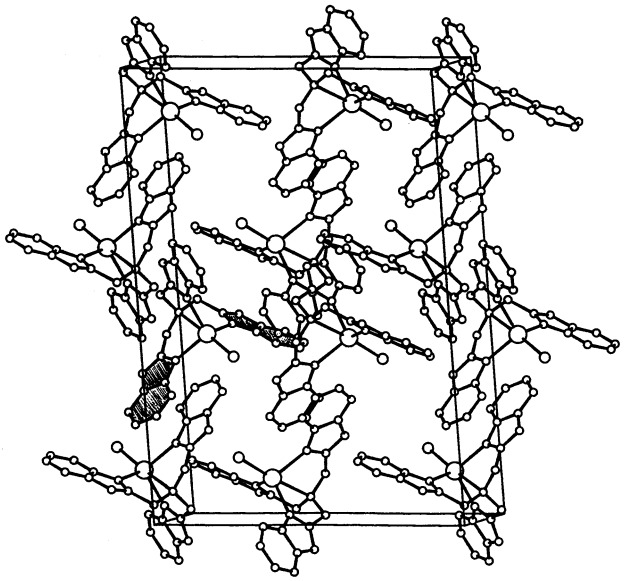


Fig. 2. View of the packing in compounds **2** and **8**. The phenylene ring of one molecule is stacked with an imidazolic ring of a neighbouring molecule (grey shading).

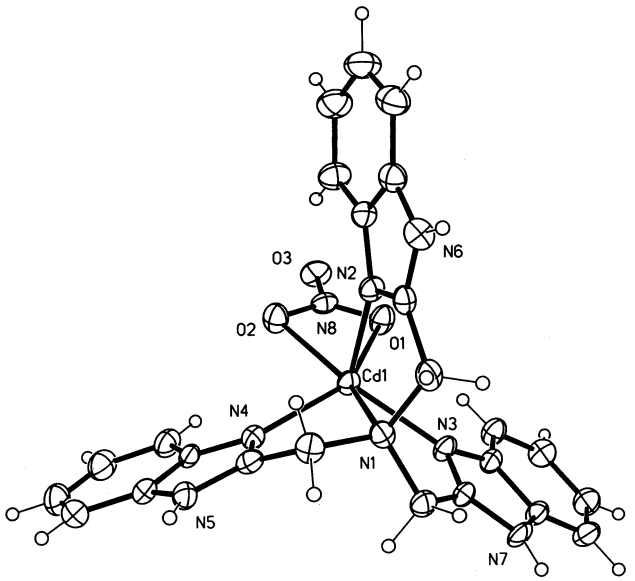


Fig. 3. View of the solid state structure of cadmium cation in compound **7**.

Weak hydrogen bonds between the imidazole protons and the oxygen atom of the nitrate group are observed in the crystal packing. In addition, intermolecular stacking is observed between the benzimidazole rings of **7** with the shortest separation between the centroid of the benzene rings being 4.245 Å.

A regular variation for angles N–M–N for these three compounds when moving from Zn(II) to Hg(II) (Table 3) is observed: the angles decrease in that order due to the M–N1 bond. The nature of the coordinated ion (Cl^-, NO_3^-) does not contribute to this effect.

4. Conclusions

The diamagnetic nature of the metals allowed a study of the coordination behaviour of these compounds in solution. The Zn(II), Cd(II) and Hg(II) halide complexes contain distorted trigonal bipyramidal cations $[M(ntb)X]^+$ and tetrahedral anions $[MX_4]^{2-}$. On the other hand, the hexacoordinated $[Cd(ntb)(\mu_2\text{-}NO_3)]NO_3 \cdot 2DMSO$ complex may be considered to have trigonal bipyramidal geometry. The ligand is coordinated to the metal through the imidazolic nitrogen atoms and has a weak coordination with the tertiary amine. The counterion (halide or nitrate) remains bonded to the metal ion in solution and in the solid state as was evidenced by NMR spectroscopy and X-ray diffraction. The compounds presented interactions between the coordinated counterion and the nearest C–H of the

aromatic rings stabilising the complexes. The distortions found in the solid state were attributed to stacking interactions between aromatic rings of different molecules. From NMR it is clear that in solution the ligand is tetracoordinated as it was also found in the solid state.

5. Supplementary material

Crystallographic data (excluding structure factors) for the structures reported in this paper have been deposited with the Cambridge Crystallographic Data Centre as supplementary publication nos. CCDC-138103–138105. Copies of the data can be obtained free of charge on application to: The Director, CCDC, 12 Union Road, Cambridge, CB2 1EZ, UK (fax: +44-1223-336-033; e-mail: deposit@ccdc.cam.ac.uk or www: http://www.ccdc.cam.ac.uk).

Acknowledgements

E.Q.-C. acknowledges the CONACYT scholarship. S.B. is grateful to the UNAM for financial support. Financial support by CONACYT (grant no. 25564-E) is acknowledged.

References

[1] Y. Chiou, L. Que, J. Am. Chem. Soc. 117 (1995) 3999.
[2] G.J. Koolhaas, W.L. Driessen, J. Reedijk, H. Kooijman, A.L. Spek, J. Chem. Soc., Chem. Commun. (1995) 517.
[3] K.K. Nanda, E. Sinn, A.W. Addison, Inorg. Chem. 35 (1996) 1.
[4] H. Oka, Y. Nakao, Inorg. Chim. Acta 165 (1989) 111.
[5] H. Pandey, Y. Sharma, P. Mathur, Polyhedron 11 (1992) 2631.
[6] H. Pandey, P. Mathur, Indian J. Chem. 31A (1992) 666.
[7] U. Sivagnanam, T. Pandiyan, M. Palaniandavar, Indian J. Chem. 32B (1993) 572.
[8] H. Pandey, P. Mathur, Transition Met. Chem. 20 (1995) 144.
[9] D.E. Fenton, H. Adams, Q.Y. He, Acta Crystallogr., Sect. C 54 (1998) 286.
[10] R. Burth, H. Vahrenkamp, Z. Anorg. Allg. Chem. 624 (1998) 381.
[11] M. Soo Lah, H. Chun, Inorg. Chem. 36 (1997) 1782.
[12] J. Sletten, H. Grove, Acta Chem. Scand. 51 (1997) 822.
[13] T. Brandsch, A. Schell, K. Weis, M. Ruf, B. Müller, H. Vahrenkamp, Chem. Ber. 130 (1997) 283.
[14] C.Y. Su, B.S. Kang, T.B. Wen, Y.X. Tong, X.P. Yang, C Zhang, H.Q. Liu, J. Sun, Polyhedron 18 (1999) 1577.
[15] U. Hartmann, R. Gregorzik, H. Vahrenkamp, Chem. Ber. 127 (1994) 2123.
[16] R. Gregorzik, U. Hartmann, H. Vahrenkamp, Chem. Ber. 127 (1994) 2117.
[17] R. Oki, R. Bommarreddy, H. Zhang, N. Hosmane, Inorg. Chim. Acta 231 (1995) 109.
[18] C. Nazikkol, R. Wegner, J. Bremer, B. Krebs, Z. Anorg. Allg. Chem. 622 (1996) 329.
[19] M. Soo Lah, M. Moon, Bull. Korean Chem. Soc. 18 (1997) 406.
[20] L.K. Thompson, B.S. Ramaswamy, E.A. Seymour, Can. J. Chem. 55 (1976) 878.
[21] G.M. Sheldrick, SHELX-97 Users Manual, University of Göttingen, Germany, 1997.
[22] K. Nakamoto, Infrared and Raman Spectra of Inorganic and Coordination Compounds, fourth ed., Wiley, New York, 1986, p. 245.
[23] I. Padilla-Martínez, N. Andrade-López, M. Gama-Goicochea, E. Aguilar-Cruz, A. Cruz, R. Contreras, H. Tlahuext, Heteroat. Chem. 7 (1996) 323.
[24] S.G. Wilkinson, R.D. Gillard, J.A. McCleverty, Comprehensive Coordination Chemistry. The Synthesis, Reactions, Properties and Applications of Coordination Compounds, vol. 5, first ed., Pergamon, Oxford, 1987, p. 1078.
[25] N.N. Greenwood, A. Earnshaw, Chemistry of Elements, first ed., Pergamon, Oxford, 1986, p. 304.

PERGAMON

www.elsevier.nl/locate/poly

Polyhedron 19 (2000) 1485–1492

POLYHEDRON

Binuclear copper(II), nickel(II), cobalt(II) and zinc(II) complexes of the macrocycle 1,4,7,16,19,22-hexaaza[9.9]metacyclophane (L). Crystal structure of $[Cu_2LCl_4]_{0.5}\cdot[Cu_2LCl_3]ClO_4\cdot$dmf and the copper complex catalysed hydrolysis of the phosphotriester 2,4-dinitrophenyldiethylphosphate

Robert W. Hay [1], Thomas Clifford, David T. Richens *, Philip Lightfoot

School of Chemistry, University of St Andrews, KY16 9ST, UK

Received 4 January 2000; accepted 17 April 2000

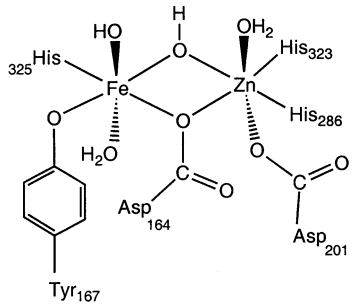
Abstract

Copper(II), nickel(II), cobalt(II) and zinc(II) complexes of the 22-membered hexa-aza macrocycle 1,4,7,16,19,22-hexaaza[9.9]metacyclophane (L) have been prepared and characterised. The crystal structure of a copper(II) chloro complex has been determined. The complex exists in two forms, one form (Type 1) with an inversion centre has both copper atoms in essentially square pyramidal stereochemistry with an N_3Cl_2 donor set and a Cu···Cu distance of 5.82 Å. The other form (Type II) has one square pyramidal copper with an N_3Cl_2 donor set and one planar copper with an N_3Cl donor set. The Type II Cu···Cu distance is 6.13 Å. The structure is best described as $[Cu_2LCl_4]_{0.5}\cdot[Cu_2LCl_3]ClO_4\cdot$dmf (dmf = *N*,*N*-dimethylformamide). The copper(II) complex catalyses the hydrolysis of the phosphotriester 2,4-dinitrophenyldiethylphosphate to give diethyl phosphate and the mechanism of the reaction is discussed. © 2000 Elsevier Science Ltd. All rights reserved.

Keywords: Binucleating hexa-aza macrocycle; Copper(II); Nickel(II); Cobalt(II); Zinc(II); Crystal structures; Phosphotriester; Hydrolysis

1. Introduction

Recently there has been considerable interest in the area of binucleating macrocycles capable of incorporating two metal centres [1]. In part, this interest has arisen due to the occurrence of binuclear metal centres in several enzymes such as purple acid phosphatase [2] (**1**) and urease [3]. In addition, several marine natural products have been shown recently to involve binucleating macrocycles [4] and binuclear copper(II) centres are well established in marine oxygen carrying proteins such as hemocyanin [5]. For this reason we have been interested in the coordination chemistry of binucleating ligand systems. In the present paper we describe the synthesis of a series of metal complexes of the hexa-aza macrocycle (**2**) = L including the crystal structure of a binuclear copper(II) complex. In the context of binuclear phosphatases, the binuclear copper complex of L has catalytic activity above pH 7 for the hydrolysis of the water soluble phosphotriester 2,4-dinitrophenyldiethylphosphate (**3**) to give diethyl phosphate. The nature of the catalytically active complex is discussed.

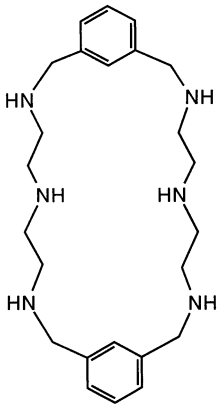


(1)

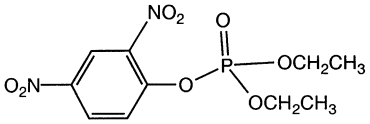
* Corresponding author. Fax: +44-1334-463-808.
E-mail address: dtr@st-andrews.ac.uk (D.T. Richens).

[1] Deceased 8th January 1999 and submitted in his memory.

0277-5387/00/$ - see front matter © 2000 Elsevier Science Ltd. All rights reserved.
PII: S0277-5387(00)00410-1



(2) L



(3)

The chemistry of L has attracted a number of previous studies. Martell and co-workers [6–9] have studied host–guest interactions between *ortho*-, pyro- and triphosphate anions and the mono and dinuclear copper(II) complexes of L by potentiometric methods. Ternary complexes are formed in aqueous solution as a result of coordinate bonding, hydrogen bond formation and electrostatic attraction between host and guest. The ligand also forms binary complexes with the nucleotides AMP, ADP and ATP due to electrostatic attraction and hydrogen bonding interactions. The protonated forms of L are capable of recognising the nucleotides in solution and the strength of the binding follows the order ATP > ADP > AMP. The mono- and dinuclear copper(II) complexes of L also form stable ternary complexes with ADP and ATP in solution although the formation constants are somewhat less than those of the macrocycle alone. The conversion of ATP to ADP and orthophosphate at 70°C has been shown to occur with the rates of hydrolysis increasing with decreasing pH. The presence of copper(II) ions has an inhibitory effect on the hydrolysis of ATP by L.

2. Experimental

2.1. Synthesis

2.1.1. $L \cdot 6HBr \cdot 5H_2O$

The macrocycle 1,4,7,16,19,22-hexa-aza[9.9]metacyclophane L (**2**) was prepared by the non-template [2 + 2] condensation of 1,5-diamino-3-azapentane with *iso*-phthalaldehyde to give the macrocyclic tetra-imine which was reduced with sodium borohydride essentially as described previously [7,8]. The hexahydrobromide salt was prepared by the addition of concentrated hydrobromic acid to a solution of the free base macrocycle in methanol and was recrystallised three times from aqueous methanol (40:190). Yield 9.56 g, 61%. m.p. 164–168, FAB MS (m/z), 655 ($LH_4Br_3^+$), 573 ($LH_3Br_2^+$), 491 (LH_2Br^+), 411 (LH^+). IR (cm^{-1}) 3450s (H_2O), 2800–2940m (C–H), 2450m (NH_2^+), 1590s (arom C–C), 1450s (C–H), 710, 810s (*m*-substituted Ph). $\delta(^1H)$ (ppm from sodium 3-trimethylsilyl-1-propane sulfonate in D_2O) 7.4 s (2H, arom.), 7.5 s (6H, arom.) 4.2 s (8H, CH_2–Ph), 3.2–3.4 m (16H, CH_2). *Anal*. Found: C, 29.6; H, 5.7; Br 48.8; N, 8.35. Calc. for $C_{24}H_{38}N_6 \cdot 6HBr \cdot 5H_2O$: C, 29.2; H, 5.5; Br 48.6; N, 8.5%. The free base form of the ligand was prepared by the addition of a concentrated potassium hydroxide solution to an aqueous solution of the HBr salt followed by extraction with dichloromethane. The stepwise protonation constants for the free base L have been determined previously to be 9.43(2), 8.68(2), 7.94(1), 7.07(1), 3.77(2) and 3.36(2) [8].

2.1.2. $[Cu_2LCl_4](Cu_2Cl_4)_{0.33}(EtOH)_{0.165}$

Copper(II) chloride dihydrate (0.99 g, 4.82 mmol) was dissolved in ethanol (20 cm^3) and added dropwise to a boiling solution of the free base ligand L (1.20 g, 2.93 mmol) in ethanol (20 cm^3). A fine blue–green precipitate began to form when half of the copper solution had been added. The complex was filtered off, washed with ethanol, then diethyl ether and dried in vacuo at 50°C (yield 1.70 g, 75%). *Anal*. Found: C, 37.5; H, 5.1; N, 10.8. Calc. for $C_{24}H_{38}N_6Cu_2 \cdot (Cu_2Cl_4)_{0.33} \cdot (C_2H_5OH)_{0.165}$: C, 37.6; H, 5.1; N, 10.8%. IR (KBr) 3434(OH), 3186 (NH), 1614 (aromatic) cm^{-1}. In DMF solution, the complex has λ_{max} 692 nm (ε = 304 $dm^3\ mol^{-1}\ cm^{-1}$) and 437 nm (ε = 116 $dm^3\ mol^{-1}\ cm^{-1}$) and a molar conductance (Λ_M) of 46 S $cm^2\ mol^{-1}$ per dimer at 25°C.

2.1.3. $[Cu_2L](ClO_4)_4 \cdot H_2O$

(**CAUTION**: Perchlorate salts are potentially explosive and should be handled with care.)

A solution of $L \cdot 6HBr \cdot 5H_2O$ (0.55 g, 0.56 mmol.) in distilled water (50 cm^3) was stirred with a suspension of excess $CuCO_3$ (0.2 g, 1.68 mmol) at room temperature (r.t.) for 3–4 h. The excess $CuCO_3$ was removed by filtration to leave a deep blue filtrate. Treatment of the filtrate at 0°C with $NaClO_4$ (0.3 g, 2.8 mmol in 5 cm^3 H_2O) resulted in precipitation of a blue solid which was removed by filtration and dried briefly in a desiccator over a silica gel. Yield 0.3 g, 60%. *Anal*. Found (%): C, 30.63; H, 4.13; N, 8.87. Calc. for $C_{24}H_{40}Cl_4N_6O_{17}Cu_2$ (M_r = 953.21): C, 30.22; H, 4.20; N 8.81%. IR (cm^{-1}), 3450s (νOH, H_2O), 3280m (νNH), 2900–2950w (νCH), 1450m (δCH), 1070, 1105, 1135vs (ν_3 ClO_4), 730m, 795m (*m*-Ph), 640, 650s (ν_4 ClO_4). In aqueous solution, the complex has λ_{max} 646 nm (ε = 308 $dm^3\ mol^{-1}\ cm^{-1}$) and Λ_M = 440 S $cm^2\ mol^{-1}$ per dimer (4:1

electrolyte). The solid complex possesses a μ/μ_B value (per Cu) of 1.53 at 18°C.

2.1.4. $[Zn_2LCl_4]\cdot 2H_2O$

Anhydrous zinc(II) chloride (0.86 g, 6.3 mmol) was dissolved in ethanol (20 cm^3) and added dropwise to a boiling ethanolic solution of the free base L (1.3 g, 3.2 mmol). A flocculent white precipitate formed immediately but slowly dissolved. On complete addition of the ligand, a white solid began to form. The solution was cooled and the complex filtered off, washed with ethanol then diethyl ether and dried in vacuo for 24 h at 50°C (yield 1.65 g, 73%). *Anal.* Found: C, 40.2; H, 5.4; N, 11.2. Calc. for $C_{24}H_{38}N_6Zn_2Cl_4\cdot 2H_2O$: C, 40.1; H, 5.9; N, 11.7%. IR (KBr), 3475 (OH), 3217 (NH), 1615 (aromatic) cm^{-1}. In DMF solution the complex has $\Lambda_M = 30$ S cm^2 mol^{-1} per dimer at 25°C.

2.1.5. $[Ni_2LCl_4](NiCl_2)_{0.167}\cdot H_2O$

Nickel(II) chloride hexahydrate (1.23 g, 5.2 mmol) in ethanol (20 cm^3) was added dropwise to a refluxing solution of the free base L (1.07 g, 2.4 mmol) in ethanol (30 cm^3). A pale-green precipitate formed during the addition. The solution was cooled and the complex filtered off, washed with ethanol and dried in vacuo for 24 h at 50°C (yield 1.35 g, 73%). *Anal.* Found: C, 40.5; H, 5.7; N, 11.5. Calc. for $C_{24}H_{44}N_6O_2Ni_2Cl_4\cdot(NiCl_2)_{0.167}\cdot H_2O$: C, 40.6; H, 5.7; N, 11.8%. IR (KBr) cm^{-1}, 3434–3194 (OH and NH), 1635 (aromatic and OH). In aqueous solution the complex has λ_{max} 390 nm ($\varepsilon = 33$ dm^3 mol^{-1} cm^{-1}) and 628 nm ($\varepsilon = 20$ dm^3 mol^{-1} cm^{-1}). In DMF solution the complex has $\Lambda_M =$ 67 S cm^2 mol^{-1} per dimer at 25°C.

2.1.6. $[Co_2LCl_2](CoCl_4)_{0.25}(Cl)_{1.5}$

Anhydrous cobalt(II) chloride (0.65 g, 4.98 mmol) was dissolved in ethanol (20 cm^3) and added dropwise to a boiling solution of the ligand (1.02 g, 2.49 mmol) in ethanol (20 cm^3) under argon. A blue precipitate formed and was filtered off and washed with ethanol (3×10 cm^3) then diethyl ether (1×10 cm^3). The complex was dried in vacuo for 24 h at 50°C (yield 1.31 g, 75%). *Anal.* Found: C, 41.45; H, 5.4, N, 11.8. Calc. for $C_{24}H_{38}N_6Co_2Cl_2\cdot(CoCl_4)_{0.25}(Cl)_{1.5}$: C, 41.0; H, 5.4; N, 11.95%. IR (KBr), 3397 (OH), 3235 (NH), 1616 (aromatic). In DMF solution the complex has λ_{max} 524 nm ($\varepsilon = 112$ dm^3 mol^{-1} cm^{-1}) 609 nm ($\varepsilon = 122$ dm^3 mol^{-1} cm^{-1}), 661 nm ($\varepsilon = 143$ dm^3 mol^{-1} cm^{-1}) and 802 nm ($\varepsilon = 18$ dm^3 mol^{-1} cm^{-1}) and $\Lambda_M = 3.4$ S cm^2 mol^{-1} per dimer at 25°C.

2.2. Crystal structure determination of $[Cu_2LCl_4]_{0.5}[Cu_2LCl_3]ClO_4\cdot dmf$

Crystals suitable for X-ray diffraction were grown by diffusion of diethyl ether into a solution of the chloro-complex prepared in DMF containing added sodium perchlorate. Small dark blue blocks were obtained. The diffraction measurements were carried out at 220 K.

2.2.1. Crystal data

$C_{39}H_{64}N_{10}Cu_3Cl_6O_5$, $M = 1156.5$, primitive monoclinic, $a = 10.504(4)$, $b = 38.68(2)$, $c = 12.962(6)$ Å, $\beta = 110.35(3)°$, $U = 4937(3)$ $Å^3$, space group $P2_1/c$ (no. 14), $Z = 4$, $D_{calc} = 1.556$ g cm^{-3}, $F(000) = 2388$. Approximate crystal dimensions $0.30 \times 0.20 \times 0.15$ mm, μ(Mo Kα) = 16.57 cm^{-1}.

2.2.2. Data collection and processing

Rigaku AFC7S diffractometer, ω–2θ scan type, graphite monochromated Mo Kα radiation; 8688 reflections measured (max $2\theta = 45.1°$) of which 6275 were unique ($R_{int} = 0.045$). No decay correction was required. Corrections for absorption (trans. factors: 0.7596–1.0000) were required. Corrections were made for Lorentz and polarisation effects.

2.2.3. Structure analysis and refinement

Direct methods were employed [10] and expanded using Fourier techniques [11]. All non-hydrogen atoms were refined anisotropically. Hydrogen atoms were included but not refined. The final cycle of full-matrix least-squares refinement was based on 4241 observed reflections ($I > 3\sigma(I)$) and 568 variable parameters and converged (largest parameter shift was 0.04 times its e.s.d.) with unweighted agreement factors of $R = 0.048$ and $R_w = 0.055$. The weighting scheme was based on counting statistics and included a factor ($\rho = 0.027$) to downweight the intense reflections. The maximum and minimum peaks in the final difference Fourier map corresponded to 0.68 and -0.49 e A^{-3}, respectively. All calculations were carried out using the TEXSAN [12] crystallographic software package of the Molecular Structure Corporation.

2.3. Kinetic measurements

The water-soluble phosphotriester 2,4-dinitrophenyldiethylphosphate was prepared as described previously [13]. The release of 2,4-dinitrophenolate was monitored by the absorbance increase at 360 nm using a Perkin–Elmer lambda-14 spectrophotometer in 1 cm quartz cells. Plots of $\ln(A_\infty - A_t)$ versus time (t) were linear for at least two half-lives. All measurements were made at 25 ± 0.1°C. Solutions of varying pH were prepared by the adjustment of a 4.65×10^{-3} mol dm^{-3} solution of copper(II), 2.52×10^{-3} mol dm^{-3} L and 0.1 mol dm^{-3} KCl to the required pH by the addition of NaOH or HCl. Reactions were initiated by the addition of 2 μdm^3 of a solution of 2,4-dinitrophenyldiethylphosphate in acetonitrile to 2 cm^3 of the metal complex solution in a 1 cm cuvette. The final phosphotriester concentration was 2×10^{-4} mol dm^{-3}. For

slow reactions (pH < 7) absorbance data were collected over one half-life and the final value of A_∞ was obtained after 2 weeks at r.t. Above pH 7, absorbance data were collected for up to three half-lives. The absorbance versus time curves were fitted to a first order rate equation using a linear least-squares method. Rate constants could be replicated to within 5%. The quoted rate constants are the average of duplicate runs.

Infra-red spectra were recorded on a Perkin–Elmer Paragon 1000 FT spectrometer as KBr pellets. Cyclic voltammetric measurements were recorded using a PAR model 170 electrochemistry system with built in sweep generator and $X-Y$ plotter. A standard three-electrode system was employed comprising Pt disc working electrode, Pt wire counter electrode and a Ag/AgCl reference electrode. Potentials are reported relative to the Ag/AgCl electrode. The solvent was dry deoxygenated acetonitrile (distilled from P_2O_5 onto 4 Å molecular sieves) and the electrolyte was 0.1 M tetra-*n*-butylammonium hexafluorophosphate. All metal salts and other solvents/materials were used as supplied.

3. Results and discussion

The 22-membered hexa-aza macrocycle 1,4,7,16,-19,22-hexa-aza[9.9]metacyclophane L (**2**) was readily prepared by the [2 + 2] condensation of 1,5-diamino-3-azapentane with isophthalaldehyde followed by sodium borohydride reduction. The macrocycle could not be readily recrystallised and it was found most convenient to purify the ligand as the hexahydrobromide salt which could be recrystallised from aqueous methanol. The free base was then prepared by the addition of a concentrated KOH solution to an aqueous solution of the hexahydrobromide followed by extraction into dichloromethane.

Complexes with Cu(II), Ni(II), Co(II) and Zn(II) could be prepared by the reaction of the metal chlorides with the free base ligand in ethanol or by use of the metal carbonate with the ligand hydrobromide salt. Analytical data was not consistent with the formation of simple binuclear chloro-complexes. The percentage of carbon, hydrogen and nitrogen was consistently lower than expected. Similar problems were also encountered with the larger 28-membered metacyclophane [14]. Chloride analysis indicated a higher percentage of chloride than predicted, which could be explained by the presence of bridging metal-chloro clusters or the presence of tetrachlorometallate anions. In view of the large size of the metal complex, it is not surprising that large anions are required to stabilise the structure. In addition, it is also known that large macrocyclic complexes of this type readily incorporate solvent molecules within their structure [15].

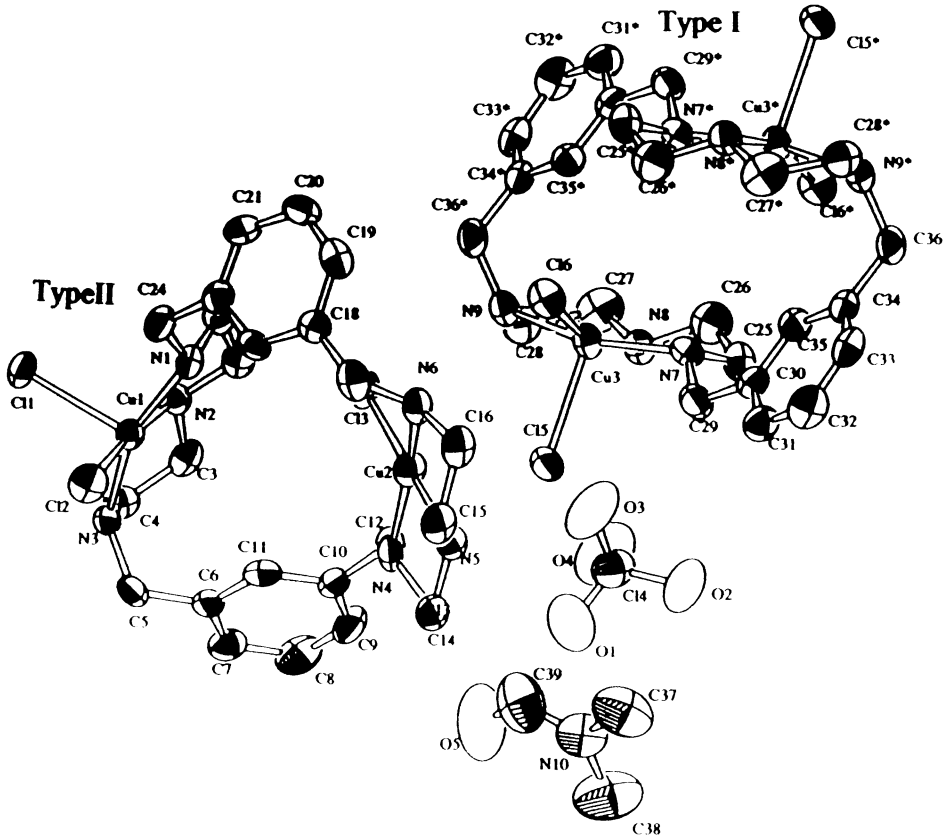


Fig. 1. ORTEP of the complex, $[Cu_2LCl_4]_{0.5}\cdot[Cu_2LCl_3]ClO_4\cdot$dmf with the atomic numbering scheme.

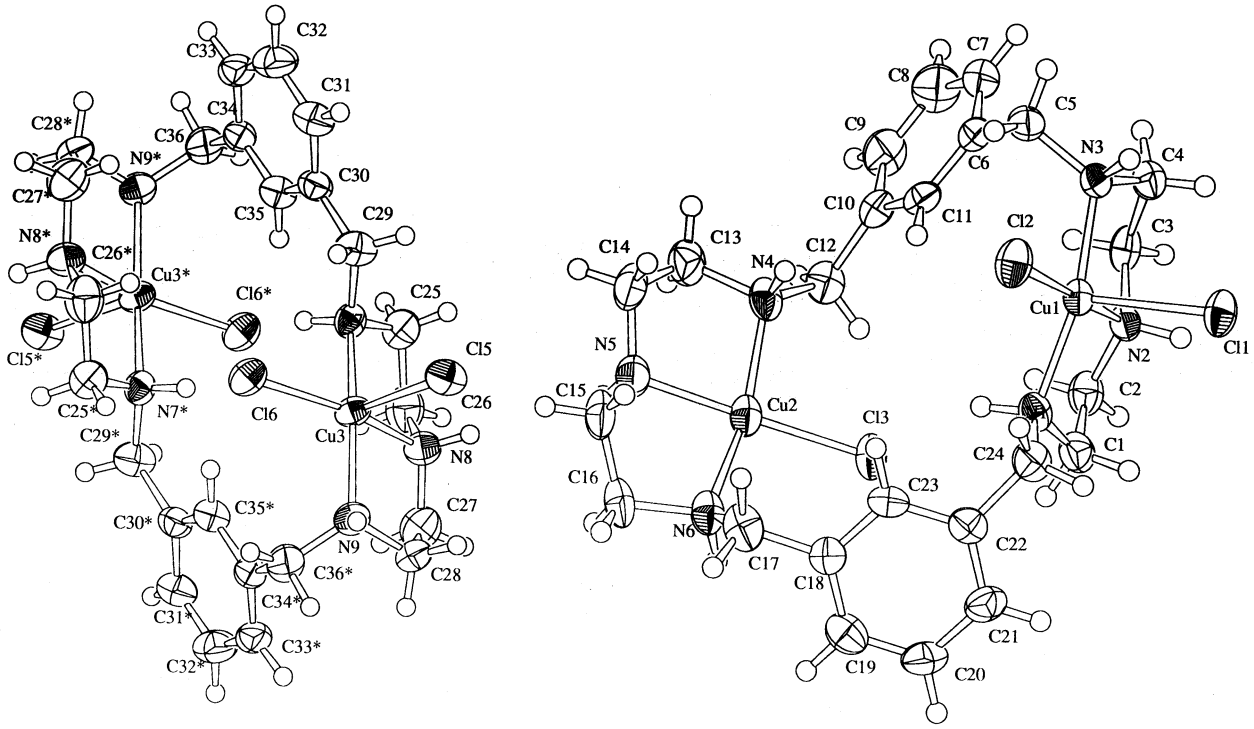


Fig. 2. Close up of the structure of the Type I (a) and Type II (b) dicopper units in the structure of $[Cu_2LCl_4]_{0.5}\cdot[Cu_2LCl_3]ClO_4\cdot dmf$.

3.1. Crystal structure of $[Cu_2LCl_4]_{0.5}[Cu_2LCl_3]ClO_4\cdot dmf$

The crystal structure (Fig. 1) shows the presence of two different binuclear copper complexes. One third of the complex has the Type 1 structure and two thirds the Type II structure. These two structures will be discussed separately.

3.1.1. Type I

The complex lies on a crystallographic centre of inversion (at 1, 0, 1/2) and displays C_i symmetry. The bond lengths and angles of half of this molecule relate to the other half as a result of this centre of symmetry. The copper centres can best be described as square pyramidal; three nitrogen donors from the macrocycle and one chloride make up the base of the pyramid (Fig. 2(a)). The copper atom is somewhat displaced from the basal plane towards the apical chloride as is frequently observed in square pyramidal complexes. The apical chloride is directed away from the macrocyclic cavity to form a long bond with a copper centre in the Type II structure. The copper–nitrogen bond distances fall within the range 2.021–2.045 Å, values which are fairly typical for five-coordinate secondary amine complexes of copper(II) where the mean value found in the Cambridge data file is 2.029 Å. The copper–chloride bond distance is 2.287 Å which is quite normal for the basal chloride, but the bond to the apical chloride (2.491 Å) is quite long and there is probably a small degree of electron withdrawal from the bond to form a bridge to the Type II structure. The Cu–Cu distance within the Type I structure is 5.82 Å. Bond lengths and angles for the Type I structure are summarised in Table 1.

Table 1
Assorted bond lengths (Å), angles (°) and Cu···Cu separation for the Type I dicopper unit

Cu(3)–Cl(6)	2.287(2)	Cl(6)–Cu(3)–Cl(5)	102.95(8)
Cu(3)–Cl(5)	2.491(2)	N(7)–Cu(3)–Cl(6)	90.6(2)
Cu(3)–N(8)	2.021(6)	N(8)–Cu(3)–Cl(5)	96.1(2)
Cu(3)–N(7)	2.043(6)	N(8)–Cu(3)–Cl(6)	160.8(2)
Cu(3)–N(9)	2.045(6)	N(9)–Cu(3)–Cl(6)	97.0(2)
Cu(3)···Cu(3)*	5.82	N(7)–Cu(3)–N(8)	83.3(2)
		N(8)–Cu(3)–N(9)	84.1(2)
		N(7)–Cu(3)–N(9)	162.0(2)

Table 2
Assorted bond lengths, angles and Cu···Cu separation for the Type II dicopper unit

Cu(1)–N(1)	2.033(6)	N(1)–Cu(1)–N(2)	83.8(2)
Cu(1)–N(2)	2.015(6)	N(1)–Cu(1)–N(3)	158.1(2)
Cu(1)–N(3)	2.040(6)	N(4)–Cu(2)–N(5)	83.7(3)
Cu(1)–Cl(1)	2.543(2)	N(6)–Cu(2)–N(4)	161.9(2)
Cu(1)–Cl(2)	2.256(2)	N(6)–Cu(2)–N(5)	83.7(3)
Cu(2)–N(4)	2.063(6)	N(1)–Cu(1)–Cl(1)	105.0(2)
Cu(2)–N(5)	2.008(6)	N(1)–Cu(1)–Cl(2)	96.5(2
Cu(2)–N(6)	2.093(6)	N(2)–Cu(1)–Cl(1)	88.0(2)
Cu(2)–Cl(3)	2.257(2)	N(6)–Cu(2)–Cl(3)	98.6(2)
Cu(2)–Cl(5)	2.845(2)	Cl(1)–Cu(1)–Cl(2)	98.24(7)
Cu(1)···Cu(2)	6.13		

3.1.2. Type II

As with the Type I structure one of the copper centres has square pyramidal stereochemistry; however, the other copper centre is best described as square planar or Jahn–Teller distorted square pyramidal (Fig. 2(b)), the apical chloride bridging from the Type I structure. The Cu–N bond distances are similar to those observed in the Type I structure although somewhat shorter distances occur in the Jahn–Teller distorted copper centre (Table 2). The planar character of this centre is reflected in the donor–copper–donor angles which are close to the ideal 90 or 180°. The Cu–Cu distance observed in the Type II structure is 6.13 Å.

The structure also includes one dmf molecule and a perchlorate anion to balance the charge on the four coordinate copper in the Type II structure. The *N*,*N*-dimethylformamide is not hydrogen bonded to any of the components of the structure and the bond lengths and angles are quite normal.

The crystal structure of the related sulfato complex $Cu_2L(SO_4)_2$ has been determined recently [6]. Crystals were prepared by slow diffusion of acetone into an aqueous solution of L·6HBr and copper(II) sulfate in a 1:2 molar ratio adjusted to pH 6.3 with KOH. The macrocycle binds two copper(II) ions via the two diethylenetriamine moieties which provide three nitrogen donors to each metal ion. The copper has square pyramidal stereochemistry with the coordination sphere being completed by one sulfate oxygen in an equatorial site and another sulfate oxygen from a different sulfate anion in the apical site. The Cu–N distances range from 1.99(1) to 2.06(1) Å and are typical of interactions of this type [16–19]. The equatorial Cu–O bond distance is 1.947(8) Å while the axial Cu–O bond distance is considerably longer at 2.262(10) Å consistent with the expected Jahn–Teller distortion. As the sulfate anions bridge the two copper centres in neighbouring molecules the crystal has an extended polymeric structure.

The solid state structure of $Cu_2L(SO_4)_2$ establishes that the macrocycle has a chair conformation with one dien moiety flipped down and the other flipped up. This conformation may not necessarily be that adopted in solution.

3.2. Electrochemical studies on $[Cu_2L(solv)_x]^{2+}$ ($solv = CH_3CN$ or H_2O)

Cyclic voltammograms recorded on solutions of freshly made up solutions of $[Cu_2L](ClO_4)_4$ in dry deoxygenated acetonitrile show a quasi-reversible oxidation wave to Cu(III) centred at $+0.99$ V (vs. Ag/AgCl) and a broad quasi-reversible reduction wave to Cu(I) centred at ~ -0.1 V. Exposure of the solution to air over a period of 12 h, however, results in the slow appearance of a new quasi-reversible oxidation wave to Cu(III) at $\sim +0.72$ V. At the same time the reduction wave to Cu(I) moves more negative towards -0.5 V and becomes largely irreversible. The deliberate addition of a few drops of water resulted in the new waves becoming dominant. It is concluded that the acetonitrile-solvated complex $[Cu_2L(NCCH_3)_x](ClO_4)_4$ ($x = 1$–4) is immediately formed upon dissolution of the presumed complex, $[Cu_2L(OClO_3)_x](ClO_4)_{4-x}$, which then slowly aquates in the air to give the aqua complex, $[Cu_2L(OH_2)_x](ClO_4)_4$ ($x = 1$–4), the rate-determining process of which is the diffusion of atmospheric moisture into the acetonitrile solvent in the electrochemical cell. On the basis of the observed potentials it can be concluded that replacement of CH_3CN by H_2O in the coordination sphere of the copper results in stabilisation of the Cu(III) state to the extent of ~ 0.23 eV and correspondingly destabilises the Cu(I) state to the extent of 0.5 eV.

3.3. Other metal complexes

The nickel(II) complex isolated is green in colour and presumably has octahedral stereochemistry at each nickel ion. This view is supported by the d–d spectrum which displays two bands at 390 nm ($\varepsilon = 33$ dm^3 mol^{-1}) and 628 nm ($\varepsilon = 20$ dm^3 mol^{-1} cm^{-1}) in the wavelength range 350–900 nm.

The d–d spectrum of the cobalt(II) complex excludes tetrahedral geometry and is consistent with a trigonal bipyramidal stereochemistry of the type observed in $[Co(Et_4dien)Cl_2]$ [20] which exhibits three bands between 950 and 520 nm with absorption coefficients in the range 20–100 dm^3 mol^{-1} cm^{-1}. The low conductivity of the complex in dmf solution also suggests that two chlorides are bound to each cobalt.

3.4. Kinetic studies

Recent investigations [13,21] have established that simple aqua-hydroxo copper(II) complexes such as $[Cu(tmen)(OH)OH_2)]^+$ (tmen = *N*,*N*,*N*′,*N*′-tetramethylenediamine) are excellent catalysts for the hydrolysis of phosphodiesters and phosphotriesters. Red kidney bean purple acid phosphatase [2] (**1**) is a binuclear Fe^{III}–Zn^{II} metalloenzyme resembling the mammalian Fe^{III}–Fe^{II} version. As a result, we were interested to establish whether the binuclear copper(II) complex of L exhibited any equivalent, or even enhanced, catalytic activity in such reactions to those of related mononuclear copper(II) systems.

Measurements were made using the water-soluble phosphotriester 2,4-dinitrophenyldiethylphosphate (**3**). In order to avoid complications due to general base catalysis which can arise from the use of buffers, the copper(II) complex of L was employed as the buffer

Table 3
The pH dependence of the hydrolysis of 2,4-dinitrophenyldiethylphosphate by the binuclear copper complex at 25°C and $I = 0.1$ mol dm^{-3}

pH	$10^5\ k_{obs}$ (s^{-1})	pH	$10^5\ k_{obs}$ (s^{-1})
5.05	1.9	8.00	6.3
5.52	2.5	8.50	8.5
6.01	2.2	9.00	12.2
6.52	1.85	9.48	23.6
7.00	2.15	10.06	24.3
7.50	2.5	10.5	26.8

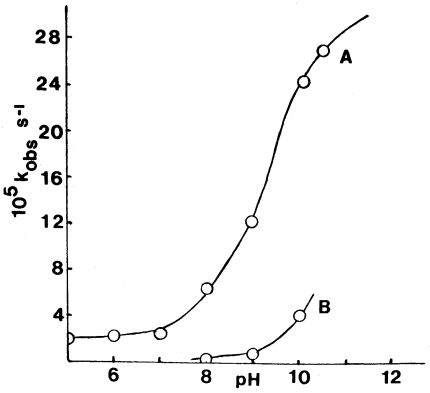
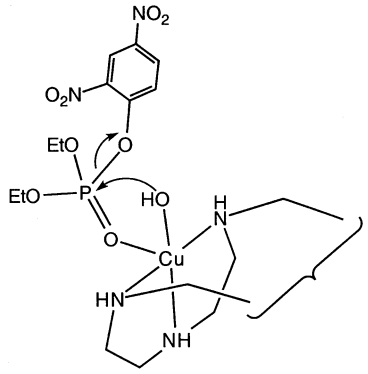


Fig. 3. Plot of k_{obs} versus pH for the binuclear copper(II) L-catalysed hydrolysis of 2,4-dinitrophenyldiethylphosphate (curve A). Curve B is the plot for the uncatalysed reaction. Measurements were made at 25°C and $I = 0.1$ mol dm^{-3} KCl.

and the pH adjusted by the dropwise addition of acid or base. The concentration of the copper complex was 2.5×10^{-3} mol dm^{-3} and the phosphotriester 2×10^{-4} mol dm^{-3}. The kinetic measurements are summarised in Table 3. The pH-rate profile is sigmoidal (Fig. 3) suggesting that the catalytically active species have a pK of ca. 9. The pH-rate profile for the uncatalysed reaction was calculated from the expression $k_{obs} = k_o + k_{OH}[OH^-]$ where k_o is the rate constant for the spontaneous water hydrolysis and k_{OH} relates to base hydrolysis. At 25°C and $I = 0.1$ mol dm^{-3}, $k_o = 1.2 \times 10^6$ s^{-1} and $k_{OH} = 0.305$ dm^3 mol^{-1} s^{-1} [13]. Using the formation constants reported by Martell and co-workers [8] for copper(II) complexes of the ligand L it is possible to construct the speciation diagram shown in Fig. 4. Formation of the dihydroxo complex $[Cu_2L(OH)_2(OH_2)_{x-2}]^{2+}$ occurs with a pK of ca. 9 and its formation mirrors the hydrolysis rate profile observed. The aqua complex $[Cu_2L(OH_2)_x]^{4+}$ also appears to exert a significant catalytic effect at pH 6 where it is the predominant species. At pH 6, in the presence of the metal complex $k_{obs} = 2.20 \times 10^{-5}$ s^{-1} while the uncatalysed reaction has $k = 1.2 \times 10^{-6}$ s^{-1}, a rate enhancement of some 20-fold. Although the rate enhancement observed with the aqua complex is not



(4)

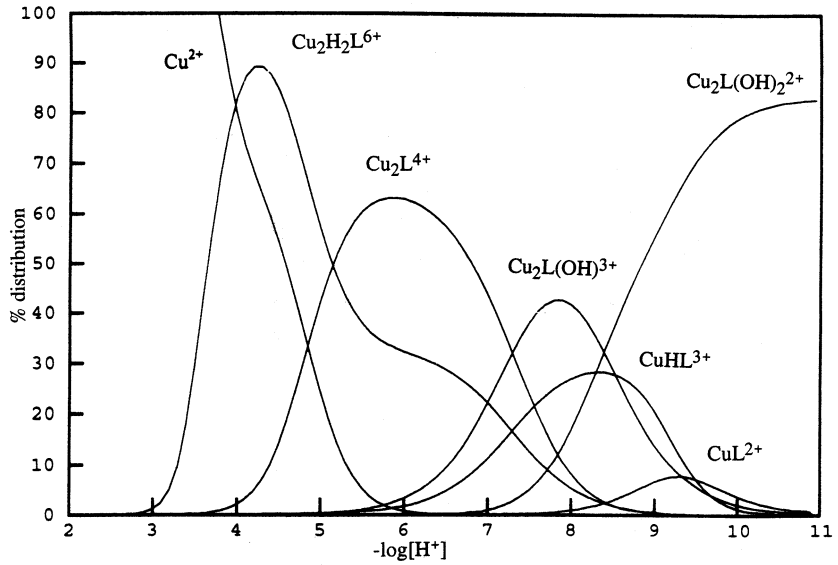


Fig. 4. Speciation curves for the copper(II) complexes of L at a 2:1 copper to ligand ratio at 25°C (constructed from the data of Martell et al. [8]).

large, the effect on the half-life of the phosphate ester is quite substantial. At pH 6 the half-life of the ester is ca. 160 h which is reduced to some 8 h in the presence of the copper complex.

In copper complexes of this type, it appears that a square pyramidal stereochemistry on copper tends to be favoured. As the distance between the copper centres in the complexes is quite large (5.8–6.0 Å), a co-operative mechanism involving both centres appears unlikely. Hydrolysis almost certainly takes place at a single copper site by formation of a ternary complex with the phosphotriester via the P=O group which then undergoes intramolecular attack by a coordinated water molecule or hydroxide ion (**4**). Such a mechanism is now well recognised in a variety of such reactions catalysed by copper(II) complexes [13,21].

4. Supplementary material

Supplementary crystallographic data are available from the CCDC, 12 Union Road, Cambridge CB2 1EZ, UK (fax: +44-1223-336033; e-mail: deposit@ccdc.cam.ac.uk or www: http://www.ccdc.cam.ac.uk) on request, quoting the deposition no. CCDC 138257.

References

[1] See for example (a) D.E. Fenton, H. Okawa, in: R.W. Hay, J.R. Dilworth, K.B. Nolan (Eds.), Perspectives in Bioinorganic Chemistry, vol. 2, Jai Press, Connecticut, 1993. (b) T. Sorrel, Tetrahedron 45 (1989) 3.
[2] N. Strater, T. Klabunde, P. Tucker, H. Witzel, B. Krebs, Science 268 (1995) 1489.
[3] See for example, P.A. Clark, D.E. Wilcox, Inorg. Chem. 28 (1989) 1326.
[4] A.L. van den Brenk, K.A. Byrel, D.P. Fairlie, L.A. Gahan, G.R. Hanson, C.J. Hawkins, A. Jones, C.H.L. Kennard, B Moubaraki, K.S. Murray, Inorg. Chem. 33 (1993) 3549.
[5] H. Ton-That, K.A. Magnus, J. Inorg. Biochem. 51 (1993) 65.
[6] D.A. Nation, A.E. Martell, R.I. Carroll, A. Clearfield, Inorg. Chem. 35 (1996) 7246.
[7] D.A. Nation, Q. Lu, A.E. Martell, Inorg. Chim. Acta 263 (1997) 209.
[8] R. Menif, A.E. Martell, P.J. Squattrito, A. Clearfield, Inorg. Chem. 29 (1990) 4723.
[9] R. Menif, A.E. Martell, J. Chem. Soc., Chem. Commun. (1989) 1522.
[10] A. Altomare, M.C. Burla, M. Camalli, M. Cascarano, C. Giacovazzo, A. Gugliardi, G. Polidori, SIR 92, J. Appl. Crystallogr. 26 (1993) 343.
[11] P.T. Beurskens, G. Admiraal, G. Beurskens, W.P. Bosman, R. de Gelder, R. Israel, J.M.M. Smitts, The DIRDIF-94 Program System, Technical Report of the Crystallography Laboratory, University of Nijmegan, The Netherlands, 1994.
[12] TEXSAN, Crystal Structure Analysis package, Molecular Structure Corporation, Houston, TX, 1985, 1992.
[13] R.W. Hay, N. Govan, Polyhedron 16 (1997) 4233.
[14] R.W. Hay, T. Clifford, unpublished work.
[15] D.A. Nation, J. Reibenspies, A.E. Martell, Inorg. Chem. 35 (1996) 4597.
[16] P.K. Coughlin, S.J. Lippard, J. Am. Chem. Soc. 106 (1984) 2328.
[17] A.E. Martin, S.J. Lippard, J. Am. Chem. Soc. 106 (1984) 2579.
[18] C.L. O'Young, J.C. Dewan, H.R. Lithenthal, S.J. Lippard, J. Am. Chem. Soc. 100 (1978) 7291.
[19] C. Bazzicalupi, A. Bencini, A. Bianchi, V. Fusi, C. Giorgi, P. Paoletti, B. Valtancoli, Inorg. Chem. 34 (1995) 552.
[20] Z. Dori, H.B. Gray, Inorg. Chem. 7 (1968) 889.
[21] R.W. Hay, N. Govan, K.E. Parchment, E. Kiss, T. Clifford, Inorg. React. Mech. 1 (1998) 33.

PERGAMON

www.elsevier.nl/locate/poly

Polyhedron 19 (2000) 1493–1502

POLYHEDRON

The spectroscopic characterisation of *cis*-$Fe(CO)_4IBr$ and *cis*-$Fe(CO)_4ICl$ and an investigation of their halogen exchange reactions in solution and the vapour

Einhard W. Robertson, Owen M. Wilkin, Nigel A. Young *

Department of Chemistry, The University of Hull, Hull, HU6 7RX, UK

Received 14 February 2000; accepted 19 April 2000

Abstract

Infrared spectra of the iron carbonyl halides, *cis*-$Fe(CO)_4X_2$ (X = I, Br, Cl) and *cis*-$Fe(CO)_4XY$ (XY = IBr, ICl), have been studied in the 4000–150 cm^{-1} region. Solution ^{13}C NMR, mass spectrometry and matrix isolation infrared studies have provided evidence of cross halogenation reactions of *cis*-$Fe(CO)_4I_2$ and *cis*-$Fe(CO)_4Br_2$ to yield *cis*-$Fe(CO)_4IBr$ in both the solution and the vapour phases and have facilitated the characterisation of the mixed halide species for the first time. Improved structural data for *cis*-$Fe(CO)_4I_2$ and the first for *cis*-$Fe(CO)_4Br_2$ have been obtained using iron K-edge X-ray absorption fine structure (XAFS) spectroscopy. © 2000 Elsevier Science Ltd. All rights reserved.

Keywords: Iron carbonyl halides; NMR; XAFS spectroscopy; Halogen exchange reactions; Matrix isolation

1. Introduction

Iron carbonyl halides, and in particular *cis*-$Fe(CO)_4I_2$, have been well studied using infrared [1–9], Mössbauer [10–13], ^{13}C NMR [14] and photoelectron [15,16] spectroscopies along with mass spectrometric [17] and calorimetric studies [18]. Whilst the *cis*-$Fe(CO)_4X_2$ (X = I, Br, Cl) complexes are well documented, little or no attention has been given to the mixed halide complexes such as *cis*-$Fe(CO)_4IBr$ and *cis*-$Fe(CO)_4ICl$ since the original reports of their synthesis in 1940 [19]. Of the *trans* complexes, only *trans*-$Fe(CO)_4I_2$ has been obtained in solution [1,5,8,9,20], the solid [9] and in a matrix [21], with the only reports of *trans*-$Fe(CO)_4Br_2$ [22] and *trans*-$Fe(CO)_4Cl_2$ [23] being limited to matrix isolation experiments. Previous work on the *cis*-$Fe(CO)_4X_2$ complexes has concentrated on the infrared spectra and in particular the ν_{CO} region with assignments of the four fundamental frequencies now being generally agreed upon [1,2,5,6]. Work has also been carried out on the infrared spectra of the metal–carbon and metal–halogen stretching vibrations (ν_{MC} and ν_{MX}) and the metal–carbon–oxygen deformation modes, δ_{MCO} [6–9]. Whilst Bennett and Clark [7] did not distinguish between the ν_{MC} and δ_{MCO} vibrations, Pankowski and Bigorgne [8,9] assigned some of those for *cis*-$Fe(CO)_4I_2$. In neither report were the ν_{MX} modes of *cis*-$Fe(CO)_4I_2$ identified. To our knowledge, only *cis*-$Fe(CO)_4I_2$ has been characterised by solution ^{13}C NMR spectroscopy, yielding two equally intense carbonyl resonances at room temperature [14]. Structural data on these compounds is limited to *cis*-$Fe(CO)_4I_2$ using Fe K-edge X-ray absorption fine structure (XAFS) spectroscopy [24], although *trans*-$Fe(CO)_4Cl_2$ [23] and *trans*-$Fe(CO)_4Br_2$ [22] have been characterised by Fe K-edge XAFS from the co-condensation of $FeCl_2$ or $FeBr_2$ into a carbon monoxide matrix. The mass spectra of *cis*-$Fe(CO)_4X_2$ showed fragmentation involving the loss of both carbon monoxide and halogen [17].

Therefore, the aim of this work was to characterise *cis*-$Fe(CO)_4IBr$ and *cis*-$Fe(CO)_4ICl$ for the first time, and to improve the structural data available for *cis*-$Fe(CO)_4I_2$ and also to provide the first structural data for *cis*-$Fe(CO)_4Br_2$.

* Corresponding author. Tel.: +44-1482-465-442; fax: +44-1482-466-410.

E-mail address: n.a.young@chem.hull.ac.uk (N.A. Young).

0277-5387/00/$ - see front matter © 2000 Elsevier Science Ltd. All rights reserved.
PII: S0277-5387(00)00412-5

2. Experimental

All compounds were prepared from iron pentacarbonyl and the appropriate halogen or interhalogen by literature methods [19,25]. *cis*-$Fe(CO)_4Br_2$ and *cis*-$Fe(CO)_4I_2$ were vacuum sublimed before further analysis. Infrared spectra were acquired using a Bruker IFS66 FTIR spectrometer. Mid-infrared (MIR) spectra (4000–400 cm^{-1}) were recorded as Nujol mulls or as solutions in NaCl or KBr windowed cells with a KBr beamsplitter and DTGS detector at 1 cm^{-1} resolution. Far-infrared (FIR) spectra (600–150 cm^{-1}) were recorded as Nujol mulls between polythene sheets (1 mm) using a 6 μm Mylar beamsplitter and DTGS detector at 2 cm^{-1} resolution. ^{13}C NMR spectra were recorded in $CDCl_3$ at 20°C on a JEOL JNM-GX270 FT NMR spectrometer at 67.8 MHz with the chemical shifts reported relative to TMS. Mass spectra were recorded using a VG SXP-1000 quadrupole mass spectrometer at 70 eV.

Matrix isolation IR spectroscopy was carried out by co-condensation of *cis*-$Fe(CO)_4X_2$ with a large excess of matrix gas on a caesium iodide window held at 15 K during deposition and 9 K during data acquisition by an APD Cryogenics DE-204SL Displex closed cycle refrigerator. No heating of the samples was necessary and deposition times were typically 20–30 min. The IR spectra were acquired on a Bruker IFS 66 FTIR spectrometer as above. Light was excluded from the samples to prevent conversion to the *trans*-species [1,5,8,9]. Details of the XAFS matrix isolation experiments, performed at the Daresbury Laboratory Synchrotron Radiation Source (SRS), have been described previously [24] and were similar to the infrared matrix isolation experiments described above except that (i) the deposition substrate was aluminium, (ii) deposition was monitored by observing the increase in the Fe K-absorption edge (2.5–4 h) and (iii) the co-condensed gas was methane at an approximate rate of 1 mmol h^{-1}. The Fe K-edge spectra were collected in fluorescence mode (NaI/Tl scintillator detector) on station 9.2 of the Daresbury Laboratory SRS (operating at 2 GeV with circulating currents of ca. 200 mA) using a Si(220) double crystal monochromator detuned by ca. 50% to remove harmonic contamination. Four to seven spectra were collected for each sample, averaged and calibrated using the first maximum in the first derivative of the Fe K-edge of Fe foil (7111.2 eV [26]). Background subtraction was carried out using PAXAS [27] by fitting the pre-edge region to a quadratic polynomial, subtracting this from the data and approximating the atomic component of the post-edge region with a high (typically sixth) order polynomial. This approximation was optimised in order to minimise the low-*r* features in the Fourier transforms by an iterative process. In the case of *cis*-$Fe(CO)_4Br_2$ it was necessary to truncate the data at 12.5 $Å^{-1}$ due to unnormalised glitches. Fitting of the experimental data was carried out with EXCURV98 [28–30] making use of the single and multiple scattering curved wave theory with linear Fe–C–O units, a von-Barth ground state and a Hedin–Lundqvist exchange potential. The same potentials and phase-shifts were used for all samples and included both bromine and iodine backscatterers as well as carbon and oxygen around a central absorbing iron atom.

3. Results and discussion

3.1. IR solution studies in the ν_{CO} region

In the ν_{CO} region, *cis*-$Fe(CO)_4X_2$ complexes have four IR active modes, and in line with previous studies [3–6], the *z* axis is taken to bisect the two Fe–X bonds which lie in the *yz* plane, the two CO ligands *trans* to each other (also called axial) lie in the *xz* plane and the 2 CO ligands *cis* to each other (equatorial) lie in the *yz* plane. Assuming no coupling, the ν_{CO} modes of the CO ligands *trans* to each other transform as $A_1^{(2)}$ and B_1, whereas the ν_{CO} modes of the CO ligands *cis* to each other transform as $A_1^{(1)}$ and B_2, and this is shown schematically below. The $A_1^{(2)}$ mode is expected to be very weak, but its intensity will be enhanced by coupling with the $A_1^{(1)}$ mode.

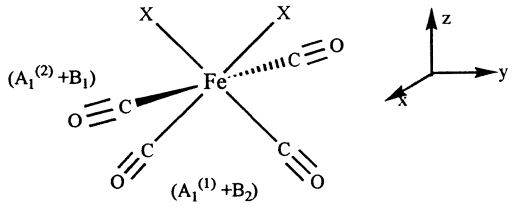


Fig. 1(a) shows the cyclohexane solution infrared spectrum of *cis*-$Fe(CO)_4I_2$ in the ν_{CO} region, and the 2129.8 cm^{-1} band can readily be assigned to the $A_1^{(2)}$ mode on the basis of its relative intensity. In agreement with Noack's findings [1] we observed only three bands instead of the expected four and he suggested that the fourth absorption was either weak at 2047 cm^{-1} or accidentally degenerate with the strong band at 2084 cm^{-1}. The overlapping of the $A_1^{(1)}$ and B_1 modes was later confirmed by Johnson et al. [5] and Butler and Spendjian [6] with the use of $C^{18}O$ and ^{13}CO isotopic exchange experiments, respectively, and it is clear from our spectra that the band at 2085 cm^{-1} is asymmetric, indicating the presence of more than one band. The solution infrared data for *cis*-$Fe(CO)_4I_2$ in the ν_{CO} region are given in Table 1 and are in good agreement with those previously reported [1,2,5,6]. In the spectrum of *cis*-$Fe(CO)_4Br_2$ (Fig. 1(b), Table 1), the four fundamental absorption bands were resolved, and in this case the relative intensity of the peaks allows for the unam-

biguous assignment of the 2149.5 and 2107.7 cm^{-1} bands to the $A_1^{(2)}$ and B_1 modes, respectively. The assignment of the two remaining peaks at 2097.4 and 2073.6 cm^{-1} to the $A_1^{(1)}$ and B_2 modes, respectively, is based on the work of Johnson et al. [5] and Butler and Spendjian [6] on the basis of the values of the principal and interaction force constants required to fit the data. As to be expected [3,31–34] the ν_{CO} modes of *cis*-$Fe(CO)_4Br_2$ are at higher wavenumbers than those of *cis*-$Fe(CO)_4I_2$, but all the modes are not affected by the same amount, with the $A_1^{(2)}$ and B_1 modes of the *trans* COs being more affected than the $A_1^{(1)}$ and B_2 modes of the *cis* CO ligands. This behaviour has been rationalised previously [3,31] to be due to the differing extent of metal dπ-orbital sharing by the *cis* and *trans* CO ligands.

The IR spectrum of *cis*-$Fe(CO)_4IBr$ shown in Fig. 1(c) clearly has features due to both *cis*-$Fe(CO)_4I_2$ and

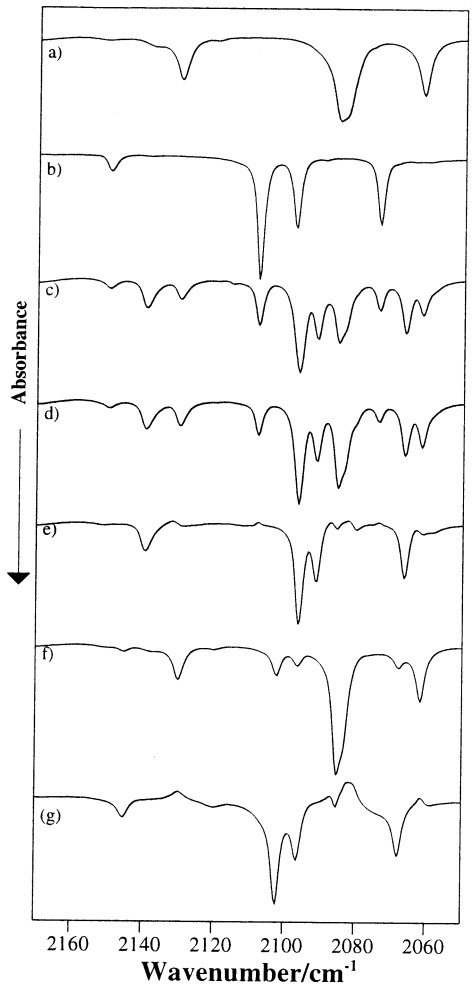


Fig. 1. Infrared spectra of *cis*-iron carbonyl halides in cyclohexane solution in the ν_{CO} region (a) *cis*-$Fe(CO)_4I_2$, (b) *cis*-$Fe(CO)_4Br_2$, (c) *cis*-$Fe(CO)_4IBr$, (d) mixture of *cis*-$Fe(CO)_4I_2$ and *cis*-$Fe(CO)_4Br_2$, (e) *cis*-$Fe(CO)_4IBr$ (obtained by subtracting (a) and (b) from (c)), (f) *cis*-$Fe(CO)_4ICl$ and (g) *cis*-$Fe(CO)_4ICl$ (obtained by subtracting (a) from (f)).

cis-$Fe(CO)_4Br_2$, as well as new bands which are from *cis*-$Fe(CO)_4IBr$. This is confirmed in Fig. 1(e) where the spectral features of the parent molecules (Fig. 1(a)) and (Fig. 1(b)) have been subtracted from Fig. 1(c) to reveal the bands solely due to *cis*-$Fe(CO)_4IBr$, and these lie approximately midway between the comparable bands of the parent species. All four of the ν_{CO} modes are observable, but are not as well separated as in *cis*-$Fe(CO)_4Br_2$, with those at 2139.3 and 2096.0 cm^{-1} being assigned to the modes of the COs *trans* to each other, whereas those at 2091.2 and 2066.2 cm^{-1} arise from the CO ligands *cis* to each other. For the case of *cis*-$Fe(CO)_4ICl$, the main features present in Fig. 1(f) are clearly due to *cis*-$Fe(CO)_4I_2$ with a set of weaker bands assigned to *cis*-$Fe(CO)_4ICl$ shown in Fig. 1(g), which was obtained by subtraction of the spectrum of *cis*-$Fe(CO)_4I_2$ and again four modes are clearly present. No absorptions due to *cis*-$Fe(CO)_4Cl_2$ were observed in this spectrum because *cis*-$Fe(CO)_4Cl_2$ was particularly unstable in solution and very insoluble in cyclohexane.

Whilst we were able to use the SOTONVIB program [35] and the force field of Butler and Spendjian [6] to calculate the positions of the ν_{CO} modes of *cis*-$Fe(CO)_4I_2$ and *cis*-$Fe(CO)_4Br_2$ and could also generate values of the force constants for *cis*-$Fe(CO)_4IBr$ and *cis*-$Fe(CO)_4ICl$, there is no unique solution in the absence of isotopic data, because it is necessary to define five force constants for *cis*-$Fe(CO)_4X_2$ and seven force constants for *cis*-$Fe(CO)_4XY$ molecules with only four observed frequencies for each molecule.

The bands due to *cis*-$Fe(CO)_4I_2$ and *cis*-$Fe(CO)_4Br_2$ observed in the spectra of *cis*-$Fe(CO)_4IBr$ and *cis*-$Fe(CO)_4ICl$ posed the questions: (i) whether the starting materials IBr and ICl existed in significant equilibrium with the parent halogens to such an extent as to carry over to the final product, or (ii) whether halogen exchange occurred in solution, or a combination of the two. The degree of dissociation of IBr into I_2 and Br_2 in carbon tetrachloride has been investigated by Christian and co-workers [36] and was found to be around 8%. A far greater proportion of the parent complexes was seen in our spectra than would be expected due to dissociation of the interhalogen alone. The extent of halogen exchange between the complexes in solution was demonstrated by recording infrared spectra of a 1:1 mixture of *cis*-$Fe(CO)_4I_2$ and *cis*-$Fe(CO)_4Br_2$. In this case a significant amount of *cis*-$Fe(CO)_4IBr$ formed instantly (Fig. 1(d)) with no time-dependent intensity changes being observed. Comparison of this spectrum with that of the material prepared from IBr shown in Fig. 1(c) is very good, showing that halogen exchange in solution produced very similar proportions of *cis*-$Fe(CO)_4I_2$, *cis*-$Fe(CO)_4Br_2$ and *cis*-$Fe(CO)_4IBr$ compared with the solution of *cis*-$Fe(CO)_4IBr$ prepared directly from $Fe(CO)_5$ and IBr. Therefore, it appears that there is indeed halogen exchange between the

Table 1
Infrared data and assignments for *cis*-$Fe(CO)_4X_2$ complexes in the 2200–2000 cm^{-1} region

Complex	N_2 matrix [a]	Ar matrix [a]	Solution [a]	Johnson et al. [d]	Butler and Spendjian [e]	Taylor and Horrocks [f]	Assignment
cis-$Fe(CO)_4I_2$	2139.2	2133.5	2129.8 [b]	2128.8 [b]	2128.4 [b]	2134.7 [c]	ν_{CO} $A_1^{(2)}$
	2093.6	2090.0	2084.9 [b]	2083.5 [b]	2083.5 [b]	2089.4 [c]	ν_{CO} B_1, $A_1^{(1)}$
	2070.7	2064.5	2061.5 [b]	2060.3 [b]	2060.0 [b]	2068.4 [c]	ν_{CO} B_2
cis-$Fe(CO)_4Br_2$	2158.9	2153.6	2149.5 [b]	2148.5 [b]	2148.6 [b]	2155.0 [c]	ν_{CO} $A_1^{(2)}$
	2116.8	2110.4	2107.7 [b]	2106.7 [b]	2108.7 [b]	2108.6 [c]	ν_{CO} B_1
	2106.2	2100.7	2097.4 [b]	2097.2 [b]	2098.6 [b]	2112.4 [c]	ν_{CO} $A_1^{(1)}$
	2081.6	2076.2	2073.6 [b]	2073.8 [b]	2074.4 [b]	2081.6 [c]	ν_{CO} B_2
cis-$Fe(CO)_4Cl_2$			2168.2 [c]			2166.9 [c]	ν_{CO} $A_1^{(2)}$
			2127.6 [c]			2125.8 [c]	ν_{CO} B_1
			2115.5 [c]			2125.8 [c]	ν_{CO} $A_1^{(1)}$
			2091.5 [c]			2081.7 [c]	ν_{CO} B_2
cis-$Fe(CO)_4IBr$ [g]	2148.9	2143.4	2139.3 [b]				ν_{CO} $A'^{(2)}$
	2105.2	2098.6	2096.0 [b]				ν_{CO} A''
	2100.6	2094.9	2091.2 [b]				ν_{CO} $A'^{(1)}$
	2074.7	2068.9	2066.2 [b]				ν_{CO} $A'^{(3)}$
cis-$Fe(CO)_4ICl$ [g]			2145.2 [b]				ν_{CO} $A'^{(2)}$
			2102.2 [b]				ν_{CO} A''
			2096.3 [b]				ν_{CO} $A'^{(1)}$
			2067.7 [b]				ν_{CO} $A'^{(3)}$

[a] This work.
[b] Cyclohexane solution.
[c] Chloroform solution.
[d] Ref. [5].
[e] Ref. [6].
[f] Ref. [2].
[g] For *cis*-$Fe(CO)_4IBr$ and *cis*-$Fe(CO)_4ICl$ only the features belonging to these species are tabulated.

complexes when in solution. Previous kinetic studies [37] on ^{14}CO exchange with *cis*-$Fe(CO)_4I_2$ have shown that all four CO ligands exchange at the same rate via a S_N2 (associative) mechanism, with a proposed seven-coordinate transition state. We have not carried out IR kinetic experiments for the halogen exchange due to the limited time resolution available, and isotopic labelling would produce complex spectra with many overlapping bands in both the mid and far infrared that would be hard to disentangle with confidence.

3.2. IR solution and mull studies in the δ_{MCO}, ν_{MC} and ν_{MX} region

For *cis*-$Fe(CO)_4X_2$ complexes, a total of 12 infrared active bands are expected in the FIR region, and these can be described as six infrared-active δ_{MCO} vibrations ($2A_1 + 2B_1 + 2B_2$), four infrared-active ν_{MC} vibrations ($2A_1 + B_1 + B_2$), and two infrared-active ν_{MX} vibrations ($A_1 + B_2$). However, as noted by Bennett and Clark [7] unambiguous assignment of the spectra is not easy, especially as the various modes lie close together in frequency, allowing the coupling of those with the same symmetry, but Pankowski and Bigorgne [8] have assigned a few of the spectral features. It is however instructive to compare the spectra for the analogous *trans*-$Fe(CO)_4X_2$ complexes as the higher symmetry results in fewer IR bands which are much easier to assign with confidence, especially in conjunction with isotopic data. The ν_{MC} (E_u, assuming D_{4h}) modes for *trans*-$Fe(CO)_4X_2$ were observed at 414 (X = I, solution [8]), 394.9 (X = Br, CO matrix [22]) and 380.4 cm^{-1} (X = Cl, CO matrix [23]), with the expected shift to lower energy for more electronegative halogen, which is the reverse of the trend observed for the ν_{CO} modes. The δ_{MCO} modes ($A_{2u} + E_u$) at 606 and 600 (X = I, solution [8,9]), 612 and 598 (X = I, CO matrix [21]), 608.7 and 589.0 (X = Br, CO matrix [22]), 606.6 and 582.3 (X = Cl, CO matrix [23]) were less sensitive to a change of halogen, but much more intense than the ν_{MC} modes. Therefore, for the *cis*-$Fe(CO)_4X_2$ complexes we might expect some relatively intense δ_{MCO} modes not very sensitive to halogen around 600 cm^{-1} and some weaker ν_{MC} modes much more sensitive to halogen at about 400 cm^{-1} in addition to ν_{MX} modes which would be very sensitive to a change in halogen.

The FIR data for the *cis*-$Fe(CO)_4X_2$ complexes are shown in Fig. 2. The data in Fig. 2(a) and Fig. 2(c) were collected as cyclohexane solutions, whereas for all the other spectra the samples were presented as Nujol

mulls. As there is little difference between the spectrum of *cis*-$Fe(CO)_4I_2$ (Fig. 2(a)) and *cis*-$Fe(CO)_4Br_2$ (Fig. 2(c)) in the 630–480 cm^{-1} region, the spectra of the mixed complexes are not shown in this region. It is clear from Fig. 2(a) to (d) that not all of the 12 IR active modes are clearly identifiable, with some being either too weak to observe, or overlapped by other bands. The ν_{MX} vibrations below 330 cm^{-1} are readily identified due to their large shifts on change of halogen, and the presence of triplets in the mixed halogen species at 245–215 cm^{-1} and 210–180 cm^{-1} for *cis*-$Fe(CO)_4IBr$ and 330–290 cm^{-1} and 210–180 cm^{-1} for *cis*-$Fe(CO)_4ICl$. The three intense features at ca. 600 cm^{-1}, which are not greatly affected by a change in halogen, can be assigned to δ_{MCO} modes on the basis of the arguments above, which is in agreement with Pankowski and Bigorgne [8] who also assigned the weaker feature at 505 cm^{-1} to a δ_{MCO} mode. The spectra between 470–350 cm^{-1} are complex with many bands being sensitive to a change of halogen. In some cases (460–420 cm^{-1} for *cis*-$Fe(CO)_4IBr$ Fig. 2(f)) triplets are clearly observed confirming that these are most probably due to the ν_{MC} modes, although it is possible that there are also some weak δ_{MCO} modes in this spectral region. Whilst it may be possible to make firmer assignments on the basis of the relative intensities expected for the ν_{MC} modes, there is the severe problem of mixing of the vibrational modes of the same symmetry, so that even assignments of the features as exclusively ν_{MC} modes should be treated with care. In particular, the ν_{MX} modes may mix with three of the ν_{MC} modes and four of the δ_{MCO} modes to cause both intensity and energy perturbations that will be different for each complex. Therefore, whilst the assignment of the δ_{MCO}, ν_{MC} and ν_{MX} modes is reasonable, we do not believe that it is possible or meaningful to assign any of the individual δ_{MCO}, ν_{MC} and ν_{MX} modes to their respective normal modes.

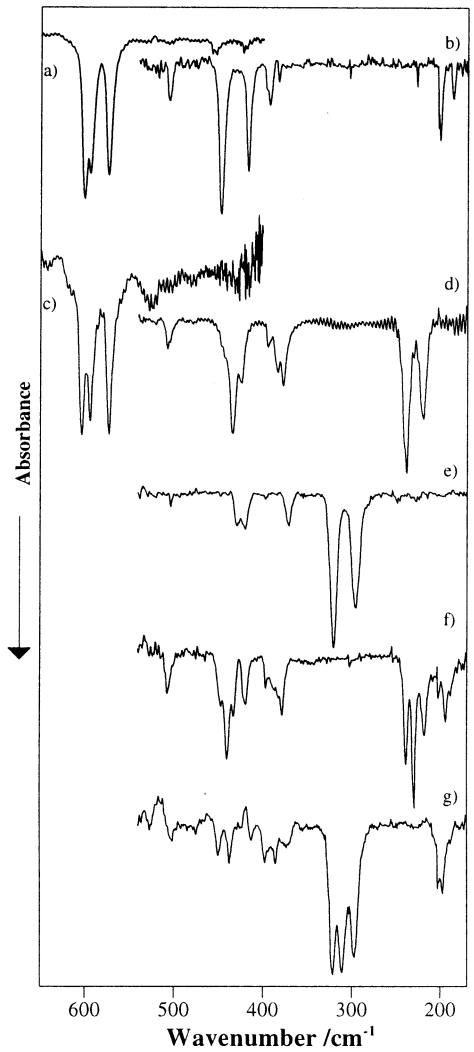


Fig. 2. Infrared spectra in the $\delta_{M\text{-}C\text{-}O}$, $\nu_{M\text{-}C}$ and $\nu_{M\text{-}X}$ regions of (a) *cis*-$Fe(CO)_4I_2$ (cyclohexane solution), (b) *cis*-$Fe(CO)_4I_2$ (Nujol mull) (c) *cis*-$Fe(CO)_4Br_2$ (cyclohexane solution), (d) *cis*-$Fe(CO)_4Br_2$ (Nujol mull) (e) *cis*-$Fe(CO)_4Cl_2$ (Nujol mull), (f) *cis*-$Fe(CO)_4IBr$ (Nujol mull) and (g) *cis*-$Fe(CO)_4ICl$ (Nujol mull).

3.3. Solution ^{13}C NMR studies

The ^{13}C NMR spectra from the *cis*-$Fe(CO)_4X_2$ (X = I, Br,) complexes yielded two equally intense resonances at 204.2 and 197.7 ppm (X = I) and 199.4 and 194.1 ppm (X = Br) in good agreement with the literature values for *cis*-$Fe(CO)_4I_2$ given in Table 3 [14]. The marked shift to lower frequency of both resonances observed for *cis*-$Fe(CO)_4Br_2$ compared with *cis*-$Fe(CO)_4I_2$ has been observed previously for related platinum and palladium carbonyl complexes [38]. Spectra of *cis*-$Fe(CO)_4Cl_2$ were unobtainable due to significant decomposition involving the loss of CO during analysis. The mixed halide complexes also proved difficult to analyse due to their lack of stability, and in the case of *cis*-$Fe(CO)_4IBr$ this problem was remedied by combining *cis*-$Fe(CO)_4Br_2$ and *cis*-$Fe(CO)_4I_2$ in a 1:1 mixture in the NMR tube just prior to spectral acquisition. For *cis*-$Fe(CO)_4IBr$ three ^{13}C NMR resonances are expected in a 2:1:1 intensity ratio; one signal for the two CO ligands *trans* to each other (axial) and one signal each for the *cis* CO ligands (equatorial) but *trans* to different halogens. Therefore, the spectrum of a 1:1 mixture of *cis*-$Fe(CO)_4Br_2$ and *cis*-$Fe(CO)_4I_2$ would be expected to contain seven peaks if the halogen exchange is slow on the NMR timescale, and this was indeed the case, as shown in Fig. 3 with the features due to the different complexes marked. This spectrum also allows for the direct assignment of the *cis*-$Fe(CO)_4IBr$ resonances at 202.6, 201.3 and 196.3 ppm due to their different intensities. Therefore, as the signal at 196.3 ppm has approximately twice the intensity of those at 202.6 and 201.3 ppm, it must arise from the axial CO ligands *trans* to each other, with those at

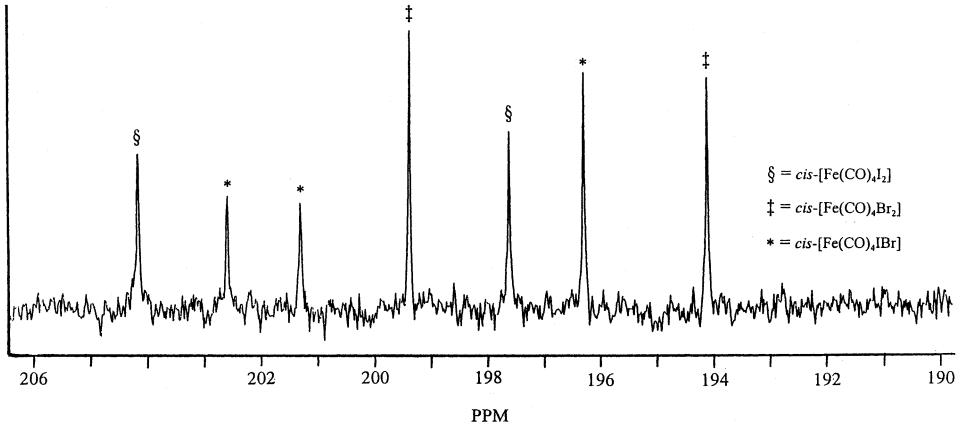


Fig. 3. $CDCl_3$ solution ^{13}C NMR of a mixture of *cis*-$Fe(CO)_4I_2$ and *cis*-$Fe(CO)_4Br_2$.

202.6 and 201.3 ppm from the equatorial CO ligands *cis* to each other, but *trans* to I and Br, respectively. This assignment can then be extended to *cis*-$Fe(CO)_4I_2$ and *cis*-$Fe(CO)_4Br_2$ where the 204.2 and 199.4 ppm signals can be assigned to the equatorial CO ligands *trans* to the halogen, whereas the 197.7 and 194.1 ppm features can be assigned to the axial CO ligands *trans* to CO. These assignments are the reverse of those given previously for *cis*-$Fe(CO)_4I_2$ [14], but as this was based on the coupling patterns in the analogous *cis*-$Os(CO)_4H_2$ complexes, we believe that our assignments based on the mixed halogen complexes are more likely to be the correct ones. The ^{13}C NMR spectrum of *cis*-$Fe(CO)_4ICl$ was very noisy due to the lack of sample stability, and this should be borne in mind when consulting the data in Table 3.

3.4. Matrix isolation infrared studies

Having observed halogen exchange in solution, experiments were performed to check whether halogen exchange also occurred in the vapour phase. Mass spectrometry was initially employed, firstly with *cis*-$Fe(CO)_4IBr$ to see if it was sufficiently stable as a vapour phase species, and subsequently, the vapour phase combination of *cis*-$Fe(CO)_4I_2$ and *cis*-$Fe(CO)_4Br_2$. All complexes gave fragmentation patterns involving the loss of both carbon monoxide and halogen as previously reported [17]. When *cis*-$Fe(CO)_4I_2$ and *cis*-$Fe(CO)_4Br_2$ were combined in the vapour phase in the mass spectrometer, the fragmentation pattern characteristic of *cis*-$Fe(CO)_4IBr$ was observed, in addition to those characteristic of *cis*-$Fe(CO)_4I_2$ and *cis*-$Fe(CO)_4Br_2$. Whilst this is reasonable evidence of halogen exchange in the vapour, it should be remembered that the ionisation process for mass spectrometry is very energetic, and the apparent composition may not be representative of the true vapour phase behaviour. Therefore, infrared studies of the vapour phase combination of *cis*-$Fe(CO)_4I_2$ and *cis*-$Fe(CO)_4Br_2$ were also conducted using matrix isolation techniques. Argon and nitrogen were used as the matrix gases and the absorption bands observed in the 4000–550cm^{-1} region are given in Tables 1 and 2. As to be expected, the ν_{CO} modes are shifted to slightly higher frequency for the matrix isolated species compared with the solution data, and with the N_2 matrix data blue shifted with respect to the Ar matrix data. Because the argon matrix IR spectra of *cis*-$Fe(CO)_4Br_2$ and *cis*-$Fe(CO)_4IBr$ were complicated by site effects, the vapour phase combination of *cis*-$Fe(CO)_4I_2$ and *cis*-$Fe(CO)_4Br_2$ was only carried out in dinitrogen matrices. Fig. 4 shows the nitrogen matrix infrared spectra in the ν_{CO} region from samples of (a) *cis*-$Fe(CO)_4I_2$, (b) *cis*-$Fe(CO)_4Br_2$, (c) *cis*-$Fe(CO)_4IBr$ and (d) the vapour phase combination of *cis*-$Fe(CO)_4I_2$ and *cis*-$Fe(CO)_4Br_2$. Matrix isolation experiments with *cis*-$Fe(CO)_4Cl_2$ were not possible due to extensive sample decomposition under vacuum. The spectrum showing the vapour phase combination of *cis*-$Fe(CO)_4I_2$ and *cis*-$Fe(CO)_4Br_2$ (Fig. 4(d)) illustrates that whilst the spectral components from *cis*-$Fe(CO)_4I_2$ predominate, bands due to the formation of *cis*-$Fe(CO)_4IBr$ are clearly visible and are marked with an asterisk. Therefore, this is clear evidence that vapour phase halogen exchange is occurring between *cis*-$Fe(CO)_4I_2$ and *cis*-$Fe(CO)_4Br_2$ resulting in the formation of *cis*-$Fe(CO)_4IBr$, and that the most likely mechanism in this case involves a seven-coordinate, halogen bridged, dimeric intermediate.

3.5. Fe K-edge XAFS studies

In order to obtain structural data for these complexes, Fe K-edge XAFS experiments were carried out on *cis*-$Fe(CO)_4I_2$ and *cis*-$Fe(CO)_4Br_2$, but not on *cis*-$Fe(CO)_4IBr$ because the presence of very significant proportions of *cis*-$Fe(CO)_4I_2$ and *cis*-$Fe(CO)_4Br_2$ would

Table 2
Infrared data and assignments for *cis*-$Fe(CO)_4X_2$ complexes in the 650 –150 cm^{-1} region

Complex		δ_{MCO} (cm^{-1})	ν_{MC} (cm^{-1})	ν_{MX} (cm^{-1})
cis-$Fe(CO)_4I_2$	N_2 matrix [a]	607.7, 594.0, 580.4		
	Ar matrix [a]	605.8, 594.9, 579.6		
	cyclohexane solution [a]	601, 594, 575	456, 423	
	Nujol mull [a]	505	447, 417, 393, 383,	200, 186
	Bennett & Clark [b] (not assigned)	631, 592, 587, 575, 504	445, 415, 391, 382	<200
	Pankowski & Bigorgne [c]	600, 594, 573, 507	454, 421	
cis-$Fe(CO)_4Br_2$	N_2 matrix [a]	610.5,596.5, 579.5		
	Ar matrix [a]	609.6, 597.2, 579.2		
	cyclohexane solution [a]	603, 594, 573		
	Nujol mull [a]	507	434, 424, 394, 383, 377	238, 219
	Bennett and Clark [b] (not assigned)	593, 585, 575, 503	440, 430, 422, 392, 375	237, 217
cis-$Fe(CO)_4Cl_2$	chloroform solution [a]	602, 587, 570		
	Nujol mull [a]	503	429, 420, 397, 371	320, 295
	Bennett and Clark [b] (not assigned)	622, 593, 583, 570, 502	437, 427, 419, 391, 368	318, 294
cis-$Fe(CO)_4IBr$ [d]	N_2 matrix [a]	608.7, 596.4, 580.1		
	Ar matrix [a]	607.4, 596.8, 579.9		
	cyclohexane solution [a]	601, 594, 574		
	Nujol mull [a]	506	447, 440, 432, 419, 396, 388, 383, 377	238, 229, 217 202, 193, 187
cis-$Fe(CO)_4ICl$ [d]	cyclohexane solution [a]	602, 594, 572		
	Nujol mull [a]	502	450, 437, 413, 397, 385, 373	321, 310, 296 201, 197, 188

[a] This work.
[b] Ref. [7].
[c] Refs. [8,9].
[d] For *cis*-$Fe(CO)_4IBr$ and *cis*-$Fe(CO)_4ICl$ all the features are tabulated.

make the analysis effectively impossible. In order to obtain the XAFS data from the highest purity sample, and to reduce the problems of self-absorption by the iodine in *cis*-$Fe(CO)_4I_2$, the samples were vacuum sublimed in-situ into a methane matrix at 15 K. The experimental Fe K-edge XAFS and Fourier transforms as well as the theoretical fits for *cis*-$Fe(CO)_4I_2$ and *cis*-$Fe(CO)_4Br_2$ isolated in methane matrices at 9 K are shown in Fig. 5, with values of the refined parameters given in Table 4. Also included in Table 4 are the literature structural values for $Fe(CO)_5$ from the most recent gas-phase electron diffraction [39] and single-crystal X-ray diffraction studies [40]. Fe K-edge XAFS data for $Fe(CO)_5$ have been obtained and analysed previously by us using EXCURV90 [23] and this data has now been refitted using EXCURV98 using the same phase shifts as for the iron carbonyl halides. Although small differences (ca. 0.01–0.02 Å) in the axial and equatorial Fe–C bond lengths have been observed in the diffraction studies [39,40], the ordering was actually reversed between the two techniques. A recent theoretical study [41] has tried to reconcile these differences, and indicates slightly longer (0.068 Å) axial Fe–C bond lengths than equatorial Fe–C bond lengths, but only when a relatively high level of theory (DZP B3LYP) was used. The differences in the axial and equatorial Fe–C bond lengths from the diffraction experiments or theory are too small to be detected by XAFS (to resolve a difference of 0.02 Å requires a data set of ca. 75 $Å^{-1}$ [42]) and therefore as expected there was no statistical improvement in the quality of the fit when two shells of CO ligands were used rather than one. However, it is clear that the agreement between Fe K-edge XAFS and the other structural methods for the Fe–C distances is

Table 3
^{13}C NMR data for *cis*-$Fe(CO)_4X_2$ complexes in solution

Complex	^{13}C chemical shift (ppm) and assignment
cis-$Fe(CO)_4I_2$ [a]	204.6 ($CO_{trans\ CO}$) 198.5 ($CO_{trans\ I}$)
cis-$Fe(CO)_4I_2$ [b]	204.8 ($CO_{trans\ CO}$) 198.5 ($CO_{trans\ I}$)
cis-$Fe(CO)_4I_2$ [c]	204.2 ($CO_{trans\ I}$) 197.7 ($CO_{trans\ CO}$)
cis-$Fe(CO)_4Br_2$ [c]	199.4 ($CO_{trans\ Br}$) 194.1 ($CO_{trans\ CO}$)
cis-$Fe(CO)_4IBr$ [c]	202.6 ($CO_{trans\ I}$) 201.3 ($CO_{trans\ Br}$) 196.3 ($CO_{trans\ CO}$)
cis-$Fe(CO)_4ICl$ [c]	200.7 ($CO_{trans\ I}$) 200.4 ($CO_{trans\ Cl}$) 196.1 ($CO_{trans\ CO}$)

[a] Ref. [14], toluene d^8.
[b] Ref. [14], CD_2Cl_2.
[c] This work, $CDCl_3$.

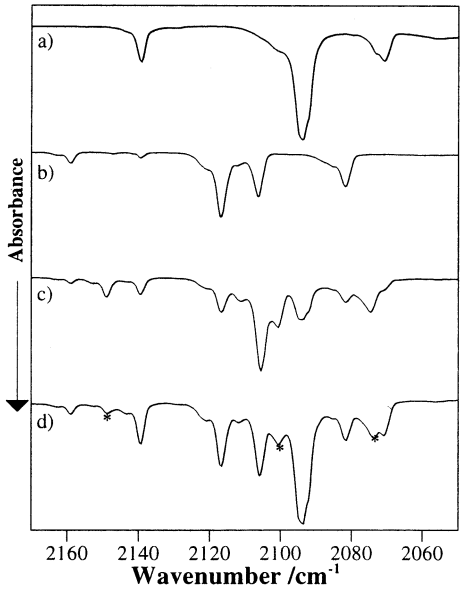


Fig. 4. Nitrogen matrix infrared spectra in the ν_{CO} region for (a) *cis*-$Fe(CO)_4I_2$, (b) *cis*-$Fe(CO)_4Br_2$, (c) *cis*-$Fe(CO)_4IBr$ and (d) vapour phase combination of *cis*-$Fe(CO)_4I_2$ and *cis*-$Fe(CO)_4Br_2$.

better for the refinements using EXCURV98 rather than EXCURV90, therefore an even better improvement would be expected in the quality of the refined parameters for *cis*-$Fe(CO)_4I_2$ as the previous analysis made use of EXCURV88. The only structurally characterised iron(II) complex which has carbonyl ligands both *trans* to CO and *trans* to a halogen is $[Fe(CO)_3I_2(C(O)CH_3)]^-$ [43]. This has Fe–C bond lengths of 1.781 Å for CO *trans* to I, and 1.826 and 1.869 Å for the two CO ligands *trans* to each other, as well as Fe–I bond lengths of 2.632 and 2.686 Å. Although a difference of ca. 0.1 Å could just be resolved, any spread of distances would rule this out. Therefore, in the case of *cis*-$Fe(CO)_4I_2$ and *cis*-$Fe(CO)_4Br_2$ the data would only fit to one significant Fe–C shell. The shorter average Fe–C bond length for $Fe(CO)_5$ (1.81(2) Å) compared with *cis*-$Fe(CO)_4I_2$ (1.87(2) Å) or *cis*-$Fe(CO)_4Br_2$ (1.85(2) Å) is expected on the basis of the relative position of the ν_{CO} modes. The small difference between the Fe–C bond lengths for *cis*-$Fe(CO)_4I_2$ and *cis*-$Fe(CO)_4Br_2$ are about the same as the confidence limits, and therefore their significance should not be over interpreted. Like-

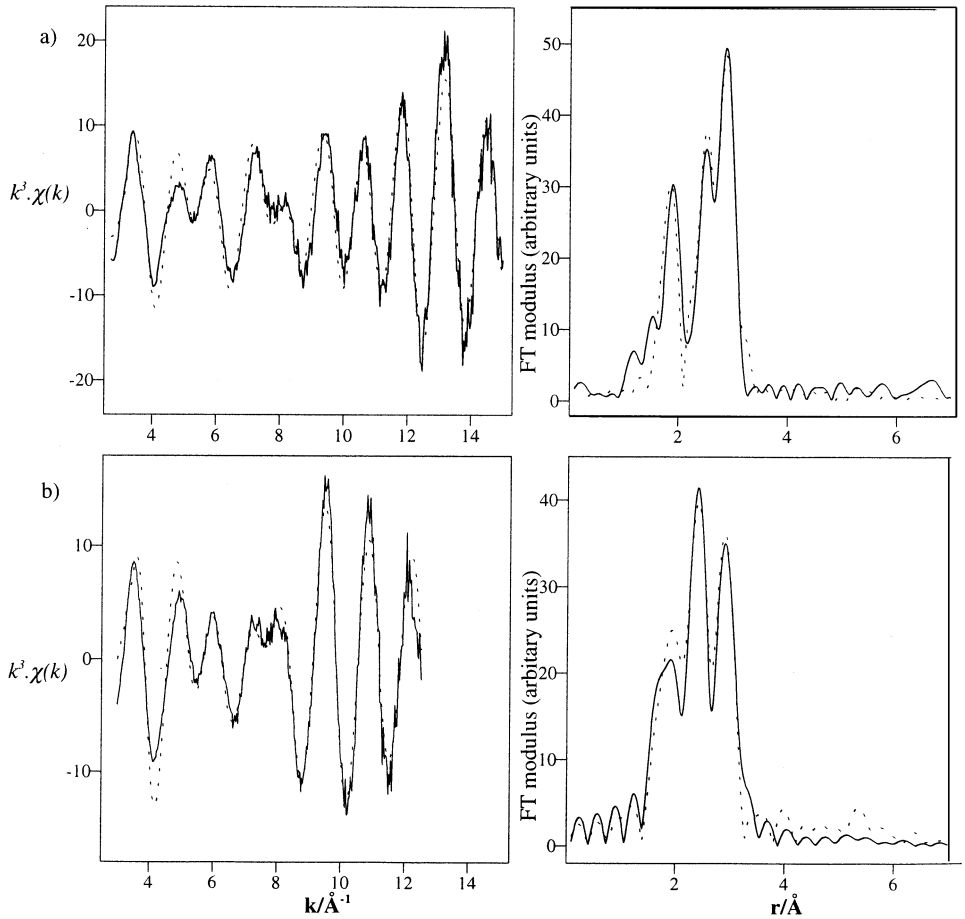


Fig. 5. Fe K-edge XAFS and Fourier transforms for (a) *cis*-$Fe(CO)_4I_2$ and (b) *cis*-$Fe(CO)_4Br_2$ isolated in CH_4 matrices at 9 K.

Table 4
Refined Fe K-edge XAFS parameters [a] for $Fe(CO)_5$, *cis*-$Fe(CO)_4Br_2$ and *cis*-$Fe(CO)_4I_2$

	r_{Fe-C} [g] (Å)	$2\sigma^2_{Fe-C}$ [h] (Å^2)	$r_{Fe\cdots O}$ (Å)	$2\sigma^2_{Fe\cdots O}$ (Å^2)	r_{Fe-X} (Å)	$2\sigma^2_{Fe-X}$ (Å^2)	E_f [i] (eV)	FI [j]	R [k]
$Fe(CO)_5$									
Electron diffraction [b]	1.8273 (eq)		2.9719 (eq)						
	1.8068 (ax)		2.9515 (ax)						
X-ray diffraction [c]	1.801 (eq)		2.929 (eq)						
	1.804 (eq)		2.940 (eq)						
	1.811 (ax)		2.928 (ax)						
Fe K-edge XAFS [d]	1.796	0.0028	2.917	0.0077					
Fe K-edge XAFS [e]	1.813(2)	0.0046(8)	2.948(4)	0.0072(6)			0.66	0.329	30.0
cis-$Fe(CO)_4I_2$									
Fe K-edge XAFS [f]	1.81	0.005	2.97	0.015	2.60	0.010			
Fe K-edge XAFS [e]	1.874(6)	0.0051(12)	2.961(3)	0.0121(13)	2.627(2)	0.0031(3)	−1.25	0.384	33.8
cis-$Fe(CO)_4Br_2$									
Fe K-edge XAFS [e]	1.851(8)	0.0099(17)	2.963(6)	0.0109(11)	2.429(3)	0.0032(4)	0.49	0.36699	27.6

[a] Standard deviation in parentheses.
[b] Ref. [39].
[c] Ref. [40].
[d] Ref. [23], EXCURV90.
[e] This work, EXCURV98.
[f] Ref. [24], EXCURV88.
[g] Estimated systematic errors in XAFS bond lengths are ±1.5% for well-defined co-ordination shells.
[h] $2\sigma^2$ is the Debye–Waller factor.
[i] E_f is a single refined parameter to reflect differences in the theoretical and experimental Fermi levels.
[j] $FI = \Sigma_i[(\chi_i^T - \chi_i^E)k_i^3]^2$.
[k] $R = [\int|\chi^T - \chi^E|k^3dk \Big/ \int|\chi^E|k^3dk] \times 100\%$.

wise the differences in Fe–C bond lengths between *cis*-$Fe(CO)_4Br_2$ and *trans*-$Fe(CO)_4Br_2$ (Fe–C, 1.87 Å) [22] are also probably not statistically significant. However, because our current analysis methods give better values for $Fe(CO)_5$, we believe that the bond lengths reported herein for *cis*-$Fe(CO)_4I_2$ are more accurate than those we have published previously [24]. The Fe–I bond length of 2.63(3) Å in *cis*-$Fe(CO)_4I_2$ obtained from the XAFS data is in very good agreement with those for related complexes derived from crystallography [43–49]. The accuracy of Fe–Br distances from Fe K-edge XAFS has been demonstrated previously, where the Fe–Br bond lengths from a single-crystal X-ray study [50] published after our XAFS study [51] were within 0.01 Å of our values for both the high- and low-spin states of $Fe(dppen)Br_2 \cdot 2Me_2CO$. Therefore, we believe that the Fe–Br bond length of 2.43(3) Å is accurate.

4. Conclusions

Using a range of spectroscopic techniques, this work has shown that both solution and vapour phase halogen exchange reactions occur between *cis*-$Fe(CO)_4I_2$ and *cis*-$Fe(CO)_4Br_2$ leading to the formation of *cis*-$Fe(CO)_4IBr$. Although we have not been able to elucidate the detailed mechanism of the halogen exchange, on the basis that both solution and vapour phase exchange has been observed, it is most likely an associative mechanism with a seven-coordinate transition state probably involving halogen bridging ligands. The fact that a *cis* complex results from the halogen exchange indicates that in the absence of light this must be the thermodynamically preferred isomer. In addition, this work has provided the first spectroscopic characterisation of *cis*-$Fe(CO)_4IBr$ and *cis*-$Fe(CO)_4ICl$ and has also assisted in resolving a number of unanswered questions for the well known, *cis*-$Fe(CO)_4X_2$ (X = I, Br, Cl) complexes. An unambiguous assignment of the solution ^{13}C NMR resonances for these compounds is proposed with carbonyl groups *trans* to halogens having a higher chemical shift than those *cis* to halogens. The cross halogenation reaction of *cis*-$Fe(CO)_4I_2$ and *cis*-$Fe(CO)_4Br_2$ leading to the formation of *cis*-$Fe(CO)_4IBr$ has assisted in this characterisation. XAFS studies have provided the first structural data for *cis*-$Fe(CO)_4Br_2$ and improved structural data for *cis*-$Fe(CO)_4I_2$.

Acknowledgements

We gratefully acknowledge the support of: the SERC/EPSRC for the award of an Advanced Fellow-

ship (NAY), equipment and SRS beamtime (GR/H 29117, GR/K 17514), a post-graduate studentship (OMW) and for access to the Chemical DataBase Service at Daresbury Laboratory [52,53]; The University of Hull for equipment; and the Director of the Synchrotron Radiation Department at Daresbury Laboratory for access to synchrotron and computing facilities.

References

[1] K. Noack, Helv. Chim. Acta 45 (1962) 1847.
[2] R.C. Taylor, W.D. Horrocks Jr., Inorg. Chem. 3 (1964) 584.
[3] L.A.W. Hales, R.J. Irving, J. Chem. Soc. A (1967) 1389.
[4] E.W. Abel, I.S. Butler, Trans. Faraday Soc. 63 (1967) 45.
[5] B.F.G. Johnson, J. Lewis, P.W. Robinson, J.R. Miller, J. Chem. Soc. A (1968) 1043.
[6] I.S. Butler, H.K. Spendjian, J. Organomet. Chem. 18 (1969) 145.
[7] M.A. Bennett, R.J.H. Clark, J. Chem. Soc. (1964) 5560.
[8] M. Pankowski, M. Bigorgne, C.R. Acad. Sci. Paris. 263 (1966) 239.
[9] M. Pankowski, M. Bigorgne, J. Organomet. Chem. 19 (1969) 393.
[10] E. Fluck, W. Kerler, W. Neuwirth, Angew. Chem., Int. Ed. Engl. 2 (1963) 277.
[11] R.L. Collins, R. Pettit, J. Chem. Phys. 39 (1963) 3433.
[12] R.H. Herber, R.B. King, G.K. Wertheim, Inorg. Chem. 3 (1964) 101.
[13] P. Vasudev, C.H.W. Jones, Can. J. Chem. 51 (1973) 405.
[14] L. Vancea, W.A.G. Graham, J. Organomet. Chem. 134 (1977) 219.
[15] R.A. Levenson, J.L. Cihonski, P. Milazzo, G.P. Ceasar, Inorg. Chem. 14 (1975) 2578.
[16] M.C. Böhm, Inorg. Chim. Acta 68 (1983) 63.
[17] K. Edgar, B.F.G. Johnson, J. Lewis, I.G. Williams, J.M. Wilson, J. Chem. Soc. A (1967) 379.
[18] J.A. Connor, C.P. Demain, H.A. Skinner, M.T. Zafarani-Moattar, J. Organomet. Chem. 170 (1979) 117.
[19] W. Hieber, A. Wirsching, Z. Anorg. Allg. Chem. 245 (1940) 35.
[20] M. Bigorgne, R. Poilblanc, M. Pankowski, Spectrochim. Acta, Part A 26 (1970) 1217.
[21] I.R. Beattie, S.D. McDermott, E.A. Mathews, K.R. Millington, A.D. Willson, Angew. Chem., Int. Ed. Engl. 27 (1988) 1161.
[22] O.M. Wilkin, PhD thesis, The University of Hull, 1999.
[23] I.R. Beattie, P.J. Jones, N.A. Young, J. Am. Chem. Soc. 114 (1992) 6146.
[24] I.R. Beattie, N. Binsted, W. Levason, J.S. Ogden, M.D. Spicer, N.A. Young, High Temp. Sci. 26 (1990) 71.
[25] W. Hieber, G. Bader, Chem. Ber. 61 (1928) 1717.
[26] C. Cartier, M. Momenteau, E. Dartyge, A. Fontaine, G. Tourillon, A. Michalowicz, M. Verdaguer, J. Chem. Soc., Dalton Trans. (1992) 609.
[27] N. Binsted, PAXAS, Program for the Analysis of X-Ray Absorption Spectra, University of Southampton, 1988.
[28] N. Binsted, EXCURV98, CCLRC Daresbury Laboratory Computer Program, 1998.
[29] S.J. Gurman, N. Binsted, I. Ross, J. Phys. C: Solid State Phys. 17 (1984) 143.
[30] S.J. Gurman, N. Binsted, I. Ross, J. Phys. C: Solid State Phys. 19 (1986) 1845.
[31] M.B. Hall, R.F. Fenske, Inorg. Chem. 11 (1972) 1619.
[32] A.S. Goldman, K. Krogh-Jespersen, J. Am. Chem. Soc. 118 (1996) 12159.
[33] H. Willner, F. Aubke, Angew. Chem., Int. Ed. Engl. 36 (1997) 2403.
[34] A.J. Lupinetti, G. Frenking, S.H. Strauss, Angew. Chem., Int. Ed. Engl. 37 (1998) 2113.
[35] I.R. Beattie, N. Cheetham, M. Gardiner, D.E. Rogers, J. Chem. Soc. A (1971) 2240.
[36] J.D. Childs, L.-N. Lin, S.D. Christian, J. Inorg. Nucl. Chem. 37 (1975) 757.
[37] A. Wojcicki, F. Basolo, J. Am. Chem. Soc. 83 (1961) 525.
[38] J. Browning, P.L. Goggin, R.J. Goodfellow, M.G. Norton, A.J.M. Rattray, B.F. Taylor, J. Mink, J. Chem. Soc., Dalton Trans. (1977) 2061.
[39] B. Beagley, D.W.J. Cruickshank, P.M. Pinder, A.G. Robiette, G.M. Sheldrick, Acta Crystallogr., Sect. B 25 (1969) 737.
[40] D. Braga, F. Grepioni, A.G. Orpen, Organometallics 12 (1993) 1481.
[41] J.H. Jang, J.G. Lee, H. Lee, Y. Xie, H.F. Schaefer, J. Phys. Chem. A 102 (1998) 5298.
[42] K. Clark-Baldwin, D.L. Tierney, N. Govindaswamy, E.S. Gruff, C. Kim, J. Berg, S.A. Koch, J.E. Penner-Hahn, J. Am. Chem. Soc. 120 (1998) 8401.
[43] T. Mitsudo, A. Ishihara, T. Suzuki, Y. Watanabe, Organometallics 9 (1990) 1357.
[44] W.-F. Liaw, M-H Chiang, C.-H. Lai, S.-J. Chiou, G.-H. Lee, S.-M. Peng, Inorg. Chem. 33 (1994) 2493.
[45] H. Berke, R. Birk, G. Huttner, L. Zsolnai, Z. Naturforsch., Teil B 39 (1984) 1380.
[46] G. Cardaci, G. Bellachioma, P. Zanazzi, Organometallics 7 (1988) 172.
[47] P. Johnston, L. Denner, C.F. Marais, J.C.A. Boegens, N.J. Coville, J. Cryst. Spectrosc. Res. 18 (1988) 403.
[48] D. Sellman, G. Mahr, F. Knoch, M. Moll, Inorg. Chim. Acta 224 (1994) 45.
[49] Z.-Z. Zhang, J.-K. Zhang, W.-P. Zhang, H.-P. Xi, H. Cheng, H.-G. Wan, J. Organomet. Chem. 515 (1996) 1.
[50] C-C. Wu, J. Jung, P.K. Gantzel, P. Gütlich, D.N. Hendrickson, Inorg. Chem. 36 (1997) 5339.
[51] N.A. Young, J. Chem. Soc., Dalton Trans. (1996) 1275.
[52] D.A. Fletcher, R.F. McMeeking, D. Parkin, J. Chem. Inf. Comput. Sci. 36 (1996) 746.
[53] F.H. Allen, O. Kennard, Chem. Design Automat. News 8 (1993) 1, 31.

PERGAMON

www.elsevier.nl/locate/poly

Polyhedron 19 (2000) 1503–1509

POLYHEDRON

Preparation and characterisation of $[M(CN)_4O(pz)]^{2-}$ complexes (M = Mo or W) and their reactivity towards molecular oxygen

Dariusz Matoga [a], Janusz Szklarzewicz [a], Alina Samotus [a,*], John Burgess [b], John Fawcett [b], David R. Russell [b]

[a] *Department of Inorganic Chemistry, Faculty of Chemistry, Jagiellonian University, R. Ingardena 3, 30-060 Cracow, Poland*
[b] *Department of Chemistry, University of Leicester, Leicester, LE1 7RH, UK*

Received 14 February 2000; accepted 29 March 2000

Abstract

The synthesis and characterisation of $(PPh_4)_2[M(CN)_4O(pz)]\cdot 3H_2O$ (M = Mo or W; pz = pyrazine) are presented. The salts are reactive towards molecular oxygen, both in solution and in the solid state, with formation of $(PPh_4)_2[M(CN)_4O(O_2)]$. The X-ray crystal structure of the molybdenum compound confirmed the presence of a peroxo ligand *cis* to the M=O bond; the O–O bond distance is 1.41 Å. The IR spectra exhibit two absorption bands in the 950–850 cm^{-1} region assigned to the terminal M=O group [917 (Mo) and 933 (W) cm^{-1}] and the peroxo group [893 (Mo) and 871 (W) cm^{-1}]. The possible mechanism of molecular oxygen uptake by pyrazine complexes is discussed. © 2000 Elsevier Science Ltd. All rights reserved.

Keywords: Molybdenum complexes; Tungsten complexes; Pyrazine complexes; Peroxo ligands; Crystal structures

1. Introduction

It is well known that in aqueous solutions tetracyanodioxometallates(IV), $[M(CN)_4O_2]^{4-}$ (M = Mo, W) undergo stepwise protonation reactions

$$[M(CN)_4O_2]^{4-} + H^+ \overset{K_1}{\rightleftharpoons} [M(CN)_4O(OH)]^{3-} \quad (1)$$

$$[M(CN)_4O(OH)]^{3-} + H^+ \overset{K_2}{\rightleftharpoons} [M(CN)_4O(H_2O)]^{2-} \quad (2)$$

with the equilibrium constants given by: $\log K_1 = 13.00$, $\log K_2 = 9.70$ and $\log K_1 = 11.60$, $\log K_2 = 7.76$ for M = Mo and W, respectively [1,2]. It is also known that the $[M(CN)_4O(H_2O)]^{2-}$ ion easily undergoes a considerable number of substitution reactions. It reacts with a variety of monodentate ligands yielding complexes of general formula $[M(CN)_4O(L)]^{(n+2)-}$, where $L = CN^-$, NCS^-, F^-, N_3^-, HCN and pyridine (py) [2–5].

$$[M(CN)_4O(H_2O)]^{2-} + L^{n-} \rightarrow [M(CN)_4O(L)]^{(n+2)-} + H_2O \quad (3)$$

Bidentate ligands are coordinated according to the reaction

$$[M(CN)_4O(H_2O)]^{2-} + LL^{n-} \rightarrow [M(CN)_3O(LL)]^{(n+1)-} + H_2O + CN^- \quad (4)$$

where LL = 2,2′-bipyridyl (bipy), 1,10-phenanthroline (phen), pyridine-2-carboxylate (pic) and several Schiff bases [6]. There is also one known example of a neutral seven-coordinate complex $[M(CN)_2O(LLLL)]$ formed in the reaction

$$[M(CN)_4O(H_2O)]^{2-} + LLLL \rightarrow [M(CN)_2O(LLLL)] + H_2O + 2CN^- \quad (5)$$

where the tetradentate ligand LLLL = *N*,*N*′-bis[1-(pyridin-2-yl)ethylidene]ethane-1,2-diamine [7].

The considerable number of relatively fast reactions of $[M(CN)_4O(H_2O)]^{2-}$ with different ligands prompted us to use a similar procedure to obtain tetracyanocomplexes with pyrazine (pz), which forms a variety of complexes with different transition metals [8,9]. The pyrazine ligand seemed interesting for us due to its small dimensions, which imply that the steric factor does not interfere with its coordination and, moreover, it can act as a monodentate ligand or as a bridging ligand. We have found, however, that the only species formed under our experimental conditions was

* Corresponding author. Fax: +48-12-6340-515.
E-mail address: samotus@chemia.uj.edu.pl (A. Samotus).

0277-5387/00/$ - see front matter © 2000 Elsevier Science Ltd. All rights reserved.
PII: S0277-5387(00)00413-7

$[M(CN)_4O(pz)]^{2-}$, in which pyrazine is monodentate. The syntheses of new complexes, with their spectroscopic and physicochemical characterisation, and their reactivity towards molecular oxygen are the subject of this report. There is only one known example of molecular oxygen uptake by a similar type of complex. The anhydrous salt $(PPh_4)_3[Mo(CN)_5O]$ has been reported [10] to react with dioxygen according to the equation

$$(PPh_4)_3[Mo^{IV}(CN)_5O] + O_2 \rightarrow (PPh_4)_2[Mo^{VI}(CN)_4O(O_2)] + (PPh_4)CN \quad (6)$$

In this paper we present the spectroscopic and physicochemical characteristics of peroxo complexes of formula $(PPh_4)_2[M(CN)_4O(O_2)]$ obtained by us in the reaction of hydrated pyrazine salts with molecular oxygen. We also discuss the mechanism of molecular oxygen incorporation, our proposal differing from that presented earlier [11].

2. Experimental

2.1. Materials

$K_3Na[M(CN)_4O_2]\cdot 6H_2O$ (M = Mo or W) were prepared as described in the literature [12], and their purity confirmed by their IR spectra. Tetraphenylphosphonium chloride [$(PPh_4)Cl$], pyrazine (pz), triphenylphosphine (PPh_3) and standard laboratory reagents were of analytical grade (Sigma, Aldrich) and used as supplied.

2.2. Syntheses

Tetraphenylphosphonium tetracyanooxopyrazinemolybdate(IV) was prepared as its trihydrate, $(PPh_4)_2[Mo(CN)_4O(pz)]\cdot 3H_2O$ (**1**), by dissolving 2.80 g (5.8 mmol) of $K_3Na[Mo(CN)_4O_2]\cdot 6H_2O$ and 1.92 g (24 mmol) of pz in 15 ml of water. The pH of the solution was adjusted to ca. 8 with 1 M HCl and a solution of 4.5 g (12 mmol) of $(PPh_4)Cl$ in 15 ml of water added. The resulting green crystals were filtered off, washed four times with water and dried in air. Yield: 5.80 g (97%). *Anal.* Found: C, 65.80; H, 4.96; N, 8.09. Calc. for $C_{56}H_{50}MoN_6O_4P_2$: C, 65.37; H, 4.90; N, 8.17%.

Tetraphenylphosphonium tetracyanooxopyrazine tungstate(IV) was prepared as its trihydrate, $(PPh_4)_2[W(CN)_4O(pz)]\cdot 3H_2O$ (**2**), by dissolving 3.3 g (5.8 mmol) of $K_3Na[W(CN)_4O_2]\cdot 6H_2O$ and 1.92 g (24 mmol) of pz in 15 ml of water. The pH of the solution was adjusted to ca. 7 with 1 M HCl. It was heated to 50°C for ca. 20 min, followed by addition of 4.5 g (12 mmol) of $(PPh_4)Cl$ in 15 ml of water. The resulting dark green crystals were filtered off, washed four times with water and dried in air. Yield: 2.46 g (38%). *Anal.* Found: C, 60.40; H, 4.77; N, 7.53. Calc. for $C_{56}H_{50}N_6O_4P_2W$: C, 60.22; H, 4.51; N, 7.52%.

Tetraphenylphosphonium tetracyanooxoperoxomolybdate(VI), $(PPh_4)_2[Mo(CN)_4O(O_2)]$ (**3**), was prepared by extraction of 1.1 g (1.07 mmol) of **1** three times with 30 ml of acetone and filtering the extracts. The resulting yellow filtrates were combined and the solvent was evaporated in air at room temperature within 20 min. The yellow crystals were washed three times with ethanol and dried in air. Yield: 0.46 g (46%). *Anal.* Found: C, 67.38; H, 4.25; N, 5.94. Calc. for $C_{52}H_{40}MoN_4O_3P_2$: C, 67.39; H, 4.35; N, 6.05%.

Tetraphenylphosphonium tetracyanooxoperoxotungstate(VI), $(PPh_4)_2[W(CN)_4O(O_2)]$ (**4**), was prepared by dissolving 0.45 g (0.4 mmol) of **2** in 30 ml of acetonitrile. After 60 min, the initially yellow solution turned colourless; it was evaporated in air at room temperature. The resulting white product was washed three times with ethanol and dried in air. Yield: 0.35 g (85%). *Anal.* Found: C, 61.34; H, 3.92; N, 5.29. Calc. for $C_{52}H_{40}N_4O_3P_2W$: C, 61.55; H, 3.97; N, 5.52%.

2.3. Reaction of $(PPh_4)_2[M(CN)_4O(O_2)]$ with molecular oxygen

The salts **3** or **4** were dissolved in acetonitrile and left in air for about 2 h. In the case of salt **4** no changes were observed and after evaporation of solvent **4** was quantitatively recovered. In the case of **3** its yellow colour disappeared, and after removal of solvent by evaporation a white product of formula $(PPh_4)_2[Mo_2O_7]$ was isolated. IR: $\nu(Mo{=}O) = 880\ cm^{-1}$, $\nu(Mo{-}O{-}Mo) = 790\ cm^{-1}$. *Anal.* Found: C, 58.06; H, 3.92; N, 0.06. Calc. for $C_{48}H_{40}Mo_2O_7P_2$: C, 58.66; H, 4.07; N, 0.00%.

2.4. Analytical methods and physical measurements

Carbon, nitrogen and hydrogen were determined by organic microanalysis. UV–Vis absorption spectra (Shimadzu 2101 PC) were recorded in the normal way. Reflectance spectra were measured in $BaSO_4$ pellets versus $BaSO_4$ as a reference (Shimadzu 2101 PC equipped with ISR-260 attachment). IR spectra were measured in KBr pellets on a Bruker IFS 48 spectrometer. ^1H NMR spectra in $CDCl_3$ were recorded on a Tesla BS-567A spectrometer. ESR spectra were measured on a Bruker ELEXSYS spectrometer at room and liquid nitrogen temperatures using diphenylpicrylhydrazide (dpph) as an internal standard. To estimate the amount of paramagnetic centres, $VOSO_4$ was used as standard.

2.5. Crystal structure determination

Crystals of **3** suitable for X-ray crystallography were selected from the recrystallised material prepared as described above. Crystal data for **3**, and a summary of

data collection and structure refinement parameters, are given in Table 1. The positions of Mo and P atoms were determined by Patterson methods; the remaining non-hydrogen atoms were located in successive difference Fourier syntheses. Hydrogen atoms were included in the structure factor calculations at idealised positions and were not refined. In the final refinement cycle all non-hydrogen atoms were refined anisotropically. The largest peaks in the final difference maps were located near the Mo atom. All calculations were performed using SHELXTL-PC [13]; scattering factors and anomalous dispersion factors were those given in SHELXTL.

3. Results

3.1. Characterisation of the complexes

The reaction of $[M(CN)_4O(H_2O)]^{2-}$ with pyrazine under appropriate conditions results in aqua ligand substitution and pyrazine coordination according to the equation

$$[M(CN)_4O(H_2O)]^{2-} + pz \leftrightarrows [M(CN)_4O(pz)]^{2-} + H_2O \quad (7)$$

Table 1
Crystal data and structure refinement for **3**

Complex	**3**
Empirical formula	$C_{52}H_{40}N_4O_3P_2Mo$
Formula weight	926.76
Temperature (K)	200(2)
Wavelength (Å)	0.71073
Crystal system	triclinic
Space group	$P\bar{1}$
Unit cell dimensions	
a (Å)	10.235(4)
b (Å)	10.912(3)
c (Å)	22.557(8)
α (°)	84.44(2)
β (°)	82.21(3)
γ (°)	63.64(2)
Volume (Å^3)	2234.6(13)
Density (Mg m^{-3})	1.377
Absorption coefficient (mm^{-1})	0.413
Min./max. transmission	0.863, 0.934
$F(000)$	952
Crystal size (mm)	$0.54 \times 0.32 \times 0.08$
ϑ range data collection (°)	1.82–26.00
Reflection collected	9174
Independent reflections	8688
Observed data [$I > 2\sigma(I)$]	3828
Free parameters	464
R_1	0.1127
wR_2	0.2437
Goodness-of-fit	1.058
$\Delta\rho_{max}$, $\Delta\rho_{min}$ (e Å^{-3})	+1.271, −3.017

The equilibrium lies strongly towards the reactants — formation of the product complex can be observed only in concentrated solutions in the presence of a large excess of pyrazine. Complexes **1** and **2** were isolated as tetraphenylphosphonium salts. The $(PPh_4)^+$ cation forms insoluble salts only with the product complex thus shifting equilibrium (7) to the right.

The results of analysis and physicochemical measurements indicate that pyrazine acts as a monodentate ligand; the possibility of its acting as a bridging ligand between two complex units can be excluded. On the basis of the crystal structure data of all known $[M(CN)_4O(L)]^{n-}$ type complexes [3,5,11], the pyrazine ligand is expected to be in the position *trans* to the M=O bond.

Both light green **1** and dark green **2** are diamagnetic. In the solid state they are stable when kept under restricted anaerobic conditions. The salts are almost insoluble in water, but soluble in polar organic solvents such as MeCN, CH_2Cl_2 and DMSO. In dilute aqueous solutions, the only species which can be detected by visible spectroscopy is the $[M(CN)_4O(H_2O)]^{2-}$ ion, even in the presence of a large excess of pyrazine. In organic solvents in the presence of air, a fast change of colour from green to yellow is observed. After evaporating the solvent, yellow **3** and white **4** were isolated, indicating that the colour change is connected with molecular oxygen uptake:

$$[M(CN)_4O(pz)]^{2-} + O_2 \rightarrow [M(CN)_4O(O_2)]^{2-} + pz \quad (8)$$

Similar colour changes were observed when solid salts **1** and **2** were kept in air. The final products of solid state reactions were found to be identical with those isolated from the solutions. They were found not to be contaminated with free pyrazine thanks to its high volatility. The salts **3** and **4** are insoluble in water and alcohols and soluble in common organic solvents, such as MeCN, $CHCl_3$, CH_2Cl_2, DMSO and DMF. As solids they are stable in air at room temperature. In solution, complex **4** is thermally stable, whereas salt **3** undergoes slow decomposition to $(PPh_4)_2[Mo_2O_7]$ as confirmed by the elemental analysis and IR spectra of the product formed.

Molecular oxygen uptake by cyano-oxo complexes of Mo(IV) was found only for anhydrous $(PPh_4)_3[Mo(CN)_5O]$, and was postulated to be impossible for hydrated salts [11]. Here we have succeeded, for the first time, in demonstrating molecular oxygen uptake by the hydrated oxotetracyano complexes and in isolating the tungsten salt analogous to $(PPh_4)_2[Mo(CN)_4O(O_2)]$ described in the literature [10].

3.2. Description of the structure of **3**

The structure of **3** is presented in Fig. 1 and selected bond distances and angles are collected in Table 2. The

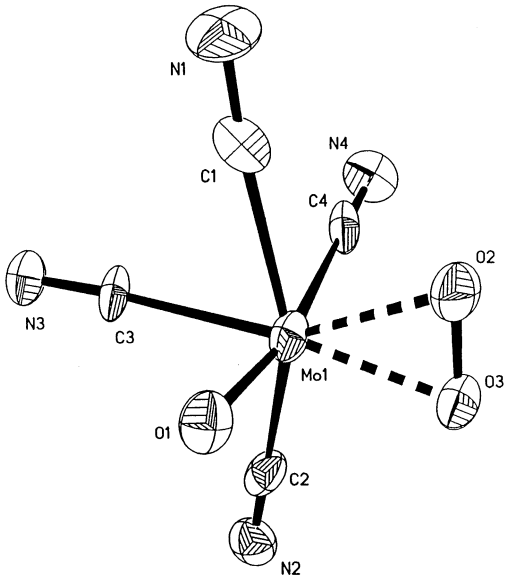


Fig. 1. Structure of the $[Mo(CN)_4O(O)_2]^{2-}$ ion in **3**.

anion has a distorted pentagonal bipyramidal geometry with the O–O group *cis* to the Mo=O bond. The O–O bond distance of 1.41 Å is typical for the peroxo group [14–17] and thus the formal oxidation state of the metal is +6.

A salt of the same formula was obtained earlier by Arzoumanian et al. [10] in the reaction of $(PPh_4)_3[Mo(CN)_5O]$ in CH_2Cl_2 with molecular oxygen and its structure was determined by X-ray crystal analysis. There are, however, some differences in the bond distances and angles between salt **3** and that described in the literature. The Mo(1)–O(1) bond distance is shorter (1.671(10) compared with 1.694(3) Å) and the Mo(1)–C(4) and Mo(1)–C(3) bond distances are longer (2.296(16) compared with 2.197(4) Å and 2.196(11) compared with 2.167(5) Å, respectively). It is difficult to compare the bond angles with the literature data due to some mistakes in the assignments of angles (e.g. the O(1)–Mo(1)–C(4) angle (O3–Mo–C4 in their numbering scheme) was reported to be 88.20°, which is impossible for atoms in *trans* positions). It seems, however, that there are probably some differences in bond angles in the structures of both salts, though the angle subtended by the peroxo ligand is the same in both determinations (43.1(4)° in **3**, 43.2(2) in Ref. [10]). The O–O bond distance in our crystal, 1.410(14) Å, is the same as that in the earlier reference, 1.416(5) Å; these distances do not differ significantly from that in the analogous complex $[Mo(CN)_3O(O_2)(hmpa)]^-$, 1.397(10) Å [10].

Table 2
Selected bond distances (Å) and angles (°) for $(PPh_4)_2[Mo(CN)_4O(O_2)]$ (**3**), with estimated standard deviations in parentheses

Mo(1)–O(1)	1.671(10)	Mo(1)–O(2)	1.914(9)
Mo(1)–O(3)	1.927(9)	Mo(1)–C(1)	2.156(16)
Mo(1)–C(2)	2.188(16)	Mo(1)–C(3)	2.196(11)
Mo(1)–C(4)	2.296(16)	O(2)–O(3)	1.410(14)
C(1)–N(1)	1.145(18)	C(2)–N(2)	1.156(17)
C(3)–N(3)	1.150(14)	C(4)–N(4)	1.145(17)
O(1)–Mo(1)–O(2)	106.5(4)	O(1)–Mo(1)–O(3)	106.7(4)
O(2)–Mo(1)–O(3)	43.1(4)	O(1)–Mo(1)–C(1)	97.0(5)
O(2)–Mo(1)–C(1)	81.1(5)	O(3)–Mo(1)–C(1)	123.2(5)
O(1)–Mo(1)–C(2)	92.3(5)	O(2)–Mo(1)–C(2)	123.7(5)
O(3)–Mo(1)–C(2)	80.9(5)	C(1)–Mo(1)–C(2)	149.7(5)
O(1)–Mo(1)–C(3)	87.9(5)	O(2)–Mo(1)–C(3)	153.5(5)
O(3)–Mo(1)–C(3)	153.5(5)	C(1)–Mo(1)–C(3)	75.1(5)
C(2)–Mo(1)–C(3)	76.5(5)	O(1)–Mo(1)–C(4)	166.2(4)
O(2)–Mo(1)–C(4)	86.6(4)	O(3)–Mo(1)–C(4)	85.8(4)
C(1)–Mo(1)–C(4)	80.3(5)	C(2)–Mo(1)–C(4)	83.8(5)
C(3)–Mo(1)–C(4)	78.3(5)	O(3)–O(2)–Mo(1)	69.0(5)
O(2)–O(3)–Mo(1)	68.0(5)	N(1)–C(1)–Mo(1)	175.4(13)
N(2)–C(2)–Mo(1)	178.1(13)	N(3)–C(3)–Mo(1)	176.1(13)
N(4)–C(4)–Mo(1)	177.6(12)		

3.3. IR spectra

Selected IR data for salts **1** to **4** are presented in Table 3. For comparison data for pyrazine and $(PPh_4)Cl$ are also included.

The IR spectra of salts **1** and **2** show bands at 974 cm^{-1} (**1**) and at 969 cm^{-1} (**2**) which can be assigned to the stretching vibrations of the M=O group. The pyrazine complexes have higher values of ν(M=O) than analogous six-coordinate cyano-oxo complexes of Mo(IV) and W(IV) with monodentate ligands having the nitrogen atom in the *trans* position to the M=O bond [3,5,11,18] (for $L = N_3^-$, CH_3CN, HCN band positions are at 953, 940 and 940 cm^{-1} for Mo and for $L = N_3^-$, NCS^-, py at 952, 954 and 964 cm^{-1} for W, respectively). This suggests weak bonding of pyrazine and locates the pyrazine ligand between pyridine (ν(W=O) = 964 cm^{-1}) and H_2O (ν(W=O) = 980 cm^{-1}) in the series of ligands arranged according to the decreasing value of ν(W=O), viz.

$$OH^- > CN^- > F^- > N_3^- > NCS^- > \text{pyridine} > \textit{pyrazine} > H_2O$$

given in the literature [5]. The analogous series for Mo complexes [3,10,11,19] is:

$$OH^- > CN^- > HCN > CH_3CN > N_3^- > \textit{pyrazine} > H_2O.$$

In the CN stretching region four bands are observed (Table 3). The larger number of bands with respect to analogous complexes of the $[M(CN)_4O(L)]^{n-}$ type indicates lower symmetry for the anions in **1** and **2**.

The 400–1800 cm^{-1} region is dominated by overlapping bands of $(PPh_4)^+$ and pyrazine. There are four bands assigned to coordinated pyrazine, at 1017, 1037, 1147 and 1415 cm^{-1} for salt **1** and at 1017, 1040, 1148 and 1415 cm^{-1} for salt **2**. The positions of the bands

Table 3
Selected IR absorption bands (cm^{-1}) [a]

Compound	ν(O–O)	ν(M=O)	ν(C≡N)	Others
				712 s, 816 s, 870 s, 1010 s, 1036 w, 1145 m, 1183 vs, 1351 vs, 1408 vs, 1613 vs, 3077 s
1		974 s	2085 m, 2088 s, 2094 s, 2103 vw	444 m, 527 vs, 620 vw, 690 vs, 723 vs, 757 m, 763 m, 814 vw, 853 vw, 998 w, 1017 vw, 1027 vw, 1037 w, 1083 vw, 1108 vs, 1147 vw, 1162 vw, 1187 vw, 1316 w, 1338 vw, 1415 m, 1436 vs, 1442 vs, 1484 m, 1586 w, 1620 vw, 3061 vw, 3407 m, b, 3490 w, sh, 3654 w
2		969 vs	2071 s, 2079 sh, 2082 s, 2092 w	444 m, 527 vs, 623 vw, 690 vs, 722 vs, 757 m, 763 m, 814 w, 853 vw, 998 m, 1017 vw, 1027 vw, 1040 w, 1085 vw, 1108 vs, 1148 vw, 1162 vw, 1188 w, 1318 w, 1340 vw, 1415 m, 1436 vs, 1441 vs, 1484 s, 1584 w, 1620 vw, 3061 vw, 3400 m, b, 3470 w, sh, 3651 w
3	893 s	917 s	2127 vvw, 2150 vvw, 2201 vvw	415 w, 527 vs, 620 vw, 690 vs, 722 vs, 754 m, 761 m, 852 vw, 996 m, 1027 vw, 1085 vw, sh, 1108 vs, 1164 vw, 1186 vw, 1315 w, 1340 vw, 1437 s, 1443 s, sh, 1484 m, 1586 w, 1615 vw, 3061 vw
4	871 m	933 s	2132 vvw, 2154 vvw, 2199 vvw	422 w, 526 vs, 623 w, 688 vs, 722 vs, 753 m, 762 m, 853 vw, 995 m, 1029 vw, 1086 vw, sh, 1107 vs, 1163 vw, 1185 vw, 1314 w, 1341 vw, 1435 s, 1441 s, 1483 m, 1585 w, 1612 w, 3056 vw

[a] s, strong; m, medium; w, weak; v, very; sh, shoulder; b, broad.

are only slightly shifted in comparison with free pyrazine (1010, 1036, 1145 and 1408 cm^{-1} [20]) in agreement with weak bonding of pyrazine to the metal centre.

The IR spectra of **3** and **4** exhibit bands at 917 and 933 cm^{-1}, assigned to the respective M=O stretching vibrations. The bands at 893 cm^{-1} (**3**) and 871 cm^{-1} (**4**) correspond to the stretching vibrations of side on bonded peroxo group [17,21]. The positions of the ν(M=O) and ν(O–O) bands are close to those of peroxo complexes of molybdenum(VI) and tungsten(VI) without cyanide ligands [14,15,22].

In the CN stretching region the IR spectra show bands of very low intensity at 2127, 2150 and 2201 cm^{-1} for **3** and 2132, 2154 and 2199 cm^{-1} for **4**. The unusually high position of these CN vibrations in comparison with the cyano-oxo complexes of Mo(IV) and W(IV) is consistent with an increase of the formal oxidation state of the central atom resulting in the decrease of π-back donation which shifts the CN stretching band towards higher energy.

3.4. ^1H NMR spectra

^1H NMR spectra for solutions of salts **1** and **2** exhibit signals of protons of pyrazine, aromatic rings of $(PPh_4)^+$ cations and water molecules. The four pyrazine protons give a singlet at 8.48 ppm for **1** and at 8.60 ppm for **2**, in comparison with 8.60 ppm for free pyrazine [23]. One could expect that pyrazine coordinated as a monodentate ligand should exhibit two doublets of two groups of protons, positioned farther and closer to the metal centre, respectively [9]. The singlet resonances for salts **1** and **2** indicate very weak bonding of pyrazine which causes the protons of pyrazine to be chemically equivalent. The upfield shift of the signal for salt **1** shows that in $CDCl_3$ solution weakly bonded pyrazine is still coordinated whereas for salt **2** decomposition accompanied by the release of pyrazine occurs.

3.5. UV–Vis spectra

In the solid state reflection spectra show bands at 232, 270, 303 and 650 nm for salt **1** and at 229, 270, 309 and 620 nm for salt **2**. In aqueous solutions, the bands observed in the visible region at 610 and 562 nm (for salts **1** and **2**, respectively) can be attributed to the $[M(CN)_4O(H_2O)]^{2-}$ ions which are formed according to equilibrium (7). In organic solvents such as MeCN, CH_2Cl_2 and acetone fast formation of **3** and **4** is observed.

Fig. 2 presents typical spectral changes observed for a solution of **1** in dichloromethane in the presence of air, together with the spectrum of **3** in the same solvent. The decrease of the band at ca. 621 nm, characteristic of a d–d transition in **1**, and the growth of a new band at ca. 393 nm, connected with dioxygen uptake and formation of **3**, are observed. The diffuse isosbestic point (Fig. 2) indicates that two species are dominant in the system.

The reflection spectra of salts **3** and **4** consist of bands originating from the respective cations at 231 and 276 nm and at 237 and 281 nm, and bands at 420 and 336 nm which can be assigned to charge-transfer to metal (CTTM) transitions. In organic solvents the latter bands are shifted towards higher energy, e.g. in acetonitrile the band maximum is observed at 393 (**3**) and 323 nm (4) (Fig. 3) with molar absorptivity equal to 465 and 635 M^{-1} cm^{-1}, respectively.

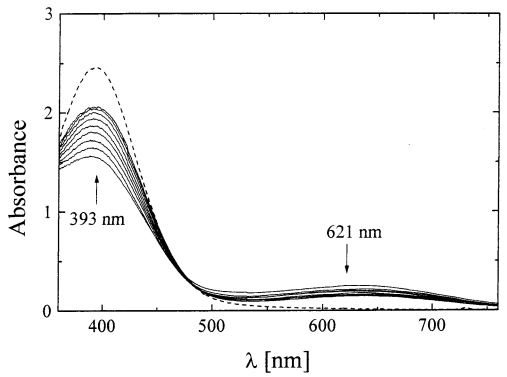


Fig. 2. Spectral changes of **1** in dichloromethane solution. The arrows show the direction of changes with time (first spectrum measured after 30 s from dissolution, time interval = 90 s). For comparison the spectrum of **3** is given (dashed curve). Conc. = 5.3×10^{-3} M, optical path = 1 cm.

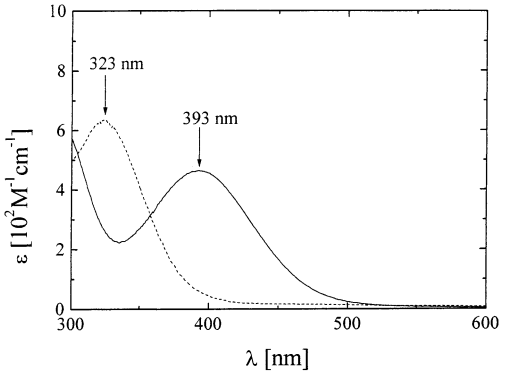


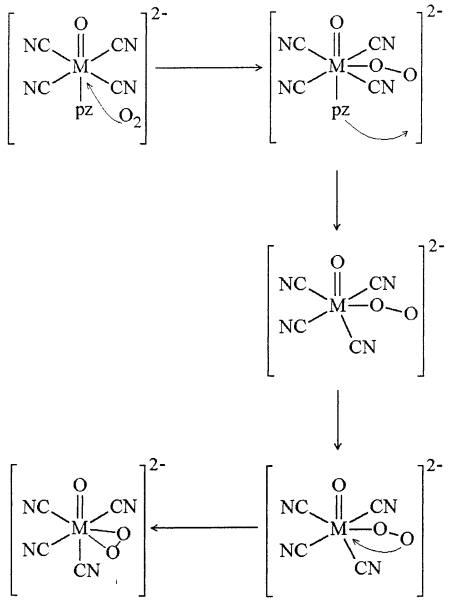
Fig. 3. Electronic spectra of **3** (solid curve) and of **4** (dashed curve) in acetonitrile.

3.6. ESR spectra

The ESR spectra for salts **3** and **4** consist of very weak signals, which are typical for paramagnetic centres M(V)–d^1 [24] with g factors (at room temperature) equal to 1.970 and 1.915, respectively. In the case of salt **3** in liquid nitrogen (77 K) an anisotropic signal is observed with $g = 1.915$ and 1.943 indicating the axial symmetry of the complex anion. The amount of M(V) centres in salts **3** and **4** is equal to 0.32 and 0.82%, respectively. This indicates that to some extent thermal charge transfer from the O_2^{2-} ligand to the metal occurs, resulting in M(V) and O_2^- formation.

4. Discussion

It was found earlier that anhydrous $(PPh_4)_3[Mo(CN)_5O]$ can react with molecular oxygen giving $(PPh_4)_2[Mo(CN)_4O(O_2)]$ [10]. It was also found that this reaction is possible only for the anhydrous salt and that hydrated salts are not reactive towards molecular oxygen [11]. We have now found that the hydrated tetracyano complexes of Mo(IV) and W(IV) of formula $[M(CN)_4O(pz)]^{2-}$ can react with molecular oxygen, both in solution and in the solid state. The presence of water molecules does not interfere with the reaction with dioxygen. This is probably caused by the fact that the weakly bonded pyrazine ligand does not participate in the network of hydrogen-bonds. Thus, the best site for nucleophilic attack of dioxygen seems to be in the vicinity of pyrazine, whereas the rest of the complex ion is surrounded by water molecules, hydrogen-bonded to cyano and oxo ligands, which hinder the reaction with O_2. It seems also that the dissociative mechanism proposed by Arzoumanian et al. [11] is not valid. In this case the incoming dioxygen should be in the *trans* position to the M=O bond, as found for all substitution reactions leading to the $[M(CN)_4O(L)]^{n-}$ ($n = 2, 3$) type complexes. In all these cases the coordinatively unsaturated $[M(CN)_4O]^{2-}$ does not undergo rearrangement in the coordination sphere and does not react with dioxygen. The associative mechanism presented in Scheme 1 seems more probable. In the first step the coordination of dioxygen occurs with the increase of coordination number to seven. Such a structure (distorted pentagonal bipyramid) was found by us earlier in $[Mo(CN)_2O(LLLL)]\cdot H_2O$ [7]. Release of pyrazine followed by a rearrangement in which a cyano group is transferred to the vacant *trans* position and the second oxygen of dioxygen is bonded to the metal centre could lead to the observed *cis*-tetracyanooxoperoxomolybdate(VI) anion.



Scheme 1. Proposed mechanism for molecular oxygen incorporation into the $[M(CN)_4O(pz)]^{2-}$ ion.

5. Supplementary material

Full crystallographic data may be obtained from the Cambridge Crystallographic Data Centre, where CIF files have been deposited (deposition no. 139915) Copies of this information may be obtained free of charge from The Director, CCDC, 12 Union Road, Cambridge CB2 1EZ, UK (fax: +44-1223-336033; e-mail: deposit@ccdc.cam.ac.uk or www: http://www.ccdc.cam.ac.uk).

Acknowledgements

This work was supported in part by the Polish Research Committee, KBN, Grant no. 3T09A 057 17.

References

[1] (a) E. Hejmo, A. Kanas, A. Samotus, Bull. Acad. Polon. Sci. Ser. Sci. Chim. 21 (1973) 311. (b) A. Kanas, M. Dudek, A. Samotus, Bull. Acad. Polon. Sci. Ser. Sci. Chim. 24 (1976) 43.
[2] M. Dudek, A. Samotus, Transition Met. Chem. 10 (1985) 271.
[3] (a) S.S. Basson, J.G. Leipoldt, I.M. Potgieter, A. Roodt, Inorg. Chim. Acta 103 (1985) 121. (b) J.G. Leipoldt, R. van Eldik, S.S. Basson, A. Roodt, Inorg. Chem. 25 (1986) 4639. (c) J.P. Smit, W. Purcell, A. Roodt, J.G. Leipoldt, J. Chem. Soc., Chem. Commun. (1993) 1388.
[4] (a) J.G. Leipoldt, S.S. Basson, A. Roodt, I.M. Potgieter, S. Afr. J. Chem. 39 (1986) 179. (b) I.M. Potgieter, S.S. Basson, A. Roodt, J.G. Leipoldt, Transition Met. Chem. 13 (1988) 209.
[5] A. Roodt, J.G. Leipoldt, S.S. Basson, I.M. Potgieter, Transition Met. Chem. 13 (1988) 336.
[6] (a) S.S. Basson, J.G. Leipoldt, I.M. Potgieter, Inorg. Chim. Acta 87 (1984) 71. (b) S.S. Basson, J.G. Leipoldt, I.M. Potgieter, Inorg. Chim. Acta 90 (1984) 57. (c) J.G. Leipoldt, S.S. Basson, A. Roodt, I.M. Potgieter, Transition Met. Chem. 11 (1986) 323. (d) J. Szklarzewicz, A. Samotus, N.W. Alcock, M. Moll, J. Chem. Soc., Dalton Trans. (1990) 2959. (e) B. Burda, J. Burgess, S.A. Parsons, A. Samotus, J. Szklarzewicz, Transition Met. Chem. 20 (1995) 291. (f) B. Nowicka, A. Samotus, J. Szklarzewicz, F. Heinemann, H. Kisch, J. Chem. Soc., Dalton Trans. (1998) 4009. (g) J. Szklarzewicz, A. Samotus, D. Matoga, J. Burgess, J. Fawcett, D.R. Russell, Coordination Chemistry at the Turn of the Century, Slovak Technical University Press, Bratislava, vol. 7, 1999, p. 139.
[7] J. Szklarzewicz, A. Samotus, J. Burgess, J. Fawcett, D.R. Russell, J. Chem. Soc., Dalton Trans. (1995) 3057.
[8] (a) C. Creutz, H. Taube, J. Am. Chem. Soc. 91 (1969) 3988. (b) C. Creutz, H. Taube, J. Am. Chem. Soc. 95 (1973) 1086.
[9] C.G. Johnson, R.E. Shepherd, Inorg. Chem. 22 (1983) 1117.
[10] H. Arzoumanian, J.F. Petrignani, M. Pierrot, F. Ridouane, J. Sanchez, Inorg. Chem. 27 (1988) 3377.
[11] H. Arzoumanian, M. Pierrot, F. Ridouane, J. Sanchez, Transition Met. Chem. 16 (1991) 422.
[12] (a) J.P. Smit, W. Purcell, A. Roodt, J.G. Leipoldt, Polyhedron 12 (1993) 2271. (b) A. Roodt, S.S. Basson, J.G. Leipoldt, Polyhedron 13 (1994) 599.
[13] G.M. Sheldrick, SHELXTL-PC Release 4.2, Siemens Analytical X-ray Instruments, Madison, WI, 1991.
[14] A.C. Dengel, W.P. Griffith, R.D. Powell, A.C. Skapski, J. Chem. Soc., Dalton Trans. (1987) 991.
[15] (a) W.P. Griffith, B.C. Parkin, A.J.P. White, D.J. Williams, J. Chem. Soc., Dalton Trans. (1995) 3131. (b) N.M. Gresley, W.P. Griffith, B.C. Parkin, A.J.P. White, D.J. Williams, J. Chem. Soc., Dalton Trans. (1996) 2039.
[16] (a) M.H. Dickman, M.T. Pope, Chem. Rev. 94 (1994) 569. (b) M. Sivak, V. Sucha, L. Kuchta, J. Marek, Polyhedron 18 (1998) 93 and references therein. (c) M. Kosugi, S. Hikichi, M. Akita, Y. Moro-oka, J. Chem. Soc., Dalton Trans. (1999) 1369.
[17] A. Butler, M.J. Clague, G.E. Meister, Chem. Rev. 94 (1994) 625.
[18] A. Roodt, J.G. Leipoldt, S.S. Basson, I.M. Potgieter, Transition Met. Chem. 15 (1990) 439.
[19] (a) M. Dudek, A. Kanas, A. Samotus, J. Inorg. Nucl. Chem. 41 (1979) 1135. (b) M. Dudek, A. Kanas, A. Samotus, J. Inorg. Nucl. Chem. 42 (1980) 1701.
[20] B. Klein, J. Berkowitz, J. Am. Chem. Soc. 81 (1959) 5160.
[21] L.J. Bellamy, The Infra-red Spectra of Complex Molecules, Chapman and Hall, London, 1975, p. 135.
[22] R. Bandyopadhyay, S. Biswas, S. Guha, A.K. Mukherjee, R. Bhattacharyya, Chem. Commun. (1999) 1627.
[23] C.J. Pouchert, J. Behnke, The Aldrich Library of ^{13}C and ^{1}H FT NMR Spectra, vol. III, Aldrich Chemical Company Inc., 1993.
[24] (a) B.R. McGarvey, Inorg. Chem. 5 (1966) 476. (b) R.A. Pribush, R.D. Archer, Inorg. Chem. 13 (1974) 2556. (b) P.M. Kiernan, W.P. Griffith, J. Chem. Soc., Dalton Trans. (1975) 2489. (c) T.J. Kemp, M.A. Shand, D. Rehorek, J. Chem. Soc., Dalton Trans. (1988) 285. (d) J. Szklarzewicz, A. Samotus, O. Traverso, S. Sostero, Polyhedron 13 (1994) 1755.

PERGAMON

www.elsevier.nl/locate/poly

Polyhedron 19 (2000) 1511–1517

POLYHEDRON

The synthesis and characterisation of $[Pd(S_2CNEt_2)\{Ph_2P(CH_2)_nPPh_2\}]^+$ salts of some chlorometallate anions ($n = 1, 3, 4$): X-ray crystal structures of the salts $[Pd(S_2CNEt_2)\{Ph_2P(CH_2)_nPPh_2\}]_2[MCl_4]$ ($n = 1, 4$; M = Cd; $n = 3$; M = Hg)

George Exarchos, Stephen D. Robinson *, Jonathan W. Steed

Department of Chemistry, King's College London, Strand, London, WC2R 2LS, UK

Received 17 February 2000; accepted 25 April 2000

Abstract

The palladium complexes $[PdCl_2\{Ph_2P(CH_2)_nPPh_2\}]$ ($n = 1, 3, 4$) react with the bi- and tri-valent metal diethyldithiocarbamates $[M(S_2CNEt_2)_2]$ (M = Zn, Cd, Hg, Pb) and $[Mn(S_2CNEt_2)_3]$ in cold dichloromethane solution to afford salts of the general form $[Pd(S_2CNEt_2)\{Ph_2P(CH_2)_nPPh_2\}]_2[MCl_4]$ in almost quantitative yield. X-ray crystal structures are reported for the salts $[Pd(S_2CNEt_2)\{Ph_2P(CH_2)_nPPh_2\}]_2[MCl_4]$ ($n = 1, 4$; M = Cd: $n = 3$, M = Hg). Structural parameters, IR and NMR spectroscopic data for these salts are compared with similar data previously reported for salts of the related cation $[Pd(S_2CNEt_2)\{Ph_2P(CH_2)_2PPh_2\}]^+$. © 2000 Elsevier Science Ltd. All rights reserved.

Keywords: Palladium; Diethyldithiocarbamate; Diphosphines; Tetrachlorometallate anions; X-ray crystal structures

1. Introduction

While attempting the synthesis of heteronuclear bimetallic complexes containing bridging dithiocarbamate ligands we observed that many class b metal diethyldithiocarbamates react readily with the palladium(II) halide complexes $[PdX_2\{Ph_2P(CH_2)_2PPh_2\}]$ (X = Cl, Br) to afford halometallate salts containing the $[Pd(S_2CNEt_2)\{Ph_2P(CH_2)_2PPh_2\}]^+$ cation in essentially quantitative yield [1]. Two of these salts, $[Pd(S_2CNEt_2)\{Ph_2P(CH_2)_2PPh_2\}][MCl_2]$ (M = Cu, Ag) were characterised by X-ray diffraction methods [1]. Given the tendency of soft class b metal ions to bind strongly to S-donor ligands, the ease with which some of the softer metal ions investigated, notably Cd(II), Hg(II) and Ag(I), relinquished their dithiocarbamate ligands in favour of halide anions was somewhat unexpected. We have therefore sought to investigate the generality of this behaviour by examining the reactions of some metal dithiocarbamates with a range of other transition metal halide complexes. In the present paper we describe the synthesis and characterisation of a series of halometallate complexes containing the cations $[Pd(S_2CNEt_2)\{Ph_2P(CH_2)_nPPh_2\}]^+$ ($n = 1, 3, 4$) and report X-ray crystal structures for the salts $[Pd(S_2CNEt_2)\{Ph_2P(CH_2)_nPPh_2\}]_2[MCl_4]$ ($n = 1$, 4; M = Cd: $n = 3$, M = Hg). We also examine the effect of chelate ring size on the structural and spectroscopic parameters of the complex cations $[Pd(S_2CNEt_2)\{Ph_2P(CH_2)_nPPh_2\}]^+$ ($n = 1$–4).

2. Experimental

2.1. Materials and measurements

Bis(diphenylphosphino)methane was purchased from Lancaster Synthesis, 1,3-bis(diphenylphosphino)-

* Corresponding author. Tel.: +44-208-546-7940; fax: +44-207-848-2810.

E-mail address: stephen.robinson@ukgateway.net (S.D. Robinson).

0277-5387/00/$ - see front matter © 2000 Elsevier Science Ltd. All rights reserved.
PII: S0277-5387(00)00415-0

propane and 1,4-bis(diphenylphosphino)butane from Avocado and palladium chloride from Johnson Matthey. Metal dithiocarbamates were prepared from the metal nitrates and the sodium salt of the ligand in aqueous media and recrystallised from dichloromethane/petroleum spirit 60–80. Dichloro[bis(diphenylphosphino)methane]palladium(II), dichloro[1,3-bis(diphenylphosphino)propane]palladium and dichloro[1,4 - bis(diphenylphosphino)butane]palladium were prepared by dissolving palladium(II) chloride in acetonitrile under reflux and adding the stoichiometric amount of diphosphine to the filtered solution thus obtained. All complexes were recrystallised from dichloromethane. Instrumentation and other experimental details were as described in a preceding paper [1]. Analytical, IR and NMR data are given in Tables 1–3, respectively.

2.1.1. (*N*,*N*-Diethyldithiocarbamato)-[bis(diphenylphosphino)methane]palladium(II) tetrachlorozincate

Dichloro[bis(diphenylphosphino)methane]palladium (0.169 g, 0.30 mmol) and bis(*N*,*N*-diethyldithiocarbamato)zinc (0.054 g, 0.15 mmol) were stirred in dichloromethane (60 cm^3) for 1 h. The solution obtained was filtered and concentrated under reduced pressure to a small volume (ca. 5 cm^3). Diethyl ether (70 cm^3) was added to the concentrated solution and the precipitate obtained was filtered, washed with diethyl ether (3 × 10 cm^3) and dried in vacuo for 3 h. The product appears as a yellowish–white fine powder (yield 0.211 g, 94%; m.p. 148–150°C).

The following complexes were obtained by the same method and on a similar scale:

(*N*,*N* - Diethyldithiocarbamato)[bis(diphenylphosph-

Table 1
Analytical data for halometallate salts of the $[Pd(S_2CNEt_2)\{Ph_2P(CH_2)_nPPh_2\}]^+$ cations ($n = 1, 3, 4$)

n	Anion	Solvent	C (%) [a]	H (%) [a]	N (%) [a]
1	$ZnCl_4^{2-}$		48.10 (48.50)	4.25 (4.35)	1.75 (1.90)
1	$CdCl_4^{2-}$	[b]	45.20 (47.00)	3.95 (4.20)	1.70 (1.85)
1	$HgCl_4^{2-}$	[c]	43.55 (43.70)	3.75 (3.95)	1.50 (1.70)
1	$MnCl_4^{2-}$	[c]	48.10 (48.10)	4.25 (4.35)	1.80 (1.85)
1	$ZnBr_4^{2-}$	[c]	42.85 (42.60)	3.45 (3.85)	1.70 (1.65)
3	$PbCl_4^{2-}$	[c]	44.15 (44.90)	4.20 (4.25)	1.55 (1.60)
3	$ZnCl_4^{2-}$	[c]	49.20 (48.90)	4.60 (4.65)	1.75 (1.75)
3	$CdCl_4^{2-}$	[c]	47.40 (47.50)	4.50 (4.50)	1.55 (1.70)
3	$HgCl_4^{2-}$	[d]	44.35 (43.90)	4.25 (4.30)	1.55 (1.55)
3	$MnCl_4^{2-}$	[c]	49.05 (49.25)	4.70 (4.70)	1.80 (1.80)
4	$PbCl_4^{2-}$	[c]	44.90 (45.70)	4.45 (4.45)	1.50 (1.60)
4	$ZnCl_4^{2-}$	[c]	49.85 (49.55)	4.75 (4.80)	1.70 (1.75)
4	$CdCl_4^{2-}$		49.00 (49.00)	4.70 (4.75)	1.65 (1.75)
4	$HgCl_4^{2-}$	[c]	45.25 (45.70)	4.30 (4.45)	1.50 (1.60)

[a] Calculated figures in parentheses.
[b] The compound readily loses $CHCl_3$ of crystallisation in air, calculated values given are for the unsolvated species.
[c] Solvated with $0.5CH_2Cl_2$ per anion.
[d] Solvated with $1.0CH_2Cl_2$ and $1.0H_2O$ per anion.

Table 2
IR spectroscopic data for halometallate salts of the $[Pd(S_2CNEt)_2\{Ph_2P(CH_2)_nPPh_2\}]^+$ cations ($n = 1, 3, 4$)

Biphosphine	Anion	ν(C–N)	ν(C–S)	ν(Pd–S)	ν_3(M–X)
$Ph_2PCH_2PPh_2$	$ZnCl_4^{2-}$	1525s	1026, 998s	363m	273m
	$CdCl_4^{2-}$	1523s	1026, 998s	363m	249m
	$HgCl_4^{2-}$	1525s	1027, 998s	363m	219m
	$MnCl_4^{2-}$	1525s	1027, 998s	364m	286m
$Ph_2P(CH_2)_3PPh_2$	$PbCl_4^{2-}$	1522s	1028, 999s	371m	214w [a]
	$ZnCl_4^{2-}$	1524s	1027, 999s	371m	274m
	$CdCl_4^{2-}$	1526s	1027, 999s	371m	247m
	$HgCl_4^{2-}$	1525s	1027, 999s	370m	219m
	$MnCl_4^{2-}$	1525s	1027, 999s	370m	281m
$Ph_2P(CH_2)_4PPh_2$	$PbCl_4^{2-}$	1527s	1027, 999s	371m	199w [a]
	$ZnCl_4^{2-}$	1527s	1027, 999s	371m	279m
	$CdCl_4^{2-}$	1522s	1027, 999s	371m	243m
	$HgCl_4^{2-}$	1527s	1027, 999s	371m	216m

[a] Tentative assignment. w, weak; m, medium; s, strong.

Table 3
^{1}H and ^{31}P NMR data for halometallate salts of the $[Pd(S_2CNEt_2)\{Ph_2P(CH_2)_nPPh_2\}]^+$ cations ($n = 1, 3, 4$) [a]

n	Anion	$(CH_3CH_2)_2NCS_2^-$	$(CH_3CH_2)_2NCS_2^-$	$Ph_2P(CH_2)_nPPh_2$	$Ph_2P(CH_2)_n\ PPh_2$	$Ph_2P(CH_2)_nPPh_2$
1	$ZnCl_4^{2-}$	1.25 (t)	3.81 (q)	2.50 (t)	7.50, 7.72 (m)	−36.31 (s)
1	$CdCl_4^{2-}$	1.26 (t)	3.83 (q)	2.50 (t)	7.52, 7.75 (m)	−36.34 (s)
1	$HgCl_4^{2-}$	1.26 (t)	3.83 (q)	2.50 (t)	7.52, 7.76 (m)	−36.34 (s)
3	$PbCl_4^{2-}$	1.19 (t)	3.65 (q)	2.29, 3.09 (b)	7.39, 7.58 (m)	10.77 (s)
3	$ZnCl_4^{2-}$	1.14 (t)	3.62 (q)	2.38, 3.15 (b)	7.33, 7.56 (m)	10.86 (s)
3	$CdCl_4^{2-}$	1.14 (t)	3.62 (q)	2.25, 3.11 (b)	7.34, 7.56 (m)	10.91 (s)
3	$HgCl_4^{2-}$	1.16 (t)	3.65 (q)	2.27, 3.05 (b)	7.39, 7.55 (m)	10.66 (s)
4	$PbCl_4^{2-}$	1.17 (t)	3.64 (q)	2.07, 2.76 (b)	7.45, 7.53 (m)	27.36 (s)
4	$ZnCl_4^{2-}$	1.16 (t)	3.65 (q)	2.08, 2.87 (b)	7.43, 7.52 (m)	28.07 (s)
4	$CdCl_4^{2-}$	1.16 (t)	3.64 (q)	208, 2.87 (b)	7.43, 7.53 (m)	28.09 (s)
4	$HgCl_4^{2-}$	1.19 (t)	3.65 (q)	2.08, 2.74 (b)	7.47, 7.55 (m)	27.25 (s)

[a] s, singlet; t, triplet; q, quartet; m, multiplet; b, unresolved broadened multiplet.

ino)methane]palladium(II) tetrachlorocadmate as yellowish–white fine powder (yield 94%; m.p. 146–148°C).

(*N*,*N* - Diethyldithiocarbamato)[bis(diphenylphosphino)methane]palladium(II) tetrachloromercurate(II) as yellowish–white fine powder (yield 92%; m.p. 150–152°C).

2.1.2. (*N*,*N*-Diethyldithiocarbamato)[bis(diphenylphosphino)methane]palladium(II) tetrachloromanganate

Dichloro[bis(diphenylphosphino)methane]palladium (0.169 g, 0.30 mmol) and tris(*N*,*N*-diethyldithiocarbamato)manganese (0.075 g, 0.15 mmol) were stirred in dichloromethane (60 cm^3) for 1 h. The solution obtained was filtered and concentrated under reduced pressure to a small volume (ca. 5 cm^3). Diethyl ether (70 cm^3) was added to the concentrated solution and the precipitate obtained was filtered, washed several times with diethyl ether to remove all the tetraethylthiuram disulfide byproduct formed and dried in vacuo for 3 h. The product appears as a yellowish fine powder (yield 0.194 g, 88%; m.p. 131–133°C).

2.1.3. (*N*,*N*-Diethyldithiocarbamato)[1,3-bis(diphenylphosphino)propane]palladium(II) tetrachlorozincate

Dichloro[1,3 - bis(diphenylphosphino)propane]palladium (0.177 g, 0.30 mmol) and bis(*N*,*N*-diethyldithiocarbamato)zinc (0.054 g, 0.15 mmol) were stirred in dichloromethane (60 cm^3) for 1 h. The solution obtained was filtered and concentrated under reduced pressure to a small volume (ca. 5 cm^3). Diethyl ether (70 cm^3) was added to the concentrated solution and the precipitate obtained was filtered, washed with diethyl ether (3×10 cm^3) and dried in vacuo for 3 h. The product appears as a yellowish–white fine powder (yield 0.214 g, 92%; m.p. 167–170°C).

The following complexes were obtained by the same method and on a similar scale:

(*N*,*N*-Diethyldithiocarbamato)[1,3-bis(diphenylphosphino)propane]palladium(II) tetrachlorocadmate as yellowish–white fine powder (yield 94%; m.p. 178–180°C).

(*N*,*N*-Diethyldithiocarbamato)[1,3-bis(diphenylphosphino)propane]palladium(II) tetrachloromercurate(II) as yellowish–white fine powder (yield 94%; m.p. 163–165°C).

(*N*,*N*-Diethyldithiocarbamato)[1,3-bis(diphenylphosphino)propane]palladium(II) tetrachloroplumbate(II) as yellowish–white fine powder (yield 94%; m.p. 250–253°C).

2.1.4. (*N*,*N*-Diethyldithiocarbamato)[1,3-bis(diphenylphosphino)propane]palladium(II) tetrachloromanganate

Dichloro[1,3 - bis(diphenylphosphino)propane]palladium (0.177 g, 0.30 mmol) and tris(*N*,*N*-diethyldithiocarbamato)manganese (0.075 g, 0.15 mmol) were stirred in dichloromethane (60 cm^3) for 1 h. The solution obtained was filtered and concentrated under reduced pressure to a small volume (ca. 5 cm^3). Diethyl ether (70 cm^3) was added to the concentrated solution and the precipitate obtained was filtered, washed several times with diethyl ether to remove all the tetraethylthiuram disulfide byproduct formed and dried in vacuo for 3 h. The product appears as a yellowish fine powder (yield 0.214 g, 93%; m.p. 190–192°C).

2.1.5. (*N*,*N*-Diethyldithiocarbamato)[1,4-bis(diphenylphosphino)butane]palladium(II) tetrachlorozincate

Dichloro[1,4 - bis(diphenylphosphino)butane]palladium (0.181 g, 0.30 mmol) and bis(*N*,*N*-diethyldithiocarbamato)zinc (0.054 g, 0.15 mmol) were stirred in dichloromethane (60 cm^3) for 1 h. The solution obtained was filtered and concentrated under reduced pressure to a small volume (ca. 5 cm^3). Diethyl ether (70 cm^3) was added to the concentrated solution and the precipitate obtained was filtered, washed with diethyl ether (3×10 cm^3) and dried in vacuo for 3 h. The product appears as a yellowish–white fine powder (yield 0.218 g, 93%; m.p. 170–172°C).

The following complexes were obtained by the same method and on a similar scale:

(*N*,*N*-Diethyldithiocarbamato)[1,4-bis(diphenylphosphino)butane]palladium(II) tetrachlorocadmate as yellowish–white fine powder (yield 94%; m.p. 154–156°C).

(*N*,*N*-Diethyldithiocarbamato)[1,4-bis(diphenylphosphino)butane]palladium(II) tetrachloromercurate(II) as yellowish–white fine powder (yield 94%; m.p. 162–164°C).

(*N*,*N*-Diethyldithiocarbamato)[1,4-bis(diphenylphosphino)butane]palladium(II) tetrachloroplumbate(II) as yellowish–white fine powder (yield 93%; m.p. 158–160°C).

2.2. Crystallography

X-ray crystal structures have been determined for the complexes $[Pd(S_2CNEt_2)(Ph_2PCH_2PPh_2)]_2[CdCl_4]$. 4.0 $CHCl_3$ (**1**), $[Pd(S_2CNEt_2)(Ph_2PCH_2CH_2CH_2PPh_2)]_2$-$[HgCl_4]\cdot CH_2Cl_2\cdot H_2O$ (**2**) and $[Pd(S_2CNEt_2)(Ph_2PCH_2$-$CH_2CH_2CH_2PPh_2)]_2[CdCl_4]$ (**3**). Crystals of **1** were grown by the slow evaporation of a $CHCl_3$ solution, while crystals of **2** and **3** were obtained by the slow evaporation of $CH_2Cl_2/C_6H_5CH_3$ solutions. For the X-ray determination yellow plates of **1**, and yellow needles of **2** and **3**, were mounted on thin glass fibres using a fast setting epoxy resin. A total of 90 oscillation frames of 90 s exposure time with 2° rotation in ϕ were recorded using a Nonius Kappa CCD diffractometer, with detector to crystal distance of 25 mm. The crystals were indexed from the first ten frames using the DENZO package [2] and positional data were refined along with diffractometer constants to give the final unit cell parameters. Integration and scaling of the whole data-sets resulted in a total of 57 655 data (10 152 unique) for **1**, 16 765 data (7036 unique) for **2** and 61 497 data (6399 unique) for **3**, which were corrected for Lorentz and polarisation effects. The structures were solved using the direct methods option of SHELXS-86 [3] and developed via alternating least square cycles and difference Fourier synthesis (SHELXL-97 [4]) with the aid of the program RES2INS [5]. All non-hydrogen atoms were modelled anisotropically, while hydrogen atoms were assigned an isotropic thermal parameter 1.2 times

Table 4
Crystal data and structure refinement for complexes **1**–**3**

	1	**2**	**3**
Empirical formula	$C_{60}H_{64}CdC_4N_2P_4Pd_2S_4\cdot 4CHCl_3$	$C_{64}H_{72}Cl_4HgN_2P_4Pd_2S_4\cdot CH_2Cl_2\cdot H_2O$	$C_{66}H_{76}CdCl_4N_2P_4Pd_2S_4$
Formula weight (g)	2009.72	1779.64	1616.41
Temperature (K)	293(2)	293(2)	293(2)
Wavelength (Å)	0.71070	0.71070	0.71070
Crystal system, space group	monoclinic, $C2/c$	monoclinic, $C2/c$	orthorhombic, $P2_1cn$
Unit cell dimensions			
a (Å)	30.4170(12)	30.5597(6)	17.2827(3)
b (Å)	14.5680(5)	14.2645(4)	19.2972(2)
c (Å)	20.1850(9)	21.4656(6)	21.1728(3)
α (°)	90	90	90
β (°)	107.1650(10)	129.061(1)	90
γ (°)	90	90	90
Volume (Å^3)	8545.9(6)	7265.7(3)	7061.29(17)
Z	4	4	4
D_{calc} (g cm^{-3})	1.562	1.629	1.520
Absorption coefficient (mm^{-1})	1.373	3.062	1.202
F(000)	4008	3552	3272
Crystal size (mm)	$0.3\times0.1\times0.05$	$0.4\times0.2\times0.2$	$0.1\times0.05\times0.05$
θ Range for data collection (°)	3.53–28.27	3.33–26.00	3.58–25.00
Index ranges	$0\le h\le40$, $0\le k\le18$, $-26\le l\le24$	$0\le h\le37$, $0\le k\le17$, $-26\le l\le20$	$0\le h\le20$, $0\le k\le22$, $0\le l\le25$
Reflections collected/unique	57 655/10 152 ($R_{int}=0.040$)	16 765/7036 ($R_{int}=0.0470$)	61 497/6399 ($R_{int}=0.076$)
Refinement method	full-matrix least-squares on F^2	full-matrix least-squares on F^2	full-matrix least-squares on F^2
Data/restraints/parameters	10 152/0/420	7036/0/381	6399/1/747
Goodness-of-fit on F^2	1.056	1.086	1.064
Final R indices	$R_1=0.0644$ $wR_2=0.1593$	$R_1=0.0295$ $wR_2=0.0698$	$R_1=0.0289$ $wR_2=0.0642$
R indices (all data)	$R_1=0.0951$ $wR_2=0.1846$	$R_1=0.0367$ $wR_2=0.0755$	$R_1=0.0333$ $wR_2=0.0668$
Largest difference peak and hole (e Å^{-3})	1.161 and –0.897	0.706 and −1.030	0.293 and −0.326

Table 5
Selected bond lengths (Å) and bond angles (°) for the $[Pd(S_2CNEt_2)\{Ph_2P(CH_2)_nPPh_2\}]^+$ cations ($n = 1$–4)

	Ph_2PCH_2-PPh_2	$Ph_2P(CH_2)_2$-PPh_2 [a]	$Ph_2P(CH_2)_3$-PPh_2	$Ph_2P(CH_2)_4$-PPh_2
Pd–S1	2.3522(14)	2.332(4)	2.3560(9)	2.3382(17) [Pd1] 2.3482(15) [Pd2]
Pd–S2	2.3430(15)	2.334(4)	2.3412(9)	2.3532(15) [Pd1] 2.3471(16) [Pd2]
Pd–P1	2.2869(14)	2.279(4)	2.2770(8)	2.2930(15) [Pd1] 2.2871(14) [Pd2]
Pd–P2	2.2707(13)	2.248(4)	2.2695(9)	2.2986(15) [Pd1] 2.2978(15) [Pd2]
C1–S1	1.725(6)	1.700(14)	1.728(3)	1.715(6)
C1–S2	1.735(6)	1.737(15)	1.728(3)	1.708(6)
C34–S3				1.720(6)
C34–S4				1.717(6)
C1–N1	1.310(7)	1.323(20)	1.314(4)	1.326(8)
C34–N2				1.319(8)
∠SPdS	75.30(6)	75.59(14)	75.36(3)	74.43(6)[Pd1] 74.59(5) [Pd2]
∠PPdP	72.90(5)	85.61(14)	91.24(3)	94.82(6) [Pd1] 95.93(6) [Pd2]

[a] In the $[Pd(S_2CNEt_2)(Ph_2PCH_2CH_2PPh_2)][CuCl_2]$ complex [1].

Table 6
^{31}P NMR data [a] for free and coordinated diphosphine ligands in the $[Pd(S_2CNEt_2)\{Ph_2P(CH_2)_nPPh_2\}]^+$ cations ($n = 1$–4)

n	Free ligand (ppm)	Coordinated ligand (ppm)	Δ (ppm) [b]
1	−21.5	−36.3	−14.8
2	−12.0	+59.5	+71.5
3	−14.0	+10.8	+24.8
4	−15.4	+27.7	+43.1

[a] Recorded using $CDCl_3$ solution, referenced to external 85% H_3PO_4.
[b] Δ (ppm) $= P_{coordinated} - P_{free}$.

(1.5 for CH_3 groups) that of the parent atom and allowed to ride. Refinement converged with $wR_2 = 0.1846$ which corresponds to a conventional R-factor of 0.0644 for data with $I > 2\sigma(I)$ for **1**, $wR_2 = 0.0755$ ($R_1 = 0.0295$) and $wR_2 = 0.0668$ ($R_1 = 0.0289$) for **2** and **3**, respectively. Crystal data and structural refinement parameters are given in Table 4, and selected bond angles and bond lengths are presented in Table 5.

3. Results and discussion

After the synthesis and characterisation of halometallate salts containing the $[Pd(S_2CNEt_2)\{Ph_2P(CH_2)_2PPh_2\}]^+$ cation [1] we sought to extend our investigations further by using a number of similar chelating diphosphines in place of dppe. The aim was to study the effect of varying the ring size formed upon coordination, investigate the relative coordinating abilities of these diphosphines and confirm whether the nature of the resulting products was similar to the ones already synthesised. The reaction stoichiometries were kept the same, however it was necessary to modify the solvent medium and reaction temperature. It was found that especially in the case of the dppm ligand, substantial decomposition of products occurred under reflux conditions. The reactions were therefore modified to take place in dichloromethane at room temperature. These conditions gave clean products and were therefore used for all the diphosphine starting materials employed. The products precipitated from the filtered and concentrated reaction solutions on addition of diethyl ether, and were isolated in essentially quantitative yield as air-stable powders. The complexes were characterised by elemental analyses, IR and NMR spectra, and X-ray diffraction methods. Their IR spectra displayed absorptions characteristic of coordinated dithiocarbamate ligands [ν(C–N) ca. 1525 cm^{-1}] [6] and of the tetrahedral $[MCl_4]^{2-}$ anions [ν_3(M–Cl) ca. 280 cm^{-1} (M = Zn) to ca. 220 cm^{-1} (M = Hg, Pb)] [7]. We were not able to unambiguously identify the ν_4(M–Cl) absorptions since these are relatively weak and occur very low (usually below 130 cm^{-1}), near the detection limit of the instrument employed. The proton NMR spectra are consistent with the stoichiometries and structures proposed for the complex cations. The $^{31}P\{^1H\}$ NMR spectra establish the chemical and magnetic equivalence of the two phosphorus atoms present in each complex cation, and confirm that the bis-(chelate) cations structurally characterised by X-ray diffraction methods for representative examples are common to all the complexes reported here. They also display the well-established relationship between ^{31}P chemical shifts and chelate ring size, in particular the anomalously low field resonances previously observed for chelated $Ph_2PCH_2CH_2PPh_2$ ligands, and attributed to a large deshielding effect characteristic of phosphorus nuclei in five member chelate rings [8]. This can be seen in Table 6, which includes data for both free and coordinated ligands.

X-ray crystal structure determinations were performed on representative examples of salts containing each of the three cations $[Pd(S_2CNEt_2)\{Ph_2P(CH_2)_nPPh_2\}]^+$ ($n = 1$, 3 or 4). All three were found to contain square planar cations and tetrahedral $[MCl_4]^{2-}$ anions. The salient bond length and bond angle data for these structures are recorded in Table 5. For comparison purposes similar data previously collected [1] for salts containing the related $[Pd(S_2CNEt_2)\{Ph_2P(CH_2)_2PPh_2\}]^+$ cation are also included. Molecular structures showing atomic labelling schemes for compounds **1**–**3** are shown in Figs. 1–3, respectively.

Bond length and bond angle data for the four complex cations are similar to those previously reported for other dithiocarbamate and diphosphine complexes of

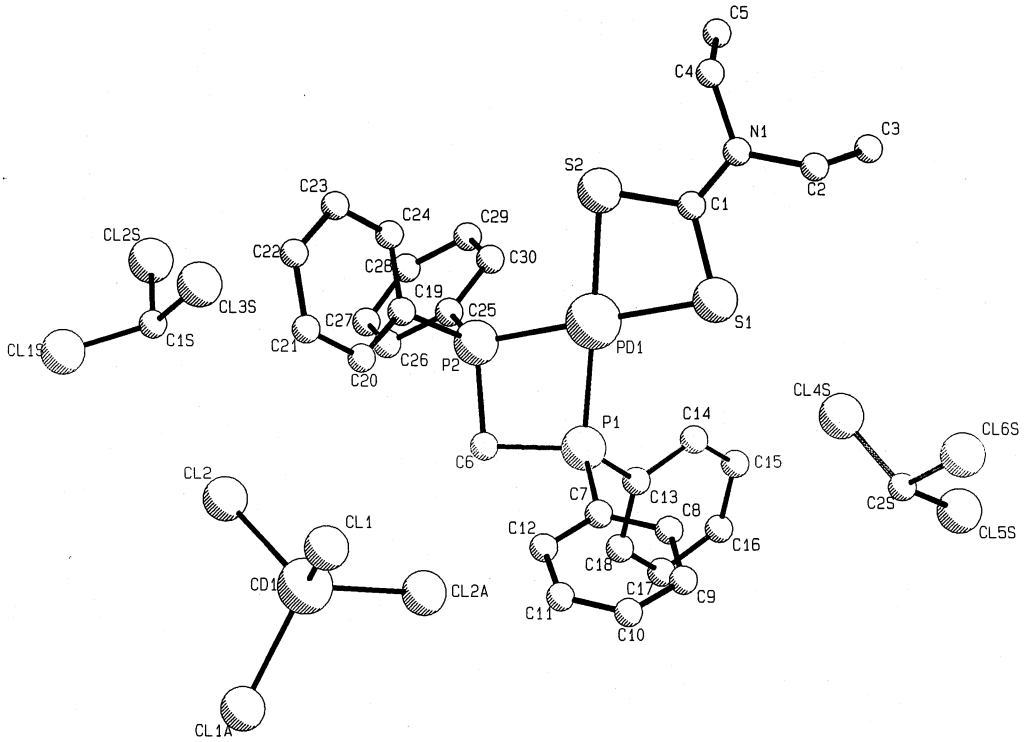


Fig. 1. Molecular structure for $[Pd(S_2CNEt_2)(Ph_2PCH_2PPh_2)]_2[CdCl_4]\cdot 4.0CHCl_3$ (**1**) showing atom labelling scheme.

palladium(II) [9]. In each case the relatively short S_2C–NEt_2 distance (ca. 1.310–1.329 Å) indicates the presence of a significant degree of double bond character arising from the $^{2-}S_2C{=}NEt_2^+$ tautomer of the dithiocarbamate ligand. The 'bite' angles of the dithiocarbamate and diphosphine ligands obviously impose considerable strain on the geometry of the square planar cation. The angles subtended at palladium by the two phosphorus donor atoms of the various diphosphines, $Ph_2P(CH_2)_nPPh_2$, increase from 72.90(5)° ($n = 1$) to 94.82(6)° ($n = 4$). However, these changes are accommodated within the coordination sphere of the palladium without any deviation from the strict planarity of the P_2PdS_2 moiety or any significant change in the coordination geometry of the dithiocarbamate ligand. In particular the angle subtended at palladium by the two sulfur atoms which reflects the narrow 'bite' angle of the dithiocarbamate ligand, remains essentially constant at 75.30–75.75°.

The tetrachlorometallate anions $[MCl_4]^{2-}$ (M = Cd, Hg) are essentially tetrahedral and display bond length and angle data similar to those previously reported for these species [10–13]. Metal chlorine distances range from 2.4482(19) to 2.4681(19) Å for M = Cd and from 2.4735(12) to 2.5093(11) Å for M = Hg. In each case the angles subtended at the metal centre by pairs of chloride ligands deviate from the ideal tetrahedral value of 109°28′ by ca. ± 5° (M = Cd) or ca. ± 7° (M = Hg).

Finally, the structures reveal the presence of a number of short contact distances between the chloride ligands of the MCl_4^{2-} anions and the phenyl hydrogens of the complex cations and the hydrogens of solvent molecules, which can be attributed to H-bonding interactions. The observed C–H···Cl distances found for complexes **1**–**3** are within the range of values associated

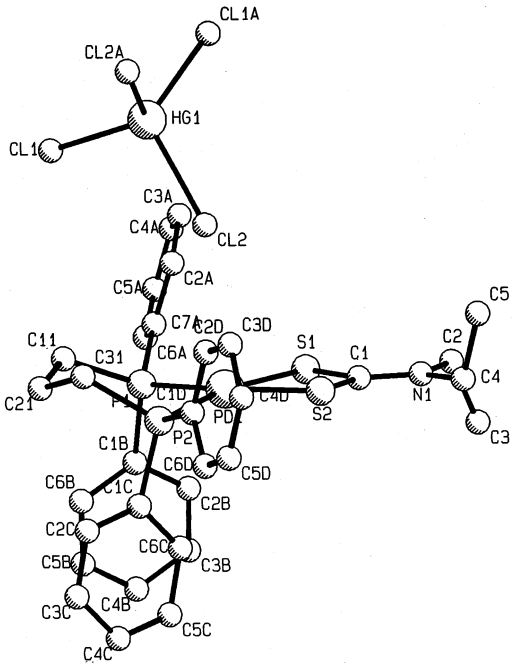


Fig. 2. Molecular structure for $[Pd(S_2CNEt_2)(Ph_2PCH_2CH_2CH_2PPh_2)]_2[HgCl_4]\cdot CH_2Cl_2\cdot H_2O$ (**2**) showing atom labelling scheme.

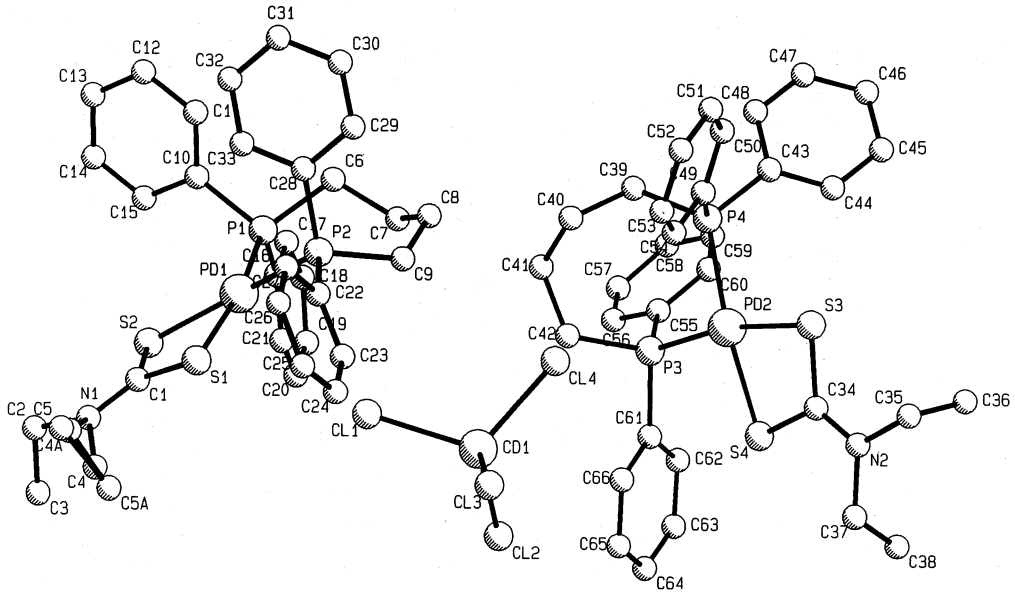


Fig. 3. Molecular structure for $[Pd(S_2CNEt_2)(Ph_2PCH_2CH_2CH_2CH_2PPh_2)]_2[CdCl_4]$ (**3**) showing atom labelling scheme.

with this type of interaction (H···Cl = 2.568–2.944 Å) [14–17]. Indeed the C–H···Cl distances are all at the lower end of the range, and suggest the presence of relatively strong C–H···Cl interactions, especially when $CHCl_3$ solvent molecules are involved.

The spectroscopic data recorded for the other complex salts of the general form $[Pd(S_2CNEt_2)\{Ph_2P(CH_2)_nPPh_2\}]_2[MCl_4]$ all appear to indicate the presence of essentially tetrahedral $[MCl_4]^{2-}$ anions similar to those found for the structurally characterised examples. Given the wide variety of cation dependent stoichiometries and coordination geometries known to exist for the various halometallate anions of zinc, cadmium and mercury [18] this observation was rather disappointing. Therefore, a small number of complexes containing cations of the general form $[Pd(S_2CNR_2)\{Ph_2P(CH_2)_nPPh_2\}]^+$ (R = Me, Bu^n, Morph) in which the identity of the dithiocarbamate ligand varied were prepared. However, IR data strongly suggested that these salts also contain tetrahedral $[MCl_4]^{2-}$ anions similar to those described above. Their characterisation was therefore not pursued further.

4. Supplementary data

Supplementary data are available from CCDC, 12 Union Road, Cambridge CB2 1EZ, UK on request quoting the deposition numbers 139279–139281.

References

[1] G. Exarchos, S.C. Nyburg, S.D. Robinson, Polyhedron 17 (1998) 1257.
[2] Z. Otwinowski, W. Minor, in: C.W. Carter, R.M. Sweet (Eds.), Methods in Enzymology, Academic Press, New York, 1996.
[3] G.M. Sheldrick, Acta Crystallogr., Sect. A 46 (1990) 467.
[4] G.M. Sheldrick, SHELXL-97, University of Göttingen, Germany, 1997.
[5] L.J. Barbour, University of Missouri-Columbia, USA, 1995.
[6] J. Chatt, L.A. Duncanson, L.M. Venanzi, Nature 177 (1956) 1042.
[7] D.M. Adams, Metal–Ligand and Related Vibrations, Edward Arnold, London, 1967, pp. 26–83 and Refs. therein.
[8] P.E. Garrou, Chem. Rev. 81 (1981) 229.
[9] P.T. Beurskens, J.A. Cras, T.W. Hummelink, J.H. Noordik, J. Cryst. Mol. Struct. 1 (1971) 253.
[10] Q. Ye, Q.J. Meng, X.Z. You, X.Y. Huang, Acta Crystallogr., Sect. C 52 (1996) 33.
[11] L.J. Zompa, R. Haidar, Acta Crystallogr., Sect. C 52 (1996) 1188.
[12] R. Spengler, F. Zouari, A. BenSalah, H. Burzlaff, Acta Crystallogr., Sect. C 53 (1997) 1407, 1566.
[13] I.M. Vezzosi, A. Benedetti, A. Albinati, F. Ganazzoli, F. Cariati, L. Pellicciari, Inorg. Chim. Acta 90 (1984) 1.
[14] R. Taylor, O. Kennard, J. Am. Chem. Soc. 104 (1982) 5063.
[15] R.D. Bailey, W.T. Pennington, Polyhedron 16 (1997) 417 and Refs. therein.
[16] P.B. Hitchcock, K.R. Seddon, T. Welton, J. Chem. Soc., Dalton Trans. (1993) 2639 and Refs. therein.
[17] C.B. Aakeröy, K.R. Seddon, Z. Naturforsch., Teil B 48 (1993) 1023 and Refs. therein.
[18] G. Wilkinson, R.D. Gillard, J.A. McCleverty (Eds.), Comprehensive Coordination Chemistry, vol. 5, Pergamon, Oxford, 1987, pp. 981–985, 1059–1062 and Refs. therein.

PERGAMON

www.elsevier.nl/locate/poly

Polyhedron 19 (2000) 1519–1526

POLYHEDRON

Optically active transition metal complexes☆ Part 125. Preparation and epimerization of chiral-at-metal pentamethylcyclopentadienyl-rhodium(III) and iridium(III) half-sandwich complexes

H. Brunner *, A. Köllnberger, T. Burgemeister, M. Zabel [1]

Institut für Anorganische Chemie, Universität Regensburg, D-93040 Regensburg, Germany

Received 7 February 2000; accepted 25 April 2000

Abstract

The optically active bidentate Schiff base ligands (+)-2-*N*-[(*S*)-1-phenylethyl]pyrrolcarbaldimine NN*H and (+)-*N*-[(*S*)-1-phenylethyl]salicylaldimine ON*H react with $[Cp^*MCl_2]_2$ (M = Rh, Ir) to give the half-sandwich complexes Cp*Rh(NN*)Cl (**1**), Cp*Ir(NN*)Cl (**2**), Cp*Rh(ON*)Cl (**3**) and Cp*Ir(ON*)Cl (**4**). In all four cases two diastereomers (R_M,S_C) and (S_M,S_C) arise, differing only in the metal configuration. However, in each of the systems **1**–**4**, only the (R_M,S_C) diastereomer crystallized. X-ray structure analyses established the absolute configuration in the crystals of all four complexes. In solution the compounds epimerize via a change of the metal configuration and approach equilibria (R_M,S_C) (S_M,S_C) in which for **1** and **2** the (S_M,S_C) diastereomers dominate. Time dependent integration of ^{1}H NMR signals of the complexes **1** and **2** revealed that the epimerization is a clean first-order reaction. The half-lives in CD_2Cl_2 solution at −50°C were 19.4 min for **1** and 30.6 min for **2**. From the temperature dependence $\Delta H^{\neq}$ was determined as 62.4 kJ mol^{-1} for **1** and 44.3 kJ mol^{-1} for **2** and $\Delta S^{\neq}$ as 148 J K^{-1} mol^{-1} for **1** and 65 J K^{-1} mol^{-1} for **2**. For the compounds **3** and **4**, the kinetic data for the epimerization with respect to the metal center were derived from ^{1}H NMR coalescence experiments: half lives 35 ms for **3** at 21 ± 3° (CH_2Cl_2 solution) and 58 ms for **4** at −1.8 ± 3°C ($CHCl_3$ solution). These epimerization studies show that the metal configuration is labile in complexes **1** and **2** and extremely labile in complexes **3** and **4**. © 2000 Elsevier Science Ltd. All rights reserved.

Keywords: Chiral-at-metal complexes; Configurational stability; Epimerisation; Equilibria; X-ray structure analyses

1. Introduction

In 1997 in this journal a communication entitled 'Diastereoselective preparation of chiral-at-metal pentamethylcyclopentadienyl iridium(III) and rhodium(III) complexes' was published by Loza et al. [1]. They claimed that in the reaction of (+)-*N*-[(*S*)-1-phenylethyl]salicylaldimine ON*H with $[Cp^*MCl_2]_2$ (M = Rh, Ir) in the presence of KO^{t}Bu only one diastereomer of the complexes **3** and **4** was formed with high diastereomeric excess. The X-ray crystallographic analysis of complex **4,** performed by the authors, was used to assign R-configuration to the only isomer observed in solution. These conclusions turned out to be unsafe, because the authors had overlooked the configurational instability of the complexes **3** and **4** at the metal center. On the basis of additional experiments we present here a rectification [2].

2. Experimental

2.1. Physical measurements

^{1}H NMR spectra: Bruker ARX 400 spectrometer, the solvent signal acting as an internal standard. Elemental analyses: Microanalytical laboratory, University of Re-

☆ Part 124. H. Brunner, J. Klankermayer, M. Zabel, J. Organomet. Chem. 601 (2000) 211.

* Corresponding author. Tel.: +49-941-943-4440; fax: +49-941-943-4439.

E-mail address: henri.brunner@chemie.uni-regensburg.de (H. Brunner).

[1] X-ray structure analyses.

0277-5387/00/$ - see front matter © 2000 Elsevier Science Ltd. All rights reserved.
PII: S0277-5387(00)00416-2

gensburg. MS: MAT 311 A (EI) and MAT 95 (FD), both Finnigan. Vibrational spectra: Beckman spectrometer IR 4240 (KBr pellets).

2.2. Ligands and precursors

The ligands (+)-2-*N*-[(*S*)-1-phenylethyl]pyrrolcarbaldimine NN*H [3,4] and (+)-*N*-[(*S*)-1-phenylethyl]-salicylaldimine ON*H [5] were prepared by condensation of pyrrol-2-carbaldehyde and salicylaldehyde, respectively, with (−)-(*S*)-1-phenylethylamine. $[Cp^*MCl_2]_2$ (M = Rh, Ir) were synthesized by a published method [6].

2.3. Cp*Rh(NN*)Cl (1)

NN*H (233 mg, 1.175 mmol) was dissolved in CH_2Cl_2 (10 ml) and NaH (25 mg, 1.05 mmol) was added at 0°C. After 1 h $[Cp^*RhCl_2]_2$ (404 mg, 0.654 mmol) was added. The solution was stirred for 20 h at room temperature. By filtering the mixture over Celite, evaporating the solvent, picking up in toluene and adding petroleum ether, red single crystal prisms could be obtained in a yield of 74%. The crystals only consisted of the (R_{Rh},S_C) diastereomer. A solution of the powdered crystals in CD_2Cl_2 was prepared at −80°C for ^{1}H NMR investigations. At this temperature the ^{1}H NMR spectrum mainly showed the diastereomer (R_{Rh},S_C), whereas measurements at 21°C gave a ratio (R_{Rh},S_C):(S_{Rh},S_C) = 13:87 (CD_2Cl_2).

Anal. Calc. for Cp*Rh(NN*)Cl, $C_{23}H_{28}ClN_2Rh$ (470.84): C, 58.67; H, 5.99; N, 5.95. Found: C, 58.87; H, 6.09; N, 5.88%. $[\alpha]_D^{23} = +74.5°$ ($c = 0.36$, $CHCl_3$). MS-FD: $m/z = 470$ (100, M). IR: 1575 cm^{-1} (vs, $\nu_{C=N}$). ^{1}H NMR (250 MHz, $CDCl_3$) of (S_{Rh},S_C)–Cp*Rh(NN*)Cl (the values of the thermodynamically less stable diastereomer (R_{Rh},S_C)–Cp*Rh(NN*)Cl are given in brackets): $\delta = 1.67$ (1.66) (s, 15H, C_5Me_5), 1.81 (1.86) (d, ^3J(H,H) = 7.0 Hz, 3H, CH_3), 5.31 (5.17) (q, ^3J(H,H) = 7.0 Hz, CH), 6.32 (6.33) (ddd, $^3J(H^3,H^4)$ = 3.7 Hz, $^4J(H^3,H^5) = 1.8$ Hz, $^4J(H^3,CH) = 0.4$ Hz, 1H, H^3-pyrr), 6.61 (6.64) (dd, $^3J(H^4,H^3) = 3.7$ Hz, $^3J(H^4,H^5) = 1.1$ Hz, 1H, H^4-pyrr), 7.23–7.44 (m, 6H, H^5-pyrr, Ph), 7.45 (m, 1H, N=CH).

2.4. Cp*Ir(NN*)Cl (2)

Cp*Ir(NN*)Cl (**2**) was synthesized in the same way as Cp*Rh(NN*)Cl (**1**). The orange crystals of **2**, which formed in a toluene/petroleum ether solution in a yield of 96%, only consisted of the (R_{Ir},S_C) diastereomer as confirmed by X-ray analyses. Crystals of **2** were dissolved in CD_2Cl_2 at −80°C and analyzed by ^{1}H NMR spectroscopy. At −80°C only the (R_{Ir},S_C) diastereomer was observed. At room temperature, the diastereomer ratio was (R_{Ir},S_C):(S_{Ir},S_C) = 12:88 (CD_2Cl_2).

Anal. Calc. for Cp*Ir(NN*)Cl, $C_{23}H_{28}ClIrN_2$ (560.15): C, 49.32; H, 5.04; N, 5.00. Found: C, 49.08; H, 5.09; N, 4.66%. $[\alpha]_D^{23} = -47.5°$ ($c = 0.40$, $CHCl_3$). MS: $m/z = 560$ (100, M). IR: 1590 cm^{-1} (vs, $\nu_{C=N}$). ^{1}H NMR (400 MHz, $CDCl_3$) of (S_{Ir},S_C)–Cp*Ir(NN*)Cl (the values of the thermodynamically less stable diastereomer (R_{Ir},S_C)–Cp*Ir(NN*)Cl are given in brackets): $\delta = 1.62$ (1.63) (s, 15 H, C_5Me_5), 1.76 (1.72) (d, ^3J(H,H) = 7.0 Hz, 3H, CH_3), 5.22 (5.16) (q, ^3J(H,H) = 7.0 Hz, CH), 6.23 (6.26) (dd, $^3J(H^3,H^4) = 3.8$ Hz, $^4J(H^3,H^5) = 1.8$ Hz, 1H, H^3-pyrr), 6.52 (6.54) (dd, $^3J(H^4,H^3) = 3.8$ Hz, $^3J(H^4,H^5) = 1.1$ Hz, 1H, H^4-pyrr), 7.04 – 7.38 (m, 6H, H^5-pyrr, Ph), 7.47 (7.48) (s, 1H, N=CH).

2.5. Cp*Rh(ON*)Cl (3)

Cp*Rh(ON*)Cl (**3**) was synthesized in the same way as Cp*Rh(NN*)Cl (**1**), except that KO^{t}Bu instead of NaH was used as the base. Red plate-like crystals of the (R_{Rh},S_C) diastereomer were obtained in a yield of 84% by crystallization from a toluene/petroleum ether solution. The 400 MHz ^{1}H NMR spectrum in $CDCl_3$ at room temperature showed broad signals (coalescence regime). Therefore, the ^{1}H NMR spectrum was measured at −80°C in CD_2Cl_2. At this temperature the diastereomer ratio was 81:19.

Anal. Calc. for Cp*Rh(ON*)Cl, $C_{25}H_{29}ClNORh$ (497.86): C, 60.31; H, 5.87; N, 2.81. Found: C, 59.93; H, 5.86; N, 2.59%. $[\alpha]_D^{23} = +25.8°$ ($c = 0.44$, $CHCl_3$). MS: $m/z = 497$ (100, M), 462 (30, M–Cl). IR: 1610 cm^{-1} (vs, $\nu_{C=N}$). ^{1}H NMR (−80°C, 400 MHz, $CDCl_3$) of the thermodynamically more stable diastereomer (the values of the thermodynamically less stable diastereomer are given in brackets): $\delta = 1.33$ (1.47) (s, 15H, C_5Me_5), 1.72 (1.81) (d, ^3J(H,H) = 7.0 Hz, 3H, CH_3), 5.57 (q, ^3J(H,H) = 7.0 Hz, 1H, CH), 6.42 (dd, $^3J(H^3,H^4) = 7.1$ Hz, $^3J(H^5,H^4) = 7.1$ Hz, 1H, H^4-sal), 6.90–7.50 (m, 8H, H^3,H^5,H^6-sal, Ph), 7.95 (7.81) (s, 1H, N=CH).

2.6. Cp*Ir(ON*)Cl (4)

Cp*Ir(ON*)Cl (**4**) was synthesized in the same way as Cp*Rh(ON*)Cl (**3**). The orange crystals of **4**, which formed in a toluene/petroleum ether solution in a yield of 65%, only consisted of the (R_{Ir},S_C) diastereomer. The 400 MHz ^{1}H NMR spectrum at room temperature showed broad signals (coalescence regime). Therefore, the ^{1}H NMR spectrum was measured at −50°C in $CDCl_3$. At this temperature the diastereomer ratio was 85:15.

Anal. Calc. for Cp*Ir(ON*)Cl, $C_{25}H_{29}ClIrNO$ (587.17): C, 51.14; H, 4.98; N, 2.39. Found: C, 51.15; H, 5.15; N, 2.02%. $[\alpha]_D^{23} = +18.6°$ ($c = 0.43$, $CHCl_3$). MS: $m/z = 587$ (100, M). IR: 1610 cm^{-1} (vs, $\nu_{C=N}$). ^{1}H

NMR (-50°C, 400 MHz, $CDCl_3$) of the thermodynamically more stable diastereomer (the values of the thermodynamically less stable diastereomer are given in brackets): $\delta = 1.53$ (1.64) (s, 15 H, C_5Me_5), 1.97 (1.78) (d, $^3J(H,H) = 7.0$ Hz, 3H, CH_3), 5.60 (q, $^3J(H,H) = 7.0$ Hz, 1H, CH), 6.43 (dd, $^3J(H^3,H^4) = 7.1$ Hz, $^3J(H^5,H^4) = 7.1$ Hz, 1H, H^4-sal), 6.90–7.50 (m, 8H, H^3,H^5,H^6-sal, Ph), 7.86 (7.72) (s, 1H, N=CH).

2.7. X-ray

Diffraction data were collected on a STOE-IPDS diffractometer using Mo Kα radiation ($\lambda = 0.7107$ Å). The unit cells for **1**–**4** were determined from 8000 randomly selected reflections. Intensity data were collected for Lorentz and polarization effects. For the two iridium compounds absorption effects must be calculated. Crystal data and details of the structure determination are shown in Table 1. The structures **1**–**4** were solved by direct methods and SIR-97 [7]. All were refined on F^2 by the full-matrix least-squares technique (SHELXL-97 [8]). All non-hydrogen atoms were refined anisotropically. The hydrogen atoms were calculated geometrically and a riding model was used during the refinement process.

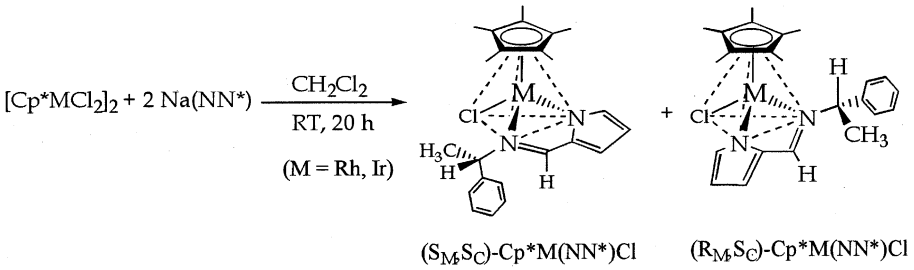
3. Cp*Rh(NN*)Cl (1) and Cp*Ir(NN*)Cl (2)

3.1. Synthesis and X-ray structure analyses

The deprotonated ligand NN*H is reacted with $[Cp^*MCl_2]_2$ (M = Rh, Ir) to give the compounds Cp*M(NN*)Cl (M = Rh, Ir) (**1** and **2**) (Scheme 1). The

Table 1
Crystallographic data of complexes**1**–**4**

Compound	Cp*Rh(NN*)Cl (**1**)	Cp*Ir(NN*)Cl (**2**)	Cp*Rh(ON*)Cl (**3**)	Cp*Ir(ON*)Cl (**4**)
Crystal data				
CCDC number	139216	139217	139218	139215
Empirical formula	$C_{23}H_{28}ClN_2Rh$	$C_{23}H_{28}ClIrN_2$	$C_{25}H_{29}ClNORh$	$C_{25}H_{29}ClIrNO$
Formula weight	470.83	560.14	497.85	587.16
Crystal size (mm)	$0.16 \times 0.10 \times 0.08$	$016 \times 0.10 \times 0.06$	$0.28 \times 0.12 \times 0.05$	$0.30 \times 0.14 \times 0.08$
Crystal color, habit	red, prism	orange, prism	red, plate-like	orange, prism
Crystal system	monoclinic	monoclinic	orthorhombic	orthorhombic
Space group	$P2_1$	$P2_1$	$P2_12_12_1$	$P2_12_12_1$
a (Å)	8.6523(13)	8.5620(6)	8.3889(5)	13.5843(9)
b (Å)	7.9959(9)	8.0390(5)	13.6062(7)	8.4600(4)
c (Å)	16.109(2)	15.9370(10)	19.6297(9)	19.5653(11)
α (°)	90	90	90	90
β (°)	105.339(17)	105.410(7)	90	90
γ (°)	90	90	90	90
V (Å^3)	1074.8(2)	1057.51	2240.6(2)	2248.51(19)
Z	2	2	4	4
D_{calc} (g cm^{-3})	1.455	1.759	1.476	1.735
F(1526), absorption coefficient (mm^{-1})	484, 0.93	548, 6.45	1024, 0.90	1152, 6.07
Data collection				
T (K)	293(1)	173(1)	173(1)	173(1)
Θ range for data collection (°)	2.44–25.81	2.47–25.78	1.82–25.79	1.83–25.75
Index ranges	$-10 \le h \le 10$ $-9 \le k \le 9$ $-19 \le l \le 19$	$-10 \le h \le 10$ $-9 \le k \le 9$ $-19 \le l \le 19$	$-10 \le h \le 10$ $-16 \le k \le 16$ $-20 \le l \le 23$	$-16 \le h \le 16$ $-10 \le k \le 10$ $-23 \le l \le 23$
Reflections collected	15 259	14 057	13 914	20 992
Independent reflections	4114	4035	4284	4289
Observed reflections [$I > 2\sigma(I)$]	3647	3784	3820	4111
Absorption correction	none	numerical	none	numerical
Refinement				
Hydrogen treatment	mixed	mixed	refall	refall
Data/restraints/parameters	4114/1/284	4035/1/276	4284/0/378	4289/0/378
Goodness-of-fit on F^2	1.051	1.036	0.888	1.072
Final R indices [$I > 2\sigma(I)$]	$R_1 = 0.0256$ $wR_2 = 0.0587$	$R_1 = 0.0217$ $wR_2 = 0.0510$	$R_1 = 0.0235$ $wR_2 = 0.0507$	$R_1 = 0.0135$ $wR_2 = 0.0311$
R indices (all data)	$R_1 = 0.0296$ $wR_2 = 0.0592$	$R_1 = 0.0240$ $wR_2 = 0.0514$	$R_1 = 0.0289$ $wR_2 = 0.0519$	$R_1 = 0.0147$ $wR_2 = 0.0313$
Absolute structure parameter	$-0.04(3)$	$-0.01(1)$	$-0.03(3)$	$-0.01(1)$
Largest difference peak and hole (e Å^{-3})	0.767 and -0.233	1.990 and -0.515	0.681 and -0.256	0.827 and -0.261



Scheme 1. Synthesis of Cp*M(NN*)Cl (M = Rh, Ir) **1** and **2**.

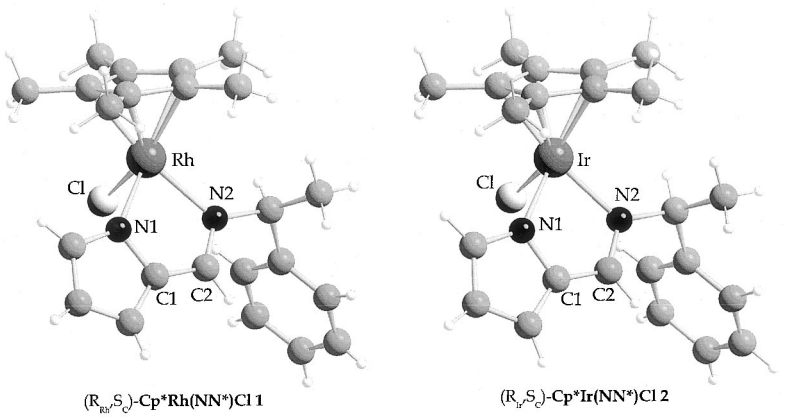


Fig. 1. Crystal structures of (R_{Rh},S_C)–Cp*Rh(NN*)Cl (**1**) and (R_{Ir},S_C)–Cp*Ir(NN*)Cl (**2**).

ligand NN*H contains an asymmetric carbon atom in S_C configuration. In the complexes **1** and **2** a new stereogenic center arises at the metal center. Consequently, there are two diastereomers (R_M,S_C) and (S_M,S_C) which differ in their ^{1}H NMR spectra. The (R_M,S_C):(S_M,S_C) ratio was 13:87 for **1** and 12:88 for **2** (CD_2Cl_2 solution) at ambient temperature obtained by integration of the Cp* signals.

Petroleum ether was added to a solution of Cp*Rh(NN*)Cl (**1**) and Cp*Ir(NN*)Cl (**2**), respectively, in toluene to obtain single crystals. The X-ray analyses showed, that the absolute configuration at the metal atom was R in both cases using the ligand priority sequence Cp* > Cl > N(imine) > N(pyrrolate) [9,10]. Thus, crystals of the two compounds only contain the (R_M,S_C) diastereomer (Fig. 1).

Table 2 summarizes selected bold lengths [Å], angles [°] and torsional angles of (R_{Rh},S_C)–Cp*Rh(NN*)Cl (**1**) and (R_{Ir},S_C)–Cp*Ir(NN*)Cl (**2**), which turn out to be very similar.

3.2. Epimerization studies

In the epimerization studies of (R_{Rh},S_C)–Cp*Rh(NN*)Cl (**1**) and (R_{Ir},S_C)–Cp*Ir(NN*)Cl (**2**) the samples stayed within the Bruker ARX 400 spectrometer. During the kinetic measurements the temperature varied from series to series by approximately ± 2°C. Within one series of measurements the temperature was much more constant. The evaluation was done by integration of the Cp* ^{1}H NMR signals.

Powdered crystals of (R_{Rh},S_C)-**1** or (R_{Ir},S_C)-**2,** dissolved at − 80°C in CD_2Cl_2, mainly showed the signals of the diastereomer (R_M,S_C) in the ^{1}H NMR spectrum as shown for Cp*Ir(NN*)Cl (**2**) in Fig. 2. In both cases on raising the temperature the signals of the (S_M,S_C)-diastereomers grew — a process which continued on further warming up. Obviously, the reason for this behavior is an epimerization at the metal center which

Table 2
Selected bond lengths (Å), bond angles (°) and torsional angles (°) of **1** and **2**

	(R_{Rh}, S_C)–Cp*-Rh(NN*)Cl (**1**)	(R_{Ir},S_C)–Cp*-Ir(NN*)Cl (**2**)
M–Cl	2.3956(14)	2.4017(16)
M–N1(pyrrolate)	2.068(3)	2.068(5)
M–N2(imine)	2.136(3)	2.121(3)
M–C(Cp*)(average):	2.16	2.17
Cl–M–N1(pyrrolate)	88.05(10)	86.07(14)
Cl–M–N2(imine)	86.37(9)	84.49(12)
N1(pyrrolate)–M–N2(imine)	76.97(11)	76.54(17)
M–N1–C1–C2	1.3(4)	1.6(6)
N1–C1–C2–N2	1.3(5)	0.2(8)
M–N1–C2–C1	−3.1(5)	−1.8(6)

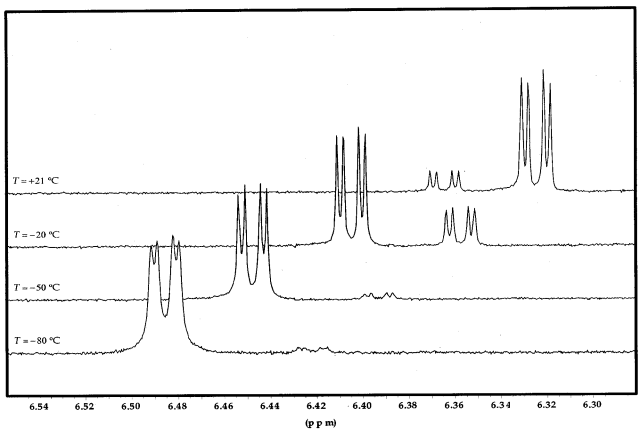


Fig. 2. ^{1}H NMR spectra of Cp*Ir(NN*)Cl (**2**) (400 MHz, CD_2Cl_2) in temperature range −80 to 21°C.

leads to an equilibrium between the two diastereomers (R_M,S_C) and (S_M,S_C). Measurements at 21°C gave the equilibrium ratios (R_{Rh},S_C):(S_{Rh},S_C) = 13:87 and (R_{Ir},S_C):(S_{Ir},S_C) = 12:88.

Kinetic studies of the epimerization were made on the basis of the integration of the Cp* signals. After dissolving the powdered crystals at −80°C in CD_2Cl_2, ^{1}H NMR spectra were recorded at defined time intervals for more than 1.5 half-lives at the temperatures −35, −50 and −65°C, leaving the samples in the NMR spectrometer. The data analyzed perfectly according to first-order kinetics (Fig. 3), the half-lives for the approach to equilibrium of Cp*Rh(NN*)Cl (**1**) (Cp*Ir(NN*)Cl (**2**)) being 247 (225) min at −65°C, 19.4 (30.6) min at −50°C and 2.66 (7.63) min at −35°C (Table 3).

The Eyring-plots show the temperature dependence of the epimerization (Fig. 4), giving the activation enthalpies $\Delta H^{\neq}$ 62.4 (44.3) kJ mol^{-1} and the activation entropies $\Delta S^{\neq}$ 148 (65) J K^{-1} mol^{-1} for **1** (**2**).

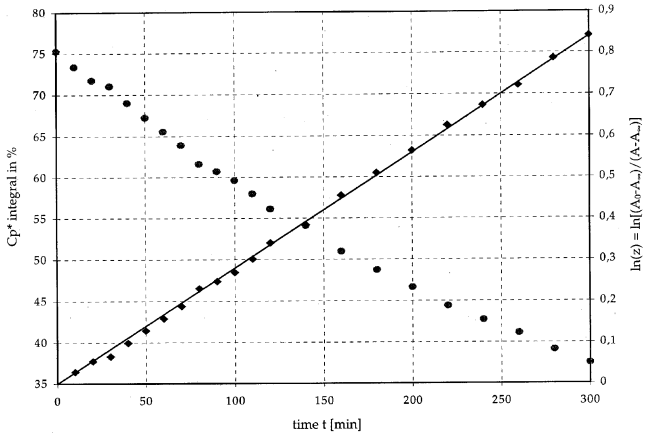


Fig. 3. The epimerization of Cp*Rh(NN*)Cl (**1**) at −65°C in CD_2Cl_2.

Table 3
Kinetic data of the epimerization of **1** and **2** in CD_2Cl_2

ϑ (°C)	Cp*Rh(NN*)Cl (**1**)		Cp*Ir(NN*)Cl (**2**)	
	$k \times 10^5$ (s^{-1})	τ (min)	$k \times 10^5$ (s^{-1})	τ (min)
−36°C (**1**), −35°C (**2**)	434	2.66	151.3	7.63
−50°C	59.6	19.4	37.7	30.6
−65°C	4.78	247	5.12	225

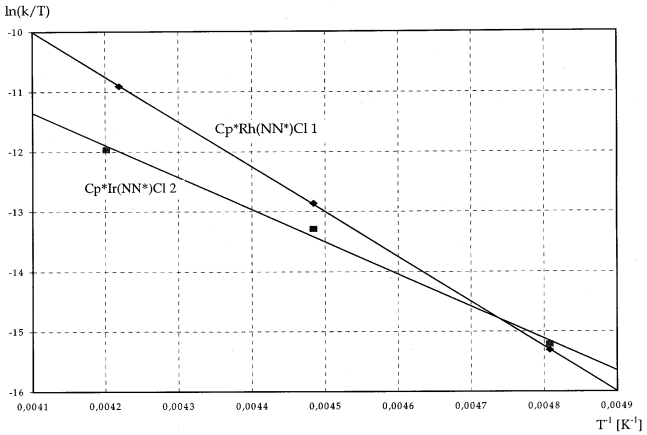


Fig. 4. Eyring-plot for Cp*Rh(NN*)Cl (**1**) and Cp*Ir(NN*)Cl (**2**).

4. Cp*Rh(ON*)Cl (3) and Cp*Ir(ON*)Cl (4)

4.1. Synthesis and X-ray structure analyses

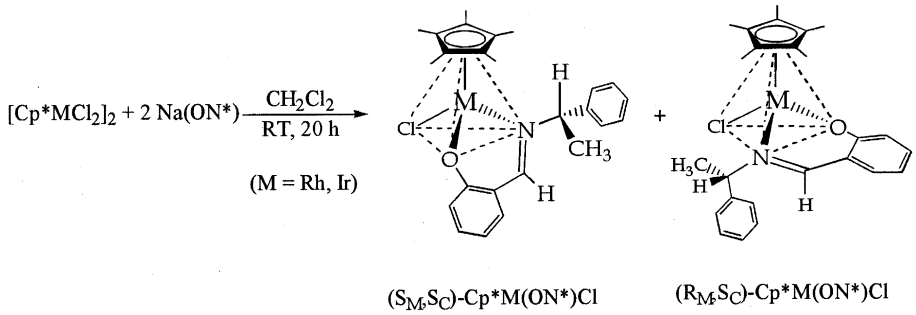
The deprotonated ligand ON*H is reacted with [Cp*MCl_2]$_2$ (M = Rh, Ir) to give the complexes Cp*M(ON*)Cl (M = Rh, Ir) **1** and **2** (Scheme 2). Again, two diastereomers are possible. The diastereomer ratio can only be determined at low temperatures. In CD_2Cl_2 solution the ratio is 81:19 for 3 at −80°C and 85:15 for **4** at −40°C in $CDCl_3$ solution.

To a toluene solution of Cp*Rh(ON*)Cl (**3**) and Cp*Ir(ON*)Cl (**4**), respectively, petroleum ether was added to obtain single crystals. In both cases the absolute configuration at the metal atom was R as shown by X-ray analyses (Fig. 5).

In Table 4 selected bond lengths [Å], angles [°] and torsional angles of (R_{Rh},S_C)–Cp*Rh(ON*)Cl (**3**) and (R_{Ir},S_C)–Cp*Ir(ON*)Cl (**4**) are summarized.

4.2. Coalescence measurements

As for Cp*Rh(ON*)Cl (**3**) and Cp*Ir(ON*)Cl (**4**), respectively, the interconversion of the two possible diastereomers is too fast, the rate constants cannot be



Scheme 2. Synthesis of Cp*M(ON*)Cl (M = Rh, Ir) **3** and **4**.

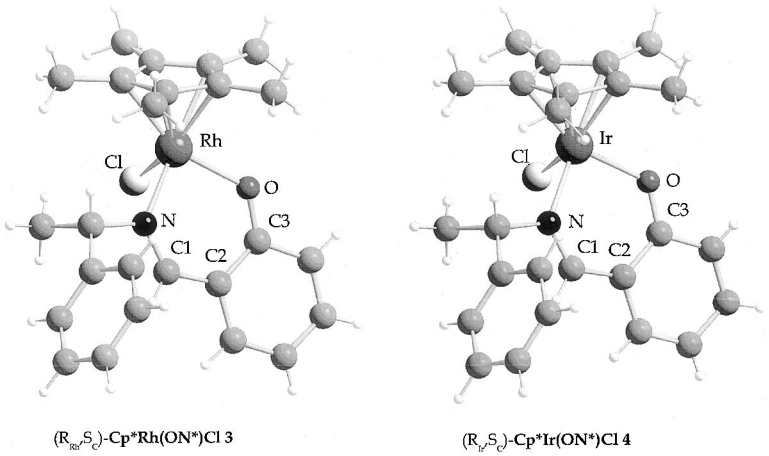


Fig. 5. Crystal structures of (R_{Rh},S_C)–Cp*Rh(ON*)Cl (**3**) and (R_{Ir},S_C)–Cp*Ir(ON*)Cl (**4**).

determined by time dependent integration of suitable ^{1}H NMR signals as in the complexes **1** and **2**. Therefore, in case of **3** and **4** the kinetic parameters were determined from the coalescence of the ^{1}H NMR spectra. At low temperatures the signals of the two diastereomers are clearly recognizable as shown for the imine protons of Cp*Rh(ON*)Cl (**3**) at −80°C in Fig. 6. On raising the temperature the signals broaden. At the coalescence temperature T_c there is a horizontal connection between the two peaks. The coalescence temperature T_c is +21°C for Cp*Rh(ON*)Cl (**3**) (Fig. 6) and −1.8°C for Cp*Ir(ON*)Cl (**4**).

Table 4
Selected bond lengths (Å), bond angles (°) and torsional angles (°) of **3** and **4**

	(R_{Rh},S_C)–Cp*Rh(ON*)-Cl (**3**)	(R_{Ir},S_C)–Cp*Ir(ON*)-Cl (**4**)
M–Cl	2.4245(8)	2.42(8)
M–O	2.074(2)	2.082(2)
M–N	2.097(2)	2.092(2)
M–C(Cp*) (average)	2.16	2.16
Cl–M–O	88.47(5)	85.87(7)
Cl–M–N	85.51(6)	83.94(7)
O–M–N	89.05(9)	88.38(10)
O–M–N–C1	−17.0(3)	−15.5(2)
M–N–C1–C2	11.4(5)	9.9(4)
N–C1–C2–C3	5.1(5)	6.1(5)
C1–C2–C3–O	−9.6(4)	−10.3(5)
N–M–O–C3	14.0(2)	12.4(3)
M–O–C3–C2	−3.8(4)	−2.4(5)

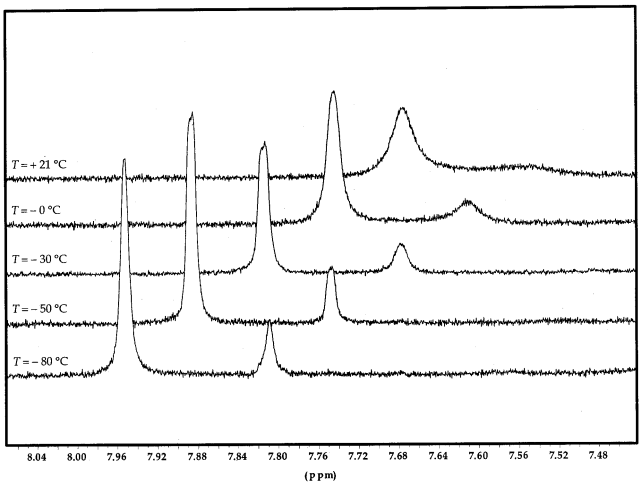


Fig. 6. ^{1}H NMR spectra of (400 MHz, CD_2Cl_2) of Cp*Rh(ON*)Cl (**3**) (imine proton).

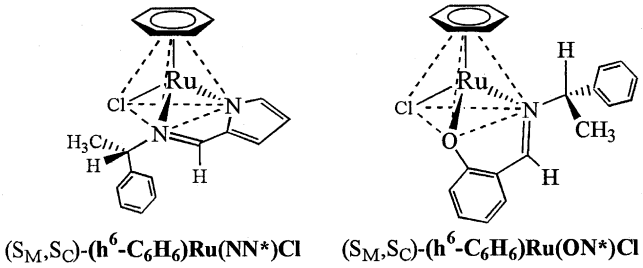
Table 5
Results of the coalescence measurements of Cp*Rh(ON*)Cl (**3**) and Cp*Ir(ON*)Cl (**4**)

	Cp*Rh(ON*)Cl (**3**)	Cp*Ir(ON*)Cl (**4**)
Coalescence temperature T_c (°C)	21 ± 3	-1.8 ± 3
$\Delta\nu$ at T_c (extrapolated) (Hz)	52.60	39.04
Equilibrium constant K	0.24	0.18
Rate constant k_A (s^{-1})	24.7	13.7
Half-life τ (A) (ms)	28	50
Rate constant k_B (s^{-1})	102.8	76.9
Half-life τ (B) (ms)	6.7	8
Rate constant k (s^{-1})	127.5	90.6
^{1}H NMR parameters	400 MHz, CD_2Cl_2	400 MHz, $CDCl_3$

For a first-order reaction it is possible to compute the rate constants k_A, k_B, k, the half-lives τ_A, τ_B and the free enthalpies of activation $\Delta G_A^{\neq}$, $\Delta G_B^{\neq}$ (A = forward reaction, B = back reaction) using the equilibrium constant K, the coalescence temperature T_c, the line widths b_E [Hz] and the chemical shift difference $\Delta\nu$ [Hz] of the signals of the two diastereomers at different temperatures below T_c [2,11]. A linear extrapolation has to be made to calculate the value of $\Delta\nu$ at T_c. Table 5 summarizes the results of the coalescence measurements.

5. Discussion

As outlined in the Introduction, the complexes **3** and **4** had been prepared before and complex **4** had been characterized by an X-ray structure analysis [1]. However, the authors had characterized the complexes **3** and **4** only by room temperature ^{1}H NMR spectra. Our investigations demonstrated that the room temperature ^{1}H NMR spectra are the averaged high temperature limiting spectra (fast exchange regime of two diastereomers in diastereomer equilibria). Therefore, the authors of Ref. [2] missed to recognize the configurational lability of the complexes **3** and **4** with respect to the metal configuration. As the consequence, their overall result 'The complex **4** forms with R configuration at the metal centre exclusively, as confirmed by X-ray crystallography and comparison of the ^{1}H-NMR spectra of the reaction mixtures from the preparation with those of the crystallised material' [1] is an oversimplification and misinterpretation of the systems **3** and **4**. The X-ray structure analyses of the complexes **3** and **4** unequivocally establish the stereochemistry in the solid state. However, metal configurations in solution cannot be assigned because of the configurational instability at the metal center. The complexes **1** and **2** demonstrate how questionable such assignments can be. Although



Scheme 3. (η^6-C_6H_6)Ru(NN*)Cl and (η^6-C_6H_6)Ru(ON*)Cl (only one diastereomer shown).

for both **1** and **2**, there is a major isomer dominating the minor isomer by about 90:10 in the diastereomer equilibrium established in solution, it is the minor diastereomer which crystallizes in both cases. Thus, the major diastereomers are converted into the less soluble minor diastereomers in a second-order asymmetric transformation [12].

(η^5-C_5H_5)Rh and (η^5-C_5H_5)Ir complexes are isolobal with the corresponding (η^6-C_6H_6)Ru and (η^6-C_6H_6)Os complexes [13]. Therefore, a comparison of their configurational stability at the metal atom seems appropriate. Whereas the compound (η^6-C_6H_6)Ru(ON*)Cl (Scheme 3) undergoes fast epimerization in solution [14], the half-life of the equilibration of the diastereomers of (η^6-C_6H_6)Ru(NN*)Cl (Scheme 3) was determined to be 9.2 min at 27°C in $CDCl_3$ solution [15]. Thus, the rhodium complexes **1** and **3** seem to be more labile in the configuration at the metal center than the corresponding ruthenium counterparts.

6. Supplementary material

Crystallographic data for the structural analyses have been deposited with the Cambridge Crystallographic Centre. Supplementary data are available from the CCDC, 12 Union Road, Cambridge CB2 1EZ, UK (fax: +44-1223-336033; e-mail: deposit@ccdc.cam.ac.uk or www: http://www.ccdc.cam.ac.uk) on request, quoting the deposition nos. 139215–139218.

References

[1] M.L. Loza, J. Parr, A.M.Z. Slawin, Polyhedron 16 (1997) 2321.
[2] A. Köllnberger, Diplomarbeit, Universität Regensburg, Germany, 1999.
[3] I. Bernal, G.M. Reisner, H. Brunner, G. Riepl, Inorg. Chim. Acta 103 (1985) 1799.
[4] H. Brunner, G. Riepl, R. Benn, A. Rufinska, J. Organomet. Chem. 253 (1983) 93.
[5] H.E. Smith, S.L. Cook, M.E. Warren Jr., J. Org. Chem. 29 (1964) 2265.
[6] C. White, A. Yates, P.M. Maitlis, Inorg. Synth. 29 (1992) 228.
[7] A. Altomare, G. Cascarano, C. Giacovazzo, A. Guagliardi, J. Appl. Cryst. 26 (1993) 343.

[8] G.M. Sheldrick, SHELXL-97, University of Göttingen, Germany, 1997.
[9] C. Lecompte, Y. Dusausoy, J. Protas, J. Tirouflet, A. Dormond, J. Organomet. Chem. 73 (1974) 67.
[10] H. Brunner, Enantiomer 2 (1996) 133.
[11] A. Jaeschke, H. Muensch, H.G. Schmid, H. Friebolin, A. Mannschreck, J. Mol. Spectrosc. 31 (1969) 14.
[12] E.E. Turner, M.M. Harris, Quart. Rev. 1 (1947) 299.
[13] R. Hoffmann, Angew. Chem. 94 (1982) 725; Angew. Chem., Int. Ed. Engl. 21 (1982) 711.
[14] R. Oeschey, Ph.D. Thesis, University of Regensburg, Germany, 1995.
[15] H. Brunner, R. Oeschey, B. Nuber, Organometallics 15 (1996) 3616.

PERGAMON

www.elsevier.nl/locate/poly

Polyhedron 19 (2000) 1527–1537

POLYHEDRON

Synthesis, structural characterization and potentiometric studies of divalent metal complexes with an octadentate tetraazamacrocyclic ligand and their DNA cleavage ability

De-Yuan Kong [a,*], Yu-Yuan Xie [b]

[a] *Department of Chemistry, Texas A&M University, College Station, TX 77842-3012, USA*
[b] *Shanghai Institute of Materia Medica, Chinese Academy of Sciences, Taiyuan Road 294, Shanghai 200031, PR China*

Received 13 December 1999; accepted 18 April 2000

Abstract

Four new metal complexes with an octadentate macrocyclic ligand [L = 1,4,7,10-tetrakis(2-carbamoylethyl)-1,4,7,10-tetraazacyclododecane] were synthesized and characterized by elemental analyses, IR and MS. These complexes have the general formula: $M(L)(NO_3)_2{\cdot}nH_2O$ [M = Co (**1**), Ni (**2**), $n = 2$; M = Cu (**3**), Zn (**4**), $n = 1$]. The structures of complexes **1**, **2** and **3** have been determined by X-ray diffraction. $[Co(L)(NO_3)](NO_3){\cdot}2H_2O$ (**1**) crystallizes in the triclinic space group $P\bar{1}$. The refinement converges with $R = 0.045$ and $R_w = 0.057$ for 3233 reflections with ($I > 2.5\sigma(I)$). The Co has an octahedral geometry, and was coordinated with four amine nitrogen atoms of macrocyclic ligand and two or one acylate oxygen atoms derived from amide pendant groups. Two water molecules crystallize in the lattice cell and two kinds of hydrogen bonds exist between the coordinated acylate group and the water molecules: N(6)–H(27)···O(11) 2.158, N(8)–H(40)···O(12) 2.158 Å or exist between the uncoordinated acylate group and the nitrate ion: N(5)–H(21)···O(8) 2.452, N(7)–H(33)···O(5) 2.256 Å. $[Ni(L)(NO_3)](NO_3){\cdot}2H_2O$ (**2**) crystallizes in the monoclinic space group $C2/c$. The refinement converges with $R = 0.044$ and $R_w = 0.059$ for 2726 reflections with ($I > 3\sigma(I)$). The crystal of complex **2** has high symmetry with a C_{2v} symmetric operation. The central Ni atom is coordinated to four amine nitrogen atoms of macrocyclic skeleton and two acylate oxygen atoms of pendant amide groups. The polyhedron of the central atom can be described as a pseudo-octahedron. Two water molecules crystallized in the cell lattice. $[Cu(L)](NO_3)_2{\cdot}H_2O$ (**3**) crystallizes in the monoclinic space group $P2_1/n$. The refinement converges with $R = 0.037$ and $R_w = 0.048$ for 3174 reflections with ($I > 2.5\sigma(I)$). Complex **3** has a five-coordinated pyramid. The bond lengths of Co–O (av.) 2.088(3), Ni–O 2.089(2) Å are almost equal, and are shorter than Cu–O 2.137(3) Å. On the other hand, the bond lengths of Co–N (av.) and Ni–N (av.) are 2.194(3) and 2.153(2) Å, respectively. Both of them are longer than Cu–N (av.) 2.0465(3) Å. The potentiometric experiments in aqueous solution showed that the stability constants of three complexes were in the range of $\log K_{ML} = 17.11–15.00$. The DNA cleavage results showed that the cobalt complex can effectively cleave supercoiled DNA to form nicked or linear DNA by performing single strand and double strand scissions under aerobic conditions in the presence of hydrogen peroxide as co-oxidant. Electron paramagnetic resonance results with the aid of DMPO as trapping agent demonstrated that the cleavage mechanism possibly occurred via hydroxy radical attacking. © 2000 Elsevier Science Ltd. All rights reserved.

Keywords: Tetraazamacrocyclic ligand; Transition metal; Synthesis; Structural characterization; Stability constants; DNA cleavage activities

1. Introduction

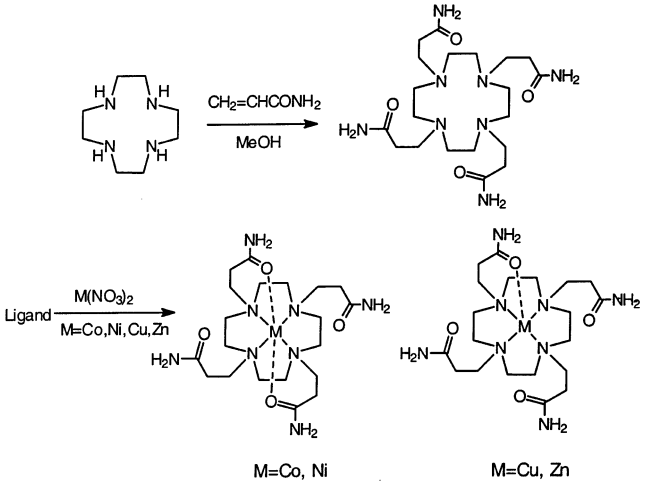
Cyclen-based macrocyclic metal complexes have been of interest for many years. With the recent elucidation of more and more biological activities of these complexes, researchers have started to concentrate on their antitumor and anti-HIV activities [1–3].

A variety of pendant arm ligands, such as CH_2CH_2COOH [4], $CH_2CH_2PO_3H_2$ [5], CH_2CH_2OH [6], $CH_2C_6H_4COOH$ [7], $CH_2C_6H_5$ [8], CH_2CH_2CN [9], $CH_2CH_2NH_2$ [10], $CH_2CH(OH)C_6H_5$ [11], $CH_2CH_2CONH_2$ [12], $CH_2CH(OH)CH_3$ [13] and CH_2CONH(naphthyl)CH_3 [14], have been prepared. These ligands possess divergent steric and electronic properties

* Corresponding author. Tel.: +1-979-8452-232; fax: +1-979-8454-719.
E-mail address: kong@mail.chem.tamu.edu (D.-Y. Kong).

0277-5387/00/$ - see front matter © 2000 Elsevier Science Ltd. All rights reserved.
PII: S0277-5387(00)00420-4

and coordination environments. Several types of tetraazamacrocyclic lanthanide complex have been developed, which are inert to the dissociation of metal ions, and can hydrolyze the phosphodiester backbone of RNA as free complexes in solution [15] as well as conveniently attach to antisense oligonucleotides [16–18]. These complexes have at least one coordination site available for binding a small molecule or substrate. Since the Morrow group reported their results on the specific cleavage of RNA with tetraazamacrocyclic lanthanide complexes [19], a wide range of metal complexes have become available for the scission of nucleic acids. One of the most effective metal-based nucleases is the copper complex of 1,10-phenanthroline, which has been extensively studied and used for mapping protein and drug binding sites on DNA as well as for studying DNA structure [20]. Ligands with pendant amide groups are particularly interesting. Because they can form complexes in which the NH_2 group can remain protonated and the metal coordination to the CH_2CONH_2 group occurs through the carbonyl oxygen, or the NH_2 group can be deprotonated and so act as a deprotonated amide nitrogen, thus providing a strong metal binding site. This coordination behavior is very similar to that of the CONH group in small peptides. This kind of ligand has the advantage of having carbonyl oxygen and amide nitrogens as donor atoms at the same time. This characteristic was found in the complexes with 1,4,7-tri(carbamoylmethyl)-1,4,7-triazacyclonanone [21]. In order to screen new metal complexes for cancer chemotherapy, we synthesized these four complexes. However, compared with other analogous complexes reported with ligands: 1,4,7,10-tetrakis(benzyl)-1,4,7,10-tetraazacyclododecane [8] or 1,4,7,10-tetrakis(2-cycanoethyl)-1,4,7,10-tetraazacyclododecane [22], four metal complexes showed little activities against P388 or A549 tumor cell lines in vitro. In the research on the antitumor mechanism of these complexes, we found unexpectedly that complex **1** can effectively cleave supercoiled DNA into nicked and linear DNA in the presence of hydrogen peroxide at different concentrations.



Scheme 1. Synthetic route of L and its complexes.

2. Results and discussion

2.1. Spectrum analyses

The ligand and complexes were synthesized according to Scheme 1. All metal complexes dissolved well in water, DMF, DMSO and CH_3OH, but were insoluble in ether or acetone. The characteristic absorption of the ionic nitrate can be found in the IR spectrum of four complexes at ca. 1385 cm^{-1} [23]. Two vibration bands of the acylate of N–H pendant groups exist in the ligand at ca. 3155 and 3379 cm^{-1}. When the ligand coordinated with metal ions, this band was overlapped with O–H vibration absorption of the water molecule and only existed as a broader band at ca. 3377, 3411, 3408 and 3348 cm^{-1} for Co, Ni, Cu and Zn, respectively. The carbonyl group C=O of the amide of the ligand has a characteristic absorption at 1672 cm^{-1}, but in Co and Ni complexes this band shifted to 1676 cm^{-1} after the two carboxamide oxygen atoms coordinated to the central metal ions. However, this band is absent and strong bands are observed in Cu and Zn complexes at lower wavelengths: ca. 1666 and 1670 cm^{-1}, respectively. In the case of Cu and Zn complexes, the carboxamide oxygen atom also coordinated to the central metal ions then decreased the electronic density of the delocalized double bond. The absorption bands shifted to low wavelengths. The same phenomenon was observed in $[Cr(L'–H)]^{2+}$ reported by Weyhermüller et al. [21].

In the EI MS spectrum of complex **4** the base peak is m/z 71 $[CHCH_2CONH_2]^+$. Other peaks correspond to the loss of one or more pendant groups, which are m/z 503 $[M^+ - 2CHCH_2CONH_2]$, 429 $[M^+ - 3CH_2CH_2CONH_2]$, 369 $[M^+ - 3(CH_2CH_2CONH_2)–NO_3]$, 357 $[M^+ - 4CH_2CH_2CONH_2]$ and 295 $[M^+ - 4(CH_2CH_2CONH_2)–NO_3]$. The molecular peak does not exist because the pendant group $CH_2CH_2CONH_2$ is easily lost under EI source conditions. However, the FAB MS spectrum of complex **2** shows different characteristics to the above-mentioned. The molecular peak: M^+ m/z 639 $[Ni(L)(NO_3)_2]^+$ easily lost the non-coordination ionic nitrate to form the peak $[Ni(L)(NO_3)]^+$ m/z 577, which can lose the coordinating nitrate further to form a fragment peak at m/z 515 corresponding to $[Ni(L)]^+$. Then the ligand decomposes with the loss of several pendant groups to generate fragmentation peaks: m/z 443, 299, 229.

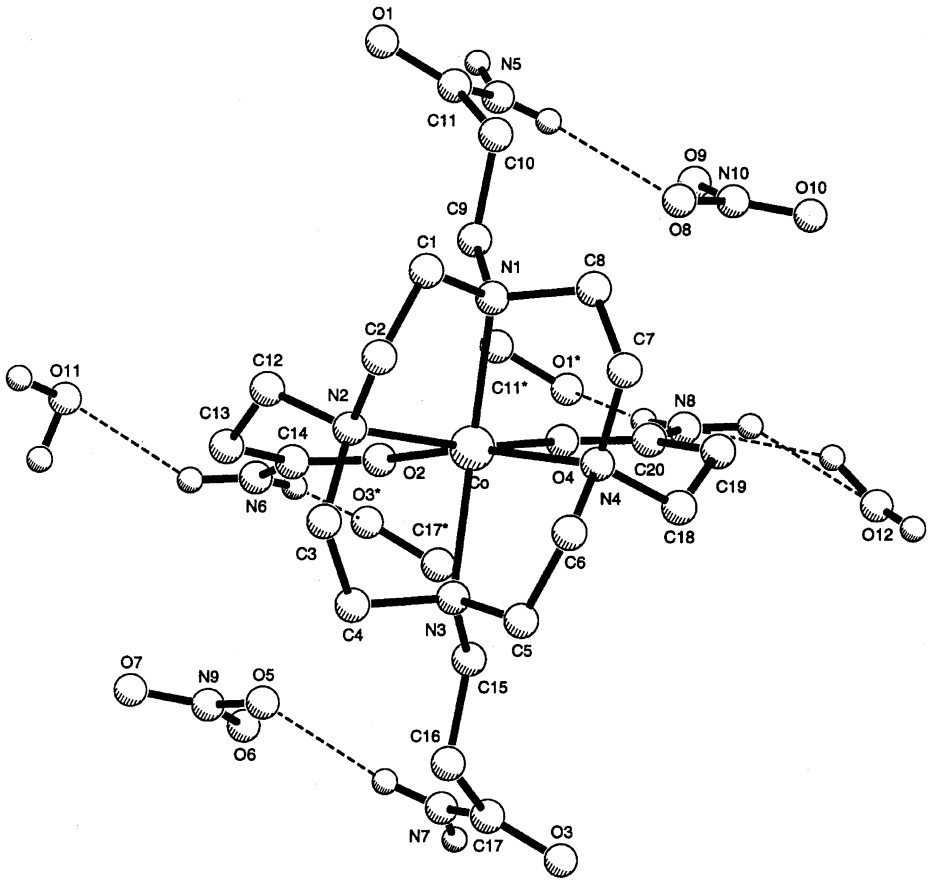


Fig. 1. The ORTEP drawing of the cation part in complex **1** with ellipsoid 40%.

2.2. Structural analyses

The ORTEP drawings for crystal structures of complexes **1**, **2** and **3** are depicted as Figs. 1–3, respectively. The crystallographic data and important parameters are given in Table 1. The selected bond distances and bond angles of two crystals are listed in Tables 2–4, respectively.

Complex **1** consists of ion pairs. In the cationic part, the central Co atom was surrounded by four imino nitrogen and two acylato oxygen atoms, which were defined as an octahedral polyhedron. Two water molecules crystallize in the lattice cell and two kinds of hydrogen bonds exist between the coordinated acylate group and water molecules: N(6)–H(27)···O(11) 2.158, N(8)–H(40)···O(12) 2.158 Å, or exist between an uncoordinated acylate group and a nitrate ion: N(5)–H(21)···O(8) 2.452, N(7)–H(33)···O(5) 2.256 Å. The four nitrogen atoms of the macrocycle are coplanar with a mean deviation 0.3337 Å and the Co atom departed from this plane −0.974 Å. Two oxygen atoms have similar distances separated from this plane −2.556 Å. The bond lengths between Co and O(2), O(4) are 2.087(3) and 2.089(3) Å. Co–N distances exist in the range 2.169(3)–2.222(3) Å, which are longer than

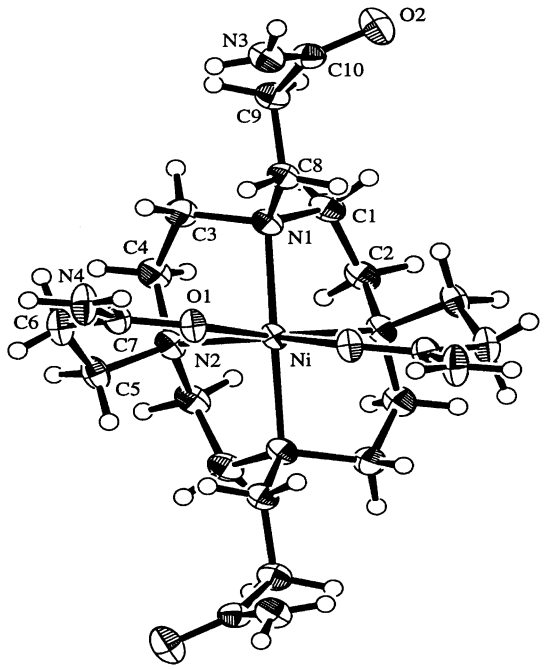


Fig. 2. The ORTEP drawing of the dication part in complex **2** with ellipsoid 40%.

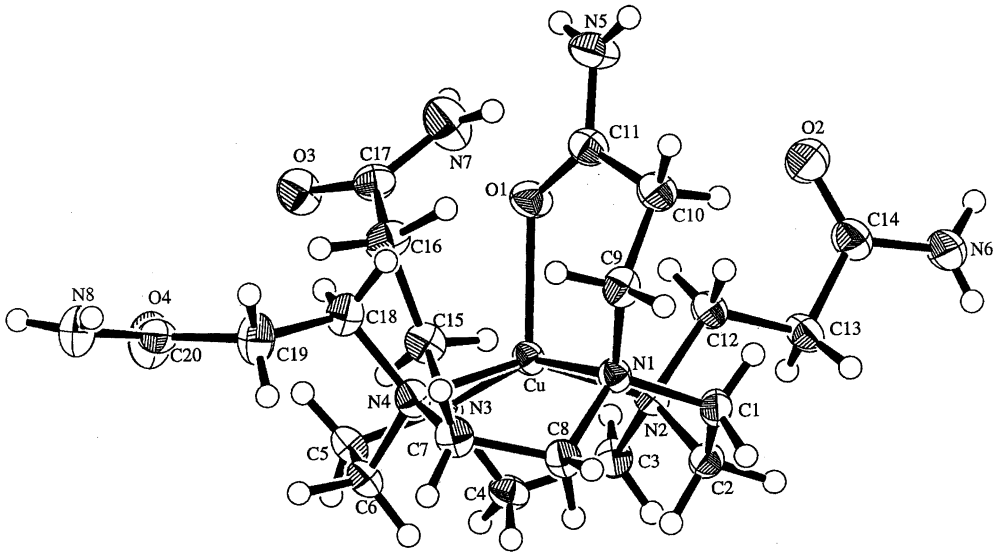


Fig. 3. The ORTEP drawing of the cation part in complex **3** from side view with ellipsoid 50%.

Table 1
The crystallographic data of complexes **2** and **3**

Molecular formula	$C_{20}H_{44}N_{10}O_{12}Co$ (**1**)	$C_{20}H_{44}N_{10}O_{12}Ni$ (**2**)	$C_{20}H_{42}N_{10}O_{11}Cu$ (**3**)
Formula weight	675.56	675.33	662.16
Crystal color; habit	red; prismatic	green; prismatic	blue; prismatic
Crystal dimensions (mm)	$0.20\times0.20\times0.30$	$0.20\times0.20\times0.30$	$0.20\times0.20\times0.30$
Crystal system	triclinic	monoclinic	monoclinic
Lattice type	primitive	primitive	primitive
Lattice parameters			
a (Å)	10.531(2)	13.070(2)	12.618(2)
b (Å)	3.689(3)	16.380(2)	16.108(7)
c (Å)	10.529(3)	13.771(1)	14.411(4)
α (°)	93.93(2)		
β (°)	102.82(2)	96.45(1)	104.07(2)
γ (°)	94.07(2)		
V (Å^3)	1470.7(5)	2929.4(1)	2841(1)
Space group	$P\bar{1}$ ($\#2$)	$C2/c$ ($\#15$)	$P2_1/n$ ($\#14$)
Z	2	4	4
D_{calc} (g cm^{-3})	1.525	1.531	1.548
$F(3499)$	714	1432	1396
θ Max. (°)	27	27	27
μ (cm^{-1})	6.60	7.39	8.43
Function minimized	$\Sigma\varpi(\lvert F_o\rvert-\lvert F_c\rvert)^2$	$\Sigma\varpi(\lvert F_o\rvert-\lvert F_c\rvert)^2$	$\Sigma\varpi(\lvert F_o\rvert-\lvert F_c\rvert)^2$
p-factor	0.03	0.03	0.03
No. of reflections measured	total: 4336; unique 4025 ($R_{int}=0.029$)	total: 3512; unique 3361 ($R_{int}=0.023$)	total: 4380; unique 4132 ($R_{int}=0.054$)
No. of observations	3233 ($I>2.5\sigma(I)$)	2726 ($I>3\sigma(I)$)	3174 ($I>2.5\sigma(I)$)
No. of variables	389	196	380
Residuals: R; R_w	0.045; 0.057	0.044; 0.059	0.037; 0.048
Goodness-of-fit indicator	2.28	2.13	1.76
Maximum shift of final cycle	0.00	0.04	0.00
Peak, hole in final difference map (e Å^{-3})	0.60; −0.54	0.67; −0.62	0.32; −0.52

Co–O bond lengths. This result is consistent with our former reports.

The crystal of complex **2** has high symmetry with a C_{2v} symmetric operation. The central Ni atom is coordinated to four amine nitrogen atoms of macrocyclic skeleton and two acylate oxygen atoms of pendant amide groups. The polyhedron of the central atom can be described as a pseudo-octahedron. Two water molecules crystallized in the cell lattice. The bond length between the central nickel and the coordinated

oxygen is Ni–O(1) 2.089(1) Å, and the distances of Ni–N(1) and Ni–O(2) are 2.192(2), 2.114(2) Å, respectively. Because the acylate oxygen atoms coordinate with the nickel atom, the bond length of C(7)–N(4) 1.306(3) Å is shorter than the other bond length C(3)–N(10) 1.329(4) Å existing in non-coordinating pendant groups. This decrease in bond length is due to the unpaired electrons of nitrogen atoms at amide residues transferring to the C–N single bond. And this delocalization of electronic density made the C=O double bonds lengthen [from C(10)–O(2) 1.234(3) to C(7)–O(1) 1.255(3) Å]. The ligand serves as a N_4O_2 donor for the nickel atom. Two non-coordinating pendant amide groups may adopt a clockwise or anticlockwise fashion for a given arrangement. O(1), Ni and N(2) atoms are nearly in one line with an angle of 161.00(8)°.

Table 2
Selected bond distances (Å) and bonds angles (°) for complex **1**

Co–O(2)	2.087(3)	N(3)–C(4)	1.490(5)
Co–O(4)	2.089(3)	N(3)–C(5)	1.498(5)
Co–N(1)	2.214(3)	N(3)–C(15)	1.492(5)
Co–N(2)	2.169(3)	N(4)–C(6)	1.492(5)
Co–N(3)	2.222(3)	N(4)–C(7)	1.488(5)
Co–N(4)	2.169(3)	N(4)–C(18)	1.496(5)
O(1)–C(11)	1.226(5)	N(5)–C(11)	1.325(5)
O(2)–C(14)	1.260(5)	N(6)–C(14)	1.300(5)
O(3)–C(17)	1.227(5)	N(7)–C(17)	1.321(5)
O(4)–C(20)	1.250(5)	N(8)–C(20)	1.310(5)
O(2)–Co–O(4)	78.2(1)	C(2)–N(2)–C(3)	110.5(3)
O(2)–Co–N(1)	110.1(1)	C(2)–N(2)–C(12)	107.4(3)
O(2)–Co–N(2)	87.5(1)	C(3)–N(2)–C(12)	111.2(3)
O(2)–Co–N(3)	94.3(1)	Co–N(3)–C(4)	104.8(2)
O(2)–Co–N(4)	161.7(1)	Co–N(3)–C(5)	109.5(2)
O(4)–Co–N(1)	94.1(1)	Co–N(3)–C(15)	108.6(2)
O(4)–Co–N(2)	161.7(1)	N(1)–Co–N(3)	148.8(1)
O(4)–Co–N(3)	110.2(1)	Co–N(4)–C(7)	109.4(2)
O(4)–Co–N(4)	87.4(1)	N(2)–Co–N(3)	81.9(1)
N(1)–Co–N(2)	80.1(1)	Co–N(4)–C(6)	105.4(2)
N(1)–Co–N(4)	81.9(1)	Co–N(4)–C(18)	112.8(2)
N(2)–Co–N(4)	108.7(1)	N(3)–Co–N(4)	80.1(1)
Co–O(2)–C(14)	135.6(3)	Co–O(4)–C(20)	135.6(3)
Co–N(1)–C(1)	110.0(2)	Co–N(1)–C(8)	105.2(2)
Co–N(1)–C(9)	109.1(2)	Co–N(2)–C(2)	105.4(2)
Co–N(2)–C(3)	109.3(2)	Co–N(2)–C(12)	112.8(2)

Table 3
Selected bond distances (Å) and bonds angles (°) for complex **2**

Ni–O(1)	2.089(2)	N(1)–C(8)	1.487(3)
Ni–N(1)	2.191(2)	N(2)–C(4)	1.490(4)
Ni–N(2)	2.114(2)	N(2)–C(5)	1.499(3)
O(1)–C(7)	1.255(3)	N(3)–C(10)	1.330(4)
O(2)–C(10)	1.234(3)	C(1)–C(2)	1.520(4)
O(3)–N(5)	1.203(5)	C(3)–C(4)	1.518(4)
O(4)–N(5)	1.276(6)	C(5)–C(6)	1.510(4)
O(5)–N(5)	1.134(5)	C(6)–C(7)	1.505(4)
N(1)–C(1)	1.495(3)	C(8)–C(9)	1.532(4)
N(1)–C(3)	1.489(3)	C(9)–C(10)	1.505(4)
O(1)–Ni–O(1)	76.2(1)	Ni–N(2)–C(4)	109.2(2)
O(1)–Ni–N(1)	93.26(8)	Ni–N(2)–C(5)	113.1(1)
O(1)–Ni–N(1)	107.49(8)	C(2)–N(2)–C(4)	111.5(2)
O(1)–Ni–N(2)	87.95(7)	C(2)–N(2)–C(5)	106.3(2)
O(1)–Ni–N(2)	161.00(8)	C(4)–N(2)–C(5)	111.5(2)
O(1)–Ni–N(1)	107.49(8)	O(3)–N(5)–O(4)	114.3(5)
O(1)–Ni–N(1)	93.26(8)	O(3)–N(5)–O(5)	125.5(7)
O(1)–Ni–N(2)	161.00(8)	O(4)–N(5)–O(5)	120.2(7)
O(1)–Ni–N(2)	87.95(7)	N(1)–C(1)–C(2)	112.7(2)
N(1)–Ni–N(1)	153.7(1)	N(2)–C(2)–C(1)	111.2(2)
N(1)–Ni–N(2)	83.49(8)	N(1)–C(3)–C(4)	111.4(2)
N(1)–Ni–N(2)	81.42(8)	N(2)–C(4)–C(3)	111.1(2)
N(1)–Ni–N(2)	81.42(8)	N(2)–C(5)–C(6)	117.0(2)
N(1)–Ni–N(2)	83.49(8)	C(5)–C(6)–C(7)	113.6(2)
N(2)–Ni–N(2)	109.4(1)	Ni–O(1)–C(7)	135.0(2)
Ni–N(1)–C(3)	104.0(1)	Ni–N(1)–C(1)	108.7(2)
Ni–N(1)–C(8)	111.9(2)	Ni–N(2)–C(2)	105.1(2)

Table 4
Selected bond distances (Å) and bonds angles (°) for complex **3**

Cu–O(1)	2.137(3)	N(3)–C(5)	1.511(5)
Cu–N(1)	2.017(3)	N(3)–C(15)	1.500(5)
Cu–N(2)	2.072(3)	N(4)–C(6)	1.492(5)
Cu–N(3)	2.043(3)	N(4)–C(7)	1.501(5)
Cu–N(4)	2.054(3)	N(4)–C(18)	1.482(5)
O(1)–C(11)	1.254(4)	N(5)–C(11)	1.312(5)
O(2)–C(14)	1.218(5)	N(6)–C(14)	1.331(5)
O(3)–C(17)	1.221(4)	N(7)–C(17)	1.307(5)
O(4)–C(20)	1.213(4)	N(8)–C(20)	1.333(5)
O(1)–Cu–N(1)	92.6(1)	C(4)–N(3)–C(5)	110.3(3)
O(1)–Cu–N(2)	107.2(1)	C(4)–N(3)–C(15)	108.8(3)
O(1)–Cu–N(3)	113.0(1)	C(5)–N(3)–C(15)	109.5(3)
O(1)–Cu–N(4)	102.9(1)	Cu–N(4)–C(6)	101.9(2)
N(1)–Cu–N(2)	86.9(1)	Cu–N(4)–C(7)	107.9(2)
N(1)–Cu–N(3)	154.4(1)	Cu–N(4)–C(18)	112.2(2)
N(1)–Cu–N(4)	86.1(1)	C(6)–N(4)–C(7)	111.3(3)
N(2)–Cu–N(3)	86.2(1)	C(6)–N(4)–C(18)	112.5(3)
N(2)–Cu–N(4)	149.4(1)	C(7)–N(4)–C(18)	110.6(3)
N(3)–Cu–N(4)	87.4(1)	O(5)–N(9)–O(6)	119.2(4)
Cu–O(1)–C(11)	127.5(2)	Cu–N(1)–C(1)	108.1(2)
Cu–N(1)–C(8)	101.9(2)	Cu–N(1)–C(9)	115.5(2)
Cu–N(2)–C(2)	101.1(2)	Cu–N(2)–C(3)	106.8(2)
Cu–N(2)–C(12)	112.0(2)	Cu–N(3)–C(4)	99.5(2)
Cu–N(3)–C(5)	106.6(2)	Cu–N(3)–C(15)	121.5(2)
Cu–N(4)–C(7)	107.9(2)	Cu–N(4)–C(5)	101.9(2)
Cu–N(4)–C(18)	112.2(2)		

The blue crystal of complex **3** consists of the dication $[Cu(L)]^{2+}$, two non-coordinated nitrates and a water molecule of crystallization. Fig. 3 shows the cation together with the atom-labeling scheme. The geometry about the copper atom is tetragonal pyramid. For the smaller ion radii of the copper atom, only one acylate oxygen together with four amine nitrogen atoms coordinate to the central metal atom. The bond length of the coordinated acylate oxygen to the copper, Cu–O(1) 2.137(3) Å, is significantly longer than the Cu–N(amine) bonds, average 2.0465(3) Å. This is different from the nickel complex, the bond length of Ni–O(1) is shorter than the Ni–N(amine) bonds, average 2.153(2) Å. Four amine nitrogen atoms are copla-

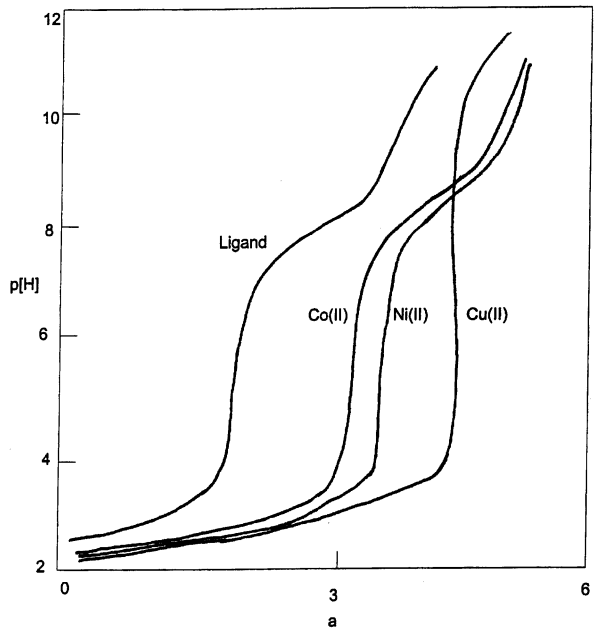


Fig. 4. Potentiometric equilibrium curves for ligand and metal complexes.

nar with a mean deviation of 0.0477 Å. Co and Ni atoms are prone to coordinate to the oxygen atom, and the Cu atom is more likely to form a coordination bond with the nitrogen atom. This similar bond relationship can be observed in the analogous complexes with the ligand 1,4,7,10-tetrakis(2-cycanoethyl)-1,4,7,10-tetraazacyclododecane [22]. The copper atom and O(1) are at the same side of this plane with distances of 0.496 and 2.579 Å, respectively. The angles between the oxygen, central copper atom and nitrogen atoms are in the range 92.6 ~ 113.0°, which forms a slightly distorted tetragonal pyramid coordination environment.

2.3. Potentiometric titrations

The potentiometric equilibrium curve of this ligand as shown in Fig. 4, is found to have two inflections at $a = 2$ and $a = 3$ (where $a =$ moles of base per mole of ligand). From $a = 0$ to $a = 2$, and $a = 3$ to $a = 4$, there are two buffer regions. In the first buffer region, two substituted ammonium ions were neutralized. Between the first and second inflection, the third substituted ammonium ion was neutralized. Fig. 5 gives the species distribution plot of ligand, at pH < 2, $[H_3L]^{3+}$ reaches the highest concentration (79.7%). The distribution of $[H_2L]^{2+}$ arrives at maximum value of 99.9% at pH 5.7. In more basic conditions, pH 11.4, the ligand exits in free base type. The probable processes of stepwise deprotonation constants are listed in Table 5. Compared with the famous ligand, Cyclen, the first deprotonated constant is lower than 0.29 logarithm units, which resulted from the electron-withdrawing pendant groups existing at nitrogen atoms of this ligand [24]. Using the direct titration method, the stability constants of three complexes were determined. Co and Ni complexes have a similar titration curve: both of them have two inflections of $a = 3$ and $a = 4$. [ML](M = Co, Ni) form and are stable at pH 2 ~ 6.5, and $\log K_{[ML]}$(M = Co, Ni) = 17.11 and 16.83, respectively. The hydroxo species $[Co(OH)L]^{+}$ form from pH 7, then the $[Co(OH)_2L]$ dominated. However, the stability constants of the Cu complex are lower than these by about two logarithm units ($\log K_{[CuL]} = 15.00$) and the Cu complex had one inflection at $a = 4$; [CuL] reaches maximum concentration at pH 3.9. This species is stable in the range 3 ~ 11.5, and then a hydroxy species $[Cu(OH)L]^{+}$ forms. Fig. 6 gives the species distribution plot of a Co complex as an example.

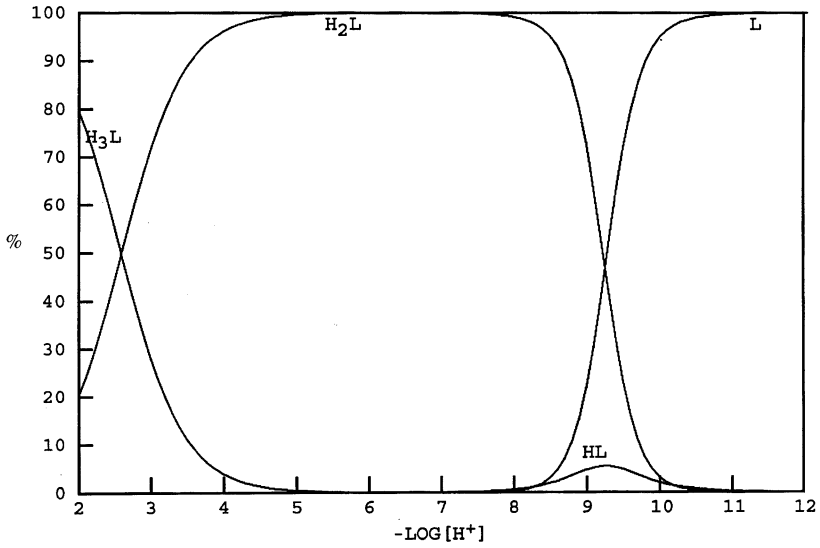


Fig. 5. Species distribution diagram for the ligand.

Table 5
Logarithms of deprotonation constants of ligand and stability constants of complexes ($\mu = 0.100$ M KCl, $T = 25$°C, under argon)

Equilibrium quotient, K	log K				
	L	Cyclen	Co(II)	Ni(II)	Cu(II)
[HL]/[L][H]	10.31	10.6			
[H_2L]/[HL][H]	6.83	9.6			
[H_3L]/[H_2L][H]	1.34	1.5			
[ML]/[M][L]			17.11	16.8	15.00
[ML(OH)][H]/[ML]			−7.67	−6.74	−12.3
[$ML(OH)_2$][H]/[ML(OH)]			−6.59	−5.25	

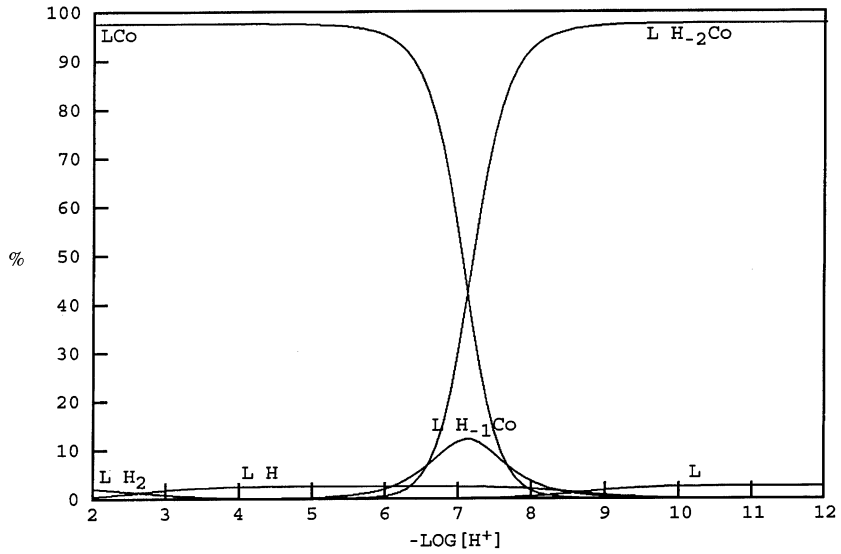


Fig. 6. Species distribution diagram for the Co complex.

2.4. Cleavage of pBR 322 DNA analyses

For the cobalt complex, DNA cleavage was analyzed by monitoring the conversion of supercoiled DNA (Form I) to the nicked circular molecules (Form II) and linear DNA (Form III). The tests were performed under aerobic conditions with H_2O_2 as a reducing agent. No cleavage occurs in the absence of H_2O_2 or with uncomplexed Co atoms (not shown). As shown in Figs. 7 and 8, complex **1** can effectively cleave duplex DNA. Incubation of the pBR 322 DNA at 37°C for 2 h with 6.25 μM of complex **1** causes the complete conversion of Form I to Form II. It is clear that the degradation of pBR 322 DNA is highly dependent on the concentration of complex **1** used. As complex **1** concentration increases the probability of double strand scissions is enhanced once the DNA has undergone a single strand break. This is manifested in the gel by the appearance of linear DNA molecules (Form III) from 6.25 μM. The percentage of linear DNA molecules observed with Co complex increases with the increase of the concentration as shown in Fig. 7. The percentage of Form III demonstrates a linear correlation with

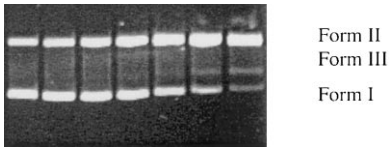


Fig. 7. The cleavage result of cobalt complex **1** in the presence of H_2O_2. Line 1: DNA + 1/100 DMSO + H_2O_2; line 2: DNA + H_2O_2 + complex **1** 0.195 μmol l^{-1}; line 3: DNA + H_2O_2 + complex **1** 0.39 μmol l^{-1}; line 4: DNA + H_2O_2 + complex **1** 0.78 μmol l^{-1}; line 5: DNA + H_2O_2 + complex **1** 1.56 μmol l^{-1}; line 6: DNA + H_2O_2 + complex **1** 3.125 μmol l^{-1}; line 7: DNA + H_2O_2 + complex **1** 6.25 μmol l^{-1}.

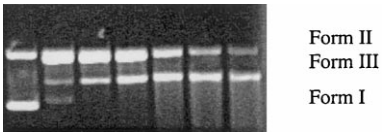


Fig. 8. The cleavage result of cobalt complex **1** in the presence of H_2O_2. Line 1: DNA + 1/100 DMSO; line 2: DNA + H_2O_2 + complex **1** 6.25 μmol l^{-1}; line 3: DNA + H_2O_2 + complex **1** 12.5 μmol l^{-1}; line 4: DNA + H_2O_2 + complex **1** 25 μmol l^{-1}; line 5: DNA + H_2O_2 + complex **1** 50 μmol l^{-1}; line 6: DNA + H_2O_2 + complex **1** 100 μmol l^{-1}; line 7: DNA + H_2O_2 + complex **1** 200 μmol l^{-1}.

Table 6
Cleavage percentage dependence on the concentration of complex **1** (μmol l^{-1})

Line	1	2	3	4	5	6	7
Concentration	1% DMSO	0.195	0.39	0.78	1.56	3.125	6.25
Form II	41.28	46.18	48.80	53.34	64.55	78.81	93.38
Form III						3.46	4.49
Form I	58.72	53.82	51.20	45.66	35.45	17.73	2.13

Table 7
Cleavage percentage dependence on the concentration of complex **1** (μmol l^{-1})

Line	1	2	3	4	5	6	7
Concentration	1% DMSO	6.25	12.5	25	50	100	200
Form II	44.83	91.76	78.41	62.75	40.95	23.12	8.67
Form III		8.14	21.09	37.25	59.05	76.88	91.33
Form I	55.17	0.10					

concentration. The analytical results are listed in Table 6. At the same time, when the concentration of complex **1** increased from 6.25 to 200 μM, the supercoiled DNA could be completely cleaved to form linear DNA as shown in Fig. 8. The cleavage percentages and respective concentrations are listed in Table 7. From the above results, we therefore conclude that the activation of the cobalt complex leads mainly to single strand cleavage of duplex DNA in lower concentration (< 6.25 μM). When the concentration of cobalt complex increases, the linear DNA appears, which exhibits the double strand cleaving ability of this complex. This phenomenon is first reported in comparison with famous DNA cleaving agents, such as Cu–phen or Co–salen complexes, which only showed single strand cleaving ability. In conclusion, complex **1** has the promising possibility to be developed into a chemical nuclease if the detailed mechanism can be clearly elucidated in further experiments.

The possible mechanism of this cleavage may be due to the Fenton type chemistry, which involves the release of diffusible hydroxyl radical or molecular oxygen or other active intermediates. This conclusion will be supported by further experiments in which the degradation products should be detected. When Bhattacharya and Mandal [25] treated plasmid pTZ 19R with Co–salen complex, they thought that in the presence of co-reductant, DTT, Co(II) complex could form an air-stable adduct: Co(II)–complex–O_2, which can induce efficient DNA damage under physiological conditions. They also concluded that the co-oxidant induced product [Co^{III}–complex] lacked the O_2 binding ability and failed to induce DNA nicking. This is consistent with Bailly's results [26]. Bailly et al. showed that the Co-2,9-bis(2-hydroxyphenyl)-1,10-phenanthroline complex, in the presence of MPA as reductant, can cleave pUC12 DNA to form nicked or linear DNA at different concentrations. In this case, we performed electron paramagnetic resonance (EPR) measurements to detect the production of hydroxyl radicals or oxygen molecules by means of the spin-trapping technique (using DMPO as trapping agent, DMPO = 5,5′-dimethylpyrroline *N*-oxide). The spin-trapping experiment showed that the cleavage occurred possibly via an OH radical mechanism. From Fig. 9, the EPR spectrum of the Co complex exhibited four hyperfine patterns with the parameter $g = 2.005$ in DMSO solution with a concentration of 5 mM, which is consistent with results observed in Co–BLM [27]. Because of the existence of water molecules, both in Co complex and H_2O_2 solution, the DMPO–OH spin adduct showed the typical four-line spectrum. Water appears to exert a leveling effect in the sense that only hydroxyl radicals could be detected in the aqueous solutions.

The other three complexes did not show similar cleaving ability under similar conditions.

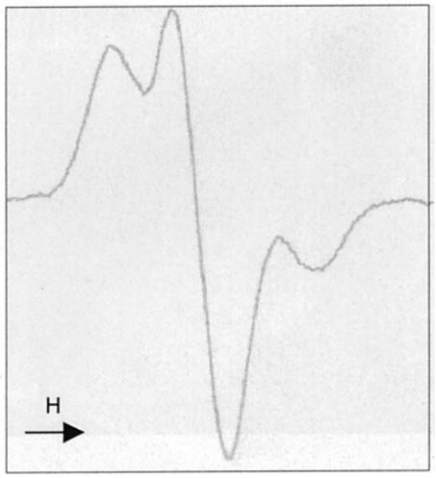


Fig. 9. EPR spectrum.

3. Experimental

The macrocyclic amine, Cyclen, was synthesized according to the method described by Richman and Atkins [28]. The ligand was prepared as reported [12]. All other chemicals were obtained from commercial sources and used as received.

3.1. Preparation of ligand

Cyclen (3 mmol, 500 mg) and acrylamide (14 mmol, 1.0 g) were dissolved in CH_3OH (5 ml), the mixture reacted under nitrogen at 60°C for 48 h. To the obtained solution ether was added until the separation of oily substances. After standing for one more hour, white crystals were deposited. The crystals were filtered and washed with CH_3Cl (20 ml) and dried over P_2O_5 in vacuum.

Yield: 1.1 g, 80.4%. m.p. 175°C. (Found: C, 50.65; H, 8.65; N. 23.76; *Anal*. Calc. for $C_{20}H_{40}N_8O_4$: C, 50.61; H, 8.92; N, 23.61%). ^{1}H NMR (300 Hz, D_2O): δ 2.4–2.6, t, 8H (N–CH_2); δ 2.6–2.8, m, 16H (CH_2 of macrocycle); δ 2.8–3.0, q, 8H (–CH_2–C=O). IR (KBr pellet): 3379s, 3155s, 2426w, 1672s, 1442s, 1358s, 1086m, 725s, 557m, 461m.

3.2. Preparation of complexes

3.2.1. $Co(NO_3)_2C_{20}H_{40}N_8O_4{\cdot}2H_2O$ (1)

To $Co(NO_3)_2{\cdot}6H_2O$ (0.5 mmol, 145 mg) in EtOH (15 ml) was added L (0.5 mmol, 228 mg), the reaction mixture was stirred at room temperature overnight. Red precipitate formed quickly. After filtration, the solids were washed with ether and dried with P_2O_5 in vacuum.

Yield: 136 mg, 40.3%. m.p. 186°C.(dec.) (Found: C, 35.38; H, 6.61; N, 20.67; *Anal*. Calc. for $Co(NO_3)_2C_{20}H_{40}N_8O_4{\cdot}2H_2O$: C, 35.56; H, 6.56; N, 20.73%). IR (KBr pellet): 3411s, 3180m, 2426w, 1676s, 1620s, 1385s, 1074m, 567m.

3.2.2. $Ni(NO_3)_2C_{20}H_{40}N_8O_4{\cdot}2H_2O$ (2)

To $Ni(NO_3)_2{\cdot}6H_2O$(0.5 mmol, 146 mg) in MeOH (20 ml) was added L (0.5 mmol, 228 mg), the reaction mixture was stirred at room temperature overnight. The solution turned green and clear, the solvent was evaporated under vacuum. The green solids collected were washed with ether repeatedly and dried with P_2O_5 in vacuum. The crystal suitable for X-ray diffraction was obtained from the slow diffusion of ether into the DMF solution of complex.

Yield: 312 mg, 95.5%. m.p. 205°C (dec.) (Found: C, 36.61; H, 6.37; N, 21.31; *Anal*. Calc. for $Ni(NO_3)_2C_{20}H_{40}N_8O_4{\cdot}2H_2O$: C, 36.54; H, 6.44; N, 20.31%). IR (KBr pellet): 3408s, 3180m, 2426w, 1676s, 1620s, 1385s, 1078m, 579m. FAB-MS: m/z 577 [$M^+ - NO_3$], 515 [$M^+ - 2NO_3$], 443, 227.

3.2.3. $Cu(NO_3)_2C_{20}H_{40}N_8O_4{\cdot}H_2O$ (3)

To $Cu(NO_3)_2{\cdot}3H_2O$ (0.5 mmol, 121 mg) in H_2O (20 ml) was added L (0.5 mmol, 228 mg), the reaction mixture was stirred at room temperature overnight. The solution was blue and clear, the solvent was evaporated under vacuum. The blue solids were collected, washed with ether repeatedly and dried with P_2O_5 in vacuum. The crystal suitable for X-ray diffraction was obtained from the slow diffusion of ether into the DMF solution of complex.

Yield: 225 mg, 68%. m.p. 225°C (dec.) (Found: C, 36.37; H, 6.36; N, 21.15; *Anal*. Calc. for $Cu(NO_3)_2C_{20}H_{40}N_8O_4{\cdot}H_2O$: C, 36.28; H, 6.39; N, 20.15%). IR (KBr pellet): 3377s, 3199s, 2426w, 1666s, 1385s, 1072s, 557m.

3.2.4. $Zn(NO_3)_2C_{20}H_{40}N_8O_4{\cdot}H_2O$ (4)

To $Zn(NO_3)_2{\cdot}6H_2O$ (0.5 mmol, 148 mg) in EtOH (20 ml) was added L (0.5 mmol, 228 mg), white precipitate formed quickly. The reaction mixture was stirred at room temperature overnight. After filtration, the solids were washed with ether and dried with P_2O_5 in vacuum.

Yield: 234 mg, 71.5%. m.p. 234°C (dec.) (Found: C, 36.64; H, 6.34; N, 21.28; *Anal*. Calc. for $Zn(NO_3)_2C_{20}H_{40}N_8O_4{\cdot}H_2O$: C, 36.68; H, 6.31; N, 20.38%). IR (KBr pellet): 3348s, 3160s, 2426w, 1670s, 1620s, 1385s, 1082m, 579m, 463m. EI MS: m/z 503, 429, 369, 357, 295.

3.3. Crystallographic

Red–green–blue prismatic crystals of $C_{20}H_{44}N_{10}O_{12}Co$ (**1**) $C_{20}H_{44}N_{10}O_{12}Ni$ (**2**) and $C_{20}H_{42}N_{10}O_{11}Cu$ (**3**) having approximate dimensions of $0.20 \times 0.20 \times 0.30$ mm were mounted on a glass filter. All measurements were made on a Rigaku AFC 7R automated four-circle diffractometer with graphite-monochromated Mo Kα radiation ($\lambda = 0.71069$ Å) and a 12 kW rotating anode generator. The cell parameters were determined by 25 reflections in the 2θ range $18.77° < 2\theta < 21.55°$ for **1**, $16.12 < 2\theta < 25.78°$ for **2**, $13.56 < 2\theta < 21.48°$ for **3**. For the intensity data collection, the φ–2θ scan mode was used to a maximum 2θ value of 50.0° for **1**, 55.0° for **2** and 50.0° for **3** at a scan rate of 16° min^{-1}. The weak reflections ($I < 13\sigma(I)$) were rescanned (maximum of four scans) and the counts were accumulated to ensure good counting statistics. Stationary background counts were recorded on each side of the reflection. The ratio of peak counting time to background counting time was 2:1. The diameter of the incident beam collimator was 1.0 mm, the crystal to detector distance was 235 mm, and the computer-controlled detector aperture was set to 9.0×13.0 mm (horizontal × vertical). The intensities of three respective reflections were measured after every 200 reflections. Over the course of data collection, the standards decreased or increased by

−0.9% for **1**, 0.1% for **2** and 0.0% for **3**. A linear correction factor was applied to the data to account for this phenomenon. The linear absorption coefficient, μ, for Mo Kα radiation was 6.60 cm^{-1} for **1**, 7.4 cm^{-1} for **2** and 8.4 cm^{-1} for **3**. An empirical absorption correction based on azimuthal scans of several reflections was applied which resulted in transmission factors ranging from 0.93 to 1.00 for **1** and **2**, using the program DIFABS, which resulted in transmission factors ranging from 0.88 to 1.15 for **3**. The data were corrected for Lorentz and polarization effects. Pertinent crystallographic parameters for **1**, **2** and **3** are given in Table 1.

The structure was solved by heavy atom Patterson and expanded using Fourier techniques [29–31]. The non-hydrogen atoms were refined anisotropically [32]. Hydrogen atoms were included but not refined [33]. Refinements were carried out by the full-matrix least-squares method, where the function minimized is $\Sigma w(|F_o| - |F_c|)^2$ with $w = 1/\sigma(F_o)$.

Neutral atom scattering factors were taken from Cromer and Waber. Anomalous dispersion effects were included in F_{calc}; the values for $\Delta f'$ and $\Delta f''$ were those of Creagh and McAuley. The values for the mass attenuation coefficients are those of Creagh and Hubbel. All calculations were performed using the TEXAN crystallographic software of the Molecular Structure Corporation.

3.4. Potentiometric equilibrium measurements and computation

Stock solutions of Co(II), Ni(II) and Cu(II) nitrate were used for potentiometric experiments, and the concentrations of metal ions were close to 0.02 M in all cases. A carbonate-free KOH solution was prepared from a Dilute-it ampoule and standardized with potassium acid phalate. Reagent grade potassium chloride was used as supporting electrolyte for all the experiments. The potentiometric equilibrium measurements in the absence of and in the presence of metal ions were carried out with a Corning 250 digital pH meter. The ionic strength of the medium was maintained at 0.100 M by the titration of a KCl solution. The potentiometric cell was fitted with glass and calomel electrodes in a water-jacketed reaction vessel maintained at 25.0 ± 0.1°C, and was calibrated with standard aqueous HCl and KOH solution to read −log[H] directly. The measurements were carried out under an atmosphere of Argon gas. The equilibrium constants were determined with the program BEST, the species distribution diagrams were obtained with the programs SPE and SPEPLOT [34].

3.5. Cleavage of pBR 322 DNA

DNA(supercoiled pBR 322) was purchased from Huamei Chemicals. In a typical run, each reaction mixture contained 0.15 μg of supercoiled pBR322 DNA, 5 μl of the tested complexes at the desired concentration in 1% DMSO as solvent, and 5 μl hydrogen peroxide (40 mmol l^{-1}) was added as a co-oxidant reagent. After incubation at 37°C for 2 h, 1 μl of loading buffer (0.25% bromophenol blue, 0.25% xylene cyanol, 30% glycerol in H_2O) was added to each tube and the mixed solution was loaded on 1% agarose gel. The electrophoresis was carried out for 2 h at 50 V in TBE buffer (89 mM Tris–borate, pH 8.3, 1 mmol l^{-1} EDTA). Gels were stained with ethidium bromide (1 μg ml^{-1}) for 30 min prior to being photographed under UV light. Figs. 8 and 9 give the DNA cleavage results of the electrophoresis on agarose gel.

3.6. EPR measurement

The X-band EPR spectra of the metal complex (5 mM in DMSO) were recorded at 77 K using a Bruker ESP-300 spectrometer operating with a 100 kHz magnetic field modulation. For spin-trapping experiments, 3 mM DMPO was added to the metal complex solution at 5 mM.

4. Supplementary material

Atomic coordinates, bond angles, bond distances and thermal parameters assisted to these three complexes have been deposited at the Cambridge Crystallographic Data Center. Data are available on request from The Director, CCDC, 12 Union Road, Cambridge CB2 1EZ, UK (fax: +44-1223-336033; e-mail: deposit@ccdc.cam.ac.uk or www: http://www.ccdc.cam.ac.uk) with CIF deposition codes: 137312, 137554 and 137555.

Acknowledgements

We thank Jie Sun of the Shanghai Institute of Organic Chemistry for helping in the structure determination, and Hauy Keng Loke and Gang Xing for EPR experimental assistance and Dr Paul Lindahl for helpful discussion.

References

[1] (a) A. Shin, Y. Honda, E. Kimura, J. Am. Chem. Soc. 120 (1998) 10018. (b) A. Shin, C. Sngimura, E. Kimura, J. Am. Chem. Soc. 120 (1998) 10094.

[2] E. Kimura, H. Kitamura, T. Koike, M. Shiro, J. Am. Chem. Soc. 119 (1997) 10909.
[3] (a) Y. Inouye, T. Kanamori, T. Yoshida, X.H. Bu, M. Shionoya, T. Koike, E. Kimura, Biol. Pharm. Bull. 17 (1994) 243. (b) Y. Inouye, T. Kanamori, T. Yoshida, T. Koike, M. Shionoya, H. Fujika, E. Kimura, Biol. Pharm. Bull. 17 (1994) 243.
[4] (a) X. Wang, T. Jin, V. Comblin, A. Lopez-Mut, E. Merciny, J.F. Desreux, Inorg. Chem. 31 (1992) 1095. (b) E.T. Clarke, A.E. Martell, Inorg. Chim. Acta 190 (1991) 37. (c) S. Aime, M. Botta, G. Eronondi, Inorg. Chem. 31 (1992) 4291. (d) P.A. Pittet, D. Foüh, V. Tissières, J.C.G. Bünzli, J. Chem. Soc., Dalton Trans. (1997) 895.
[5] (a) R. Delgado, L.C. Siegfried, T.A. Kaden, Helv. Chim. Acta 73 (1990) 140. (b) I. Lazár, D.C. Hrncir, W.D. Kim, G.E. Kiefer, A.D. Sherry, Inorg. Chem. 31 (1992) 4422. (c) J.G. Dingwall, C.D. Champell, E.K. Baylis, J. Chem. Soc., Perkin Trans. 1 (1984) 2845.
[6] J.R. Morrow, K.O.A. Kin, Inorg. Chem. 32 (1993) 3357.
[7] K.L.T. Edwards, N.W. Alcock, D.H. Busch, Acta Crystallogr., Sect. C 54 (1998) 340.
[8] D.Y. Kong, L.H. Meng, L. Song, Y.Y. Xie, Transition Met. Chem. 24 (1999) 553.
[9] (a) D.Y. Kong, C. Qing, L.H. Meng, Y.Y. Xie, Bioorg. Med. Chem. Lett. 9 (1999) 1087. (b) C. Gros, H. Chollet, A.K. Mishra, R. Guilard, Synth. Commun. 26 (1996) 35.
[10] Y. Liu, G.P. Xue, C.T. Wu, S.B. Luo, Chin. J. Chem. 16 (1998) 16.
[11] P. Valente, S.F. Linciln, K.P. Wainwright, Inorg. Chem. 37 (1998) 2846.
[12] J.R. Morrow, S. Amin, C.H. Lake, M.R. Churchill, Inorg. Chem. 32 (1993) 4566.
[13] K.O.A. Chin, J.R. Morrow, C.H. Lake, M.R. Churchill, Inorg. Chem. 33 (1994) 656.
[14] R.S. Dickins, J.A.K. Howard, J.M. Moloney, D. Parkers, R.D. Peacock, G. Siligardi, Chem. Commun. (1997) 1747.
[15] (a) K.O.A. Chin, J.R. Morrow, Inorg. Chem. 33 (1994) 5036. (b) S. Amine, J.R. Morrow, C.H. Lake, M.R. Churchill, Angew Chem., Int. Ed. Engl. 33 (1994) 773.
[16] D. Magda, M. Wright, S. Crofts, A. Lin, J.L. Sessler, J. Am. Chem. Soc. 119 (1997) 6947.
[17] M. Komiyama, J. Inokawa, K. Yoshinari, J. Chem. Soc., Chem. Commun. (1995) 77.
[18] J. Hall, D. Hüsken, U. Pieles, H.E. Moser, R. Haner, Chem. Biol. 1 (1994) 185.
[19] (a) L.L. Chappell, D.A. Voss Jr., W.D. Horrocks Jr., J.R. Morrow, Inorg. Chem. 37 (1998) 3989. (b) B.F. Baker, H. Khalili, N. Wei, J.R. Morrow, J. Am. Chem. Soc. 119 (1997) 8749.
[20] (a) D.S. Sigman, A. Mazumder, D.M. Perrin, Chem. Rev. 93 (1993) 2295. (b) D.S. Sigman, Acc. Chem. Res. 19 (1986) 180.
[21] T. Weyhermüller, K. Weighardt, P. Chauhuri, J. Chem. Soc., Dalton Trans. (1998) 3805.
[22] D.Y. Kong, L.H. Meng, J. Ding, Y.Y. Xie, X.Y. Huang, Polyhedron 19 (2000) 217.
[23] K. Nakamoto, Infrared and Raman Spectra of Inorganic and Coordination Compounds, third ed., Wiley-Interscience, New York, 1978.
[24] (a) M. Kodama, E. Kimura, J. Chem. Soc., Chem. Commun. (1975) 326. (b) M. Kodama, E. Kimura, J. Chem. Soc., Dalton Trans. (1976) 116.
[25] S. Bhattacharya, S.S. Mandal, J. Chem. Soc., Chem. Commun. (1995) 2489.
[26] (a) S. Routier, J.L. Bernier, M.J. Waring, P. Colson, C. Houssier, C. Bailly, J. Org. Chem. 61 (1996) 2326. (b) S. Routier, V. Joanny, A. Zaparucha, H. Vezin, J.P. Catteau, J.L. Bernier, C. Bailly, J. Chem. Soc., Perkin Trans. 2 (1998) 863.
[27] J.D. Tan, S.E. Hudson, S.J. Brown, M.M. Olmstead, P.K. Mascharak, J. Am. Chem. Soc. 114 (1992) 3841.
[28] J.E. Richman, T.J. Atkins, J. Am. Chem. Soc. 96 (1974) 2268.
[29] N. Walker, D. Stuart, DIFABS, Acta Crystallogr., Sect. A 39 (1983) 158.
[30] Fan Hai-Fu, SAPI 91, Structure analysis programs with intelligent control, Rigaku, Tokyo, 1991.
[31] P.T. Beurskens, G. Admirael, G. Beurskens, W.P.S. Bosman, R. Garcia-Granda, O. Gould, J.M.M. Smits, C. Smykalla, DIRDIF 92, The DIRDIF system, Technical report of the crystallography laboratory, University of Nijmegen, The Netherlands, 1992.
[32] D.T. Cromer, J.T. Waber, International Tables for X-Ray Crystallography, vol. 4, Kynoch, Birmingham, UK, 1974, Table 2A.
[33] TEXAN, Crystal Structure of Analysis Package, Molecular Structure Corporation, Houston, TX, 1985–1992.
[34] A.E. Martell, R.J. Motekaitis, The Determination and Use of Stability Constants, second ed., VCH, New York, 1992.

PERGAMON

www.elsevier.nl/locate/poly

Polyhedron 19 (2000) 1539–1543

POLYHEDRON

Organometallic tin(IV) derivatives of the ambidentate *O*-cholesteryl-*O*-phenyl phosphorothioate ligand

Marcela López-Cardoso [a], Patricia García y García [a], Alejandro Rogers-Sakuma [a], Raymundo Cea-Olivares [b,*]

[a] *Centro de Investigaciones Químicas, Universidad Autónoma del Estado de Morelos, Av. Universidad 1001, Cuernavaca 62210, Morelos, Mexico*

[b] *Instituto de Química, Universidad Nacional Autónoma de México, Circuito Exterior, Ciudad Universitaria, Mexico 04510, D.F., Mexico*

Received 1 December 1999; accepted 21 March 2000

Abstract

Organotin(IV) compounds of the potentially ambidentate *O*-cholesteryl-*O*-phenyl phosphorothioate ligand formulated as $Me_3SnOSPR'R''$ (**1**), $Ph_3SnOSPR'R''$ (**2**), $O(CH_2CH_2S)_2Sn(n\text{-Bu})OSPR'R''$ (**3**), $S(CH_2CH_2S)_2Sn(n\text{-Bu})OSPR'R''$ (**4**), ($R' = O$-Ph; $R'' = O$-cholesteryl) were obtained and characterized by elemental analyses, IR, MS and multinuclear NMR (^1H, ^{13}C, ^{31}P and ^{119}Sn) spectroscopy. The spectroscopic data are consistent with bonding of the phosphorothioate ligand through both sulfur and oxygen atoms to the Sn(IV) center. © 2000 Elsevier Science Ltd. All rights reserved.

Keywords: Phosphorothiates; Organotin(IV); Bioactive groups; Cholesteryl

1. Introduction

The coordination chemistry of Tin(IV) derivatives towards phosphorus-based acids continues to receive attention mainly due to the reactivity, interesting structural features and anticancer activity of some organotin(IV) compounds [1,2]. The structural chemistry of such compounds presents a great diversity and is influenced by factors such as the number and nature of organic groups bonded to the tin and phosphorus atoms, as well as the type of donor atom (O, S, Se) [3]. Recently, we have reported the preparation of a new ambidentate phosphorothioate ligand, containing a bioactive group, Na[OSPR′R″], [R = *O*-Ph, R″ = *O*-cholesteryl] [4]. In order to investigate the coordinating ability of this new ligand towards different organotin(IV) entities, the ligand was reacted with the following monochlorotin(IV) compounds: Me_3SnCl, Ph_3SnCl, $O(CH_2CH_2S)_2Sn(n\text{-Bu})Cl$ and $S(CH_2CH_2S)_2Sn(n\text{-Bu})Cl$. The resulting phosphorothioatotin(IV) derivatives (**1**–**4**) were characterized by elemental analyses, as well as IR, MS and multinuclear NMR (^1H, ^{13}C, ^{31}P, ^{119}Sn) spectroscopy.

2. Results and discussion

The organotin(IV)-*O*-cholesteryl-*O*-phenyl phosphorothioate compounds reported here were synthesized by the following reaction route, using stoichiometric ratios in refluxing chloroform. Compounds **1**–**4**, are soluble in common organic solvents and were characterized by elemental analyses (C, H, P) as well as IR, mass and multinuclear NMR (^1H, ^{13}C, ^{31}P, ^{119}Sn) spectroscopy.

$$R_nSnCl + Na[OSPR'R''] \rightarrow R_nSnOSPR'R'' + NaCl$$

[R′ = *O*-Ph, R″ = *O*-cholesteryl]

[$R_n = Me_3$ (**1**), Ph_3 (**2**), $O(CH_2CH_2S)_2(n\text{-Bu})$ (**3**), $S(CH_2CH_2S)_2(n\text{-Bu})$ (**4**)].

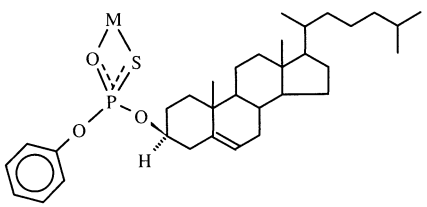
* Corresponding author. Tel.: +52-5-616-2203; fax: +52-5-616-2217.

E-mail address: cea@servidor.unam.mx (R. Cea-Olivares).

0277-5387/00/$ - see front matter © 2000 Elsevier Science Ltd. All rights reserved.
PII: S0277-5387(00)00396-X

Table 1
Infrared data for some derivatives of tin(IV) compounds of **1–4** and related compounds

Compound	ν(P–O)	ν(P=O)	ν(P–S)	ν(P=S)	ν(Sn–S)	ν(Sn–C)	Ref.
$Me_3SnOSPMe_2$	1085s		549s			540s	[7]
$Me_2Sn(OSPPh_2)_2$	948s			646s		576w	[8]
$Ph_3SnOSPPh_2$	1063s		595s				[6]
$Ph_3SnOSPEt_3$	1100s		535m				[6]
$Me_2P(S)OMe$	1038			581			[6]
$Me_2P(O)SMe$		1184	510				[6]
Me_2PSONa	1075vs		562s				[6]
$O(CH_2CH_2S)_2Sn$ (*n*-Bu)OSPR′R″	1113		510		340		this work
$S(CH_2CH_2S)_2Sn$ (*n*-Bu)OSPR′R″	1132		529		310 and 340		this work
$Ph_3SnOSPR'R''$	1025		595			520	this work
$Me_3SnOSPR'R''$	1023		551			580	this work
Na[OSPR′R″]	1028		560				this work



M = -$SnMe_3$,-$SnPh_3$, -Sn(*n*-Bu)$(SCH_2CH_2)_2$X
X = O,S

2.1. Infrared spectra

Infrared spectra were interpreted by comparison with reported spectra of known *O*- and *S*-alkyl esters of monothiophosphinic acids, their sodium salts and other analogous derivatives (Table 1). The new compounds showed strong bands in the regions 1030–1170, 950–970, and 510–570 cm^{-1}, assigned to ν(P)–O–C, νP–O–(C) and ν(P–S), respectively [5]. The absence of bands in the regions 1200–1180 cm^{-1} due to ν(P=O) as well as in 630–580 cm^{-1} for ν(P=S) suggests that the ligand is coordinated to Sn(IV) in **1–4** through the sulfur and oxygen donor atoms. When the phosphorothioate ligand is bonded through both donor atoms it is possible that it displays either a chelating binding mode (type (a)) or a bridge binding mode (type (b)), (Fig. 1). In the present cases of compounds **1–4**, it is not possible to know from IR data if the interaction is of the type (a) or (b).

2.2. Mass spectra

The mass spectra of the four organotin(IV) derivatives (**1–4**) were recorded with FAB positive source. The spectra do not show the molecular ion, but the data are easily related to the proposed structures, with the normal loss of *n*-Bu, the presence of polymeric species, due to the FAB method and fragments arising from the R_nSn entity and the ligand.

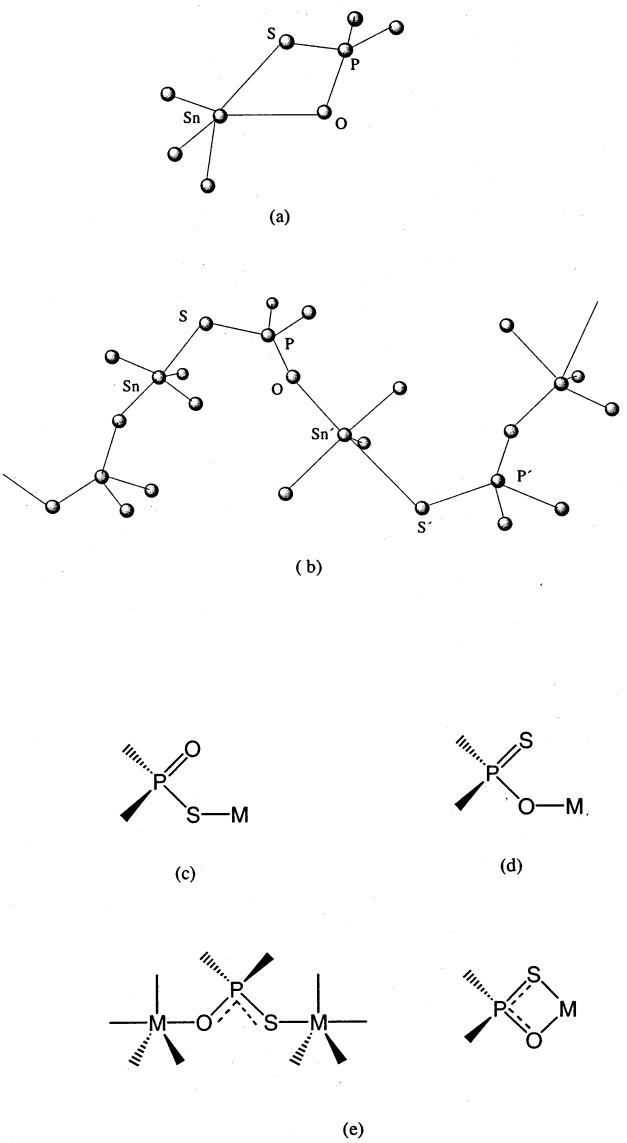


Fig. 1. Binding modes of tin(IV) phosphorothioates.

Table 2(a)
^{1}H NMR data of $Me_3SnOSPR'R''$, $Ph_3SnOSPR'R''$, $O(CH_2CH_2S)_2Sn(n\text{-Bu})OSPR'R''$, $S(CH_2CH_2S)_2Sn(n\text{-Bu})OSPR'R''$ derivatives

Compound	PhO–P	ColO–P	R–Sn
Na[OSPR′R″]	6.96(dd, 1H, POC_6H_5(*p*-H), 8.16, 3.84 Hz), 7.18 (dd, 2H, POC_6H_5(*m*-H), 7.41, 6.8 Hz), 7.26 (dd, 2H, POC_6H_5(*o*-H), 7.41, 4.14 Hz)	0.66 (s, 3H), 0.85 (d, 6H, 6.6 Hz), 0.90 (d, 3H, 6.3 Hz), 0.97 (s, 3H), 1.10–2.61 (m, 28H), 4.26 (m, 1H), 5.26 (d, 1H, 5.22 Hz)	
$Me_3SnOSPR'R''$	7.10 (dd, 1H, POC_6H_5(*p*-H), 8.16, 3.84 Hz), 7.20 (dd, 2H, POC_6H_5(*m*-H), 7.31, 6.8 Hz), 7.31 (dd, 2H, POC_6H_5(*o*-H), 7.41, 4.14 Hz)	0.67 (s, 3H), 0.84 (d, 6H, 6.6 Hz), 0.90 (d, 3H, 6.3 Hz), 1.0 (s, 3H), 1.1–2.6 (m, 28H), 4.38 (m, 1H), 5.9 (d, 1H, 5.3 Hz)	0.622 (s, 9H)
$Ph_3SnOSPR'R''$	7.0 (dd, 1H, POC_6H_5(*p*-H), 8.16, 3.84 Hz), 7.11 (dd, 2H, POC_6H_5(*m*-H), 7.41, 6.8 Hz), 7.20 (dd, 2H, POC_6H_5(*o*-H), 7.0, 3.9 Hz)	0.69 (s, 3H); 0.88 (d, 6H, 6.6 Hz); 0.90 (d, 3H, 6.3 Hz); 0.95 (s, 3H); 1.1–2.6 (m, 28H); 4.20 (m, 1H), 5.25 (dd, 1H, 4.5 Hz, 4.5 Hz)	7.4 (m, 9H), 7.7 (m, 6H)
$O(CH_2CH_2S)_2$-Sn(*n*-Bu)-OSPR′R″	7.1 (dd, 1H, POC_6H_5(*p*-H), 8.16, 3.84 Hz), 7.2 (dd, 2H, POC_6H_5(*m*-H), 7.41 Hz, 6.8 Hz), 7.25 (dd, 2H, POC_6H_5(*o*-H), 7.0, 3.9 Hz)	0.66 (s, 3H); 0.86 (d, 6H, 6.6 Hz); 0.89 (d, 3H, 6.3 Hz); 0.99 (s, 3H); 1.0–2.6 (m, 28H); 4.35 (m, 1H), 5.35 (d, 1H, 5.2 Hz)	3.95 (compl, 2H); 3.58 (compl, 2H); 2.94(compl, 4H); 2.0–1.6 (m, 6H); 0.87 (t, 3H)
$S(CH_2CH_2S)_2$-Sn(*n*-Bu)-OSPR′R″	7.1 (dd, 1H, POC_6H_5(*p*-H), 8.16, 3.84 Hz), 7.25 (dd, 2H, POC_6H_5(*m*-H), 7.41, 6.8 Hz), 7.28 (dd, 2H, POC_6H_5(*o*-H), 7.0, 3.9 Hz)	0.66 (s, 3H); 0.85 (d, 6H, 6.6 Hz); 0.90 (d, 3H, 6.3 Hz); 0.99 (s, 3H); 1.06–2.6 (m, 28H); 4.4 (m, 1H), 5.35 (d, 1H, 5.2 Hz)	3.1 (compl, 4H); 2.95 (compl, 2H); 2.7 (compl, 2H); 2.2–1.6 (compl, 6H); 0.87 (t, 3H)

Table 2(b)
^{13}C NMR data of Na[OSPR′R″], $Me_3SnOSPR'R''$, $Ph_3SnOSPR'R''$, $O(CH_2CH_2S)_2Sn(n\text{-Bu})OSPR'R''$, $S(CH_2CH_2S)_2Sn(n\text{-Bu})OSPR'R''$ [R′ = *O*-Ph, R″ = *O*-cholesteryl]

Compound	PhO–P	ColO–P	R–M
Na[OSPR′R″]	152.0 (C*i*) ($^2J_{pc}$ = 8.25 Hz), 127.5 (C*o*), 120.3 (C*m*), 119.72 (C*p*)	139.5, 121.1, 74.6 ($^2J_{pc}$ = 4.5 Hz), 55.4, 54.7, 48.8, 41.0, 39.4, 39.1, 35.9, 35.2, 34.8, 34.4, 30.6, 28.6, 26.9, 26.6, 23.0, 22.4, 21.6, 21.3, 19.7, 18.1, 17.5, 10.6	
$Me_3SnOSPR'R''$	151.6 (C*i*) ($^2J_{pc}$ = 8.8 Hz), 129.24 (C*o*), 124.4 (C*m*), 122.68 (C*p*)	139.8, 121.0, 78.7 ($^2J_{pc}$ = 4.3 Hz), 56.6, 56.1, 50.0, 42.3, 39.7, 39.5, 37.0, 36.4, 36.1, 35.7, 31.8, 29.6, 28.2, 27.9, 24.2, 23.8, 22.8, 22.5, 21.0, 19.3, 18.7, 11.8	0.533
$Ph_3SnOSPR'R''$	151.4 (C*i*) ($^2J_{pc}$ = 8.6 Hz), 128.4 (C*o*), 124.5 (C*m*), 121.0 (C*p*)	139.5, 122.7, 78.5 ($^2J_{pc}$ = 4.6 Hz), 56.7, 56.1, 50.0, 42.3, 39.5, 39.0, 37.0, 36.8, 35.1, 35.7, 31.8, 29.1, 29.0, 28.0, 24.3, 24.0, 22.8, 22.5, 21.0, 19.1, 18.7, 11.8	138.5 (C*i*), 137.0 (C*o*), 130.5 (C*m*), 129.5 (C*p*)
$O(CH_2CH_2S)_2$-Sn(*n*-Bu)-OSPR′R″	151.7 (C*i*) ($^2J_{pc}$ = 8.9 Hz), 129.2 (C*o*), 122.5 (C*m*), 121.0 (C*p*)	140.1, 122.5, 72.0 ($^2J_{pc}$ = 4.4 Hz), 56.7, 56.2, 50.0, 42.4, 39.8, 39.5, 37.1, 36.5, 36.2, 35.8, 31.9, 26.9, 26.2, 26.0, 24.3, 23.8, 22.8, 22.6, 21.1, 19.4, 18.7, 11.9	71.5 (C4, C6), 28.3 (C3, C7), 27.8 (C9), 27.5 (C10), 27.3 (C11), 13.7 (C12)
$S(CH_2CH_2S)_2$-Sn(*n*-Bu)-OSPR′R″	151.9 (C*i*) ($^2J_{pc}$ = 8.5 Hz), 129.1 (C*o*), 122.4 (C*m*), 121.4 (C*p*)	142.3, 124.2, 78.5 ($^2J_{pc}$ = 4.6 Hz), 56.8, 56.2, 50.1, 42.4, 39.8, 39.5, 36.0, 36.5, 36.0, 35.5, 31.9, 31.0, 24.5, 24.0, 22.8, 22.6, 21.4, 19.4, 18.7, 11.9	28.4 (C3, C7), 28.0 (C9, C4, C6), 26.0 (C10, C11), 13.6 (C12)

2.3. NMR spectra

The ^{1}H and ^{13}C NMR spectra of compounds **1**–**4**, confirmed the identity of the compounds, showing the expected integration and multiplicities. (Table 2(a)). Compounds **1** and **2** presented the corresponding signal sets for the groups attached to Sn, indicating the equivalence of such groups (Table 2(b)), while the stannocanes **3** and **4** showed the complex signals characteristic of these rings [9]. As expected, the ^{13}C NMR signal of the C*i* of *O*-Ph and the C_{base} of *O*-cholesteryl appeared as doublets, due to phosphorus coupling.

The ^{31}P NMR spectra for **1**–**4** correspond to a singlet (Table 3). In a ^{31}P NMR spectroscopy study of a series of di-isopropylthiophosphate derivatives, Glidewell [10] suggested that when the derivative is *S*-bonded (binding mode type (c)) the value of δ ^{31}P is $< +30$ ppm, while for *O*-bonding (binding mode type

Table 3
^{31}P and ^{119}Sn NMR data of Na[OSPR′R″], $Me_3SnOSPR'R''$, $Ph_3SnOSPR'R''$, $O(CH_2CH_2S)_2Sn(n\text{-Bu})OSPR'R''$, $S(CH_2CH_2S)_2Sn(n\text{-Bu})OSPR'R''$ [R′ = *O*-Ph, R″ = *O*-cholesteryl]

Derivative	δ (^{31}P) (ppm)	δ (^{119}Sn) (ppm)
Na[OSPR′R″]	50.16	
$Me_3SnOSPR'R''$	49.45	−146.76
$\varnothing_3SnOSPR'R''$	34.29	−80.87
$O(CH_2CH_2S)_2Sn(n\text{-Bu})OSPR'R''$	51.21	−45.18
$S(CH_2CH_2S)_2Sn(n\text{-Bu})OSPR'R''$	51.91	−50.75

(d)) δ ^{31}P is $> +58$ ppm and if it is both *O*- and *S*-bonded (binding mode type (e)) the value corresponds to $+58 > \delta$ $^{31}P > +30$ (Fig. 1).

Compounds **1**–**4** fall in the range from 34.74 to 51.91 ppm and the bonding through both oxygen and sulfur is suggested for each one of this new organotin compounds. It is interesting to note, that ^{31}P chemical shift of these compounds showed differences compared with complexes of related metal centers; for example some organogermanium [6], organoantimony(V) [11] and organotin(IV) [12] compounds, primary bonded through oxygen, present values for ^{31}P from 40.0 to 80.0 ppm. The ^{119}Sn chemical shifts is influenced by the variation in the coordination number and bond angles at tin, by any dπ–pπ bonding effect and by the presence of electronegative substituents [13–15]. When the tin coordination number increases from four to five or six to seven, the ^{119}Sn signal gradually moves to lower field. Thus, for five-coordinate compounds, δ ^{119}Sn has a value from 0 to -200, six-coordinated δ ^{119}Sn from -125 to -365 and seven-coordinated δ ^{119}Sn from -400 to -700 ppm. The δ ^{119}Sn of compounds **1**–**4**, fall in the range from 0 to -200 ppm (Table 3) and it is suggested that both the sulfur and the oxygen atom participate in the bonding to Sn. It is interesting to note that anisobidentate behavior is present in related organotin(IV) derivatives such as dialkyltin(IV) bis(dialkyldithiophosphates) [13] or diorganotin(IV) diphenylphosphinothioates [8] and these compounds have a ^{119}Sn NMR chemical shift close to those of ours. The NMR data suggest that **1**–**4** are penta-coordinated; however, the situation is more complex in the stannocane derivatives **3** and **4**, where the Sn–O or Sn–S intramolecular interaction is able to increase the coordination number to six. However, such interaction is of the secondary type and possibly is not very strong in solution.

In conclusion, data from both the ν(P–O), ν(P–S) infrared bands and the ^{31}P chemical shifts, indicate that the ligand in these new compounds is most probably bonded in an ambidentate fashion through oxygen and sulfur atoms and the ^{119}Sn NMR data point to the presence of five-coordinated tin species in solution.

3. Materials and methods

All reagents and solvents were of commercial grade and the starting material. $O(CH_2CH_2S)_2Sn(n\text{-Bu})Cl$ [9], $S(CH_2CH_2S)_2Sn(n\text{-Bu})Cl$ [9] and Na[OSPR′R″][4], were prepared by literature methods. Elemental analyses (C, H, P) were performed by Galbraith Laboratories, Inc. (Knoxville, TN). IR spectra (4000–200 cm^{-1}) were recorded on KBr discs using a Perkin–Elmer 282B Spectrophotometer; FAB(+) mass spectra using a JEOL SX-102A instrument. ^1H, ^{13}C, ^{31}P and ^{119}Sn NMR spectra were obtained at room temperature in $CDCl_3$ solution using a Varian VXR-300S spectrometer operating at 300, 75.4, 121.4 and 111.85 MHz, respectively. TMS, H_3PO_4 85% and Me_4Sn 33% were used as external standards.

*3.1. Preparation of $Me_3SnOSPR'R''$ (**1**), $Ph_3SnOSPR'R''$ (**2**), $O(CH_2CH_2S)_2Sn(n\text{-Bu})OSPR'R''$ (**3**) and $S(CH_2CH_2S)_2Sn(n\text{-Bu})OSPR'R''$ (**4**)*

To a chloroform solution of sodium *O*-cholesteryl-*O*-phenyl-phosphorothioate Na[OSPR′R″] (0.25 g, 0.43 mM), was added a stoichiometric solution of the corresponding Me_3SnCl, Ph_3SnCl, $O(CH_2CH_2S)_2Sn(n\text{-Bu})Cl$ or $S(CH_2CH_2S)_2Sn(n\text{-Bu})Cl$ also in chloroform (10 ml). The mixture was stirred under reflux for 4 h. The precipitated sodium chloride was filtered off and the filtrate after drying over anhydrous Na_2SO_4 was con-

Table 4
Analytical data for organotin derivatives $Me_3SnOSPR'R''$ (**1**), $Ph_3SnOSPR'R''$ (**2**), $O(CH_2CH_2S)_2Sn(n\text{-Bu})OSPR'R''$ (**3**), $S(CH_2CH_2S)_2Sn(n\text{-Bu})OSPR'R''$ (**4**) [R′ = *O*-Ph, R″ = *O*-cholesteryl]

Starting materials		Derivative	M.p. (°C)	Yield (%)	Elemental analyses. Found(Calc.) %		
Ligand g(mmol)	Reagent g(mmol)				C	H	P
0.25(0.429)	0.08(0.429)	**1**	80	70	61(59.81)	8.19(8.2)	4.31(4.30)
0.25(0.429)	$(\phi_3)_3SnCl$ 0.16(0.429)	**2**	219	65	67.2(67.4)	7.24(7.21)	3.44(3.41)
0.25(0.429) $O(CH_2CH_2S)_2Sn$	(*n*-Bu)Cl 0.15(0.429)	**3**	111	65	56.40(56.53)	7.75(7.76)	3.60(3.56)
0.25(0.429) $S(CH_2CH_2S)_2Sn$	(*n*-Bu)Cl 0.15(0.429)	**4**	126	57	55.35(55.51)	7.6(7.62)	3.45(3.49)

centrated in a vacuum. The remaining solid was then recrystallized from $CHCl_3$–hexane mixture. Analytical and preparation data for these derivatives are given in Table 4. Unfortunately all attempts to grow single crystals of compounds **1**–**4** failed.

Acknowledgements

We thank the Mexican National Council of Science and Technology (CONACYT) Grant No. 47-3100-5-1428P-N for financial support.

References

[1] (a) A.G. Davies, P.J. Smith, in: G. Wilkinson, F.G.A. Stone, E.W. Abel (Eds.), Comprehensive Organometallic Chemistry, vol. 2, Pergamon Press, Oxford, 1982. (b) S.J. Blunden, A.H. Chapman, in: P.J. Craing. (Ed.), Organometallic Compounds in the Environment, Longman, Harlow, London, 1986. (c) M.A. Champ, P.F. Seligman, Organotin: Environmental Fate and Effects, Chapman and Hall, London, 1996 (Chapter 1). (d) C.E. Holloway, M.M. Melnik, Main Group Met. Chem. 21 (1998) 371.
[2] M. Gielen, Coord Chem Rev. 151 (1996) 41.
[3] K.J. Vimal, Coord. Chem. Rev. 135/136 (1994) 809.
[4] M. López-Cardoso, P. García y García, V. García-Montalvo, R. Cea-Olivares, Heteroatom Chem. 11 (2000) 6.
[5] B.P. Singh, G. Srivastava, R.C. Mehrotra, J. Organomet. Chem. 171 (1979) 35.
[6] C. Silvestru, I. Haiduc, E. Drake, J. Yang, F. Caruso, Polyhedron 16 (1997) 949.
[7] A. Shihada, I. Jassim, F. Weller, J. Organomet. Chem. 268 (1984) 125.
[8] C. Silvestru, I. Haiduc, F. Caruso, M. Rossi, B. Mahieu, M. Gielen, J. Organomet. Chem. 448 (1993) 75.
[9] R. Cea-Olivares, V. García-Montalvo, A. Toscano, A. Gómez, R. Ferrari, P. García y García, A.M. Cotero, M. López-Cardoso, J. Organomet. Chem. 587 (1999) 215.
[10] C. Glidewell, Inorg. Chim. Acta 24 (1977) 255.
[11] S.S. Garje, V.K. Jain, Main Group Met. Chem. 18 (1995) 387.
[12] V.B. Mokal, V.K. Jain, E.R.T. Tiekink, J. Organomet. Chem. 471 (1994) 53.
[13] H.C. Clark, V.K. Jain, R.C. Mehrotra, B.P. Singh, G. Srivastava, T. Birchall, J. Organomet. Chem. 279 (1985) 385.
[14] P.J. Smith, A.P. Tupciauskas, Ann. Rep. NMR Spectrosc. 8 (1978) 291.
[15] H.C. Clark, V.K. Jain, I.J. McMahon, R.C. Mehrotra, J. Organomet. Chem. 243 (1983) 299.

PERGAMON

www.elsevier.nl/locate/poly

Polyhedron 19 (2000) 1545–1549

POLYHEDRON

Synthesis, crystal structure and third-order optical nonlinearity of a 'flywheel'-shaped cluster, $[MoS_4Cu_3(dppm)_3][BF_4]\cdot 2H_2O$

Weilian Tan [a], Hegen Zheng [b], Qionghua Jin [c], Guocheng Jin [b], Wei Ji [a], Deliang Long [d], Xinquan Xin [b,*]

[a] *Department of Physics, National University of Singapore, Singapore 119260, Singapore*
[b] *State Key Laboratory of Coordination Chemistry Institute, Nanjing University, Nanjing 210093, PR China*
[c] *Department of Chemistry, Capital Normal University, Beijing 100037, PR China*
[d] *State Key Laboratory of Structural Chemistry, Fujian Institute of Research on the Structure of Matter, Chinese Academy of Sciences, Fuzhou 350002, PR China*

Received 16 November 1999; accepted 10 April 2000

Abstract

The title compound $[MoS_4Cu_3(dppm)_3][BF_4]]\cdot 2H_2O$ (dppm = $Ph_2PCH_2PPh_2$) was synthesized for nonlinear optical studies by the reaction of $(Et_4N)_2MoS_4$ and $[Cu_2(dppm)_2(MeCN)_4][BF_4]_2$ in CH_3CN solution. Single-crystal X-ray analysis revealed that three copper atoms and the MoS_4^{2-} form a distorted 'flywheel' array with W–Cu separations of 2.7754(14), 2.792(2) and 2.820 (2) Å. The third-order nonlinear optical properties were investigated by a Z-scan technique with 7 ns laser pulses at 532 nm. It was observed that the nonlinear absorption is very small, but it has considerable third-order large nonlinear refractive index.
© 2000 Elsevier Science Ltd. All rights reserved.

Keywords: Tetrathiometalate; Nonlinear optical properties; Synthesis; Copper compounds; Crystal structures; Dppm

The tetrathiometallates MS_4^{2-} (M = Mo, W) have been shown to be able to act as multidentate ligands with a variety of transition metal ions [1]. They have been used extensively as starting materials in synthesizing Mo(W) containing inorganic clusters [2,3] and in catalytic studies [4,5]. Studies on these clusters have been expanded to include their third-order nonlinear optical (NLO) properties in our laboratory. Traditionally, NLO research has been largely focused on conjugated polymers, semiconductors and discrete organic molecules [6,7]. In our search for better NLO materials we have undertaken a series of studies on the structure and NLO properties of Mo(W)–Cu(Ag, Au, Pd)–S clusters [8–14]. In this article, we report the synthesis, X-ray crystal structure and nonlinear optical properties of a novel cluster compound containing μ_4-S: $[MoS_4Cu_3(dppm)_3][BF_4]\cdot 2H_2O$. We also compare its third-order NLO absorptive and refractive properties with those of other reported cluster compounds.

1. Experimental

1.1. Reagents

The reaction was performed under anaerobic conditions using standard Schlenk techniques; solvents were purified, distilled and degassed prior to use. The reagents $[Et_4N]_2[MoS_4]$ and $[Cu_2(dppm)_2(MeCN)_4][BF_4]_2$ were prepared according to the literature [15,16].

1.2. Physical measurements

Infrared spectra were recorded on a Fourier Nicolet FT-170SX spectrophotometer with pressed KBr pellets and the electronic spectrum of the title cluster was measured with a Hitachi U-3410 spectrophotometer. Carbon and hydrogen analyses were performed on a PE 240C Elemental Analyser.

* Corresponding author. Tel.: +86-25-359-3132; fax: +86-25-331-4502.
E-mail address: xxin@netra.nju.edu.cn (X. Xin).

0277-5387/00/$ - see front matter © 2000 Elsevier Science Ltd. All rights reserved.
PII: S0277-5387(00)00399-5

1.3. Nonlinear optical (NLO) measurements

The dimethylforminade (DMF) solution of the title cluster was contained in a 1-mm thick quartz cuvette with concentration of 3.6×10^{-4} M. The sample was irradiated by a Q-switched frequency-doubled Nd:YAG laser, which produced linearly polarized 7 ns (FWHM) optical pulses at 532 nm. The laser was operated at a pulse repetition rate of 10 Hz. The spatial profiles of the optical pulses were nearly Gaussian after passing through a spatial filter. The laser beam was then divided by a beam splitter into two parts: one was used as a reference for the incident energy and the other was focused onto the sample by a focusing mirror of 25 cm focal length. The minimum beam radius of the focused laser beam was determined to be 30 ± 5 μm. Both incident and transmitted pulse energies were measured simultaneously by two energy detectors (Rjp-735 energy probes, Laser Precision), which were linked to a computer by an IEEE interface. The NLO properties of the sample were determined by performing the Z-scan measurements [17]. The sample was mounted on a translation stage that was controlled by a computer to move along the Z-axis with respect to the focal point. To determine both the sign and magnitude of the nonlinear refraction, a 1.0 mm diameter aperture was placed in front of the transmission detector and the transmittance was recorded as a function of the sample position on the Z-axis (closed-aperture Z-scan). For measuring the nonlinear absorption, the Z-dependent sample transmittance was taken without the aperture (open-aperture Z-scan).

1.4. Syntheses

1.4.1. $[MoS_4Cu_3(dppm)_3][BF_4]\cdot 2H_2O$

A mixture of $[Cu_2(dppm)_2(MeCN)_4][BF_4]_2$ (237.3 mg, 0.1923 mmol) and $(Et_4N)_2MoS_4$ (93 mg, 0.1923 mmol) in acetonitrile (25 ml) was stirred at room temperature for 2 h. The volume of the solution was reduced to 5 ml and an orange precipitate was obtained upon the addition of diethyl ether. Vapor diffusion of diethyl ether into a CH_2Cl_2 solution gave a product isolated as an air-stable orange crystalline solid. *Anal.* Calc. for $C_{75}H_{70}BCu_3F_4MoO_2P_6S_4$: C, 53.28; H, 4.17; Found: C, 53.60; H, 4.20%. IR spectra (KBr pellet): Mo–S, 480.0 and 454.8 cm^{-1}.

1.5. X-ray structure determination

An orange crystal with dimension of $0.45 \times 0.25 \times 0.10$ mm was stuck to the end of a glass fiber by using neutral jelly, which was mounted on a Siemens SMART CCD area-detecting diffractometer. The structure was solved by using a direct method and expanded with subsequent Fourier syntheses. The quality of the solution was comprised somewhat by disorder in the BF_4^- ion and solvent water molecules. Rotational disorder about the B–F_1 bond of the BF_4^- ion was modeled with another three F atoms each occupying two half-weighted sites. All B–F distances were restrained to be similar with a standard deviation of 0.03 Å using SADI instruction (SHELXTL Version 5) [18], as were all F···F distances within each idealized tetrahedron. The four solvent water oxygen atoms contained a site-occupancy factor of 0.5. All non-hydrogen atoms in the cation portion were refined anisotropically. Hydrogen atoms riding on carbon atoms (C–H = 0.95 Å) were introduced in ideal positions and refined with an isotropic temperature factor 20% greater than that of the parent atoms. No attempts were made to generate hydrogen atoms for solvent water molecules. Refinement of the structure was carried out by full-matrix least-squares methods, and the final cycle of full-matrix least-squares refinement converged to give $R = 0.0678$ and $wR = 0.1661$. The crystallographic data and details concerning the intensity are summarized in Table 1.

2. Results and discussion

2.1. Structure of the title compound

The ORTEP diagram of the cation $[MoS_4Cu_3(dppm)_3]^+$ of the title compound is depicted in Fig. 1. The selected bond lengths and angles are given in Tables 2 and 3. The Mo atom has retained its initial tetrahedral coordination, with S–Mo–S angles in the range of 107.06(11)–112.79(12)°. The three Cu

Table 1
Crystal data and data collection parameters

Formula	$C_{75}H_{70}O_2MoCu_3S_4P_6BF_4$
Formula weight	1686.71
Crystal system	monoclinic
Space group	$P2(1)$
a (Å)	13.0481(2)
b (Å)	16.9413(2)
c (Å)	17.8930(1)
β (°)	93.255(1)
V (Å^3)	3948.9(8)
Z	2
Crystal size (mm)	$0.45 \times 0.25 \times 0.10$
T (K)	296
D_{calc} (g cm^{-3})	1.419
$F(000)$	1712
μ (cm^{-1})	1.231
Reflections measured	15976
Unique reflections	9800
Observation	7895 ($I > 2.0\sigma(I)$)
Parameters refined	851
Goodness-of-fit	1.067
Largest shift	0.000

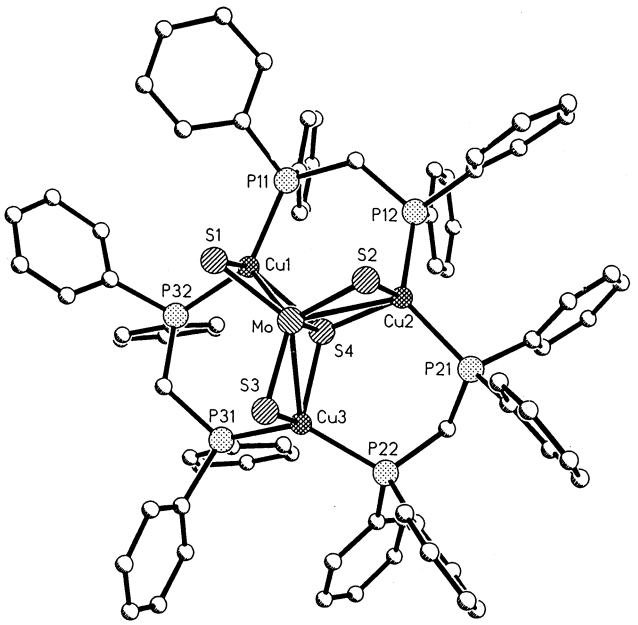


Fig. 1. The ORTEP diagram of the cation $[MoS_4Cu_3(dppm)_3]^+$ of the title compound.

atoms and the MoS_4^{2-} form a distorted 'flywheel' array. There are two different coordination modes of the bridging S atom. The atoms S_1, S_2 and S_3 are bonded to Mo and only one Cu atom, but S_4 adopts a μ_4-bridging mode, being bonded to Mo and the three Cu atoms. Each of the three Cu atoms is in a distorted tetrahedron. Compounds with a μ_4-S moiety asymmetrically bonded to two kinds of metal ion are not unprecedented in the literature. Examples include $(n\text{-}Bu_4N)_2[MoOS_3Cu_3(NCS)_3]$, $[MoCu_2OS_3(PPh_3)_3]$ and $[NEt_4]_3[WOS_3(CuBr)_3(\mu\text{-}Br)]\cdot 2H_2O$ [19–21]. The Mo–Cu bond lengths [2.7754(14), 2.792(2) and 2.820(2) Å] are longer than those observed in $[Et_4N]_4[Mo_2O_2S_6Cu_6I_6]$ (av. 2.661 Å) [22], but comparable with those of $(n\text{-}Bu_4N)_2[MoOS_3Cu_3(NCS)_3]$. Each of the three copper atoms is in a distorted tetrahedron. The six-membered ring comprising Cu, S, Cu, P, C and P has a boat conformation, whereas the other related rings have a chair conformation. This is probably due to the rigidity of the $[MoS_4]^{2-}$ group and the steric crowding of the phenyl groups of dppm.

Table 2
Selected bond lengths (Å) for the title compound

Mo–S_1	2.191(3)	Mo–S_2	2.192(3)
Mo–S_3	2.205(3)	Mo–S_4	2.286(3)
Mo–Cu_1	2.820(2)	Mo–Cu_2	2.7754(14)
Mo–Cu_3	2.792(2)	Cu_1–S_1	2.358(4)
Cu_1–S_4	2.317(3)	Cu_2–S_2	2.326(3)
Cu_2–S_4	2.310(2)	Cu_3–S_3	2.335(3)
Cu_3–S_4	2.309(3)	Cu_1–P_{11}	2.302(3)
Cu_1–P_{32}	2.300(3)	Cu_2–P_{21}	2.294(3)
Cu_2–P_{12}	2.300(3)	Cu_3–P_{22}	2.293(3)
Cu_3–P_{31}	2.309(3)		

Table 3
Selected angles (°) for the title compound

S_1–Mo–S_2	110.37(13)	S_1–Mo–S_3	111.77(13)
S_2–Mo–S_3	112.79(12)	S_1–Mo–S_4	107.06(11)
S_2–Mo–S_4	107.41(10)	S_3–Mo–S_4	107.11(11)
S_1–Mo–Cu_2	126.07(10)	S_2–Mo–Cu_2	54.31(9)
S_3–Mo–Cu_2	121.84(10)	S_4–Mo–Cu_2	53.24(6)
S_1–Mo–Cu_3	125.62(9)	S_2–Mo–Cu_3	123.60(11)
S_3–Mo–Cu_3	54.18(9)	S_4–Mo–Cu_3	52.97(7)
Cu_2–Mo–Cu_3	84.96(4)	P_{32}–Cu_1–P_{11}	132.86(12)
P_{32}–Cu_1–S_4	105.46(12)	P_{11}–Cu_1–S_4	108.75(11)
P_{32}–Cu_1–S_1	99.24(12)	P_{11}–Cu_1–S_1	105.07(13)
S_4–Cu_1–S_1	100.75(1)	P_{21}–Cu_2–P_{12}	120.56(11)
P_{21}–Cu_2–S_4	106.12(11)	P_{12}–Cu_2–S_4	101.75(10)
P_{21}–Cu_2–S_2	114.49(12)	P_{12}–Cu_2–S_2	109.07(12)
S_4–Cu_2–S_2	102.30(10)	P_{22}–Cu_3–P_{31}	124.21(12)
P_{22}–Cu_3–S_4	104.94(10)	P_{31}–Cu_3–S_4	100.72(10)
P_{22}–Cu_3–S_3	116.78(12)	P_{31}–Cu_3–S_3	104.62(11)
S_4–Cu_3–S_3	102.17(11)		

2.2. The third-order NLO properties of the title compound

The electronic spectrum of the title compound in DMF is depicted in Fig. 2. It was noted that the compound has relatively low linear absorption in the visible and near-IR region. The lowest absorption peak is located at 560 nm. The Z-scan results for the compound are shown in Fig. 3, where the filled circles were the Z-scan data measured without the aperture and the open circles were the results obtained from the division of the closed aperture Z-scan data by the open aperture Z-scan data. To obtain the NLO parameters we employed a Z-scan theory [17], which considers nonlinearities of third-order nature. The total absorption coefficient can be written as $\alpha = \alpha_0 + \alpha_2 I$, where α_0 and

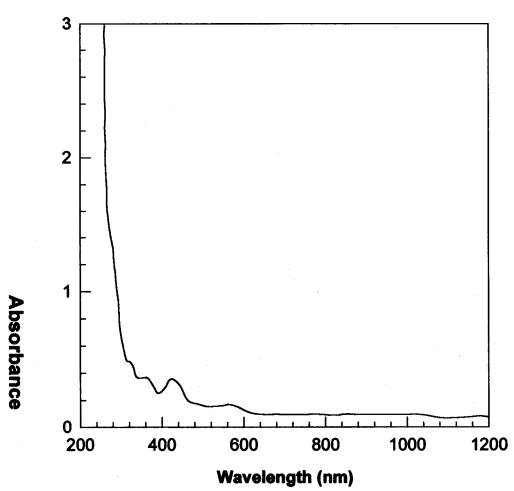


Fig. 2. Electronic spectrum of $[MoS_4Cu_3(dppm)_3][BF_4]\cdot 2H_2O$ (3.6×10^{-4} M) (_) DMF. The optical path is 1 mm.

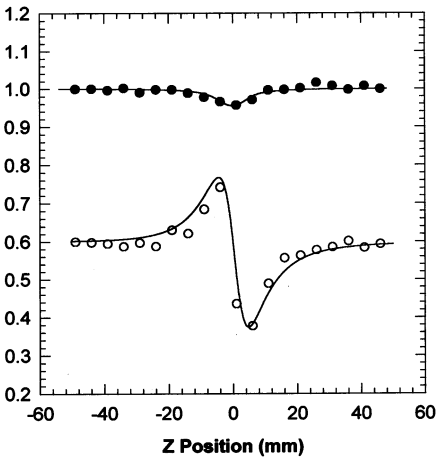


Fig. 3. The normalised Z-scan data $[MoS_4Cu_3(dppm)_3][BF_4]\cdot 2H_2O$ (3.6×10^{-4} M) in DMF solution with 532 nm, 7 ns laser pulses. The optical path is 1 mm. The peak incident irradiance of the pulses at focus is 420 MW cm^{-2}. The experimental data were measured without (●) an aperture. The open circles (○) were obtained by dividing the Z-scan data collected with the aperture by those collected without the aperture, they have been vertically displaced by -0.4 for clarity. The solid curves are the theoretical fits based on the Z-scan theory.

α_2 are the linear and nonlinear absorption coefficients, respectively, and I is the irradiance of the laser beam within the sample. The total refractive coefficient can be expressed as $n = n_0 + n_2 I$, where n_0 and n_2 are the linear and nonlinear refractive indices. The good fits between the theory and our experimental data suggest that the observed NLO phenomena can be expressed effectively by third-order susceptibilities. In Fig. 3, it was observed that the compound shows a negative sign for n_2. This indicates that the laser beam propagating in it undergoes a self-defocusing process. Table 4 lists the measured nonlinear absorption coefficient, α_2, and nonlinear refractive index, n_2, for the title compound. In accordance with the observed α_2 and n_2 values, the modulus of the third-order molecular susceptibility γ can be calculated using Eq. (1)

$$|\gamma| = \frac{1}{NF^4}\sqrt{\left(\left|\frac{9\times 10^8 \varepsilon_0 n_0^2 c^2 \alpha_2}{4\pi\omega}\right|^2 + \left|\frac{c n_0^2 n_2}{80\pi^2}\right|^2\right)} \quad (1)$$

where ε_0 and c are the permittivity and the speed of light in a vacuum, respectively, ω is the angular frequency of the light, N the concentration of the cluster (in cm^3) and $F^4 = 3$ is the local Lorentz field factor. We calculated that $|\gamma| = 2.4 \times 10^{-29}$ esu for the title compound. This calculated value is several orders of magnitude greater than the well known NLO materials (for example 1×10^{-32}–1×10^{-31} esu for metallophthalocyanines at 1064 nm [23] and 7.5×10^{-34} esu for C_{60} at 1910 nm [24]). It should be noted that the Z-scan measurements reported here could not reveal the origin of the measured α_2 and n_2 values for the title compound. Excited-state effects, two-photon absorption, third-order bound-electronic effect and nonlinear scattering are the possible mechanism behind the observed nonlinearities [25–27]. The observed self-defocusing property possessed by the compound shows that it can be a promising material for applications such as protection of optical sensors. It is also interesting to compare this compound with other different structural clusters such as twin-nested, nested and butterfly-shaped clusters [9,19,20,22]. Table 4 shows that the title compound is comparable with most of the other clusters in terms of the effective n_2 value.

3. Supplementary data

Supplementary data are available from the Cambridge Crystallographic Data Centre, 12 Union Road, Cambridge, CB2 1EZ, UK on request, quoting the deposition number 135206.

Acknowledgements

This research was supported by the National Natural Science Foundation of China and the National University of Singapore.

Table 4
The NLO parameters for cluster compounds [a]

Compound	Structure	α_o (cm^{-1} M^{-1})	α_2 (cm W^{-1} M^{-1})	n_2 (cm^2 W^{-1} M^{-1})
$[MoS_4Cu_3(dppm)_3][BF_4]]\cdot 2H_2O$ [b]	flywheel	5.50×10^3	1.1×10^{-5}	-5.5×10^{-10}
$(n\text{-}Bu_4N)_2[MoOS_3Cu_3(NCS)_3]$ [19]	nested	0.40×10^3	1.8×10^{-6}	-3.8×10^{-10}
$[MoOS_3Cu_3I(py)_5]$ [9]	nested	0.04×10^3	2.5×10^{-5}	-1.3×10^{-10}
$[WOS_3Cu_3I(py)_5]$ [9]	nested	2.10×10^3	15.0×10^{-5}	16.0×10^{-10}
$[Et_4N][Mo_2O_2S_6Cu_6I_6]$ [22]	twin-nested	0.74×10^3	2.0×10^{-5}	-3.0×10^{-10}
$[WOS_3Cu_2(PPh_3)_3]$ [20]	butterfly	2.50×10^3		6.7×10^{-10}

[a] Note: α_o is the linear absorption coefficient; α_2 is the nonlinear absorption coefficient; n_2 is the nonlinear refractive index. The dashed line represents negligible nonlinear absorption coefficient.
[b] This Work.

References

[1] A. Muller, E. Diemann, R. Jostes, H. Bogge, Angew. Chem., Int. Ed. Engl. 20 (1981) 934.
[2] J.P. Lang, X.Q. Xin, J. Solid State Chem. 108 (1994) 118.
[3] J.G. Li, X.Q. Xin, Z.Y. Zhou, K.B. Yu, J. Chem. Soc., Chem. Commun. (1991) 250.
[4] R.H. Holm, Chem. Soc. Rev. 10 (1981) 455.
[5] L. Bremner, C.F. Mills, B.W. Young, J. Inorg. Biochem. 16 (1982) 109.
[6] D.S. Chenla, J. Zyss (Eds.), Nonlinear Optical Properties of Organic Molecules and Crystals, Academic Press, Orlando, FL, 1987.
[7] H. Haug (Ed.), Optical Nonlinearities and Instabilities in Semiconductors, Academic Press, Boston, MA, 1988.
[8] H.G. Zheng, W. Ji, M.K.M. Low, G. Sakane, T. Shibahara, X.Q. Xin, J. Chem. Soc., Dalton Trans. (1997) 2537.
[9] P. Ge, S.H. Tang, W. Ji, S. Shi, H.W. Hou, D.L. Long, X.Q. Xin, S.F. Lu, Q.J. Wu, J. Phys. Chem. B. 101 (1997) 27.
[10] S. Shi, W. Ji, S.H. Tang, J.P. Lang, X.Q. Xin, J. Am. Chem. Soc. 116 (1994) 3615.
[11] W. Ji, S. Shi, H.J. Du, P. Ge, S.W. Tang, X.Q. Xin, J. Phys. Chem. 99 (1995) 17297.
[12] M.K.M. Low, H.W. Hou, H.G. Zheng, W.T. Wong, G.X. Jin, X.Q. Xin, W. Ji, Chem. Commun. 4 (1998) 505.
[13] D.X. Zeng, W. Ji, W.T. Wong, W.Y. Wong, X.Q. Xin, Inorg. Chim. Acta 279 (1998) 172.
[14] H.W. Hou, H.G. Zheng, H.G. Ang, Y.T. Fan, M.K.M. Low, Y. Zhu, W.L. Wang, X.Q. Xin, W. Ji, W.T. Wong, J. Chem. Soc., Dalton Trans. (1999) 2953.
[15] J.W. McDonald, G.D. Friesen, L.D. Rosenhein, W.E. Newton, Inorg. Chem. Acta 72 (1983) 205.
[16] J. Diez, M.M.P. Gamcia, J. Gimeno, A. Tiripicchio, M.T. Camellini, J. Chem. Soc., Dalton Trans. (1987) 1275.
[17] M. Sheik-Bahae, A.A. Said, T.H. Wei, D.J. Hagan, E.W. Van Stryland, IEEE J. Quant. Electron. 26 (1990) 760.
[18] Siemens (1994), SHELXTL, Version 5 Reference Manual, Siemens Energy & Automation Inc., Madison, WI, USA.
[19] S. Shi, W. Ji, W. Xie, T.C. Chong, H.C. Zeng, J.P. Lang, X.Q. Xin, Mater. Chem. Phys. 39 (1995) 298.
[20] H.W. Hou, X.Q. Xin, J. Liu, M.Q. Chen, S. Shi, J. Chem. Soc., Dalton Trans. (1994) 3211.
[21] S. Shi, H.W. Hou, X.Q. Xin, J. Phys. Chem. 99 (1995) 4050.
[22] H.W. Hou, D.L. Long, X.Q. Xin, X.Y. Huang, B.S. Kang, P. Ge, W. Ji, S. Shi, Inorg. Chem. 35 (1996) 5363.
[23] J.S. Shirk, J.R. Lindle, F.J. Bartoli, Z.H. Kafafi, A.W. Snow, in: S.R. Marder, J.E. Sohn, G.D. Stucky (Eds.), Materials for Nonlinear Optics, American Chemical Society, Washington, 1992, p. 626.
[24] Y. Wang, L.T. Cheng, J. Phys. Chem. 96 (1992) 1530.
[25] W. Ji, W. Xie, S.H. Tang, S. Shi, Mater. Chem. Phys. 43 (1995) 1.
[26] M. Sheik-Bahae, D.C. Hutching, D.J. Hagan, E.W. Van Stryland, Phys. Rev. Lett. 65 (1991) 96.
[27] K. Mansour, M.J. Soileau, E.W. Van Stryland, J. Opt. Soc. Am. B 9 (1992) 1100.

PERGAMON

www.elsevier.nl/locate/poly

Polyhedron 19 (2000) 1551–1557

POLYHEDRON

X-ray structure determination of two related uranyl phosphate crown ether compounds

Janet A. Danis [a], Heather T. Hawkins [b], Brian L. Scott [a], Wolfgang H. Runde [a], Barry E. Scheetz [c], Bryan W. Eichhorn [d,*]

[a] *Chemical Science and Technology Divisions, Los Alamos National Laboratory, Los Alamos, NM 87545, USA*
[b] *Nuclear Materials Technology Divisions, Los Alamos National Laboratory, Los Alamos, NM 87545, USA*
[c] *Materials Research Laboratory, The Pennsylvania State University, University Park, PA 16802, USA*
[d] *Department of Chemistry and Biochemistry, The University of Maryland, College Park, MD 20742, USA*

Received 8 December 1999; accepted 21 March 2000

Abstract

Two new uranyl phosphate compounds have been prepared and their structures determined. $[UO_2(H_2PO_4)_2(H_2O)]_2\cdot$(18-crown-6)$\cdot 5H_2O$ (**1**) and $UO_2(H_2PO_4)_2(H_2O)\cdot$(18-crown-6)$\cdot 3H_2O$ (**2**) contain neutral one-dimensional $[UO_2(H_2PO_4)_2(H_2O)]_\infty$ chains that are nearly identical to those of a previously reported binary phosphate, $UO_2(H_2PO_4)_2(H_2O)\cdot 2H_2O$ (**3**). The new compounds, however, crystallized with either one-half or one 18-crown-6 molecule per uranium atom for **1** and **2**, respectively. The seven-coordinate uranium(VI) assumes a pentagonal bipyramidal configuration, which is common for uranyl compounds. Empty 18-crown-6 molecules are hydrogen bonded to the uranyl phosphate chains as well as to lattice water molecules and function as 'packing-directing' agents. © 2000 Elsevier Science Ltd. All rights reserved.

Keywords: Uranium; Uranyl; Phosphate; Crown; Crystal structures

1. Introduction

Phosphate coordination plays a significant role in several areas of uranium chemistry. Various forms of phosphate are used in the processing of uranium both before and after its use as a nuclear fuel [1,2]. Phosphate matrices have been proposed as potential hosts for uranium and the light actinides to reduce solubility or as secondary barriers to enhance adsorption of mobile species [3–5]. In addition, the phosphate anion is prevalent in natural systems [6–8] and must be considered when evaluating the environmental complexation possibilities for uranium(IV, VI) ions. In order to predict and understand the formation and behavior of actinide phosphate complexes in solution and phosphate-mediated actinide migration in waste streams, it is important to examine the structure, bonding, stability, and spectroscopic properties of these species. Surprisingly, the few uranium phosphates characterized to date show a remarkable array of structural and chemical diversity [9–11]. For example, uranium can exist in multiple oxidation states (most commonly $+4$ and $+6$ in aqueous systems) and assume coordination numbers that can vary from six to nine inclusive. In addition, frameworks can be charged or neutral and of variable dimensionality (zero-, one-, two- or three-). Finally, the phosphate-binding mode can be bridging or terminal, unidentate or bidentate. Combinations of the aforementioned features quickly result in a vast number of new structural possibilities. What conditions dictate the occurrence of each of these features remain unclear and are the subject of ongoing research.

One approach to devising novel uranium phosphate structure types is to exert influence over structural features through the introduction of co-crystallites or templating agents. Crown ethers have historically been used as ion sequestering, separation and crystallizing agents, but they occasionally act as neutral addition species. In the present study, their usefulness as crystal-

* Corresponding author. Tel.: +1-301-405-1864; fax: +1-301-304-9121.
E-mail address: b._eichhorn@umail.umd.edu (B.W. Eichhorn).

0277-5387/00/$ - see front matter © 2000 Elsevier Science Ltd. All rights reserved.
PII: S0277-5387(00)00408-3

lizing agents was employed to encourage single-crystal growth of new phases. Their effectiveness in this area has been proven through the many uranium-crown complexes previously reported [12–18]. Uranium and the uranyl cation (UO_2^{2+}) can interact with crown ether molecules in a number of ways. For example, in UO_2(18-crown-6)$(CF_3SO_3)_2$, the uranyl ion resides within the crown ether cavity [18]. In [(dicyclohexano-18-crown-6)$(H_3O)]_2[UCl_6]$, the hydronium cation resides within the crown ether molecule and functions as a countercation to the UCl_6^{2-} anion [14]. In neutral coordination compounds, empty crown ether molecules have been known to hydrogen bond to the uranyl moieties, as shown by crystalline $UO_2(NO_3)_2(H_2O)_2{\cdot}2H_2O{\cdot}$(18-crown-6) [12] and $UO_2(SO_4)(H_2O)_3{\cdot}0.5$(18-crown-6) [15].

Herein we report the synthesis and structural characterization of $[UO_2(H_2PO_4)_2(H_2O)]_2{\cdot}$(18-crown-6)$\cdot 5H_2O$ (**1**) and $UO_2(H_2PO_4)_2(H_2O){\cdot}$(18-crown-6)$\cdot 3H_2O$ (**2**). Compounds **1** and **2** contain neutral one-dimensional uranyl phosphate chains that crystallized with either one-half or one 18-crown-6 molecule per uranium atom, respectively. Despite the variability in 18-crown-6 content, the two compounds both contain $[UO_2(H_2PO_4)_2(H_2O)]_\infty$ chains that are nearly identical to each other and to those of a previously reported binary phosphate, $UO_2(H_2PO_4)_2(H_2O){\cdot}2H_2O$ (**3**) [19].

2. Experimental

2.1. General procedures

Chemicals of reagent grade quality were obtained commercially (uranyl nitrate hexahydrate, Fluka; 85% H_3PO_4, Fisher; 1,4,7,10,13,16-hexaoxacyclooctadacane (18-crown-6), Aldrich) and used without further purification. Uranium tetrachloride was prepared by methods previously described [20]. Water was purified in a Millipore Milli-Q Ultra-pure water purification system. Elemental analyses were performed in our laboratories on a Perkin–Elmer series II 2400 CHN analyzer.

2.2. Synthesis

2.2.1. Preparation of $[UO_2(H_2PO_4)_2(H_2O)]_2{\cdot}$(18-crown-6)$\cdot 5H_2O$ (1)

UCl_4 (11.0 mg, 0.003 mmol), 85% H_3PO_4 (38.8 mg, 0.03 mmol PO_4) and 18-crown-6 (75.6 mg, 0.03 mmol) were added to 2.6817 g of H_2O in a glass vial and briefly stirred. The resulting solution was allowed to evaporate slowly. After approximately 60 days, gold crystals precipitated from the solution (crystalline yield, 5 mg, 25%). A crystal of suitable size for single-crystal X-ray diffraction was isolated, briefly dried in air, and then transferred to a mineral oil matrix for analysis.

Compound **1** was also prepared by an alternate synthesis. $UO_2(NO_3)_2{\cdot}6H_2O$ (15.1 mg, 0.003 mmol), 85% H_3PO_4 (38.8 mg, 0.03 mmol PO_4) and 18-crown-6 (75.6 mg, 0.03 mmol) were added to 2.6817 g of H_2O in a glass vial and briefly stirred. After approximately 21 days, gold crystals precipitated from the solution (crystalline yield, 20 mg, 83%). Crystals of **1** appear to be moderately stable in air at room temperature (r.t.). *Anal.* Calc. for $C_{12}H_{46}O_{33}P_4U_2$: C, 10.93; H, 3.52. Found: C, 11.82; H, 3.71%. A crystal of suitable size for single-crystal X-ray diffraction was isolated, briefly dried in air, and then transferred to a mineral oil matrix for analysis.

2.2.2. Preparation of $UO_2(H_2PO_4)_2(H_2O){\cdot}$(18-crown-6)$\cdot 3H_2O$ (2)

A procedure identical to that described for the preparation of **1** from UCl_4 was followed. After approximately 30 days, gold crystals separated from the solution (crystalline yield 5 mg, 21%). A crystal of suitable size for single-crystal X-ray diffraction was isolated, briefly dried in air, and then transferred to a mineral oil matrix for analysis. *Anal.* Calc. for $C_{12}H_{36}O_{20}P_2U$: C, 18.00; H, 4.54. See **1** above for analysis results on crystal mixtures. The crystals decompose within hours of isolation at r.t. and within 2 weeks when left in the reaction solution.

2.3. Crystallography

The crystallographic data for both compounds **1** and **2** were collected using a sealed, graphite monochromatized Mo Kα X-ray source ($\lambda = 0.71073$ Å) on a Bruker P4/CCD/PC diffractometer. The crystals were mounted from a matrix of mineral oil and cooled to 203 K using a Bruker LT-2 temperature device. A hemisphere of data was collected using a combination of φ and ω scans, with 30 s frame exposures and 0.3° frame widths. Data collection and initial indexing and cell refinement was handled using SMART [21] software. Frame integration and final cell parameter calculation were carried out using SAINT [22] software. The data were corrected for absorption using the SADABS [23] program. Decay of reflection intensity was not observed. The structures were refined by full-matrix least-squares technique on F^2. Structure solutions and refinements were performed using SHELXTL PC [24] and SHELX-93 [25], respectively.

2.3.1. $[UO_2(H_2PO_4)_2(H_2O)]_2{\cdot}$(18-crown-6)$\cdot 5H_2O$ (1)

A small pale gold plate was attached to a glass fiber with silicone grease. The data were collected and processed as described above. The selection of the space group $P\bar{1}$ was confirmed by the subsequent successful solution and refinement of the structure by direct methods and difference Fourier techniques. The initial solution revealed the uranium, phosphorus, and the

majority of all non-hydrogen atom positions. The remaining atomic positions were determined from subsequent Fourier synthesis. Hydrogen atom positions were fixed (C–H = 0.97 Å). The hydrogen atoms were refined using the riding model, with isotropic temperature factors fixed to 1.2 times the equivalent isotropic U of the carbon atom to which they were bound. Water and phosphate hydrogen atoms were not included in the final model. The final refinement included anisotropic temperature factors on all non-hydrogen atoms. Additional details of data collection and structure refinement are listed in Table 1.

2.3.2. $UO_2(H_2PO_4)_2(H_2O)\cdot$(18-crown-6)$\cdot 3H_2O$ (2)

A large gold crystal was attached to a glass fiber with silicone grease. The data were collected and processed as described above. The space group $P2_12_12_1$ was uniquely determined by its systematic absences. The structure was solved by direct methods and difference Fourier techniques. The initial solution revealed the uranium, phosphorus, and the majority of all non-hydrogen atom positions. The remaining atomic positions were determined from subsequent Fourier synthesis and refinement was performed as described above. Water and phosphate hydrogen atoms were not included in the final model. A racemic twin was refined using the TWIN command, and the scale factor refined to 0.5811(8). The final refinement included anisotropic temperature factors on all non-hydrogen atoms. Additional details of data collection and structure refinement are listed in Table 1.

Table 1
Crystallographic data for $[UO_2(H_2PO_4)_2(H_2O)]_2\cdot$(18-crown-6)$\cdot 5H_2O$ (**1**) and $UO_2(H_2PO_4)_2(H_2O)\cdot$(18-crown-6)$\cdot 3H_2O$ (**2**)

Compound	**1**	**2**
Empirical formula	$C_{12}H_{46}O_{33}P_4U_2$	$C_{12}H_{36}O_{20}P_2U$
Formula weight	1318.43	800.38
Space group	$P1$	$P2_12_12_1$
Unit cell dimensions		
a (Å)	11.0973(6)	11.1578(6)
b (Å)	13.0004(7)	14.0641(7)
c (Å)	14.7557(8)	16.7742(9)
α (°)	107.823(1)	
β (°)	102.765(1)	
γ (°)	103.965(1)	
V (Å^3)	1863.9(2)	2632.3(2)
Z	2	4
Absorption coefficient (mm^{-1})	8.957	6.372
D_{calc} (Mg m^{-3})	2.349	2.020
Crystal size (mm)	$0.12\times0.14\times0.20$	$16\times0.16\times0.21$
θ Range for data collection (°)	1.53–26.52	1.89–26.43
Index ranges	$-13\le h\le13$, $-16\le k\le15$, $0\le l\le18$	$0\le h\le13$, $0\le k\le17$, $0\le l\le20$
Reflections collected	9465	13910
Independent reflections	6892 [$R_{int}=0.0254$]	3041 [$R_{int}=0.0462$]
Data/restraints/parameters	6892/0/460	3041/0/317
Goodness-of-fit on F^2	1.527	1.271
Final R indices [$I>2\sigma(I)$]	R_1 [a] = 0.0489, wR_2 [b] = 0.1043	R_1 [a] = 0.0189, wR_2 [c] = 0.0572
R indices (all data)	$R_1=0.0636$, w$R_2=0.1091$	$R_1=0.0198$, w$R_2=0.0574$
Largest difference peak and hole (e Å^{-3})	1.834 and −2.605 [0.959 Å from U2]	0.643 and −1.061 [0.793 Å from P2]

[a] $R_1=\sigma||F_o|-|F_c||/\sigma|F_o|$.
[b] $wR_2=[\Sigma[w(F_o^2-F_c^2)^2]/\Sigma[w(F_o^2)^2]]^{1/2}$. The parameter $w=1/[\sigma^2(F_o^2)+(0.0310*P)^2]$.
[c] $wR_2=[\Sigma[w(F_o^2-F_c^2)^2]/\Sigma[w(F_o^2)^2]]^{1/2}$. The parameter $w=1/[\sigma^2(F_o^2)+(0.0249*P)^2]$.

3. Results and discussion

3.1. Synthesis and characterization

Aqueous phosphoric acid solutions react with UCl_4 or $UO_2(NO_3)_2\cdot6H_2O$ in the presence of 18-crown-6 to form transparent gold-colored crystals of **1** and **2**. Single crystals were isolated from these solutions that were prepared at different times, but in an identical fashion. Single-crystal X-ray diffraction analyses revealed that both **1** and **2** form under these conditions. Repeated elemental analyses carried out on single crystals prepared from uranyl nitrate consistently gave C and H results intermediate for the two compounds, but were always closer to the calculated percentages for **1**. These data suggest that both species are present simultaneously and that **1** may form preferentially to **2**. We have been unable to prepare the two compounds in a pure form.

It is interesting to note that the formulas of **3**, **1** and **2** are suggestive of a solid solution having the formula $[UO_2(H_2PO_4)_2(H_2O)]\cdot x$(18-crown-6), where $0\le x\le1$. However, X-ray analysis shows that the compounds are non-isomorphic and each represents a unique line in the $[UO_2(H_2PO_4)_2(H_2O)]\cdot$(18-crown-6) phase diagram.

3.2. Structural studies

3.2.1. $[UO_2(H_2PO_4)_2(H_2O)]_2\cdot$(18-crown-6)$\cdot 5H_2O$ (1)

Compound **1** crystallizes in the triclinic space group $P\bar{1}$ and consists of one-dimensional $[UO_2(H_2PO_4)_2(H_2O)]_\infty$ chains (Fig. 1) that hydrogen bond to empty crown ether molecules and water solvate molecules in the lattice (Fig. 2). A summary of the crystallographic data is given in Table 1 and a list of selected bond distances and angles is given in Table 2. The asymmetric unit contains one 18-crown-6 molecule, five solvate water molecules, and two crystallographically distinct $UO_2(H_2PO_4)_2(H_2O)$ subunits. Each uranium is coordinated by two uranyl oxygen atoms at the average bonding distance of 1.76(1) Å to form linear

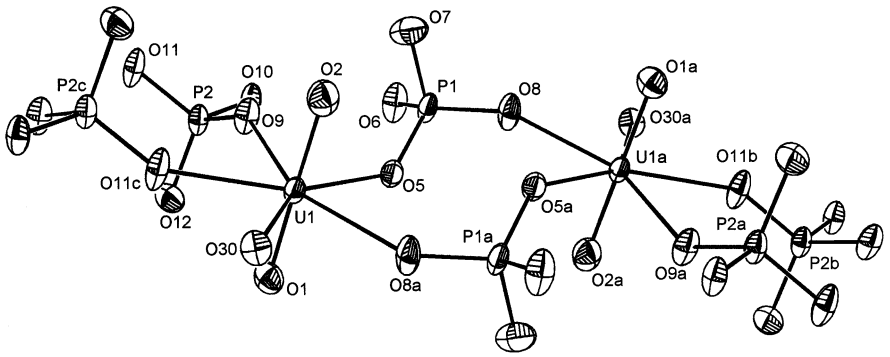


Fig. 1. ORTEP view of a portion of a $[UO_2(H_2PO_4)_2(H_2O)]_\infty$ chain of **1**.

UO_2^{2+} ions (O1–U1–O2, O3–U2–O4 angles, 178.9(3) and 177.7(3)°, respectively). The uranyl oxygen atoms form the apices of a pentagonal bipyramid, while the equatorial positions are occupied by the oxygens of a water molecule and four $(H_2PO_4)^-$ groups that bind in an μ-η^1 fashion. The mean U–O distance for all equatorial bonds is 2.38(1) Å. The equatorial and uranyl bond distances and angles are typical of the U(VI) uranyl species and comparable with those of $UO_2(H_2PO_4)_2(H_2O)\cdot 2H_2O$ (**3**) [26].

There are four crystallographically independent phosphate tetrahedra (P1, P2, P3, P4). In each tetrahedron there are two long P–O bonds and two short P–O bond distances. For P1 these distances are, respectively, 1.569(8), 1.569(7), 1.487(1) and 1.510(7) Å. For P2 the long P–O bond distances are 1.583(6) and 1.551(8) Å and the short distances are 1.492(7) and 1.515(7) Å. A similar pattern is exhibited for P3 and P4. The P–O bond distances longer than 1.55 Å are indicative of protonated phosphate oxygens, as described in related complexes [26,27]. The structural data suggest that the phosphate tetrahedra are all doubly protonated (as in **3**), and establish the necessary charge balance.

The bond distances and angles of the 18-crown-6 moiety are virtually identical to other crystallographically characterized examples [12]. As shown in Fig. 2, the crown and lattice water molecules participate in an extensive system of hydrogen bonding that cohesively binds the structure. A list of hydrogen bonding distances is given in Table 4. Two of the lattice water molecules (Ow1 and Ow2) are hydrogen bonded to the crown ether, the protonated phosphate oxygen atoms and the coordinated water molecule, O31. Three additional lattice water molecules (Ow3, Ow4 and Ow5) connect adjacent chains along a line that diagonally bisects the *bc* plane. These water solvates form hydrogen bonds to the protonated phosphate oxygen atoms O7, O12, O16, and O20 (bond distances span a range 2.590(4)–3.032(2) Å), but do not interact with the crown molecules.

The uranyl phosphate portion of **1** is quite similar to that in $UO_2(H_2PO_4)_2(H_2O)\cdot 2H_2O$ (**3**). The metric parameters of **3** [19] (uranyl bond distances of 1.774(1) and 1.773(1) Å, the O1–U1–O2 bond angle of 177.6(5)°, average equatorial bond distance of 2.38(1) Å) compare closely to those of **1** (see Table 2). The uranyl phosphate chains of **3** are spatially related to one another in

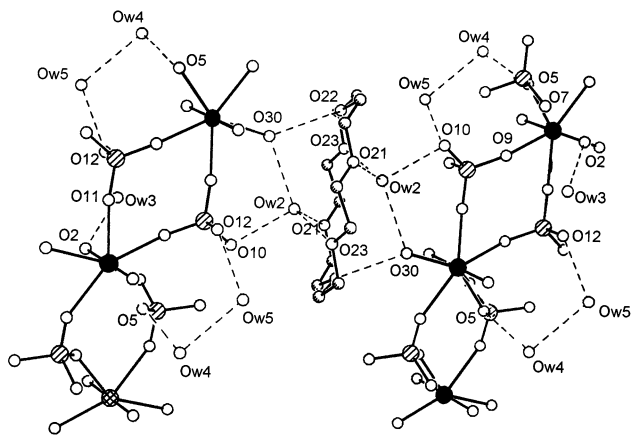


Fig. 2. Ball and stick view of a portion of **1** showing hydrogen bonding interactions (indicated by dashed bonds) between the lattice water molecules, crown ether molecules and phosphate chains. The filled balls represent uranium, the striped ones phosphorous and the empty ones oxygen.

Table 2
Selected bond lengths (Å) and angles (°) for **1**

U(1)–O(1)	1.754(7)	O(1)–U(1)–O(2)	178.9(3)
U(1)–O(2)	1.765(8)	O(3)–U(2)–O(4)	177.7(3)
U(1)–O(30)	2.508(6)	O(1)–U(1)–O(30)	92.9(3)
U(1)–O(5)	2.364(6)	O(2)–U(1)–O(30)	88.2(3)
U(1)–O(8)	2.351(7)	O(3)–U(2)–O(31)	91.0(3)
U(1)–O(9)	2.358(6)	O(4)–U(2)–O(31)	87.4(3)
U(1)–O(11)	2.322(6)		
U(2)–O(3)	1.760(7)		
U(2)–O(4)	1.765(6)		
U(2)–O(31)	2.528(6)		
U(2)–O(14)	2.315(7)		
U(2)–O(15)	2.338(7)		
U(2)–O(17)	2.343(6)		
U(2)–O(18)	2.344(6)		

Table 3
Selected bond lengths (Å) and angles (°) for **2**

U(1)–O(1)	1.766(5)	O(3)–P(1)	1.485(5)
U(1)–O(2)	1.772(4)	O(4)–P(1)	1.489(5)
U(1)–O(7)	2.331(4)	O(5)–P(1)	1.587(4)
U(1)–O(3)	2.333(4)	O(6)–P(1)	1.564(5)
U(1)–O(4)	2.341(5)	O(7)–P(2)	1.490(5)
U(1)–O(10)	2.356(4)	O(8)–P(2)	1.574(5)
U(1)–O(11)	2.570(4)	O(9)–P(2)	1.556(6)
		O(10)–P(2)	1.504(4)
O(1)–U(1)–O(2)	177.6(2)		
O(1)–U(1)–O(11)	91.9(2)		
O(2)–U(1)–O(11)	85.7(2)		

Table 4
Hydrogen bond lengths (Å) for **1** and **2**

1		**2**	
Ow1–O13	2.603(2)	Ow1–O6	2.692(2)
Ow1–O29	2.712(0)	Ow1–Ow3	2.813(4)
Ow1–O31	2.737(8)	Ow1–O14	2.839(2)
Ow1–O28	2.753(3)	Ow1–O12	2.943(2)
Ow1–O27	2.989(8)	Ow1–O13	3.066(8)
Ow2–O10	2.612(1)	Ow2–O5	2.605(7)
Ow2–O23	2.742(2)	Ow2–O15	2.687(1)
Ow2–O21	2.753(3)	Ow2–O17	2.832(1)
Ow2–O30	2.784(9)	Ow2–O11	2.838(4)
Ow2–O22	2.963(2)	Ow2–O16	2.954(5)
Ow3–O16	2.711(3)	Ow3–O9	2.617(2)
Ow3–O2	2.896(5)	Ow3–O11	2.962(7)
Ow3–O12	2.953(6)	Ow3–O1	3.146(2)
Ow3–O31	2.986(5)		
Ow4–Ow5	2.834(0)		
Ow4–O20	2.843(9)		
Ow4–O5	2.858(9)		
Ow4–O16	3.032(2)		
Ow4–O1	3.065(1)		
Ow5–O12	2.590(4)		
Ow5–O4	3.029(2)		

a manner reminiscent of **1**. The lattice arrangement is discussed below.

3.2.2. $UO_2(H_2PO_4)_2(H_2O)\cdot$(18-crown-6)$\cdot 3H_2O$ (2)

Compound **2** crystallizes in the orthorhombic space group $P2_12_12_1$. As in **1**, the structure of **2** consists of one-dimensional $[UO_2(H_2PO_4)_2(H_2O)]_\infty$ chains that run along the crystallographic *a* axis and hydrogen bond to empty crown ether molecules and water solvate molecules in the lattice. The asymmetric unit contains one 18-crown-6 molecule, three solvate water molecules, and a pentagonal bipyramidal $UO_2(H_2PO_4)_2(H_2O)$ subunit. U1 is coordinated by two axial uranyl oxygen atoms (1.766(5), 1.772(4) Å; O1–U1–O2 bond angle, 177.6(2)°) and five equatorial oxygen atoms, which include the oxygens of a water molecule and four $(H_2PO_4)^-$ groups that bind in an μ-η^1 fashion. The mean U–O distance for all equatorial bonds is 2.386(9) Å. There are two crystallographically independent phosphate tetrahedra, P1 and P2, with protonation schemes identical to that of compound **1**. In **2**, P–O bond distances range from 1.485(5) to 1.587(4) Å in P1 and 1.490(5) to 1.574(5) Å in P2. As in **1**, the $[UO_2(H_2PO_4)_2(H_2O)]_\infty$ chains are virtually identical to those in the binary phosphate **3** [19].

The bond distances and angles of the 18-crown-6 molecules are typical and the structure is rendered cohesive by a network of hydrogen bonds (Table 3). The lattice waters Ow1 and Ow2 are positioned above and below the plane of the crown ether rings. Ow1 is hydrogen bonded to the protonated phosphate oxygen, O6, the crown ether oxygen atoms, O12, O13 and O14 and Ow3 (see Table 4). Ow2 is hydrogen bonded to the protonated phosphate oxygen, O5, the crown ether oxygen atoms, O15, O16 and O17 and the uranium bound water, O11. Ow3 is hydrogen bonded to the protonated phosphate oxygen, O9, and the uranium bound water, O11.

The differences between **1**, **2**, and **3** are best illustrated by analyzing the general packing around the $[UO_2(H_2PO_4)_2(H_2O)]_\infty$ chains. Views down the chain axis of the three compounds are given in Fig. 3. The structures can be viewed as parallel chains of $[UO_2(H_2PO_4)_2(H_2O)]_\infty$ that pack with one dimensional 'chains' of 18-crown-6 molecules. In all three compounds, each $[UO_2(H_2PO_4)_2(H_2O)]_\infty$ chain has six nearest neighbor chains that form pseudo-hexagonal arrays. In **2**, each $[UO_2(H_2PO_4)_2(H_2O)]_\infty$ unit is surrounded by six 18-crown-6 chains, which separate them from the other uranyl phosphate chains (Fig. 3(b)). In contrast, the $[UO_2(H_2PO_4)_2(H_2O)]_\infty$ chains of **3** are hydrogen bonded to six identical $[UO_2(H_2PO_4)_2(H_2O)]_\infty$ chains through lattice water molecules to form a cohesive, three-dimensional network (Fig. 3(c)). The hydrogen bonds to the lattice water molecules are apparently optimized when the interchain uranyl units are roughly parallel (in the direction normal to the chains). In compound **1**, each $[UO_2(H_2PO_4)_2(H_2O)]_\infty$ chain is surrounded by four 18-crown-6 chains and two $[UO_2(H_2PO_4)_2(H_2O)]_\infty$ chains. As in **3**, the hydrogen bonding between adjacent $[UO_2(H_2PO_4)_2(H_2O)]_\infty$ chains is mediated through lattice water molecules and, therefore, the relative orientations of the interchain uranyl units in the two compounds are quite similar. Since the direct $[UO_2(H_2PO_4)_2(H_2O)]_\infty$ interchain interactions are absent in **2**, the lattice packing reflects the optimization of the interactions between the 18-crown-6 molecules and the $[UO_2(H_2PO_4)_2(H_2O)]_\infty$ chains. As a result, the uranyl phosphate chains in **2** have a different packing motif relative to **1** or **3** and the 18-crown-6 molecules can be viewed as 'packing directing' agents.

4. Conclusions

The crystal chemistry of the $[UO_2(H_2PO_4)_2(H_2O)]\cdot$18-crown$\cdot 6H_2O$ system is governed by the manner in which the lattice water and crown ether molecules interact with the $[UO_2(H_2PO_4)_2(H_2O)]_\infty$ chains. Compound **1** has one-half of a crown ether molecule and 2.5 molecules of lattice water per uranium, while **2** has one crown ether and three lattice water molecules per uranium. Compound **3** has two lattice waters per uranium and represents the optimized packing of the inorganic binary phosphate.

Because the 18-crown-6 molecules interrupt the direct interactions between the $[UO_2(H_2PO_4)_2(H_2O)]_\infty$ chains, they also lower the dimensionality of the crystal lattice. Compound **3** has coordinate linkages along the chain axes and can be viewed as a three-dimensional structure in view of the strong interchain hydrogen bonding contacts. In contrast, the direct interchain hydrogen bonding interactions in compound **1** only extend in two

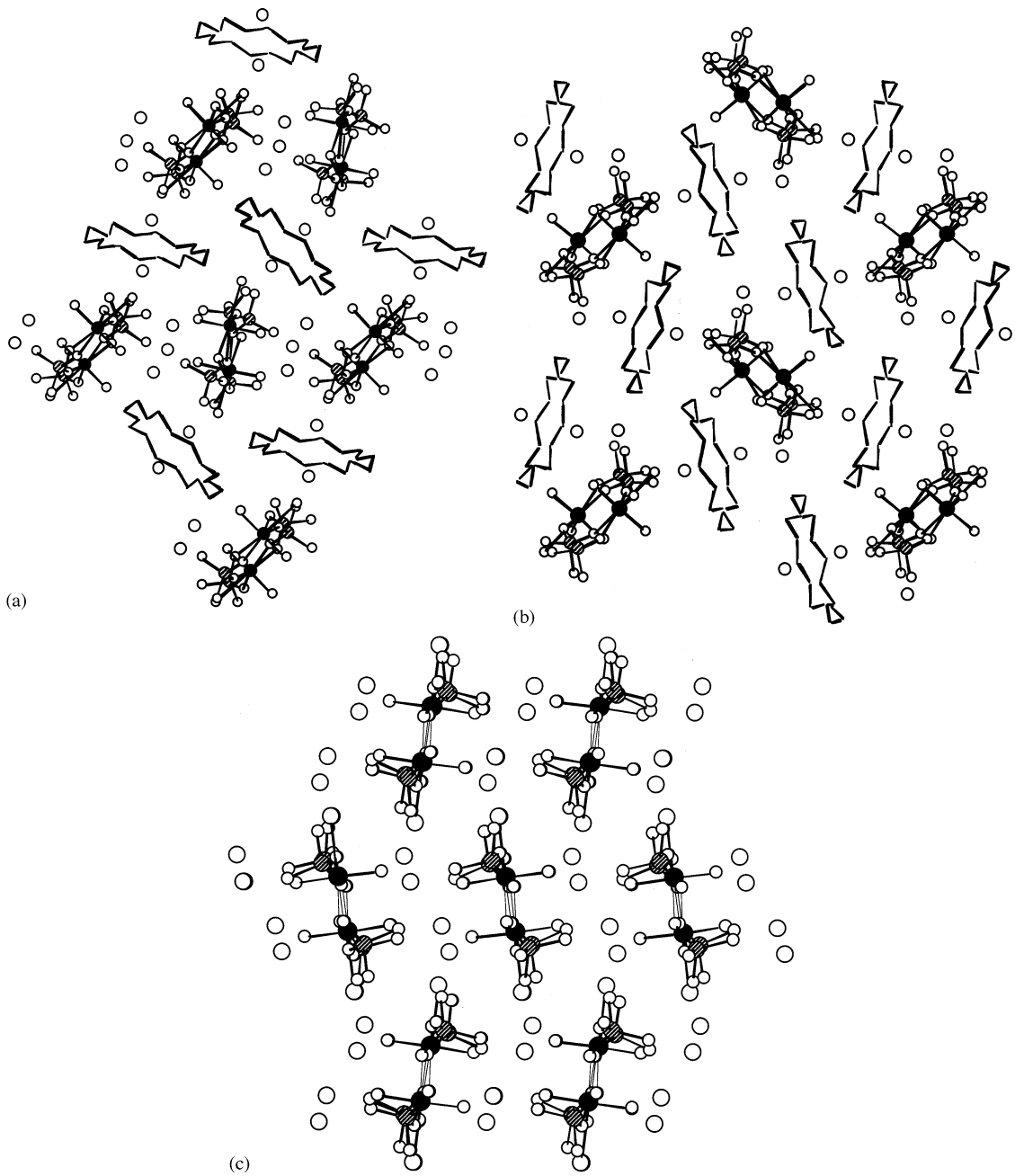


Fig. 3. Ball and stick views of the structures of **1** (3a), **2** (3b) and **3** (3c) viewed down the phosphate chains. The crown ether molecules are shown as stick drawings for clarity. The filled balls represent uranium, the striped ones phosphorous and the empty ones oxygen.

directions and, as such, the structure can be viewed as alternating layers of organic (18-crown-6) and inorganic lamellae. Finally, the $[UO_2(H_2PO_4)_2(H_2O)]_\infty$ chains in **2** are isolated and can be viewed as one-dimensional. The 18-crown-6 acts as a 'packing-directing agent' and controls the dimensionality of the structure. This effect may be reproducible with other neutral molecules that have a tendency to form hydrogen bonds.

5. Supplementary material

Crystallographic data have been deposited with the CCDC, 12 Union Road, Cambridge, CB2 1EZ, UK, and are available on request quoting the deposition numbers 136233 for $[UO_2(H_2PO_4)_2(H_2O)]_2 \cdot$(18-crown-6)$\cdot 5H_2O$ and 136232 for $UO_2(H_2PO_4)_2(H_2O) \cdot$(18-crown-6)$\cdot 3H_2O$.

Acknowledgements

Funding for this effort was made possible through the Nuclear Materials Stabilization Task Group, EM-66 of the US Department of Energy under contract W-7405-ENG-36. The authors would like to thank Dr David L. Clark, Professor Peter Dorhout, Professor Dermot O'Hare and Dr D. Kirk Veirs for helpful discussions.

References

[1] M. Benedict, T.H. Pigford, H.W. Levi, Nuclear Chemical Engineering, McGraw-Hill, New York, 1981.
[2] K.C. Buschbeck (Ed.), Gmelin Handbook of Inorganic Chemistry 8th ed., Supplement Volume A4, Springer-Verlag, New York, 1982.
[3] L.A. Boatner, B.C. Sales, in: W. Lutze, R.C. Ewing (Eds.), Radioactive Waste Forms for the Future, North-Holland, Amsterdam, 1988, p. 495.
[4] B.E. Scheetz, D.K. Agrawal, E. Breval, R. Roy, Waste Manag. 14 (1994) 489.
[5] H.T. Hawkins, D.R. Spearing, D.K. Veirs, J.A. Danis, D.M. Smith, C.D. Tait, W.H. Runde, M.N. Spilde, B.E. Scheetz, Chem. Mater. 11 (1999) 2851.
[6] D.E. White, J.D. Hem, G.A. Waring, Data of Geochemistry, US Geological Survey, 1963.
[7] D. Langmuir, Geochim. Cosmochim. Acta 42 (1978) 547.
[8] A. Sandino, J. Bruno, Geochim. Cosmochim. Acta 56 (1992) 4135.
[9] H.T. Evans, Science 141 (1963) 154.
[10] J.O. Nriagu, P.B. Moore, Phosphate Minerals, first ed., Springer-Verlag, New York, 1984.
[11] P.C. Burns, M.L. Miller, R.C. Ewing, Can. Mineral. 34 (1996) 845.
[12] P.G. Eller, R.A. Penneman, Inorg. Chem. 15 (1976) 2439.
[13] G. Bombieri, G. De Paoli, A. Immirzi, J. Inorg. Nucl. Chem. 40 (1978) 1889.
[14] W. Wang, L. Jie, S. Hong, Z. Peiju, W. Ming, W. Boyi, Radiochim. Acta 40 (1986) 199.
[15] R.D. Rogers, A.H. Bond, W.G. Hipple, A.N. Rollins, R.F. Henry, Inorg. Chem. 30 (1991) 2671.
[16] J. Berthet, C. Villiers, J. Le Maréchal, B. Delavaux-Nicot, M. Lance, M. Nierlich, J. Vigner, M. Ephritikhine, J. Organomet. Chem. 440 (1992) 53.
[17] R.D. Rogers, M.M. Benning, R.D. Etzenhouser, A.N. Rollins, J. Coord. Chem. 26 (1992) 299.
[18] L. Deshayes, N. Keller, M. Lance, A. Navaza, M. Nierlich, J. Vigner, Polyhedron 13 (1994) 1725.
[19] R. Mercier, M. Pham Thi, Ph. Colomban, Solid State Ionics (1985) 113.
[20] J.A. Hermann, J.F. Suttle, Inorganic Syntheses, vol. V, McGraw-Hill, New York, 1957.
[21] SMART Data collection software, Bruker Analytical X-Ray Systems, Inc., Madison, WI, Ver 4.210, 1996.
[22] SAINT Software: frame integration and final cell parameter calculation; Bruker Analytical X-Ray Systems, Inc., Madison, WI, Ver 4.05, 1996.
[23] G.M. Sheldrick, SADABS absorption correction program, University of Göttingen, Germany, Ver 1st release, 1996.
[24] SHELXTL PC, Bruker Analytical X-ray Instruments, Inc., Madison, WI, Ver 4.2/360, 1994.
[25] G.M. Sheldrick, SHELX-93 crystal structure solution program, University of Göttingen, Germany, 1993.
[26] M. Pham Thi, Ph. Colomban, Less-Common Met. (1985) 189.
[27] R.J. Francis, M.J. Drewitt, P.S. Halasyamani, C. Ranganathachar, D. O'Hare, W. Clegg, S.J. Teat, Chem. Commun. (1998) 279.

PERGAMON

www.elsevier.nl/locate/poly

Polyhedron 19 (2000) 1559–1566

POLYHEDRON

Synthesis, crystal structure and properties of two new binuclear complexes bridged by end-to-end azido: $[Ni_2(TLA)_2(N_3)_3]^+$ and $[Mn_2(TLA)_2(N_3)_3]^+$, [TLA = tris(6-methyl-2-pyridylmethyl)amine]

Zhi-Hui Zhang [a,*], Xian-He Bu [a], Zhi-Hong Ma [a], Wei-Ming Bu [b], Yu Tang [a], Qi-Hua Zhao [a]

[a] *Department of Chemistry, Nankai University, Tianjin 300071, China*
[b] *Key Laboratory on Supramolecular Structure and Spectra, Jilin University, Changchun 130023, China*

Received 4 February 2000; accepted 19 April 2000

Abstract

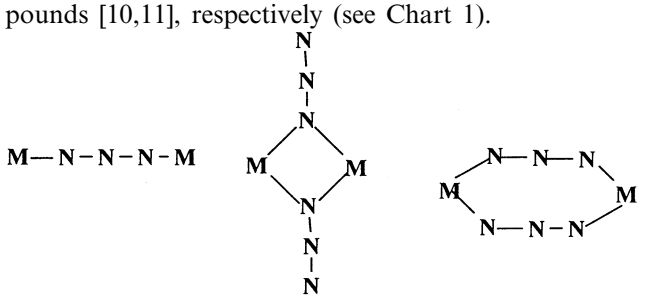
Two new binuclear complexes bridged by end-to-end azido, $[Ni_2(TLA)_2(N_3)_3]\cdot(ClO_4)$ (**1**) and $[Mn_2(TLA)_2(N_3)_3]\cdot(ClO_4)$ (**2**), where TLA is tris(6-methyl-2-pyridylmethyl)amine, have been synthesized and characterized. The structures of the two complexes have been studied by X-ray diffraction analysis. The complex **1** cation is a dimeric structure consisting of two $[(TLA)Ni(N_3)]^+$ units linked by an end-to-end (μ-1,3-N_3^-) bridging azide anion. There is an inversion center at the center N(2) of the bridged azido group. Each of the Ni^{II} atoms is in a distorted octahedral configuration. The crystal structure of **2** is very similar to that of **1**, in which the Mn^{II} atoms by bridging the azide group are also in the distorted octahedral environment. The variable temperature magnetic susceptibilities of the title complexes have been studied. For **1**, the exchange integral is $J = -20.45\ cm^{-1}$, $g = 2.23$; for **2**, $J = -2.99\ cm^{-1}$, $g = 2.04$, indicating the existence of an intramolecular antiferromagnetic interaction between the two metal ions in both complexes. The spectral properties of the two complexes have been studied further by UV–Vis techniques, and the results have been discussed in detail. © 2000 Elsevier Science Ltd. All rights reserved.

Keywords: Binuclear nickel(II) complex; Binuclear manganese(II) complex; Crystal structures; Magnetic properties; Tris(6-methyl-2-pyridylmethyl)amine

1. Introduction

Studies on the coordination properties of bi- and polynuclear nickel(II) and manganese(II) complexes have attracted a lot of attention in recent years [1–4]. The investigation of the magnetic properties of such compounds has been an active field of research, since the study on the correlation between magnetism and structure for nickel(II) and manganese(II) complexes can help not only in further understanding the interaction between magnetic coupling centers in metalloproteins and enzymes, but also to develop the field of molecular magnetism.

With regard to the factors that affect magnetic exchange pathways between paramagnetic centers, the choice of bridging ligands is of great importance because the magnetic-exchanging interaction in these compounds might be propagated or affected by the bridging ligand through various pathways and exhibit different magnetic strengths of the molecules. The pseudohalide ion, azide anion N_3^-, shows a great tendency to act as a bridging ligand between metallic centers [5–7]. As is well-known, the azido ligand stabilizes either end-on or end-to-end coordination modes when it links two metal centers, giving ferromagnetic [8,9] or antiferromagnetic compounds [10,11], respectively (see Chart 1).



(I) (II) (III)

(Chart 1)

* Corresponding author. Tel.: +86-22-2350-3075; fax: +86-22-2350-2458.
E-mail address: tangqi@public.tpt.tj.cn (Z.-H. Zhang).

0277-5387/00/$ - see front matter © 2000 Elsevier Science Ltd. All rights reserved.
PII: S0277-5387(00)00411-3

The binuclear complexes of tris(2-pyridylmethyl)-amine (TPA) and its derivatives, bridged by various groups as the model compounds for understanding the oxygen-transporting process in metal protein, have made significant contributions [12–14]. The crystal structure and magnetism of several mononuclear and binuclear metal complexes of TPA have been reported by this group [15]. In order to further explore the relationship between the bridging ligand and substituted groups on the ligand with the properties of TPAs complexes, we report herein the synthesis, crystal structures, magnetism, and spectral characters of the new binuclear nickel(II) and binuclear manganese(II) complexes of TLA and azido mixing ligands (Scheme 1).

2. Experimental

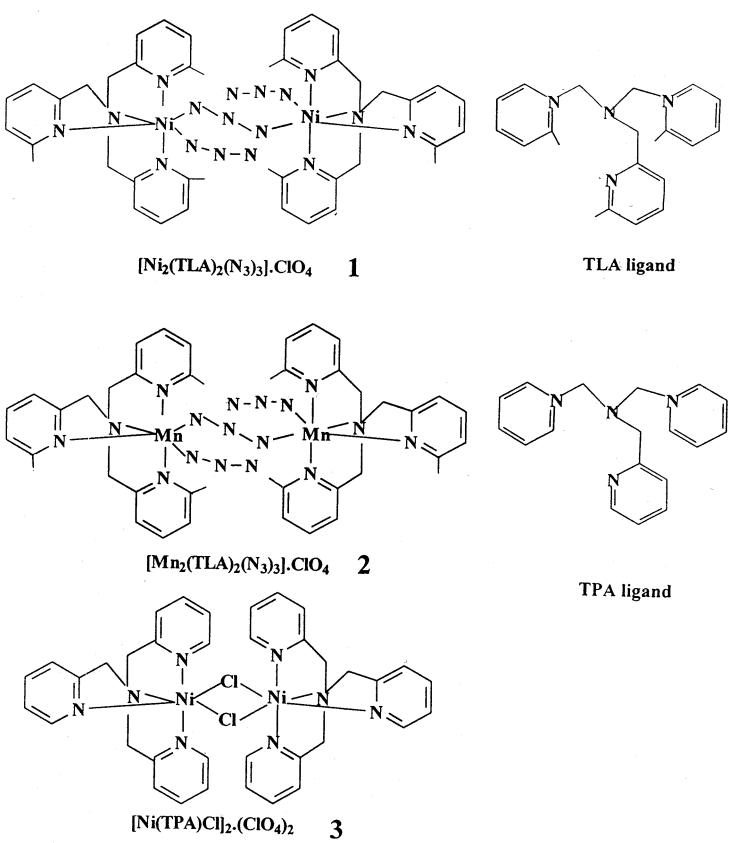
2.1. Materials and general methods

All the starting materials and organic solvents for synthesis were of analytical grade as purchased commercially and purified by standard methods prior to use. The TLA ligand was prepared by using the published procedure [16]. IR spectra were recorded on a Nicolet 170 SX FTIR spectrophotometer. Electronic spectra were measured in acetonitrile solution on a Shimadzu UV-365 for complex **1** and UV-240 spectrophotometer for complex **2**. Variable temperature magnetic susceptibility was measured on a MPMS 7 Quantum Design SQUID magnetometer in the temperature range 4–300 K, and diamagnetic corrections were made by using Pascal's constants [17]. Elemental analysis was carried out on a Perkin–Elmer model 240 analyzer. X-band ESR spectra were performed at room temperature (r.t.) on a JES-FEIXG spectrometer.

2.2. Syntheses

2.2.1. $[Ni_2(TLA)_2(N_3)_3]\cdot ClO_4$ (1)

A solution of TLA (33.2 mg, 0.1 mmol) in MeOH (10 cm^3) was added dropwise into a solution of $Ni(ClO_4)_2\cdot 6H_2O$ (36.6 mg, 0.1 mmol) in absolute methanol (10 cm^3) under stirring, and a solution of NaN_3 (26.0 mg, 0.4 mmol) in MeOH (5 cm^3) was added to the solution mentioned above. The resulting green solution was further stirred for ca. 30 min, and then it was filtered. The filtration was left to stand for over 2 weeks under ambient conditions, and green needle crystals of **1** were obtained (85 mg, 85%). IR (KBr pellets): 3445 (H_2O), 2952, 2924, 2120, 2042 (N_{3asym}^-), 1606, 1577 (py-ring), 1452, 1353, 1298 (N_{3sym}), 1095, 1005, 790,



Scheme 1. The molecular structures of the compounds used in this paper.

Table 1
The crystal data and data collection summary for **1** and **2**

	1	**2**
Empirical formula	$C_{42}H_{48}N_{17}Ni_2ClO_4$	$C_{42}H_{48}N_{17}Mn_2ClO_4$
Formula weight	1007.73	1000.30
Space group	$P\bar{1}$	$P\bar{1}$
a (Å)	8.286(2)	8.406(3)
b (Å)	8.5818(5)	8.659(2)
c (Å)	16.339(2)	16.524(5)
α (°)	93.424(10)	94.52(3)
β (°)	97.12(2)	97.55(3)
γ (°)	100.032(14)	99.56(4)
V (Å^3)	1131.3(3)	1169.6(7)
Z	1	1
D_{calc} (g cm^{-3})	1.479	1.420
$F(000)$	524	518
Crystal dimensions (mm)	$0.18\times0.38\times0.5$	$0.16\times0.40\times0.06$
μ(Mo Kα) (mm^{-1})	0.954	0.658
λ (Å)	0.71073	0.71073
Temperature (K)	293 ± 2	293 ± 2
θ (°)	2.42–25.48	1.25–25
Independent reflections	2188 [$R_{int}=0.0267$]	3329 [$R_{int}=0.0699$]
Data/restraints/parameters	1488/0/302	3329/0/310
R, wR	0.0435, 0.1299	0.0608, 0.0838
R, wR (all data)	0.0638, 0.1017	0.0812, 0.1033
GOF	0.913	1.095
Largest difference peak and hole (e Å^{-3})	0.515/−0.465	0.381/−0.476

623, 469 cm^{-1}. *Anal.* Calc. for $C_{42}H_{48}N_{17}Ni_2ClO_4$: C, 50.0; H, 4.80; N, 23.6. Found: C, 49.6; H, 4.70; N, 24.1%.

2.2.2. $[Mn_2(TLA)_2(N_3)_3]\cdot(ClO_4)$ (2)

For the synthesis of complex **2**, similar procedures to that of complex **1** were followed, and the colorless needle crystals of **2** suitable for X-ray structure determination were obtained (80 mg, 80%). IR (KBr pellets): 3473, 3417, 3369, 3073, 2963, 2853, 2121, 2045 (N_{3asym}), 1604, 1577 (py-ring), 1453, 1387, 1353, 1296 (N_{3asym}^{-}), 1094, 1007, 790, 624, 557, 453 cm^{-1}. *Anal.* Calc. for $C_{42}H_{48}Mn_2N_{17}ClO_4$: C, 50.4; H, 4.80; N, 23.8. Found: C, 49.7; H, 4.50; N, 23.8%.

CAUTION: Perchlorate salts and azide compounds are potentially explosive. Treat the compounds with great care.

2.3. Crystallographic studies

The crystals of complexes **1** and **2** were mounted on a Siemens P4 diffractometer equipped with a graphite crystal monochromator for data collection. The determination of unit cell parameters and the data collection were performed with Mo Kα radiation ($\lambda=0.71073$ Å). Unit cell dimensions were obtained by least-square refinements of setting angles of 25 reflections. The structure was solved by direct methods and the metal atoms were located from E-maps. The other non-H atoms were determined with successive Fourier difference synthesis. Final refinement by full-matrix least-squares methods was carried out with anisotropic thermal parameters for non-H atoms. The H atoms were treated as riding on their attached atoms, refined isotropically and placed at calculated positions. All the calculations were performed on a computer using the SHELXL-93 and SHELXL-86 program packages [18]. The crystal data of complex **1** are not good since the quality of the crystal we obtained was not good, although many attempts were made under different conditions. The crystal data and data collection details are summarized in Table 1.

3. Results and discussions

3.1. Synthesis of the metal complexes

There are two types of azido group-linked metal center as the bridged ligand by end-to-end or end-on fashions. According to the above, the dimeric molecule could be obtained. However, when all the azido groups incorporate the metal centers as a terminal ligand, the monomer complex with mixing ligands is obtained. Thus, the ratio of ligand to azido salt and the reaction conditions are the important factors for the synthesis of polynuclear metal complexes.

The monomeric complex of general formula $(M\cdot L)\cdot ClO_4$ (L = TLA) can be considered as precursors in the synthesis of polynuclear metal systems with the azido anion. The synthetic strategy is based on the following equations:

$$M(ClO_4)_2 + TLA \rightarrow [M(TLA)]ClO_4 \quad (1)$$

$$[M(TLA)]ClO_4 + N_3^- \rightarrow [M(TLA)\cdot(N_3)]\cdot ClO_4 \quad (2)$$

$$2[M(TLA)\cdot N_3]\ ClO_4 + N_3^- \rightarrow [M_2(TLA)_2(N_3)_3]\cdot ClO_4 \quad (3)$$

(M = Ni^{II} and Mn^{II})

3.2. Crystal structure of $[Ni_2(TLA)_2(N_3)_3]\cdot ClO_4$ (1)

Fig. 1 shows an ORTEP view of complex **1**, and the selected bond distances and angles are given in Table 2. From Fig. 1, it can be seen that there are two unique units $[(TLA)Ni(N_3)]^+$ linked by single μ-end-to-end azide bridging groups with an inversion center at the N(2) center of the bridged azide group. Another two azide groups act as terminal ligands. Each nickel atom is in a distorted octahedral environment consisting of four nitrogen atoms from TLA and two nitrogen atoms from a bridging azide and coordinated terminal azide groups, respectively.

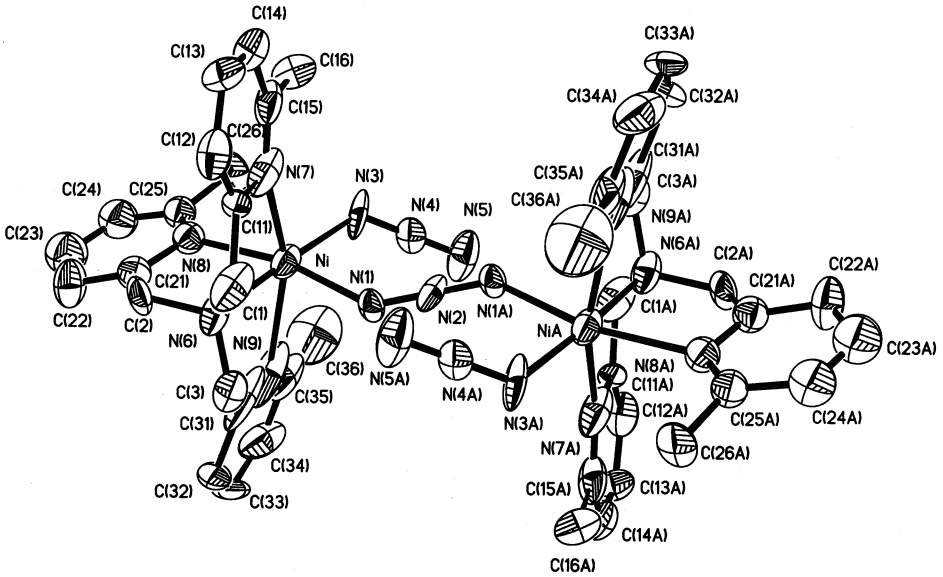


Fig. 1. ORTEP view and labelling scheme of complex **1**.

The intramolecular distance of Ni^{II}–Ni^{II} in complex **1** is 6.188 Å, being longer than the Ni^{II}–Ni^{II} distances found for bis(μ-1,3-azido) nickel(II) complexes (5.220 Å) [19], and also much longer than that of $[Ni(TPA)Cl]_2$ $(ClO_4)_2$ (**3**) [15a] bridged by bis(μ-Cl) (3.523 Å). The geometry of **1** is similar to **3** except for the bridging ligand and the substituted methyl groups on TPA.

In complex **1**, the average Ni–N_{py} bond length is 2.23 Å, which is ~0.15 Å longer than that of Ni–N_{py} in **3**. It might arise from the presence of the 6-methyl groups on the pyridine rings, whose steric interactions prevent the pyridine nitrogen from coordinating to the nickel(II) center at the optimum bond length. However, the Ni–N_{amine} distance is 0.067 Å shorter than that of Ni–N_{amine} in **3**. The Ni-μ-N_{azido} bond length is 2.117 Å, which is longer than that found for bis(μ-azido) nickel(II) complexes (2.069 Å) [19]. The Ni–N(terminal azido) bonds have lengths of 2.047 Å, which is shorter than that of Ni–N(bridged azido) bonds [2.117(7) Å] in **1**, it might be due to the repulsion of the two unique units in **1** as well as the stronger *trans* influence of the 6-methylpyridine than that of the tertiary amine group of TLA ligand [20].

The bridging angles of the binuclear complexes are directly related to the magnetic coupling. Most end-to-end (EE) bridging modes of azido lead to antiferromagnetic coupling except the nickel(II) complex reported recently by Hong and Do [21]. The bridging angle of Ni–N(1)–N(2) in **1** is 139.1 (5)°, which is smaller than that found for other singly bridged nickel(II) complexes, for instance $[Ni_2(macro)_2(N_3)_3]^+$ (142°) [22], and is bigger than that found for the bis(μ-azido)nickel(II) complex (135°) [19]. The N(7)–Ni–N(9) angle of 156.6(3)° in **1** is smaller than the corresponding angle of **3** (the N21–Ni–N31 angle is 161.8(7)° in **3**), indicating stronger repulsion of the 6-methyl groups on the pyridine rings of TLA and the flexibility of the singly bridged azide group in comparison to the doubly bridged chlorine atoms.

3.3. Crystal structure of $[Mn_2(TLA)_2(N_3)_3]\cdot(ClO_4)$ (2)

The ORTEP structure of complex **2** is shown in Fig. 2, and the selected bond distances and angles are listed in Table 3.

The structure of **2** is quite similar to that of **1**, and the local geometry around each Mn^{II} center is also in a distorted octahedron environment with one of the bridging azide nitrogens [N(2)] and the pyridine nitrogen [N(9)] occupying the axial positions. The equatorial positions are occupied by the other terminal azide nitrogen [N(3)], two pyridine nitrogens [N(8) and N(7)]

Table 2
Selected bond distances (Å) and angles (°) for complex **1**

Ni–N(3)	2.047(7)	N(1)–N(2)	1.167(7)
Ni–N(1)	2.117(7)	N(3)–N(4)	1.170(9)
Ni–N(6)	2.077(7)	N(4)–N(5)	1.174(9)
Ni–N(7)	2.208(8)	N(2)–N(1A)	1.167(7)
Ni–N(8)	2.191(7)	N(6)–C(2)	1.471(10)
Ni–N(9)	2.249(8)	N(6)–C(3)	1.494(1)
N(3)–Ni–N(6)	173.5(3)	N(8)–Ni–N(7)	91.2(3)
N(1)–Ni–N(3)	88.3(3)	N(3)–Ni–N(9)	103.9(3)
N(6)–Ni–N(1)	86.0(3)	N(6)–Ni–N(9)	79.2(3)
N(3)–Ni–N(8)	102.4(3)	N(1)–Ni–N(9)	89.7(3)
N(6)–Ni–N(8)	83.6(3)	N(8)–Ni–N(9)	82.7(3)
N(1)–Ni–N(8)	168.0(3)	N(7)–Ni–N(9)	156.6(3)
N(3)–Ni–N(7)	99.4(3)	N(4)–N(3)–Ni	125.4(6)
N(6)–Ni–N(7)	77.7(3)	N(2)–N(1)–Ni	139.1(5)
N(1)–Ni–N(7)	92.3(3)	N(1)–N(2)–N(1A)	180.0(4)

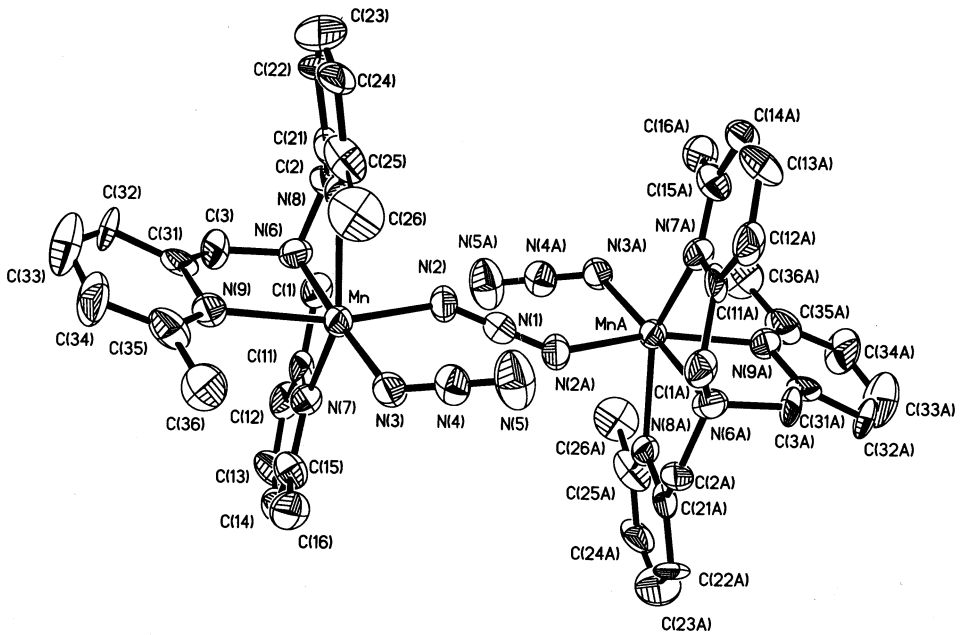


Fig. 2. ORTEP view and labelling scheme of complex **2**.

and the amine nitrogen [N(6)] of TLA. The two Mn^{II} centers are linked by a bridging azido (end-to-end, μ-1,3-N_3 coordination mode). The intramolecular Mn^{II}–Mn^{II} distance in **2** is 6.367 Å, being slightly longer than that of Ni^{II}–Ni^{II} in **1**. The average Mn–N_{py} bond length of **2** is 2.37 Å, being longer than those of Mn–N_{bipy} [2.255 (4) Å] [23], while the distance of Mn–N(8) [2.420(13) Å] is longer than other the two Mn–N_{py} distances [Mn–N(7) = 2.295(13) and Mn–N(9) = 2.375(13) Å] due to the steric hindrance of the coordinated terminal azido groups. The bond length of Mn–N(bridging azido) [2.210(13) Å] is much longer than that of Mn–N(terminal azido) [2.073(14) Å] being the result of repulsion of the two units $[(TLA)Mn(N_3)]^+$ in **2**. The bridged angle N(1)–N(2)–Mn [141.2(10)°] is larger than that in **1** [N(2)–N(1)–Ni] (139.1°), and this might be one of the factors leading to the difference in magnetic properties of **1** and **2**.

3.4. Magnetic properties

The magnetic behavior of complex **1** and **2** was measured throughout the temperature range 4–300 K. The temperature dependence of the magnetic susceptibility and the magnetic moments for the title complexes are shown in Figs. 3 and 4, respectively.

From Fig. 3, it can be seen that the effective magnetic moment (μ_{eff}) of complex **1** decreases slowly in the 300–50 K temperature range, but sharply decreases below 50 K. This behavior is characteristic of antiferromagnetic spin-exchange interactions between paramagnetic ions. The observed magnetic behavior clearly demonstrates the existence of intramolecular antiferromagnetic spin-exchange interactions through the N–N–N bridging ligand in this complex. The downturn in the effective magnetic moment plots may be attributed to zero-field splitting of the triplet Ni^{II} in complex **1**.

In order to quantitatively understand the magnitude of the spin-exchange interaction between the intramolecular Ni^{II}–Ni^{II} ions, the magnetic data of complex **1** were fit to the susceptibility Eq. (4), which is

Table 3
Selected bond distances (Å) and angles (°) for complex **2**

Mn–N(2)	2.210(13)	N(3)–N(4)	1.181(17)
Mn–N(3)	2.073(14)	N(4)–N(5)	1.150(17)
Mn–N(6)	2.260(13)	N(6)–C(1)	1.466(16)
Mn–N(7)	2.295(13)	N(6)–C(2)	1.463(16)
Mn–N(8)	2.420(13)	N(6)–C(3)	1.519(16)
Mn–N(9)	2.375(13)	N(7)–C(11)	1.310(2)
N(1)–N(2)	1.145(13)	N(7)–C(15)	1.346(18)
N(1)–N(2) #	1.145(13)	N(8)–C(21)	1.340(19)
N(3)–Mn–N(2)	89.1(5)	N(9)–Mn–N(8)	81.1(4)
N(3)–Mn–N(6)	174.5(5)	N(2)–N(1)–N(2) #	180(2)
N(2)–Mn–N(6)	85.6(5)	N(1)–N(2)–Mn	141.2(10)
N(3)–Mn–N(7)	104.3(5)	N(4)–N(3)–Mn	128.1(12)
N(2)–Mn–N(7)	91.3(5)	N(5)–N(4)–N(3)	178.6(11)
N(6)–Mn–N(7)	74.2(5)	C(1)–N(6)–Mn	106.5(9)
N(3)–Mn–N(9)	106.7(6)	C(2)–N(6)–Mn	106.4(9)
N(2)–Mn–N(9)	163.5(6)	C(3)–N(6)–Mn	108.6(9)
N(6)–Mn–N(9)	78.7(5)	C(11)–N(7)–Mn	113.9(11)
N(7)–Mn–N(9)	89.2(4)	C(15)–N(7)–Mn	130.8(12)
N(3)–Mn–N(8)	106.8(6)	C(21)–N(8)–Mn	111.2(12)
N(2)–Mn–N(8)	90.0(5)	C(25)–N(8)–Mn	131.0(14)
N(6)–Mn–N(8)	74.8(5)	C(31)–N(9)–Mn	108.8(11)
N(7)–Mn–N(8)	148.8(6)	C(35)–N(9)–Mn	129.1(13)

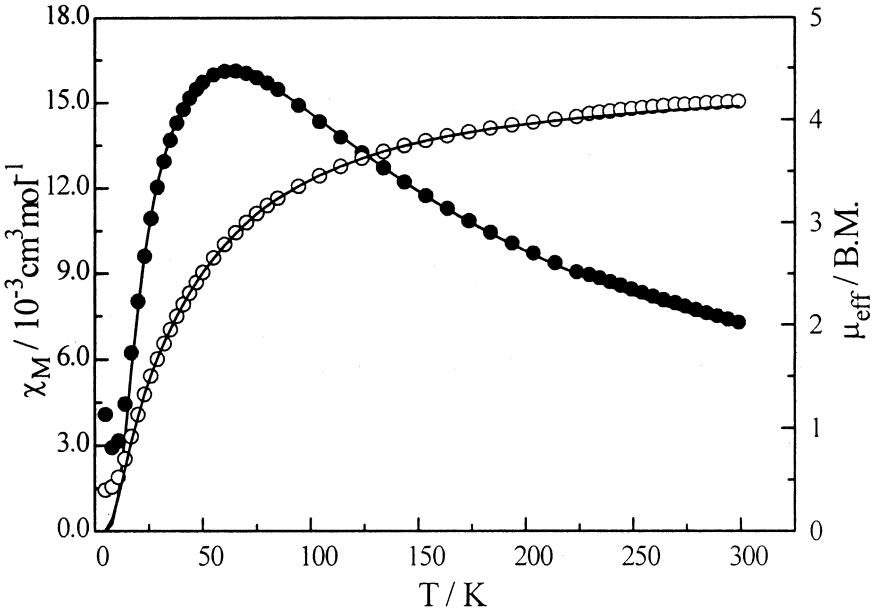


Fig. 3. The temperature variation of magnetic susceptibility (●) and magnetic moment (○) for complex **1**.

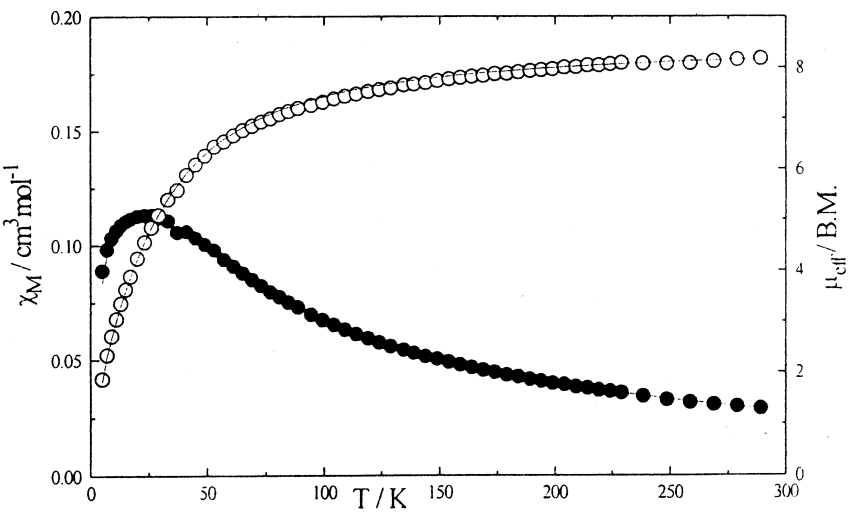


Fig. 4. The temperature variation of magnetic susceptibility (●) and magnetic moment (○) for complex **2**.

based on the Heisenberg spin-exchange operator: $\hat{H} = -2J\hat{S}_1\hat{S}_2$.

$$\chi_M = \{2Ng^2\beta^2 \times [5 + \exp(-4J/kT)]\} / \{kT \times [5 + 3\exp(-4J/kT) + \exp(6J/kT)]\} \quad (4)$$

where χ_M denotes the susceptibility per binuclear complex molecule, and other symbols have their usual meanings. As shown in Fig. 3, a good least-squares fit to the experimental data was attained from Eq. (4). The magnetic parameters thus obtained are $J = -20.5$ cm^{-1}, $g = 2.2$ and the agreement factor defined by $F = \Sigma(\chi i_{obs} - \chi i_{cald})^2(\chi i_{obs})^{-1}$ is equal to 5.3×10^{-5}. The results further indicate that there exists an intramolecular antiferromagnetic spin-exchange interaction between two Ni^{II} ions in complex **1**. The magnetic behavior is in good agreement with this fact, where the super-exchange interaction in the M–N–N–N–M mode is antiferromagnetic coupling. It is also in good agreement with those of metal binuclear complexes with μ-1,3-azide-bridged [19,24]. In complex **3**, there is a ferromagnetic spin-exchange interaction. However, complex **1** shows an antiferromagnetic spin-exchange interaction between Ni^{II} ions. From the magnetic behavior of complexes **1** and **3**, it is obvious that the magnetic properties of the binuclear complexes of the same system ligands can be adjusted by altering the bridging ligands.

For complex **2**, the magnetic behavior is similar to that of complex **1**. It adopted a susceptibility equation based on the Hamiltonian: $\hat{H} = -2J\hat{S}_1\hat{S}_2$. The molar magnetic susceptibility is given by Eq. (5):

$$\chi_M = [(2Ng^2\beta^2)/kT]\cdot \{[(55 + 30\exp(-10J/kT) + 14\exp(-18J/kT) + 5\exp(-24J/kT) + \exp(-28J/kT))]/ [11 + 9\exp(-10J/kT) + 7\exp(-18J/kT) + 5\exp(-24J/kT) + 3\exp(-28J/kT) + \exp(-30J/kT)]\} \quad (5)$$

The temperature dependence of the magnetic susceptibility for **2** is shown in Fig. 4. The μ_{eff} value is 8.30 BM at r.t., which is slightly lower than the spin-only value of 8.36 BM excepted for two uncoupled high-spin Mn^{II} ions. Upon cooling, the magnetic moment value decreases slowly from 8.30 BM (300 K) to 6.45 BM (50 K), indicating the presence of a weak antiferromagnitic exchange interaction. The magnetic susceptibility of **2** was obtained by using Eq. (5), and the least-squares fitting with an assumed g value of 2.04 ($g_{exp} = 2.018$ by EPR) gives the parameters: $J = -2.99\ cm^{-1}$ and $F = 2.87 \times 10^{-5}$, $R = 3.58 \times 10^{-4}$ $[R = (\chi_{calc} - \chi_{obs})^2]/\Sigma(\chi_{obs})^2]$. The J value is much smaller than that of complex **1**.

The weaker antiferromagnetic interaction can be further illustrated by the fact that in complex **1** the unpaired electrons are in molecular orbitals that are probably dominantly nickel $3_{dx^2-y^2}$ and 3_{dz^2} in character. The four orbits, two on each nickel center, will interact with the azido orbit of the correct symmetry and thereby provide a potential 'pathway' for antiferromagnetic exchange between the two nickel centers [25].

For complex **2**, the $|J|$ value is much smaller than that of **1**. This situation may be illustrated as follows: in the Ni^{II} complex there are two magnetic orbits on each nickel atom, but there are five magnetic orbits on each atom in the case of Mn^{II}. However, the interaction between only a part of the magnetic orbits can be considered for the contribution of magnetic behavior. The other unpaired electrons that do not participate on manganese atom 'dilute' the magnetic coupling action [26].

3.5. Electronic spectra

The electronic spectra of the title complexes in methanol solution have been studied, these have been assigned and summarized in Table 4. The spectral data of complex **3** and listed for comparison. For complex **1**, three absorption bands have been observed. The two bands in the visible and infrared range are assigned to d–d spin-allowed transition of the Ni^{II} ion in an octahedral crystal field and the stronger absorption band in the UV range is assigned to the charge-transfer band [27]. According to Lever's transition energy ratio [28], some coordination field parameters of the complexes have been obtained by using two observed bands v_1 and v_2, and the calculated results are summarized in Table 4. From the data of Table 4, it has been observed that the Dq value of **1** is lower than that of **3**, indicating the stronger coordination field strength of TPA in comparison to that of TLA. The values of $\beta < 1$ show strongly covalent bonding of Ni^{II} in complex **1** [29], and the covalent property of metal–nitrogen bonds in **1** is greater than that in **3** from the β value [β value of **1** (0.785) is lower than that of **3** (0.838)]. It might be illustrated that although the substituted methyl groups on the pyridines of TLA as the electron-donating groups increase the electronic density on the ligand, they meanwhile increase the space hindrance. Both electronic and hindrance effects result in **1** being less

Table 4
Electronic spectral data and some coordination field parameters of **1**, **2** and **3** in MeOH solution

Complex	λ (nm)	$\varepsilon \times 10^{-3}$ ($M^{-1}\ cm^{-1}$)	Assignment	Dq (cm^{-1})	B	β
1	312	1.840	L → M (CT) $^3A_{2g} \rightarrow {}^3T_{1g}(P)$; v_3			
	655	0.035	d → d $^3A_{2g} \rightarrow {}^3T_{1g}(F)$; v_2	940	817	0.785
	1064	0.056	d → d $^3A_{2g} \rightarrow {}^3T_{2g}(F)$; v_1			
2	264	18.44	π → π*			
	206	16.97	n → π*			
3 [15a]	323	1.108 (v_3)	L → M (CT) $^3A_{2g} \rightarrow {}^3T_{1g}(P)$; v_3			
	595	0.043 (v_2)	d → d $^3A_{2g} \rightarrow {}^3T_{1g}(F)$; v_2	1046	872	0.838
	955	0.042 (v_1)	d → d $^3A_{2g} \rightarrow {}^3T_{2g}(F)$; v_1			

stable than **3**, implying the space effect as the main factor.

For complex **2**, two bands around 264 and 206 nm with high intensity in UV-range have been observed, which can be assigned to the transitions in the ligands themselves. The d–d transition band of **2** is not observed in the dilute solution.

4. Supplementary material

Supplementary data are available from the Cambridge Crystallographic Data Centre, 12 Union Road, Cambridge CB2 1EZ, UK on request, quoting the deposition numbers CCDC 132443 and 132442 for **1** and **2**, respectively.

Acknowledgements

This work was financially supported by the Tianjin Natural Science Foundation of PR China (No. 973602311) and the National Natural Science Foundation of PR China (No. 29771022).

References

[1] C.P. Landee, R.D. Willet, Inorg. Chem. 20 (1981) 2521.
[2] R. Cortes, J.I.R. Larramendi, L. Lezama, T. Rojo, K. Urtiaga, M.I. Arriortua, J. Chem. Soc., Dalton Trans. (1992) 2723.
[3] C.S. Hong, Y. Do, Inorg. Chem. 29 (1997) 5684.
[4] A.R. Oki, J. Glerup, D.J. Hodgson, Inorg. Chem. 29 (1990) 2435.
[5] Z. Dori, R.F. Ziolo, Chem. Rev. 73 (1973) 247.
[6] J. Ribas, M. Monfort, C. Diaz, C. Bastos, X. Solans, Inorg. Chem. 33 (1994) 484.
[7] J. Commarmond, P. Plumere, J.M. Lehn, Y. Agnus, R. Louis, R. Weiss, O. Kahn, I. Morgenstern-Badarall, J. Am. Chem. Soc. 23 (1982) 490.
[8] A. Escuer, R. Vicente, M.S.EI. Fallah, J. Ribas, X. Soloms, M. Font-Bardia, J. Chem. Soc., Dalton Trans. (1993) 2975.
[9] R. Cortes, J.L. Pizarro, L. Lezama, M.I. Arriortua, T. Rojo, Inorg. Chem. 33 (1994) 2697.
[10] P. Chaudhuri, M. Guttmann, D. Ventur, K. Weighardt, B. Nuber, J. Weiss, J. Chem. Soc., Chem. Commun. (1985) 1618.
[11] R.E. Sikorav, I. Bkouche-Waksman, O. Kahn, Inorg. Chem. 23 (1984) 490.
[12] (a) T. Sasaki, N. Nakamura, Y. Naruta, Chem. Lett. (1998) 351. (b) T. Kojima, T. Amano, Y. Ishii, M. Ohba, Y. Okaue, Y. Matsuda, Inorg. Chem. 37 (1998) 4076. (c) A. Ghosh, J. Almtof, L. Que Jr, Angew. Chem., Int. Ed. Engl. 35 (1996) 770.
[13] (a) A. Nanthakumar, S. Fox, N.N. Murthy, K.D. Karlin, J. Am. Chem. Soc. 119 (1997) 3898. (b) Y. Zang, J. Kim, Y. Dong, E.C. Wilkinson, E.H. Appleman, L. Que Jr., J. Am. Chem. Soc. 119 (1997) 4197.
[14] (a) K.J. Oberhausen, R.J. O'Brien, J.F. Richardson, R.M. Buchanan, R. Costa, J.M. Latour, H. Tsai, D.J. Hendrickson, Inorg. Chem. 32 (1994) 4561, and refs. therein. (b) J. Ribas, M. Monfort, I. Resino, X. Solans, P. Raly, F. Maingot, M. Drillon, Angew Chem., Int. Ed. Engl. 21 (1996) 2520.
[15] (a) Z.H. Zhang, X.H. Bu, Z.A. Zhu, Z.H. Jiang, Y.T. Chen, Transition Met. Chem. 21 (1996) 235. (b) Z.H. Zhang, X.H. Bu, Z.A. Zhu, Y.T. Chen, Polyhedron. 16 (1996) 2787. (c) Z.H. Zhang, Z.A. Zhu, X.H. Bu, Y.T. Chen, Polyhedron 3 (1997) 527.
[16] M.M. De Mota, J. Rodgers, S.M. Nelson, J. Chem. Soc., A (1969) 2036.
[17] P.W. Selwood, Magnetochemistry, Interscience, New York, 1956, pp. 78–91.
[18] (a) G.M. Sheldrick, SHELXTL-plus, structure determination software programs, Simense Analytical X-ray Instruments Inc., Madison, WI, USA, 1990. (b) G.M. Sheldrick, SHELXTL93 programs for crystal structures, University of Gottingen, Germany, 1990.
[19] (a) J. Ribas, M. Monfort, X. Solans, Inorg. Chem. 32 (1993) 3557. (b) R. Vicente, A. Escuer, J. Ribas, X. Solan, Inorg. Chem. 31 (1992) 1726. (c) A. Escure, R. Vicente, M.S.El. Fallah, J. Ribas, X. Solans, M. Font-Bardia, J. Chem. Soc., Dalton Trans. (1993) 2975.
[20] J.E. Huheey, Inorgorganic Chemistry, third ed., Harper and Row, New York, 1983.
[21] C.S. Hong, Y. Do, Angew Chem., Int. Ed. Engl. 38 (1999) 193.
[22] C.G. Pierpont, D.N. Hendrickson, D.M. Duggan, F. Wagner, E.K. Barefield, Inorg. Chem. 3 (1975) 604.
[23] D.F. Xiang, X.S. Tan, W.X. Tang, F. Xue, T.C.W. Mark, Polyhedron 17 (1998) 1375.
[24] M.A.S. Geher, N.A. Al-Salem, F.A. Mautner, K.O. Klepp, Polyhedron 16 (1997) 825.
[25] A.P. Ginsberg, Inorg. Chim. Acta, Rev. 5 (1971) 45.
[26] J. Glerup, P.A. Goodson, D.J. Hodgson, K. Michelsen, Inorg. Chem. 34 (1995) 495.
[27] Y. Journeaux, O. Kahn, J. Chem. Soc., Dalton Trans. (1979) 1575.
[28] O. Kahn, Angew. Chem., Int. Ed. Engl. 24 (1985) 384.
[29] A.B.P. Lever, Inorganic Electronic Spectroscopy, Second ed., Elsevier, Amsterdam, 1984, pp. 816–818.

PERGAMON

www.elsevier.nl/locate/poly

Polyhedron 19 (2000) 1567–1574

POLYHEDRON

Complexes of praseodymium(III) with D-gluconic acid

Sébastien Giroux, Patrice Rubini *, Bernard Henry, Sabrina Aury

Laboratoire de Chimie Physique Organique et Colloïdale, Université Henri Poincaré-Nancy I, Unité Mixte CNRS-UHP (SRSMC, UMR no. 7565), BP 239, 54506 Vandoeuvre-Les-Nancy Cedex, France

Received 25 February 2000; accepted 8 May 2000

Abstract

The complexation of the praseodymium(III) ion with D-gluconic acid was studied by potentiometry, UV–Vis spectrophotometry, circular dichroism (CD) experiments and ^{1}H and ^{13}C NMR. In order to determine the coordination sites, the study of the complexation with D-galactonic and D-gulonic acids was also achieved. It was found that six different complexes are formed in solution from pH 2 to 11.5. The formation constants were determined. For four species among the six, D-gluconic acid binds the cation with deprotonated hydroxylic group(s) in addition to the carboxylate group. On the basis of the spectroscopic results, the structures of the complexes are discussed. © 2000 Elsevier Science Ltd. All rights reserved.

Keywords: D-Gluconic acid; D-Galactonic acid; D-Gulonic acid; Praseodymium(III); Complexation

1. Introduction

Gluconic acid is used more and more in the industrial domain for its complexing properties. Gluconate is non-toxic and fully biodegradable. It is prepared from maize or wheat starch [1] and available potentially in great quantity.

If the complexing ability of gluconic acid for metallic cations is largely accepted [2–6], detailed studies on the nature of the complexes formed in solution and their structures are not so numerous. It was shown that gluconic acid binds to cations in basic solutions by the carboxylate group and deprotonated hydroxyl functions, but the exact coordination sites are difficult to determine in solution, although some NMR [7–9] and circular dichroism [10] studies on a few systems have been performed in order to solve this problem.

Among the cations studied, the lanthanides ions have not been studied much [2,10,11], particularly the lanthanide(III) ions. Nevertheless, as they are hard acids, the complexation with D-gluconic acid, which binds to cations by oxygen atoms, must be strong. This work is devoted to the study of the complexation of D-gluconic acid with the cation Pr(III) in aqueous solutions from pH 2 to 11.5. The stoichiometry and the formation constants of the complexes were determined by pH-potentiometry. The system was ascertained by spectroscopic studies such as UV–Vis spectrophotometry and NMR and by CD experiments. For the CD study, a comparison with D-gulconic and D-galactonic acids, which are epimers of D-gluconic acid, was made in order to know which oxygens of the ionized hydroxyl groups are bound to the cation.

This work is the first step in the study of the complexation of D-gulonic acid (and other polyhydroxylated carboxylic acids) with the series of the lanthanide(III) ions. Besides the thermodynamical and the structural aspects, we are interested also in the search for ligands which present selectivity along the lanthanide series.

2. Experimental

2.1. Materials

Potassium D-gluconate (Fluka 99%), D-galactonic acid γ-lactone (Fluka 99%), D-gulonic acid γ-lactone

* Corresponding author. Fax: 33-3-839-12532.
E-mail address: rubini@lesoc.u-nancy.fr (P. Rubini).

0277-5387/00/$ - see front matter © 2000 Elsevier Science Ltd. All rights reserved.
PII: S0277-5387(00)00422-8

(Fluka 97%) and praseodymium(III) nitrate (Strem Chem 99.9%) were used without further purification. The concentration of Pr(III) was determined by a standard procedure using EDTA (Merck). pH-metric titrations were performed with NaOH (Merck or SDS) standard solutions.

2.2. pH-metric measurements

pH-metric titrations were performed in aqueous solutions for the investigation of the protonation and coordination equilibria at $T = 298.0 \pm 0.1$ K and at an ionic strength $I = 0.1$ mol l^{-1} ($NaClO_4$) under an argon atmosphere. An automatic titration set, including a Dosimat 665 (Metrohm) autoburette, an Orion-525 A precision digital pH-meter and a Mettler Toledo Inlab 422 type combined glass electrode, was used for the titrations. The species formed in the systems were characterized by the following general equilibrium process:

$$pM + qL + rH \rightleftharpoons M_pL_qH_r \quad (\beta_{pqr})$$

$$\beta_{pqr} = \frac{[M_pL_qH_r]}{[M]^p[L]^q[H]^r}$$

where M denotes the lanthanide(III) ion and L denotes the non-protonated ligand molecules (L^-). Charges are omitted for simplicity, but can be easily calculated taking into account that the fully protonated ligand is LH. The detailed description of the experimental procedure and data evaluation, using the PSEQUAD computer program [12] were described earlier [13,14]. The protonation and the complex formation constants were determined from four and eight independent titrations (~ 100 data points per titration), respectively. The metal-to-ligand ratio was varied between 1:1 and 1:6, using praseodymium(III) concentration ranging from 1.3×10^{-3} to 5.6×10^{-3} mol l^{-1}. The pH-metric data between pH 2 and 11.3 were used for the evaluation.

For the analysis of the titration curves, the formation of the hydroxo complex MOH^{2+} (MH_{-1}) was taken into consideration with a formation constant value ($\log \beta_{10-1}$) equal to -8.82 [14].

It must be noted that the accurate determination of the acidity constant of D-gluconic, D-galactonic and D-gulonic acids is not so easily calculated because of the lactonization of these molecules in acidic solutions. The gluconate solution must be acidified just before the beginning of the titration and the speed of the titration before the equivalence point must be adjusted to avoid lactone formation at the maximum on one hand, and to allow a good stabilization of the measurements on the other hand. The value obtained in this work ($pK_a = 3.472 \pm 0.007$) is in agreement with those reported in the literature for identical experimental conditions ($t = 25°C$, $I = 0.1$ mol l^{-1}) [16–18].

2.3. UV–Vis spectrophotometry

The visible absorption spectra were recorded on a Varian Cary 3E UV–Vis spectrophotometer. The Pr(III) concentration was 3×10^{-2} mol l^{-1} initially and the ligand (D-gluconic acid) to metal ratios 1.1:1 and 2.1:1. pH was varied by the addition of soda or perchloric acid. The different spectra were normalized by considering the band of the nitrate anions, the intensity of which depends only on the concentration of these ions (and not on pH).

As the concentrations of the seven possible species present in solution (Pr^{3+}, PrL^{2+}, $PrLH^{+}_{-1}$, $PrLH_{-2}$, $PrLH_2^{+}$, PrL_2H_{-1} and $PrL_2H^{2-}_{-3}$) are known from the potentiometric results and by using the Beer–Lambert equation, the ε values of each complex as a function of the wavelength could be computed, taking into account the spectra recorded at different pH values and L:M ratios:

$$D_i(\lambda) = \sum_J \varepsilon_j(\lambda) \cdot C_{ji} \cdot 1$$

where j denotes one of the seven species ($j = 1$–7) and $i = 1$–7, seven different spectra. Therefore the determination of the seven ε values consists in the matricial resolution of seven equations with seven unknown quantities.

2.4. Circular dichroism experiments

CD spectra were recorded on a Jobin-Yvon DGG circular dichroism spectrophotometer on solutions of Pr(III) with a concentration equal to 5×10^{-2} mol l^{-1}, for ligand to metal ratios equal to 1:1 and 5:1 and for different pH values. Only the domain 430–500 nm was observed.

2.5. NMR spectroscopy

^1H and ^{13}C NMR spectra were recorded on a Bruker DRX 400 apparatus at 400 and 100.6 MHz, respectively. ^1H chemical shifts were measured relatively to DSS, the chemical shift of which is the same as that of TMS; the concentration of the ligand was 0.1 mol l^{-1} and the solvent D_2O. ^{13}C NMR chemical shifts were measured with respect to dioxane and converted to the TMS scale using the value $\delta_{dioxane} = 67.4$ ppm. The concentration of the ligand was fixed to 0.3 mol l^{-1} and the solvent was a mixture of H_2O and D_2O (80/20 v/v)

In D_2O solutions, the pD value was obtained by adding 0.40 to the value read on the pH-meter [19].

3. Results

3.1. pH-metric measurements

From potentiometric experiments, a set of six complexes formed between Pr(III) and D-gluconic acid can be determined: ML^{2+}, MLH^{+}_{-1}, MLH_{-2}, ML_2^{+}, ML_2H_{-1} and $ML_2H^{2-}_{-3}$ (the ligand, under its acidic form, is noted LH). The corresponding formation constants are: $\log \beta_{110} = 2.78 \pm 0.03$, $\log \beta_{11-1} = -3.34 \pm 0.02$, $\log \beta_{11-2} = -10.09 \pm 0.01$, $\log \beta_{120} = 5.57 \pm 0.03$, $\log \beta_{12-1} = -0.67 \pm 0.05$ and $\log \beta_{12-3} = -19.13 \pm 0.08$. From these values, some characteristic protonation constants can be calculated:

$$ML^{2+} \rightarrow MLH^{+}_{-1} + H^{+} \qquad pK = 6.12$$

$$MLH^{+}_{-1} \rightarrow MLH_{-2} + H^{+} \qquad pK = 6.75$$

$$ML_2^{+} \rightarrow ML_2H_{-1} + H^{+} \qquad pK = 6.24$$

Some representative distribution diagrams of these complexes in function of pH are represented in Fig. 1. The complexation starts at pH 2 with the formation of the complex ML. The formation constant of this species is of the same order of magnitude as those for comparable polyhydroxylated carboxylic acids [20,21]. ML and ML_2 complexes are present together in solution up to pH 7–8 but ML_2 predominates over ML for ligand to metal ratios higher than 2:1 from pH ~ 3–4. At neutral pH values, MLH_{-1} or ML_2H_{-1} are the major species (ML_2H_{-1} for high ligand to metal L:M ratios). From pH ~ 8, MLH_{-2} becomes the predominant species up to pH ~ 11. Beyond this value, ML_2H_{-3} predominates. It must be noted that, for low L:M ratios, a precipitate is observed at pH ~ 8–9.

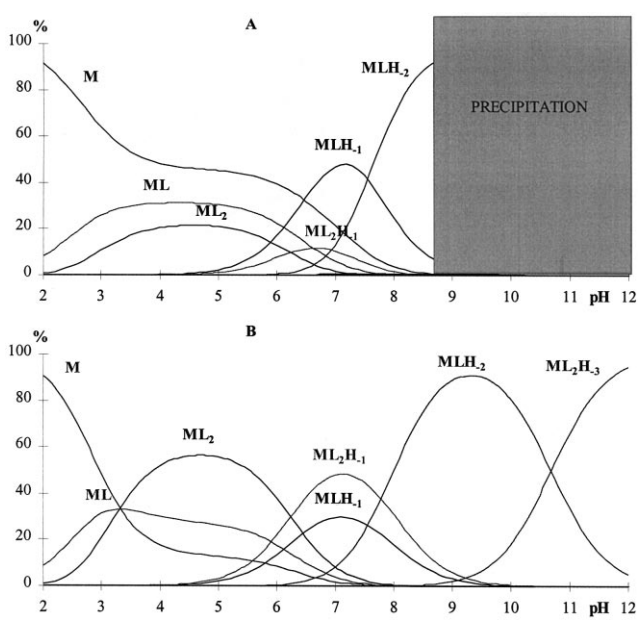


Fig. 1. Distribution diagrams for the Pr(III):D-gluconic acid system. $[Pr(III)] = 5 \times 10^{-3}$ mol l^{-1}. Ligand to metal ratio L:M = 1:1 (A) and L:M = 5:1 (B).

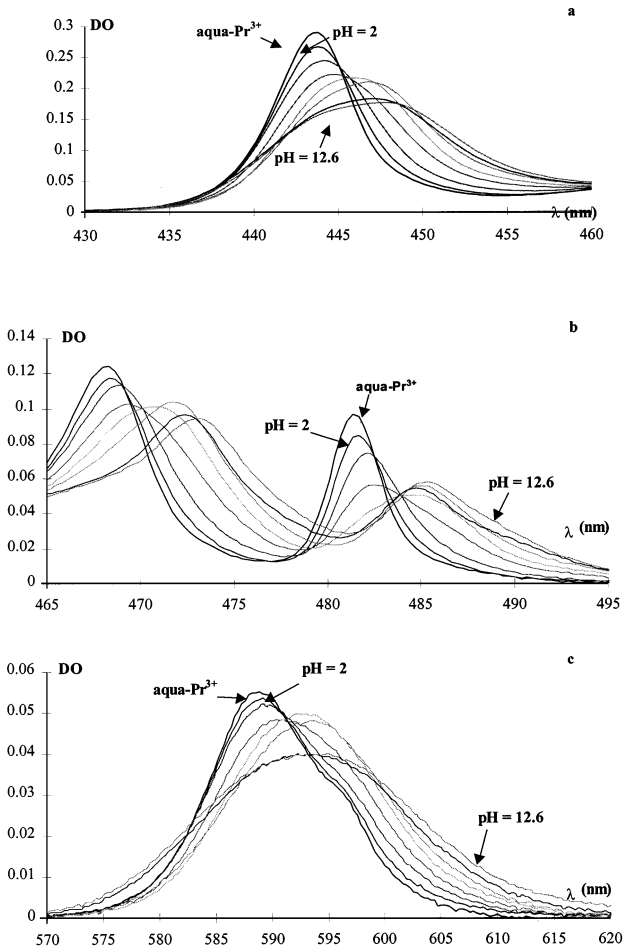


Fig. 2. Visible spectrophotometic spectra of the system Pr(III):D-gluconic acid in a 2.1:1 ratio ($Pr(III) = 0.03$ mol l^{-1}) corresponding to the $^3P_2$ (a), $^3P_1$ and $^3P_0$ (b) and $^1D_2$ (c) transitions. Evolution of the spectra from pH 2 to 12.6.

3.2. UV–Vis spectroscopy

UV–Vis spectra of Pr(III)/D-gluconic acid solutions present band absorptions in the visible region (solutions are pale green) corresponding to $^3P_2$, $^3P_1$, $^3P_0$ (around 450–490 nm) and $^1D_2$ (around 590 nm) transitions. This spectroscopy can be used to study the complexation at different pH values, but it is well known that the shifts due to complexation are weak for lanthanides ions [22]. Nevertheless spectra show clearly an evolution when pH is varied (Fig. 2). At pH 4.2 where the species ML_2 is predominant, it can be seen on the spectra for L:M = 2.1:1 that the peak corresponding to M^{3+} without ligand is slightly (but surely) shifted and its intensity decreases. At pH 7, where ML_2H_{-1} is the major complex, the shift of the bands is more pronounced (~ 4 cm^{-1} towards the high wavelengths) and distinct peaks from those of the free metal are clearly

observed. Around pH ~ 8 where MLH_{-2} arises, a decrease in the intensity of the peaks and a broadening are observed. Finally, for high pH values (11–12), spectra do not much differ from those recorded at pH ~ 8. It is clearly shown, by varying pH, that four major species are formed in solutions, exactly as the potentiometric results proved (the four complexes: ML_2, ML_2H_{-1}, MLH_{-2} and ML_2H_{-3} are found to be dominant for L:M = 2.1:1, successively from pH 2 to 12). From the spectra recorded for different pH values and two different L:M ratios and from the knowledge of the proportions of the different complexes from the pH-metric results, the ε values of the seven species (six complexes plus the M^{3+} aquo-cation) can be calculated. The results are presented in Fig. 3. It is clear that, if the system found from the potentiometric experiments was wrong, it would not be possible to fit all these results and to obtain reasonable ε values and a correct peak shape for all the species.

3.3. Complexation of Pr(III) by D-galactonic and D-gulonic acids

D-Gluconic acid has four asymmetric carbons and the interaction of this ligand with Pr(III) which presents

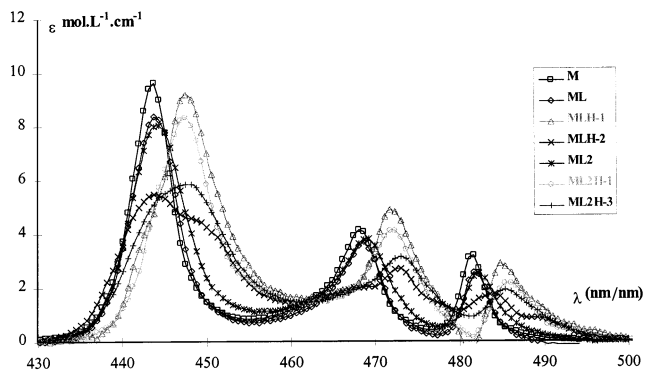
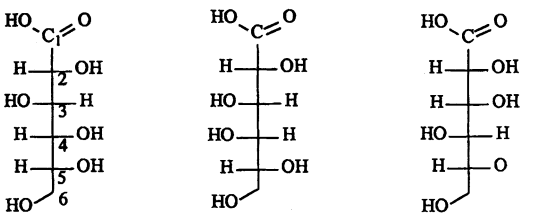


Fig. 3. Calculated ε values for the different complexes formed in the system Pr(III):D-gluconic acid as a function of λ.

Table 1
Logarithm of the formation constant β_{pqr} of the complexes $Pr_pL_qH_r$ for the different ligands studied

	D-Galactonic acid	D-Gulonic acid	D-Gluconic acid
PrL	2.60 ± 0.03	2.67 ± 0.02	2.78 ± 0.03
$PrLH_{-1}$	-3.47 ± 0.02	-3.21 ± 0.01	-3.34 ± 0.02
$PrLH_{-2}$	-10.19 ± 0.01	-9.80 ± 0.01	-10.09 ± 0.01
PrL_2	5.53 ± 0.02	5.32 ± 0.02	5.57 ± 0.03
PrL_2H_{-1}	-0.56 ± 0.03	–	-0.67 ± 0.03
PrL_2H_{-3}	–	–	-19.13 ± 0.08
$Pr_2L_2H_{-3}$	–	-10.50 ± 0.03	–
$Pr_2L_2H_{-5}$	–	-26.76 ± 0.05	–
LH	3.52	3.45	3.47

absorption bands in the UV–vis domain may generate effects in the circular dichroism (CD) spectra providing that the asymmetry centers are not too far from the complexation sites. CD studies may be very useful to determine these sites and to obtain information about the coordination mode of D-gluconic acid with the lanthanide(III) ions. In order to have elements of comparison and a better information on the coordination sites, it was decided to study the complexation of Pr(III) with two epimers of D-gluconic acid:D-galactonic acid which differs from D-gluconic acid only by the configuration of the C_4 carbon (carbon in γ position relative to the carboxylic function) and D-gulonic acid which differs from D-galactonic acid by the configuration of the C_3 atom.



It is necessary, before recording CD spectra with these ligands, to know which complexes are formed with Pr(III) and if they are different from those found for D-gluconic acid. A potentiometric study was made and the nature of the complexes and their formation constants are summarized in Table 1. The complexes ML, MLH_{-1}, MLH_{-2} and ML_2 are shared by the three ligands. ML_2H_{-1} does not exist for the system Pr(III)/D-gulonic acid. The bigger differences are observed in basic media. For D-galactonic acid, no complex at basic pH was determined since a precipitate is systematically observed from pH ~ 9.5. For D-gulonic acid, the dimeric species $M_2L_2H_{-3}$ and $M_2L_2H_{-5}$ replace the complex ML_2H_{-3} for D-gluconic acid. The respective distribution diagrams for D-galactonic and D-gluconic acids are not so different from each other, as can be seen in Fig. 4 (drawn for L:M = 5:1): ML_2 predominates at pH 2–6 and ML_2H_{-1} at pH ~ 6 – 8. The distribution diagram for D-gulonic acid is a little different from the two others, particularly in the pH domain ~ 6–8.

3.4. CD experiments

Katzin performed circular dichroic studies [10] of hydroxy acids complexes with the praseodymium ion but he did not know exactly the repartition of the different species according to pH. He worked on acidic, neutral and basic complexes. Furthermore, our detailed work on the formation of complexes as a function of pH, resumed this CD study. Spectra were recorded for

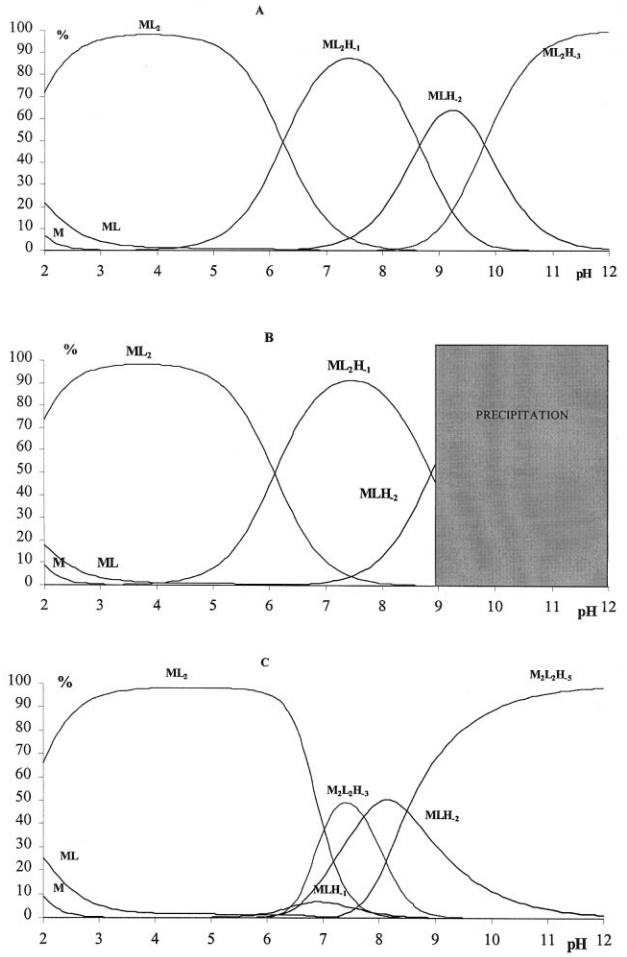


Fig. 4. Distribution diagrams for the systems Pr^{3+}:D-gluconic acid (A), Pr^{3+}:D-galactonic acid (B) and Pr^{3+}:D-gulonic acid (C) for L:M = 5:1 and [M] = 0.05 mol l^{-1}.

L:M = 5:1 (Pr(III) = 0.05 mol l^{-1}) as well for D-gluconic acid as for D-gulonic and D-galactonic acids (Fig. 5). At pH 4, the complex ML_2 is predominant and there is practically no dichroic effects. At pH ~ 6–7, strong CD effects are seen. This pH domain corresponds to the existence of the complex ML_2H_{-1} for D-gluconic and D-galactonic acid. It can be noted that the spectra are inverted as already reported by Katzin [10]. This probably denotes the participation to the complexation of a hydroxyl or a deprotonated hydroxyl group. It must also kept in mind that D-gluconic acid and D-galactonic acid only differ from the configuration of the C_4 carbon. It can be concluded that the hydroxyl group or the hydroxylate in γ position relative to the carboxylate is probably involved in the coordination. For D-gulonic acid, the complexes present at pH 6.5–7.5 are $M_2L_2H_{-3}$ and MLH_{-2}; the CD spectrum is quite different from those observed for the other molecules but strong CD effects are also observed. It must be noted that, for D-gluconic and D-galactonic acids, there is at the most one deprotonated OH function in the complex ML_2H_{-1} whereas, for $M_2L_2H_{-3}$ and MLH_{-2} complexes with D-gulonic acid, the ligand is potentially under the form LH_{-2} with two ionized OH functions.

The spectrum obtained at pH 11.0 with D-gluconic acid is quite different from those obtained at pH 6–7. It corresponds to the domain of existence of the complex ML_2H_{-3}, the structure of which is discussed below. The corresponding UV–Vis spectrum shows broader absorption bands than those observed at lower pH values.

3.5. ^1H and ^{13}C NMR

Solutions of D-gluconic acid and praseodymium(III) ion for various L:M ratios and pH values were examined by ^1H and ^{13}C NMR. Pr(III) cation is paramagnetic and leads to broadenings of the peaks in the NMR spectra, particularly for the nuclei which are close to the binding sites. The assignment of the peaks for free D-gluconic in ^{13}C NMR spectra has been made already [7,23].

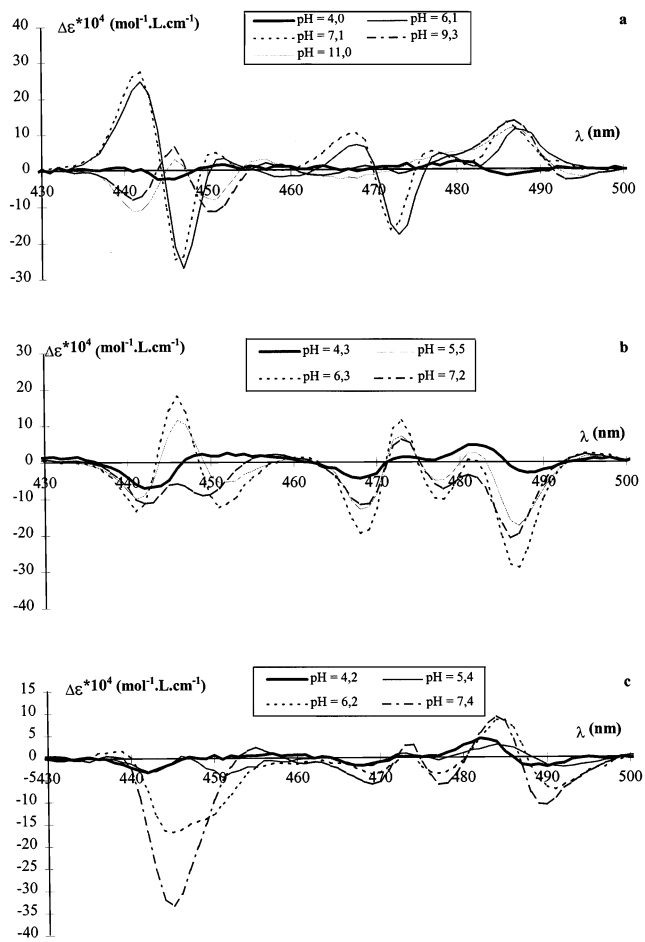


Fig. 5. CD spectra of Pr(III):D-gluconic acid (A), Pr(III):D-galactonic acid (B) and Pr(III):D-gulonic acid (C) solutions for different pH values (L:M = 5:1 and [M] = 0.05 mol l^{-1}).

Table 2
Chemical shifts, in ppm, of the ^{13}C NMR (A) and ^{1}H NMR (B) signals of D-gluconic acid for different metal to ligand M:L ratios [a]

M:L	C_1	C_2	C_4	C_5	C_3	C_6
(A)						
1:1	~212.2	~93.3	70.46	70.46	76.83	62.06
1:2.5	201.93	89.26	71.19	70.80	74.58	62.44
1:5	191.91	82.84	71.84	71.29	73.04	62.89
1:25	181.62	76.30	72.89	71.90	72.02	63.41
1:33	180.92	75.86	72.97	71.94	71.94	63.44
1:50	180.18	75.39	73.04	71.99	71.90	63.48
$\delta_{1:2,5}-\delta_{1:50}$	21.75	13.87	−1.85	−1.19	2.68	−1.04
	C_2H	C_3H	$C_{4.5}H$	C_6H'	C_6H''	
(B)						
1:5	8.32	5.62	(3.20)	3.30	−3.10	
1:10	5.17	4.42	3.65	3.72	3.55	
1:20	–	4.25	3.70	3.77	3.59	
1:30	4.57	4.18	3.72	3.78	3.62	
0:1	4.14	4.04	3.77	3.84	3.67	
$\delta_{1:5}-\delta_{0:1}$	4.18	1.58	−0.57	−0.54	−0.57	

[a] [L] = 0.1 mol l^{-1}; pH 4.0.

At pH 4, where ML_2 is present at 100% for these experimental conditions, ^{13}C NMR spectra as well as ^{1}H NMR spectra show clearly that the peak, the most affected by the presence of Pr(III), corresponds to the carbon of the carboxylate group and the hydrogen on the carbon C_2, in ^{13}C and ^{1}H NMR, respectively. The effect plays as well on the line-width as on the shift of the signals. The further from the carboxylate the carbon or proton nuclei are, the less their shifts and line-width are affected (Table 2). This indicates clearly a coordination by the carboxylate group for the complex ML_2.

At pH 7.5 (complex ML_2H_{-1} after the potentiometric results), the peaks are much broadened, even for large L:M ratios, but very little shifted. Probably the exchange between free and bound ligand molecules is slow relative to the NMR time scale. The signal due to bound molecules is very broad and probably much shifted and cannot be detected. The signals of the free ligand are broadened because the exchange with bound molecules (the signal of which are very broad) occurs at a rate allowing the observation of separate free signals but generating, nevertheless, a broadening of the peaks. The most disturbed signals are, in order: C_1, C_2, C_3 and C_4.

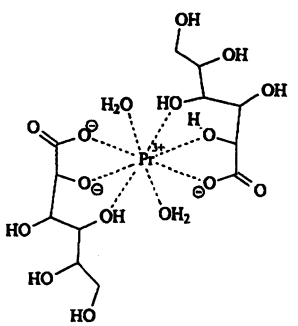
In the domain of existence of the species ML_2H_{-3}, at pH 11.4, the ^{1}H and ^{13}C NMR spectra correspond to that of the free ligand: signals are narrow and not shifted. It was verified that the complex is paramagnetic by measuring the magnetic susceptibility. The signals observed are those of the free ligand only, as proved by the measurements of the integrals of the peaks compared to those of an external reference (contained in a capillary tube). The signals of the bound molecules do not appear in the spectrum: they are probably very broad and shifted. The exchange rate between bound and free ligands is slow relative to the NMR time scale, slower than that observed in the case of the complex ML_2H_{-1}.

4. Discussion

The calculations from potentiometric experiments allowed us to show that six different complexes are formed in aqueous solutions containing the praseodymium(III) cation and D-gluconic acid. In acidic domains, the species ML^{2+} and ML_2^{+} are present. ML_2^{+} is predominant where L:M is higher than 2:1, except for low cation concentrations at low pH values. The site of coordination in these complexes is the carboxylate group as revealed mainly by ^{1}H and ^{13}C NMR (Table 2). It can be noted that the peak of the carbon C_2 is also broadened and shifted, indicating that, the corresponding hydroxyl group gives probably rise to an interaction with the cation. This interaction is weak since no CD effect is observed. The formation constant of the complex PrL^{2+} ($\log \beta_{110} = 2.78$) is higher than that found for the complex AlL^{2+} ($\log \beta_{110} = 1.98$) [16]. This observation could confirm the participation of the hydroxyl group of the carbon C_2 to the coordination in the case of Pr(III) since, if it is considered that the interaction between the carboxylate group and the trivalent cation is essentially electrostatic, the formation constant of the species AlL^{2+} should be higher than that of PrL^{2+}.

Around pH ~ 6–8 appear the complexes MLH_{-1} and ML_2H_{-1}. For high L:M ratios, ML_2H_{-1} is pre-

dominant. The ionization constants of ML and ML_2 are very close together (6.12 and 6.24, respectively) indicating that the same process of deprotonation occurs in both cases. The loss of a proton can be due to the deprotonation of a OH group of the ligand or to the ionization of a coordinated water molecule. The pK for the latter process is 8.82 [15] for the aqua-complex $Pr(H_2O)_n^{3+}$ and is probably higher in ML or ML_2 as the result of the weakening of the Pr–OH_2 bond due to the coordination of the negatively charged carboxylate group [14]. It can be said that, in the complexes MLH_{-1} and ML_2H_{-1}, a OH group of D-gluconic acid is deprotonated and bound to the cation. These species give rise to absorption bands in the visible spectrum clearly shifted with respect to those relative to ML or ML_2 complexes. The coordination of an hydroxylate is also proved by the CD experiments. A clear CD effect occurs at pH 6–7; this indicates that the cation is bound to an atom close to a chiral center. ^1H and ^{13}C NMR spectra show that the exchange between free and bound molecules is slow relatively to the NMR time scale and much slower than in the case of the ML and ML_2 complexes, due to a stronger complexation. NMR seems to indicate that the coordination sites of D-gluconic acid are the carboxylate and the hydroxylate on carbon 2, forming a five-membered ring chelate for LH_{-1}. Nevertheless our dichroic studies on D-gluconic and D-galactonic acids show that the CD spectra for these two ligands are inverted at pH 6. Since D-galactonic and D-gluconic acids differ only by the configuration of the C_4 carbon, it seems that the OH group of the carbon C_4 plays a role in the coordination of these molecules with Pr(III). The following structure for ML_2H_{-1} can be proposed:

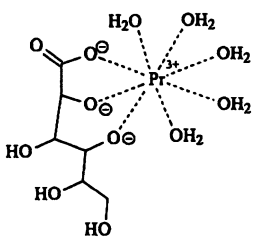


It must be noted that the coordination by the C_2–O^- group has been proposed already for the complexes of D-gluconic acid with Co(II), W(VI) and Mo(VI) by Escandar et al. [9] and by Ramos et al. [6].

For ligand to metal ratios L:M lower than 2:1, a precipitate appears systematically at pH 8. For L:M > 2:1, it is possible to go through the pH domain 8–11 without observing precipitation, but, if the pH is adjusted in this domain, a green precipitate appeared after a few minutes. We could not obtain crystals from this solid and a characterization by X-ray analysis was not possible. The ^1H NMR spectrum of an acidic aqueous solution in which the precipitate is dissolved, is identical to the NMR spectrum of a 1:1 cation/ligand solution at the same pH. The ^1H NMR analysis of the supernatant solution, which results from the precipitation of a 1:1 ligand to cation mixture at pH 8–10, indicates that there is no ligand in this phase. These two results and the microanalysis of the precipitate allow confirmation of the 1:1 stoichiometry of the solid complex which can be written MLH_{-2} as proved by the potentiometric study. The neutral character of the species explains its non-solubility in water. The acidity constant of MLH_{-1} corresponding to the reaction:

$$MLH^+_{-1} \rightarrow MLH_{-2} + H^+$$

has a value equal to 6.75. It is higher than the pK_a of ML^{2+} and smaller than the hydrolysis constant of the aqua-complex $Pr(H_2O)_n^{3+}$. This is consistent with the deprotonation of a second OH group of the ligand. As the CD experiments seem to prove that the OH group of the carbon C_4 plays a role in the coordination of D-gluconic acid in the species MLH_{-1} (see above), it can be concluded that it is probably this group which is deprotonated. The following structure for MLH_{-2} can be proposed:



For high pH values, the potentiometric results indicate the formation of the complex $(ML_2H_{-3})^{2-}$. The NMR spectra showed that the exchange between free and bound ligand molecules is slow relative to the NMR time scale as for the complexes MLH_{-1} or ML_2H_{-1}. For ML_2H_{-3}, the simultaneous presence of LH_{-1} and LH_{-2} (D-gluconate with one or two deprotonated alcoholic functions, respectively) can be envisaged. A coordination sphere including two LH_{-1} ligands and a hydroxyl ion OH^- can be also taken into consideration. It is not possible to conclude the structure of this complex from our spectroscopic studies but the latter assumption seems to be the most plausible. Indeed, as a result of the studies on the complexation of other trivalent lanthanide ions by D-gluconic acid (results to be published), it was found that, for some cations, a gel is formed at basic pH. An explanation could be the formation of a polymeric structure of entities ML_2H_{-2} linked together by OH^- bridges.

5. Conclusions

From a combination of pH-potentiometry and various spectroscopic methods we have shown that D-gluconic acid forms with Pr(III) six different complexes in aqueous solutions. At low pH, D-gluconic acid binds with the carboxylate group in the species ML and ML_2. At higher pH values, deprotonated OH groups participate to the coordination, that in α to the carboxylate group and, probably, for MLH_{-2} that in γ-position to the carboxylate group too. At $pH > 11$, the species ML_2H_{-3} is predominant and there is a strong presumption that a polymeric structure is formed where entities ML_2H_{-2} would be bound together by ions OH^-.

The existence of the complex MLH_{-2} at neutral pH values makes possible the extraction of this species in an organic phase (since this species is neutral), but the ligand must be more hydrophobic. In this field, we reported the preparation of hydrophobic derivatives of tartaric acid [21]: HOOC–CHOH–CHOH–CONHR where R is a long alkyl chain, to be used in the liquid–liquid extraction of lanthanide(III) ions (these compounds have the same complexing sites as D-gluconic acid).

The study of the complexation of other lanthanide(III) ions with D-gluconic acid is in progress in order to know if selectivity is observed along the series.

Acknowledgements

NMR spectra and a part of the CD spectra were recorded on the apparatus of 'Service Commun de RMN' and 'Service Commun de Biophysicochimie des Interactions Moléculaires' of University Henri Poincaré-Nancy I, respectively. Some of the CD experiments were also performed at the Jozsef Attila University, Department of Inorganic and Analytical Chemistry, Szeged, Hungary. The authors are grateful to Bela Gyurcsik and to Attila Jancso for their assistance and competence. The authors would like to thank Dr D. Champmartin for her help in NMR experiments.

References

[1] S. Gosset, Inf. Chim 296 (1988) 41.
[2] D.T. Sawyer, Chem. Rev. 6 (1964) 633 and references cited therein.
[3] K. Burger, L. Nagy, in: K. Burger (Ed.), Biocoordination Chemistry, Ellis Horward Series in Inorganic Chemistry, J. Burgess (Series Ed.), Ellis Horward, Chichester, UK, 1990, Chapter III and references cited therein.
[4] W.R. Carper, D.B. Coffin, Inorg. Chim. Acta 167 (1990) 261.
[5] R.E. Sheperd, Y. Isaacson, L. Chensny, S. Zhang, R. Kortes, J. Kevin, Inorg. Biochem. 49 (1993) 23.
[6] M.L. Ramos, M.M. Caldeira, V.M.S. Gil, Carbohydr. Res. 304 (1997) 97.
[7] T. Gajda, B Gyurcsik, T. Jakusch, K. Burger, B. Henry, J.J. Delpuech, Inorg. Chim. Acta 275–276 (1998) 130.
[8] G.D. Bailey, W.R. Carper, J. Inorg. Nucl. Chem. 52 (1993) 99.
[9] M.E. Escandar, L.F. Scala, M.G. Sierra, Polyhedron 13 (1994) 143.
[10] L.I. Katzin, Inorg. Chem. 7 (1968) 1183.
[11] D.T. Sawyer, R.T. Ambroise, Inorg. Chem. 1 (1962) 296.
[12] L. Zékány, L. Nagypal, in: D. Legget (Ed.), Computational Methods for the Determination of Stability Constants, Plenum, New York, 1995, Chapter 8.
[13] T. Gajda, B. Henry, S. Aubry, J.J. Delpuech, Inorg. Chem. 35 (1996) 586.
[14] P. Surdy, P. Rubini, N. Buzas, B. Henry, L. Pellerito, T. Gajda, Inorg. Chem. 38 (1999) 346.
[15] (a) U.K. Frolova, V.N. Kumok, V.V. Serebrennikov, Izv. Vyssh. Uchebn. Zaved. SSSR Khim. Khim. Tekhnol. 9 (1966) 176. (b) ibid., Chem. Abstr. 65 (1966) 9816c.
[16] R.J. Motekaitis, A.E. Martell, Inorg. Chem. 23 (1984) 18.
[17] A.E. Martell, R.M. Smith, Critical Stability Constants, Plenum, New York, 1982.
[18] M.F. Escandar, L.F. Scala, Can. J. Chem. 70 (1992) 2053.
[19] (a) P.K. Glasoe, F.A. Long, J. Phys. Chem. 64 (1960) 188. (b) D.T. Sawyer, J.R. Brannan, Inorg. Chem. 5 (1966) 65.
[20] J.E. Powell, J.L. Fawell, S. Kulprathipanja, Inorg. Chem. 4 (1975) 786.
[21] S. Giroux, P. Rubini, C. Gérardin, C. Selve, B. Henry, New J. Chem. 24 (2000) 173.
[22] S. Cotton, Lanthanides and Actinides, MacMillan Education, London, 1991.
[23] G.D. Bailey, W.R. Carper, J. Inorg. Biochem. 52 (1993) 99.

PERGAMON

www.elsevier.nl/locate/poly

Polyhedron 19 (2000) 1575–1578

POLYHEDRON

A new one-dimensional $[Ni(phen)(N_3)_2]_n$ compound with alternating end-on and end-to-end bridging azido ligands

Licun Li* [a,1], Daizheng Liao [b], Zonghui Jiang* [a,2], Shiping Yan [a]

[a] *Department of Chemistry, Nankai University, Tianjin 300071, People's Republic of China*
[b] *State Key Laboratory of Structural Chemistry, Fujian Institute of Research on Structure of Matter, Chinese Academy of Sciences, Fujian 350002, People's Republic of China*

Received 1 February 2000; accepted 3 May 2000

Abstract

A new azido-nickel(II) one-dimensional (1D) compound of $[Ni(phen)(N_3)_2]_n$ (phen = 1,10-phenanthroline) was prepared and characterized by X-ray crystallography and magnetic measurement. Its structure consists of nickel chains in which the nickel(II) ions are alternatively bridged by double end-on and double end-to-end azido bridges. The nickel(II) ions have a distorted octahedral environment, completed by the two nitrogen atoms of the phen ligand. The variable temperature magnetic susceptibility of the title compound has been investigated in the temperature range 4–300 K and revealed alternating antiferromagnetic ($J_{AF} = -4.77$ cm^{-1}) and ferromagnetic ($J_F = +28.08$ cm^{-1}) interactions. © 2000 Elsevier Science Ltd. All rights reserved.

Keywords: Azido-bridged nickel(II) compounds; Crystal structures; Magnetic properties

1. Introduction

One-dimensional (1D) magnetic chain compounds have been a very active area of magnetic materials and have been widely investigated from both experimental and theoretical viewpoints [1]. The azido group is a versatile bridging ligand which can generate complexes from binuclear [2], tetranuclear [3], cubane [4], 1D [5–7], 2D [8,9] to 3D compounds [10], and specifically for nickel(II) a large number of 1D compounds have been reported [7]. The coordination modes generally observed for the bridging azido groups are end-on with ferromagnetic interaction and end-to-end with antiferromagnetic interaction. The end-to-end nickel–azide system has been extensively studied from synthetic and magnetic points of view and suitable models were proposed to explain and predict the magnitude of the antiferromagnetic coupling as a function of the bond parameters in the bridge region [2,11]. Non-azido chain complexes with alternating ferromagnetic and antiferromagnetic couplings have been reported [12]. To the best of our knowledge, 1D nickel–azide systems with alternating ferromagnetic (through end-on bridges) and antiferromagnetic (through end-to-end bridges) interactions are very scarce. In the present paper, we describe the preparation of single crystal of the 1D compound $[Ni(phen)(N_3)_2]_n$ (phen = 1,10-phenanthroline) and we investigated its magnetic properties as a function of the temperature. The exchange interactions between nickel(II) ions through the double end-on and double end-to-end azido bridges are also analyzed.

2. Experimental

2.1. Materials

1,10-Phenanthroline and nickel(II) nitrate hexahydrate and sodium azide were purchased from commercial sources and used as received.

2.2. Preparation of a single crystal of $[Ni(phen)(N_3)_2]_n$

A single crystal of $[Ni(phen)(N_3)_2]_n$ was grown in aqueous solution by a slow-diffusion method using a

[1] *Corresponding author. E-mail: coord@sun.nankai.edu.cn
[2] *Corresponding author. E-mail: coord@sun.nankai.edu.cn

0277-5387/00/$ - see front matter © 2000 Elsevier Science Ltd. All rights reserved.
PII: S0277-5387(00)00424-1

H-double-tube glass vessel. The starting solution was an aqueous solution of $Ni(phen)(NO_3)_2$ (0.01 M) in one arm and an aqueous solution of NaN_3 (0.02 M) in the other one. After 1 month, green crystals separated out of solution. *Anal.* Calc. for $C_{12}H_8N_8Ni$: C, 44.63; H, 2.50; N, 34.70; Ni, 18.71. Found: C, 44.75; H, 2.69; N, 34.96; Ni, 18.84%. The occurrence in the IR spectrum of two strong peaks at 2050 and 2075 cm^{-1}, corresponding to $\nu_{as}(N_3)$ stretching vibrations, suggests the presence of different types of azide ligand.

2.3. Measurements

Elemental analysis for carbon, hydrogen and nitrogen were carried out on a Perkin–Elmer model 240 elemental analyzer. Metal contents were determined by EDTA titration. The IR spectra were recorded on a Shimadzu model 408 IR spectrophotometer using KBr pellets. Variable temperature magnetic susceptibilities were measured on an MPMS-7 SQUID magnetometer.

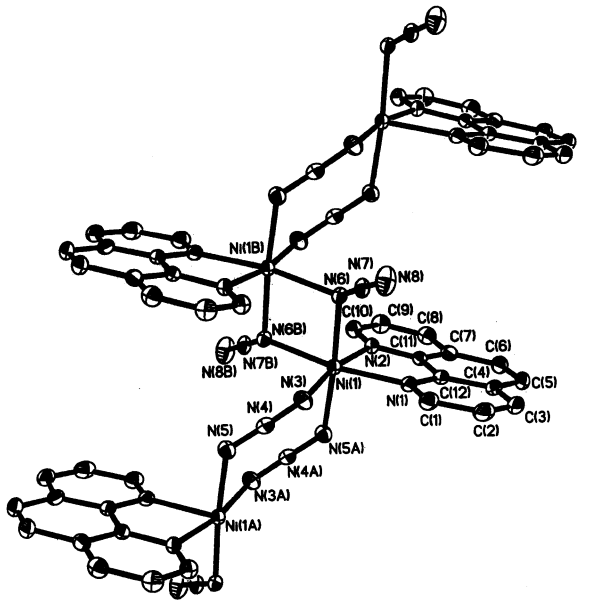


Fig. 1. A labeled diagram of $[Ni(phen)(N_3)_2]_n$. Thermal ellipsoids are at the 30% probability level.

Table 1
Crystallographic data and processing parameters for $[Ni(phen)(N_3)_2]_n$

Formula	$C_{12}H_8N_8Ni$
Formula weight	322.97
Crystal system	triclinic
Space group	$P\bar{1}$
a (Å)	6.9237(7)
b (Å)	9.9651(10)
c (Å)	10.4360(11)
α (°)	109.309(2)
β (°)	104.143(2)
γ (°)	105.889(2)
V (Å^3)	607.47(11)
Z	2
D_{calc} (g cm^{-3})	1.766
$F(000)$	328
R_1	0.0293
wR_2	0.0803

Table 2
Selected bond distances (Å) and bond angles (°) for $[Ni(phen)(N_3)_2]_n$

Ni(1)–N(1)	2.076(2)	Ni(1)–N(6B)	2.092(2)
Ni(1)–N(2)	2.095(2)	Ni(1)–N(3)	2.116(2)
Ni(1)–N(6)	2.139(2)	Ni(1)–N(5A)	2.163(2)
N(3)–N(4)	1.186(3)	N(4)–N(5)	1.169(3)
N(6)–N(7)	1.184(3)	N(7)–N(8)	1.157(3)
N(1)–Ni(1)–N(6B)	170.97(8)	N(1)–Ni(1)–N(2)	79.76(8)
N(1)–Ni(1)–N(3)	91.89(9)	N(6B)–Ni(1)–N(3)	91.88(9)
N(2)–Ni(1)–N(3)	169.78(8)	Ni(1B)–N(6)–Ni(1)	100.53(8)
N(1)–Ni(1)–N(6)	92.17(8)	N(6B)–Ni(1)–N(6)	79.47(8)
N(2)–Ni(1)–N(6)	93.78(8)	N(3)–Ni(1)–N(6)	92.40(8)
N(3)–Ni(1)–N(5A)	89.15(9)	N(6)–Ni(1)–N(5A)	175.00(8)
N(4)–N(3)–Ni(1)	116.95(17)	N(5)–N(4)–N(3)	177.8(2)
N(4)–N(5)–Ni(1A)	128.33(17)	N(8)–N(7)–N(6)	179.0(3)

Diamagnetic corrections were made with Pascal's constants for all constituent atoms, and the magnetic moments were calculated using the equation $\mu_{eff} = 2.828(\chi_M T)^{1/2}$.

2.4. Crystal structure determination and refinement

A single green crystal of the title compound having the approximate dimensions $0.30 \times 0.25 \times 0.20$ mm was put on Bruker Smart 1000 diffractometer equipped with graphite-monochromated Mo Kα radiation ($\lambda =$ 0.71073 Å). Data were collected at room temperature to $2\theta_{max}$ of 25.02° index ranges $-8 \le h \le 7$, $-10 \le k \le 11$ and $-12 \le l \le 6$ with a total of 2547 reflections collected including 2132 independent reflections ($R_{int} =$ 0.0153). A summary of the crystallographic data is given in Table 1. The structure was solved with direct methods using the SHELXS-97. Full-matrix least-squares refinement on F^2 was carried out using SHELXL-97. The final agreement factor values are $R_1 = 0.0293$ and $wR_2 = 0.0803$ $(I > 2\sigma)$ where $R_1 = \Sigma(||F_o| - |F_c||)/\Sigma|F_o|$, $wR_2 = (\Sigma w(|F_o|^2 - |F_c|^2)^2/\Sigma w|F_o|^2)^2$, and $w = 1/[\sigma^2(F_o^2) + (0.0602P)^2 + 0.0102P]$ where $P = (F_o^2 + 2F_c^2)/3$. Selected bond distances and angles are given in Table 2.

3. Result and discussion

3.1. Description of the crystal structure

A labeled diagram of $[Ni(phen)(N_3)_2]_n$ is shown in Fig. 1. The crystal structure is made of chains of Ni(II)

ions alternatively linked by double end-on and double end-to-end azido bridges. The 1D nickel(II) chains are interconnected by weak hydrogen bonding contacts involving the azide nitrogens in end-on mode and the C–H groups of the phen molecules. A sketch of the unit cell is shown in Fig. 2.

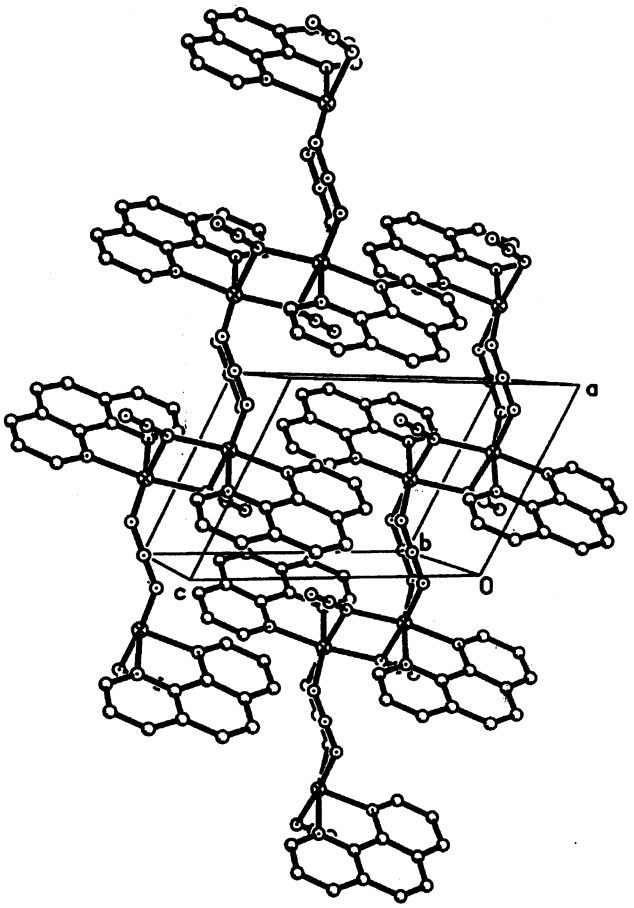


Fig. 2. A sketch of the unit cell of $[Ni(phen)(N_3)_2]_n$.

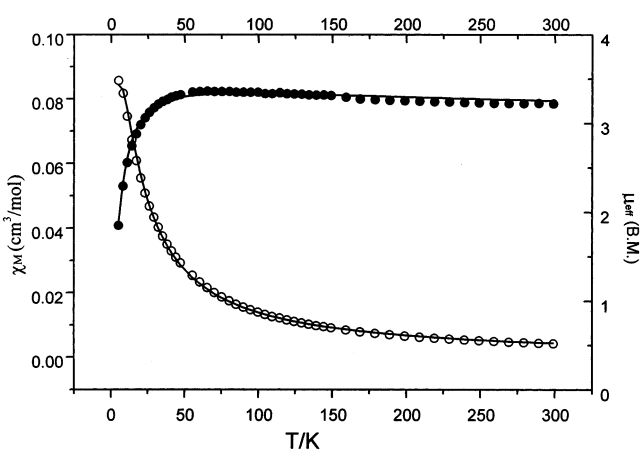


Fig. 3. Molar susceptibility (○) and effective magnetic moment (●) values per Ni(II) atom for $[Ni(phen)(N_3)_2]_n$ as a function of temperature. Solid lines represent the best theoretical fits.

Two nitrogen atoms of the phen ligand complete a distorted NiN_6 octahedral environment. Four nitrogen atoms N(1), N(2), N(3), N(6B), two from azide groups and the other two from phen, form a basal plane and the nickel(II) ion is in this least-squares plane. The values of the two axial Ni–N(azide) bonds are 2.139(2) and 2.163(2) Å for Ni(1)–N(6) and Ni(1)–N(5A), respectively, which are longer than the equatorial ones. The phen ligand is planar and the Ni–N(phen) average bond length is 2.086 Å. The end-on and end-to-end azido bridges are propagated within the chain with a mutual perpendicular arrangement. The end-on bridging azides are quasi-linear (N(6)–N(7)–N(8), 179.0(3)°) and the Ni(1)–N(6)–Ni(1B) angle in end-on mode is 100.53(8)°, which is in good agreement with the results usually obtained for these kind of bridges [13]. The end-to-end azido bridges adopt a chair conformation for the Ni–$(N_3)_2$–Ni unit. The Ni(1)–N(3)–N(4) and Ni(1A)–N(5)–N(4) angles are 116.95(17)° and 128.33(17)°, respectively. The torsion angle (τ) formed by Ni–N–N–N–Ni is 65.8° and the dihedral angle (δ) is 39.0° (as defined as the dihedral angle between the plane defined the six *N*-azido atoms of end-to-end bridges and the N(3)–Ni(1)–N(5A) plane). The intrachain Ni···Ni separations are 3.2541(6) and 5.0933(8) Å in the end-on and end-to-end azido bridges, respectively. The shortest interchain Ni···Ni distance is 7.108(5) Å.

3.2. Magnetic properties

Magnetic susceptibility data of the title compound in the range 4–300 K were collected. The molar susceptibility data is plotted in Fig. 3. In this figure, the μ_{eff} values and the results of the fitting procedure are also included. The effective magnetic moment (μ_{eff}) was found to be 3.22 BM at room temperature which is greater than the value expected for an uncoupled Ni(II) ion. This value slightly increased when the temperature was lowered and attained a shoulder in the temperature range 75–20 K. It reached a maximum of 3.36 BM at 65.20 K, then it decreased with decreasing temperature.

This compound should exhibit alternating ferromagnetic and antiferromagnetic interactions, since end-on azido bridges with a bridging angle (100.53(8)°) as observed here are able to mediate a ferromagnetic interaction between the Ni(II) magnetic centers, and the end-to-end azido bridges with an Ni–N–N bond angle 116.95(17)/128.33(17)° lead to antiferromagnetic coupling [2]. Consequently, the magnetic behavior of the title compound must be explained by assuming a positive J_F for end-on bridges and a negative J_{AF} for end-to-end bridges. The magnetic data were analyzed through the alternating ferromagnetic and antiferromagnetic Heisenberg chain model using the Hamiltonian

$$\hat{H} = -\sum_{i=1}^{N-1} (J_{AF}\hat{S}_{2i}\hat{S}_{2i+1} - J_F\hat{S}_{2i}\hat{S}_{2i-1})$$

where N is the number of spin pairs. J_{AF} and J_F are the nearest neighbor antiferro- and ferromagnetic exchange interactions. Escuer et al. [13] developed an expression for the $N =$ infinite extrapolation with $S = 1$ spins. We used this expression to fit the experimental data. However, at temperatures below ca. 10 K, the calculated molar susceptibility values are less than the experimental values. Taking into account interchain interaction, we modified the molar magnetic susceptibility by employing the equation

$$\chi_M = \chi_{chain}/[1 - \chi_{chain}(2zJ'/Ng^2\beta^2)]$$

where J' is the interchain coupling constant and $z = 2$, the number of nearest Ni(II) neighbors. Other symbols have the usual meanings. The fitting result is perfect. The best-fitting parameters are: $J_{AF} = -4.77$ cm^{-1}, $J_F = +28.08$ cm^{-1}, $\alpha = 5.88$, $g = 2.12$, $zJ' = -0.21$ cm^{-1} and $R = 2.03 \times 10^{-5}$ (R is an agreement factor defined as $R = \Sigma[(\chi_M)_{obs} - (\chi_M)_{calc}]^2/\Sigma[(\chi_M)_{obs}]^2$ and the alternating parameter α defined as $J_F/|J_{AF}|$). The best fitting J_F is almost consistent with the J_F value obtained in a similar compound [14], which was not determined accurately due to poor fitting results below 50 K. The fitting result is also agreement with the calculations performed by Ruiz et al. [15] by means of density functional methods, which predict a maximum ferromagnetic coupling around the bond angle Ni–N–Ni = 104° (end-on bridges) and a narrow range of this bond parameter, in which a minor J_F value is expected. The antiferromagnetic superexchange J_{AF} through double end-to-end azido bridges has been modeled as a function of the dihedral angle δ and J_{AF} should decrease with increasing dihedral δ [7]. In the current case, δ is 39.0° and J_{AF} value is -4.77 cm^{-1}, which is almost in agreement with the regulation.

4. Supplementary data

Supplementary data are available upon request from: The Director, CCDC, 12 Union Road, Cambridge, CB2 1EZ, UK (fax: +44-1223-336-033; e-mail: deposit@ccdc.cam.ac.uk or www: http://www.ccdc.cam.ac.uk), quoting the deposition number CCDC-139111.

Acknowledgements

This project was supported by the Tianjin Natural Science Foundation (No. 983700511).

References

[1] O. Kahn, Molecular Magnetism, VCH, New York, 1993.
[2] J. Ribas, M. Monfort, C. Diaz, C. Bastos, X. Solans, Inorg. Chem. 32 (1993) 3557.
[3] J. Ribas, M. Monfort, R. Costa, X. Solans, Inorg. Chem. 32 (1993) 695
[4] M.A. Halcrow, J.C. Huffman, G. Christou, Angew. Chem. 107 (1995) 971; Angew. Chem., Int. Ed. Engl. 34 (1995) 889.
[5] A. Escuer, R. Vicente, J. Ribas, M.S. El Fallah, X. Solans, M. Font-Bardía, Inorg. Chem. 33 (1994) 1842.
[6] R. Vicente, A. Escuer, J. Ribas, M.S. El Fallah, X. Solans, M. Font-Bardía, Inorg. Chem. 34 (1995) 1278.
[7] J. Ribas, M. Monfort, B.K. Ghosh, R. Cortés, X. Solans, M. Font-Bardía, Inorg. Chem. 35 (1996) 864.
[8] M. Monfort, J. Ribas, X. Solans, J. Chem. Soc., Chem. Commun. (1993) 350.
[9] J. Ribas, M. Monfort, X. Solans, M. Drillon, Inorg. Chem. 33 (1994) 742.
[10] F.A. Mautner, R. Cortés, L. Lezama, T. Rojo, Angew. Chem. 108 (1996) 96; Angew. Chem., Int. Ed. Engl. 35 (1996) 78.
[11] (a) R. Vicente, A. Escuer, Polyhedron 14 (1995) 2133. (b) A. Escuer, R. Vicente, M.A.S. Goher, F.A. Mautner, Inorg. Chem. 37 (1998) 782.
[12] R.J. Butcher, C.J. O'Connor, E. Sinn, Inorg. Chem. 20 (1981) 3486.
[13] A. Escuer, R. Vicente, M.S. El Fallah, S.B. Kumar, F.A. Mautner, D. Gatteschi, J. Chem. Soc., Dalton Trans. (1998) 3905.
[14] G. Viau, M. Lombardi, G. De Munno, M. Julve, F. Lloret, J. Faus, A. Caneschi, J.M. Clemente-Juan, Chem. Commun. (1997) 1195.
[15] E. Ruiz, J. Cano, S. Alvarez, P. Alemany, J. Am. Chem. Soc. 120 (1998) 11122.

PERGAMON

www.elsevier.nl/locate/poly

Polyhedron 19 (2000) 1579–1583

POLYHEDRON

Synthesis, crystal structure and reactivity of the dihydroborate $[Li(Et_2O)][B(C_6F_5)_2(H)_2]$

Richard E. Douthwaite *

Inorganic Chemistry Laboratory, South Parks Road, Oxford, OXI 3QR, UK

Received 21 February 2000; accepted 10 May 2000

Abstract

The new dihydroborate $[Li(Et_2O)][B(C_6F_5)_2(H)_2]$ (**1**) has been prepared and characterised by single-crystal X-ray diffraction. In the solid state **1** exhibits a one-dimensional chain structure that is a result of intermolecular Li–F interactions. Reaction between **1** and one equivalent of Cp_2TiCl or 0.5 equivalents of Cp_2TiCl_2 gives the violet compound $Cp_2Ti\{(\mu\text{-}H)_2B(C_6F_5)_2\}$ (**2**), which has also been characterised by single-crystal X-ray diffraction. Addition of two equivalents of PMe_3 to **2** does not result in elimination of a borane:phosphine adduct, but yields the ionic compound $[Cp_2Ti(PMe_3)_2][H_2B(C_6F_5)_2]$ (**3**). © 2000 Elsevier Science Ltd. All rights reserved.

Keywords: Hydroborates; Lithium; Titanium(IV); Bonding; Crystal structures

1. Introduction

Tetrahydroborate $[BH_4]^-$ and its derivatives are used extensively as reducing agents in organic chemistry [1]. In addition d- and f-block metal complexes of BH_4^- have a rich chemistry and have been investigated as pre-catalysts for olefin polymerisation, hydrogenation and as precursors for transition metal hydrides and borides [2]. Reported herein is the synthesis, characterisation and some reactivity of the dihydroborate $[BH_2(C_6F_5)_2]^-$, a compound related to the C_6F_5 substituted boranes $B(C_6F_5)_3$ and $B(C_6F_5)_2H$, which have been investigated as co-catalysts for Zeigler–Natta polymerisation [3].

2. Results and discussion

Reaction at 25°C between $B(C_6F_5)_2Cl$ and excess LH in Et_2O gave $[(Et_2O)Li][(\mu\text{-}H)_2B(C_6F_5)_2]$ (**1**) in 90% yield. Compound **1** decomposes slowly in air and is very soluble in ethers and has good solubility in aromatic solvents such as benzene. The $^{11}B\{^1H\}$ NMR spectrum of **1** shows a single resonance at $\delta = -29.9$, indicative of borate species and the ^1H coupled spectrum a triplet ($J = 81$ Hz) ascribed to two protons directly bonded to a boron atom. In addition, elemental analysis and integration of the ^1H NMR spectrum of several independently prepared samples of **1** showed a constant ratio of 1:1 between Et_2O and $[(H)_2B(C_6F_5)_2]^-$. IR spectroscopy of **1** shows two absorptions at 2318 and 2380 cm^{-1} attributed to B–H vibrations. This was determined from comparison with the IR spectrum (H/D 1.37) of the deuterated isotopomer $[(Et_2O)Li][(\mu\text{-}D)_2B(C_6F_5)_2]$ (D_2-**1**) prepared from $B(C_6F_5)_2Cl$ and excess LiD. Attempts to synthesize the mixed isotopomer $[(Et_2O)Li][(\mu\text{-}D)(\mu\text{-}H)B(C_6F_5)_2]$ from $BH(C_6F_5)_2$ and LiD and also reaction between $B(C_6F_5)_2D$ and LiH gave mixtures of $[(Et_2O)Li][(\mu\text{-}D)_{2-x}(\mu\text{-}H)_xB(C_6F_5)_2]$ (where $x = 0$–2), a result of H/D exchange similar to that reported between BH_4^- and BD_4^- [4].

Determination of the single-crystal X-ray structure of **1** confirmed the proposed formulation (Fig. 1). The asymmetric unit of **1** contains half of the molecule and the remainder of the molecular structure is generated by mirror symmetry. The geometry about each lithium atom is a pseudo-trigonal bipyramid with a B–H hydro-

* Present address: School of Chemistry, University of Birmingham, Edgbaston, Birmingham, B15 2TT, UK. Tel.: +44-121-414-7816; fax: +44-121-414-4403.

E-mail address: r.e.douthwaite@bham.ac.uk (R.E. Douthwaite).

0277-5387/00/$ - see front matter © 2000 Elsevier Science Ltd. All rights reserved.
PII: S0277-5387(00)00428-9

gen atom and Et_2O oxygen atom occupying apical positions. The equatorial sites are comprised of the remaining B–H hydrogen and two *ortho* fluorine atoms from an adjacent $[(H)_2B(C_6F_5)_2]^-$ moiety (Li1–F1 1.972(7) Å). This intermolecular bonding interaction gives rise to a very unusual one-dimensional chain structure shown in the packing diagram (Fig. 2). A few examples of solid state Li–F interactions have been structurally characterised, including fluorobenzenes coordinated to lithium hexamethyldisilazide dimers, one of which incorporating *para*-difluorobenzene, crystallises in a one-dimensional polymer structure (Li–F 1.999(8) Å) [5].

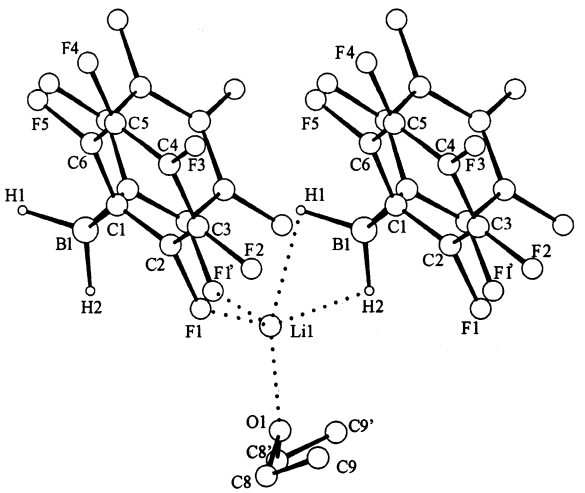


Fig. 1. Structure of **1**. Et_2O hydrogen atoms have been removed for clarity. Selected bond lengths (Å) and angles (°): Li(1)–H(1) 2.139(9), Li(1)–H(2) 1.884(6), Li(1)–F(1) 1.972(7), H(1)–B(1)–H(2) 111.6(5), Li(1)–O(1) 1.879(7), H(1)–Li(1)–H(2) 55.2(5), H(1)–Li(1)–O(1) 159.9(6), F(1)–Li(1)–O(1) 106.3(5), H(1)–Li(1)–F(1) 85.9(4).

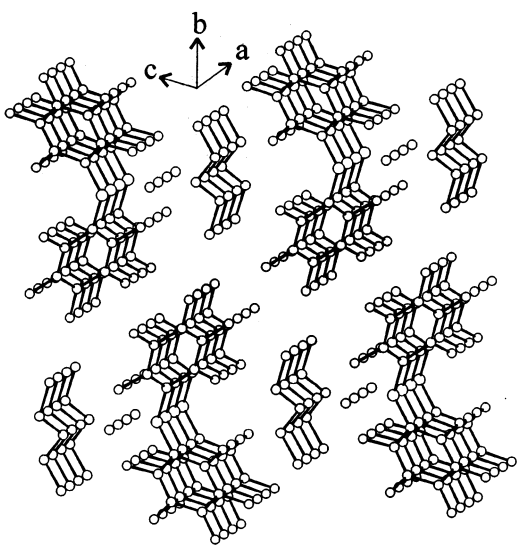


Fig. 2. Packing diagram of **1** illustrating 1-D chain structure along *a* axis. All hydrogen atoms have been removed for clarity.

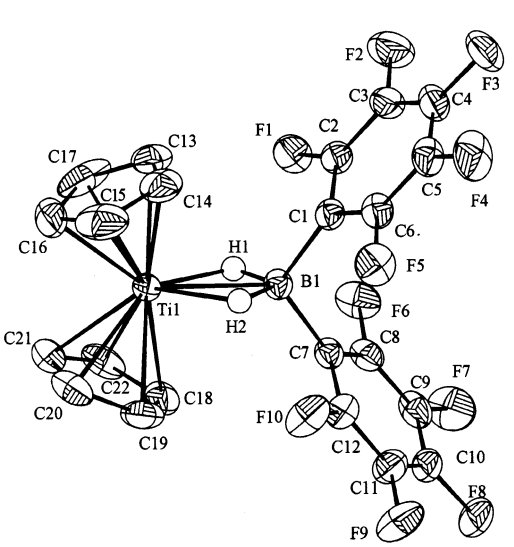


Fig. 3. Molecular structure of **2**. All hydrogen atoms were calculated. Cp hydrogen atoms have been removed for clarity. Selected bond lengths (Å) and angles (°): Ti(1)–B(1) 2.440(3), Ti(1)–H(1) 1.91(1), B(1)–H(1) 1.21(1), Cp_{cent}–Ti(1) 2.03 H(1)–B(1)–H(2) 100.8(7), H(1)–Ti(1)–H(2) 58.1(2), Cp_{cent}–Ti(1)–Cp_{cent} 138.0.

Initial exploration of the chemistry of **1** shows it to be effective as a reagent for the preparation of transition metal complexes of $[(H)_2B(C_6F_5)_2]^-$. An example has been previously described from reaction between Cp_2ZrH_2 and two equivalents of the borane $BH(C_6F_5)_2$ to give $Cp_2Zr\{(\mu\text{-}H)_2B(C_6F_5)_2\}_2$ [6]. However, **1** is a reagent of more general utility for the preparation of this class of compound. For example, reaction between Cp_2TiCl and **1** in C_6H_6 yields the violet Ti(III) complex $Cp_2Ti\{(\mu\text{-}H)_2B(C_6F_5)_2\}$ (**2**). Compound **2** is stable as a solid in air for hours and has good solubility in aromatic and ether solvents. No signals in the ^1H or ^{11}B spectrum of **2** could be observed; however, ^{19}F NMR spectroscopy did yield relatively sharp resonances at δ −158.9 and −166.2, facilitating assessment of product purity. The IR spectrum of **2** displays bands attributable to B–H vibrations at 2073, 2008 and 1367 cm^{-1} assigned from comparison with the deuterium isotopomer $Cp_2Ti\{(\mu\text{-}D)_2B(C_6F_5)_2\}$ ([D_2]-**2**) prepared from [D_2]-**1** and Cp_2TiCl. The IR spectrum of **2** is indicative of bidentate coordination of the dihydroborate [2] and the molecular structure obtained from a single-crystal X-ray diffraction study corroborates this (Fig. 3). The μ-H atoms were calculated; however, it is clear from the disposition of the $B(C_6F_5)_2$ fragment relative to Cp_2Ti that the hydrogen atoms occupy sites in a plane containing Ti(1) and B(1).

Comparison between the IR and structural data of **2** and the known tetrahydroborate $Cp_2Ti\{(\mu\text{-}H)_2BH_2\}$ (Ti–B 2.440(3) Å, IR $\nu = 1936$ cm^{-1}) [7] indicate greater ionic character in the bonding between Cp_2Ti and $[(H)_2B(C_6F_5)_2]$ [8]. Perhaps the clearest evidence of this is reaction between **2** and strong σ-donor ligands

such as PMe_3. Under ambient conditions it has been reported that no reaction occurs between $Cp_2Ti\{(\mu\text{-}H)_2BH_2\}$ and PMe_3 [7]. In contrast, on addition of two equivalents of PMe_3 to a toluene solution of **2**, a blue viscous oil immediately precipitates that can be crystallised from THF/pentane to give a blue microcrystalline solid (**3**). Compound **3** is extremely sensitive to air and is insoluble in non-polar organic solvents, sparingly soluble in diethyl ether and very soluble in THF. Spectroscopic data and elemental analysis are consistent with the formulation $[Cp_2Ti(PMe_3)_2][H_2B(C_6F_5)_2]$. No ^1H NMR resonance was observed for **3** that could be ascribed to the $[Cp_2Ti(PMe_3)_2]^+$ fragment and the ^{31}P NMR spectrum was featureless. The ^1H NMR did however contain a 1:1:1:1 signal at δ 2.40 ($^1J(B, H) = 86.0$ Hz) and the ^{11}B NMR a triplet at δ −26.0. In addition, IR spectroscopy showed B–H stretches (confirmed by reaction between $[D_2]$-**2** and two equivalents of PMe_3) at 2314 and 2361 cm^{-1}. On steric grounds and the similarity between the IR data of compounds **1** and **3** in comparison to **2**, and the observation of NMR signals attributable to $[H_2B(C_6F_5)_2]^-$, an ionic formulation for **3** seems likely. This is a surprising result as reaction between transition metal tetrahydroborates and σ-donors (L) invariably result in formation of borane adducts $L{:}BH_3$. This reaction type has however been observed in an alternative preparation of **2** that gives the adduct $Et_2O{:}B(C_6F_6)H$ as a by-product. Addition of two equivalents of **1** to Cp_2TiCl_2 in benzene gave **2** and $Et_2O{:}B(C_6F_5)_2H$ with concomitant elimination of H_2 (Eq. (1)), illustrating that in this system **1** acts as a reducing agent in a similar manner to $LiBH_4$.

$$2\ (\mathbf{1}) + Cp_2TiCl_2 \rightarrow (\mathbf{2}) + Et_2O{:}B(C_6F_5)_2H + 0.5H_2 + 2LiCl \quad (1)$$

In conclusion, the high yield synthesis of **2** shows that the new dihydroborate **1** is an effective reagent for the simple preparation of transition metal derivatives of $[H_2B(C_6F_5)_2]^-$. It was further observed that unusual reactivity is exhibited by compound **2** in comparison to the $[BH_4]^-$ analogue, presumably a consequence of the electron withdrawing effect of the C_6F_5 groups. The presence of two bulky electron withdrawing C_6F_5 groups will also attenuate the propensity of $[H_2B(C_6F_5)_2]^-$ to act as a reducing agent. Compound **1** and transition metal derivatives of $[H_2B(C_6F_5)_2]^-$ may therefore find use in the selective reduction of organic substrates [1].

3. Experimental

All manipulations were performed under nitrogen in a dry box or using standard Schlenk techniques. All solvents were dried over the appropriate drying agent and distilled under nitrogen. LiH, LiD, PMe_3, and Cp_2TiCl_2 were purchased from Aldrich and used as received. Cp_2TiCl [9] and $(C_6F_5)BCl$ [3] were prepared according to a literature method. ^1H, ^{13}C, ^{11}B and ^{19}F NMR spectra were recorded at 500, 125.7, 160.6 and 470.4 MHz, respectively, at probe temperature on a Varian Unity 500 spectrometer. Proton and carbon spectra were referenced internally to the residual solvent proton and ^{13}C resonance, respectively, relative to tetramethylsilane. Boron spectra were referenced externally to $Et_2O{:}BF_3$ and fluorine externally to $CClF_3$. Infrared spectra were recorded on a Mattson–Polaris FT interferometer. Microanalyses were obtained at the Inorganic Chemistry Laboratory, Oxford.

3.1. $[(Et_2O)Li][(\mu\text{-}H)_2B(C_6F_5)_2]$ (1)

To a solid mixture of $(C_6F_5)_2BCl$ (20 g, 52.6 mmol) and LiH (2 g, 251.8 mmol) was added Et_2O (100 ml) and the white mixture stirred at room temperature (r.t.) for 12 h. The volatiles were removed under reduced pressure and the resulting white solid extracted with Et_2O (2 × 50 ml) to give a colourless solution. Removal of the volatiles and washing with pentane (2 × 20 ml) gave **1** as a white powder (90% yield). Crystals were obtained by crystallisation from benzene. *Anal.* Found: C, 45.00; H, 2.87; B, 2.50; Li, 1.64. Calc. C, 44.90; H, 2.83; B, 2.53; Li, 1.62.%. ^1H NMR (500 MHz, benzene-d_6): $\delta = 2.89$ (q, $^3J(H, H) = 7$ Hz, 4H, OCH_2CH_3), 2.00 (1:1:1:1, $^1J(B, H) = 81.0$ Hz, 2H, BH_2), 0.71 (t, $^1J(H, H) = 7$ Hz, 6H, OCH_2CH_3); ^{11}B NMR (160.6 MHz, benzene-d_6): $\delta = -29.9$ (t, $^1J(B, H) = 81.0$ Hz); ^{19}F NMR (470.4 MHz, benzene-d_6): $\delta = -135.5$ (m, 2F), −160.6 (m, 1F), −164.3 (m, 2F); $^{13}C\{^1H\}$ NMR (125.8 MHz, benzene-d_6): $\delta = 148.48$ (d, $^1J(C, F) = 231.0$ Hz), 139.06 (d, $^1J(C, F) = 246.7$ Hz), 137.5 (d, $^1J(C, F) = 250.5$ Hz), 120.6 (br. s), 66.1, 13.9; IR (KBr pellet): $\nu(BH_2) = 2380$ cm^{-1} (br m), 2314 (br m).

3.2. $Cp_2Ti\{(\mu\text{-}H)_2B(C_6F_5)_2]$ (2): method 1

To solid mixture of $[(Et_2O)Li][(\mu\text{-}H)_2B(C_6F_5)_2]$ (500 mg, 1.17 mmol) and Cp_2TiCl (290 mg, 1.17 mmol) was added benzene (30 ml) and the green mixture stirred at r.t. for 90 min to give a white solid and violet supernatant. The volatiles were removed under reduced pressure and the resulting violet solid was extracted with benzene (2 × 30 ml) or until the washings were colourless. Removal of the volatiles and washing with ice cold Et_2O (2 × 5 ml) gave **2** as a violet microcrystalline solid (82% yield). Crystals were obtained by crystallisation from hot toluene. *Anal.* Found: C, 50.37; H, 2.28; B, 2.04; Ti, 9.03. Calc.: C, 50.33; H, 2.30; B, 2.06; Ti, 9.12%. ^{19}F NMR (470.4 MHz, benzene-d_6): $\delta = -158.9$ (br s, 1F), −166.2 (br s, 2F) (only two resonances could be found); IR (KBr pellet): $\nu(BH_2) = 2075$ cm^{-1} (br m), 2008 (br m), 1373 (s).

3.3. Method 2

At r.t. benzene was added (30 ml) to a solid mixture of $[(Et_2O)Li][(\mu\text{-}H)_2B(C_6F_5)_2]$ (500 mg, 1.17 mmol) and Cp_2TiCl_2 (136 mg, 0.55 mmol). On stirring, the red reaction mixture immediately became green with evolution of a gas. Over a further period of 1 h, gas evolution ceased and a violet supernatant developed with precipitation of a white solid. The volatiles were removed under reduced pressure and the solid washed with pentane (2×10 ml). Final work-up was as described in method 1 (80% yield).

3.4. $[Cp_2Ti(PMe_3)_2][H_2B(C_6F_5)_2]$ (3)

To a violet benzene (20 ml) solution of $Cp_2Ti\{(\mu\text{-}H)_2B(C_6F_5)_2\}$ (200 mg, 0.30 mmol) was added a benzene (10 ml) solution of PMe_3 (46 mg, 0.70 mmol). Immediately the reaction developed a dark blue colour and after 5 min gave an oily blue solid precipitate and colourless supernatant. The volatiles were removed under reduced pressure and the blue powder was washed with pentane (2×10 ml) and crystallised from 3:1 THF–pentane (3 ml) at -80°C to give **3** as a blue crystalline solid (95% yield). *Anal.* Found: C, 50.85; H, 3.30; B 1.55; P, 8.97; Ti, 6.93. Calc.: C, 50.32; H, 3.15, B, 1.62; P, 9.28; Ti, 7.17%. ^{1}H NMR (500 MHz, THF-d_8): $\delta = 2.40$ (1:1:1:1, ^1J(B, H) = 86.0 Hz, BH_2); ^{11}B NMR (160.6 MHz, THF-d_6): $\delta = 26.0$ (t, ^3J(B, H) = 86.0 Hz); IR (KBr pellet): $\nu(BH_2) = 2361$ cm^{-1} (br m), 2314 (br m).

4. Structural studies

Crystals of $[(Et_2O)Li][(\mu\text{-}H)_2B(C_6F_5)_2]$ (**1**) and $Cp_2Ti\{(\mu\text{-}H)_2B(C_6F_5)_2\}$ (**2**) were isolated under dinitrogen. Crystals of **1** were flame sealed in glass capillaries and crystals of **2** were covered with a polyfluoroether and mounted on glass fibres. Data were collected on an Enraf–Nonius DIP2000 image plate diffractometer with graphite monochromated Mo Kα radiation ($\lambda =$ 0.71069 Å). The images were processed with the DENZO and SCALEPACK programs [10]. All solution, refinement and graphical calculations were performed using the CRYSTALS and CAMERON software packages [11,12]. Crystal structures were solved by direct methods using the SIR92 program [13] and were refined by full-matrix least-squares on *F*. All non-hydrogen atoms were refined with anisotropic displacement parameters unless otherwise stated below.

4.1. Crystal data for 1

$C_{16}H_{12}B_1F_{10}Li_1O_1$, $M = 418$, monoclinic, $a =$ 5.0060(4), $b = 19.068(3)$, $c = 9.6780(13)$ Å, $\beta =$ 99.151(8)°, $V = 912.1(2)$ Å^3, $T = 294$ K, space group $P2_1/m$, $Z = 4$, μ(Mo Kα) = 0.16 mm^{-1}, 3512 measured reflections, 1688 independent ($R_{int} = 0.046$), 958 reflections with $I > 3\sigma(I)$, $R(F) = 0.055$, $wR(F) = 0.076$, disorder is present in the ethyl groups of Et_2O. The best results were obtained by refining over two sites the occupancies of each carbon atom adjacent to oxygen. Hydroborate hydrogens were located and refined isotropically. The remaining Et_2O hydrogens were placed in calculated positions and allowed to ride on their corresponding carbon atoms with fixed thermal parameters.

4.2. Crystal data for 2

$C_{22}H_{12}B_1F_{10}Ti_1$, $M = 525.03$, triclinic, $a = 11.6410(9)$, $b = 12.7490(12)$, $c = 15.7680(13)$ Å, $\alpha = 90.754(9)$, $\beta =$ 109.448(11), $\gamma = 110.35(1)$°, $V = 2046.8(8)$ Å^3, $T = 220$ K, space group $P\bar{1}$, $Z = 2$, μ(Mo Kα) = 0.51 mm^{-1}, 10197 measured reflections, 7713 independent ($R_{int} =$ 0.045), 5972 reflections with $I > 3\sigma(I)$, 626 parameters, $R(F) = 0.058$, $wR(F) = 0.062$. Hydroborate hydrogen atoms were placed in calculated positions with fixed thermal parameters and then refined with anisotropic displacement parameters. The remaining Cp hydrogens were placed in calculated positions and allowed to ride on their corresponding carbon atoms with fixed thermal parameters.

5. Supplementary material

Supplementary data are available from the Cambridge Crystallographic Data Centre, 12 Union Road, Cambridge CB2 1EZ, UK, on request, quoting the deposition numbers CCDC 137188 (**1**) and 137187 (**2**).

Acknowledgements

I would like to thank St. John's College, Oxford for a Junior Research Fellowship and Professor M.L.H. Green FRS for additional financial support.

References

[1] J. Seyden-Penne, Reductions by the Alumino- and Borohydrides in Organic Synthesis, Wiley-VCH, New York, 1997.
[2] (a) T.J. Marks, J.R. Kolb, Chem. Rev. 77 (1977) 263. (b) M. Ephritikhine, Chem. Rev. 97 (1997) 2193.
[3] (a) X.M. Yang, C.L. Stem, T.J. Marks, J. Am. Chem. Soc. 116 (1994) 10015. (b) D.J. Parks, R.E. von H. Spence, W.E. Piers, Angew Chem., Int. Ed. Engl. 34 (1995) 809.
[4] B.D. James, B.E. Smith, J. Chem. Soc., Chem. Commun. (1974) 294. (b) B.E. Smith, B.D. James, R.M. Peachey, Inorg. Chem. 16 (1977) 2057.

[5] (a) P.G. Willard, Q-Y. Liu, J. Org. Chem. 59 (1994) 1596. (b) D. Stalke, K.H. Whitmire, J. Chem. Soc., Chem. Commun. (1990) 833.
[6] R.E. von, H. Spence, D.J. Parks, W.E. Piers, M.-A. MacDonald, M.J. Zaworotko, S.J. Rettig, Angew Chem., Int. Ed. Engl. 34 (1995) 1230.
[7] (a) H. Nöth, R. Hartwimmer, Chem. Ber. 93 (1960) 2238. (b) K.M. Melmed, D. Coucouvanis, S.J. Lippard, Inorg. Chem. 12 (1973) 232.
[8] J.A. Jensen, G.S. Girolami, Inorg. Chem. 28 (1989) 2107.
[9] R.J. Angelici, Inorg. Synth. 28 (1995) 263.
[10] Z. Otwinowski, W. Minor, Methods Enzymol. 276 (1997) 307.
[11] D.J. Watkin, C.K. Prout, J.R. Carruthers, P.W. Betteridge, Crystals, Chemical Crystallography Laboratory, Oxford, UK, 1996.
[12] D.J. Watkin, C.K. Prout, L.J. Pearce, Cameron, Chemical Crystallography Laboratory, Oxford, UK, 1996.
[13] A. Altomare, G. Cascarano, G. Giacovazzo, A. Guagliardi, M.C. Burla, G. Polidori, M. Camalli, J. Appl. Cryst. 27 (1994) 435.

PERGAMON

www.elsevier.nl/locate/poly

Polyhedron 19 (2000) 1585–1588

POLYHEDRON

Synthesis and spectral properties of some new cobalt/tungsten chain triphos {$PhP(CH_2CH_2PPh_2)_2$} bridged multimetallic complexes

Paul K. Baker *, Margaret M. Meehan

Department of Chemistry, University of Wales, Bangor, Gwynedd, LL57 2UW, UK

Received 27 March 2000; accepted 15 May 2000

Abstract

Reaction of $[Co_2(CO)_8]$ with two equivalents of L, L′ or L″ {L, L′ or L″ = $[WI_2(CO)\{PhP(CH_2CH_2PPh_2)_2$-*P*,*P*′$\}(\eta^2$-$RC_2R')]$; L, R = R′ = Me; L′, R = R′ = Ph; L″, R = Me, R′ = Ph} in CH_2Cl_2 at room temperature gives the new chain triphos bridged salts, *trans*-$[Co(CO)_3$(L, L′ or L″)$_2][Co(CO)_4]$ (**1**–**3**) in high yield. Refluxing complexes **1**–**3** in toluene for 2 h gives the neutral metal–metal bonded complexes $[Co_2(CO)_6$(L, L′ or L″)$_2]$ (**4**–**6**). All the new multimetallic complexes have been characterised by elemental analysis (C, H and N), IR, ^1H and $^{31}P\{^1H\}$ NMR spectroscopy. © 2000 Elsevier Science Ltd. All rights reserved.

Keywords: Multimetallic; Cobalt carbonyl complexes; Tungsten(II); Alkyne complexes; Chain triphos-bridged

1. Introduction

Multimetallic organotransition-metal complexes containing bridging phosphine ligands have received considerable attention over the years [1–10]. Although examples throughout the range of transition-metal chemistry have been described, very few examples involving phosphine-bridges between cobalt and tungsten have been reported. A cobalt dppe-bridged example is $[\{Co(CO)_2(\eta^3$-$C_3H_4R)\}_2(\mu$-dppe)] {dppe = bis(diphenylphosphino)ethane}, which has been prepared by reacting $[Co(CO)_3(\eta^3$-$C_3H_4R)]$ (R = H, Me) with dppe [11]. Hitherto, until our work described herein, no examples containing chain triphos {$PhP(CH_2CH_2PPh_2)_2$} bridging cobalt and tungsten centres have been reported.

In 1996 [12], we described the preparation and crystallographic characterisation (R = R′ = Me; R = Me, R′ = Ph), of the bidentately attached chain triphos complexes, $[WI_2(CO)\{PhP(CH_2CH_2PPh_2)_2$-*P*,*P*′$\}(\eta^2$-$RC_2R')]$ which have the potential to act as monodentate phosphine ligands to a further metal centre. In this paper we describe the reactions of $[WI_2(CO)$-$\{PhP(CH_2CH_2PPh_2)_2$-*P*,*P*′$\}(\eta^2$-$RC_2R')]$ as monodentate phosphines with $[Co_2(CO)_8]$ to give a range of new multimetallic complexes.

2. Experimental

All reactions described in this paper were carried out using standard vacuum/Schlenk line techniques. The starting materials, $[WI_2(CO)\{PhP(CH_2CH_2PPh_2)_2$-*P*,*P*′$\}(\eta^2$-$RC_2R')]$ (R = R′ = Me or Ph; R = Me, R′ = Ph) were prepared by the literature method [12]. All chemicals used were purchased from commercial sources, and CH_2Cl_2 was dried over calcium hydride and distilled before use.

Elemental analyses (C, H and N) were recorded on a Carlo Erba Elemental analyser MOD 1108 (helium used as a carrier gas). IR spectra were recorded on a Perkin–Elmer 1600 FT-IR spectrophotometer. ^1H and $^{31}P\{^1H\}$ NMR spectra were recorded on a Bruker AC 250 MHz NMR spectrometer. Molecular weights of selected complexes were determined using Rast's method [13], using camphor as the standard. Physical and analytical data are given in Table 1.

* Corresponding author. Tel.: +44-1248-382-379; fax: +44-1248-370-528.

E-mail address: p.k.baker@bangor.ac.uk (P.K. Baker).

0277-5387/00/$ - see front matter © 2000 Elsevier Science Ltd. All rights reserved.
PII: S0277-5387(00)00431-9

Table 1
Physical and analytical data [a], Infrared data [b], ^{1}H NMR data [c], ^{31}P{^{1}H} NMR data [d], and molecular weight studies [e] for the linear triphos-bridged Co/W multimetallic complexes **1**–**6** [f]

Complex	Yield (%)	Colour	C (%)	H (%)	ν(C≡O) (cm^{-1})	ν(C≡C) (cm^{-1})	^{1}H (δ) (ppm)	^{31}P (δ)(ppm)	Molecular weight
1 $[Co(CO)_3L_2][Co(CO)_4]$	97	green	42.7 (42.1)	3.7 (3.3)	1999(s), 1958(br), 1888(s)	1574(w)	7.8–7.4 {m, 50H, *Ph*}; 3.1 {s, 12H, C_2Me}; 2.9–2.7 {m, 16H, CH_2}	31.4 {m, 1P, Co–PPh_2}; 24.2 {m, 1P, Co–PPh_2}; 22.7 {m, 1P, W–PPh}; 20.2 {m, 1P, W–PPh}; 3.8{m, $J_{w-p}=202$ Hz, W–PPh_2}; −2.2 {m, 1P, $J_{wp-}=162$ Hz,W–PPh_2}	2461 (2423)
2 $[Co(CO)_3L'_2][Co(CO)_4]$	91	green	47.3 (47.2)	3.6 (3.3)	2004(s), 1959(br), 1889(m)	1573(w)	7.8–7.4 {m, 70H, *Ph*}; 2.6–2.4 {m, 16H, CH_2}	31.3 {m, 1P, Co–PPh_2}; 25.1 {m, 1P, Co–PPh_2}; 20.0 {m, 2P, W–PPh}; 4.0 {m, 1P, W–PPh_2}; −2.3{m, 1P,W–PPh_2}	2700 (2671)
3 $[Co(CO)_3L''_2][Co(CO)_4]$	80	green	45.3 (44.8)	3.4 (3.3)	1973(sh), 1958(s), 1892(sh)	1571(w)	7.7–7.4 {m, 60H, *Ph*}; 3.0 {s, 6H, C_2Me}; 2.6–2.4 {m, 16H, CH_2}	31.0 {m, 1P, Co–PPh_2}; 23.4 {m, 1P, Co–PPh_2}; 21.8 {m, 1P, W–PPh_2}; 19.9 {m, 1P, W–PPh_2}; 6.6 {m, 1P, W–PPh_2}; −0.5 {m, 1P, W–PPh}	2556 (2547)
4 $[Co_2(CO)_6L_2]$	74	green	42.3 (42.2)	3.3 (3.0)	1974(sh), 1958(br)	1574(w)	7.8–7.4 {m, 50H, *Ph*}; 3.6 {s, 12H, C_2Me}; 2.6–2.4 {m, 16H, CH_2}	31.4 {m, 1P, Co–PPh_2}; 24.2 {m, 1P, W–PPh_2}; 22.8 {m, 1P, W–PPh}; 20.3 {m, 1P, W–PPh}; 4.2 {m, 1P, W–PPh_2}; –2.2 {m, IP, $J_{w-p}=197$ MHz, W–PPh_2}	2410 (2395)
5 $[Co_2(CO)_6L'_2]$	95	green	47.3 (47.3)	3.4 (3.3)	1980(sh), 1958(s)	1601(w)	7.8–7.4 {m, 70H, *Ph*}; 2.6–2.4 {m, 16H, CH_2}	30.4 {m, 1P, Co–PPh_2}; 25.1 {m, 1P, Co–PPh_2}; 20.7 {m, 1P, W–PPh}; 19.8 {m, 1P, W–PPh}; −2.8 {m, 1P, W–PPh_2}; −4.2 {m, 1P, W–PPh_2}	2654 (2643)
6 $[Co(CO)_3L''_2]$	83	green	44.5 (44.8)	3.7 (3.4)	1974(sh), 1958(s)	1571(w)	7.8–7.4 {m, 60H, *Ph*}; 3.0 {s, 6H, C_2Me}; 2.6–2.4 {m, 16H, CH_2}	31.0 {m, 1P, Co–PPh_2}; 23.4 {m, 1P, Co–PPh_2}; 21.8 {m, 1P, W–PPh}; 19.9 {m, 1P, W–PPh}; 6.6{m, 1P, W–PPh_2}; −0.5 {m, 1P, $J_{w-p}=260$ Hz, W–PPh_2}	2523 (2519)

[a] Calculated values in parentheses.
[b] Spectra recorded as thin $CHCl_3$ films between NaCl plates. Br, broad; s, strong; w, weak.
[c] Spectra recorded in $CDCl_3$ (+25°C) and referenced to $SiMe_4$. m, multiplet; s, singlet.
[d] Spectra recorded in $CDCl_3$ (+25°C) and referenced to 85% H_3PO_4. m, multiplet.
[e] Camphor was used as the standard in these measurements.
[f] L = $[WI_2(CO)\{PhP(CH_2CH_2PPh_2)_2$-*P*,*P*′$\}(\eta^2$-$MeC_2Me)]$; L′ = $[WI_2(CO)\{PhP(CH_2CH_2PPh_2)_2$-*P*,*P*′$\}(\eta^2$-$PhC_2Ph)]$; L″ = $[WI_2(CO)\{PhP(CH_2CH_2PPh_2)_2$-*P*,*P*′$\}(\eta^2$-$MeC_2Ph)]$.

2.1. Preparation of *trans*-[Co(CO)$_3$L$_2$][Co(CO)$_4$] (1)

To a stirred solution of [Co$_2$(CO)$_8$] (0.04 g, 0.12 mmol) dissolved in CH_2Cl_2 (30 cm^3) in a Schlenk tube at room temperature, [WI$_2$(CO){PhP(CH$_2$CH$_2$PPh$_2$)$_2$-*P*,*P*′}(η^2-MeC$_2$Me)] (L) (0.24 g, 0.23 mmol) was added, and the reaction mixture was stirred for 24 h. The resulting green solution was filtered through celite, and the solvent was removed in vacuo giving a green crystalline powder of *trans*-[Co(CO)$_3$L$_2$][Co(CO)$_4$] (**1**). Complex **1** was recrystallised from CH_2Cl_2–Et_2O. Yield of pure product = 0.27 g, 97%.

Similar reactions of [Co$_2$(CO)$_8$] with two equivalents of [WI$_2$(CO){PhP(CH$_2$CH$_2$PPh$_2$)$_2$-*P*,*P*′}(η^2-RC$_2$R′)] {L′ = R and R′ = Ph; L″ = R = Me, R′ = Ph} gives the complexes *trans*-[Co(CO)$_3$(L′ or L″)$_2$][Co(CO)$_4$] (**2**) and (**3**).

2.2. Refluxing *trans*-[Co(CO)$_3$L$_2$][Co(CO)$_4$] (1) in toluene to give [Co$_2$(CO)$_6$L$_2$] (4)

A toluene solution of *trans*-[Co(CO)$_3$L$_2$][Co(CO)$_4$] (**1**) (0.17 g, 0.07 mmol) was refluxed for 90 min under an N_2 atmosphere to give, after cooling and filtering, the green complex [Co$_2$(CO)$_6$L$_2$] (**4**). Complex **4** was recrystallised from CH_2Cl_2–Et_2O, to give a yield of pure product = 0.12 g, 74%.

Similar reflux reactions of *trans*-[Co(CO)$_3$(L′ or L″)$_2$][Co(CO)$_4$] in toluene for 2 and 7 h, respectively gave the neutral complexes [Co$_2$(CO)$_6$(L′)$_2$] (**5**) and [Co$_2$(CO)$_6$(L″)$_2$] (**6**).

3. Results and discussion

The tungsten phosphine complex, [WI$_2$(CO){PhP(CH$_2$CH$_2$PPh$_2$)$_2$-*P*,*P*′}(η^2-RC$_2$R′)] [12], are prepared by treating the bis(alkyne) complexes [WI$_2$(CO)(NCMe)(η^2-RC$_2$R′)$_2$] (R = R′ = Me, Ph; R = Me, R′ = Ph) [14] with one equivalent of chain triphos {PhP(CH$_2$CH$_2$PPh$_2$)$_2$}. Previous studies [15–21], have shown that reaction of [Co$_2$(CO)$_8$] with monodentate phosphines (L) generally gives *trans*-[Co(CO)$_3$L$_2$][Co(CO)$_4$], which can be converted to the Co–Co bonded complexes [Co$_2$(CO)$_6$L$_2$] by refluxing in benzene [22–25]. Equimolar quantities of [Co$_2$(CO)$_8$] and L [L = WI$_2$(CO){PhP(CH$_2$CH$_2$PPh$_2$)$_2$-*P*,*P*′}(η^2-MeC$_2$Me)] react in CH_2Cl_2 for 2 h to give, as identified by IR spectroscopy, a mixture of products, namely *trans*-[Co(CO)$_3$L$_2$][Co(CO)$_4$], [Co$_2$(CO)$_7$L] and a third product, possibly [Co$_2$(CO)$_6$L$_2$] {ν(CO) = 1958(br) and 1974(br) cm^{-1}}. Similar IR spectra were obtained from the reactions of equimolar quantities of [Co$_2$(CO)$_8$] and L′ or L″ [L′ = WI$_2$(CO){PhP(CH$_2$CH$_2$PPh$_2$)$_2$-*P*,*P*′}(η^2-PhC$_2$Ph); L″ = WI$_2$(CO){PhP(CH$_2$CH$_2$PPh$_2$)$_2$-*P*,*P*′}(η^2-MeC$_2$Ph)]. In view of these observations, we decided to investigate the reactions of [Co$_2$(CO)$_8$] with two equivalents of L, L′ and L″.

Reactions of [Co$_2$(CO)$_8$] with two equivalents of L, L′ or L″ in CH_2Cl_2 at room temperature gave the new salts, *trans*-[Co(CO)$_3$(L, L′ or L″)$_2$][Co(CO)$_4$] (**1**–**3**) in very good yield. Complexes **1**–**3** have been characterised fully by elemental analysis (C, H and N), ^{1}H and ^{31}P{^{1}H} NMR spectroscopy. Molecular weight studies by Rast's method [13] confirm the trimetallic ionic nature of these complexes. Complexes **1**–**3** are soluble in polar solvents such as $CHCl_3$ and CH_2Cl_2, but as they are salts they are insoluble in Et_2O and hydrocarbon solvents. They are very air-sensitive in solution, but can be kept in the solid state if stored under nitrogen in the dark.

The infrared spectrum of complex **1** (L, R = R′ = Me), in $CHCl_3$ shows bands at 1888 cm^{-1} (vs) due to the tetrahedral anion, [Co(CO)$_4$]$^-$, a very strong band at 1958 cm^{-1} due to L {L = [WI$_2$(CO){PhP(CH$_2$CH$_2$PPh$_2$)$_2$-*P*,*P*′}(η^2-MeC$_2$Me)] has ν(CO)($CHCl_3$) = 1957 cm^{-1}}, and a strong band at 1999 cm^{-1} due to the cation, *trans*-[Co(CO)$_3$L$_2$]$^+$ {cf. *trans*-[Co(CO)$_3$(P^{i}Pr$_3$)$_2$]$^+$ has ν(CO)($CHCl_3$) = 1990 cm^{-1}} [26]. The ^{31}P{^{1}H} NMR spectra of **1**–**3** generally show six resonances. For example, the but-2-yne complex **1**, has resonances at δ = 22.7 and 20.2 ppm due to the central phosphorus atom, and two sets at δ = 31.4 due to the two different diastereoisomers for the *trans*-phosphines at-

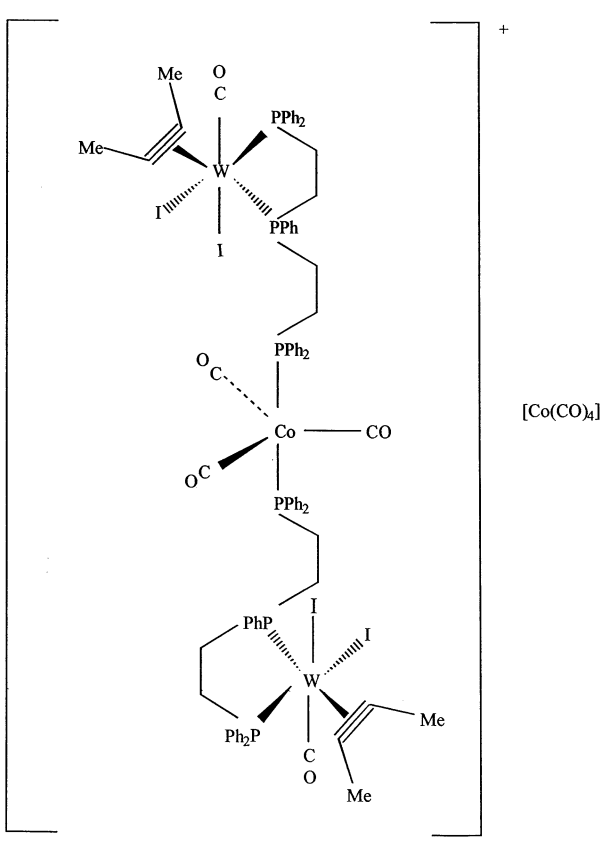


Fig. 1. Proposed structure for the complex *trans*-[Co(CO)$_3$L$_2$]-[Co(CO)$_4$] (**1**).

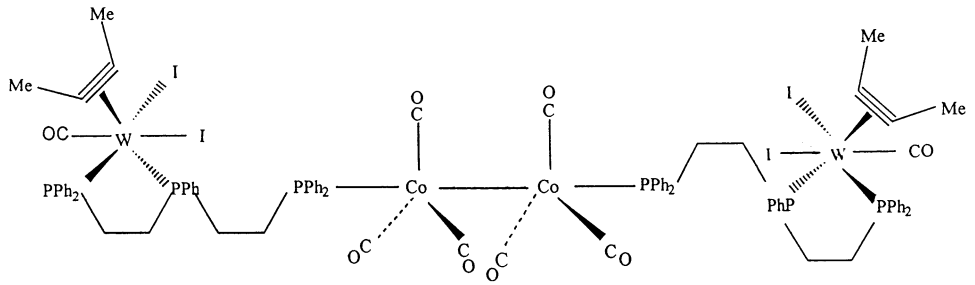


Fig. 2. Proposed structure for the complex $[Co_2(CO)_6L_2]$ (**4**).

tached to the cobalt, and two resonances at $\delta = 3.8$ and -2.2 ppm due to the two diastereoisomers of the end phosphorus atoms on the chain triphos attached to the tungsten. It should be noted that the X-ray crystal structure of the but-2-yne complex $[WI_2(CO)\{PhP(CH_2CH_2PPh_2)_2\text{-}P,P'\}(\eta^2\text{-}MeC_2Me)]$ (L) has two diastereoisomers in the asymmetric unit [12]. One possible isomer of **1** is shown in Fig. 1. We have made a number of unsuccessful attempts to grow suitable single crystals for X-ray analysis of complexes **1**–**3**, by using a wide range of different solvent and temperature conditions.

Refluxing complexes **1**–**3** in toluene, gave the dinuclear Co–Co bonded complexes $[Co_2(CO)_6(L, L' \text{ or } L'')_2]$ (**4**–**6**) in good yield. Complexes **4**–**6** were more soluble than **1**–**3** in chlorinated solvents and slightly soluble in diethyl ether. They are air-sensitive in solution and the solid state, but less sensitive than the salts **1**–**3**. The carbonyl band at ≈ 1888 cm^{-1}, due to the tetrahedral anion $[Co(CO)_4]^-$, has as expected disappeared, and the bands at 1974 and 1958 cm^{-1} in **4** due to the complex $[Co_2(CO)_6L_2]$ are related to the bands for the bis(triphenylphosphine) complex, $[Co_2(CO)_6(PPh_3)_2]$ $\{\nu(CO)(CHCl_3) = 1977, 1957 \text{ cm}^{-1}\}$ [25]. The very strong band at 1958 cm^{-1} also masks the single carbonyl band in L $\{\nu(CO) = 1957 \text{ cm}^{-1}$ [12]$\}$. Manning [25] has carried out a detailed IR analysis of $[Co_2(CO)_6L_2]$ type complexes and shows the 2000 cm^{-1} region of the spectrum is compatible with local D_{3h} or D_{3d} symmetry of the $[Co_2(CO)_6]$ unit [27]. As with complexes **1**–**3**, the $^{31}P\{H\}$ NMR spectra are complex and show that there are several isomers of these complexes in solution. One possible isomer of **4**–**6** is shown in Fig. 2. As for complexes **1**–**3**, no suitable single crystals of **4**–**6** were grown for X-ray analysis despite numerous attempts. This may be due to the high molecular weights of these complexes.

In conclusion, we have described the synthesis and characterisation of the new multimetallic chain triphos-bridged complexes, *trans*-$[Co(CO)_3(L, L' \text{ or } L'')_2][Co(CO)_4]$ and $[Co_2(CO)_6(L, L' \text{ or } L'')_2]$. In the future we will explore the nature of these complexes as potentially mixed hydroformylation (Co centres)/metathesis (W centres) homogeneous catalysts.

Acknowledgements

M.M.M. thanks the EPSRC for a studentship.

References

[1] E.W. Stern, P.K. Maples, J. Catal. 27 (1972) 134.
[2] C.T. Hunt, A.L. Balch, Inorg. Chem. 20 (1981) 2267.
[3] A.P. Gaughan, R.F. Ziolo, Z. Dori, Inorg. Chem. 10 (1971) 2776.
[4] B.F. Hoskins, R.J. Stern, T.W. Turnery, Inorg. Chim. Acta 77 (1983) L69.
[5] H. Schmidbaur, A. Wohlleben, F. Wagner, P. Orama, G. Huttner, Chem. Ber. 110 (1977) 1748.
[6] L. Manojlovíc-Muir, K.W. Muir, A.A. Frew, S.S.M. Ling, M.A. Thomson, R.J. Puddephatt, Organometallics 3 (1984) 1637.
[7] A.T. Hutton, P.G. Pringle, B.L. Shaw, J. Chem. Soc., Dalton Trans. (1985) 1677.
[8] F.S. Hassan, D.P. Markham, P.G. Pringle, B.L. Shaw, J. Chem. Soc., Dalton Trans. (1985) 279.
[9] K.R. Pörschke, Y.-H. Tsay, C. Krüger, Inorg. Chem. 25 (1986) 2097.
[10] P.K. Baker, M.M. Meehan, Coord. Chem. Rev. (submitted for publication).
[11] C. Loubser, H.M. Roos, S. Lotz, J. Organomet. Chem. 402 (1991) 393.
[12] P.K. Baker, S.J. Coles, D.E. Hibbs, M.M. Meehan, M.B. Hursthouse, J. Chem. Soc., Dalton Trans. (1996) 3995.
[13] F.G. Mann, B.C. Saunders, Practical Organic Chemistry, Longmans Green and Co, New York, 1954, pp. 342–344.
[14] E.M. Armstrong, P.K. Baker, M.G.B. Drew, Organometallics 7 (1988) 319.
[15] G. Capron-Cotigny, R. Poilblanc, Bull. Soc. Chim. Fr. (1967) 1440.
[16] W. Hieber, W. Freyer, Chem. Ber. 91 (1958) 1230.
[17] W. Hieber, W. Freyer, Chem. Ber. 93 (1960) 462.
[18] A. Sacco, M. Freni, Ann. Chim. (Rome) 48 (1958) 218.
[19] F. Bonati, S. Cerini, P. Morelli, R. Ugo, J. Chem. Soc. A (1966) 1052.
[20] W. Hieber, J. Sedlmeier, Chem. Ber. 87 (1954) 789.
[21] W. Reppe, W.J. Schweckendiek, Justus. Leibigs. Ann. Chem. 560 (1948) 104.
[22] A. Sacco, Ann. Chim. 43 (1953) 495.
[23] A. Sacco, N. Freni, J. Inorg. Nucl. Chem. 8 (1958) 566.
[24] L. Marco, G. Bor, E. Klumpp, Angew. Chem. 75 (1963) 248.
[25] A.R. Manning, J. Chem. Soc. A (1968) 1135.
[26] N.P. Forbus, T.L. Brown, Inorg. Chem. 20 (1981) 4343.
[27] O. Vohler, Chem. Ber. 91 (1958) 1235.

PERGAMON

www.elsevier.nl/locate/poly

Polyhedron 19 (2000) 1589–1592

POLYHEDRON

Ruthenium carboxylate complexes $[Ru(O_2CR)_2(H_2O)(Me_2SO)_3]$ (R = Me, CF_3)-synthesis and X-ray crystal structures.

Kausar Z. Malik, Stephen D. Robinson *, Jonathan W. Steed

Department of Chemistry, King's College London, Strand, London, WC2R 2LS, UK

Received 22 March 2000; accepted 26 April 2000

Abstract

Reactions of $[RuCl_2(Me_2SO)_4]$ with silver carboxylates, $[Ag(O_2CR)]$ (R = Me, CF_3) in cold dichloromethane afford the title compounds, $[Ru(O_2CR)_2(H_2O)(Me_2SO)_3]$ in good yield as pale cream crystals. X-ray crystal structure determinations have been performed on both complexes. In each case the geometry about the ruthenium centre is essentially octahedral with three S-bonded Me_2SO ligands arranged in a fac configuration, two monodentate carboxylate anions and a coordinated H_2O molecule. The carboxylate ligands are H-bonded to the H_2O ligand via their non-coordinated oxygen atoms. The structures are compared with those previously reported for the alcohol dehydrogenation catalyst $[Ru(O_2CCF_3)_2(MeOH)(CO)(PPh_3)_2]$ and a closely related ruthenium carboxylate complex $[Ru(O_2CCF_3)_2(H_2O)(PMe_3)_3]$. © 2000 Elsevier Science Ltd. All rights reserved.

Keywords: Crystal structures; Ruthenium; Dimethyl sulfoxide; Carboxylates; Complexes; Catalysis

1. Introduction

Dialkyl sulfoxides, notably dimethyl sulfoxide (dmso), are important in coordination chemistry as excellent solvents and versatile ambidentate S-, O- or S,O-donor ligands [1,2]. The chemistry of ruthenium sulfoxide complexes is particularly well developed, largely because of their potential in the fields of homogeneous catalysis [3–5] and antitumour activity [6–8], and their utility as intermediates in the synthesis of a wide range of ruthenium coordination compounds [9–11]. However to the best of our knowledge no ruthenium complexes containing sulfoxide and simple carboxylate ligands in the same coordination sphere have been characterised. We became interested in such complexes because of our earlier work on the development of ruthenium carboxylate based alcohol dehydrogenation catalysts $[Ru(O_2CR)_2(H_2O)(CO)(PPh_3)_2]$ [12]. In this paper we report the synthesis and characterisation of two new ruthenium–dmso–carboxylate complexes $[Ru(O_2CR)_2(H_2O)(Me_2SO)_3]$ closely related to our previously reported alcohol dehydrogenation catalysts.

2. Experimental

Ruthenium trichloride trihydrate was obtained from Johnson Matthey, dimethylsulfoxide, silver acetate and silver trifluoroacetate were purchased from Avocado. Dichlorotetrakis(dimethylsulfoxide)ruthenium was prepared using a literature procedure [11].

2.1. Bis(acetato)aquatris(dimethylsulfoxide)ruthenium(II)

Dichlorotetrakis(dimethylsulfoxide)ruthenium (2.00 g, 4.2 mmol) was dissolved in dichloromethane (100 cm^3) contained in a 250 cm^3 conical flask covered with aluminium foil to exclude light. Silver acetate (1.6 g, 9.6 mmol) was added and the mixture stirred for 24 h. Filtration to remove silver salts left an almost colourless solution, which was evaporated to dryness under reduced pressure. Crystallisation of the residue from dichloromethane–light petroleum (b.p. 60–80°C) afforded cream needle crystals (Yield 1.69 g, 87%) *Anal.* Found: C, 25.50; H, 5.35. Calc. for $C_{10}H_{26}O_8RuS_3$: C, 25.45; H 5.55%.

* Corresponding author. Tel.: +44-208-546-7940; fax: +44-207-848-2810.

E-mail address: stephen.robinson@ukgateway.net (S.D. Robinson).

0277-5387/00/$ - see front matter © 2000 Elsevier Science Ltd. All rights reserved.
PII: S0277-5387(00)00432-0

2.2. Bis(trifluoroacetato)aquatris(dimethylsulfoxide)-ruthenium(II)

Bis(trifluoroacetato)aquatris(dimethylsulfoxide)ruthenium was similarly prepared using silver trifluoroacetate, with a shorter reaction time (3 h), and obtained as cream micro crystals from dichloromethane–light petroleum (b.p. 60–80°C). Yield 76%: *Anal*. Found: C, 20.85; H, 3.35. Calc. for $C_{10}H_{20}F_6O_8RuS_3$: C, 20.7; H, 3.5%.

2.3. Crystallography

X–ray crystal structures have been determined for $[Ru(O_2CMe)_2(H_2O)(Me_2SO)_3]$ (**1**) and $[Ru(O_2CCF_3)_2(H_2O)(Me_2SO)_3]$ (**2**). In both cases crystals suitable for X-ray diffraction study were grown from dichloromethane–light petroleum solutions. Pale cream needles of (**1**) and pale cream crystals of (**2**) were mounted on thin glass fibres using a fast setting epoxy resin. A total of 180 oscillation frames of 90 s exposure time with 1° in θ were recorded using a Nonius Kappa CCD diffractometer, with a detector to crystal distance of 35 mm. The crystals were indexed for the first ten frames using a DENZO package [13] and positional data were refined along with diffractometer constants to give the final unit cell parameters. Integration and scaling of the whole data sets resulted in a total of 6412 data (3281 unique) for **1** and 17 565 data (3733 unique) for **2** which were corrected for Lorentz and polarisation effects. The structures were solved using the direct methods option of SHELXS-86 [14] and developed via alternating least squares cycles and difference Fourier synthesis [SHELXL-97] [15] with the aid of the program RES2INS [16]. All non-hydrogen atoms were modelled anisotopically, while hydrogen atoms were assigned an isotopic parameter 1.2 times (1.5 times for CH_3 groups) that of the parent atom and allowed to ride. Crystal data and structural refinement details for **1** and **2** are given in Table 1.

3. Results and discussion

The new ruthenium(II) carboxylate complexes $[Ru(O_2CR)_2(H_2O)(Me_2SO)_3]$ were prepared by the reaction of $[RuCl_2(Me_2SO)_4]$ with the appropriate silver carboxylate in dichloromethane at room temperature and in the absence of light. Crystallisation from dichloromethane–light petroleum afforded the complexes in good yield as very pale cream coloured, air stable crystals. The complexes are soluble in a range of organic solvents, notably chloroform and dichloromethane, but the solutions show some tendency to darken on standing. The ambient temperature ^{1}H NMR spectrum of the acetate complex **1** displayed a sharp singlet at δ 2.05 attributable to the acetate protons, and three singlets-one at δ 3.30 and a partially resolved pair at ca. δ 3.25-attributable to the protons of the dmso ligands. The 1:3 integration ratio corresponds with the proposed stoichiometry. On cooling the sample to 214 K the signals arising from the dmso ligands separated out into three rather broad but well resolved singlets of equal intensity δ 3.39, 3.35 and 3.30. These are consistent with fac arrangement of three S-bonded dmso ligands. One singlet can be attributed to the methyl protons of the unique dmso ligand *trans* to H_2O, the remaining two singlets arise from the stereochemically non-equivalent methyl groups attached to each of the remaining two chemically and magnetically equivalent dmso ligands. The ambient temperature ^{1}H NMR spectrum of the trifluoroacetate complex (**2**) likewise displayed three partially resolved singlets at ca. δ 3.32, 3.30 and 3.29. The corresponding ^{19}F NMR spectrum consisted of a strong, rather broad singlet at

Table 1
Crystal data and structure refinement for **1** and **2**

	1	**2**
Empirical formula	$C_{10}H_{26}O_8RuS_3$	$C_{10}H_{20}F_6O_8RuS_3$
Formula weight	471.56	579.51
Temperature (K)	100 (2)	100 (2)
Wavelength	0.71070	0.71070
Crystal system	monoclinic	monoclinic
Space group	$P2_1/n$	$P2_1/c$
Unit cell dimensions		
a (Å)	8.4040 (12)	8.5925 (3)
b (Å)	25.0992 (6)	17.8819 (12)
c (Å)	8.6274 (8)	13.1956 (8)
β (Å)	100.0750 (10)	92.459 (2)
Volume (Å^3)	1791.7	(3) 2025.6 (2)
Z	4	4
D_{calc} (mg m^{-3})	1.748	1.900
Absorption coefficient (mm^{-1})	1.256	1.171
F(000)	968	1160
Crystal size (mm)	$0.4\times0.3\times0.2$	$0.3\times0.1\times0.02$
θ Range (°)	3.42–25.98	3.59–26.00
Index ranges	$-9\le h\le 9$, $-30\le k\le 30$, $-10\le l\le 10$	$-10\le h\le 10$, $-22\le k\le 22$, $-16\le l\le 16$
Reflections collected/unique	6412, 3281 [$R_{int}=0.0246$]	17565, 3733[$R_{int}=0.0348$]
Refinement method	full-matrix least-square on F^2	full-matrix least-square on F^2
Data/restraints/parameters	3281/0/208	3733/0/261
Final R indices [$I>2\sigma(I)$]	$R_1=0.0297$, $wR_2=0.0776$	$R_1=0.0366$, $wR_2=0.0761$
R indices (all data)	$R_1=0.0314$, $wR_2=0.0787$	$R_1=0.0468$, $wR_2=0.0793$
Largest difference peak and hole (e Å^{-3})	0.765 and −0.663	0.612 and −0.711

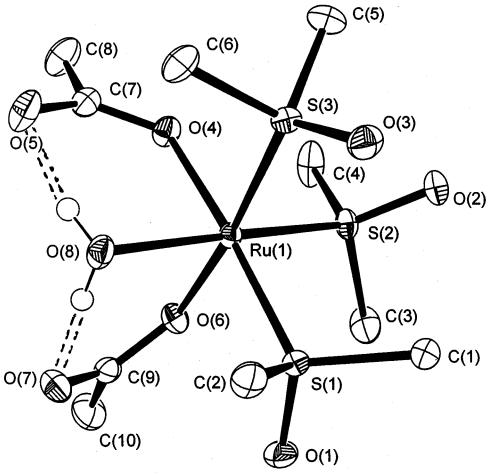


Fig. 1. Molecular structure and atom numbering scheme for $[Ru(O_2CMe)_2(H_2O)(Me_2SO)_3]$ (**1**) (methyl hydrogen atoms omitted for clarity).

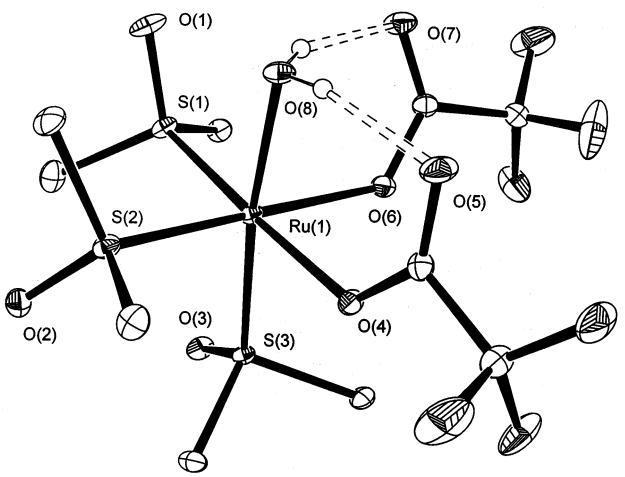


Fig. 2. Molecular structure and atom numbering scheme for $[Ru(O_2CCF_3)_2(H_2O)(Me_2SO)_3]$ (**2**) (methyl hydrogen atoms omitted for clarity).

δ −73.6, and a sharp but much weaker singlet at δ −76.4. We attribute the former to the coordinated trifluoroacetate, and the latter to traces of free trifluoroacetic acid. No signals attributable to the protons of the water ligand were observed, presumably they were shifted by H-bonding effects and broadened by exchange reactions.

Evidence concerning the nature of the complexes was also provided by infrared spectroscopy. The acetato complex (**1**) has values of 1570 and 1338 cm^{-1} for $\upsilon(OCO)_{asym}$ and $\upsilon(OCO)_{sym}$, respectively giving a value of 232 cm^{-1} for $\Delta\upsilon$, consistent with monodentate acetate [17]. Corresponding data for the trifluoroacetato complex (**2**) are 1693, 1450 and 243 cm^{-1}, respectively, again indicating monodentate coordination. The infrared spectra also show absorptions at ca. 1160–1050 cm^{-1} attributable to υ(S=O) for S-bonded dmso. Similar assignments for the parent compound, $[RuCl_2(S\text{–}Me_2SO)_3(O\text{–}Me_2SO)]$ were 1120 and 1090 cm^{-1} [11].

In order to facilitate an investigation of H-bonding interactions between coordinated water and carboxylate ligands, and to make comparisons with related ruthenium carboxylate complexes, notably the dehydrogenation catalysts $[Ru(O_2CCF_3)_2(ROH)(CO)(PPh_3)_2]$ (R = H, alkyl), X-ray crystal structures determinations were performed on **1** and **2**. Molecular structures and atomic labelling schemes for **1** and **2** are shown in Figs. 1 and 2, respectively, selected bond length and bond angle data are presented in Tables 2 and 3. The two complexes display similar overall geometry, in each case

Table 2
Selected bond length (Å) and bond angle (°) data for fac-$[Ru(O_2CMe)_2(H_2O)(Me_2SO)_3]$ (**1**)

Ru–O(4)	2.1050 (18)	S(2)–O(2)	1.4897 (18)
Ru–O(6)	2.1173 (19)	S(2)–C(3)	1.782 (3)
Ru–O(8)	2.1262 (18)	S(2)–C(4)	1.773 (3)
Ru–S(1)	2.2465 (7)	S(3)–O(3)	1.481 (2)
Ru–S(2)	2.2462 (6)	S(3)–C(5)	1.772 (3)
Ru–S(3)	2.2735 (7)	S(3)–C(6)	1.785 (3)
S(1)–O(1)	1.4890 (19)	O(4)–C(7)	1.272 (3)
S(1)–C(1)	1.795 (3)	O(5)–C(7)	1.251 (3)
S(1)–C(2)	1.784 (3)	O(6)–C(9)	1.278 (3)
		O(7)–C(9)	1.250 (4)
O(4)–Ru–O(6)	83.51 (8)	O(6)–Ru–S(1)	92.36 (6)
O(4)–Ru–O(8)	89.29 (8)	O(8)–Ru–S(1)	89.10 (6)
O(6)–Ru–O(8)	89.72 (8)	S(2)–Ru–S(1)	92.94 (2)
O(4)–Ru–S(2)	88.28 (5)	O(4)–Ru–S(3)	89.60 (6)
O(6)–Ru–S(2)	84.81 (5)	O(6)–Ru–S(3)	173.09 (5)
O(8)–Ru–S(2)	174.24 (6)	O(8)–Ru–S(3)	89.60 (6)
O(4)–Ru–S(1)	175.58 (6)	S(2)–Ru–S(3)	95.61 (2)
		S(1)–Ru–S(3)	94.50 (2)

Table 3
Selected bond lengths (Å) and bond angles (°) data for fac-$[Ru(O_2CCF_3)_2(H_2O)(Me_2SO)_3]$ (**2**)

Ru–O(4)	2.121 (2)	S(2)–O(2)	1.482 (3)
Ru–O(6)	2.135 (2)	S(2)–C(5)	1.792 (4)
Ru–O(8)	2.152 (3)	S(2)–C(6)	1.784 (4)
Ru–S(1)	2.2607 (9)	S(3)–O(3)	1.483 (3)
Ru–S(2)	2.2481 (9)	S(3)–C(3)	1.780 (4)
Ru–S(3)	2.2600 (9)	S(3)–C(4)	1.774 (4)
S(1)–O(1)	1.475 (3)	O(4)–C(7)	1.261 (4)
S(1)–C(1)	1.775 (4)	O(5)–C(7)	1.226 (4)
S(1)–C(2)	1.782 (4)	O(6)–C(9)	1.275 (4)
		O(7)–C(9)	1.229 (4)
O(4)–Ru–O(6)	84.52 (10)	O(6)–Ru–S(3)	86.52 (7)
O(4)–Ru–O(8)	90.10 (11)	O(8)–Ru–S(3)	173.23 (9)
O(6)–Ru–O(8)	88.51 (10)	S(2)–Ru–S(3)	96.11 (3)
O(4)–Ru–S(2)	91.33 (7)	O(4)–Ru–S(1)	176.79 (7)
O(6)–Ru–S(2)	174.88 (7)	O(6)–Ru–S(1)	92.31 (7)
O(8)–Ru–S(2)	88.51 (8)	O(8)–Ru–S(1)	89.31 (9)
O(4)–Ru–S(3)	84.86 (7)	S(2)–Ru–S(1)	91.81 (3)
		S(3)–Ru–S(1)	95.47 (3)

the octahedral ruthenium(II) centre is coordinated to a fac set of three S-bonded dmso ligands, similar to that found in the parent complex $[RuCl_2(S–Me_2SO)_3(O–Me_2SO)]$ [18]. Two monodentate carboxylate ligands and a water molecule complete the coordination sphere. Angles subtended at ruthenium by adjacent pairs of donor atoms range from 83.51 (8)° to 95.61 (2)° for **1** and from 84.52 (10)° to 96.11 (3)° for **2**. Ruthenium–sulfur bond lengths which range from 2.2462 (6) to 2.2735 (7) Å for **1** and from 2.2481 (9) to 2.2607 (9) Å for **2**, are very typical for dmso S-bonded to ruthenium(II) [18]. However, in each case one Ru–S bond, *trans* to carboxylate, differs significantly in length from the other two, *trans* to carboxylate and aqua ligands. If these differences were attributable to *trans* effects, the Ru–S bond *trans* to the aqua ligand would be expected to have the anomalous value. Since this is clearly not the case in either complex it seems likely that intramolecular steric interactions between adjacent ligands, rather than *trans* effects, are responsible for the differing Ru–S bond lengths. In the acetate complex (**1**) where the anomalous Ru–S(3) bond (2.2735 (7) Å) is ca. 0.027 Å longer than the other two, the difference is tentatively attributed to steric interactions involving ligands in the O(4)–O(6)–S(1)–S(3) plane. For the trifluoroacetate complex (**2**) where the anomalous Ru–S(2) bond (2.2481(9) Å) is ca 0.012 Å shorter than the other two the dominant steric interactions appear to involve ligands in the O(4)–O(8)–S(1)–S(3) plane.

The ruthenium oxygen bond lengths for **1** and **2** are significantly shorter than those reported for the closely related complex fac-$[Ru(O_2CCF_3)_2(H_2O)(PMe_3)_3]$. The differences, ca. 0.05 Å for Ru–O_2CR and ca. 0.09 Å for Ru–OH_2, no doubt reflect the greater *trans* effect of PMe_3 relative to S-bound Me_2SO. In each complex the aqua ligand is oriented to permit H-bonding to the non-coordinated oxygen atoms of the two adjacent carboxylate ligands. The O (carboxylate)···O (aqua) distances are 2.579 (3) and 2.631 (3) Å for **1** and 2.654 (4) and 2.690 (4) Å for **2**. Corresponding O (carboxylate)···H (aqua) distances are 1.78 (4) and 1.89 (4) Å for **1** and 1.91 (7) and 2.04 (6) Å for **2**. These values are similar to those previously reported for fac-$[Ru(O_2CCF_3)_2(H_2O)(PMe_3)_3]$ [19] which displays an analogous pattern of H-bonding interactions.

The ability of water to complete successfully with the non-coordinated oxygen atoms of the carboxylate ligands for coordination sites in these complexes is no doubt largely due to the strong RCO_2^-–H_2O H-bonding interactions. A similar stereochemical arrangement of H-bonded carboxylate and aqua or alcohol ligands also prevails in the alcohol dehydrogenation catalysts $[Ru(O_2CCF_3)_2(ROH)(CO)(PPh_3)_2]$ (R = H, alkyl), and is thought to play a key role in the initial step of the catalytic cycle, namely transfer of oxygen bound hydrogen from the alcohol to a carboxylate ligand [12].

4. Supplementary data

Supplementary data for the structural analyses has been deposited with the Cambridge Crystallographic Data Centre, CCDC Nos. 141469 and 141468 for compounds **1** and **2.** Copies of this information may be obtained free of charge from The Director, CCDC, 12 Union Road, Cambridge, CB2 1EZ, UK (fax: +44-1223-336-033; e-mail: deposit@ccdc.cam.ac.uk or www: http://www.ccdc.cam.ac.uk).

References

[1] W.L. Reynolds, Prog. Inorg. Chem. 12 (1970) 1.
[2] J.A. Davies, Adv. Inorg. Chem. Radiochem. 24 (1981) 115 and references therein.
[3] B.R. James, R.S. McMillan, R.H. Morris, D.K.W. Wang, Adv. Chem. Ser. 167 (1978) 122.
[4] D.P. Riley, Inorg. Chem. 22 (1983) 1965.
[5] R.S. Srivastava, B. Milani, E. Alessio, G. Mestroni, Inorg. Chim. Acta 191 (1992) 15.
[6] G. Mestroni, G. Zassinovich, E. Alessio, A. Bontempi, Inorg. Chim. Acta 137 (1987) 63.
[7] N.P. Farrell, Transition Metal Complexes as Drugs and Chemotherapeutic Agents, Kluwer Academic, Dordrecht, 1989.
[8] E. Alessio, G. Mestroni, G. Nardin, W.M. Attia, M. Calligaris, G. Sava, S. Zorzet, Inorg. Chem. 27 (1988) 4099.
[9] S.F. Lessing, S. Lotz, H.M. Roos, P.H. van Rooyen, J. Chem. Soc., Dalton Trans. (1999) 1499.
[10] Y. Yamamoto, K. Sugawara, T. Aiko, J.F. Ma, J. Chem. Soc., Dalton Trans. (1999) 4003.
[11] I.P. Evans, A. Spencer, G. Wilkinson, J. Chem. Soc., Dalton Trans. (1973) 204.
[12] A. Dobson, S.D. Robinson, Inorg. Chem. 16 (1977) 137.
[13] Z. Otwinowski, W. Minor, Methods Enzymol. 276 (1996) 307.
[14] G.M. Sheldrick, SHELXS 86, Program for the solution of crystal structures, University of Göttingen, 1986.
[15] G.M. Sheldrick, SHELXL 97, Program for refinement of crystal structures, University of Göttingen, 1997
[16] L.J. Barbour, RES2INS, University of Missouri-Columbia, 1995.
[17] K. Nakamoto, Infrared and Raman Spectra of Inorganic and Coordination Compounds, fourth ed., Wiley, New York, 1986, p. 232.
[18] A. Mercer, J. Trotter, J. Chem. Soc., Dalton Trans. (1975) 2480.
[19] M.O. Albers, D.C. Liles, E. Singleton, Acta Crystallogr., Sect. C 43 (1987) 860.

PERGAMON

www.elsevier.nl/locate/poly

Polyhedron 19 (2000) 1593–1600

POLYHEDRON

Dimeric and polymeric square-pyramidal copper(II) complexes containing equatorial–apical chloride or acetate bridges

Nimma Rajaiah Sangeetha, Samudranil Pal *

School of Chemistry, University of Hyderabad, Hyderabad 500 046, India

Received 20 March 2000; accepted 15 May 2000

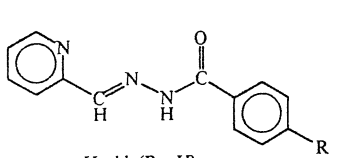
Abstract

Syntheses, crystal structures and physical properties of four new copper(II) complexes of deprotonated aroylhydrazones of 2-pyridine-carboxaldehyde are reported. Two of the complexes contain chloride as a coligand and the other two contain acetate as a coligand. In each complex, the planar tridentate monoanionic ligand binds the metal ion via the pyridine-N, the imine-N and the amide-O atoms. The fourth site is satisfied by the chloride or the acetate-O to form a square-plane. In the solid state, both complexes containing the acetate as the coligand exist as centrosymmetric dimeric species with the metal ion in a distorted square-pyramidal coordination sphere and the acetate group acting as a monoatomic equatorial–apical bridge. One of the complexes containing chloride is a similar centrosymmetric dichloro-bridged dinuclear species. However, the other one exists as a polymeric chain species via equatorial–apical chloride bridges. The electronic spectra of the complexes in methanol solutions display a ligand-field band in the visible region (687–713 nm). The complexes are redox active and, in each case, two reduction responses are observed in the potential range -0.06 to -0.29 and -0.60 to -0.70 V (vs. Ag/AgCl) in methanol solutions. Cryomagnetic studies revealed that no significant spin–spin interaction is operative between the metal ions in any of these four complexes. © 2000 Elsevier Science Ltd. All rights reserved.

Keywords: Copper(II) complexes; Dinuclear and polynuclear; Crystal structures; Equatorial–apical bridge; Paramagnetic

1. Introduction

Dinuclear copper complexes are of interest mainly due to their structural, magnetic, catalytic and electron transfer properties [1–4]. Such complexes are also important as models for copper proteins containing dimetallic active sites [5–9]. Tridentate Schiff-bases are very efficient as binucleating ligands for metal ions which prefer square-planar based geometry. Aroylhydrazones of 2-pyridine-carboxaldehyde (HL **I**, H represents the dissociable amide proton) can coordinate a given metal ion via the pyridine-N, the imine-N and the amide-O centres. In addition, the deprotonated monobasic hydrazones can also form amide-O bridged dinuclear copper complexes. We have been interested in such monomeric and dimeric species with a specific aim of studying the effect of amide protonation state on the coordination geometry, redox and interaction between the two metal ions [10–14]. During our recent attempts to prepare such species, we have isolated four new copper(II) complexes. Two of them have chloride and the other two have acetate as the coligand. In solid state, one of the chloride containing complexes exists as a chain-like polymer formed via equatorial–apical single chloride bridges. On the other hand, rest of the complexes are dimers formed through equatorial–apical chloro- or rare monoatomic acetato-bridges. Herein, we report the syntheses, X-ray structures, spectroscopic, electrochemical and magnetic properties of these complexes.



Hpabh (R = H)
Hpamh (R = OMe)

I

* Corresponding author. Tel.: +91-40-301-0500; fax: +91-40-301-0120.

E-mail address: spsc@uohyd.ernet.in (S. Pal).

0277-5387/00/$ - see front matter © 2000 Elsevier Science Ltd. All rights reserved.
PII: S0277-5387(00)00433-2

2. Experimental

The hydrazones, Hpabh and Hpamh were prepared in ~90% yields by condensing equimolar quantities of 2-pyridine-carboxaldehyde and the corresponding aroylhydrazine in methanol. All other solvents and chemicals used were of analytical grade available commercially.

2.1. Preparation of $[Cu_2(\mu\text{-}Cl)_2(pabh)_2]$ (1)

A methanol solution (5 cm^3) of $CuCl_2 \cdot 2H_2O$ (170 mg, 1.0 mmol) was added to a solution (15 cm^3) of Hpabh (225 mg, 1.0 mmol) and KOH (56 mg, 1.0 mmol) in methanol. The mixture was stirred at room temperature in air for 30 min. The green solid which separated was collected by filtration, washed with water and dried in vacuum over anhydrous $CaCl_2$. Yield 220 mg (68%). *Anal.* Found: C, 48.0; H, 3.0; N, 12.8. Calc. for $C_{13}H_{10}N_3OCuCl$: C, 48.31; H, 3.12; N, 12.99%. Selected IR bands (cm^{-1}): 1601s, 1561w,1487s, 1462s, 1425m, 1375s, 1294m, 1215w, 1148s, 1082s, 920m, 775m, 714s, 417w.

2.2. Preparation of $[Cu(pamh)Cl]_n$ (2)

This was synthesised by the procedure described for **1** from Hpamh, KOH and $CuCl_2 \cdot 2H_2O$ in 70% yield. *Anal.* Found: C, 47.4; H, 3.3; N, 11.8. Calc. for $C_{14}H_{12}N_3O_2CuCl$: C, 47.60; H, 3.42; N, 11.89%. Selected IR bands (cm^{-1}): 1605s, 1557w, 1532w, 1508m, 1483m, 1447m, 1370s, 1252s, 1167s, 1076m, 1020m, 912w, 847m, 762m, 675w, 623m, 505w.

2.3. Preparation of $[Cu_2(\mu\text{-}O_2CCH_3)_2(pabh)_2]$ (3)

Hpabh (225 mg, 1.0 mmol) was added to a methanol solution (15 cm^3) of $Cu(O_2CCH_3)_2 \cdot H_2O$ (200 mg, 1.0 mmol) and the mixture was boiled under reflux for 1 h. The reaction mixture was then cooled to room temperature. The complex, which separated as a dark green crystalline solid, was collected by filtration, washed with ice-cold methanol and dried under vacuum.. Yield 230 mg (66%). *Anal.* Found: C, 51.8; H, 3.8; N, 12.0. Calc. for $C_{15}H_{13}N_3O_3Cu$: C, 51.94; H, 3.78; N, 12.11%. Selected IR bands (cm^{-1}): 1626s, 1606s, 1557w, 1489s, 1464s, 1425m, 1366s, 1213w, 1145s, 1082s, 920s, 800w, 768s, 716s, 681s, 575w, 521m, 463m, 415m.

2.4. Preparation of $[Cu_2(\mu\text{-}O_2CCH_3)_2(pamh)_2]$ (4)

This complex was prepared by the procedure described for **3** from Hpamh and $Cu(O_2CCH_3)_2 \cdot H_2O$ in 65% yield. *Anal.* Found: C, 50.8; H, 4.0; N, 11.1. Calc. for $C_{16}H_{15}N_3O_4Cu$: C, 50.99; H, 4.01; N, 11.15%. Selected IR bands (cm^{-1}): 1625s, 1604s, 1556w, 1512m, 1483m, 1451s, 1362s, 1254s, 1167s, 1080s, 920s, 843m, 764s, 679s, 621m, 509m, 417m.

2.5. Physical measurements

A Perkin–Elmer model 240C elemental analyser was used to obtain microanalytical (C, H, N) data. Infrared spectra were collected on a JASCO-5300 FT IR spectrophotometer using KBr pellets. Electronic spectra were recorded on a JASCO-7800 UV–Vis spectrophotometer. A JEOL FE-3X spectrometer was used to obtain the ESR spectra. The spectra were calibrated with the help of DPPH. A Cypress model CS-1090/CS-1087 electroanalytical system was used for cyclic voltammetric experiments with methanol solutions of the complexes containing tetrabutylammonium perchlorate as supporting electrolyte. The three electrode measurements were carried out at 298 K under a dinitrogen atmosphere with platinum disk working electrode, a platinum wire auxiliary electrode and a Ag/AgCl reference electrode. The potentials reported in this work are uncorrected for junction contributions. The variable temperature (17–300 K) magnetic susceptibility measurements were performed using the Faraday technique with a set-up comprising a George Associates Lewis coil force magnetometer, a CAHN microbalance and an Air Products cryostat. $Hg[Co(NCS)_4]$ was used as the standard. Diamagnetic corrections, calculated from Pascal's constants [15], were used to obtain the molar paramagnetic susceptibilities.

2.6. Crystallographic studies

Single crystals were obtained by slow evaporation of methanol solutions of the complexes. Complex **1** crystallises as a tetrahydrate. In each case, the data were collected on an Enraf–Nonius Mach-3 single crystal diffractometer using graphite monochromated Mo Kα radiation ($\lambda = 0.71073$ Å) by ω-scan method at 293 K. Unit cell parameters were determined by the least-squares fit of 25 reflections having 2θ values in the range 18–30°. Stability of the crystal was monitored by measuring the intensities of three check reflections after every 1.5 h during the data collection. None of the crystals displays any decay during data collection. The data were corrected for Lorentz-polarisation effects. No absorption correction was applied. The structures were solved by direct methods and refined by full-matrix least-squares on F^2 and Fourier techniques. Due to insufficient data, only Cu, N and O atoms were refined anisotropically for **3**. For the other three complexes, all the non-hydrogen atoms were refined anisotropically. Hydrogen atoms were added at calculated positions by using riding model for structure factor calculation, but not refined. Calculations were done using the programs of XTAL software [16] for data reduction and SHELX-97

programs [17] for structure solution and refinement. ORTEX6a package [18] was used for molecular graphics. Significant crystal data for all the complexes are listed in Table 1.

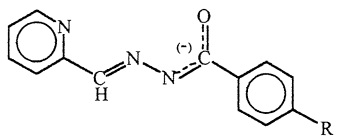
3. Results and discussion

3.1. Synthesis

The complexes **1** and **2**, of empirical formula CuLCl (L = pabh$^-$ for **1**; L = pamh$^-$ for **2**), were synthesised in good yields by reacting one equivalent each of HL, $CuCl_2{\cdot}2H_2O$ and KOH in methanol. Other two complexes, **3** and **4**, containing acetate as the coligand were obtained as $CuL(O_2CCH_3)$ (L = pabh$^-$ for **3**; L = pamh$^-$ for **4**) in comparable yields from reaction of equimolar quantities of $Cu(O_2CCH_3)_2{\cdot}H_2O$ and HL in methanol. While for the chloro-complexes (**1** and **2**) KOH was required to deprotonate the amide functionality, in the latter cases (**3** and **4**), the acetate of the metal salt appears to be sufficient for the deprotonation of the amide functionality. Elemental analysis data for the complexes are consistent with the empirical formulae mentioned above.

3.2. Spectroscopic properties

Infrared spectrum of each of the two complexes containing chloride as coligand displays a strong peak with a shoulder near 1603 cm^{-1}. The origin of a peak in this region might involve the stretching due to the HC=N–N---C(---O)– moiety of the deprotonated ligands (**II**) [19–21]. In addition to the same peak at $\sim$1605 cm^{-1}, the spectra of the complexes containing acetate show a peak near 1625 cm^{-1} possibly due to the ν_{as} stretch of the unidentate acetate group [22]. All the complexes display a strong peak in the range 1362–1375 cm^{-1}. However, this peak is significantly stronger for acetate coordinated complexes compared to the peak observed for chloride containing complexes. This difference is most likely due to the ν_s stretch of the acetate in this region [22].



II

The electronic spectra of the complexes display a weak absorption in the range 687–713 nm (Table 2). Absorptions in this region observed for other square-planar or square-pyramidal copper(II) complexes of Schiff bases and similar ligands have been assigned to d–d transition [12,13,23,24]. In addition to this weak band, the complexes of pabh$^-$ display two strong absorptions and the complexes of pamh$^-$ exhibit three intense bands in the range 385–252 nm. These higher energy absorptions are most probably due to the ligand-to-metal charge transfer and intraligand transitions [24].

The room temperature powder ESR spectral profiles of the complexes investigated in this study are very similar. For all the complexes $g_{\|} > g_{\perp}$ (Table 2) which is typical of square-planar or square-pyramidal copper(II) complexes [25,26]. Thus the unpaired electron resides in the $d_{x^2-y^2}$ orbital.

Table 1
Crystallographic data for complexes **1**, **2**, **3** and **4**

Complex	**1**	**2**	**3**	**4**
Empirical formula	$Cu_2Cl_2C_{26}H_{28}N_6O_6$	$CuClC_{14}H_{12}N_3O_2$	$Cu_2C_{30}H_{26}N_6O_6$	$Cu_2C_{32}H_{30}N_6O_8$
Crystal size (mm)	0.48 × 0.45 × 0.45	0.48 × 0.40 × 0.35	0.28 × 0.15 × 0.12	0.40 × 0.16 × 0.12
Crystal system	triclinic	orthorhombic	monoclinic	monoclinic
Space group	$P\bar{1}$	$Pca2_1$	$P2_1/c$	$P2_1/n$
a (Å)	8.605(2)	6.9561(11)	10.773(4)	13.7425(15)
b (Å)	9.199(3)	12.2621(13)	8.766(3)	8.6684(11)
c (Å)	9.858(3)	16.3550(19)	15.952(5)	14.0568(19)
α (°)	76.30(2)	90.0	90.0	90.0
β (°)	78.35(2)	90.0	101.60(3)	105.705(10)
γ (°)	75.20(2)	90.0	90.0	90.0
V (Å^3)	724.6(3)	1395.0(3)	1475.7(9)	1612.0(3)
Z	1	4	2	2
Reflections measured	2530	2347	2347	3169
Reflections unique	2530	2095	2299	2839
Reflections [$I>2\sigma(I)$]	2207	1575	914	1226
Parameters	190	191	125	219
R_1, wR_2 [$I>2\sigma(I)$]	0.0282, 0.0773	0.0364, 0.0788	0.0562, 0.0875	0.0479, 0.0718
R_1, WR_2 (all data)	0.0336, 0.0834	0.0536, 0.0896	0.1454, 0.1257	0.1252, 0.1015

Table 2
Electronic spectral data [a], ESR g values [b], reduction potentials [c] and magnetic moments [b]

Complex	λ_{max} (nm) ($10^{-3} \times \varepsilon$ (M^{-1} cm^{-1})) [d]	$g_{\parallel}$	$g_{\perp}$	$E_{1/2}$ (V) (ΔE_p (mV))	E_{pc} (V)	μ_{eff} [d]/μ_B
1	707 (0.08), 378 (17.9), 261 (16.0)	2.26	2.09	−0.07 (180)	−0.60	1.90
2	713 (0.09), 385 (20.5), 295 (11.6), 252 (15.0)	2.29	2.11	−0.06 (200)	−0.70	1.84
3	694 (0.09), 376 (17.5), 258 (16.1)	2.32	2.19	−0.29 [e]	−0.66	1.90
4	687 (0.08), 383 (19.0), 285 (12.0), 253 (15.1)	2.33	2.18	−0.22 (140)	−0.68	1.92

[a] In methanol.
[b] In powder phase at 300 K.
[c] E_{pa}, anodic peak potential; E_{pc}, cathodic peak potential; $E_{1/2} = (E_{pa} + E_{pc})/2$; $\Delta E_p = E_{pa} - E_{pc}$.
[d] Per monomer.
[e] E_{pc}.

3.3. Redox potentials

In methanol solutions cyclic voltammograms of the complexes display two reduction responses (Table 2). The first response is observed in the potential range −0.06 to −0.29 V and the second one appears in the range −0.60 to −0.70 V (vs. Ag/AgCl). In each case, assuming a monomeric species in solution, the current height of the first reduction is comparable with that of the known one-electron redox processes under identical conditions [27]. However, the current height of the second reduction is two to three times larger than that of the first reduction. The potential of the first response for chloride containing complexes is higher than that observed for the complexes containing acetate. There is no such trend in the potentials for the second reduction (Table 2). It has been observed earlier that with the increase of the basicity of the coordinating atom, the metal–ligand σ-bond strength increases and as a result the metal centred reduction potential decreases [28]. The basicity of the acetate-O is much higher than that of chloride. Thus the first reduction response most probably involves the metal centre and the second reduction is associated with the coordinated ligand.

3.4. Description of structures

The molecular structures of **1**, **2**, **3** and **4** are illustrated in Figs. 1–4, respectively. The corresponding selected bond parameters for the complexes are listed in Tables 3–6. The asymmetric unit of complex **1** includes one Cu(pabh)Cl fragment and two water molecules. The water molecules are hydrogen bonded to the oxygen (O1) and the nitrogen (N3) centres (Fig. 1) of the deprotonated amide functionality. The O1–O(water) and N3–O(water) distances are 3.069(3) and 2.939(3) Å, respectively. The asymmetric units of the other three complexes contain the CuLX ($X = Cl^-$ or $CH_3CO_2^-$) moiety. In each of the four complexes the planar ligand coordinates the metal ion via the pyridine-N, the imine-N and the amide-O atoms forming two five-membered chelate rings. In **1** and **2** the fourth site of the square-plane around the metal ion is occupied by a chloride ion. An acetate-O completes the square-plane in **3** and **4**. The chelate bite angles in the five-membered rings formed by the amide-O and the imine-N, and the pyridine-N and the imine-N are in the range 78.61(14)–79.2(2) and 80.04(15)–80.55(19)°, respectively. The N–N, C–N and C–O distances in the =N–N---C(---O)– fragment of the coordinated ligands are in the range 1.353(5)–1.380(7), 1.321(7)–1.331(6) and 1.278(8)–1.289(6) Å, respectively. These distances are consistent with the deprotonated form of the amide functionality [10–14,29,30]. The Cu–N(pyridine) distance is significantly longer than the Cu–N(imine) distance. The former is in the range 2.028(2)–2.045(4) Å, whereas the latter is within 1.915(4)–1.933(3) Å. This difference is possibly due to the rigidity of the tridentate ligand [31] and the better π-backbonding in the Cu–N(imine) bond than that in the Cu–N(pyridine) bond [29,30,32]. The Cu–O(amide) distance (1.971(3)–1.989(5) Å) is shorter than that observed in copper(II) complexes where the

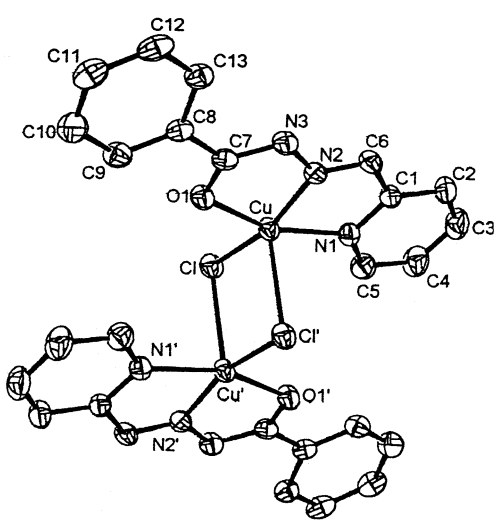


Fig. 1. Structure of $[Cu_2(\mu\text{-}Cl)_2(pabh)_2]$ (**1**) showing the 40% probability thermal ellipsoids and the atom-labelling scheme. Hydrogen atoms are omitted for clarity.

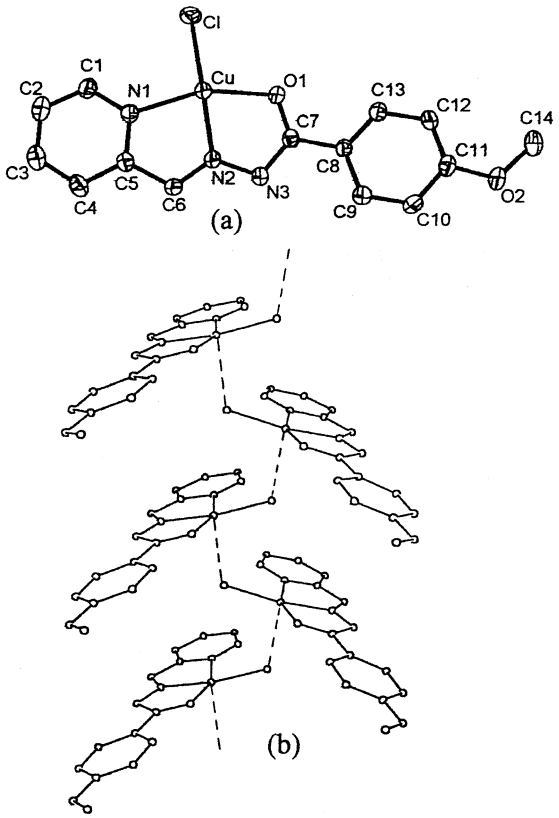


Fig. 2. (a) View of the asymmetric unit of $[Cu(pamh)Cl]_n$ (**2**) with the atom-labelling scheme. Atoms are represented by their 40% probability thermal ellipsoids. (b) Single chloride bridged chain structure of **2**. For clarity hydrogen atoms are not included.

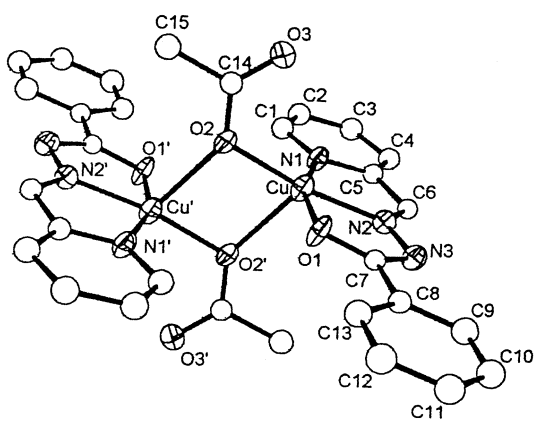


Fig. 3. Structure of $[Cu_2(\mu\text{-}O_2CCH_3)_2(pabh)_2]$ (**3**) with the atom labelling scheme. All atoms are represented by their 20% probability thermal ellipsoids. Hydrogen atoms are omitted for clarity.

metal ion is coordinated to the oxygen of a protonated amide functionality [13,33–35].

In solid state, **2** forms a one-dimensional chain of copper(II) ions via equatorial–apical chloride bridges (Fig. 2b). This type of single chloride bridged polymeric species is unique for copper(II) containing a tridentate coligand. The Cu···Cl(apical) and inter-monomer metal···metal distances are 2.7821(13) and 4.2866(7) Å, respectively. The Cu–Cl–Cu bridge angle is 117.60(5)°. The four coordinating atoms O1, N2, N1 and Cl are nearly coplanar (Fig. 2a). The largest deviation from the mean plane is 0.012 Å. The metal centre is at 0.126 Å from the mean plane towards the apical chloride bridge.

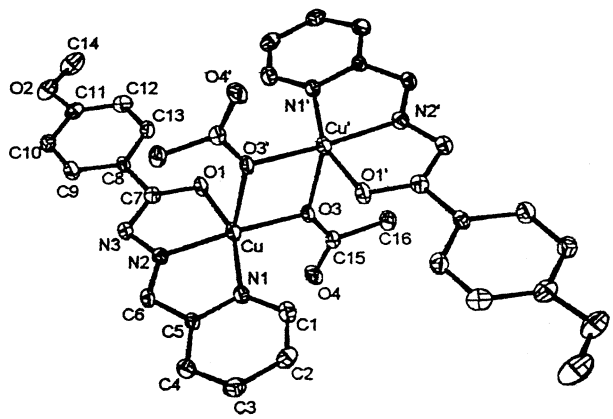


Fig. 4. Structure of $[Cu_2(\mu\text{-}O_2CCH_3)_2(pamh)_2]$ (**4**) depicting the 30% probability thermal ellipsoids and the atom-labelling scheme. Hydrogen atoms are omitted for clarity.

Table 3
Selected bond distances (Å) and angles (°) for $[Cu_2(\mu\text{-}Cl)_2(pabh)_2]\cdot 4H_2O$ (**1**·$4H_2O$) [a]

Cu–Cl	2.2440(9)	Cu–O(1)	1.9853(17)
Cu–N(1)	2.028(2)	Cu–N(2)	1.9299(19)
Cu–Cl′	2.6682(10)	O(1)–C(7)	1.288(3)
N(3)–C(7)	1.324(3)	N(2)–N(3)	1.369(3)
N(2)–C(6)	1.276(3)		
N(2)–Cu–O(1)	78.93(8)	N(2)–Cu–N(1)	80.15(8)
O(1)–Cu–N(1)	158.59(8)	N(2)–Cu–Cl	162.28(6)
O(1)–Cu–Cl	98.81(6)	N(1)–Cu–Cl	99.72(6)
N(2)–Cu–Cl′	104.60(6)	O(1)–Cu–Cl′	97.34(6)
N(1)–Cu–Cl′	92.28(6)	Cl–Cu–Cl′	93.11(3)
Cu–Cl–Cu′	86.89(3)		

[a] Symmetry transformation used to generate equivalent atoms: $1-x, 1-y, 1-z$.

Table 4
Selected bond distances (Å) and angles (°) for $[Cu(pamh)Cl]_n$ (**2**) [a]

Cu–Cl	2.2177(11)	Cu–O(1)	1.978(3)
Cu–N(1)	2.045(4)	Cu–N(2)	1.933(3)
Cu–Cl′	2.7821(13)	N(2)–C(6)	1.278(5)
N(2)–N(3)	1.353(5)	N(3)–C(7)	1.331(6)
O(1)–C(7)	1.279(5)		
O(1)–Cu–Cl	102.16(10)	O(1)–Cu–N(1)	158.03(15)
O(1)–Cu–N(2)	78.61(14)	N(1)–Cu–N(2)	80.04(15)
N(1)–Cu–Cl	98.31(11)	N(2)–Cu–Cl	172.37(11)
N(1)–Cu–Cl′	91.59(11)	N(2)–Cu–Cl′	87.23(11)
O(1)–Cu–Cl′	92.52(10)	Cl–Cu–Cl′	100.29(3)
Cu–Cl′–Cu′	117.60(5)		

[a] Symmetry transformation used to generate equivalent atoms: $1/2+x, 2-y, z$.

Table 5
Selected bond distances (Å) and angles (°) for $[Cu_2(\mu\text{-}O_2CCH_3)_2(pabh)_2]$ (**3**) [a]

Cu–O(1)	1.989(5)	Cu–O(2)	1.935(5)
Cu–O(2)′	2.286(6)	Cu–N(1)	2.033(6)
Cu–N(2)	1.924(6)	O(2)–C(14)	1.266(9)
O(3)–C(14	1.224(9)	N(2)–C(6)	1.246(9)
N(2)–N(3)	1.380(7)	N(3)–C(7)	1.321(9)
O(1)–C(7)	1.278(8)		
N(2)–Cu–O(2)	170.8(3)	O(2)–Cu–O(1)	100.0(2)
N(2)–Cu–O(1)	79.2(2)	N(2)–Cu–N(1)	80.1(2)
O(2)–Cu–N(1)	100.2(2)	O(1)–Cu–N(1)	159.3(2)
N(2)–Cu–O(2)′	110.6(2)	N(1)–Cu–O(2)′	93.5(2)
O(1)–Cu–O(2)′	95.3(2)	O(2)–Cu–O(2)′	78.6(2)
Cu–O(2)–Cu′	101.4(2)		

[a] Symmetry transformation used to generate equivalent atoms: $1-x, -y, -z$.

Table 6
Selected bond distances (Å) and angles (°) for $[Cu_2(\mu\text{-}O_2CCH_3)_2(pamh)_2]$ (**4**) [a]

Cu–O(1)	1.971(3)	Cu–O(3)	1.922(3)
Cu–O(3)′	2.282(4)	Cu–N(1)	2.040(4)
Cu–N(2)	1.915(4)	O(3)–C(15)	1.282(6)
O(4)–C(15)	1.223(6)	O(1)–C(7)	1.289(6)
N(3)–C(7)	1.321(6)	N(2)–C(6)	1.279(6)
N(2)–N(3)	1.361(5)		
N(2)–Cu–O(3)	171.83(17)	N(2)–Cu–O(1)	79.16(17)
O(3)–Cu–O(1)	98.90(15)	N(2)–Cu–N(1)	80.55(19)
O(3)–Cu–N(1)	100.80(17)	O(1)–Cu–N(1)	159.52(16)
N(1)–Cu–O(3)′	95.05(16)	N(2)–Cu–O(3)′	109.94(15)
O(1)–Cu–O(3)′	94.42(14)	O(3)–Cu–O(3)′	78.06(15)
Cu–O(3)–Cu′	101.94(15)		

[a] Symmetry transformation used to generate equivalent atoms: $1-x, -y, 1-z$.

The other three complexes crystallise as centrosymmetric dinuclear species in which each copper(II) is in a distorted square-pyramidal coordination sphere. In **1**, the chloride ions act as equatorial–apical bridges (Fig. 1). The acetate ions perform the role of monoatomic bridges in the same fashion in **3** and **4** (Figs. 3 and 4). The metal···metal distance in the diacetato-bridged complexes, **3** (3.273(2) Å) and **4** (3.273(1) Å) are identical. However the same (3.3918(9) Å) in **1** is significantly longer. The O1, N2, N1 and Cl atoms form the base (largest deviation from the mean plane, 0.11 Å) of the square-pyramid in **1**. The metal centre is displaced from this base towards the apical bridging Cl′ by 0.23 Å. In **3** and **4**, the planar N,N,O-coordinating ligand and the acetate-O comprise the square-base of the pyramid. The largest deviations from the NNOO mean planes are 0.06 Å (**3**) and 0.04 Å (**4**). In **3**, the displacement of the metal ion towards the apical bridging acetate-O is 0.11 Å and that in **4** is 0.10 Å. Such displacement is very common in square-pyramidal copper(II) complexes [12,13,36,37]. A few structurally characterised dicopper(II) complexes of planar tridentate ligands containing equatorial–apical bridging chloride [38–50] or acetate [51–60] groups are known. In **1**, Cu–Cl and Cu–Cl′ distances are 2.2440(9) and 2.6682(10) Å. The Cu–Cl–Cu′ bridge angle is 86.89(3)°. In similar dichloro-bridged dicopper(II) complexes, the Cu–Cl(equatorial) and Cu–Cl(apical) distances are in the range 2.218–2.329 and 2.526–3.129 Å, respectively. In these complexes the Cu–Cl–Cu bridge angle varies from 83.291–91.989° [38–50]. In **3** and **4**, the bond parameters of the Cu_2O_2 unit are very similar. The Cu–O and Cu–O′ distances observed are 1.935(5) and 2.286(6) Å and 1.922(3) and 2.282(2) Å for **3** and **4**, respectively. The Cu–O–Cu′ bridge angles are 101.4(2)° (**3**) and 101.94(15)° (**4**). The values of Cu–O(equatorial) and Cu–O(apical) distances and the Cu–O–Cu bridge angles reported for similar diacetato-bridged complexes are in the range 1.951–1.987, 2.427–2.572 and 95.338–106.681°, respectively [51–60].

An interesting observation in the structures of the two diacetato-bridged complexes is the distances between the uncoordinated acetate oxygen atoms and the azomethine (–HC=N–) carbon atoms of the adjacent dimers (3.162(10) Å for **3** and 3.199(6) Å for **4**). Thus a one dimensional assembly of the dimer is formed by involvement of the molecule in two pairs of reciprocal C–H···O interactions with its two neighbours on both sides.

3.5. Magnetic properties

Magnetic susceptibility measurements for powdered samples of the four complexes were carried out in the temperature range 17–300 K at a constant magnetic field of 5 kG. The room temperature effective magnetic moments (μ_{eff}/monomer) are in the range 1.84–1.92 μ_B (Table 2). On cooling there is no significant change in the magnetic moments. At 17 K the magnetic moments are within 2.07–2.19 μ_B. That each complex behaves essentially as a Curie paramagnet is readily apparent from the linear plots of inverse magnetic susceptibility values (per monomer) against temperature. The data were fit using the expression for Curie–Weiss law. The Curie (C) and the Weiss constants (θ in K) are 0.45 and -3.57, 0.42 and 1.98, 0.45 and -1.41, and 0.46 and -1.04 for **1**, **2**, **3**, and **4**, respectively.

Magnetostructural studies on equatorial–apical dichloro-bridged copper(II) dimers have been reported [41,61]. The exchange coupling constant (J) in such complexes cover a wide range ($+6$ to -41.3 cm^{-1}) [41–43,46,61]. An empirical relationship has been observed between the extent of the Cu···Cu interaction and the ratio ϕ/R, where ϕ is the Cu–Cl–Cu bridge angle and R is the longer Cu–Cl distance [41,61]. With the increase of the ratio ϕ/R the value of $-2J$ decreases and reaches a minimum and then again in-

creases. The magnitude of J is very small for most of the complexes in which $\phi/R \approx 33$. In **1** this ratio is 32.6. The paramagnetic nature of **1** is consistent with this ratio.

Magnetic properties of very few single chloride bridged polymeric copper(II) complexes analogous to **2** are reported [62]. In all of them the intrachain magnetic interaction is very weak ($J = -6.1$–1.58 cm^{-1}). However a trend in the Cu–Cl–Cu bridge angle (ϕ) and the value of J has been observed [62]. The coupling constant (J) decreases with the increase of ϕ. For large ϕ (144.6°), the J is negative (-6.1 cm^{-1}). Weak ferromagnetic interaction is observed for species with smaller Cu–Cl–Cu angle ($\phi = 113.58(5)°$, $J = 1.58$ cm^{-1}; $\phi = 128.1°$, $J = 0.48$ cm^{-1}). Although the small positive Weiss constant (1.98 K) observed for **2** indicates the near paramagnetic nature, it is interesting that ϕ (117.60(5)°) in **2** is intermediate of the above two values.

Compared to the dichloro-bridged complexes magnetic data for diacetato-bridged dimeric species similar to **3** and **4** are scarce. The coupling constants J reported for the previously studied complexes are very small and within the range -1.54 to $+0.63$ cm^{-1} [51,53,54,56]. The small values of θ observed for **3** and **4** suggest a similar situation where no significant spin–spin interaction exists between the metal ions.

4. Conclusions

One polymeric and three dimeric copper(II) complexes with N,N,O-donor ligands have been synthesised and structurally characterised by X-ray crystallography. Metal ions are in distorted square-pyramidal N_2OCl_2 or N_2O_3 coordination sphere in these complexes. The polymeric chain complex is formed via single chloride bridges. In the dimers, chloride or acetate ions act as the monoatomic bridging units. In all the complexes the bridging units are in equatorial–apical fashion. The spectral properties (UV–Vis and ESR) are similar to those of other complexes containing square-planar or square-pyramidal copper(II). The complexes are redox active in methanol solutions. Variable temperature magnetic susceptibility measurements revealed the paramagnetic nature of the complexes.

5. Supplementary material

Crystallographic data are available from the Cambridge Crystallographic Data Centre, 12 Union Road, Cambridge CB2 1EZ, UK (fax: +44-1223-336033; e-mail: deposit@ccdc.cam.ac.uk or www: http://www.ccdc.cam.ac.uk) on request, quoting the deposition Nos. CCDC 141222–141225.

Acknowledgements

Financial assistance for this work was provided by the Council of Scientific and Industrial Research, New Delhi (Grant no. 01(1422)/96/EMR-II). N.R.S thanks the University Grants Commission, New Delhi for a research fellowship. We are grateful to Professor A.R. Chakravarty for providing the variable temperature magnetic susceptibility data and to Professor P.S. Zacharias for allowing the use of the electroanalytical system. The X-ray crystallographic studies were performed at the National Single Crystal Diffractometer Facility, School of Chemistry, University of Hyderabad. We thank the Department of Science and Technology, New Delhi, for setting up this facility.

References

[1] D.J. Hodgson, Prog. Inorg. Chem. 19 (1975) 182.
[2] O. Kahn, Angew. Chem., Int. Ed. Engl. 24 (1985) 834.
[3] P.A. Vigato, T. Samburini, D.E. Fenton, Coord. Chem. Rev. 106 (1990) 25.
[4] E. Spodin, J. Manzur, Coord. Chem. Rev. 119 (1992) 171.
[5] E. Bouwman, W.L. Driessen, J. Reedijk, Coord. Chem. Rev. 104 (1990) 143.
[6] K.D. Karlin, Z. Tyeklár, Adv. Inorg. Biochem. 9 (1994) 123.
[7] N. Kitajima, Y. Moro-oka, Chem. Rev. 94 (1994) 737.
[8] E.I. Solomon, U.M. Sundaram, T.E. Machonkin, Chem. Rev. 96 (1996) 2563.
[9] W.B. Tolman, Acc. Chem. Res. 30 (1997) 227.
[10] N.R. Sangeetha, C.K. Pal, P. Ghosh, S. Pal, J. Chem. Soc., Dalton Trans. (1996) 3293.
[11] A.V. Lakshmi, N.R. Sangeetha, S. Pal, Indian J. Chem. 36A (1997) 844.
[12] N.R. Sangeetha, K. Baradi, R. Gupta, C.K. Pal, V. Manivannan, S. Pal, Polyhedron 18 (1999) 1425.
[13] N.R. Sangeetha, S. Pal, J. Chem. Crystallogr. 29 (1999) 287.
[14] N.R. Sangeetha, S. Pal, Bull. Chem. Soc. Jpn. 73 (2000) 357.
[15] W.E. Hatfield, in: E.A. Boudreaux, L.N. Mulay (Eds.), Theory and Applications of Molecular Paramagnetism, Wiley, New York, 1976, p. 491.
[16] S.R. Hall, G.S.D. King, J.M. Stewart (Eds.), XTAL3.4 User's Manual, University of Western Australia, Perth, 1995.
[17] G.M. Sheldrick, SHELX-97, Structure Determination Software, University of Göttingen, Göttingen, Germany, 1997.
[18] P. McArdle, J. Appl. Crystallogr. 28 (1995) 65.
[19] L. El-Sayed, M.F. Iskander, J. Inorg. Nucl. Chem. 33 (1971) 435.
[20] K. Nakamoto, Infrared and Raman Spectra of Inorganic and Coordination Compounds, Wiley, New York, 1986, p. 244.
[21] S. Choudhury, M. Kakoti, A.K. Deb, S. Goswami, Polyhedron 11 (1992) 3183.
[22] K. Nakamoto, Infrared and Raman Spectra of Inorganic and Coordination Compounds, Wiley, New York, 1986, p. 233.
[23] H.S. Maslen, T.N. Waters, Coord. Chem. Rev. 17 (1975) 137.
[24] S. Karunakaran, M. Kandaswamy, J. Chem. Soc., Dalton Trans. (1995) 1851.
[25] B.J. Hathaway, D.E. Billing, Coord. Chem. Rev. 5 (1970) 143.
[26] P. O'Brien, J.R. Thornback, Inorg. Chim. Acta 64 (1981) 135.
[27] S. Pal, D. Bandyopadhyay, D. Datta, A. Chakravorty, J. Chem. Soc., Dalton Trans. (1985) 159.
[28] S. Dutta, P. Basu, A. Chakravorty, Inorg. Chem. 30 (1991) 4031.

[29] S. Seth, S. Chakraborty, Acta Crystallogr., Sect. C 40 (1984) 1530.
[30] G.V. Karunakar, N.R. Sangeetha, V. Sushila, S. Pal, J. Coord. Chem. 50 (2000) 51.
[31] G.D. Storrier, S.B. Colbran, D.C. Craig, J. Chem. Soc., Dalton Trans. (1997) 3011.
[32] A. Seal, S. Ray, Acta Crystallogr., Sect. C 40 (1984) 929.
[33] Y. Shiping, C. Peng, L. Diazeng, J. Zonghui, W. Honggen, Y. Xinkan, Polyhedron 11 (1992) 879.
[34] E.W. Ainscough, A.M. Brodie, A.J. Dobbs, J.D. Ranford, J.M. Waters, Inorg. Chim. Acta 267 (1998) 27.
[35] V.V. Lukov, V.A. Kogan, S.I. Levchenkov, L.V. Zavada, K.A. Lyssanko, O.V. Shisbkin, Zh. Neorg. Khim. 43 (1998) 421.
[36] D.L. Lewis, K.T. McGregor, W.E. Hatfield, D.J. Hodgson, Inorg. Chem. 13 (1974) 1013.
[37] S.K. Mandal, L.K. Thompson, M.J. Newlands, E.J. Gabe, K. Nag, Inorg. Chem. 29 (1990) 1324.
[38] G.R. Desiraju, H.R. Luss, D.L. Smith, J. Am. Chem. Soc. 100 (1978) 6375.
[39] X. Xiaojie, S. Meichang, Y. Zhiyao, Y. Qingchuan, T. Shenyang, Acta Chim. Sin. 40 (1982) 353.
[40] S.K. Hoffmann, D.K. Towle, W.E. Hatfield, K. Weighardt, P. Chaudhuri, J. Weiss, Mol. Cryst. Liq. Cryst. 107 (1984) 161.
[41] T. Rojo, M.I. Arriortua, J. Ruiz, J. Darriet, G. Villeneuve, D. Beltran-Porter, J. Chem. Soc., Dalton Trans. (1987) 285.
[42] S.J. Brown, X. Tao, T.A. Wark, D.W. Stephan, P.K. Mascharak, Inorg. Chem. 27 (1988) 1581.
[43] E. Kwiatkowski, M. Kwiatkowski, A. Olechnowicz, J. Mrozinski, D.M. Ho, E. Deutsch, Inorg. Chim. Acta 158 (1989) 37.
[44] M.B. Ferrari, G.G. Fava, P. Tarasconi, C. Pelizzi, J. Chem. Soc., Dalton Trans. (1989) 361.
[45] M. Zoeteman, E. Bouwman, R.A.G. de Graaff, W.L. Driessen, J. Reedijk, Inorg. Chem. 29 (1990) 3487.
[46] M. Kwiatkowski, E. Kwiatkowski, A. Olechnowicz, G. Bandoli, Inorg. Chim. Acta 182 (1991) 117.
[47] M. Bukowska-Strzyzewska, W. Maniukiewicz, J. Crystallogr. Spectrosc. Res. 22 (1992) 43.
[48] W. Maniukiewicz, M. Bukowska-Strzyzewska, J. Chem. Crystallogr. 24 (1994) 133.
[49] M.K. Urtiaga, M.I. Arriorfua, R. Cortes, T. Rojo, Acta Crystallogr., Sect. C 52 (1996) 3007.
[50] W. Maniukiewicz, M. Bukowska-Strzyzewska, J. Chem. Crystallogr. 26 (1996) 43.
[51] A.M. Greenaway, C.J. O'Connor, J.W. Overman, E. Sinn, Inorg. Chem. 20 (1981) 1508.
[52] R. Hämäläinen, M. Ahlgrén, U. Tupeinen, Acta Crystallogr., Sect. B 38 (1982) 1577.
[53] B. Chiari, W.E. Hatfield, O. Piovesana, T. Tarantelli, L.W. Ter Haar, P.F. Zanazzi, Inorg. Chem. 22 (1983) 1468.
[54] J.-P. Costes, F. Daham, J.-P. Laurent, Inorg. Chem. 24 (1985) 1018.
[55] N.A. Bailey, D.E. Fenton, J.R. Tate, P.M. Thomas, J. Chem. Soc., Dalton Trans. (1985) 1471.
[56] B. Chiari, J.J. Helms, O. Piovesana, T. Tarantelli, P.F. Zanazzi, Inorg. Chem. 25 (1986) 870.
[57] S.J. Brown, X. Tao, D.W. Stephan, P.K. Masharak, Inorg. Chem. 25 (1986) 3377.
[58] A.G. Bingham, H. Bögge, A. Müller, E.W. Ainscough, A.M. Brodie, J. Chem. Soc., Dalton Trans. (1987) 493.
[59] B. Chiari, O. Piovesana, T. Tarantelli, P.F. Zanzzi, Inorg. Chem. 27 (1988) 3246.
[60] M. Becht, T. Gerfin, K.-H. Dahmen, Helv. Chim. Acta 77 (1994) 1288.
[61] W.E. Marsh, K.C. Patel, W.E. Hatfield, D.J. Hodgson, Inorg. Chem. 22 (1983) 511.
[62] W.E. Estes, W.E. Hatfield, J.A.C. van Ooijen, J. Reedijk, J. Chem. Soc., Dalton Trans. (1980) 2121.

PERGAMON

www.elsevier.nl/locate/poly

Polyhedron 19 (2000) 1601–1605

POLYHEDRON

Palladium(II) complexes bearing ethylene-bridged S∩As and S∩P donor ligands: synthesis, crystal structure and reactivity towards the polymerization of norbornene

Adnan S. Abu-Surrah [a,*], Kristian Lappalainen [a], Timo Repo [a], Martti Klinga [a], Markku Leskelä [a], Hamdallah A. Hodali [b]

[a] *Laboratory of Inorganic Chemistry, University of Helsinki, PO Box 55, 00014 Helsinki, Finland*
[b] *Department of Chemistry, Faculty of Science, University of Jordan, Amman, Jordan*

Received 2 March 2000; accepted 19 May 2000

Abstract

Palladium(II) complexes of the general type $[Pd(L\cap L)Cl_2]$ (**4**–**6**) and their corresponding dicationic complexes $[Pd(L\cap L)(NCCH_3)_2](BF_4)_2$ (**7**–**9**) (L∩L = [(1-(thiomethyl)-2-(diphenylarsino)ethane] (S∩As, **1**) (**4**, **7**) [1-(thiomethyl)-2-(diphenylphosphino)ethane] (S∩P, **2**) (**5**, **8**) and [1,2-bis(diphenylphosphino)ethane] (P∩P, **3**) (**6**, **9**) have been synthesized and utilized as catalysts for the polymerization reaction of bicyclo[2.2.1]hept-2-ene (norbornene). The dichloride complexes can be activated with methylaluminoxane (MAO), while the corresponding dicationic compounds were used as single component catalysts for the polymerization reactions. Catalytic performance of the new type of catalyst can be altered by modifying the donor atoms in the bidentate ligand. The activity of the Pd(II) complexes towards the polymerization reaction increases with increasing the *trans*-influence of the donor atoms (P∩P > S∩P > S∩As). The influence of donor atoms on the length of the Pd–Cl bonds was elucidated by X-ray structure analysis carried out on the palladium(II) complex $[Pd(S\cap As)Cl_2]$ (**4**). © 2000 Elsevier Science Ltd. All rights reserved.

Keywords: Palladium(II) complexes; Mixed donor ligands; *Trans*-influence; X-ray crystallography; Methylaluminoxane (MAO); Norbornene; Polymerization

1. Introduction

Different methods for polymerization of bicyclo[2.2.1]hept-2-ene (norbornene) are known: ring-opening metathesis polymerization (ROMP) [1], cationic polymerization, radical polymerization [2] and the vinyl-type olefin addition (1,2-insertion), where the polymerization involves exclusively the π bond and leaves the bicyclic monomer unit intact [3]. Polymerization of norbornene to poly(2,3-bicyclo[2.2.1]heptene) was first reported in the early 1960s [4]. In addition to Ti(IV)- and Zr(IV)-based catalysts [5], Pd(II) compounds have also been applied successfully for the polymerization of norbornene to amorphous, transparent polymer products, which consist of 2,3-linked bicyclic units (Fig. 1) [3]. The first generation of the palladium catalysts consisted of neutral palladium(II) halides [6]. These compounds required long polymerization time and elevated temperatures and resulted in low yields and lower molecular weights materials. Cationic palladium(II) complexes in which the Pd(II) center is surrounded by four weakly coordinated nitrile ligands [3] (e.g. $[Pd(NCCH_3)_4](BF_4)_2$) represent the current catalyst generation of highly increased activity. However, by using these chelate-free solvated complexes, no control on the polymer microstructure is feasible. Furthermore, this type of catalyst is not soluble in chlorinated solvents such as CH_2Cl_2 and chlorobenzene. A catalyst system consisting of palladium(II) based catalyst precursor and methylaluminoxane as activator was also reported to catalyze efficiently the polymerization reaction [7].

* Corresponding author. Tel.: +358-9-1914-0236; fax: +358-9-1914-0198.
E-mail address: adnan.surrah@helsinki.fi (A.S. Abu-Surrah).

0277-5387/00/$ - see front matter © 2000 Elsevier Science Ltd. All rights reserved.
PII: S0277-5387(00)00436-8

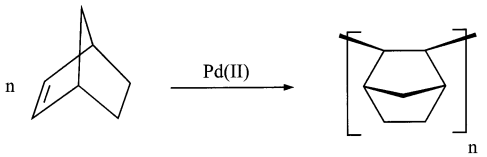


Fig. 1. Structure of poly(2,3-bicyclo[2.2.1]heptene).

In a previous report we presented new palladium(II) complexes with ethylene-bridged bisindolinyl nitrogen ligands together with weakly coordinated acetonitrile moieties as active, single component catalysts for the polymerization of norbornene. Using this catalyst system a monomer conversion up to 70% could be reached [8]. As an extension of our studies upon both the coordination chemistry of heteroatom-containing ligands and the polymerization of cyclic olefines [8–10] we report here on the application of palladium(II) complexes stabilized with ethylene-bridged bidentate ligands that contain different donor atoms (S∩As, **1** and S∩P, **2**) as a new type of catalyst for the polymerization reaction of norbornene. Their catalytic behavior was compared with that for the symmetrical P∩P based Pd(II) complexes. In addition, the influence of the donor atoms P, As, and S on the catalytic conduct of the complexes has been rationalized.

2. Experimental

2.1. Materials

All reactions were carried out under dry Argon using standard Schlenk techniques. The ligands (S∩As) (**1**), (S∩P) (**2**) [11], and the palladium(II) complexes $[Pd(S\cap As)Cl_2]$ (**4**) [9b], $[Pd(S\cap P)Cl_2]$ (**5**) [9b] and $[Pd(P\cap P)Cl_2]$ (**6**) [12] were prepared according to literature procedures. MAO was purchased from WITCO. Toluene was purified by distillation over $LiAlH_4$. CH_2Cl_2 and CH_3CN were purified by distillation over CaH_2 and P_2O_5, respectively. Reagent grade chemicals were used as received unless otherwise stated

2.2. Physical measurements

Elemental analyses was performed by the Microanalytical Laboratories of Ulm University, Germany. ^1H NMR spectra were recorded on a Bruker AC 200 spectrometer. Infrared spectra (KBr film) were measured on a Bruker model IFS113V spectrometer. Molecular weights and molecular weight distributions were determined by a Waters 150-C GPC chromatograph relative to polystyrene standards. Thermogravimetric analysis (TGA) data were collected by a Perkin–Elmer DSC-7 with a 20 K min^{-1} heating rate.

2.3. Synthesis of the complexes

The complexes $[Pd(S\cap As)(NCCH_3)_2](BF_4)_2$ (**7**), $[Pd(S\cap P)(NCCH_3)_2](BF_4)_2$ (**8**) and $[(P\cap P)Pd(NCCH_3)_2](BF_4)_2$ [13] (**9**) were prepared following a previously published procedure [14]. The corresponding dichloride complex **4**, **5**, or **6** (0.89 mmol) was mixed with $AgBF_4$ (0.35 g, 1.79 mmol) in CH_3CN (50 ml). After the mixture had been stirred for 12 h at room temperature (r.t.), the resulting agile precipitate was removed by filtration and the filtrate was evaporated under reduced pressure. The residue was dissolved in CH_2Cl_2 (40 ml), filtered and the filtrate was evaporated to dryness under reduced pressure and dried under vacuum.

2.3.1. $[Pd(S\cap As)(NCCH_3)_2](BF_4)_2$ (7)

Yield: 85%. Found: C, 33.7; H, 3.25; N, 3.74. *Anal.* Calc. for $C_{19}H_{23}AsB_2F_8N_2PdS$: C, 34.2; H, 3.48; N, 4.20%. ^1H NMR (200 MHz, CD_3CN): δ 7.80–7.50 (m, 10H, $H_{arom.}$), 3.48–2.93 (m, 4H, $C_2H_{4\ bridg.}$), 2.67 (s, 3H, S–CH_3), 1.93 (s, $NCCH_3$). IR (CsI, cm^{-1}): 2299 (m), 2327 (m) (C≡N), 1061 (s, br) (BF_4).

2.3.2. $[Pd(S\cap P)(NCCH_3)_2](BF_4)_2$ (8)

Yield: 91%. Found: C, 36.9; H, 3.51; N, 4.35. *Anal.* Calc. for $C_{19}H_{23}B_2F_8N_2PPdS$: C, 36.7; H, 3.72; N, 4.50%. ^1H NMR (200 MHz CD_3CN): δ 7.62–7.43 (m, 10H, $H_{arom.}$), 3.56 (m, 4H, $C_2H_{4\ bridg.}$), 2.98 (s, 3H, S–CH_3), 2.09 (s, $NCCH_3$). IR (CsI, cm^{-1}): 2299 (w), 2325 (w) (C≡N), 1062 (s, br) (BF_4).

2.4. X-ray crystal structure determination for 4

Crystal data for compound **4** was collected on a Rigaku AFC7S single-crystal diffractometer at 193(2) K using graphite monochromatized Mo Kα radiation (0.71073 Å). The intensities were corrected for Lorentz and polarization effects. An experimental absorption correction (ψ-scan) was performed. The structures were solved by direct methods (SHELXTL/PC program). All non-hydrogen atoms were refined anisotropically and hydrogen atoms isotropically on calculated positions. Final calculations were performed with SHELXTL/PC and SHELXL-93 program systems. The final cell parameters and specific data collection parameters are summarized in Table 1.

2.5. Polymerization experiments

To a solution of the palladium(II) complex (**4**–**6**) (50 mg) in CH_2Cl_2 (50 ml), 1,2-dichlorobenzene (5.0 ml) and nitrobenzene (2 ml), norbornene was added (Table 2, entries 4–6). When MAO-activation was utilized

Table 1
Crystallographic data and parameters for data collection and refinement of complex **4**

Formula	$C_{15}H_{17}AsCl_2PdS$
Formula weight	481.57
T (K)	193(2)
Crystal system	monoclinic
Space group	$P2_1/n$
a (Å)	11.531(2)
b (Å)	12.327(2)
c (Å)	11.677(2)
α (°)	90
β (°)	92.98(3)
γ (°)	90
V (A^3)	1657.6(5)
Z	4
D_{calc} (g cm^{-3})	1.930
Absorption coefficient (mm^{-1})	3.536
Crystal dimensions (mm)	$0.60 \times 0.53 \times 0.50$
θ Range (°)	2.55–26.51
Scan mode	ω–2θ
Scan range (°)	1.80
Number of data collected	3546
Number of unique data	3379 [$R_{int} = 0.0478$]
Number of data refined	3370
Observed criterion	$F > 4\sigma(F)$
Number of parameters	199
R [a]	0.0283
wR_2 [b]	0.0745
Residual density [c]	1.047, −0.632

[a] $R = \Sigma||F_o| - |F_c||/\Sigma|F_o|$.
[b] $wR_2 = \{\Sigma[w(F_o^2 - F_c^2]^2\}/\Sigma[w(F_o^2)^2]^{0.5}$.
[c] Maximum residual electron density of 1.047 e $Å^{-3}$ is 0.89 Å from the Pd atom.

(Table 2, entries 1–3) the polymerization reaction was performed in toluene (80 ml). The reaction mixture was stirred at r.t. for 2 h. At the end of the reaction period the reaction was quenched by addition of methanol and the polymer was isolated by filtration, washed with excess methanol and dried under vacuum at 80°C. *Anal.* Found: C, 89.00; H, 10.58. Calc. for $[C_7H_{10}]_n$: C, 89.29; H 10.7%.

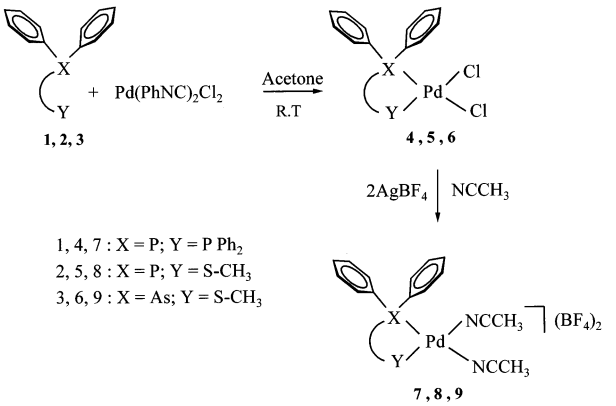


Fig. 2. Structure of the palladium(II) complexes **4**–**9**.

3. Results and discussion

The air- and moisture-stable palladium(II) complexes $[Pd(S \cap As)Cl_2]$ (**4**), $[Pd(S \cap P)Cl_2]$ (**5**) and $[Pd(P \cap P)Cl_2]$ (**6**) were prepared by stirring the ligands **1**–**3**, respectively, with $Pd(NCPh)Cl_2$ in acetone following literature procedures [9b]. Chloride abstraction from compounds **4**–**6** with $AgBF_4$ afforded the solvated diacetonitrile complexes **7**–**9**, respectively (Fig. 2). The complexes were characterized by elemental analysis, ^1H NMR and IR spectroscopy.

3.1. Crystal structure of complex *4*

Suitable crystals of $[Pd(S \cap As)Cl_2]$ (**4**) (Fig. 3) were obtained by crystallization from acetone. Selected bond lengths and angles are given in Table 3. The Pd atom is at the center of approximately square-planar arrangement. The complex form monoclinic crystals with space group $P2_1/n$ which also similar to that for the complexes $[Pd(S \cap P)Cl_2]$ (**5**) [15] and $[Pd(P \cap P)Cl_2]$ (**6**) [12].

A comparison among the X-ray structural data of complexes **4**–**6** showed that the Pd–Cl bond is obviously sensitive to the nature of the *trans* donor atom. The Pd–Cl_1 and Pd–Cl_2 bond lengths in the compound **4** are 2.3143(8) and 2.3575(9) Å, respectively, the first is *trans* to S and the second is *trans* to As. The distances

Table 2
Polymerization results [a]

Entry	Ligand	Catalyst	Al/Pd (mol ratio)	$\bar{M}_w$ (g mol^{-1}) [b]	$\bar{M}_w/\bar{M}_n$ [b]	Yield (g)	Conversion (%)
1	S∩As	**4**	200	1.50×10^4	1.65	0.77	15.8
2	S∩P	**5**	200	2.86×10^5	1.81	2.29	42.6
3	P∩P	**6**	200	2.82×10^5	1.34	2.56	62.6
4	S∩As	**7**		7.67×10^5	1.92	3.04	86.1
5	S∩P	**8**		5.71×10^5	1.87	3.51	92.9
6	P∩P	**9**		4.73×10^5	1.91	3.43	98.4

[a] Polymerization conditions: solvent, toluene (entries 1–3), CH_2Cl_2 (50 ml), 1,2-dichlorobenzene (5.0 ml), nitrobenzene (1.0 ml); norbornrne/Pd(II) mol ratio, 500; T, r.t; time, 2 h.
[b] Measured by GPC (relative to polystyrene).

in compound **5** are 2.3719(13) Å (Pd–Cl_1) and 2.3116(12) Å (Pd–Cl_2), which are *trans* to P and S, respectively [12]. These bonds are shorter than those in [Pd(P∩P)Cl_2] (**6**) (2.415(3) Å (Pd–Cl_1) and 2.394(3) Å (Pd–Cl_2)) [13] which suggest that with increasing the *trans*-influence of the donor atom the length of Pd–Cl bond *trans* to it increases. The variation of Pd–Cl distances shown above are in agreement with the *trans*-influence orderings (P > As > S) [9]. In summary, we could say that the ligands exert a stronger influence in the order (P∩P) > (S∩P) > (S∩As).

The higher weakening effect caused on the Pd–Cl bond when phosphorus is the *trans* donor atom is in harmony with previous NMR investigations carried out on the corresponding dialkyl complexes (the methyl signals are shifted up field with increasing *trans*-influence) [9b]. This was explained in terms of weakening effect caused by the donor atom on the Pd–CH_3 bond *trans* to it.

3.2. Polymerization behavior

Polymerization reactions of norbornene were carried out using the MAO activated palladium(II) chloride complexes (**4**–**6**) in toluene or by utilizing the self-activated dicationic species (**7**–**9**) in a reaction medium consisting of a mixture of dichloromethane, 1,2-dichlorobenzene and nitrobenzene (Table 2). The amorphous, transparent polymer products consist of 2,3-linked norbornene units. Monomer conversion up to 98% can be reached by the right choice of the ligand and the catalyst system.

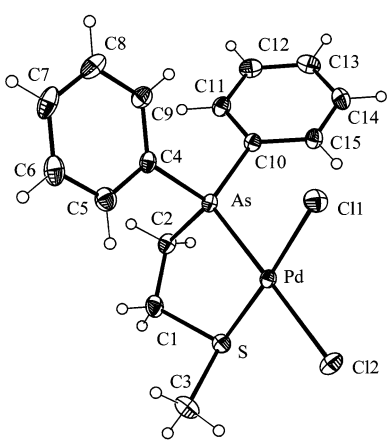


Fig. 3. ORTEP plot of the molecular structure of compound **4**. Displacement ellipsoids are drawn at the 50% probability level.

Table 3
Selected bond lengths (Å) and angles (°) for complex **4**

Pd–S	2.2785(8)	As–C(4)	1.929(3)
Pd–Cl(1)	2.3143(8)	As–C(2)	1.961(3)
Pd–As	2.3190(6)	S–C(3)	1.809(3)
Pd–Cl(2)	2.3575(9)	S–C(1)	1.840(3)
S–Pd–Cl(1)	175.86(3)	Cl(1)–Pd–Cl(2)	93.86(4)
S–Pd–As	87.55(3)	As–Pd–Cl(2)	177.60(2)
Cl(1)–Pd–As	88.31(3)	C(1)–S–Pd	106.84(11)
S–Pd–Cl(2)	90.28(4)	C(2)–As–Pd	105.47(10)

Higher polymer yields were obtained by using the single-component Pd(II) catalysts **7**–**9** (Table 2, entries 4–6) compared to the Pd(II)/MAO catalyst systems **4**–**6** (Table 2, entries 1–3). The complexes with phosphine ligands [Pd(S∩P)$(NCCH_3)_2$]$(BF_4)_2$ (**8**) and [Pd(P∩P)$(NCCH_3)_2$]$(BF_4)_2$ (**9**) showed a considerably higher activity for norbornene polymerization than the corresponding complex [Pd(S∩As)$(NCCH_3)_2$]$(BF_4)_2$ (**7**) under similar reaction conditions (Table 2). The same behavior was also observed when utilizing the Pd(II)/MAO catalyst systems **4**–**6**. However, a decrease in the yield of polymer was observed using these catalysts for polymerization in toluene that can be attributed to precipitation of the polymer in toluene before all the monomer had been consumed.

The higher rate of monomer conversion using complex **9** might be due to the stronger *trans*-influence of the ligand (P∩P, **3**) compared to that for the mixed ligands (S∩P, **2**) and (S∩As, **1**), which leads to the weakening of the in situ formed Pd–alkyl bond, allowing therefore faster monomer insertion. Previous investigations on the corresponding alkyl palladium(II) and platinum(II) complexes showed also that the weakening effect on the metal–alkyl bond *trans* to the donor atom increases in the order P > As > N > S [9a,b].

No change in the color of the polymerization media due to the decomposition of the palladium catalysts was observed in either system, which indicates a rare ligand dissociation under the applied polymerization conditions. The IR spectra of the polymers are similar to those of the previously described vinyl-type poly(norbornene)s, prepared by Pd(II) catalysis [3e,8]. No absorption bands due to double bonds resulting from ring opening (ROMP) were observed. According to thermogravimetric analysis (TGA) under nitrogen, the poly(norbornene)s prepared utilizing the complexes that carry phosphorus donor atom (**5**, **6**, **8** and **9**) show higher stability; the polymer products start to decompose at temperatures above 425°C. This is about 100°C higher compared to the polymers produced by **4** and **7** or [Pd$(NCCH_3)_4$]$(BF_4)_2$, where decomposition commences at 335°C [3a].

4. Conclusion

Palladium(II) complexes bearing bidentate ligands with different donor atoms were used successfully as

catalysts for the polymerization reaction of norbornene. These compounds are a new type of Pd(II)-based catalyst for the polymerization of cyclic monomers. Higher catalytic activity was observed for the dicationic Pd(II) single-component catalysts (**7**–**9**) compared to the Pd(II)/MAO catalyst system (**4**–**6**). By maintaining the structural features of the complexes (**4** and **5** or **7** and **8**) we have been able to look into the influence of the donor atoms on their catalytic conduct. With increasing the *trans*-influence of the donor atom, the in situ formed Pd–alkyl bond *trans* to it is weakened and thus catalytic activity of the compound is increased.

5. Supplementary material

Crystallographic data for the structure reported in this paper have been deposited at the Cambridge Crystallographic Data Center as supplementary publication number CCDC-134953. Copies of the data can be obtained on application to: The Director, CCDC, 12 Union Road, Cambridge, CB2 1EZ, UK (fax: +44-1223-336-033; e-mail: deposit@ccdc.cam.ac.uk or www: http://www.ccdc.cam.ac.uk).

Acknowledgements

Financial support from the International Center for Mobility (CIMO) and University of Helsinki, Finland is gratefully acknowledged. The authors wish to thank E. Aitola for GPC measurements of the polymer samples.

References

[1] (a) K.J. Ivin, J.C. Mol, Olefin Metathesis and Metathesis Polymerization, Academic, London 1997. (b) V. Dragutan, A.T. Balaban, M. Dimonie, Olefin Metathesis and Ring-Opening Polymerization of Cycloolefins, Wiley, Chichester 1985.
[2] N.G. Gaylord, A.B. Deshpanda, B.M. Mandal, M. Martan, J. Macromol. Sci., Chem. A 11 (1977) 1053.
[3] (a) N. Seehof, C. Mehler, S. Breunig, W. Risse, J. Mol. Catal. 76 (1992) 219. (b) A. Sen, T.-W. Lai, Organometallics 1 (1982) 415. (c) A. Sen, T.-W. Lai, R.R. Thomas, J. Organomet. Chem. 358 (1988) 567. (d) A.L. Safir, B.M. Novak, Macromolecules 28 (1995) 5396. (f) Chem. Week 20 (1996) 56.
[4] G. Sartori, F.C. Ciampelli, N. Cameli, Chim. Ind. (Milan) 45 (1963) 1478.
[5] (a) T. Tsujino, T. Saegusa, J. Furukawa, Makromol. Chem. 85 (1965) 71. (b) W. Kaminsky, A. Bark, M. Arndt, Makromol. Chem., Macromol. Symp. 47 (1991) 83.
[6] (a) R.G. Schultz, J. Polym. Sci., Polym. Lett. 4 (1966) 541. (b) J.E. McKeon, P.S. Stracher, US Pat. 3330815, 1967; Chem. Abstr. 67 (1967) 64884g. (c) R.G. Schultz, Polym. Lett. 4 (1966) 541.
[7] B.S. Heinz, F.P. Alt, W. Heitz, Macromol. Rapid Commun. 19 (1998) 251. (b) M. Arndt, M. Gosmann, Polym. Bull. 41 (1998) 433.
[8] A.S. Abu-Surrah, B. Rieger, J. Mol. Catal A: Chem. 128 (1998) 239.
[9] (a) A.S. Abu-Surrah, H.A. Hodali, Inorg. Chim. Acta 174 (1990) 223. (b) A.S. Abu-Surrah, H.A. Hodali, Transition Met. Chem. 16 (1991) 458.
[10] (a) A.S. Abu-Surrah, B. Rieger, M. Geprägs, J. Queisser, DE Pat. App. 19714532.9, 1997. (b) A.S. Abu-Surrah, U. Thewalt, B. Rieger, J. Organomet. Chem. 587 (1999) 58.
[11] (a) P. Rigo, M. Bressan, Inorg. Chem. 14 (1975) 1491. (b) H.A. Hodali, J. Chem. Eng. Data 32 (1987) 382.
[12] (a) W.L. Steffen, G.J. Palenik, Inorg. Chem. 15 (1976) 2432. (b) S. Singh, N.K. Jha, Acta Crystallogr., Sect. C 51 (1995) 593
[13] F.Y. Xu, A.X. Zhao, J.C.W. Chien, Makromol. Chem. 149 (1993) 2579.
[14] A.S. Abu-Surrah, R. Fawzi, M. Steimann, B. Rieger, J. Organomet. Chem. 512 (1996) 243.
[15] A.S. Abu-Surrah, K. Lappalainen, M. Klinga, M. Leskelä, H.A. Hodali, B. Rieger, Acta Crystallogr., Sect. C 55 (1999) 188.

PERGAMON

www.elsevier.nl/locate/poly

Polyhedron 19 (2000) 1607–1614

POLYHEDRON

Direct electrochemical synthesis of cobalt(II) complexes of tosylamides: crystal structures of $[CoL_2py_2]$, $[CoL_2DMF_2]$, $[CoL_2bipy]$ and $[CoL_2phen]$, L = [(4-methylphenyl)sulfonyl]-2-pyridylamide

Santiago Cabaleiro [a], Jesús Castro* [a,1], José A. García-Vázquez [b], Jaime Romero [b], A. Sousa* [b,2]

[a] *Departamento de Química Inorgánica, Universidade de Vigo, E-36200 Vigo, Galicia, Spain*
[b] *Departamento de Química Inorgánica, Universidade de Santiago, E-15706 Santiago de Compostela, Galicia, Spain*

Received 7 February 2000; accepted 17 May 2000

Abstract

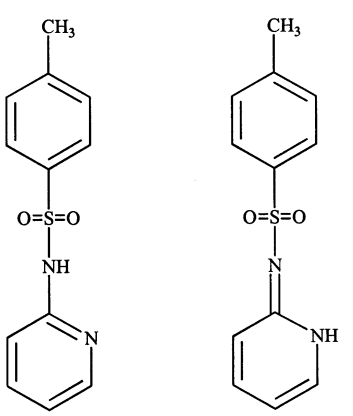
Several complexes with tosylamides were synthesised by the electrochemical oxidation of cobalt in an acetonitrile solution of [(4-methylphenyl)sulfonyl]-imino-1*H*-pyridine (HL) and the appropriate neutral coligand: L′ (pyridine, 2,2′-bipyridine, 1,10-phenanthroline or *N*,*N*-dimethylformamide). The structures of bis-(*N*,*N*-dimethylformamide)bis{[(4-methylphenyl)sulfonyl]-2-pyridyl-amide}cobalt(II), bis-(pyridine)bis{[(4-methylphenyl)sulfonyl]-2-pyridyl-amide}cobalt(II), 2,2′-bipyridine bis{[(4-methylphenyl)sulfonyl]-2-pyridyl-amide}cobalt(II) and 1,10-phenanthroline bis{[(4-methylphenyl)sulfonyl]-2-pyridyl-amide}cobalt(II) were determined by X-ray diffraction methods. In these monomeric complexes, the cobalt atom is in a distorted octahedral environment. The vibrational and electronic spectra of the complexes are discussed and are shown to agree with the structures.
© 2000 Elsevier Science Ltd. All rights reserved.

Keywords: Electrochemical synthesis; Cobalt(II) complexes; Crystal structures; Tosylamide complexes

1. Introduction

The coordination chemistry of amides is scarce due to the difficulty of the substitution of a metal ion for an amide proton. However, if a sulfonamide group substitutes the amide group, the electron withdrawal of the sulfonyl group causes important changes and the formation of the complexes is facilitated [1].

This is one of the reasons why the coordination chemistry of sulfonamide ligands has been investigated in recent years [2,3]. Electron withdrawal of the sulfonyl group causes important changes in both the neutral ligand and in the complexes. Free molecules, such as tosylsulfonylimino-1*H*-pyridine, are expected to exist in



(I) (II)

the form **I**. However, crystallographic and spectroscopic data show that the most stable is **II** [3]. This electron withdrawal of the sulfonyl group increases the acidity of the hydrogen on the pyridine group and complexes are easily obtained by the deprotonation of

[1] *Corresponding author. Fax: +34-986-813-798; e-mail: fojo@uvigo.es

[2] *Corresponding author. Tel.: +34-981-594-488/14255; fax: +34-981-597-525; e-mail: qiansoal@usc.es

0277-5387/00/$ - see front matter © 2000 Elsevier Science Ltd. All rights reserved.
PII: S0277-5387(00)00437-X

the ligand. This deprotonation may be carried out with an electrochemical procedure.

Electrochemical methods have been widely used for the synthesis of metallic complexes, especially those of weakly acid organic ligands [4–8]. Of particular relevance to the present work are metal complexes with heterocyclic ligands, such as pyridine derivatives containing, apart from the nitrogen atom, sulfur [9,10], oxygen and sulfur [11] or selenium [12] atoms as additional donor atoms.

In this paper, we now report the electrochemical synthesis and characterisation of several cobalt(II) complexes with the mentioned ligand, where an *N*-tosylamido group substitutes a pyridine ring, and the additional atom is another nitrogen atom.

2. Experimental

Acetonitrile, dichloromethane, 2-aminopyridine, tosyl chloride, pyridine, 2,2′-bipyridine, 1,10-phenanthroline, *N*,*N*-dimethylformamide and all other reagents were commercial products and were used as supplied. Cobalt (Aldrich Chemie) was used as 2 × 2 cm plates.

The proligand, HL, was prepared by reaction of the amine and the tosyl chloride following the method previously described [3]. Before its use, the product was recrystallized from $CH_3CN/(CH_3)_2CO$.

2.1. Preparation of complexes. General procedure

The complexes were obtained following an electrochemical procedure [8]. A solution of the proligand and the appropriated coligand (either pyridine, DMF, 2,2′-bipyridine or 1,10-phenanthroline) in a mixture of acetonitrile–dichloromethane containing about 20 mg of tetraethylammonium perchlorate as a current carrier was electrolysed using a platinum wire as the cathode and a cobalt plate as the sacrificial anode. In all cases, hydrogen was evolved at the cathode.

2.1.1. *[CoL_2py_2] (**1**)*

Electrolysis of an acetonitrile–dichloromethane (25 + 25 ml) solution containing the proligand HL (201.4 mg, 0.81 mmol), pyridine (ca. 1 ml) and tetraethylammonium perchlorate (ca. 20 mg) at 10 mA and 14 V for 2 h dissolved 21.1 mg of cobalt (E_f = 0.48). At the end of the experiment the pale pink solid product was filtered, washed with hot acetonitrile and ether and dried in vacuo. The compound was characterised as [CoL_2py_2]: *Anal.* Found: H, 4.7; C, 57.2; N, 11.8; S, 8.7. Calc. for [$C_{34}H_{32}CoN_6O_4S_2$]: C, 57.4; H, 4.5; N, 11.8; S, 9.0%. IR (KBr, cm^{-1}): 3071(m), 3069(m), 2973(sh), 1593(s), 1463(s), 1315(b), 1135(b), 1038(s), 981(vb), 702(s), 662(s), 579(s), 559(b), 531(s), 430(m). Crystals suitable for X-ray diffraction studies were obtained by crystallisation from $(CH_3)_2CO$–CH_3CN.

2.1.2. *[$CoL_2(DMF)_2$] (**2**)*

Electrolysis of an acetonitrile–*N*,*N*-dimethylformamide (50 + 10 ml) solution containing HL (327.8 mg, 1.3 mmol) and tetraethylammonium perchlorate (ca. 20 mg) at 10 mA and 14 V for 2.2 h dissolved 22.2 mg of cobalt (E_f = 0.46). At the end of the experiment the pale pink solid product was filtered, washed with hot acetonitrile and ether and dried in vacuo. The compound was characterised as [CoL_2DMF_2]: *Anal.* Found: H, 4.93; C, 51.6; N, 12.09; S, 9.52. Calc. for [$C_{30}H_{36}CoN_6O_6S_2$]: C, 51.50; H, 5.19; N, 12.01; S, 9.17%. IR (KBr, cm^{-1}): 3082(w), 3064(vw), 2923(m), 2851 (w), 1650(s), 1596(m), 1466(s), 1450(m), 1392(m), 1321(s), 1265(m), 1137(m), 1090(m), 784(m), 661(m), 577(m), 554(m). Crystals were obtained by recrystallisation from $(CH_3)_2CO$–CH_3CN.

2.1.3. *[CoL_2bipy] (**3**)*

Electrolysis of an acetonitrile–dichloromethane (25 + 25 ml) solution containing HL (201.0 mg, 0.81 mmol), 2,2′-bipyridine (67.2 mg, 0.43 mmol) and tetraethylammonium perchlorate (ca. 20 mg) at 10 mA and 10 V for 2.16 h dissolved 22.1 mg of cobalt (E_f = 0.47). At the end of the experiment the pale pink solid was filtered, washed with hot acetonitrile and ether and dried in vacuo. The compound was characterised as [CoL_2bipy]. *Anal.* Found: C, 57.5; H, 4.5; N, 11.8; S, 8.9. Calc. for [$C_{34}H_{30}CoN_6O_4S_2$]: C, 57.5; H, 4.3; N, 11.8; S, 9.0%. IR (KBr, cm^{-1}): 3107(w), 3064(vw), 2919(m), 1595(s), 1465(s), 1319(s), 1138(s), 1138(s), 1088(m), 1011(m), 976 (m), 764(m), 736(s), 667(s). Crystals were obtained by crystallisation from $(CH_3)_2CO$–CH_3CN.

2.1.4. *[CoL_2phen] (**4**)*

Electrolysis of an acetonitrile–dichloromethane (25 + 25 ml) solution containing HL (202.1, 0.81 mmol), 1,10-phenanthroline (83.3 mg, 0.46 mmol) and tetraethylammonium perchlorate (ca. 20 mg) at 10 mA and 13.5 V for 2.12 h dissolved 21.7 mg of cobalt (E_f = 0.46). At the end of the experiment the pale pink solid was filtered, washed with hot acetonitrile and ether and dried in vacuo. The compound was characterised as [CoL_2phen]: *Anal.* Found: C, 58.74; H, 4.23; N, 11.52, S, 8.41. Calc. for [$C_{36}H_{30}CoN_6O_4S_2$]: C, 58.93; H, 4.12; N, 11.45; S, 8.74%. IR (KBr, cm^{-1}): 3062(w), 3023(w), 2921(sh), 1588(s), 1559(s), 1515(m), 1495(m), 1315(m), 1178(m), 1134(m), 1038 (m), 981(m), 847(m), 727(s), 702(s), 662(m). Crystals by crystallisation from $(CH_3)_2CO$–CH_3CN.

2.2. Physical measurements

The C, N, H and S contents of the compounds were determined on a Carlo–Erba EA 1108 microanalyser. IR spectra were recorded as KBr mulls on a Bruker Vector-22 spectrophotometer. The ^{1}H NMR spectrum of the ligand was recorded on a Bruker ARX-400 MHz spectrometer using Cl_3CD as solvent. Solid-state electronic spectra were recorded on a Shimadzu UV 3101 PC. Magnetic measurements were made using a DMS VSM 1160 instrument.

2.3. Crystal structure determination

The data collection, in all the cases at room temperature, was taken on a MACH3 Enraf–Nonius using Mo Kα radiation for $[CoL_2py_2]$ and for $[CoL_2bipy]$. Data were corrected for polarization and Lorentz effects. Ψ-scan absorption corrections were applied [13]. The data collection for $[CoL_2DMF_2]$ and $[CoL_2phen]$ was taken on a Siemens Smart CCD area-detector diffractometer with graphite-monochromated Mo Kα radiation. Absorption corrections were carried out using SADABS [14].

All the structures were solved by direct methods and refined by a full-matrix least-squares based on F^2 [15]. Non-hydrogen atoms were refined with anisotropic displacement parameters. Hydrogen atoms were included in idealised positions and refined with isotropic displacement parameters. Correct absolute structures of $[CoL_2phen]$ were determined by using the Flack parameter [16]. Atomic scattering factors and anomalous dispersion corrections for all atoms were taken from the International Tables for X-ray Crystallography [17]. Details of crystal data and structural refinement are given in Table 1.

3. Results and discussion

Anodic oxidation of cobalt metal in a non-aqueous solution containing (4-methylphenyl)sulfonyl]imino-1*H*-pyridine and one coligand as pyridine (py), *N*,*N*-dimethylformamide (DMF), 2,2′-bipyridine (bipy) or 1,10-phenanthroline (phen) yields crystalline products of formulae $[CoL_2py_2]$, $[CoL_2DMF_2]$, $[CoL_2bipy]$ and $[CoL_2phen]$, respectively. The values of the electrochemical efficiency, defined as the amount of metal dissolved per number of Faradays, were close to 0.5 mol F^{-1} in all cases. This value is compatible with the mechanism

Cathode: $2HL + 2e^- \rightarrow 2L^- + H_2$

Anode: $Co \rightarrow Co^{2+} + 2e^-$

The overall reactions can be described as

$Co + 2HL + nL' \rightarrow [CoL_2L'_n] + H_2$

$n = 1$; L′ = bipy or phen.

$n = 2$; L′ = py or DMF.

3.1. Description of the structures of $[CoL_2py_2]$ (1), $[CoL_2DMF_2]$ (2), $[CoL_2bipy]$ (3), and $[CoL_2phen]$ (4)

The molecular structures are shown in Figs. 1–4. Selected bond lengths and angles are given in Tables

Table 1
Summary of crystal data and structure refinement

Compound	$[CoL_2py_2]$	$[CoL_2DMF_2]$	$[CoL_2bipy]$	$[CoL_2phen]$
Empirical formula	$C_{17}H_{16}Co_{0.5}N_3O_2S$	$C_{15}H_{18}Co_{0.5}N_3O_3S$	$C_{34}H_{30}CoN_6O_4S_2$	$C_{36}H_{30}CoN_6O_4S_2$
Formula weight	355.85	349.85	709.69	733.71
Crystal system	monoclinic	monoclinic	monoclinic	monoclinic
Space group	$P2_1/n$ (no 14)	$P2_1/n$ (no 14)	$P2_1/n$ (no. 14)	$P2_1$ (no. 4)
Unit cell dimensions				
a (Å)	9.5603(11)	9.5240(2)	10.8443(19)	9.4524(5)
b (Å)	18.934(2)	18.5979(3)	21.2416(6)	19.6321(10)
c (Å)	9.7615(15)	10.21420(10)	14.386(4)	9.6993(5)
β (°)	109.457(9)	111.4133(7)	93.90(3)	109.8834(11)
Volume (Å^3)	1666.0(4)	1684.32(5)	3306.0(11)	1692.6(2)
Z	4	4	4	2
Absorption coefficient (mm^{-1})	0.688	0.683	0.693	0.680
Reflections collected	4226	11983	7059	9376
Independent reflections	4001 [$R_{int} = 0.0750$]	4113 [$R_{int} = 0.0226$]	6704 [$R_{int} = 0.1331$]	7312 [$R_{int} = 0.0410$]
Reflections observed [$>2\sigma(I)$]	1546	3452	2297	4864
Data/restraints/parameters	4001/0/266	4113/0/205	6703/0/424	7312/1/442
Final R indices [$I>2\sigma(I)$]	$R_1 = 0.0495$, $wR_2 = 0.0853$	$R_1 = 0.0363$, $wR_2 = 0.0955$	$R_1 = 0.0642$, $wR_2 = 0.1276$	$R_1 = 0.0718$, $wR_2 = 0.1294$
Absolute structure parameter				−0.03(2)
Largest difference peak and hole (e Å^{-3})	0.345 and −0.340	0.290 and −0.423	0.540 and −0.556	0.287 and −0.506

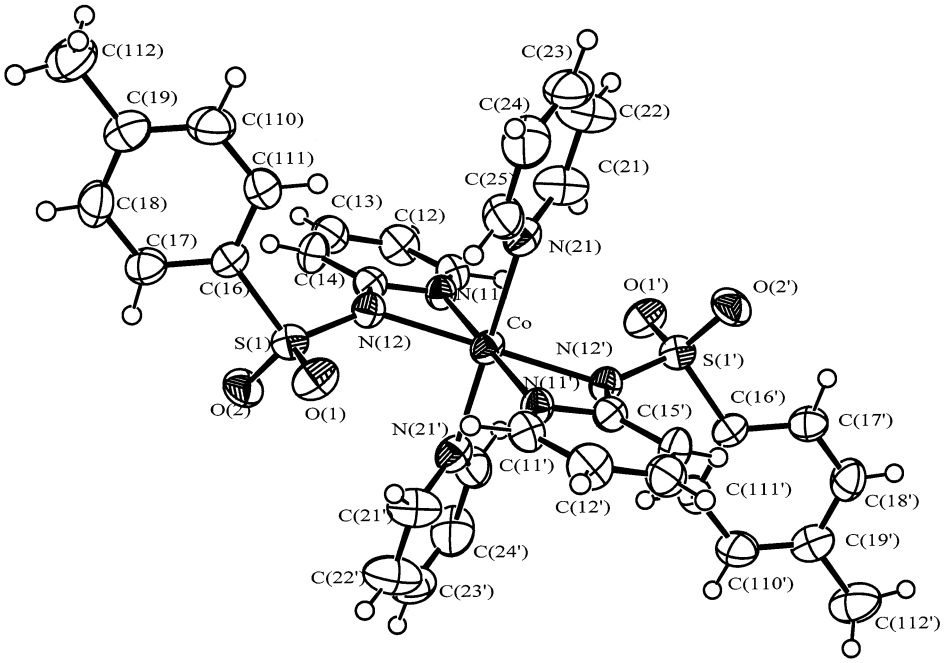


Fig. 1. Molecular structure of $[CoL_2py_2]$ (**1**).

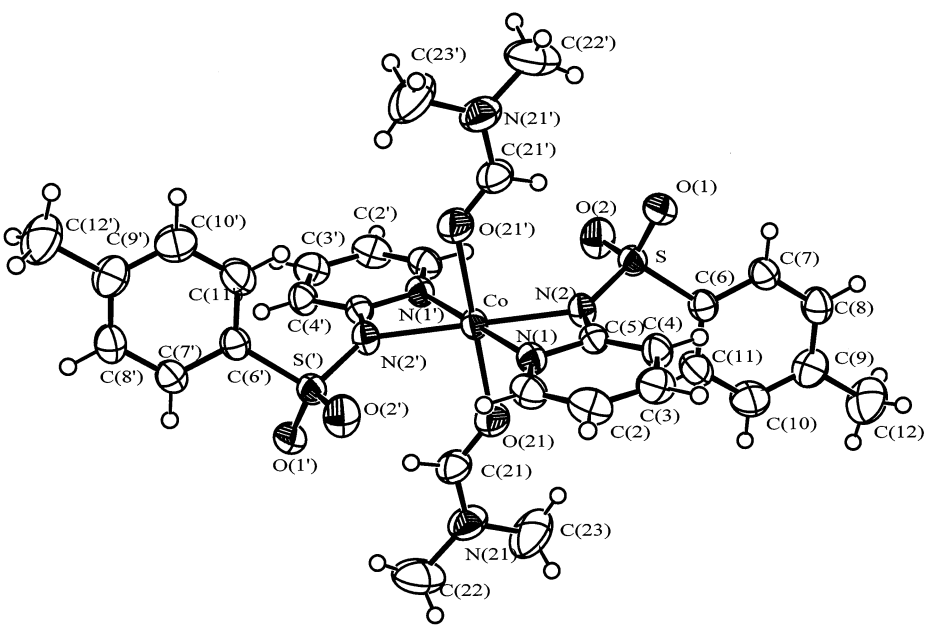


Fig. 2. Molecular structure of $[CoL_2DMF_2]$ (**2**).

2–5 for each compound. In the four complexes the cobalt atom is in a highly distorted octahedral environment but they are different to each other. In the case of **1**, **3** and **4**, the environment is $[CoN_6]$, and in **2** is $[CoO_2N_4]$. Compounds **1** and **2** contain two N–N anionic ligands and two monodentate ligands, but **3** and **4** have three bidentate N–N ligands, two anionic and one neutral.

3.1.1. Molecular structure of $[CoL_2py_2]$ (1)

The cobalt atom in $[CoL_2py_2]$ is in an octahedral environment $[CoN_6]$. The nitrogen atoms of the two neutral pyridine molecules are in *trans* positions, and the nitrogen atoms of the two anionic tosylato ligands are in the equatorial plane. As the cobalt atom is in a symmetry center, the equivalent nitrogen atoms of the tosylato ligands are in *trans* positions.

The Co–N bond lengths of the apical positions are slightly longer, 2.164(3) Å, than the Co–N bonds lengths on the equatorial plane, 2.125(3) and 2.138(3) Å. This is probably because the apical ligands are neutral, but the ligands in the equatorial plane are anionic. Similar behaviour has been found in the pyridine complex containing other anionic ligands, such as in diaqua-dipyridyl-bis(*N*-(4-methyl-2-sulfamoyl-Δ^2-1,3,4-thiadiazolin-5-ylidene)acetamide)cobalt(II) [18], with a Co(II)–N_{py} distance of 2.198(2) Å and other

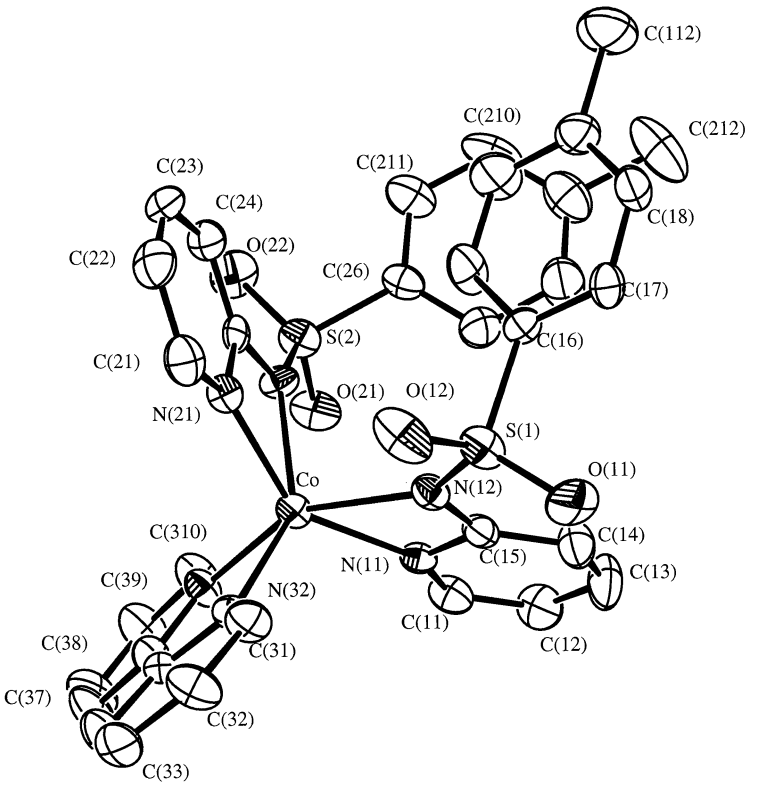


Fig. 3. Molecular structure of [CoL_2bipy] (**3**).

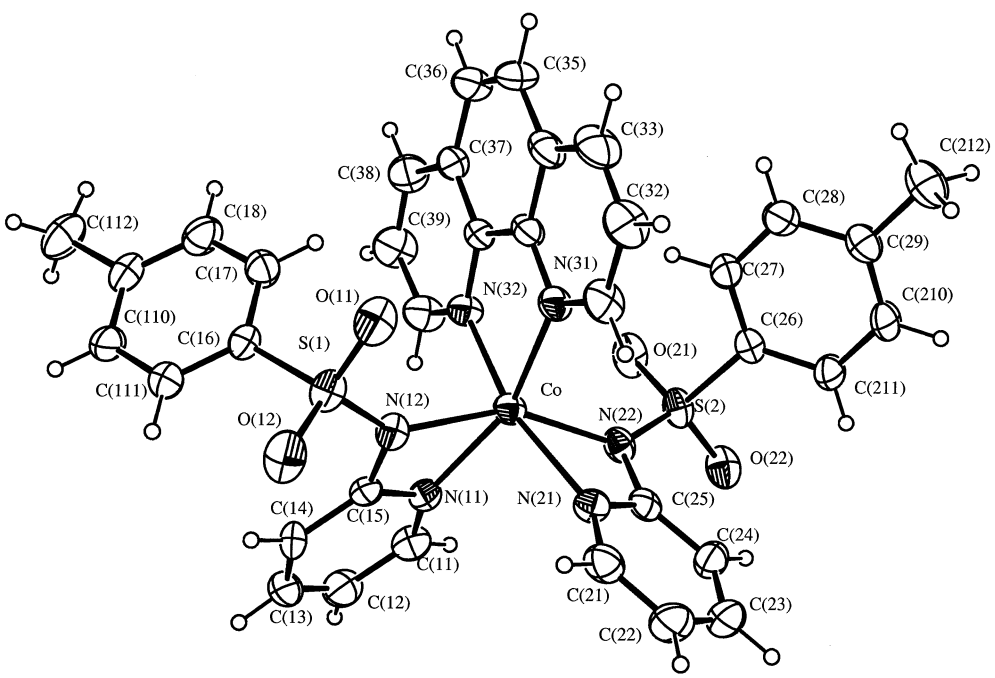


Fig. 4. Molecular structure of [CoL_2phen] (**4**).

Table 2
Selected bond lengths (Å) and angles (°) for $[CoL_2py_2]$

Co–N(11)	2.125(3)	Co–N(11 [a])	2.125(3)
Co–N(12 [a])	2.138(3)	Co–N(12)	2.138(3)
Co–N(21)	2.164(3)	Co–N(21 [a])	2.164(3)
S(1)–N(12)	1.588(3)	S(1)–C(16)	1.772(4)
N(11)–C(11)	1.330(5)	N(11)–C(15)	1.350(5)
N(12)–C(15)	1.383(5)	N(21)–C(25)	1.323(5)
N(21)–C(21)	1.316(5)		
N(11)–Co–N(11 [a])	180.0	N(11)–Co–N(12 [a])	117.07(11)
N(11)–Co–N(12)	62.93(11)	N(12 [a])–Co–N(12)	180.0
N(11)–Co–N(21)	91.71(13)	N(12)–Co–N(21)	87.93(12)
N(11)–Co–N(21 [a])	88.29(13)	N(12)–Co–N(21 [a])	92.07(13)
N(21)–Co–N(21 [a])	180.0	N(12)–S(1)–C(16)	107.82(18)
C(11)–N(11)–C(15)	118.6(4)	C(15)–N(12)–S(1)	123.7(3)
N(11)–C(11)–C(12)	123.6(5)	N(11)–C(15)–N(12)	108.9(3)
C(21)–N(21)–C(25)	117.2(4)	N(21)–C(21)–C(22)	123.3(5)
N(21)–C(25)–C(24)	122.5(5)		

[a] Symmetry transformations used to generate equivalent atoms: $-x+1, -y+1, -z+1$.

Co–N distance of 2.108(2) Å. Nevertheless, there are some examples where the Co–N_{py} bond lengths are longer than the other Co–N bond lengths and all the ligands are neutral. That is the case for (1,3,5-tris-(pyridine-2-carboxaldimino)-cyclohexane-N^1,N^2,N^3,N^4,N^5,N^6)cobalt(II) diperchlorate [19], with average bond distances Co–N_{py} of 2.231 Å and Co–N_{imino} of 2.131 Å, or (1,1,1-tris(pyridine-2-aldiminomethyl)ethane)-cobalt(II) diperchlorate [20] with average bond distances Co–N_{py} of 2.150 Å and Co–N_{imino} of 2.097 Å.

A tetrahedral coordination around the cobalt atom has been found for bis{[(4-methylphenyl)sulfonyl][2-(2-pyridyl)phenyl]amine}cobalt(II) [2]. In this case, the Co–N distances are shorter, average Co–N_{amide} = 1.963(2) and Co–N_{py} = 2.042(2) Å, as expected for a complex with a lower coordination number.

The ligand bond distances and angles are normal and do not deserve special discussion. The neutral pyridine is almost perpendicular to the pyridine ring belonging to the anionic ligand, with a dihedral angle of 86.93(12)°. The pyridine ring of the anionic ligand is almost coplanar with the small chelate ring Co–N(12)–C(15)–N(11), with a dihedral angle of 3.92(14)°.

The most important deviation of the octahedron from regularity is the small bite of the ligand, 62.93(11)°. This value is in the range for a four-member chelate ring found for complexes of cobalt(II): 55.3° in hexakis[(μ^2-methoxo)-(μ^2-σ^3-1,5-di-*p*-tolyl-1,4-pentaazadienido)cobalt(II)] mesitylene solvate [21] and 65.8° in diaqua-bis[(*N*,*N*′-methylene-bis(L-prolinato)]-cobalt(II) sesquihydrate [22] or 65.5° in diaqua-[*N*,*N*′-methylene-bis(4-hydroxy-L-prolinato)]cobalt(II) [23].

3.1.2. Molecular structure of $[CoL_2DMF_2]$ (2)

In this compound, the metal environment is $[CoN_4O_2]$. The cobalt atom is in a centre of symmetry coordinated by two *N*,*N*-bidentate anionic ligands and by two molecules of DMF through the oxygen atom. The coordination polyhedron can be described as an octahedron with the neutral DMF ligands in the axial positions and the anionic ligands in the equatorial plane. As happens in $[CoL_2py_2]$, the ligands in the apical positions are slightly farther than the ligands in the equatorial plane. All the other features are very

Table 3
Bond lengths (Å) and angles (°) for $[CoL_2DMF_2]$

Co–N(1 [a])	2.1194(15)	Co–N(1)	2.1194(15)
Co–N(2 [a])	2.1415(14)	Co–N(2)	2.1415(13)
Co–O(21 [a])	2.1635(14)	Co–O(21)	2.1635(14)
S–N(2)	1.5856(14)	S–C(6)	1.7808(18)
N(1)–C(1)	1.344(2)	N(1)–C(5)	1.353(2)
N(2)–C(5)	1.387(2)	N(21)–C(22)	1.473(3)
O(21)–C(21)	1.229(3)	N(21)–C(21)	1.321(2)
N(21)–C(23)	1.434(3)		
N(1 [a])–Co–N(2 [a])	62.97(5)	N(1)–Co–N(2 [a])	117.03(5)
N(1 [a])–Co–N(2)	117.03(5)	N(1)–Co–N(2)	62.97(5)
N(2 [a])–Co–N(2)	180.0	N(1 [a])–Co–O(21 [a])	87.97(6)
N(1)–Co–O(21 [a])	92.03(6)	N(2 [a])–Co–O(21 [a])	86.41(6)
N(2)–Co–O(21 [a])	93.59(6)	N(1 [a])–Co–O(21)	92.03(6)
N(1)–Co–O(21)	87.97(6)	N(2 [a])–Co–O(21)	93.59(6)
N(2)–Co–O(21)	86.41(6)	O(21 [a])–Co–O(21)	180.0
N(1 [a])–Co–N(1)	180.0	N(2)–S–C(6)	108.91(8)
C(23)–N(21)–C(22)	117.8(2)	C(21)–O(21)–Co	127.91(14)
O(21)–C(21)–N(21)	125.5(2)	C(21)–N(21)–C(23)	121.1(2)
C(21)–N(21)–C(22)	121.0(2)		

[a] Symmetry transformations used to generate equivalent atoms: $1-x+, 1-y, 1-z$.

Table 4
Selected bond lengths (Å) and angles (°) for $[CoL_2bipy]$

Co–N(21)	2.065(5)	Co–N(31)	2.107(6)
Co–N(32)	2.120(5)	Co–N(11)	2.120(5)
Co–N(12)	2.185(5)	Co–N(22)	2.259(5)
S(1)–N(12)	1.606(6)	S(1)–C(16)	1.774(7)
S(2)–N(22)	1.586(5)	S(2)–C(26)	1.774(7)
N(11)–C(11)	1.345(8)	N(11)–C(15)	1.353(8)
N(12)–C(15)	1.357(8)	N(21)–C(21)	1.332(8)
N(21)–C(25)	1.361(8)	N(22)–C(25)	1.369(8)
N(31)–C(36)	1.336(8)	N(31)–C(310)	1.347(8)
N(32)–C(31)	1.332(8)	N(32)–C(35)	1.341(8)
N(21)–Co–N(31)	111.3(2)	N(21)–Co–N(32)	94.3(2)
N(31)–Co–N(32)	76.6(2)	N(21)–Co–N(11)	145.0(2)
N(31)–Co–N(11)	96.4(2)	N(32)–Co–N(11)	113.1(2)
N(21)–Co–N(12)	96.0(2)	N(31)–Co–N(12)	152.0(2)
N(32)–Co–N(12)	95.7(2)	N(11)–Co–N(12)	61.4(2)
N(21)–Co–N(22)	61.36(19)	N(31)–Co–N(22)	94.0(2)
N(32)–Co–N(22)	149.1(2)	N(11)–Co–N(22)	97.01(19)
N(12)–Co–N(22)	105.0(2)	N(12)–S(1)–C(16)	108.3(3)
N(22)–S(2)–C(26)	107.3(3)	C(11)–N(11)–C(15)	119.2(6)
C(11)–N(11)–Co	144.1(5)	C(15)–N(11)–Co	96.6(4)
C(15)–N(12)–S(1)	123.4(5)	N(11)–C(15)–N(12)	108.5(6)
N(11)–C(15)–C(14)	120.6(7)	N(12)–C(15)–C(14)	131.0(7)

Table 5
Selected bond lengths (Å) and angles (°) for [CoL_2phen]

Co–N(31)	2.113(5)	Co–N(22)	2.120(6)
Co–N(32)	2.122(5)	Co–N(12)	2.140(5)
Co–N(11)	2.143(5)	Co–N(21)	2.215(6)
S(1)–N(12)	1.587(5)	S(1)–C(16)	1.782(7)
S(2)–N(22)	1.586(6)	S(2)–C(26)	1.779(6)
N(12)–C(15)	1.399(8)	N(11)–C(15)	1.349(8)
N(11)–C(11)	1.351(8)	N(21)–C(21)	1.341(9)
N(21)–C(25)	1.342(8)	N(22)–C(25)	1.390(8)
N(31)–C(31)	1.339(8)	N(31)–C(311)	1.340(8)
N(32)–C(310)	1.329(8)	N(32)–C(312)	1.363(7)
N(31)–Co–N(22)	100.6(2)	N(31)–Co–N(32)	78.4(2)
N(22)–Co–N(32)	104.5(2)	N(31)–Co–N(12)	99.0(2)
N(22)–Co–N(12)	154.2(2)	N(32)–Co–N(12)	95.6(2)
N(31)–Co–N(11)	159.4(2)	N(22)–Co–N(11)	99.7(2)
N(32)–Co–N(11)	93.8(2)	N(12)–Co–N(11)	62.5(2)
N(31)–Co–N(21)	96.6(2)	N(22)–Co–N(21)	61.8(2)
N(32)–Co–N(21)	164.7(2)	N(12)–Co–N(21)	99.5(2)
N(11)–Co–N(21)	95.3(2)	O(11)–S(1)–N(12)	106.9(3)
O(12)–S(1)–N(12)	112.0(3)	O(11)–S(1)–C(16)	107.3(3)
O(12)–S(1)–C(16)	106.3(3)	N(12)–S(1)–C(16)	106.1(3)
N(22)–S(2)–C(26)	105.8(3)	C(15)–N(12)–S(1)	122.6(4)
C(15)–N(11)–C(11)	118.5(6)		

similar to those in [CoL_2py_2]. The Co–O bond length (2.1635(14) Å) and the angles C–O–Co (127.91(14)°) are in the range for Co(II) complexes with DMF as the ligand, like, for example, *trans*-bis(benzo(1,3)-thiazole)-bis(*N*,*N* - dimethylformamide) - bis(isothiocyanato)cobalt(II) [24], with values of 2.118 Å and 126.14°, respectively.

3.1.3. Molecular structure of [CoL_2 bipy] (3)

The cobalt atom in **3** is in a distorted octahedral environment [CoN_6], with the two anionic tosyl ligands and the neutral bipyridine molecule as *N*,*N*-bidentate ligands. The small bite angles of the ligands, especially in the case of the anionic ligand, are the main reason for the distortion. So, the angles N_{amide}–Co–$N_{pyridine}$ are 61.3(2) and 61.4(2)° in each anionic ligand, with a chelate ring of four members (see above) and 76.6(2)° in the bipyridine, with a chelate ring of five members. The pyridine fragments of the anionic ligands are in *trans* positions, and consequently if these are considered as the apical positions, the equatorial plane is formed by the amide nitrogen atoms of the tosylamide ligands and the nitrogen atoms of the bipyridine molecule. The cobalt atom is 0.024(3) Å out of this equatorial plane. The pyridine rings in *trans* positions are also almost perpendicular between them, dihedral angle of 80.5(2)°, and form dihedral angles with the equatorial plane of 76.5(2) and 79.3(2)°. It is worth noting that while the Co–N bond distances in the case of one of the tosyl ligands are quite similar, 2.121(6) and 2.185(6) Å, for the other one, one of the distances is significantly shorter than the other, 2.259(6) and 2.066(6) Å. Such disposition of the ligands around the metal corresponds approximately to non-crystallographic two-fold point symmetry.

The distances Co–N_{bipy}, 2.106(6) and 2.119(6) Å, are slightly shorter that those found in tris(2,2′-bipyridine)cobalt(II) dichloride [25], average 2.130 Å, or in *cis*-dichloro-bis(2,2′-bipyridyl-*N*,*N*′)cobalt(II) [26], average 2.154 Å.

The distances and angles of the anionic ligands are normal, with dihedral angles between the rings of 83.5(2) and 78.2(2)°, this last one in the case of the anisodentate ligand. The free ligand shows dihedral angles of 83.7(1) and 87.6(1)° [3].

3.1.4. Molecular structure of [CoL_2 phen] (4)

Compound **4** contains a cobalt atom in a distorted octahedral geometry coordinated by two nitrogen atoms of an neutral ligand (phen), and by four nitrogen atoms of two anionic ligands. This is similar to **3**, but there is an important difference between these compounds in the disposition of the ligands around the metal. In the case of **4**, the amide nitrogen atoms of the anionic ligands occupy the axial positions, and the equatorial plane is formed by the pyridine nitrogen atoms of the anionic ligands and the nitrogen atoms of the phenanthroline molecule. This structure corresponds to that of the Λ isomer. This geometry has also been found in the corresponding Ni(II) complexes with this ligands and either bipyridine or phenanthroline [3].

The Co–N distances to one of the anionic ligands are very similar, 2.140(5) and 2.143(5) Å, but the other anionic ligand again shows an anisobidentate behaviour, Co–N distances 2.120(6) and 2.215(6) Å. The dihedral angle between the pyridine ring and the phenyl ring is 85.12(18) and 81.98(23)° in each ligand, respectively. The disposition of the pyridine rings of the ligands are almost perpendicular, with a dihedral angle between the pyridine rings of 89.95(22)°.

The distances Co–N_{phen} (2.113(5) and 2.122(5) Å) are quite similar to those found in 1,10-phenanthroline bis{2-[(2-pyrrole)methylimino]phenolato}cobalt(II) [27], 2.22 and 2.16 Å, and in tris(1,10-phenanthroline)-cobalt(II) diperchlorate monohydrate [28] (average 2.128 Å, max. 2.141 Å, min. 2.109 Å).

3.2. Spectroscopic and magnetic studies

The IR spectra of the complexes do not show the band attributable to ν(N–H), which in the free ligand appears at 3230 cm^{-1}, confirming that the hydrogen atom of the amide group is lost during the electrolysis. The IR spectra of the mixed complexes show IR absorptions typical of coordinated pyridine (662 and 430

cm^{-1}), *N*,*N*-dimethylformamide (2923, 2850, 1650 and 1392 cm^{-1}), 2,2′-bipyridine (764 and 736 cm^{-1}) and 1,10-phenanthroline (1515, 847 and 727 cm^{-1}).

The magnetic moments of $[CoL_2py_2]$, 4.49 BM $[CoL_2DMF_2]$, 4.39 BM $[CoL_2bipy]$, 4.41 BM and $[CoL_2phen]$ 4.66 BM, are in the low limit for high-spin Co(II) complexes (4.7–5.2 BM). The solid reflectance spectra of $[CoL_2py_2]$, $[CoL_2DMF_2]$, $[CoL_2bipy]$ and $[CoL_2phen]$ show three bands at 28 170, 21 500, 9700, 28 450, 20 325, 8740, 25 757, 20 800, 8830 and 25 850, 20 600, 8925 cm^{-1}, respectively. They can be assigned to the $^4T_{1g}(P) \leftarrow {}^4T_{1g}(F)$, $^4A_{2g} \leftarrow {}^4T_{1g}$ and $^4T_{2g} \leftarrow {}^4T_{1g}$ transitions, and are in accordance with an octahedral geometry for the complex. These conclusions are in keeping with the X-ray diffraction results.

4. Supplementary material

The atomic positions, full list of bond lengths and angles and other crystallographic data are available on request from the CCDC, 12 Union Road, Cambridge CB2 1EZ, UK (fax: +44-1223-336-033; e-mail: deposit@ccdc.cam.ac.uk or www: http://www.ccdc.cam.ac.uk), quoting the deposition numbers CCDC 139406–139409.

Acknowledgements

This work was supported by the Xunta de Galicia under the grant XUGA20302B97. We thank angus.uvigo.es (http://angus.uvigo.es/) for X-ray solution and refinement facilities.

References

[1] (a) L. Antonili, L.P. Battaglia, A. Bonamartini Corradi, G. Marcotrigliano, L. Menablue, G.C. Pellacani, J. Am. Chem. Soc. 107 (1985) 1369. (b) A. Bonamartini Corradi, E. Gozzoli, L. Menablue, M. Saladini, L.P. Battaglia, P. Sgarabotto, J. Chem. Soc., Dalton Trans. (1994) 273.
[2] C.A. Otter, S.M. Couchman, J.C. Jeffery, K.L.V. Mann, E. Psillakis, M.D. Ward, Inorg. Chim. Acta 278 (1998) 178, and Refs. therein.
[3] S. Cabaleiro, J. Castro, E. Vázquez-López, J.A. García-Vázquez, J. Romero, A. Sousa, Polyhedron 18 (1999) 1669.
[4] A.D. Garnovskii, B.I. Kharisov, G. Gojón-Zorrilla, D.A. Garnovskii, Russ. Chem. Rev. 64 (1995) 201.
[5] M.C. Chakravorti, G.V.B. Subrahmanyam, Coord. Chem. Rev. 135/136 (1994) 65.
[6] A.M. Vecchio-Sadus, J. Appl. Electrochem. 23 (1993) 401.
[7] J.A. Davies, C.M. Hokensmith, V.Yu Kukushkin, Yu N. Kukushkin, Synthetic Coordination Chemistry. Principles and Practice, Word Scientific, Singapore, 1996 (Chapter. 7).
[8] D.G. Tuck, Pure Appl. Chem. 51 (1979) 2005.
[9] (a) E.S. Raper, Coord. Chem. Rev. 61 (1985) 115. (b) E.S. Raper, Coord. Chem. Rev. 153 (1996) 199. (c) E.S. Raper, Coord. Chem. Rev. 165 (1997) 475.
[10] J.A. García-Vázquez, J. Romero, A. Sousa, Coord. Chem. Rev. 193–195 (1999) 691.
[11] A. Rodríguez, J. Romero, J.A. García-Vázquez, A. Sousa, K. Maresca, D.J. Rose, J. Zubieta, Inorg. Chim. Acta 281 (1998) 70.
[12] J. Romero, M.L. Durán, J.A. García-Vázquez, A. Castiñeiras, A. Sousa, L. Christiaens, J. Zubieta, Inorg. Chim. Acta 255 (1997) 307 and Refs. therein.
[13] A.C.T. North, D.C. Phillips, F. Scott Mathews, Acta Crystallogr., Sect. A 24 (1968) 351.
[14] G.M. Sheldrick, SADABS. An empirical absorption correction program for area detector data, University of Göttingen, Germany, 1996.
[15] G.M. Sheldrick, SHELX-97, Program for the solution and refinement of crystal structures, University of Göttingen, Germany, 1997.
[16] H.D. Flack, Acta Crystallogr., Sect. A 39 (1983) 876.
[17] International Tables for X-ray Crystallography, vol. C, Kluwer, Dordrecht, 1992.
[18] G. Alzuet, S. Ferrer, J. Borrás, A. Castiñeiras, X. Solans, M. Font-Bardía, Polyhedron 11 (1992) 2849.
[19] R.A.D. Wentworth, P.S. Dahl, C.J. Huffman, W.O. Gillum, W.E. Streib, J.C. Huffman, Inorg. Chem. 21 (1982) 3060.
[20] P.B. Donaldson, P.A. Tasker, N.W. Alcock, J. Chem. Soc., Dalton Trans. (1977) 1160.
[21] R. Schmid, J. Beck, J. Strahle, Z. Naturforsch., Teil B 42 (1987) 911.
[22] S.B. Teo, C.H. Ng, S.G. Teoh, C. Wei, J. Coord. Chem. 36 (1995) 141.
[23] S.B. Teo, S.G. Teoh, C.H. Ng, H.K. Fun, J.P. Declercq, Polyhedron 14 (1995) 1447.
[24] E.S. Raper, R.E. Oughtred, J.R. Creighton, I.W. Nowell, Inorg. Chim. Acta 87 (1984) 201.
[25] D.J. Szalda, C. Creutz, D. Mahajan, N. Sutin, Inorg. Chem. 22 (1983) 2372.
[26] T. Kramer, J. Strahle, Z. Naturforsch., Teil B 41 (1986) 692.
[27] J.A. Castro, J. Romero, J.A. García-Vázquez, A. Sousa, A. Castiñeiras, J. Chem. Crystallogr. 24 (1994) 469.
[28] D. Boys, C. Escobar, O. Wittke, Acta Crystallogr., Sect. C 40 (1984) 1359.

PERGAMON

www.elsevier.nl/locate/poly

Polyhedron 19 (2000) 1615–1620

POLYHEDRON

Binuclear copper(I) complexes containing bis(diphenylphosphino)ethane bridges: the crystal structure of bis[{μ-bis(diphenylphosphino)ethane}(pyridine-2-thione)copper(I) bromide]

P.J. Cox [a], P. Aslanidis [b,*], P. Karagiannidis [b]

[a] *School of Pharmacy, Robert Gordon University, Schoolhill, Aberdeen, AB10 1FR, Scotland, UK*

[b] *Inorganic Chemistry Laboratory, Faculty of Chemistry, Aristotle University of Thessaloniki, PO Box 135, GR-540 06 Thessaloniki, Greece*

Received 4 January 2000; accepted 18 May 2000

Abstract

Treatment of copper(I) bromide with one equivalent of 1,2-bis(diphenylphosphino)ethane (dppe), followed by the addition of one equivalent of heterocyclic thione L {L = pyridine-2-thione (py2SH), pyrimidine-2-thione (pymtH), imidazole-2-thione (imtH), benz-1,3-imidazoline-2-thione ($bzimtH_2$), benz-1,3-thiazoline-2-thione (bztztH), 2-mercapto-1-methylimidazole (meimtH), 4,6-dimethylpyrimidine-2-thione (dmpymtH), and 6-ethoxybenz-1,3-thiazoline-2-thione (etObztztH) in dry acetone affords the dinuclear complexes $[CuBr(dppe)(L)]_2$ in ca. 60–80% yield. These compounds have been characterized by their IR, far-IR, UV–Vis and ^1H NMR spectroscopic data. The crystal structure of $[CuBr(dppe)(py2SH)]_2$ has been determined by single-crystal X-ray diffraction methods. In the dinuclear complex in which the two monomers are related by inversion, each Cu(I) centre exhibits a tetrahedral coordination sphere involving, besides the bromine, the exocyclic sulfur of one thione molecule and two phosphor atoms from two different diphosphine units. Vibrational, electronic and ^1H NMR spectral data of the complexes are discussed in relation to the structure. © 2000 Elsevier Science Ltd. All rights reserved.

Keywords: Copper(I) bromide complexes; Heterocyclic thione complexes; Diphosphine complexes; Dinuclear complexes; Crystal structures

1. Introduction

Owing to their relevance in biological systems, heterocyclic thiones have attracted considerable attention as ligands in metal complexes [1]. Because of their application in catalytic functions, transition metal complexes with phosphine ligands have also been studied extensively [2]. In recent years, we have explored the group IB metal complexes blending both heterocyclic thione and tertiary arylphosphine ligands. In the course of our investigations, whose major target was the study of the factors that govern the coordination geometry of the metal atom, a large set of compounds with an interesting and in some cases unpredictable structural variety has been observed [3]. Although the interplay of several parameters like the geometrical flexibility of the coinage metals and electronic properties or bulkiness on the part of the ligands make structural prediction of these complexes virtually impossible, steric demands of the phosphine ligands seems to be of major importance causing significant changes on the coordination geometry of the metal atom [4]. To obtain further insight into this very interesting field of research we, therefore, decided to initiate a comparative investigation on substituting the unidentate triarylphosphines with acyclic multidentate phosphine ligands.

Recent interest in copper(I) bis(diphosphine) complexes, which are mostly polynuclear species containing bridging diphosphines, stems from their potential biological significance [5]. In this work, we report on the reaction of copper(I) bromide with 1,2-bis(diphenylphosphino)ethane (dppe) and several heterocyclic thione ligands, as well as the structure of $[CuBr(dppe)(py2SH)]_2$.

* Corresponding author. Tel.: +30-31-997-694; fax: +30-31-997-738.

E-mail address: aslanidi@auth.gr (P. Aslanidis).

0277-5387/00/$ - see front matter © 2000 Elsevier Science Ltd. All rights reserved.
PII: S0277-5387(00)00438-1

2. Experimental

2.1. Materials and instruments

Copper(I) bromide, 1,2-bis(diphenylphosphino)-ethane and all solvents are commercially available and were used as obtained, while the thiones (E. Merck or Aldrich) were recrystallized from hot ethanol prior to their use. IR, UV, Vis and NMR spectra, conductivities, melting points and elemental analyses of carbon, nitrogen and hydrogen were performed as described previously [6].

2.2. Preparation of the complexes

The complexes of the formula $[CuBr(dppe)(L)]_2$ were prepared according to the following general procedure. A solution of 1,2-bis(diphenylphosphino)ethane (99.6 mg, 0.25 mmol) in dry acetone (20 ml) was added to a stirred suspension of CuBr (35.3 g, 0.25 mmol) in 15 ml of the same solvent and the mixture was stirred and moderately heated. After the formation of a complete clear solution, 0.25 mmol of the appropriate thione, dissolved in dry acetone (30 ml), was added slowly and the stirring was continued for 2 h. The resulting solution was filtered off and allowed to cool. Slow evaporation of the solvent at room temperature (r.t.) gave the microcrystalline solid, which was filtered off and dried in vacuo.

2.2.1. $[CuBr(dppe)(py2SH)]_2$

Yellow crystals. Yield: 80%, m.p. 220°C. *Anal.* Calc. for $C_{62}H_{58}Br_2Cu_2N_2P_4S_2$: C, 57.0; H, 4.5; N, 2.1. Found: C, 56.3; H, 4.5; N, 2.1%. UV–Vis (λ, log ε): 295 (4.46); 244 (4.52). IR (cm^{-1}): 3048 m, 2960 m, 2897 s, 1610 s, 1577 vs, 1500 s, 1433 vs, 1366 s, 1132 vs, 1097 s, 882 m, 745 vs, 695 vs, 518 s, 479 s, 448 s, 336 m. ^1H NMR: δ 14.25 (s, >NH), 7.60–7.10 (m, aromatic), 2.17 (s, P–CH_2CH_2–P).

2.2.2. $[CuBr(dppe)(pymtH)]_2$

Orange–red crystals. Yield: 80%, m.p. 148°C. *Anal.* Calc. for $C_{60}H_{56}Br_2Cu_2N_4P_4S_2$: C, 55.1; H, 4.3; N, 4.2. Found: C, 55.9; H, 4.4; N, 4.2%. UV–Vis (λ, log ε): 290 (4.69); 247 (4.66). IR (cm^{-1}): 3066 m, 2923 w, 1606 m, 1564 vs, 1480 s, 1432 vs, 1324 s, 1175 vs, 1091 s, 1025 m, 744 vs, 697 vs, 511 s, 481 m, 448. ^1H NMR: δ 14.80 (s, >NH), 7.50–7.20 (m, aromatic), 2.17 (s, P–CH_2CH_2–P).

2.2.3. $[CuBr(dppe)(bzimtH_2)]_2$

Pale-yellow crystals. Yield: 60%, m.p. 146°C. *Anal.* Calc. for $C_{66}H_{60}Br_2Cu_2N_4P_4S_2$: C, 57.3; H, 4.4; N, 4.1. Found: C, 57.8; H, 4.2; N, 4.1%. UV–Vis (λ, log ε): 309 (4.95); 248 (5.09). IR (cm^{-1}): 3049 s, 2925 m, 1618 m, 1500 vs, 1463 s, 1434 vs, 1359 s, 1172 s, 1099 s, 1026 m, 740 vs, 694 vs, 512 s, 478 m, 418 m. ^1H NMR: δ 12.43 (s, >NH), 7.65–7.15 (m, aromatic), 2.17–2.50 (m, P–CH_2CH_2–P).

2.2.4. $[CuBr(dppe)(bztzH)]_2$

Yellow crystals. Yield: 66%, m.p. 177°C. *Anal.* Calc. for $C_{66}H_{58}Br_2Cu_2N_2P_4S_4$: C, 55.9; H, 4.5; N, 2.0. Found: C, 54.8; H, 4.1; N, 2.1%. UV–Vis (λ, log ε): 328 (4.38); 244 (4.58). IR (cm^{-1}): 3057 m, 2953 m, 1597 m, 1490 vs, 1458 s, 1428 vs, 1321 vs, 1170 s, 1099 s, 1076 m, 1031 vs, 1013 s, 745 vs, 693 s, 512 s, 423 m. ^1H NMR: δ 12.90 (s, >NH), 7.70–7.26 (m, aromatic), 2.03–2.59 (m, P–CH_2CH_2–P).

2.2.5. $[CuBr(dppe)(meimtH)]_2$

Pale-yellow crystals. Yield: 75%, m.p. 225°C. *Anal.* Calc. for $C_{60}H_{60}Br_2Cu_2P_4N_4S_2$: C, 54.9; H, 4.6; N, 4.3. Found: C, 55.3; H, 4.9; N, 4.1%. UV–Vis (λ, log ε): 266 (4.31); 245 (4.25). IR (cm^{-1}): 3131 m, 3046 m, 2940 w, 1572 vs, 1478 vs, 1433 vs, 1281 vs, 1254 m, 1153 s, 1095 s, 1025 m, 998 m, 883 m, 756 vs, 670 vs, 514 vs, 487 s, 416 m, 341 m. ^1H NMR: δ 12.50 (s, >NH), 7.80–7.26 (m, aromatic), 6.80–6.75 (m, –CH=CH–), 3.67 (s, >N–CH_3), 2.03–2.17 (m, P–CH_2CH_2–P).

2.2.6. $[CuBr(dppe)(imtH)]_2$

Red–brown crystals. Yield: 65%, m.p. 171°C. *Anal.* Calc. for $C_{58}H_{60}Br_2Cu_2N_4P_4S_2$: C, 54.1; H, 4.7; N, 4.3. Found: C, 53.7; H, 4.4; N, 4.9%. UV–Vis (λ, log ε): 290 (4.54); 243 (4.42). IR (cm^{-1}): 3138 m, 3055 m, 2950 w, 1582 vs, 1480 s, 1438 vs, 1306 m, 1169 vs, 1115 vs, 989 m, 738 vs, 730 vs, 697 vs, 618 s, 535 vs, 511 vs, 406 m, 340 m. ^1H NMR: δ 13.10 (s, >NH), 7.76–7.26 (m, aromatic), 2.52 (s, N–CH_2CH_2–N), 2.09–2.17 (m, P–CH_2CH_2–P).

2.2.7. $[CuBr(dppe)(dmpymtH)]_2$

Yellow crystals. Yield: 76%, m.p. 246°C. *Anal.* Calc. for $C_{64}H_{64}Br_2Cu_2N_4P_4S_2$: C, 56.3; H, 4.7; N, 4.1. Found: C, 55.8; H, 4.5; N, 4.0%. UV–Vis (λ, log ε): 294 (4.80); 247 (4.74). IR (cm^{-1}): 3148 m, 2910 w, 1614 vs, 1560 vs, 1483 s, 1433 vs, 1320 m, 1227 vs, 1189 s, 1098 s, 1027 m, 982 m, 885 m, 741 vs, 694 vs, 512 vs, 484 s, 416 m, 341 m. ^1H NMR: δ 13.95 (s, >NH), 7.66–7.08 (m, aromatic), 2.30 (s, C–CH_3), 2.17 (s, P–CH_2CH_2–P).

2.2.8. $[CuBr(dppe)(etObztztH)]_2$

Pale-yellow crystals. Yield: 70%, m.p. 177°C. *Anal.* Calc. for $C_{70}H_{66}Br_2Cu_2N_2O_2P_4S_4$: C, 55.8; H, 4.4; N, 1.8. Found: C, 55.3; H, 4.6; N, 2.0%. UV–Vis (λ, log ε): 331 (4.37); 247 (4.30). IR (cm^{-1}): 3033 m, 2925 w, 1601 vs, 1483 vs, 1427 vs, 1398 s, 1332 s, 1260 s, 1224 vs, 1099 s, 1044 vs, 1026 vs, 943 m, 877 m, 740 vs, 692 vs, 668 s, 584 s, 512 vs, 489 s, 421 m. ^1H NMR: δ 13.84 (s, >NH), 7.86–7.05 (m, aromatic), 4.07 (q, O–CH_2–C), 2.16 (s, P–CH_2CH_2–P), 1.45 (t, CH_3–C).

2.3. Collection and reduction of X-ray data

The unit cell and intensity data were collected on a Delft Instruments FAST diffractometer using the routines ENDEX, REFINE and MADONL in the MADNES software [7] and processed using ABSMAD [8]; detailed procedures are described by Darr et al. [9]. Absence of crystal decay in the X-ray beam was confirmed by checking equivalent reflections at the beginning and end of data collection, which lasted about 8 h. The structure was solved with SIR-92 [10] and refined with SHELX93 [11]. Details of crystal data and structure refinement and bond lengths (Å) and angles (°) are given in Tables 1 and 2, respectively. The copper, bromine, sulfur, phosphorus, nitrogen and carbon atoms were refined with anisotropic temperature factors. The hydrogen atoms were allowed to ride on their attached atoms with common isotropic temperature factors for methyl and non-methyl hydrogens. An absorption correction was made with DIFABS [12].

Table 1
Crystal data and structure refinement

Empirical formula	$C_{31}H_{29}BrCuNP_2S$
Formula weight	653.00
Temperature (K)	150(2)
Wavelength (Å)	0.71073
Crystal system	monoclinic
Space group	$P2_1/n$
Unit cell dimensions	
a (Å)	11.783(5)
b (Å)	15.539(5)
c (Å)	16.157(5)
β (°)	93.375(5)
Volume (Å^3)	2953(2)
Z	4
D_{calc} (Mg m^{-3})	1.469
Absorption coefficient (mm^{-1})	2.293
$F(000)$	1328
Crystal size (mm)	$0.21 \times 0.14 \times 0.05$
θ range for data collection (°)	1.82–25.05
Index ranges (°)	$-13 \le h \le 10$
	$-16 \le k \le 17$
	$-16 \le l \le 18$
Reflections collected	12213
Independent reflections	4526 [$R_{int} = 0.0761$]
Observed reflections [$I > 2\sigma(I)$]	3171
Refinement method	full-matrix least squares on F^2
Number of parameters	335
Goodness-of-fit on F^2 (S)	0.884
Final R indices [$I > 2\sigma(I)$]	$R_1 = 0.0335$, $wR_2 = 0.0709$
R indices (all data)	$R_1 = 0.0521$, $wR_2 = 0.0815$
Final weighting scheme	Calc.
	$w = 1/[\sigma^2(F_o^2) + (0.0146P)^2]$
	where $P = (F_o^2 + 2F_c^2)/3$
Residual diffraction max. (e Å^{-3})	0.371
Residual diffraction min. (e Å^{-3})	−0.342

Table 2
Bond lengths (Å) and angles (°)

Br–Cu	2.5693(12)	C(9)–C(10)	1.373(7)
Cu–P(2) # 1 [a]	2.2564(13)	C(10)–C(11)	1.380(6)
Cu–P(1)	2.2778(12)	C(12)–C(13)	1.359(6)
Cu–S	2.3456(13)	C(12)–C(17)	1.403(6)
S–C(1)	1.709(4)	C(13)–C(14)	1.400(7)
P(1)–C(6)	1.827(4)	C(14)–C(15)	1.350(8)
P(1)–C(12)	1.830(4)	C(15)–C(16)	1.377(7)
P(1)–C(18)	1.843(4)	C(16)–C(17)	1.373(7)
P(2)–C(20)	1.824(4)	C(18)–C(19)	1.525(5)
P(2)–C(26)	1.838(4)	C(20)–C(25)	1.389(5)
P(2)–C(19)	1.837(4)	C(20)–C(21)	1.398(6)
P(2)–Cu(1) # 1	2.2564(13)	C(21)–C(22)	1.370(6)
N(1)–C(1)	1.331(5)	C(22)–C(23)	1.372(6)
N(1)–C(2)	1.356(5)	C(23)–C(24)	1.380(6)
C(1)–C(5)	1.409(6)	C(24)–C(25)	1.387(6)
C(2)–C(3)	1.352(6)	C(26)–C(27)	1.372(5)
C(3)–C(4)	1.391(6)	C(26)–C(31)	1.393(5)
C(4)–C(5)	1.375(6)	C(27)–C(28)	1.390(5)
C(6)–C(11)	1.362(6)	C(28)–C(29)	1.354(6)
C(6)–C(7)	1.399(6)	C(29)–C(30)	1.374(7)
C(7)–C(8)	1.394(6)	C(30)–C(31)	1.391(5)
C(8)–C(9)	1.350(7)		
P(2) # 1–Cu–P(1)	123.14(4)	C(4)–C(5)–C(1)	119.5(5)
P(2) # 1–Cu–S	105.64(5)	C(11)–C(6)–C(7)	117.6(4)
P(1)–Cu–S	109.06(5)	C(11)–C(6)–P(1)	119.3(3)
P(2) # 1–Cu–Br	107.38(4)	C(7)–C(6)–P(1)	123.0(3)
P(1)–Cu–Br	101.25(3)	C(8)–C(7)–C(6)	120.3(5)
S–Cu–Br	109.98(3)	C(9)–C(8)–C(7)	120.2(5)
C(1)–S–Cu	108.7(2)	C(8)–C(9)–C(10)	120.2(5)
C(6)–P(1)–C(12)	102.7(2)	C(9)–C(10)–C(11)	119.5(5)
C(6)–P(1)–C(18)	99.5(2)	C(6)–C(11)–C(10)	122.1(4)
C(12)–P(1)–C(18)	107.3(2)	C(13)–C(12)–C(17)	117.8(4)
C(6)–P(1)–Cu	118.54(13)	C(13)–C(12)–P(1)	125.6(4)
C(12)–P(1)–Cu	111.62(12)	C(17)–C(12)–P(1)	116.6(4)
C(18)–P(1)–Cu	115.63(13)	C(12)–C(13)–C(14)	121.3(5)
C(20)–P(2)–C(26)	104.5(2)	C(15)–C(14)–C(13)	119.7(6)
C(20)–P(2)–C(19)	103.0(2)	C(14)–C(15)–C(16)	120.6(5)
C(26)–P(2)–C(19)	101.8(2)	C(17)–C(16)–C(15)	119.5(5)
C(20)–P(2)–Cu # 1	109.71(14)	C(16)–C(17)–C(12)	121.1(5)
C(26)–P(2)–Cu # 1	117.06(13)	C(19)–C(18)–P(1)	115.2(2)
C(19)–P(2)–Cu # 1	119.00(14)	C(18)–C(19)–P(2)	112.3(2)
C(1)–N(1)–C(2)	125.4(4)	C(25)–C(20)–C(21)	117.6(4)
N(1)–C(1)–C(5)	116.1(4)	C(25)–C(20)–P(2)	123.9(3)
N(1)–C(1)–S	121.6(3)	C(21)–C(20)–P(2)	117.9(3)
C(5)–C(1)–S	122.3(4)	C(22)–C(21)–C(20)	121.2(4)
C(3)–C(2)–N(1)	119.6(4)	C(21)–C(22)–C(23)	120.9(4)
C(2)–C(3)–C(4)	117.9(4)	C(22)–C(23)–C(24)	118.9(4)
C(5)–C(4)–C(3)	121.5(5)	C(23)–C(24)–C(25)	120.7(4)
C(24)–C(25)–C(20)	120.6(4)	C(29)–C(28)–C(27)	120.4(4)
C(27)–C(26)–C(31)	119.8(4)	C(28)–C(29)–C(30)	120.8(4)
C(27)–C(26)–P(2)	122.3(3)	C(29)–C(30)–C(31)	119.6(4)
C(31)–C(26)–P(2)	117.7(3)	C(30)–C(31)–C(26)	119.6(4)
C(26)–C(27)–C(28)	119.8(4)		

[a] Atomic coordinates transposed by $-x+3/2$, $-y+1/2$, $-z+1$.

3. Results and discussion

The complexes were prepared by reacting equimolar quantities of copper(I) bromide and 1,2-bis-(diphenylphosphino)ethane (dppe), followed by the addition of one equivalent of the appropriate thione (L) in

dry acetone solution. This procedure, frequently used for the preparation of copper(I) halide complexes containing both heterocyclic thiones and triphenyl- or tritolylphosphine ligands, gave monomeric complexes of the formula $[CuX(PPh_3)_2L]$ [3] or dimers $[CuX(PPh_3)L]_2$ with the two copper centres being bridged either by the halogen [13] or by the thione-S atom [14]. In this work we expected that replacement of the monodentate phosphine by the bidentate dppe would lead to the formation of chelated products; however, this was not the case.

All the complexes are coloured solids soluble in chloroform, methanol, ethanol, acetone and acetonitrile. They are stable in air and moisture and can be, after the isolation, manipulated in air without appreciable decomposition. Their solutions are non-conducting in acetone and chloroform. Room temperature magnetic measurements confirm the diamagnetic nature of the compounds.

3.1. Spectroscopy

The electronic absorption spectra of the complexes in chloroform solutions are dominated by broad bands in the regions 240–250 and 280–330 nm attributable to intraligand transitions of the dppe, since the uncoordinated dppe also absorbs strongly in this region.

The infrared spectra of the compounds, recorded in the range 4000–250 cm^{-1}, show, apart from the existence of strong phosphine bands, all of the bands required by the presence of the heterocyclic thione ligands. In detail they exhibit the usual four 'thioamide bands' in the regions $\sim$1510, 1320, 1000 and 750 cm^{-1}, although in some cases partly masked by strong phosphine absorptions, as well as the characteristic NH stretching vibrations observed in the 3050–3160 cm^{-1} region. The shifts observed for these bands due to coordination (upward shifts of 15–35 cm^{-1} for thioamide I, downward shifts of 10–30 cm^{-1} for thioamide II and III) in combination with the lack of ν(SH) bands at ca. 2500–2600 cm^{-1} [15] signify the exclusive S-coordination mode of the thione ligands.

The prevailance of the thione tautomer in the complexes is further confirmed by the ^1H NMR spectra of the compounds, which display, apart from the signals expected for the phosphine and thione ligands, a single resonance at $\delta \sim 12$–14 ppm attributed to the NH proton.

3.2. Description of the structure

The ability of 1,2-bis(diphenylphosphino)ethane (dppe) to chelate Cu(I) is well known and a few double-chelated cationic $Cu(dppe)_2^+$ species have been observed [16,17]. Most of the structurally characterized binuclear copper(I) complexes involving dppe ligands are, however, of the type $[Cu_2(dppe)_3L_2]$ [18–23], in which the diphosphine units act at the same time both as chelating ligands for each of the copper atoms and as a bridge between them. The double bridging coordination mode realized in the case of the complex under investigation is quite common for univalent Group 1B metal complexes of bis(diphenylphosphino)methane (dppm) [24–27].

Bond lengths and angles are given in Table 2. The atomic arrangement in the complex is shown in Fig. 1. The basic structural unit of $[Cu(dppe)(py2SH)Br]_2$ is a dimer in which the two monomers are related by inversion. The two copper atoms are doubly bridged by two dppe ligands to form a ten-membered $Cu_2P_4C_4$ ring. The slightly distorted tetrahedral coordination around copper is completed by one sulphur atom from the thione ligand and one bromine atom.

The Cu–S and Cu–Br bond lengths lie in the range normally observed for tetrahedrally coordinated copper(I) complexes with terminal bromine and thione-sulphur donors [28]. The two individual Cu–P distances of 2.2564(13) and 2.2778(12) Å are somewhat shorter than those found for bridging dppe in other dimeric copper(I) complexes, e.g. $[Cu_2Cl_2(dppe)_3]$ (2.284(6) Å) [20] and $[Cu_2(3\text{-}Me_3Sipyt)_2(dppe)_3]$ (2.294(3) Å) [23].

The irregularities in the tetrahedral coordination geometry about the copper(I) centre are best reflected in the values of the bond angles, since only three of them are close to the ideal tetrahedral value. As expected, the largest angle [P–Cu–P = 123.14(4)°] arises between the two most bulky ligands, whereas the presence of intramolecular hydrogen bonds between the bromine and the N(1)H, C(4)H(4) and C(19)H(19A) hydrogen [N(1)···Br = 3.226(3) Å, N(1)–H = 0.880(4) Å, H···Br = 2.367(3) Å, N(1)–H–Br = 165.1(3)°; C(4)···Br = 3.585(5) Å, C(4)–H(4) = 0.951(7) Å, H(4)···Br = 2.902(5) Å, C(4)–H(4)–Br = 129.6(5)°; C(19)···Br = 3.582(4) Å, C(19)–H(19) = 0.990(5) Å, H(19)···Br = 2.703(4) Å, C(19)–H(19)–Br = 148.1(4)°] could be responsible for the moderate narrowing of the P(1)–Cu–Br angle [101.25(3)°]. It is interesting to note that all these angles are in qualitative agreement with the corresponding values already observed for a series of monomeric copper(I) halide complexes that contain one heterocyclic thione and two monodentate triphenylphosphine ligands, exhibiting the same $CuSP_2X$ core [28]. Given that steric constrains between the ligands are of significance in achieving minimum energy arrangements around the metal centre, this fact indicates that the steric requirements of the bridging dppe units within the dimer $[Cu(dppe)(py2SH)Br]_2$ are approximately of the same magnitude as those of the triphenylphosphine ligands in the monomeric complexes $[Cu(PPh_3)_2(S)X]$ [29]. It seems plausible, therefore, to invoke steric reasons in order to explain the feature of the complex under investigation, the most energetically favourable

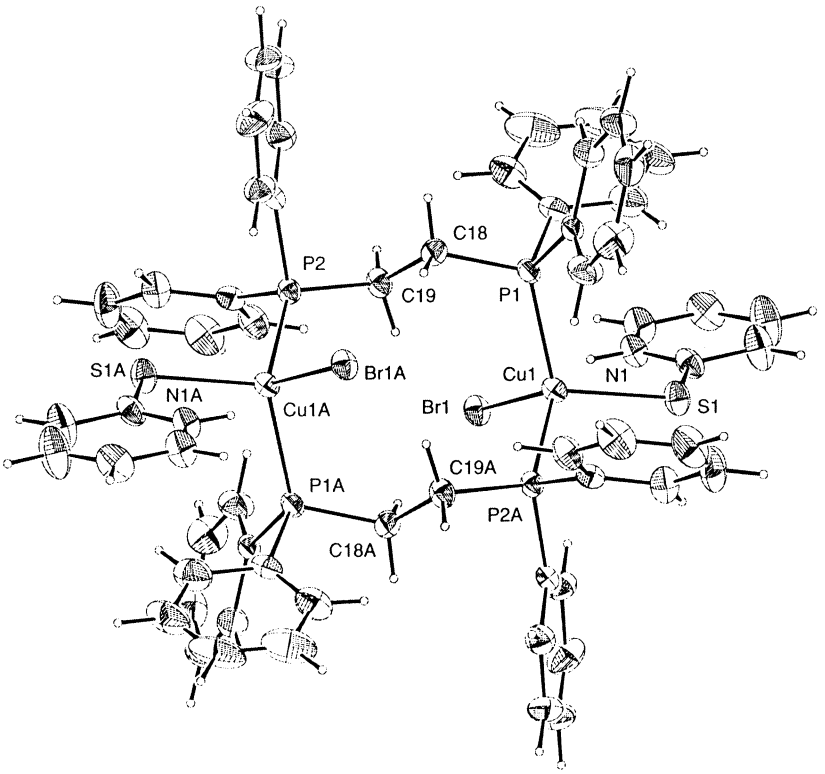


Fig. 1. A view of the complex with atom labels. Displacement ellipsoids are shown at the 50% probability level.

situation being manifested by the appearance of doubly bridged dppe ligands but not by the formation of five-membered chelate rings.

4. Supplementary material

Supplementary data are available free of charge from: The Director, CCDC, 12 Union Road, Cambridge, CB2 1EZ, UK (fax: +44-1223-336-033; e-mail: deposit@ccdc.cam.ac.uk or www:http://www.ccdc.cam.ac.uk) quoting the deposition number CCDC-114060.

Acknowledgements

We thank the EPSRC X-ray crystallographic service at the University of Wales, Cardiff for data collection.

References

[1] E.S. Raper, Coord. Chem. Rev. 129 (1994) 91.
[2] (a) F.A. Cotton, K.R. Dunbar, M.G. Verbruggen, J. Am. Chem. Soc. 109 (1987) 5498. (b) R.J. Puddephatt, Chem. Soc. Rev. 12 (1983) 99. (c) R.V. Kiress, R. Eisenberg, Inorg. Chem. 28 (1989) 3372.
[3] P. Aslanidis, S.K. Hadjikakou, P. Karagiannidis, M. Gdaniec, Z. Kosturkiewicz, Polyhedron 12 (1993) 2221, and Refs. therein.
[4] S.K. Hadjikakou, P. Aslanidis, P. Karagiannidis, A. Aubry, S. Skoulika, Inorg. Chim. Acta 193 (1992) 129.
[5] (a) S.J. Berners-Price, P.J. Sandler, Struct. Bonding 70 (1988) 70. (b) J.S. Lewis, J. Zweit, J.L.J. Dearling, B.C. Rooney, P.J. Blower, Chem. Commun. (1996) 1093. (b) J. Lewis, S.L. Heath, A.K. Powell, J. Zweit, P.J. Blower, J. Chem. Soc., Dalton Trans. (1997) 855.
[6] P. Karagiannidis, S.K. Hadjikakou, P. Aslanidis, A. Hountas, Inorg. Chim. Acta 178 (1990) 27.
[7] J.W. Pflurgrath, A. Messerschmidt, MADNES, Version 11 September 1989, Distributed by Delft Instruments, Delft, The Netherlands.
[8] A.I. Karaulov, ABSMAD, Program for FAST data Processing, University of Wales, Cardiff, 1992.
[9] J.A. Darr, S.R. Drake, M.B. Hursthouse, K.M.A. Malik, Inorg. Chem. 32 (1993) 5704.
[10] A. Altomare, M.C. Burla, M.C. Camalli, G. Cascarano, C. Giacovazzo, A. Guagliardi, G. Polidori, J. Appl. Cryst. 27 (1994) 435.
[11] G.M. Sheldrick, SHELXL-93, Program for the Refinement of Crystal Structures, University of Göttingen, Germany, 1994.
[12] N. Walker, D. Stuart, Acta Crystallogr., Sect. A 39 (1983) 158.
[13] S.K. Hadjikakou, P. Aslanidis, P. Karagiannidis, A. Hountas, A. Terzis, Inorg. Chim. Acta 184 (1991) 161.
[14] S.K. Hadjikakou, P. Aslanidis, P.D. Akrivos, P. Karagiannidis, B. Kojic-Prodic, M. Luic, Inorg. Chim. Acta 197 (1992) 31.
[15] R. Battistuzzi, G. Peyronel, Can. J. Chem. 59 (1981) 591.
[16] S.J. Rettig, A. Storr, J. Trotter, Can. J. Chem. 66 (1988) 2194.
[17] J.S. Lewis, J. Zweit, P.J. Blower, Polyhedron 17 (1998) 513.
[18] A.P. Gaughan, R.P. Ziolo, Z. Dori, Inorg. Chem. 10 (1971) 2776.
[19] A.P. Gaughan, C.S. Bowman, Z. Dori, Inorg. Chem. 11 (1972) 601.

[20] V.G. Albano, P.L. Bellon, G. Ciani, J. Chem. Soc., Dalton Trans. (1972) 1938.
[21] E.W. Ainscough, E.N. Baker, A.G. Bingham, A.M. Brodie, C.A. Smith, J. Chem. Soc., Dalton Trans. (1989) 2167.
[22] B. Mohr, E.E. Brooks, N. Rath, E. Deutsch, Inorg. Chem. 30 (1991) 4541.
[23] R. Castro, J. Romero, J.A. Garcia-Vazquez, A. Sousa, Y.D. Chang, J. Zubieta, Inorg. Chim. Acta 345 (1996) 119.
[24] J. Diez, M.P. Gamasa, J. Gimeno, J. Chem. Soc., Dalton Trans. (1987) 1275.
[25] A.M. Manotti Lanfredi, F. Ugozzoli, A. Gamus, N. Marsich, R. Capelletti, Inorg. Chim. Acta 206 (1993) 173.
[26] E.R.T. Tiekink, Acta Crystallogr., Sect. C 46 (1990) 235.
[27] L.C. Porter, M.N.I. Khan, C. King, J.P. Fackler Jr., Acta Crystallogr., Sect C 45 (1989) 949.
[28] (a) P. Karagiannidis, P. Aslanidis, D.P. Kessissoglou, B. Krebs, M. Dartmann, Inorg. Chim. Acta 156 (1989) 47. (b) P. Aslanidis, S.K. Hadjikakou, P. Karagiannidis, B. Kojic-Prodic, M. Luic, Polyhedron 13 (1994) 3119. (c) P. Karagiannidis, P. Aslanidis, S. Papastefanou, D. Mentzafos, A. Hountas, A. Terzis, Polyhedron 9 (1990) 981. (d) S.K. Hadjikakou, P. Aslanidis, P. Karagiannidis, D. Mentzafos, A. Terzis, Inorg. Chim. Acta 186 (1991) 199.
[29] G.P. Voutsas, S.C. Kokkou, C.J. Cheer, P. Aslanidis, P. Karagiannidis, Polyhedron 14 (1995) 2287.

PERGAMON

www.elsevier.nl/locate/poly

Polyhedron 19 (2000) 1621–1626

POLYHEDRON

The synthesis and characterisation of two mononuclear tungsten pentacarbonyl complexes of 4,4′-bipyridine and 1,2-bis(4-pyridyl)ethane

Annette Nel [a], James Chapman [a,b], Nicholas Long [b], Gabriel Kolawole [a], Majid Motevalli [c], Paul O'Brien [d,*]

[a] *Department of Chemistry, University of Zululand, Private Bag X1001, Kwa-Dlangezwa, Natal, South Africa*
[b] *Department of Chemistry, Imperial College of Science Technology and Medicine, South Kensington, London, SW7 2AY, UK*
[c] *Department of Chemistry, Queen Mary and Westfield College, Mile End Road, London, E1 4NS, UK*
[d] *Department of Chemistry and Manchester Materials Science Centre, University of Manchester, Oxford Road, Manchester, M13 9PL, UK*

Received 17 February 2000; accepted 25 April 2000

Abstract

The mononuclear tungsten pentacarbonyl complexes with 1,2-bis(4-pyridyl)ethane and 4,4′-bipyridine were synthesised by the irradiation, with a UV source, of solutions of tungsten hexacarbonyl and the relevant N-containing ligand. Both complexes were characterised by single-crystal X-ray diffraction and in both structures, the coordination geometry of the tungsten atom is slightly distorted from octahedral. © 2000 Elsevier Science Ltd. All rights reserved.

Keywords: Mononuclear; Tungsten pentacarbonyl complexes; 1,4-Bipyridine; 1,2-Bis(4-pyridyl)ethane

1. Introduction

Organometallic complexes between transition metal carbonyls and N-containing heterocycles have been the subject of considerable interest in recent years. Their photochemical and electronic properties and potential for industrial applications have led to many studies for use as photosensitisers, catalysts and conducting coordinating polymers [1–6]. It is known that the photochemical properties of these transition metal complexes are dominated by low-lying charge-transfer (MLCT), excited states, which have been extensively investigated [7–18]. Attention has also been given to the electronic interactions across ligands that bridge the binuclear complexes [19–27]; on photoexcitation they provide a relatively simple route for the study and understanding of intramolecular electron transfer processes [6,28–31], magnetic coupling interactions from one metal to another and inner-sphere electron-transfer mechanisms [32–40]. Binuclear systems are particularly interesting in that electron transfer can be studied between one metal centre and another across a conjugated system. These interactions can be varied using different ligands, which will change the metal–metal distance, the extent of conjugation between metal sites, complex planarity and π-acceptor–donor ligand interactions.

Most of the studies of such complexes involve metals with different oxidation states. However, at the moment, there is substantial interest in the photochemical and optical properties of binuclear zero valent Group 6 metal carbonyl complexes [5]. Bridged complexes of the type $(OC)_5M–L–M'(CO)_5$ and $(OC)_4M–L–M'(CO)_4$ have been synthesised containing two $(OC)_5M–$ and two $(OC)_4M–$ moieties, respectively, where M, M′ = Cr, Mo or W. It is interesting to attempt to understand the photophysical and photochemical changes that occur when forming these binuclear compounds and the effect of changing the shape and degree of conjugation of the binucleating ligand between the metal centres.

Creutz and Taube first reported the synthesis of the complex Ru(II)–L–Ru(III) where the ligand [19] acts as a bridge between the two metal centres in which elec-

* Corresponding author. Tel. +44-161-275-4653; fax: +44-161-275-4616.
E-mail address: paul.obrien@man.ac.uk (P. O'Brien).

0277-5387/00/$ - see front matter © 2000 Elsevier Science Ltd. All rights reserved.
PII: S0277-5387(00)00439-3

tron transfer can take place via an inner sphere mechanism. Such metallorganic dimers have been synthesised by a variety of routes in attempts to further elucidate the mechanism of electron transfer. Work on these ligand-bridged systems using tungsten in heteronuclear complexes has been reported [5]. These complexes were found to be stable in solid form, but in solution are air and/or light sensitive. The instability of these complexes is thought to be due to cleavage of the M–L–M bond as shown in the bridged dimer $(OC)_5Mo(pyz)Mo(CO)_5$. There is interest in pyrazine-type-bridged dimers where the two nitrogen donors are *trans*- to each other which focuses on the electronic, photochemical and photophysical properties of these complexes. Binuclear 4,4′-bipyridine systems have also been synthesised, and show similar light and air sensitivity but as yet, have not been the subject of investigation. Similarly to pyrazine, the nitrogen donors in 4,4′-bipyridine are *trans*- to each other where the metal–metal separation is increased from 6.9 Å for pyrazine to 11.2 Å for 4,4′-bipyridine, and so far no X-ray crystal structure has been reported for these complexes.

Our work has been concerned with the synthesis of complexes between various substituted pyridine derivatives and tungsten hexacarbonyl (see Scheme 1). In this paper, we report the crystal and molecular structures of pentacarbonyl-1,2-bis(4-pyridyl)ethanetungsten (**1**) and pentacarbonyl-4,4′-bipyridinetungsten (**2**). The synthesis and characterisation of such 1:1 adducts is a step towards a route to synthesise binuclear hetreonuclear complexes which may have interesting electronic properties.

2. Experimental

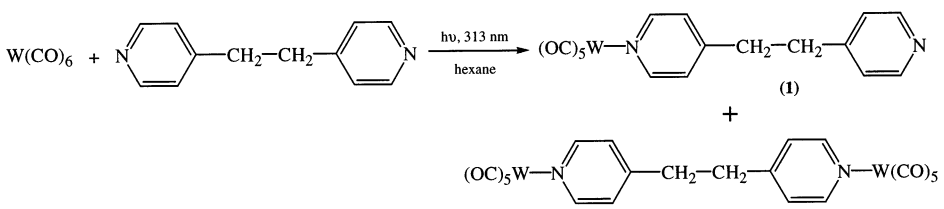
2.1. Pentacarbonyl-1,2-bis(4-pyridyl)ethanetungsten (*1*)

A solution of 1,2-bis(4-pyridyl)ethane (0.368 g, 2 mmol) and finely ground tungsten hexacarbonyl (1.407 g, 4 mmol) in dry N_2 purged hexane (150 ml) was irradiated at $\lambda = 313$ nm using a 200 W medium pressure tungsten lamp. After 2 h reaction time a green solution and a yellow precipitate were obtained. The yellow precipitate was isolated and the solution taken to dryness. The residual solid contained a mixture of the mononuclear and binuclear materials, which were separated by column chromatography (alumina, 50:50 hexane–benzene) the monomer crystallised from this as fine yellow needles. m/z 508 [M^+], 480 [$M^+ - CO$] and 452 [$M^+ - 2 \times CO$]. Found: C, 37.4; H, 1.6; N 6.0; Calc.: C, 37.5; H, 1.7; N, 5.9%.

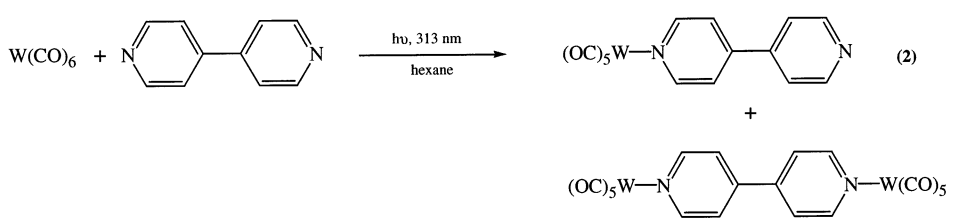
2.2. Pentacarbonyl-4,4′-bipyridinetungsten (*2*)

The reaction of 4,4′-bipyridine (0.312 g, 2 mmol) with finely ground tungsten hexacarbonyl (1.41 g, 4 mmol) in dry N_2 purged hexane (150 ml) was carried out with UV irradiation at $\lambda = 313$ nm, 200 W medium pressure tungsten lamp, and after 1.5 h afforded a yellow coloured suspension containing the mononuclear and binuclear complexes. The reaction was monitored by FTIR spectroscopy. During this reaction the binuclear complex precipitated from solution as an orange crystalline solid and the mononuclear complex remained in solution and was isolated by column chromatography

Synthesis of pentacarbonyl-1,2-bis(4-pyridyl)ethanetungsten (**1**)



Synthesis of pentacarbonyl-4,4'-bipyridinetungsten (**2**)



Scheme 1.

Table 1
Crystal data and structure refinement for complexes **1** and **2**

	Complex **1**	Complex **2**
Formula	$C_{17}H_{12}N_2O_5W$	$C_{15}H_9N_2O_5W$
Molecular weight	508.14	481.09
Crystal system	monoclinic	monoclinic
Crystal size (mm)	$0.4\times0.2\times0.1$	$0.3\times0.3\times0.1$
Space group	$P2_1/n$	$C2/c$
a (Å)	14.113(2)	12.497(2)
b (Å)	11.064(1)	16.632(2)
c (Å)	11.724(2)	7.620(1)
α (°)	90	90
β (°)	102.02(2)	90.19(2)
γ (°)	90	90
Volume (Å^3)	1790.6(4)	1583.9(4)
Z	4	4
D_{calc} (g cm^{-1})	1.885	2.018
$F(000)$	968	908
Temperature (K)	293(2)	293(2)
Radiation	Mo Kα ($\lambda=0.71073$ Å)	Mo Kα ($\lambda=0.71073$ Å)
Absorption coefficient μ (mm^{-1})	6.48	7.319
2θ Range (°)	2.06–24.97	2.04–24.95
Data/restraints/parameters	3135/0/236	1398/0/113
Observed reflections [$I>2\sigma(I)$]	2354	1309
Refinement method	full-matrix least squares on F^2	full-matrix least squares on F^2
Goodness-of-fit on F^2	1.046	1.066
Final R_1	0.0241	0.0232
Final wR_2	0.0547	0.0609
Largest difference peak and hole (e Å^{-3})	0.354 and −0.382	0.641 and −0.880

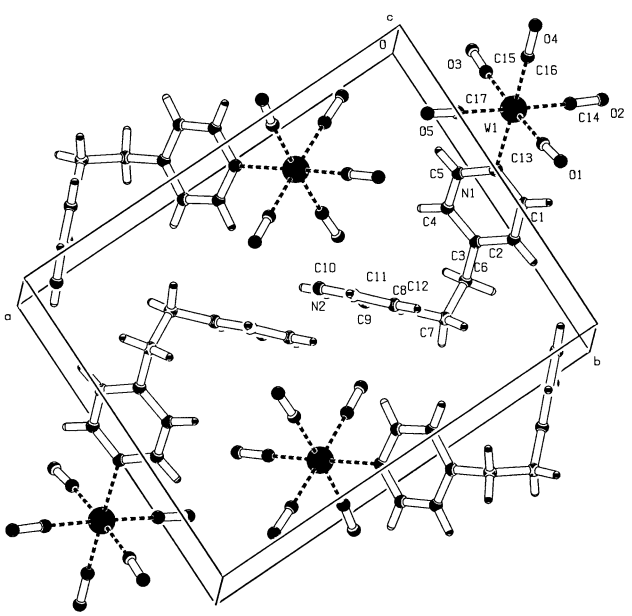


Fig. 1. The unit cell of pentacarbonyl-1,2-bis(4-pyridyl)ethane-tungsten.

(alumina, 50:50 hexane–benzene), to yield a product which crystallised as needles from a 50:50 hexane–benzene mixture. m/z 480 [M^+], 452 [$M^+ - CO$] and 424 [$M^+ - 2\times CO$]. Found: C, 40.1; H, 2.3; N, 5.7; Calc.: C, 40.2; H, 2.4, N, 5.5%.

2.3. X-ray crystallography

The structure of the subject compounds were determined by single X-ray methods. Measurements were made on samples mounted on a glass capillary. The intensity data were collected with a CAD4 diffractometer in a $\omega/2\theta$ scan mode with graphite-monochromated Mo Kα, and corrected for absorption by the empirical method (ψ-scan) [41]. The unit cell parameters were determined by a least squares refinement on diffractometer angles for automatically centred reflections. The structure was solved by the heavy atom method using the SHELX-97 program package [42] and then refined anisotropically (non-hydrogen atoms) by a full-matrix least-square on F^2. All hydrogen atoms were calculated geometrically (riding model) using the AFIX command on the SHELX-97 program. The program PLATON for Windows [43] was used for drawing molecular structures. Crystal data and details of the intensity measurements are given in Table 1. Atomic coordinates, thermal parameters and bond lengths and angles have been deposited at the Cambridge Crystallographic Data Centre.

3. Results and discussion

A two-stage reaction is often used in the synthesis of these binuclear complexes where usually the initial photolysis of tungsten hexacarbonyl in 0.1 M THF in hexane yields a mononuclear THF adduct. This on further thermochemical reaction with the same or a different pyridine ligand derivative gives a binuclear metal complex plus some of the mononuclear component [6,28–31]. In this instance the synthesis of the THF adduct was bypassed and direct photolysis of 2 mol of the pyridine derivative with 1 mol of tungsten hexacarbonyl in dry hexane was used as a synthetic route to the mononuclear complex.

The structure of complex **1** was determined by single-crystal X-ray diffraction methods. The unit cell and molecular structures are shown in Figs. 1 and 2, respectively. Selected bond distances and angles are given in Table 2. The structure is based on mononuclear units with four molecules of the complex in the unit cell. The tungsten atoms lie on the faces of the cell. The structure shows coordination at one nitrogen atom of 1,2-bis(4-pyridyl)ethane to the tungsten atom $(WCO)_5$ leaving the other nitrogen uncoordinated. The non-coordinated pyridyl ring lies almost perpendicular to the complexed ring and probably maximises packing. The molecule

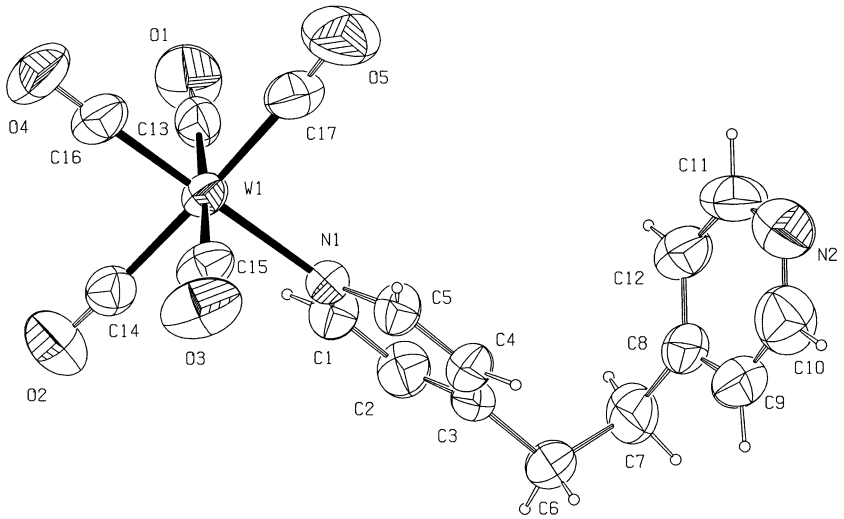


Fig. 2. The molecular structure of pentacarbonyl-1,2-bis(4-pyridyl)ethanetungsten.

has C_1 symmetry. The tungsten is hexacoordinated through the ring nitrogen atom, an axial carbon monoxide group and four equatorial carbon monoxide groups, the metal can be defined as distorted octahedral. The W1–N1 bond distance is 2.271(4) Å whilst the corresponding axial W1–C16 carbon monoxide bond length is 1.955(6) Å which is somewhat shorter. The four axial carbon monoxide bond lengths W1–C13, W1–C15, W1–C14 and W1–C17 are 2.029(6), 2.025(6), 2.025(7) and 2.037(7) Å, respectively, which are all comparable. It is interesting to note that the bond angles C13–W1–C15 177.2(2)° and C14–W1–C17 177.8(2)° both deviate away from linearity. Van der Waals repulsions between the H atoms on the complexed ring and the equatorial carbon monoxide groups attached to the tungsten atom may cause distortion away from octahedral.

The structure of complex **2** (Fig. 3) was also determined by single-crystal X-ray diffraction methods. Selected bond lengths and bond angles are given in Table 3. The complex has a C_2 axis through the central atoms C3–W1–N1–N2. Tungsten is hexacoordinated with a single ring nitrogen atom, a corresponding axial carbon monoxide group and four equatorial carbon monoxide groups. The W1–N1 bond length is 2.273(5) Å, which is identical to that found in the pentacarbonyl-1,2-bis(4-pyridyl)ethane tungsten analogue, complex **1**. The tungsten-axial carbon monoxide bond length is 1.954(8) Å, which is similar to the related bond length in complex **1** (1.955(6) Å). The four axial carbon monoxide bond lengths, W1–C1, W1–C1a, W1–C2 and W1–C2a are 2.025(6), 2.025(6), 2.031(6) and 2.031(6) Å, respectively, and are almost identical in length. The *trans*-equatorial bond lengths C1–W1–C1a 176.2(3)° and C2–W1–C2a 176.7(3)° again both deviate away from linearity of 180° and very slightly more than in complex **1.** Similarly this exhibits an distorted octahedral environment for the tungsten atom whereby this distortion is again thought to be due to van der Waals repulsion between the H atoms of the complexed ring and the equatorial carbon monoxide groups coordinated to the tungsten atom.

4. Conclusions

The single-crystal X-ray structures of complexes **1** and **2** have been successfully carried out and analysed. Further photochemical studies will be carried out on these complexes. Complex **2** has a linear conjugated system but complex **1** is non-linear where the two methylene groups break the π-conjugation within this complex. The tungsten–nitrogen bond lengths in complex **1** and complex **2** are almost identical 2.271(4) and 2.273(5) Å, which compares well with that observed in the bidentate metallacycle $Me_2Sn(CHSiMe_3C_5H_3N)_2$-$W(CO)_4$ [44] of 2.215(7) and 2.228(7) Å.

Table 2
Selected bond lengths (Å) and bond angles (°) for complex **1**

W(1)–C(13)	2.029(6)	C(6)–C(7)	1.519(9)
W(1)–C(14)	2.025(7)	C(7)–C(8)	1.505(9)
W(1)–C(15)	2.025(6	N(1)–C(1)	1.337(6)
W(1)–C(17)	2.037(7)	N(1)–C(5)	1.345(6)
W(1)–C(16)	1.955(6)	N(2)–C(10)	1.307(9)
W(1)–N(1)	2.271(4)	N(2)–C(11)	1.305(9)
C(3)–C(6)	1.514(8)		
C(13)–W–C(15)	177.5(3)	C(13)–W–C(17)	92.6(3)
C(14)–W–C(17)	177.7(3)	C(13)–W–C(14)	87.5(2)
C(16)–W–N(1)	179.0(3)		

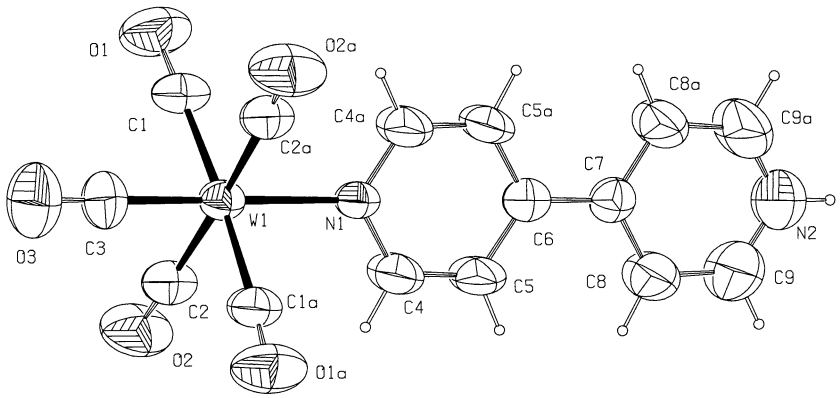


Fig. 3. The molecular structure of pentacarbonyl-4,4′-bipyridinetungsten.

Table 3
Selected bond lengths (Å) and bond angles (°) for complex **2**

W(1)–C(1)	2.025(6)	C(6)–C(7)	1.451(9)
W(1)–C(1)a	2.025(6)	N(1)–C(4)	1.323(7)
W(1)–C(2)	2.031(6)	N(1)–C(4)a	1.323(7)
W(1)–C(2)a	2.031(6)	N(2)–C(9)	1.283(10)
W(1)–C(3)	1.954(8)	N(2)–C(9)a	1.283(101)
W(1)–N(1)	2.273(5)		
C(1)–W–C(1)a	176.2(3)	C(1)–W–C(2)a	89.9(2)
C(2)–W–C(2)a	176.7(3)	C(1)–W–C(3)	88.10(14)
C(3)–W–N(1)	180.0		

Other similar complexes containing the π-system, tetracarbonyl-2,2-bipyridinetungsten and pentacarbonyl-1,2-bis(4-pyridyl)ethenetungsten have been synthesised and we are awaiting the X-ray crystallographic analysis. This will permit further studies of mononuclear substitution and π-conjugation within these complexes.

5. Supplementary material

Complete bond lengths and angles, and co-ordinates and displacement parameters have been deposited at the Cambridge Crystallographic Centre. Crystallographic data for the structural analysis has been deposited with the Cambridge Crystallographic Data Centre, CCDC Nos. 140616 and 146017. Copies of this information may be obtained free of charge from: The Director, CCDC, 12 Union Road, Cambridge, CB2 1EZ, UK (Fax: +44-1223-336-033; e-mail: deposit@ccdc.cam.ac.uk or www: http://www.ccdc.cam.ac.uk).

Acknowledgements

We would like to thank the Royal Society, UK, and the Foundation for Research and Development, SA, for grants supporting work on this project. P.O'B. was the Sumitomo/STS Professor of Materials Chemistry and the Royal Society Amersham International Research Fellow during the time this work was carried out (1997/98).

References

[1] C.A. Hunter, Angew. Chem., Int. Ed. Engl. 34 (1995) 1079.
[2] P.J. Stang, D.H. Cao, S. Saito, A.M. Arif, J. Am. Chem. Soc. 117 (1995) 6273 and references therein.
[3] A.J. Blake, N.R. Champness, P. Hubberstey, W.-S. Li, M.A. Withersby, M. Schroder, Coord. Chem. Rev. 183 (1999) 117.
[4] S.R. Battern, R. Robson, Angew. Chem., Int. Ed. Engl. 37 (1998) 1460.
[5] I-Y. Wu, J.T. Lin, J. Luo, S-S. Sun, C-S. Li, K.J. Lin, C. Tsai, C-C. Hsu, J.-L. Lin, Organometallics 16 (1997) 2038.
[6] J.A. Gelroth, J.E. Figard, J.D. Peterson, J. Am. Chem. Soc. 101 (1979) 3649.
[7] G.L. Geoffroy, M.S. Wrighton, Organometallic Photochemistry, Academic Press, New York, 1979.
[8] P.C. Ford, Rev. Chem. Intermed. 2 (1979) 267.
[9] A.W. Adamson, Pure Appl. Chem. 51 (1979) 313.
[10] G. Schwenger, M.Y. Darensbourg, D.J. Darensbourg, Inorg. Chem. 11 (1972) 1967.
[11] D.J. Darensbourg, M.A. Murphy, Inorg. Chem. 17 (1978) 884.
[12] G. Boxhoorn, G.C. Schoemaker, D.J. Stufkens, A. Oskam, A.J. Rest, D.J. Darensbourg, Inorg. Chem. 19 (1980) 3455.
[13] G. Boxhoorn, A. Oskam, E.P. Gibson, R. Narayanaswamy, A.J. Rest, Inorg. Chem. 20 (1981) 783.
[14] G. Boxhoorn, A. Oskam, T.M. McHugh, A.J. Rest, Inorg. Chim. Acta 44 (1980) L1.
[15] R.M. Dahlgren, J.L. Zinc, Inorg. Chem. 16 (1977) 3154.
[16] (a) R.M. Dahlgren, J.I. Zinc, Inorg. Chem. 18 (1979) 597. (b) R.M. Dahlgren, J.I. Zinc, J. Am. Chem. Soc. 101 (1979) 1448.
[17] J.E. Figard, J.D. Peterson, Inorg. Chem. 17 (1979) 2736.
[18] C.C. Frazier, H. Kirsh, Inorg. Chem. 17 (1978) 2736.
[19] (a) C. Creutz, H. Taube, J. Am. Chem. Soc. 91 (1969) 3988. (b) C. Creutz, H. Taube, J. Am. Chem. Soc. 95 (1973) 1086.
[20] A Haim, Acc. Chem. Res. 8 (1975) 264.
[21] T.J. Meyer, Acc. Chem. Res. 11 (1978) 94.
[22] E. Brown (Ed.), Mixed Valence Chemistry, Reidal, Dordrecht, The Netherlands, 1980.
[23] R.D. Cannon, Electron Transfer Reactions, Butterworths, London, 1980, p. 1980.

[24] K.Y. Wong, P.N. Schatz, Prog. Inorg. Chem. 28 (1981) 370.
[25] K.R. Seddon, Coord. Chem. Rev. 41 (1982) 79.
[26] C. Creutz, Prog. Inorg. Chem. 30 (1983) 1.
[27] U. Fürholtz, H.-B. Burghi, F.E. Wagner, A Stebler, J.H. Ammeter, E. Krausz, R.J.H. Clark, M.J. Stead, A. Lundi, J. Am. Chem. Soc. 106 (1984) 121.
[28] J.C. Curtis, J.S. Bernstein, R.H. Schmehl, T.J. Meyer, Chem. Phys. Lett. 48 (1981) 81.
[29] R. Ruminski, J.D. Peterson, Inorg. Chem. 21 (1982) 3706.
[30] K.J. Moore, L. Lee, J.E. Figard, J.A. Gelroth, A.J. Stinson, H.D. Wohlers, J.D. Peterson, J. Am. Chem. Soc 105 (1983) 2274.
[31] J.D. Peterson, W.R. Murphy, R. Sahai, K.J. Brewer, R.R Ruminski, Coord. Chem. Rev. 64 (1985) 261.
[32] J.K. Farr, L.G. Hulett, R.H. Lane, J.K. Hurst, J. Am Chem. Soc. 97 (1975) 2654.
[33] V.A. Durante, P.C. Ford, J. Am. Chem. Soc. 97 (1975) 6898.
[34] D.A. Piering, J.M. Malin, J. Am. Chem. Soc. 98 (1976) 6043.
[35] J.M. Malin, D.A. Ryan, T.V O'Halloran, J. Am. Chem. Soc. 100 (1976) 2097.
[36] C. Creutz, P. Kroger, T. Matsubara, T.L. Netzel, N. Sutin, J. Am. Chem. Soc. 101 (1979) 5442.
[37] K.A. Norton, J.K. Hurst, J. Am. Chem. Soc. 104 (1982) 5960.
[38] C.A. Bignozzi, S. Roffia, F. Scandola, J. Am. Chem. Soc. 107 (1985) 1644.
[39] J.C. Curtis, J.S. Bernstein, T.J. Meyer, Inorg. Chem. 24 (1985) 385.
[40] K.S. Schanze, G.A. Neyhart, T.J. Meyer, J. Phys. Chem. 90 (1986) 2182.
[41] A.C.T. North, D.C. Phillips, F.S. Matthews, Acta Crystallogr., Sect A 24 (1968).
[42] G.M. Sheldrick, SHELX-97, Program for Solution and Refinement of Crystal Structures, University of Göttingen, Germany, 1998.
[43] A.L. Spek, PLATON, A Multipurpose Crystallographic Tool, Utrecht University, Utrecht, The Netherlands, 1998
[44] W.-P. Leung, K.S.M. Poon, T.C.W. Mak, R.-J. Wang, Z.-Y. Zhou, Organometallics 16 (1997) 4839.

PERGAMON

www.elsevier.nl/locate/poly

Polyhedron 19 (2000) 1627–1631

POLYHEDRON

Synthesis and characterization of heterodinuclear thiolate complexes containing the Pd(η^3-allyl)$^+$ moiety. Crystal structure of [(dppe)Pd(μ-SC_6H_4Me-*p*)$_2$Pd(η^3-C_3H_5)][ClO_4]

José Ruiz [a], José Giner [a], Venancio Rodríguez [a], Gregorio López [a,*], Jaume Casabó [b], Elies Molins [c], Carles Miravitlles [c]

[a] *Departamento de Química Inorgánica, Universidad de Murcia, 30071 Murcia, Spain*
[b] *Departament de Química, Universitat Autònoma de Barcelona, Campus Universitari de Bellaterra, 08193-Cerdanyola, Barcelona, Spain*
[c] *Institut de Ciència de Materials de Barcelona, CSIC, Campus Universitari de Bellaterra, 08193-Cerdanyola, Barcelona, Spain*

Received 1 February 2000; accepted 22 May 2000

Abstract

Heterodinuclear complexes of the types [(dppe)M(μ-$SR)_2$Pd(η^3-allyl)][ClO_4] (M = Pd or Pt) and [(dppe)Pt(μ-SC_2H_4S)Pd(η^3-allyl)][ClO_4] [dppe = 1,2-bis(diphenylphosphino)ethane; allyl = C_3H_5 or C_4H_7] have been obtained by reaction of the corresponding *cis*-dithiolato complexes, [M($SR)_2$ (dppe)] or [Pt(SC_2H_4S)(dppe)], and [Pd(η^3-allyl)($PhCN)_2$][ClO_4]. The identity of these complexes has been established by NMR (^{1}H and ^{31}P) spectroscopy. The crystal structure of [(dppe)Pd(μ-SC_6H_4Me-*p*)$_2$Pd(η^3-C_3H_5)][ClO_4] has been determined by single-crystal X-ray methods. The *p*-tolyl groups on the sulfur atoms adopt a *syn* conformation with respect to the central Pd–S_2–Pd core. © 2000 Elsevier Science Ltd. All rights reserved.

Keywords: Palladium; Platinum; Thiolate complexes; Allyl complexes

1. Introduction

The relevance of transition-metal complexes with S-donor ligands as models of biologically redox-active metalloproteins [1] has stimulated interest in the chemistry of metal thiolates [2,3]. Platinum and palladium μ-thiolate complexes are also of recent interest due to their possible use in homogeneous catalysis [4–6]. For example, systems of the type [Pt_2(μ-SR)(μ-$Cl)Cl_2(PR'_3)_2$]/$SnCl_2 \cdot H_2O$ have a high catalytic activity in the hydrogenation of styrene [7].

We have recently described the synthesis of di- and tri-nuclear nickel(II), palladium(II) or platinum(II) complexes with bridging thiolato groups of the types [NBu_4]$_2$[$M_2(C_6F_5)_4$(μ-$SR)_2$], [NBu_4]$_2$[$M_3(C_6F_5)_4$(μ-$SR)_4$] (M = Ni, Pd or Pt) [8,9] and [{Pd($CH_2C_9H_6N$)}$_2$(μ-SR)(μ-O_2CR'')] ($CH_2C_9H_6N$ = 8-quinolylmethyl) [10]. Dinuclear thiolato-bridged allylpalladium complexes have been reported recently [11]. On the other hand, the synthesis and study of heterobinuclear complexes have been the subject of active research over the past years, as they can serve as models for active intermediates in heterobimetallic catalysis [12].

In this paper we report the preparation of a variety of heterodinuclear MM′ (M = Pd, Pt; M′ = Pd) complexes with bridging thiolato ligands by using *cis*-dithiolato complexes [M($SR)_2$ (dppe)] [M = Pd or Pt; dppe = 1,2-bis(diphenylphosphino)ethane] and [Pd(η^3-allyl)($PhCN)_2$]$^+$, which contain the readily removable PhCN ligands, as building blocks.

2. Experimental

The C, H, N, S analyses were performed with a Carlo Erba model EA 1108 microanalyzer. Decomposition temperatures were determined with a Mettler TG-50 thermobalance at a heating rate of 5°C min^{-1} and the solid sample under nitrogen flow (100 ml min^{-1}). Molar conductivities were measured in acetone solution (c Å 5×10^{-4} mol dm^{-3}) with a Crison 525 conducti-

* Corresponding author. Fax: +34-68-36-4148.
E-mail address: gll@fcu.um.es (G. López).

0277-5387/00/$ - see front matter © 2000 Elsevier Science Ltd. All rights reserved.
PII: S0277-5387(00)00440-X

meter. The NMR spectra were recorded on a Bruker AC 200E or Varian Unity 300 spectrometer, using $SiMe_4$ and H_3PO_4 as standards, respectively. Infrared spectra were recorded on a Perkin–Elmer 1430 spectrophotometer using Nujol mulls between polyethylene sheets. Solvents were dried by the usual methods. The starting complexes $[M(SR)_2](dppe)$ (M = Pd or Pt), $[Pt(SC_2H_4S)(dppe)]$ [13] and $[Pd(\eta^3\text{-allyl})(PhCN)_2][ClO_4]$ (allyl = C_3H_5 or C_4H_7) [14] were prepared by procedures described elsewhere.

Safety note. **Caution!** Perchlorate salts of metal complexes with organic ligands are potentially explosive. Only small amounts of these materials should be prepared, and they should be handled with great caution.

2.1. Preparation of complexes *1–11*

To a solution of the corresponding benzonitrile complex $[Pd(\eta^3\text{-allyl})(PhCN)_2][ClO_4]$ (0.3 mmol) in methanol (20 cm^3) was added the corresponding *cis*-dithiolato complex $[M(SR)_2$ (dppe)] or $[Pt(SC_2H_4S)(dppe)]$ (0.3 mmol) with constant stirring at room temperature (r.t.) (2 h for the palladium compounds or 4 h for the platinum complexes) to afford a suspension from which the solvent was partially evaporated under reduced pressure and, after addition of water, filtered-off. The desired yellow complex was air-dried.

Complex **1**: Yield 54%; m.p. 154°C (dec.). *Anal.* Calc. for $C_{41}H_{39}ClO_4P_2Pd_2S_2$: C, 50.8; H, 4.1; S, 6.6. Found: C, 50.8; H, 4.1; S, 6.3%. Λ_M 130 S cm^2 mol^{-1}. ^1H NMR ($CDCl_3$): δ 7.6–7.3 (m, 20H, aromatics dppe), 6.99 (d, 4H, H_o of SPh, $J_{om} = 7.7$ Hz), 6.88 (t, 2H, H_p of SPh, $J_{mp} = 7.7$), 6.69 (pseudo-t, 4H, H_m of SPh), 5.56 (m, 1H, CC*H*C allyl), 3.76 (d, 2H, H_{syn}, $J = 6.9$), 3.25 (d, 2H, H_{anti}, $J = 12.6$), 2.39 (d, 4H, CH_2 dppe, $J_{HP} = 22.5$). ^{31}P NMR ($CDCl_3$) δ 60.8 (s).

Complex **2**: Yield 55%; m.p. 189°C (dec.). *Anal.* Calc. for $C_{43}H_{43}ClO_4P_2Pd_2S_2$: C, 51.7; H, 4.3; S, 6.4. Found: C, 52.0; H, 4.5; S, 6.4%. Λ_M 145 S cm^2 mol^{-1}. ^1H NMR ($CDCl_3$): δ 7.6–7.3 (m, 20H, aromatics dppe), 6.86 (d, 4H, H_o of SC_6H_4Me, $J_{om} = 7.8$ Hz), 6.48 (d, 4H, H_m of SC_6H_4Me, $J_{om} = 7.8$), 5.57 (m, 1H, CC*H*C allyl), 3.76 (d, 2H, H_{syn}, $J = 6.9$), 3.24 (d, 2H, H_{anti}, $J = 12.7$), 2.38 (d, 4H, CH_2 dppe, $J_{HP} = 22.6$), 2.12 (s, 6H, Me). ^{31}P NMR ($CDCl_3$): δ 60.0 (s).

Complex **3**: Yield 56%; m.p. 175°C (dec.). *Anal.* Calc. for $C_{33}H_{39}ClO_4P_2Pd_2S_2$: C, 45.4; H, 4.5; S, 7.3. Found: C, 45.1; H, 4.5; S, 7.3%. Λ_M 150 S cm^2 mol^{-1}. ^1H NMR ($CDCl_3$): δ 8.0–7.4 (m, 20H, aromatics dppe), 5.46 (m, 1H, CC*H*C allyl), 3.93 (d, 2H, H_{syn}, $J = 6.9$ Hz), 3.03 (d, 2H, H_{anti}, $J = 12.4$), 2.59 (d, 4H, CH_2 dppe, $J_{HP} = 23.4$), 2.03 (m, 4H, CH_2S), 0.88 (t, 6H, CH_3 CH_2S, $J = 7.2$). ^{31}P NMR ($CDCl_3$): δ 60.5 (s).

Complex **4**: Yield 59%; m.p. 175°C (dec.). *Anal.* Calc. for $C_{34}H_{41}ClO_4P_2Pd_2S_2$: C, 46.0; H, 4.7; S, 7.2. Found: C, 45.5; H, 4.7; S, 7.1%. Λ_M 148 cm^2 S mol^{-1}. ^1H NMR ($CDCl_3$): δ 7.8–7.4 (m, 20H, aromatics dppe), 3.64 (s, 2H, H_{syn}), 2.87 (s, 2H, H_{anti}), 2.59 (d, 4H, CH_2 dppe, $J_{HP} = 24.0$ Hz), 2.03 (m, 4H, CH_2S), 1.98 (s, 3H, CH_3 allyl), 0.86 (t, 6H, CH_3 CH_2S, $J = 7.2$). ^{31}P NMR ($CDCl_3$): δ 60.7 (s).

Complex **5**: Yield 68%; m.p. 188°C (dec.). *Anal.* Calc. for $C_{41}H_{39}ClO_4P_2PdPtS_2$: C, 46.5; H, 3.7; S, 6.1. Found: C, 46.8; H, 3.8; S, 5.8%. Λ_M 135 S cm^2 mol^{-1}. ^1H NMR ($CDCl_3$): δ 7.7–7.3 (m, 20H, aromatics dppe), 6.96 (d, 4H, H_o of SPh, $J_{om} = 7.3$ Hz), 6.81 (t, 2H, H_p of SPh, $J_{mp} = 7.3$), 6.67 (pseudo-t, 4H, H_m of SPh), 5.52 (m, 1H, CC*H*C allyl), 3.76 (d, 2H, H_{syn}, $J = 6.9$), 3.23 (d, 2H, H_{anti}, $J = 12.6$), 2.25 (d, 4H, CH_2 of dppe, $J_{HP} = 19.8$). ^{31}P NMR ($CDCl_3$): δ 45.6 (s, $J_{PtP} = 3108$ Hz).

Complex **6**: Yield 73%; m.p. 194°C (dec.). *Anal.* Calc. for $C_{43}H_{43}ClO_4P_2PdPtS_2$: C, 47.5; H, 4.0; S, 6.0. Found: C, 47.1; H, 4.0; S, 5.8%. Λ_M 136 S cm^2 mol^{-1}. ^1H NMR ($CDCl_3$): δ 7.7–7.3 (m, 20H, aromatics dppe), 6.88 (d, 4H, H_o of SC_6H_4Me, $J_{om} = 7.8$ Hz), 6.49 (d, 4H, H_m of SC_6H_4Me, $J_{om} = 7.8$), 5.57 (m, 1H, CC*H*C allyl), 3.81 (d, 2H, H_{syn}, $J = 6.9$), 3.26 (d, 2H, H_{anti}, $J = 12.6$), 2.28 (d, 4H, CH_2 dppe, $J_{HP} = 19.1$), 2.14 (s, 6H, Me). ^{31}P NMR ($CDCl_3$): δ 45.2 (s, $J_{PtP} = 3110$ Hz).

Complex **7**: Yield 74%; m.p. 191°C (dec.). *Anal.* Calc. for $C_{33}H_{39}ClO_4P_2PdPtS_2$: C, 41.2; H, 4.1; S, 6.7. Found: C, 41.3; H, 4.0; S, 7.1%. Λ_M 131 S cm^2 mol^{-1}. ^1H NMR ($CDCl_3$): δ 8.0–7.5 (m, 20H, aromatics dppe), 5.47 (m, 1H, CC*H*C allyl), 4.01 (d, 2H, H_{syn}, $J = 6.7$ Hz), 3.05 (d, 2H, H_{anti}, $J = 12.5$), 2.50 (d, 4H, CH_2 dppe, $J_{HP} = 19.7$), 2.17 (m, 4H, CH_2S), 0.89 (t, 6H, CH_3 CH_2S, $J = 6.6$). ^{31}P NMR ($CDCl_3$): δ 46.8 (s, $J_{PtP} = 3055$ Hz).

Complex **8**: Yield 57%; m.p. 168°C (dec.). *Anal.* Calc. for $C_{42}H_{41}ClO_4P_2PdPtS_2$: C, 47.0; H, 3.9; S, 6.0. Found: C, 46.7; H, 3.7; S, 5.8%. Λ_M 133 S cm^2 mol^{-1}. ^1H NMR ($CDCl_3$): δ 7.8–7.2 (m, 20H, aromatics dppe), 6.94 (d, 4H, H_o of SPh, $J_{om} = 7.3$ Hz), 6.83 (t, 2H, H_p of SPh, $J_{mp} = 7.3$), 6.68 (pseudo-t, 4H, H_m of SPh), 3.59 (s, 2H, H_{syn}), 3.12 (s, 2H, H_{anti}), 2.33 (d, 4H, CH_2 dppe, $J_{HP} = 18.9$), 1.96 (s, 3H, CH_3 allyl). ^{31}P NMR ($CDCl_3$): δ 45.9 (s, $J_{PtP} = 3105$ Hz).

Complex **9**: Yield 67%; m.p. 153°C (dec.). *Anal.* Calc. for $C_{34}H_{41}ClO_4P_2PdPtS_2$: C, 41.8; H, 4.2; S, 6.6. Found: C, 41.6; H, 4.2; S, 6.4%. Λ_M 145 S cm^2 mol^{-1}. ^1H NMR ($CDCl_3$): δ 8.0–7.3 (m, 20H, aromatics dppe), 3.71 (s, 2H, H_{syn}), 2.89 (s, 2H, H_{anti}), 2.49 (d, 4H, CH_2 dppe, $J_{HP} = 20.4$ Hz), 2.12 (m, 4H, CH_2S), 1.99 (s, 3H, CH_3 allyl), 0.87 (t, 6H, CH_3 CH_2S, $J = 7.2$). ^{31}P NMR ($CDCl_3$): δ 47.1 (s, $J_{PtP} = 3056$ Hz).

Complex **10**: Yield 46%; m.p. 170°C (dec.). *Anal.* Calc. for $C_{31}H_{33}ClO_4P_2PdPtS_2$: C, 39.9; H, 3.6; S, 6.9. Found: C, 39.3; H, 3.6; S, 6.8%. Λ_M 120 S cm^2 mol^{-1}. ^1H NMR ($CDCl_3$): δ 7.9–7.3 (br m, 20H, aromatics dppe), 5.1 (br, 1H, CC*H*C allyl), 4.08 (br, 2H, H_{syn}),

Table 1
Crystal data and structure refinement for **2**

Empirical formula	$C_{43}H_{43}ClO_4P_2Pd_2S_2$
Formula weight	998.08
Temperature (K)	294(2)
Wavelength (Mo Kα) (Å)	0.71073
Crystal system	triclinic
Space group	$P\bar{1}$ (# 2)
Unit cell dimensions	
a (Å)	10.873(1)
b (Å)	11.698(1)
c (Å)	17.353(2)
α (°)	84.733(9)
β (°)	88.052(8)
γ (°)	77.284(8)
Volume (Å^3)	2143.7(4)
Z	2
Density (calculated) (Mg m^{-3})	1.546
Absorption coefficient (mm^{-1})	1.113
$F(000)$	1008
θ Range for data collection (°)	2.23–30.42
Index ranges	$0 \le h \le 15$, $-16 \le k \le 16$, $-24 \le l \le 24$
Reflections collected	13 602
Independent reflections	12 973 ($R_{int} = 0.0127$)
Refinement method	Full-matrix least-squares on F^2
Data/restraints/parameters	12 973/1/468
Goodness-of-fit on F^2	1.047
Final R indices [$I > 2\sigma(I)$]	$R_1 = 0.0383$, $wR_2 = 0.1184$
R indices (all data)	$R_1 = 0.0580$, $wR_2 = 0.1306$
Largest difference peak and hole (e Å^{-3})	1.543 and −1.058

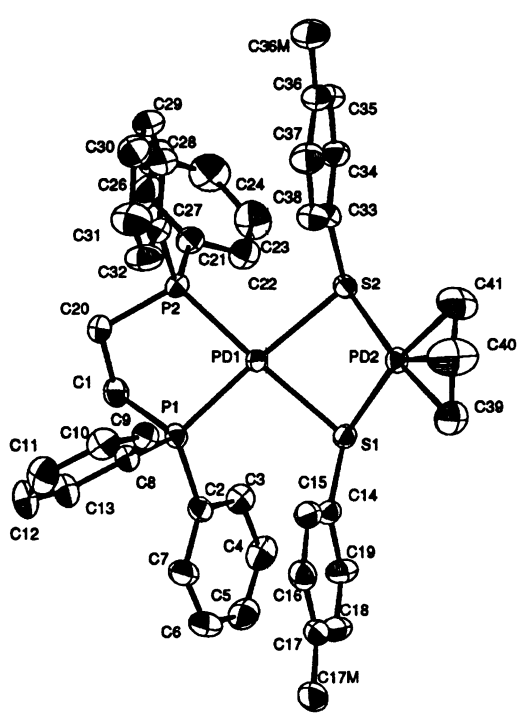
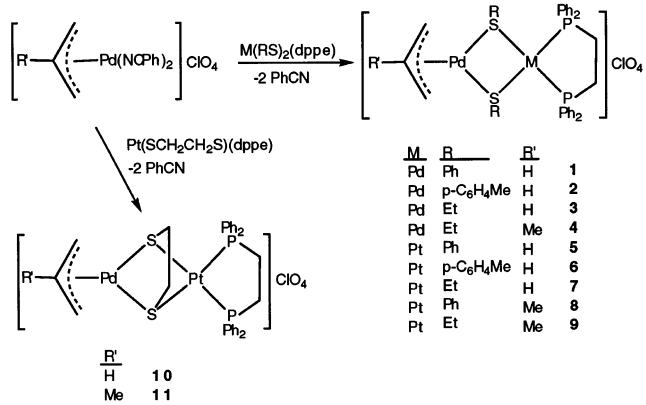


Fig. 1. Perspective view of the molecular structure of **2**.



Scheme 1.

3.0–2.5 (br m, 10H, $H_{anti} + CH_2$ dppe + SCH_2CH_2S). ^{31}P NMR ($CDCl_3$): δ 46.3 (s, $J_{PtP} = 2748$ Hz).

Complex **11**: Yield 45%; m.p. 125°C (dec.). *Anal.* Calc. for $C_{32}H_{35}ClO_4P_2PdPtS_2$: C, 40.6; H, 3.7; S, 6.8. Found: C, 40.3; H, 3.7; S, 6.6%. Λ_M 135 S cm^2 mol^{-1}. ^1H NMR ($CDCl_3$): δ 7.8–7.3 (m, 20H, aromatics dppe), 3.81 (br, 2H, H_{syn}), 3.0–2.5 (br m, 10H, $H_{anti} + CH_2$ dppe + SCH_2CH_2S), 1.80 (br, 3H, CH_3 allyl). ^{31}P NMR ($CDCl_3$): δ 45.2 (s, $J_{PtP} = 3050$ Hz).

2.2. Determination of the X-ray crystal structure of complex **2**

A single crystal of complex **2** (approximate dimensions 0.55 × 0.37 × 0.24 mm) was mounted on an Enraf–Nonius CAD4 diffractometer equipped with a graphite monochromator for Mo Kα radiation. The crystallographic data are shown in Table 1 (Fig. 1). Accurate cell parameters were determined by least-squares fitting of 25 high-angle reflections. The scan method was ω–2Θ and the empirical Psi scan mode absorption correction was applied. The structure was solved by heavy atom methods SHELXS-86 [15] and refined anisotropically on F^2 [16]. Hydrogen atoms were introduced in calculated positions. The residual peaks in the final Fourier difference synthesis were located close to the metal atoms.

3. Results and discussion

The mononuclear palladium and platinum complexes [M(SR)$_2$ (dppe)] (M = Pd or Pt) or [Pt(SC$_2$H$_4$S)(dppe)] [dppe = 1,2-bis(diphenylphosphino)ethane] react with [Pd(η^3-allyl)(PhCN)$_2$][ClO$_4$] (allyl = C$_3$H$_5$ or C$_4$H$_7$) in a 1:1 molar ratio to give heterodinuclear complexes of the types [(dppe)M(μ-SR)$_2$Pd(η^3-allyl)][ClO$_4$] (M = Pd or Pt) (**1**–**9**) and [(dppe)Pt(μ-SC$_2$H$_4$S)Pd(η^3-allyl)][ClO$_4$] (**10** and **11**) with the concomitant release of PhCN (Scheme 1).

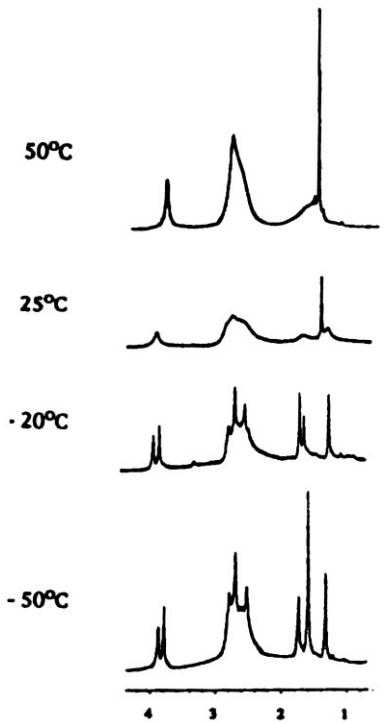


Fig. 2. Variable-temperature ^{1}H NMR spectrum of **11**.

The new complexes **1**–**11** have been characterized on the basis of partial elemental analyses and spectroscopic data and they behave in acetone as 1:1 electrolytes [17], in accordance with the formulas given.

The ^{31}P NMR spectra show a single resonance and those of the platinum complexes are flanked by the satellites due to coupling to ^{195}Pt, the coupling constant being in the range 2700–3100 Hz.

The ^{1}H NMR spectra of complexes **1**–**9** show a single set of resonances, indicating that both thiolate ligands are equivalent and the free rotation of the thiolate aryl or alkyl group around the C–S bond. The ^{1}H NMR spectra of complexes **1**–**3** and **5**–**7** show also three resonances with the expected intensity ratio (1:2:2) and peak multiplicities in the allylic group region (multiplet for CC*H*C, doublet for *syn* protons, and doublet for *anti* protons) whereas the spectra of complexes **4** and **8**–**9** show three singlet resonances for the methylallyl group with the expected intensity ratio of 2:2:3.

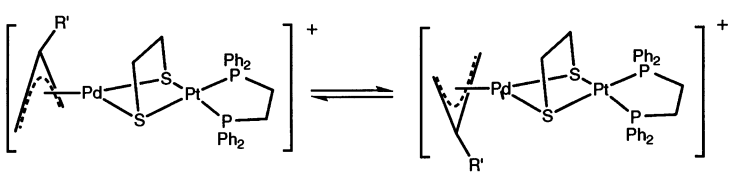
However, the ^{1}H NMR spectra of complexes **10** and **11** show broad bands at room temperature, which suggests a fluxional behavior in the ^{1}H NMR scale of time. Rotation of the η^{3}-allyl group has been suggested as a possible dynamic process [18]. The ^{1}H NMR spectrum of complex **11** at -50°C (Fig. 2) shows two different singlets at δ 3.91 and 3.83 assigned to *syn* protons and two additional singlets at δ 1.86 and 1.80 due to the Me protons of the allyl groups of the two conformational isomers tentatively shown in Scheme 2 (signals due to the *anti* protons are obscured by resonances of dppe and SC_2H_4S ligands).

Table 2
Selected distances (Å) and bond angles (°) for complex **2**

Bond distances		Bond angles	
Pd(1)–P(1)	2.2777(8)	P(1)–Pd(1)–P(2)	85.34(3)
Pd(1)–P(2)	2.2871(8)	P(1)–Pd(1)–S(1)	96.87(3)
Pd(1)–S(1)	2.3742(8)	P(2)–Pd(1)–S(1)	172.13(3)
Pd(1)–S(2)	2.3783(8)	P(1)–Pd(1)–S(2)	172.45(3)
Pd(1)···Pd(2)	3.2428(4)	P(2)–Pd(1)–S(2)	95.85(3)
Pd(2)–C(40)	2.085(5)	S(1)–Pd(1)–S(2)	80.98(3)
Pd(2)–C(39)	2.137(4)	Pd(2)–S(1)–Pd(1)	86.77(3)
Pd(2)–C(41)	2.140(4)	Pd(2)–S(2)–Pd(1)	86.54(3)
Pd(2)–S(1)	2.3465(8)	S(1)–Pd(2)–S(2)	82.10(3)
Pd(2)–S(2)	2.3524(9)	C(40)–Pd(2)–S(1)	140.5(2)
		C(39)–Pd(2)–S(1)	105.58(14)
		C(41)–Pd(2)–S(1)	171.3(2)
		C(40)–Pd(2)–S(2)	137.1(2)
		C(39)–Pd(2)–S(2)	172.24(14)
		C(41)–Pd(2)–S(2)	105.1(2)
		C(41)–C(40)–C(39)	142.4(8)

Suitable crystals of complex **2** were grown from acetone–ethanol. The structure of **2** is shown in Fig. 1 and selected lengths and angles in Table 2. Both metal atoms, Pd(1) and Pd(2), are coordinated in a slightly distorted square-planar geometry and the phenyl groups on the sulfur atoms adopt a *syn* arrangement with respect to the central Pd–S_2–Pd core. The same conformation has been recently found in $[(C_6F_5)_2Ni(\mu\text{-}SPh)_2Pd(dppe)]$ [19], $[\eta^5\text{-}C_5H_4SiMe_3)_2Ti(\mu\text{-}SPh)_2Pd(C_6F_5)_2]$ [20] and $[\eta^5\text{-}C_5H_5)Ti(\mu\text{-}SMe)_2PtMe_2]$ [21].

The Pd(1)–S distances are 2.3742(3) and 2.3783(8) Å, significantly longer than Pd(2)–S distances, 2.3465(8) and 2.3524(9) Å. This is due to the strong *trans* influence of the phosphine ligand [19]. The Pd···Pd distance is 3.2428(4) Å, showing no significant metal–metal interaction. The PdSPdS ring adopts a hinged square-planar geometry with a dihedral angle of 129.9° along



Scheme 2.

the S···S line. As expected, the PdP_2C_2 chelate ring is non-planar. The Pd-η^3-allyl distances are in the range expected for a Pd(II)-allyl.

4. Supplementary material

Supplementary data for complex **2** are available from the CCDC, 12 Union Road, Cambridge CB2 1EZ, UK on request, quoting the deposition number CCDC 139771. Copies of this information may be obtained free of charge from: The Director, CCDC, 12 Union Road, Cambridge, CB2 1EZ, UK (Fax: +44-1223-336-033; e-mail: deposit@ccdc.cam.ac.uk or www: http://www.ccdc.cam.ac.uk).

Acknowledgements

Financial support from the DGICYT (project PB97-1036), Spain, is gratefully acknowledged. V.R. thanks CajaMurcia, Spain, for a research grant.

References

[1] P.P. Power, S.C. Shoner, Angew. Chem., Int. Ed. Engl. 30 (1991) 330.
[2] I.G. Dance, Polyhedron 5 (1986) 1037.
[3] P.G. Blower, J.R. Dilworth, Coord. Chem. Rev. 76 (1987) 121.
[4] E.M. Padilla, C.M. Jensen, Polyhedron 10 (1991) 89.
[5] Y.K. Jim, K. Osakada, K. Sugita, T. Yamamoto, A. Yamamoto, Organometallics 7 (1988) 2182.
[6] V.K. Jain, G.S. Rao, Inorg. Chim. Acta 127 (1987) 161.
[7] H.C. Clark, V.K. Jain, G.S. Rao, J. Organomet. Chem. 279 (1985) 181.
[8] G. Sánchez, F. Ruiz, M.D. Santana, G. García, G. López, J.A. Hermoso, M. Martínez-Ripoll, J. Chem. Soc., Dalton Trans. (1994) 19.
[9] J. Ruiz, C. Vicente, V. Rodríguez, G. López, Polyhedron 17 (1998) 1503.
[10] J. Ruiz, N. Cutillas, J. Torregrosa, G. García, G. López, P.A. Chaloner, P.B. Hitchcock, R.M. Harrison, J. Chem. Soc., Dalton Trans. (1994) 2353.
[11] A. Singhal, V.K. Jain, J. Organomet. Chem. 494 (1995) 75.
[12] J. Fawcett, W. Henderson, R.D.W. Kemmitt, D.R. Rusell, A. Upreti, J. Chem. Soc., Dalton Trans. (1996) 1897.
[13] R.G. Hayter, F.S. Humiec, J. Inorg. Nucl. Chem. 26 (1964) 807.
[14] I.A. Zakharova, Y.L. Gaft, N.T. Kuznetsov, Y.V. Salyn, L.A. Leytes, A.P. Kurbakova, M.M. Kagansky, Inorg. Chim. Acta 47 (1981) 181.
[15] G.M. Sheldrick, Crystallogr. Comp. 5 (1991) 145.
[16] G.M. Sheldrick, SHELXL-93, Program for Crystal Structure Refinement, University of Göttingen, 1993.
[17] W.J. Geary, Coord. Chem. Rev. 7 (1971) 81.
[18] S. Trofimenko, Inorg. Chem. 10 (1971) 1372.
[19] G. Sánchez, F. Momblona, M. Sánchez, J. Pérez, G. López, J. Casabó, E. Molins, C. Miravitlles, Eur. J. Inorg. Chem. (1998) 1199.
[20] U. Amador, E. Delgado, J. Forniés, E. Hernández, E. Lalinde, M.T. Moreno, Inorg. Chem. 34 (1995) 5279.
[21] N. Nakahara, M. Hirano, A. Fukuoka, S. Komiya, J. Organomet. Chem. 572 (1999) 81.

PERGAMON

www.elsevier.nl/locate/poly

Polyhedron 19 (2000) 1633–1637

POLYHEDRON

Cadmium(II) complexes of fully condensed Schiff-base ligands derived from two different symmetrical and asymmetrical tripodal tetraamines and 2-acetylpyridine; the novel observations for heptadentate mono-capped trigonal antiprismatic Schiff-base complexes

Hassan Keypour [a,*], Sadegh Salehzadeh [a], Robin G. Pritchard [b], R.V. Parish [b]

[a] *Department of Chemistry, Bu-Ali Sina University, Hamadan, Iran*
[b] *Department of Chemistry, UMIST, PO Box 88, Manchester, M60 1QD, UK*

Received 20 March 2000; accepted 26 April 2000

Abstract

In the presence of cadmium(II), 2-acetylpyridine condenses with tris(3-aminopropyl)amine, tpt, and bis(3-aminopropyl)(2-aminoethyl)amine, ppe, in absolute methanol to produce two fully condensed potentially heptadentate Schiff-base complexes, $[Cd(py_3tpt)](ClO_4)_2$ and $[Cd(py_3ppe)](ClO_4)_2$. X-ray structure analysis of the former complex shows mono-capped distorted trigonal antiprism geometry wherein the Cd–unique nitrogen distance is 2.486 Å. In comparison with the weighted mean of other Cd–N distances, 2.425 Å, this indicates a 'bonding' interaction. The mean of the bond angles about the bridging amine atom (C–N1–C), 107.43°, is quite close to sp^3 hybridization as expected for an unconstrained tertiary amine nitrogen atom. The ^1H NMR, COSY and HMQC spectra shows six inequivalent protons, two for each methylene group caused by the rigidity of resulting six-membered chelate rings. © 2000 Elsevier Science Ltd. All rights reserved.

Keywords: Cadmium(II) complexes; Schiff-base ligands; Symmetrical complexes; Asymmetrical complexes; Heptadentate ligands

1. Introduction

Schiff-base complexes are considered to be among the most important stereochemical models in main group and transition metal coordination chemistry due to their preparative accessibility and structural variety [1,2]. We have prepared some symmetrical and asymmetrical tripodal tetraamines and their macrocyclic and acyclic Schiff-base complexes of Ni(II) and Cu(II) [3–5]. Other workers and we have reported the synthesis of fully condensed potentially heptadentate Schiff-base complexes [6–8]. N.J. Rose suggested a monocapped trigonal antiprismatic coordination polyhedron for latter complexes [9] and X-ray analysis have shown that these complexes are considerably distorted from trigonal antiprism (TAP), toward trigonal prism (TP). The metal–unique nitrogen distance is much longer than other metal nitrogen distances and there is the intriguing question about the nature of this bond. Some of the important features of these complexes are now described in text books and reviews where particular attention is given to the relationship between the M–N bond distances and the electronic configuration of the metal ion [7,10,11]. We now report usage of one symmetrical and one asymmetrical tetraamine, tris(3-aminopropyl)amine, tpt, and bis(3-aminopropyl)(2-aminoethyl)amine, ppe, to prepare two acyclic potentially heptadentate Schiff-base complexes of Cd(II). We also make a comparison with previous data, in order to study the influence of the nature of the ligand as well as the metal ion on the metal–ligand distances and geometry of this type of complex.

* Corresponding author. Tel.: +98-81-822-3283; fax: +98-81-223-404.

E-mail address: keypour@basu.ac.ir (H. Keypour).

0277-5387/00/$ - see front matter © 2000 Elsevier Science Ltd. All rights reserved.
PII: S0277-5387(00)00444-7

2. Experimental

2-Acetylpyridine was obtained from Aldrich and was used without further purification. The tripodal tetraamine ligands, tpt and ppe, were synthesized according to methods that we have earlier reported [3,5]. IR and NMR spectra were measured on Schimadzu IR-435, Bruker DPX 300 and 400 NMR spectrometer, respectively.

Table 1
Crystal data and structure refinement for complex **1**

Empirical formula	$C_{30}H_{39}CdCl_2N_7O_8$
Formula weight	808.98
Temperature (K)	293(2)
Wavelength (Å)	0.71073
Crystal system	monoclinic
Space group	P_21/a
Unit cell dimensions	
a (Å)	25.017(8)
b (Å)	10.197(3)
c (Å)	13.246(2)
α (°)	90
β (°)	93.97(4)
γ (°)	90
V (Å^3)	3370.7(16)
Z	4
D_{calc} (Mg m^{-3})	1.594
μ (mm^{-1})	0.867
$F(000)$	1656
Crystal size (mm)	$0.25 \times 0.2 \times 0.1$
θ Range for data collection (°)	2.16–25.04
Index ranges	$0 \le h \le 29$, $0 \le k \le 12$, $-15 \le l \le 15$
Reflections collected	5955
Independent reflections	5821
R_{int}	0.0636
Refinement method	full-matrix least-squares on F^2
Data/restrains/parameters	5821/0/436
Goodness-of-fit on F^2	0.974
Final R indices	$R_1 = 0.0879$
$[I > 2\sigma(I)]$	$wR_2 = 0.1853$
R indices (all data)	$R_1 = 0.2328$, $wR_2 = 0.2625$
Largest difference peak and hole (e Å^3)	0.587 and −0.615

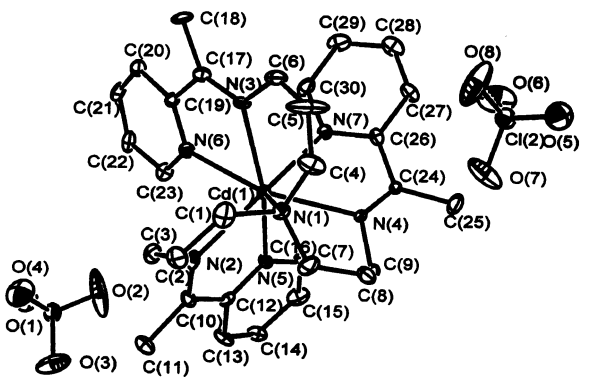


Fig. 1. Crystal structure of compound **1**. Hydrogen atoms are omitted for clarity.

2.1. [Cd(py$_3$tpt)](ClO$_4$)$_2$·H$_2$O (1)

2-Acetylpyridine (0.182 g, 1.5 mmol) was added to a solution of tpt·4HCl (0.177 g, 0.5 mmol) and $Cd(NO_3)_2 \cdot 4H_2O$ (0.111 g, 0.5 mmol) and NaOMe (0.216 g, 4 mmol) in absolute MeOH (150 cm^3). The resulting colorless solution was boiled under reflux and stirred for 36 h, during which time it changed to pink. $NaClO_4$ (0.4 g) was added, the solution was filtered and the filtrate reduced to ca. 10 cm^3. Crystalline compound was obtained by slow diffusion of Et_2O vapor into this solution, yielding 0.2 g (60%) of the complex, $[Cd(py_3tpt)](ClO_4)_2 \cdot H_2O$ (**1**). *Anal.* Found: C, 43.5; H, 4.6; N, 11.3. Calc. for $C_{30}H_{41}N_7Cl_2O_9Cd$: C, 43.56; H, 4.96; N, 11.8%. FAB MS (positive FAB in nitrobenzyl alcohol): m/z 710 [M − ClO_4^+], isotopic pattern corresponds to the proposed formulation. IR (Nujol mull, cm^{-1}): 3500, 3590, 1630, 1589,1566, 1100vs. ^{1}H NMR (CD_3CN, ppm, 300 MHZ, py = pyridine): δ 2.54 (9H, s, 5H), 1.8(3H, m, 2H$_\alpha$), 1.91(3H, m, 2H$_\beta$), 2.32(3H, bt, 1H$_\alpha$), 2.66(3H, bt, 3H$_\alpha$), 2.91(3H, bt, 1H$_\beta$), 3.78 (3H, m, 3H$_\beta$), 7.58(3H, t, py H), 7.9(3H, d, py H), 8.25(6H, m, py H). ^{13}C NMR (CD_3CN, ppm, 300 MHz): δ 14.9(C5), 25.4(C2), 52.2(C1), 57.0(C3), 124.8, 127.7, 140.1, 148.4(C7 to C10), 149.9(C6), 167.1(C4).

2.2. [Cd(py$_3$ppe)](ClO$_4$)$_2$ (2)

This compound was prepared analogously using ppe·4HCl. After the concentration and cooling stages, a yellowish powder was obtained and recrystallized by slow diffusion of Et_2O vapor into a solution in methanol producing white powder. yielding 0.11 g (32%) of the complex, $[Cd(py_3ppe)](ClO_4)_2$. *Anal.* Found: C, 43.5; H, 4.5; N, 12.1. Calc. for $C_{29}H_{37}N_7Cl_2O_8Cd$: C, 43.8; H, 4.7; N, 12.4%. FAB MS (positive FAB in nitrobenzyl alcohol): m/z 696 [M − ClO_4^+], isotopic pattern corresponds to the proposed formulation. IR (Nujol mull, cm^{-1}): 1640, 1589,1566, 1100 vs.

2.3. X-ray crystal structure determination

Suitable crystals of **1** were obtained by slow diffusion of diethyl ether vapor into a methanol solution. Three-dimensional X-ray data were collected at room temperature in the $4.32 < 2\theta < 50.08°$ range on a Rigaku AFC65 diffractometer by the ω–2θ method, using Mo Kα radiation ($\lambda = 0.71073$ Å). The structures was solved by Patterson and Fourier techniques and refined by full-matrix least-squares regression (SHELX97) [12]. Complex scattering factors were taken from [13] and from SHELX97. The parameters of the crystal, data collection, solution and refinement are given in Table 1.

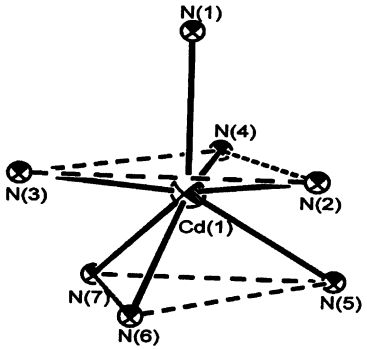


Fig. 2. The nitrogen atoms arrangement around the metal ion in compound **1**.

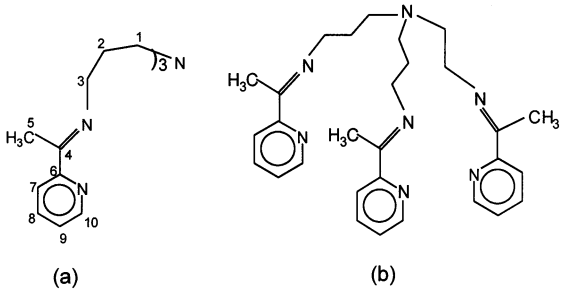


Fig. 3. Two potentially heptadentate ligands; py_3tpt (a) and py_3ppe (b).

3. Results and discussion

The synthesis of both complexes is confirmed by elemental analysis IR and FAB mass spectroscopy. Condensation of all primary amine groups is confirmed by the lack of N–H stretching bands in the IR region 3150–3450 cm^{-1} and the presence of strong C=N (Schiff-base) stretching bands at 1630 and 1640 cm^{-1} for compounds **1** and **2**, respectively. The presence of lattice water for compound **1** was shown by bands at 3500 and 3590 cm^{-1}. Broad intense bands at ca. 1100 cm^{-1} due to ClO_4^- shows no splitting, indicating the absence of coordination of ClO_4^- for both complexes. The structure of compound **1** is also determined by NMR techniques and X-ray crystal structure analysis.

3.1. X-ray crystal structure analysis

X-ray crystal structure analysis of complex **1** shows that the three imine, three pyridine and unique tertiary nitrogen donor atoms arranged at apices of a distorted capped trigonal antiprism (Figs. 1 and 2). Selected bond lengths and bond angles of this complex together with some TAP structural model parameters [7] are given in Table 2. The Cd–N bond lengths are in the

Table 2
Selected bond lengths (Å) and bond angles (°) and some TAP structural parameters for compound **1**

Cd(1)–N(3)	2.339(12)	Cd(1)–N(1)	2.486(11)	N(1)–C(1)	1.48(2)
Cd(1)–N(2)	2.344(14)	Cd(1)–N(7)	2.572(12)	N(2)–C(10)	1.28(2)
Cd(1)–N(4)	2.364(11)	N(1)–C(7)	1.43(2)	N(3)–C(17)	1.275(19)
Cd(1)–N(5)	2.454(11)	N(1)–C(4)	1.45(2)	N(4)–C(24)	1.259(17)
Cd(1)–N(6)	2.470(13)				
N(3)–Cd(1)–N(2)	115.6(5)	N(5)–Cd(1)–N(1)	124.4(4)	C(1)–N(1)–Cd(1)	109.6(10)
N(3)–Cd(1)–N(4)	115.4(4)	N(6)–Cd(1)–N(1)	133.4(5)	C(3)–N(2)–Cd(1)	118.5(13)
N(2)–Cd(1)–N(4)	121.2(4)	N(3)–Cd(1)–N(7)	78.4(4)	C(6)–N(3)–Cd(1)	118.7(11)
N(3)–Cd(1)–N(5)	152.7(4)	N(2)–Cd(1)–N(7)	151.8(5)	C(9)–N(4)–Cd(1)	113.1(10)
N(2)–Cd(1)–N(5)	68.2(5)	N(4)–Cd(1)–N(7)	65.9(4)	N(1)–C(1)–C(2)	121.2(19)
N(4)–Cd(1)–N(5)	79.3(4)	N(5)–Cd(1)–N(7)	88.3(4)	C(3)–C(2)–C(1)	119.7(19)
N(3)–Cd(1)–N(6)	68.0(5)	N(6)–Cd(1)–N(7)	83.7(5)	N(2)–C(3)–C(2)	114.4(17)
N(2)–Cd(1)–N(6)	79.9(4)	N(1)–Cd(1)–N(7)	125.5(5)	C(5)–C(4)–N(1)	121.1(17)
N(4)–Cd(1)–N(6)	146.9(4)	C(7)–N(1)–C(4)	113.4(16)	C(6)–C(5)–C(4)	141(3)
N(5)–Cd(1)–N(6)	87.1(5)	C(7)–N(1)–C(1)	105.3(15)	C(5)–C(6)–N(3)	122.5(17)
N(3)–Cd(1)–N(1)	82.2(4)	C(4)–N(1)–C(1)	103.9(16)	N(1)–C(7)–C(8)	118.1(17)
N(2)–Cd(1)–N(1)	82.0(5)	C(7)–N(1)–Cd(1)	111.1(11)	C(7)–C(8)–C(9)	119.5(19)
N(4)–Cd(1)–N(1)	78.0(5)	C(4)–N(1)–Cd(1)	112.9(10)	N(4)–C(9)–C(8)	110.7(15)

Coordination polyhedron values [a]	$Cd(py_3tpt)^{2+}$ (this work)	$Cd(py_3tren)^{2+}$ [b]	$Zn(py_3tren)^{2+}$ [c]
Twist angle Φ (°)	52	47	45.9
M–N(unique nitrogen) (Å)	2.486	2.778	3.013
M–N_6 (Å)	2.425	2.412	2.180
a	4.01	3.36	3.29
c	3.73	3.29	3.14
a/*c*	1.07	1.02	1.05
b (bite)	2.89	2.79	2.64

[a] For definition of model, see [7].
[b] See [8].
[c] See [7].

normal range, and the Cd(II)–unique nitrogen distance, 2.486 A°, is about the weighted mean of the other Cd–N distances, 2.425 Å, and is even shorter than one of the Cd–N distances (Cd–N7). In other similar complexes of py_3tren with Cd(II) and other metal ions, $[M(py_3tren)]^{2+}$ the metal–unique nitrogen distance is long for an actual bond. In both $[Cd(py_3tpt)]^{2+}$ and $[Cd(py_3tren)]^{2+}$ the Cd–imine bond lengths are shorter than Cd–pyridine bond lengths. As can be seen in Fig. 2 the Cd(II) ion is displaced toward the imine nitrogen triangle and the mean of Cd–imine distances, 2.350 Å, is shorter than that of Cd–py distances, 2.497 Å. The cadmium ion is so near to imine nitrogen plane that the mean of three imine–Cd–imine angles, 117.6°, and three N1–Cd–imine angles, 80.96°, are near to 120 and 90°, respectively. In the cases of py_3tren complexes, the mean of the metal–imine distances is shorter than that of the metal–pyridine distances but there is not such a noticeable displacement toward the imine nitrogen triangle. The mean of the bond angles about the bridging amine atom (C–N1–C), 107.43°, is close to sp^3 hybridization as expected for an unconstrained tertiary amine nitrogen atom, but for $[M(py_3tren)]^{2+}$ complexes this angle varies from 112° in the Mn(II) and Cd(II) complexes up to a maximum value of 120° in the Fe(II) complex.

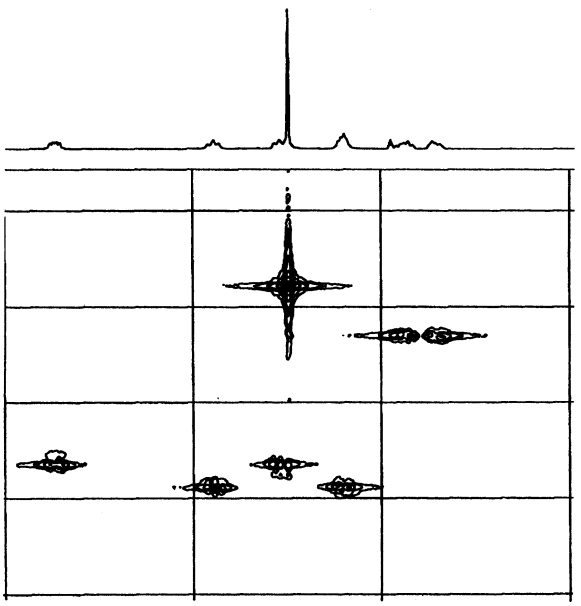


Fig. 4. The HMQC spectrum of compound **1** at the aliphatic region.

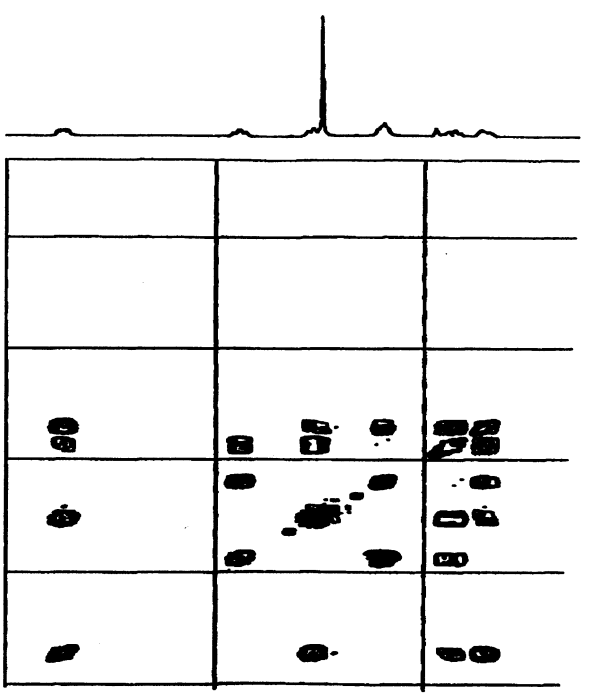


Fig. 5. The COSY spectrum of compound **1** at the aliphatic region.

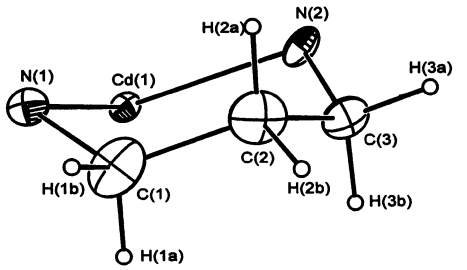


Fig. 6. One of the rigid six-membered chelate rings in compound **1**.

3.2. NMR spectra

Compound **1** was studied with ^1H NMR, ^{13}C NMR, DEPT, COSY and HMQC spectroscopy. While the ^{13}C NMR spectrum shows that there are, as we expect, three distinct methylene carbons but its ^1H NMR, COSY and HMQC spectra shows six kinds of protons two for each methylene groups (Figs. 4 and 5). The COSY spectrum confirms the geminal coupling of two protons of each methylene group. Such geminal coupling of protons will occur in the rigid six-membered rings and we observed this even up to 60° (maximum limit of temperature in actonitrile solution). It seems from COSY spectrum that both protons of C3 (Fig. 3a) have a coupling to protons of C2 but between protons of C1 and C2 the protons with higher chemical shifts couple with each other and there is also similar coupling between protons with smaller chemical shifts. One of these six-membered rings of compound **1** is shown in Fig. 6. The protons H1a, H2a and H3b are axial and protons H1b, H2b and H3a are equatorial. The N1 is a unique tertiary nitrogen atom and N2 is one of the three imine nitrogen atoms. There is no plane of symmetry through any of the carbon atoms, so that the methylene protons are in principle all non-equivalent. This is of course true for all other tren and tpt derivatives but the effects are not seen in their NMR spectra.

The additional factor in the present case is the rigidity of the chelate rings, which is forced by the strong co-ordinating of N(1) and the anchoring effect of the pyridine units.

4. Conclusion

The existence of a 'bonding' interaction between the capping unique nitrogen atom and the cadmium ion in **1** was confirmed by X-ray analysis and NMR investigations. The stronger co-ordination of the unique nitrogen atom to the metal ion in this complex than in the previously prepared $[M(py_3tren)]^{2+}$ complexes is probably due to the great intrinsic flexibility of the tri-methylene chains in $[Cd(py_3tpt)]^{2+}$ complex. The NMR spectrum of this complex shows the three resulting six-membered chelate rings are so rigid that two axial and equatorial protons of each methylene group are non-equivalent.

5. Supplementary data

Crystallographic data for the structural analyses have been deposited with the Cambridge Crystallographic Data Centre, CCDC No. 141926. Copies of this information may be obtained free of charge from The Director, CCDC, 12 Union Road, Cambridge, CB2 1EZ, UK (fax: +44-1223-336-033; e-mail: deposit@ccdc.cam.ac.uk or www: http://www.ccdc.cam.ac.uk).

References

[1] A.D. Garnovskii, A.L. Nivorozhkin, V.I. Minkin, Coord. Chem. Rev. 126 (1993) 1.
[2] V. Alexander, Chem. Rev. 95 (1995) 273.
[3] H. Keypour, D.A. Stotter, Inorg. Chim. Acta 33 (1979) 141.
[4] H. Keypour, R.G. Pritchard, R.V. Parish, Transition Met. Chem. 23 (1998) 609.
[5] H. Keypour, S. Salehzadeh, Transition Met. Chem. 25 (2000) 205.
[6] H. Keypour, S. Salehzadeh, R.G. Pritchard, R.V. Parish, Transition Met. Chem. 23 (1998) 605.
[7] R.M. Kirchner, C. Mealli, M. Bailey, N. Howe, L.P. Torre, L.J. Wilson, L.C. Andrews, N.J. Rose, E.C. Lingafelter, Coord. Chem. Rev. 77 (1987) 89.
[8] A. Jantti, M. Wagner, R. Suontamo, E. Kolehmainen, K. Rissanen, Eur. J. Inorg. Chem. (1998) 1555.
[9] L.J. Wilson, N.J. Rose, J. Am. Chem. Soc. 90 (1968) 6041.
[10] J.E. Huheey, Inorganic Chemistry, third ed., Harper and Row, New York, 1983, p. 389, 507.
[11] J.K. Bardett, Molecular Shapes, Wiley, New York, 1980, pp. 166–167.
[12] G.M. Sheldrick, SHELX93, Computer Program for Crystal Structure Refinement, University of Göttingen (1997).
[13] International Tables for X-ray Crystallography, Kynoch Press, Birmingham, vol. 4 (1994).

PERGAMON

www.elsevier.nl/locate/poly

Polyhedron 19 (2000) 1639–1642

POLYHEDRON

Homoleptic silyl complexes of arsenic and antimony

Claire J. Carmalt [a,*], Jonathan W. Steed [b]

[a] *Department of Chemistry, Christopher Ingold Laboratories, University College London, 20 Gordon Street, London, WC1H 0AJ, UK*
[b] *Department of Chemistry, Kings College London, Strand, London, WC2R 2LS, UK*

Received 18 February 2000; accepted 19 May 2000

Abstract

Several homoleptic silyl complexes of arsenic(III) and antimony(III), namely $As(SiR_2R')_3$ (R = Me, R′ = cyclohexyl (Cy); R = Me, R′ = Ph; R = R′ = Ph) and $Sb(SiPh_3)_3$, have been prepared via salt elimination reactions of $R_2R'SiCl$ and Na_3E (E = As or Sb). The structures of two complexes, $As(SiMe_2Cy)_3$ and $Sb(SiPh_3)_3$, have been determined by X-ray crystallography. Both structures possess a three-coordinate Group 15 element centre with a pyramidal geometry of the ESi_3 core. © 2000 Elsevier Science Ltd. All rights reserved.

Keywords: Homoleptic silyl complexes; Arsenic; Antimony

1. Introduction

There has been a significant amount of interest in the chemistry of silyl complexes of arsenic(III) and antimony(III) over the last few decades. These compounds, in combination with Group 13 species (e.g. halides and alkyls), are excellent starting materials for preparing molecules containing Group 13 element-arsenic or -antimony bonds [1]. Such compounds have attracted a great deal of attention due to their potential applications as single-source precursors for the deposition of thin films of the corresponding semiconductor material by organometallic chemical vapour deposition (OMCVD) [1,2]. Silylarsines have also been used for the preparation of inter-Group 15 element phases [3].

Tris(silyl)arsenic and antimony complexes were first synthesised about 30 years ago [4–10], with further developments occurring some years later [11–15]. Although there have been studies into the synthesis and reactivity of silyl Group 15 complexes [4], structural characterisation of these compounds have emerged only very slowly. Until recently, single crystal X-ray diffraction studies of silyl complexes of As and Sb were limited to $E_2(SiMe_3)_4$ (E = As or Sb) [16,17] and the lithium–arsenide and antimonide salts, $[Li(L)_n][E(SiMe_3)_2]$ (where $n = 1$, E = As or Sb, L = DME; $n = 2$, E = As, L = thf) and $[Li(thf)_2][As(SiPr^i_3)(SiFAr_2)]$ (Ar = 2,4,6-triisopropylphenyl) [18–20]. The only examples of structures of tris(silyl)arsenic and antimony complexes include $As(SiMe_2Bu^t)_3$ (**1**) [21], $As(SiMe_3)_2(SiPh_3)$ (**2**) [21], and $Sb(SiMe_2Ph)_3$ (**3**) [22].

In this contribution, we present the synthesis and characterisation of a series of tris(silyl) complexes of arsenic(III) and antimony(III). Our motivation was to explore further the structural characteristics of these complexes and to isolate a range of stable silyl complexes.

2. Results and discussion

The reaction between Na_3As (generated in situ from arsenic powder and sodium metal in thf) and chlorodimethylcyclohexylsilane in thf at reflux temperature afforded, after work-up, colourless crystals of the complex $As(SiMe_2Cy)_3$ (**4**) (Cy = cyclohexyl), according to Eq. (1):

$$Na_3E + 3R_2R'SiCl \rightarrow E(SiR_2R')_3 + 3NaCl \quad (1)$$

4; E = As, R = Me, R′ = Cy
5; E = As, R = Me, R′ = Ph

* Corresponding author. Tel.: +44-20-7679-7528; fax: +44-20-7679-7463.
E-mail address: c.j.carmalt@ucl.ac.uk (C.J. Carmalt).

0277-5387/00/$ - see front matter © 2000 Elsevier Science Ltd. All rights reserved.
PII: S0277-5387(00)00446-0

6; E = As, R = Ph, R′ = Ph
7; E = Sb, R = Ph, R′ = Ph

Similar methods for the preparation of other tris(silyl)arsenic complexes have been described previously [14,15]. Spectroscopic and analytical data were consistent with the anticipated formula of **4** and the structure was confirmed by X-ray crystallography, the results of which are shown in Fig. 1. Selected bond lengths and angles are given in Table 1. The solid state structure of **4** consists of individual molecules with no unusually short intermolecular contacts between the monomeric units. Although not required crystallographically, individual molecules of **4** possess approximate C_3 symmetry. The geometry about the arsenic centre is pyramidal [av. Si–As–Si 101.6(3)°] with the average As–Si bond length of 2.361(7) Å being similar to those observed in **1** and **2** [21]. The relative orientation of the three dimethylcyclohexylsilyl groups at the arsenic centre is all-staggered with each cyclohexyl group placed between two methyl groups of a neighbouring silyl group. As such, the structure is similar to that observed for **1** [21] and the related antimony complex $Sb(SiMe_2Ph)_3$ (**3**) [22].

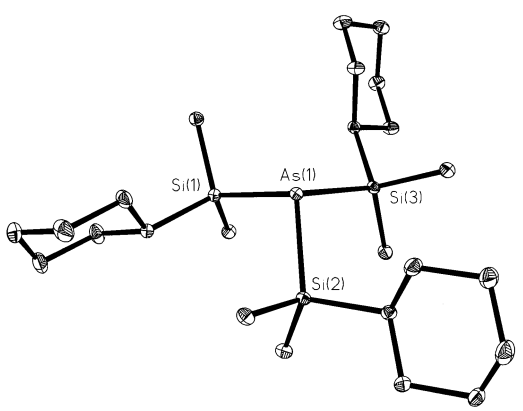


Fig. 1. Molecular structure of compound **4** showing the atom numbering scheme. Atoms are drawn as 30% probability ellipsoids. Hydrogen atoms are omitted for clarity.

Table 1
Selected bond distances (Å) and angles (°) for **4** and **7**

$As(SiMe_2Cy)_3$ (**4**)		$Sb(SiPh_3)_3$ (**7**)	
Bond lengths			
As(1)–Si(1)	2.3567(8)	Sb(1)–Si(1)	2.5977(12)
As(1)–Si(2)	2.3609(7)	Sb(1)–Si(2)	2.5992(12)
As(2)–Si(3)	2.3664(7)	Sb(1)–Si(3)	2.6037(12)
Bond angles			
Si(1)–As(1)–Si(2)	102.22(3)	Si(1)–Sb(1)–Si(2)	103.33(4)
Si(1)–As(1)–Si(3)	100.94(3)	Si(1)–Sb(1)–Si(3)	110.09(4)
Si(2)–As(1)–S(3)	101.74(3)	Si(2)–Sb(1)–S(3)	106.48(4)

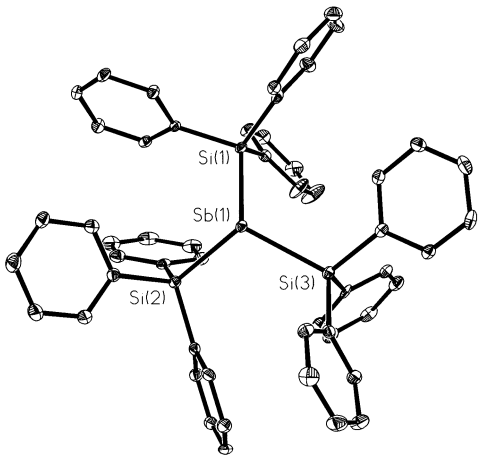


Fig. 2. Molecular structure of compound **7** showing the atom numbering scheme. Atoms are drawn as 30% probability ellipsoids. Hydrogen atoms are omitted for clarity.

A similar reaction between Na_3As and chlorodimethylphenylsilane in thf at reflux temperature afforded, after work-up, colourless crystals of the complex $As(SiMe_2Ph)_3$ (**5**) (Eq. (1)). Spectroscopic and analytical data for **5** were consistent with the expected formula. Unfortunately, an attempted crystal structure determination was only partially successful due to disorder problems. However, the structure of **5** is apparently similar to that of compound **1** [21], **4** and the related antimony derivative **3** [22].

The analogous reaction between Na_3As and chlorotriphenylsilane in thf at reflux temperature (Eq. (1)) resulted in a cream crystalline solid, spectroscopic and analytical data for which were consistent with the formula $As(SiPh_3)_3$ **6**. Unfortunately X-ray quality crystals of **6** could not be isolated. Interestingly, previous attempts to prepare **6** and the antimony analogue, $Sb(SiPh_3)_3$ (**7**), via the reaction between 3 equivalents of triphenylsilyllithium and the appropriate element(III) chloride were reported to be unsuccessful [23]. However, compound **7** has reportedly been prepared from the reaction of $SbEt_3$ and 3 equivalents of triphenylsilane, although **7** was poorly characterised [9]. A related reaction between $Sb(SiEt_3)_3$ and 3 equivalents of triphenylsilane was also reported to result in the formation of **7**; no characterisation of this material was published [7]. However, compound **7** can be prepared in a similar manner to the arsine complexes **4**–**6** as described in Section 3. Spectroscopic and analytical data for **7** were consistent with the expected formula and the structure was confirmed by X-ray crystallography, the results of which are shown in Fig. 2. Selected bond distances and angles are given in Table 1. The solid state structure of **7** consists of individual molecules with no unusually short intermolecular contacts between the monomeric units. Although not required crystallographically, individual molecules of **7** possess approxi-

mate C_3 symmetry. The geometry about the antimony centre is pyramidal [av. Si–Sb–Si 106.60(4)°] with the average Sb–Si bond length of 2.600(12) Å being slightly longer than that observed in **3** [av. Sb–Si 2.559 Å] [22]. The greater deviation from ideal tetrahedral coordination geometry and the longer Sb–Si bond lengths observed in **7** are probably a result of the increased steric requirements of the Ph_3Si ligand. A similar effect was noted on comparison of the As–Si bond distances and Si–As–Si angles in compounds **1** and **2** [21].

In conclusion, several homoleptic silyl arsenic(III) and antimony(III) compounds have been synthesised and characterised. Two of the compounds, $As(SiMe_2Cy)_3$ and $Sb(SiPh_3)_3$ were structurally characterised. Complexes **4**–**7** are possible precursors for the preparation of arsenides and antimonides and the reactivity of these complexes is currently being investigated.

3. Experimental

3.1. General procedures

All manipulations were performed under a dry, oxygen-free dinitrogen atmosphere using standard Schlenk techniques or in a MBraun Unilab glove box. All solvents were distilled from appropriate drying agents prior to use (sodium–toluene and hexanes; potassium–THF; CaH_2 for CH_2Cl_2). All other reagents were procured commercially from Aldrich and used without further purification. Microanalytical data were obtained at University College London.

3.2. Physical measurements

NMR spectra were recorded on Brüker AMX300 or DRX500 spectrometers at UCL. The NMR spectra are referenced to CD_2Cl_2 or $CDCl_3$, which were degassed and dried over molecular sieves prior to use; ^1H and ^{13}C chemical shifts are reported relative to $SiMe_4$ (0.00 ppm). Mass spectra (CI) were run on a micromass ZABSE instrument, and IR spectra on a Nicolet 205 instrument. Melting points were obtained in sealed glass capillaries under argon and are uncorrected.

3.3. Preparations

All of the compounds were synthesised by the same general procedures, hence only one example is described in detail below.

3.3.1. Synthesis of compound *4*

A mirror of sodium metal is generated on the inner surface of a Schlenk flask by heating and stirring sodium (1.00 g, 43.5 mmol). After cooling to room temperature (r.t.) arsenic powder (1.09 g, 14.5 mmol) and a few crystals of naphthalene were added. THF (40 ml) was added and the resulting black slurry was heated at reflux for 24 h. After cooling to r.t. chlorodimethylcyclohexylsilane (8 ml, 43.2 mmol) was added dropwise with stirring and the reaction mixture was refluxed for a further 12 h. The resulting black slurry was cooled to r.t. and pumped to dryness in vacuo. Toluene (40 ml) was added to the remaining black–grey solid and the mixture was filtered through Celite. The volume of the filtrate was reduced to ca. 15 ml and cooling of this solution to −20°C afforded a 67% yield of colourless crystalline **4**. M.p. 80–82°C. ^1H NMR ($CDCl_3$): δ 0.29 (s, 18H, $SiMe_2$), 0.72–1.83 (m, 33H, SiCy). $^{13}C\{^1H\}$ NMR ($CDCl_3$): δ 0.01 ($SiMe_2$), 26.8, 27.7, 28.1, 28.4 (SiCy). CIMS: m/z 499 [M^+], 359 [$M^+ - SiMe_2Cy$]. *Anal.* Calc. for $C_{24}H_{51}AsSi_3$: C, 57.79; H, 10.30. Found: C, 57.48; H, 10.44%.

3.3.2. Compound *5*

Yield: 52% of colourless crystalline **5**. M.p. 122–124°C. ^1H NMR (CD_2Cl_2): δ 0.35 (s, 18H, $SiMe_2$), 7.25–7.55 (m, 15H, SiPh). $^{13}C\{^1H\}$ NMR ($CDCl_3$): δ 1.7 ($SiMe_2$), 127.5 (*m*-C of SiPh), 128.8 (*p*-C of SiPh), 133.7 (*o*-C of $SiPh_3$), *ipso* carbon not detected. CIMS: m/z 481 [M^+]. *Anal.* Calc. for $C_{24}H_{33}AsSi_3 \cdot 0.5CH_2Cl_2$: C, 56.25; H, 6.55. Found: C, 56.25; H, 6.54%.

3.3.3. Compound *6*

Yield: 65% of pale yellow crystalline **6**. M.p. 180°C (dec.). ^1H NMR ($CDCl_3$): δ 6.98–7.30 (m, 45H, $SiPh_3$). $^{13}C\{^1H\}$ NMR ($CDCl_3$): δ 127.2 (*m*-C of $SiPh_3$), 128.8 (*p*-C of $SiPh_3$), 136.2 (*o*-C of $SiPh_3$), *ipso* carbon not detected. CIMS: m/z 853 [M^+], 595 [$M^+ - SiPh_3$]. *Anal.* Calc. for $C_{54}H_{45}AsSi_3$: C, 76.03; H, 5.32. Found: C, 75.98; H, 5.45%.

3.3.4. Compound *7*

Yield: 58% of colourless crystalline **7**. M.p. 127°C (dec.). ^1H NMR (CD_2Cl_2): δ 6.87–7.54 (m, 45H, $SiPh_3$). $^{13}C\{^1H\}$ NMR ($CDCl_3$): δ 126.2 (*m*-C of $SiPh_3$), 128.2 (*p*-C of $SiPh_3$), 135.5 (*o*-C of $SiPh_3$), *ipso* carbon not detected. CIMS: m/z 901 [M^+]. *Anal.* Calc. for $C_{54}H_{45}SbSi_3$: C, 72.07; H, 5.04. Found: C, 72.61; H, 5.08%.

3.4. Structure determinations

Crystals of **4** and **7** were mounted on a glass fibre using silicones grease and cooled on the diffractometer. Crystallographic measurements were carried out with a Nonius Kappa CCD diffractometer equipped with graphite-monochromated Mo Kα radiation using a combination of ϕ and ω scans with 2° frames and a detector-to-crystal distance of 30 mm. Integration was carried out by the program DENZO-SMN [24]. Data sets were corrected for Lorentz and polarisation effects and for the effects of absorption using the program SCALEPACK [24]. The structure was solved using the

Table 2
Crystallographic data for **4** and **7**

	4	**7**
Empirical formula	$C_{24}H_{51}AsSi_3$	$C_{58}H_{50}ClSbSi_3$
Crystal system	triclinic	monoclinic
Space group	$P\bar{1}$	$P2_1/n$
a (Å)	6.3863(3)	13.3164(6)
b (Å)	14.2940(6)	21.6196(7)
c (Å)	16.1607(8)	17.6477(8)
α (°)	72.897(3)	90
β (°)	89.005(3)	109.198(3)
γ (°)	88.017(3)	90
V (Å^3)	1409.12(11)	4798.1(3)
D_{calc} (g cm^{-3})	1.176	1.368
Z	2	4
T (K)	100(2)	100(2)
λ (Å)	0.71073	0.71073
Reflections collected	10474	23285
No. unique reflections	6451	9011
Crystal size (mm)	$0.80 \times 0.15 \times 0.10$	$0.40 \times 0.10 \times 0.10$
θ Range (°)	2.64–27.50	2.48–26.00
R [a] ($I>2\sigma(I)$)	0.0429	0.0519
wR' [b] ($I>2\sigma(I)$)	0.0837	0.1008

[a] $R = \Sigma(\Delta F)/\Sigma(F_o)$.

[b] $wR' = [\Sigma\{w(\Delta F^2)^2\}/\Sigma\{w(F_o^2)^2\}]^{1/2}$. $w = 1/[\sigma^2(F_o^2)+(aP)^2]$ where $P = [\max(F_o^2)+2(F_c^2)]/3$ and $a = 0.0003$.

direct methods option of SHELXS-97 [25] and developed using conventional alternating cycles of least-squares refinement and difference Fourier synthesis (SHELXL-97) [25] with the aid of XSeed [26]. All non-hydrogen atoms were refined anisotropically, while hydrogen atoms were fixed in idealised positions and allowed to ride. Hydrogen atom thermal parameters were tied to those of the atom to which they were attached. All calculations were carried out on a Silicon Graphics Indy workstation or an IBM-PC compatible personal computer. Crystal data and details of the data collections and refinements are given in Table 2.

4. Supplementary material

Crystallographic data have been deposited with the CCDC and are available on request from: The Director, CCDC, 12 Union Road, Cambridge, CB2 1EZ, UK (fax: +44-1223-336033; e-mail: deposit@ccdc.cam.ac.uk or www: http://www.ccdc.cam.ac.uk) by quoting the deposition numbers 140720 and 140721.

Acknowledgements

C.J.C. is grateful to the Royal Society for a Dorothy Hodgkin fellowship and financial support. We thank Kings College London and EPSRC for provision of the diffractometer system. Dr D. Tocher is thanked for his assistance with X-ray crystallography.

References

[1] See for example the following and references therein: (a) E.E. Foos, R.J. Jouet, R.L. Wells, A.L. Rheingold, L.M. Liable-Sands, J. Organomet. Chem. 582 (1999) 45. (b) J.F. Janik, R.L. Wells, P.S. White, Inorg. Chem. 37 (1998) 3561. (c) E.E. Foos, R.L. Wells, A.L. Rheingold, G.P.A. Yap, L.M. Liable-Sands, P.S. White, Organometallics 17 (1998) 2361. (e) R.L. Wells, E.E. Foos, P.S. White, A.L. Rheingold, L.M. Liable-Sands, Organometallics 16 (1997) 4771 (f) R.L. Wells, Coord. Chem. Rev. 112 (1992) 273.
[2] See for example: (a) E.E. Foos, R.L. Wells, A.L. Rheingold, J. Cluster Sci. 10 (1999) 121. (b) J.F. Janik, R.L. Wells, V.G. Young, A.L. Rheingold, I.A. Guzei, J. Am. Chem. Soc. 120 (1998) 532 (c) S.R. Aubuchon, M.S. Lube, R.L. Wells, Chem. Vap. Depos. 1 (1995) 28 (d) R.L. Wells, S.R. Aubuchon, S.S. Kher, M.S. Lube, P.S. White, Chem. Mater. 7 (1995) 793.
[3] G.C. Allen, C.J. Carmalt, A.H. Cowley, A.L. Hector, S. Kamepalli, Y.G. Lawson, N.C. Norman, I.P. Parkin, L.K. Pickard, Chem. Mater. 9 (1997) 1385.
[4] For reviews on organosilicon arsenic and antimony complexes see: (a) D.A. Armitage, in: E.W. Abel, F.G.A. Stone, G. Wilkinson (Eds.), Comprehensive Organometallic Chemistry, vol. II, Elsevier, Oxford, 1995, pp. 27–31. (b) E.W. Abel, S.M. Illingworth, Organomet. Chem. Rev. (A) 5 (1970) 143. (c) S.N. Borisov, M.G. Voronkov, E.Ya. Lukevits, Organosilicon Heteroploymers and Heterocompounds, Plenum, New York, 1990, pp. 455–486 (Chapter 5).
[5] E. Amberger, H.D. Boeters, Chem. Ber. 97 (1964) 1999.
[6] E. Amberger, R.W. Salazar, J. Organomet. Chem. 8 (1967) 111.
[7] N.S. Vyazankin, G.A. Razuvaev, O.A. Kruglaya, G.S. Semchikova, J. Organomet. Chem. 6 (1966) 474.
[8] N.S. Vyazankin, O.A. Kruglaya, G.A. Razuvaev, G.S. Semchikova, Dokl. Akad. Nauk. SSSR 166 (1966) 99.
[9] N.S. Vyazankin, G.S. Kalinina, O.A. Kruglaya, G.A. Razuvaev, Zhur. Obshchei Khim. 38 (1968) 205 [J. Gen. Chem. USSR 38 (1968) 211].
[10] H. Bürger, U. Goetze, J. Organomet. Chem. 12 (1968) 451.
[11] H.J. Breunig, Z. Naturforsch., Teil B 33 (1978) 244, 990.
[12] H.J. Breunig, V. Breunig-Lyriti, Z. Naturforsch., Teil B 34 (1979) 926.
[13] H.J. Breunig, W. Fichtner, J. Organomet. Chem. 222 (1981) 97.
[14] G. Becker, G. Gutekunst, H.J. Wessely, Z. Anorg. Allg. Chem. 462 (1980) 113.
[15] R.L. Wells, M.F. Self, J.D. Johansen, J.A. Laske, S.A. Aubuchon, L.J. Jones III, Inorg. Synth. 31 (1996) 150.
[16] (a) G. Becker, G. Gutekunst, C. Witthauer, Z. Anorg. Allg. Chem. 486 (1982) 90. (b) See also: G. Becker, H. Freudenblum, C. Witthauer, Z. Anorg. Allg. Chem. 492 (1982) 37.
[17] (a) G. Becker, M. Meiser, O. Mundt, J. Weidlein, Z. Anorg. Allg. Chem. 569 (1989) 62. (b) S. Roller, M. Dräger, H.J. Breunig, M. Ates, S. Guelec, J. Organomet. Chem. 378 (1989) 327.
[18] (a) G. Becker, C. Witthauer, Z. Anorg. Allg. Chem. 492 (1982) 28. (b) See also: L.J. Jones, A.T. McPhail, R.L. Wells, J. Coord. Chem. 34 (1995) 119.
[19] G. Becker, A. Münch, C. Witthauer, Z. Anorg. Allg. Chem. 492 (1982) 15.
[20] M. Driess, H. Pritzkow, Angew. Chem., Int. Ed. Engl. 31 (1992) 316.
[21] R.A. Baldwin, H. Rahbarnoohi, L.J. Jones III, A.T. McPhail, R.L. Wells, Heteroatom Chem. 7 (1996) 409.
[22] A. Sladek, H. Schmidbaur, Chem. Ber. 128 (1995) 565.
[23] M.V. George, B.J. Gaj, H. Gilman, J. Org. Chem. 24 (1959) 624.
[24] Z. Otwinowski, W. Minor, in: C.W. Carter, R.M. Sweet (Eds.), Methods in Enzymology, Academic, New York, 1996.
[25] G.M. Sheldrick, SHELX-97, University of Göttingen, Germany, 1997.
[26] L.J. Barbour, XSEED—A Graphical Interface for the Solution and Refinement of X-ray Crystal Structures, University of Missouri, Columbia, SC, 1999.

PERGAMON

www.elsevier.nl/locate/poly

Polyhedron 19 (2000) 1643–1648

POLYHEDRON

Magnetic and spectral properties of two five-coordinate Lewis-base adducts of cobalt(II) Schiff-base complexes with a N_3O_2 ligand environment

Floriana Tuna [a], Luminita Patron* [a,1], Eric Rivière [b], Marie-Laure Boillot* [b,2]

[a] *Coordination Chemistry Laboratory, Institute of Physical Chemistry, Splaiul Independentei nr. 202, 77208 Bucharest, Romania*
[b] *Laboratoire de Chimie Inorganique, Université de Paris-Sud, UMR 8613, Bâtiment 420, F-91405 Orsay, France*

Received 21 March 2000; accepted 30 May 2000

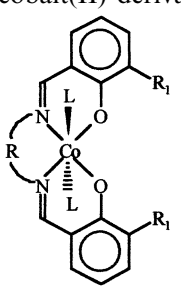
Abstract

Two new five-coordinate Lewis-base adducts of cobalt(II) N_2O_2 Schiff-base complexes, [Co(Salpad)$_2$(*t*-MeStpy)] and [Co(H$_2$(fsa)$_2$phn)(*t*-MeStpy)]·0.5H$_2$O (where H(Salpad) = 2-[*N*-(4-phenylaminophenyl)formimidoyl]phenol, H$_4$(fsa)$_2$phn = *N*,*N*′-*o*-phenylenebis(3-carboxysalicylaldimine), and *t*-MeStpy = *trans*-1-(4-methylphenyl)-2-(4-pyridyl)ethene), have been synthesized in order to investigate the influence of the in-plane donor atom topology on the spin-state of the cobalt(II) ion. The compounds have been characterized by analytical and spectroscopic methods. The spin-state behavior of cobalt(II) was investigated by variable-temperature magnetic susceptibility measurements over the temperature range 10–380 K. For [Co(Salpad)$_2$(*t*-MeStpy)] the magnetic data indicate a spin-quartet ground state which can be described using an axial spin Hamiltonian ($D = 16.57$ cm^{-1}, $g = 2.39$ for CoN_2O_2N') with additional temperature-independent paramagnetism ($N\alpha = 360 \times 10^{-6}$ cm^3 mol^{-1}). The compound [Co(H$_2$(fsa)$_2$phn)(*t*-MeStpy)]·0.5H$_2$O undergoes a thermally-induced $S = 1/2 \leftrightarrow S = 3/2$ spin equilibrium at high temperatures. The magnetic properties of the four-coordinate [Co(Salpad)$_2$] precursor are also reported here. © 2000 Elsevier Science Ltd. All rights reserved.

Keywords: Schiff bases; Cobalt complexes; Spin crossover; Photosensitive ligands; LD-LISC effect

1. Introduction

There is much current interest in five- and six-coordinate transition-metal Schiff-base complexes because these species can display a variety of structural and magnetic properties [1]. Depending on the chemical environment, the metal ion can exist in different spin states. When the high-spin (HS) and low-spin (LS) states of a d^4–d^7 transition metal ion are in close energy proximity, it may also undergo a HS↔LS conversion under the effect of an external perturbation (temperature, pressure). Then the magnetic behavior depends on small inductive, geometrical and sterical effects. In comparison to the vast number of papers dealing with iron(II) [2–6] and iron(III) [7,8] spin-crossover complexes, there are relatively few studies dealing with cobalt(II) complexes [9–12]. In these compounds, the cobalt(II) ion can display a $S = 3/2 \leftrightarrow S = 1/2$ spin crossover. In a few cases it lies in an oxygen–nitrogen closest environment, as in five- or six-coordinated Lewis-base adducts of cobalt(II) chelates derived from the phenolic anions of the *N*,*N*′-bridged Schiff-bases of salicylaldehyde [10,11] (see **I**) or 3-formylsalicylic acid [9] (see **II**). The family of compounds Co(H$_2$(fsa)$_2$R)L$_x$ ($x = 1$ or 2, L = H$_2$O or pyridines; see **II**) is particularly attractive because it displays not only various structural and magnetic properties, but it also exhibits the most abrupt thermally-induced spin transitions ever observed for cobalt(II) derivatives [13–16].



Ia: R_1 = H; R = $(CH_2)_2$
Ib: R_1 = H; R = C_6H_4
IIa: R_1 = COOH; R = $(CH_2)_2$
IIb: R_1 = COOH; R = C_6H_4

[1] *Corresponding author. Tel.: +40-1-650-7615; fax: +40-1-312-1147; e-mail: ftuna@pcnet.pcnet.ro
[2] *Corresponding author. E-mail: mboillot@icmo.u-psud.fr

0277-5387/00/$ - see front matter © 2000 Elsevier Science Ltd. All rights reserved.
PII: S0277-5387(00)00450-2

For most spin-crossover metal complexes, the transition was triggered by varying temperature or pressure. It is now possible to observe the switching of spin states of some transition metal complexes with an optical excitation according to the so-called ligand-driven light-induced spin change (LD-LISC) effect [4]. It consists in the *trans*/*cis* photoisomerization of the ligands and the subsequent change of the ligand-field strength and the spin state of the metal center. A spin conversion triggered by the ligand isomerization has been evidenced for the first time in iron(II) complexes [4–6] and recently in an iron(III) complex [7]. From the basic concept of LD-LISC, it is expected that the spin change can also be observed in d^7 transition-metal complexes, which contains one or two photosensitive ligands in the molecule. For this purpose, we have prepared Co(II) complexes containing a 4-styrylpyridine derivative as a photoisomerizable ligand in an axial position and polydentate Schiff-base ligands.

In this paper, we report the synthesis and magnetic properties of a new five-coordinate species from the family of compounds $[Co(H_2(fsa)_2phn)L_x]$ (see **IIb**), namely $[Co(H_2(fsa)_2phn)(t\text{-MeStpy})]\cdot 0.5H_2O$ (**3**), where $H_2(fsa)_2phn^{2-}$ denotes the phenolic dianion of the Schiff-base *N*,*N*′-*o*-phenylenebis(3-carboxysalicylaldimine) and *t*-MeStpy is *trans*-1-(4-methyl-phenyl)-2-(4-pyridyl)ethene. In this compound, the cobalt(II) ion undergoes a gradual high-spin (HS)↔low-spin (LS) interconversion, in the range of high temperatures, that can be described in terms of spin equilibrium.

We also focus on another five-coordinate cobalt(II) complex, $[Co(Salpad)_2(t\text{-MeStpy})]$ (**2**), which is derived from the bidentate Schiff-base 2-[*N*-(4-phenylaminophenyl)formimidoyl]phenol, H(Salpad). We report here the magnetic and spectral properties of the five-coordinate adduct, as well as those of the four-coordinate cobalt(II) parent complex, $[Co(Salpad)_2]$ (**1**).

2. Experimental

2.1. Solvents and reagents

All the reagents and solvents were purchased from commercial sources (Aldrich) and used as received. The photosensitive ligand, *trans*-1-(4-methylphenyl)-2-(4-pyridyl)ethene (or *t*-MeStpy) was prepared as reported in Ref. [5]. The Schiff-base, 2-[*N*-(4-phenylaminophenyl)formimidoyl]phenol, H(Salpad), and its metal chelate, $[Co(Salpad)_2]$ (**1**), were obtained according to the procedures described previously [17]. The Schiff base, *N*,*N*′-*o*-phenylenebis(3-carboxysalicylaldimine), $H_4(fsa)_2phn$, was prepared according to the literature [15]. Part of the experiments were carried out under an atmosphere of dried argon and in the dark in order to prevent both metal ion oxidation and ligand photoisomerization.

2.2. Preparation of $[Co(Salpad)_2(t\text{-MeStpy})]$ (2)

To a suspension of **1** (0.5 mmol, 316 mg) in 15 ml of toluene was added with stirring an methanolic solution (10 ml) containing 3 mmol of *t*-MeStpy (585 mg). The mixture was then heated at 60°C for 5 h. The resulting brown precipitate was collected, washed with ether, and dried under vacuum. Yield 273 mg ($\sim$66%). *Anal.* Calc. for $C_{52}H_{43}CoN_5O_2$ ($F_w = 828.88$): C, 75.35; H, 5.23; Co, 7.11; N, 8.45. Found: C, 76.58; H, 5.28; Co, 7.42; N, 8.27%.

2.3. Preparation of $[Co(H_2(fsa)_2phn)(t\text{-MeStpy})]\cdot 0.5H_2O$ (3)

The synthesis of **3** implies, as a first step, the preparation of $[Co(H_2(fsa)_2phn)(H_2O)_2]$ according to the procedure described previously by Zarembowitch et al. [16]. Both water molecules of $[Co(H_2(fsa)_2phn)(H_2O)_2]$ are removed by heating the solid phase at $\sim$65°C for 3 h, and a square-planar compound, $[Co(H_2(fsa)_2phn)]$, is formed, as shown by thermogravimetric analysis. The mixture of 0.5 mmol (240 mg) of $[Co(H_2(fsa)_2phn)]$ and 2.5 mmol (488 mg) of *t*-MeStpy in 10 ml of anhydrous ethanol was heated in the dark (to prevent ligand photoisomerization) at 40°C for 5 h. A brown precipitate was formed. The excess of *t*-MeStpy was removed by washing with ethanol. The precipitate of $[Co(H_2(fsa)_2phn)(trans\text{-MeStpy})]\cdot 0.5H_2O$ was isolated by filtration and dried under an argon stream. *Anal.* Calc. for $C_{36}H_{28}CoN_3O_{6.5}$ ($F_w = 665.57$): C, 64.96; H, 4.24; Co, 8.85; N, 6.31; O, 15.62. Found: C, 64.46; H, 4.19; Co, 8.93; N, 6.08; O, 15.32%.

2.4. Physical measurements

IR spectra (KBr pellets) were recorded on a BIO RAD FTS-135 spectrophotometer. Diffuse reflectance UV–Vis spectra were obtained with a VSU-2P (Carl Zeiss) spectrophotometer. UV electronic spectra, in non-aqueous solutions, were recorded with a UV4 Unicam spectrophotometer. Magnetic measurements were performed on polycrystalline samples, using a Quantum Design MPMS-5S SQUID magnetometer. The independence of susceptibility, with regard to the strength of the applied magnetic field, was checked for each compound at room temperature (r.t.). Diamagnetic correction was estimated at -357×10^{-6}, -478×10^{-6} and -340×10^{-6} $cm^3\ mol^{-1}$ for $[Co(Salpad)_2]$ (**1**), $[Co(Salpad)_2(t\text{-MeStpy})]$ (**2**) and $[Co(H_2(fsa)_2phn)(t\text{-MeStpy})]\cdot 0.5H_2O$ (**3**), respectively. Elemental analyses were performed on a Carlo Erba model 1108 CHNS-O elemental analyzer. The electric

conductivities were determined in DMF (10^{-3} M) on an OK 102/l Radelkis conductometer.

3. Results and discussion

In previous papers [17] we have showed that bidentate Schiff-base 2-[*N*-(4-phenyl-aminophenyl)formimidoyl]phenol, H(Salpad), is a very suitable ligand to form neutral 3d metal complexes corresponding to a stoichiometry of M(II):Salpad (1:2) type. In these complexes, the Schiff-base acts as a chelate monoanionic ligand with coordination involving phenolato oxygen and imino nitrogen atoms. The reaction of 1 equiv. of cobalt(II) acetate with 2 equiv. of H(Salpad), in a slightly basic solution, yields the complex [Co(Salpad)$_2$] (**1**), as shown in Scheme 1. By treating 1 equiv. of **1** with 1 equiv. of *t*-MeStpy (where *t*-MeStpy = *trans*-1-(4-methylphenyl)-2-(4-pyridyl)ethene), a five-coordinate adduct, [Co(Salpad)$_2$(*t*-MeStpy)] (**2**), is obtained (see Scheme 1 and Section 2).

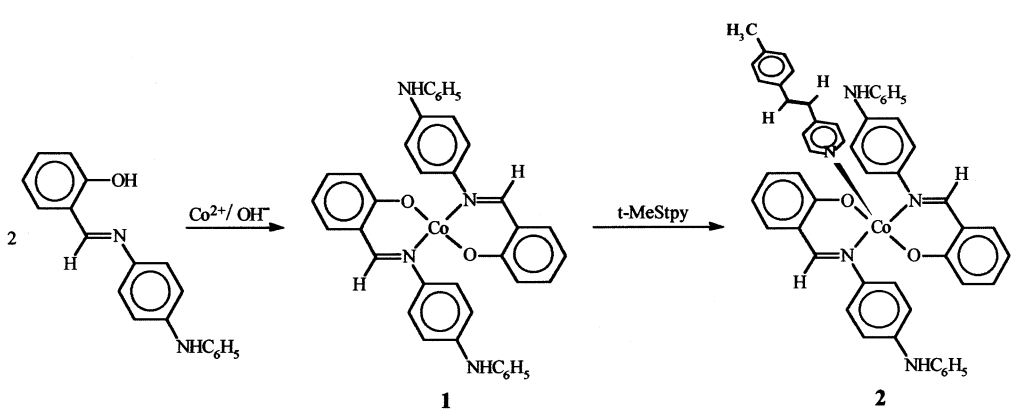
[Co(H$_2$(fsa)$_2$phn)(*t*-MeStpy)]·0.5H$_2$O (**3**) was prepared according to Section 2 and the reactions shown in Scheme 2. All the experiments have been carried out under an argon atmosphere in order to avoid the oxidation to the cobalt(III) species.

We were not able to obtain single crystals suitable for X-ray crystallographic studies; however, useful information regarding the structures of compounds **1**–**3** was derived from spectroscopic and magnetic measurements (vide infra). The non-electrolytic nature of these compounds was established from conductance measurements carried out in DMF solutions (10^{-3} M). The three compounds show very small molar electric conductivity values ($\Lambda_M = 6$–14 ohm^{-1} cm^2 mol^{-1}).

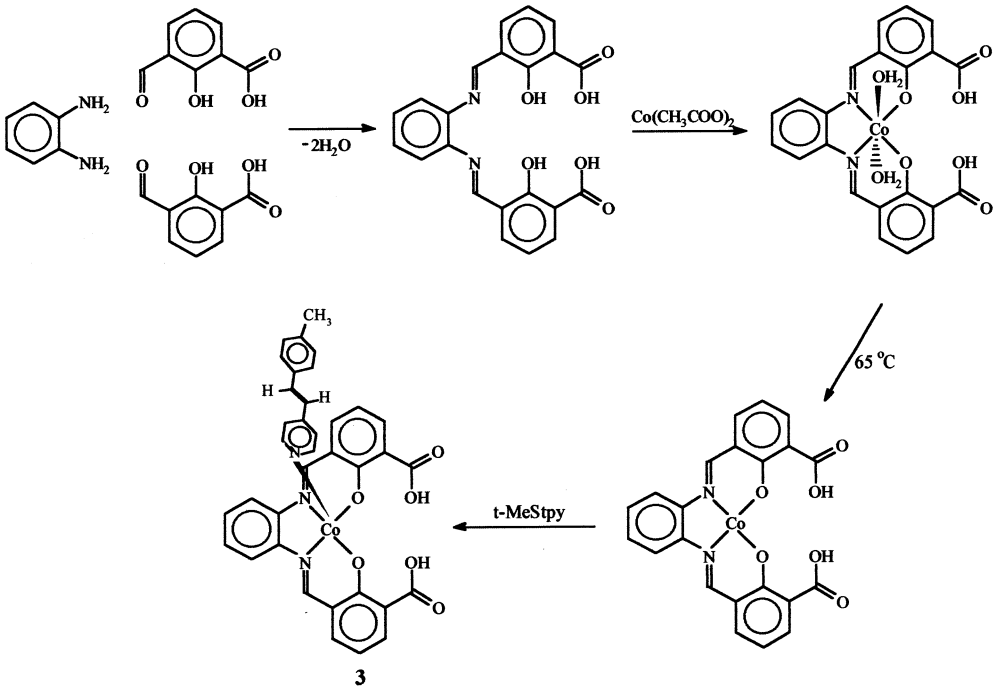
3.1. Infrared and electronic spectra

The IR spectra of compounds **1**–**3** show absorptions characteristic of coordinated ligands. Our discussion is confined to the most important vibrations of the 4000–400 cm^{-1} region in relation to structure. The mode ν(C=N), present as a strong band at 1620 cm^{-1} in the free ligand spectrum of H(Salpad), lies at 1600 and 1602 cm^{-1}, respectively, in the spectra of compounds **1** and **2**, suggesting an imino–nitrogen coordination [18]. The free ligand exhibits a medium band around 3030 cm^{-1} is due to the intra-molecularly hydrogen bonded OH group. The absence of this band in the spectra of compounds **1** and **2**, as well as the shift to higher energy by 20–30 cm^{-1} of the phenolic ν(C–O) bands, can be interpreted as proving the involvement of the phenolato oxygen atom in coordination [19]. In the case of compound **3**, the band due to the ν(C=N) mode lies at 1607 cm^{-1}. This band is shifted considerablly to lower frequencies when compared with that (1630 cm^{-1}) of the ligand H$_4$(fsa)$_2$phn [15], suggesting that the cobalt atom is bounded in the N_2O_2 coordination site provided by this ligand. This conclusion is supported further by an intense band located at 1705 cm^{-1} in the IR spectrum of compound **3**, which is due to the ν_{asym}(C=O) mode associated with the two uncoordinated –COOH groups of the Schiff-base ligand. A similar band was previously observed [13,18] with the IR spectra of several mononuclear 3d metal complexes from the family [M(H$_2$(fsa)$_2$R)L$_x$] (see **II**), where H$_2$(fsa)$_2$R^{2-} is the dianion of the Schiff base resulting from 2:1 condensation of 3-formylsalicylic acid with various diamine and L is a pyridine derivative. Another solid argument for the formation of five-coordinate adducts **2** and **3** consists in the appearance in their IR spectra of the very characteristic bands of *t*-MeStpy (near 810, 970 and 1600 cm^{-1}) [20]. In the case of **3**, the presence of water results in a strong IR absorption at 3433 cm^{-1}.

Further evidence for the formation of the two *t*-MeStpy adducts is provided by UV–Vis spectrometry. The electronic spectrum of compound **2**, recorded in acetonitrile solution at r.t., clearly indicates the presence of a broad intense band with maximum around 313 nm ($\sim$31 950 cm^{-1}), which corresponds to the



Scheme 1. Synthesis of [Co(Salpad)$_2$] (**1**) and [Co(Salpad)$_2$(*t*-MeStpy)] (**2**).



Scheme 2. Stepwise synthesis of $[Co(H_2(fsa)_2phn)(t\text{-MeStpy})]\cdot 0.5H_2O$ (**3**).

t-MeStpy $\pi \rightarrow \pi^*$ absorbtion, according to the previous assignments [4,5]. A band of the same nature was also observed in the r.t. spectrum of compound **3** (in dimethylformamide solution) around 315 nm ($\sim$ 31 750 cm^{-1}).

The electronic spectrum of compound **1**, recorded by diffuse reflectance technique, clearly indicates the presence of a *pseudo*-tetrahedral Co(II) chromophore, while those of compounds **2** and **3** show the characteristic features of five-coordinated cobalt(II) ions, with a distorted square-pyramidal stereochemistry. The tetrahedral compound is distinguished by its relative intense ligand field band, the maximum at 10 900 cm^{-1} (Fig. 1) corresponding to a splitted component of the second spin-allowed transition ($^4T_1$ (F) $\leftarrow {}^4A_2$) of the ideal tetrahedron, while the third band, due to the spin-allowed $^4T_1$ (P) $\leftarrow {}^4A_2$ transition, should be located on the side of high energies, in overlapping with the charge transfer bands.

The square pyramidal stereochemistry of compound **2** may be also established from UV–Vis spectral data, by comparison with similar literature spectra [21]. The two bands centered at 8110 and 11 050 cm^{-1} in the UV–Vis spectrum of **2** are assigned to the spin-allowed transitions $^4B_1 \leftarrow {}^4A_2$ and $^4B_2 \leftarrow {}^4A_2$, respectively. Though the available spectral data are not enough detailed to indicate the *cis* or *trans* disposal of $[N_2O_2]$ set of the equatorial plane, we assumed that a *trans* arrangement is adopted, where the steric effects should be reduced [22]. In addition, this arrangement can be governed by packing effects because of the more symmetrical molecular unity and a subsequent gain in the lattice energy. The diffuse reflectance spectrum of compound **3** also shows two bands of moderate intensity in the visible region, at 7610 and 12 300 cm^{-1}. It can be inferred that the coordination polyhedron around the cobalt(II) ion is an axially elongated square-pyramid, with the donor atom *cis*-$[N_2O_2]$ set provided by the Schiff base $H_4(fsa)_2phn$ occupying the basal plane and with *t*-MeStpy as an axial ligand. This result is in accordance with the X-ray crystal structure of the similar complex [Co(salen)(py)] [11].

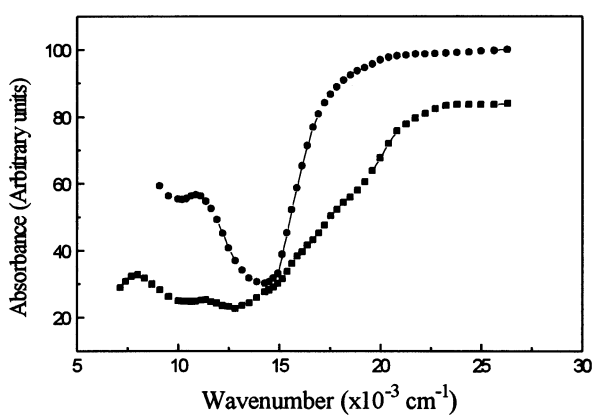


Fig. 1. Diffuse reflectance spectra of (●) $[Co(Salpad)_2]$ (**1**) and (■) $[Co(Salpad)_2(t\text{-MeStpy})]$ (**2**).

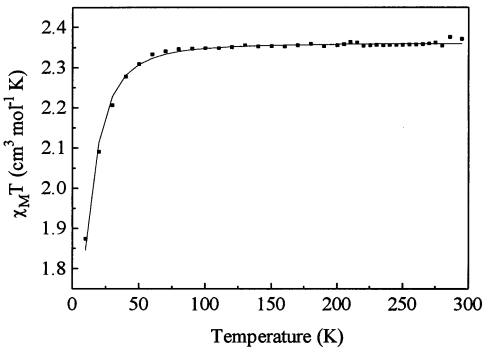


Fig. 2. Plot of $\chi_M T$ vs. T for [Co(Salpad)$_2$] (**1**).

3.2. Magnetic properties

Variable-temperature magnetic susceptibility measurements were carried out for complexes **1** and **2** in the temperature range 10–300 K. The $\chi_M T$ versus T plots (χ_M denoting the molar magnetic susceptibility) are given in Figs. 2 and 3, respectively. The $\chi_M T$ product of [Co(Salpad)$_2$] (**1**) is quasi-independent of temperature in the range of high temperatures, passing from 2.37 cm^3 mol^{-1} K at 295 K to 2.33 cm^3 mol^{-1} K at 60 K (Fig. 2).

Below 60 K it decreases more rapidly, reaching 1.87 cm^3 mol^{-1} K at 10 K. The high-temperature values corresponding to the plateau are in the range expected for a *pseudo*-tetrahedral Co(II) complex with an orbitally non-degenerate $^4A_2$ ground state. For [Co(Salpad)$_2$(*t*-MeStpy)] (**2**), the $\chi_M T$ values slightly vary from 2.79 cm^3 mol^{-1} K at 295 K to 2.68 cm^3 mol^{-1} K at 70 K and then drop more rapidly reaching 2.09 cm^3 mol^{-1} K at 10 K (Fig. 3). The higher magnetic moments suggest a supplementary contribution, aside from the pure spin one. A second-order orbital contribution is possible, as it is qualitatively argued in the following. For the actual C_{2v} symmetry the set of lowest quartet states, A_2, B_1, B_2 formed by the splitting of the T_1 parent allows a nonvanishing expectation value for the orbital momentum operator, which spans the same set of representations, a_2, b_1, b_2. In each nondiagonal matrix element is contained a contribution behaving like the triple product, $A_2 \otimes B_1 \otimes B_2 \equiv A_1$, as indicative of a nonvanishing quantity. For a *trans*-[Co(II)N$_2$O$_2$N′] chromophore, the lowest first and second spin quartet states are quite close forming a quasidegenerate ground state. This results in a second order contribution from these elements to the ground state orbital moment.

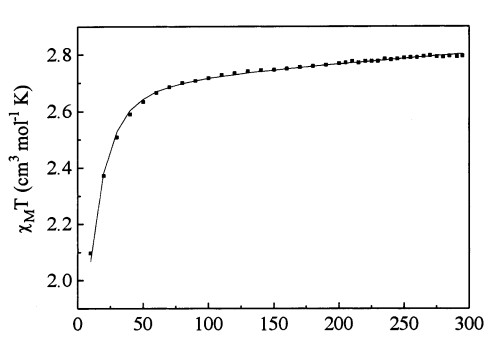


Fig. 3. Plot of $\chi_M T$ vs. T for [Co(Salpad)$_2$(*t*-MeStpy)] (**2**).

We interpret the magnetic behaviors of **1** and **2** in terms of a large zero field splitting (ZFS) of a $^4A_2$ ground-state with no contribution from a doublet state even at low temperature. The ZFS Hamiltonian can be taken in the simplified axial form: $H = g\beta HS + D[S_z^2 - 1/3S(S+1)]$, and for $S = 3/2$ the susceptibility data are described by Eq. (1):

$$\chi_M T = \frac{g^2}{8}\left[\frac{9}{4} + \frac{3}{x}\frac{1-e^{-x}}{1+e^{-x}}\right] + N\alpha T \quad (1)$$

where, $x = 2D/kT$ and $N\alpha$ is the temperature independent paramagnetism (TIP).

By a least-squares fitting, the following parameters were found: $g = 2.24$ and $D = 14.91$ cm^{-1} ($N\alpha$ being assumed to be zero) for **1**, and $g = 2.39$, $D = 16.57$ cm^{-1} and $N\alpha = 360 \times 10^{-6}$ emu, for **2**. The values are in line with similar systems [10,14] and the reliability factors defined as $R(\chi_M T) = \{\Sigma[(\chi_M T)_{obs} - (\chi_M T)_{calc}]^2 / \Sigma[(\chi_M T)_{obs}]^2\}^{1/2}$ are below 10^{-4}.

It is worth noting that the perturbational term of orbital magnetism is not important for a five-coordinate cobalt(II) compound with a *cis*-[N$_2$O$_2$] configuration of the equatorial plane, because the orbitally non-degenerate ground state of the metal ion is quite spaced from the following ones. This affirmation is corroborated with the magnetic behavior of the square-pyramidal compound [Co(H$_2$(fsa)$_2$phn)(*t*-MeStpy)]·0.5H$_2$O (**3**) (where H$_2$(fsa)$_2$phn^{2-} denotes the phenolic dianion of the Schiff-base *N*,*N*′-*o*-phenylenebis(3-carboxysalicylaldimine); see Scheme 2), as well as with those of the well known [Co(Saloph)(2-MeImd)] [10] (Saloph^{2-} being the phenolic dianion of the Schiff-base *N*,*N*′-*o*-phenylenebis(salicylaldimine)), where the high-temperature magnetic moments are very close to the spin-only value. The molar magnetic susceptibilities (χ_M) of **3** were measured over the temperature range 10–380 K. The cobalt(II) ion exhibits a rather smooth thermally-induced spin crossover without any detectable hysteresis.

As shown in Fig. 4, the temperature dependence of the $\chi_M T$ product is more pronounced in the interval 380–200 K decreasing from 1.61 cm^3 mol^{-1} K at 380 K to 0.93 cm^3 mol^{-1} K at 200 K. The curve then has a plateau between 160 and 40 K, at $\sim$0.82 cm^3 mol^{-1} K, and $\chi_M T$ values drop again at lower temperatures, reaching 0.66 cm^3 mol^{-1} K at 10 K. The latter decrease may be due to a weak intermolecular exchange coupling between neighboring cobalt atoms. It is worth pointing out that this behavior is very different from

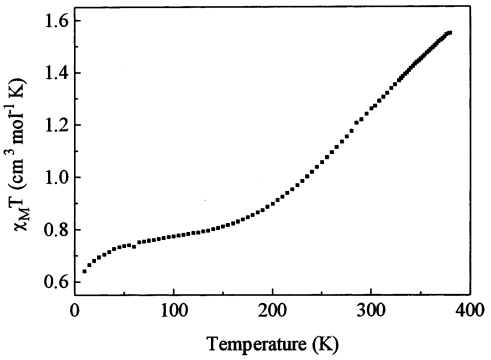


Fig. 4. Plot of $\chi_M T$ vs. T for $[Co(H_2(fsa)_2phn)(t\text{-MeStpy})]\cdot 0.5H_2O$ (**3**).

that of the compound **2**, which is also square-pyramidal, but with a *trans* arrangement for the equatorial plane.

4. Conclusion

By combining the results described here with previously published work it is possible to rationalize new synthetic routes leading to cobalt(II) spin-crossover compounds. The compound $[Co(H_2(fsa)_2phn)(t\text{-MeStpy})]\cdot 0.5H_2O$ (**3**) is particularly attractive since, to the best of our knowledge, this is the first five-coordinate species containing a photosensitive ligand in the molecule which displays a thermally-induced spin conversion. In addition, its transition temperature range ($T_{1/2} \sim 270$ K) is significantly shifted towards higher values, as compared with the critical temperatures of 101 K ($T\downarrow$) and 105 K ($T\uparrow$) reported [16] for the precursor compound $[Co(H_2(fsa)_2phn)(H_2O)_2]$. There is a possibility that this complex, like other square-pyramidal Co(II) complexes, presents noticeable distortion of the coordination core by moving the metal out of the equatorial plane. The dependence of the spin states on this distortion precludes the comparison of the properties of the complexes containing *trans* and *cis* ligand isomers.

Acknowledgements

We gratefully acknowledge the financial support from the Conseil National de la Recherche Scientifique, France and the Romanian Academy. We thank Dr F. Cimpoesu for fruitful discussions during the preparation of this manuscript.

References

[1] (a) O. Kahn, Molecular Magnetism, VCH, New York, 1993. (b) L. Banci, A. Bencini, C. Benelli, D. Gatteschi, C. Zanchini, Struct. Bond. (Berlin) 52 (1982) 37.
[2] (a) P. Gütlich, A. Hauser, H. Spiering, Angew. Chem., Int. Ed. Engl. 33 (1994) 2024. (c) E. König, Prog. Inorg. Chem. 35 (1987) 527. (d) J.K. Beattie, Adv. Inorg. Chem. 32 (1988) 1. (e) H. Toftlund, Coord. Chem. Rev. 67 (1989) 108.
[3] J.F. Létard, P. Guinneau, L. Rabardel, J.A.K. Howard, A.E. Goeta, D. Chasseau, O. Kahn, Inorg. Chem. 37 (1998) 4432.
[4] C. Roux, J. Zarembowitch, B. Gallois, T. Granier, R. Claude, Inorg. Chem. 33 (1994) 2273.
[5] M.L. Boillot, C. Roux, J.P. Audière, A. Dausse, J. Zarembowitch, Inorg. Chem. 35 (1996) 3975.
[6] (a) M.L. Boillot, S. Chantraine, J. Zarembowitch, J.Y. Lallemand, J. Prunet, New J. Chem. 2 (1999) 179. (b) M.L. Boillot, H. Soyer, New. J. Chem. 21 (1997) 889.
[7] A. Sour, M.L. Boillot, E. Rivière, P. Lesot, Eur. J. Inorg. Chem. (1999) 2117.
[8] (a) M.D. Timken, A.M. Abdel-Mawgoud, D.N. Hendrickson, Inorg. Chem. 25 (1986) 160. (b) S. Hayami, K. Inoue, S. Osaki, Y. Maeda, Chem. Lett. (1998) 987.
[9] J. Zarembowitch, New J. Chem. 16 (1992) 255 and references therein.
[10] B.J. Kennedy, G.D. Fallon, B.M.K.C. Gatehouse, K.S. Murray, Inorg. Chem. 23 (1984) 580.
[11] K.S. Murray, R.M. Sheahan, J. Chem. Soc., Dalton Trans. (1976) 999.
[12] (a) A.L. Nivorozhkin, H. Toflund, M. Nielsen, J. Chem. Soc., Dalton Trans. (1994) 361. (b) J. Faus, M. Julve, F. Lloret, J.A. Real, J. Sletten, Inorg. Chem. 33 (1994) 5535.
[13] (a) J. Zarembowitch, R. Claude, O. Kahn, Inorg. Chem. 24 (1985) 1576. (b) J. Zarembowitch, O. Kahn, Inorg. Chem. 23 (1984) 589.
[14] P. Thuéry, J. Zarembowitch, Inorg. Chem. 25 (1986) 2001.
[15] R. Claude, J. Zarembowitch, M. Philoche-Levisalles, F. d'Yvoire, New J. Chem. 15 (1991) 635.
[16] J. Zarembowitch, R. Claude, P. Thuéry, Nouv. J. Chim. 9 (1985) 467.
[17] (a) F. Tuna, L. Patron, A. Meghea, G. Aivanese, Rev. Roum. Chim. 42 (1997) 961. (b) F. Tuna, L. Patron, Rev. Roum. Chim. 42 (1997) 677.
[18] M. Tanaka, M. Kitaoka, H. Okawa, S. Kida, Bull. Chem. Soc. Jpn. 49 (1976) 2469.
[19] S.K. Mandal, K. Nag, J. Chem. Soc., Dalton Trans. (1984) 2141.
[20] K. Nakamoto, Infrared and Raman Spectra of Inorganic Coordination Compounds, third ed., Wiley, New York, 1978.
[21] A.P.B. Lever, Inorganic Electronic Spectroscopy, Elsevier, New York, 1984.
[22] F. Tuna, L. Patron, Y. Journaux, M. Andruh, W. Plass, J.-C. Trombe, J. Chem. Soc., Dalton Trans. (1999) 539.

PERGAMON

www.elsevier.nl/locate/poly

Polyhedron 19 (2000) 1649–1661

POLYHEDRON

Polyhedron Report No. 67

Primary alanes and alanates: useful synthetic reagents in aluminum chemistry

Rudolf J. Wehmschulte [a,*1], Philip P. Power [b,*2]

[a] *Department of Chemistry and Biochemistry, University of Oklahoma, 620 Parrington Oval, Room 208, Norman, OK 72019, USA*
[b] *Chemistry Department, University of California, One Shields Avenue, Davis, CA 95616, USA*

Received 7 February 2000; received in revised form 2 June 2000; accepted 7 June 2000

Abstract

Primary alanes $[RAlH_2]_2$ can be stabilized kinetically by employment of very bulky alkyl or aryl substituents. They are easily prepared by reacting the appropriate lithium trihydroalanate precursor with organic halides, anhydrous hydrogen halides or halogens. Reactions of these aluminum hydrides with a wide variety of substrates ranging from protic reagents such as water, alcohols, amines, phosphines or thiols over ketones, nitriles or isonitriles to silylated species such as siloxanes or silyl halides are presented. Primary alanes were shown to be unique starting materials for a number of interesting compounds that were otherwise not accessible, or only available in low yields. In addition, postulated intermediates of aluminum hydride reductions of organic substrates such as ketones or nitriles can be isolated when using bulky primary alanes. © 2000 Elsevier Science Ltd. All rights reserved.

Keywords: Alane; Aluminum hydride; Alanate; Alumoxane; Reduction

1. Introduction

Hydrides of the Group 13 metals are considerably less well investigated than their lighter boron counterparts. Nonetheless, recent years have seen a much-increased level of interest in the area. Various aspects of their chemistry and applications have been the subject of a number of reviews [1–8]. The metal hydrides are of course of inherent interest since they are compounds of a fundamental type. In this regard it is interesting to note that although AlH_3 has been known for almost 60 years [9], GaH_3 has only been well characterized within the last decade [4]. However, in this review we focus on a specific class of Group 13 metal hydrides which up until recently had received little attention. These are the monosubstituted (or primary) alanes of the general formula $RAlH_2$ and the related alanate ions $[RAlH_3]^-$ (R = organo or related group). Traditionally, such compounds have been regarded as unstable owing to their tendency to undergo redistribution reactions (vide infra, Eq. (1)). However, the employment of large R substituents has enabled several examples to be stabilized. These have proven to not only have interesting structures, but also a rich chemistry which allows access to several other classes of aluminum compounds that were either unavailable or difficult to synthesize by other routes.

The field of aluminum hydride chemistry could be said to have been inaugurated when AlH_3 was first synthesized as an impure solid by Stecher and Wiberg [9] in 1942. It was obtained by thermolysis of crystalline $H_3Al{\cdot}NMe_3$, which itself was obtained by fractional crystallization of NMe_3 solutions of the residue from glow-discharge reactions of mixtures of $(Me_3Al)_2$ and H_2 [9]. The subsequent synthesis of $LiAlH_4$ from the reaction of LiH with $AlCl_3$ by Schlesinger and co-workers in 1946 [10] introduced aluminum hydrides as new, powerful and easy to handle reducing and/or hydride-

[1] *Corresponding author. Tel.: +1-405-325-2388; fax: +1-405-325-6111; e-mail: rjwehmschulte@chemdept.chem.ou.edu

[2] *Corresponding author. Fax: +1-530-752-8995; e-mail: pppower@ucdavis.edu

0277-5387/00/$ - see front matter © 2000 Elsevier Science Ltd. All rights reserved.
PII: S0277-5387(00)00455-1

transfer reagents for organic and inorganic chemistry [11,12]. It was subsequently recognized that the reducing power and selectivity could be modified by substitution of some of the hydrides by other groups such as amides, alkoxides, alkyls, aryls, etc. [13–15]. Typical examples include the ubiquitous diisobutylaluminum hydride (DIBALH), diethylaluminum hydride, lithium aluminum tri-*tert*-butoxyhydride and sodium bis(2-methoxyethoxy)aluminum hydride (Red-Al), all of which are commercially available. While the synthesis, structure and reactivity of these and related compounds are well documented and understood [12,16], until recently there was only scant information available for primary alanes $(RAlH_2)_n$ and their related alkali metal hydride adducts (or alanates) $[M][RAlH_3]$ (M = alkali metal), which also feature one organic substituent on aluminum. This was due to the difficulty in obtaining pure compounds owing to the ease of ligand distribution reactions (Eq. (1)).

$$2RAlH_2 \rightleftharpoons R_2AlH + AlH_3 \quad (1)$$

Although the synthesis, structure and reactivity of unsolvated primary alanes $(RAlH_2)_n$ and their related alanates $[RAlH_3]^-$ (R = alkyl or aryl) form the main theme of this review, data on related solvated species and primary aluminum hydride compounds with other substituents will be provided when they are relevant to the discussion.

2. Synthesis and structures

Early investigations of aluminum hydrides utilized electrical glow discharges in mixtures of Me_3Al and H_2 as a synthetic approach [9]. Addition of NMe_3 to the resulting mixtures afforded several fractions which were identified as the base stabilized adducts $Me_nAlH_{3-n}\cdot NMe_3$ ($n = 0–3$). Only $H_3Al\cdot NMe_3$ was obtained as a crystalline solid. Some 20 years later Peters and Bartocha [17,18] reported the synthesis of what were described as pure $MeAlH_2\cdot NMe_3$ and $EtAlH_2\cdot NMe_3$ by three different methods:

Alkylation of $H_3Al\cdot NMe_3$ with mercury dialkyl R_2Hg (R = Me, Et).

$$R_2Hg + 2H_3Al\cdot NMe_3 \rightarrow 2RAlH_2\cdot NMe_3 + Hg + H_2 \quad (2)$$

'Syn-proportionation' of $H_3Al\cdot NMe_3$ with $R_3Al\cdot NMe_3$.

$$2H_3Al\cdot NMe_3 + R_3Al\cdot NMe_3 \rightarrow 3RAlH_2\cdot NMe_3 \quad (3)$$

Reduction of R_2AlCl with $LiAlH_4$ in the presence of NMe_3.

$$R_2AlCl + LiAlH_4 \xrightarrow{NMe_3} 2RAlH_2\cdot NMe_3 + LiCl \quad (4)$$

However, later investigations suggested that Peters' and Bartocha's '$MeAlH_2\cdot NMe_3$' consisted of an equilibrium mixture of 4.3% $Me_3Al\cdot NMe_3$, 21.8% $Me_2AlH\cdot NMe_3$, 38.5% $MeAlH_2\cdot NMe_3$ and 35.4% $AlH_3\cdot NMe_3$ [19]. In agreement with this finding, freshly prepared $PhAlH_2\cdot NMe_3$ was shown to rearrange easily at room temperature (r.t.) into mixtures containing Ph_2AlH and $Ph_3Al_2H_3\cdot NMe_3$ [20]. In light of these results the reported $PhAlH_2$ [21] is also likely to be a mixture of species. So far the only structurally authenticated primary organoalanes $[RAlH_2]_n$ with simple organic groups such as methyl are those which are stabilized by complexation with BH_3 or Cp_2TiH as in $MeAl(BH_4)_2$ [22] or $MeAl(Cp_2TiH_2)_2$ [23]. Both compounds feature five-coordinate aluminum with a terminal Me group and two bridging $Ti/B(\mu\text{-}H)_2Al$ units.

Another method for the stabilization of primary alanes employs the chelate effect, i.e. intramolecular base stabilization. Typical ligands include mono- and bis-*o*-(aminomethyl)phenyl and 3-aminopropyl. These ligands have permitted the isolation of five-coordinate monomeric and dimeric aluminum hydrides 2,6-$(R_2NCH_2)_2C_6H_3AlH_2$ (R = Me [24], Et [25]), [2-$(Me_2NCH_2)C_6H_4AlH_2]_2$ [26] and $[Me_2NCH_2CH_2\text{-}CH_2AlH_2]_2$ [27]. The latter two species dimerize via $Al\text{-}(\mu\text{-}H)_2\text{-}Al$ bridges. The synthesis was effected by reacting the dihalide precursors with $LiAlH_4$ or MH (M = Li, Na).

$$RAlCl_2 \xrightarrow{LiAlH_4 \text{ or } MH} RAlH_2 \quad (5)$$

Heterosubstituted, unsolvated primary alanes such as $[H_2AlNMe_2]_3$ [28–30], $[H_2Al(\mu\text{-}N(CH_2CH_2)_2S)]_2$ [31] $[H_2AlO\textit{t}\text{-}Bu]_2$ [32], $[(\textit{t}\text{-}Bu_2MeCO)AlH_2]_2$, $[(\textit{t}\text{-}BuMe\text{-}CHO)AlH_2]_4$ [33], $[H_2AlOCH\textit{t}\text{-}Bu_2]_4$ [34], or $[H_2AlP(SiMe_3)_2]_3$ [35] have been synthesized by aminolysis, alcoholysis, ketone reduction or dehydrosilylation reactions involving amine or ether solvated AlH_3 and the appropriate substrate. These compounds are associated through bridging of the aluminums through the heteroatoms.

Finally, employment of bulky substituents like Mes* and 2,6-$Ar_2C_6H_3$– (Ar = Mes, Trip = 2,4,6-*i*-$Pr_3C_6H_2$–, Mes* = 2,4,6-*t*-$Bu_3C_6H_2$–) allowed access to the first stable, base-free primary organoalanes $[Mes^*AlH_2]_2$ and $[2,6\text{-}Ar_2C_6H_3AlH_2]_2$. In contrast to the heterosubstituted primary alanes these compounds are associated through hydride bridges (vide infra). They can be conveniently synthesized by a simple two-step reaction sequence as shown in Eqs. (6) and (7). Reaction of the bulky aryllithium starting material RLi with $AlH_3\cdot NMe_3$ affords the dimeric lithium trihydroalanates $[RAl(H)(\mu\text{-}H)_2LiL_2]_2$ (L = Et_2O, THF) [36]. Removal of LiH from the alanates by reaction with organic or silyl halides such as MeI and *n*-BuBr or Me_3SiCl gave the primary alanes [37,38].

$$2RLi + 2AlH_3\cdot NMe_3 \xrightarrow{L} [RAl(H)(\mu\text{-}H)_2LiL_2]_2 + 2NMe_3 \quad (6)$$

$$[RAl(H)(\mu\text{-}H)_2LiL_2]_2 + 2R'X \rightarrow [RAlH_2]_2 + 2R'H + 2LiX \quad (7)$$

Trihydroalanates $[M][RAlH_3]$ were first described in the 1960s by Zakharkin and Gavrilenko [39], but it was not until 1994 that the first crystal structures were reported [36,40]. Their common feature is a puckered eight-membered ring $[Li(\mu\text{-}H)Al(\mu\text{-}H)]_2$ skeleton which arises from the association of two $RAlH_3^-$ anions through two ether solvated Li^+ cations, which affords $Al(\mu\text{-}H)Li(\mu\text{-}H)Al$ linkages (Fig. 1).

The ^1H NMR data for crystals of $[Mes^*AlH_3Li(THF)_2]_2$, which were recrystallized in the presence of excess THF, suggest the formation of a putative monomeric species $Mes^*AlH_3Li(THF)_3$ [41]. If the bidentate ligand tetramethylethane-1,2-diamine (TMEN) was used instead of THF, crystals of $[(Me_3Si)_3CAlH_3]^-$ $[Li(TMEN)_2]^+$ with discrete anions and cations were obtained (Fig. 2) [42]. The recently published trihydroalanate $BmtAlH_3Li(DME)_2$ (Bmt = 4-*t*-butyl-2,6-bis[(2,2′,6,6′-tetramethyl-*m*-terphenyl-2′-yl)-methyl]phenyl, DME = 1,2-dimethoxyethane) features only one Li–H–Al bridge between the ions [43]. Table 1 lists the crystallographically characterized trihydroalanates. The coordination environment at the aluminum atoms is generally distorted tetrahedral with the $Al–H_{term}$ distances being only slightly shorter than the $Al–H_{bridg}$ distances. In general, it appears that the aggregation state of the lithium trihydroalanates — dimeric, monomeric, monomeric ion pairs — does not significantly affect the metric parameters at the aluminum centers.

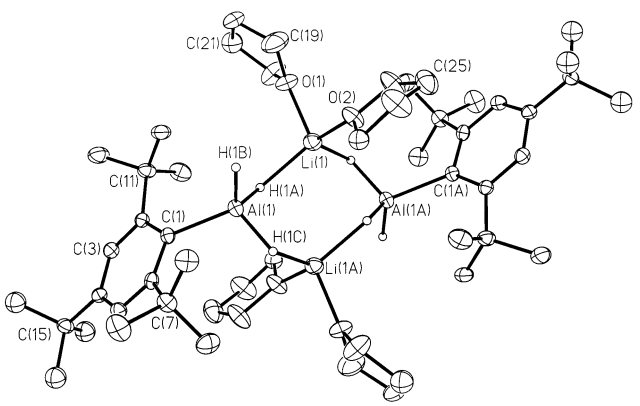


Fig. 1. Thermal ellipsoid plot (35%) of $[Mes^*AlH_3Li(THF)_2]_2$. H-atoms except of those bound to aluminum are not shown for clarity [36].

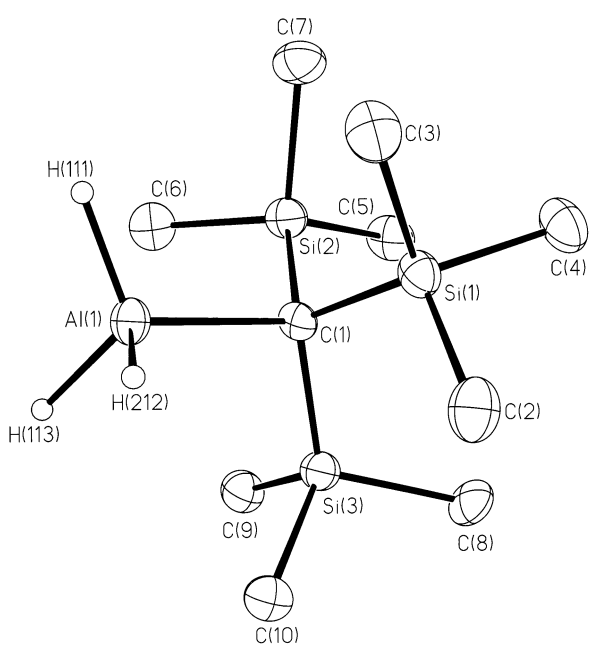


Fig. 2. Thermal ellipsoid plot (35%) of the anion $[(Me_3Si)_3CAlH_3]^-$ in $[(Me_3Si)_3CAlH_3]^-[Li(TMEN)_2]^+$. H-atoms except of those bound to aluminum are not shown for clarity [42].

At present, the $(Me_3Si)_3C$ group is the smallest alkyl substituent that has been shown to stabilize the organotrihydroalanate structure $RAlH_3^-$ against rearrangement to $R_2AlH_2^-$ and AlH_4^- (Eq. (8)).

$$2RAlH_3^- \rightarrow R_2AlH_2^- + AlH_4^- \quad (8)$$

Attempted isolation of $t\text{-}BuAlH_3^-$ only afforded the rearranged species $t\text{-}Bu_2AlH_2Li(THF)_2$ [40]. The least bulky aryl substituent capable of effecting the stabilization of compounds of this class appears to be the Trip-substituent in the species $[TripAlH_3Li(OEt_2)]_n$ [38].

The aryltrihydroalanates $[ArAl(H)(\mu\text{-}H)_2LiL_2]_2$ (Ar = Mes*, 2,6-$Mes_2C_6H_3$–, 2,6-$Trip_2C_6H_3$–, L = Et_2O, THF) have proven to be excellent starting materials for the syntheses of the primary alanes $[ArAlH_2]_2$ (see Eq. (7) and Table 2). These compounds are the only base free primary organoalanes that have been completely characterized. The reaction of $[(Me_3Si)_3CAlH_3Li(THF)_2]_2$ with 1 equiv. of Me_3SiCl afforded $[(Me_3Si)_3C]_2Al_2H_5Li(THF)_2$ whose cyclic structure is similar to the corresponding indium compound [44]. The addition of a further equivalent of Me_3SiCl gave the base stabilized alane $[(Me_3Si)_3CAlH_2{\cdot}THF]$ [45]. However, treatment of $[TripAlH_3Li(OEt_2)]_n$ with Me_3SiCl afforded only the known secondary alane $[Trip_2AlH]_2$ [38]. Ligand migration in these systems appears to be facile and it can only be suppressed by the use of the very bulky trisilylmethyl, Mes* or terphenyl substituents.

The structures of the three crystallographically characterized primary organoalanes are very similar: all are dimeric via hydrogen bridges and the aryl substituents are *trans* to each other. The $Al–H_{term}$ distances are in the range 1.46–1.50 Å, whereas the $Al–H_{bridg}$ distances are significantly longer at 1.65–1.74 Å. The internal angles $H_{bridg}–Al–H_{bridg}$ are narrow at 77–81°, while the widest angles are $H_{term}–Al–C_{ipso}$ at 127–135.5°, proba-

Table 1
Bond distances (Å) and angles (°) for lithium trihydroalanates.

Compound	Al–C	Al–H_{term}	Al–H_{bridg}	Li–H	H_{bridg}–Al–H_{bridg}	H–Li–H	Ref.
$[TriphAlH_3Li(OEt_2)_{1.5}]_2$	2.018(4)	1.54(4)	1.62 av [a]	1.77 av	107(2)	120 av	[36]
$[Mes^*AlH_3Li(thf)_2]_2$	2.030(5)	1.54(6)	1.58 av	2.00 av	103(3)	104(2)	[36]
$[(PhMe_2Si)_3CAlH_3Li(thf)_2]_2$	2.045 av	1.58 av	1.61 av	1.93 av	103 av	117 av	[40]
$[(Me_3Si)_3CAlH_3]^-[Li(tmen)_2]^+$	2.059 av	1.56 av			108 av		[42]
$BmtAlH_3Li(DME)_2$ [b]	2.021(6)	1.58(7)	1.64(5)	1.94(5)	107 av		[43]
$[(Me_3Si)_2(Me_2SiOMe)CAlH_3Li(thf)]$	2.020(6)	1.62 av	1.66(7)	1.94(7)			[99]
$[(Me_3Si)_2NAlH_3Li(OEt_2)_2]_2$	1.858 av [c]	1.60 av	1.62 av	1.77 av	106 av	107 av	[100]
$[(2,6\text{-}t\text{-}Bu_2C_6H_3O)AlH_3Li(OEt_2)_2]_2$	1.739(2) [d]	1.51(2)	1.57 av	1.88 av	106(1)	97(1)	[101]

[a] av = average.
[b] bmt = 4-*t*-butyl-2,6-bis[(2,2″,6,6″-tetramethyl-*m*-terphenyl-2′-yl)-methyl]phenyl.
[c] Al–N distance.
[d] Al–O distance.

Table 2
Bond distances (Å) and angles (°) for primary alanes.

Compound	Al–C	Al–H_{term}	Al–H_{bridg}	H_{bridg}–Al–H_{bridg}	H_{term}–Al–H_{bridg}	Ref.
$[Mes^*AlH_2]_2$	1.966(3)	1.50(4)	1.69 av [a]	77(2)	106 av	[37]
$[2,6\text{-}Mes_2C_6H_3AlH_2]_2$	1.956(3)	1.44(4)	1.65(5)	75(2)	108(1)	[38]
$[2,6\text{-}Trip_2C_6H_3AlH_2]_2$	1.963(4)	1.46(4)	1.74 av	81(3)	109 av	[38]
$2,6\text{-}(4\text{-}t\text{-}BuC_6H_4)_2C_6H_3AlH_2{\cdot}NMe_3$	2.018	1.60 av			108(1) [b]	[36]
$2,6\text{-}Mes_2C_6H_3AlH_2{\cdot}OEt_2$	2.002(3)	1.54 av			108(2) [b]	[38]
$2,6\text{-}Trip_2C_6H_3AlH_2{\cdot}OEt_2$	1.983(5)	1.68 av			115(3) [b]	[38]
$[2\text{-}(Me_2NCH_2)C_6H_4AlH_2]_2$ [c]	1.974(5)	1.52	1.69 1.93	79	116 87	[26]
$[Me_2NCH_2CH_2CH_2AlH_2]_2$ [c]	1.977(2)	1.56(1)	1.60(1) 1.95(2)	77(1)	116(7)	[27]
$2\text{-}(Me_2NCH_2)_2C_6H_3AlH_2$ [c]	1.949(5)	1.50 av			119(2) [b]	[24]

[a] av = average.
[b] H_{term}–Al–H_{term}.
[c] Five-coordinate Al.

bly indicative of some steric strain as shown in the structure of $[Mes^*AlH_2]_2$ (Fig. 3).

The terphenyl substituted primary alanes form stable adducts with Et_2O and NMe_3 (Table 2) although the Et_2O may be removed by gentle warming under reduced pressure. On the other hand, $[Mes^*AlH_2]_2$ does not form stable adducts with Et_2O, THF, NMe_3 or NEt_3, although its NMR spectrum in C_6D_6 solutions displays a drastically changed chemical shift in the presence of 1 or 2 equiv. of THF. This, together with a large increase of its solubility, may be interpreted as a result of a weak adduct formation. So far, only the very strong donor HMPA has afforded a monomeric adduct ($MesAlH_2^*OP(NMe_2)_3$) as a stable solid (vide infra) [46]. The feeble reactivity of $[Mes^*AlH_2]_2$ towards Lewis bases may be explained by the presence of the bulky *o*-*t*-Bu groups that display short C–H···Al contacts (ca. 2.25–2.40 Å) and thus hinder access to the metal center [37].

It is interesting to note that these primary alanes are considerably more thermally stable than the 'simple' aluminum hydrides $H_3Al{\cdot}NMe_3$ or $LiAlH_4$. Decomposition occurs at or above the melting points at 173–177°C (Mes*–) [37], 219–221°C (2,6-$Mes_2C_6H_3$–) and 310–320°C (2,6-$Trip_2C_6H_3$–) [38], cf. ca. 105°C for $H_3Al{\cdot}NMe_3$ [9] or 125°C for $LiAlH_4$ [10].

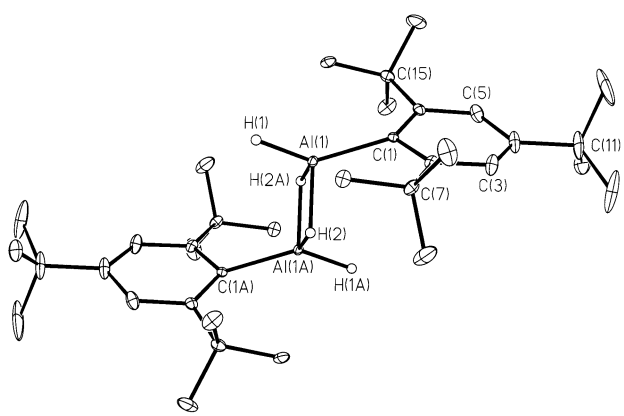


Fig. 3. Thermal ellipsoid plot (35%) of $[Mes^*AlH_2]_2$. H-atoms except of those bound to aluminum are not shown for clarity [37].

3. Reactivity

The availability of stable, well-defined primary alanes and their lithium hydride adducts has allowed for the first time the systematic study of their chemistry. As will be discussed in more detail later, these aluminum hydrides have proven to be important starting materials for a wide variety of compounds, some of which are difficult to synthesize by other routes.

4. Organoaluminum dihalides and pseudohalides

Sterically crowded primary alanes offer a potentially facile route to bulky organoaluminum dihalides $RAlX_2$, which are often difficult to synthesize by more obvious traditional routes. For example, the less sterically crowded organoaluminum dihalides are generally obtained by ligand exchange reactions between R_3Al and AlX_3 [47,48] as shown in Eq. (9).

$$R_3Al + 2AlX_3 \rightarrow 3RAlX_2 \quad (9)$$

In contrast, large, bulky substituents have a low tendency to migrate and in many cases it is not possible to synthesize the required R_3Al or R_2AlX starting materials. For example, $Trip_2AlBr$ does not react with $AlBr_3$ at r.t., but the reaction which proceeded at ca. 150°C was complicated by side reactions such as C–H activation [49]. The alternative 'direct' reaction of organolithium or -magnesium compounds with AlX_3 (Eq. (10)) affords the desired product only in a few cases and often in low yield.

$$RLi + AlX_3 \rightarrow RAlCl_2 + LiCl \quad (10)$$

Among the problems encountered in this reaction are ether or THF cleavage reactions (as seen in the reaction of $(Me_3Si)_3CLi(THF)_2$ and AlX_3 [50]), low yields and difficulty in purification ($< 30\%$ for $Mes^*Li(THF)_2 + AlBr_3$ [51]), formation of lithium halide adducts (e.g. $(2,6\text{-}Mes_2C_6H_3AlBr_3Li)_2$ [52]) and lack of organo group transfer, e.g. $Mes^*MgBr(THF) + AlCl_3$ yields two-coordinate Mes^*_2Mg instead of Mes^*AlCl_2 [53].

In contrast, the lithium trihydroalanates $RAlH_3Li(L)_n$ have proven efficient starting materials for the synthetically very useful organoaluminum dihalides $RAlX_2$ via reaction with alkyl or silyl halides as described in Eq. (11).

$$RAlH_3Li(L)_n + 3R'X \rightarrow 2RAlX_2 + 3R'H + LiX \quad (11)$$

$R' = \text{alkyl or } SiMe_3,\ X = \text{halide}$

In a related reaction Roesky and co-workers have recently found that $(Me_3Si)_3CAlMe_2(THF)$ was also a source for $(Me_3Si)_3CAlX_2(THF)$ [54]. Here the halide was introduced by reaction with Me_3SnX (X = F, Cl) or X_2 (X = Br, I). Interestingly, the halide transfer reagent reacted preferentially with the Al–Me bond.

Reaction of HX (X = Cl, Br) with the lithium trihydroalanate $[(Me_3Si)_3CAlH_3Li(THF)_2]_2$ leads cleanly to the appropriate organoaluminum dihalides $(Me_3Si)_3CAlX_2(THF)$ at r.t. with concomitant H_2 evolution [42]. Hydrogen fluoride also reacted smoothly, but gave the tetrameric LiF adduct $[(Me_3Si)_3CAlF_3Li(THF)]_4$, which features a cube-like $Al_4Li_4F_8$ core with bridging fluorides [55]. Treatment of $[(Me_3Si)_3CAlH_3Li(THF)_2]_2$ with Br_2 or I_2 also affords the dibromide or diiodide compounds, but in lower yields [42]. Similarly, a low yield of Mes^*AlI_2 may be isolated from the reaction of $[Mes^*AlH_3Li(THF)_2]_2$ with I_2 [41].

$$[RAlH_3Li(THF)_2]_2 + 6HX \rightarrow 2RAlX_2(THF) + 6H_2 + 2LiX + 2THF \quad (12)$$

$$[RAlH_3Li(THF)_2]_2 + 3X_2 \rightarrow 2RAlX_2(THF) + 3H_2 + 2LiX + 2THF \quad (13)$$

In these reactions the more reactive Al–H bond is cleaved preferentially. In the case of the Mes* substituted aluminum hydrides the steric strain caused by the bulky substituent apparently decreases the reactivity difference so that other methods of Al–X bond formation were investigated.

The elimination of Me_3SiH from the reaction of $ArAlH_3Li(L)_2$ or $[ArAlH_2]_2$ with Me_3SiCl (Eqs. (14) and (15)) is currently the most effective and clean method for the synthesis of $ArAlCl_2$ (Ar = Mes*, 2,6-$Mes_2C_6H_3$, 2,6-$Trip_2C_6H_3$) compounds [38,53].

$$[ArAlH_3Li(L)_2]_2 + 6Me_3SiCl \rightarrow 2ArAlCl_2(L) + 6Me_3SiH + 2LiCl + 2L \quad (14)$$

$$[ArAlH_2]_2 + 4Me_3SiCl \xrightarrow{L} 2ArAlX_2(L) + 4Me_3SiH \quad (15)$$

This reaction proceeds smoothly at r.t. over a period of several hours. The presence of 1 or 2 equiv. of Et_2O or THF seems to be required, especially if $[ArAlH_2]_2$ is reacted with the chlorosilane (Eq. (15)). The aryl aluminum dichlorides are isolated in the form of their THF (Ar = Mes* [53]) or Et_2O adducts (Ar = 2,6-$Mes_2C_6H_3$, 2,6-$Trip_2C_6H_3$ [38]), $ArAlCl_2{\cdot}L$. The coordinated donor molecule can be removed under mild conditions to give the base free monomeric (Ar = Mes*) or dimeric (Ar = 2,6-$Mes_2C_6H_3$, 2,6-$Trip_2C_6H_3$) aryl aluminum dichlorides. By using only 2 equiv. of Me_3SiCl the potentially useful mixed aryl aluminum hydride halide $Mes^*Al(H)Cl{\cdot}THF$ can be isolated in good yield [53].

$$[Mes^*AlH_3Li(THF)_2]_2 + 4Me_3SiCl \rightarrow 2Mes^*Al(H)Cl{\cdot}THF + 4Me_3SiH + 2LiCl + 2THF \quad (16)$$

The major advantage of these reactions is that the Al–C bond remains unaffected, i.e. there is high selectivity

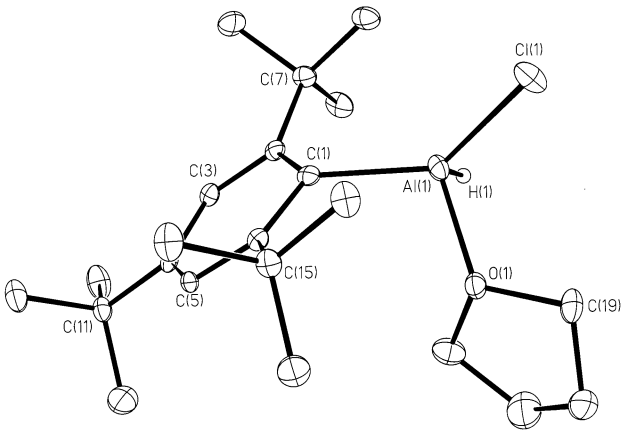


Fig. 4. Thermal ellipsoid plot (35%) of Mes*Al(H)Cl·THF. H-atoms except those bound to aluminum are not shown for clarity [53].

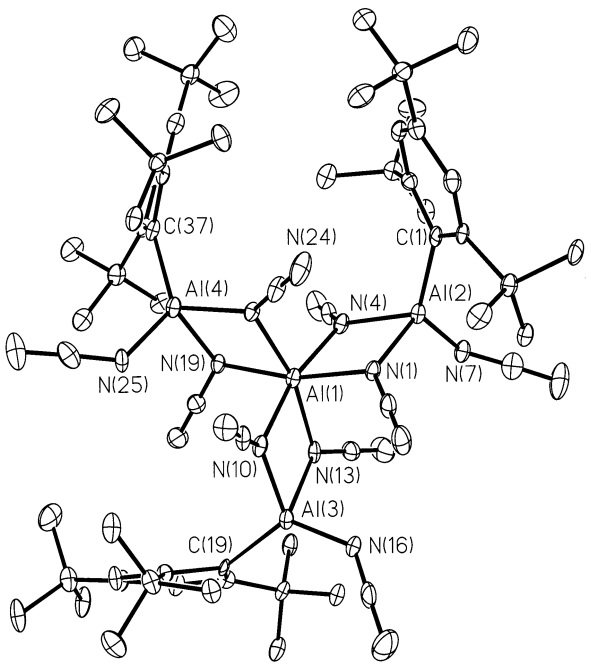


Fig. 5. Thermal ellipsoid plot (35%) of $[Mes*Al(N_3)]_3Al$. H-atoms are not shown for clarity [41].

even in the presence of high steric congestion. The steric crowding is illustrated in Fig. 4, which shows the distorted Mes* substituent in Mes*Al(H)Cl·THF. An additional practical advantage of the use of Me_3SiCl is that it can be used as a neat liquid, whereas the use of HX usually requires the setup of calibrated stock solutions.

Dehydrosilylation (Me_3SiH elimination) reactions have also led to novel organoaluminum azide and cyanide derivatives. Aluminum azides are currently of interest as possible precursors for AlN, an important ceramic material [56,57]. Aluminum cyanides may be of interest in the area of crystal engineering (cf. $Ga(CN)_3$ [58]).

The reaction of $[Mes*AlH_3Li(THF)_2]_2$ with Me_3SiN_3 afforded $[Mes*Al(N_3)_3Li(THF)_m]_n$ on the basis of NMR spectroscopic data, but no pure material could be isolated. However, the use of $[Mes*AlH_2]_2$ as starting material in the presence of at least 1 equiv. of THF resulted in the isolation of colorless, crystalline $Mes*Al(N_3)_2·THF$. The THF can easily be removed at 60–80°C under reduced pressure to give $[Mes*Al(N_3)_2]_n$ with a so far unknown structure. Repeated attempts at crystallization resulted in the isolation of a few colorless crystals of the unexpected azide $[Mes*Al(N_3)_3]_3Al$ (Fig. 5). However, the synthesis of this compound is difficult to reproduce [41].

Investigations on the NMR scale showed that $[Mes*AlH_2]_2$ reacted rapidly with Me_3SiCN at r.t., even in the absence of THF to give $[Mes*Al(CN)_2]_n$ and the concomitant Me_3SiH [41].

5. Aluminum chalcogen compounds

5.1. Aluminum alcoholates and thiolates

Aluminum alcoholates (i.e. alkoxides and aryloxides) are an industrially important class of compounds which may be illustrated by their use in, e.g. the Meerwein–Ponndorf–Verley reduction, i.e. the reduction of aldehydes to alcohols (Eq. (17)) [59], or as Lewis-acid catalysts in organic transformations such as Aldol reactions, Diels–Alder reactions [60] and polymerizations [61].

$$R{-}\overset{\overset{O}{\|}}{C}{-}R' + CH_3{-}\overset{\overset{OH}{|}}{CH}{-}CH_3 \xrightleftharpoons{Al(OCHMe_2)_3} R{-}\overset{\overset{OH}{|}}{CH}{-}R' + CH_3{-}\overset{\overset{O}{\|}}{C}{-}CH_3 \quad (17)$$

Their structure is generally not well defined and often consists of a mixture of oligomers connected by Al–O–Al linkages [62,63]. The coordination number at aluminum is four or higher, whereas that of oxygen is three. Large substituents and, sometimes, careful control of the reaction conditions can limit the amount of oligomerization and crystalline species may be isolated.

Common synthetic approaches to alcoholates have included the alcoholysis of Al–C and Al–H bonds, oxidation of organoaluminum compounds and reduction of carbonyl compounds. Until recently, low coordinate aluminum alcoholates were limited to bulky alkoxides or aryl oxides [64,65].

It was expected that the bulky primary alanes and alanates would be convenient starting materials for low coordinate and well-defined aluminum alcoholates $RAl(OR)_2$, which could be of interest as Lewis-acid catalysts in organic transformations [60].

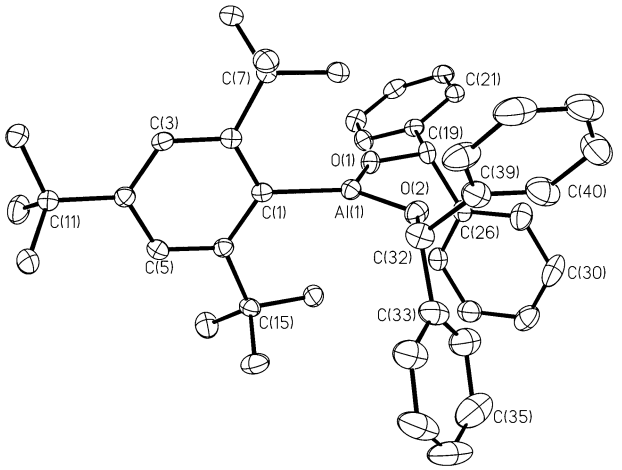


Fig. 6. Thermal ellipsoid plot (35%) of Mes*Al(OCH_2Ph)$_2$. H-atoms are not shown for clarity [41].

The compound [(Me_3Si)$_3$$CAlH_3Li(THF)_2$]$_2$ reacted with alcohols to give the organotrisalkoxy (or aryloxy) alanates (Me_3Si)$_3$$CAl(OR)_3Li(THF)_n$ ($n = 1$, R = Me, *i*-Pr, *t*-Bu, CH_2-*t*-Bu, CH_2Ph, $CHPh_2$; $n = 2$, R = Et, Ph; $n = 4$, R = Me) [66].

$$[(Me_3Si)_3CAlH_3Li(THF)_2]_2 + 6ROH \rightarrow 2(Me_3Si)_3CAl(OR)_3Li(THF)_n + 6H_2 \quad (18)$$

Reaction of [Mes*AlH_2]$_2$ with the geminal diol $Ph_2Si(OH)_2$ afforded only low yields of [Mes*Al-(μ-O)$_2$$SiPh_2$]$_n$. The main product was identified as the Al–C bond cleavage product Mes*H. A similar result was also observed in the reaction of [Mes*AlH_2]$_2$ with *i*-PrOH [67]. Again, the Al–C bond in [(Me_3Si)$_3$$CAlH_3$-$Li(THF)_2$]$_2$ remains intact, whereas significant bond cleavage was observed for [Mes*AlH_2]$_2$.

The reaction of aldehydes and ketones with aluminum hydrides provides an alternative and aprotic route to aluminum alcoholates [68].

$$>Al–H + O{=}CRR' \rightarrow >Al–OC(H)RR' \quad (19)$$

The lithium alanate [(Me_3Si)$_3$$CAlH_3Li(THF)_2$]$_2$ reacts smoothly with acetaldehyde, acetone, trimethylacetaldehyde, benzaldehyde and benzophenone to give the appropriate lithium trisalkoxy alanates [66]. As already seen, a LiOR elimination is not observed. Similarly, $BmtAlH_3Li(DME)_2$ was shown to reduce Ph_2CO and $PhCO_2Ph$ quantitatively to $PhCH_2OH$. The intermediate $BmtAl(OCH_2Ph_2)_3Li$ was characterized by ^1H and ^{27}Al NMR spectroscopy [43].

The lithium free alane [Mes*AlH_2]$_2$ afforded Mes*Al($OCHPh_2$)$_2$ upon treatment with benzaldehyde (Fig. 6). However, use of acetone at r.t. led to considerable Al–C bond cleavage, which was explained by formation of the corresponding enol, $CH_2{=}C(OH)CH_3$, a protic reagent. The ester ethyl acetate was cleanly reduced to [Mes*Al(OEt)$_2$]$_n$ and styrene oxide was regioselectively opened to [Mes*Al(H)OCH_2CH_2Ph]$_n$ [41].

Thiols and disulfides react with [(Me_3Si)$_3$$CAlH_3Li$-$(THF)_2$]$_2$ to afford the lithium tristhiolato aluminum compounds (Me_3Si)$_3$$CAl(SR)_3Li(THF)_2$, which have a structure similar to the related alkoxide derivatives [69]. The compound [Mes*AlH_2]$_2$ smoothly cleaved the Se–Se bond in diphenyl diselenide to give colorless crystals of [Mes*Al(H)$SePh$]$_n$, which can react with additional diphenyl diselenide to afford Mes*Al($SePh$)$_2$ [41].

5.2. Alumoxanes

The development of so-called 'single-site' olefin polymerization catalysts has increased the demand for alumoxanes (RAlO)$_n$ [70]. Despite of the huge quantities of alumoxanes, especially methyl alumoxane (MAO), being produced and consumed each year, their structure is only partially understood [71]. It is now clear that MAO probably consists of a mixture of oligomers with four-coordinate aluminum centers and three-coordinate oxygen donors [72]. In addition, there is also a significant portion that consists of complexed and free $AlMe_3$ present in commercial MAO solutions [73,74].

Controlled hydrolysis of *t*-Bu_3Al has afforded discrete and stable alumoxane molecules [*t*-BuAlO]$_n$ (n = 6–12), most of which were characterized by X-ray crystallography [75,76]. This work also established that even four-coordinate aluminum in these alumoxanes is sufficiently Lewis-acidic for use as a co-catalyst in the polymerization systems, and the term 'latent Lewis-acidity' was coined [77]. It was therefore of interest to learn if an alumoxane with three-coordinate aluminum centers (as was originally proposed for MAO) could be synthesized and what properties it would have. The Mes* substituent was thought to be bulky enough to stabilize a three-coordinate aluminum center in [Mes*AlO]$_n$. Initial attempts using [Mes*AlH_2]$_2$ and water or [2,6-$Mes_2C_6H_3AlH_2$]$_2$ and dry air only led to intractable mixtures [46]. Using HMPA as the oxygen source in Mes*AlH_2·$OP(NMe_2)_3$ required temperatures of ca. 135°C for a reaction to occur and resulted in the formation of the metallated alumoxane [2,4-*t*-Bu_2-(6-CMe_2CH_2)$C_6H_2Al(OP(NMe_2)_3)]_2O$ (Fig. 7). The sulfoxides DMSO and Ph_2SO reacted rapidly with [Mes*AlH_2]$_2$ to afford the desired alumoxane, [Mes*AlO]$_4$ (Fig. 8), in low to moderate yields. A high yield (ca. 80%) route was found by using the silane elimination method. The cyclic siloxane (Me_2SiO)$_3$ cleanly formed the alumoxane in refluxing benzene within a period of 12 h (Eq. (20))[78].

$$6[Mes^*AlH_2]_2 + 4(Me_2SiO)_3 \rightarrow 3[Mes^*AlO]_4 + 12Me_2SiH_2 \quad (20)$$

The more sterically encumbered siloxane (Me_3Si)$_2$O did not show any reactivity toward [Mes*AlH_2]$_2$. Interest-

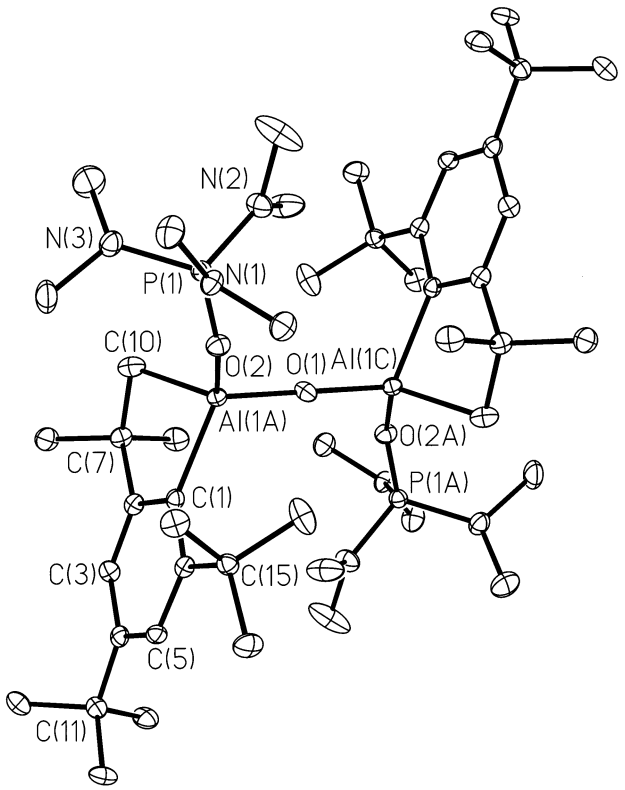


Fig. 7. Thermal ellipsoid plot (35%) of [2,4-*t*-Bu_2-(6-CMe_2CH_2)C_6H_2-$Al(OP(NMe_2)_3)]_2O$. H-atoms are not shown for clarity [46].

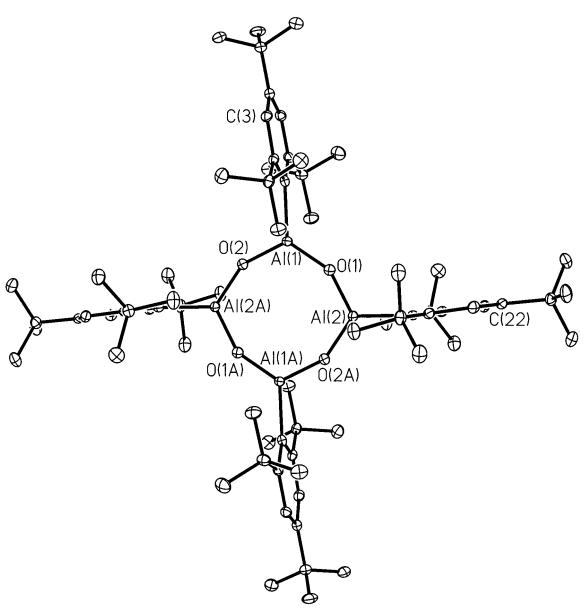


Fig. 8. Thermal ellipsoid plot (35%) of $[Mes*AlO]_4$. H-atoms are not shown for clarity [78].

ingly, the reaction of the terphenyl substituted primary alane $[2,6\text{-}Mes_2C_6H_3AlH_2]_2$ with $(Me_2SiO)_3$ required temperatures of 110–130°C and resulted in mixtures from which only $[2,6\text{-}Mes_2C_6H_3Al(Me)(\mu\text{-}H]_2$ could be isolated in crystalline form. In this case, a methyl group was transferred from silicon to aluminum by an, as yet, unknown pathway [41].

The structure of $[Mes*AlO]_4$ features a unique, almost planar, eight-membered Al_4O_4 ring with three-coordinate aluminum and two-coordinate oxygen (Fig. 8). Despite the low coordination number, no catalytic activity was observed in ethene polymerization experiments with Cp_2ZrMe_2. There was also no complex formation between $[Mes*AlO]_4$ and Cp_2ZrMe_2 or Cp_2ZrCl_2. However, the Lewis acidic $AlMe_3$ and $AlEt_3$ react with $[Mes*AlO]_4$ to give 'mixed' alumoxanes. One of the products of the $AlEt_3$ reaction was characterized by X-ray diffraction as $[Mes*(Et)AlOAlEt_2(Mes*AlO)]_2$ (Fig. 9), which is the only structurally characterized product formed by the reaction of an alumoxane with a trialkylalane [78]. A possible pathway may be initial complexation of AlR_3 by the oxygen donors of $[Mes*AlO]_4$ (cf. crown ethers and $AlMe_3$ [79]) followed by alkyl group migration and rearrangement.

The sulfur analogue, the dimeric $[Mes*AlS]_2$, whose structure is shown in Fig. 10, can also be obtained in

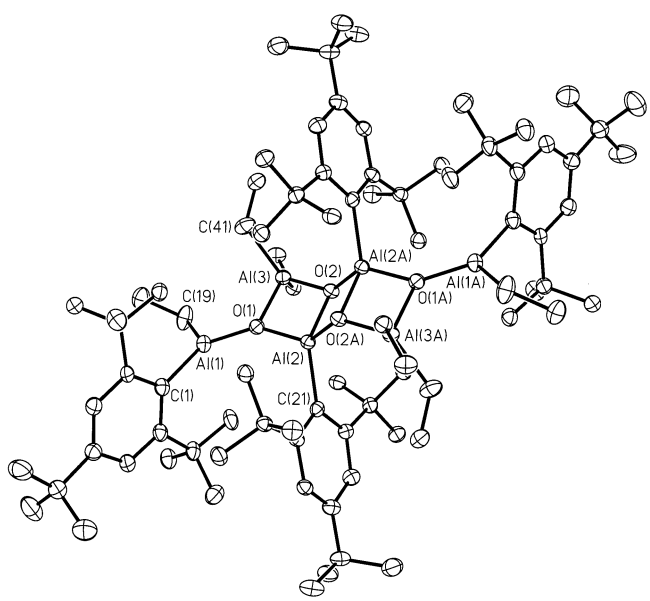


Fig. 9. Thermal ellipsoid plot (35%) of $[Mes*(Et)AlOAlEt_2$-$(Mes*AlO)]_2$. H-atoms are not shown for clarity [78].

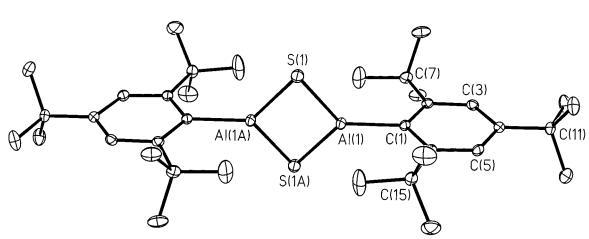


Fig. 10. Thermal ellipsoid plot (35%) of $[Mes*AlS]_2$. H-atoms are not shown for clarity [80].

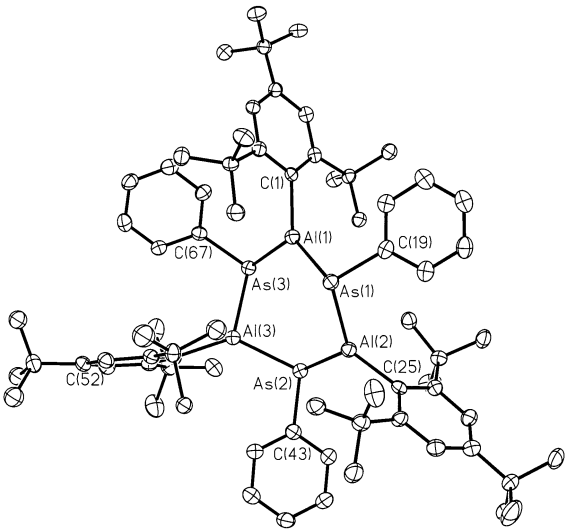


Fig. 11. Thermal ellipsoid plot (35%) of $[Mes^*AlAsPh]_3$. H-atoms are not shown for clarity [85].

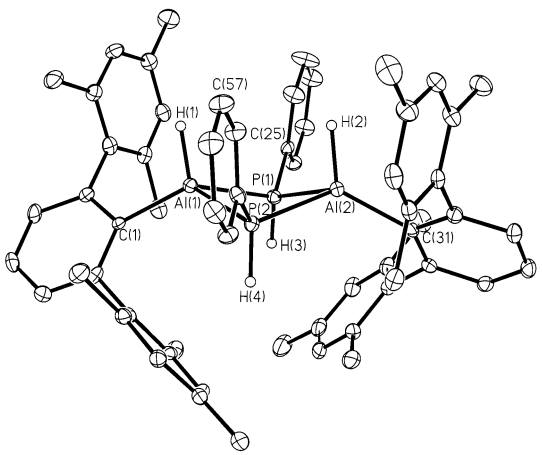


Fig. 12. Thermal ellipsoid plot (35%) of $[2,6\text{-}Mes_2C_6H_3Al(H)P(H)Ph]_2$. H-atoms except those bound to aluminum or phosphorus are not shown for clarity [87].

high yields by the dehydrosilylation method. Here, $(Me_3Si)_2S$ is sufficiently reactive to afford the product in almost quantitative yields [80].

6. Aluminum pnictogen compounds

The synthesis of the 'alumazene' $[MeAlNDipp]_3$ ($Dipp = C_6H_3\text{-}2,6\text{-}i\text{-}Pr_2$) in 1988 [81] sparked interest in the synthesis of low-coordinate aluminum pnictogen compounds to study the possibility of multiple bonding between these elements [65]. In addition, some work has concentrated on finding (molecular) precursors for the synthesis of AlE insulators (E = N) [82,83] and semiconductors (E = P, As, Sb) [35,84]. Primary alanes with bulky substituents were therefore expected to be ideal starting materials for the synthesis of low-coordinate aluminum pnictogen compounds $[RAlER']_n$ or $RAl(EHR')_2$ (Eqs. (21) and (22)).

$$RAlH_2 + H_2ER \xrightarrow{-H_2} RAl(H)E(H)R' \xrightarrow{-H_2} 1/n[RAlER']_n \quad (21)$$

$$RAlH_2 + 2H_2ER \xrightarrow{-2H_2} RAl(EHR')_2 \quad (22)$$

Accordingly, $[Mes^*AlH_2]_2$ was found to react cleanly at elevated temperatures with H_2NPh and H_2NSiPh_3 to give the dimeric imides $[Mes^*AlNPh]_2$ [85] and $[Mes^*AlNSiPh_3]_2$ [86], which have planar Al_2N_2 cores. The trimeric aluminum phosphide and arsenide compounds $[Mes^*AlEPh]_3$ (E = P, As) were produced similarly [85]. The latter two compounds are formally heavier element Group 13–15 analogs of benzene. The crystal structures, however, showed a significant degree of pyramidalization at the phosphorus or arsenic atoms (Fig. 11), so that extensive aromatic delocalization can be largely ruled out.

The intermediate, a mixed hydride pnictide RAl(H)E(H)R′, could not be isolated. In fact, ^1H NMR studies on the $[Mes^*AlH_2]_2$–H_2NPh system showed an equilibrium involving $[Mes^*AlH_2]_2$, $[Mes^*Al(H)N(H)NPh]_n$ and $Mes^*Al(N(H)Ph)_2$. The latter compound could be crystallized and characterized by X-ray diffraction. The reaction of the bulkier amine $DippNH_2$ with $[Mes^*AlH_2]_2$ afforded the bisamide $Mes^*Al(N(H)Dipp)_2$ as the only isolable product [85]. Interestingly, the benzylamine H_2NCH_2Mes does not form the expected imide either. C–H activation is observed instead [86].

The terphenyl substituted primary alane $[2,6\text{-}Mes_2C_6H_3AlH_2]_2$ reacts smoothly with H_2NPh and H_2AsPh at r.t. For the reaction with H_2PPh a temperature of ca. 160°C was required. Here, the products are the dimeric mixed hydride pnictide compounds $[2,6\text{-}Mes_2C_6H_3Al(H)E(H)Ph]_2$ (Fig. 12). Elimination of the 2nd equiv. of H_2 was accompanied by decomposition. However, in the presence of excess H_2AsPh at 150–160°C $[2,6\text{-}Mes_2C_6H_3AlH_2]_2$ reacted to form an interesting Al–As cage compound $[(2,6\text{-}Mes_2C_6H_3Al)_2\{\mu\text{-}As(H)Ph\}_2(\mu\text{-}PhAsAsPh)]$ with an As–As bond [87].

In order to probe the feasibility of dehydrosilylation for the synthesis of Al–N compounds (with the goal of making AlN) the mixed aluminum hydride amide $Mes^*Al(H)N(SiMe_3)_2$ was synthesized (Eq. (23)). An alternative method, the reaction of $LiN(SiMe_3)_2$ with $[Mes^*AlH_2]_2$ also gave $Mes^*Al(H)N(SiMe_3)_2$, but in yields of less than 40% due to competing Mes*Li elimination.

$$[Mes^*AlH_2]_2 + 2HN(SiMe_3)_2 \rightarrow 2Mes^*Al(H)N(SiMe_3)_2 + H_2 \quad (23)$$

The crystal structure revealed a planar C(*ipso*)Al(H)N core with the hydride and one of the Me_3Si substituents in a *cis* configuration, an orientation which should

support Me_3SiH elimination. However, at the temperatures required for a reaction to occur, competing reactions such as C–H activation and ligand migration also take place. The formal dehydrosilylation product was formed in only 7% yield [88]. An unusually high rotational barrier around the Al–N bond of 18.5(2) kcal mol^{-1} was measured for $Mes^*Al(H)N(SiMe_3)_2$. Crystal structure data indicate that this is more likely due to steric constraints than Al–N π-bonding.

The lithium alanate $[(Me_3Si)_3CAlH_3Li(THF)_2]_2$ reacts with aniline to give the lithium alkylbis(amido)-hydroalanate $(Me_3Si)_3CAlH(\mu\text{-}N(H)Ph)_2Li(THF)_2$ or the alkyltris(amido)alanate $(Me_3Si)_3CAl\{N(H)Ph\}_3Li(THF)_4$, depending on the amount of aniline added [42].

Aluminum nitrogen bonds may also be formed by the reaction of aluminum hydrides with nitriles or isonitriles. The former reaction, i.e. the reduction of nitriles, is a general procedure in organic chemistry (Eq. (24)) [89].

$$>Al\text{–}H \xrightarrow{N\equiv CR} \text{–}Al(H)N{=}C(H)R \rightarrow \text{‘–}Al{=}NCH_2R\text{’} \quad (24)$$

Reaction of $[Mes^*AlH_2]_2$ with nitriles RCN (R = Me, *t*-Bu, Mes) gives the *ortho*-metalated dimers, *cis* and *trans* $[AlC_6H_2\text{-}2,4\text{-}t\text{-}Bu_2\text{-}6\text{-}CMe_2CH_2\{\mu^2\text{-}N(H)CH_2R\}]_2$. In the case of R = *t*-Bu the intermediate $[Mes^*Al(H)N{=}C(H)R]_2$ can be isolated. The formation of an aluminum imide $[Mes^*AlNCH_2R]_n$ was not observed [86]. Similarly, the lithium alanate $BmtAlH_3Li(DME)_2$ was reported to reduce PhCN in a stepwise fashion to PhCH=NH and then $PhCH_2NH_2$ [43]. The isonitrile *t*-BuNC is cleanly reduced to $[Mes^*AlN(t\text{-}Bu)CH_2]_2$, a C- and N-metalated methylbutylamine. No intermediate was isolated. The dimeric compound, which features a six-membered $(AlNC)_2$ ring can be described as a heavier analog of a substituted 1,4-cyclohexadiene (Fig. 13). Refluxing in benzene for 1 h also led to C–H activation of the *o*-*t*-Bu groups of the Mes* substituent [86].

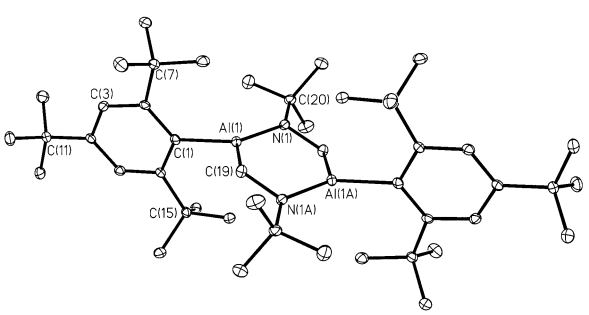


Fig. 13. Thermal ellipsoid plot (35%) of to $[Mes^*AlN(t\text{-}Bu)CH_2]_2$. H-atoms are not shown for clarity [86].

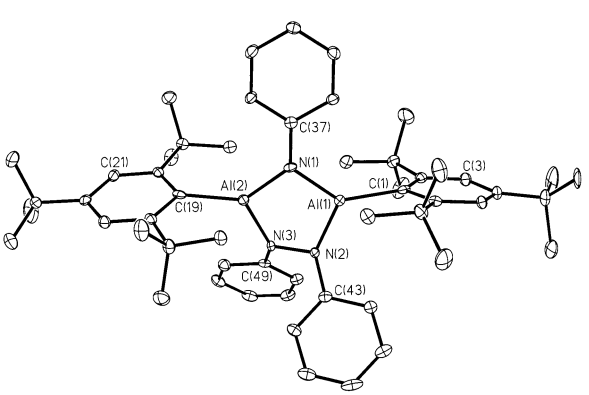


Fig. 14. Thermal ellipsoid plot (35%) of $Mes^*AlN(Ph)Al(Mes^*)N(Ph)NPh$. H-atoms are not shown for clarity [90].

The alane $[Mes^*AlH_2]_2$ also reacts with azobenzene (Eq. (25)) or 1,2-diphenyl hydrazine (Eq. (26)) to give the unique five-membered ring compound $Mes^*\overline{AlN(Ph)Al(Mes^*)N(Ph)N}Ph$, which is a formal aluminum–nitrogen analog of the cyclopentadienide anion, and $[Mes^*AlNPh]_2$ [90].

$$3/2[Mes^*AlH_2]_2 + 2PhNNPh \rightarrow Mes^*\overline{AlN(Ph)Al(Mes^*)N(Ph)N}Ph + 1/2[Mes^*AlNPh]_2 + 3H_2 \quad (25)$$

$$3/2[Mes^*AlH_2]_2 + 2Ph(H)NN(H)Ph \rightarrow Mes^*\overline{AlN(Ph)Al(Mes^*)N(Ph)N}Ph + 1/2[Mes^*AlNPh]_2 + 5H_2 \quad (26)$$

The five-membered ring compound can be viewed as an intermediate in the reduction of diazenes and hydrazines to amines. Fig. 14 shows that the product has a nonplanar Al_2N_3 core indicating little if any π-electron delocalization. This result is in agreement with recent theoretical calculations on the parent compound $H\overline{AlN(H)AlN(H)N}H$ [91].

An NMR experiment to investigate the donor properties of pyridine towards $[Mes^*AlH_2]_2$ showed a rapid 1,2 and 1,4 addition of the Al–H group to give Mes*Al(1,2-dihydropyridyl)- and Mes*Al(1,4-dihydropyridyl)-containing compounds. Isomerization to primarily the 1,4 addition products occurs over a period of 14 days [92]. A similar reaction has also been observed for $LiAlH_4$ and pyridine [93,94]. This reaction was found to be reversible, so that lithium tetrakis-(*N*-dihydropyridyl)-alanate could be used as a mild hydride donor for the reduction of ketones.

7. Miscellaneous reactions

A synthetically very useful reaction is the hydroalumination of alkenes and alkynes, i.e. the formal addition of Al–H across a double or triple bond [95,96].

$$>Al\text{–}H + R_2C{=}CR_2 \rightarrow >Al\text{–}CR_2\text{–}C(H)R_2 \quad (27)$$

The most common reagent employed is the secondary alane $(i\text{-}Bu_2AlH)_3$ and the reaction may be promoted

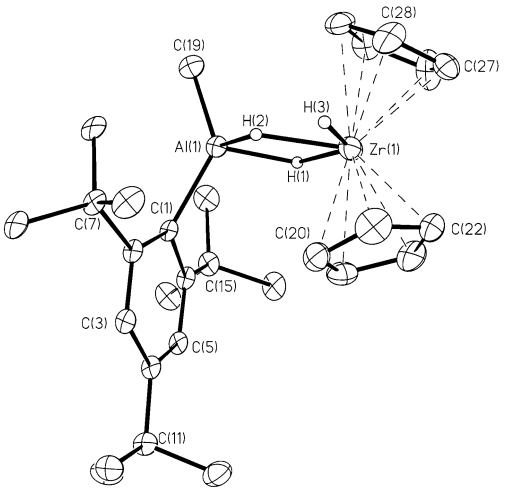


Fig. 15. Thermal ellipsoid plot (35%) of Mes*Al(Me)(μ-H)$_2$Zr(H)Cp$_2$. H-atoms except of those bound to aluminum or zirconium are not shown for clarity [97].

by transition-metal catalysts. Interestingly, [Mes*AlH$_2$]$_2$ does not react with internal alkynes RC≡CR (R = Me, Ph, Me$_3$Si) at temperatures below its melting/decomposition point. A complicated product mixture was obtained when [Mes*AlH$_2$]$_2$ and Me$_3$SiC≡CSiMe$_3$ were reacted at 170°C. The addition of donors like THF did not influence the outcome of these reactions [92].

Similary, there was also no reaction between the weak organic acid CpH and [Mes*AlH$_2$]$_2$, even in refluxing benzene with or without THF added [67].

Addition of Cp$_2$ZrMe$_2$ to [Mes*AlH$_2$]$_2$ in hexane or benzene resulted in methyl and hydride exchange to give a mixture of Cp$_2$ZrH$_2$, Mes*AlMe$_2$ and Mes*Al(Me)(μ-H)$_2$Zr(H)Cp$_2$. The latter compound was characterized by X-ray crystallography (Fig. 15) [97]. It can be viewed as an intermediate in the methyl and hydride exchange reaction. A related methyl free mixed hydride species, Mes*Al(H)(μ-H)$_2$Zr(H)Cp$_2$, can be obtained by the reaction of Cp$_2$Zr(H)Cl with [Mes*AlH$_3$Li(THF)$_2$]$_2$. Its structure is probably similar to the methyl-containing compound according to IR and NMR spectroscopic results. Preliminary experiments concerning the reaction of Mes*Al(H)(μ-H)$_2$-Zr(H)Cp$_2$ with PhC≡CPh or its use as a catalyst in the reaction of [Mes*AlH$_2$]$_2$ with PhC≡CPh afforded only complicated intractable mixtures.

Reactions of [Mes*AlH$_2$]$_2$ with other transition-metal complexes like Cp$_2$MoH$_2$ or (Cy$_3$P)$_2$Ni with the goal of synthesizing compounds with metal–aluminum bonds led to decomposition of the alane [92].

8. Summary

Aluminum hydrides have been widely used in many areas of chemistry since their first isolation in the 1940s. The employment of large sterically protecting substituents has only recently allowed the synthesis and systematic study of the reactivity and structures of primary alanes RAlH$_2$ and the related trihydroalanates RAlH$_3$Li. These new compounds are crystalline and thermally stable. The steric bulk of the substituents makes it possible to isolate intermediates in a variety of 'organic' reductions. In addition, the compound [Mes*AlH$_2$]$_2$ has been shown to be a uniquely suitable starting material for low coordinate aluminum compounds, which could not be synthesized by alternative routes. These species with Al–N, Al–P, Al–As, Al–O and Al–S bonds have contributed significantly to the current knowledge of the ability of aluminum to engage in multiple bonding [65]. Finally, the dehydrosilylation reaction has proven to be a convenient method for the formation of aluminum heteroelement bonds. This is also transferable to 'simple' systems such as the reaction of H$_3$Al·NMe$_3$ with (Me$_3$Si)$_2$S to afford the cluster (Me$_3$NAl)$_4$S$_6$, essentially a solvated form of the inorganic salt Al$_2$S$_3$ [98].

Acknowledgements

We thank the National Science Foundation and the donors of the Petroleum Research Fund administered by the American Chemical Society for financial support.

References

[1] S. Cucinella, A. Mazzei, W. Marconi, Inorg. Chim. Acta Rev. 4 (1970) 51.
[2] C. Jones, G.A. Koutsantonis, C.R. Raston, Polyhedron 12 (1993) 1829.
[3] A.J. Downs, C.R. Pulham, Chem. Soc. Rev. 23 (1994) 175.
[4] A.J. Downs, C.R. Pulham, Adv. Inorg. Chem. 41 (1994) 171.
[5] C.L. Raston, J. Organomet. Chem. 475 (1994) 15.
[6] A.H. Cowley, F.P. Gabbaï, H.S. Isom, A. Decken, J. Organomet. Chem. 500 (1995) 81.
[7] M.G. Gardiner, C.R. Raston, Coord. Chem. Rev. 166 (1997) 1.
[8] A.J. Downs, Coord. Chem. Rev. 189 (1999) 59.
[9] O. Stecher, E. Wiberg, Ber. Dtsch. Chem. Ges. 75 (1942) 2003.
[10] A.E. Finholt, J.A.C. Bond, H.I. Schlesinger, J. Am. Chem. Soc. 69 (1947) 1199.
[11] N.G. Gaylord, Reduction with Complex Metal Hydrides, Interscience, New York, 1956, p. 1046.
[12] M. Hudlicky, Reductions in Organic Chemistry, second ed., American Chemical Society, Washington, DC, 1996, p. 429.
[13] A.P. Davis, in: G. Helmchen, R.W. Hoffmann, J. Mulzer, E. Schaumann (Eds.), Methods of Organic Chemistry, Vol. E21d, Ch. 2.3.3.1, Georg Thieme, Stuttgart, 1995.
[14] J. Málek, Org. React. 34 (1985) 1.
[15] J. Málek, Org. React. 36 (1988) 249.
[16] M.J. Taylor, P.J. Brothers, in: A.J. Downs (Ed.), Chemistry of Aluminum, Gallium, Indium and Thallium, Blackie-Chapman Hall, London, 1993, p. 118.
[17] F.M. Peters, B. Bartocha, Chem. Ind. (1961) 1271.

[18] F.M. Peters, B. Bartocha, A.J. Bilbo, Can. J. Chem. 41 (1963) 1051.
[19] A. Storr, V.G. Wiebe, Can. J. Chem. 47 (1969) 674.
[20] R. Ehrlich, C.B. Parisek, G. Rice, Inorg. Chem. 4 (1965) 1075.
[21] J.R. Surtees, Chem. Ind. (1964) 1260.
[22] M.T. Barlow, C.J. Dain, A.J. Downs, P.D.P. Thomas, D.W.H. Rankin, J. Chem. Soc., Dalton Trans. (1980) 1374.
[23] A.I. Sizov, I.V. Molodnitskaya, B.M. Bulychev, E.V. Evdokimora, V.K. Bel'skii, G.L. Soloveichik, J. Organomet. Chem. 344 (1988) 293.
[24] L. Contreras, A.H. Cowley, F.P. Gabbaï, R.A. Jones, C.J. Carrano, M.R. Bond, J. Organomet. Chem. 489 (1995) C1.
[25] M. Stender, U. Segerer, J. Sieler, E. Hey-Hawkins, Z. Anorg. Allg. Chem. 624 (1998) 85.
[26] H.S. Isom, A.H. Cowley, A. Decken, F. Sissingh, S. Corbelin, R.J. Lagow, Organometallics 14 (1995) 2400.
[27] U. Dümichen, K.-H. Thiele, T. Gelbrich, J. Sieler, J. Organomet. Chem. 495 (1995) 71.
[28] K.N. Semenenko, E.B. Lobkovshii, A.L. Dorosinskii, J. Struct. Chem. (USSR) 13 (1972) 696.
[29] K. Ouzounis, H. Riffel, H. Hess, U. Kohler, J. Weidlein, Z. Anorg. Allg. Chem. 504 (1983) 67.
[30] A.J. Downs, D. Duckworth, J.C. Machell, C.R. Pulham, Polyhedron 11 (1992) 1295.
[31] C. Jones, F.C. Lee, G.A. Koutsantonis, M.G. Gardiner, C.L. Raston, J. Chem. Soc., Dalton Trans. (1996) 829.
[32] M. Veith, S. Faber, H. Wolfanger, V. Huch, Chem. Ber. 129 (1996) 381.
[33] H. Nöth, A. Schlegel, J. Knizek, H. Schwenk, Angew. Chem., Int. Ed. Engl. 36 (1997) 2640.
[34] G.A. Koutsantonis, F.C. Lee, C.L. Raston, Main Group Chem. 1 (1995) 21.
[35] J.F. Janik, R.L. Wells, P.S. White, Inorg. Chem. 37 (1998) 3561.
[36] R.J. Wehmschulte, J.J. Ellison, K. Ruhlandt-Senge, P.P. Power, Inorg. Chem. 33 (1994) 6300.
[37] R.J. Wehmschulte, P.P. Power, Inorg. Chem. 33 (1994) 5611.
[38] R.J. Wehmschulte, W.J. Grigsby, B. Schiemenz, R.A. Bartlett, P.P. Power, Inorg. Chem. 35 (1996) 6694.
[39] L.I. Zakharkin, V.V. Gavrilenko, Bull. Acad. Sci. USSR, Chem. Sci. Ser. (1965) 624.
[40] C. Eaborn, I.B. Gorrell, P.B. Hitchcock, J.D. Smith, K. Tavakkoli, Organometallics 13 (1994) 4143.
[41] R.J. Wehmschulte, P.P. Power, unpublished results, 1997.
[42] S.S. Al-Juaid, C. Eaborn, I.B. Gorrell, S.A. Hawkes, P.B. Hitchcock, J.D. Smith, J. Chem. Soc., Dalton Trans. (1998) 2411.
[43] K. Goto, J. Kobayashi, R. Okazaki, Organometallics 18 (1999) 1357.
[44] A.A. Avent, C. Eaborn, P.B. Hitchcock, J.D. Smith, A.C. Sullivan, J. Chem. Soc., Chem. Commun. (1986) 988.
[45] C. Eaborn, S.M. El-Hamruni, M.S. Hill, P.B. Hitchcock, M. Hopman, A. Le Gouic, J.D. Smith, J. Organomet. Chem. 597 (2000) 3.
[46] R.J. Wehmschulte, P.P. Power, unpublished results, 1996.
[47] G.E. Coates, M.L.H. Green, K. Wade, Organometallic Compounds, third ed., Methuen, London, 1967, p. 337.
[48] J.J. Eisch, in: G. Wilkinson, F.G.A. Stone, E.W. Abel (Eds.), Comprehensive Organometallic Chemistry, Pergamon Press, Oxford, 1982, p. 631.
[49] R.J. Wehmschulte, P.P. Power, unpublished results, 1993.
[50] C. Eaborn, M.N. El-Kheli, N. Retta, J.D. Smith, J. Organomet. Chem. 249 (1983) 23.
[51] M.A. Petrie, P.P. Power, H.V.R. Dias, K. Ruhlandt-Senge, K.M. Waggoner, R.J. Wehmschulte, Organometallics 12 (1993) 1086.
[52] X.-W. Li, J. Su, G.H. Robinson, Chem. Commun. (1998) 1281.
[53] R.J. Wehmschulte, P.P. Power, Inorg. Chem. 35 (1996) 3262.
[54] C. Schnitter, K. Klimek, H.W. Roesky, T. Albers, H.-G. Schmidt, C. Roepken, E. Parisini, Organometallics 17 (1998) 2249.
[55] A.G. Avent, W.-Y. Chen, C. Eaborn, I.B. Gorrell, P.B. Hitchcock, J.D. Smith, Organometallics 15 (1996) 4343.
[56] R.A. Fischer, A. Miehr, H. Sussek, H. Pritzkow, E. Herdtweck, J. Müller, O. Ambacher, T. Metzger, J. Chem. Soc., Chem. Commun. (1996) 2685.
[57] M.-A. Munoz-Hernandez, D. Rutherford, H. Tiainen, D.A. Atwood, J. Organomet. Chem. 582 (1999) 103.
[58] L.C. Brousseau, D. Williams, J. Kouvetakis, M. O'Keeffe, J. Am. Chem. Soc. 119 (1997) 6292.
[59] J. March, Advanced Organic Chemistry, fourth ed., Wiley, New York, 1992, p. 913 and 917.
[60] S. Saito, H. Yamamoto, J. Chem. Soc., Chem. Commun. (1997) 1585.
[61] T. Kitayama, T. Hirano, K. Hatada, Tetrahedron 53 (1997) 15263.
[62] D.C. Bradley, R.C. Mehrotra, D.P. Gaur, Metal Alkoxides, Academic, New York, 1978.
[63] K. Folting, W.E. Streib, K.G. Caulton, O. Poncelet, L.G. Hubert-Pfalzgraf, Polyhedron 10 (1991) 1639.
[64] M.D. Healy, A.R. Barron, Angew. Chem., Int. Ed. Engl. 31 (1992) 921.
[65] P.J. Brothers, P.P. Power, Adv. Organomet. Chem. 39 (1996) 1.
[66] W.-Y. Chen, C. Eaborn, I.B. Gorrell, P.B. Hitchcock, M. Hopman, J.D. Smith, J. Chem. Soc., Dalton Trans. (1997) 4689.
[67] R.J. Wehmschulte, P.P. Power, unpublished results, 1995.
[68] J. March, Advanced Organic Chemistry, fourth ed., Wiley, New York, 1992, pp. 910–918.
[69] C. Eaborn, J.D. Smith, Coord. Chem. Rev. 154 (1996) 125.
[70] P.M. Morse, Chem. Eng. News 76 (49) (1998) 25.
[71] F.A. Cotton, G. Wilkinson, C.A. Murillo, M. Bochmann, Advanced Inorganic Chemistry, sixth ed., Wiley, New York, 1999, p. 198.
[72] H. Sinn, Macromol. Symp. 97-Alumoxanes 97 (1995) 27.
[73] D.W. Imhoff, L.S. Simeral, S.A. Sangokoya, J.H. Peel, Organometallics 17 (1998) 1941.
[74] A.R. Barron, Organometallics 14 (1995) 3581.
[75] M.R. Mason, J.M. Smith, S.G. Bott, A.R. Barron, J. Am. Chem. Soc. 115 (1993) 4971.
[76] C.J. Harlan, M.R. Mason, A.R. Barron, Organometallics 13 (1994) 2957.
[77] C.J. Harlan, S.G. Bott, A.R. Barron, J. Am. Chem. Soc. 117 (1995) 6465.
[78] R.J. Wehmschulte, P.P. Power, J. Am. Chem. Soc. 119 (1997) 8387.
[79] J.L. Atwood, D.C. Hrncir, R. Shakir, M.S. Dalton, R.D. Priester, R.D. Rogers, Organometallics 1 (1982) 1021.
[80] R.J. Wehmschulte, P.P. Power, J. Chem. Soc., Chem. Commun. (1998) 335.
[81] K.M. Waggoner, H. Hope, P.P. Power, Angew. Chem., Int. Ed. Engl. 27 (1988) 1699.
[82] J.F. Janik, E.N. Duesler, R.T. Paine, J. Organomet. Chem. 539 (1997) 19.
[83] M.G. Gardiner, G.A. Koutsantonis, S.M. Lawrence, F.-C. Lee, C.L. Raston, Chem. Ber. 129 (1996) 545.
[84] S. Schulz, M. Nieger, Organometallics 17 (1998) 3398.
[85] R.J. Wehmschulte, P.P. Power, J. Am. Chem. Soc. 118 (1996) 791.
[86] R.J. Wehmschulte, P.P. Power, Inorg. Chem. 37 (1998) 6906.
[87] R.J. Wehmschulte, P.P. Power, New J. Chem. 22 (1998) 1125.
[88] R.J. Wehmschulte, P.P. Power, Inorg. Chem. 37 (1998) 2106.
[89] J. Seyden-Penne, Reductions by the Alumino- and Borohydrides in Organic Synthesis, VCH, New York, 1991, pp. 129–135.

[90] R.J. Wehmschulte, P.P. Power, Inorg. Chem. 35 (1996) 2717.
[91] L. Nyulaszi, J. Chem. Soc., Dalton Trans. (1997) 2373.
[92] R.J. Wehmschulte, P.P. Power, unpublished results, 1994.
[93] P.T. Lansbury, J.O. Peterson, J. Am. Chem. Soc. 85 (1963) 2236.
[94] K. Hensen, A. Lemke, T. Stumpf, M. Bolte, H. Fleischer, C.R. Pulham, R.O. Gould, S. Harris, Inorg. Chem. 38 (1999) 4700.
[95] J.J. Eisch, in: B.M. Trost, I. Fleming (Eds.), Comprehensive Organic Synthesis, Pergamon, New York, 1991, pp. 733–761.
[96] G. Zweifel, J.A. Miller, Org. React. 32 (1984) 375.
[97] R.J. Wehmschulte, P.P. Power, Polyhedron 18 (1999) 1885.
[98] R.J. Wehmschulte, P.P. Power, J. Am. Chem. Soc. 119 (1997) 9566.
[99] C. Eaborn, P.B. Hitchcock, J.D. Smith, S.E. Sözerli, Organometallics 17 (1998) 4322.
[100] A. Heine, D. Stalke, Angew. Chem., Int. Ed. Engl. 31 (1992) 854.
[101] H. Nöth, A. Schlegel, J. Knizek, I. Krossing, W. Ponikwar, T. Seifert, Chem. Eur. J. 4 (1998) 2191.

PERGAMON

www.elsevier.nl/locate/poly

Polyhedron 19 (2000) 1663–1672

POLYHEDRON

Chemistry of ruthenium with some phenolic ligands: synthesis, structure and redox properties

Falguni Basuli[a], Anjan Kumar Das [a], Golam Mostafa [b], Shie-Ming Peng [c], Samaresh Bhattacharya [a,*]

[a] *Department of Chemistry, Inorganic Chemistry Section, Jadavpur University, Calcutta 700032, India*
[b] *Department of Physics, Krishnath College, Berhampur, West Bengal, India*
[c] *Department of Chemistry, National Taiwan University, Taipei, Taiwan, ROC*

Received 11 January 2000; accepted 11 April 2000

Abstract

Reaction of three phenolate ligands, viz. salicylaldehyde (HL^1), 2-hydroxyacetophenone (HL^2) and 2-hydroxynaphthylaldehyde (HL^3), (abbreviated in general as HL, where H stands for the phenolic proton) with $[Ru(PPh_3)_3Cl_2]$ in 1:1 mole ratio gives complexes of the type $[Ru(PPh_3)_2(L)Cl_2]$. The structure of the $[Ru(PPh_3)_2(L^2)Cl_2]$ complex has been solved by X-ray crystallography. The coordination sphere around ruthenium is $O_2P_2Cl_2$ with a *cis–trans–cis* geometry, respectively. The $[Ru(PPh_3)_2(L)Cl_2]$ complexes are one-electron paramagnetic (low-spin d^5, $S = 1/2$) and show rhombic ESR spectra in 1:1 dichloromethane–toluene solution at 77 K. In dichloromethane solution the $[Ru(PPh_3)_2(L)Cl_2]$ complexes show several intense LMCT transitions in the visible region. Reaction between the phenolic ligands and $[Ru(PPh_3)_3Cl_2]$ in 2:1 mole ratio in the presence of a base affords the $[Ru(PPh_3)_2(L)_2]$ complexes in two isomeric forms. ^1H NMR spectra of one isomer shows that it does not have any C_2 symmetry and has the *cis–cis–cis* disposition of the three sets of donor atoms. ^1H NMR spectra of the other isomer shows that it has C_2 symmetry. The structure of the isomer of the $[Ru(PPh_3)_2(L^1)_2]$ complex has been solved by X-ray crystallography. The coordination sphere around ruthenium is O_4P_2 with a *cis–trans–cis* disposition of the carbonylic oxygens, phenolate oxygens and phosphorus atoms, respectively. The $[Ru(PPh_3)_2(L)_2]$ complexes are diamagnetic (low-spin d^6, $S = O$) and show intense MLCT transitions in the visible region. Cyclic voltammetry on the $[Ru(PPh_3)_2(L)Cl_2]$ complexes shows a ruthenium(III)–ruthenium(II) reduction near -0.3 V versus SCE and a ruthenium(III)–ruthenium(IV) oxidation in the range 1.08–1.24 V versus SCE. Cyclic voltammetry on both isomers of the $[Ru(PPh_3)_2(L)_2]$ complexes shows a ruthenium(II)–ruthenium(III) oxidation within 0.09–0.41 V versus SCE, followed by a ruthenium(III)-ruthenium(IV) oxidation within 1.31–1.52 V versus SCE. © 2000 Elsevier Science Ltd. All rights reserved.

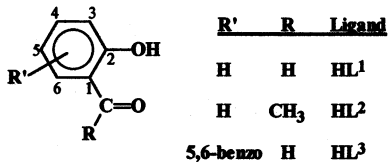
Keywords: Ruthenium; Phenolic ligands; Synthesis; Structure; Redox properties

1. Introduction

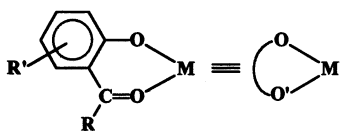
The chemistry of ruthenium has currently been receiving a lot of attention [1–10] primarily because of the fascinating electron-transfer and energy-transfer properties displayed by the complexes of this metal. Ruthenium offers a wide range of oxidation states and the reactivities of the ruthenium complexes depend on the stability and interconvertibility of these oxidation states, which in turn depend on the nature of ligands bound to the metal. Complexation of ruthenium by ligands of different types has thus been of particular interest. In the present study, which has originated from our interest in the chemistry of ruthenium in different coordination environments [11–18], we have chosen phenolic ligands of type **1** as the principal ligand, which are abbreviated in general as HL where H stands for the dissociable phenolic proton. The deprotonated ligands are known to coordinate metal ions as bidentate O,O-donor forming six-membered chelate rings (**2**) [19,20]. Three different phenolic ligands have been used in this study, which are shown in **1** along with their specific abbreviations.

* Corresponding author. Fax: +91-33-473-4266.
E-mail address: samaresh_b@hotmail.com (S. Bhattacharya).

0277-5387/00/$ - see front matter © 2000 Elsevier Science Ltd. All rights reserved.
PII: S0277-5387(00)00404-6



1



2

While phenolate oxygen is a recognized hard donor, and coordination by it is known to stabilize the higher oxidation states of ruthenium [21–23], coordination of metals by carbonylic oxygen has also recently been of considerable interest in bioinorganic chemistry [24–28]. It may be mentioned here that ruthenium chemistry of these ligands has not been explored much [19]. Stability of different oxidation states of ruthenium is expected to depend on the number of phenolate and carbonylic oxygen in the coordination sphere and in the case of mixed-ligand complexes, on the nature of coligands also. Herein we have restricted our studies to some mono- and bis-phenolate complexes of ruthenium, which have been synthesized by reacting the phenolic ligands with $[Ru(PPh_3)_3Cl_2]$ under different experimental conditions. The chemistry of complexes of the type $[Ru(PPh_3)_2(L)Cl_2]$ and $[Ru(PPh_3)_2(L)_2]$ has been described in this paper with special reference to synthesis, stereoisomerism and electron-transfer properties.

2. Experimental

2.1. Materials

Commercial ruthenium trichloride was purchased from Arora Matthey, Calcutta, India, and was converted into $RuCl_3 \cdot 3H_2O$ by repeated evaporation with concentrated hydrochloric acid. Triphenylphosphine (PPh_3), triethylamine (NEt_3) and salicylaldehyde (HL^1) were obtained from SD, India. 2-Hydroxyacetophenone (HL^2) and 2-hydroxynaphthaldehyde (HL^3) were purchased, respectively, from Spectrochem, India and Aldrich. All other chemicals and solvents were reagent grade commercial materials and were used as received. $[Ru(PPh_3)_3Cl_2]$ was prepared following a reported procedure [29]. Purification of acetonitrile and preparation of tetraethylammonium perchlorate (TEAP) for electrochemical work were performed as before [30,31].

2.2. Preparation of complexes

2.2.1. $[Ru(PPh_3)_2(L^1)Cl_2]$

HL^1 (15 mg, 0.12 mmol) was added to a suspension of $[Ru(PPh_3)_3Cl_2]$ (100 mg, 0.10 mmol) in ethanol (40 cm^3) and the mixture was stirred for 5 h to produce a green solution. On partial evaporation of the solvent, $[Ru(PPh_3)_2(L^1)Cl_2]$ separated out as a green crystalline solid, which was collected by filtration, washed with ethanol and dried in air. The yield was 55 mg (64%).

2.2.2. $[Ru(PPh_3)_2(L^2)Cl_2]$

This was synthesized by following the same procedure above using HL^2 instead of HL^1. The yield was 60 mg (69%).

2.2.3. $[Ru(PPh_3)_2(L^3)Cl_2]$

Dichloromethane (40 cm^3) was added to a solid mixture of $[Ru(PPh_3)_3Cl_2]$ (100 mg, 0.10 mmol) and HL^3 (20 mg, 0.12 mmol) and the solution was stirred for 3 h to afford a green solution. On evaporation of the solvent, a green solid was obtained, which was washed with ethanol and dried in air. Purification of this product was achieved by chromatography through a silica gel column. Using toluene as the eluent a green band resulted, which was collected. Evaporation of the eluate gave $[Ru(PPh_3)_2(L^3)Cl_2]$ as a green microcrystalline solid. The yield was 55 mg (61%).

2.2.4. ctc and ccc isomers of $[Ru(PPh_3)_2(L^1)_2]$

2.2.4.1. Method A. $[Ru(PPh_3)_3Cl_2]$ (100 mg, 0.10 mmol) was added to a hot solution of HL^1 (30 mg, 0.24 mmol) in ethanol (40 cm^3), followed by NEt_3 (30 mg, 0.30 mmol). The mixture was refluxed for 2 h to produce a red solution. On partial evaporation of solvent, a microcrystalline red solid precipitated, which was collected by filtration, washed thoroughly with water and dried in vacuo over P_4O_{10}. Purification was achieved by chromatography through silica gel column. Using toluene and 1:4 acetonitrile–toluene as the eluents, two different red bands resulted, which were collected separately and evaporation of the eluates, respectively, gave the ctc and ccc isomers of $[Ru(PPh_3)_2(L^1)_2]$. The yield was 30 mg (33%) for the ctc isomer and 32 mg (35%) for the ccc isomer.

2.2.4.2. Method B. $[Ru(PPh_3)_2(L^1)Cl_2]$ (50 mg, 0.06 mmol) was dissolved in a minimum volume of dichloromethane and to it a solution of HL^1 (10 mg, 0.08 mmol) in ethanol (30 cm^3) was added, followed by NEt_3 (10 mg, 0.10 mmol). The solution was refluxed for 4 h. Upon evaporation of the solution, a red crystalline solid was obtained, which was washed with water and dried in vacuo over P_4O_{10}. The solid was then purified as in Method A. The ctc and ccc isomers of $[Ru(PPh_3)_2(L^1)_2]$ were obtained in 36 and 32% yields, respectively.

2.2.5. ctc and ccc isomers of $[Ru(PPh_3)_2(L^2)_2]$

These isomers have been prepared by following the above procedures. In method A, HL^2 was used instead of HL^1. The ctc and ccc isomers of $[Ru(PPh_3)_2(L^2)_2]$ were obtained in 30 and 34% yields. In method B $[Ru(PPh_3)_2(L^2)Cl_2]$ and HL^2 were used instead of $[Ru(PPh_3)_2(L^1)Cl_2]$ and HL^1, respectively. Yields of the ctc and ccc isomers were 35 and 33%, respectively.

2.2.6. ctc and ccc isomers of $[Ru(PPh_3)_2(L^3)_2]$

These isomers have been prepared by following the above procedures (Section 2.2.4). In method A, HL^3 was used instead of HL^1. The ctc and ccc isomers of $[Ru(PPh_3)_2(L^3)_2]$ were obtained in 32 and 36% yields. In method B, $[Ru(PPh_3)_2(L^3)Cl_2]$ and HL^1 were used instead of $[Ru(PPh_3)_2(L^1)Cl_2]$ and HL^1, respectively. Yields of the ctc and ccc isomers were 32 and 34%, respectively.

2.3. Physical measurements

Microanalyses (C, H, N) were performed using a Perkin–Elmer 240C elemental analyzer. IR spectra were obtained on a Perkin–Elmer 783 spectrometer with samples prepared as KBr pellets. Electronic spectra were recorded on Shimadzu UV 240 spectrophotometer. Magnetic susceptibilities were measured using a PAR 155 Vibrating sample magnetometer fitted with a Walker scientific L75FBAL magnet. ^1H NMR spectra were recorded on a Bruker AC-200 spectrometer using TMS as the internal standard. ESR spectra were recorded on a Varian Model 109C E-line X-band spectrometer fitted with a quartz Dewar for measurements at 77 K (liquid dinitrogen). All spectra were calibrated with the help of DPPH ($g = 2.0037$). Electrochemical measurements were made using a PAR model 273 potentiostat. A platinum disc working electrode, a platinum wire auxiliary electrode and an aqueous saturated calomel reference electrode (SCE) were used in a three electrode configuration. Dinitrogen gas was purified by successively bubbling it through alkaline dithionite and concentrated sulfuric acid. All electrochemical experiments were performed under a dinitrogen atmosphere. All electrochemical data were collected at 298 K and are uncorrected for junction potentials. An RE 0089 X-Y recorder was used to trace the voltammograms.

Table 1
Crystallographic data

	$[Ru(PPh_3)_2(L^2)Cl_2]$	ctc-$[Ru(PPh_3)_2(L^1)_2]$
Formula	$C_{44}H_{37}Cl_2O_2P_2Ru$	$C_{50}H_{40}O_4P_2Ru$
Formula weight	831.65	867.87
Space group	orthorhombic, *Pnma*	triclinic, $P\bar{1}$
a (Å)	10.5844(10)	10.7368(19)
b (Å)	23.817(2)	11.637(4)
c (Å)	15.407(2)	16.732(7)
α (°)	90	96.18(3)
β (°)	90	91.78(3)
γ (°)	90	99.44(3)
V (Å^3)	3884.0(8)	2047.7(12)
Z	4	2
Crystal size (mm)	$0.50 \times 0.30 \times 0.15$	$0.40 \times 0.30 \times 0.20$
T (K)	293(2)	298
μ (cm^{-1})	6.60	4.951
R	$R_1 = 0.0522$ [a]	$R_f = 0.046$ [d]
	$wR_2 = 0.1390$ [b]	$R_w = 0.047$ [c]
GOF	1.082 [e]	2.01 [f]

[a] $R_1 = \Sigma\|F_o|-|F_c\|/\Sigma|F_o|$.
[b] $wR_2 = [\Sigma[w(F_o^2-F_c^2)^2]/\Sigma[w(F_o^2)^2]]^{1/2}$.
[c] GOF $= [\Sigma[w(F_o^2-F_c^2)^2]/(M-N)^{1/2}$, where M is the number of reflections and N is the number of parameters refined.
[d] $R_f = \Sigma\|F_o|-|F_c\|/\Sigma|F_o|$.
[e] $R_w = [\Sigma w(|F_o|-|F_c|)^2/\Sigma w(F_o)^2]^{1/2}$.
[f] GOF $= [\Sigma w(|F_o|-|F_c|)^2/(M-N)]^{1/2}$, where M is the number of reflections and N is the number of parameters refined.

2.4. Crystallography

Single crystals of $[Ru(PPh_3)_2(L^2)Cl_2]$ were grown by slow diffusion of hexane into a dichloromethane solution of the complex. Selected crystal data and data collection parameters are given in Table 1. Data were collected on a Siemens Smart CCD diffractometer using graphite monochromated Mo Kα radiation ($\lambda = 0.71073$ Å) by ω scans within the angular range $1.57 < \theta < 25.00°$. X-ray data reduction, structure solution and refinement were done using SHELXTL-PLUS package. The structure was solved by direct methods.

Single crystals of ctc-$[Ru(PPh_3)_2(L^1)_2]$ were grown by slow diffusion of benzene into an acetonitrile solution of the complex. Selected crystal data and data collection parameters are given in Table 1. The unit cell dimensions were determined by a least-squares fit of 25 centered reflections ($10.80 \le \theta \le 20.94°$). Data were collected on an Enraf–Nonius CAD-4 diffractometer using graphite monochromated Mo Kα radiation ($\lambda = 0.71073$ Å) by $\theta - 2\theta$ scans within the angular range $3.0 < 2\theta < 45.0°$. Three standard reflections, used to check the crystal stability towards X-ray exposure, showed no significant intensity variation over the course of data collection. X-ray data reduction, and structure solution and refinement were carried out using the SHELXS-97 package. The structure was solved by the direct methods.

3. Results and discussion

3.1. Preparation and characterization

3.1.1. $[Ru(PPh_3)_2(L)Cl_2]$ complexes

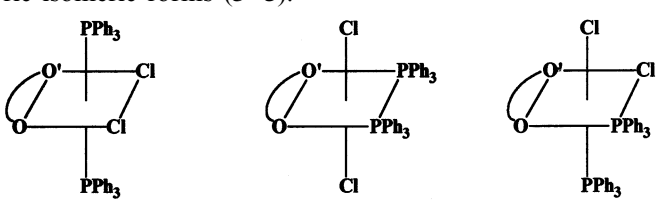
Reaction of $[Ru(PPh_3)_3Cl_2]$ with an equimolar quantity of each phenolic ligand (HL) proceeds smoothly in dichloromethane solution at ambient temperature to

Table 2
Microanalytical, electronic spectral and cyclic voltammetric data

Compound	Microanalytical data [a]		Electronic spectral data [b] λ_{max} (nm) (ε, M^{-1} cm^{-1})	Cyclic voltammetric date [c] $E_{1/2}$ (V) (ΔE_p, mV)
	%C	%H		
$[Ru(PPh_3)_2(L^1)Cl_2]$	63.5 (63.2)	4.4 (4.3)	656 (423), 492 [d] (966), 396 (4700), 304 (19300), 272 [d] (22 000) 240 (25 600)	−0.28 (120), 1.16 (120)
$Ru(PPh_3)_2(L^2)Cl_2]$	62.6 (63.5)	4.9 (4.5)	624 (907), 388 (5200), 300 [d] (15 100), 268 [d] (23 100), 236 (38800)	−0.37 (120), 1.08 (120)
$[Ru(PPh_3)_2(L^3)Cl_2]$	65.3 (65.1)	4.5 (4.3)	588 (855), 400 [d] (2000), 312 [d] (3300), 260 [d] (10700), 232 (19300)	−0.30 (120), 1.24 (120)
ctc-$[Ru(PPh_3)_2(L^1)_2]$	69.7 (69.2)	4.7 (4.6)	504 (2300), 404 [d] (7000), 364 (10 400), 232 (78 300)	0.23 (80), 1.35 (100)
ccc-$[Ru(PPh_3)_2(L^1)_2]$	69.5 (69.2)	4.5 (4.6)	500 (1300), 408 [d] (3700), 356 (5000), 232 (38600)	0.28 (80), 1.41 (100)
ctc-$[Ru(PPh_3)_2(L^2)_2]$	70.1 (69.7)	5.0 (4.9)	492 (1800), 388 [d] (5000), 340 (7800), 260 (22 900), 236 (23600)	0.09 (80), 1.31 (110)
ccc-$[Ru(PPh_3)_2(L^2)_2]$	69.9 (69.7)	4.9 (4.9)	500 [d] (2300), 400 (6300), 336 (8200), 232 (64 600)	0.21 (80), 1.52 (120)
ctc-$[Ru(PPh_3)_2(L^3)_2]$	72.1 (72.0)	4.7 (4.6)	490 (3000), 390 (9600), 340 [d] (12 200), 320 [d] (17 700), 280 (32 700), 232 (77 600)	0.35 (80), 1.46 (100)
ccc-$[Ru(PPh_3)_2(L^3)_2]$	72.2 (72.0)	4.6 (4.6)	490 (3000), 398 (7400), 340 (11 200), 320 [d] (17 200), 276 (30 000), 232 (61 300)	0.41 (80), 1.52 (110)

[a] Calculated values are in parenthesis.
[b] Dichloromethane solution.
[c] Solvent, acetonitrile; supporting electrolyte, TEAP; reference electrode, SCE; $E_{1/2} = 0.5(E_{pa} + E_{pc})$, where E_{pa} and E_{pc} are anodic and cathodic peak potentials, respectively; $\Delta E_p = E_{pa} - E_{pc}$; scan rate, 50 mV s^{-1}.
[d] Shoulder.

afford complexes of the type $[Ru(PPh_3)_2(L)Cl_2]$. It is interesting to note here that ruthenium has undergone a one-electron oxidation during the course of this synthetic reaction. In view of the ruthenium(III)–ruthenium(II) reduction potentials in these complexes (vide infra), oxygen in air appears to have served as the oxidant. Compositions of the complexes have been confirmed by their microanalytical data (Table 2). As all the three phenolate ligands used in the present study are asymmetric bidentate in nature, the $[Ru(PPh_3)_2(L)Cl_2]$ complexes may exist in three geometric isomeric forms (**3**–**5**).



3 **4** **5**

To distinguish between the possible three isomers, molecular structure of a representative complex, viz. $[Ru(PPh_3)_2(L^2)Cl_2]$, has been determined by X-ray crystallography. The structure is shown in Fig. 1 and selected bond distances and angles are presented in Table 3. The $O_2P_2Cl_2$ coordination sphere around ruthenium is distorted octahedral in nature, which is

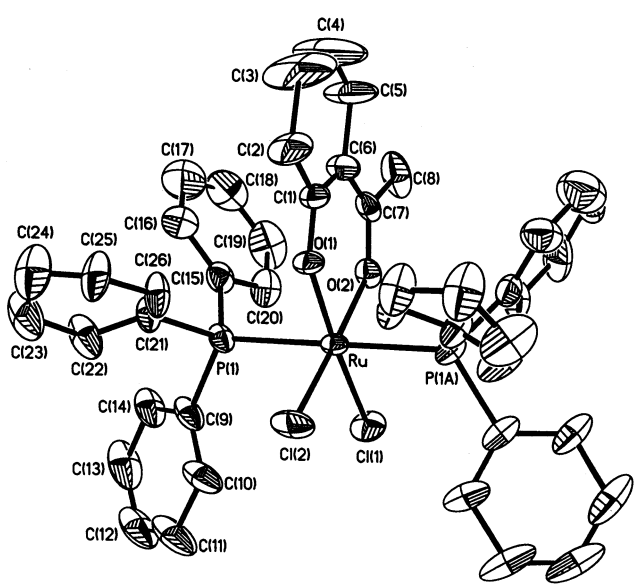


Fig. 1. View of the $[Ru(PPh_3)_2(L^2)Cl_2]$ molecule.

Table 3
Selected bond distances (Å) and bond angles (°) for $[Ru(PPh_3)_2(L^2)Cl_2]$

Ru–Cl(1)	2.324(2)	O(2)–C(7)	1.298(12)
Ru–Cl(2)	2.304(2)	O(1)–C(1)	1.267(10)
Ru–P(1)	2.415(2)	C(1)–C(2)	1.405(14)
Ru–O(1)	1.995(5)	C(2)–C(3)	1.45(3)
Ru–O(2)	2.025(6)	C(3)–C(4)	1.39(5)
		C(4)–C(5)	1.22(4)
		C(5)–C(6)	1.44(2)
		C(6)–C(7)	1.42(2)
		C(1)–C(6)	1.38(2)
		C(7)–C(8)	1.494(13)
O(2)–Ru–Cl(2)	176.9(2)		
P(1)–Ru–P(1A)	179.41(8)		
O(1)–Ru–Cl(1)	173.2(2)		
O(1)–Ru–O(2)	86.4(2)	O(1)–Ru–Cl(2)	90.5(2)
O(2)–Ru–Cl(1)	86.9(2)	C(2)–Ru–Cl(1)	96.27(11)
O(1)–Ru–P(1)	89.73(4)	O(2)–Ru–P(1)	90.10(5)
Cl(2)–Ru–P(1)	89.88(5)	Cl(1)–Ru–P(1)	90.28(4)

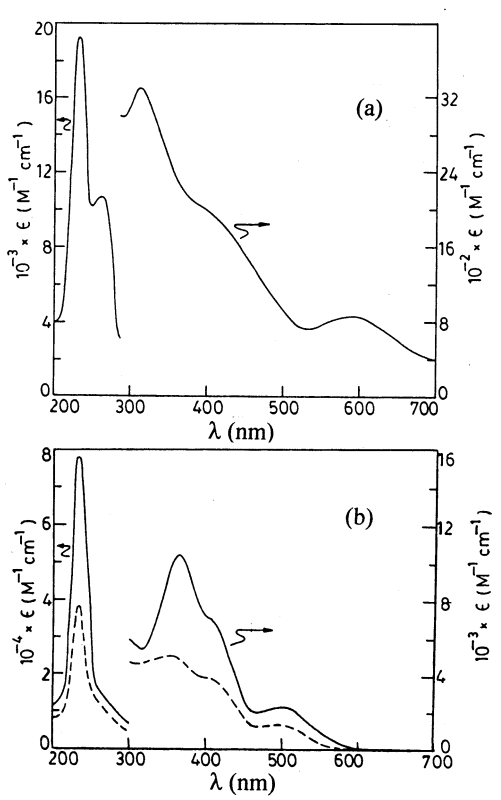


Fig. 2. Electronic spectra of (a) $[Ru(PPh_3)_2(L^3)Cl_2]$ and (b) ctc-$[Ru(PPh_3)_2(L^1)_2]$ (—) and ccc-$[Ru(PPh_3)_2(L^1)_2]$ (------) in dichloromethane solution.

reflected in the bond parameters. The two bulky PPh_3 ligands are in *trans* positions, as is usually observed in complexes of ruthenium(III) having the $Ru(PPh_3)_2$ moiety [32–34], while the two chloride ligands have occupied *cis* positions. The observed bond distances are all quite normal as observed in structurally characterized complexes of ruthenium containing similar ligands [19,32–34]. This structure determination thus shows that $[Ru(PPh_3)_2(L^2)Cl_2]$ has structure **3**. As all the three $[Ru(PPh_3)_2(L)Cl_2]$ complexes display similar properties (vide infra), the other two $[Ru(PPh_3)_2(L)Cl_2]$ complexes are assumed to have a similar structure as $[Ru(PPh_3)_2(L^2)Cl_2]$.

Infrared spectra of the $[Ru(PPh_3)_2(L)Cl_2]$ complexes show many sharp and strong vibrations in the 1600–300 cm^{-1} region, of which the vibrations near 520, 700 and 745 cm^{-1} are also observed in $[Ru(PPh_3)_3Cl_2]$ and hence these are attributable to the $Ru(PPh_3)_2$ fragment of the $[Ru(PPh_3)_2(L)Cl_2]$ complexes. One new band, observed near 1580 cm^{-1} in all these complexes, is assigned to the ν(C=O) vibration of the coordinated phenolate ligand. The ν(Ru–Cl) stretching vibration appears as a strong band in all the complexes near 330 cm^{-1}. The infrared spectral data thus correspond to the composition of the complexes. The $[Ru(PPh_3)_2(L)Cl_2]$ complexes are soluble in common polar organic solvents, like dichloromethane, chloroform, acetonitrile, etc., producing green solutions. Electronic spectra of these complexes have been recorded in dichloromethane solution. A selected spectrum is shown in Fig. 2 and spectral data are listed in Table 2. Each complex shows few intense absorptions in the visible region together with some very intense absorptions in the ultraviolet region. The absorptions in the ultraviolet region may be assigned to transitions occurring within the ligand orbitals. To have an insight into the nature of transitions appearing in the visible region, qualitative EHMO calculations have been performed [35,36] on a model of the $[Ru(PPh_3)_2(L)Cl_2]$ complexes, which was computer generated from $[Ru(PPh_3)_2(L^1)Cl_2]$ by replacing the phenyl groups of the PPh_3 ligands with hydrogen. A partial MO diagram is shown in Fig. 3. The highest occupied (singly occupied) molecular orbital (MO-1) and the next two filled orbitals (MO-2 and MO-3) of this model are predominantly ($\geq 80\%$) ruthenium t_2 in character. There are two filled molecular orbitals (MO-4 and MO-5) below these metal t_2 orbitals, which are localized almost entirely ($\geq 96\%$) on the phenolate ligand. The intense absorptions observed in the visible region may therefore be assigned to the allowed ligand-to-metal charge-transfer transitions occurring from the filled orbitals of the phenolate ligand (MO-4 and MO-5) to the half-filled ruthenium t_2 orbital (MO-1).

Magnetic susceptibility show that all the three $[Ru(PPh_3)_2(L)Cl_2]$ complexes are one-electron paramagnetic, which is in accordance with the +3 oxidation state of ruthenium (low-spin d^5, $S = 1/2$) in these complexes. Electron spin resonance spectra of the $[Ru(PPh_3)_2(L)Cl_2]$ complexes, recorded in 1:1 dichloromethane–toluene solution at 77 K, show rhombic spectra with three distinct signals (g_1, g_2 and g_3 in the order of decreasing magnitude). A representative spectrum is shown in Fig. 4 and the spectral data are

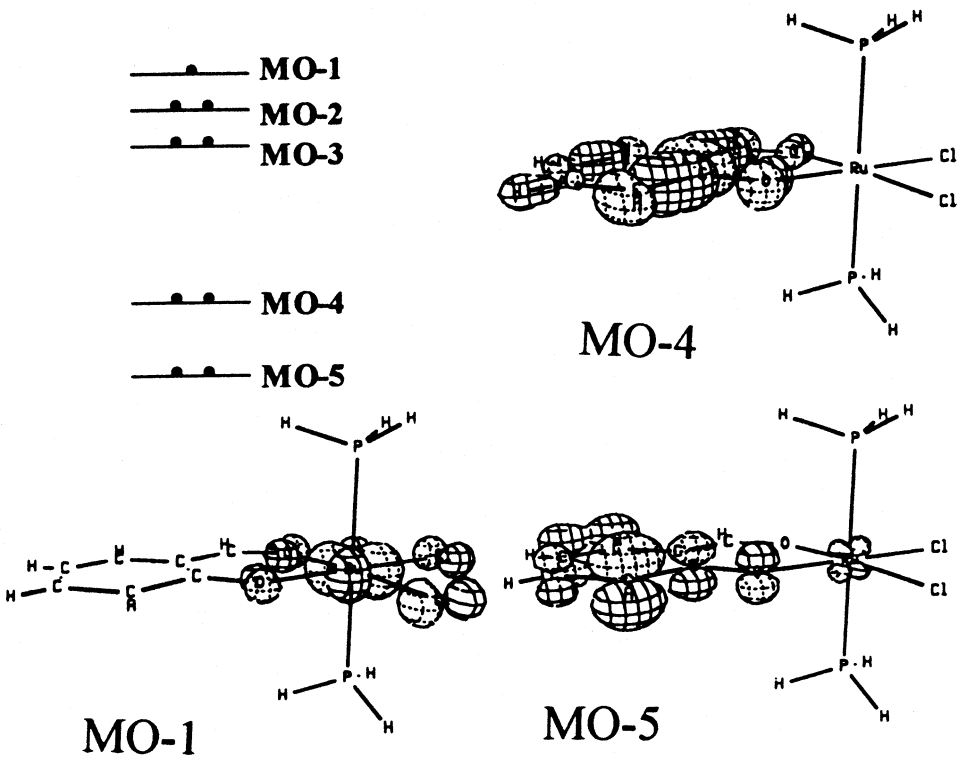


Fig. 3. Qualitative molecular orbital diagram of $[Ru(PPh_3)_2(L)Cl_2]$.

presented in Table 4. The observed rhombicity of the ESR spectra is understandable in terms of the gross molecular symmetry of these complexes containing the three non-equivalent P–Ru–P, O(phenolic)–Ru–Cl and O(carbonylic)–Ru–Cl axes. The rhombic distortion can be thought of a combination of axial distortion (Δ, which splits t_2 into **a** and **e**) and rhombic distortion (V, which splits **e**). The splitting pattern is illustrated in Fig. 4. Spin-orbit coupling causes further changes in the energy gaps. Thus two electronic transitions (transition energies ΔE_1 and ΔE_2; $\Delta E_1 < \Delta E_2$) are possible within these three levels. All these energy parameters have been computed (Table 4) using the observed g values, the g tensor theory of low-spin d^5 complexes and a reported method [37–39]. The axial distortion is observed to be much stronger than the rhombic one. The ΔE_1 transition falls in the infrared region (3200–3700 cm^{-1}) and could not be detected. The ΔE_2 transition, which is expected to occur near 6000 cm^{-1} ($\sim$1667 nm), could not be verified either because of the non-transparency of the solvent in this region. However, the ESR data analysis shows that the $[Ru(PPh_3)_2(L)Cl_2]$ complexes are significantly distorted from ideal octahedral geometry, which was also observed in the structural analysis of $[Ru(PPh_3)_2(L_2)Cl_2]$.

3.1.2. $[Ru(PPh_3)_2(L)_2]$ complexes

These complexes have been prepared in two different ways (Scheme 1). Direct reaction of the phenolic ligands (HL) with $[Ru(PPh_3)_3Cl_2]$ in 2:1 mole ratio proceeds smoothly in refluxing ethanol in the presence of a base to afford the bis complexes of type $[Ru(PPh_3)_2(L)_2]$. These complexes can also be prepared from $[Ru(PPh_3)_2(L)Cl_2]$ by reacting them with one equivalent of the respective phenolic ligand (HL) in the presence of a base. Thin layer chromatographic experiments indicated the presence of two isomers (isomer-I and isomer-II) in all $[Ru(PPh_3)_2(L)_2]$ complexes, which have

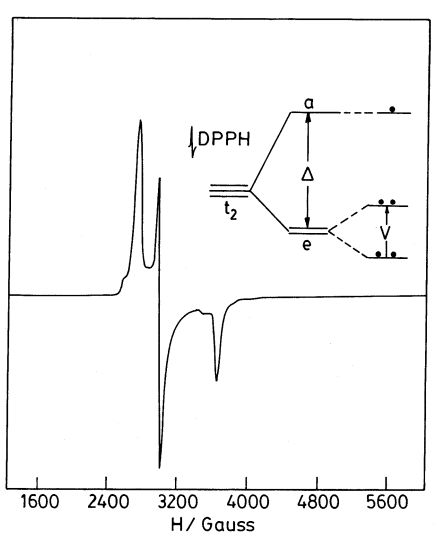


Fig. 4. ESR spectrum of $[Ru(PPh_3)_2(L^2)Cl_2]$ in 1:1 dichloromethane–toluene solution at 77 K.

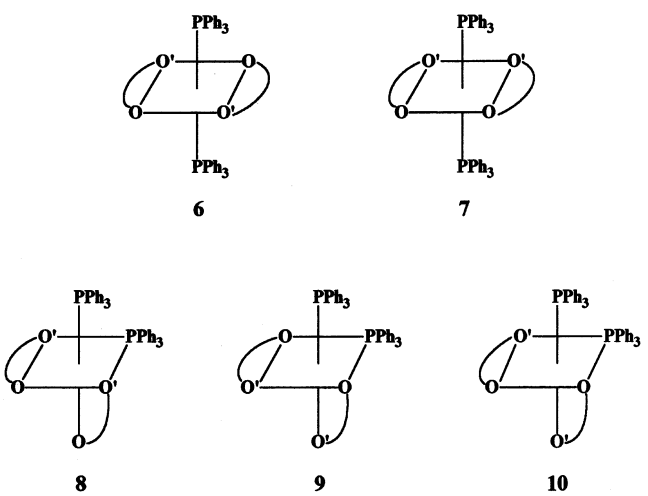
Table 4
Magnetic moment and ESR g values [a] and derived parameters [b] of the $[Ru(PPh_3)_2(L)Cl_2]$ complexes

Compound	μ_{eff} (BM)	g_1	g_2	g_3	Δ/λ	V/λ	$\Delta E_1/\lambda$	$\Delta E_2/\lambda$
$[Ru(PPh_3)_2(L^1)Cl_2]$	1.85	2.497	2.212	1.791	4.313	−2.450	3.236	5.801
$[Ru(PPh_3)_2(L^2)Cl_2]$	1.93	2.428	2.233	1.828	4.574	−1.976	3.691	5.830
$[Ru(PPh_3)_2(L^3)Cl_2]$	1.97	2.407	2.258	1.795	4.065	−1.264	3.515	5.029

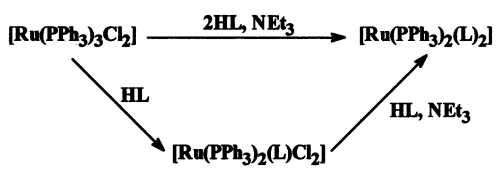
[a] In 1:1 dichloromethane–toluene solution at 77 K.
[b] Spin-orbit coupling constant (λ) for complexed ruthenium(III) is $\sim$1000 cm^{-1}.

been separated by column chromatography. Microanalytical data of these complexes are in good agreement with their compositions (Table 2). Both isomers of these complexes are diamagnetic, which corresponds to the bivalent state of ruthenium (low-spin d^6, $S = O$) in these complexes.

As all three phenolate ligands used in the present study are asymmetric, the $[Ru(PPh_3)_2(L)_2]$ complexes may exist in five geometrical isomeric forms (**6**–**10**). Isomers **6**–**9** have a C_2 axis, while isomer **10** does not have any C_2 symmetry. ^1H NMR spectra have been recorded on both isomers of all three $[Ru(PPh_3)_2(L)_2]$ complexes in $CDCl_3$ solution. Isomer-I of all three complexes clearly shows the presence of a C_2 axis, while isomer-II indicates the absence of C_2 symmetry. For example, isomer-I of $[Ru(PPh_3)_2(L^1)_2]$ shows only one aldehydic proton signal at 8.68 ppm, while isomer-II of $[Ru(PPh_3)_2(L^1)_2]$ shows two aldehydic proton signals (1H each) at 8.36 and 8.53 ppm. This shows that isomer-II has structure **10**, where the three sets of donor atoms are in *cis* positions and henceforth this isomer will be labeled as the *cis*–*cis*–*cis* or ccc isomer.



It has not been possible to assign specific stereochemistry of isomer-I on the basis of ^1H NMR spectral results alone. However, as complexes of ruthenium with the $Ru(PPh_3)_2$ are known to Prefer *cis*-disposition of PPh_3 ligands [33,34,40], these $[Ru(PPh_3)_2(L)_2]$ complexes may be assumed to have either structure **8** or **9**. To sort out this problem of stereochemistry of isomer-I, the molecular structure of isomer-I of $[Ru(PPh_3)_2(L^1)_2]$ has been determined by X-ray crystallography. The structure is shown in Fig. 5 and selected bond distances and angles are presented in Table 5. Ruthenium has a distorted octahedral O_4P_2 coordination sphere with the two PPh_3 ligands in *cis* positions, the two phenolate oxygens in *trans* positions and the two carbonylic oxygens in *cis* positions. Therefore isomer-I of $[Ru(PPh_3)_2(L^1)_2]$ has structure **9** (henceforth referred to as the ctc isomer to indicate the *cis*–*trans*–*cis* dispositions of the carbonylic oxygens, phenolate oxygens and phosphines, respectively). The observed bond parameters are all quite normal. In view of the similarity in synthetic procedure and properties, isomer-I of the other two $[Ru(PPh_3)_2(L)_2]$ complexes are assumed to have similar ctc structure.



Scheme 1.

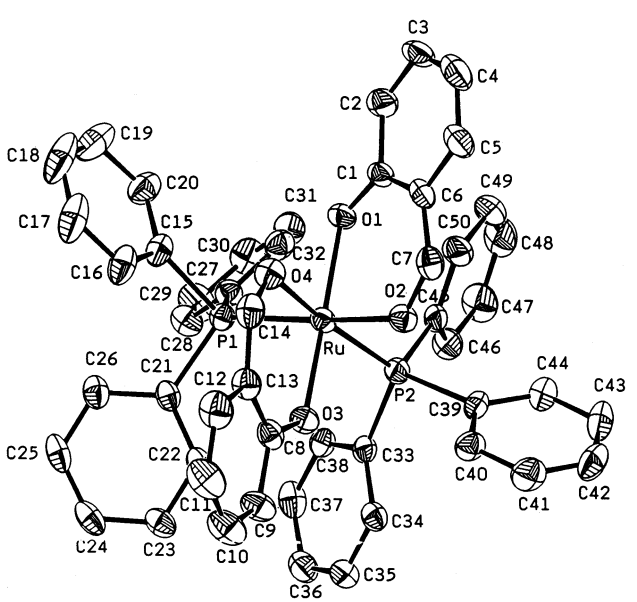


Fig. 5. View of the ctc-$[Ru(PPh_3)_2(L^1)_2]$ molecule.

Table 5
Selected bond distances (Å) and bond angles (°) for $[Ru(PPh_3)_2(L^1)_2]$

Ru–P(1)	2.2929(18)	O(1)–C(1)	1.295(6)
Ru–P(2)	2.3031(17)	O(2)–C(7)	1.239(7)
Ru–O(1)	2.057(3)	O(3)–C(8)	1.313(6)
Ru–O(2)	2.090(4)	O(4)–C(14)	1.262(7)
Ru–O(3)	2.052(3)		
Ru–O(4)	2.128(4)		
P(1)–Ru–O(2)	169.48(11)		
P(2)–Ru–O(4)	169.69(11)		
O(1)–Ru–O(3)	173.61(14)		
P(1)–Ru–P(2)	99.22(6)	P(2)–Ru–O(3)	87.90(11)
P(1)–Ru–O(1)	90.17(11)	O(1)–Ru–O(2)	90.75(14)
P(1)–Ru–O(3)	93.05(11)	O(1)–Ru–O(4)	83.48(14)
P(1)–Ru–O(4)	91.07(11)	O(2)–Ru–O(3)	85.08(14)
P(2)–Ru–O(1)	97.04(11)	O(2)–Ru–O(4)	78.62(14)
P(2)–Ru–O(2)	91.08(11)	O(3)–Ru–O(4)	90.94(14)

Infrared spectra of ctc and ccc isomers of the $[Ru(PPh_3)_2(L)_2]$ complexes are very similar. Each shows characteristic vibrations near 500, 700, 750 cm^{-1}, indicating the presence of the $Ru(PPh_3)_2$ moiety. The ν(C=O) vibration is observed as a strong band near 1580 cm^{-1} in all these complexes. The $[Ru(PPh_3)_2(L)_2]$ complexes are soluble in common organic solvents like dichloromethane, chloroform, acetone, acetonitrile, etc., forming intense red solutions. Electronic spectra of these complexes, recorded in dichloromethane solution, show several intense absorptions in the visible region and few absorptions of very high intensity in the ultraviolet region (Fig. 2, Table 2). The latter absorptions are assigned to transitions within the ligand orbitals. The former absorptions in the visible region are probably due to allowed metal-to-ligand charge-transfer transitions. Multiple charge-transfer transitions are common in such mixed ligand complexes, primarily because of the lower symmetry splitting of the metal orbitals and presence of different accepting orbitals. For proper assignment of the absorptions in the visible region, qualitative EHMO calculations have been performed as before on models of the ctc and ccc isomersa of $[Ru(PPh_3)_2(L^1)_2]$, where phenyl groups of the PPh_3 ligands have been replaced by hydrogen. The results of these calculations are qualitatively very similar for both the isomers. A partial MO diagram for one isomer is shown in Fig. 6. The highest occupied molecular orbital (HOMO) and the next two filled orbitals (HOMO-1 and HOMO-2) are basically ($>75\%$) ruthenium t_2 orbitals. There are two relatively close vacant molecular orbitals above these filled orbitals, the lowest unoccupied molecular orbital (LUMO) and the next unoccupied orbital (LUMO + 1), which are primarily ($>95\%$) π-orbitals of the phenolate ligands. The intense absorptions observed in the visible region may therefore be assigned to the charge-transfer transitions occurring from the filled ruthenium t_2 orbitals to the vacant π-orbitals of the phenolate ligands.

3.2. Electron-transfer properties

Electron-transfer properties of the $[Ru(PPh_3)_2(L)Cl_2]$ and $[Ru(PPh_3)_2(L)_2]$ have been studied in acetonitrile solution by cyclic voltammetry. Representative voltammograms are shown in Fig. 7 and voltammetric data are presented in Table 2.

Each $[Ru(PPh_3)_2(L)Cl_2]$ complex shows a reductive response on the negative side of SCE and an oxidative response on the positive side. Both responses are quasi-reversible in nature. The reduction, observed near -0.3 V (all potentials are referenced to SCE), is tentatively assigned to ruthenium(III)-ruthenium(II) reduction and the oxidation, which occurs within 1.08–

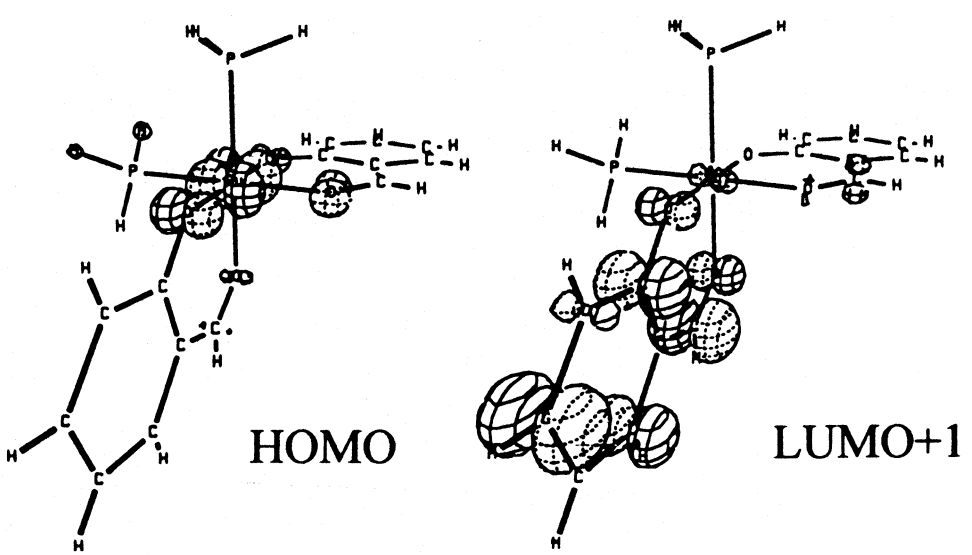


Fig. 6. Qualitative molecular orbital diagram of $[Ru(PPh_3)_2(L)_2]$.

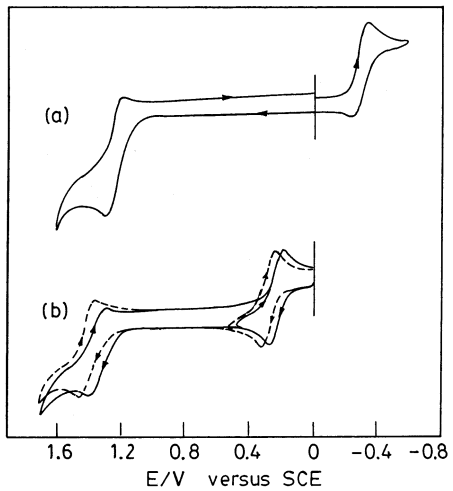


Fig. 7. Cyclic voltammograms of (a) $[Ru(PPh_3)_2(L^3)Cl_2]$ and (b) ctc-$[Ru(PPh_3)_2(L^1)_2]$ (—) and ccc-$[Ru(PPh_3)_2(L^1)_2]$ (-------) in acetonitrile solution (0.1 M TEAP) at a scan rate of 50 mV s^{-1}.

1.24 V, is tentatively assigned to ruthenium(III)–ruthenium(IV) oxidation. Both potentials have shifted to a little more negative values in $[Ru(PPh_3)_2(L^2)Cl_2]$ relative to $[Ru(PPh_3)_2(L^1)Cl_2]$, which may be attributed to the electron donating character of the methyl group in L^2.

Both isomers of $[Ru(PPh_3)_2(L)_2]$ complexes show two oxidative responses on the positive side of SCE. The first oxidation, which is observed within 0.09–0.41 V, is reversible in nature and is assigned to ruthenium(II)–ruthenium(III) oxidation. The second quasi-reversible oxidation appears within 1.31–1.52 V and is tentatively assigned to the ruthenium(III)–ruthenium(IV) oxidation. Potentials of both oxidations have been observed to shift to lower values in the ctc isomer than the ccc isomer, which indicates that the lower oxidation states are more comfortable in the ccc isomer than in the ctc isomer. This is in accordance with the higher probability of dπ-pπ backbonding in the ccc isomer [41–43]. The oxidation potentials are observed to be a little lower in $[Ru(PPh_3)_2(L^2)_2]$ than in $[Ru(PPh_3)_2(L^1)_2]$, as before. The cyclic voltammetric studies indicate that the +3 state of ruthenium is stable in the $O_2P_2Cl_2$ coordination sphere in the $[Ru(PPh_3)_2(L)Cl_2]$ complexes and so is the +2 state of ruthenium in the O_4P_2 coordination sphere in the $[Ru(PPh_3)_2(L)_2]$ complexes.

4. Supplementary data

Supplementary data are available from the Cambridge Crystallographic Data Center, 12 Union Road, Cambridge, CB2 1EZ, UK, on request, quoting the deposition numbers CCDC 138541 and 138542.

Acknowledgements

Financial assistance received from the Council of Scientific and Industrial Research, New Delhi [Grant No. 01(1408)/96/EMR-II] is gratefully acknowledged. Thanks are also due to the Third World Academy of Sciences for financial support for the purchase of an electrochemical cell system. F.B. thanks the University Grants Commission, New Delhi, for her fellowship.

References

[1] S.-M. Lee, W.-T. Wong, Coord. Chem. Rev. 164 (1997) 415.
[2] I. Ortmanes, C. Moucheron, A.K.-D. Mesmaeker, Coord. Chem. Rev. 168 (1998) 233.
[3] A. Islam, N. Ikeda, K. Nozak, Y. Okamoto, B. Gholamkhass, A Yoshimura, T. Ohno, Coord. Chem. Rev. 171 (1998) 355.
[4] J.W.-S. Hui, Y.-T. Wong, Coord. Chem. Rev. 172 (1998) 389.
[5] P.J. Dyson, B.F.G. Johnson, C.M. Martin, Coord. Chem. Rev. 175 (1998) 59.
[6] D.J. Stufkens, A. Vlcek Jr., Coord. Chem. Rev. 177 (1998) 127.
[7] L.D. Cola, P. Belser, Coord. Chem. Rev. 177 (1998) 301.
[8] S. Sabo-Etienne, B. Chaudret, Coord. Chem. Rev. 178–180 (1998) 381.
[9] D. Touchard, P.H. Dixneuf, Coord. Chem. Rev. 178–180 (1998) 409.
[10] G. Jia, C.-P. Lau, Coord. Chem. Rev. 190–192 (1999) 83.
[11] N.C. Pramanik. S. Bhattacharya, J. Chem. Res. (S) (1997) 98.
[12] F. Basuli, S.M. Peng, S. Bhattacharya, Inorg. Chem. 36 (1997) 5645.
[13] N.C. Pramanik, K. Pramanik, P. Ghosk, S. Bhattacharya, Polyhedron 17 (1998) 1525.
[14] F. Basuli, M. Ruf, C.G. Pierpont, S. Bhattacharya, Inorg. Chem. 37 (1998) 6113.
[15] N.C. Pramanik, S. Bhattacharya, Transition Met. Chem. 24 (1999) 95.
[16] K. Sui, S.M. Peng, S. Bhattacharya, Polyhedron 18 (1999) 631.
[17] A.K. Das, S.M. Peng, S. Bhattacharya, J. Chem. Soc., Dalton Trans. (2000) 181.
[18] F. Basuli, S.M. Peng, S. Bhattacharya, Inorg. Chem. 39 (2000) 1120.
[19] N. Bag, G.K. Lahiri, S. Bhattacharya, L.R. Falvello, A. Chakravorty, Inorg. Chem. 27 (1988) 4396.
[20] F. Basuli, S.M. Peng, S. Bhattacharya, Polyhedron 17 (1998) 2191.
[21] G.K. Lahiri, S. Bhattachaya, B.K. Ghosh, A. Chakravorty, Inorg. Chem. 26 (1987) 4324.
[22] S. Bhattacharya, S.R. Boone, G.A. Fox, C.G. Pierpont, Inorg. Chem. 29 (1990) 1088.
[23] S. Bhattacharya, Polyhedron 12 (1993) 235.
[24] B. Muller, H. Vahrenkamp, Chem. Eur. J. (1998) 117.
[25] B. Muller, H. Vahrenkamp, Chem. Eur. J. (1998) 129.
[26] B. Muller, H. Vahrenkamp, Chem. Eur. J. (I998) 137.
[27] B. Muller, A. Schneider, M. Tesmer, H. Vahrenkamp, Inorg. Chem. 38 (1999) 1900.
[28] T.R. Ward, A. Lutz, S.P. Parel, J. Ensling, P. Gutlich, P. Buglyo, C. Orvig, Inorg. Chem. 38 (1999) 5007.
[29] T.A. Stephenson, G. Wilkinson, J. Inorg. Nucl. Chem. 28 (1966) 945.
[30] D.T. Sawyer, J.L. Roberts Jr., Experimental Electrochemistry for Chemists, Wiley, New York, 1974, pp. 167–215.
[31] M. Walter, L. Ramaley, Anal. Chem. 45 (1973) 165.
[32] S. Chattopadhyay, N. Bag, G.K. Lahiri, A. Chakravorty, J. Chem. Soc., Dalton Trans. (1990) 3389.

[33] S. Bhattacharya, C.G. Pierpont, Inorg. Chem. 30 (1991) 1511.
[34] M. Menon, A. Pramanik N. Bag, A. Chakravorty, J. Chem. Soc., Dalton Trans. (1995) 1417.
[35] C. Mealli, D.M. Proserpio, CACAO Version 4.0, Firenze, Italy, July 1994.
[36] C. Mealli, D.M. Proserpio, J. Chem. Educ. 67 (1990) 399.
[37] B. Bleany, M.C.M. O'Brien, Proc. Phys. Soc. Lond., Sect B 69 (1956) 1216.
[38] J.S. Griffith, The Theory of Transition Metal Ions, Cambridge University Press, London, 1961, p. 364.
[39] S. Bhattacharya, A. Chakravorty, Proc. Indian Acad. Sci. 95 (1985) 159.
[40] A. Pramanik, N. Bag, G.K. Lahiri, A. Chakravorty, J. Chem. Soc., Dalton Trans. (1990) 3823.
[41] R.A. Krause, K. Krause, Inorg. Chem. 19 (1980) 2600.
[42] S. Goswami, A.R. Chakravarty, A. Chakravorty, Inorg. Chem. 20 (1981) 2246.
[43] R.A. Krause, K. Krause, Inorg. Chem. 21 (1982) 1714.

PERGAMON

www.elsevier.nl/locate/poly

Polyhedron 19 (2000) 1673–1680

POLYHEDRON

Chemistry of some ruthenium phenolates: synthesis, structure and redox properties

Prasanta Kumar Sinha [a], Larry R. Falvello [b], Shie-Ming Peng [c], Samaresh Bhattacharya [a,*]

[a] *Department of Chemistry, Inorganic Chemistry Section, Jadavpur University, Calcutta 700032, India*
[b] *Department of Inorganic Chemistry, Faculty of Science, University of Zaragoza, E-50009 Zaragoza, Spain*
[c] *Department of Chemistry, National Taiwan University, Taipei, Taiwan, ROC*

Received 16 March 2000; accepted 28 April 2000

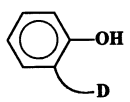
Abstract

Reaction of three phenolate ligands, viz. 2,4,6-tribromophenol (HL^1, where H stands for the phenolic proton), 2-nitrophenol (HL^2) and 2,4,6-trinitrophenol (HL^3O), with $[Ru(PPh_3)_3Cl_2]$ in a 2:1 molar ratio in the presence of a base gives complexes of type $[Ru(PPh_3)_2(L)_2]$ ($L = L^1$, L^2 and L^3). The 2,4,6-tribromophenolate ligand (L^1) binds to ruthenium as a bidentate O,Br-donor, while the 2-nitrophenolate ligand (L^2) acts as a bidentate O,O-donor. 2,4,6-Trinitrophenol (HL^3O) undergoes oxygen loss from one nitro group at the *ortho* position and coordinates to ruthenium in the 2-nitroso-4,6-dinitrophenolate (L^3) form through the nitroso nitrogen and phenolate oxygen. The structures of the $[Ru(PPh_3)_2(L^1)_2]$ and $[Ru(PPh_3)_2(L^3)_2]$ complexes have been solved by X-ray crystallography. In $[Ru(PPh_3)_2(L^1)_2]$ the coordination sphere around ruthenium is $O_2P_2Br_2$ with a *trans–cis–cis* disposition of the three sets of donor atoms, respectively. In $[Ru(PPh_3)_2(L^3)_2]$ ruthenium has a $N_2O_2P_2$ coordination sphere with a *cis–cis–trans* arrangement of the three sets of donor atoms, respectively. The $[Ru(PPh_3)_2(L)_2]$ complexes are diamagnetic (low-spin d^6, $S = 0$) and in acetonitrile solution show intense MLCT transitions in the visible region. Cyclic voltammetry on the $[Ru(PPh_3)_2(L)_2]$ complexes shows a reversible ruthenium(II)–ruthenium(III) oxidation within 0.63–0.71 V versus SCE followed by an irreversible ruthenium(III)–ruthenium(IV) oxidation near 1.5 V versus SCE. © 2000 Elsevier Science Ltd. All rights reserved.

Keywords: Ruthenium; Phenolic ligands; Synthesis; Structure; Redox properties

1. Introduction

There is much current interest in the chemistry of ruthenium [1–10], most of which is due to the fascinating electron-transfer and energy-transfer properties displayed by the complexes of this metal. The coordination environment around the metal primarily dictates properties of the ruthenium complexes. Complexation of ruthenium by ligands of different types has thus been of particular interest. In the present work, which has emerged from our continued interest in the chemistry of ruthenium in different coordination environments [11–25], our objective has been to explore the chemistry of ruthenium bound to phenolate oxygens. Phenolate oxygen is a recognized hard donor and hence coordination of ruthenium by phenolate oxygen is of particular importance with regard to stabilization of the higher oxidation states of this metal [26–29]. The initial goal of the present study was to investigate the coordinating ability of simple phenols with no additional donor atoms. As a source of ruthenium, $[Ru(PPh_3)_3Cl_2]$ has been used, which is well known for its efficiency in binding to ligands of different types via dissociation of PPh_3 and chloride ligands [29–33]. However, we have observed that until a second donor site is incorporated at the *ortho* position of the phenyl ring, no tractable phenolate complex is formed.



1

* Corresponding author. Tel.: +91-33-483-6223; fax: +91-33-473-4266.
E-mail address: samaresh_b@hotmail.com (S. Bhattacharya).

0277-5387/00/$ - see front matter © 2000 Elsevier Science Ltd. All rights reserved.
PII: S0277-5387(00)00459-9

When phenols of type **1** (abbreviated in general as HL, where H stands for the dissociable phenolic proton) are used, where D is the second donor atom linked to the *ortho* carbon directly or via one intervening atom, stable complexes of general formula $[Ru^{II}(PPh_3)_2(L)_2]$ are formed. The chemistry of these complexes is described in this paper with special reference to synthesis, structure and redox properties.

2. Experimental

2.1. Materials

Commercial ruthenium trichloride was purchased from Arora Matthey, Calcutta, India and was converted to $RuCl_3{\cdot}3H_2O$ by repeated evaporation with concentrated hydrochloric acid. Triphenylphosphine, triethylamine, 2,4,6-tribromophenol (HL^1), 2-nitrophenol (HL^2) and 2,4,6-trinitrophenol (HL^3O) were obtained from SD Fine Chemicals, Mumbai, India. $[Ru(PPh_3)_3Cl_2]$ was prepared following a reported procedure [34]. Purification of acetonitrile and preparation of tetraethylammonium perchlorate (TEAP) for electrochemical work were performed as reported in the literature [35,36]. All other chemicals and solvents were reagent grade commercial materials and were used as received.

2.2. Preparation of complexes

2.2.1. $[Ru(PPh_3)_2(L^1)_2]$

$[Ru(PPh_3)_3Cl_2]$ (100 mg, 0.10 mmol) and 2,4,6-tribromophenol (85 mg, 0.26 mmol) were taken up in 30 cm^3 methanol and triethylamine (42 mg, 0.42 mmol) was added. The resulting mixture was stirred for 2 h. A dark-red microcrystalline solid separated out, which was collected by filtration, washed with methanol and dried in vacuo. Recrystallization from 1:4 dichloromethane–hexane solution afforded shiny red crystals of $[Ru(PPh_3)_2(L^1)_2]$. The yield was 94 mg (70%).

2.2.2. $[Ru(PPh_3)_2(L^2)_2]$

This compound was prepared by following the same above procedure using 2-nitrophenol instead of 2,4,6-tribromophenol. The yield was 70 mg (75%).

2.2.3. $[Ru(PPh_3)_2(L^3)_2]$

To a solution of 2,4,6-trinitrophenol (50 mg, 0.22 mmol) in ethanol (30 cm^3) was added $[Ru(PPh_3)_3Cl_2]$ (100 mg, 0.10 mmol) and triethylamine (42 mg, 0.42 mmol). The resulting mixture was heated at reflux for 2.5 h to produce a red solution. Upon cooling the solution to room temperature, a dark red crystalline solid separated out, which was collected by filtration, washed with ethanol and dried in air. Recrystallization from dichloromethane–benzene afforded shiny red crystals of $[Ru(PPh_3)_2(L^3)_2]$. The yield was 34 mg (30%).

2.3. Physical measurements

Microanalyses (C, H, N) were performed using a Perkin–Elmer 240C elemental analyzer. IR spectra were obtained on a Perkin–Elmer 783 spectrometer with samples prepared as KBr pellets. Electronic spectra were recorded on a Shimadzu UV 240 spectrophotometer. Magnetic susceptibilities were measured using a PAR 155 vibrating sample magnetometer fitted with a Walker scientific L75FBAL magnet. Electrochemical measurements were made using a PAR model 273 potentiostat. A platinum disc working electrode, a platinum wire auxiliary electrode and an aqueous saturated calomel reference electrode (SCE) were used in a three-electrode configuration. A RE 0089 X-Y recorder was used to trace the voltammograms. Dinitrogen gas was purified by successively bubbling it through alkaline dithionite and concentrated sulfuric acid. All electrochemical experiments were performed under a dinitrogen atmosphere. All electrochemical data were collected at 298 K and are uncorrected for junction potentials.

2.4. Crystallography

Single crystals of $[Ru(PPh_3)_2(L^1)_2]$ were grown by slow diffusion of hexane into a dichloromethane solution of the complex. Selected crystal data and data collection parameters are given in Table 1. The unit cell dimensions were determined by a least-squares fit of 25 centered reflections ($11.4 \leq \theta \leq 25.5°$). Data were collected on an Enraf–Nonius CAD-4 diffractometer using graphite-monochromated Mo Kα radiation ($\lambda = 0.71073$ Å) by ω scans within the angular range $2.15 < \theta < 27.49°$. Three standard reflections were used to check the crystal stability towards X-ray exposure and they showed no significant intensity variation over the course of data collection. X-ray data reduction, structure solution and refinement were done using the SHELXS-97 and SHELXL-97 packages. The structure was solved by the direct method.

Single crystals of $[Ru(PPh_3)_2(L^3)_2]$ were grown by slow diffusion of benzene into a dichloromethane solution of the complex. Selected crystal data and data collection parameters are given in Table 1. The unit cell dimensions were determined by a least-squares fit of 25 centered reflections ($10.84 < \theta < 19.80°$). Data were collected on an Enraf–Nonius CAD-4 diffractometer using graphite-monochromated Mo Kα radiation ($\lambda = 0.71073$ Å) by θ–2θ scans within 2θ max 50.0°. Three standard reflections, used to check the crystal stability towards X-ray exposure, showed no significant

intensity variation over the course of data collection. X-ray data reduction, and structure solution and refinement were done using the NRCVAX package. The structure was solved by the direct method.

Table 1
Crystallographic data

	$[Ru(PPh_3)_2(L^1)_2]$	$[Ru(PPh_3)_2(L^3)_2]$
Formula	$C_{48}H_{34}Br_6O_2P_2Ru$	$C_{54}H_{40}N_6O_{12}P_2Ru$
Formula weight	1285.22	1049.0
Space group	monoclinic, $P21/c$	orthorhombic, $Pccn$
a (Å)	12.8954(18)	11.766(4)
b (Å)	16.334(2)	14.613(3)
c (Å)	21.572(6)	28.395(5)
β (°)	97.071(15)	90
V (Å^3)	4509.2(15)	4882.1(21)
Z	4	4
Crystal size (mm)	$0.42\times0.27\times0.02$	$0.50\times0.10\times0.10$
T (K)	299	298
μ (cm^{-1})	5.775	4.487
R indices	$R_1 = 0.0740$ [a]	$R_f = 0.038$ [c]
	$wR_2 = 0.1300$ [b]	$R_w = 0.037$ [d]
GOF	0.993 [e]	1.15 [f]

[a] $R_1 = \Sigma||F_o|-|F_c||/\Sigma|F_o|$.
[b] $wR_2 = [\Sigma[w(F_o^2-F_c^2)^2]/\Sigma[w(F_o^2)^2]]^{1/2}$.
[c] $R_f = \Sigma||F_o|-|F_c||/\Sigma|F_o|$.
[d] $R_w = [\Sigma w(|F_o|-F_c|)2/\Sigma w(F_o^2]^{1/2}$.
[e] GOF $= [\Sigma[w(F_o^2-F_c^2)^2]/(M-N)]^{1/2}$, where M is the number of reflections and N is the number of parameters refined.
[f] GOF $= [\Sigma w(|F_o|-|F_c|)^2/(M-N)]^{1/2}$, where M is the number of reflections and N is the number of parameters refined.

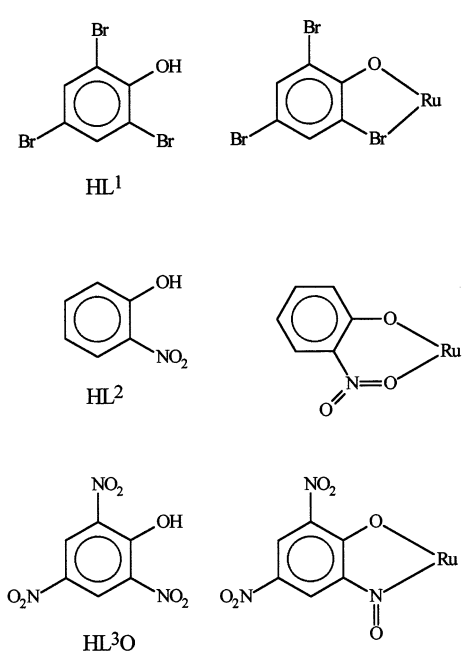


Fig. 1. The phenolic ligands and their coordination modes.

3. Results and discussion

Three phenolic ligands have been used in the present study which are shown, along with their individual abbreviation and coordination mode, in Fig. 1. The phenolic ligands react smoothly with $[Ru(PPh_3)_3Cl_2]$ in the presence of a base to afford complexes of type $[Ru(PPh_3)_2(L)_2]$. It may be noted here that unlike in the reactions of the first two phenolic ligands, heating of the reaction mixture at reflux was necessary in the reaction of 2,4,6-trinitrophenol with $[Ru(PPh_3)_3Cl_2]$ for obtaining the phenolate complex. It is also interesting to note that 2,4,6-trinitrophenol undergoes oxygen loss from one nitro group during the course of the synthetic reaction and coordinates in the nitrosophenolate fashion. Hence 2,4,6-trinitrophenol is abbreviated as HL^3O (see Fig. 1) to underline this oxo-transfer reaction. Mechanism of this oxygen loss reaction is not yet clear. However, oxygen from the nitro group is probably transferred to the PPh_3, dissociated from $[Ru(PPh_3)_3Cl_2]$. Indirect evidence of this oxo-transfer comes from detection of $OPPh_3$ in the residue of the synthetic reaction (after isolation of $[Ru(PPh_3)_2(L^3)_2]$), identified by its characteristic infrared spectrum (ν_{P-O} observed at 1185 cm^{-1}). Triphenylphosphine is well known to act as an oxygen-scavenger in many oxo-transfer reactions [37–40]. The role of $[Ru(PPh_3)_3Cl_2]$ in this oxo-transfer reaction is not yet clear, but that it does not act as a mere supplier of PPh_3 is clear from the fact that a mixture of PPh_3 and 2,4,6-trinitrophenol is unable to bring about any oxo-transfer reaction. Prior coordination of the 2,4,6-trinitrophenolate ligands to ruthenium in the nitrophenolate fashion followed by oxo-transfer from the metal-bound ligands appears to be probable. It may also be noted here that the yield of

$$2[Ru(PPh_3)_3Cl_2] + 2HL^3O \rightarrow [Ru(PPh_3)_2(L^3)_2] + 2HCl + 2OPPh_3 + [Ru(PPh_3)_2Cl_2] \quad (1)$$

$[Ru(PPh_3)_2(L^3)_2]$ is rather low, which might be attributed to the fact that $[Ru(PPh_3)_3Cl_2]$ dissociates in solution yielding free PPh_3 and an unstable $[Ru(PPh_3)_2Cl_2]$ species [41,42]. Hence 2 mol of $[Ru(PPh_3)_3Cl_2]$ (which supply 2 mol of PPh_3) are required for the reduction of 2 mol of 2,4,6-trinitrophenol. The 2 mol of reduced ligand (L^3) utilize only 1 mol of $[Ru(PPh_3)_2Cl_2]$ for complex formation (Eq. (1)). The other mole of $[Ru(PPh_3)_2Cl_2]$ probably undergoes decomposition [41,42]. Some characterization data of the complexes are given in Table 2. Elemental (C, H, N) analytical data agree well with the compositions of the $[Ru(PPh_3)_2(L)_2]$ complexes. All three complexes are diamagnetic, which corresponds to the bivalent state of ruthenium (low-spin d^6, $S = 0$) in these complexes.

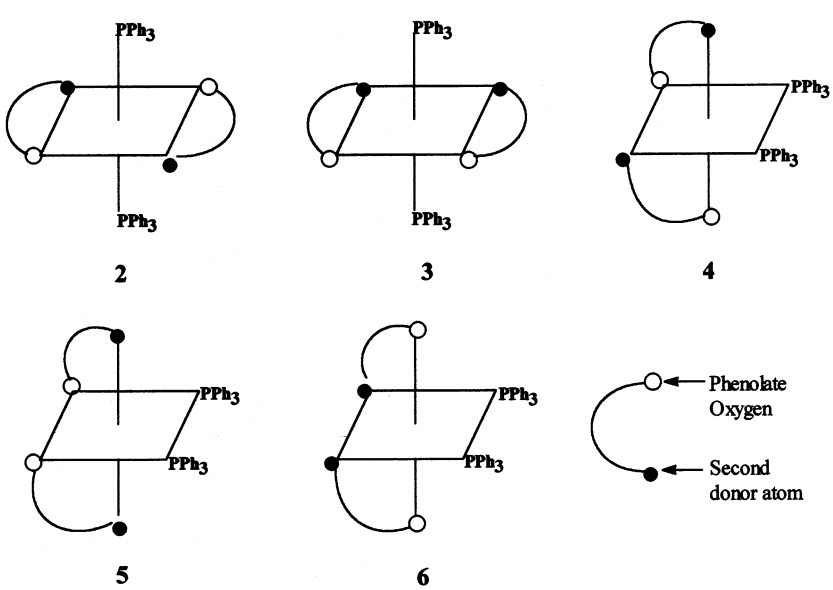
Table 2
Microanalytical, electronic spectral and cyclic voltammetric data

Compound	Microanalytical data [a]			Electronic spectral data [b] λ_{max} (nm), ε (M^{-1} cm^{-1})	Cyclic voltammetric data [c] $E_{1/2}$ (V), ΔE_p (mV)
	%C	%H	%N		
$[Ru(PPh_3)_2(L^1)_2]$	44.82 (44.83)	2.68 (2.65)		495(1200), 310(6200), 250(27 900), 220(43 300)	0.63(60), 1.48 [d]
$[Ru(PPh_3)_2(L^2)_2]$	63.94 (63.93)	4.16 (4.22)	3.06 (3.11)	490(5900), 390(8800), 250(28 700), 224(46 000)	0.64(70), 1.50 [d]
$[Ru(PPh_3)_2(L^3)_2]$	54.91 (54.99)	3.24 (3.25)	7.98 (8.02)	530(11 300), 340(21 520), 285(34 440), 224(55 960)	0.71(60), 1.55 [d]

[a] Calculated values are in parentheses.
[b] Dichloromethane solution.
[c] Solvent, acetonitrile; Supporting electrolyte, TEAP; reference electrode, SCE; $E_{1/2} = 0.5(E_{pa} + E_{pc})$, where E_{pa} and E_{pc} are anodic and cathodic peak potentials, respectively; $\Delta E_p = E_{pa} - E_{pc}$; scan rate, 50 mV s^{-1}.
[d] E_{pa} value.

From the composition of the complexes and also from the fact that ruthenium(II) prefers to be hexacoordinated, the phenolic ligands appear to have served as bidentate ligands. Five geometrical isomers (**2**–**6**) are then possible for the $[Ru(PPh_3)_2(L)_2]$ complexes.

To sort out the problem of stereochemistry and also to authenticate coordination mode of the phenolic ligands, molecular structures of $[Ru(PPh_3)_2(L^1)_2]$ and $[Ru(PPh_3)_2(L^3)_2]$ have been solved by X-ray crystallography [43]. The structures are shown in Fig. 2 and selected bond parameters are given in Table 3. In $[Ru(PPh_3)_2(L^1)_2]$, 2,4,6-tribromophenol is coordinated to ruthenium via loss of the phenolic proton, as a bidentate O,Br-donor ligand forming a five-membered chelate ring with a bite angle of 80.55°. While the phenolate oxygens are mutually *trans*, the PPh_3 ligands are mutually *cis* and the two bromines are also mutually *cis*. Hence the $O_2P_2Br_2$ coordination sphere around ruthenium has a *trans–cis–cis* geometry (**6**) with regard to mutual dispositions of the three pairs of donor atoms. The coordination sphere around ruthenium is distorted octahedral in nature, which is reflected in the bond parameters around ruthenium. While the Ru–O and Ru–P distances are quite normal [18,21,44,45], the Ru–Br lengths are a bit longer than is usually observed [46–48]. The C–Br lengths corresponding to the coordinated bromines are slightly longer than the other two C–Br distances in the same ligand and this may be attributed to coordination of the bromine to ruthenium(II). The phenolate C–O lengths are also quite usual [44,45]. The $[Ru(PPh_3)_2(L^2)_2]$ complex could not be characterized crystallographically [43]. However, the 2-nitrophenolate ligand is known to coordinate as bidentate O,O-donor forming a six-membered chelate ring [49] as shown in Fig. 1. The same coordination mode of the 2-nitrophenolate ligand is assumed in $[Ru(PPh_3)_2(L^2)_2]$.



Structure determination of $[Ru(PPh_3)_2(L^3)_2]$ shows that 2,4,6-trinitrophenol is coordinated, via loss of the phenolic proton and reduction of one nitro group at the *ortho* position, as a 2-nitroso-4,6-dinitrophenolate anion. Chelation takes place from the nitroso nitrogen and phenolate oxygen forming a five-membered chelate ring with a bite angle of 80.85°. The coordinated nitrogens are mutually *cis*, the phenolate oxygens are also mutually *cis* and the two coordinated PPh_3 ligands are mutually *trans*. The coordination sphere around ruthenium is slightly distorted octahedral $N_2O_2P_2$ with a *cis–cis–trans* geometry, respectively (**3**). While the Ru–P distances are normal [50,51], the bond distances within the N–O chelates are rather unusual. The Ru–N bonds are significantly shorter than usually observed [15,16,18]. Such a short Ru–N distance is known to result only from very strong π-interaction [52]. The Ru–O bonds are longer than usually observed [21,45]. The observed C–O lengths are shorter than usual phenolate C–O distances [44,45]. The unusual nature of observed bond distances in $[Ru(PPh_3)_2(L^3)_2]$ appears to result from the combined effect of the possible resonance in the nitrosophenolate ligand (**7**) and the π-bonding interaction [52–54] between ruthenium(II) and the imine-oxo moiety of the nitrosophenolate ligand.

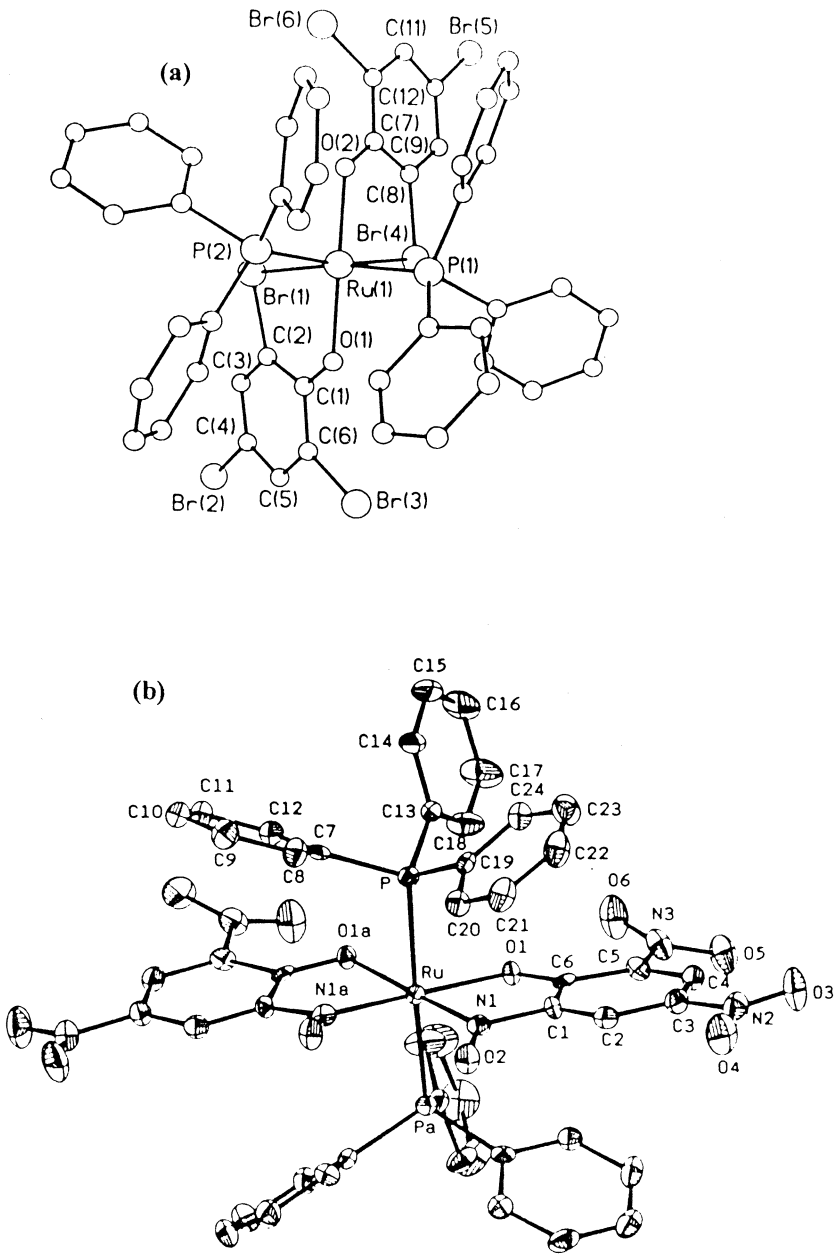
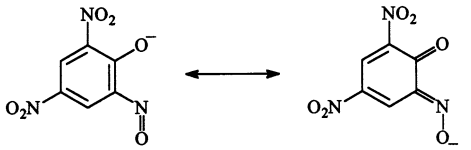


Fig. 2. View of the (a) $[Ru(PPh_3)_2(L^1)_2]$ and (b) $[Ru(PPh_3)_2(L^3)_2]$ molecules.



7

This strong π-interaction is also reflected in the *cis* disposition of this imine nitrogens [53,54]. In complexes containing the $Ru^{II}(PPh_3)_2$ moiety, the two triphenylphosphines usually take up *cis* positions [15,18,45,55,56], which has also been observed in $[Ru(PPh_3)_2(L^1)_2]$ (vide supra). In $[Ru(PPh_3)_2(L^3)_2]$ the imine-oxo group appears to be a stronger π-acceptor than PPh_3 and thus forces the bulky PPh_3 ligands to take up *trans* positions for less steric hindrance.

The IR spectra of these complexes show many sharp bands of different intensities in the 1700–400 cm^{-1} region due to vibrations arising from the coordinated PPh_3 and phenolic ligands and are therefore complex in nature. No attempt has been made to assign individual bands. However, the strong vibrations near 520, 700, and 740 cm^{-1} displayed by all the complexes indicate the presence of the $Ru(PPh_3)_2$ fragment [15,18,44,45]. The $[Ru(PPh_3)_2(L)_2]$ complexes are soluble in polar solvents like acetonitrile, dichloromethane, chloroform, etc, producing intense red solutions. Electronic spectra of the complexes have been recorded in dichloromethane solution. All these complexes show several intense absorptions in the visible and ultraviolet region. Spectral data are presented in Table 2. The intense absorptions in the ultraviolet region are attributable to transitions within the ligand orbitals and those in the visible region are probably due to allowed metal-to-ligand charge-transfer transitions. Multiple charge-transfer transitions in such mixed-ligand complexes are known to result from lower symmetry splitting of the metal level, the presence of different acceptor orbitals and from the mixing of singlet and triplet configurations in the excited state through spin-orbit coupling [57–60].

Table 3
Selected bond distances (Å) and bond angles (°)

$[Ru(PPh_3)_2(L^1)_2]$		$[Ru(PPh_3)_2(L^3)_2]$	
Ru–O(1)	2.091(6)	Ru–P	2.4205(18)
Ru–O(2)	2.086(6)	Ru–O1	2.100(4)
Ru–Br(1)	2.6354(13)	Ru–N1	1.927(5)
Ru–Br(4)	2.6343(12)	O1–C6	1.269(7)
Ru–P(1)	2.282(3)	O2–N1	1.243(6)
Ru–P(2)	2.299(2)	O3–N2	1.208(8)
O(1)–C(1)	1.281(10)	O4–N2	1.224(8)
O(2)–C(7)	1.299(10)	O5–N3	1.230(7)
C(2)–Br(1)	1.914(9)	O6–N3	1.208(8)
C(4)–Br(2)	1.899(11)	N1–C1	1.437(7)
C(6)–Br(3)	1.895(11)	N2–C3	1.457(8)
C(8)–Br(4)	1.906(8)	N3–C5	1.465(7)
C(10)–Br(5)	1.893(9)	C1–C2	1.359(8)
C(12)–Br(6)	1.895(9)	C2–C3	1.382(9)
		C3–C4	1.385(9)
		C4–C5	1.363(2)
		C5–C6	1.428(8)
		C6–C1	1.426(8)
O(1)–Ru–O(2)	171.6(2)	P–Ru–Pa	171.59(6)
P(1)–Ru–Br(1)	168.12(7)	O1–Ru–N1a	177.93(17)
P(2)–Ru–Br(4)	169.08(7)	O1a–Ru–N1	177.93(17)
P(1)–Ru–P(2)	96.16(9)	O1–Ru–N	80.85(17)
Br(1)–Ru–Br(4)	83.54(4)	O1a–Ru–N1a	80.85(17)
O(1)–Ru–Br(1)	80.55(17)		
O(2)–Ru–Br(4)	80.93(16)		

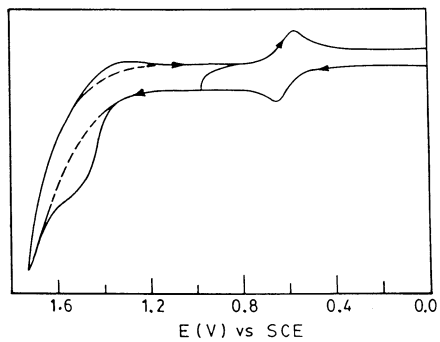


Fig. 3. Cyclic voltammogram of $[Ru(PPh_3)_2(L^1)_2]$ in acetonitrile solution (0.1 M TEAP) at a scan rate of 50 mV s^{-1}.

Electrochemical properties of all the complexes have been studied in acetonitrile solution (0.1 M TEAP) by cyclic voltammetry. A selected voltammogram is shown in Fig. 3 and the voltammetric data are presented in Table 2. Each complex shows two oxidative responses on the positive side of SCE. The first oxidative response is observed within 0.63–0.71 V versus SCE and is assigned to the ruthenium(II)–ruthenium(III) oxidation (Eq. (2)) This oxidation is reversible in nature with a peak-to-peak separation (ΔE_p) of 60–70 mV, which does not change when the scan rate is changed.

$$[Ru^{II}(PPh_3)_2(L)_2] \rightleftharpoons [Ru^{III}(PPh_3)_2(L)_2]^+ + e^- \quad (2)$$

$$[Ru^{III}(PPh_3)_2(L)_2]^+ \rightarrow [Ru^{IV}(PPh_3)_2(L)_2]^{2+} + e^- \quad (3)$$

The anodic peak current (i_{pa}) is also equal to the cathodic peak current (i_{pc}) as expected for a reversible electron-transfer process. The one-electron nature of this oxidation has been verified by comparing its current heights with those of the standard ferrocene–ferrocenium couple under identical experimental conditions. The second oxidative response, which appears near 1.5 V versus SCE, is irreversible and is tentatively assigned to ruthenium(III)–ruthenium(IV) oxidation (Eq. (3)). One-electron stoichiometry of the oxidation is verified by comparing its current height (i_{pa}, calculated after deduction of solvent contribution from the observed current at E_{pa}) with that of the ruthenium (II)–ruthenium(III) oxidation.

4. Conclusions

The present study shows that coordination of phenols to ruthenium as simple monodentate oxygen donor ligands is probably not possible, but phenols having a second donor site linked to the *ortho* position can bind to ruthenium as a bidentate ligand affording stable complexes.

5. Supplementary data

Copies of supplementary data can be obtained free of charge from The Director, Cambridge Crystallographic Data Centre, 12 Union Road, Cambridge, CB2 1EZ, UK (Fax: +44-1223-336-033; e-mail: deposit@ccdc.cam.ac.uk or www: http://www.ccdc.cam.ac.uk), quoting the deposition numbers CCDC 141332 and CCDC 141333.

Acknowledgements

Financial assistance received from the Council of Scientific and Industrial Research, New Delhi [Grant No. 01(1408)/96/EMR-II] and the Directorate General for Higher Education (Spain) under Grant PB98-1593 is gratefully acknowledged. Thanks are also due to the Third World Academy of Sciences for financial support enabling the purchase of an electrochemical cell system.

References

[1] S.-M. Lee, W.-T. Wong, Coord. Chem. Rev. 164 (1997) 415.
[2] I. Ortmanes, C. Moucheron, A.K.-D. Mesmaeker, Coord. Chem. Rev. 168 (1998) 233.
[3] A. Islam, N. Ikeda, K. Nozaki, Y. Okamoto, B. Gholamkhass, A. Yoshimura, T. Ohno, Coord. Chem. Rev. 171 (1998) 355.
[4] J.W.-S. Hui, Y.-T. Wong, Coord. Chem. Rev. 172 (1998) 389.
[5] P.J. Dyson, B.F.G. Johnson, C.M. Martin, Coord. Chem. Rev. 175 (1998) 59.
[6] D.J. Stufkens, A. Vlcek Jr., Coord. Chem. Rev. 177 (1998) 127.
[7] L.D. Cola, P. Belser, Coord. Chem. Rev. 177 (1998) 301.
[8] S. Sabo-Etienne, B. Chaudret, Coord. Chem. Rev. 178–180 (1998) 381.
[9] D. Touchard, P.H. Dixneuf, Coord. Chem. Rev. 178–180 (1998) 409.
[10] G. Jia, C-P. Lau, Coord. Chem. Rev. 190–192 (1999) 83.
[11] P.K. Sinha, J. Chakravarty, S. Bhattacharya, Polyhedron 16 (1997) 81.
[12] N.C. Pramanik, S. Bhattacharya, J. Chem. Res. (S) (1997) 98.
[13] N.C. Pramanik, S. Bhattacharya, Polyhedron 16 (1997) 1755.
[14] N.C. Pramanik, S. Bhattacharya, Polyhedron 16 (1997) 3047.
[15] F. Basuli, S.M. Peng, S. Bhattacharya, Inorg. Chem. 36 (1997) 5645.
[16] N.C. Pramanik, K. Pramanik, P. Ghosh, S. Bhattacharya, Polyhedron 17 (1998) 1525.
[17] N.C. Pramanik, S. Bhattacharya, Transition Met. Chem. 23 (1998) 429.
[18] F. Basuli, M. Ruf, C.G. Pierpont, S. Bhattacharya, Inorg. Chem. 37 (1998) 6113.
[19] N.C. Pramanik, S. Bhattacharya, Transition Met. Chem. 24 (1999) 95.
[20] K. Sui, S.M. Peng, S. Bhattacharya, Polyhedron 18 (1999) 631.
[21] A.K. Das, A. Rueda, L.R. Falvello, S.M. Peng, S. Bhattacharya, Inorg. Chem. 38 (1999) 4365.
[22] K. Majumder, S. Bhattacharya, Polyhedron 18 (1999) 3669.
[23] A.K. Das, S.M. Peng, S. Bhattacharya, J. Chem. Soc., Dalton Trans. (2000) 181.
[24] S. Dutta, N.C. Pramanik, S. Bhattacharya, J. Ind. Chem. Soc. 77 (2000) 1.
[25] F. Basuli, S.M. Peng, S. Bhattacharya, Inorg. Chem. 39 (2000) 1120.
[26] G.K. Lahiri, S. Bhattacharya, B.K. Ghosh, A. Chakravorty, Inorg. Chem. 26 (1987) 4324.
[27] S. Bhattacharya, S.R. Boone, G.A. Fox, C.G. Pierpont, J. Am. Chem. Soc. 112 (1990) 1088.
[28] H. Aneetha, C.R.K. Rao, K.M. Rao, P.S. Zacharias, X. Feng, T.C.W. Mak, B. Srinivas, M.Y. Chiang, J. Chem. Soc., Dalton Trans. (1997) 1697.
[29] M.G. Bhowon, H.L.K. Wah, R. Narain, Polyhedron 18 (1998) 341.
[30] H.J. Yao, C.H. Hu, J.M. Duo, J.D. Wei, R.S. Jin, W. Li, P.J. Zheng, Polyhedron 18 (1999) 631.
[31] M. Hossain, M. Maji, S.K. Chottopadhyay, S. Ghosh, A.J. Blake, Polyhedron 17 (1998) 1897.
[32] K. Wohnrath, A.A. Batista, A.G. Ferreira, J.Z. Spectra, L. Antonio, A.D. Oliveira, E. Castellano, Polyhedron 17 (1998) 2013.
[33] E.A. Seddon, K.R. Seddon, The Chemistry of Ruthenium, Elsevier, Amsterdam, 1994.
[34] T.A. Stephenson, G. Wilkinson, J. Inorg. Nucl. Chem. 28 (1966) 945.
[35] D.T. Sawyer, J.L. Roberts, Experimental Electrochemistry for Chemists, Wiley, New York, 1974, pp. 167–215.
[36] M. Walter, L. Ramaley, Anal. Chem. 45 (1973) 165.
[37] S. Chattopadhyay, N. Bag, G.K. Lahiri, A. Chakravorty, J. Chem. Soc., Dalton Trans. (1990) 3389.
[38] B.A. Moyer, B.K. Sipe, T. Meyer, J. Inorg. Chem. 20 (1981) 1475.
[39] M.E. Mormoin, T.J. Takeuchi, J. Am. Chem. Soc. 110 (1988) 1472.
[40] C.M. Che, K.Y. Wong, J. Chem. Soc., Dalton Trans. (1989) 2065.
[41] S. Cenini, A. Fusi, G. Capparella, J. Inorg. Nucl. Chem. 33 (1971) 3576.
[42] B.R. James, L.R. Markham, Inorg. Chem. 13 (1974) 1997.
[43] Single crystals of $[Ru(PPh_3)_2(L^2)_2]$ could not be grown.
[44] S. Bhattacharya, C.G. Pierpont, Inorg. Chem. 30 (1991) 1511.
[45] F. Basuli, A.K. Das, G. Mostafa, S.M. Peng, S. Bhattacharya, Polyhedron 19 (2000) 1663.
[46] R.H.B. Mais, H.M. Powell, J. Chem. Soc. (1965) 7471.
[47] S. Merlino, G. Montagnoli, Acta Crystallogr., Sect. B 24 (1968) 424.
[48] M.A. Bennet, G.B. Robertson, I.B. Tomkins, P.O. Whimp, J. Organomet. Chem. 32 (1971) C19.
[49] R.G. Little, Acta Crystallogr., Sect. B 35 (1979) 2398.
[50] G.K. Clark, T.J. Collins, S.M. James, W.R. Roper, J. Organomet. Chem. 125 (1977) C23.
[51] G.K. Clark, S.M. James, J. Organomet. Chem. 134 (1977) 229.
[52] I.M. Treitel, M.T. Flood, R.E. Marsh, H.B. Gray, J. Am. Chem. Soc. 91 (1969) 6512.
[53] A.R. Krause, K. Krause, Inorg. Chem. 19 (1980) 2600.
[54] A. Goswami, A.R. Chakravorty, A. Chakravorty, Inorg. Chem. 20 (1981) 2246.

[55] M. Menon, A. Pramanik, N. Bag, A. Chakravorty, J. Chem. Soc., Dalton Trans. (1995) 1417.
[56] A. Pramanik, N. Bag, G.K. Lahiri, A. Chakravorty, J. Chem. Soc., Dalton Trans. (1990) 3823.
[57] B.J. Pankuch, D.E. Lacky, G.A. Crosby, J. Phys. Chem. 84 (1980) 2061.
[58] A. Ceulemans, L.G. Vanquickenborne, J. Am. Chem. Soc. 103 (1981) 2238.
[59] S. Decurtins, F. Felix, J. Ferguson, H.U. Gudel, A. Ludi, J. Am. Chem. Soc. 102 (1980) 4102.
[60] E.M. Kober, T.J. Meyer, Inorg. Chem. 21 (1982) 5645.

PERGAMON

www.elsevier.nl/locate/poly

Polyhedron 19 (2000) 1681–1685

POLYHEDRON

Competitive lithium-7 NMR study of the complexation of some alkaline earth and transition metal ions with 18-crown-6 in acetonitrile and its 50:50 mixtures with nitrobenzene and nitroethane

Mojtaba Shamsipur *, Tayyebeh Madrakian

Department of Chemistry, Razi University, Kermanshah, Iran

Received 21 January 2000; accepted 27 April 2000

Abstract

Lithium-7 NMR spectroscopy was used to investigate the stoichiometry and stability of a Li^+ complex with 18-crown-6 (18C6) in pure acetonitrile and its 50:50 (w/w) mixtures with nitrobenzene and nitromethane. A competitive ^7Li NMR method was also employed to probe the complexation of Mg^{2+}, Ca^{2+}, Ba^{2+}, Co^{2+}, Ni^{2+}, Cu^{2+}, Zn^{2+} and Cd^{2+} ions with 18C6 in the same solvent systems. In all solvents, the stability of the resulting 1:1 complexes was found to vary in the order $Ba^{2+} > Ca^{2+} > Cd^{2+} > Mg^{2+} \approx Cu^{2+} > Ni^{2+} > Co^{2+} > Zn^{2+}$. © 2000 Elsevier Science Ltd. All rights reserved.

Keywords: Macrocyclic polyether 18-crown-6; Acetonitrile; Alkaline earth metal ions; Transition metal ions

Because of the vital importance of recognition and binding of ionic substrates to organic hosts, such as enzymes, antibodies and membrane carriers, model studies on the recognition of cations using synthetic host compounds, such as macrocyclic polyethers and their aza- and thia-substituted derivatives, are of special interest [1–3]. There is an extensive amount of literature reported on the study of macrocyclic ligands and their interaction with a wide variety of cations, anions and neutral guests [4–7]. Structural, spectral, electrochemical, thermodynamic and kinetic properties of macrocyclic complexation have been investigated [4], and detailed thermodynamic and kinetic data for different macrocyclic complexes evaluated by different physico–chemical methods in various solvent media are reported [5–7]. During their formation, the selectivity and stability of metal ion complexes with macrocyclic ligands is of special importance in their use as suitable neutral carriers for the selective transport across liquid membranes [8–10] and for constructing membrane-selective sensors for different metal ions [11–13].

In recent years, we have introduced some competitive spectrophotometric [14–17], polarographic [18] and potentiometric [19] methods to investigate the thermodynamics and kinetics of complexation of a variety macrocycle–metal ion systems which possess no spectrophotometric or electrochemical properties under the experimental conditions used. In this paper, we used ^7Li NMR as a very sensitive probe to study the complexation of Mg^{2+}, Ca^{2+}, Ba^{2+}, Co^{2+}, Ni^{2+}, Cu^{2+}, Zn^{2+} and Cd^{2+} ions with 18-crown-6 (18C6) in acetonitrile (AN) and its 50:50 (w/w) mixtures with nitrobenzene (NB) and nitromethane (NM) by a competitive technique. It should be noted that the alkaline earth and transition metal ions used have unsuitable NMR properties such as low receptivity, high quadrupole moment, insensitive chemical shifts, etc.

1. Experimental

The macrocyclic polyether 18-crown-6 (18C6, Merck) was precipitated as its acetonitrile complex [20]. The resulting crystals were isolated and kept under vacuum at room temperature for several days to remove the

* Corresponding author. Tel.: +98-831-94-066; fax: +98-831-831-618.

0277-5387/00/$ - see front matter © 2000 Elsevier Science Ltd. All rights reserved.
PII: S0277-5387(00)00417-4

acetonitrile. Lithium perchlorate (Merck) was purified and dried as reported elsewhere [21]. The nitrate salts of all other cations used were of the highest purity available from Fluka and used without any further purification except for vacuum drying over P_2O_5. Spectroscopic grade acetonitrile, nitrobenzene and nitromethane (Merck) were used as received.

All NMR measurements were made on a Jeol FX90Q FT-NMR spectrometer with a field strength of 21.13 kG. At this field, lithium-7 resonates at 33.74 MHz. An aqueous 4.0 M LiCl solution was used as the external reference and the reported lithium-7 chemical shifts are referenced to this solution. The paramagnetic (downfield) shift from the reference is designated as being positive. The concentration of all cations used was 0.005 M. All chemical shift measurements were carried out at a temperature of 27.0 ± 0.1°C.

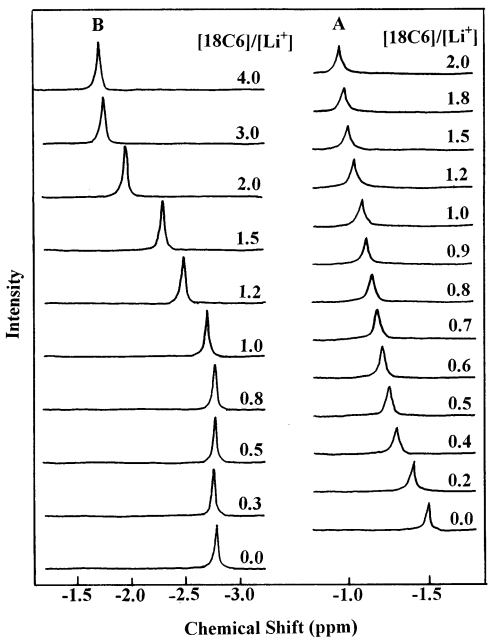


Fig. 1. Lithium-7 NMR spectra for Li^+–18C6–acetonitrile (A) and Li^+–18C6–Ba^{2+}–acetonitrile–nitrobenzene (B) systems.

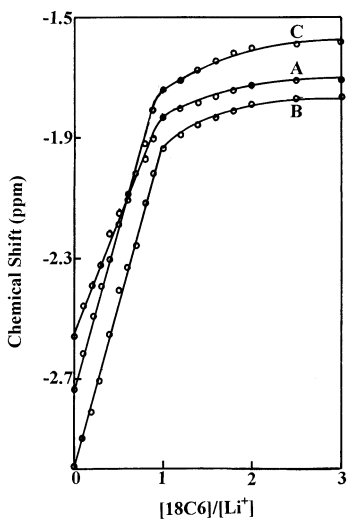


Fig. 2. Lithium-7 chemical shifts as a function of the 18C6/Li^+ mole ratio in acetonitrile (A), acetonitrile–nitrobenzene (B) and acetonitrile–nitromethane (C) solutions.

2. Results and discussion

Lithium-7 chemical shifts were measured as a function of the mole ratio of complexant 18C6 to lithium ion in acetonitrile, acetonitrile–nitrobenzene and acetonitrile–nitromethane solutions. In all cases, only one population-averaged resonance was observed, indicating that the exchange rate of the cation between the bulk solution and the complexed site is fast on the NMR time scale (Fig. 1). The resulting mole data are shown in Fig. 2. As can be seen, in all three cases, addition of 18C6 to the Li^+ ion solution causes an almost linear paramagnetic shift that begins to level off at mole ratios greater than unity. The slope of the corresponding mole ratio plots changes significantly at the point where the ligand-to-cation mole ratio is equal to one, showing the formation of a relatively stable complex.

The formation constants of 1:1 complexes were calculated from the variation of the ^7Li chemical shift crown/Li^+ mole ratio. It was been shown previously [22] that the observed chemical shift is given by

$$\delta_{obs} = \{[(K_{Li}C_{Li}C_{18C6} - 1) + (K_{Li}^2C_{18C6}^2 + K_{Li}^2C_{Li}^2 - 2K_{Li}^2C_{18C6}C_{Li} + 2K_{Li}C_{18C6} + 2K_{Li}C_{Li} + 1)^{1/2}](\delta_{Li} - \delta_{Li-18C6})/2K_{Li}C_{Li}\} + \delta_{Li-18C6} \quad (1)$$

where K_{Li} is the formation constant for the 1:1 complex, C_{18C6} and C_{Li} are the analytical concentrations of the crown ether and Li^+ ion, respectively, and δ_{Li} and $\delta_{Li-18C6}$ are the respective chemical shifts of the free and complexed lithium ion. The non-linear least-squares curve-fitting program KINFIT [23] was used to evaluate K_{Li} and $\delta_{Li-18C6}$ values for the 1:1 complexes by fitting the δ_{obs} versus C_{18C6} data (at constant $C_{Li} =$ 0.005 M) to Eq. (1).

A sample computer fit of the ^7Li chemical shift–mole ratio data is shown in Fig. 3(A), and the calculated $\log K_f$ values are given in Table 1. A fair agreement between the observed and calculated chemical shifts shown in Fig. 3(A) further supports the formation of a complex with 1:1 stoichiometry between Li^+ and 18C6.

In contrast to ^7Li and other NMR active alkali metals, most alkaline earth and transition metal nuclei cannot be accurately used in an NMR study of their macrocyclic complexes. This is mainly because of their high quadrupole moments and low receptivities [24].

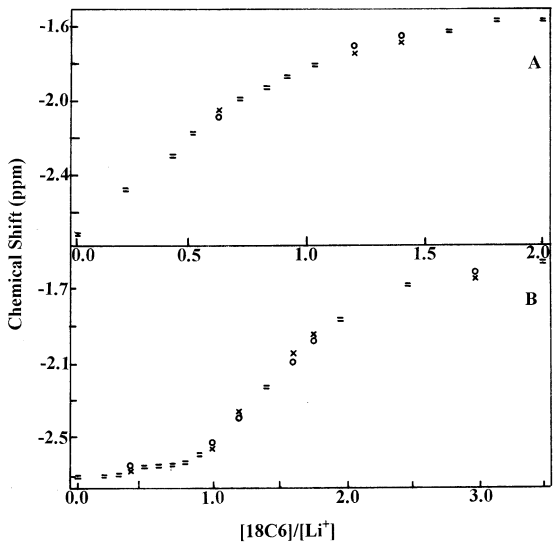


Fig. 3. Computer fit of lithium-7 chemical shift vs. 18C6/Li^+ mole ratio for Li^+–18C6 (A) and Li^+–18C6–Ca^{2+} (B) systems in acetonitrile–nitrobenzene solution. (×) Experimental point; (○) calculated point; (=) experimental and calculated points are the same within the resolution of the plot.

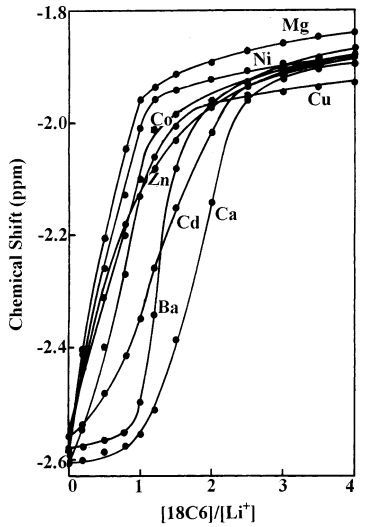


Fig. 4. Lithium-7 chemical shifts as function of 18C6/Li^+ mole ratio in acetonitrile solution in the presence of different M^{2+} ions.

Thus, in this work, we decided to employ ^7Li NMR as a very sensitive probe [21,22,25–27] to investigate the complex formation of Co^{2+}, Ni^{2+}, Cu^{2+}, Zn^{2+}, Cd^{2+}, Mg^{2+}, Ca^{2+} and Ba^{2+} ions with 18C6 in the solvent media used. The variation of lithium-7 chemical shift in the presence of an equimolar concentration of different alkaline earth and transition metal ions (0.005 M) as a function of 18C6/Li^+ mole ratio in different solvent systems was measured. Typical spectra are shown in Fig. 1(B) and the resulting chemical shift–mole ratio plots are illustrated in Figs. 4–6.

As is obvious from Figs. 4–6, unlike the cases involved in the formation of 1:1 Li^+–18C6 complex (Fig. 2) in which the change in chemical shift with the 18C6/Li^+ mole ratio is quite linear at mole ratios < 1, the ^7Li chemical shift shows a curved relationship for 18C6/Li^+ mole ratios between 0 and 2. However, in all cases, a plateau in the chemical shift is reached at mole ratios > 2. This is obviously indicative of the quantitative formation of 1:1 complexes of 18C6 with both Li^+ and M^{2+} ions. It is worthwhile noting that in the cases of Cd^{2+}, Ca^{2+} and Ba^{2+} ions, the corresponding mole ratio plots (Figs. 4–6) also show a distinct infection point at a 18C6/Li^+ mole ratio of ca. 1, most probably due to significant differences in the stability of the 18C6 complexes of these cations with that of Li^+–18C6 in solution [5,6].

The competitive complexation equilibria for the case of 1:1 complexation between 18C6 and Li^+ and M^{2+} ions can be written as:

$$Li^+ + 18C6 = Li^+–18C6$$

$$K_{Li} = [Li^+–18C6]/[Li^+][18C6] \quad (2)$$

Table 1
Formation constants of different metal ion complexes with 18C6 in various solvents [a]

Metal ion [b]	Log K_f		
	Acetonitrile	Acetonitrile–nitrobenzene	Acetonitrile–nitromethane
Co^{2+} (0.75)	2.15 ± 0.03	2.38 ± 0.07	2.59 ± 0.04
Ni^{2+} (0.69)	2.34 ± 0.06	2.59 ± 0.04	2.77 ± 0.04
Cu^{2+} (0.77)	2.48 ± 0.02	2.67 ± 0.08	2.94 ± 0.04
Zn^{2+} (0.74)	2.07 ± 0.05	2.33 ± 0.02	2.48 ± 0.06
Cd^{2+} (0.95)	3.07 ± 0.04	3.16 ± 0.05	3.91 ± 0.20
Mg^{2+} (0.72)	2.31 ± 0.02	2.62 ± 0.04	3.05 ± 0.04
Ca^{2+} (1.00)	4.14 ± 0.16	4.21 ± 0.06	4.34 ± 0.08
Ba^{2+} (1.35)	4.24 ± 0.30	4.58 ± 0.16	5.39 ± 0.30
Li^+ (0.76)	2.52 ± 0.07	2.80 ± 0.10	2.98 ± 0.06

[a] The errors associated with log K_f values are ± S.D.
[b] The values in parentheses are the ionic radii in angstroms [31].

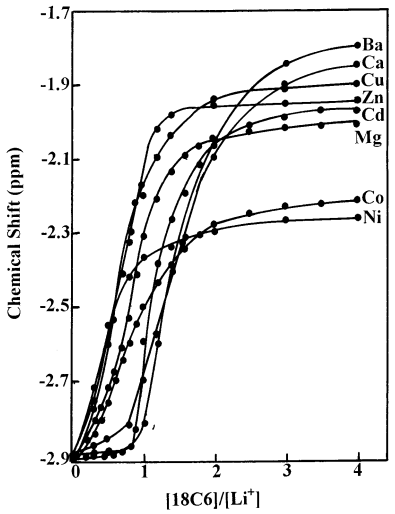


Fig. 5. Lithium-7 chemical shifts as a function of 18C6/Li^+ mole ratio in acetonitrile–nitrobenzene solution in the presence of different M^{2+} ions.

$$M^{2+} + 18C6 = M^{2+}\text{–}18C6$$

$$K_M = [M^{2+}\text{–}18C6]/[M^{2+}]/[18C6] \quad (3)$$

The free 18C6 concentration, [18C6], is then obtained from Eq. (4) [14]:

$$K_{Li}K_M[18C6]^3 - \{K_{Li}K_M(C_{18C6} - C_{Li} - C_M) - K_{Li} - K_M\}[18C6]^2 - \{K_{Li}(C_{18C6} - C_{Li}) + K_M(C_{18C6} - C_{Li}) - 1\}[18C6] - C_{18C6} = 0 \quad (4)$$

where C_{18C6}, C_{Li} and C_M are the analytical concentrations of 18C6, Li^+ ion and M^{2+} ion, respectively. In this case, the observed ^7Li chemical shift is obtained from Eq. (5) [22]:

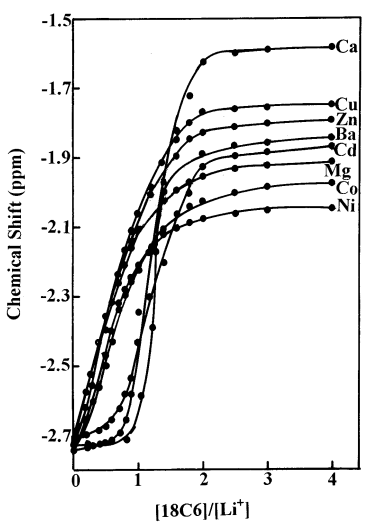


Fig. 6. Lithium-7 chemical shifts as a function of 18C6/Li^+ mole ratio in acetonitrile–nitromethane solution in the presence of different M^{2+} ions.

$$\delta_{obs} = P_{Li}\delta_{Li} + P_{Li\text{–}18C6}\delta_{Li\text{–}18C6} \quad (5)$$

where P_{Li} and $P_{Li\text{–}18C6}$ are the mole fractions of the free and complexed Li^+ ion, respectively. By substitution from Eq. (2) and the mass balance equation $C_{Li} = [Li^+] + [Li^+\text{–}18C6]$, Eq. (5) can be written as:

$$\delta_{obs} = \{\delta_{Li} + \delta_{Li\text{–}18C6}[18C6]K_{Li}\}/\{1 + K_{Li}[18C6]\} \quad (6)$$

The K_M values were evaluated by obtaining the free [18C6] from Eq. (4) and fitting the chemical shift–mole ratio data to Eq. (6) using the KINFIT program.

A sample computer fit of the mole ratio data for a remary Li^+–18C6–M^{2+} system is shown in Fig. 3(B) and the resulting log K_f values for all M^{2+}–18C6 complexes are also included in Table 1. Our assumption that the 1:1 stoichiometry of both Li^+–18C6 and M^{2+}–18C6 complexes seems reasonable in the light of a fair agreement between the observed and calculated chemical shifts [5,6]. It should be noted that the curve-fitting method used in this study is not able to evaluate the K_f values accurately at values $> 10^6$.

The data given in Table 1 clearly indicate the influence of solvent properties on the stability of the resulting 18C6 and Li^+ complexes, and all M^{2+} ions used. Amongst the different factors affecting the stability of macrocyclic crown ethers in solution [5,6], the ability of solvent to solvate ionic species and, thus, compete with the ligands for the cation is of vital importance [14,19,21,22,25–27]. Of course, the interaction of some solvents with macrocyclic ligands [7,20,28] is of equal importance, although much less appreciated. Thus, the thermodynamic stability of metal ion–macrocycle complexes is not just a measure of the absolute strength of ion–dipole interactions between the cation and the donating oxygen atoms of crown ethers, but it is also a measure of the relative strength as compared with ionic solvation.

From Table 1, it is obvious that the stability of all 18C6 complexes increases in the order acetonitrile < acetonitrile–nitrobenzene < acetonitrile–nitromethane. It is well known that the Gutmann donor number of solvents [29] is an important measure in complexation reactions [5,6,14–19,21,22,25–27]. It should be noted that acetonitrile, nitrobenzene and nitromethane possess similar dielectric constants (i.e. $\varepsilon_{AN} = 37.5$, $\varepsilon_{NM} = 34.8$ and $\varepsilon_{NM} = 35.6$), but have quite different donor numbers (i.e. $DN_{AN} = 14.1$, $DN_{NB} = 4.4$ and $DN_{NM} = 2.7$) [29]. Acetonitrile, as a solvent of intermediate solvating ability, can thus compete with the crown ether for metal ions more readily than nitrobenzene and, especially, nitromethane as low donicity solvents. In addition, it has been shown that acetonitrile can solvate the macrocyclic ligand to a large extent [20,28], while nitrobenzene and nitromethane have no significant interaction with the ligand [7]. Thus, it is not unexpected to observe a rather large increase in the stability of the

metal ion–18C6 complexes with addition of nitrobenzene and, especially, nitromethane to acetonitrile solutions.

The data given in Table 1 revealed that the stability of M^{2+}–18C6 complexes vary in the order $Ba^{2+} > Ca^{2+} > Cd^{2+} > Mg^{2+} \approx Cu^{2+} > Ni^{2+} > Co^{2+} > Zn^{2+}$. As is obvious, with the exception of the Cd^{2+} ion, transition metal complexes form weaker complexes with 18C6 than the alkaline earth metal ions used. This is not only due to the soft character of the transition metal ions, which result in weaker interactions with the donating oxygens of the macrocyclic ring as hard bases [30], but also because of the small ionic radii (i.e. 0.69–0.77 Å) [31] for the cavity of 18C6 (with an anionic radius of 1.3–1.6 Å) [32]. However, the Cd^{2+} ion ($r = 0.95$ Å) [31], despite its weaker soft–hard interaction with the macrocycle, forms a more stable complex than the hard Mg^{2+} ion, most probably due to its more suitable size for the 18C6 cavity than the magnesium ion ($r = 0.72$ Å) [31]. On the other hand, as expected [5,6], the hard Ba^{2+} ion with the most suitable ionic size for the cavity of 18C6 ($r = 1.35$ Å) [31] forms the most stable complex in the series. Finally, the Ca^{2+} ion ($r = 1.00$ Å) [31] with a similar ionic size to Cd^{2+}, but possessing a hard character [30], forms the second most stable 18C6 complex among the cations used.

It is worth noting that, in the case of 18C6 complexes with the metal ions of the first transition series, the stability of the resulting complexes decrease in the order $Cu^{2+} > Ni^{2+} > Co^{2+} > Zn^{2+}$. This sequence follows the Irving–Williams order [33] which generally holds for equilibrium constants of different complexes of the metal ions of first transition series [14,34].

References

[1] M.W. Hosseini, J.M. Lehn, Helv. Chim. Acta 69 (1986) 587.
[2] R. Menif, A.E. Martell, P.J. Sqnattrito, A. Clearfield, Inorg. Chem. 29 (1990) 4723.
[3] E. Kimura, Pure Appl. Chem. 65 (1993) 355 and Refs. cited therein.
[4] L.F. Lindoy, The Chemistry of Macrocyclic Ligand Complexes, Cambridge University Press, New York, 1989.
[5] R.M. Izatt, J.S. Bradshaw, S.A. Nielsen, J.D. Lamb, J.J. Christensen, D. Sen, Chem. Rev. 85 (1985) 271.
[6] R.M. Izatt, K. Pawlak, J.S. Bradshaw, R.L. Bruening, Chem. Rev. 91 (1991) 1721.
[7] R.M. Izatt, K. Pawlak, J.S. Bradshaw, R.L. Bruening, B.J. Tarbet, Chem. Rev. 92 (1992) 1261.
[8] R.M. Izatt, G.A. Clark, J.S. Bradshaw, J.D. Lamb, J.J. Christensen, Sep. Purif. Methods 15 (1986) 21.
[9] M. Dozol, in: Cecille, M. Casaraci, L. Pictelli (Eds.), New Separation Chemistry Techniques for Radio Active Waste and Other Specific Applications, Elsevier, Amsterdam, 1991.
[10] H.C. Visser, D.N. Reinhoudt, F. DeJong, Chem. Soc. Rev. (1994) 75.
[11] D. Ammann, W.E. Morf, P. Anker, P.C. Meier, E. Pretsch, W. Simon, Ion-Selective Electrode Rev. 5 (1983) 3.
[12] M.A. Arnold, M.E. Meyerhoff, Crit. Rev. Anal. Chem. 20 (1988) 149.
[13] P. Bühlmann, E. Pretsch, E. Bakker, Chem. Rev. 98 (1998) 1593.
[14] J. Ghasemi, M. Shamsipur, J. Coord. Chem. 31 (1994) 265.
[15] H. Khajeshrifi, M. Shamsipur, J. Coord. Chem. 35 (1995) 289.
[16] J. Ghasemi, M. Shamsipur, Polyhedron 15 (1996) 923.
[17] G. Azimi, M. Shamsipur, J. Coord. Chem. 47 (1999) 581.
[18] M.R. Ganjali, M. Shamsipur, Incl. Phenom. 23 (1995) 41.
[19] H.R. Pouretedal, M. Shamsipur, J. Chem. Eng. Data 43 (1998) 742.
[20] G.W. Gokel, D.J. Cram, C.L. Liotta, H.P. Harris, F.L. Cook, Org. Synth. 56 (1977) 30.
[21] M. Shamsipur, A.I. Popov, Inorg. Chim. Acta 43 (1980) 1243.
[22] E.T. Poach, P.R. Handy, A.I. Popov, Inorg. Nucl. Chem. Lett. 9 (1973) 359.
[23] V.A. Nicely, J.L. Dye, J. Chem. Educ. 48 (1971) 443.
[24] R.K. Harris, B.E. Mann, NMR and the Periodic Table, Academic, New York, 1978.
[25] T. Madrakian, A. Afkhami, M. Shamsipur, Polyhedron 15 (1996) 3647.
[26] M. Shamsipur, E. Karkhaneei, A. Afkhami, Polyhedron 17 (1998) 3809.
[27] M. Shamsipur, E. Karkhaneei, A. Afkhami, J. Coord. Chem. 44 (1998) 23.
[28] P.A. Mosier-Boss, A.I. Popov, J. Am. Chem. Soc. 107 (1985) 6168.
[29] V. Gutmann, The Donor–Acceptor Approach to Molecular Interactions, Plenum, New York, 1978.
[30] R.G. Pearson, J. Am. Chem. Soc. 84 (1963) 3533.
[31] R.D. Shannon, Acta Crystallogr., Sect. A 32 (1976) 731.
[32] C.J. Pedersen, H.K. Frensdorff, Angew. Chem., Int. Ed. Engl. 11 (1972) 16.
[33] H. Irving, R.J.P. Williams, J. Chem. Soc. (1953) 3192.
[34] M.R. Ganjali, A. Rouhollahi, A.R. Mardan, M. Shamsipur, J. Chem. Soc., Faraday Trans. 94 (1998) 1959.

PERGAMON

www.elsevier.nl/locate/poly

Polyhedron 19 (2000) 1687–1692

POLYHEDRON

Transition metal complexes of benzil-α-monoxime (BMO); X-ray structure determination of $Co(BMO)_3$

P. Sambasiva Reddy, K. Hussain Reddy *

Department of Chemistry, Sri Krishnadevaraya University, Anantapur 515 003, India

Received 28 January 2000; accepted 8 May 2000

Abstract

Cobalt(III), nickel(II) and copper(II) complexes of benzil-α-monoxime (BMO) have been synthesized and characterized by elemental analyses, conductivity, magnetic susceptibility measurements, IR and electronic spectral data. The molar conductivity data show them to be non-electrolytes. The monoanionic bidentate behavior of BMO is inferred from IR spectral studies. The electronic spectral data suggest planar geometry for nickel(II) and copper(II) complexes. The nickel complex assumes an octahedral structure in a coordinating solvent (*N*,*N*-dimethylformamide (DMF)). The $[Co(BMO)_3]$ complex has been isolated as a single crystal and its structure was determined by X-ray diffraction. X-ray data confirms the presence of a *fac*-octahedral configuration for this complex. Electrochemical studies suggest that the cobalt complex undergoes two single one-electron reduction steps corresponding to $Co(III) \rightarrow Co(II)$ and $Co(II) \rightarrow Co(I)$. © 2000 Elsevier Science Ltd. All rights reserved.

Keywords: Transition metal complexes; Electronic spectral data; Oximes; Benzil-α-monoxime

1. Introduction

Oximes are widely recognized ligands [1,2]. In general, monoxime is known to coordinate in three different ways (structures **I**, **II** and **III**). In structure **III** monoxime acts as a bridging ligand. Among carbonyl oximes diacetylmonoxime is the most studied ligand. Ni(II), Cu(II) and Co(III) complexes of diacetyl monoxime have been reported [3–5]. There is considerable confusion in the literature [6] about the nickel complexes of benzil-α-monoxime (BMO). Because of this, no report is available on Co(III), Ni(II) and Cu(II) complexes of BMO. In continuation of our ongoing research [7–11] on the metal complexes of benzil-based derivatives, we report herein the synthesis and characterization of metal complexes with BMO. The structure of $Co(BMO)_3$ is determined by X-ray single-crystal diffraction. Variety in structural features of BMO metal complexes is presented in this paper.

2. Experimental

2.1. Materials and methods

Benzil and hydroxylamine hydrochloride were of reagent grade. Solvents used for the synthesis of ligands and their metal complexes were redistilled. All other chemicals were of AR grade and used as supplied.

2.2. Preparation of ligand

BMO was prepared according to the procedure described previously [12].

2.3. Preparation of complexes

Attempts to prepare a cobalt(II) complex of BMO were not successful. Cobalt(III), nickel(II) and copper(II) complexes were prepared by mixing a hot methanolic solution of metal chlorides (1 mol) and ligand (2 mol). To the boiling solution of the ligand (0.01776 mol) in methanol (100 cm^3) was added metal chloride dissolved in a minimum quantity of methanol and refluxed for 30 min. NaOAc (2 g) was added to the

* Corresponding author. Tel.: +91-8554-55367-73; fax: +91-8554-29043.

0277-5387/00/$ - see front matter © 2000 Elsevier Science Ltd. All rights reserved.
PII: S0277-5387(00)00429-0

Table 1
Analytical data of ligand and their metal complexes

Ligand/complex	Color (m.p. ° C)	Percentage [a] of		
		Carbon	Hydrogen	Nitrogen
BMO	light pink (140–141)	74.00 (74.66)	4.57 (4.80)	6.50 (6.20)
$[Co(BMO)_3]$	orange red (195–197)	68.20 (68.94)	4.15 (4.10)	5.70 (5.74)
$[Ni(BMO)_2]$	light green (215–218)	65.95 (66.40)	3.72 (3.75)	5.48 (5.53)
$[Cu(BMO)]_n$	dark green (175–177)	65.67 (65.75)	3.85 (3.91)	5.49 (5.47)

[a] Calculated values are in parentheses.

reaction mixture (in the case of the copper complex CH_3ONa is added) and refluxed for another 30 min. Crystalline complexes which separated from the solution were collected by filtration, washed with hot water and a small quantity of methanol and dried under vacuum over $CaCl_2$. The analytical data of the ligand and their complexes are presented in Table 1.

2.4. Physical measurements

The elemental microanalyses were carried out at the RSIC, CDRI, Lucknow, India. The molar conductance of the complexes in *N*,*N*-dimethylformamide (DMF) (1×10^{-3} M) solution were measured at 28°C with a Systronic model 303 direct reading conductivity bridge. Magnetic measurements were carried out in the polycrystalline state on a PAR model 155 vibrating sample magnetometer operating at a field strength between 2 and 8 KG. High purity Ni metal (saturation moment 55 emu g^{-1}) was used as a standard. The electronic spectra were recorded in DMF and $CHCl_3$ with a Shimadzu UV-160 A spectrophotometer. The FT-IR spectra were recorded in the range 4600–50 cm^{-1} with a JASCO FT/IR-5300 in KBr and polyethylene medium. ^1H NMR spectra were obtained using a JEOL-GSX-400 NMR instrument at r.t. The voltammetric measurements were performed on Bio-analytical Systems (BAS) CV-27 assembly in conjunction with an X-Y recorder. These measurements were made on the degassed (N_2 bubbling for 5 min) solution in dimethylformamide (1×10^{-3} M) containing 0.1 M tetraethylammonium perchlorate as the supporting electrolyte. The system consisted, working (glass carbon), an auxiliary (Pt wire) and reference (Ag/AgCl) electrodes.

2.5. X-ray crystallography and structure solution

A diffraction quality crystal of cobalt(III) complex was grown at room temperature (r.t.) by slow evaporation of the complex in dimethylformamide solvent. Intensity data for a dark orange crystal with approximate dimensions $0.3 \times 0.2 \times 0.2$ mm were measured at r.t. 273(2) K on an Enraf–Nonius CAD4 diffractometer using monochromated Mo Kα radiation ($\lambda = 0.71073$ Å) with a scan mode of ω–2θ. No decomposition of the crystal occurred during the data collections. The Co atom was located from an E-map . The other non-hydrogen atoms were determined with successive difference Fourier syntheses. Final refinement by full-matrix least-squares methods was carried out with anisotropic thermal parameters for non-hydrogen atoms. The hydrogen atoms, included in the refinement were located in succeeding difference Fourier synthesis after the non-hydrogen atoms were refined anisotropically.

3. Results and discussion

The analytical data of the ligand (Table 1) is consistent with its proposed molecular formula. All the complexes are insoluble in water and methanol, but readily soluble (except copper complex) in $CHCl_3$, DMF and DMSO. The copper complex is sparingly soluble in DMF and DMSO. The physico-chemical and analytical data for all the complexes are given in Table 1. The analytical data (Table 1) are consistent with the proposed molecular formula. The molar conductivity data reveal the nonelectrolytic nature of all the complexes. Cobalt(III) and nickel(II) complexes are diamagnetic and the magnetic moment of the copper(II) complex is found to be 1.24 BM indicating the presence of one unpaired electron. The value is subnormal because it is quite less than the experimental magnetic moment (1.9–2.1 BM) values. It may suggest the existence of polymeric species.

3.1. Electronic spectra

The electronic spectra (Table 2) of the cobalt complex are recorded in $CHCl_3$ and DMF. The most intense band in the highest energy region has been assigned to π–π* transition of ligand. The next lowest energy band found at 27 397 cm^{-1} (in $CHCl_3$), 27 777 cm^{-1} (in DMF) has been assigned to charge transfer transitions [13].

In the electronic spectrum of the nickel complex in DMF, three bands are observed at 10 152 cm − 1 (ν_1); 17 094 (ν_2); 22 772 cm^{-1} (ν_3) assigned to $^3A_{2g}(F) \rightarrow {}^3T_{2g}(F)$; $^3A_{2g}(F) \rightarrow {}^3T_{1g}(F)$ and $^3A_{2g}(F) \rightarrow {}^3T_{1g}(P)$ transitions [14], respectively. The ratio of ν_1:ν_2 lies at 1.68 as required for an octahedral Ni(II) complex. The ligand field parameters, field splitting energy (10 Dq), Racah interelectronic repulsion parameter β, covalent factor and ligand field stabilization energy (LFSE) have been calculated and presented in Table 3. The electronic data (in DMF) suggest an octahedral geometry for the nickel

Table 2
Electronic spectral band (cm^{-1}) for the metal complexes of BMO

Complex	$CHCl_3$		DMF	
	Intraligand and charge transfer	d–d	Intraligand and charge transfer	d–d
$[Co(BMO)_3]$	33 222 27 397		33 222 27 777	
$[Ni(BMO)_2]$	33 898 28 901 27 777	16 806	34 482 28 901 27 777	17 094 10 152
$[Cu(BMO)]_n$	33 557	16 949	23 333 24 390	16 863

Table 3
Electronic spectral data and ligand field parameters for the nickel complex

Method of evaluation	ν_1 (cm^{-1})	ν_2 (cm^{-1})	ν_3 (cm^{-1})	B	B_{35} [b]	δ_V [a]	10 Dq	$\nu_2-\nu_1$	ν_2/ν_1	LFSE (K cal^{-1} mol^{-1})
Observed	10 152	17 094	27 777				10 152	6942	1.68	29.00
Calculated	10 Dq	19 702	25 168	961	0.923	2607	10 152	9550	1.94	

[a] Difference in the observed and calculated value of frequencies.
[b] Ratio of the free ion and the complex.

Table 4
Important IR spectral bands and their assignments

Ligand/complex	ν(OH)	ν(C=O)	ν(C=N)	ν(N–O)	ν_{asy}(C–C_6H_5)	ν_{sym}(C–C_6H_5)	ν(M–O)	ν(M–N)
BMO	3389	1647	1597	1211	1493	1373	–	–
$[Co(BMO)_3]$	–	1597	1576	1277	1493	1377	490	445
$[Ni(BMO)_2]$	–	1589	1562	1269	1446	1346	459	424
$[Cu(BMO)]_n$	–	1583	1556	1271	1439	1336	456	422

complex. DMF is a known coordinating solvent and presumably coordinates nickel in both axial positions to complete the octahedral structure.

The electronic spectrum of the nickel complex is also recorded in chloroform. The spectral behavior in chloroform is in agreement with the square-planar coordination of nickel. The electronic spectrum of the copper complex is recorded in DMF covering a 50 000–125 000 cm^{-1} range. The absorption band is observed at 33 330 cm^{-1} is due to π–π^*/charge transfer transition. However, the low intensity band is observed at 16 863 cm^{-1}. This band is assigned to the $^2B_{1g} \rightarrow {}^2A_{1g}$ transition [14,15] suggesting the presence of square-planar geometry.

3.2. IR spectra

Important IR spectral bands of BMO and its complexes are given in Table 4. A broad band of medium intensity is observed at 3389 cm^{-1} in the spectrum of the free ligand. This band is absent in the spectra of all complexes suggesting the deprotonation of oxime proton in complex formation. The downward shift of ν(C=N) and ν(C=O) bands in the spectra of all complexes suggests the coordination of the metal ion through the azomethine nitrogen and the oxygen atom of the C=O group. The non ligand bands in the 456–490 and 422–445 cm^{-1} regions are tentatively assigned to ν(M–O) and ν(M–N) stretching vibrations [16], respectively.

3.3. ^1H NMR spectra

Cobalt(III) and nickel(II) complexes are characterized by high resolution (400 MHz) ^1H NMR spectra in $CDCl_3$ solvent. In the case of the ligand a singlet is observed in the low field region of the spectra at δ 8.227 ppm, but it is absent in the cobalt and nickel complexes, which indicates the absence of an oxime proton in these complexes.

Table 5
Cyclic voltammetric data of cobalt, nickel and copper complexes (10^{-3} M) in DMF containing 0.1 M $TEAClO_4$ at 1.0 V/S^{-1} at glassy carbon electrode (Temp. 26°C)

Complex	Scan rate	Redox couple	E_{pc} (V)	E_{pa} (V)	DE (mV)	$E_{1/2}$ (V)	$-i_c/i_a$
$[Co(BMO)_3]$	100	III/II	−0.52	−0.18	340	0.35	
		II/I	−0.128				
$[Ni(BMO)_2]$	100	II/I	−1.20				
$[Cu(BMO)]_n$	100	III/II	+0.28	+0.55	270	0.415	0.651

3.4. Cyclic voltammetric studies

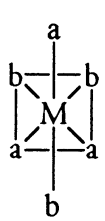
The cyclic voltammograms for cobalt, nickel and copper complexes are recorded in dimethylformamide. The cyclic voltammetric data for all the complexes are given in Table 5.

The cyclic voltammogram of the present cobalt complex has a single reversible electron [Co(III) → Co(II)] couple with $E_{1/2} = -0.35$ V. This complex also has an irreversible cathodic peak at $E_{pc} = -1.28$ V, corresponding to Co(II) → Co(I).

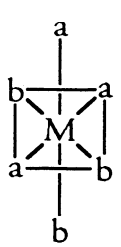
The cyclic voltammogram data for the copper complex show a single reduction wave at $E_{1/2} = +0.415$ V and have a quasi reversible behavior [17] as indicated by the non-equivalent current intensity of cathodic and anodic peaks ($-i_c/i_a = 0.615$ at 100 mV s^{-1}). The reversible couple is assigned to Cu(III) → Cu(II), which is similar to values reported earlier [18–21].

Electronic spectral data together with magnetic moment data suggest an octahedral structure of the $[Co(BMO)_3]$ complex. Thus, it is a tris(benzil-α-monoximato)cobalt(III) complex.

No isomers are possible for tris-chelated complexes with symmetrical ligands. However, cobalt complexes with unsymmetrical ligands give facial and meridonial isomers.



facial



meridonial

The present ligand, BMO is unsymmetrical ligand. Now the question is whether the $Co(BMO)_3$ has facial configuration or meridonial configuration. The ^1H NMR spectrum of $Co(BMO)_3$ gave no information about the configuration of the complex. Hence it is considered worthwhile to study the complex using the X-ray diffraction technique. The results obtained in the X-ray structure determination of the complex are presented herein.

3.5. X-ray crystal and molecular structure of the cobalt(III) complex of BMO

The crystallographic data and data collection details for$[Co(BMO)_3]$ are summarized in Table 6. The molecular structure of $[Co(BMO)_3]$ is shown in Fig. 1 and the important bond lengths and bond angles are listed in Table 7.

From Fig. 1, it can be seen that cobalt is six-coordinate with three nitrogen atoms [N(1), N(2), N(3)] and three oxygen atoms [O(2), O(4), O(6)], thus giving an octahedral configuration from three unsymmetrically bonding bidentate ligands.

As expected, the three imino nitrogen atoms give stronger coordination bonds. This is evident by shorter Co–N bond lengths (1.868–1.901 Å). The Co–O bond

Table 6
Crystal data collection parameter for $[Co(BMO)_3]$

Empirical formula	$C_{42}H_{30}CoN_3O_6$
Crystal color	orange
Formula weight	731.62
Temperature (K)	293(2)
λ (Å)	0.71073
Crystal system	monoclinic
Space group	$P21/c$
a (Å)	18.165(2)
b (Å)	10.0260(12)
c (Å)	19.962(4)
α (°)	90
β (°)	98.638(13)
γ (°)	90
V (Å^3)	3594.3(9)
Z	4
D_{calc} (mg cm^{-3})	1.352
μ(Mo Kα) (cm^{-1})	0.530
F(000)	1512
Crystal (dimension mm)	$0.3 \times 0.2 \times 0.2$
Index ranges: h, k, l	−21–21, 0–11, 0–23
Number of reflections collected	6288
Unique reflections	6288
Absorption correction	Psi scan
Max. and min. transmission	0.99 and 0.9
Final R, R_w	$R_1 = 0.0547$, $wR_2 = 0.1395$
R indices (all data)	$R_1 = 0.0949$, $wR_2 = 0.1534$
Extinction coefficient	0.0000(4)
Largest difference peak and hole (e Å^{-3})	0.523 and −0.555

Table 7
Selected bond lengths (Å) and angles (°) for $[Co(BMO)_3]$ with e.s.d values in parentheses [a]

Co–N(1)	1.868(3)
Co–N(2)	1.881(3)
Co–N(3)	1.901(3)
Co–O(4)	1.906(2)
Co–O(2)	1.918(2)
Co–O(6)	1.933(3)
O(1)–N(1)	1.266(4)
O(2)–C(8)	1.279(4)
O(3)–N(2)	1.236(4)
O(4)–C(22)	1.300(4)
O(5)–N(3)	1.275(4)
O(6)–C(36)	1.301(4)
N(1)–C(1)	1.328(4)
N(2)–C(15)	1.364(4)
N(3)–C(29)	1.295(4)
C(15)–C(22)	1.443(5)
C(29)–C(36)	1.434(5)
N(1)–Co–N(2)	94.79(14)
N(1)–Co–N(3)	96.91(12)
N(2)–Co–N(3)	94.48(12)
N(1)–Co–O(4)	177.52(12)
N(2)–Co–O(4)	83.71(11)
N(3)–Co–O(4)	85.19(11)
N(1)–Co–O(2)	82.56(11)
N(2)–Co–O(2)	88.75(12)
N(3)–Co–O(2)	176.76(13)
O(4)–Co–O(2)	95.43(9)
N(1)–Co–O(6)	90.38(13)
N(2)–Co–O(6)	174.27(11)
N(3)–Co–O(6)	82.43(11)
O(4)–Co–O(6)	91.21(10)
O(2)–Co–O(6)	94.38(11)
C(8)–O(2)–Co	112.4(2)
C(22)–O(4)–Co	111.2(2)
C(36)–O(6)–Co	110.9(2)
O(1)–N(1)–C(1)	121.1(3)
O(1)–N(1)–Co	122.8(2)
C(1)–N(1)–Co	116.1(2)
O(3)–N(2)–C(15)	120.5(3)
O(3)–N(2)–Co	123.9(2)
C(15)–N(2)–Co	115.5(3)
O(5)–N(3)–C(29)	123.3(3)
O(5)–N(3)–Co	119.8(2)
C(29)–N(3)–Co	116.5(2)
N(1)–C(1)–C(8)	110.9(3)
N(1)–C(1)–C(2)	119.3(3)
O(2)–C(8)–C(1)	117.7(3)
O(2)–C(8)–C(9)	114.8(3)
N(2)–C(15)–C(22)	109.0(3)
N(2)–C(15)–C(16)	122.1(3)
O(4)–C(22)–C(15)	119.0(3)
O(4)–C(22)–C(23)	115.1(3)
N(3)–C(29)–C(36)	111.0(3)
N(3)–C(29)–C(30)	120.5(3)
O(6)–C(36)–C(29)	118.8(3)
O(6)–C(36)–C(37)	116.4(3)

[a] Symmetry transformations used to generate equivalent atoms.

lengths fall in the 1.906–1.933 Å range. The Co–N and Co–O bond lengths are comparable to those of the

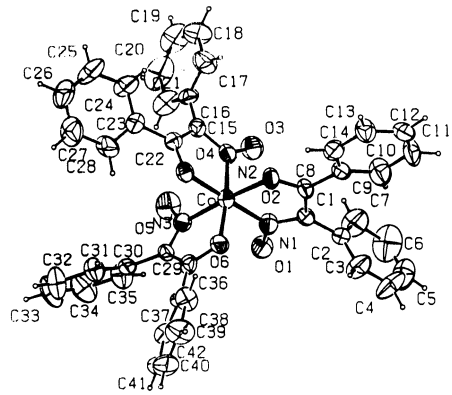


Fig. 1. Molecular structure of $[Co(BMO)_3]$ with numbering scheme.

cobalt(III) complexes containing nitrogen and oxygen donor atoms.

The distances of C(1)–C(8) (1.424 Å), C(15)–C(22) (1.443 Å) and C(29)–C(36) (1.434 Å) are shorter than the normal C–C single bond and larger than the C=C, suggesting the delocalization of electrons in the complexed ligand systems.

The ligand acts as an uninegative unsymmetrical bidentate ligand. The oxime hydrogen is absent in the structure. The ligands are arranged in facial configuration at the metal center.

4. Supplementary material

Supplementary data are available on request from The Director, CCDC, 12 Union Road, Cambridge, CB2 1EZ, UK (fax: +44-1223-336033; e-mail: deposit@ccdc.cam.ac.uk or www: http://www.ccdc.cam.ac.uk) by quoting the deposition number CCDC 138847.

Acknowledgements

P.S.R. acknowledges support from the CSIR (New Delhi) who provided the financial support in the form of a senior research fellowship.

References

[1] M. Akbar Ali, S.F. Livingstone, Coord. Chem. Rev. 13 (1974) 101.
[2] A. Chakravorty, Coord. Chem. Rev. 13 (1974) 1.
[3] T.W.J. Taylor, E.K. Ewbank, J. Chem. Soc., Lond. (1926) 2818.
[4] A. Okac, M. Simek, Collect. Czech. Chem. Commun. 15 (1950) 445.
[5] D.A. White, J. Chem. Soc. A. (1971) 233.
[6] J.V. Quagliano, D.H. Wilkins, in: J.C. Bailor Jr. (Ed.), Chemistry of the Coordination Compounds, Reinhold, New York, 1956, p. 672.

[7] A. Krishna, K. Hussain Reddy, D. Venkata Reddy, Inorg. Chim. Acta 177 (1990) 13.
[8] K. Hussain Reddy, Y. Lingappa, Transition Met. Chem. 19 (1994) 487.
[9] M. Radhakrishna Reddy, K. Mohana Raju, K. Hussain Reddy, Indian J. Chem. 35A (1996) 677.
[10] K. Hussain Reddy, M. Radhakrishna Reddy, Y. Lingappa, Indian J. Chem. 35A (1996) 775.
[11] K. Hussain Reddy, M. Radhakrishna Reddy, K. Mohana Raju, Indian J. Chem. 38A (1999) 299.
[12] A.I. Vogel, Text Book of Practical Organic Chemistry, 4th ed., ELBS, UK, 1984, p. 811.
[13] A.B.P. Lever, Inorganic Electronic Spectroscopy, 2nd ed., Elsevier, Amsterdam, 1984.
[14] J. Bjerrum, C.J. Balahauisen, C.K. Jorgenson, Acta Chem. Scand. (1984) 1273.
[15] W. Byers, A.B.P. Lever, R.D. Parish, Inorg. Chem. 7 (1968) 1835.
[16] K. Nakamoto, Infrared and Raman Spectra of Inorganic and Coordination Compounds, Wiley-Interscience, New York, 1978.
[17] R.S. Nicholson, I. Shain, Anal. Chem. 36 (1964) 706.
[18] R. Shukla, S. Mandal, P.K. Bharadwaj, Polyhedron 12 (1993) 83.
[19] X.H. Bu, Z.H. Zhang, X. Cao, S. Ma, Y. Tichen, Polyhedron 16 (1997) 3525.
[20] A. Pasini, E. Bermini, M. Scaglia, Polyhedron 15 (1996) 4461.
[21] S. Djebbar-Sid, Benali-Baitich, J.P. Deloume, Polyhedron 16 (1997) 2175.

PERGAMON

www.elsevier.nl/locate/poly

Polyhedron 19 (2000) 1693–1698

POLYHEDRON

Isomerization of 2-methyl-3-butyn-2-ol into prenal: mechanistic observations on tricomponent catalyst systems of the type $Ti(OR)_4$–CuCl–$R'CO_2H$. Crystal structure of $[CuCl(Me_2C(OH)C{\equiv}CH)]_4$

Christian Y. Lorber *, Marie-Thérèse Youinou, Jacky Kress, John A. Osborn [1]

Laboratoire de Chimie des Métaux de Transition et de Catalyse, UMR du CNRS 7513, Université Louis Pasteur, Institut Le Bel, 4 rue Blaise Pascal, 67000 Strasbourg, France

Received 28 February 2000; accepted 22 May 2000

Abstract

The mechanism of the title catalytic system was investigated, in particular by synthesizing several compounds that model the postulated metal–oxo–propargyloxo intermediates, such as $[Ti(\mu\text{-}O)(O\text{–}Bu^t)(O_2CTol)]_2$ (Tol = *p*-MeC_6H_4), $Ti(OCMe_2C{\equiv}CH)_4$ and $[CuCl(Me_2C(OH)C{\equiv}CH)]_4$. The molecular structure of $[CuCl(Me_2C(OH)C{\equiv}CH)]_4$ was determined by X-ray crystallography and heterobimetallic Ti–Cu complexes comprising the 2-methyl-3-butyn-2-oxo fragment are reported. © 2000 Elsevier Science Ltd. All rights reserved.

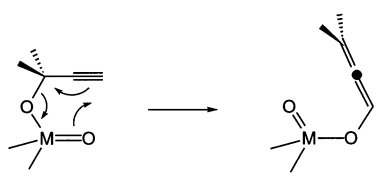
Keywords: α-Acetylenic alcohols; Isomerization; Rearrangement; Heterobimetallic titanium–copper systems

1. Introduction

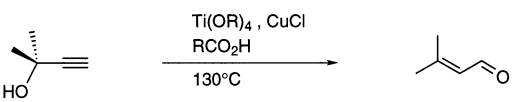
α,β-Ethylenic carbonyl compounds such as prenal (3-methyl-2-butenal) are important intermediates in the manufacture of fragrances, carotenoids or vitamins [1], and their synthesis via isomerization of α-acetylenic alcohols has been known for many years [2,3]. This type of reaction was initially catalysed in protic media, as first shown by Meyer and Schuster [2], before oxo complexes of early transition metals such as vanadium, rhenium and molybdenum were found to be efficient catalysts [4–6]. The oxo ligands were supposed to play a key mechanistic role as receptors of migrating propargyl groups, in the [3,3] sigmatropic rearrangement of metal–oxo–propargyloxo entities (Scheme 1).

More recently however, Chabardès has shown [7] that efficient and selective isomerization of α-acetylenic alcohols such as 2-methyl-3-butyn-2-ol (1,1-dimethylpropargyl alcohol) can be achieved homogeneously in the presence of mixtures of titanium alkoxides, copper (I) chloride and carboxylic acids. Despite the absence of an oxo ligand, these tricomponent catalyst systems are even more efficient than the previous oxo catalysts (Scheme 2).

The mechanism suggested for the operation of these new systems is summarized in Scheme 3 [7]. By analogy



Scheme 1.



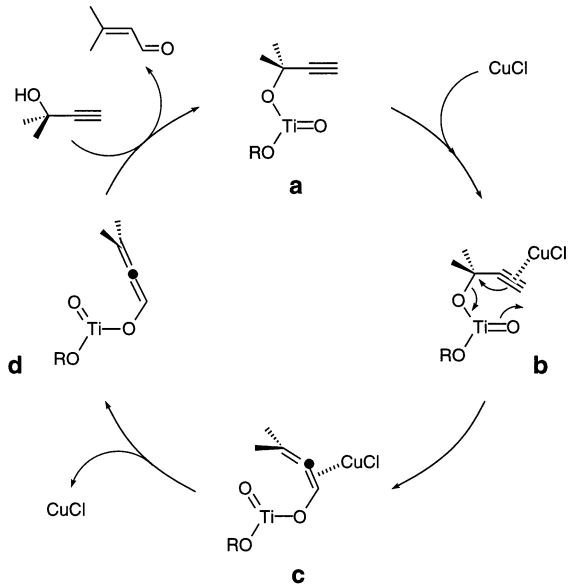
Scheme 2.

* Current address: Laboratoire de Chimie de Coordination, UPR du CNRS 8241, 205 route de Narbonne, 31077 Toulouse Cedex, France. Fax: +33-5-6155-3003.

E-mail address: lorber@lcc-toulouse.fr (C.Y. Lorber).

[1] Deceased 23 April, 2000. Address further correspondence to C.Y. Lorber.

0277-5387/00/$ - see front matter © 2000 Elsevier Science Ltd. All rights reserved.
PII: S0277-5387(00)00441-1



Scheme 3.

with the metal–oxo catalysts, it involves initial formation of a titanium propargyloxo complex **a** via reaction of the carboxylic acid and titanium precursor. Copper chloride, which is necessary for activity, activates the propargyloxide ligand by interaction with the carbon–carbon triple bond **b**. Such an interaction would favour the [3,3] sigmatropic rearrangement leading to **c**. Decoordination of CuCl from the allenyloxo ligand of **c** would then give **d**, and displacement of the rearranged ligand by a further molecule of propargyl alcohol, followed by its spontaneous isomerization, yields the α,β-ethylenic carbonyl product and regenerates **a**.

In this paper, we wish to discuss the initial steps of this mechanism on the basis of reactivity and model studies.

2. Experimental

All manipulations were carried out under an atmosphere of argon using standard dry box, vacuum line, or Schlenk tube techniques. Solvents were distilled under nitrogen in the presence of a suitable drying agent. Copper(I) chloride (Strem) was purified via a known method [14]. Titanium tetraisopropoxide and titanium tetratertiobutoxide (Aldrich) were purified by fractional distillation. Carboxylic acids were dried under vacuum over P_2O_5. 2-Methyl-3-butyn-2-ol (Aldrich) was refluxed over CaH_2, fractionally distilled, and stored over molecular sieves (4 Å) in a dry box. Elemental analyses were performed by the CNRS Microanalytical Laboratory at Strasbourg or Lyon, France. Infrared (IR) spectra were recorded as nujol mulls on a Perkin–Elmer 597 or a Perkin–Elmer 1650 (FTIR) spectrometer; absorption bands are listed in reciprocal cm as weak (w), medium (m), or strong (s). 200 MHz ^{1}H NMR and 50 MHz ^{13}C{^{1}H} NMR spectra were recorded on a Bruker SY200 instrument; chemical shifts (δ) are given in parts per million relative to TMS.

2.1. Experimental procedure for catalytic isomerisation of 2-methyl-3-butyn-2-ol

In a typical experiment, 2-methyl-3-butyn-2-ol (8.41 g, 100 mmol), *n*-nonane (3.41 g) (internal standard for GC analysis), crotonic acid (1.47 g, 17 mmol), copper(I) chloride (150 mg, 1.5 mmol), Ti(O–Pr^i)$_4$ (42 ml, 1.4 mmol) and *o*-dichlorobenzene (13 ml) were introduced into a round-bottom flask fitted with a reflux condenser, under an atmosphere of argon. The mixture was heated to 100°C, after 1 h reaction, GC analysis of the reaction mixture indicated 98% conversion of 2-methyl-3-butyn-2-ol into prenal.

2.2. Preparation and characterization of [Ti(μ-O)(O–Bu^t)(O$_2$CTol)]$_2$ (1)

Under an atmosphere of argon, a solution of Ti(^{t}O–Bu)$_4$ (2.50 g, 7.35 mmol) and TolCO$_2$H (1.00 g, 36.72 mmol) (Tol = *p*-MeC$_6$H$_4$) in 20 ml of dry C$_6$H$_6$ was refluxed for 9 h. After removal of the volatiles under vacuum and extraction of the residue in pentane (10 ml), the solution was kept at −20°C overnight. The resulting white precipitate was filtered and redissolved in 10 ml of pentane, and the solution was maintained at −20°C for a few hours. The solution was then filtered, and the white solid was dried in vacuo to give 1.20 g of **1** (yield 60%). *Anal.* Calc. for $C_{24}H_{32}O_8Ti_2$ (**1**): C, 52.96; H, 5.93. Found: C, 54.50; H, 5.62%. IR (nujol mull, cm^{-1}) 1607 s ($\nu_{C=C}$); 1526 s ($\nu_{as\ COO}$); 1412 s ($\nu_{s\ COO}$); 1237 s, 1130 s, 1000 s (ν_{C-O}); 869 s; 764 s (ν_{Ti-O}); 628 m; 592 m; 464 m. ^{1}H NMR (200 MHz, C$_6$D$_6$; δ (ppm)) 8.18 (d, $^3J_{Ha-Hb}$ = 8 Hz, 2H, H$_{a\ Tol}$); 6.76 (d, $^3J_{Ha-Hb}$ = 8 Hz, 2H, H$_{b\ Tol}$); 1.86 (s, 3H, Me$_{Tol}$); 1.49 (s, 9H, ^{t}Bu). ^{13}C{^{1}H} NMR (50 MHz, CDCl$_3$; δ (ppm)) 155.5 (CO$_2$H); 144.5, 130.0, 129.0, 127.1 (C$_{aromatic}$); 31.0 (*C*Me$_3$); 31.1 (C*Me*$_3$); 21.9 (Me$_{Tol}$).

2.3. Preparation and characterization of Ti(OCMe$_2$C≡CH)$_4$ (2)

To a solution of TiCl$_4$ (556 mg, 2.93 mmol) in pentane (20 ml) was added dropwise at −30°C a solution of 2-methyl-3-butyn-2-ol (1.11 g, 13.2 mmol) and triethylamine (1.30 g, 13.2 mmol) in pentane (20 ml), under an atmosphere of argon. The mixture was stirred overnight (−20°C) and then filtered to give a colorless solution. The volatiles were removed under vacuum to yield the product as pale yellow oil (880 mg, 79%). Further purification was achieved by vacuum

distillation. *Anal*. Calc. for $C_{20}H_{28}O_4Ti$ (**2**): C, 63.16; H, 7.42. Found: C, 63.17; H, 7.44%. IR (nujol mull, cm^{-1}) 3290 s ($\nu_{\equiv C-H}$); 2090 w ($\nu_{C\equiv C}$); 1210 s, 1130 s, 1000 s (ν_{C-O}). ^1H NMR (200 MHz, C_6D_6; δ (ppm)) 2.10 (s, 1H, ≡C–H); 1.67 (s, 6H, Me). $^{13}C\{^1H\}$ NMR (50 MHz, C_6D_6; δ (ppm)) 89.2 (*C*≡CH); 76.3 (C–O); 70.0 (≡CH); 33.2 (Me).

2.4. Preparation and characterization of $[CuCl(Me_2C(OH)C\equiv CH)]_4$ (3)

Under an atmosphere of argon, 500 mg of freshly purified CuCl was stirred at about 50°C with 2 ml of 2-methyl-3-butyn-2-ol until a clear solution was obtained. After hot filtration over celite, the colorless filtrate was allowed to cool slowly to room temperature to give, after a few days, colorless crystals of **3**, which were suitable for X-ray analysis. Crystals were washed with pentane (3 × 2 ml) and dried under vacuum (yield 45%). *Anal*. Calc. for $C_{20}H_{32}O_4Cl_4Cu_4$ (**3**): C, 32.80; H, 4.40. Found: C, 32.82; H, 4.32%. IR (nujol mull, cm^{-1}) 3500–3200 m (ν_{OH}); 3180 s ($\nu_{\equiv C-H}$); 1940 m ($\nu_{C\equiv C}$); 1205 s, 1160 s (ν_{C-O}); 240 w ($\nu_{Cu-Cl-Cu}$). ^1H NMR (200 MHz, C_6D_6; δ (ppm)) 2.22 (s, 1H, ≡C–H); 1.57 (s, 1H, OH); 1.31 (s, 6H, Me). $^{13}C\{^1H\}$ NMR (50 MHz, C_6D_6; δ (ppm)) 89.54 (*C*≡CH); 70.07 (≡CH); 64.70 (C–O); 31.35 (Me).

2.5. Crystal structure determination

Crystal data were obtained at −100°C using a Philips PW1100/16 diffractometer with Cu Kα graphite-monochromated radiation ($\lambda = 1.5418$ Å). The scan width (°) in the $\theta/2\theta$ mode used was $\Delta\theta = 0.80 + 0.14 \tan\theta$. A total of 953 *hkl* reflections were recorded within $3 < \theta < 52°$, and 823 reflections having $I > 3\sigma(I)$ were used for determining and refining the structure. The structure was determined using direct methods and refined using full-matrix least-squares to $R(F) = 0.039$ and $R_w(F) = 0.056$, GOF = 1.478, maximum electronic density = 0.765 $eÅ^{-3}$, 145 variables. The Nonius Open-Molen/Alpha package [15] was used for all calculations. Selected crystal data for **3**: $C_{10}H_{16}O_2Cl_2Cu_2$, $M_r = 366.22$, orthorhombic, space group *Pba*2, $a = 9.170(2)$, $b = 18.544(5)$, $c = 8.188(2)$ Å, $V = 1392(1)$ $Å^3$, $Z = 4$, $D_{calc} = 1.75$ g cm^{-3}, $\mu = 7.231$ mm^{-1}.

2.6. Reaction between $TiCl_4$ and 3

In an NMR tube containing 15 mg of **3** (0.014 mmol) in 0.45 ml $CDCl_3$ were added 10 ml of $TiCl_4$ (0.055 mmol). The solution became pink after a few minutes at 20°C. ^1H NMR (200 MHz, $CDCl_3$): δ 2.80 (s, 1H, ≡CH); 1.87 (s, 6H, Me). When the solution was kept at room temperature for 24 h, it turned blue. GC analysis and ^1H NMR spectroscopy showed complete conversion into prenal: ^1H NMR (200 MHz, $CDCl_3$): δ 9.95 (d, $^3J_{H-H} = 8$ Hz, 1H, CHO); 5.89 (m, 1H, =CH); 2.17 (d, $^4J_{H_a-H} = 1$ Hz, 3H, Me_a); 1.98 (d, $^4J_{H_b-H}$ 1 Hz, 3H, Me_b).

2.7. Reaction between CuCl and 2

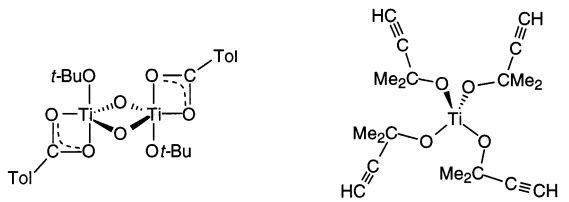
CuCl (104 mg, 1.06 mmol) was added to a solution of **2** (400 mg, 1.06 mmol) in 15 ml CH_2Cl_2. The mixture was stirred at 20°C for 1 h and then filtered to eliminate unreacted CuCl. Removal of volatiles under vacuum yielded orange oil (450 mg). ^1H NMR (200 MHz, CD_2Cl_2) δ 2.69 (s, 1H, ≡CH); 1.65 (s, 6H, Me) and peaks from residual **2**. IR (nujol mull, cm^{-1}) 3190 s ($\nu_{\equiv CH}$); 1940 m ($\nu_{C\equiv C}$) and bands from residual **2**. The reaction was also followed in situ by ^1H NMR in $CDCl_3$.

3. Results and discussion

3.1. Formation of titanium–oxo functions

To investigate the initiation step of the mechanism, we first measured the influence of the nature of the carboxylic acid on the catalytic efficiency of a given pair of titanium and copper compounds. Using a mixture of $Ti(O–Pr^i)_4$ and CuCl (1:1), isomerization of 2-methyl-3-butyn-2-ol (50 equivalents) at 100°C, in the presence of five equivalents of various carboxylic acids, reaches the following conversion percentages after 30 min: 3,3-dimethylacrylic acid ($pK_a = 5.12$), 98%; crotonic acid ($pK_a = 4.69$), 97%; *p*-methoxybenzoic acid ($pK_a = 4.49$), 88%; *p*-*t*-butylbenzoic acid ($pK_a = 4.39$), 82%; *p*-toluic acid ($pK_a = 4.37$), 72%; acetic acid ($pK_a = 4.75$), 48%; benzoic acid ($pK_a = 4.19$), 42%; *p*-chlorobenzoic acid ($pK_a = 3.97$), 10%; *p*-nitrobenzoic acid ($pK_a = 3.41$), 3%. The reaction rates therefore decrease with decreasing pK_a values. This implies that, if carboxylic acids are necessary for the formation of titanium oxo species, too strong an acid will be less favourable; the lower activity obtained with acetic acid demonstrates that other factors contribute.

On the other hand, we have found that the reaction of $Ti(O–Bu^t)_4$ with *p*-toluic acid (benzene, 80°C) yields significant amounts of a bridged oxo species which could be separated and formulated as $\{Ti(\mu\text{-}O)(O–Bu^t)(O_2CTol)\}_2$ (**1**), and whose structure is proposed in Scheme 4 on the basis of spectroscopic data. This confirms that titanium alkoxides can be effectively convert into oxo species in the presence of carboxylic acids [8,9]. Complex **1** is analogous to earlier compounds such as $\{Ti(\mu\text{-}O)(\mu\text{-}O_2CR)_2\}_2$ [8b–c, 9e] and catalyses the rearrangement of 2-methyl-3-butyn-2-ol into prenal as efficiently as its titanium tetraalkoxide precursor. However, analogous substrates or reactants



1 2

Scheme 4.

lead to less clear-cut results. For example, addition of crotonic acid to $Ti(O–Pr^i)_4$ only affords mixtures of carboxylato and *i*-propyloxo complexes, in which the presence of an oxo function could not be firmly established.

3.2. Formation of titanium–propargyl oxide complexes

In species **a**, a 1,1-dimethyl-propargyloxo ligand bound to titanium is also involved. This would arise from alkoxide exchange between OR ligands initially present in $Ti(OR)_4$ and 2-methyl-3-butyn-2-ol. Such an exchange process has literature precedent [10] and, with R = *i*-Pr, we obtained a mixture of products of general formula $Ti(O–Pr^i)_{4-n}(OCMe_2C{\equiv}CH)_n$ ($n = 0–4$). A well-defined propargyl oxide complex was synthesized by reacting four equivalents of 2-methyl-3-butyn-2-ol with $TiCl_4$ in the presence of triethylamine, leading to $Ti(OCMe_2C{\equiv}CH)_4$ (**2**) in good yield. The bulkiness of the dimethylpropargyloxo ligands probably prevents association by means of oxygen bridges, allowing a monomeric geometry similar to that of $Ti(O–Bu^t)_4$ [10] to be proposed for this compound (Scheme 4). Reaction of 1,1-dimethylpropargyl alcohol to form the tetraalkoxide **2** is revealed by a chemical shift variation of $^1H_{Me}$ from 1.32 to 1.67 ppm, and of $^1H_{C{\equiv}CH}$ from 2.02 to 2.10 ppm (in C_6D_6), the infrared $\nu_{C{\equiv}C}$ being only slightly modified. It is worth noting that complex **2** is as active as other $Ti(OR)_4$ catalysts, and that, in the absence of 1,1-dimethylpropargyl alcohol, its ligands isomerize as expected into prenal (100°C, Ti:Cu:acid = 1:1:5).

Further comparison of the ability of various titanium complexes to catalyse the rearrangement of 2-methyl-3-butyn-2-ol has led to following qualitative sequence (CuCl:crotonic acid:2-methyl-3-butyn-2-ol = 1:5:50, 100°C, 30 min reaction):

$Ti(O–Bu^t)_4 \approx Ti(O–Pr^i)_4 > TiCl(O–Pr^i)_3 \approx TiO(acac)_2 > TiCl_2(O–Pr^i)_2 > Cp_2TiCl_2 > TiCl_3(O–Pr^i)$. Such a result is consistent with rapid alkoxide exchange on titanium, and completes earlier results [7] by showing, in particular, the negative effect of chloro ligands.

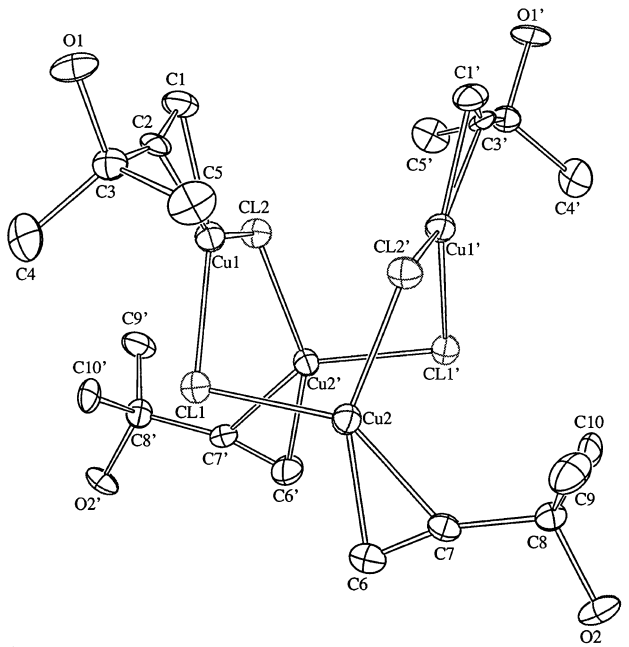
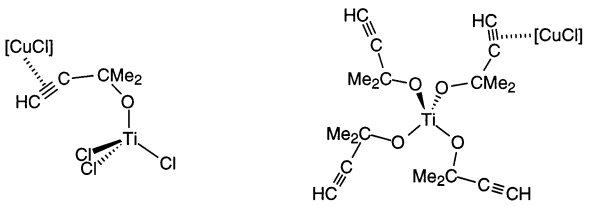


Fig. 1. ORTEP diagram of compound **3**. Hydrogen atoms are omitted. Selected bond distances (Å): Cu(1)–Cl(1) = 2.263(3), Cu(1)–Cl(2) = 2.286(2), Cu(2)–Cl(1) = 2.258(2), Cu(2)–Cl(2') = 2.266(3), Cu(1)–C(1) = 2.01(1), Cu(1)–C(2) = 2.037(8), Cu(2)–C(6) = 1.97(1), Cu(2)–C(7) = 2.021(9), C(1)–C(2) = 1.19(1), C(6)–C(7) = 1.18(1). Selected bond angles (°): Cl(1)–Cu(1)–Cl(2) = 105.9(1), C(1)–Cu(1)–C(2) = 34.2(3), C(6)–Cu(2)–C(7) = 34.3(4), C(1)–C(2)–C(3) = 161.1(9), C(6)–C(7)–C(8) = 164(1).

3.3. Formation of copper(I)–chloride complexes of 2-methyl-3-butyn-2-ol

The role of the copper chloride component of the catalyst system would be to interact with, and hence activate, the carbon–carbon triple bond of α-acetylenic alcohols, as in species **b** (Scheme 3). The affinity of copper (I) complexes for alkynes, resulting in the formation of π-adducts, is well-established [11], and we have verified that various propargylic alcohols effectively coordinate through their triple bond to copper (I). Complexes such as $[CuCl(2\text{-butyn-1-ol})]_4$, $[Cu(CF_3CO_2)(2\text{-methyl-3-butyn-2-ol})]_2$, and $[Cu(bipy)(2\text{-methyl-3-butyn-2-ol})]PF_6$ were appropriately synthesized [5b]. In particular, dissolution of CuCl into 2-methyl-3-butyn-2-ol, followed by filtration and slow crystallization, yielded colorless, air-sensitive crystals of $\{CuCl(Me_2C(OH)C{\equiv}CH)\}_4$ (**3**). The ^1H NMR spectrum of **3** in C_6D_6 showed the terminal acetylenic proton of the 2-methyl-3-butyn-2-ol shifted downfield on coordination, from 2.02 to 2.22 ppm (and from 2.42 to 2.60 ppm in $CDCl_3$), whereas the methyl signal is hardly shifted. This feature characterizes bonding of the carbon–carbon triple bond to copper, which is further defined by the shift of the infrared C≡C stretching band from 2110 cm^{-1} for the free ligand to 1940 cm^{-1} for **3**.



Scheme 5.

The crystal structure of **3** has been determined by single-crystal X-ray diffraction. An ORTEP drawing is shown in Fig. 1, along with selected interatomic distances and angles. The molecular structure consists of two $Cu_2Cl_2(C_5H_8O)_2$ units crystallographically related by a twofold symmetry axis, yielding an overall tetrameric arrrangement of four copper atoms lying at the vertices of a slightly distorted tetrahedron. The two metal centers of the dimeric units are linked through a nearly symmetrical chloride bridge, with Cu(1)–Cl(1) = 2.263(3) and Cu(2)–Cl(1) = 2.258(2) Å. The two dimeric units are associated similarly one to each other, with Cu(1)–Cl(2) = 2.286(2) and Cu(2)–Cl(2′) = 2.266(3) Å, leading to an eight-membered ring possessing a boat configuration. Each copper atom is further bound to the carbon–carbon triple bond of a 2-methyl-3-butyn-2-ol molecule, thus adopting an approximate trigonal planar geometry, as already observed in other copper(I)–alkyne compounds [12]. The copper–alkyne interaction is weak, as revealed by the short carbon–carbon bonds of 1.19(1) and 1.18(1) Å, but strong enough to deviate the propargyl skeleton from linearity by 18.9(9) and 16(1)°.

This shows how coordination of CuCl to the carbon–carbon triple bond of a catalytic intermediate such as **b** may facilitate subsequent rearrangement step (Scheme 3) by favoring nucleophilic attack of the titanium–oxo function on the terminal acetylenic carbon: besides making the triple bond more reactive, it also brings the terminal acetylenic carbon closer to the oxo ligand [13].

3.4. Formation of heterobimetallic Ti–Cu–propargyl oxide complexes

In order to model more precisely species **b**, we attempted to synthesize titanium–propargyl oxide complexes such as **2** in which the carbon–carbon triple bond of the propargyl oxide ligand would be bound to copper (I) chloride as in **3**. Thus, addition of four equivalents of $TiCl_4$ to tetrameric **3** was followed by ^1H NMR in $CDCl_3$. Rapid reaction occurs, as revealed by the significant shift of the methyl and acetylenic proton signals from respectively 1.54 and 2.60 ppm to 1.87 and 2.80 ppm, and by the disappearance of the hydroxyl proton. Such downfield displacements are similar to those observed on conversion of 1,1-dimethylpropargyl alcohol into **2**, suggesting that the four hydroxy functions of the copper tetramer have reacted, each with one molecule of $TiCl_4$, to yield the bimetallic complex $[CuCl(Me_2C(OTiCl_3)C{\equiv}CH)]_4$ (**4**). However, the degree of association in **3** may be modified during the course of reaction, especially if chlorides bridge titanium centers. A simple representation of a monomeric unit of **4** is given in Scheme 5.

On the other hand, addition of one equivalent of CuCl to **2** in $CDCl_3$ results in the emergence of a new 1,1-dimethylpropargyl oxide spectrum in which the acetylenic proton signal is shifted downfield to 2.69 ppm, although features of **2** are still observed. This suggests that a fraction of the carbon–carbon triple bonds of **2** coordinates to CuCl, as depicted in **5** for instance (Scheme 5). The spectrum of the uncomplexed propargyl oxide ligands of **5** would be identical to that of **2**, itself certainly still present. The infrared spectrum of the orange oil obtained after removal of all volatiles under vacuum, showing two $\nu_{C\equiv C}$ bands at 2100 and 1940 cm^{-1}, confirms this conclusion.

Unfortunately, neither **4** nor **5** was stable enough to be isolated. Interestingly, **4** decomposed at room temperature within 24 h with liberation of prenal, mimicking not only the structure of intermediate **b**, but also its reactivity.

In conclusion, our results are consistent with the mechanistic proposal of Scheme 3. The respective role of titanium, copper and carboxylic acid in the catalytic system has been confirmed, and the observation of heterobimetallic Ti–Cu complexes of 2-methyl-3-butyn-2-ol, in particular, is unprecedented to our knowledge.

4. Supplementary data

Further details of the structure investigation have been deposited with the Cambridge Crystallographic Data Centre, CCDC No. 141001. Copies of this information may be obtained free of charge from The Director, CCDC, 12 Union Road, Cambridge, CB2 1EZ, UK (fax: +44-1223-336-033; e-mail: deposit@ccdc.cam.ac.uk or www: http://www.ccdc.cam.ac.uk).

Acknowledgements

We thank Dr P. Chabardès and Dr C. Mercier for helpful discussions and we gratefully acknowledge the support of this work by the Centre National de la Recherche Scientifique and Rhône-Poulenc.

References

[1] (a) G.W. Parshall, W.A. Nugent, Chemtech (US) (1988) 376 and references therein. (b) C. Mercier, P. Chabardès, Pure Appl. Chem. 66 (1994) 1509. (c) H. Bienaymé, Bull. Soc. Chim. Fr. 132 (1995) 696.

[2] K.H. Meyer, K. Schuster, Chem. Ber. 55 (1922) 819.

[3] (a) H. Rupe, E. Kambli, Helv. Chim. Acta 9 (1926) 672. (b) S. Swaminathan, K.V. Narayan, Chem. Rev. 71 (1971) 429 and references therein. (c) S.A. Vartayan, S.O. Babanyan, Russ. Chem. Rev. 36 (1967) 670. (d) R. Heilmann, R. Glenat, Ann. Chim. 8 (1963) 175. (e) M. Apparu, M. Glenat, Bull. Soc. Chim. Fr. 3 (1968) 1106. (f) N.K. Chaudhuri, M. Gut, J. Am. Chem. Soc. 87 (1965) 3737. (g) M. Edens, D. Boerner, C.R. Chase, D. Nass, M.D. Schiavelli, J. Org. Chem. 42 (1977) 3403. (h) M.V. Mavrov, V.F. Kucherov, Russ. Chem. Rev. 36 (1967) 233. (i) O. Tapia, J.M. Lluch, R. Cardenas, J. Andres, J. Am. Chem. Soc. 111 (1989) 829.

[4] (a) P. Chabardès, E. Kuntz, J. Varagnat, Tetrahedron 33 (1977) 1775. (b) H. Pauling, D.A. Andrews, N.C. Hindley, Helv. Chim. Acta 59 (1976) 1233. (c) G.L. Olson, K.D. Morgan, G. Saucy, Synthesis (1976) 25. (d) G.L. Olson, H.C. Cheung, K.D. Morgan, R. Borer, G. Saucy, Helv. Chim. Acta 59 (1976) 567. (e) M.B. Erman, I.S. Aul'chenko, L.A. Keiffith, V.G. Dulova, J.N. Novikov, M.E. Vol'pin, Tetrahedron Lett. 34 (1976), 2981. (f) M.B. Erman, S.E. Gulyi, I.S. Aul'chenko, Mendeleev Commun. (1994) 89.

[5] (a) K. Narasaka, H. Kusama, Y. Hayashi, Chem. Lett. (1991) 1413. (b) C.Y. Lorber, J.A. Osborn, unpublished results.

[6] C.Y. Lorber, J.A. Osborn, Tetrahedron Lett. 37 (1996) 853.

[7] P. Chabardès, Tetrahedron Lett. 29 (1988) 6253.

[8] see for example: (a) K.C. Pande, R.C. Mehrotra, Z. Anorg. Allg. Chem. 290 (1957) 87 and 95. (b) R. Kapoor, B.K. Bahl, P. Kapoor, Indian J. Chem. Sect. A, 25 (1986) 271. (c) H. Barrow, D.A. Brown, N.W. Alcock, H.J. Clase, M.G.H. Wallbridge, J. Chem. Soc., Chem. Commun. (1995) 1231. (d) H. Barrow, D.A. Brown, N.W. Alcock, W. Errington, M.G.H. Wallbridge, J. Chem. Soc., Dalton Trans. (1994) 3533. (e) N.W. Alcock, D.A. Brown, S.M. Roe, M.G.H. Wallbridge, J. Chem. Soc., Chem. Commun. (1992) 846.

[9] The Ti–Cu system is in fact slightly active in the absence of carboxylic acid. Titanium–oxo complexes may be obtained in this case by reaction of $Ti(OR)_4$ with traces of water, a commonly observed reaction. See for example: (a) F. Botomley, L. Sutin, Adv. Organomet. Chem. 28 (1988) 346. (b) S. Doeuff, Y. Dromzee, F. Taulelle, C. Sanchez, Inorg. Chem. 28 (1989) 4439. (c) D.C. Bradley, R.C. Mehrotra, D.P. Gaur, Metal Alkoxide, Academic Press, New York, 1978. (d) G.S. Hermann, G.H. Alt, U. Thewalt, J. Organomet. Chem. 393 (1990) 83. (e) N.W. Alcock, D.A. Brown, T.F. Illson, S.M. Roe, M.G.H. Wallbridge, J. Chem. Soc., Dalton Trans. (1991) 873. (f) N.W. Alcock, P.N. Bartlett, D. Gordon, T.F. Illson, M.G.H. Wallbridge, J. Chem. Soc., Chem. Commun. (1986) 614. (g) D.C. Bradley, R. Gaze, W. Wardlaw, J. Chem. Soc. (1955) 721, 3977, (1957) 469.

[10] M.H. Chisholm, I.P. Rothwell, in: G. Wilkinson, R.D. Gillard, J.A. McCleverty (Eds.), Comprehensive Coordination Chemistry, vol. 2, Pergamon, Oxford, 1987, pp. 335–364.

[11] see for example: H. Lang, K. Köhler, S. Blau, Coord. Chem. Rev. 143 (1995) 113.

[12] (a) F.L. Carter, E.W. Hughes, Acta Crystallogr. 10 (1957) 801. (b) G.G. Aleksandrov, I.R. Gol'ding, S.R. Sterlin, A.M. Sladkov, I.T. Struchkov, I.A. Garbuzova, V.T. Aleksanyan, Isv. Akad. Nauk., Ser. Khim. (1980), 2679. (c) D.W. Macomber, M.D. Rausch, J. Am. Chem. Soc. 105 (1983) 5325. (d) K. Brantin, M. Hakansson, S. Jagner, J. Organomet. Chem. 474 (1994) 229. (e) M. Pasquali, P. Leoni, C. Floriani, A. Gaetani-Manfredotti, Inorg. Chem. 21 (1982) 4324. (f) D.L. Reger, M.F. Huff, T.A. Wolfe, R.D. Adams, Organometallics 8 (1989) 848.

[13] Copper (I) chloride assistance would be needed in the case of titanium catalysts, as opposed to the vanadium ones [4], because of the lower nucleophilicity of Ti=O versus V=O functions.

[14] A.F. Armington, Inorg. Synth. 20 (1983) 10.

[15] C.K. Fair, An Interactive Intelligent System for Crystal Structure Analysis, MOLEN, Nonius, Delft, The Netherlands, 1990.

PERGAMON

www.elsevier.nl/locate/poly

Polyhedron 19 (2000) 1699–1705

POLYHEDRON

Synthesis and characterization of thorium and uranium tetraphenylimidophosphinate complexes. Crystal and molecular structures of $Th(tpip)_4$, $U(tpip)_4$ and $UCl(tpip)_3$

Adelaide Carvalho [a], Verónica García-Montalvo [b], Ângela Domingos [a], Raymundo Cea-Olivares [b], Noémia Marques [a], António Pires de Matos [a,*]

[a] *Departamento de Química, ITN, Estrada Nacional 10, 2686-953 Sacavém, Portugal*

[b] *Instituto de Química, Universidad Nacional Autónoma de México, Circuito Exterior, Ciudad Universitaria, Coyoacán, Mexico OF, Mexico*

Received 18 February 2000; accepted 26 May 2000

Abstract

Tetra(tetraphenylimidophosphinato)thorium, $Th(tpip)_4$ (**1**), was obtained from $Th(NO_3)_4{\cdot}4H_2O$ and Ktpip in aqueous medium. The analogous uranium compound, $U(tpip)_4$ (**2**), has been prepared by reacting UCl_4 with Ktpip in a 1:4 stoichiometric ratio, either in THF or in aqueous solution. X-ray diffraction analysis showed that compounds **1** and **2** were isostructural. The metal center is eight-coordinate by way of four bidentate tetraphenylimidophosphinate ligands in a square antiprismatic configuration. $UCl(tpip)_3$ (**3**) has been isolated from the reaction of uranium tetrachloride with 3 equiv. of Ktpip in aqueous solution. When this reaction was run in THF both compounds, $U(tpip)_4$ and $UCl(tpip)_3$, were obtained. The molecular structure of **3** has been determined by X-ray crystallography. The uranium atom is seven-coordinate in a pentagonal bipyramidal configuration. These compounds were also characterized by infrared and ^1H and ^{31}P NMR spectroscopies. © 2000 Elsevier Science Ltd. All rights reserved.

Keywords: Uranium; Thorium; Coordination compounds; Tetraphenylimidophosphinate ligand; X-ray crystal structures

1. Introduction

Bidentate oxygen ligands, such as carboxylates, tropolonates, β-ketoenolates, and oxalates have been used extensively in actinide chemistry [1]. They usually chelate to a single metal center, but they can also bridge dimetal units. Due to the large ionic radii of the actinide metals the coordination number of the metal atom is increased frequently by the presence of additional small molecules.

The synthesis of tris(tetraphenylimidodiphosphonato)lanthanide complexes ($Ln(tpip)_3$) has been reported before [2a]. The X-ray crystal structure of the praseodymium compound free from any external ligand has been determined, but the compound readily forms adducts with water, carboxylic acids, and carboxylates [2b]. It was reported that $Pr(tpip)_3$ induces important shifts in the ^1H NMR spectra of carboxylic acids and carboxylates, as a result of the formation of labile adducts, which makes this compound a useful NMR-shift reagent [2b–d]. Recently, long-lived highly luminescent terbium and europium complexes with these ligands were reported [3]. Although there is no evidence of water coordination in the structure, addition of water in the acetonitrile solution of $Tb(tpip)_3$ and $Eu(tpip)_3$ leads to shortening of the emission lifetime, which indicates some involvement of the water molecules in the coordination sphere of the lanthanide.

Due to the great flexibility of the chelating rings observed for these ligands which show wide variations in the ring angles (P–N–P, M–O–P, O–P–N), and also to its larger bite compared with other bidentate oxygen ligands, we decided to study the complexes of the early actinides, thorium and uranium, with the tetraphenylimidophosphinate ligand to determine how the different sizes of the metal ions would influence the

* Corresponding author. Tel.: +351-21-994-6000; fax: +351-21-994-1455.

E-mail address: pmatos@itn1.itn.pt (A. Pires de Matos).

0277-5387/00/$ - see front matter © 2000 Elsevier Science Ltd. All rights reserved.
PII: S0277-5387(00)00462-9

molecular structure of the complexes and if additional ligands would be needed to stabilize them. Herein we wish to report the synthesis of the first actinide tetraphenylimidophosphinate complexes.

2. Experimental

2.1. General procedures and techniques

The preparation and manipulation of the uranium compounds were carried out using standard Schlenk-line and dry-box techniques in an atmosphere of dinitrogen. UCl_4 was prepared as described previously [4]. $Th(NO_3)_4{\cdot}4H_2O$ was purchased from BDH Ltd. and used as received. $HN[P(O)(C_6H_5)_2]_2$ was prepared as reported previously [5]. THF and TDF were distilled from Na–benzophenone ketyl under nitrogen. NMR spectra were recorded at 27°C on a Varian 300 spectrometer in TDF. All ^1H NMR chemical shifts are reported in ppm relative to the ^1H impurity in TDF at δ 3.70 and the ^{31}P chemical shift to an external reference of H_3PO_4. Infrared spectra were recorded on a Perkin–Elmer 577 spectrophotometer as Nujol mulls between CsI plates. Elemental analyses were performed on a CE Instruments EA 1110 CHN analyzer.

2.2. Preparation of the compounds

2.2.1. Ktpip

To a suspension of $HN[P(O)(C_6H_5)_2]_2$ in methanol was slowly added a solution of KOH (10%) in water. After addition of the stoichiometric amount of KOH the suspension gives a clear solution, which was used in this form for the preparation of the compounds isolated in aqueous solution. For the reactions run in THF, the solution of Ktpip was evaporated to dryness to yield a white solid which was further recrystallized from ethanol.

2.2.2. $Th(tpip)_4$ (**1**)

Addition of an aqueous solution of the potassium salt of the ligand tpip (205 mg, 0.45 mmol) to an aqueous solution of $Th(NO_3)_4{\cdot}4H_2O$ (62 mg, 0.11 mmol) results in immediate formation of a white precipitate. This was collected over a filter, washed with water several times and dried under vacuum. Yield: 77% (160 mg, 0.084 mmol). The compound could be recrystallized from a THF–hexane solution yielding transparent crystals of **1**. IR spectrum (Nujol, cm^{-1}): $\nu(P_2N)$ 1210, 800; ν(PC) 745, 720, 695. ^1H NMR (THF-d_8, 27°C, δ ppm): 7.64 (2H, dd, 7.8, 4.6 Hz), 7.08 (1H, m), and 6.86 (2H, m). $^{31}P\{^1H\}$ NMR (THF-d_8, 27°C, δ ppm): 20.37. *Anal.* Calc. for $C_{96}H_{80}N_4O_8P_8Th$ (1897.55): C, 60.77; H, 4.25; N, 2.95. Found: C, 59.77; H, 4.33; N, 2.67%.

2.2.3. $U(tpip)_4$ (**2**)

Compound **2** was prepared by two methods.

2.2.3.1. Method a. An aqueous solution of Ktpip (437 mg, 0.96 mmol) was slowly added to 90 mg (0.24 mmol) of UCl_4, under nitrogen. There was an immediate formation of a light-green precipitate. The mixture was stirred for 10 min and evaporated to dryness. The compound was extracted with THF. Removal of the solvent under vacuum yielded a green solid in ca. 70% yield (319 mg, 0.17 mmol). *Anal.* Calc. for $C_{96}H_{80}N_4O_8P_8U$ (1903.54): C, 60.57; H, 4.24; N, 2.94. Found: C, 58.39; H, 3.96; N, 2.68%.

2.2.3.2. Method b. A stoichiometric amount of Ktpip (214 mg, 0.47 mmol) was added to a THF solution of UCl_4 (47 mg, 0.12 mmol) in a glove box. After separation of the KCl precipitate, removal of the solvent under vacuum yielded a light-green compound, which was washed with *n*-hexane and dried under vacuum. Yield: 76% (90 mg, 0.047 mmol). Crystals suitable for X-ray diffraction analysis were obtained by recrystallization from a concentrated THF solution, layered with *n*-hexane. IR spectrum (Nujol, cm^{-1}): $\nu(P_2N)$ 1208, 795; ν(PC) 745, 725, 690. ^1H NMR (THF-d_8, 27°C, δ ppm): 7.35 (1H, m), 6.97 (2H, m), 6.43 (2H, br). $^{31}P\{^1H\}$ NMR (THF-d_8, 27°C, δ ppm): −11.79. *Anal.* Calc. for $C_{96}H_{80}N_4O_8P_8U$: C, 60.57; H, 4.24; N, 2.94. Found: C, 58.42; H, 3.92; N, 2.68%.

2.2.4. $UCl(tpip)_3$ (**3**)

Addition of an aqueous solution of Ktpip (246 mg, 0.54 mmol) to UCl_4 (70.4 mg, 0.18 mmol), under a nitrogen atmosphere, resulted in immediate formation of a light-green precipitate. After stirring for a few minutes, the mixture was dried under vacuum, and the compound was extracted with THF. Removal of the solvent under vacuum yielded the green compound with a yield of 50% (137 mg, 0.09 mmol). Green crystals of **3** suitable for X-ray diffraction analysis were obtained from a THF–hexane solution. IR spectrum (Nujol, cm^{-1}): $\nu(P_2N)$ 1235, 1205 and 815; ν(PC) 750, 725, 690. ^1H NMR (THF-d_8, 27°C, δ ppm): 8.15 (2H, dd, 7.4, 4.6 Hz), 7.30 (1H, m), 7.05 (2H, m). $^{31}P\{^1H\}$ NMR (THF-d_8, 27°C, δ ppm): −14.12. *Anal.* Calc. for $C_{72}H_{60}ClN_3O_6P_6U$ (1522.61): C, 56.80; H, 3.97; N, 2.76. Found: C, 56.29; H, 3.61; N, 2.63%.

2.3. X-ray crystallographic analysis of $Th(tpip)_4$ (**1**), $U(tpip)_4$ (**2**) and $UCl(tpip)_3$ (**3**)

Crystals were mounted in thin-walled glass capillaries in a nitrogen-filled glove box. Data were collected at room temperature on an Enraf–Nonius CAD-4 diffractometer with graphite-monochromatized Mo Kα radiation. A summary of the crystallographic data is given in

Table 1. Data were corrected for Lorentz-polarization effects, for decay (no decay was observed for **3**) and for absorption by empirical corrections based on ψ scans [6].

The structures were solved by Patterson methods [7] and subsequent difference Fourier techniques and refined by full-matrix least-squares procedures on F^2 using SHELXL-93 [8]. Compounds **1** and **2** are isomorphous. In their lattice there is one molecule of THF of crystallization per asymmetric unit. Aditionally, the three strongest peaks in the difference Fourier map, severely disordered across a center of symmetry, were indicative of another solvent present, possibly hexane, the disorder of which could not be modelled, and so they were taken into account as full-occupancy carbon atoms (they were excluded from the formula, from the molecular weight and from the calculation of the density in Table 1). All but the solvent atoms were refined anisotropically and the contributions of the hydrogen atoms were included in calculated positions (except those of the solvent). Atomic scattering factors and anomalous dispersion terms were taken as in Ref. [8].

3. Results and discussion

3.1. Synthesis

$Th(tpip)_4$ (**1**) was obtained as a white precipitate by reacting an aqueous solution of $Th(NO_3)_4{\cdot}4H_2O$ with 4 equiv. of an aqueous solution of Ktpip. Compound **1** is insoluble in common aromatic and aliphatic hydrocarbons and in halogenated solvents, but dissolves in THF from where transparent crystals suitable for X-ray diffraction analysis could be obtained.

Addition of 4 equiv. of an aqueous solution of potassium tetraphenylimidophosphinate to UCl_4, under a nitrogen atmosphere, resulted in immediate formation of a light green precipitate. After drying under vacuum, the solid was extracted with THF giving a green compound, $U(tpip)_4$ (**2**), in good yield. **2** could also be obtained by reacting anhydrous potassium tetraphenylimidophosphinate with UCl_4, in THF solution, in the appropriate amounts. $UCl(tpip)_3$ (**3**) was obtained as a light-green precipitate when 3 equiv. of Ktpip in aqueous solution were added to UCl_4. When this reaction was run in THF solution there is concomitant formation of $UCl(tpip)_3$ and $U(tpip)_4$, as shown by its ^1H and ^{31}P NMR spectra. Recrystallization from THF did not allow the separation of the compounds.

Attempts to obtain the analogous $ThCl(tpip)_3$ failed. When $ThCl_4$ reacts with 3 equiv. of Ktpip, either in aqueous or THF solution, a mixture of compounds is obtained. One compound could be identified as $Th(tpip)_4$ by its ^1H and ^{31}P NMR spectra. The other species is probably $ThCl(tpip)_3$, by comparison with the result obtained in the uranium case. To support this hypothesis the typical Th–Cl vibration could be identified in the

Table 1
Crystallographic data for complexes $[Th(tpip)_4]{\cdot}OC_4H_8$ (**1**·OC_4H_8), $[U(tpip)_4]{\cdot}OC_4H_8$ (**2**·OC_4H_8), and $[UCl(tpip)_3]$ (**3**)

	1·OC_4H_8	**2**·OC_4H_8	**3**
Formula	$C_{96}H_{80}N_4O_8P_8Th{\cdot}OC_4H_8$	$C_{96}H_{80}N_4O_8P_8U{\cdot}OC_4H_8$	$C_{72}H_{60}ClN_3O_6P_6U$
Crystal system	triclinic	triclinic	triclinic
Space group	$P\bar{1}$	$P\bar{1}$	$P\bar{1}$
a (Å)	14.536(3)	14.486(2)	13.518(1)
b (Å)	14.615(2)	14.568(2)	14.222(4)
c (Å)	24.595(3)	24.525(2)	19.283(2)
α (°)	74.52(1)	74.75(1)	108.96(1)
β (°)	87.40(1)	87.88(1)	91.31(1)
γ (°)	67.04(2)	67.08(1)	107.45(1)
V (Å^3)	4626(1)	4587(1)	3315(1)
Z	2	2	2
μ (mm^{-1})	1.809	1.969	2.688
Crystal size (mm)	$0.54\times0.20\times0.12$	$0.63\times0.27\times0.03$	$0.54\times0.31\times0.22$
Crystal color	colorless	green	green
Scan mode	ω–2θ	ω–2θ	ω–2θ
θ Range (°)	1.5–23.1	1.5–24.0	1.5–24.0
Number of reflections collected	13 188	14 996	10 393
Number of independent reflections (R_{int})	12 832 (0.0390)	14 347 (0.0716)	9785 (0.0307)
Observed [$I>2\sigma(I)$]	9281	9505	7619
Number of parameters	1086	1086	802
R_1[a]	0.0586	0.0689	0.0529
wR_2[b]	0.0984	0.1237	0.0995
Largest difference peak and hole (e Å^{-3})	1.39 and −0.93	1.47 and −1.44	1.39 and −1.53

[a] $R_1=\Sigma||F_o|-|F_c||/\Sigma|F_o|$.
[b] $wR_2=\{\Sigma[w(F_o^2-F_c^2)^2]/\Sigma[w(F_o^2)^2]\}^{1/2}$; $w=1/[\sigma^2(F_o^2)+(aP)^2+bP]$, where $P=(F_o^2+2F_c^2)/3$. The values were calculated for data with $I>2\sigma(I)$.

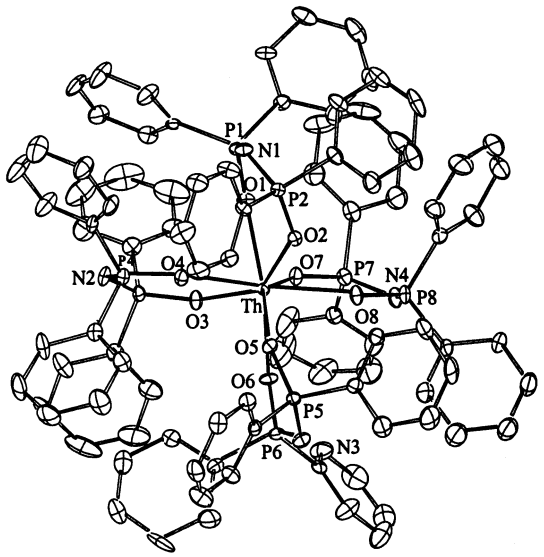


Fig. 1. ORTEP diagram of [Th(tpip)$_4$] (**1**), using 30% probability ellipsoids.

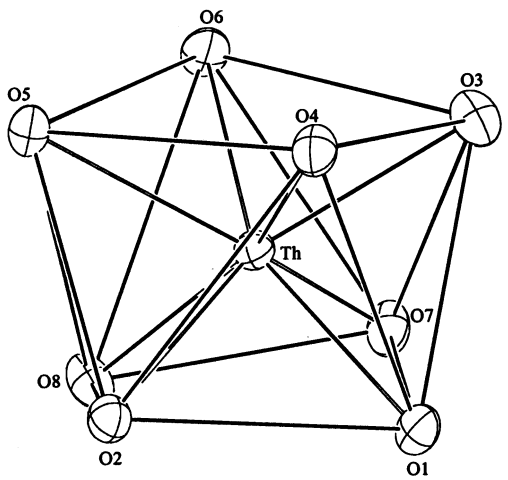


Fig. 2. View of the coordination geometry around the Th atom in [Th(tpip)$_4$].

IR spectrum of the mixture. Attempts to recrystallize the compound yielded always crystals of **1**.

3.1.1. IR spectroscopy

The solid state IR spectra of the complexes show absorptions characteristic of P–N bonds [9,10]. The absorptions due to the phosphazenic stretching vibration (PNP) appear as a doublet centered at 1210 cm^{-1} in complex **1**, whereas this band is centered at 1208 cm^{-1} in complex **2**. The spectrum of **3** is more complex in this region, with bands centered at 1230, 1200 and 1190 cm^{-1}. Bands in the region 775–690 cm^{-1} are assigned to the P–C(phenyl) vibrations [10]. In addition the spectrum of **3** shows the U–Cl stretching vibration at 270 cm^{-1}.

3.1.2. NMR spectroscopy

The room temperature ^{1}H NMR spectra of all the complexes are deceptively simple exhibiting only one set of complex multiplets associated with the aromatic protons of the ligands and one single resonance in the ^{31}P{^{1}H} NMR spectra. The magnetic equivalence of the chelating ligands indicates a fluxional process which is fast in the NMR time scale. By lowering the temperature the resonances broaden and shift but a limit static spectrum is not obtained. The assignment of the resonances could be done on the basis of their relative intensity and multiplicity. In the ^{1}H NMR spectrum of **1** the resonances due to the *o*-, *p*-, and *m*-protons of the aromatic rings appear as complex multiplets centered at 7.64, 7.08 and 6.86 ppm, respectively, and the ^{31}P NMR spectrum showed one single resonance at 20.37 ppm. In the spectrum of **2** the *p*- and the *m*-protons appear as complex triplets centered at 7.35 and 6.97 ppm, respectively, and the *o*-protons as a broad resonance at 6.43 ppm. The ^{31}P NMR spectrum displays one resonance at -11.79 ppm. The resonances due to the *o*-, *p*-, and *m*-protons of **3** are multiplets centered at 8.15, 7.30 and 7.05 ppm, respectively, and the resonance due to the phosphorus atoms is located at -14.12 ppm.

A stoichiometric amount of pyridine was added to the less crowded compound **3** in TDF in a NMR tube. The NMR spectrum of the mixture displays the resonances due to compound **3** and free pyridine only, in contrast with the tris(tetraphenylimidodiphosphonato)lanthanide complexes (Ln(tpip)$_3$) [2], which form adducts with neutral small ligands.

To confirm the identity of **1**, **2**, and **3** and to establish their coordination geometry the solid state structures of the compounds were determined by single crystal X-ray diffraction.

3.2. Crystallographic studies

3.2.1. Complexes *1* and *2*

Compounds **1** and **2** are isostructural and crystallized from THF as monomeric molecules. The metal center is eight-coordinate by way of four bidentate tetraphenylimidophosphinate groups and displays distorted square antiprismatic (SAP) geometry. Fig. 1 shows a perspective view of the molecule **1** (**2** is isomorphous and is not illustrated, but equal atomic numbering schemes are used for **1** and **2**). Each two tpip ligands are chelated along the edges of the square faces of the SAP polyhedron (Fig. 2). Both 'square' faces, O(1)–O(2)–O(8)–O(7) and O(3)–O(4)–O(5)–O(6), are quite bent (dihedral angles of its diagonals are 16.8, 12.6°, and 15.7, 13.1° for **1** and **2**, respectively), which together with the ϕ values (20.8, 18.9° and 21.4, 19.2° for **1** and **2**, respectively) leads to distortion of the SAP along the pathway towards dodecahedron (DD), as shown in Table 2, where the values of the shape

Table 2
Values [a] of the δ and ϕ shape parameters (°) for $[Th(tpip)_4]\cdot OC_4H_8$ and $[U(tpip)_4]\cdot OC_4H_8$

		$\mathbf{1}\cdot OC_4H_8$	$\mathbf{2}\cdot OC_4H_8$	SAP	BCTP	DD
δ_s	O(2) [O(1) O(8)] O(7)	16.8	15.7	0.0	0.0	29.5
δ_s	O(4) [O(3) O(5)] O(6)	12.6	13.1	0.0	21.8	29.5
δ_l	O(4) [O(1) O(3)] O(7)	46.7	44.3	52.5	48.2	29.5
δ_l	O(2) [O(5) O(8)] O(6)	45.7	45.9	52.5	48.2	29.5
ϕ	O(1)–O(2)–O(5)–O(6)	20.8	21.4	24.5	14.1	0.0
ϕ	O(8)–O(7)–O(3)–O(4)	18.9	19.2	24.5	14.1	0.0

[a] Values referred to the normalized polyhedron. δ_s, dihedral angles referred to the diagonals of the square faces of the polyhedron; δ_l, dihedral angles referred to the lateral edges of the polyhedron; ϕ, values for the planarity of the two orthogonal trapezoids.

parameters [11] for the normalized polyhedra are shown.

Selected bond lengths and angles are given in Table 3. Only one tpip ligand (containing the O(7) and O(8) atoms) is symmetrically bonded to the metal center, whilst the others are asymmetrically bonded. The An–O bond lengths average 2.41(3) Å for **1**, (range: 2.376(7)–2.459(6) Å) and 2.37(3) Å for **2** (range: 2.324(7)–2.425(7) Å), which is consistent with the difference of the ionic radii of Th(IV) and U(IV).

The O–An–O bond angles are similar and average 71.8(2)° for **1** and 72.3(2)° for **2**. The Th–O bond lengths and the O–Th–O bond angles are comparable to the values 2.40(2) Å and 70.5(4)° of the eight-coordinate tetrakis(thenoyltrifluoroacetonato)thorium(IV), $Th(TTA)_4$ [12], which presents a dodecahedral geometry. The U–O bond length and the O–U–O bond angles in **2** compare with the values of 2.32(3) Å and 71(1)° in the eight-coordinate SAP [β-$U(acac)_4$] [13] and with the values of 2.34(1) Å and 70.8(2)° in [U(PhCOCHCOPh)$_4$] [14].

The more relevant parameters for the tpip ligands are the P–O and P–N bond distances, which are equivalent in both compounds (average P–O and P–N: 1.518(11) and 1.583(6) Å in **1**, 1.517(7) and 1.584(11) Å in **2**). These distances are shorter than the corresponding single bonds, suggesting electron delocalization over the chelate rings, as already observed by other authors for analogous complexes with the tetraphenyldithioimidophosphinate ligand [15]. The maximum variations observed in the ring angles P–N–P, O–P–N and An–O–P within the four chelate rings in compounds **1** and **2** are similar, as expected, as they are isomorphous (compound **1**: 2.4, 2.0, 4.6°; compound **2**: 2.1, 2.1, 4.4°). In **1** and **2** the O_2P_2N chelate rings show significant deviations from planarity (atomic deviations in the range −0.142 to 0.188 Å). All the six-membered AnO_2P_2N rings are non-planar with the rings containing the O3/O4 and O7/O8 atoms being almost planar within AnO_2P_2 with some folding about the P···P axis (fold angles: 16.9 and 25.7° for **1**, 18.1 and 27.0° for **2**). The different deformations observed for each chelate ring reflects the flexible nature of these ligands.

3.2.2. Complex **3**

The uranium atom is in a pentagonal bipyramidal configuration (PB) in complex **3**, with two chelating rings (O(3)/O(4) and O(5)/O(6)) and the O(1) atom of the third chelating ring occupying the equatorial plane, while the chlorine and the O(2) atoms are in the axial positions (Cl–U–O(2) angle of 176.1(2)°). An ORTEP drawing of **3** is shown in Fig. 3, selected bond lengths and angles are listed in Table 4.

The U–O bond lengths and the O–U–O bond angles range from 2.268(6) to 2.355(5) Å (average 2.31(3) Å) and from 72.0(2) to 79.0(2)° (average 74.6(2)°), respectively. The ligand containing oxygens in equatorial and axial positions presents the largest O–U–O bond angle

Table 3
Selected bond lengths (Å) and angles (°) for $\mathbf{1}\cdot OC_4H_8$ and $\mathbf{2}\cdot OC_4H_8$

$\mathbf{1}\cdot OC_4H_8$		$\mathbf{2}\cdot OC_4H_8$	
Th–O(1)	2.392(6)	U–O(1)	2.349(7)
Th–O(2)	2.459(6)	U–O(2)	2.425(7)
Th–O(3)	2.376(7)	U–O(3)	2.324(7)
Th–O(4)	2.418(6)	U–O(4)	2.377(7)
Th–O(5)	2.440(6)	U–O(5)	2.412(6)
Th–O(6)	2.398(6)	U–O(6)	2.351(7)
Th–O(7)	2.409(6)	U–O(7)	2.374(7)
Th–O(8)	2.399(6)	U–O(8)	2.352(7)
Average P–O	1.518(11)	Average P–O	1.517(7)
Average P–N	1.583(6)	Average P–N	1.584(11)
O(1)–Th–O(2)	72.9(2)	O(1)–U–O(2)	73.1(2)
O(3)–Th–O(4)	71.6(2)	O(3)–U–O(4)	71.9(2)
O(5)–Th–O(6)	71.1(2)	O(5)–U–O(6)	72.0(2)
O(7)–Th–O(8)	71.7(2)	O(7)–U–O(8)	72.0(2)
O(1)–Th–O(3)	80.8(2)	O(1)–U–O(3)	80.7(2)
O(1)–Th–O(4)	78.5(2)	O(1)–U–O(4)	78.5(2)
O(1)–Th–O(7)	75.7(2)	O(1)–U–O(7)	75.5(2)
O(2)–Th–O(4)	81.7(2)	O(2)–U–O(4)	81.7(2)
O(2)–Th–O(5)	70.7(2)	O(2)–U–O(5)	70.5(2)
O(2)–Th–O(8)	72.0(2)	O(2)–U–O(8)	72.0(2)
O(3)–Th–O(6)	73.9(2)	O(3)–U–O(6)	73.3(2)
O(3)–Th–O(7)	69.4(2)	O(3)–U–O(7)	69.4(2)
O(4)–Th–O(5)	76.1(2)	O(4)–U–O(5)	75.5(2)
O(5)–Th–O(8)	82.9(2)	O(5)–U–O(8)	82.7(2)
O(6)–Th–O(7)	80.0(2)	O(6)–U–O(7)	79.8(2)
O(6)–Th–O(8)	83.8(2)	O(6)–U–O(8)	83.8(3)

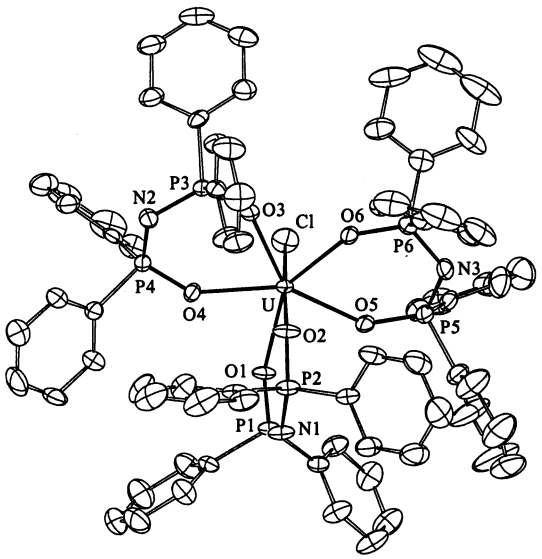


Fig. 3. ORTEP diagram of $[UCl(tpip)_3]$ (**3**), using 30% probability ellipsoids.

Table 4
Selected bond lengths (Å) and angles (°) for **3**

U–O(1)	2.355(5)	U–O(4)	2.341(6)
U–O(2)	2.276(6)	U–O(5)	2.327(6)
U–O(3)	2.317(6)	U–O(6)	2.268(6)
U–Cl	2.624(3)		
Average P–O	1.516(11)	Average P–N	1.581(12)
O(1)–U–O(2)	79.0(2)	O(2)–U–O(5)	90.6(2)
O(3)–U–O(4)	72.0(2)	O(2)–U–O(6)	85.2(2)
O(5)–U–O(6)	72.9(2)	O(1)–U–Cl	97.8(2)
O(1)–U–O(4)	73.0(2)	O(2)–U–Cl	176.1(2)
O(1)–U–O(5)	74.8(2)	O(3)–U–Cl	93.9(2)
O(3)–U–O(6)	68.6(2)	O(4)–U–Cl	89.7(2)
O(2)–U–O(3)	90.1(2)	O(5)–U–Cl	86.4(2)
O(2)–U–O(4)	91.4(2)	O(6)–U–Cl	96.3(2)

(O(1)–U–O(2) angle of 79.0(2)°). The U–O bond lengths in **3** are shorter than in complex **2**, as it would be expected for a complex with a lower coordination number and compares with the value of 2.32(2) Å in the seven-coordinate (PB) $UCl_2(acac)_2(OPPh_3)$ [16]. The U–Cl bond length in **3** (2.624(3) Å) is comparable with the value of 2.617(8) Å found in $UCl_2(acac)_2(OPPh_3)$ [16].

As in compounds **1** and **2**, the P–O and P–N bond distances are similar (average P–O and P–N: 1.516(11), 1.581(12) Å) but shorter than the corresponding single bonds. **3** shows higher values for the maximum variations in the ring angles P–N–P, O–P–N and U–O–P within the three chelate ring (6.8, 3.8. and 5.3°) reflecting again the large flexibility of the ligand. This flexibility is also manifested by the folding of some rings along the P···P axis, as already mentioned for **1** and **2**, as well as by the folding of some rings along the O···O axis. One of the O_2P_2N chelate rings (the one containing the O3/O4 atoms) shows significant deviations from planarity, while the other two are almost planar. The UO_2P_2N rings containing the O1/O2 and the O5/O6 atoms, show folding angles of 11.1 and 12.1° about the O···O and P···P axes, respectively.

4. Conclusions

So far, the structures reported here are the first structurally characterized actinide complexes with tpip ligands. The complexes isolated demonstrate the influence of the ionic radii of the actinide ions in the structure of the resulting complexes nicely. For the smaller uranium ion both compounds $U(tpip)_4$ and $UCl(tpip)_3$ could be synthesized while for the thorium ion only the more coordinative saturated $Th(tpip)_4$ could be isolated.

5. Supplementary data

Supplementary data are available free of charge from: The Director, CCDC, 12 Union Road, Cambridge, CB2 1EZ, UK (fax: +44-1223-336-033; e-mail: deposit@ccdc.cam.ac.uk or www: http://www.ccdc.cam.ac.uk) on request, quoting the deposition numbers CCDC-137427 (**1**), CCDC-137428 (**2**), and CCDC-137429 (**3**).

Acknowledgements

Financial support from PRAXIS XXI (2/2.1/QUI/386/94) is gratefully acknowledged.

References

[1] K.W. Bagnall, in: G. Wilkinson (Ed.), Comprehensive Coordination Chemistry, vol. 3, Pergamon, Oxford, 1987, p. 1129.
[2] (a) I. Rodriguez, C. Alvarez, J. Gómez-Lara, R. Cea-Olivares, Lanthanide Actinide Res. 1 (1985–1986) 253. (b) N. Platzer, H. Rudler, C. Alvarez, L. Barkaoui, B. Denise, N. Goasdoue, M.N. Rager, J. Vaissermann, J.C. Daran, Bull. Soc. Chim. Fr. 132 (1995) 95. (c) C. Alvarez, N. Goasdoue, N. Platzer, I. Rodriguez, H. Rudler, J. Chem. Soc., Chem. Commun. (1988) 1002. (d) I. Rodriguez, C. Alvarez, J. Gomez-Lara, R.A. Toscano, N. Platzer, C. Mulheim, H. Rudler, J. Chem. Soc., Chem. Commun. (1987) 1502.
[3] S.W. Magennis, S. Parsons. A. Corval, J.D. Woolins, Z. Pikramenou, J. Chem. Soc., Chem. Commun. (1999) 61.
[4] J.A. Hermann, J.F. Suttle, Inorg. Synth. 5 (1957) 143.
[5] F.T. Wang, J. Najdzionek, K.L. Leneker, H. Wasserman, D.M. Braitsch, Synth. React. Met-Org. Chem. 8 (2) (1978) 119.

[6] C.K. Fair, MOLEN, Enraf–Nonius, Delft, The Netherlands, 1990.
[7] G.M. Sheldrick, SHELXS-86: Program for the Solution of Crystal Structure, University of Göttingen, Germany, 1986.
[8] G.M. Sheldrick, SHELXL-93: Program for the Crystal Structure Refinement, University of Göttingen, Germany, 1986.
[9] G.P. Quillan, I.A. Oxton, Inorg. Chim. Acta 29 (1979) 69.
[10] O. Siiman, J. Vetuskey, Inorg. Chem. 19 (1980) 1672.
[11] (a) E.L. Muetterties, L.J. Guggenberger, J. Am. Chem. Soc. 96 (1974) 1748. (b) M.G.B. Drew, Coord. Chem. Rev. 24 (1977) 179.
[12] M. Lenner, O. Lindqvist, Acta Crystallogr., Sect. B 35 (1979) 600.
[13] H. Titze, Acta Chem. Scand. 24 (1970) 405.
[14] D.L. Kepert, J.M. Patrick, A.H. White, J. Chem. Soc., Dalton Trans. (1983) 567.
[15] (a) N. Zúñiga-Villarreal, C. Silvestru, M.R. Lezama, S. Hernández-Ortega, C.A. Toledano, J. Organomet. Chem. 496 (1995) 169. (b) R. Rossi, A Marchi, L. Marvelli, L. Magon, M. Peruzzini, U. Casellato, R. Graziani, J. Chem. Soc., Dalton Trans. (1993) 723.
[16] C. Baudin, P. Charpin, M. Ephritikine, M. Lance, M. Nierlich, J. Vigner, J. Organomet. Chem. 345 (1988) 263.

PERGAMON

www.elsevier.nl/locate/poly

Polyhedron 19 (2000) 1707–1712

POLYHEDRON

Synthesis, luminescence studies and crystal structures of two europium(II) hydrotris(pyrazol-1-yl)borate complexes: $Eu(HBpz_3)_2 \cdot 2DPSO$ and $Eu(HBpz_3)_2 \cdot 2BPMU$

Adelaide Carvalho [a], Ângela Domingos [a], Paulo C. Isolani [b], Noémia Marques [a], António Pires de Matos [a,*], Geraldo Vicentini [b]

[a] *Departamento de Química, ITN, Estrada Nacional 10, 2686-953 Sacavém, Portugal*
[b] *Instituto de Química, Universidade de São Paulo, C.P. 26077, São Paulo, SP 05513-970, Brazil*

Received 29 March 2000; accepted 23 May 2000

Abstract

Europium(II) hydrotris(pyrazol-1-yl)borate complexes, $Eu(HBpz_3)_2L_2$ (L = diphenylsulfoxide (**1**) and bis(pentamethylene)urea (**2**)), have been synthesized. Characterization of **1** and **2** by infrared absorption spectroscopy points to coordination of the neutral ligands through the sulfoxide and carbonyl oxygens, respectively. This was corroborated by X-ray diffraction analysis. In both compounds the metal centre is eight-coordinate by way of the six nitrogens of the two tridentate pyrazolyl ligands and the oxygen atoms of the diphenylsulfoxide or bis(pentamethylene) urea ligands, in a square antiprismatic configuration. Both complexes are luminescent at 77 K and display emission bands with maxima at 610 and 632 nm for **1** and **2**, respectively. © 2000 Elsevier Science Ltd. All rights reserved.

Keywords: Europium compounds; Hydrotris(pyrazolyl)borate ligands; Luminescence studies; X-ray crystal structures

1. Introduction

The chemistry of the lanthanides in low-oxidation states is being widely studied because of their potential in organic synthesis [1] and the luminescent properties of complexes containing Eu^{2+} ions [2].

Most of the chemistry of the lanthanide ions in low oxidation states has been mainly based on the cyclopentadienyl type ligands, but recently an increasing interest has been directed towards other ligand frameworks [3]. One of the ligand systems that has been explored is based on polypyrazolylborate ligands, which have been considered similar to the cyclopentadienyls. Some years ago we and others initiated an extensive investigation into the synthesis of hydrotris(pyrazolyl)borate ($Tp^{R,R'}$) anchored lanthanide(II) complexes. $Ln(Tp^{Me,Me})_2$ (Ln = Sm, Yb, Eu) [4], $Ln(HBpz_3)_2 \cdot 2THF$ and $Ln(Bpz_4)_2 \cdot 2THF$ (Ln = Sm, Yb, Eu) [5], $Ln(Tp^{Ph,Me})_2$ and $Ln(Tp^{thyenyl,Me})_2$ (Ln = Sm, Yb) [6], $Ln(Tp^{tBu,Me})_2$ (Ln = Sm, Yb) [7] are among the compounds which have been isolated upon reaction of the appropriate di-iodides with the wide variety of accessible hydrotrispyrazolylborate ligands. The luminescent behaviour of $Eu(HBpz_3)_2 \cdot 2THF$ and $Eu(Bpz_4)_2 \cdot 2THF$ have also been reported [5]. $Eu(HBpz_3)_2 \cdot 2THF$ proved to be a very good emitter and, therefore, a potentially good phosphor.

This paper describes the synthesis, characterization, spectroscopic studies and structural determination of europium bishydrotris(pyrazol-1-yl)borate complexes with the neutral ligands diphenylsulfoxide (DPSO) and bis(pentamethylene)urea (BPMU).

* Corresponding author. Tel.: +351-21-944-6000; fax: +351-21-994-1455.
E-mail address: pmatos@itn1.itn.pt (A. Pires de Matos).

0277-5387/00/$ - see front matter © 2000 Elsevier Science Ltd. All rights reserved.
PII: S0277-5387(00)00445-9

2. Experimental

2.1. Materials and instrumentation

All synthetic procedures were carried out under nitrogen using glove box and Schlenk-line techniques. Solvents used were purified by distillation from sodium benzophenone ketyl and degassed immediately before use. $KHBpz_3$ [8] and $Eu(HBpz_3)_2{\cdot}2THF$ [5] were prepared as previously described. Europium(II) iodide solutions were prepared according to literature procedures [9]. Diphenylsulfoxide and bis(pentamethylene)urea were purified by sublimation under vacuum. Infrared absorption spectra were recorded on a Perkin–Elmer 577 spectrophotometer using Nujol mulls between CsI plates. Emission spectra were recorded on a Hitachi Perkin–Elmer MPF-4 spectrofluorimeter with modifications for solid samples positioning and thermostating at low temperatures [10]. As all the samples were oxygen and water sensitive they were sealed in quartz tubes under vacuum. Although no quantum emission efficiencies could be obtained in our laboratories, the experimental conditions followed allowed a comparison of relative emission efficiencies.

2.2. Preparation of the complexes

2.2.1. $Eu(HBpz_3)_2{\cdot}2DPSO$ (1)

To a solution of $Eu(HBpz_3)_2{\cdot}2THF$ (200 mg, 0.277 mmol) in THF was added diphenylsulfoxide (112 mg, 0.554 mmol). After the addition the solution turns immediately from yellow to orange. Stirring was continued for 16 h. Removal of the solvent under reduced pressure yielded a yellow solid, which was further crystallized from toluene. Yield: 60% (163 mg, 0.166 mmol). IR (Nujol, cm^{-1}): ν(BH) 2395, 2435. *Anal.* Calc. for $C_{42}H_{40}B_2N_{12}O_2S_2Eu$: C, 51.34; H, 4.10; N, 17.11. Found: C, 49.70; H, 3.94; N, 16.57%.

2.2.2. $Eu(HBpz_3)_2{\cdot}2BPMU$ (2)

The compound was prepared as described for **1**, by reacting $Eu(HBpz_3)_2{\cdot}2THF$ (255 mg, 0.353 mmol) in THF with bis(pentamethylene)urea (139 mg, 0.706 mmol). Yield: 60% (205 mg, 0.211 mmol). IR (Nujol, cm^{-1}): ν(BH) 2390, 2430. *Anal.* Calc. for $C_{40}H_{60}N_{16}B_2O_2Eu$: C, 49.50; H, 6.23; N, 23.09. Found: C, 49.27; H, 6.82; N, 23.11%.

2.3. X-ray crystallographic analysis of $Eu(HBpz_3)_2{\cdot}2DPSO$ and $Eu(HBpz_3)_2{\cdot}2BPMU$

Orange crystals of **1** and **2**, of approximate dimensions $0.54 \times 0.18 \times 0.14$ mm and $0.43 \times 0.22 \times 0.14$ mm, respectively, were mounted in thin-walled glass capillaries in a nitrogen-filled glove-box. Data were collected at room temperature (r.t.) on an Enraf–Nonius CAD-4 diffractometer with graphite-monochromated Mo Kα radiation, using a ω–2θ scan mode. Unit cell parameters were obtained by least-square refinement of the setting angles of 25 reflections with $16.6 < 2\theta < 25.1°$ for **1** and $15.9 < 2\theta < 25.8°$ for **2**. A summary of the crystallographic data is given in Table 1.

Table 1
Crystallographic data for complexes $Eu(HBpz_3)_2{\cdot}2DPSO$ (**1**) and $Eu(HBpz_3)_2{\cdot}2BPMU$ (**2**) [a]

	1	**2**
Formula	$C_{42}H_{40}B_2N_{12}O_2S_2Eu$	$C_{40}H_{60}B_2N_{16}O_2Eu$
Crystal system	monoclinic	triclinic
Space group	$P2/c$	$P\bar{1}$
a (Å)	18.509(4)	12.601(2)
b (Å)	12.268(1)	12.786(3)
c (Å)	22.464(5)	17.183(3)
α (°)		83.27(2)
β (°)	113.64(2)	74.07(1)
γ (°)		62.58(1)
V (Å^3)	4673(2)	2363(l)
Z	4	2
θ Range (°)	1.5–24.0	1.5–26.0
Reflections collected	6709	9316
Independent (R_{int})	6512 (0.0430)	8992 (0.0348)
Observed [$I > 2\sigma(I)$]	5465	8169
Number of parameters	431	550
R_1 [a]	0.0751	0.0575
wR_2 [b]	0.1394	0.0904

[a] $R_1 = \Sigma||F_o|-|F_o||/\Sigma|F_o|$.

[b] $wR_2 = [\Sigma(w(F_o^2-F_c^2)^2)/\Sigma(w(F_o^2)]^{1/2}$; $w = 1/[\sigma^2(F_o^2)+(aP)^2+bP]$, where $P = (F_o^2+2F_c^2)/3$. The values were calculated for data with $I > 2\sigma(I)$.

Data were corrected [11] for Lorentz and polarization effects, for linear decay and for absorption by empirical corrections based on ψ scans. The heavy atom positions were located by Patterson methods using SHELXS-86 [12]. The remaining atoms were located by successive difference Fourier maps and refined by least-squares refinements on F^2 using SHELXS-93 [13]. All the non-hydrogen atoms (except the phenyl carbon atoms, which showed large U_{iso} values) were refined with anisotropic thermal motion parameters, and the contribution of the hydrogen atoms was included in calculated positions. The relatively weak diffraction of crystal **1** limited the accuracy of the structural analysis. The final difference Fourier syntheses revealed electron densities between 0.80 and -0.57 e Å^3 for **1** and 1.06 and -0.49 e Å^3 for **2**, near the heavy atoms. Atomic scattering factors and anomalous dispersion terms were taken as in [13]. Drawings were made with ORTEPII [14] and all the calculations were performed on a Dec α 3000 computer.

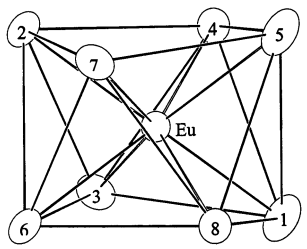


Fig. 1. Coordination polyhedron for the molecules of $Eu(HBpz_3)_2{\cdot}2DPSO$ (**1**). Polyhedra vertices were defined thus: **1** [O(l), O(2)], **2** [N(1), N(4)], **3** [N(2), N(5)], **4** [N(3), N(6)], **5** [O(1a), O(2a)], **6** [N(1a), N(4a)], **7** [N(2a), N(5a)], **8** [N(3a), N(6a)]

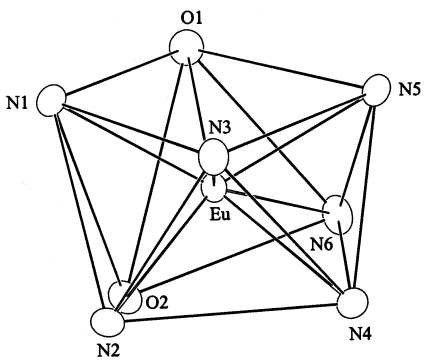


Fig. 2. Coordination polyhedron of $Eu(HBpz_3)_2{\cdot}2BPMU$ (**2**).

3. Results and discussion

3.1. Synthesis and characterization of complexes $Eu(HBpz_3)_2{\cdot}2L$ ($L = DPSO$, $BPMU$)

Replacement of the two molecules of THF in $Eu(HBpz_3)_2{\cdot}2THF$ by DPSO or BPMU was readily achieved by adding 2 equiv. of the appropriate reagent to one equivalent of $Eu(HBpz_3)_2{\cdot}2THF$ in THF solution. After addition, the yellow solution of $Eu(HBpz_3)_2{\cdot}2THF$ turned immediately to orange. Recrystallization from toluene afforded the expected $Eu(HBpz_3)_2{\cdot}2DPSO$ (**1**) and $Eu(HBpz_3)_2{\cdot}2BPMU$ (**2**), as orange crystalline materials in reasonable yield.

The compounds are soluble in common aromatic and ether type solvents. The infrared spectra exhibit the ν(B–H) stretching vibration between 2390 and 2435 cm^{-1} consistent with tridentate ($HBpz_3$) ligands. In the spectrum of **1** ν(SO) appears at 967 cm^{-1}, whereas in neat DPSO it appears at 1000 cm^{-1}. This is within the range of observed ν(SO) shifts towards lower energies that occur in other DPSO complexes [15,16] and it is indicative of coordination through the oxygen of the sulfoxide group. Infrared spectra of **2** show ν(CO) at 1620 cm^{-1}. The CO stretching in neat BPMU appears at 1648 cm^{-1}. This shift to lower energy has also been observed in other complexes containing ligands with the carbonyl group [17] and is indicative of coordination through the carbonyl oxygen.

Due to the poor elemental analysis and to the Eu(II) ion paramagnetism, which hampered characterization of the complexes by NMR spectroscopy, unambiguous characterizations of the complexes were not possible. In order to confirm the identity of **1** and **2** and establish the coordination geometry at the metal single crystal X-ray studies of the compounds were undertaken.

3.2. Crystal structures of *1* and *2*

In both compounds the crystal structures consist of discrete molecular units. In the structure of **1** there are two crystallographically independent molecules in the asymmetric unit in which both molecules have imposed C_2 symmetry with the europium atoms lying on a two-fold rotation axis. The europium atoms are eight-coordinate, by six nitrogen atoms of the two tridentate ligands and two oxygen atoms of the DPSO/BPMU groups. The coordination geometries are best described as distorted square antiprismatic (SAP), as shown in Figs. 1 and 2.

Each tridentate ligand occupies two triangular faces of the SAP polyhedra while the oxygen atoms are in adjacent sites along a lateral edge. Polytopal analysis [18] of these structures reveals a substantial distortion of the SAP geometry towards dodecahedral (DD), as shown in Table 2, where the values of the shape parameters, δ and ϕ, are listed for both compounds along with the values for the idealized polyhedra.

The 'square' faces of the polyhedra are quite bent (**1**, 9.6° for molecule 1 and 8.4° for molecule 2; **2**, 5.8 and 25.6°), which together with the average ϕ values (**1**, 22.6° for molecules 1 and 2; **2**, 26.3°) takes the coordination polyhedra along the geometric pathway towards DD. In the structure of **2** the δ values of 5.8 and 25.6° show that one 'square' face is quite bent when compared with the other. As can be seen in Table 2 the coordination polyhedra for the two independent molecules of **1** are very similar. Also, the structures of **1** and **2** are similar in terms of both the disposition of the ligands and the coordination geometry. However, a more irregular polyhedron is observed in **2** to allow the same set of the two tripodal ligands to accomodate the more sterically demanding BPMU group relatively to DPSO. The SAP geometry observed for these complexes is in contrast to that observed in the related eight-coordinate $Eu(Bpz_4)_2{\cdot}2THF$ complex in which a bicapped trigonal prismatic (BCTP) geometry was found [5].

Tables 3 and 4 show selected bond lengths and bond angles for **1** and **2**. Within three standard deviations the two independent molecules of **1** have similar molecular dimensions.

The molecular structure of one of the molecules of **1** is shown in Fig. 3 along with the numbering scheme for the atoms around the Eu(1) atom. Fig. 4 shows the molecular structure of **2**.

Table 2
Normalized shape parameters (°) for Eu[HB(pz)$_3$]$_2$·2DPSO (**1**) and Eu[HB(pz)$_3$]$_2$·2BPMU (**2**) [a]

	Atoms	1		2		SAP	BCTP	DOD
		Molecule 1 [b]	Molecule 2 [b]	Atoms				
δ_S [c]	[4(25)7]	9.6	8.4	N(1)[O(1)N(3)]N(5)	5.8	0.0	0.0	29.5
δ_S	[3(16)8]	9.6	8.4	N(2)[O(2)N(4)]N(6)	25.6	0.0	21.8	29.5
δ_1 [d]	[3(26)7]	47.1	48.2	N(l)[O(1)O(2)]N(6)	50.7	52.5	48.2	29.5
δ_1	[4(15)8]	46.0	53.0	N(2)[N(3)N(4)]N(5)	46.7	52.5	48.2	29.5
ϕ [e]	2–7–8–1	17.9	20.7	N(3) N(5) N(6) O(2)	11.0	24.5	14.1	0.0
ϕ	5–4–3–6	17.9	20.7	O(1) N(l) N(2) N(4)	25.5	24.5	14.1	0.0
ϕ	2–4–1–8	28.5	24.1	O(1) N(5) N(4) N(2)	31.8	24.5	14.1	0.0
ϕ	5–7–6–3	25.9	24.8	N(3) N(1) O(2) N(6)	36.9	24.5	14.1	0.0

[a] All data refer to normalized polyhedra.
[b] The numbering of atoms is as shown in Fig. 1.
[c] δ_S = dihedral angles referred to the diagonals of the square faces of the polyhedron.
[d] δ_1 = dihedral angles referred to the lateral edges of the polyhedron.
[e] ϕ = values for the planarity of the two orthogonal trapezoids.

The average Eu–N bond distances (2.69 for **1** and 2.72 Å for **2**) compare with the value of 2.70 Å observed for Eu(Bpz$_4$)$_2$·2THF [5].

The average Eu–O bond distances (2.58(1) for **1** and 2.604(4) for **2**) are comparable with the values of 2.649(5) observed for Eu(Bpz$_4$)$_2$·2THF [5] and with the value of 2.64(2) Å in the eight-coordinate complex $Cp^*_2Sm(THF)_2$ [19]. The O–Eu–O bond angle in **1** is 84.8(5) and 80.6(5)° (av. 82.7(5)°) which is smaller than the value of 88.1(1)° found in **2**, reflecting the more sterically demanding nature of the BPMU ligand imposed by the nonplanarity of their rings.

3.3. Luminescence studies

Luminescence spectra were studied for complexes synthesized in this work as well as for the previously reported complex Eu(Tp^{Me,Me})$_2$ [4]. The results obtained were compared with the spectra already studied for Eu(Bpz$_4$)$_2$·2THF and Eu(HBpz$_3$)$_2$·2THF [5], in order to evaluate their spectral characteristics and relative emission efficiencies.

Eu(HBpz$_3$)$_2$·2DPSO is not luminescent at r.t., however a weak emission is observed at 77 K. It is a broad band with a maximum at 610 nm, very similar to the one observed for Eu(HBpz$_3$)$_2$·2THF. Eu(HBpz$_3$)$_2$·2BPMU is also not luminescent at r.t., but at 77 K is strongly luminescent presenting a broad band with maximum at 632 nm. Eu(Tp^{Me,Me})$_2$ is a very strong emitter, either at r.t. or at 77 K. It shows a broad band with maximum emission at 587 nm at 298 K, which shifts to 600 nm at 77 K maintaining its line shape. This wavelength shift with temperature was also observed in Eu(HBpz$_3$)$_2$·2THF [5] which is also a very strong emitter, presenting at r.t. a broad band with maximum at 586 nm. This maximum shifts to 607 nm at 77 K. In the same study, Eu(Bpz$_4$)$_2$·2THF was found to be a weaker emitter, showing a relatively narrow band with maximum at 460 nm [5].

Excitation spectra were also recorded. The spectrum of Eu(HBpz$_3$)$_2$·2DPSO is very similar to the spectrum obtained for the complex with coordinated THF, showing a large band between 320 and 400 nm with a shoulder at 330 nm. The spectrum of Eu(HBpz$_3$)$_2$·2BPMU shows a broad peak from 310 to 560 nm, with shoulders at 380 and 520 nm. For Eu(Tp^{Me,Me})$_2$ this peak appears between 390–490 nm, with a shoulder at 320 nm. Previous work [5] showed that the excitation band for the complexes Eu(HBpz$_3$)$_2$·2THF is very broad, extending from 285 to ca. 500 nm.

Table 3
Selected bond lengths (Å) and angles (°) for Eu[HB(pz)$_3$]$_2$·2DPSO (**1**)

Molecule 1		Molecule 2	
Eu(1)–N(1)	2.703(12)	Eu(2)–N(4)	2.672(12)
Eu(1)–N(2)	2.703(12)	Eu(2)–N(5)	2.712(12)
Eu(1)–N(3)	2.658(12)	Eu(2)–N(6)	2.689(11)
Eu(1)–O(1)	2.612(9)	Eu(2)–O(2)	2.551(9)
O(1)–S(1)	1.501(9)	O(2)–S(2)	1.508(9)
O(1)–Eu(1)–O(1) [a]	84.8(5)	O(2)–Eu(2)–O(2) [b]	80.6(5)
O(1)–Eu(1)–N(3)	77.1(3)	O(2)–Eu(2)–N(4) [b]	113.9(3)
O(1) [a]–Eu(1)–N(3)	73.8(4)	N(4)–Eu(2)–N(4) [b]	78.4(5)
N(3)–Eu(1)–N(2) [a]	122.7(4)	N(6)–Eu(2)–O(2)	79.8(3)
N(2)–Eu(1)–N(3)	72.1(4)	N(6)–Eu(2)–O(2) [b]	75.0(3)
O(1)–Eu(1)–N(2)	73.2(3)	N(4)–Eu(2)–N(6)	70.4(4)
N(1)–Eu(1)–N(3)	70.3(4)	N(4)–Eu(2)–N(5)	70.1(4)
N(1)–Eu(1)–N(2) [a]	81.1(4)	N(4)–Eu(2)–N(5) [b]	77.4(4)
N(1)–Eu(1)–N(2)	69.1(4)	N(6)–Eu(2)–N(5) [b]	122.6(4)
O(1)–Eu(1)–N(1) [a]	112.6(4)	N(5)–Eu(2)–N(6)	70.5(4)
N(1)–Eu(1)–N(I) [a]	83.3(5)	O(2)–Eu(2)–N(5)	76.6(3)
Eu(1)–O(1)–S(1)	124.9(5)	Eu(2)–O(2)–S(2)	126.6(5)
O(1)–S(1)–C(lA)	107.0(7)	O(2)–S(2)–C(2A)	105.2(7)
O(1)–S(1)–C(lB)	104.4(8)	O(2)–S(2)–C(2B)	106.2(7)

[a] Atoms related by the symmetry operation: $-x$, y, $-z+0.5$.
[b] Atoms related by the symmetry operation: $-x+1$, y, $-z+0.5$.

Table 4
Selected bond lengths (Å) and angles (°) for $Eu[HB(pz)_3]_2 \cdot 2BPMU$ (**2**)

Eu–N(1)	2.696(5)	Eu–N(4)	2.679(6)
Eu–N(2)	2.791(5)	Eu–N(5)	2.702(5)
Eu–N(3)	2.741(5)	Eu–N(6)	2.703(5)
Eu–O(1)	2.611(4)	Eu–O(2)	2.596(4)
O(1)–C(1)	1.230(7)	O(2)–C(2)	1.233(7)
N(1)–Eu–N(2)	73.5(2)	O(1)–Eu–O(2)	88.08(14)
N(1)–Eu–N(3)	68.9(2)	O(1)–Eu–N(1)	73.48(14)
N(2)–Eu–N(3)	66.8(2)	O(1)–Eu–N(3)	120.7(2)
N(4)–Eu–N(5)	68.7(2)	O(1)–Eu–N(5)	81.8(2)
N(4)–Eu–N(6)	71.3(2)	O(1)–Eu–N(6)	74.1(2)
N(5)–Eu–N(6)	70.4(2)	O(2)–Eu–N(1)	93.3(2)
N(1)–Eu–N(5)	115.4(2)	O(2)–Eu–N(2)	70.7(2)
N(2)–Eu–N(4)	79.2(2)	O(2)–Eu–N(4)	100.8(2)
N(2)–Eu–N(6)	128.6(2)	O(2)–Eu–N(6)	74.5(2)
N(3)–Eu–N(4)	77.7(2)	Eu–O(1)–C(1)	163.8(5)
N(3)–Eu–N(5)	75.2(2)	Eu–O(2)–C(2))	157.3(5)
O(1)–C(1)–N(7)	121.6(6)	O(2)–C(2)–N(9)	120.6(7)
O(1)–C(1)–N(8)	122.1(6)	O(2)–C(2)–N(10)	117.2(6)

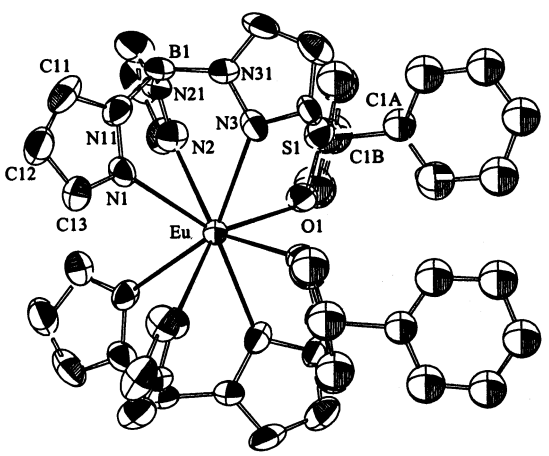


Fig. 3. ORTEP diagram of molecule 1 of $Eu(HBpz_3)_2 \cdot 2DPSO$ (**1**), using 30% probability ellipsoids.

The results obtained indicate the antenna effect of the coordinated polypyrazolyl ligands. Whereas the solvent free europium complex with the 3,5-dimethylpolypyrazolyl ligand, $Eu(Tp^{Me,Me})_2$, and the complex with the less bulky pyrazolyl borate ligand, $Eu(HBpz_3)_2 \cdot THF$, show strong luminescence, the complex with the tetrapolypyrazolyl ligand $Eu(Bpz_4)_2 \cdot 2THF$, as reported before is a very weak emitter [5]. This complex has one of the pyrazolyl rings of the ligand not coordinated to the metal, and the weak luminescence was explained by the vibrations or even rotations (in the solid state) which can provide very efficient internal conversion channels.

When, in $Eu(HBpz_3)_2 \cdot 2THF$, the tetrahydrofuran molecules are replaced by diphenylphosphine oxide or bispentamethyleneurea no luminescence is observed at r.t.

An explanation for this phenomenon is possibly the fact that donor ligands, more strongly bound than THF, present less isolation between the excited ion and ligand moieties, making energy transfer to the latter easier. At r.t. quenching of the emitting level is facilitated via thermal excitation back to a lower energy state of the ligand. At low temperature this effect is diminished and emission is observed for both complexes, being the complex with BMPU the stronger emitter. Recent studies on dissociation in the gas phase of several $Eu(HBpz_3)_2 \cdot 2L$ (L = neutral ligand) positive ions, made by Fourier transform ion cyclotron resonance spectrometry, showed that BMPU is weakly bonded [20]. Moreover, if the structures of both compounds are compared it can be seen that the BMPU adduct is more stereochemically congested, so non-radiative quenching due to vibration should be more difficult.

It has been observed in Eu(II) complexes that increasing the distance between absorbing groups and the Eu(II) ion causes an strengthening in emission intensity [2]. Considering the energy of the excited state of Eu(II), the neutral ligand absorption is in the vicinity of a $\pi \rightarrow \pi^*$ transition.

On the other hand, one can not discard the possibility of mixing of electronic states of Eu(II) and ligand vibrational states. This mixing can open an internal conversion channel for energy relaxation, which can account for the quantum efficiency lowering. It has been observed in Eu(III) complexes with β-diketonates that the substitution of methyl for phenyl groups in the diketonate ligands lowers both emission lifetimes and emission quantum yields [21]. These lifetimes are further lowered by introduction of substituents in the phenyl groups.

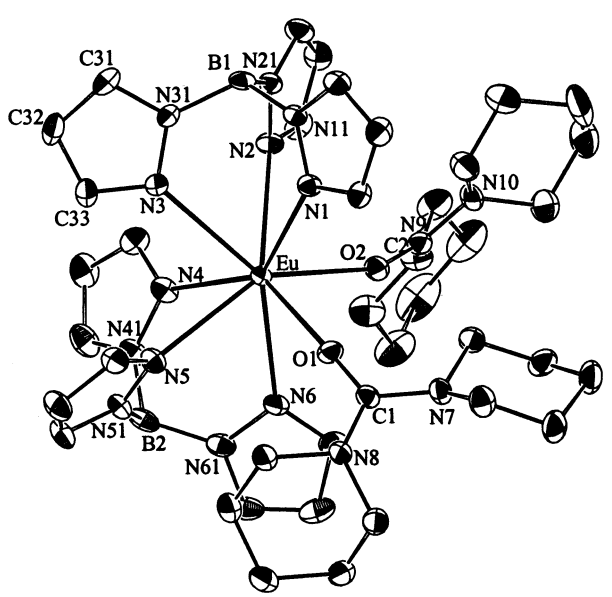


Fig. 4. ORTEP diagram of $Eu(HBpz_3)_2 \cdot 2BPMU$ (**2**), using 30% probability ellipsoids.

Concluding polypyrazolylborate ligands seemed to provide an interesting antenna effect for the luminescence of the europium complexes studied. The choice of the polypyrazolylborate ligand type and the choice of the neutral ligand, when needed to stabilise the complex should determine the emission quantum efficiencies of this type of europium compound.

4. Supplementary data

Atomic co-ordinates, bond lengths and angles and thermal parameters have been deposited with the Cambridge Crystallographic Data Centre, CCDC Nos. 140084 and 140085. Copies of this information may be obtained free of charge from The Director, CCDC, 12 Union Road, Cambridge, CB2 1EZ, UK (fax: +44-1223-336-033; e-mail: deposit@ccdc.cam.ac.uk or www: http://www.ccdc.cam.ac.uk).

Acknowledgements

The authors would like to thank gratefully Conselho Nacional de Desenvolvimento Científico e Tecnológico (Brazil) and Instituto de Cooperação Científica e Tecnológica Internacional (Portugal), whose support made this work possible.

References

[1] G.A. Molander, Chem. Rev. 92 (1992) 29.
[2] J. Jiang, N. Higashiyama, K. Machida, G. Adachi, Coord. Chem. Rev. 170 (1998) 1.
[3] F.T. Edelmann, Angew. Chem., Int. Ed. Engl. 34 (1995) 2466.
[4] (a) J. Takats, X.W. Zhang, V.W. Day, T.A. Eberspacher, Organometallics 12 (1993) 4286. (b) G.H. Maunder, A. Sella, D.A. Tocher, J. Chem. Soc., Chem. Commun. (1994) 885. (c) M.A.J. Moss, R.A. Kresinki, C.J. Jones, W.J. Evans, Polyhedron 12 (1993) 1953.
[5] A. Domingos, J. Marçalo, N. Marques, A. Pires de Matos, A. Galvão, P.C. Isolani, G. Vicentini, K. Zinner, Polyhedron 14 (1995) 3067.
[6] J. Takats, J. Alloys Compd. 249 (1997) 52.
[7] X.W. Zhang, R. McDonald, J. Takats, New J. Chem. 19 (1995) 573.
[8] S. Trofimenko, J. Am. Chem. Soc. 89 (1967) 3170.
[9] P. Girard, J.L. Namy, H. Kagan, J. Am. Chem. Soc. 102 (1980) 2693.
[10] P.C. Isolani, K. Zinner, Quim. Nova 17 (1994) 65.
[11] C.K. Fair, MOLEN, Enraf–Nonius, Delft, The Netherlands, 1990.
[12] G.M. Sheldrick, SHELXS-86, Program for Solution of Crystal Structure, University of Göttingen, Germany, 1986.
[13] G.M. Sheldrick, SHELXS-93, Program for Crystal Structure Refinement, University of Göttingen, Germany, 1993.
[14] C.K. Johnson, ORTEPII, Report ORNL-5138, Oak Ridge National Laboratory, Oak Ridge, TN, 1976.
[15] P.W.N.M. van Leeuwen, Rec. Trav. Chim. Pays-Bas 86 (1967) 201.
[16] P.W.N.M. van Leeuwen, W.L. Groenweld, Rec. Trav. Chim. Pays-Bas 86 (1967) 721.
[17] H.A. Alvarez, J.R. Matos, P.C. Isolani, G. Vicentini, E.E. Castellano, J. Zukerman-Schpector, J. Coord. Chem. 43 (1998) 349.
[18] (a) E.L. Muetterties, L.J. Guggenberger, J. Am. Chem. Soc. 96 (1974) 1748. (b) M.G.B. Drew, Coord. Chem. Rev. 24 (1977) 179.
[19] W.J. Evans, J.W. Grate, H.W. Choi, I. Bloom, W.E. Hunter, J.L. Atwood, J. Am. Chem. Soc. 107 (1985) 941.
[20] M. Freitas, N. Marques, A. Pires de Matos, A.G. Marshall, unpublished results.
[21] J.C.G. Bunzli, E. Moret, V. Foiret, K.J. Schenk, W. Mingzhao, I. Linpei, J. Alloy. Comp. 207 (1994) 107.

PERGAMON

www.elsevier.nl/locate/poly

Polyhedron 19 (2000) 1713–1717

POLYHEDRON

Ni(II)-piperidinedithiocarbamate complexes with bidentate phosphorus-donor ligands

Richard Pastorek [a], Zdeněk Trávníček [a,*], Jaromír Marek [b], Dalibor Dastych [b], Zdeněk Šindelář [a]

[a] *Department of Inorganic and Physical Chemistry, Palacký University, Křížkovského 10, 771 47 Olomouc, Czech Republic*
[b] *Department of Inorganic Chemistry, Masaryk University, Kotlářská 2, 611 37 Brno, Czech Republic*

Received 10 January 2000; accepted 7 June 2000

Abstract

Nickel(II) piperidinedithiocarbamate complexes of the composition [Ni(pipdtc)(P-P)]X and $[Ni_2(pipdtc)_2(NCS)_2(dpph)]$ (X = NCS, ClO_4, I; P-P = 1,2-bis(diphenylphosphino)ethane (dppe), 1,4-bis(diphenylphosphino)butane (dppb), 1,6-bis(diphenylphosphino)hexane (dpph), 1,4-bis(diphenylphosphino)ferrocene (dppf); pip = C_5H_{10}; dtc = S_2CN^-) have been synthesized. The compounds have been characterized by elemental analyses, IR, electron and ^1H, $^{13}C\{^1H\}$ and $^{31}P\{^1H\}$ NMR spectroscopies, thermal analysis, magneto-chemical and conductivity measurements. A single-crystal X-ray analysis of the $[Ni(pipdtc)(dppf)]ClO_4$ complex proved four-coordinated nickel in a deformed square-planar arrangement with a S_2P_2 donor set. © 2000 Elsevier Science Ltd. All rights reserved.

Keywords: Nickel(II) piperidinedithiocarbamate complexes; Synthesis; X-ray structure

1. Introduction

To date, no nickel(II) piperidinedithiocarbamate complexes with bidentate P-P donor ligands in the coordination sphere have been prepared. Only diamagnetic complexes with triphenylphosphine (PPh_3) as a monodentate phosphorus donor ligand of composition $[Ni(pipdtc)(PPh_3)_2]ClO_4$ [1] and $[NiX(pipdtc)(PPh_3)]$ (X = Cl, Br, I, NCS) [1–3] have been synthesized. In both above complexes it was found that the central nickel atom is four-coordinated in a distorted square-planar arrangement of donor atoms with a NiS_2P_2, and NiS_2PX chromophore, respectively. This fact was proved by single-crystal X-ray analysis of the $[Ni(pipdtc)(PPh_3)_2]ClO_4 \cdot PPh_3 \cdot H_2O$ complex [4] in the case of the NiS_2P_2 chromophore.

In the framework of systematic study of dithiocarbamates at our department we focused attention to preparation and study of nickel(II) piperidinedithiocarbamates with bidentate phosphorus donor ligands in the coordination sphere. The aim of the present work was to study the influence of ligands used on structure and physico-chemical properties of the synthesized complexes.

2. Experimental

2.1. Materials

Nitromethane, acetone, 1,2-bis(diphenylphosphino)-ethane (dppe), 1,4-bis(diphenylphosphino)butane (dppb), 1,6-bis(diphenylphosphino)hexane (dpph) and 1,4-bis(diphenylphosphino)ferrocene (dppf) were supplied by Fluka Co. All other reagents were obtained from Lachema Co. and were of p.a. purity.

2.2. Syntheses

Caution! Perchlorate salts of metal complexes with organic ligands are potentially explosive. Only a small amount of the material should be prepared and it should be handled with care.

* Corresponding author. Tel.: +420-68-563-4361; fax: +420-68-522-5737.
E-mail address: trav@risc.upol.cz (Z. Trávníček).

0277-5387/00/$ - see front matter © 2000 Elsevier Science Ltd. All rights reserved.
PII: S0277-5387(00)00449-6

2.2.1. Preparation of [Ni(pipdtc)(P-P)]X (P-P = dppe, dppb, dpph, dppf; X = ClO_4, NCS, I)

Fine pulverized $NiX_2 \cdot nH_2O$ (1 mmol, i.e. 0.21 g $Ni(NCS)_2 \cdot 2H_2O$, 0.37 g $Ni(ClO_4)_2 \cdot 6H_2O$, 0.42 g $NiI_2 \cdot 6H_2O$) and P-P ligand (1 mmol, i.e. 0.40 g dppe, 0.43 g dppb, 0.46 g dpph, 0.56 g dppf) was added to a suspension of fine pulverized [Ni(pipdtc)$_2$] [5] (1 mmol, 0.39 g) in 50 cm^3 of absolute EtOH. The mixture was intensively stirred under reflux for 5–6 h till the reaction components were dissolved and then filtered. The solid formed after standing for 3 days at room temperature (r.t.) in all cases (except of **1**). It was filtered off, washed with Et_2O and dried under an IR lamp at 40°C. A volume of the reaction solution of complex **1** was reduced to 1/5 and then an excess of water was added to it. The solid substance was obtained by freezing out of the above mixture to −25°C. It was separated by filtration, washed with water and dried under an IR lamp at 40°C. (Yields: 0.52 g (75%) for **1**, 0.57 g (80%) for **2**, 0.56 g (78%) for **3**, 0.61 g (82%) for **4**, 0.64 g (79%) for **5**, 0.63 g (76%) for **7**, 0.71 g (81%) for **8**, 0.70 g (78%) for **9**).

*2.2.1.1. NMR data for **1**.* ^{1}H NMR: δ aromatic region: 7.40–7.90 (m), methylene region: 3.81(t), 3.70(t), 3.48(s), 2.77(d), 2.58(s), 2.55(s), 2.52(s), 2.16(s), 1.78(m), 1.68(m), 1.52(m), 1.27(m), 0.88(t); $^{13}C\{^1H\}$ NMR: δ 199.1(s), aromatic region: 133.1(t), 132.8(t), 132.3(s), 129.6(t), 127.6(s), 127.0(s), methylene region: 48.2(s), 47.5(2 x s), 31.4(s), 26.3(t), 25.5(s), 25.3(s), 25.2(s), 23.9(s), 23.8(s); $^{31}P\{^1H\}$ NMR: δ 63.0(m).

*2.2.1.2. NMR data for **2**.* ^{1}H NMR: δ aromatic region: 7.74(s), 7.56(s), methylene region: 3.80(s), 2.66(d), 1.97(s), 1.76(s), 1.68(s); $^{13}C\{^1H\}$ NMR: δ 198.8(s), aromatic region: 132.7(t), 132.3(s), 129.6(t), 127.4(s), 126.8(s), methylene region: 48.2(s), 26.19(t), 25.5(s), 23.7(s); $^{31}P\{^1H\}$ NMR: δ 62.8(m).

*2.2.1.3. NMR data for **3**.* ^{1}H NMR: δ aromatic region: 7.74(s), 7.46(s), methylene region: 3.70(s), 3.54(s), 2.30(s), 2.06(s), 2.06(s), 1.68(s), 1.62(s); $^{13}C\{^1H\}$ NMR: δ 201.2(s), aromatic region: 133.1(d), 130.9(s), 129.1(s), 128.8(d), 128.5(s), methylene region: 47.9(unres.), 26.3(s), 26.1(s), 25.4(s), 24.9(s), 24.0(s); $^{31}P\{^1H\}$ NMR: δ 20.7(s).

*2.2.1.4. NMR data for **4**.* ^{1}H NMR: δ aromatic region: 7.2–7.9(m), methylene region: 3.73(q), 3.63(t), 3.28(s), 2.52(s), 2.13(t), 1.72(m), 1.61(m), 1.25(t); $^{13}C\{^1H\}$ NMR: δ 197.8(unres.), aromatic region: 133.0(t), 131.7(s), 129.4(s), 129.2(t), 128.8(s), methylene region: 48.1(s), 26.1(t), 25.4(s), 24.0(t), 23.8(s); $^{31}P\{^1H\}$ NMR: δ 30.0(s).

*2.2.1.5. NMR data for **5**.* ^{1}H NMR: δ aromatic region: 7.2–7.8(m), methylene region: 4.91(m), 3.68(s), 3.19(s), 2.47(unres.), 2.17(s), 1.96(s), 1.73(s), 1.64(s), 1.50(s), 1.40(s), 1.28(s), 1.05(s), 0.89(t); $^{13}C\{^1H\}$ NMR: δ aromatic region: 132.9(unres.), 132.05(s), 131.4(unres.), 131.2(s), 129.0(unres.), methylene region: 48.01(s), 48.5(s), 31.5(s), 30.0(unres.), 25.8(s), 25.4(unres.), 25.3(s), 23.8(s), 22.5(s), 14.0(s); $^{31}P\{^1H\}$ NMR: δ 25.0(s).

*2.2.1.6. NMR data for **7**.* ^{1}H NMR: δ aromatic region: 7.70(s), 7.51(s), methylene region: 5.08(s), 4.53(s), 3.64(s), 2.13(s), 1.81(s), 1.65(s), 1.28(s), 0.90(t); $^{13}C\{^1H\}$ NMR: δ aromatic region: 133.8(s), 132.4(s), 131.6(s), 131.5(s), 131.3(s), 131.2(2 × s), 128.7(s), 128.2(s), 128.1(s), methylene region: 47.9(s), 31.4(s), 25.3(s), 23.9(s), 22.4(s), 13.9(s); $^{31}P\{^1H\}$ NMR: δ 29.4(s).

*2.2.1.7. NMR data for **8**.* ^{1}H NMR: δ aromatic region: 7.79(s), 7.59(s), 7.50(s), methylene region: 4.59(s), 4.41(s), 3.63(s), 2.18(s), 1.93(s), 1.74(s), 1.61(s), 1.25(t); $^{13}C\{^1H\}$ NMR: δ 196.4(s), aromatic region: 134.0(t), 132.0(s), 129.7(s), 129.0(t), 128.7(s), methine region: 76.0(t), 74.6(t), 71.8(s), 71.0(s), methylene region: 48.2(s), 25.5(s), 23.7(s); $^{31}P\{^1H\}$ NMR: δ 32.7(s).

*2.2.1.8. NMR data for **9**.* ^{1}H NMR: δ aromatic region: 8.79(s), 7.80(s), 7.62(s), 7.53(s), 7.28(s), 7.00(s), 6.85(s), 6.64(s), methylene region: 4.91(s), 4.60(s), 4.43(s), 3.73(s), 3.52(s), 3.34(s), 3.27(s), 2.53(s), 2.19(s), 2.08(s), 1.67(s); $^{13}C\{^1H\}$ NMR: δ aromatic region: 134.4(t), 133.7(s), 133.6(s), 132.8(unres.), 132.0(s), 130.2(s), 130.0(s), 129.6(s), 129.0(t), 127.9(s), 127.8(s), methine region: 76.00(s), 74.5(s), methylene region: 48.3(s), 47.5(s), 25.5(s), 25.3(s), 25.2(s), 24.1(s), 23.8(s); $^{31}P\{^1H\}$ NMR: δ 32.6(s).

*2.2.2. Preparation of [Ni_2(pipdtc)$_2$(NCS)$_2$(dpph)]·2H_2O (**6**)*

Fine pulverized $Ni(NCS)_2 \cdot 2H_2O$ (1 mmol, 0.21 g) and dpph (1 mmol, 0.46 g) was added to a suspension of fine pulverized [Ni(pipdtc)$_2$] (1 mmol, 0.39 g) in 50 cm^3 of absolute EtOH. The solid formed during intensive stirring of the reaction mixture under reflux (6 h). The substance was dissolved in CH_2Cl_2 and then filtered. Red microcrystals formed after standing of solution for 3 days at r.t. They were filtered off, washed with Et_2O and dried under an IR lamp at 40°C. (Yield: 0.75 g (72%)).

NMR data for **6**: ^{1}H NMR: δ aromatic region: 7.53 (s), 7.42 (m), methylene region: 3.57 (s), 2.78 (s), 2.40 (s), 2.00 (s), 1.66 (s), 1.53 (s), 1.16 (t); $^{13}C\{^1H\}$ NMR: δ 198.4 (s), aromatic region: 132.7 (s), 131.0 (s), 130.5 (s), 130.4 (s), 129.6 (s), 128.8 (s), 128.4 (unres.), 128.2 (s), methylene region: 57.7 (s), 47.7 (s), 25.7 (unres.), 25.15 (s), 24.3 (s), 23.5 (s), 18.2 (s); $^{31}P\{^1H\}$ NMR: δ 25.4 (s).

2.3. Physical measurements

The content of nickel was determined by the chelatometric titration on murexid as an indicator. Chlorine and bromine were determined by the Schöniger method [6]. The elemental analyses (C, H, N, S) were performed on an EA 1108 instrument (FISONS). The r.t. magnetic susceptibilities of all complexes were measured by the Faraday method. $Co[Hg(NCS)_4]$ was used as a calibrant. Diamagnetic corrections were made with Pascal's constants [7]. Conductivities were measured with an OK 102/1 conductivity meter (Radelkis, Budapest) at 25°C. Diffuse-reflectance electronic absorption spectra (45 000–11 000 cm^{-1}) were carried out on a Specord M40 (Carl Zeiss, Jena). IR spectra (4000–400 cm^{-1}) were recorded on a Specord M80 (Carl Zeiss, Jena) using Nujol mulls. ^1H, $^{13}C\{^1H\}$ and $^{31}P\{^1H\}$ NMR spectra of the complexes were recorded in $CDCl_3$ on a Bruker AVANCE DRX 300 or 500 instruments. Chemical shifts of ^1H and ^{13}C spectra were given upfield with respect to $SiMe_4$, chemical shifts of ^{31}P spectra were given upfield with respect to 85% aqueous solution of H_3PO_4.

2.4. Crystal structure determination of **8**

Single crystals of **8** were obtained direct from reaction mixture. A crystal of size $0.80 \times 0.20 \times 0.20$ mm was used for data collection. All geometric and intensity data were collected on a κ-axis four-circle diffractometer KUMA KM-4CCD equipped with a OXFORD Cryostream cooler at temperature 150 K. A total of 23 686 reflections (of which 6 482 [$R_{int} = 0.0831$] were unique) in the range $7.28 < 2\theta < 50.00°$ were collected at 150(2) K with monochromatic Mo Kα radiation ($\lambda = 0.71073$ Å, $V = 55$ kV, $I = 30$ mA) and 0.7 mm collimator. A distance of 50 mm between the crystal and CCD detector was chosen. All rotations were performed around omega axis perpendicular to the direction of the X-ray beam. Six different orientations of diffractometer axis (ϕ, κ and θ) were chosen in sequence for covering of practically full 2–50° 2θ hemisphere. A total of 1800 frames were recorded. The exposure time was 20 s for each 0.33° rotation step. The cell parameters were retrieved from all frames using KM4 software and refined on all strong reflections. Data reduction was processed by 3D profile analysing software KM4RED, which corrects intensities for Lorentz and polarization effects too.

Crystal data and structure refinement: $C_{40}H_{38}ClFeNNiO_4P_2S_2$: monoclinic, $P2_1/n$, $a = 10.056(2)$, $b = 15.813(2)$, $c = 24.000(3)$ Å, $\beta = 101.70(2)°$, $V = 3737.1(10)Å^3$, $Z = 4$, $D_{X\text{-ray}} = 1.551$ g cm^{-3}, $\mu = 1.205$ mm^{-1}, $F(000) = 1800$, GOF = 1.018, extinction coefficient = 0.00083(13), 632 parameters, $R_1(obs.) = 0.0617$, $wR_2(obs.) = 0.1220$, $R_1(all) = 0.0761$, $wR_2(all) = 0.1341$, $\Delta F_{max} = 0.612$ e $Å^{-3}$, $\Delta F_{min} = -0.788$ e $Å^{-3}$.

The structure was solved by the direct methods using the program SHELXS-97 [8]. The structure was refined anisotropically by the full-matrix least-squares procedure on F^2 with weight: $w = 1/[\sigma^2(F_o^2) + (0.0250P)^2 + 27.0000P]$, where $P = (F_o^2 + 2F_c^2)/3$, using the SHELXL-97 program [9]. All H-atoms were found from differential Fourier maps and all their parameters were left free for refinement. The O(1), O(2) and O(3) atoms of perchlorate anion are disordered and their positions and U_{eq}-factors were refined using a combination of FVAR and EADP instructions. Additional calculations were made using PARST95 [10].

3. Results and discussion

Composition and analytical data for the complexes are listed in Table 1. The results of physico-chemical studies are summarized in Table 2. All the [Ni(p-ipdtc)(P-P)]X complexes are diamagnetic and behave as electrolytes of the 1:1 type [11]. An ionic binding of the ClO_4 and NCS anions is also supported by IR spec-

Table 1
The results of elemental analyses

Compound		Found (Calc.) (%)					
		Ni	C	H	N	S	X [a]
1	[Ni(pipdtc)(dppe)](NCS)·H_2O	8.5(8.8)	57.1(56.6)	5.2(4.9)	4.0(3.9)	13.9(13.5)	
2	[Ni(pipdtc)(dppe)]ClO_4	8.2(8.1)	53.6(53.2)	4.8(5.2)	2.0(1.7)	9.0(8.7)	5.0(4.6)
3	[Ni(pipdtc)(dppb)](NCS)·H_2O	8.1(9.0)	58.3(58.0)	5.6(5.6)	3.9(4.2)	13.3(12.7)	
4	[Ni(pipdtc)(dppb)]ClO_4	7.9(7.6)	1.9(1.8)	54.8(54.7)	5.1(4.9)	8.6(8.1)	4.8(4.2)
5	[Ni(pipdtc)(dpph)]ClO_4·$2H_2O$	7.2(7.1)	53.4(53.0)	5.7(5.5)	1.7(1.6)	7.9(8.0)	4.4(3.9)
6	[Ni_2(pipdtc)$_2$(NCS)$_2$(dpph)]·$2H_2O$	11.2(10.8)	50.6(50.1)	5.4(5.1)	5.4(5.1)	18.4(17.8)	
7	[Ni(pipdtc)(dppf)](NCS)	7.1(7.0)	59.2(58.8)	4.6(4.4)	3.4(3.4)	11.6(11.0)	
8	[Ni(pipdtc)(dppf)]ClO_4	6.7(6.7)	55.1(54.5)	4.4(4.4)	1.6(1.5)	7.4(6.5)	4.1(4.4)
9	[Ni(pipdtc)(dppf)]I	6.5(7.0)	53.4(53.6)	4.2(4.2)	1.6(1.6)	7.1(6.4)	14.1(13.5)

[a] X = Cl, I

Table 2
The results of physico-chemical studies

Compound	Color	μ_{eff}/μ_B	λ_M (S cm^2 mol^{-1})	(C–S)	IR (cm^{-1}) (C–N) [d]		UV–Vis [d] ($\times 10^3$ cm^{-1})	T [e]	TA (°C) Plateau	E [f]
1	Light brown	dia	100.3 [a]	996w	1528w	ν(C≡N) ν(C–S)	2052m, 745w	20.9, 32.5, 41.0	60 100–180	95
2	Orange–red	dia	141.1 [a]	996m	1534m	$\nu_3(ClO_4^-)$, $\nu_4(ClO_4^-)$	1084s, 622m	21.6, 32.6	no study	
3	Violet	dia	66.1 [c]	995w	1510w	ν(C≡N), ν(C–S)	2044m, 750w	21.0, 32.2	60 100–160	90
4	Dark red	dia	u [g]	994m	1534m	$\nu_3(ClO_4^-)$, $\nu_4(ClO_4^-)$	1086s, 622m	21.0, 32.4	no study	
5	Orange	dia	u [g]	985m	1515w	$\nu_3(ClO_4^-)$, $\nu_4(ClO_4^-)$	1080m, 615m	20.0	no study	
6	Red	dia	u [g]	995w	1536w	ν(C≡N), ν(C–S)	2092s, 842w	20.8, 30.8, 41.1	60	80
7	Red	dia	103.7 [a]	998w	1534m	ν(C≡N), ν(C–S)	2055vs, 740s	20.6, 31.8	190	
8	Red	dia	127.2[a]	992m	1528s	$\nu_3(ClO_4^-)$, $\nu_4(ClO_4^-)$	1082vs, 620s	18.8, 31.6	no study	
9	Red	dia	77.8 [b]	988s	1522s			20.8, 31.4	180	

[a] Measured in acetone solution, $[Ni^{2+}] = 10^{-3}$ mol.dm^{-3}.
[b] Measured in nitromethane solution, $[Ni^{2+}] = 10^{-3}$ mol.dm^{-3}.
[c] Measured in dimethylformamide solution, $[Ni^{2+}] = 5.10^{-4}$ mol.dm^{-3}.
[d] Measured using the Nujol technique.
[e] The beginning of thermal decomposition.
[f] The peak of *endo*-effect.
[g] u, insoluble.

troscopy. Strong maxima at 1085 cm^{-1} [$\nu_3(ClO_4)$], 620 cm^{-1} [$\nu_4(ClO_4)$] were found in the IR spectra of the [Ni(pipdtc)(P-P)]ClO_4 complexes (**2**, **4**, **5**, **8**) which can characterize an ionic nature of the perchlorate anion [12]. Maximum at 2050 cm^{-1} may be connected with the ν(C≡N) vibration of the ionic binding NCS group [13].

The binuclear complex $[Ni_2(pipdtc)_2(NCS)_2(dpph)]\cdot 2H_2O$ (**6**) is also diamagnetic. Maxima observed in the IR spectrum of this complex at 2092 and 842 cm^{-1} can be attributable to the ν(C≡N) and ν(C–S) vibrations. The presence of these maxima indicates that the NCS group is coordinated to nickel through the N atom [13].

An assumption of square-planar geometry around the central atom in both types of the above complexes (**1**–**9**) may be also supported by electronic absorption spectra. Medium strong maxima found in the 18 800–21 600 cm^{-1} region in the electronic spectra of all complexes can be attributed to the $^1A_{1g} \rightarrow {}^1B_{1g}$ electron transition [14]. The maxima above 30 000 cm^{-1} are assignable to intraligand transitions in the S_2CN group [15,16]. In the IR spectra of all the complexes characteristic maxima at 1536–1510 cm^{-1} [ν(C–N)] and 998–988 cm^{-1} [ν(C–S)] were observed for dithiocarbamate ligands [13,15].

The thermal decompositions of the hydrated complexes (**1**, **3**, **6**) begin at 60°C. The dehydratation is accompanied by *endo*-effects on DTA-curves (see Table 2). Further thermal decompositions of **1**, **3** and **6** proceed without formation of thermally stable intermediates. Thermal decays of **7** and **9** begin at 190 and 180°C, respectively. The next process of decomposition also proceeds without formation of thermally stable intermediates. The decomposition of the complexes containing the perchlorate anion (**5**) were not performed owing to their possible explosivity.

The structure of [Ni(pipdtc)(dppf)]ClO_4 (**8**) was determined by a single-crystal X-ray analysis. Selected bond lengths and angles are listed in Table 3. The complex [Ni(pipdtc)(dppf)]$^+$ cation is shown in Fig. 1. As excepted, X-ray structure analysis proved that the nickel(II) atom is four-coordinated by two sulfur atoms from pipdtc and by two phosphorus atoms from dppf in distorted square-planar arrangement. The NiS_2P_2 chromophore is nearly planar even if the group of atoms deviates significantly from planarity [$\Sigma((d/s)^2 = 2758.04$, $\chi^2 = 5.99$ at 95% probability level for 3 degrees of freedom]. A degree of the distortion is also apparent from displacements of the Ni(1), S(1), S(2), P(1) and P(2) atoms from a least-squares plane fitted through the above atoms [10]. The deviations are as follows: Ni(1) −0.0153(5), S(1) 0.030(12), S(2) 0.0345(12), P(1) 0.0352(12) and P(2) 0.096(2) Å. An increase of π-electron density over the S_2CN^- moiety was also proved. This delocalization of electron density is obvious from shortening of the C–S [1.733(5) and 1.727(4) Å] and

Table 3
Selected bond lengths (Å) and angles (°) for [Ni(pipdtc)(dppf)]ClO_4 (**8**)

Ni(1)–S(2)	2.2161(13)	S(2)–Ni(1)–P(2)	91.78(5)
Ni(1)–P(2)	2.2164(13)	S(2)–Ni(1)–S(1)	78.75(5)
Ni(1)–S(1)	2.2260(13)	P(2)–Ni(1)–S(1)	170.48(5)
Ni(1)–P(1)	2.2279(13)	S(2)–Ni(1)–P(1)	168.78(5)
Fe(1)–C(36)	2.014(5)	P(2)–Ni(1)–P(1)	99.11(5)
Fe(1)–C(37)	2.028(5)	S(1)–Ni(1)–P(1)	90.32(5)
Fe(1)–C(32)	2.036(5)	C(1)–S(1)–Ni(1)	85.62(16)
Fe(1)–C(40)	2.037(5)	C(1)–S(2)–Ni(1)	86.08(16)
Fe(1)–C(33)	2.040(5)	C(1)–N(1)–C(6)	122.0(4)
Fe(1)–C(31)	2.040(5)	C(1)–N(1)–C(2)	122.5(4)
Fe(1)–C(35)	2.042(5)	C(6)–N(1)–C(2)	113.8(4)
Fe(1)–C(34)	2.053(6)	N(1)–C(1)–S(2)	126.1(4)
Fe(1)–C(38)	2.067(6)	N(1)–C(1)–S(1)	124.8(3)
Fe(1)–C(39)	2.068(6)	S(2)–C(1)–S(1)	109.1(3)
S(1)–C(1)	1.733(5)	N(1)–C(2)–C(3)	108.5(4)
S(2)–C(1)	1.727(4)	C(2)–C(3)–C(4)	110.3(4)
N(1)–C(1)	1.307(6)	C(5)–C(4)–C(3)	112.3(4)
N(1)–C(6)	1.477(6)	C(4)–C(5)–C(6)	111.3(4)
N(1)–C(2)	1.480(6)	N(1)–C(6)–C(5)	108.5(4)
C(2)–C(3)	1.518(7)		
C(3)–C(4)	1.524(7)		
C(4)–C(5)	1.518(7)		
C(5)–C(6)	1.530(7)		

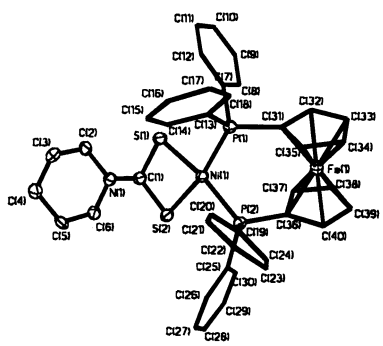


Fig. 1. Molecular structure of the $[Ni(pipdtc)(dppf)]^+$ cation. The hydrogen atoms and ClO_4^- anion are omitted for clarity.

C(1)–N(1) [1.307(6) Å] bond lengths considering the typical C–N (1.47 Å) and C–S (1.81 Å) single bonds [17]. An ionic binding of perchlorate anion is also supported by X-ray structure determination. A direct distance between Ni(1) and Cl(1) atoms is equal to 8.3363(19) Å.

The ligand coordination in [Ni(pipdtc)(P-P)]X complexes is identical to that in the [Ni(plddtc)(dppb)]I·H_2O complex (plpddtc = pyrrolidinedithiocarbamate anion) which structure was elucidated by single-crystal X-ray analysis [18]. In the case of $[Ni_2(pipdtc)_2(NCS)_2(dppf)]\cdot 2H_2O$ we assume that dppf forms a bridge between neighbouring nickel(II) ions to which is coordinated through phosphorus atoms. Unfortunately, any attempts to prepare single crystals of this complex have not been successful yet.

As expected, the $^{31}P\{^1H\}$ NMR spectra measured for selected complexes exhibit one signal at 63.0 ppm (**1**), 62.8 ppm (**2**), 20.7 (**3**), 30.0 ppm (**4**), 25.0 ppm (**5**), 25.4 ppm (**6**), 29.4 ppm (**7**), 32.7 ppm (**8**), and 32.6 ppm (**9**), respectively, corresponding to one kind of phosphorus atoms in the molecule.

4. Supplementary material

Supplementary data have been deposited with the Cambridge Crystallographic Data Centre under deposition number 137218. Copies of this information may be obtained free of charge from The Director, CCDC, 12 Union Road, Cambridge, CB2 1EZ, UK (fax: +44-1223-336-033; e-mail: deposit@ccdc.cam.ac.uk or www: http://www.ccdc.cam.ac.uk).

Acknowledgements

We are grateful to the FRVŠ (Project No. 31702007/1999) for financial support.

References

[1] K. Ramalingam, G. Aravamudan, M. Seshasayee, Inorg. Chim. Acta 128 (1987) 231.
[2] R. Pastorek, J. Kameníček, F. Březina, M. Hamrusová, Z. Šindelář, J. Lasovský, Chem. Pap. 47 (1993) 210.
[3] R. Pastorek, J. Kameníček, F. Březina, Z. Šindelář, E. Jehlářová, N.V. Duffy, T. Glowiak, Chem. Pap. 48 (1994) 317.
[4] V. Ventachalam, K. Ramalingam, R. Akilan, K. Sivakumar, K. Chinnakali, F. Hoong-Kun, Polyhedron 15 (1996) 1289.
[5] Gmelins Handbuch der Anorganischen Chemie, Nickel, Teil C, Lief. 2, Verlag Chemie, Weinheim, 1969, p. 997.
[6] M. Jureček, Organická analýza II, CSAV, Praha, 1957, p. 140.
[7] E.A. Boudreaux, L.N. Mulay, Theory and Applications of Molecular Paramagnetism, Wiley, New York, 1976, p. 491.
[8] G.M. Sheldrick, SHELXS-97, Acta Crystallogr., Sect. A 46 (1990) 467.
[9] G.M. Sheldrick, SHELXL-97, Program for crystal structure refinement, University of Göttingen, Germany, 1997.
[10] M. Nardelli, PARST95, J. Appl. Crystallogr. 28 (1995) 659.
[11] W.J. Geary, Coord. Chem. Rev. 7 (1971) 81.
[12] R.P. Scholer, A.E. Merbach, Inorg. Chim. Acta 15 (1975) 15.
[13] E. Černikova, I.A. Chartonik, D.S. Umrejko, A.B. Kavrikov, V.I. Afanov, Koord. Chim. 15 (1989) 1695.
[14] A.B.P. Lever, Inorganic Electronic Spectroscopy, Elsevier, Amsterdam, 1984, p. 534.
[15] C.A. Tsipis, D.P. Kessissoglou, G.A. Katsoulos, Chem. Chron. New Series 14 (1985) 195.
[16] C.A. Tsipis, I.J. Meleziadis, D.P. Kessissoglou, G.A. Katsoulos, Inorg. Chim. Acta 90 (1984) L19.
[17] D.R. Lide (Ed.), Handbook of Chemistry and Physics, 73rd Edn., CRC, Boca Raton, FA, 1992.
[18] R. Pastorek, Z. Trávníek, P. Ptošek, Z. Šindelář, F. Březina, J. Marek, J. Coord. Chem. 44 (1998) 247.

PERGAMON

www.elsevier.nl/locate/poly

Polyhedron 19 (2000) 1719–1726

POLYHEDRON

Mercury halide complexes of tertiary phosphines. Part XVI. Dimer–monomer trend in the 1:1 complexes of mercury(II) halides with bulky tris(2,6-dimethoxyphenyl)phosphine (DMPP)

Norman A. Bell [a,*], Simon J. Coles [b], Michael B. Hursthouse [b], Mark E. Light [b], K. Abdul Malik [c], Rafizah Mansor [a]

[a] *Division of Chemistry, Sheffield Hallam University, Pond Street, Sheffield, S1 1WB, UK*
[b] *Department of Chemistry, University of Southampton, Highfield, Southampton, SO17 1BJ, UK*
[c] *Department of Chemistry, University of Wales Cardiff, PO Box 912, Cardiff, CF1 3TB, UK*

Received 25 April 2000; accepted 23 May 2000

Abstract

Reactions of HgX_2 (X = Cl, Br, I) with the very bulky tertiary phosphine, tris(2,6-dimethoxyphenyl)phosphine (DMPP), in either a 1:1 or a 1:2 ratio, result in only the isolation of the 1:1 adducts. The structures adopted in the solid state are markedly influenced by the steric requirement of the phosphine. In contrast to the 1:1 triphenylphosphine adducts reported earlier, which are dimeric, the DMPP mercury(II) chloride and bromide complexes are weakly linked dimers while the iodide is the first example of a mercury iodide–phosphine complex with a monomeric distorted trigonal-planar arrangement around mercury. All three complexes contain secondary interactions with the *o*-methoxy groups. © 2000 Elsevier Science Ltd. All rights reserved.

Keywords: Mercury(II) halides; Phosphine complexes; Crystal structures

1. Introduction

Following Mann's seminal work in 1940 [1], mercury(II) halides are now known to form a wide range of stoichiometries with tertiary phosphine ligands. By far the most common are the 1:1 and 2:1 complexes, $(R_3P)_nHgX_2$ ($n = 1,2$; X = Cl, Br, I). The 2:1 complexes have a monomeric pseudo-tetrahedral structure with the degree of distortion depending on the σ-donor ability and steric requirement of the phosphine [2–6]. In contrast the 1:1 complexes exhibit a remarkable variety of structures in the solid state, ranging from weakly linked polymeric units with strong σ-donors such as Me_3P and Et_3P, to discrete dimeric structures for weak donors such as Ph_3P [6–13]. The nature of the halide also has an effect on the adopted structure, exemplified by the series Pr_3PHgX_2 (X = Cl, Br, I) in which the chloride and bromide are halogen-bridged dimers with increasing asymmetry in the HgX_2Hg bridge, whereas the β-iodide has a polymeric loosely linked trigonal-planar arrangement [13] (the α-iodide is unique in having both phosphines coordinated to the same mercury atom in a dimeric arrangement [11]). These variations stem from the increased donor capacity from chloride to iodide towards mercury, resulting in a weakening association from chloride to iodide.

Both tris(2,4,6-trimethoxyphenyl)phosphine (TMPP) and tris(2,6-dimethoxyphenyl)phosphine (DMPP) are sterically demanding ligands (cone angle 184° [14]) and have very high basicities ($pK_a = 11.02$ and 9.33, respectively [15]) and are therefore likely to result in the formation of complexes with low coordination numbers [14,16]. Transition-metal chemistry of TMPP has been studied extensively by Dunbar and co-workers and the phosphine has been shown to behave as a mono-, di- and tri-dentate ligand [17]. Tertiary phosphines con-

* Corresponding author. Tel.: +44-114-2253002; fax: +44-114-2253066.
E-mail address: n.a.bell@shu.ac.uk (N.A. Bell).

0277-5387/00/$ - see front matter © 2000 Elsevier Science Ltd. All rights reserved.
PII: S0277-5387(00)00451-4

taining 2,6-dimethoxyphenyl groups, including DMPP, have also been the subject of study, forming transition-metal complexes with a variety of modes of coordination of the ligand [18]. However, interest in these types of extremely bulky ligands with non-transition metals has been very limited. Bowmaker and co-workers [19] have formed only complexes of unusual stoichiometry (e.g. of empirical formula $TMPPHg_2X_4$ and $(TMPP)_2Hg_3X_6$) with TMPP and suspensions of HgX_2 in acetonitrile and our studies with this ligand and the Group 12 metal halides will be reported elsewhere. Herein we report the formation and structures of a series of 1:1 complexes of HgX_2 (X = Cl, Br, I) with DMPP.

2. Experimental

DMPP was prepared using the Aldrich as supplied reagents, 1,3-dimethoxybenzene, butyllithium and triphenylphosphite, by the previously described method [14]. Melting points were obtained using an electrothermal melting point apparatus and are uncorrected. ^{31}P-$\{^1H\}$ NMR spectra were recorded as solutions in acetone and acetonitrile using a Bruker AC250 spectrometer with 85% H_3PO_4 as external reference. Far IR spectra were recorded with background subtraction using a Magna-IR750 Nicolet spectrometer from 600–50 cm^{-1}, to a resolution of 2 cm^{-1} on samples dispersed in a paraffin wax disk. Raman spectra were obtained from a Renishaw Ramascope 1000 Raman Microscope using a 780 nm near IR laser. All spectra were recorded using a 200 exposure 'extended' scan between 3400 and 300 cm^{-1} and a 0.5 s static scan down to 50 cm^{-1}. Elemental analyses were carried out by the Sheffield University Centre for Chemical Instrumental Analytical Services.

2.1. Preparations

2.1.1. Tris(2,6-dimethoxyphenylphosphine)-dichloromercury(II) (1)

To a solution of mercury(II) chloride (0.270 g, 1.0 mmol), dissolved in warm ethanol (30 cm^3), was added DMPP (0.442 g, 1.0 mmol) also dissolved in warm ethanol (25 cm^3) with stirring. The white precipitate which formed immediately was filtered off under suction and dried in vacuo, yielding a white powder; m.p. 273–275°C (Found: C, 40.21; H, 3.80. $C_{24}H_{27}O_6PHgCl_2$ requires C, 40.37; H, 3.81%) ^{31}P-$\{^1H\}$ NMR (MeCN solution) δ −31.19 (s).

2.1.2. Tris(2,6-dimethoxyphenylphosphine)-dibromomercury(II) (2)

DMPP (0.442 g, 1.0 mmol), dissolved in warm ethanol (25 cm^3), was added to a warm ethanolic solution (30 cm^3) of mercury(II) bromide (0.360 g, 1.0 mmol). The immediate white precipitate was filtered off under suction and dried in vacuo, yielding a white powder; m.p. 265–268°C (Found: C, 35.15; H, 3.35. $C_{24}H_{27}O_6PHgBr_2$ requires C, 35.89; H, 3.36%) ^{31}P-$\{^1H\}$ NMR (MeCN solution) δ −27.88(s).

2.1.3. Tris(2,6-dimethoxyphenylphosphine)-diiodomercury(II) (3)

A warm ethanolic solution (25 cm^3) of DMPP (0.442 g, 1.0 mmol) was added to a similar solution (30 cm^3) of mercury(II) iodide. A slight cream precipitate was formed, which increased as the solution was steadily evaporated down to 30 cm^3. Filtration under suction yielded very pale cream crystals which were dried in vacuo; m.p. 194–197°C (Found: C, 32.15; H, 3.03. $C_{24}H_{27}O_6PHgI_2$ requires C, 32.13; H, 3.01%) ^{31}P-$\{^1H\}$ NMR (MeCN solution) δ −26.31(s).

2.2. X-ray crystallography

Crystals suitable for X-ray analysis were grown by slow evaporation of ethanolic solutions of the complexes, mounted on glass fibres and intensity data was collected. A summary of crystal data, data collection strategy and model refinement parameters are given in Table 1.

The structures were solved via direct methods and then subjected to full-matrix least-squares refinement on F_o^2 using the SHELXL-97 [20] suite of programs. For all structures non-hydrogen atoms were made anisotropic, with hydrogens in calculated positions (C–H = 0.96 Å, with U_{iso} tied to U_{eq} of the parent atoms). Absorption corrections were applied using the RefDelf approach of DIFABS [21] for $DMPPHgCl_2$ and the semi-empirical comparison of multiple and symmetry equivalent reflections employed in SORTAV [22] for $DMPPHgBr_2$ and $DMPPHgI_2$. Large residual electron density is observed as satellite peaks around mercury in all three structures. These are commonly attributed to the inability to correctly account for the large absorption effects of heavy metal centres.

3. Results and discussion

Reaction of mercury(II) halides in ethanol solution with DMPP, also dissolved in ethanol, in a 1:1 mole ratio resulted in the formation of solid deposits of complexes having 1:1 stoichiometry. The addition of a solution of 1 mol of the mercury(II) halides to 2 mol of the phosphine also resulted in the formation of the 1:1 complexes: clearly the bulk of the phosphine precludes the formation of the 2:1 complexes, which are readily formed with triphenylphosphine [1] ($pK_a = 2.73$ [23]) and several other tertiary phosphines [2–6].

Colourless crystals of all three complexes, suitable for X-ray analysis, were grown by slow evaporation from ethanolic solutions. In the only other complete series of 1:1 tertiary phosphine–mercury(II) halides structurally characterised, the tripropylphosphine series [13], the structures vary from a slightly asymmetrically bridged dimer for the chloride, through a much more asymmetric bromide, to a weakly linked polymeric arrangement for the iodide reflecting the stronger donor ability $I^- > Br^- > Cl^-$ to mercury. In marked contrast the structures of the DMPP complexes are overwhelmingly dominated by the steric bulk of the phosphine ligand with the Hg–P bond length increasing along the series chloride to iodide (Table 2), all being longer than in the corresponding Pr_3P [13] and Ph_3P [7,12] complexes due to the buttressing effect of the *ortho* methoxy groups. The chloride (Fig. 1) is a very weakly linked centrosymmetric dimer with a much greater degree of asymmetry in the bridging region (Hg–Cl_{br}; 2.475(3), 2.902(4) Å cf. Hg–Cl_{term}, 2.514(4) Å) than in the corresponding Ph_3P [7] (2.623(8), 2.658(8) Å) or Pr_3P [13] complexes (2.638(4), 2.780(4) Å) and with the angles P–Hg–Cl_{term} (113.11(12)°) and P–Hg–Cl_{br} (105.78(11)°) to the longer bridging bond being much smaller than the angle between phosphorus and the shorter bridging chloride (138.95(14)°). The bromide (Fig. 2) shows an even closer similarity in the Hg–Br_{term} (2.6129(6) Å) and the shorter of the two bridging distances (2.6272(6) Å) (c.f. the longer bridging Hg–Br distance of 2.9195(6) Å) and with similar angles to the chloride, indicating that this is an even weaker linked dimeric structure.

The trend is complete with the iodide which shows a completely monomeric structure (Fig. 3), with both Hg–I distances agreeing to within ca. 0.04 Å, the $PHgI_2$ unit being planar and there being no intermolecular Hg···I distances less than 4 Å. This represents the first structurally characterised tertiary phosphine–mercury(II) iodide complex which has a monomeric essentially trigonal-planar arrangement, with angles around mercury varying from 107.95(3) to 132.86(4)°. However, the two PHgI angles are quite different (119.12(4) and 132.86(4)°), which is due to some particularly strong interactions between the central mercury atom and oxygens [O(2), O(4) and O(6)] of the methoxy groups (3.089, 3.268 and 2.672 Å, respectively). These contacts are within the sum of the van der Waals radii for the interacting atoms and may be considered to be bonding, resulting in six-coordinate mercury. The geometry about Hg(1), when considering the interactions with methoxy group oxygens, is very distorted from idealised octahedral geometry (see Table 2).

The dimeric Cl and Br complexes also exhibit weak secondary interaction with the *ortho* methoxy groups at around the sum of the van der Waal's radii [24], as seen

Table 1
Crystal data, data collection strategy and model refinement parameters

	$DMPPHgCl_2$	$DMPPHgBr_2$	$DMPPHgI_2$
Empirical formula	$C_{24}H_{27}O_6PHgCl_2$	$C_{24}H_{27}O_6HgBr_2$	$C_{24}H_{27}O_6PHgI_2$
Formula weight	713.92	802.84	896.82
Temperature (K)	293(2)	150(2)	150(2)
Crystal system	triclinic	triclinic	monoclinic
Space group	$P\bar{1}$	$P\bar{1}$	$P2_1/n$
a (Å)	10.056(2)	10.1414(2)	12.607(3)
b (Å)	10.849(2)	11.0219(2)	14.050(3)
c (Å)	14.211(2)	14.4192(2)	16.354(3)
α (°)	78.783(14)	78.6299(9)	90.0
β (°)	69.49(2)	69.7350(7)	107.96(3)
γ (°)	64.680(10)	64.6536(7)	90.0
Volume (Å^3)	1310.8(4)	1364.16(4)	2755.6(10)
Z	2	2	4
D_{calc} (Mg m^{-3})	1.809	1.955	2.162
Absorption coefficient (mm^{-1})	6.173	8.644	7.920
$F(000)$	696	768	1680
Crystal size (mm)	$0.22 \times 0.16 \times 0.12$	$0.25 \times 0.2 \times 0.1$	$0.2 \times 0.2 \times 0.01$
Diffractometer	Nonius FAST	Nonius KappaCCD	Nonius KappaCCD
θ_{max} (°)	24.95	25.03	30.48
Reflections collected	5211	26 242	35 933
Independent reflections	3589	4811	7750
R_{int}	0.1147	0.0689	0.0642
Absorption correction/transmission factors	DIFABS [21]	SORTAV [22]	SORTAV [22]
	0.794/1.024	0.578/0.306	0.970/0.623
Final R indices	$R_1 = 0.0569$	$R_1 = 0.0349$	$R_1 = 0.0503$
	$wR_2 = 0.1516$	$wR_2 = 0.0861$	$wR_2 = 0.1301$
ρ max/min (e Å^{-3})	1.872/−1.799	1.259 and −1.801	3.581/−2.750

Table 2
Selected bond lengths (Å) and angles (°)

	$DMPPHgCl_2$	$DMPPHgBr_2$	$DMPPHgI_2$
Hg–P	2.436(3)	2.4490(12)	2.4656(16)
Hg–X_{term}	2.514(4)	2.6129(6)	2.7428(11)
			2.7016(7)
Hg–X_{br}	2.475(3)	2.6272(6)	
	2.902(4)	2.9195(6)	
Hg···O	3.106(6)	3.157(6)	3.0895(45)
	3.126(4)	3.140(5)	3.1678(46)
	2.805(6)	2.825(6)	2.6718(39)
P–Hg–X_{term}	113.11(12)	112.41(3)	119.12(4)
	132.86(4)		
P–Hg–X_{br}	105.78(11)	107.79(3)	
	138.95(14)	136.09(3)	
X_{ter}–Hg–X_{ter}		107.95(3)	
X_{ter}–Hg–X_{br}	109.23(14)	109.13(2)	
	102.0(2)	96.145(18)	
X_{br}–Hg–X_{br}	80.71(11)	83.855(18)	
P–Hg···O	58.74(9)	58.22(8)	59.36(11)
	58.16(10)	57.59(8)	57.02(10)
	67.82(9)	66.94(10)	69.85(10)
X_{br}–Hg···O	153.00(11)	158.15(8)	
	91.53(10)	87.87(11)	
	84.58(8)	84.20(8)	
X_{ter}–Hg···O	170.04(9)	168.48(9)	129.49(9)
	91.38(11)	89.98(9)	76.45(9)
	79.48(11)	80.05(7)	103.90(10)
			86.84(10)
			71.08(13)
			96.33(10)

in Table 2. A comparison of the phosphine moiety, with the previously determined structure [25] shows some distortions, due to the interaction of the methoxy groups with the mercury centre.

3.1. Solution ^{31}P NMR spectra

The spectra of all three complexes were recorded as solutions in acetone and acetonitrile solutions, though the solubility was low in both solvents. The spectra all contained a single line due to species which contain the non-magnetic isotope of mercury. The expected satellites due to $^1J(^{199}Hg^{31}P)$ coupling (^{199}Hg 16.84% natural abundance, nuclear spin $I = 1/2$) were not observed in acetone solution due to the weak intensity of the spectra because of the very low solubility of the complexes. The chemical shifts in acetonitrile were slightly larger (Table 3) and also the slightly greater solubility allowed observation of mercury–phosphorus coupling. The $\delta(^{31}P)$ and $^1J(^{199}Hg^{31}P)$ coupling constants are listed in Table 3, together with the results reported by Bowmaker et al. for 1:1 mixtures of HgX_2 and TMPP in MeCN solution for comparison [19]. The signals are clearly halogen-dependent with chemical shifts and coupling constants increasing from iodide to chloride, in accordance with observations elsewhere [26]. These results, together with the non-electrolytic behaviour of the complexes in MeCN solution, clearly show the presence of only one phosphorus-containing species in solution. This is in marked contrast to Bowmaker's work [19] on the very similar TMPP–HgX_2 system in which NMR studies (Table 3) of equimolar mixtures in MeCN solution showed the presence of halogen-dependent parameters assigned to $[TMPPHgX]^+$ and a non-halogen-dependent parameter due to $[(TMPP)_2Hg]^{2+}$, both associated with $[Hg_2X_6]^{2-}$ anions. For the chloride these two species were present in approximately equal amounts, decreasing to $\sim 13\%$ of the latter for the iodide.

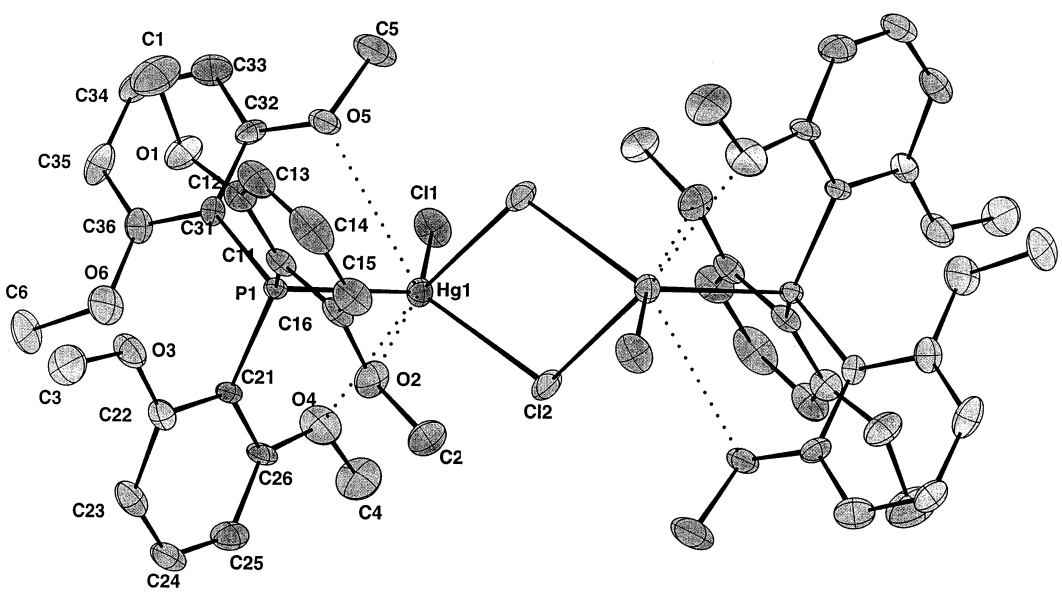


Fig. 1. The molecular structure of $DMPPHgCl_2$ with ellipsoids at 30% probability.

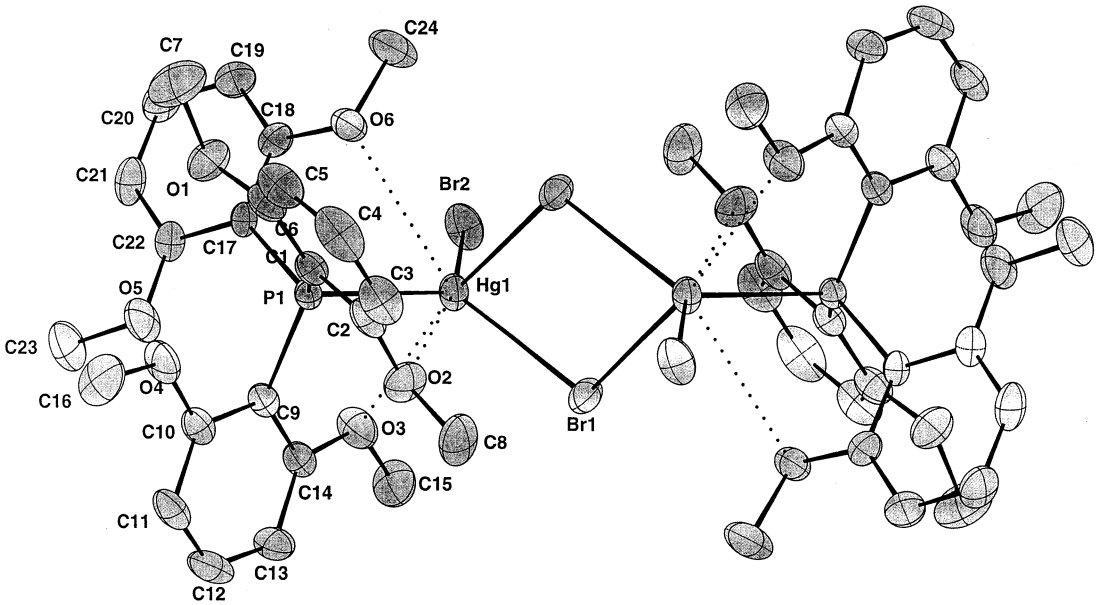


Fig. 2. The molecular structure of $DMPPHgBr_2$ with ellipsoids at 30% probability.

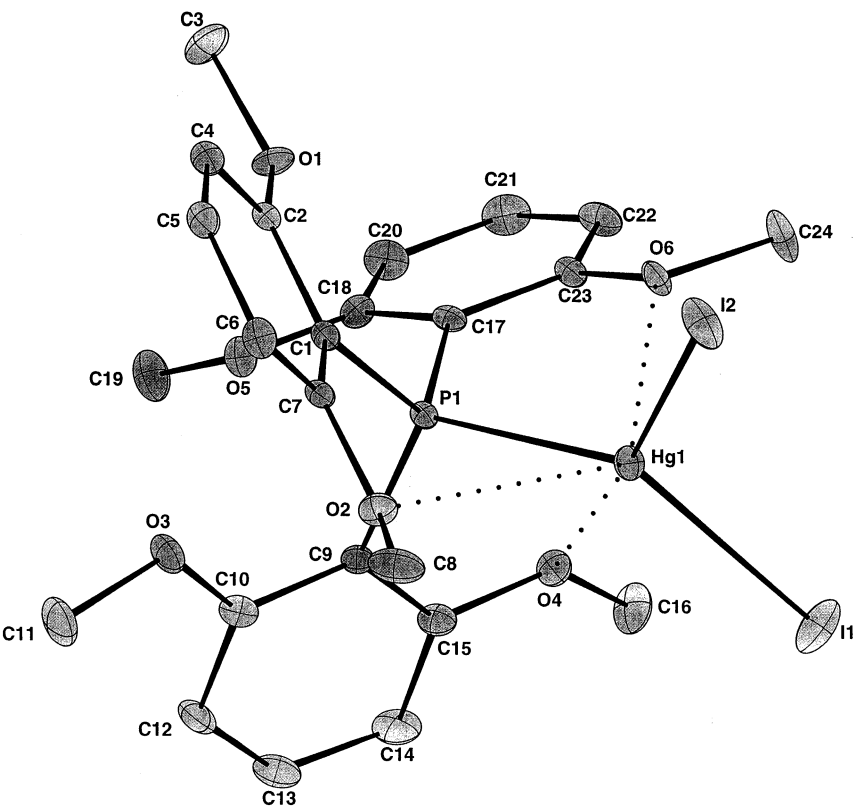


Fig. 3. The molecular structure of $DMPPHgI_2$ with ellipsoids at 30% probability.

3.2. Vibrational spectra

The assignment of vibrational spectral features of a range of R_3PHgX_2 complexes has previously been correlated with their full crystal and molecular structures [26]. The structural variety found for these complexes gives rise to differences in vibration spectra. For example terminal and bridging Hg–Cl stretching frequencies [26] in symmetrical (or near symmetrical) halogen bridged dimers are usually separated by $\sim 120\ cm^{-1}$. The absorptions below $600\ cm^{-1}$ found in the IR and Raman spectra of $DMPPHgX_2$ are listed in Table 4 and

Table 3
^{31}P NMR parameters for $DMPPHgX_2$ in MeCN solution with data in acetone solution in parentheses [a]

	$DMPPHgX_2$		$[TMPPHgX]^+$		$[(TMPP)_2Hg][Hg_2X_6]$	
X	δ	$^1J(^{199}Hg^{31}P)$ (Hz)	δ	$^1J(^{199}Hg^{31}P)$ (Hz)	δ	$^1J(^{199}Hg^{31}P)$ (Hz)
Cl	−31.19 (−30.17)	9022	−30.21	9190	−30.70	5217
Br	−27.87 (−26.61)	8030	−26.62	8405	−30.84	5219
I	−26.31 (−25.29)	7066	−24.59	6839	−30.76	5275

[a] Data for $[TMPPHgX]^+$ and $[(TMPP)_2Hg]^{2+}$ shown for comparison [19].

the Raman spectra are shown in Fig. 4. There are several bands common to all three spectra which must be due to skeletal vibrations of the phosphine ligand, but the halogen-dependent bands can readily be identified. In the spectra of the chloride the closeness of the two νHg–Cl vibrations at 250(vs) and its shoulder at 230 cm^{-1} (Raman) may be ascribed to the weak nature of chloride bridging in the complex.

For the bromide a similar picture emerges with peaks which are clearly associated with νHg–Br vibrations occurring at 161(vs) cm^{-1} and a strong shoulder at 142 cm^{-1}, again illustrating the weak association of the dimer as confirmed by the crystallographic data. The monomeric nature of the iodide results in two much sharper, very strong absorption bands at 148 and 118 cm^{-1}, which may be ascribed to the νHg–I symmetric and asymmetric stretching vibrations, respectively. Terminal Hg–I vibrations have been assigned [27] at ~ 150/135 cm^{-1} in $[Hg_2I_6]^{2-}$ and 160/154 cm^{-1} in $[HgI_3]^-$.

Table 4
IR and Raman spectral data for $DMPPHgX_2$ (cm^{-1}) [a]

X	Cl		Br		I	
	Raman	IR	Raman	IR	Raman	IR
	531w	525m	528w	525m	529w	524m
	519vw		520vw			
	509mw		509mw		509w	
	431mw	448vs	428mw	447vs	423mw	451m
	372m		370mw		372mw	
	338vw					
	250vs*	265s*	251w		249w	
	230msh*	245s*				
		217w				
		206w				
			161vs*	161m*		
					148vs*	146m
			142msh*	147m*		
	154m					
			119m		118vs*	124m
	109vs		106ms		111s	
	94s		91ms		92m	

[a] *Mercury–halogen vibrations.

4. Conclusions

The bulky nature of DMPP precludes the formation of the well known 2:1 tertiary phosphine–mercury(II) halide complexes and only 1:1 complexes have been isolated. This is in marked contrast to the structurally similar TMPP system where only ionic complexes of somewhat unusual stoichiometry ($L_2Hg_2X_8$ and $L_2Hg_3X_6$) have been isolated [19]. X-ray structures of $DMPPHgX_2$ (X = Cl, Br, I) display a trend from weakly linked dimers for the chloride and bromide, while the iodide is unique in being the first example of a monomeric tertiary phosphine–mercury(II) iodide complex, having a distorted trigonal-planar arrangement around mercury. ^{31}P NMR and conductance studies show the presence of only one non-ionic species in solution and vibrational spectral data are consistent with the structural results.

5. Supplementary material

Full details of atomic coordinates, bond lengths and angles and thermal parameters have been deposited as supplementary material; CCDC reference numbers, CCDC 133199–133201. Supplementary data are available on request from The Director, CCDC, 12 Union Road, Cambridge, CB2 1EZ, UK (fax: +44-1223-336033; e-mail: deposit@ccdc.cam.ac.uk or www: http://www.ccdc.cam.ac.uk).

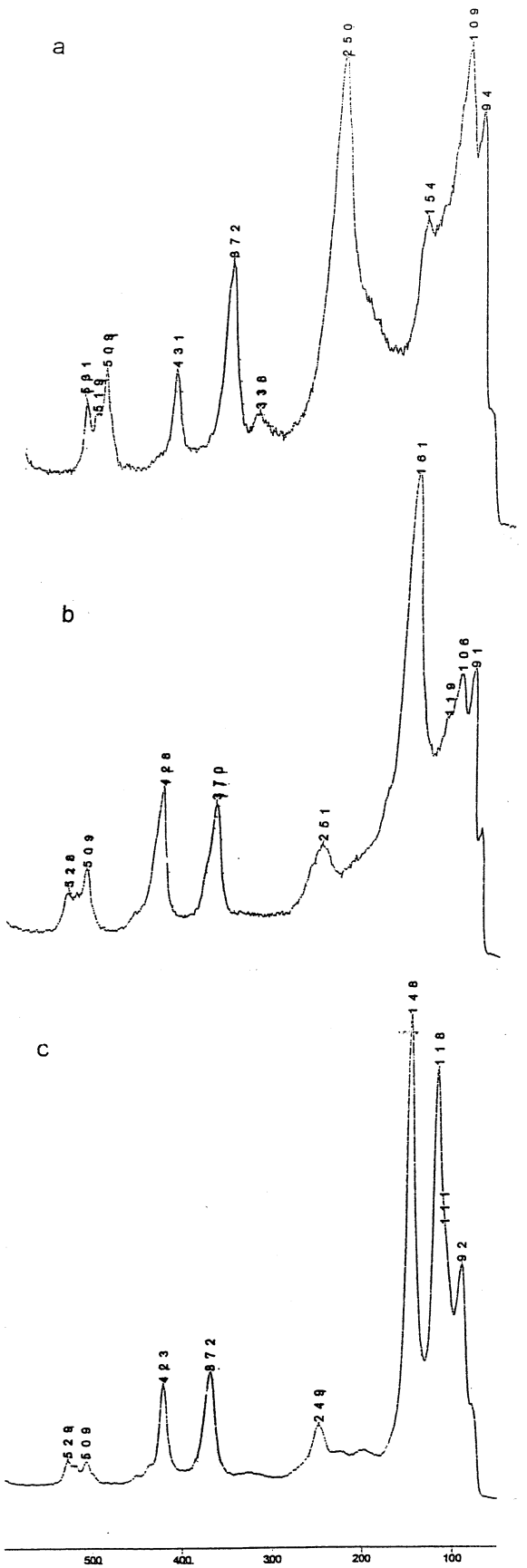


Fig. 4. Raman spectra (600–50 cm^{-1}) of **1** (a), **2** (b) and **3** (c).

References

[1] R.C. Evans, F.G. Mann, H.S. Peiser, D. Purdie, J. Chem. Soc. (1940) 1209.

[2] N.A. Bell, T.D. Dee, M. Goldstein, P.J. McKenna, I.W. Nowell, Inorg. Chim. Acta 71 (1983) 135.

[3] N.A. Bell, T.D. Dee, M. Goldstein, T. Jones, I.W. Nowell, P.L. Goggin, R.J. Goodfellow, K. Kessler, D.M. McEwan, J. Chem. Res. (S) 2 (1981) (M) 0201.

[4] D.W. Allen, N.A. Bell, S.T. Fong, L.A. March, I.W. Nowell, Inorg. Chim. Acta 99 (1985) 157.

[5] N.A. Bell, L.A. March, I.W. Nowell, Inorg. Chim. Acta 156 (1989) 195.

[6] N.A. Bell, M. Goldstein, L.A. March, I.W. Nowell, J. Chem. Soc., Dalton Trans. (1984) 1621.

[7] N.A. Bell, M. Goldstein, T. Jones, I.W. Nowell, Inorg. Chim. Acta 43 (1980) 87.

[8] N.A. Bell, M. Goldstein, T. Jones, I.W. Nowell, Inorg. Chim. Acta 48 (1981) 185.

[9] N.A. Bell, M. Goldstein, T. Jones, L.A. March, I.W. Nowell, Inorg. Chim. Acta 61 (1982) 83.

[10] N.A. Bell, T.D. Dee, M. Goldstein, I.W. Nowell, Inorg. Chim. Acta 70 (1983) 215.

[11] N.A. Bell, N.A. Chudley, L.A. March, I.W. Nowell, Inorg. Chim. Acta 141 (1988) 155.

[12] N.A. Bell, L.A. March, I.W. Nowell, Inorg. Chim. Acta 156 (1989) 201.

[13] N.A. Bell, L.A. March, I.W. Nowell, Inorg. Chim. Acta 162 (1989) 57.

[14] M.S. Wada, S. Higashizaki, A. Tsubo, J. Chem. Res. (S) 38 (1985) (M) 0467.

[15] Y. Yamashoji, T. Matsushita, M. Tanaka, T. Shono, M. Wada, Polyhedron 8 (1989) 1053.

[16] M.S. Wada, S. Higashizaki, J. Chem. Soc., Chem. Commun. (1984) 482.

[17] (a) K.R. Dunbar, S.C. Haefner, L.E. Pence, J. Am. Chem. Soc. 111 (1989) 5504. (b) K.R. Dunbar, S.C. Haefner, D.J. Burzynski, Organometallics 9 (1990) 1347. (c) S.-J. Chen, K.R. Dunbar, Inorg. Chem. 29 (1990) 588. (d) K.R. Dunbar, S.C. Haefner, A. Quillevere, Polyhedron 9 (1990) 1695. (e) K.R. Dunbar, S.C. Haefner, P.M. Swepston, J. Chem. Soc., Chem. Commun. (1991) 460. (f) S.-J. Chen, K.R. Dunbar, Inorg. Chem. 29 (1990) 2018. (g) K.R. Dunbar, A. Quillevere, S.C. Haefner, Acta Crystallogr., Sect. C 47 (1991) 2319. (h) K.R. Dunbar, L.E. Pence, Acta Crystallogr., Sect. C 47 (1991) 23. (i) S.C. Haefner, K.R. Dunbar, C. Bender, J. Am. Chem. Soc. 113 (1991) 9540. (j) S.C. Haefner, K.R. Dunbar, Organometallics 11 (1992) 1431. (k) J.I. Dulebophn, S.C. Haefner, K.R. Dunbar, K.A. Berglund, Chem. Mater. 4 (1992) 506. (l) K.R. Dunbar, Comments Inorg. Chem. 6 (1992) 313. (m) K.R. Dunbar, A. Quillevere, Polyhedron 12 (1993) 807. (n) K.R. Dunbar, J.H. Matonic, V.P. Saharan, Inorg. Chem. 33 (1994) 25. (o) K.R. Dunbar, S.C. Haefner, C.E. Uzelmeier, A. Howard, Inorg. Chim. Acta 240 (1995) 527. (p) L.-J. Baker, R.C. Bott, G.A. Bowmaker, P.C. Healey, B.W. Skelton, P.A. Schwerdtfeger, A.H. White. J. Chem. Soc., Dalton Trans. (1995) 1341, and references therein. (q) K.R. Dunbar, J.-S. Sun, J. Chem. Soc., Chem. Commun. (1994) 2387. (r) J.-S. Sun, C.E. Uzelmeier, D.L.Ward, K.R. Dunbar, Polyhedron 11/12 (1998) 2049. (s) K.R. Dunbar, J.-S. Sun, A. Quillevere, Inorg. Chem. 33 (1994) 3598.

[18] Y. Yamamoto, K. Sugawara, T. Aiko, J.-F. Ma, J. Chem. Soc., Dalton Trans. (1999) 4003.

[19] L.-J. Baker, G.A. Bowmaker, B.W. Skelton, A. H. White. J. Chem. Soc., Dalton Trans. (1993) 3235.

[20] G.M. Sheldrick, SHELXL-97. Program for the refinement of crystal structures, University of Göttingen, 1997.

[21] N.P.C. Walker, D. Stuart, Acta Crystallogr., Sect. A 39 (1983) 158; adapted for FAST geometry by A. Karaulov, University of Wales, Cardiff, 1991.
[22] (a) R.H. Blessing, Acta Crystallogr., Sect A 51 (1995) 33. (b) R.H. Blessing, J. Appl. Cryst. 30 (1997) 421.
[23] T. Allman, R.G. Goel, Can. J. Chem. 60 (1982) 716.
[24] A. Bondi, J. Phys. Chem. 68 (1964) 441.
[25] P. Livant, Y.J. Sun, T.R. Webb, Acta Crystallogr., Sect. C 47 (1991) 1003.
[26] N.A. Bell, M. Goldstein, T. Jones, I.W. Nowell, Inorg. Chim. Acta 75 (1983) 21.
[27] P.L. Goggin, P. King, D.M. McEwan, G.E. Taylor, P. Woodward, M. Sandström, J. Chem. Soc., Dalton Trans. (1972) 647.

PERGAMON

www.elsevier.nl/locate/poly

Polyhedron 19 (2000) 1727–1736

POLYHEDRON

Coordination modes of hydroxamic acids in copper(II), nickel(II) and zinc(II) mixed-ligand complexes in aqueous solution

Etelka Farkas [a,*], Éva A. Enyedy [a], Giovanni Micera [b], Eugenio Garribba [b]

[a] *Institute of Inorganic and Analytical Chemistry, University of Debrecen, H-4010 Debrecen, Hungary*
[b] *Department of Chemistry, University of Sassari, I-07100 Sassari, Italy*

Received 13 April 2000; accepted 5 June 2000

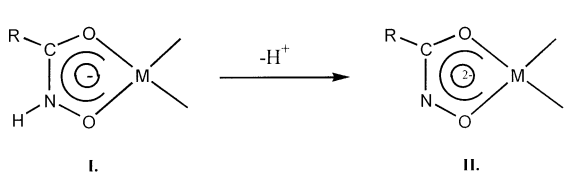
Abstract

The stability constants and coordination modes of the mixed-ligand complexes formed by Cu(II), Ni(II), Zn(II), ethylenediamine (en), 2,2′-bipyridine (bpy), glycinate (Gly), disodium salt of 4,5-dihydroxybenzene 1,3-disulfonate (Tiron), diethylenetriamine (dien) or 2,2′:6,2″-terpyridine (terpy) (= ligand B) and acetohydroxamate (Aha), *N*-methylacetohydroxamate (MeAha) or *N*-phenylacetohydroxamate (PhAha) (= ligand A) were determined in water (25°C, $I = 0.2$ M KCl) by pH-metric, spectrophotometric, EPR and calorimetric methods. Mixed-ligand complexes with typical hydroxamate type chelation mode involving the NHO^- moiety are formed in all systems. However, further copper(II) induced deprotonation of the NHO^- moiety of Aha in the presence of en or bpy results in the formation of mixed-ligand complexes with hydroximato chelates at high pH. The results show the favoured coordination of a hydroxamate to metal(II)–en and especially to a metal(II)–bpy moiety. If ligand B is Gly, the increase of stability of the mixed-ligand complexes is as expected on statistical basis, whereas the formation of complexes involving O,O-coordinated hydroxamate and O,O-coordinated Tiron is unfavoured. The tridentate coordination of dien or terpy results in five-coordinated mixed-ligand copper(II) complexes in which, most probably, the hydroxamate moiety adopts an equatorial–axial coordination mode. This quite unstable hydroxamate chelate can not hinder the hydrolysis of the complex above pH 8. Under very basic conditions acetohydroximato moieties ($-CONO^{2-}$) displace the rigid terpy ligand from the coordination sphere and complexes, $[Cu(AhaH_{-1})_2]^{2-}$ involving hydroximato chelates are formed. © 2000 Elsevier Science Ltd. All rights reserved.

Keywords: Mixed-ligand complexes; Solution equilibrium; Hydroxamic acid; Copper(II), nickel(II) and zinc(II) complexes

1. Introduction

Hydroxamate molecules, one of the major classes of naturally occurring metal complexing agents, have been thoroughly studied as ligands. Numerous papers showed that monohydroxamic acids adopt a typical binding mode. As disclosed first by an X-ray diffraction study of the benzohydroxamate complex of iron(III), the chelation involves the oxygens belonging to carbonyl and NHOH groups [1]. Complexes of simple hydroxamic acids have been studied both in solution and in solid state [2–9]. First of all Fe(III) but also some other metal ions, e.g. Co(II), Co(III), Ni(II), Zn(II), Cu(II) and V(IV) were involved in studies. The relevancy of the results to siderophore-mediated iron uptake by microorganisms was discussed in reviews [10,11].



Scheme 1.

Investigations on the complex formation with simple primary hydroxamic ligands in aqueous solution demonstrated clearly that, depending on pH, two (O,O) bonding modes of the ligands are accessible to metal ions like Cu(II) and VO(IV) [8,9]. The hydroxamato(1 −) type mode arises from the first deprotonation step and involves the coordination of the NHO^- moi-

* Corresponding author. Tel.: +36-52-512-900; fax: +36-52-489-667.
E-mail address: efarkas@delfin.klte.hu (E. Farkas).

0277-5387/00/$ - see front matter © 2000 Elsevier Science Ltd. All rights reserved.
PII: S0277-5387(00)00453-8

ety (**I**, see Scheme 1). The hydroximato(2 −) form of the ligand is produced by further metal-induced deprotonation of NHO^- (**II**).

The coordination of the nitrogen atom of hydroxamic moiety was never found in metal complexes formed by simple hydroxamic acids even if this nitrogen atom can be converted into very effective binding site in aminohydroxamates, as demonstrated by studies on aminohydroxamates both in solution and in the solid state [12].

In contrast with binary systems of hydroxamic acids or aminohydroxamic acids, their ternary systems have been studied only in a few cases [12–15]. Nevertheless, mixed ligand complexes are better models for understanding the reactivity of hydroxamic acids in biological systems (e.g. inhibition of metalloenzymes). We have performed a systematic study in solution aimed at establishing the coordination modes of hydroxamic acids and the stability of the resulting chelates in the presence of additional ligands. The ternary systems examined involve metal(II), hydroxamate (ligand A) and an additional ligand (ligand B) like ethylenediamine (en), 2,2′-bipyridine (bpy), glycinate (Gly), the disodium salt of 4,5-dihydroxybenzene 1,3-disulfonate (Tiron), diethylenetriamine (dien), or 2,2′:6,2″-terpyridine (terpy).

2. Experimental

2.1. Chemicals

Acetohydroxamic acid (Aha), en, bpy, Gly, Tiron, dien, and terpy were pure commercially available chemicals (Sigma, Reanal, Aldrich and Fluka). *N*-Methylacetohydroxamic (MeAha) and *N*-phenylacetohydroxamic (PhAha) acids were prepared by standard procedures from the corresponding carboxylic esters and hydroxylamine [16]. Freshly distilled en and dien were dissolved in known amounts of HCl solutions. The purity of the ligands and the concentration of the ligand stock solutions were determined by Gran's method [17]. The metal ion stock solutions were prepared from $CuCl_2{\cdot}2H_2O$, $NiCl_2{\cdot}5H_2O$ (Reanal). ZnO (Reanal) was dissolved in a known amount of HCl solution. The concentrations of the copper(II), nickel(II) and zinc(II) stock solutions were determined gravimetrically via the precipitation of quinolin-8-olates.

2.2. Potentiometric, spectrophotometric, calorimetric and EPR studies

All the measurements were carried out at 0.2 M ionic strength (KCl) and 25°C. Carbonate-free KOH solution of known concentration (ca. 0.2 M) was used as titrant. The binary systems were studied previously [8,18–22], however most of the constants were redetermined in the present work. The pH-metric titrations were performed over the pH range 2.0–10.5, or below precipitation, on 10.00 cm^3 samples. The ligand concentration varied in the range 2×10^{-3}–8×10^{-3} M. In the binary systems, the metal–ligand ratios were, generally, in the range 1:1–1:8, and samples at four or five different ratios were measured. The metal:ligand A:ligand B ratios were 1:1:1, 1:2:1, 1:1:2 and 1:2:2. The pH-metric titrations were made with a Radiometer pHM84 instrument equipped with a Metrohm 6.0234.100 combined electrode. The titrant was added from a Metrohm 715 Dosimat autoburette. The electrode system was calibrated by the method of Irving et al. [23] so that the pH-meter readings could be converted into hydrogen ion concentration. A pK_w value of 13.756 was determined in the present work. The pH-metric results were used to establish the stoichiometry of the species and to calculate the stability constants. Calculations were performed with the program PSEQUAD [24]. In the pH regions where the experimental findings indicated hydrolysis (a continuous decrease in the pH or the formation of a precipitate) calculations were not performed. The volume of the titrant was fitted and the accepted fittings were below 1×10^{-2} cm^3.

UV–Visible measurements were carried out on systems containing copper(II) and nickel(II). The metal ion to ligand ratios were 1:1, 1:2 and 1:5 for the binary systems and the metal:ligand A:ligand B ratios were 1:1:1 and 1:2:1 for the ternary systems. Titrations were made on samples containing the metal(II) ion at $3–5 \times 10^{-3}$ M. A HP 8453 spectrophotometer was used to record the spectra in the region of 300–800 nm.

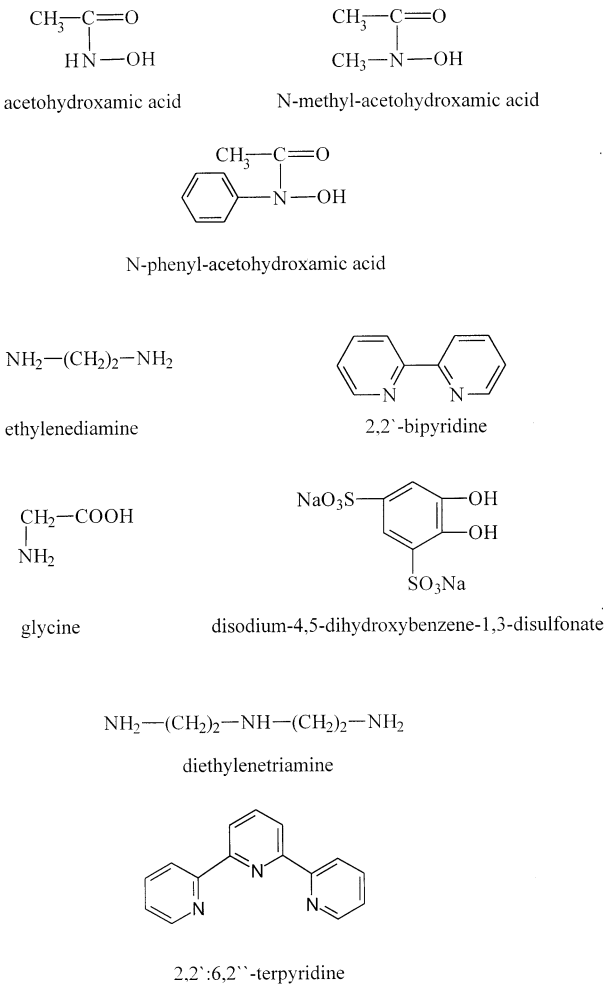
Calorimetric measurements were performed to determine the enthalpy changes of the reaction of the [CuB] complex (B = bpy, dien or terpy) with Aha and KOH using an LKB 8700 solution calorimeter. Samples of the [CuB] species (25 cm^3, $c = 3.0 \times 10^{-3}$ M, pH 10) were reacted with ampoules containing a known amount of Aha or KOH.

EPR spectra were recorded on a Varian E9 spectrometer at the X-band frequency (9.15 GHz) at 120 K. Ethylene glycol was added to aqueous samples to ensure glass formation.

3. Results and discussion

3.1. Solution equilibria

Among the hydroxamic acids (ligand A), the primary derivative Aha was studied with copper(II), nickel(II) and zinc(II), whereas the secondary ones, MeAha and PhAha were studied only with copper(II). The type of donor atom (nitrogen donors, oxygen donors or mixed,



Scheme 2.

in alyphatic or in aromatic compounds) and number of donor atoms (two or three) were varied in ligands B. The formulae of the neutral ligands are shown in Scheme 2.

3.1.1. Binary systems

The copper(II), nickel(II) and zinc(II) complexes of the hydroxamic ligands were already studied in previous works of ours and most of the systems containing copper(II) were characterised by EPR, too [8,18]. Stability constants for the metal ion–ligand B complexes were determined in former works [19–22], but those for the copper(II)–dien, copper(II)–terpy, nickel(II)–Tiron and zinc(II)–Tiron complexes were redetermined in the present work. Owing to oxidation reactions involving the ligand, the copper(II)–Tiron system could not be investigated. On the other hand, as the formation of $[Cu(terpy)]^{2+}$ occurs below the measurable pH range, overall stability constant was not obtained for this species. Instead, the equilibrium process

$$[Cu(terpy)]^{2+} + H_2O \rightleftharpoons [Cu(terpy)(OH)]^{+} + H^{+} \quad (1)$$

what takes place in a measurable pH range (ca. 7–10) was characterised. The equilibrium models and corresponding stability constants ($\log \beta$) are summarised in Table 1. EPR and electron absorption parameters for copper(II) simple complexes are shown in Table 2 (Cu(II)–Aha hydroximate species which formed beyond the capability of glass electrode potentiometry were detected only by EPR).

The main conclusions drawn for the coordination modes of hydroxamic ligands in the binary systems are as follows: exclusively hydroxamate-type (O,O) coordination (the ligand chelates the metal ion via the monoanionic form R–CO–NR′–O$^-$) exists in all the nickel(II)– and zinc(II)–hydroxamate complexes as well as in copper(II)–MeAha (R′ = Me) and –PhAha (R′ = Ph) complexes [18]. Hydroximate-type chelated complexes arising from a further deprotonation process of the hydroxamic moiety (the dianionic form R–CO–N–O^{2-} is involved) exist only in the copper(II)–Aha (R′ = H) system at high pH [8]. The hydroximate chelation is significantly more stable than the hydroxamate one and is clearly indicated by EPR spectra. The decrease of $g_{\|}$ and increase of $A_{\|}$ parameters of EPR spectra, in comparison to the hydroxamate species (see Table 2), substantiate a significant strengthening of the in plane bonds in the copper(II) coordination sphere.

3.1.2. Ternary systems

The stability constants for mixed-ligand complexes giving the best fit of the pH-metric titration curves are listed in Table 3.

Table 3 lists the logarithmic overall constants expressed by the equation

$$pM + qA + rB + sH \rightleftharpoons M_pA_qB_rH_s \quad (2)$$

except for mixed-ligand complexes containing terpy, for which data related to the equilibrium

$$MB + A \rightleftharpoons MAB \quad (3)$$

have been determined. As Table 3 shows, mixed-ligand complexes with stoichiometry [MAB] are formed in all systems. In addition, $[MABH_{-1}]$ species exist in metal(II)–Aha–bpy/en systems, and also $[MA_2B]$ and/or $[MAB_2]$ complexes exist in some nickel(II) and zinc(II) containing systems.

The relative stability of the mixed-ligand complexes, as compared with the corresponding binary species, could be evaluated in different ways. In most cases the relative stability of [MAB] is expressed in terms of $\Delta\log K_{MAB}$, the logarithmic stability constant for the equilibrium

$$MA + MB \rightleftharpoons MAB + M \quad (4)$$

The equilibrium constant for Eq. (4) can be calculated from the experimentally measured stability constants according to equation:

Table 1
Models and stability constants (log β) for the complexes formed in proton–, copper(II)–, nickel(II)– and zinc(II)–ligand A and B binary systems * ($T = 25$°C; $I = 0.2$ M KCl)

Log β	M_p	L_q	H_r	Aha [a]	MeAha [a]	PhAha [a]	en	bpy	Gly	Tiron	dien	terpy
H^+	0	1	1	9.27	8.70	8.44	10.12(1)	4.43(1)	9.60(1)	11.93(1)	9.91(6)	4.54(3)
	0	1	2				17.37(2)		11.92(1)	19.34(1)	19.04(6)	8.11(2)
	0	1	3								23.50(1)	
Cu(II)	1	1	1								18.42(4)	
	1	1	0	7.89	7.40	7.31	10.57 [b]	9.06 [d]	8.07 [b]		16.10(2)	
	1	2	1								29.50(4)	
	1	2	0	13.80	13.3	12.90	19.68 [b]	14.96 [d]	14.84 [b]		20.98(2)	
	1	3	0					18.21 [d]				
	1	1	−1								6.86(1)	8.60(1) [f]
	1	1	−2					−9.10 [d]				
	1	2	−1	4.4				5.38 [d]				
	2	2	−2					7.27 [d]				
	2	4	−1					23.46 [d]				
Ni(II)	1	1	0	5.37	4.73	4.68	7.36 [c]	7.07 [e]	5.65 [c]	9.21(1)		
	1	2	0	9.50	8.27	8.28	13.52 [c]	13.93 [e]	10.40 [c]	15.87(3)		
	1	3	0	13.32		10.16	17.78 [c]	20.13 [e]	13.78 [c]	18.8(1)		
	1	1	−1							−0.1(2)		
	1	2	−1	−0.87	−3.2	−2.42						
Zn(II)	1	1	0	5.32	4.51	4.34	5.75 [c]	5.04 [e]	4.84 [c]	9.65(1)		
	1	2	0	9.64	8.35	8.12	10.79 [c]	9.39 [e]	9.02 [c]	17.70(1)		
	1	3	0	12.8				12.96 [e]		20.3(4)		
	1	2	−1	−0.32		−1.9						

[a] Ref. [18].
[b] Ref. [19].
[c] Ref. [20].
[d] Ref. [21].
[e] Ref. [22].
[f] Log K value relates to the process: $[Cu(terpy)] + H_2O \rightleftharpoons [Cu(terpy)OH] + H^+$.
* Standard deviations are shown in parentheses for the complexes determined in the present work.

Table 2
EPR and absorption parameters for the complexes formed in the copper(II)–ligand A and B binary systems

Ligand	Species	$g_\parallel$	$A_\parallel$ ($\times 10^{-4}$ cm^{-1})	Coordination mode [a]	λ_{max} (nm)	ε (M^{-1} cm)
Aha	$[MA]^+$	2.336	168	ha (O,O)		
	$[MA_2]$	2.282	181	2 × ha (O,O)	653	30
	$[MA_2H_{-1}]^-$	2.258	192	ha (O,O, hi (O,O)		
	$[MA_2H_{-2}]^{2-}$	2.219	206	2 × hi (O,O)		
	$[MAH_{-1}(OH)_2]^{2-}$	2.230	204	hi (O,O), 2 (OH^-)		
MeAha	$[MA]^+$	2.327	169	ha (O,O)		
	$[MA_2]$	2.267	185	2 × ha (O,O)	647	36
PhAha	$[MA_2]$			2 × ha (O,O)	651	42
en	$[MB_2]^{2+}$			2 × 2 (N)	548	75
bpy	$[MB]^{2+}$	2.307	170	2 (N)	700	32
	$[MB_2]^{2+}$	2.263	162	2 × 2 (N)	731	91
	$[MBH_{-1}]$	2.253	177	2 (N); (OH^-)	640	42
	$[MBH_{-2}]$	2.233	197	2 (N); 2 (OH^-)	619	49
Gly	$[MB_2]$			2 × (N,O)	615	38
dien	$[MB]^{2+}$	2.230	191	3 (N)	615	70
	$[MBOH]^+$	2.240	171	3 (N), (OH^-)	608	65
terpy	$[MB]^{2+}$	2.262	178	3 (N)	685	90
	$[MBOH]^+$	2.262	156	3 (N), (OH^-)	674	72

[a] ha, hydroxamato; hi, hydroximato.

Table 3
Models and stability constants ($\log \beta$) for the mixed-ligand complexes formed in metal ion–ligand A–ligand B systems [a]

Ligand B	Ligand A	Cu(II)		Ni(II)				Zn(II)			
		[MAB]	[MABH$_{-1}$]	[MAB]	[MA$_2$B]	[MAB$_2$]	[MABH$_{-1}$]	[MAB]	[MA$_2$B]	[MAB$_2$]	[MABH$_{-1}$]
en	Aha	17.65(1)	7.49(2)	12.62(1)	15.89(9)	17.85(4)	1.8(2)	11.15(1)	14.07(9)	14.4(1)	1.77(6)
	MeAha	17.07(2)									
	PhAha	17.38(2)									
bpy	Aha	16.90(2)	7.31(2)	12.78(4)	17.31(3)			10.65(4)	14.3(1)	14.93(3)	2.08(8)
	MeAha	16.67(1)									
	PhAha	16.52(1)									
Gly	Aha	14.92(1)		10.20(2)		14.18(2)		9.78(4)		13.08(5)	
	MeAha	14.36(3)									
	PhAha										
Tiron	Aha			13.36(5)				13.57(5)			
	MeAha										
	PhAha										
dien	Aha	19.70(1)									
	MeAha	19.30(1)									
	PhAha	19.85(1)									
terpy	Aha	4.21 [b]									
	MeAha	3.89 [b]									
	PhAha	3.67 [b]									

[a] Standard deviations are shown in parenthesis for the complexes determined in the present work.
[b] Log K values related to the following process: MB + A $\rightleftharpoons$ MAB.

$$\Delta\log K_{MAB} = \log \beta_{MAB} - (\log \beta_{MA} + \log \beta_{MB}) \quad (5)$$

The differences between $\Delta\log K_{MAB}$ data calculated by Eq. (5) and its statistical values are evaluated. If bidentate ligands are coordinated to the metal ion, depending on the geometry of the complex, the following statistical values can be calculated for $\Delta\log K_{MAB}$: -0.4 for complexes with nearly octahedral geometry, e.g. nickel(II) and zinc(II) complexes, and -0.9 for distorted copper(II) complexes [25]. $\Delta\log K_{MAB}$ values calculated by Eq. (5) are listed in Table 4.

The results in Table 4 substantiate that the formation of mixed-ligand complexes with N-donor bidentate ligands B is favoured ($\Delta\log K_{MAB}$ values are higher than statistical). It is true especially with the aromatic bpy. Formation of mixed-ligand complexes involving hydroxamate and an other O-donor ligand B like Tiron is unfavoured ($\Delta\log K_{MAB}$ values are significantly lower than statistical).

The relative stability of the mixed-ligand complexes with compositions [MA$_2$B] and [MAB$_2$], could be also evaluated in different ways, e.g. it is possible to calculate the stability constants expected on a statistical basis [26] through the equations:

$$\log \beta^{stat}_{MA_2B} = 2/3\log \beta_{MA_3} + 1/3\log \beta_{MB_3} + \log 3 \quad (6)$$

$$\log \beta^{stat}_{MAB_2} = 2/3\log \beta_{MB_3} + 1/3\log \beta_{MA_3} + \log 3 \quad (7)$$

The values of $\log \beta^{stat}_{MA_2B}$ (15.28 for [Ni(Aha)$_2$(en)] and 16.07 for [Ni(Aha)$_2$(bpy)]) and $\log \beta^{stat}_{MAB_2}$ (16.77 for [Ni(Aha)(en)$_2$]$^+$ and 14.10 for [Ni(Aha)(Gly)$_2$]$^-$) are calculated by use of the corresponding constants listed in Table 1. From a comparison of these data with the experimentally measured constants ($\log \beta^{meas}$) in Table 3 we conclude that the formation of [Ni(Aha)(Gly)$_2$]$^-$ is as expected on the statistical basis, but the formation of en and bpy containing mixed-ligand species is much more favoured. Similar calculations for the zinc(II) containing species lead to the same conclusion. Concentration distribution curves for zinc(II)–Aha–bpy (a) and zinc(II)–Aha–Tiron (b) are shown in Fig. 1.

Fig. 1 clearly indicates that mixed-ligand species dominate in zinc(II)–Aha–bpy above pH 7, whereas no significant mixed-ligand complex formation occurs in the zinc(II)–Aha–Tiron system. These results are in agreement with the general finding that the formation

Table 4
$\Delta\log K_{MAB}$ values calculated for copper(II)–, nickel(II)– and zinc(II)–ligand A–bidentate ligand B complexes

	Cu(II)			Ni(II)	Zn(II)
Ligands	Aha	MeAha	PhAha	Aha	Aha
en	−0.81	−0.90	−0.50	−0.11	0.08
bpy	−0.05	0.21	0.15	0.34	0.29
Gly	−1.04	−1.11		−0.82	−0.38
Tiron				−1.22	−1.40

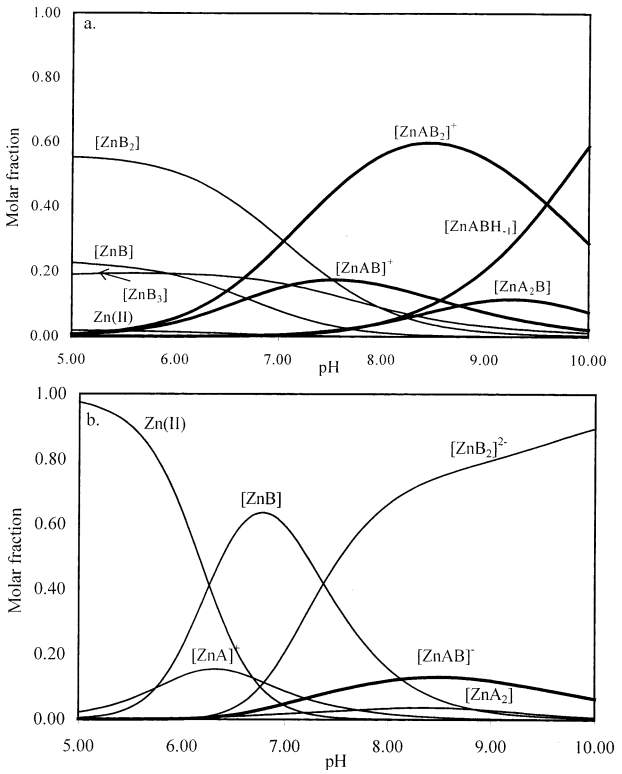


Fig. 1. Concentration distribution curves for zinc(II)–Aha–bpy (a) and zinc(II)–Aha–Tiron (b) mixed-ligand complexes ($c_{Zn(II)} = 2 \times 10^{-3}$ M, $c_{Aha} = 4 \times 10^{-3}$ M, $c_{bpy} = c_{Tiron} = 4 \times 10^{-3}$ M).

Table 5
Stepwise equilibrium constants (log K) for the mixed-ligand complexes containing copper(II)

Equilibrium process	Log K	Equilibrium process	Log K
$[Cu(en)]^{2+} + Aha$	7.08	$[Cu(dien)]^{2+} + Aha$	3.60
$[Cu(en)]^{2+} + MeAha$	6.50	$[Cu(dien)]^{2+} + MeAha$	3.20
$[Cu(en)]^{2+} + PhAha$	6.81	$[Cu(dien)]^{2+} + PhAha$	3.75
$[Cu(bpy)]^{2+} + Aha$	7.84	$[Cu(terpy)]^{2+} + Aha$	4.21
$[Cu(bpy)]^{2+} + MeAha$	7.61	$[Cu(terpy)]^{2+} + MeAha$	3.89
$[Cu(bpy)]^{2+} + PhAha$	7.46	$[Cu(terpy)]^{2+} + PhAha$	3.67
$[Cu(Gly)]^{+} + Aha$	6.85		
$[Cu(Gly)]^{+} + MeAha$	6.29		

of mixed-ligand complexes is favoured with ligands having different types of donor atom [27].

The situation is somewhat different when the coordinating ligand B is tridentate, terpy or dien. $\Delta\log K_{MAB}$ values were not calculated in these cases (equilibrium constant for Cu + terpy $[Cu(terpy)]^{2+}$ is not available which prevents the calculation of $\Delta\log K_{MAB}$ for the copper(II)–hydroxamate–terpy complexes); however, a comparison of the stepwise stability constants of the mixed-ligand species (see Table 5) shows much lower constants for the complexes involving dien or terpy than for the species containing en, bpy or Gly. There are significant differences in the calorimetric results, too. Namely, the ΔH value is -19.4 kJ mol^{-1} for the process $[Cu(bpy)]^{2+}$ + Aha and those of $[Cu(terpy)]^{2+}$ + Aha and $[Cu(dien)]^{2+}$ + Aha are $+2.8$ and -0.2 kJ mol^{-1}, respectively. The corresponding ΔS values, in turn, are 87, 90 and 68 J mol^{-1} K^{-1}.

In order to interpret the above results one must take into account that tridentate terpy and dien ligands occupy three equatorial positions of copper(II) in their [CuB] complexes. It means that only one position remains available for the coordination of a second ligand in the plane. Possible modes of coordination of a hydroxamate ligand in the mixed-ligand complexes are: (i) monodentate coordination at the fourth equatorial position; (ii) formation of a (O,O) chelate in the plane by the replacement of one of the three N atoms of dien/terpy; (iii) formation of a (O,O) chelate through equatorial–axial binding mode. Thermodynamic results do not allow us to differentiate the above three possibilities. It is known, however, that the axial coordination in copper(II) complexes results in a red shift of the electron absorption maximum λ_{max} [28]. The pH dependence of λ_{max} in the visible spectra collected on all copper(II)–terpy/dien–hydroxamate systems indicates a significant red shift in the pH region corresponding to the formation of species CuAB. This is clearly demonstrated in Fig. 2 which shows the pH–λ_{max} plot together with the species distribution curves for the copper(II)–Aha–dien. The value of λ_{max} increases from 615 (at pH ca. 7) to 685 nm (at pH 8.8), but starts to decrease above pH 9. Consequently, the red shift which parallels the formation of $[Cu(Aha)(dien)]^{+}$ supports a significant axial interaction in copper(II)–terpy/dien–hydroxamate mixed-ligand complexes.

$[MABH_{-1}]$ is detected only with the Aha ligand in which hydrogen is the R_N substituent, but it is not formed in measurable concentration with MeAha and PhAha secondary derivatives. As an illustration of the different behaviour of the complexes formed by primary and secondary hydroxamates, Fig. 3 shows the electron absorption spectra obtained as a function of pH for copper(II)–Aha–en (a) and copper(II)–MeAha–en (b) systems.

In nickel(II)– and zinc(II)–Aha systems, the species $[MABH_{-1}]$ is formed just before the precipitation so that it can be considered a mixed hydroxo species, denotated better as [MAB(OH)]. Instead, the complex remains in solution and is a dominant species in copper(II)–Aha–en/bpy systems. Parallel with its formation, a significant blue shift in the λ_{max} values is observed (see Fig. 3(a)) which supports the strengthening of the equatorial bonds in the chelated species. A comparison of the above findings with the results for the corresponding binary systems supports that the coordinated hydroxamate moiety of Aha looses a proton in the $[CuAB]^{+} \rightleftharpoons [CuABH_{-1}] + H^{+}$ process resulting in the formation of very stable copper(II)–hydroximato–en/bpy complexes.

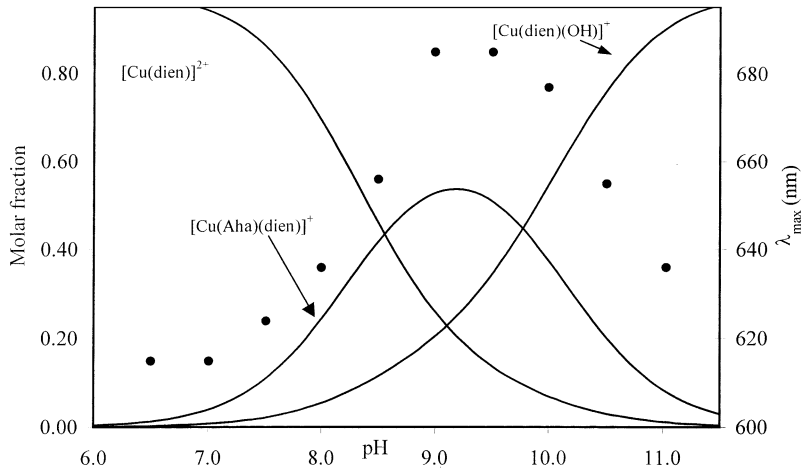


Fig. 2. Concentration distribution curves for copper(II)–Aha–dien mixed-ligand complexes are plotted together with the λ_{max} values in dependence of pH (●) ($c_{Cu(II)} = c_{terpy} = 3 \times 10^{-3}$ M, $c_{Aha} = 6 \times 10^{-3}$ M).

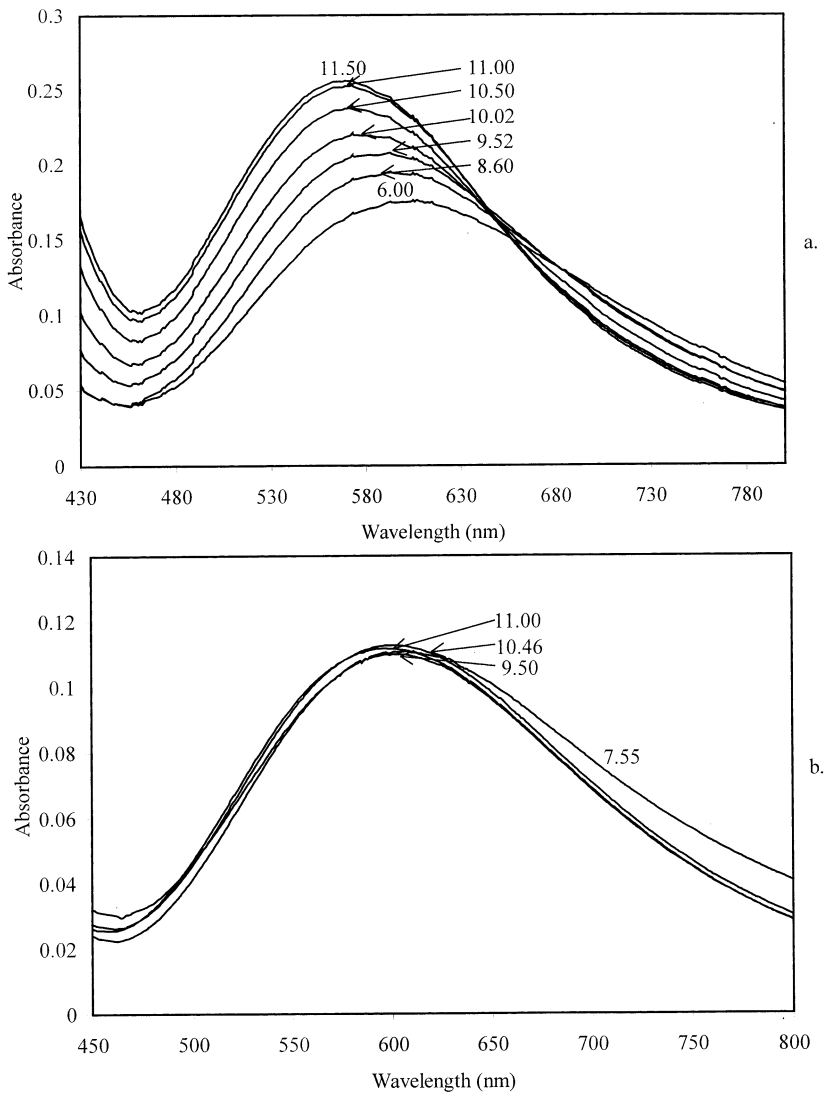


Fig. 3. UV–Vis spectra for copper(II)–Aha–en (a) and copper(II)–MeAha–en (b) at different pH values in the range 430–800 nm ($c_{Cu(II)} = 5 \times 10^{-3}$ M, $c_{Aha} = c_{en} = c_{MAha} = 5 \times 10^{-3}$ M).

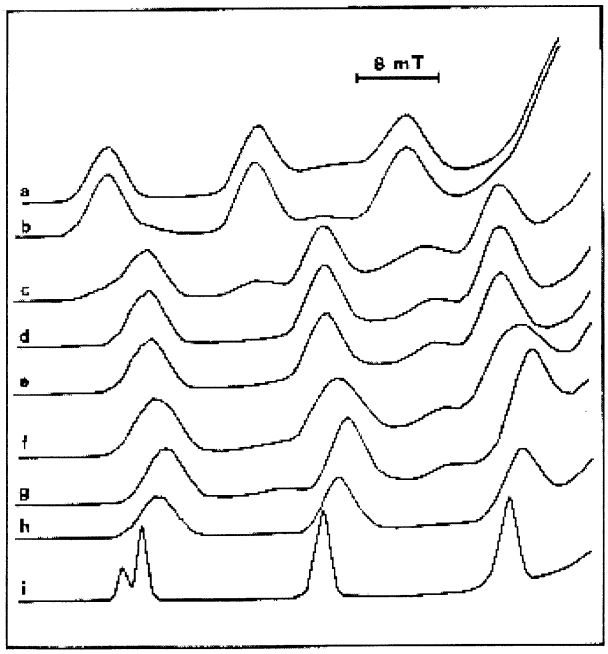


Fig. 4. Parallel region of frozen-solution EPR spectra recorded on copper(II)–Aha–bpy system at the 1:2:1 molar ratio ($c_{Cu(II)} = 5 \times 10^{-3}$ M) at different pH values: (a) 2.55, (b) 3.60, (c) 4.60, (d) 6.50, (e) 9.50, (f) 10.45, (g) 11.25 and (h) 12.48. Spectrum (i) belongs to $[Cu(OH)_4)]^{2-}$. Main species: (a,b) $[CuB]^{2+}$, (c–f) $[CuAB]^{+}$, (g) $[CuABH_{-1}]$ and (h) $[CuBH_{-2}]$.

3.2. EPR results

In order to get more complete information about the bonding modes in mixed ligand complexes formed in the copper(II)–Aha/MeAha–bpy/terpy/dien systems, EPR measurements were also performed and spectra were recorded at different pH values. Selected spectra for the Cu(II)–Aha–bpy system at the 1:2:1 molar ratio are shown in Fig. 4.

The measured $g_{\|}$ and $A_{\|}$ parameters and the proposed bonding modes in the various complexes are listed in Table 6.

The conclusions that can be drawn from the EPR results are substantially in agreement with those derived from equilibrium studies, but interesting new information has been got also in some cases. Details for the individual systems are described below.

3.2.1. Copper(II)–Aha/MeAha–bpy systems

Following the formation of the monochelated copper(II)–bpy complex, a new species starts to form at pH ca. 4.5 in copper(II)–Aha–bpy (see Fig. 4) and at pH lower than 3 in copper(II)–MeAha–bpy. This species, $[CuAB]^{+}$, predominates until pH 10.5 in the latter system and only the hydrolysis of this species can be found at higher pH. The donor atoms in the equatorial plane are the same in the $[Cu(Aha)(bpy)]^{+}$ and $[Cu(MeAha)(bpy)]^{+}$ species, as indicated by their similar spectral values. A further complex $[CuABH_{-1}]$ is formed in the copper(II)–Aha–bpy system at pH ca. 10. For this species, $g_{\|}$ is lower and $A_{\|}$ higher (see Table 5), supporting the presence of a stronger in-plane field than in the preceding complex $[CuAB]^{+}$. Therefore, the spectral changes could be assumed as the distinctive features for the second proton dissociation from the hydroxamic group of Aha and the formation of a hydroximato-type chelate in the species $[CuABH_{-1}]$. All the above findings are in complete agreement with equilibrium studies.

In both ternary systems involving MeAha and Aha EPR spectra show the signals due to a dimeric species present as a minor component in solution over the pH range 6–11. The species is distinguished, in the region of the spectrum corresponding to $\Delta M = 1$ resonances, by two peaks centred at 0.295 and 0.338 T attributable to the perpendicular features. A g factor of 2.07 is measured at the middle point between these two resonances and a value of 0.042 cm^{-1} is calculated for the 'zero-field splitting' value, D. A $\Delta M = 2$ transition, without resolved hyperfine structure, is observed in the range 0.150–0.170 T. Similar spectral features were not observed in the binary systems; therefore, it is likely

Table 6
EPR parameters for the Cu(II)–ligand A–ligand B mixed complexes [a]

Ligand A	Ligand B	Species	$g_{\|}$	$A_{\|}$ ($\times 10^{-4}$ cm^{-1})	Donor atoms
Aha	bpy	[MAB]	2.239	192	ha (O,O), 2 (N)
		$[MABH_{-1}]$	2.219	199	hi (O,O), 2 (N)
		$[M_2AB]$			
		$[M_2A_2B_2]$			
MeAha	bpy	[MAB]	2.235	193	ha (O,O), 2 (N)
Aha	dien	[MAB]	2.240	181	ha (O,O), 3 (N)
MeAha	dien	[MAB]	2.241	182	ha (O,O), 3 (N)
Aha	terpy	[MAB]	2.267	158	ha (O,O), 3 (N)
MeAha	terpy	[MAB]	2.266	160	ha (O,O), 3 (N)

[a] ha, hydroxamato; hi, hydroximato.

that the dimer is a mixed-ligand species. As judged from the signal intensity, the concentration of the dimer is quite low and this could be the reason why the species was not detected by solution equilibrium studies and their structure not fully characterised.

The most likely hypothesis is that the dimer is formed by bridging of $[Cu(bpy)]^{2+}$ and $[Cu(Aha)]^{+}$ by two OH^{-} ions. In the copper(II)–bpy binary system the hydrolysis starts at pH 6 with the formation of a dimeric complex $[Cu_2(bpy)_2(OH)_2]^{2+}$. In the presence of hydroxamate it is probable that one of the bpy molecules is replaced by a hydroxamate ligand. Since the species is observed both with Aha and MeAha, the hydroxamate form of the ligands seems involved.

An examination of molecular models shows that the interatomic distance in a $[(bpy)Cu(\mu\text{-}OH)_2Cu(Aha)]^{+}$ complex is of ca. 3 Å. If we assume that the structure is nearly planar, we can apply the Steven's equation [29] (a value of 90° for ϑ, the angle formed by Cu–Cu axis and the direction of the magnetic field is used) to correlate the D parameter to the Cu–Cu distance R in the dimer.

$$R^3 = \frac{0.325 g_{\perp}^2}{D} |1 - 3\cos^2 \vartheta|$$

By use of this equation we calculate a Cu–Cu distance of 3.2 Å.

For the sake of comparison, it must be observed that in $[Cu_2(\mu\text{-}OH)_2(bpy)_2]SO_4 \cdot 5H_2O$, the copper separation is ca. 2.9 Å in the solid state [30–32], while it changes to ca. 3.4 Å in solution [33].

3.2.2. Copper(II)–Aha/MeAha–dien/terpy systems

The dien and terpy ligands chelate the metal ion in the $[CuB]^{2+}$ species by use of three nitrogen atoms. The basicity of their nitrogens is, however, significantly different from each other (see Table 1). As a result, their mixed-ligand complexes are formed in significantly different pH ranges. Namely, the EPR parameters that can be calculated from the spectra recorded in copper(II)–Aha/MeAha–terpy at 1:3:1 molar ratio below pH 7 are consistent with the presence of the $[Cu(terpy)]^{2+}$ complex (see Table 2) and signals characteristic of complexes $[CuAB]^{+}$ are observed above pH 7. Instead, the monochelated $[Cu(hydroxamato)]^{+}$ species predominates in the pH range 4–4.5 if dien is ligand B, and is replaced by $[Cu(dien)]^{2+}$ and, to a smaller extent, by the bis chelated hydroxamato complex $[CuA_2]$ as the pH is raised. Mixed-ligand complexes $[CuAB]^{+}$ are formed above pH 8. The EPR spectra for these complexes are of the tetragonal type and substantiate a five-coordinated metal ion with approximate square pyramidal geometry. As EPR results show (Table 6), the geometry is more distorted with the more sterically rigid terpy ligand. However, to establish which groups are bound in the plane and which are in an axial position is a rather difficult task.

If the pH is increased further, the replacement of hydroxamates by OH^{-} is documented by both pH-metric and spectrophotometric results (see Fig. 2). The EPR results indicate again the significant differences existing at very high pH (above 11) between the behaviour of Aha and MeAha and also between dien and terpy. The formation of the hydroximato bis-chelated complex $[CuA_2H_{-2}]^{2-}$ takes place in the copper(II)–Aha–terpy system, as it is supported by its characteristic EPR parameters ($g_{\|} = 2.217$ and $A_{\|} = 203 \times 10^{-4}$ cm^{-1}) and the hydrolysed species of terpy $[CuBH_{-1}]^{+}$ appears only as a minor species. At pH values higher than 12, the formation of the hydrolysed species of Aha, $[CuAH_{-1}(OH)_2]^{2-}$, is observed. However, in the copper(II)–Aha–dien system the hydrolysed complex of dien is the predominant species. With MeAha $[CuBH_{-1}]$ is formed in both the copper(II)–MeAha–dien and copper(II)–MeAha–terpy systems at high pH.

Acknowledgements

E.F. is grateful for support from OTKA T023612 and EU COST D8.

References

[1] H.J. Lindner, S. Goettlicher, Acta Crystallogr., Sect. B 25 (1969) 832.
[2] D.A. Brown, D. McKeith, W.K. Glass, Inorg. Chim. Acta 35 (1979) 5.
[3] D.A. Brown, D. McKeith, W.K. Glass, Inorg. Chim. Acta 35 (1979) 57.
[4] C.P. Brink, A.L. Crumbliss, Inorg. Chem. 23 (1984) 4708.
[5] M.T. Caudle, A.L. Crumbliss, Inorg. Chem. 33 (1994) 4077.
[6] A. Evers, R.D. Hancock, A.E. Martell, R.J. Motekaitis, Inorg. Chem. 28 (1989) 2189.
[7] P.C. Parekh, S.K. Manon, Y.K. Agrawal, J. Chem. Soc., Perkin Trans. II (1989) 1117.
[8] E. Farkas, E. Kozma, M. Pethő, K.M. Herlihy, G. Micera, Polyhedron 17 (1998) 3331.
[9] A. Dessì, G. Micera, D. Sanna, L. Strinna-Erre, J. Inorg. Biochem. 48 (1992) 27.
[10] A.L. Crumbliss, in: G. Winkellmann (Ed.), CRC Handbook of Microbial Iron Chelates, CRC, Boca Raton, FL, 1991 (Chapter 7).
[11] A.-M. Albrecht-Gary, A.L. Crumbliss, in: A. Sigel, H. Sigel (Eds.), Metal Ions in Biological Systems, vol. 35, Marcel Dekker, New York, 1999 (Chapter 7).
[12] B. Kurzak, H. Kozłowski, E. Farkas, Coord. Chem. Rev. 114 (1992) 169.
[13] B. Kurzak, D. Kroczewska, J. Jerzierska, Polyhedron 17 (1998) 1831.
[14] F. Dallavalle, G. Folesani, E. Leporati, R. Borromei, J. Coord. Chem. 44 (1998) 225.
[15] E. Farkas, B. Kurzak, J. Coord. Chem. 22 (1990) 145.
[16] A.H. Blatt, Organic Syntheses, Wiley, New York, 1963.
[17] G. Gran, Acta Chem. Scand. 4 (1950) 599.
[18] E. Farkas, É.A. Enyedy, H. Csóka, J. Inorg. Biochem. 79 (2000) 205.

[19] I. Sóvágó, A. Gergely, Inorg. Chim. Acta 20 (1976) 27.
[20] I. Sóvágó, A. Gergely, Inorg. Chim. Acta 37 (1979) 233.
[21] I. Fábián, Inorg. Chem. 28 (1989) 3805.
[22] H. Irving, D. Mellor, J. Chem. Soc. (1962) 5222.
[23] H.M. Irving, M.G. Miles, L.D. Petit, Anal. Chim. Acta 38 (1967) 475.
[24] L. Zékány, I. Nagypál, in: D. Leggett (Ed.), Computational Methods for the Determination of Stability Constants, Plenum, New York, 1985.
[25] H. Sigel, Angew. Chem., Int. Ed. Engl. 14 (1975) 394.
[26] M.T. Beck, I. Nagypál, Chemistry of Complex Equilibria, Ellis Horwood, London, 1990.
[27] H. Sigel, in: A. Sigel, H. Sigel (Eds.), Metal Ions in Biological Systems, vol. 2, Marcel Dekker, New York, 1990 (Chapter 2).
[28] H. Gampp, H. Sigel, A.D. Zuberbühler, Inorg. Chem. 21 (1982) 1190.
[29] K.W.H. Stevens, Proc. R. Soc. (Lond.) A214 (1952) 237.
[30] A.T. Casey, B.F. Hoskins, F.D. Whillans, J. Chem. Soc., Chem. Commun. (1970) 904.
[31] A.T. Casey, Aust. J. Chem. 25 (1972) 2311.
[32] B.F. Hoskins, F.D. Whillans, J. Chem. Soc., Dalton Trans. (1975) 1267.
[33] E. Garribba, G. Micera, D. Sanna, L. Strinna-Erre, Inorg. Chim. Acta 299 (2000) 253.

PERGAMON

www.elsevier.nl/locate/poly

Polyhedron 17 (2000) 1737–1740

POLYHEDRON

Synthesis and structure of a complex with the coordinated triaminoguanidinium(2 +) ion, $[Cu(TAGH_2)Cl_3]Cl \cdot H_2O$

Zoya A. Savel'eva, Galina V. Romanenko*, Liliya A. Sheludyakova, Stanislav V. Larionov

Institute of Inorganic Chemistry, Siberian Branch of the Russian Academy of Sciences, Lavrentjev prospect 3, Novosibirsk 630090, Russia

Received 27 July 1999; accepted 29 May 2000

Abstract

The title compound has been isolated upon the reaction of copper(II) chloride and triaminoguanidine hydrochloride in concentrated HCl. An X-ray study has shown that the crystal structure of this complex is composed of $[Cu(TAGH_2)Cl_3]^+$ cations, Cl^- anions and water molecules. The complex cation involved the coordinated triaminoguanidinium(2 +) cation bonded to the Cu(II) ion via N atoms of the amino group and the C=N moiety as a chelate bidentate ligand. The square-planar environment of the Cu atom is formed by two Cl atoms (2.2769(9) and 2.3002(9) Å) and two N atoms (Cu–N 1.987(2) and 2.043(2) Å). The long Cu–Cl bonds (2.728(1) and 2.941(1) Å) which complement the environment to a distorted square bipyramid allow us to separate the staggered cation chains. μ_{ef} values are 1.83 and 1.86 μB at 78 and 300 K, respectively. © 2000 Elsevier Science Ltd. All rights reserved.

Keywords: Cu(II) complex; Structure; Triaminoguanidinium(2 +) ion

1. Introduction

The research on the reaction products of guanidine and its amino derivatives (aminoguanidine $NH_2NHC(NH)NH_2$ (AG), diaminoguanidine $NH_2NHC(NH)NHNH_2$ (DAG), and triaminoguanidine $NH_2NHC(NNH_2)NHNH_2$ (TAG) and copper(II) salts is of considerable interest. Information on these is useful, in particular, for the inhibiting properties of guanidines and their amino derivatives for the formation of the nitrogen oxide in the human body [1,2].

The structure and acid–base properties of AG, DAG and TAG motivate their potential participation in complexation as protonated, deprotonated and neutral forms depending on pH. All these potential compounds have been realized for AG, e.g. the prepared complex $Cu(AG)_2(NO_3)_2$ containing the AG molecules [3]. This compound was taken as a copper precursor [4]. The complex $[Co(AGH)_2Cl_4]$ involves the coordinated aminoguanidinium(1 +) cations [5]. The compounds $(AGH_2)_2[CuCl_6]$ and $(AGH_2)_2[CuBr_6]$ have been synthesized containing the isolated $[CuCl_6]^{4-}$ or $[CuBr_6]^{4-}$ anions and counterions — the aminoguanidinium(2 +) cations [6–8]. The first compound possesses reversible low-temperature thermochromism. Finally, the chelate nickel(II) compound with the deprotonated AG form has been prepared [9].

Little data on the DAG and TAG forms which participate in the coordination exist. The complexes $Cu(DAG)(NO_3)_2$, $Cu(DAG)_2(NO_3)_2$, and $Cu(DAG)_2(NO_3)_2 \cdot HNO_3$ have been prepared previously [10]. In the first two compounds, the DAG molecules are coordinated; for the latter complex it has been proposed that both the DAG molecule and the diaminoguanidinium(1 +) cation may be coordinated. This assumption has received further support: the coordinated cation mentioned has been revealed in the crystal structure of $[Cu(DAGH)Cl_3]$[11]. The reaction between the copper(II) nitrate and TAG in aqueous solution at ca. pH 1 resulted in the compound $Cu(TAG)(NO_3)_2$ containing the TAG molecule [10]. Ref. [9] reports on the preparation of unstable chelate nick-

* Corresponding author. Tel.: + 7-3832-344-466; fax: + 7-3832-344-466.

E-mail address: romanenk@che.nsk.su (G. V. Romanenko).

0277-5387/00/$ - see front matter © 2000 Elsevier Science Ltd. All rights reserved.
PII: S0277-5387(00)00460-5

el(II) compounds with the deprotonated DAG and TAG forms. Data on complex compounds containing the protonated coordinated TAG form are not available. This article reports on the synthesis and properties of the compound prepared upon the reaction of the copper(II) chloride and TAG in concentrated HCl. In the structure of this compound the form mentioned has been revealed.

2. Experimental

We used 'p' grade $CuCl_2 \cdot 2H_2O$, triaminoguanidine hydrochloride (TAG·HCl) synthesized by the reaction of AG·HCl and hydrazine hydrate similarly to the preparation procedure for $TAG \cdot HNO_3$ [12]. The Cu content was found by complexonometric titration with Trilon B solution; the C, H, N analysis was performed at the Analytical Laboratory of the Novosibirsk Institute of Organic Chemistry.

The thermal curves were obtained in air on a MOM derivatigraph (heating rate 2.5°C min^{-1}, for a 50 mg sample). IR spectra were recorded on SPECORD 75IR and BOMEN MB-102 spectrophotometers from samples as suspensions in vaseline and fluorinated oils and pellets with polyethylene, respectively. Magnetic susceptibility was measured by the Faraday method over the range 78–300 K.

2.1. Preparation of $[Cu(TAGH_2)Cl_3]Cl \cdot H_2O$

To a solution of 0.35 g (0.0025 mol) of TAG·HCl in 5 ml of water was added 10 ml of concentrated HCl and then a solution of 0.43 g (0.0025 mol) of $CuCl_2 \cdot 2H_2O$ in 10 ml of concentrated HCl. The solution were mixed, and the light-green precipitate was filtered off with suction, washed with a cool mixture of 5 ml of H_2O and 20 ml of concentrated HCl, dried and held in an desiccator over $Mg(ClO_4)_2$. Yield 0.7 g (90%). Found: C, 3.6; H, 3.6; Cu, 19.1; N 25.5. Calc. for $CH_{12}Cl_4CuN_6O$: C, 3.7; H, 3.6; Cu, 19.3; N, 25.5%. IR spectrum (ν, cm^{-1}): 3490, 3240, 3160, ~3000(br), 1660, 1645, 1600, 1570, 1500, 1420, 1230, 1180, 1150, 1120, 1100, 1070, 880, 675, 645, 570, 460, 313, 307(sh), 288, 210.

Table 1
Bond lengths (Å) and angles (°)

Cu–N(21)	1.987(2)	N(21)–Cu–N(12)	79.16(8)
Cu–N(12)	2.043(2)	N(21)–Cu–Cl(3)	171.65(7)
Cu–Cl(3)	2.2769(9)	N(12)–Cu–Cl(2)	171.50(6)
Cu–Cl(2)	2.3002(9)	Cl(1)–Cu–Cl(1) [a]	168.81(1)
Cu–Cl(1)	2.728(1)	N(21)–C(1)–N(11)	118.7(2)
Cu–Cl(1) [a]	2.941(1)	N(21)–C(1)–N(31)	123.6(2)
C(1)–N(21)	1.288(3)	N(11)–C(1)–N(31)	117.3(2)
C(1)–N(11)	1.354(3)	C(1)–N(11)–N(12)	114.7(2)
C(1)–N(31)	1.363(3)	N(11)–N(12)–Cu	110.4(1)
N(11)–N(12)	1.410(3)	C(1)–N(21)–N(22)	116.5(2)
N(21)–N(22)	1.419(3)	C(1)–N(21)–Cu	115.4(2)
N(31)–N(32)	1.407(3)	N(22)–N(21)–Cu	125.1(2)
C(1)–N(31)–N(32)	121.4(2)		

[a] Symmetry transformations used to generate equivalent atoms: $-x+3/2$, $-y+1/2$, $-z$.

2.2. Crystal structure determination

X-ray quality crystals were selected from sets of materials obtained from solutions containing smaller concentrations of initial reagents by slow crystallization. The identity of solid phases obtained by different methods was checked by X-ray phase analysis. The orthorhombic unit cell parameters are $a = 10.070(2)$, $b = 11.603(2)$, $c = 18.390(4)$ Å, $V = 2148.7(7)$ $Å^3$, space group $Pbca$, $Z = 8$, $D_{calc} = 2.037$ g cm^{-3}, $\mu = 3.001$ mm^{-1}. The set of reflections from a single crystal ($0.04 \times 0.07 \times 0.52$ mm, color light-green) was obtained on a CAD-4 automatic diffractometer (λ Mo Kα, graphite monochromator, the 1–25° θ range, 2177 collected I_{hkl}, absorption was accounted for by transmission curves) using the standard technique. The structure was solved by direct methods and refined by the full-matrix least-squares method in an anisotropic approximation for all non-hydrogen atoms and isotropically for H atoms with positions located on a difference electron density map. The final R indices are $R_1 = 0.0310$, $wR_2 = 0.0589$ for 1322 non-zero unique I_{hkl} (167 parameters) with $I > 2\sigma(I)$; GOOF = 0.422. The bond lengths and bond angles and hydrogen bond parameters are reported in Tables 1 and 2, respectively. All calculations were performed by using the SHELX-97 program package.

3. Results and discussion

The reaction of the triaminoguanidine hydrochloride and the Cu(II) chloride in dilute solutions of HCl is complicated by the intense redox reaction (gassing). The compound $[Cu(TAGH_2)Cl_3]Cl \cdot H_2O$ was isolated by using highly concentrated HCl ($C \approx 10$ mol l^{-1}). This substance is stable in dry air and decomposes in water. According to the TG curve, on heating at ca. 40°C, the mass of the complex gradually begins to decrease, perhaps, due to the elimination process of water (estimated content 5.1%). After a partial elimination (mass loss ca. 2%) at 110°C, the mass loss is observed to be sharply defined owing to the decomposition of the substance. An extreme rate of mass loss is observed at 150°C from the DTG data.

The structure is composed of $[Cu(TAGH_2)Cl_3]^+$ cations, Cl^- anions and H_2O molecules. Triaminoguanidine enters into the composition of the complex cation as the $TAGH_2^{2+}$ cation (protonated at

Table 2
Hydrogen bonds (Å and °) [a]

D–H···A	d(D–H)	d(H···A)	d(D···A)	∠(DHA)
O(1)–H(1)···Cl(1) [2]	0.71(2)	2.43(2)	3.098(2)	157(2)
O(1)–H(2)···Cl(4) [3]	1.05(3)	2.21(3)	3.223(2)	161(2)
N(11)–H(111)···Cl(4) [4]	0.84(2)	2.34(2)	3.179(2)	175(2)
N(12)–H(121)···Cl(3) [5]	1.08(5)	2.49(5)	3.385(2)	140(3)
N(12)–H(122)···Cl(2) [1]	0.85(2)	2.62(2)	3.456(2)	169(2)
N(22)–H(221)···Cl(1) [3]	1.04(3)	2.27(4)	3.003(2)	126(3)
N(22)–H(221)···Cl(2)	1.04(3)	2.42(4)	3.126(2)	124(3)
N(22)–H(222)···Cl(2) [6]	0.86(2)	2.47(2)	3.230(2)	147(2)
N(22)–H(222)···Cl(4) [3]	0.86(2)	2.79(2)	3.313(2)	120(2)
N(22)–H(223)···Cl(3) [7]	0.92(4)	2.26(4)	3.137(2)	159(3)
N(31)–H(311)···Cl(4) [3]	0.82(2)	2.35(2)	3.158(2)	172(2)
N(32)–H(321)···O(1)	0.87(3)	1.83(3)	2.644(3)	153(3)
N(32)–H(322)···Cl(4) [4]	0.97(4)	2.46(4)	3.340(2)	151(3)
N(32)–H(323)···Cl(4)	0.96(3)	2.21(3)	3.122(2)	159(3)
N(32)–H(321)···Cl(2) [2]	0.87(3)	2.83(3)	3.108(2)	100(2)
N(32)–H(321)···Cl(3) [2]	0.87(3)	2.90(3)	3.284(2)	108(2)

[a] Symmetry transformations used to generate equivalent atoms: [1] $x-1/2,\ -y+1/2\ ,-z$; [2] $x,-y+1/2,\ z-1/2$; [3] $-x+3/2,\ y+1/2,\ z$; [4] $x-1/2,\ y,\ -z-1/2$; [5] $-x+1,\ -y,\ -z$; [6] $-x+1,\ -y+1,\ -z$; [7] $x+1/2,\ -y+1/2,\ -z$.

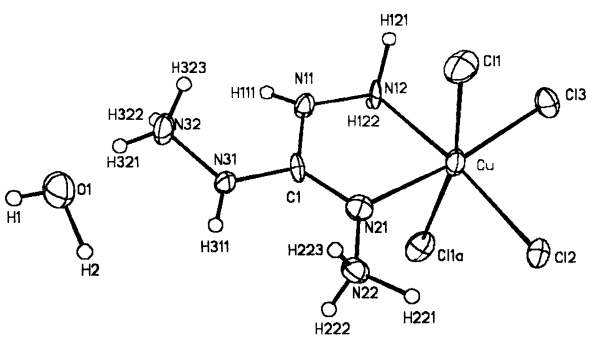


Fig. 1. Cation structure and numbering scheme in the crystal structure of $[Cu(TAGH_2)Cl_3]Cl{\cdot}H_2O$.

two amino groups). The latter is connected to the copper(II) ion by N atoms of the amino group and the C=N moiety (Fig. 1) as a chelate bidentate ligand. The protonated amino groups are distant from the Cu atom. Its square-planar environment is formed by two Cl atoms (2.2769(9) and 2.3002(9) Å) and two N atoms of the triaminoguanidinium(2 +) cation forming a five-membered chelate cycle CuN_3C (Cu–N 1.987(2) and 2.043(2) Å, N–Cu–N 79.16(8)°). The Cl atoms (2.728(1) and 2.941(1) Å) alter the square geometry to a distorted square bipyramid. Taking into account these bonds, one can separate the staggered cation chains along [100] with the outerspheric Cl^- ions and water molecules located in between (Fig. 2). All structure moieties are connected by strong hydrogen bonds (Table 2).

In the only known compound with the coordinated aminoguanidium(1 +) cation, $[Co(AGH)_2Cl_4]$, no chelate cycle is formed and the cation is bonded to the cobalt(II) ion by the N atom of the hydrazine amino group as a monodentate ligand [5]. In $[Cu(DAGH)Cl_3]$ investigated by us [11], the $DAGH^+$ cation, along with $TAGH_2^{2+}$, and the Cu(II) ion form the same five-membered chelate cycle but the molecule contains only the coordinated Cl^- ions [11]. An increase in the charge of the intraspheric cations ($TAGH_2^{2+}$ rather than $DAGH^+$) necessitates an extra anion. As is shown in the present study, it is located just in the outer sphere. Besides, in $[Cu(DAGH)Cl_3]$, the distance to the chlorine atom which formally complements CN of Cu (4 + 1) to 6 is significantly larger (3.178(2) Å), suggesting the molecules of the complex are isolated. Note that the chelate bond lengths are close in $[Cu(DAGH)Cl_3]$ and $[Cu(TAGH_2)Cl_3]Cl{\cdot}H_2O$ but in the latter the character of the multiple C=N bond in the cation CN 3 mode is more clearly defined, i.e. C=N is 1.288(3) and C–N are 1.354(3) and 1.363(3) Å while the corresponding bond lengths in $[Cu(DAGH)Cl_3]$ are 1.309, 1.337 and 1.342 Å and 1.311, 1.333 and 1.336 Å in $[Co(AGH)_2Cl_4]$, respectively.

The IR spectrum of TAG·HCl shows two peaks at 3340 and 3220 cm^{-1} over the ν(NH) range while the absorptions at 1690 and 1620 cm^{-1} are due to ν(CN) and $\delta(NH_2)$ vibrations. The protonated of TAG by one proton proceeds the N atom of C=N moiety [13]. Spectroscopic characteristics of $[Cu(TAGH_2)Cl_3]Cl{\cdot}H_2O$ are in good agreement with XRD analysis data. The appearance of a broad band at ca. 3000 cm^{-1}, typical of the $\nu(NH_3^+)$ group, confirms data on the protonation of two TAG amino groups. The novel bands (compared to TAG·HCl) at 1570 and 1500 cm^{-1} are assigned to $\delta(NH_3^+)$ [14]. The 3240 and 3160 cm^{-1} bands belong to the coordinated amino group; vibrations of the water of crystallization manifest themselves in the intense absorption band at 3490 cm^{-1}. Changes in spectrum (as compared to TAG·HCl) over the ν(CN) and $\delta(NH_2)$ range — a low-energy frequency shift — are associated with the coordination of the amino group and the N atom of the C=N moiety of the protonated amidrazone group. Over this interval (1600–1660 cm^{-1}), a picture is complicated by the superposition of the $\delta(H_2O)$ absorption bands. The 313, 307(sh), 288 cm^{-1} bands are assigned to ν(Cu–Cl) vibrations and 460 cm^{-1} to the Cu–N bond vibrations [15]. A comparison of data on the crystal structures and IR spectra for TAG·HCl and $[Cu(TAGH_2)Cl_3]Cl{\cdot}H_2O$ shows that chelation influences the protonation mode of the amidrazone –C=N–NH_2 group. If the nitrogen atom of the C=N moiety is protonated in TAG·HCl, the protonation of TAG proceeds at two amino groups in the complex because this atom is coordinated to the Cu(II) ion. The compound $[Cu(TAGH_2)Cl_3]Cl{\cdot}H_2O$ is paramagnetic, μ_{ef} values are 1.83 and 1.86 μB at 78 and 300 K, respectively, and correspond to the d^9 configura-

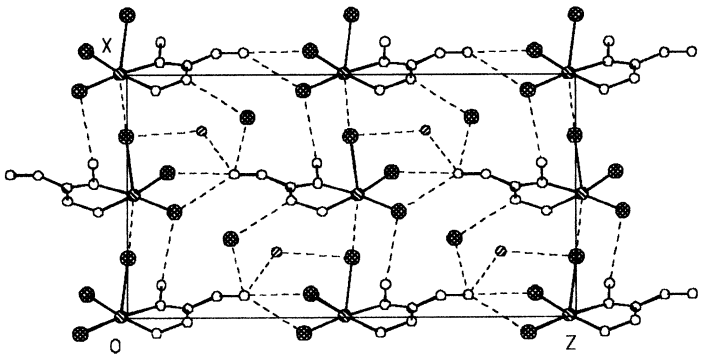


Fig. 2. Projection of crystal structure onto (010) plane.

tion. These data show the lack of exchange interaction between the unpaired electrons of the Cu(II) ions. The compound possesses low-temperature thermochromism: its color changes from light-green to blue upon cooling to liquid nitrogen temperature.

A decrease in temperature does not change the color of the blue complex $[Cu(DAGH)Cl_3]$. A difference in the properties of the complexes containing the coordinated diaminoguanidinium(1 +) and triaminoguanidinium(2 +) cations may be associated with differences in the coordination environment of the copper atom. It is likely that in the $TAGH_2^{2+}$ complex a temperature decrease causes the shortening of the longest Cu–Cl bond in the cation chains while this is not the case in the $DAGH^+$ complex because its molecules are isolated.

4. Conclusions

The compound synthesized is the first complex cation containing the coordinated triaminoguanidinium(2 +) cation. The chelate bidentate coordination of the diaminoguanidinium(1 +) and triaminoguanidinium(2 +) cations to the Cu(II) ion give grounds for the preparation of similar compounds with other metal ions.

5. Supplementary material

Crystallographic data for the structural analysis have been deposited with the Cambridge Crystallographic Data Centre, CCDC 131489. Copies of this information may be obtained free of charge from: The Director, CCDC, 12 Union Road, Cambridge, CB2 1EZ, UK (Fax: + 44-1223-336-033; e-mail: deposit@ccdc.cam.ac.uk or www: http://www.ccdc.cam.ac.uk).

Acknowledgements

The authors thank Dr V.N. Ikorskii for performing the magnetochemical study. This work was financially supported by the Russian Basic Research Foundation (grant 98-03-32470).

References

[1] V.G. Granik, S.Yu. Ryabova, N.B. Grigor'ev, Uspekhi Khim. 66 (8) (1997) 792.
[2] J.R. Williamson, J.A. Corbett, M.L. Daniel, R.G. Tilton, Patent 5358969 USA.
[3] A.V. Nikolaev, S.V. Larionov, L.G. Lavrenova, T.G. Leonova, Izvestiya SO RAN SSSR, Ser. Khim. Nauk. 1 (1977) 38.
[4] R.K. Tukhtaev, A.I. Gavrilov, S.V. Larionov, Z.A. Savel'eva, L.G. Lavrenova, V.V. Boldyrev, J. Mater. Synth. Process. 5 (5) (1997) 371.
[5] A.E. Shvelashvili, E.B. Miminishvili, V.K. Bel'skii, T.O. Vardosanidze, Zh. Neorg. Khim. 43 (2) (1999) 255.
[6] S.V. Larionov, Z.A. Savel'eva, G.V. Romanenko, N.V. Podberezskaya, L.A. Sheludyakova, E.G. Boguslavskii, S.A. Gromilov, Zh. Neorg. Khim. 37 (12) (1993) 1661.
[7] G.V. Romanenko, Z.A. Savel'eva, N.V. Podberezskaya, V.I. Alekseev, S.V. Larionov, Zh. Strukt. Khim. 35 (3) (1994) 48.
[8] Z.A. Savel'eva, G.V. Romanenko, N.V. Podberezskaya, S.V. Larionov, Polyhedron 15 (20) (1996) 3581.
[9] K.A. Jensen, B. Nygaard, Acta Chem. Scand. 3 (1949) 481.
[10] Z.A. Savel'eva, S.V. Larionov, V.N. Ikorskii, Izvestiya SO RAN SSSR, Ser. Khim. Nauk. 2 (1982) 89.
[11] Z.A. Savel'eva, S.V. Larionov, G.V. Romanenko, N.V. Podberezskaya, O.V. Shishkin, Yu.T. Struchkov, Zh. Strukt. Khim. 36 (5) (1995) 936.
[12] W. Sauermilch, Explosivstoffe 9 (1964) 197.
[13] Y. Okaya, R. Pepinsky, Acta Crystallogr., Sect. C 10 (1957) 681.
[14] L.J. Bellamy, Advances in Infrared Group Frequencies, World, Moscow, 1971, p. 444 (Russian Edition).
[15] K. Nakamoto, Infrared and Raman Spectra of Inorganic and Coordination Compounds, World, Moscow, 1991, p. 536 (Russian Edition).

PERGAMON

www.elsevier.nl/locate/poly

Polyhedron 19 (2000) 1741–1748

POLYHEDRON

The reaction of rhenium nitrido complexes with $^{+}CPh_3$. Synthesis, structures and EPR spectra of rhenium imido compounds

Ulrich Abram[a,*], Andreas Voigt[b], Reinhard Kirmse[b]

[a] *Division of Radiochemistry, Institute of Chemistry, Freie Universität Berlin, Fabeckstraße 34-36, D-14195 Berlin, Germany*
[b] *Institute of Inorganic Chemistry, University of Leipzig, Johannisallee 29, D-04103 Leipzig, Germany*

Received 25 February 2000; accepted 26 May 2000

Abstract

The reactions of triphenylcarbonium hexafluorophosphate, $(CPh_3)(PF_6)$, with the terminal nitrido ligands of $[ReN(Et_2dtc)_2(Me_2PhP)]$ ($Et_2dtc^- = N,N$-diethyldithiocarbamate) and $(Bu_4N)[ReNCl_4]$ are described. The resulting imido complexes $[Re(NCPh_3)(Et_2dtc)_2(Me_2PhP)](PF_6)$ and $(Bu_4N)[Re(NCPh_3)Cl_4(OReO_3)]$ have been studied by X-ray crystallography showing short rhenium–nitrogen multiple bond lengths of 1.706(6) and 1.686(6) Å, respectively. Nevertheless, the structural trans influence due to the imido ligand is significantly smaller than that of 'N^{3-}' which leads to a decreasing of the trans Re–S bond length by 0.24 Å in $[Re(NCPh_3)(Et_2dtc)_2(Me_2PhP)](PF_6)$. Despite the addition of the bulky $^{+}CPh_3$ to the nitrido ligand, the $N{\equiv}Re{-}L_{(equatorial)}$ angles are only slightly increased in $[Re(NCPh_3)(Et_2dtc)_2(Me_2PhP)]^+$, whereas those in $[Re(NCPh_3)Cl_4(OReO_3)]^-$ are smaller compared with the values in the starting complex which may also be attributed to the occupation of the sixth coordination position by perrhenate. The rhenium(VI) compounds ($5d^1$) $[Re(NCPh_3)X_4Y]^-$ (X = F, Cl, Br, NCS; Y = X or $OReO_3$) were studied by EPR spectroscopy indicating a noticeable loss of electron density in the central '$ReNX_4$' moiety upon addition of $^{+}CPh_3$ to the nitrido site of the $[ReNX_{4(5)}]^{-,(2-)}$ starting complexes. The EPR parameters of mixed-ligand intermediates of the general composition $[Re(NCPh_3)Br_{4-n}Cl_nY]^-$ (Y = Cl, Br or $OReO_3$) which are formed during ligand exchange reactions are clearly correlated to the composition of the coordination sphere and can be used to characterize the mixed-ligand species unambiguously. © 2000 Elsevier Science Ltd. All rights reserved.

Keywords: Rhenium; Nitrido complexes; Imido complexes; EPR spectroscopy; X-ray structures

1. Introduction

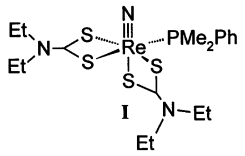
Rhenium complexes with terminal nitrido ligands readily undergo reactions with electrophilic reagents [1–3]. Following this approach numerous compounds containing nitrido bridges between the transition metal and boron [4], gallium [5], gold [6], tin [7], zinc [8], molybdenum [9] or rhenium [10] have been prepared and characterized. Similar reactions with disulfur dichloride, phosphines or F_2 (or XeF_2) lead to thionitrosyls [11], phosphorane iminates [12] or *N*-halogenoimido complexes [13].

The conversion of the nitrido ligand to an imido function succeeds upon reactions with carbonium ions. Recently, we demonstrated that nitrido ligands can trap carbonium cations which arise from the condensation of two acetone molecules in the presence of an acid [14] as has been suggested by Bishop et al. [15]. Alkylation of nitrido ligands with $^{+}CPh_3$ salts has been proved for molybdenum, tungsten and osmium complexes [16]. The formation of complexes with the $Re(NCPh_3)$ moiety has been reported in [15], but no crystallographical data are available up to now.

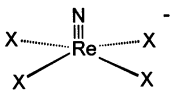
In the present paper we describe the reactions of $(CPh_3)(PF_6)$ with bis(diethyldithiocarbamato)(dimethylphenylphosphine)nitridorhenium(V), $[ReN(Et_2dtc)_2(Me_2PhP)]$ (**I**), and (pseudo)halogenonitridorhenates(VI), $[ReNX_{4(5)}]^{-,(2-)}$ (X = F, Cl, Br, NCS) (**II**), which lead to triphenylmethylimido complexes of Re(V) and Re(VI), respectively, as well as the crystal structures of the products $[Re(NCPh_3)(Et_2dtc)_2(Me_2PhP)]^+$ and $[Re(NCPh_3)Cl_4(OReO_3)]^-$.

* Corresponding author. Tel.: +49-30-838-54002; fax: +49-30-838-52676.
E-mail address: abram@chemie.fu-berlin.de (U. Abram).

0277-5387/00/$ - see front matter © 2000 Elsevier Science Ltd. All rights reserved.
PII: S0277-5387(00)00463-0



I



II

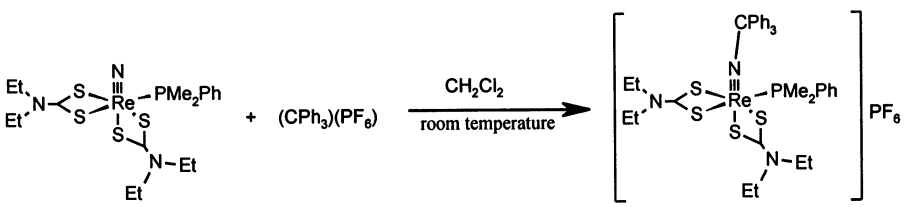
X = F, Cl, Br, NCS

We show that the nitridorhenate(VI) compounds **II** are suitable starting materials for the formation of new rhenium(VI) imido complexes containing the $Re(NCPh_3)$ moiety. EPR spectroscopy appears to be a valuable method to study these reactions. The hyperfine structure and ligand hyperfine structure data are used to characterize the bonding properties in the molecular orbital of the unpaired electron and are compared with the results of the starting complexes **II**.

2. Results and discussion

Treatment of $[ReN(Et_2dtc)_2(Me_2PhP)]$ or $(Bu_4N)[ReNCl_4]$ with $(CPh_3)(PF_6)$ in dichloromethane results in the formation of triphenylmethylimido complexes. The formal oxidation states of the metal, '+5' and '+6' remain unchanged. Thus, the $[Re(NCPh_3)(Et_2dtc)_2(Me_2PhP)]^+$ cation is formed and the occupation of the sixth position of the rhenium(VI) compound by a perrhenate ligand yields $[Re(NCPh_3)Cl_4(OReO_3]^-$. The products have been isolated as PF_6^- and Bu_4N^+ salts, respectively. The crystalline solids are stable in air. Solutions of $(Bu_4N)[Re(NCPh_3)Cl_4(OReO_3)]$, however, slowly decompose even at room temperature. Thus, the crystallization procedure has been performed at low temperatures for this compound. Infrared bands between 1150 and 1200 cm^{-1} have been assigned to the imido vibrations which is in accord with previous findings [1].

The formation of $[Re(NCPh_3)(Et_2dtc)_2(Me_2PhP)](PF_6)$ from complex **I** and $(CPh_3)(PF_6)$ in dichloromethane (Eq. (1)) is almost quantitative. The blue crystals obtained are readily soluble in organic solvents like CH_2Cl_2, $CHCl_3$ or acetone.



(1)

No decomposition of the complex has been observed as solid or in solution. The compound has been identified by common spectroscopic methods and the formation of the imido ligand '$NCPh_3^{2-}$' was confirmed by both IR and NMR spectroscopy and by X-ray crystallography.

The preferred electrophilic attack at the nitrido ligands does not necessarily mean that this is the most nucleophilic site of the molecule with respect to a study at an nitridoosmium thiolato complex where alkylation was achieved at the nitrido site or the thiolato site in dependence on the steric requirements of the attacking electrophile [16]. Similar results have been derived from the reactions of compound **I** with boranes where nitrido bridges are formed with bulky alkyl or aryl boranes [17,18] or boron halides [5b], whereas a preferred attack at the sulfur donors is observed when BH_3 is applied [4].

Single crystals of $[Re(NCPh_3)(Et_2dtc)_2(Me_2PhP)](PF_6)$ have been obtained by slow diffusion of *n*-hexane into a solution of the complex in CH_2Cl_2. They contain one molecule of the solvent per complex molecule. The structure consists of well-separated complex cations and PF_6^- anions. Two crystallographically independent ion pairs are contained in the asymmetric unit of the triclinic unit cell. Since there are no significant differences between them, only one arbitrarily chosen $[Re(NCPh_3)(Et_2dtc)_2(Me_2PhP)]^+$ cation is shown in Fig. 1 [19]. Table 1 contains selected bond lengths and angles. The rhenium atom has a distorted octahedral coordination environment. Main distortions are due to the restricting bite angle of the dithiocarbamato ligands which form four-membered chelate rings. The rhenium–nitrogen multiple bond is only slightly lengthened by the conversion of a nitrido site into an imido one, but the structural trans influence due to the multiply bonded ligand decreases significantly. The Re–S(32) bond length (averaged value from both molecules) in $[Re(NCPh_3)(Et_2dtc)_2(Me_2PhP)]^+$ is shorter by 0.24 Å compared with the value in the nitrido compound **I** [20]. The Re=N–C angles of 172.5° (averaged from both molecules) is in the range of values which have been found for the other structurally characterized transition metal complexes with $NCPh_3^{2-}$ units (163.3–179° [14–16]). The same holds true for the N(10)–C(10) bond length.

In a recently published short communication [21] we reported on the existence of tetrahalogeno(triphenylmethylimido)rhenium(VI) species which we have detected spectroscopically using EPR in reaction mixtures containing $[ReNX_4]^-$ complexes (X = Cl, Br) and $^+CPh_3$. Solutions of the complexes were sufficiently stable for detailed EPR spectroscopic studies. A slow decomposition that accompanied a decrease of the in-

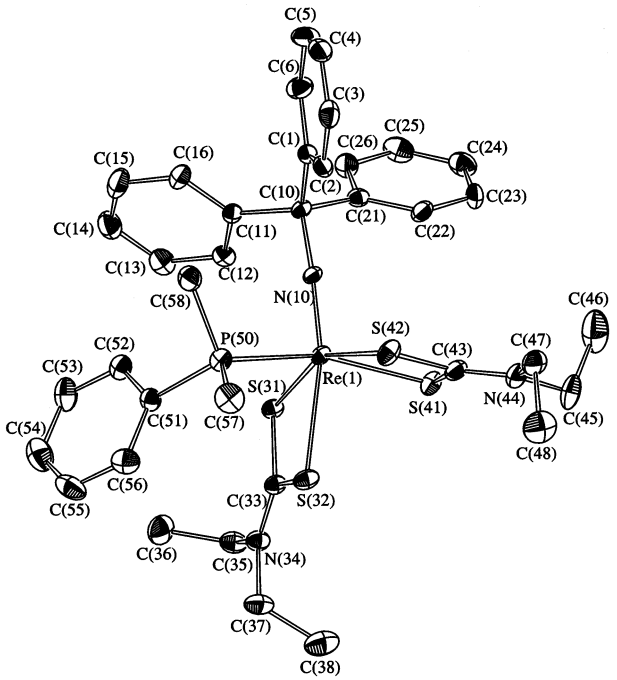


Fig. 1. ZORTEP representation [19] of one of the crystallographically independent complex cations in $[Re(NCPh_3)(Et_2dtc)_2(Me_2PhP)](PF_6)$. Thermal ellipsoids represent 50% probability. H atoms have been omitted for clarity.

tensity of the EPR signals, however, was observed over a period of hours and we were not able to isolate pure, crystalline samples which allowed crystallographic studies and an unambiguous assignment of the structures of the new compounds. Considerable amounts of perrhenate has been detected spectroscopically in the decomposition products which suggested a disproportionation of the rhenium(VI) complexes to diamagnetic rhenium(V) compounds and perrhenate. The rate of decomposition

Table 1
Selected bond lengths (Å) and angles (°) in the complex cation of $[Re(NCPh_3)(Et_2dtc)_2(Me_2PhP)](PF_6)\cdot CH_2Cl_2$ [a]

Re(1)–N(10)	1.706(6)	Re(1)–P(50)	2.421(3)
N(10)–C(10)	1.483(10)	S(31)–C(33)	1.718(8)
Re(1)–S(31)	2.461(2)	S(32)–C(33)	1.724(8)
Re(1)–S(32)	2.552(2)	S(41)–C(43)	1.729(9)
Re(1)–S(41)	2.417(3)	S(42)–C(43)	1.737(9)
Re(1)–S(42)	2.372(2)		
Re(1)–N(10)–C(10)	172.2(5)	P(50)–Re(1)–S(41)	158.24(8)
N(10)–Re(1)–P(50)	97.2(2)	P(50)–Re(1)–S(42)	92.66(9)
N(10)–Re(1)–S(31)	96.5(2)	S(31)–Re(1)–S(32)	69.64(7)
N(10)–Re(1)–S(32)	164.1(2)	S(31)–Re(1)–S(41)	91.30(8)
N(10)–Re(1)–S(41)	102.6(2)	S(31)–Re(1)–S(42)	153.67(8)
N(10)–Re(1)–S(42)	107.4(2)	S(32)–Re(1)–S(41)	85.47(9)
P(50)–Re(1)–S(31)	95.19(8)	S(32)–Re(1)–S(42)	87.90(8)
P(50)–Re(1)–S(32)	77.48(9)	S(41)–Re(1)–S(42)	73.10(8)

[a] The values for the second, crystallographically independent, molecule show no significant deviations.

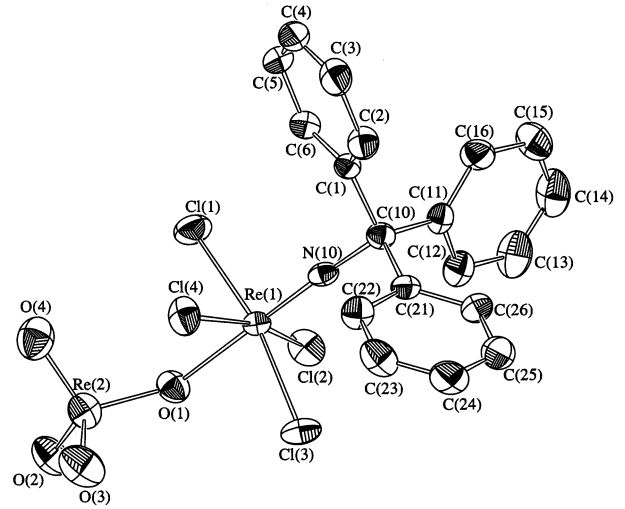


Fig. 2. ZORTEP representation [19] of the complex anion in $(Bu_4N)[Re(NCPh_3)Cl_4(OReO_3)]$. Thermal ellipsoids represent 50% probability. H atoms have been omitted for clarity.

can be decreased at low temperature. Thus, we were able to isolate yellow–brown single crystals of $(Bu_4N)[Re(NCPh_3)Cl_4(OReO_3)]$ by overlayering a CH_2Cl_2 solution of the complex with *n*-hexane at low temperatures.

The structure of $(Bu_4N)[Re(NCPh_3)Cl_4(OReO_3)]$ is built up of well separated $[Re(NCPh_3)Cl_4(OReO_3)]^-$ anions and tetrabutylammonium cations. An ellipsoid representation [19] of the complex anion is given in Fig. 2. Selected distances and angles are listed in Table 2. The rhenium atom is six-coordinate with a short Re=N bond of 1.686(6) Å. The occupation of the sixth position by perrhenate leads to smaller N–Re–Cl angles (mean value 96.4°) compared with the situation in $[ReNCl_4]^-$ (102.8° [22]). Thus, the rhenium atom is situated 0.260(1) Å above a least-square plane which is formed by the four Cl atoms. The Re(1)–O(1) distance of 2.091(5) Å is shorter than the values found for the bonds to coordinated water molecules in [Re{NB-

Table 2
Selected bond lengths (Å) and angles (°) in the complex anion of $(Bu_4N)[Re(NCPh_3)Cl_4(OReO_3)]$

Re(1)–N(10)	1.686(6)	Re(1)–O(1)	2.091(5)
N(10)–C(10)	1.475(9)	Re(2)–O(1)	1.769(5)
Re(1)–Cl(1)	2.332(2)	Re(2)–O(2)	1.696(6)
Re(1)–Cl(2)	2.326(2)	Re(2)–O(3)	1.688(6)
Re(1)–Cl(3)	2.327(2)	Re(2)–O(4)	1.668(7)
Re(1)–Cl(4)	2.350(2)		
Re(1)–N(10)–C(10)	173.6(5)	N(10)–Re(1)–O(1)	176.7(2)
N(10)–Re(1)–Cl(1)	97.7(1)	Re(1)–O(1)–Re(2)	140.5(3)
N(10)–Re(1)–Cl(2)	99.1(2)	O(1)–Re(2)–O(2)	107.2(3)
N(10)–Re(1)–Cl(3)	94.1(2)	O(1)–Re(2)–O(3)	111.5(3)
N(10)–Re(1)–Cl(4)	94.7(2)	O(1)–Re(2)–O(4)	111.2(3)

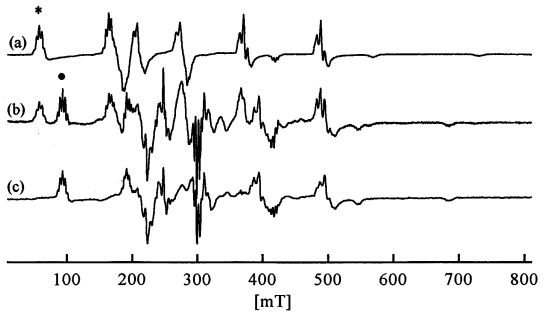


Fig. 3. Experimental X-band EPR spectra of a $[ReNF_4]^-/^+CPh_3$ mixture in CH_2Cl_2 at $T = 130$ K. (a) Immediatly after treatment of $[ReNF_4]^-$ with an excess of $(CPh_3)(PF_6)$. (b) After standing for 3 min at r.t. (c) After standing for 8 min at r.t. (*) $[ReNF_4]^-$. (●) $[Re(NCPh_3)F_4Y]^-$; Y = F or $OReO_3$.

$(C_6F_5)_3\}Cl_4(OH_2)]^-$ (2.282(4) Å [23]) or $[(H_2O)Br_4Re{\equiv}N{-}ReBr_4{-}N{\equiv}ReBr_4(OH_2)]^{2-}$ (2.41(2) Å [24]) and can be compared with the coordinated perrhenate ions in $[Re(NO)Cl_2(PPh_3)(OPPh_3)(OReO_3)]$ (2.058(8) Å [25]) or $[Re(NO)Cl_2(OPPh_3)_2(OReO_3)]$ (2.068(1) Å [25]). This indicates a significantly lower *trans* influence of the imido ligand compared with the situation in complexes with terminal nitrido ligands (Re–O bond in *mer*,*cis*-$[ReN(Cl)(Me_2PhP)_3(OSO_2CF_3)]$: 2.403(5) Å [26]) and explains the formation of a six-coordinate complex despite the addition of the bulky CPh_3 unit to the nitrido ligands. Similar results have been found for nitrogen bridges between rhenium and boron [4,18].

During the formation of $[Re(NCPh_3)X_4Y]^-$ complexes (X = F, Cl, Br, NCS; Y = X or $OReO_3$) by reactions of nitridorhenate(VI) compounds **II** with an excess of triphenylmethylcarbonium salt $(CPh_3)(PF_6)$ in dichloromethane solutions the formal oxidation state of the Re, '+6', remains unchanged. Thus, the triphenylmethylimido complexes as well as the nitridorhenate(VI) starting complexes $[ReNX_{4(5)}]^{-,\,(2-)}$ (X = F, Cl, Br, NCS) are favored for EPR spectroscopy because of their $5d^1$ ($S = 1/2$) configuration. The EPR spectra of the $\{Re^{VI}N\}$ starting compounds **II** are well characterized [22,27–29]. As found for the recently published tetrahalogeno(triphenylmethylimido)rhenium(VI) species (halide = Cl, Br) [21] the complexes $[Re(NCPh_3)X_4Y]^-$ (X = F, NCS; Y = X or $OReO_3$) give well resolved frozen solution X-band EPR spectra. For the characterization of chemical reactions of the nitridorhenate(VI) species **II** with $^+CPh_3$ the experimental EPR spectra of frozen solutions ($T = 130$ K) of a $[ReNF_4]^-/^+CPh_3$ mixture are given in Fig. 3(a–c). Fig. 3(a) shows the EPR spectrum of the starting complex $[ReNF_4]^-$ [28]. In the spectrum of $[ReNF_4]^-$ with an excess of $^+CPh_3$ (recorded 3 min after mixing of the reactants) in addition to the signals of the $[ReNF_4]^-$ species there are new signals which indicate the formation of $[Re(NCPh_3)F_4Y]^-$ (Y = F or $OReO_3$) (Fig. 3(b)). After standing for 8 min at room temperature only the signals of the triphenylmethylimido complex were observed (Fig. 3(c)). The EPR spectra of the $[Re(NCPh_3)X_4Y]^-$ imido complexes (X = F, Cl, Br, NCS; Y = X or $OReO_3$) show a typical axially symmetric pattern with six ^{185,187}Re hyperfine structure (hfs) lines (nuclear spin ^{185,187}Re: $I^{Re} = 5/2$, natural abundance ^{185}Re 37.4% and ^{187}Re 62.6%) in the parallel and the perpendicular part. Due to the large ^{185,187}Re hfs coupling constants and the nuclear quadrupole moments of the rhenium isotopes the equidistant hfs lines are disturbed.

The rhenium(VI) compounds of the general formulae $[Re(NCPh_3)X_4Y]^-$ (X = F, Cl, Br, NCS; Y = X or $OReO_3$) can be described by the spin Hamiltonian (2):

$$\mathbf{H}_{sp} = \mathbf{g}\cdot\mu_B\cdot\mathbf{S}\cdot\mathbf{B}_0 + \mathbf{S}\cdot\mathbf{A}^{Re}\cdot\mathbf{I}^{Re} + \mathbf{I}^{Re}\cdot\mathbf{Q}^{Re}\cdot\mathbf{I}^{Re} + \sum_{i=1}^{4}\mathbf{S}\cdot\mathbf{A}_i^X\cdot\mathbf{I}_i^X \quad (2)$$

with X = F, Br; all other symbols have their usual meaning. The last term stands for the ligand hfs interaction with the ^{19}F nuclei (^{19}F: $I^F = 1/2$) and the ^{79,81}Br nuclei (^{79,81}Br: $I^{Br} = 3/2$, natural abundance ^{79}Br 50.7% and ^{81}Br 49.3%), respectively. ^{19}F ligand hfs couplings are well-resolved in the parallel part (quintets with 1:4:6:4:1 intensity ratio) as well as in the perpendicular part (distorted 1:2:1 multiplets) of the above mentioned EPR spectra (see Fig. 3). The notation of the ligand hfs tensor components is the commonly used one for d^1 systems [21,28,29]. All spectral parameters determined for the triphenylmethylimido complexes $[Re(NCPh_3)X_4Y]^-$ (X = F, Cl, Br, NCS; Y = X or $OReO_3$) are summarized in Table 3 and are compared with those of the $\{Re^{VI}N\}$ starting compounds **II**. The comparison of the EPR parameters yields the following results:

1. For the $\{Re^{VI}N\}$ species **II** as well as for the triphenylmethylimido complexes typical axially symmetric spectra were detected. This indicates a electrophilic attack of the $^+CPh_3$ to the nitrido ligand of **II**.
2. On going from the $\{Re^{VI}N\}$ to the $\{Re^{VI}(NCPh_3)\}$ complexes an increase of the $g_\parallel$ values and an decrease of the $g_\perp$ values is observed.
3. The magnitudes of the Re hfs coupling constants $A_\parallel^{Re}$ and $A_\perp^{Re}$ of the imido compounds are about 10–20% smaller than those of the starting complexes **II**.
4. After the addition of $^+CPh_3$ to the nitrido site of the starting compounds **II** the magnitudes of the ligand hfs coupling parameters A_i^X (X = F, Br) are slightly increased.

The differences outlined in the statements (1)–(4) suggest a noticeable loss of spin-density of the central '$ReNX_4$' moiety (X = F, Cl, Br, NCS) upon formation of the $\{Re(NCPh_3)\}$ complexes. In order to account for the changes of the bonding situation in the compounds under study we calculated the molecular orbital (MO) coefficients α and α' of the MO of the unpaired electron for the $[ReNX_{4(5)}]^{-,\,(2-)}$ [27–29] and the $[Re(NCPh_3)$-

Table 3
EPR parameter [a] for $[Re(NCPh_3)X_4Y]^-$ and $[ReNX_{4(5)}]^{-,\,(2-)}$ with X = F, Cl, Br, NCS and Y = X, $OReO_3$ (hyperfine coupling constants are given in 10^{-4} cm^{-1})

	$[ReNF_4]^-$	$[Re(NCPh_3)F_4Y]^-$	$[ReNCl_4]^-$	$[Re(NCPh_3)Cl_4Y]^-$	$[ReNBr_4]^-$	$[Re(NCPh_3)Br_4Y]^-$	$[ReN(NCS)_5]^{2-}$	$[Re(NCPh_3)(NCS)_4Y]^-$
$g_\perp$	1.870	1.810	1.957	1.883	1.973	1.912	1.958	1.882
$g_\parallel$	1.649	1.678	1.908	1.969	2.069	2.145	1.817	1.831
g_{av} [b]	1.796	1.766	1.941	1.912	2.005	1.990	1.911	1.865
$A_\perp^{Re}$	546	503	410	333	357	281	379	311
$A_\parallel^{Re}$	1027	926	768	664	660	542	687	579
A_{av}^{Re} [b]	706	644	529	443	458	368	482	400
A_σ^X	≤14.2 [c]	≤21.1 [c]	[d]	[d]	≤2.1 [c]	≤3.8 [c]	[d]	[d]
A_π^X	53.4	65.1	[d]	[d]	25.5	28.3	[d]	[d]
A_z^X	30.9	29.0	[d]	[d]	≤7.7 [c]	≤8.9 [c]	[d]	[d]
A_{av}^X [b]	32.8	38.4			11.8	13.7		

[a] Experimental error: $g_i \pm 0.003$; $A_i^{Re} \pm 3$; $A_i^X \pm 1.0$ (X = F, Br).
[b] $g_{av} = (g_\parallel + 2g_\perp)/3$; $A_{av}^{Re} = (A_\parallel^{Re} + 2A_\perp^{Re})/3$; $A_{av}^X = (A_\sigma^X + A_\pi^X + A_z^X)/3$.
[c] Estimated from linewidth considerations.
[d] Not resolved.

for the $[ReNX_{4(5)}]^{-,\,(2-)}$ [27–29] and the $[Re(NCPh_3)X_4Y]^-$ complexes (X = F, Cl, Br, NCS; Y = X or $OReO_3$) [21] from the experimental hfs parameters. The molecular orbital of the unpaired electron (C_{4v} symmetry assumed) is of 'in-plane π-type' as given in Eq. (3):

$$\psi_{MO}(b_2) = \alpha|5d_{xy}\rangle - \alpha'|\phi_L\rangle \quad (3)$$

where ϕ_L represents a linear combination of mainly p orbitals of the donor atoms of the (pseudo)halide ligands (L). The squared coefficients α^2 and $(\alpha')^2$ are a measure of covalency of the Re–ligand$_{(equatorial)}$ bonds in this MO. Applying the generally accepted formalism of Morton and Preston [30], the s, p and d spin-densities $(c_s^X)^2$, $(c_p^X)^2$ and $(c_d^X)^2$ are calculated by means of Eqs. (4a) and (4b):

$$(c_s^X)^2 = (a_{iso,exp}^X / a_{iso,th}^X) \quad (4a)$$

$$(c_{p,d}^X)^2 = (b_{dip,exp}^X / b_{dip,th}^X) \quad (4b)$$

In these equations, $a_{iso,th}^X$ and $b_{dip,th}^X$ are the isotropic and dipolar parts of the (ligand) hyperfine tensor and have been calculated by Morton and Preston [30] for the case when the unpaired electron is completely localized in the corresponding s, p and d function of the nucleus X under discussion. $a_{iso,exp}^X$ and $b_{dip,exp}^X$are the experimentally obtained values. The spin-densities calculated are listed in Table 4.

From the values given in Table 4 the following conclusions can be drawn:

1. They indicate a predominant Re $5d_{xy}$ character in the highest occupied molecular orbital (HOMO). For the α^2 values of the fluoro and chloro species we estimated values larger than 100%. The discrepancies in the α^2 values may be due to inaccuracies in the atomic orbitals of the heavy Re atom. Also, relativistic effects as discussed for Au^{II} compounds [31,32] may have an influence.
2. The α^2 values decrease, as expected, with an increase of the 'heaviness' of the equatorial donor atoms. The isothiocyanato complexes shows a noticeably small α^2 value which is attributed to the π-acceptor behavior of the NCS^- ligands.
3. For the triphenylmethylimido complexes a remarkable decrease of the α^2 values was observed.

Table 4
Experimentally obtained spin-density distribution [a] for $[Re(NCPh_3)X_4Y]^-$ and $[ReNX_{4(5)}]^{-,\,(2-)}$ complexes (X = F, Cl, Br, NCS, Y = X, $OReO_3$)

Spin-density		$[ReNX_{4(5)}]^{-,\,(2-)}$	$[Re(NCPh_3)X_4Y]^-$
X = F			
Re	c_s^2	6.0	5.4
	c_d^2	145.0	127.8
	α^2	151.0	133.2
X	c_s^2	0.2	0.2
	c_p^2	1.8	2.7
	$(\alpha')^2$	8.0	11.6
X = Cl			
Re	c_s^2	4.4	3.8
	c_d^2	108.8	99.8
	α^2	113.2	103.6
X = Br			
Re	c_s^2	3.8	3.3
	c_d^2	91.6	78.9
	α^2	95.4	82.2
X	c_s^2	0.1	0.1
	c_p^2	2.5	2.7
	$(\alpha')^2$	10.4	11.2
X = NCS			
Re	c_s^2	3.9	3.4
	c_d^2	91.4	80.9
	α^2	95.3	84.3

[a] Contributions of a sixth ligand coordinated in a trans position to the 'N^{3-}' or '$NCPh_3^{2-}$' are small and therefore neglected.

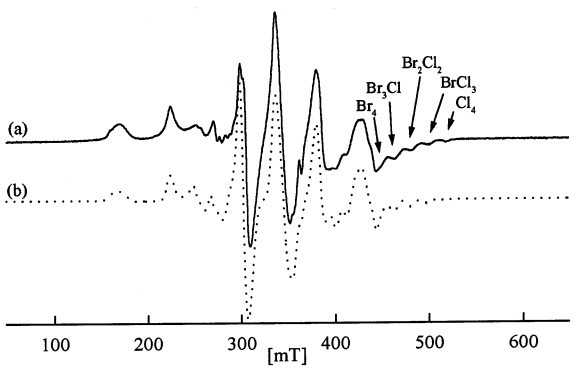


Fig. 4. (a) Experimental X-band EPR spectrum of $[Re(NCPh_3)Br_{4-n}Cl_nY]^-$ complexes ($n = 0$–4; Y = Cl, Br or $OReO_3$) in CH_2Cl_2 at $T = 130$ K. In the high-field region of the parallel part all three mixed-ligand species and the parent compounds are detected. (b) Simulated spectrum.

Table 5
Experimentally obtained [a] and calculated [b] EPR parameters $g_\parallel$ and $A_\parallel^{Re}$ for $[Re(NCPh_3)$–$Br_{4-n}Cl_nY]^-$ mixed-ligand complexes ($n = 1$–3; Y = Cl, Br or $OReO_3$) (hyperfine coupling constants are given in 10^{-4} cm^{-1})

	$g_\parallel$		$A_\parallel^{Re}$	
	Found	Calculated	Found	Calculated
$[Re(NCPh_3)Br_4Y]^-$	2.145	2.145	542	542
$[Re(NCPh_3)$-$Br_3ClY]^-$	2.104	2.101	569	573
$[Re(NCPh_3)$ $\times Br_2Cl_2Y]^-$	2.057	2.057	601	603
$[Re(NCPh_3)$-$BrCl_3Y]^-$	2.013	2.013	633	633
$[Re(NCPh_3)Cl_4Y]^-$	1.969	1.969	664	664

[a] Experimental error: $g_\parallel \pm 0.003$; $A_\parallel^{Re} \pm 5$.
[b] $p = ([Re(NCPh_3)Br_{4-n}Cl_nY]^-) = \{(4-n)p([Re(NCPh_3)$-$Br_4Y]^-) + np([Re(NCPh_3)Cl_4Y]^-)\}$ with $p = g_\parallel$ and $A_\parallel^{Re}$; Y = Cl, Br or $OReO_3$.

4. On going from the nitrido to the imido complexes a slightly increase of the $(\alpha')^2$ values was found.
5. On going from nitrido to imido nitrogen (i.e. changing the formal charge from '−3' to '−2') spin-density will be transferred from Re to the added CPh_3 unit.

In the frozen solution EPR spectra of $[ReNCl_4]^-$/$[ReNBr_4]^-$ mixtures containing an excess of $(CPh_3)(PF_6)$, in addition to the signals of the parent imido complexes $[Re(NCPh_3)X_4Y]^-$ (X = Cl, Br; Y = X or $OReO_3$), new signals are to be seen in the high-field region ($m_I^{Re} = -5/2$) of the parallel part. These are attributed to rhenium(VI) imido mixed-ligand complexes of the general formulae $[Re(NCPh_3)Br_{4-n}Cl_nY]^-$ ($n = 1$–3; Y = Cl, Br or $OReO_3$). A typical experimental EPR spectrum and its simulation is reproduced in Fig. 4. The perpendicular part of the spectrum is very complex due to many lines overlapping. Therefore, no attempts were made to derive the EPR parameters $g_\perp$ and $A_\perp^{Re}$. The tensor components $g_\parallel$ and $A_\parallel^{Re}$ of the parallel part of the spectra are summarized in Table 5. Due to the large linewidths ($\Delta B_{pp} \geq 7$ mT) $^{35,37}Cl$, $^{79,81}Br$ and ^{14}N hfs interactions were not resolved.

The investigation of ligand-exchange reactions by means of EPR requires knowledge about the dependence of the EPR parameters on the type (composition, symmetry) of the coordination sphere. Extensive investigations have been made e. g. on the nitridorhenate(VI) complexes of the general formulae $[ReNX_4]^-$ (X = F, Cl, Br) [22,33]. According to this a nearly linear dependence of the EPR spectral quantities $g_\parallel$ and $A_\parallel^{Re}$ on the 'heaviness' of the first coordination sphere is expected. This can be defined for the $[Re(NCPh_3)Br_{4-n}Cl_nY]^-$ complexes ($n = 0$–4; Y = Cl, Br or $OReO_3$) under study as given in Eq. (5):

$$g_\parallel,\ A_\parallel^{Re} \sim \lambda_L/\lambda_{Re} = (1/4)[n\lambda_{Cl} + (4-n)\lambda_{Br}]/\lambda_{Re} \quad (5)$$

where λ_{Cl}, λ_{Br} and λ_{Re} are the spin-orbit coupling constants of chlorine, bromine and rhenium, respectively.

The proportionality (Eq. (5)) holds true if there are no significant differences concerning the structure and bonding properties of the complexes considered. Thus, if the $g_\parallel$ values and the hfs coupling parameters $A_\parallel^{Re}$ of the parent complexes are known, the $g_\parallel$ and $A_\parallel^{Re}$ values of the mixed-ligand complexes can be estimated simply using the 'additivity rule' given in Eq. (6):

$$\begin{aligned} p &= ([Re(NCPh_3)Br_{4-n}Cl_nY]^-) \\ &= \{(4-n)p([Re(NCPh_3)Br_4Y]^-) \\ &\quad + np([Re(NCPh_3)Cl_4Y]^-)\} \end{aligned} \quad (6)$$

with $p = g_\parallel$ and $A_\parallel^{Re}$. In Table 5 the $g_\parallel$ and $A_\parallel^{Re}$ values estimated for $[Re(NCPh_3)Br_{4-n}Cl_nY]^-$ mixed-ligand complexes ($n = 1$–3; Y = Cl, Br or $OReO_3$) according to Eq. (6) are compared with the experimentally derived ones. It can be seen that the experimental values are well reproduced by Eq. (6). Fig. 5 illustrates the nearly linear dependence of the observed EPR quantities of the $[Re(NCPh_3)Br_{4-n}Cl_nY]^-$ complexes ($p = 0$–4; Y = Cl, Br or $OReO_3$) on the composition of the first coordination sphere.

3. Experimental

$(NBu_4)[ReNCl_4]$ [22] and $[ReN(Et_2dtc)_2)(Me_2PhP)]$ [20] have been prepared by literature procedures. $(CPh_3)(PF_6)$ has been purchased from ALDRICH and used without further purification. IR spectra have been recorded on a Perkin–Elmer Spectrum 1000. NMR spectra have been measured on a Bruker DRX-250

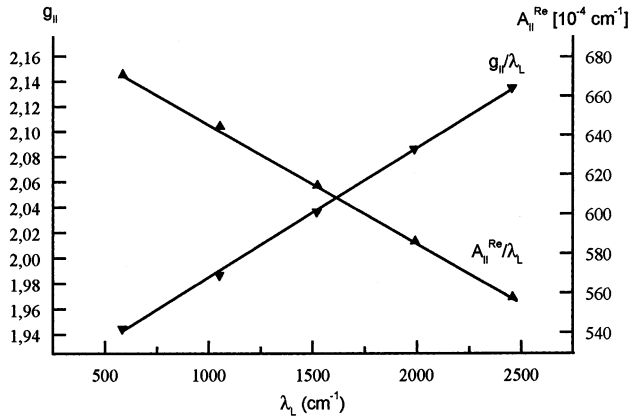


Fig. 5. Dependence of $g_{\|}$ and $A_{\|}^{Re}$ of $[Re(NCPh_3)Br_{4-n}Cl_nY]^-$ complexes ($n = 0$–4; Y = Cl, Br or $OReO_3$) on the effective spin-orbit coupling $\lambda_L = 1/4[(4-n)\lambda_{Br} + \lambda_{Cl}]$. $\lambda_{Cl} = 586$ cm^{-1} and $\lambda_{Br} = 2460$ cm^{-1}.

instrument with TMS and H_3PO_4 as standards. FAB mass spectra have been obtained using a TSQ 70 (Finnigan MAT) with nitrobenzylalcohol as matrix (8 keV, xenon). EPR spectra have been recorded for CH_2Cl_2 solutions at $T = 130$ K in the X-band ($\nu \approx 9.5$ GHz) with a Bruker ESP 300E spectrometer under standard conditions (typically modulation frequency 100 kHz, modulation amplitude 5 G, microwave power 4 mW).

3.1. *[Re(NCPh$_3$)(Et$_2$dtc)$_2$(Me$_2$PhP)](PF$_6$)*

[ReN(Et_2dtc)$_2$(Me_2PhP)] (63 mg, 0.1 mmol) was dissolved in ca. 5 ml CH_2Cl_2 and (CPh_3)(PF_6) (44 mg, 0.11 mmol) was added. The color of the solution immediately changed to blue. The volume was reduced to about 2 ml after stirring at room temperature (r.t.) for 1 h and overlayered with *n*-hexane. Blue needles deposited upon diffusion of *n*-hexane into the dichloromethane solution. Yield: 94 mg (85%). *Anal.* Found: C, 42.0; H, 3.9; N, 3.8; S, 11.2. Calc. for $C_{38}H_{48}Cl_2F_6N_3P_2ReS_4$: C, 41.2; H, 4.3; N, 3.8; S, 11.5%. IR (ν_{max}/cm^{-1}): 1192 s (Re=N). ^{1}H NMR (acetone-d_6/ppm): 1.12–186 (18H, CH_3); 3.32–3.85 (8H, CH_2); 7.01–7.26 (20H, phenyl). ^{13}C NMR (acetone-d_6/ppm): 12.1, 12.5 (CH_3, phosphine); 14.1, 14.3, 14.4, 14.6 (CH_3, Et_2dtc^-); 45.0, 45.3, 45.9, 47.0 (CH_2); 94.5 (CPh_3); 128.4, 12.6, 128.9, 129.3, 129.4, 131.0, 131.4, 140.7 (phenyl).

3.2. *(Bu$_4$N)[Re(NCPh$_3$)Cl$_4$(OReO$_3$)]*

(Bu_4N)[$ReNCl_4$] (59 mg, 0.1 mmol) was dissolved in 3 ml CH_2Cl_2 and solid (CPh_3)(PF_6) (39 mg, 0.1 mmol) was added at −20°C. The mixture was carefully overlayered with *n*-hexane and kept for crystallization at −20°C. Yellow–brown crystals deposited during a period of several days which were removed by filtration and dried in vacuum. Yield: 48 mg (45%). *Anal.* Found: C, 39.2; H, 4.9; Cl, 11.2; N, 2.9. Calc. for $C_{35}H_{51}Cl_4N_2O_4Re_2$: C, 39.0; H, 4.7; Cl, 13.0; N, 2.6%. IR (ν_{max}/cm^{-1}): 1163 s (Re=N).

3.3. *X-ray structural determinations*

The intensities for the X-ray structural determinations were collected on an automated single crystal diffractometer (Enraf–Nonius, Delft, The Netherlands) with Mo Kα radiation ($\lambda = 0.71073$ Å) at −65°C. HELENA [34] was used for data reduction. The structures were solved by direct methods using SHELXS-97 [35]. Subsequent Fourier-difference map analyses yielded the positions of the non-hydrogen atoms. Refinement was performed using SHELXL-97 [36]. Hydrogen atoms have been included at calculated positions and refined using the 'riding model' option of SHELXL-97. Crystal data and more details of the data collections and refinements are contained in Table 6.

Table 6
X-ray structure data collection and refinement parameters

	[Re(NCPh$_3$)(Et$_2$dtc)$_2$-(Me$_2$PhP)](PF$_6$)·CH_2Cl_2	(Bu$_4$N)[Re(NCPh$_3$)-Cl$_4$(OReO$_3$)]
Crystal dimensions (mm)	0.4 × 0.2 × 0.2	0.6 × 0.1 × 0.1
Formula	$C_{38}H_{48}Cl_2F_6N_3P_2S_4Re$	$C_{35}H_{51}Cl_4N_2O_4Re_2$
M (g mol^{-1})	1108.07	1077.98
Crystal system	triclinic	triclinic
Space group	$P\bar{1}$	$P\bar{1}$
Unit cell dimensions		
a (Å)	10.340(2)	9.433(1)
b (Å)	14.317(4)	10.205(2)
c (Å)	30.26(2)	22.906(50
α (°)	84.31(3)	77.77(1)
β (°)	89.44(4)	79.36(2)
γ (°)	81.87(3)	67.83(1)
V (Å^3)	4413(3)	1982(1)
Z	4	2
D_{calc} (g cm^{-3})	1.668	1.806
Linear absorption coefficient, μ (mm^{-1})	3.194	6.408
Absorption correction	ψ scans	ψ scans
T_{min}/T_{max}	0.8137/0.9671	0.634/0.871
Measured reflections	16475	7523
Independent reflections	15516	6964
Independent reflections [$I > 2\sigma(I)$]	11224	5790
Refined parameters	1009	424
R_1 (F)/wR_2 (F^2)	0.0535/0.1166	0.0355/0.0887
GOF	1.058	1.052

4. Supplementary material

Additional information on the structural determinations is available free of charge from: The Director, CCDC, 12 Union Road, Cambridge, CB2 1EZ, UK (fax: +44-1223-336033; e-mail: deposit@ccdc.cam.ac.uk or www: http://www.ccdc.cam.ac.uk), quoting the deposition numbers CCDC-134361 ($[Re(NCPh_3)(Et_2dtc)_2(Me_2PhP)](PF_6)\cdot CH_2Cl_2$) and CCDC-134360 $\{(Bu_4N)[Re(NCPh_3)Cl_4(OReO_3)]\}$

Acknowledgements

The authors would like to thank Herrmann-Starck AG for generously providing the rhenium metal and they gratefully acknowledge financial support from the Deutsche Forschungsgemeinschaft and the Fonds der Chemischen Industrie. U.A. would also like to thank Professor J. Strähle (Tübingen) for his hospitality and the opportunity to collect the X-ray data sets.

References

[1] W.A. Nugent, J.M. Mayer, Metal–Ligand Multiple Bonds, Wiley, New York, 1988.
[2] K. Dehnicke, J. Strähle, Angew. Chem. 93 (1981) 451; Angew. Chem., Int. Ed. Engl. 20 (1981) 413.
[3] K. Dehnicke, J. Strähle, Angew. Chem. 104 (1992) 978; Angew. Chem., Int. Ed. Engl. 31 (1992) 955.
[4] U. Abram, Inorg. Chem. Commun. 2 (1999) 227 and Refs. cited therein.
[5] (a) S. Ritter, R. Hübener, U. Abram, J. Chem. Soc., Chem. Commun. (1995) 2047. (b) S. Ritter, U. Abram, Z. Anorg. Allg. Chem. 611 (1996) 965.
[6] G. Beuter, U. Englert, J. Strähle, Z. Naturforsch., Teil. B 43 (1988) 145.
[7] B. Schmid, J. Strähle, Z. Anorg. Allg. Chem. 624 (1998) 1429.
[8] A. Hagenbach, J. Strähle, Z. Anorg. Allg. Chem. 625 (1999) 1181.
[9] B. Schmid, E. Schweda, J. Strähle, Z. Anorg. Allg. Chem. 624 (1998) 1111.
[10] (a) D.V. Griffiths, S.J. Parrott, M. Togrou, J.R. Dilworth, Yifan Zheng, S. Ritter, U. Abram, Z. Anorg. Allg. Chem. 624 (1998) 1409. (b) A. Haug, J. Strähle, Z. Anorg. Allg. Chem. 624 (1998) 931.
[11] (a) T. Chivers, F. Edelman, Polyhedron 5 (1983) 1661. (b) P.F. Kelly, J.D. Woolins, Polyhedron 6 (1986) 607 and Refs. cited therein.
[12] (a) K. Dehnicke, J. Strähle, Polyhedron 8 (1989) 707. (b) K. Dehnicke, F. Weller, Coord. Chem. Rev. 158 (1997) 103 and Refs. cited therein.
[13] K. Dehnicke, J. Strähle, Chem. Rev. (1993) 981.
[14] S. Ritter, U. Abram, Z. Anorg. Allg. Chem. 629 (1994) 1786.
[15] M.W. Bishop, J. Chatt, J.R. Dilworth, B.D. Neaves, P. Dahlstrom, J. Hyde, J. Zubieta, J. Organomet. Chem. 213 (1981) 109.
[16] (a) D. Fenske, R. Kujanek, K. Dehnicke, Z. Anorg. Allg. Chem. 507 (1983) 51. (b) D. Sellmann, M.W. Wemple, W. Donaubauer, F.W. Heinemann, Inorg. Chem. 36 (1997) 1397.
[17] S. Ritter, U. Abram, Inorg. Chim. Acta 231 (1995) 245.
[18] U. Abram, B. Schmidt-Brücken, unpublished results.
[19] L. Zsolnai, ZORTEP, A Programme for the Ellipsoid Presentation of Crystal Structures, University of Heidelberg, Germany, 1995.
[20] S. Ritter, U. Abram, Z. Anorg. Allg. Chem. 620 (1994) 1443.
[21] A. Voigt, U. Abram, R. Kirmse, Inorg. Chem. Commun. 1 (1998) 203.
[22] U. Abram, M. Braun, S. Abram, R. Kirmse, A. Voigt, J. Chem. Soc., Dalton Trans. (1998) 231.
[23] U. Abram, F.J. Kohl, K. Öfele, W.A. Herrmann, A. Voigt, R. Kirmse, Z. Anorg. Allg. Chem. 624 (1998) 934.
[24] U. Abram, A. Voigt, R. Kirmse, Inorg. Chem. Commun. 1 (1998) 213.
[25] U. Abram, A. Voigt, R. Kirmse, K. Ortner, R. Hübener, R. Carballo, E. Vazquez-Lopez, Z. Anorg. Allg. Chem. 624 (1998) 1662.
[26] U. Abram, I. Walker, Acta Crystallogr., Sect. C 51 (1995) 1250.
[27] A. Voigt, U. Abram, R. Böttcher, U. Richter, J. Reinhold, R. Kirmse, Chem. Phys. 253 (2000) 171.
[28] A. Voigt, U. Abram, R. Kirmse, Inorg. Chem. Commun. 1 (1998) 141.
[29] A. Voigt, U. Abram, P. Strauch, R. Kirmse, Inorg. Chim. Acta 271 (1998) 199.
[30] J.R. Morton, K.F. Preston, J. Magn. Reson. 30 (1978) 577.
[31] O.D. Häberlein, H. Schmidbaur, N. Rösch, J. Am. Chem. Soc. 116 (1994) 8241.
[32] L. Ihlo, R. Böttcher, R.-M. Olk, R. Kirmse, Inorg. Chim. Acta 281 (1998) 160.
[33] A. Voigt, U. Abram, R. Kirmse, Z. Naturforsch., Teil B 53 (1998) 1183.
[34] A. Spek, PLATON and HELENA, Programs for Data Reduction and Handling of Crystal Structure Data, University of Utrecht, The Netherlands, 1994.
[35] G.M. Sheldrick, SHELXS-97, A Program for the Solution of Crystal Structures, University of Göttingen, Germany, 1997.
[36] G.M. Sheldrick, SHELXL-97, A Program for the Refinement of Crystal Structures, University of Göttingen, Germany, 1997.

PERGAMON

www.elsevier.nl/locate/poly

Polyhedron 19 (2000) 1749–1756

POLYHEDRON

Complexes of sodium and caesium perrhenates with calix[4]arene bis(crown-6): a model for pertechnetate ion extraction

Pierre Thuéry [a,*], Martine Nierlich [a], Zouhair Asfari [b], Jacques Vicens [b], Jean-François Dozol [c]

[a] *CEA/Saclay, SCM (CNRS URA 331), Bâtiment 125, 91191 Gif-sur-Yvette, France*
[b] *ECPM, Laboratoire de Chimie des Interactions Moléculaires Spécifiques (CNRS UMR 7512), 25 rue Becquerel, 67087 Strasbourg, France*
[c] *CEA/Cadarache, DESD/SEP, 13108 Saint-Paul-lez-Durance, France*

Received 14 March 2000; accepted 23 May 2000

Abstract

The ability of calix[4]arene bis(crown-6) in the 1,3-alternate conformation (BC6) to co-extract caesium and pertechnetate ions from acidic or basic aqueous to organic solutions, which is of interest for nuclear waste reprocessing, has previously been demonstrated. We report the crystal structures of the complexes formed by this ligand with sodium and caesium ions with perrhenate (isoelectronic to pertechnetate) counter-ions, in an acidic medium. The sodium complex $[(Na^+\cdot H_2O)_2BC6](ReO_4^-)_2$ (**1**) differs from the previously reported sodium nitrate complex mainly by the dissociation of the anion–cation pair. Three forms of the caesium complex are described, $[(Cs^+)_2(ReO_4^-)BC6](ReO_4^-)\cdot H_2O$ (**2**), $[(Cs^+)_2(ReO_4^-)(H_2O)BC6](ReO_4^-)(H_2O)_{0.5}$ (**3**) and $[(Cs^+)_{1.5}(ReO_4^-)BC6](ReO_4^-)_{0.5}$ (**4**), which differ one from the other by the coordination mode of the perrhenate ions (monodentate, bidentate, bridging) and the position of the caesium ion in the crown. © 2000 Elsevier Science Ltd. All rights reserved.

Keywords: Calixcrowns; Caesium ion; Sodium ion; Perrhenate ion; Pertechnetate ion; Nuclear reprocessing

1. Introduction

Nuclear fission provides an almost infinite source of energy but presents the important drawback of generating nuclear wastes, which are presently the subject of much concern. The wastes produced during reprocessing are divided into two classes: (i) low- and medium-level liquid wastes (LLLW and MLLW) and (ii) high-level liquid wastes (HLLW). Recovery of technetium (high-yield fission product ^{99}Tc, present as TcO_4^- ions in aqueous acid solution) from HLLW is one of the important new challenges, not only because of its environmental impact due to its long half-life of 2.13×10^5 years and its relative mobility in disposals [1], but also because it is the most important of the radionuclides in nuclear medicine [2]. A lot of work has been devoted to the development of extractants selective for this anion. The close relationship between TcO_4^- and the isoelectronic perrhenate ion ReO_4^- makes the latter a convenient and widely used model for the former [2].

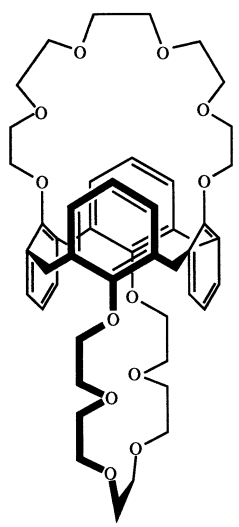
With the advent of macrocyclic ligands such as crown ethers, cryptands and calixarenes, supramolecular chemistry has developed rapidly in a wide range of application fields. Although development of anionic complexation has been slower than that of cations, recent studies have shown that this field of research could have already found applications for industrial purposes [3]. In the particular area of concern, the extraction of the tetrahedral pertechnetate anion TcO_4^- from aqueous solutions by several crown ether compounds has been reported. For example, dicyclohexyl-18-crown-6 has been shown to extract TcO_4^- from water acidified with nitric acid into trichlorobenzene [4], as well as dibenzo-crown-6 from an acid medium into 1,2-dichloroethane or dibenzo-crown-6 and a series of related crown ethers and cryptands from alkaline media into various organic solvents [5]. In all those cases, the

* Corresponding author. Tel.: +33-1-6908-6329; fax: +33-1-6908-6640.
E-mail address: thuery@drecam.cea.fr (P. Thuéry).

0277-5387/00/$ - see front matter © 2000 Elsevier Science Ltd. All rights reserved.
PII: S0277-5387(00)00464-2

extracted species is $[M^+/H^+$: crown ether$]TcO_4^-$ ($M^+ = Na^+$, K^+). Di-*tert*-butylcyclohexyl-18-crown-6 co-extracts Sr^{2+} and TcO_4^- from a nitric acid solution into octanol [6]. Benzo-15-crown-5 (B15C5) and dibenzo-18-crown-6 (DB18C6) extract ReO_4^- into 1,2-dichloroethane by forming the compounds $[M^+(B15C5)_n]ReO_4^-$ and $[M^+DB18C6]ReO_4^-$ ($M^+ = Na^+$, K^+, NH_4^+; $n = 1, 2$), respectively [7]. The existence of such crown ether complexes was confirmed by the determination of some crystalline structures in the case of $Na^+ReO_4^-$, in which the perrhenate ion is bound to the sodium ions included in the crown ether [8,9a,b], or not bound in the case of the large wrapping tetrabenzo-24-crown-8 [9c]. Recently, the ability of a tripodal tris(amido benzo-15-crown-5) to co-extract sodium and pertechnetate ions has been demonstrated [10]. Macrocycles other than crown ethers have also been investigated for perrhenate or pertechnetate extraction. A calix[4]arene functionalized with amido groups at the 1,3-positions of the upper rim was reported to act as a poor complexant for ReO_4^- [11]. Recently, the presence of Na^+ ions in the aqueous phase has been shown to be necessary for the extraction of perrhenate ions by 25,26,27,28-tetrakis[(ethoxycarbonyl)methoxy]-*p*-*tert*-butylcalix[4]arene (L) into 1,2-dichloroethane and the corresponding extracted complex $[Na^+L]ReO_4^- \cdot H_2O$ has been prepared and characterized [12]. However, the presence of an alkali metal counter-ion may not be a requisite: the positively charged, bowl-shaped, π-metalated calix[*n*]arenes ($n = 4, 5$) and cyclotriveratrylene (CTV) have been shown to be versatile anion complexants, the latter being selective for large tetrahedral species such as ReO_4^- and TcO_4^- [13].

The simultaneous removal of technetium and caesium ions from nuclear wastes by using calix[4]arene bis(crown-6) (BC6, represented on Scheme 1) in the 1,3-alternate conformation has recently been reported by Moyer et al. in the case of alkaline solutions [14] and by some of us in the case of acidic ones [15]. The extraction experiments performed in an acidic (HNO_3) medium demonstrate that trace amounts of technetium could be recovered with different calix[4]arenes mono or bis(crown-6). All the calixcrowns investigated give distribution coefficients close to 8 except for calix[4]arene bis(naphtho-crown-6) which coextracts pertechnetate ions to a lesser extent [16]. This result is related to the ability of BC6 to selectively complex caesium ions [17]. Crystal structure determinations and molecular modeling have shown that caesium ions are held in the crown ether loops by six Cs–O bonds and are also bound to a counter-ion (generally a bidentate nitrate ion, but also iodide, which is close to TcO_4^- in terms of size and charge density [10]) [18]. It was anticipated that the interactions between caesium and pertechnetate ions were the result of the replacement of nitrate by pertechnetate counter-ions. We report in this paper the crystal structures of sodium and caesium ion (both present in nuclear wastes) complexes of BC6 obtained in an acidic medium with perrhenate counter-ions, as a model for pertechnetate ones.



Scheme 1. Calix[4]arene bis(crown-6), BC6.

2. Experimental

2.1. Synthesis

The 1,3-alternate calix[4]arene bis(crown-6) (BC6) ligand has been synthesized as already reported [17].

2.1.1. $[(Na^+ \cdot H_2O)_2BC6](ReO_4^-)_2$ (1)

A mixture of BC6 (0.13 mmol) and a large excess of $NaNO_3$ (4 mmol) and perrhenic acid (1 ml; water solution, 65–70% in weight) in 30 ml of 1:1 methanol–chloroform was refluxed for 5 h. The unreacted residue was then filtered off and the solution allowed to slowly evaporate, leading to colorless single crystals of complex **1**.

2.1.2. $[(Cs^+)_2(ReO_4^-)BC6](ReO_4^-) \cdot H_2O$ (2), $[(Cs^+)_2(ReO_4^-)(H_2O)BC6](ReO_4^-)(H_2O)_{0.5}$ (3) and $[(Cs^+)_{1.5}(ReO_4^-)BC6](ReO_4^-)_{0.5}$ (4)

A mixture of BC6 (0.12 mmol), a large excess of $CsNO_3$ (1 mmol) and perrhenic acid (100 μl; water solution, 65–70% in weight) in 20 ml of 1:1 chloroform–acetonitrile was refluxed for 2 h. The unreacted residue was then filtered off and the solution allowed to slowly evaporate. Three types of single crystal were collected in the same batch, corresponding to complexes **2**–**4**.

All the single crystals investigated in the present study were of rather low quality (particularly those of **2**), which resulted in crystal structure determinations of moderate quality (even for data collected at 100 K).

Table 1
Crystal data and structure refinement details

	1	2	3	4
Empirical formula	$C_{48}H_{64}Na_2O_{22}Re_2$	$C_{48}H_{62}Cs_2O_{21}Re_2$	$C_{96}H_{126}Cs_4O_{43}Re_4$	$C_{48}H_{60}Cs_{1.5}O_{18}Re_1.5$
M (g mol^{-1})	1411.37	1629.21	3244.41	1403.62
T (K)	100(2)	100(2)	100(2)	100(2)
Crystal system	monoclinic	monoclinic	monoclinic	monoclinic
Space group	$C2/c$	$C2/c$	$P2_1$	$C2/c$
a (Å)	17.867(2)	24.932(2)	13.856(3)	33.354(1)
b (Å)	14.7439(7)	11.4994(7)	11.514(1)	11.7655(6)
c (Å)	20.876(2)	38.348(3)	33.948(6)	26.543(1)
α (°)	90	90	90.	90
β (°)	92.225(3)	100.757(3)	96.872(6)	96.150(3)
γ (°)	90.	90	90	90
V (Å^3)	5495(4)	10 801(4)	5377(3)	10 356(4)
Z	4	8	2	8
μ (mm^{-1})	4.494	5.886	5.910	4.619
Reflections collected	17781	32190	26479	32541
Independent reflections	4826	8534	7868	8718
Observed reflections [$I>2\sigma(I)$]	3036	3902	4728	5814
R_{int}	0.079	0.076	0.092	0.142
R_1	0.076	0.098	0.070	0.085
wR_2	0.192	0.238	0.129	0.201

2.2. Crystallography

The data were collected on a Nonius Kappa-CCD area detector diffractometer [19] using graphite monochromated Mo Kα radiation (0.71073 Å). The crystals were introduced in Lindemann glass capillaries with a protecting 'Paratone' oil (Exxon Chemical Ltd.) coating. The data were processed with the HKL package [20]. The structures were solved by direct methods with SHELXS-97 [21], expanded by subsequent Fourier-difference synthesis and refined by full-matrix least-squares on F^2 with SHELXL-97 [22]. Absorption effects were corrected empirically with the program MULABS from PLATON [23]. The geometrically constrained hydrogen atoms were introduced at calculated positions (unless those of water molecules) as riding atoms, with a displacement parameter equal to 1.2 times that of the parent atom. All non-hydrogen atoms were refined anisotropically in complexes **1**, **2** and **4**, and Re, Cs and O atoms only in **3**, in order to keep a number of parameters compatible with the number of reflections. Some soft restraints on bond distances had to be applied in all four structures, particularly in the ether chains. The correct enantiomorph in **3** has been determined from the value of the Flack parameter [0.069(15)] [24]. Crystal data and structure refinement parameters are given in Table 1. The molecular drawings were done with SHELXTL [25]. All calculations were performed on a Silicon Graphics R5000 workstation.

3. Results and discussion

The asymmetric unit in **1** comprises half a molecule with a binary symmetry axis including two diametrically opposed methylene bridge carbon atoms. Such an overall geometry has already been observed, in several caesium ion and acetonitrile complexes of BC6 [18]. In the binuclear sodium nitrate complex of BC6 previously reported (**6**) [26], the complexed species is $Na^+(NO_3^-)\cdot H_2O$, the sodium atom being bound to three ether oxygen atoms, to a bidentate nitrate ion and to the water molecule. The water molecule is itself hydrogen bonded to the two ether oxygen atoms nearer to the calixarene core (hydrogen bonds inferred from the O···O distances). The main difference observed in complex **1** is that the perrhenate counter-ion is not bound to the cation. As illustrated in Fig. 1, each of the two sodium cations is loosely bound to three ether oxygen atoms with a non-optimal mean Na–O distance of 2.8(2) Å (Table 2), larger than that in **6** [distances in the range 2.44(2)–2.86(2), mean value 2.6(1) Å], in spite of the lower temperature used for the data recording in the present case. This mean value corresponds to the largest Na–O distances in crown ether complexes [9,27]. The Na–O_{water} distance is also larger in **1** [2.39(1) Å, compared to 2.18(2) and 2.24(2) Å in **6**] and corresponds to the largest of previously published values [27,28]. Conversely, the O···O hydrogen bond distances in **1** [mean value 2.69(8) Å] are lower than in **6** [mean value 2.86(3) Å]. The resulting four-coordination is rare in sodium complexes; however, one example has been given in the domain of calixarene chemistry, which is

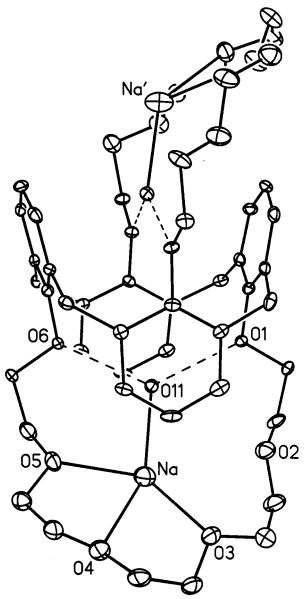


Fig. 1. Complex of BC6 with $(Na^+\cdot H_2O)ReO_4^-$ (**1**). Hydrogen bonds in dashed lines. Hydrogen atoms and perrhenate ions omitted for clarity. Primed atoms are related to unprimed ones by the binary axis.

the sodium complex of tetrakis[(ethoxycarbonyl)methoxy]calix[4]arene in the 1,3-alternate conformation [29]: in this case, the Na–O bond lengths [2.288–2.434 (mean value 2.36(6)) Å] are shorter than in **1**, probably as a result of a less rigid ligand geometry. In both cases, the existence of π-interactions involving the aromatic rings is unlikely. The sodium cation and the three bound ether oxygen atoms in **1** define a plane within ±0.290(6) Å, which makes a dihedral angle of 129.3(3)° with the mean plane defined (within ± 0.143(6) Å) by the sodium cation, the water oxygen atom and the two ether oxygen atoms hydrogen bonded to it. The concave region of the space defined by these two planes, which was occupied by the nitrate ion in **6**, is free in **1**. However, neighboring molecules are arranged so that their $Na[O_{ether}]_3$ planes are roughly parallel, with a Na···Na distance of 4.09(2) Å, comparable to those in a recently reported different sodium–calixarene complex [3.182 and 4.203 Å] [28]. The structures of **1** and **6** present some analogies with those of 18-crown-6 complexes of $(Na^+\cdot H_2O)$ recently published [30], in which intramolecular hydrogen bonds influence the sodium ion position and contribute to the stability of the complex, with the difference that the water molecule is located close to the mean plane of the crown in **1** and **6**, whereas it is positioned out of the crown in the other cases. The two perrhenate ions, which occupy voids in the lattice, are unremarkable, with a mean Re–O distance of 1.68(4) Å and a mean O–Re–O angle of 109(7)°. The conformation of the ether chain can be characterized by the sequence of torsion angles it defines, and particularly the *gauche* O–C–C–O angles sequence [31], which, in the present case, is $g^-g^+g^+g^-g^+$ (Table 3). This conformation (or its equivalent $g^+g^-g^+g^+g^-$), with *gauche* angles that may be rather far from their ideal value of 60° [departure up to 21° in **1**] and in some cases one of the *anti* C–O–C–C angles far from its ideal value [100(1)° in **1**], is the second most frequent conformation in BC6 complexes and is also observed in one of the two crowns of complex **6** [32]. On the whole, in spite of the absence of any bound counter-ion in **1**, there are only slight differences between the location of the $(Na^+\cdot H_2O)$ moiety and the ether chain conformation in **1** and **6**. We had previously assumed that, due to the lack of complemen-

Table 2
Selected bond distances (Å) [a]

1	Na–O(3)	2.75(1)	Na–O(4)	2.95(1)	Na–O(5)	2.63(1)	Na–O(11)	2.39(1)
	O(11)···O(1)	2.634(9)	O(11)···O(6)	2.748(9)				
2	Cs(1)–O(1)	3.42(1)	Cs(1)–O(2)	3.08(2)	Cs(1)–O(3)	3.53(3)	Cs(1)–O(4)	3.40(3)
	Cs(1)–O(5)	3.07(2)	Cs(1)–O(6)	3.21(1)	Cs(1)–O(14′)	3.39(2)		
	Cs(2)–O(7)	3.30(1)	Cs(2)–O(8)	2.94(3)	Cs(2)–O(9)	3.25(2)	Cs(2)–O(10)	3.21(3)
	Cs(2)–O(11)	3.19(1)	Cs(2)–O(12)	3.43(1)	Cs(2)–O(13)	3.28(2)		
3	Cs(1A)–O(1A)	3.25(2)	Cs(1A)–O(2A)	3.18(3)	Cs(1A)–O(3A)	3.25(4)	Cs(1A)–O(4A)	3.53(3)
	Cs(1A)–O(5A)	3.15(2)	Cs(1A)–O(6A)	3.36(3)	Cs(1A)–O(13A)	3.21(5)		
	Cs(2A)–O(7A)	3.77(2)	Cs(2A)–O(8A)	3.18(2)	Cs(2A)–O(9A)	3.23(2)	Cs(2A)–O(10A)	3.43(2)
	Cs(2A)–O(11A)	3.02(3)	Cs(2A)–O(12A)	3.18(2)	Cs(2A)–O(14A)	3.37(4)	Cs(2A)–O(15A)	3.38(3)
	Cs(1B)–O(1B)	3.15(2)	Cs(1B)–O(2B)	3.11(3)	Cs(1B)–O(3B)	3.22(4)	Cs(1B)–O(4B)	3.37(3)
	Cs(1B)–O(5B)	3.03(2)	Cs(1B)–O(6B)	3.22(3)		Cs(1B)–O(13B)	3.28(3)	
	Cs(2B)–O(7B)	3.49(3)	Cs(2B)–O(8B)	3.25(3)	Cs(2B)–O(9B)	3.53(3)	Cs(2B)–O(10B)	3.24(3)
	Cs(2B)–O(11B)	3.18(3)	Cs(2B)–O(12B)	3.30(2)	Cs(2B)–O(14B)	3.13(4)	Cs(2B)–O(15B)	3.55(4)
4	Cs(1)–O(1)	3.05(1)	Cs(1)–O(2)	3.16(1)	Cs(1)–O(3)	3.82(1)	Cs(1)–O(4)	4.34(2)
	Cs(1)–O(5)	3.35(1)		Cs(1)–O(6)	3.02(1)			
	Cs(2)–O(7)	3.51(1)	Cs(2)–O(8)	3.09(1)	Cs(2)–O(9)	3.36(1)	Cs(2)–O(10)	3.44(1)
	Cs(2)–O(11)	2.90(1)	Cs(2)–O(12)	3.34(1)	Cs(2)–O(13)	3.50(2)		

[a] Symmetry code: $' = x-1/2,\ 1/2+y,\ z$.

Table 3
Selected torsion angles (°)

	1	2	3		4
			Molecule A	Molecule B	
O(1)–C(1)–C(2)–O(2)	−69(1)	−62(3)	73(4)	−66(3)	−72(2)
O(2)–C(3)–C(4)–O(3)	63(2)	14(6)	−73(4)	−59(4)	77(2)
O(3)–C(5)–C(6)–O(4)	63(2)	45(4)	62(4)	63(5)	−75(1)
O(4)–C(7)–C(8)–O(5)	−57(2)	−75(3)	70(4)	68(4)	−73(2)
O(5)–C(9)–C(10)–O(6)	81(1)	61(3)	−69(3)	−63(3)	73(1)
O(7)–C(11)–C(12)–O(8)		−70(3)	62(4)	73(4)	−64(1)
O(8)–C(13)–C(14)–O(9)		35(7)	−85(4)	−70(8)	72(2)
O(9)–C(15)–C(16)–O(10)		76(3)	61(4)	−71(5)	−61(2)
O(10)–C(17)–C(18)–O(11)		−68(3)	−62(5)	60(5)	66(2)
O(11)–C(19)–C(20)–O(12)		63(3)	−60(6)	−66(4)	68(2)

tarity between Na^+ and BC6, the electrostatic interactions between the cation and its counter-ion were playing a major role [26]. Besides, molecular dynamics simulations have been reported which show evidence of a 'pulling' effect of the picrate counter-ion in the case of the sodium complex of BC6 in chloroform [33]. Even if the formation of other species in solution cannot be ruled out, the present structure can be considered as a counter-example, the nature of the complex being only slightly perturbed by the absence of a coordinated counter-ion, and, in particular, the relative positioning of Na^+ and H_2O being retained. However, this solid state structure does not give any clue concerning the complexation mechanism, in which the counter-ion might be present as an active species.

The asymmetric unit in **2** comprises one complete BC6 molecule (Fig. 2). One caesium ion is located at the center of each crown, with a mean Cs–O distance of 3.3(2) Å, comparable to those previously obtained in complexes with nitrate, thiocyanate or iodide counter-ions [18]. One of the perrhenate ions is bridging the caesium ions of neighboring molecules, which gives rise to infinite chains made of parallel molecules related one to the other by the (1/2, 1/2, 0) translation (i.e. the chains are parallel to the [110] direction). Such a formation of polymeric species has already been encountered in the caesium nitrate complex of calix[4]arene bis[-bis(1,2-phenylene)-crown-6] [34]. The coordinated anion is monodentate towards each ion, giving a resulting coordination number of 7 for the caesium cation, with $Cs–O_{perrhenate}$ distances of 3.39(2) and 3.28(2) Å. To the best of our knowledge, no crystal structure comprising a caesium–perrhenate bond has been reported up to now [35]. The two caesium ions are displaced by 0.783(8) and 0.654(8) Å from the mean planes defined by the six bonding oxygen atoms (with deviations of 0.26 and 0.15 Å, respectively), which are usual values [18]. The dihedral angles between each of the four aromatic rings and the mean plane defined by the four methylene carbon atoms are 76.7(5), 78.1(6), 79.5(4) and 77.4(5)° [mean value 78(1)°]. As in the previous structures of caesium complexes with 1,3-alternate calixarenes, the short $Cs\cdots C_{aromatic}$ distances are indicative of possible cation···π interactions, the π-cloud acting as a donor towards the soft caesium cation; among those distances, the shortest ones [3.21(3) and 3.17(3) Å for Cs(1) and Cs(2), respectively] involve the aromatic carbon atoms diametrically opposite to those bearing the oxygen atoms. The O–C–C–O torsion angles define a $g^-g^+g^+g^-g^+$ sequence in both crowns, with a low value for the first g^+ angle. Some C–O–C–C angles are rather far from the ideal value of 180°, the lowest value being 121(3)°. Such a conformation is close to that observed in **1**, and also in the caesium complexes of BC6 with other monodentate counter-ions such as NCS^- and I^- [36,37]. The second, non-bonding, per-

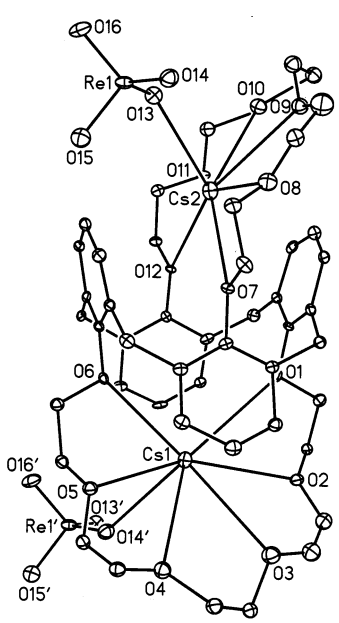


Fig. 2. View of the polymeric caesium complex **2**. Hydrogen atoms and non-coordinated perrhenate ions omitted for clarity. Symmetry code: ′ = $x - 0.5$, $0.5 + y$, z.

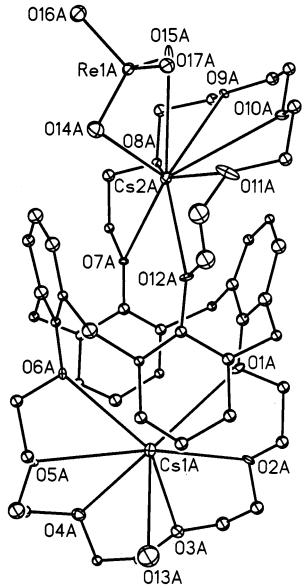


Fig. 3. View of the caesium complex **3**. Hydrogen atoms and non-coordinated perrhenate ion and water molecule omitted for clarity.

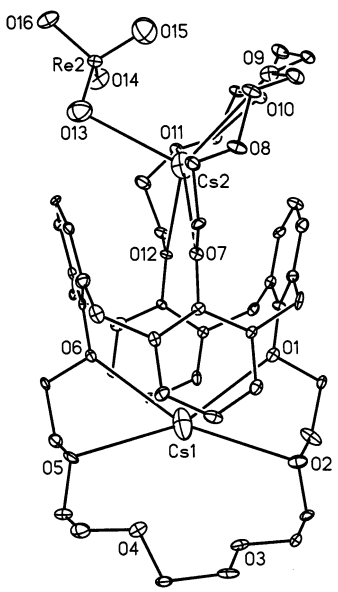


Fig. 4. View of the caesium complex **4**. Hydrogen atoms and non-coordinated perrhenate ion omitted for clarity.

rhenate ion is located on two sites with crystallographically imposed 0.5 occupation. One of them, on a symmetry center, has been interpreted as transformed from the tetrahedral ReO_4^- to an octahedral $ReO_4(H_2O)_2^-$ species, with two short Re–O distances [1.64(5) Å] and four longer ones [2.02(5) and 2.07(6) Å], two of which are likely associated with water molecules. This bis(aquo) complex of ReO_4^- can be compared with the bis(aquo) complexes of Re_2O_7, in which the $Re–O_{water}$ distances are somewhat larger (2.16–2.22 Å) [38].

The asymmetric unit in the second form obtained for the caesium perrhenate complex, **3**, comprises two independent molecules with nearly similar geometries (noted A and B). One of them is represented in Fig. 3. The coordination environment of the two caesium cations is different from the one in **2**. In both molecules A and B, the two caesium ions are located at the center of the crowns, with identical mean $Cs–O_{ether}$ distances of 3.2(1) Å for Cs(1) and 3.3(2) Å for Cs(2). One of the caesium ions [Cs(2)] is bound to a bidentate perrhenate ion with a mean Cs–O distance of 3.4(2) Å (the bonding mode is more symmetrical in molecule A than in molecule B), which results in a coordination number of 8. The other cation [Cs(1)] is bound to a water molecule (7-coordination), with Cs–O distances of 3.21(5) and 3.28(3) Å in molecules A and B, respectively (few crystal structures displaying $Cs–O_{water}$ bonds have been reported, the corresponding distances being in the range 3.013–3.660 Å [39]). This is the first occurrence of a water molecule coordinated to caesium ions in the present family of compounds. By contrast with the case of sodium ions, this water molecule occupies the usual location of the counter-ion and is not included within the calixcrown cavity, which is filled by the cation. The Cs(2) ions are located at 0.84(1) and 0.77(1) Å from the mean planes defined by the six ether oxygen atoms (deviations of 0.31 and 0.58 Å), in molecules A and B, respectively. The corresponding values for the Cs(1) ions are 0.605(7) and 0.320(8) Å (deviations of 0.35 and 0.22 Å). The dihedral angles between the aromatic rings and the mean planes defined by the methylene bridges are 74.9(7), 73.3(6), 78.1(7) and 82.5(6)° [mean value 77(4)°] in molecule A and 77.7(7), 76.4(7), 76.3(7) and 77.3(7)° [mean value 76.9(7)°] in molecule B. The crowns define the O–C–C–O torsion angles sequences $g^+g^-g^+g^+g^-$ and $g^+g^-g^+g^-g^-$ in molecule A and $g^-g^-g^+g^+g^-$ and $g^+g^-g^-g^+g^-$ in molecule B. The sequence $g^+g^-g^+g^-g^-$, with one C–O–C–C value far from 180°, is also observed in the sodium ion complex of BC6. Finally, the sequence $g^-g^-g^+g^+g^-$, with two C–O–C–C values far from 180°, has already been encountered in caesium complexes with monodentate nitrate [40] and thiocyanate [36] as counter-ions. The two non-bonding perrhenate counter-ions associated with molecules A and B are hydrogen bonded to a water molecule, which is also hydrogen bonded to one of the oxygen atoms of the complexed anion.

The case of complex **4** is even more unusual (Fig. 4). The asymmetric unit comprises one complete molecule. Two caesium ions, one of them with a 0.5 occupation factor (which corresponds to the location of the corresponding perrhenate ion on a binary axis), are complexed with different environments. Cs(2) is bound as usual to the six ether oxygen atoms [mean Cs–O distance 3.3(2) Å] and to a monodentate perrhenate ion [Cs–O distance 3.50(2) Å]. Its distance with respect to

the mean plane defined by the six oxygen atoms (deviation 0.38 Å) is 0.777(4) Å. The second cation [Cs(1)] is only bound to four ether oxygen atoms [mean Cs–O distance 3.1(1) Å, the other two distances can be considered too large for a coordinative bond] and displaced towards the calixarene aromatic cavity. The displacement of Cs(1) with respect to the usual location evidences the pulling effect of coordinated counter-ions or solvent molecules, whereas this effect was hindered in the sodium complex **1** by the co-complexation of a water molecule in the inner part of the calixcrown coordination site. This is the first occurrence of such a coordination mode in this family of compounds. The resulting coordination number is 4, which is unusual and presumably only possible in this case due to the Cs···π interactions involving the aromatic rings: the shortest $Cs(1)\cdots C_{aromatic}$ distances, involving the three carbon atoms of each ring opposite to the phenolic oxygen atom are in the range 3.14(2)–3.66(2) [mean value 3.4(2)] Å, which is the usual range. The complexation of caesium ions by polyhapto interactions in calix[4]arene systems in cone conformations has been described, with shortest Cs···C distances of 3.545(3) [41] and 3.53(1) Å [39a]. Cs(1) is located at 0.604(5) Å from the mean plane defined by the four bonding oxygen atoms (rms deviation 0.06). The calixarene core is no more distorted than in **2** and **3**, with dihedral angles between the aromatic rings and the plane defined by the four methylene bridges of 80.1(3), 76.2(3), 74.7(3) and 80.1(3)° [mean value 78(3)°], i.e. two rings more tilted than the others. The ether chains conformations correspond to O–C–C–O torsion angles sequences $g^-g^+g^-g^-g^+$ and $g^-g^+g^-g^+g^+$, for the crowns associated with Cs(1) and Cs(2), respectively, with in each case only one C–O–C–C angle value far from 180°. The peculiar coordination mode of Cs(1) is not associated with a particularly distorted crown conformation. The non-coordinated perrhenate ion is unremarkable. As a final remark, one can notice that the unit cells of **3** and **4** appear related one to the other, the expression of the cell parameters of **4** in terms of those of **3** being *c*, *b*, 2*a*, which reflects rather similar crystal packing, in spite of the chemical differences between the two compounds.

4. Conclusion

Some general conclusions can be drawn from this work, which are of interest in the scope of the perrhenate (or pertechnetate) extraction. In all the alkali-metal ion complexes reported herein, the perrhenate ion, present in excess in solution, has completely replaced the nitrate ion. ReO_4^- presents the same variety of coordination modes than NO_3^-, with a more current tendency to be non-coordinating (at least one cation is not bound in each of the caesium complexes structures **2**–**4**, whereas it has been observed only once among numerous caesium nitrate complexes [18]). An unusual phenomenon is the observation of all those coordination modes in different crystals from the same batch, which indicates that various forms are present in solution. The dissociation of the anion/cation pair observed in the case of the sodium cation is to be compared to the crystal structures reported in the cases of the tetrabenzo-24-crown-8 [9c] and 25,26,27,28-tetrakis[(ethoxycarbonyl)methoxy]-*p*-*tert*-butylcalix[4]arene [12] complexes, in which the perrhenate ion is not bound to sodium. However, in the last two cases, the origin of the dissociation is likely to be found in the high coordination number provided by the ligand (8 in both complexes) and in steric effects (the geometry of the ligand does not permit a close approach of the anion), whereas, in complex **1**, the very low coordination number and the geometry would make the anion bonding likely. These results give some clues to explain the extraction experiments. When one or two benzenic units are included in the crowns of calix[4]arene mono or bis(crown-6), a strong decrease in sodium nitrate or nitric acid extraction occurs, which is linked to the lipophilic character of the aromatic units, thus enhancing the selectivity for caesium ions [34]. On the other hand, as indicated above, the pertechnetate (or perrhenate) ions are less extracted by calix[4]arene bis(naphthocrown-6) than by the other members of the series, which all give similar extraction results. The explanation which can be proposed is that those anions, which can be more distant from the calixarene than nitrate ions, are likely to be less sensitive to the presence of aromatic units on the crown, except for the bulky and very lipophilic naphtho units.

5. Supplementary data

Crystallographic data for the structural analysis has been deposited with the Cambridge Crystallographic Data Center, deposition numbers CCDC 141077 (**1**), 141078 (**2**), 141079 (**3**) and 141080 (**4**). Copies of this information may be obtained free of charge from: The Director, CCDC, 12 Union Road, Cambridge, CB2 1EZ, UK (Fax: +44-1223-336-033; e-mail: deposit@ccdc.cam.ac.uk or www: http://www.ccdc.cam.ac.uk).

References

[1] (a) K.H. Leiser, Radiochim. Acta 63 (1993) 5. (b) E. Holm, Radiochim. Acta 63 (1993) 57. (c) M. Kubota, Radiochim. Acta 63 (1993) 91.

[2] See the special issue devoted to the chemistry of technetium and rhenium in: K. Yoshihara, T. Omori, eds., Topics Curr. Chem. 176 (1996).

[3] (a) J.L. Pierre, P. Barret, Bull. Chem. Soc. Fr. (1983) 367. (b) J. Scheeder, J.F.J. Engbersen, D.N. Reinhoudt, Rec. Trav. Chim. Pays-Bas (1996) 307. (c) P.D. Beer, Chem. Commun. (1996) 689.
[4] G.V. Korpusov, Y.S. Krylov, Radiokhimiya 26 (1984) 408.
[5] (a) M.G. Jalhoom, Radiochim. Acta 39 (1986) 195. (b) M.G. Jalhoom, J. Radioanal. Nucl. Chem. Lett. 104 (1986) 131.
[6] E.P. Horwitz, M.L. Dietz, D.E. Fisher, Solv. Extr. Ion Exch. 9 (1991) 1.
[7] X. Zhang, Z. Zhou, S. Ma, C. Shu, Solv. Extr. Ion Exch. 11 (1993) 585.
[8] (a) W.A. Herrmann, J.G. Kuchler, G. Weichselbaumer, E. Herdtweck, P. Kiprof, J. Organomet. Chem. 372 (1989) 351. (b) F. Weller, H. Borgholte, H. Stenger, S. Vogler, K. Dehnicke, Z. Naturforsch., Teil B 44 (1989) 1524.
[9] (a) J.C. Bryan, Acta Crystallogr., Sect. C 54 (1998) 1569. (b) J.C. Bryan, R.A. Sachleben, J.M. Lavis, M.C. Davis, J.H. Burns, B.P. Hay, Inorg. Chem. 37 (1998) 2749. (c) J.C. Bryan, R.A. Sachleben, B.P. Hay, Inorg. Chim. Acta 290 (1999) 86.
[10] P.D. Beer, P.K. Hopkins, J.D. McKinney, Chem. Commun. (1999) 1253.
[11] B.R. Cameron, S.J. Loeb, Chem. Commun. (1997) 573.
[12] Z. Zhou, Y. Xing, Y. Wu, J. Incl. Phenom. Macr. Chem. 34 (1999) 219.
[13] J.L. Atwood, K.T. Holman, J.W. Steed, Chem. Commun. (1996) 1401 and references therein.
[14] B.A. Moyer, P.V. Bonnesen, L.H. Delmau, T.J. Haverlock, R.A. Sachleben, R.A. Leonard, C. Conner, G.J. Lumetta, The International Solvent Extraction Conference (ISEC 99), Barcelona, Spain, July 11–16, 1999.
[15] M. Grunder, J.F. Dozol, Z. Asfari, J. Vicens, J. Radioanal. Nucl. Chem. 241 (1999) 59.
[16] J.F. Dozol, N. Simon, V. Lamare, A. Garcia Carrera, D. de Marc, S. Eymard, H. Rouquette, B. Tournois, Proceedings of the International Solvent Extraction Symposium, Moscow, Russia, June 21–27, 1998, pp. 99–108.
[17] Z. Asfari, C. Bressot, J. Vicens, C. Hill, J.F. Dozol, H. Rouquette, S. Eymard, V. Lamare, B. Tournois, Anal. Chem. 67 (1995) 3133.
[18] For a review, see: P. Thuéry, M. Nierlich, V. Lamare, J.F. Dozol, Z. Asfari, J. Vicens, J. Incl. Phenom. Macr. Chem. 36 (2000) 375.
[19] Kappa-CCD Software, Nonius B.V., Delft, The Netherlands, 1998.
[20] Z. Otwinowski, W. Minor, Methods Enzymol. 276 (1997) 307.
[21] G.M. Sheldrick, Acta Crystallogr., Sect. A 46 (1990) 467.
[22] G.M. Sheldrick, SHELXL-97: Program for the Refinement of Crystal Structures, University of Göttingen, Germany, 1997.
[23] A.L. Spek, PLATON, University of Utrecht, The Netherlands, 1998.
[24] H.D. Flack, Acta Crystallogr., Sect. A 39 (1983) 876.
[25] G.M. Sheldrick, SHELXTL, Version 5.1. University of Göttingen, Germany (distributed by Bruker AXS, Madison, Wisconsin), 1999.
[26] P. Thuéry, M. Nierlich, V. Lamare, J.F. Dozol, Z. Asfari, J. Vicens, Supramol. Chem. 8 (1997) 319.
[27] See, for example: (a) M.A. Bush, M.R. Truter, Chem. Commun. (1970) 1439. (b) M.A. Bush, M.R. Truter, J. Chem. Soc. B (1971) 1440. (c) M.A. Bush, M.R. Truter, J. Chem. Soc., Perkin Trans. 2 (1972) 341. (d) M. Mercer, M.R. Truter, J. Chem. Soc., Dalton Trans. (1973) 2215. (e) J.D. Dunitz, M. Dobler, P. Seiler, R.P. Phizackerley, Acta Crystallogr., Sect. B 30 (1974) 2733. (f) M. Dobler, J.D. Dunitz, P. Seiler, Acta Crystallogr., Sect. B 30 (1974) 2741. (g) R.D. Rogers, A.H. Bond, R.F. Henry, A.N. Rollins, Supramol. Chem. 4 (1995) 191.
[28] Z. Asfari, J.M. Harrowfield, P. Thuéry, M. Nierlich, J.E. Vicens, Aust. J. Chem. 52 (1999) 403.
[29] A. Ikeda, H. Tsuzuki, S. Shinkai, Tetrahedron Lett. 35 (1994) 8417.
[30] J.W. Steed, P.C. Junk, J. Chem. Soc., Dalton Trans. (1999) 2141.
[31] T.M. Fyles, R.D. Gandour, J. Incl. Phenom. Mol. Rec. Chem. 12 (1992) 313.
[32] P. Thuéry, M. Nierlich, J.C. Bryan, V. Lamare, J.F. Dozol, Z. Asfari, J. Vicens, J. Chem. Soc., Dalton Trans. (1997) 4191.
[33] A. Varnek, G. Wipff, Theochem. J. Mol. Struct. 363 (1996) 67.
[34] V. Lamare, J.F. Dozol, S. Fuangswasdi, F. Arnaud-Neu, P. Thuéry, M. Nierlich, Z. Asfari, J. Vicens, J. Chem. Soc., Perkin Trans. 2 (1999) 271.
[35] April 1999 release of the Cambridge Structural Database System; F.H. Allen, O. Kennard, Chem. Des. Autom. News 8 (1993) 31.
[36] P. Thuéry, M. Nierlich, C. Bressot, V. Lamare, J.F. Dozol, Z. Asfari, J. Vicens, J. Incl. Phenom. Mol. Rec. Chem. 23 (1996) 305.
[37] P. Thuéry, M. Nierlich, V. Lamare, J.F. Dozol, Z. Asfari, J. Vicens, Acta Crystallogr., Sect. C 52 (1996) 2729.
[38] (a) B. Krebs, D. Fischer, G. Paul, Z. Anorg. Allg. Chem. 622 (1996) 448. (b) W.A. Herrmann, J.D.G. Correia, F.E. Kühn, G.R.J. Artus, C.C. Romão, Chem. Eur. J. 2 (1996) 168.
[39] (a) R. Assmus, V. Böhmer, J.M. Harrowfield, M.I. Ogden, W.R. Richmond, B.W. Skelton, A.H. White, J. Chem. Soc., Dalton Trans. (1993) 2427. (b) P.J. Dutton, T.M. Fyles, V.V. Suresh, F.R. Fronczek, R.D. Gandour, Can. J. Chem. 71 (1993) 239. (c) D. Whang, J. Heo, J.H. Park, K. Kim, Angew. Chem. Int. Ed. Engl. 37 (1998) 78.
[40] Z. Asfari, C. Naumann, J. Vicens, M. Nierlich, P. Thuéry, C. Bressot, V. Lamare, J.F. Dozol, New J. Chem. 20 (1996) 1183.
[41] J.M. Harrowfield, M.I. Ogden, W.R. Richmond, A.H. White, J. Chem. Soc., Chem. Commun. (1991) 1159.

PERGAMON

www.elsevier.nl/locate/poly

Polyhedron 19 (2000) 1757–1767

POLYHEDRON

Synthesis, spectroscopic, and X-ray crystallographic characterisation of thorium(IV) and uranium(IV) malonato and substituted malonato compounds

Y.-J. Zhang [a,1], D. Collison [a], F.R. Livens [a,*], A.K. Powell [b,2], S. Wocadlo [b], H. Eccles [c]

[a] *Department of Chemistry, University of Manchester, Oxford Road, Manchester, M13 9PL, UK*
[b] *School of Chemical Sciences, University of East Anglia, Norwich, NR4 7TJ, UK*
[c] *Research and Technology, BNFL, Springfields, Salwick, Preston, PR4 0XJ, UK*

Received 15 February 2000; accepted 23 May 2000

Abstract

With doubly protonated piperazine or ethylenediamine as cations, eight Th(IV) malonato or substituted malonato complexes have been prepared and characterised by elemental analysis, thermal analysis, IR and ^{13}C CPMAS NMR spectroscopy. One polymeric U(IV) malonato complex has also been prepared and characterised by elemental analysis, thermal analysis and IR spectroscopy. $(C_4H_{12}N_2)_2[Th(C_3H_2O_4)_4]\cdot H_2O$ (**2**), $(C_2H_{10}N_2)_2[Th(C_3H_2O_4)_4(H_2O)]$ (**3**), $(C_4H_{12}N_2)_2[Th(C_4H_4O_4)_4]\cdot 2H_2O$ (**4**), $(C_2H_{10}N_2)_2[Th(C_5H_6O_4)_4]\cdot 5H_2O$ (**6**) and $[U(C_3H_2O_4)_2(H_2O)_3]_n$ (**9**) have been further characterised by single-crystal X-ray diffraction. Two types of monomeric anion structure are identified in the Th compounds: four 1,5-bidentate ligands in a distorted square antiprismatic geometry, giving coordination number (CN) 8; and four 1,5-bidentate ligands and a coordinated H_2O molecule in a capped square antiprismatic geometry, giving CN 9. The U compound has a 3D polymeric structure, with U in an approximately capped square antiprismatic geometry, achieving CN 9 from two 1,5-bidentate ligands, each of which also bridges through a carbonyl oxygen to an adjacent U centre, and three H_2O molecules. In the crystallographically-characterised Th compounds, the Th–O and C–O distances are correlated with the carbonyl resonance positions in the ^{13}C CPMAS NMR spectra, allowing prediction of structural types in the non-crystalline compounds. © 2000 Elsevier Science Ltd. All rights reserved.

Keywords: Thorium(IV); Uranium(IV); Dicarboxylate complexes; CPMAS ^{13}C NMR spectroscopy; X-ray crystallography

1. Introduction

Uranyl carboxylato complexes have been extensively studied for many years and a wide variety of structural types, including monomers, dimers, 1D infinite chains, 2D sheets and 3D polymers have been identified. It has been suggested that the structures of uranyl carboxylate compounds may be rationalised in relation to ligand size, additional functionality and stoichiometry [1]. To test this hypothesis, a systematic study of the coordination chemistry of uranyl with malonate and substituted malonates has recently been undertaken [2,3]. Structural diversity in the solid state can be achieved by varying counter-cations and by slight modification of the ligand substituent groups [2,3]. The two axial oxygen atoms of the uranyl ion confine coordination of the ligands to the equatorial plane and thus exert a considerable influence on the coordination chemistry, giving overall coordination numbers (CNs) of 6, 7 or 8. By contrast, there is no such stereochemical restriction of the coordination sphere for tetravalent actinide ions [An(IV)] [4], so a comparative study of the coordination chemistry of An(VI) and An(IV) with malonate-type ligands may aid the identification of the general principles governing of complexation of actinides by hard, O-donor chelating ligands. Unfortunately there is little relevant information in the literature and, indeed, there are no reports of structurally characterised Th(IV) or U(IV) malonato complexes. By contrast, several ox-

* Corresponding author. Tel.: +44-161-275-4642; fax: +44-161-275-4598.

E-mail address: francis.livens@man.ac.uk (F.R. Livens).

[1] Present address: ANSTO, PMB 1, Menai, NSW 2234, Australia.

[2] Present address: Institut für Anorganische Chemie, Universität Karlsruhe, Engesserstrasse Gelo 30.45, D-76128 Karlsruhe, Germany.

0277-5387/00/$ - see front matter © 2000 Elsevier Science Ltd. All rights reserved.
PII: S0277-5387(00)00465-4

alato complexes of U(IV) and Th(IV) are well-characterised [5–7], although synthetic and structural differences from the malonato analogues might now be expected. In this paper we report the synthesis of eight Th(IV) and one U(IV) malonato or substituted malonato compounds, the further characterisation of these compounds by spectroscopic techniques and, in five cases, by X-ray crystallography.

2. Experimental

2.1. Synthesis

All chemicals were reagent grade, purchased from Strem Chemicals, Aldrich or Lancaster and used without further purification unless otherwise specified. Reactions were carried out in hydroxylic media (H_2O and MeOH) with an initial metal to ligand ratio of 1:2 for **1** and 1:4 for the other preparations. All manipulations of U(IV) were carried out in a dinitrogen atmosphere.

2.2. Preparation of bis(malonato)thorium(IV) trihydrate

$Th(C_3H_2O_4)_2{\cdot}3H_2O$ (**1**). A solution of thorium nitrate tetrahydrate (0.55 g, 1 mmol in 5 cm^3 H_2O) was added to a solution of malonic acid (0.21 g, 2 mmol) in H_2O (30 cm^3). A white solid product formed after a few hours, was collected by filtration and dried in air, yield 95%. *Anal.* Found: C, 15.00, H, 2.00, Th, 47.55. Calc. for $C_6H_{10}O_{11}Th$: C, 14.70, H, 2.08, Th, 47.34%. IR (KBr disc, cm^{-1}): 3373 s(br), 1592 vs(br), 1553 w, 1452 m, 1384 w, 1360 m, 1272 m, 1186 w, 988 w, 956 w, 801 w, 709 m, 610 w, 541 w, 450 w). TG/DTA: 186°C (-11.0%, endo, $-3H_2O = 10.8\%$), 334°C (-24.4%, exo), residue 56.0%, $ThO_2 = 53.8\%$).

2.3. Preparation of bis(piperazinium) tetrakis(malonato)thorate(IV) monohydrate

$(C_4H_{12}N_2)_2[Th(C_3H_2O_4)_4]{\cdot}H_2O$ (**2**). A solution of thorium nitrate tetrahydrate (0.55 g, 1 mmol in 5 cm^3 H_2O) was added to a solution of malonic acid and piperazine (0.42 g, 4 mmol and 0.76 g, 4 mmol, respectively) in H_2O (30 cm^3). The solution was left to stand for a week. A colourless crystalline product, formed by dropwise addition of MeOH (ca. 20 cm^3), was collected by filtration and dried in air, yield 50%. *Anal.* Found: C, 28.52, H, 4.27, N, 6.59, Th, 27.30. Calc. for $C_{20}H_{34}N_4O_{17}Th$: C, 28.78, H, 4.11, N, 6.71, Th, 27.81%. IR (KBr disc, cm^{-1}): 3374 m, 3248 w, 3026 w, 1673 m, 1613 vs (br), 1413 w, 1381 m, 1316 w, 1289 w, 1203 w, 1086 w, 953 m, 934 m, 866 w, 702 s, 583 m). TG/DTA: 107°C (-4.3%, endo, $-H_2O = 4.2\%$), 214°C (endo), 309 and 399°C (-62.5%, both exo), residue 33.2%, $ThO_2 = 31.0\%$).

2.4. Preparation of bis(ethylenediammonium) tetrakis(malonato)aquathorate(IV)

$(C_2H_{10}N_2)_2[Th(C_3H_2O_4)_4(H_2O)]$ (**3**). A solution of thorium nitrate tetrahydrate (0.55 g, 1 mmol in 5 cm^3 H_2O) was added to a solution of malonic acid and ethylenediamine (0.42 g, 4 mmol and 0.28 cm^3, 4 mmol, respectively) in H_2O (30 cm^3). The solution was left to stand for a week. A white crystalline product, formed by dropwise addition of MeOH (ca. 20 cm^3), was collected by filtration and dried in air, yield 85%. *Anal.* Found: C, 24.63, H, 4.00, N, 7.27, Th, 29.52. Calc. for $C_{16}H_{30}N_4O_{17}Th$: C, 24.56, H, 3.86, N, 7.16, Th, 29.65%. IR (KBr disc, cm^{-1}): 3457 vs (br), 1593 vs (br), 1426 m, 1350 w, 1274 w, 1197 w, 963 w, 936 w, 713 w). TG/DTA: 172°C (-2.5%, endo, $-H_2O = 2.2\%$), 204°C (endo), 342 and 419°C (-61.2%, both exo), residue 36.3%, $ThO_2 = 33.7\%$).

2.5. Preparation of bis(piperazinium) tetrakis(methylmalonato)thorate(IV) dihydrate

$(C_4H_{12}N_2)_2[Th(C_4H_4O_4)_4]{\cdot}2H_2O$ (**4**). A solution of thorium nitrate tetrahydrate (0.55 g, 1 mmol in 5 cm^3 H_2O) was added to a solution of methylmalonic acid and piperazine (0.48 g, 4 mmol and 0.76 g, 4 mmol, respectively) in H_2O (30 cm^3). A white solid product formed after few days, was collected by filtration and dried in air, yield 85%. *Anal.* Found: C, 32.00, H, 5.00, N, 6.26, Th, 25.69. Calc. for $C_{24}H_{44}N_4O_{18}Th$: C, 31.72, H, 4.88, N, 6.16, Th, 25.54%. IR (KBr disc, cm^{-1}): 3478 m (br), 3248 w, 3004 w, 1625 s, 1597 s, 1414 s, 1350 m, 1281 m, 1011 m, 931 m, 869 w, 768 w, 684 m, 585 w). TG/DTA: 140°C (-3.7%, endo, $-2H_2O = 3.9\%$), 226°C (endo), 320°C (exo, -64.4%), residue 31.7%, $ThO_2 = 29.1\%$).

2.6. Preparation of bis(piperazinium)tetrakis(dimethylmalonato)thorate(IV)

$(C_4H_{12}N_2)_2[Th(C_5H_6O_4)_4]$ (**5**). A solution of thorium nitrate tetrahydrate (0.55 g, 1 mmol in 5 cm^3 H_2O) was added to a solution of dimethylmalonic acid and piperazine (0.52 g, 4 mmol and 0.76 g, 4 mmol, respectively) in H_2O (30 cm^3). A white solid product formed overnight, was collected by filtration and dried in air, yield 80%. *Anal.* Found: C, 35.93, H, 5.14, N, 5.98, Th, 24.61. Calc. for $C_{28}H_{48}N_4O_{16}Th$: C, 36.21, H, 5.21, N, 6.03, Th, 24.98%. IR (KBr disc, cm^{-1}): 3458 m (br), 3000 w, 2454 w, 1636 vs, 1596 w, 1562 m, 1466 m, 1406 s, 1353 s, 1299 m, 1206 s, 1089 w, 897 s, 803 w, 768 w, 689 m, 586 w, 504 w). TG/DTA: 259°C [-42.9%, endo, $-2(\text{cation} + \text{ligand}) = 42.7\%$], 383°C (exo, -27.0%), residue 30.1%, $ThO_2 = 28.4\%$).

2.7. Preparation of bis(ethylenediammonium) tetrakis(dimethylmalonato)thorate(IV) pentahydrate

$(C_2H_{10}N_2)_2[Th(C_5H_6O_4)_4]\cdot 5H_2O$ (**6**). A solution of thorium nitrate tetrahydrate (0.55 g, 1 mmol in 5 cm^3 H_2O) was added to a solution of dimethylmalonic acid and ethylenediamine (0.52 g, 4 mmol and 0.28 cm^3, 4 mmol, respectively) in H_2O (30 cm^3). A white crystalline product formed after a week, was collected by filtration and dried in air, yield 65%. *Anal.* Found: C, 30.30, H, 5.65, N, 6.00, Th, 24.01. Calc. for $C_{24}H_{54}N_4O_{21}Th$: C, 29.82, H, 5.63, N, 5.79, Th, 24.00%. IR (KBr disc, cm^{-1}): 3451 vs (br), 1632 vs, 1561 w, 1460 w, 1402 s, 1385 w, 1352 m, 1200 m, 892 m, 795 w, 720 w, 688 w, 582 w). TG/DTA: 55°C (-2.1%, endo, $-H_2O = 2.0$%), 228°C (endo), 362°C (exo, -66.8%), residue 31.2%, $ThO_2 = 29.5$%).

2.8. Preparation of bis(piperazinium) tetrakis(diethylmalonato)thorate(IV) hexahydrate

$(C_4H_{12}N_2)_2[Th(C_7H_{10}O_4)_4]\cdot 6H_2O$ (**7**). A solution of thorium nitrate tetrahydrate (0.55 g, 1 mmol in 5 cm^3 H_2O) was added to a solution of diethylmalonic acid and piperazine (0.64 g, 4 mmol and 0.76 g, 4 mmol, respectively) in H_2O (30 cm^3). After a few hours, a white solid product formed, which was collected by filtration and dried in air, yield 70%. *Anal.* Found: C, 37.35, H, 6.35, N, 4.74, Th, 19.94. Calc. for $C_{36}H_{76}N_4O_{22}Th$: C, 37.63, H, 6.67, N, 4.88, Th, 20.19%. IR (KBr disc, cm^{-1}): 3468 vs (br), 3247 m, 2975 w, 1636 m, 1613 s, 1461 w, 1441 w, 1381 s, 1316 m, 1271 w, 1176 w, 1087 w, 1061 w, 950 m, 814 m, 742 w, 704 w, 570 w). TG/DTA: 64°C (-9.5%, endo, $-6\ H_2O = 9.4$%), 235°C (-39.3%, endo, -2(cation + ligand) = 40.0%], 390°C (exo, -24.4%), residue 25.8%, $ThO_2 = 23.0$%).

2.9. Preparation of bis(ethylenediammonium) tetrakis(diethylmalonato)thorate(IV) monohydrate

$(C_2H_{10}N_2)_2[Th(C_7H_{10}O_4)_4]\cdot H_2O$ (**8**). A solution of thorium nitrate tetrahydrate (0.55 g, 1 mmol in 5 cm^3 H_2O) was added to a solution of diethylmalonic acid and ethylenediamine (0.64 g, 4 mmol and 0.28 cm^3, 4 mmol, respectively) in H_2O (30 cm^3). A white crystalline product formed after a few days, and was collected by filtration and dried in air, yield 75%. *Anal.* Found: C, 37.98, H, 5.86, N, 5.33, Th, 23.23%. Calc. for $C_{32}H_{62}N_4O_{17}Th$: C, 38.32, H, 5.83, N, 5.59, Th, 23.14%. IR (KBr disc, cm^{-1}): 3475 vs (br), 1638 s, 1619 s, 1384 s, 1318 w, 1274 w, 946 m, 818 m, 704 w, 581 w). TG/DTA: 61°C (-2.3%, endo, $-H_2O = 2.2$%), 239°C [-37.7%, endo, -2(cation + ligand) = 38.5%], 400°C (exo, -32.5%), residue 27.5%, $ThO_2 = 26.3$%).

2.10. Preparation of triaquabis(malonato)uranium(IV)

$[U(C_3H_2O_4)_2\cdot(H_2O)_3]_n$ (**9**). Uranium(IV) chloride (UCl_4) was prepared following a published method by reaction of UO_3 with excess hexachloropropene [8]. A solution of uranium(IV) chloride (0.38 g, 1 mmol in 5 cm^3 H_2O) was added to a solution of malonic acid and ethylenediamine (0.42 g, 4 mmol and 0.28 cm^3, 4 mmol, respectively) in H_2O (35 cm^3) under a dinitrogen atmosphere. A grey precipitate formed immediately and was redissolved by adding malonic acid (0.21 g, 2 mmol in 5 cm^3 H_2O). A dark green crystalline product formed after few weeks and was collected by filtration and vacuum dried in a desiccator, yield 50%. *Anal.* Found: C, 14.72, H, 2.00, U, 47.71. Calc. for $C_6H_{10}O_{11}U$: C, 14.53, H, 2.02, U, 47.98%. IR (cm^{-1}): 3317 s (br), 1589 s, 1563 s, 1449 m, 1361 m, 1264 w, 1168 w, 953 m, 808 w, 768 w, 649 w). TG/DTA: 61°C (-2.3%, endo, $-H_2O = 2.2$%), 239°C (-37.7%, endo, -2(cation + ligand) = 38.5%), 400°C (exo, -32.5%), residue 27.5%, $UO_2 = 26.3$%).

2.11. Crystallography, thermoanalysis and ^{13}C CPMAS NMR spectroscopy

Crystallographic data for compounds **2**–**4**, **6** and **9** were collected and analysed as summarised in Table 1. Thermogravimetric and differential thermal analysis was carried out on a Seiko (TG/DTA 220) Thermal Analyser over a temperature range from ambient to approximately 600°C, at a heating rate of 10 C min^{-1} and an air flow rate of 100 cm^3 min^{-1}. High resolution ^{13}C NMR spectra were recorded at 75.4 MHz using the cross polarisation-magic angle spinning (CPMAS) technique on a Varian Unity-300 spectrometer with a spinning speed of ca. 4.0 kHz. The acquisition time was 0.050 s, spectral width was 30 007.5 Hz, contact time was 1.5 ms and recycle time was 3.000 s. The chemical shift scale was referenced by setting the CH_3 peak in a sample of solid hexamethylbenzene, run using the same conditions, to 16.5 ppm.

3. Results

3.1. Synthesis

The effects of initial metal:ligand (M:L) ratio and of the presence of N-base can be illustrated using malonic acid as proligand and piperazine as an N-base. In the case of Th, if the proligand is not neutralised to produce a countercation, the neutral product **1** with M:L = 1:2 forms, regardless of the initial M:L ratio. If the malonic acid is neutralised by piperazine, the products vary according to the initial M:L ratio. The 1:2 neutral product forms from a starting stoichiometry of

Table 1
X-ray crystallographic results for **2**, **3**, **4**, **6** and **9**

	2	**3**	**4**	**6**	**9**
Crystal	colourless block	white block	white block	white block	dark green block
Dimensions (mm)	$0.15\times0.13\times0.11$	$0.11\times0.0870.03$	$0.15\times0.1070.06$	$0.11\times0.06\times0.04$	$0.11\times0.08\times0.06$
Molecular formula	$(C_4H_{12}N_2)_2$-$[Th(C_3H_2O_4)_4]\cdot H_2O$	$(C_2H_{10}N_2)_2$-$[Th(C_3H_2O_4)_4(H_2O)]$	$(C_4H_{12}N_2)_2$-$[Th(C_4H_4O_4)_4]\cdot 2H_2O$	$(C_2H_{10}N_2)_2$-$[Th(C_5H_6O_4)_4]\cdot 5H_2O$	$[U(C_3H_2O_4)_2$-$(H_2O)_3]_n$
Unit cell parameters					
a (Å)	16.6110(10)	9.649(2)	10.378(1)	11.760(5)	15.9170(10)
b (Å)	8.8530(10)	11.150(2)	16.699(1)	11.901(4)	15.9170(4)
c (Å)	20.4630(10)	11.805(2)	19.138(1)	14.399(9)	8.9100(4)
α (°)	90.00	96.408(12)	90.00	106.34(2)	90.00
β (°)	105.700(4)	96.130(13)	90.00	99.87(4)	90.00
γ (°)	90.00	98.390(13)	90.00	109.36(2)	90.00
Wavelength (Å)	0.71073	0.71073	0.71073	0.71073	0.71073
Crystal system	monoclinic	triclinic	orthorhombic	triclinic	tetragonal
Space group	$C2/c$	P	$Ccca$	P	I-42d
N	4	2	4	2	8
Diffractometer	Rigaku Raxis II	Rigaku Raxis II	Rigaku Raxis II	Rigaku Raxis II	Rigaku Raxis II
Method (θ range, °)	ω–2θ (2.63–24.72)	ω–2θ (2.15–23.00)	ω–2θ (3.14–24.69)	ω–2θ (1.95–24.73)	ω–2θ (2.57–24.82)
Reflections collected	3882	4156	9593	10 658	3517
Number of unique reflections	2220	3438	1415	5560	967
R_{int}	0.0147	0.0315	0.0528	0.0358	0.0449
Number of observed reflections	2142 [$I>2\sigma(I)$]	3141 [$I>2\sigma(I)$]	1184 [$I>2\sigma(I)$]	4755 [$I>2\sigma(I)$]	964 [$I>2\sigma(I)$]
Absorption correction	empirical	empirical	empirical	empirical	empirical
R	0.0163	0.0314	0.0181	0.0304	0.0168
R_w	0.0409	0.0737	0.0492	0.0786	0.0428
Number of parameters	195	363	109	416	83
Refinement	full least-squares on F^2	full least-squares on F^2	full least-squares on F^2	full least-squares on F^2	full least-squares on F^2
H atom positions	calculated	calculated	calculated	calculated	calculated

1:2, while the 1:4 anionic product forms with an initial stoichiometry of 1:4 or higher. In all cases, there is no evidence of NO_3^- being retained as a ligand in the resultant solid products. By contrast, the U compound **9**, with M:L = 1:2, forms under conditions which, in the case of Th, led to the 1:4 compound **3**.

3.2. Crystallography

Selected bond lengths and angles for **2**–**4**, **6** and **9** are listed in Tables 2–6. The asymmetric unit of **2** contains half of the molecule and the other half can be generated by a twofold symmetry operation. The cation is unexceptional. The anion structure is shown in Fig. 1. The thorium atom is eight-coordinate with four terminal 1,5-bidentate ligands, giving a monomeric structure. It has a distorted square antiprismatic geometry with significantly different Th–O distances, 2.337(2) Å for O(1), an average of 2.395(2) Å for the O(5) and O(7) atoms from the same ligand and 2.450(2) Å for O(3). The ligands have boat conformations flattened at the Th end.

The asymmetric unit of **3** contains a whole molecule with one cation unexceptional and the other disordered. The anion structure is shown in Fig. 2. The thorium atom is coordinated by four 1,5-bidentate malonate ligands and one H_2O molecule, giving the thorium atom a CN of 9. It has approximately a mono-capped

Table 2
Selected bond lengths (Å) and angles (°) for **2** (A - symmetry equivalent atoms)

Th(1)–O(1)	2.337(2)	Th(1)–O(7)	2.392(2)
Th(1)–O(5)	2.395(2)	Th(1)–O(3)	2.450(2)
O(1)–C(1)	1.296(4)	O(3)–C(3)	1.265(4)
O(5)–C(4)	1.274(3)	O(7)–C(6)	1.266(4)
O(1)–Th(1)–O(3)	70.79(8)	O(1)–Th(1)–O(3A)	75.43(9)
O(5)–Th(1)–O(3)	138.59(8)	O(5)–Th(1)–O(3A)	72.19(8)
O(1)–Th(1)–O(1A)	100.3(2)	O(7)–Th(1)–O(7A)	100.06(13)
O(1)–Th(1)–O(7)	146.16(8)	O(1)–Th(1)–O(7A)	89.57(9)
O(1)–Th(1)–O(5)	81.35(8)	O(1)–Th(1)–O(5A)	141.13(7)
O(7)–Th(1)–O(3)	142.90(8)	O(7)–Th(1)–O(3A)	77.56(9)
O(7)–Th(1)–O(5)	71.19(7)	O(7)–Th(1)–O(5A)	72.10(8)
O(3)–Th(1)–O(3A)	126.12(13)		

Table 3
Selected bond lengths (Å) and angles (°) for **3**

Th(1)–O(2)	2.400(5)	Th(1)–O(13)	2.404(5)	Th(1)–O(6)	2.422(5)
Th(1)–O(1)	2.424(5)	Th(1)–O(5)	2.429(5)	Th(1)–O(9)	2.447(5)
Th(1)–O(14)	2.449(5)	Th(1)–O(10)	2.469(5)	Th(1)–O(17)	2.564(5)
O(1)–C(1)	1.272(8)	O(2)–C(3)	1.278(9)	O(5)–C(4)	1.272(8)
O(6)–C(6)	1.270(8)	O(9)–C(7)	1.276(8)	O(10)–C(9)	1.257(9)
O(13)–C(10)	1.241(11)	O(14)–C(12)	1.280(9)		
O(2)–Th(1)–O(13)	141.6(2)	O(2)–Th(1)–O(6)	137.3(2)	O(13)–Th(1)–O(6)	77.6(2)
O(2)–Th(1)–O(1)	69.8(2)	O(13)–Th(1)–O(1)	137.8(2)	O(6)–Th(1)–O(1)	90.5(2)
O(2)–Th(1)–O(5)	99.7(2)	O(13)–Th(1)–O(5)	74.9(2)	O(6)–Th(1)–O(5)	70.1(2)
O(1)–Th(1)–O(5)	138.6(2)	O(2)–Th(1)–O(9)	74.4(2)	O(13)–Th(1)–O(9)	85.3(2)
O(6)–Th(1)–O(9)	139.8(2)	O(1)–Th(1)–O(9)	78.2(2)	O(5)–Th(1)–O(9)	139.4(2)
O(2)–Th(1)–O(14)	129.7(2)	O(13)–Th(1)–O(14)	68.9(2)	O(6)–Th(1)–O(14)	69.9(2)
O(1)–Th(1)–O(14)	68.9(2)	O(5)–Th(1)–O(14)	130.4(2)	O(9)–Th(1)–O(14)	70.0(2)
O(2)–Th(1)–O(10)	71.8(2)	O(13)–Th(1)–O(10)	70.5(2)	O(6)–Th(1)–O(10)	134.4(2)
O(1)–Th(1)–O(10)	134.9(2)	O(5)–Th(1)–O(10)	70.7(2)	O(9)–Th(1)–O(10)	69.3(2)
O(14)–Th(1)–O(10)	123.7(2)	O(2)–Th(1)–O(17)	68.3(2)	O(13)–Th(1)–O(17)	137.3(2)
O(6)–Th(1)–O(17)	69.5(2)	O(1)–Th(1)–O(17)	70.2(2)	O(5)–Th(1)–O(17)	68.8(2)
O(9)–Th(1)–O(17)	137.3(2)	O(14)–Th(1)–O(17)	120.8(2)	O(10)–Th(1)–O(17)	115.5(2)

square antiprismatic geometry (Fig. 3), with the capped square face of the antiprism being more planar than the uncapped one. The average Th–O distances are 2.416(5) Å for O(2), O(1), O(6) (which comprise the capped face) and O(5), 2.448(5) Å for O(9) and O(14), 2.469(5) Å for O(10) and 2.564(5) Å for O(17), the H_2O molecule. One ligand has a boat conformation while the other three are puckered.

The asymmetric unit of **4** contains a quarter of the molecule and the other three quarters can be generated by three twofold symmetry operations. The cation is unexceptional. The anion structure is shown in Fig. 4. The thorium atom is coordinated by four 1,5-bidentate methylmalonate ligands, giving a monomeric structure with the thorium atom in eight-coordination and Th–O distances of 2.393(2) Å for O(1) and 2.406(2) Å for O(2). It has a distorted square antiprismatic geometry and the ligand is puckered, so no typical conformation can be assigned to it.

The asymmetric unit of **6** contains a whole molecule with two slightly different cations. The anion structure is shown in Fig. 5. The thorium atom is coordinated by four 1,5-bidentate ligands giving the thorium atom a CN of 8. It has a distorted square antiprismatic geometry with Th–O distances ranging from 2.372(5) Å for O(5) to 2.448(5) Å for O(2). One ligand has a boat conformation flatted at the Th end, but the other three ligands are puckered and no typical conformations can be assigned to them.

Selected bond lengths and angles for **9** are listed in Table 5. The asymmetric unit consists of a uranium atom located on a twofold axis along the U–O(6) direction, a 1,5-bidentate ligand and two-coordinated H_2O molecules. The full structure is generated by the twofold symmetry and the coordination polyhedron of uranium is shown in Fig. 6. The uranium atom has, approximately, a mono-capped square antiprismatic geometry (Fig. 7), with the two remaining coordination positions filled by carbonyl oxygen atoms, O(4) and O(4A), one of which, O(4), is the capping atom. The CN of 9 [2 O(1), 2 O(2), 2 O(3), 2 O(4) and 1 O(6)] is achieved through two tridentate ligands (1,5-bidentate to one uranium atom and μ_1 bridging to another uranium atom through a third O atom of one carboxylate group) and three H_2O molecules, forming a 3D polymeric structure. The U–O distances for the chelate malonate ligand are 2.315(4) Å for O(3) and 2.434(4) Å for O(2). For the bridging O atom, O(4), the U–O distance is 2.420(4) Å. There are two kinds of coordinated H_2O molecules, one O(6) with a U–O distance of 2.414(5) Å and two symmetry equivalent O(1)'s with a longer U–O distance (2.483(4) Å). The chelate malonate ligand has a boat conformation flattened at the U end.

4. Discussion

4.1. Structural comparison

Several tetrakis(oxalato)thorate(IV) and uranate(IV) compounds have been previously characterised by X-

Table 4
Selected bond lengths (Å) and angles (°) for **4** (A, B, C - symmetry equivalent atoms)

Th(1)–O(1)	2.393(2)	Th(1)–O(2)	2.406(2)
O(1)–C(1)	1.283(4)	O(2)–C(3)	1.284(4)
O(1)–Th(1)–O(2)	69.60(6)	O(1)–Th(1)–O(1A)	74.22(8)
O(1)–Th(1)–O(1B)	122.18(8)	O(1)–Th(1)–O(1C)	137.69(8)
O(2A)–Th(1)–O(2)	148.52(8)	O(1)–Th(1)–O(2B)	75.65(6)
O(1)–Th(1)–O(2C)	79.35(6)		

Table 5
Selected bond lengths (Å) and angles (°) for **6**

Th(1)–O(5)	2.372(5)	Th(1)–O(14)	2.391(5)	Th(1)–O(6)	2.396(5)
Th(1)–O(9)	2.398(5)	Th(1)–O(13)	2.408(5)	Th(1)–O(1)	2.416(6)
Th(1)–O(10)	2.430(5)	Th(1)–O(2)	2.448(5)	O(1)–C(1)	1.274(10)
O(2)–C(3)	1.295(9)	O(5)–C(6)	1.297(9)	O(6)–C(8)	1.252(9)
O(9)–C(13)	1.251(9)	O(10)–C(11)	1.282(9)	O(13)–C(18)	1.293(9)
O(14)–C(16)	1.302(10)				
O(5)–Th(1)–O(14)	74.5(2)	O(5)–Th(1)–O(6)	69.9(2)	O(14)–Th(1)–O(6)	102.6(2)
O(5)–Th(1)–O(9)	141.4(2)	O(14)–Th(1)–O(9)	92.9(2)	O(6)–Th(1)–O(9)	148.4(2)
O(5)–Th(1)–O(13)	122.3(2)	O(14)–Th(1)–O(13)	70.3(2)	O(6)–Th(1)–O(13)	75.1(2)
O(9)–Th(1)–O(13)	84.8(2)	O(5)–Th(1)–O(1)	81.4(2)	O(14)–Th(1)–O(1)	149.7(2)
O(6)–Th(1)–O(1)	85.5(2)	O(9)–Th(1)–O(1)	94.9(2)	O(13)–Th(1)–O(1)	139.5(2)
O(5)–Th(1)–O(10)	72.6(2)	O(14)–Th(1)–O(10)	79.2(2)	O(6)–Th(1)–O(10)	140.3(2)
O(9)–Th(1)–O(10)	69.2(2)	O(13)–Th(1)–O(10)	138.7(2)	O(1)–Th(1)–O(10)	76.3(2)
O(5)–Th(1)–O(2)	134.9(2)	O(14)–Th(1)–O(2)	142.8(2)	O(6)–Th(1)–O(2)	75.8(2)
O(9)–Th(1)–O(2)	75.3(2)	O(13)–Th(1)–O(2)	73.5(2)	O(1)–Th(1)–O(2)	
O(10)–Th(1)–O(2)	125.9(2)				

Table 6
Selected bond lengths (Å) and angles (°) for **9** (A, B, C, D - symmetry equivalent atoms)

U(1)–O(3)	2.315(4)	U(1)–O(6)	2.414(5)	U(1)–O(4B)	2.420(4)
U(1)–O(2)	2.434(4)	U(1)–O(1)	2.483(4)	O(2)–C(3)	1.260(6)
O(3)–C(1)	1.265(6)	O(4)–C(3)	1.262(7)	O(5)–C(1)	1.248(7)
O(3)–U(1)–O(3A)	144.9(2)	O(3)–U(1)–O(6)	72.43(10)	O(3)–U(1)–O(4B)	128.4(2)
O(6)–U(1)–O(4B)	115.25(10)	O(3)–U(1)–O(4C)	68.7(2)	O(4B)–U(1)–O(4C)	129.5(2)
O(3)–U(1)–O(2A)	97.99(13)	O(3)–U(1)–O(2)	70.10(13)	O(6)–U(1)–O(2)	70.52(10)
O(4B)–U(1)–O(2)	66.26(12)	O(4C)–U(1)–O(2)	133.39(13)	O(2A)–U(1)–O(2)	141.0(2)
O(3)–U(1)–O(1A)	136.11(14)	O(2)–U(1)–O(1A)	137.15(14)	O(3)–U(1)–O(1)	75.1(2)
O(6)–U(1)–O(1)	140.23(11)	O(4B)–U(1)–O(1)	69.68(14)	O(4C)–U(1)–O(1)	72.04(13)
O(2)–U(1)–O(1)	77.3(2)	O(1A)–U(1)–O(1)	79.5(2)	C(3)–O(2)–U(1)	137.2(3)
C(1)–O(3)–U(1)	141.6(4)	C(3)–O(4)–U(1D)	147.4(4)	O(5)–C(1)–O(3)	121.2(5)
O(5)–C(1)–C(2)	119.7(5)	O(3)–C(1)–C(2)	119.1(5)	C(1)–C(2)–C(3)	115.5(4)
O(2)–C(3)–O(4)	123.4(5)	O(2)–C(3)–C(2)	119.4(5)	O(4)–C(3)–C(2)	117.2(5)

ray crystallography [5–7]. Structural data for $K_4[Th(C_2O_4)_4]\cdot 4H_2O$ (**10**), $K_4[U(C_2O_4)_4]\cdot 4H_2O$ (**11**) and $Ba_2[U(C_2O_4)_4(H_2O)]\cdot 7H_2O$ (**12**) together with those of the thorium(IV) malonato and substituted malonato compounds characterised in this study are summarised in Table 7. Compounds **10** and **11** are isostructural, with the metal centres coordinated by three 1,4-bidentate oxalate ligands and two tetradentate bridging ligands, forming an infinite chain structure with thorium or uranium in ten-coordination, approximately in a bicapped square antiprismatic geometry. With this relatively high CN, the coordination sphere is crowded, giving long average M–O distances (2.49(2) Å for Th–O and 2.467(8) Å for U–O). For the barium compound (**12**), monomeric $[U(C_2O_4)_4(H_2O)]^{4-}$ anions with four 1,4-bidentate oxalate ligands and a coordinated H_2O molecule were identified [7], suggesting that the size and coordination polyhedron of the cations are an important control on structural type. In the Th malonates, the size of the protonated N-base cations may thus lead to the eight- and nine-coordinate monomeric structures observed.

There is a strong correlation between CN and mean Th–O distance (Fig. 8), with an increase of 1 in CN

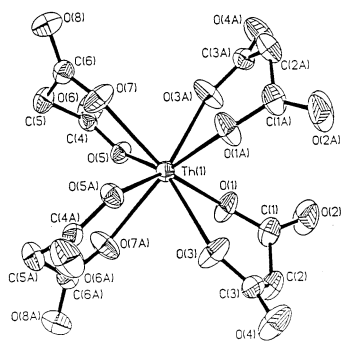


Fig. 1. An ORTEP drawing of the anion structure in **2** (50% probability ellipsoids).

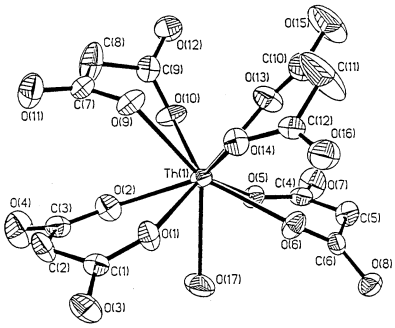


Fig. 2. An ORTEP drawing of the anion structure in **3** (50% probability ellipsoids).

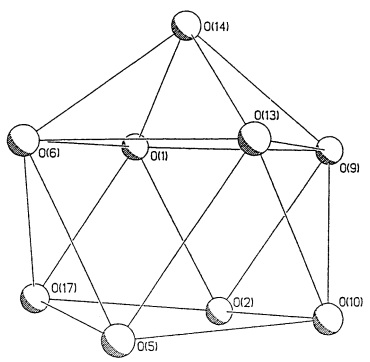


Fig. 3. Coordination polyhedron of Th in **3**.

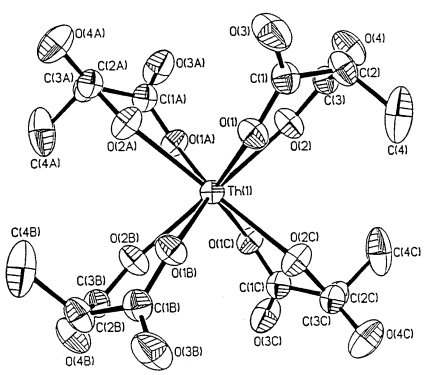


Fig. 4. An ORTEP drawing of the anion structure in **4** (50% probability ellipsoids).

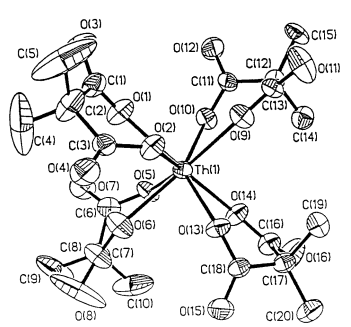


Fig. 5. An ORTEP drawing of the anion structure in **6** (50% probability ellipsoids).

leading to an increase of around 0.04 Å in mean interatomic distance. There is also apparently a similar relationship for the U compounds although, for a given CN, the U–O distance is around 0.04 Å shorter than the Th–O distance, consistent with the smaller radius of the U^{4+} cation. This relationship also suggests that the mean U–O distance in an eight-coordinate U^{4+} oxalate or malonate complex would be around 2.36 Å, which is perhaps a little short to permit easy adoption of such a CN.

Recent EXAFS studies of the coordination of tetravalent actinide ions with water and carbonate ligands have given first shell coordination numbers and distances of 10.8 at 2.45 for Th with H_2O [9], 10.8 at 2.42 for U with H_2O [9], 11.2 at 2.40 for Np with H_2O [10] and 10 at 2.42 for $[Pu(CO_3)_5]^{6-}$ [11]. There is no obvious reflection of the actinide contraction in these CNs although this may be a result of the uncertainties in the EXAFS analysis, which is typically ± 1. However, in the aquo complexes there is perhaps evidence of a decrease in interatomic distance from Th to Np. These ligands are clearly much more compact than malonate and in the malonate complexes described here, the larger size of the ligands would be expected to lead to longer interatomic distances for relatively lower CNs.

4.2. Thermogravimetric and differential thermoanalysis

The compounds decompose in two main steps, the first being dehydration and the second decomposition of organic components to leave a final residue of the dioxide [12,13]. In principle, this gives a method of distinguishing between ligating and lattice water molecules and hence can give an indication of CN.

Compounds **2**, **4** and **6** have monomeric anion structures with CN 8 and lose their lattice H_2O molecules at 107, 140 and 55°C, respectively. The higher dehydration temperature for **4** (140 C) is probably due to the lattice H_2O molecules being trapped in the crystal packing (see above). Compound **3** also has a monomeric anion structure but includes a coordinated H_2O molecule to give a CN of 9. This is only lost at 172°C. The DTA curve of **9** is complex, with several overlapping features, although the first change is endothermic and starts at 185°C. This relatively high temperature is consistent with the presence of coordinated H_2O molecules, as identified by X-ray crystallography.

Compound **1** loses three H_2O molecules at 186°C, suggesting that in **1** the three H_2O molecules are coordinated to the thorium centre and that it may be structurally similar to **9**. By contrast, **6**, **7** and **8** lose their H_2O molecules at low temperature (about 60°C), suggesting that they do not contain coordinated H_2O molecules and therefore have a CN of 8. The final residual mass from all the Th compounds is generally

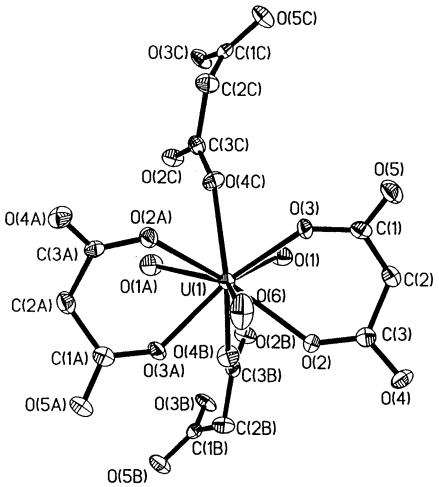


Fig. 6. An ORTEP drawing of the structure of **9** (50% probability ellipsoids).

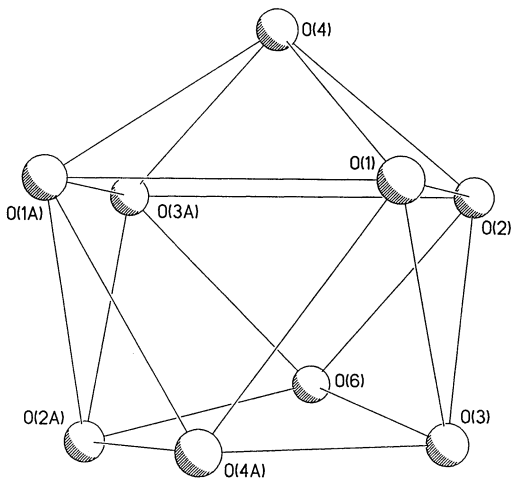


Fig. 7. Coordination polyhedron of U in **9**.

2–3% higher than expected for a pure ThO_2 product, suggesting that the final residue could be a mixture, for example, of thorium oxide and carbonate. Elemental analysis of the TGA/DTA residues confirms that there is a trace of carbon in the final products. Compound **9** decomposes to UO_2, again containing a trace of carbon.

4.3. ^{13}C CPMAS NMR spectroscopy

Expansions of the carbonyl region of the ^{13}C CPMAS NMR spectra of **1**–**8** are shown in Fig. 9 and the chemical shifts are listed in Table 8. Generally, the chemical shift, $\delta_{C=O}$, increases with the bulk of the substituent groups on the ligand. The stoichiometry, TG/DTA data and ^{13}C CPMAS NMR for **7** and **8** are similar to those of **2**, suggesting they have similar monomeric anion structures. Compounds **4** and **5** have very similar ^{13}C CPMAS NMR spectra although the former has H_2O molecules in the lattice. Compound **1** has a different stoichiometry to the rest. Compound **9** is paramagnetic and it was not possible to obtain a ^{13}C CPMAS NMR spectrum.

The ^{13}C CPMAS NMR results can be related to the known crystal structures using the crystallographic data and carbonyl (^{13}C CPMAS) patterns summarised in Table 9. The anionic structure of **2** has a twofold symmetry axis, so that four carbonyl peaks might be expected in its ^{13}C CPMAS NMR spectrum. Experimentally three carbonyl peaks are observed, and these correlate with three distinct groups of Th–O and/or C–O distances. The anion in **4** has three twofold symmetry axes, so two carbonyl peaks may be expected in its ^{13}C CPMAS NMR spectrum. One carbonyl peak is actually observed, reflecting the similarity of the Th–O and/or C–O distances. The anionic structures of **3** and **6** have no crystallographically imposed symmetry so, in principle, eight carbonyl peaks might be expected. In practice, four distinct groups of Th–O and C–O distances can be identified in the crystal structure and these correspond to the four carbonyl peaks observed in the ^{13}C CPMAS NMR spectra. The groupings of Th–O and C–O distances are not directly correlated, so consideration of either or both could account for the structure of the ^{13}C NMR spectra. There is no obvious relationship between C=O distances and the patterns in the carbonyl region of the ^{13}C NMR spectra.

Table 7
Structural comparisons of dicarboxylato compounds of U(IV) and Th(IV)

Compound	structural type	CN	M–O distances (Å)	Average (Å)	Ref.
$K_4[Th(C_2O_4)_4]\cdot 4H_2O$ (**10**)	infinite chain	10	2.41(2)–2.62(2)	2.49(2)	[5]
$K_4[U(C_2O_4)_4]\cdot 4H_2O$ (**11**)	infinite chain	10	2.406(5)–2.641(4)	2.467(8)	[6]
$Ba_2[U(C_2O_4)_4(H_2O)]\cdot 7H_2O$ (**12**)	monomeric	9	2.366(4)–2.569(6)	2.407(6)	[7]
3	monomeric	9	2.400(5)–2.564(5)	2.445(5)	this work
2	monomeric	8	2.337(2)–2.450(2)	2.394(2)	this work
4	monomeric	8	2.393(2)–2.406(2)	2.400(2)	this work
6	monomeric	8	2.372(5)–2.448(5)	2.401(5)	this work
9	3D polymer	9	2.315(4)–2.487(4)	2.413(4)	this work

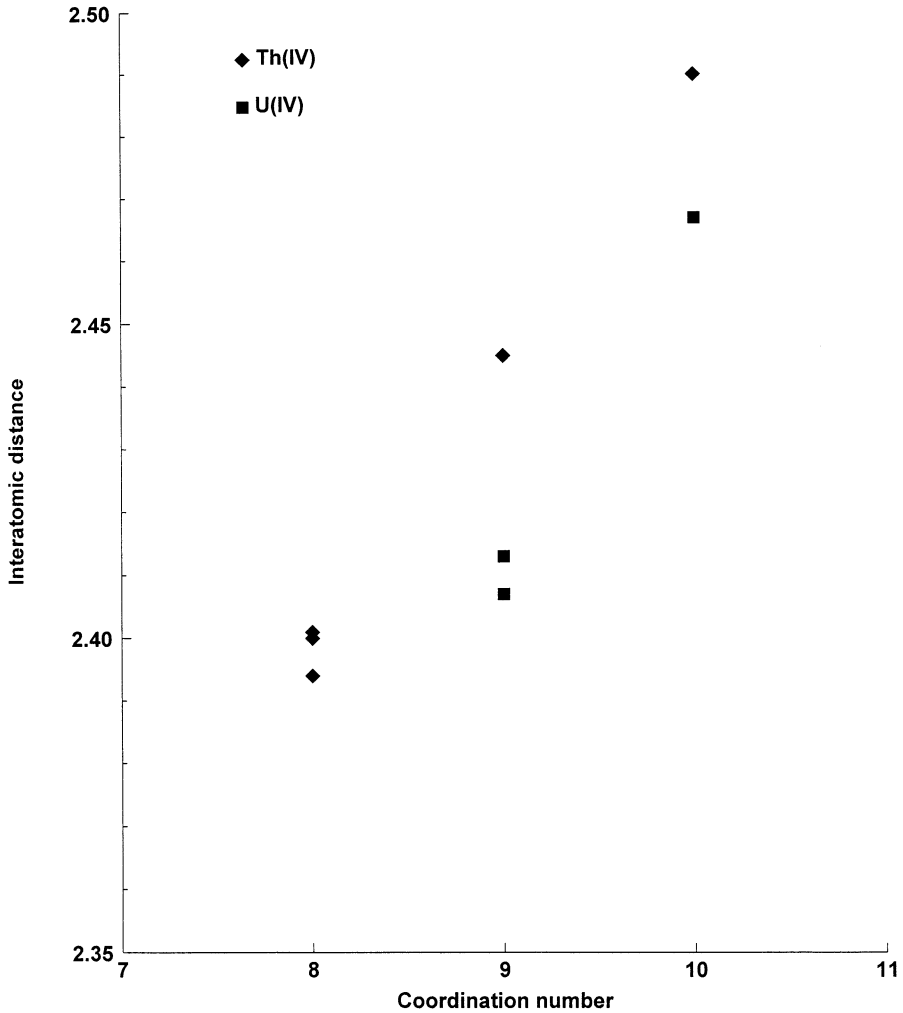


Fig. 8. Relationship between CN and mean interatomic distance in U(IV) and Th(IV) dicarboxylate complexes.

4.4. Infrared spectroscopy

Infrared spectroscopy has been widely used as a fingerprint method for metal carboxylates, with the difference in wavenumber between the antisymmetric and symmetric carboxylate mode, $\Delta\nu$ ($=\nu_{as}-\nu_{s}$), often being used to estimate bonding types [14–19]. Several attempts have been made to rationalise and distinguish structures of carboxylate groups by values [18–20]. Since the symmetric and antisymmetric stretching frequencies are highly sensitive to the structures and environments of the carboxylate groups, the nature of the accompanying ligands and the identity of the central metal ion, the bonding type predicted with IR spectroscopic data is often at variance with the real bonding, as determined from the crystal structures [21,22]. IR spectra of some Th(IV) acetato and halogenoacetato complexes have been reported [23], but no attempt has been made to predict bonding modes. Because of the generally low symmetry, the antisymmetric and symmetric stretching frequencies are normally split. The carboxylate stretching frequencies for the compounds studied here are summarised in Table 10. The values range from 140 to 260 cm^{-1} and perhaps fall into two groups, 160–211 and 230–260 cm^{-1}. However, the crystallographically characterised compounds, all of which contain 1,5-bidentate ligands, cover a wide range of values from 167 to 260 cm^{-1}, which suggests that any grouping of the values is fortuitous. Only compounds **1** and **9** have values as low as 140 cm^{-1}, which may be a characteristic of the slightly different bonding type in **9**, where bridging carbonyl groups are present. The similarity in values for **1** and **9** (Table 10), which have the same stoichiometry, supports the suggestion, from thermal analysis, that **1** could have a similar 3D polymeric structure to **9**.

5. Conclusions

Dicarboxylate complexes of the early actinides are readily formed in aqueous media, with oxalate and malonate being good examples. In the case of UO_2^{2+}, CN 4, 5 or 6 in the equatorial plane has been observed and a range of structural types has been identified in the solid state. Variable CN (8, 9 or 10) is also possible for Th^{4+}, while CN 9 and 10 have been identified for U^{4+}, but without the stereochemical control exerted by the axial O groups in UO_2^{2+}. Under reaction conditions in which bridging occurs in UO_2^{2+} complexes, CN of 8 or 9 are observed for Th^{4+} without any tendency to form bridges. By contrast, there appears to be a single favoured, bridging structure for U^{4+} in these conditions. Metal–ligand bond distances in Th^{4+} and U^{4+} malonate and oxalate complexes, determined from X-ray crystallography, are strongly correlated

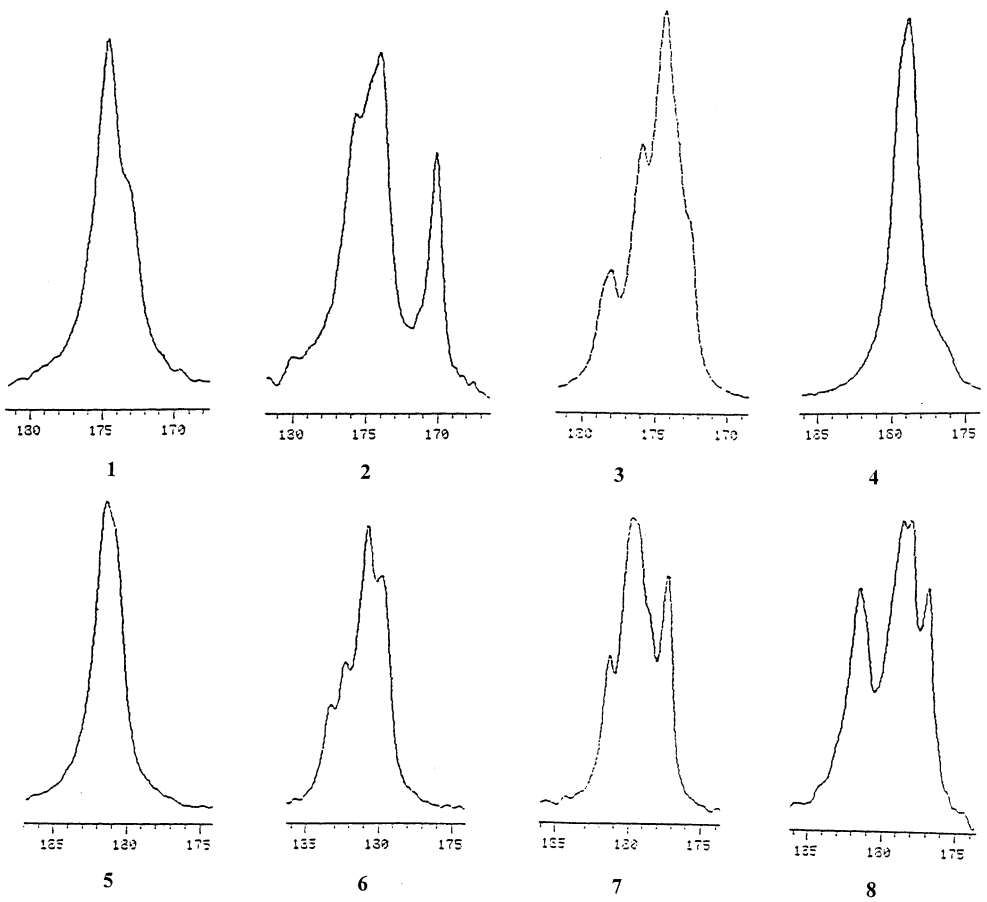


Fig. 9. Expansion of the carbonyl regions in the ^{13}C CPMAS NMR spectra of **1**–**8**.

Table 8
^{13}C CPMAS NMR data for **1** to **8**.

	δ (ppm)				
Compound	C=O	C_q [a]	CH	CH_2	CH_3
1	174.7, 173.2			40–44	
2	175.7, 174.0			38–42	
3	178.2, 176.2, 174.9, 172.5			35.2, 40.0	
4	178.8		45.3	39.1	13.5
5	181.7	47.6		35–40	22.6, 18.6
6	183.2, 182.2, 180.8, 179.8	47.6		38.3	22.6, 18.6
7	181.5, 180.1, 177.6	57.6		30.0	8.2
8	182.0, 179.2, 178.7, 177.3	58.3, 57.8		30.7	7.8

[a] C_q, quaternary carbon.

Table 9
Correlation of crystallographic and ^{13}C CPMAS NMR spectroscopic data (letters in square brackets represent possible groupings of bond distances)

Compound	O atom	Th–O (Å)	C–O (Å)	$\delta_{C=O}$; number (intensity ratio)
2	O1	2.337(2) [a]	1.296(4) [a]	3 (1:2:1)
	O3	2.450(2) [b]	1.265(4) [b]	
	O7	2.392(2) [c]	1.266(4) [b]	
	O5	2.395(2) [c]	1.274(3) [c]	
3	O1	2.424(5) [a]	1.272(8) [a]	4 (1:2:3:2)
	O2	2.400(5) [b]	1.278(9) [b]	
	O5	2.429(5) [a]	1.272(8) [a]	
	O6	2.422(5) [a]	1.270(8) [a]	
	O9	2.447(5) [c]	1.276(8) [b]	
	O10	2.469(5) [d]	1.257(9) [c]	
	O13	2.404(5) [b]	1.241(11) [d]	
	O14	2.449(5) [c]	1.280(9) [b]	
4	O1	2.393(2) [a]	1.283(4)[a]	1
	O2	2.406(2) [a]	1.284(4)[a]	
6	O1	2.416(6) [a]	1.274(10) [a]	4 (1:2:3:2)
	O2	2.448(5) [b]	1.295(9) [b]	
	O5	2.372(5) [c]	1.297(9) [b]	
	O6	2.396(5) [d]	1.252(9) [c]	
	O9	2.398(5) [d]	1.251(9) [c]	
	O10	2.430(5) [b]	1.282(9) [d]	
	O13	2.408(5) [a]	1.293(9) [d]	
	O14	2.391(5) [d]	1.302(10) [b]	

Table 10
$\Delta\nu$ ($=\nu_{as}-\nu_{s}$) values (cm^{-1}) for **1**–**9**

Compound	$\Delta\nu$ (cm^{-1})	Compound	$\Delta\nu$ (cm^{-1})
1	140, 193	**6**	230, 209
2	260, 232	**7**	175, 232
3	167	**8**	254, 235
4	211, 240	**9**	140, 202
5	160, 209		

with CN and suggest that CN 8 for U^{4+} may be unlikely in complexes of this type.

6. Supplementary data

Crystallographic data have been deposited with the CCDC and are available on request quoting the deposition numbers (CCDC 139360, 139361, 139362, 139363 and 102800 for **2**, **3**, **4**, **6** and **9**, respectively). Copies of this information are available free of charge from The Director, Cambridge Crystallographic Data Centre, 12 Union Road, Cambridge, CB2 1EZ, UK (Fax: +44-1223-336-033; e-mail: deposit@ccdc.cam.ac.uk or www: http://www.ccdc.cam.ac.uk).

Acknowledgements

We are grateful to M. Hart (Manchester University) for microanalysis; J. Friend and Dr F. Heatley (Manchester University) for solid-state ^{13}C CPMAS NMR; to BNFL (Y.J.Z. and F.R.L.), CVCP (Y.J.Z.) and the University of Manchester (Y.J.Z.) for financial support.

References

[1] J. Leciejewicz, N.W. Alcock, T. Kemp, J. Struct. Bond. 82 (1995) 43.
[2] Y.-J. Zhang, D. Collison, F.R. Livens, M. Helliwell, N. Tinker, H. Eccles, J. Alloys Comp. 271 (1998) 139.
[3] Y.-J. Zhang, Ph.D. Thesis, University of Manchester, 1998.
[4] N.W. Alcock, T.J. Kemp, S. Sostero, O. Traverso, J. Chem. Soc., Dalton Trans. (1980) 1182.
[5] M.N. Akhtar, A.J. Smith, Acta Crystallogr., Sect. B 31 (1975) 1361.
[6] M.C. Favas, D.L. Kepert, J.M. Patrick, A.H. White, J. Chem. Soc., Dalton Trans. (1983) 571.
[7] M.R. Spirlet, J. Rebizant, B. Kanellakopulos, E. Dornberger, Acta Crystallogr., Sect. C 43 (1987) 19.
[8] T. Moeller, Inorg. Synth. 5 (1957) 45.
[9] H. Moll, M.A. Denecke, F. Jalilehvand, M. Sandstrom, I. Grenthe, Inorg. Chem. 38 (1999) 1795.
[10] P.G. Allen, J.J. Bucher, D.K. Shuh, N.M. Edelstein, T. Reich, Inorg. Chem. 36 (1997) 4676.
[11] D.L. Clark, S.D. Conradson, D.W. Keogh, P.D. Palmer, B.L. Scott, C.D. Tait, Inorg. Chem. 37 (1998) 2893.
[12] A.K. Molodkin, T.A. Balakaeva, A.N. Kuchumova, Russ. J. Inorg. Chem. 13 (1968) 1095.
[13] G.B. Deacon, R.J. Phillips, Coord. Chem. Rev. 33 (1980) 227.
[14] K. Nakamoto, Infrared and Raman Spectra of Inorganic and Coordination Compounds, third ed., Wiley-Interscience, New York, 1978.
[15] M.L. Morris, D.H. Busch, J. Am. Chem. Soc. 78 (1956) 5178.
[16] M.J. Schmelz, T. Nakagawa, S. Mizushima, J.V. Quagliano, J. Am. Chem. Soc. 81 (1959) 287.
[17] M.J. Schmelz, T. Miyazuwa, S. Mizushima, T.J. Lane, J.V. Quagliano, Spectrochim. Acta 9 (1957) 51.
[18] M.G. Zaitseva, S.A. Stepanyan, V.V. Kravchenko, K.I. Petrov, Russ. J. Inorg. Chem. 21 (1976) 1820.
[19] J.R. Ferraro, M. Becker, J. Inorg. Nucl. Chem. 32 (1970) 1495.
[20] M. Kakihana, T. Nagumo, M. Okamoto, H. Kakihana, J. Phys. Chem. 91 (1987) 6128.
[21] K. Nakamoto, J. Fujita, S. Tanaka, M. Kobayshi, J. Am. Chem. Soc. 79 (1957) 4904.
[22] J.D. Donaldson, J.F. Knifton, S.D. Ross, Spectrochim. Acta 21 (1965) 1043.
[23] R.C. Mehrotra, R. Bohra, Metal Carboxylates, Academic, London, 1983.

PERGAMON

www.elsevier.nl/locate/poly

Polyhedron 19 (2000) 1769–1775

POLYHEDRON

Synthesis, spectral, electrochemical and magnetic properties of new phenoxo-bridged dicopper(II) complexes derived from unsymmetrical binucleating ligands with imino and amino side arms

P. Amudha, P. Akilan, M. Kandaswamy *

Department of Inorganic Chemistry, School of Chemical Sciences, University of Madras, Guindy Campus, Chennai 25, India

Received 8 February 2000; accepted 27 April 2000

Abstract

New unsymmetrical binuclear copper(II) complexes of the general formula $[Cu_2L(X)]ClO_4$, (X = OH, OAc) have been prepared by in situ complexation of the compound 3-[*N*-methyl-*N*-(2-hydroxy-3,5-dichlorobenzyl)aminomethyl]-5-bromosalicylaldehyde (**mhdab**) with various primary amines, copper(II) perchlorate and appropriate sodium salt. Positive ion FAB mass spectral studies of the complexes show the presence of a dicopper core in the complexes. Electronic spectra of the complexes show a broad band for the d–d transition in the region around 635–685 nm. A cyclic voltammetric study of the complexes shows two quasi-reversible reduction waves in the range $E^1_{pc} = -0.52$ to -0.86 V and $E^2_{pc} = -1.02$ to -1.16 V, and the reduction potentials are sensitive towards the chemical environment around the copper atoms. Cryomagnetic investigation of the complexes shows a moderately strong antiferromagnetic spin exchange interaction between the two copper(II) ions ($-2J$ 60–170 cm^{-1}). ESR spectra of the complexes show a broad band at room temperature. The electrochemical and magnetic properties of the complexes are compared on the basis of the rigidity and conjugation of the ligands H_2L^1, H_2L^2 and H_2L^3. © 2000 Elsevier Science Ltd. All rights reserved.

Keywords: Binuclear Cu(II) complexes; Magnetic properties; Electrochemistry; ESR

Interest in the synthesis of new binuclear copper(II) complexes is mainly due to their applications in bioinorganic chemistry, magnetochemistry and homogeneous catalysis. Copper is an essential trace element for life processes and several copper-containing proteins have been identified. In particular, a dicopper active center is found in many copper proteins like hemocyanin, tyrosinase and also in multinuclear proteins like laccase, ceruloplasmin, catechol oxidases and ascorbate oxidase [1–4]. Although all these proteins contain binuclear copper active sites, their functions, nature of the amino acid coordination and stereochemistry of the active site vary. Understanding the functional and structural properties of these binuclear active site by developing small dicopper complexes as models for these metalloproteins is the main objective of bioinorganic chemistry, which links the chemistry of coordination complexes and life processes. In magnetochemistry, the study of magnetic properties of these dicopper complexes offered considerable information about the basic factors governing the superexchange phenomenon, which is very much important in understanding the physics of magnetic materials, superconductivity and in the construction of molecular ferromagnets [5]. From Robson's pioneering work on binuclear copper(II) complexes, most of the work is concerned with the studies of symmetrical dicopper complexes and the study of unsymmetrical dicopper complexes is sparse [4,6]. Synthesis of unsymmetrical binucleating ligands and their copper(II) complexes has gained attention in recent years with the establishment of the unsymmetrical nature of the active site of hemocyanin [7] and tyrosinase [8]. The present work deals with the synthesis, spectral, electrochemical and magnetic properties of a few unsymmetrical binuclear copper(II) complexes.

* Corresponding author. Tel.: +91-44-245-4515; fax: +91-44-235-2494.

E-mail address: mkands@unimad.ernet.in (M. Kandaswamy).

0277-5387/00/$ - see front matter © 2000 Elsevier Science Ltd. All rights reserved.
PII: S0277-5387(00)00418-6

1. Experimental

1.1. Materials and methods

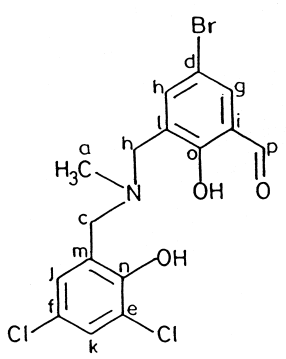
All the chemicals were obtained from commercial sources and used without any further purifications. 2-Aminophenylbenzimidazole [9] and 2-methylaminoethyl-4,6- dichlorophenol [10] were prepared by following the literature procedures. Commercial grade methanol was distilled from quick lime and used. HPLC grade dimethylformamide was purchased from Qualigens's fine chemicals. Elemental analyses were carried out using a Carlo Erba elemental Analyser Model 1106. ^{1}H and ^{13}C NMR spectra were recorded in $CDCl_3$ using a JOEL GSX 400 NMR spectrometer. Mass (EI) spectra were recorded on a JMS-DX303 HF Mass spectrometer. Positive ion fast atom bombardment (FAB) mass spectra were recorded on a SX 102/DA-6000 mass spectrometer in which the matrix solvent used was 3-nitrobenzyl alcohol. IR spectra were recorded on a Hitachi 270-50 spectrophotometer in the spectral range 400–4000 cm^{-1} using KBr discs. Electronic spectra of the complexes were recorded using a Hewlett–Packerd 8452A spectrophotometer. Molar conductivity was measured by using an Elico model SX80 conductivity bridge using freshly prepared solution of the complex in DMF. Cyclic voltammograms were obtained on an apparatus comprising a PAR model 173 potentiostat/galvanostat, model 175 universal programmer, model 176 current/voltage convertor, 179 coulometer and a Perkin–Elmer Hitachi 057 X-Y recorder. The measurements were carried out under oxygen free condition using a three electrode cell in which the working and auxiliary electrodes were small platinum foils (1 × 1 cm) and the reference electrode was saturated Ag/AgCl. Tetra(*n*-butyl)ammonium perchlorate was used as supporting electrolyte. The magnetic susceptibility of the complexes was measured in the temperature range 77–300 K using a PAR model 155 vibrating sample magnetometer, and the instrument was calibrated with the use of metallic nickel. Room temperature magnetic moment of the complexes was measured using Guoy balance, in which $Hg[Co(SCN)_4]$ was used as the calibrant. X-band ESR spectra of the complexes were recorded on Varian EPR-E 112 spectrophotometer using DPPH as the reference.

1.2. Preparation of the precursor ligands

1.2.1. 3-[N-Methyl-N-(2-hydroxy-3,5-dichlorobenzyl)-aminomethyl]-5-bromosalicylaldehyde (**mhdab**)

2-Methylaminomethyl-4,6-dichlorophenol (2.05 g, 0.01 mol) and paraformaldehyde (0.33 g, 0.011 mol) were stirred in 75 cm^3 glacial acetic acid for 24 h. To this mixture 5-bromosalicylaldehyde (2.0 g, 0.02 mol) was added and stirred for 48 h. The mixture was heated on a water bath for 7 h and neutralized with solid Na_2CO_3. The residue was extracted with CH_2Cl_2. The solvent was evaporated. Column chromatographic separation on silica gel (4:1 CH_2Cl_2–MeOH) afforded the product. M.p. 97°C, Yield 1 g, (25%), IR KBr disc 1680 cm^{-1} for CHO, Mass (EI) $m/z = 416$ [M − 2]. *Anal.* Calc. for $C_{16}H_{14}BrCl_2NO_3$: C, 45.83; H, 3.34; N, 3.34. Found: C, 45.95; H, 3.43; N, 3.41%. Table 1 accounts the ^{1}H and ^{13}C NMR peak assignment of the compound.

Table 1
^{1}H and ^{13}C NMR spectral assignment for **mhdab**



	^{13}C NMR ($CDCl_3$)	^{1}H NMR ($CDCl_3$)
a	45.2	2.5 (s, 3H, N–CH_3)
b	54.3	3.5 (s, 2H, CH_2)
c	60.6	3.8 (s, 2H, CH_2)
d	111.3	6.8 (s, 1H, Ar–H)
e	118.5	6.9 (s, 1H, Ar–H)
f	119.7	7.5 (s, 1H, Ar–H)
g	121.7	7.6 (s, 1H, Ar–H)
h	125.8	7.8 (s, 1H, CHO)
i	128.7	
j	129.6	
k	133.5	
l	135.6	
m	139.6	
n	154.0	
o	160.5	
p	194.5	

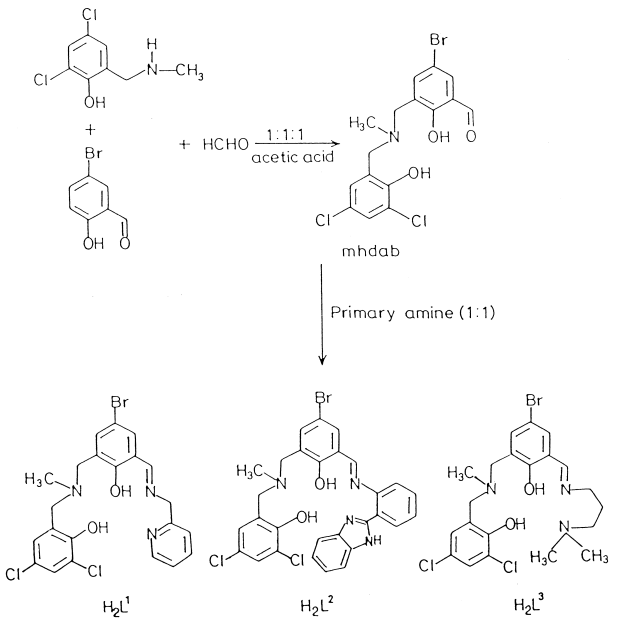


Fig. 1. Schematic diagram for the synthesis of the intermediate **mhdab** and ligands.

1.3. Preparation of the complexes

The μ-phenoxo-μ-(X)-dicopper(II) complexes $[Cu_2L^{1-3}(X)]ClO_4$ (**1**–**6**) were prepared by following the general procedure [11]. To the precursor compound **mhdab** (0.42 g, 1 mmol), dissolved in 75 cm^3 of methanol, primary amine (1 mmol) (2-aminomethylpyridine for H_2L^1 or 2-aminophenylbenzimidazole for H_2L^2 or *N*,*N*-dimethylpropanediamine for H_2L^3) was added and refluxed for 2 h. The resulting solution was added to a solution of copper(II) perchlorate hexahydrate (0.75 g, 2 mmol) dissolved in 50 ml of methanol and refluxed for a further hour. The mixture was then reacted with one equivalent of NaX (X = OH, OAc), dissolved in 5 cm^3 of 1:4 water–methanol and refluxed for a further hour. The solid complex that deposited on slow evaporation of the solvent was filtered, washed with diethyl ether and dried.

1.3.1. $[Cu_2L^1(OH)]ClO_4 \cdot H_2O \cdot MeOH$ (1)

Dark green plates were deposited, which were filtered and dried, whereupon the crystals turned to green powder. *Anal.* Calc. for $C_{23}H_{25}BrCl_3Cu_2N_3O_9$: C, 34.45; H, 3.12; N, 5.24. Found: C, 34.55; H, 3.23; N, 5.42%. Selected IR (KBr): 3450, 1630, 1100 and 620 cm^{-1}. Conductance (Λ_m/S cm^2 mol^{-1}) in DMF 65. λ_{max} (nm) (ε/M^{-1} cm^{-1}) in DMF 658(219), 384(1015), 274(15876).

1.3.2. $[Cu_2L^1(OAc)]ClO_4 \cdot 2H_2O$ (2)

Dark green solid. *Anal.* Calc. for $C_{24}H_{25}BrCl_3Cu_2N_3O_{10}$: C, 34.76; H, 3.02; N, 5.07. Found: C, 34.63; H, 3.15; N, 5.12%. Selected IR (KBr): 3450, 1620, 1540, 1100 and 620 cm^{-1}. Conductance (Λ_m/S cm^2 mol^{-1}) in DMF 60. λ_{max} (nm) (ε/M^{-1} cm^{-1}) in DMF 685(276), 410(s), 275(15110).

1.3.3. $[Cu_2L^2(OH)]ClO_4 \cdot 2H_2O$ (3)

Dark brown solid. *Anal.* Calc. for $C_{29}H_{26}BrCl_3Cu_2N_4O_9$: C, 39.21; H, 2.93; N, 6.31. Found C, 39.63; H, 2.95; N, 6.42%. Selected IR (KBr): 3450, 1620, 1100 and 620 cm^{-1}. Conductance (Λ_m/S cm^2 mol^{-1}) in DMF 55. λ_{max} (nm) (ε/M^{-1} cm^{-1}) in DMF 623(216), 386(2709), 290(12123).

1.3.4. $[Cu_2L^2(OAc)]ClO_4 \cdot H_2O$ (4)

Dark green solid. *Anal.* Calc. for $C_{31}H_{26}BrCl_3Cu_2N_4O_9$: C, 40.83; H, 2.85; N, 6.15. Found C, 40.54; H, 2.88; N, 6.26%. Selected IR (KBr): 3450, 1610, 1540, 1100 and 620 cm^{-1}. Conductance (Λ_m/S cm^2 mol^{-1}) in DMF 65. λ_{max} (nm) (ε/M^{-1} cm^{-1}) in DMF 641(213), 391(s), 286(15110).

1.3.5. $[Cu_2L^3(OH)]ClO_4 \cdot 2H_2O$ (5)

Green solid. *Anal.* Calc. for $C_{21}H_{29}BrCl_3Cu_2N_3O_9$: C, 32.31; H, 3.72; N, 5.39. Found C, 32.52; H, 3.81; N, 5.45%. Selected IR (KBr): 3450, 1610, 1100 and 620 cm^{-1}. Conductance (Λ_m/S cm^2 mol^{-1}) in DMF 65. λ_{max} (nm) (ε/M^{-1} cm^{-1}) in DMF 664(275), 410(s), 276(16032).

1.3.6. $[Cu_2L^3(OAc)]ClO_4 \cdot MeOH$ (6)

Dark green solid. *Anal.* Calc. for $C_{24}H_{31}BrCl_3Cu_2N_3O_9$: C, 35.20; H, 3.79; N, 5.13. Found: C, 35.26; H, 3.95; N, 5.21%. Selected IR (KBr): 1630, 1540, 1100 and 620 cm^{-1}. Conductance (Λ_m/S cm^2 mol^{-1}) in DMF 55. λ_{max} (nm) (ε/M^{-1} cm^{-1}) in DMF 681(168), 398(s), 298(18139).

2. Results and discussion

2.1. Syntheses

Reaction of 5-bromosalicylaldehyde, 2-methylaminomethyl-4,6-dichlorophenol and paraformaldehyde in acetic acid medium afforded the desired precursor compound **mhdab**. The IR spectra of the compound showed the characteristic peak at 1680 cm^{-1} for the aldehyde group.

Condensation of the aldehyde **mhdab** with 2-aminomethylpyridine, 2-aminophenyl-benzimidazole and *N*,*N*-dimethylpropanediamine gave the ligands H_2L^1, H_2L^2 and H_2L^3, respectively (Fig. 1), which were complexed in situ with copper(II) perchlorate hexahydrate and appropriate sodium salt in methanol medium. In all the complexes the characteristic IR peak for the CHO group at 1680 cm^{-1} is absent and the characteristic peak for the C=N around 1610–1630 cm^{-1} is

observed, which indicates the effective condensation of the aldehyde group with the primary amines.

2.2. Spectroscopy

The positive ion FAB mass spectral study was carried out for selected complexes **1**, **4** and **6** to confirm the binuclearity of the complexes. All three complexes show the molecular ion peak assignable to the $[Cu_2L(X)]^+$ fragment. The molecular ion peak for complex **1** is observed at $m/z = 668$ for the $[Cu_2L^1(OH)H_2O]^+$ fragment, the molecular ion peak for complex **4** is observed at $m/z = 792$ for the fragment $[Cu_2L^2(OAc)]^+$ and complex **6** shows the molecular ion peak for the fragment $[Cu_2L^3(OAc)MeOH]^+$ at $m/z = 719$. The FAB mass spectrum of complex **4** is given in Fig. 2.

IR spectra of the complexes show the characteristic peak for the C=N group around 1610–1630 cm^{-1}, along with a broad band centered around 3400 cm^{-1}, indicating the presence of coordinated or lattice water and a strong symmetrical peak around 1100 cm^{-1}, indicating the presence of an uncoordinated ClO_4 ion in the complexes. A characteristic peak for the acetate of the complexes **2**, **4** and **6** was observed in the region 1540 cm^{-1}. The electronic spectra of the complexes were recorded in DMF, which show a weak band in the region around 635–685 nm for the d–d transition along with shoulders around 375–430 nm, which are most probably due to the charge transfer transitions originated from the phenolate to copper [12] or benzimidazole to copper [13]. The intense peak observed below 300 nm is assigned to the ligand–ligand charge transfer transition. Appearance of a single d–d band in the region around 650 nm indicates that the coordination geometry around the copper atoms is basically four-coordinated planar with weak axial interactions and the red shift in the λ_{max} value for complexes **1**, **2** and **5**, **6** with respect to the complexes **3**, **4**, indicates that the complexes of the ligands H_2L^1 and H_2L^3 have relatively more distorted geometry than the complexes of the ligand H_2L^2 [14].

2.3. Electrochemical studies

All the complexes show a molar conductance value in the range 45–60 Λ_m/S cm^2 mol^{-1} in DMF, which indicates that the complexes are 1:1 electrolyte in nature [15]. The cyclic voltammograms of the complexes show two redox waves in the cathodic potential region and the data are given in Table 2. Constant potential electrolysis of complexes **2** and **5** at 100 mV more negative to their first reduction potential consumed one electron per molecule and consumed two electrons per molecule at the potential −1.25 V, which indicates the involvement of two single electron transfers in the reduction processes. Based on the coulometric results,

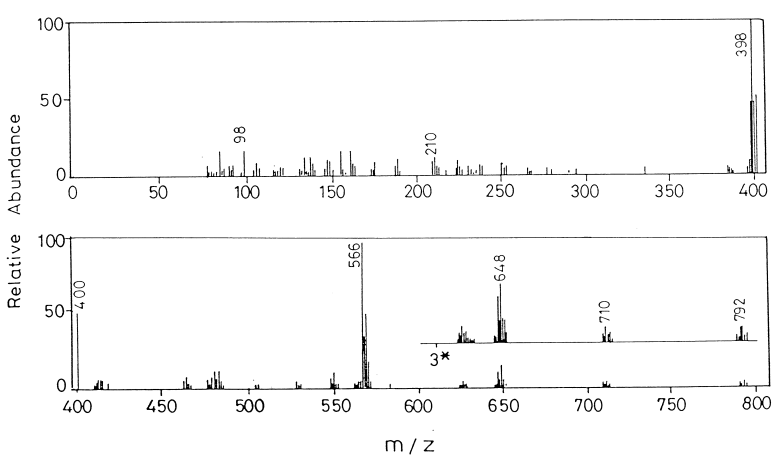


Fig. 2. FAB mass spectra for complex **4**.

Table 2
Electrochemical data for the complexes

Complex	E^1_{pc} (V)	E^1_{pa} (V)	$E^1_{1/2}$ (V)	ΔE (mV)	E^2_{pc} (V)	E^2_{pa} (V)	$E^2_{1/2}$ (V)	ΔE (mV)
1	−0.64	−0.50	−0.57	140	−1.15	−1.00	−1.07	150
2	−0.58	−0.46	−0.52	120	−1.05	−0.79	−0.92	260
3	−0.86	−0.62	−0.74	240	−1.11	−1.02	−1.06	90
4	−0.81	−0.55	−0.68	270	−1.10	−1.00	−1.05	100
5	−0.62	−0.34	−0.48	280	−1.12	−0.96	−1.02	280
6	−0.52	−0.32	−0.40	200	−1.02	−0.68	−0.85	340

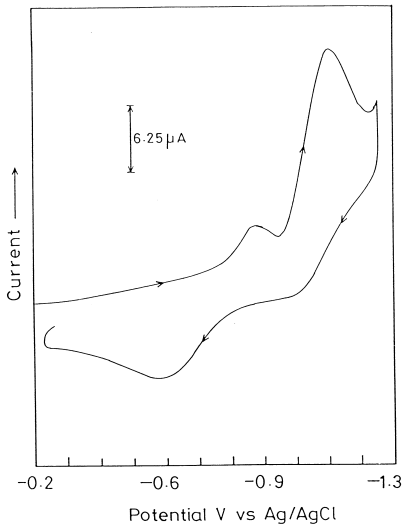


Fig. 3. Cyclic voltammogram for complex **3**.

the two reduction peaks observed in the cyclic voltammograms are attributed to the two stepwise one electron transfers as given below

$$[Cu(II)Cu(II)] \leftrightharpoons [Cu(II)Cu(I)] \leftrightharpoons [Cu(I)Cu(I)]$$

The cyclic voltammetric response of the complexes follow the typical characteristics of a quasi-reversible redox process. The cyclic voltammogram for complex **3** was given in Fig. 3.

A closer observation of the electrochemical data of the complexes of the ligands H_2L^1, H_2L^2 and H_2L^3 will be interesting to identify which end of the present unsymmetrical complexes is reduced first in one electron reductive processes. Although all the complexes undergo reduction at negative potentials, it is interesting to note that for all the complexes, irrespective of their exogenous bridging donor, there is a notable shift in the first reduction potential and there is only a minor shift in the second reduction potential. Since nitrogen is a soft donor when compared with the phenoxide oxy-gen [16], it is reasonable to say that the first reduction is associated with the copper atom in the ONN compartment in these ligands. The pronounced shift in the reduction potential is most probably due to the chemically different environments of this compartment. The second reduction peak observed at almost same potential seems to be associated with the copper atom in the ONO compartment, where the chemical environment is identical for all the three ligands.

From the table it is observed that the order of first reduction potential for the complexes of the ligand is $H_2L^3 < H_2L^1 < H_2L^2$. The NNO compartment comprises a *N*,*N*-dimethylpropanediamine side arm in the ligand H_2L^3, 2-methylpyridine in ligand H_2L^1 and 2′-phenylbenzimidazole in the ligand H_2L^2. The reduction observed at high negative potential for the complexes of the ligand H_2L^2 (**3**–**4**) may be the result of the greater planarity of the complexes induced by the rigidity [17] due to direct attachment of the benzimidazole group [18] to the phenyl ring and conjugation [19] of the phenylbenzimidazole side arm. Further, the complexes of the ligand H_2L^3 undergo reduction at less negative potential when compared with the complexes of the H_2L^1 ligand. The easy reduction of the complexes of the ligand H_2L^3 may be due to the more flexible [20] nature of the *N*,*N*-dimethylpropanediamine side arm when compared with the 2-methylpyridine side arm.

A comparison of the reduction potentials of the complexes of a particular ligand indicates that the reduction potential is exogenous, bridging donor dependent and the acetato bridged complexes undergo reduction at less negative potential when compared with the hydroxo bridged complexes. This behaviour seems to be associated with the increased number of atoms (–O–C–O–) involved in the acetate bridge, which may provide more flexibility for the acetato bridged complexes as against the hydroxo bridged complexes.

2.4. Magnetic properties

The magnetic moments of the complexes are subnormal at room temperature, suggesting the presence of an antiferromagnetic interaction within the complex. A variable temperature magnetic moment measurement was carried out for complexes **1**–**3**, **5** and **6** in the temperature range 77–300 K to evaluate the temperature dependence of magnetic properties of the complexes. Analyses were carried out by fitting the experimental

Table 3
Temperature dependence magnetic parameters and ESR spectrum data for the complexes

Complex	μ_{eff} (BM per molecule)		$-2J$ (cm^{-1})	P (%)	ESR data (g)	
	298 K	77 K			$g_{\|\|}$	$g_{\perp}$
1	2.19	1.17	82	0.25	2.19	2.06
2	2.35	1.06	59	0.18	2.18	2.02
3	1.86	1.10	167	0.51	2.05	
4	1.92				2.20	
5	2.15	1.08	97	0.19	2.08	2.02
6	2.64	1.56	56	0.45	2.20	2.01

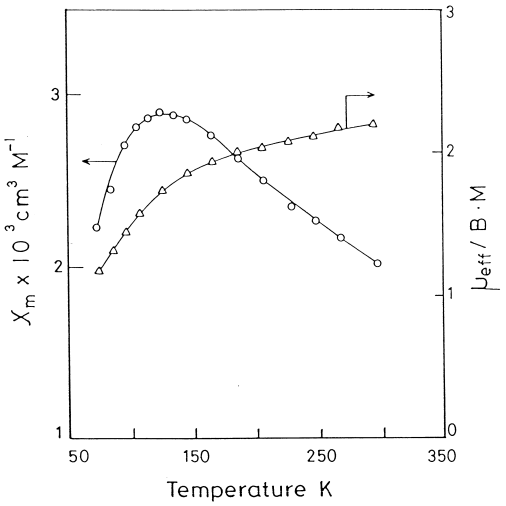


Fig. 4. Temperature dependence of magnetic properties for **1**.

susceptibility values to the modified Bleaney–Bowers equation.

$$\chi_m = (Ng^2\beta^2/3kT)\,[3 + \exp(-2J/kT)]^{-1}\,(1 - P) + (0.45P/T) + N\alpha$$

where χ_m is the molar magnetic susceptibility of the complex, P is the percentage of monomeric impurities and other symbols have their usual meanings. $N\alpha$ and g have been fixed as 120×10^{-6} cm^3 mol^{-1} and 2.20, respectively for all magnetic simulations. The best fit parameters are tabulated in Table 3. Temperature dependence of the magnetic properties for complexes **1** is given in Fig. 4.

The exchange integral values ($-2J$) observed for the complexes is in the range 60–170 cm^{-1}, which indicates the presence of antiferromagnetic coupling between the copper atoms. A comparison of the observed $-2J$ value of the complexes **1**, **3** and **5** shows that for the phenylbenzimidazole substituted complex **3**, the $-2J$ value is 167 cm^{-1}, indicating the strong antiferromagnetic coupling between the copper atoms when compared with complexes **1** and **5** ($-2J = 82$ and 97 cm^{-1}, respectively). In the complexes of all the three ligands reported in the present work, the geometry around the phenolic side arm (ONO) would be the same, but the geometry around the other copper atom (ONN) will be different due to the variations in chemical environments. As observed in the electrochemical properties of the complexes, the most probable reason for the strong exchange interaction may be the planarity of the phenylbenzimidazole compartment due to rigidity and conjugation of the phenylbenzimidazole side arm, which seems to reduce the dihedral angle between the two copper planes, thereby causing effective antiferromagnetic coupling in the complex. Relatively less exchange interaction observed in complexes **1** and **5** may be due to the flexibility of the *N*,*N*′-dimethylpropanediamine side arm of the ligand H_2L^3 and five membered ring formation in complex **1** of the ligand H_2L^1, which may increase the dihedral angle between the copper planes, resulting in a weak exchange interaction in these complexes. The variation in the $-2J$ values of complexes **1**, **2** or **5**, **6** is due to the effect of the exogenous bridging donor. The higher $-2J$ value observed for the acetato-bridged complexes when compared with their corresponding hydroxo bridged complexes is possibly due to the counter-complementary nature of the overlap of the magnetic orbitals involving the monoatomic and three atom bridging ligands [21–23].

2.5. EPR spectroscopy

Room temperature ESR spectra of the complexes were studied. The ESR spectra of complexes **1**, **3** and **5**

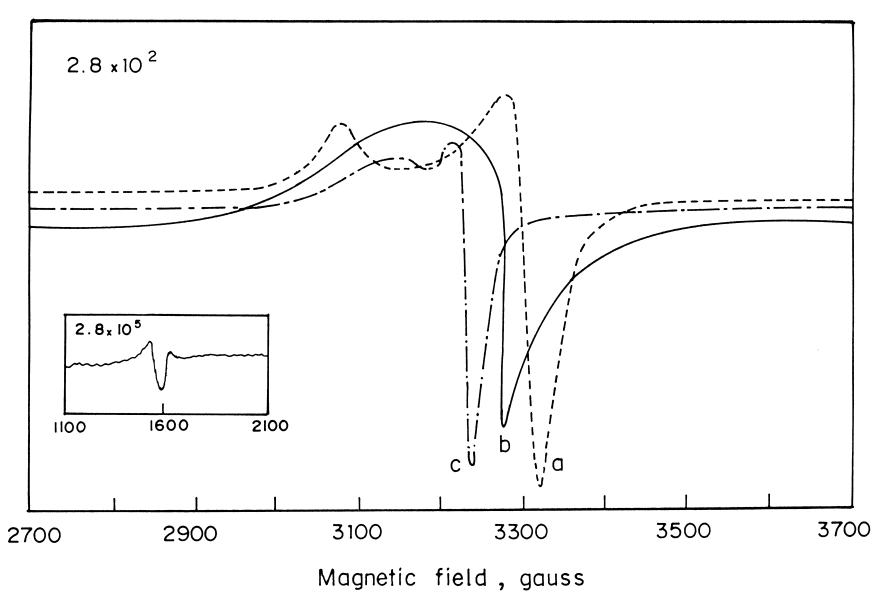


Fig. 5. ESR spectra for complex (a) **1**; (b) **3** and (c) **5**. The half-field signal for complex **3** is inserted.

are given in Fig. 5. The g value of the complexes was evaluated using the relationship $h\upsilon = g\beta H$ and given in Table 3. The ESR spectra of the complexes of the ligands H_2L^1 and H_2L^3 show asymmetric signal with poorly resolved hyperfine splitting signals; however' the complexes of the ligand H_2L^2 show only a broad signal. In addition, all the complexes show a signal for $\Delta Ms = 2$ transition at the low field region around 1600 G, with $g \approx 4$.

$g_{\|} > g_{\perp}$ values observed for the complexes suggest a planar-based geometry with $d_{x^2-y^2}$ ground state [24]. Appearance of a hyperfine splitting component for the complexes of the ligands H_2L^1 and H_2L^3 indicates that the antiferromagnetic coupling in the complexes is weak when compared with the complexes of the ligand H_2L^2.

References

[1] H. Holden Thorp, in: H. Holden Thorp, V.L. Pecoraro (Eds.), Mechanistic Bioinorganic Chemistry, The American Chemical Society, Washington, DC, 1995, p. 1.

[2] E.I. Solomon, V.M. Sundaram, T.E. Machonkin, Chem. Rev. 96 (1996) 2563.

[3] E.I. Solomon, M.J. Baldwin, M.D. Lowery, Coord. Chem. Rev. 92 (1992) 521.

[4] P.A. Vigato, S. Tamburini, Coord. Chem. Rev. 106 (1990) 25.

[5] (a) D. Willett, G. Gatteschi, O. Kahn (Eds.), Magnetostructural Correlations in Exchange Coupled Systems, NATO-ASI Series, Reidal, Dordrecht, The Netherlands, 1985. (b) O. Kahn, Molecular Magnetism, VCH, New York, 1993.

[6] E. Spodine, J. Manzur, Coord. Chem. Rev. 119 (1992) 171.

[7] W.P.J. Gaykema, A. Volbeda, W.G.H. Hol, J. Mol. Biol. 187 (1985) 2255.

[8] K.J. Lerch, M. Huber, H.-J. Schneider, R. Drexel, B. Linzen, J. Inorg. Biochem. 26 (1986) 213.

[9] D.W. Hein, R.J. Alhem, J.J. Leavitt, J. Am. Chem. Soc. 79 (1957) 427.

[10] W.J. Burke, E.L.M. Glennie, C. Weatherbee, J. Org. Chem. 29 (1962) 909.

[11] V. McKee, M. Zvagulis, J.V. Dogdigian, M.G. Patch, C.A. Reed, J. Am. Chem. Soc. 106 (1984) 4765.

[12] A.B.P. Lever, Electronic Spectra of Inorganic and Coordination Compounds, 2nd Ed., Elsevier, Amsterdam, 1984, 1986.

[13] L. Casella, O. Carugo, M. Gullotti, S. Doldi, M. Frassoni, Inorg. Chem. 35 (1995) 1101.

[14] B.J. Hathway, in: G. Wilkinson (Ed.), Comprehensive Coronation Chemistry, vol. 5, Pregamon, New York, 1987, p. 353.

[15] W.J. Geary, Coord. Chem. Rev. 7 (1971) 85.

[16] A. Benzekeri, J. Dudourdeaux, J.M. Latour, P. Rey, J. Laugier, J. Chem. Soc., Dalton Trans. (1991) 3359.

[17] (a) R.L. Lintvedt, L.S. Kramer, Inorg. Chem. 22 (1983) 796. (b) R.R. Gagne, C.L. Spiro, T.J. Smith, C.A. Hamann, A.K. Shiemke, J. Am. Chem. Soc. 103 (1981) 4073.

[18] A.K. Mishra, S.K. Dogra, Bull. Chem. Soc. Jpn. 58 (1985) 3587.

[19] N.A. Bailey, D.E. Fenton, J. Lay, P.B. Roberts, J.M. Latour, D. Limosin, J. Chem. Soc., Dalton Trans. (1986) 2681.

[20] (a) G.C. Patterson, R.H. Holm, Bioinorg. Chem. 4 (1975) 257. (b) D.E. Fenton, R.L. Lintvedt, J. Am. Chem. Soc. 100 (1978) 6368.

[21] Y. Nishida, S. Kida, J. Chem. Soc., Dalton Trans. (1986) 2633.

[22] K. Geetha, M. Netahji, A.R. Chakravarthy, N.Y. Vasanthacharya, Inorg. Chem. 35 (1996) 7666.

[23] T.N. Sorrell, C.J. O'Connor, D.P. Anderson, J.H. Reibenspies, J. Am. Chem. Soc. 107 (1985) 4199.

[24] R.C. Agarwal, N.K. Singh, R.P. Singh, Inorg. Chem. 20 (1981) 2794.

PERGAMON

www.elsevier.nl/locate/poly

Polyhedron 19 (2000) 1777–1781

POLYHEDRON

Syntheses of *nido*-9,11-X_2-7,8-$C_2B_9H_{10}^-$ anions (X = Cl, Br or I) and the synthesis and structural characterization of $N(C_2H_5)_4$[*commo*-3,3′-Co(4,7-Br_2-3,1,2-$CoC_2B_9H_9)_2$]

Erich C. Santos [a], Anthony B. Pinkerton [a], Scott A. Kinkead [a], Paul K. Hurlburt [a], Steve A. Jasper [b], Christopher W. Sellers [b], John C. Huffman [b], Lee J. Todd [b,*]

[a] *Mailstop J514, Los Alamos National Laboratory, Los Alamos, NM 87545, USA*
[b] *Department of Chemistry and Molecular Structure Center, Indiana University, Bloomington, IN 47405-7201, USA*

Received 17 May 2000; accepted 24 May 2000

Abstract

Treatment of *nido*-7,8-$C_2B_9H_{12}^-$ with *N*-halosuccinimide (halo = chloro, bromo or iodo) formed the corresponding *nido*-9,11-(halo)$_2$-7,8-$C_2B_9H_{10}^-$ ion in good yield. The *nido*-9,11-Br_2-7,8-$C_2B_9H_{10}^-$ ion was deprotonated with *n*-butyllithium and then reacted with cobalt(II) chloride to form the *commo*-3,3′-Co(4,7-Br_2-3,1,2-$CoC_2B_9H_9)_2^-$ ion. A single-crystal X-ray structure determination of this cobalt complex is reported. © 2000 Elsevier Science Ltd. All rights reserved.

Keywords: Halogenated carborane anions; Cobalt bis(dicarbollide); Boron; Carborane; Halogenation

1. Introduction

A few halogenated derivatives of the *nido*-[7,8-$C_2B_9H_{12}]^-$ ion are known [1–3,5,8,12]. Reaction of [$(CH_3)_3$NH][*nido*-7,8-$C_2B_9H_{12}$] with I_2 in refluxing MeOH formed [$(CH_3)_3$NH)][*nido*-9,11-I_2-7,8-$C_2B_9H_{10}$] in good yield [2]. The positions of iodination were determined by a single-crystal X-ray diffraction study [2].

There have been several studies of direct halogenation of *commo*-3,3′-Co(3,1,2-$CoC_2B_9H_{11})_2$ anion [also referred to as the cobalt bis(dicarbollide) anion] and these are outlined in a recent review [10]. Halogenation of 1,2-$C_2B_{10}H_{12}$ followed by conversion of this icosahedral molecule to its *nido*-[7,8-$C_2B_9H_{12}$] anion derivatives and then deprotonation and complexation with $CoCl_2$ has formed the *commo*-3,3′-Co(9-X-3,1,2-$CoC_2B_9H_{10})_2^-$ ion, X = Cl or Br as well as other halogenated derivatives [9].

Reaction of Me_3NH[*commo*-3,3′-Co(3,1,2-$CoC_2B_9H_{11})_2$] (**1**) with *N*-chlorosuccinimide or *N*-bromosuccinimide in THF formed the dihalogenated derivatives Me_3NH[*commo*-3,3′-Co(8-X-3,1,2-$CoC_2B_9H_{10})_2$], X = Cl or Br, respectively [4]. A single-crystal X-ray study of the dichloro derivative has been reported [4]. Treatment of **1** in refluxing glacial acetic acid solution with excess bromine formed [*commo*-3,3′-Co(8,9,12-Br_3-3,1,2-$CoC_2B_9H_8)_2]^-$ [7]. A single-crystal X-ray determination of this hexabromo derivative has been reported [11]. This hexabromo-derivative has been studied as a weakly coordinating anion [13]. Reaction of **1** with six equivalents of iodine monochloride in refluxing methylene chloride gave [*commo*-3,3′-Co(8,9,12-I_3-3,1,2-$CoC_2B_9H_8)_2]^-$ [6].

In this report, we describe the syntheses of the *nido*-9,11-X_2-7,8-$C_2B_9H_{10}^-$ anions (X = Cl, Br and I) employing *N*-halosuccinimide as the halogenation reagent. We also report the synthesis, characterization and single-crystal X-ray structure determination of a new brominated cobalt dicarbollide anion obtained by complexation of two *nido*-9,11-Br_2-7,8-$C_2B_9H_9^{2-}$ dianions with cobalt(II) chloride.

* Corresponding author. Tel.: +1-812-855-8733; fax: +1-812-855-8300.
E-mail address: toddlj@indiana.edu (L.J. Todd).

0277-5387/00/$ - see front matter © 2000 Elsevier Science Ltd. All rights reserved.
PII: S0277-5387(00)00461-7

2. Experimental

2.1. Physical measurements

Boron (^{11}B) NMR spectra were recorded at 128.4 MHz using a Varian Unity INOVA 400 spectrometer or at 80.21 MHz using a Bruker AF 250SY spectrometer. ^{11}B chemical shift values were reported relative to BF_3(diethylether). Proton (^{1}H) NMR were obtained on the same instruments and referenced to the protio solvent impurities. Proton chemical shift values were reported relative to tetramethylsilane. Elemental analysis for [$(CH_3)_3NH$][*nido*-9,11-Br_2-7,8-$C_2B_9H_{10}$] was performed at Los Alamos National Laboratories.

2.1.1. Synthesis of [$(CH_3)_4N$][*nido*-9,11-Cl_2-7,8-$C_2B_9H_{10}$]

In a 150-ml beaker, [$(CH_3)_3NH$][7,8-$C_2B_9H_{12}$] (0.50 g, 2.6 mmol) was dissolved in 25 ml CH_3CN. A solution of *N*-chlorosuccinimide (1.04 g, 7.8 mmol, three equivalents) in 25 ml of CH_3CN was added to the reaction beaker and the mixture was stirred at 25°C for 2 h. Evaporation of the CH_3CN gave a white crystalline solid that was dissolved in 120 ml of H_2O. Precipitation at 25°C with $(CH_3)_4NCl$ (0.86 g, 7.8 mmol, three equivalents) yielded 0.59 g (81%) of product. HRMS (positive ion FAB with glycerol matrix) (m/z) observed 350.2969, calculated 350.2973 [$(Me_4N)_2(C_2B_9H_{10}Cl_2)^+$] ($\Delta = 0.4$ mmu, 1.2 ppm).

2.1.2. Synthesis of [$(CH_3)_3NH$][*nido*-9,11-Br_2-7,8-$C_2B_9H_{10}$]

A THF solution of trimethylammonium dicarbollide [$(CH_3)_3NH$][7,8-$C_2B_9H_{12}$] was refluxed with 2.2 equivalents of *N*-bromosuccinimide for 15 min. After evaporation of the solution to dryness, the resulting white solid was dissolved in water giving a clear, colorless solution. The addition of two equivalents of $(CH_3)_3NHCl$ produced a flocculent white solid which was recovered by filtration. The compound identified as [$(CH_3)_3NH$][9,11-Br_2-7,8-$C_2B_9H_{10}$] was formed in 82% yield. Elemental analysis: Found: C, 17.19; H, 5.72; N, 4.15. *Anal*. Calc. For $C_5H_{20}B_9Br_2N$: C, 17.09; H, 5.74; N, 3.99%. HRMS (positive ion FAB with glycerol matrix) (m/z) observed 412.1621, calculated 412.1631 [$(Me_3NH)_2(C_2B_9H_{10}Br_2)^+$] ($\Delta = 1.0$ mmu, 1.2 ppm). ^{1}H NMR: acetone-d_6 solvent, 2.2 ppm, carborane CH.

2.1.3. Synthesis of [$(CH_3)_3NH$][*nido*-9,11-I_2-7,8-$C_2B_9H_{10}$]

A magnetic stir bar was placed in a 150-ml beaker to which [$(CH_3)_3NH$][7,8-$C_2B_9H_{12}$] (1.98 g, 10 mmol) and 12.5 ml THF were then added. A solution of *N*-iodosuccinimide (4.66 g, 21 mmol, 2.1 equivalents) in 12.5 ml of THF was added to the reaction beaker and the mixture was stirred at 25°C for 20 min. Evaporation of the THF gave a white crystalline solid that was dissolved in 200 ml H_2O. Precipitation at 25°C with $(CH_3)_3NHCl$ (2.4 g, 25 mmol, 2.5 equivalents) yielded 3.6 g (78%) of product.

2.1.4. Preparation of [Et_4N^+][*commo*-3,3′-Co(4,7-Br_2-3,1,2-$CoC_2B_9H_9)_2$]

To a two-neck, round-bottom flask equipped with a magnetic stir bar and nitrogen inlet, 0.1052 g (0.2994 mmol) of [Me_3NH] [9,11-Br_2-7,8-$C_2B_9H_{10}$] and 2.4 ml of dry THF were added. The vessel was flushed with nitrogen and cooled to -78°C using a dry ice–acetone bath; then 1.8 ml of 2.5 M (4.5 mmol) *n*-butyllithium were added and the vessel was warmed to room temperature. Upon warming, 0.0712 g (0.549 mmol) of dry cobalt(II) chloride was added, which resulted in a black liquid. The THF was removed by rotary evaporation and the remaining residue was washed with methylene chloride. After suction filtration to remove any cobalt or cobalt chloride, the methylene chloride solution was slowly evaporated and gave an orange crystalline solid. The yield was not established. The compound appeared to slowly decompose upon prolonged exposure to moist air at room temperature. ^{11}B and ^{1}H NMR data are summarized in Tables 2 and 3, respectively.

2.1.5. X-ray structure determination for [Et_4N^+][(*commo*-3,3′-Co(4,7-Br_2-3,1,2-$CoC_2B_9H_9)_2$]

A thin orange crystal of dimensions $0.03 \times 0.22 \times 0.40$ mm was affixed to the end of a glass fiber using

Table 1
^{11}B NMR chemical shift data for 9,11-*dihalo*-7,8-$C_2B_9H_{10}^-$ ions

Compound	Numbered positions of boron atoms					
	9,11	5,6	3	2,4	10	1
[$(CH_3)_3NH$][7,8-$C_2B_9H_{12}$]	−11.0	−16.9	−16.9	−22.3	−33.3	−37.9
[$(CH_3)_3NH$][9,11-Cl_2-7,8-$C_2B_9H_{10}$]	0.2	−17.4	−18.8	−24.2	−33.3	−38.5
[$(CH_3)_3NH$][9,11-Br_2-7,8-$C_2B_9H_{10}$]	−5.8	−15.5	−17.5	−21.9	−31.5	−37.4
[$(CH_3)_3NH$][9,11-I_2-7,8-$C_2B_9H_{10}$]	−21.3	−14.3	−16.9	−19.9	−29.5	−36.6
	−21.2	−13.9	−16.6	−19.6	−29.2	−36.5 [a]

[a] From Ref. [2].

Table 2
Boron ^{11}B NMR chemical shift data (ppm) for some brominated [*commo*-3,3′-Co(3,1,2-$CoC_2B_9H_{11})_2]^-$ ions

Compound	Numbered positions of boron atoms					
	8	10	9,12	4,7	5,11	6
[Et_4N][*commo*-3,3′-Co(3,1,2-$CoC_2B_9H_{11})_2$]	6.8 (d)[a]	1.6 (d)	−5.0 (d)	−6.0 (d)	−17.0 (d)	−22.5 (d)
Cs[*commo*-3,3′-Co(8,9,12-Br_3-3,1,2-$CoC_2B_9H_8)_2$]	6.0 (s)	4.0 (d)	−1.4 (s)	−4.3 (d)	−16.9 (d)	−23.1 (d)
[Et_4N][*commo*-3,3′-Co(4,7-Br_2-3,1,2-$CoC_2B_9H_9)_2$]	8.6 (d)	0.8 (d)	−4.4 (d)	3.0 (s)	−13.2 (d)	−23.6 (d)
				−1.4 (s)	−16.1 (d)	

[a] d = doublet, s = singlet

silicon grease and transferred to the goniostat where it was cooled to −170°C. A systematic search of a limited hemisphere of reciprocal space was used to determine that the crystal possessed no symmetry or systematic absences, indicating a triclinic space group. Subsequent solution and refinement confirmed the centrosymmetric choice, $P\bar{1}$ (see Table 4).

The diffractometer utilized for data collection was designed and constructed locally. A Picker four-circle goniostat equipped with a Furnas monochromator (HOG crystal) was modified by addition of stepping motors (Slo-Syn) on each of the four axes, and a fifth motor drives a 20-position filter/attenuator wheel. The latter allows top/bottom-left/right alignment of reflections. All motors are driven by a locally designed ISA board in an IBM PC compatible computer. The computer also has a timer/scalar board that is used to accumulate the counts from the scintillation counter used with the goniostat. The control software, PCPS is the Picker software written by Streib of the IUMSC. The software for the structure solution and refinement include SHELXTL-PC, and other versions of SHELX, as well as the XTEL program library.

Data were collected using a standard moving crystal–moving detector technique with fixed backgrounds at each extreme of the scan. Data were corrected for Lorentz and polarization effects and equivalent reflections were then averaged after application of an analytical absorption correction. The structure was readily solved using direct methods (SHELXTL-PC) and Fourier techniques. The cobalt and four bromine atoms were clearly visible, and the remaining atoms appeared in subsequent difference Fourier maps. The hydrogen atoms associated with the anion were located in difference Fouriers and included as fixed atom contributors in the final cycles of refinement. A final difference Fourier was featureless, the largest peak being 0.7 e $Å^{-3}$.

3. Results and discussion

The reaction of [$(CH_3)_3NH$][7,8-$C_2B_9H_{12}$] with 2.5–3.0 equivalents of *N*-halosuccinimide provided a convenient route to the series of compounds [$(CH_3)_3NH$]-[9,11-X-7,8-$C_2B_9H_{10}$] where X = Cl, Br or I. The compound [$(CH_3)_3NH$][9,11-Cl_2-7,8-$C_2B_9H_{10}$] was obtained in 81% yield when the reaction was carried out using three equivalents of *N*-chlorosuccinimide in acetonitrile solvent. Other solvents (benzene, CH_2Cl_2,

Table 3
^1H NMR chemical shift data for some brominated [*commo*-3,3′-Co(3,1,2-$CoC_2B_9H_{11})_2]^-$ ions

Compound	Solvent	Metallacarborane CH resonance (ppm)
[Et_4N][*commo*-3,3′-Co(3,1,2-$CoC_2B_9H_{11})_2$]-[$Co(C_2B_9H_{11})_2^-$]	Acetone-d_6	4.40
Cs[*commo*-3,3′-Co(8,9,12-Br_3-3,1,2-$CoC_2B_9H_8)_2$]	Acetone-d_6	4.62
[Et_4N][*commo*-3,3′-Co(4,7-Br_2-3,1,2-$CoC_2B_9H_9)_2$]	CD_2Cl_2	4.60
		4.80

Table 4
Crystallographic data for [Et_4N^+][*commo*-3,3′-Co(4,7-Br_2-3,1,2-$CoC_2B_9H_9)_2$]

Formula	$C_{12}H_{38}B_{18}CoBr_4N$
Formula weight	769.57
Space group	$P\bar{1}$
a (Å)	10.660(8)
b (Å)	16.048(14)
c (Å)	8.225(5)
α (°)	91.49
β (°)	105.33(3)
γ (°)	72.87(5)
V ($Å^3$)	1294.81
Z	2
T (K)	103
λ (Å)	0.71069
$D_{calc.}$ (g cm^{-1})	1.974
μ (Mo Kα) (cm^{-1})	67.858
R	0.0548
R_w	0.0482

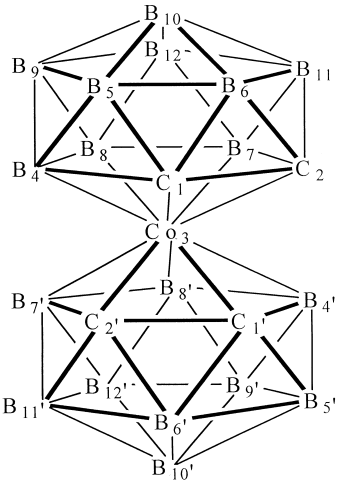


Fig. 1. Numbering system for the [*commo*-3,3′-Co(3,1,2-$CoC_2B_9H_{11})_2]^-$ ion.

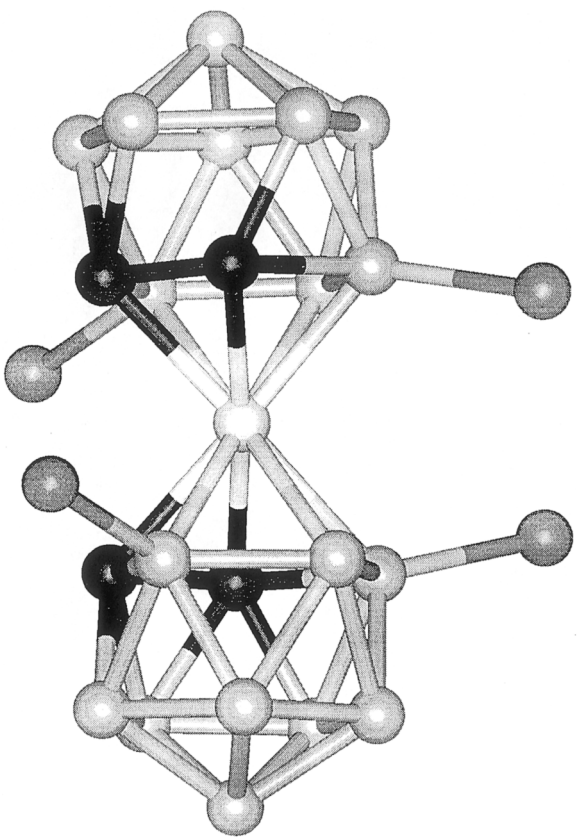


Fig. 2. A drawing illustrating the structure of the [*commo*-3,3′-Co(4,7-Br_2-3,1,2-$CoC_2B_9H_9)_2]^-$ ion.

DMF and DMSO) gave a mixture of monochloro- and dichloro-dicarbollide anions and decomposition products.

The compound $[(CH_3)_3NH][9,11\text{-}I_2\text{-}7,8\text{-}C_2B_9H_{10}]$ had been prepared previously from $[(CH_3)_3NH][7,8\text{-}C_2B_9H_{12}]$ and I_2 in refluxing methanol [2]. The ^{11}B NMR spectra of our diiodo product (in acetone-d_6) (see Table 1) and that of Ref. [2] (in ethanol) are in good agreement. The positions of iodination were determined by a single-crystal X-ray diffraction study of $[(CH_3)_3NH][9,11\text{-}I_2\text{-}7,8\text{-}C_2B_9H_{10}]$ [2].

The high-resolution mass spectra (FAB^+) are in agreement with the dihalo (halo = Cl or Br) *nido*-carborane cage formulae.

A comparison of the ^{11}B NMR chemical shift data is presented in Table 1. The assignments for the parent $7,8\text{-}C_2B_9H_{12}^-$ ion [2] and the $9,11\text{-}Br_2\text{-}7,8\text{-}C_2B_9H_{10}^-$ ion (study done here) are based on ^{11}B–^{11}B COSY NMR experiments. Previously, other face-substituted $7,8\text{-}C_2B_9H_{12}^-$ ions were analyzed by this 2D method [2]. The ^{11}B NMR assignments for the dichloro- and diido-$7,8\text{-}C_2B_9H_{10}^-$ ions were made based on the similarity to the other existing NMR studies. The chemical shift for the 9,11-halogen substituted boron nuclei shows the only significant variation. This change is similar to that found for other halogen-substituted cage-boron series.

3.1. $[Et_4N^+][Co(4,7\text{-}Br_2\text{-}1,2\text{-}C_2B_9H_9)_2^-]$

Deprotonation of $[(CH_3)_3NH^+][4,7\text{-}Br_2\text{-}1,2\text{-}C_2B_9H_{10}]$ with excess *n*-butyllithium in dry THF at −78.5°C, followed by warming to room temperature and the addition of cobalt(II) chloride, yielded the first 4,7-bromine substituted cobalt dicarbollide anion; (see numbering scheme for this anion in Fig. 1).

The structure of $[Et_4N^+][$*commo*-3,3′-Co(4,7-Br_2-3,1,2-$CoC_2B_9H_9)_2]$ was determined by a single-crystal X-ray study and is illustrated in Fig. 2. The cobalt atom is complexed in an η^5 fashion to each of the two ligands. The Co–B and Co–C bond distances of this new brominated cobalt *nido*-$C_2B_9H_9Br_2$ dicarbollide anion were found to be in the range 2.099(14)–2.168(13) and 2.044(11)–2.058(9) Å, respectively (see Table 5). These values are similar to the reported Co–B

Table 5
Selected bond distances for $[Et_4N^+][$*commo*-3,3′-Co(4,7-Br_2-3,1,2-$CoC_2B_9H_9)_2]$

Br(4)–B(4)	1.996(8)	C(2′)–B(7′)	1.686(4)
Br(7)–B(7)	1.968(3)	C(2′)–B(6′)	1.753(21)
Br(4′)–B(4′)	1.993(7)	C(2′)–B(11′)	1.688(19)
Br(7′)–B(7′)	1.975(9)	C(2)–C(1)	1.652(4)
Co(3)–C(2)	2.044(11)	C(2)–B(7)	1.695(8)
Co(3)–C(11)	2.058(9)	C(2)–B(11)	1.705(26)
Co(3)–C(1′)	2.054(11)	C(2)–B(6)	1.803(20)
Co(3)–C(2′)	2.046(11)	C(1)–B(4)	1.676(10)
Co(3)–B(7′)	2.121(12)	C(1)–B(6)	1.759(22)
Co(3)–B(8′)	2.168(13)	C(1)–B(5)	1.707(21)
Co(3)–B(4′)	2.139(15)	B(7′)–B(8′)	1.810(11)
Co(3)–B(4)	2.126(13)	B(7′)–B(11′)	1.782(22)
Co(3)–B(80)	2.147(17)	B(7′)–B(12′)	1.771(24)
Co(3)–B(7)	2.099(14)		
C(1′)–C(2′)	1.654(8)		
C(1′)–B(4′)	1.691(8)		
C(1′)–B(5′)	1.711(21)		
C(1′)–B(6′)	1.717(18)		

Table 6
Selected bond angles for $[Et_4N^+][commo\text{-}3,3'\text{-}Co(4,7\text{-}Br_2\text{-}3,1,2\text{-}CoC_2B_9H_9)_2]$

	4	4′	7	7′
Br–B–Co	116.2(8)	116.1(7)	122.7(8)	121.5(9)
Br–B–C	122.0(6)	122.10(26)	122.2(5)	122.6(6)
$Br–B–B_{8,8'}$	126.0(5)	126.5(5)	129.7(3)	129.3(4)
$Br–B–B_{5,5',11,11'}$	111.3(3)	112.4(6)	108.7(5)	109.3(5)
$Br–B–B_{9,9',12,12'}$	117.8(6)	117.3(7)	113.7(7)	115.5(5)

and Co–C distances of $[(CH_3)_4N^+][commo\text{-}3,3'\text{-}Co(8,9,12\text{-}Br_3\text{-}3,1,2\text{-}CoC_2B_9H_8)_2]$, which are in the range 2.05(2)–2.17(3) and 1.98(2)–2.09(2) Å, respectively [11].

Two enantiomers of this species exist by definition of the determined space group, $P\bar{1}$. These two mirror images are a result of the steric interference of the 4,7-position bromine atoms, which inhibits free rotation of the two dicarbollide ligands about the axis running through B(10), the cobalt atom and B(10′). The ^{11}B NMR spectrum (see Table 2) exhibits two unique environments for the 4,7-positioned boron atoms (two singlets) as well as for the 5,11-positioned boron atoms (two doublets). The ^{1}H NMR spectrum also exhibits two unique environments for the cage carbons (see Table 3). The structural effect of the steric interference of the bromine atoms is observed in the large bond angles of $Br–B_7–B_8$ and $Br–B_{7'}–B_{8'}$ (Table 6). Attempts to unlock the cage have so far proven unsuccessful. Observance of the ^{11}B NMR spectrum at 100°C showed no convergence of the two 4,7-peaks.

The $commo\text{-}3,3'\text{-}Co(4,7\text{-}Cl_2\text{-}3,1,2\text{-}CoC_2B_9H_9)_2^-$ ion was prepared by a similar reaction. It was not fully characterized; however, the ^{11}B NMR spectrum contained resonances at (multiplicity, intensity); 9.0 (s, 2B), 6.0 (d, 2B), 4.2 (s, 2B), −0.4 (d, 4B), −3.0 (d, 2B), −5.5 (d, 2B), −14.5 (d, 2B), −21 ppm (d, 2B). This spectrum is consistent with the expected structure of the complex and similar to the spectrum obtained for the tetrabromo derivative.

4. Supplementary material

Full crystallographic details, positional and thermal parameters, and bond lengths and angles (13 pages) have been deposited with the Cambridge Crystallographic Data Centre, CCDC No. 144461. Copies of this information may be obtained free of charge from: The Director, CCDC, 12 Union Road, Cambridge, CB2 1EZ, UK (fax: +44-1223-336033; e-mail: deposit@ccdc.cam.ac.uk or www: http://www.ccdc.cam.ac.uk).

References

[1] S. Hermanek, Chem. Rev. 92 (1992) 350.
[2] R.H. Pak, R.R. Kane, C.B. Knobler, M.F. Hawthorne, Inorg. Chem. 33 (1994) 5355.
[3] F.P. Olsen, M.F. Hawthorne, Inorg. Chem. 4 (1965) 1839.
[4] P.K. Hurlburt, R.L. Miller, K.D. Abney, T.M. Foreman, R.J. Butcher, S.A. Kinkead, Inorg. Chem. 34 (1995) 5215.
[5] E.A. Mizusawa, M.R. Thompson, M.F. Hawthorne, Inorg. Chem. 24 (1985) 1911.
[6] M.D. Mortimer, C.B. Knobler, M.F. Hawthorne, Inorg. Chem. 35 (1996) 5750.
[7] M.F. Hawthorne, D.C. Young, T.D. Andrews, D.V. Howe, R.L. Pilling, A.D. Pitts, M. Reintjes, L.F. Warren, P.A. Wegner, J. Am. Chem. Soc. 90 (1968) 879.
[8] L. Matel, F. Macasek, P. Rajec, S. Hermanek, J. Plesek, Polyhedron 1 (1982) 511.
[9] A.R. Siedle, G.M. Bodner, A.R. Garber, D.C. Beer, L.J. Todd, Inorg. Chem. 13 (1974) 2321.
[10] I.B. Sivaev, V.I. Bregadze, Collect. Czech. Chem. Commun. 64 (1999) 783.
[11] D.G. DeBoer, A. Zalkin, D.H. Templeton, Inorg. Chem. 1 (1968) 2288.
[12] A.R. Siedle, G.M. Bodner, L.J. Todd, J. Organomet. Chem. 33 (1971) 137.
[13] Z. Xie, T. Jelinek, R. Bau, C.A. Reed, J. Am. Chem. Soc. 116 (1994) 1907.

PERGAMON

www.elsevier.nl/locate/poly

Polyhedron 19 (2000) 1783–1789

POLYHEDRON

H-bonded polymer structures of different dimensionality: syntheses and crystal structures of $[Ca(DME)_n(H_2O)_m]I_2 \cdot (DME)_x$ (**1**: $n = 3$, $m = 3$, $x = 1$; **2**: $n = 2$, $m = 4$, $x = 0$) and $[Ca\{CH_3(OCH_2)_3OCH_3\}(H_2O)_4]I_2$

Katharina M. Fromm [a,*], Helmut Goesmann [b], Gérald Bernardinelli [c]

[a] *Department of Inorganic Chemistry, Sciences II, University of Geneva, CH-1211 Geneva 4, Switzerland*
[b] *Institut für Anorganische Chemie, Universität Karlsruhe, Engesserstrasse, Geb. 30.45, D-76128 Karlsruhe, Germany*
[c] *Laboratory of Crystallography, University of Geneva, CH-1211 Geneva 4, Switzerland*

Received 14 March 2000; accepted 26 May 2000

Abstract

From the non-covalent binding modes used in supramolecular chemistry, metal ion complexation and hydrogen bonding are combined in order to synthesise new inorganic polymers as precursors for thin layer deposition. With the same coordinating ligands, DME and water, but in varying stoichiometries, two different dimensional compounds are obtained. The synthesis and crystal structures of the one- and three-dimensional polymers are described together with a third example for better control of the supramolecular products formed. © 2000 Elsevier Science Ltd. All rights reserved.

Keywords: Calcium; H-bonding; Inorganic Polymers; Alkaline Earth; X-ray structure

1. Introduction

The bonding modes used in supramolecular chemistry provide elegant tools to design and synthesise architectures of nanoscopic dimensions with novel structural and functional properties [1]. Non-covalent interactions, such as hydrogen bonding, metal ion coordination, electrostatic and hydrophobic forces, permit precise positioning of molecular components in a well-defined supramolecular architecture [2]. The final product is built up following a series of spontaneous recognition, growth, and termination steps of suitable components and specified interaction schemes.

Whereas the underlying principles of non-covalent interactions are generally well understood, the next challenge in the implementation of supramolecular devices in molecular based materials lies in the generation of spatially confined and macroscopically ordered compounds. In our aim to develop new precursors for thin metal oxide films, especially high-temperature superconductors, we study the formation of inorganic polymers of alkaline earth metal halide derivatives based on metal ion complexation and covalent or hydrogen bonding in organic donor solvents [3]. For both cases, it is in general very difficult to control and predict the coordination sphere of the metal, the bridging mode of the anions and the resulting overall dimensionality of the compound [4–8]. The latter is influenced by the donor ligand, that is its size, strength, polarizability and concentration, its capacity to build non-covalent bonds in order to obtain a network, as well as thermodynamic conditions during the reaction and crystallisation. In the case of mixed ligand systems, the product that is formed also depends on the orientation and arrangement of the donors around the metal ion. In this work, two calcium compounds will be presented, $[Ca(DME)_3(H_2O)_3]I_2 \cdot DME$ (**1**) and $[Ca(DME)_2(H_2O)_4]I_2$ (**2**), which feature the same type of ligands in their coordination sphere but in different stoichiometries and spatial arrangements, thus leading

* Corresponding author. Tel.: +41-22-702-6421; fax: +41-22-702-6069.
E-mail address: katharina.fromm@chiam.unige.ch (K.M. Fromm).

0277-5387/00/$ - see front matter © 2000 Elsevier Science Ltd. All rights reserved.
PII: S0277-5387(00)00466-6

to H-bridged polymers of different dimensionality. They might be regarded as early intermediate species on the formation of sol–gels via solvation by water and following hydrolysis starting from $[Ca(DME)_3I_2]$, and leading to $[Ca(OH)_2(H_2O)_y]$. The third compound $[Ca\{CH_3(OCH_2)_2OCH_3\}(H_2O)_4]I_2$ (**3**) is an example derived from **2** which shows how an isosteric ligand to the two DME molecules of **2** can maintain the same overall structure.

2. Experimental

All reactions were carried out under an atmosphere of dried nitrogen using standard inert atmosphere and Schlenk techniques, unless otherwise stated. DME (1,2-dimethoxy ethane) was distilled from sodium benzophenone under N_2, *n*-hexane was distilled from $LiAlH_4$ under N_2, and distilled water was degassed with N_2. Triethylene glycol dimethyl ether (triglyme) was obtained p.a. from Fluka and distilled from sodium benzophenone under vacuum. $CaI_2{\cdot}5H_2O$ obtained from Aldrich Chemicals Co. was dried under vacuum at 200°C. IR spectra were taken on CsI plates in Nujol on a Perkin–Elmer Spectrum-One.

2.1. $[Ca(DME)_3(H_2O)_3]I_2{\cdot}DME$ (1)

Dried CaI_2 (0.4 g, 1.36 mmol) was dissolved in 50 ml of a 100:1 mixture of DME and water. The slightly yellow solution was filtered and evaporated to 35 ml under vacuum, layered with *n*-hexane and left at 243 K overnight. Colourless crystals of **1** in a yield of 84% referring to CaI_2 were collected. More product could be isolated from the mother liquid by concentrating the solution. The crystals are stable at room temperature. However, they lose solvent after several hours of exposure to air. IR of **1**: 3802(vw), 3415(vs, sh), 3210(s), 2926 (Nujol), 2114(w, sh), 1641(m), 1609(s), 1454 (Nujol), 1367 (Nujol), 1303(vw), 1281(m), 1246(m), 1116(vs), 1060(s), 1025(s), 982(m), 940(m), 864(s), 840(sh), 722 (Nujol) 553(s, sh), 376(m), 301(m). Elemental analysis of **1**. Found: C, 24.92; H, 5.92; Ca, 6.23. *Anal.* Calc.:C, 25.35; H, 6.23; Ca, 6.04%.

2.2. $[Ca(DME)_2(H_2O)_4]I_2$ (2)

Dried CaI_2 (0.32 g, 1.09 mmol) was dissolved in 30 ml of a 100:5 mixture of DME and water. The pale yellow solution was filtered, stored at room temperature, and after 3 days colourless single crystals of **2** were obtained in a yield of 72% referring to CaI_2. The compound is stable at air and room temperature. IR of **2**: 3383(m, sh), 3020(w), 2926 (Nujol), 1607(vs), 1460 (Nujol), 1376 (Nujol), 1247(w), 1192(m), 1114(s), 1061(m), 1025(m), 979(w), 864(m), 790(w), 722 (Nujol), 551(m), 315(m, sh). Elemental analysis of **2**. Found: C, 17.31; H, 4.80; Ca, 7.55. *Anal.* Calc.: C, 17.60; H, 5.17; Ca, 7.34%.

2.3. $[Ca\{CH_3(OCH_2)_3OCH_3\}(H_2O)_4]I_2$ (3)

$CaI_2(H_2O)_5$ (0.46 g, 1.23 mmol) were dissolved in 50 ml triglyme. The light yellow solution was layered with *n*-hexane and left to diffuse at room temperature. Colourless single crystals of **3** were obtained after 3 days in a yield of 23% referring to Ca. The same product **3** is obtained when recrystallising **2** from triglyme in 88% yield. The compound is very stable at air and room temperature. IR of **3**: 3381(m), 3182(m), 2929 (Nujol), 1958(w), 1603(s), 1456 (Nujol), 1350 (Nujol), 1285(m), 1247(s), 1199(vs), 1110(vs), 1028(sh), 982(m), 943(s), 848(vs, sh), 723 (Nujol), 540(s, sh), 389(w), 347(m), 238 (m). Elemental analysis. Found: C, 17.52; H, 4.68; Ca, 7.48. *Anal.* Calc.: C, 17.66; H, 4.82; Ca, 7.37%.

2.4. X-ray crystallographic structural solution of $[Ca(DME)_3(H_2O)_3]I_2{\cdot}DME$ (1), $[Ca(DME)_2(H_2O)_4]I_2$ (2) and $[Ca\{CH_3(OCH_2)_3OCH_3\}(H_2O)_4]I_2$ (3)

A colourless cube-like crystal of **1** having the dimensions $0.46 \times 0.38 \times 0.38$ mm was mounted on a glass fibre. For **2**, a colourless crystal with a rhombic habitus of dimensions $0.37 \times 0.32 \times 0.12$ mm was chosen. The needle-like crystal chosen from **3** had the dimensions $0.07 \times 0.07 \times 0.58$ mm. All measurements were carried out on a STOE STADI 4 four circle diffractometer with graphite monochromated Mo Kα radiation and at 200 K. Pertinent data collection and reduction information as well as selected bond distances and angles are given in Tables 1 and 2. Cell constants and an orientation matrix for data collection, obtained from a least-squares refinement using the setting angles of 25 carefully centred reflections corresponded to a triclinic cell for **1** and **2**, the space group being $P\bar{1}$. For **3**, the monoclinic space group $C2/c$ was found. The intensities of two standard reflections measured every 2 h showed no significant change throughout the measurements. The structures were solved with direct methods and refined using the programme SHELX [9]. The hydrogen positions in the water molecules could in all three cases be determined by difference Fourier maps.

3. Results

Dry CaI_2 dissolves quite well in etheral solvents like THF, DME (monoglyme, $CH_3OC_2H_4OCH_3$) and higher glymes (diglyme, triglyme, tetraglyme) but even better in the presence of traces of water. Excess water leads to the formation of sol–gels of composition of $[Ca(OH)_2(H_2O)_y]$.

Dissolving CaI_2 in a 100:1 mixture of DME and water yields a slightly yellow solution from which colourless crystals of $[Ca(DME)_3(H_2O)_3]I_2 \cdot DME$ (**1**) were obtained at −30°C after layering with *n*-hexane. **1** crystallises in the triclinic space group $P\bar{1}$ with one molecule per unit cell. The calcium atoms in **1** feature a coordination number of seven (CN = 7) with two molecules of DME and three water ligands (Fig. 1). With respect to the oxygen atoms of the donor molecules, the coordination geometry can be described as a distorted pentagonal bipyramid with two of the water molecules in axial positions (O7 and O9), the oxygen atoms of the third water and the two DME ligands occupying approximately the five positions around the almost planar equator. The Ca–O(H_2O) bond lengths are with 2.348(3)–2.351(3) Å by 0.7–1.0 Å shorter than the Ca–O(DME) distances, the difference as expected between mono- and bidentate ligands.

Table 1
Crystallographic data for **1**, **2** and **3**

	1	**2**	**3**
Formula	$C_{14}H_{41}CaI_2O_{10}$	$C_8H_{28}CaI_2O_8$	$C_8H_{26}CaI_2O_8$
Formula weight	663.21	546.10	544.17
Colour	colourless	colourless	colourless
Crystal size	0.46 × 0.38 × 0.38	0.37 × 0.32 × 0.12	0.07 × 0.07 × 0.58
Space group	$P\bar{1}$	$P\bar{1}$	$C2/c$
Crystal system	triclinic	triclinic	monoclinic
a (Å)	9.014(2)	9.511(2)	9.572(2)
b (Å)	13.577(3)	9.524(2)	16.306(3)
c (Å)	13.647(3)	13.120(3)	12.981(3)
α (°)	60.75(3)	98.34(3)	90
β (°)	75.46(3)	98.73(3)	105.32(3)
γ (°)	88.98(3)	118.87(3)	90
V (Å^3)	1399.6(5)	995.4(3)	1954.1(7)
Z	2	2	4
D_{calc} (g cm^{-3})	1.574	1.822	1.850
μ (Mo Kα) (mm^{-1})	2.467	3.440	3.504
λ (Mo Kα) (Å)	0.71069	0.71069	0.71069
Theta range	1.73–25.99	2.49–25.97	2.50–27.01
Reflections collected	4180	6540	1774
Independent reflections	4180	3285	1774
Parameters	275	208	104
Refinement method	Full matrix least squares on F^2		
Final R indices [a] R_1, wR_2	0.0258, 0.0709	0.0258, 0.0632	0.0396, 0.0872
GOOF[b]	1.116	1.163	1.147

[a] $R_1 = \Sigma||F_o|-|F_c||/\Sigma|F_o|$. $wR_2 = \{\Sigma[w(F_o^2-F_c^2)^2]/\Sigma[w(F_o^2)^2]\}^{1/2}$.
[b] GOOF = $S = \{\Sigma[w(F_o^2-F_c^2)^2]/(n-p)\}^{1/2}$; n = number of reflections, p = number of parameters. Weighting scheme: $w = 1/[\sigma^2(F_o^2)+(aP)^2+bP]$ where $P = [2F_c^2+\max(F_o^2,0)]/3$.

Table 2
Comparison of the most important structural data and features of **1**, **2** and **3** [a]

	1	**2**	**3**
Coordination number	7	8	8
Ca–O(DME)	2.427(2)–2.471(3)	2.503(2)–2.514(3)	
Ca–O(triglyme)			2.487(5)–2.506(4)
Ca–O(H_2O)	2.348(3)–2.351(3)	2.417(2)–2.436(2)	2.393(4)–2.424(5)
O(H)–I	3.492(4)–3.611(3)	3.510(2)–3.586(2)	3.514(5)–3.579(5)
O(H)–O(DME3)	2.756(4)–2.820(4)		
O–Ca–O(DME)	66.94(9)–67.72(9)	65.52(8)–65.55(8)	
O–Ca–O(triglyme)			62.3(2)–65.1(1)
O–Ca–O(H_2O)	80.4(1)–96.5(1)	71.07(8)–73.52(9)	70.0(3)–71.43(2)
H–I–H	87.21(7), 130.57(9)	49.27(6)–84.79(8)	50.77(6)–82.55(7)
I–O–I	95.16(9)	96.30(8)–100.77(9)	99.09(5)
Valence bond sum	2.24	2.15	2.24

[a] Bond distances (Å) and angles (°).

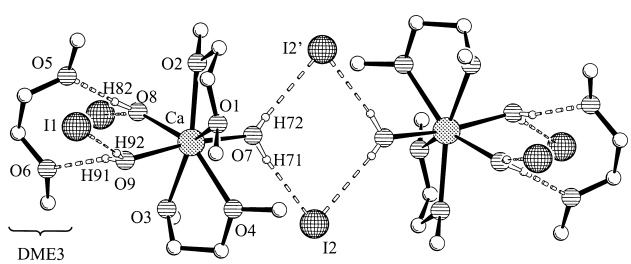


Fig. 1. Excerpt from the band structure of **1** showing two cationic units linked together to dimers via hydrogen bonding by I2.

With these five ligands, the closer coordination sphere of seven oxygen atoms around the calcium atom is fully described. However, a second, outer coordination sphere must be taken into account. In fact, a third solvent molecule, DME3, is bound to the cationic complex. Whereas the Ca–O(DME3) distances are 4.198(3) and 4.369(3) Å, much too long for direct interactions, the ligand is actually bound via hydrogen bonding between two of the water molecules involving O8–H82 and O9–H91 and the oxygen atoms of the third DME3, O5 and O6, respectively. The two water molecules O8 and O9 are both classified as class 1′, and type J concerning their hydrogen bonding [10,11]. The corresponding bond lengths are O8(H82)–O5, 2.756(4)

Å (1.90(4) Å) and O9(H91)–O6, 2.820(4) Å (1.99(6) Å). This complex, containing an inner and outer coordination sphere around the alkaline earth metal, describes the cationic fraction of the unit cell, and is part of the polymer structure.

Two such cationic units form dimers via hydrogen bonding involving both hydrogen atoms H71 and H72 of the water molecule O7 and the anion I2 as well as their symmetry equivalents O7' and I2'. The iodide acts as μ_2-bridge between two calcium complexes, featuring a H71–I2–H72′ angle of 87.21(8)°. The hydrogen bonds are O7(H71)–I2 3.611(3) Å (2.70(6) Å) and O7(H72)–I2′ 3.502(3) Å (2.78(5) Å) long. The water molecule O7 is of class 1, type D in the classification of hydrogen bonded water molecules with respect to its lone pair coordination [10,11]. A crystallographic inversion center is found in the geometric middle of the rhombus formed by O7–I2–O7′–I2′. Opposite to the axial water O7, in the *trans* position on the pentagonal bipyramid,

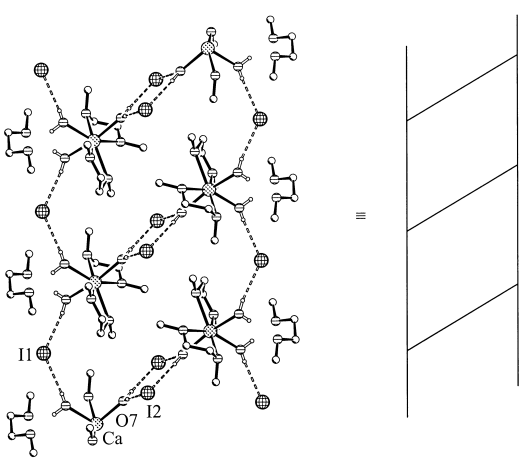


Fig. 2. View onto the band structure of **1**, compared to a railway or ladder arrangement.

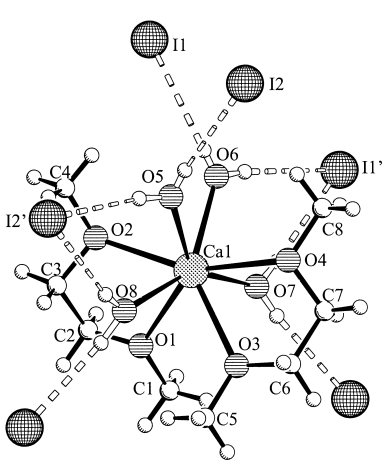


Fig. 3. Square antiprismatic coordination sphere of **2** and corresponding H-bonding.

the water molecule O9 is partially blocked by H-bonds of H92 to the third DME molecule. It thus cannot form the same type of hydrogen bonding as O7, hindering the structure from the formation of strands along this axis and restraining it to dimers.

These cationic dimers are linked to each other to form a ladder structure by hydrogen bonding of the water molecules O8(H81) and O9(H92) via one hydrogen atom to I1 which acts as μ_2-bridging ligand between the dimers with I1–O(H) distances of 3.492(4) (2.75(5)) Å and 3.514(4) (2.74(5)) Å, respectively (Fig. 2). The O8(H81)–I1–O9(H92) angle is with 134.07(9)° (130.57(9)°) about 40° wider than the O7–I2–O7′ angle. Thus, **1** builds up a one-dimensional polymer, the dimers forming a ribbon-like structure. In the crystal, these bands are stacked onto each other alternating in an ABAB fashion. The cavities of approximate average diameter of 6 Å thus formed are filled with one free DME molecule per asymmetric unit.

Higher concentrations of water yield a different adduct. From a solution of dry CaI_2 in a mixture 100:5 DME–water, compound $[Ca(DME)_2(H_2O)_4]I_2$ (**2**) is obtained at room temperature. Colourless blocks crystallise in the triclinic space group $P\bar{1}$ with two cationic units and four iodide per unit cell. Again, two DME molecules are directly coordinated to the alkaline earth cation, and the angles between the DME molecules are very similar to the ones in **1**, leaving the rest of the coordination sphere to four water molecules instead of three. The calcium thus reaches a coordination number of eight (CN = 8) with a distorted square antiprismatic geometry, two water molecules and one DME in each square plane (Fig. 3). The Ca–O distances in **2** reach from 2.417(2) to 2.436(2) Å for water and from 2.503(2) to 2.514(3) Å for the DME ligands. All water molecules are involved in hydrogen bonding, each of them being linked to two iodide. Two of them, O6 and O7, of one square face of the antiprism and I1 thus build up a ribbon-like structure in one direction. A second strand is formed by the other two water molecules O5 and O8 of the second square face and their hydrogen bonding to I2, featuring a direction vector of the ribbon almost perpendicular to the first (Fig. 4(a)). The corresponding O(H)–I distances are between 3.510(3) and 3.586(3) Å long. The water molecules O5 and O6 are of class 1, type D, whereas the water ligands O7 and O8 are of class 1′, type J concerning their hydrogen bonding modes [10,11]. In total, a three-dimensional network results with channels along the *c*-axes with a diameter of approximately 5 Å (Fig. 4(b)).

Each of the anions I1 and I2 is μ_4-bridging between three cationic units $[Ca(DME)_2(H_2O)_4]^{2+}$, having contacts with two water molecules of one cationic unit and one water of a second and a third unit. Crystallo-

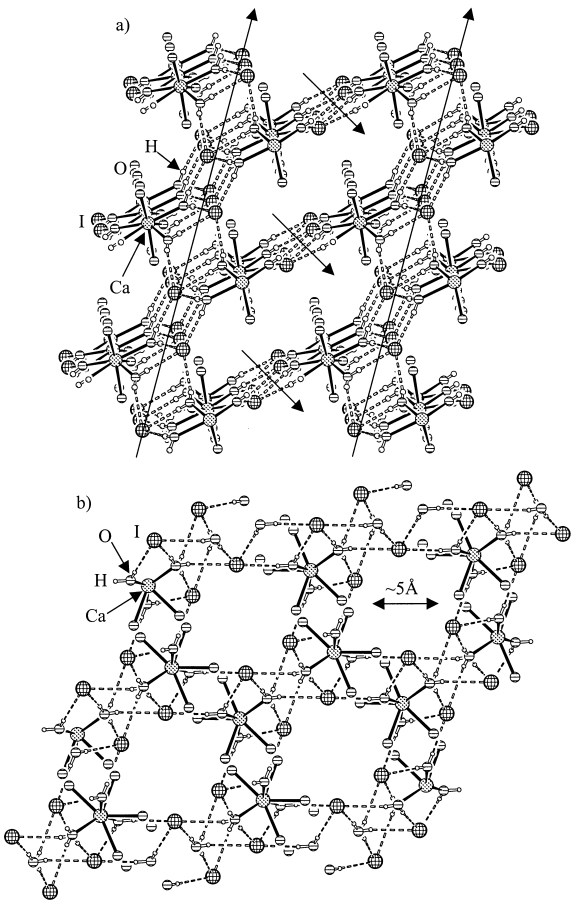


Fig. 4. (a) View of **2** along *b*, onto the *ac*-plane showing the orientation of the bands formed by hydrogen bonding; (b) View of **2** along *c*, onto *ab*-plane.

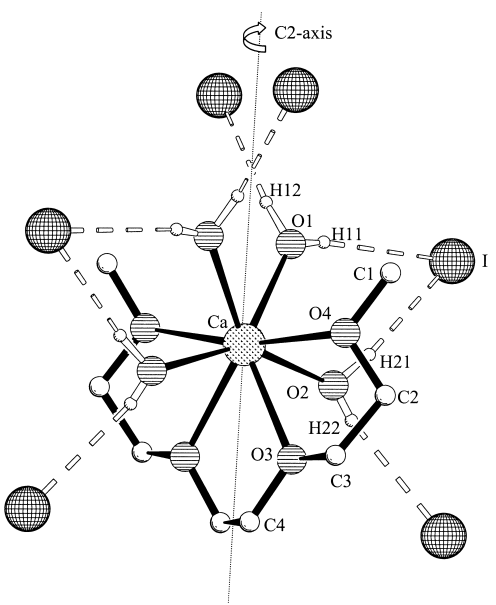


Fig. 5. Square antiprismatic coordination sphere of **3** and corresponding H-bonding, the H-atoms of the triglyme ligand are omitted for clarity.

graphic inversion centres are found in the geometric middle of each O*n*–I*m*–O*n*′–I*m*′ rhombus (*m* = 1; *n* = 6, 7 and *m* = 2; *n* = 5, 8).

In order to preorganise the positioning of the two DME molecules to each other in **2**, they were formally replaced by a triglyme ligand. The compound $[Ca\{CH_3(OCH_2)_3OCH_3\}(H_2O)_4]I_2$ (**3**) was obtained in form of colourless blocks and crystallises in the monoclinic space group *C*2/*c* (no. 15). In the cationic part of the structure, the calcium lies on a crystallographic two-fold axis which also passes through the geometrical middle of the triglyme ligand (0, *y*, 1.4 (e)) (Fig. 5).

The metal ion has a coordination number of eight, and presents the coordination geometry of a distorted square antiprism like **2** with two water molecules and two oxygen atoms of the triglyme in one square plane, the other two oxygen atoms and the two water molecules are situated in the other plane of the prism. As a result, the hydrogen bonds that are built up between the water ligands and the iodides are very similar to the ones in **2** and again lead to a three-dimensional network (Fig. 6). The hydrogen bonds maintained by O1 and O1′ correspond to the ones built by O5 and O6 in **2** and are also of type D, class 1, whereas O2 and O2′ are of type J, class 1′ similar to O7 and O8 in **2** [10,11].

4. Discussion

Comparing **1** and **2** reveals a surprisingly similar close coordination of the alkaline earth cation by the two DME molecules both in angles and in orientation. Formally, the third H-bound DME in **1** has been taken off, and one of the water molecules in the axial positions of the distorted pentagonal bipyramid of **1** has been replaced by two water molecules in **2**. However, the Ca–O bond lengths in **1** are almost 0.1 Å shorter than in **2** (Table 2). A similar trend is observed for the Ca–O distances concerning the water ligands. This is due to the difference in the coordination number varying from seven in **1** to eight in **2** and explains the elongation of bond lengths for the latter. As the iodide anions in **2** are shared between four water molecules, the O(H)–I hydrogen bonds are by up to 0.08 Å longer than in **1** where the anion acts as μ_2-bridging ligand.

The presence of a further DME molecule in **1** sterically hinders the approach of the strands to each other, and the formation of a sheet-like or three-dimensional structure via μ_4-bridging iodide is excluded. In **2**, the absence of the H-bound DME3 allows the mutual approach of two parallel ribbons. The space left by the elimination of DME3 is filled by the iodide of the neighbour strand, leading to new H-bonding and allowing the iodide to act as an μ_4-bridging ligand. By the additional water molecule in **2**, networking is improved

in the opposite direction as well, which finally leads to the three-dimensional structure in contrast to **1**.

Both compounds can be regarded as early intermediates on the way to sol–gels starting from $[Ca(DME)_3I_2]$ [12,13] towards $[Ca(OH)_2(H_2O)_y]$. A following reaction mechanism can be proposed.

On addition of water ligands to $[Ca(DME)_3I_2]$, the iodides which are directly linked to the alkaline earth cation will be formally replaced by H_2O molecules, the halide being displaced into the outer coordination sphere, linked by hydrogen bonding (Scheme 1). As the coordination sphere around the equatorial positions is dense, one DME molecule is formally substituted by a third H_2O ligand which can be placed more easily at the metal center and allow the type of hydrogen bonding to a third DME in an outer ligand sphere as is shown in the crystal structure of **1**. Higher concentrations of H_2O will displace DME from the second coordination sphere and lead to compound **2**. On further addition of water to compound **2**, hydrolysis occurs, and the formation of a white sol–gel of composition $[Ca(OH)_2(OH_2)_y]$ can be observed. More investigations are on the way in order to identify other intermediates of this hydrolysis reaction.

As **2** and **3** have very similar structural features, the only difference being the formal replacement of two DME molecules in **2** by a triglyme ligand in **3**, one should expect similar bond lengths in both compounds. However, the average Ca–O distances in **3** are up to 0.02 Å shorter than in **2**. The bite angles of the triglyme ligand and the $O(H_2O)$–Ca–$O(H_2O)$ angles of **3** between neighbouring water molecules are on average smaller than in **2**. Concerning the hydrogen bonding part of the two structures, the parameters such as H–I–H and I–O–I angles as well as O(H)–I distances are in the same order of magnitude. The difference between **2** and **3** is thus found in the metal ion complexation and can be expressed in the valence bond sum [14,15] for calcium which can be calculated to be 2.15 for **2** and 2.24 for **3**, meaning a stronger, more efficient complexation for **3** by the triglyme ligand than for **2** by the two DME ligands. The same valence bond sum as for **3** is calculated for **1** which has a lower coordination number for calcium than **3**, meaning that the DME and water ligands are more strongly bound than in **2** due to the lower coordination number for calcium.

Other polymer structures built from alkali or alkaline earth metal ion complexation and hydrogen bonding have been described in the literature, without however rationalising the influences of the ligands and their concentrations on the final dimensionality of the structures. Thus, the complex $[Na\{N(CH_2CH_2OH)_3\}I]$ features a coordination number of seven for the sodium cation which is coordinated by four heteroatoms of one ligand, two oxygen atoms of neighbouring ligands and the iodide, and builds one-dimensional chains via additional hydrogen bonding between the ligands [16]. A parallel sheet structure is obtained when replacing the iodide by a perchlorate anion which offers a wider, yet directed range of hydrogen bonding possibilities due to its tetrahedral arrangement of oxygen atoms [17]. Infinite chains of dimers, cross-linked via ClO_4^- into sheets by van der Waals contacts, are observed in the barium compound $[Ba\{N(CH_2CH_2OH)_3\}_2(ClO_4)_2]$ [17]. Hydro-

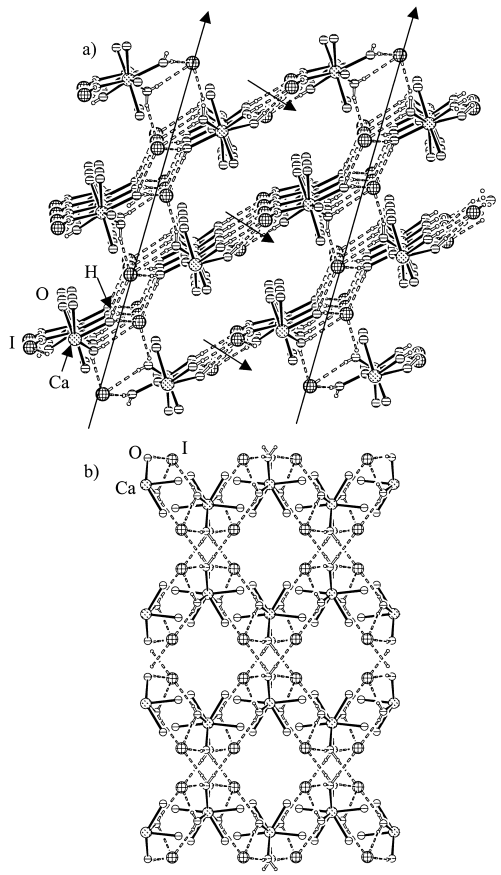
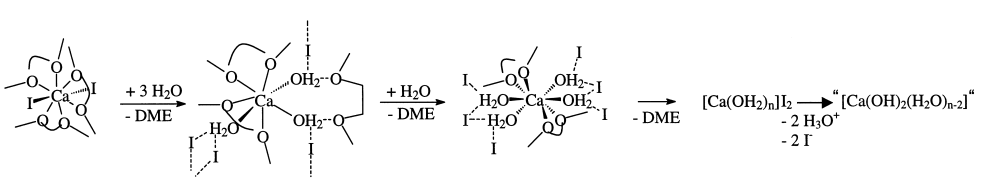


Fig. 6. Three-dimensional network formed by **3**.



Scheme 1.

gen bonding due to water ligands is described in $[(py)_4Mg(OH_2)_2]I_2$2py, yielding dimeric units, and $[Ba(ClO_4)_2(OH_2)(py)]$ which forms two-dimensional sheets (py = pyridine) [6]. Three-dimensional networks are observed by hydrogen bonding between water molecules and halide anions in the compounds $[(dien)_2Ca(OH_2)Cl]Cl$, $[(dien)_2Ca(OH_2)_2]Br_2$ and $[(en)_4Ba(OH_2)]Br_2$ [8]. In all cases described, the final structure and dimensionality were unpredictable. A study of two calcium complexes $[Ca(OH_2)_2(L)_4]I_2$ with a very similar octahedral coordination geometry with L = THF (tetrahydrofurane) for one and CH_3-$COOC_2H_5$ (ethyl acetate) for the other compound shows that even slight differences in the coordination sphere lead to a two-dimensional sheet structure in the first case and a one-dimensional polymer in the second case [3]. The determination of the strength of hydrogen bonds from IR spectra and X-ray data was attempted for intramolecular O–X bond lengths for which X = H or D [18]. For O–H···Y with Y = F, Cl, Br or I however, more reliable data are still needed before it will be possible to rationalise the strength of hydrogen bonding in compounds such as **1**, **2** and **3**.

5. Conclusions

It can be seen from **1**, **2**, **3** and the examples known from the literature that the ligands, their size and number as well as the type of counter ion play an important role in the building of hydrogen bonds. Two new structures, **1** and **2**, are presented that clearly show the dependence of stoichiometry for a pair of given ligands on the network formation. Reorganisation of the cationic building block can be achieved by the utilisation of a polyether ligand that is very similar in coordination and size to the diethers used in **1** and **2**. This allows one to predict with high probability the same hydrogen bonding structure for **3** that was obtained in **2**. It is still however a long way away from an efficient rationalisation of the pathway behind the formation of inorganic polymers based on complexation and hydrogen bonding, especially of the type O(H)···X, where X = halide.

6. Supplementary material

Crystallographic data have been deposited with the CCDC deposition numbers CCDC 141463 for **1**, CCDC 141464 for **2** and CCDC 141688 for **3**. Copies of this information may be obtained free of charge from: The Director, CCDC, 12 Union Road, Cambridge, CB2 1EZ, UK (Fax: +44-1223-336033; e-mail: deposit@ccdc.cam.ac.uk or www: http://www.ccdc.cam.ac.uk).

Acknowledgements

We thank the Swiss National Foundation and the University of Geneva for supporting this work. We are grateful to Professor Dr A.F. Williams and Professor Dr C. Piguet, University of Geneva, for their generosity and help.

References

[1] J.M. Lehn, Supramolecular Chemistry — Concepts and Perspectives, VCH, Weinheim, 1995.
[2] G.M. Whitesides, J.P. Mathias, C.T. Seto, Science 254 (1991) 1312.
[3] (a) K.M. Fromm, Angew. Chem. 109 (1997) 2876; Angew. Chem. Int. Ed. 36 (1997) 2799. (b) K.M. Fromm, G. Bernardinelli, M.-J. Mayor-López, J. Weber, H. Goesmann, Z. Anorg. Allg. Chem. 7 (2000) 1685.
[4] R. Sarma, F. Ramirez, B. McKeever, Y. Fen Chaw, J.F. Maracek, D. Nierman, T.M. McCaffrey, J. Am. Chem. Soc. 99 (1977) 5289.
[5] C. Bois, S. Halut-Desportes, J. Inorg. Nucl. Chem. 41 (1979) 414.
[6] D.L. Kepert, B.W. Skelton, A.F. Waters, A.H. White, Aust. J. Chem. 49 (1996) 47.
[7] A.F. Waters, A.H. White, Aust. J. Chem. 49 (1996) 61.
[8] A.F. Waters, A.H. White, Aust. J. Chem. 49 (1996) 87.
[9] G.M. Sheldrick, Program for Single-Crystal Structure Solution and Refinement, University of Göttingen, 1997
[10] G. Ferraris, M. Franchini-Angela, Acta Crystallogr., Sect. B 28 (1972) 3572.
[11] R. Chidambaram, A. Sequeira, S.K. Sikka, J. Chem. Phys. 41 (1964) 3616.
[12] K.M. Fromm, unpublished results.
[13] K.M. Fromm, Chem. Commun. 17 (1999) 1659.
[14] M. O'Keeffe, N.E. Brese, J. Am. Chem. Soc. 113 (1991) 3226.
[15] G.J. Palenik, Inorg. Chem. 36 (1997) 122.
[16] J.C. Voegele, J. Fischer, R. Weiss, Acta Crystallogr., Sect B 30 (1974) 62.
[17] A.A. Naiini, J. Pinkas, W. Plass, V.G. Young Jr., J.G. Verkade, Inorg. Chem. 33 (1994) 2137.
[18] H.D. Lutz, C. Jung, M. Trömel, J. Lösel, J. Mol. Struct. 351 (1995) 205.

PERGAMON

www.elsevier.nl/locate/poly

Polyhedron 19 (2000) 1791–1798

POLYHEDRON

Synthesis and X-ray single crystal study of the bi- and trimetallic alkoxides of molybdenum(VI) and tantalum, $Mo_2Ta_4O_8(OMe)_{16}$, $Mo_4Ta_4O_{16}(O^iPr)_{12}$ and $LiMo_4Ta_3O_{14}(O^iPr)_9(OC_2H_4OMe)_3$

Anders Johansson, Vadim G. Kessler *

Department of Chemistry, Swedish University of Agricultural Sciences, PO Box 7015, S-75007 Uppsala, Sweden

Received 1 November 1999; accepted 31 May 2000

Abstract

The partial hydrolysis of a mixture of molybdenum and tantalum methoxides (Mo:Ta = 1:2) with stoichiometric amounts of water yields a new bimetallic complex $Mo_2Ta_4O_8(OMe)_{16}$ (**I**) on crystallization from toluene. The molecules of **I** appear to be a combination of two $MoO_2(O^iPr)_2$ units with the earlier described $Ta_4O_4(O^iPr)_{12}$ core. The thermal reduction of a mixture of $MoO(O^iPr)_4$ and $Ta_2(O^iPr)_{10}$ (in a 1:1 Mo:Ta ratio) followed by oxidation of the products by dry oxygen, provides access to $Mo_4Ta_4O_{16}(O^iPr)_{12}$ (**II**). The same procedure, using $LiMo_2O_4(O^iPr)_4(OC_2H_4OMe)$ instead of $MoO(O^iPr)_4$, yielded trimetallic $LiMo_4Ta_3O_{14}(O^iPr)_9(OC_2H_4OMe)_3$ (**III**) in minor yields. The molecular structure of **II** can be described as a distorted cube, the corners of which are occupied in turn by $[(^iPrO)_3Ta(\mu\text{-}O)_3]$ octahedra and $[MoO(\mu\text{-}O)_3]$ tetrahedra sharing common vertexes. The molecular structure of **III** can be derived from that of **II** by replacing one $[(^iPrO)_3Ta(\mu\text{-}O)_3]$ octahedron with an $[Li(\mu,\eta^2\text{-}OC_2H_4OMe)_3]$ trigonal prism (the coordination number of the three Mo atoms is then increased to six). © 2000 Elsevier Science Ltd. All rights reserved.

Keywords: Molybdenum; Tantalum; Trimetallic alkoxides; Crystal structures

1. Introduction

Heterometallic alkoxides of heavy transition elements appear to be potent precursors of fine powders of the mixed-metal oxides and corresponding metal alloys having a broad range of applications [1,2]. We have reported earlier the isolation and characterization of the mixed-metal molybdenum(VI) and Group 4, e.g. $Zr_3Mo_8O_{24}(O^iPr)_{12}(^iPrOH)_4$ [3], and Group 7, e.g. $ReMoO_2(OMe)_7$ [4], derivatives. It appeared challenging to extend this study to the Group 5 derivatives and we report here the isolation and structural characterization of the bimetallic alkoxides of molybdenum(VI) and tantalum and of the related trimetallic complex of these elements and lithium. A preliminary communication reporting the isolation and a short description of the molecular structure of $Mo_2Ta_4O_8(OMe)_{16}$ has been published [5].

* Corresponding author. Tel.: +46-18-671-541; fax: +46-18-673-476.

E-mail address: vadim.kessler@keuvi.slu.se (V.G. Kessler).

2. Experimental

All manipulations were carried out in a dry nitrogen atmosphere using the Schlenk technique or a dry box. The alcohols were purified by distillation over $Al(O^iPr)_3$ or $Mg(OMe)_2$ under argon. IR spectra of Nujol mulls were registered with a Bruker IFS-55 spectrometer. The ^1H NMR spectra were obtained with a Varian 400 MHz spectrometer, using dry deaerated toluene as solvent (using TMS as internal and 20 vol% solution of $CDCl_3$ as external standards). The metal ratio in the samples was determined, exploiting the facilities of Arrhenius Laboratory, Stockholm University, Sweden, on a JEOL-820 scanning electron microscope (SEM), supplied with a Link AN-10000 energy dispersive spectrometer (EDS). The total contents of the incombustible residues for the samples was determined using Perkin–Elmer TGA-7 device (in air, 10°C min^{-1}, final temperature 800°C).

The starting reagents used in this work ($MoO(OMe)_4$ and $LiMo_2O_4(O^iPr)_4(OC_2H_4OMe)$ [6] $Ta(OMe)_5$, and

0277-5387/00/$ - see front matter © 2000 Elsevier Science Ltd. All rights reserved.
PII: S0277-5387(00)00443-5

$Ta(O^iPr)_5$ [7]) were prepared by anodic oxidation of metals in alcohols and purified according to conventional techniques. An alcohol interchange reaction with isopropanol was used to obtain $MoO(O^iPr)_4$ and was performed by repeated (three times) dissolution of a measured quantity of methoxide in an excess of ^{i}PrOH with subsequent evaporation to dryness.

2.1. Preparation of $Mo_2Ta_4O_8(OMe)_{16}$ (I)

$MoO(OMe)_4$ (0.584 g, 2.47 mmol) and $Ta(OMe)_5$ (1.734 g, 5.16 mmol) were dissolved in 20 ml MeOH and then a solution of H_2O (0.13 ml, 7.2 mmol) in 20 ml MeOH was added dropwise to the bright yellow solution over a period of 1 h. The transparent colorless solution formed was then evaporated to dryness in vacuo and the glassy residue was redissolved in 5 ml of toluene and left to crystallize at −30°C for 2 days. The colorless crystals obtained were separated by decantation, washed with 1 ml toluene and dried in vacuo. Yield: 1.353 g (71%). IR (cm^{-1}): 1160 s, 1155 s, 1146 s, 1133 s, 1059 s br, 1035 sh, 1028 s, 935 s, 912 s, 837 sh, 826 s br, 732 w, 616 s br, 578 m, 547 s, 540 s, 527 s br, 502 s, 494 s, 449 m br. The ^{1}H NMR spectrum of **I** is shown in Fig. 1.

2.2. Preparation of $Mo_4Ta_4O_{16}(O^iPr)_{12}$ (II)

$MoO(O^iPr)_4$ (0.472 g, 1.36 mmol) and $Ta(O^iPr)_5$ (0.674 g, 1.41 mmol) were dissolved in 5 ml of toluene and the bright yellow solution obtained was refluxed for 30 min. The brownish–orange viscous liquid thus formed was left at room temperature (r.t.) for 2 weeks in a flask covered by a serum cup and it changed color slowly to light brown. The solvent was evaporated in vacuo and the light-brown glassy residue redissolved in 3 ml of hexane and left overnight to crystallize. The colorless transparent crystals formed were separated by filtration and dried in vacuo. Yield: 0.127 g (18%). IR (cm^{-1}): 1381 m, 1367 m, 1337 w, 1262 w, 1179 s, 1168 m, 1120 s br, 1007 s br, 966 w, 904 sh, 877 s, 840 s, 810 s br, 684 sh, 583 s br, 565 sh, 455 m br. ^{1}H NMR (ppm): 5.28 septet (1H, C*H*), 1.56 doublet (6H, CH_3).

2.3. Preparation of $LiMo_4Ta_3O_{14}(O^iPr)_9(OC_2H_4OMe)_3$ (III)

The procedure used was analogous to that for the preparation of **II** except that $LiMo_2O_4(O^iPr)_4$-(OC_2H_4OMe) was used instead of $MoO(O^iPr)_4$. The crystals of **III** were obtained in minor yields after prolonged storage in toluene solution in contact with dry air (about 2 months) of the products of thermal reduction.

2.4. Crystallography

2.4.1. Crystal data for $C_{16}H_{48}O_{24}Mo_2Ta_4$ (I)

$M = 1450.22$, monoclinic, space group $P2_1/n$, $a = 9.3422(18)$, $b = 9.455(2)$, $c = 22.621(6)$ Å, $b = 99.94(3)°$, $V = 1968.3(8)$ Å^3, $D_{calc} = 2.599$ g cm^{-3} for $Z = 2$, λ(Mo Kα) = 0.71073 Å, 4414 [$R_{int} = 0.1053$] independent reflections with $I > 2\sigma(I)$ were collected at 22°C up to $2\theta_{max} = 56.58°$ with a Bruker SMART CCD 1K diffractometer. The structure was solved by standard direct methods; the coordinates of tantalum and molybdenum

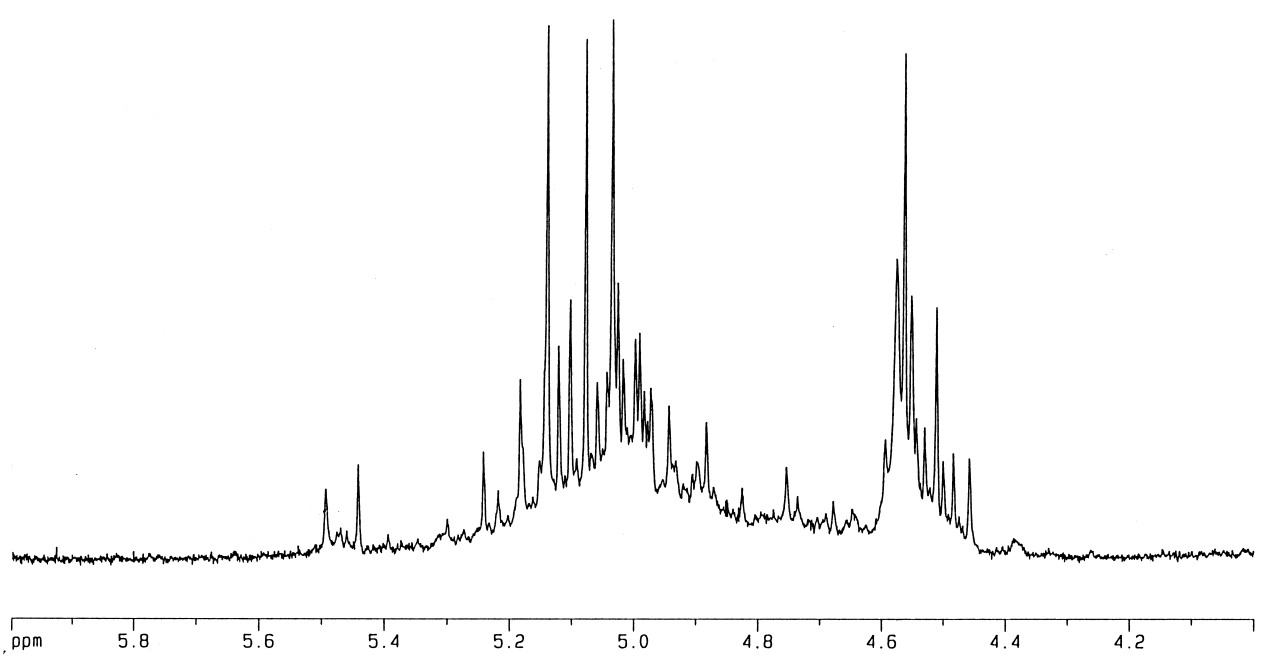


Fig. 1. The ^{1}H NMR spectrum of $Mo_2Ta_4O_8(OMe)_{16}$ (**I**) (toluene, 300 K).

atoms were taken from the initial solution and the other non-hydrogen atoms were located in subsequent Fourier syntheses. The structure was refined by full-matrix least-squares in an isotropic and then anisotropic approximation. Final discrepancy factors are $R = 0.0501$ and $wR_2 = 0.0711$.

*2.4.2. Crystal data for $C_{36}H_{84}O_{28}Mo_4Ta_4$ (**II**)*

$M = 2072.59$, tetragonal, space group $I\bar{4}$, $a = b = 14.998(6)$, $c = 14.974(8)$ Å, $V = 3368(3)$ Å^3, $D_{calc} = 2.044$ g cm^{-3} for $Z = 2$, λ(Mo Kα) = 0.71073 Å, 785 [$R_{int} = 0.0000$] independent reflections with $I > 2\sigma(I)$ were collected at 22°C up to $2\theta_{max} = 41.58°$ with a Bruker SMART CCD 1K diffractometer. The structure was solved by direct methods, applying HKLF 5 option for the experimental data file because of the presence of two twinning domains (creating a pseudo 3-fold axis and a pseudo-symmetry plane, the crystal thus having six individual components with an ideal crystallographic symmetry). The coordinates of tantalum and molybdenum atoms were taken from the initial solution and refined anisotropically. The other non-hydrogen atoms were located in subsequent Fourier syntheses and refined isotropically, the geometrical restraints being applied to conserve the idealized geometry for the ^{i}Pr-radicals (subjected to rotational disorder at r.t.). Final discrepancy factors are $R_1 = 0.0766$ and $wR_2 = 0.1933$.

*2.4.3. Crystal data for $C_{36}H_{84}O_{29}Mo_4Ta_3Li$ (**III**)*

$M = 1914.58$, triclinic, space group $P\bar{1}$, $a = 14.628(4)$, $b = 14.721(4)$, $c = 17.238(6)$ Å, $\alpha = 90.620(17)$, $\beta = 95.908(18)$, $\gamma = 118.354(9)°$, $V = 3241.6(17)$ Å^3, $D_{calc} = 1.962$ g cm^{-3} for $Z = 2$, λ(Mo Kα) = 0.71073 Å, 8399 [$R_{int} = 0.0534$] independent reflections with $I > 2\sigma(I)$ were collected at 22°C up to $2\theta_{max} = 45.00°$ with a Bruker SMART CCD 1K diffractometer. The coordinates of tantalum and molybdenum atoms were taken from the initial solution and refined anisotropically. The coordinates of all other non-hydrogen atoms were located in subsequent Fourier synthese and refined in anisotropic approximation for the oxygen atoms and isotropically for the carbon atoms. Final discrepancy factors are $R_1 = 0.0636$ and $wR_2 = 0.1516$.

The positions of the hydrogen atoms in the structures **I**–**III** were calculated geometrically and included in the final cycles of the refinement in isotropic approximation. All calculations were performed with an IBM PC using SHELXTL-NT programs [8].

3. Results and discussion

Taking into account the absence of complex formation between the monooxoalkoxides of molybdenum(VI), $MoO(OR)_4$, and tantalum alkoxides, $Ta(OR)_5$, [9] we decided to apply the microhydrolysis as the latter leads to oxoalkoxide species [10,11] that might have unsaturated coordination and thus be prone to aggregation with the formation of heterometallic products. The Mo:Ta = 1:2 ratio was chosen initially taking into account the existence of a bimetallic oxoalkoxotantalate of $I_2Zn_2Ta_4O_4(O^iPr)_{14}$ [12] composition, in which molecular structure the ZnI(μ-OR)$_2$(μ_3-O) tetrahedra appeared to be as sterically demanding as should be necessary for the $MoO_2(OR)(\mu\text{-}OR)_2(\mu_3\text{-}O)$ octahedra. When the hydrolysis of a mixture of methoxides with stoichiometric amounts of water was carried out in MeOH and the transparent solution obtained was left overnight to crystallize, the amorphous solid product collected did not contain tantalum (according to EDS analysis) and displayed an IR spectrum identical with that described for $MoO_2(OMe)_2$ [13]. To enhance the formation of heterometallic species, which could occur only via the Lewis acid–base interaction mechanism, a non-donor solvent was used (thus removing the concurrent Lewis base, MeOH). Evaporation of the reaction mixture produced by the hydrolytic treatment, to dryness and redissolution of the residue in toluene produced a clear solution from which the expected heterometallic complex, $Mo_2Ta_4O_8(OMe)_{16}$ (**I**), was obtained by crystallization at low temperatures.

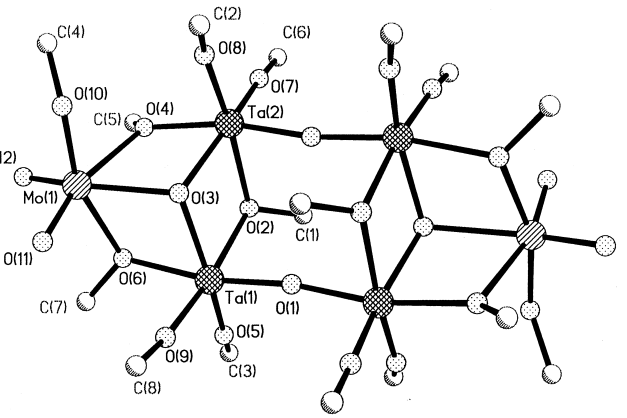


Fig. 2. The molecular structure of $Mo_2Ta_4O_8(OMe)_{16}$ (**I**).

The molecular structure of **I**, determined by an X-ray single crystal study (see Fig. 2 and Tables 1 and 2), was analogous to that of the chosen structural prototype, $I_2Zn_2Ta_4O_4(O^iPr)_{14}$ [12]. It is composed of centrosymmetric hexanuclear molecules, with the Ta–O distances (see Table 2) divided into two large groups, the first of which includes the bonds with the bridging alkoxoligands (Ta(1)–O(2) 2.125(7), Ta(2)–O(2) 2.128(7), Ta(1)–O(6) 2.125(7), Ta(2)–O(4) 2.043(7) Å) and the triply-bridging oxoatom (Ta(1)–O(3) 2.044(7), Ta(2)–O(3) 2.026(7) Å), and the second includes the bonds to the terminal alkoxide ligands (Ta(1)–O(5) 1.859(8), Ta(1)–O(9) 1.859(8), Ta(2)–O(7) 1.852(8),

Ta(2)–O(8) 1.865(8) Å) and the doubly-bridging oxoatom (Ta(1)–O(1) 1.890(7) and Ta(2)–O(1)# 1.931(7) Å). The Ta(1)–Ta(2) distance of 3.155(9) Å is quite short (compared with 3.31 Å in the Zn–Ta complex). The coordination of the doubly-bridging oxogroups is also almost linear, Ta(1)–O(1)–Ta(2)# 172.0(4)°. The coordination of the Mo atom is rather distorted in comparison with that usually observed [14]. The Mo–O distances themselves fall into the common ranges: 1.686–1.700(9) for the double bonds, 1.883(8) for the terminal alkoxide one and 2.134–2.279(8) for the alkoxide and oxo-bridging groups. However, the sum of the bond lengths in the *trans*-position differ noticeably (3.873(15), 3.979(17) and 4.017(16) Å) and the bond angles deviate strongly from 180° (O(10)–Mo(1)–O(6) 161.3(3), O(11)–Mo(1)–O(4) 164.1(4) and O(12)–Mo(1)–O(3) 151.7(4)°).

The IR spectrum of **I** is in good agreement with its molecular structure: there is a strong doublet present at 935 and 912 cm^{-1}, corresponding to vibrations in the *cis*-MoO_2 fragment [14], a very strong and broad band at 837 cm^{-1}, that can be attributed to vibrations with participation of oxobridging ligands, and a number of strong and well-defined bands in the area corresponding to the M–OR vibrations (616 s br, 578 m, 547 s, 540 s, 527 s, 502 s, 494 s, 449 m br). It should be mentioned that **I** supposedly does not exist in solution: it is almost insoluble in toluene at r.t. and when dissolved under reflux does not crystallize on cooling for several weeks. The ^1H NMR spectra of **I** (see Fig. 1) are strikingly complex: at least 20 sharp and well defined signals are observed between 4.40 and 5.20 ppm indicating presumably the destruction of the molecules on dissolution and the coexistence in solution of different molecular aggregates. The dissolution in MeOH in contrast occurs easily at r.t. and a very high solubility can in fact be observed on dissolution, but after several hours precipitation of an insoluble sediment characterized as $MoO_2(OMe)_2$ takes place (see above). Compound **I** is almost insoluble in hexane even on heating.

Analogous experiments to those used in the preparation of **I** were carried out with the isopropoxides of the title elements but did not lead to isolation of any crystalline product. At the same time it was found that oxidation of the bimetallic alkoxides of molybdenum(V) and tantalum, such as $Mo_4Ta_2O_8(O^iPr)_{14}$ or $Mo_3Ta_2O_8(O^iPr)_{10}$, with dry air led to the formation of a colorless crystalline product containing Mo and Ta in

Table 1
Crystal data and structure refinement parameters for compounds **I–III**

Empirical formula	$C_8H_{24}MoO_{12}Ta_2$	$C_{36}H_{84}Mo_4O_{28}Ta_4$	$C_{36}H_{84}LiMo_4O_{29}Ta_3$
Formula weight	770.11	2072.59	1914.58
Temperature (K)	295(2)	295(2)	295(2)
Wavelength (Å)	0.71073	0.71073	0.71073
Crystal system	monoclinic	tetragonal	triclinic
Space group	$P2_1/n$	$I\bar{4}$	$P\bar{1}$
Unit cell dimensions			
a (Å)	9.3422(18)	14.998(6)	14.628(4)
b (Å)	9.455(2)	14.998(6)	14.721(4)
c (Å)	22.621(6)	14.974(8)	17.238(6)
α (°)	90	90	90.620(17)
β (°)	99.94(3)	90	95.908(18)
γ (°)	90	90	118.354(9)
Volume (Å^3)	1968.3(8)	3368(3)	3241.6(16)
Z	4	2	2
D_{calc} (g cm^{-3})	2.599	2.044	1.962
Absorption coefficient (mm^{-1})	11.766	7.255	5.862
$F(000)$	1424	1968	1844
Crystal size (mm)	$0.50\times0.15\times0.10$	$0.5\times0.2\times0.15$	$1.1\times0.4\times0.3$
θ Range for data collection (°)	1.83–28.29	1.92–20.79	1.59–22.50
Index ranges (°)	$-11\le h\le12$, $-12\le k\le12$, $-25\le l\le29$	$-10\le h\le14$, $-10\le k\le14$, $-14\le l\le14$	$-15\le h\le15$, $15\le k\le15$, $15\le l\le18$
Reflections collected	11 104	785	12 866
Independent reflections	4414 [$R_{int}=0.1053$]	785 [$R_{int}=0.0000$]	8399 [$R_{int}=0.0534$]
Completeness to $\theta=28.29°$ (%)	90.1	84.9	99.1
Refinement method	full-matrix least-squares on F^2	full-matrix least-squares on F^2	full-matrix least-squares on F^2
Data/restraints/parameters	4414/0/208	785/33/88	8399/0/473
Goodness-of-fit on F^2	0.867	1.039	0.838
Final R indices [$I>2\sigma(I)$]	$R_1=0.0501$, $wR_2=0.0711$	$R_1=0.0766$, $wR_2=0.1933$	$R_1=0.0636$, $wR_2=0.1516$
R indices (all data)	$R_1=0.1342$, $wR_2=0.0865$	$R_1=0.0867$, $wR_2=0.2081$	$R_1=0.1080$, $wR_2=0.1612$
Largest difference peak and hole (e Å^{-3})	1.224 and −1.299	0.800 and −1.201	1.848 and −3.048
Absolute structure parameter		0.14(11)	

Table 2
Selected bond distances (Å) and angles (°) of compound **I** [a]

Ta(1)–O(5)	1.859(8)	Ta(2)–O(4)	2.043(7)
Ta(1)–O(9)	1.859(8)	Ta(2)–O(2)	2.128(7)
Ta(1)–O(1)	1.890(7)	O(1)–Ta(2) # 1	1.931(7)
Ta(1)–O(3)	2.044(7)	Ta(1)–Ta(2)	3.3155(9)
Ta(1)–O(2)	2.125(7)	Mo(1)–O(12)	1.686(8)
Ta(1)–O(6)	2.125(7)	Mo(1)–O(11)	1.700(9)
Ta(2)–O(7)	1.852(8)	Mo(1)–O(10)	1.883(8)
Ta(2)–O(8)	1.865(8)	Mo(1)–O(6)	2.134(8)
Ta(2)–O(1) # 1	1.931(7)	Mo(1)–O(3)	2.187(7)
Ta(2)–O(3)	2.026(7)	Mo(1)–O(4)	2.279(8)
O(5)–Ta(1)–O(9)	100.2(3)	O(7)–Ta(2)–O(8)	101.3(3)
O(5)–Ta(1)–O(1)	99.5(3)	O(7)–Ta(2)–O(1) # 1	97.9(3)
O(9)–Ta(1)–O(1)	94.7(3)	O(8)–Ta(2)–O(1) # 1	92.0(3)
O(5)–Ta(1)–O(3)	154.7(3)	O(7)–Ta(2)–O(3)	159.4(3)
O(9)–Ta(1)–O(3)	97.1(3)	O(8)–Ta(2)–O(3)	93.9(3)
O(1)–Ta(1)–O(3)	97.3(3)	O(1) # 1–Ta(2)–O(3)	95.3(3)
O(5)–Ta(1)–O(2)	88.9(3)	O(7)–Ta(2)–O(4)	89.2(3)
O(9)–Ta(1)–O(2)	170.4(3)	O(8)–Ta(2)–O(4)	94.4(3)
O(1)–Ta(1)–O(2)	86.7(3)	O(1) # 1–Ta(2)–O(4)	169.3(3)
O(3)–Ta(1)–O(2)	73.4(3)	O(3)–Ta(2)–O(4)	75.8(3)
O(5)–Ta(1)–O(6)	87.7(3)	O(7)–Ta(2)–O(2)	91.8(3)
O(9)–Ta(1)–O(6)	90.5(3)	O(8)–Ta(2)–O(2)	166.8(3)
O(1)–Ta(1)–O(6)	170.2(3)	O(1) # 1–Ta(2)–O(2)	85.0(3)
O(3)–Ta(1)–O(6)	73.8(3)	O(3)–Ta(2)–O(2)	73.6(3)
O(2)–Ta(1)–O(6)	86.9(3)	O(4)–Ta(2)–O(2)	86.9(3)
O(12)–Mo(1)–O(11)	105.6(5)	O(10)–Mo(1)–O(3)	92.3(3)
O(12)–Mo(1)–O(10)	100.9(4)	O(6)–Mo(1)–O(3)	70.8(3)
O(11)–Mo(1)–O(10)	99.8(4)	O(12)–Mo(1)–O(4)	88.0(4)
O(12)–Mo(1)–O(6)	91.4(4)	O(11)–Mo(1)–O(4)	164.1(4)
O(11)–Mo(1)–O(6)	90.3(4)	O(10)–Mo(1)–O(4)	85.2(3)
O(10)–Mo(1)–O(6)	161.3(3)	O(6)–Mo(1)–O(4)	81.1(3)
O(12)–Mo(1)–O(3)	151.7(4)	O(3)–Mo(1)–O(4)	68.0(3)
O(11)–Mo(1)–O(3)	96.6(4)		

[a] Symmetry transformations used to generate equivalent atoms: # 1 $-x$, $-y+1$, $-z$.

1:1 composition (according to EDS analysis) in minor yields [9]. The solution containing $MoO(O^iPr)_4$ and $Ta(O^iPr)_5$ in a 1:1 molar ratio in toluene was then prepared and subjected to thermal tretament in an analogous manner to that used for the complete reduction of Mo(VI) to Mo(V). It was then left at r.t. in a flask covered by a serup cup that provides good protection against moisture but not against oxygen in air. Complete oxidation, accompanied by the appropriate color change, occurred in 2 weeks and the bimetallic complex $Mo_4Ta_4O_{16}(O^iPr)_{12}$ (**II**) was obtained on crystallization from hexane in rather low yields. One of the major difficulties in the isolation of **II** appears to be its very high solubility in hydrocarbon solvents (achieving at least 50 wt% in both toluene and hexane).

The molecular structure of **II** (see Figs. 3 and 4 and Tables 1 and 3) is composed of non-centrosymmetric octanuclear molecules, the arrangement of the metal atoms in which can be described best as a distorted cube. The vertexes of this cube contain the molybdenum and tantalum atoms in turn. The former are tetracoordinated, building tetraoxomolybdate anions,

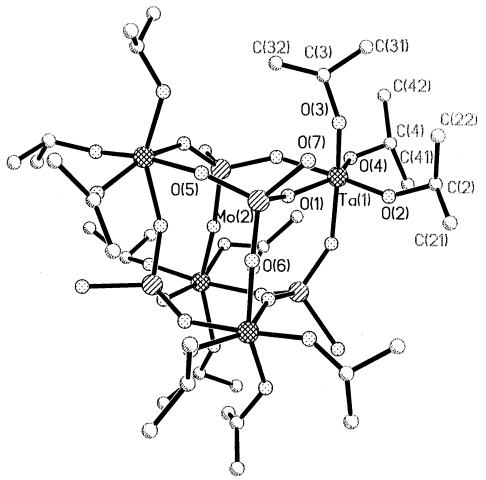


Fig. 3. The molecular structure of $Mo_4Ta_4O_{16}(O^iPr)_{12}$ (**II**).

Mo(2)O(7){μ-O(1)}{μ-O(5)}{μ-O(6)}, the latter hexacoordinated, forming Ta(1){μ-O(1)}{μ-O(5)}{μ-O(6)}O(2)O(3)O(4) octahedral units. The bonding parameters (Table 3) inside the tetraoxomolybdate unit are quite close to those usually observed for such fragments in polyoxometallate structures [15] (Mo–O 1.76(3)–1.77(3) for Mo–O–Ta bridging fragments and Mo(2)–O(7) 2.04(6) for the terminal Mo=O bond, the O–Mo–O angles being quite close to the tetrahedral ones, i.e. 110(4)–116(3)°). The bond lengths and angles inside the $Ta(\mu\text{-}O)_3(OR)_3$ octahedron (see Table 3) are within the ranges usually observed for tantalum oxoalkoxides [7]. The metal–oxygen core in structure **II** can be considered as the first representative of an unusual oxometallate core composed by four tetrahedra

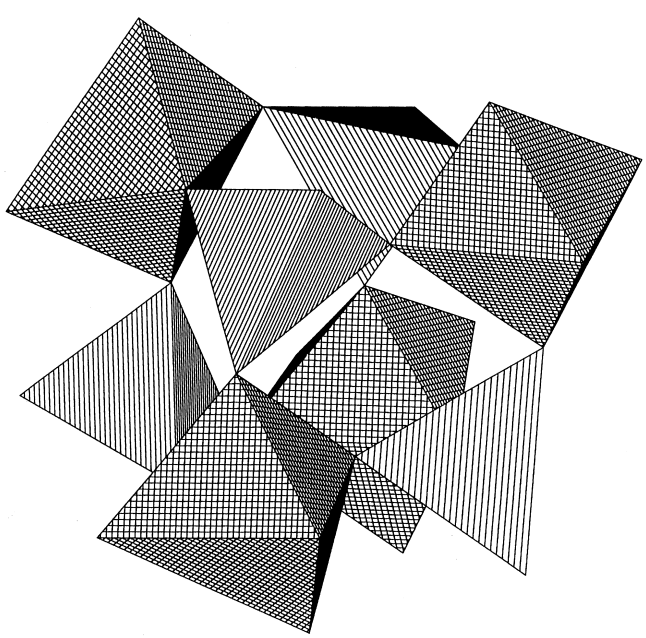


Fig. 4. A polyhedral presentation of the metal–oxygen core in the structure of **II**.

Table 3
Selected bond distances (Å) and angles (°) of compound **II** [a]

O(1)–Ta(1)	2.09(3)	O(5)–Ta(1) # 3	2.09(3)
Ta(1)–O(2)	1.83(6)	O(6)–Ta(1) # 1	2.08(3)
Ta(1)–O(3)	1.97(11)	Mo(2)–O(1)	1.77(3)
Ta(1)–O(6) # 1	2.08(3)	Mo(2)–O(6)	1.76(3)
Ta(1)–O(5) # 2	2.09(3)	Mo(2)–O(5)	1.77(3)
Ta(1)–O(4)	2.08(7)	Mo(2)–O(7)	2.04(6)
Mo(2)–O(1)–Ta(1)	158(4)	O(6)–Mo(2)–O(5)	110(4)
O(2)–Ta(1)–O(3)	85(4)	O(6)–Mo(2)–O(1)	116(3)
O(2)–Ta(1)–O(6) # 1	84(3)	O(5)–Mo(2)–O(1)	110(4)
O(3)–Ta(1)–O(6) # 1	156(4)	O(6)–Mo(2)–O(7)	111(3)
O(2)–Ta(1)–O(5) # 2	172(3)	O(5)–Mo(2)–O(7)	113(4)
O(3)–Ta(1)–O(5) # 2	93(4)	O(1)–Mo(2)–O(7)	97(3)
O(6) # 1–Ta(1)–O(5) # 2	95(3)	Mo(2)–O(5)–Ta(1) # 3	149(3)
O(2)–Ta(1)–O(1)	97(3)	Mo(2)–O(6)–Ta(1) # 1	142(2)
O(3)–Ta(1)–O(1)	78(3)		

[a] Symmetry transformations used to generate equivalent atoms: # 1 $-x+2$, $-y+1$, z; # 2 $-y+3/2$, $x-1/2$, $-z+3/2$; # 3 $y+1/2$, $-x+3/2$, $-z+3/2$.

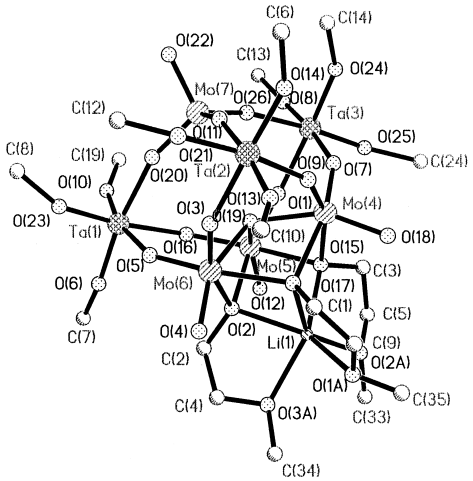


Fig. 5. The molecular structure of $LiMo_4Ta_3O_{14}(O^iPr)_9(OC_2H_4OMe)_3$ (**III**): the β-carbon atoms of the isopropoxide groups are omitted for clarity.

and four octahedra, sharing vertexes with each other (see Fig. 4).

The IR spectrum of **II** appears to be in good agreement with its molecular structure described above: it displays three broad and intensive lines that correspond to the vibration of the tetraoxomolybdate core at 877, 840 and 840 cm^{-1} and two strong lines at 583 and 455 cm^{-1} typical of Ta–OR bond vibration. Structure of **II** is preserved in hydrocarbon solution because the NMR spectra obtained in toluene display only one kind of well-defined signal for both methyne and methyl protons (all the isopropoxide groups in the solid state structure of **II** are terminal and have analogous bonding parameters), while the dissociation in solution would supposedly lead to the appearance of several different signals.

An attempt to prepare a trimetallic alkoxide complex using $LiMo_2O_4(O^iPr)_4(OC_2H_4OMe)$ instead of $MoO(O^iPr)_4$ yielded trimetallic $LiMo_4Ta_3O_{14}(O^iPr)_9(OC_2H_4OMe)_3$ (**III**) in minor yields (only a small crop of single crystals could be isolated from the viscous liquid media on complete removal of the solvent). Compound **III**, in analogy with **II**, possesses very high solubility in hydrocarbon solvents. The molecular structure of **III** (see Figs. 5 and 6 and Tables 1 and 4) is closely related to that of **II** and can be obtained from the latter by replacement of one of the $[(^iPrO)_3Ta(\mu\text{-}O)_3]$ octahedra with a $[Li(\mu,\eta^2\text{-}OC_2H_4OMe)_3]$ trigonal prism and demonstrates a distorted trigonal symmetry. The three $[MoO(\mu\text{-}O)_3]$ tetrahedra that were in contact with the $[(^iPrO)_3Ta(\mu\text{-}O)_3]$ octahedron that is removed get their μ-O groups, which became 'free', fused to one μ_3-O ligand. The molybdenum atoms complete their coordination number to six by coordinating two additional μ-OR 2-methoxyethoxide groups each. The coordination of the tantalum atoms is very close to that observed in **II** (the distances to the oxygen atoms of the terminal O^iPr-groups are essentially the same 1.832(14)–1.865(11) Å, while the lengths of the oxo-bridges vary a little more 1.988(10)–2.114(10) Å, with no obvious difference observed between the bridges to the tetrahedrally coordinated Mo(7) and 'pseudooctahedrally'-'4 + 2' coordinated Mo(4), Mo(5) and Mo(6) atoms). The bonding parameters for Mo(7) indicate a rather regular tetrahedral coordination (Mo(7)–O 1.697(13)–1.772(13) Å, the O–Mo(7)–O angles usual for a tetrahedron 105.8(6)–113.6(6)°). The bonding

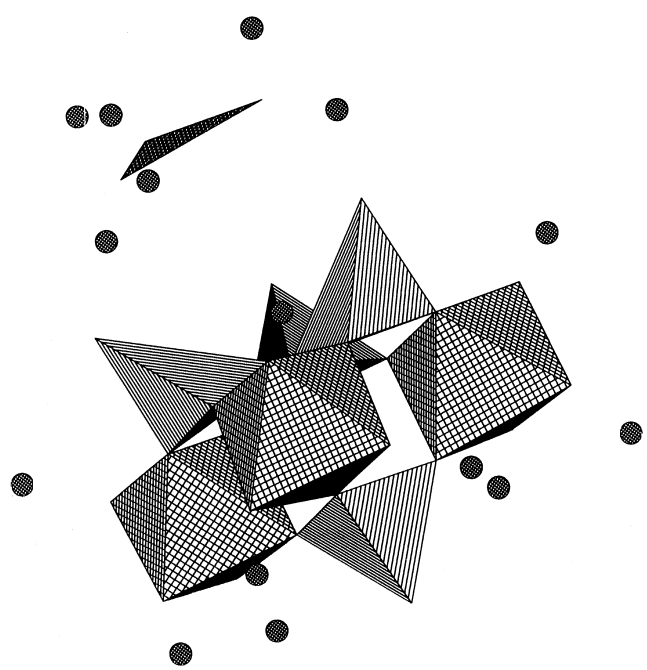


Fig. 6. A polyhedral presentation of the metal–oxygen core in the structure of **III**.

Table 4
Selected bond distances (Å) and angles (°) of compound **III**

Ta(1)–O(10)	1.832(13)	Mo(5)–Li(1)	3.30(4)
Ta(1)–O(23)	1.846(13)	Mo(6)–Li(1)	3.35(3)
Ta(1)–O(6)	1.861(11)	Mo(4)–O(18)	1.739(10)
Ta(1)–O(5)	1.988(10)	Mo(4)–O(7)	1.771(11)
Ta(1)–O(16)	2.065(11)	Mo(4)–O(9)	1.823(11)
Ta(1)–O(20)	2.124(11)	Mo(4)–O(19)	2.065(10)
Ta(2)–O(13)	1.850(13)	Mo(4)–O(17)	2.155(12)
Ta(2)–O(14)	1.857(13)	Mo(4)–O(15)	2.184(9)
Ta(2)–O(21)	1.856(13)	Mo(5)–O(12)	1.690(11)
Ta(2)–O(9)	2.020(11)	Mo(5)–O(16)	1.815(10)
Ta(2)–O(11)	2.091(12)	Mo(5)–O(1)	1.831(11)
Ta(2)–O(3)	2.114(10)	Mo(5)–O(19)	2.075(10)
Ta(3)–O(25)	1.814(14)	Mo(5)–O(15)	2.170(10)
Ta(3)–O(8)	1.849(12)	Mo(5)–O(2)	2.168(11)
Ta(3)–O(24)	1.868(13)	Mo(6)–O(4)	1.721(12)
Ta(3)–O(1)	2.026(10)	Mo(6)–O(3)	1.781(10)
Ta(3)–O(26)	2.089(13)	Mo(6)–O(5)	1.840(10)
Ta(3)–O(7)	2.100(11)	Mo(6)–O(19)	2.045(11)
O(2)–Li(1)	2.16(3)	Mo(6)–O(17)	2.164(10)
O(15)–Li(1)	2.08(3)	Mo(6)–O(2)	2.168(11)
O(17)–Li(1)	2.17(3)	Mo(7)–O(22)	1.697(13)
O(1A)–Li(1)	2.17(4)	Mo(7)–O(20)	1.748(11)
O(2A)–Li(1)	2.09(3)	Mo(7)–O(11)	1.771(12)
O(3A)–Li(1)	2.16(3)	Mo(7)–O(26)	1.772(13)
Mo(4)–Li(1)	3.33(3)		
O(10)–Ta(1)–O(23)	96.1(6)	O(18)–Mo(4)–O(19)	152.5(5)
O(10)–Ta(1)–O(6)	95.6(6)	O(7)–Mo(4)–O(19)	91.5(4)
O(23)–Ta(1)–O(6)	98.1(5)	O(9)–Mo(4)–O(19)	93.4(4)
O(10)–Ta(1)–O(5)	165.2(5)	O(18)–Mo(4)–O(17)	89.7(5)
O(13)–Ta(2)–O(14)	96.4(6)	O(7)–Mo(4)–O(17)	158.8(4)
O(13)–Ta(2)–O(21)	94.4(6)	O(9)–Mo(4)–O(17)	86.7(5)
O(14)–Ta(2)–O(21)	97.8(5)	O(19)–Mo(4)–O(17)	69.8(4)
O(13)–Ta(2)–O(9)	93.6(5)	O(18)–Mo(4)–O(15)	86.8(5)
O(14)–Ta(2)–O(9)	93.1(5)	O(7)–Mo(4)–O(15)	89.0(4)
O(21)–Ta(2)–O(9)	165.7(5)	O(9)–Mo(4)–O(15)	159.5(4)
O(13)–Ta(2)–O(11)	171.1(5)	O(19)–Mo(4)–O(15)	70.8(4)
O(22)–Mo(7)–O(20)	105.8(6)	O(17)–Mo(4)–O(15)	75.8(4)
O(22)–Mo(7)–O(11)	106.7(6)	O(15)–Li(1)–O(2A)	80.4(12)
O(20)–Mo(7)–O(11)	113.6(6)	O(15)–Li(1)–O(2)	79.1(13)
O(22)–Mo(7)–O(26)	106.5(6)	O(2A)–Li(1)–O(2)	127.8(17)
O(20)–Mo(7)–O(26)	111.2(5)	O(15)–Li(1)–O(17)	77.8(12)
O(11)–Mo(7)–O(26)	112.5(6)	O(2A)–Li(1)–O(17)	142.2(16)
O(18)–Mo(4)–O(7)	104.3(5)	O(2)–Li(1)–O(17)	77.4(12)
O(18)–Mo(4)–O(9)	103.8(5)	O(15)–Li(1)–O(3A)	144.1(17)
O(7)–Mo(4)–O(9)	104.8(5)	O(2A)–Li(1)–O(3A)	91.7(13)

parameters for Mo(4), Mo(5) and Mo(6) are very similar and indicate the same kind of distortion for the octahedra: the shortest bonds are those to the terminal oxygen atoms (1.690(11)–1.739(10) Å), the oxobridges to the tantalum atoms are also rather short (1.771(11)–1.840(10) Å), the triply bridging oxoatom has a longer Mo–O(19) distance, essentially same for all the three Mo atoms (2.045(10)–2.075(10) Å) and the longest distances are those to the alkoxobridges (2.155(12)–2.168(11) Å). It is very interesting to note that the lithium atoms definitely do not have an octahedral coordination but, indeed, have a trigonal prismatic coordination analogous to that observed for one of the symmetrically independent Li atoms in the structure of $[\{LiWO_2(OC_2H_4OCH_3)_3\}_2{\cdot}2Li(HOC_2H_4OCH_3)_2]^{2+}$ cations [6]. In both cases, this coordination appears to be forced by the parallel arrangement of the three 2-methoxyethoxide groups providing a pair of donor atoms each.

The molecule of **III** also represents a new type of a polyoxometallate core with a combination of octahedral and tetrahedral elements via sharing the common vertexes.

4. Supplementary material

Supplementary data are available from: The Director, CCDC, 12 Union Road, Cambridge, CB2 1EZ, UK (fax: +44-1223-336033; e-mail: deposit@ccdc.cam.ac.uk or www: http://www.ccdc.cam.ac.uk) on request, quoting the deposition numbers CCDC-139287 (**I**), CCDC-142959 (**II**), and CCDC-142960 (**III**).

Acknowledgements

The authors express their sincerest gratitude to Dr Regine Herbst-Irmer, who succeeded in resolving the twinning in the structure of **II** and provided a lot of help with its refinement. The authors are grateful to Dr C. Sandström for the assistance with the NMR experiments, to Dr G. Westin for providing access to EDS-analysis and to the Swedish Council for Natural Science Research for financial support of this work.

References

[1] M.T. Pope, A. Muller (Eds.), Polyoxometallates: From Platonic Solids to Anti-retroviral Activity, Kluwer, Dordrecht, 1993.
[2] G.A. Seisenbaeva, V.G. Kessler, M. Sundberg, M. Nygren, D.V. Drobot, in: B.D. Bryskin (Ed.), Rhenium and Rhenium Alloys, The Minerals, Metals & Materials Society, USA, 1997, p. 159.
[3] V.G. Kessler, A.N. Panov, A.Yu. Borissevitch, N.Ya. Turova, J. Sol-Gel Sci. Tech. 12 (1998) 81.
[4] V.G. Kessler, G.A. Seisenbaeva, A.V. Shevelkov, G.V. Khvorykh, J. Chem. Soc., Chem. Commun. (1995) 1779.
[5] A. Johansson, V.G. Kessler, Inorg. Chem. Commun. 3 (2000) 5.
[6] V.G. Kessler, A.N. Panov, N.Ya. Turova, Z.A. Starikova, A.I. Yanovsky, F.M. Dolgushin, A.P. Pisarevsky, Yu.T. Struchkov, J. Chem. Soc., Dalton Trans. (1998) 21.
[7] N.Ya. Turova, A.V. Korolev, D.E. Tcheboukov, A.I. Belokon, Polyhedron 15 (1996) 3869.
[8] SHELXTL-NT Reference manual, Bruker AXS, 1997.
[9] A. Johansson, M. Roman, G. Seisenbaeva, L. Kloo, Z. Szabo, V.G. Kessler, J. Chem. Soc., Dalton Trans. (2000) 387.

[10] L.G. Hubert-Pfalzgraf, Polyhedron 13 (1994) 1181.
[11] N.Ya. Turova, E.P. Turevskaya, V.G. Kessler, M.I. Yanovskaya, J. Sol-Gel Sci. Tech. 2 (1994) 17.
[12] S. Boulmaaz, L.G. Hubert-Pfalzgraf, S. Halut, J.C. Daran, J. Chem. Soc., Chem. Commun. (1994) 601.
[13] N.Ya. Turova, V.G. Kessler, Russ. J. Gen. Chem. (Russ.) 60 (1990) 1, 113.
[14] M.H. Chisholm, K. Folting, J.C. Huffman, C.C. Kirkpatric, Inorg. Chem. 23 (1984) 1021.
[15] M.I. Khan, J. Zubieta, Prog. Inorg. Chem. 43 (1995) 1.

PERGAMON

www.elsevier.nl/locate/poly

Polyhedron 19 (2000) 1799–1802

POLYHEDRON

Crown ether complexation of Te(IV): formation and crystal structure of $[(18\text{-crown-6})Te(Cl)(\mu\text{-}O)_2Te(Cl)(18\text{-crown-6})][SbCl_6]_2$ ☆

Gerald R. Willey *, Marcus P. Spry, William Errington

Department of Chemistry, University of Warwick, Coventry, CV4 7AL, UK

Received 3 April 2000; accepted 5 June 2000

Abstract

The product isolated as colourless crystals from the reaction system $TeCl_4$–$SbCl_5$–18-crown-6–MeCN has been identified (X-ray diffraction studies) as the ionic salt $[(18\text{-crown-6})Te(Cl)(\mu\text{-}O)_2Te(Cl)(18\text{-crown-6})][SbCl_6]_2$. The μ-oxo-bridged cations have a centre of inversion and feature a distorted eight-coordinate metal environment involving two bridging oxygen atoms (Te–O 1.960(4) Å), one terminal chlorine atom (Te–Cl 2.361(2) Å) and five of the six oxygen atoms of the crown ligand (Te–O 2.549(4)–2.886(5) Å). The question of stereochemical involvement of the lone pair of electrons associated with each Te(IV) centre is considered. © 2000 Elsevier Science Ltd. All rights reserved.

Keywords: μ-oxo-Bridged cations; Crown ether complexation; Crystal structures; Bridging oxygen atoms

1. Introduction

In the solid state $TeCl_4$ has a cubane-like tetrameric structure wherein each metal centre is six-coordinate (distorted O_h) and the lone pair electrons associated with Te(IV) are visualised as pointing to the centre of the cube [1]. In solution, lattice breakdown can provide neutral mononuclear species and solvated $TeCl_3^+$ and Cl^- ions. Although a number of $TeCl_4(L)_n$ adducts have been noted, very few have been studied by X-ray crystallography, e.g. $TeCl_4[(Me_2N)_2C{=}S]_2$ [2], $TeCl_4[Ph_3P{=}O]_2$ and $TeCl_4[Ph_2P(S)\cdot CH_2\cdot P(S)Ph_2]\cdot MeCN$ [3]. Salts of the pyramidal cation $TeCl_3^+$ have been reported, e.g. $[TeCl_3][AlCl_4]$ α-form (A) [4], $[TeCl_3][AlCl_4]$ β-form (B) [5], $[TeCl_3][SbF_6]$ (C) [5] and $[TeCl_3][AsF_6]$ (D) [5]. In all of these examples the tetrahedral $TeCl_3E$ (E = lone pair) primary bond geometry becomes expanded as a result of significant secondary bonding interactions (Te···Y) involving halogen atom(s) (Y) of the complex anion, e.g. $TeCl_3Y_3E$ (distorted monocapped octahedron), (A) and (B); $TeCl_3Y_4E$ (C); $TeCl_3Y_5E$ (D). Our interest in macrocyclic complexation of p-block metallo-species has featured crown ether, crown thioether and aza ligands with Ga(III), In(III), Ge(IV), Sn(IV), As(III), Sb(III) and Bi(III) [6]. In this study of the $TeCl_4$–18-crown-6–$SbCl_5$–MeCN system we probe the binding of Te(IV) with a typical crown ether ligand; rather than the expected entrapment of the $TeCl_3^+$ cation, as formed by direct halide transfer $TeCl_4 \rightarrow SbCl_5$, a novel μ-oxo-Te(IV)–18-crown-6 complex was isolated. Specifically for Te(IV)–crown ether complexes there are three examples in the literature, viz. $[TeCl_3(15\text{-crown-5})][TeCl_5]$ [7], $[TeCl_3(15\text{-crown-5})]_2[TeCl_6]$ [7] and $[TeCl_3(15\text{-crown-5})][SbCl_6]$ [8]. Structural characterisation of the latter reveals the tellurium atom positioned over the ring cavity and linked symmetrically to the five oxygen atoms of the crown ligand.

2. Materials and methods

Manipulations were carried out using a Schlenk high-vacuum system in conjunction with a standard di-nitrogen-filled glove-box. Acetonitrile was pre-dried over molecular sieves and then freshly distilled from CaH_2 under a di-nitrogen atmosphere prior to use. $TeCl_4$, 18-crown-6 and $SbCl_5$ were used as supplied (Aldrich).

☆ 18-crown-6 = 1,4,7,10,13,16-hexaoxacyclooctadecane.

* Corresponding author. Tel.: +44-247-6523227; fax: +44-247-6524112.

E-mail address: msrep@snow.csvwarwick.ac.uk (G.R. Willey).

0277-5387/00/$ - see front matter © 2000 Elsevier Science Ltd. All rights reserved.
PII: S0277-5387(00)00452-6

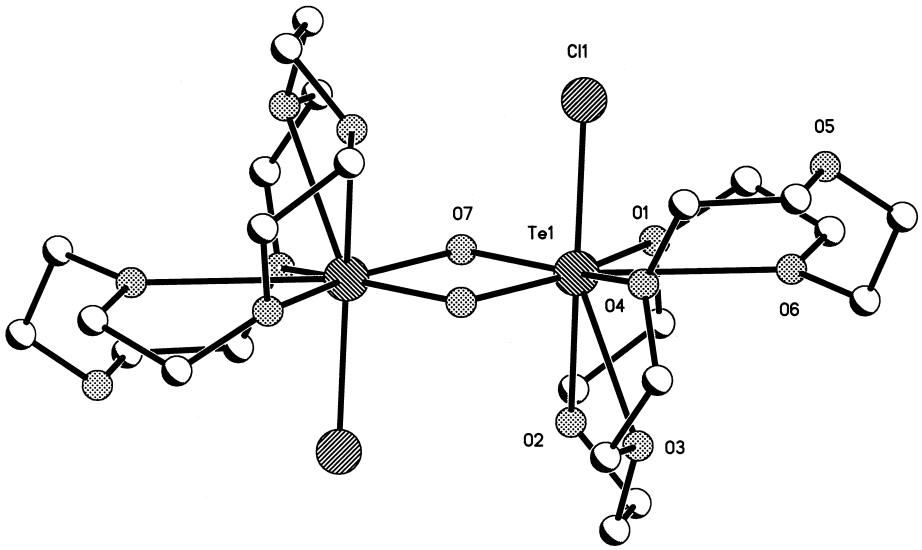


Fig. 1. The structure of the cation $[(18\text{-crown-6})Te(Cl)(\mu\text{-}O)_2Te(Cl)(18\text{-crown-6})]^{2+}$ showing atom notation used.

IR spectra were recorded using a Perkin–Elmer 580B spectrometer with samples as Nujol mulls placed between CsI discs. Elemental analyses were carried out using a CE440 elemental (C, H, N) analyser.

2.1. [(18-crown-6)Te(Cl)(μ-O)$_2$Te(Cl)(18-crown-6)][SbCl$_6$]$_2$

A solution of $SbCl_5$ (0.80 g, 2.68 mmol) in acetonitrile (20 cm^3) was added dropwise to a stirred solution of $TeCl_4$ (0.72 g, 2.67 mmol) in acetonitrile (20 cm^3) maintained at 0 °C. Directly afterwards a solution of 18-crown-6 (0.71 g, 2.69 mmol) in acetonitrile (20 cm^3) was further added and the resulting solution was stirred for 12 h at room temperature. Gradual removal of solvent in vacuo (ca. 50% by volume) provided a crop of colourless needle crystals. Yield 0.22 g, 5.3%. Found: C, 18.26; H, 3.02. Calc. for $C_{24}H_{48}O_{14}Cl_{14}Sb_2Te_2$: C, 18.53; H, 3.11%.

IR: $\bar{\nu}_{max}$ (cm^{-1}) (Nujol): 1287 (m), 1250 (m), 1141 (m), 1094 (s), 1077 (s), 970 (s), 946 (m), 839 (w), 723 (w), 340 (vs, $SbCl_6$).

2.2. X-ray crystallography

Data were collected using a Siemens SMART CCD area-detector diffractometer. Absorption corrections were applied using SADABS [9]. The structure was solved by direct methods and refined by full-matrix least-squares on F^2 for all data using SHELXL-97 [10].

2.2.1. Crystal data

$TeClC_{12}H_{24}O_7SbCl_6$, $M = 777.81$, monoclinic, $a = 8.4328(12)$, $b = 12.3141(15)$, $c = 23.764(2)$ Å, $\beta = 96.169(3)°$, $U = 2453.5(5)$ Å^3, $T = 180(2)$ K, space group $P2(1)/n$, $Z = 4$, μ(Mo Kα) = 3.082 mm^{-1}, wavelength = 0.71073 Å, 12 475 reflections measured, 4285 unique ($R_{int} = 0.044$). The final values of R_1 [$I > 2\sigma(I)$] and wR_2 are 0.0408 and 0.0984, respectively.

3. Results and discussion

Reaction of $TeCl_4$ and $SbCl_5$ in acetonitrile in the presence of 18-crown-6 provided colourless crystals of $[(18\text{-crown-6})Te(Cl)(\mu\text{-}O)_2Te(Cl)(18\text{-crown-6})][SbCl_6]_2$, which are highly sensitive to the merest trace of air/moisture. Partial hydrolysis of the 'direct' halide abstraction cation $[TeCl_3(18\text{-crown-6})]^+$ is seen as the root cause for the formation of the oxo-species. The ionic structure of the title compound has been established by X-ray diffraction; the cation is depicted in Fig. 1 (with atom notation) and selected bond dimensions are listed in Table 1. The dinuclear μ-oxo-bridged cations possess a two-fold axis of symmetry and feature a distorted eight-coordinate metal environment com-

Table 1
Bond lengths (Å) and angles (°) for the cation $[(18\text{-crown-6})Te(Cl)(\mu\text{-}O)_2Te(Cl)(18\text{-crown-6})]^{2+}$ [a]

Te(1)–Cl(1)	2.3609(16)	Te(1)–O(1)	2.5814(44)
Te(1)–O(2)	2.5490(44)	Te(1)–O(3)	2.6512(46)
Te(1)–O(4)	2.7148(45)	Te(1)–O(6)	2.8858(46)
Te(1)–O(7)	1.960(4)		
O(7) # 1–Te(1)–O(7)	77.29(17)	O(1)–Te(1)–Cl(1)	88.49(11)
O(2)–Te(1)–Cl(1)	151.75(13)	O(3)–Te(1)–Cl(1)	141.34(12)
O(4)–Te(1)–Cl(1)	82.80(11)	O(6)–Te(1)–Cl(1)	87.83(12)

[a] Symmetry transformations used to generate equivalent atoms: # 1 $-x, -y+1, -z$.

Table 2
Bond dimensions of [Te(μ-O)$_2$Te] subunits

	Te–O (Å)	Te–O–Te (°)	O–Te–O (°)	Ref.
[(18-crown-6)Te(Cl)(μ$_2$-O)]$_2$[SbCl$_6$]$_2$	1.960(4)	102.7(2)	77.3(2)	this work
[(cyclenH$_3$)Te(μ$_2$-O)]$_2$Cl$_2$	1.998(13)		77.3(6)	[11]
[(2,4,6-Ph$_3$C$_6$H$_2$)Te(Br)(μ$_2$-O)]$_2$	2.084(5)	102.4(2)	77.6(2)	[12]
	1.898(4)			
[(2,4,6-Ph$_3$C$_6$H$_2$)Te(I)(μ$_2$-O)]$_2$	2.086(2)	102.3(1)	77.8(1)	[12]
	1.914(2)			

prising the two bridging oxygen atoms, a terminal chlorine atom Te–Cl 2.361(2) Å (for comparison [TeCl$_3$][AlCl$_4$] Te–Cl 2.279, 2.281, 2.277 Å [5], [TeCl$_4$]$_4$ Te–Cl 2.31 Å [1]) and five of the oxygen atoms of the oxacrown ligand. Although the [Te(μ-O)$_2$Te] subunit is rare, with only three structures listed, viz. [(cyclenH$_3$)Te(μ$_2$-O)]$_2$Cl$_2$·2MeOH·4CHCl$_3$ [11] and [(2,4,6-Ph$_3$C$_6$H$_2$)Te(X)(μ$_2$-O)]$_2$ where X = Br, I [12], the bond dimensions show a high degree of uniformity with the Te–O$_{bridge}$ distances in the region 1.9–2.0 Å (see Table 2).

Of the six donor oxygen atoms of the ring, five are within binding distance of the metal with Te–O$_{crown}$ distances 2.549(5)–2.886(5) Å (van der Waal radii, Te 2.06 and O 1.52 Å [13]); for direct comparison the Te–O$_{crown}$ bond distances in [TeCl$_3$(15-crown-5)][SbCl$_6$] are found in the range 2.66(3)–2.79(3) Å. The remaining oxygen atom lies well outside this region and is clearly not involved in coordination to the metal Te···O(5) 4.144(5) Å. The resulting distorted crown conformation is seen as a direct consequence of stereochemical activity of the lone pair associated with Te(IV) pointing towards the O(5) region. Thus, the metal coordination geometry can be described as a distorted ψ-capped square antiprism with the lone pair occupying a capped (rectangular) face to the exclusion of O(5), (see Fig. 2).

The SbCl$_6^-$ anions are unexceptional with regular octahedral coordination about Sb atoms, Sb–Cl (mean) 2.364(2) Å, Cl–Sb–Cl (mean) 89.94(7) and 179.21(7)°.

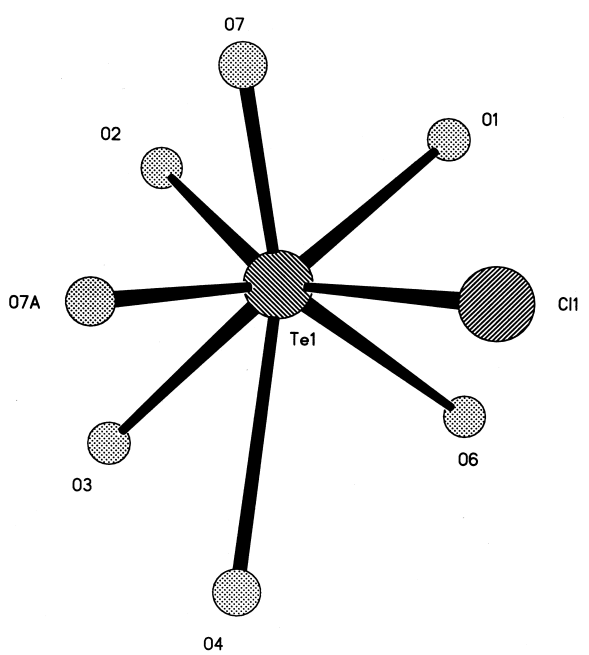


Fig. 2. The coordination geometry of the Te(IV) centres in the cation [(18-crown-6)Te(Cl)(μ-O)$_2$Te(Cl)(18-crown-6)]$^{2+}$.

4. Supplementary material

Additional material containing non-hydrogen and hydrogen atomic coordinates, thermal parameters, and the remaining bond lengths and angles are available from The Director, Cambridge Crystallographic Data Centre, 12 Union Road, Cambridge CB2 1EZ, UK (fax: +44-1223-336033; e-mail: deposit@ccdc.cam.ac.uk or www: http://www.ccdc.cam.ac.uk) on request, quoting the Deposition Number 141855.

Acknowledgements

We thank the EPSRC for a postgraduate studentship (M.P.S.) and acknowledge the contributions from Siemens plc, the EPSRC and the University of Warwick for funding of the X-ray facilities.

References

[1] B. Buss, B. Krebs, Inorg. Chem. 10 (1971) 2795.
[2] S. Esperas, J.W. George, S. Husebye, O. Mikalsen, Acta Chem. Scand. 29 (1975) 141.
[3] C.J. Carmalt, N.C. Norman, L.J. Farrugia, Polyhedron 14 (1995) 1405.
[4] B. Krebs, B. Buss, D. Altena, Z. Anorg. Allg. Chem. 386 (1971) 257.
[5] B.H. Christian, M.J. Collins, R.J. Gillespie, J.F. Sawyer, Inorg. Chem. 25 (1986) 777.
[6] See, e.g. (a) G.R. Willey, M.P. Spry, M.G.B. Drew, Polyhedron 15 (1996) 4497. (b) G.R. Willey, L.T. Daly, P.R. Meehan, M.G.B. Drew, J. Chem. Soc., Dalton Trans. (1996) 4045. (c) G.R. Willey, T.J. Woodman, U. Somasundaram, D.R. Aris, W.

Errington, J. Chem. Soc., Dalton Trans. (1998) 2573. (d) G.R. Willey, D.R. Aris, A.L. Beamont, W. Erringtom, Main Group Met. Chem. 22 (1999) 515. (e) G.R. Willey, D.R. Aris, W. Errington, Inorg. Chim. Acta 300–302 (2000) 1004, and references therein.
[7] B. Borgsen, F. Weller, K. Dehnicke, Z. Anorg. Allg. Chem. 596 (1991) 55.
[8] M. Shäfer, K. Dehnicke, Z. Anorg. Allg. Chem. 614 (1992) 21.
[9] G.M. Sheldrick, SADABS, Program for Absorption Corrections, University of Göttingen, 1996.
[10] G.M. Sheldrick, SHELXL-97, Program for Crystal Structure Refinement, University of Göttingen, 1997.
[11] R.B. King, S.A. Sangokoya, E.M. Holt, Inorg. Chem. 26 (1987) 4307.
[12] E. Schulz Lang, U. Abram, J. Strähle, Z. Anorg. Allg. Chem. 623 (1997) 1968.
[13] A. Bondi, J. Phys. Chem. 68 (1964) 441.

PERGAMON

www.elsevier.nl/locate/poly

Polyhedron 19 (2000) 1803–1807

POLYHEDRON

Synthesis and characterization of *cis* and *trans* isomers of $[NiL_2(NCS)_2]$ [L = 1-(2-aminoethyl)pyrrolidine]: X-ray single-crystal structures

Inamur Rahaman Laskar [a], Tapas Kumar Maji [b], Siddhartha Chaudhuri [c], Ashutosh Ghosh [d], Nirmalendu Ray Chaudhuri [b,*]

[a] *Department of Chemistry, Ananda Mohan College, 102/1 Raja Ram Mohan Sarani, Calcutta 700 009, India*
[b] *Department of Inorganic Chemistry, Indian Association for the Cultivation of Science, Calcutta 700 032, India*
[c] *Regional Sophisticated Instrumentation Centre, Bose Institute, Calcutta 700 009, India*
[d] *Department of Chemistry, Calcutta University, 92, A.P.C. Road, Calcutta 700 009, India*

Received 20 January 2000; accepted 5 June 2000

Abstract

The isomeric complexes *trans*-$[NiL_2(NCS)_2]$ (violet) (**1**) and *cis*-$[NiL_2(NCS)_2]$ (blue) (**2**) [L = 1-(2-aminoethyl)pyrrolidine] have been synthesized, varying solvents and temperature, and their X-ray crystal structures have been determined. Both the isomers possess the same space group, $P2_1/c$, having distorted octahedral geometry. © 2000 Elsevier Science Ltd. All rights reserved.

Keywords: Nickel(II)thiocyanate; 1-(2-Aminoethyl)pyrrolidine; Crystal structures; *cis*/*trans* Isomers

1. Introduction

The chemistry of amine with nickel(II)thiocyanate is well documented, but the examples for the formation of both *cis* and *trans* isomers with the same amine are rare. The mutual interaction between the amine ligands is found to be responsible for the stability of the *cis* or *trans* isomer as in the case of 1,2-bis(2-imidazolinyl)benzene which yields the *cis* species whereas 1,2-bis(2-imidazolinyl)ethane generates the *trans* species [1]. The amine, phenylethylamine, is reported to yield *cis* as well as *trans* species but the latter is stabilized only as clathrates with *sec*-butylbenzene or *o*-xylene [2]; thus, they are not isomers. Ethane-1,2-diamine and its derivatives which form five-membered chelate rings with nickel(II)thiocyanate always produce the *trans* species [3–5], but propane-1,3-diamine [6] and *N*-methylpropane-1,3-diamine [7] which form six-membered chelate rings result the *cis*-diisothiocyanato species. Recently, there has been a report of the reaction of ethane-1,2-diamine and nickel(II)selenocyanate where a pure *trans* species has been synthesized, although on variation of preparative method a new species has been derived whose unit cell contains two moieties of *cis* species along with one moiety of tris-(ethane-1,2-diamine)nickel(II) selenocyanate [8]. The foregoing facts lead us to pursue the reaction of nickel(II)thiocyanate with the ethane-1,2-diamine analogue to synthesize *trans* as well as *cis* isomers in pure form altering the preparative procedure. We were able to synthesize both the *cis*- and *trans*-diisothiocyanato species with 1-(2-aminoethyl)pyrrolidine as ligand on variation of temperature as well as reaction medium. The present paper reports the synthesis, characterization and single-crystal X-ray diffraction studies of *cis* and *trans* isomers of diisothiocyanato bis[1-(2-aminoethyl)-pyrrolidine]nickel(II).

* Corresponding author. Tel.: +91-33-473-4971; fax: +91-33-473-2805.
E-mail address: icnrc@mahendra.iacs.res.in (N. Ray Chaudhuri).

0277-5387/00/$ - see front matter © 2000 Elsevier Science Ltd. All rights reserved.
PII: S0277-5387(00)00476-9

2. Experimental

2.1. Materials

High-purity (98%) 1-(2-aminoethyl)pyrrolidine (L) was purchased from Lancaster Chemical Company and used as received and all the non-aqueous solvents were dried before use.

2.2. Physical measurements

Elemental analyses (carbon, hydrogen and nitrogen) were performed using a Perkin–Elmer 240C elemental analyzer and nickel(II) content was estimated gravimetrically [9]. IR-spectra (4000–400 cm^{-1}) were taken at 27°C using a Perkin–Elmer IR 783 where KBr was used as medium. Electronic spectra (1400–200 nm) were obtained at 27°C using a Hitachi UV–Vis–NIR model U-3410 where Nujol was used as a medium as well as a reference. The magnetic susceptibility was measured at 27°C using an EG and G PAR 155 vibrating sample magnetometer, where $[HgCo(SCN)_4]$ was used as a reference material and diamagnetic corrections were made using Pascal's constants. Molar conductivity values were measured using a Systronics 304 conductivity meter, where the cell constant was calibrated with 0.02 M KCl.

2.3. Synthesis of the complexes

trans-$[NiL_2(NCS)_2]$ (**1**) (violet) was synthesized by adding diamine (2 mmol) (L) in methanol (5 cm^3) to the nickel(II)thiocyanate (1 mmol) dissolved in methanol (10 cm^3) at a temperature lower than 10°C. The resulting solution was stirred for a few minutes. A violet complex was separated out, filtered, washed with isopropanol and dried in a $CaCl_2$-desiccator (yield, 81%). Found for **1**: C, 41.6; H, 6.7; N, 20.8; Ni, 14.5. Calc. for $NiC_{14}H_{28}N_6S_2$: C, 41.7; H, 6.9; N, 20.8; Ni, 14.6%. $\mu_{eff} = 2.97$ μB. λ_{max} (Nujol): 936, 566 and 362 nm. Single crystals suitable for X-ray analysis were obtained by slow evaporation of the methanolic solution of **1** by maintaining the temperature < 10°C.

cis-$[NiL_2(SCN)_2]$ (**2**) (blue), was synthesized using the same method as above but keeping the temperature above 30°C. The blue complex formed was kept in a $CaCl_2$-desiccator (yield, 76%). Found for **2**: C, 41.5; H, 6.9; N, 20.7; Ni 14.6. Calc. for $NiC_{14}H_{28}N_6S_2$: C, 41.7; H, 6.9; N, 20.8; Ni, 14.6%. $\mu_{eff} = 2.98$ μB. λ_{max} (Nujol): 979, 580 and 370 nm. Single crystals suitable for X-ray analysis were obtained by slow evaporation of the methanolic solution of **1** by maintaining the temperature > 30°C.

2.4. X-ray data collection and structure determination

The data for complex **1** were collected on a Nonius CAD4 diffractometer using the $\omega - 2\theta$ scan technique while the diffraction data for complex **2** were collected similarly on a Nonius MACH3 diffractometer. Both sets of data were corrected for Lorentz and polarization factors and empirical absorption corrections were carried out using ψ-scan data of some selected reflections using the NRCVAX suite of programs [10]. The structures were solved by direct methods and partial difference Fourier techniques using the SHELXS-86 [11] program and refined using SHELXL-93 [12].

3. Results and discussion

Both the temperature and solvents have very important role in the syntheses of the isomers (Table 1). Treatment of nickel(II)thiocyanate with diamine in 1:2 ratio in alcohol (MeOH/EtOH/2-PrOH)–water mixture (99:1) above 30°C yields the pure *cis* isomer whereas if the temperature is maintained below 10°C the *trans* species is the only product. The mixture of *cis* and *trans* isomers results in the temperature range, 10–30°C; with an increasing percentage of the *cis* isomer with increasing temperature. When the above reaction is carried out in alcohol (dried before use by distillation with Mg) the pure *trans* isomer is obtained till the temperature is raised up to 50°C, a mixture of the *cis* and *trans* isomer results in the temperature range 50–55°C, and above 55°C the *cis* complex is the only product. The reaction was also carried out in dry non-alcoholic solvent, e.g. CH_3CN, CH_2Cl_2 and $CHCl_3$ (where the nickel(II)-thiocyanate is taken in suspension due to its insolubility in these solvents) and the results were found to be the same as in dry alcohol. When the same reaction is performed in water medium the *cis* isomer is the only

Table 1
Effect of solvent and temperature on the syntheses of *cis* and *trans* isomers

Solvents	*trans* Isomer (°C)	Mixture (*cis* and *trans* isomers) (°C)	*cis* Isomer (°C)
H_2O			2–90
Alcohol (MeOH/EtOH/2-PrOH)[a]–water (99:1)	<10	10–30	>30
MeOH/EtOH/2-PrOH/CH_2Cl_2/$CHCl_3$/CH_3CN	<50	50–55	>55

[a] Any of the alcohols mixed individually with water.

Table 2
Molar conductance data (S cm^{-1}) of complexes **1** and **2**

Solvent	Complex	Λ_m (S cm^{-1})		
		~0°C	~30°C	~55°C
H_2O	**1**	56	90	165
H_2O	**2**	54	93	164
MeOH–H_2O (99:1)	**1**	9	36	117
MeOH–H_2O (99:1)	**2**	12	34	111
MeOH	**1**	9	21	77
MeOH	**2**	10	18	80

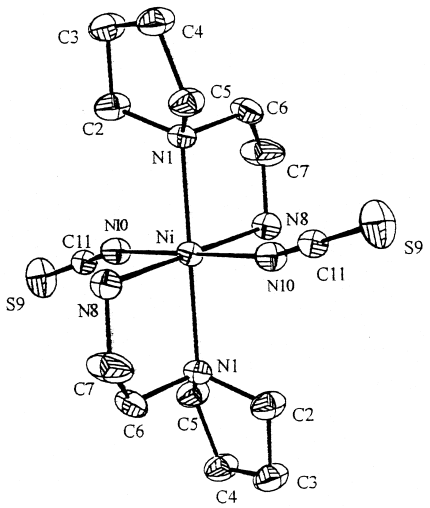


Fig. 1. ORTEP diagram of *trans*-[$NiL_2(SCN)_2$]. Ellipsoids are drawn at 50% probability.

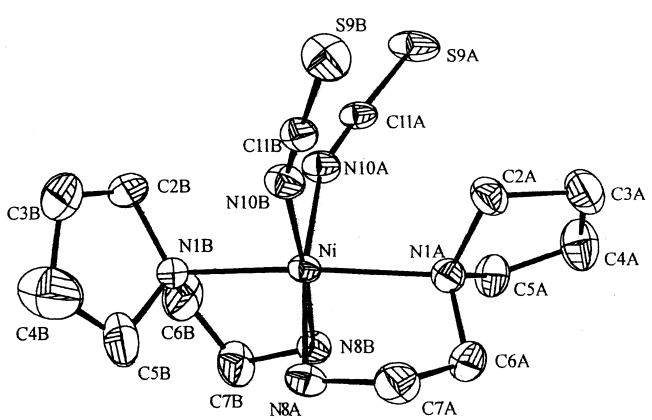


Fig. 2. ORTEP diagram of *cis*-[$NiL_2(SCN)_2$]. Ellipsoids are drawn at 50% probability.

product, irrespective of temperature. From the foregoing facts it is apparent that water, with the highest dielectric constant among the solvents used in the synthesis, stabilizes the more polar *cis* isomer, and the *trans* isomer is obtained from the less polar solvents. Temperature plays a very important role in the synthesis of the complexes. Molar conductivity data (Table 2) show that both the *cis* and *trans* isomers are almost nonconducting at low temperatures (~0°C) but their conductivity increases with temperature indicating appreciable solvation at higher temperature:

$$NiL_2(NCS)_2 + \text{solvent} \rightleftharpoons [NiL_2(\text{solvent})(NCS)]^+ + NCS^-$$

The synthesis of *cis* or *trans* complexes at different temperature seems to be related to the solvation of the complex; the greater the level of solvation, the higher the yield of the *cis* complex. As for example in ethanol, where solvation is much less compared to water, the *trans* isomer is obtained only at high temperatures (>50°C).

The composition of the complexes $NiL_2(NCS)_2$ (violet) (**1**) and $NiL_2(NCS)_2$ (blue) (**2**) has been confirmed by elemental analyses. The complexes exhibit IR bands comparable to those of the diamine systems whose chelate character has been established by X-ray single-crystal structure analyses [13,14]. The magnetic and electronic spectral data of the complexes are in good agreement with octahedral nickel(II). The IR bands for complex **1** (ν_{C-N} at 2077 cm^{-1}) and for complex **2** (ν_{C-N} at 2081 and 2096cm^{-1}) suggest that the violet species is *trans* and the blue is *cis* [15].

Figs. 1 and 2 show ORTEP [16] views of the complexes with the atom numbering schemes. Crystal data are summarized in Table 3. Selected bond distances and angles involving the Ni ions are shown in Table 4. In both the complexes the Ni coordination is distorted-octahedral with the four N-atoms of two bidentate 1-(2-aminoethyl)pyrrolidine and two N-atoms of two isothiocyanate groups. In **1** the isothiocyanato groups are *cis* and in **2** they are *trans* to each other. The pyrrolidine groups of the two diamines remains *trans* in both the isomers. There are still other possible isomers with this ligand set that would be obtained by flipping the orientation of one of the chelating ligands in each of the products with pyrrolidine *cis* to pyrrolidine configuration. However, they could not be synthesized because there would be severe steric interaction between the pyrrolidine groups. It is seen that the two ligands coordinate to the metal ion in the *trans* configuration in **1** and in the *cis* configuration in **2**. The shorter Ni–N coordination distances involving the thiocyanate nitrogens can be explained by the fact that these nitrogen atoms are sp^2 hybridized. Also, the relatively longer Ni–N bonds involving the ring nitrogen atoms (N1) can be attributed to strong steric hindrance caused by the bulky pyrrolidine ring. The Ni–N distances are consistent with the corresponding nickel(II)-amine complexes [14,17].

The coordinating ligands (L) in both the complexes are disordered. The C6 atom of the ethylamine moiety in **1** has alternative positions, with partial occupancies

of 0.76 and 0.24. In complex **2**, three atoms (C3B, C4B, C5B) of ligand B are disordered with partial occupancies of 0.51 and 0.49 in two alternative sets of coordinates.

In **1**, the corresponding crystallographically independent five-membered ring is disordered and flips between the twist [$q_2 = 0.385(6)$ Å, $\phi_2 = -130.4(5)°$] and envelope [$q_2 = 0.302(10)$ Å, $\phi_2 = -1.3(12)°$] conformations. The pyrrolidine ring in the crystallographic asymmetric unit of **1** is in the envelope conformation [$q_2 = 0.389(3)$ Å, $\phi_2 = -178.9(5)°$]. The pyrrolidine ring in ligand A of **2** is in the envelope conformation [$q_2 = 0.331(4)$ Å, $\phi_2 = -0.8(9)°$] while in ligand B it flips between the twist [$q_2 = 0.205(16)$ Å, $\phi_2 = -127.4(44)°$] and the envelope [$q_2 = 0.242(9)$ Å, $\phi_2 = 6.9(33)°$] conformations. In complex **2**, the five-membered ring (N1–C6–C7–N8–Ni), formed by the coordination of the pyrrolidine and ethylamine nitrogen atoms to the Ni ion, is in the twist conformation [$q_2 = 0.441(4)$ Å, $\phi_2 = 60.1(4)°$] for ligand A and in the envelope conformation [$q_2 = 0.458(5)$ Å, $\phi_2 = -145.2(5)°$] for ligand B [18]. Although no hydrogen bonds are present in the crystal structure of **1**, the crystal structure of **2** is stabilized by two intermolecular N–H···S hydrogen bonds between screw related molecules (N8B···S9B($-x+1, y-\frac{1}{2}, -z+\frac{1}{2}$), 3.537(3); H8B1···S9B, 2.67; N8B···S9A($-x+1, y-\frac{1}{2}, -z+\frac{1}{2}$), 3.618(3); H8B2···S9A, 2.76 Å; ∠N8B–H8B1···S9B 162.8(3)°; ∠N8B–H8B2···S9A 160.6(3)°).

Table 3
Crystallographic data and structure refinement for **1** and **2**

	Complex **2** (*cis*)	Complex **1** (*trans*)
Formula	$C_{14}H_{28}N_6S_2Ni$	$C_{14}H_{28}N_6S_2Ni$
Color	Blue	Violet
Formula weight	403.2	403.2
Space group	$P2_1/c$	$P2_1/c$
Temperature (°C)	22(±1)	20(±1)
Unit cell dimensions		
a (Å)	8.559(1)	6.550(1)
b (Å)	12.775(2)	10.270(3)
c (Å)	18.091(2)	14.223(4)
β (°)	97.33(1)	101.71(1)
Cell volume (Å^3)	1962.0(4)	936.8(4)
Z	4	2
D_{calc} (g cm^{-3})	1.3	1.43
m_{calc} (cm^{-1})	12.09	36.32
Diffractometer/scan	Nonius MACH3	Nonius CAD4
Radiation, graphite monochromated	Mo Kα ($\lambda = 0.71073$ Å)	Cu Kα (1.5418 Å)
Maximum crystal dimensions, mm	$0.40 \times 0.40 \times 0.20$	$0.88 \times 0.75 \times 0.44$
Scan width	$1.0 + 0.35 \tan\theta$	$1.2 + 0.14 \tan\theta$
Reflections measured	3658	2071
Unique reflections	3442	1786
Observed reflections [$I > 2\sigma(I)$]	2650	1686
2θ Range (°)	$4 \le 2\theta \le 50$	$4 \le 2\theta \le 150$
Programs for structure solution and refinement	SHELXS, SHELXL	
Number of parameters varied	233	117
Number of restraints	40	10
Weights	$1/\sigma^2(F_o)$	$1/\sigma^2(F_o)$
Goodness-of-fit	1.09	1.07
$R = \Sigma\|\|F_o\| - \|F_c\|\|/\Sigma\|F_o\|$	0.045	0.046
R_w	0.126	0.129
Largest features in final difference map (e Å^{-3})	+0.68 to −0.44	+0.43 to −0.53

Table 4
Selected bond distances (Å) and bond angles (°)

*Bond lengths (**1**)*			
Ni–N10	2.090(2)		
Ni–N1	2.189(2)		
Ni–N8	2.101(3)		
Bond angles			
N1–Ni–N8	82.9(1)	N10–Ni–N1	91.6(1)
N10–Ni–N8	90.5(1)		
*Bond lengths (**2**)*			
Ni–N10B	2.064(3)	Ni–N10A	2.080(3)
Ni–N1B	2.172(3)	Ni–N1A	2.219(3)
Ni–N8B	2.111(3)	Ni–N8A	2.108(3)
Bond angles			
N1B–Ni–N8B	82.1(1)	N10B–Ni–N8A	87.1(1)
N8A–Ni–N8B	93.4(1)	N10B–Ni–N1A	92.8(1)
N8A–Ni–N1B	97.9(1)	N10A–Ni–N8B	91.0(1)
N1A–Ni–N8B	90.8(1)	N10A–Ni–N1B	91.1(1)
N1A–Ni–N1B	172.9(1)	N10A–Ni–N8A	170.5(1)
N1A–Ni–N8A	82.2(1)	N10A–Ni–N1A	89.3(1)
N10B–Ni–N8B	176.4(1)	N10A–Ni–N10B	89.1(1)
N10B–Ni–N1B	94.3(1)		

4. Conclusion

The present report reveals that by using the ligand 1-(2-aminoethyl)pyrrolidine, both the *cis*-diisothiocyanato species (which is a rather uncommon geometrical isomer among the bis-complexes of ethane-1,2-diamine derivatives with Ni(II)), and the usual *trans* isomer, can be both synthesized in pure form; one has to simply choose the proper solvent and vary the reaction temperature to get the desired isomer.

5. Supplementary data

Crystallographic data have been deposited with the Cambridge Crystallographic Data Centre, deposition numbers 132798/132799. Copies of this information may be obtained free of charge from: The Director, CCDC, 12 Union Road, Cambridge, CB2 1EZ, UK (Fax: +44-1223-336033; e-mail: deposit@ccdc.cam.ac.uk or www: http://www.ccdc.cam.ac.uk).

Acknowledgements

We thank the Regional Sophisticated Instrumentation Centre, Bose Institute, Calcutta-700 009, for the single-crystal X-ray diffractometer facility. Financial support by the Council of Scientific and Industrial Research, New Delhi, as a grant to N.R.C. is also gratefully acknowledged.

References

[1] A.B.P. Lever, B.S. Ramaswamy, S.H. Simonsen, L.K. Thompson, Can. J. Chem. 48 (1970) 3076.
[2] L.R. Nassimbeni, M.L. Niven, K. Zemke, Acta Crystallogr., Sect. B 42 (1986) 453.
[3] C. Pariya, A. Ghosh, N. Ray Chaudhuri, S. Ghosh, M. Mukherjee, A.K. Mukherjee, Polyhedron 15 (1996) 1643.
[4] D. Das, A. Ghosh, N. Ray Chaudhuri, Thermochim. Acta 287 (1996) 155.
[5] I.R. Laskar, D. Das, G. Mostafa, A.J. Welch, N. Ray Chaudhuri, Acta Chem. Scand. 52 (1998) 702.
[6] S.L. Moore, P.J. Squattrito, Acta Crystallogr., Sect. C 55 (1999) 332.
[7] A.K. Mukherjee, M. Mukherjee, S. Ray, A. Ghosh, N. Ray Chaudhuri, J. Chem. Soc., Dalton Trans. (1990) 2347.
[8] J. Ribas, M. Monfort, I. Resino, B.K. Ghosh, X. Solans, M. Font-Bardia, Polyhedron 17 (1998) 1735.
[9] A.I. Vogel, A Text Book of Quantitative Inorganic Analysis, fourth ed., Longman, New York, 1978.
[10] E.J. Gabe, Y. Le Page, J-P Charland, F.L. Lee, P.S. White, J. Appl. Crystallogr. 22 (1989) 384.
[11] G.M. Sheldrick, SHELXS-86, Program for the Solution of Crystal Structure, University of Göttingen, Germany, 1985.
[12] G.M. Sheldrick, SHELXL-93, Program for the Solution of Crystal Structure, Universityof Göttingen, Germany, 1993.
[13] A.K. Mukherjee, M. Mukherjee, A.J. Welch, A. Ghosh, N. Ray Chaudhuri, J. Chem. Soc., Dalton Trans. (1987) 997.
[14] D. Das, N.P. Nayak, A.K. Mukherjee, A. Ghosh, N. Ray Chaudhuri, Polyhedron 16 (1997) 2361.
[15] K. Nakamoto, Infrared Raman Spectra of Inorganic and Coordination Compounds, Wiley, New York, 1978, p. 271.
[16] C.K. Johnson, ORTEP. Report ORNL-5138, Oak Ridge National Laboratory, Tenessee, 1976.
[17] M. Soriano-Garcia, T. Pandiyan, C. Druan de Bazua, Acta Crystallogr., Sect. C 51 (1995) 1107.
[18] D. Cremer, J.A. Pople, J. Am. Chem. Soc. 97 (1975) 1354.

PERGAMON

www.elsevier.nl/locate/poly

Polyhedron 19 (2000) 1809–1814

POLYHEDRON

Synthesis and structures of two-dimensional coordination polymers constructed by metal salts and 4,4′-bipyridine

Ming-Liang Tong, Shao-Liang Zheng, Xiao-Ming Chen *

School of Chemistry and Chemical Engineering, Zhongshan University, Guangzhou 510275, PR China

Received 23 February 2000; accepted 5 June 2000

Abstract

Two nitrate compounds, $[Cu(4,4'\text{-bpy})_2(NO_3)_2]\cdot(paba)_3$ (**1**) and $[Cd(4,4'\text{-bpy})_2(H_2O)_2](NO_3)_2\cdot 4H_2O$ (**2**) (4,4′-bpy = 4,4′-bipyridine; paba = 4-aminobenzic acid), were obtained from the reactions of different metal salts and 4,4′-bpy. Compounds **1** and **2** are made up of two-dimensional square $[M_4(4,4'\text{-bpy})_4]$ grids in which the cavity has dimensions of 11.01×11.02 and 11.69×11.81 Å for **1** and **2**, respectively. In **1**, the guest paba molecules are enclathrated in the hydrophobic host cavities or situated between the coordination layers and interlinked into one-dimensional hydrogen-bonding chains through hydrogen bonding and C–H···π interactions, which further interpenetrate and contact the square grids through their functional moieties (pyridyl rings, amine groups and carboxylic groups), resulting in a new three-dimensional molecular network. In **2**, the lattice water molecules and nitrate ions are situated between the coordination layers, and extensive hydrogen bonds between the host grid and guest molecules extend the two-dimensional coordination layer into a three-dimensional molecular network. © 2000 Elsevier Science Ltd. All rights reserved.

Keywords: 4,4′-Bipyridine; Coordination polymers; Copper(II) complexes; Cadmium(II) complexes

1. Introduction

The synthesis of coordination polymers with large channels or cavities has been rapidly expanding due to their intriguing structural diversity and potential functions as microporous solids for molecular adsorption, ion exchange, and heterogeneous catalysis [1–3]. The construction of such cavities, mainly surrounded by aromatic edges, is very attractive since their shape, size and function may be controlled by the different oxidation states, the coordination preference of the metal ions, the types of ligands and solvents and the molar ratio of the metal ions and the ligands. On the other hand, the design of supramolecular architectures is also of interest in the field of host–guest chemistry. A number of the infinite frameworks well meet these requirements, because the hosts employed are relatively rigid, contain large cavities and the van der Waals surfaces and electrostatic potential surfaces of the host and guest may be complementary [4]. Although a wide range of infinite one-, two- and three-dimensional coordination frameworks have already been generated with simple, linear spacers such as 4,4′-bipyridine (4,4′-bpy) and pyrazine [5], it is somewhat surprising that very few frameworks have been reported to enclathrate larger organic guest molecules [6,7].

We have recently reported a series of non-interpenetrating open-frameworks with variable cavities or channels, in which the rod-like rigid spacers such as 4,4′-bpy, pyrazine and the related species are chosen as the building blocks [7,8]. We report herein the preparation and crystal structures of two layer-type coordination networks constructed by metal(II) salts with 4,4′-bpy, namely $[Cu(4,4'\text{-bpy})_2(NO_3)_2]\cdot(paba)_3$ (**1**) and $[Cd(4,4'\text{-bpy})_2(H_2O)_2](NO_3)_2\cdot 4H_2O$ (**2**) (paba = 4-aminobenzic acid).

* Corresponding author. Tel.: +86-20-8411-2074; fax: +86-20-8411-2245.

E-mail address: cescxm@zsu.edu.cn (X.-M. Chen).

0277-5387/00/$ - see front matter © 2000 Elsevier Science Ltd. All rights reserved.
PII: S0277-5387(00)00477-0

2. Experimental

2.1. Materials and physical measures

All reagents were commercially available and used as received. The C, H, N microanalyses were carried out with a Perkin–Elmer 240 elemental analyzer. The FTIR spectra were recorded from KBr pellets in range 4000–400 cm^{-1} on a Nicolet 5DX spectrometer.

2.2. Synthesis of metal complexes

2.2.1. $[Cu(4,4'\text{-bpy})_2(NO_3)_2]\cdot(paba)_3$ (1)

To a solution of $Cu(NO_3)_2\cdot 3H_2O$ (0.242 g, 1.0 mmol) in 4:1 (v/v) MeOH–H_2O (10 cm^3), a solution of 4,4′-bpy (0.156 g, 1.0 mmol) in MeOH (5 cm^3) was slowly added with stirring for 15 min at 60°C, and the solution was adjusted to pH 4.5 by addition of dilute HNO_3 solution, then a solution of paba (2.0 mmol, 0.274 g) in MeOH (5 cm^3) was slowly added. Dark blue block-like crystals were deposited within five days in 78% yield based on 4,4′-bpy (*Anal.* Calc. for $C_{41}H_{37}CuN_9O_{12}$: C, 54.04; H, 4.09; N, 13.83. Found: C, 53.89; H, 4.02; N, 13.72%). Infrared data (ν cm^{-1}): 3461m, 3363m, 3336m, 3232m, 3100m, 3061m, 2957m, 2918m, 2850m, 1673s, 1601vs, 1568m, 1517m, 1494w, 1409s, 1385vs, 1343s, 1313vs, 1285s, 1222s, 1168s, 1120m, 1071m, 1042w, 1017w, 932w, 855w, 818m, 776m, 726w, 696w, 644m, 609m, 547m, 498m.

2.2.2. $[Cd(4,4'\text{-bpy})_2(H_2O)_2](NO_3)_2\cdot 4H_2O$ (2)

A methanolic solution (10 cm^3) of 4,4′-bpy (0.156 g, 1.0 mmol) was added dropwise to a stirring aqueous solution (5 cm^3) of $Cd(NO_3)_2\cdot 4H_2O$ (0.308 g, 1.0 mmol) at 50°C for 15 min. An ethanolic solution (10 cm^3) of 4,4′-bpy (0.156 g, 1.0 mmol) was then added. The resulting colorless solution was allowed to stand in air at r.t. for 3 weeks, yielding colorless block-like crystals (64% yield based on 4,4′-bpy). *Anal.* Calc. for $C_{20}H_{28}CdN_6O_{12}$: C, 36.57; H, 4.30; N, 12.79. Found: C, 36.45; H, 4.21; N, 12.65%. Infrared data (ν cm^{-1}): 3409m, 3107w, 3057w, 1609s, 1539w, 1489s, 1384vs, 1278s, 1222m, 1075m, 1039m, 1011w, 983w, 807m, 723w, 674w, 632m, 568w, 491w.

2.3. X-ray crystallography

A summary of selected crystallographic data for **1** and **2** is given in Table 1. The data collections for the two complexes were carried out on a Siemens R3m diffractometer using graphite-monochromatized Mo Kα (λ 0.71073 Å) radiation at 298(2) K. Lorentz-polarization and absorption corrections were applied [9]. The structures were solved with direct methods and refined with full-matrix least-squares technique using the SHELXS-97 and SHELXL-97 programs, respectively [10,11]. Non-hydrogen atoms were refined anisotropically. The organic hydrogen atoms were generated geometrically (C–H = 0.96 Å); the aqua hydrogen atoms were located from difference maps and refined with isotropic temperature factors. Analytical expressions of neutral-atom scattering factors were employed, and anomalous dispersion corrections were incorporated [12]. The non-hydrogen atomic coordinates and selected bond lengths (Å) and angles (°) for complexes **1** and **2** are given in Table 2. Drawings were produced with SHELXTL [13].

Table 1
Crystallographic data

	1	2
Empirical formula	$C_{41}H_{37}CuN_9O_{12}$	$C_{20}H_{28}N_6O_{12}Cd$
Formula weight	911.34	656.88
Temperature	293(2) K	293(2) K
Wavelength (Mo Kα)	0.71073 Å	0.71073 Å
Crystal system	triclinic	monoclinic
Space group	$P\bar{1}$	$C2/c$
Unit cell dimensions		
a (Å)	11.008(5)	18.931(13)
b (Å)	13.057(4)	11.688(5)
c (Å)	15.752(5)	12.101(10)
α (°)	99.07(1)	90
β (°)	100.22(1)	96.65(10)
γ (°)	105.39(1)	90
Volume ($Å^3$)	2097.6(13)	2660(3)
Z	2	4
D_{calc} (Mg m^{-3})	1.443	1.641
Absorption coefficient	0.595	0.893
$F(000)$	942	1336
Crystal size (mm)	$0.46\times0.38\times0.32$	$0.42\times0.36\times0.24$
θ Range for data collection	2.0–26	2.0–28
Reflections collected	7688	4010
Independent reflections	7671 ($R_{int}=0.0259$)	3198 ($R_{int}=0.0212$)
Absorption correction	ψ-scan	ψ-scan
Max and min transmission coefficients	0.898 and 0.782	0.878 and 0.582
Data/parameters	7671/568	3198/177
Goodness-of-fit on F^2	1.039	1.102
R_1 indices ($I>2\sigma(I)$)	0.0724	0.0335
wR_2 indices (all data)	0.2226	0.0955
Largest difference peak and hole (e $Å^{-3}$)	0.737 and −0.923	0.814 and −0.495

3. Results and discussion

3.1. Preparation

Generally, with a 1:1 molar ratio of metal–4,4′-bpy, one-dimensional polymeric products or two- and three-dimensional interpenetrating networks should be expected in absence of suitable guest molecules [7a, 14]. However, only the two-dimensional coordination net-

Table 2
Selected bond lengths (Å) and angles (°) [a]

1			
Cu(1)–N(2a)	1.989(3)	Cu(1)–N(3)	2.014(3)
Cu(1)–N(1)	1.996(3)	Cu(1)–O(1)	2.461(3)
Cu(1)–N(4)	2.009(3)	Cu(1)–O(6)	2.762(3)
N(2a)–Cu(1)–N(1)	178.39(11)	N(4)–Cu(1)–O(1)	96.92(10)
N(2a)–Cu(1)–N(4)	92.52(12)	N(3)–Cu(1)–O(1)	87.68(10)
N(1)–Cu(1)–N(4)	87.86(12)	N(2a)–Cu(1)–O(6)	89.10(10)
N(2a)–Cu(1)–N(3)	89.77(12)	N(1)–Cu(1)–O(6)	89.33(10)
N(1)–Cu(1)–N(3)	89.72(12)	N(4)–Cu(1)–O(6)	91.06(10)
N(4)–Cu(1)–N(3)	174.93(12)	N(3)–Cu(1)–O(6)	84.45(10)
N(2a)–Cu(1)–O(1)	87.71(10)	O(1)–Cu(1)–O(6)	171.52(8)
N(1)–Cu(1)–O(1)	93.80(11)		
Hydrogen bonding			
N(7)···O(4c)	3.032(6)	N(8)···O(3e)	3.087(5)
N(8)···O(7d)	3.083(6)	N(9)···O(9c)	3.047(6)
O(5)···O(10)	2.673(5)	O(12)···O(7f)	2.657(6)
O(8)···O(11f)	2.614(6)	C(39)–N(9)···O(9c)	113.1(4)
O(4)–N(6)···O(10)	166.6(2)	N(6)–O(5)···O(10)	112.0(3)
C(32)–N(7)···O(4c)	120.3(4)	C(28)–O(8)···O(11f)	114.3(3)
C(25)–N(8)···O(7d)	107.2(3)	C(21)–O(10)···O(5)	113.1(3)
C(25)–N(8)···O(3e)	104.3(3)	C(35)–O(12)···O(7f)	112.4(3)
O(7d)···N(8)···O(3e)	148.19(17)		
2			
Cd(1)–O(1w)	2.305(3)	Cd(1)–N(2)	2.326(3)
Cd(1)–N(1)	2.371(3)	Cd(1)–N(3)	2.345(3)
O(1w)–Cd(1)–O(1wa)	178.50(11)	O(1wa)–Cd(1)–N(1)	87.58(11)
O(1w)–Cd(1)–N(2)	89.25(6)	N(2)–Cd(1)–N(1)	88.60(5)
O(1w)–Cd(1)–N(3)	90.75(6)	N(3)–Cd(1)–N(1)	91.40(5)
O(1w)–Cd(1)–N(1)	92.38(11)	N(1)–Cd(1)–N(1a)	177.21(10)
Hydrogen bonding			
O(1w)···O(2we)	2.663(4)	O(2w)···O(2)	2.814(6)
O(1w)···O(3w)	2.664(4)	O(3w)···O(1g)	2.855(6)
O(2w)···O(3f)	2.765(6)	Cd(1)–O(1w)···O(2we)	118.00(11)
Cd(1)–O(1w)···O(3w)	117.14(11)	O(3f)···O(2w)···O(2)	114.53(18)
O(2we)···O(1w)···O(3w)	110.09(13)	N(4)–O(3)···O(2w)	122.8(3)

[a] Symmetry codes: (a) $x+1$, y, z; (b) $x-1$, y, z; (c) $-x$, $-y+1$, $-z+1$; (d) $-x-1$, $-y$, $-z+1$; (e) $-x$, $-y$, $-z+1$; (f) $-x-1$, $-y$, $-z$; (g) $-x$, $-y+1$, $-z$ for (**1**). (a) $-x$, y, $-z+1/2$; (b) $-x+1/2$, $-y+1/2$, $-z$; (c) x, $y-1$, z; (d) x, $y+1$, z; (e) x, $-y$, $z+1/2$; (f) $-x+1/2$, $y+1/2$, $-z+1/2$; (g) $-x+1/2$, $-y+1/2$, $-z+1$ for (**2**).

work of **1** was isolated in high yield when the reactions were conducted with equivalents of the copper salt, 4,4′-bpy and paba, in an MeOH–H_2O mixture. Therefore, the presence of guest paba molecules in the reaction system may be very important in the formation of the two-dimensional polymeric structures, which is similar to other recently observed phenomena [7b, 8]. On performing the above reactions with a 1:2:3 molar ratio of Cu–4,4′-bpy–paba, crystals of **1** were also isolated in high yield, suggesting that the guest paba molecules present here may serve as templates to exclude self-inclusion or interpenetration [14].

Four metal-4,4′-bpy compounds having the similar formula to **2**, $M(4,4'\text{-bipy})_2(H_2O)_mX_2\cdot nH_2O$ (M = Cu(II), Zn(II) or Mn(II); X = ClO_4^-, NO_3^-, BF_4^-, or SCN^-), have been recently synthesized and structurally characterized [7a, 15]. However, their coordination structures are greatly different from that of **2**. In the former case one-dimensional coordination chains are generated first, and are further extended into higher dimensional networks by hydrogen bonding interactions. The difference may result from the different reaction conditions. The formers were synthesized by one-pot methods, whereas **2** was obtained by addition of the 4,4′-bpy ligand in two steps.

3.2. Crystal structures

3.2.1. $[Cu(4,4'\text{-bpy})_2(NO_3)_2]\cdot(paba)_3$ (*1*)

Compound **1** is made up of neutral two-dimensional square grids and guest paba molecules. Each layer is constructed of a common planar square with a Cu(II) atom and a 4,4′-bpy at each corner and side, respectively. The square cavity has dimensions of 11.01 × 11.02 Å, which are very similar to that of a recently reported Cu(II)–4,4′-bpy compound [7b]. The Cu(II) atom in Jahn–Teller tetragonally elongated distorted octahedral geometry, similar to those in two reported Cu-4,4′-bpy coordination networks [7b, 8g], is ligated by four pyridyl groups in the equatorial positions [Cu–N = 1.996(3)–2.014(3) Å] and weakly by two monodentate NO_3^- groups in the apical positions [Cu–O = 2.461(3) and 2.762(3) Å, respectively].

The most interesting structural features are the host–guest interactions between the host square $[Cu_4(4,4'\text{-bpy})_4(NO_3)_8]_n$ grids and the guest paba molecules, as shown in Fig. 1. The guest paba molecules are enclosed in the hydrophobic host cavities or situated between the coordination layers, and also make contact with the host grids through hydrogen bonding and C–H···π interactions [16]. Each cavity accommodates a pair of centrosymmetrically-orientated paba molecules, which are parallel to each other with a face-to-face distance of ca. 3.68 Å, indicating significant π–π interactions. Each guest paba molecule in the cavity forms three types of hydrogen bonds. The carboxylic group forms a pair of intermolecular hydrogen bonds (O···O = 2.614(6) and 2.657(6) Å) with a carboxylic group of another guest paba molecule occupying the cavity of an adjacent upper or lower coordination layer, as well as an acceptor hydrogen bond (N···O = 3.083 Å) between one of its carboxylic oxygen atom and the amine group of paba situated between the coordination layers. The paba amine group forms a donor hydrogen bond with the carboxylic group of an adjacent paba molecule situated between the coordination layers (N···O = 3.032 Å). Furthermore, there is close edge-to-face C–H···π interaction with carbon-to-carbon contacts at ca. 3.75–3.89 Å, between the aromatic rings of each guest paba molecule in the cavity and a pair of opposite edges of the host

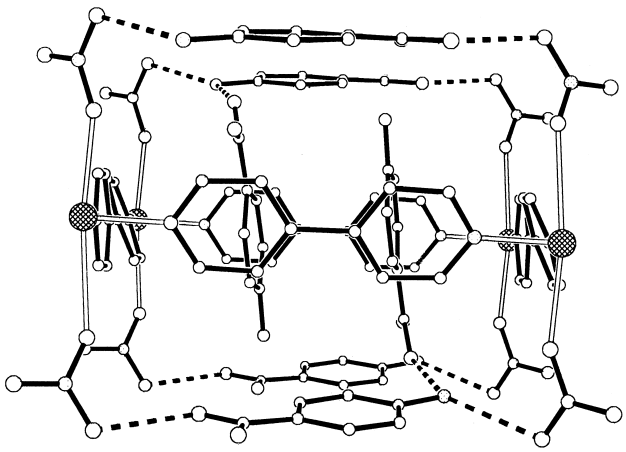


Fig. 1. Side view showing the host–guest interactions in **1**. Hydrogen bonds are represented by broken lines.

square grid, and the pyridyl rings of a pair of edges are therefore ideally coplanar. On the other hand, the guest paba molecules situated between the coordination layers similarly form extensive hydrogen bonds among the amine groups, carboxylic groups and the uncoordinated nitrate oxygen atoms (O···O = 2.673, N···O = 3.078–3.083 Å). These hydrogen bonding and C–H···π interactions rationally influence the crystalline architecture. The guest molecules are interlinked into one-dimensional hydrogen-bonding chains with two types of hourglass shaped holes, which interpenetrate and contact with the square grids through their functional moieties such as pyridyl rings, amine groups and carboxylic groups, resulting in a three-dimensional molecular networks (Fig. 2).

3.2.2. *[Cd(4,4′-bpy)$_2$(H$_2$O)$_2$](NO$_3$)$_2$·4H$_2$O* (**2**)

Compound **2** is made up of cationic two-dimensional square grids, lattice water molecules and nitrate anions. Each layer features a perfectly planar, though slightly distorted, square with a Cd(II) atom and a 4,4′-bpy at each corner and side, respectively (*cis* N–Cd–N = 88.60(5), 91.40(5)°) (see Fig. 3(a)). The Cd(II) atom, being located on a two-fold crystallographic axis, has slightly distorted octahedral geometry, being ligated by four pyridyl groups [Cd–N = 2.326(3)–2.371(3) Å] and two aqua ligands [Cd–O = 2.305(3) Å]. The square cavity has dimensions of 11.69 × 11.81 Å, which are comparable to those of closely related compounds such as [Cd(4,4′-bpy)$_2$(H$_2$O)$_2$](PF$_6$)$_2$·2(4,4′-bpy)·4H$_2$O [6a],

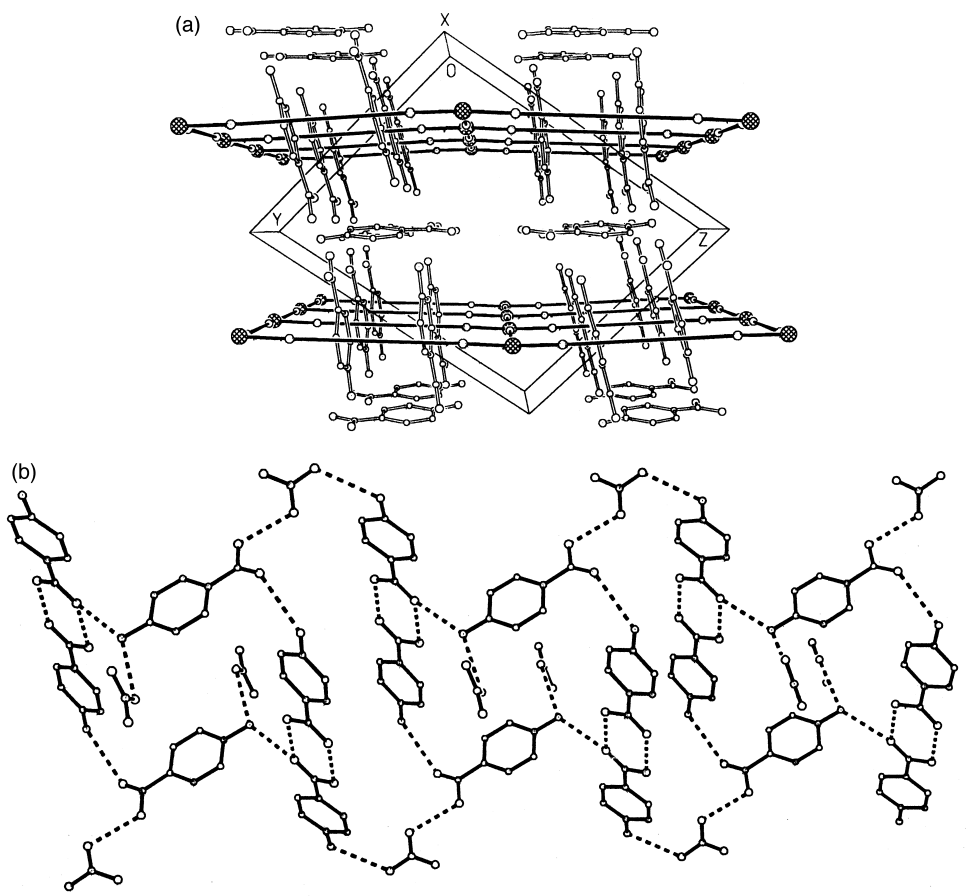


Fig. 2. (a) The 3-D network of **1** viewed from *a*-axis direction (hydrogen bonds are omitted for clarity); (b) 1-D hydrogen-bonded chains in **1**. Carbon and hydrogen atoms are omitted for clarity, the 4,4′-bpy molecular rods are shown as single bold lines. Hydrogen bonds are represented by broken lines.

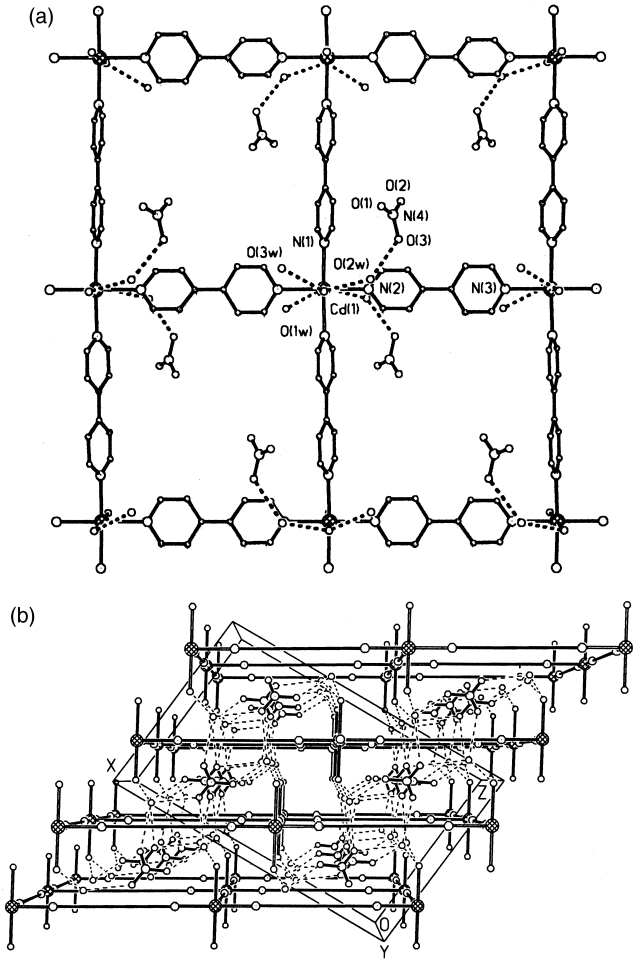


Fig. 3. (a) Top view of the square grids of **2**; (b) side view of the molecular packing of **2**. Carbon and hydrogen atoms are omitted for clarity, the 4,4′-bpy molecular rods are shown as single bold lines. Hydrogen bonds are represented by broken lines.

$[Cd(4,4'\text{-bpy})_2(NO_3)_2]\cdot 2(o\text{-}C_6H_4Br_2)$ [6b], $[Cd(4,4'\text{-bpy})_2(H_2O)_2](ClO_4)_2\cdot 1.5(4,4'\text{-bpy})\cdot(C_6H_4NO_3Cl)\cdot H_2O$ [6c] and $[Cd(4,4'\text{-bpy})_2(H_2O)_2](ClO_4)_2\cdot 2(2,4'\text{-bpy})\cdot H_2O$ [7b]. It is noteworthy that the pyridyl rings of a pair of opposite edges are ideally parallel though no larger guest molecule is enclathrated in each hydrophobic host cavity. This may be attributed to C–H···O hydrogen bonding interaction between the nitrate ions and the related 4,4′-bpy ligands (the shortest C···O distance = 3.214(3) Å), which has recently been documented elsewhere [17]. The offset superposition [8a] of each pair of adjacent layers by half of the noncoplanar edges divides the square voids into rectangular channels. The nitrate ions and lattice water molecules are situated between the coordination layers and form extensive hydrogen bonds among the aqua ligands, nitrate ions and the lattice water molecules (O···O = 2.663(4)–2.855(6) Å), which extend the two-dimensional coordination layers into a three-dimensional molecular network (Fig. 3(b)).

4. Conclusions

Two two-dimensional coordination polymers assembled by metal(II) salts and 4,4′-bpy have been prepared and characterised. Compound **1** is made up of neutral two-dimensional square $[Cu_4(4,4'\text{-bpy})_4]$ grids, in which the cavity has dimensions of 11.01×11.02 Å and are occupied by large guest paba molecules. The guest molecules are interlinked into one-dimensional hydrogen-bonding chains, which interpenetrate and contact with the square grids, resulting in a three-dimensional molecular network. Compound **2** is made up of cationic two-dimensional square $[Cd_4(4,4'\text{-bpy})_4]$ grids in which the square cavity has dimensions of 11.69×11.81 Å. The lattice water molecules and nitrate ions are situated between the coordination layers and hydrogen-bonded to the host grids.

5. Supplementary data

Supplementary data have been deposited with the Cambridge Crystallographic Centre, CCDC Nos. 139161 and 139162. Copies of this information may be obtained free of charge from The Director, CCDC, 12 Union Road, Cambridge, CB2 1EZ, UK (fax: +44-1223-336033; e-mail: deposit@ccdc.cam.ac.uk or www: http://www.ccdc.cam.ac.uk).

Acknowledgements

This work was supported by the National Natural Science Foundation of China (No. 29625102). We are indebted to the Chemistry Department of the Chinese University of Hong Kong for the donation of the R3m diffractometer.

References

[1] (a) B.F. Hoskins, R. Robson, J. Am. Chem. Soc.112 (1990) 1564. (b) A. Stein, S.W. Keller, T.E. Mallouk, Science 259 (1993) 1558.
[2] (a) S. Subramanian, M.J. Zaworotko, Angew. Chem., Int. Ed. Engl. 34 (1995) 2127. (b) C. Janiak, Angew. Chem., Int. Ed. Engl. 36 (1997) 1431.
[3] (a) O.M. Yaghi, G. Li, Angew. Chem., Int. Ed. Engl. 34 (1995) 207. (b) O.M. Yaghi, H. Li, J. Am. Chem. Soc. 117 (1995) 10401. (c) O.M. Yaghi, in: T.J. Pinnavaia, M.F. Thorpe (Eds.), Access in Nanoporous Materials, Plenum, New York, 1995, p. 111.
[4] C.A. Hunter, Angew. Chem., Int. Ed. Engl. 34 (1995) 1079.
[5] (a) S.R. Batten, R. Robson, Angew. Chem., Int. Ed. 37 (1998) 1460. (b) S. Kitagawa, M. Kondo, Bull. Chem. Soc. Jpn. 71 (1998) 1735. (c) A.J. Blake, N.R. Champness, P. Hubberstey, W.S. Li, M.A. Withersby, M. Schröder, Coord. Chem. Rev. 183 (1999) 117. (d) O.M. Yaghi, H. Li, C. Davis, D. Richardson, T.L. Groy, Acc. Chem. Res. 31 (1998) 474.

[6] (a) R. Robson, B.F. Abrahams, S.R. Batten, R.W. Gable, B.F. Hoskins, J. Liu, Supramolecular Architecture, ACS, Washington DC, p. 256, 1992. (b) M. Fujita, Y.J. Kwon, S.W. Ashizu, K. Ogura, J. Am. Chem. Soc. 116 (1994) 1151. (c) C.M. Liu, R.G. Xiong, X.Z. You, W. Chen, J. Coord. Chem. 46 (1998) 211. (d) C.M. Liu, R.G. Xiong, X.Z. You, W. Chen, J. Acta Chem. Scand. 52 (1998) 1353. (e) K. Biradha, K.V. Domasevitch, B. Moulton, C. Seward, M.J. Zaworotko, Chem. Commun. (1999) 1327. (f) S. Noro, S. Kitagawa, Chem. Lett. (1999) 727.

[7] (a) X.M. Chen, M.L. Tong, Y.J. Luo, Z.N. Chen, Aust. J. Chem. 49 (1996) 835. (b) M.L. Tong, B.H. Ye, J.W. Cai, X.M. Chen, S.W. Ng, Inorg. Chem. 37 (1998) 2645.

[8] (a) M.L. Tong, X.M. Chen, X.L. Yu, T.C.W. Mak, J. Chem. Soc., Dalton Trans. (1998) 5. (b) M.L. Tong, J.W. Cai, X.L. Yu, X.M. Chen, S.W. Ng, T.C.W. Mak, Aust. J. Chem. 51 (1998) 637. (c) M.L. Tong, X.M. Chen, B.H. Ye, S.W. Ng, Inorg. Chem. 37 (1998) 5278. (d) M.L. Tong, S.L. Zheng, X.M. Chen, Chem. Commun. (1999) 561. (e) M.L. Tong, X.M. Chen, B.H. Ye, L.N. Ji, Angew. Chem., Int. Ed. 38 (1999) 2237. (f) M.L. Tong, H.K. Lee, X.M. Chen, R.B. Huang, T.C.W. Mak, J. Chem. Soc., Dalton Trans. (1999) 3657. (g) M.L. Tong, H.J. Chen, X.M. Chen, Inorg. Chem. 39 (2000) 2235. (h) M.L. Tong, X.M. Chen, Cryst. Eng. Commun. (2000) 1.

[9] A.C.T. North, D.C. Phillips, F.S. Mathews, Acta Crystallogr., Sect. A 24 (1968) 351.

[10] G.M. Sheldrick, SHELXS-97, Program for X-ray Crystal Structure Solution, University of Göttingen, Germany, 1997.

[11] G.M. Sheldrick, SHELXL-97, Program for X-ray Crystal Structure Refinement, University of Göttingen, Germany, 1997.

[12] International Tables for X-ray Crystallography, Vol. C, Tables 4.2.6.8 and 6.1.1.4, Kluwer Academic, Dordrecht, 1992.

[13] G.M. Sheldrick, SHELXTL Version 5, Siemens Industrial Automation Inc., Madison, WI, USA, 1995.

[14] T.L. Hennigar, D.C. MacQuarrie, P. Losier, R D.and Rogers, M.J. Zaworotko, Angew. Chem., Int. Ed. Engl. 36 (1997) 972.

[15] (a) A.J. Blake, S.J. Hill, P. Hubberstey, W.S. Li, J. Chem. Soc., Dalton Trans. (1997) 913. (b) L. Carlucci, G. Ciani, D.M. Proserpio, A. Sironi, J. Chem. Soc., Dalton Trans. (1997) 1801. (c) M.X. Li, G.Y. Xie, Y.D. Gu, J. Chen, P.J. Zheng, Polyhedron 14 (1995) 1235.

[16] (a) T. Steiner, M. Tamm, B. Lutz, J. Van der Mass, J. Chem. Soc., Chem. Commun. (1996) 1127. (b) N.N.L. Madhavi, A.K. Katz, H.L. Carrell, A. Nangia, G.R. Desiraju, J. Chem. Soc., Chem. Commun. (1997) 1953. (c) H.C. Weiss, D. Bläser, R. Boese, B.M. Doughan, M.M. Haley, J. Chem. Soc., Chem. Commun. (1997) 1703. (d) K. Biradha, C. Seward, M.J. Zaworotko, Angew. Chem., Int. Ed. 38 (1999) 492.

[17] (a) C.V. Krishnamohan, S.T. Griffin, R.D. Rogers, Chem. Commun. (1998) 215. (b) C.J. Kepert, M.J. Rosseinsky, Chem. Commun. (1999) 375.

PERGAMON

www.elsevier.nl/locate/poly

Polyhedron 19 (2000) 1815–1820

POLYHEDRON

Zinc bis(pyrazolyl)silane complexes

Lauakia M. Richburg [a,b], Jamshaid A. Farouq [a], Christopher D. Incarvito [c], Arnold L. Rheingold [c,*1], Daniel Rabinovich [a,*2]

[a] *Department of Chemistry, University of North Carolina at Charlotte, 9201 University City Boulevard, Charlotte, NC 28223, USA*
[b] *Department of Natural Sciences, Johnson C. Smith University, Charlotte, NC 28216, USA*
[c] *Department of Chemistry and Biochemistry, University of Delaware, Newark, DE 19716, USA*

Received 27 May 2000; accepted 7 June 2000

Abstract

The first two members of a new family of nitrogen-donor ligands, the bis(pyrazolyl)silanes $Me_2Si(3,5\text{-}R_2pz)_2$ (R = H, Me), have been readily synthesized in almost quantitative yield from Me_2SiCl_2 and the alkali metal pyrazolates M(3,5-R_2pz) (M = Li or Na). Both bidentate ligands, abbreviated Bps and Bps^{Me_2}, respectively, have been used to prepare the zinc derivatives $LZnX_2$ (L = Bps, Bps^{Me_2}; X = Cl, Br, I), all of which have been characterized by a combination of analytical and spectroscopic techniques and, in the case of $(Bps^{Me_2})ZnI_2$, also by single-crystal X-ray diffraction. © 2000 Elsevier Science Ltd. All rights reserved.

Keywords: Zinc; Bis(pyrazolyl)silanes; Crystal structures; Nitrogen-donor ligands

1. Introduction

Trofimenko's poly(pyrazolyl)borates or scorpionates (Fig. 1) are among the most conspicuous ligands in modern coordination chemistry [1]. Their popularity stems from the distinctive steric and electronic effects that can be obtained by changing the nature, number, and position of the substituents in the pyrazole rings, thus allowing the reactivity at the metal centers they support to be fine-tuned. Not surprisingly, these ligands have been used to prepare complexes with metals all across the periodic table, some of which have found interesting applications in catalysis and bioinorganic chemistry [2,3]. In contrast, the synthesis and reactivity of their neutral and isosteric carbon-centered analogues, the poly(pyrazolyl)methanes $H_nC(3,5\text{-}R_2pz)_{4-n}$ ($n = 1, 2$), is considerably less developed [4,5], perhaps due to the relatively small number of such ligands currently available. However, recent developments in bis(pyrazolyl)methane chemistry, including the synthesis of potential platinum anticancer agents [6] and the preparation of asymmetric allylic alkylation [7], olefin hydrogenation [8], and alkyne hydroamination catalysts [9], prompted us to seek a high-yield, straightforward route to alternative neutral analogues of the bis(pyrazolyl)borates. We envisioned that the closely related but hitherto unknown bis(pyrazolyl)silanes $Me_2Si(3,5\text{-}R_2pz)_2$ (Fig. 2) would be excellent candidates to meet this demand and could be readily prepared in excellent yields given the enhanced reactivity of the Si–Cl versus C–Cl bonds towards nucleophiles (see below). Based on

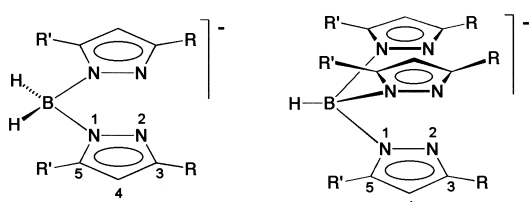


Fig. 1. Bis–(Bp) and tris(pyrazolyl)borate (Tp) ligands.

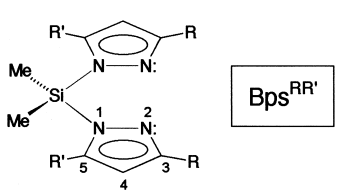


Fig. 2. Bis(pyrazolyl)silane (Bps) ligands.

[1] *Corresponding author. E-mail: arnrhein@udel.edu
[2] *Corresponding author. Tel.: +1-704-547-4442; fax: +1-704-547-3151; e-mail: drabinov@email.uncc.edu

0277-5387/00/$ - see front matter © 2000 Elsevier Science Ltd. All rights reserved.
PII: S0277-5387(00)00470-8

nomenclature introduced a few years ago for the tris(pyrazolyl)borates [1], we will abbreviate the new ligands $Bps^{RR'}$, where R and R′ are the alkyl or aryl substituents in the 3- and 5-positions of the pyrazolyl rings, respectively and two methyl groups are assumed to be attached to the silicon center.

In this paper we present the synthesis and characterization of the first two representatives of this new family of bidentate ligands, namely the bis(pyrazolyl)dimethylsilane $Me_2Si(pz)_2$ (Bps) and the bis(3,5-dimethylpyrazolyl)dimethylsilane $Me_2Si(3,5\text{-}Me_2pz)_2$ (Bps^{Me_2}). Given the role that nitrogen-donor groups such as pyrazolyl or imidazolyl play in model compounds of the active sites in a number of zinc enzymes (e.g. carbonic anhydrase, carboxypeptidase A) [10,11], an initial investigation of the binding properties of the new ligands was centered on simple derivatives of this metal, as described below.

2. Results and discussion

2.1. Ligand synthesis

The bis(pyrazolyl)silanes Bps and Bps^{Me_2} were readily prepared from the reactions of dichlorodimethylsilane and two molar equivalents of the corresponding alkali metal pyrazolates M(3,5-R_2pz) (M = Li or Na), as illustrated in Eq. (1):

$$Me_2SiCl_2 + 2M(3,5\text{-}R_2pz) \xrightarrow[\substack{M=Li,\ Na\\ R=H,\ Me}]{\text{pentane}} Bps^{RR} + 2MCl \quad (1)$$

Both compounds were isolated in excellent yield (90–95%) as white powders after separating the alkali chloride by-products by filtration. They are stable in dry air for at least 6 months and they are soluble in aliphatic and aromatic hydrocarbons, acetonitrile, ethers and dichloromethane. However, they slowly decompose in acetone or in the presence of solvents with acidic protons such as water and alcohols, an important difference with respect to the analogous $H_2C(3,5\text{-}R_2pz)_2$ ligands. It is also important to note that we have recently used a similar approach to prepare the tridentate ligands $MeSi(3,5\text{-}Me_2pz)_3$ (Tps^{Me_2}) [12] and $MeSi(3\text{-}^tBupz)_3$ ($Tps^{^tBu}$) [13] from the reactions of $MeSiCl_3$ and three molar equivalents of the corresponding lithium pyrazolates, an observation that illustrates the general applicability of our methodology.

2.2. Preparation of zinc complexes

The zinc(II) derivatives $LZnX_2$ (L = Bps, Bps^{Me_2}; X = Cl, Br, I) were prepared by mixing equimolar amounts of the zinc halides and the ligands dissolved in diethyl ether or tetrahydrofuran (THF), as represented in Eq. (2), and isolated as white or off-white

$$ZnX_2 + Bps^{RR} \xrightarrow[\substack{X=Cl,\ Br,\ I\\ R=H,\ Me}]{Et_2O \text{ or } THF} (Bps^{RR})ZnX_2 \quad (2)$$

diamagnetic solids in 65–85% yield. While the $(Bps)ZnX_2$ complexes are insoluble in all common organic solvents of low to medium polarity, the $(Bps^{Me_2})ZnX_2$ derivatives are slightly soluble in THF or dichloromethane, solvents in which their solubilities increase in the order Cl < Br < I. Dissolution of both series of complexes in more polar or coordinating solvents such as acetone, acetonitrile, or dimethylsulfoxide (DMSO) results in significant decomposition or the immediate displacement of the ligands, as established by ^{1}H NMR spectroscopy.

The new $LZnX_2$ complexes were characterized by a combination of analytical and spectroscopic techniques, with elemental analyses (CHN) being consistent with the formation of simple 1:1 adducts. All the complexes were characterized by solid-state infrared (IR) spectroscopy and, in the case of the Bps^{Me_2} derivatives, by both ^{1}H NMR and $^{13}C\{^1H\}$ NMR spectroscopy in solution. In general, both IR and NMR data for the new compounds are similar to those reported for a number of related zinc bis(pyrazolyl)alkane complexes [14–20]. For example, in the ^{1}H NMR spectra of the series $(Bps^{Me_2})ZnX_2$, all the signals are downfield shifted between 0.14 and 0.54 ppm relative to the corresponding values obtained for the free ligand in the same solvent. The deshielding effect (Δ) observed upon complexation is more pronounced for the pyrazolyl methyl groups ($\Delta \approx 0.47$ ppm) than for either the 4-H ($\Delta \approx 0.27$ ppm) or the methylsilyl protons ($\Delta \approx 0.15$ ppm). Similarly, downfield shifts of between 2 and 7 ppm relative to the free ligand are found for all the resonances in the ^{13}C NMR spectra of the Bps^{Me_2} complexes, an observation that is unlike the data published for the bis(pyrazolyl)alkane analogues, which typically show both positive and negative Δ values.

2.3. Structure of $(Bps^{Me_2})ZnI_2$

Single crystals suitable for an X-ray diffraction study of $(Bps^{Me_2})ZnI_2$ were obtained by slow evaporation at room temperature of a concentrated THF solution of the title compound (Fig. 3). A selection of bond lengths and angles is given in Table 1. The four-coordinate complex exhibits a slightly distorted tetrahedral geometry in the solid state that resembles those of the related bis(pyrazolyl)alkane complexes $\{H_2C(3,4,5\text{-}Me_3pz)_2\}ZnBr_2$ [20] and $\{Me_2C(pz)_2\}ZnX_2$ (X = Cl, Br, I, O_2CCF_3) [16,18,21]. However, the angles subtended at zinc in $(Bps^{Me_2})ZnI_2$, in the approximate range 99–115°, deviate less from the ideal tetrahedral values than those found in the bis(pyrazolyl)alkane complexes. Specifically, the N–Zn–N angle in $(Bps^{Me_2})ZnI_2$ (ca. 99.2°) is significantly larger than the corresponding values

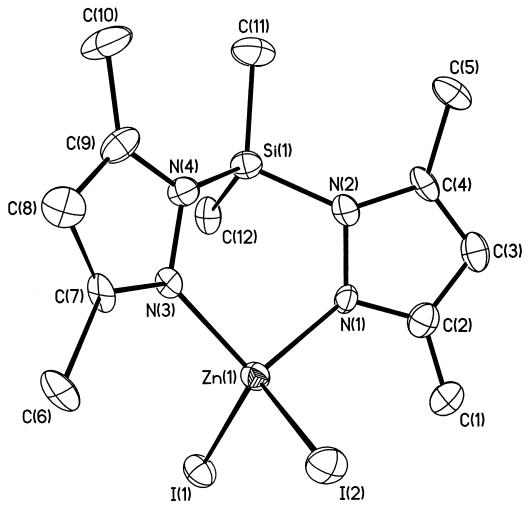


Fig. 3. ORTEP showing one of the two independent molecules of $(Bps^{Me_2})ZnI_2$, with hydrogen atoms omitted for clarity and thermal ellipsoids at the 30% probability level.

Table 1
Selected bond lengths (Å) and angles (°) for $(Bps^{Me_2})ZnI_2$

Zn(1)–I(1)	2.5484(9)	Zn(1)–N(1)	2.044(6)
Zn(1)–I(2)	2.5981(10)	Zn(1)–N(3)	2.047(6)
I(1)–Zn(1)–I(2)	113.48(3)	N(1)–Zn(1)–N(3)	99.3(2)
N(1)–Zn(1)–I(1)	112.38(16)	N(1)–Zn(1)–I(2)	106.85(15)
N(3)–Zn(1)–I(1)	115.56(16)	N(3)–Zn(1)–I(2)	108.05(16)

found in bis(pyrazolyl)alkane derivatives, typically between 84 and 89° [16,18,20,21]. It is likely that this observation is a consequence of the larger size of the silicon atom in the bis(pyrazolyl)silane derivatives relative to that of the carbon centers in the alkane analogues, a phenomenon that may have implications in the reactivity of the complexes that these ligands support.

The average Zn–I and Zn–N bond distances in $(Bps^{Me_2})ZnI_2$, 2.571 and 2.042 Å, respectively, are within the range of the corresponding values observed in $\{Me_2C(pz)_2\}ZnI_2$ [18], in the bis(pyrazole) complex $\{3,5\text{-}(^tBuph)_2pzH\}_2ZnI_2$ [22], and in various other nitrogen-donor adducts of ZnI_2 [23–31]. All the remaining interatomic distances (i.e. Si–N, Si–C, C–N and C–C bond lengths) are also normal.

3. Conclusions

In summary, the bis(pyrazolyl)silanes Bps and Bps^{Me_2}, two new bidentate nitrogen-donor ligands representing alternative neutral analogues of the corresponding anionic bis(pyrazolyl)borates, have been readily synthesized and their first transition metal derivatives have been prepared. While continuing to investigate the coordination chemistry of Bps and Bps^{Me_2}, we have also extended our methodology to the syntheses of more sterically demanding ligands, in particular those having no bis(pyrazolyl)methane analogues. In this regard, we have already prepared the 3-*tert*-butyl- and 3,5-diphenyl-substituted bis(pyrazolyl)silanes $Bps^{^tBu}$ and Bps^{Ph_2}, the synthesis and reactivity of which will be reported in due course.

4. Experimental

4.1. General considerations

All reactions were performed under dry oxygen-free nitrogen in an Innovative Technology System One-M-DC glovebox or under argon using a combination of high-vacuum and Schlenk techniques [32–34]. Solvents were purified and degassed by standard procedures and all commercially available reagents were used as received. The lithium pyrazolates Li(3,5-R_2pz) (R = H, Me) were prepared by deprotonation of the corresponding pyrazoles with *n*-butyllithium in pentane and isolated as white solids in ca. 90% yield [12]. ^1H and ^{13}C NMR spectra were obtained on General Electric QE 300 or Varian Gemini (300 MHz) FT spectrometers. Chemical shifts (δ) are reported in parts per million relative to $SiMe_4$ ($\delta = 0$ ppm) and were referenced internally with respect to the solvent resonances (δ 5.32 for $CDHCl_2$, 7.15 for C_6D_5H, 53.8 for CD_2Cl_2, 128.0 for C_6D_6,); coupling constants are given in hertz (Hz). IR spectra were recorded as KBr pellets on a Midac Collegian FT spectrophotometer and data are reported in cm^{-1}; relative intensities of the absorptions are indicated in parentheses (vs = very strong, s = strong, m = medium, w = weak, sh = shoulder). Elemental analyses were determined by Atlantic Microlab, Inc. (Norcross, GA) or Desert Analytics (Tucson, AZ).

4.2. Synthesis of Bps

Me_2SiCl_2 (0.41 ml, 3.38 mmol) was slowly added via syringe to a stirred suspension of Na(pz) (0.61 g, 6.77 mmol) in pentane (75 ml). After stirring for 1 h, the suspension was filtered using a fritted funnel and the collected solid (NaCl) washed with pentane (2 × 20 ml). The solvent was removed under reduced pressure from the combined filtrate and washings to give an analytically and spectroscopically pure white solid, which was dried in vacuo for 1 h (0.59 g, 91%). M.p. = 48–49°C. NMR data (in C_6D_6): ^1H δ 0.62 (s, 6 H, CH_3Si), 6.09 (dd, $^3J_{H-H} = 1.4$ and 2.4, 2 H, 4-*H* in pz), 7.28 (d, $^3J_{H-H} = 2.4$, 2 H, 3-*H* or 5-*H* in pz), 7.77 (d, $^3J_{H-H} = 1.4$, 2 H, 3-*H* or 5-*H* in pz); ^{13}C δ −2.6 (q, $^1J_{C-H} = 122$, 2 C, CH_3Si), 107.4 (d, $^1J_{C-H} = 177$, 2 C, 4-*C* in pz), 134.9 (d, $^1J_{C-H} = 185$, 2 C, 3-*C* or 5-*C* in pz), 144.4 (d,

$^1J_{C-H} = 184$, 2 C, 3-*C* or 5-*C* in pz). IR data (cm^{-1}): 3092 (w), 2964 (w), 1767 (w), 1512 (m), 1403 (m), 1382 (m), 1375 (m), 1277 (s), 1269 (s), 1173 (s), 1165 (s), 1075 (s), 1037 (s), 951 (m), 916 (m), 900 (m), 842 (sh), 816 (vs), 785 (s), 768 (vs), 691 (s), 668 (w), 618 (s), 498 (vs), 421 (vs). *Anal*. Calc. for $C_8H_{12}N_4Si$: C, 50.0; H, 6.3; N, 29.1. Found: C, 49.8; H, 6.5; N, 28.9%.

4.3. Synthesis of (Bps)$ZnCl_2$

A solution of Bps (0.164 g, 0.853 mmol) in tetrahydrofuran (5 ml) was added to a stirred, filtered solution of $ZnCl_2$ (0.116 g, 0.851 mmol) in the same solvent (10 ml), resulting in the immediate formation of an off-white precipitate. The suspension was stirred for 45 min, concentrated under reduced pressure to ca. 5 ml, and treated with pentane (10 ml). The product was isolated by filtration, washed with pentane (3×5 ml), and dried in vacuo for 1 h (0.186 g, 67%). M.p. = 238°C (dec.). IR data (cm^{-1}): 3144 (m), 3121 (m), 3102 (m), 3013 (w), 2963 (m), 2899 (w), 1784 (w), 1652 (w), 1513 (m), 1422 (s), 1408 (m), 1389 (vs), 1378 (m), 1283 (vs), 1272 (s), 1182 (vs), 1169 (s), 1122 (w), 1089 (vs), 1065 (vs), 979 (m), 920 (w), 913 (w), 847 (vs), 826 (vs), 785 (vs), 691 (s), 611 (s), 488 (s), 429 (s). *Anal*. Calc. for $C_8H_{12}Cl_2N_4SiZn$: C, 29.2; H, 3.7; N, 17.1. Found: C, 28.8; H, 3.9; N, 16.9%.

4.4. Synthesis of (Bps)$ZnBr_2$

A solution of Bps (0.095 g, 0.494 mmol) in tetrahydrofuran (3 ml) was added to a stirred solution of $ZnBr_2$ (0.111 g, 0.493 mmol) in the same solvent (5 ml), resulting in the immediate formation of an off-white precipitate. The suspension was stirred for 20 min and the product separated by decantation, washed with tetrahydrofuran (5 ml), and dried in vacuo for 1 h (0.148 g, 72%). M.p. = 268°C (dec.). IR data (cm^{-1}): 3153 (m), 3140 (m), 3118 (m), 3102 (m), 2962 (m), 2895 (w), 1524 (m), 1511 (m), 1475 (s), 1421 (s), 1406 (s), 1388 (s), 1350 (s), 1289 (sh), 1282 (s), 1266 (s), 1181 (s), 1169 (m), 1121 (vs), 1088 (s), 1063 (vs), 1046 (s), 979 (m), 912 (m), 845 (s), 823 (vs), 782 (vs), 690 (s), 611 (s), 588 (m), 487 (m), 429 (m). *Anal*. Calc. for $C_8H_{12}Br_2N_4SiZn$: C, 23.0; H, 2.9; N, 13.4. Found: C, 23.1; H, 2.9; N, 13.4%.

4.5. Synthesis of (Bps)ZnI_2

A solution of Bps (0.144 g, 0.749 mmol) in diethylether (3 ml) was added to a stirred solution of ZnI_2 (0.240 g, 0.752 mmol) in the same solvent (5 ml), resulting in the immediate formation of an off-white precipitate. The suspension was stirred for 20 min and the product separated by decantation, washed with diethylether (2×5 ml), and dried in vacuo for 30 min (0.275 g, 72%). M.p. = 282°C (dec.). IR data (cm^{-1}): 3144 (w), 3116 (w), 2964 (w), 1522 (w), 1510 (w), 1474 (m), 1420 (w), 1405 (m), 1389 (m), 1356 (m), 1282 (m), 1264 (s), 1181 (w), 1121 (s), 1089 (s), 1064 (vs), 1046 (vs), 978 (w), 948 (w), 910 (w), 843 (w), 831 (m), 816 (s), 793 (s), 779 (m), 770 (s), 703 (w), 674 (m), 609 (m). *Anal*. Calc. for $C_8H_{12}I_2N_4SiZn$: C, 18.8; H, 2.4; N, 11.0. Found: C, 18.5; H, 2.3; N, 11.0%.

4.6. Synthesis of Bps^{Me_2}

Me_2SiCl_2 (2.40 ml, 19.8 mmol) was slowly added via syringe to a stirred suspension of Li(3,5-Me_2pz) (4.03 g, 39.5 mmol) in pentane (150 ml). After being stirred for 2 h, the suspension was filtered using a fritted funnel and the collected solid (LiCl) was washed with pentane (2×20 ml). The solvent was removed under reduced pressure from the combined filtrate and washings to give an analytically and spectroscopically pure white solid, which was dried in vacuo for 1 h (4.62 g, 94%). M.p. = 44–45°C. ^{1}H NMR data (in C_6D_6): δ 0.85 (s, 6 H, CH_3Si), 1.80 [s, 6 H, (CH_3)$_2$pz], 2.24 [s, 6 H, (CH_3)$_2$pz], 5.72 (s, 2 H, 4-*H* in 3,5-Me_2pz); ^{1}H NMR data (in CD_2Cl_2): δ 0.87 (s, 6 H, CH_3Si), 1.91 [s, 6 H, (CH_3)$_2$pz], 2.19 [s, 6 H, (CH_3)$_2$pz], 5.87 (s, 2 H, 4-*H* in 3,5-Me_2pz); ^{13}C NMR data (in C_6D_6): δ −0.2 (q, $^1J_{C-H} = 121$, 2 C, *C*H$_3$Si), 11.6 [q, $^1J_{C-H} = 126$, 2 C, (*C*H$_3$)$_2$pz], 13.9 [q, $^1J_{C-H} = 128$, 2 C, (*C*H$_3$)$_2$pz], 108.7 (d, $^1J_{C-H} = 172$, 2 C, 4-*C* in 3,5-Me_2pz), 146.9 (s, 2 C, 3-*C* or 5-*C* in 3,5-Me_2pz), 152.4 (s, 2 C, 3-*C* or 5-*C* in 3,5-Me_2pz); ^{13}C NMR data (in CD_2Cl_2): δ −0.1 (q, $^1J_{C-H} = 122$, 2 C, *C*H$_3$Si), 11.7 [q, $^1J_{C-H} = 128$, 2 C, (*C*H$_3$)$_2$pz], 13.7 [q, $^1J_{C-H} = 127$, 2 C, (*C*H$_3$)$_2$pz], 108.8 (d, $^1J_{C-H} = 172$, 2 C, 4-*C* in 3,5-Me_2pz), 147.5 (s, 2 C, 3-*C* or 5-*C* in 3,5-Me_2pz), 152.8 (s, 2 C, 3-*C* or 5-*C* in 3,5-Me_2pz). IR data (cm^{-1}): 3201 (m), 3131 (m), 3109 (m), 3038 (m), 2960 (m), 2878 (m), 2791 (w), 2729 (w), 2610 (w), 1595 (m), 1555 (m), 1484 (m), 1465 (m), 1420 (m), 1370 (w), 1327 (m), 1308 (s), 1261 (s), 1149 (m), 1091 (m), 1029 (vs), 966 (w), 810 (vs), 781 (s), 738 (m), 692 (m), 662 (m), 587 (m). *Anal*. Calc. for $C_{12}H_{20}N_4Si$: C, 58.0; H, 8.1; N, 22.6. Found: C, 57.7; H, 8.2; N, 22.4%.

4.7. Synthesis of (Bps^{Me_2})$ZnCl_2$

A solution of Bps^{Me_2} (0.365 g, 1.469 mmol) in THF (10 ml) was added to a stirred, slightly cloudy solution of $ZnCl_2$ (0.200 g, 1.468 mmol) in the same solvent (20 ml), resulting in the formation of a white precipitate. After being stirred for 30 min, the solution was concentrated under reduced pressure to ca. 10 ml and pentane (20 ml) added. The white product was isolated by filtration, washed with pentane (30 ml), and dried in vacuo for 18 h (0.403 g, 71%). M.p. = 242°C (dec.). NMR data (in CD_2Cl_2): ^{1}H δ 1.04 (s, 6 H, CH_3Si), 2.43

[s, 6 H, (CH_3)$_2$pz], 2.55 [s, 6 H, (CH_3)$_2$pz], 6.14 (s, 2 H, 4-*H* in 3,5-Me$_2$pz); ^{13}C{^{1}H} δ 1.9 (s, 2 C, *C*H$_3$Si), 14.3 [s, 2 C, (*C*H$_3$)$_2$pz], 14.5 [s, 2 C, (*C*H$_3$)$_2$pz], 111.1 (s, 2 C, 4-*C* in 3,5-Me$_2$pz), 151.0 (s, 2 C, 3-*C* or 5-*C* in 3,5-Me$_2$pz), 159.2 (s, 2 C, 3-*C* or 5-*C* in 3,5-Me$_2$pz). IR data (cm^{-1}): 3341 (m), 3317 (m), 3125 (w), 3004 (w), 2971 (w), 2922 (w), 1570 (m), 1555 (s), 1485 (w), 1440 (m), 1416 (m), 1381 (w), 1328 (m), 1305 (m), 1266 (m), 1146 (s), 1139 (s), 1048 (s), 1032 (w), 983 (w), 850 (s), 825 (vs), 804 (s), 762 (m), 694 (m), 668 (w), 591 (w), 505 (m), 478 (w), 440 (m), 414 (w). *Anal.* Calc. for $C_{12}H_{20}Cl_2N_4SiZn$: C, 37.5; H, 5.2; N, 14.6. Found: C, 37.1; H, 5.3; N, 14.9%.

4.8. Synthesis of (Bps^{Me_2})ZnBr$_2$

A solution of Bps^{Me_2} (0.221 g, 0.890 mmol) in THF (10 ml) was added to a stirred solution of $ZnBr_2$ (0.200 g, 0.888 mmol) in the same solvent (20 ml), resulting in the formation of a white precipitate. After being stirred for 15 min, the solution was concentrated under reduced pressure to ca. 5 ml and pentane (25 ml) added. The white product was isolated by filtration, washed with pentane (20 ml), and dried in vacuo for 1 h (0.370 g, 88%). M.p. = 192°C (dec.). NMR data (in CD_2Cl_2): ^{1}H δ 1.01 (s, 6 H, CH_3Si), 2.43 [s, 6 H, (CH_3)$_2$pz], 2.59 [s, 6 H, (CH_3)$_2$pz], 6.14 (s, 2 H, 4-*H* in 3,5-Me$_2$pz); ^{13}C{^{1}H} δ 2.0 (s, 2 C, *C*H$_3$Si), 14.3 [s, 2 C, (*C*H$_3$)$_2$pz], 15.0 [s, 2 C, (*C*H$_3$)$_2$pz], 111.5 (s, 2 C, 4-*C* in 3,5-Me$_2$pz), 151.5 (s, 2 C, 3-*C* or 5-*C* in 3,5-Me$_2$pz), 159.6 (s, 2 C, 3-*C* or 5-*C* in 3,5-Me$_2$pz). IR data (cm^{-1}): 3358 (m), 3344 (m), 3340 (sh), 2967 (w), 1574 (m), 1572 (m), 1555 (s), 1474 (w), 1438 (m), 1420 (m), 1327 (m), 1301 (m), 1266 (m), 1184 (w), 1145 (m), 1136 (m), 1047 (vs), 984 (w), 849 (m), 826 (vs), 803 (m), 762 (m), 693 (m), 668 (m), 657 (m), 564 (w), 503 (m), 478 (m), 439 (m). *Anal.* Calc. for $C_{12}H_{20}Br_2N_4SiZn$: C, 30.4; H, 4.3; N, 11.8. Found: C, 30.1; H, 4.3; N, 11.9%.

Table 2
Crystallographic data for (Bps^{Me_2})ZnI$_2$

Formula	$C_{12}H_{20}I_2N_4SiZn$
Formula weight	567.58
Crystal system	triclinic
Space group	$P\bar{1}$ (no. 2)
Temperature (K)	244(2)
a (Å)	8.8701(16)
b (Å)	15.305(3)
c (Å)	15.6865(19)
α (°)	66.948(10)
β (°)	85.581(14)
γ (°)	76.924(11)
V (Å^3)	1908.6(5)
Z	4
D_{calc} (g cm^{-3})	1.975
μ(Mo Kα) (mm^{-1})	4.581
θ_{max} (°)	25
Number of data	6202
Number of parameters	361
R_1 ($I>2\sigma(I)$) [a]	0.0420
wR_2 ($I>2\sigma(I)$) [a]	0.1032

[a] $R_1 = \Sigma(|F_o|-|F_c|)/\Sigma|F_o|$; $\{\Sigma[w(F_o^2-F_c^2)^2]/\Sigma[w(F_o^2)^2\}^{1/2}$.

4.9. Synthesis of (Bps^{Me_2})ZnI$_2$

A solution of Bps^{Me_2} (0.200 g, 0.805 mmol) in diethyl ether (10 ml) was added to a stirred solution of ZnI_2 (0.257 g, 0.805 mmol) in the same solvent (20 ml), resulting in the formation of a white precipitate. After being stirred for 1 h, the solution was concentrated under reduced pressure to ca. 10 ml and pentane (10 ml) added. The white product was isolated by filtration, washed with pentane (20 ml), and dried in vacuo for 1 h (0.390 g, 85%). M.p. = 210°C (dec.). NMR data (in CD_2Cl_2): ^{1}H δ 1.01 (s, 6 H, CH_3Si), 2.45 [s, 6 H, (CH_3)$_2$pz], 2.64 [s, 6 H, (CH_3)$_2$pz], 6.15 (s, 2 H, 4-*H* in 3,5-Me$_2$pz); ^{13}C{^{1}H} δ 2.2 (s, 2 C, *C*H$_3$Si), 14.3 [s, 2 C, (*C*H$_3$)$_2$pz], 15.7 [s, 2 C, (*C*H$_3$)$_2$pz], 111.8 (s, 2 C, 4-*C* in 3,5-Me$_2$pz), 151.3 (s, 2 C, 3-*C* or 5-*C* in 3,5-Me$_2$pz), 159.8 (s, 2 C, 3-*C* or 5-*C* in 3,5-Me$_2$pz). IR data (cm^{-1}): 3337 (s), 3134 (w), 2965 (w), 1570 (s), 1555 (s), 1547 (s), 1476 (m), 1474 (m), 1439 (m), 1420 (m), 1381 (w), 1326 (m), 1301 (m), 1267 (m), 1182 (w), 1142 (s), 1133 (s), 1046 (vs), 1029 (w), 983 (w), 846 (s), 824 (vs), 800 (s), 761 (m), 692 (w), 655 (m), 589 (w), 562 (m), 499 (m), 477 (w), 439 (m). *Anal.* Calc. for $C_{12}H_{20}I_2N_4SiZn$: C, 25.4; H, 3.6; N, 9.9. Found: C, 25.4; H, 3.4; N, 10.0%.

4.10. X-ray structure determination

A summary of crystal data collection and refinement parameters is given in Table 2. A crystal suitable for data collection was selected and mounted with epoxy glue on the tip of a fine glass fiber. Data were collected on a Siemens P4 diffractometer equipped with a SMART/CCD detector using Mo Kα radiation (λ = 0.71073 Å). No evidence of symmetry higher than triclinic was observed in either the axial views or diffraction data. *E*-statistics suggested the centrosymmetric space group option $P\bar{1}$, which yielded chemically reasonable and computationally stable results of refinement. The structure was solved by direct methods, completed by subsequent difference Fourier syntheses, and refined by full-matrix, least-squares procedures. An empirical absorption correction was applied to the data using DIFABS [35]. There are two crystallographically independent but chemically equivalent molecules in the asymmetric unit. All non-hydrogen atoms were refined with anisotropic displacement parameters and hydrogen atoms were treated as idealized contributions. All software and sources of the scattering factors are contained in the SHELXTL (version 5.10) program library [36].

5. Supplementary data

Crystallographic data (excluding structure factors) for $(Bps^{Me_2})ZnI_2$ have been deposited with the Cambridge Crystallographic Data Centre, CCDC No. 142657. Copies of this information may be obtained free of charge from The Director, CCDC, 12 Union Road, Cambridge, CB2 1EZ, UK (fax: +44-1223-336033; e-mail: deposit@ccdc.cam.ac.uk or www: http://www.ccdc.cam.ac.uk).

Acknowledgements

We thank the Camille and Henry Dreyfus Foundation Faculty Start-Up Grant Program for Undergraduate Institutions, Research Corporation for a Cottrell College Science Award, the donors of the Petroleum Research Fund, administered by the American Chemical Society, and the University of North Carolina at Charlotte for support of this research. L.M.R. also acknowledges the National Institute of General Medical Sciences and its MBRS/RISE program at Johnson C. Smith University (grant # GM58042) for financial support.

References

[1] S. Trofimenko, Scorpionates: The Coordination Chemistry of Polypyrazolylborate Ligands, Imperial College Press, London, 1999.
[2] N. Kitajima, W.B. Tolman, Prog. Inorg. Chem. 43 (1995) 419.
[3] G. Parkin, Adv. Inorg. Chem. 42 (1995) 291.
[4] P.K. Byers, A.J. Canty, R.T. Honeyman, Adv. Organomet. Chem. 34 (1992) 1.
[5] S. Trofimenko, Prog. Inorg. Chem. 34 (1986) 115.
[6] J.A. Broomhead, M.J. Lynch, Inorg. Chim. Acta 240 (1995) 13.
[7] M. Bovens, A. Togni, L.M. Venanzi, J. Organomet. Chem. 451 (1993) C28.
[8] F.A. Jalón, A. Otero, A. Rodríguez, M. Pérez-Manrique, J. Organomet. Chem. 508 (1996) 69.
[9] S. Burling, L.D. Field, B.A. Messerle, Organometallics 19 (2000) 87.
[10] I. Bertini, C. Luchinat, W. Maret, M. Zeppezauer (Eds.), Zinc Enzymes, Progress in Inorganic Biochemistry and Biophysics, vol. 1, Birkhäuser, Boston, MA, 1986.
[11] T.G. Spiro (Ed.), Zinc Enzymes, Krieger, Malabar, FL, 1991.
[12] E.E. Pullen, D. Rabinovich, C.D. Incarvito, T.E. Concolino, A.L. Rheingold, Inorg. Chem. 39 (2000) 1561.
[13] E.E. Pullen, A.L. Rheingold, D. Rabinovich, Inorg. Chem. Commun. 2 (1999) 194.
[14] A. Lorenzotti, A. Cingolani, G. Gioia Lobbia, D. Leonesi, F. Bonati, Gazz. Chim. Ital. 117 (1987) 191.
[15] D. Leonesi, A. Cingolani, G. Gioia Lobbia, A. Lorenzotti, F. Bonati, Gazz. Chim. Ital. 117 (1987) 491.
[16] B. Bovio, A. Cingolani, C. Pettinari, G. Gioia Lobbia, F. Bonati, Z. Anorg. Allg. Chem. 602 (1991) 169.
[17] C. Pettinari, C. Santini, D. Leonesi, P. Cecchi, Polyhedron 13 (1994) 1553.
[18] C. Pettinari, A. Cingolani, B. Bovio, Polyhedron 15 (1996) 115.
[19] C. Pettinari, A. Lorenzotti, M. Pellei, C. Santini, Polyhedron 16 (1997) 3435.
[20] C. Pettinari, F. Marchetti, A. Cingolani, D. Leonesi, M. Colapietro, S. Margadonna, Polyhedron 17 (1998) 4145.
[21] B. Bovio, A. Cingolani, F. Bonati, Z. Anorg. Allg. Chem. 610 (1992) 151.
[22] E. Libertini, K. Yoon, G. Parkin, Polyhedron 12 (1993) 2539.
[23] J.F. Le Querler, M.M. Borel, A. Leclaire, Acta Crystallogr., Sect. B 33 (1977) 2299.
[24] F. Raubacher, F. Weller, Z. Kristallogr. 211 (1996) 576.
[25] K. Davarski, J. Macicek, L. Konovalov, J. Coord. Chem. 38 (1996) 123.
[26] L.F. Lindoy, H.C. Lip, J.H. Rea, R.J. Smith, K. Henrick, M. McPartlin, P.A. Tasker, Inorg. Chem. 19 (1980) 3360.
[27] H. Adams, N.A. Bailey, D.E. Fenton, I.G. Ford, S.J. Kitchen, M.G. Williams, P.A. Tasker, A.J. Leong, L.F. Lindoy, J. Chem. Soc., Dalton Trans. (1991) 1665.
[28] C.M. Hughes, M.C. Favas, B.W. Skelton, A.H. White, Aust. J. Chem. 38 (1985) 1521.
[29] C.A. Grapperhaus, T. Tuntulani, J.H. Reibenspies, M.Y. Darensbourg, Inorg. Chem. 37 (1998) 4052.
[30] A.A. Freer, G. McDermott, J.C. Melville, D.J. Robins, Acta Crystallogr., Sect. C 49 (1993) 2115.
[31] S. Htoon, M.F.C. Ladd, J. Cryst. Mol. Struct. 4 (1974) 357.
[32] R.J. Errington, Advanced Practical Inorganic and Metalorganic Chemistry, Blackie Academic & Professional, London, 1997.
[33] A.L. Wayda, M.Y. Darensbourg (Eds.), Experimental Organometallic Chemistry, American Chemical Society, Washington, DC, 1987.
[34] D.F. Shriver, M.A. Drezdzon, The Manipulation of Air-sensitive Compounds, 2nd ed., Wiley-Interscience, New York, 1986.
[35] N. Walker, D. Stuart, Acta Crystallogr., Sect. A 39 (1983) 158.
[36] G.M. Sheldrick, Siemens XRD, Madison, WI.

PERGAMON

www.elsevier.nl/locate/poly

Polyhedron 19 (2000) 1821–1827

POLYHEDRON

Synthesis, X-ray and spectroscopic characterisation of chromium(III) coordination compounds with benzimidazolic ligands

Agueda E. Ceniceros-Gómez [a], Norah Barba-Behrens [a], M. Elba Quiroz-Castro [a], Sylvain Bernès [b], Heinrich Nöth [c], Silvia E. Castillo-Blum [a,*]

[a] *Departimento de Química Inorgánica, Facultad de Química, UNAM, Ciudad Universitaria, 04510 Mexico D.F., Mexico*
[b] *USAI, Facultad de Química, UNAM, Ciudad Universitaria, 04510 Mexico D.F, Mexico*
[c] *Institute of Inorganic Chemistry, University of Munich, Bütenandtstraße 5-13, Haus D, D-81377 Munich, Germany*

Received 6 June 2000; accepted 7 June 2000

Abstract

The syntheses and characterisation of chromium(III) complexes with tris(2-benzimidazolylmethyl)amine (ntb), 2-guanidinobenzimidazole (2gb), 2,6-bis(2-benzimidazolyl)pyridine (bbimpy) and 2-(2-pyridyl)benzimidazole (2pb), of composition $[Cr(ntb)Cl_2]Cl\cdot 4.5H_2O$ (**1**), $[Cr(2gb)_3]Cl[ZnCl_4]\cdot CH_3OH$ (**2**), $[Cr(2gb)_3]Cl_3\cdot 4H_2O$ (**3**), $[Cr_2(2gb)_4(\mu\text{-}OH)_2](ClO_4)_4\cdot 5H_2O$ (**4**), $[Cr(bbimpy)Cl_3]$ (**5**) and $[Cr(2pb)_2Cl_2]Cl\cdot C_2H_5OH\cdot 0.5H_2O$ (**6**) are presented. The compounds are obtained from Cr(III) in alcoholic solution, or a Cr(II) aqueous acidic solution. The latter were carried out under air-free conditions. The reaction of 2gb with Cr(II) in aqueous solution yielded a dinuclear compound. The X-ray crystal structures of **1** and **4** are discussed. © 2000 Elsevier Science Ltd. All rights reserved.

Keywords: Chromium(III) complexes; Tris(2-benzimidazolylmethyl)amine; 2-Guanidinobenzimidazole; 2,6-Bis(2-benzimidazolyl)pyridine; 2-(2-Pyridyl)benzimidazole; Crystal structures

1. Introduction

Imidazole is a typical heterocyclic ligand with nitrogen as the donor atom. It is also a component of biologically important molecules [1]. Because of this, the coordination chemistry of related ligands has been the subject of numerous investigations [1]. Amongst them, the coordinating behaviour of chelating benzimidazolic ligands has been studied by several research groups, some of them with an interest in mimicking biological activities [2–6]. Benzimidazoles exhibit a wide variety of pharmacological activities like fungicides or anti-helminthics amongst others [7]. Studies about the coordination chemistry of benzimidazolic ligands have been carried out mainly on labile metal ions [1,8–10]. It is worth mentioning that there are only a limited number of reports on chromium(III) complexes containing imidazoles [11–14] or benzimidazoles [14,15]. The synthesis, reactivity and magnetic properties of dinuclear chromium(III) species containing OH^- bridges have been studied for the last two decades [16,17]. However, none of them contained imidazolic or benzimidazolic ligands.

We have been interested in the coordinating ability of benzimidazolic ligands towards transition metal ions [8,18,19]. Here we describe the synthesis and characterisation of substitution inert chromium(III) coordination compounds with four benzimidazolic ligands. The X-ray crystal structures of $[Cr(ntb)Cl_2]Cl\cdot 2H_2O\cdot C_2H_5OH$ and $[Cr_2(2gb)_4(\mu\text{-}OH)_2](ClO_4)_4\cdot 4.67H_2O$ are discussed.

* Corresponding author. Tel.: +52-5-622-3812; fax: +52-5-622-3724.
E-mail address: blum@servidor.unam.mx (S.E. Castillo-Blum).

0277-5387/00/$ - see front matter © 2000 Elsevier Science Ltd. All rights reserved.
PII: S0277-5387(00)00458-7

2. Experimental

2.1. Materials

Metallic chromium, zinc and mercury, anhydrous $CrCl_3$, $CrCl_2$, $CrCl_3{\cdot}nH_2O$, 2-guanidinobenzimidazole (2gb), 2,6-bis(2-benzimidazolyl)pyridine (bbimpy), 2-(2-pyridyl)benzimidazole (2pb) and tris(2-benzimidazolylmethyl)amine (ntb), methanol, ethanol and $HClO_4$ were used as analytical reagents and obtained from Aldrich. They were used without further purification.

2.2. Syntheses

2.2.1. $[Cr(ntb)Cl_2]Cl{\cdot}4.5H_2O$ (1)

Anhydrous $CrCl_3$ (0.158 g, 1.00 mmol) was placed in the filter thimble of a Soxhlet extractor together with Zn–Hg amalgam (1 cm^3), and a solution of ntb (0.407 g, 1.00 mmol) in anhydrous methanol (50 cm^3) was added to the reservoir flask. N_2 was bubbled through the ntb solution for 10 min before heating and chromium chloride was then extracted as a green solution that reacted with ntb. A green precipitate formed and was isolated by vacuum filtration (0.270 g, 42.3%). (Found: C, 44.65; H, 4.20; N, 14.90. $C_{24}H_{20}N_7CrCl_3{\cdot}4.5H_2O$ requires C, 44.56; H, 4.67; N, 15.16%). Green crystals of **1** (minimum formula $C_{26}H_{31}O_3N_7CrCl_3$) were obtained simply by mixing the solutions of $CrCl_3{\cdot}nH_2O$ and ntb in ethanol and leaving the solution to stand for few days.

2.2.2. $[Cr(2gb)_3]Cl[ZnCl_4]{\cdot}CH_3OH$ (2), $[Cr(2gb)_3]Cl_3{\cdot}4H_2O$ (3)

Anhydrous $CrCl_3$ (1.0 g, 6.3 mmol) and Zn powder (10 mg) were stirred together in anhydrous methanol (50 cm^3). A solution of 2gb (3.31 g, 18.9 mmol) in hot anhydrous methanol was added with stirring. The mixture was heated (40°C) with stirring for 3 h. A pink solid precipitated immediately **2**, which was filtered off. The red solution deposited small red crystals of **3** by slow evaporation. Compound **2**: (0.128 g, 2.4%). (Found: C, 35.20; H, 4.47; N, 25.38. $C_{25}H_{31}ON_{15}CrZnCl_5$ requires C, 35.23; H, 3.68; N, 24.65%). Compound **3**: (4.50 g, 95.2%). (Found: C, 38.13; H, 4.15; N, 27.16. $C_{24}H_{35}O_4N_{15}CrCl_3$ requires C, 38.13; H, 4.67; N, 27.79%).

2.2.3. $[Cr_2(2gb)_4(\mu\text{-}OH)_2](ClO_4)_4{\cdot}5H_2O$ (4)

A solution of 2gb (0.525 g, 3.00 mmol) in methanol (30 cm^3) was deoxygenated with N_2 in a vacuum line. Chromium metal (0.32 g, 6.00 mmol), or $CrCl_2$ (0.737 g, 6.00 mmol), was dissolved in 6 cm^3 of deoxygenated 2.0 M $HClO_4$. 1.0 cm^3 of this chromium(II) solution was injected into the 2gb solution. Air was allowed into the flask, and 2.0 g of $NaClO_4$ was added. X-ray quality purple crystals deposited from the solution, which were filtered off (0.635 g, 48.1%). (Found: C, 28.74; H, 3.41; N, 20.85. $C_{32}H_{48}O_{23}N_{20}Cr_2Cl_4$ requires C, 28.97; H, 3.65; N, 21.12%).

2.2.4. $[Cr(bbimpy)Cl_3]$ (5)

Anhydrous $CrCl_3$ (0.158 g, 1.00 mmol) was placed in the filter thimble of a Soxhlet extractor together with Zn–Hg amalgam (1 cm^3). A solution of bbimpy (0.622 g, 2.00 mmol) in anhydrous ethanol (60 cm^3) was placed into the reservoir flask. N_2 was bubbled through the ligand solution for 10 min before heating and chromium chloride was then extracted as a green solution that reacted with the bbimpy ligand. A green solid precipitated and was isolated by vacuum filtration (0.435 g, 92.6%). (Found: C, 48.77; H, 2.95; N, 14.82. $C_{19}H_{13}N_5CrCl_3$ requires C, 48.59; H, 2.80; N, 14.90%).

2.2.5. $[Cr(2pb)_2Cl_2]Cl{\cdot}C_2H_5OH{\cdot}0.5H_2O$ (6)

Anhydrous $CrCl_3$ (0.158 g, 1.0 mmol) was placed in the filter thimble of a Soxhlet extractor together with Zn–Hg amalgam (1 cm^3) and a solution of 2pb (0.585 g, 3.0 mmol) in anhydrous ethanol (60 cm^3) was added to the reservoir flask. N_2 was bubbled through the ligand solution for 10 min before heating and the chromium chloride was then extracted as a green solution that reacted with the 2pb ligand. A green precipitate formed and was isolated by vacuum filtration (0.294 g, 49.5%). (Found: C, 51.65; H, 4.02; N, 13.99. $C_{24}H_{18}N_6CrCl_3{\cdot}C_2H_5OH{\cdot}0.5H_2O$ requires C, 51.71; H, 4.17; N, 13.92%).

2.3. Physical measurements

An FT-IR spectrometer (Perkin–Elmer 1600) was used for obtaining IR spectra of solid samples in KBr pellets (4000–400 cm^{-1}). The UV–Vis spectra (diffuse reflectance) were recorded on a Cary-5E (Varian) spectrometer (250–2500 nm). Elemental analyses were carried out with a Fisons EA 1180 analyser. Magnetic susceptibility measurements of powdered samples were recorded on a Johnson–Matthey DG8 5HJ balance using the Gouy method. Magnetic susceptibilities were measured on powdered samples of **4** in the temperature range 17–280 K using a Vibrating Sample Magnetometer Model 4500 from EG & G PARC.

2.4. Crystallography

Pertinent crystal data for **1** and **4** are given in Table 1. The diffraction data for **4** were collected at 298 K on a Siemens P4 diffractometer in the 2θ range 3–50° ($\lambda = 0.71073$ Å) at variable scan speed in ω (4–60° min^{-1}). Data were corrected for absorption using 12 ψ-scans with χ close to 90° (min = 0.712, max = 0.758). Data for **1** were collected at 183 K with the crystal mounted on a glass fibre coated with perfluorpolyether

Table 1
Crystallographic data for compounds **1** and **4**

	1	**4**
Formula	$[Cr(C_{24}H_{21}N_7)Cl_2]Cl$ $(C_2H_5OH)(H_2O)_2$	$[Cr_2(C_8H_9N_5)_4(OH)_2]$ $(ClO_4)_4(H_2O)_{4.67}$
M	647.93	1320.70
Crystal system	monoclinic	triclinic
Space group	$P2_1/c$	$P\bar{1}$
a (Å)	10.3057(2)	12.156(2)
b (Å)	13.4632(3)	14.035(2)
c (Å)	21.5037(3)	16.733(3)
α (°)		90.04(1)
β (°)	103.103(1)	110.18(1)
γ (°)		106.96(1)
U (Å^3)	2905.91(9)	2546.7(6)
Z	4	2
D_{calc} (Mg m^{-3})	1.481	1.722
$F(000)$	1340	1353
μ(Mo Kα) (mm^{-1})	0.711	0.738
Crystal dimensions (mm)	$0.32\times0.25\times0.18$	$0.6\times0.4\times0.4$
Total reflections measured	16 066	10 303
Number of unique reflections	5802	8917
Number of observed reflections [$F_o>4\sigma(F_o)$]	3791	6646
Number of variables	362	739
Goodness of fit [a]	1.501	1.034
R_1 (observed data) [a]	6.62	5.91
wR_2 (all data) [a]	12.64 [b]	18.24 [c]

[a] $R_1=\Sigma\|F_o|-|F_c\|/\Sigma|F_o|$, $wR_2=\sqrt{\Sigma w(F_o^2-F_c^2)^2/\Sigma w(F_o^2)^2}$, $S=\sqrt{\Sigma w(F_o^2-F_c^2)^2/m-n}$.
[b] $w=[\sigma^2(F_o^2)+(0.0210P)^2+7.6749P]^{-1}$.
[c] $w=[\sigma^2(F_o^2)+(0.0959P)^2+4.42P]^{-1}$.

oil. 1200 frames were measured on a Siemens P4 diffractometer equipped with an area detector in the hemisphere scan mode ($\phi=0$–360°, 10 s exposure per frame), which corresponds to the 2θ range 3–58° ($\lambda=$ 0.71073 Å). Absorption correction was applied using SADABS [20] (min = 0.804, max = 0.883). Both structures were solved and refined using SHELXTL 5.03 [21] and SHELX-97-2 [22], without constraints or restraints for non-H atoms. Most of the H atoms were placed on idealised positions and refined using a riding model with a fixed isotropic U factor. H atoms for the OH groups in **4** and for the water molecules in **1** were found on difference maps and refined as remaining H. In the case of **4**, H atoms were omitted for the water molecules.

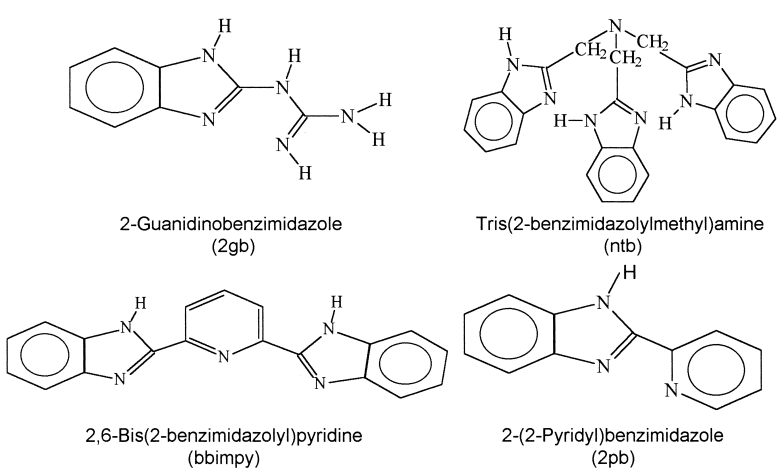


Fig. 1. Structures of the benzimidazolic ligands.

Table 2
Spectroscopic UV–Vis, IR and magnetic data for **1**–**6**

Compound	Uv–Vis			IR				μ_{eff}
	ν_1 (cm^{-1})	ν_2	ν_3	ν(N–H) (cm^{-1})	ν(C=C)+ν(C=N)	δ(N–H)	δ(C–H)	M.B.
ntb				3384	1622, 1536	1438	742	
1 $[Cr(ntb)Cl_2]Cl{\cdot}4.5H_2O$	16 650	23 050	28 580	3384	1622, 1594	1450	744	3.9
2gb				3140	1648 [a], 1598 [a], 1540	1450	740	
2 $[Cr(2gb)_3]Cl(ZnCl_4){\cdot}CH_3OH$	20 050	25 050	28 650	3190	1666 [a], 1634 [a], 1556	1486	744	3.9
3 $[Cr(2gb)_3]Cl_3{\cdot}4H_2O$	19 723	25 320	28 010	3190	1668 [a], 1634 [a], 1556	1486	744	3.9
4 $[Cr_2(2gb)_4(\mu\text{-}OH)_2](ClO_4)_4{\cdot}5H_2O$	17 360	24 570	36 100	3194	1667 [a], 1560	1466	749	4.96 [b]
bbimpy				3055	1599, 1588, 1571	1459	741	
5 $[Cr(bbimpy)Cl_3]$	16 660	20 000	25 000	3068	1607, 1590, 1575	1467	753	3.8
2pb				3056	1593, 1567,	1442, 1400	743	
6 $[Cr(2pb)_2Cl_2]Cl{\cdot}0.5H_2O{\cdot}C_2H_5OH$	17 240	20 490	25 970	3072	1608, 1593	1457, 1445	752	3.9

[a] There is also contribution from $\delta(NH_2)$ and ν(C=N) from the guanidine group.
[b] Calculated for the dinuclear compound.

3. Results and discussion

3.1. Synthesis and characterisation of the coordination compounds

Six coordination compounds with the benzimidazolic ligands: ntb, 2gb, bbimpy and 2pb Fig. 1, were synthesised and characterised by spectroscopic and analytical methods.

Two different synthetic routes were used for preparing the coordination compounds. In the first technique, chromium(III) is extracted, in anhydrous methanol or ethanol, from $CrCl_3$ by means of a Soxhlet and then reacted with the ligand, as previously reported for chelating ligands [23]. For the second method, a chromium(II) acidic aqueous solution is reacted with the ligand under oxygen-free conditions, followed by air oxidation [24]. The solution of chromium(II) is made from $CrCl_2$ or chromium metal in $HClO_4$ under a nitrogen atmosphere.

Compounds **1**, **5** and **6** can be prepared by either of these techniques, i.e. from Cr(II) or $CrCl_3$; however, yields are better when using the Soxhlet method.

The reactions with the 2gb ligand yielded two different types of chromium(III) compound, i.e. two mononuclear compounds **2** and **3**, and a dinuclear species **4**. The dinuclear compound is bridged by two hydroxo moieties and was obtained when a chromium(II) acid aqueous solution was reacted with a methanolic solution of 2gb. The coordination sphere of each chromium(III) contains two chelating 2gb molecules. It is known that the synthesis of the chromium(III) dinuclear species containing hydroxo bridges requires the addition of a base; however, in some instances this is not necessary, depending on the basicity of the ligand and the molar ratio of ligand to metal ion [16,17]. We here suggest that the basicity of 2gb is responsible for the formation of the hydroxo bridges. The same method of synthesis gave mononuclear species when ntb, bbimpy or 2pb were reacted with an acidic aqueous Cr(II) solution, indicating that they are less basic than 2gb.

Table 2 shows some of the main IR vibrational frequencies, UV–Vis absorption bands and magnetic moments.

3.2. Spectroscopy

The main vibrational frequencies observed for the benzimidazolic ring are those due to the ν(N–H), ν(C=C)+ν(C=N) vibrations, δ(N–H) and δ(C–H) benzimidazolic ring out of plane [8,10,25,26]. All the IR spectra of the coordination compounds show these vibrations, however in all cases the bands are shifted towards higher energy as compared with the position in the free ligand, Table 2. These results are indicative of ligand coordination through the imidazolic nitrogen. For the 2gb complexes the band due to ν(NH···N) from the guanidine group in the ligand [8] is shifted from 3444 to 3300 cm^{-1} for **2** and **3**, and to 3341 cm^{-1} for **4**.

The strong band at 1317 (bbimpy) and 1314 cm^{-1} (2pb) in the spectra of the ligands is shifted towards higher energy and splitted upon chelation, indicating coordination through the pyridinic nitrogen [27,28]. The split band appears at 1321 and 1310 cm^{-1} for **5** and at 1323 and 1302 cm^{-1} for **6**. In the low-frequency infrared spectra of **1**, **5** and **6** the vibrational bands at 360, 343 and 361 cm^{-1}, respectively, were assigned as ν(Cr–Cl) [29], corroborating the presence of coordinated chlorides.

For Cr(III) hexacoordinated complexes there are three spin-allowed transitions in the electronic spectrum, ν_1 $^4T_{2g} \leftarrow {}^4A_{2g}$, ν_2 $^4T_{1g}(F) \leftarrow {}^4A_{2g}$ and ν_3 $^4T_{1g}(P) \leftarrow {}^4A_{2g}$

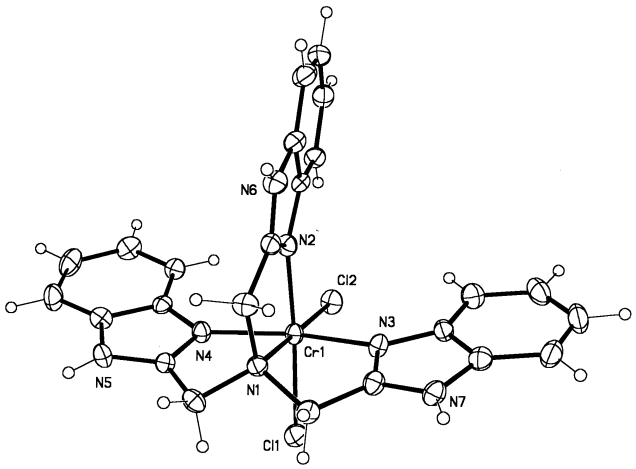


Fig. 2. Geometry for the cation $[CrCl_2ntb]^+$ in complex **1**. Thermal ellipsoids are at 50% probability level.

Table 3
Selected bond lengths (Å) and angles (°) with s.u. in parentheses for compound **1**

Cr1–N2	2.047(3)	Cr1–N4	2.050(3)
Cr1–N3	2.062(3)	Cr1–N1	2.154(3)
Cr1–Cl2	2.2909(13)	Cr1–Cl1	2.3180(13)
N2–Cr1–N4	88.26(13)	N2–Cr1–N3	87.82(13)
N4–Cr1–N3	157.18(14)	N2–Cr1–N1	82.95(13)
N4–Cr1–N1	78.30(13)	N3–Cr1–N1	78.91(13)
N2–Cr1–Cl2	95.75(10)	N4–Cr1–Cl2	103.23(10)
N3–Cr1–Cl2	99.52(10)	N1–Cr1–Cl2	177.98(10)
N2–Cr1–Cl1	172.76(11)	N4–Cr1–Cl1	89.30(10)
N3–Cr1–Cl1	91.80(10)	N1–Cr1–Cl1	89.88(10)
Cl2–Cr1–Cl1	91.45(5)		

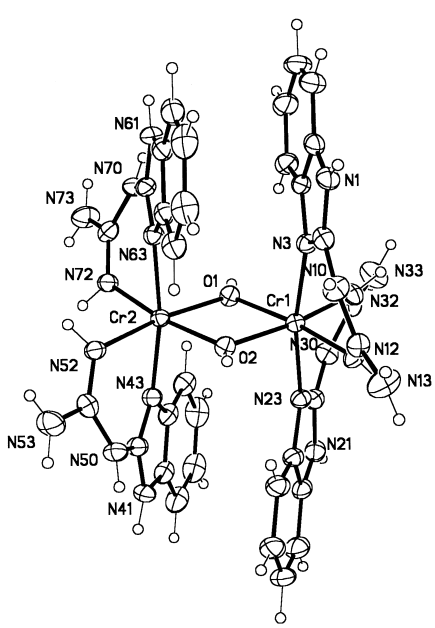


Fig. 3. Geometry for the cation $[Cr_2(2gb)_4(\mu\text{-}OH)_2]^{4+}$ in complex **4**. Thermal ellipsoids are at 30% probability level.

[30]. The diffuse reflectance spectra of compounds **1**–**6**, show three absorption bands, the first one in the region from 16 600 to 20 050 cm^{-1}, the second band from 20 000 to 25 400 cm^{-1} and the third from 25 000 to 36 100 cm^{-1}, where ν_1 correspond to 10 Dq for each complex (Table 2). The third band for compounds **1**, **3**, **4**, **5** and **6** appears as a shoulder obscured by CT bands. The electronic spectra of the compounds reported here are in reasonable agreement with those in the literature [30,31].

The magnetic moments at room temperature for compounds **1**, **2**, **3**, **5** and **6** correspond to the expected values for mononuclear chromium(III) compounds. Compound **4** has a magnetic moment at room temperature of 4.96 MB, smaller than the expected value (5.43 MB spin only) for a Cr(III) dinuclear species [32]. Studies of the variable temperature magnetic susceptibility of **4** were made at 3500 Oe and in the temperature range 17–280.15 K. Least-squares analysis was used to fit the data to a susceptibility expression based on the isotropic spin Hamiltonian [33]:

$$H = -2J(S_1 \cdot S_2)$$

The best fit of the susceptibility data reveals that the dinuclear compound has weak antiferromagnetic coupling ($J = -2.05$ cm^{-1}). This value is within the range of those for other dinuclear di-μ-hydroxo-chromium(III) complexes [17].

3.3. Description of the structures

3.3.1. Complex *1*

The cation $[CrCl_2ntb]^+$ is depicted in Fig. 2. Ntb acts as a tetradentate ligand coordinating through the amine N atom and the three benzimidazole N atoms to the metal ion, as reported for a number of ntb complexes [2]. Two Cl atoms in a *cis* configuration complete the coordination sphere, yielding an hexacoordinated arrangement for the metal. It should be mentioned that only two related ntb-containing complexes with an hexacoordinated metal environment have been reported up to now, with Fe(II) [34] and Ni(II) [9]. On the other hand, **1** is the first reported X-ray characterised Cr(III)–ntb complex.

As expected, the tertiary N atom presents a bond length about 0.10 Å longer than those for the benzimidazole N atoms (see Table 3). The tripodal ntb ligand is forced to adopt a planar geometry in order to retain the octahedral geometry on the metal–dihedral angle between the aromatic moieties containing the rings [N3, N7] and [N4, N5] is 10.1°, while angles of these planes with the third moiety [N2, N6] are 89.6 and 79.6°. This uncommon spatial arrangement for ntb reflects the great versatility of this tripodal ligand in order to take in the preferred geometry of the metal ion. On the other

Table 4
Selected bond lengths (Å) and angles (°) for compound **4**

Cr1–O2	1.960(3)	Cr1–O1	1.961(3)
Cr1–N12	2.021(3)	Cr1–N32	2.023(4)
Cr1–N3	2.045(3)	Cr1–N23	2.052(3)
Cr2–O1	1.953(3)	Cr2–O2	1.955(3)
Cr2–N72	2.019(3)	Cr2–N52	2.020(4)
Cr2–N63	2.056(3)	Cr2–N43	2.060(3)
O2–Cr1–O1	75.83(11)	O2–Cr1–N12	92.50(14)
O1–Cr1–N12	168.30(14)	O2–Cr1–N32	168.65(13)
O1–Cr1–N32	92.86(13)	N12–Cr1–N32	98.82(15)
O2–Cr1–N3	93.25(13)	O1–Cr1–N3	95.54(13)
N12–Cr1–N3	84.10(14)	N32–Cr1–N3	88.72(14)
O2–Cr1–N23	95.31(13)	O1–Cr1–N23	92.78(13)
N12–Cr1–N23	89.10(14)	N32–Cr1–N23	84.14(14)
N3–Cr1–N23	169.29(14)		
O1–Cr2–O2	76.12(11)	O1–Cr2–N72	93.49(14)
O2–Cr2–N72	169.49(14)	O1–Cr2–N52	169.32(14)
O2–Cr2–N52	93.30(14)	N72–Cr2–N52	97.13(15)
O1–Cr2–N63	92.25(13)	O2–Cr2–N63	94.87(13)
N72–Cr2–N63	83.81(14)	N52–Cr2–N63	90.01(14)
O1–Cr2–N43	95.06(13)	O2–Cr2–N43	92.23(13)
N72–Cr2–N43	90.25(14)	N52–Cr2–N43	83.82(14)
N63–Cr2–N43	170.85(14)		
Cr2–O1–Cr1	104.03(12)	Cr2–O2–Cr1	104.01(12)

hand, the Cr ion lies in the plane formed by N1, N3, N4 and Cl2 (calculated maximal deviation: 0.025 Å). As a result of these features, the deviations from an ideal octahedral geometry around the Cr ion are the following: *trans* angles range from 157.18(14) to 177.98(10)° and *cis* angles from 78.30(13) to 99.52(10)°.

Ethanol and water molecules included in the cell form a complex tri-dimensional network of hydrogen bonds using benzimidazolic N atoms and chlorine atoms as acceptors (H···A separations in the range 1.854–2.468 Å), which probably greatly stabilises the crystal.

3.3.2. Complex *4*

Complex **4** is the first X-ray characterised Cr(III) complex including 2gb as ligand. The dinuclear cation $[Cr_2(2gb)_4(\mu\text{-}OH)_2]^{4+}$ is depicted in Fig. 3. It should be mentioned that the charge of the cation is in line with the four ClO_4^- anions present in the asymmetric unit and with the fact that the H atoms of the OH groups were found on difference Fourier maps. The $(\mu\text{-}OH)_2$ bridge is symmetric, with Cr–O bond lengths in the range 1.953(3)–1.961(3) Å. The metal–metal separation, 3.085 Å, is similar to that reported for other complexes containing the $Cr_2(\mu\text{-}OH)_2$ fragment, as well as the Cr–O–Cr angles, 104.02° [35–38] (Table 4). Each Cr(III) ion coordinates two 2gb ligands with Cr–N bond lengths in the short range 2.019(3)–2.060(3) Å, as expected. For each ligand, the N atom bonded to the benzimidazolic moiety lies in the plane of the imidazole: deviations for N10, N30, N50 and N70 from the mean planes formed by the benzimidazolic groups are in the range 0.040–0.048 Å. This point confirms that the coordinated 2gb ligand in **4** is the same as the free ligand depicted in Fig. 1. However, deviations from an ideal octahedral geometry are smaller than in the case of **1**, because 2gb acts as a bidentate ligand while ntb is tetradentate: *cis* and *trans* angles for Cr1 are from 75.83(11) to 95.54(13)° and from 168.30(14) to 169.29(14)°, respectively, and ranges are similar for Cr2. This distortion is reflected in the dihedral angles between the benzimidazolic rings for two 2gb coordinated on the same metal centre: 29.0° between planes [N1, N3] and [N21, N23] and 29.6° between planes [N41, N43] and [N61, N63]. In spite of the parallel arrangement of the benzimidazolic rings in the complex, no intramolecular interactions are observed: the shortest calculated separation between the centroids of the benzene rings is 4.13 Å.

As in the previous case, numerous hydrogen bonds which involve five water molecules, μ-OH groups, NH of imidazole, NH and NH_2 of 2gb stabilise, the crystals (H···A separations from 1.971 to 2.624 Å).

4. Supplementary data

Supplementary data are available from the CCDC on request, quoting the deposition numbers CCDC 140724 (**1**) and 140725 (**4**). The information can be obtained free of charge from The Director, Cambridge Crystallographic Data Centre, 12 Union Road, Cambridge, CB2 1EZ, UK (Fax: +44-1223-336033; e-mail: deposit@ccdc.cam.ac.uk or www: http://www.ccdc.cam.ac.uk).

Acknowledgements

We acknowledge grant DGAPA-UNAM IN 222096 for financial support. S.B. is grateful to Dr Cecilia Rodríguez de Barbarín (Monterrey, México) for diffractometer time and UNAM for financial support. A.E.C.-G. thanks CONACyT and DGEP for a scholarship. We thank M. Franco-Gutiérrez, R.P. Fierro and Antonio Morales for technical support.

References

[1] J. Reedijk, Comprehensive Coordination Chemistry, vol. 2, Pergamon, Oxford, 1987 (Chapter 13.2).
[2] R. Rajan, R. Rajaram, B.U. Nair, T. Ramasami, S.K. Mandal, J. Chem. Soc., Dalton Trans. (1996) 2019.
[3] J. García-Lozano, J. Server-Carrió, E. Coret, J.-V. Folgado, E. Escrivà, R. Ballesteros, Inorg. Chim. Acta 245 (1996) 75.
[4] T.J. Cardwell, A.J. Edwards, J.M. Hartshorn, R.J. Holmes, W.D. McFadyen, Aust. J. Chem. 50 (1997) 1009.
[5] R.W. Gable, R.M. Hartshorn, W.D. McFadyen, L. Nunno, Aust. J. Chem. 49 (1996) 625.
[6] C. Piguet, B. Bocquet, E. Müller, A.F. Williams, Helv. Chim. Acta 72 (1989) 323.

[7] T.M. Aminabhavi, N.S. Biradar, S.B. Patil, D.E. Hoffman, Inorg. Chim. Acta 125 (1986) 125.
[8] N. Barba-Behrens, A. Vázquez-Olmos, S.E. Castillo-Blum, G. Höjer, S. Meza- Höjer, R.M. Hernández, M.J. Rosales-Hoz, R. Vicente, A. Escuer, Transition Met. Chem. 21 (1996) 31.
[9] M.E. Quiroz-Castro, H. Nöth, S. Bernès, N. Barba-Behrens, Polyhedron 19 (2000) 1479.
[10] S. Wang, S. Yu, Q. Luo, Q. Wang, J. Shi, Q. Wu, Transition Met. Chem. 19 (1994) 205.
[11] J. Chatlas, S. Kaizaki, E. Kita, P. Kita, N. Sakagami, R. van Eldik, J. Chem. Soc., Dalton Trans. (1999) 91, and references therein.
[12] J.A. Winter, D. Caruso, R.E. Shepherd, Inorg. Chem. 27 (1988) 1086.
[13] J.R. Bocarsly, M.Y. Chiang, L. Bryant, J.K. Barton, Inorg. Chem. 29 (1990) 4898.
[14] H. Bhushan, L.K. Mishra, Ind. J. Chem. 21A (1982) 1135.
[15] A. Mishra, J.P. Singh, J. Ind. Chem. Soc. 56 (1979) 771.
[16] S.J. Brudenell, S.J. Crimp, J.K.E. Higgs, B. Moubaraki, K.S. Murray, L. Spiccia, Inorg. Chim. Acta 247 (1996) 35.
[17] L. Spiccia, G.D. Fallon, A. Markiewicz, K.S. Murray, H. Riesen, Inorg. Chem. 31 (1992) 1066, and references therein.
[18] A.E. Ceniceros-Gómez, N. Barba-Behrens, S. Bernès, H. Nöth, S.E. Castillo-Blum, Inorg. Chim. Acta 304 (2000) 230.
[19] A.E. Ceniceros-Gómez, A. Ramos-Organillo, J. Hernández-Díaz, J. Nieto-Martínez, R. Contreras, S.E. Castillo-Blum, Heteroatom. Chem. (2000), in press.
[20] SADABS, Siemens Area Detector Absorption Corrections, Siemens Analytical X-ray Instruments Inc., Madison, WI, USA.
[21] G.M. Sheldrick, SHELXTL-plus, release 5.03, Siemens Analytical X-ray Instruments Inc., Madison, WI, USA, 1995.
[22] G.M. Sheldrick, SHELX-97 Users Manual, University of Göttingen, Germany, 1997.
[23] V. Ugalde-Saldivar, M.A. Luna-Canut, M.E. Sosa-Torres, M.J. Rosales-Hoz, R.A. Toscano, M.L. Tobe. J. Chem. Soc., Dalton Trans. (1990) 3629.
[24] C.S. Lee, E.M. Gorton, H.M. Neumann, H.R. Hunt, Inorg. Chem. 5 (1966) 1397.
[25] L.K. Thompson, B.S. Ramaswamy, E.A. Seymour, Can. J. Chem. 55 (1977) 878.
[26] T.J. Lane, I. Nakagawa, J.L. Walter, J. Kandathil, Inorg. Chem. 1 (1962) 267.
[27] J.R. Sams, T.B. Tsin, J. Chem. Soc., Dalton Trans. (1976) 488.
[28] T.A. Kabanos, A.D. Keramidas, D. Mentzafos, U. Russo, A. Terzis, J.M. Tsangaris. J. Chem. Soc., Dalton Trans. (1992) 2729.
[29] J.R. Ferraro, Low-Frequency Vibrations of Inorganic and Coordination Compounds, Plenum, New York, 1971, pp. 111–183.
[30] A.B.P. Lever, Inorganic Electronic Spectroscopy, 2nd ed., Elsevier, Amsterdam, 1984.
[31] D.J. Hodgson, M.H. Zietlow, E. Pedersen, H. Toflund, Inorg. Chim. Acta 149 (1988) 111.
[32] C.J. O'Connor, Prog. Inorg. Chem. 29 (1982) 203.
[33] T. Fujihara, A. Fuyuhiro, S. Kaizaki. J. Chem. Soc., Dalton Trans. (1995) 1813.
[34] S. Wang, Q. Luo, X. Wang, L. Wang, K. Yu. J. Chem. Soc., Dalton Trans. (1995) 2045.
[35] H.R. Fischer, D.J. Hodgson, K. Michelsen, E. Pedersen, Inorg. Chim. Acta 88 (1984) 143.
[36] M.A. Heinrichs, D.J. Hodgson, K. Michelsen, E. Pedersen, Inorg. Chem. 23 (1984) 3174.
[37] M. Ardon, A. Bino, K. Michelsen, J. Am. Chem. Soc. 109 (1987) 1986.
[38] B.G. Gafford, R.A. Holwerda, Inorg. Chem. 28 (1989) 60.

PERGAMON

www.elsevier.nl/locate/poly

Polyhedron 19 (2000) 1829–1835

POLYHEDRON

Studies of dirhodium(II) tetrakis(trifluoroacetate). Part 8. One-dimensional polymers of $Rh_2(O_2CCF_3)_4$ with aromatic ligands: benzene, *p*-xylene and naphthalene

F. Albert Cotton *, Evgeny V. Dikarev, Marina A. Petrukhina, Salah-Eddine Stiriba

Laboratory for Molecular Structure and Bonding, Department of Chemistry, PO Box 30012, Texas A&M University, College Station, TX 77842-3012, USA

Received 30 May 2000; accepted 7 June 2000

Abstract

The interaction of benzene, *p*-xylene, and naphthalene with a strong two-ended Lewis acid, $Rh_2(O_2CCF_3)_4$, led to one-dimensional linear polymers of 1:1 composition, $[Rh_2(O_2CCF_3)_4 \cdot L]_\infty$, where $L = C_6H_6$ (**1**), p-$(CH_3)_2C_6H_4$ (**2**), and $C_{10}H_8$ (**3**). Compounds **1**–**3** have been characterized by elemental analysis and IR spectroscopy and their structures have been determined by X-ray diffraction. In the crystal structures of the compounds the alternating arrangement of the dirhodium(II) tetrakis(trifluoroacetate) units with the aromatic ligands coordinated to their axial positions forms infinite chains extended along one direction of the unit cell. The rare bridging off-centered, η^2:η^2 coordination of arene groups by the Rh(II) centers was found to be preferred in all three cases with the two closest Rh–C_{arene} distances averaged to 2.662(6) Å in the benzene complex (**1**), to 2.684(7) Å in the *p*-xylene analogue (**2**), and to 2.588(9) Å in the naphthalene product (**3**). © 2000 Elsevier Science Ltd. All rights reserved.

Keywords: Dirhodium(II) compounds; Trifluoroacetate; One-dimensional polymers; Arene coordination; π-Complexes; Crystal structures

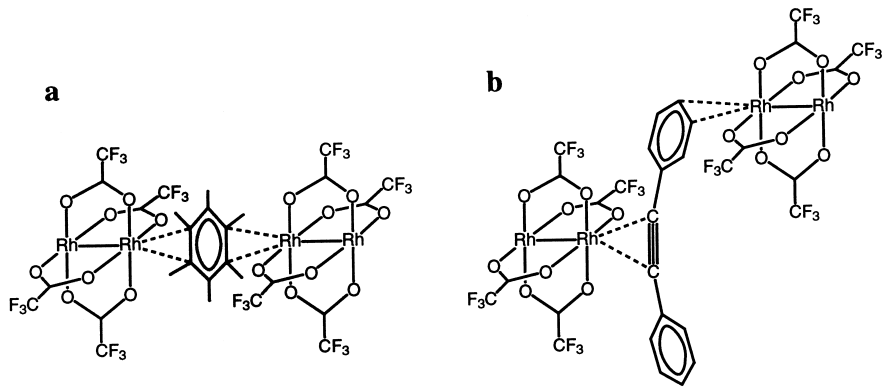
1. Introduction

Dirhodium(II) tetrakis(trifluoroacetate) exhibits an extensive axial coordination chemistry with a variety of strong N, O, P-containing bases [1]. Our research interest has been recently focused on studies of weak axial interactions by the powerful two-ended Lewis acid, $Rh_2(O_2CCF_3)_4$ [2]. We introduced a solid state deposition technique ('solventless' synthesis) [2] as an efficient way to study these interactions and to avoid competitive coordination of solvents in solutions. Our recent results have included the first structurally characterized π-complex with an aromatic ligand (hexamethylbenzene), $[Rh_2(O_2CCF_3)_4 \cdot (C_6Me_6)]_\infty$ [2a] and a compound $[Rh_2(O_2CCF_3)_4 \cdot (C_2Ph_2)]_\infty$ [2e] with both a triple carbon–carbon bond and an arene system from the bifunctional diphenylacetylene ligand involved in coordination (Scheme 1). A rare off-centered orientation of the aromatic ligands at the Rh(II) centers has been found in both dirhodium trifluoroacetate chain compounds, with the C_6Me_6 and the Ph_2C_2 ligands. We believe systematic research is needed in order to get more insight into complexation of arenes by the electron-deficient dirhodium(II) carboxylate molecules, as these interactions have an important role in some catalytic and aromatic substitution reactions [3]. Therefore, we have extended the number of arene ligands to benzene, *p*-xylene and naphthalene and report here on their interactions with $Rh_2(O_2CCF_3)_4$. The first two ligands are commonly used as non-coordinating solvents for studying weak interactions in the Lewis acid–Lewis base systems. Naphthalene is the first conjugated arene molecule used for such reactions with the dirhodium moiety. With all three ligands the products are analogous one-dimensional linear polymers of 1:1 composition, namely $[Rh_2(O_2CCF_3)_4 \cdot C_6H_6]_\infty$ (**1**), $[Rh_2(O_2CCF_3)_4 \cdot (p\text{-}(CH_3)_2C_6H_4)]_\infty$ (**2**) and $[Rh_2(O_2CCF_3)_4 \cdot C_{10}H_8]_\infty$ (**3**). They have been crystallographically characterized and their structures have been compared.

* Corresponding author. Tel.: +1-979-845-4432; fax: +1-979-845-9351.

E-mail address: cotton@tamu.edu (F.A. Cotton).

0277-5387/00/$ - see front matter © 2000 Elsevier Science Ltd. All rights reserved.
PII: S0277-5387(00)00472-1



Scheme 1.

2. Experimental

2.1. General

All manipulations were carried out under an atmosphere of dry, oxygen-free dinitrogen by employing Schlenk techniques. Solvents were dried and deoxygenated by refluxing over appropriate agents before use. The anhydrous form of $Rh_2(O_2CCF_3)_4$ was prepared using a literature procedure [4]. Naphthalene ($C_{10}H_8$) was purchased from Aldrich and sublimed before use. The IR spectra were recorded on a Perkin–Elmer 16PC FTIR spectrophotometer using KBr pellets. Elemental analysis was done by Canadian Microanalytical Services, Ltd.

2.2. Synthesis of $Rh_2(O_2CCF_3)_4 \cdot C_6H_6$ (1)

A few drops of distilled benzene were added to the solid unligated $Rh_2(O_2CCF_3)_4$ (0.10 g, 0.15 mmol) in a Pyrex tube. The excess of benzene was removed under vacuum. The tube was then sealed and left in a furnace at 90°C for 24 h. Green crystals of **1** were deposited on the walls after slow cooling of the tube over 48 h to r.t. Yield: 0.030 g, 27%.

2.3. Synthesis of $Rh_2(O_2CCF_3)_4 \cdot (p\text{-}(CH_3)_2C_6H_4)$ (2)

2.3.1. $Rh_2(O_2CCF_3)_4$ in benzene containing p-xylene

The solution containing $Rh_2(O_2CCF_3)_4$ (0.10 g, 0.15 mmol) in 5 ml of benzene containing *p*-xylene (the ratio of $p\text{-}(CH_3)_2C_6H_4$ to C_6H_6 was found by NMR to be about 1:100) was layered with 10 ml of hexanes at r.t. This resulted in deposition of a few crystals of **2** in a week.

2.3.2. $Rh_2(O_2CCF_3)_4$ in p-xylene

The vial containing solution of $Rh_2(O_2CCF_3)_4$ (0.10 g, 0.15 mmol) in 5 ml of *p*-xylene was placed in the Ar glovebox. After keeping the solution for one week at 0°C light-green plates of **2** had appeared. Yield: 0.089 g, 77%.

2.3.3. p-Xylene added to unligated $Rh_2(O_2CCF_3)_4$

A few drops of anhydrous *p*-xylene were added to the solid unligated $Rh_2(O_2CCF_3)_4$ (0.10 g, 0.15 mmol) in a Pyrex tube. The excess of solvent was removed under vacuum. The tube was then sealed and left in a furnace at 95°C for 2 days. Green crystals of **2** were deposited on the walls after slow cooling of the tube over 24 h to r.t. Yield: 0.046 g, 40%.

Anal. Calc. for $C_{16}H_{10}F_{12}O_8Rh_2$: C, 25.25; H, 1.32. Found: C, 24.98; H, 1.32%. IR (KBr, cm^{-1}): 1665.6 (s), 1191.4 (s), 868.4 (s), 840.9 (m), 794.9 (m), 739.4 (s), 540.8 (s).

2.4. Synthesis of $Rh_2(O_2CCF_3)_4 \cdot C_{10}H_8$ (3)

Unligated $Rh_2(O_2CCF_3)_4$ (0.066 g, 0.10 mmol) was mixed with freshly sublimed naphthalene (0.012 g, 0.10 mmol) under an inert atmosphere. The mixture was sealed in an evacuated Pyrex tube and the tube was placed in a furnace at 90°C. Green block-shaped crystals of **3** were deposited over two days in the 'cold' zone of the tube, where the temperature was about 5°C lower. Yield: 0.027 g, 35%. *Anal.* Calcd. for $C_{18}H_8F_{12}O_8Rh_2$: C, 27.50; H, 1.03. Found: C, 27.47; H, 1.03%. IR (KBr, cm^{-1}): 1683.9 (m), 1669.6 (s), 1653.0 (m), 1558.3 (s), 1540.0 (m), 1506.4 (m), 1456.7 (m), 1192.2 (s), 1167.5 (s), 861.0 (m), 784.8 (m), 739.8 (s), 525.9 (m), 457.8 (m), 418.0 (m).

2.5. X-ray structure determinations

Single crystals of compounds **1**–**3** were obtained as described above. X-ray diffraction experiments were carried out on a Nonius FAST diffractometer with an area detector using Mo Kα radiation. Details concern-

ing data collection have been fully described elsewhere [4]. Each crystal was mounted on the tip of a quartz fibre with silicone grease, and the set-up was quickly placed in the cold N_2 stream (-60°C) of a low-temperature controller. Fifty reflections were used in the cell indexing and about 200 reflections in the cell refinement.

All calculations were done on a DEC Alpha running VMS. The coordinates of rhodium and oxygen atoms for the structures were found in direct method *E* maps using the structure solution program SHELXTL [5]. The positions of the remaining atoms were located after an alternating series of least-squares cycles and difference Fourier maps using the SHELXL-93 package [6]. The fluorine atoms of all CF_3 groups were found to be disordered over two or three different rotational orientations. Anisotropic displacement parameters were assigned to all non-hydrogen atoms, except the disordered fluorine atoms. Hydrogen atoms of aromatic ligands were included in the structure factor calculations at idealized positions. Relevant crystallographic data for compounds **1**–**3** are summarized in Table 1.

3. Results and discussion

3.1. Synthesis

Our experimental procedure included both the solid state deposition approach (**1**–**3**) and solution synthesis (**2**). Preparations of **1** and **2** are good examples of using a solid deposition technique for studying interactions of $Rh_2(O_2CCF_3)_4$ with liquid ligands, benzene and *p*-xylene in this case. The key factor in this synthesis is the use of extremely small amounts of suitable solvent, almost close to the equimolar ratio of the arene to the dirhodium molecules. This solid state approach was recently shown to be an effective route for obtaining unusual structures and compositions unattainable in solutions for the systems containing solvents, for example, $Rh_2(O_2CCF_3)_4$–THF [2b] and $Rh_2(O_2CCF_3)_4$–DMSO [2d]. The fact that dirhodium trifluoroacetate was forming an adduct with benzene became obvious a few years ago [4], but at that time suitable crystals had not been obtained from solution. The solid state approach (Section 2.2) applied here for benzene produced crystals of $Rh_2(O_2CCF_3)_4{\cdot}C_6H_6$ (**1**) in moderate yield and of quality suitable for X-ray diffraction study.

Table 1
Crystal data and details on data collection and refinement for $Rh_2(O_2CCF_3)_4{\cdot}C_6H_6$ (**1**), $Rh_2(O_2CCF_3)_4{\cdot}(p\text{-}(CH_3)_2C_6H_4)$ (**2**) and $Rh_2(O_2CCF_3)_4{\cdot}C_{10}H_8$ (**3**)

	1	**2**	**3**
Formula	$C_{14}H_6F_{12}O_8Rh_2$	$C_{16}H_{10}F_{12}O_8Rh_2$	$C_{18}H_8F_{12}O_8Rh_2$
Crystal system	monoclinic	monoclinic	triclinic
Space group	$P2_1/n$ (No. 14)	$P2_1/n$ (No. 14)	$P\bar{1}$ (No. 2)
a (Å)	8.2818(5)	8.3121(9)	8.573(2)
b (Å)	15.624(2)	15.896(6)	9.069(9)
c (Å)	8.574(2)	8.6884(9)	9.332(6)
α (°)			69.71(2)
β (°)	103.81(1)	91.59(1)	63.50(2)
γ (°)			77.62(3)
V (Å^3)	1077.4(3)	1147.5(5)	607.5(7)
Z	2	2	1
Crystal size (mm)	$0.25\times0.15\times0.05$	$0.23\times0.20\times0.03$	$0.25\times0.12\times0.10$
Radiation Mo Kα (λ, Å)	(0.71073)	(0.71073)	(0.71073)
Temperature (°C)	-60	-60	-60
Data collection range, 2θ (°)	5.22–45.00	5.12–45.48	4.80–45.10
Reflections collected/unique	4830/1382 ($R_{int}=0.0515$)	4750/1512 ($R_{int}=0.0391$)	3303/1524 ($R_{int}=0.0672$)
Data/observ/restraints/params	1382/1272/30/157	1512/1410/54/191	1524/1409/12/175
R_1 [a], wR_2 [b] [$I\geq2\sigma(I)$]	0.0381, 0.0891	0.0403, 0.0957	0.0546, 0.1382
R_1 [a], wR_2 [b] (all data)	0.0420, 0.0933	0.0436, 0.1004	0.0603, 0.1517
Goodnes-of-fit [c]	1.116	1.119	1.107
Largest difference peak and hole (e Å^{-3})	1.004 and -0.574	0.735 and -0.589	1.201 and -0.813

[a] $R_1=\Sigma(|F_o|-|F_c|)/\Sigma|F_o|$.
[b] $wR_2=[\Sigma[w(F_o^2-F_c^2)^2]/\Sigma[w(F_o^2)^2]]^{1/2}$.
[c] Goodness-of-fit $=[\Sigma[w(F_o^2-F_c^2)^2]/(N_{observns}-N_{params})]^{1/2}$, based on all data.

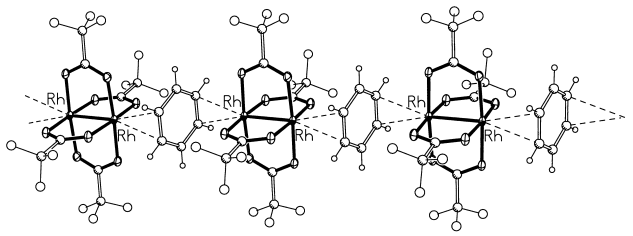


Fig. 1. Fragment showing the alternating arrangement of $Rh_2(O_2CCF_3)_4$ and C_6H_6 in the chain structure of **1**. Rhodium and oxygen atoms are represented by thermal ellipsoids at the 40% probability level. Carbon, fluorine and hydrogen atoms are shown as spheres of arbitrary radii. Axial contacts to Rh atoms are drawn by dashed lines. Only rhodium atoms are labeled for clarity.

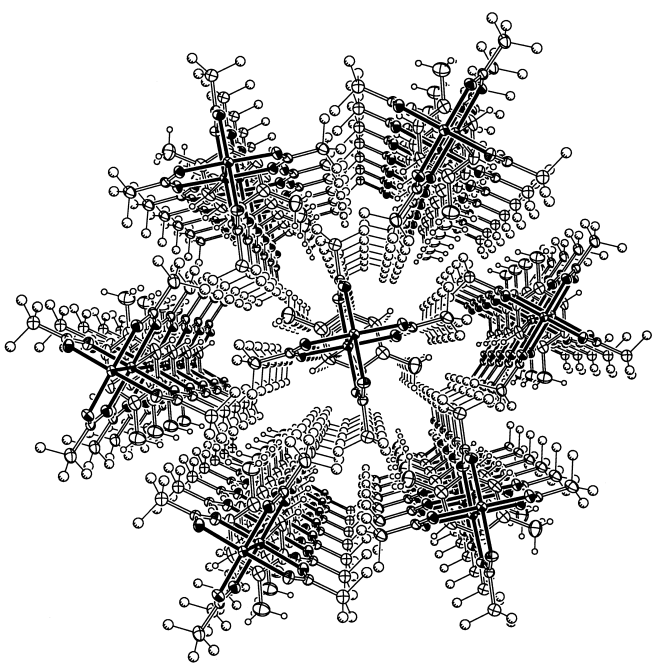


Fig. 2. Crystal packing of 1D chains of **2** viewed along the [100] direction of the unit cell.

The formation of complex **2**, $Rh_2(O_2CCF_3)_4\cdot(p\text{-}(CH_3)_2C_6H_4)$, was first observed accidentally in the benzene–hexane solution system (Section 2.3.1). The presence of *p*-xylene was explained by the fact that it is added to both benzene and hexanes stills at the stage of the preparation the Na–K amalgam. Later the yield of **2** was increased by using neat *p*-xylene as a solvent (Section 2.3.2); in addition, product **2** was also obtained by the solid state approach (Section 2.3.3). The first synthesis of **2** (Section 2.3.1) is an interesting example of a competition in solution of weak π-donor ligands for coordination by the strong Lewis acid, $Rh_2(O_2CCF_3)_4$. The *p*-xylene, being a stronger donor than benzene (even though present in solutions as a minor component), binds preferentially to axial positions of dirhodium trifluoroacetate units to form **2**. This fact should be taken into account when studying weak interactions in so-called 'noncoordinating' solvents such as benzene, toluene or xylenes, which can be considered as weak Lewis bases themselves, as we clearly observed for the systems containing $Rh_2(O_2CCF_3)_4$. Similar observations were made when studying weakly coordinating anions, which have about the same nucleophilicity toward various cations as toluene [7]. Interestingly, in the case of *p*-xylene ligand, both solution and solid state techniques yielded the same product, the chain polymer of 1:1 composition in which the aromatic ring is acting as a bidentate ligand, while for THF and DMSO [2b,d], solution reactions always resulted only in the formation of the discrete bis-adduct molecules with monodentate coordination of ligands.

The solid state deposition approach ('solventless' technique, indeed, in this case) has been used (Section 2.4) for studying complexation of $Rh_2(O_2CCF_3)_4$ with the solid sublimable ligand, naphthalene, to give crystals of $Rh_2(O_2CCF_3)_4\cdot C_{10}H_8$ (**3**). In contrast to the single ring aromatic ligands, benzene and *p*-xylene, naphthalene, the simplest compound having fused arene rings, was used for coordination with $Rh_2(O_2CCF_3)_4$. From previous reports on transition-metal–naphthalene complexes, (η^6-naphthalene) sandwiches containing a metal in the zero-valent state (Cr, Mo, etc) have been traditionally prepared by metal vapor synthesis technique [8]. Recently, the naphthalene radical anion reductions of a variety of transition metal precursors have been introduced as a convenient method for the synthesis of anionic bis or tris(naphthalene) metal complexes [9], with examples such as $[(\eta^6\text{-}C_{10}H_8)_2Ti]^{2-}$ [9b], or structurally characterized $[(\eta^4\text{-}C_{10}H_8)_3Zr]^{2-}$ [9c]. Some mixed ligand naphthalene complexes have been also obtained using this technique, as for example $[Ru(\eta^6\text{-}C_{10}H_8)(1,5\text{-cyclooctadiene})]$ [10] and $[Fe(\eta^6\text{-}C_{10}H_8)(Cy_2PC_2H_4PCy_2)]$ [11].

3.2. Crystal structures

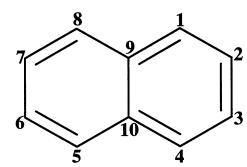
Three new complexes **1**–**3** have been obtained as green crystals, which were extremely unstable for **1** (loss of benzene), relatively stable for **3**, with **2** being an intermediate case; any exposure to solvent media led to the solvolytic cleavage of **1**–**3**. All products have been examined by X-ray crystallography and the 1:1 composition was confirmed by elemental analysis. All three structures consisted of the dirhodium(II) tetrakis(trifluoroacetate) molecules alternating with aromatic ligands, C_6H_6 (**1**), $p\text{-}(CH_3)_2C_6H_4$ (**2**), and $C_{10}H_8$ (**3**), which are bound at axial positions of the Rh_2 units thus forming linear one-dimensional chains (Fig. 1). These chains lying parallel in the crystal are extended in the structure along the [100] direction ([001] in the case of **3**) of the unit cell (Fig. 2). Selected distances and angles for **1**–**3** are given in Table 2. The coordination of arene

Table 2
Selected distances (Å) and angles (°) for $[Rh_2(O_2CCF_3)_4 \cdot arene]$ coordination polymers

Arene	Rh–Rh	Rh–C_{arene}	Rh–$arene_{center}$	C–C_{aver}	Rh–Rh–C_{arene}	Ref.
C_6H_6	2.4115(9)	2.646(6), 2.678(6)	2.98	1.39(1)	164.2(2), 164.1(2)	this work
$(CH_3)_2C_6H_4$	2.417(1)	2.598(7), 2.770(7)	2.99	1.39(1)	167.6(2), 161.1(2)	this work
$C_{10}H_8$	2.422(2)	2.609(9), 2.567(9)	2.97	1.39(1)	164.1(2), 166.1(2)	this work
$(CH_3)_6C_6$	2.422(1)	2.770(6), 2.787(6)	2.98	1.40(1)	165.4(1), 164.1(1)	[2a]
$(C_6H_5)_2C_2$	2.4256(6)	2.696(5), 2.750(6)	3.06	1.369(9)	165.1(1), 164.7(1)	[2e]

ligands in **1**–**3** was found to be off-center (Fig. 3) as in the cases of the C_6Me_6 and the Ph_2C_2 dirhodium complexes reported earlier [2a,e]. For benzene and *p*-xylene ligands (**1** and **2**) two opposite edges of the arene ring approach the axial sites of the neighboring dirhodium dimers in the $\eta^2(1,2):\eta^2(4,5)$ bridging fashion. For the single-ring aromatic ligands, in addition to the common η^6-binding mode, there are only a few examples with benzene and *p*-xylene ligands bonding two metal centers in the off-centered way, for example, $[(^tBu_3SiO)_3Ta]_2[\mu\text{-}\eta^2(1,2):\eta^2(4,5)\text{-}C_6H_6]$ [12] and $[(Cy_2PC_2H_4PCy_2)Co]_2[\mu\text{-}\eta^3:\eta^3\text{-}C_6H_4(CH_3)_2]$ [13]. There was also a systematic study of the Ag(I)-aromatic interactions, including benzene, xylenes and naphthalene ligands [14], which were all examples of an η^2 off-centered donation of π-electrons to Ag^+, including one unusual η^1-benzene compound [15].

In complex **3** both arene rings of the naphthalene molecule are engaged in coordination to the different Rh(II) centers in the $\eta^2(1,2):\eta^2(5,6)$ mode (see numbering in Scheme 2, Fig. 4). This is a rare unsymmetrical mode for the μ^2-naphthalene in transition metal complexes [16–18]. The two coordination modes of naphthalene mentioned above, the most common for the discrete transition metal complexes obtained so far, were η^4 and η^6. Several different bridging, μ^2 modes of naphthalene have been found [16–18] in a number of the multidecker compounds with different d- and f-block transition metals: $CpV(\mu^2\text{-}\eta^6:\eta^6\text{-}C_{10}H_8)VCp$ [16a], $[CpV(\mu^2\text{-}\eta^6:\eta^2\text{-}C_{10}H_8)Yb(THF)Cp]_n$ ($Cp = \eta^5\text{-}C_5H_5$) [16b], $(C_6H_6)Ru(\mu^2\text{-}\eta^4:\eta^6\text{-}C_{10}H_8)Cr(CO)_3$ [17].



Scheme 2.

The two closest Rh–C_{arene} distances average to 2.662(6) in (**1**), 2.684(7) in (**2**) and to 2.588(9) Å in (**3**) indicating the tightest metal–arene interaction in the naphthalene compound. At first glance, this contrasts to the general assumption that naphthalene binds less strongly to a metal than benzene [19], and to the data on bond-dissociation energies via calorimetric methods revealing that the naphthalene–Cr bond in the $Cr(CO)_3$ complex is 6 kcal mol^{-1} weaker than the benzene–Cr bond [8c]. However, it is worth emphasizing that those data were valid for the discrete η^6-compounds, while in the chain polymers **1** and **2** each arene ring coordinates two metal centers, and in **3** different rings of naphthalene are involved in coordination. This means that axial

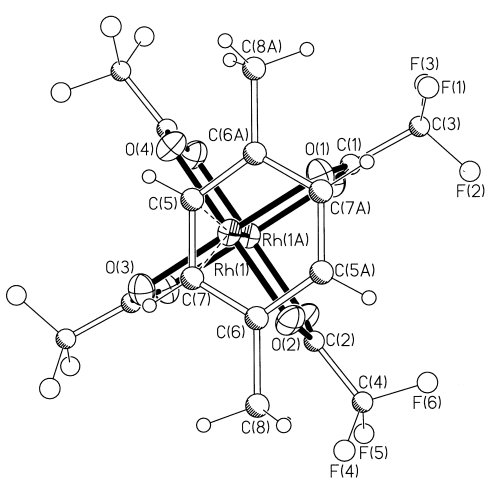


Fig. 3. The view almost down the Rh–Rh axis of the $Rh_2(O_2CCF_3)_4 \cdot (p\text{-}(CH_3)_2C_6H_4)$ unit in the chain structure of **2**. Rhodium and oxygen atoms are represented by thermal ellipsoids at the 40% probability level. Carbon, fluorine and hydrogen atoms are shown as spheres of arbitrary radii. Two closest axial contacts to Rh atoms are drawn by dashed lines.

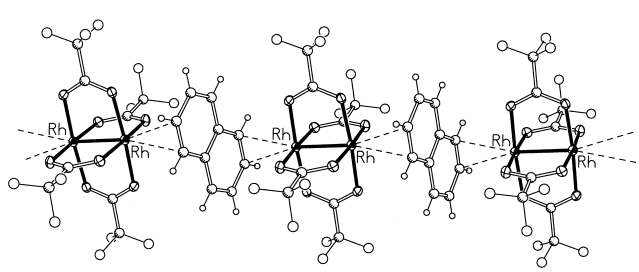
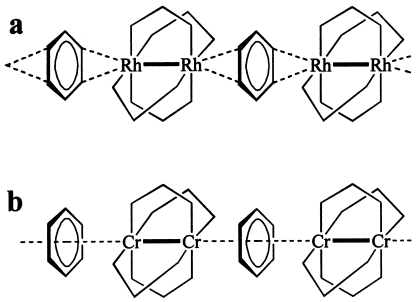


Fig. 4. Fragment showing the alternating arrangement of $Rh_2(O_2CCF_3)_4$ and $C_{10}H_8$ in the chain structure of **3**. Rhodium and oxygen atoms are represented by thermal ellipsoids at the 40% probability level. Carbon, fluorine and hydrogen atoms are shown as spheres of arbitrary radii. The shortest Rh–C_{arene} contacts are drawn by dashed lines. Only rhodium atoms are labeled for clarity.



Scheme 3.

contacts to arene are expected to be shorter in **3** than in **1** and **2**. Actually the Rh–arene center distances are very close, being in the range of 2.97–2.99 Å, for all dirhodium polymers mentioned in Table 2, except in the diphenylacetylene compound where the distance is 3.06 Å. All of the arene complexes, **1**–**3**, demonstrate asymmetry in the two nearest metal–carbon distances. The difference in these two Rh–C_{arene} contacts is the most significant (0.172 Å) in complex **2** with *p*-xylene compared to the benzene (0.032 Å) and to the naphthalene (0.042 Å) polymers. It was 0.017 Å in the $[Rh_2(O_2CCF_3)_4{\cdot}C_6Me_6]_\infty$ compound [2a].

The unsymmetrical $\eta^2{:}\eta^2$ complexation of arene groups (Scheme 3a) seems to be preferred for the dirhodium(II) trifluoroacetate one-dimensional polymers based on the several examples obtained so far. This contrasts to the dichromium carboxylates with coordinated aromatic ligands of the 1:1 composition, including benzene and p-xylene analogues, in which arene rings were lying centrically on the line between two dimetal units and thus having a η^6 (Scheme 3b) symmetrical coordination [20]. In $[Bi_2(O_2CCF_3)_4{\cdot}C_6Me_6]_\infty$, the only arene adduct of a main group element tetracarboxylate, the C_6Me_6 molecules are also acting in an η^6 coordination mode [21].

The unsymmetrical complexation of aromatics in **1**–**3** causes no detectable distortion of the arene rings. The mean C–C distances are the same, averaged to 1.39(1) in **1**–**3**.

There was an attempt to compare the inductive effect of different substituents of arene ligands on the Cr–Cr and the Cr–ring center distances [20]. One might expect that the stronger the nucleophile substituent is, the stronger is the interaction of an axial ligand with the dimetal moiety (which, in turn, would result in the elongation of the metal–metal distance). However, there was no simple relationship found for a number of relative compounds between the ionization potentials of arenes and the Cr–Cr distances [20]. The latter was shown to be influenced by other variables, packing forces being the most important one. This is also the case for a number of dirhodium tetrakis(trifluoroacetate) chain polymers with coordinated arenes studied here. The present results show that the electronic properties of aromatic ligands in donor–acceptor complexes with $Rh_2(O_2CCF_3)_4$ are not simply correlated with their coordination strength. For example, the relatively strong donor, hexamethylbenzene, has the longest Rh–C_{arene} contacts (averaged to 2.779(6) Å [2a]) among the arenes studied (Table 2). The difference, 0.19 Å, in these two shortest Rh–C_{arene} contacts in $[Rh_2(O_2CCF_3)_4{\cdot}(C_6Me_6)]_\infty$ compared to the naphthalene analogue (2.588(9) Å) is significant, while the Rh–Rh distances are exactly the same for two compounds. Obviously, packing forces and other stereochemical factors are very important in these arene–metal interactions, capable of overriding electronic factors.

In **3** the naphthalene molecule approaches the rhodium atoms via the 1,2 and 5,6 C–C bonds. This could well be an electronic effect since it is these bonds that have the highest π-bond order, 0.73, compared to 0.61 for the 2,3 and 6,7 bonds (Scheme 2), according to Hückel calculations [22].

3.3. Conclusions

In summary, complexation of π-arene ligands, benzene, *p*-xylene and naphthalene, with the dirhodium unit has been examined by preparing a number of 1:1 coordination polymers with $Rh_2(O_2CCF_3)_4$. It is found that dirhodium tetrakis (trifluoroacetate) exhibits a selective coordination toward weak donor bases, such as benzene and *p*-xylene, in solutions. The crystalline complexes **1**–**3** have a one-dimensional framework constructed by the dirhodium units and arene ligands bound to its axial positions through two carbon atoms at each end. The geometry of coordinated arene bridges is unsymmetrical, an $\eta^2{:}\eta^2$ type, in all cases. Complex **3**, $[Rh_2(O_2CCF_3)_4{\cdot}(C_{10}H_8)]_\infty$ constitutes the first example of such products with a dicyclic arene system. We think that related and novel compounds with polycyclic aromatic ligands having an extended delocalized π-system will generally be accessible by the technique introduced, and studies on arene ligands with multicoordination-site possibilities are under way.

4. Supplementary Material

Crystallographic data (excluding structure factors) for the structures reported in this paper have been deposited with the Cambridge Crystallographic Data Centre CCDC Nos. 140762, 140763 and 140764 for compounds **1**, **2** and **3**, respectively. Copies of the data can be obtained free of charge from The Director, CCDC, 12 Union Road, Cambridge, CB2 1EZ, UK (fax: +44-1223-336033; e-mail: deposit@ccdc.cam.ac.uk or www: http://www.ccdc.cam.ac.uk).

Acknowledgements

This work was supported by the Robert A. Welch Foundation. We thank the Johnson Matthey Company for the loan of rhodium.

References

[1] (a) F.A. Cotton, R.A. Walton, Multiple Bonds Between Metal Atoms, second ed., Oxford University Press, Oxford, 1993, pp. 432–443. (b) C.A. Crawford, J.H. Matonic, W.E. Streib, J.C. Huffman, K.R. Dunbar, G. Christou, Inorg. Chem. 32 (1993) 3125. (c) J. Lu, W.T.A. Harrison, A.J. Jacobson, Chem. Commun. (1996) 399. (d) F.A. Cotton, Y Kim, J. Lu, Inorg. Chem. Acta 221 (1994) 1.

[2] (a) Part 2. F.A. Cotton, E.V. Dikarev, S.E. Stiriba, Organometallics 18 (1999) 2724. (b) Part 3. F.A. Cotton, E.V. Dikarev, S.E. Stiriba, Inorg. Chem. 38 (1999) 4877. (c) Part 4. F.A. Cotton, E.V. Dikarev, M.A. Petrukhina, J. Organomet. Chem. 596 (2000) 130. (d) Part 5. F.A. Cotton, E.V. Dikarev, M.A. Petrukhina, S.E. Stiriba, Inorg. Chem. 39 (2000) 1748. (e) Part 6. F.A. Cotton, E.V. Dikarev, M.A. Petrukhina, S.E. Stiriba, Organometallics 19 (2000) 1402. (f) Part 7. F.A. Cotton, E.V. Dikarev, M.A. Petrukhina, Angew. Chem., Int. Ed. 39 (2000) 2362.

[3] (a) T.R. Felthouse, Progr. Inorg. Chem. 29 (1982) 73. (b) A.F. Noels, A.J. Hubert, P.H. Teyssie, J. Organomet. Chem. 166 (1979) 79. (c) A. Padwa, D.J. Austin, A.T. Price, M.A. Semones, M.P. Doyle, M.N. Protopopova, W.R. Winchester, A. Tran, J. Am. Chem. Soc. 115 (1993) 8669. (d) M.P. Doyle, M.A. McKervey, Chem. Commun. (1997) 983. (e) T.H. Black, Aldrichim. Acta 15 (1982) 13.

[4] F.A. Cotton, E.V. Dikarev, X. Feng, Inorg. Chim. Acta 237 (1995) 19.

[5] SHELXTL V.5, Siemens Industrial Automation Inc., Madison, WI, 1994.

[6] G.M. Sheldrick, in: H.D. Flack, L. Parkanyi, K. Simon (Eds.), Crystallographic Computing, vol. 6, Oxford University Press, Oxford, 1993, p. 111.

[7] (a) Z. Xie, R. Bau, C. Reed, Angew. Chem., Int. Ed. Engl. 33 (1994) 2433. (b) C.A. Reed, Acc. Chem. Res. 31 (1998) 133.

[8] (a) C. Elschenbroich, R. Möckel, Angew. Chem., Int. Ed. Engl. 16 (1977) 870. (b) E.P. Kündig, P.L. Timms, J. Chem. Soc., Chem. Comm. (1977) 912. (c) N.P.D. Thi, S. Spichiger, P. Paglia, G. Bernardinelli, E.P. Kündig, P.L. Timms, Helv. Chim. Acta 75 (1992) 2593.

[9] (a) M.K. Pomije, C.J. Kurth, J.E. Ellis, M.V. Barybin, Organometallics 16 (1997) 3582. (b) J.E. Ellis, D.W. Blackburn, P. Yuen, M. Jang, J. Am. Chem. Soc. 115 (1993) 11616. (c) M. Jang, J.E. Ellis, Angew. Chem., Int. Ed. Engl. 33 (1994) 1973.

[10] M. Crocker, M. Green, J.A.K. Howard, N.C. Norman, D.M. Thomas, J. Chem. Soc., Dalton Trans. (1990) 2299.

[11] H. Kubo, M. Hirano, S. Komiya, J. Organomet. Chem. 556 (1998) 89.

[12] D.R. Neithamer, L. Parkanyi, J.F. Mitchell, P.T. Wolczanski, J. Am. Chem. Soc. 110 (1988) 4421.

[13] K. Jonas, G. Koepe, L. Schieferstein, R. Mynott, C. Krüger, Y.H. Tsay, Angew. Chem., Int. Ed. Engl. 22 (1983) 620.

[14] E.A.H. Griffith, E.L. Amma, J. Am. Chem. Soc. 96 (1974) 743 and references therein.

[15] K. Shelly, D.C. Finster, Y.J. Lee, W.R. Scheidt, C.A. Reed, J. Am. Chem. Soc. 107 (1985) 5955.

[16] (a) M.N. Bochkarev, I.L. Fedushkin, H. Schumann, J. Loebel, J. Organomet. Chem. 410 (1991) 321. (b) M.N. Bochkarev, I.L. Fedushkin, V.K. Cherkasov, V.K. Nevodchikov, H. Schumann, F.H. Görlitz, Inorg. Chim. Acta 201 (1992) 69. (c) I.L. Fedushkin, V.K. Nevodchikov, V.K. Cherkasov, M.N. Bochkarev, H. Schumann, F. Girgsdies, F.H. Görlitz, G. Kociok-Köhn, J. Pickardt, J. Organomet. Chem. 511 (1996) 157.

[17] J.W. Hull, W.L. Gladfelter, Organometallics 3 (1984) 605.

[18] B.F. Bush, V.M. Lynch, J.J. Lagowski, Organometallics 6 (1987) 1267.

[19] M. Randić, Tetrahedron 31 (1975) 1477.

[20] (a) F.A. Cotton, X. Feng, P.A. Kibala, M. Matusz, J. Am. Chem. Soc. 110 (1988) 2807. (b) F.A. Cotton, L.M. Daniels, P.A. Kibala, Inorg. Chem. 31 (1992) 1865.

[21] W. Frank, V. Reiland, G.J. Reiss, Angew. Chem., Int. Ed. Engl. 37 (1998) 2984.

[22] F.A. Cotton, Chemical Applications of Group Theory, 3rd ed., Wiley, New York, 1990, p. 176.

PERGAMON

www.elsevier.nl/locate/poly

Polyhedron 19 (2000) 1837–1841

POLYHEDRON

Gold(I) complexes containing the cationic ylide ligand bis(methyldiphenylphosphonio)methylide

Inocencio Romeo, Manuel Bardají, M. Concepción Gimeno, Mariano Laguna *

Departamento de Química Inorgánica, Instituto de Ciencia de Materiales de Aragón, Universidad de Zaragoza-CSIC, 50009 Zaragoza, Spain

Received 9 March 2000; accepted 15 June 2000

Abstract

The ylide $Ph_2PCH{=}PPh_2Me$ can be selectively P-alkylated by MeI or MeO_3SCF_3 to form the bis(methyldiphenylphosphonio)methylide salts $[MePPh_2CHPPh_2Me]A$ (A=I (**1**), CF_3SO_3 (**2**)). The ylidic carbon shows a weak nucleophilicity and does not give typical reactions with common organic electrophiles, including Wittig type reactions, but it is able to displace tetrahydrothiophene in [AuX(tht)] to give the corresponding C-coordinated gold(I) compounds $[Au\{CH(PPh_2Me)_2\}X]CF_3SO_3$ (X=Cl (**3**), C_6F_5 (**4**)). The crystal structure of (**4**) displays a linear coordination for the gold atom, single P–C bond lengths and a PCP angle of 119.1(3)° for the ligand. © 2000 Elsevier Science Ltd. All rights reserved.

Keywords: Gold(I) complexes; Cationic ylide ligand; Bis(methyldiphenylphosphonio)methylide salts; P-alkylation

1. Introduction

Carbodiphosphorane chemistry has attracted much attention not only because of the synthesis and geometry of the P=C=P fragment [1] but also for the synthesis of metallic complexes. Therefore several mononuclear copper, gold, silver [2,3], iridium [4], platinum [5,6], rhenium [7,8], tungsten [6,8,9], manganese, chromium, iron and nickel [8] or dinuclear gold [10] and iron [11] derivatives have been prepared.

On the contrary the mesomeric phosphonium ylides $R_3PCHPR_3^+$ have often been overlooked because of their intermediate position on the carbodiphosphoranes and not C_{ylidic}-bonded metallic complexes have been described so far. Some complexes containing the unit $-CH_2PR_2CHPR_2CH_2-$ have been reported with the ligand acting as quelate through the CH_2 groups [10,12,13].

In this paper, the synthesis of the phosphoranium salts $[MePPh_2CHPPh_2Me]A$ (A=I, CF_3SO_3) and their first metallic complexes $[Au[CH(PPh_2Me)_2)X]CF_3SO_3$ (X=Cl, C_6F_5) are reported, which in spite of the weak nucleophilic character of the ylidic carbon are stable. X-ray diffraction studies of the pentafluorophenyl derivative were carried out to fully characterize their geometry.

2. Experimental

All the reactions were carried out under a dry nitrogen atmosphere at room temperature (r.t.). IR spectra were recorded on a Perkin–Elmer 883 spectrophotometer, over the range 4000–200 cm^{-1}, by using Nujol mulls between polyethylene sheets. ^1H, ^{19}F and $^{31}P\{^1H\}$ NMR spectra were recorded on a Varian UNITY 300 or Bruker ARX-300 apparatus in $CDCl_3$ solutions; chemical shifts are quoted relative to $SiMe_4$ (external, ^1H), $CFCl_3$ (external, ^{19}F) and 85% H_3PO_4 (external, ^{31}P). C, H, N and S analyses were performed with a Perkin–Elmer 2400 microanalyzer. Mass spectra were recorded on a VG Autospec using LSIMS technique (with cesium gun) and 3-nitrobenzyl alcohol as matrix.

2.1. Preparation of the ligands

2.1.1. $[MePh_2PCHPPh_2Me]I$ (**1**)

To a diethyl ether suspension (10 ml) of $[Ph_2PCH_2PPh_2Me]I$ [14] (0.54 g, 1 mmol) was added an

* Corresponding author. Tel.: +34-976-761-181; fax: +34-976-761-187.

E-mail address: mlaguna@posta.unizar.es (M. Laguna).

0277-5387/00/$ - see front matter © 2000 Elsevier Science Ltd. All rights reserved.
PII: S0277-5387(00)00467-8

excess of sodium hydride (1.2 g of a 60% paraffin suspension, 3 mmol). After stirring for 5 h, the excess of NaH and the formed NaI are filtered off, obtaining a yellow solution of the ylide. The addition of MeI (0.142 g, 1 mmol) immediately afforded a white solid which was filtered off and washed with diethyl ether (3×5 ml). Yield of **1**: 55%. ^{1}H NMR: δ 7.8–7.2 (m, 20H, Ph), 2.13 (d, 6H, $^2J_{HP} = 12.0$, Me–P), 1.39 (t, 1H, $^2J_{HP} = 4.6$ Hz, P–CH–P); ^{31}P{^{1}H} NMR: δ 16.5. Anal. Calc. $C_{27}H_{27}IP_2$: C, 60.0; H, 5.05. Found: C, 59.85; H, 4.9.

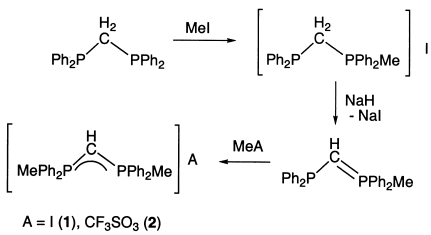
Table 1
Details of data collection and structure refinement for complex **4**

Compound	**4**
Chemical formula	$C_{34}H_{27}AuF_8O_3P_2S$
Crystal habit	colourless needle
Crystal size (mm)	$0.65 \times 0.20 \times 0.10$
Crystal system	triclinic
Space group	$P\bar{1}$
a (Å)	9.641(2)
b (Å)	11.538(2)
c (Å)	16.696(3)
α (°)	77.91(3)
β (°)	77.69(3)
γ (°)	81.05(3)
U (Å^3)	1762.3(6)
Z	2
D_{calc} (Mg m^{-3})	1.746
M	926.52
$F(000)$	904
T(°C)	25
$2\theta_{max}$ (°)	50
μ (Mo Kα) (mm^{-1})	4.400
Transmission	0.649–0.970
Number of reflections measured	7767
Number of unique reflections	6179
R_{int}	0.023
R [a] (F, $F>4\sigma(F)$)	0.040
wR [b] (F^2, all reflections)	0.098
Number of parameters	442
Number of restraints	0
S [c]	0.959
Max. $\Delta\rho$ (eÅ^{-3})	1.81

[a] $R(F) = \Sigma \| |F_o| - |F_c| \| / \Sigma |F_o|$.

[b] $wR \quad (F^2) = [\Sigma\{w(F_o^2 - F_c^2)2\}/\Sigma\{w(F_o^2)^2\}]^{0.5}$; $\quad w^{-1} = \sigma^2(F_o^2) + (aP)^2 + bP$, where $P = [F_o^2 + 2F_c^2]/3$ and a and b are constants adjusted by the program.

[c] $S = [\Sigma\{w(F_o^2 - F_c^2)^2\}/(n-p)]^{0.5}$, where n is the number of data and p the number of parameters.



Scheme 1.

2.1.2. [$MePh_2PCHPPh_2Me$]CF_3SO_3 (2)

As stated for (**1**) but adding drop by drop MeO_3SCF_3 instead of MeI till all the white solid has precipitated. Yield of 2: 65%. ^{1}H NMR: 8 7.8–7.2 (m, 20H, Ph), 2.04 (d, 6H, $^2J_{HP} = 12.3$, Me–P), 1.30 (t, 1H, $^2J_{HP} = 5.6$ Hz, P–CH–P); ^{31}P{^{1}H} NMR: δ 16.5. Anal. Calc. $C_{28}H_{27}F_3O_3P_2S$: C, 59.8; H, 4.85;S, 5.7. Found: C, 60.0; H, 4.65; S, 5.55.

2.2. Preparation of the gold(I) complexes

2.2.1. [$Au\{CH(PPh_2Me)_2\}X$]CF_3SO_3; X=Cl (3), C_6F_5 (4)

To a dichloromethane solution (20 ml) of 2 (0.11 g, 0.2 mmol) was added 0.2 mmol of [AuX(tht)] (X=Cl 0.064 g, C6F5 0.09 9) [15,16]. The mixture was stirred for 90 min, then concentrated to ca. 5 ml and the addition of diethyl ether (15 ml) afforded complexes **3**–**4** as white solids, which were washed with diethyl ether (3×5 ml). Yield of (**3**): 88%. ^{1}H NMR: 6 7.8–7.2 (m, 20H, Ph), 4.66 (t, 1H, $^2J_{HP} = 16.8$, P–CH–P), 2.14 (d, 6H, $^2J_{HP} = 12.4$ Hz, Me–P); ^{31}P{^{1}H} NMR: δ 22.1. Anal. Calc. $C_{28}H_{27}ClF_3O_3P_2SAu$: C, 42.3; H, 3.4; S, 4.05. Found: C, 42.35; H, 3.75; S, 4.0. Yield of (**4**): 87%. ^{1}H NMR: δ 7.8–7.2 (m, 20H, Ph), 4.28 (t, 1H, $^2J_{HP} = 16.7$, P–CH–P), 2.22 (d, 6H, $^2J_{HP} = 11.9$ Hz, Me–P); ^{19}F NMR: δ −78.0 (s, 3F, CF_3), −117.0 (m, $2F_o$), −161.3 (t, $1F_p$), −164.8 (m, $2F_m$); ^{31}P{^{1}H} NMR: δ 22.7. Anal. Calc. $C_{34}H_{27}F_8O_3P_2SAu$: C, 44.1; H, 2.95; S, 3.45. Found: C, 44.35; H, 3.0; S, 3.3.

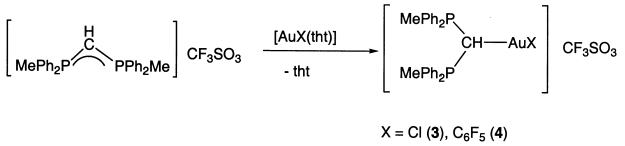
2.3. X-ray crystallography

The crystal was mounted in inert oil on a glass fibre and transferred to the cold gas stream of a Siemens P4 diffractometer equipped with an Oxford low temperature attachment. Data were collected using monochromated Mo Kα radiation ($\lambda = 0.71073$). Scan type theta-2theta. Absorption correction was applied based on Ψ-scans. The structure was solved by the heavy-atom method, and refined on F^2 using the program SHELXL-93 [17]. Non hydrogen atoms were refined anisotropically. Hydrogen atoms were included using a riding model. Further details are given in Table 1.

3. Results and discussion

3.1. Ligand synthesis

The phosphoranium salts were prepared following the Scheme 1. First it was carried out the reaction of bis(diphenylphosphino)methane (dppm) with MeI to give the monomethylated product. This compound was deprotonated in the presence of an excess of sodium hydride to afford a yellow solution of the mono-ylide



Scheme 2.

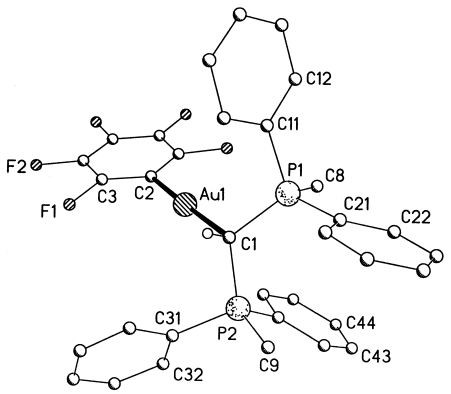


Fig. 1. Structure of the cation of complex **4** in the crystal with the numbering scheme. Radii are arbitrary; hydrogen atoms except at C1 are omitted for clarity.

$Ph_2PCH{=}PPh_2Me$, air and moisture sensitive, which had been already prepared by a transylidation reaction [14]. Ylides can be easily alkylated although a mixture of the C-alkylated and the P-alkylated derivatives are usually obtained [18,19]. The alkylation of our ylide affords purely the P-alkylated derivative, by using MeI or methyl triflate as reagents, which is probably due to the stability of the bisphosphonium fragment. Even by adding 100% excess of MeI the P-alkylated derivative was the only compound obtained. However the addition of methyltriflate to the ylide in a 2:1 molar ratio leads mainly to a mixture of the P-alkylated derivative (**2**) and the phosphonium salt $PPh_2Me_2^+$ coming from the cleavage of (**2**).

These derivatives are air- and moisture-stable white solids at room temperature. The IR spectrum of (**2**) shows absorptions at 1266, 1222 and 638 cm^{-1} from the triflate anion [20]. The ^1H NMR spectra of (**1**) and (**2**) are very similar showing a doublet around 2 ppm for the methyl group and a higher field triplet (about 1.35 ppm) for the methylide bridge. In the $^{31}P\{^1H\}$ NMR spectra it can be observed, in both cases, a singlet at 16.5 ppm as expected for two equivalent phosphorus atoms.

These phosphoranium salts are very stable, which has been explained by the very weak nucleophilicity of the ylidic carbon which prevents nucleophilic substitution or addition reactions. In fact, typical Wittig reactions for these ylides are only known if hydrogen is replaced by fluor in the carbanion, that has been explained because fluor destabilizes negative charges in an alfa position [21,22]. That is why to our knowledge there is no metallic complexes containing the ligand $R_3P{=}CH{-}PR_3^+$. On the contrary and as stated before for the corresponding carbodiphosphorane ligands $R_3P{=}C{=}PR_3$, of which the ylidic carbon is a stronger nucleophile, coordination compounds are well known, although most of them are only mononuclear C-coordinated complexes. Reactions of ylides with electrophiles such as benzaldehyde, acetyl chloride, benzoyl chloride, benzyl chloride and carbon disulfide gave no reaction.

3.2. Gold(I) complexes synthesis

We have previously reported several gold(I) complexes with C-coordination to ylides coming from the dppm [23]. For instance we have prepared the corresponding C-bonded gold complexes by coordination to $[Au(C_6F_5)SPPh_2CH(PPh_2Me)]$ [24] or to $[Au(C_6F_5)$-$PPh_2CH(PPh_2Me)]$ [25] which are very close to ligands **1**–**2** (equals by substituting the P- or S-coordinated gold(I) fragment for methyl) and they also are very stable ylides. Therefore we carried out the same reactions between the phosphoranium salts **1**–**2** and gold(I) complexes (see Scheme 2). The reactions evolve with displacement of tetrahydrothiophene (tht) to afford complexes **3**–**4** as white solids air and moisture stable.

Their IR spectra show absorptions at 335 cm^{-1} (**3**) due to ν(Au–Cl) [26], 955 and 797 cm^{-1} from the pentafluorophenyl groups (**4**) [27], and 1265, 1222, 638 (**3**), 1250,1224 and 638 cm^{-1} (**4**) from triflate anions. The ^1H NMR spectra show an almost unchanged doublet around 2.1 ppm for the methyl group and a triplet at 4.66 ppm for (**3**) and 4.28 ppm for (**4**) due to the methylide bridge, clearly low-field shifted from (**2**) ($\Delta\delta$ is 3.36 ppm for (**3**) and 2.98 ppm for (**4**)). The $^{31}P\{^1H\}$ NMR spectra show a singlet around 22 ppm and again about 6 ppm low-field shifted after gold coordination. The ^{19}F NMR spectrum of (**4**) shows the pattern of a pentafluorophenyl group besides of the triflate counterion. The LSIMS mass spectra show the base peak at $m/z = 413$ due to the bis(phosphonium)methylide ligand and at 645 (20%, for (**3**)) and at 777 (65%, for (**4**)) corresponding to $[M{-}CF_3SO_3]^+$.

3.3. Crystal structure of $[Au\{CH(PPh_2Me)_2\}(C_6F_5)]CF_3SO_3$

The structure of the cation is shown in Fig. 1, with selected bond lengths and angles in Table 2. It consists of a gold(I) center bonded to two kinds of carbon atoms, one coming from a pentafluorophenyl group and the other from an ylidic ligand. Both distances Au–C are very different; $Au^I{-}C_6F_5$ is 2.029(6), which is of the same order as that found in related complexes such as $[Au(C_6F_5)_2\{(PPh_2)_2CH\}Au(C_6F_5)]$ (2.048(8) Å)

Table 2
Selected bond lengths (Å) and angles (°) for complex **4**

Au(1)–C(2)	2.029(6)	P(1)–C(21)	1.795(6)
Au(1)–C(1)	2.112(6)	P(1)–C(11)	1.799(7)
C(1)–P(2)	1.781(6)	P(2)–C(9)	1.794(7)
C(1)–P(1)	1.792(6)	P(2)–C(41)	1.794(7)
P(1)–C(8)	1.788(7)	P(2)–C(31)	1.797(7)
C(2)–Au(1)–C(1)	175.9(2)	C(1)–P(2)–C(31)	106.6(3)
P(2)–C(1)–P(1)	119.1(3)	C(9)–P(2)–C(31)	106.6(3)
P(2)–C(1)–Au(1)	109.1(3)	C(41)–P(2)–C(31)	110.4(3)
P(1)–C(1)–Au(1)	105.7(3)	C(16)–C(11)–P(1)	121.2(5)
C(8)–P(1)–C(1)	111.4(3)	C(12)–C(11)–P(1)	119.9(7)
C(8)–P(1)–C(21)	108.5(3)	C(22)–C(21)–P(1)	123.2(5)
C(1)–P(1)–C(21)	112.6(3)	C(26)–C(21)–P(1)	118.1(5)
C(8)–P(1)–C(11)	108.9(4)	C(36)–C(31)–P(2)	119.7(5)
C(1)–P(1)–C(11)	108.4(3)	C(32)–C(31)–P(2)	121.3(6)
C(21)–P(1)–C(11)	107.0(3)	C(42)–C(41)–P(2)	120.7(5)
C(1)–P(2)–C(9)	112.3(3)	C(46)–C(41)–P(2)	119.9(5)
C(1)–P(2)–C(41)	111.8(3)	C(3)–C(2)–Au(1)	125.9(5)
C(9)–P(2)–C(41)	109.0(4)	C(7)–C(2)–Au(1)	120.3(5)

[28] or $[(F_5C_6)AuCH(PPh_2AuPPh_2)_2CHAu(C_6F_5)]$ (2.012(13) Å) [29] or to the one for the Au–C_6F_5 group *trans* to the ylidic carbon in $[(F_5C_6)AuPPh_2CH(PPh_2Me)Au(C_6F_5)]$ (2.011(11) Å) [25]. In the latter the Au–C_6F_5 distance *trans* to the phosphorus ligand is longer, 2.053(15) Å, as corresponds to the higher *trans* influence of the phosphine ligand. The Au–C_{ylidic} bond length is 2.112(6) Å and the value agrees well with those in the complexes mentioned. The gold atom displays an almost linear coordination (175.9(2)°). There are not short gold–gold interactions presumably because steric effects of the bulky ligand prevent the intimate approach required for metal–metal contacts, as have been observed for other complexes with crowded ligands [30].

The P–C_{ylidic} bond lengths are 1.781(6) and 1.792(6) Å, far from those found in $MePPh_2P{=}C{=}PPh_2Me$ (1.645 Å) [31,32] or in $[Au(C_6F_5)PPh_2CH(PPh_2Me)]$ [25] (1.692 Å), as expected because of the absence of double bond character in complex **4**. In fact the distances compare well with the other P–C single bond lengths found in the ligand (from 1.788(7) to 1.799(7) Å), although they are shorter than those reported in $[PPh_3CH_2PPh_3][FeCl_4]$ (1.822(4) and 1.816(4) Å) [33].

The P–C–P angle is 119.1(3)°, slightly smaller than that found in $MePPh_2P{=}C{=}PPh_2Me$ (121.8°) or $[Au(C_6F_5)PPh_2CH(PPh_2Me)]$ (126.0(4)°) due to hybridization state, also smaller than that found in $[PPh_3CH_2PPh_3][FeC1_4]$ (123.4(2)°), probably because of electrostatic repulsion in the latter [33] but bigger than that in $[(F_5C_6)AuPPh_2CH(PPh_2Me)AuC_6F_5]$ 114.9(6)° presumably because the major steric repulsion of an Au–C_6F_5 unit compared to a methyl group. The P–C–Au angles, 109.1(3) and 105.7(3)°, are close to a tetrahedral disposition.

4. Supplementary material

Crystallographic data for complex **4** (excluding structure factors) have been deposited with the Cambridge Crystallographic Data Centre, CCDC No. 141436. Copies can be obtained free of charge from The Director, CCDC, 12 Union Road, Cambridge, CB2 1EZ, UK (Fax: +44-1123-336033; e-mail: deposit @ccdc.cam.ac.uk or www: http://www.ccdc.cam.ac.uk).

Acknowledgements

We thank the Dirección General de Enseñanza Superior (Project PB98-0542) for financial support.

References

[1] A.W. Johnson, Ylides and Imines of Phosphorus, Wiley, New York, 1993, p. 64 and references therein.
[2] H. Schmidbaur, C.E. Zybill, G. Müller, C. Krüger, Angew. Chem., Int. Ed. Engl. 22 (1983) 729.
[3] C.E. Zybill, G. Müller, Organometallics 6 (1987) 2489.
[4] W.C. Kaska, R.F. Reichelderfer, J. Organomet. Chem. 78 (1974) C47.
[5] J.C. Baldwin, W.C. Kaska, Inorg. Chem. 18 (1979) 686.
[6] W.C. Kaska, D.K. Mitchell, R.F. Reichelderfer, J. Organomet. Chem. 47 (1973) 391.
[7] J. Sundermeyer, K. Weber, K. Peters, H. Georg von Schnering, Organometallics 13 (1994) 2560.
[8] W.C. Kaska, D.K. Mitchell, R.F. Reichelderfer, W.D. Korte, J. Am. Chem. Soc. 96 (1974) 2847.
[9] A.E. Bruce, A.S. Gamble, T.L. Tonker, J.L. Templeton, Organometallics 6 (1987) 1350.
[10] H. Schmidbaur, O. Gasser, Angew. Chem., Int. Ed. Engl. 15 (1976) 502.
[11] W.C. Kaska, K.A.O. Starzewski, D.A. Dixon, in: A.W. Johnson (Ed.), Ylides and Imines of Phosphorus, Wiley, New York, 1993, p. 521.
[12] C. Krüger, J.C. Sekutowski, R. Goddard, H.J. Fuller, O. Gasser, H. Schmidbaur, Isr. J. Chem. 15 (1977) 149.
[13] H. Schmidbaur, O. Gasser, C. Krüger, J.C. Sekutowski, Chem. Ber. 110 (1977) 3517.
[14] H. Schmidbaur, U. Deschler, Chem. Ber. 116 (1983) 1386.
[15] R. Usón, A. Laguna, M. Laguna, Inorg. Synth. 26 (1989) 85.
[16] R. Usón, A. Laguna, J. Vicente, J. Chem. Soc., Chem. Commun. (1976) 353.
[17] G.M. Sheldrick, SHELXL-93: a program for crystal structure refinement, University of Göttingen, Göttingen, Germany, 1993.
[18] R. Appel, G. Hambrich, F. Knoch, Chem. Ber. 117 (1984) 2063.
[19] L.R. Falvello, J. Forniés, R. Navarro, A. Rueda, E.P. Urriolabeitia, Organometallics 15 (1996) 309.
[20] P.J. Stang, Y. Huang, A.M. Arif, Organometallics 11 (1992) 231.
[21] D.G. Cox, D.J. Burton, J. Am. Chem. Soc. 105 (1983) 650.
[22] D.G. Cox, D.J. Burton, N. Gurusamy, J. Am. Chem. Soc. 107 (1985) 2811.

[23] A. Laguna, M. Laguna, J. Organomet. Chem. 394 (1990) 743 and references therein.
[24] R. Usón, A. Laguna, M. Laguna, M.N. Fraile, I. Lázaro, M.C. Gimeno, P.G. Jones, C. Reihs, G.M. Sheldrick, J. Chem Soc., Dalton Trans. (1990) 333.
[25] R. Usón, A. Laguna, M. Laguna, I. Lázaro, A. Morata, P.G. Jones, G.M. Sheldrick, J. Chem Soc., Dalton Trans. (1986) 669.
[26] R. Usón, A. Laguna, M. Laguna, M.N. Fraile, P.G. Jones, G.M. Sheldrick, J. Chem Soc., Dalton Trans. (1986) 291.
[27] R. Usón, A. Laguna, J. García, M. Laguna, Inorg. Chim. Acta 37 (1979) 201.
[28] R. Usón, A. Laguna, M. Laguna, B.R. Manzano, P.G. Jones, G.M. Sheldrick, J. Chem Soc., Dalton Trans. (1984) 839.
[29] R. Usón, A. Laguna, M. Laguna, M.C. Gimeno, P.G. Jones, C. Fittschen, G.M. Sheldrick, J. Chem. Soc., Chem. Commun. (1986) 509.
[30] M. Bardají, P.G. Jones, A. Laguna, Eur. J. Inorg. Chem. (1998) 989 and references therein.
[31] U. Schubert, C. Kappenstein, B. Malewski-Mahrla, H. Schmidbaur, Chem. Ber. 114 (1981) 3070.
[32] M.S. Hussain, H. Schmidbaur, Z. Naturforsch., Teil B 31 (1976) 721.
[33] J.D. Walker, R. Poli, Polyhedron 8 (1989) 1293.

PERGAMON

www.elsevier.nl/locate/poly

Polyhedron 19 (2000) 1843–1848

POLYHEDRON

Complexes of Cu(II) with α-[(ethylamino)methyl]-3-hydroxy, benzenemethanol (Effortil). Crystal structure of the mononuclear Cu(II) complex with Effortil

P.R. Bontchev [a,*], B.B. Ivanova [a], R.P. Bontchev [b], D.R. Mehandjiev [c], D.S. Ivanov [d]

[a] *Faculty of Chemistry, Sofia University, 1, J. Bourchier Boulevard, Sofia 1164, Bulgaria*
[b] *Department of Chemistry, University of Houston, Houston, TX 77204-5641, USA*
[c] *Institute of Inorganic Chemistry, Bulgarian Academy of Sciences, Sofia, Bulgaria*
[d] *Faculty of Pharmacy, Medical University-Sofia, Sofia, Bulgaria*

Received 22 February 2000; accepted 15 June 2000

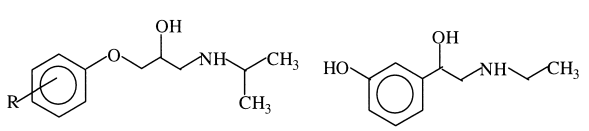
Abstract

The complexation processes between Cu(II) and the antihypotension drug Effortil (HEff) at different reaction conditions lead to the formation of two types of complex — a mononuclear violet one, $CuEff_2{\cdot}2CH_3OH$, and the binuclear green $Cu_2Eff_2Cl_2$. Monocrystals of the mononuclear $CuEff_2{\cdot}2CH_3OH$ complex were isolated and their structure determined by X-ray diffraction. Copper is coordinated through O^- and N of OH and NH groups from the ligands in a perfectly flat tetragon. The crystal structure also includes two solvent CH_3OH molecules per $CuEff_2$ unit. The $CuEff_2$ fragments are linked by hydrogen bonds. The binuclear $Cu_2Eff_2Cl_2$ complex was characterized using electronic and IR spectra, EPR, magnetochemical, calorimetric, thermogravimetric methods and elemental analysis. The complex contains bidentately bound monoanionic ligands and chloride ions. Each Cu atom is coordinated with NH, and bridged by the deprotonated OH group of Effortil with the second Cu center. The chloride ions are coordinated with copper as terminal ligands. © 2000 Elsevier Science Ltd. All rights reserved.

Keywords: Effortil; Cu(II) complexes; Structures; Stability constants; EPR; Magnetochemical data

1. Introduction

Recently it was assumed and found that arterial blood pressure is a process regulated by the biometals copper and zinc [1–4]. On the other hand, the drugs for treatment of arterial hypertension are effective ligands and it could be presumed that their action is at least partially related to complexation with the two metals, causing a shift in their homeostasis. From this point of view, we have already studied the complex formation between Cu(II) and different anti-hypertensives such as ACE-inhibitors [5], vasodilators [6] and diuretics [7,8]. Special attention was paid to the β-blockers [8–13], the drugs most widely used for this purpose, which represent aminoalcohols of type **I**, and differ by the substituent R in the phenyl ring.



(I) **(II)**

It seems worth noting however, that one of the most efficient drugs used against arterial hypotension, Effortil, **II** also represents an aminoalcohol of the same type. It was interesting therefore, to study whether its behavior towards copper is analogous and why its effect on the blood pressure is just the opposite.

Hence, the aim of the present study was investigation of the complexation processes between copper(II) and Effortil.

* Corresponding author. Tel.: +35-92-628-323; fax: +35-92-962-5438.
E-mail address: prbontchev@chem.uni-sofia.bg (P.R. Bontchev).

0277-5387/00/$ - see front matter © 2000 Elsevier Science Ltd. All rights reserved.
PII: S0277-5387(00)00468-X

2. Experimental

2.1. Apparatus and analysis

The IR spectra in the 4000–100 cm^{-1} range were recorded on a Perkin–Elmer 893 spectrometer both in Nujol and CsI, the X-band EPR spectra on a Bruker ER 420 spectrometer and the electronic spectra were obtained on a Specord UV–Vis (Carl–Zeiss, Jena). The calorimetric and gravimetric studies were performed on DSC-2C and TGS-2 Perkin–Elmer equipment in argon. The magnetic measurements were carried out in argon atmosphere by the Faraday balance. The elemental analysis was performed according to the standard methods: C and H were determined as CO_2 and H_2O, N through the Duma's method, chlorine by titration with $Hg(NO_3)_2$ after wet digestion of the sample. Copper(II) was determined after ignition of a sample, dissolution of the residue in diluted HNO_3 and titration with standard solution of EDTA using indicator Murexide at pH 8 (ammonia buffer). The potentiometric measurements were provided with aqueous solutions of $(Cu(ClO_4)_2 \cdot 6H_2O)$ containing 5×10^{-4} Cu(II) and 1×10^{-3} mol dm^{-3} of Effortil base (HEff). Aliquots of these solutions with Cu–HEff molar ratio 1:2 were titrated with 9.95×10^{-3} mol dm^{-3} $HClO_4$ to obtain the stability constants. The ionic strength was adjusted to 0.1 mol dm^{-3} with $NaClO_4 \cdot H_2O$. Argon was bubbled through the samples to remove O_2 and CO_2 and for stirring the solution. Measurements were performed on a Radiometer PHM84 pH-meter with accuracy of ± 0.001 pH units, equipped with a GK240C combined electrode and an ABU80 automatic burette for potentiometric titration. The stability constants were calculated by means of a general computation program (PSEQUAD) [14]. X-ray diffraction was studied on a monocrystal using an Enraf–Nonius CAD-4 diffractometer. A transparent violet crystal of $CuEff_2 \cdot 2CH_3OH$ was selected and mounted on an Enraf–Nonius CAD-4 diffractometer. A hemisphere of 1743 independent reflections, of which 1620 with $I > 2\sigma(I)$, was collected at r.t. using graphite monochromated Mo Kα radiation ($\lambda = 1.71073$ Å). The structure was solved by direct methods (SHELXTL) [15] and refined by least squares on F^2 (SHELX-96) [16]. First the Cu, N and O atoms were located according to the difference Fourier map and their positions refined isotropically. Next the C atoms were found and all the atoms refined anisotropically. Finally the H atoms were refined using a riding model. The main crystal and refinement data are listed in Table 1.

Table 1
Crystal data and structure refinement for the mononuclear complex $CuEff_2 \cdot 2CH_3OH$

Empirical formula	$Cu(C_{10}NO_2H_{14})_2 \cdot 2CH_3OH$
Formula weight	488.08
Temperature (K)	293(2)
Wavelength (Å)	0.71073
Crystal system	monoclinic
Space group	$P2_1/n$ (no. 14)
Unit cell dimensions	
a (Å)	7.7373(6)
b (Å)	13.5607(10)
c (Å)	11.7331(9)
α (°)	90
β (°)	99.1470(10)
γ (°)	90
Volume ($Å^3$)	1215.4(2)
Z	2
D_{calc} (g cm^{-3})	1.295
Absorption coefficient (mm^{-1})	0.935
$F(000)$	518
Crystal size (mm)	$0.20 \times 0.15 \times 0.10$
θ Range for data collection (°)	2.31–23.26
Index ranges	$-8 \le h \le 8$, $0 \le k \le 15$, $0 \le l \le 13$
Reflections collected	1743
Independent reflections	1743 [$R_{int} = 0.052$]
Refinement method	full-matrix least-squares on F^2
Data/restraints/parameters	1743/0/143
Goodness-of-fit on F^2	1.139
Final R indices [$I > 2\sigma(I)$]	$R_1 = 0.0442$, $wR_2 = 0.1267$
R indices (all data)	$R_1 = 0.0470$, $wR_2 = 0.1290$
Largest difference peak and hole (e $Å^{-3}$)	0.634 and −0.269

2.2. Synthesis

The ligand was obtained from Sopharma, Bulgaria, $CuCl_2 \cdot 2H_2O$ and CH_3OH (both of analytical grade) were supplied by Riedel E. de Haën AG.

2.2.1. The mononuclear complex

HEff·HCl (0.0541 g) was dissolved in 10 ml methanol. The addition of 1 ml methanolic Cu(II) solution containing 0.0043 g $CuCl_2 \cdot 2H_2O$ and NaOH (0.0200 g in 20 ml methanol) at molar ratio Cu–HEff·HCl–NaOH = 1:10:20 leads to the formation of a violet solution from which a crystalline violet mononuclear complex was obtained after four months. It was filtered, washed with methanol and dried over P_2O_5. *Anal.* Found: C, 54.21; H, 6.97; N, 5.63; Cu, 12.01. Calc. for $CuEff_2 \cdot 2CH_3OH$: C, 54.36; H, 7.05; N, 5.76; Cu, 12.07%. The mononuclear complex was also obtained in aqueous solution, at excess of the ligand, Cu–HEff·HCl = 1:2–1:10 and pH 10.5.

The synthesis of the binuclear complex was realized using 0.0541 g HEff·HCl in 10 ml methanol, Cu(II) salt (0.0213 g $CuCl_2 \cdot 2H_2O$ in 5 ml methanol) and NaOH (0.0100 g in 10 ml methanol). The molar ratio was Cu–HEff·HCl–NaOH = 1:2:2. After three days a green precipitate was formed and it was filtered, washed with methanol and dried over P_2O_5. *Anal.* Found: C, 42.94; H, 5.00; N, 5.04; Cu, 22.61. Calc. for $Cu_2Eff_2Cl_2$: C, 43.02; H, 5.05; N, 5.02; Cu, 22.76%.

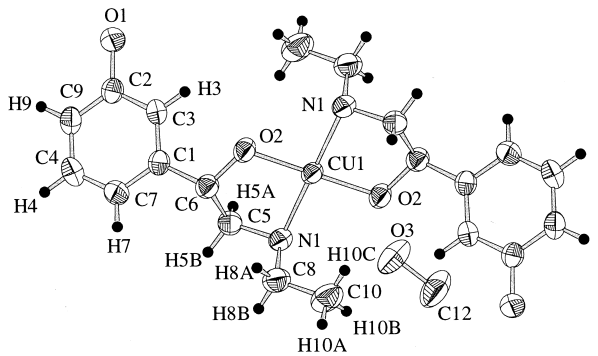


Fig. 1. The asymmetric unit and coordination of the copper atoms in $CuEff_2{\cdot}2CH_3OH$, 50% thermal ellipsoids.

Table 2
Selected bond lengths (Å) and angles (°) for $CuEff_2{\cdot}2CH_3OH$ [a]

Cu coordination		Effortil	
Cu(1)–O(2)	1.905(2)	C(8)–N(1)	1.489(5)
Cu(1)–O(2)	1.905(2)	C(5)–N(1)	1.484(4)
Cu(1)–N(1)	2.042(3)	C(2)–O(1)	1.370(4)
Cu(1)–N(1)	2.042(3)	C(6)–O(2)	1.412(4)
C–C range within 1.375(5)–1.528(5) Å			
O(2)–Cu(1)–O(2)	180.0		
O(2)–Cu(1)–N(1)	85.65(10)		
O(2)–Cu(1)–N(1)	94.35(10)		
O(2)–Cu(1)–N(1)	94.35(10)		
O(2)–Cu(1)–N(1)	85.65(10)		
N(1)–Cu(1)–N(1)	180.0		

[a] Symmetry transformation used to generate equivalent atoms: $1-x, -y+1, -z$.

3. Results and discussion

3.1. Mononuclear $CuEff_2{\cdot}2CH_3OH$ complex

3.1.1. X-ray data and crystal structure

The structure is shown in Fig. 1, and selected bond lengths and angles in Table 2.

In the structure the Cu atoms occupy one crystallographically independent special position. Each Cu atom is coordinated by two OH groups and two N atoms from two ligand molecules in a perfectly flat tetragon. The Cu–O and Cu–N distances (1.905 and 2.042 Å) and O–Cu–N angles (85.60 and 94.40°) are typical for a four-fold square coordination and compare well with the distances reported for similar copper complexes [17]. The $CuEff_2$ and the solvent methanol molecules are arranged in layers parallel to the b-axis. A complex network of hydrogen bonds links these layers in a 3D structure (Fig. 2). The closest Cu–Cu separation corresponds to the a-axis (7.737 Å) which clearly indicates that there is no direct magnetic interaction between the Cu centers in the structure. The C–C, C–N and C–O distances in the Effortil and methanol molecules range from 1.375 to 1.528 Å and the C–H distances are of the order 0.8–1.1 Å.

3.1.2. Electronic spectra

In methanolic solution the mononuclear complex shows an absorbence at 519 nm ($\varepsilon = 92$ l mol^{-1} cm^{-1}) and 626 nm ($\varepsilon = 75$ l mol^{-1} cm^{-1}). These data are in accordance with the assumption for the formation of Cu–N and Cu–O bonds. As a rule the first ones are

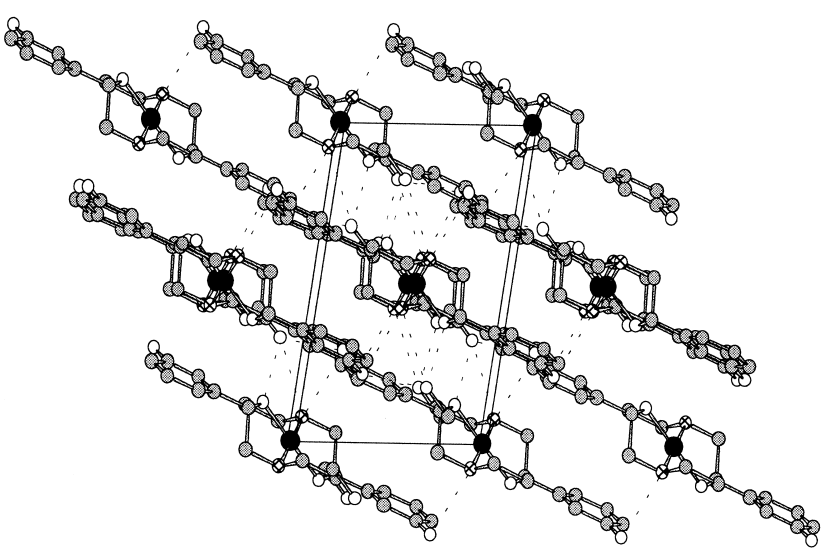


Fig. 2. The 3D structure of $CuEff_2{\cdot}2CH_3OH$, view along the b-axis. Copper, nitrogen, carbon and oxygen atoms are depicted as black, hatched, filled and open circles, respectively, hydrogen atoms are omitted for clarity. The hydrogen bonds are shown as dotted lines.

connected with absorbencies at wavelengths below 600 nm and the second type in the range 600–750 nm, but quite often these regions are not so strictly localized and separated. The position and the intensity of the bands observed are characteristic for Cu(II) complexes with a tetragonal geometry [18,19].

3.1.3. Magnetic measurements

The temperature dependence of the magnetic susceptibility is typical for a normal mononuclear paramagnetic complex (Fig. 3(a)), without any measurable exchange interaction between the Cu(II) centers. The Curie–Weiss law is not obeyed in the temperature range studied and in such conditions the magnetic moment was calculated using the equation $\mu_{eff} = 2.828(\kappa_M T - \theta)^{1/2}$; $\theta = -80$. At low temperatures, the magnetic moment μ is temperature dependent and corresponds to a tetrahedral coordination of copper(II) (Fig. 4) but at higher temperatures (>253 K), the μ-value differs from the theoretical one. Most probably the deviation observed is due to a deformation of the tetrahedral structure to a nearly square-planar one, a fact supported by the obtained EPR data, is also observed in other similar complexes [10,11] and is directly confirmed in the present work by X-ray diffraction data.

3.1.4. EPR spectra

The methanolic solution of the complex at room temperature shows an isotropic spectrum with a resolved hyperfine structure from ^{63,65}Cu and parameters $g_{iso} = 2.103$, $A_{iso} = 86$ at $H_{iso} = 3300$ G. The spectrum of the same solution at 77 K exhibits an anisotropic signal with an additional resolved SHFS from ^{14}N in the perpendicular region of the magnetic field due to the formation of Cu–N bonds. The EPR parameters ($g_{//} = 2.23$, $g_{\perp} = 2.07$, $A_{//} = 204$, $A_{\perp} = 24$, $A_N = 14$ G) are typical for Cu(II) complexes with a nearly square-planar symmetry. The EPR data for the solid state complex at ambient temperature are analogous to those for frozen solutions at 77 K as in other similar cases [10,11,13].

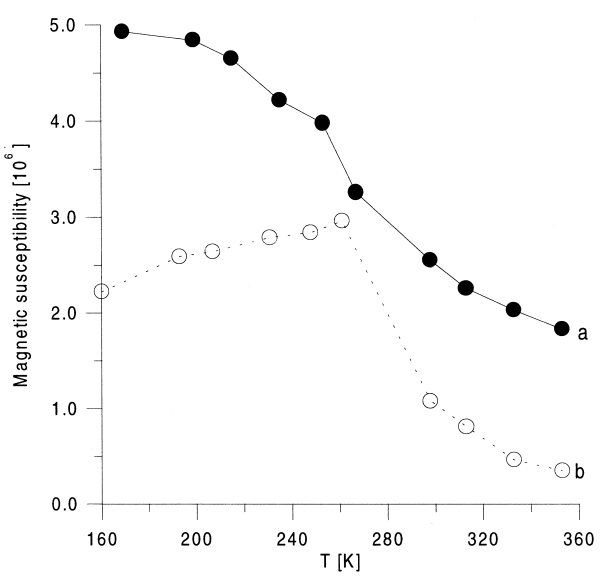


Fig. 3. Magnetic susceptibility vs. T for (a) mononuclear complex $CuEff_2{\cdot}2CH_3OH$ and (b) binuclear $Cu_2Eff_2Cl_2$ complex.

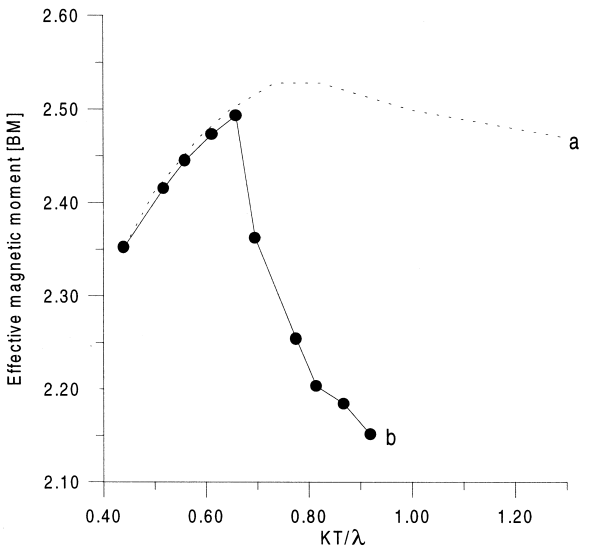


Fig. 4. Graphs μ_{eff} vs. T for the monouclear complex (a) theoretical dependence for a tetrahedral Cu(II) complex; (b) experimental data ($\theta = -80$).

3.1.5. IR spectra

The Effortil base shows absorption bands at 3450 and 3200 cm^{-1} corresponding to ν(OH) and ν(NH), a broad band in the 2600–2800 cm^{-1} range, that can be attributed to $\nu(NH_2^+)$ and a band at 1600 cm^{-1} assigned to δ(NH). In the complex the band at 3450 cm^{-1} is observed with a low intensity, as a result of OH group deprotonation in the aminoalcohol fragment and the presence of CH_3OH. The coordination of NH follows from the shift of the bands of the complex to 3180 and 1650 cm^{-1}. The absorbence in the 2600–2800 cm^{-1} range practically disappears in the complex, which is also an indication for coordination of NH. In the far IR spectrum of the complex, new bands at 475 and 370 cm^{-1} are observed, corresponding to ν(Cu–N) and ν(Cu–O) respectively [20].

3.1.6. Calorimetric and thermogravimetric data

The thermogravimetric study of the complex shows a reduction of the sample weight with about 13.20% in the temperature range 350–430 K. This fact correlates well with the expected value of 13.17% that corresponds to the elimination of two methanol molecules. It is also supported by the DSC data obtained (Fig. 5) showing an endothermic effect at about 400 K, with an enthalpy change of 13.3 cal g^{-1}. The value is higher than the expected one, probably due to another endothermic process at the same temperature interval, indications for which are observed in the DSC curve in Fig. 5.

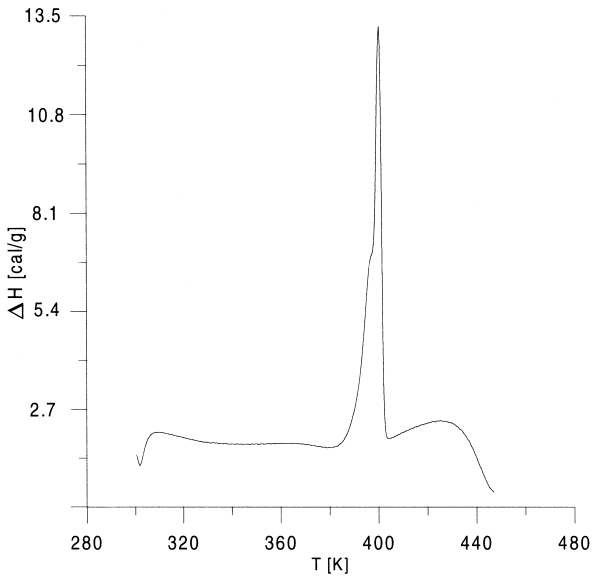


Fig. 5. DSC data for the mononuclear complex $CuEff_2{\cdot}2CH_3OH$.

3.1.7. Dissociation and stability constant

The dissociation (acidity) constant of Effortil using a free base was determined as $pK_a = 8.83 \pm 0.09$. For a molar ratio Cu–HEff = 1:2, two stability constants were calculated: $lg\beta_1[Cu(Eff)]^+ = 5.52 \pm 0.05$; $lg\beta_2[Cu(Eff)_2] = 10.55 \pm 0.04$.

Two Effortil molecules are coordinated to Cu(II), consequently forming the complexes $[Cu(Eff)]^+$ and $[Cu(Eff)_2]$.

3.2. Binuclear complex — $Cu_2Eff_2Cl_2$

3.2.1. Electronic spectra

The methanolic solution of the green complex shows absorbance at 700 nm ($\varepsilon = 96$ l mol^{-1} cm^{-1}) and 385 nm ($\varepsilon = 106$ l mol^{-1} cm^{-1}). The first band is associated with d–d transitions in Cu(II), engaged in Cu–O bonds. The second band at 385 nm is attributed to a ligand-to-metal charge-transfer when a polynuclear copper(II) complex with oxygen-bridge ligand is formed [10,11,13]. It is interesting to notice that in such binuclear complexes, with both Cu–N and Cu–O bonds there is usually no separate bond at $\lambda < 600$ nm, typical for Cu–N bond, but only one broad complex band at 600–700 nm [9–13,22].

3.2.2. Magnetic data

The temperature dependence of the magnetic susceptibility (Fig. 3(b)) is typical for cases of antiferromagnetic exchange interaction between copper(II) centers (see for example [21]). In complexes of that type, the intramolecular antiferromagnetism leads first to an increase of the magnetic susceptibility to a maximum (at the Neel's temperature) and then it decreases as a result of disturbance of the exchange interaction. At high temperatures the complex exhibits a normal paramagnetic character.

These results are in accordance with the other spectral and EPR data indicating the formation of binuclear species in this case, namely the EPR signals at lower and higher fields (1350 and 5470 G, respectively) and the absorbence at 385 nm in the electronic spectra as well.

3.2.3. EPR spectra

In methanolic solution at room temperature, the complex is EPR silent. The spectrum of the same solution at 77 K shows a weak signal at 3300 G and two signals at 1350 and 5470 G. The last two signals are connected with an antiferomagnetic coupling between Cu(II) centers in bi- and polynuclear structures [22]. The spectrum of the solid phase complex shows the same signals as the frozen solution. Similar EPR spectra for Cu(II) complexes with a nearly square-planar geometry were already reported [10,13].

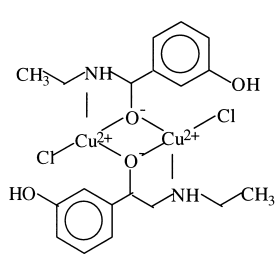
3.2.4. IR spectra

The absorption bands at 3450 and 3200 cm^{-1} (ν(OH) and ν(NH)) of the Effortil base are transformed into one broad band at 3400–3250 cm^{-1} in the spectrum of the complex. The band at 1600 cm^{-1} (δ(NH)) shifts to 1620 cm^{-1} in the complex and the absorbance in the 2600–2800 cm^{-1} range ($\nu(NH_2^+)$) practically disappears. The far IR spectrum of the complex shows three new bands at 538, 420 and 251 cm^{-1} assigned to ν(Cu–N), ν(Cu–O) and ν(Cu–Cl), respectively [20].

3.2.5. Calorimetric and thermogravimetric data

The calorimetric and thermogravimetric studies were provided in the 300–500 K range. The results obtained have shown that no solvent molecules are present in the structure of the solid binuclear green complex.

All data obtained for the $Cu_2Eff_2Cl_2$ complex indicate that they are similar to those for the analogous binuclear Cu(II) complexes of pindolol and oxprenolol, studied by X-ray diffraction [12,13,23]. On the grounds of all these considerations, structure **III** was suggested for the $Cu_2Eff_2Cl_2$ binuclear complex **III**.



(III)

4. Discussion

Effortil forms two types of complex, depending on the solvent and the metal-to-ligand molar ratio. At excess of the ligand, the mononuclear soluble violet complex $Cu(Eff)_2 \cdot 2CH_3OH$ was formed in alkaline methanolic solution, from which the neutral complex very slowly spontaneously precipitated.

The violet complex, however, was obtained in aqueous alkaline solution in a soluble form only, a fact indicating that most probably in such conditions it includes hydroxyl ions instead of solvent molecules and the charged complex thus formed remains in solution. The negative charge of this complex was confirmed by its sorption on anionite (Amberlite IRA-400, Merck). That was the reason for isolating the mononuclear complex in a solid phase only from methanol.

On the other hand the binuclear complex is formed at compatible amounts of the metal and the ligand (1:1–1:2) and only in alkaline methanolic media. In this case, the deprotonated oxygens of the two coordinated ligands act as bridges between the two copper atoms in the framework of the binuclear complex. Each Cu atom is bound also with NH from one ligand, thus forming a chelate ring with one Cl^- present as a terminal ligand. This configuration of the binuclear complex was already proved by us with different methods, including X-ray diffraction for Cu(II) complexes of some β-blockers with similar chemical composition and structure [23]. Unfortunately, in the present case we were unable to obtain crystals of proper size for X-ray study.

The mononuclear violet complex precipitated from methanolic solution can be transformed slowly in excess of the ligand into the green binuclear one after addition of proper amount of Cu(II) in the solution. The reciprocal process, however, is much slower and occurs only partially when excess of Heff is added to the solvent containing the green precipitate. These experiments show that the two complexes can be transformed into each other by changing the reaction conditions in an appropriate way.

5. Supplementary data

Crystallographic data have been deposited with the Cambridge Crystallographic Centre, CCDC No. 140618. Copies of this information may be obtained free of charge from The Director, CCDC 12 Union Road, Cambridge, CB2 1EZ, UK (fax: +44-1223-336-033; e-mail: deposit@ccdc.cam.ac.uk or www: http://www.ccdc.cam.ac.uk).

Acknowledgements

The authors greatly acknowledge the financial support given by the National Research Fund of Bulgaria.

References

[1] L.M. Klevay, Biol. Trace Elem. Res. 5 (1983) 245.
[2] D. Gantenand and E. Ritz (Eds.), Lehrbuch der Hypertonie: Pathophysiologie, Klinik, Therapie, Epidemiologie, Schattauer, Frankfurt, 1985, p. 628.
[3] Ch. Nachev, Dr. Sci. Diss., Medical Academy, Sofia, 1988.
[4] B. Sarkar, in: H.G. Seiler, H. Sigel (Eds.), Handbook on Toxicity of Inorganc Compounds, Marcel Dekker, New York, 1988.
[5] P.R. Bontchev, G. Gochev, B. Evtimova, H. Kadum, Ch. Nachev, J. Inorg. Biochem. 46 (1992) 23.
[6] P.R. Bontchev, Ch. Nachev, B. Evtimova, N.D. Yordanov, E. Zhecheva, D.R. Mehandjiev, Proceedings of the 12th Conference Coordinate Chemistry, Smolenice, CSSR, 1989, pp. 47–52.
[7] P.R. Bontchev, H. Kadum, G. Gochev, B. Evtimova, J. Macicek, Ch. Nachev, Polyhedron 11 (1992) 1973.
[8] P.R. Bontchev, B. Ivanova, K. Koicheva, Proceedings of the Fifth International Symposium on Applied Inorganic and Bioinorganic Chemistry, Corfu, Greece, 1999.
[9] P.R. Bontchev, H. Kadum, B. Evtimova, Ch. Nachev, E. Zecheva, D. Mehandjiev, D. Ivanov, J. Inorg. Biochem. 48 (1992) 153.
[10] I. Pantcheva, P.R. Bontchev, Ch. Nachev, in: G. Ondrejovic, A. Sirota (Eds.), Progress in Coordination and Organometallic Chemistry, Slovac Technical University Press, Bratislava, 1997, pp. 209–214.
[11] P.R. Bontchev, I. Pantcheva, B.B. Ivanova, D. Mehandjiev, Bulg. Chem. Commun. 31 (1999) 59.
[12] P.R. Bontchev, in: G. Ondrejovic, A. Sirota (Eds.), Coordination Chemistry at the Turn of the Century, Slovac Technical University Press, Bratislava, 1999, pp. 53–66.
[13] P.R. Bontchev, I. Pantcheva, B.B. Ivanova, Proceedings of the Fifth International Symposium on Applied Inorganic and Bioinorganic Chemistry, Corfu, Greece, 1999.
[14] D.J. Leggett, Computational Methods for the Determination of Formation Constants, Plenum, New York, 1985, p. 291.
[15] G.M. Sheldrick, SHELXTL, Version 5.03, Siemens Analytical X-ray Instruments, Madison, WI, 1995.
[16] G.M. Sheldrick, SHELX-96, Program for Crystal Structure Determination, University of Göttingen, Germany, 1996.
[17] M. Melnik, M. Kabesova, M. Dunaj-Jurco, C.E. Holloway, J. Coord. Chem. 41 (1997) 35.
[18] E.I. Solomon, W.P. Kevin, E.W. Dean, Structure and Bonding, Springer–Verlag, Berlin, 1983, p. 3.
[19] C. Oldham, in: G. Wilkinson (Ed.), Comprehensive Coordination Chemistry, vol. 5, Pergamon, Oxford, 1987, p. 663.
[20] K. Nakamoto, Infrared and Raman Spectra of Inorganic and Coordination Compounds, 5th ed., Wiley, New York, 1997.
[21] F.E. Mabbs, D.J. Machin, Magnetism and Transition Metal Complexes, Chapman and Hall, London, 1973, p. 172.
[22] P.R. Bontchev, I. Pantcheva, G. Gochev, D. Mehandjiev, D. Ivanov, Trans. Met. Chem. 25 (2000) 196.
[23] P.R. Bontchev, Proceedings of the Fifth International Symposium on Applied Inorganic and Bioinorganic Chemistry, Corfu, Greece, 1999.

PERGAMON

www.elsevier.nl/locate/poly

Polyhedron 19 (2000) 1849–1857

POLYHEDRON

Solution equilibria and structural characterisation of the transition metal complexes of glycyl-L-cysteine disulfide

Csaba G. Ágoston [a], Katalin Várnagy [a], Attila Bényei [b], Daniele Sanna [c], Giovanni Micera [d], Imre Sóvágó [a,*]

[a] *Department of Inorganic and Analytical Chemistry, University of Debrecen, H-4010 Debrecen, Hungary*
[b] *Department of Physical Chemistry, University of Debrecen, H-4010 Debrecen, Hungary*
[c] *Instituto CNR per l'Applicazione delle Tecniche Chimiche Avanzate ai Problemi Agrobiologici, Via Vienna 2, I-07100 Sassari, Italy*
[d] *Department of Chemistry, University of Sassari, Via Vienna 2, I-07100 Sassari, Italy*

Received 5 May 2000; accepted 16 June 2000

Abstract

Stoichiometry, stability constants and structure of the complexes formed in the reaction of copper(II), nickel(II), zinc(II), cobalt(II) and cadmium(II) with $(GlyCys)_2$ containing disulfide bond were determined by potentiometric, UV–Vis, NMR and EPR spectroscopic methods. The complex $[Ni(GlyCys)_2 \cdot H_2O]$ was prepared in the solid state and its structure determined by single crystal X-ray diffraction method. Disulfide sulfur atoms of $(GlyCys)_2$ were not metal-binding sites in any of the systems studied in solution or in the solid state. It was found that copper(II) is able to induce deprotonation and coordination of the peptide amide nitrogen donor atoms. This resulted in the formation of [CuL], $[Cu_2H_{-2}L]$ and $[CuH_{-1}L]^-$ as the major species in solution. In the case of nickel(II), cobalt(II), zinc(II) and cadmium(II) the complex [ML] predominates, and the outstanding stability of this species was explained by the formation of a macrochelate between the (NH_2, CO)-coordinated five-membered chelates in solution. Crystal structure of $[Ni(GlyCys)_2 \cdot H_2O]$ revealed the octahedral geometry of nickel(II) in a polymeric structure. © 2000 Elsevier Science Ltd. All rights reserved.

Keywords: Disulfide; Peptides; Transition metal ions

1. Introduction

Disulfide bonds (S–S) have an outstanding significance in the stabilisation of protein structures. As a consequence, both complex formation and redox reactions of this moiety are of much biological importance. In general the disulfide bond easily undergoes reductive cleavage giving rise to sulfur radicals, thiols, thioethers or thiolate anions. The metal ion promoted disproportionation of disulfides has already been well clarified [1], while the insertion of a metal-bond nitrogen atom into a disulfide bond has been described recently [2]. The various redox reactions of disulfide bridges are often involved in the catalytic activity of various metalloenzymes including nickel containing methyl-coenzyme M reductase [3].

There are many examples in the literature of the interactions of metal ions and organic ligands containing disulfide bonds and the most important aspects of the coordination chemistry of organodisulfide ligands have already been reviewed [4]. It is also obvious from these studies that apart from the soft metal ions the stable coordination of disulfide sulfur atoms generally takes place in aprotic solvents or in the absence of other strongly coordinating donor groups. Consequently, in the case of the simplest and biologically important disulfide ligands (cystine, oxidized glutathione and D-penicillamine disulfide) the amino, carboxylate and amide functions are the major metal binding sites for the 3d divalent metal ions, while the disulfide sulfur atoms are uncoordinated or take part in a weak interaction. The structure of the dimeric species obtained in the reaction of copper(II) and D-penicillamine disulfide has been described via the equatorial coordination of the amino acid binding sites with a

* Corresponding author. Tel.: +36-52-512-900; fax: +36-52-489-667.
E-mail address: sovago@tigris.klte.hu (I. Sóvágó).

0277-5387/00/$ - see front matter © 2000 Elsevier Science Ltd. All rights reserved.
PII: S0277-5387(00)00469-1

weak axial interaction of sulfur atoms [5]. In the case of oxidised glutathione a 2:1 = Cu(II):GSSG complex was prepared with (ON_3) equatorial binding sites and weak axial interaction of both sulfur atoms [6]. Copper(II) complexes of pyridine- or imidazole-containing disulfide ligands were also characterised by the formation of Cu–S(disulfide) bonds in solution on the basis of charge transfer transition around 310–330 nm [7]. The existence of a relatively short Cu(II)–S bond length was reported in the complexes of dithiodipropanoate [8] and synthetic macrocyclic bis(disulfide) tetramine ligands, while other examples of copper(II) complexes of disulfides have been reviewed by Fox et al. [9]. As concerns the other 3d transition metal ions a strong interaction of nickel(II) and sulfur atom was reported in the nickel(II) complex of a ligand containing both pyridine and disulfide donor functions [10].

In a previous study we reported the results of potentiometric and spectroscopic studies in solution on the cobalt(II), nickel(II), copper(II) and zinc(II) complexes of three disulfide ligands: D-penicillamine disulfide, oxidised glutathione and L-cysteinylglycine disulfide [11]. The amino, carboxylate and the amide functions were detected as the exclusive metal binding sites and no indication on the formation of M–S bonds was obtained. In the case of the copper(II)-oxidised glutathione system many other studies have been performed in solution, but the Cu(II)–S interaction was excluded in all cases [12–15]. The peptide hormones oxytocin and vasopressin are other examples of simple peptides containing disulfide bonds. The twenty-membered ring linked by the disulfide bridges (between Cys^1 and Cys^6 residues) provides a unique conformation of these molecules. This resulted in the increased stability of metal complexes [16–18]. The enhancement of thermodynamic stability was, however, not attributed to a significant Cu(II)–S interaction, which was only detected in the 2N complexes of oxytocin [16]. The development of a more intense charge transfer band around 380 nm in the 2N complex of the copper(II)–glipressin (GlyGlyGly-Lys^8–vasopressin) system also was explained by the formation of Cu(II)–S(disulfide) bond [18]. In contrast with the above-mentioned 3d transition metal ions the soft palladium(II) and platinum(II) interact easily with disulfides and the existence of strong Pd–S and Pt–S bonds were reported in the complexes of cystine or oxidized glutathione [19–21].

The survey of the literature data obtained for the complexes of disulfide derivatives of peptides with 3d transition element reveals that the formation of M–S bonds are generally negligible in solution. On the other hand, the results obtained for the copper(II) complexes of glipressin suggest that the formation of this bond requires a specific arrangement of donor groups in the peptide chain [18]. The role of specific amino acid sequences in the enhanced metal binding ability of peptide molecules is well known and it is probably best represented by the C-terminal His peptides, e.g. GlyHis and GlyGlyHis [22,23]. Similar increased stability of the copper(II) or nickel(II) complexes of peptides were reported with several other peptide sequences including GlyGlyCys [24], X–X–Asp [25] and to a smaller extent with the tripeptides of methionine [26]. The oxidised form of the dipeptide glycyl-L-cysteine, $(GlyCys)_2$, contains the disulfide sulfur atoms in a chelating position with the amide nitrogen. Therefore this molecule can be a promising candidate for the metal ion promoted formation of disulfide complexes. In this paper we report the results of combined potentiometric and spectroscopic studies on the copper(II), nickel(II), cobalt(II), zinc(II) and cadmium(II) complexes of $(GlyCys)_2$ in solution. The crystal structure of the nickel complex of $(GlyCys)_2$ also has been determined by single crystal X-ray diffraction method.

2. Experimental

2.1. Materials

The peptides glycyl-L-cysteine disulfide, $(GlyCys)_2$, and glycineamide were purchased from Bachem and their purity checked via potentiometric titrations. Stock solutions of the metal ions ($CoCl_2$, $NiCl_2$, $CuCl_2$, $ZnCl_2$ and $Cd(NO_3)_2$) were prepared from analytical grade reagents and their concentrations were checked gravimetrically via precipitation of oxinates.

2.2. Potentiometric studies

The pH-potentiometric titrations were performed in 5 cm^3 samples in the metal ion concentration range 2–4×10^{-3} mol dm^{-3} and with metal ion to ligand ratios between 2:1 and 1:2. The measurements were made with a Radiometer pHM64 pH-meter equipped with a Russel CWR/320/757 combined electrode and an ABU-13 automatic burette containing a carbonate free stock solution of potassium hydroxide. 40–60 titration points were recorded for all different ratios. During the titration argon was bubbled through the samples to ensure the absence of oxygen and carbon dioxide, and stirring of the solutions. All pH-potentiometric measurements were carried out at a constant ionic strength of 0.2 mol dm^{-3} KCl (KNO_3 for cadmium(II)) and at constant temperature (298 K). The pH-readings were converted to hydrogen ion concentration and the overall stability constants ($\log \beta_{pqr}$) were calculated by means of a general computational program (PSEQUAD) [27].

$$pM + qH + rL \rightleftharpoons M_pH_qL_r$$

$$\beta_{pqr} = \frac{[M_pH_qL_r]}{[M]^p[H]^q[L]^r}$$

2.3. Spectroscopic studies

UV–Vis absorption spectra of copper(II) and nickel(II) complexes were recorded on an HP 8453 diode array spectrophotometer in the concentration range of 4×10^{-3} mol dm^{-3} for copper(II) and 10^{-2} mol dm^{-3} for nickel(II). Anisotropic X-band EPR spectra of copper(II) complexes were recorded at 120 K using a Varian E-9 spectrometer in frozen solution after addition of ethylene glycol to ensure good glass formation. Proton NMR spectra of the free ligand and zinc(II) complexes ($c_L = c_{Zn} = 10^{-2}$ mol dm^{-3}) were measured in D_2O as a function of pD. The spectra were recorded on a Bruker MA 360 MHz instrument using TSP (sodium 3-trimethylsilylpropionate) as internal standard.

2.4. Crystallisation of [Ni(GlyCys)$_2$·H$_2$O] ($C_{10}H_{18}N_4NiO_7S_2$)

One equivalent of $(GlyCys)_2$ was added to a solution of $NiCl_2$ in water ($c = 0.1$ mol dm^{-3}) and the pH was adjusted to 8.50. The solution was transferred into a glass tube and methanol was layered on it. Green crystals were formed at the interface which were filtered off, washed with a mixture of cold water and methanol and dried in air.

2.5. Structure analysis and refinement

Green prism crystals ($0.3 \times 0.25 \times 0.2$ mm) of $C_{10}H_{18}N_4NiO_7S_2$, $M = 429.11$, trigonal, $a = 12.988(4)$, $b = 12.988(6)$, $c = 20.665(7)$ Å, $V = 3019$ Å^3, $Z = 6$, space group: $P3_121$, $\rho_{calc} = 1.416$ g cm^{-3}. Data were collected at 293(1) K, Enraf Nonius MACH3 diffractometer, Mo Kα radiation $\lambda = 0.71073$ Å, ω-2θ motion, $\theta_{max} = 25.5°$, 2017 measured, 2017 unique reflections of which 1519 were with $I > 2\sigma(I)$, decay: 1%. The structure was solved using the SIR-92 software [28] and refined on F^2 using SHELX-97 [29] program, publication material was prepared with the WINGX-97 suite [30]. $R(F) = 0{,}0853$ and $wR(F^2) = 0.246$ for 2017 reflections, 220 parameters. The maximum and minimum residual electron densities are 1.057 and -0.607 e Å^{-3}, respectively.

3. Results and discussion

Stability constants of the proton and metal ion complexes of $(GlyCys)_2$ were determined by pH-potentiometric titrations of the samples containing the metal ion and ligands at different ratios. The stability constants of the complexes and the corresponding pK values are included in Table 1.

The lowest pK values (around 2–3) correspond to the deprotonation of the carboxylic groups, while the other two deprotonation processes in the pH range 7–9 results from the ammonium groups. The potentiometric titration curves provide an unambiguous proof that extra deprotonation processes occur only in the copper(II) containing systems. In the copper(II)–$(GlyCys)_2$ = 2:1 system two equivalents of base are titrated in addition to the carboxylic and ammonium groups suggesting that copper(II) is able to induce deprotonation and coordination of amide nitrogen donor atoms. In the case of cobalt(II), nickel(II), zinc(II) and cadmium(II) the parent mono and bis complexes can form and the coordination of the amide groups can be ruled out below pH 10. On the other hand, stable pH values cannot be determined in more alkaline solutions, because all metal ions are able to induce disproportionation of disulfide bonds in alkaline solutions as was reported for oxidised glutathione [1]. As a consequence, only the experimental points below pH 10 were used for calculation of stability constants of metal complexes.

Table 1
pK values and stability constants ($\log \beta_{pqr}$) of the metal complexes of $(GlyCys)_2$[a]

		Cu(II)	Ni(II)	Co(II)	Zn(II)	Cd(II)
pK_1	2.06(4)					
pK_2	3.21(2)					
pK_3	7.75(2)					
pK_4	8.77(2)					
$[MHL]^+$		14.55(4)	12.85(3)	12.01(5)	12.55(9)	11.70(20)
[ML]		10.35(3)	7.41(2)	5.51(1)	6.69(2)	5.40(3)
$[MH_{-1}L]^-$		3.55(4)	−2.83(7)			
$[MH_{-2}L]^{2-}$		−7.03(9)				
$[ML_2]^{2-}$				8.87(8)		8.40(10)
$[M_2H_{-1}L]^+$		8.13(8)				
$[M_2H_{-2}L]$		3.55(3)				
$[M_2H_{-3}L]^-$		−4.27(6)				
$[M_2H_{-4}L]^{2-}$		−14.63(7)				

[a] $I = 0.2$ mol dm^{-3}, $T = 298$ K (standard deviations are in parenthesis).

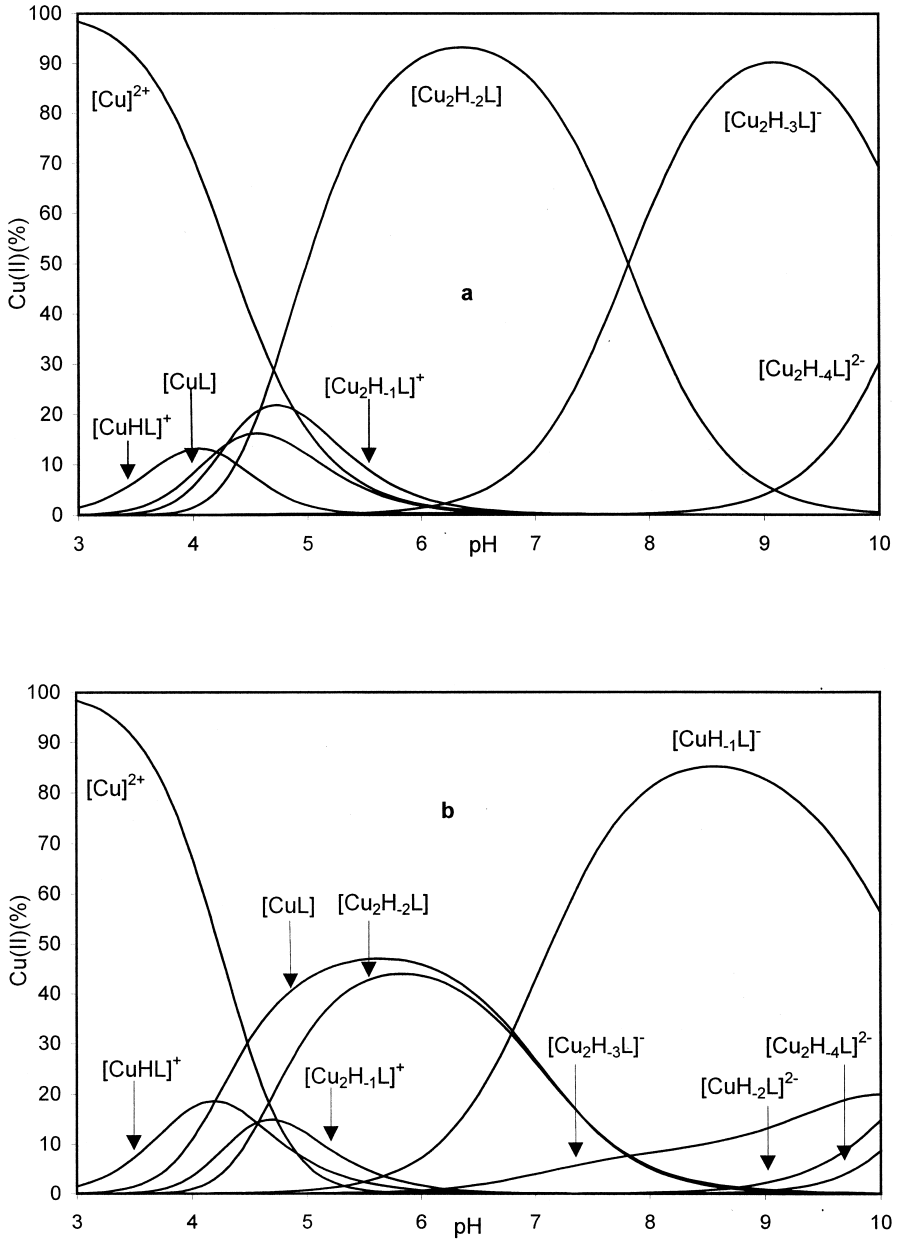


Fig. 1. Concentration distribution of the complexes formed in the copper(II)–$(GlyCys)_2$ system. (a) $c_{Cu} = 8 \times 10^{-3}$ mol dm^{-3}, $c_L = 4 \times 10^{-3}$ mol dm^{-3}; and (b) $c_{Cu} = c_L = 4 \times 10^{-3}$ mol dm^{-3}.

In agreement with the conclusions drawn from the titration curves, Table 1 shows a significant difference in the complex formation processes of copper(II) and the other metal ions. Namely, in the case of copper both mono- and dinuclear species can form, while the other systems are characterised by the formation of [ML] as the major species. Concentration distributions of the various complexes formed in the copper(II)–$(GlyCys)_2$ system at 1:1 and 2:1 ratios are shown in Fig. 1.

It can be seen from Fig. 1 that in the copper(II)–$(GlyCys)_2$ system the complex formation starts above pH 3 and the stoichiometry of the first species is $[CuHL]^+$, which can correspond to the coordination of the terminal amino and neighbouring carbonyl oxygen donor atoms in a five-membered chelate, while the amino group at the other side of the disulfide bridge remains uncoordinated and protonated. EPR spectra of equimolar solutions support this conclusion (see Table 2), because the parallel region of EPR spectra provides the parameters reminescent to those of (NH_2, CO) species of GlyGly [31].

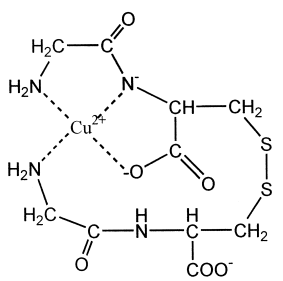
The species [CuL] is present in the pH range 4.5–6.5 and its spectral parameters show a close similarity to those of $[CuH_{-1}L]$ of GlyGly or other common dipeptides. It supports that one dipeptide unit of the

molecule is coordinated as the common dipeptides, (NH_2, N^-, COO^-), while the other side is still free with protonated amino group. The visible spectra of equimolar solutions do support this conclusion, because $\lambda_{max} = 635$ and 640 nm and $\varepsilon = 74$ and 84 $dm^3\ mol^{-1}\ cm^{-1}$ can be obtained for the [CuL] of $(GlyCys)_2$ and $[CuH_{-1}L]$ of GlyGly, respectively [31]. Further increase of pH results in a blue shift of absorption spectra ($\lambda_{max} = 612$ nm and $\varepsilon = 80$ $dm^3\ mol^{-1}\ cm^{-1}$) and it is accompanied with a characteristic change of EPR parameters. The most reasonable explanation for the binding sites of the species $[CuH_{-1}L]^-$ that one more nitrogen donor from the other dipeptide unit of the molecule coordinates to copper(II) as it is represented by Scheme 1.

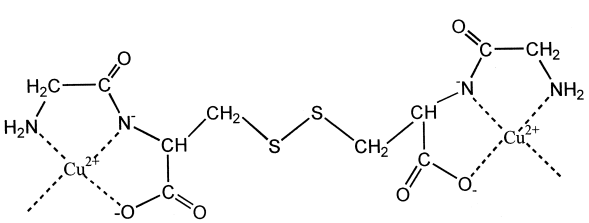
Table 2
Parameters of the parallel region of EPR spectra of the complexes formed in copper(II)–$(GlyCys)_2$ and copper(II)–GlyGly systems[a]

Species	Coordination	$g_{\|}$	$10^{-4}A_{\|}/cm^{-1}$
Cu(II)–$(GlyCys)_2$			
$[CuHL]^+$	(NH_2, CO)	2.330	153
[CuL]	(NH_2, N^-, COO^-)	2.236	193
$[CuH_{-1}L]^-$	(NH_2, N^-, COO^-) + (NH_2, CO)	2.215	171
Cu(II)–GlyGly [b]			
$[CuL]^+$	(NH_2, CO)	2.332	161
$[CuH_{-1}L]$	(NH_2, N^-, COO^-)	2.248	185
$[CuH_{-1}L_2]^-$	(NH_2, N^-, COO^-) + (NH_2, CO)	2.232	168

[a] For the $[CuH_{-1}LB]^-$ complex of GlyGly and *N*-acetyllysine $g_{\|} = 2.226$ and $A_{\|} = 168 \times 10^{-4}$ cm^{-1} were measured.
[b] Data are taken from Ref. [31]



Scheme 1.



Scheme 2.

The binding mode in Scheme 1 is similar to that of GlyGly in $[CuH_{-1}L_2]^-$, but in the case of GlyGly the second ligand coordinates via the amino-N and carbonyl-O donor atoms in an equatorial-axial equilibrium. The mixed complex $[CuH_{-1}LB]^-$ provides a good model for the structure of $[CuH_{-1}L]^-$ of $(GlyCys)_2$. In the ternary species B represents *N*-acetyllysine, which is a monodentate amino donor via the ε-amino group and the spectral parameters $A_{\|} = 168 \times 10^{-4}$ cm^{-1}, $g_{\|} = 2.226$ and $\lambda_{max} = 612$ nm, $\varepsilon = 96$ $dm^3\ mol^{-1}\ cm^{-1}$ were reported for the mixed ligand complex [32]. The spectral data for the species $[CuH_{-1}L]^-$ of $(GlyCys)_2$ are slightly different from those of the complexes described above. However, the spectral trend observed on passing from (NH_2, N^-, COO^-) to (NH_2, N^-, COO^-) + (NH_2, CO) coordination, namely the simultaneous decrease of both $A_{\|}$ and $g_{\|}$, is the same in all the three systems. This trend is unusual for a regular geometry and indicates the achievement of a distorted structure even if further data are needed for a complete understanding of the details of structural changes. In any case, it means that in the species $[CuH_{-1}L]^-$ the two dipeptide residues linked by the disulfide bridge are not identical, being tridentately coordinated from one end and monodentately from the other one. This binding mode, of course, should result in some enhancement of the thermodynamic stability of the complexes and suppresses the hydroxo complex formation. It is reflected in the increase of p*K* for the formation of the hydroxo complexes $[CuH_{-2}L]^{2-}$, because the values 9.37 and 10.58 can be obtained for GlyGly and $(GlyCys)_2$, respectively.

The potentiometric titration curves indicate that in the copper(II)–$(GlyCys)_2$ system two additional equivalents of base can be titrated in the presence of excess of metal ion. In principle, the extra base consumption can correspond to both deprotonation of the second amide nitrogen or only hydrolytic processes. The spectral changes during titration definitely support the amide coordination above pH 5 and it results in dinuclear complex formation as it is shown by Fig. 1. A comparison of Fig. 1(a, b) reveals that the dimeric species are also present in equimolar solution but their concentration will predominate only in the presence of metal ion excess. The absorption maximum of the complex $[Cu_2H_{-2}L]$ appears at $\lambda_{max} = 639$ nm, which corresponds to the assumption that both copper(II) is coordinated in the (NH_2, N^-, COO^-) environment as it is depicted by Scheme 2. The dimeric complex $[Cu_2H_{-2}L]$ has two free coordination sites, which are occupied by water molecules or hydroxide ions in slightly basic media (see Fig. 1).

EPR spectra of the samples containing metal ion excess are poorly resolved, but the signals of free copper(II) ions disappear by pH 6 and the significant line

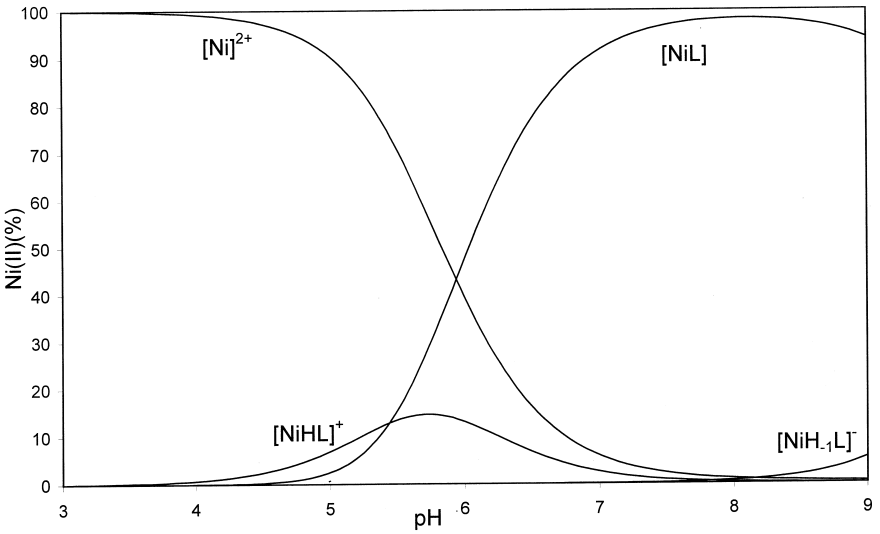


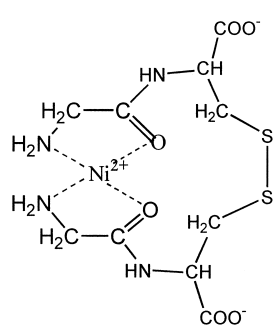
Fig. 2. Concentration distribution of the complexes formed in the nickel(II)–$(GlyCys)_2$ system. $c_{Ni} = c_L = 4 \times 10^{-3}$ mol dm^{-3}.

broadening can be explained by the dipolar coupling between the copper(II) units of the species $[Cu_2H_{-2}L]$.

Another question which arises in connection with the structural characterisation of the copper(II) complexes of $(GlyCys)_2$ is whether the disulfide moiety took part in any interaction with the metal ion. The absence of any characteristic charge transfer band below 400 nm and the clear evidence for the existence of the (NH_2, N^-, COO^-) binding site seem to rule out the involvement of sulfur atom in metal binding in solution. In part this is in contradiction with our expectations, but can be explained by the more effective coordination of the charged carboxylate residue. On the other hand, it should be emphasized that this result was obtained in solution and a weak metal ion interaction with the disulfide bond is still a possibility in the solid state as it was found for the copper(II) complex of D-penicillamine disulfide [5,11].

The pH-potentiometric titration curves of nickel(II)–$(GlyCys)_2$ system at different metal ion to ligand ratios show that there is no any extra base consuming process below pH 9. This is clear evidence that the amide nitrogen is not a metal binding site and the 1:1 complex should have an outstanding thermodynamic stability as compared to that of the bis complex. Equilibrium data in Table 1 reveal that the formation of only three species $[NiHL]^+$, [NiL] and $[NiH_{-1}L]^-$ can be detected in this system. The corresponding species distribution curves are shown by Fig. 2 and it can be seen that $[NiHL]^+$ and $[NiH_{-1}L]^-$ are only minor species and the interaction of nickel(II) and $(GlyCys)_2$ can be described almost exclusively by the formation of the species [NiL]. A reasonable explanation for the outstanding thermodynamic stability of the species [NiL] and for the lack of bis(ligand) complex formation can be given by the assumption of the binding mode shown by Scheme 3. The enhanced thermodynamic stability of the complex [NiL] probably stems from the formation of 16-membered loop around the central metal ion. This loop is a consequence of the presence of the disulfide bond in the molecule supporting that this residue affects the thermodynamic stability of the complexes via the change of the conformation of the molecules without the formation of a direct Ni–S bond. The increased nickel binding ability of $(GlyCys)_2$ as compared to that amino acid amides is reflected in the corresponding stability constants, too. Namely, $\log \beta_1 = 7.41$ was obtained for [NiL] of $(GlyCys)_2$, while $\log \beta_2 = 4.93$ was reported for $[NiL_2]^{2+}$ of valineamide [33]. The formation of a similar loop or macrochelate and extra stabilization of the complex was reported in the copper(II)-oxidised glutathione system [11].

According to Scheme 3 the species [NiL] has the same binding sites as that of $[NiL_2]^{2+}$ of glycineamide [33,34]. The absorption spectra of the complexes show the presence of octahedral central metal ions in both species and in the visible range the spectral parameters $\lambda_1 = 373$ and 373 nm and $\lambda_2 = 620$ and 621 nm were measured for [NiL] of $(GlyCys)_2$ and $[NiL_2]^{2+}$ of



Scheme 3.

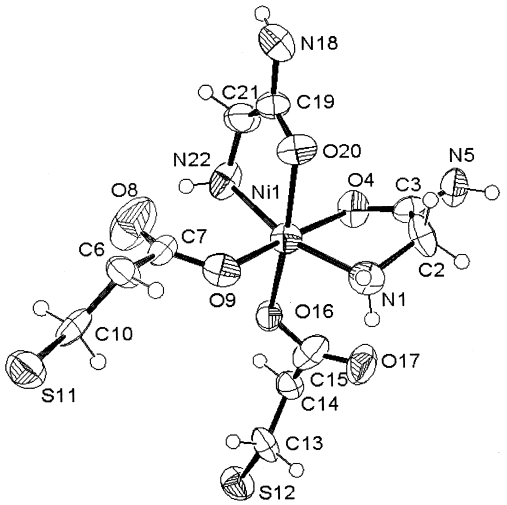


Fig. 3. ORTEP view and numbering scheme of $[Ni(GlyCys)_2 \cdot H_2O]$ (50% probability displacement ellipsoids).

glycineamide, respectively. These parameters show a very close similarity in the binding sites, but on the other hand there is a big difference in the complex formation processes of $(GlyCys)_2$ and glycineamide. Namely, in the nickel(II)–glycineamide system the species $[NiL_2]^{2+}$ is present only in a narrow pH range (around pH 8) and by pH 9 it is followed by the complete formation of the square planar and diamagnetic $[NiH_{-2}L_{-2}]$ complex with the cooperative deprotonation of two amide nitrogens. This reaction and the formation of square planar complexes, however, can not be detected at any pH or metal ion to ligand ratios in the nickel(II)–$(GlyCys)_2$ system. It supports that the binding mode presented by Scheme 3 prevents deprotonation and coordination of the amide groups and also prevents the interaction with the disulfide bond.

The exclusive formation of the species [NiL] in the pH range of 6–9 and its structural peculiarity stimulated us to prepare the complex in the solid state. The compound was obtained with the stoichiometric composition of $C_{10}H_{18}N_4NiO_7S_2$ ($[Ni(GlyCys)_2 \cdot H_2O]$) and X-ray quality crystals were grown from a mixture of methanol and water. The crystal structure of the complex $[Ni(GlyCys)_2 \cdot H_2O]$ shows octahedral nickel(II) ions (Fig. 3), but in contrast with Scheme 3 in a coordinatively saturated environment. Four coordination sites of the octahedron are occupied by two amino-N and two carbonyl-O donor atoms, while the remaining two co-ordination sites are occupied by the carboxylate residues. Thus all coordination sites of the metal ions and all possible donor functions of the ligands take part in binding in the solid state. The other difference between the structures obtained in solution and in the solid state is that the $(NH_2, CO)_2$ coordination environment exists in a polymeric network in the solid state and that the two five-membered chelate rings come from two different ligands. Selected examples of bond lengths and angles are collected in Table 3.

It can be seen from Fig. 3 and also from Table 3 that coordination geometry of the central Ni(II) ion corresponds to a slightly distorted octahedron. The bond lengths of the three different types of metal–ligand bond (Ni–N(amino), Ni–O(carbonyl) and Ni–O-(carboxylate)) are quite close to each other being in the range 2.070–2.111 Å. There are more significant differences in the bond angles. The smallest values are obtained for the chelating sites N(22)–Ni(1)–O(20) and N(1)–Ni(1)–O(4) are 78.2 and 80.7°, respectively. The monodentate carboxylate donor functions are more separated, but they are in *cis* arrangement, while the two nitrogen donors occupy *trans* positions. The Ni(II)–S distance ranges from 5.864 to 6.603 Å, supporting that the disulfide donors are not involved in metal binding in the solid state either. The complex crystallizes in space group of $P3_121$ with significant solvent accessible void volumes. However, only one solvent water molecule with high isotropic atomic displacement parameter for oxygen (O1w) could be located on the electron density map. The void space can be explained by the polymeric nature of the structure. N1, N5, N18, N22, O18 and O1w donors participate in

Table 3
Selected bond lengths (Å) and angles (°) for the compound $[Ni(II)(GlyCys)_2 \cdot H_2O]$

Ni1–N22	2.070(10)
Ni1–O4	2.074(10)
Ni1–N1	2.081(12)
Ni1–O16	2.092(9)
Ni1–O9	2.104(9)
Ni1–O20	2.111(9)
S12–C13	1.817(15)
S12–S12 [a]	2.017(9)
S11–C10	1.803(17)
S11–S11 [a]	2.043(9)
O9–C7	1.267(17)
O20–C19	1.222(15)
O4–C3	1.292(16)
O17–C15	1.220(18)
O16–C15	1.282(17)
N22–Ni1–O4	86.1(5)
N22–Ni1–N1	163.5(5)
O4–Ni1–N1	80.7(4)
N22–Ni1–O16	94.9(4)
O4–Ni1–O16	90.3(4)
N1–Ni1–O16	95.0(4)
N22–Ni1–O9	98.4(4)
O4–Ni1–O9	174.1(4)
N1–Ni1–O9	94.2(4)
O16–Ni1–O9	93.0(4)
N22–Ni1–O20	78.2(4)
O4–Ni1–O20	88.8(4)
N1–Ni1–O20	91.6(4)
O16–Ni1–O20	173.2(4)
O9–Ni1–O20	88.5(4)

[a] $-x, -x+y, 4/3-z$.

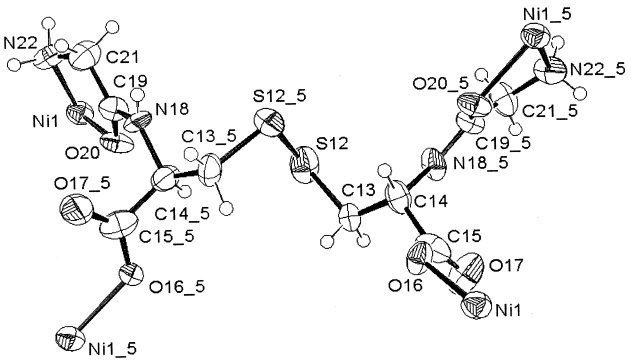


Fig. 4. Coordination modes of nickel on one $(GlyCys)_2$ ligand. Symmetry code:_5: $-x, -x+y, 4/3-z$.

an infinite H-bond network while N1 and N22 form intramolecular H-bonds, too. For the numbering scheme see Fig. 3. There are 14 and 26 membered macrocycles in the structure formed by the sigma bond network of ligands coordinated to Ni(II). Fig. 4 is another view of the complex showing that one ligand is coordinated to four independent metal ions providing a polymeric network, in which all coordination sites of the metal ions and all donor groups of the ligands (except disulfide sulfur atoms) are involved in coordinative bonds.

The results obtained for the structure of [NiL] in the solid state seem to be in contradiction with those suggested in solution. However, it should be considered that the structure presented in Scheme 3 was suggested for rather diluted solutions, where the existence of coordinatively unsaturated metal ions is quite common. Steric requirements rule out the binding of free carboxylate residues to the same metal ion in the monomeric complex, but they can act as additional binding sites for another [NiL] unit in more concentrated solutions. As a consequence, the coordinatively unsaturated loop structure will be destroyed during crystallisation, but the major metal binding sites (NH_2, $CO)_2$ will remain the same.

The complex formation processes of cobalt(II), zinc(II) and cadmium(II) with $(GlyCys)_2$ are rather similar to those of nickel(II). Namely, the species [ML] predominates in all cases and it should have the same binding sites as reported for the nickel(II) complexes. The corresponding stability constants are, however, smaller than those of nickel(II). This results in two major differences between nickel(II) and the other metal ions. On the one hand, the lower thermodynamic stability of the complexes is not able to prevent metal ion hydrolysis and results in precipitation in slightly basic media. On the other hand, there is an increased tendency for the formation of bis(ligand) complexes. This is especially true for cobalt(II) and cadmium(II), but the ratio of stepwise stability constants is rather high even with these metal ions ($\log(K_1/K_2) = 2.15$ and 2.40 for cobalt(II) and cadmium(II), respectively) supporting the fact that [ML] is the major species with all metal ions. Proton NMR spectra of the ligand and zinc(II) containing systems provided further evidence for the existence of [ZnL] as major species in zinc(II)–$(GlyCys)_2$ system. Protons of CH_2(Gly) moieties are detected as a singlet both in the free ligand and in the zinc(II) complex, but the chemical shift of their protons is a function of pD and the extent of complexation. The NMR peaks were obtained as follows: 3.892 and 3.893 ppm (pD 3.90), 3.871 and 3.674 ppm (pD 6.50), 3.783 and 3.659 ppm (pD 7.40), 3.639 and 3.643 ppm (pD 8.05) for the free ligand and Zn(II): $(GlyCys)_2 = 1{:}1$ solutions, respectively. These data clearly indicate that there is no complex formation below pH ~ 4 while the very small changes of CH_2 peaks in the zinc(II) containing systems between pD 6.50 and 8.05 suggest the existence of one major species in agreement with the complexation with nickel(II) shown by Fig. 2. None of the above mentioned results provided evidence for the existence of M–S bond in complexes. In some sense it contradicts with our previous expectations based upon the location of disulfide bond in the amino acid sequence of the peptide. After the coordination of the first two nitrogen donors (amino and amide) both carboxylate-O and disulfide-S atoms are in favourable position for metal ion coordination. The preference of (NH_2, N^-, COO^-)-binding to that of (NH_2, N^-, S) probably comes from the charge neutralization and from the higher flexibility of the small carboxylate function. On the other hand, these results indicate that sulfur atoms of disulfide bonds are even weaker donors towards 3d transition metal ions than the thioether sulfur atoms [26].

To summarize the results obtained for the metal complexes of the disulfide bridged peptide molecule $(GlyCys)_2$ it can be concluded that in the case of 3d transition elements including copper(II), nickel(II), cobalt(II) and zinc(II) the stable coordination of nitrogen and oxygen donors in chelates rules out the formation of M–S bonds both in solution and, at least in the case of nickel(II), in the solid state. The complex formation processes of $(GlyCys)_2$ are, however, significantly different from those of simple di- or tetrapeptides (e.g. from diglycine or tetraglycine), which is caused by the presence of the disulfide bonds. In the case of copper(II) it results in the enhanced stability of the species with (N_3O) donor sites, $[CuH_{-1}L]^-$, in equimolar solution and in the formation of dinuclear complexes in the presence of excess of copper(II). As concerns the other 3d transition metal ions the stable coordination of the amino and carbonyl functions prevent amide and disulfide coordination and this results in the formation of a sixteen-membered loop around the central metal ion (see Scheme 3 for nickel(II)). The complexes of cadmium(II) are very similar to those of

zinc(II) or especially cobalt(II) and the sulfur coordination was ruled out with this metal ion, too. Cadmium(II) generally prefers the coordination of sulfur donor atoms [35], but in this case the binding in a stable chelate should be accompanied by the formation of Cd(II)–N(amide) bond, which has not yet been reported in peptides.

4. Supplementary data

Crystallographic data have been deposited with the Cambridge Crystallographic Data Centre, CCDC No. 143861. Copies of this may be obtained free of charge from The Director, CCDC, 12 Union Road, Cambridge, CB2 1EZ, UK (Fax: +44-1223-336033; e-mail: deposit@ccdc.cam.ac.uk or www: http://www.ccdc.cam.ac.uk).

Acknowledgements

This work was supported by the Hungarian Scientific Research Fund (OTKA T19337) and by the Ministry of Education (Hungary, FKP0507). The postdoctoral fellowship of A.B. is sponsored by OTKA D25136.

References

[1] M. Ostern, J. Pelczar, H. Kozlowski, B. Jezowska-Trzebiatowska, Inorg. Nucl. Chem. Lett. 16 (1980) 251.
[2] H. Nakayama, K. Prout, H.A.O. Hill, D. Datta, Chem. Commun. (1999) 695.
[3] U. Ermler, W. Grabarse, S. Shima, M. Goubeaud, R.K. Thauer, Science 278 (1997) 1457.
[4] D. Carillo, Coord. Chem. Rev. 119 (1992) 137.
[5] J.A. Tich, D. Mastropaolo, J. Potenza, H.J. Schugar, J. Am. Chem. Soc. 96 (1974) 726.
[6] K. Miyoshi, Y. Sugiura, K. Ishizu, Y. Iitaka, H. Nakamura, J. Am. Chem. Soc. 102 (1980) 6130.
[7] O. Yamauchi, H. Seki, T. Shoda, Bull. Chem. Soc. Jpn. 56 (1983) 3258.
[8] M.L. Brader, E.W. Ainscough, E.N. Baker, A.M. Brodie, D.A. Lewandoski, J. Chem. Soc., Dalton Trans. (1990) 2089.
[9] S. Fox, J.A. Potenza, S. Knapp, H.J. Schugar, in: K.D. Karlin, Z. Tyeklár (Eds.), Bioinorganic Chemistry of Copper, Chapman and Hall, New York, 1993.
[10] P.E. Riley, K. Seff, Inorg. Chem. 11 (1972) 2993.
[11] K. Várnagy, I. Sóvágó, H. Kozlowski, Inorg. Chim. Acta 151 (1988) 117.
[12] M-J. Blais, G. Berthon, J. Chem. Soc., Dalton Trans. (1982) 1803.
[13] W.S. Postal, E.J. Vogel, C.M. Young, F.T. Greenaway, J. Inorg. Biochem. 25 (1985) 25.
[14] P. Piu, G. Sanna, M.A. Zoroddu, R. Seeber, R. Basosi, R. Pogni, J. Chem. Soc., Dalton Trans. (1995) 1267.
[15] P. Piu, G. Sanna, A. Masia, M.A. Zoroddu, R. Seeber, J. Chem. Soc., Dalton Trans. (1997) 2369.
[16] W. Bal, H. Kozlowski, B. Lammek, L.D. Pettit, K. Rolka, J. Inorg. Biochem. 45 (1992) 193.
[17] H. Kozlowski, B. Radomska, G. Kupryszewski, B. Lammek, C. Livera, L.D. Pettit, S. Pyburn, J. Chem. Soc., Dalton Trans. (1989) 173.
[18] P. Danyi, K. Várnagy, I. Sóvágó, I. Schon, D. Sanna, G. Micera, J. Inorg. Biochem. 60 (1995) 69.
[19] H. Kozlowski, G. Formicka-Kozlowska, B. Jezowska-Trzebiatowska, Bull. Acad. Pol. Sci. 26 (1978) 153.
[20] L.D. Pettit, M. Bezer, Coord. Chem. Rev. 61 (1985) 97.
[21] E.L.M. Lempers, K. Inagaki, J. Reedijk, Inorg. Chim. Acta 152 (1988) 201.
[22] H. Kozlowski, W. Bal, M. Dyba, T. Kowalik-Jankowska, Coord. Chem. Rev. 184 (1999) 319.
[23] K. Várnagy, J. Szabó, I. Sóvágó, G. Malandrinos, N. Hadjiliadis, D. Sanna, G. Micera, J. Chem. Soc., Dalton Trans. (2000) 467.
[24] H. Kozlowski, B. Decock-Le Reverend, D. Ficheux, C. Loucheux, I. Sóvágó, J. Inorg. Biochem. 29 (1987) 187.
[25] I. Sóvágó, B. Radomska, I. Schon, O. Nyéki, Polyhedron 9 (1990) 825.
[26] K. Várnagy, B. Bóka, I. Sóvágó, D. Sanna, P. Marras, G. Micera, Inorg. Chim. Acta 275-276 (1998) 440.
[27] L. Zékány, I. Nagypál, in: D. Leggett (Ed.), Computational Methods for the Determination of Stability Constants, Plenum, New York, 1985.
[28] A. Altomare, G. Cascarano, C. Giacovazzo, A. Guagliardi, J. Appl. Crystallogr. 26 (1993) 343.
[29] G. M. Sheldrick, SHELXL-97, Universität Göttingen, Göttingen, Germany, 1997.
[30] L. J. Farrugia, WINGX-97 system, University of Glasgow, Scotland, UK, 1996.
[31] I. Sóvágó, D. Sanna, A. Dessi, K. Várnagy, G. Micera, J. Inorg. Biochem. 63 (1996) 99.
[32] I. Sóvágó, A. Kiss, E. Farkas, D. Sanna, P. Marras, G. Micera, J. Inorg. Biochem. 65 (1997) 103.
[33] F. Dallavalle, G. Folesani, E. Leporati, L.H. Abdel-Rahman, J. Coord. Chem. 42 (1997) 189.
[34] T.F. Dorigatti, E.J. Billo, J. Inorg. Nucl. Chem. 37 (1975) 1515.
[35] H. Kozlowski, J. Urbanska, I. Sóvágó, K. Várnagy, A. Kiss, J. Spychala, K. Cherifi, Polyhedron 9 (1990) 831.

PERGAMON

www.elsevier.nl/locate/poly

Polyhedron 19 (2000) 1859–1866

POLYHEDRON

Coordination chemistry of sulfamethizole: crystal structures of $[Cu(sulfamethizolate)_2(py)_2(OH_2)]\cdot H_2O$, $[M(sulfamethizolate)_2(py)_2(OH_2)_2]$ [M = Co and Ni] and $\{Cu(sulfamethizolate)_2(dmf)_2\}_\infty$

Elisa Borrás [a], Gloria Alzuet [b], Joaquín Borrás [b,*], Juan Server-Carrió [b], Alfonso Castiñeiras [c], Malva Liu-González [d], Francisco Sanz-Ruiz [d]

[a] *Departamento de Bioquímica y Biologia Molecular, Facultad de Medicina y Odontología, Universidad de Valencia, Avda. Vicente Blasco Ibáñez, 17, E-46010 Valencia, Spain*

[b] *Departamento de Química Inorgánica, Facultad de Farmacia, Universidad de Valencia, Avda. Vicent Andrés Estellés s/n, E-46100 Burjassot, Spain*

[c] *Departamento de Química Inorgánica, Facultad de Farmacia, Universidad de Santiago de Compostela, E-15703 Santiago de Compostela, Spain*

[d] *Departamento de Termología, Facultad de Fisicas, Universidad de Valencia, Dr Moliner, 50, 46100 Burjassot, Spain*

Received 2 March 2000; accepted 16 June 2000

Abstract

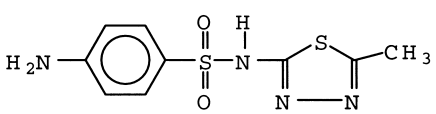
The synthesis and characterisation of copper, cobalt, nickel and zinc compounds with sulfamethizole (4-amino-*N*-(5-methyl-1,3,4-thiadiazole-2-yl)sulfanilamide) (Hsmtz) are described. The first crystal structures of ternary sulfamethizole complexes are reported. The crystal structures of $Cu(smtz)_2(py)_2(OH_2)\cdot H_2O$ (**1**), $M(smtz)_2(py)_2(OH_2)_2$ [M = Co (**2**), Ni (**3**)] and $\{Cu(smtz)_2(dmf)_2\}_\infty$ (**5**) were determined by X-ray diffraction. The Cu(II) ion exhibits a square pyramidal geometry in complex **1**, while in the other compounds the metal ion presents a distorted octahedral environment. In compounds **1**, **2** and **3** the deprotonated sulfamethizole acts as monodentate ligand coordinating through the thiadiazole N atom and in compound **5** it behaves as a bridge linking two metal cations via the thiadiazole and the amino nitrogen atoms. The IR, electronic, EPR and thermal data are consistent with the crystal structures. © 2000 Elsevier Science Ltd. All rights reserved.

Keywords: Sulfamethizole; Metal complexes; Crystal structures; Spectroscopic properties

1. Introduction

Among the N-substituted sulfanilamides, sulfamethizole (4-amino-*N*-(5-methyl-1,3,4-thiadiazole-2-yl)sulfanilamide) (Hsmtz) (Scheme 1) is one of the most used antibacterial drugs. It is expended as 'thiosulfil'. Sulfamethizole is extensively used in the treatment of the urinary tract infections [1]. The mechanism of action is based on the competitive antagonism of PABA (*p*-aminobenzoic acid) and the sulfanilamide derivative. Recently, sulfamethizole has been used as capsules containing contrast medium for assessment of gastric emptying in functional dyspepsia patients [2].

The Hsmtz has several groups with donor atoms that are able to interact with metal ions. Metal complexes of Hsmtz have been reported [3], but until now no crystal structure of binary or ternary sulfamethizole metal complexes had been determined. Previously, we have undertaken an investigation on the coordination properties of the sulfathiazole [4-amino-*N*-2-thiazolylbenzenosulfonamide, Hstz], a sulfonamide closely related



Scheme 1. 4-amino-*N*-(5-methyl-1,3,4-thiadiazole-2-yl)sulfanilamide (sulfamethizole).

* Corresponding author. Tel.: +34-6-386-4530; fax: +34-6-386-4960.

E-mail address: joaquin.borras@uv.es (J. Borrás).

0277-5387/00/$ - see front matter © 2000 Elsevier Science Ltd. All rights reserved.
PII: S0277-5387(00)00474-5

to sulfamethizole. We have found that it presents different coordination behaviour as a ligand, acting as: (i) monodentate through the amino group [4,5]; (ii) monodentate via the thiazole N atom [6]; (iii) bidentate bridging two metal ions through the N_{amino} and the $N_{thiazole}$ [7]; (iv) bidentate through the $N_{thiazole}$ and the $N_{sulfonamido}$ [8]; (v) bidentate to one Cu(II) through the $N_{thiazole}$ and the $N_{sulfonamido}$ and bridging to an adjacent Cu(II) through the N_{amino} [9].

The different coordination abilities of the sulfathiazole have led us to study the chelating properties of the sulfamethizole in order to compare the behaviour of both sulfanilamides. In this work we synthesise and characterise Cu, Co, Ni and Zn complexes of sulfamethizole and report the first crystal structures of sulfamethizolate complexes.

2. Experimental

2.1. Physical measurements

All reagents were of the highest grade commercially available and used without further purification. Elemental analyses (C, H, N) were done at the microanalytical laboratory of the University of Salamanca. IR spectra were recorded on a Mattson Satellite FTIR spectrometer. Samples were prepared using the KBr technique. Electronic spectra were registered on a Shidmazu UV 2101PC spectrophotometer using the diffuse reflectance technique. EPR spectra were carried out with a Brucker ER 200 D spectrometer. Magnetic susceptibility measurements at r.t. were taken with a fully automatized AZTEC DSM8 pendulum-type susceptometer. Mercury tetrakis(thyocianato)cobaltate(II) was used as a susceptibility standard. Data were corrected for diamagnetic contribution, which were estimated from Pascal's constants. Thermogravimetric analyses were made in air atmosphere using a Shimadzu TGA-50H.

2.2. Synthesis of the complexes

2.2.1. $Cu(smtz)_2(py)_2(OH_2)\cdot H_2O$ (1)

A 50 ml sample of a 1:1 aqueous pyridine solution containing 5 mmol of Hsmtz was added to an equal volume of an aqueous solution of $CuSO_4\cdot 5H_2O$ (10 mmol) containing 25% per volume of pyridine, slowly and with continuous stirring. Immediately, the mixture took on an intense blue colour. After 3 days prismatic blue crystals were obtained. They were filtered, washed and dried at vacuum. *Anal.* Calc. for $C_{28}H_{30}N_{10}O_5S_4$: C, 43.2; H, 3.8; N, 18.0; Cu, 8.2. Found: C, 42.4; H, 4.0; N, 17.7; Cu, 8.1%.

2.2.2. $M(smtz)_2(py)_2(OH_2)_2$ [M = Co (2), Ni (3), Zn (4)]

The compounds were obtained by a procedure similar to that described for the copper complex but using $CoCl_2\cdot 6H_2O$, $NiCl_2\cdot 6H_2O$ and $ZnCl_2\cdot 2H_2O$ instead of $CuSO_4\cdot 5H_2O$. The resulting solutions were orange, blue and white, respectively. They were left to stand at r.t. and after few days single crystals suitable for X-ray diffraction were obtained for the Co and Ni complexes, while a white solid was obtained for the Zn complex. *Anal.* Calc. for $C_{28}H_{32}CoN_{10}O_6S_4$: C, 42.5; H, 4.0; N, 17.7. Found: C, 42.8; H, 4.0; N, 17.6%. *Anal.* Calc. for $C_{28}H_{32}N_{10}O_6S_4$: C, 43.2; H, 3.8; N, 18.0. Found: C, 42.4; H, 4.0; N, 17.7%. *Anal.* Calc. for $C_{28}H_{32}ZnN_{10}O_6S_4$ C, 42.1; H, 4.0; N, 17.5. Found: C 42.6; H 3.9; N 17.8%.

2.2.3. $\{Cu(smtz)_2(dmf)_2\}_\infty$ (5)

Sulfamethizole (3 mmol) was added to 1 mmol of copper acetate in 30 ml of dimethylformamide. The resulting solution was left to stand at r.t. and after few days prismatic green crystals were obtained. *Anal.* Calc. for $C_{24}H_{32}CuN_{10}O_6S_4$: C, 38.5; H, 4.3; N, 18.7. Found: C, 38.9; H, 4.1; N, 18.9%.

2.3. Crystallographic data and structure determination

2.3.1. $Cu(smtz)_2(py)_2(OH_2)\cdot H_2O$ (1) and $Ni(smtz)_2(py)_2(OH_2)_2$ (3)

Diffraction measurements of the selected blue (Cu) and pale green (Ni) prismatic crystals, with approximate sizes $0.10 \times 0.20 \times 0.25$ mm (Cu) and $0.15 \times 0.25 \times 0.25$ mm (Ni), were carried out at 290 K using an Enraf–Nonius CAD-4 single-crystal diffractometer with graphite monochromated Mo Kα radiation ($\lambda = 0.7107$ Å). The unit cell dimensions were determined from the angular settings of 25 reflections with $9 < \theta < 13°$ (Cu) and $8 < \theta < 14°$ (Ni). The intensity data of 6965 (Cu) and 3281 (Ni) reflections were measured in the limits $1 < \theta < 25°$ using ω–2θ scan technique, variable speed, width $(0.80 + 0.35\tan\theta)°$ in ω and maximum scan time of 60 s per reflection in the *hkl* ranges 0–18, 0–13, −23–23 (Cu) and 0–9, −12–12, −12–12 (Ni). Three reflections were measured every hour as intensity controls without significant decay. Some double measured reflections were averaged, $R_{int} = 0.025$ (Cu) and 0.007 (Ni), resulting in 6079 (Cu) and 2957 (Ni) independent reflections of which 3673 (Cu) and 2441 (Ni) were considered, observed with the $[I > 2\sigma(I)]$ criterion. Absorption correction was not applied. The structure was solved by direct methods using the program SIR92 [10]. All non-hydrogen atoms were anisotropically refined by least-squares on F_{obs} using the X-RAY76 System [11]. The hydrogen atoms, kept fixed in the refinement with a common isotropic thermal parameter, were located by difference synthesis. In the

Table 1
Crystal data and structure refinement for $Cu(smtz)_2(py)_2(OH_2)\cdot H_2O$ (**1**), $M(smtz)_2(py)_2(OH_2)_2$ (M = Co (**2**), Ni(**3**)) and $\{Cu(smtz)_2(dmf)_2\}_\infty$ (**5**)

	1	**2**	**3**	**5**
Formula	$C_{28}H_{32}CuN_{10}O_6S_4$	$C_{28}H_{32}CoN_{10}O_6S_4$	$C_{28}H_{32}N_{10}NiO_6S_4$	$C_{24}H_{32}N_{10}O_6S_4Cu$
Symmetry	monoclinic	triclinic	triclinic	monoclinic
Space group	$P2_1/a$	$P\bar{1}$	$P\bar{1}$	$P2_1/c$
a (Å)	15.668(3)	8.4013(14)	8.3700(4)	9.408
b (Å)	11.279(1)	10.5612(17)	10.520(1)	14.737
c (Å)	19.559(2)	10.7828(12)	10.831(1)	11.882
α (°)	90.0	75.099(13)	75.16(1)	90.0
β (°)	90.75(1)	76.034(12)	76.01(1)	111.27
γ (°)	90.0	68.555(12)	68.48(1)	90.0
V (Å^3)	3456.2(8)	848.9(2)	846.0(1)	1535.2
Z	4	1	1	2
D_{calc} (g cm^{-3})	1.53	1.549	1.55	1.619
M	796.4	791.81	791.6	748.36
$F(000)$	1644	409	410	774
μ (cm^{-1})	9.31	8.09	8.78	10.29
Goodness-of-fit	0.85	1.044	1.24	1.0152
R	0.053	0.0330	0.046	0.0440
Rw	0.058	0.0779	0.051	0.1470

final stages an empirical weighting scheme was chosen as to give no trends in $\langle w\Delta^2F\rangle$ versus $\langle F_o\rangle$ and versus $\langle \text{sen}\,\theta/\lambda\rangle$ using the program PESOS [12]. Geometrical calculations were made with PARST [13]. Atomic scattering factors and anomalous dispersion corrections were taken from reference [14]. All calculations were performed on a VAX6410. Graphical manipulations were produced by the ORTEP-3 for Windows program [15]. Other relevant parameters of the crystal structure determination are listed in Table 1.

2.3.2. *Co(smtz)$_2$(py)$_2$(OH$_2$)$_2$ (**2**)*

A rose-coloured prismatic crystal of $Co(smtz)_2(py)_2(H_2O)_2$ was mounted on a glass fibre and used for data collection. Cell constants and an orientation matrix for data collection were obtained by least-squares refinement of the diffraction data from 25 reflections in the range of $11.00 < \theta < 18.12°$ in an Enraf–Nonius MACH3 automatic diffractometer [16]. Data were collected at 293 K using Mo Kα radiation ($\lambda = 0.71073$ Å) and the ω-scan technique, and corrected for Lorentz and polarisation effects [17]. A semi-empirical absorption correction (ψ-scans) was made [18]. The structure was solved by direct methods [19] and subsequent difference Fourier maps, and refined on F^2 by a full-matrix least-squares procedure using anisotropic displacement parameters [20]. All hydrogen atoms were located from difference Fourier maps and were refined isotropically. Atomic scattering factors from International Tables for X-ray Crystallography [14]. Molecular graphics from PLATON-98 [21]. A summary of the crystal data, experimental details and refinement results are listed in Table 1.

2.3.3. *{Cu(smtz)$_2$(dmf)$_2$}$_\infty$ (**5**)*

A green crystal, size 0.2 × 0.2 × 0.2 mm was mounted on an Enraf–Nonius CAD-4 single-crystal diffractometer with graphite monochromated Mo Kα radiation ($\lambda = 0.7173$ Å). The unit cell dimensions were determined from the angular settings of 25 reflections with $3.57 < \theta < 25.98°$. The space group was determined to be $P2_1/c$ from systematic absences. The intensity data of 3025 reflections, in the hkl range (0, 0, −14) to (11, 18, 13) and limits ($0 < \theta < 25°$) were measured using the ω–2θ scan technique and variable scan rate with a maximum scan time of 60 s per reflection. The intensity of the primary beam was checked throughout the data collection by monitoring three standard reflections every 60 min. On all reflections profile analysis was performed [22]. Lorentz-polarization corrections were applied and then the data were reduced to F_o^2 values. The structure was solved by Patterson methods using DIRDIF [23]. Isotropic least squares refinement on F^2 was made using SHELX-93[24]. During the final stages of the refinement on F^2 the positional parameters and the anisotropic thermal parameters of the non-H atoms were refined. All non-hydrogen atoms were anisotropically refined. All hydrogen atoms were geometrically placed and isotropically refined. The final conventional agreement factors were $R = 0.044$ and $wR_2 = 0.147$ for 3016 observed reflections and 236 variables. The function minimised was $\Sigma w(F_o^2 - F_c^2)/\Sigma wF_o^2]^{1/2}$, $w = 1/[\sigma 2(F_o^2 + 0.0828P)^2]$ with σF_o^2 from counting statistic and $P = (\max(F_o^2) + 2F_c^2)/3$. The final difference Fourier map showed a peak of 0.54 Å^3 very close to the C11′, the others peak no deeper than −0.39 Å^3. Atomic scattering factors were taken from International Tables for X-ray Crystallography [14]. Geometrical calculations were made with PARST [13]. Graphical manipulations were performed with EUCLID [25]. All calculations were made at the University of Valencia on the S.C.S.I.E. X-ray section VAX-computers. Other relevant parameters are collected in Table 1.

3. Results and discussion

3.1. *Crystal structures of Cu(smtz)$_2$(py)$_2$(OH$_2$)·H$_2$O (**1**), Co(smtz)$_2$(py)$_2$(OH$_2$)$_2$·(**2**) and Ni(smtz)$_2$(py)$_2$(OH$_2$)$_2$ (**3**)*

Selected bond distances and angles of the three crystal structures are shown in Table 2. Figs. 1–3 show ORTEP drawings of compounds **1**, **2** and **3**, respectively.

In compound **1** the copper atom is five co-ordinated with a geometry near to a regular square pyramidal.

Table 2
Selected bond distances (Å) and angles (°) for compounds $Cu(smtz)_2(py)_2(OH_2)\cdot H_2O$ (**1**) and $M(smtz)_2(py)_2(OH_2)_2$ (M = Co (**2**), Ni (**3**))

1		**2**		**3**	
Cu–O(3)	2.183(4)	Co–O(3)	2.0457(18)	Ni–O(3)	2.040(2)
Cu–N(11)	2.002(4)	Co–N(1)	2.2110(18)	Ni–N(1)	2.163(2)
Cu–N(12)	2.001(5)	Co–N(11)	2.157(2)	Ni–N(11)	2.100(3)
Cu–N(111)	2.045(5)				
Cu–N(112)	2.046(5)				
O(3)–Cu–N(11)	95.7(2)	O(3)1–Co–N(1)	90.61(7)	O(3)–Ni–N(1)	90.7(1)
O(3)–Cu–N(111)	97.9(2)				
O(3)–Cu–N(12)	97.8(2)	O(3)–Co–N(11)	90.44(8)	O(3)–Ni–N(11)	90.7(1)
O(3)–Cu–N(112)	91.4(2)				
N(11)–Cu–N(111)	88.4(2)	N(1)–Co–N(11)	90.25(7)	N(1)–Ni–N(11)	89.6(1)
N(11)–Cu–N(12)	166.5(2)				
N(11)–Cu–N(112)	90.6(2)				
N(111)–Cu–N(12)	88.4(2)				
N(111)–Cu–N(112)	170.7(2)				
N(12)–Cu–N(112)	90.4(2)				

The equatorial plane is defined by two thiadiazole N atoms from two sulfamethizolate ligands in *trans* position and by two pyridine N atoms. The axial site is occupied by a water O atom at longer distance, 2.183(4) Å. The $Cu–N_{thiadiazole}$ bond length 2.002(4) Å, is significantly shorter than the $Cu–N_{thiadiazole}$ of the related $[Cu(Hacm)_2(tn)_2]$ compound (H_2acm = acetazolamide, tn = propylenediamine) [26]. The $Cu–N_{py}$, 2.045(5) Å ones are comparable to those found in other pyridine compounds [6]. The *cis* angles in the equatorial plane ranging from 90.6(2) to 88.4(2)° do not deviate significantly from 90°. The τ value of 0.07 [$\tau = (\alpha - \beta/60)$] indicates a small distortion from a regular square pyramidal geometry [27].

The Co(II) ion in compound **2** and the Ni(II) ion in compound **3** are six co-ordinated by two pyridine N atoms and two thiadiazole N pertaining to two sulfamethizolate ligands in the equatorial sites and two water O atoms are in the apical positions. In both complexes the $M–N_{thiadiazole}$ and the $M–N_{py}$ are markedly longer than the $M–O_w$ distance. So, the geometry of the complexes can be described as compressed distorted octahedral. As expected from the ionic radii of the divalent metal ions the $Co–N_{thiadiazole}$, 2.2110(18) Å and the $Co–N_{py}$, 2.157(2) Å are longer than the $Ni–N_{thiadiazole}$, 2.163(2) Å and the $Ni–N_{py}$, 2.100(3) Å. However, the corresponding $M–O_w$ are practically the same [$Co–O_w$, 2.0457(18) Å and $Ni–O_w$, 2.040(2) Å]. The $Ni–N_{thiadiazole}$ bond is slightly longer than the same distance in the $[Ni(Hacm)_2(NH_3)_4]$ complex [28]. The $M–N_{py}$ are similar to those of the $M(macm)_2(py)_2(OH_2)_2$ (M = Co, Ni; macm = methazolamidate) [29]. Angles around the metal do not differ significantly from those of a regular octahedron.

Several interesting aspects can be deduced from a comparison of bond distances of the **2** and **3** complexes with those of the compound **1**. The equatorial Cu–N lengths are significantly shorter than the Co–N and the Ni–N ones. In particular, the $M–N_{thiadiazole}$ is the short-

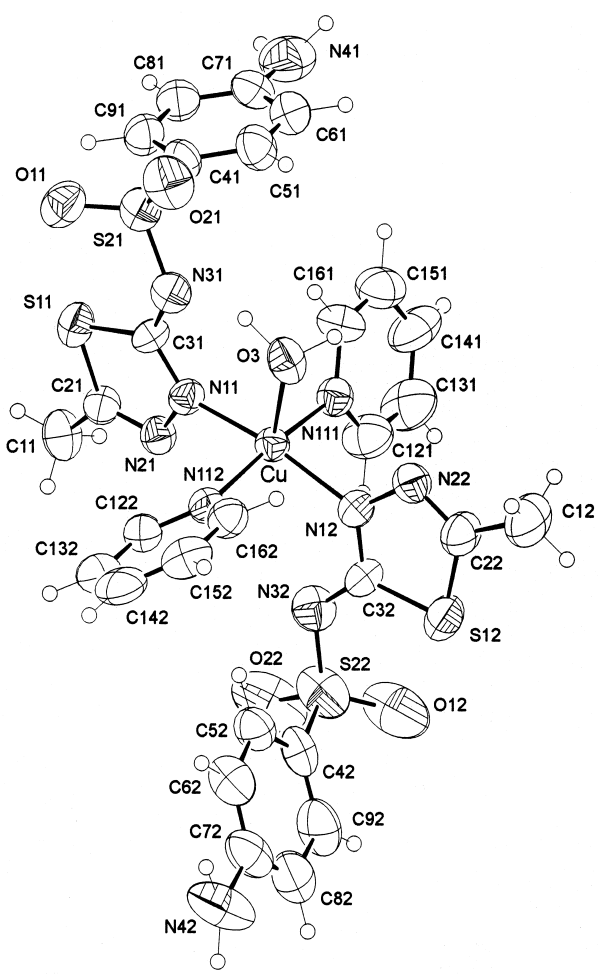


Fig. 1. ORTEP drawing of $Cu(smtz)_2(py)_2(OH_2)\cdot H_2O$ (**1**).

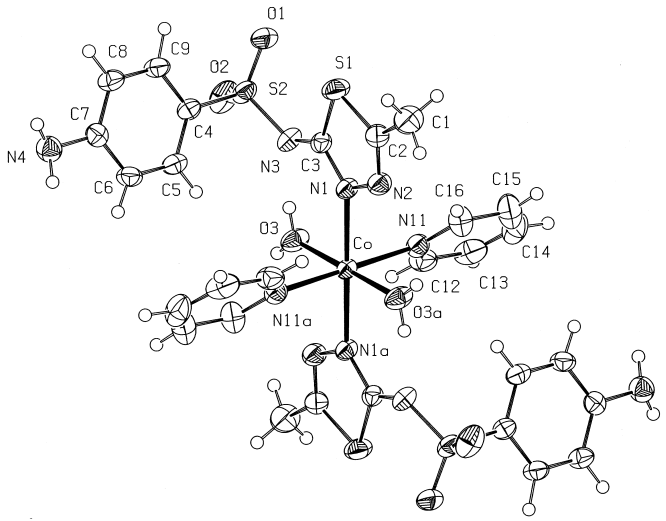


Fig. 2. ORTEP drawing of $Co(smtz)_2(py)_2(OH_2)_2$ (**2**).

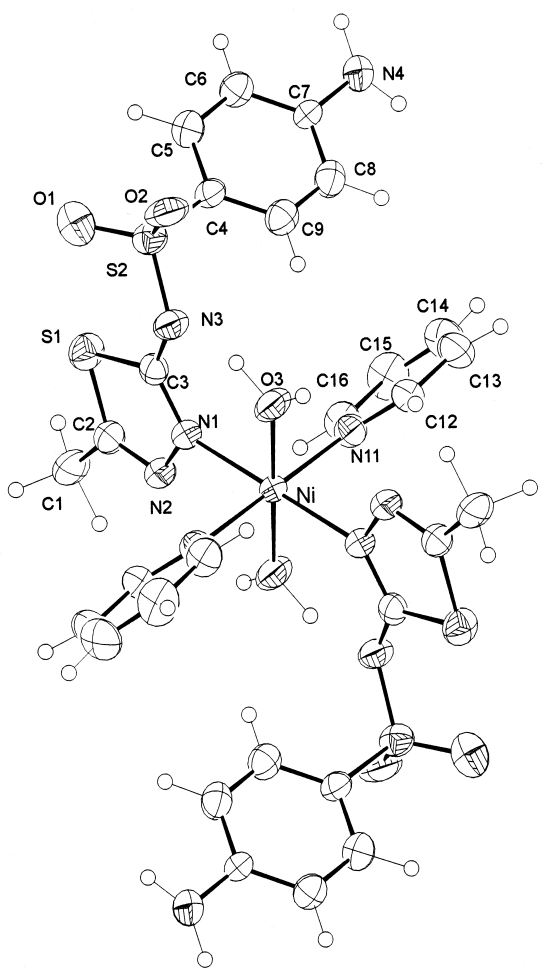


Fig. 3. ORTEP drawing of $Ni(smtz)_2(py)_2(OH_2)_2$ (**3**).

est bond distance in the copper complex, whereas it is the longest one in the nickel and cobalt compounds.

It must be noted that the sulfamethizole ligand acts as monodentate coordinating through the thiadiazole N atom closest to the deprotonated sulfonamido group although it presents several donor atoms and therefore it offers different coordination possibilities. The same coordination behaviour has been exhibited by the related acetazolamide in the octahedral $[Cu(Hacm)_2(tn)_2]$ and $[Ni(Hacm)_2(NH_3)_4]$ complexes [26,28] and by the sulfathiazole in the $[Cu(stz)(py)_3Cl]$ and $[Cu(stz)_2(mim)_2]\cdot H_2O$ compounds [6,9].

3.2. Crystal structure of $\{Cu(smtz)_2(dmf)_2\}_\infty$ (5)

A drawing of the complex is presented in Fig. 4. Selected bond and angles of the coordination polyhedron are listed in Table 3.

The structure is a coordination polymer in which each Cu(II) ion presents an octahedral geometry. The equatorial plane is defined by two $N_{thiadiazole}$ atoms *trans* one another and two N_{amino} atoms from four sulfamethizolate ligands. Two O atoms of two disordered dimethylformamide molecules are placed in the apical positions at the distance of 2.391(4) Å. Each cupric ion is connected with the other Cu ions by four sulfamethizolate anions acting as bridges via the $N_{thiadiazole}$ and N_{amino} atoms.

The four in-plane Cu–N bond distances [Cu–$N_{thiadiazole}$, 2.083(4); Cu–N_{amino}, 2.056(4) Å] are similar. The Cu–$N_{thiadiazole}$ is longer than this distance in compound **1**. Regarding to the Cu–N_{amino} length it is in the range found for the corresponding distances in Cu complexes of the sulfathiazole ligand [from 2.020 to 2.071 Å] [4]. The Cu–O_{dmf} bond lengths can be regarded as normal [30].

The largest deviation from a regular octahedral geometry is found in the axial angles involving the amino N atoms [94.8(2) and 85.2(2)°].

The sulfamethizolate anion behaves as a bridging ligand through the $N_{thiadiazole}$ and N_{amino} atoms. This coordination behaviour is different to that exhibit by the ligand in the complexes described above, although is similar to that observed for the sulfathiazole in the $[Zn(stz)_2]\cdot H_2O$ complex [7].

A comparison of the four crystal structures described in this paper shows that no remarks can be noted as far as the sulfamethizole bond distances are concerned. From a different coordination behaviour of the sulfamethizole in compound **5** with respect to complexes **1**, **2** and **3**, only a slight difference can be observed in the N(4)–C(7) bond lengths [1.424(6) compound **5**, 1.382(9) compound **1**, 1.398(3) complex **2** and 1.402(5) Å complex **3**]. Moreover, the different strength binding of the $N_{thiadiazole}$ does not modify significantly the N–N distance [1.390(5) compound **5**, 1.376(9) compound **1**, 1.387(3) complex **2** and 1.386(3) Å complex **3**]. This fact could be related to the charge delocalization through the thiadiazole ring as a consequence of the deprotonation of the sulfonamide group.

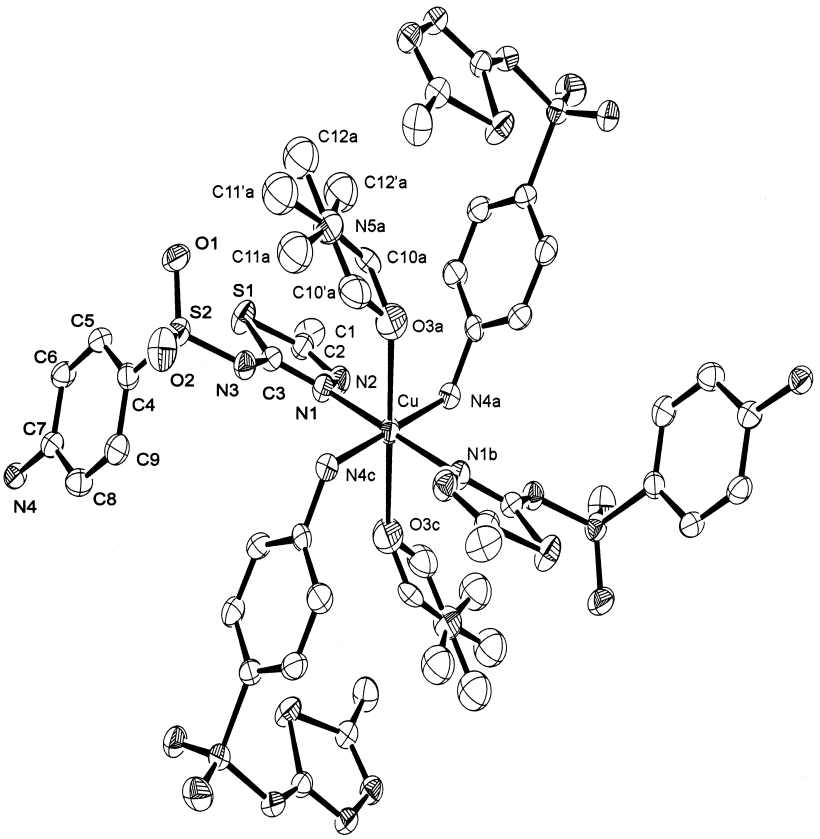


Fig. 4. ORTEP drawing of $\{Cu(smtz)_2(dmf)_2\}_\infty$ (**5**).

3.3. IR spectra

A comparative study of the IR spectra of the complexes with that of the free ligand and those of the complexes of related ligands gives some positive information regarding the binding sites of the sulfamethizole. All the complexes show very similar spectral pattern. The strong bands at 3440, 3360 and 3250 cm^{-1} in the IR of the ligand attributed to $\nu_{as}(NH_2)$, $\nu_s(NH_2)$ and $\nu(NH)$ of the amino group appear at the same range in the IR spectra of complexes **1**, **2**, **3** and **4**. However, these bands are modified in the IR spectrum of the compound **5** as a consequence of the interaction of the amino group with the copper(II) ion.

With respect to the 1,3,4-thiadiazole ring modes, because of the rigidity of the penta-atomic ring, the vibrational spectra can not be interpreted in terms of localised vibrations, being many atoms involved in several vibration modes. The strong band at 1550 cm^{-1} in the ligand is shifted to 1450–1440 cm^{-1} in the complexes. On the one hand this is due to deprotonation of the sulfonamido group that gives rise to a delocalization of the negative charge between the $N_{sulfonamidate}$ and the thiadiazole ring and on the other hand, to the interaction of the $N_{thiadiazole}$ with the metal ions.

The SO_2 group modes of the ligand appear as strong bands at 1325 (ν_{as}) and 1128 cm^{-1} (ν_s). In the complexes, the asymmetric mode is shifted to 1290–1260 cm^{-1} and the symmetric vibration gives rise a band practically unchanged with respect to that of the ligand.

Table 3
Selected bond distances (Å) and angles (°) for $\{Cu(smtz)_2(dmf)_2\}_\infty$ (**5**) [a]

Cu–O(3) # 1	2.391(4)
Cu(1)–O(3) # 2	2.391(4)
Cu–N(1)	2.083(4)
Cu(1)–N(1) # 3	2.083(4)
Cu–N(4) # 1	2.056(4)
Cu(1)–N(4) # 2	2.056(4)
O(3) # 1–Cu–O(3) # 2	180.0
N(4) # 1–Cu–N(1)	88.4(2)
N(4) # 2–Cu–N(1)	91.6(2)
N(4) # 1–Cu–N(4) # 2	180.0
N(4) # 1–Cu–O(3) # 1	94.8(2)
N(4) # 2–Cu–O(3) # 1	85.2(2)
N(1)–Cu–O(3) # 1	89.2(2)
N(1) # 1–Cu–O(3) # 1	90.8(2)
N(1)–Cu–N(1) # 3	180.0

[a] Symmetry transformations used to generate equivalent atoms # 1: $-x+2$, $y-1/2$, $-z+5/2$; # 2: x, $-y+1/2$, $z-1/2$; # 3 $-x+2$, $-y$, $-z+2$; # 4: $-x+2$, $y+1/2$, $-z+5/2$.

In spite of the coordination of one of the $N_{thiadiazole}$ to metal ions, the complexes present the same N–N bond distances so, the band located at 990 cm^{-1} assigned to a ν(N–N) mode does not change in the IR spectra of the complexes.

A shift of the ν(S–N) band is observed in the IR spectra of the complexes (940–930 cm^{-1}) with respect to that of the ligand (920 cm^{-1}). This could be attributed to deprotonation of the sulfonamido group and consequently the shortening of the S–N bond distance.

A band at 3470 cm^{-1} in the IR spectra of the compounds **1** and **4** is attributed to ν(O–H) vibration. The IR spectrum of the complex **5** shows a strong band at 1650 cm^{-1} assigned to a ν(C=O) vibration of the dmf molecules. The pyridine ring breathing band in compounds **1**, **2**, **3** and **4** is found at 1040 cm^{-1}, according to the fact that the pyridine molecules are coordinated [31].

3.4. Magnetic properties, electronic and EPR spectra

At room temperature the Cu(II) complexes have magnetic moment (2.01 BM for **1** and 1.94 BM for **5**) somewhat higher than the spin-only value. Such divergence is not uncommon in mononuclear Cu(II) complexes due to mixing-in of some angular momentum from the closely lying excited states via spin–orbit coupling [32]. The cobalt complex presents a magnetic moment (4.11 BM) slightly lower than the common values of octahedral complexes. This fact could be attributed to the distortion of the coordination polyhedra that leads to a minor orbital contribution to the magnetic moment. The magnetic moment value for the Ni(II) compound (2.90 BM), indicative of a slight orbital contribution, is in the range found for octahedral complexes.

The diffuse reflectance (DR) spectra of the $Cu(smtz)_2(py)_2(OH_2)\cdot H_2O$ (**1**) and the $\{Cu(smtz)_2(dmf)_2\}_\infty$ (**5**) with a well-defined d–d maximum at 595 (compound **1**) and 660 nm (compound **5**) agree well with the square pyramidal geometry and the octahedral geometry deduced from their crystal structures. The DR spectra of compounds **2** and **3** (with maxima at 490 and 600 nm, respectively) fit for an octahedral environment according to their crystal structures.

Intense absorption in the ultraviolet region (ca. 300 nm) is a feature common to all the complexes and it is attributed to an intra-ligand transition.

The polycrystalline powder EPR spectrum at room temperature of the compound **1** is axial in nature with a poorly resolved parallel component. The EPR spectrum of the zinc copper-doped compound is also axial anisotropy with a four-line hyperfine structure due to the interaction of the unpaired electron with the nuclear spin of the copper nucleus. The ground state parameters extracted from the experimental spectrum by simulation [33], $g_\parallel = 2.26$, $g_\perp = 2.07$ and $A_\parallel = 140 \times 10^4$ cm^{-1} are in good agreement with a square pyramidal geometry. The compound **5** shows a rhombic polycrystalline powder EPR spectrum with $g_3 = 2.20$; $g_2 = 2.13$ and $g_1 = 2.08$ values, according to the copper coordination polyhedron.

3.5. Thermal analyses of compounds *1–4*

The thermal study of the compound **1** has a first step at 120°C corresponding to the loss of two water molecules (% experimental weight 4.78; calculated weight 4.52). The second step, that take place at 180°C, corresponds to a loss of the two pyridine molecules (% experimental weight 17.94; calculated weight 19.86). There is a third step at 350°C where the two aniline groups of the sulfonamidate are lost (% experimental weight 25.62, calculated 23.38) and a fourth step where the pyrolytic decomposition takes place leaving a percentage residual weight of 12.85% that can be attributed to a mixture of CuO and $CuSO_4$.

The compound **2** is stable to 110–120°C. At this temperature range the first step of the thermal decomposition starts. This step corresponds to the loss of the two pyridine ligands (% experimental weight 19.06, calculated weight for two pyridines 19.98). Between 200–250°C a second step occurs where the weight loss corresponds to a water molecules and aniline groups of the sulfonamidate ligand (% experimental weight 34.25, calculated weight 31.62). In a third step the pyrolytic decomposition of the rest takes place, yielding a residue that it is a mixture of cobalt sulphate and cobalt oxide.

The TG curve of the compound **3** presents a first step (150°C) where the loss of the pyridine and water molecules takes place at the same time (% experimental weight 23.07. calculated weight 24.54). The second (250–500°C) and third (500–600°C) steps agree with the pyrolytic decomposition of the compound. As in the other processes the residue is a mixture of nickel sulphate and nickel oxide.

The TG curve of the compound **4** shows two separate thermal events. Until 150°C the compound does not present any loss of weight. Between 150–400°C a first step takes place with a weight loss of 52.68% that can be attributed to a loss of two pyridine, two water molecules and two aniline groups. The second step corresponds to the pyrolytic decomposition of the compound. The residue is composed of a mixture of zinc sulphate and zinc oxide.

From a comparison of the first step of the thermal process we can observe a different stability of the water molecules between the compound **1** and the rest of the complexes. The lower temperature of water loss in the compound **1** can be related with the larger Cu–OH_2 bond length observed in this compound with respect to

the other M–OH_2 bond distances (M = Co and Ni) in the compounds **2** and **3**.

4. Supplementary data

Supplementary crystallographic data have been deposited with the Cambridge Crystallographic Data Centre, CCDC Nos. 140608, 140609, 140610 and 140611. Copies of this information may be obtained free of charge from The Director, CCDC, 12 Union Road, Cambridge, CB2 1EZ, UK (fax: +44-1223-336-033; e-mail: deposit@ccdc.cam.ac.uk or www: http://www.ccdc.cam.ac.uk).

Acknowledgements

G.A. and J.B. would like to thank the Spanish CICYT (PM97-0105-C02-01) for financial support. A.C. thanks the Xunta de Galicia (Project XUGA20309B97) for financial support. The authors thank Professor J. Niclós-Gutierrez (University of Granada) for the thermal studies.

References

[1] E.R. Barnhart (Ed.), Physician's Desk Reference, PDR, 43rd ed., Medical Economics, New York, 1989.
[2] T. Suzuki, Y. Yamamoto, K Abe, M. Hirano, H. Oka, Dig. Dis. Sci. 44 (1999) 1741.
[3] A. Bult, Metal complexes of sulfanilamides, in: Metal Ions in Biological Systems, Sigel ed., Marcel Dekker, New York, 1983.
[4] J. Casanova, G. Alzuet, J. Borrás, J. Timoneda, S. García-Granda, I. Cándano-González, J. Inorg. Biochem 56 (1994) 65.
[5] J. Casanova, G. Alzuet, J. Borrás, J.M. Amigó, T. Debaerdemaeker, Z. Kristallogr. 209 (1994) 271.
[6] J. Casanova, G. Alzuet, J. Borrás, J. Latorre, M. Sanaú, S. García-Granda, J. Inorg. Biochem 60 (1995) 219.
[7] J. Casanova, G. Alzuet, S. Ferrer, J. Borrás, J. Timoneda, S. García-Granda, E. Pérez-Carreño, J. Inorg. Biochem. 51 (1993) 689.
[8] J. Casanova, G. Alzuet, J. Latorre, J. Borrás, Inorg. Chem. 36 (1997) 2052.
[9] J. Casanova, G. Alzuet, J. Borrás, O. Carugo, J. Chem. Soc., Dalton Trans. (1996) 2239.
[10] A. Altomare, M.C. Burla, M. Camalli, G. Cascarano, G. Giacovazzo, A. Guagliardi, G. Polidori, J. Appl. Crystallogr. 27 (1994) 435.
[11] J.M. Stewart, P.A. Machin, C.W. Dickinson, H.L. Ammon, H. Heck, H. Flack, The X-RAY76 system, in: Technical Report TR-446, Computer Science Center, University of Maryland, College Park, MD, 1976.
[12] Martínez-Ripoll, M. Cano, F.H. PESOS Computer Program, Instituto Rocasolano, C.S.I.C., Madrid, Spain, 1975.
[13] M. Nardelli, Comput. Chem. 7 (1983) 95.
[14] International Tables for X-ray Crystallography, vol. 4, Kynoch Press, Birmingham, 1974, p. 71–79, 149.
[15] L.J. Farrugia, J. Appl. Crystallogr. 30 (1997) 565.
[16] B.V. Nonius, CAD4-Express Software, Ver. 5.1/1.2. Enraf Nonius, Delft, The Netherlands, 1994.
[17] M. Kretschmar, GENHKL Program for the Reduction of CAD4 Diffractometer Data, University of Tübingen, Germany, 1997.
[18] A.C.T. North, D.C. Phillips, F.S. Mathews, Acta Crystallogr., Sect. A 24 (1968) 351.
[19] G.M. Sheldrick, Acta Crystallogr., Sect. A 46 (1990) 467.
[20] G.M. Sheldrick, SHELXL-97, Program for the Refinement of Crystal Structures, University of Göttingen, Germany, 1997.
[21] A.L. Spek, PLATON, A Multipurpose Crystallographic Tool, Utrecht University, Utrecht, The Netherlands, 1999.
[22] M.S. Lehman, F.K. Larsen, Acta Crystallogr., Sect. A 30 (1974) 580.
[23] P.T. Beurskens, P.T. Admiraall, G. Beurskens, W.P. Bosman, S. García-Granda, R.O. Gould, J. M.M. Smits, C. Smykalla, DIRDIF User's Guide Technical Report, Crystallography Laboratory, University of Nijmegen, The Netherlands, 1992.
[24] G.M. Sheldrick, in: H.D. Flack, P. Parkanyi, K. Simon (Eds.), SHELX-93, Crystallographic Computing 6deIUCr, Oxford University Press, Oxford, 1993.
[25] A.L. Speck, in: D. Sayre (Ed.), The EUCLID Package, Computational Crystallography, Claredon, Oxford, 1999, p. 528.
[26] S. Ferrer, J.G. Haasnoot, R.A.G. de Graaff, J. Reedijk, J. Borrás, Inorg. Chim. Acta 192 (1992) 129.
[27] A.W. Addison, T.N. Rao, J. Reedijk, J. van Rijn, G.C. Verschoor, J. Chem. Soc., Dalton. Trans. (1984) 1349.
[28] S. Ferrer, J. Borrás, C. Miratvilles, A. Fuertes, Inorg. Chem. 28 (1989) 160.
[29] G. Alzuet, S. Ferrer, J. Borrás, A. Castiñeiras, X. Solans, M. Font-Bardía, Polyhedron 11 (1992) 2849.
[30] E. Müller, G. Bernardinelli, J. Reedijk, Inorg. Chem. 34 (1995) 5979.
[31] A.R. Katritzky, A.R. Hands, J. Chem. Soc. (1958) 2202.
[32] B.N. Figgis, J. Lewis, in: J. Lewis, R.G. Wilkins (Eds.), Modern Coordination Chemistry: Principles and Methods, Interscience, New York, 1960, p. 400.
[33] WINEPR-SimFonia. I.25, Bruker Analytik GmbH, Karlsruhe, Germany, 1994–1996.

PERGAMON

www.elsevier.nl/locate/poly

Polyhedron 19 (2000) 1867–1872

POLYHEDRON

Aza–oxa macrocyclic ligands functionalised with naphthylmethyl fluorescent groups

Youseff Al Shihadeh [a], Angel Benito [a], José Manuel Lloris [a], Ramón Martínez-Máñez [a,*], Teresa Pardo [a], Juan Soto [a], M[a] Dolores Marcos Martínez [b]

[a] *Departamento de Química, Universidad Politécnica de Valencia, Camino de Vera s/n, E-46071 Valencia, Spain*
[b] *Institut de Ciència dels Materials de la Universitat de València (ICMUV), PO Box 2085, Valencia, Spain*

Received 2 May 2000; accepted 16 June 2000

Abstract

Compounds L^1 and L^2 were obtained by reaction of 2-(bromomethyl)naphthalene with 1,4,10-trioxa-7,13-diazacyclopentadecane and 1,4,7-trioxa-10-azacyclododecane, respectively. These receptors contain aza–oxa crowns attached covalently to fluorescent groups. The protonation and coordination behaviour of L^1 and L^2 against metal ions has been studied in dioxane:water (70:30 v/v, 25°C, 0.1 M potassium nitrate) using potentiometric methods. All metal ions studied form complexes with L^1 and L^2 with the logarithm of the formation constants $L + M^{2+} = [M(L)]^{2+}$ in the sequence $Cd^{2+} \cong Pb^{2+}$, $Zn^{2+} < Hg^{2+}$ for L^1 and $Zn^{2+} < Ni^{2+} < Pb^{2+} < Cd^{2+} < Cu^{2+}$ for L^2. The fluorescent behaviour of L^1 and L^2 was studied in dioxane:water (70:30, v/v) and in acetonitrile in the presence of Ni^{2+}, Cu^{2+}, Zn^{2+}, Cd^{2+}, Hg^{2+}, Pb^{2+} cations and chloride, bromide, sulfate and phosphate anions. The most significant feature is the quenching of the fluorescence produced by Cu^{2+} in acetonitrile. © 2000 Elsevier Science Ltd. All rights reserved.

Keywords: Macrocyclic ligands; Naphthylmethyl fluorescent groups; Aza–oxa crowns

1. Introduction

The development of new chemical sensors based on the application of supramolecular concepts is an area of current interest. The fundamentals involve the functionalisation of suitable coordination sites with appropriate groups that are able to switch their state upon guest binding [1–9]. When the switching process is followed by a change in an easily observable macroscopic parameter (such as redox potential, absorption or emission sprectrum, etc.), then monitoring results in information on the presence or absence of a certain guest [10–16]. The recognition process in these molecules operates as follows: in the first step there is a guest–receptor interaction usually governed by well-known binding rules. In the second step there is a non-covalent, generally supramolecular in nature, interaction between the guest attached to the binding sites of the receptor and the signalling subunit. The latter interaction produces a macroscopically observable change in an easily to measure physical property. The nature of the signalling subunit not only determines the type of macroscopic signal but it also has a control on the selectivity. In fact, some factors can be controlled easily to obtain selectivity against a target guest: (i) the nature of the binding sites; (ii) the nature of the signalling unit, and (iii) the solvent in which the receptor–guest interaction takes place. We recently described [17] that the functionalisation of aza–oxa macrocycles with either ferrocenyl or anthracenyl subunits leads to molecules that can sense mercury selectively in an aqueous environment. With the aim of continuing those studies, we functionalised the cyclic aza crown ethers 1,4,10-trioxa-7,13-diazacyclopentadecane and 1,4,7-trioxa-10-azacyclododecane with naphthylmethyl groups and studied the fluorescent emission of the pendant signalling subunits in the presence of metal ions and anions in dioxane:water (70:30, v/v) and acetonitrile.

* Corresponding author. Tel.: +34-96-387-7343; fax: +34-96-387-7349.
E-mail address: rmaez@qim.upv.es (R. Martínez-Máñez).

0277-5387/00/$ - see front matter © 2000 Elsevier Science Ltd. All rights reserved.
PII: S0277-5387(00)00475-7

2. Experimental

2.1. Physical measurements

Potentiometric titrations were carried out in dioxane:water (70:30 v/v, 0.1 M potassium nitrate, 25°C) for L^1 and L^2, using a reaction vessel with a water thermostat at 25.0 ± 0.1°C under nitrogen. The titrant was added using a Crison 2031 microburete. Potentiometric measurements were carried out using a Crison 2002 pH meter and a combined glass electrode. A PC was used to control the titration system automatically. The electrode was calibrated using a known hydrogen concentration by titrating known amounts of HCl with CO_2-free KOH solution and determining the equivalent point by the Gran's method [18] which gives the standard potential $E'°$ and the ionic product of the solvent ($K'_w = [H^+][OH^-]$, $\log K = -16.20$ for dioxane:water 70:30 v/v, 0.1 M potassium nitrate, 25°C). The computer program SUPERQUAD [19] was used to calculate the protonation and stability constants. The titration curves for each system (ca. 250 experimental points corresponding to at least three titration curves; pH range investigated 2.5–10; concentration of the ligand and cations was ca. 1.2×10^{-3} M) were treated either as a single set or separate entities without significant variations in the values of the stability constants. Fluorescence measurements were made on an Edinburgh analytical instrument using L^1 and L^2 at a concentration of ca. 3.00×10^{-5} M in dioxane:water (70:30, v/v) or acetonitrile.

2.2. Synthesis of L^1 and L^2

The corresponding aza–oxa macrocycle (0.91 mmol) and 2-(bromomethyl)naphthalene (1.81 mmol for L^1 and 1.14 mmol for L^2) were refluxed in dichloromethane for 72 h in the presence of K_2CO_3. The solvent was removed, the residue dissolved in dichloromethane and then purified by column chromatography on alumina using CH_2Cl_2:CH_3OH (98:2) as eluent. A pale yellow oil was obtained.

L^1: Yield 385 mg, 85%. *Anal.* Found: C, 71.55; H, 7.84; N, 5.51. Calc. for $C_{32}H_{38}N_2O_3 \cdot 2H_2O$: C, 71.91; H, 7.86; N, 5.24%. ^{1}H NMR ($CDCl_3$): δ 2.76 (s, CH_2N, 4H), 2.80 (s, CH_2, 4H), 3.50–3.70 (m, CH_2O, 12H), 4.6 (s, CH_2–$C_{10}H_7$, 2H), 7.33 (m, $C_{10}H_7$, 4H), 7.41 (d, $C_{10}H_7$, 2H), 7.70 (d, $C_{10}H_7$, 2H). FABMS (R_{int}, %): 521 $[M + Na]^+$ (25), 499 (100), 46 (5).

L^2: Yield 269 mg, 75%. *Anal.* Found: C, 68.49; H, 7.82; N, 4.19. Calc. for $C_{19}H_{25}NO_3 \cdot H_2O$: C, 68.46; H, 8.10; N, 4.20%. ^{1}H NMR ($CDCl_3$): δ 2.75 (t, CH_2N, 4H), 2.83 (t, CH_2N, 4H), 3.5–3.7 (m, CH_2O, 12H), 4.60 (s, CH_2–$C_{10}H_7$, 2H), 7.50 (m, $C_{10}H_7$, 4H), 8.01 (d, $C_{10}H_7$, 2H), 8.60 (d, $C_{10}H_7$, 2H). FABMS (R_{int}, %): 338 $[M + Na]^+$ (90), 316 (100), 154 (10), 141 (80).

Table 1
Stepwise protonation constants in dioxane:water (70:30 v/v, 0.1 M potassium nitrate, 25°C) for L^1 and L^2 [a]

Reaction	Log K	
	L^1	L^2
$L + H^+ \rightleftharpoons [HL]^+$	8.17(4)	7.64(3)
$L + 2H^+ \rightleftharpoons [H_2L]^{2+}$	14.08(4)	

[a] Values in parentheses are standard deviations on the last significant digit.

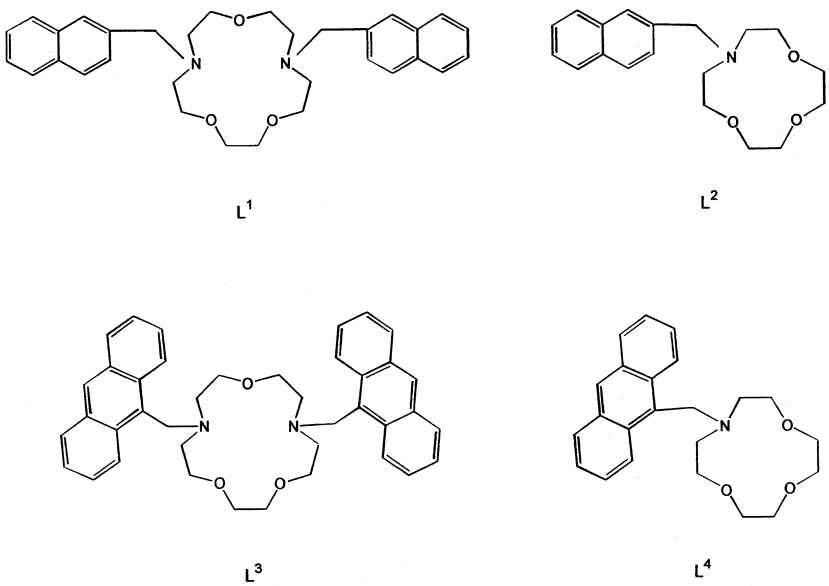
3. Results and discussion

L^1 and L^2 where synthesised by reaction of 2-(bromomethyl)naphthalene with 1,4,10-trioxa-7,13-diazacyclopentadecane and 1,4,7-trioxa-10-azacyclododecane, respectively. ^{1}H and ^{13}C NMR, mass spectra and elemental analysis are in agreement with the proposed formulation. L^1 and L^2 are aza–oxa macrocycles containing pendant fluorescent naphthylmethyl groups [20–22]. We studied the fluorescent behaviour of receptors L^3 and L^4 in dioxane:water mixtures recently. It was found that L^3 sense the presence of Hg^{2+} at basic pH selectively [23]. We also studied the electrochemical sensing behaviour of similar ligands to L^1 and L^2 but functionalised with ferrocenylmethyl groups and found that both could sense the presence of Hg^{2+} selectively and electrochemically [23]. Bearing this in mind, we synthesised and studied the coordination and emission behaviour of the L^1 and L^2 ligands which are analogous to those functionalised previously with anthracenyl or ferrocenyl but having the naphthyl group as fluorescent groups.

3.1. Coordination behaviour

The protonation and coordination behaviour of L^1 and L^2 against metal ions was studied in dioxane:water (70:30 v/v, 25°C, 0.1 M potassium nitrate) using potentiometric methods. Table 1 shows the protonation constants of L^1 and L^2. As expected, these display two and one protonation processes, respectively. Protonation constants are similar to those obtained for the analogous anthracenyl-functionalised ligands L^3 and L^4 (Scheme 1). For instance, the logarithms of the first protonation process $L + H^+ \rightleftharpoons HL^+$ for L^1 and L^2 are $\log K = 8.17$ and 7.64, whereas the logarithms for L^3 and L^4 for the same process are 8.30 and 7.80, respectively.

Table 2 shows the stability constants for the formation of the Zn^{2+}, Cd^{2+}, Pb^{2+} and Hg^{2+} complexes of L^1 in dioxane:water (70:30, v/v). All metal ions form complexes with L^1 with the logarithm of the formation



Scheme 1.

constants $L^1 + M^{2+} \rightleftharpoons [M(L^1)]^{2+}$ in the sequence $Zn^{2+} \cong Cd^{2+}$, $Pb^{2+} < Hg^{2+}$. For instance, the logarithm of the formation constant of the complex $[M(L^1)]^{2+}$ with $M = Zn^{2+}$, Cd^{2+}, Pb^{2+} is $\log K = 7.10$, 6.93, 6.91, respectively, whereas the value for the formation of the $[Hg(L^1)]^{2+}$ complex is $\log K = 12.25$. Therefore, the stability constant for the formation of the $[M(L^1)]^{2+}$ complex ($M^{2+} + L^1 \rightleftharpoons [M(L^1)]^{2+}$) is ca. 10^5 times larger for Hg^{2+} than those for Zn^{2+}, Cd^{2+} and Pb^{2+}. The presence of naphthylmethyl groups attached to the coordination sites does not modify the coordination behaviour of the aza–oxa macrocyclic cavity substantially. For instance, the logarithms of the stability constants for the formation of $[M(L)]^{2+}$ complexes (with L = 1,4,10-trioxa-7,13-diazacyclopentadecane and $M = Zn^{2+}$, Cd^{2+} and Pb^{2+} in water) have been reported to be $\log K = 5.19$, 6.46 and 5.85, respectively [24,25].

The stability constants of L^3 in dioxane:water (70:30, v/v) mixtures with several metal ions have also been determined recently. L^3 forms complexes with transition metal ions with stability constants for the formation of the $[M(L^3)]^{2+}$ species in the sequence $Zn^{2+} \cong Cd^{2+}$, $Pb^{2+} < Hg^{2+}$. The stability constant for the formation of the $[Hg(L)]^{2+}$ complex is very similar for both L^1 and L^3 receptors ($\log K = 12.25$ and 12.70, respectively). In contrast, the stability constants for the formation of the $[M(L)]^{2+}$ complexes ($M = Zn^{2+}$, Cd^{2+} and Pb^{2+}) are approximately ten times larger for the L^1 ligand than the L^3 ligand.

We also studied the solution behaviour of the ligand L^2 in dioxane:water (70:30, v/v) in the presence of the metal ions Ni^{2+}, Cu^{2+}, Zn^{2+}, Cd^{2+} and Pb^{2+}. Table 1 gives the stability constants of the complexes with L^2. L^2 forms stronger complexes with Cu^{2+} than with other metal ions studied. Fig. 1 shows the distribution diagram of the L^2–H^+–Cu^{2+} system. The constants for the formation of the $[M(L^2)]^{2+}$ complexes are in the sequence $Zn^{2+} < Ni^{2+} < Pb^{2+} < Cd^{2+} < Cu^{2+}$. The coordination behaviour of the non-functionalised receptor 1,4,7-trioxa-10-azacyclododecane was reported in methanol:water against the metal ions Zn^{2+}, Cd^{2+} and Hg^{2+} with values of the logarithms of the formation constants of the $[M(L)]^{2+}$ complexes of 3.7, < 4.5 and > 11 for Zn^{2+}, Cd^{2+} and Hg^{2+}, respectively [26]. The stability constants for the formation of the Zn^{2+} and

Table 2
Stability constants ($\log K$) for the formation of Zn^{2+}, Cd^{2+}, Pb^{2+} and Hg^{2+} complexes of L^1 in dioxane:water (70:30, v/v) at 25°C in 0.1 M KNO_3 [a]

Reaction	Zn^{2+}	Cd^{2+}	Pb^{2+}	Hg^{2+}
$M^{2+} + L^1 + H^+ \rightleftharpoons [M(HL^1)]^{3+}$	13.92(2)	13.18	11.91(9)	15.47(7)
$M^{2+} + L^1 \rightleftharpoons [M(L^1)]^{2+}$	7.10(4)	6.93	6.91(3)	12.25(5)
$M^{2+} + L^1 + H_2O \rightleftharpoons [M(L^1)(OH)]^+ + H^+$	0.38(2)	0.39	0.42(3)	4.20(5)
$M^{2+} + L^1 + 2H_2O \rightleftharpoons [M(L^1)(OH)]_2^+ + 2H^+$	−7.40(2)	−7.48(6)	−8.18(4)	5.77(5)

[a] Values in parentheses are standard deviations on the last significant digit.

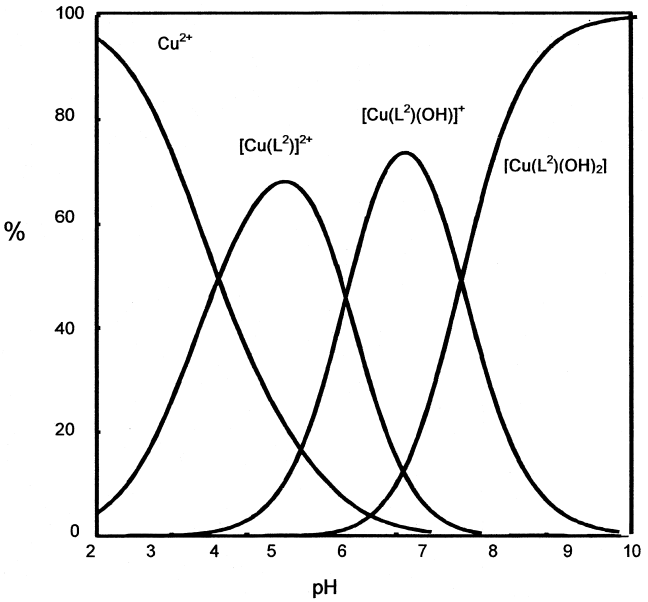


Fig. 1. Distribution diagram of the L^2–H^+–Cu^{2+} system.

Cd^{2+} complexes with the ligand 1,4,7-trioxa-10-azacyclododecane are analogous to those obtained here with L^2 (log $K = 3.96$ and 5.38, respectively, for the formation of $[Zn(L^2)]^{2+}$ and $[Cd(L^2)]^{2+}$ complexes, see Table 3). The coordination behaviour of L^4 in dioxane:water (70:30, v/v) mixtures using potentiometric methods with the Cd^{2+} and Pb^{2+} metal ions was also reported recently. Logarithms of the stability constants for the formation of the $[Cd(L^4)]^{2+}$ and $[Pb(L^4)]^{2+}$ complexes are 3.63 and 4.02, respectively.

3.2. Fluorescent behaviour

The fluorescent behaviour of L^1 and L^2 was studied in dioxane:water mixtures as a function of the pH and in the presence of the cations Ni^{2+}, Cu^{2+}, Zn^{2+}, Cd^{2+}, Hg^{2+} or Pb^{2+}. The fluorescent response of both L^1 and L^2 is pH dependent. Disappointingly, the emission intensity as a function of the pH is not modified in the presence of any of the metal ions studied and therefore neither L^1 nor L^2 display sensing properties in this medium. This contrasts strongly with the selective sensing properties of L^3 under similar experimental conditions [17].

As was stated above, selectivity could be investigated by modifying the coordination core, using a different signalling subunit or carrying out the experiment in a different solvent. Aza crown ethers are known to coordinate transition metal ions and the naphthyl group has been used satisfactorily as a fluorescent signalling subunit [20–22]. Therefore, both L^1 and L^2 appear to be good candidates for metal signalling and, although dioxane:water mixtures did not give any conclusion of interest, a change in the solvent would probably lead to positive results. Therefore, the fluorescent behaviour of L^1 and L^2 was also studied in acetonitrile in the presence of acid and transition metal ions. Addition of one equivalent of acid to L^1 produces an enhancement of the fluorescence with $I_{acid}/I_{L^1} = 1.286$. Addition of a second equivalent gave an I_{acid}/I_{L^1} ratio of 1.693. Further addition of acid does not change the fluorescence band intensity significantly. For L^2, addition of one equivalent of acid gave only a slight enhancement of the fluorescence intensity with an I_{acid}/I_{L^2} ratio of 1.103. No further modification was observed by addition of more acid.

In the presence of transition metals both L^1 and L^2 display a similar behaviour. All metal ions produced a partial quenching of the intensity fluorescent band of L^1 at 360 nm in the order $Pb^{2+} < Cd^{2+} < Hg^{2+} < Zn^{2+} < Ni^{2+} \ll Cu^{2+}$ with $I_{complex}/I_{L^1}$ ratios of 0.793, 0.600, 0.520, 0.362, 0.187 and ca. 0, respectively. The intensity of the band at 335 nm of L^2 is reduced in the order $Hg^{2+} < Zn^{2+} < Pb^{2+} < Ni^{2+} < Cd^{2+} \ll Cu^{2+}$ with $I_{complex}/I_{L^2}$ ratios of 1.124, 1.124, 1.052, 1.052, 0.575 and ca. 0, respectively. Fig. 2 shows the fluorescent spectrum of L^2 in the presence of various metal ions. The most significant feature is the total quenching that produces the presence of Cu^{2+} selectively.

In order to compare the effect of using a different signalling subunit, the fluorescent behaviour of L^3 and L^4 was also studied in acetonitrile in the presence of acid and metal ions.

Addition of one equivalent of trifluoroacetic acid to L^3 modified the fluorescence spectrum of the free recep-

Table 3
Stability constants (log K) for the formation of Ni^{2+}, Cu^{2+}, Zn^{2+}, Cd^{2+} and Pb^{2+} complexes of L^2 in dioxane:water (70:30, v/v) at 25°C in 0.1 M KNO_3 [a]

Reaction	Cu^{2+}	Zn^{2+}	Cd^{2+}	Pb^{2+}	Ni^{2+}
$M^{2+} + L^2 \rightleftharpoons [M(L^2)]^{2+}$	5.72(2)	3.96(5)	5.38(3)	4.86(1)	4.79(3)
$M^{2+} + L^2 + H_2O \rightleftharpoons [M(L^2)(OH)]^{+} + H^{+}$	0.41(1)	−3.42(1)	−2.51(3)	−2.18(1)	−2.43(2)
$M^{2+} + L^2 + 2H_2O \rightleftharpoons [M(L^2)(OH)]_2^{+} + 2H^{+}$	−6.46(2)	−10.42(2)	−11.03(3)	−10.17(1)	−11.05(3)

[a] Values in parentheses are standard deviations on the last significant digit.

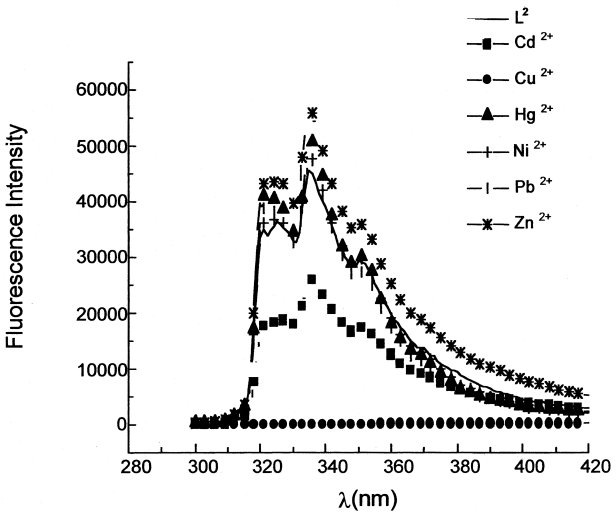


Fig. 2. Fluorescent spectra of L^2 in the presence of the metal cations Ni^{2+}, Cu^{2+}, Zn^{2+}, Cd^{2+}, Hg^{2+} and Pb^{2+}.

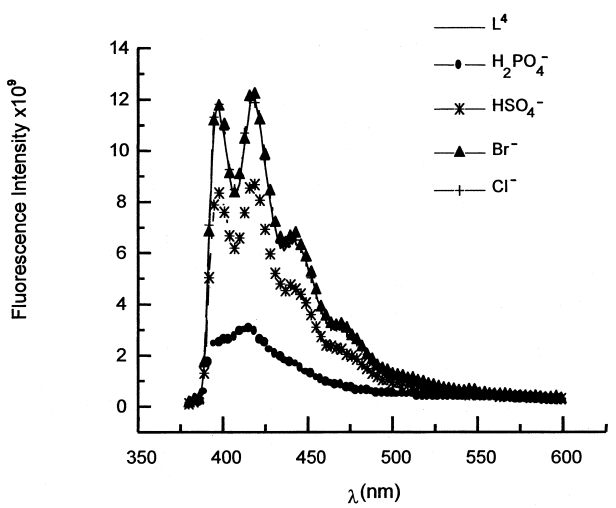


Fig. 3. Fluorescent spectra of L^4 in the presence of the anions $H_2PO_4^-$, HSO_4^-, Br^- and Cl^-.

tor significantly, with the presence of a new band centred at ca. 475 nm due probably to the formation of an exciplex. Whereas Ni^{2+} and Cu^{2+} enhances the emission intensity of the anthracenyl groups ($I_{complex}/I_{L^3} = 2.216$ and 1.859 for Ni^{2+} and Cu^{2+}, respectively), the presence of Zn^{2+}, Cd^{2+}, Hg^{2+} and Pb^{2+} gave a similar spectrum to that obtained in the presence of trifluoroacetic acid.

In the presence of one equivalent of trifluoroacetic acid, L^4 gave an enhancement of the fluorescence with an I_{acid}/I_{L^4} ratio of 3.163. In the presence of metal ions (one equivalent) the fluorescence band is very close to that found in the presence of one equivalent of acid.

The fluorescent behaviour of L^1, L^2, L^3 and L^4 was also studied in dioxane:water mixtures as a function of the pH in the presence of chloride, bromide, sulfate, phosphate and adenosine triphosphate anions. However, the emission fluorescent intensity versus pH curve is not modified in the presence of any of the anions studied. In order to complete the study, the emission properties of the ligands L^1, L^2, L^3 and L^4 were also monitored in acetonitrile in the presence of anions. The most interesting feature is that shown by the receptor L^4 whose fluorescent behaviour was studied in the presence of the tetrabutylammonium salts of Cl^-, Br^-, HSO_4^- and $H_2PO_4^-$ (see Fig. 3). Whereas the emission intensity of the fluorescent band is not modified in the presence of chloride or bromide, addition of HSO_4^- produces a slight decrease in the fluorescence intensity with $I_{complex}/I_{L^4} = 0.723$. The quenching induced by the addition of $H_2PO_4^-$ with $I_{complex}/I_{L^4} = 0.252$ is most noticeable.

Acknowledgements

The authors would like to thank the DGICYT (proyecto PB95-1121-C02-021 and FD97-0508-C03-01) and Generalitat Valenciana (proyecto GV97-CB-11-62 and GV98-2-65) for their support.

References

[1] P.D. Beer, P.A. Gale, G.Z. Chen, J. Chem. Soc., Dalton Trans. (1999) 1897.
[2] J.E. Kingston, L. Ashford, P.D. Beer, M.G.B. Drew, J. Chem. Soc., Dalton Trans. (1999) 251.
[3] P.L. Boulas, M. Gómez-Kaifer, L. Echegoyen, Angew. Chem., Int. Ed. Engl. 37 (1998) 216.
[4] P.D. Beer, Acc. Chem. Res. 31 (1998) 71.
[5] P.D. Beer, Chem. Commun. (1999) 689.
[6] P.D. Beer, Chem. Soc. Rev. 18 (1989) 409.
[7] A.W. Czarnik, Acc. Chem. Res. 27 (1994) 302.
[8] V. Balzani, S.F. Candola, Supramolecular Photochemistry, Ellis Horwood, Chichester, UK, 1991.
[9] A.W. Czarnik, Top. Fluoresc. Spectrosc. 4 (1994) 49.
[10] J.M. Lloris, R. Martínez-Máñez, T. Pardo, J. Soto, M.E. Padilla-Tosta, Chem. Commun. (1998) 837.
[11] J.M. Lloris, R. Martínez-Máñez, T. Pardo, J. Soto, M.E. Padilla-Tosta, J. Chem. Soc., Dalton Trans. (1998) 2635.
[12] J.M. Lloris, A. Benito, R. Martínez-Máñez, M.E. Padilla-Tosta, T. Pardo, J. Soto, M.J.L. Tendero, Helv. Chim. Acta 81 (1998) 2024.
[13] M.E. Padilla-Tosta, J.M. Lloris, R. Martínez-Máñez, T. Pardo, J. Soto, A. Benito, M.D. Marcos, Inorg. Chem. Commun. (2000) 45.
[14] E.V. Akkaya, M.E. Huston, A.W. Czarnik, J. Am. Chem. Soc. 112 (1990) 3590.
[15] T.D. James, H. Shimmori, M. Takenchi, Suji Shinkai, Chem. Commun. (1996) 705.
[16] F. Arnand-Neu, B. Spiess, M.J. Schwing-Weill, Helv. Chim. Acta 60 (1977) 2633.

[17] Y. Al Shihadeh, A. Benito, J.M. Lloris, R. Martínez-Máñez, T. Pardo, J. Soto, J. Chem. Soc., Dalton Trans. (2000) 1.
[18] (a) G. Gran, Analyst (London) 77 (1952) 661. (b) F.J. Rossotti, H.J. Rossotti, J. Chem. Educ. 42 (1965) 375.
[19] P. Gans, A. Sabatini, A. Vacca, J. Chem. Soc., Dalton Trans. (1985) 1195.
[20] D.T. James, H. Shimmori, S. Shinkai, Chem. Commun. (1997) 71.
[21] K. Kubo, R. Ishige, T. Sakurai, Heterocycles 48 (1998) 347.
[22] K. Kubo, R. Ishige, N. Kato, E. Yamamoto, T. Sakurai, Heterocycles 45 (1997) 2365.
[23] J.M. Lloris, R. Martínez-Máñez, M.E. Padilla-Tosta, T. Pardo, J. Soto, P.D. Beer, J. Cadman, D.K. Smith, J. Chem. Soc., Dalton Trans. (1999) 2359.
[24] K.A. Byriel, K.R. Dunster, L.R. Gahan, C.H.L. Kennard, J.L. Latten, I.L. Swann, P.A. Duckworth, Inorg. Chim. Acta 205 (1993) 191.
[25] A.E. Martell, R.M. Smith, R.M. Motekairis, NIST Critical Stability Constants of Metals Complexes Database, Texas A&M University, College Station, TX, 1993.
[26] E. Luboch, A. Cygan, J.F. Biernat, Inorg. Chim. Acta 68 (1983) 201.

PERGAMON

www.elsevier.nl/locate/poly

Polyhedron 19 (2000) 1873–1880

POLYHEDRON

Structures of 2-pyridineformamide thiosemicarbazone and its complexes with cadmium halides

Alfonso Castiñeiras [a,*], Isabel Garcia [a], Elena Bermejo [a], Douglas X. West [b]

[a] *Departamento de Química Inorgánica, Universidad de Santiago de Compostela, E-15706 Santiago de Compostela, Spain*
[b] *Department of Chemistry, Illinois State University, Normal, IL 61790-4160, USA*

Received 9 March 2000; accepted 20 June 2000

Abstract

Reduction of 2-cyanopyridine by sodium in dry methanol in the presence of thiosemicarbazide produces 2-pyridineformamide thiosemicarbazone, HAm4DH. Complexes of HAm4DH with cadmium(II) chloride, bromide and iodide have been prepared and spectroscopically characterized, and crystal structures of $[Cd(HAm4DH)Cl_2]\cdot DMSO$, $[Cd(HAm4DH)Br_2]\cdot H_2O$ and $[Cd(HAm4DH)I_2]$ have been determined by X-ray diffractometry. In each of these complexes neutral HAm4DH coordinates via its pyridyl and imine nitrogens and sulfur, and the cadmium atom is pentacoordinated to the thiosemicarbazone and the two halo ligands. The coordination polyhedra of the three complexes are best described as square pyramidal, with $[Cd(HAm4DH)Br_2]$ having the greatest distortion toward a trigonal bipyramid. The hydrogens attached to nitrogens in coordinated HAm4DH form hydrogen bonds with oxygen atoms in solvent molecules and with halo ligands on adjacent molecules. © 2000 Elsevier Science Ltd. All rights reserved.

Keywords: 2-Pyridineformamide; Thiosemicarbazone; Crystal structures; Cadmium halides

1. Introduction

Although N(4)-substituted 2-formyl-, 2-acetyl- and 2-benzoylpyridine thiosemicarbazones [1–3] possess substantial in vitro activity against various human tumor lines [4], they are poorly soluble in water. Therefore, these thiosemicarbazones and their metal complexes are less promising when tested in vivo. In an attempt to enhance the water solubility of thiosemicarbazones and their complexes, a new series in which the thiosemicarbazone moiety is attached to an amide carbon rather than an aldehyde or ketone carbon has been prepared. Following our studies of complexes of 2-pyridineformamide *N*(4)-methylthiosemicarbazone, HAm4M [5,6], and of Group 12 metal complexes of various 2-acetylpyridine thiosemicarbazones [7–9], we recently communicated the structures of 2-pyridineformamide thiosemicarbazone (HAm4DH) (Fig. 1) and of its complexes with zinc chloride, bromide and iodide [10]. Here we present the structures of complexes of HAm4DH with cadmium chloride, bromide and iodide, and compare them to their zinc analogues and to previously studied cadmium complexes of heterocyclic thiosemicarbazones [11].

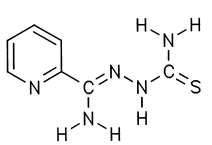


Fig. 1. 2-Pyridineformamide thiosemicarbazone, HAm4DH.

2. Experimental

Infrared spectra in KBr pellets (4000–400 cm^{-1}) and Nujol mulls (500–100 cm^{-1}) were recorded in a Bruker IFS 66V spectrometer. ^1H and ^{13}C NMR spectra were recorded in DMSO-d_6 solutions in a Bruker WM-300 spectrometer using TMS as internal reference. Elemental analysis was performed with a Carlo Erba 1108 elemental analyzer. The melting point was determined with a Büchi apparatus.

* Corresponding author. Tel.: +34-981-594-636; fax: +34-981-547-163.
E-mail address: qiac01@usc.es (A. Castiñeiras).

0277-5387/00/$ - see front matter © 2000 Elsevier Science Ltd. All rights reserved.
PII: S0277-5387(00)00473-3

Table 1
Colors, melting points and partial elemental analyses of cadmium complexes of HAm4DH

Compound	Color	M.p. (°C)	%Found (Calc.)			
			C	H	N	S
$[Cd(HAm4DH)Cl_2]\cdot 0.25H_2O$	white	284	21.76 (21.95)	2.27 (2.50)	18.32 (18.28)	7.92 (8.37)
$[Cd(HAm4DH)Br_2]$	yellow	240	18.13 (17.99)	1.89 (1.94)	14.86 (14.98)	6.76 (6.86)
$[Cd(HAm4DH)I_2]$	yellow	210	15.12 (14.97)	1.57 (1.62)	12.47 (12.47)	5.48 (5.71)

The details of the preparation of HAm4DH were communicated in our earlier report on its zinc complexes [10]. The cadmium complexes were prepared as follows. A solution of $CdCl_2$, $CdBr_2$ or CdI_2 (0.002 mol) in EtOH (30 mL) was mixed with a solution of HAm4DH (0.002 mol) in the same solvent (30 mL) and the mixture was stirred under reflux for 2 h. The resulting solids were filtered out, washed with anhydrous ether to apparent dryness, and placed on a warm plate at 35°C. Yields were 97.4, 94.3 and 83.5% for $[Cd(HAm4DH)Cl_2]\cdot 0.25H_2O$, $[Cd(HAm4DH)Br_2]$ and $[Cd(HAm4DH)I_2]$, respectively. Their partial elemental analyses are listed in Table 1 with their melting points.

Crystals of $[Cd(HAm4DH)Cl_2]\cdot$DMSO were grown from a 1:1 v/v DMSO–EtOH mixture, and crystals of $[Cd(HAm4DH)Br_2]\cdot H_2O$ and $[Cd(HAm4DH)I_2]$ from 96% ethanol. The crystals were mounted on glass fibers and used for data collection in an automatic diffractometer (Enraf–Nonius MACH3 for $[Cd(HAm4DH)Cl_2]\cdot$DMSO and $[Cd(HAm4DH)I_2]$; CAD4 for $[Cd(HAm4DH)Br_2]\cdot H_2O$). Cell constants and an orientation matrix for data collection were obtained by least-squares refinement of the diffraction data from 25 reflections in the ranges 9.422–20.833° for $[Cd(HAm4DH)Cl_2]\cdot$DMSO, 7.921–45.065° for $[Cd(HAm4DH)Br_2]\cdot H_2O$ and 9.327–21.137° for $[Cd(HAm4DH)I_2]$. Data for $[Cd(HAm4DH)Br_2]\cdot H_2O$ were collected at 293(2) K using Cu Kα radiation ($\lambda =$ 1.54184 Å), and data for $[Cd(HAm4DH)Cl_2]\cdot$DMSO and $[Cd(HAm4DH)I_2]$ using Mo Kα radiation ($\lambda = 0.71073$ Å). The ω-scan technique were employed for the three crystals and the data were corrected for Lorentz and polarization effects [12]. A semi-empirical absorption correction was made for the three crystals [13]. The structures were solved by direct methods [14], which showed the positions of all non-hydrogen atoms, and refined on F^2 by a full-matrix least-squares procedure using anisotropic displacement parameters [15]. The positions of most hydrogens were calculated (C–H 0.93–0.97 Å) and refined using a riding model; the exceptions were the H_2O hydrogens in the bromo complex, which were located from difference Fourier maps and refined isotropically. In $[Cd(HAm4DH)Cl_2]\cdot$DMSO a weak peak found near Cd(11) in the Fourier difference synthesis at 1.052 Å was included in the final model as a Cd(12) atom; the occupancy factors refined to 0.93(1) for Cd(11) and 0.07(1) for Cd12. Atom scattering factors were taken from the International Tables for X-ray Crystallography [16]. Molecular graphics were generated with PLATON-98 [17] for $[Cd(HAm4DH)Cl_2]\cdot$DMSO and $[Cd(HAm4DH)I_2]$, and with ZORTEP [18] for $[Cd(HAm4DH)Br_2]\cdot H_2O$.

3. Results and discussion

Crystal and structure refinement data for the three cadmium complexes are summarized in Table 2. Selected bond lengths and angles are listed in Tables 3 and 4. Perspective views of $[Cd(HAm4DH)Cl_2]\cdot$DMSO, $[Cd(HAm4DH)Br_2]\cdot H_2O$ and $[Cd(HAm4DH)I_2]$ are shown in Figs. 2–4, respectively. Hydrogen bonding parameters are compiled in Table 5, and the root-mean-square plane data in Table 6.

3.1. Structures of the $[Cd(Am4DH)X_2]$ complexes

In all three complexes HAm4DH coordinates via its pyridyl and imine nitrogens and its sulfur, and the two halo ligands bring the coordination number to five. As found previously with metal complexes of heterocyclic thiosemicarbazones [1–3], in $[Cd(HAm4DH)Cl_2]$ and $[Cd(HAm4DH)Br_2]$ the Cd–N(2) bond is shorter than the Cd–N(1) bond, by ca. 0.08 and 0.06 Å, respectively. The two Cd–X bond distances also differ, by ca. 0.06 Å in the chloro complexes and ca. 0.07 Å in the bromo compound. However, in $[Cd(HAm4DH)I_2]$ neither the two Cd–N bond lengths nor the two Cd–I distances differ significantly. Cd–N(1) is significantly shorter in the iodo complex than in the others (as also in the $[Zn(HAm4DH)X_2]$ series [10]), but the Cd–N(2) and Cd–S bond lengths are similar in all three. The average Cd–X distance increases in the expected order Cd–Cl < Cd–Br < Cd–I. Comparison of $[Cd(HAm4DH)Cl_2]$ with $[Cd(HFo4DH)Cl_2]$, where HFo4DH is 2-formylpyridine thiosemicarbazone, shows that Cd–N(2) is much shorter in the former, 2.307(6) compared to 2.350(3) Å [11], but the lengths of the other bonds are similar in the two compounds. The difference in Cd–N(2) is presumably due to the N(2) amino group of

Table 2
Crystal and structure refinement data for $[Cd(HAm4DH)Cl_2]\cdot(CH_3)_2SO$, $[Cd(HAm4DH)Br_2]\cdot H_2O$ and $[Cd(HAm4DH)I_2]$ (HAm4DH = 2-pyridineformamide N(4)-thiosemicarbazone)

Empirical formula	$C_9H_{15}CdCl_2N_5OS_2$	$C_7H_{11}Br_2CdN_5OS$	$C_7H_9CdI_2N_5S$
Color, habit	yellow, prism	yellow, prism	yellow, plate
Formula weight	456.68	485.49	561.45
Crystal size (mm)	$0.25\times0.20\times0.15$	$0.35\times0.25\times0.15$	$0.30\times0.30\times0.10$
Crystal system	monoclinic	triclinic	monoclinic
Space group	$P2_1/c$ (no. 14)	$P\bar{1}$ (no. 2)	$P2_1/c$ (no. 14)
Unit cell dimensions			
a (Å)	11.970(2)	7.525(2)	7.627(5)
b (Å)	10.737(2)	9.772(4)	14.980(4)
c (Å)	13.559(2)	10.398(4)	14.356(3)
α (°)	90.00(-)	80.856(17)	90.00(-)
β (°)	108.19(1)	76.391(18)	121.978(1)
γ (°)	90.00(-)	67.944(11)	90.00(-)
Volume (Å^3)	1655.4(4)	686.6(4)	1391.3(10)
Z	4	2	4
D_{calc} (g cm^{-3})	1.832	2.348	2.680
Absorption coefficient (mm^{-1})	1.895	20.936	6.140
θ Range for data collection (°)	2.47–27.97	4.39–75.89	2.72–27.97
Index ranges (°)	$-15\le h\le0$, $0\le k\le14$, $-17\le l\le17$	$-9\le h\le6$, $-12\le k\le11$, $-13\le l\le6$	$0\le h\le10$, $0\le k\le19$, $-10\le l\le16$
Absorption correction	ψ-scan	ψ-scan	ψ-scan
Reflections collected	4166	2986	1869
Independent reflections (R_{int})	3984(5.67%)	2867(7.74%)	1869(0.00%)
Data/parameters	3984/193	2867/161	1869/145
Final R indices [$I>2\sigma(I)$]	$R_1=0.0518$, $wR_2=0.1252$	$R_1=0.0668$, $wR_2=0.1849$	$R_1=0.0372$, $wR_2=0.0692$
R Indices (all data)	$R_1=0.1824$, $wR_2=0.1580$	$R_1=0.0682$, $wR_2=0.1867$	$R_1=0.1275$, $wR_2=0.0861$
Goodness-of-fit	0.977	1.086	0.970
Largest difference peak and hole (e Å^{-3})	0.891 and −0.791	2.338 and −2.193	0.689 and −0.537

HAm4DH having a larger inductive effect than the hydrogen in HFo4DH.

In the analogous series of zinc complexes only bond angles involving halogen atoms differed significantly [10]. The same is essentially true for the cadmium series, the greatest bond angle differences concerning X(1)–Cd–N(2) and X(2)–Cd–N(2), which respectively increase and decrease with increasing halogen size. The N(1)–Cd–S(1) angles, which reflect the two bite angles of the bichelate bonding system, average 142.6(3)°, as against 148.6(2)° for the analogous zinc complexes. These ligands may not be able to maintain N,N,S-coordination with larger metal ions: in $[Hg(HAm4DH)_2Br_2]$ only the sulfurs are coordinated [19].

In all three complexes the thiosemicarbazone bond lengths (Table 3) differ slightly from their values in HAm4DH [10]. As in the zinc series [10], the S(1)–C(7) bonds shorten with increasing halogen size, and other bonds involving C(7) are consequently altered. By contrast, C(6)–N(2) is longest in $[Cd(HAm4H)I_2]$, which suggests that coordination via the thione sulfur is weakest, and bonding via the imine nitrogen strongest, in this sterically more crowded complex. Of the six known Group 12 metal complexes of HAm4DH, $[Cd(HAm4DH)I_2]$ differs most from HAm4DH in its thiosemicarbazone bond distances: for example, the S(1)–C(7) distance is 1.671(15) Å in the complex and 1.698(2) Å in the ligand, and the C(6)–N(2) distance 1.322(16) Å in $[Cd(HAm4DH)I_2]$ and 1.293(2) Å in HAm4DH. The fact that the C–S bond is shorter in $[Cd(HAm4DH)I_2]$ than HAm4DH indicates the importance of intermolecular hydrogen bonding in the latter. Coordination also alters bond angles in the vicinity of the coordinating imine nitrogen, N(2), and the thione sulfur, S(1).

Table 3
Selected bond lengths (Å) in $[Cd(HAm4DH)Cl_2]\cdot(CH_3)_2SO$, $[Cd(HAm4DH)Br_2]\cdot H_2O$ and $[Cd(HAm4DH)I_2]$

Bond	$[Cd(HAm4DH)Cl_2]$	$[Cd(HAm4DH)Br_2]$	$[Cd(HAm4DH)I_2]$
Cd(1)–N(1)	2.384(6)	2.385(7)	2.325(12)
Cd(1)–N(2)	2.307(6)	2.327(6)	2.313(12)
Cd(1)–S(1)	2.596(3)	2.579(2)	2.601(3)
Cd(1)–X(1)	2.455(2)	2.654(1)	2.7784(13)
Cd(1)–X(2)	2.515(2)	2.587(1)	2.780(2)
S(1)–C(7)	1.706(8)	1.693(7)	1.671(15)
C(6)–N(2)	1.281(9)	1.288(9)	1.322(16)
N(2)–N(3)	1.380(9)	1.375(8)	1.399(11)
N(3)–C(7)	1.332(9)	1.337(10)	1.340(15)
C(7)–N(4)	1.292(10)	1.333(9)	1.344(14)
C(6)–N(5)	1.367(9)	1.335(9)	1.342(18)

Table 4
Selected bond angles (°) in $[Cd(HAm4DH)Cl_2]\cdot(CH_3)_2SO$, $[Cd(HAm4DH)Br_2]\cdot H_2O$ and $[Cd(HAm4DH)I_2]$

Bond	$[Cd(HAm4DH)Cl_2]$	$[Cd(HAm4DH)Br_2]$	$[Cd(HAm4DH)I_2]$
S(1)–Cd(1)–N(11)	142.76(17)	143.60(16)	141.5(3)
S(1)–Cd(1)–N(2)	75.62(17)	75.97(15)	73.5(2)
S(1)–Cd(1)–X(1)	107.98(7)	101.38(5)	100.41(10)[c]
S(1)–Cd(1)–X(2)	106.30(8)	108.76(6)	108.06(8)[c]
X(1)–Cd(1)–N(1)	92.87(17)	91.97(16)	97.3(3)
X(1)–Cd(1)–N(2)	110.92(17)	115.45(15)	133.36(18)
X(1)–Cd(1)–X(2)	107.84(8)	120.87(4)	109.85(6)
N(1)–Cd(1)–N(2)	68.1(2)	67.7(2)	69.4(4)
X(2)–Cd(1)–N(1)	95.60(17)	92.32(16)	97.5(2)
X(2)–Cd(1)–N(2)	138.36(17)	120.54(15)	116.02(18)
Cd(1)–S(1)–C(7)	99.3(3)	99.2(2)	101.0(4)
Cd(1)–N(2)–C(6)	122.6(5)	122.6(5)	123.5(8)
Cd(1)–N(2)–N(3)	119.2(5)	118.5(4)	121.5(8)
N(5)–C(6)–N(2)	124.8(7)	126.6(7)	126.7(12)
C(5)–C(6)–N(2)	116.5(7)	115.8(6)	110.1(13)
C(6)–N(2)–N(3)	118.0(7)	118.9(6)	115.0(12)
N(2)–N(3)–C(7)	121.7(6)	121.3(6)	118.5(13)
N(3)–C(7)–N(4)	116.5(7)	115.3(7)	114.1(14)
N(3)–C(7)–S(1)	123.7(6)	124.8(5)	124.1(10)
N(4)–C(7)–S(1)	119.8(6)	119.9(6)	121.7(10)

In $[Cd(HAm4DH)I_2]$, which crystallized without an accompanying solvent molecule, N(3)–H(3), N(4)–H(4A) and N(5)–H(5B) all form hydrogen bonds with I(1) of one neighboring molecule while N(4)–H(4B) hydrogen bonds to I(2) of a second neighboring molecule (Table 5). In $[Cd(HAm4DH)Cl_2]\cdot DMSO$, N(3)–H(3) and N(5)–H(5A) form hydrogen bonds with the oxygen of the DMSO molecule and N(4)–H(4A), N(4)–H(4B) and N(5)–H(5B) with Cl atoms on three different neighboring molecules. The hydrogen bonding in $[Cd(HAm4DH)Br_2]\cdot H_2O$ is similar to that of $[Cd(HAm4DH)Cl_2]\cdot DMSO$, with the water molecule supplying the oxygen instead of DMSO; additionally, the hydrogens of the water molecule interact with the bromo ligands. The crystals of these cadmium complexes thus feature dense hydrogen bond networks, which contributes to their stability and helps to promote crystal growth.

The planarity in HAm4DH of the pyridine ring and the thiosemicarbazone moiety is generally retained in the cadmium complexes; the greatest change in the thiosemicarbazone moiety occurs in $[Cd(HAm4DH)I_2]$ (Table 6). As in the zinc series [10], the angle between the best planes of the pyridine ring and the thiosemicarbazone moiety increases in the order $[Cd(HAm4DH)Cl_2] < [Cd(HAm4DH)Br_2] < [Cd(HAm4DH)I_2]$. In the chloro and iodo complexes this angle is smaller for Cd than for Zn, while the reverse holds for the bromo complexes: $[Cd(HAm4DH)Cl_2]$, 2.04(24)°; $[Zn(HAm4DH)Cl_2]$, 5.46(11)°; $[Zn(HAm4DH)Br_2]$, 6.92(16)°; $[Cd(HAm4DH)Br_2]$, 8.22(36)°; $[Cd(HAm4DH)I_2]$, 9.25(61)° and $[Zn(HAm4DH)I_2]$, 11.44(58)°.

The values of the geometrical parameter $\tau = (\beta - \alpha)/60$ [20], where $\alpha = Cl(2)–Cd–N(2)$ and $\beta = N(1)–Cd–S(1)$, show that, like the Zn complexes, all three Cd complexes are closer to ideal square pyramid with X(1) apical than to a trigonal bipyramid (Table 7). However, $[Cd(HAm4DH)Br_2]$ ($\tau = 0.39$) is closer to a trigonal bipyramid than any of the Group 12 complexes prepared with HAm4DH or any of the other Group 12 complexes listed in Table 7, which includes $[Cd(HAc4DH)Cl_2]$ [11] and six cadmium complexes of N(4)-substituted 2-acetylpyridine thiosemicarbazones [7–9].

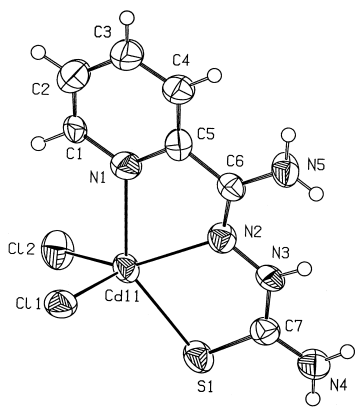


Fig. 2. Perspective view of dichloro(2-pyridineformamide thiosemicarbazone) cadmium(II), $[Cd(Am4DH)Cl_2]$, showing 50% probability ellipsoids for the nonhydrogen atoms and the numbering scheme of the atoms in the molecule.

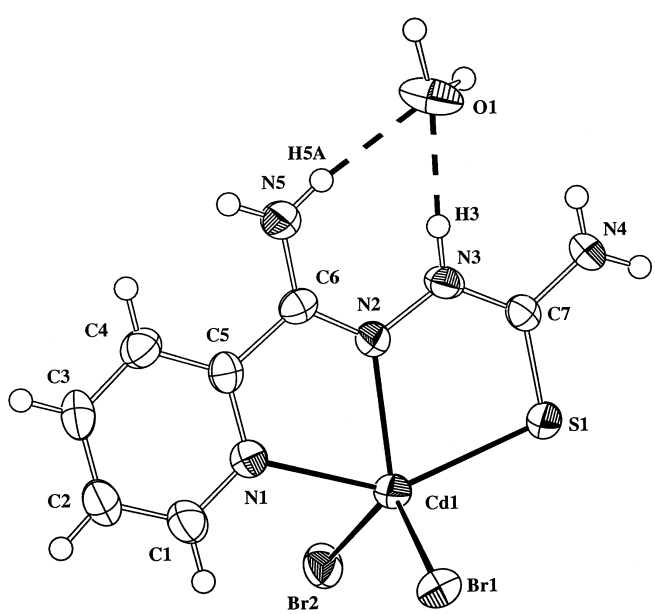


Fig. 3. Perspective view of dibromo(2-pyridineformamide thiosemicarbazone) cadmium(II) monohydrate, $[Cd(Am4DH)Br_2]\cdot H_2O$, drawn with 50% probability ellipsoids. Some of the hydrogen bonds are shown by dashed lines.

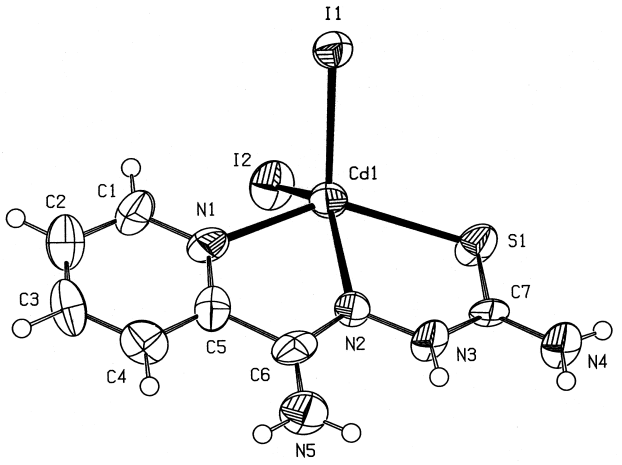


Fig. 4. Perspective view of diiodo(2-pyridineformamide thiosemicarbazone) cadmium(II), [Cd(Am4DH)I_2] with thermal ellipsoids at 50% probability. The hydrogen atoms (○) are drawn with an arbitrary radius of 0.1 Å.

3.2. Infrared spectra

The IR bands that are most useful for determining the coordination mode of the thiosemicarbazone are given in Table 8. As many as four bands can be assigned to ν(NH). The highest energy band in the spectrum of HAm4DH at 3421 cm^{-1}, is attributable to $\nu_a(N14H_2)$ on the basis of previous studies of thiosemicarbazones [11]. In the complexes there are substantial shifts to lower energy of the other three bands, which in view of the distances listed in Table 5 is probably due to the stronger hydrogen bonding interactions of coordinated HAm4DH. The fact that the ν(C=N) band at 1590 cm^{-1} in the spectrum of HAm4DH shifts to smaller wavenumbers in the spectra of the cadmium complexes indicates coordination of the imine nitrogen, as does the band in the 344–400 cm^{-1} range assigned to ν(CdN(2)) [21]. This range for ν(CdN(2)) is lower than is found for cobalt(II), nickel(II) and copper(II) complexes of related thiosemicarbazones [5,6], which is consistent with the larger size and longer bonds of cadmium. Coordination of the sulfur is indicated by a similar decrease in energy of the thioamide IV band, which derives considerable intensity from ν(CS), and by the appearance of a band in the 247–316 cm^{-1} range assignable to ν(CdS) [22,23]. Coordination of the pyridyl nitrogen shifts the out-of-plane ring deformation ρ(py) some 18–21 cm^{-1} to higher frequencies. In the 100–500 cm^{-1} region, assignation to ν(Cd–X) of two strong bands whith energies increasing in the order [Cd(HAm4DH)I_2] < [Cd(HAm4DH)Br_2] < [Cd(HAm4DH)-Cl_2] affords ν(Cd–Br)/ν(Cd–Cl) and ν(Cd–I)/ν(Cd–Cl) ratios of ca. 0.63 and 0.60, respectively (Table 8).

3.3. NMR spectra

Also included in Table 8 are ^{1}H, ^{13}C and ^{113}Cd NMR spectral assignments for HAm4DH and its cadmium complexes. As in other studies of heterocyclic thiosemicarbazones [1–3], N(13)H interacts with the solvent

Table 5
Hydrogen bond parameters (Å, °) in [Cd(HAm4DH)Cl_2]·$(CH_3)_2$SO, [Cd(HAm4DH)Br_2]·H_2O and [Cd(HAm4DH)I_2]

Compound	D–H···A	d(D–H)	d(H···A)	d(D···A)	>(DHA)
[Cd(HAm4DH)Cl_2] [a]	N(3)–H(3)–O(1) # 1	0.86	1.96	2.779(9)	158.3
	N(4)–H(4A)–Cl(2) # 2	0.86	2.90	3.531(7)	132.0
	N(4)–H(4B)–Cl(1) # 3	0.86	2.49	3.300(7)	156.5
	N(5)–H(5A)–O(1) # 1	0.86	2.05	2.862(9)	157.9
	N(5)–H(5B)–Cl(1) # 4	0.86	2.48	3.224(6)	145.6
[Cd(HAm4DH)Br_2] [b]	N(3)–H(3)–O(1)	0.86	1.96	2.818(9)	176.7
	N(4)–H(4A)–Br(2) # 1	0.86	3.02	3.722(7)	139.9
	N(4)–H(4B)–Br(1) # 2	0.86	2.82	3.588(7)	149.1
	N(5)–H(5A)–O(1)	0.86	2.07	2.921(11)	172.3
	N(5)–H(5B)–Br(1) # 3	0.86	2.76	3.526(7)	148.6
	O(1)–H(1A)–Br(2) # 4	1.06(1)	2.70(1)	3.507(8)	132(9)
	O(1)–H(1A)–Br(2) # 1	1.06(1)	2.71(1)	3.524(8)	133(9)
	O(1)–H(1B)–Br(1) # 4	0.69(5)	2.64(2)	3.329(7)	177(16)
[Cd(HAm4DH)I_2] [c]	N(3)–H(3)–I(1) # 1	0.86	2.82	3.623(12)	156.7
	N(4)–H(4A)–I(1) # 1	0.86	3.10	3.859(13)	148.8
	N(4)–H(4B)–I(2) # 2	0.86	2.92	3.711(11)	169.0
	N(5)–H(5A)–I(1) # 1	0.86	3.06	3.849(12)	153.7

[a] Symmetry transformations used to generate equivalent atoms: # 1: $x-1$, $-y+1/2$, $z-1/2$; # 2: $-x$, $-y+1$, $-z$; # 3: $-x$, $y+1/2$, $-z+1/2$; # 4: $-x$, $y-1/2$, $-z+1/2$.

[b] Symmetry transformations used to generate equivalent atoms: # 1: $-x+1$, $-y+1$, $-z+1$; # 2: $-x$, $-y+1$, $-z+1$; # 3: $-x+1$, $-y+1$, $-z$; # 4: x, $y+1$, z.

[c] Symmetry transformations used to generate equivalent atoms: # 1: x, $-y+1/2$, $z-1/2$; # 2: $-x+1$, $y-1/2$, $-z+3/2$.

Table 6
Root-mean square planes in $[Cd(HAm4DH)Cl_2]\cdot(CH_3)_2SO$, $[Cd(HAm4DH)Br_2]\cdot H_2O$ and $[Cd(HAm4DH)I_2]$

Compound	Plane	Root-mean square deviation	Largest deviation	Angle with previous plane
$[Cd(HAm4DH)Cl_2$	C(6)/N(2)/N(3)/C(7)/N(4)/S(1)	0.0176	N(3), 0.035(6)	
	N(1)/C(1)/C(2)/C(3)/C(4)/C(5)	0.0105	C(2), 0.017(7)	2.0(2)
$[Cd(HAm4DH)Br_2$	C(6)/N(2)/N(3)/C(7)/N(4)/S(1)	0.0118	N(3), 0.022(6)	
	N(1)/C(1)/C(2)/C(3)/C(4)/C(5)	0.0023	C(5), 0.004(5)	8.2(4)
$[Cd(HAm4DH)I_2$	C(6)/N(2)/N(3)/C(7)/N(4)/S(1)	0.0578	N(2), 0.097(6)	
	N(1)/C(1)/C(2)/C(3)/C(4)/C(5)	0.0050	C(4), 0.007(7)	9.3(6)

Table 7
Deviation from tetragonal-pyramidal coordination in Group 12 metal thiosemicarbazone complexes $[M(NNS)X_2]$ {M = Zn(II), Cd(II), Hg(II); X = Cl, Br, I}

Compound	β(N–M–X)	α(S–M–N)	$\beta-\alpha$	$\tau=(\beta-\alpha)/60$	Ref.
$[Cd(HAm4DH)Cl_2]$	142.8	138.4	4.4	0.07	this work
$[Cd(HAm4DH)Br_2]$	143.6	120.5	23.1	0.39	this work
$[Cd(HAm4DH)I_2]$	141.5	133.4	8.1	0.14	this work
$[Cd(HAc4DH)Cl_2]$	141.5	137.7	3.8	0.06	[11]
$[Cd(HAc4M)Cl_2]$	139.8	136.7	3.1	0.05	[7]
$[Cd(HAc4M)Br_2]$	139.9	135.3	4.6	0.08	[7]
$[Cd(HAc4M)I_2]$	140.1	135.2	4.9	0.08	[7]
$[Cd(HAc4DM)Cl_2]$	145.2	135.5	9.7	0.16	[9]
$[Cd(HAc4DM)I_2]$	145.4	131.6	13.8	0.23	[9]
$[Cd(HAc4Ph)Br_2]$	136.1	139.5	3.4	0.06	[8]
$[Zn(HAm4DH)Cl_2]$	149.7	141.8	7.9	0.13	[10]
$[Zn(HAm4DH)Br_2]$	146.0	148.4	2.4	0.04	[10]
$[Zn(HAm4DH)I_2]$	150.1	136.3	13.8	0.23	[10]
$[Hg(HAc4M)Cl_2]$	138.7	132.4	6.3	0.11	[7]

and is assigned to the signal furthest downfield, and the $N(14)H_2$ protons are assigned to the two resonances in the region around 7.85 ppm, which disappear on addition of D_2O to the sample. The $N(15)H_2$ protons are assigned to the resonance at 6.91 ppm, which is similar to the chemical shift found for HAm4M, 6.86 ppm [6]. None of these signals shifts significantly upon coordination to cadmium. Of the ^{13}C NMR signals of the free ligand, the signal for the thione carbon, C(7), does not shift significantly on complexation, but the signal of the imine carbon, C(6), shifts from 142.0 to 144.6–144.8 ppm in the complexes, as has also been observed for other thiosemicarbazone complexes with Group 12 dihalides [7–9].

The ^{113}Cd NMR spectra show a single signal between 387 ppm, for $[Cd(HAm4DH)Cl_2]$, and 291 ppm, for $[Cd(HAm4DH)I_2]$. The metal atom is in each case less deshielded than in the corresponding dihalide (CdX_2) in DMSO [24]. These findings are consistent with those obtained for other complexes of cadmium(II) halides with thiosemicarbazones [6–9] and are compatible with pentacoordination of the metal [25].

4. Conclusion

These three cadmium complexes are similar in their structural and spectral properties. The results presented here form a basis for future comparison with complexes of the same ligand with other metals, and with cadmium complexes of N(4)-substituted 2-pyridineformamide thiosemicarbazones. The strong intermolecular hydrogen bonds of HAm4DH become even stronger in the cadmium complexes, particularly when a solvate molecule is present in the crystal.

5. Supplementary material

Crystallographic data for $C_{10}H_{15}CdCl_2N_5OS_2$ {$[Cd(HAm4DH)Cl_2]\cdot$DMSO, CCDC-139834}, $C_7H_{11}Br_2CdN_5OS$ {$[Cd(HAm4DH)Br_2]\cdot H_2O$, CCDC-139835} and $C_7H_9CdI_2N_5SCd$ {$[Cd(HAm4DH)I_2]$, CCDC-139836} have been deposited with the Cambridge Crystallographic Data Centre as supplementary publication No. CCDC-1003/m. Copies of available material can be

Table 8
IR and ^{1}H, ^{13}C and ^{113}Cd NMR data ([$^{6}d_2$]-DMSO) for HAm4DH and its cadmium complexes [a]

Assignment	HAm4DH	[Cd(HAm4DH)Cl_2] [b]	[Cd(HAm4DH)Br_2]	[Cd(HAm4DH)I_2]
IR				
ν(NH)	3421s	3370s	3422m	3461w
	3360s	3288s	3385m	3389s
	3283s	3191s	3315s	3281s
	3234s		3235s	3173m
	3208m			
	3184m			
ν(NH)	1663m	1704s	1697s	1664s
			1674m	
ν(CN)+ν(CC)	1612m	1635sh	1610s	
	1590s	1623s	1587s	1598s
	1568m	1583s	1569m	1542s
	1524s			
ν(CS)	854m	857m	845m	831w
ρ(py)	618m	636m	636w	639w
ν(CdN)		400m	368m	344m
ν(CdS)		316s	261m	247s
ν_a(CdX)		256s	160s	154m
ν_s(CdX)		225s	148s	147s
NMR				
N13H	10.05	10.05	10.05	10.05
$N14H_2$	7.93	7.95	7.94	7.94
	7.78 [c]	7.81 [c]	7.81 [c]	7.81 [c]
$N15H_2$	6.91	6.92	6.92	6.92
$C(7)_{(thioamide)}$	176.7	176.7	177.1	177.1
$C(6)_{(imine)}$	142.0	144.6	144.8	144.6
^{133}Cd		387.27	361.06	291.39

[a] Recorded as ground crystals.
[b] ν(SO) at 997 cm^{-1}, ν(CS) at 829 cm^{-1} for DMSO.
[c] Overlapping.

obtained, free of charge, on application to: The Director, CCDC, 12 Union Road, Cambridge, CB2 1EZ, UK (fax: +44-1223-336033; e-mail: deposit@ccdc.cam.ac.uk or www: http://www.ccdc.cam.ac.uk).

References

[1] D.X. West, C.E. Ooms, J.S. Saleda, H. Gebremedhin, A.E. Liberta, Transition Met. Chem. 19 (1994) 553 and references cited therein.
[2] D.X. West, H. Gebremedhin, R.J. Butcher, J.P. Jasinski, A.E. Liberta, Polyhedron 12 (1993) 2489 and references cited therein.
[3] D.X. West, J.S. Ives, J. Krejci, M.M. Salberg, T.L. Zumbahlen, G.A. Bain, A.E. Liberta, J. Valdés-Martínez, S. Hernández-Ortega, R.A. Toscano, Polyhedron 14 (1995) 2189.
[4] (a) M.C. Miller, C.N. Stineman, J.R. Vance, D.X. West, I.H. Hall, Anticancer Res. 18 (1998) 4131. (b) M.C. Miller, C.N. Stineman, J.R. Vance, D.X. West, I.H. Hall, Appl. Organomet. Chem. 13 (1999) 9.
[5] D.X. West, J.K. Swearingen, A.K. El-Sawaf, Transition Met. Chem. 25 (2000) 80.
[6] D.X. West, J.K. Swearingen, J. Valdés-Martínez, S. Hernández-Ortega, A.K. El-Sawaf, F. van Meurs, A. Castiñeiras, I. Garcia, E. Bermejo, Polyhedron 18 (1999) 2919.
[7] E. Bermejo, R. Carballo, A. Castiñeiras, R. Domínguez, A.E. Liberta, C. Maichle-Mössmer, M.M. Salberg, D.X. West, Eur. J. Inorg. Chem. (1999) 965.
[8] E. Bermejo, A. Castiñeiras, R. Domínguez, R. Carballo, C. Maichle-Mössmer, J. Strähle, D.X. West, Z. Anorg. Allg. Chem. 625 (1999) 961.
[9] E. Bermejo, R. Carballo, A. Castiñeiras, R. Domínquez, C. Maichle-Mössmer, A.E. Liberta, D.X. West, Z. Naturforsch., Teil. B 54 (1999) 777.
[10] A. Castiñeiras, I. Garcia, E. Bermejo, D.X. West, Z. Naturforsch, Teil. B 55 (2000) 511.
[11] J.S. Casas, M.V. Castaño, M.S. Garcia-Tasende, I. Martínez-Santamarta, J. Sordo, E.E. Castellano, J. Zuckerman-Schpector, J. Chem. Res. (S) (1992) 324; (M) (1992) 2626.
[12] H. Kretschmar, GENHKL: A Program for the Reduction of CAD4 Diffractometer Data, University of Tübingen, Germany, 1997.
[13] A.C.T. North, D.C. Phillips, F.S. Mathews, Acta Crystallogr., Sect. A 24 (1968) 351.
[14] G.M. Sheldrick, Acta Crystallogr., Sect. A 46 (1990) 467.
[15] G.M. Sheldrick, SHELX-97: Program for the Refinement of Crystal Structures, University of Göttingen, Germany, 1997.
[16] A.J.C. Wilson, in: International Tables for X-ray Crystallography, vol. C, Kluwer Academic, Dordrecht, The Netherlands, 1995, Tables 4.2.6.8 and 6.1.1.4.

[17] A.L. Spek, PLATON: A Multipurpose Crystallographic Tool, Utrecht University, Utrecht, The Netherlands, 1998.
[18] L. Zsolnai, ZORTEP: A Program for the Presentation of Thermal Ellipsoids, University of Heidelberg, Germany, 1997.
[19] A. Castiñeiras, I. Garcia, E. Bermejo, D.X. West, unpublished results.
[20] A.W. Addison, T.N. Rao, J. Reedijk, J. van Rijn, C.C. Verschoor, J. Chem. Soc., Dalton Trans. (1984) 1349.
[21] (a) S.K. Nag, D.S. Joarder, Can. J. Chem. 54 (1976) 2827. (b) S.K. Sengupta, S.K. Sahni, R.N. Kapoor, Acta Chim. Acad. Sci. Hung. 104 (1990) 89. (c) R. Roy, M. Chaudhury, S.K. Mondal, S.K. Nag, J. Chem. Soc., Dalton Trans. (1984) 1681. (d) A.Z. El-Sonbati, E.M. Mabrouk, H.E. Megahed, Transition Met. Chem. 16 (1991) 280.
[22] K. Nakamoto, Infrared and Raman Spectra of Inorganic and Coordination Compounds, 5th ed., Wiley, New York, 1997.
[23] J. Weidlein, U. Müller, K. Dehnicke, Schwingungsfrequenzen II, Verlag, Stuttgart, 1986.
[24] T. Drakenberg, N.-O. Björk, R. Portanova, J. Phys. Chem. 82 (1978) 2423.
[25] J.J.H. Ackerman, T. Vorr, V.J. Bartuska, G.E. Maciel, J. Am. Chem. Soc. 101 (1979) 341.

PERGAMON

www.elsevier.nl/locate/poly

Polyhedron 19 (2000) 1881–1885

POLYHEDRON

Synthesis, characterisation and crystal structure of a 1,4-diazacycloheptane complex of copper(II)

Sutapa Sen [a], Manas Kumar Saha [a], Samiran Mitra* [a,1], Andrew J. Edwards [b], William Clegg* [b,2]

[a] *Department of Chemistry, Jadavpur University, Calcutta 700032, India*
[b] *Department of Chemistry, University of Newcastle, Newcastle upon Tyne, NE1 7RU, UK*

Received 28 February 2000; accepted 26 June 2000

Abstract

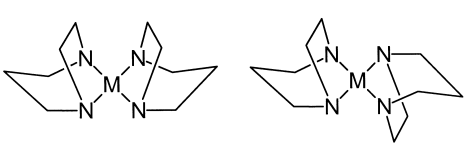
A new complex of formula $[Cu(dach)_2(CCl_3CO_2)]CCl_3CO_2$ (dach = 1,4-diazacycloheptane) has been synthesised and its crystal structure determined by single-crystal X-ray diffraction. The crystal structure contains two independent copper(II)-centred cations (one disordered) and two trichloroacetate ions. Both copper(II) atoms are pentacoordinate. The chelated 1,4-diazacycloheptane moieties are in a double boat conformation and represent the first structurally characterised example of a *trans* configuration for two such ligands at a metal centre. The compound was also characterised by IR, electronic and EPR spectra, cyclic voltammetry, and magnetic susceptibility studies. © 2000 Elsevier Science Ltd. All rights reserved.

Keywords: Copper(II); 1,4-Diazacycloheptane; Trichloroacetate; Crystal structures

1. Introduction

Acyclic diamines having a $N(CH_2)_nN$ grouping in their molecular framework have long been accepted as excellent chelating agents for transition metal ions and many results on these diamine complexes in solution and also in the solid state have been reported [1,2]. Reports on complexed cyclic diamines are, however, still scarce [1,3]. The seven-membered ring diamine 1,4-diazacycloheptane (dach) was examined as a chelating agent for nickel(II) and copper(II). Nickel(II) complexes of dach were planar, but the geometry of both tetra- and pentacoordinate complexes of copper(II) was dependent on the solvent and the anions present [4]. Comparing the formation constants of acyclic diamine complexes of Ni(II) and Cu(II), it is seen that complexes of ethylenediamine and its N- and C-substituted derivatives [5a–c] are more stable than those of 1,3-diaminopropane and higher homologues [5d]. Although *N*-alkylation of ethylenediamines might increase the complex stability due to increased basicity, it was actually found that the resulting steric effects caused a decrease in stability [5]. *C*-Alkylation of ethylenediamine gave increased complex stability, although the basicity of the amine was not significantly changed [5c]. This effect was attributed to a shielding of the metal–nitrogen bonds from polar solvents by the C-substituents, thus enhancing interactions between the metal ion and nitrogen dipoles [5e]. A combination of effects leading to enhanced stability might be expected if, in the chelated structure, the metal ion forms part of a bicyclic system rather than a single ring upon coordination with a secondary amine [5].

The dach ligand can assume a boat-chair conformation to minimise all non-bonded interactions [6]. In this conformation, the axial positions of the metal ion are markedly shielded and additional coordination is restricted.



Scheme 1.

[1] *Corresponding author. E-mail: pkbose@cal.vsnl.net.in
[2] *Corresponding author. Tel.: +44-191-222-6649; fax: +44-191-222-6929; e-mail: w.clegg@ncl.ac.uk

0277-5387/00/$ - see front matter © 2000 Elsevier Science Ltd. All rights reserved.
PII: S0277-5387(00)00480-0

In bis-dach complexes the two dach ligands can coordinate to the central metal ion in two different ways. The two carbon chains can be on the same side of the plane formed by the four nitrogen atoms to give a *cis* configuration, or on opposite sides of the plane, resulting in a *trans* configuration (Scheme 1).

The crystal structural analysis of the pyramidal complex $[Cu(dach)_2(NO_3)_2]\cdot 0.5H_2O$ shows the *cis* configuration to exist with each ring in a double boat form [7]. In the presence of non-coordinating solvents and anions, the four planar nitrogen atoms exert a major influence on the metal atoms with the carbon chains playing a passive role. The *cis* form can easily accommodate a fifth ligand on the metal, giving a pyramidal structure. On the other hand, the *trans* form can coordinate with two additional ligands, forming a tetragonally distorted octahedral structure. Hence, under certain conditions there may be an equilibrium between the *cis* and *trans* forms of the diamine complexes and in certain complexes the *trans* form may predominate. However, no evidence of a *trans* form has yet been obtained.

We report here the X-ray crystal structure of a copper trichloroacetate complex of 1,4-diazacycloheptane together with its IR, electronic and ESR spectra, magnetic susceptibility and electrochemical data. This shows the so far elusive *trans* configuration, but with only one additional ligand to give a five-coordinate structure.

2. Experimental

2.1. Synthesis

Copper trichloroacetate was synthesised as reported earlier [8]. 1,4-Diazacycloheptane was purchased from Fluka Chemie, Switzerland, and used as received.

Copper trichloroacetate (0.85 g, 2 mmol) was dissolved in methanol (15 ml). The solution was added to a solution of the dach ligand (0.44 g, 4 mmol) in methanol (20 ml) over a period of 10 min at 0°C with constant stirring. The reaction mixture was then stirred for about 2 h at 0°C and the solvent was allowed to evaporate slowly at room temperature (r.t.). Dark blue prismatic crystals of the title compound suitable for X-ray analysis were obtained after 3–4 days. They were collected and dried under vacuum. Found: C, 28.4; H, 3.9; N, 9.3; Cu, 10.8. $C_{14}H_{24}Cl_6CuN_4O_4$ requires C, 28.6; H, 4.1; N, 9.5; Cu, 10.8%.

2.2. Measurements

Infrared spectra were obtained from KBr discs on a Perkin–Elmer 883 spectrophotometer; electronic spectra were recorded from methanol solutions with a Hitachi U-3400 (UV–Vis, NIR) spectrophotometer. Cyclic voltammograms were obtained with an EG and G Princeton Applied Research Potentiostat/Galvanostat and a BAS X-Y recorder by using a three-electrode configuration, including a platinum-coil working electrode, a platinum-coil auxiliary electrode, and a saturated calomel electrode as a reference electrode; dichloromethane was used as the solvent and tetrabutylammonium perchlorate as a supporting electrolyte. X-band ESR spectra were measured on a JEOL JES-RE1X ESR spectrometer (X-band microwave unit, 100 kHz field modulation); the band frequency was calibrated with 1,1-diphenyl-2-picrylhydrazyl (DPPH, $g = 2.0036$).

2.3. X-ray crystallography

Crystal data: $C_{14}H_{24}Cl_6CuN_4O_4$, $M = 588.6$, orthorhombic, space group $P2_12_12_1$, $a = 11.0134(10)$, $b = 14.7433(13)$, $c = 27.292(3)$ Å, $V = 4431.5(7)$ Å^3, $Z = 8$, $D_{calc} = 1.764$ g cm^{-3}, λ(Mo Kα) = 0.71073 Å, $\mu = 1.74$ mm^{-1}, $T = 160$ K, crystal size $0.30 \times 0.13 \times 0.11$ mm. Measurements were made on a Bruker AXS SMART CCD area-detector diffractometer. Measured intensity data covered more than a hemisphere of reciprocal space. Semi-empirical absorption corrections were based on symmetry-equivalent and repeated reflections (transmission 0.663–0.862). 27 787 reflections were measured ($\theta_{max} = 28.37°$), giving 10 112 unique data with $R_{int} = 0.0476$.

The structure was solved by direct methods and refined on F^2 values, with anisotropic displacement parameters and riding hydrogen atoms. Twofold disorder was resolved for the coordinated trifluoroacetate in one of the two independent cations; no restraints were required. At convergence $R_w = \{\Sigma[w(F_o^2 - F_c^2)^2]/\Sigma[w(F_o^2)^2]\}^{1/2} = 0.0734$ for all data, conventional $R = 0.0460$ on F values of 8238 reflections having $F_o^2 > 2\sigma(F_o^2)$, goodness-of-fit = 1.102 for all F^2 values and 571 refined parameters. A final difference synthesis contained no features outside ± 0.47 e Å^{-3}. The crystal was probably racemically twinned, with an enantiopole parameter of 0.599(11) [9].

Programs were standard Bruker AXS control and integration software, and SHELXTL [10].

3. Results and discussion

3.1. IR spectra

The ν(C=O) band at 1683 cm^{-1} is assigned to the free trichloroacetate ion [11]. The ν_{asym}(C=O) band at 1688 cm^{-1} and ν_{sym}(C=O) band at 1310 cm^{-1} give $\Delta\nu = 378$ cm^{-1}, indicating the presence of trichloroacetate as a monodentate ligand [12]. Both coordinated and uncoordinated trichloroacetate are confirmed by the crystal structure analysis.

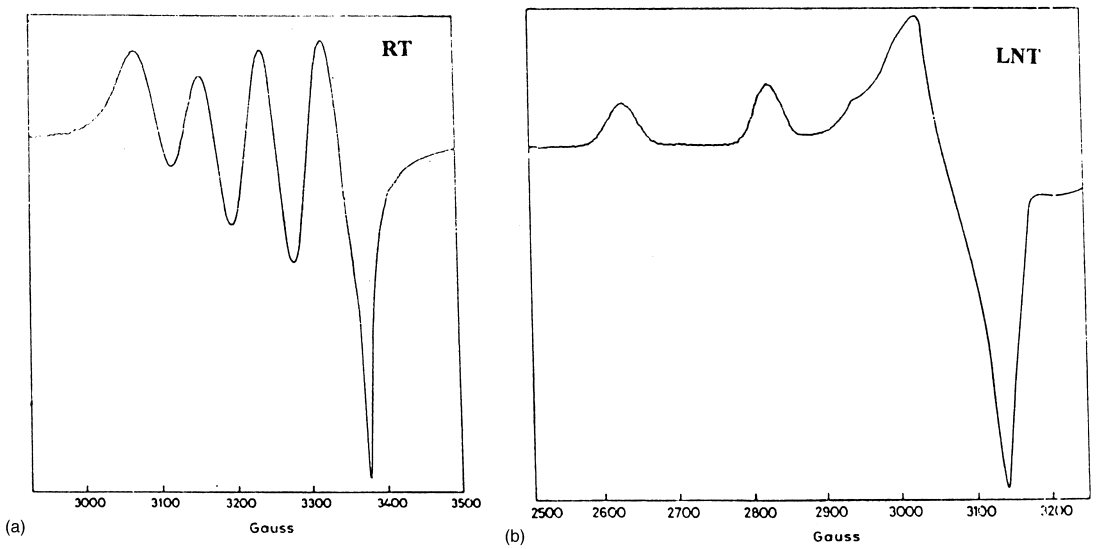


Fig. 1. ESR spectra in methanol solution: (a) at room temperature; (b) at liquid nitrogen temperature.

The bands resulting from the NH stretching vibrations in the complex are at 3289 and 3217 cm^{-1}. It is reasonable to assign the two bands at 431 and 502 cm^{-1} as ν(Cu–N) stretching modes [13]. The characteristic IR bands of the dach ligand are at 2978, 2891, 1494, 1475, 1462, 1446, 1349, 1286, 1127, 1107, 980, 969, 825, and 730 cm^{-1} [13].

3.2. Electronic spectra

The title compound in methanol solution exhibits a sharp absorption band at 28 490 cm^{-1}, along with a broad absorption band having a maximum at 16 273 cm^{-1}. Due to the Jahn–Teller distortion, the majority of copper(II) complexes are tetragonally distorted with four short and two long metal–ligand bonds and are usually expected to absorb near 16 000 cm^{-1} [14,15]. From the observed values it is evident that the absorption is due to the $^2B_{1g} \rightarrow {}^2A_{1g}$ transition in a tetragonally distorted octahedral geometry having CuN_4O_2 chromophores. The other high energy transition at 28 490 cm^{-1} is attributed to ligand-to-metal charge transfer (LMCT) transitions.

From the electronic spectra, it seems that copper(II) is in octahedral coordination in this complex in methanol solution. This is probably due to weak coordination of a second anion as an extra ligand in solution.

3.3. ESR spectra

The ESR spectra of the complex were recorded from powder samples and from methanol solution at r.t. and at liquid nitrogen temperature.

When measured on powder samples at r.t., the spectrum showed an axially symmetric pattern with $g_{\parallel} = 2.20$ and $g_{\perp} = 2.02$. No hyperfine structure was resolved for either $g_{\parallel}$ or $g_{\perp}$, even at liquid nitrogen temperature. The ESR spectrum of the copper(II) complex in solution is shown in Fig. 1. It exhibits a set of four well resolved peaks in the high field region. The g tensor values of copper(II) complexes can be used to derive the ground state [16]. In axially elongated octahedral and square-planar complexes, the unpaired electron occupies the $d(x^2 - y^2)$ orbital with a $^2B_{1g}$ ground state resulting in $g_{\parallel} > g_{\perp}$. However, in a compressed octahedron the unpaired electron occupies the $d(z^2)$ orbital with a $^2A_{1g}$ ground state having $g_{\parallel} > g_{\perp}$. The observed g values suggest that the unpaired electron lies predominantly in the $d(x^2 - y^2)$ orbital. The higher g values are due to a greater elongation in the z axis of the complex with the $^2B_{1g}$ ground state.

3.4. Magnetic measurements

The r.t. magnetic moment of the complex (1.99 BM) is a little larger, which should be associated with some orbital contribution and should be dependent on temperature [17]. Variable temperature magnetic susceptibility measurements are more helpful in this respect. The magnetic behaviour of the complex was studied over the temperature range 300–10 K. Correction for the diamagnetism of the complex was estimated from Pascal's constants to be 271.57 $cm^3\ mol^{-1}$. The magnetic susceptibility data for the complex may be interpreted in terms of the Curie–Weiss law

$$\chi_M^{corr} = Ng^2\beta^2/4K(T - \theta) + N_\alpha$$

where χ_M^{corr} is the molar susceptibility corrected for diamagnetism, $N_\alpha = 60 \times 10^{-6}$ cgs unit is the corrected value of temperature-independent paramagnetism, and the remaining symbols have their usual meanings. It

was found that the complex follows the Curie–Weiss law; the $1/\chi_M$ versus T plot is linear. The values are in the range expected for copper(II) complexes in a magnetically dilute environment [17].

3.5. Electrochemical data

The cyclic voltammogram of the complex exhibits one reduction wave at -1.07 V versus SCE, which appears to correspond to the Cu(II)/Cu(I) couple. The reduction is quasi-reversible. The ratio of the anodic to cathodic peak currents (I_{pa}/I_{pc}) is nearly 1 [18].

3.6. Crystal structure

The title compound contains two copper-centred complex ions of very similar stereochemistry, which are nonetheless crystallographically distinct. Perspective drawings of each molecule **A** and **B** are shown in Fig. 2. Selected bond lengths and angles are listed in Table 1.

In each cation the two dach ligands apparently enforce a distorted square-based pyramidal geometry, which can be assessed using the structural index parameter $\tau = (\beta - \alpha)/60$, where β and α are the two largest coordination angles; $\tau = 0$ for perfect square pyramidal and 1 for trigonal bipyramidal geometry [19]. The value of τ is 0.12 for **A** and 0.08 for **B**, indicating the geometry to be square pyramidal. The complex cation comprises copper(II) coordinated by a pair of dach ligands and a trichloroacetate anion in the primary coordination sphere. In each molecule four nitrogen atoms of two dach ligands form the approximate square-planar arrangement, with a trichloroacetate anion occupying the apex of a distorted square pyramid. The copper atoms lie out of the two N_4 basal planes by 0.317 and 0.308 Å in the direction of the axially bonded ligand.

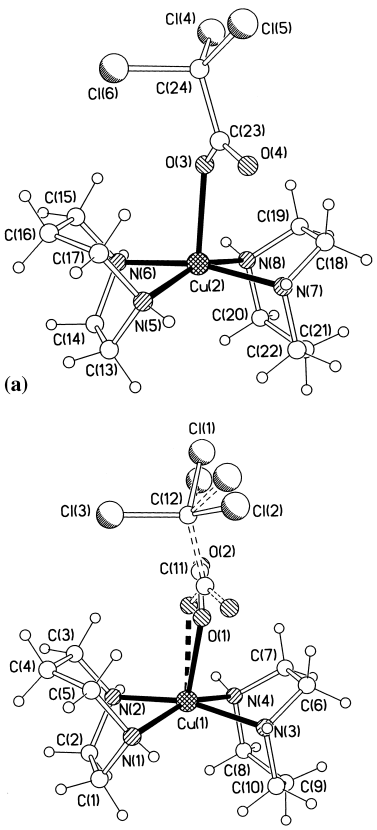


Fig. 2. Perspective view of cations **A** and **B**.

Table 1
Selected bond lengths (Å) and angles (°)

Molecule A			
Cu(2)–N(7)	2.010(3)	Cu(2)–N(6)	2.008(3)
Cu(2)–N(5)	2.024(3)	Cu(2)–N(8)	2.030(3)
Cu(2)–O(3)	2.220(2)		
N(6)–Cu(2)–N(7)	166.14(14)	N(6)–Cu(2)–N(5)	78.01(13)
N(7)–Cu(2)–N(5)	99.83(12)	N(6)–Cu(2)–N(8)	99.31(12)
N(7)–Cu(2)–N(8)	77.68(14)	N(5)–Cu(2)–N(8)	158.82(13)
N(6)–Cu(2)–O(3)	96.93(12)	N(7)–Cu(2)–O(3)	96.80(12)
N(5)–Cu(2)–O(3)	106.63(12)	N(8)–Cu(2)–O(3)	94.54(12)
Molecule B			
Cu(1)–N(2)	2.008(3)	Cu(1)–N(3)	2.006(3)
Cu(1)–N(4)	2.022(3)	Cu(1)–N(1)	2.025(3)
Cu(1)–O(1)	2.233(7)	Cu(1)–O(2X)	2.266(11)
N(2)–Cu(1)–N(3)	164.13(14)	N(2)–Cu(1)–N(4)	98.44(12)
N(3)–Cu(1)–N(4)	77.33(14)	N(2)–Cu(1)–N(1)	77.81(14)
N(3)–Cu(1)–N(1)	100.74(13)	N(4)–Cu(1)–N(1)	159.61(14)
N(2)–Cu(1)–O(1)	108.44(18)	N(3)–Cu(1)–O(1)	87.43(18)
N(4)–Cu(1)–O(1)	105.12(17)	N(1)–Cu(1)–O(1)	95.00(17)
N(2)–Cu(1)–O(2X)	90.5(2)	N(3)–Cu(1)–O(2X)	104.7(2)
N(4)–Cu(1)–O(2X)	89.9(3)	N(1)–Cu(1)–O(2X)	110.1(3)

The four Cu–N bond lengths fall within the range usually observed for heterocyclic ligands [20]. The fifth position is occupied at a longer distance by an oxygen atom of a trifluoroacetate ligand; this is disordered over two orientations in the case of complex **B**. Similar disorder has also been observed in other ions [21].

The overall single positive charge on the complex cation is balanced by a second, uncoordinated, trifluoroacetate anion, which appears to be coordinated in methanol solution (see above). Even though the copper ion is only pentacoordinate in the solid state, the two dach ligands are arranged in a *trans* configuration, which in principle renders the two axial positions equally accessible for ligand attachment.

4. Supplementary material

Supplementary data are available on request from the The Director, CCDC, 12 Union Road, Cambridge, CB2 1EZ, UK (fax: +44-1223-336033; e-mail: deposit@ccdc.cam.ac.uk or www: http://www.ccdc.cam.ac.uk), quoting the deposition number 140664.

Acknowledgements

This work was financially supported by UGC and CSIR, New Delhi, India, and by EPSRC, UK.

References

[1] W.K. Musker, M.S. Hussain, Inorg. Chem. 8 (1969) 528.
[2] G. De, P.K. Biswas, N. Raychoudhuri, J. Chem. Soc., Dalton Trans. (1984) 2591.
[3] P.J. Hendra, D.B. Powell, J. Chem. Soc. (1960) 5105.
[4] W.K. Musker, M.S. Hussain, Inorg. Nucl. Chem. Lett. 3 (1967) 271.
[5] (a) F. Basolo, R.K. Murmann, J. Am. Chem. Soc. 74 (1952) 5243. (b) F. Basolo, Y.T. Chen, R.K. Murmann, J. Am. Chem. Soc. 76 (1954) 956. (c) H. Irving, J.M.M. Griffiths, J. Chem. Soc. (1954) 213. (d) G.B. Hares, W.C. Fernilius, D.E. Douglas, J. Am. Chem. Soc. 78 (1956) 1816. (e) D.L. Leussing, Inorg. Chem. 2 (1963) 77.
[6] W.K. Musker, M.S. Hussain, Inorg. Chem. 5 (1966) 1416.
[7] M.S. Hussain, H. Hope, Acta Crystallogr., Sect. B 25 (1969) 1866.
[8] S. Mitra, L.K. Singh, Thermochim. Acta 176 (1991) 327.
[9] H.D. Flack, Acta Crystallogr., Sect. A 39 (1983) 876.
[10] G.M. Sheldrick, SHELXTL version 5, Bruker AXS, Madison, WI, USA, 1994.
[11] K. Nakamoto, Infrared and Raman Spectra of Inorganic and Coordination Compounds, 3rd ed., Wiley Interscience, New York, USA, 1978, p. 233.
[12] A.V.R. Warrier, R.S. Krishnan, Spectrochim. Acta 27A (1971) 1243.
[13] L.K. Singh, S. Mitra, J. Chem. Soc., Dalton Trans. (1987) 2089.
[14] B.N. Figgis, Introduction to Ligand Fields, Wiley, New York, 1967.
[15] C.S. Alleyne, R.C. Thompson, Can. J. Chem. 52 (1974) 3211.
[16] C.J. Ballhausen, Introduction to Ligand Field Theory, McGraw-Hill, New York, 1962.
[17] B.J. Hathaway, in: G. Wilkinson, R.D. Gillard, J.A. McCleverty, Comprehensive Coordination Chemistry, vol. 5, Pergamon, Oxford, 1987, p. 533 and refs. therein.
[18] Pr. Athappan, G. Rajagopal, Polyhedron 15 (1996) 527.
[19] (a) A.W. Addison, T.N. Rao, J. Reedijk, J. van Rijn, G.C. Verschoor, J. Chem. Soc., Dalton Trans. (1984) 1349. (b) M. Zoeteman, E. Bouwman, R.A.G. deGraaff, W.L. Driessen, J. Reedijk, P. Zanello, Inorg. Chem. 29 (1990) 3487.
[20] C.Y. Wu, C.C. Su, Polyhedron 16 (1997) 383 and refs. therein.
[21] (a) C. Glidewell, D.C. Liles, J. Organomet. Chem. 243 (1983) 291. (b) J.M. Dominguez-Vera, E. Colacio, A. Escuer, M. Klinga, R. Kivekäs, A. Romerosa, Polyhedron 16 (1997) 281.

PERGAMON

www.elsevier.nl/locate/poly

Polyhedron 19 (2000) 1887–1894

POLYHEDRON

Dimetallic thiolate-bridged complexes: synthesis and rich electrochemistry of dinickel(II) and dizinc(II) monothiolate complexes

Sally Brooker *, Paul D. Croucher, Tony C. Davidson, Paul D. Smith

Department of Chemistry, University of Otago, PO Box 56, Dunedin, New Zealand

Received 29 February 2000; accepted 5 May 2000

Abstract

The synthesis of the two-armed amine precursor 2,6-di[*N*-(3′-aminopropyl)aminomethyl]-4-methylphenol (**1**) is detailed. Zinc(II) and nickel(II) templated Schiff base condensation reactions of **1** and 2,6-diformyl-4-methylthiophenolate (obtained by base hydrolysis of *S*-(2,6-diformyl-4-methylphenyl)dimethylthiocarbamate (**2**)), in IPA, yield the macrocyclic complexes $Zn_2L1(CH_3CO_2)_2(H_2O)_2$ (**3**) and $[Ni_2L1(MeCN)_2](ClO_4)_2$ (**4**), respectively. Addition of two equivalents of NaNCS to **4**, in DMF, gives the complex $[Ni_2L1(NCS)_2(DMF)]$ (**5**). An acyclic complex, $[Ni_2L2(C_3H_3N_2)](CF_3SO_3)_2$ (**6**), is formed by reaction of two equivalents of nickel(II) ions with 2,6-diformyl-4-methylthiophenolate, pyrazole and two equivalents of 2-(2-aminoethyl)pyridine. Single crystal X-ray diffraction studies of **4** and **5** revealed differing environments for the nickel(II) ions within the macrocycle: in the case of **4** one nickel ion is square planar whilst the other is octahedral, whereas in **5** both nickel ions are high spin but one is square pyramidal whilst the other is octahedral. In contrast, the structure determination carried out on **6** shows that both of the nickel ions are square planar. ^1H and ^{13}C NMR studies show that the diamagnetic compounds $Zn_2L1(CH_3CO_2)_2(H_2O)_2$ (**3**) and $[Ni_2L2(C_3H_3N_2)](CF_3SO_3)_2$ (**6**) remain intact in $MeNO_2$-d_3 solution. In MeCN-d_3 solution the dizinc complex **3** again retains its integrity. In contrast, the dinickel complex **6** has some tendency to coordinate MeCN in the otherwise vacant axial sites leading to traces of paramagnetic species in solution and to very broad signals in the ^1H NMR spectrum. Electrochemical studies, in MeCN, on the soluble dinickel(II) complexes **4** and **6**, revealed a series of one electron processes (-1.23^{QR}, $+0.65^{I}$ and $+1.00^{R}$ V versus 0.01 M $AgNO_3$–Ag for **4**; -1.46^{I}, -0.96^{R}, $+1.03^{I}$ and $+1.50^{I}$ V versus 0.01 M $AgNO_3$–Ag for **6**; where R, reversible; I, irreversible; QR, quasireversible), in contrast to the dizinc(II) complex **3** which is redox inactive over this range. © 2000 Elsevier Science Ltd. All rights reserved.

Keywords: Thiolate; Electrochemistry; Macrocycle; Crystal structures

1. Introduction

In order to provide distinctive coordination environments for transition metal ions we have developed routes to ligands which contain unusual mixtures of donors [1–6]. A key strategy has been the tailoring of new classes of unsymmetrical macrocycles, which incorporate two different head units. In contrast to the usual one-pot syntheses of symmetrical macrocycles from two relatively simple difunctionalised starting materials [7] most of the unsymmetrical polynucleating macrocycles prepared to date have been built up in a stepwise, controlled, manner [8]. The use of mono-N-protected diaminoalkanes to facilitate the stepwise formation of two-armed amine precursors was reported by Martell and coworkers [9] and we have subsequently extended the use of this approach with some success [1–4,10]. Here we detail the synthesis of **1** which incorporates a phenol head unit and provides access to an unsymmetrical macrocyclic ligand, $(L1)^{2-}$, which possesses an unprecedented combination of phenolate and thiophenolate head units, along with imine and amine nitrogen groups (Fig. 1). In contrast to all of the other macrocyclic complexes derived from **2** [11–18] the complexes of $(L1)^{2-}$ described here, $Zn_2L1(CH_3CO_2)_2(H_2O)_2$ (**3**), $[Ni_2L1(MeCN)_2](ClO_4)_2$ (**4**) and $[Ni_2L1(NCS)_2(DMF)]$

* Corresponding author. Tel.: +64-3-479-7908; fax: +64-3-479-7906.

E-mail address: sbrooker@alkali.otago.ac.nz (S. Brooker).

0277-5387/00/$ - see front matter © 2000 Elsevier Science Ltd. All rights reserved.
PII: S0277-5387(00)00506-4

(**5**), incorporate a single bridging thiolate donor atom and the impact of this change is significant (vide infra) [2,3]. Prior to these macrocyclic studies [2,3,11–18], Robson and co-workers had investigated the coordination chemistry of acyclic ligands prepared from **2** [19–26], including the palladium(II) complex $[Pd_2L2Cl_2]Cl$ [22]. Here we describe the nickel(II) complex $[Ni_2L2(C_3H_3N_2)](CF_3SO_3)_2$ (**6**) of the acyclic ligand $(L2)^-$. This was prepared because, like $(L1)^{2-}$, it provides only a single thiolate bridge, and because it is closely related to the dinickel(II) complexes of the Schiff-base macrocyclic ligand $(L3)^{2-}$ (Fig. 1) which have exhibited rich, reversible redox chemistry. The electrochemistry of these complexes is presented and discussed.

2. Experimental

CAUTION: *perchlorate salts are potentially explosive and should therefore be handled with appropriate care.*

Measurements were carried out, and solvents purified, as previously described [12,13], with the exception of the NMR spectra of **6**, which were obtained on a Varian 500 MHz spectrometer. *S*-(2,6-Diformyl-4-methylphenyl)dimethylthiocarbamate (**2**) [12] and *N*-acetyldiaminopropane [4] were prepared as previously described. Ethanol was distilled from magnesium ethoxide before use (5 g magnesium and 0.5 g iodine per litre of ethanol). Reactions to produce complexes **3**–**6** were carried out under nitrogen using Schlenk techniques.

2.1. 2,6-Di[*N*-(3′-aminopropyl)aminomethyl]-4-methylphenol hydrochloride (1·4HCl)

Step 1. A solution of *N*-acetyldiaminopropane (7.06 g, 58.1 mmol) in EtOH (50 ml) was added to a suspension of 2,6-diformyl-4-methylphenol (4.77 g, 29.0 mmol) in EtOH (50 ml) and the resulting dark brown solution was refluxed (4 h). The reaction mixture was then cooled (273 K) and an excess of sodium borohydride (4.83 g, 128 mmol) added in three approximately equal portions over 1 h. The pale mixture was stirred and allowed to warm up to room temperature over 4 h, followed by refluxing for a further 4 h. Water (50 ml) was then added to the cloudy yellow mixture. The mixture became thick and waxy in appearance. After cooling the solution was concentrated (50 ml) and then extracted with CH_2Cl_2 (150 ml) in a continuous extractor (18 h). The CH_2Cl_2 fraction was removed, concentrated (50 ml), washed with H_2O (3 × 50 ml), dried with anhydrous $MgSO_4$ and then taken to dryness under vacuum to yield the *N*-protected precursor as a yellow oil. ^1H NMR (300 MHz, solvent $CDCl_3$, reference TMS) 6.80 (s, 2H), 6.7 (s, 1H), 3.83 (s, 4H), 3.30 (dd, 4H), 2.69 (t, 4H), 2.22 (s, 3H), 1.94 (s, 6H), 1.69 (quintet, 4H); ^{13}C NMR (75 MHz, $CDCl_3$ reference TMS) 170.4, 154.1, 127.6, 124.1, 128.8, 50.9, 46.6, 38.0, 29.0, 23.2, 20.4.

Step 2. Isolation of **1**, as the HCl salt, was via hydrolysis of the *N*-acetyl groups in the above oil by refluxing with 20% HCl (200 ml) for 12 h. The excess HCl was removed under vacuum, the resulting tacky

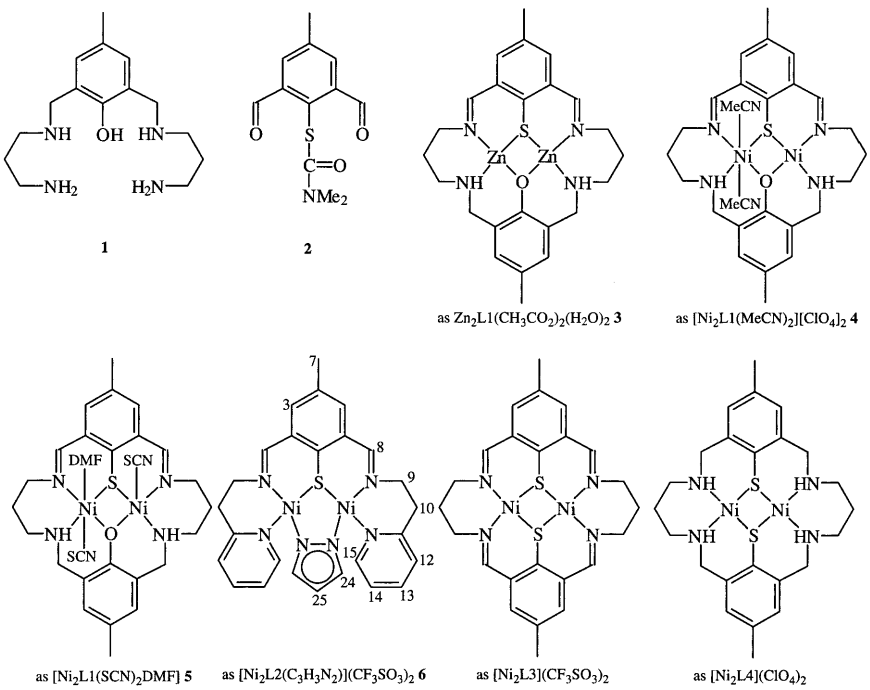


Fig. 1. The two-armed amine precursor **1**, the masked-thiolate head unit **2** and complexes $Zn_2L1(CH_3CO_2)_2(H_2O)_2$ (**3**), $[Ni_2L1(MeCN)_2](ClO_4)_2$ (**4**), $[Ni_2L1(NCS)_2(DMF)]$ (**5**), $[Ni_2L2(C_3H_3N_2)](CF_3SO_3)_2$ (**6**), $[Ni_2L3](CF_3SO_3)_2$ and $[Ni_2L4](ClO_4)_2$.

brown solid extracted into MeOH (100 ml), filtered and the clear solution evaporated to dryness under vacuum to give a white powder. Yield 8.00 g, 64%. Found: C, 42.3; H, 7.7; N, 12.8. $C_{15}H_{32}N_4OCl_4$ requires C, 42.3; H, 7.6; N, 13.1%. ν_{max} (cm^{-1}) (KBr disk, inter alia) 3359, 3000, 2338, 2005, 1604, 1487 cm^{-1}; ^1H NMR (300 MHz, solvent D_2O, reference DSS) 7.26 (s, 2H), 4.26 (s, 4H), 3.18 (dd, 4H), 3.06 (dd, 4H), 2.24 (s, 3H), 2.09 (q, 4H); ^{13}C NMR (75 MHz, solvent D_2O, reference DSS) 153.8, 134.9, 122.8, 136.6, 49.4, 46.8, 39.3, 26.3, 22.1.

2.2. 2,6-Di[N-(3′-aminopropyl)aminomethyl]-4-methylphenol (**1**)

This was prepared prior to use by reacting the above HCl salt (0.43 g, 1 mmol) with KOH (0.04 g, 4 mmol) in EtOH (40 ml). The mixture was stirred at 298 K (1 h), evaporated to dryness under vacuum and the resulting residue was taken up in $CHCl_3$ (20 ml), dried over anhydrous $MgSO_4$ then filtered to remove both the desiccant and the KCl by product. Finally the $CHCl_3$ was removed under vacuum to yield **1** as a pale yellow oil which was used promptly, without further purification.

2.3. $Zn_2L1(CH_3CO_2)_2(H_2O)_2$ (**3**)

NaOH (0.04 g, 1 mmol) and **2** (0.25 g, 1 mmol) were dissolved in IPA (50 ml) and refluxed for 5 h under a nitrogen atmosphere. To this was added a solution of zinc(II) acetate dihydrate (0.444 g, 2 mmol) in IPA. Compound **1** (0.28 g, 1 mmol) in IPA (10 ml) was then added dropwise to produce a bright yellow solution which was refluxed for 1 h under nitrogen. The reaction mixture was cooled to room temperature, filtered and evaporated to dryness under vacuum to give a yellow residue. This solid was extracted into CH_2Cl_2 (50 ml), filtered and concentrated (10 ml). A yellow powder was obtained from a CH_2Cl_2 solution via slow vapour diffusion of pentane. The solid was collected and dried under vacuum. Yield 0.30 g, 45%. Found: C, 47.2; H, 5.8; N, 7.9; S, 4.1. $C_{28}H_{40}N_4SO_7Zn_2$ requires C, 47.5; H, 5.7; N, 7.9; S, 4.5%. ν_{max} (cm^{-1}) (KBr disk, inter alia) 3236, 1631. ^1H NMR (300 MHz, solvent $CDCl_3$, reference TMS) 8.18 (s, 2H), 7.09 (s, 2H), 6.79 (s, 2H), 4.68 (t, 4H), 4.47 (t, 4H), 3.59 (d, 2H), 3.22 (m, 4H), 2.97 (m, 4H), 2.59 (s, 3H), 2.29 (s, 3H), 2.15 (s, 6H), 1.78 (m, 4H); ^{13}C NMR (75 MHz, $CDCl_3$ reference TMS) 179.4, 166.0, 158.7, 136.8, 134.9, 133.1, 132.3, 127.9, 126.4, 62.2, 54.3, 50.9, 36.2, 30.3, 25.4, 20.3; Λ_m (MeCN), 35 mol^{-1} cm^2 Ω^{-1} (cf. 220–300 mol^{-1} cm^2 $^{-1}$ for a 2:1 electrolyte in MeCN) [31]; FAB mass spectrum m/z 612 $[Zn_2L1(CH_3CO_2)]^+$, 553 $[Zn_2L1]^+$.

2.4. $[Ni_2L1(MeCN)_2](ClO_4)_2$ (**4**)

NaOH (0.04 g, 1 mmol) and **2** (0.25 g, 1 mmol) were dissolved in IPA (50 ml) and refluxed for 5 h under a nitrogen atmosphere. To this was added a solution of nickel(II) perchlorate hexahydrate (0.73 g, 2 mmol) in IPA (10 ml), which produced a brown solution. Compound **1** (0.28 g, 1 mmol) in IPA (10 ml) was then added dropwise and the resulting mixture was refluxed under nitrogen for 3 h. The solution was filtered, concentrated to 10 ml and cooled (253 K, 18 h), yielding a red–brown powder which was collected, washed with IPA (10 ml) and dried under vacuum. Yield 0.17 g, 20%. Found: C, 40.6; H, 4.5; N, 10.2; S, 3.9. $C_{28}H_{36}N_6SO_9Cl_2Ni_2$ requires C, 41.0; H, 4.4; N, 10.2; S, 3.9%. ν_{max} (cm^{-1}) (KBr disk, inter alia) 3238, 1631, 1093, 624. Λ_m (MeCN), 280 mol^{-1} cm^2 Ω^{-1} (cf. 220–300 mol^{-1} cm^2 Ω^{-1} for a 2:1 conductor in MeCN) [31]; λ_{max} (MeCN) nm (ε dm^{-3} mol^{-1} cm^{-1}) 800 (19); FAB mass spectrum m/z 540, $[Ni_2L1]^+$; $\mu = 3.0$ BM per complex.

2.5. $[Ni_2L1(NCS)_2(DMF)]\cdot 2H_2O$ (**5**$\cdot 2H_2O$)

Sodium thiocyanate (0.05 g, 0.51 mmol) was added to a solution of **4** (0.21 g, 0.25 mmol) in DMF (5 ml). Addition of IPA (60 ml) precipitated a green–brown powder that was collected, washed with IPA (10 ml) and dried under vacuum. Yield 0.09 g, 52%. A small number of brown plate-like crystals of $[Ni_2L1(NCS)_2$-(DMF)], suitable for X-ray diffraction, were obtained from DMF via slow vapour diffusion of Et_2O. Found: C, 45.7; H, 5.2; N, 13.1. $C_{29}H_{41}N_7S_3O_4Ni_2$ requires C, 45.5; H, 5.4; N, 12.8% ν_{max} (cm^{-1}) (KBr disk, inter alia) 3244, 2083, 1630. Λ_m (DMF), 76 mol^{-1} cm^2 Ω^{-1} (cf. 50–90 mol^{-1} cm^2 Ω^{-1} for a 1:1 conductor in DMF) [31]; λ_{max} (DMF) nm (ε dm^{-3} mol^{-1} cm^{-1}) 850 (15), 650 (46); FAB mass spectrum m/z 598 $[Ni_2L1(NCS)]^+$, 540 $[Ni_2L1]^+$; $\mu = 4.5$ BM per complex.

2.6. $[Ni_2L2(C_3H_3H_2)](CF_3SO_3)_2$ (**6**)

NaOH (0.02 g, 0.5 mmol) and **2** (0.13 g, 0.5 mmol) were dissolved in IPA (60 ml) and refluxed for 5 h under a nitrogen atmosphere. To this was added a solution of pyrazole (0.04 g, 0.5 mmol) and NaOH (0.02 g, 0.5 mmol) in IPA (30 ml) followed by a solution of nickel(II) trifluoromethanesulfonate hexahydrate (0.39 g, 1 mmol) in IPA (10 ml), which produced a red–brown solution. 2-(2-Aminoethyl)pyridine (0.11 g, 1 mmol) in IPA (50 ml) was added dropwise. No colour change was observed. The solution was refluxed for a further 2 h under nitrogen, filtered hot to remove a trace of powder, and on cooling the filtrate a brown powder precipitated. Red–brown crystals were obtained from MeCN via slow vapour diffusion of Et_2O. Yield 0.87 g, 42%. Found: C, 39.1; H, 3.3; N, 9.5; S,

10.7. $C_{28}H_{26}N_6S_3O_6F_6Ni_2$ requires C, 38.7; H, 3.0; N, 9.6; S, 11.0% ν_{max} (cm^{-1}) (KBr disk, inter alia) 1630, 1611, 1268, 1028, 632. λ_m (MeCN), 280 mol^{-1} cm^2 Ω^{-1} (cf. 220–300 mol^{-1} cm^2 Ω^{-1} for a 2:1 conductor in MeCN) [31]; λ_{max} (MeCN) nm (ε dm^{-3} mol^{-1} cm^{-1}) 365 (1900), 463 (620) shoulder, 540 (390) shoulder; ^1H NMR (500 MHz, solvent $MeNO_2$-d_3, referenced to solvent) 8.52 (d, 2H), 8.12 (t, 2H), 7.90 (s, 2H), 7.70 (d, 2H), 7.60 (s, 2H), 7.45 (t, 2H), 6.24 (d, 2H), 5.88 (t, 1H), 5.36 (t, 2H), 4.20 (d, 2H), 3.70 (d, 2H), 3.40 (t, 2H), 2.4 (s, 3H); ^{13}C NMR (125 MHz, solvent $MeNO_2$-d_3, referenced to solvent) 172.9, 160.6, 153.0, 145.0, 142.9, 141.2, 140.7, 135.5, 126.0, 125.5, 125.1, 109.3, 54.2, 37.4, 20.5; FAB mass spectrum m/z 570 $[Ni_2L2(C_3H_3H_2)]^+$, 503 $[Ni_2L2]^+$; $\mu = 0.0$ BM. Crystal data: $C_{28}H_{26}N_6Ni_2O_6S_3F_6$, red block, $0.70 \times 0.40 \times 0.22$ mm^3, monoclinic, space group $P2_1/c$; $a = 15.7537(3)$; $b = 14.0559(3)$; $c = 16.8208(3)$ Å, $\beta = 115.6990(10)°$; $V = 3356.24(16)$ $Å^3$; $Z = 4$. A total of 23 171 reflections were collected on a Bruker SMART diffractometer at 142 K in the range $2 < 2 < 61°$, and the 7698 independent reflections were used in the structural analysis after a semi-empirical absorption correction had been applied ($T_{min} = 0.75$, $T_{max} = 1.00$). The structure was solved by direct methods (SHELXS-97) [32,33] and refined against all F^2 data (SHELXL-97) [34] to $R_1 = 0.0439$ (for 7449 $F > 4\sigma(F)$; $wR_2 = 0.0905$ and goodness-of-fit = 1.320 for all 7698 F^2; 461 parameters, all non-hydrogen atoms anisotropic; $+0.47/-0.65$ e $Å^{-3}$).

3. Results and discussion

3.1. Synthesis

The Schiff base condensation of two equivalents of *N*-acetyldiaminopropane with one equivalent of 2,6-diformyl-4-methylphenol was followed by reduction of the imine bonds by sodium borohydride and hydrolysis of the protecting groups with aqueous acid to yield **1** as the tetrahydrochloride salt.

The deprotection of the masked-thiolate head unit **2** (Fig. 1), to produce the unmasked thiophenolate head unit, was carried out in situ using NaOH in IPA [12], and then the appropriate metal salt and **1** were added to form the complexes $Zn_2L1(CH_3CO_2)_2(H_2O)_2$ (**3**) (45% yield) and $[Ni_2L1(MeCN)_2](ClO_4)_2$ (**4**) (20% yield). The infrared spectra of **3** and **4** were consistent with macrocycle formation: an imine stretch was present at 1631 cm^{-1} for both **3** and **4**, and no peaks corresponding to unreacted primary amine or carbonyl were present. The addition of 2.2 equivalents of sodium thiocyanate to an acetonitrile solution of complex **4** causes the precipitation of a solid which on recrystallisation from DMF by vapour diffusion of diethylether yields $[Ni_2(L1)(NCS)_2(DMF)]$ (**5**).

Complex $[Ni_2L2(C_3H_3N_2)](CF_3SO_3)_2$ (**6**) (Fig. 1) was prepared from the reaction of two equivalents of nickel(II) ions with hydrolysed **2**, pyrazole and two equivalents of 2-(2-aminoethyl)pyridine, in 42% yield. An imine stretch was present at 1630 cm^{-1} in the infrared spectrum and no carbonyl or amine peaks were observed. The ease of synthesis and stability of **6** contrast with the instability of one of the two imine bonds in the dipalladium(II) complex $[Pd_2L2Cl_2]Cl$ [22].

Complex **3** is a non-conductor in freshly prepared MeCN solution, indicating that the acetate ions are coordinated in solution. As expected, complex **4** is a 2:1 conductor in MeCN. Complex **5** takes some time to dissolve in DMF and is a 1:1 conductor in this solvent, indicating that on dissolution of this neutral complex a thiocyanate ion dissociates. Complex **6** is a 2:1 conductor in MeCN, indicating that the pyrazolate anion remains coordinated in solution.

3.2. Crystal structures

The X-ray crystal structures of the dinickel(II) complexes **4** [2] and **5** [3] have been presented in preliminary communications and in both cases differing environments for the nickel(II) ions within the $L1^{2-}$ macrocycle were revealed (Fig. 1). In the case of complex **4** one nickel ion is square planar whilst the other is octahedral, whereas in complex **5** both nickel ions are high spin but one is square pyramidal whilst the other is octahedral.

Dark red single crystals of $[Ni_2L2(C_3H_3N_2)](CF_3SO_3)_2$ (**6**) were obtained by diethylether vapour diffusion into an MeCN solution of **6** and the structure determined (Fig. 2). There is one complete molecule, containing two square planar nickel(II) ions, in the asymmetric unit. Each nickel atom is bound to a bridging thiolate sulfur, an imine nitrogen, a pyridine nitrogen and a pyrazolate nitrogen, giving a N_3S coordination sphere. In order to accommodate the geometries of the nickel ions the two square planes are at an angle of 46.32(4)° to each other and the complex adopts a bowed shape with the thiophenolate head unit almost perpendicular to the two pyridine rings (85.4 and 84.7°). Examination of the dihedral angles between the respective $Ni(N_{L2-})_2$ and $NiSN_{pyrazolate}$ planes reveals a similar degree of tetrahedral distortion away from square planar (12.9–16.2°) to that found in the butylene chain analogue of $[Ni_2L3]^{2+}$ (15.4–18.9°) [13]. Due to the two atom pyrazolate bridge and the flexible nature of the acyclic ligand the Ni···Ni separation is greater, by 0.08–0.36 Å, than that observed in related macrocyclic complexes (Fig. 1) [2,3,11–13]. There are π–π stacking interactions between adjacent complexes with the thiophenolate ring of one complex lying over that of another (3.46–3.89 Å apart).

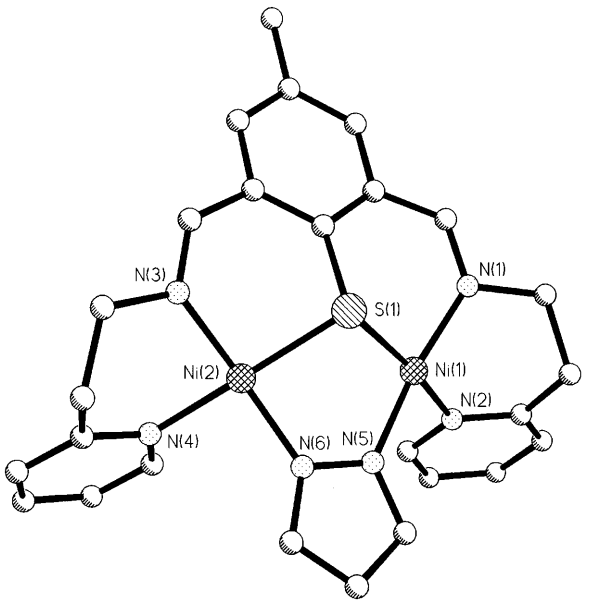


Fig. 2. Perspective view of the cation of **6**, $[Ni_2L2(C_3H_3N_2)]^{2+}$ (hydrogen atoms and triflate ions omitted for clarity). Selected bond lengths (Å) and angles (°): Ni(1)–N(5) 1.870(2), Ni(1)–N(1) 1.894(2), Ni(1)–N(2) 1.917(2), Ni(1)–S(1) 2.1872(6), Ni(2)–N(6) 1.875(2), Ni(2)–N(3) 1.898(2), Ni(2)–N(4) 1.930(2), Ni(2)-S(1) 2.1944(6), S(1)–C(1) 1.766(2), Ni(1)···Ni(2) 3.376(1), N(5)–Ni(1)–N(1) 170.50(9), N(5)–Ni(1)–N(2) 90.83(9), N(1)–Ni(1)–N(2) 89.56(8), N(5)–Ni(1)–S(1) 87.75(7), N(1)–Ni(1)–S(1) 93.26(6), N(2)–Ni(1)–S(1) 171.28(7), N(6)–Ni(2)–N(3) 168.54(9), N(6)–Ni(2)–N(4) 91.56(9), N(3)–Ni(2)–N(4) 90.17(9), N(6)–Ni(2)–S(1) 87.48(6), N(3)–Ni(2)–S(1) 93.03(6), N(4)–Ni(2)–S(1) 168.59(7), C(1)–S(1)–Ni(1) 103.68(8), C(1)–S(1)–Ni(2) 103.02(8), Ni(1)–S(1)–Ni(2) 100.79(2).

Comparison of the structure of **6** with that of the two complexes in the asymmetric unit of $[Pd_2L2Cl_2]Cl$ [22] reveals significant differences between them. In the case of **6** the two-atom pyrazolate bridge helps to pin the structure together, something which has been seen before in complexes of related two-armed thiophenolate ligands [23–25]. This bridge also requires the two arms to be held such that the two pyridine rings are almost parallel to each other. In contrast, in $[Pd_2L2Cl_2]Cl$ the two non-bridging chloride ions twist away from one another and hence force the two arms to twist in opposite directions with respect to the plane of the bridging thiophenolate moiety (the pyridine and phenyl ring planes intersect at 21.9 and 93.9° in the Pd(1)–Pd(2) complex and 14.9 and 87.2° in the Pd(3)/Pd(4) complex) [22]. The two square planes of donor atoms within each dipalladium complex are at much greater angles to each other (75.3° Pd(1)/Pd(2); 77.0° Pd(3)/Pd(4)) than is the case in **6**. Another consequence of the non-bridging chloride ions is that the metal ions are separated by a greater distance in the case of the palladium(II) complex (3.798 and 3.893 Å) [22] than in **6**.

3.3. NMR studies

Inspection of the ^1H and ^{13}C NMR data obtained for **3** and **6** establishes that both complexes have two-fold symmetry in solution (Fig. 1). For the macrocyclic dizinc complex **3** similar spectra were obtained in both MeCN-d_3 and $MeNO_2$-d_3. In the non-coordinating solvent $MeNO_2$-d_3 the acyclic dinickel complex **6** gave easily assigned diamagnetic ^1H and ^{13}C NMR spectra (Fig. 3). In coordinating solvents such as MeCN-d_3 **6** has some tendency to coordinate solvent molecules in the otherwise vacant axial sites leading to traces of paramagnetic species in solution. The ^1H NMR spectrum obtained for **6** in MeCN-d_3 is too broad to be assigned.

3.4. Electrochemical studies

Electrochemical studies were performed in MeCN, versus a 0.01 M $AgNO_3$–Ag reference electrode, on all complexes except the dinickel(II) complex **5** which was not soluble enough. The macrocyclic dizinc(II) complex **3** shows no electrochemical response within the solvent limits of MeCN (-2.4 to $+1.6$ V, Fig. 4). In contrast, the dinickel(II) complexes **4** and **6** both exhibit a series

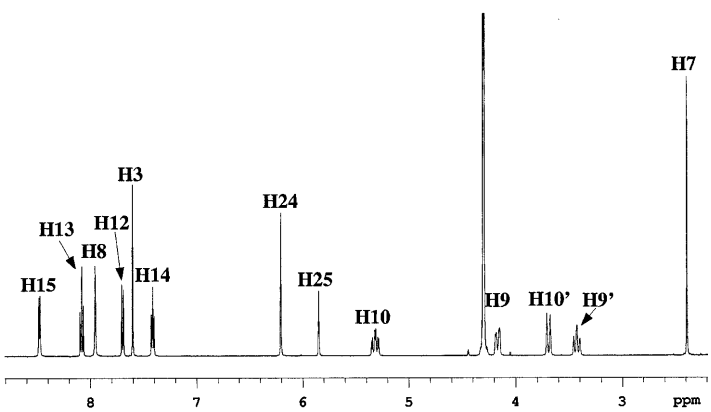


Fig. 3. ^1H NMR spectrum of $[Ni_2L2(C_3H_3N_2)](CF_3SO_3)_2$ (**6**) in $MeNO_2$-d_3 (numbering scheme as in Fig. 1).

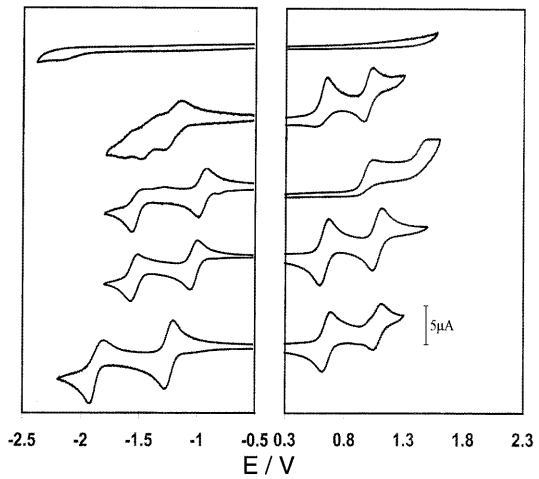


Fig. 4. Cyclic voltammograms of complexes (listed from top to bottom): $Zn_2L1(CH_3CO_2)_2(H_2O)_2$ (**3**), $[Ni_2L1(MeCN)_2](ClO_4)_2$ (**4**), $[Ni_2L2(C_3H_3N_2)](CF_3SO_3)_2$ (**6**), $[Ni_2L3](CF_3SO_3)_2$ and $[Ni_2L4](ClO_4)_2$ as 1 mmol l^{-1} solutions in MeCN (200 mV s^{-1}, 0.1 M NEt_4ClO_4, platinum electrode, versus 0.01 M $AgNO_3$–Ag).

of redox processes. The macrocyclic complex **4** has three redox processes between -1.3 and $+1.3$ V and the acyclic complex **6** has four redox processes between -1.8 and $+1.7$ V (Fig. 4). All of these approximately one-electron processes are believed to be largely metal-centred (Table 1) [11–13]. Two further reduction processes occur for the macrocyclic complex **4**, at -1.50 and -1.61 V (Fig. 4).

The two oxidation processes of the macrocyclic complex $[Ni_2L1(MeCN)_2](ClO_4)_2$ (**4**) occur at remarkably similar potentials to those of the two macrocyclic complexes $[Ni_2L3](CF_3SO_3)_2$ and $[Ni_2L4](ClO_4)_2$ (Fig. 1) [11–13], which are also 2:1 conductors in MeCN solution [26]. This is despite considerable differences in the macrocyclic donors, the most significant of which is changing one of the two thiophenolate bridges to a phenolate bridge. This is consistent with the electron being removed from the axial nickel(II) orbital, which is more sensitive to the ability of the MeCN solvent to coordinate axially (as nickel(III) is expected to have a coordination number greater than four) than to changes in the macrocyclic donors in the equatorial plane. Curiously, the first oxidation process for **4** is irreversible, independent of scan speed and of whether or not the second oxidation process is included in the scan.

The two oxidation processes of the acyclic complex **6** occur at significantly higher potentials than those of the macrocyclic complexes **4**, $[Ni_2L3](CF_3SO_3)_2$ and $[Ni_2L4](ClO_4)_2$, and both processes are irreversible. This indicates that the combination of losing the macrocyclic cavity and of replacing one thiophenolate or phenolate bridge by a pyrazolate bridge has significantly reduced the ability of the ligand to stabilise nickel(III). We have previously shown that replacement of both thiophenolate bridges by phenolate bridges also significantly increases the potential of these processes [13]. Interestingly the first process in the diphenolate macrocyclic complex occurs at a similar potential to that observed here for the acyclic complex **6**. The irreversibility of both of these processes for complex **6** may be due to a structural rearrangement occurring on removal of an electron from the nickel(II) ions, which are no longer constrained in a macrocyclic ring, leading to the pyrazolate dissociating from at least one nickel ion [20].

As expected, the reduction processes are more dependent on the nature of the donors in the equatorial plane (Fig. 4) [13]. In general, changing from a thiophenolate to a phenolate donor makes it harder to reduce the nickel(II) ion [13,20]. Likewise, changing from an imine to an amine donor also destabilises the nickel(I) oxidation state due to a reduction in the π-acceptor ability of the ligand [11,27,28].

As anticipated, replacing a thiophenolate diimine unit in $[Ni_2L3](CF_3SO_3)_2$ by a phenolate diamine unit in **4** has, as is seen from the potential of the first reduction process, significantly reduced the ability of the ligand to stabilise nickel(I). It is interesting to note that the potential of the first reduction process observed for complex **4** is very similar to that observed for the tetra-amine macrocyclic complex $[Ni_2L4](CF_3SO_3)_2$.

The two reduction processes observed for the acyclic complex **6**, are well separated and occur at very similar potentials to those observed for the tetra-imine complex

Table 1
Potentials ($E_{1/2}$, V) for the dinickel complexes [a]

	$Ni(I)_2 \Leftrightarrow Ni(I)Ni(II)$	$Ni(I)Ni(II) \Leftrightarrow Ni(II)_2$	$Ni(II)_2 \Leftrightarrow Ni(II)Ni(III)$	$Ni(II)Ni(III) \Leftrightarrow Ni(III)_2$
$[Ni_2L1(MeCN)_2](ClO_4)_2$	-1.50^{I}	-1.23^{QR}	$+0.65^{I}$	$+1.00^{R}$
$[Ni_2L2(C_3H_3H_2)](CF_3SO_3)_2$	-1.46^{I}	-0.96^{R}	$+1.03^{I}$	$+1.50^{I}$
$[Ni_2L3](CF_3SO_3)_2$	-1.46^{R}	-1.01^{R}	$+0.63^{R}$	$+1.07^{R}$
$[Ni_2L4](ClO_4)_2$	-1.86^{QR}	-1.18^{R}	$+0.69^{R}$	$+1.10^{QR}$

[a] R, reversible; QR, quasireversible; I, irreversible (hence in this case $E_{pa/pc}$ is quoted not $E_{1/2}$); these assignments were made on the basis of peak separation ΔE (cf. ferrocene), analysis of the ratio of peak currents and scan rate dependence of $E_{1/2}$ [35]. Controlled potential electrolysis of **4** at -1.30 V and of **6** at -1.10 V transferred ca. one electron equivalent of charge (0.90 and 0.93, respectively) and, by comparisons of the peak height currents, the remaining processes are therefore also assigned to be one-electron processes.

$[Ni_2L3](CF_3SO_3)_2$. This indicates that the replacement of N_{imine} by $N_{pyridine}$, both π-acceptors, and of S by $N_{pyrazolate}$ has had minimal overall effect on the reduction processes. The biggest difference is that the second process is less reversible for the acyclic complex **6** than for the macrocyclic complex $[Ni_2L3](CF_3SO_3)_2$. It is quite common for macrocyclic complexes to exhibit more reversible redox behaviour than acyclic analogues [13].

4. Conclusions

A series of dinuclear complexes incorporating a single bridging-thiolate donor have been prepared and characterised. Interestingly the redox potentials observed for the soluble dinickel(II) complexes **4** and **6**, do not simply fall in between those observed for the dinickel(II) complexes containing either none or two such bridging-thiolate donors. Complexes **4** and **5** are interesting first generation structural models for the [Ni–Fe] hydrogenases as they incorporate bridging thiolate sulfur and oxygen donors between two transition metal ions as is thought to be the case in the oxidised inactive forms of this enzyme. More importantly, they are uncommon examples of complexes in which the nickel ions have adopted two different geometries (and indeed spin states in the case of 4) despite the fact that the ligand provided potentially equivalent binding sites. Finally, complex **5** is a rare example of a high-spin square-pyramidal thiolate-coordinated nickel(II) ion [29]. These results illustrate the ability of macrocyclic ligands to provide unusual donor environments to the incorporated metal ions, resulting in complexes with intriguing structures and/or properties [30].

5. Supplementary material

Atomic coordinates, thermal parameters, and bond lengths and angles have been deposited at the Cambridge Crystallographic Data Centre, CCDC No. 137369. See Instructions for Authors, Polyhedron, 2000, Issue 1. Any request to the CCDC for this material should quote the full literature citation and the deposition number. Copies of this information can be obtained free of charge from The Director, CCDC, 12 Union Road, Cambridge, CB2 1EZ, UK (fax: +44-1223-336033; e-mail: deposit@ccdc.cam.ac.uk or www: http://www.ccdc.cam.ac.uk).

Acknowledgements

This work was supported by grants from the University of Otago, including a bridging grant (to T.C.D.) which has greatly facilitated the preparation of this paper. We are grateful to B.M. Clark for the FAB mass spectra and to Professor W.T. Robinson and Dr J. Wikaira for the X-ray data collection (University of Canterbury). We thank G.B. Caygill (University of Otago) for useful discussions during the course of this work.

References

[1] S. Brooker, P.D. Croucher, J. Chem. Soc., Chem. Commun. (1993) 1278.
[2] S. Brooker, P.D. Croucher, J. Chem. Soc., Chem. Commun. (1995) 2075.
[3] S. Brooker, P.D. Croucher, Chem. Commun. (1997) 459.
[4] S. Brooker, T.J. Simpson, J. Chem. Soc., Dalton Trans. (1998) 1151.
[5] S. Brooker, D.J. de Geest, G.S. Dunbar, Inorg. Chim. Acta 282 (1998) 222.
[6] S. Brooker, G.S. Dunbar, G.B. Jameson, Polyhedron 18 (1999) 679.
[7] S.M. Nelson, Pure Appl. Chem. 52 (1980) 2461.
[8] F.C.J.M.v. Veggel, M. Bos, S. Harkema, H.v.d. Bovenkamp, W. Verboom, J. Reedijk, D.N. Reinhoudt, J. Org. Chem. 56 (1991) 225.
[9] W.R. Harris, I. Murase, J.H. Timmons, A.E. Martell, Inorg. Chem. (1978) 889.
[10] S.R. Aspinall, J. Am. Chem. Soc. (1941) 852.
[11] (a) S. Brooker, T.C. Davidson, Chem. Commun. (1997) 2007. (b) S. Brooker, P.D. Croucher, T.C. Davidson, G.S. Dunbar, A.J. McQuillan, G.B. Jameson, Chem. Commun. (1998) 2131.
[12] (a) S. Brooker, P.D. Croucher, F.M. Roxburgh, J. Chem. Soc., Dalton Trans. (1996) 3031. (b) S. Brooker, G.B. Caygill, P.D. Croucher, T.C. Davidson, D.L.J. Clive, S.R. Magnuson, S.P. Cramer, C.Y. Ralston, Dalton Trans. (2000) in press.
[13] S. Brooker, P.D. Croucher, T.C. Davidson, G.S. Dunbar, C.U. Beck, S. Subramanian, Eur. J. Inorg. Chem. (2000) 169.
[14] A.J. Atkins, A.J. Blake, M. Schroder, J. Chem. Soc. Chem. Commun. (1993) 1662.
[15] A.J. Atkins, D. Black, A.J. Blake, A. Marin-Becerra, S. Parsons, L. Ruiz-Ramirez, M. Schroder, Chem. Commun. (1996) 457.
[16] N.D.J. Branscombe, A.J. Blake, A. Marin-Becerra, W.S. Li, S. Parsons, L. Ruiz-Ramirez, M. Schroder, Chem. Commun. (1996) 2573.
[17] P.E. Kruger, V. McKee, Chem. Commun. (1997) 1341.
[18] A. Christensen, H.S. Jensen, V. McKee, C.J. McKenzie, M. Munch, Inorg. Chem. 36 (1997) 6080.
[19] J.G. Hughes, R. Robson, Inorg. Chim. Acta 35 (1979) 87.
[20] A.M. Bond, M. Haga, I.S. Creece, R. Robson, J.C. Wilson, Inorg. Chem. 27 (1988) 712.
[21] A.M. Bond, M. Haga, I.S. Creece, R. Robson, J.C. Wilson, Inorg. Chem. 28 (1989) 559.
[22] B.F. Hoskins, C.J. McKenzie, R. Robson, L. Zhenrong, J. Chem. Soc., Dalton Trans. (1990) 2637.
[23] B.F. Hoskins, I.A.S. McDonald, Aust. J. Chem. 37 (1984) 1395.
[24] P. Illiopoulos, K.S. Murray, R. Robson, J. Wilson, G.A. Williams, J. Chem. Soc., Dalton Trans. (1987) 1585.
[25] B.F. Hoskins, C.J. McKenzie, I.A.S. MacDonald, R. Robson, J. Chem. Soc., Dalton Trans. (1996) 2227.
[26] T. Beissel, F. Birkelbach, E. Bill, T. Glaser, F. Kesting, C. Krebs, T. Weyhermuller, K. Wieghardt, C. Butzlaff, A.X. Trautwein, J. Am. Chem. Soc. 118 (1996) 12376.
[27] D.H. Busch, E.S. Gore, F.V. Lovecchio, J. Am. Chem. Soc. 96 (1974) 3109.
[28] A.G. Lappin, A. McAuley, Adv. Inorg. Chem. 32 (1988) 241.

[29] M.S. Ram, C.G. Riordan, R. Ostrander, A.L. Rheingold, Inorg. Chem. 34 (1995) 5884.
[30] V. McKee, Adv. Inorg. Chem. 40 (1993) 323.
[31] W.J. Geary, Coord. Chem. Rev. 7 (1971) 81.
[32] G.M. Sheldrick, Acta Crystallogr. 46 (1990) 467 Sect. A.
[33] G.M. Sheldrick, Methods Enzymol. 276 (1997) 628.
[34] G.M. Sheldrick, T.R. Schneider, Methods Enzymol. 277 (1997) 319.
[35] T.J. Kemp (Ed.), Southampton Electrochemistry Group: Instrumental Methods in Electrochemistry, Ellis Horwood, Chichester, UK, 1985.

PERGAMON

www.elsevier.nl/locate/poly

Polyhedron 19 (2000) 1895–1901

POLYHEDRON

Versatile chelating behavior of aliphatic thiosemicarbazones in zinc and cobalt complexes

Marisa Belicchi Ferrari, Giovanna Gasparri Fava *, Giorgio Pelosi, Pieralberto Tarasconi

Dipartimento di Chimica Generale ed Inorganica, Chimica Analitica, Chimica Fisica, Centro di Studio per la Strutturistica Diffrattometrica del CNR, Parco Area delle Scienze 17A, 43100 Parma, Italy

Received 10 March 2000; accepted 5 June 2000

Abstract

In this paper we report the synthesis of three new complexes of Zn(II) and Co(III) with two ligands, methyl pyruvate thiosemicarbazone (Hmpt) and α-ketoglutaric acid thiosemicarbazone (H_3ct). The three compounds [Zn(H_2pt)(Hpt)Cl] (**A**), [Zn(H_2ct)$_2$]·H_2O (**B**), [Co(H_2ct)(Hct)]·H_2O (**C**), are characterized by IR spectroscopic techniques and the structures determined by single-crystal X-ray diffraction analysis. In **A** an interesting feature is the different behavior of the two ligand molecules, one terdentate and the other monodentate. The coordination geometry about zinc is better described as intermediate between an ideal square pyramid and trigonal bipyramid, while in **B** and **C** the metals are six-coordinated in a distorted octahedral geometry. All compounds are monomeric. © 2000 Elsevier Science Ltd. All rights reserved.

Keywords: Zinc complexes; Cobalt complex; α-Ketoglutaric acid; Thiosemicarbazones; Crystal structures; Spectroscopic properties

1. Introduction

Recently we described the synthesis, the spectroscopic characterization and X-ray structural analysis of some zinc and cobalt complexes with mono- and bisthiosemicarbazones [1,2], with the aim to understand the correlation between structural features and the biological properties of these classes of compounds [3], under different experimental conditions. Continuing this program of research we have synthesized a new complex [Zn(H_2pt)(Hpt)Cl] (**A**) starting from $ZnCl_2$ and the ligand Hmpt (Hmpt = methylpyruvate thiosemicarbazone) [4]. Upon preparative conditions, in alcoholic medium, Hmpt is converted to its hydrolyzed form (H_2pt). An interesting result of the present study is the different behavior of the two ligand molecules, the first terdentate, the second unusually monodentate through the sulfur atom. In the course of our investigation this latter coordinating behavior has only been found in two copper(I) complexes [5,6]. The aliphatic nature of the Hmpt ligand gives unsatisfactory biological results due to poor solubility in biological solvents and therefore a different aliphatic thiosemicarbazone, the α-ketoglutaric acid (H_3ct) derivative has also been synthesized. This ligand presents more potential donor atoms and a variety of potential conformations; its complexes with zinc [Zn(H_2ct)$_2$]·H_2O (**B**) and cobalt [Co(H_2ct)(Hct)]·H_2O (**C**) have been synthesized and characterized with the aim to elucidate the correlation between the structure and the induced differentiation by these compounds in Friend erythroleukemia cells (FLC).

2. Experimental

2.1. Synthesis of ligands and complexes

The preparation of the ligand Hmpt·0.5H_2O was the same as previously described [4].

* Corresponding author: Tel.: +39-521-905-420; fax: +39-521-905-557.

E-mail address: chimic8@ipruniv.cce.unipr.it (G. Gasparri Fava).

0277-5387/00/$ - see front matter © 2000 Elsevier Science Ltd. All rights reserved.
PII: S0277-5387(00)00454-X

The ligand H_3ct (α-ketoglutaric acid thiosemicarbazone) was prepared according to a procedure previously reported [7] and achieved as transparent crystals (m.p. = 184.8°C). Found: C, 33.01; H, 4.17; N, 18.86; S, 14.90. $C_6H_9N_3O_4S$ requires: C, 32.87; H, 4.14; N, 19.17; S, 14.63%.

2.1.1. [Zn(H$_2$pt)(Hpt)Cl] (A)

A batch of 0.25 g (1.83 mmol) of anhydrous $ZnCl_2$ was added with stirring to an absolute ethanol solution (30 ml) of 0.34 g (1.83 mmol) of Hmpt·0.5H_2O. After 60 min of stirring at room temperature (r.t.) the clear solution (ca. pH 5) was allowed to stand. Pale yellow crystals of the product **A** were grown by slow evaporation of the solvent. Analytical data and complete structural determinations showed that the ligand (in its hydrolyzed form) to metal ratio in the product was 2:1. Found: C, 22.64; H, 3.76; N, 19.96, S, 15.22. $C_8H_{13}ClN_6O_4S_2Zn$ requires: C, 22.76; H, 3.10; N, 19.91; S, 15.19%.

We have observed that the nature of the product obtained by this procedure depends on the amount of water involved in the synthesis. Molecules of water were present in the medium because we employed an undryed appreciably hygroscopic organic solvent (EtOH abs.), a deliquescent inorganic salt and a hemihydrate ligand. Upon these conditions the reaction proceeds through different new ligand forms as a function of temperature and these new ligands are converted into products of different nature. The driving force of the reaction is the formation of the most stable product. At 'high' temperature Hept (ethyl pyruvate thiosemicarbazone) is formed by transesterification of the ligand precursor Hmpt·0.5H_2O, at r.t. the ligand Hmpt is hydrolyzed into H_2pt (pyruvic acid thiosemicarbazone). So this reaction, sensitive to a change in temperature and in the amount of water present, can be used to generate zinc complexes containing different ligands. Alternatively compound **A** was obtained by reaction of $ZnCl_2$ with Hmpt·0.5H_2O in a 1:1 molar ratio, in MeOH at reflux for 2 h (pH of resulting solution 5–6), as confirmed by analytical and spectroscopic data.

2.1.2. Preparations of [Zn(H$_2$ct)$_2$]·H$_2$O (B) and [Co(H$_2$ct)(Hct)]·H$_2$O (C)

A solution of $ZnCl_2$ (0.1 g) in 20 ml of water was added to a warm aqueous solution (20 ml) of H_3ct (ratio metal:H_3ct = 2:1) and then stirred for 5 min. The resulting clear solution (ca. pH 1) was allowed to stand at r.t. and after evaporation gave pale yellow crystals of **B** (m.p. = 247.6°C). Found: C, 28.01; H, 4.02; N, 16.20; S, 12.39. $C_{12}H_{18}N_6O_9S_2Zn$ requires: C, 27.73; H, 3.49; N, 16.17; S. 12.33%.

The complex [Co(H_2ct)(Hct)]·H_2O (**C**) was similarly obtained as deep brown crystals by aerobic oxidation of the starting material, $CoCl_2·6H_2O$ in refluxing aqueous solution for 1 h (pH 2) (m.p. = 260.4°C). Found: C, 28.42; H, 3.54; N, 16.14; S, 12.65. $C_{12}H_{17}N_6O_9S_2Co$ requires: C, 28.13; H, 3.34; N, 16.40; S, 12.52%.

Compound **B** was also obtained as a crystalline product by evaporation of (i) an aqueous solution (pH 3) and (ii) an EtOH (abs.) solution (pH 1) containing the reactant in an equimolar amount previously refluxed for 30 min. Despite the ratio employed upon the experimental conditions described above, these reactions gave only monometallic compounds containing two independent ligand molecules.

2.2. Physical measurements

The FT IR spectra were recorded on a Nicolet 5PC spectrophotometer in the frequency range 4000–400 cm^{-1} using KBr discs. Microanalyses (C, H, N and S) were made on Carlo Erba instruments CHNS-O EA 1108 automatic equipment.

2.3. X-ray structure determination

The crystal and instrumental parameters used in the unit-cell determination and data collection are summarized in Table 1. All intensity data were collected on a CAD4 diffractometer for **A**, on a Siemens AED for **B** and on a Philips for **C** by the θ–2θ technique. The structures were solved by the heavy-atom technique starting from a three-dimensional Patterson analysis for compounds **A** and **C**, and by direct methods for **B** using the SHELX-86 [8] programs. For all compounds successive Fourier syntheses gave coordinates of non-hydrogen atoms which were refined by full-matrix least-squares with anisotropic thermal parameters for compounds **B** and **C**. In compound **A** however, the carbon atoms were isotropically refined. Hydrogen atoms were located from a ΔF map and introduced in the last refinement cycles for **B** and **C**, while for **A** were partly located and partly (methyl groups) calculated at their geometrical positions and maintained as fixed contributors in the last calculation. The hydrogen atoms of the carboxylic groups O(4)–C(7)–O(3) in **A** and O(6)–C(6)–O(5) in **C** have not been located, but the interaction O(3)···N(6) = 2.58(3) Å and the distances C(7)–O(3) = 1.30(4) Å in **A** and C(6)–O(5) = 1.311(4) Å in **C** indicate O(3) and O(5), respectively, as hydroxylic moieties. The absorption correction was neglected in **A** and **C** in view of small crystal dimensions. In **A** a correction for secondary extinction [9] was applied owing to an unsuccessful absorption correction. In compound **B** the absorption correction was applied following the method of Walker and Stuart [10]. The final atomic coordinates are given as supplementary material (see Section 4). Atomic scattering factors were taken from Ref. [11]. All calculations were performed on a Gould 6440 Powernode computer of the Centro di

Table 1
Experimental data for the crystallographic analyses [a]

Compound	[Zn(H_2pt)(Hpt)Cl] (**A**)	[Zn(H_2ct)$_2$]·H_2O (**B**)	[Co(H_2ct)(Hct)]·H_2O (**C**)
Formula	$C_8H_{13}ClN_6O_4S_2Zn$	$C_{12}H_{18}N_6O_9S_2Zn$	$C_{12}H_{17}CoN_6O_9S_2$
Molecular weight	422.2	519.8	512.4
Space group	$P2_1/n$	$P2_1/n$	$P2_1/n$
a (Å)	9.775(2)	14.883(2)	9.558(1)
b (Å)	14.120(3)	9.513(1)	16.566(2)
c (Å)	12.616(3)	14.302(2)	12.188(2)
β (°)	103.09(3)	91.43(2)	91.32(2)
V (Å^3)	1696.0(5)	2024.3(4)	1929.3(4)
Z	4	4	4
D_{calc} (mg m^{-3})	1.65	1.70	1.76
$F(000)$	856	1064	1048
μ (cm^{-1})	19.0	41.7	11.7
Crystal size (mm)	$0.20\times0.23\times0.05$	$0.80\times0.50\times0.10$	$0.10\times0.13\times0.29$
θ Range (°)	3–21	2.5–70	3–27
Number of measured reflections	2010	4238	4547
Maximum/minimum height in final difference map (e Å^{-3})	0.23; −0.23	0.57; −0.59	0.12; −0.10
Number of refined parameters	151	343	335
Number of unique reflections	715	3374	2672
R	0.064	0.057	0.033
R'	0.087	0.082	0.038
λ	0.71070 (Mo Kα)	1.54178 (Cu Kα)	0.71070 (Mo Kα)
$w = k[\sigma^2(F_o)+\lvert g\rvert(F_o)^2]^{-1}$	1; 0.00378	1; 0.02107	1.3429; 0.00029

[a] Data common to all compounds: $T = 293 \pm 1$ K, condition for observed reflections: $I > 3\sigma(I)$.

Studio per la Strutturistica Diffrattometrica del C.N.R. (Parma) using the PARST [12] program for the geometrical description of the structure, and ORTEP [13] and PLUTO [14] for the structure drawings.

3. Results and discussion

3.1. Description of the structure

The structure of **A** is shown in Fig. 1 and consists of discrete molecular units. Although the metal can be formally described as having a square-pyramidal coordination, the distortion around the zinc center gives it a structure intermediate between the five-coordinated extremes of an ideal square pyramid and a trigonal bipyramid [15]. An interesting result of the present study is the different behavior of the two ligand molecules, the first terdentate via the S,N (iminic) and O (carboxylic) donor atoms as earlier found in [Zn(Hpt)$_2$], [Zn(Hept)Cl$_2$] (Hept = ethyl pyruvate thiosemicarbazone) [1] and in other Mn(II), Zn(II), Co(III) and Cu(II) complexes [1,2,4,16], the second unusually monodentate through the sulfur atom. This latter coordinating behavior has been found in the course of our investigations only in two copper(I) complexes with Hmpt and H_2mpipt (methyl pyruvate-hydrazinopyruvoylthiosemicarbazone) [5,6]. The terdentate ligand shows a Z configuration about the C(1)–N(2) bond and the carboxylate oxygen *cis* to N(3), while the monodentate molecule shows an E configuration about C(5)–N(5) bond as the free ligand and the carboxylic oxygen O(3) *cis* to N(6).

In the copper(I) compounds however, the ligand shows different configurations [5,6]. The versatility of this ligand, involving the change of its configuration, suggests that different factors, such as electronic effects, play essential roles in determining the formation of the metal complexes and their related biological properties. Experiments concerning the biological activity (as erythroid differentiation, cell proliferation, potential antiviral action) have been undertaken, but the poor solubility of the complexes with Hmpt causes some difficulties in the reproducibility of the experimental data.

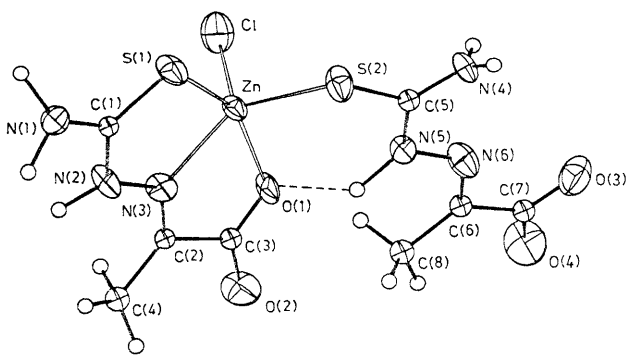


Fig. 1. ORTEP drawing of **A** with thermal ellipsoids at 50% probability level.

Table 2
Selected bond lengths (Å) and angles (°) of **A**

Zn–Cl	2.283(7)	N2–N3	1.39(3)
Zn–S1	2.476(8)	N2–C1	1.35(3)
Zn–S2	2.368(7)	N3–C2	1.25(3)
Zn–O1	2.082(18)	N4–C5	1.31(3)
Zn–N3	2.116(20)	N5–N6	1.41(3)
S1–C1	1.68(3)	N5–C5	1.31(3)
S2–C5	1.74(3)	N6–C6	1.31(4)
O1–C3	1.24(3)	C2–C3	1.58(4)
O2–C3	1.22(4)	C2–C4	1.51(4)
O3–C7	1.30(4)	C6–C7	1.47(4)
O4–C7	1.21(4)	C6–C8	1.51(4)
N1–C1	1.34(3)		
Cl–Zn–S1	106.9(3)	S1–Zn–N3	78.2(6)
Cl–Zn–S2	108.3(3)	S2–Zn–O1	98.1(5)
Cl–Zn–O1	97.6(5)	S2–Zn–N3	133.4(6)
Cl–Zn–N3	118.3(6)	O1–Zn–N3	74.9(7)
S1–Zn–S2	90.5(3)		
S1–Zn–O1	149.9(5)		

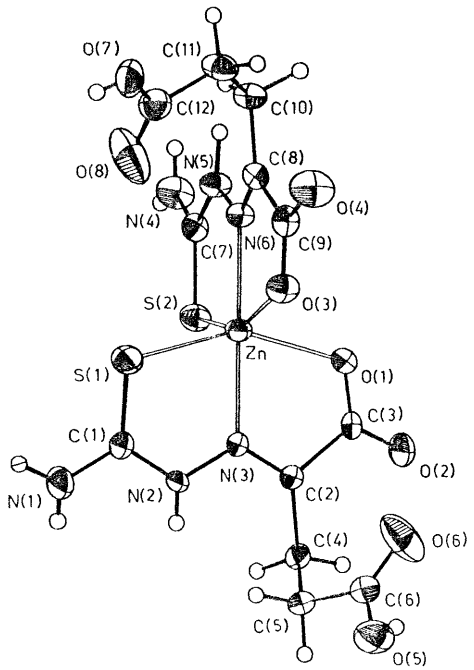


Fig. 2. ORTEP drawing of **B** with thermal ellipsoids at 50% probability level.

In solution and in the presence of metal ions the ligand may exist in equilibrium with the two thione and thiol tautomeric forms. In the solid state the terdentate exists in the thione form, while the monodentate one is in the thiol form (see Table 2).

The thione ligand is singly deprotonated but the thiol molecule is neutral and its iminic nitrogen forms an intramolecular hydrogen bond with the O(1) oxygen coordinated to zinc (Fig. 1). The thiol ligand is bound more tightly to the zinc ion than the thione chelate (Zn–S(2) = 2.368(7), Zn–S(1) = 2.476(8) Å).

The terdentate molecule is nearly planar, the largest deviation from the best plane being for the terminal O(2), probably due to the hydrogen bond with N(1) (N(1)–H(11)···O(2) = 2.71(3) Å). The monodentate ligand deviates considerably from planarity. In fact the thiosemicarbazide moiety and the pyruvic group are planar, but the dihedral angle between them is 11.4(7)°.

The zinc **B** and cobalt **C** complexes with H_3ct are monomeric and the metal coordination in both cases is distorted octahedral with two terdentate ligands (Figs. 2 and 3).

In the zinc complex both ligands are monodeprotonated, while in the cobalt complex one of the ligands is mono and the second is bideprotonated, in accordance with the oxidation state III for cobalt. In both compounds the two ligands are in the meridional configuration (S and O atom *cis* to each other and the N atoms *trans*) as found in other octahedral cobalt and zinc complexes [1,2,17].

A crystallization water molecule is present in both compounds and even if the environment of the metal is

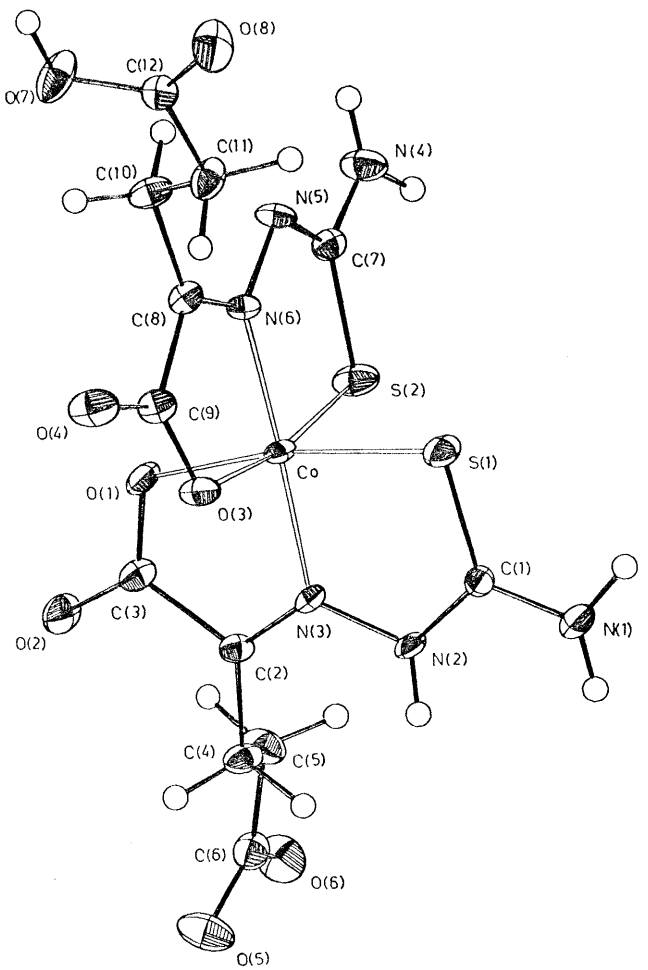


Fig. 3. ORTEP drawing of **C** with thermal ellipsoids at 50% probability level.

Table 3
Selected bond lengths (Å) and angles (°) of **B**

Zn–S1	2.482(1)	O1–C3	1.269(4)
Zn–S2	2.498(1)	O2–C3	1.240(4)
Zn–N3	2.137(2)	O3–C9	1.266(4)
Zn–N6	2.157(2)	O4–C9	1.222(3)
Zn–O1	2.174(2)	O5–C6	1.308(4)
Zn–O3	2.114(2)	O6–C6	1.193(5)
S1–C1	1.690(3)	O8–C12	1.197(5)
S2–C7	1.683(3)	C2–C3	1.526(4)
N1–C1	1.334(4)	C2–C4	1.508(4)
N2–N3	1.376(3)	C4–C5	1.532(4)
N2–C1	1.356(3)	C5–C6	1.506(4)
N3–C2	1.284(3)	C8–C9	1.530(4)
N4–C7	1.322(4)	C8–C10	1.492(4)
N5–N6	1.368(3)	C10–C11	1.523(4)
N5–C7	1.355(3)	C11–C12	1.497(4)
N6–C8	1.279(3)	O7–C12	1.299(5)
O1–Zn–O3	88.6(1)	S2–Zn–O1	93.3(1)
N6–Zn–O3	74.3(1)	S2–Zn–N6	78.7(1)
N6–Zn–O1	101.9(1)	S2–Zn–N3	89.8(1)
N3–Zn–O3	116.7(1)	S1–Zn–O3	91.5(1)
N3–Zn–O1	74.0(1)	S1–Zn–O1	150.1(1)
N3–Zn–N6	167.6(1)	S1–Zn–N6	106.9(1)
S2–Zn–O3	152.7(1)	S1–Zn–N3	79.3(1)
		S1–Zn–S2	100.0(0)

very similar they are not isostructural. The charge and radium of the cations and the ligands different charge delocalization probably change the electronic and steric situation and therefore the packing.

In the Zn complex, **B**, the two ligands, both monodeprotonated, are in the thione form (S(1)–C(1) = 1.690(3), S(2)–C(7) = 1.683(3) Å, Table 3) and not planar even though the thiourea moiety and the carboxylic group are planar as previously found in other similar compounds [3]. The dihedral angles between them are 11.6(1) and 6.8(1)°, respectively, for S(1)– and S(2)-molecules.

The oxidation state three of cobalt is shown by its coordination bond lengths Co–S, Co–N and Co–O (Table 4) which are in the expected ranges of 2.201–2.230, 1.891–1.901 and 1.945–1.968 Å, respectively, as already noted for several Co(III) complexes [2,17]. The loss of the proton originally bound to N(5) produces a negative charge which is delocalized in the N6–N5–C7 system as indicated by the bond distances and in particular S(2)–C(7) = 1.744(3) Å and C(7)–N(5) = 1.326(4) Å. The other ligand not deprotonated on N(2), is in the thione form [S(1)–C(1) = 1.711(3), C(1)–N(2) = 1.357(4) Å]. The dihedral angles between the thiourea moiety and the carboxylic group are 1.6(1) (thione) and 9.6(1)° (thiol), respectively.

The $–CH_2–CH_2–COOH$ groups adopt different conformation (C(6) and C(12) are synclinal in **B**, and antiperiplanar in **C** with regard to C(2) and C(8), respectively) as shown by the torsion angles (C(2)–C(4)–C(5)–C(6) = −63.6(3), −169.7(3); C(8)–C(10)–C(11)–C(12) = −46.3(4), −165.1(3)°). These conformations are probably adopted in order to form intermolecular hydrogen bonds.

The large steric constraints in the two five-membered chelate rings distort the coordination to metal in complex **B** much more than that in complex **C**, probably as a consequence of the large size of the Zn(II) cation with respect to Co(III). In fact N(3)–Zn–N(6) = 167.6(1)°; N(3)–Co–N(6) = 177.9(1)°, S(1)–Zn–O(1) = 150.1(1)°; S(1)–Co–O(1) = 170.5(1)°; S(2)–Zn–O(3) = 152.7(1)°, S(2)–Co–O(3) = 170.2(1)°. The dihedral angle between Zn–S(1)–N(3)–O(1) and Zn–S(2)–N(6)–O(3) planes is 82.8(1)°, while the corresponding angle in the Co complex is 90°. This easy deformation of the geometry of the ligands in the coordination sphere to the Zn atom seems to be connected with a structural or a catalytic role of the metal.

In **A** the packing interactions are very important. Chains of molecules determined by hydrogen bonds N(1)–H(11)···O(2) $(x-1/2,\ 1/2-y,\ 1/2+z)$ = 2.71(3) Å are joined together with N–H···Cl bonds (N(1)–H(21)···Cl $(1/2-x,\ 1/2+y,\ 1/2-z)$, N(2)–H(2)···Cl $((1/2-x,\ 1/2+y,\ 1/2-z))$ to form ribbons parallel to (2 0 2) planes. These ribbons are linked by N(4)–H(42)···O(4) $(x-1/2,\ -y-1/2,\ 1/2+z)$ bonds.

In **B** and **C** the packing is determined essentially by hydrogen bonds between nitrogens of amine groups, the carboxylate oxygen atoms and the water molecules which have different neighbors in the two compounds.

Table 4
Selected bond lengths (Å) and angles (°) of **C**

Co–S1	2.205(1)	N1–C1	1.318(4)
Co–S2	2.201(1)	N2–N3	1.374(3)
Co–O1	1.958(2)	N2–C1	1.357(4)
Co–O3	1.968(2)	N3–C2	1.287(4)
Co–N3	1.894(2)	N4–C7	1.344(4)
Co–N6	1.878(3)	N5–N6	1.366(3)
S1–C1	1.711(3)	N5–C7	1.326(4)
S2–C7	1.744(3)	N6–C8	1.309(4)
O1–C3	1.276(4)	C2–C3	1.525(4)
O2–C3	1.231(4)	C2–C4	1.486(4)
O3–C9	1.279(4)	C4–C5	1.536(5)
O4–C9	1.244(4)	C5–C6	1.496(5)
O5–C6	1.311(4)	C8–C9	1.493(4)
O6–C6	1.218(4)	C8–C10	1.492(4)
O7–C12	1.302(4)	C10–C11	1.534(5)
O8–C12	1.214(4)	C11–C12	1.506(5)
N3–Co–N6	177.9(1)	S2–Co–O3	170.2(1)
O3–Co–N6	84.1(1)	S2–Co–N3	94.2(1)
O3–Co–N3	95.1(1)	S2–Co–O1	91.1(1)
O1–Co–N6	95.1(1)	S1–Co–N6	94.3(1)
O1–Co–N3	82.9(1)	S1–Co–N3	87.7(1)
O1–Co–O3	87.0(1)	S1–Co–O3	92.6(1)
S2–Co–N6	86.6(1)	S1–Co–S2	90.9(1)
		S1–Co–O1	170.5(1)

Table 5
Selected infrared spectroscopic data (cm^{-1})

	ν(NH), ν(OH)	ν(C=O), $\nu_{as}(CO_2^-)$	ν(C=N)	$\nu_s(CO_2^-)$	ν(C–OH)	ν(NCS)	ν(C=S)
[Zn(H_2pt)(Hpt)Cl] (**A**)	3400 m	1708 s	1601 vs	1449 m	1414 ms	1184 s	867 ms
	3292 s	1667 vs	1552 s		1330 ms	1172 s	776 ms
	3180 m	1651 s					
	3131 ms	1636 vs					
H_3ct	3352 s	1728 s	1612 (sh)		1368 ms	1175 vs,br	784 vs,br
	3270 s	1699 vs	1513 s		1330 ms		776 (sh)
	3167 vs	1631 s, br			1273 s		
[Zn(H_2ct)$_2$]H_2O (**B**)	3480 (sh)	1726 ms	1600 (sh)	1432 ms	1381 m	1201 vs,br	765 s
	3380 m,br	1694 m	1554 s		1333 ms		
	3290 m	1654 s			1271 mw		
	3172 vs	1629 s,br			1241 m		
[Co(H_2ct)(Hct)H_2O] (**C**)	3580 (sh)	1704 s	1616 (sh)	1496 ms	1380 m	1182 s	749 mw
	3482 m,br	1636 vs,br	1576 s		1275 m		
	3369 ms				1254 ms		
	3283 s						
	3170 vs						

A comparison of the structures of the complexes with both ligands, Hmpt and H_3ct, and those of similar zinc and cobalt compounds, suggests the following considerations: (a) a greater variation in the bonding geometry of the zinc complexes is observed; (b) both ligands have aliphatic properties, but the complexes with H_3ct are more soluble in biological solvents; (c) both ligands yield complexes with different stoichiometry depending on the inorganic ion or on the ligand whether it is in a neutral or monoanionic form.

The correlation between structural analysis and biological activity (induced differentiation in FLC, assay carried out as previously reported in Refs. [18,19]) shows that the studied complexes with H_3ct do not have biological activity, probably due to the complete octahedral coordination sphere and the presence of polar acid groups which could prevent transfer through the cellular membrane.

However the action mechanism of these molecules will have to be clarified.

3.2. IR spectra

As reported in the experimental, the ligand molecule Hmpt·0.5H_2O upon preparative conditions hydrolyzed in its derivative H_2pt (pyruvic acid thiosemicarbazone) still containing SNO potential coordinating sites. The ligands H_2pt and H_3ct differ from each other only by the groups (–CH_3 or –$(CH_2)_2$–COOH, respectively) bonded to the imminic carbon atom of the thiosemicarbazone moiety. Consequently the IR spectra of their metal complexes namely **A**, **B** and **C**, exhibit some similarities and distinct differences. In particular significant spectra differences are observed for the octahedral neutral metal chelates of H_3ct, despite their structural analogies and similar molecular formula [Zn(H_2ct)$_2$]·H_2O and [Co(H_2ct)(Hct)]·H_2O. On the contrary, **A** and **B**, the zinc complexes of H_2pt and H_3ct, respectively, which have different coordination numbers, produce similar features in their spectra. This can be explained in terms of electronic and steric effects. The zinc compounds that contain a d^{10} metal center, do not feel the ligand field stabilization effects so their spectral features are a result of steric forces between parts of the molecules. On the contrary, in the Co(III) complex with a geometric structure imposed by ligand field requirements, are most important the electronic effects.

On the basis of the above observations we assigned the selected bands present in the infrared spectra of compounds (reported in Table 5) in agreement with the X-ray structural data.

Strong broad structured bands spanning from 3700–2600 cm^{-1} which appear in the spectra of all compounds are due to νOH, νNH and νCH stretching vibrations. The three medium–strong intensity bands at around 3366, 3280 and 3169 cm^{-1} in the spectra of H_3ct, **B** and **C** are assigned to $\nu_{as}NH_2$, ν_sNH_2 and νNH, respectively. These bands are overlapped with the broad lattice water bands (compounds **B** and **C**) and are superimposed upon the broader more intense O–H stretching absorption typical of the carboxylic acid functions. For complex [Zn(H_2pt)(Hpt)Cl] (**A**), the $\nu_{as}NH_2$ modes give rise to a band with maximum intensity at 3400 cm^{-1}. Its position is shifted by 34 cm^{-1} toward higher frequencies with respect to those previously observed at ca. 3366 cm^{-1} for H_3ct **B** and **C**. Such a shift can be interpreted as being due to the presence of a coordinated chloride anion. Moreover the new νNH band observed at 3131 cm^{-1} may be due to the effect of simultaneous interactions of the NH group of the monodentate ligand with the neighboring $–COO^-$ and C=S coordinated groups. A comparison of the bands present in the 1720–1630 cm^{-1} region of the

spectrum of [Zn(H_2pt)(Hpt)Cl] with those observed for [Zn(Hpt)$_2$] [1] and {[Cu(Hpt)Cl]·2H_2O}$_n$ [4] can provide information about the different situation (free or coordinated) of the carboxylic groups. The C=O bands of compound **A** at 1651 (s) and 1636 (vs) cm^{-1} are attributed to the stretching modes of the coordinate carboxylate groups as the *anti*monodentate terminal, while the other two, that show the same features, at 1708 (s) and 1667 (vs) cm^{-1} are indicative of an uncoordinated carboxylic group. On the basis of this observation attempts can be made to related values of carbon–oxygen stretching frequencies to the nature of the complexes **B** and **C** as reported in Table 5. In the zinc complexes and also in compound **B** the shifts of the C=O bands are most likely caused by the vibrational coupling of the C=O in the solid state H-bonded structure. This phenomenon is, at least in part, eliminated in the Co(III) complexes by the field effect of the charge delocalization due to the loss of the azomethyne hydrogen. The IR spectrum obtained by crystals of ligand H_3ct which present the same X-ray crystallographic data published in Ref. [20], indicates that H_3ct forms both intra- and intermolecular hydrogen bond networks. These are responsible for the positions of the bands corresponding to the modes which involve νNH_2 and νNH vibrations (found at lower frequencies with respect to those in the spectra of **B** and **C**) and probably cause the multiply-split bands due to the C=O stretching vibrations. The significant IR bands of $\nu_s(COO^-)$ and of those arising from interaction between C–O stretching and O–H bending of the carboxylic acid function appear in the range 1496–1241 cm^{-1}. Absorptions in the region 1616–1552 cm^{-1} are associated with carbon–nitrogen double bond stretching vibration. For the other compounds, the spectrum of complex **A** presents a strong doublet located between 1601 and 1552 cm^{-1} in agreement with the structural data. On coordination of complex **C** deprotonation of the imino-hydrogen of the ligand H_3ct occurs such that the strong bands associated with the ν(C=N) are observed at higher frequencies with respect to those of the free ligand and complex **B**. Strong bands corresponding to normal modes in which the stretching vibration of the C=S groups are involved, appeared in the range 1201–1172 cm^{-1} for all the compounds studied. Finally, other bands which contains ν(CS) character, indicative of the involvement of the sulfur atom in binding the metal coordination center, are found at lower frequencies.

4. Supplementary material

Supplementary data have been deposited with the Cambridge Crystallographic Data Center, deposition numbers CCDC 137145, 137146 and 137147 for compounds **A**, **B** and **C**, respectively. Copies of this information may be obtained free of charge from: The Director, CCDC, 12 Union Road, Cambridge, CB2 1EZ, UK (Fax: +44-1223-336033; e-mail: deposit@ccdc.cam.ac.uk or www: http://www.ccdc.cam.ac.uk).

Acknowledgements

This work was supported by Italian MURST (COFIN 98) as part of the project 'Pharmacological and Diagnostic Properties of Metal Complexes' (Coordinator Professor G. Natile). We also thank D. Belletti, A. Cantoni and G. Pasquinelli for their valuable technical assistance.

References

[1] M. Belicchi Ferrari, G. Gasparri Fava, C. Pelizzi, P. Tarasconi, J. Chem. Soc., Dalton Trans. (1992) 2153.
[2] M. Belicchi Ferrari, G. Gasparri Fava, G. Pelosi, M.C. Rodriguez-Argüelles, P. Tarasconi, J. Chem. Soc., Dalton Trans. (1995) 3035.
[3] D.X. West, A.E. Liberta, S.B. Padhyè, R.C. Chikate, P.B. Sonawane, A.S. Kumbhar, R.G. Yerande, Coord. Chem. Rev. 49 (1993) 123.
[4] M. Belicchi Ferrari, G. Gasparri Fava, C. Pelizzi, P. Tarasconi, G. Tosi, J. Chem. Soc., Dalton Trans. (1989) 361.
[5] M. Belicchi Ferrari, A. Bonardi, G. Gasparri Fava, C. Pelizzi, P. Tarasconi, Inorg. Chim. Acta 223 (1994) 77 and references therein.
[6] M. Belicchi Ferrari, G. Gasparri Fava, M. Lanfranchi, C. Pelizzi, P. Tarasconi, Inorg. Chim. Acta 181 (1991) 253.
[7] J. Slouka.v., Pharmazie (Ber.) 15 (1960) 317.
[8] G.M. Sheldrick, SHELX-86, Crystallographic Computing 3, Oxford University Press, 1985.
[9] W.H. Zachariasen, Acta Crystallogr. 16 (1963) 1139.
[10] F. Ugozzoli, ABSORB, A Program for Walker and Stuart's absorption correction, University of Parma, 1983.
[11] International Tables for X-ray Crystallography, vol. 4, Kynoch Press, UK, 1974.
[12] M. Nardelli, Comput. Chem. 7 (1983) 95.
[13] C.K. Johnson, ORTEP, Rep. ORNL-3794, Oak Ridge National Laboratory, Oak Ridge, TN, 1965.
[14] W.D.S. Motherwell, PLUTO, University of Cambridge, 1976.
[15] R.J. Gillespie, J. Chem. Soc. (1963) 4672.
[16] M. Belicchi Ferrari, G. Gasparri Fava, C. Pelizzi, P. Tarasconi, G. Tosi, J. Chem. Soc., Dalton Trans. (1987) 227.
[17] M. Belicchi Ferrari, G. Gasparri Fava, M. Lanfranchi, C. Pelizzi, P. Tarasconi, J. Chem. Soc., Dalton Trans. (1991) 1951.
[18] M. Belicchi Ferrari, G. Gasparri Fava, P. Tarasconi, R. Albertini, S. Pinelli, R. Starcich, J. Inorg. Biochem. 53 (1994) 13.
[19] M.C. Rodriguez-Argüelles, M. Belicchi Ferrari, G. Gasparri Fava, C. Pelizzi, P. Tarasconi, R. Albertini, P.P. Dall'Aglio, P. Lunghi, S. Pinelli, J. Inorg. Biochem. 58 (1995) 157.
[20] B.Ya. Antosyak, V.N. Byushkin, N.I. Belichuk, T.I. Malinovskii, Dokl. Akad. Nauk. SSSR 273 (1983) 1375.

PERGAMON

www.elsevier.nl/locate/poly

Polyhedron 19 (2000) 1903–1907

POLYHEDRON

Synthesis, characterization of triamine complexes of nickel(II)selenocyanate and their thermally induced dimerization: X-ray single crystal structures of $[Ni(dpt)(SeCN)_2(H_2O)]$ and $[Ni(aepn)(SeCN)_2(H_2O)]$ (dpt = bis (3-aminopropyl)amine and aepn = (2-aminoethyl)(3-aminopropyl)amine)

Tapas K. Maji [a], Golam Mostafa [b], Partha S. Mukherjee [a], Arunendu Mondal [a], Alan J. Welch [c], Ken-ichi Okamoto [d], Nirmalendu Ray Chaudhuri [a,*]

[a] *Deparment of Inorganic Chemistry, Indian Association for the Cultivation of Science, Jadavpur, Calcutta 700 032, India*
[b] *Department of Physics, Krishnath College, Berhampur 742101, India*
[c] *Department of Chemistry, Heriot-Watt University, Edinburgh, EH14 4AS, UK*
[d] *Department of Chemistry, University of Tsukuba, Tsukuba, Ibaraki 305, Japan*

Received 22 March 2000; accepted 5 June 2000

Abstract

$[NiL(SeCN)_2(H_2O)]$ [L = bis(3-aminopropyl)amine (dpt), (**1**), (2-aminoethyl)(3-aminopropyl)amine (aepn), (**2**) and bis(2-aminoethyl)methylamine) (medien), (**3**)] have been synthesized and characterized in the solid state by X-ray single crystal analysis (**1** and **2**), IR, electronic spectra and magnetic measurement. Structure analyses of (**1**) and (**2**) reveal that the nickel(II) center is coordinated in a distorted octahedral fashion and the two SeCN groups are attached in *trans* position. Upon heating they undergo deaquation followed by color change, yielding dinuclear species bridging through selenocyanate. The deaquated dinuclear complexes have been characterized by IR, electronic spectra and magnetic susceptibility measurement. © 2000 Elsevier Science Ltd. All rights reserved.

Keywords: Nickel(II)selenocyanate; Bis(3-aminopropyl)amine; (2-Aminoethyl)(3-aminopropyl)amine; Bis(2-aminoethyl)methylamine; Thermochromism

1. Introduction

Exploitation of thiocyanate anion as bridging ligand between nickel(II) centers has attracted much attention from chemists in recent years. A large number of dinuclear and polynuclear nickel(II) amine complexes with thiocyanate anion have been structurally and magnetically characterized [1–5]. Recently this laboratory also reported [6,7] a number of interesting thiocyanato bridged dinuclear and polynuclear complexes of nickel(II) with linear chain triamine ligand. In contrast, the number of selenocyanate bridged complexes of Ni(II) is negligible in the literature [8,9] as (i) destabilization of selenocynate anion separating selenium and (ii) the weak affinity of selenium towards nickel(II), though Vicente et al. [9] reported first structurally and magnetically characterized bis(μ-selenocyanate) nickel(II) dinuclear compound, $(\mu\text{-}SeCN)_2[Ni(medpt)(SeCN)_2]_2$ where medpt = *N*,*N*-bis(3-aminopropyl)methylamine. This led us to pursue the chemistry of nickel(II) selenocyanate with other linear chain triamines in search of complexes having bridging selenocyanate. Here we report the synthesis and characterization of $[NiL(SeCN)_2(H_2O)]$ and, $(\mu\text{-}SeCN)_2[NiL(SeCN)_2]_2$ (where L = bis(3-aminopropyl)amine (dpt), (2-aminoethyl)(3-aminopropyl)-amine (aepn), and bis(2-aminoethyl)methylamine) (medien), and X-ray single crystal structures of $[Ni(dpt)(SeCN)_2(H_2O)]$ and $[Ni(aepn)(SeCN)_2(H_2O)]$.

* Corresponding author. Tel.: +91-33-473-4971; fax: +91-33-473-2805.
E-mail address: icnrc@mahendra.iacs.res.in (N. Ray Chaudhuri).

0277-5387/00/$ - see front matter © 2000 Elsevier Science Ltd. All rights reserved.
PII: S0277-5387(00)00478-2

2. Experimental

2.1. Materials

High purity bis(3-aminopropyl)amine (dpt), (2-aminoethyl)(3-aminopropyl)amine (aepn), bis(2-aminoethyl)methylamine (medien) and potassium selenocyanate were purchased from Aldrich Chemical Company Inc. and used as received. All other chemicals were AR grade.

2.2. Physical measurement

Elemental analyses (carbon, hydrogen, nitrogen) were performed using Perkin–Elmer 240C elemental analyzer and Ni(II) content was estimated gravimetrically [10]. IR spectra (4000–400 cm^{-1}) were taken at 27°C using Nicolet Magna-IR 750 spectrometer series -II, electronic spectra (1600–200 nm) at 27°C using a Hitachi UV–VIS–NIR model U-3410 spectrometer where Nujol was used as medium as well as reference. The magnetic susceptibility was measured at 27°C using an EG and G PAR155 vibrating sample magnetometer, where $Hg[Co(SCN)_4]$ was used as a reference material and diamagnetic correction was made by using Pascal's constants. Molar conductance was measured using a systronics 304 conductivity meter where the cell constant was calibrated with 0.02 M KCl solution and dry methanol was used as solvent. The thermal analysis (TG-DTA) was carried out on a Shimadzu DT-30 thermal analyzer in dynamic atmosphere of dinitrogen (flow rate, 30 cm^3 min^{-1}). The sample particle size was within 150–200 mesh.

2.3. Preparation of the complexes

2.3.1. *[Ni(dpt)(SeCN)$_2$(H$_2$O)] (blue) (**1**), [Ni(aepn)(SeCN)$_2$(H$_2$O)] (violet) (**2**) and [Ni(medien)(SeCN)$_2$(H$_2$O)] (sky blue) (**3**)*

An aqueous solution (5 cm^3) of triamine (1 mmol) was added dropwise with constant stirring to an aqueous solution (10 cm^3) of $Ni(ClO_4)_2{\cdot}6H_2O$ (0.365 g, 1 mmol). KSeCN (0.288 g, 2 mmol) dissolved in water (5 cm^3) was added slowly to it with stirring. The resulting mixture after filtration was kept in a $CaCl_2$ desiccator. After a few days desired complexes were separated, washed with chilled water and dried in a $CaCl_2$ desiccator. Yield: 80%. (Found (**1**): C, 22.9; H, 4.3; N, 16.8; Ni, 14.1%, $\mu_{eff} = 3.16$ BM; λ_{max} (nm) (Nujol) 480, 820, 1520; IR spectrum (cm^{-1}) in KBr: 3348 br (νO–H, νNH_2); 2088 (νCN); 733 ($\rho_r H_2O$), 626 ($\rho_w H_2O$). Calc. $C_8H_{19}N_5Se_2ONi$ (**1**) C, 22.9; H, 4.5; N, 16.7; Ni, 14.0%). (Found (**2**): C, 20.7; H, 4.3; N, 17.5; Ni, 14.3%, $\mu_{eff} = 3.07$ BM, λ_{max} (nm) (Nujol) 480, 820,1450; IR spectrum (cm^{-1}) in KBr:3250, 3311, 3422,br (νO–H, νNH_2); 2088 (νCN); 770 ($\rho_r H_2O$), 613 ($\rho_w H_2O$). Calc. $C_7H_{17}N_5Se_2ONi$ (**2**): C, 20.8; H, 4.2; N, 17.3; Ni, 14.5%.). (Found (**3**): C, 20.6; H, 4.3; N, 17.2; Ni, 14.5%, $\mu_{eff} = 3.23$ B.M, λ_{max} (nm) (Nujol) 570, 895,1580, IR spectrum (cm^{-1}) in KBr: 3237, 3332, 3400 br (νO–H, νNH_2); 2101 (νCN); 760 ($\rho_r H_2O$), 657 ($\rho_w H_2O$). Calc. $C_7H_{17}N_5Se_2ONi$ (**3**): C, 20.8; H, 4.2; N, 17.2; Ni, 14.7%).

2.3.2. *(μ-SeCN)$_2$[Ni(dpt)(SeCN)$_2$]$_2$ (violet) (**1a**), (μ-SeCN)$_2$[Ni(aepn)(SeCN)$_2$]$_2$ (bluish green) (**2a**) and (μ-SeCN)$_2$ [Ni(medien)(SeCN)$_2$]$_2$ (violet) (**3a**)*

These were synthesized in the solid state by careful temperature arrest technique at temperature $\sim$110, $\sim$150 and $\sim$140°C, respectively. (Found (**1a**): C, 24.04; H, 4.1; N, 17.3; Ni, 14.45%, $\mu_{eff} = 3.32$ BM; λ_{max} (nm) (Nujol) 490, 790, 1400; IR spectrum (cm^{-1}) in KBr: 3256, 3312 (νNH_2); 2072, 2119 (νCN). Calc. $C_8H_{17}N_5Se_2Ni$ (**1a**): C, 24.02; H, 4.35; N, 17.3; Ni, 14.68%). (Found (**2a**): C, 21.9; H, 4.0; N, 18.0; Ni, 14.3%, $\mu_{eff} = 3.12$ BM, λ_{max} (nm) (Nujol) 540, 890, 1570; IR spectrum (cm^{-1}) in KBr: 3251, 3309 (νNH_2); 2087, 2109 (νCN). Calc. $C_7H_{15}N_5Se_2Ni$ (**2a**): C, 21.78; H, 3.88; N, 18.15; Ni, 15.4%). (Found (**3a**): C, 21.5; H, 3.7; N, 18.3; Ni, 15.4%, $\mu_{eff} = 3.26$ BM, λ_{max} (nm) (Nujol) 580, 895,1550, IR spectrum (cm^{-1}) in KBr: 3236, 3270, 3332 (νNH_2); 2078, 2103 (νCN). Calc. $C_7H_{15}N_5Se_2Ni$ (**3a**): C, 21.78; H, 3.88; N, 18.15; Ni, 15.22%).

2.4. X-ray diffraction structural study

Single crystals suitable for X-ray analysis were obtained by recrystallization of **1** and **2** from water. A single crystal of complex **1** was mounted on a Rigaku/AFC 7 diffractometer, while the crystal of complex **2** was mounted on a Siemens P4 diffractometer. Lattice constants and orientation matrices were determined by least-squares refinement of the angular settings of 25 well-centred reflections. Crystal data collection and structure solution parameters for both the complexes are summarized in Table 1. Intensity data were collected using Mo Kα radiation ($\lambda = 0.7107$ Å) with ω–2θ scan mode for both the complexes. For both (**1**) and (**2**), the stability of crystals was measured during X-ray exposures by monitoring three standard reflections at a regular interval. The intensity data were corrected for Lorentz and Polarisation effects [11]. Both structures were solved by Patterson techniques followed by Fourier synthesis and refined through full matrix least-square calculations. Both the structures were analogous but the unsymmetrical molecule of complex **2** showed disorder about the twofold axis. As N3 atom of complex **2** occupied general position and the twofold axis passed through near N3 atom, both N3 and C4 showed symmetry imposed disorder. So their occupancy factors were taken as 0.5. Anisotropic refine-

ments were carried out for the non-hydrogen atoms. Hydrogen atoms on water oxygen were located from difference map for complex **1**, but were unsuccessful for complex **2**. The hydrogen atoms were introduced in the final structure-factor calculations at idealized position with fixed isotropic thermal parameters. Complex neutral atom scattering factors [12] were used throughout. All calculations were carried out using TEXSAN [13], PLATON-99 [14], and ZORTEP [15] programs for complex **1** and SHELXS-86 [16], SHELXL-93 [17], PLATON-99 [14] and ZORTEP [15] programs for complex **2**. Selected bond distances and bond angles are listed in Table 2.

Table 1
Crystal data and structure refinement for complexes **1** and **2**

	1	**2**
Chemical formula	$C_8H_{19}N_5NiOSe_2$	$C_7H_{17}N_5NiOSe_2$
Formula weight	417.88	403.88
Temperature (K)	293(2)	293(2)
Crystal system	orthorhombic	orthorhombic
Space group	*Pbcn*	*Pbcn*
Unit cell dimensions		
a (Å)	9.411(3)	8.7020(10)
b (Å)	10.532(2)	10.6600(10)
c (Å)	15.269(2)	14.950(2)
V (Å^3)	1513.3(9)	1386.8(3)
Z	4	4
D_{calc}	1.821	1.934
F(000)	820.00	792.00
Radiation (λ, Å)	Mo Kα 0.7107	Mo Kα 0.7107
Crystal size (mm)	$0.25\times0.25\times0.50$	$0.20\times0.40\times0.50$
θ Range (°)	2.2–27.5	3.0–25.0
Total data	1736	1470
Unique data	1736	1096
R_{int}	0.067	0.040
Observed data [$I>2\sigma(I)$]	987	945
Max. Δ	0.08	0.01
Estimated S.D.	0.01	0.00
δ_{max}	0.78	0.68
δ_{min}	−0.49	−0.95

Table 2
Selected bond lengths (Å) and bond angles (°) of complexes **1** and **2**

Ni–O	2.150(6)	2.101(5)
Ni–N1	2.094(6)	2.065(5)
Ni–N2	2.089(6)	2.102(5)
Ni–N3	2.100(7)	2.127(10)
N1–C1	1.136(8)	1.148(8)
Se–C1	1.790(6)	1.796(6)
O–Ni–N1	90.08 (15)	89.51(18)
N1–Ni–N2	90.8(2)	90.2(2)
N2–Ni–N3	93.85(18)	94.8(3)
Ni–N1–C1	158.4(5)	158.4(6)
Se–C1–N1	178.3(5)	177.2(5)

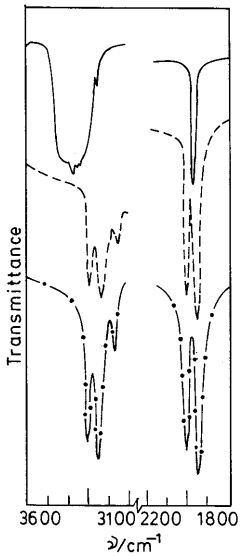


Fig. 1. IR-spectra (KBr) of [Ni(dpt)(SeCN)$_2$(H$_2$O)] (**1**) (——); (μ-SeCN)$_2$[Ni(dpt)(SeCN)$_2$]$_2$ (**1a**) (– – – –); and (μ-SeCN)$_2$[Ni(medpt)(SeCN)$_2$]$_2$ [9] (— · — · — · —).

3. Results and discussion

We obtained the complexes by having one molecule of water in case of other triamines, i.e. dpt, aepn and medien following the method of synthesis for (μ-SeCN)$_2$[Ni(medpt)(SeCN)$_2$]$_2$ (medpt = *N*,*N*-bis(3-aminopropyl)methylamine) adopted by Vicente et al. [9]. The IR-spectrum of the aquated species (**1**, **2** and **3**) shows broad band in the region 3200–3400 cm^{-1} (νOH, νNH$_2$) which is assumed to be due to the overlapping of νOH with νNH$_2$ band (Fig. 1). The presence of IR band ρ_r(H$_2$O) at ~800 cm^{-1} and ρ_w(H$_2$O) at ~645 cm^{-1} [18] suggests that the water molecule is coordinated to nickel(II). The complexes also exhibit IR bands (νCH$_2$, δNH$_2$, δCH$_2$) comparable to analogous system whose chelate character has been authenticated by X-ray single crystal structure analysis [6]. The single band for νCN at ~2100 cm^{-1} (Fig. 1) suggests that two SeCN groups are linked to Ni(II) in *trans* position [18]. The conductance datum shows that the complexes are nonelectrolyte. Above facts suggest that all aquated species are mononuclear and the nickel(II) is surrounded by one tridentate amine, two isoselenocyanate groups and one molecule of water having N$_5$O chromophore. The magnetic susceptibility and electronic spectral data are in good agreement with the octahedral geometry around nickel(II). It is to note that the slight difference in color amongst the aquated species reflected in electronic spectral band position has arisen due to the difference in the ligand field strength of the respective triamine.

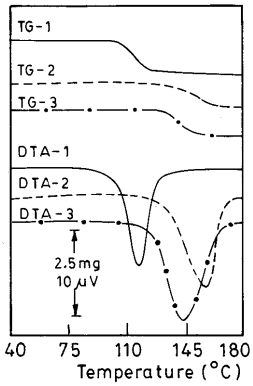


Fig. 2. TG-DTA curves: [Ni(dpt)(SeCN)$_2$(H$_2$O)] (**1**) (sample mass, 14.39 mg) (—); [Ni(aepn)(SeCN)$_2$(H$_2$O)] (**2**) (sample mass, 14.38 mg) (– – – –); and [Ni(medien)(SeCN)$_2$(H$_2$O)] (**3**) (sample mass, 11.2 mg) (— · — · —).

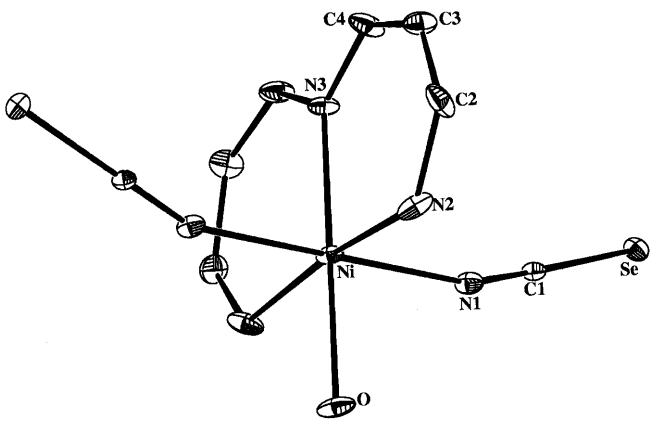


Fig. 3. ZORTEP diagram of [Ni(dpt)(SeCN)$_2$(H$_2$O)]. Ellipsoids are drawn at 50% probability.

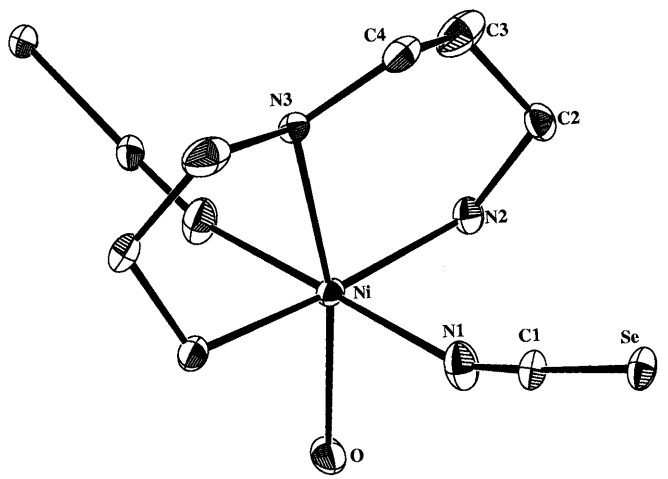


Fig. 4. ZORTEP diagram of [Ni(aepn)(SeCN)$_2$(H$_2$O)]. Ellipsoids are drawn at 50% probability.

*3.1. Molecular structures of [Ni(dpt)(SeCN)$_2$(H$_2$O)] (**1**) and [Ni(aepn)(SeCN)$_2$(H$_2$O)] (**2**)*

The structural analyses of **1** and **2** reveal that both the crystal structures consist of discrete mononuclear molecules. Crystal lattices are having same space group and almost same parameters. The only difference between them is the chain length of the triamine ligand. Molecular structure of the two complexes are similar and the ZORTEP diagrams are shown in Figs. 3 and 4. The selected bond distances and angles are tabulated in Table 2.

In both the complexes the coordination polyhedra around the metal centres are best described as distorted octahedron with N_5O chromophore. The distortion from ideal octahedral geometry is due to assymetric nature of the binding ligand and the deviations of the refine angles formed at the metal centres (Table 2) from 90°. Four nitrogen atoms (N1, N1*, N2, N2*) define as equatorial plane and the remaining one nitrogen atom (N3) and one oxygen atom (O) are in axial positions. The two SeCN ligands are *trans* to each other. Ni–N distances are in the range [2.065(5)–2.127(10) Å] which are consistent with corresponding values of analogous octahedrally coordinated nickel (II) complexes [6,7]. The bond angles between terminal nitrogen atoms (N2–Ni–N2*) are 172.3(3) and 174.69(17)° for complexes **1** and **2**, respectively. The angles between secondary nitrogen atom and aqua O-atom are 180.0(8)° for (**1**) and 168.4 (2)° for (**2**). The corresponding angles N1–Ni–N1* are 179.84(14)° for (**1**) and 179.0(3)° for (**2**). The mean plane of the four equatorial atoms passes through the Ni atom. The maximum deviations of Ni atom from the mean planes passed through four equatorial N atoms are 0.069 Å for (**1**) and 0.038 Å for (**2**). Thus the structural analyses corroborate the geometry proposed based on physicochemical studies.

The aquated species (**1**, **2** and **3**) upon careful (to inhibit selenium separation) heating undergo deaquation in the temperature range ~100–150°C (Fig. 2) and transform to respective deaquated species (**1a**, **2a** and **3a**) with visual color change. The deaquation temperature ranges also corroborate the presence of coordinated water molecule (vide infra). The deaquated species are stable in humid atmosphere (90% RH) but they revert on crystallization from boiling water. IR spectra show (i) the absence of bands responsible for water moiety; (ii) well resolved νNH_2 band; and (iii) the splitting of νCN band into two sharp peaks (Fig. 1). It is interesting to note that the IR spectral profile has unique resemblance to (μ-SeCN)$_2$[Ni(medpt)(SeCN)$_2$]$_2$ [9] (Fig. 1). The electronic spectral band position shifts also slightly corroborating the respective color of the deaquated species. We have calculated ratio ν_2/ν_1 (where ν_1 is assigned to $^3A_{2g} \rightarrow {}^3T_{2g}$ and the second main peak ν_2 to $^3A_{2g} \rightarrow {}^3T_{1g}$) bands which are found to

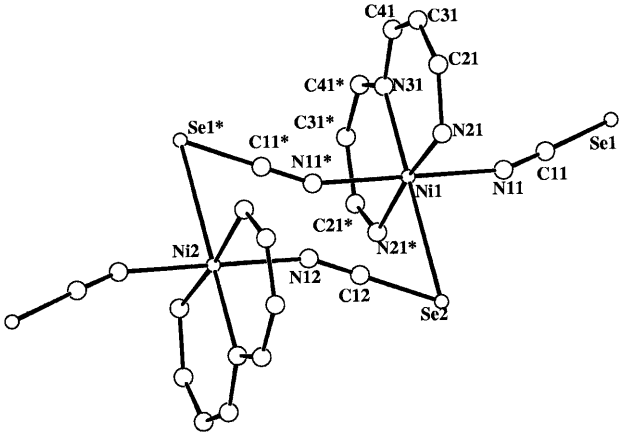


Fig. 5. Proposed ball and stick diagram of $(\mu\text{-SeCN})_2$-$[Ni(dpt)(SeCN)_2]_2$ (**1a**) (model structure is achieved after translating one of the two closest monomers in the unit cell of $[Ni(dpt)(SeCN)_2(H_2O)]$ (**1**) by -0.43, -0.59 and -0.33 (fractional) and keeping other monomer fixed).

be 1.77 (**1a**), 1.76 (**2a**) and 1.73 (**3a**) suggesting octahedral geometry [19] in them rather than penta coordinated species, if at all generated after deaquation. The magnetic susceptibility values also corroborate it. In order to satisfy the proposed geometry one of the SeCN groups must bridge the two nickel(II) centers resulting dinuclear species in them. We tried to prepare their single crystals but ultimately failed as they are not soluble in suitable solvents. As a result we propose the structure suggested by Vicente et al. [9] for the corresponding medpt complex. This tell us that the triamine, medpt in reaction with nickel(II) selenocyanate creates an unique environment which activates Se coordination which is rare in the literature. Whereas in the case of the other three triamines, Se coordination does not take place in aquated species but after withdrawal of the water moiety from the coordination sphere the environment suits Se coordination to nickel(II). The proposed model structure of dinuclear compound formed after deaquation is shown in Fig. 5.

4. Supplementary data

Supplementary data have been deposited with the Cambridge Crystallographic Data Centre, CCDC No. 141092 and 141093. Copies of this information can be obtained free of charge from The Director, CCDC, 12 Union Road, Cambridge, CB2 1EZ, UK (fax: +44-1223-336033; e-mail: deposit@ccdc.cam.ac.uk or www: http://www.ccdc.cam.ac.uk).

Acknowledgements

The authors thank the Council of Scientific and Industrial Research, New Delhi (grant to N.R.C.) for providing financial support.

References

[1] R. Vicente, A. Escuer, J. Ribas, X. Solans, J. Chem. Soc., Dalton Trans. (1994) 259.
[2] M. Monfort, C. Bastos, C. Diaz, J. Ribas, X. Solans, Inorg. Chim. Acta 218 (1994) 185.
[3] A. Escuer, R. Vicente, J. Ribas, M.S. El Fallah, X. Solans, M. Font-Bardia, Inorg. Chem. 32 (1993) 3727.
[4] A. Escuer, R. Vicente, J. Ribas, M.S. El Fallah, X. Solans, M. Font-Bardia, Inorg. Chim. Acta 216 (1994) 5.
[5] A. Escuer, S.B. Kumar, F. Mautner, R. Vicente, Inorg. Chim. Acta 269 (1998) 313.
[6] A. Mondal, C. Pariya, N. Ray Chaudhuri, N.P. Nayak, A.K. Mukherjee, A. Ghosh, Polyhedron 16 (1997) 39.
[7] A.K. Mukherjee, N.P. Nayak, A. Mondal, N. Ray Chaudhuri, Acta Crystallogr., Sect. C 55 (1999) 365.
[8] U. Turpeinen, Finn. Chem. Lett. (1997) 75.
[9] R. Vicente, A. Escuer, J. Ribas, X. Solans, M. Font-Bardia, Inorg. Chem. 32 (1993) 6117.
[10] A.I. Vogel, A Text Book Quantitative Inorganic Analysis, 4th ed., Longman, New York, 1978.
[11] A.C.T. North, D.C. Philips, F.S. Mathews, Acta Crystallogr., Sect. A 24 (1986) 351.
[12] International Tables for Crystallography, vol. C., Tables 4.2.6.8 and 6.1.1.4, 1992.
[13] TEXSAN crystal structure analysis package, Molecular Structure Corporation, Houston, TX, 1985, 1992.
[14] A.L. Spek, PLATON-99, molecular geometry program, University of Utrecht, The Netherlands, 1999.
[15] Zsolani, ZORTEP, a program for the presentation of thermal ellipsoids, University Heidelberg, Germany, 1994.
[16] G.M. Sheldrick, SHELXS-86, Program for the solution of crystal structure, University of Göttingen, Göttingen, Germany, 1985.
[17] G.M. Sheldrick, SHELXL-93, Program for the solution of crystal structure, University of Göttingen, Göttingen, Germany, 1993.
[18] K. Nakamoto, Infrared and Raman Spectra of Inorganic and Coordination Compounds, third ed., Wiley-Interscience, New York, 1978, p. 227 and 275.
[19] M. Nonoyama, Inorg. Chim. Acta 20 (1976) 53.

PERGAMON

www.elsevier.nl/locate/poly

Polyhedron 19 (2000) 1909–1915

POLYHEDRON

Dicopper(II) complexes of a phenolate-hinged ditopic ligand with solvent-derived ancillary ligands bound at the potentially dimetallic exogenous site

Pia Dalgaard [a], Alan Hazell [b], Christine J. McKenzie [a,*], Boujemaa Moubaraki [c], Keith S. Murray [c]

[a] *Department of Chemistry, University of Southern Denmark, Odense Campus, Campusvej 55, DK-5230 Odense M, Denmark*
[b] *Department of Chemistry, Aarhus University, DK-8000 Aarhus C, Denmark*
[c] *Department of Chemistry, Monash University, Clayton, Vic. 3800, Australia*

Received 14 April 2000; accepted 5 June 2000

Abstract

Copper complexes based on the $[Cu_2(bpbp)]^{3+}$ core (bpbp$^-$ = 2,6-bis((*N*,*N*′-bis-(2-picolyl)amino)methyl)-4-tertbutylphenolate) containing methoxide or water ancillary ligands, $[Cu_2(bpbp)(OCH_3)](ClO_4)_2$ (**1**), $[Cu_2(bpbp)(OH_2)_2](ClO_4)_3$ (**2**) and $Cu_2(bpbpH)(OH_2)_4(ClO_4)_4$ (**3**), were isolated from methanol–water solutions above pH 3, between pH 2–3, and below pH 2, respectively. ESR and magnetochemistry reveal that the copper ions are antiferromagnetically ($J = -156$ cm^{-1}) and weakly ferromagnetically ($J = +5.3$ cm^{-1}) coupled in the doubly-bridged **1** and its singly-bridged pseudo acid congener **2**, respectively. They are uncoupled in **3**, consistent with each copper atom being bound only by an amine and two pyridine donors of bpbpH and oxygen donors of water and/or perchlorate. Thus the phenol residue of the dinucleating ligand is protonated and uncoordinated. Further, the ESR spectra show that complexes **1**, **2** and **3** retain their integrity in solution. ESI mass spectra demonstrate that, as expected, the cations are labile in solution. However, the patterns that emerge support the formulations; numerous ions containing the $[Cu_2(bpbp)]^{3+}$ core plus water, hydroxide and methoxide ligands are observed. The intensities of the more protonated species increase in the spectra going from complex **1** to **3**. The only complex to give a molecular ion for the intact cation was **1**, and only from methanol solutions. However, the dominant ion observed in the mass spectra of **1** is $[Cu_2(bpbp)(OH)]^{2+}$ from all solvents tried. Thus in solution, the methoxide complex, **1**, is in equilibrium with the isoelectronic hydroxide complex, $[Cu_2(bpbp)(OH)](ClO_4)_2$, with the latter favored. Complex **1** was used to provide a labile preformed core for bridge replacement reactions, and the acetate and pyrazolate complexes, $[Cu_2(bpbp)(CH_3CO_2)](ClO_4)_2$ (**4**) and $[Cu_2(bpbp)(C_3H_3N_2)](ClO_4)_2$ (**5**), were prepared in this manner. © 2000 Elsevier Science Ltd. All rights reserved.

Keywords: Dicopper complexes; Solvent-derived ancillary ligands; Acid–base congeners

1. Introduction

Metal-solvent species are often proposed as labile intermediates in the reaction cycles of enzymes and catalysts, since solvent (usually water)-derived ligands can be replaced easily by incoming substrates. Water-derived species can also be reactants: coordinated hydroxide ligands are often proposed to be the nucleophilic hydroxides in hydrolytic enzymatic processes, e.g. in carbonic hydratase. The solid state characterisation of simple coordination compounds incorporating these motifs, i.e. weak solvent or hydroxide ligands, can be difficult due to (i) their lability; (ii) a necessity for extensive lattice water of crystallisation or (iii) their propensity for polymerisation reactions or carbonate formation. Dimetallic activation of substrates is a particular fascinating area and mechanisms for the dinuclear catalysis of hydrolysis reactions have been proposed for both enzymes and coordination complexes. For example, dipalladium systems are capable of high turnover catalysis in nitrile hydration reactions [1]. The crucial intermediate containing the

* Corresponding author. Tel.: +45-65-502-518; fax: +45-66-158-780.
E-mail address: chk@chem.sdu.dk (C.J. McKenzie).

0277-5387/00/$ - see front matter © 2000 Elsevier Science Ltd. All rights reserved.
PII: S0277-5387(00)00482-4

hydroxide nucleophile was proposed to contain the M–(HOH···OH)–M motif; however, this intermediate could not be isolated. This structural motif has now been crystallographically characterised in several dinuclear complexes [2], two of which promote hydrolysis reactions [2a,b]. Species containing this motif and related dimetallic/solvent motifs are likely to be relevant to dinuclear hydrolysis enzymes like phosphatases and urease in which two metal ions are within 4 Å of each other [3].

A study of the copper complexes of the acyclic phenolate-hinged dinucleating ligand 2,6-bis[(bis-(2-pyridylmethyl)amino)methyl]-4-tertbutylphenolato-(1−) (bpbp$^-$) [4] is described here, for which compounds with solvent ligands bound at the exogenous, potentially dimetallic, site have been isolated. Dicopper complexes of related dinucleating alkoxo- and phenoxo-hinged ligands containing exogenous oxo-acid bridging groups supporting the dimetallic structures are well-known. Complexes with solvent species are much rarer.

2. Experimental

IR spectra were measured as KBr discs using a Hitachi 270-30 IR spectrometer.

Electrospray ionization mass spectra (ESIMS) were obtained using a Finnigan TSQ 700 triple quadrupole instrument equipped with a Finnigan API source in the nanoelectrospray mode. Electron spin resonance (ESR) measurements at X-band frequency were obtained using a Bruker ESP-380E FT-EPR spectrometer. Elemental analyses were carried out at the microanalytical laboratory of the H.C. Ørsted Institute, Copenhagen. 2,6-Bis[(bis-(2-pyridylmethyl)amino)methyl]-4-tertbutylphenol (bpbpH) was prepared as described previously [4].

CAUTION! Although no problems were encountered in the preparation of the perchlorate salt, suitable care should be taken when handling such potentially hazardous compounds.

2.1. $[Cu_2(bpbp)(OCH_3)](ClO_4)_2$ (1)

$Cu(ClO_4)_2{\cdot}6H_2O$ (0.3639 g, 0.98 mmol) dissolved in methanol (5 ml) was added to bpbpH (0.2813 g, 0.49 mmol) dissolved in methanol (10 ml) to give a green–brown solution (pH 2). A suspension of $(NH_4)_2CO_3$ (0.102 g, 1.1 mmol) in methanol (15 ml) was added dropwise to give clear dark green solution (pH ~ 7). The mixture was filtered and dark green crystals of the title compound deposited. Yield 0.368 g (81%). Found: C, 46.71; H, 4.69; N, 8.71. *Anal.* Calc. for $C_{37}H_{42}N_6O_{10}Cl_2Cu_2{\cdot}0.72H_2O$: C, 46.94; H, 4.68; N, 8.88%.

2.2. $[Cu_2(bpbp)(H_2O)_2](ClO_4)_3{\cdot}H_2O$ (2)

$[Cu_2(bpbp)(OMe)](ClO_4)_2$ (31.7 mg, 0.0334 mmol) was dissolved in a warm water–acetone mixture (1:1, 5 ml). One drop of concentrated perchloric acid (0.02 g, 0.2 mmol) was added to give a brown solution (pH ≈ 2). On standing in an open vessel, long thin brown needles of the product were deposited. Yield 67%. Found: C, 41.23; H, 4.30; N, 7.79; Cl, 10.38. *Anal.* Calc. for $C_{36}H_{45}Cl_3Cu_2N_6O_{16}$: C, 41.13; H, 4.31; N, 7,99; Cl, 10.12%.

2.3. $Cu_2(bpbpH)(OH_2)_4(ClO_4)_4$ (3)

$[Cu_2(bpbp)(OMe)](ClO_4)_2$ (21.1 mg, 0.0223 mmol) was dissolved in 4 ml of warm acetone. Two drops of concentrated perchloric acid (0.04 g, 0.4 mmol) were added to give a blue solution (pH ≈ 1). On standing in an open vessel, blue crystals of the product were deposited. Yield 43%. Found: C, 36.80; H, 4.35; N, 7.19; Cl, 14.03. *Anal.* Calc. for $C_{36}H_{49}Cl_4Cu_2N_6O_{21}$: C, 36.93; H, 4.22; N, 7.18; Cl, 12.11%.

2.4. $[Cu_2(bpbp)(CH_3CO_2)](ClO_4)_2$ (4)

A solution of sodium acetate (87.7 mg, 1.07 mmol) and a single drop of concentrated perchloric acid in 10 ml of methanol was added to a solution of $[Cu_2(bpbp)(OMe)](ClO_4)_2$ (26.7 mg, 0.0282 mmol) dissolved in 5 ml of warm methanol to give a green solution (pH ~ 6). On standing in an open vessel, olive green crystals of the product were deposited. These were collected and washed with water. Yield 73%. Found: C, 47.40; H, 4.53; N, 8.68; Cl, 7.48. *Anal.* Calc. for $C_{38}H_{42}Cl_2Cu_2N_6O_{11}$: C, 47.70; H, 4.42; N, 8.77; Cl, 7.41%.

2.5. $[Cu_2(bpbp)(C_3H_3N_2)](ClO_4)_2$ (5)

Pyrazole (0.901 g, 13.43 mmol) was added to a suspension of $[Cu_2(bpbp)(OMe)](ClO_4)_2$ (68.7 mg, 0.0726 mmol) in methanol (20 ml). The solution became clear dark green on heating. On standing in an open vessel, olive green crystals of the product were deposited. These were collected and washed with methanol. Yield 48%. Found: C, 48.47; H, 4.41; N, 11.64; Cl, 7.48. *Anal.* Calc. for $C_{39}H_{42}Cl_2Cu_2N_8O_9$: C, 48.55; H, 4.39; N, 11.61; Cl, 7.35%.

2.6. X-ray crystal structure determination

The structure of **1** was determined with data measured at 120 K using an area detector [5], data were processed using SAINT [5] and XPREP [5]. Absorption corrections were made by integration using XPREP [5]. The structure was determined using SIR97 [6] and

Table 1
Crystal data and structure refinement details for **1**

Empirical formula	$C_{37}H_{43.44}N_6O_{10.72}Cl_2Cu_2$
M (g mol^{-1})	941.80
T (K)	120
Crystal system	monoclinic
Space group	$C2/c$
a (Å)	22.414(1)
b (Å)	16.1527(8)
c (Å)	22.236(1)
β (°)	91.160(1)
V (Å^3)	8049(1)
Z	8
μ (mm^{-1})	1.25
Reflections collected	32 113
Independent reflections	11 571
R_{int}	0.066
Observed reflections [$I>3\sigma(I)$]	6345
Parameters	530
$R(F)$	0.043
$wR(F)$	0.057

refined using the local modification of ORFLS [7] in the KRYSTAL [8] package. Non-hydrogen atoms were refined with anisotropic displacement parameters, hydrogen atoms of the ligands were kept fixed in calculated positions (C–H = 0.95 Å) and given isotropic displacement parameters 20% larger than those of the atoms to which they were attached. There were two waters of crystallization, one of the sites being only partially occupied, the hydrogen atoms for these were not included in the calculations. Atomic scattering factors were taken from Ref. [9]. Crystal data and details of the structure determinations are given in Table 1.

2.7. Magnetochemistry

A Quantum design MPMS5 Squid magnetometer was used to obtain magnetic susceptibility in a field of 1 T. Samples of mass ca. 20 mg were contained in a calibrated gelatine capsule, which was held in the centre of a plastic drinking straw fixed to the sample oval. The instrument was calibrated by use of a standard palladium sample supplied by Quantum Design Inc.

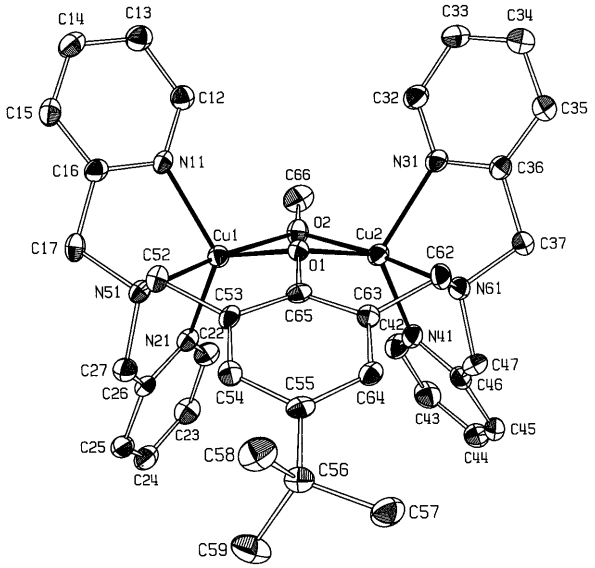
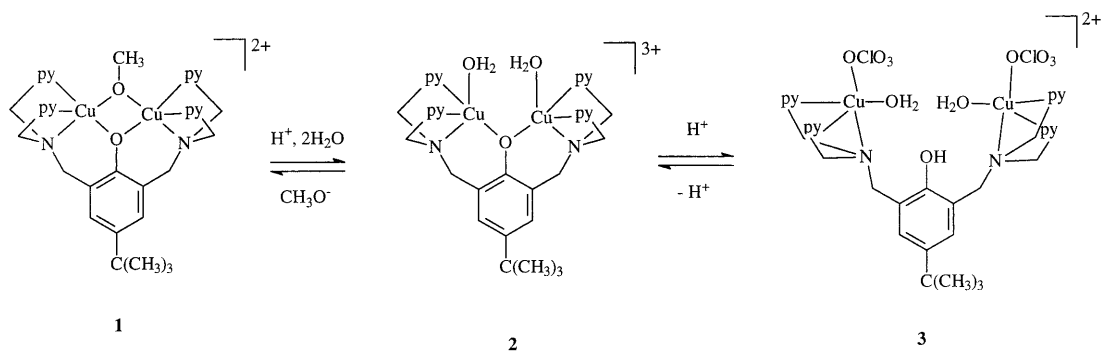


Fig. 1. Drawing of $[Cu_2(bpbp)(CH_3O)]^{2+}$ (**1**) showing the atom numbering scheme, thermal ellipsoids are drawn at the 50% probability level.

3. Results and discussion

The reaction of bpbpH with two equivalents of copper perchlorate in a methanol–water solvent system was investigated over a range of acid strengths, and three different crystalline dicopper complexes were recovered (Scheme 1). The green crystalline compound isolated above pH 3 is the methoxide complex, $[Cu_2(bpbp)(OCH_3)](ClO_4)_2$ (**1**), which is structurally analogous to $[Cu_2(bmbp)(OCH_3)](ClO_4)_2$ (bmbp$^-$ = 2,6-bis[(bis-(2-pyridylmethyl)amino)methyl]-4-methylphenolato(1−) [10]. The X-ray crystal structure of **1** is shown in Fig. 1. Selected distances and angles are shown in Table 2. The geometry about the copper atoms is trigonal bipyramidal, with the methoxide O atom and amine N atoms and each Cu atom defining the threefold axes; O2–Cu1–N51 = 172.2° and O2–Cu2–N61 = 172.9°. Cu–N distances are in the range 2.020(3)–2.089(3) Å, with the bonds to the amine N



Scheme 1.

atoms being the shorter than those to the pyridine N atoms, whereas they would normally be expected to be longer. Similarly the axial Cu–O(2) distances are about 0.1 Å shorter than the equatorial Cu–O(1) bonds. Attempts were made to obtain the hydroxide complex, $[Cu_2(bpbp)(OH)](ClO_4)_2$, which is isoelectronic with **1**, as a solid product. No solid compound could be isolated from aqueous solutions above pH 3 in the absence of methanol. At pH values between 2 and 3 a brown crystalline compound was isolated and formulated as the diaqua complex $[Cu_2(bpbp)(OH_2)_2](ClO_4)_3$ (**2**). This compound is the pseudo acid congener (protonation of the bridging methoxide and replacement by two terminal water ligands) of **1** (Scheme 1). Below pH 2 solutions are blue and a blue compound, formulated as $Cu_2(bpbpH)(OH_2)_4(ClO_4)_4$ (**3**), was obtained. It is proposed that the phenoxide hinge of the ligand is protonated and no longer coordinated to the copper atoms. The structure for the cation in **3** is depicted in Scheme 1 with a perchlorate and a water ligand on each copper ion. We believe this to be the most likely arrangement for the stoichiometry; however, this cannot be confirmed without a crystal structure analysis. Two terminal waters on each copper and uncoordinated perchlorate is a feasible alternative arrangement. However, the splitting of the perchlorate stretch in the IR spectrum of **3** compared with **1** and **2**, is consistent with the structural proposal in Scheme 1. Otherwise the IR spectra are of **1**, **2** and **3** are essentially indistinguishable. Also, ions in the ESI mass spectra provide circumstantial evidence for the presence of coordinated perchorates in **3**, since ions bearing two pechlorates were prevalent in the spectra of **3** and not in the spectra of **1** and **2**.

Table 2
Selected bond distances (Å) and angles (°) for **1**

Cu1–O1	2.068(2)	Cu2–O1	2.056(2)
Cu1–O2	1.923(3)	Cu2–O2	1.929(3)
Cu1–N11	2.064(3)	Cu2–N31	2.089(3)
Cu1–N21	2.024(3)	Cu2–N41	2.041(3)
Cu1–N51	2.022(3)	Cu2–N61	2.020(3)
Cu1–Cu2	3.002(1)		
O1–Cu1–O2	79.5(1)	O1–Cu2–O2	79.6(1)
O1–Cu1–N11	106.0(1)	O1–Cu2–N31	110.0(1)
O1–Cu1–N21	128.1(1)	O1–Cu2–N41	129.8(1)
O1–Cu1–N51	94.2(1)	O1–Cu2–N61	95.1(1)
O2–Cu1–N11	102.6(1)	O2–Cu2–N31	102.9(1)
O2–Cu1–N21	98.2(1)	O2–Cu2–N41	97.8(1)
O2–Cu1–N51	172.2(1)	O2–Cu2–N61	172.9(1)
N11–Cu1–N21	124.7(1)	N31–Cu2–N41	119.2(1)
N11–Cu1–N51	83.6(1)	N31–Cu2–N61	83.3(1)
N21–Cu1–N51	81.9(1)	N41–Cu2–N61	81.9(1)
Cu1–O1–Cu2	93.4(1)	Cu1–O2–Cu2	102.4(1)

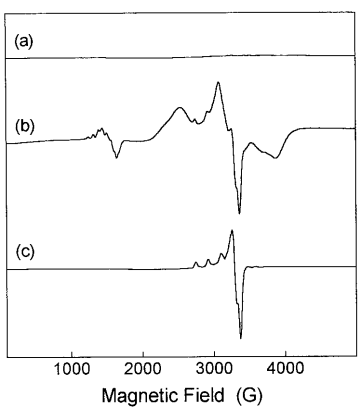


Fig. 2. The ESR spectra of (a) complex **1**; (b) complex **2**; (c) complex **3**, in a 9:1 methanol–water solution at 102 K.

Complex **1** was used to prepare 'bridge-substituted' products: the reaction of **1** with the acid forms of the potential 3-atom and 2-atom bridging groups, acetate and pyrazolate gave the compounds $[Cu_2(bpbp)(CH_3CO_2)](ClO_4)_2$ (**4**) and $[Cu_2(bpbp)(C_3H_3N_2)](ClO_4)_2$ (**5**). The methoxide/hydroxide leaving group is capable of deprotonating the incoming bridged ligands. This type of chemistry is well documented.

3.1. ESR and magnetic properties

ESR spectra and magnetic susceptibility measurements are consistent with the X-ray structure of **1** and the proposed structures of **2** and **3**. Fig. 2 shows the solution ESR spectrum of **1**, **2** and **3**, respectively, recorded in 9:1 methanol–water at 102 K. The ESR spectra obtained for neat powdered samples are slightly broader. No signal was observed for **1** (Fig. 2(a)) due to the strong intramolecular antiferromagnetic coupling. The ESR spectrum of **2** in Fig. 2(b) gave the first indication of a ferromagnetic coupling between the copper atoms of this complex. Signals at 'half field' (1500 G) are due to $\Delta M_s = 2$ transitions in the coupled $S = 1$ state, the frozen solution spectrum shows Cu hyperfine splitting [11]. The lines at 2700 and 3800 G are due to the $\Delta M_s = \pm 1$ transitions and the strong line at 3300 G is probably due to monomer impurity. The ESR spectrum of **3** in Fig. 2(c) shows an unperturbed axial signal consistent with non-interacting square-pyramidal copper atoms.

Magnetic susceptibility measurements on powdered samples show an interesting variation in the sign and size of exchange coupling in compounds **1**–**3**. Complex **1** is antiferromagnetically coupled (Fig. 3) with best fit parameter values obtained using a $-2J\bar{S}_1 \cdot \bar{S}_2$ Hamiltonian of $g = 2.03$, $J = -156\ cm^{-1}$, $N_\alpha = 60 \times 10^{-6}\ cm^3\ mol^{-1}$ and % monomer = 1%. In the figure it can be seen that a contaminating spin-coupled species, possibly the μ-OH bridged analogue (see also Ref. [10]) is present and gives rise to the humps in μ_{eff} between 30 and 120 K. The rapid increase in χ below 25 K (not

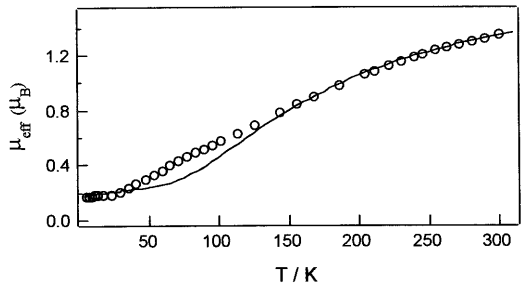


Fig. 3. Plots of magnetic moment (O) per Cu for complex **1**. The solid line shows the best fit for parameters (see text).

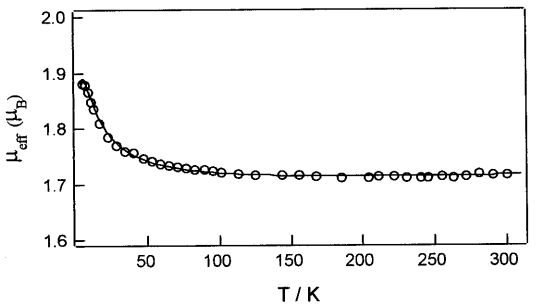


Fig. 4. Plots of magnetic moment (O) per Cu for complex **2**. The solid line shows the best fit for parameters (see text).

shown) is due to monomer impurity, a common phenomenon in such dinucleated systems.

There are a number of factors contributing to the medium sized negative J values obtained for **1**. The primary influence is the symmetry and disposition of the magnetic orbitals on each Cu centre in relation to the bridging phenoxide and methoxide oxygen orbitals. The Cu···Cu distance and Cu–O–Cu angles then play important roles, while effects such as steric strain around Cu and the trigonal planar versus pyramidal geometry around the phenolate oxygen atom play minor, but sometimes important roles. A review of {Cu(μ-*O*-alkoxo)$_2$Cu} [12] and {Cu(μ-*O*-alkoxo-μ-*O*-phenoxo)Cu} [13] systems in which the co-ligands allow non-strained square-pyramidal geometry around each Cu, show that very large negative J values are quite common, the compounds often approaching diamagnetic behaviour at room temperature ($J \geq -500$ cm^{-1}). Complex **1** has r(Cu···Cu) = 3.002(1) Å, Cu–O(CH$_3$)–Cu = 102.4(1)° and Cu–O(Ph)–Cu = 93.4(1)° and the sum of the angles around the phenoxo oxygen, O(1), is 337.9°, the pyramidal distortion arising through steric strain. As in [Cu$_2$(bmbp)(OCH$_3$)](ClO$_4$)$_2$ [10], the coordination geometry around Cu(1) and Cu(2) is closer to trigonal bipyramidal than to square pyramidal, with the apical ligands being OCH_3^- and N(amine), and the phenoxo O(1) bridging atom being in the trigonal plane. Thus, the Cu(1)d$_{z^2}$–O(2)–Cu(2)d$_{z^2}$ pathway will yield weaker antiferromagnetic coupling than in related Cu(1)d$_{x^2-y^2}$–O(2)–Cu(2)d$_{x^2-y^2}$ systems, and the Cu–O(Ph)–Cu pathway will contribute little to J, perhaps even a ferromagnetic contribution, vide infra. Nishida et al. [14] have shown that the bmbp$^-$ analogue of **4**, which has a longer r(Cu…Cu) value of 3.55 Å because of the acetate bridge, also has a lower than normal J value (-80 cm^{-1}), largely because of negligible overlap via the O(phenoxo).

Interestingly, complex **2**, which possesses only the O(phenoxo) bridge, shows weak ferromagnetic coupling, in agreement with the EPR triplet state spectrum. A characteristic increase in μ_{Cu} occurs at low temperature on account of thermal population of the $S = 1$ state (Fig. 4). The best fit parameters are $g = 1.95$, $J = +5.4$ cm^{-1}, $N_\alpha = 60 \times 10^{-6}$ cm^3 mol^{-1} and % monomer = 2%. It was found that inclusion of a small ϑ value of -0.2 K in to the $(T - \vartheta)$ term of susceptibility improved the fitting of the plateau in the μ_{eff} values noted below 6 K. This suggests some weak intermolecular effects are occurring in **2**. In the absence of a crystal structure, one can only speculate on the reason for weak ferromagnetic coupling in **2**. The related singly-bridged complex [Cu$_2$(bmbp)(Cl)$_2$](ClO$_4$) showed $J = 0$ cm^{-1} [14]. It is likely that **2** also has the O(phenoxo) bridge occupying the common apical positions of the square pyramidal chromophores adopted by each Cu. The lack of a methoxo bridge in **2** compared with **1** relieves the strain and allows a change in coordination geometry. We have observed more strongly antiferromagnetically coupled effects in other phenoxo-only bridged dinucleated complexes but in such cases the phenoxo oxygen provided good overlap with the Cud$_{x^2-y^2}$ orbitals [15].

Finally, complex **3** is uncoupled, as expected because of the lack of any endogenous bridging group.

3.2. Electrospray ionization mass spectrometry (ESI MS)

The labile complexes **1**, **2** and **3** give ESI mass spectra significantly more complicated than complexes **4** and **5**. Perusal of the species observed in spectra recorded in methanol (Table 3) support an increase in the state of protonation of ions in going from complex **1** to **3**. Hydroxide (and methoxide for **1**)-containing ions were observed as base peaks for complexes **1** and **2**, but not detected for **3**. Also, a tendency for ions bearing two perchlorates was seen in the spectra of **3**, suggesting a stronger association than ion pairing, i.e. coordination. Notably, dominant ions in the spectra of **3** include only one copper ion. Loss of copper is not unexpected from the protonated species **3**. The ESI mass spectra of methanol solutions of **1** show that the cation present in the solid state structure is observed only as a minor peak at m/z 364.1 along with [(bpbp)Cu$_2$(OH)]$^{2+}$ at m/z 357.1 as the major ion. Variation in source conditions show that the hydroxide ion is present in solution

Table 3
Distribution and intensity of ions in the ESI mass spectra of complexes **1**, **2** and **3**

m/z	Assignment	**1**	**2**	**3**
364.1	$(bpbp)Cu_2(OCH_3)]^{2+}$	20		
357.1	$(bpbp)Cu_2(OH)^{2+}$	100	100	
365.8	$(bpbp)Cu_2(OH)(H_2O)^{2+}$		75	
399.2	$(bpbp)Cu_2(ClO_4)^{2+}$		70	10
367.7	$(bpbpH)Cu(ClO_4)^{2+}$			100
815.3	$(bpbp)Cu_2(OH)(ClO_4)^{+}$	20		
833.3	$(bpbp)Cu_2(OH)(H_2O)(ClO_4)^{+}$		5	
897.3	$(bpbp)Cu_2(ClO_4)_2^{+}$		18	7
734.2	$(bpbpH)Cu(ClO_4)^{+}$			15
836.2	$(bpbpH)Cu(ClO_4)_2^{+}$			20
936.3	$(bpbpH_2)Cu(ClO_4)_2^{+}$			3

and not generated in the gas phase. The ESMS spectrum of **1** recorded in acetonitrile show no signal at the m/z value expected for $[(bpbp)Cu_2(OCH_3)]^{2+}$, rather the base peak is always at m/z 357.1 due to $[(bpbp)Cu_2(OH)]^{2+}$. This result suggests that the dominant solution species is the hydroxide complex, despite the fact that crystallization of a methoxide-bridged complex occurs in the presence of methanol. Crystal packing forces probably drive the crystallisation of a methoxide complex, despite the higher pK_a for methanol compared with water. Collision activation of the $[(bpbp)Cu_2(OCH_3)]^{2+}$ ion results in one daughter ion, $[Cu_2(bpbp)]^{2+}$ at m/z 348.5, which corresponds to the loss of neutral radical methoxide with concomitant reduction of a copper centre by one electron.

The ESI mass spectrum of the acetate complex **4** shows the expected cation $[Cu_2(bpbp)(CH_3CO_2)]^{2+}$, as the base peak at m/z 379.0 and its ion pair $[Cu_2(bpbp)(CH_3CO_2)](ClO_4)^{+}$ as the base peak at m/z 857.4. Also, isoelectronic species were detected; $[Cu_2(bpbp)(OH)]^{2+}$, $[Cu_2(bpbp)(OH)(H_2O)]^{2+}$, and $[Cu_2(bpbp)(OH)](ClO_4)]^{2+}$, demonstrating that there is a considerable exchange of the acetate ligand in solution. By contrast, the ESI mass spectrum of the less labile complex **5** is very simple by comparison with peaks for $[Cu_2(bpbp)(C_3H_3N_2)]^{2+}$ and its ion pair, $[Cu_2(bpbp)(C_3H_3N_2)](ClO_4)^{+}$ at m/z 382.1 and m/z 865.3, respectively.

4. Conclusions

Labile complexes with the $[Cu_2(bpbp)]^{2+}$ core and an ancillary methoxide ligand (antiferromagnetic green complex **1**) or two ancillary water ligands (ferromagnetic brown complex **2**) were isolated depending on the pH of reaction solutions. From acidic solutions below pH **2**, a blue dinuclear complex, **3**, in which the phenol group of the dinucleating is uncoordinated, is isolated and the magnetic properties confirm this arrangement. The series show an interesting variation in magnetic coupling between the copper ions, from antiferromagnetic for **1**, ferromagnetic for **2** and uncoupled for **3**. Complex **1** can be used for substitution reactions in which the methoxide is replaced by bridging groups. Unfortunately investigations into the possible biomimetic activity of these complexes in the promotion or catalysis of the hydrolysis of nitriles, amides and esters have not yielded observations of unusual reactivity.

5. Supplementary material

Supplementary data are available upon request from: The Director, CCDC, 12 Union Road, Cambridge, CB2 1EZ, UK (fax: +44-1223-336033; e-mail: deposit@ccdc.cam.ac.uk or www: http://www.ccdc.cam.ac.uk), quoting the deposition number CCDC-143540.

Acknowledgements

Support from the Danish Natural Science Council (grant No. 28808 to C.J.M.) and from the Carlsberg Foundation is acknowledged (A.H.). We are grateful to Jens Zacho Pederson for recording the ESR spectra.

References

[1] C.J. McKenzie, R. Robson, J. Chem. Soc., Chem. Commun. (1988) 112.
[2] (a) A. Hazell, K.B. Jensen, C.J. McKenzie, H. Toftlund, Inorg. Chem. 33 (1994) 3127. (b) E.C. Wilkinson, Y. Dong, L. Que Jr., J. Am. Chem. Soc. 116 (1994) 8394. (c) M. Ardon, A. Bino, K. Michelsen, J. Am. Chem. Soc.109 (1987) 1986. (d) F. Glasbøl, S. Larsen, B. Rasmussen, J. Springborg, Inorg. Chem. 25 (1986) 290. (e) M. Arden, A. Bino, Inorg. Chem. 24 (1985) 1343.
[3] (a) D.E. Wilcox, Chem. Rev. 96 (1996) 2435. N. Strater, W.N. Lipscomb, T. Klabunde, B. Krebs, Angew. Chem., Int. Ed. Engl. 35 (1996) 2024.
[4] M. Ghiladi, C.J. McKenzie, A. Meier, A.K. Powell, J. Ulstrup, S. Wocaldo, J. Chem. Soc., Dalton Trans. (1997) 4011.
[5] SMART, SAINT and XPREP, Area-Detector Control and Integration Software, Siemens Analytical X-ray Instruments Inc., Madison, WI, USA, 1995.
[6] G. Cascarano, A. Altomare, C. Giacovazzo, A. Guagliardi, A.G.G. Moliterni, D. Siliqi, M.C. Burla, G. Polidori, M. Camalli, Acta Crystallogr., Sect. A 52 (1996) C-79.
[7] W.R. Busing, K.O. Martin, H.A. Levy, ORFLS, Report ORNL-TM-305, Oak Ridge National Laboratory, TN, USA. 1962.
[8] A. Hazell, KRYSTAL, Aarhus University, Denmark, 1995.
[9] International Tables for X-ray Crystallography, vol. IV, Kynoch Press, Birmingham (present distributor, Kluwer, Dordrecht), 1974.

[10] J.J. Maloney, M. Glogowski, D.F. Rohrbach, F.L. Urbach, Inorg. Chim. Acta 127 (1987) L33.
[11] (a) J.R. Pilbrow, T.D. Smith, Coord. Chem. Rev. 13 (1974) 173. (b) A. Bencini, D. Gatteschi, EPR of Exchange Coupled Systems, Springer, New York, 1990.
[12] M. Melnik, Coord. Chem. Rev. 42 (1982) 259.
[13] W. Mazurek, K.J. Berry, K.S. Murray, M.J. O'Connor, M.R. Snow, A.G. Wedd, Inorg. Chem. 21 (1982) 3071.
[14] Y. Nishida, H. Shimo, H. Maehara, S. Kida, J. Chem. Soc., Dalton Trans. (1985) 1945.
[15] K. Bertoncello, G.D. Fallon, J.H. Hodgkin, K.S. Murray, Inorg. Chem. 27 (1988) 4750.

PERGAMON

www.elsevier.nl/locate/poly

Polyhedron 19 (2000) 1917–1923

POLYHEDRON

Spectroscopic and electrochemical investigations of the $K_8[P_2VMoW_{16}O_{62}]\cdot 31H_2O$ heteropolyoxometalate

L. David [a,*], Cora Crăciun [a], Mariana Rusu [b], O. Cozar [a], P. Ilea [b], D. Rusu [c]

[a] *Department of Physics, 'Babeş-Bolyai' University, 1, M. Kogalniceanu, 3400 Cluj-Napoca, Romania*
[b] *Department of Chemistry, 'Babeş-Bolyai' University, 3400 Cluj-Napoca, Romania*
[c] *Department of Chemical-Physics, Medical and Pharmacy University, 3400 Cluj-Napoca, Romania*

Received 25 February 2000; accepted 7 June 2000

Abstract

The $K_8[P_2VMoW_{16}O_{62}]\cdot 31H_2O$ heteropolyoxometalate complex was synthesized and investigated by electrochemistry measurements and IR, UV–Vis and EPR spectroscopy. The substitution of one $W{=}O_d$ unit by the VO^{2+} group was inferred from the shift of the $\nu_{as}(M{=}O_{a,d})$ and $\nu_{as}(M{-}O_{b,c}{-}M)$ vibrational bands (M = W, Mo) and the appearance of $\nu_{as}(V{=}O_d) \approx 960\ cm^{-1}$ vibration in the IR spectrum of the complex and from the electrochemistry studies. The three transitions in the electronic spectra were assigned to $^2B_2 \rightarrow {}^2E$ (13 700 cm^{-1}), $^2B_2 \rightarrow {}^2B_1$ (16 490 cm^{-1}) and $^2B_2 \rightarrow {}^2A_1$ (23 140 cm^{-1}), indicating a six coordination of the vanadium(IV) ion in an axial C_{4v} environment. EPR spectrum of the complex obtained at room temperature shows resolved hyperfine features in the parallel and perpendicular regions typical for monomeric V^{4+} ion. EPR parameters ($g_{\|} = 1.940$, $g_{\perp} = 1.982$, $A_{\|} = 178.5$, $A_{\perp} = 62.9$ G) and the values of LCAO–MO coefficients ($\beta_1^2 = 0.863$, $\beta_2^2 = 0.875$ and $\beta_3^2 = 0.935$) correspond to a dominant ionic character of the σ and π V–O bondings and to an important delocalization of the electrons towards the $O_{b,c}$ atoms. © 2000 Elsevier Science Ltd. All rights reserved.

Keywords: Vanadium; Molybdenum; Heteropolyoxometalate; IR spectroscopy; UV–Vis spectroscopy; EPR spectroscopy

1. Introduction

Heteropolyoxometalates (HPOM) are intensely studied for their use in catalysis, biology and materials science. When these polyanions contain vanadium and molybdenum atoms near the tungsten and oxygen atoms, they exhibit important catalytic activities for redox reactions [1]. In this paper we investigate the $K_8[P_2VMoW_{16}O_{62}]\cdot 31H_2O$ complex by electrochemical and spectroscopic methods. This complex has an α-Dawson–Wells structure [1,2] with one tungsten atom substituted by one easier molybdenum atom and another tungsten atom replaced by one vanadium ion (Fig. 1). The two phosphorus atoms are tetrahedrally coordinated in the center of the investigated heteropolyoxometalate complex.

Usually, the oxygen atoms of α-Dawson–Wells structure coordinate octahedrally the vanadium and molybdenum ions, similarly to the fundamental WO_6 units [3,4]. The MoO_6 and VO_6 substitute WO_6 octahedra in a 6W belt or in a 3W cap regions of the α-Dawson–Wells structure [3]. On the other hand, these could be in the vicinity, sharing a corner oxygen atom or an edge, or could be nonadjacent. Previous studies revealed the affinity of the molybdenum ion to coordinate in the 'cap' region [3,5] and the affinity of vanadyl ions for the 'belt' region of the complex [5]. Also, the vanadium ion is more easily reducible (to V^{4+}) compared to molybdenum ion (to Mo^{5+}) [6]. The electron trapped on the vanadium ion is slightly delocalized, more into the V–O–Mo bond than into the V–O–W bond [7].

2. Experimental

2.1. Synthesis of $K_8[P_2VMoW_{16}O_{62}]\cdot 31H_2O$ complex

A solution of 0.163 g (1 mmol) of $VOSO_4$ in 20 ml acetate buffer was added to 4.81 g (1 mmol) of

* Corresponding author. Fax: +40-64-191906.
E-mail address: leodavid@phys.ubbcluj.ro (L. David).

0277-5387/00/$ - see front matter © 2000 Elsevier Science Ltd. All rights reserved.
PII: S0277-5387(00)00448-4

$K_{10}[P_2MoW_{16}O_{61}]\cdot 19H_2O$ (obtained as described in [8]) in 50 ml acetate buffer solution (pH 4.7) at 60–70°C, under vigorous stirring for 1 h. After cooling at room temperature (r.t.), KCl saturated solution was added to blue polyoxometalate complex solution.

The dark blue precipitate was collected on a medium frit, dried for 30 min under vacuum, washed with saturated KCl solution and dried again under vacuum. The chemical analysis was carried out by atomic absorption methods after the complex decomposition by boiling with 6 M NaOH solution. The chemical analysis data are: *Anal*. Calc.: H_2O, 11.14; K, 6.21; Mo, 1.95;P, 1.24; V, 1.02; W, 58.68%. Found: H_2O, 11.05; K, 6.16; Mo, 1.87; P, 1.26; V, 1.00; W, 58.42%.

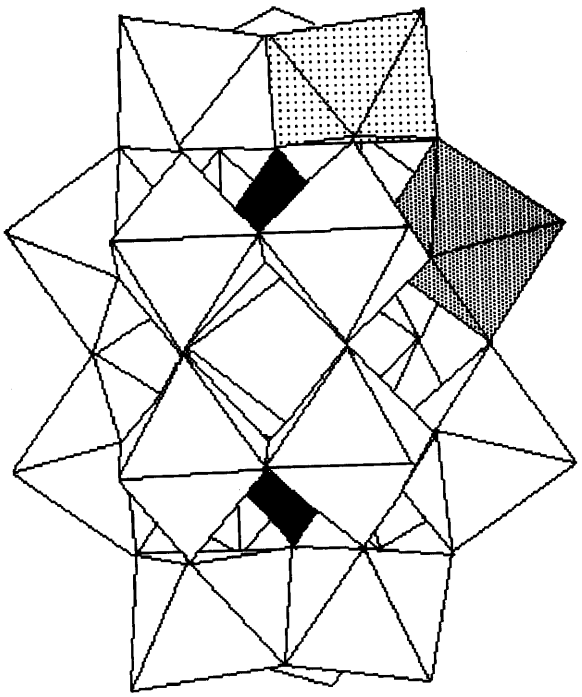


Fig. 1. The structure of the $K_8[P_2VMoW_{16}O_{62}]\cdot 31H_2O$ heteropolyoxometalate (Shaded octahedron in the 'belt' position represents VO_6 site. Pointed octahedron in the 'cap' position represents the MoO_6 site).

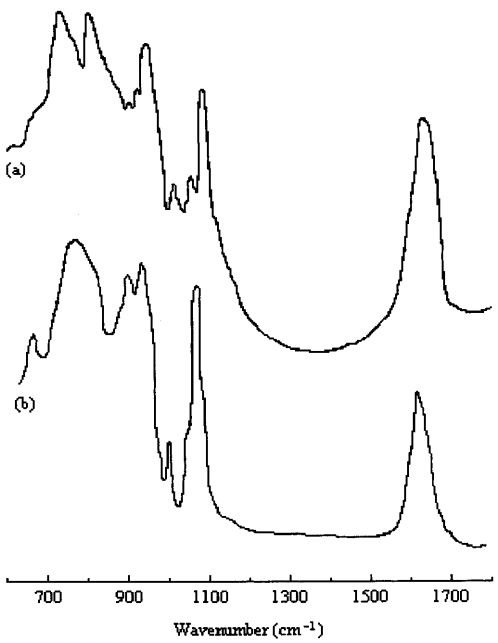


Fig. 2. IR spectra of the ligand (a) and vanadium–HPOM complex (b).

2.2. Physical measurements

UV and visible electronic spectra were performed in $\lambda = 200$–800 nm range in aqueous solutions, using a standard Specord UV–Vis spectrometer. IR spectra were obtained in KBr pellets in the 4000–400 cm^{-1} range with a Carl Zeiss Jena model UR-20 spectrophotometer. Cyclic voltammetry experiments were performed using a computer-controlled potentiostat AUTOLAB 10. A conventional three-electrode cell was used. The working electrode (WE) was a vitreous carbon disk ($\phi = 3$ mm), the reference electrode was a saturated calomel electrode (SCE, $\varepsilon^0 = 0.244$ V NHE) and the counter electrode was a platinum plate ($S = 1$ cm^2). The WE was polished before use on abrasive paper 1200, followed with a paste of Al_2O_3 (Struers, Denmark). The electrolyte solutions were prepared from distilled water and heteropolyoxometalates. All measurements were performed in phosphates buffer at pH 3. EPR measurements were performed at 9.4 GHz (X band) using a standard JEOL-JES-3B equipment at r.t.

3. Results and discussion

3.1. IR spectra

By compairing the IR frequencies of the monolacunary $K_{10}[P_2MoW_{16}O_{61}]\cdot 19H_2O$ ligand with those of the vanadium–polyoxometalate complex, we have obtained information concerning the coordination of the vanadium ion at the polyoxometalate. Fig. 2 presents the main part of the IR spectra and the most important IR absorption bands and their assignments are shown in Table 1.

The shoulder at ≈ 960 cm^{-1} in the IR spectrum of the complex is due to the stretching vibration of a vanadyl group, whose oxygen is a terminal atom [7,9].

The bands of the $\nu_{as}(W{=}O_d)$ and $\nu_{as}(Mo{=}O_d)$ strechings vibrations [10] are supperposed in the IR spectrum of the ligand. One of the two shoulders (at 910 cm^{-1})

Table 1
Some IR bands (cm^{-1}) of the ligand and vanadium–HPOM complex [a]

Band	Ligand (cm^{-1})	V(IV)–HPOM (cm^{-1})
$\nu(H_2O)$	3500 (s,b)	3470 (s,b)
		3570 (s,b)
δ(H–O–H)	1643 (m,sp)	1620 (m,sp)
ν_{as}(P–O_a)	1082 (s,sp)	1080 (s,sp)
	1064 (m,sp)	1060 (m,sh)
	1021 (m,sh)	1015 (m,sp)
	1054 (m,sh)	
ν_{as}(V=O_d)		960 (m,sh)
ν_{as}(W=O_d) + ν_{as}(Mo=O_d)	945 (s,sp)	945 (s,sp)
	923 (m,sp)	910 (s,sp)
ν_{as}(W–O_c–W)	895 (m,sp)	890 (m,sh)
ν_{as}(W–O_b–W)	807 (s,b)	795 (s,b)
	839 (m,sh)	840 (s,sh)
ν_{as}(W–O_a)	730 (s,sp)	745 (m,sh)
ν_{as}(O–W–O)	677 (m,sh)	685 (m,b)
ν_{as}(P–O–W)	603 (w,b)	603 (w,sp)
	586 (w,sp)	565 (w,sp)

[a] w, weak; m, medium; s, strong; sh, shoulder; b, broad; sp, sharp; vs, very strong; vw, very weak.

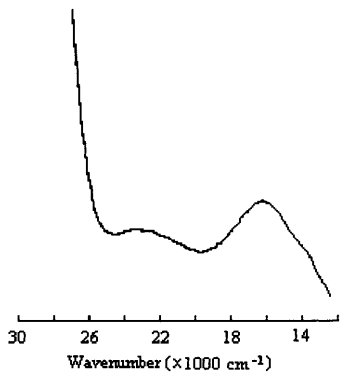


Fig. 3. Visible electronic spectra of the vanadium–HPOM complex in 10^{-2} mol l^{-1} aqueous solution.

is red-shifted with ~ 13 cm^{-1} due to the coordination of the vanadyl group at the polyoxometalate [11].

In the IR spectrum of the complex the streching vibration of the tricentric W–O_c–W bonds of the edge-sharing WO_6 octahedra [12] appears as shoulder and is shifted with 5 cm^{-1} to lower frequencies than the corresponding value in the IR spectrum of the ligand.

Due to the coordination of the vanadium ion at O_a and O_b atoms, the shape of the spectra is modified in the 700–850 cm^{-1} region [13]. IR spectrum of the monolacunary ligand presents two distinct bands, one at 807 cm^{-1} (with a shoulder at 839 cm^{-1}) assigned to ν_{as}(W–O_b–W) vibration and another at 730 cm^{-1} corresponding to ν_{as}(W–O_a) vibration, while in the IR spectrum of the complex there is only a broad band with some features at 840, 795 and 745 cm^{-1}.

The frequency of the ν_{as}(W–O_a) vibration is shifted with 15 cm^{-1} to smaller frequencies in the IR spectrum of the complex. This is due to the coordination of the vanadyl group at the ligand which also affects the neighboring octahedra of the structure [14].

The WO_6 octahedra from the equatorial regions have three O_b atoms and one O_c, O_a and O_d atom, while the WO_6 octahedra from the polar regions have two O_b, two O_c, one O_a and one O_d atoms. The value of the ν_{as}(W–O_b–W) vibration and the shape of its band are more affected by the vanadium coordination than those of ν_{as}(W–O_c–W) vibration. We conclude that the vanadium ion coordinates in the region with more O_b atoms (the equatorial region) of the α-Dawson–Wells structure.

The three absorption bands assigned to ν_{as}(P–O_a) vibrations [7,15] correspond to distorted PO_4 tetrahedra whose symmetry decreases to C_s. These frequencies are red-shifted with 2–6 cm^{-1} comparatively to the ligand spectrum. The shoulder at ≈ 1054 cm^{-1} arrises from the nonequivalent character of the two PO_4 distorted tetrahedra [16]. The shifts of the ν_{as}(P–O_a) frequencies and the lowering of the local symmetry around the phosphorus atoms are due to the vanadium coordination at O_a type atoms.

The frequency of the deformation band of the water molecules changes because of the raising of basic character of the O_d atom bounded to the vanadium ion [17]. The terminal O_d oxygen could be involved in hydrogen bonds with the neighbouring water molecules [18]. This fact is confirmed by the shape of the ν_{as}(OH) vibration band, which spreads in the 3100–3700 cm^{-1} range and presents two separate shoulders, at 3460 and 3570 cm^{-1}, respectively. The first shoulder, which is also less intense, corresponds to the coordination water involved in hydrogen bonds, while the other is due to the crystalization water.

The IR spectrum of vanadium–HPOM complex indicates the coordination of the vanadyl ion at O_a, O_b and O_c type oxygen atoms, in the equatorial region of Dawson–Wells structure.

3.2. Electronic spectra

The visible electronic spectrum of the complex in aqueous solution (Fig. 3) presents typical absorptions for vanadium(IV) ion in C_{4v} local symmetry [19,20]. In terms of the Ballhausen and Gray molecular orbital theory [21], these bands can be assigned to the transitions indicated in Table 2 and are consistent with the $d_{xy} < d_{xz,yz} < d_{x^2-y^2} < d_{z^2}$ energetical orbital ordering [22].

The absorption band centered at $\approx 13\,700$ cm^{-1} is due to the transition into V=O_d double bond. The second absorption band ($\approx 16\,490$ cm^{-1}) is a measure of the nonaxial ligand field strength. The smaller value

comparative to the other vanadium–HPOM complexes [19] indicates the presence of one important ligand field in the oxy plane (ortogonal to V=O_d direction).

For the assignment of the band centered at $\approx 23\ 140\ cm^{-1}$, there are two posibilities: this can arise from a $d_{xy} \rightarrow d_{z^2}$ transition [22] or can be a heteronuclear charge-transfer transition ($V^{4+} \rightarrow W^{6+}$, Mo^{6+}) [23]. For some vanadium–heteropolyoxometalates, M.T. Pope [24] and E. Cadot [19] have assigned the bands at $\approx 20\ 000$ and $\approx 25\ 000\ cm^{-1}$ to the charge-transfer transitions, owing to their important intensity comparative to d–d transitions. Because in the present case the absorption at $\approx 23\ 140\ cm^{-1}$ is less intense than the other two bands and also than the charge-transfer band appearing up to $25\ 000\ cm^{-1}$ (responsible for the intense colour of the anion), we attribute this band to a d–d transition [25].

The UV electronic spectra of the vanadium complex and of the ligand are similar in shape and number of bands (Fig. 4). The band centered at $47\ 040\ cm^{-1}$ in the ligand spectrum is assigned to p_π–d_π transitions into the W=O and Mo=O bonds [26]. The shift of the maximum of this band for the complex is due to the distortions introduced by the weaker vanadium(IV) ion into its neighbouring MO_6 octahedra (M = W, Mo).

Table 2
UV–Vis spectral features (cm^{-1}) of the vanadium–HPOM complex [a]

Electronic transition	ν (cm^{-1})
$^2B_2(d_{xy}) \rightarrow {}^2E(d_{xz,yz})$	13700 (sh)
$^2B_2(d_{xy}) \rightarrow {}^2B_1(d_{x^2-y^2})$	16490 (s)
$^2B_2(d_{xy}) \rightarrow {}^2A_1(d_{z^2})$	23140 (m)
$d_\pi \rightarrow p_\pi \rightarrow d_\pi$ (M–O–M′)	34000 (m)
$p_\pi \rightarrow d_\pi$(M=O)	47440 (s)

[a] sh, shoulder; s, strong; m, medium.

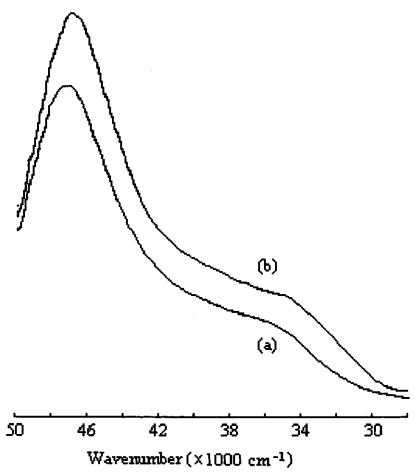


Fig. 4. UV spectra of the ligand (a) and vanadium–HPOM complex (b) obtained in 5×10^{-5} mol l^{-1} aqueous solution.

The broad bands centered at $\approx 34\ 040\ cm^{-1}$ for the ligand and at $\approx 34\ 000\ cm^{-1}$ for the complex (Fig. 4) are due to electron transition between the energetic levels of the M–O–M′ tricentric bonds (M, M′ = Mo, W) [27]. The two shoulders arrising from different M–O–M′ bonds are more resolved in the vanadium complex spectrum.

3.3. Electrochemistry

To establish the electrochemical behaviour of the $K_8[P_2VMoW_{16}O_{62}]\cdot 31H_2O$ heteropolyoxometalate, the cyclic voltammograms of the heteropolyanions: α_2-$[P_2W_{17}O_{61}]^{10-}$ (abbreviated P_2W_{17}), α_2-$[P_2MoW_{16}O_{61}]^{10-}$ (abbreviated P_2MoW_{16}) and α_2-$[P_2VMoW_{16}O_{62}]^{8-}$ (abbreviated P_2VMoW_{16}) were performed at different potential scan rates (Fig. 5).

The four pairs of peaks in the case of voltammograms obtained for P_2W_{17} (Fig. 5a) showed clearly three reduction reversible processes (peaks I, II, and III) confirmed by a linear dependence between the peak current (I_{pc}) logarithm and the scan rate logarithm, and by the fact that the peak potentials are independent of scan rates. In the case of peak IV, the behaviour is less clear due to the fact that the maximum corresponding to anodic peak is in cathodic current range. For the four pairs of peaks the charge transfer and protonation reactions are the same with those confirmed by literature [28–31]:

$$\alpha_2\text{-}[P_2W_{17}O_{61}]^{10-} + 1e^- \rightarrow \alpha_2\text{-}[P_2W_{16}W^{5+}O_{61}]^{11-} \text{ (peak I)} \quad (1)$$

$$\alpha_2\text{-}[P_2W_{16}^{6+}W^{5+}O_{61}]^{11-} + 1e^- \rightarrow \alpha_2\text{-}[P_2W_{15}^{6+}W_2^{5+}O_{61}]^{12-} \text{ (peak II)} \quad (2)$$

$$\alpha_2\text{-}[P_2W_{15}^{6+}W_2^{5+}O_{61}]^{12-} + 2e^- + 2H^+ \rightarrow \alpha_2\text{-}[H_2P_2W_{15}^{6+}W_2^{5+}O_{61}]^{12-} \text{ (peak III)} \quad (3)$$

$$\alpha_2\text{-}[H_2P_2W_{15}^{6+}W_2^{5+}O_{61}]^{12-} + 2e^- + 2H^+ \rightarrow \alpha_2\text{-}[H_4P_2W_{15}^{6+}W_2^{5+}O_{61}]^{12-} \text{ (peak IV)} \quad (4)$$

The voltammetric behaviour of the compound P_2MoW_{16} (Fig. 5b) is similar to that of the P_2W_{17} anion but the peak for Mo^{6+}–Mo^{5+} appears at a potential about +0.2 V SCE and the corresponding reaction is:

$$\alpha_2\text{-}[P_2Mo^{6+}W_{16}^{6+}O_{61}]^{10-} + 1e^- \rightarrow \alpha_2\text{-}[P_2Mo^{5+}W_{16}^{6+}O_{61}]^{11-} \quad (5)$$

For the P_2VMoW_{16} compound (Fig. 5c) a new peak for the V^{5+}–V^{4+} appears at +0.36 V SCE and the corresponding reaction is:

$$\alpha_2\text{-}[P_2V^{5+}Mo^{6+}W_{16}^{6+}O_{62}]^{7-} + 1e^- \rightarrow \alpha_2\text{-}[P_2V^{4+}Mo^{6+}W_{16}^{6+}O_{62}]^{8-} \quad (6)$$

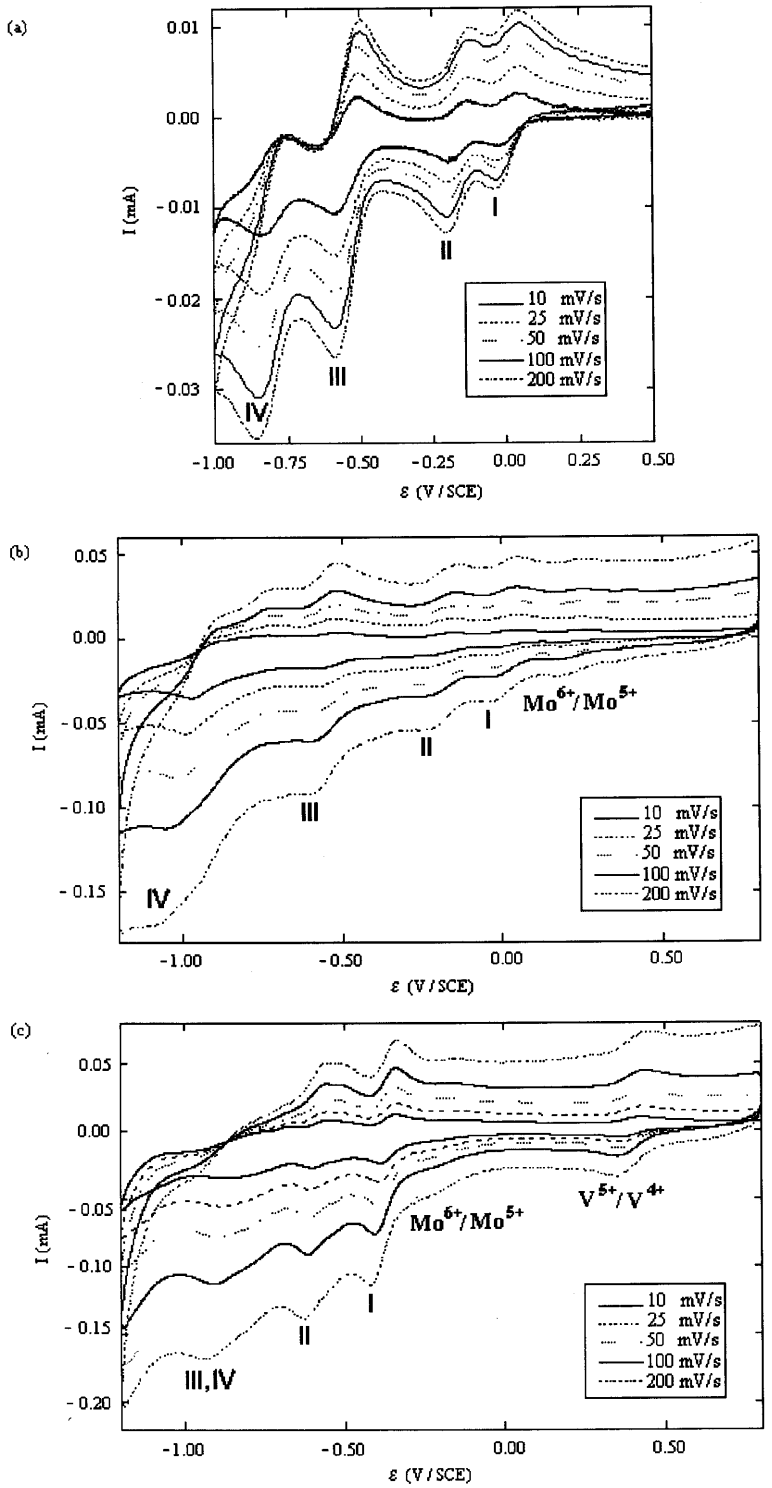


Fig. 5. Experimental cyclic voltammograms of 10^{-3} M $K_{10}P_2W_{17}O_{61}$ (a), 2×10^{-3} M $K_{10}P_2MoW_{16}O_{61}$ (b) and 2×10^{-3} M $K_8P_2VMoW_{16}O_{62}$ (c) complexes at different scan rates at pH 3.

Our results are in good agreement with those proposed by Pope [32]. Both iso and heteropolyoxometalates containing vanadium, molybdenum or tungsten shows the ability to form reduced species only when the metal atom is coordinated by the oxygen terminal atom. The presence of the three cations (vanadium, molybdenum and tungsten) in the same polyoxometalate structure leads first to electrochemical reductions of

vanadium (V^{5+}), this being more easy reducible, then to that of molybdenum (Mo^{6+}) and finally to that of tungsten (W^{6+}) [33,34].

Voltammetric study of P_2VMoW_{16} in acid media showed the modification of the electrochemical behaviour compared with that of the P_2W_{17} anion because of the vanadium and molybdenum addenda presence.

The electrochemical signal of vanadium is very distinct and creates favorable views for using it as a redox mediator for electrochemical polyoxometalate modified electrodes.

3.4. EPR spectra

The powder EPR spectrum of the complex recorded at r.t. (Fig. 6, normal line) is typical for mononuclear oxovanadium species in an axial environment. This spectrum can be described by an axial spin Hamiltonian for a d^1 system Eq. (7) [27]:

$$H = \beta[g_{\|}B_zS_z + g_{\perp}(B_xS_x + B_yS_y)] + A_{\|}S_zI_z + A_{\perp}(S_xI_x + S_yI_y) \quad (7)$$

The spectrum exhibits eight components, both in the perpendicular and in the parallel bands, due to the metallic hyperfine coupling of the electron spin with the nuclear spin ($I = 7/2$) of the 99.75% natural abundant ^{51}V isotope. The absence of Mo^{5+} and W^{5+} EPR signals confirms that all the molybdenum and tungsten atoms are in the $+6$ oxidation state [35]. The best fitting simulated EPR parameters are: $g_{\|} = 1.940$, $g_{\perp} = 1.982$, $A_{\|} = 178.5$, $A_{\perp} = 62.9$ G, with the line widths $\Delta B_{pp}(\|) = 52$ and $\Delta B_{pp}(\perp) = 38$ G in the parallel and perpendicular bands, respectively. The principal axis of g and A tensors have been presumed coincident, with the $g_{\|}$ and $A_{\|}$ directions parallel to the V=O_d bond. Differences between the experimental and simulated spectra indicate a small rhombic distortion of the VO_6 octahedron.

The electronic ground state for V^{4+} ion in a C_{4v} local symmetry is the antibonding B_2 molecular orbital, formed by the d_{xy} orbital of the vanadium ion. The LCAO–MO approach gives the spin Hamiltonian parameters (Eq. (8)) [21,37]:

$$g_{\|} = g_0 - \frac{8\beta_1^2\beta_2^2\lambda}{\Delta E(d_{xy} \rightarrow d_{x^2-y^2})}$$

$$g_{\perp} = g_0 - \frac{2\beta_2^2\beta_3^2\lambda}{\Delta E(d_{xy} \rightarrow d_{xz,yz})}$$

$$A_{\|} = -P\left[\beta_2^2\left(K + \frac{4}{7}\right) + (g_0 - g_{\|}) + \frac{3}{7}(g_0 - g_{\perp})\right]$$

$$A_{\perp} = -P\left[\beta_2^2\left(K - \frac{2}{7}\right) + \frac{11}{14}(g_0 - g_{\perp})\right] \quad (8)$$

where λ is the spin-orbit coupling constant for the vanadium(IV) ion, $P = 2.0023\beta_e g_N \beta_N \langle r^{-3} \rangle$ is the dipolar interaction term, K is the isotropic Fermi contact term, β_1^2, β_2^2 and β_3^2 are the fractional contributions of $d_{x^2-y^2}$, d_{xy}, $d_{xz,yz}$ vanadium orbitals to the molecular orbitals. Using $P = 0.0128$ [38] and $\lambda = 170$ cm^{-1} [39], we obtained $\beta_1^2 = 0.863$, $\beta_2^2 = 0.875$ and $\beta_3^2 = 0.935$ for the in-plane σ-bonding, in-plane π-bonding and out-of-plane π bonding, respectively.

The out-of-plane π bonding has a dominant ionic character, with the unpaired electron spending more time into the $d_{xz,yz}$ orbitals of the vanadium ion. The not too high values of β_1^2 and β_2^2 coefficients suggest that the VO_6 and MoO_6 octahedra could share a corner, as previous studies of polyoxometalates with vanadyl and molybdenum ions have indicated [19]. The calculation was made by considering all the possibilities for the signs of $A_{\|}$ and $A_{\perp}$, but only the case $A_{\|} < 0$,

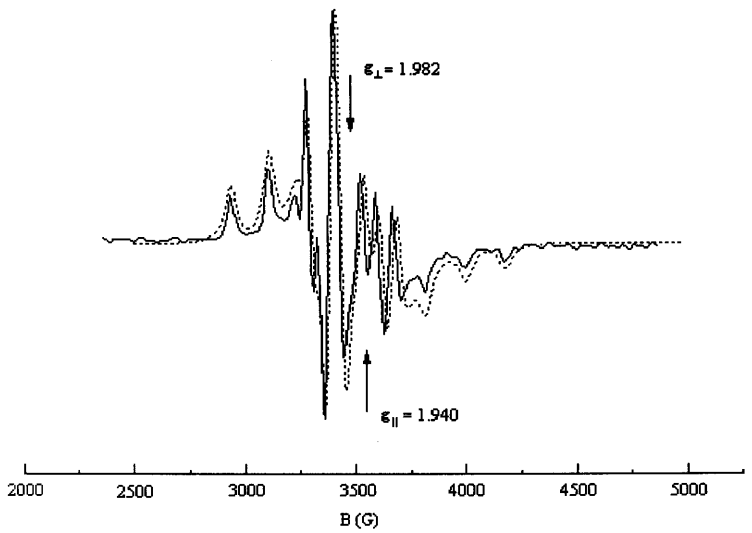


Fig. 6. Experimental (normal line) and simulated (dashed line) EPR spectra of the powder vanadium–HPOM complex, at room temperature.

$A_{\perp} < 0$ gives rise to acceptable values for the molecular orbital coefficients (for $A_{\parallel} > 0$, $A_{\perp} > 0$ and $A_{\parallel} > 0$, $A_{\perp} < 0$ we obtained the negative $\beta_2^2 = -1.003$ and $\beta_2^2 = -2.060$ values respectively and for $A_{\parallel} < 0$, $A_{\perp} < 0$, the $\beta_2^2 = 1.932$ exceed the $\beta_2^2 = 1$ superior limit). This fact together with the low $K = 0.785$ value are in good agreement with the presence of a negative charge on the $O_{b,c}$ oxygen atoms, resulted from the delocalization of the unpaired electron of the vanadium(IV) ion [24,36,38].

4. Conclusions

The spectroscopic and electrochemical investigations of $K_8[P_2VMoW_{16}O_{62}]\cdot 31H_2O$ complex indicate the coordination of the vanadyl group at the monolacunary α-Dawson–Wells fragment. The vanadium(IV) ion is six coordinated by oxygen atoms in a C_{4v} local environment, with a $^2B_2(d_{xy})$ ground state. EPR parameters obtained from the simulated spectrum confirm the axial symmetry. The values of the molecular orbital coefficients for the in-plane σ and π bondings show the electron delocalization towards the oxygen atoms from $V–O_{b,c}$ bonds.

References

[1] N. Casañ-Pastor, C. Louis, W. Baker, J. Am. Chem. Soc. 114 (1992) 10384.
[2] Y.P. Jeannin, Chem. Rev. 98 (1998) 51.
[3] A. Müller, F. Peters, M.T. Pope, D. Gatteschi, Chem. Rev. 98 (1998) 239.
[4] J.B. Tommasino, R. Contant, J.P. Michaut, J. Roncin, Polyhedron 17 (1998) 357.
[5] C. Rong, F.C. Anson, Inorg. Chem. 33 (1994) 1064.
[6] M. Cindric, B. Kamenar, N. Strukan, Polyhedron 14 (8) (1995) 1045.
[7] C.J. Gómez-Garcia, C. Giménez-Saiz, S. Triki, E. Coronado, P. Le Magueres, L. Ouahab, L. Ducasse, C. Sourisseau, P. Delhaes, Inorg. Chem. 34 (1995) 4139.
[8] R. Contant, J.P. Ciabrini, Chem. Res. (M), 2601 (1977).
[9] A. Müller, R. Sessoli, E. Krickemeyer, H. Bögge, J. Meyer, D. Gatteschi, L. Pardi, J. Westphal, K. Hovemeier, R. Rohlfing, J. Döring, F. Hellweg, C. Beugholt, M. Schmidtmann, Inorg. Chem. 36 (1995) 5239.
[10] R. Thouvenot, M. Fournier, R. Franck, C. Rocchiccioli-Deltcheff, Inorg. Chem. 23 (1984) 598.
[11] M. Abbessi, R. Contant, R. Thouvenot, G. Hervé, Inorg. Chem. 30 (1991) 1695.
[12] C. Rocchiccioli-Deltcheff, M. Fournier, R. Franck, R. Thouvenot, Inorg. Chem. 22 (1983) 207.
[13] M. Fournier, C. Rocchiccioli-Deltcheff, L.P. Kazanskii, Chem. Phys. Lett. 223 (1994) 297.
[14] J.Y. Niu, J.P. Wang, X.Z. You, Polyhedron 15 (1996) 3963.
[15] M.H. Alizadeh, S.P. Harmalker, Y. Jeannin, J. Martin-Frère, M.T. Pope, J. Am. Chem. Soc. 107 (1985) 2662.
[16] T.J.R. Weakley, J. Chem. Soc., Dalton Trans. 3 (1973) 341.
[17] C.W. Lee, H. So, Bull. Korean Chem. Soc. 9 (1988) 362.
[18] R. Massart, R. Contant, J.M. Fruchart, J.F. Ciabrini, M. Fournier, Inorg. Chem. 16 (1977) 2916.
[19] E. Cadot, M. Fournier, A. Tézé, G. Hervé, Inorg. Chem. 35 (1996) 282.
[20] D.P. Smith, M.T. Pope, Inorg. Chem. 12 (1973) 331.
[21] A. Bencini, D. Gatteschi, Transition Metal Chemistry, vol. 8, Marcel Dekker, New York, 1982.
[22] J.I. Zink, R.S. Drago, J. Am. Chem. Soc. 94 (1972) 4550.
[23] C. Sanchez, J. Livage, J.P. Launay, M. Fournier, Y. Jeannin, J. Am. Chem. Soc. 104 (1982) 3194.
[24] D.P. Smith, H. So, J. Bender, M.T. Pope, Inorg. Chem. 12 (1973) 685.
[25] R. Neumann, I. Assael, J. Chem. Soc. Chem. Commun (1988) 1285.
[26] T. Yamase, Chem. Rev. 98 (1998) 307.
[27] H. So, M.T. Pope, Inorg. Chem. 11 (1972) 1441.
[28] M. Sadakane, E. Steckhan, Chem. Rev. 98 (1998) 219.
[29] X. Xi, G. Wang, B. Liu, S. Dong, Electrochim. Acta 40 (1995) 105.
[30] X. Xi, S. Dong, J. Mol. Catal. A: Chem. 114 (1996) 257.
[31] S. Dong, X. Xi, M. Tian, J. Electroanal. Chem. 385 (1994) 227.
[32] M.T. Pope, Heteropoly and Isopoly Oxometalates, Springer–Verlag, Berlin, 1983.
[33] M. Otake, Y. Komiyama, T. Otaki, J. Phys. Chem. 77 (1973) 2896.
[34] J.B. Tommasino, R. Contant, J.P. Michaut, J. Roncin, Polyhedron 17 (1998) 357.
[35] U. Kortz, M.T. Pope, Inorg. Chem. 33 (1994) 5643.
[36] J. Park, H. So, Bull. Korean Chem. Soc. 15 (1994) 752.
[37] H. So, C.M. Flynn Jr., M.T. Pope, J. Inorg. Nucl. Chem. 36 (1974) 329.
[38] B.R. Mc Garvey, J. Phys. Chem. 71 (1967) 51.
[39] D. Kivelson, S.K. Lee, J. Chem. Phys. 41 (1964) 1896.

PERGAMON

www.elsevier.nl/locate/poly

Polyhedron 19 (2000) 1925–1933

POLYHEDRON

Ruthenium(II) complexes of α-diimines: synthesis, spectral characterisation, electrochemical properties and single-crystal X-ray structure of bis(2,2′-bipyridine){1-benzyl-2-(*p*-tollylazo)imidazole}-ruthenium(II) perchlorate

Sanjib Pal [a], Tarun K. Misra [a], Chittaranjan Sinha [a,*], Alexander M.Z. Slawin [b], J. Derek Woollins [b]

[a] *Department of Chemistry, The University of Burdwan, Burdwan 713 104, India*
[b] *Department of Chemistry, University of St. Andrews, St. Andrews, KY16 9ST, UK*

Received 27 March 2000; accepted 8 June 2000

Abstract

Mixed-ligand tris-chelates, $[Ru(bpy)_2(RaaiR')](ClO_4)_2 \cdot H_2O$ (bpy = 2,2′-bipyridine; RaaiR′ = 1-alkyl-2-(arylazo)imidazole) have been synthesized by a silver-assisted route $[Ru(bpy)_2Cl_2 + RaaiR' + AgNO_3 + NaClO_4/Ru(bpy)_2Cl_2 + [Ag(RaaiR')_2](ClO_4)]$. The structures of the complexes have been supported by the single-crystal X-ray diffraction study and the stereochemistry are assessed by ^1H NMR spectral data. All the complexes show two metal-to-ligand charge transfer (MLCT) transitions in the visible region at ca. 400 and 500 nm and their emission spectra are also described here. Cyclic voltammetric studies exhibit high-potential $Ru^{III/II}$ (1.4 V vs. SCE) and three successive ligand reductions at negative to SCE in acetonitrile solution. The difference in the first metal and successive ligand redox potentials are linearly correlated with the ν_{CT} of MLCT band. © 2000 Elsevier Science Ltd. All rights reserved.

Keywords: Azoimine; Ru–bipyridine; Tris-chelates; X-ray structures; Electrochemistry; Emission spectra

1. Introduction

For the past several years we have been engaged [1–11] in the exploration of the chemistry of arylazoimidazoles (RaaiR′) (**1**–**3**). The ligand behaves as N,N′-chelator with azoimine, –N=N–C=N–, function. Dichloro-bis(arylazoimidazoles)-ruthenium(II), $Ru(RaaiR')_2Cl_2$, have been structurally characterized in two isomeric forms although the complexes, in principle, may exist in five isomeric forms [11]. The present study is concerned with the heteroleptic tris-chelates of ruthenium(II)-bipyridine and RaaiR′. The chemistry of ruthenium–bipyridine complexes has been widely studied during the last few years [12–33]. Recently there has been a growing interest [20–30] in modifying the properties of Ru–bpy complexes by substituting ligands of other donor centres, altering the steric and electronic properties of the ligands, differently substituted polypyridines, other heterocycles, etc. Herein we wish to report the synthesis, structural characterisation, redox activities, absorption and emission spectroscopic properties of ruthenium complexes of 1-alkyl-2-(arylazo)imidazoles (RaaiR′) with $Ru(bpy)_2$–core.

2. Experimental

2.1. Materials

$RuCl_3 \cdot nH_2O$ was obtained from Arrora Matthey, Calcutta and was digested thrice with concentrated HCl

* Corresponding author. Tel.: +91-342-57-683; fax: +91-342-64-452.
E-mail address: bdnuvlib@giascl01.vsnl.net.in (C. Sinha).

0277-5387/00/$ - see front matter © 2000 Elsevier Science Ltd. All rights reserved.
PII: S0277-5387(00)00447-2

before use [1]. 1-Alkyl-2-(arylazo)imidazoles (RaaiR′) and $[Ag(RaaiR')_2](ClO_4)$ were synthesized as before [3]. *Cis*-$Ru(bpy)_2Cl_2$ was prepared by a published procedure [34]. The purification of dry solvents for electrochemical spectral work and preparation of $[Bu_4N][ClO_4]$ were done as described earlier [1]. All other chemicals and solvents used for the preparative work were of reagent grade and were used as received.

2.2. Instrumentation

Infra-red spectra were obtained on KBr discs (4000–200 cm^{-1}) with JASCO FTIR model 420 spectrophotometer. Solution electronic spectra were received on a Shimadzu UV 160A spectrophotometer and solution emission spectra were recorded with Hitachi F-4500 fluorescence spectrophotometer. The room temperature (298 K) spectra were taken in MeOH–EtOH (1:4, v/v) mixture using a 1 cm pathlength quartz cell. The spectra at 77 K were recorded in liquid nitrogen. Quantum yields were calculated using Eq. (1) [35].

$$\varphi_s = \varphi_{std} \frac{A_{std} I_s \eta_s^2}{A_s I_{std} \eta_{std}^2} \quad (1)$$

where φ_s = quantum yield of unknown sample; φ_{std} = quantum yield of $Ru(bpy)_3^{2+}$: 0.089 at 298 K [36] and 0.35 at 77 K [37] in MeOH–EtOH (1:4, v/v) at λ_{ex} = 450 nm; A_s and A_{std} are the solution absorbencies at the excitation wavelength (λ_{ex}); I_s and I_{std} are the integrated emission intensities and η_s and η_{std} are the refractive indices of the solvent.

Solution electrical conductivity of the complexes were collected from a Systronics digital conductivity meter model 304 with a solute concentration of ca. 10^{-3} mol dm^{-3}. ^1H NMR spectra in $CDCl_3$ were obtained on a Brucker 300 MHz FT NMR spectrometer using $SiMe_4$ as internal standard. The magnetic susceptibilities of the samples were measured on a PAR 155 vibration sample magnetometer. Electrochemical measurements were carried out using EG&G PAR Versastat computer controlled model 270 electrochemical system. All experiments were done under a dinitrogen atmosphere in a three-electrode configuration by using glassy carbon disc milli-electrode and Pt-wire auxiliary electrode. All results were collected at 298 ± 1 K and are referenced to a saturated calomel electrode. The reported potential and the instrument are internally IR compensated.

2.3. Preparation of complexes

2.3.1. Bis(2,2′-bipyridine)[1-methyl-2-(phenylazo)imidazole]ruthenium(II) perchlorate, monohydrate $[Ru(bpy)_2(HaaiMe)](ClO_4)_2 \cdot H_2O$ (**4a**)

(i) To a suspension of *cis*-$Ru(bpy)_2Cl_2$ (1 mmol) in acetone (15 ml) was added aqueous solution of $AgNO_3$ (2 mmol) and was refluxed for 15 min, AgCl so precipitated was filtered off by G-4 crucible. The acetone solution (10 ml) of HaaiMe (0.2g, 1.08 mmol) was then added and the resulting mixture was heated to reflux for 1 h under nitrogen atmosphere. The solution volume was then evaporated to half of its original volume by N_2 bubbling and an aqueous solution of $NaClO_4$ (ca. 1 g in 20 ml water) was added. The reddish brown precipitate thus obtained was filtered and dried in vacuo over P_4O_{10}. The dry mass was then dissolved in minimum volume of CH_2Cl_2 and was subjected to column chromatography on a silica gel column (60–120 mesh). A reddish brown band was eluted with C_6H_6–MeCN (3:2, v/v). This was collected and evaporated. Crystals were collected by layering a solution of the complex in CH_2Cl_2 with hexane. Yield, 68%. *Anal*. Found (Calc.): (**4a**): C, 38.02 (38.24); H, 3.19 (3.43); N, 13.85 (13.73)%; IR: ν(N=N) 1316 cm^{-1}, $\nu(ClO_4^-)$ 1089, 623 cm^{-1}.

Other complexes were also prepared following the same general route as discussed above and the yields were varied 60–75%. *Anal*. Found (Calc.): $[Ru(bpy)_2(p$-MeaaiMe)$](ClO_4)_2 \cdot H_2O$ (**4b**): C, 39.29 (39.04); H, 3.48 (3.61); N, 13.38 (13.50)%; IR: ν(N=N) 1314, $\nu(ClO_4^-)$ 1088, 622 cm^{-1}. $[Ru(bpy)_2(p$-ClaaiMe)$]$ $(ClO_4)_2 \cdot H_2O$ (**4c**): C, 36.50 (36.68); H, 3.31 (3.17); N, 13.33 (13.17)%; ν(N=N) 1318, $\nu(ClO_4^-)$ 1090, 625 cm^{-1}. $[Ru(bpy)_2$-(HaaiEt)$]$ $ClO_4)_2 \cdot H_2O$ (**5a**): C, 38.89 (39.04); H, 3.49 (3.61); N, 13.39 (13.50)%; ν(N=N) 1311, $\nu(ClO_4^-)$ 1086, 624 cm^{-1}. $[Ru(bpy)_2(p$-MeaaiEt)$](ClO_4)_2 \cdot H_2O$ (**5b**): C, 46.28 (46.45); H, 3.92 (3.79); N, 13.08 (13.27)%; ν(N=N) 1312, $\nu(ClO_4^-)$ 1087, 626 cm^{-1}. $[Ru(bpy)_2(p$-ClaaiEt)$](ClO_4)_2 \cdot H_2O$ (**5c**): C, 37.32 (37.48); H, 3.48 (3.35); N, 12.79 (12.96)%; ν(N=N) 1313, $\nu(ClO_4^-)$ 1089, 625 cm^{-1}. $[Ru(bpy)_2(HaaiCH_2Ph)](ClO_4)_2 \cdot H_2O$ (**6a**): C, 42.89 (43.05); H, 3.47 (3.59); N, 12.68 (12.56)%; ν(N=N) 1310, $\nu(ClO_4^-)$ 1087, 626 cm^{-1}. $[Ru(bpy)_2(p$-MeaaiCH$_2$Ph)$](ClO_4)_2 \cdot H_2O$ (**6b**): C, 43.93 (43.71); H, 3.66 (3.75); N, 12.44 (12.36)%; ν(N=N) 1309, $\nu(ClO_4^-)$ 1088, 625 cm^{-1}. $[Ru(bpy)_2(p$-ClaaiCH$_2$Ph)$](ClO_4)_2 \cdot H_2O$ (**6c**): C, 41.61(41.45); H, 3.41 (3.35); N, 12.28 (12.09)%; ν(N=N) 1313, $\nu(ClO_4^-)$ 1090, 626 cm^{-1}.

2.3.2. Reaction of *cis*-$Ru(bpy)_2Cl_2$ with $[Ag(RaaiR')_2](ClO_4)$

General procedure [38] for synthesis of $[Ru(bpy)_2(p$-MeaaiMe)$](ClO_4)_2 \cdot H_2O$. To a methanolic suspension of *cis*-$Ru(bpy)_2Cl_2$, $[Ag(MeaaiMe)_2](ClO_4)$ in acetone was added and refluxed for 1 h under nitrogen atmosphere. Solution was filtered through a G-4 sintered glass funnel. Insoluble AgCl was filtered, the solution was evaporated to dryness and washed thoroughly with cold water (20 $cm^3 \times 4$). The dried mass was dissolved in methanol and an aqueous solution of $NaClO_4$ (ca. 1 g in 15 cm^3) was added. The reddish brown product was filtered and purified as before (yield: 74%).

All other complexes were prepared similarly (yield: 70–80%).

CAUTION! Perchlorate salts of metal complexes are generally explosive. Care should be taken in handling the samples.

2.4. X-ray crystal structure and analysis

Crystal suitable for X-ray work was grown by slow diffusion of hexane–benzene (1:1, v/v) into a dichloromethane solution of $[Ru(bpy)_2(p\text{-MeaaiCH}_2\text{-Ph})](ClO_4)_2.H_2O$ (**6b**). Crystal size was $0.1 \times 0.2 \times 0.2$ mm^3. Data were collected on a Siemens SART CCD diffractometer with graphite monochromatized Mo Kα radiation ($\lambda = 0.71073$ Å) at 293(2) K. Crystal data and collection parameters are listed in Table 1. The data were corrected for absorption effects by empirical method using azimuthal scan data. Systematic absences led to the identification of space group $P\bar{1}$ (triclinic crystal system). Of the 10 532 collected reflections, 5889 with $I > 2\sigma(I)$ were used for structure solution. The structure was solved by conventional heavy-atom method and refined by full-matrix least-square method on all F_o^2 data using the SHELXTL 5.03 package on silicon graphics Indigo-R4000 computers. Hydrogen atoms were included in calculated positions and refined with isotropic thermal parameters which were ~ 1.04 (aromatic (H)) times the equivalent isotopic thermal parameters of their parent carbon atoms. Atomic coordinates (SHELXTL 5.03 program system; Siemens analytical X-ray instruments, Madison, WI, 1995) and isotropic thermal parameters are available as Section 4.

Table 1
Crystallographic data for (**6b**)

Chemical formula	$C_{39.25}H_{34.25}Cl_2N_8O_8Ru$
Formula weight	917.97
T (K)	293 (2)
Crystal system	Triclinic
Space group	$P\bar{1}$
μ (mm^{-1})	0.571
A (Å)	11.3859 (6)
B (Å)	13.6144 (8)
c (Å)	13.9414 (8)
α (°)	93.992 (1)
β (°)	106.681(1)
γ (°)	91.584 (1)
Unit cell volume (Å^3)	2062.6 (2)
Z	2
D_{calc} (g cm^{-3})	1.478
Measured reflections	10 532
Independent reflection (R_{int})	5889 (0.0327)
$R[I>2\sigma(I)]$	5.59
wR	14.43
Goodness-of-fit on F^2	0.944

3. Results and discussion

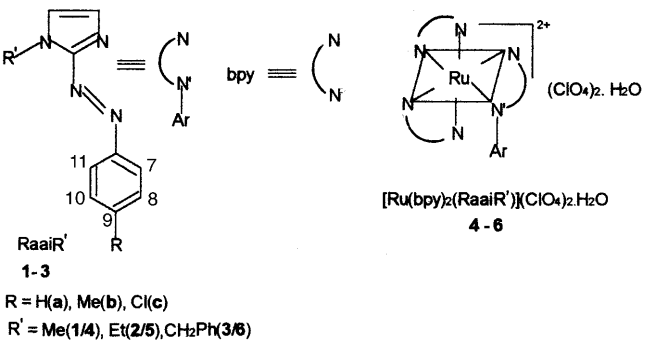
3.1. Synthesis

1-Alkyl-2-(arylazo)imidazoles (RaaiR′) are unsymmetric N,N′-chelating ligands [1] and the donor centres are abbreviated as N(imidazole), N and N(azo), N′. The complexes are isolated as perchlorate salt, $[Ru(bpy)_2(RaaiR')](ClO_4)_2$, by nucleophilic substitution of chloride from *cis*-$Ru(bpy)_2Cl_2$ by RaaiR′ via Ag^+-assisted route. The same reaction is also carried out by reacting $Ag(RaaiR')_2^+$ with *cis*-$Ru(bpy)_2Cl_2$ [18,19].

$$cis\text{-}Ru(bpy)_2Cl_2 + RaaiR' \xrightarrow[(2)\ NaClO_4]{(1)\ Ag^+,\ MeOH,\ reflux} [Ru(bpy)_2(RaaiR')](ClO_4)_2 + 2AgCl\downarrow \quad (2)$$

$$cis\text{-}Ru(bpy)_2Cl_2 + Ag(RaaiR')_2^+ \xrightarrow[(2)\ NaClO_4]{(1)\ MeOH,\ reflux} [Ru(bpy)_2(RaaiR')](ClO_4)_2 + RaaiR' + 2AgCl\downarrow \quad (3)$$

Reaction (3) has been particularly useful for the synthesis of heteroleptic tris-chelate. The products were purified by chromatographic process. Although the tris-chelate may exist in different isomeric forms [19] but they have not been separated by chromatographic separation process and the mixed chelate cation $[Ru(bpy)_2(RaaiR')]^{2+}$ may exist in one chiral structure (**4**–**6**).



The composition of the compounds was formulated by elemental analyses. The complexes are expectedly diamagnetic (d^6) and 1:2 electrolyte in MeCN. The mixed tris-chelate cation $[Ru(bpy)_2(RaaiR')]^{2+}$ can have one chiral structure (**4**–**6**).

3.2. Molecular structure

View of the molecular unit $[Ru(bpy)_2(p\text{-Meaai-CH}_2\text{Ph})]^{2+}$ is shown in Fig. 1 and the bond parameters are given in Table 2. The distorted RuN_6 octahedron is due to the coordination from two N-donor centres of a 1-benzyl-2-(*p*-tolylazo)imidazoles and four N-donor centres of two bpy units. Molecular packing view down the *b* axis shows trapped benzene at

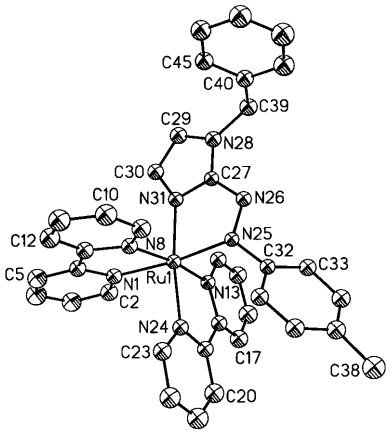


Fig. 1. Single crystal structure of $[Ru(bpy)_2(p\text{-}MeaaiCH_2ph)]^{2+}$ showing the atom numbering scheme. For clarity, all hydrogen atoms have been omitted.

special position and disorder in ClO_4 unit. The three atomic groups Ru, N(1), C(6), C(7), N(8); Ru, N(4), C(19), C(18), N(13) and Ru, N(25), N(26), C(27), N(31) separately constitute three chelate planes (mean deviation < 0.02 Å). The planes are mutually orthogonal (dihedral angle 86–90°). The N(1)–Ru–N(25), N(8)–Ru–N(13), N(24)–Ru–N(31) angles are 173.3(2), 171.7(2), 172.1(2)°, respectively. The angles are deviated from *trans*-angular value (180°), this deviation originates undoubtedly from the acute chelate bite angles: N(1)–Ru–N(8), 78.0(2); N(13)–Ru–N(24) 78.6(2); N(25)–Ru–N(31), 76.5(2)°. The chelate ring constituted by azoimine (N(25)–Ru–N(31)) group has experienced heavy perturbation and is responsible for the deviation from octahedral geometry. The N–N distance is 1.296(6) Å and is longer than the free azo bond length [8] (1.25 Å). The increase in bond length is undoubtedly due to coordination of N(azo) that can lead to a decrease in the N–N bond order due to both σ- and

Table 2
Selected bond distances (Å) and angles (°) and their estimated standard deviations for $[Ru(bpy)_2(p\text{-}MeaaiCH_2Ph)](ClO_4)_2$ (**6b**)

Distances		*Angles*	
Ru–N(1)	2.082(5)	N(1)–Ru–N(8)	78.0(2)
Ru–N(8)	2.068(5)	N(13)–Ru–N(24)	78.6(2)
Ru–N(13)	2.060(5)	N(25)–Ru–N(31)	76.5(2)
Ru–N(24)	2.068(4)	N(1)–Ru–N(31)	97.2(2)
Ru–N(25)	2.023(4)	N(1)–Ru–N(25)	173.3(2)
Ru–N(31)	2.038(4)	N(8)–Ru–N(31)	89.8(2)
N(25)–N(26)	1.296(6)	N(8)–Ru–N(25)	99.6(2)
Cl(1)–O(1)	1.417(6)	N(8)–Ru–N(13)	171.7(2)
Cl(1)–O(2)	1.391(5)	N(1)–Ru–N(24)	88.3(2)
Cl(1)–O(3)	1.407(5)	N(1)–Ru–N(13)	94.8(2)
Cl(1)–O(4)	1.423(7)	O(1)–Cl(1)–O(2)	110.5(4)
		O(1)–Cl(1)–O(3)	108.9(4)
		O(2)–Cl(1)–O(3)	110.2(3)
		O(2)–Cl(1)–O(4)	108.7(5)

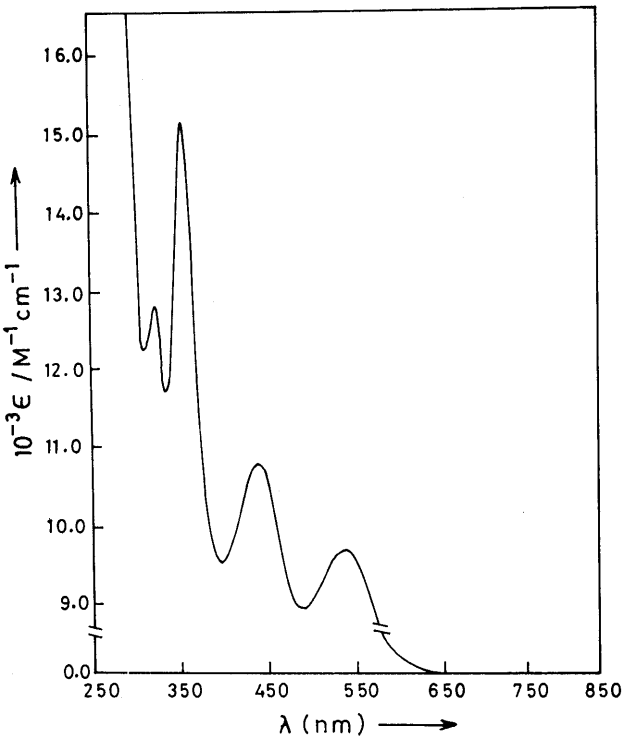


Fig. 2. Absorption spectra of $[Ru(bpy)_2(p\text{-}ClaaiCH_2Ph)](ClO_4)_2$ in methanol at 298 K.

π-acceptor character of the ligands — the latter character having a more pronounced effect and may be the reason for elongation [1]. The pendent *p*-tolyl ring is planar and is inclined at angle 57.1° with the chelate azoimine group N(25)–Ru–N(31).

The average Ru–N(bpy) distance (2.07 Å) is longer than Ru–N(imidazole) (2.038(4) Å) and Ru–N(azo) (2.023(4) Å) distances. The shortening of Ru–N(azo) distance as opposed to Ru–N(imidazole)/Ru–N(bpy) is the indication of metal–ligand π-interaction that is localised in the M–azo fragment [39–41].

3.3. Spectra and bonding mode

The complexes exhibit characteristic IR transmission [1,14,18,33] for ν(N=N), 1360; ν(C=N), ~ 1596; $\nu(H_2O)$, ~ 3400; $\nu(ClO_4^-)$, ~ 1100 and 625 cm^{-1}. The solution spectral studies of the complexes within 200–900 nm (Table 3, Fig. 2) reveal the free ligand absorption < 400 nm and are not considered further. The transitions in the visible region are of typical metal to ligand charge transfer type (MLCT) in the range 400–510 nm with high absorption coefficients ($\sim 10^4$ dm^3 $mol^{-1}cm^{-1}$). The spectra of the complexes are very similar to that of other $[Ru(bpy)_2(L)]^{2+}$ (L = bpy, aryl(2-pyridylmethylene)amine [19]/2-(arylazo)pyridine [42]) in intensity and profile pattern. The MLCT transitions may be compared with reported results [1,37] and is concluded that the absorption at 400–420 nm is

Table 3
UV–Vis, fluorescence and cyclic voltammetric data of the complexes

Compound	Absorption spectra [a] λ_{max} (nm) ($10^{-3}\varepsilon$ M^{-1} cm^{-1})	ν_{CT} [c]	Emission spectra [a]				Cyclic voltammetric data [b]				
			298 K		77 K		$E^{M}_{1/2}$,V	$-E^{L1}_{1/2}$	$-E^{L2}_{1/2}$	$-E^{L3}_{1/2}$	$\Delta E^{\circ}_{1/2}$
			λ_{max} (nm)	$\varphi \times 10^3$	λ_{max} (nm)	$\varphi \times 10^3$	(ΔE_P, mV)				
$[Ru(bpy)_2(HaaiMe)](ClO_4)_2 \cdot H_2O$ (**4a**)	500(9.8), 406(10.55), 380(14.90)	2.482	585	1.1	560	30	1.47 (70)	0.65 (90)	1.43 (90)	1.72 (90)	2.12
$[Ru(bpy)_2(p-MeaaiMe)](ClO_4)_2 \cdot H_2O$ (**4b**)	495(9.90), 420(11.73), 392(17.12)	2.507	576	1.4	550	30	1.45 (90)	0.67 (90)	1.47 (90)	1.73 (110)	2.12
$[Ru(bpy)_2(p\text{-}Claai\text{-}Me)](ClO_4)_2 \cdot H_2O$ (**4c**)	504(9.67), 412(12.79), 386(19.15)	2.462	578	1.0	555	28	1.48 (80)	0.62 (80)	1.48 (100)	1.72 (100)	2.10
$[Ru(bpy)_2(HaaiEt)](ClO_4)_2 \cdot H_2O$ (**5a**)	500(9.49), 408(9.35), 380(13.35)	2.482	585	1.3	558	35	1.49 (80)	0.62 (90)	1.43 (100)	1.72 (110)	2.11
$[Ru(bpy)_2(p\text{-}MeaaiEt)](ClO_4)_2 \cdot H_2O$ (**5b**)	498(9.60), 410(11.12), 395(16.82)	2.492	570	1.5	535	38	1.46 (90)	0.66 (70)	1.47 (110)	1.62 (110)	2.12
$[Ru(bpy)_2(p\text{-}ClaaiEt)](ClO_4)_2 \cdot H_2O$ (**5c**)	503(9.66), 416(7.17), 378(9.15)	2.467	590	1.1	560	32	1.50 (90)	0.60 (80)	1.39 (100)	1.71 (110)	2.10
$[Ru(bpy)_2(HaaiCH_2Ph)](ClO_4)_2 \cdot H_2O$ (**6a**)	502(10.76), 412(11.31), 381(16.02)	2.472	550	1.1	520	31	1.50 (100)	0.61 (100)	1.41 (90)	1.71 (110)	2.11
$[Ru(bpy)_2(p\text{-}MeaaiCH_2Ph)](ClO_4)_2 \cdot H_2O$ (**6b**)	500(8.79), 408(10.84), 395(15.23)	2.482	550	1.3	520	34	1.48 (100)	0.63 (100)	1.45 (85)	1.73 (110)	2.11
$[Ru(bpy)_2(p\text{-}ClaaiCH_2Ph)](ClO_4)_2 \cdot H_2O$ (**6c**)	506(9.73), 414(10.82), 386(15.22)	2.998	555	1.0	520	30	1.53 (100)	0.56 (90)	1.36 (100)	1.69 (90)	2.09

[a] In CH_3OH.

[b] Meaning and units of the symbols are as in text; solvent is CH_3CN, supporting electrolyte Bu_4NClO_4 (0.1 M), solute concentration 10^{-3} M; scan rate 0.05 V s^{-1}; $E^{L1}_{1/2}$ for azo$^-$/azo, $E^{L2}_{1/2}$ and $E^{L3}_{1/2}$ for the reduction of two bpy unit; $\Delta E_p = (E_{pc} - E_{pa})/2$, E_{pc} and E_{pa} are cathodic and anodic peak potentials; $\Delta E^0_{1/2} = E^{M}_{1/2} - E^{L1}_{1/2}$.

[c] $\nu_{CT} = 1241/\lambda$ (nm) e V.

attributed to d(Ru)→π*(bpy) and at 500–510 nm is diagnostic feature in d(Ru)→π*(RaaiR′) transition.

The emission spectral behaviour of the complexes have been studied at room temperature (298 K) and 77 K using MeOH–EtOH (1:4, v/v) solution or glass. The emission spectra in frozen glass are sharper and considerably more intense relative to solution spectra. The emission peaks and quantum yields are given in Table 1 and a representative spectrum is shown in Fig. 3. The spectral behaviour is basically similar to the reported mononuclear analogues, $[Ru(bipy)_2(L)]^{n+}$ (L = phenolic Schiff bases, $n=1$ [16]; 3,5-bis(benzimidazole-2-yl)pyrazole, $n=2$ [33]; aryl-(2-pyridylmethylene)amine, $n=2$ [19]). The complexes on excitation at the wavelengths where their two MLCT absorption maxima are observed, exhibit three to four luminiscent bands in the range 400–600 nm. The peak of the longer wavelength band, which lies between 550 and 590 nm at 298 K, remains unchanged with the energy of excitation radiation. However, the peak positions of the luminescent bands observed at 420–500 nm are affected by the irradiation wavelength; they undergo a blue shift on lowering of the excitation wavelength. The emission band occurring at the longer wavelength part has the characteristic of emission from the ^{3}MLCT excited state, which corresponds to a spin forbidden Ru→bpy transition [3]. In solution, at room temperature, all the complexes are weak emitters with their quantum yields in the range 1.0×10^{-3} to 1.5×10^{-3}. On the other hand, in frozen glass the longer wavelength peak observed at 520–560 nm shows a significant increase of quantum yield 0.028–0.035. The blue shift of the emission band and the enhancement of intensity on lowering of temperature are typical of MLCT emitters [43,44]. The emission observed between 420 and 500 nm is highly unusual and is not expected for ruthenium complexes. It could be either due to emission from the ^{1}MLCT state or from an impurity, free ligand or similar [45]. The fact that peak positions are affected by the excitation wavelength and may suggest that scattered light is the cause of this observation.

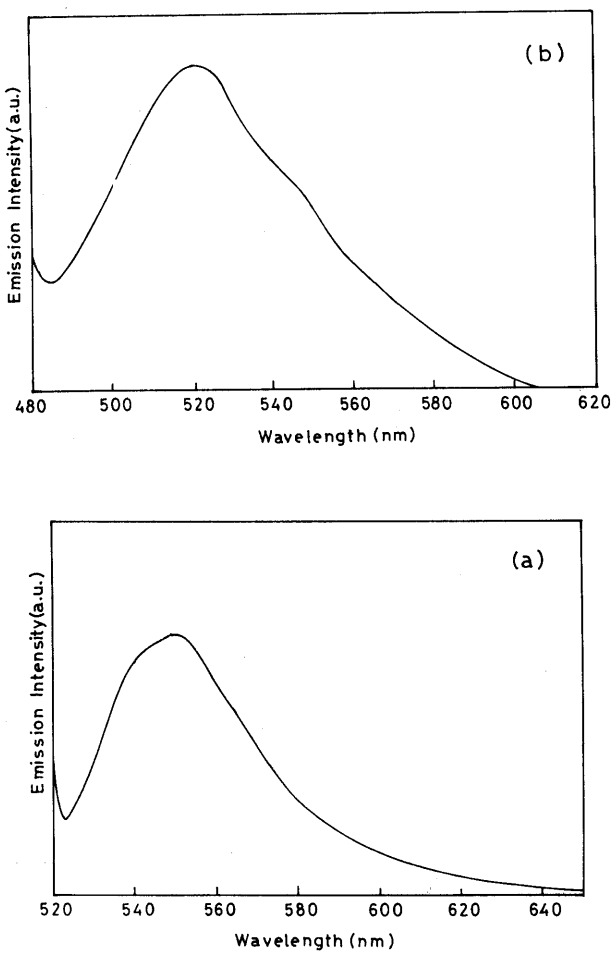


Fig. 3. Emission spectra of $[Ru(bpy)_2(p\text{-}ClaaiCH_2Ph)](ClO_4)_2$ in methanol–ethanol (1:4) (a) at 298 K and (b) frozen glass at 77 K.

3.4. ^{1}H NMR spectra

The ^{1}H NMR spectra were collected in $CDCl_3$. The proton numbering pattern is shown in structure **1** and spectral data are given in Table 4. The N–Me signal appears at 4.3 ppm and is downfield shifted by 0.3 ppm compared to free ligand values (free ligand δ(Me): 4.0 ppm) [1]. N–CH_2CH_3 shows usually a quartet and triplet for –CH_2– and –CH_3 groups respectively in free ligand. In the present complexes methylene protons –CH_2–, appear as AB type complex multiplet (Fig. 4) with geminal coupling constant ca. 24 Hz. The $[Ru(bpy)_2(RaaiCH_2Ph)]^{2+}$ compounds show quartet (AB type, Fig. 4) for methylene, –CH_2–(Ph), protons at ca. 5.8 ppm ($J=18.0$ Hz). The complex does not possess neighbouring chiral centres but there exist a distorted coordination around the metal ion (vide supra, X-ray structure, Fig. 1). This overall distortion leads to the molecular dissymmetry [1,2]. The imidazolic 4- and 5-H protons appear at 7.0–7.2 and 6.8–7.0 ppm, respectively. The coordination of N(3) to ruthenium(II) may lead to downfield shifting of 4-H signal [3–7]. The aryl protons 8,10-H resonate symmetrically at a single position and are perturbed by the substituents at C-9 position. The signal movement is in accordance with the electronic effects of the group. The protons 7-H and 11-H resonate asymmetrically, indicative of a magnetically inequivalent environment. The 11-H is assigned as stereochemically nearer than 7-H to the metal centre. Bipyridine protons are assigned as reported elsewhere [33].

3.5. Redox studies and correlation with electronic spectra

The redox properties of the complexes were examined cyclic voltammetrically at a glassy carbon working

Table 4
^{1}H NMR spectra of the complexes [a]

Compound	δ ppm [b]									
	4-H[c]	5-H [c]	7-H [c]	11-H [c]	8,10-H	12-CH_3	13-H	9-R	9-Me	bpy-H
4a	6.92	6.79	7.70	7.99	7.18 [d]	4.33		7.32 [d]		8.80, 7.50-7.75, 8.0–8.50, 8.80–8.90
4b	6.90	6.82	7.63	7.92	7.00 [c]	4.26			2.82, 2.89	7.50–7.80, 8.00–8.40, 8.70–8.85
4c	6.91	6.87	7.75	8.04	7.29	4.35				7.50–7.75, 8.01–8.45, 8.75–8.85
5a	7.07	6.74	7.52	7.81	7.30 [c]	4.48	1.32	7.30		7.40–7.70, 8.00–8.50, 8.70–8.80
5b	7.08	6.70	7.76	7.91	7.14	4.65	1.61		2.28, 2.89	7.5 0–7.80, 8.00–8.20, 8.60–8.80
5c	7.11	7.01	7.88	8.01	7.55	4.70	1.61			7.60–7.80, 8.20–8.30, 8.50–8.80
6a	7.14	6.84	7.72	7.89	7.24	5.76		7.30		8.5, 7.60–8.00, 8.10 –8.20
6b	7.15	6.89	7.68	7.83	7.05	5.86			2.58, 2.68	7.60–7.70, 7.95–8.25, 8.77, 8.80
6c	7.20	6.95	7.78	7.94	7.37	5.85				8.20–8.25, 8.87, 7.70–8.0 8.80–8.90

[a] In $CDCl_3$ with Me_4Si as internal standard.
[b] J values lie between 7.5 and 9.0 Hz for doublet and triplet signals.
[c] Doublet.
[d] Triplet.

electrode and the potentials are reported with reference to SCE. The voltammograms display $Ru^{III/II}$ couple at the positive side and the ligand reductions at the negative side to SCE. The results are in Table 3, and a representative voltammogram is shown in Fig. 5.

In the potential range + 0.5 to 1.8 V at the scan rate 50 mV s^{-1} in MeCN a reversible to quasireversible (peak-to-peak separation $\Delta E = 70–120$ mV) oxidative response is observed corresponding to the redox reaction (Eq. (4)).

$$[Ru(bpy)_2(RaaiR')]^{3+} + e \rightleftharpoons [Ru(bpy)_2(RaaiR')]^{2+} \quad (4)$$

$$[Ru(bpy)_2(RaaiR')]^{2+} + e \rightleftharpoons [Ru(bpy)_2(RaaiR'^{-})]^{2+} \quad (5)$$

$$[Ru(bpy)_2(RaaiR')]^{2+} + e \rightleftharpoons [Ru(bpy)(bpy^{-})(RaaiR'^{-})]^{2+} \quad (6)$$

$$[Ru(bpy)(bpy^{-})(RaaiR'^{-})]^{2+} + e \rightleftharpoons [Ru(bpy^{-})(bpy^{-})(RaaiR'^{-})]^{2+} \quad (7)$$

The i_{pa}/i_{pc} ratio (i_{pa} = anodic peak current and i_{pc} = cathodic peak current) is close to 1.0, as expected for reversible couples. The $Ru^{III/II}$ redox potential ($E_{1/2}$ = 1.4 V, Table 2) is expectedly higher than that of $Ru(RaaiR')_2Cl_2$ (0.6–0.9 V vs. SCE) [1]. Some $Ru^{III/II}$ formal potential data in tris-chelates $[Ru(bpy)_2(L)]^{2+}$ for L = N,N-bidentate neutral donor are as follows: $Ru(bpy)_3^{2+}$ in CH_2Cl_2 1.29 V [46]; $[Ru(bpy)_2(2\text{-(arylazo)pyridine})]^{2+}$ in MeCN 1.60 V [42]; $[Ru(bpy)_2\text{-(camphorquinonemono–oximato)}]^{+}$ in MeCN 0.85 V [18]. The relative values of the potential support the π-acidity order [1,47] bipyridine < arylazoimidazoles < arylazopyridines. Thus azoimidazole ligands stabilise (with respect to oxidation) Ru(II) better than bipyridine but less effectively than azopyridines.

In the potential range − 0.5 to − 2.4V three successive reductive responses are observed under similar conditions. The literature reports on the redox properties of *cis*-$Ru(bpy)_2Cl_2$ [46], $[Ru(bpy)_2(L)]^{2+}$ (L = 2-(arylazo)pyridines [42], aryl-(2-pyridylmethylene)amine [19]), and $Ru(RaaiR')_2Cl_2$ [1] suggest the cathodic responses those are due to reductions of the coordinated ligands. Redox data in Table 2 reveal that the first reduction potential of the coordinated ligand occurs at a much less negative potential than that of other two responses. The first reduction may be expected to involve the ligand having the most stable lowest unoccupied molecular orbital (LUMO) [18–21]. We believe that this is for arylazoimidazole than bpy and it is due to the acceptance of electron at the azo function (Eq. (5)). The present values are less negative by 0.1–0.2 V than previously reported azo reduction potential in $Ru(RaaiR')_2Cl_2$ [1]. This may be due to coligand effect of π-acidic bpy groups. The first reduction in $[Ru(bpy)_2(2\text{-(arylazo)pyridine})]^{2+}$ has been observed [42] at ca. − 0.5 V and in $[Ru(bpy)(aryl\text{-(2-pyridyl methylene)amine})]^{2+}$ at ca. − 1.0 V [19]. This is certainly due to π-acidity of the ligands, 2-arylazopyridines > 2-arylazoimidazoles > aryl-(2-pyridyl methylene)-amine. In the potential range − 1.4 to − 1.8 V two reductive responses are observed. These are referred to the reduction of bpy in $Ru(bpy)_2$ motif (Eqs. (6) and (7)) [48]. The one-electron nature of these processes was assigned from the comparison of current height with couple (Eq. (4)). The potential is sensitive to the substituent in the aryl ring and is linearly related with Hammett σ values of the substituent. It is interesting to note that the potential, ruthenium(III)/ruthenium(II) and first bound ligand reduction potential correlate linearly (with the slope less than unity). This observation is justified with the extent of perturbation of the ligand π*-orbital due to direct bonding of the substituent in the ligand frame. The effect is more pronounced in the ligand than the metal centre.

It is observed that the MLCT absorption energies for the complexes $[Ru(RaaiR')(bpy)_2]^{2+}$ show a linear cor-

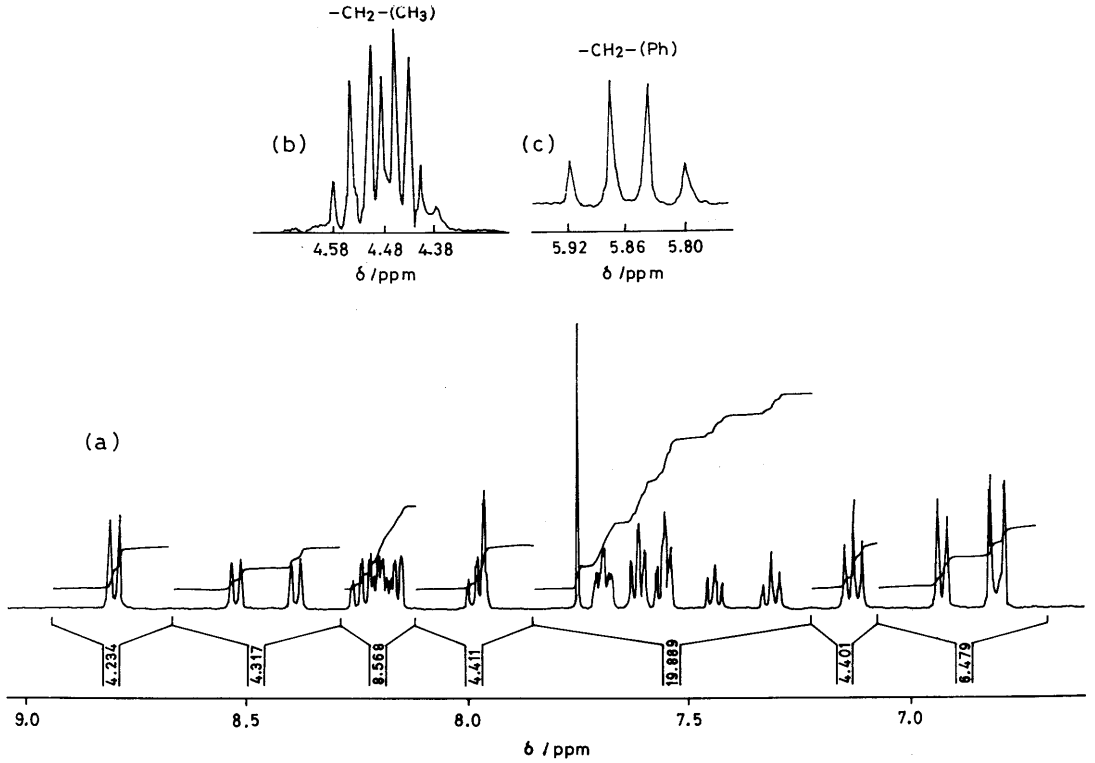


Fig. 4. ^{1}H NMR spectra of (a) aromatic region of $[Ru(bpy)_2(HaaiMe)](ClO_4)_2$ (**4a**), (b) methylene part ($–CH_2–(CH_3)$) of $[Ru(bpy)_2(HaaiEt)](ClO_4)_2$ (**5a**) and (c) methylene part ($–CH_2–(Ph)$) of $[Ru(bpy)_2(p\text{-}MeaaiCH_2Ph)](ClO_4)_2$.

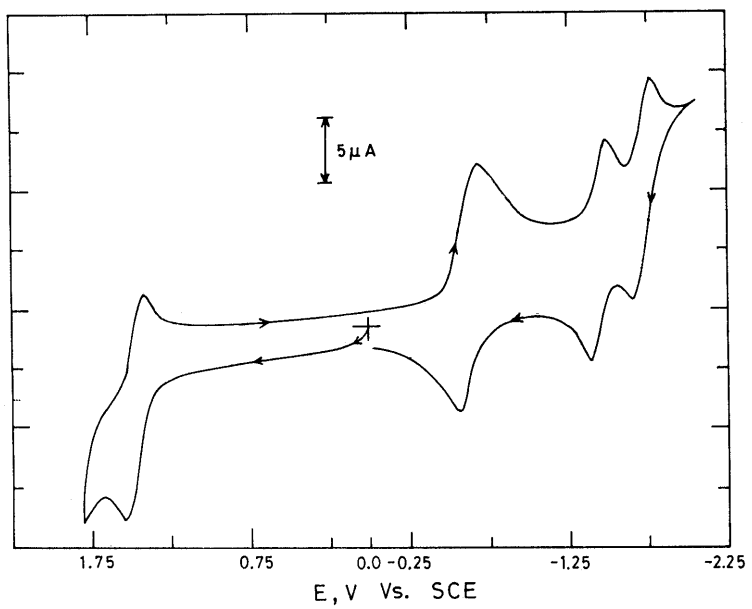


Fig. 5. Cyclic voltammogram of $[Ru(bpy)_2(p\text{-}MeaaiCH_2ph)](ClO_4)_2$ in acetonitrile at GC-milli electrode (0.1 M Bu_4NClO_4) at 298 K using SCE as reference.

relation with $\Delta E°$ values. The difference in potential between the $Ru^{III/II}$ couple and the first ligand reduction couple ΔE_1° ($= E_{1/2}^{M}$ (Eq. (4)) $- E_{1/2}^{L1}$ (Eq. (5))) is linearly related (Eq. (8)) with the longer wavelength MLCT transition (ca. 500 nm). Similarly the potential difference ΔE_2° ($= E_{1/2}^{M}$ (Eq. (4)) $- E_{1/2}^{L1}$ (Eq. (5))) is linearly

$$\nu_1 = 1.39\Delta E_1^\circ - 0.46 \quad (8)$$

correlated with the MLCT transition at ca. 400 nm. (Eq. (9)). The plots are not exactly parallel but their

trend (slopes of same sign) support equivalent intramolecular redox process.

$$v_2 = 1.67\Delta E_2^{\circ} - 1.82 \quad (9)$$

Therefore, the low-energy MLCT transition (ca. 500 nm) for these complexes involves excitation to the π* (RaaiR′) and high-energy transition (ca. 400 nm) is associated with electron excitation to the π* (bpy). It may also be noted that other examples of ruthenium(II) complexes with similar ligands, e.g. the 2,2′-bipyridine [14–16], 2-(arylazo)pyridines [42], 2-(arylazo)imidazoles [1] and aryl-(2-pyridyl methylene)amine [19] also show similar relationships.

4. Supplementary data

Supplementary data for the structural analyses have been deposited with the Cambridge Crystallographic Data Centre, CCDC No. 142090. Copies of this information are available free of charge from The Director, CCDC, 12 Union Road, Cambridge, CB2 1EZ, UK (fax: +44-1223-336033; e-mail: deposit@ccdc.cam.ac.uk or www: http://www.ccdc.cam.ac.uk).

Acknowledgements

Financial support from the Council of Scientific and Industrial Research (CSIR), New Delhi is gratefully acknowledged. We thank Dr B.B. De, University of Massachusetts, Lowell, USA, for recording some NMR spectra. Our sincere thanks are also due to Professor S. Bagchi, Department of Chemistry, Burdwan University, Burdwan, for helpful discussion.

References

[1] T.K. Misra, D. Das, C. Sinha, P. Ghosh, C.K. Pal, Inorg. Chem. 37 (1998) 1672.
[2] T.K. Misra, C. Sinha, Trans. Met. Chem. 24 (1999) 168; 172.
[3] T.K. Misra, D. Das, C. Sinha, Polyhedron 16 (1997) 4163.
[4] D. Das, T.K. Misra, C. Sinha, Trans. Met. Chem. 23 (1998) 73.
[5] D. Das, M.K. Nayak, C. Sinha, Trans. Met. Chem. 22 (1997) 172.
[6] D. Das, T.K. Misra, C. Sinha, Trans. Met. Chem. 23 (1998) 233.
[7] D. Das, C. Sinha, Trans. Met. Chem. 23 (1998) 517.
[8] D. Das, PhD. Thesis, Burdwan University, Burdwan, India, 1998.
[9] D. Das, A.K. Das, C. Sinha, Talanta 48 (1999) 1013.
[10] D. Das, A.K. Das, C. Sinha, Anal. Lett. 32 (1999) 567.
[11] T.K. Misra, C. Sinha, Transition Met. Chem. 24 (1999) 467.
[12] G. Wilkinson, R.D. Gillard, J.A. McCleverty, Comprehensive Coordination Chemistry, Pergamon, Oxford, 1987, vol. 2, p. 43; vol., 4, p. 277.
[13] W.T. Wong, Coord. Chem. Rev. 131 (1994) 45.
[14] K.D. Keerthi, B.K. Santra, G.K. Lahiri, Polyhedron 17 (1998) 1387.
[15] S. Chakraborty, P. Munshi, G.K. Lahiri, Polyhedron 18 (1999) 1437.
[16] N.C. Pramanik, S. Bhattacharya, Polyhedron 16 (1997) 1755.
[17] G.B. Deacon, C.M. Kepert, N. Sahely, B.W. Skelton, L. Spiccia, N.C. Thomas, A.H. White, J. Chem. Soc., Dalton Trans. (1999) 275.
[18] S. Sinha, P.K. Das, B.K. Ghosh, Polyhedron 13 (1994) 2665.
[19] S. Choudhury, A.K. Deb, S. Goswami, J. Chem. Soc., Dalton Trans. (1994) 1305.
[20] B.T. Farrer, H.H. Thorp, Inorg. Chem. 38 (1999) 2492.
[21] A.D. Shukla, B. Whittle, H.C. Bajaj, A. Das, M.D. Ward, Inorg. Chim. Acta 285 (1999) 89.
[22] V.W.W. Yan, B.W.K. Chu, K.K. Cheung, Chem. Commun. (1998) 2773.
[23] K. Kalyansundaram, Coord. Chem. Rev. 46 (1982) 159.
[24] K. Kalyansundaram, M.S. Lakeeruddin, M.K. Nazeeruddin, Coord. Chem. Rev. 132 (1994) 259.
[25] P.D. Beer, Acc. Chem. Res. 31 (1998) 71.
[26] Y. Segawa, M. Kira, Chem. Lett. (1997) 1163.
[27] M. Fukushima, K. Tatsimi, S. Tanaka, H. Wakamura, Environ. Sci. Technol. 32 (1998) 3948.
[28] P. Lincoln, B. Norden, J. Phys. Chem. 102 (1998) 9583.
[29] Y. Xiong, X.F. He, X.H. Zon, J.Z. Wu, X.M. Chen, L.N. Ji, R.H. Li, J.Y. Zhou, K.B. Yu, J. Chem. Soc., Dalton Trans. (1999) 19.
[30] K.M. Maness, H. Masui, R.M. Wightman, R.W. Murray, J. Am. Chem. Soc. 119 (1997) 3987.
[31] J.R. Schoonover, C.A. Bignozzi, T.J. Meyer, Coord. Chem. Rev. 165 (1997) 239.
[32] P.K. Dutta, S.K. Das, J. Am. Chem. Soc. 119 (1997) 4311.
[33] (a) S. Baitalik, U. Florke, K. Nag, J. Chem. Soc., Dalton Trans. (1999) 719. (b) S. Baitalik, U. Florke, K. Nag, Inorg. Chem. 38 (1999) 3296.
[34] F. Beeston, W.S. Aldridge, J.A. Treadway, M.C. Fitzgerald, B.A. De-Graff, S.E. Stitzel, Inorg. Chem. 37 (1998) 4368.
[35] C.J. Van Houten, R.J. Watts, J. Am. Chem. Soc. 98 (1976) 4853.
[36] M.J. Cook, A.P. Lewis, G.S.G. McAuliffe, V. Sharda, A.J. Thomson, J.L. Glasper, D.J. Robbins, J. Chem. Soc., Perkin Trans. 2 (1984) 293.
[37] G.A. Crosby, W.H. Elfring Jr., J. Phys. Chem. 80 (1976) 2206.
[38] S. Choudhury, A.K. Deb, W. Kharmawphalang, S. Goswami, Proc. Indian Acad. Sci. (Chem. Sci.) 100 (1994) 665.
[39] A. Seal, S. Roy, Acta Crystallogr. Sect. C: Struct. Commun. C40 (1984) 929.
[40] B.K. Ghosh, A Mukhopadhyay, S. Goswami, S. Roy, A. Chakravorty, Inorg. Chem. 23 (1984) 4633.
[41] S. Goswami, L.F. Falvello, A. Chakravorty, Inorg. Chem. 26 (1987) 3365.
[42] S. Goswami, A.R. Chakravarty, A. Chakravorty, Inorg. Chem. 20 (1981) 2246.
[43] K. Kalyansundaram, Photochemistry of Polypyridines and Porphyrin Complexes, Academic Press, London, 1992.
[44] R.S. Lumpkin, T.J. Meyer, J. Phys. Chem. 90 (1986) 5307.
[45] J.A. Bolger, G. Ferguson, J.P. James, C. Long, P. McArdle, J.G. Vos, J. Chem. Soc., Dalton Trans. (1993) 1577.
[46] E.C. Johnson, B.P. Sullivan, D.J. Salmon, S.A. Adeyemi, T.J. Meyer, Inorg. Chem. 17 (1978) 2211.
[47] E.C. Constable, Coord. Chem. Rev. 93 (1989) 205.
[48] A.A. Vlyek, Coord. Chem. Rev. 43 (1982) 39.

PERGAMON

www.elsevier.nl/locate/poly

Polyhedron 19 (2000) 1935–1939

POLYHEDRON

Synthesis, characterization and crystal structure of cyano-bridged dinuclear copper–iron complexes

Nijhuma Mondal [a], Manas Kumar Saha [a], Samiran Mitra [a,*], Volker Gramlich [b], Mohamed Salah El Fallah [c]

[a] *Department of Chemistry, Faculty of Science, Jadavpur University, Calcutta 700 032, India*
[b] *Laboratorium für Kristallographie ETH, Eidgenössische Technische Hochschule Zürich, CH-8092 Zurich, Switzerland*
[c] *Department de Química Inorganica, Universitat de Barcelona, Diagonal 647, E-08028 Barcelona, Spain*

Received 11 February 2000; accepted 8 June 2000

Abstract

Two new cyano-bridged dinuclear complexes $[Cu(dmen)_2Fe(CN)_5(NO)]$ (**1**) and $[Cu(dmpn)_2Fe(CN)_5(NO)]$ (**2**) (where dmen = 2-dimethylaminoethylamine and dmpn = 1 dimethylamino-2-propylamine) have been synthesized. The complexes have been characterized by elemental analyses, spectroscopic studies and magnetic moment measurements, and the structures were determined using single-crystal X-ray diffraction. In both complexes the copper(II) ion is coordinated by five nitrogen atoms and has distorted square-pyramidal geometry. The iron(II) center is in a distorted octahedral environment and is linked to copper(II) through a cyano-bridge. © 2000 Elsevier Science Ltd. All rights reserved.

Keywords: Copper–iron complexes; Cyano-bridge; Crystal structures; IR spectra

1. Introduction

Interaction of ferrocyanide with copper proteins was studied and it is suggested that outer sphere charge-transfer (CT) complexes are formed during the electron transfer between two metals. The binding in such complexes is proposed to occur via electrostatic interaction and hydrogen bonding, but direct information is not available [1]. In some cases CT complexes without electron transfer take place as is the case for ferrocyanide with bovine superoxide dismutase, copper substituted carbonic anhydase [2,3] and also in the complex of copper(II) with tris(2-aminoethylamine) [4]. It is well known that the cyanide ion may coordinate through the carbon atom acting as a monodentate ligand or through both the carbon and nitrogen atoms acting as a bridging ligand [5,6]. Recently, there has been a growing interest in the field of coordination polymers based on hexacyanometalate $[M(CN)_6]^{3-}$ as a building block, due to the generation of anomalous structures, magnetic behavior and electron transfer properties [7–11]. Electron transfer is a fundamental and important chemical process with important applications in the field of photosynthesis, disease control and catalysis. Previously, we have reported synthesis and thermally induced electron transfer properties of some cyano-bridged complexes [12]. Zhan and others have reported few cyano-bridged complexes by controlling the reaction conditions [13–17].

Several works have been carried out with the $[Fe(CN)_5(NO)]^{2-}$ anion [18–20], but the interesting polymeric network using nitroprusside as building block was developed very recently [21–23]. Tang and co-workers [21] reported an antiferromagnetic 2D polymeric complex $[Cu_2(oxpn)Fe(CN)_5(NO)]_n$ (oxpn = *N*,*N*′-bis(3-aminopropyl)oxamide) in which the copper(II) and iron(III) centers are bridged by both oxpn and cyanide. Recently, Wei and co-workers [22] reported a double complex $[Ni(bpy)_3][Fe(CN)_5(NO)]\cdot 3H_2O$ and an antiferromagnetic 1D polymeric complex $[Ni(en)_2Fe(CN)_5(NO)]\cdot H_2O$, in which the nickel(II) and iron(II) centers are linked by two cyanide groups. Fur-

* Corresponding author. Tel.: +91-33-668-4193; fax: +91-33-473-4266.
E-mail address: pkbose@cal.vsnl.net.in (S. Mitra).

0277-5387/00/$ - see front matter © 2000 Elsevier Science Ltd. All rights reserved.
PII: S0277-5387(00)00456-3

thermore, Zhan et al. [23] reported three complexes of general formula $[Cu(L)_2\{Fe(CN)_5(NO)\}_2][Cu(L)_2]\cdot nH_2O$ [where L = ethylenediamine, 1,2-diaminopropane and 1,3-diaminopropane and $n = 0–2$] in which the anionic moiety proceeds with the formation of a trinuclear zigzag chain. Attempts have been made to clarify the structural correlation with the magnetic property of dinuclear complexes with the $[Fe(CN)_5(NO)]^{2-}$ anion. In an attempt to achieve this goal, we have synthesized two new cyano-bridged heterometallic complexes $[Cu(dmen)_2Fe(CN)_5(NO)]$ (**1**) and $[Cu(dmpn)_2Fe(CN)_5(NO)]$ (**2**), which have been characterized by X-ray analysis, IR, ESR, electronic spectroscopy and magnetic measurements.

Table 1
Crystallographic data for **1** and **2**

	1	**2**
Chemical formula	$C_{13}H_{24}CuFeN_{10}O$	$C_{15}H_{28}CuFeN_{10}O$
a (Å)	9.252(10)	10.484(3)
b (Å)	20.15(2)	19.960(9)
c (Å)	10.980(11)	11.048(4)
α (°)	90.00	90.00
β (°)	96.70(8)	101.89(3)
γ (°)	90.00	90.00
V (Å^3)	2033(4)	2262(2)
Z	4	4
Space group	$P2(1)/n$	$P2(1)/n$
Crystal size (mm)	$0.2\times0.2\times0.02$	$0.3\times0.15\times0.03$
θ Range (°)	4.39–49.99	4.43–50.00
Reflections collected	2083	2325
R indices (all data)	$R_1 = 0.0554$, $wR_2 = 0.0932$	$R_1 = 0.0476$, $wR_2 = 0.1068$
Final R indices $[I>2\sigma(I)]$	$R_1 = 0.0350$, $wR_2 = 0.0838$	$R_1 = 0.0381$, $wR_2 = 0.0994$
Goodness-of-fit on F^2	1.020	1.016
Parameters	247	260

Table 2
Selected bond lengths (Å) and bond angles (°) for **1** and **2**

	1	**2**
Cu(1)–N(7)	2.003(4)	1.989(3)
Cu(1)–N(8)	2.097(4)	2.123(4)
Cu(1)–N(9)	1.989(4)	1.988(3)
Cu(1)–N(10)	2.120(4)	2.133(3)
Fe(1)–C(1)	1.929(6)	1.945(5)
Fe(1)–C(2)	1.936(5)	1.949(5)
Fe(1)–C(3)	1.936(6)	1.949(5)
Fe(1)–C(4)	1.936(6)	1.939(5)
Fe(1)–C(5)	1.935(6)	1.939(5)
N(1)–C(1)	1.148(5)	1.139(5)
N(2)–C(2)	1.148(6)	1.128(6)
N(3)–C(3)	1.142(6)	1.127(5)
N(4)–C(4)	1.152(6)	1.146(6)
C(5)–N(5)	1.150(6)	1.139(6)
N(6)–O	1.144(4)	1.143(4)
Fe(1)–N(6)	1.631(4)	1.641(4)
N(9)–Cu(1)–N(7)	161.6(2)	166.0(2)
N(9)–Cu(1)–N(8)	94.7(2)	95.10(14)
N(7)–Cu(1)–N(8)	83.9(2)	83.18(13)
N(9)–Cu(1)–N(10)	83.8(2)	83.50(13)
N(7)–Cu(1)–N(10)	94.6(2)	95.15(13)
N(8)–Cu(1)–N(10)	170.6(2)	167.4(2)
N(6)–Fe(1)–C(3)	176.5(2)	177.1(2)
C(1)–N(1)–Cu(1)	146.5(4)	147.5(3)
O–N(6)–Fe(1)	176.6(4)	176.3(4)
N(1)–C(1)–Fe(1)	175.7(4)	176.2(4)
N(2)–C(2)–Fe(1)	176.9(4)	176.6(4)
N(3)–C(3)–Fe(1)	178.0(5)	178.4(4)
N(4)–C(4)–Fe(1)	179.0(4)	178.0(4)
N(5)–C(5)–Fe(1)	176.0(4)	176.6(4)

2. Experimental

2.1. Materials

All chemicals and solvents used for synthesis were of reagent grade. 2-Dimethylaminoethylamine and 1-dimethylamino-2-propylamine (Fluka), $Cu(NO_3)_2\cdot3H_2O$ (Lancaster) and $Na_2[Fe(CN)_5(NO)]\cdot2H_2O$ (Aldrich) were used as received.

2.2. Physical measurements

Elemental analyses were carried out using a Perkin–Elemer 2400 II elemental analyzer. Infrared spectra were recorded on a Perkin–Elemer 883-Infrared spectrophotometer in the range 4000–200 cm^{-1} as KBr pellets. Electronic spectra were recorded from an aqueous solution on a Hitachi U-3400 (UV–Vis–NIR) spectrophotometer. ESR spectra of the crystalline compound were recorded at X-band frequency using a Bruker ESP 300E automatic spectrometer. Magnetic susceptibility measurements in the temperature range 2–300 K were carried out using MPMS SQUID magnetometer.

2.3. X-ray crystallography

The air-stable crystals of **1** and **2** were mounted on glass fiber. Crystallographic data for **1** and **2** are listed in Table 1 and selected bond lengths and angles are listed in Table 2. The data were measured at 293(2) K on a Syntex $P2_1$ four-circle diffractometer fitted with graphite-monochromated Cu Kα radiation, $\lambda = 1.54178$ Å. The stability of the crystals was checked by measuring standard reflections at fixed intervals during the data collection. However, no significant loss of intensity was noted for the crystals. All the reflections collected were independent, satisfied the $I > 2\sigma(I)$ criterion of observability and were used in the subsequent structure determination and refinement. The structures were solved by direct methods using SHELXTL-PLUS [24] and

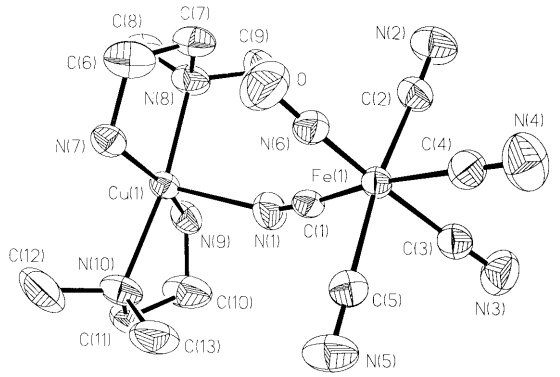


Fig. 1. View of $[Cu(dmen)_2Fe(CN)_5(NO)]$ (**1**) with atom numbering scheme.

refined by a full-matrix least-squares procedure based on F^2 using SHELXL-93 [25].

2.4. Synthesis of the complexes

$[Cu(dmen)_2Fe(CN)_5(NO)]$ (**1**): a 10 ml aqueous solution of $Na_2[Fe(CN)_5(NO)]\cdot 2H_2O$ (0.29 g, 1 mmol) was added slowly to an aqueous solution of $[Cu(dmen)_2](NO_3)_2$ (0.36 g, 1 mmol) and the mixture was kept in a dark place. The deep blue square-shaped crystals of **1** appeared after 2 days, from which crystals suitable for X-ray analysis were separated. The crystals were collected by suction filtration, washed with water and dried in air. *Anal*. Found: C, 34.5; H, 5.4; N, 30.5. Calc. for $C_{13}H_{24}CuFeN_{10}O$: C, 34.2; H, 5.3; N, 30.7%.

$[Cu(dmpn)_2Fe(CN)_5(NO)]$ (**2**): the synthesis was carried out using the same procedure as in **1**, by using $[Cu(dmpn)_2](NO_3)_2$. The blue prismatic crystals of **2** appeared after 1 day. *Anal*. Found: C, 37.0; H, 5.9; N, 28.8. Calc. for $C_{15}H_{28}CuFeN_{10}O$ requires: C, 37.2; H, 5.8; N, 28.9%.

3. Results and discussion

3.1. IR spectra

The characteristic IR active bands for ν(NH) of the NH_2 groups appeared at 3275, 3231 and 3151 cm^{-1} for complex **1** and at 3246, 3230 and 3137 cm^{-1} for complex **2**. In general, IR absorption bands in the region 2200–1900 cm^{-1} are due to the presence of CN^- and NO^+ stretching vibrations [22]. The low intensity bands that appeared at 2162 and 2154 cm^{-1} for **1** and **2**, respectively, was assigned to the intermetallic bridging ν(C≡N), and the high intensity band that appeared at 2143 and 2144 cm^{-1} for **1** and **2**, respectively, was assigned to the terminal ν(C≡N) stretching mode. Our results suggest that the contribution of the terminal cyanide group is high. The band of ν(NO) appeared at 1928 and 1916 cm^{-1} for **1** and **2**, respectively, in accordance with the literature [22].

3.2. Electronic spectra

The binuclear complexes exhibit two broad peaks at 673 and 545 nm for **1** and at 675 and 549 nm for **2**. The high-energy peaks are assigned as a d–d transition of copper(II) ions and the low-energy absorptions are assigned to iron(II)–copper(II) [3,4,23] charge transfer.

3.3. ESR spectra

The ESR spectra for the complexes show a symmetric feature with the g values, $g_\parallel = 2.21$, $g_\perp = 2.06$ and there is no change on lowering the temperature for compound **1** except a simple decrease in intensity. For compound **2** some ill-defined hyperfine splits were observed. The ESR spectra of the complexes are typically the same as the copper(II) ion, and the data suggest square-pyramidal geometry with $g_\parallel > g_\perp > g_e$ in both cases, and the unpaired electron occupies the $d_{x^2-y^2}$ orbital.

3.4. Magnetic measurements

Both the complexes follow the Curie law due to the presence of copper(II) ion, and the plot of $\chi_M T$ versus T remains invariant. In each case the $\chi_M T$ values are 0.5, typical for one unpaired electron of copper(II) ion with a g value of 2.06–2.21. Magnetic results indicate that exchange interaction between copper(II)–iron(II) is absent in both the complexes as the $[Fe(CN)_5(NO)]^{2-}$ anion is diamagnetic. This is also supported by the reported complexes $[Cu_2(oxpn)Fe(CN)_5(NO)]_n$ and $[Ni(en)_2Fe(CN)_5(NO)]\cdot H_2O$ [21,22], which were found to exhibit an antiferromagnetic behavior due to the interaction of M(II) [Cu, Ni] ions through oxpn in the former and cyano-bridge in the latter, but the exchange interaction between the M(II)–Fe(II) through cyano-bridge is negligible.

3.5. Description of structures

The crystal structures of **1** and **2** with atom numbering schemes are presented in Figs. 1 and 2, respectively. The copper(II) ions in both the complexes are pentacoordinated. The coordination number five is very common and possesses either square-based pyramid (SP) or trigonal-bipyramid (TBP) geometry. Recently some complexes have been reported in which the copper(II) ion adopts geometry that is intermediate between SP and TBP [4,11]. Several parameters are used to specify the geometry, one of which is the parameter τ [26]. The

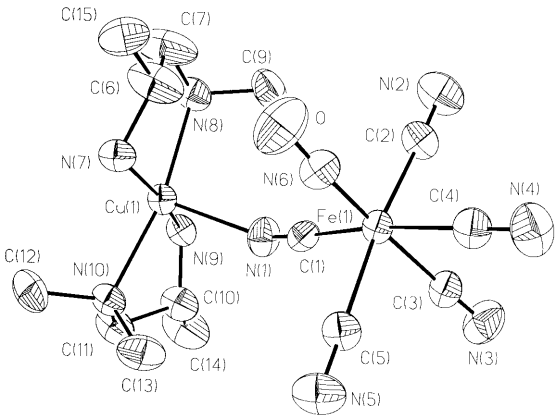


Fig. 2. View of $[Cu(dmpn)_2Fe(CN)_5(NO)]$ (**2**) with atom numbering scheme.

value of τ is 0.15 for **1** and 0.023 for **2**, which indicates that the coordination environment of the copper atom in both complexes is distorted square-pyramidal. The distortion towards TBP geometry is smaller for **2** than for **1**. The basal plane is constructed by the coordination of two primary nitrogen atoms [Cu(1)–N(7), Cu(1)–N(9) are 2.003(4) and 1.989(4) Å for **1** and 1.989(3) and 1.988(3) Å for **2**] and two tertiary nitrogen atoms [Cu(1)–N(8), Cu(1)–N(10) are 2.097(4) and 2.120(4) Å for **1** and 2.123(4) and 2.133(3) Å for **2**] and the nitrogen atom of the cyanide group occupies the axial position [Cu(1)–N(1) is 2.234(5) Å for **1** and 2.223(4) Å for **2**]. The axial Cu(1)–N(1) bond is elongated, as in the case of $[Cu_2(oxpn)Fe(CN)_5(NO)]_n$ and $[Cu(en)_2\{Fe(CN)_5(NO)\}][Cu(en)_2]$ [21,23], in which the values are 2.25(1) and 2.477(3) Å, respectively. The deviation of the Cu(1) from the mean basal plane N(7) N(8) N(9) N(10) is 0.24(1) Å for **1** and 0.25(1) Å for **2**. The bond angles and bond distances of **1** and **2** do not differ significantly and compare well with the related pentacoordinated complexes [4,10,11].

In both cases the iron(II) atom is in a distorted octahedral arrangement with a coordination of four carbon atoms of cyanide groups occupying the equatorial positions, whereas a carbon atom of cyanide group and a nitrogen atom of nitrosyl group from $[Fe(CN)_5(NO)]^{2-}$ anion, occupying the axial positions. According to MO theory, $M–NO^+$ will be nearly linear which is proved by the bond angles of Fe–N–O 176.6(4) and 176.3(4)° for **1** and **2**, respectively. The bond angles of Fe–C–N (ranging from 175.7 to 179° for **1** and from 176.2 to 178.4° for **2**) are nearly linear. The bond angle of C(1)–N(1)–Cu(1) for **1** and **2** are 146.5(4) and 147.5(3)°, respectively, indicating a nonlinear linkage between the nitrogen atom of the cyanide ligand and the copper(II) atom. The average Fe–C and C–N bond distances are 1.934 and 1.148 Å for **1** and 1.944 and 1.135 Å for **2**, respectively. The N(6)–O distances for **1** and **2** are 1.143(4) and 1.144(4) Å, respectively. All of these bond distances are comparable with those found in reported multinuclear complexes of $[Fe(CN)_5(NO)]^{2-}$ [21–23] and also in accordance with other nitroprusside metal salts [19].

4. Supplementary data

Supplementary data have been deposited with the CCDC under deposition numbers 139244 and 139243. Copies of this information are available free of charge from The Director, Cambridge Crystallographic Data Center, 12 Union Road, Cambridge, CB2 1EZ, UK (Fax: +44-1223-336033; e-mail: deposit@ccdc.cam.ac.uk or www: http://www.ccdc.cam.ac.uk).

Acknowledgements

We acknowledge the financial assistance from the Council of Scientific and Industrial Research and University Grants commission (New Delhi, India).

References

[1] M. Goldberg, I. Pecht, Biochemistry 15 (1976) 4197.
[2] L. Morpurgo, I. Mavelli, L. Carabreses, A. Finazzi, G. Rotilio, Biochem. Biophys. Res. Commun. 70 (1976) 607.
[3] G.O. Morpurgo, V. Mosini, P. Porte, J. Chem. Soc., Dalton Trans. (1980) 1272.
[4] Z.L. Lu, C.Y. Duan, Y.P. Tian, Z.W. Wu, J.J. You, Z.Y. Zhou, T.C.-W. Mak, Polyhedron 16 (1997) 909.
[5] A.G. Sharpe, The Chemistry of Cyano Complexes of the Transition Metals, Academic, London, 1976.
[6] D.T. Cramer, A.C. Larson, R.B. Roof, Acta Crystallogr. 19 (1965) 192.
[7] H.-Z. Kou, W.-M. Bu, D.-Z. Liao, Z.-H. Jiang, S.-P. Yan, Y.-G. Fan, G.L. Wang, J. Chem. Soc., Dalton Trans. (1998) 4161.
[8] M. Ohba, N. Usuki and H. Ōkawa, Inorg. Chem. 37 (1998) 3349, and references therein.
[9] B. O'Regan, M. Gratzel, Nature 353 (1991) 737.
[10] H.Z. Kou, D.-Z. Liao, P. Cheng, Z.-H. Jiang, S.-P. Yan, G.-L. Wang, X.-K. Yao, H.-G. Wang, J. Chem. Soc., Dalton Trans. (1997) 1503.
[11] M. Ferbinteanu, S. Tanase, M. Andruh, Y. Journaux, F. Compoesu, I. Strenger, E. Riviere, Polyhedron 18 (1999) 3019.
[12] P. Kundu, M.K. Saha, S. Sen, S. Mitra, S. Kumar, D. Banerjee, R. Bhattarcharya, Polyhedron 15 (1996) 3353, and references therein.
[13] F. Scandola, R. Argazzi, C.A. Bignozzi, C. Chiorboli, M.T. Indelli, M.A. Rampi, Coord. Chem. Rev. 125 (1993) 283.
[14] S.Z. Zhan, X.Y. Chun, Q.J. Meng, Transition Met. Chem. 21 (1996) 181.
[15] A. Vogler, H. Kunkely, Inorg. Chim. Acta 150 (1988) 1.
[16] S.Z. Zhan, Q.J. Meng, Spectrosc. Lett. 29 (1996) 127.
[17] S.Z. Zhan, X.Y. Chun, Q.J. Meng, W. Xie, Synth. React. Inorg. Met.-Org. Chem. 26 (1996) 277.
[18] Y.Y. Yang, J.I. Zink, J. Am. Chem. Soc. 107 (1985) 4799.

[19] M.R. Pressrich, M.A. White, Y. Vekhter, P. Coppens, J. Am. Chem. Soc. 116 (1994) 5233.
[20] J.A. Olabe, L.A. Gentil, G. Rigotti, A. Navaza, Inorg. Chem. 23 (1984) 4297.
[21] Z.N. Chen, J.L. Wang, J. Qiu, F.M. Miao, W.X. Tang, Inorg. Chem. 34 (1995) 2255.
[22] H.L. Shyu, H.H. Wei, Y. Wang, Inorg. Chim. Acta 258 (1997) 81.
[23] S. Zhan, X. Chen, A. Vij, D. Guo, Q. Meng, Inorg. Chim. Acta 292 (1999) 157.
[24] G.M. Sheldrick, SHELXTL-PLUS, Siemens X-ray Analytical X-ray Instruments Inc., Madison, USA, 1990.
[25] G.M. Sheldrick, SHELXL-93, Program for Solution of Crystal Structure Refinement, University of Göttingen, Germany, 1993.
[26] D. Fenton, H. Ōkawa, Chem. Ber./Recueil 130 (1997) 433.

PERGAMON

www.elsevier.nl/locate/poly

Polyhedron 19 (2000) 1941–1947

POLYHEDRON

Synthesis and crystal structures of unbridged bis(4-R-1,2-diphenylcyclopentadienyl)zirconium dichlorides (R = phenyl, cyclohexyl), and catalysis for olefin polymerization

Fan Zhang [a], Ying Mu [a,*], Jianhui Wang [a], Zhan Shi [a,b], Weiming Bu [c], Shirong Hu [a], Yuetao Zhang [a], Shouhua Feng [a,b]

[a] *Department of Chemistry, Jilin University, Changchun 130023, PR China*
[b] *Key Laboratory of Inorganic Hydrothermal Synthesis, Department of Chemistry, Jinlin University, Changchun 130023, PR China*
[c] *Key Laboratory of Supramolecular Structure and Spectroscopy, Jilin University, Changchun 130023, PR China*

Received 31 March 2000; accepted 9 June 2000

Abstract

Zirconocene complexes carrying sterically bulky tri-substituted cyclopentadienyl ligands, $(\eta^5\text{-4-R-1,2-Ph}_2\text{C}_5\text{H}_2)_2\text{ZrCl}_2$ [R = phenyl (**3**), cyclohexyl (**4**)], were synthesized by the reaction of $ZrCl_4$ with lithio salt of 1,2,4-triphenylcyclopentadiene (**1**) or 4-cyclohexyl-1,2-diphenylcyclopentadiene (**2**), respectively. The single-crystal X-ray structure analysis reveals that both complexes crystallize in C_2-symmetric conformation in solid state. When activated with methylaluminoxane (MAO), complexes **3** and **4** polymerize ethylene with moderate activities to produce ultra-high-molecular-weight polyethylenes with high melting transition temperatures at low Al/Zr ratios. Under ambient conditions, both systems of **3**–MAO and **4**–MAO show relatively high activities in propylene oligomerization. The molecular weight of the polypropylene produced from the **3**–MAO system is lower than that from the **4**–MAO system. In comparison with **4**, complex **3** is more active in both ethylene and propylene polymerization. © 2000 Elsevier Science Ltd. All rights reserved.

Keywords: Zirconocene; Crystal structures; Catalysis; Olefin polymerizations

1. Introduction

Group 4 metallocenes have attracted extensive research attention in recent years because of their application as catalysts in olefin polymerization [1–4]. In the development of new metallocene catalysts, modification of the cyclopentadienyl ligand is an effective means of optimizing catalyst activity as well as polymer properties such as molecular weight, stereoregularity and microstructure, etc. [5–10]. Recently, unbridged zirconocenes bearing trisubstituted cyclopentadienyl or mono-substituted indenyl ligands have drawn much attention because some of this type of zirconocenes produce semi-isotactic polypropylene elastomers [11–16]. The design of this type of catalyst was based on the consideration that the conformation conversion of the metallocene molecule could be controlled by the introduction of appropriate substituents on the cyclopentadienyl or indenyl ligand to block the rotation of the ligand during polymerization, so that the stereospecificity of the polymer could be controlled. It was believed that the π-stacking between the aryl substituents plays a crucial role in blocking the conversion between the *rac*-like and *meso*-like conformations of the catalyst molecule [13,17]. On the other hand, it has been demonstrated that modification of the ligand with phenyl substituent whether on the ligand ring [8,12–19] or even on the bridging moiety [20] has a considerably strong influence on the catalytic properties of metallocenes due to the special steric and electronic characteristics of phenyl group. In these respects, we have concentrated our efforts on designing a series of unbridged sterically hindered metallocenes containing phenyl substituents and investigating their polymeriza-

* Corresponding author. Tel.: +86-431-892-2331 ext. 3120; fax: +86-431-894-9334.
E-mail address: ymu@mail.jlu.edu.cn (Y. Mu).

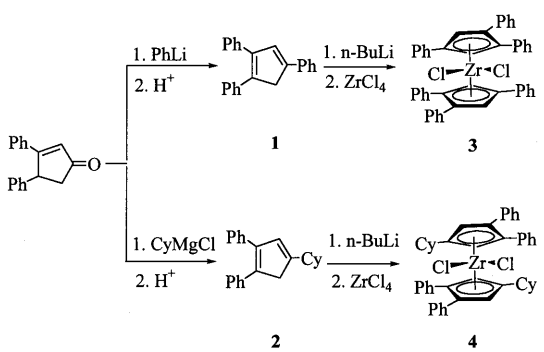
0277-5387/00/$ - see front matter © 2000 Elsevier Science Ltd. All rights reserved.
PII: S0277-5387(00)00484-8

tion behavior. The present paper describes the synthesis and structure characterization of two new C_2-symmetric unbridged zirconocenes (η^5-4-R-1,2-$Ph_2C_5H_2)_2ZrCl_2$ [R = phenyl (**3**), cyclohexyl (**4**)], as well as their catalytic properties for ethylene and propylene polymerizations.

2. Results and discussion

2.1. Synthesis

1,2,4-Triphenyl-1,3-cyclopentadiene (**1**) was synthesized by a modified literature procedure [21]. Treatment of 3,4-diphenyl-2-cyclopenten-1-one with phenyl lithium in THF formed the intermediate 1-hydroxy-1,3,4-triphenyl-2-cyclopentene, which was then converted into **1** by dehydration with *p*-toluenesulfonic acid monohydrate (Scheme 1). Pure **1** was obtained as pale yellow needles by recrystallization from 1:3 CH_2Cl_2–hexane in a good yield (70%). THF was used as solvent because of the good solubility of 3,4-diphenyl-2-cyclopenten-1-one and the increased reactivity of the addition of phenyllithium to the keto group of α–β unsaturated ketone. 4-cyclohexyl-1,2-diphenyl-1,3-cyclopentadiene (**2**) was prepared in a similar manner to **1** by the reaction of 3,4-diphenyl-2-cyclopenten-1-one with cyclohexyl magnesium chloride. Compound **2** was obtained in low yields (less than 30%) presumably due to that the bulky cyclohexyl Grignard reagent disfavors 1,2-addition to the keto group of the α–β unsaturated ketone. Pure **2** was obtained by column chromatography as a yellow oil which solidified slowly at room temperature. Attempts to prepare **2** with cyclohexyl lithium instead of cyclohexyl magnesium chloride were unsuccessful. ^{1}H NMR spectroscopic analysis indicates that both **1** and **2** were obtained in single isomer form (as depicted in Scheme 1). The chemical shifts of the cyclopentadiene ring protons of **2** (δ 3.47 and 6.31 ppm) are shifted up-field 0.5–0.8 ppm compared with those (δ 3.95 and 7.06 ppm) of **1** due to the electronic donating effect of the cyclohexyl substituent.



Scheme 1.

The ligand precursor **1** is well soluble in toluene, while only slightly soluble in other common organic solvents. Therefore, **1** was deprotonated with butyllithium in toluene. The produced lithium salt was easily isolated from solvent as white precipitate in ca. 90% yield. Interestingly, the ligand precursor **2** has a pretty good solubility in hexane. The lithium salt of **2** was therefore prepared in hexane in high yields ($\sim$95%) with convenient isolation and purification. THF was found to be an unsuitable solvent for the lithiation reaction due to low yield and difficulty in isolation. The zirconocene dichlorides **3** and **4** were prepared from the reaction of two equivalents of lithium salt of corresponding ligand with $ZrCl_4$ in toluene. The reaction mixture was heated at 60–70°C for hours until a bright yellow solution was formed, which indicates the completion of the reaction. Pure complexes **3** and **4** were obtained by recrystallization of the crude products from hexane–toluene in high yields (80% for **3** and 74% for **4**). Both **3** and **4** were found to be stable to air and moisture for several days.

^{1}H and ^{13}C NMR spectra reveal that **3** and **4** both exhibit C_{2v} symmetry in solution due to the rapid rotation of the cyclopentadienyl ligands around the Cp–Zr axis and all phenyl groups in both complexes are in free rotating fashion at room temperature. In complex **3**, the down-field shift of the Cp ring proton resonance (δ 6.75 ppm) compared to that (δ 6.64 ppm) in **4** is in agreement with the result mentioned above for their ligand precursors **1** and **2**. In ^{13}C NMR spectra, down-field shifts of the resonances (δ 125.1 and 125.4 ppm in **3**, 128.0 ppm in **4**) assigned to the Cp ring carbons linked to phenyl groups compared to resonances of other Cp ring carbons were also observed due to the electron-withdrawing effect of the phenyl substituents.

2.2. X-ray crystal structures analyses

The molecular structures of **3** and **4** determined by X-ray diffraction are shown in Figs. 1 and 2, respectively. Selected bond distances and angles are given in Table 1. The geometry about zirconium in **3** or **4** can be described as pseudo-tetrahedral and the whole molecule adopts a C_2-symmetric conformation. The two adjacent phenyl substituents at each Cp ring lie in the front open side of the zirconocene molecule, one of which is staggered nearly over one of the two Cl atoms and the other is oriented away from the corresponding phenyl group at another Cp ring. The third phenyl substituent at each Cp ring in **3** and the cyclohexyl group in **4** are arranged backwards from the front side of the metallocene.

In complex **3**, the Cl–Zr–Cl # angle of 94.08(9)° is a typical value for unbridged zirconocenes [22,23]. The Cent–Zr–Cent angle (Cent is the centroid of Cp ring)

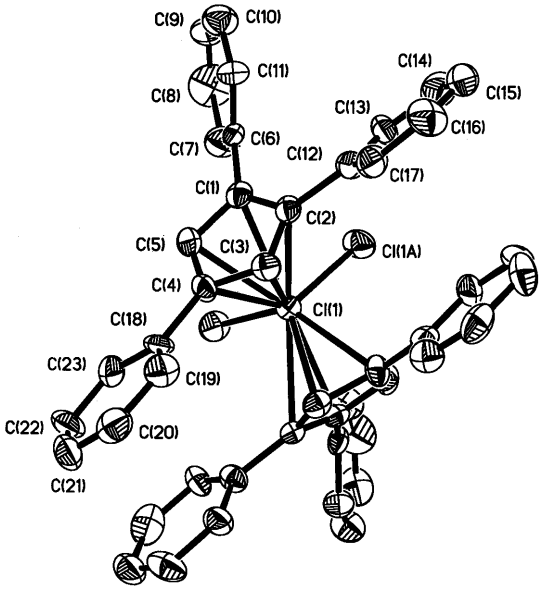


Fig. 1. ORTEP plot of complex **3** at 50% probability ellipsoids. The solvent molecules and hydrogen atoms were omitted for clarity reasons.

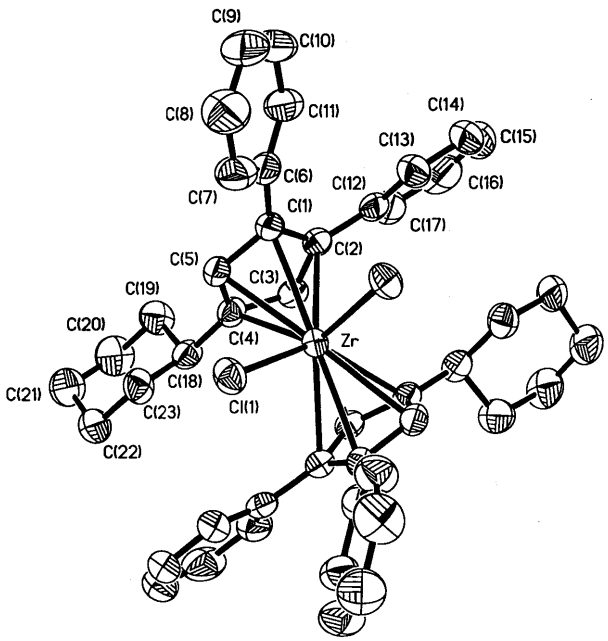


Fig. 2. ORTEP plot of complex **4** at 50% probability ellipsoids. The solvent molecules and hydrogen atoms were omitted for clarity reasons.

129.3° is almost identical to that (129.7°) observed in $[\eta^5\text{-}C_5H_3\text{-}1,3\text{-}(CMe_3)_2]_2ZrCl_2$ [24], smaller than the one of 131.3° for bis(2-phenylindenyl)zirconium dichoride [12], but much larger than that of 119.4° found in [bis(η^5-7,9-diphenylcyclopenta[*a*]acenaphthadienyl)] zirconium dichloride [19]. The angle (φ) between two Cp ring planes (56.6°) is larger than the one (51.4°) observed for $(Me_3CCp)_2ZrCl_2$ and analogous metallocenes [25]. The angles between the Cp and the phenyl planes are separately 56.9, 33.3 and 24.1°. Compared with the value (less than 10°) of the angle between the phenyl and indenyl planes in bis(2-phenylindenyl)zirconium dichloride [13], the angle (24.1°) between the Cp plane and the phenyl ring at the 4-position in **3** is quite large. This angle is also larger than those for complexes $(1,2\text{-}Me_2\text{-}4\text{-}Ph\text{-}C_5H_2)ZrCl_2$ (18.8, 13.6°) [15], while close to that (22.5°) in $(1,2\text{-}Me_2\text{-}4\text{-}p\text{-}tolyC_5H_2)_2ZrCl_2$ [13].

The Zr–Cl bond distance of 2.441(3) Å is in a normal range for zirconocene dichloride [25]. The distance from Zr atom to the centriod of cyclopentadienyl ring (2.245 Å) is longer than those (2.215–2.223 Å) found in analogous bulky zirconocene compounds [19,26]. The C(1)–C(2) bond has the longest bond length [1.458(9) Å] among five wedges of the Cp ring. It seems likely that the two adjacent phenyl substituents sterically force the C–C bond longer. The bond lengths for C(1)(sp^2)–C(6)(sp^2) [1.495(9) Å] and C(2)(sp^2)–C(12)(sp^2) [1.510(9) Å] are longer than that of C(4)(sp^2)–C(18)(sp^2) [1.490(9) Å], which might be attributed to that the bonds C(1)–C(6) and C(2)–C(12) are in more sterically congest environments.

The structure of **4** is similar to that of **3** with the substituted cyclohexyl group at each Cp ring adopting a

Table 1
Selected bond lengths (Å) and angles (°) for complexes **3** and **4**

	3	**4**
Zr–Cl(1)	2.439(2)	2.4303(7)
Zr–C(1)	2.617(6)	2.605(2)
Zr–C(2)	2.612(7)	2.583(2)
Zr–C(3)	2.497(7)	2.502(3)
Zr–C(4)	2.472(6)	2.516(2)
Zr–C(5)	2.539(5)	2.551(3)
C(5)–C(1)	1.406(8)	1.413(4)
C(5)–C(4)	1.423(9)	1.411(4)
C(4)–C(3)	1.427(9)	1.417(4)
C(3)–C(2)	1.371(9)	1.411(4)
C(2)–C(1)	1.458(9)	1.433(4)
C(1)–C(6)	1.495(9)	1.479(4)
C(2)–C(12)	1.510(9)	1.488(4)
C(4)–C(18)	1.490(8)	1.507(4)
Cent–Zr	2.245	2.251
Cl(1)–Zr–Cl(1) #	94.08(9)	93.71(4)
C(1)–C(5)–C(4)	109.3(6)	110.3(2)
C(5)–C(4)–C(3)	106.2(5)	105.6(2)
C(2)–C(3)–C(4)	110.1(6)	110.3(2)
C(3)–C(2)–C(1)	107.8(6)	106.7(2)
C(5)–C(1)–C(2)	106.6(5)	107.0(2)
C(5)–C(4)–C(18)	126.9(6)	126.6(2)
C(3)–C(4)–C(18)	126.6(6)	126.4(2)
C(3)–C(2)–C(12)	126.4(6)	123.8(2)
C(1)–C(2)–C(12)	125.6(5)	129.1(2)
C(2)–C(1)–C(6)	129.5(6)	130.1(2)
C(5)–C(1)–C(6)	122.4(6)	122.4(2)
Cent(1)–Zr–Cent(1) #	129.3	131.6
φ	56.6	53.1

Table 2
Polymerization of ethylene with **3**–MAO, **4**–MAO and Cp_2ZrCl_2–MAO under similar conditions [a]

Catalyst	Al–Zr	Activity $\times 10^{-3}$ [b]	$M_\eta \times 10^{-6}$ [c]	T_m (°C) [d]
3	300	1.28	1.41	140.9
	1000	1.87	1.18	140.0
	1500	1.92	0.91	138.4
4	300	1.01	1.35	140.6
	1000	1.12	1.05	140.2
	1500	1.26	0.87	138.1
Cp_2ZrCl_2	300	1.09	0.47	132.9
	1000	2.26	0.43	131.9
	1500	3.69	0.42	131.5

[a] Polymerization conditions: catalyst 1.7 μmol, volume of toluene 50 ml, time 1 h, temp. 18°C, ethylene pressure 6 bar.
[b] kg PE (mol Zr)$^{-1}$ h^{-1}.
[c] Measured in decahydronaphthalene at 135°C.
[d] Determined with DSC at a heating rate of 10°C min^{-1}.

twist-chair conformation. The Cl–Zr–Cl angle of 93.71(4)° is smaller than that for **3**. The Cent–Zr–Cent (131.6°) is nearly equal to the value of 131.5° for (1,2-Me_2-4-Ph-C_5H_2)$_2$$ZrCl_2$ [15] and close to those (130.3 and 131.0°) in bis(2-phenyl-4,5,6,7-tetrahydroindenyl)(2-cyclohexylindenyl)zirconium dibromide [13]. In comparison with complex **3**, the Cent–Zr–Cent angle in **4** is increased by 2.3° and the angle between the Cp ring planes (53.1°) is reduced by 3.5°. The angles between the substituted phenyl and Cp planes (42.6 and 30.8°) are quite different from those (56.9 and 33.3°) for complex **3**. Obviously, the bulky cyclohexyl groups demand more space at the back part of the zirconocene molecule and result in these differences.

The Zr–Cl bond length [2.4303(7) Å] is also a typical value. The distance (2.251 Å) of Zr–Cent is somewhat larger than that in **3**. The bond lengths for C(1)(sp^2)–C(6)(sp^2) [1.479(4) Å] and C(2)(sp^2)–C(12)(sp^2) [1.488(4) Å] are smaller than those for C(1)(sp^2)–C(6)(sp^2) [1.495(9) Å] and C(2)(sp^2)–C(12)(sp^2) [1.510(9) Å] in **3**, probably due to stronger π-binding resulted from the smaller angle between the substituted phenyl and Cp planes in **4**.

2.3. Polymerization

Complexes **3** and **4** were studied as ethylene polymerization catalysts. For comparison purposes, some polymerization experiments were also carried out with Cp_2ZrCl_2 as catalyst under the same conditions (Table 2). Upon activation with MAO, both **3** and **4** polymerize ethylene with moderate activities at lower Al/Zr ratios. Unlike Cp_2ZrCl_2, the catalytic activities of **3** and **4** do not decrease very much when the Al/Zr ratio changes from 1500 to 300, which suggests that the concentration of cationic active species formed by the activation of MAO does not change very much with the change in Al/Zr ratios. In addition, the samples of polyethylene produced by **3** and **4** show high molecular weights and melting transition temperatures. These results could be explained on the basis of steric effects of the complexes. X-ray structures of **3** and **4** exhibit that the bulky substituents at the Cp ring construct a sterically crowded environment around the metal center, which could weaken the interaction between cationic zirconium center and anionic cocatalyst and therefore could efficiently prevent the active catalyst from bimolecular deactivation. Therefore, a smaller amount of MAO is needed to keep the catalyst in the active state. On the other hand, the large steric hindrance of the complexes could effectively block the chain termination by β-H transfer, thus long polymer chains could be formed.

The results in Table 2 also reveal that replacement of the phenyl group (in **3**) at the 4-position of Cp ring by a cyclohexyl group (in **4**) leads to a decrease in catalytic activities. As can be seen from their structures, complex **3** has a smaller angle of Cent–Zr–Cent and a larger angle of Cp–Cp than **4**. This means that the steric hindrance of **4** in the front side of Zr atom is larger and the coordination gap aperture for the monomer is smaller, and hence the catalytic activity of **4** is lower than that of **3**. Obviously, the steric effect of the ligands in **3** and **4** seems to play a predominant role in ethylene polymerization. Otherwise, the electron donating effect of the cyclohexyl group should increase the catalytic activity of **4**.

Complexes **3** and **4** were also tested for propylene polymerization under ambient conditions. From two typical experiments, 2.5 g of colorless oily propylene oligomer (catalytic activity: 1470 kg PP (mol Zr)$^{-1}$ h^{-1} was obtained from **3**, and 1.2 g of similar product (catalytic activity: 706 kg PP (mol Zr)$^{-1}$ h^{-1} was obtained from **4**. From the ^{1}H NMR spectra of the oligomer samples, resonances (δ 4.65, s; 4.72, s) for vinylidene end group were observed as the only signals in the unsaturated end group region, which indicates that β-H elimination is the single detectable chain termination pathway. The number average molecular weights (M_n) of propylene oligomers produced by **3** and **4** were calculated by end group analysis. It was found that the molecular weight of the propylene oligomer (M_n: 1.89×10^3 g mol^{-1}) produced by **3** is lower than that (M_n: 2.52×10^3 g mol^{-1}) of the sample from **4**. ^{13}C NMR spectra revealed that the polypropylene samples produced by **3** and **4** are highly regioregular and no 2,1-insertion takes place during the polymerization reaction. The reason for the lower catalytic activity of **4** would be the same as above mentioned for ethylene polymerization. Compared with **3**, the increased steric hindrance of **4** would result in a decline in the rates of chain propagation and chain termination, while the decrease in the chain termination rate seems to be more

remarkable, and thus longer polymer chains are produced.

It was demonstrated that the stereospecificity of polypropylene could be improved by introducing a bulky substituent at the appropriate position of the Cp ring to restrict the rotation of the ligand ring, e.g. polypropylene with high isotacticity (49.8%) was produced by *rac*-(1-Me-3-^{t}BuC_5H_3)$_2$ZrCl_2–MAO [15]. At ambient conditions, the lack of stereospecificity for **3** and **4** suggests that the bulky substituents at their Cp rings could not efficiently block the rapid rotation of the Cp rings to make the catalyst molecule maintain an isospecific coordination site-switching model with a long enough life-time during the polymerization [27,28]. On the other hand, it has been reported that high stereoregularity could be obtained with analogous complex bis(2-aryindenyl)zirconium dichloride [12–14]. In this case, the phenyl group and the rigid indenyl moiety have been believed to be two crucial factors for generating appropriate π-stacking and establishing a balance between two conformational isomers (from *rac* to *meso*) of the catalyst [12–14,17]. In the present case, there seems to be no effective π-stacking interaction in both **3** and **4** during polymerization. Investigations on the propylene polymerization under different conditions are currently underway in our laboratory.

3. Experimental

3.1. General procedures and material

All reactions with moisture- and air-sensitive compounds were carried out under argon with use of Schlenk techniques. Toluene and THF were refluxed over sodium benzophenone ketyl and distilled prior to use. Hexane and CH_2Cl_2 were refluxed and distilled from CaH_2 under nitrogen. Polymerization grade ethylene and propylene were further purified by passage through columns of 10 Å molecular sieves and MnO. 3,4-Diphenyl-2-cyclopenten-1-one was prepared by a known procedure [29]. Methylaluminoxane (MAO, 10 wt.% solution in toluene, $M = 800$ g mol^{-1}, Al = 5.3 wt.%) was purchased from Witco. Cyclohexylmagnesium chloride (2.0 M in diethyl ether), phenyllithium (1.8 M in cyclohexane–ether) and ^{n}BuLi (1.6 M in hexanes), $ZrCl_4$, and Cp_2ZrCl_2 were purchased from Aldrich. NMR spectra were recorded on Varian Unity-400 (FT 400 MHz, ^{1}H; 100 MHz, ^{13}C) spectrometer. Elemental analyses were carried out on Perkin–Elmer 240 C elemental analyzer. Viscosity-average molecular weights of the polyethylenes were determined in decahydronaphthalene at 135°C using Schott Gerate Mod. AVS/T2 Ubbelohde viscosimeter. Melting transition temperatures (T_m) of the polyethylenes were determined by DSC (Du Pont 910 differential scanning calorimeter) at a heating rate of 10°C min^{-1}.

3.2. 1,2,4-Triphenyl-1,3-cyclopentadiene (1)

To a solution of phenyl lithium (25 ml, 1.8 M in cyclohexane–ether, 0.045 mol) was added dropwise a solution of 3,4-diphenyl-2-cyclopenten-1-one (10 g, 0.043 mol) in THF (70 ml) at −10°C. The deep reddish solution was allowed to warm to r.t. and stirred for 6 h. After quenching with 40 ml of ice–water, the organic layer was separated and the aqueous phase was extracted with diethyl ether (2 × 30 ml). The combined organic phases were stirred with *p*-toluenesulfonic acid monohydrate (1 g) for 2 h. The mixture was neutralized by addition of 30 ml acqueous NH_4Cl and then the organic solution was dried over $MgSO_4$. After removal of the solvent, pure **1** was obtained as a pale yellow needle solid by recrystallization from hexane–CH_2Cl_2 (3:1). Yield 7.73 g (61.1%). ^{1}H NMR ($CDCl_3$, 400 MHz): δ 3.95 (s, 2H, C_5H_3), 7.06 (s, 1H, C_5H_3), 7.1–7.6 (m, 15H, Ph) ppm.

3.3. 4-Cyclohexyl-1,2-diphenyl-1,3-cyclopentadiene (2)

THF (40 ml) was added to a dry 200 ml Schlenk flask under argon. Cyclohexylmagnesium chloride (21.5 ml, 2.0 M in diethyl ether, 0.043 mol) was added, followed by dropwise addition of a solution of 3,4-diphenyl-2-cyclopenten-1-one (10 g, 0.043 mol) in THF (50 ml) at −10°C. The mixture was allowed to warm to r.t. and stirred for 5 h. After the solution was quenched with 40 ml of ice water, the organic layer was extracted with diethyl ether (2 × 30 ml). The combined organic phases were treated with concentrated HCl (3 × 20 ml). The mixture was washed with saturated NH_4Cl (aq). After drying with $MgSO_4$ and filtering, the solvent was evaporated under reduced pressure. Pure **2** was obtained as yellow–brown oil by chromatography over silica gel (eluent: hexane–CH_2Cl_2 (15:1), which was gradually made more polar to a ratio of 6:1). Yield: 3.26 g, 25.3%. ^{1}H NMR ($CDCl_3$, 400 MHz): δ 0.95–1.98 (br m, 10H, Cy), 2.40 (br m, 1H, Cy), 3.47 (s, 2H, C_5H_3), 6.31 (s, 1H, C_5H_3), 7.02–7.40 (m, 10H, Ph).

3.4. Bis(1,2,4-triphenylcyclopentadienyl)zirconium dichloride (3)

1,2,4-Triphenyl-1,3-cyclopentadiene (0.88 g, 2.99 mmol) was dissolved in toluene (40 ml). ^{n}BuLi (2.0 ml, 1.6 M, 3.20 mmol) was added dropwise at −78°C to give a creamy suspension. The mixture was stirred for 18 h at r.t. After the solvent had been removed by filtration, the solid residue was washed with hexane (20 ml) and then suspended in toluene (40 ml). $ZrCl_4$ powder (0.34 g, 1.46 mmol) was added slowly at −15°C and the suspension was allowed to warm to r.t. The mixture was stirred over night and heated to 70°C for further 18 h. The precipitate was filtered off and the solution was

concentrated in vacuo. Recrystallization from toluene–hexane (1:3) afforded **3** as a yellow crystalline powder. Yield: 0.89 g (80.3%). ^{1}H NMR ($CDCl_3$, 400 MHz): δ 6.75 (s, 4H, Cp), 7.00–7.20 (m, 30H, Ph). ^{13}C NMR ($CDCl_3$, 100 MHz): δ 116.1, 125.1, 125.4 (Cp), 127.4, 127.6, 127.8, 129.0, 129.5, 130.8, 131.9, 133.0 (Ph). $C_{46}H_{34}Cl_2Zr$ (748.85): *Anal.* Calc. C, 73.78; H, 4.58. Found: C, 73.98; H, 4.65%.

3.5. Bis(4-cyclohexyl-1,2-diphenylcyclopentadienyl)zirconium dichloride (4)

To a solution of 4-cyclohexyl-1,2-diphenyl-1,3-cyclopentadiene (0.78 g, 2.65 mmol) in hexane (30 ml) was added BuLi (1.8 ml, 1.6 M in hexane, 2.88 mmol) at −78°C. The mixture was allowed to warm to r.t. and stirred overnight. The solvent was removed by filtration and the solid was suspended in toluene (50 ml) and cooled to −15°C. $ZrCl_4$ (0.30 g, 1.3 mmol) was added to the suspension. The mixture was stirred overnight at r.t. and for 18 h at 70°C. The resulting suspension was filtered to remove precipitate. The solution was concentrated in vacuo and pure **4** was given as green–yellow micro-crystals by recrystallization from toluene–hexane (1:3). Yield: 0.73 g (73.8%). ^{1}H NMR ($CDCl_3$, 400 MHz): δ 0.71–0.82, 1.02–1.10, 1.37–1.61 (br m Cy, 20H), 1.78 (br m, Cy, 2H), 6.64 (s, 4H, Cp), 7.26–7.44 (m, 20 H, Ph). ^{13}C NMR ($CDCl_3$, 100 MHz): δ 25.6 (double intensity), 33.2, 36.2 (Cy), 117.4, 127.3, 128.0 (Cp), 128.7, 129.8, 133.3, 133.6 (Ph). $C_{46}H_{46}Cl_2Zr$ (760.95): *Anal.* Calc. C, 72.61, H, 6.09. Found: C, 72.99, H, 6.18%.

Table 3
Crystallographic data and parameters of the crystal structure determinations

	3·2CH_2Cl_2	**4**·CH_2Cl_2
Formula	$C_{48}H_{38}Cl_6Zr$	$C_{47}H_{48}Cl_4Zr$
*F*w	918.70	845.87
Temperature (K)	293 (2)	293 (2)
Crystal system	trigonal	monoclinic
Space group	*P*3(1)21	*P*2/*c*
a (Å)	12.2157 (13)	8.8746 (7)
b (Å)	12.2157 (13)	11.1902 (9)
c (Å)	24.245 (6)	21.0399 (18)
α (°)	90	90
β (°)	90	91.7260 (10)
γ (°)	120	90
V (Å^3)	3133.2 (9)	2088.5 (3)
Z	3	2
Absorption coefficient (mm^{-1})	0.454	0.551
F(000)	936	876
D_{calc} (Mg m^{-3})	1.461	1.345
Crystal size (mm)	0.36 × 0.38 × 0.4	0.40 × 0.12 × 0.12
Wavelength (Å)	0.71073	0.71073
Collection region	$-1<h<14$; $-14<k<1$; $-1<l<28$	$-9<h<9$; $-12<k<11$; $-22<l<23$
θ Range (°)	$1.92<\theta<25.00$	$3.48<\theta<23.26$
Scan type	ω–2θ	ω–2θ
Absorption correction	semi-empirical	empirical
Max and min transmission	0.923 and 0.599	0.882 and 0.658
Number of reflections collected	4860	9092
Number of uniqe reflections	3674 ($R_{int}=0.0388$)	2999 ($R_{int}=0.0425$)
Reflections with ($F_o^2>3\sigma(F_o^2)$)	2401	2498
Number of variables	311	341
Goodness-of-fit on F^2	1.160	1.002
R_1 (wR_2) [a]	0.0431 (0.0879)	0.0320 (0.0773)
Largest difference peak and hole (e Å^{-3})	0.963 and −0.671	0.382 and −0.256

[a] $R_1=\Sigma|F_o-F_c|/\Sigma|F_o|$, $wR_2=\{[\Sigma w(F_o^2-F_c^2)^2]/\Sigma wF_o^4\}^{0.5}$, $w=1/[\sigma^2(F_o^2)+(mP)^2+0.0000P]$, $P=(F_o^2+2F_c^2)/3$, (**3**, $m=0.0508$; **4**, $m=0.0536$).

3.6. X-ray structural determination of complex 3

Crystals of **3** with two CH_2Cl_2 solvent molecules were obtained by recrystallization from a solution of hexane–CH_2Cl_2 (4:1). A yellow crystal suitable for X-ray diffraction sealed in a glass capillary was used. Data were collected on a Siemens P_4 four-circle diffractometer with a graphite monochromator using Mo Kα radiation. The structure was solved by direct methods and refined by full-matrix least-squares methods on F^2. The hydrogen atoms were located by combination of difference Fourier map and HYDROHEN program. All calculations were performed using SHELX-93 [30]. Crystallographic data and parameters are summarized in Table 3.

3.7. X-ray structural determination of complex 4

A yellow crystal of **4** with one CH_2Cl_2 solvent molecule crystallized from hexane–CH_2Cl_2 (5:1) was mounted in a thin-walled glass capillary under nitrogen. Data collection was performed using a standard Siemens SMART CCD diffractometer with graphite-monochromated Mo Kα radiation. Hydrogen atoms were located by combination of difference Fourier map and HYDROGEN program. Except for CH_2Cl_2 molecular, all non-hydrogen atoms were refined with anisotropic thermal parameters, while hydrogen atoms were refined isotropically. The disorder CH_2Cl_2 molecule founded in the lattice as a solvent of recrystallization exhibited high thermal parameters. The disorder CH_2Cl_2 was refined as 50/50 disordered. All calculations were performed using SHELX crystallographic package [31]. Crystallographic data and parameters are summarized in Table 3.

3.8. Polymerizations

A dry 250 ml steel reactor equipped with a magnetic stirrer was evacuated and pressurized with ethylene to 1.0 bar. Toluene and appropriate amount of MAO were added to the reactor through a septum port via syringe. After the solution was saturated with ethylene for 30 min, a solution of catalyst (1.7 μmol) in toluene was injected (total volume of the polymerization solution is 50 ml after the addition of catalyst). The vessel was repressurized to the required pressure with ethylene as soon as the catalyst was injected and the pressure was maintained by continuously feeding monomer. After the mixture was stirred for the desired reaction time, the reactor was vented and the polymerization was terminated by injecting acidified methanol [HCl (3 M)–methanol = 1:1]. The polymer was stirred in acidified methanol overnight, washed with water and methanol, dried in vacuo at 60°C. Polymerization of propylene was performed under ambient conditions (1 bar, temperature 20°C, time 1 h, Al/Zr = 1000/1, catalyst = 1.7 μmol). The procedure was similar to that for ethylene polymerization. After the reaction mixture was treated with acidified methanol and stirred overnight, the organic layer was separated and the aqueous phase was extracted with toluene. The organic layers were combined and dried over $MgSO_4$. After the solvent was removed, the propylene oligomer was obtained as a colorless oil.

4. Supplementary data

Crystallographic data (excluding structure factors) for the structures reported in this paper have been deposited with the Cambridge Crystallographic Data Centre, CCDC Nos. 140596 and 140597. Copies of the data can be obtained free of charge from The Director, CCDC, 12 Union Road, Cambridge, CB2 1EZ, UK (fax: +44-1223-336033; e-mail: deposit@ccdc.cam.ac.uk or www: http://www.ccdc.cam.ac.uk).

Acknowledgements

This work was supported by the National Natural Science Foundation of China (No. 29734143 and No. 29672013) and the Sinopec.

References

[1] H.H. Brintzinger, D. Fischer, R. Mülhaupt, B. Rieger, R.M. Waymouth, Angew. Chem., Int. Ed. Engl. 34 (1995) 1143.
[2] M. Bochmann, J. Chem. Soc., Dalton Trans. (1996) 255.
[3] W. Kaminsky, J. Chem. Soc., Dalton Trans. (1998) 1413.
[4] H.G. Alt, E. Samuel, Chem. Soc. Rev. 27 (1998) 323.
[5] N. Schneider, M.E. Huttenloch, U. Stehling, R. Kirsten, F. Schaper, H.H. Brintzinger, Organometallics 16 (1997) 3413.
[6] Y. Mu, W.E. Piers, L.R. MacGillivray, M.J. Zaworotko, Polyhedron 14 (1995) 1.
[7] W. Spaleck, M. Antberg, J. Rohrmann, A. Winter, B. Bachmann, P. Kiprof, J. Behm, W.A. Herrmann, Angew. Chem., Int. Ed. Engl. 31 (1992) 1347.
[8] W. Spaleck, F. Küber, A. Winter, J. Rohrmann, B. Bachmann, M. Antberg, V. Dolle, E.F. Paulus, Organometallics 13 (1994) 954.
[9] E.J. Thomas, J.C.W. Chien, M.D. Rausch, Organometallics 18 (1999) 1439.
[10] W. Kaminsky, Macromol. Chem. Phys. 197 (1996) 3907.
[11] G. Erker, M. Aulbach, M. Knickmerier, D. Wingbermühle, C. Krüger, M. Nolte, S. Werner, J. Am. Chem. Soc. 115 (1993) 4590.
[12] G.W. Coates, R.M. Waymouth, Science 267 (1995) 217.
[13] J.L. Maciejewski-Petoff, M.D. Bruce, R.M. Waymouth, A. Masood, T.K. Lal, R.W. Quan, S.J. Behrend, Organometallics 16 (1997) 5909.
[14] C.D. Tagge, R.L. Kravchenko, T.K. Lal, R.M. Waymouth, Organometallics 18 (1999) 380.
[15] K. Kimura, K. Takaishi, T. Matsukawa, T. Yoshimura, H. Yamazaki, Chem. Lett. (1998) 571.
[16] B.Y. Lee, J.W. Han, Y.K. Chung, S.W. Lee, J. Organomet. Chem. 587 (1999) 181.
[17] M.A. Pietsch, A.K. Rappé, J. Am. Chem. Soc. 118 (1996) 10908.
[18] B. Rieger, T. Repo, G. Jany, Polym. Bull. 35 (1995) 87.
[19] T. Repo, G. Jany, K. Hakala, M. Klinga, M. Polamo, M. Leskelä, B. Rieger, J. Organomet. Chem. 549 (1997) 177.
[20] K. Patsidis, H.G. Alt, W. Milius, S.J. Palackal, J. Organomet. Chem. 509 (1996) 63.
[21] W. Dilthey, W. Schommer, J. Prakt. Chem. 136 (1933) 293.
[22] A. Antiñolo, M.F. Lappert, A. Singh, D.J.W. Winterborn, L.M. Engelhardt, C.L. Raston, A.H. White, A.J. Carty, N.J. Taylor, J. Chem. Soc., Dalton Trans. (1987) 1463.
[23] B.J. Grimmond, J.Y. Corey, N.P. Rath, Organometallics 18 (1999) 404.
[24] P.J. Chirik, M.W. Day, J.E. Bercaw, Organometallics 18 (1999) 1873.
[25] G. Erker, S. Wilker, C. Krüger, M. Nolte, Organometallics 12 (1993) 2140.
[26] G. Erker, R. Nolte, R. Aul, S. Wilker, C. Krüger, R. Noe, J. Am. Chem. Soc. 113 (1991) 7594.
[27] W. Kaminsky, K. Külper, H.H. Brintzinger, F.R.W.P. Wild, Angew. Chem. 97 (1985) 507.
[28] W. Spaleck, M. Antberg, J. Rohrmann, A. Winter, B. Bachmann, P. Kiprof, J. Behm, W.A. Herrmann, Angew. Chem., Int. Ed. Engl. 31 (1992) 1347.
[29] T.A. Geissmann, C.F. Koelsch, J. Org. Chem. 3 (1939) 489.
[30] (a) G.M. Sheldrick, SHELXTL-Plus, Structure Determination Software Programs, Siemens Analytical X-ray Instruments Inc., Madison, WI, USA, 1990. (b) G.M. Sheldrick, SHELXL-93, Programs for the Refinement of Crystal Structures, University of Göttingen, Germany, (1993).
[31] SHELXTL, Version 5.1; Siemens Industrial Automation, Inc., 1997.

PERGAMON

www.elsevier.nl/locate/poly

Polyhedron 19 (2000) 1961–1966

POLYHEDRON

Electronic and NMR properties of *meso*-monosubstituted ferrocenylporphyrin: evidence of π-conjugation between porphyrin and ferrocene

Seog Woo Rhee [b], Byung Bin Park [a], Youngkyu Do [b,*1], Jinkwon Kim[a,*2]

[a] *Department of Chemistry and RRC/NMR, Kongju National University, Kongju 314-701, South Korea*
[b] *Department of Chemistry, School of Molecular Science-BK21 and Center for Molecular Design and Synthesis, Korea Advanced Institute of Science and Technology, Taejon 305-701, South Korea*

Received 29 February 2000; accepted 26 June 2000

Abstract

The reaction of dipyrrylmethane with an equimolar mixture of ferrocenecarboxaldehyde and benzaldehyde in dry acetonitrile in the presence of a catalytic amount of trichloroacetic acid leads to the formation of 5-ferrocenyl-15-phenyl-2,8,12,18-tetraethyl-3,7,13,17-tetramethylporphyrin (**1**) with a yield of 27%. The metallation of **1** with $Zn(OAc)_2 \cdot 2H_2O$ and $MnCl_2 \cdot 4H_2O$ gives Zn·**1** and MnCl·**1**, respectively. Cyclic voltammograms of **1**, Zn·**1** and MnCl·**1** show reversible one-electron oxidation processes for the oxidation of ferrocene at 0.29, 0.22, and 0.37 V, respectively. Variable temperature ^{1}H NMR spectra of **1** in toluene-d_8 show two distinct singlets of equal intensities and line widths for NH protons. From the plot of $\ln(k/T)$ versus $1/T$ according to the Eyring equation, gave straight line with $\Delta G^{\ddagger} = 51$ kJ mol^{-1}. © 2000 Elsevier Science Ltd. All rights reserved.

Keywords: Ferrocenylporphyrin; π-Conjugation; Electrochemical communication; Intramolecular hydrogen bonding; NH tautomerism

1. Introduction

Many discrete molecules in which two photo- and redox-active sites are linked by π-conjugation have been developed with great interest for applications in molecular electronic devices [1,2]. In particular, porphyrins [3,4] or ferrocenes [5] are the most frequently used molecules for this purpose. However, examples of covalently linked π-conjugates of these two units are quite rare [6,7]. These facts and the recent demonstration on the significant substituent effect on electronic properties in porphyrins prompted us to explore new porphyrin–ferrocene conjugates. Herein we describe the synthesis, structure and conjugated feature of 5-ferrocenyl-15-phenyl-2,8,12,18-tetraethyl-3,7,13,17-tetramethylporphyrin (**1**).

2. Experimental

2.1. Materials

Solvents were purified according to standard methods where applicable [8]. Tetra-*n*-butylammonium perchlorate (TBAP) was synthesized and purified by procedure described in the literature [9]. 3,3′-Diethyl-4,4′-dimethyl-2,2′-dipyrrylmethane was synthesized according to procedures described in the literature [10]. All other reagents were purchased from Aldrich Chemical Co. or Sigma Chemical Co. and were used as received.

2.2. Preparations

5-Ferrocenyl-15-phenyl-2,8,12,18-tetraethyl-3,7,13,17-tetramethylporphyrin (**1**) was synthesized by a procedure similar to that described by Osuka et al. for the preparation of 5,15-diarylporphyrins [11]. The ferrocenecarboxaldehyde (0.79 g, 3.7 mmol) and benzaldehyde (0.39 g, 3.7 mmol) were dissolved in dry acetonitrile (84 ml) containing trichloroacetic acid (0.56 g,

E-mail address: jkim@knu.kongju.ac.kr (J. Kim).
[1] *Corresponding author
[2] *Corresponding author. Tel.: +82-41-850-8496; fax: +82-41-850-8479

0277-5387/00/$ - see front matter © 2000 Elsevier Science Ltd. All rights reserved.
PII: S0277-5387(00)00481-2

3.4 mmol). The mixture was stirred for 30 min under nitrogen. Then, the 3,3′-diethyl-4,4′-dimethyl-2,2′-dipyrrylmethane (1.8 g, 7.4 mmol) in acetonitrile (20 ml) was added through cannula under positive nitrogen pressure. After stirring for 60 h under nitrogen in the dark, *p*-chloranil (2.93 g, 12 mmol) in THF (100 ml) was added and stirred for 5 h under same conditions. The solvent was evaporated to dryness, and the residual solid was suspended on aqueous NaOH solution (10%, 100 ml) to dissolve the hydroquinone impurities. After stirring for 2 h, filtered on a glass frit, washed with water and then methanol. The crude products were separated and purified by flash chromatography (SiO_2, 3.8×25 cm, $CHCl_3$). The first red band was 5,15-diphenyl-2,8,12,18-tetraethyl-3,7,13,17-tetramethylporphyrin (**2**), and the second olive green band was the desired 5-ferrocenyl-15-phenyl-2,8,12,18-tetraethyl-3,7,13,17-tetramethylporphyrin (**1**). Recrystallization from toluene–methanol mixture gave purple crystals of **1**·0.5C_6H_5Me (0.70 g, 27% based on the amount used dipyrrylmethane). *Anal.* Calc. for $C_{48}H_{50}N_4Fe{\cdot}0.5C_6H_5Me$ (MW 784.87): C, 78.81; H, 6.93; N, 7.14. Found: C, 77.58; H, 6.93; N, 7.19. ^{1}H NMR (δ ppm, $CDCl_3$) 9.86 (s, 2H, *meso*-H), 8.25 (d, 1H, phenyl), 7.75 (m, 3H, phenyl), 7.64 (d, 1H, phenyl), 7.25–7.16 (m, 2.5H, phenyl of C_6H_5Me), 4.70 (t, 2H, ferrocenyl), 4.60 (t, 2H, ferrocenyl), 3.90 (m, 8H, CH_2CH_3), 3.72 (s, 5H, ferrocenyl), 3.35 (s, 6H, CH_3), 2.39 (s, 6H, CH_3), 2.35 (s, 1.5H, C_6H_5Me), 1.72 (t, 6H, CH_2CH_3), 1.66 (t, 6H, CH_2CH_3), −1.06 (s, 1H, NH), −1.32 (s, 1H, NH). UV–Vis (C_6H_5Me) [λ_{max}, nm (log ε, mol^{-1} dm^3 cm^{-1})] 421 (5.19), 505 (4.05), 527 (4.01), 581 (3.94), 601 (3.95), 662 (3.53).

Zn·**1** was obtained by treatment of refluxing chloroform solution of **1** with saturated methanolic $Zn(OAc)_2{\cdot}2H_2O$ solution. Recrystallization from chloroform–methanol mixture gave purple crystals of Zn·**1** (77%). MnCl·**1** were obtained by treatment of refluxing chloroform solution of **1** with saturated methanolic $MnCl_2{\cdot}4H_2O$ solution and then by air-oxidation (58%).

Table 1
Details of the crystallographic data collection for **1**·0.5C_6H_5Me

Chemical formula	$C_{48}H_{50}N_4Fe{\cdot}0.5C_6H_5Me$
Chemical formula weight	784.87
Space group	$C2/c$
a (Å)	50.557(5)
b (Å)	14.611(5)
c (Å)	23.593(3)
β (°)	101.54(2)
V (Å^3)	17076(7)
Z	16
ρ_{calc} (g cm^{-3})	1.255
μ (mm^{-1})	0.395
λ (Mo Kα) (Å)	0.71073
2θ max. (°)	44
Parameters refined	955
$R(F_o)$	0.0780
$wR(F_o^2)$ [a]	0.2032
Goodness-of-fit	1.070

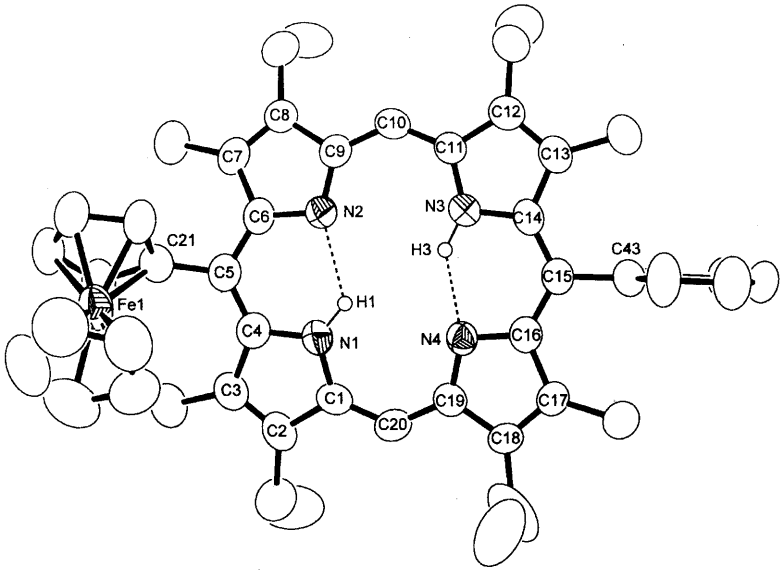
[a] $w = 1/[\sigma^2(F_o^2) + (0.1197P)^2 + 37.5443P]$ where $P = (F_o^2 + 2F_c^2)/3$.

2.3. Physical measurements

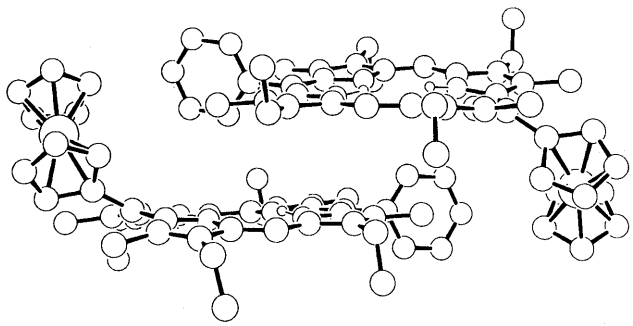
Elemental analyses (C, H, and N) were performed by Fisons EA 1110 analyzer. ^{1}H NMR spectra were recorded on a Bruker Spectrospin 400 instrument with chemical shifts being referenced against the signal of the deuterated NMR solvents. Electronic spectra were measured on a Shimadzu UV-3100S spectrophotometer. Thermogravimetric analyses were performed under nitrogen atmosphere at a heating rate of 10°C min^{-1} with DuPont TGA 2050 instrument. Electrochemical measurements were carried out on a BAS-100W system. Cyclic voltammetry was performed with 1×10^{-3} mol dm^{-3} solution of sample in dry CH_2Cl_2 containing 0.1 mol dm^{-3} of $(n\text{-}C_4H_9)_4NClO_4$ as supporting electrolyte. The potentials were determined with reference to the Ag–AgCl electrode at room temperature. Under these conditions ferrocene shows a reversible one-electron oxidation wave ($E_{1/2} = 0.37$ V).

2.4. X-ray crystallography

A purple crystal of **1**·0.5 C_6H_5Me with dimensions $0.5 \times 0.4 \times 0.25$ mm, obtained from toluene–methanol solution, was mounted on a thin glass fiber and intensity data were collected on an Enraf–Nonius CAD4 diffractometer equipped with monochromated Mo Kα ($\lambda = 0.71073$ Å) radiation. Unit cell parameters were determined from a least-squares fit of 25 accurately centered reflections ($22.45 < 2\theta < 27.22$). These dimensions and other parameters, including conditions of data collection, are summarized in Table 1. Data were collected at 293 K in the ω–2θ scan mode. Three intense reflections were monitored every 200 reflections to check stability. Of the 9932 unique reflections measured, 6198 were considered observed ($F_o > 4\sigma(F_o)$) and were used in subsequent structure analysis. Data were corrected for Lorentz and polarization effects. Empirical absorption correction using the ψ scan technique was applied. Maximum and minimum transmissions were 99.83 and 96.21%, respectively. The SHELXS-86 program was utilized for the direct method. The structure refinements were performed with the SHELXL-93 program on F^2 data. Anisotropic thermal parameters for all non-hydrogen atoms were included in the refinements. All hydrogen atoms bonded to carbon atoms were included in calculated positions. This C–H bond distance was fixed and U values were assigned based approximately on the U value of the attached atom. The other hydrogens (N–H) were included in located positions with $U = 0.08$ Å^2. The toluene molecule is



(a)



(b)

Fig. 1. Molecular structure of **1**, monomeric (a), and dimeric (b) structure.

refined with the regular hexagon model ($d_{C-C} = 1.39$ Å). A final difference Fourier map revealed several random features (< 0.627 eÅ^{-3}). The full-matrix least-squares refinement finally converged with $R_1 = 0.0780$ (based on F) and $wR_2 = 0.2032$ (based on F^2) for observed reflections ($F_o > 4\sigma(F_o)$).

3. Results and discussion

Compound **1** was synthesized by condensation of dipyrrylmethane with an equimolar mixture of benzaldehyde and ferrocenecarboxaldehyde. Pure **1** was separated from crude mixtures by column chromatography, and 5,15-diphenyl-2,8,12,18-tetraethyl-3,7,13,17-tetramethylporphyrin (**2**) was also obtained as a side-product in 28% yield but 5,15-diferrocenyl-2,8,12,18-tetraethyl-3,7,13,17-tetramethylporphyrin was not formed, because of steric demand.

The X-ray study of **1** shows that an asymmetric cell consists of one toluene solvent molecule and two ferrocenylporphyrins to form a dimer owing to a π–π interaction between the porphyrin planes. As shown in Fig. 1, the linked cyclopentadienyl (Cp) ring of the ferrocene substituent and the porphyrin plane twisted with dihedral angles of 47.1(3) and 49.3(3)°. The unusually small dihedral angles caused by large steric hindrance of β-pyrrolic methyl group imply that there might be a chance for a weak π-overlap between the Cp and the porphyrin rings. Furthermore, large steric hindrance of the β-pyrrolic methyl groups not only prevents the ferrocenyl moiety from rotating around the *meso* carbon but also results in distortion of the porphyrin ring. The C–C distance (1.50 Å) between the Cp and *meso* carbon of porphyrin is not significantly shorter than the pure single bond distance (1.52 Å) found in the 5,15-diferrocenylporphodimethene [12]. However, It should be considered that this bond distance of other ferrocenyl porphyrin complexes characterized by our and other

group was in the range of 1.477(5) ~ 1.498(8) Å which are significantly shorter than 1.52(1) Å. [6a,13] The conjugated feature of **1** was further explored by spectroscopic and electrochemical means. Selected bond distances and angles are listed in Table 2.

Table 2
Selected bond distances (Å) and angles (°) of **1**·0.5C_6H_5Me

Fe1–C21	2.072(6)	Fe1–C22	2.050(7)
Fe1–C23	2.038(7)	Fe1–C24	2.009(7)
Fe1–C25	2.013(7)	Fe1–C26	2.024(8)
Fe1–C27	2.026(8)	Fe1–C28	2.03(1)
Fe1–C29	2.02(1)	Fe1–C30	2.015(9)
C4–C5	1.383(8)	C5–C6	1.427(8)
C5–C21	1.505(9)	C15–C43	1.503(8)
C14–C15	1.391(8)	C15–C16	1.397(8)
N1–H1	0.948	N3–H3	0.952
C4–C5–C6	122.1(6)	C4–C5–C21	124.1(6)
C6–C5–C21	113.1(5)	C16–C15–C14	124.9(5)
C16–C15–C43	117.8(5)	C14–C15–C43	117.1(5)
Hydrogen bonding parameters			
N2…H1	2.021(5)	N4…H3	1.910(5)
N1…N2	2.692(7)	N3…N4	2.718(7)
N1…N4	3.160(7)	N2…N3	3.123(7)

Table 3
Half-wave potentials of porphyrin **1**, Zn·**1**, MnCl·**1**

Compound	$E_{1/2}$ (V) [a]		
	Ferrocene oxidation	Porphyrin oxidation	
1	0.29	0.61	1.05
Zn·**1**	0.22	0.45	0.83
MnCl·**1**	0.37	0.97 [b]	
Ferrocene	0.37		

[a] Obtained in CH_2Cl_2 solution containing 0.1 mol dm^{-3} TBAP as supporting electrolyte. Solutions were 1×10^{-3} mol dm^{-3} in compound and potentials were determined with reference to a Ag–AgCl electrode with 0.1 V s^{-1} scan rate.

[b] Two-electron process.

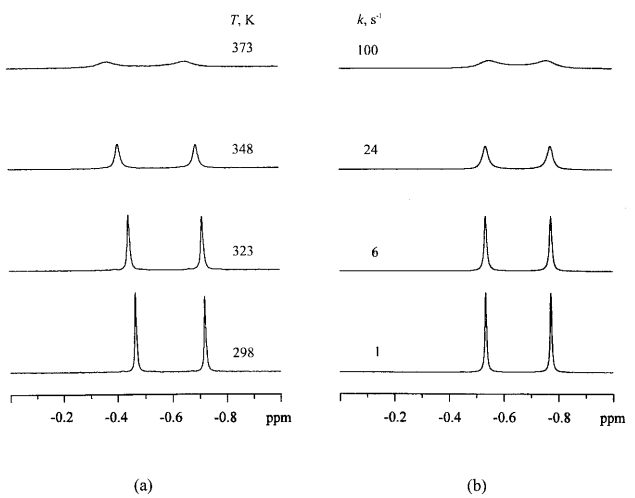
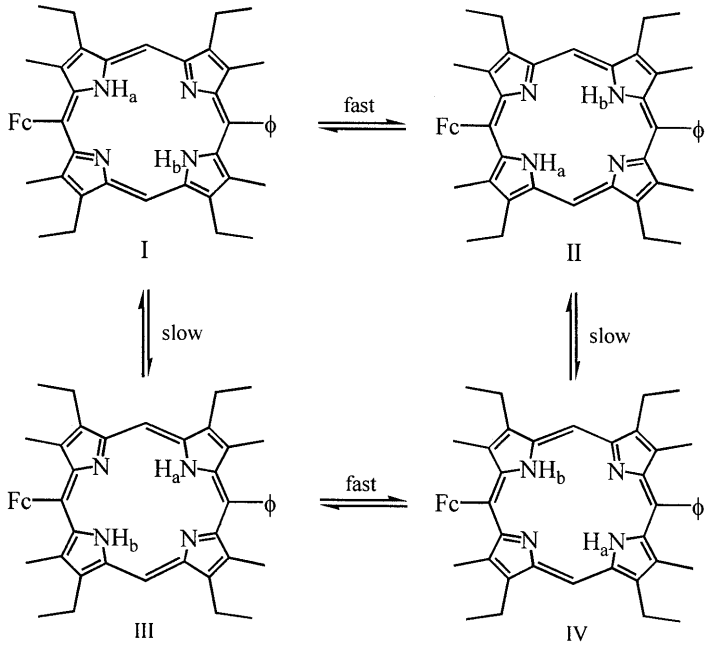


Fig. 2. Variable temperature ^1H NMR spectra for the nitrogen-bonded inner protons of porphyrin **1** in dry toluene-d_8. (a) observed and (b) calculated.

Electrochemical properties of **1** and its metal complexes Zn·**1** and MnCl·**1** in dichloromethane solution are summarized in Table 3. The ferrocenyl groups of compounds **1** and Zn·**1** undergo a reversible one-electron transfer process at 0.29 and 0.22 V, respectively. The values of half-wave oxidation potentials indicate that the ferrocenyl groups in these compounds are more susceptible for the oxidation than the free ferrocene. The easier ferrocenyl oxidation might be considered as a consequence of the great electron releasing ability of the porphyrin ring. In the case of MnCl·**1**, the higher oxidation state of Mn(III) is expected to reduce the electron releasing tendency of the porphyrin ring and thus make the ferrocene oxidation difficult. In fact, the oxidation potential of MnCl·**1** shifts to positive direction. The foregoing electrochemical analyses show that the oxidation of the ferrocene subunit is strongly affected by porphyrin ring as well as the central metal through extended π-conjugation.

^1H NMR data further support the strong electronic interaction of the ferrocenyl group with the porphyrin ring. In the case of **1** in chloroform, an electron withdrawing effect of ferrocenyl group through π-conjugation with the porphyrin ring was suggested to account for the large downfield shift of β-pyrrolic methyl protons adjacent to ferrocenyl group (3.35 ppm) compared to those adjacent to phenyl group (2.39 ppm). Furthermore, the chemical shifts for *meso* CH (9.86 ppm) and NH (−1.06 and −1.32 ppm) protons of **1** are quite different from the chemical shift for *meso* CH (10.22 ppm) and NH (−2.41 ppm) protons of **2**. This indicates that the ring current in **1** might be partially reduced due to the ring distortion [14]. Notably, the large downfield shift of NH for **1** compared to **2** can be interpreted by the N–H···N intramolecular hydrogen bonding [15].

The NH tautomerism in porphyrin is an intramolecular proton transfer process coupled with migration of double bonds. The two NH protons of the porphyrin **1** are situated on different chemical environments. Variable temperature ^1H NMR spectra of **1** in toluene-d_8 show two distinct singlets of equal intensities and line widths for NH protons as shown in Fig. 2. The chemical shifts are −0.47 and −0.72 ppm at 298 K. The presence of ferrocenyl substituent at only C5 position renders the two nitrogen-bonded protons magnetically nonequivalent at room temperature. The coalescence of the two NH peaks was unobserved up to the higher temperature limit of 373 K and only line broadening occurred, indicating that the exchange rate is very slow. This observation can be explained by considering that one kind of intramolecular N–H···N hydrogen bonding is prevailing against the other due to a rectangular



Scheme 1. Schematic representation of NH tautomerism.

elongation of porphyrin core. The X-ray analysis shows that **1** has two sets of short (2.69 and 2.72 Å) and long (3.12 and 3.16 Å) N···N distances and the short N···N distances lie in the known range (2.71 Å) observed for the N–H···N hydrogen bonding units of porphyrin [15]. Thus, the tautomerisations between tautomer I and III as well as between II and IV are not energetically favorable (Scheme 1) [16]. Based on the assumption that exchange is only responsible for the temperature-dependent line broadening, the rate constants for exchange can be determined. From plot of $\ln(k/T)$ versus $1/T$ according to Eyring equation [17], a straight line with $\Delta G^{\ddagger} = 51$ kJ mol^{-1} was obtained. This is similar to values reported in the literatures [18]. The exchange rate for NH protons depends on the solution conditions. When anhydrous chloroform is employed as a NMR solvent for **1**, the coalescing of the two NH peaks is not observed up to the higher temperature limit of 328 K. This is similar to the result observed in dry toluene as shown in Fig. 3. However, two NH signals are coalesced below room temperature in chloroform containing trace amount of residual water. It implies that the NH tautomerism of **1** in wet chloroform may be mediated by the trace amount of water in solvent. In dilute solution (0.04 mmol dm^{-3}) of porphyrin, the signal of NH protons is a singlet at 298 K. However, in concentrated solution (0.5 mmol dm^{-3}), the signals of NH protons split into two peaks because the rate of exchange becomes slower. Such result suggests that the rate of dynamic exchange of NH protons is accelerated in proportion to the water concentration of solution.

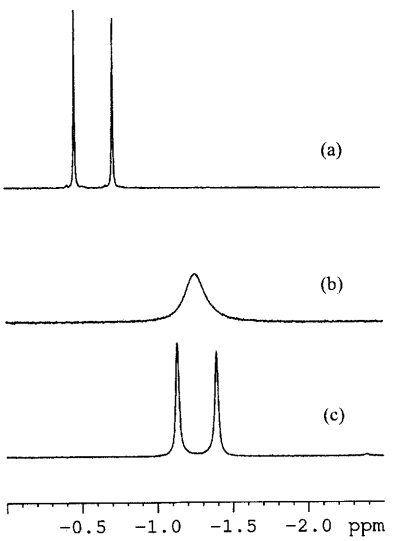


Fig. 3. ^{1}H NMR spectra of **1** in various solvent conditions at 298 K. (a) H_2**1**·0.5C_6H_5Me in anhydrous toluene-d_8, (b) H_2**1** in wet chloroform-*d*, and (c) H_2**1** in anhydrous chloroform-*d*.

4. Supplementary material

Crystallographic data for the structural analysis have been deposited with the Cambridge Crystallographic Data Centre, CCDC No. 140998. Copies of this information may be obtained free of charge from The Director, CCDC, 12 Union Road, Cambridge, CB2 1EZ, UK (fax: +44-1223-336033; e-mail: deposit@ccdc.cam.ac.uk or www: http://www.ccdc.cam.ac.uk).

Acknowledgements

This work was supported by the Korea Science and Engineering Foundation (981-0308-135-2).

References

[1] J. Jortner, M. Ratner (Eds.), Molecular Electronics, IUPAC, Blackwell, Oxford, 1997.
[2] (a) M.A. Fox, Acc. Chem. Res. 32 (1999) 201. (b) I. Willner, B. Willner, J. Mater. Chem. 8 (1998) 2543.
[3] (a) H. Kurreck, M. Huber, Angew. Chem., Int. Ed. Engl. 34 (1995) 849. (b) M.R. Wasielewski, Chem. Rev. 92 (1992) 435.
[4] (a) S.I. Yang, J. Seth, T. Balasubramanian, D. Kim, J.S. Lindsey, D. Holten, D.F. Bocian, J. Am. Chem. Soc. 121 (1999) 4008. (b) J.P. Strachan, S. Gentemann, J. Seth, W.A. Kalsbeck, J.S. Lindsey, D. Holten, D.F. Bocian, Inorg. Chem. 37 (1998) 1191. (c) S.I. Yang, R.K. Lammi, J. Seth, J.A. Riggs, T. Arai, D. Kim, D.F. Bocian, D. Holten, J.S. Lindsey, J. Phys. Chem., Part B 102 (1998) 9426.
[5] (a) T. Yamamoto, T. Morikita, T. Maruyama, K. Kubota, M. Katada, Macromolecules 30 (1997) 5390. (b) B. Bildstein, M. Schweige, H. Kopacka, K.-H. Ongania, K. Wurst, Organometallics 17 (1998) 2414. (c) J.T. Lin, J.J. Wu, C.-S. Li, Y.S. Wen, K.-J. Lin, Organometallics 15 (1996) 5028. (d) D. Posselt, W. Badur, M. Steiner, M. Baumgarten, Synthetic Metals 55 (1993) 3299. (e) M.J. Cohn, M.D. Timken, D.N.J. Hendrickson, Am. Chem. Soc. 106 (1984) 6683.
[6] (a) P.D.W. Boyd, A.K. Burrell, W.M. Campbell, P.A. Cocks, K.C. Gordon, G.B. Jamneson, D.L. Officer, Z. Zhao, Chem. Commun. (1999) 637. (b) A.K. Burrell, W.M. Campbell, D.L. Officer, Tetrahedron Lett. 38 (1997) 1249. (c) N.L. Loim, N.V. Abromova, V.I. Sokolov, Mendeleev Commun. (1996) 46. (d) R.G. Wollmann, D.N. Hendrickson, Inorg. Chem. 16 (1977) 3079.
[7] E.S. Schmidt, T.S. Calderwood, T.C. Bruice, Inorg. Chem. 25 (1986) 3718.
[8] D.D. Perrin, W.L.F. Armarego, Purification of Laboratory Chemicals, Pergamon Press, NewYork, 1988.
[9] D.T. Sawyer, A. Sobkowiak, J.L. Roberts Jr., Electrochemistry for Chemists, Wiley, New York, 1995.
[10] (a) R. Young, C.K. Chang, J. Am. Chem. Soc. 107 (1985) 898. (b) G.M. Sanders, M. van Dijk, A. van Veldhuizen, H. van der Plas, U. Hofstra, T.J. Schaafsma, J. Org. Chem. 53 (1988) 5272.
[11] A. Osuka, T. Nagata, F. Kobayashi, K. Maruyama, J. Heterocycl. Chem. 27 (1990) 1657.
[12] S.W. Rhee, Y.H. Na, Y. Do, J. Kim, Inorg. Chim. Acta (in press).
[13] S.W. Rhee, Y.H. Na, Y. Do, J. Kim (unpublished results).
[14] J.A. Shelnutt, X.-Z. Song, J.-G. Ma, S.-L. Jia, W. Jentzen, C.J. Medforth, Chem. Soc. Rev. 27 (1998) 31, and references therein.
[15] M.S. Somma, C.J. Medforth, N.Y. Nelson, M.M. Olmstead, R.G. Khoury, K.M. Smith, Chem. Commun. (1999) 1221.
[16] M. Asakawa, H. Toi, Y. Aoyama, H. Ogoshi, J. Org. Chem. 57 (1992) 5796.
[17] (a) H. Eyring, Chem. Rev. 17 (1935) 65. (b) S. Glasstone, K.J. Laidler, H. Eyring, The Theory of Rate Processes, McGraw-Hill, New York, 1941. (c) J. Sandström, Dynamic NMR Spectroscopy, Academic Press, New York, 1982.
[18] (a) R.J. Abraham, G.E. Hawkes, K.M. Smith, Tetrahedron Lett. 16 (1974) 1483. (b) K.M. Kadish, K.M. Smith, R. Guilard, The Porphyrin Handbook; Academic Press, Burlington, MA, 1999.

PERGAMON

www.elsevier.nl/locate/poly

Polyhedron 19 (2000) 1967–1973

POLYHEDRON

Synthesis and characterization of a new molecular magnet, $[Ni(ampy)_2]_3[Fe(CN)_6]_2 \cdot 6H_2O$, and synthesis, crystal structure and magnetic properties of its mononuclear precursor, *trans*-$[Ni(ampy)_2(NO_3)_2]$ (ampy = 2-aminomethylpyridine)

Stefania Tanase [a], Marilena Ferbinteanu [a], Marius Andruh [a,*], Corine Mathonière [b], Irina Strenger [c], Guillaume Rombaut [b]

[a] *Inorganic Chemistry Laboratory, Faculty of Chemistry, University of Bucharest, Str. Dumbrava Rosie nr. 23, 70254 Bucharest, Romania*
[b] *Laboratoire des Sciences Moléculaires, Institut de Chimie de la Matière Condensée de Bordeaux, 33608 Pessac, France*
[c] *Fachbereich Biologie/Chemie der Universität Kassel, Kassel, Germany*

Received 25 April 2000; accepted 30 June 2000

Dedicated to Professor Herbert W. Roesky, on the occasion of his 65th anniversary.

Abstract

The reaction of *trans*-$[Ni(ampy)_2(NO_3)_2]$ (**1**) (ampy = 2-aminomethylpyridine) with $K_3[Fe(CN)_6]$ affords a cyano-bridged bimetallic system, $[Ni(ampy)_2]_3[Fe(CN)_6]_2 \cdot 6H_2O$ (**2**). The crystal structure of compound **1** has been solved. It crystallizes in the monoclinic space group $P121/c1$ and consists of neutral mononuclear entities with the nickel atom located on an inversion center. The nickel atom exhibits a (pseudo)octahedral stereochemistry with the two nitrato ligands coordinated in *trans* positions. The Ni–N bond distances vary from 2.0690(15) to 2.0811(15) Å, while the *trans*-Ni–O distances are 2.1665(13) Å. The cryomagnetic investigation of compound **1** reveals an intermolecular ferromagnetic coupling ($\theta = +3.7$ K), which is mediated by the π–π stacking interactions between the mononuclear entities. Compound **2** is a soft ferromagnet with $T_c = 7.5$ K and a coercive field of 330 G at 2 K. © 2000 Elsevier Science Ltd. All rights reserved.

Keywords: Molecular magnets; Cyano-bridged heteropolynuclear complexes; Iron complexes; Nickel complexes; Ferromagnetic coupling

1. Introduction

In the past decade or so, we have been facing a spectacular revival of the chemistry generated by the hexacyanometallate anions [1,2]. This is due to the discovery of the spontaneous 3-D long-range magnetic ordering exhibited by the Prussian Blue (PB) analogues, $M'_q[M(CN)_6]_m \cdot nH_2O$ and $C^IM'^{II}[M^{III}(CN)_6] \cdot nH_2O$ [3–9]. It has been found that, for certain combinations of paramagnetic metal ions in the cubic PB framework, room-temperature molecule-based magnets can be obtained [7,10]. The interesting magnetic and photomagnetic properties of these materials gave a strong impulse to the development of an extremely rich coordination chemistry, which is based on self-assembly processes involving $[M(CN)_6]^{q-}$ templates and $[M'L_x(H_2O)_y]^{m+}$ assembling cations. The presence of ancillary (usually polydentate) ligands, L, in the coordination sphere of the assembling cation influences the topology of the spin carriers in the lattice, and, consequently, the magnetic properties. The M′(II)–M(III) pairs are chosen in order to achieve the strict orthogonality of the magnetic orbitals, which affords a ferromagnetic interaction between the nearest-neighbor metal ions (M′(II) = Cu(II), Ni(II); M(III) = Cr(III), l.s.–Fe(III)).

For the particular Ni(II)–Fe(III) pair, a survey of the recent literature reveals numerous polynuclear complexes, with interesting structures and physical properties. Depending on the nature of the ancillary ligands attached to the nickel ion, discrete entities or 1-D, 2-D and 3-D bimetallic assemblies are obtained. One

* Corresponding author. Tel.: +40-1-94-870656.
E-mail address: marius.andruh@dnt.ro (M. Andruh).

0277-5387/00/$ - see front matter © 2000 Elsevier Science Ltd. All rights reserved.
PII: S0277-5387(00)00497-6

Ni(II)–Fe(III) pentanuclear cluster, $[(Ni(bpm)_2)_3(Fe(CN)_6)_2]\cdot 7H_2O$ (bpm = bis(1-pyrazolyl)methane), has been characterized [11]. Its low nuclearity permitted accurate calculation of the value of the exchange coupling constant between cyano-bridged Ni(II) and low-spin Fe(III) ions ($J_{NiFe} = +5.3\ cm^{-1}$). Three types of compound exhibiting extended structures have been characterized in the Ni^{2+}–polydentate ligand–$[Fe(CN)_6]^{3-}$ system. They have the following stoichiometries: (a) $[Ni(LL)_2]_3[Fe(CN)_6]_2$ (Ni_3Fe_2) with a 1-D rope-ladder structure (LL = ethylenediamine) [12,13]; (b) $PPh_4[Ni(LL)_2][Fe(CN)_6]$ (NiFe) with a 1-D zig-zag chain structure (LL = propylenediamine) [14]; (c) $[Ni(LL)_2]_2[Fe(CN)_6]X$ (Ni_2Fe) with a 2-D square sheet structure (LL = 1,1-dimethylethylenediamine, propylenediamine; $X = ClO_4^-$, BF_4^-, PF_6^-, $CF_3SO_3^-$, $C_6H_5COO^-$, NO_3^-) [15–18]. By using tetradentate macrocyclic ligands, two $[Ni(MAC)]_3[Fe(CN)_6]_2$ compounds have been obtained, both with a 2-D honeycomb-like structure (MAC = cyclam, 1,4,8,11-tetraazacyclotetradecane [19]; 3,10-dimethyl-1,3,5,8,10,12-hexaazacyclotetradecane [20]). Finally, when the tripodal tetradentate ligand tris(2-aminoethyl)amine (tren) is used, the self-assembly between $[Ni(tren)]^{2+}$ and $[Fe(CN)_6]^{3-}$ ions leads to a cyano-bridged compound, $[Ni(tren)]_3[Fe(CN)_6]_2.6H_2O$, with a 3-D structure [21].

Beyond the beauty of their solid-state architectures, all these compounds played a very important role in gaining insights into the magnetostructural correlation of the cyano-bridged heteropolynuclear complexes. Magnetic ordering occurs in all compounds exhibiting 2-D and 3-D structures. As a matter of fact, it has been observed that the incorporation of an organic ligand in the $M'^{n+}/[M(CN)_6]^{q-}$ systems leads to materials undergoing magnetic phase transitions at lower temperatures than the PB analogue.

Table 1
Crystal data and structure refinement for crystal **1**

Empirical formula	$C_{12}H_{16}N_6NiO_6$
Formula weight	399.02
Crystal system	monoclinic
Space group	$P121/c1$
a (Å)	8.7300(10)
b (Å)	8.7320(10)
c (Å)	10.2620(10)
β (°)	101.547(7)
V (Å^3)	764.44(14)
Z	2
$F(000)$	412
D_{calc} (g cm^{-3})	1.729
Absorption coefficient (μ) (mm^{-1})	1.313
Final R indices	$R_1(I>2\sigma(I)) = 0.0261$; wR_2 (all data) = 0.0730
Goodness-of-fit	1.152

We report here on the magnetic properties of a new $Ni(II)_3Fe(III)_2$ cyano-bridged bimetallic complex, $[Ni(ampy)_2]_3[Fe(CN)_6]_2\cdot 6H_2O$, as well as on the crystal structure and magnetic properties of its mononuclear precursor, *trans*-$[Ni(ampy)_2(NO_3)_2]$ (ampy = 2-aminomethylpyridine) (Table 1).

2. Experimental

2.1. Synthesis

The chemicals were purchased from Aldrich and all manipulations were performed using materials as received.

trans-$[Ni(ampy)_2(NO_3)_2]$ (**1**) was prepared by mixing an aqueous solution of $Ni(NO_3)_2\cdot 6H_2O$ (10 ml, 1 mmol) with 2 mmol of 2-aminomethylpyridine. The slow evaporation of the resulting mixture led to a highly crystalline blue material. IR data (KBr, cm^{-1}): 3337m, 3283m, 3258m, 2927w, 2858vw, 1607m, 1569w, 1496w, 1416m, 1383vs, 1315s, 1287m, 1180w, 1147w, 1117w, 1100w, 1035m, 939vw, 886vw, 774m, 725w, 638w, 571w. Elemental analyses: Found: C, 35.6; H, 4.1; N, 14.4%; Calc.: C, 36.08; H, 4.00; N, 14.71%.

$[Ni(ampy)_2]_3[Fe(CN)_6]_2\cdot 6H_2O$ (**2**): an aqueous solution containing compound **1** (30 ml; 1 mmol) was added to an aqueous solution of $K_3[Fe(CN)_6]$ (20 ml; 0.6 mmol). The resulting brown precipitate was filtered off and washed with water. IR data (KBr, cm^{-1}): 3424vs, 3355vs, 3286vs, 2920w, 2144s, 2114s, 1606vs, 1484m, 1442s, 1380m, 1155m, 1077m, 1023vw, 771s, 638m. Elemental analyses: Found: C, 42.7; H, 4.4; N, 24.3; Fe, 7.9; Ni, 13.1%; Calc.: C, 42.48; H, 4.22; N, 24.78; Fe, 8.23; Ni, 12.98%.

$[Ni(ampy)_2]_3[Co(CN)_6]_2\cdot 6H_2O$ (**3**) was obtained following the same procedure as for compound **2**. Violet powder. IR data (KBr, cm^{-1}): 3421vs, 3355vs, 3281vs, 2924m, 2854m, 2154vs, 2124vs, 1606vs, 1570m, 1484m, 1441s, 1379m, 1283m, 1154m, 1111w, 1076m, 1021vs, 932m, 811w, 770s, 731w. Elemental analyses: Found: C, 41.7; H, 4.2; N, 24.2; Co, 8.1; Ni, 12.1%; Calc.: C, 41.92; H, 4.36; N, 24.45; Co, 8.57; Ni, 12.81%.

2.2. Physical measurements

The IR spectra (KBr pellets) were measured on a BIO-RAD FTS 135 spectrometer. UV–Vis spectra (diffuse reflectance technique) were recorded with a VSU2 spectrophotometer with MgO as a standard. Magnetic measurements were carried out on a Quantum Design MPMS-5S SQUID magnetometer.

2.3. Crystallography

The data collection for **1** was made at room temperature on an Enraf–Nonius CAD4 diffractometer with a

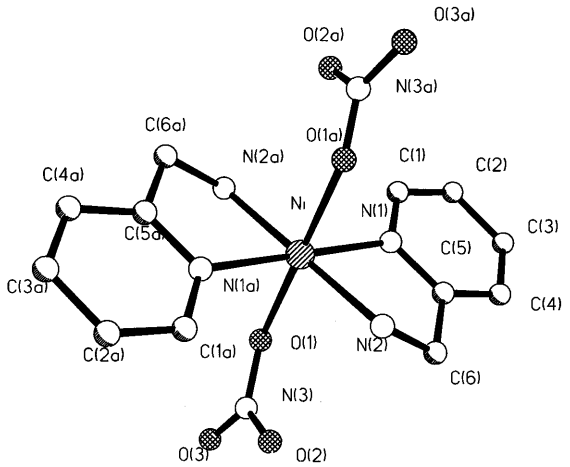


Fig. 1. Perspective view of compound **1** with the atom numbering scheme.

Table 2
Selected bond lengths (Å) and angles (°) for **1**[a]

Ni–N(1)	2.0811(15)	Ni–N(1) # 1	2.0811(15)
Ni–N(2)	2.0690(15)	Ni–N(2) # 1	2.0690(15)
Ni–O(1)	2.1665(13)	Ni–O(1) # 1	2.1665(13)
N(2)–Ni–N(1)	79.92(6)	N(1) # 1–Ni–N(1)	180.0
N(2)–Ni–O(1)	94.99(6)	N(2)–Ni–O(1) # 1	85.01(6)
N(1)–Ni–O(1)	88.65(6)	N(3)–O(1)–Ni	127.15(10)
N(2) # 1–Ni–N(2)	180.0	C(5)–N(1)–Ni	113.88(11)
N(2)–Ni–N(1) # 1	100.08(6)	C(1)–N(1)–Ni	127.86(13)
N(1) # 1–Ni–O(1)	91.35(6)	C(6)–N(2)–Ni	109.06(11)

[a] Symmetry transformations to generate equivalent atoms: # $1-x$, $-y$, $z+1$.

graphite-monochromatized Mo Kα radiation ($\lambda =$ 0.71073 Å). The $\omega-2\theta$ scan technique was used ($\theta_{max} =$ 25.00°). A total of 1434 reflections were collected, of which 1351 independent reflections ($R_{int} = 0.0080$). The coordinates of the heavy atoms were determined from direct methods and the positions of all non-hydrogen atoms were found by usual Fourier techniques. The refinement of the structure was done by full-matrix least-squares techniques) on F^2 (SHELX-97) and converged to R_1 ($I > 2\sigma(I)$) = 0.0261, wR_2 (all data) = 0.0730, Goodness-of-fit = 1.152, largest difference peak and hole 0.273 and -0.614 Å^{-3}.

3. Results and discussion

The synthesis of the cyano-bridged polynuclear compound, $[Ni(ampy)_2]_3[Fe(CN)_6]_2 \cdot 6H_2O$, is based on the observation that bis-chelated Ni(II) complexes, $[Ni(chelate)_2X_2]$, are very good candidates for self-assembly processes with $[M(CN)_6]^{3-}$ templates. These processes consist in the replacement of the weakly bound anions, X^-, with bridging cyano groups. Therefore, the first step in our work was the synthesis of a bis-chelated nickel(II) complex with 2-aminomethylpyridine (ampy) as a bidentate ligand. Indeed, the reaction between $Ni(NO_3)_2 \cdot 6H_2O$ with ampy in a metal:ligand molar ratio of 1:2 leads to the mononuclear complex $[Ni(ampy)_2(NO_3)_2]$ (**1**).

Let us discuss first the crystal structure and the magnetic properties of the nickel(II) precursor. The structure in itself has nothing exceptional and consists of neutral mononuclear $[Ni(ampy)_2(NO_3)_2]$ entities. However, the crystal structure proves that this compound, with only two molecules of chelating ligands and two potentially free coordination sites, is a suitable starting material in synthesizing cyano-bridged Ni(II)–Fe(III) polynuclear complexes. The nickel atom lies on an inversion center and the nitrato ligands occupy the *trans* positions (Fig. 1). Selected bond distances and angles are given in Table 2. The nickel atom is coordinated to four nitrogen atoms of the chelating ampy ligands and two oxygen atoms, from two nitrato ligands, in a distorted octahedral geometry. The distortion of the octahedron arises mainly from the short bite of the ampy ligands (79.92(6)°). The Ni–N distances are very close; Ni–N(py) = 2.0811(15) and Ni–N(NH_2) = 2.0690(15) Å). The Ni–O bond lengths are slightly longer (2.1665(13) Å) in comparison with the Ni–N. Compound **1** crystallizes as one of the five possible isomers, [22], namely the α-*trans* isomer (*trans*-NO_3, *trans*-py, *trans*-NH_2).

The solid-state electronic spectrum of **1** is typical for a (pseudo)octahedral Ni(II) complex, showing the expected d–d bands at: 989, 644, and 422 nm. These bands are assigned to following transitions: $^3A_{2g} \rightarrow {}^3T_{2g}$ and $^3A_{2g} \rightarrow {}^3T_{1g}$, and $^3A_{2g} \rightarrow {}^3T_{1g}(P)$, respectively.

Surprisingly, the cryomagnetic investigation of **1** reveals an intermolecular ferromagnetic coupling. The magnetic properties are shown in Fig. 2 in the form of $\chi_M T$ versus T plot. The value of the $\chi_M T$ product at room temperature (1.202 cm^3 mol^{-1} K) corresponds to the expected value for non-interacting Ni(II) ions. By lowering the temperature, $\chi_M T$ increases, reaching a maximum value at 30 K (1.283 cm^3 mol^{-1} K), then abruptly decreases to a value of 0.93 cm^3 mol^{-1} K at 5 K.

In order to understand the magnetic behavior of **1**, we have analyzed the packing diagram of the molecules in the crystal. The most interesting structural feature, at the supramolecular level, consists in the stacking interactions involving the pyridyl moieties of neighboring mononuclear entities. The weak intermolecular π–π overlap leads to infinite chains (Fig. 3) and thus provides an exchange pathway. Weak magnetic interactions across π-stacking have been already observed with several compounds [23–25]. In one case, namely between Mn(II) ions, the intermolecular interaction was found to be ferromagnetic [23]. The magnetic behavior

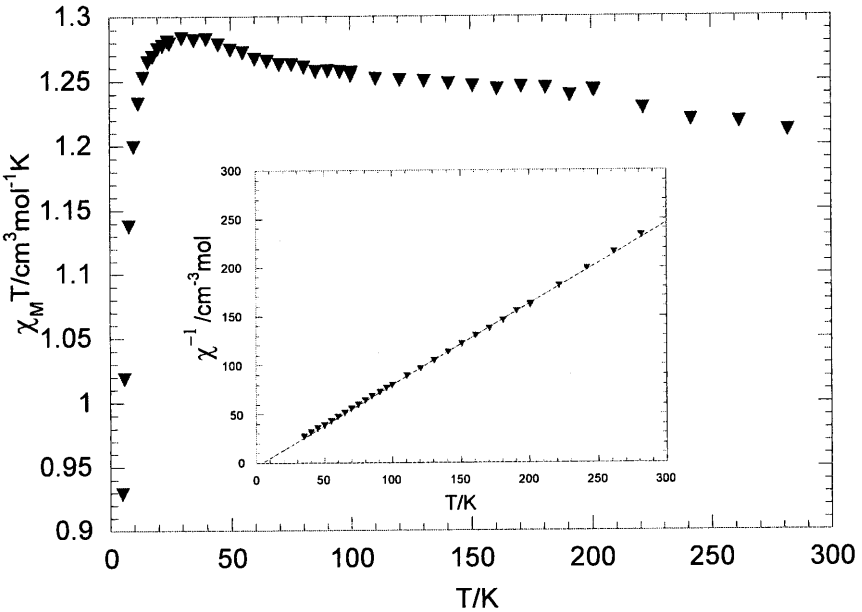


Fig. 2. Temperature dependence of $\chi_M T$ and χ_M^{-1} (inset) for compound **1**.

of **1** below 30 K could be explained by the onset of long-range antiferromagnetic ordering and/or by a zero-field splitting of the ground state of the Ni(II) ion. The data between 300 and 30 K have been fitted through the Curie–Weiss law, $\chi^{-1} = (T - \theta)/C$ (see the inset in Fig. 2). The fit leads to $\theta = +3.7$ K, $C = 1.205$ cm^3 mol^{-1} K, and $g = 2.19$. Given that $\theta = zJ'S(S+1)/3k$ and $S = 1$, it follows that $zJ' = 3.8$ cm^{-1}. As the packing of **1** shows, z is equal to 2 and, consequently, $J' = +1.9$ cm^{-1}. By fitting with the Curie–Weiss law the data below 30 K, one obtains $\theta = -1.7$ K.

The bimetallic assembly, $[Ni(ampy)_2]_3[Fe(CN)_6]_2 \cdot 6H_2O$ (**2**), has been obtained as brown crystals by the reaction of **1** with $K_3[Fe(CN)_6]$ in water. The infrared spectrum shows two characteristic bands of the CN^- groups in the region between 2100 and 2200 cm^{-1}, indicating both their terminal and bridging functions. The band located at 2144 cm^{-1} is assigned to the bridging cyano groups, while the other one (2114 cm^{-1}) is assigned to the terminal cyano ligands. The diffuse reflectance electronic spectrum shows a shoulder at 920 nm and one band at 520 nm. These are characteristic for the Ni(II) ions in a (pseudo)octahedral environment and are assigned to the $^3A_2 \rightarrow {}^3T_2$ and $^3A_2 \rightarrow {}^3T_1$ spin-allowed transitions (assuming the O site symmetry) [26]. The band located at 440 nm is due to a ligand-to-metal charge transfer within the $\{Fe(CN)_6\}$ chromophore. The cobalt(III) derivative, $[Ni(ampy)_2]_3[Co(CN)_6]_2 \cdot 6H_2O$ (**3**), exhibits a very similar infrared spectrum with compound **2**, with bridging and terminal cyano groups (ν(CN) = 2154, and 2124 cm^{-1}).

The magnetic properties of compound **2** have been investigated in the temperature range 2–300 K. The $\chi_M T$ versus T plot is given in Fig. 4. At room tempera-

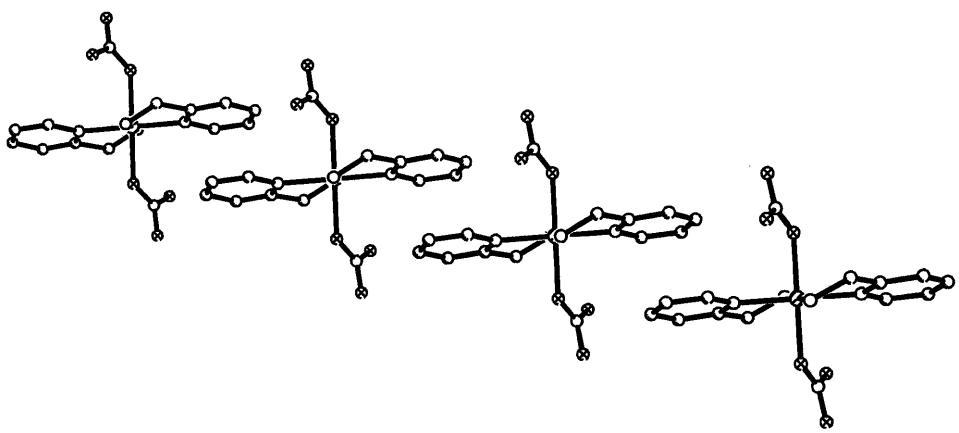


Fig. 3. Packing diagram for compound **1** showing the π–π stacking interactions.

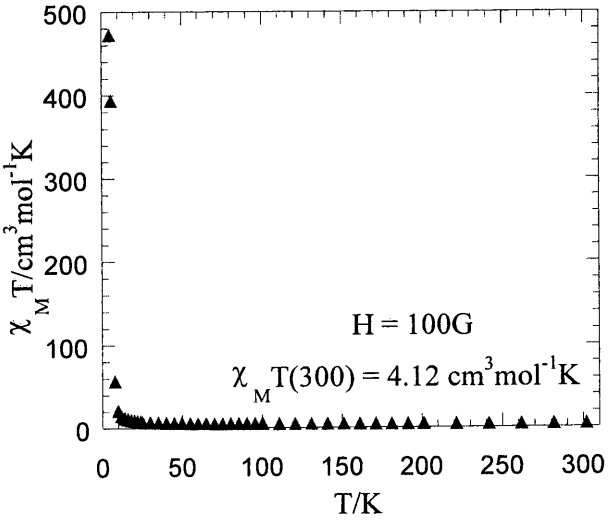


Fig. 4. $\chi_M T$ versus T plot for compound **2**.

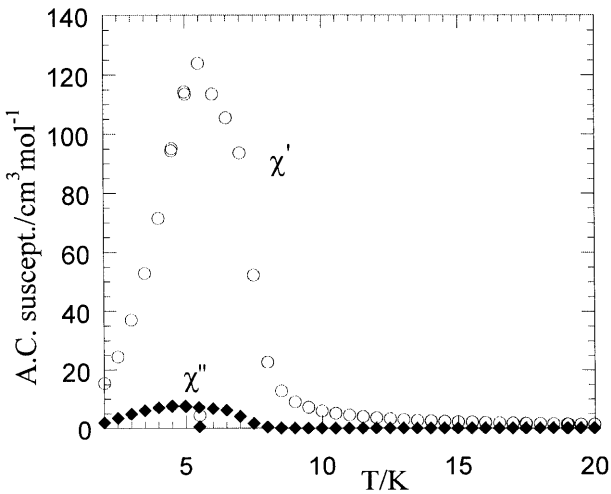


Fig. 5. In-phase(χ') and out-of-phase (χ'') ac magnetic susceptibility as a function of temperature for compound **2**.

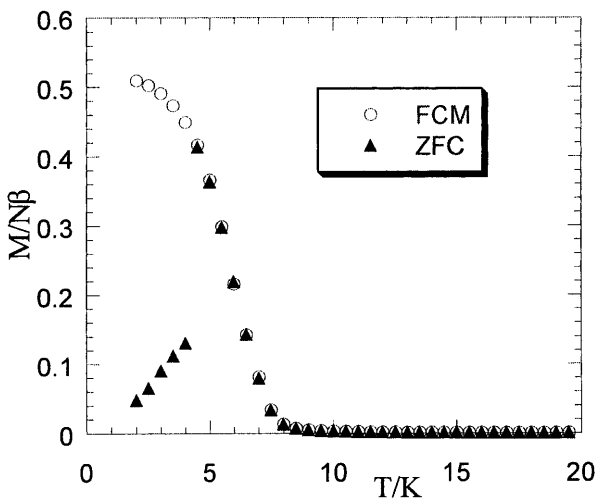


Fig. 6. Temperature dependence of the FCM and ZFCM curves for compound **2**.

ture, the value of the $\chi_M T$ product is 4.12 $cm^3\ mol^{-1}$ K (per Ni_3Fe_2), being close to the value expected for an uncoupled Ni_3Fe_2 system (4.13 $cm^3\ mol^{-1}$ K, with $g = 2.1$). Down to 30 K, $\chi_M T$ is constant, then diverges reaching a maximum value of 470 $cm^3\ mol^{-1}$ K at 2 K. This behavior suggests that a long-range ferromagnetic ordering occurs. The ferromagnetic interaction is rationalized by the strict orthogonality of the e_g(Ni(II)) and t_{2g}(low spin-Fe(III)) orbitals [27].

The ferromagnetic transition in compound **2** is further confirmed by ac magnetic susceptibility measurements in the temperature range 2–20 K ($\nu_{ac} = 125$ Hz, $H_{ac} = 1$ G) (Fig. 5). The in-phase (real) component, χ', increases sharply when the sample is cooled below 9 K, reaching a maximum around 5.5 K. The out-of-phase (imaginary) χ'' component shows a broad hump with maximum at 5 K. The non-zero value of χ'' is another indication of the bulk magnetic ordering in **2**. Usually, the T_c temperature is defined as the inflexion point in the increasing part of the χ' curve, as well as the point where χ'' becomes non-zero. In our case the two points are coincident, $T_c = 7.5$ K.

The magnetization studies are also in line with the ferromagnetic nature of **2** (Fig. 6). The field-cooled magnetization (FCM) curve, which is obtained on cooling the sample within a field of 10 G, exhibits a break at $T_c = 7.5$ K and begins to saturate below 4 K. The zero-field-cooled magnetization (ZFCM) curve, measured upon cooling down in zero field, shows also a break at $T_c = 7.5$ K. The field dependence of the magnetization, $M = f(H)$, was measured at 2 K up to 50 kG (Fig. 7). The material begins to saturate at high fields, but not completely ($M = 7.2\ N\beta$ at 50 kG, the theoretical saturation value being $M_s = 8\ N\beta$). The M versus H curve shows hysteresis behavior (see the inset in Fig. 7), which is observed upon cycling the applied field.

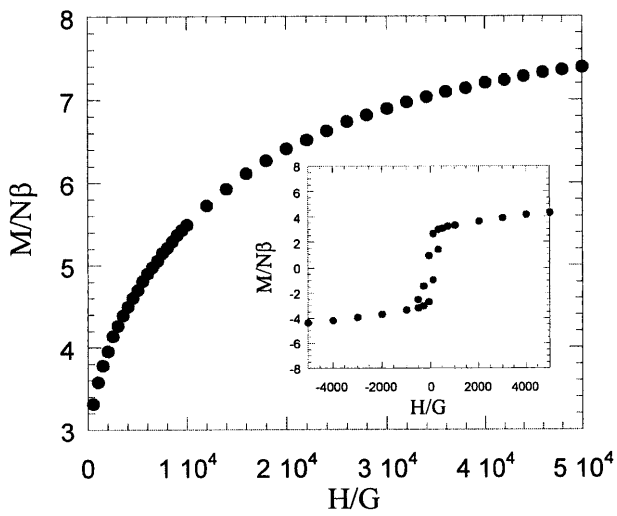


Fig. 7. Magnetization and hysteresis loop (inset) at 2 K as a function of the applied field for compound **2**.

Table 3
$Ni(II)_3Fe(III)_2$ cyano bridged complexes with long-range magnetic ordering

Compound	Structure	Magnetic behavior	T_c (K)	Reference
$[Ni(en)_2]_3[Fe(CN)_6]_2 2H_2O$	1-D (rope-ladder)	metamagnet	18.6	[12,13]
$[Ni(cyclam)_2]_3[Fe(CN)_6]_2 22.5H_2O$	2-D (honeycomb)	ferromagnet	3	[19]
$[Ni(mac)_2]_3[Fe(CN)_6]_2 9H_2O$ [a]	2-D (honeycomb)	metamagnet	5	[20]
$[Ni(tren)_2]_3[Fe(CN)_6]_2 6H_2O$	3-D	ferrimagnet	8	[21]
$[Ni(pn)_2]_3[Fe(CN)_6]_2 12H_2O$	unknown	ferromagnet	19	[28]
$[Ni(bpm)(H_2O)_2]_3[Fe(CN)_6]_2 2H_2O$ [b]	unknown	ferromagnet	19	[29]
$[Ni(ampy)_2]_3[Fe(CN)_6]_2 6H_2O$	unknown	ferromagnet	7.5	this work

[a] mac = 3,10-dimethyl-1,3,5,8,10,12-hexaazacyclotetradecane.
[b] bpm = bispyrazolylmethane.

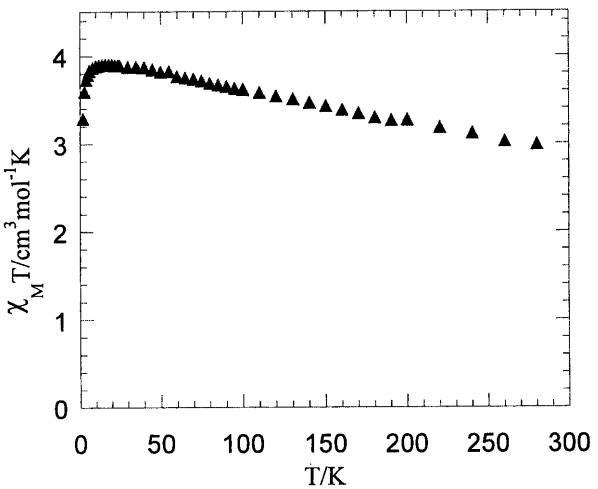


Fig. 8. $\chi_M T$ versus T plot for compound **3**.

According to the value of the coercive field, $H_c = 330$ G, compound **2** may be considered as a soft magnet.

Compound **3**, $[Ni(ampy)_2]_3[Co(CN)_6]_2 \cdot 6H_2O$, is most probably isostructural with compound **2**. Such families of isostructural $[M(CN)_6]^{3-}$–M′(II)-chelate bimetallic compounds (M = Fe(III), Cr(III), Co(III)) are already known [13,30]. The cryomagnetic investigation of the Co(III) derivative, since $[Co(CN)_6]^{3-}$ is diamagnetic, gives information about the pure Ni(II)–Ni(II) exchange interactions. The magnetic properties of compound **3** are shown in the form of $\chi_M T$ versus T plot (Fig. 8). The value of the $\chi_M T$ product at room temperature (2.92 cm^3 mol^{-1} K) corresponds to three uncoupled Ni(II) ions. By lowering the temperature, $\chi_M T$ increases reaching a maximum value (3.90 cm^3 mol^{-1} K) at 18 K. Below this temperature, $\chi_M T$ decreases. Such a behavior is characteristic of dominant ferromagnetic interactions to which antiferromagnetic interactions are superimposed.

Only a few cyano-bridged polynuclear complexes with the stoichiometry $[Ni(polydentate\ ligand)_x]_3[Fe(CN)_6]_2 \cdot nH_2O$ and extended structures have been reported so far (Table 3). Some of them have been structurally characterized.

The analysis of the magnetic properties of the compounds presented in Table 3 shows that the critical temperatures are always lower than for the corresponding PB analogue, $Ni_3[Fe(CN)_6]_2 \cdot xH_2O$ ($T_c = 23$ K, [31]). To date, this seems to be true for all the systems obtained by introducing an organic ligand in PB-like phases, irrespective of the nature of the paramagnetic metal ions.

4. Supplementary material

Crystallographic data for the structural analysis has been deposited with the Cambridge Crystallographic Data Centre, CCDC No. 142419. Copies of this information may be obtained free of charge from The Director, CCDC, 12 Union Road, Cambridge, CB2 1EZ, UK (fax: +44-1223-336033; e-mail deposit@ccdc.cam.ac.uk or www: http://www.ccdc.cam.ac.uk).

Acknowledgements

We are grateful to the Romanian Ministry of National Education for financial support of this research (Grants 30C/CNCSIS and 1D/CNCSIS).

References

[1] K.R. Dunbar, R.A. Heintz, Progr. Inorg. Chem. 45 (1997) 283 and references therein.
[2] M. Verdaguer, A. Bleuzen, V. Marvaud, J. Veissermann, F. Tournilhac, C. Train, R. Ouahès, R. Garde, F. Fabrizi de Biani, C. Desplanches, A. Scuiller, in: G. Ondrejovic, A. Sirota (Eds.), Coordination Chemistry at the Turn of the Century, STU Press, Bratislava, 1999, p. 67 and references therein.
[3] D. Babel, Comments Inorg. Chem. 5 (1982) 285.
[4] V. Gadet, T. Mallah, I. Castro, M. Verdaguer, J. Am. Chem. Soc. 114 (1992) 9213.
[5] T. Mallah, S. Thiebaut, M. Verdaguer, P. Veillet, Science 262 (1993) 1554.
[6] W.R. Entley, G.S. Girolami, Science 268 (1995) 397.
[7] S. Ferlay, T. Mallah, R. Ouhès, P. Veillet, M. Verdaguer, Nature 378 (1995) 701.

[8] O. Sato, T. Iyoda, A. Fujishima, K. Hashimoto, Science 271 (1996) 49.
[9] O. Kahn, Nature 378 (1995) 667.
[10] R. Garde, C. Desplanches, A. Bluezen, P. Veillet, M. Verdaguer, Mol. Cryst. Liq. Cryst. 334 (1999) 587 and references therein.
[11] K. Van Langenberg, S.R. Batten, K.J. Berry, D.C.R. Hockless, B. Moubaraki, K.S. Murray, Inorg. Chem. 36 (1997) 5006.
[12] M. Ohba, N. Maruono, H. Okawa, T. Enoki, J.-M. Latour, J. Am. Chem. Soc. 116 (1994) 11566.
[13] M. Ohba, N. Fukita, H. Okawa, J. Chem. Soc., Dalton Trans. (1997) 1733.
[14] M. Ohba, N. Usuki, N. Fukita, H. Okawa, Inorg. Chem. 37 (1998) 3349.
[15] M. Ohba, H. Okawa, N. Fukita, Y. Hashimoto, J. Am. Chem. Soc. 119 (1997) 1011.
[16] M. Ohba, H. Okawa, T. Ito, A. Ohto, J. Chem. Soc., Chem. Commun. (1995) 1545.
[17] M. Ohba, H. Okawa, Mol. Cryst. Liq. Cryst. 286 (1996) 101.
[18] H.-Z. Kou, W.-M. Bu, D.-Z. Liao, Z.-H. Jiang, S.-P. Yan, Y.-G. Fan, G.-L Wang., J. Chem. Soc., Dalton Trans. (1998) 4161.
[19] E. Colacio, J.M. Dominguez-Vera, M. Ghazi, R. Kivekäs, F. Lloret, J.M. Moreno, H. Stoeckli-Evans, Chem. Commun. (1999) 987.
[20] H.-Z. Kou, S. Gao, W.-M. Bu, D.-Z. Liao, B.-Q. Ma, Z.-H. Jiang, S.-P. Yan, Y.-G. Fan, G.-L. Wang, J. Chem. Soc., Dalton Trans. (1999) 2477.
[21] S. El Fallah, E. Rentschler, A. Caneschi, R. Sessoli, D. Gatteschi, Angew. Chem., Int. Ed. Engl. 35 (1996) 1947.
[22] (a) D.J. Ayres, D.A House, W.T. Robinson, Inorg. Chim. Acta 277 (1998) 177. (b) H. Kooijman, A.L. Spek, D. Rehorst, W.L. Driessen, J. Reedijk, Acta Cryst., Sect. C 53 (1997) 1596.
[23] M. Wesolek, D. Meyer, J.A. Osborn, A. De Cian, J. Fischer, A. Derory, P. Legoll, M. Drillon, Angew. Chem., Int. Ed. Engl. 33 (1994) 1592.
[24] A.J. Amoroso, J.C. Jeffery, P.L. Jones, J.A. McCleverty, P. Thornton, M.D. Ward, Angew. Chem., Int. Ed. Engl. 34 (1995) 1443.
[25] M.C. Muñoz, M. Julve, F. Lloret, J. Faus, M. Andruh, J. Chem. Soc., Dalton Trans. (1998) 3125.
[26] A.B.P. Lever, Inorganic Electronic Spectroscopy, 2nd ed., Elsevier, Amsterdam, 1984, p. 511.
[27] O. Kahn, Molecular Magnetism, VCH, New York, 1993.
[28] E.V.K. Suresh Kumar, S.A. Chavan, A.K. Sra, M.K. Bhide, M.D. Sastry, R. Ganguly, H.B. Singh, J.V. Yakhmi, Philos. Mag., Sect B 79 (1999) 127.
[29] K.S. Murray, G.D. Fallon, D.C.R. Hockless, K.D. Lu, B. Moubaraki, K. Van Langenberg, in: M.M. Turnbull, T. Sugimoto, L.K. Thompson (Eds.), Molecule-Based Magnetic Materials, ACS, Washington, 1996, p. 201.
[30] M. Ferbinteanu, S. Tanase, M. Andruh, Y. Journaux, F. Cimpoesu, I. Strenger, E. Rivière, Polyhedron 18 (1999) 3019.
[31] V. Gadet, M. Bujoli-Doeuff, L. Force, M. Verdaguer, K.E. Malkhi, A. Deroy, J.P. Besse, C. Chappert, P. Veillet, J.P. Renard, P. Beauvillain, in: D. Gatteschi, O. Kahn, J.S. Miller (Eds.), Magnetic Molecular Materials, vol. 198, Plenum, New York, 1991, p. 281 NATO ASI Series.

PERGAMON

www.elsevier.nl/locate/poly

Polyhedron 19 (2000) 1975–1983

POLYHEDRON

Synthesis, electrochemical and spectroscopic properties of ruthenium(II) complexes containing 1,3-bis([1,10]phenanthroline-[5,6-*d*]imidazol-2-yl)benzene

Hui Chao, Bao-Hui Ye, Hong Li, Run-Hua Li, Jian-Ying Zhou, Liang-Nian Ji *

State Key Laboratory of Ultrafast Laser Spectroscopy, Department of Chemistry, Zhongshan University, Guangzhou 510275, PR China

Received 22 February 2000; accepted 30 June 2000

Abstract

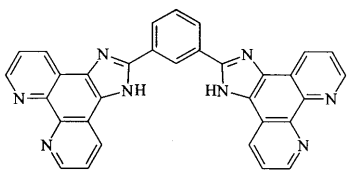
1,3-Bis([1,10]phenanthroline-[5,6-*d*]imidazol-2-yl)benzene ($mbpibH_2$) and its $(bpy)_2Ru^{2+}$ complexes (bpy = 2,2′-bipyridine) have been synthesized and characterized. The electrochemical and spectroscopic studies of the mono- and dinuclear complexes have shown that there is very little or no interaction between the linked metal centers. The absorption spectra of the mono- and dinuclear complex are both strongly dependent on the solution pH. The deprotonation of the bridging ligand $mbpibH_2$ also induces a pertubation on the spectral and redox properties of the dinuclear complex. © 2000 Elsevier Science Ltd. All rights reserved.

Keywords: Bpy ligands; Polypyridine ligands; Ruthenium(II) complexes

1. Introduction

Photoinduced energy- and electron-transfer in supramolecular systems have attracted much current attention in connection with the design of molecular electronic devices [1–3]. Ruthenium(II) complexes of polypyridine-type ligands are excellent building blocks for the construction of such devices due to their rich photochemical and photophysical properties [4]. Thus, it is not surprising that the number of investigations concerning the photochemical and photophysical behavior of dinuclear or polynuclear ruthenium(II) polypyridine complexes is rapidly growing [5–16]. In most cases, the spacer between the metal centers is a polychelating ligand and it plays an important role in the polynuclear complex, since the interaction between the bridged units, and thereby the properties of the polynuclear complex, are critically dependent on the size, shape and electronic nature of the spacer.

Recently, protonation has been shown to induce the switching of fluorescence, redox properties, and electron transfer reactions [17–21]. This motivated us to design a new phen-based bridging ligand: 1,3-bis([1,10]-phenanthroline-[5,6-*d*]imidazol-2-yl)benzene ($mbpibH_2$) (Chart 1). A unique feature of this bridging ligand is its two imidazole intervening fragments, which can undergo reversible acid–base interversion by protonation and deprotonation to induce a large energy perturbation. Although several diruthenium(II) complexes containing imidazole fragment have been reported [10,22–25], in most cases the imidazole ring is coordinated to the metal ion and not protonated. We describe here the synthesis, electrochemical and spectroscopic properties of ruthenium(II) complexes containing the ligand $mbpibH_2$.



(Chart 1)

* Corresponding author. Tel.: +86-20-8411-0115, fax: +86-20-8403-5497.

E-mail address: cesjln@zsu.edu.cn (L.-N. Ji).

0277-5387/00/$ - see front matter © 2000 Elsevier Science Ltd. All rights reserved.
PII: S0277-5387(00)00500-3

2. Experimental

2.1. Materials and preparations

The compounds *cis*-$[Ru(bpy)_2Cl_2]\cdot 2H_2O$ [26] and 1,10-phenanthroline-5,6-dione [27] were synthesized according to literature methods. Other materials were commercially available and of reagent grade.

(**Caution**: perchlorate complexes are potential explosives. These complexes must be handled in small quantities and with great care.)

2.1.1. Synthesis of 2-(3-formylphenyl)imidazo[4,5-f]-[1,10]phenanthroline (mfmp)

A mixture of isophthalic aldehyde (0.201 g, 1.5 mmol), 1,10-phenanthroline-5,6-dione (0.315 g, 1.5 mmol), ammonium acetate (2.31 g, 30 mmol) and glacial acetic acid (30 cm^3) was refluxed for about 2 h, and then cooled to room temperature (r.t.) and diluted with water (ca. 60 cm^3). Dropwise addition of concentrated aqueous ammonia gave a yellow precipitate, which was collected and washed with water. The crude product in ethanol was purified by silica gel filtration (60–100 mesh, ethanol). The principal yellow band was collected. A yellow crystalline solid was obtained by slow evaporation of the solution, then were dried in vacuo. Yield 0.369 g, 76% (Found: C, 74.0; H, 3.9; N, 16.9. $C_{20}H_{12}N_4O$ requires C, 74.1; H, 3.7; N, 17.3%). ν (cm^{-1}) 3374m, 3064s, 1693s 1609m, 1546m, 1507m, 1400m, 805s, 737s and 674m. ^{1}H NMR data (300 M, DMSO-d_6): δ 13.94 (s, 1H), 10.17 (s, 1H), 9.04 (d, 2H, $J = 4.5$), 8.94 (d, 2H, $J = 8$), 8.81 (s, 1H), 8.62 (d, 1H, $J = 7.8$), 8.04 (d, 1H, $J = 7.5$), 7.84 (q, 3H). FABMS: $m/z = 325$ ($C_{20}H_{12}N_4O$ requires 324).

2.1.2. Synthesis of 1,3-bis([1,10]phenanthroline-[5,6-d]-imidazol-2-yl)benzene (mbpibH$_2$)

A mixture of 1,10-phenanthroline-5,6-dione (0.63 g, 3 mmol), ammonium acetate (4.62 g, 60 mmol), isophthalic aldehyde (0.201 g, 1.5 mmol) and glacial acetic acid (50 cm^3) was refluxed for about 2 h and then cooled to r.t. The precipitate was collected and washed with H_2O. The crude product was recrystallized from DMF and produced a greenish yellow powder. Yield 0.347 g, 45% (Found: C, 74.3; H, 3.8; N, 21.5. $C_{32}H_{18}N_8$ requires C, 74.7; H, 3.5; N, 21.8%) ν (cm^{-1}) 3403s, 3065m, 1616m, 1559m, 1501m, 1452s, 1398m, 807s, 737s and 672m. ^{1}H NMR data (300 M, DMSO-d_6): δ 14.05 (s, 2H), 9.24 (s, 1H), 9.07 (d, 4H, $J = 4.5$), 9.05 (d, 4H, $J = 8$), 8.42 (d, 2H, $J = 7.8$), 7.89 (t, 5H, $J = 7.7$). FABMS: $m/z = 515$ ($C_{32}H_{18}N_8$ requires 514).

2.1.3. Synthesis of [Ru(bpy)$_2$(mbpibH$_2$)](ClO$_4$)$_2\cdot 3H_2O$ (**1**)

A mixture of $[Ru(bpy)_2Cl_2]\cdot 2H_2O$ (0.261 g, 0.5 mmol), mfmp (0.162 g, 0.5 mmol), methanol (20 cm^3) and water (10 cm^3) was refluxed under argon for 5 h to give a clear red solution. The solvent was removed by rotory evaporation, and the residue was dissolved in glacial acetic acid (5 cm^3). This solution was then added dropwise under argon to a mixture of 1,10-phenanthroline-5,6-dione (0.084 g, 0.4 mmol) and ammonium acetate (0.616 g, 8 mmol) in glacial acetic acid (5 cm^3). The mixture was refluxed under argon for 2 h. After neutralization with concentrated aqueous ammonia, a red precipitate was obtained by dropwise addition of aqueous $NaClO_4$ solution. The product was purified by column chromatography on alumina with acetonitrile as eluent and dried in vacuo. Yield: 0.248 g, 55% (Found: C, 51.03; H, 3.12; N, 13.98. $RuC_{52}H_{40}N_{12}Cl_2O_{11}$ requires C, 52.88; H, 3.39; N, 14.24%) ν (cm^{-1}) 3389w(br), 3064w, 1603m, 1559m, 1465m, 1082vs (ClO_4), 807m, 765s, 723m and 625s. ^{1}H NMR data (500 M, DMSO-d_6): δ 14.08 (s, 1H), 9.34 (s, 1H), 9.05 (d, 4H, $J = 7.5$), 9.00 (d, 2H, $J = 7$), 8.89 (d, 2H, $J = 8$), 8.85 (d, 2H, $J = 8.5$), 8.53 (d, 1H, $J = 6.5$), 8.27 (d, 1H, $J = 6.5$), 8.22 (t, 2H, $J = 8$), 8.11 (t, 2H, $J = 8$), 7.89 (d, 2H, $J = 5.5$), 7.85 (m, 4H), 7.79 (d, 2H, $J = 6$), 7.71 (m, 1H), 7.67 (d, 2H, $J = 5.5$), 7.60 (t, 2H, $J = 6.5$), 7.39 (t, 2H, $J = 6.5$). FABMS: $m/z = 1028$ [$M - ClO_4$] and 928 [$M - 2ClO_4$].

2.1.4. Synthesis of [(bpy)$_2$Ru(mbpibH$_2$)Ru(bpy)$_2$](ClO$_4$)$_4\cdot 3H_2O$ (**2**)

A solution of $[Ru(bpy)_2Cl_2]\cdot 2H_2O$ (0.25 g, 0.58 mmol) in ethylene glycol was heated for 30 min. Solid mbpibH_2 (0.149 g, 0.29 mmol) was added to the reddish–violet solution, and the resulting mixture was refluxed for 12 h. During the period, the solution turned dark red. The solution was cooled to r.t., and 60 cm^3 H_2O was added. After filtration, a dark red precipitate was obtained by dropwise addition of aqueous $NaClO_4$ solution. The product was purified by column chromatography on alumina with 4:1 acetonitrile–ethanol (v/v) as eluent. Yield: 0.404 g, 80.2%. (Found: C, 47.90; H, 3.14; N, 12.38; $Ru_2C_{72}H_{56}N_{16}C_{14}O_{19}$ requires C, 48.21; H, 3.12; N, 12.49%). ν (cm^{-1}) 3483w(br), 3071m, 1602m, 1549m, 1444m, 1082vs (ClO_4), 807m, 765s, 723m and 625s. ^{1}H NMR data (500 M, DMSO-d_6): δ 9.37 (s, 1H), 9.10 (d, 4H, $J = 8.5$), 8.85 (d, 4H, $J = 8.5$), 8.81 (d, 4H, $J = 8$), 8.40 (d, 2H, $J = 7.5$), 8.20 (t, 4H, $J = 8$), 8.09 (t, 4H, $J = 8$), 7.89 (d, 4H, $J = 5.5$), 7.88 (d, 4H, $J = 5.6$), 7.81 (dd, 4H, $J_1 = 5.5$, $J_2 = 2.5$), 7.63 (d, 4H, $J = 5.5$), 7.59 (t, 5H, $J = 6.5$), 7.38 (t, 4H, $J = 6.5$). ESMS [CH_3OH, m/z] 769.7 ([$M - 2ClO_4$]$^{2+}$), 478.8 ([$M - 3ClO_4$]$^{3+}$), 446.9 ([$M - 4ClO_4 - H$]$^{3+}$), 335.7 ([$M - 4ClO_4$]$^{4+}$).

2.1.5. Synthesis of [(bpy)$_2$Ru(mbpib)Ru(bpy)$_2$](ClO$_4$)$_2\cdot 5H_2O$ (**3**)

A solution of complex **2** (0.15 g, 0.084 mmol) in methanol was added to a sodium methoxide solution,

which was made in situ by dissolving sodium metal (0.04 g, 1.7 mmol) in methanol (10 cm^3). The solution was heated while stirring for 1 h and then cooled to 0–5°C in a refrigerator. A red microcrystalline solid was collected by filtration. Yield: 0.109 g, 85%. (Found: C, 53.06; H, 3.78; N, 13.62; $Ru_2C_{72}H_{58}N_{16}Cl_2O_{13}$ requires C, 53.09; H, 3.56; N, 13.77%). ^1H NMR data (500 M, DMSO-d_6): δ 9.43 (s, 1H), 9.02 (d, 4H, $J = 8$), 8.87 (d, 4H, $J = 8$), 8.83 (d, 4H, $J = 8.5$), 8.33 (d, 2H, $J = 7.5$), 8.20 (t, 4H, $J = 8.5$), 8.08 (t, 4H, $J = 8$), 7.89 (d, 4H, $J = 5$), 7.74 (d, 4H, $J = 5.5$), 7.71 (t, 4H, $J = 5.5$), 7.61 (d, 4H, $J = 6$), 7.60 (t, 4H, $J = 6$), 7.45 (t, 1H, $J = 8$), 7.38 (t, 4H, $J = 6.5$). ESMS [CH_3OH, m/z] 669.7 ($[M - 2ClO_4]^{2+}$), 447.0 ($[M - 2ClO_4 + H]^{3+}$).

2.2. Physical measurements

Microanalyses (C, H and N) were carried out with a Perkin–Elmer 240Q elemental analyzer. Infrared spectra were recorded on a Nicolet 170SX-FTIR spectrometer as KBr discs. UV–Vis spectra were measured on a Shimadzu MPS-2000 spectrophotometer. Emission spectra were obtained for each complex in CH_3CN at r.t. with a Hitachi F-4500 spectrofluorometer and ^1H NMR spectra were recorded on a Bruker ARX-300 NMR spectrometer and a Varian-500 NMR spectrometer with $(CD_3)_2SO$ as solvent at r.t. and $SiMe_4$ as an internal standard. Fast atomic bombardment mass spectra (FABMS) were obtained on a VG ZAB-HS spectrometer in a 3-nitrobenzyl alcohol matrix. Electrospray mass spectra (ESMS) were recorded on a LCQ system (Finnigan MAT, USA) using methanol as mobile phase. The spray voltage, tube lens offset, capillary voltage and capillary temperature were set at 4.50 kV, 30.00 V, 23.00 V and 200°C, respectively, and the quoted m/z values are for the major peaks in the isotope distribution.

Cyclic voltammetry was performed on an EG&G PAR Model 173 potentiostat/175 universal programmer. The supporting electrolyte was 0.1 mol dm^{-3} tetrabutylammonium perchlorate in acetonitrile freshly distilled from phosphorus pentaoxide and deaerated by purging with nitrogen. A standard three-electrode system was used comprising a platinum microcyclinder working electrode, platinum-wire auxiliary electrode and a saturated calomel reference electrode (SCE).

The pH measurements were made with a TOA mode HM-20E pH meter standardized with buffers of pH 4.01 and 6.86. To facilitate dissolution of samples in aqueous solutions a minimal volume of acetonitrile was added. The readings of the pH meter in this mixture are referred to as apparent pH unless otherwise stated. Spectrophotometric titrations were performed in buffer solution, The titration experiment were conducted with Gilson P20 Pipetman microburettes by using a 2.0 mol dm^{-3} NaOH aqueous solution. Buffer systems and pH ranges employed were as follows: $HClO_4$–$NaClO_4$, pH 0–2; Robinson-Britton buffer, pH 2–11 [28]. The pK values of the protonation and deprotonation in the complexes were calculated by using the equation:

$$\mathrm{pH} = \mathrm{p}K - \log\frac{A - A_o}{A_f - A}$$

where A_o and A_f are the initial and final absorbances, respectively. Some A_o and A_f values were evaluated from the graphical method of Coleman et al. [29], because two closely spaced protonation or deprotonation equilibria exist in this system.

The luminescence lifetime measurements were done with an excimer laser (Lambda Physics EMG 201MSC)-pumped dye laser (Lambda Physics model FL2002) system. The nominal pulse width and the line width of the dye-laser output were 10 ns and 0.18 cm^{-1}, respectively. The excitation wavelength was fixed at 455 nm, The emission of a sample was collected by two lenses into a monochromator, detected by a photomultiplier and processed by a Boxcar Average (EG&G model 162) in line with a microcomputer.

3. Results and discussion

3.1. Synthesis

An outline of the synthesis of the ligands and complexes is presented in Scheme 1. The ligands were synthesized on the basis of the method for imidazole ring preparation established by Steck et al. [30]. The ligand mfmp and $mbpibH_2$ were obtained through condensation of 1,10-phenanthroline-5,6-dione with isophthalic aldehyde in refluxing glacial acetic acid containing ammonium acetate at a molar ratio of 1:1 or 2:1, respectively. The ligand $mbpibH_2$ is hardly soluble in common organic solvents, but partly soluble in hot DMF and DMSO. The low solubility of $mbpibH_2$ in most solvents prevents efficient synthesis of the mononuclear complex **1** since it is much more soluble than the ligand $mbpibH_2$. Even when the reaction between $Ru(bpy)_2Cl_2$ and $mbpibH_2$ was run in a 1:1 molar ratio in glycerol, only the dinuclear complex was formed. Therefore, to prepare the mononuclear complex **1**, we carried out the condensation of 1,10-phenanthroline-5,6-dione with the precoordinated mfmp in $[(bpy)_2Ru(mfmp)]^{2+}$ to avoid the formation of the dinuclear complex (Scheme 1). Deprotonation was achieved by reaction of sodium methoxide with the dinuclear complex in methanol. The deprotonated complex completely reverted to the corresponding protonated complex by the addition of acid. All these compounds were characterized by IR, FABMS, ESMS, ^1H NMR and elemental analyses.

3.2. ^1H NMR spectra

The ^1H NMR spectra of the bridging ligand mbpibH_2 and two representative complexes **2** and **3** in $(CD_3)_2SO$ solvent are shown in Fig. 1. The observed ^1H NMR spectra indicate that each half of the ligand is equivalent due to the presence of internal symmetry. In the ^1H NMR spectrum of free mbpibH_2 the proton signals at δ 14.05, 9.24, 9.07, 9.05, 8.42 and 7.89 can be easily assigned to H(NH), H_d, H_a, H_c, H_e and H_b/H_f, respectively, according to $^1H-{}^1H$ COSY experiments and comparison with those of oligopyridine. The proton on the nitrogen atom of the imidazole resonates at ca δ 14.05 for the free ligand mbpibH_2 as a broad singlet, but it is unobserved for the ruthenium complexes because of quickly exchanging between the two nitrogens of the imidazole ring.

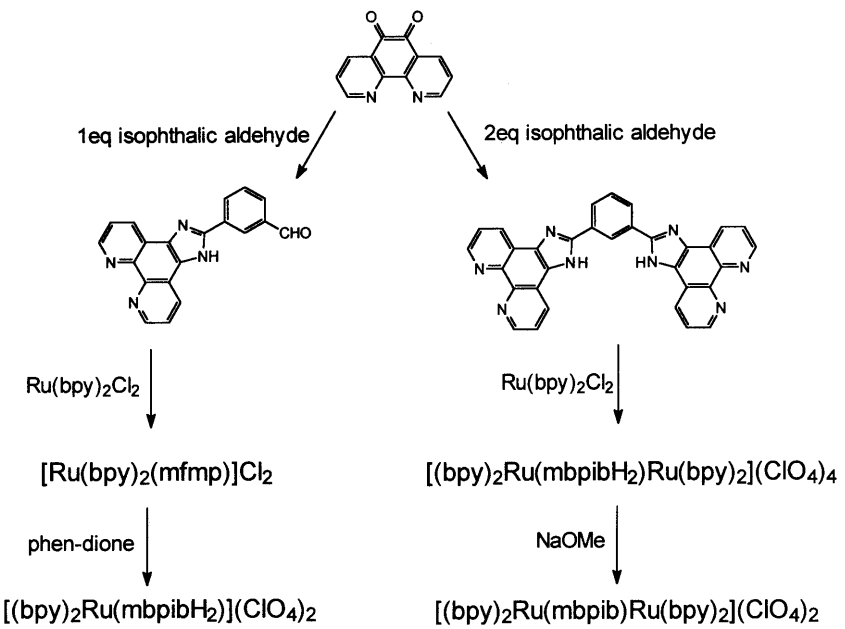
It is easy to assign the chemical shifts of the protons of the bridging ligand mbpibH_2 in its complexes, bearing in mind the free mbpibH_2 data. On coordination to two ruthenium ions to form complex **2**, the protons on the mbpibH_2 all experience shifts by comparison with those of free mbpibH_2: H_c and H_d show 0.05 and 0.13 ppm downfield shifts, H_b, H_e and H_f show 0.08, 0.02 and 0.30 ppm upfield shifts, respectively, while H_a experiences surprising upfield shifts of 1.19 ppm. Similar behaviors have been observed for the mononuclear complex **1** and its ^1H NMR spectrum exhibits two distinct sets of aromatic resonances for both coordinated and uncoordinated parts of mbpibH_2, which is especially clear for H_a. The dramatic upfield shifts of H_a may be due to the effect of the ring current of the bpy ligands.

Deprotonation of the dinuclear complex has a strong influence on the resonance frequency of the protons in the bridging ligand (Fig. 1). Resonances for H_a, H_b, H_c, H_d, H_e and H_f appear at δ 7.74, 7.71, 9.02, 9.43, 8.33 and 7.45, respectively. Shifts in the bpy resonances are small but nevertheless significant. The shift in the resonance positions of mbpibH_2 protons can be explained by the increased electron density in the imidazole ring, which probably also affects the electron density in the phen ring and phenyl ring of mbpibH_2. Also, the change in the overall charge of the compound is likely to influence the resonance frequencies. A similar example has been reported [31].

3.3. Electrochemistry

The electrochemical behaviors of the complexes have been studied in CH_3CN by cyclic voltammetry. Results are collected in Table 1. Due to the poor solubility of free mbpibH_2, it has not been possible to study its electrochemical behavior. Each complex exhibits well shaped oxidation (one) and reduction (three) waves in the sweep range from -1.8 to $+1.6$ V, as shown in Fig. 2 for the dinuclear complex $[(bpy)_2Ru(mbpibH_2)Ru(bpy)_2]^{4+}$. This pattern is common to most d^6 metal polypyridyl complexes where the redox orbitals are localized on the individual ligands [32].

For all of the three complexes, the first reduction potential may be assigned to the bridging ligand mbipbH_2 by comparison with the reduction potential of $[Ru(bpy)_3]^{2+}$ in CH_3CN [33]. It is concluded that reductions of the three complexes occur first on the mbipbH_2 ligand and then on each bpy ligand. Coordi-



Scheme 1.

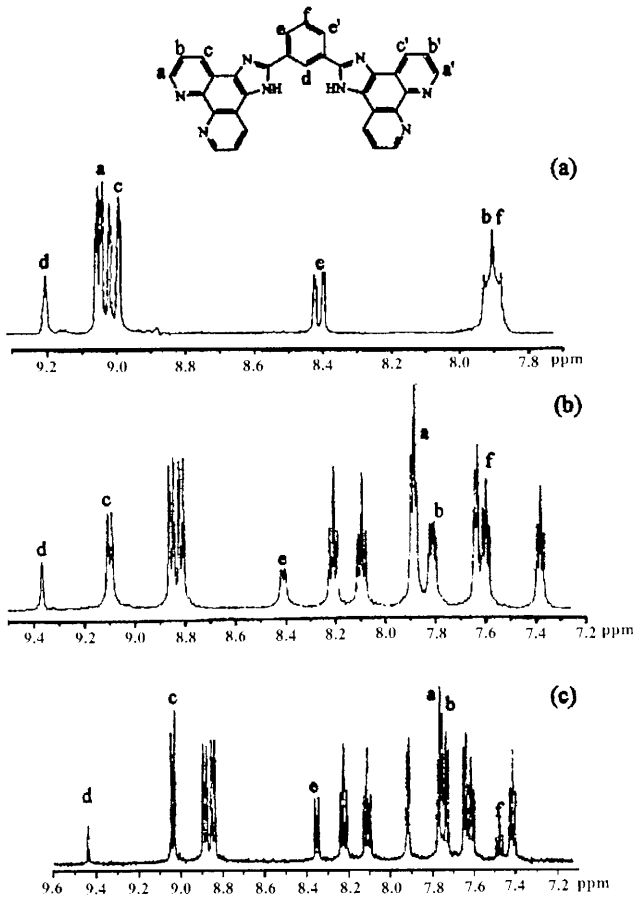


Fig. 1. ^{1}H NMR spectra of $mbpibH_2$ (a), $[(bpy)_2Ru(bpibH_2)Ru(bpy)_2]^{4+}$ (b) and $[(bpy)_2Ru(bpib)Ru(bpy)_2]^{2+}$ (c) in the aromatic region between $\delta = 7.0$ and $\delta = 9.6$ ppm [$(CD_3)_2SO$ solvent, TMS reference].

nation of the second $[Ru(bpy_3)]^{2+}$ ion to the remote nitrogen atoms of the mononuclear $[(bpy)_2Ru(mbpibH_2)]^{2+}$ causes a shift to more positive values in the reduction potential of the $mbpibH_2$ ligand, reflecting the stabilization of the $mbpibH_2$ π^* orbital in the dinuclear complex.

For dinuclear complexes, investigation of the oxidation behavior is very useful to determine the extent of electronic interaction between the metal units. In the absence of any metal–metal interaction, one would anticipate that symmetric bimetallic complexes should exhibit metal-based oxidations at the same potential for both metal centers. If there is metal–metal communication through the bridging ligand, such symmetric bimetallic complex would be expected to exhibit two oxidations since the oxidation of one metal center will be influenced by the oxidation of the other. In the current study, only a single anodic wave is observed for complex **2**. No difference in the oxidation potential was observed between the mononuclear and the dinuclear complex (Table 2). Coulometry indicates that two electrons are involved in this process. From the separation between the anodic and cathodic peak potential (65 mV), it is concluded that two simultaneously independent one-electron processes are involved in this oxidation. This indicates that in the present system the electrostatic interaction between metal sites plays a negligible role, which is attributed to the large distance of separation between the two $Ru(bpy)_2$ units and free rotation around the C–C bond of $mbpibH_2$. Upon deprotonation of the dinuclear complex, the oxidation potential of complex **3** shifts to a more negative potential (about 70 mV).

Table 1
Redox potentials for the ruthenium(II) complexes [a]

Complex	$E_{1/2}$, V (ΔE, mV) [b]			
	Oxidations		Reductions	
1	1.29 (56)	−0.31 (63)	−1.36 (63)	−1.59 (75)
2	1.31 (65)	−0.23 (63)	−1.35 (63)	−1.59 (75)
3	1.24 (60)	−0.39 (63)	−1.40 (63)	−1.63 (75)

[a] All complexes measured in 0.1 M TBAP/CH_3CN, error in potentials was ± 0.02 V, $T = 20 \pm 1$°C, scan rate = 100 mV s^{-1}.
[b] Peak-to-peak separation is given in parentheses.

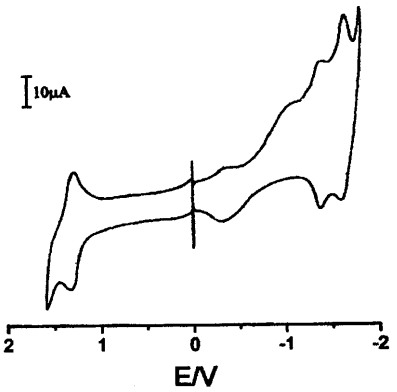


Fig. 2. Cyclic voltammogram of complex **2** in acetonitrile at room temperature.

3.4. Electronic absorption spectra

Absorption spectra were obtained in CH_3CN for all complexes at room temperature (Fig. 3), and the ab-

Table 2
Absorption spectral data for the ruthenium(II) complexes [a]

Complex	λ_{max}, nm (ε, M^{-1} cm^{-1})
1	457 (9800), 285 (70 350), 244 (28 000)
2	457 (21 600), 285 (119 450), 243 (41 600)
3	461 (20 050), 427 (18 050), 339 (49 700), 288 (105 200), 243 (45 850)

[a] In CH_3CN, $T = 298 \pm 1$ K.

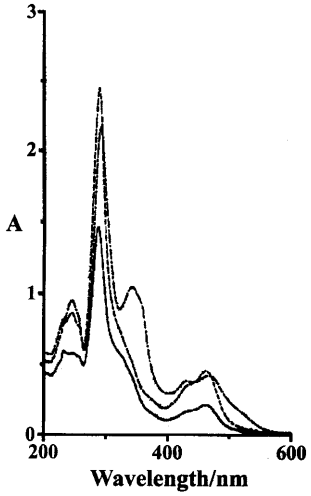


Fig. 3. Absorption spectra of complex **1** (solid line), complex **2** (dotted line) and complex **3** (dashed line) in CH_3CN at room temperature.

sorption data listing energy maxima and the absorption coefficients are summarized in Table 2. The absorption spectra of complexes having a polyunsaturated bridging ligand represent a composite of intraligand ($\pi \rightarrow \pi^*$) and metal to bridging ligand charge transfer (MLCT). By comparison with the spectrum of $[Ru(bpy)_3]^{2+}$ [34], the lowest energy band at 458 nm is assigned to metal–ligand charge transfer (MLCT) transition and consists of overlapping $Ru(d\pi) \rightarrow mbpibH_2(\pi^*)$ and $Ru(d\pi) \rightarrow bpy(\pi^*)$ transitions. The lowered symmetry removes the degeneracy of the π^* levels, which results in the appearance of broad MLCT bands.

When the mononuclear complex **1** is treated with another ruthenium center to form the dinuclear complex, the MLCT absorption maximum around 458 nm remained almost unaltered, except that it becomes twice as intense compared with the mononuclear complex (Fig. 3). This is in sharp contrast to a π-accepting bridging system such as bbdb [bbdb = 1,4-bis(4′-methyl-2,2(bipyridin-4-yl)buta-1,3-diene] [35], dpp [dpp = 2,3-bis(2-pyridyl)pyrazine] [36]. A shift to longer wavelength of the MLCT band compared with that of the mononuclear complex has been reported when the latter containing such a π-accepting ligand forms a dinuclear complex. It suggests that in the present $mbpibH_2$ system the metal–metal interaction is very small, which is consistent with the electrochemistry results. Similar cases were observed between $[Ru(bpy)_2(tpbq)]^{2+}$ and $[(bpy)_2Ru(tpbq)Ru(bpy)_2]^{4+}$ [tpdq = 2,2′,3,3′-tetra(2-pyridyl)-6,6′-biquinoxaline] [37].

Deprotonation of $mbpibH_2$ in the dinuclear complex induces a marked change in the absorption spectrum. Compared with the absorption spectrum of complex **2**, the deprotonated dinuclear complex **3** exhibits the MLCT absorption maxima at 427 and 461 nm, which are much broader with a tail extending out to nearly 600 nm. The red shift of the MLCT band may be explained by an increase in the σ-donor properties of the deprotonated ligand [31]. The band at 339 nm is attributed to the $\pi-\pi^*$ (mbpib) transition in comparison with the absorption spectrum of complex **2**, which suggests that the deprotonated bridging ligand has a larger extent of π delocalization.

The influence of pH on the absorption spectral behavior has been studied for complexes **1** and **2**. The changes that occur for **1** in buffer over the pH range 2–11 are shown in Fig. 4. From pH 2.30 to 6.05, the MLCT band at 458 nm decreases and has a small red-shifts. A further increase of pH from 6.05 to 7.51 leads an increase of the minimum at 380 nm and the band at 500 nm, but a further decrease of the 460 nm

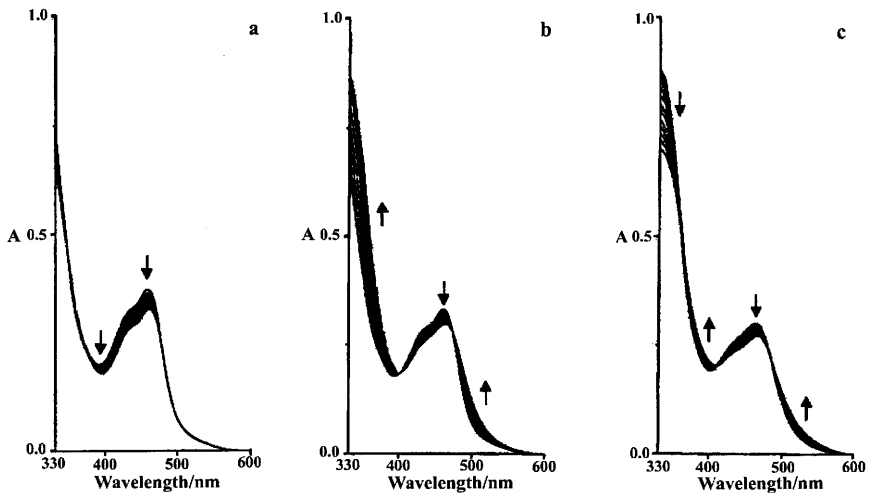


Fig. 4. Absorption spectra of complex **1** (1.00×10^{-5} mol dm^{-3}) at 20°C in buffer at various pH values: (a) pH 2.32 → 6.05; (b) pH 6.05 → 7.51; (c) pH 7.51 → 11.

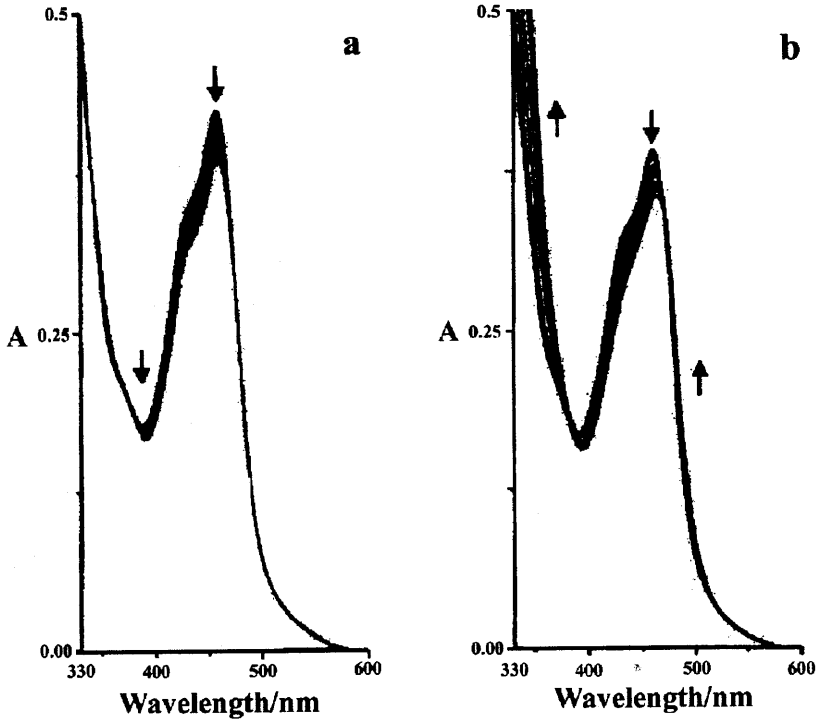


Fig. 5. Absorption spectra of complex **2** (1.00×10^{-5} mol dm^{-3}) at 20°C in buffer at various pH values: (a) pH 2.90→6.49; (b) pH 6.49→9.86.

band, and two well-defined isosbestic points at 400 and 470 nm can be seen. In the range pH 7.51–11 the MLCT band at 465 nm still decreases and shifts to a longer wavelength (470 nm), three well-defined isosbestic points at 360, 410 and 485 nm can be seen. Above the spectral changes are attributed to the following acid–base equilibria. The pK values obtained are $pK_{b1} = 3.43$, $pK_{b2} = 6.45$ and $pK_{a1} = 9.48$.

$$[(bpy)_2Ru(mbpibH_4)]^{4+} \overset{K_{b1}}{\rightleftharpoons} [(bpy)_2Ru(mbpibH_3)]^{3+} \quad (1)$$

$$[(bpy)_2Ru(mbpibH_3)]^{3+} \overset{K_{b2}}{\rightleftharpoons} [(bpy)_2Ru(mbpibH_2)]^{2+} \quad (2)$$

$$[(bpy)_2Ru(mbpibH_2)]^{2+} \overset{K_{a1}}{\rightleftharpoons} [(bpy)_2Ru(mbpibH)]^{+} \quad (3)$$

The bridging ligand $bpibH_2$ has two protonated sites and two depronated sites. The first protonation ($pK_{b2} = 6.45$), according to the spectral changes, should take place at the imidazole group of uncoordinated subunit. On the contrary, only the dissociation of the imidazole group in the coordinated subunit was observed in the pH range 2–11. This result is rationalized by the fact that the pK_a of the imino NH protons of free benzimidazole derivatives is usually around 14. Therefore, it shows clearly that in complex **1** the imidazole of the coordinated subunit is a stronger acid or a weaker base in comparison with that of the uncoordinated subunit.

The dinuclear complex **2** in buffer (pH 2.07) exhibits a MLCT band at 458 nm. The pH dependence of the absorption spectra is shown in Fig. 5. Since the two imidazole groups in $mbpibH_2$ only act as intervening units and are uncoordinated to metal ion, the spectral changes of complex **2** can be attributed to the acid–base equilibria analogous with those of complex **1**. The pK values obtained are 3.23 and 9.28.

3.5. Emission spectra

The steady-state emission spectra of the three complexes in MeCN are shown in Fig. 6. The observed bands correspond to emission from what is assumed to be a Ru(II)-based ^{3}MLCT excited state, similar to that observed for $[Ru(bpy)_3]^{2+}$ [38]. The emission band

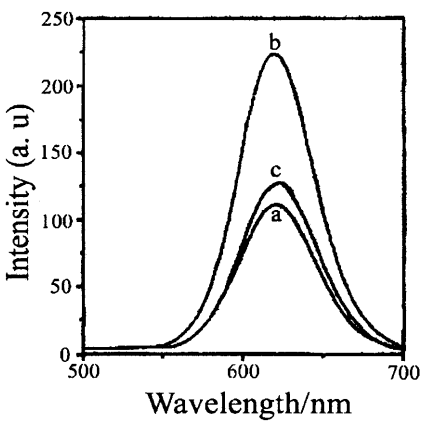


Fig. 6. Room temperature emission spectra of complex **1** (a), complex **2** (b) and complex **3** (c) in CH_3CN excited at 460 nm.

Table 3
Emission spectral data for ruthenium(II) complexes [a]

Complex	λ_{max} (nm)	τ (ns)	Φ_{em} ($\times 10^2$) [b]
1	618	520	5.2
2	618	880	10.2
3	623	545	5.8

[a] In CH_3CN, $T = 298 \pm 1$ K.
[b] Quantum yields of the complexes were determined by a relative method using $[Ru(bpy)_3]^{2+}$ ($\Phi_{em} = 0.062$) as the standard.

maxima, quantum yields and selected excited-state lifetimes of the ruthenium complexes are given in Table 3.

The mono- and dinuclear complexes in CH_3CN all emit at the same wavelength (618 nm). It is interesting to observe that the emission intensity of the dinuclear complex **2** is nearly twice that of the mononuclear complex **1**. At the same time, the excited state lifetime (τ) at room temperature for the dinuclear complex **2** is larger than that observed for the mononuclear complexes **1** (Table 3). In the $[(bpy)_2Ru(mbpibH_2)Ru(bpy)_2]^{4+}$ dinuclear system, the MLCT state is greatly stabilized relative to the ligand field state. This prevents thermal population of the LF state in the dinuclear complex at room temperature. On the other hand, the metal–metal interaction is very weak in the $mbpibH_2$ system. The two reasons result in the emission intensity and lifetime of the chromophore in the dinuclear complex **2** being enhanced relative to the mononuclear complex **1** when measured at room temperature. Deprotonation of the dinuclear complex **2** results in decreasing of the emission intensity (Fig. 6), with less than 60% of the original emission intensity remaining. The emission wavelength also shifts to a longer wavelength (623 nm). This may be involved in the rapid radiationless decay [4]. It has been known that the energy of the metal-centered (MC) excited states depends on the ligand field strength, which in turn depends on the σ-donor and π-acceptor properties of the ligands [4]. The negative charge on the deprotonated imidazol substituent may be delocalized over the whole π framework, which decreases the σ-donor and increases the π-acceptor capacity of the $mbpib^{2-}$ ligand, resulting in weakening of the ligand-field strength around the metal center and in turn lowering the metal σ* orbitals [39–41].

4. Conclusions

A new bridging ligand $mbpibH_2$ [$mbpibH_2$ = 1,3-bis([1,10]phenanthroline-[5,6-*d*]imidazol-2-yl)benzene] and its mono- and dinuclear complexes have been synthesized and characterized. Electrochemical and spectroscopic data clearly suggest that in $mbpibH_2$ system the properties of each metal-based component are essentially maintained and the metal–metal interaction is very weak between the linked metal centers. The longer lifetime and larger emission intensity of the bimetallic chromophore make it a useful component in the design of supramolecular complexes. In addition, since the bridging ligand enables the mono- and dinuclear complexes to act not only as a diprotic acid, but also as a diprotic base, the two complexes show quite interesting proton-dependent photophysical properties.

Acknowledgements

We are grateful to the National Natural Science Foundation Of China, the Natural Science Foundation of Guangdong Province and the State Key Laboratory of Coordination Chemistry in Nanjing University for their financial support.

References

[1] J.M. Lehn, Angew. Chem., Int. Ed. Engl. 29 (1990) 1304.
[2] V. Bazani, F. Scandola, Supramolecular Photochemistry, Horwood, Chichester, 1991.
[3] L. Fabbrizzi, A. Poggi (Eds.), Transition Metals in Supramolecular Chemistry, Kluwer, Dordrecht, 1994.
[4] A. Juris, V. Balzani, F. Barigelletti, S. Campagna, P. Belser, A. Von Zelewsky, Coord. Chem. Rev. 84 (1988) 85.
[5] V. Balzani, A. Juris, M. Venturi, S. Campagna, S. Serroni, Chem. Rev. 96 (1996) 756.
[6] L. De Cola, P. Belser, Coord. Chem. Rev. 177 (1998) 301.
[7] C. Patoux, J.P. Launay, M. Beley, S. Chodorowski-kimmes, J.P. Collin, S. James, J.P. Sauvage, J. Am. Chem. Soc. 120 (1998) 3717.
[8] E. Ishow, A.-P. Gourdon, J. Launay, C. Chiorboli, F. Scandola, Inorg. Chem. 38 (1999) 1504.
[9] Y.X. Wang, W.J. Perez, G.Y. Zheng, D.P. Rillema, C.L. Huber, Inorg. Chem. 37 (1998) 2227.
[10] S. Baitalik, U. Florke, K. Nag, J. Chem. Soc., Dalton Trans. (1999) 719.
[11] G.D. Storrier, S.B. Colbran, Inorg. Chim. Acta 284 (1999) 76.
[12] R.L. Cleary, K.J. Byrom, D.A. Bardwell, J.C. Jeffery, M.D. Ward, G. Carlogero, N. Armaroli, L. Flamigni, F. Barigelletti, Inorg. Chem. 36 (1997) 2601.
[13] A.D. Shukla, B. Whittle, H.C. Bajaj, A. Das, M.D. Ward, Inorg. Chim. Acta 285 (1999) 89.
[14] S. Bodige, A.S. Torres, D.J. Maloney, D. Tate, G.R. Kinsel, A.K. Walker, F.M. MacDonnell, J. Am. Chem. Soc. 119 (1997) 10364.
[15] S. Chakraborty, P. Munshi, G.K. Lahiri, Polyhedron 18 (1999) 1437.
[16] X.H. Zou, B.H. Ye, H. Li, J.G. Liu, Y. Xiong, L.N. Ji, J. Chem. Soc., Dalton Trans. (1999) 1423.
[17] A.P. de Silva, H.Q.N. Gunaratne, T. Gunnlangasson, A.J.M. Huxley, C.P. McCoy, J.P. Rademacher, T.E. Rice, Chem. Rev. 97 (1997) 1515.
[18] M. Haga, M.M. Ali, R. Arakawa, Angew. Chem., Int. Ed. Engl. 35 (1996) 76.
[19] G.A. Neyhart, T.J. Meyer, Inorg. Chem. 25 (1986) 4808.
[20] V. Goulle, A. Harriman, J.M. Lehn, J. Chem. Soc., Chem. Commun. (1993) 1034.

[21] H. Chao, B.H. Ye, Q.L. Zhang, L.N. Ji, Inorg. Chem. Commun. 2 (1999) 338.
[22] M. Haga, T. Matsumura-Inoue, S. Yamabe, Inorg. Chem. 26 (1987) 4148.
[23] M. Haga, T. Ano, K. Kano, S. Yamabe, Inorg. Chem. 30 (1991) 3843.
[24] T. Ohno, K. Nozaki, M. Haga, Inorg. Chem. 31 (1992) 548.
[25] M. Haga, M.M. Ali, S. Koseki, K. Fujimoto, A. Yoshimura, K. Nozaki, T. Ohno, K. Nakajima, D.J. Stufkens, Inorg. Chem. 35 (1996) 3335.
[26] B.P. Sullivan, D.J. Salmon, T.J. Meyer, Inorg. Chem. 17 (1978) 3334.
[27] M. Yamada, Y. Tanaka, Y. Yoshimato, S. Kuroda, I. Shimao, Bull. Chem. Soc. Jpn. 65 (1992) 1006.
[28] H.T.S. Britton, R.A. Robinson, J. Chem. Soc. 458 (1931) 1456.
[29] J.S. Coleman, L.P. Varga, S.H. Mastin, Inorg. Chem. 9 (1970) 1015.
[30] E.A. Steck, A.R. Day, J. Am. Chem. Soc. 65 (1943) 452.
[31] R. Hage, R. Prins, J.G. Haasnoot, J. Reedijk, J.G. Vos, J. Chem. Soc., Dalton Trans. (1987) 1389.
[32] S. Zalis, V. Drchal, Chem. Phys. 118 (1987) 313.
[33] T. Matsumura-Inoue, J. Electroanal. Chem. 95 (1979) 109.
[34] G.M. Bryant, J.E. Fergusson, H.K.J. Powell, Aust. J. Chem. 24 (1971) 257.
[35] A.I. Baba, H.E. Ensleg, R.H. Schmehl, Inorg. Chem. 34 (1995) 1198.
[36] W.R. Murphy, K.J. Brewer, G. Gettliffe, J.D. Petersen, Inorg. Chem. 28 (1989) 81.
[37] D.P. Rillema, R.W. Callahan, K.B. Mack, Inorg. Chem. 21 (1982) 2589.
[38] J.M. Calvert, J.V. Caspar, R.A. Binstead, T.D. Westmoreland, T.J. Meyer, J. Am. Chem. Soc. 104 (1982) 6620.
[39] R.H. Fabian, D.M. Klassen, R.W. Sonntag, Inorg. Chem. 19 (1980) 1977.
[40] J.M. Kelly, C. Long, C.M. O'Connell, J.G. Vos, A.H.A. Tinnemans, Inorg. Chem. 22 (1983) 2818.
[41] E.C. Constable, M.J. Hannon, A.M.W. Cargill Thompson, D.A. Tocher, J.V. Walker, Supramol. Chem. 2 (1993) 243.

PERGAMON

www.elsevier.nl/locate/poly

Polyhedron 19 (2000) 1985–1994

POLYHEDRON

Hexanuclear manganese metallamacrocycles with tripled hydrophobic tails

Byunghoon Kwak, Hakjune Rhee, Myoung Soo Lah *

Department of Chemistry, College of Science, Hanyang University, 1271 Sa-1-dong, Ansan, Kyunggi-do 425-791, South Korea

Received 2 May 2000; accepted 4 July 2000

Abstract

A series of hexanuclear manganese(III) metallamacrocycles were synthesized using *N*-acylsalicylhydrazides (H_3xshz) (where H_3xshz = H_3ashz, *N*-acetylsalicylhydrazide; H_3pshz, *N*-propionylsalicylhydrazide; H_3hshz, *N*-hexanoylsalicylhydrazide; H_3lshz, *N*-lauroylsalicylhydrazide), where the pentadentate ligands bridged the metal ions. The triple deprotonated *N*-acylsalicylhydrazidate (xshz^{3-}) could bridge the metal ions by using a hydrazide N–N group and form the hexanuclear manganese metallamacrocycle with a hole in the center. Depending on the ligands used, the tripled hydrophobic tails of different lengths are attached at both chiral faces of the metallamacrocycles. In the complex $[Mn_6(ashz)_6(DMF)_6]$ (**2**), both sides of the hole are closed by the three methyl groups of the ligands. In the complex $[Mn_6(pshz)_6(DMF)_6]$ (**3a**), one ethyl side chain of the ligands is located inside the hole. In complexes $[Mn_6(hshz)_6(DMF)_6]$ (**4**) and $[Mn_6(lshz)_6(MeOH)_6]$ (**5**), three alternating long alkyl side chains aligned at an approximately right angle to the plane of the metallamacrocycle in one direction, while the other three alkyl side chains aligned in the opposite direction. The stability of the metallamacrocycles in the solution was addressed using ^{1}H NMR spectroscopy. Three phenyl protons of the bridging ligands in the metallamacrocycles were observed in the upfield region. © 2000 Elsevier Science Ltd. All rights reserved.

Keywords: Metallamacrocycles; Hexanuclear clusters; Manganese complexes; Pentadentate ligands; Hydrophobic aliphatic tripled tails

1. Introduction

Self-assembly is one of the most efficient methods for the synthesis of the variety of supramolecular species [1,2]. Recently, several research groups have been synthesizing and characterizing new types of inorganic cluster that can serve as inorganic counterparts of the macrocyclic organic host molecules, where the metal centers are connected by the bridging ligand. Depending on the metal ions, the bridging ligands and the additional ligands used, the self-assembled metallamacrocycles were obtained by the cyclic repeat of the metal ions and the bridging ligands. Macrocyclic squares [3], mercuracarborand cyclic species [4], metal analogue of calix[4]arene [5], and other types of metallamacrocycle [6–8] have appeared as new types of the macrocyclic inorganic host molecule, where the bidentate bridging ligands connect two metal centers.

Another type of metallamacrocycle, known as metallacrowns [9,10], has also emerged as inorganic host molecules. The tetradentate ligands, salicylhydroximate (shi^{3-}), not only serve as a bridging ligand between the metal centers, but also form the five-membered chelate ring using a hydroximate group and the six-membered chelate ring using a iminophenolate group. The chelation gave the metallamacrocycles additional stabilization. Depending on the chelation mode of the ligands around the metal center, the metal centers of the metallamacrocycle could have two different configurations,

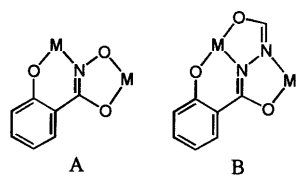


Fig. 1. (A) Binding site of shi^{3-}: 6-, 5-membered chelating rings. (B) Binding sites of fshz^{3-}: 6-, 5-, 5-membered chelating rings.

* Corresponding author. Tel.: +82-31-400-5496; fax: +82-31-400-3863.

E-mail address: mslah@email.hanyang.ac.kr (M.S. Lah).

0277-5387/00/$ - see front matter © 2000 Elsevier Science Ltd. All rights reserved.
PII: S0277-5387(00)00499-X

the planar configuration and the propeller configuration [9a,c].

We have recently synthesized a new type of metallamacrocycle [11], where the pentadentate ligand, *N*-formylsalicylhydrazide (H_3fshz), bridged the metal ions using a hydrazide N–N group (instead of a hydroximate N–O group of the salicylhydroximate) and formed three chelate rings in each metal center (Fig. 1). In addition, the chelation mode of the ligands enforced the metal centers only into the propeller configuration. The metallamacrocycle $[Mn(III)_6(fshz)_6(MeOH)_6]$ (**1**) [11], prepared by using a trianionic pentadentate ligand $fshz^{3-}$, has a large, vacant and hydrophobic hole in the center of the metallamacrocycle. The chiralities of the metal center in metallamacrocycle **1** alternate between Λ and Δ forms. As a result of the alternation, two faces of the donut-shaped hexanuclear manganese metallamacrocycle have opposite chiralities to each other.

In this study, we synthesized a series of pentadentate ligands with various lengths of hydrophobic alkyl chains and their corresponding hexanuclear manganese metallamacrocycles. We report here the general method of synthesizing the series of pentadentate ligands and the features of the corresponding hexanuclear manganese metallamacrocycles with tripled hydrophobic tails. These metallamacrocycles have been characterized using X-ray crystallography and spectroscopic methods.

2. Experimental

2.1. Materials

The following were used as received with no further purification: Salicylhydrazide, dimethylsulfoxide-d_6 (DMSO) and acetone-d_6, acetic anhydride, propionic anhydride, hexanoyl chloride, lauroyl chloride and triethylamine from Aldrich, Inc.; manganese acetate tetrahydrate from Yakuri; acetone, diethylether, chloroform, hexane, methanol (MeOH), ethanol (EtOH), dimethylformamide (DMF) and tetrahydrofuran (THF) from Carlo Erba.

2.2. Instrumentation

The Elemental Analysis Laboratory of the Korean Institute of Basic Science performed C, H, N and Mn determinations. Infrared spectra were recorded as KBr pellets in the range 4000–600 cm^{-1} on a Bio-Rad FTIR spectrometer. Absorption spectra were obtained using a Perkin Elmer Lambda spectrometer. NMR spectra were obtained using a Varian-300 spectrometer. Positive-ion FAB mass spectra were obtained using a JEOL HX110A/HX110A tandem mass spectrometer in a 3-nitrobenzyl alcohol matrix. Room temperature (r.t.) magnetic susceptibilities of well-ground solid samples were measured by using an Evans balance. The measurements were calibrated against a $Hg[Co(SCN)_4]$ standard.

2.3. Synthesis

2.3.1. Ligand synthesis

2.3.1.1. N-Acetylsalicylhydrazide (H_3ashz). Salicylhydrazide (2.017 g, 13.3 mmol) was added to acetic anhydride (8.00 ml) at an ambient temperature. A white suspension was immediately obtained. The suspension was diluted with diethylether, filtered, and rinsed with diethylether (2.453 g, 95% yield). M.p. = 174–176°C. IR (KBr pellet): 3187, 1605, 1573, 1487, 1235, 753 cm^{-1}. ^{1}H NMR (300 MHz, DMSO-d_6): δ 11.90, 10.54, 10.18 (br s, br s, s, 3H, Hs at amides and phenolic OH), 7.90 (dd, 1H, $J = 7.9$, 1.5 Hz, H at phenyl), 7.44 (td, 1H, $J = 7.8$, 1.6 Hz, H at phenyl), 7.03–6.91 (m, 2H, Hs at phenyl), 1.96 (s, 3H, H at methyl). ^{13}C NMR (75.5 MHz, DMSO-d_6): δ 168.29, 167.06, 159.21, 134.36, 128.78, 119.39, 117.65, 115.02, 20.81. *Anal.* Calc. for $C_9H_{10}N_2O_3$: C, 55.67; H, 5.19; N, 14.43. Found: C, 55.74; H, 5.22; N, 14.69%.

2.3.1.2. N-Propionylsalicylhydrazide (H_3pshz). The ligand, *N*-propionylsalicylhydrazide was prepared in an analogous manner to that used for *N*-acetylsalicylhydrazide. Propionic anhydride (8.00 ml) was used. 91% yield. M.p. = 148–151°C. IR (KBr pellet): 3333, 3302, 3201, 2976, 1675, 1640, 1607, 1485, 1236, 752 cm^{-1}. ^{1}H NMR (300 MHz, DMSO-d_6): δ 11.93, 10.54, 10.12 (s, s, s, 3H, Hs at amides and phenolic OH), 7.91 (dd, 1H, $J = 7.9$, 1.5 Hz, H at phenyl), 7.44 (td, 1H, $J = 7.7$, 1.5 Hz, H at phenyl), 6.99–6.91 (m, 2H, Hs at phenyl), 2.25 (q, 2H, $J = 7.6$ Hz, H at –CH_2–), 1.09 (t, 3H, $J = 7.6$ Hz, H at –CH_3). ^{13}C NMR (75.5 MHz, DMSO-d_6): δ 172.14, 167.19, 159.27, 134.35, 128.71, 119.36, 117.66, 114.98, 26.81, 9.96. *Anal.* Calc. for $C_{10}H_{12}N_2O_3$: C, 57.69; H, 5.81; N, 13.45. Found: C, 57.48; H, 5.68; N, 12.75%.

2.3.1.3. N-Hexanoylsalicylhydrazide (H_3hshz). Hexanoyl chloride (2.76 ml, 19.7 mmol) was added to a solution of chloroform (100 ml) containing water (0.36 ml, 19.7 mmol) and triethylamine (5.5 ml, 39.4 mmol) at 0°C. The reaction mixture was slowly warmed to ambient temperature. Another hexanoyl chloride (2.76 ml, 19.7 mmol) was added to the mixture. Then, salicylhydrazide (2.500 g, 16.4 mmol) was added to the reaction mixture. The resulting reaction mixture was stirred at ambient temperature for 1 day. The white suspension was diluted with hexane (200 ml), filtered, and rinsed with water (50 ml × 3) and hexane (50 ml × 5). 3.450 g of the product was obtained (84% yield). M.p. = 163–

165°C. IR (KBr pellet): 3323, 3195, 2963, 2935, 1610, 1576, 1490, 1235, 756 cm^{-1}. ^1H NMR (300 MHz, DMSO-d_6): δ 11.89, 10.48, 10.07 (s, s, s, 3H, Hs at amides and phenolic OH), 7.83 (dd, 1H, $J = 7.9$, 1.3 Hz, H at phenyl), 7.36 (td, 1H, $J = 7.7$, 1.4 Hz, H at phenyl), 6.95–6.83 (m, 2H, Hs at phenyl), 2.14 (t, 2H, $J = 7.4$ Hz, H at $-CH_2-$), 1.49 (m, 2H, H at $-CH_2-$), 1.22 (m, 4H, H at $-CH_2-CH_2-$), 0.80 (t, 3H, $J = 6.8$ Hz, H at $-CH_3$). ^{13}C NMR (75.5 MHz, DMSO-d_6): δ 172.57, 168.41, 160.69, 135.57, 129.90, 120.55, 118.87, 116.10, 34.70, 32.46, 26.29, 23.43, 15.40. *Anal.* Calc. for $C_{13}H_{18}N_2O_3$: C, 62.38; H, 7.25; N, 11.90. Found: C, 62.17; H, 7.18; N, 11.73%.

2.3.1.4. N-Lauroylsalicylhydrazide (H_3lshz). The ligand *N*-lauroylsalicylhydrazide was prepared in an analogous manner to that used for *N*-hexanoylsalicylhydrazide. Lauroyl chloride (2.76 ml, 19.7 mmol) was used. 93% yield. M.p. = 145–147°C. IR (KBr pellet): 3328, 3195, 2919, 2850, 1604, 1576, 1490, 1234, 751 cm^{-1}. ^1H NMR (300 MHz, DMSO-d_6): δ 11.97, 10.56, 10.15 (br s, br s, s, 3H, Hs at amides and phenolic OH), 7.91 (dd, 1H, $J = 7.9$, 1.5 Hz, H at phenyl), 7.44 (td, 1H, $J = 7.8$, 1.5 Hz, H at phenyl), 7.00–6.90 (m, 2H, Hs at phenyl), 2.22 (t, 2H, $J = 7.3$ Hz, H at $-CH_2-$), 1.54 (m, 2H, H at $-CH_2-$), 1.26 (m, 16H, H at $-(CH_2)_8-$), 0.86 (t, 3H, $J = 6.6$ Hz, H at $-CH_3$). ^{13}C NMR (75.5 MHz, DMSO-d_6): δ 171.28, 167.12, 159.48, 134.32, 128.69, 119.30, 117.64, 114.89, 33.53, 31.70, 29.42, 29.35, 29.18, 29.13, 28.96, 25.43, 22.49.14.28. *Anal.* Calc. for $C_{19}H_{30}N_2O_3$: C, 68.23; H, 9.04; N, 8.38. Found: C, 67.97; H, 9.02; N, 8.39%.

2.3.2. Synthesis of metallamacrocycles

*2.3.2.1. [Mn(fshz)(MeOH)]$_6$ (**1**).* The metallamacrocycle, [Mn(fshz)(MeOH)]$_6$, was synthesized as previously described [11]. ^1H NMR (acetone-d_6): δ −10.14, −21.64, −34.94 (Hs at phenyl); 3.03 (Hs for H_2O).

*2.3.2.2. [Mn(ashz)(DMF)]$_6$ (**2**).* A 0.588 g (3.0 mmol) sample of *N*-acetylsalicylhydrazide was dissolved in 30 ml of DMF and 0.735 g (3.0 mmol) of manganese(II) acetate tetrahydrate was dissolved in 30 ml of DMF in another flask. The two solutions were mixed and the combined solution was allowed to stand for 4 days, whereupon dark brown rectangular crystals were obtained (0.935 g, 90.7% yield). *Anal.* Calc. for [Mn(ashz)(DMF)]$_6$·2DMF ($C_{78}H_{98}Mn_6N_{20}O_{26}$) (fw = 2061.38): C, 45.45; H, 4.79; Mn, 15.99; N, 13.59. Found: C, 45.32; H, 5.20; Mn, 16.55; N, 14.25%. ^1H NMR (acetone-d_6): δ −10.03, −20.40, −33.12 (Hs at phenyl); 37.94 (H at C9); 8.01, 2.95, 2.79 (Hs for DMF); 2.99 (Hs for H_2O). FABMS, m/z: $[Mn_6(ashz)_6 + H]^+$, 1477.6. UV–Vis ($CHCl_3$) $\lambda_{max}(\varepsilon)$: 249 nm (36 500 M^{-1} cm^{-1}); 298 nm (20 100 M^{-1} cm^{-1}); 364 nm (10 600 M^{-1} cm^{-1}). μ_{eff}: 11.84 μ_B (4.83 μ_B/metal).

*2.3.2.3. [Mn(pshz)(DMF)]$_6$ (**3a**).* A 0.365 g (2.0 mmol) sample of *N*-propionylsalicylhydrazide was dissolved in 15 ml of DMF and 0.49 g (2.0 mmol) of manganese(II) acetate tetrahydrate was dissolved in 15 ml of DMF in another flask. The two solutions were mixed and the combined solution was allowed to stand for 4 days, whereupon dark brown rectangular crystals were obtained (0.58 g, 87.0% yield). *Anal.* Calc. for [Mn(pshz)(DMF)]$_6$ ($C_{78}H_{96}Mn_6N_{18}O_{24}$) ($F_w = 1999.35$): C, 46.86; H, 4.84; Mn, 16.49; N, 12.61. Found: C, 46.56; H, 5.58; Mn, 16.18; N, 13.23%. ^1H NMR (acetone-d_6): δ −2.76(br); −10.10, −20.26, −32.90 (Hs at phenyl); 49.90 (H at C9); 8.10, 2.99, 2.82 (Hs for DMF); 3.11 (Hs for H_2O). UV–Vis (acetone) $\lambda_{max}(\varepsilon)$: 328 nm (27400 M^{-1} cm^{-1}); 372 nm (17 500 M^{-1} cm^{-1}); 467 nm (2460 M^{-1} cm^{-1}). μ_{eff}: 11.13 μ_B (4.55 μ_B/metal).

*2.3.2.4. [Mn(pshz)(EtOH)]$_6$ (**3b**).* A 0.10 g (0.5 mmol) sample of *N*-propionylsalicylhydrazide was dissolved in 5 ml of DMF and 0.123 g (0.5 mmol) of manganese(II) acetate tetrahydrate was dissolved in 5 ml of DMF in another flask. The two solutions were mixed and the combined solution was allowed to stand for 4 days, whereupon dark brown rectangular crystals were obtained (0.10 g, 67% yield). *Anal.* Calc. for [Mn_6(pshz)$_6$(EtOH)$_5$] ($C_{70}H_{84}Mn_6N_{12}O_{23}$) ($F_w = 1791.13$): C, 46.94; H, 4.73; Mn, 18.40; N, 9.38. Found: C, 46.25; H, 4.51; Mn, 18.46; N, 9.36%. UV–Vis (THF) $\lambda_{max}(\varepsilon)$: 239 nm (233 000 M^{-1} cm^{-1}); 278 nm (193 000 M^{-1} cm^{-1}); 327 nm (45 600 M^{-1} cm^{-1}); 369 nm (26 700 M^{-1} cm^{-1}); 439 nm (3850 M^{-1} cm^{-1}); 739 nm (2640 M^{-1} cm^{-1}).

*2.3.2.5. [Mn(hshz)(DMF)]$_6$ (**4**).* A 0.250 g (1.0 mmol) sample of *N*-hexanoylsalicylhydrazide was dissolved in 15 ml of DMF and 0.245 g (1.0 mmol) of manganese (II) acetate tetrahydrate was dissolved in 15 ml of DMF in another flask. The two solutions were mixed and the combined solution was allowed to stand for 5 days, whereupon dark brown rectangular crystals were obtained (0.352 g, 93.8% yield). *Anal.* Calc. for [Mn(hshz)(DMF)]$_6$ ($Mn_6C_{96}H_{132}N_{18}O_{24}$) ($F_w$ = 2251.84): C, 51.21; H, 5.91; Mn, 14.64; N, 11.20. Found: C, 51.04; H, 5.88; Mn, 14.00; N, 11.25. ^1H NMR (acetone-d_6): δ -12.0(shoulder); −10.63, −20.61, −32.56 (Hs at phenyl); 54.73 (H at C9); 8.43, 3.102, 2.926 (Hs for DMF); 3.351 (Hs for H_2O); 1.30, 0.51 (Hs for alkyl chains). UV–Vis (THF) $\lambda_{max}(\varepsilon)$: 239 nm (247 000 M^{-1} cm^{-1}); 278 nm (208 000 M^{-1} cm^{-1}); 369 nm (24 000 M^{-1} cm^{-1}); 456 nm (4060 M^{-1} cm^{-1}). UV − Vis (acetone) $\lambda_{max}(\varepsilon)$: 326 nm (31 000 M^{-1} cm^{-1}); 374 nm (19 200 M^{-1} cm^{-1}); 458 nm (2200 M^{-1} cm^{-1}). μ_{eff}: 11.59 μ_B (4.73 μ_B/metal).

*2.3.2.6. [Mn(lshz)(MeOH)]$_6$ (**5**).* A 0.668 g (2.0 mmol) sample of *N*-lauroylsalicylhydrazide was dissolved in 80 ml of MeOH and 0.490 g (2.0 mmol) of manganese(II) acetate tetrahydrate was dissolved in 20 ml of MeOH in another flask. When the two solutions were mixed precipitate formed immediately. After a day of stirring, the solution was filtered to obtain 0.56 g of undissolved powder. The filtrate was allowed to stand for 3 days, whereupon dark brown rectangular crystals were obtained (0.10 g, 11.9% yield). The undissolved powder obtained from the early stage of the reaction was added to 200 ml of MeOH. After a week of the stirring, most of powders were dissolved. Slow evaporation of the solution yielded the same dark rectangular crystals (0.34 g, 40.6% yield). *Anal.* Calc. for [Mn(lshz)(MeOH)]$_6$ ($Mn_6C_{120}H_{186}N_{12}O_{24}$) ($F_w$ = 2510.49): C, 57.41; H, 7.47; Mn, 13.13; N, 6.70. Found: C, 57.06; H, 8.07; Mn, 13.77; N, 7.03%. ^{1}H NMR (acetone-d_6): δ −10.44, −20.35, −31.18 (Hs at phenyl); 52.95 (H at C9); 3.837(Hs for H_2O); 5.792, 1.296, 0.915 (Hs for alkyl chains). UV–Vis (THF) $\lambda_{max}(\varepsilon)$: 239 nm (249 000 M^{-1} cm^{-1}); 278 nm (214 000 M^{-1} cm^{-1}); 368 nm (24 000 M^{-1} cm^{-1}); 466 nm (4020 M^{-1} cm^{-1}); 742 nm (360 M^{-1} cm^{-1}). UV–Vis (acetone) $\lambda_{max}(\varepsilon)$: 328 nm (34 200 M^{-1} cm^{-1}); 375 nm (21 900 M^{-1} cm^{-1}); 465 nm (3500 M^{-1} cm^{-1}). μ_{eff}: 11.63 μ_B (4.75 μ_B/metal).

2.4. Crystallographic data collection and refinement of structures

Because crystals of **2**–**5** lose their structural solvents of crystallization within 1 min, they were mounted in a glass capillary with the mother liquor to prevent the loss of the structural solvents during data collection. Preliminary examination and data collection for crystals of **2**–**4** were performed with Mo Kα radiation (λ = 0.71069 Å) on an Enraf–Nonius CAD4 computer-controlled κ-axis diffractometer equipped with a graphite crystal, incident-beam monochromator. Cell constants and orientation matrices for data collection were obtained from least-squares refinement, using the setting angles of 25 reflections. Data were collected at r.t. using the ω scan technique. Three standard reflections were monitored every hour, but no intensity variations were monitored. Lorentz and polarization corrections were applied to the data; however, no corrections were made for absorption. Preliminary examination and data collection for the crystal of **5** were performed with Mo Kα radiation (λ = 0.71069 Å) on a Siemens SMART CCD equipped with a graphite crystal, incident-beam monochromator. Data were collected at r.t. Lp correction and absorption correction were applied to the data. All structures were solved by direct methods using SHELXS-86 [12] and refined by full-matrix least-squares calculations with SHELX-97 [13].

*2.4.1. Complex [Mn(ashz)(DMF)]$_6$ (**2**).*

All non-hydrogen atoms except one solvent molecule were refined anisotropically; hydrogen atoms were allowed to ride on geometrically ideal positions with isotropic temperature factors 1.2 times those of the attached non-hydrogen atoms. One DMF molecule coordinated to the ring metal ion is statically disordered. This disordered site was refined with two partially occupied DMF molecules (0.47 occupancy site: O4C, C101, N3C, C111, C121; 0.53 occupancy site: O4C, C102, N3C, C112, C122). Two solvent sites were identified; one of them performed very poorly. Refinement without any geometrical restraint or with disordered modelling produced bad geometry. So the geometry of this solvent molecule was restrained the same as the geometry of the other solvent molecule.

*2.4.2. Complex [Mn(pshz)(DMF)]$_6$ (**3a**).*

All non-hydrogen atoms (except disordered sites) were refined anisotropically; hydrogen atoms were allowed to ride on geometrically ideal positions with isotropic temperature factors 1.2 times those of the attached non-hydrogen atoms. All ethyl side chains of the ligands were disordered. These disordered sites were refined with partial occupancy. One disordered ethyl side chain showed abnormal bond distances (C9A–C10A 1.73; C9A–C11A 1.86 Å). The restrained refinement with an ideal geometry gave similar result. Two solvent sites were identified, one of them performed very badly. Refinement without any geometrical restraint or with disordered modelling produced bad geometry. So the geometry of this solvent molecule was restrained the same as the geometry of the other solvent molecule.

*2.4.3. Complex [Mn(hshz)(DMF)]$_6$ (**4**).*

All non-hydrogen atoms were refined anisotropically; hydrogen atoms were allowed to ride on geometrically ideal positions with isotropic temperature factors 1.2 times those of the attached non-hydrogen atoms. Two solvent sites were identified; one of which yield an abnormal bond distance (1.78 Å) between O1DE–C1DE. So the geometry of this solvent molecule was restrained the same as the geometry of the other solvent molecule.

*2.4.4. Complex [Mn(lshz)(MeOH)]$_6$ (**5**).*

All non-hydrogen atoms were refined anisotropically; hydrogen atoms were allowed to ride on geometrically ideal positions with isotropic temperature factors 1.2 times those of the attached non-hydrogen atoms. In the crystal structures, only portions of the long alkyl side chains could be identified in the difference Fourier map. The remaining terminal carbon atoms were disordered. During the least-squares refinement of the crystal **5**, the alkyl side chains of the ligands were restrained as an

Table 1
Crystallographic data for $[Mn(III)(ashz)(DMF)]_6 \cdot 4DMF$ (**2**), $[Mn(III)(pshz)(DMF)]_6 \cdot 4DMF$ (**3a**), $[Mn(III)(hshz)(DMF)]_6 \cdot 4DMF$ (**4**), $[Mn(III)(lshz)(MeOH)]_6 \cdot 4.67MeOH$ (**5**)

	Complex **2**	Complex **3a**	Complex **4**	Complex **5**
Formula	$C_{42}H_{56}Mn_3N_{11}O_{14}$	$C_{45}H_{62}Mn_3N_{11}O_{14}$	$C_{54}H_{80}Mn_3N_{11}O_{14}$	$C_{187}H_{307}Mn_9N_{18}O_{43}$
Formula weight	1103.80	1145.88	1272.11	3989.97
Space group	$P\bar{1}$	$P\bar{1}$	$P\bar{1}$	$P\bar{1}$
Z	2	2	2	6
a (Å)	12.866(2)	13.039(2)	14.685(2)	16.4398(3)
b (Å)	14.608(2)	14.691(3)	15.737(2)	28.0779(5)
c (Å)	15.957(2)	16.238(4)	16.178(2)	28.6136(5)
α (°)	63.94(1)	110.64(2)	61.708(6)	118.772(1)
β (°)	73.82(2)	94.85(2)	81.529(8)	93.650(1)
γ (°)	76.46(2)	109.43(2)	75.808(8)	100.871(1)
V (Å^3)	2565.7(6)	2672.3(9)	3189.5(6)	11185.0(3)
Max θ value (°)	20	20	20	20
Crystal size (mm)	$0.54 \times 0.40 \times 0.30$	$0.70 \times 0.32 \times 0.28$	$0.50 \times 0.40 \times 0.10$	$0.60 \times 0.25 \times 0.20$
Number reflections collected	4790	4986	5933	34 154
Number independent reflections	4790[$R_{int} = 0.00$]	4986[$R_{int} = 0.00$]	5930[$R_{int} = 0.008$]	20 479[$R_{int} = 0.072$]
Goodness-of-fit on F^2	1.121	1.086	1.081	1.011
Final R [$I > 2\sigma(I)$]	$R_1 = 0.0697$ [a]	$R_1 = 0.0727$	$R_1 = 0.0535$	$R_1 = 0.0914$
	$wR_2 = 0.1727$ [b]	$WR_2 = 0.1784$	$wR_2 = 0.1283$	$wR_2 = 0.2607$
R (all data)	$R_1 = 0.0932$	$R_1 = 0.1293$	$R_1 = 0.0924$	$R_1 = 0.1512$
	$wR_2 = 0.1866$	$WR_2 = 0.2198$	$wR_2 = 0.1541$	$wR_2 = 0.3107$

[a] $R_1 = \Sigma(|F_o| - |F_c|)/\Sigma|F_o|$.
[b] $wR_2 = [\Sigma w(F_o^2 - F_c^2)^2/\Sigma wF_o^4]^{1/2}$.

ideal geometry. Seven solvent sites were identified and refined as methanol molecules but some of them might be part of the unconnected long alkyl side chains.

Crystal and intensity data are given in Table 1.

3. Results and discussion

In this study, a series of potential pentadentate ligands, *N*-acylsalicylhydrazides (H_3xshz) (–$COCH_3$, *N*-acetylsalicylhydrazide; –$COCH_2CH_3$, *N*-propionylsalicylhydrazide; –$CO(CH_2)_2CH_3$, *N*-hexanoylsalicylhydrazide; and, –$CO(CH_2)_{10}CH_3$, *N*-lauroylsalicylhydrazide) were synthesized by the coupling of the salicylhydrazide and the corresponding acyl chloride or acyl anhydrides. The triple deprotonated *N*-acylsalicylhydrazidate (xshz^{3-}) with a linear aliphatic chain were able to bridge the metal ions using a hydrazide N–N group and form the isostructural hexanuclear manganese metallamacrocycle. Depending on the ligands used, the tripled hydrophobic aliphatic tails of different lengths are attached at both chiral faces of the hexanuclear manganese metallamacrocycle (Fig. 2).

3.1. Crystal structure of $[Mn(ashz)(DMF)]_6$ (2)

Hexanuclear manganese metallamacrocycle $[Mn(ashz)(DMF)]_6$, **2** were able to be synthesized using manganese(II) acetate tetrahydrate as a metal source and ashz^{3-} as a trianionic pentadentate ligand. An ORTEP diagram of complex **2** is shown in Fig. 3. This neutral hexanuclear manganese metallamacrocycle is similar to the previously reported hexanuclear manganese metallamacrocycle $[Mn(fshz)(DMF)]_6$ (**1**) (Tables 2 and 3) [11]. Complex **2** with noncrystallographic local pseudo-C_{3i} symmetry is in the crystallographic inversion center. As in complex **1**, the pentadentate ligand *N*-acetylsalicylhydrazidate also bridges the ring metal ions using a hydrazide N–N group. An iminophenolate group (O1 and N1 atoms) and an iminoacetyl group (N1 and O3 atoms) of the ligand are coordinated to the metal ion in the meridional mode to form the six-membered and five-membered chelating rings. A hydrazidate group (O2 and N2 atoms) occupies two of the three remaining coordination sites of the octahedral

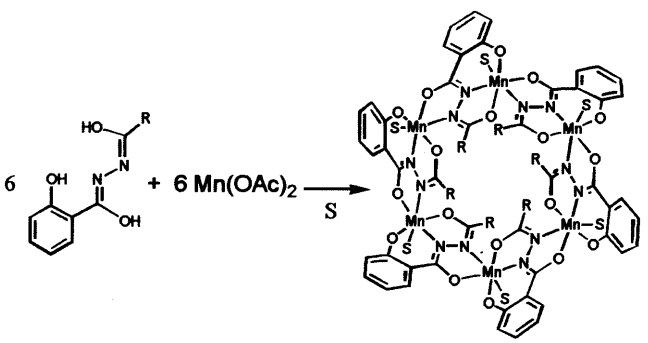


Fig. 2. Synthesis of metallamacrocycles.

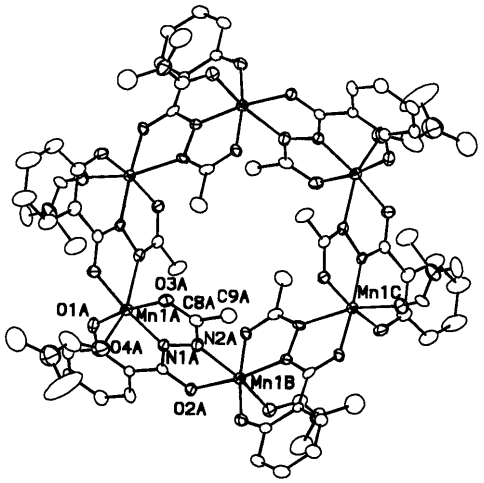


Fig. 3. An ORTEP drawing of complex **2**, $[Mn(ashz)(DMF)]_6$. The complex is in the crystallographic inversion center. A, B, and C in manganese ions could be related to each other by using a noncrystallographic S_6 symmetry operation. Hydrogen atoms have been omitted for clarity.

Table 2
Selected bond lengths (Å) [a] and angles (°) [a] for **1**, **2**, **3a**, **4** and **5**

	1 [b]	**2**	**3a**	**4**	**5**
Mn1–O1	1.852	1.851	1.859	1.852	1.858
Mn1–O2 [c]	1.967	1.967	1.971	1.973	1.967
Mn1–O3	1.945	1.929	1.925	1.915	1.923
Mn1–N1	1.929	1.942	1.93	1.935	1.932
Mn1–O4	2.233	2.248	2.260	2.239	2.268
Mn1–N2 [c]	2.246	2.251	2.27	2.265	2.251
O1A–Mn1A–O2C [c]	94.6	96.5	96.2	95.7	96.5
O1A–Mn1A–O3A	169.9	170.7	170.3	170.0	170.5
O1A–Mn1A–O4A	92.1	91.6	91.3	91.4	89.7
O1A–Mn1A–N1A	90.5	90.8	90.6	90.5	91.0
O1A–Mn1A–N2C [c]	96.7	93.9	93.1	95.7	94.4
O2C [b]–Mn1A–O3A	95.0	92.7	93.4	93.9	92.5
O2C [b]–Mn1A–O4A	83.6	86.8	86.0	85.8	86.7
O2C [b]–Mn1A–N1A	172.7	172.5	173.0	173.4	172.3
O2C [b]–Mn1A–N2C [c]	74.7	75.1	74.3	74.3	74.8
O3A–Mn1A–O4A	86.0	88.5	88.3	86.5	88.5
O3A–Mn1A–N1A	80.2	80.1	79.7	80.1	80.0
O3A–Mn1A–N2C[c]	88.7	88.9	89.7	89.5	90.2
O4A–Mn1A–N1A	101.5	94.6	95.0	95.9	94.0
O4A–Mn1A–N2C[c]	157.0	161.3	159.3	159.2	161.0
N1A–Mn1A–N2C[c]	99.6	102.9	104.3	103.4	104.1

[a] The geometry data are the average values of the bond distances and angles related by the noncrystallographic S_6 symmetry operation.
[b] Ref. [11].
[c] Symmetry transformation used to generate equivalent atoms: $1-x, -y+2, -z$

manganese ions to form the five-membered chelating ring. A solvent molecule DMF (O4 atom), coordinated at the Jahn–Teller elongation axis, finishes the octahedral geometry of the manganese ion (Table 2). The binding mode of the ligand enforces the stereochemistry of the metal ions only into a propeller configuration in the complex **2**. The resulting chiralities of the metal centers in complex **2** alternate between Λ and Δ forms. The alternation of the chiralities of the metal centers generates two chiral faces with opposite chiralities in the hexanuclear manganese metallamacrocycle. Complex **2** also has a vacant, hydrophobic hole in the center of the metallamacrocycle. The approximate dimensions of the hydrophobic hole are similar to those in the previously reported complex **1**, $[Mn(fshz)(DMF)]_6$ (Table 3). However, in complex **2** the entrance of the hole at each face is closed by three methyl groups of the *N*-acetyl side chains of the ligands. The diameter of the entrance of the hole, formed by the pseudo-C_3 symmetry-related three methyl carbon atoms (C9), is about 1.3 Å smaller than that of the entrance of the hole formed by the pseudo-C_3 symmetry-related three C8 carbon atoms (Table 3).

3.2. Crystal structure of $[Mn(pshz)(DMF)]_6$ (3a)

Hexanuclear manganese metallamacrocycle $[Mn(pshz)(DMF)]_6$ (**3a**) could be synthesized using manganese(II) acetate tetrahydrate as a metal source and $pshz^{3-}$ as a trianionic pentadentate ligand. An ORTEP diagram of complex **3a** is shown in Fig. 4. This neutral hexanuclear manganese metallamacrocycle is also similar to the previously reported hexanuclear manganese metallamacrocycle $[Mn(fshz)(DMF)]_6$ (**1**) and $[Mn(ashz)(DMF)]_6$ (**2**). Complex **3a** with noncrystallographic local pseudo-C_{3i} symmetry is also in the crystallographic inversion center. In the crystal structure, ethyl side chains of the ligands (three ethyl side chains in the asymmetric unit) are disordered. In the complex **3a**, only one entrance of the hole is blocked by three ethyl groups of the *N*-propionyl side chains of the ligands. At the other entrance of the hole, one ethyl group is located on the inside of the hole and the remaining two ethyl groups are at the face of the hole. When the ethyl group located in the inside of the hole was omitted during crystallographic refinement, the difference Fourier map showed about 1.5 residual electron density per $Å^2$. In addition, the hole of the metallamacrocycle

Table 3
Selected lengths (Å) and hole sizes (Å) for **1**, **2**, **3a**, **4** and **5**

	1 [a]	**2**	**3**	**4**	**5**
Mn1A···Mn1B	4.805	4.819	4.891	4.880	4.877
Mn1A···Mn1C	8.031	8.208	8.256	8.183	8.268
Hole size [b]	6.89	7.10	7.15	7.07	7.17
C8A···C8C	5.026	5.226	5.405	5.235	5.355
Hole size	2.70	2.93	3.14	2.94	3.08

[a] Ref. [11].
[b] The hole was formed by the three pseudo-C_3 symmetry-related atoms and the size of the hole was calculated by the subtraction of the Van der Waals radii of the constituting atoms.

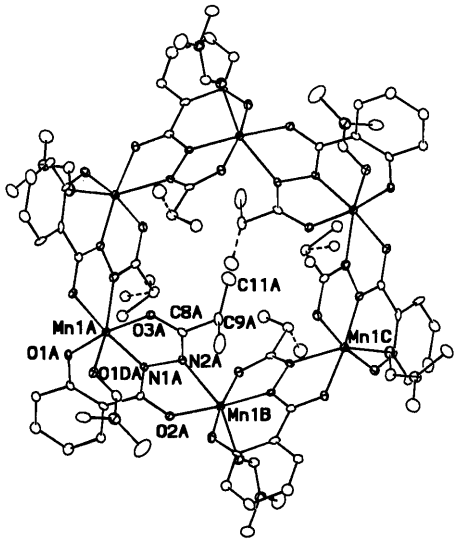


Fig. 4. An ORTEP drawing of complex **3a**, $[Mn(pshz)(DMF)]_6$. The complex is in the crystallographic inversion center. A, B, and C in manganese ions could be related to each other by using a noncrystallographic S_6 symmetry operation. The dotted lines are for the disordered ethyl groups. Hydrogen atoms have been omitted for clarity.

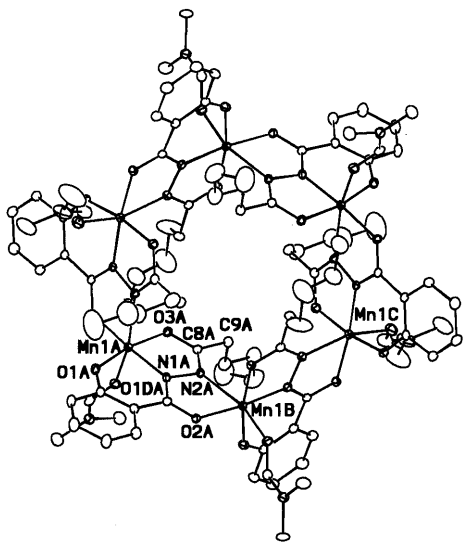


Fig. 5. An ORTEP drawing of complex **4**, $[Mn(hshz)(DMF)]_6$. The complex is in the crystallographic inversion center. A, B, and C in manganese ions could be related to each other by using a noncrystallographic S_6 symmetry operation. Hydrogen atoms have been omitted for clarity.

expanded slightly. The diameter of the entrance formed by the pseudo C_3 symmetry related three C8 atoms in the complex **3a** increased approximately 0.4 Å compared to the corresponding diameter in the complex **1** (Table 3). The incorporation of the ethyl group resulted in the expansion of the hole. This shows that the hexanuclear manganese metallamacrocycle has some degree of flexibility.

3.3. Crystal structure of $[Mn(hshz)(DMF)]_6$ (4)

Hexanuclear manganese metallamacrocycle $[Mn(hshz)(DMF)]_6$ (**4**) could be synthesized using manganese(II) acetate tetrahydrate as a metal source and $hshz^{3-}$ as a trianionic pentadentate ligand. An ORTEP diagram of complex **4** is shown in Fig. 5. The complex has two sets of tripled hydrophobic tails at each face of the donut shaped metallamacrocycles. In the crystal structure, three alternating pentyl side chains aligned at an approximately right angle to the plane of the metallamacrocycle in one direction, while the other three alternating pentyl side chains aligned in the opposite direction (Fig. 6).

3.4. Crystal structure of $[Mn(lshz)(MeOH)]_6$ (5)

Hexanuclear manganese metallamacrocycle $[Mn(lshz)(MeOH)]_6$ (**5**) could be synthesized using manganese(II) acetate tetrahydrate as a metal source and $lshz^{3-}$ as a trianionic pentadentate ligand. The crystal structure showed three crystallographically independent, but chemically identical, molecules. In the crystal structure, only a portion of the long alkyl side chains could be identified. Depending on the alkyl side chains in the three crystallographically independent molecules, three to seven carbon atoms among eleven could be found in the difference Fourier map. The remaining terminal carbon atoms were disordered. An ORTEP drawing of one of these molecules (complex **5**) is shown in Fig. 7. The three alternating hydrophobic alkyl chains aligned at an approximately right angle to the plane of the metallamacrocycle, and the other three alkyl chains aligned in the opposite direction as in

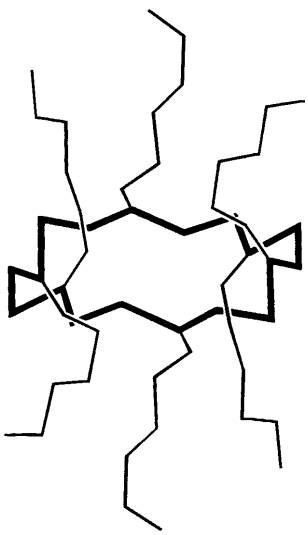


Fig. 6. Side view of complex **4**, $[Mn(hshz)(DMF)]_6$. Cyclic $(Mn–N–N–)_6$ linkage is drawn in bold. The alternating side chains aligned at an approximately right angle to the plane of the metallamacrocycle.

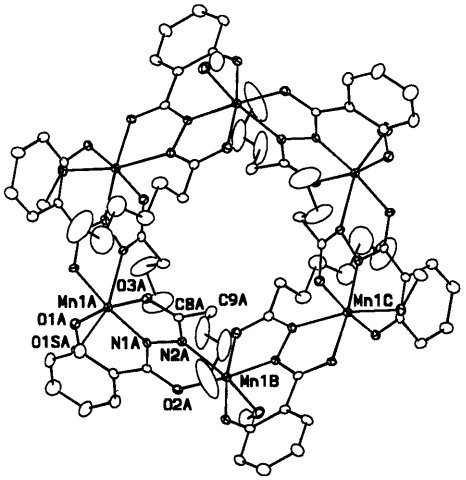


Fig. 7. An ORTEP drawing of complex **5**, $[Mn(lshz)(MeOH)]_6$. Only parts of the alkyl chains could be identified in the difference Fourier map. A, B and C in manganese ions could be related to each other by using a noncrystallographic S_6 symmetry operation. Hydrogen atoms have been omitted for clarity.

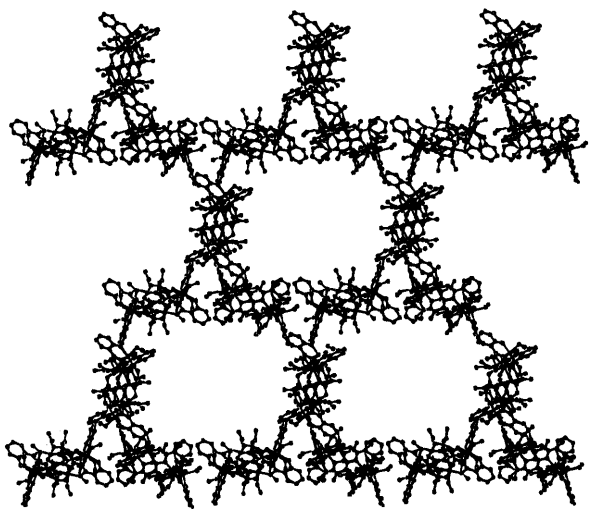


Fig. 8. Packing diagram of complex **5**, $[Mn(lshz)(MeOH)]_6$. Complex **5** serves as unit for the gigantic hexagonal packing of the hexanuclear metallamacrocycles. Only the part of the alkyl chains (C9 and C10 atoms) are represented in this packing diagram. The disordered hydrophobic alkyl chains of the hexanuclear metallamacrocycles are gathered at the centers of the gigantic hexagonal network.

complex **4**. In the crystal packing structure, the hexanuclear metallamacrocycle **5** serves as a unit for the gigantic hexagonal packing of the metallamacrocycles. The disordered hydrophobic alkyl chains of the hexanuclear metallamacrocycles are gathered at the centers of the gigantic hexagon (Fig. 8).

The charge balance of the metallamacrocycles in the crystal structures suggests that the oxidation state of the manganese ion is $+3$. The oxidation state of the manganese ion is also confirmed by room temperature magnetic susceptibililty measurement. The magnetic moments per metal center in the metallamacrocycles are in the range of 4.55 to 4.83 μ_B. The values correspond to the spin-only value, 4.9, for the high spin manganese(III) d^4 ions.

The methanol solution of the complex **2** in a 3-nitrobenzyl alcohol matrix gave a peak at m/z 1477.6 in the FABMS. This peak corresponds to the hexanuclear metallamacrocycle ion $[Mn_6(ashz)_6 + H]^+$. A similar peak at m/z 1393.5 in complex **1**, corresponding to the hexanuclear metallamacrocycle ion $[Mn_6(fshz)_6 + H]^+$, was previously reported [11]. The solution integrity of the metallamacrocycle was confirmed using paramagnetically shifted ^1H NMR spectroscopy. In the ^1H NMR spectra of all hexanuclear manganese metallamacrocycles in acetone-d_6, three distinctive peaks around -10, -20 and -33 ppm were observed (Fig. 9). These peaks were tentatively assigned to the phenyl protons of the bridging ligands. Similar upfield peaks of the manganese metallacrowns were observed and assigned to the phenyl protons of the salicylhydroximate (shi^{3-}) ligand using deuterium exchange experiments [9g]. The peaks around 38–55 ppm were observed for all complexes with alkyl side chains. The peak at 37.9 ppm was assigned to the methyl protons in the complex **2**, and the peak at 49.9, 54.7, and 53.0 ppm was

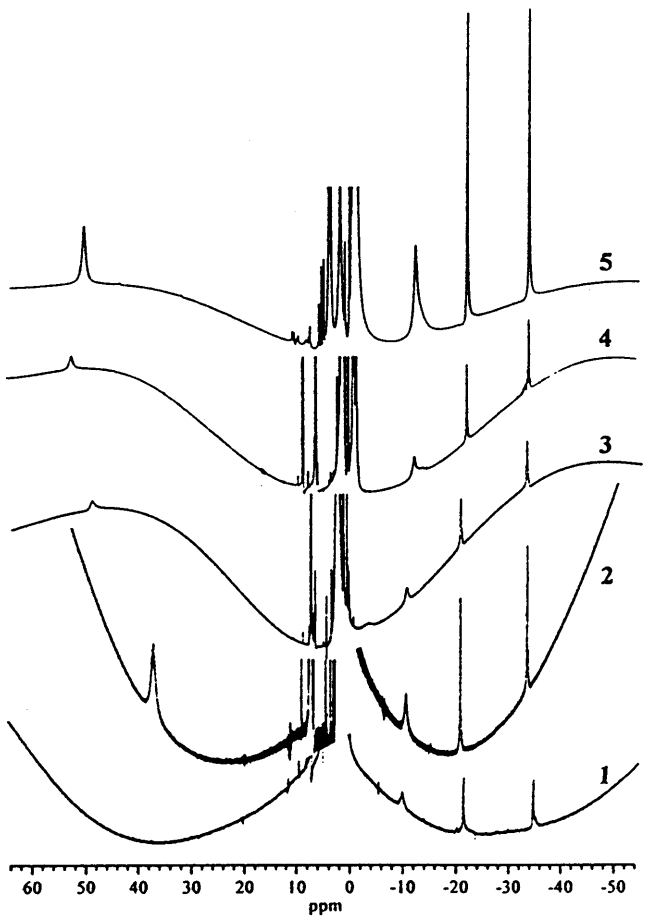


Fig. 9. ^1H NMR spectra of macrocyclic hexanuclear manganese complexes, **1**–**5** in acetone-d_6.

assigned to the methylene protons at the C9 position for the complex **3a**, **4** and **5**, respectively. However, no corresponding peak was observed in the complex **1** (Fig. 9) [11].

All hexanuclear manganese metallamacrocycles with various lengths of hydrophobic aliphatic linear chains are isostructural. The introduction of the side chain to the ligand does not disturb the formation of the hexanuclear manganese metallamacrocycle. Depending on the ligand used, two sets of triple hydrophobic tails of different lengths aligned at a right angle to the plane of the metallamacrocycle in opposite directions to each other. In general, the metallamacrocycle is only slightly soluble in various organic solvents. This might come from the large molecular weight of the metallamacrocycle. However, the solubility of the metallamacrocycle with long hydrophobic alkyl side chains is reasonably good in organic solvent. The ligands with the various functional groups might yield the isostructural metallamacrocycles with the interesting functional groups.

All metallamacrocycles are stable in the solid state. Even in solution, the metallamacrocycles were fairly stable. The ^{1}H NMR spectra of the metallamacrocycles did not change for at least a few months. The stability of the metallamacrocycles might come from the formation of the three chelating rings around the metal ions. The variation of the diameters of the holes (Table 3) implies that the metallamacrocycles have some degree of flexibility. Five donor atoms (from two chelating pentadentate ligands) and an additional donor atom (from a solvent molecule) have coordinated each metal center in the metallamacrocycle. In addition to the stability and flexibility of the metallamacrocycles, the presence of the replaceable solvent site suggests that the hexanuclear manganese metallamacrocycles could be used as a building block for the molecular frameworks [14] or a new type of molecular recognition agent.

4. Supplementary material

Crystallographic data (excluding structure factors) for the structure reported in this paper have been deposited with the Cambridge Crystallographic Data Centre, CCDC Nos. 136344 and 136347. Copies of the data can be obtained free of charge from The Director, CCDC, 12 Union Road, Cambridge, CB2 1EZ, UK (fax: +44-1223-336033; e-mail: deposit@ccdc.cam.ac.uk or www: http://www.ccdc.cam.ac.uk).

Acknowledgements

We thank the Korean Institute of Basic Science for elemental and mass spectroscopy analyses, and the National Institute of Technology and Quality, Dr Y. Park and Dr M. Choi, for the use of their X-ray diffractometers. The authors wish to acknowledge the financial support of the Korea Research Foundation (KRF-99-041-D00280).

References

[1] (a) J.M. Lehn, Supramolecular Chemistry: Concepts and Perspectives, VCH, New York, 1995. (b) D.J. Cram, J.M. Cram, Container Molecules and Their Guests, The Royal Society of Chemistry, Cambridge, UK, 1994.

[2] (a) K.N. Houk, K. Nakamura, C. Sheu, A.E. Keating, Science 273 (1996) 627. (b) J.M. Rivera, T. Martin, J. Rebek Jr., Science 279 (1998) 1021. (c) M. Asakawa, P.R. Ashton, R. Ballardini, V. Balzani, M. Belohradsky, M.T. Gandolfi, O. Kocian, L. Prodi, F.M. Raymo, J.F. Stoddart, M. Venturi, J. Am. Chem. Soc. 119 (1997) 302. (d) Y.M. Jeon, J. Kim, D. Whang, K. Kim, J. Am. Chem. Soc. 118 (1996) 9790. (e) S.S. Zhu, P.J. Carroll, T.M. Swager, J. Am. Chem. Soc. 118 (1996) 8713. (f) M. Berger, F.P. Schmidtchen, J. Am. Chem. Soc. 118 (1996) 8947. (g) C.F. van Nostrum, R.J.M. Nolte, J. Chem. Soc., Chem. Commun. (1996) 2385.

[3] (a) M. Fujita, O. Sasaki, T. Mitsuhashi, T. Fujita, J. Yazaki, K. Yamaguchi, K. Ogura, J. Chem. Soc., Chem. Commun. (1996) 1535. (b) P.J. Stang, B. Olenyuk, Acc. Chem. Res. 30 (1997) 502. (c) R.V. Slone, J.T. Hupp, C.L. Stern, T.E. Albrecht-Schmitt, Inorg. Chem. 35 (1996) 4096. (d) R.V. Slone, D.I. Yoon, R.M. Calhoun, J.T. Hupp, J. Am. Chem. Soc. 117 (1995) 11813.

[4] M.F. Hawthorne, Z. Zheng, Acc. Chem. Res. 30 (1997) 267.

[5] H. Rauter, E.C. Hillgeris, A. Erxleben, B. Lippert, J. Am. Chem. Soc. 116 (1994) 616.

[6] (a) M.J. Hannon, C.L. Painting, A. Jackson, J. Hamblin, W. Errington, J. Chem. Soc., Chem. Commun. (1997) 1807. (b) P.N.W. Baxter, J.M. Lehn, K. Rissanen, J. Chem. Soc., Chem. Commun. (1997) 1323.

[7] M. Clemente-León, E. Coronado, J.R. Galán-Mascarós, C.J. Gómez-García, J. Chem. Soc., Chem. Commun. (1997) 1727.

[8] (a) W. Clegg, A.M. Drummond, R.E. Mulvey, P. O'Shaughnessy, J. Chem. Soc., Chem. Commun. (1997) 1301. (b) F.S. McQuillan, H. Chen, T.A. Hamor, C.J. Jones, K. Paxton, Inorg. Chem. 36 (1997) 4458. (c) A.E. Pullen, J. Piotraschke, K.A. Abboud, J.R. Reynolds, Inorg. Chem. 35 (1996) 793. (d) Q. Huang, X. Wu, Q. Wang, T. Sheng, J. Lu, Inorg. Chem. 35 (1996) 893.

[9] (a) V.L. Pecoraro, A.J. Stemmler, B.R. Gibney, J.J. Bodwin, H. Wang, J.W. Kampf, A. Barwinski, in: K.D. Karlin (Ed.), Progress in Inorganic Chemistry, vol. 45, Wiley, 1997, pp 83. (b) M.S. Lah, V.L. Pecoraro, M.L. Kirk, W.E. Hatfield, in: R.P. Buck, W.E. Hatfield, M. Umaña, E.F. Bowden (Eds.), Biosensor Technology; Marcel Dekker Inc., 1991; pp. 201. (c) M.S. Lah, V.L. Pecoraro, Comments Inorg. Chem. 11 (1990) 59. (d) B.R. Gibney, A.J. Stemmler, S. Pilotek, J.W. Kampf, V.L. Pecoraro, Inorg. Chem. 32 (1993) 6008. (e) M.S. Lah, M.L. Kirk, W. Hatfield, V.L. Pecoraro, J. Chem. Soc., Chem. Commun. (1989) 1606. (f) V.L. Pecoraro, Inorg. Chim. Acta 155 (1989) 171. (g) B.R. Gibney, H. Wang, J.W. Kampf, V.L. Pecoraro, Inorg. Chem. 35 (1996) 6184. (h) B.R. Gibney, J.W. Kampf, D.P. Kessissiglou, V.L. Pecoraro, Inorg. Chem. 33 (1994) 4840. (i) M.S. Lah, V.L. Pecoraro, Inorg. Chem. 30 (1991) 878. (j) M.S. Lah, V.L. Pecoraro, J. Am. Chem. Soc. 111 (1989) 7258. (k) B. Kurzak, E. Farkas, T. Glowiak, H. Kozlowski, J. Chem. Soc., Dalton Trans. (1991) 163. (l) A.J. Stemmler, J.W. Kampf, V.L.

Pecoraro, Inorg. Chem. 34 (1995) 2771. (m) M.S. Lah, B.R. Gibney, D.L. Tierney, J.E. Penner-Hahn, V.L. Pecoraro, J. Am. Chem. Soc. 115 (1993) 5857. (n) A.J. Stemmler, A. Barwinski, M.J. Baldwin, Y. Victor, V.L. Pecoraro, J. Am. Chem. Soc. 118 (1996) 11962. (o) A.J. Stemmler, J.W. Kampf, V.L. Pecoraro, Angew. Chem., Int. Ed. Engl. 35 (1996) 2841. (p) D.P. Kessissiglou, J.W. Kampf, V.L. Pecoraro, Polyhedron 13 (1994) 1379.

[10] (a) A.J. Blake, R.O. Gould, C.M. Grant, P.E. Milne, D. Reed, E.P. Winpenny, Angew. Chem. Int. Ed. Engl. 33 (1994) 195. (b) A.J. Blake, R.O. Gould, P.E. Milne, E.P. Winpenny, J. Chem. Soc., Chem. Commun. (1991) 1453.

[11] B. Kwak, H. Rhee, S. Park, M.S. Lah, Inorg. Chem. 37 (1998) 3599.

[12] G.M. Sheldrick, Acta Crystallogr., Sect. A 46 (1990) 467.

[13] G.M. Sheldrick, SHELX-97; University of Göttingen, Göttinggen, Germany, 1997.

[14] M. Moon, I. Kim, M.S. Lah, Inorg. Chem 39 (2000) 2710.

PERGAMON

www.elsevier.nl/locate/poly

Polyhedron 19 (2000) 1995–2002

POLYHEDRON

Solvothermal synthesis and structure of iron tellurido carbonyl clusters

Birinchi K. Das [1], Mercouri G. Kanatzidis *

Department of Chemistry, Michigan State University, East Lansing, MI 48824, USA

Received 27 May 2000; accepted 7 June 2000

Abstract

Three compounds prepared solvothermally from a mixture of $Fe_3(CO)_{12}$, Na_2Te_2, and Ph_4PBr in the 1:5:6 molar ratio are described. The compound $(Ph_4P)_2[Fe_6Te_{14}(CO)_{12}]\cdot 2H_2O$ (**1**) was obtained by heating the reaction mixture in water at 130°C for 16 h. With 0.5 ml ethanol as the solvent for a reaction carried out at 110°C for 12 h, $(Ph_4P)_2[Fe_4Te_6(TeC_2H_5)_2(CO)_8]$ (**2**) was obtained. $(Ph_4P)_2[Fe_2Te_3(CO)_6]$ (**3**) was obtained as the only product in 4 h with 0.5 ml methanol heated at 80°C. These high-yield preparations illustrate vividly how strongly the identity of product is dependent on the conditions of a solvothermal reaction. X-ray structural studies reveal a variety of coordination modes for the Te_x^{2-} ligands present in these anionic polynuclear clusters.
© 2000 Elsevier Science Ltd. All rights reserved.

Keywords: Solvothermal synthesis; Polytelluride; Iron telluride; Iron cluster; Iron carbonyl; Carbonyl clusters

1. Introduction

The solvothermal preparation of metal carbonyl clusters containing polytelluride ligands is now well demonstrated as a synthesis technique [1]. A host of products can be obtained in high yield from reactions involving a mixture of a metal carbonyl compound, an alkali metal polytelluride and a suitable quaternary ammonium or phosphonium cation in an appropriate molar ratio. The improved solvent properties under hydrothermal (or solvothermal for nonaqueous solvents) conditions help in crystal growth [2] and thus in this preparative method lengthy purification procedures can often be avoided by way of the simple filtration of the only desired solid product. By developing this technique we have been successful in obtaining several anionic metal tellurido carbonyl clusters, both homo as well as heterometallic, in very good yield and high level of purity and crystallinity [3]. The nature of exact product formed is highly dependent on the various reaction parameters such as molar ratio of the reactants, solvent, and the temperature and duration of the reaction. We have already published our results on the unusual cluster anions $[M_4Te_6(TeCH_3)_2(CO)_8]^{2-}$ (M = Fe, Ru) [3e], $[Fe_2MTe_3(CO)_{11}]^{2-}$ (M = Mo, W) [3d], $[Fe_3W_2Te_8(TeCH_3)(CO)_{12}]^{3-}$ [3d], $[Fe_4Te_2(CO)_{14}]^{2-}$ [3b], $[HFe_3Te(CO)_9]^-$ [3b], $[Ru_4Te_2(CO)_{10}]^{2-}$ [3a], and $[Ru_5Te(CO)_{14}]^{2-}$ [3a]. The potency of the solvothermal reactions in generating metal clusters is also illustrated by our isolation of $[Fe_2(AsS)(CO)_6]^-$ and $[Fe_5As_2(CO)_{17}]^{2-}$ from reactions involving $Fe_3(CO)_{12}$, $NaAsO_2$, and Ph_4PBr [3c]. The sulfur atom in the former complex is derived from $Na_2S_2O_4$ which was added into the reaction mixture in order to reduce As^{3+} to As^0. In this paper we describe the solvothermal preparation and structural characterization of two new compounds $(Ph_4P)_2[Fe_6Te_{14}(CO)_{12}]\cdot 2H_2O$ (**1**) and $(Ph_4P)_2[Fe_4Te_6(TeC_2H_5)_2(CO)_8]$ (**2**) along with $(Ph_4P)_2[Fe_2Te_3(CO)_6]$ (**3**) which was previously isolated as $[(K.crypt)_2][Fe_2Te_3(CO)_6]\cdot 0.5en$ by reacting $Fe(CO)_3(\eta^4$-butadiene) with K_2Te_4 and crypt (4,7,13,16,21,24 - hexaoxa - 1,10 - diazabicyclo[8,8,8]hexacosane) in ethylenediamine (en) [4]. The present report highlights how an identical mixture consisting of $Fe_3(CO)_{12}$, Na_2Te_2 and Ph_4PBr under three different sets of reaction

* Corresponding author. Tel.: +1-517-355-9715; fax: +1-517-353-1793.

E-mail address: kanatzid@cem.msu.edu (M.G. Kanatzidis).

[1] Present address: Department of Chemistry, Gauhati University, Guwahati 781 014, India.

0277-5387/00/$ - see front matter © 2000 Elsevier Science Ltd. All rights reserved.
PII: S0277-5387(00)00471-X

conditions leads to the formation of three entirely different anionic iron-tellurido carbonyl clusters of nuclearities six, four and two.

2. Experimental

Solids were handled in an inert atmosphere glove box. Triiron dodecacarbonyl (Strem Chemicals Inc) and tetraphenylphosphonium bromide (Lancaster) were used as received. Sodium ditelluride was prepared by reacting stoichiometric amounts of the elements in liquid ammonia.

Solution IR spectra were recorded using a cell with NaCl windows on a Nicolet IR/42 FT Spectrometer. For obtaining the solid-state spectra also the same instrument was used. A Varian VXR-300 NMR spectrometer was used to obtain the ^{1}H NMR spectrum of **2**. ^{125}Te NMR spectra were obtained on a Varian VXR-500 spectrometer operating at approximately 157.9 MHz for ^{125}Te resonances. Spectral data were referenced to a signal for $TeCl_4$, dissolved in D_2O–HCl, at 1237 ppm with respect to Me_2Te at 0.0 ppm [5]. Elemental analyses for P, Fe and Te were performed by Energy Dispersive Spectroscopy (EDS) of X-rays using a JEOL JSM-6400V Scanning Electron Microscope. Instruments and experimental procedures of single crystal X-ray work are described in a separate section below.

2.1. Preparation of $(Ph_4P)_2[Fe_6Te_{14}(CO)_{12}]\cdot 2H_2O$ (1)

A mixture of 50 mg $Fe_3(CO)_{12}$ (0.1 mmol), 150 mg Na_2Te_2 (0.5 mmol) and 250 mg Ph_4PBr (0.6 mmol) was loaded into a thick-walled Pyrex tube of 9 mm outer diameter. The tube was frozen in liquid N_2 after adding 0.3 ml water (under nitrogen) into it and subsequently it was flame-sealed under vacuum. The sealed tube was heated at 130°C and the solid product was isolated after 16 h by washing with MeOH several times. The dark brown crystals of **1** were separated from the needle-shaped crystals of elemental tellurium by suspending the mixture in bromoform which is lighter than the Te crystals, but heavier than the triclinic plate-like crystals of **1**. Yield: 145 mg (ca. 90% based on Fe). EDS analysis gave a P:Fe:Te ratio close to the expected ratio of 1:3:7. IR data: (ν_{CO}, cm^{-1}; KBr pellet) 1978(sh), 1965(s), 1942(w), 1936(m), 1927(m).

2.2. Preparation of $(Ph_4P)_2[Fe_4Te_6(TeC_2H_5)_2(CO)_8]$ (2)

A mixture of 50 mg $Fe_3(CO)_{12}$ (0.1 mmol), 150 mg Na_2Te_2 (0.5 mmol) and 250 mg Ph_4PBr (0.6 mmol) was loaded into a thick-walled Pyrex tube of 9 mm outer diameter. The tube was frozen in liquid N_2 after adding 0.5 ml ethanol into it and subsequently it was flame-sealed under vacuum. The sealed tube was heated at 110°C and the dark brown crystals of **2** were isolated after 12 h by washing with MeOH. Yield: 127 mg (77% based on Fe). EDS analysis gave a P:Fe:Te ratio close to the expected ratio of 1:2:4. IR data: (a) (ν_{CO}, cm^{-1}; KBr pellet) 1948(s), 1997(s) (b) (ν_{CO}, cm^{-1}, DMF solution) 1971(w), 1945(m), 1907(vs). ^{1}H NMR (δ, ppm; DMSO-d_6 solution) 2.79(quartet), 1.61(triplet). UV–visible spectral data: (nm, DMF solution) 331(sh), 438(sh), 565(sh).

2.3. Preparation of $(Ph_4P)_2[Fe_2Te_3(CO)_6]$ (3)

A mixture of 50 mg $Fe_3(CO)_{12}$ (0.1 mmol), 150 mg Na_2Te_2 (0.5 mmol) and 250 mg Ph_4PBr (0.6 mmol) was loaded into a thick-walled Pyrex tube of 9 mm outer diameter. The tube was frozen in liquid N_2 after adding 0.5 ml methanol into it and subsequently it was sealed under vacuum. The sealed tube was heated at 80°C and the red brown, hexagonal plate-like crystals of **3** were isolated after 4 h by washing with small aliquots of MeOH. Yield: 130 mg (65% based on Fe). EDS analyses carried out on well defined crystals showed expected P:Fe:Te ratios. IR data: (a) (ν_{CO}, cm^{-1}; KBr pellet) 2024(w), 2018(w), 1993(s), 1951(s), 1914(s), 1903(s), 1892(vs), 1882(sh); (b) (ν_{CO}, cm^{-1}, DMF solution) 2002(m), 1973(m), 1923(s), 1908(s). UV–Vis spectrum in DMF solution: λ_{max}, 515 nm ($\varepsilon = 7230\ M^{-1}\ cm^{-1}$). ^{125}Te NMR spectral data (δ, ppm; DMSO-d_6 solution): 241, −32, −613.

2.4. X-ray crystallography

The single crystals used for X-ray diffraction experiments were chosen from the products formed during the solvothermal reactions employed for preparing the compounds. Intensity data of **1** were collected on a Rigaku AFC-6S diffractometer using Mo Kα ($\lambda =$ 0.7107 Å). A crystal sealed inside a glass capillary was used as the specimen for doing the experiments at room temperature. For the crystal of **2** also, similar arrangements were made. To collect the intensity data on **3**, a glass fiber mounted crystal was cooled with a cold stream of nitrogen gas and it was seen that no ice crystals had developed over the crystal surfaces during the data collection process. Intensities of three standard reflections were measured repeatedly after every 200 reflections in all three cases during the collection of intensity data. No significant decay of intensities was observed, however. The structures were solved by direct methods using SHELXS-86 [6] and were refined on a VAXstation 3100/76 computer by least squares techniques using the TEXSAN crystallographic software package [7]. Intensity data were corrected for absorption effects using the empirical method of Walker and Stuart [8]. These corrections were applied to the data by

using the refined parameters obtained after refining the non-hydrogen atom structure isotropically to convergence. For all structures the non-hydrogen atoms barring the carbon atoms belonging to the tetraphenylphosphonium cations were refined anisotropically and the carbon-bonded hydrogen atoms were placed at calculated positions, but not refined. The hydrogen atoms belonging to the water molecules in **1** were ignored. Relevant crystal data on **1**, **2**, and **3** are presented in Table 1. Positional coordinates and geometric data on the structurally important portions of **1**, **2**, and **3** have been deposited (see below).

3. Results and discussion

The preparative reaction explored in this work has been classified previously as *oxidative decarbonylation* wherein chalcogenide fragments oxidatively replace some or all of the CO ligands of a neutral metal carbonyl compound [1b,9]. However, partial substitution of CO ligands may also occur without any concomitant oxidation of the central metal atom as shown by the report on the $[M(CO)_4Te_4]^{2-}$ (M = Cr, Mo, W) anions, which were prepared by reacting $M(CO)_6$ with K_2Te_4 [9]. On the other hand, Se_3^{2-} anions were shown to completely decarbonylate $Mn_2(CO)_{10}$ at 100°C in DMF so as to form $[Mn(Se_4)_2]^{2-}$ [10]. However, under solvothermal (albeit more drastic) conditions we have invariably observed only partial decarbonylation reactions which have resulted in the isolation of several anionic metal-chalcogenido clusters including $[Mn_3(Q_2)_2(QCH_3)(CO)_9]^{2-}$ (Q = S, Se, Te), [1b,11], $[Re_4(Te_2)_3(TeCH_3)(CO)_{12}]^{3-}$ (this compound was prepared from $CpRe(CO)_3$ and as such no CO ligands have been removed during the reaction) [1b,11]) $[Fe_4Se_2(Se_2)(CO)_{12}]^{2-}$ [3f], $[Fe_8Te_8(Te_2)(CO)_{20}]^{2-}$ [3f], and $[Ru_6(Te_2)_7(CO)_{12}]^{2-}$ [3g]. These and other routes to the synthesis of metal carbonyl clusters containing main-group element based ligands have been extensively reviewed [1,9,12].

In the present reactions, Na_2Te_2 has been used to decarbonylate $Fe_3(CO)_{12}$ in the presence of the large Ph_4P^+ cations. Syntheses, molecular structures and properties of **1**, **2**, **3** are discussed below under separate headings.

3.1. $[Fe_6Te_{14}(CO)_{12}]^{2-}$

Compound **1** has been obtained as the only insoluble crystalline species other than the crystals of elemental tellurium using a 1:5:6 reaction mixture of $Fe_3(CO)_{12}$,

Table 1
Crystal data for $(Ph_4P)_2[Fe_6Te_{14}(CO)_{12}]\cdot 2H_2O$ (**1**), $(Ph_4P)_2[Fe_4Te_6(TeC_2H_5)_2(CO)_8]$ (**2**) and $(Ph_4P)_2[Fe_2Te_3(CO)_6]$ (**3**)

	1	**2**	**3**
Formula	$C_{60}H_{44}O_{14}Fe_6P_2Te_{14}$	$C_{60}H_{50}O_8Fe_4P_2Te_8$	$C_{54}H_{40}O_6P_2Fe_2Te_3$
Unit cell dimensions			
a (Å)	13.528(4)	13.010(5)	19.981(8)
b (Å)	14.561(5)	13.647(4)	12.110(6)
c (Å)	13.351(3)	11.466(5)	21.519(6)
α (°)	115.14(2)	114.79(3)	90
β (°)	90.85(3)	112.29(3)	106.92(2)
γ (°)	116.30(2)	80.57(3)	90
Z	1	1	4
V (Å^3)	2067(1)	1710(3)	4981(6)
Space group	$P\bar{1}$ (No. 2)	$P\bar{1}$ (No. 2)	$P2_1/a$ (No. 14)
D_{calc} (g cm^{-3})	2.549	2.141	1.788
Crystal size (mm)	$0.1\times0.2\times0.2$	$0.1\times0.2\times0.3$	$0.06\times0.3\times0.3$
$2\theta_{max}$ (°)	50	50	45
Temperature (°C)	23	23	−96
Number of data collected (independent)	7262	4495	4726
Number of data used ($F_o^2>3\sigma F_o^2$)	4696	2875	3264
Number of variables	436	250	364
λ (Mo Kα) (cm^{-1})	59.752	42.816	24.211
Minimum and maximum absorption	0.875, 1.040	0.809, 1.120	0.855, 1.305
Final R, R_w [a]	0.033, 0.044	0.045, 0.053	0.039, 0.042
Goodness-of-fit [b]	1.566	1.987	1.717
Largest shift/error	0.001	0.002	0.001
Highest electron density in final difference Fourier map	ca. 1.0 in the diffuse water region	1.7 (1.34 Å from less than 1 e Te(1))	

[a] $R=\Sigma(|F_o|-|F_c|)/\Sigma|F_o|$; $R_w=\{\Sigma w(|F_o|-|F_c|)^2/\Sigma w|F_o|^2\}^{1/2}$
[b] $S=\{\Sigma(|F_o|-|F_c|)/\sigma\}/(n-m)$; for n reflections and m variables.

Table 2
Bond distances (Å) and angles (°) for $(Ph_4P)_2[Fe_6Te_{14}(CO)_{12}]\cdot 2H_2O$ (**1**)

Te(1)–Te(1)′	2.726(2)
Te(1)–Fe(1)	2.639(2)
Te(1)–Fe(2)	2.640(2)
Te(1)–Fe(3)	2.645(3)
Te(2)–Fe(1)	2.588(2)
Te(2)–Fe(2)′	2.654(2)
Te(2)–Te(5)	2.771(2)
Te(3)–Fe(1)	2.649(2)
Te(3)–Fe(3)′	2.577(2)
Te(3)–Te(7)	2.769(2)
Te(4)–Fe(1)	2.603(2)
Te(4)–Te(6)	2.779(1)
Te(5)–Fe(3)	2.596(2)
Te(6)–Fe(2)	2.589(2)
Te(6)–Fe(3)′	2.661(2)
Te(7)–Fe(2)′	2.614(3)
Fe(1)–C(1)	1.80(1)
Fe(1)–C(2)	1.75(1)
Fe(2)–C(3)	1.76(1)
Fe(2)–C(4)	1.78(1)
Fe(3)–C(5)	1.81(1)
Fe(3)–C(6)	1.72(1)
O(1)–C(1)	1.11(1)
O(2)–C(2)	1.16(1)
O(3)–C(3)	1.15(1)
O(4)–C(4)	1.12(1)
O(5)–C(5)	1.08(1)
O(6)–C(6)	1.17(1)
Fe(1)–Te(1)–Fe(2)	118.52(7)
Fe(1)–Te(1)–Fe(3)	118.52(7)
Fe(1)–Te(2)–Fe(2)	108.95(6)
Fe(1)–Te(3)–Fe(3)	109.71(6)
Fe(2)–Te(1)–Fe(3)	118.27(7)
Fe(2)–Te(6)–Fe(3)	109.37(7)
Te(1)–Fe(1)–Te(2)	86.12(7)
Te(1)–Fe(1)–Te(3)	99.32(7)
Te(1)–Fe(1)–Te(4)	94.81(7)
Te(1)–Fe(2)–Te(2)	99.27(6)
Te(1)–Fe(2)–Te(6)	86.32(7)
Te(1)–Fe(2)–Te(7)	94.47(7)
Te(1)–Fe(3)–Te(3)	86.61(7)
Te(1)–Fe(3)–Te(5)	94.50(7)
Te(1)–Fe(3)–Te(6)	99.02(7)
Te(1)′–Te(1)–Fe(1)	96.99(6)
Te(1)′–Te(1)–Fe(2)	97.10(6)
Te(1)′–Te(1)–Fe(3)	97.12(6)
Te(2)–Fe(1)–Te(3)	91.72(6)
Te(2)–Fe(1)–Te(4)	170.49(8)
Te(2)–Fe(2)–Te(6)	90.04(9)
Te(2)–Fe(2)–Te(7)	79.82(6)
Te(2)–Te(5)–Fe(3)	96.99(6)
Te(3)–Fe(1)–Te(4)	78.79(6)
Te(3)–Fe(3)–Te(5)	170.39(8)
Te(3)–Fe(3)–Te(6)	90.30(6)
Te(3)–Te(7)–Fe(2)	97.47(6)
Te(4)–Te(6)–Fe(2)	100.75(6)
Te(4)–Te(6)–Fe(3)	103.65(5)
Te(5)–Fe(3)–Te(6)	80.09(6)
Te(5)–Te(2)–Fe(1)	100.41(6)
Te(5)–Te(2)–Fe(2)	105.19(6)
Te(6)–Fe(2)–Te(7)	169.83(8)
Te(6)–Te(4)–Fe(1)	97.24(6)
Te(7)–Te(3)–Fe(1)	103.59(6)
Te(7)–Te(3)–Fe(3)	100.30(6)
Fe(1)–C(1)–O(1)	176(1)
Fe(1)–C(2)–O(2)	175(1)
Fe(2)–C(3)–O(3)	175(1)
Fe(2)–C(4)–O(4)	177(1)
Fe(3)–C(5)–O(5)	174(1)
Fe(3)–C(6)–O(6)	178(1)

Na_2Te_2 and Ph_4PBr at 130°C in water. The same compound has also been found to form at 110°C, which is incidentally the temperature at which the ruthenium analogue of **1** was prepared [3g], but the product in the present instance is microcrystalline in nature. The tellurium crystals are conveniently separated from the desired product by taking advantage of their different densities with respect to that of the heavy organic liquid bromoform where compound **1** is not soluble. Crystals of **1** are fairly stable in air and these have appreciable solubility only in DMF and DMSO among common organic solvents. The $[Fe_6Te_{14}(CO)_{12}]^{2-}$ anion in **1** is isostructural (Fig. 1) with $[Ru_6Te_{14}(CO)_{12}]^{2-}$ and the powder X-ray diffraction patterns of both compounds are nearly superimposable. The structural relationship of the $\{Ru_6(Te_2)_7\}^{2-}$ core in the latter with the pyrite structure type has been emphasized earlier [3g] and the same arguments are valid in the case of compound **1** as well. The ethane-like staggered geometry of the central μ_3,μ_3-Te_2 fragment is a notable feature of this type of structure. This ditelluride ligand in **1** and its ruthenium analogue have nearly the same Te–Te distance. Other

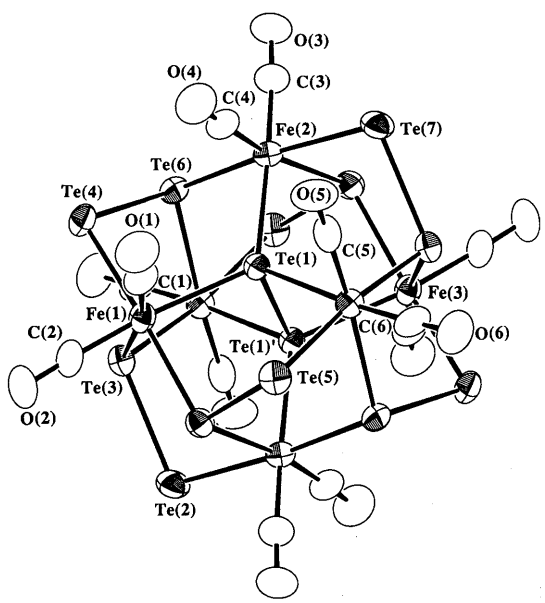


Fig. 1. An ORTEP view of the $[Fe_6Te_{14}(CO)_{12}]^{2-}$ cluster anion in **1**.

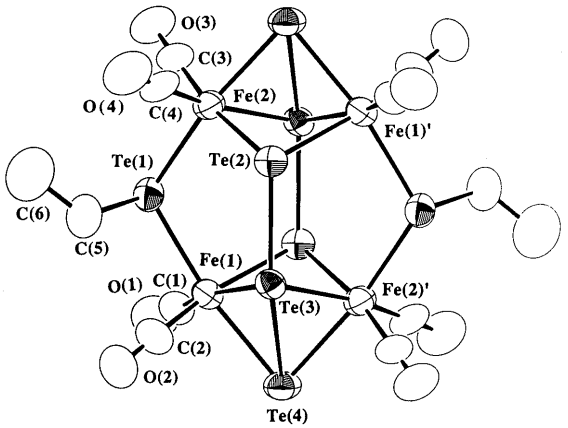


Fig. 2. An ORTEP view of the $[Fe_4Te_6(TeC_2H_5)_2(CO)_8]^{2-}$ cluster anion in **2**.

Te–Te distances are also comparable in magnitude. Selected bond distances and angles are given in Table 2.

The Fe–C bonds in **1** (ca. 1.77 Å) are uniformly shorter compared to those in $[Ru_6Te_{14}(CO)_{12}]^{2-}$ (ca. 1.9 Å) and this difference is reflected appropriately in the carbonyl region IR spectra of the compounds. While the two pairs of ν(CO) doublets in **1** center around 1967 and 1929 cm^{-1}, those in the ruthenium compound appear at ca. 1997 and 1950 cm^{-1}. Although three ^{125}Te NMR signals were reported [3g] to occur for $[Ru_6Te_{14}(CO)_{12}]^{2-}$ at -1606, -2978, and -3616 ppm, no such signals could be recorded under similar conditions for **1**. The dark brown crystals of **1** dissolve slowly in DMF to give a dark solution, which may not contain much of $[Fe_6Te_{14}(CO)_{12}]^{2-}$ as evidenced by the rather poorly defined IR spectrum of the solution. It is likely to behave in deuterated DMF in a similar manner and during the long hours of ^{125}Te signal acquisition, the sample must have decomposed to a mixture of unknown species. Solution IR spectra of $[Ru_6Te_{14}(CO)_{12}]^{2-}$ were not reported. The above results, however, indicate a difference in solution stability between the iron and ruthenium clusters having identical solid state structures. Perhaps due to the same inherent reasons we were previously unable to isolate the iron analogues of the pseudo-octahedral ruthenium clusters $[Ru_5(\mu_4\text{-Te})(CO)_{14}]^{2-}$ and $[Ru_4(\mu_4\text{-Te})_2(CO)_{10}]^{2-}$ [3a].

3.2. $[Fe_4Te_6(TeC_2H_5)_2(CO)_8]^{2-}$

The synthesis and characterization of two chemical analogues of **2** have been previously reported [3e]. In spite of the triclinic symmetry of the crystals of **2**, the structure of the $[Fe_4Te_6(TeC_2H_5)_2(CO)_8]^{2-}$ anion (Fig. 2) present in this compound is closely related to the $[M_4Te_6(TeCH_3)_2(CO)_8]^{2-}$ anions [3e] present in its analogues described below. Selected bond distances and angles are given in Table 3. The compound $(Me_4N)_2[Fe_4Te_6(TeCH_3)_2(CO)_8]$ was made using a set of near identical conditions ($Fe_3(CO)_{12}/Na_2Te_2/Me_4NBr$ in a 1:5:6 ratio, 110°C, 12 h, 0.5 ml MeOH) with those of **2**, while $(Ph_4P)_2[Ru_4Te_6(TeCH_3)_2(CO)_8]$ was prepared at a lower temperature. In the formation of these two structurally unique compounds a novel telluride alkyla-

Table 3
Bond distances (Å) and angles (°) for $(Ph_4P)_2[Fe_4Te_6(TeC_2H_5)_2(CO)_8]$ (**2**)

Te(1)–Fe(1)	2.582(3)
Te(1)–Fe(2)	2.596(2)
Te(1)–C(5)	2.17(2)
Te(2)–Te(3)′	2.817(2)
Te(2)–Fe(1)	2.604(2)
Te(2)–Fe(2)	2.614(3)
Te(3)···Te(4)	3.233(2)
Te(3)–Fe(1)	2.611(2)
Te(3)–Fe(2)	2.595(3)
Te(4)–Fe(1)	2.662(3)
Te(4)–Fe(2)	2.650(2)
Fe(1)–C(1)	1.75(2)
Fe(1)–C(2)	1.72(2)
Fe(2)–C(3)	1.77(2)
Fe(2)–C(4)	1.76(2)
O(1)–C(1)	1.17(2)
O(2)–C(2)	1.17(2)
O(3)–C(3)	1.14(2)
O(4)–C(4)	1.15(2)
C(5)–C(6)	1.52(3)
Te(2)···Te(4)	3.361(2)
Fe(1)···Fe(2)′	4.360(3)
Fe(1)···Fe(2)	3.482(4)
Fe(1)–Te(1)–Fe(2)	114.71(8)
Te(3)–Te(2)–Fe(1)	106.46(7)
Te(3)–Te(2)–Fe(2)	107.04(7)
Fe(1)–Te(2)–Fe(2)	83.72(8)
Te(2)–Te(3)–Te(4)	149.73(4)
Te(2)–Te(3)–Fe(1)	107.32(6)
Te(2)–Te(3)–Fe(2)	108.08(7)
Te(4)–Te(3)–Fe(1)	52.90(6)
Te(4)–Te(3)–Fe(2)	52.72(6)
Fe(1)–Te(3)–Fe(2)	83.97(8)
Te(3)–Te(4)–Fe(1)	51.46(6)
Te(3)–Te(4)–Fe(2)	51.18(5)
Fe(1)–Te(4)–Fe(2)	81.92(7)
Te(1)–Fe(1)–Te(2)	93.56(8)
Te(1)–Fe(1)–Te(3)	99.31(8)
Te(1)–Fe(1)–Te(4)	171.4(1)
Te(2)–Fe(1)–Te(3)	86.03(7)
Te(2)–Fe(1)–Te(4)	79.31(8)
Te(3)–Fe(1)–Te(4)	75.64(7)
Te(1)–Fe(2)–Te(2)	99.10(8)
Te(1)–Fe(2)–Te(3)	92.75(8)
Te(1)–Fe(2)–Te(4)	168.8(1)
Te(2)–Fe(2)–Te(3)	86.14(8)
Te(2)–Fe(2)–Te(4)	79.35(8)
Te(3)–Fe(2)–Te(4)	76.11(7)
Fe(1)–C(1)–O(1)	178(2)
Fe(1)–C(2)–O(2)	178(2)
Fe(2)–C(3)–O(3)	178(1)
Fe(2)–C(4)–O(4)	179(1)
Te(1)–C(5)–C(6)	112(2)

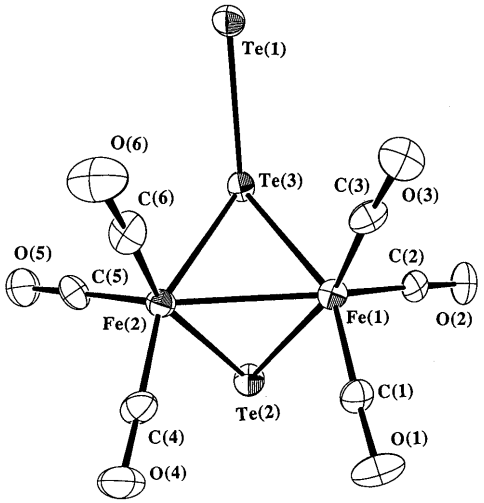


Fig. 3. An ORTEP view of the $[Fe_2Te_3(CO)_6]^{2-}$ cluster anion in **3**.

Table 4
Bond Distances(Å) and Angles(°) for $(Ph_4P)_2[Fe_2Te_3(CO)_6]$ (**3**)

Te(1)–Te(3)	2.736(2)
Te(2)···Te(3)	3.307(2)
Te(2)–Fe(1)	2.590(2)
Te(2)–Fe(2)	2.594(2)
Te(3)–Fe(1)	2.551(1)
Te(3)–Fe(2)	2.560(2)
Fe(1)–Fe(2)	2.651(2)
Fe(1)–C(1)	1.756(8)
Fe(1)–C(2)	1.78(1)
Fe(1)–C(3)	1.77(1)
Fe(2)–C(4)	1.757(9)
Fe(2)–C(5)	1.747(8)
Fe(2)–C(6)	1.78(1)
O(1)–C(1)	1.16(1)
O(2)–C(2)	1.14(1)
O(3)–C(3)	1.16(1)
O(4)–C(4)	1.17(1)
O(5)–C(5)	1.17(1)
O(6)–C(6)	1.14(1)
Fe(1)–Te(2)–Fe(2)	61.49(5)
Te(1)–Te(3)–Fe(1)	113.24(3)
Te(1)–Te(3)–Fe(2)	115.15(4)
Fe(1)–Te(3)–Fe(2)	62.48(4)
Te(2)–Fe(1)–Te(3)	80.07(4)
Te(2)–Fe(1)–Fe(2)	59.33(4)
Te(3)–Fe(1)–Fe(2)	58.93(4)
Te(2)–Fe(2)–Te(3)	79.83(5)
Te(2)–Fe(2)–Fe(1)	59.18(4)
Te(3)–Fe(2)–Fe(1)	58.59(4)
Fe(1)–C(1)–O(1)	178.7(8)
Fe(1)–C(2)–O(2)	178.6(7)
Fe(1)–C(3)–O(3)	177.0(7)
Fe(2)–C(4)–O(4)	177.6(7)
Fe(2)–C(5)–O(5)	178.3(7)
Fe(2)–C(6)–O(6)	175.1(8)

tion reaction was found to occur in methanolic media. In order to learn more about the mechanistic pathway involved in this process the present reaction involving a 1:5:6 mixture of $Fe_3(CO)_{12}$, Na_2Te_2, Ph_4PBr in *ethanol* was carried out. Isolation of **2**, with its $TeCH_2CH_3$ ligand, has thus established the involvement of the alcoholic media in the telluride alkylation process.

The ethyl group is easily identified in the ^1H NMR spectrum of **2**. Although it was not possible to observe a ^{125}Te NMR spectrum of the present compound, considering the fact that its methyl analogue $[Fe_4Te_6(TeCH_3)_2(CO)_8]^{2-}$ was found to display four instead of the expected three signals, the solution stability of $[Fe_4Te_6(TeC_2H_5)_2(CO)_8]^{2-}$ is also suspect [1,3e]. The solution IR spectrum of the later displays three ν(CO) bands and the spectrum in the carbonyl stretching region is nearly identical with that of the former [3e]. The color of the solution of **2** in DMF or DMSO is yellowish green and the UV–Vis spectral behavior of the solution is similar to that of $(Me_4N)_2[Fe_4Te_6(TeCH_3)_2(CO)_8]$.

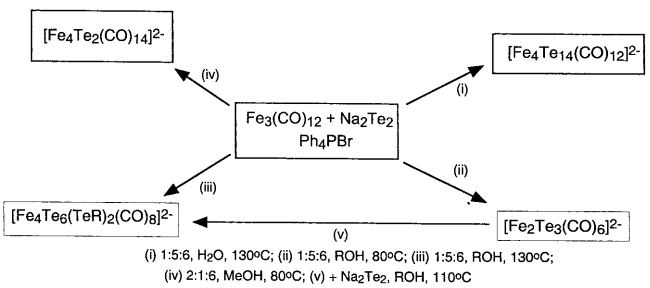
3.3. $[Fe_2Te_3(CO)_6]^{2-}$

The simpler cluster anion $[Fe_2Te_3(CO)_6]^{2-}$ was previously made from the reaction of $Fe(CO)_3(\eta^4$-butadiene) with the soluble Te_4^{2-} ions in ethylenediamine [4]. This compound is structurally quite novel because of the presence of a dangling tellurium atom from a η^1,μ_2-Te_2^{2-} ligand. Following the isolation and structural characterization of the alkylated tetranuclear clusters we saw the obvious structural relationship between $[Fe_2Te_3(CO)_6]^{2-}$ and $[M_4Te_6(TeR)_2(CO)_8]^{2-}$ and it was found interesting to probe if the former could be involved in the formation of the latter. By carrying out methanothermal reactions at lower temperatures and for shorter duration, it was possible to isolate red-brown hexagon-shaped crystals of a single product that was moderately soluble in methanol. This is unlike other tetraphenylphosphonium salts of iron-carbonyl telluride anions are sparingly soluble in methanol. The IR spectrum for the carbonyl stretching vibrations of this product differed somewhat from the one reported for $[(K.crypt)_2][Fe_2Te_3(CO)_6]\cdot 0.5en$ (**4**) and as a result, its crystal structure was determined. Notwithstanding this minor difference, the X-ray structure of **3** (Fig. 3) shows that the anionic cluster contained in our crystal is essentially the same with that of the K.crypt-compound. The residuals for the X-ray diffraction analysis on $(Ph_4P)_2[Fe_2Te_3(CO)_6]$ (**3**) are, however, considerably better than those of **4** and thus more accurate geometrical parameters of $[Fe_2Te_3(CO)_6]^{2-}$ are now available.

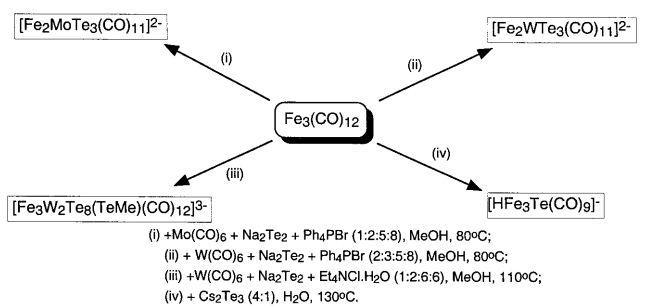
An ORTEP representation of the $[Fe_2Te_3(CO)_6]^{2-}$ cluster anion present in **3** is shown in Fig. 3. The Fe–Fe distance of 2.651(2) Å in **3** is longer than the corresponding distance (2.614(4) Å) in **4**. Similarly, the Te–Te distance in the ditelluride ligand is also longer (2.736(2) and 2.705(3) Å). The non-bonding Te(2)···Te(3) distances are however significantly differ-

ent (by 0.09 Å) in the two structures, the distance in **3** being longer at 3.307(2) Å. Selected bond distances and angles are given in Table 4. We have previously noticed [3b,e] short, non-bonding contacts between tellurium atoms in similar clusters and from a comparison of those results with the present ones it appears to us that such distances may be quite sensitive to crystal packing effects. Thus Te–Te bonding interactions are likely to be significant only when the distances are about 3.1 Å or shorter. Another structural difference of note in **4** and **3** is that in the latter, all the Fe–C distances are roughly equal ($\sim$ 1.76 Å), but these are found in the range of 1.683–1.814 Å in the former. This difference could explain the small departures between the number and positions of the ν(CO) vibrations in the IR spectrum. Our work, on the other hand, proves that compound **3** is a true intermediate in the reaction that leads to the formation of the tetranuclear clusters, as evidenced by our isolation of $(Ph_4P)_2[Fe_4Te_6(TeCH_3)_2(CO)_8]$ in the reaction between **3** and Na_2Te_2 at 110°C [3e]. The dangling tellurium atom in $[Fe_2Te_3(CO)_6]^{2-}$ thus acts as a center of high reactivity as shown by the conversion of two $[Fe_2Te_3(CO)_6]^{2-}$ clusters into $[M_4Te_6(TeR)_2(CO)_8]^{2-}$ [1a,3e].

We have already noted the moderate solubility of **3** in methanol. This compound gives reddish solutions in most of the polar organic solvents. The DMF solution displays a moderately intense absorption band at 515 nm that is of as yet unknown origin. Bands of similar origin were also observed for the clusters $[Fe_2MoTe_3(CO)_{11}]^{2-}$ and $[Fe_2WTe_3(CO)_{11}]^{2-}$ at 509 nm [3d].



Scheme 1.



Scheme 2.

These solutions are stable in an inert atmosphere. The carbonyl region of the IR spectrum recorded for a DMF solution of **3** is much more simplified. From its similarity with the solution spectrum previously reported for **4**, and from the fact that $(Ph_4P)_2[Fe_2Te_3(CO)_6]$ (**3**) can be recovered from a solution of **3** in DMF by adding diethyl ether, leaves no doubt that the dinuclear $[Fe_2Te_3(CO)_6]^{2-}$ cluster anion remains intact in solution. Moreover, three ^{125}Te resonances are observable for a solution of **3** in DMSO-d_6 corresponding to the three different types of tellurium environment.

4. Summary and conclusions

The synthetic results obtained from our studies are summarized in Schemes 1 and 2. These highlight the usefulness of the solvothermal technique in the synthesis of anionic metal chalcogenido carbonyl clusters. Of particular note is the extensive chemistry that has been generated on this type of reaction for the $Fe_3(CO)_{12}/Te_x^{2-}$ system. Clearly, the right set of conditions must be used for synthesizing a particular cluster compound solvothermally. Thus in the present reactions involving $Fe_3(CO)_{12}$, Na_2Te_2, and Ph_4PBr in the 1:5:6 molar ratio, the hexanuclear cluster **1** containing as many as fourteen tellurium atoms (as ditelluride ligands) is the product when water is the solvent of choice; on the other hand, the tetranuclear cluster **2** with ethyl tellurolate ligands (in addition to mono and ditellurides) is obtained just by changing the solvent to ethanol. In methanol, the cluster species formed is $[Fe_4Te_6(TeCH_3)_2(CO)_8]^{2-}$. Observation of telluride alkylation reactions in alcoholic media suggests the participation of the solvents in these reactions. This fact also indicates why compound **1** cannot form in alcoholic solvents. That a non-alcoholic solvent is necessary for the preparation of **1** is also confirmed by our isolation of **1** using CH_3CN.

Solvothermal preparation of **1** and its ruthenium analogue $[Ru_6Te_{14}(CO)_{12}]^{2-}$ as well as **2** and its chemical analogues $[Fe_4Te_6(TeCH_3)_2(CO)_8]^{2-}$ and $[Ru_4Te_6(TeCH_3)_2(CO)_8]^{2-}$ proves that the syntheses described are rational and reproducible and not mere serendipities. Thus this method can provide planned routes to the preparation of desired products. For the isolation of intermediate compounds, the reaction temperature must be controlled as shown by our isolation of **3**.

Choice of the starting metal carbonyl compound also appears to play an important role in the formation of a particular complex. For example, the double cubane cluster [13] $[Fe_8Te_{10}(CO)_{20}]^{2-}$ is obtained by reacting $Fe(CO)_5$ with Na_2Te_2 [3f], but the same cluster anion has never been found to form in reactions where $Fe_3(CO)_{12}$ is the starting carbonyl compound, except in the isolated instance of its formation as a byproduct

along with $[Fe_2MoTe_3(CO)_{11}]^{2-}$ [3d]. Similarly, compound **1** is not obtainable from $Fe(CO)_5$. Furthermore, reactant ratios do play a crucial role in determining the nature of the product formed. Thus, while a 2:3:5 mixture of $Fe_3(CO)_{12}$, $W(CO)_6$ and Na_2Te_2 leads to the formation of $[Fe_2WTe_3(CO)_{11}]^{2-}$, a change of the ratio to 1:2:6 results in the isolation of the cluster $[Fe_3W_2Te_8(TeCH_3)(CO)_{12}]^{3-}$ [3d]. For obtaining the tellurium-poor species $[Fe_4Te_2(CO)_{14}]^{2-}$ we must use an $Fe_3(CO)_{12}$: Na_2Te_2 ratio of 2:1, and to make $[HFe_3Te(CO)_9]^-$, the $Fe_3(CO)_{12}$:Cs_2Te_3 ratio of 4:1 must be used [3b]. Slight change in reactant ratio and reaction time during the preparation of the former resulted in the formation of yet another cluster anion $[Fe_5Te_4(CO)_{14}]^{2-}$. However, values of x in the range of 2–4 in the telluride fragment Te_x^{2-} of the starting alkali telluride appears to have no influence on the identity of products. This is only to be expected because the chalcogenide species (Q_x^{2-}) formed in solutions prepared by dissolving a solid alkali metal chalcogenide may correspond to $x = 1$–6, depending on the conditions. Synthetic methods of the type described here may also be useful for the synthesis of other molecular organometallic and coordination compounds.

5. Supplementary data

Crystallographic data (excluding structure factors) for the structural analysis have been deposited with the Cambridge Crystallographic Data Centre, CCDC Nos. 145390 and 145392. Copies of this information may be obtained free of charge from: The Director, CCDC, 12 Union Road, Cambridge, CB2 1EZ, UK (fax: +44-1223-336033; e-mail: deposit@ccdc.cam.ac.uk or www: http://www.ccdc.cam.ac.uk).

Acknowledgements

Financial support for this work was made available by the National Science Foundation. B.K.D. thanks Gauhati University for a leave which enabled him to carry out this work.

References

[1] (a) M.G. Kanatzidis, B.K. Das, Comments Inorg. Chem. 21 (1999) 29. (b) S.-P. Huang, M.G. Kanatzidis, Coord. Chem. Rev. 130 (1994) 509.
[2] (a) R.A. Laudise, Chem. Eng. News, September 28, 1987, 30. (b) A. Rabenau, Angew. Chem., Int. Ed. Engl. 24 (1985) 1026.
[3] (a) B.K. Das, M.G. Kanatzidis, Polyhedron 16 (1997) 3061. (b) B.K. Das, M.G. Kanatzidis, J. Organomet. Chem. 513 (1996) 1. (c) B.K. Das, M.G. Kanatzidis, Inorg. Chem. 34 (1995) 6505. (d) B.K. Das, M.G. Kanatzidis, Inorg. Chem. 34 (1995) 5721. (e) B.K. Das, M.G. Kanatzidis, Inorg. Chem. 34 (1995) 1011. (f) S.-P. Huang, M.G. Kanatzidis, Inorg. Chem. 32 (1993) 821. (g) S.-P. Huang, M.G. Kanatzidis, J. Am. Chem. Soc. 114 (1992) 5477.
[4] B.W. Eichhorn, R.C. Haushalter, J.S. Merola, Inorg. Chem. 29 (1990) 728.
[5] H. Schumann, M.J. Magerstodt, J. Organomet. Chem. 232 (1982) 147.
[6] G.M. Sheldrick, SHELXS-86: A Computer Program for Automatic Crystal Structures, Universität Göttingen.
[7] TEXSAN: Single Crystal Structure Analysis Software, Version 5.0, Molecular Structure Corp., The Woodlands, TX.
[8] N. Walker, D. Stuart, Acta Crystallogr., Sect. A 39 (1983) 158.
[9] (a) L.C. Roof, J.W. Kolis, Chem. Rev. 93 (1993) 1037. (b) J.W. Kolis, Coord.
[10] S.C. O'Neal, W.T. Pennington, J.W. Kolis, Inorg. Chem. 29 (1990) 3134.
[11] S.-P. Huang, Ph.D. Thesis, Michigan State University, USA (1993).
[12] (a) M. Shieh, J. Cust. Sc. 10 (1999) 3. (b) N.A. Compton, R.J. Errington, N.C. Norman, Adv. Organomet. Chem. 31 (1990) 91. (c) K.H. Whitmire, J. Coord. Chem. 17 (1988) 95.
[13] L.C. Roof, W.T. Pennington, J.W. Kolis, Angew. Chem., Int. Ed. Engl. 31 (1992) 153.

PERGAMON

www.elsevier.nl/locate/poly

Polyhedron 19 (2000) 2003–2010

POLYHEDRON

Ligand reactivity, substituent effects and solvent interactions in the spectra and structure of some oxovanadium(V) chelates with Schiff bases. Proof for dimeric species

Chris Tsiamis *, Byron Voulgaropoulos, Dimitrios Charistos, George P. Voutsas, Constantin A. Kavounis

Department of Chemistry and Department of Physics, University of Thessaloniki, 54006 Thessaloniki, Greece

Received 29 September 1999; accepted 9 June 2000

Abstract

The reaction of bis(β-dionato)oxovanadium(IV) chelates, $VO\beta_2$, with substituted benzoylhydrazines, $XbhH_2$, was explored in alcoholic solutions and oxovanadium(V) compounds with Schiff bases as ligands were obtained in high yield. These VOL(OR) compounds have alkoxide as coligand and the asymmetic tridentate Schiff base ligands, L^{2-}, bind to the oxovanadium core through the carbonyl oxygens and the imine nitrogen. Substituents attached to benzoylhydrazines affect the electron density about the oxovanadium core. While electron attracting substituents appear to favour monomeric square pyramidal chelates, the derivatives having electron repelling groups seem to encourage formation of dimeric structures and alkoxo bridged dimers are obtained. The crystal structures of the products of the reaction of bis(1-phenyl-1,3-butanedionato)oxovanadium(IV), $VO(bzac)_2$, with *o*-nitrobenzoylhydrazine (*o*-O_2NbhH_2) and *m*-methoxybenzoylhydrazine (*m*-CH_3ObhH_2) that are reported demonstrate the influence of the substituents as well as the role of the solvent. © 2000 Elsevier Science Ltd. All rights reserved.

Keywords: Alkoxo compounds of oxovanadium(V); Crystal structure of compounds of oxovanadium(V); Hydrazonato compounds of oxovanadium(V); Oxovanadium(V) dimers; Reactivity of bis(β-dionato)oxovanadium(IV) chelates; Hydrazonato tridentate Schiff base ligands

1. Introduction

Vanadium exists in a plethora of oxidation states and its coordination compounds play an important role in nitrogen activation and fixation and other biologically important reactions [1–3]. This revelation has stimulated interest in the stereochemistry and reactivity of its coordination compounds that contain the diazo and hydrazido group because they may provide some understanding of the mechanism of metalloenzymatic reduction of dinitrogen. Substituted aroylhydrazones possessing a suitably disposed amino group, whilst often bind directly to the metal [4], they may also interact with compounds containing carbonyl groups, for example salicylaldehydes and β-diones [5–10]. Such reactions have been exploited adroitly to form Schiff bases that are capable of confining metal atoms and controlling their properties and functionality [11]. Regarding β-diones and the oxovanadium(IV) core, the 1-phenyl-1,3-propanedione [6–9] has been gainfully employed in studies involving the Schiff bases resulting from the condensation reaction with aroylhydrazines [4–9]. Recent studies have indicated that solvent interactions with the moieties resulting from the ligation of such tridentate Schiff bases to the oxovanadium(IV) core have significant repercussions on the structure of the resulting chelates since solvent molecules or solvent fragments participate as coligands [6–9]. Other β-diones have not been utilised in similar studies, even though seemingly minor changes in ligand structure incurred by groups within the β-dionato moiety have a profound effect on the stereochemistry, the spacing of the energy levels, the redox potentials and other distinctive physicochemical properties of the β-dionato chelates [12]. The effects of substituents attached to the phenyl ring of benzoylhydrazines on the electron distri-

* Corresponding author. Tel.: +30-31-997-863; fax: +30-31-427-218.

E-mail address: tsiamis@chem.auth.gr (C. Tsiamis).

0277-5387/00/$ - see front matter © 2000 Elsevier Science Ltd. All rights reserved.
PII: S0277-5387(00)00483-6

bution of the Schiff bases have not been explored sufficiently. Further, the reactivity of the bis(β-dionato)oxovanadium(IV) chelates, $VO\beta_2$, has not been probed adequately in the preparation of tridentate Schiff base ligands, even though the $VO\beta_2$ chelates have been engaged successfully in ligand addition and ligand exchange reactions and are often used as starting material in syntheses [13,14].

This investigation was undertaken in order to explore the reactivity of certain bis(β-dionato)oxovanadium(IV) chelates with aroylhydrazines, to assess the influence of the reaction medium in the formation of products, to appraise the effect of substituents in the structure and the spectroscopic properties of the chelates formed, to assay the possibility of oxygen bridge creation and formation dimeric structures and to determine the stereochemistry of the resulting compounds. In this work the preparation of some β-dionate(benzoyl)hydrazonato(2-)oxovanadium(V) chelates is reported, the structures of [ethoxo(4-phenyl-2,4-butanedione(2′-nitrobenzoyl)hydrazonato(2-))oxo-vanadium(V)] and the anticoplanar bis[μ_2-methoxo(4-phenyl-2,4-butanedione(3′-methoxybenzoyl)hydrazonato(2-))oxovanadium(V)] are described and the results of the investigation are presented and discussed.

2. Experimental

2.1. Preparation and characterisation of the *VO(βbh)OR* compounds

The β-diones, βH, namely 2,4-pentanedione (acetylacetone, acacH), 1-phenyl-1,3-butanedione (benzoylacetone, bzacH), 1-phenyl-4,4,4-trifluoro-1,3-butanedione (trifluorobenzoylacetone, bztfH) and 1-thenyl-4,4,4-trifluoro-1,3-butanedione (trifluorothenoylacetone, thtfH), were purchased from Sigma–Aldrich. The bis(β-dionato)oxovanadium(IV) chelates ($VO\beta_2$), that were used as starting materials, were prepared and purified as described in the literature [15,16]. The compound $(n\text{-}C_4H_9)_4NVO_3$ was prepared by established procedures [17]. The substituted aroylhydrazines, $XbhH_2$, were procured from Fluka. Certain Schiff bases resulting from the reaction of benzoylacetone or trifluorobenzoylacetone with substituted benzoylhydrazines were prepared by literature methods [18] and characterised. The synthesis of the new vanadium chelates was accomplished as follows:

In a 200 cm^3 conical flask containing a magnetic follower are placed 10 mmol of $VO\beta_2$ and ~ 80 cm^3 alcohol and the mixture is stirred at ambient temperature until complete dissolution. Then 20 mmol of aroylhydrazine (also dissolved in the same alcohol) are added while stirring and the colour of the reaction mixture changes from brown to red–brown. The stirring continued for an additional 20 h. The VO(Xbh)OR compounds precipitated as red–brown solids. Recrystallisation was achieved by redissolving the solid in alcohol and allowing crystals to grow under refrigeration.

The chelates prepared, their stoichiometry and melting points are given in Table 1.

2.2. X-ray crystallographic analysis of *[VO(o-O_2Nbhbzac)OC_2H_5]* and of *[VO(m-CH_3Obhbzac)(μ_2-OCH_3)]$_2$*

Intensities of X-ray reflections within two octants of the reciprocal sphere were collected by means of a four-circle Philips-STOE computer-controlled X-ray diffractometer employing graphite-filtered Mo Kα radiation. The orientation matrix and refined unit cell dimensions of the crystal of [ethoxo(4-phenyl-2,4-

Table 1
Elemental analyses and physicochemical data of some aroylhydrazonato(2-)oxovanadium(V) chelates containing alkoxo ligands, VOL(OR)

	Compound	Yield (%)	M.p. (°C) [a]	C (%)	H (%)	N (%)
1	VO(*p*-NO_2bhacac)OMe	73	131d	43.7 (43.47)	3.93 (3.93)	11.4 (11.70)
2	VO(*p*-NO_2bhacac)OEt	77	153d	44.7 (45.05)	4.27 (4.32)	11.8 (12.26)
3	VO(*p*-NO_2bhacac)$OCHMe_2$	91	251d	46.7 (46.49)	4.72 (4.68)	11.1 (10.84)
4	VO(*p*-NO_2bhbzac)OMe	95	180d	51.3 (51.32)	3.79 (3.83)	9.87 (9.97)
5	VO(*p*-NO_2bhbzac)OEt	83	210d	52.3 (52.42)	4.20 (4.17)	9.75 (9.65)
6	VO(*p*-NO_2bhbzac)$OCHMe_2$	87	180d	53.8 (53.46)	4.52 (4.49)	9.47 (9.35)
7	VO(*o*-NO_2bhbzac)OMe	93	207d	51.1 (51.32)	3.86 (3.83)	10.2 (9.97)
8	VO(*o*-NO_2bhbzac)OEt	90	180d	51.9 (52.42)	4.21 (4.17)	9.57 (9.65)
9	VO(*o*-NO_2bhbzac)$OCHMe_2$	82	202d	53.2 (53.46)	4.37 (4.49)	9.29 (9.35)
10	VO(*p*-NO_2bhbztf)$OCHMe_2$	81	177d	47.7 (47.73)	3.37 (3.40)	8.39 (8.35)
11	VO(*p*-NO_2bhthtf)OEt	71	230d	41.3 (41.22)	2.68 (2.65)	8.44 (8.48)
12	VO(*p*-NO_2bhthtf)$OCHMe_2$	74	184d	42.4 (42.45)	3.01 (2.97)	8.28 (8.25)
13	[VO(*m*-CH_3Obhbzac)OMe]$_2$	91	219d	55.8 (56.17)	4.71 (4.71)	6.84 (6.89)
14	[VO(*m*-CH_3Obhthtf)OMe]$_2$	81	185d	44.1 (43.79)	3.01 (3.03)	5.94 (6.01)

[a] d, decomposition.

Table 2
Crystal data and experimental details for the structural study of (a) [VO(o-O_2Nbhbzac)OC_2H_5] and (b) [VO(m-CH_3Obhbzac)(μ_2-OCH_3)]$_2$

Formula	(a) $C_{19}H_{18}N_3O_6V$	(b) $C_{19}H_{19}N_2O_5V$
Formula mass, M_r	435.31	406.31
Crystal parameters		
Crystal shape	dark brown plates	deep brown rectangular prisms
Crystal size (mm)	$0.75\times0.45\times0.25$	$0.70\times0.55\times0.32$
Crystal system	monoclinic	triclinic
Space group	$P2_1/n$	$P\bar{1}$
Unit-cell dimensions		
a (Å)	11.033(5)	7.550(3)
b (Å)	7.537(5)	10.010(3)
c (Å)	23.369(9)	13.637(5)
α (°)	90.00	106.99(2)
β (°)	93.920(5)	92.76(2)
γ (°)	90.00	105.70(3)
V_c (Å^3)	1938.7(16)	939.8(6)
Units per cell, Z	4	2
D_{calc} (Mg m^{-3})	1.4914(12)	1.43548(9)
Measurement of intensity data		
Instrument	PW100-STOE	
Radiation (Å)	Mo Kα, $\lambda = 0.71069$	
Temperature (K)	298(2)	
Monochromometer	Graphite	
Scan mode	ω–2θ	
θ Range (°)	1.76–27.57	1.58–30.00
Linear absorption coefficient, μ (mm^{-1})	1.097	1.14
Reflections measured	4233	4728
Independent reflections	3825	4671
Reflections observed ($I>2\sigma(I)$)	2647	3454
Indices limits		
h	−14–9	−10–5
k	0–9	−14–13
l	0–30	0–19
Refinement and final discrepancy factors		
Refinement	full-matrix least-squares on F^2	full-matrix least-squares on F^2
Parameters refined	323	301
Largest difference peak and hole (e Å^{-3})	0.399, −0.397	0.351, −0.416
$R = \Sigma(\|F_o\|-\|F_c\|)/\Sigma\|F_o\|$	0.0512	0.0387
$R_w = [\Sigma w(\|F_o\|-\|F_c\|)^2/\Sigma w(\|F_o\|)^2]^{1/2}$	0.0777	0.1026

butanedione(2′-nitrobenzoyl)hydrazonato(2-))oxovanadium(V)], [VO(o-O_2Nbhbzac)OC_2H_5] and of bis[μ_2-methoxo(4-phenyl-2,4-butanedione(3′-methoxybenzoyl)-hydrazonato(2-))oxovanadium(V)], [VO(m-CH_3Obhbzac)(μ_2-OCH_3)], were obtained from independent reflections of high intensity ($12 \le \theta \le 15°$). Details of crystal analysis, data collection and structure refinement are given in Table 2, together with the final values for the unit cells. All intensities were corrected as usual for Lorentz and polarization effects. In view of the low μ value no correction for absorption deemed necessary. In both cases the vanadium position was deduced by direct methods employing the SHELXS-86 and the SIR-97 programs [19,20] and used to compute a first-approximation electron-density synthesis, which revealed the position of all remaining atoms except the hydrogens. After least-squares refinements with the non-hydrogen atoms, the hydrogen atoms were also located in the difference Fourier map using the SHELX-97 program [21]. The figures of the clinographic projection were produced with the DIAMOND and ATOMS programs [22]. Refinement was carried out by full-matrix least-squares, with unit weight to all reflections.

3. Results and discussion

Many oxometallates undergo condensation reactions in which polyatomic groups replace the oxygen ligand. For example, the diazenido and the hydrazido groups are attached to molybdenum by employing oxomolybdenum compounds as precursors [23]. In the case of bis(β-dionato)oxovanadium(IV) chelates, the mixing of alcoholic solutions of $VO\beta_2$ and a substituted benzoylhydrazine, $XbhH_2$, is accompanied by a change in colour (suggesting commencement of a reaction) and formation of a precipitate as the main product. The elemental analysis of the recrystallised precipitate revealed the presence of nitrogen while the stoichiometry disclosed dependence on the alcohol employed as solvent. Interestingly, the yield is maximised when the metal-to-benzoylhydrazine molecule is 1:2 and the reaction mixture is accessible to atmospheric oxygen. Further, in a series of reactions using the same alcohol as solvent and the same $XbhH_2$ but different chelate $VO\beta_2$, the composition of the main product suggested abstraction of a β-ketoenol and entrapment of a aroylhydrazine molecule by the vanadium atom. The diamagnetic behaviour of the new compounds indicated absence of unpaired electrons while the lack of absorption in the electronic excitation spectra at wavenumber below $\sim 2.50\ \mu m^{-1}$ reaffirmed the absence of electrons localised in the d orbital manifold [12,13]. These observations suggested an oxidative displacement reaction in the oxovanadium core converting the metal to vanadium(V) with sacrificial species one of the ligated β-dionato anions and formation of chelates corresponding to the general formula VOL(OR), where OR^- is an alkoxide and L^{2-} denotes the Schiff base resulting from the partial addition-elimination reaction of the β-dionato anion with an aroylhydrazine. To verify this hypothesis, aroylhydrazones and either 1-phenyl-1,3-butanedione (bzacH) or trifluorobenzoylacetone (bztfH) were employed to obtain Schiff bases which were subsequently

reacted with $(n\text{-}C_4H_9)_4NVO_3$ to produce chelates. The later reaction afforded products identical to those obtained by the reaction of the appropriate $VO\beta_2$ chelates with aroylhydrazines. Interestingly the yield of the one-pot synthesis was appreciably higher. Further information regarding the structure of the new compounds was acquired from their electronic absorption spectra.

3.1. Electronic excitation spectra

In the electronic excitation spectra of the VOL(OR) chelates no absorptions attributable to the ligand field excitations happen. The lack of paramagnetic interactions and the absence of ligand field transitions indicate oxidation of the metal to vanadium(V) and disallow any inference about the ordering of the d orbitals. A strong broad band (or envelope) is observed at ~ 2.50 μm^{-1} and is solvent depended. The absorption in this region, for energy and intensity reasons, should be attributed to a charge transfer excitation most likely from a π ligand orbital to the manifold of the d metal orbitals. The influence of the solvent in this band is clearly evident in the spectra of the monomers in which shifts and alterations of band shape are notable upon change of solvent. Actually in the spectra of the monomers obtained from 1,2-dichloroethane solutions this LMCT excitation affords an envelope with no definite maximum. From the shape of the envelope and the preliminary analysis the occurrence of a band with maximum at ~ 2.0 μm^{-1} is deduced. In the spectra of the monomers obtained employing acetonitrile or DMSO as solvent, a well-formed band is evident at ~ 2.3 μm^{-1}. This shift suggests change of the ordering of the d orbitals effected by the occupation of the vacant coordination site. Further information regarding bonding in the chelates under consideration were sought from the infrared spectra.

3.2. Infrared spectra

In the IR spectra of the compounds resulting from the reaction of the substituted benzoylhydrazines with bis(β-dionato)oxovanadium(IV) chelates, the absence of absorptions above 3100 cm^{-1} implied that the hydrazino group, $-NHNH_2$, has taken part in an addition–elimination reaction and that proton transfer has taken place. The marginal shift in the diminished band that turns out at $\sim 1578 \pm 10$ cm^{-1} and is associated with the stretching vibration of a carbonyl group of the β-dionato anion [13] suggested that carbonyl oxygen remains bonded to vanadium since the C–O bending mode appears as a rather strong band around 1160 cm^{-1}. Further, the intense band occurring at $\sim 970 \pm 30$ cm^{-1} and assigned to the V=O stretching vibration [23–25] indicated that the V=O core stays intact, while the variation in frequency to the V=O stretching vibration suggests that the $d_\pi - p_\pi$ overlap between the vanadium and the oxygen atoms is influenced by the substituents and the coligands. The implication of these observations is that the condensation reaction of hydrazine does not involve the oxo ligand. Further, it transpires that while one of the β-dionato anions, β^-, participates in the condensation reaction, the other becomes the sacrificial species of the oxidative displacement reaction.

In addition to IR absorptions originating from V=O core and the β-dione fragment of the Schiff base, the bands may be distinguished in those arising from the entrapped hydrazine species and in those emerging from the alkoxy group. The presence of substituents attached to the β-dionato moiety and the existence of groups appended to the phenyl ring of the aroylhydrazine engender absorption bands and spectral shifts. Whenever the β-diones employed are non-symmetric the site of the attack becomes important. In the case of $bzac^-$ the phenyl ring renders the adjacent carbonyl group immune to the attack while in ($bztf^-$) the strong electron attracting ability of the trifluoro group ensures that the attack is targeted in the carbonyl neighbouring the phenyl ring. In the ensuing Schiff bases, the =NH proton is prone to form intermolecular and intramolecular hydrogen bonds as the bands observed at ~ 3400 (broad) and 1630 cm^{-1} indicated. These bands are not present whenever the bis(β-dionato)oxovanadium(IV) is employed, as the β-dione source and the chelates are obtained in the one-pot synthesis. In the chelates prepared the intense absorption observed at $\sim 1600 \pm 10$ cm^{-1} probably emanates from the azomethine (C=N) stretching mode [26] while the high intensity band occurring at $\sim 1520 \pm 15$ cm^{-1} and is tentatively assigned to the $>C{=}N{-}N{=}CPhO(^-)$ entity indicates extensive delocalisation. The prototropic $>C{=}NNHCOPh$ entity in the Schiff base apparently undergoes hydrogen abstraction from the tautomeric form, $>C{=}N{-}N{=}C(OH)Ph$, to produce the electron-rich hydrazido(2-) species because no band could be associated with vibrations of either the N–H or the O–H bonds. The process of hydrogen abstraction is accomplished presumably with the aid of atmospheric oxygen that facilitates the oxidation of the metal to vanadium(V). Taking into consideration the strongly electron-attracting nature of the metal and the availability of electron density at the nitrogen atoms the wholly reasonable assumption may be made that they may be involved in bonding interactions. On the basis of previous structural data and the geometry of the resulting Schiff base, the nitrogen atom engaged in the condensation reaction is presumed to be bonded to the metal atom. This assumption is further supported by the relatively weak bands at around 475 ± 10 cm^{-1} that are assigned to the stretching vibrations of the V–N bonds [27]. The stretching vibrations of the V–O

Table 3
Selected interatomic distances (Å) and bond angles (°) of [VO(*o*-NO_2bhbzac)OC_2H_5]

V–O(1)	1.580(2)	N(1)–N(2)	1.394(3)	C(8)–C(9)	1.374(5)
V–O(4)	1.758(2)	N(2)–C(2)	1.327(3)	C(9)–C(10)	1.380(5)
V–O(2)	1.860(2)	N(3)–C(13)	1.461(4)	C(11)–C(12)	1.475(4)
V–O(3)	1.915(2)	C(1)–C(2)	1.493(4)	C(12)–C(13)	1.391(4)
V–N(2)	2.061(2)	C(4)–C(5)	1.475(4)	C(12)–C(17)	1.393(4)
O(2)–C(4)	1.324(3)	C(2)–C(3)	1.401(4)	C(13)–C(14)	1.391(4)
O(3)–C(11)	1.318(3)	C(3)–C(4)	1.367(4)	C(14)–C(15)	1.368(5)
O(5)–N(3)	1.216(3)	C(5)–C(10)	1.391(4)	C(15)–C(16)	1.379(5)
O(6)–N(3)	1.225(3)	C(5)–C(6)	1.396(4)	C(16)–C(17)	1.373(5)
O(6)–C(18)	1.453(5)	C(6)–C(7)	1.366(5)	C(18)–C(19)	1.442(6)
N(1)–C(11)	1.286(3)	C(7)–C(8)	1.384(5)		
O(1)–V–O(4)	106.05(11)	O(5)–N(3)–O(6)	124.2(3)	C(10)–C(9)–C(8)	120.6(3)
O(1)–V–O(2)	107.15(10)	O(5)–N(3)–C(13)	118.0(2)	C(9)–C(10)–C(5)	120.5(3)
O(4)–V–O(2)	95.94(9)	O(6)–N(3)–C(13)	117.7(2)	N(1)–C(11)–O(3)	121.7(2)
O(1)–V–O(3)	107.96(10)	O(2)–C(4)–C(3)	120.8(3)	N(1)–C(11)–C(12)	119.1(2)
O(4)–V–O(3)	89.71(9)	O(2)–C(4)–C(5)	115.8(2)	O(3)–C(11)–C(12)	119.2(2)
O(2)–V–O(3)	141.26(10)	C(3)–C(4)–C(5)	123.3(3)	C(13)–C(12)–C(17)	116.5(3)
O(1)–V–N(2)	99.99(9)	C(4)–C(3)–C(2)	124.6(3)	C(13)–C(12)–C(11)	123.6(2)
O(4)–V–N(2)	152.86(10)	N(2)–C(2)–C(3)	120.9(2)	C(17)–C(12)–C(11)	119.8(3)
O(2)–V–N(2)	83.40(9)	N(2)–C(2)–C(1)	120.2(2)	C(16)–C(17)–C(12)	121.5(3)
O(3)–V–N(2)	74.90(9)	C(3)–C(2)–C(1)	118.9(2)	C(15)–C(14)–C(13)	118.7(3)
C(4)–O(2)–V	133.94(18)	C(10)–C(5)–C(6)	118.0(3)	C(14)–C(15)–C(16)	120.5(3)
C(11)–O(3)–V	117.74(16)	C(10)–C(5)–C(4)	120.3(3)	C(15)–C(16)–C(17)	120.4(4)
C(18)–O(4)–V	124.6(2)	C(6)–C(5)–C(4)	121.7(3)	C(14)–C(13)–C(12)	122.4(3)
C(11)–N(1)–N(2)	108.1(2)	C(7)–C(6)–C(5)	121.2(3)	C(14)–C(13)–N(3)	117.0(3)
C(2)–N(2)–N(1)	115.5(2)	C(6)–C(7)–C(8)	120.2(4)	C(12)–C(17)–N(3)	120.4(2)
C(2)–N(2)–V	128.24(18)	C(9)–C(8)–C(7)	119.5(3)	O(4)–C(18)–C(19)	109.6(4)
N(1)–N(2)–V	116.25(17)				

bonds appear as rather medium intensity bands around 525 ± 20 cm^{-1}. Some of the metal–ligand absorptions are not related to the Schiff base and are solvent dependent. For instance, in the IR spectra of the product of the reaction of *m*-methoxybenzoylhydrazine with $VO\beta_2$ in methanol a very broad feature centred around 340 cm^{-1} propounded the possibility of additional metal–oxygen bonds and suggested the likely occurrence of dimeric structures [27]. The broad feature appears to consist of a number of overlapping peaks attributable to deformations of bridging V–O–V bonds and vibrational coupling of low frequency modes that complicate the assignments in this region. The notion of the existence of dimeric structures was enhanced by the shift of the bands due to the C–O vibrations to higher wave-numbers by 10–30 cm^{-1} that suggested absence of additional bonding interactions of the carbonyl oxygens. The oxo ligand was not implicated in the formation of the dimeric species, because the shift of the band due to the V=O stretching vibration was imperceptible [23–25]. Since neither the infrared spectra nor the elemental analyses revealed the presence of water molecules, the alkoxo groups were implicated in the formation of dimeric species. Confirmation of their existence and details of the structures of representative compounds of the new chelates were acquired from the X-ray diffraction study.

3.3. Description of the structures

The X-ray diffraction study of [ethoxo(4-phenyl-2,4-dione(2′ - nitrobenzoyl)hydrazonato(2 -)oxovanadium-(V)], [VO(*o*-NO_2bhbzac)OC_2H_5], disclosed that in the unit cell there are four vanadium atoms. The positional parameters, the interatomic distances and the bond angles (Table 3) reveal that the coordination environment in which the vanadium atoms exist is approximately square pyramidal with the oxo ligand engaging the apical position. The oxygen of the ethoxy group, the carbonyl oxygens and the nitrogen of the primary amino group that reacted with the β-dione, are in the immediate vicinity of vanadium. While the aforementioned oxygen and nitrogen atoms are virtually in the same plane (the basal plane), the central atom is above the basal plane by 0.480(2) Å and is directed towards the oxo ligand. The $V–O_{oxo}$ interatomic distance at 1.580(2) Å is in accord with other pentacoordinate oxovanadium compounds (Table 4). These data reaffirm the indications of coordination unsaturation suggested by the solvent shifts in the electronic excitation spectra. The Schiff base ligand forms a six-membered and a five-membered chelate ring and the interatomic distances within the C(2)–N(2)–N(1)–C(11) group reassert that no hydrogen is bonded to the nitrogen atoms and that extensive electron delocalisa-

tion has taken place. The planar aromatic rings form a dihedral angle of 34.53(5)°. A clinographic projection of [VO(*o*-NO_2bhbzac)OC_2H_5] and its labelling scheme is shown in Fig. 1.

The X-ray diffraction study of bis[μ_2-methoxo-(4-phenyl-2,4-dione(3′-methoxybenzoyl)hydrazonato-(2-))oxovanadium(V)], [VO(*m*-CH_3Obhbzac)OCH_3]$_2$, disclosed that in the unit cell there are only two vanadium atoms. The positional parameters (Table 4) show that the coordination environment in which the vanadium atoms exist resembles closely that of the metal in [VO(*o*-NO_2bhbzac)OC_2H_5] and other [VO(L)OR] chelates. The vanadium atoms are separated by a distance of only 3.370(2) Å, suggesting the possibility of a dimeric structure. The oxo ligand binds to one vanadium atom but exists at a distance of 4.750(2) Å from the other vanadium centre, implying absence of bonding interactions. However, at a distance of 2.360(2) Å from the vanadium centre the position *trans* to the oxo ligand is engaged by the oxygen of another alkoxo ligand. The methoxo group is strongly ligated to one vanadium centre and interacts with the other forming a bridge. The resulting distorted octahedral structures of the oxovanadium centres are bridged by one shared edge leading to the creation of a $\{VO(\mu_2\text{-}OR)_2VO\}^{4+}$ core. As the oxygen atom of the alkoxo group becomes involved in covalent interactions with the other vanadium atom, the $V–O_{alkox}$ distance increases and the change in electron density should affect the interactions of the nitrogen atom in *trans* position. A diminution of the distance of the nitrogen atom in *trans* position from the vanadium centre is envisaged and, indeed, such a trend becomes apparent when the interatomic distances listed in Table 5 are considered. The compounds described in this work do not follow exactly the expected trend.

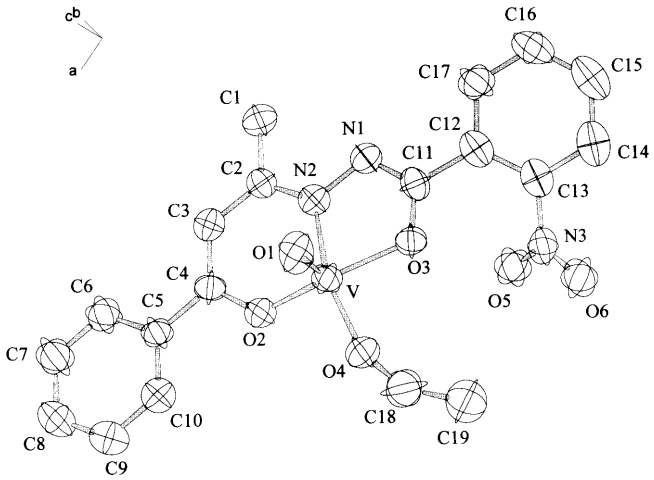


Fig. 1. A clinographic projection and labelling scheme of [ethoxo(4-phenyl-2,4-butanedione(2′-nitrobenzoyl)hydrazonato(2-))oxovanadium(V)]. The ATOMS drawing shows the thermal ellipsoids at the 50% probability level. Hydrogen atoms are omitted for clarity.

In the binuclear compound [VO(*m*-CH_3Obhbzac)-OCH_3]$_2$, the $\{VO(\mu_2\text{-}OR)_2VO\}^{4+}$ core forms a parallelepiped and the mutual steric requirements of the

Table 4
Bond lengths in some oxovanadium chelates with tridentate Schiff bases and other ligands

Compound [c]	$V–O_{oxo}$	V–N	$V–O_\beta$	$V–O_h$	$V–O_{alk}$ [a]	V–O [b]	N–N	V···V	Ref.
[VO(bhbzac)OC_2H_5]	1.595(3)	2.070(3)	1.848(2)	1.907(2)	1.750(3)		1.400(6)		[7]
[VO_2(bzacGRP)]	1.601(3)	2.133(4)	1.929(4)	1.980(4)	1.616(3)		1.405(5)		[9]
[VO(bhbzac)$O(CH_2)_2OH$]	1.583(4)	2.093(4)	1.883(3)	1.937(3)	1.789(3)	2.286(3)	1.408(5)		[10]
[VO(*m*-Cl bhbzac)OC_2H_5]	1.598(5)	2.043(6)	1.835(5)	1.893(5)	1.770(4)		1.409(7)		[28]
[VO(*o*-O_2Nbhbzac)OC_2H_5]	1.580(2)	2.061(2)	1.860(2)	1.915(2)	1.758(2)		1.394(3)		This work
[VO(*m*-CH_3Obhbzac)-OCH_3]$_2$	1.584(2)	2.083(2)	1.848(1)	1.922(2)	1.824(2)	2.360(2)	1.396(2)	3.370(2)	This work
K_4[VO(cit)]$_2$·$6H_2O$	1.608(3)		2.022(3)	2.041(3)	2.171(3)	1.977(3)		3.301(3)	[29]
[VO(SalAHE)]$_2$	1.619(10)	2.009(11)	1.892(10)	1.985(10)	1.980(9)				[14]
	1.548(9)	2.034(11)	1.888(10)	1.963(10)	1.979(9)			3.068(4)	
{[VO(SalAMHP)]$_2$}O	1.598(4)	2.130(5)	1.880(4)	1.805(4)	1.857(4)				[14]
	1.591(4)	2.115(5)	1.888(4)	1.828(4)	1.759(4)			3.06	
[VO_2(1,2-pnSal)]$_2$	1.619(6)	2.162(5)	1.915(4)	2.120(5)[s]	1.665(4)	2.427(5)		3.222(7)	[30]
[VO_2(salGRP)]·CH_3OH	1.626(4)	2.143(5)	1.894(4)	1.966(4)	1.635(4)		1.409(7)		[31]
[VO_2(salGRT)]	1.611(4)	2.128(3)	1.897(4)	1.996(3)	1.627(3)		1.403(5)		[31]

[a] Atoms in the basal position of the alkoxo oxygen.

[b] Atoms in the basal position of the oxygen of the aroyl group.

[c] bhbzac = 4-phenylbutane-2,4-dionebenzoylhydrazonato(2-); *m*-Clbhbzac = 4-phenylbutane-2,4-dione(*m*-chloro)benzoyl-hydrazonato(2-); cit = citrate; Sal = Salicylaldehyde; GRP and GRT = Girard's reagent P and T, respectively; H_2SalAHE = 2-(salicylideneamino)-1-hydroxyethane; H_2SalAMHP = 2-(salicylideneamino)-1-hydroxypropane; 1,2-pnSal = 1(*N*-salicylideneamino)-2-aminopropane; bzacGRP = 4-phenylbutane-2,4-dione((1-carboxymethyl)pyridinium chloride)hydrazonato(2-); SalGRP = 2-(salicyl(1-carboxymethyl)pyridinium chloride)hydrazonato(2-); SalGRT = 2-(salicyl(1-carboxymethyl)trimethylammonium chloride)hydrazonato(2-). 2-{2-[(2-hydroxyphenyl)methylidene]hydrazino}-*N*,*N*,*N*-trimethyl-2-oxo-1-ethanaminium chloride.

Table 5
Selected interatomic distances (Å) and bond angles (°) of [VO(*m*-CH_3Obhbzac)(μ_2-OCH_3)]$_2$

V–O(1)	1.584(2)	N(1)–C(11)	1.295(3)	C(7)–C(8)	1.382(4)
V–O(5)	1.824(2)	N(1)–N(2)	1.396(2)	C(8)–C(9)	1.384(4)
V–O(2)	1.848(1)	N(2)–C(2)	1.315(2)	C(9)–C(10)	1.378(3)
V–O(3)	1.922(2)	C(1)–C(2)	1.496(3)	C(11)–C(12)	1.475(3)
V–N(2)	2.083(2)	C(2)–C(3)	1.419(3)	C(12)–C(13)	1.388(3)
V–O(5) [a]	2.360(2)	C(3)–C(4)	1.362(3)	C(12)–C(17)	1.391(3)
O(2)–C(4)	1.322(2)	C(4)–C(5)	1.472(3)	C(13)–C(14)	1.383(3)
O(3)–C(11)	1.314(2)	C(5)–C(6)	1.399(3)	C(14)–C(15)	1.387(3)
O(4)–C(14)	1.358(3)	C(5)–C(10)	1.401(3)	C(15)–C(16)	1.363(4)
O(4)–C(18)	1.400(4)	C(6)–C(7)	1.377(3)	C(16)–C(17)	1.385(3)
O(5)–C(19)	1.418(3)				
O(1)–V–O(5)	102.43(8)	C(19)–O(5)–V	124.75(15)	C(6)–C(7)–C(8)	120.4(2)
O(1)–V–O(2)	99.69(8)	C(19)–O(5)–V [a]	122.32(14)	C(7)–C(8)–C(9)	119.9(2)
O(5)–V–O(2)	104.12(6)	V–O(5)–V [a]	106.61(7)	C(10)–C(9)–C(8)	120.1(2)
O(1)–V–O(3)	98.22(8)	C(11)–N(1)–N(2)	108.13(16)	C(9)–C(10)–C(5)	120.6(2)
O(5)–V–O(3)	89.99(6)	C(2)–N(2)–N(1)	115.71(16)	N(1)–C(11)–O(3)	122.24(18)
O(2)–V–O(3)	154.14(7)	C(2)–N(2)–V	127.58(14)	N(1)–C(11)–C(12)	119.57(18)
O(1)–V–N(2)	98.88(8)	N(1)–N(2)–V	116.29(12)	O(3)–C(11)–C(12)	118.10(18)
O(5)–V–N(2)	155.48(7)	N(2)–C(2)–C(3)	121.13(17)	C(13)–C(12)–C(17)	120.02(19)
O(2)–V–N(2)	83.91(7)	N(2)–C(2)–C(1)	120.63(19)	C(13)–C(12)–C(11)	118.90(19)
O(3)–V–N(2)	74.99(7)	C(3)–C(2)–C(1)	118.24(18)	C(17)–C(12)–C(11)	121.0(2)
O(1)–V–O(5) [a]	175.58(7)	C(4)–C(3)–C(2)	124.84(18)	C(14)–C(13)–C(12)	120.0(2)
O(5)–V–O(5) [a]	73.39(7)	O(2)–C(4)–C(3)	121.09(18)	O(4)–C(14)–C(13)	124.6(2)
O(2)–V–O(5) [a]	80.19(6)	O(2)–C(4)–C(5)	114.75(16)	O(4)–C(14)–C(15)	115.6(2)
O(3)–V–O(5) [a]	83.36(6)	C(3)–C(4)–C(5)	124.13(18)	C(13)–C(14)–C(15)	119.8(2)
N(2)–V–O(5) [a]	85.51(6)	C(6)–C(5)–C(10)	118.39(19)	C(16)–C(15)–C(14)	119.9(2)
C(4)–O(2)–V	133.70(12)	C(6)–C(5)–C(4)	121.75(18)	C(15)–C(16)–C(17)	121.4(2)
C(11)–O(3)–V	118.28(13)	C(10)–C(5)–C(4)	119.83(18)	C(16)–C(17)–C(12)	118.9(2)
C(14)–O(4)–C(18)	118.8(2)	C(7)–C(6)–C(5)	120.5(2)		

[a] Symmetry transformations used to generate equivalent atoms: $-x,-y+1,-z+1$.

metal coordination spheres exert strong influence on the V···V separation, the hybridisation of the bridging oxygen, and hence the bridge angle about oxygen which is 106.61(7)°. Since the C(19)–O(5)–V angles exceed 120°, it transpires that the hybridisation of the oxygen is rather near sp^2. Dimeric vanadium chelates with a $\{VO(\mu_2\text{-}OR)_2VO\}^{4+}$ core may exist in five possible configurations classified according to the orientation of the vanadyl groups in respect to the plane defined by the vanadium centres and the bridging oxygen atoms [32]. The configurations are *syn*-orthogonal, *anti*-orthogonal, *syn*-coplanar, *anti*-coplanar, and twist. It has been suggested [33] that, when several structures differing very little in energy are possible, the centrosymmetric structure is preferred by crystal packing requirements. In dimeric vanadium chelates with a $\{VO(\mu_2\text{-}OR)_2VO\}^{4+}$ core, the *anti*-structures are favorites. In the [VO(*m*-CH_3Obhbzac)(μ_2-OCH_3)]$_2$ chelate, the atoms of the ligands are symmetrically disposed relative to the centre of the $\{VO(\mu_2\text{-}OR)_2VO\}^{4+}$ core and the disposition of the oxovanadium groups is anti-coplanar, a configuration sporadically encountered in dimeric oxovanadium compounds [34,35]. A clinographic projection of [VO(*m*-CH_3Obhbzac)OCH_3]$_2$ is shown in Fig. 2.

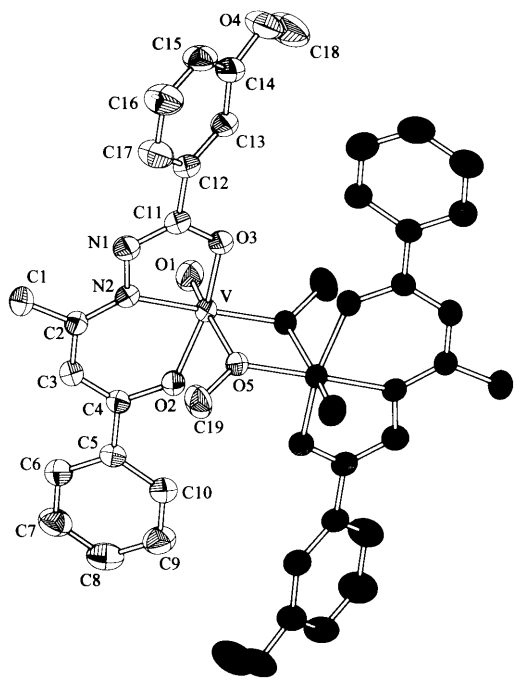


Fig. 2. A clinographic projection and labelling scheme of bis-[methoxo(4-phenyl-2,4-butanedione(3′-methoxybenzoyl)hydrazonato-(2-))-oxovanadium(V)]. The DIAMOND drawing shows the thermal ellipsoids at the 50% probability level. Hydrogen atoms are omitted for clarity.

4. Supplementary data

Crystallographic data have been deposited with the Cambridge Crystallographic Data Centre, CCDC Nos. 134611 and 134612 for bis[μ_2-methoxo(4-phenyl-2,4-dione(3′ - methoxybenzoyl)hydrazonato(2 -))oxovanadium(V)] and [ethoxo(4-phenyl-2,4-dione(2′-nitrobenzoyl)hydrazonato(2-)oxovanadium(V)], respectively. Copies of this information may be obtained free of charge from The Director, CCDC, 12 Union Road, Cambridge, CB2 1EZ, UK (fax: +44-1223-336033; e-mail: deposit@ccdc.cam.ac.uk or www: http://www.ccdc.cam.ac.uk).

References

[1] A. Butler, C.J. Carrano, Coord. Chem. Rev. 109 (1991) 61.
[2] D. Rehder, Angew. Chem., Int. Ed. 30 (1991) 148.
[3] I. Cavaco, J.C. Pessoa, M. Duarte, R.D. Gillard, P. Matias, Chem. Commun. (1996) 1365.
[4] M.F. Iskander, S. Saddek, Inorg. Chim. Acta 22 (1977) 141.
[5] D.K. Rastogi, S.K. Sahni, V.B. Rana, S.K. Dua, J. Coord. Chem. 8 (1978) 97.
[6] D.K. Rastogi, S.K. Sahni, V.B. Rana, K. Dua, S.K. Dua, J. Inorg. Nucl. Chem. 41 (1979) 21.
[7] A.A. Diamantis, J.M. Frederiksen, M.A. Salam, M.R. Snow, E.R.T. Tiekink, Aust. J. Chem. 39 (1986) 1081.
[8] K.C. Joshi, R. Bohra, B.S. Joshi, Inorg. Chem. 31 (1992) 598.
[9] H.X. Liu, W. Wang, X. Wang, M.Y. Tan, J. Coord. Chem. 33 (1994) 347.
[10] S.P. Rath, S. Mondal, A. Chakravorty, Inorg. Chim. Acta 263 (1997) 247.
[11] L.J. Boucher, V.W. Day, Inorg. Chem. 16 (1977) 1360.
[12] (a) R.C. Mehrota, R. Bohra, D.F. Gaur, Metal β-Diketonates and Allied Derivatives, Academic, London, 1978. (b) S. Di Bella, G. Lanza, A. Gulino, I. Fragala, Inorg. Chem. 35 (1996) 3885.
[13] (a) D. Ogden, J. Selbin, J. Inorg. Nucl. Chem. 30 (1968) 1227. (b) H.J. Stoklosa, J.R. Wasson, J. Inorg. Nucl. Chem. 38 (1976) 677. (c) G.E. Mannix, A.P. Zipp, J. Inorg. Nucl. Chem. 41 (1979) 59.
[14] C.J. Carrano, C.M. Nunn, R. Quan, J.A. Bonadies, V.L. Pecoraro, Inorg. Chem. 29 (1990) 944.
[15] R.A. Rowe, M.M. Jones, Inorg. Synth. 5 (1957) 114.
[16] J. Selbin, G. Maus, D.L. Johnson, J. Inorg. Nucl. Chem. 29 (1967) 1735.
[17] K.F. Jahr, J. Fuchs, R. Oberhauser, Chem. Ber. 101 (1968) 482.
[18] R.W. Layer, Chem. Rev. 63 (1963) 489.
[19] G.M. Sheldrick, Acta Crystallogr., Sect. A 46 (1990) 467.
[20] G.M. Sheldrick, SHELXL-97, Program for the Refinement of Crystal Structures, University of Göttingen, Germany, 1997.
[21] A. Altomare, M.C. Burla, M. Cmalli, G. Cascarano, C. Giacovazzo, A. Gualiardi, A.G.G. Moliterni, G. Polidori, R. Spagna, SIR-97, A Package for Crystal Structure Solution by Direct Methods and Refinement, Roma, Italy, 1997.
[22] (a) K. Bradenburg, DIAMOND (Version 2.1). Visual Crystal Structure Information System, Bonn University, 1998. (b) A. Dowltry, ATOMS (Version 4.1). A Computer Program for Displaying Molecular Structure, Shape Software, Kingsport, 1998.
[23] J. Selbin, H.R. Manning, G. Cessac, J. Inorg. Nucl. Chem. 25 (1963) 1253.
[24] E. Sinn, C.M. Harris, Coord. Chem. Rev. 4 (1969) 39.
[25] N. Choudhary, D.L. Hughes, U. Kleinkes, L.F. Larkworthy, G.J. Leigh, M. Maiwald, C.J. Marmion, J.R. Sanders, G.W. Smith, C. Sudbrake, Polyhedron 16 (1997) 1517.
[26] P.E. Figgins, D.H. Busch, J. Phys. Chem. 65 (1961) 2236.
[27] S. Arrowsmith, M.F.A. Dove, N. Logan, A. Batsanov, Polyhedron 17 (1998) 421.
[28] W. Wang, X. Wang, H.X. Liu, M.Y. Tan, J. Coord. Chem. 36 (1995) 49.
[29] M. Velayutham, B. Varghese, S. Subramanian, Inorg. Chem. 37 (1998) 1336.
[30] M. Root, J.D. Hoeschele, C.R. Cornman, J.W. Kampf, V.L. Pecoraro, Inorg. Chem. 32 (1993) 3855.
[31] X. Wang, X.M. Zhang, H.X. Liu, Inorg. Chim. Acta 223 (1994) 193.
[32] W. Plass, Angew. Chem., Int. Ed. Engl. 35 (1996) 627.
[33] M.A. Porai-Koshits, Zh. Neorg. Khim. 13 (1968) 1233.
[34] T. Carofiglio, E. Solari, C. Floriani, A. Chiesi-Villa, C. Rizzoli, Polyhedron 15 (1996) 4435.
[35] J. Salta, J. Zubieta, Inorg. Chim. Acta 257 (1997) 83.

PERGAMON

www.elsevier.nl/locate/poly

Polyhedron 19 (2000) 2011–2018

POLYHEDRON

Synthesis of mononuclear nickel(II) and copper(II) complexes using compartmental ligands: X-ray and electrochemical studies

J. Manonmani [a], R. Thirumurugan [b], M. Kandaswamy [a,*], M. Kuppayee [b], S. Shanmuga Sundara Raj [c], M.N. Ponnuswamy [b], G. Shanmugam [b], H.K. Fun [c]

[a] *Department of Inorganic Chemistry, University of Madras, Guindy Campus, Madras 600 025, India*
[b] *Department of Crystallography and Biophysics, University of Madras, Guindy Campus, Chennai-25, India*
[c] *X-ray Crystallography Unit, School of Physics, Universiti Sains Malaysia, 11800 USM, Penang, Malaysia*

Received 12 May 2000; accepted 27 June 2000

Abstract

A series of mononuclear complexes ML^1 (M = Ni, Cu) where $L^1 = N,N'$-bis[2-hydroxy-3-(piperidin-1-ylmethyl)-5-methylbenzyl]alkyldiimine (alkyl = ethylene L^{1a}, propylene L^{1b}, butylene L^{1c}) and ML^2 (M = Ni, Cu) where $L^2 = N,N'$-bis[2-hydroxy-3-(piperidin-1-ylmethyl)-5-bromobenzyl]alkyldiimine (alkyl = ethylene L^{2a}, propylene L^{2b}, butylene L^{2c}) have been synthesized and characterized by C, H, N analysis, IR, electronic and ESR spectra. The crystal structures of the complexes NiH_2L^{1a} (**1**) and CuH_2L^{1a} (**6**) were determined and the geometry around the metal ion is square planar. Electrochemical studies of the complexes show a quasi-reversible single redox wave at negative potential in the range 0 to -1.3 V. For nickel complexes (**1**–**5**) $E_{pc} = -1.0$ to -0.80 V and for copper complexes (**6**–**9**) $E_{pc} = -0.90$ to -0.72 V. The ESR spectra of nickel complexes are inactive due to square planar nature of the complexes whereas copper complexes show an ESR spectrum characteristic of square planar complex with nuclear hyperfine spin 3/2. Copper complexes show a normal magnetic moment value of $\mu_{eff} = 1.70$–1.75 B.M. which is close to the spin-only value of 1.73 B.M. © 2000 Elsevier Science Ltd. All rights reserved.

Keywords: Binucleating ligand; Nickel complexes; Copper complexes; Crystal structures; Redox chemistry

1. Introduction

The role of metal ions at the active site of proteins has been the focus of many studies by both synthetic and biological chemists. The metal ions [1,2] such as copper, nickel, manganese, cobalt and zinc are involved in biological processes like electron transfer, dioxygen binding (Fe, Cu) and catalysis (Mn, Fe, Cu, and Ni). The enzymes that depend on nickel [3] are urease, carbon monoxide dehydrogenase, hydrogenase and methyl-*S*-coenzyme-*M*-methyl reductase. The proteins such as cytochrome *C* oxidase, copper/zinc superoxide dismutase, tyrosinase, hemocyanin and laccase contain a copper ion [4]. Synthetic chemists have synthesized many copper and nickel containing mono and polynuclear complexes using several types of ligand [5] such as, pendant arm [6], acyclic and macrocycles, porphyrins [7], polydentate Schiff bases [8], polyaza macrocycles [9], scorpionate ligands [10], etc. in order to understand the function, structure and properties of active sites in proteins.

In an earlier work we synthesised homobinuclear copper(II) complexes [11] using ligands H_2L^1 where $L^1 = N,N'$-bis[2-hydroxy-3-(piperidin-1-ylmethyl)-5-methylbenzyl]alkyldiimine (alkyl = ethylene L^{1a}, propylene L^{1b}). The present work deals with the synthesis of mononuclear complexes ML^1 (M = Ni, Cu) using ligands H_2L^{1a}, H_2L^{1b} and H_2L^{1c} where $L^{1c} = N,N'$-bis[2-hydroxy-3-(piperidin-1-ylmethyl)-5-methylbenzyl] butylenediimine (Scheme 1) and ML^2 (M = Ni, Cu) where $L^2 = N,N'$-bis[2-hydroxy-3-(piperidin-1-ylmethyl)-5-bromobenzyl]alkyldiimine (alkyl = ethylene L^{2a}, propylene L^{2b}, butylene L^{2c}). In the present work we have synthesized mononuclear complexes using the binucleating ligands as we are interested in studying the effect of a single metal ion in the ligand environment.

* Corresponding author. Tel.: +91-44-235-1269; fax: +91-44-235-2494.
E-mail address: mkands@unimad.ernet.in (M. Kandaswamy).

0277-5387/00/$ - see front matter © 2000 Elsevier Science Ltd. All rights reserved.
PII: S0277-5387(00)00498-8

This will form the basis for the synthesis and studies of heterobinuclear complexes and to compare their properties. The spectral, electrochemical and magnetic properties of the complexes and crystal structure of nickel complex **1** and copper complex **6** have been discussed.

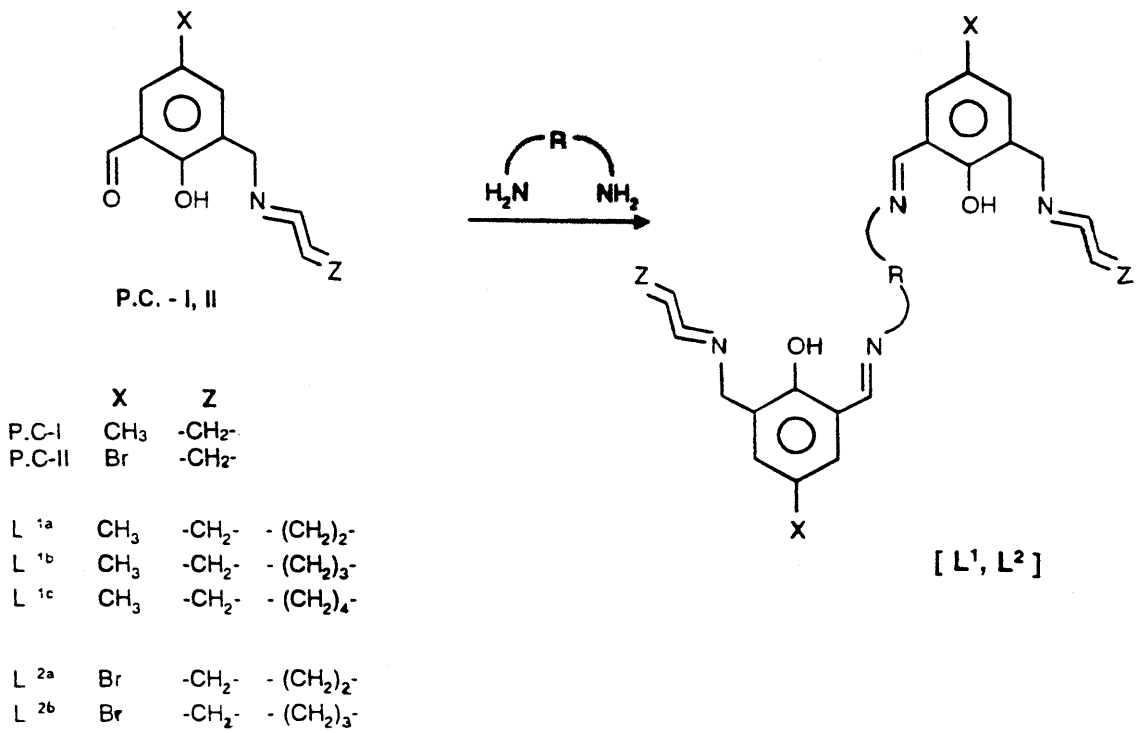
2. Experimental

2.1. Physical measurements

Elemental analyses for the complexes were obtained on a Carlo Erba Model 1106 elemental analyzer. ^{1}H NMR spectra (90 MHz) of the ligands were recorded using FX-80-Q. Fourier transform NMR spectrometer. Electronic spectra were recorded on a Hewlett-Packard 8452A spectrophotometer in the range 250–820 nm. The IR spectra were recorded on a Hitachi 270–50 spectrophotometer in the range 400–4000 cm^{-1}. The cyclic voltammograms were obtained on an apparatus comprising a PAR Model 173 potentiostat/galvanostat, 175 universal programmer, 176 current follower and 179 coulometer. For cyclic voltammetry three electrode system was used in which the counter and working electrodes were platinum foils and the reference electrode was Ag/AgCl. Ferrocene/ferricinium(1 +) couple was used as an internal standard. Room temperature (r.t.) magnetic moment was measured on a PAR vibrating sample magnetometer Model-155. The apparatus was calibrated by the use of Ni. The effective magnetic moment was calculated using the relation $\mu_{Cu} = 2.83\sqrt{\chi_{Cu}T}$, where χ_{Cu} is the molar magnetic susceptibility per Cu. X-band ESR spectra were recorded on a Varian EPR-E 112 spectrometer using diphenylpicrylhydrazine (DPPH) as the reference.

2.2. Crystal structure determination

Parallelopiped shaped orange and green coloured crystals were obtained for complex **1** and **6** by growing with DMF–ethanol by slow evaporation method at r.t. Intensity data were measured on a Siemens SMART CCD [12] area detector diffractometer with graphite monochromated Mo Kα radiation ($\lambda = 0.71073$ Å). The data collection covered over a hemisphere of reciprocal space by a combination of three sets of exposures; each set had a different ϕ angle (0, 88 and 180°) for the crystal and each exposure of 30 sec covered 0.3° in ω. The crystal-to-detector distance was 4 cm and the detector swing angle was $-35°$. Crystal decay was monitored by repeating 30 initial frames at the end of data collection and analyzing the duplicate reflections; it was found to be negligible. The structures of the complexes were solved using SHELXS-97 [13], a package for crystal structure solution using direct methods. The non-hydrogen atoms were first refined isotropically followed by anisotropic refinement by full-matrix least-squares calculation based on F^2 using SHELXL-97 [14]. Some of the hydrogen atoms were geometrically fixed and allowed to ride on the parent carbon atoms, and other



Scheme 1.

hydrogen atoms were located from the difference Fourier map and refined isotropically. Geometrical parameter calculations were performed using PARST [15].

2.3. Materials

5-Methylsalicylaldehyde was prepared by the literature method [16]. TBAP, used as the supporting electrolyte in electrochemical measurements was purchased from Fluka and recrystallized from methanol–water mixture. (Caution! TBAP is potentially explosive; hence, care should be taken in the handling of this compound). DMF (HPLC) was obtained from SD Fine Chemicals. All other chemicals and solvents were of analytical grade and were used as received.

2.4. Synthesis of precursor compounds

2.4.1. Synthesis of 4-methyl-2-formyl-6-(piperidin-1-ylmethyl)phenol (precursor compound **I**)

Piperidin (2.0 ml, 20 mmol) was added to a solution of paraformaldehyde (0.60 g, 20 mmol) dissolved in acetic acid (30 ml) and stirred for 24 h. Then 5-methylsalicyaldehyde (2.72 g, 20 mmol) was added and stirring was continued for another 24 h. The resulting compound was refluxed for 8 h and then neutralized with saturated Na_2CO_3 and extracted with $CHCl_3$. The $CHCl_3$ extract was evaporated at r.t. The resulting product was filtered, washed with methanol and recrystallized from MeOH by slow evaporation. Yield: 3 g (61%). M.p: 171°C. Selected IR data (ν cm^{-1} using KBr): 3350, 1680, 1490. ^1H NMR(δ ppm in $CDCl_3$): 2.15(s, 3H), 2.35(m, 4H), 3.45–4(m, 6H), 7.0–7.5(d, 2H), 9.8(s, H).

2.4.2. Synthesis of 4-bromo-2-formyl-6-(piperidin-1-ylmethyl)phenol (precursor compound **II**)

This precursor compound was synthesized by following the above procedure used for the synthesis of precursor compound **I** using 5-bromosalicyaldehyde instead of 5-methylsalicyaldehyde. The product was recrystallized from MeOH by slow evaporation. Yield: 4 g (70%). M.p: 185°C. Selected IR data(ν cm^{-1} using KBr): 3250, 1680, 1450. ^1H NMR (δ ppm in $CDCl_3$): 2.28(t, 4H), 3.65–4.2(m, 6H), 7.15–7.5(d, 2H), 9.8(s, H).

2.5. Synthesis of ligands

Synthesis of (*N*,*N*′ - bis - 2 - hydroxy - 3 - (piperidin - 1-yl - methyl) - 5 - methylbenzyl]ethylenediimine) (H_2L^{1a}): Ethylenediamine (0.07 ml, 10 mmol) was added to a solution of precursor compound **I** (4.7 g, 20 mmol) in methanol with stirring and refluxed for 2 h. The resulting product obtained on evaporation of the solvent at r.t. was filtered, washed with methanol and recrystallized from $CHCl_3$–MeOH (40 ml, 1:2). Yield: 4 g (81%). M.p: 193°C. Selected IR data (ν cm^{-1} using KBr): 3320, 1625, 1450. ^1H NMR(δ ppm in $CDCl_3$): 2.25(s, 6H), 2.24–2.55(m, 12H), 3.12–4.13(m, 12H), 6.85–6.90(d, 4H), 8.45(s, 2H). The X-ray crystal structure of this ligand has been reported [17].

The ligands H_2L^{1b} and H_2L^{1c} were prepared by following the above procedure used for the synthesis of H_2L^{1a} using the appropriate diamines.

2.5.1. H_2L^{1b}

Yellow coloured compound. Yield: 4.6 g (72%). M.p: 195°C. Selected IR data (ν cm^{-1} using KBr): 3340, 1625, 1510. ^1H NMR(δ ppm in $CDCl_3$): 1.12(s, 2H), 2.18(s, 6H), 2.3–2.55(m, 12H), 3.12–4.12(m, 12H), 6.67–6.89(d, 4H), 8.35(s, 2H).

2.5.2. H_2L^{1c}

Yellow coloured compound. Yield: 4.8 g (75%). M.p: 175°C. Selected IR data (ν cm^{-1} using KBr): 3290, 1635, 1480. ^1H NMR(δ ppm in $CDCl_3$): 1.17(s, 4H), 2.25(s, 6H), 2.34–2.56(m, 12H), 3.2–4.7(m, 12H), 6.75–6.86(d, 4H), 8.32(s, 2H).

2.5.3. H_2L^{2a}

Yellow coloured compound. Yield: 4 g (82%). M.p.: 165°C. ^1H NMR (δ ppm in $CDCl_3$): 2.21 (s, 6H), 2.4–2.65 (m, 14H), 3.4–4 (m, 16H), 6.95–7.10(d, 4H).

2.5.4. H_2L^{2b}

Yellow coloured compound. Yield: 3.4 g (69%). M.p: 155°C. ^1H NMR (δ ppm in $CDCl_3$): 1.15(s, 2H), 2.15(s, 6H) 2.37–2.65(d, 14H), 3.35–4.2(m, 16H), 6.89–6.95(d, 4H).

2.6. Synthesis of complexes

2.6.1. $[NiH_2L^{1a}](ClO_4)_2$ ($R = -(CH_2)_2-$) (**1**)

Ligand H_2L^{1a} (0.98 g, 2 mmol) and NaOH (0.16 g, 4 mmol) was dissolved in $CHCl_3$–MeOH (40 ml, 1:3) and added to a solution of $Ni(ClO_4)_2 \cdot 6H_2O$ (0.73 g, 2.1 mmol) in MeOH (20 ml) and refluxed for 1 h. Orange coloured crystals appeared. The crystalline product was collected by filtration and washed with MeOH. Recrystallized from CH_3CN–MeOH (40 ml, 1:3). *Anal.* Calc. for $C_{30}H_{40}N_4O_2Ni \cdot (ClO_4)_2$: C, 42.58; H, 4.75; N, 7.51. Found: C, 42.48; H, 4.62; N, 7.38%. Selected IR data (ν cm^{-1} using KBr) 3260, 1625, 1590, 1110, 625. UV–Vis [λ_{max} nm (ϵ M^{-1} cm^{-1})] in DMF: 552(228), 420(510), 270(11403). The X-ray structure of the complex has been studied and discussed in this paper (Fig. 1).

All nickel complexes given below were prepared by following the procedure used for the synthesis of complex **1** using Ni(II) perchlorate and appropriate ligands.

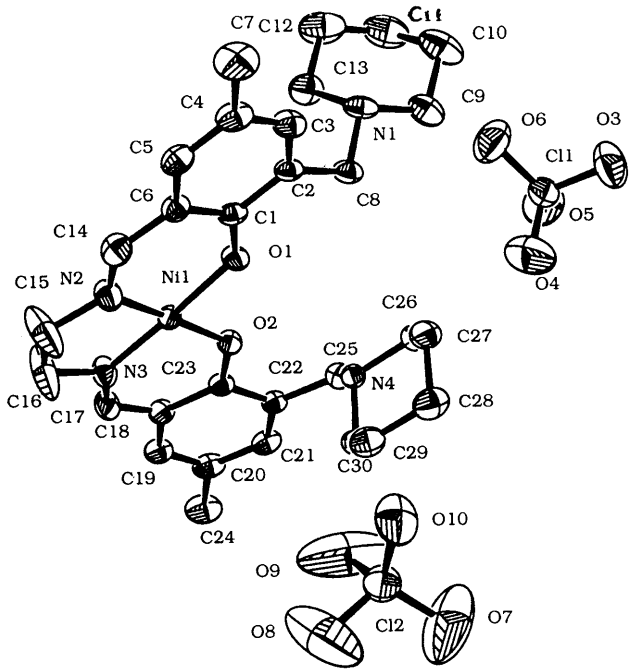


Fig. 1. ORTEP plot of $[NiH_2L^{1a}](ClO_4)_2$ (**1**) with atomic numbering scheme.

*2.6.2. $[NiH_2L^{1b}](ClO_4)_2$ ($R = -(CH_2)_3-$) (**2**)*

Anal. Calc. for $C_{31}H_{42}N_4O_2(ClO_4)$: C, 50.17; H, 5.69; N, 7.89. Found: C, 49.87; H, 5.43; N, 7.65%. Selected IR (ν cm^{-1} using KBr): 3220, 1625, 1590, 1100, 620. UV–Vis [λ_{max} nm ($\in$ M^{-1} cm^{-1})] in DMF: 595(236), 410(10688), 338(21376).

*2.6.3. $[NiH_2L^{1c}](ClO_4)_2$ ($R = -(CH_2)_4-$) (**3**)*

Anal. Calc. for $C_{32}H_{44}N_4O_2(ClO_4)$: C, 52.76; H, 5.98; N, 8.12. Found: C, 52.62; H, 5.75; N, 8.05%. Selected IR (ν cm^{-1} using KBr): 3300, 1620, 1580, 1100, 628. UV–Vis [λ_{max} nm ($\in$ M^{-1} cm^{-1})] in DMF: 615(234), 340(18378).

*2.6.4. $[NiH_2L^{2a}](ClO_4)_2$ ($R = -(CH_2)_2-$) (**4**)*

Anal. Calc. for $C_{27}H_{34}N_4O_2(ClO_4)_2$: C, 46.15; H, 4.84; N, 7.97. Found: C, 46.08; H, 4.79; N, 7.82%. Selected IR data (ν cm^{-1} using KBr): 3320, 1620, 1590, 1100, 625. UV–Vis [λ_{max} nm ($\in$ M^{-1} cm^{-1})] in DMF: 790(136), 630(146), 550(304), 375(17289).

*2.6.5. $[NiH_2L^{2b}](ClO_4)_2$ ($R = -(CH_2)_3-$) (**5**)*

Anal. Calc. for $C_{28}H_{36}N_4O_2{\cdot}(ClO_4)_2$: C, 46.93; H, 5.02; N, 7.82. Found: C, 46.85; H, 4.95; N, 7.79%. Selected IR data (ν cm^{-1} using KBr): 3330, 1640, 1100, 625. UV–Vis [λ_{max} nm ($\in$ M^{-1} cm^{-1})] in DMF: 580(217), 392(11689).

*2.6.6. $[CuH_2L^{1a}](ClO_4)_2$ ($R = -(CH_2)_2-$) (**6**)*

Ligand H_2L^{1a} (0.98 g, 2 mmol) and NaOH (0.16 g, 4 mmol) was dissolved in $CHCl_3$–MeOH (40 ml, 1:3) and added to a solution of $Cu(ClO_4)_2{\cdot}6H_2O$ (0.75 g, 2.1 mmol) in MeOH (20 ml) and refluxed for 1 h. Green coloured crystals appeared. The crystalline product was collected by filtration, washed with MeOH and recrystallized from CH_3CN–MeOH (40 ml, 1:3). *Anal*. Calc. for $C_{30}H_{40}N_4O_2{\cdot}(ClO_4)_2$: C, 48.06; H, 5.34; N, 7.47. Found: C, 47.98; H, 5.25; N, 7.38%. Selected IR data (ν cm^{-1} using KBr): 3330, 1640, 1100, 625. UV–Vis [λ_{max} nm ($\in$ M^{-1} cm^{-1})] in DMF: 570(506), 375(4726). The X-ray structure of this complex is discussed in this paper.

All the other copper complexes given below were prepared by following the procedure used for the synthesis of complex **6**, by using copper(II) perchlorarte and appropriate ligands.

*2.6.7. $[CuH_2L^{1b}](ClO_4)_2$ ($R = -(CH_2)_3-$) (**7**)*

Anal. Calc. for $C_{31}H_{42}N_4O_2{\cdot}(ClO_4)_2$: C, 43.24; H, 4.89; N, 7.20. Found: C, 43.13; H, 4.95; N, 7.24%. Selected IR data(ν cm^{-1} using KBr): 3330, 1640, 1100, 625. UV–Vis[λ_{max} nm($\in$ M^{-1} cm^{-1})] in DMF: 620(457), 372(4673), 280 (9532).

*2.6.8. $[CuH_2L^{2a}](ClO_4)_2$ ($R = -(CH_2)_2-$) (**8**)*

Anal. Calc. for $C_{27}H_{34}N_4O_2{\cdot}(ClO_4)_2$: C, 45.82; H, 4.81; N, 7.92. Found: C, 45.75; H, 4.78; N, 7.86%. Selected IR data (ν cm^{-1} using KBr): 3330, 1640, 1100, 625. UV–Vis [λ_{max} nm ($\in$ M^{-1} cm^{-1})] in DMF: 580(217), 392(11689).

*2.6.9. $[CuH_2L^{2b}](ClO_4)_2$ ($R = -(CH_2)_3-$) (**9**)*

Anal. Calc. for $C_{28}H_{36}N_4O_2{\cdot}(ClO_4)_2$: C, 46.90; H, 4.99; N, 7.76. Found: C, 46.85; H, 4.92; N, 7.66%. Selected IR data (ν cm^{-1} using KBr): 3330, 1640, 1100, 625. UV–Vis [λ_{max} nm ($\in$ M^{-1} cm^{-1})] in DMF: 680(210), 380(10689).

3. Results and discussion

3.1. X-ray structural study of the complexes

Structure of the $[NiH_2L^{1a}](ClO_4)_2$ (**1**) and $[CuH_2L^{1a}](ClO_4)_2$ (**6**): An ORTEP [18] view with crystallographic numbering scheme of complexes **1** and **6** are shown in Figs. 1 and 2. Crystallographic data and structure determination parameters are given in Table 1. Selected bond distance and angles are given in Table 2. The two structures presented in this paper are isostructural. The near equality of the bond lengths and angles of the phenyl and piperidin rings of complexes **1** and **6** indicates that the replacement of Ni by the Cu ion has not produced any extra deformation of the coordination geometry and ring system. As shown in Figs. 1 and 2, the Ni(II) and Cu(II) ions have slightly distorted square-planar coordination. The displacement

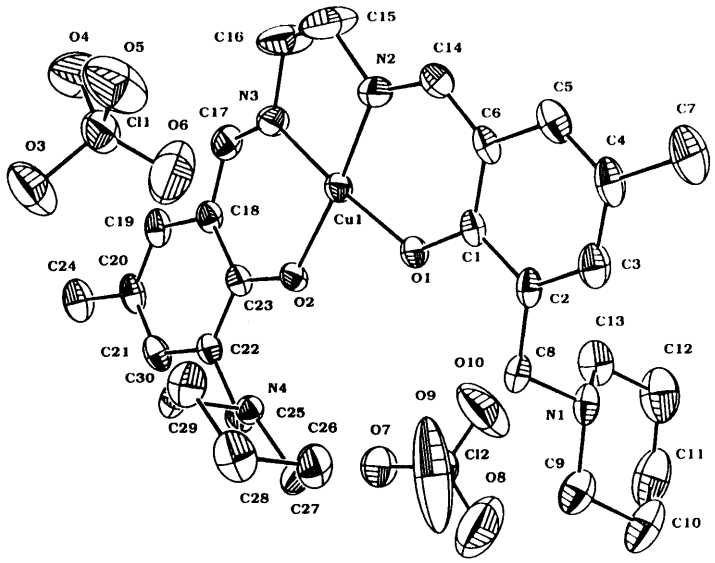


Fig. 2. ORTEP plot of $[CuH_2L^{1a}](ClO_4)_2$ (**1**) with atomic numbering scheme.

of the Ni(II) and Cu(II) ions from the best plane through the donor atoms O1, O2, N2 and N3 is −0.0004 (5) and 0.0007 Å, respectively. The coordination bond angles have values between 85.3(1) (N2–Ni1–N3) and 95.3(1)° (N2–Ni1–O1) for complex **1** and 84.5(2) (N2–Cu1–N3) and 93.6(2)° (N2–Cu1–O1) for complex **6**, their sum being 360.2(1) for **1** and 360.5(2)° for **6**. The Ni–O [1.838(3) and 1.855(2) Å] and Cu–O [1.901(4) and 1.878(4) Å] distances are equal within experimental error. There is a slight distortion of the coordination plane around the ions which can be quantified by the dihedral angle between the N2–Ni1–N3 and O1–Ni1–O2 planes [4.6(1)°] for **1** and N2–Cu1–N3 and O1–Cu1–O2 planes [7.5(2)°] for **6**.

The piperidin rings adopt chair conformation. The best plane passes through the central C atoms, leaving the N and C atoms above and below the plane. The deviations of N and C atoms are −0.485(3) and 0.318(6) Å, −0.491(4) and 0.311(8) Å for **1** and **6**, respectively. The deviations for the ring consisting of atoms C9–C13, N1 and C11 are −0.485(4) and 0.307(6), for the ring consisting of atoms C26–C30, N4 and C28 are −0.504(4) and 0.344(7) Å for **1** and **6**, respectively. The N1 and N4 atoms of the piperidin rings are protonated as shown by the degree of pyramidalization. N1 deviates from the C8, C9, C13 plane by 0.447(3) for **1** and 0.439(4) Å for **6**, and N4 deviates from the C25, C26, C30 plane by −0.423(4) for **1** and −0.429(4) Å for **6**. These two positive charges are stabilized by two lattice perchlorate anions. The hydrogen (H1–N4) of N4 is involved in intramolecular N–H···O hydrogen bonding between N4 of piperidin ring and phenoxy O2.

IR spectra of the complexes **1**–**9** shows ν(C=N) peak [19] at 1620–1640 cm^{-1}. The complexes show a broad peak at 1100 and 620 cm^{-1} characteristic of the perchlorate ion. The presence of the perchlorate ion is evident from the X-ray structure of the complexes **1** and **6** The electronic spectra of the complexes show three main transitions [20]: a weak band observed in the range 540–650 nm, due to d–d transition of the metal ion. Nickel complexes show a single d–d band in the range 550–650 nm characteristic of square planar [21] geometry around the metal ion. Copper complexes also show a d–d band in the range 550 to 620 nm characteristic of square planar geometry around the metal ion. An increase in the λ_{max} of the d–d transition of the complexes starting from **1** to **3** is observed as the number of methylene group in the imine linkage in-

Table 1
Crystal data and structure refinement for $[NiH_2L^{1a}](ClO_4)_2$ (**1**) and $[CuH_2L^{1a}](ClO_4)_2$ (**6**)

Complex	$[NiH_2L^{1a}](ClO_4)_2$ (**1**)	$[CuH_2L^{1a}](ClO_4)_2$ (**6**)
Empirical formula	$C_{30}H_{42}Cl_2N_4NiO_{10}$	$C_{30}H_{42}Cl_2CuN_4O_{10}$
Formula weight	748.29	753.12
Crystal system	triclinic	triclinic
Space group	$P\bar{1}$	$P\bar{1}$
Temperature (K)	293(2)	293(2)
Wavelength (Å)	0.71073	0.71073
a (Å)	11.4889(1)	11.5326(3)
b (Å)	12.1698(1)	12.1354(3)
c (Å)	13.3494(2)	13.4408(1)
α (°)	84.6567(9)	85.400(1)
β (°)	72.9918(7)	71.961(1)
γ (°)	75.7111(3)	76.076(1)
V (Å^3)	1729.19(3)	1736.02(6)
Z	2	2
D_{calc} (Mg m^{-3})	1.437	1.441
R_1	0.0608	0.0759
wR_2	0.1470	0.1742

Table 2
Selected bond lengths (Å) and bond angles (°) relevant to the nickel and copper coordination sphere in complexes $[NiH_2L^{1a}](ClO_4)_2$ (**1**) and $[CuH_2L^{1a}](ClO_4)_2$ (**6**)

Ni(1)–N(2)	1.837(4)	Cu(1)–O(2)	1.877(3)
Ni(1)–O(2)	1.838(3)	Cu(1)–N(1)	1.897(4)
Ni(1)–N(3)	1.849(3)	Cu(1)–O(1)	1.901(3)
Ni(1)–O(1)	1.855(2)	Cu(1)–N(2)	1.930(3)
N(2)–Ni(1)–O(2)	176.74(14)	O(2)–Cu(1)–N(1)	173.77(14)
N(2)–Ni(1)–N(3)	85.25(14)	O(2)–Cu(1)–O(1)	89.33(11)
O(2)–Ni(1)–N(3)	94.14(12)	N(1)–Cu(1)–O(1)	93.71(14)
N(2)–Ni(1)–O(1)	95.30(12)	O(2)–Cu(1)–N(2)	93.00(13)
O(2)–Ni(1)–O(1)	85.47(10)	N(1)–Cu(1)–N(2)	84.42(16)
N(3)–Ni(1)–O(1)	176.98(14)	O(1)–Cu(1)–N(2)	174.83(13)

creases [22]. The same trend has been observed for nickel(II) complexes **4** and **5** and copper(II) complexes **6** and **7**. A moderately intense peak observed in the range 400–350 nm is due to ligand to metal charge transfer transition and the very intense peak observed in the range 350–250 nm is due to ligand to ligand charge transfer transition.

3.2. Electrochemistry

Electrochemical properties of the complexes **1**–**9** were studied by cyclic voltammetry in DMF in the range + 1.2 to − 1.3 V. All the complexes **1**–**9** show a single redox wave at negative potential in the range − 0.70 to − 1.2 V. At positive potential, nickel complexes **1**–**5** show a single redox wave in the range + 0.5 to + 0.90 V. Generally, the electrochemical properties of the complexes depend on the chelate ring size [23], axial ligation [24] and substitution pattern in the chelate ring [25].

3.3. Reduction process at negative potential

The cyclic voltammogram of nickel complexes (**1**–**5**) and copper complexes (**6**–**9**) at negative potential show a single electron transfer process in the range − 0.70 to − 1.2 V. The data are given in Table 3. The reduction process is quasi-reversible in nature as is evident from the criteria: the $E_{1/2}$ value is independent of scan rate, the ΔE_p increases with increasing scan rate (10, 20, 50, 100, 150 mV s^{-1}) and is always greater than 60 mV. Repeated scanning lead to a gradual decrease in current, suggesting that the newly formed species is chemically unstable at room temperature. At a lower scan rate (10 mV s^{-1}) the oxidation process becomes irreversible. The peak currents i_{pc} and i_{pa} were not equal. Controlled potential electrolysis experiment indicates that the couple corresponds to a one-electron transfer process. Thus a quasi-reversible one-electron transfer occurred at the electrode surface, $M^{II} \rightleftharpoons M^{I}$ (M = Cu, Ni). The reduction potential of nickel complexes [23,26] of ligand L^{1a-c} (**1**–**3**) shifts anodically from $E_{pc} = -1.0$ to − 0.85 V ($E_{1/2} = -0.91$ to − 0.75 V) (vs Fc/Fc^+) as the number of methylene groups in the imine linkage is increased. A similar trend has been observed for copper complexes [27] of ligand L^{1a} (complex **6**) ($E_{1/2} = -0.84$ V) and L^{1b} (complex **7**) ($E_{1/2} = -0.71$ V) (vs Fc/Fc^+). This is because as the number of methylene group increases, the flexibility of the complex increases and the reduction process is shifted to a less negative potential.

The reduction potential for nickel complex **4** of ligand L^{2a} is observed at less a negative potential ($E_{pc} = -0.92$ V) (vs Fc/Fc^+) than complex **1** of ligand L^{1a} ($E_{pc} = -1.0$ V) (vs Fc/Fc^+). This is because complex **4**, which contains an electron-withdrawing [4] substituent (Br) at the *para* position to the phenoxide oxygen in the phenyl ring, reduces at less negative potentials than complex **1**, which contains an electron-donating substituent (CH_3) at the *para* position. A similar trend has been observed for the copper complex of ligand L^{1b} and L^{2b}. This may be due to the lesser electron density on the metal centre as a result of the poor electron donating nature of the bromine [28] at the *para* position.

Table 3
Electrochemical data for the complexes (reduction at cathodic potential) [a]

Number	Complex	E_{pc} (V)	E_{pa} (V)	ΔE_p (mV)	$E_{1/2}$ (V)
1	$[NiH_2L^{1a}](ClO_4)_2$	−1.0	−0.83	170	−0.91
2	$[NiH_2L^{1b}](ClO_4)_2$	−0.93	−0.75	180	−0.84
3	$[NiH_2L^{1c}](ClO_4)_2$	−0.86	−0.64	220	−0.75
4	$[NiH_2L^{2a}]((ClO_4)_2$	−0.92	−0.70	220	−0.81
5	$[NiH_2L^{2b}](ClO_4)_2$	−0.80	−0.62	180	−0.71
6	$[CuH_2L^{1a}](ClO_4)_2$	−0.92	−0.75	170	−0.84
7	$[CuH_2L^{1b}](ClO_4)_2$	−0.80	−0.60	200	−0.70
8	$[CuH_2L^{2a}](ClO_4)_2$	−0.85	−0.68	170	−0.76
9	$[CuH_2L^{2b}]((ClO_4)_2$	−0.72	−0.50	220	−0.61

[a] V vs. Ag/AgCl. Pt working and reference electrodes; supporting electrolyte TBAP; concentration of complex 1×10^{-3} M; concentration of TBAP 1×10^{-1} M. Scan rate: 50 mV s^{-1}.

Table 4
Electrochemical data for nickel complexes (reduction at anodic potential) [a]

Number	Complex	E_{pa} (V)	E_{pc} (V)	ΔE_p (mV)	$E_{1/2}$ (V)
1	$[NiH_2L^{1a}](ClO_4)_2$	0.50	0.35	200	0.42
2	$[NiH_2L^{1b}](ClO_4)_2$	0.75	0.55	200	0.65
3	$[NiH_2L^{1c}](ClO_4)_2$	0.84	0.62	220	0.73
4	$[NiH_2L^{2a}]((ClO_4)_2$	0.65	0.40	250	0.52
5	$[NiH_2L^{2b}](ClO_4)_2$	0.75	0.48	220	0.59

[a] V vs Pt electrode. Pt working and reference electrodes; supporting electrolyte TBAP; concentration of complex 1×10^{-3} M. concentration of TBAP 1×10^{-1} M. Scan rate: 50 mV s^{-1}.

Table 5
ESR and magnetic data (room temperature) for the complexes

Number	Complex	$g_{\|}$	$g_{\perp}$	$A_{\|} \times 10^{-4}$ cm^{-1}	μ_{eff} (B.M)
6	$[CuH_2L^{1a}](ClO_4)_2$	2.22	2.16	160	1.69
7	$[CuH_2L^{1b}](ClO_4)_2$	2.21	2.10	140	1.72
8	$[CuH_2L^{2a}](ClO_4)_2$	2.18	2.05	120	1.73
9	$[CuH_2L^{2b}](ClO_4)_2$	2.22	2.12	160	1.75

3.4. Oxidation process at positive potential

Cyclic voltammogram of nickel complexes **1**–**5** at positive potential show a single redox wave in the potential range [29] +0.50 to +0.90 V. The data are summarized in Table 4. The oxidation process is quasi-reversible in nature as is evident from the criteria: the $E_{1/2}$ value is independent of scan rate, the ΔE_p increases with increasing scan rate (10, 20, 50, 100, 150 mV s^{-1}) and is always greater than 60 mV. The peak currents I_{pa} and I_{pc} were not equal. Controlled potential electrolysis experiment indicates that the wave corresponds to one electron transfer process. The oxidation potential of nickel complexes **1**–**3** of ligand L^{1a-c} shifts towards a more positive value [23] (from $E_{pa} = +0.50$ to +0.85 V) as the number of methylene groups in the chelate ring of the complex increases. A similar trend has been observed for nickel complexes of ligand L^{2a} (complex **4**) and L^{2b} (complex **5**). This is because, as the chelate ring size of the ligand increases, the hole size provided for the coordinated ion also increases, thereby experiencing more difficulty for encompassing the smaller Ni(III) ion. Consequently, the Ni(II)/Ni(III) oxidation process of complexes with a large chelate ring size is shifted to a more positive value.

3.5. ESR and magnetic study

The ESR spectra of nickel complexes were recorded in a solution state using DMF as solvent at liquid nitrogen temperature. The data are given in Table 5. The ESR spectra of nickel complexes [30] are inactive characteristic of square-planar geometry around the metal ion. All the copper complexes (**6**–**9**) show an ESR spectrum typical of square-planar copper(II) complex [31] with nuclear hyperfine spin 3/2, three of the four expected hyperfine signals are seen, with the fourth being hidden under the $g_{\perp}$ line. For all the copper complexes the copper hyperfine $A_{\|}$ splitting falls in the range $120–160 \times 10^{-4}$ cm^{-1}, indicative of an electron interacting with only one copper nucleus. The relation $g_{\|} > g_{\perp}$ is typical of axially symmetric Cu(II) having one unpaired electron in a $d_{x^2-y^2}$ orbital. For the copper complex **7**; $g_{\|} = 2.21$, $g_{\perp} = 2.10$, $A_{\|} = 140 \times 10^{-4}$ cm^{-1}.

Magnetic moment of the complexes was observed at room temperature and the data are given in Table 5. All the nickel complexes are diamagnetic in nature due to square planar [30] geometry around the metal ion. Copper complexes (**6**–**9**) show μ_{eff} value in the range 1.70–1.75 B.M. which is close to the spin only value of 1.73 B.M. expected for copper complexes [30] with single unpaired electron located in an essentially $d_{x^2-y^2}$ orbital.

4. Supplementary material

Full crystal data and structure refinement details, atomic coordinates and equivalent isotrophic displacement parameters, full interatomic distances and angles, anisotrophic displacement parameters, hydrogen coordinates and isotrophic displacements parameters for complexes **1** and **6** are available from the Cambridge Crystallographic Data Centre, CCDC Nos. 140078 and 140079 for **1** and **6**, respectively. Copies of this information may be obtained free of charge from The Director, CCDC, 12 Union Road, Cambridge, CB2 1EZ, UK

(fax: +44-1223-336033; e-mail: deposit@ccdc.cam.ac.uk or www: http://www.ccdc.cam.ac.uk).

References

[1] D.E. Fenton, Biocoordination Chemistry, 1st ed., Oxford University Press, Oxford, 1995, p. 80.
[2] D.E. Fenton, in: A.G. Sykes (Ed.), Advances in Inorganic and Bioinorganic Mechanism, vol. 2, Academic, London, 1983, p. 187.
[3] (a) R.P. Hausinger, Biochemistry of Nickel, Plenum, New York, 1993, chapter 12, 23–50. (b) J.P. Lancaster (Ed.), The Bioinorganic Chemistry of Nickel, VCH, New York, 1998.
[4] M.J. Ettinger, in: D.R. Lontine (Ed.), Copper Proteins and Copper Enzymes, vol. 3, CRC, Boca Raton, FL, 1984, p. 175.
[5] P. Gwerriero, S. Tamburini, P.A. Vigato, Coord. Chem. Rev. 139 (1995) 17.
[6] C. Fraser, L. Johanston, A.L. Rheingold, B.S. Haggerty, G.K. Willames, J. Whelan, B. Bosnich, Inorg. Chem. 31 (1992) 1835.
[7] C. Bernard, J.P. Gisselbrecht, M. Gross, E. Vogel, M. Lausmann, Inorg. Chem. 33 (1994) 2393.
[8] P.A. Vigato, D.E. Fenton, Inorg. Chim. Acta 139 (1987) 39.
[9] J.C. Kim, J.C. Fettinger, Y.I. Kim, Inorg. Chim. Acta 286 (1999) 67.
[10] T.C. Higgs, C.J. Carrano, Inorg. Chem. 36 (1997) 298.
[11] S. Karunakaran and M. Kandaswamy, J. Chem. Soc., Dalton Trans. (1995) 1851.
[12] Siemens (1996) SMART and SAINT, Area Detector Control and Investigation Software Siemens Analytical X-Ray Instrument Inc., Maidisan, WI, USA
[13] G.M. Sheldrick, SHELXS 97. Program for the refinement of Crystal Structures University of Göttingen, Germany, 1997.
[14] G.M. Sheldrick, SHELXL-97. Program for the refinement of Crystal Structures University of Göttingen, Germany, 1997.
[15] M. Nardelli, Comput. Chem. 7 (1983) 95.
[16] J.C. Duff, J. Chem. Soc. (1941) 547.
[17] R. Thirumurgan, R. Shanmuga Sundara Raj, M. Marappan and M. Kandaswamy, Acta Crystallography, 1999 (communuicated)
[18] L. Zsolnai, (ZORTEP) An Interactive ORTEP Program for Steric Illustration, University of Heidelberg, Germany, 1997.
[19] G. Das, R. Shukala, S. Mandal, R. Singh, P.K. Bharadwaj, J.V. Singh, K.H. Whitmire, Inorg. Chem. 36 (1997) 323.
[20] P. Amudha, M. Kandaswamy, L. Govindaswamy, D. Velmurugan, Inorg. Chem. 37 (1998) 4586.
[21] T. Koga, H. Furutachi, T. Nakumura, N. Fukita, M. Ohba, K. Takahashi, H. Okawa, Inorg. Chem. 37 (1998) 989.
[22] (a) R. Bhalla, M. Helliwell, C.D. Garner, Inorg. Chem. 36 (1997) 2944. (b) H. Okawa, S. Kida, Bull. Chem. Soc. Jpn. 45 (1972) 1759.
[23] (a) F.V. Lovecchino, E.S. Gore, D.H. Bush, J. Am. Chem. Soc. 96 (1974) 3104. (b) G.K. Bareford, G.M. Freeman, D.G. Erver, Inorg. Chem. 86 (1986) 552.
[24] (a) C. Kratky, R. Tschatka, C. Augst, J.E. Johanson, Plaquvent, Helv. Chim. Acta 68 (1985) 1312. (b) P.A. Conmick, K.A. Macor, Inorg. Chem. 30 (1991) 4654.
[25] J.A. Strecky, D.G. Pillsbury, D.H. Busch, Inorg. Chem. 19 (1980) 3148.
[26] G.A. Bowmaker, J.P. Williams, J. Chem. Soc., Dalton Trans. (1993) 3593.
[27] H. Okawa, M. Tadokara, T.Y. Aretake, M. Ohba, K. Shindo, M. Mittsumi, M. Koikawa, M. Tomono, D.E. Fenton, J. Chem. Soc., Dalton Trans. (1993) 253.
[28] (a) S. Karunakaran, M. Kandaswamy, J. Chem. Soc., Dalton Trans. (1994) 1595. (b) P. Amudha, M. Thirumavalavan, M. Kandaswamy, Polyhedron 18 (1999) 1363. (c) J. Zubieta, J. Chayes, K.D. Karlin, in: K.D. Karlin, J. Zubieta (Eds.), Copper Co-ordination Chemistry Biochemical and Inorganic Perspectives, Adenine, Grilderland, New York, 1983, p. 97.
[29] (a) P. Chandhuri, H. Kuppers, K. Weighardt, S. Gehring, W. Haeser, B. Nuber, H. Weiss, J. Chem. Soc., Dalton Trans. (1988) 1367. (b) B. Kersting, G. Steinfeld, J. Hausmann, Eur. J. Inorg. Chem. (1999) 179.
[30] A. Bottcher, H. Elias, E. Jager, H. Lanffelderova, M. Mazur, L. Mullor, H. Paulus, P. Pelikan, M. Rudolph, M. Valko, Inorg. Chem. 32 (1993) 4131.
[31] S. Zhu, F. Kon, H. Lin, C. Lin, M. Lin, Y. Chen, Inorg. Chem. 35 (1996) 3851.

PERGAMON

www.elsevier.nl/locate/poly

Polyhedron 19 (2000) 2019–2025

POLYHEDRON

Syntheses, crystal structures and properties of the novel Co(II) and Ni(II) complexes with 4-(*p*-methylphenyl)-3,5-bis(pyridin-2-yl)-1,2,4-triazole

Dun-Ru Zhu [a], You Song [a], Yan Xu [a], Yong Zhang [a], S. Shanmuga Sundara Raj [b], Hoong-Kun Fun [b], Xiao-Zeng You [a,*]

[a] *Coordination Chemistry Institute, the State Key Laboratory of Coordination Chemistry, Nanjing University, Nanjing 210093, PR China*
[b] *X-ray Crystallography Unit, School of Physics, Universiti Sains Malaysia, 11800 USM, Penang, Malaysia*

Received 28 April 2000; accepted 5 July 2000

Abstract

The chelating properties of 4-(*p*-methylphenyl)-3,5-bis(pyridin-2-yl)-1,2,4-triazole (MBPT) were investigated through the study of the crystal structures of $[Co(MBPT)_2(H_2O)_2](ClO_4)_2{\cdot}4H_2O$ (**1**), $[Ni(MBPT)_2(H_2O)_2](ClO_4)_2$ (**2**) and MBPT and the analysis of IR and ESIMS spectra. The metal atom is in a distorted octahedral environment. Two bidentate chelating ligands (MBPT) coordinate to metal center equatorially and two water molecules coordinate axially. Each MBPT coordinates via one triazole nitrogen atom and one pyridine nitrogen atom. The magnetic measurements show that the complexes are high-spin species in the 75–300 K range. © 2000 Elsevier Science Ltd. All rights reserved.

Keywords: Syntheses; Crystal structures; Cobalt(II) complex; Nickel(II) complex; 4-(*p*-Methylphenyl)-3,5-bis(pyridin-2-yl)-1,2,4-triazole; ESIMS

1. Introduction

Substituted 1,2,4-triazoles have been actively studied as bridging ligands between transition metal(II) ions coordinating through their N1 and N2 atoms, since their complexes have interesting structures and specific magnetic properties [1–9]. It is interesting to note that some complexes containing substituted 1,2,4-triazole ligands have the spin-crossover properties, which could be used as molecular-based memory devices, displays and optical switches [10,11]. However, complexes containing triaryltriazole ligands have been rarely studied so far. We have synthesized some triaryltriazole compounds [12–14], which could be acted as doubly-bidentate chelating ligands because of their structural similarity to 4-amino-3,5-bis(pyridin-2-yl)-1,2,4-triazole (ABPT) [15]. It may be expected that the triaryltriazoles resulting from the substitution of 4-amino group of the ligand (ABPT) by a *p*-substituted aryl group would allow a variable structural chemistry of their complexes. Recently we have reported the crystal structure of a Ag(I) complex with 4-(*p*-methylphenyl)-3,5-bis(pyridin-2-yl)-1,2,4-triazole (MBPT), one of the triaryltriazole ligands [16]. As a continuation of our investigation of the ligand MBPT, we present here the syntheses and crystal structures of new cobalt(II) and nickel(II) complexes with MBPT and of MBPT itself. The spectroscopic and magnetic properties are also discussed in this paper.

2. Experimental

2.1. Synthesis of the compounds

All chemicals used were of analytical grade. Solvents were purified by conventional methods.

2.1.1. 4-(p-Methylphenyl)-3,5-bis(pyridin-2-yl)-1,2,4-triazol MBPT

The ligand (MBPT) was synthesized according to a similar method [14], m.p.196–198°C. Colorless single

* Corresponding author. Tel.: +86-25-359-3522; fax: +86-25-331-4502.
E-mail address: ccinu@netra.nju.edu.cn (X.-Z. You).

0277-5387/00/$ - see front matter © 2000 Elsevier Science Ltd. All rights reserved.
PII: S0277-5387(00)00501-5

crystals suitable for X-ray analysis were obtained from acetone upon slow evaporation at r.t. (*Anal.* Found: C, 72.37; H, 5.04; N, 22.64. Calc. for $C_{19}H_{15}N_5$: C, 72.82; H, 4.82; N, 22.35%). IR (cm^{-1}) $\nu(CH_3)$ 2954.7(w), 2918.9(w); ν(py ring) 1584.8(s), 1568.3(m), ν(ph) 824(s), 801.6(s); ^1H NMR δ: 2.41(s, Me), 7.18–7.34(m, 6H), 7.86–7.88(m, 2H), 8.22–8.24(m, 2H), 8.44–8.47(m, 2H).

2.1.2. Complex $[Co(MBPT)_2(H_2O)_2](ClO_4)_2\cdot 4H_2O$ (1)

To a solution of MBPT (0.6 mmol), in boiling EtOH (10 cm^3), was added a solution of $Co(OAc)_2\cdot 4H_2O$ (0.6 mmol) in EtOH (5 cm^3). The mixture was filtered into an EtOH solution containing $NaClO_4$ (1.5 mmol). The yellow crystalline solid that formed was isolated, washed with H_2O and dried in vacuo to yield 0.27 g (90%) of the perchlorate. Light-brown single crystals suitable for X-ray analysis were obtained from a methanol solution. (*Anal.* Found: C, 45.83; H, 4.56; N, 13.97. Calc. for $C_{38}H_{42}Cl_2CoN_{10}O_{14}$: C, 45.98; H, 4.26; N, 14.11%). IR (cm^{-1}): ν(O–H): 3454 (m, b); ν (CH_3): 2925.8(w); ν(py ring): 1606.6(s), 1591(m), 1572.7(w); ν(Cl–O): 1099.3(s), 929.2(w), 625.5(s).

2.1.3. Complex $[Ni(MBPT)_2(H_2O)_2](ClO_4)_2$ (2)

Complex **2** was prepared in 83% yield by a procedure similar to complex **1** but using $Ni(OAc)_2\cdot 4H_2O$ instead of $Co(OAc)_2\cdot 4H_2O$. The pale purple single crystals suitable for X-ray diffraction were obtained by evaporation from methanol solution. (*Anal.* Found: C, 49.35; H, 3.89; N, 15.09; Calc. for $C_{38}H_{34}Cl_2NiN_{10}O_{10}$: C, 49.59; H, 3.72; N, 15.22%). IR (cm^{-1}): ν(O–H): 3422.8 (m, b); $\nu(CH_3)$: 2925.6(w); ν(py ring): 1608.9(s), 1587.9(m), 1572.7(w); ν(Cl–O): 1097.7(s), 930(w), 625.4(s).

2.2. Physical measurements

Elemental analyses were performed with a Perkin–Elmer 240 instrument. IR spectra were recorded on a Nicolet 170SX FTIR instrument (KBr discs) in the 4000–400 cm^{-1} region. Electronic spectra were obtained with a Shimadzu UV3100 spectrophotometer in MeOH solution. The ^1H NMR spectra of MBPT were measured with a Bruker AM 500 spectrometer at ambient temperature in [$^2H_6$] $(CD_3)_2C{=}O$ using TMS as internal reference. Electrospray ionization mass spectra (ESIMS) were recorded with a Finnigan mat APISSQ 710 mass spectrometer, with methanol mobile phase and the flow rate of the mobile phase was 0.2 ml min^{-1}. The spray voltage was 4.5 KV and the capillary temperature was 200°C. The capillary voltage was 7.4 V for complex **1** and 28.7 V for complex **2**. Magnetic susceptibility of powder sample was collected with a CAHN 2000 magnetobalance and corrected using Pascal's constants (75–300 K).

2.3. X-ray crystallography

The well-shaped single crystals of MBPT, **1** and **2** were selected for X-ray diffraction study. The unit cell parameters and intensity data were collected at 293(2) K on a Siemens SMART CCD diffractometer with a detector distance of 4 cm and frame exposure time of 30 s using a graphite-monochromated Mo Kα (λ = 0.71073 Å) radiation. The structures were all solved by direct methods and refined on F^2 by full-matrix least-squares procedures using SHELXTL software [17]. All non-hydrogen atoms were anisotropically refined. All H atoms were located from a difference map and refined isotropically. Details on crystal data of MBPT, **1** and **2** are summarized in Table 1.

3. Results and discussion

3.1. Syntheses

The triaryltriazole ligand MBPT reacts with $M(OAc)_2\cdot 4H_2O$ ($M = Co^{II}$, Ni^{II}) and $NaClO_4$ in 2:1:2 molar ratio to form a neutral monomeric hexacoordinate complex of formula $[M(MBPT)_2(H_2O)_2](ClO_4)_2\cdot nH_2O$ ($M = Co^{II}$, $n = 4$; $M = Ni^{II}$, $n = 0$) which is stable in air. The elemental analysis is satisfactory and indicates that the complex contains one metal atom, two MBPT ligands, and six or two water molecules for complex **1** or **2**. The ligand MBPT does not seem to have any binucleating tendency towards cobalt and nickel [15].

3.1.1. Description of the structure of MBPT

For ligand MBPT the molecular structure with the atom-numbering scheme is shown in Fig. 1 and selected bond lengths and bond angles are listed in Table 2. Bond lengths and angles in the structure are comparable with those reported for related structures [12–14]. The substituted pyridyl groups and the phenyl ring lie in a propeller arrangement around the central 1,2,4-triazole ring. The dihedral angle between the phenyl and triazole rings is 53.9(3)°. The two pyridyl rings form dihedral angles of 32.0(3) and 48.0(3)° with the triazole ring.

3.1.2. Description of the structure of complex 1

The crystal structure of **1** consists of $[Co(MBPT)_2(H_2O)_2]^+$ cations, two ClO_4^- anions, and four lattice water molecules, held together by hydrogen bridges. This is consistent with the elemental analysis results. There is an inversion centre at the centre of the cation. A projection of the structure is presented in Fig. 2, together with the atomic labelling system; lattice water molecules O(2w) and O(3w) are omitted for clarity. Relevant interatomic distances and angles are given in Table 3.

Table 1
Crystallographic data for the compounds MBPT, **1** and **2**

Compound	MBPT	**1**	**2**
Empirical formula	$C_{19}H_{15}N_5$	$C_{38}H_{42}Cl_2CoN_{10}O_{14}$	$C_{38}H_{34}Cl_2NiN_{10}O_{10}$
M_r	313.36	992.65	920.36
Crystal size (mm)	$0.24\times0.14\times0.12$	$0.36\times0.26\times0.18$	$0.22\times0.16\times0.12$
Crystal color, shape	colorless, plate	light brown, slab	pale purple, slab
Crystal system	monoclinic	monoclinic	monoclinic
Space group	$P2_1/c$	$P2_1/c$	$P2_1/c$
a (Å)	11.0280(5)	9.1503(5)	9.8447(4)
b (Å)	18.5234(8)	15.4057(8)	14.8467(6)
c (Å)	8.5052(4)	16.3471(9)	14.5054(6)
β (°)	106.442(1)	95.177(1)	104.515(1)
V (Å^3)	1666.4(1)	2295.0(2)	2052.5(2)
Z	4	2	2
D_{calc} (Mg m^{-3})	1.249	1.436	1.489
$F(000)$	656	1026	948
Absorption coefficient (mm^{-1})	0.078	0.565	0.673
θ Range (°)	1.93–28.38	2.79–28.38	2.00–25.00
$h/k/l$	$-14,14/-24,24/-11,10$	$-12,10/-20,20/-19,21$	$-6,11/-17,17/-17,17$
Reflections collected	11 110	16 018	10 886
Independent reflections	4110 ($R_{int}=0.0586$)	5664 ($R_{int}=0.0988$)	3607 ($R_{int}=0.0514$)
Data/restraints/parameters	4110/0/218	5664/2/340	3607/20/268
Goodness-of-fit on F^2	1.009	0.961	1.045
R, wR indices ($I>2\sigma(I)$)	0.0592, 0.1170	0.0731, 0.1491	0.0703, 0.1733
R, wR indices (all data)	0.1392, 0.1472	0.1708, 0.1860	0.1082, 0.1990
Largest peak and hole (e Å^{-3})	0.197, −0.142	0.346, −0.863	0.775, −0.619

The cobalt atom is surrounded by four nitrogen atoms from two MBPT ligands in the equatorial plane and two oxygen atoms from two water molecules in the axial positions to form a distorted octahedral geometry. The MBPT ligand coordinates to cobalt atom via N(1) atom of a pyridyl ring and N(2) atom of the triazole moiety leaving N(4) atom of another pyridyl ring and N(3) atom of the triazole moiety uncoordinated, which is similar to the coordination mode in complex $[Ag(MBPT)(PPh_3)_2]ClO_4$ [16] and of the reported ligand (ABPT) in the mononuclear compounds [18–22]. The Co–N and Co–O distances are within the range observed for octahedral complex [23]. It is, however, noticeable that the Co–N bond to the triazole nitrogen is 0.051 Å shorter than that to the pyridyl nitrogen. This feature can be compared with those observed for the ABPT complexes [18–22]. The ligand MBPT is non-planar. The pyridyl ring of which the nitrogen is involved in coordination makes an angle of 5.6(5)° with the triazole ring, whereas the non-coordinating pyridyl ring makes 39.4(6)° with respect to the triazole plane. The same feature has been found in other mononuclear ABPT compounds. In the present compounds, however, the coordinating or non-coordinating pyridyl ring and the triazole ring are somewhat less or more twisted than those [dihedral angle: 17.0(1) or 25.2(2)°, respectively] observed for the $[Ag(MBPT)(PPh_3)_2]ClO_4$ complex [16]. On the other hand, in the free ligand MBPT, the two pyridyl rings form dihedral angles of 32.0(3) and 48.0(3)° with the triazole ring (vide ante). It appears that on complexation, a small triazole-pyridyl twist angle is required to bring the ligand in the favored conformation to obtain the coordination around the metal centre.

The packing of cations and anions in the unit cell is depicted in Fig. 3. The perchlorate ions are highly disordered (67:33) and are connected to the water ligands by O(1w)–H1B···O(1) hydrogen bridges [O(1w)···O(1) = 2.827(8) Å and O(1w)–H1B···O(1) = 168(4)°]. In addition, there are also three kinds of

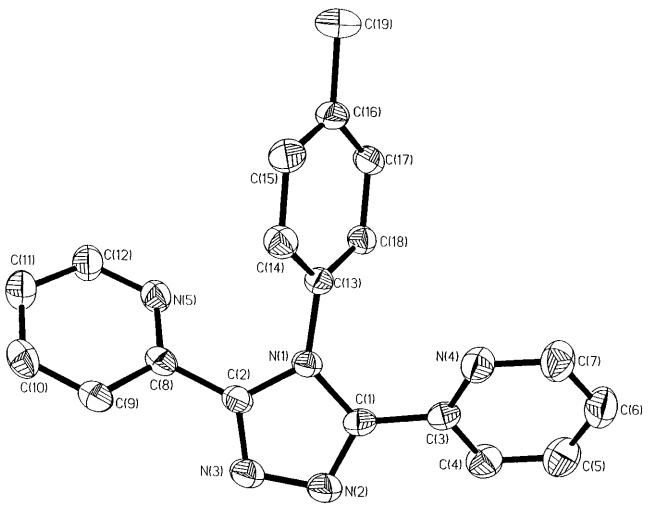


Fig. 1. The molecule of ligand MBPT with the atom-numbering scheme.

Table 2
Selected bond distances (Å) and angles (°) for MBPT

N(1)–C(1)	1.373(2)	N(3)–C(2)	1.311(3)
N(1)–C(2)	1.369(2)	N(4)–C(3)	1.335(3)
N(1)–C(13)	1.446(2)	N(4)–C(7)	1.331(3)
N(2)–C(1)	1.311(3)	N(5)–C(8)	1.339(3)
N(2)–N(3)	1.379(2)	N(5)–C(12)	1.334(3)
N(1)–C(1)–N(2)	110.3(2)	N(4)–C(3)–C(1)	117.3(2)
N(1)–C(2)–N(3)	110.3(2)	N(5)–C(8)–C(2)	117.0(2)

hydrogen bond interaction in the complex **1**: O(1w)–H1A···O(3w), O(3w)–H3A···O(2w), O(2w)–H2A···N(4). The distance of O(1w)···O(3w) is 2.625(5) Å [O(1w)–H1A···O(3w) = 160(3)°], which is shorter than those in ice [2.752(8) and 2.765(2) Å] [24]. It is clear that there is very strong hydrogen bonding between O(1) of coordinated water molecule and the lattice water molecules O(3). Moreover, O(3) interacts with another lattice water molecule, O(2), with an O···O distance of 2.810(7) Å [O(3w)–H3A···O(2w) = 132°]. Furthermore, O(2) is involved in hydrogen bonding with N(4) of the non-coordinating pyridyl group [O(2w)···N(4) = 3.264(6) Å and O(2w)–H2A···N(4) = 138.1(3)°].

3.1.3. Description of the structure of complex **2**

The structure of complex **2** is similar to that of **1** but does not contain lattice water molecules. The bond lengths and angles in the structure are in the normal range [15]. The Ni–N bond to the triazole nitrogen is 0.065 Å shorter than that to the pyridyl nitrogen. The dihedral angle between the coordinating or non-coordinating pyridyl ring and the triazole ring is 2.5(3) or 25.5(3)°, respectively. The pyridine rings are oriented at an angle of 26.2(3)° with each other. The perchlorate ion is highly disorder (56:44) and is involved in intramolecular O–H···O [O(1w)···O(2A) = 2.87(1) Å; O(1w)–H1A···O(2A) = 157°] hydrogen bonding and intermolecular C–H···O [C(18)···O(1A) = 3.43(2) Å; C(18)–H(18A)···O(1A) = 163°] hydrogen bonding thereby participating in the packing.

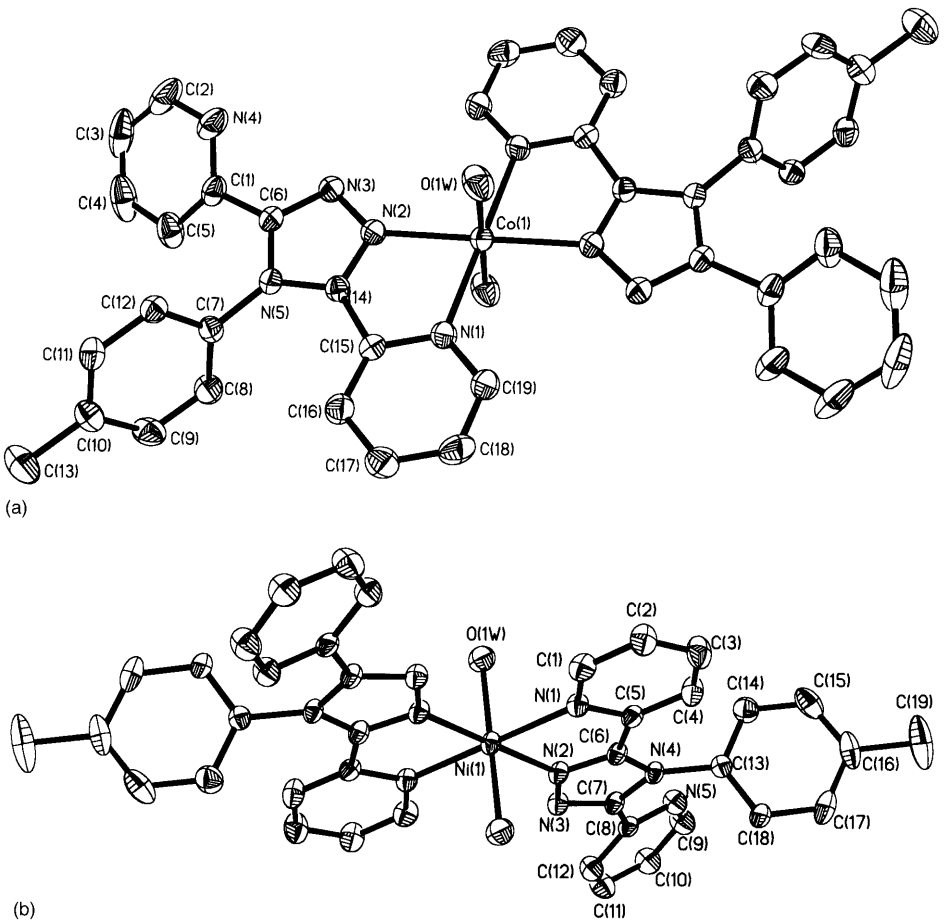


Fig. 2. Projection of the structure of $[M(MBPT)_2(H_2O)_2](ClO_4)_2 \cdot nH_2O$ with the atomic labelling system. Lattice water molecules, anions and hydrogen atoms are omitted for clarity. (a) $M = Co^{II}$, $n = 4$ for **1**; (b) $M = Ni^{II}$, $n = 0$ for **2**.

Table 3
Selected bond distances (Å) and angles (°) for the complex **1** and **2** [a]

1		**2**	
Co(1)–O(1w)	2.072(3)	Ni(1)–O(1w)	2.108(4)
Co(1)–N(2)	2.101(3)	Ni(1)–N(2)	2.052(4)
Co(1)–N(1)	2.152(3)	Ni(1)–N(1)	2.117(4)
O(1w)–Co(1)–N(2)	90.95(13)	O(1w)–Ni(1)–N(2)	89.44(17)
O(1wA)–Co(1)–N(2)	89.05(13)	O(1wA)–Ni(1)–N(2)	90.56(17)
O(1w)–Co(1)–N(1)	89.30(13)	O(1w)–Ni(1)–N(1)	88.86(17)
O(1wA)–Co(1)–N(1)	90.70(13)	O(1wA)–Ni(1)–N(1)	91.14(17)
N(2)–Co(1)–N(1A)	103.61(12)	N(2)–Ni(1)–N(1A)	101.87(16)
N(2)–Co(1)–N(1)	76.39(12)	N(2)–Ni(1)–N(1)	78.13(16)
Hydrogen bonding			
O(1w)···O(3w)[a]	2.626(5)	O(1w)···O(2A)	2.87(1)
O(3w)···O(2w)	2.810(7)	C(18)···O(1A)[c]	3.43(2)
O(2w)···N(4)	3.264(6)		
O(1w)···O(1)[b]	2.827(8)		

[a] Symmetry code: a: $-x$, $1/2+y$, $1/2-z$; b: $1-x$, $1-y$, $-z$; c: $-x$, $-y$, $-z$.

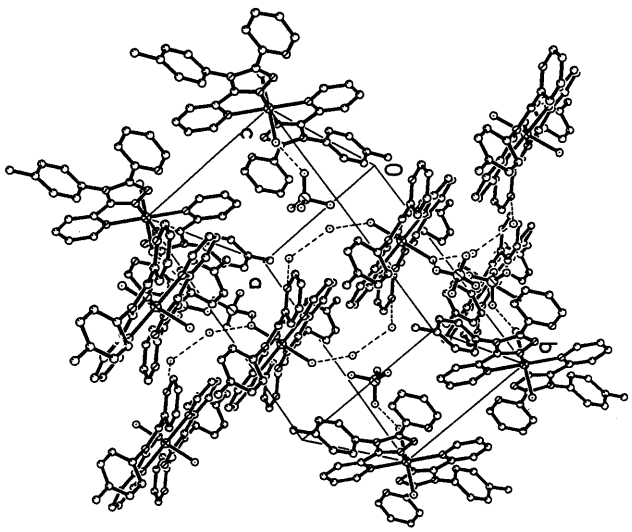


Fig. 3. The unit-cell packing of $[Co(MBPT)_2(H_2O)_2](ClO_4)_2{\cdot}4H_2O$.

3.2. Spectral characterization

In the IR spectrum of the complex **1** (or **2**), there are several broad, medium bands around 3454 (or 3423), 3250 (or 3279), 3191 (or 3110) and 3072 (or 3075) cm^{-1}, mainly attributed to H–O–H stretching vibrations, suggesting the existence of hydrogen bonding interactions [25]. This is in agreement with the results of X-ray analysis. The bands due to the ionic perchlorate groups are around 1099 (or 1098)(s), 929 (or 930)(w), 626 (or 625) cm^{-1}(s), which can be assigned as the IR-allowed ν_3 mode, IR-forbidden ν_1 mode and the nondegenerate ClO_3 symmetrical bending frequency, ν_3, respectively [26]. The IR spectrum of the complexes can also be closely related to that of free MBPT. One of the most diagnostic changes occurs in the region between 1610 and 1560 cm^{-1}. The spectrum of free MBPT shows a strong band at 1584.8 cm^{-1} and a medium band at 1568.3 cm^{-1}, attributable to the pyridine ring vibrations. Upon pyridine coordination to a metal the higher band is shifted by about +15 wavenumbers [27]. So in the spectrum of the complex **1** (or **2**), a band at 1606.6 (or 1608.9) cm^{-1}(s) and two bands at 1591 (or 1587.9)(m) and 1572.7 (or 1572.7) cm^{-1}(w) can be assigned to one coordinated and one uncoordinated pyridine ring, respectively. This means that in this 2:1 complex, each MBPT ligand uses one pyridine nitrogen and one triazole nitrogen for chelate binding, as was confirmed by the structure determination.

In the UV–Vis spectrum of the complex **1** (or **2**) in methanol solution, two intense bands at 259 (or 247) and 284 (or 293.5) nm are attributed to the MBPT $\pi-\pi^*$ and $n-\pi^*$ transitions in contrast to those (243.5 and 275 nm) in the free MBPT–methanol solution. Three bands at 531.5, 667.5 and 1133.9 nm corresponding to d–d transitions, are observed for complex **1**, whereas only a band at 532.5 nm for complex **2**.

The structures of the complex **1** and **2** in solution were also studied by electrospray ionization mass spectrometry (ESIMS) [28–30]. Fig. 4(a) displays the positive ESI mass spectrum of the complex **1** in methanol solution. Four main peaks were observed. The peak at m/z 783.9 is $[Co(MBPT)_2(ClO_4)]^{1+}$ ion and that at m/z 499.1 is $[Co(MBPT)_3]^{1+}$. The peak at m/z 358.1 is

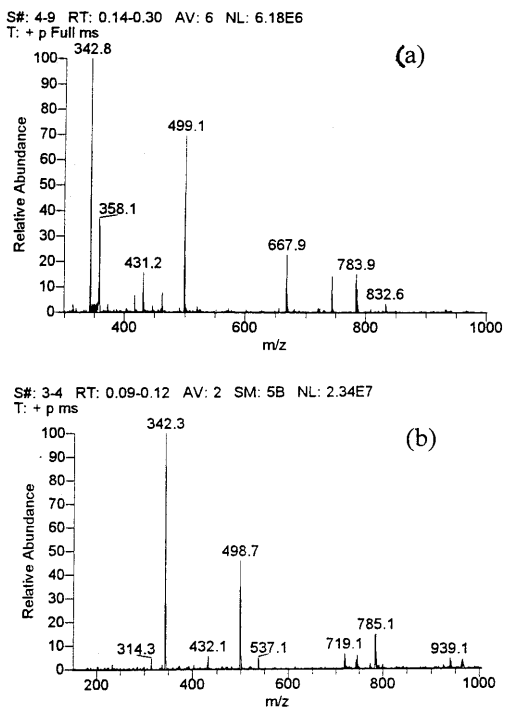


Fig. 4. Positive ion ESI mass spectrum of $[M(MBPT)_2(H_2O)_2](ClO_4)_2{\cdot}nH_2O$. (a) $M = Co^{II}$, $n = 4$ for **1**; (b) $M = Ni^{II}$, $n = 0$ for **2**.

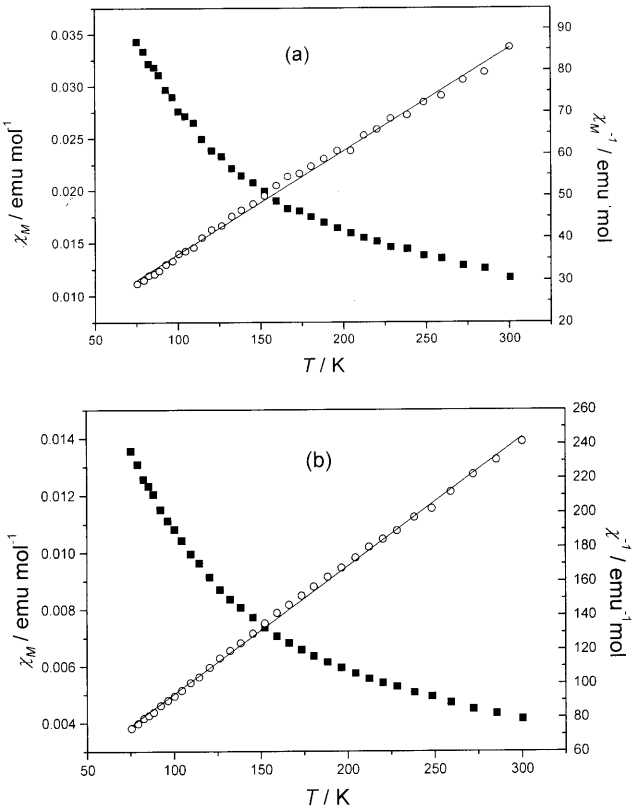


Fig. 5. The magnetic behavior of the complexes: χ_M () and χ_M^{-1} (○) vs. T plot. (a) For **1** and (b) for **2**.

probably due to $[Co(MBPT)_2(CH_3OH)]^{1+}$, which is one $[Co(MBPT)_2]$ structure unit containing a solvent molecule in it. The base peak at m/z 342.8 is $[Co(MBPT)_2]^{1+}$. Compared to that of $Co(bpy)_3(ClO_4)_3$ [29], the spectrum of the complex **1** in solution showed no sign of the presence of Co(III) complex. It clearly indicates that there is no chemical reduction/oxidation reaction in the solution and that the complex **1** is also stable in methanol solution. Fig. 4(b) displays the positive ESI mass spectrum of the complex **2** in methanol solution. Four main peaks were also observed. The peak at m/z 785.1 is $[Ni(MBPT)_2(ClO_4)]^{1+}$ ion and that at m/z 498.7 is $[Ni(MBPT)_3]^{1+}$. The base peak at m/z 342.3 is $[Ni(MBPT)_2]^{1+}$ and the peak at m/z 314.3 is $(MBPT+1)^{1+}$.

3.3. Magnetic properties

The temperature variation of the magnetic susceptibility in the form of χ_M and χ_M^{-1} versus T is shown in Fig. 5(a) and (b) for **1** and for **2**, respectively. The effective magnetic moments per molecule unit at 75–300 K range are 4.54–5.30 for **1** and 2.86–3.15 for **2**, respectively, which are in the normal range observed for a octahedral high-spin mononuclear Co(II) complex (μ_{eff} = 4.3–5.2 BM) and for a Ni(II) complex (μ_{eff} = 2.9–3.3 BM) [31]. However, the μ_{eff} values are slightly larger than the spin-only moments of 3.88 BM for **1** and of 2.83 BM for **2**. Over the whole temperature range (75–300 K), the magnetic behaviors of **1** and **2** can be interpreted by Curie–Weiss law with Curie values and Weiss constants of 4.07(5) and −47(2) for **1** and of 1.33(1) and −25(1) for **2**, respectively. The negative Weiss constants of **1** and **2** are expected for the zero-field splitting behaviors in lower temperature domain.

4. Supplementary data

Crystallographic data have been deposited with the Cambridge Crystallographic Data Centre, CCDC Nos. 137157,137158 and 137159. Copies of this information are available free of charge from The Director, CCDC, 12 Union Road, Cambridge, CB2 1EZ, UK (fax: +44-1223-336033; e-mail: deposit@ccdc.cam.ac.uk or www: http://www.ccdc.cam.ac.uk).

Acknowledgements

This work was financially supported by the State Key Project of Fundamental Research and the National Natural Science Foundation of China and the Nanjing University Talent Development Foundation. The authors would like to thank the Malaysian Government and Universiti Sains Malaysia for research grant R&D No. 305/pfizik/622004. SSSR thanks the Universiti Sains Malaysia for a Visiting Post-Doctoral Fellowship.

References

[1] P.J. van Koningsbruggen, J.G. Haasnoot, H. Kooijman, J. Reedijk, A.L. Spek, Inorg. Chem. 36 (1997) 2487.
[2] L. Antolini, A.C. Fabretti, D. Gatteschi, A. Giusti, R. Sessoli, Inorg. Chem. 29 (1990) 143.
[3] A. Bencini, D. Gatteschi, C. Zanchini, J.G. Haasnoot, R. Prins, J. Reedijk, J. Am. Chem. Soc. 109 (1987) 2926.
[4] L. Antolini, A.C. Fabretti, D. Gatteschi, A. Giusti, R. Sessoli, Inorg. Chem. 30 (1991) 4858.
[5] P.J. van Koningsbruggen, D. Gatteschi, R.A.G. de Graaff, J.G. Haasnoot, J. Reedijk, C. Zanchini, Inorg. Chem. 34 (1995) 5175.
[6] L.G. Lavrenova, N.G. Yudina, V.N. Ikorskii, V.A. Varnek, I.M. Oglezneva, S.V. Larionov, Polyhedron 14 (1995) 1333.
[7] N. Moliner, M.C. Munoz, P.J. van Koningsbruggen, J.A. Real, Inorg. Chim. Acta 274 (1998) 1.
[8] Y. Garcia, P.J. van Koningsbruggen, G. Bravic, P. Guionneau, D. Chasseau, G.L. Cascarano, J. Moscovici, K. Lambert, A. Michalowicz, O. Kahn, Inorg. Chem. 36 (1997) 6357.
[9] P.J. van Koningsbruggen, Y. Garcia, E. Codjovi, R. Lapouyade, L. Fournes, O. Kahn, L. Rabardel, J. Mater. Chem. 7 (1997) 2069.
[10] Y. Garcia, P.J. van Koningsbruggen, E. Codjovi, R. Lapouyade, O. Kahn, L. Rabardel, J. Mater. Chem. 7 (1997) 857.
[11] O. Kahn, C.J. Martinez, Science 279 (1998) 44.
[12] Z.X. Wang, Z.P. Bai, J.X. Yang, K.I. Okamoto, X.Z. You, Acta Crystallogr., Sect. C 54 (1998) 438.

[13] W. Chen, Z.X. Wang, F.F. Jian, Z.P. Bai, X.Z. You, Acta Crystallogr., Sect. C 54 (1998) 851.
[14] H.K. Fun, K. Chinnakali, S.C. Shao, D.R. Zhu, X.Z. You, Acta Crystallogr., Sect. C 55 (1999) 770.
[15] F.S. Keij, R.A.G. de Graaff, J.G. Haasnoot, J. Reedijk, J. Chem. Soc., Dalton Trans. (1984) 2093.
[16] S.C. Shao, D.R. Zhu, X.H. Zhu, X.Z. You, S.S.S. Raj, H.K. Fun, Acta Crystallogr., Sect. C 55 (1999) 1412.
[17] G.M. Sheldrick, SHELXTL, Structure Determination Software Programs. Version 5.10. Bruker Analytical X-ray Systems Inc., Madison, Wisconsin, USA, 1997.
[18] C. Faulmann, P.J. van Koningsbruggen, R.A.G. de Graaff, J.G. Haasnoot, J. Reedijk, Acta Crystallogr., Sect. C 46 (1990) 2357.
[19] U. Hartmann, H. Vahrenkamp, Inorg. Chim. Acta 239 (1995) 13.
[20] J.P. Cornelissen, J.H. van Diemen, L.R. Groeneveld, J.G. Haasnoot, A.L. Spek, J. Reedijk, Inorg. Chem. 31 (1992) 198.
[21] P.J. Kunkeler, P.J. van Koningsbruggen, J.P. Cornelissen, A.N. van der Horst, A.M. van der Kraan, A.L. Spek, J.G. Haasnoot, J. Reedijk, J. Am. Chem. Soc. 118 (1996) 2190.
[22] P.J. van Koningsbruggen, K. Goubitz, J.G. Haasnoot, J. Reedijk, Inorg. Chim. Acta 268 (1998) 37.
[23] P.B. Viossat, N.H. Dung, J.C. Lancelot, M. Robba, Acta Crystallogr., Sect. C 40 (1984) 935.
[24] S.W. Peterson, H.A. Levy, Acta Crystallogr. 10 (1957) 70.
[25] K. Nakamoto, Infrared Spectra of Inorganic and Coordination Compounds, Wiley, New York, 1970, p. 166.
[26] B.J. Hathaway, A.A.G. Tomlinson, Coord. Chem. Rev. 5 (1970) 1.
[27] M.M. da Mota, J. Rodgers, S.M. Nelson, J. Chem. Soc. A (1969) 2036.
[28] V. Katta, S.K. Chowdhury, B.T. Chait, J. Am. Chem. Soc. 112 (1990) 5348.
[29] S.R. Wilson, A. Yasmin, Y. Wu, J. Org. Chem. 57 (1992) 6941.
[30] R. Arakama, T. Matuo, H. Ito, I. Katakuse, K. Nozaki, T. Ohno, M. Haga, Org. Mass Spectrom. 29 (1994) 289.
[31] R.L. Carlin, Magnetochemistry, Springer, Berlin, 1986.

PERGAMON

www.elsevier.nl/locate/poly

Polyhedron 19 (2000) 2027–2037

POLYHEDRON

Synthesis of two N'-2-pyridylmethyl and N'-2-hydroxypropyl derivatives of diethylenetriaminepentaacetic acid and the stabilities of their complexes with Ln^{3+}, Ca^{2+}, Cu^{2+} and Zn^{2+}

Tsann-Hwang Cheng [a], Yun-Ming Wang [a,*], Wei-Thung Lee [a], Gin-Chung Liu [b]

[a] *School of Chemistry, Kaohsiung Medical University, 100 Shih-Chuan 1st Road, Kaohsiung, Taiwan 807, People's Republic of China*
[b] *Department of Radiology, Kaohsiung Medical University, 100 Shih-Chuan 1st Road, Kaohsiung, Taiwan 807, People's Republic of China*

Received 7 March 2000; accepted 11 July 2000

Abstract

Two N'-2-pyridylmethyl and N'-2-hydroxypropyl derivatives of H_5dtpa (diethylene-N,N',N''-triamine-N,N,N',N'',N''-pentaacetic acid), $H_4L^1 = N'$-(2-pyridylmethyl)-$N,N,N''N''$-diethylenetriaminetetraacetic acid and $H_4L^2 = N'$-(2-hydroxypropyl)-$N,N,N''N''$diethylenetriaminetetraacetic acid were synthesized. Their protonation constants were determined by potentiometric titration in 0.10 mol dm^{-3} Me_4NNO_3 and by NMR pH titration at 25.0 ± 0.1°C. Stability and selectivity constants were determined to evaluate the possibility of using the corresponding gadolinium(III) complexes as magnetic resonance imaging contrast agents. Low stability or selectivity constants indicate higher possibility for releasing free Gd^{3+} ion and free ligand as well from gadolinium(III) complexes. The formations of lanthanide(III), copper(II), zinc(II) and calcium(II) complexes were investigated quantitatively by potentiometry. The stability constants of lanthanides(III) complexes with H_4L^1 and H_4L^2 increase from La(III) to Nd(III) and then plateau at Sm(III) and Gd(III), before increasing again to Yb(III). The stability constant of the gadolinium(III) complex is larger than those of Ca(II), Zn(II) and Cu(II) complexes for these two ligands. The selectivity constants and modified selectivity constants of H_4L^1 and H_4L^2 for Gd^{3+} over endogenously available metal ions were calculated. Effectiveness of these two ligands in binding divalent and trivalent metal ions in biological media is assessed by comparing pM values at physiological pH 7.4. Spin-lattice relaxivity R_1 for the Gd(III) complex was also determined. The observed relaxivity values of $[GdL^1]^-$ and $[GdL^2]^-$ became invariant with respect to pH changes over the range of 2–10 and 3–10, respectively. ^{17}O NMR shifts showed that the $[DyL^1]^-$ and $[DyL^2]^-$ complexes have 1.50 and 2.51 inner-sphere water molecules, respectively. Water proton spin-lattice relaxation rates for the $[GdL^1]^-$ and $[GdL^2]^-$ complexes were also consistent with inner-sphere gadolinium(III) coordination. © 2000 Elsevier Science Ltd. All rights reserved.

Keywords: N'-2-Pyridylmethyl derivatives; N'-2-Hydroxypropyl derivatives; Stability constant

1. Introduction

Synthesis and characterization of new gadolinium-(III) complexes of poly(aminocarboxylates) ligands, as contrast agents, by magnetic resonance imaging (MRI) have been of great interest in recent years. Among paramagnetic contrast agents, stable water-soluble gadolinium(III) chelates have the ideal properties of high water relaxivity, chemical stability, and low toxicity in vivo. At present, the octachelating ligands, (carboxymethyl)iminobis(ethylenenitrilo) tetraacetic acid (H_5dtpa), N,N''-di(methylcarbamoylmethyl) diethylenetrinitrilo-N,N',N''-triacetic acid (H_3dmdtta), 10-(2-hydroxypropyl)-1,4,7,10-tetraazacyclododecane-1,4,7-triacetic acid (H_3hpdotra), 1,4,7,10-tetraazacyclododecane-$N,N',N''N'''$-tetraacetic acid (H_4dota), ethoxybenzyltriaminepentaacetic acid (H_5eob-dtpa), and benzyloxyproponic tetraacetic acid) (H_5bopta) are effective MRI contrast agents when complexed with a trivalent gadolinium ion [1–3]. These gadolinium(III) chelates possess sufficient paramagnetism and high stability. The toxic effect of uncomplexed Gd^{3+} and free pro-ligand, arising from dissociation of the metal complex, is one of the major concerns in MRI [4,5]. The

* Corresponding author. Tel.: +886-7-312-1101; fax: +886-7-312-5339.
E-mail address: m825010@cc.kmu.edu.tw (Y.-M. Wang).

0277-5387/00/$ - see front matter © 2000 Elsevier Science Ltd. All rights reserved.
PII: S0277-5387(00)00502-7

acute toxicity of gadolinium(III) complexes of poly(aminocarboxylates) correlates well with the selectivity of the latter for Gd^{3+}. The release of Gd^{3+} is related to the stability constants of the gadolinium(III) chelates [6,7]. The characterization of the complex of gadolinium(III) with bis(amide) derivatives of H_5dtpa had been investigated in a series of our studies [8–11]. In the continuing search for gadolinium(III) chelates for MRI, we have modified the carboxylate group by introducing *N*′-2-pyridylmethyl and *N*′-2-hydroxypropyl, and explored both the protonation constants of the ligands and the stability constants of the metal complexes. This report describes the synthesis of two *N*′-2-pyridylmethyl and *N*′-2-hydroxypropyl derivatives of H_5dtpa (Scheme 1). Their protonation constants, thermodynamic and conditional stability constants of complexes with lanthanides(III), Cu^{2+}, Zn^{2+}, and Ca^{2+} and their selectivity for Gd^{3+} over endogenously available metal ions are discussed. ^{17}O NMR shifts of the $[DyL^1]^-$ and $[DyL^2]^-$ complexes and water proton spin-lattice relaxivity, R_1, of the $[GdL^1]^-$ and $[GdL^2]^-$ are also discussed in this paper.

2. Experimental

2.1. Materials

Gadolinium chloride (> 99.9%) was obtained from Aldrich Chemical Co. and oven dried at 110°C for at least 24 h before use. All other reagents used for the synthesis of the ligands were purchased from commercial sources unless otherwise noted. Proton NMR spectra and elemental analyses were used to confirm the composition of the products.

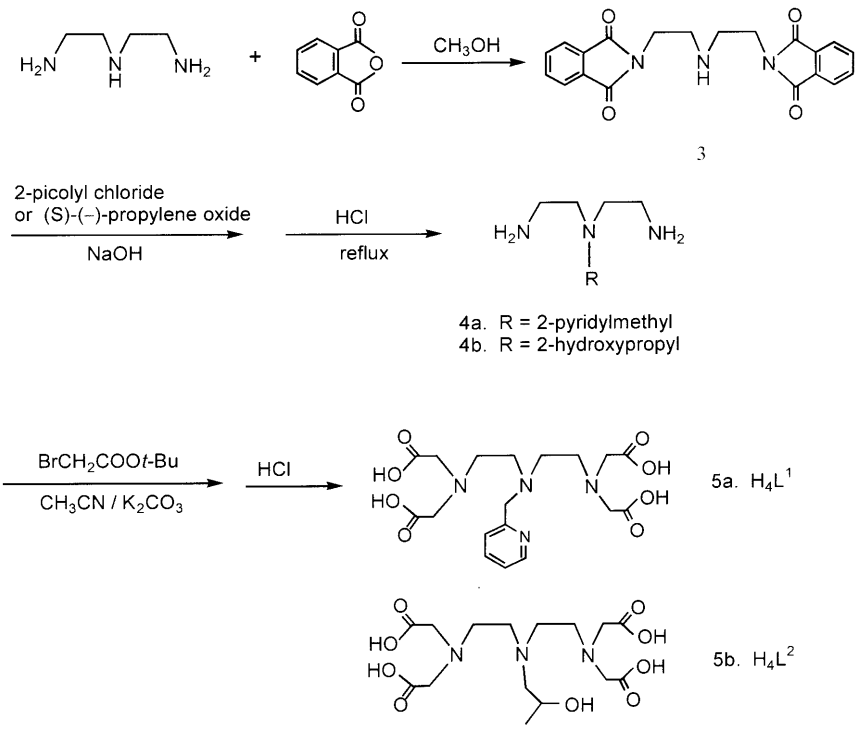
2.2. Preparations

2.2.1. Synthesis of *N*,*N*-bis(phthalimide)diethylenetriamine (**3**)

To a 500 cm^3 two-necked round-bottom flask diethylenetriamine (27.164 g, 263.30 mmol) and CH_3OH (250 cm^3) were added. The solution was heated to 60°C in an oil bath and phathalic anhydride (65.15 g, 439.85 mmol) was added. The reaction mixture became slurry within 20 min, and the mixture was stirred for 4 h. The pare yellow slurry was filtered of onto a Büchner funnel, washed with acetone (4×50 cm^3) and with MeOH (4×50 cm^3), and then vacuum dried to give 50.04 g (52.3%) of a white solid, m.p.: 181.0–181.3°C. *Anal.* Calc for $C_{20}H_{17}N_3O_4$ ($f_w = 363.37$): C, 66.12; H, 4.72; N, 11.56. *Anal.* Found: C, 66.17; H, 4.75; N, 11.37. ^1H NMR ($CDCl_3$), δ(ppm): 7.69 (m, 8H, ArH), 3.76 (t, 4H, backbone), 2.95 (t, 4H, backbone).

2.2.2. Synthesis of *N*′-(2-pyridylmethyl)diethylenetriamine (**4a**)

N,*N*-Bis(phthalimide)diethylenetriamine (**3**) (5.0 g, 13.76 mmol) was suspended in 50 cm^3 of water, with stirring, and the pH was adjusted to between 11.5 and



Scheme 1.

12.0 by addition of NaOH (2.0 mol dm^{-3}). The reaction mixture was kept at room temperature and 2-picolyl chloride (2.26 g, 13.76 mmol) was added. Then the mixture was stirred for 15 h. The mixture was evaporated by rotary evaporation to give a dark red oil, and then 6 N HCl (100 cm^3) was added and heated at reflux for 24 h to remove the protection group. The crude product was purified on an AG 50W × 8 cation exchange resin column (200–400 mesh, H^+ form, 100 cm^3 of resin, 4.2 cm column diameter). The column was eluted consecutively with 500 cm^3 of water, 250 cm^3 of 0.5 mol dm^{-3} HCl, 250 cm^3 of 1.0 mol dm^{-3} HCl, 250 cm^3 of 1.5 mol dm^{-3} HCl, 250 cm^3 of 2.0 mol dm^{-3} HCl, 250 cm^3 of 2.5 mol dm^{-3} HCl, 250 cm^3 of 3.0 mol dm^{-3} HCl and 250 cm^3 of 3.5 mol dm^{-3} HCl. The product was eluted with the 3.5 mol dm^{-3} HCl fractions, while the earlier fractions contained inorganic salts (NaCl) and impurities. All fractions containing the product were evaporated to dryness by rotary evaporation and coevaporated three times with 150 cm^3 of water to remove the excess HCl. After vacuum drying, 1.58 g (38.7%) of pure **4a** ·3HCl was obtained as a dark yellow hygroscopic powder. ^{1}H NMR (D_2O), δ(ppm): 8.64, 8.45, 7.92, 7.88 (m, 5H, pyH), 4.19 (s, 2H, N–CH_2-py), 3.20 (t, 4H, backbone), 2.98 (t, 4H, backbone).

2.2.3. Synthesis of N′-(2-pyridylmethyl)-N,N,N″N″-diethylenetriaminetetraacetic acid (*5a*, H_4L^1)

To a solution of **4a** (1.58 g, 5.5 mmol) and potassium carbonate (10 g, 72.35 mmol) in CH_3CN (150 cm^3), *tert*-butylbromoacetate (4.38 g, 22.45 mmol) was added. The reaction mixture was heated at reflux for 36 h. The potassium carbonate was removed by filtering the reaction mixture through a Büchner funnel and was washed with CH_3CN (20 cm^3). The filtrate was evaporated to dryness by rotary evaporation. To the residue H_2O was added and extracted with chloroform (3 × 50 cm^3). The chloroform phase was evaporated under reduced pressure, and 2 mol dm^{-3} HCl (50 cm^3) added. The solution was stirred for 6 h at ambient temperature, stripped to dryness, and the acid treatment repeated three times (until ^{1}H NMR showed complete removal of the *tert*-butyl group). The residue was dissolved in 50 cm^3 of distilled water, and the solution was loaded onto an AG 50W × 8 cation exchange resin column (200–400 mesh, H^+ form, 100 cm^3 of resin, 4.2 cm column diameter). The column was eluted consecutively with 500 cm^3 of water, 250 cm^3 of 0.5 mol dm^{-3} HCl, 250 cm^3 of 1.0 mol dm^{-3} HCl, 250 cm^3 of 1.5 mol dm^{-3} HCl, 250 cm^3 of 2.0 mol dm^{-3} HCl, 250 cm^3 of 2.5 mol dm^{-3} HCl and 500 cm^3 of 3.0 mol dm^{-3} HCl. The product was eluted with the 3.0 mol dm^{-3} HCl fractions. All fractions containing the product were evaporated to dryness by rotary evaporation and coevaporated three times with 150 cm^3 of water to remove the excess HCl. The product was dissolved in 50 cm^3 of distilled water and alkalized with ammonia water to pH 11.0, and the solution applied to AG1 × 8 anion exchange resin column (200–400 mesh, HCO_2H form, 60 cm^3 of resin, 3.0 cm column diameter) and the product eluted with 500 cm^3 of water, 500 cm^3 of 0.1 mol dm^{-3} formic acid, 500 cm^3 of 0.2 mol dm^{-3} formic acid, 500 cm^3 of 0.3 mol dm^{-3} formic acid, 500 cm^3 of 0.4 mol dm^{-3} formic acid and 500 cm^3 of 0.5 mol dm^{-3} formic acid. The product was eluted with the 0.5 mol dm^{-3} formic acid to yield 1.76 g (47%) of a brown hygroscopic powder. ^{1}H NMR ($CDCl_3$), δ(ppm): 8.71, 8.52, 8.03, 7.94 (m, 5H, pyH), 4.12 (s, 2H, N–CH_2-py), 3.81 (s, 8H, –CH_2–COOH), 3.44 (t, 4H, backbone), 3.00 (t, 4H, backbone).

2.2.4. Synthesis of N′-(2-hydroxypropyl)diethylenetriamine (*4b*)

N,*N*-Bis(phthalimide)diethylenetriamine (**3**) (4.72 g, 12.99 mmol) was suspended in 25 cm^3 of water, with stirring, and the pH was adjusted to between 11.5 and 12.0 by addition of NaOH (2.0 mol dm^{-3}). The reaction mixture was cooled to 2–5°C, and 1.0 cm^3 (0.86 g, 14.81 mmol, 14% excess) of (S)-(−)-propylene oxide was added. The reaction mixture was stirred for 12 h at room temperature. The mixture was evaporated by rotary evaporation to give a pale yellow oil, and then 6 mol dm^{-3} HCl (100 cm^3) was added and heated at reflux for 24 h to remove the protection group. The crude product was purified on an AG 50W × 8 cation exchange resin column (200–400 mesh, H^+ form, 100 cm^3 of resin, 4.2 cm column diameter). The column was eluted consecutively with 500 cm^3 of water, 500 cm^3 of 0.5 mol dm^{-3} HCl, 500 cm^3 of 1.0 mol dm^{-3} HCl, 500 cm^3 of 1.5 mol dm^{-3} HCl, 500 cm^3 of 2.0 mol dm^{-3} HCl, 500 cm^3 of 2.5 mol dm^{-3} HCl and 500 cm^3 of 3.0 mol dm^{-3} HCl. The product was eluted with the 2.5 mol dm^{-3} and 3.0 mol dm^{-3} HCl fractions. All fractions containing the product were evaporated to dryness by rotary evaporation and coevaporated three times with 150 cm^3 of water to remove the excess HCl. After vacuum drying, 1.58 g (45%) of pure **4b** ·3HCl was obtained as a white hygroscopic powder. ^{1}H NMR (D_2O), δ(ppm): 4.09 (m, 1H, –CH–OH), 3.37 (m, 8H, backbone), 3.08 (m, 2H, N–CH_2–CH(OH)–), 1.17 (d, 3H, –CH(OH)–CH_3).

2.2.5. Synthesis of N′-(2-hydroxypropyl)-N,N,N″N″-diethylenetriaminetetraacetic acid (*5b*, H_4L^2)

To a solution of **4b** (1.58 g, 5.84 mmol) and potassium carbonate (10 g, 72.35 mmol) in CH_3CN (150 cm^3), *tert*-butylbromoacetate (4.67 g, 23.94 mmol) was added. The reaction mixture was heated at reflux for 36 h. The potassium carbonate was removed by filtering the reaction mixture through a Büchner funnel and was washed with CH_3CN (20 cm^3). The filtrate was evapo-

rated to dryness by rotary evaporation. To the residue H_2O was added and extracted with chloroform (3×50 cm^3). The chloroform phase was evaporated under reduced pressure, and 2 mol dm^{-3} HCl (50 cm^3) added. The solution was stirred for 6 h at ambient temperature, stripped to dryness, and the acid treatment repeated three times (until ^1H NMR showed complete removal of the *tert*-butyl group). The residue was dissolved in 60 cm^3 of distilled water, and the solution was loaded onto an AG $50W \times 8$ cation exchange resin column (200–400 mesh, H^+ form, 100 cm^3 of resin, 4.2 cm column diameter). The column was eluted consecutively with 500 cm^3 of water, 500 cm^3 of 0.5 mol dm^{-3} HCl, 500 cm^3 of 1.0 mol dm^{-3} HCl, 500 cm^3 of 1.5 mol dm^{-3} HCl, 500 cm^3 of 2.0 mol dm^{-3} HCl and 500 cm^3 of 2.5 mol dm^{-3} HCl. The product was eluted with the 2.5 mol dm^{-3} HCl fractions. All fractions containing the product were evaporated to dryness by rotary evaporation and coevaporated three times with 150 cm^3 of water to remove the excess HCl. The product was dissolved in 50 cm^3 of distilled water and made alkaline with ammonia water to pH 11.0. Finally, the solution was applied to an AG 1×8 anion exchange resin column (200–400 mesh, HCO_2H form, 60 cm^3 of resin, 3.0 cm column diameter) and eluted with 500 cm^3 of water, 500 cm^3 of 0.1 mol dm^{-3} formic acid, 500 cm^3 of 0.2 mol dm^{-3} formic acid, 500 cm^3 of 0.3 mol dm^{-3} formic acid, 500 cm^3 of 0.4 mol dm^{-3} formic acid, 500 cm^3 of 0.5 mol dm^{-3} formic acid and 500 cm^3 of 0.6 mol dm^{-3} formic acid. The product was eluted with the 0.6 mol dm^{-3} formic acid to yield 1.9 g (74.2%) of a white hygroscopic free acid. *Anal.* Calc for $C_{15}H_{27}N_3O_9 \cdot 2.5\ H_2O$ ($f_w = 438.41$): C, 41.09; H, 7.36; N, 9.59. *Anal.* Found: C, 41.05; H, 7.44; N, 9.63. ^1H NMR (D_2O, pD 3.63), δ(ppm): 3.92 (m, 1H, –CH–OH), 3.79 (s, 8H, $–CH_2–COOH$), 3.41 (t, 4H, backbone), 3.09 (m, 4H, backbone), 2.68 (m, 2H, $N–CH_2–CH(OH)–$), (d, 3H, $–CH(OH)–CH_3$).

2.3. NMR experiments

Solutions of ligand (15 mmol dm^{-3}) for NMR pH titration were made up in D_2O, and p*D* was adjusted with DCl or CO_2-free NaOD. Proton NMR spectra were measured in D_2O solution on Varian Unity Plus 400 and XL-200E spectrometers. The final p*D* values of the ligand solutions were determined with a microelectrode. The final p*D* was obtained from the equation $pD = pH + 0.40$ [12]. The hydrogen electrode used in the present study allows a reliable and accurate determination of the proton activity over an extended pH range.

The ^{17}O NMR spectra were recorded by a Varian Gemini 300 spectrometer at 25°C. The induced ^{17}O shift (d.i.s.) measurements were determined with respect to D_2O as external standard. The hydration number of $[DyL^1]^-$ and $[DyL^2]^-$ was determined by the method of Alpoim et al. [13]. An equimolar solution of Dy^{3+} and ligand was prepared, and a stoichiometric amount of standardized NaOH was added so that the complex was fully formed. Six solutions of differing dysprosium concentrations were prepared by serial dilution of the stock solution.

2.4. Solution preparations

Stock solutions of trivalent lanthanides, Ca^{2+}, Zn^{2+} and Cu^{2+} were prepared between 0.010 and 0.025 mol dm^{-3} from nitrate salts with demineralized water (obtained by a Millipore/Milli-Q system) and standardized by titration with Na_2edta (disodium salt of ethylenedinitrilotetraacetic acid) or atomic absorption spectrophotometry. A stock solution was prepared by dissolving reagent grade Na_2edta (4.65 g) and diluting it to 250 cm^3 with demineralized water. This was used as a titrant to standardize the solution of lanthanides(III) and Ca^{2+}. Stock lanthanide(III) complex solutions (henceforth identified as LnL and having a concentration range of 1.5–0.5 mmol dm^{-3}) were prepared by mixing equimolar amounts of stock solution of lanthanides(III) and ligand. A slight excess (2%) of ligand was used to ensure total complexation of lanthanides(III).

2.5. Potentiometric measurements

Potentiometric titrations were performed with an automatic titrator system to determine the protonation constants of the H_4L^1 and H_4L^2, and the stability constants of the metal complexes. The autotitrating system consists of a 702 SM Titroprocessor, a 728 stirrer and a PT-100 combination pH electrode (Metrohm). The pH electrode was calibrated using two standard buffer solutions and all calibrations and titrations were carried out under a CO_2-free nitrogen atmosphere, to avoid any contact with carbon dioxide in a sealed glass vessel (20 cm^3) thermostatted at 25.0 ± 0.1°C, and an ionic strength of 0.10 mol dm^{-3} Me_4NNO_3. The concentrations of the metal–ion and ligand solutions were maintained between 2.0 and 1.0 mmol dm^{-3}. A CO_2-free 0.100 mol dm^{-3} NaOH solution was used as the titrant to minimize ionic strength change during the titration. The purity of the ligand was also confirmed by potentiometric titration with standard NaOH. Oxygen and carbon dioxide were excluded from the reaction mixtures by maintaining a positive pressure of purified nitrogen in the titration cell. Each titration was performed at least three times. Since the lanthanides(III) chelate is completely or almost completely formed at low pH, their stability constant could not be determined from the normal potentiometric titration method. Therefore, these stabil-

Table 1
Protonation constants of the ligands H_4L^1, H_4L^2, H_3dtpa-bp, H_3dmdtta and H_5dtpa at 25.0 ± 0.1°C in aqueous Me_4NNO_3 ($I = 0.10$ mol dm^{-3})

Species		Log β				
H	L	H_4L^1	H_4L^2	H_3dtpa-bp [a]	H_3dmdtta [a]	H_5dtpa [b]
1	1	9.67(0.06)	10.68(0.05)	9.53	9.37	10.49
2	1	18.44(0.02)	18.74(0.04)	15.99	13.75	19.09
3	1	23.35(0.04)	22.04(0.07)	20.75	17.06	23.37
4	1	26.33(0.01)	24.65(0.01)	24.16		26.01

[a] Data were obtained from Ref. [14].
[b] Ref. [18].

ity constants were evaluated by a ligand–ligand competition potentiometric titration in this study [14,15]. A 1:1:1 molar ratio of lanthanides(III), ligand and a reference ligand with a known metal chelate stability was titrated. A good reference ligand for the lanthanide(III) systems was found to be H_4edta. $^7H_4$edta forms complexes with lanthanides(III) ions and the stability constants are accurately known.

The potentiometric equilibrium studies were carried out on solutions of H_4L^1 and H_4L^2, in the absence of metal ions and then in the presence of each metal ion which the M:L ratio was 1:1. The E data were obtained after additions of 0.005 cm^3 increments of standard 0.100 mmol dm^{-3} NaOH solution, and after stabilization in this direction, equilibrium was then approached from the other direction by adding standard 0.100 mol dm^{-3} acid solution. The equilibria were slow to attain and it was necessary to take about 10 min for each point of the titration where the ligand–ligand competition took place. However, complexation was usually rapid (3–5 min per point to give a stable pH reading) in the Cu(II), Ca(II) and Zn(II) studies. The same values of the stability constants were obtained either by using the direct or the back titration.

2.6. Computational method

The protonation constants of the H_4L^1 and H_4L^2 were calculated using a FORTRAN computer program PKAS [16] written for polyprotonic weak acid equilibria. The overall stability constants of the various metal complexes formed in aqueous solution were determined from the titration data with the FORTRAN computer program BEST [16]. The average difference between observed and calculated log [H$^+$] was < 0.04 throughout all titration. A value of 13.78 was employed for the pK_w at 25°C. The species distribution diagrams were calculated with the FORTRAN program SPE and SPEPLOT [16].

2.7. Relaxation time measurement

The Gd(III) chelate solution was prepared by combining equal molar amounts of the stock $GdCl_3$ and the ligand solution. The Gd(III) chelate solutions under various pH values were prepared by combining the buffer solution with an appropriately diluted Gd(III) complex solution in a 1:1 (v/v) ratio. The following buffer systems (all 0.10 mol dm^{-3}) were used: chloroacetic acid–NaOH (pH 2 and 3), acetic acid–NaOH (pH 4 and 5), PIPES (PIPES = piperazine-*N*,*N*′-bis-2-ethanesulfonic acid)–NaOH (pH 6.0 and 6.8) and ammonia–HCl (pH 9 and 10). These buffer solutions were used to maintain constant ionic strength (i.e. 0.10 mol dm^{-3}). The 0.10 mol dm^{-3} buffers were sufficient to maintain the solution pH within the desired range in most cases. The buffered Gd(III) chelate solutions were all allowed to equilibrate for at least 3 h. The pH of these solutions was determined immediately before relaxation time T_1 measurements.

Relaxation times T_1 of aqueous solutions of gadolinium(III) complexes of with H_4L^1 and H_4L^2 were measured to obtain relaxivity R_1. All measurements were made using a NMR spectrometer operating at 20 MHz and 37.0 ± 0.1°C (NMS 120 Minispec, Bruker). Before each measurement the spectrometer was tuned and calibrated. The value of R_1 was measured from eight data points generated by an inversion-recovery pulse sequence. The slope of plot of $1/T_1$ versus concentration gives R_1 in dm^3 mmol^{-1} s^{-1}.

3. Results and discussion

3.1. Protonation constants

The potentiometric titration curves for H_4L^1 and H_4L^2 are deposited as supplementary material (Figs. 1S and 2S). Table 1 summarizes the protonation constants of the H_4L^1, H_4L^2, H_3dtpa-bp(*N*,*N*″-2-bis(2-pyridylmethyl)diethylenetriamine-*N*,*N*′,*N*″-triacetic acid),

H_3dmdtta and H_5dtpa [7]. The titration curves of H_4L^1 and H_4L^2 all show the increase between pH 8.5 and 3.0 (moles of base per mol ligand present equals 2). This is due to the difference between the second ($\log K_2$) and third protonation constant ($\log K_3$), i.e. 8.77 and 4.91, 8.15 and 3.17, respectively. The $\log K_1$ (first protonation constant) and the $\log K_4$ (fourth protonation constant) values of H_4L^1 and H_4L^2 are 9.67 and 10.68, 2.98 and 2.75, respectively. The cumulative protonation constant of H_4L^1 is significantly higher than those of the H_4L^2, H_3dtpa-bp and H_3dmdtta and is a slightly higher than that of the H_5dtpa.

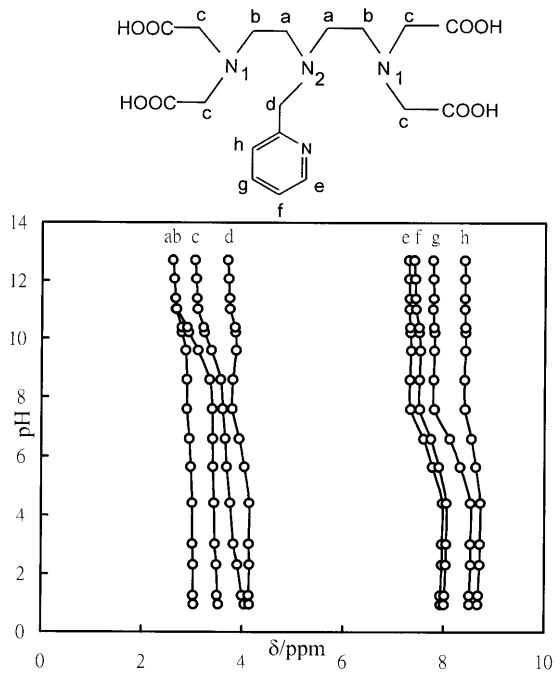


Fig. 1. Proton NMR titration curves for H_4L^1.

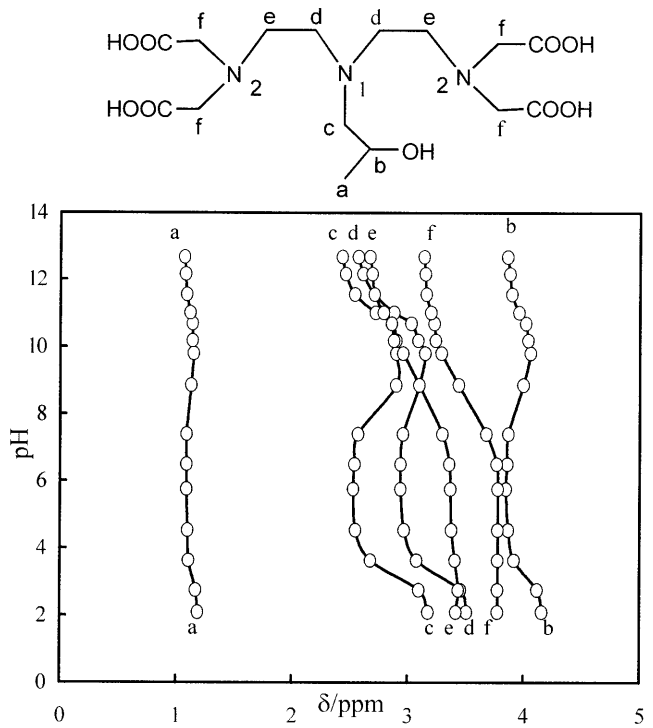


Fig. 2. Proton NMR titration curves for H_4L^2.

The replacement of the one central acetate group in H_5dtpa by the one 2-pyridylmethyl group results in a decrease in $\log K_1$ (i.e. 0.82 unit), increase in $\log K_2$ (i.e. 0.17 unit), $\log K_3$ (i.e. 0.63 unit), $\log K_4$ (i.e. 0.34 unit), and ΣpK_a value (i.e. 0.32 unit), and by the one 2-hydroxypropyl group results in an increase in $\log K_1$ (i.e. 0.19 unit), decrease in $\log K_2$ (i.e. 0.45 unit), $\log K_3$ (i.e. 1.11 unit), and ΣpK_a value (i.e. 1.36 unit).

3.2. NMR pH titration

The macroscopic protonation constants of the ligands in Table 1 are measured by the potentiometric titration technique. However, the microscopic protonation scheme is obtained by NMR spectroscopy coupled with pH titration. The proton NMR spectra of H_4L^1 and H_4L^2 as a function of pH have been deposited as supplementary material (figures 3S and 4S). Coalescence of the triplets corresponding to the ethylenic group occurs about pH > 10.0 for the H_4L^1. Plots of the proton chemical shift values (δ) of the methylenic resonance of H_4L^1 and H_4L^2 as a function of pH are shown in Figs. 1 and 2. There are four inflections centered for H_4L^2 at pH about 10.5, 8.0, 3.0 and 2.5. For H_4L^1 the chemical shift changing to lower of higher frequency in the region pH 11.0–8.3 reveals that the first and the second observed protonation occurred on the terminal nitrogen atoms, which is the first and second protonation sites. In the range pH 7.0–4.0 the chemical shift changing to lower of higher frequency shows that the third protonation occurred on the central 2-pyridylmethyl nitrogen atom. At about pH 3.0 the chemical shift changing to lower of higher frequency was also observed for the one of the carboxylate groups, which is the fourth protonation site. For H_4L^2 the chemical shift changing to lower of higher frequency in the region pH 12.0–10.2 indicates that the first observed protonation occurred on the central nitrogen atom, which is also common to H_5dtpa and bis(amide) of H_5dtpa derivatives system [7,8]. In the range of about pH 9.8–7.5 the chemical shift changing from lower of higher frequency was also observed for one of the terminal nitrogen atoms which is the second protonation site. In the range pH 3.5–2.5 the chemical shift changing from lower of higher frequency shows that the third protonation occurred on the remaining terminal nitrogen atom. At about pH 2.5 the chemical shift changing from lower of higher frequency also occurred on the central hydroxyl oxygen atom, which is the fourth protonation site. These values correlate quite

Table 2
Stability constants and selectivity constants for Gd^{3+}, Zn^{2+}, Ca^{2+} and Cu^{2+} complexes of H_4L^1, H_4L^2, H_3dtpa-bp, H_3dmdtta and H_5dtpa at 25.0 ± 0.1°C in aqueous Me_4NNO_3 ($I = 0.10$ mol dm^{-3})

	Log K				
	H_4L^1	H_4L^2	H_4dtpa-bp [a]	H_3dmdtta [a]	H_5dtpa [b]
[GdL]/[Gd][L]	21.59(0.07)	18.48(0.05)	16.83(0.11)	16.85(0.05)	22.46
Log $K_{GdL'}$ (pH 7.4)	17.53	14.38	14.65	14.88	18.14
[CaL]/[Ca][L]	8.35(0.04)	8.58(0.05)	7.97(0.05)	7.17(0.04)	10.75
Log β_{CaHL}		14.87(0.03)	13.27	11.62	
Log $K_{CaL'}$ (pH 7.4)	4.69	4.48	5.79	5.11	6.43
[CuL]/[Cu][L]	20.19(0.03)	18.09(0.02)	17.50(0.17)	13.03(0.03)	21.38
Log β_{CuHL}	26.37(0.02)	21.69(0.02)	21.14	16.39	
Log $K_{CuL'}$ (pH 7.4)	16.53	13.99	15.32	11.06	17.06
[ZnL]/[Zn][L]	17.96(0.03)	15.92(0.04)	14.02(0.14)	12.04(0.03)	18.70
Log β_{ZnHL}	23.82(0.02)	19.85(0.03)	19.38	16.08	
Log $K_{ZnL'}$ (pH 7.4)	14.30	11.82	11.84	10.02	14.38
Selectivity[log K(Gd/Zn)]	3.63	2.56	2.81	4.81	3.76
Selectivity[log K(Gd/Ca)]	13.24	9.90	8.86	9.73	11.71
Selectivity[log K(Gd/Cu)]	1.40	0.39	−0.67	3.78	1.08
Log $K_{sel'}$	7.29	6.26	5.32	9.03	7.04

[a] Ref. [14].
[b] Refs. [17,18].

well with the protonation constants of the H_4L^1 and H_4L^2 given in Table 1. This reflects stepwise protonation of the amino groups of the H_4L^2 and stepwise protonation of the amino groups and pyridyl nitrogen atom of the H_4L^1 with the formation of the species HL^{3-}, H_2L^{2-} and H_3L^-. The first protonation constant of H_4L^2 is higher than that of H_4L^1 because the first protonation site of H_4L^2 occurs on the central nitrogen atom and the H_4L^1 occurs at one of the terminal nitrogen atoms. These results seem to reveal that the methyl substituent increases the basicity of Lewis base whereas the acetate group does not. The third protonation constant of H_4L^1 is significant higher than that of corresponding value for H_4L^2 because of the protonation site of H_4L^1 being a pyridyl nitrogen atom. The species distribution curves for H_4L^1 and H_4L^2 have been deposited as supplementary material (Figs. 5S and 6S) the dominant species are the diprotonated ligand (H_2L^{2-}) between pH 5.5–8.0 and 4.0–7.5, respectively.

3.3. Thermodynamic stability constants

The metal chelate thermodynamic stability constants (K_{ML}) are expressed as in Eq. (1) where M represents the free, unhydrolyzed aquametal ion,

$$K_{ML} = [ML]/[M][L] \quad (1)$$

L is the uncomplexed, totally deprotonated form of the ligand and ML is the normal unprotonated and unhydrolyzed complex. The potentiometric titration curves for the complexes of Cu^{2+}, Ca^{2+} and Zn^{2+} with H_4L^1 and H_4L^2 have been deposited as supplement any material (Figs. 1S and 2S). The lanthanides(III) reacts strongly with H_4L^1 and H_4L^2 and at a considerably lower pH than the divalent metals. The stability constants of the complexes of lanthanides(III) with H_4L^1 and H_4L^2 were derived from the competition reaction H_4edta (not shown). In Table 2, the thermodynamic stability constants of Gd^{3+}, Cu^{2+}, Ca^{2+} and Zn^{2+} chelates are presented for the linear poly(aminocarboxylates) H_4L^1, H_4L^2, H_3dtpa-bp, H_3dmdtta and H_5dtpa [7,17,18].The similar stability constants of the complexes of Gd^{3+}, Cu^{2+} and Zn^{2+} with the H_4L^1 and H_5dtpa may indicate similar ligand basicities. The stability constants of $[GdL^2]^-$ are lower than those of $[GdL^1]^-$ and $[Gd(dtpa)]^{2-}$ and similar to that of $[Gd(deata)]^-$ (i.e. $\log K_{GdL} = 17.79$) (deata = *N*,*N*-bis-(2-aminoethyl) ethylamine-*N*′,*N*′,*N*″,*N*″tetraacetic acid) [19]. In other words, the hydroxyl group for DTPA-HP ligand does not coordinate to Gd(III) metal ion. The lower stability constants of the H_4L^2 and H_3dmdtta chelates when compared to the H_5dtpa and H_4L^1 chelates are assigned to the weaker donor ability of the hydroxyl and amide groups and the lower basicity of the ligands.

Plots of the thermodynamic stability constants ($\log K_{LnL}$) for $[LnL^1]^-$ and $[LnL^2]^-$ chelates (Ln = La^{3+}, Ce^{3+}, Nd^{3+}, Sm^{3+}, Gd^{3+}, Dy^{3+}, Ho^{3+}, Yb^{3+} and Lu^{3+}) versus lanthanide(III) ionic radius are displayed in Fig. 3. The ligand H_4L^1 forms stronger complexes with lanthanides than H_4L^2, primarily because of higher protonation constants of H_4L^1 ligand. The stability constants for $[LnL^1]^-$ and $[LnL^2]^-$ increase from La(III) to Nd(III) and then plateau at Sm(III) and Gd(III), before increasing again to Yb(III). This is a

common effect in Ln(III) solution chemistry [20]. The progressive increase in stability constants for $[LnL^1]^-$ and $[LnL^2]^-$ along the Ln(III) cation series is characteristic of ligands H_4L^1 and H_4L^2 those are higher basicity, less steric hindrance or more flexible and reveal increasing stability with enhancing the charge density of Ln(III) cation.

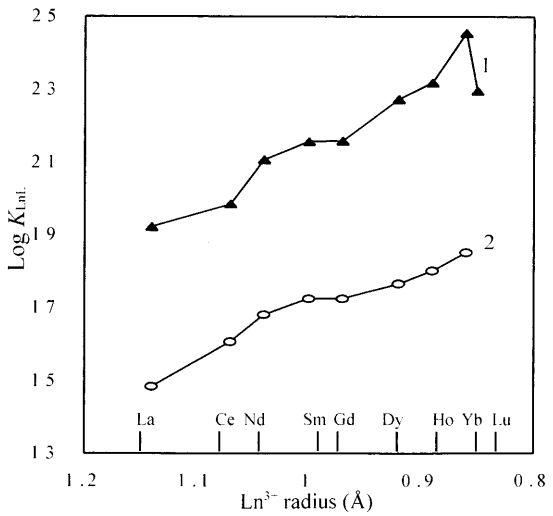


Fig. 3. Variation of stability constant with ionic radii of the lanthanides(III); (1) H_4L^1; (2) H_4L^2.

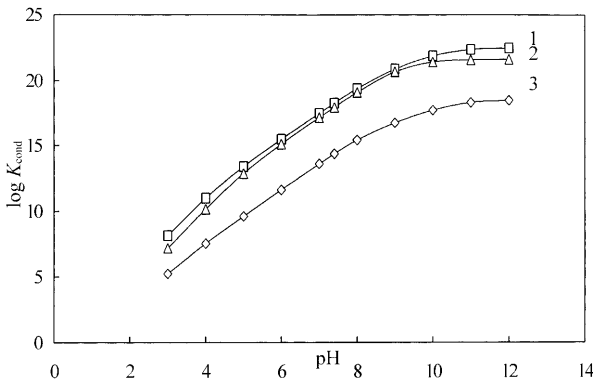


Fig. 4. Variation of the conditional stability constants for (1) $[Gd(dtpa)]^{2-}$ (□); (2) $[GdL^1]^-$ (△); (3) $[GdL^2]^-$ (◇) with pH.

Table 3
The pM values for the Gd^{3+}, Zn^{2+}, Ca^{2+}, and Cu^{2+} complexes of H_4L^1, H_4L^2, H_3dtpa-bp, H_3dmdtta and H_5dtpa at pH 7.4

	H_4L^1	H_4L^2	H_3dtpa-bp	H_3dmdtta	H_5dtpa
pGd	16.93	13.38	13.65	13.88	17.14
pCu	15.56	12.99	14.32	10.05	16.06
pCa	3.69	3.51	4.79	4.19	5.45
pZn	13.31	10.82	10.84	9.06	13.39

3.4. Conditional stability constants and selectivity constants

The conditional stability constant of a metal chelate ($K_{ML'}$) under physiological conditions (pH 7.4) is more important than the thermodynamic stability constant for biological studies. The former shows the extent of metal chelation at a pH 7.4 and can be calculated by taking regard of the thermodynamic stability constant and the stepwise ligand protonation constants [7].

Table 2 summarizes the conditional stability constants of the complexes of Gd^{3+}, Cu^{2+}, Ca^{2+} and Zn^{2+} with the five poly(aminocarboxylates), H_4L^1, H_4L^2, H_3dtpa-bp, H_3dmdtta and H_5dtpa at pH 7.4. Their order is $[Gd(dtpa)]^{2-} \approx [GdL^1]^- > [GdL^2]^- > [Gd(dtpa\text{-}bp)] \approx [Gd(dmdtta)]$. This suggests the conditional stability constants of the gadolinium(III) complexes are dependent on the ligand basicity. Fig. 4 shows the pH dependence of the conditional stability for the complexes, $[GdL^1]^-$, $[GdL^2]^-$ and $[Gd(dtpa)]^{2-}$. The results for $[GdL^1]^-$ and $[Gd(dtpa)]^{2-}$ are very similar. The conditional stability constants at pH > 11.0 for $[GdL^1]^-$ and $[Gd(dtpa)]^{2-}$ differ by a factor of $10^{0.87}$, similar to that at pH 7.4 ($10^{0.61}$). This reveals that the stability of $[GdL^1]^-$ is similar to that of $[Gd(dtpa)]^{2-}$ at pH 7.4 and 11.0, respectively. But for $[GdL^2]^-$ and $[Gd(dtpa)]^{2-}$ the conditional stability constant at pH > 11 differ by a factor of $10^{2.98}$ which is less than that at pH 7.4($10^{3.76}$). This indicates that the stability of $[GdL^2]^-$ is less significant than those of $[Gd(dtpa)]^{2-}$ and $[GdL^2]^-$ at pH 7.4.

The merit of comparing pM values $\{pM = -\log[M_f]\}$[21] rather than stability constants of the metal complexes is that the pM values give repression to the influence of ligand basicity and metal chelate protonation. The calculation of $[M_f]$ takes into consideration the protonation constants of the ligand and the stability constants of protonated metal complexes [19] The larger the pM value, the higher the affinity of that ligand for the metal ion under the specified conditions. The relative order of the stability constants may change if a different set of conditions (concentration and pH) is used to calculate the pM values. The results given in Table 3 reveal that the H_4L^1 and H_5dtpa are much stronger gadolinium(III) chelating agents than H_4L^2, H_3dtpa-bp and H_3dmdtta. The pM values of $[GdL^1]^-$ and $[GdL^2]^-$ are larger than those of $[CaL^1]^{2-}$ and $[CaL^2]^{2-}$, $[CuL^1]^{2-}$ and $[CuL^2]^{2-}$, and $[ZnL^1]^{2-}$ and $[ZnL^2]^{2-}$, respectively. However, the competition among Gd^{3+}, Ca^{2+}, Cu^{2+} and Zn^{2+} with H_4L^1 seems to favor Gd^{3+} at pH 7.4, indicating that the $[GdL^1]^-$ complex should be stable enough to avoid interference by Ca^{2+}, Cu^{2+} and Zn^{2+}. The stability constants for $[GdL^1]^-$ and $[Gd(dtpa)]^{2-}$ chelates are larger than those of the corresponding $[GdL^2]^-$ and $[Gd(dtpa\text{-}bp)]$ chelates, therefore the pGd values for $[GdL^2]^-$ and

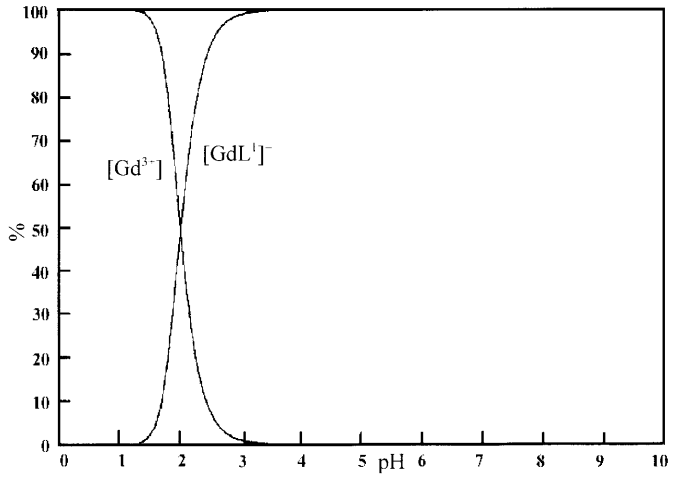


Fig. 5. Species distribution curves for 1.0×10^{-3} mol dm^{-3} $[GdL^1]^-$ system containing a 1:1 molar ratio of Gd(III) to H_4L^1. $T = 25.0 \pm 0.1$°C; $I = 0.10$ mol dm^{-3} (Me_4NNO_3); %, percent relative to 1.0×10^{-3} mol dm^{-3} total H_4L^1 species is 100%.

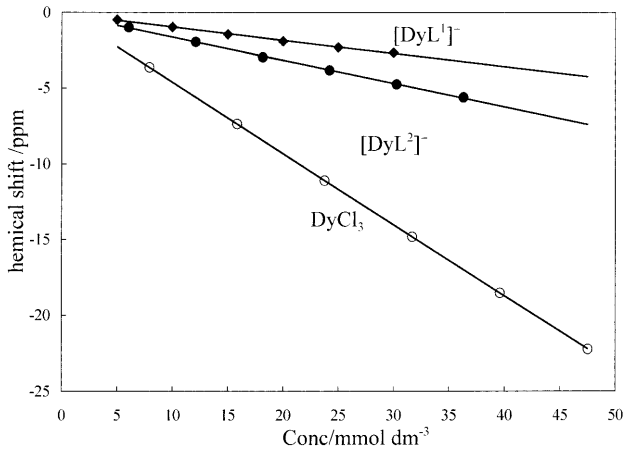


Fig. 6. The Dy(III)-induced water ^{17}O NMR shift versus Dy(III) chelate concentration for solution of (1) $[DyL^1]^-$ (◆); (2) $[DyL^2]^-$ (●); and (3) $DyCl_3$ (○) in D_2O at 25 ± 0.1°C.

[Gd(dtpa-bp)] chelates are ca. 3.55 and 2.74, 3.76 and 3.26 log units less than those of $[GdL^1]^-$ and $[Gd(dtpa)]^{2-}$, respectively. The reason is that H_4L^1 and H_5dtpa have high protonation constants, and therefore formation of their complexes is subject to stronger hydrogen ion competition. However, the p*Gd* value for $[GdL^1]^-$ is only about 0.21 log unit slightly less than that of $[Gd(dtpa)]^{2-}$, because the protonation constant of H_4L^1 is similar to that of H_5dtpa.

Species distribution curves of $[GdL^1]^-$ shown in Fig. 5, generated from the potentiometric data given in Table 2, indicate that there is still some free Gd^{3+} at pH 1, but by pH 3 the complex is fully formed. $[GdL^2]^-$ has been deposited as supplementary material (Fig. 7S). However, the $[GdL^1]^-$ and $[GdL^2]^-$ chelates are dominant species at physiological pH 7.4.

The logarithmic selectivity constant [7] of H_4L^1, H_4L^2, H_3dtpa-bp, H_3dmdtta and H_5dtpa for Gd^{3+} over Zn^{2+}, Ca^{2+} and Cu^{2+} is the difference between $\log K_{GdL}$ and $\log K_{ML}$ ($M = Zn^{2+}$, Ca^{2+} or Cu^{2+}), i.e. $\log K$(Gd–Zn), $\log K$(Gd–Ca) and $\log K$(Gd–Cu) are also listed in Table 2. From the selectivity constants, the $\log K$(Gd–Zn Gd–Ca and Gd–Cu) values of H_4L^1 are similar to that of H_5dtpa but higher than those of H_4L^2, H_3dmdtta and H_3dtpa-bp. Therefore, the H_4L^1 and H_5dtpa show more favorable selectivity toward Gd^{3+} over Zn^{2+}, Cu^{2+} and Ca^{2+} than do H_4L^2, H_3dmdtta and H_3dtpa-bp. The Gd(III) complexes of H_3dmdtta and H_3dtpa-bp have similar stability constants, but H_3dtpa-bp has a much lower selectivity for Gd(III) over Zn(II), which in turn leads to a high toxicity because of Gd(III) displacement by endogenous Zn(II) [7]. However, the selectivity constants ($\log K$(Gd/Zn)) of Gd(III) complexes with H_4L^2 and H_3dtpa-bp are similar and the toxicity of these two complexes should be similar too.

The modified selectivity constant ($K_{sel'}$) for Gd^{3+} over other endogenous metal ions (Cu^{2+}, Ca^{2+} and Zn^{2+}) and H^+ for a ligand can be calculated [14] and is obtained by the incorporation of ligand equilibria with Cu^{2+}, Ca^{2+}, Zn^{2+} and H^+. Table 2 shows the modified selectivity constants of H_4L^1, H_4L^2, H_3dtpa-bp, H_3dmdtta and H_5dtpa at pH 7.4. The concentrations of Ca^{2+}, Cu^{2+} and Zn^{2+} used were 2.5, 1.0×10^{-3} and 5.0×10^{-2} mmol dm^{-3}, respectively [7]. The $\log K_{sel'}$ of H_4L^1 (7.29) is a slightly higher than that of H_5dtpa (7.04), less than that of H_3dmdtta(9.03), but significantly higher than those of H_4L^2 (6.26) and H_3dtpa-bp (5.32). Thus, H_4L^1 forms the gadolinium(III) complex that is more stable than $[GdL^2]^-$ and [Gd(dtpa-bp)] toward transmetallation with endogenous metal ions at pH 7.4.

3.5. Dy(III)-induced ^{17}O water NMR shifts

The Dy(III)-induced water ^{17}O NMR shift versus Dy(III) chelate concentration for a solution of $DyCl_3$, $[DyL^1]^-$ and $[DyL^2]^-$ in D_2O at 25°C were shown in Fig. 6. For the H_4L^1 and H_4L^2 ligands the slopes are -88.2 ($r^2 = 0.9972$) and -154.0($r^2 = 0.9993$) ppm, respectively. The hydration number of dysprosium(III) ion has been proposed as being eight [21–23]. Under the conditions applied in the present study, the slope per Dy(III)-bound water molecule is -58.7 ppm. It can be concluded that the $[DyL^1]^-$ and $[DyL^2]^-$ complexes contain 1.50 and 2.62 inner-sphere water molecules per Dy(III) ion. The number of Ln(III)-bound water molecules in these complexes provides information on the coordination mode of the ligand. For the $[GdL^1]^-$ complex the coordination sites of Gd(III) ion is occupied by one water molecule and eight sites are available for the ligand molecule. By the

binding of three amine nitrogen atoms, four carboxylates and one 2-pyridylmethyl nitrogen atom to the H_4L^1 backbone, a similar coordination mode is found for the coordination sites of the previously studied, the bis(amide) of H_5dtpa derivative is attained [8,9,24,25]. However, two co-ordination site of Gd(III) are occupied by two water molecules and seven sites are available for the H_4L^2 ligand molecule. Therefore, the 2-hydroxypropyl oxygen atom may not coordinate to Gd(III) metal ion in the $[GdL^2]^-$ chelate. This result is also aligned with the conclusion of the thermodynamic stability studies of $[GdL^2]^-$.

3.6. Relaxometric studies of the Gd(III) complex

The rate of the chemical exchange of water from the coordination water to the bulk water could influence the inner sphere relaxation mechanism. The paramagnetic contribution of the solvent longitudinal relaxivity is obtained by the following equation [26]:

$$R_1 = Nq/[55.6\ (T_{1M} + \tau_M)] \quad (2)$$

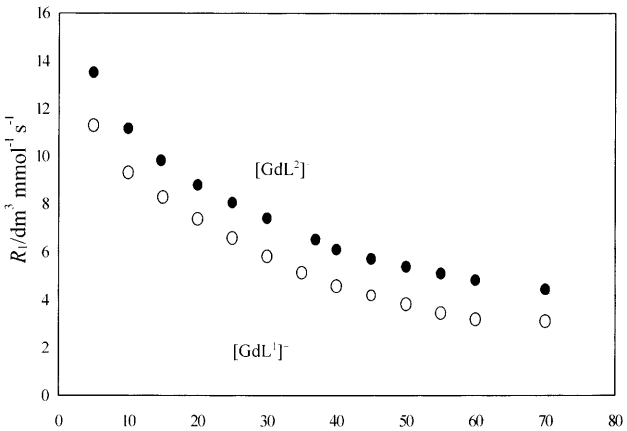


Fig. 7. Temperature dependence of the longitudinal relaxation rate for 0.5–2.0 mmol dm^{-3} solution of $[GdL^1]^-$ (○) and $[GdL^2]^-$ (●) measured at 20 MHz, pH 7.

Table 4
Relaxivities R_1 of gadolinium(III) complexes at 37.0 ± 0.1°C and 20 MHz

Complex	pH	R_1 relaxivity [a]/mmol dm^{-3} s^{-1}
$[GdL^1]^-$	6.7 ± 0.1	4.24 ± 0.03
	limiting [a]	4.27 ± 0.02
$[GdL^2]^-$	6.7 ± 0.1	6.17 ± 0.04
	limiting [a]	6.26 ± 0.03
[Gd(dmdtta)]	7.6 ± 0.1	3.89 ± 0.03
	limiting [a]	4.65 ± 0.05
$[Gd(dtpa)]^{2-}$	7.6 ± 0.1	3.89 ± 0.03
	limiting [a]	4.65 ± 0.05

[a] Average of relaxivity values over the pH range 2–10.

where N represents the molar concentration of the gadolinium(III) complex, q is the number of water molecules bound per metal ion, T_{1M} is the relaxation time of the bound water protons and τ_M is the residence lifetime of the bound water. Because of the opposite temperature dependence of T_{1M} and τ_M two cases can be considered: (1) fast chemical exchange ($T_{1M} \gg \tau_M$); R_1 increases with decreasing temperature and (2) slow chemical exchange ($T_{1M} \ll \tau_M$); R_1 decreases by decreasing the temperature. Fig. 7 shows the temperature dependence of the relaxivity for the complexes $[GdL^1]^-$ and $[GdL^2]^-$ at 20 MHz. A monoexponential decrease of the observed relaxivity upon increasing the temperature in the range 5–70°C was found for the $[GdL^1]^-$ and $[GdL^2]^-$ complexes. This is characteristic of the fast chemical exchange behavior which occurs when the residence lifetime of the coordinated water molecule (τ_M) is much shorter than the relaxation time of the bound water proton (T_{1M}).

Table 4 shows the spin-lattice relaxivity R_1 values of $[GdL^1]^-$, $[GdL^2]^-$, $[Gd(dtpa)]^{2-}$, and [Gd(dmdtta)]. The R_1 value of $[GdL^1]^-$ is similar to those of Gd(III) complexes with H_5dtpa and bis(amide) of H_5dtpa derivatives, but the $[GdL^2]^-$ is higher than those of $[Gd(dtpa)]^{2-}$, $[GdL^1]^-$ and [Gd(dmdtta)] under the same experimental conditions [7–10]. The relaxivity of a paramagnetic metal complex consists of two components: the inner-sphere and outer-sphere relaxivities. Since the basic skeleton of these ligands studied and the shapes and sizes of their gadolinium(III) complexes are similar, it is assumed that the outer-sphere relaxivities are similar. Thus, the observed relaxivity is primarily attributed to the variation in the inner-sphere contribution. The inner-sphere relaxivity is mainly dependent on the hydration number of the gadolinium(III) complex. A larger hydration number results in a higher relaxivity R_1. However, the q value of the complex of gadolinium(III) with H_4L^1 is similar to those of $[Gd(dtpa)]^{2-}$ and [Gd(dmdtta)] [14,25] leading to an almost identical R_1 value. The relaxivity R_1 of $[GdL^2]^-$ is 6.17 mmol dm^{-3} s^{-1}, higher than those of $[GdL^1]^-$, [Gd(dmdtta)] and $[Gd(dtpa)]^{2-}$, and this is undoubtedly due to the larger hydration number of the gadolinium(III) complex.

The relaxivities R_1 for the complexes $[GdL^1]^-$ and $[GdL^2]^-$ at differing pH values are shown in Fig. 8. The relaxivity R_1 curves of $[GdL^1]^-$ and $[GdL^2]^-$ complexes exhibit no pH dependence over the pH range 2–10 and 3–10, respectively. Therefore, no ligand dissociation of gadolinium(III) complexes occurred with a varying pH range of 3–10 in the solution. It is concluded that the hydration number remains constant in this pH range. When the pH range is less than 3 the $[GdL^2]^-$ complex undergoes partial dissociation. The observed relaxivity trend is qualitative agreement with the q values of the Gd(III) complexes. The dissociation of the complex

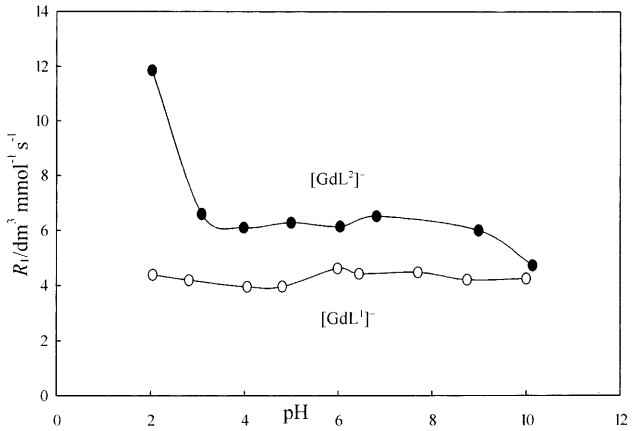


Fig. 8. pH dependence of the relaxivity for the complexes (1) $[GdL^1]^-$ (○) and (2) $[GdL^2]^-$ (●) all in 0.10 mol dm^{-3} buffers at 20 MHz and $T = 37.0 \pm 0.1$°C.

appeared to be more complete for $[GdL^2]^-$ than for $[GdL^1]^-$ in the lower pH range.

The most important prerequisites for potential use as MRI contrast agents are high relaxivity and high stability of the paramagnetic metal chelate. The Gd(III) complex of H_4L^1 is quite stable in aqueous solution, does not dissociate at physiological condition (pH 7.4) and does not exchange with Ca(II), Cu(II) and Zn(II) to an appreciable extent. However, The Gd(III) complex of H_4L^2 is not very stable and may exchange with Cu(II) and Zn(II) in aqueous solution. In conclusion, thermodynamic and relaxometric properties of $[GdL^1]^-$ chelate make it an attractive complex for the development of a new contrast agent for MRI.

4. Supplementary material

Seven figures showing potentiometric titration curves, NMR spectra, and special distribution curves are available on request from the authors (Y.-M.W.).

Acknowledgements

We are grateful to the National Science Council of the Republic of China for financial support under Contract No. NSC 88-2113-M037-016. This research was also supported in part by grants from the Department of Health under contract No. NHRI-GT-EX89B501L.

References

[1] J.C. Bousquet, S. Saini, D.D. Stark, P.F. Hahn, M. Nigam, J. Wittenberg, J.T. Ferrucci, Radiology 166 (1988) 693.
[2] G. Schuhman-Giampieri, H. Schmitt-Willich, W.R. Press, C. Negishi, H.J. Weinmann, U. Speck, Radiology 183 (1992) 59.
[3] F. Uggeri, S. Aime, P.L. Anelli, M. Botta, M. Brocchetta, C. Haen, G. Ermondi, M. Grandi, P. Paoli, Inorg. Chem. 34 (1995) 633.
[4] K. Kumar, C.A. Chang, M.F. Tweedle, Inorg. Chem. 32 (1993) 587.
[5] K. Kumar, C.A. Chang, L.C. Francesconi, D.D. Dischino, M.F. Malley, J.Z. Gougoutas, M.F. Tweedle, Inorg. Chem. 33 (1994) 3567.
[6] M.F. Tweedle, J.J. Hagan, K. Kumar, S. Mantha, C.A. Chang, Magn. Reson. Imaging 9 (1991) 409.
[7] W.P. Cacheris, S.C. Quay, S.M. Rocklage, Magn. Reson. Imaging 8 (1990) 467.
[8] Y.M. Wang, T.H. Cheng, G.C. Liu, R.S. Sheu, J. Chem. Soc., Dalton Trans. (1997) 833.
[9] Y.M. Wang, T.H. Cheng, R.S. Sheu, I.T. Chen, M.Y. Chiang, J. Chin. Chem. Soc. 44 (1997) 123.
[10] Y.M. Wang, S.T. Lin, Y.J. Wang, R.S. Sheu, Polyhedron 17 (1998) 2021.
[11] Y.M. Wang, Y.J. Wang, R.S. Sheu, G.C. Liu, W.C. Lin, J.H. Liao, Polyhedron 18 (1999) 1147.
[12] K. Mikkelsen, S.O. Nielsen, J. Phys. Chem. 64 (1960) 632.
[13] M.C. Alpoim, A.M. Urbano, C.F.G.C. Geraldes, J.A. Peters, J. Chem. Soc., Dalton Trans. (1992) 463.
[14] W.R. Harris, A.E. Martell, Inorg. Chem. 15 (1976) 713.
[15] C.H. Taliaferro, R.J. Motekaitis, A.E. Martell, Inorg. Chem. 23 (1984) 1188.
[16] A.E. Martell, R.J. Motekaitis, Determination and Use of Stability Constants, 2nd ed., VCH, New York, 1992.
[17] D.L. Wright, J.H. Holloway, C.N. Reilley, Anal. Chem. 37 (1965) 884.
[18] R.M. Smith, A.E. Martell (Eds.), Critical Stability Constants, vols. 1–4, Plenum Press, New York, 1975–1977.
[19] P.K. Tse, J.E. Powell, Inorg. Chem. 24 (1985) 2720.
[20] P. Caravan, P. Mehrhodavandi, C. Orvig, Inorg. Chem. 36 (1997) 1316.
[21] T. Kowall, F. Foglia, L. Helm, A.E. Merbach, J. Am. Chem. Soc. 36 (1995) 117, 3790.
[22] C. Cossy, C.L. Helm, D.H. Powell, A.E. Merbach, New J. Chem. 19 (1995) 27.
[23] C. Cossy, A.C. Barnes, J.E. Enderby, A.E. Merbach, J. Chem. Phys. 90 (1989) 3254.
[24] J.A. Peter, Inorg. Chem. 27 (1988) 4686.
[25] S.W.A. Bligh, A.H.M.S. Chowdhury, M. McPartlin, I.J. Scowen, R.A. Bulman, Polyhedron 14 (1995) 567.
[26] T.J. Swift, R.E. Connick, J. Chem. Phys. 37 (1962) 307.

PERGAMON

www.elsevier.nl/locate/poly

Polyhedron 19 (2000) 2039–2048

POLYHEDRON

Structures of dichloromanganese(IV) complexes with bidentate and tetradentate Schiff base ligands

Hideyuki Asada, Manabu Fujiwara, Takayuki Matsushita *

Department of Materials Chemistry, Faculty of Science and Technology, Ryukoku University, Seta, Otsu 520-2194, Japan

Received 14 April 2000; accepted 11 July 2000

Abstract

The dichloromanganese(IV) complexes with various bidentate and tetradentate Schiff base ligands, $Mn^{IV}(L')_2Cl_2$ and $Mn^{IV}(L)Cl_2$ have been obtained by the reactions of chloromanganese(III) complexes, $Mn^{III}(L')_2Cl$ and $Mn^{III}(L)Cl$ with hydrogen chloride or by the reactions of acetatomanganese(III) complexes, $Mn^{III}(L')_2OAc$, with chlorine as deep green crystals, where L′H denotes bidentate Schiff base ligands *N*-R-salH (*N*-alkyl-salicylideneamine) and R can be *n*-C_3H_7, *n*-C_6H_{13}, *n*-C_8H_{17}, or *n*-$C_{12}H_{25}$, and LH_2 denotes tetradentate Schiff base ligands X-salenH_2 (*N*,*N*′-disubstituted-salicylideneethylenediamine) or X-salpnH_2 (*N*,*N*′-disubstituted-salicylidenepropanediamine) and X can be H and 5-Br. X-ray structure analysis of the present dichloromanganese(IV) complexes has revealed that two chloride ions coordinate to the central manganese ion in a *trans*-form. © 2000 Elsevier Science Ltd. All rights reserved.

Keywords: Dichloromanganese(IV) complexes; Bidentate Schiff base ligands; Tetradentate Schiff base ligands; Crystal structures; Photosystem II

1. Introduction

The chemistry of high-valent manganese complexes, Mn(III) and Mn(IV), is interesting in relation to the biological redox systems involving manganese ions, such as oxygen-evolving center (OEC) of Photosystem II in green plants [1–10]. In the OEC of PS II, chloride ions exist near manganese ions as co-factors and it is suspected that the chloride ion may act in proton release, charge neutralization in water splitting or as a ligand to the manganese ions and facilitation of electron transfer [11–15]. However, the details have not yet been made clear. We have reported previously on the preparation and physico-chemical properties of a series of dichloromanganese(IV) complexes [16–18] and their reactivities with water [19,20]. However, their molecular structures have not yet been determined.

In this paper, we describe the molecular structures of a series of dichloromanganese(IV) complexes with bidentate and tetradentate Schiff base ligands, $Mn^{IV}(L')_2Cl_2$ and $Mn^{IV}(L)Cl_2$, respectively, together with those of the acetatomanganese(III) complexes with bidentate Schiff base ligands, $Mn^{III}(L')_2OAc$, which are starting complexes for the preparation of manganese(IV) complexes.

The structures of all $Mn^{IV}(L')_2Cl_2$ are found to be a distorted octahedron, where two bidentate Schiff base ligands (L′) coordinate to the manganese ion in a *trans*-fashion to form an equatorial plane(ONON) and two chloride ions occupy a *trans* axial position. These complexes have a high symmetry and their Cl–Mn–Cl angles are 180.0°. On the other hand, the structures of $Mn^{IV}(L)Cl_2$ are also a *trans*-distorted octahedron, where tetradentate Schiff base ligands (L) coordinate to the manganese ion by a N_2O_2 donor set to form an equatorial plane and two chloride ions occupy a *trans* axial position. However, the angles of Cl–Mn–Cl are found to be 174.5(1)° for Mn^{IV}(salen)Cl_2, 167.9(1)° for Mn^{IV}(5-Br-salen)Cl_2, and 172.6(2)° for Mn^{IV}(5-Br-salpn)Cl_2, where both chloride ions lean toward the chelate ring formed by –N–Mn–N–$(CH_2)_{2/3}$–.

The bond lengths of Mn–Cl observed for all the manganese(IV) complexes are found to be shorter than those for the corresponding chloromanganese(III) complexes, which can be explained by the stabilization effect of chloride ions at higher oxidation states of transition metal elements.

* Corresponding author. Tel.: +81-77-543-7471; fax: +81-77-543-7483.

E-mail address: matusita@chem.ryukoku.ac.jp (T. Matsushita).

0277-5387/00/$ - see front matter © 2000 Elsevier Science Ltd. All rights reserved.
PII: S0277-5387(00)00503-9

2. Experimental

2.1. Physical measurements

IR spectra were recorded on a Shimadzu Model IR-470 infrared spectrophotometer. Elemental analyses were made on a Yanaco Model CHN-CORDER MT-5.

2.2. Preparation of bidentate and tetradentate Schiff base ligands

All of the bidentate and tetradentate Schiff base ligands were prepared and identified according to the literature [16–18].

2.3. Preparation of manganese(III) complexes with bidentate Schiff base ligands

The acetatobis(*N*-dodecylsalicylideneaminato)manganese(III) complex, Mn^{III}(*N*-Dod-sal)$_2$OAc was prepared by the reaction of bidentate Schiff base ligand, *N*-dodecylsalicylideneamine, *N*-Dod-salH (Dod = *n*-$C_{12}H_{25}$) (0.58 g, 2.0 mmol) and a half molar amount of manganese(III) acetate dihydrate, $Mn^{III}(OAc)_3{\cdot}2H_2O$ (0.27 g, 1.0 mmol) in methanol at 60°C. After 2 h, the resulting precipitates were collected on a glass filter and recrystallized from acetonitrile (MeCN). Other acetatomanganese(III) complexes, Mn^{III}(*N*-R-sal)$_2$OAc, were obtained in the same manner, where R can be *n*-C_3H_7 (Pr), *n*-C_6H_{13} (Hx). The yields of these complexes were about 70%. Single crystals of Mn^{III}(*N*-Pr-sal)$_2$OAc, Mn^{III}(*N*-Hx-sal)$_2$OAc, and Mn^{III}(*N*-Dod-sal)$_2$OAc were used for X-ray crystallographic determination. *Anal.* Calc. for $C_{22}H_{27}MnN_2O_4$ {Mn^{III}(*N*-Pr-sal)$_2$OAc}: C, 60.27; H, 6.21; Mn, 12.53; N, 6.39. Found: C, 60.30; H, 6.20; Mn, 12.40; N, 6.42%. IR spectrum on KBr pellets (cm^{-1}): 2910(s), 2827(m), 1622(s), 1600(m), 1549(s), 1462(m), 1447(s), 1394(m), 1299(s), 1222(w), 1203(m), 1149(m), 1118(w), 1019(w), 1002(w), 907(w), 891(w), 803(m), 758(s), 737(w), 678(w), 647(w), 430(w). *Anal.* Calc. for $C_{28}H_{39}MnN_2O_4$ {Mn^{III}(*N*-Hx-sal)$_2$OAc}: C, 64.35; H, 7.52; Mn, 10.51; N, 5.36. Found: C, 64.40; H, 7.56; Mn, 10.33; N, 5.41%. IR spectrum on KBr pellets (cm^{-1}): 2910(m), 2827(w), 1625(s), 1600(m), 1542(s), 1467(m), 1444(s), 1393(m), 1200(s), 1201(m), 1147(m), 1121(m), 1023(w), 994(w), 912(w), 895(w), 803(m), 759(s), 738(w), 723(w), 677(m), 646(m), 461(w), 435(w). *Anal.* Calc. for $C_{40}H_{63}MnN_2O_4$ {Mn^{III}(*N*-Dod-sal)$_2$OAc}: C, 69.64; H, 9.32; Mn, 7.95; N, 4.05. Found: C, 69.58; H, 9.44; Mn, 7.99; N, 4.04%. IR spectrum on KBr pellets (cm^{-1}): 2910(s), 2825(s), 1620(s), 1600(m), 1547(s), 1464(m), 1446(s), 1387(m), 1327(w), 1301(s), 1219(w), 1202(w), 1148(m), 1116(w), 1027(w), 996(w), 899(w), 817(w), 799(w), 758(m), 738(w), 678(w), 647(w), 452(w), 421(w).

The chlorobis(*N*-alkylsalicylideneaminato)manganese(III) complexes, Mn^{III}(*N*-R-sal)$_2$Cl (R = Pr, Hx, Oct, and Dod) were prepared and identified according to the literature [16–18].

2.4. Preparation of manganese(III) complexes with tetradentate Schiff base ligands

Chloro(*N*,*N*′ - di - X - salicylideneethylenediaminato)-manganese(III) complexes, Mn^{III}(X-salen)Cl and chloro(*N*,*N*′-di-5-bromosalicylidenepropanediaminato)-manganese(III) complex, Mn^{III}(5-Br-salpn)Cl were prepared and identified according to the literature [16–18].

2.5. Preparation of dichloromanganese(IV) complexes with bidentate Schiff base ligands

Dichlorobis(*N* - dodecylsalicylideneaminato)manganese(IV) complex, Mn^{IV}(*N*-Dod-sal)$_2$Cl$_2$. To 2-propanol (150 ml) containing Mn^{III}(*N*-Dod-sal)$_2$OAc (1.38 g, 2 mmol) or Mn^{III}(*N*-Dod-sal)$_2$Cl (1.41 g, 2 mmol), a concentrated HCl solution (36%, 0.59 g, 6 mmol) was added drop by drop with stirring at 0°C. The solution changed from greenish brown to deep green with precipitation of deep green crystals. The mixture was stirred for 30 min at 0°C. The crystalline precipitates were collected on a glass filter, washed with 2-propanol and *n*-hexane, and recrystallized from a mixed solvent of dichloromethane (CH_2Cl_2) and *n*-hexane (1:1) in a refrigerator. Other dichloromanganese(IV) complexes with bidentate Schiff base ligands, Mn^{IV}(*N*-R-sal)$_2$Cl$_2$, were obtained in a similar way, where R can be *n*-C_3H_7 (Pr) or *n*-C_8H_{17} (Oct). The yields of these manganese(IV) complexes were about 40%. Dichlorobis(*N*-alkyl-salicylideneaminato)manganese(IV) complexes were also successfully obtained using a Cl_2 solution of 2-propanol instead of a conc. HCl solution. Their yields were about 70%. This means that the manganese(IV) complexes are formed by dispropotionation of the manganese(III) complex when HCl was used. Single crystals of Mn^{IV}(*N*-Pr-sal)$_2$Cl$_2$ (**4**), Mn^{IV}(*N*-Oct-sal)$_2$Cl$_2$ (**5**), and Mn^{IV}(*N*-Dod-sal)$_2$Cl$_2$ (**6**) were used for X-ray crystallographic determination. *Anal.* Calc. for $C_{20}H_{24}Cl_2MnN_2O_2$ {Mn^{IV}(*N*-Pr-sal)$_2$Cl$_2$}: C, 53.35; H, 5.37; Mn, 12.20; N, 6.22. Found: C, 53.18; H, 5.44; Mn, 12.00; N, 6.35%. IR spectrum on KBr pellets (cm^{-1}): 2948(m), 2852(w), 1611(s), 1597(m), 1541(m), 1459(m), 1438(m), 1386(w), 1297(s), 1212(w), 1143(w), 1118(w), 1029(w), 999(w), 912(w), 881(w), 812(m), 749(m), 632(m), 572(w), 515(w), 476(w), 450(w), 424(w). *Anal.* Calc. for $C_{38}H_{60}Cl_2MnN_2O_2$ {Mn^{IV}(*N*-Oct-sal)$_2$Cl$_2$}: C, 61.01; H, 7.51; Mn, 9.30; N, 4.75. Found: C, 60.90; H, 7.53; N, 4.64; Mn, 9.31%. IR spectrum on KBr pellets (cm^{-1}): 2924(s), 2840(m), 1613(s), 1598(m), 1540(m), 1457(m), 1436(m), 1299(s), 1219(w), 1142(w), 1118(w), 1107(w), 1025(w), 1001(w), 962(w), 906(m), 815(m), 749(m),

636(m), 573(w), 520(w), 472(w), 451(w), 424(w). *Anal.* Calcd for $C_{38}H_{60}Cl_2MnN_2O_2$ {Mn^{IV}(*N*-Dod-sal)$_2Cl_2$}: C, 64.94; H, 8.61; Mn, 7.82; N, 3.99. Found: C, 64.83; H, 8.66; Mn, 7.98; N, 3.96%. IR spectrum on KBr pellets (cm^{-1}): 2910(s), 2825(s), 1615(s), 1597(m), 1542(m), 1464(m), 1452(s), 1403(w), 1302(s), 1251(w), 1212(w), 1148(m), 1120(w), 1027(w), 909(m), 818(m), 753(m), 637(w), 581(w), 511(w), 480(w), 449(w), 420(w).

2.6. Preparation of dichloromanganese(IV) complexes with tetradentate Schiff base ligands

Dichloro(*N*,*N*′-disalicylideneethylenediaminato)manganese(IV) complex, Mn^{IV}(salen)Cl_2. A diethyl ether solution saturated with Cl_2 was added to a solution of dichloromethane containing Mn^{III}(salen)Cl. The solution changed from brown to deep green, which was concentrated under reduced pressure to yield deep green crystals. They were recrystallized from a mixed solvent of CH_2Cl_2 and *n*-hexane (1:1) in a refrigerator to yield Mn^{IV}(salen)Cl_2·1/2CH_2Cl_2. Moreover, in order to obtain single crystals of Mn^{IV}(salen)Cl_2, they were recrystallized from acetone under slightly reduced pressure, but mixed crystals of Mn^{III}(salen)Cl and Mn^{IV}(salen)Cl_2 were obtained. The yield of this manganese(IV) complex was low (ca. 20%), compared with those for the $Mn^{IV}(L')_2Cl_2$. Single crystals of the mixed crystals of Mn^{III}(salen)Cl and Mn^{IV}(salen)Cl_2 (**7**) were used for X-ray crystallographic determination. *Anal.* Calc. for $C_{16.5}H_{15}Cl_3MnN_2O_2$ {Mn^{IV}(salen)Cl_2·1/2CH_2Cl_2}: C, 45.60; H, 3.48; Mn, 12.64; N, 6.45. Found: C, 45.17; H, 3.55; Mn, 12.68; N, 6.49%. IR spectrum on KBr pellets (cm^{-1}): 2907(w), 1623(s), 1598(m), 1537(m), 1461(w), 1444(s), 1382(w), 1324(w), 1289(s), 1198(w), 1148(w), 1139(w), 1042(w), 1031(w), 901(m), 799(m), 762(m), 750(m), 735(w), 630(m), 584(w), 466(m).

In a similar way, Mn^{IV}(5-Br-salen)Cl_2 was prepared and identified. Single crystals of Mn^{IV}(5-Br-salen)Cl_2 (**8**) were used for X-ray crystallographic determination. *Anal.* Calc. for $C_{16}H_{12}Br_2Cl_2MnN_2O_2$ {Mn^{IV}(5-Br-salen)Cl_2}: C, 34.94; H, 2.20; Mn, 9.99; N, 5.09. Found: C, 34.91; H, 2.11; Mn, 10.2; N, 4.98%. IR spectrum on KBr pellets (cm^{-1}): 2952(w), 2905(w), 1625(s), 1592(m), 1523(m), 1455(s), 1435(m), 1430(m), 1418(m), 1369(m), 1277(s), 1192(w), 1178(w), 1135(w), 1076(w), 1041(w), 825(m), 802(m), 690(m), 683(m), 657(m), 595(w), 548(w), 486(m), 465(w).

Dichloro(*N*,*N*′-di-5-bromosalicylidenepropanediaminato)manganese(IV) complex, Mn^{IV}(5-Br-salpn)Cl_2. The concentrated HCl solution (36%, 0.59 g, 6 mmol) was added to a MeCN solution of Mn^{III}(5-Br-salpn)Cl (1.06 g, 2 mmol). The solution changed from brown to deep green with precipitation of deep green crystals. They were collected on a glass filter, washed with *n*-hexane, and recrystallized from a mixed solvent of CH_2Cl_2 and *n*-hexane (1:1) in a refrigerator. The yield of this complex was 20%. Single crystals of Mn^{IV}(5-Br-salpn)Cl_2 (**9**) were used for X-ray crystallographic determination. *Anal.* Calc. for $C_{17}H_{14}Br_2Cl_2MnN_2O_2$ {Mn^{IV}(5-Br-salpn)Cl_2}: C, 36.21; H, 2.50; Mn, 9.74; N, 4.97. Found: C, 36.37; H, 2.57; Mn, 9.86; N, 4.95%. IR spectrum on KBr pellets (cm^{-1}): 2905(w), 1612(s), 1528(m), 1455(s), 1432(m), 1378(m), 1289(s), 1196(w), 1181(w), 1131(w), 1070(w), 1062(w), 822(m), 808(m), 692(m), 685(m), 648(m), 542(w), 511(w), 454(m).

2.7. X-ray crystallographic measurements

X-ray structure analyses were taken on a Rigaku AFC-7R automatic four-circle X-ray diffractometer.

Single crystals of the manganese(III) complexes and dichloromanganese(IV) complexes were obtained by recrystallization from MeCN and from a mixed solvent of CH_2Cl_2 and *n*-hexane or acetone, respectively. The crystals were mounted on a glass capillary. All the data were collected on a Rigaku AFC-7R four circle automated diffractometer with graphite monochromated Mo Kα radiation ($\lambda = 0.71069$ Å) for **1**, **2**, **5**, **6**, **7** and **9** and Cu Kα radiation ($\lambda = 1.54178$ Å) for **3**, **4** and **8** at 23°C. Unit-cell parameters were obtained from least-squares fit of 25 reflections, $23.85 < 2\theta < 28.10°$ for **1**, $22.79 < 2\theta < 34.06°$ for **2**, $21.81 < 2\theta < 44.48°$ for **3**, $47.32 < 2\theta < 54.67°$ for **4**, $20.74 < 2\theta < 29.26°$ for **5**, $20.54 < 2\theta < 29.53°$ for **6**, $52.58 < 2\theta < 56.70°$ for **8**, $20.50 < 2\theta < 29.34°$ for **9**, and 16 reflections, $20.82 < 2\theta < 28.36°$ for **7**. Three standard reflections were measured every 150 reflections; they showed no systematic decay throughout data collection. The data were corrected for Lorentz and polarization effects. All the calculations were carried out using the TEXSAN [21] crystallographic software package. The structures of the complexes were solved using direct method for **1** (MITHRIL-84) [22], **5** (MULTAN-88) [23], **6** (SAPI-91) [24], **4**, **7**, **8**, **9** (SHELX-86) [25] or Patterson method for **2** (DIRDIF-92 PATTY) [26], **3** (SAPI) and expanded using Fourier techniques [27]. These structures were refined by the full-matrix least-squares technique with anisotropic thermal parameters for all non-hydrogen atoms. Hydrogen atoms were introduced in calculated positions but not refined. Crystallographic data for the complexes are summarized in Tables 1–3.

3. Results and discussion

Previously, we have demonstrated that some of the dichloromanganese(IV) complexes with bidentate Schiff base ligands can generate molecular oxygen by oxidation of water, which may be considered as possible models for OEC in PSII [19,20]. In this case, chloride ions, which are proposed to be an important co-factor

Table 1
Crystallographic parameters for **1**, **2** and **3**

Compound	**1**	**2**	**3**
Chemical formula	$C_{22}H_{27}MnN_2O_4$	$C_{28}H_{39}MnN_2O_4$	$C_{40}H_{63}MnN_2O_4$
Formula weight	438.40	522.57	690.89
Crystal color, habit	dark brown, prism	dark brown, prism	dark brown, prism
Crystal size	$0.50\times0.30\times0.15$	$0.40\times0.30\times0.10$	$0.25\times0.20\times0.10$
a (Å)	10.672(2)	13.723(2)	13.968(4)
b (Å)	8.688(2)	8.831(2)	8.948(3)
c (Å)	12.883(2)	23.336(1)	32.917(3)
α (°)			
β (°)	111.36(1)	91.653(7)	98.37(1)
γ (°)			
V (Å^3)	1112.5(3)	2827.0(6)	4070(1)
Z	2	4	4
Crystal system	monoclinic	monoclinic	monoclinic
Space group	$P2_1$	$C2/c$	$C2/c$
D_{calc} (g cm^{-3})	1.309	1.228	1.127
2θ max	55.0	55.0	120.1
Unique data	2724	3472	3240
Observed Δ	1857	1959	958
R [a]	0.047	0.041	0.053
R_w [b]	0.065	0.058	0.070
Goodness-of-fit	1.21	1.17	1.23

[a] $R = \Sigma(|F_o|-|F_c|)/\Sigma|F_o|$.
[b] $R_w = [\Sigma w(|F_o|-|F_c|)^2/\Sigma wF_o^2]^{1/2}$, $w = 4F_o^2/\sigma^2(F_o^2)$.

of the OEC, function to stabilize an oxidation state of manganese(IV). However, a series of dichloromanganese(IV) complexes with Schiff base ligands has been found to be usually unstable toward moisture even in the solid state and decomposes to the reduced manganese complexes. This may be caused by displacement of the coordinated chloride ions with water molecules. We have obtained single crystals of dichloromanganese(IV) with Schiff base ligands under absolutely moisture-free conditions.

3.1. Structure of $Mn^{III}(L')_2OAc$

Molecular structures of Mn^{III}(*N*-Pr-sal)$_2$OAc (**1**) and Mn^{III}(*N*-Hx-sal)$_2$OAc (**2**) and Mn^{III}(*N*-Dod-sal)$_2$OAc (**3**) are shown in Figs. 1–3, respectively. Selected bond lengths and angles are listed in Table 4. All the manganese(III) complexes, $Mn^{III}(L')_2OAc$ have a mononuclear distorted octahedral structure which comprises *cis*-form coordination of two Schiff base ligands and bidentate acetato moiety. Furthermore, these complexes belong to a $C2$ point group where a $C2$ axis passes through two carbon atoms of the acetato ligand to a manganese ion. In addition, a crystallographic $C2$ axis exists in the complexes of R = Hx and Dod. Since a significant Jahn–Teller distortion could not be observed in these complexes, the structures are considered to be trigonal bipyramidal rather than octahedral.

Table 2
Crystallographic parameters for **4**, **5** and **6**

Compound	**4**	**5**	**6**
Chemical formula	$C_{20}H_{24}Cl_2MnN_2O_2$	$C_{30}H_{44}Cl_2MnN_2O_2$	$C_{38}H_{60}Cl_2MnN_2O_2$
Formula weight	450.27	590.53	702.75
Crystal color, habit	dark green, prism	dark green, prism	dark green, prism
Crystal size	$0.05\times0.05\times0.30$	$0.20\times0.05\times0.10$	$0.20\times0.05\times0.30$
a (Å)	6.929(2)	30.428(2)	39.446(2)
b (Å)	14.0731(5)	7.968(3)	8.013(4)
c (Å)	11.4405(9)	12.827(3)	12.763(3)
α (°)			
β (°)	102.885(10)	99.68(1)	107.79(1)
γ (°)			
V (Å^3)	1087.4(2)	3065(1)	3841(2)
Z	2	4	4
Crystal system	monoclinic	monoclinic	monoclinic
Space group	$P2_1/a$	$C2/c$	$C2/c$
D_{calc} (g cm^{-3})	1.375	1.279	1.215
2θ max	120.1	55.0	55.0
Unique data	1707	3782	4738
Observed data	842	1675	1787
R [a]	0.054	0.039	0.054
R_w [b]	0.075	0.055	0.072
Goodness-of-fit	1.10	1.18	1.14

[a] $R = \Sigma(|F_o|-|F_c|)/\Sigma|F_o|$.
[b] $R_w = [\Sigma w(|F_o|-|F_c|)^2/\Sigma wF_o^2]^{1/2}$, $w = 4F_o^2/\sigma^2(F_o^2)$.

Table 3
Crystallographic parameters for **7**, **8**, and **9**

Compound	**7**·Mn(salen)Cl·Me_2CO	**8**	**9**
Chemical formula	$C_{35}H_{34}Cl_3Mn_2N_4O_5$	$C_{16}H_{12}Br_2Cl_2MnN_2O_2$	$C_{17}H_{14}Br_2Cl_2MnN_2O_2$
Formula weight	806.91	549.93	563.96
Crystal color, habit	dark green, prism	dark green, prism	dark green, prism
Crystal size	$0.20\times0.05\times0.05$	$0.20\times0.15\times0.15$	$0.20\times0.05\times0.30$
a (Å)	13.510(4)	11.175(4)	13.707(9)
b (Å)	14.865(8)	13.949(4)	11.982(3)
c (Å)	17.758(4)	11.713(4)	25.402(4)
α (°)			
β (°)	94.88(2)		102.91(2)
γ (°)			
V (Å^3)	3553(2)	1825(1)	4066(2)
Z	4	4	8
Crystal system	monoclinic	orthorhombic	monoclinic
Space group	$P2_1/a$	$Pna2_1$	$P2_1/c$
D_{calc} (g cm^{-3})	1.508	2.000	1.842
2θ max	55.0	120.1	55.0
Unique data	8145	1592	9793
Observed data	2592	1350	2780
R [a]	0.054	0.050	0.055
R_w [b]	0.072	0.079	0.070
Goodness-of-fit	1.13	1.37	1.12

[a] $R=\Sigma(|F_o|-|F_c|)/\Sigma|F_o|$.
[b] $R_w=[\Sigma w(|F_o|-|F_c|)^2/\Sigma wF_o^2]^{1/2}$, $w=4F_o^2/\sigma^2(F_o^2)$.

3.2. Structure of $Mn^{IV}(L')_2Cl_2$

Molecular structures of Mn^{IV}(*N*-Pr-sal)$_2Cl_2$ (**4**), Mn^{IV}(*N*-Oct-sal)$_2Cl_2$ (**5**) and Mn^{IV}(*N*-Dod-sal)$_2Cl_2$ (**6**) are shown in Figs. 4–6, respectively. Selected bond lengths and angles are listed in Table 5. Complex **4** crystallized in the monoclinic space group $P2_1/a$. The manganese ion located on the center of symmetry in a N_2O_2 plane. Two chloride ions occupied a *trans* axial position and two bidentate Schiff base ligands occupied an equatorial plane. Adoption of this configuration places to all the coordination atoms (Cl, N, O) *trans*-position each other: Two chloride ions and Schiff base ligands are equivalent and two bond lengths of Mn–Cl, Mn–O and Mn–N are equal. The Mn–O (1.849(6)–1.851(3) Å) and Mn–N (2.024(6)–2.039(5) Å) bond lengths are typical for several observed octahedral manganese(IV) complexes with Schiff base ligands [28–39]. The phenyl ring of the Schiff base ligand is parallel with the other one.

Complexes **5** and **6** crystallized in the monoclinic space group $C2$. The manganese ion located in a N_2O_2 plane, belonging to a $C2$ symmetry including two chloride ions and two Schiff base ligands. Adoption of this configuration places the donor atoms (Cl, N, O) to *trans*-position each other. In these cases, the two phenyl rings are bending to the same direction, forming an umbrella. Therefore, the two bond lengths of Mn–Cl are no longer equivalent: The bond length between Mn and Cl which is coordinated to the manganese ion from the top position of umbrella is slightly longer than the other. The bond lengths of Mn(1)–Cl(1) and Mn(1)–Cl(2) are 2.270(2) and 2.248(2) Å for complex **5** and 2.272(3) and 2.243(3) Å for complex **6**. Moreover, the bond lengths of Mn(1)–Cl(1) of complexes **5** and **6** are also longer than that of complex **4** (2.258(2) Å), whereas the bond lengths of Mn(1)–Cl(2) are shorter. This may be caused by the difference between the interaction of the bottom chloride ion with a phenyl group. For complexes **5** and **6**, the chloride ion placed in the bottom position of the umbrella is just wrapped

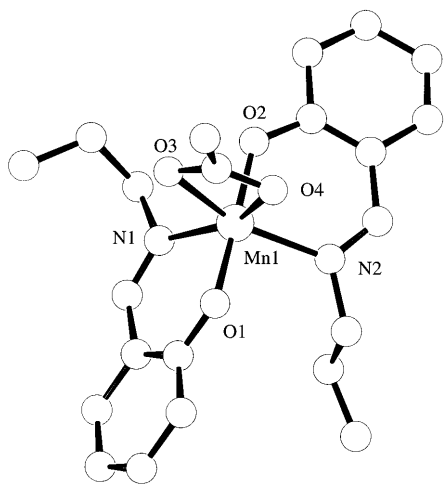


Fig. 1. The molecular structure of Mn^{III}(*N*-Pr-sal)$_2$OAc (**1**) with hydrogen atoms omitted for clarity.

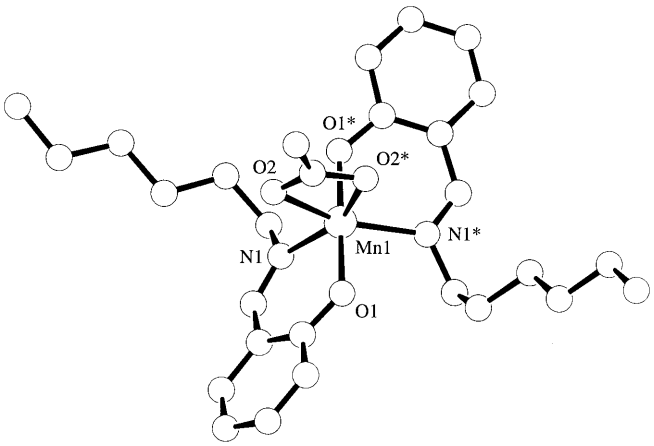


Fig. 2. The molecular structure of $Mn^{III}(N\text{-Hx-sal})_2OAc$ (**2**) with hydrogen atoms omitted for clarity.

with two phenyl rings, which may have the affect of pressing it up toward the central manganese ion, whereas for complex **4** two chloride ions may interact with only one phenyl ring. The angles between a mean plane of N_2O_2 and phenyl ring are 41.52 for complex **5** and 42.12° for complex **6** and the torsion angles of two phenyl rings are 20.76 for complex **5** and 21.06° for complex **6**, respectively. The Cl–Mn–Cl angles of these three complexes are 180.0°, and their O–Mn–O and N–Mn–N angles are close to 180.0°. Complex **4** is found to be the most symmetric among these complexes.

3.3. Structure of $Mn^{IV}(L)Cl_2$

Molecular structures of Mn^{IV}(salen)Cl_2 (**7**), Mn^{IV}(5–Br-salen)Cl_2 (**8**), and Mn^{IV}(5-Br-salpn)Cl_2 (**9**) are shown in Figs. 7–9, respectively. Their selected bond lengths and angles are listed in Table 6. Complex **8** crystallized in the orthorhombic space group $Pna2_1$. Its molecular structure has a distorted octahedral

Table 4
Selected bond lengths (Å) and angles (°) for **1**, **2** and **3**

$Mn^{III}(N\text{-Pr-sal})_2OAc$ (**1**)			
Mn(1)–O(1)	1.854(4)	Mn(1)–O(2)	1.850(4)
Mn(1)–O(3)	2.191(5)	Mn(1)–O(4)	2.220(5)
Mn(1)–N(1)	2.110(5)	Mn(1)–N(2)	2.112(5)
O(1)–Mn(1)–O(2)	178.9(3)		
O(1)–Mn(1)–N(1)	89.7(2)	O(2)–Mn(1)–N(1)	91.3(2)
O(1)–Mn(1)–N(2)	90.2(2)	O(2)–Mn(1)–N(2)	89.7(2)
O(1)–Mn(1)–O(3)	92.6(2)	O(2)–Mn(1)–O(3)	86.9(2)
O(1)–Mn(1)–O(4)	89.7(2)	O(2)–Mn(1)–O(4)	89.2(2)
N(1)–Mn(1)–N(2)	113.3(2)	O(3)–Mn(1)–O(4)	59.0(2)
$Mn^{III}(N\text{-Hx-sal})_2OAc$ (**2**)			
Mn(1)–O(1)	1.848(2)	Mn(1)–O(2)	2.192(2)
Mn(1)–N(1)	2.112(2)		
O(1)–Mn(1)–O(1)*	179.4(2)		
O(1)–Mn(1)–N(1)	89.08(9)	O(1)–Mn(1)–N(1)*	90.60(9)
O(1)–Mn(1)–O(2)	89.87(10)	O(1)–Mn(1)–O(2)*	90.62(9)
N(1)–Mn(1)–N(2)	110.4(1)	O(2)–Mn(1)–O(2)*	59.6(1)
$Mn^{III}(N\text{-Dod-sal})_2OAc$ (**3**)			
Mn(1)–O(1)	1.846(5)	Mn(1)–O(2)	2.201(7)
Mn(1)–N(1)	2.109(7)		
O(1)–Mn(1)–O(1)*	179.2(4)		
O(1)–Mn(1)–N(1)	88.8(3)	O(1)–Mn(1)–N(1)*	90.8(3)
O(1)–Mn(1)–O(2)	89.7(3)	O(1)–Mn(1)–O(2)*	91.0(3)
N(1)–Mn(1)–N(2)	109.7(4)	O(2)–Mn(1)–O(2)*	59.4(4)

configuration, in which the N_2O_2 donor set of the salen coordinated to the manganese ion to form an equatorial plane and the manganese ion displaced on a mean plane of N_2O_2 by 0.082 Å. Two chloride ions occupied a *trans* axial position and leaned toward the chelate ring formed by –N–Mn–N–$(CH_2)_2$– and the angle of Cl(1)–Mn(1)–Cl(2) was 167.9(1)°. This may be caused by the electronic repulsion between the chloride ions and the phenolic oxygen atoms, because electron negativity of oxygen atom is larger than that of nitrogen atom. Although one phenyl ring of the salen forms a co-plane with the mean plane of N_2O_2 (2.68°), the other one clearly deviates from this plane about 18.45°. Thus

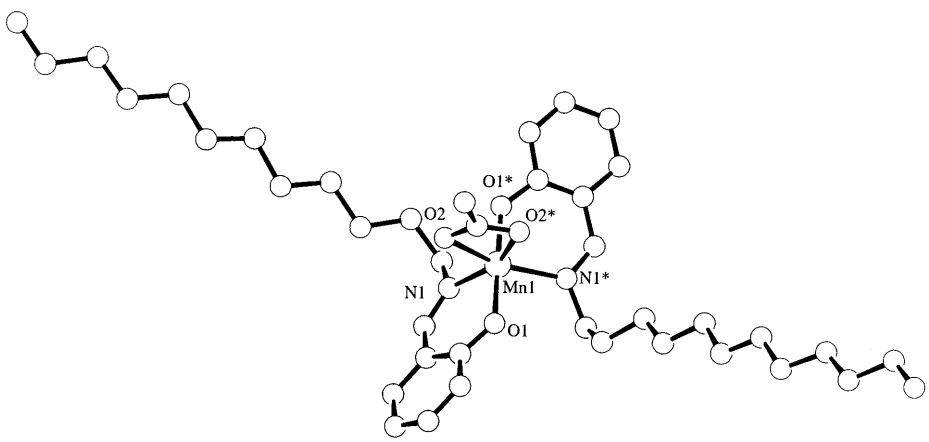


Fig. 3. The molecular structure of $Mn^{III}(N\text{-Dod-sal})_2OAc$ (**3**) with hydrogen atoms omitted for clarity.

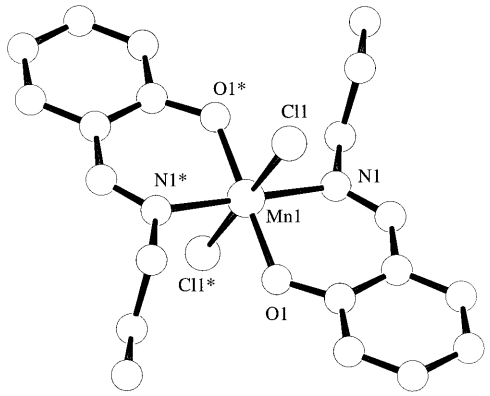


Fig. 4. The molecular structure of $Mn^{IV}(N\text{-Pr-sal})_2Cl_2$ (**4**) with hydrogen atoms omitted for clarity.

two chloride ions are no longer equivalent, which reflects difference in the Mn–Cl bond lengths: The bond length of Mn(1)–Cl(1) is 2.342(4) Å, of which the Cl(1) is coordinated to the manganese ion from the opposite site of the deviated phenyl ring, which is longer than the bond length of Mn(1)–Cl(2), 2.190(4) Å.

Complex **9** crystallized in the monoclinic space group $P2_1/c$. This complex consists of crystallographically independent two molecules. The molecular structure of complex **9** is very similar to that of $Mn^{IV}(salpn)Cl_2$ reported previously [28], in which the 5-Br-salpn coordinated to the manganese ion to form an equatorial plane by the N_2O_2 donor set and two chloride ions occupied a *trans* axial position. The central manganese ion displaced on a mean plane of N_2O_2 by 0.005 Å. Like complex **8**, two chloride ions leaned toward the chelate ring formed by –N–Mn–N–$(CH_2)_3$– and the angle of Cl(1)–Mn(1)–Cl(2) was 172.6(2)°. However, the two phenyl rings of the 5-Br-salpn are bent in the same direction, forming an umbrella, which is very similar to those observed for $Mn^{IV}(N\text{-Dod-sal})_2Cl_2$ and $Mn^{IV}(N\text{-Oct-sal})_2Cl_2$ mentioned above. The angle between one phenyl ring and a mean plane of N_2O_2 is 13.81° and the other angle is 28.81°. Moreover, the torsion angle between two phenyl rings are 42.58°, which is larger compared to those for complexes **5** and **6**. Thus, the bond lengths of Mn(1)–Cl(1) and Mn(1)–Cl(2) are not equivalent: the former is 2.281(4) and the latter 2.241(4) Å, where Cl(1) and Cl(2) denote a chloride ion coordinated to the manganese ion from the top and bottom of the umbrella, respectively. Moreover, a mean Mn–Cl bond length (2.261 Å) of this

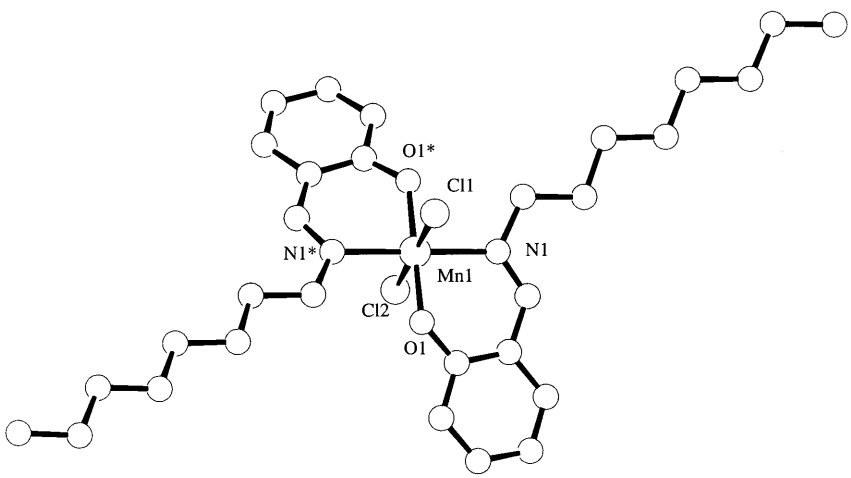


Fig. 5. The molecular structure of $Mn^{IV}(N\text{-Oct-sal})_2Cl_2$ (**5**) with hydrogen atoms omitted for clarity.

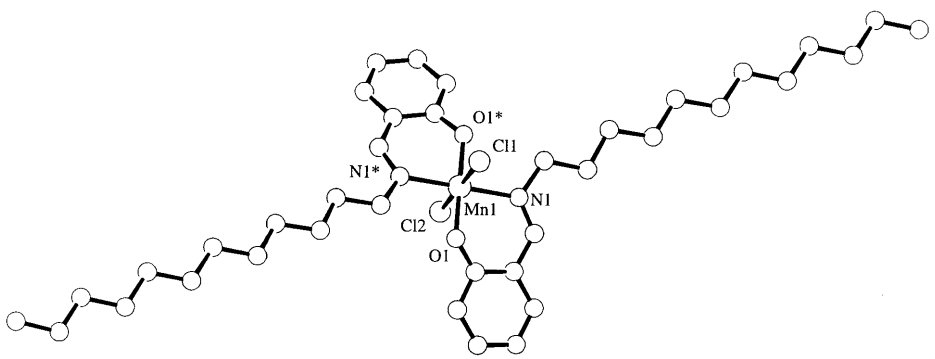


Fig. 6. The molecular structure of $Mn^{IV}(N\text{-Dod-sal})_2Cl_2$ (**6**) with hydrogen atoms omitted for clarity.

Table 5
Selected bond lengths (Å) and angles (°) for **4**, **5** and **6**

$Mn^{IV}(N\text{-Pr-sal})_2Cl_2$ (**4**)			
Mn(1)–Cl(1)	2.258(2)	Mn(1)–O(1)	1.849(6)
Mn(1)–N(1)	2.024(6)		
Cl(1)–Mn(1)–Cl(1)	180.0		
Cl(1)–Mn(1)–O(1)	89.8(2)	Cl(1)–Mn(1)–O(1)*	90.2(2)
Cl(1)–Mn(1)–N(1)	89.3(2)	Cl(1)–Mn(1)–N(1)*	90.7(2)
O(1)–Mn(1)–N(1)	89.7(3)	O(1)–Mn(1)–N(1)*	90.3(3)
O(1)–Mn(1)–O(1)*	180.0	N(1)–Mn(1)–N(1)*	180.0
$Mn^{IV}(N\text{-Oct-sal})_2Cl_2$ (**5**)			
Mn(1)–Cl(1)	2.270(2)	Mn(1)–Cl(2)	2.248(2)
Mn(1)–O(1)	1.851(3)	Mn(1)–N(1)	2.035(3)
Cl(1)–Mn(1)–Cl(2)	180.0		
Cl(1)–Mn(1)–O(1)	89.7(1)	Cl(1)–Mn(1)–N(1)	89.9(1)
Cl(2)–Mn(1)–O(1)	90.3(1)	Cl(2)–Mn(1)–N(1)	90.1(1)
O(1)–Mn(1)–N(1)	90.4(1)	O(1)–Mn(1)–N(1)*	89.6(1)
O(1)–Mn(1)–O(1)*	179.5(2)	N(1)–Mn(1)–N(1)*	179.9(2)
$Mn^{IV}(N\text{–Dod-sal})_2Cl_2$ (**6**)			
Mn(1)–Cl(1)	2.272(3)	Mn(1)–Cl(2)	2.243(3)
Mn(1)–O(1)	1.850(3)	Mn(1)–N(1)	2.039(5)
Cl(1)–Mn(1)–Cl(2)	180.0		
Cl(1)–Mn(1)–O(1)	89.6(2)	Cl(1)–Mn(1)–N(1)	90.7(2)
Cl(2)–Mn(1)–O(1)	90.4(2)	Cl(2)–Mn(1)–N(1)	89.3(2)
O(1)–Mn(1)–N(1)	90.5(2)	O(1)–Mn(1)–N(1)*	89.5(2)
O(1)–Mn(1)–O(1)*	179.1(3)	N(1)–Mn(1)–N(1)*	178.7(3)

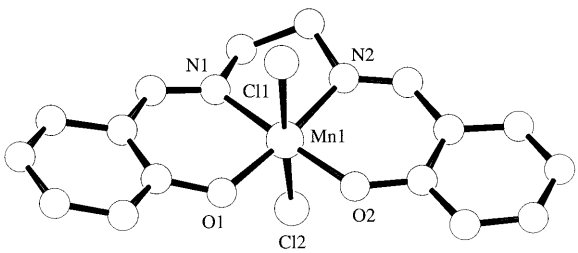


Fig. 7. The molecular structure of $Mn^{IV}(salen)Cl_2$ (**7**) with hydrogen atoms omitted for clarity.

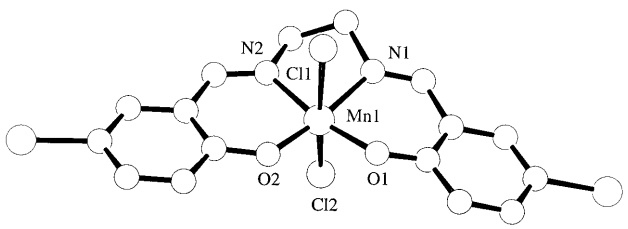


Fig. 8. The molecular structure of $Mn^{IV}(5\text{-Br-salen})Cl_2$ (**8**) with hydrogen atoms omitted for clarity.

complex is slightly shorter than that of complex **8** (2.266 Å) and that of $Mn^{IV}(salpn)Cl_2$ (2.2715 Å). This difference in the bond lengths of Mn–Cl may be caused by the difference in interaction between a chloride ion and a phenyl ring. The chloride ion placed in the bottom position is just wrapped with two phenyl rings, which may act to press it up toward the central manganese ion.

Complex **7** crystallized in the monoclinic space group $P2_1$ as mixed crystals with $Mn^{III}(salen)Cl$, which included one acetone molecule as a crystalline solvent. The molecular structure of this complex is very similar to that of complex **8**. The manganese ion displaced on a mean plane of N_2O_2 by 0.031 Å. Two chloride ions

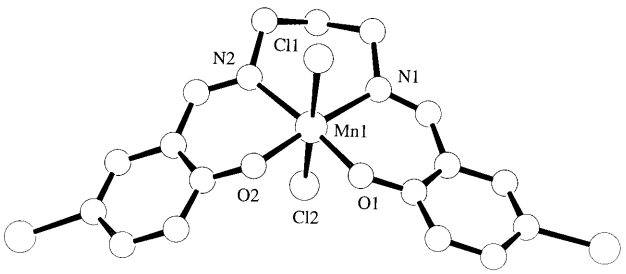


Fig. 9. The molecular structure of $Mn^{IV}(5\text{-Br-salpn})Cl_2$ (**9**) with hydrogen atoms omitted for clarity.

Table 6
Selected bond lengths (Å) and angles (°) for **7**, **8** and **9**

$Mn^{IV}(salen)Cl_2$ (**7**)			
Mn(1)–Cl(1)	2.299(3)	Mn(1)–Cl(2)	2.277(4)
Mn(1)–O(1)	1.848(6)	Mn(1)–O(2)	1.847(6)
Mn(1)–N(1)	1.974(7)	Mn(1)–N(2)	1.977(8)
Cl(1)–Mn(1)–Cl(2)	174.5(1)		
Cl(1)–Mn(1)–O(1)	88.9(3)	Cl(1)–Mn(1)–O(2)	93.2(2)
Cl(1)–Mn(1)–N(1)	86.6(3)	Cl(1)–Mn(1)–N(2)	87.2(3)
Cl(2)–Mn(1)–O(1)	93.0(2)	Cl(2)–Mn(1)–O(2)	91.9(2)
Cl(2)–Mn(1)–N(1)	88.1(2)	Cl(2)–Mn(1)–N(2)	90.5(2)
O(1)–Mn(1)–O(2)	92.1(3)	O(1)–Mn(1)–N(1)	92.1(3)
O(1)–Mn(1)–N(2)	173.6(3)	O(2)–Mn(1)–N(1)	174.4(3)
O(2)–Mn(1)–N(2)	94.2(3)	N(1)–Mn(1)–N(2)	81.5(3)
$Mn^{IV}(5\text{-Br-salen})Cl_2$ (**8**)			
Mn(1)–Cl(1)	2.342(4)	Mn(1)–Cl(2)	2.190(4)
Mn(1)–O(1)	1.837(7)	Mn(1)–O(2)	1.774(8)
Mn(1)–N(1)	2.045(8)	Mn(1)–N(2)	1.982(9)
Cl(1)–Mn(1)–Cl(2)	167.9(1)		
Cl(1)–Mn(1)–O(1)	89.7(3)	Cl(1)–Mn(1)–O(2)	92.0(3)
Cl(1)–Mn(1)–N(1)	82.2(3)	Cl(1)–Mn(1)–N(2)	85.2(3)
Cl(2)–Mn(1)–O(1)	95.0(3)	Cl(2)–Mn(1)–O(2)	98.6(3)
Cl(2)–Mn(1)–N(1)	86.6(2)	Cl(2)–Mn(1)–N(2)	88.2(3)
O(1)–Mn(1)–O(2)	95.3(4)	O(1)–Mn(1)–N(1)	89.6(3)
O(1)–Mn(1)–N(2)	169.0(4)	O(2)–Mn(1)–N(1)	172.5(4)
O(2)–Mn(1)–N(2)	94.5(4)	N(1)–Mn(1)–N(2)	80.2(3)
$Mn^{IV}(5\text{-Br-salpn})Cl_2$ (**9**)			
Mn(1)–Cl(1)	2.281(4)	Mn(1)–Cl(2)	2.241(4)
Mn(1)–O(1)	1.856(8)	Mn(1)–O(2)	1.870(8)
Mn(1)–N(1)	2.038(10)	Mn(1)–N(2)	2.036(10)
Cl(1)–Mn(1)–Cl(2)	172.6(2)		
Cl(1)–Mn(1)–O(1)	91.8(3)	Cl(1)–Mn(1)–O(2)	92.2(3)
Cl(1)–Mn(1)–N(1)	88.5(3)	Cl(1)–Mn(1)–N(2)	87.3(3)
Cl(2)–Mn(1)–O(1)	93.9(3)	Cl(2)–Mn(1)–O(2)	93.0(3)
Cl(2)–Mn(1)–N(1)	86.7(3)	Cl(2)–Mn(1)–N(2)	87.7(3)
O(1)–Mn(1)–O(2)	84.7(4)	O(1)–Mn(1)–N(1)	90.8(4)
O(1)–Mn(1)–N(2)	173.2(4)	O(2)–Mn(1)–N(1)	175.5(4)
O(2)–Mn(1)–N(2)	88.6(4)	N(1)–Mn(1)–N(2)	95.9(4)

occupied a *trans* axial position leaned toward the chelate ring formed by –N–Mn–N–$(CH_2)_2$– and the Cl(1)–Mn(1)–Cl(2) angle was 174.5(1)°. One phenyl ring of the salen is almost co-planar (4.00°) with a mean plane of N_2O_2 but the other one deviates by 16.13°. Thus, like complex **8**, two chloride ions are not equivalent: the bond lengths of Mn–Cl are 2.299(3) for Mn(1)–Cl(1) and 2.277(4) Å for Mn(1)–Cl(2), where the Cl(1) is placed at the position of the deviated phenyl ring.

All of the dichloromanganese(IV) complexes with tetradentate Schiff base ligands have a distorted octahedral structure. Comparison of the bond lengths of Mn–Cl and Mn–O between complexes **7** and **8**, and those between complex **9** and Mn^{IV}(salpn)Cl_2 has revealed that the introduction of 5-bromo substituent to the phenyl group induced shortening both bond lengths. Moreover, the Cl(1)–Mn(1)–Cl(2) angle has been found to be smaller in the complexes having 5-bromo substituent than in the non-subsituted complexes. These may be affected by both electron-withdrawing and steric effects of 5-bromo group.

4. Conclusions

X-ray crystallographic analyses have revealed that the dichloromanganese(IV) Schiff base complexes have a distorted octahedral structure, in which two chloride ions occupied a *trans* position and the N_2O_2 donor set of the Schiff base ligands coordinated to the central manganese ion to form an equatorial plane. Moreover, a configuration of the phenyl rings of the Schiff base ligands reflects the bond lengths and angles of Mn–Cl coordination environment.

5. Supplementary data

Supplementary data have been deposited with the Cambridge Crystallographic Data Centre, CCDC Nos. 142065–142073 for complexes **1**–**9**, respectively. Copies of this information are available free of charge from The Director, CCDC, 12 Union Road, Cambridge, CB2 1EZ, UK (fax: +44-1223-336033; e-mail: deposit@ccdc.cam.ac.uk or www: http://www.ccdc.cam.ac.uk).

References

[1] N.A. Law, M.T. Caudle, V.L. Pecoraro, Adv. Inorg. Chem. 46 (1998) 305.
[2] V.L. Pecoraro, Manganese Redox Enzymes, VCH, New York, 1992.
[3] V.K. Yachandra, V.J. DeRose, M.J. Latimer, I. Mukerji, K. Sauer, M.P. Klein, Science 260 (1993) 675.
[4] V.L. Pecoraro, M.J. Baldwin, A. Gelasco, Chem. Rev. 94 (1994) 807.
[5] V.K. Yachandra, K. Sauer, M.P. Klein, Chem. Rev. 96 (1996) 2927.
[6] W. Rüttinger, G.C. Dismukes, Chem. Rev. 97 (1997) 1.
[7] C.W. Hoganson, G.T. Babcock, Science 277 (1997) 1953.
[8] C. Tommos, G.T. Babcook, Acc. Chem. Res. 31 (1998) 18.
[9] P.E.M. Siegbahn, R.H. Crabtree, J. Am. Chem. Soc. 121 (1999) 117.
[10] J. Limburg, J.S. Vrettos, L.M. Liable-Sands, A.L. Rheingold, R.H. Crabtree, G.W. Brudving, Science 283 (1999) 1524.
[11] J.E. Penner-Hahn, R.M. Fronko, V.L. Pecoraro, C.F. Yocum, S.D. Betts, N.R. Bowlby, J. Am. Chem. Soc. 112 (1990) 2549.
[12] V.J. Derose, I. Mukerji, M.J. Latimer, V.K. Yachandra, K. Sauer, M.P. Klein, J. Am. Chem. Soc. 116 (1994) 5239.
[13] S. Wang, H.L. Tsai, E. Libby, K. Folting, W.E. Streib, D.N. Hendrickson, G. Christou, Inorg. Chem. 35 (1996) 7578.
[14] A. Rompel, J.C. Andrews, R.M. Cinco, M.W. Wemple, G. Christou, N.A. Law, V.L. Pecoraro, K. Sauer, V.K. Yachandra, M.P. Klein, J. Am. Chem. Soc. 119 (1997) 4465.
[15] M.R.A. Blomberg, P.E.M. Siegbahn, S. Styring, G.T. Babcock, B. Akermark, P. Korall, J. Am. Chem. Soc. 119 (1997) 8285.
[16] T. Matsushita, H. Kono, T. Shono, Bull. Chem. Soc. Jpn. 54 (1981) 2646.
[17] T. Matsushita, T. Shono, Polyhedron 2 (1983) 613.
[18] T. Matsushita, Y. Hirata, T. Shono, Bull. Chem. Soc. Jpn. 55 (1982) 108.
[19] T. Matsushita, M. Fujiwara, T. Shono, Chem. Lett. (1982) 631.
[20] M. Fujiwara, T. Matsushita, T. Shono, Polyhedron 4 (1985) 1895.
[21] TEXSAN, Crystal Structure Analysis Package, Molecular Structure Corporation (1985 and 1992).
[22] MITHRIL-84: Gilmore, C.J.; MITHRIL, an integrated direct methods computer program, J. Appl. Cryst. 17, 42–46, University of Glasgow, Scotland (1984).
[23] MULTAN-88, Debaerdemaeker, T., Germain, G., Main, P., Refaat, L.S., Tate, C. and Woolfson, M.M. (1988). Computer programs for the automatic solution of crystal structures from X-ray diffraction data, University of York, UK
[24] SAPI-91: Fan Hai-Fu (1991). Structure Analysis Programs with Intelligent Control, Rigaku Corporation, Tokyo, Japan.
[25] G.M. Sheldrick, SHELXS-86, in: G.M. Sheldrick, C. Kruger, R. Goddard (Eds.), Crystallographic Computing, vol. 3, Oxford University Press, Oxford, 1985, p. 175.
[26] P.T. Beurskens, G. Admiraal, G. Beurskens, W.P. Bosman, S. Garcia-Granda, R.O. Gould, J.M.M. Smits, C. Smykalla, PATTY, the DIRDIF program system, in: Technical Report of the Crystallography Laboratory, University of Nijmegen, The Netherlands, 1992.
[27] P.T. Beurskens, G. Admiraal, G. Beurskens, W.P. Bosman, R. de Gelder, R. Israel, J.M.M. Smits, The DIRDIF-94 program system, in: Technical Report of the Crystallography Laboratory, University of Nijmegen, The Netherlands, 1994.
[28] N.A. Law, T.E. Machonkin, J.P. McGorman, E.J. Larson, J.W. Kampf, V.L. Pecoraro, J. Chem. Soc., Chem. Commun. (1995) 2015.
[29] D.P. Kessissoglou, W.M. Butler, V.L. Pecoraro, J. Chem. Soc., Chem. Commun. (1986) 1253.
[30] S.K. Chandra, P. Basu, D. Ray, S. Pal, A. Chakravortry, Inorg. Chem. 29 (1990) 2429.
[31] E.J. Larson, V.L. Pecoraro, J. Am. Chem. Soc. 113 (1991) 3810.
[32] M. Mikuriya, D. Jie, Y. Kakuta, T. Tokii, Bull. Chem. Soc. Jpn. 66 (1993) 1132.
[33] M.R. Bermejo, A. Castineiras, J.C. Garcia-Monteagudo, M. Rey, A. Sousa, M. Watkinson, C.A. McAuliffe, R.G. Pritchard, R.L. Beddoes, J. Chem. Soc., Dalton Trans. (1996) 2935.

[34] H. Torayama, T. Nishide, H. Asada, M. Fujiwara, T. Matsushita, Chem. Lett. (1996) 387.
[35] H. Torayama, H. Asada, M. Fujiwara, T. Matsushita, Chem. Lett. (1996) 1067.
[36] H. Torayama, T. Nishide, H. Asada, M. Fujiwara, T. Matsushita, Polyhedron 16 (1997) 3787.
[37] H. Torayama, T. Nishide, H. Asada, M. Fujiwara, T. Matsushita, Polyhedron 17 (1998) 105.
[38] H. Torayama, H. Asada, M. Fujiwara, T. Matsushita, Polyhedron 17 (1998) 3859.
[39] H. Asada, M. Ozeki, M. Fujiwara, T. Matsushita, Chem. Lett. (1999) 525.

PERGAMON

www.elsevier.nl/locate/poly

Polyhedron 19 (2000) 2049–2057

POLYHEDRON

An ESR study of the copper(II)-glycyl-L-histidine system in aqueous solution by the simultaneous analysis of multi-component spectra. Formation constants and coordination modes

Terézia Szabó-Plánka [a,*], Nóra Nagy [a], Antal Rockenbauer [b], László Korecz [b]

[a] *Department of Physical Chemistry, University of Szeged, PO Box 105, H-6701 Szeged, Hungary*
[b] *Chemical Research Center, Institute of Chemistry, Hungarian Academy of Sciences, H-1525 Budapest, Hungary*

Received 20 April 2000; accepted 10 July 2000

Abstract

A series of multi-component ESR spectra of fluid aqueous solutions containing glycyl-L-histidine and copper(II) at 1:1 and 20:1 concentration ratios, taken in a circulating system at various pH, have been analysed simultaneously. The isotropic ESR parameters (g-factors, hyperfine coupling constants for the ^{63}Cu and ^{65}Cu isotopes and maximum four non-equivalent ^{14}N nuclei, and relaxation parameters) and the formation constants of the various complexes were optimized. In the acidic region, the new species $[CuLH_2]^{3+}$, has been shown and the formation of the pH-metrically identified species $[CuLH]^{2+}$, $[CuL]^{+}$ and $[CuLH_{-1}]$ has been supported. The coordination in the first three complexes is reminiscent of that in simple dipeptides: it is likely to take place at first by the carboxylate O, then by the amino N and peptide O, and then by the amino N, deprotonated peptide N and carboxylate O atoms in equatorial positions, respectively, while the imidazole ring remains protonated. In the species $[CuLH_{-1}]$, the non-protonated imidazole nitrogen displaces the carboxylate oxygen from the equatorial coordination. In the alkaline region of the equimolar solutions the spectra could be described consistently in terms of the formation of four species: three of them, the complex $[Cu_2L_2H_{-3}]^{-}$ and the two coordination isomers of the complex $[CuLH_{-2}]^{-}$ are ESR-active, while the tetramer $[Cu_4L_4H_{-8}]^{4-}$ is ESR-inactive. For the complex $[CuLH_{-2}]^{-}$, one of the isomers is the species $[CuLH_{-1}(OH)]^{-}$, while the other one has the imidazole ring deprotonated. At ligand excess the region pH 7–10 is dominated by the pH-metrically identified complexes $[CuL_2]$ and $[CuL_2H_{-1}]^{-}$. In these species the first ligand is bound equatorially by the amino, deprotonated peptide and imidazole nitrogen atoms. The second dipeptide is co-ordinated either by the amino nitrogen in equatorial and the peptide oxygen in axial position (4N isomer), or vice versa (3N isomer) in both bis complexes. © 2000 Elsevier Science Ltd. All rights reserved.

Keywords: ESR; Copper(II) complexes; Glycyl-L-histidine; Formation constants; Coordination modes; Isomerism

1. Introduction

Owing to their biological importance, the copper(II) complexes of glycyl-L-histidine [1–5] and related peptide ligands [6–9] have been extensively studied. The compositions and the formation constants of most species are known, though the formation of the various oligonuclear complexes is under debate, and the divergences in the literature formation constants of the bis complexes are unusually high. The coordination modes are less understood, since a new donor group, the imidazole ring, further increases the variety of possible structures, as compared to the simple dipeptides. Some authors stressed the similarities between the coordination properties of glycyl-L-histidine and simple dipeptides: in strongly alkaline solutions the proton loss of the equatorial water molecule was suggested to dominate, resulting in the formation of the $[CuLH_{-1}(OH)]^{-}$ complex [1,3,5,10]. Other authors [2] assumed the deprotonation of the pyrrolic NH group and the formation of the tetrameric complex $[Cu_4L_4H_{-8}]^{4-}$. For the bis complexes it is generally accepted that one of the peptide nitrogens is deprotonated, i.e. the correct formulae for these complexes are $[Cu(LH_{-1})(LH)]$ and $[Cu(LH_{-1})L]^{-}$, respectively [1–5] and a tridentate equatorial ligation of the deprotonated dipeptide is

* Corresponding author. Tel.: +36-62-544-612; fax: +36-62-544-652.
E-mail address: szabot@chem.u-szeged.hu (T. Szabó-Plánka).

0277-5387/00/$ - see front matter © 2000 Elsevier Science Ltd. All rights reserved.
PII: S0277-5387(00)00504-0

proposed. The other ligand is suggested to be bound by the imidazole nitrogen atom [1–3,8,9] in both bis complexes, i.e. the previous studies have led to the conclusion that even the non-protonated amino group of the 'L' ligand does not bind to the copper. At the same time, for the analogous $[Cu(LH_{-1})L]^{-}$ (and also $[CuL]^{+}$) complexes of the simple dipeptides, fairly stable structures are formed by the simultaneous coordination of the amino nitrogen and the peptide oxygen atoms [11].

ESR spectroscopy can provide valuable evidence on the coordination modes. In the case of minor species and/or isomeric equilibria this requires the decomposition of overlapping multi-component spectra. Previous studies were based upon the analysis of the resolved nitrogen superhyperfine structure of the high-field ^{63}Cu peak in the isotropic ESR spectra. The measured band was described in terms of two component bands [12–14]. Recently we have developed a new program [15] for the overall analysis of multi-component (up to four components) ESR spectra which was used to determine the ESR parameters and the relative concentrations of minor and major species in several copper(II)–dipeptide [16] and amino acid [17,18] systems.

Very recently we applied a basically new approach to analyse the multi-component isotropic ESR spectra: instead of the separate simulation of experimental curves we carry out a simultaneous fit for a whole series of a maximum of 36 spectra. The method allows determination of both the formation constants and the ESR parameters for a maximum of ten active species with a great confidence [19]. In the present work we report on the ESR-spectroscopic study of the copper(II)-glycyl-L-histidine system. We aimed to identify all the complexes including possible coordination and geometric isomers forming in liquid aqueous solutions, to obtain their formation constants, and to characterize the coordination modes on the basis of the ESR parameters.

2. Experimental

2.1. Reagents and solutions

The glycyl-L-histidine ligand–denoted by HL in its neutral form from FLUKA and other reagents from Reanal (Hungary) were of analytical grade and were used without further purification. The copper(II) concentration of the solutions was 2 or 5 mmol dm^{-3} at a ligand-to-metal concentration ratio 1:1, and 5 mmol dm^{-3} at a 20-fold ligand excess. The optimum conditions for the ESR measurements (concentrations and pH) were chosen according to the requirement that even the less stable species form in as high concentration as possible to obtain the most reliable parameters. Preliminary species distribution curves were calculated by the PSEQUAD program [20] from literature formation constants [1,2]. The pH was adjusted with HCl, then NaOH to an accuracy of 0.01 pH units using a Radelkis OP208/1 pH meter equipped with a Radiometer GK2401C combined glass electrode. The electrode was calibrated with IUPAC Standard Buffers from Radiometer.

2.2. ESR measurements

The ESR spectra were recorded at r.t. (291 K) under argon atmosphere in a circulating system. All the details are given in our previous work [18].

2.3. Evaluation of spectra

Before the analysis, the 'glass signal' (the curve of the capillary tube filled with distilled water, together with the manganese peaks) was subtracted from the spectra. Since the copper(II) chloride, used to make the stock solution, was a natural mixture of isotopes, the spectrum of each species was calculated as the sum of spectra containing ^{63}Cu and ^{65}Cu weighted by their abundance in nature. The different widths of copper hyperfine lines were taken into consideration by fitting the relaxation parameters α, β, γ, where $\sigma_{MI} = \alpha + \beta M_I + \gamma M_I^2$. The parameter g_o, the hyperfine (hf) coupling constant A_o, the nitrogen superhyperfine (shf) coupling constants a_{No}, the above relaxation parameters, and the formation constant of each ESR-active complexes were varied, until the overall sum of the squares of differences between the calculated and measured intensities (overall SSQD) reached its minimum. The quality of fit for each spectrum was shown by the average square deviation SQD (i.e. SSQD divided by the number of spectral points, 500). The sensitivity of the spectral fit to the various parameters was characterized by the CNF value. It is defined as the variation of the respective parameter that increases the overall SQD by the value of the average square noise, while the other parameters are kept constant. (The overall SQD is the sum of the SQD values over the whole series of spectra under analysis. The square noise obtained from the lowest- and the highest-field parts of each spectrum was averaged over the whole series, resulting in the average square noise.)

The series of 40 spectra has been evaluated by the 2D_EPR program [19]. Since in this system more than ten ESR-active species are forming (see below), the experimental curves were evaluated in two steps. At first, all the spectra of equimolar solutions in the pH range 2.5–12.2 and the curves taken at ligand excess between pH 2.5 and 6.4 were analysed simultaneously, fitting the ESR parameters and the formation constants of each ESR-active species, except for the complex $[CuL_2H_{-1}]^{-}$. In the second step the same spectra of

equimolar solutions, though only below pH 7, and the same spectra at ligand excess together with additional curves up to pH 10 (a series of 23 spectra) were evaluated simultaneously: now the data for both bis complexes and those for the mono species forming in acidic solutions (see below) were optimized. The parameters obtained for the same complexes agreed excellently: the divergences in g_o, in the parameters of field dimension, and in the formation constants were less than 0.0002, 0.3 G and 0.05 log units, respectively. Here we report their averages.

For the determination of the formation constant of the inactive species, the difference of the analytical and the calculated total copper(II) concentration was minimized.

The coupling constants and the relaxation parameters of field dimension are given in gauss (G) units throughout the paper; $1\ G = 10^{-4}$ T.

3. Results and discussion

3.1. Spectral fitting

The rate of interconversion between the various complexes was regarded to be slow on the ESR time-scale, since the experimental curves could be well described as sums of individual spectra. A Lorentzian lineshape gave a good fit in all cases: the average deviation of the calculated and measured intensities was 1.4–1.9 times as much as the noise. The spectral fit was fairly sensitive to the formation constant of each species in our model: the CNF values were 0.05–0.08 log units. The typical CNF for the g_o was $2–10 \times 10^{-4}$, while for the A_o it was 0.2–1 G. In the cases of aqua, the $[CuLH_2]^{3+}$ and $[CuLH]^{2+}$ complexes, and particularly the dimeric species of very broad spectral lines, higher CNF values (0.001–0.004 for g_o and 2–4 G for A_o) were found. The CNF values for the relaxation parameters were typically 0.2–5 G, the highest values were the α parameters of the above-mentioned four species again. In the case of the shf coupling constants, the CNF was 0.5–1.6 G (4–15% of a_{No}), with the exception of the $[CuLH]^{2+}$ complex, where the fit was only slightly sensitive to a_{No}. For isomer 1 of the $[CuLH_{-2}]^{-}$ complex the CNF values of the coupling constants and the relaxation parameters were intermediate between those of the above two groups of complexes.

3.2. Verification of the equilibrium model

According to the pH-potentiometric studies [1–9] in the acidic region the aqua complex is displaced by the mono complexes $[CuLH]^{2+}$, $[CuL]^{+}$ and $[CuLH_{-1}]$. In strongly acidic media, however, these four species proved to be insufficient for the consistent description of ESR spectra: it was necessary to also imply the complex $[CuLH_2]^{3+}$, otherwise the parameters for the aqua complex differed significantly from those obtained in the absence of the ligand, and the SQD values increased by 5–10% at ligand excess. The formation constants obtained from the ESR analysis for the above pH–potentiometrically identified species agree well with the literature values (Table 1), and so the concentration distribution curves in the acidic pH region are in good accordance with those calculated from the pH–potentiometric formation constants averaged over the data at 25°C [1,2,4] (Fig. 1).

The pH–potentiometric studies gave a controversial description for the alkaline region of equimolar solutions. According to Brookes and Pettit [1] the $[CuLH_{-1}]$ complex is displaced by the species $[Cu_2L_2H_{-3}]^{-}$, then $[CuLH_{-2}]^{-}$ with increasing pH. Other authors did not take into consideration the dimer [2–6]. Sóvágó and co-workers [2] regarded the deprotonation of the $[CuLH_{-1}]$ complex as the proton loss of the pyrrolic nitrogen, leading to the formation of the species $[Cu_4L_4H_{-8}]^{4-}$, but they did not report the formation constant for the tetramer. For other, related systems an ESR-inactive tetramer and an ESR-active monomer were shown [8,9] under similar conditions.

For the glycyl-L-histidine ligand in moderately alkaline media, where the proton loss of the $[CuLH_{-1}]$ complex starts, the measured ESR curves contain a non-resolved component spectrum which can be as-

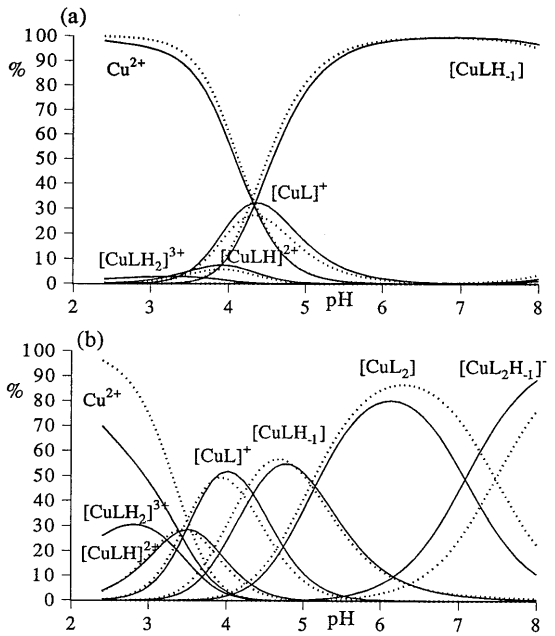


Fig. 1. Distribution of copper(II) (5 mM) amongst the pH–potentiometrically identified species as a function of pH at a ligand-to-metal concentration ratio (a) 1:1, (b) 20:1. Dotted line: curves calculated from the average literature pH–potentiometric formation constants at 25°C. Solid line: concentrations obtained from our ESR formation constants.

Table 1
Formation constants as log β for the copper(II) complexes of glycyl-L-histidine and related ligands

Method:	ESR		pH–potentiometry				
Complex	This work [a]	Ref. [7] [b,c]	Ref. [7] [b]	Ref. [5]	Ref. [1]	Ref. [2]	Ref. [4]
$[CuLH2]^{3+}$	15.86						
$[CuLH]^{2+}$	12.65	12.08		12.25		12.45	
$[CuL]^{+}$	9.17	8.76	8.93	8.68	9.14	9.06	8.83
$[CuLH_{-1}]$	4.81	4.76	4.58	4.54	4.89	4.91	4.60
$[Cu_2L_2H_{-3}]^{-}$	1.92				2.2		
$[CuLH_{-2}]^{-}$	−5.10 [d]	−4.79	−4.85	−4.94	−4.84		−5.35
Isomer 1	−5.34						
Isomer 2	−5.47						
$[Cu_4L_4H_{-8}]^{4-}$	−11.78						
$[CuL_2]$	15.62 [d]	14.93	14.66	15.41	16.53	15.96	14.67
Isomer 1	15.33						
Isomer 2	15.31						
$[CuL_2H_{-1}]^{-}$	8.63 [d]	7.42		7.68	8.44	8.02	6.31
Isomer 1	8.35						
Isomer 2	8.30						

[a] For the proton complexes [LH], $[LH_2]^{+}$ and $[LH_3]^{2+}$ the literature log β values[1] of 8.2, 14.95 and 17.41, respectively, were used.
[b] Data for the L-alanyl-L-histidine complexes at 37°C.
[c] Obtained by decomposing the ESR intensities measured at various field to the contributions of the pH–potentiometrically identified complexes, without fitting the ESR parameters.
[d] $\log \beta = (\log(\beta_{\text{isomer 1}} + \beta_{\text{isomer 2}})$.

signed to the dimeric complex $[Cu_2L_2H_{-3}]^{-}$. Omitting this species the spectral fit is poor, particularly in the region pH 9–10 (Fig. 2), where the SQD is increased by 80–100%. This species was proposed also for dipeptides with non- and weakly co-ordinating side-chains [21].

Upon a further raise in pH the spectra revealed a considerable decrease in intensity (Fig. 3) in parallel with the deprotonation of the complexes $[CuLH_{-1}]$ and $[Cu_2L_2H_{-3}]^{-}$, suggesting the formation of an ESR-inactive species: the tetramer $[Cu_4L_4H_{-8}]^{4-}$ which was suggested previously on the basis of spectroscopic evidence [2,8,9]. For the satisfactory description of the spectra of the monomer species over pH 11 a two-component model proved to be necessary: this resulted in a 20–40% reduction of the SQD compared to the one-component model (Fig. 3) which indicates a coordination isomerism in the case of the species $[CuLH_{-2}]^{-}$.

At ligand excess, in nearly neutral and moderately alkaline media the species $[CuL_2]$ and $[CuL_2H_{-1}]^{-}$ have been shown by the pH–potentiometry [1–9]. The ESR spectra reveal several kinds of coordination again

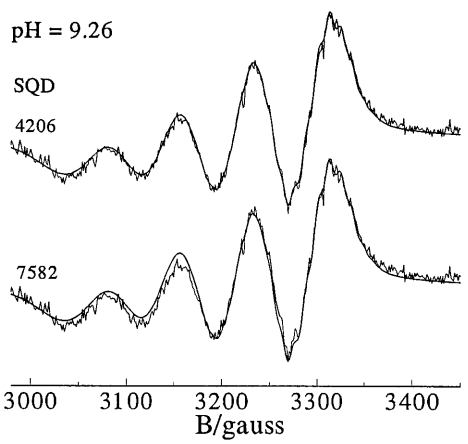


Fig. 2. Experimental ESR spectrum taken in equimolar (5 mM) solution at pH 9.26 together with the calculated curve, taking into consideration the $(Cu_2L_2H_{-3})^{-}$ complex (upper spectra), or omitting the dimer species (lower curves).

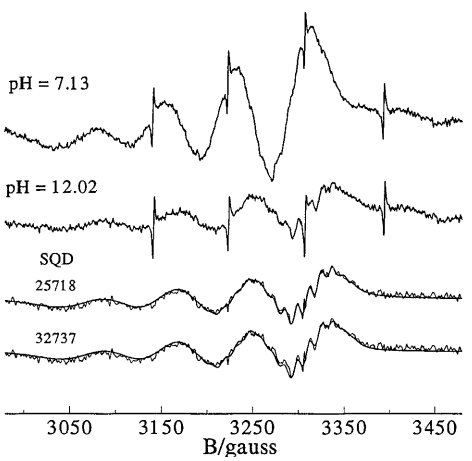


Fig. 3. ESR spectra in equimolar (5 mM) solution at pH 7.13 and 12.02. At higher pH the curves from top to bottom are the measured spectrum, then the corrected curve after subtracting the 'glass signal', together with the spectrum calculated as the sum of two component spectra, and finally the corrected curve together with a one-component calculated spectrum.

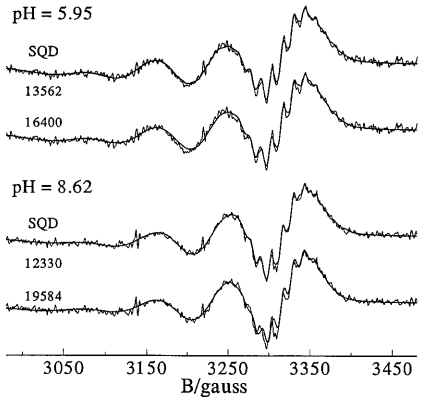


Fig. 4. ESR spectra taken at twenty-fold ligand excess at pH 5.95 and 8.62, at the maximum concentration of the $[CuL_2]$ and $[CuL_2H_{-1}]^-$ complexes, respectively, together with the curves calculated assuming two component spectra, one with a three-nitrogen, the other with a four-nitrogen shf splitting (upper spectra), or as one spectrum with a four-nitrogen shf pattern (lower curves).

for both complexes. The best spectral fit could be achieved with the assumption of two component spectra, where the ESR curve of higher g_o and A_o is described by a three-nitrogen shf pattern, while the other one by a four-nitrogen splitting ('3N + 4N' model). At ligand excess over pH 5.5, where the total concentration of the bis complexes exceeds 60%, the SQD increased by 20–50%, if one of the bis complexes was described by a one-component curve. (The spectral fit for the various models is shown in Fig. 4.)

When a 4N shf pattern ('4N + 4N' model) was applied to both component spectra of the bis complexes, the SQD values increased by about 3–4% up to pH 6.5 (near the maximum concentration of the $[CuL_2]$ complex, Fig. 1), then by 8–10% over pH 7 (where the $[CuL_2H_{-1}]^-$ complex is the major or the predominant species, Fig. 1). In the case of the $[CuL_2]$ complex, a slight impairing of the spectral fit cannot exclude alone the '4N + 4N' model. The '3N + 4N' model, in turn, was supported for this species also by the close similarity of the ESR parameters and the absorption spectra to those of the $[CuL_2H_{-1}]^-$ complex. The formation constants for the various copper(II)-glycyl-L-histidine complexes are summarized in Table 1, while their ESR parameters can be found in Table 2.

It should be noted that all the above bis and deprotonated mono complexes together with the tetramer proved to be insufficient for the consistent description of ESR spectra taken at ligand excess over pH 10. New deprotonation processes (the proton loss from the pyrrolic nitrogens or/and the second peptide nitrogen of bis complexes) may occur, resulting in even more species of similar parameters and relatively low concentration, which does not allow for an exact analysis.

3.3. Coordination modes of various species

3.3.1. Mono complexes and oligomers

For the $[CuLH_2]^{3+}$, $[CuLH]^{2+}$ and $[CuL]^+$ complexes of glycyl-L-histidine the parameters g_o and A_o (Table 2) are nearly equal to the corresponding data for the $[CuLH]^{2+}$, $[CuL]^+$ and $[CuLH_{-1}]$ complexes of glycylglycine [16] and glycyl-L-serine [18], respectively. This suggests that the imidazole ring remains protonated in the above species, and the coordination is similar to the corresponding complexes of the simple dipeptides (Fig. 5).

In the case of the $[CuLH_{-1}]$ complex the three-nitrogen shf pattern of the spectrum indicates that the carboxylate oxygen is replaced by the imidazole nitrogen atom in the equatorial coordination (Fig. 5). The tridentate equatorial ligation by nitrogen donors was proved by crystallographic studies [22] in solid state, and it was stated [22] that the carboxylate group of the equatorially co-ordinated dipeptide cannot bind to the same metal ion. In solution this structure was supported also by visible spectral evidence [2,8,9].

The ESR spectrum of unresolved hf structure (Fig. 6) for the complex $[Cu_2L_2H_{-3}]^-$ reflects on a magnetic dipole interaction between the paramagnetic centres, corresponding to the dimer structure. The coupling in the glycyl-L-histidine complex seems to be weaker than in the complexes of simple dipeptides that are diamagnetic [18,21].

For the $[CuLH_{-2}]^-$ complex it is rather difficult to assign the spectra of the isomers. Most likely the deprotonation takes place from either the pyrrolic nitrogen or the equatorial water molecule. For the analogous complexes of simple dipeptides only the latter process is possible, and mixed hydroxo complexes are formed. For these species a striking feature of the ESR spectra is the well-resolved shf splitting by equivalent nitrogen donors [10,16,18,23]. It is the spectrum of isomer 2 that shows a similar character; hence we assigned it to the mixed hydroxo complex. Accordingly, isomer 1 was regarded to have the pyrrolic nitrogen deprotonated (Fig. 5).

The tetramer $[Cu_4L_4H_{-8}]^{4-}$ is diamagnetic which indicates a strong co-operation between the copper(II) ions. This is likely to take place through the deprotonated imidazole rings which act as bidentate ligands connecting the neighbouring copper(II) ions, and simultaneously increase the number of equatorial nitrogen donors to four around the metal ions. The latter structure was assumed to explain the low wavelength of the d–d absorption band in equimolar solutions near pH

Table 2
ESR parameters for the various complexes in the copper(II)-glycyl-L-histidine system [a]

Complex		g_o	A_o (G)	a_{No} (G)	α (G)	β (G)	γ (G)
Cu^{2+}		2.1975	34.2		51.0	−1.6	0.8
$[CuLH_2]^{3+}$		2.1820	37.5		45.8	−5.6	0.4
$[CuLH]^{2+}$		2.1582	41.7	7.5	39.0	−13.7	5.4
$[CuL]^{+}$		2.1177	69.6	12.6	28.5	−8.5	2.2
				9.6			
$[CuLH_{-1}]$		2.1143	72.7	15.0	19.5	−9.8	2.2
				12.5			
				10.5			
$[Cu_2L_2H_{-3}]^{-}$		2.100	31.		58.0	0.1	7.7
$[CuLH_{-2}]^{-}$	isomer 1	2.1032	77.2	13.3	24.0	−8.6	4.5
				12.7			
				11.9			
	isomer 2	2.1063	80.0	12.9	17.2	−9.3	2.1
				12.9			
				12.9			
$[CuL_2]$	isomer 1	2.1067	82.7	14.4	23.4	−17.5	5.0
				12.7			
				9.6			
	isomer 2	2.0840	69.8	13.5	24.5	−15.4	2.7
				13.5			
				13.5			
				13.5			
$[CuL_2H_{-1}]^{-}$	isomer 1	2.1077	84.3	14.6	22.5	−17.6	5.0
				12.4			
				9.6			
	isomer 2	2.0857	71.8	13.9	25.8	−15.9	2.5
				13.9			
				13.9			
				13.9			

[a] The hyperfine coupling constants and the relaxation parameters refer to the isotope ^{63}Cu.

12 in the case of glycyl-L-histidine [2] and of related ligands [8,9].

3.3.2. Bis complexes

It is generally accepted that in the bis complexes only one of the peptide nitrogens is deprotonated, and the deprotonated ligand is bound to the copper(II) as in the ($CuLH_{-1}$) complex [1,2,8,9]. For the other ligand a monodentate coordination through the imidazole nitrogen has been suggested for both bis complexes [1,2,8,9]. The amino group was assumed to be protonated in the $[CuL_2]$ complex, and then to lose the proton simultaneously with the amino group of the free ligand, without binding to the copper(II). The arguments for this are (1) the deprotonation pK of the $[CuL_2]$ complex (7.5–8.4 from the data in Table 1) can be regarded nearly identical with the pK (8.2) for the deprotonation of the amino group in the free ligand, (2) for the glycyl-L-histidyl-glycine the deprotonation enthalpy of the $[CuL_2]$ complex is near the corresponding value for the amino group of the free ligand, and (3) the absorption [2,8,9] and CD [8] spectra of the $[CuL_2]$ and $[CuL_2H_{-1}]^{-}$ complexes are closely similar.

At the same time, many examples show that the coordination of the amino group is favoured if it can take part in a five-membered chelate ring by the bidentate binding of the ligand, even if the other group contains only a relatively weak oxygen donor, and only an equatorial–axial coordination can occur. (1) In a comprehensive ESR study of the copper(II)–histamine and L-histidine systems we have pointed out that the monodentate coordination of the histamine in its 'LH' form really takes place by the imidazole nitrogen; in the corresponding L-histidine complexes, however, a bidentate coordination by the amino and carboxylate groups occurs, with the proton loss of the amino group at significantly lower pH than in the free ligand [18]. (2) In the $[Cu(LH_{-1})L]^{-}$ complexes of simple dipeptides the amino group of the 'L' ligand, together with the peptide oxygen, binds to the metal ion at a relatively low pH where it is in a protonated state in the free ligand [11,16,19]. It occupies either the fourth equatorial position, while the oxygen is co-ordinated axially, or, in the other isomer, the above donors are interchanged [16,19]. This mode of coordination is supported by visible absorption data too [23].

As we have observed great similarities in the important features of the ESR spectra for the $[CuL_2H_{-1}]^{-}$ complex of simple dipeptides and of glycyl-L-histidine, we assume the same coordination modes, with the only

difference in the nature of the third donor atom of the deprotonated dipeptide (Fig. 5). The analogies are as follows. The ESR analysis indicates isomeric equilibria in both cases. One of the isomers is characterized by a relatively high g_o and low A_o, in accordance with the 2N [16,19] or 3N (this work) superhyperfine splitting of spectra, which suggest that from the nitrogens, only those of the 'LH$_{-1}$' ligand are co-ordinated equatorially. For the other isomer, the low g_o indicates a much stronger ligand field which shows, in agreement with the 3N [16,19] and 4N [this work] shf patterns, respectively, that all the possible nitrogen donors are bound equatorially. The A_o of this isomer is unexpectedly low for such a low g_o, indicating a considerable rhombic distortion of the ligand field. Besides, the nitrogen donors have proved to be equivalent (Refs. [16,19] and Table 2).

The wavelengths of the visible absorption maxima are in good accordance with the suggested structures. For the 4N isomer $\lambda_{max} \cong 540$ nm is calculated from the

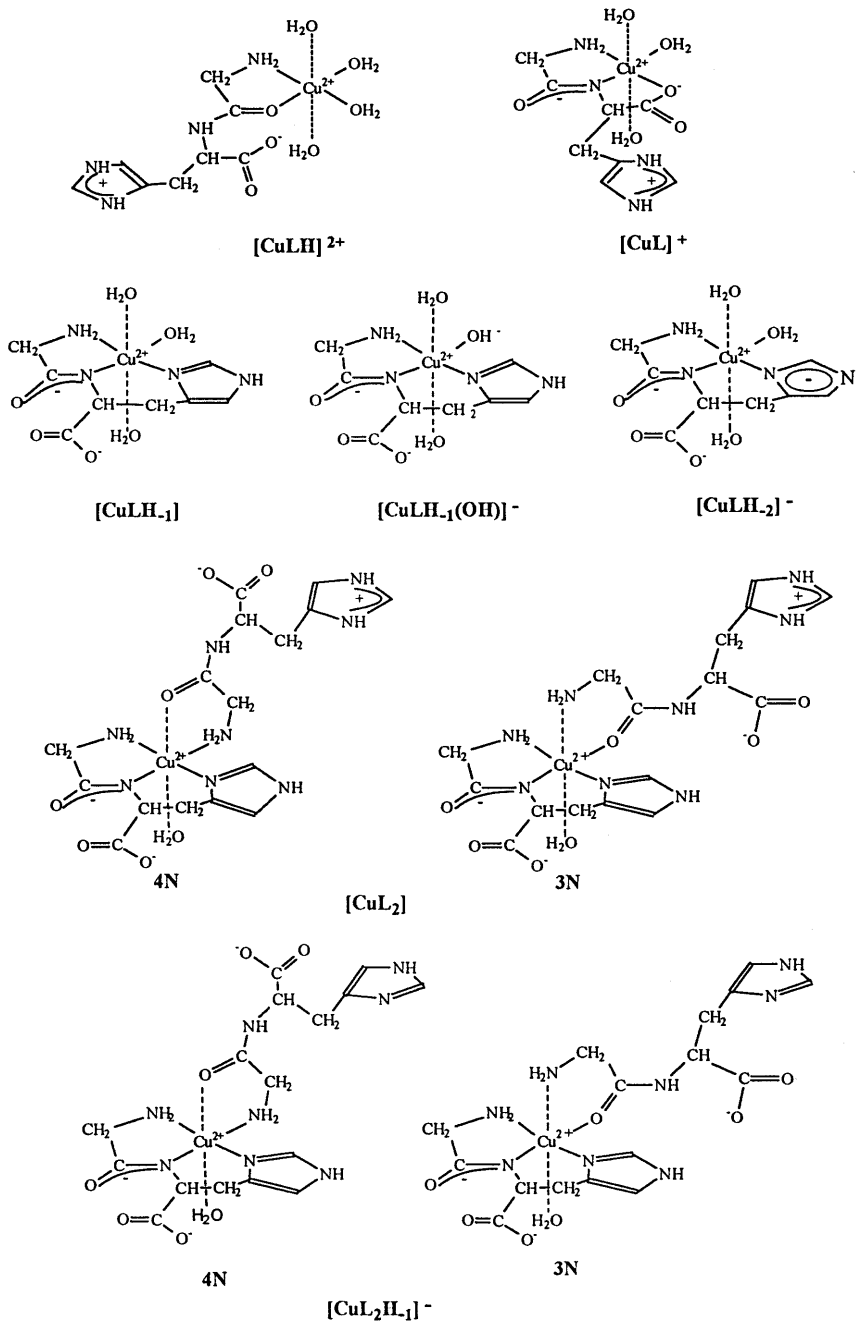


Fig. 5. Structures proposed for the various copper(II)-glycyl-L-histidine complexes.

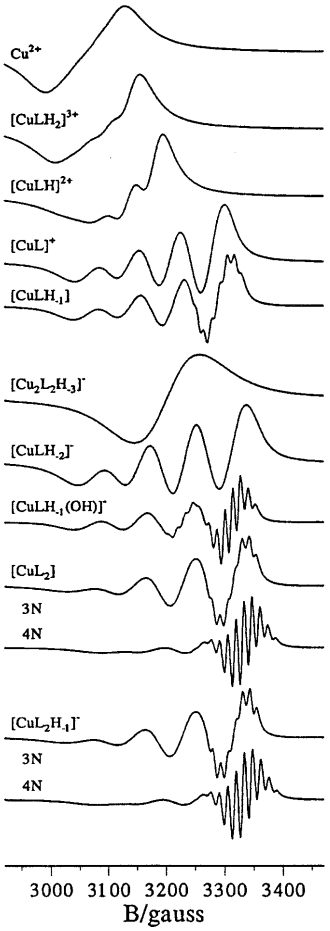


Fig. 6. ESR spectra of the various ^{63}Cu(II)-glycyl-L-histidine complexes.

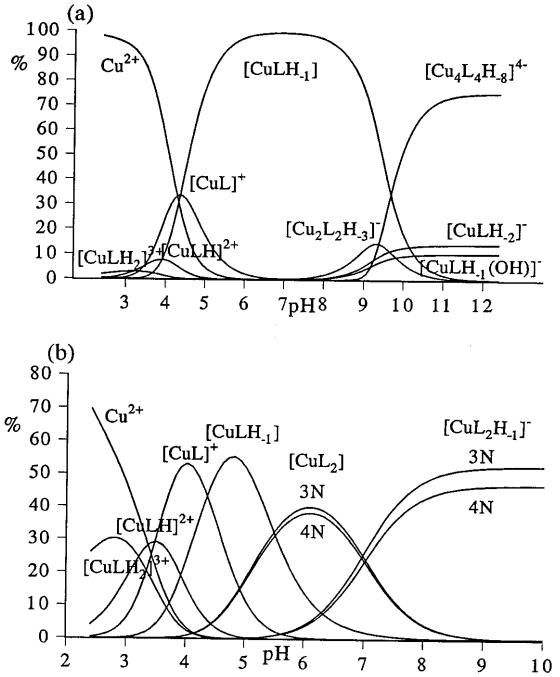


Fig. 7. Distribution of copper(II) amongst various species, including isomers, calculated from the formation constants obtained by the ESR method. The copper(II) concentration is 5 mM, the ligand-to-metal concentration ratio is (a) 1:1, (b) 20:1.

modified Billo-rule [24] while for the 3N isomer it is $\cong$ 593 nm. The experimental values are near the average of the above wavelengths: approximately 575 nm for the glycyl-L-histidine [2], 556 nm for the glycyl-L-histidyl-glycine [8] and 568 nm for the glycyl-histamine [9] complex. This is in agreement with the expectation when the measured curve is composed from a 540 and a 593 nm band of nearly equal intensity. It is worthy of note that the concentrations of the isomers were found nearly equal, and the molar absorption coefficients of the monomer species are of similar magnitude [2,8,9].

For the $[CuL_2]$ complex the close similarity of all the known characteristics (ESR parameters, the concentration ratio of the isomers, other spectroscopic data [2,8,9]) to those of the $[CuL_2H_{-1}]^-$ complex suggest the same modes of coordination (Fig. 5). The proposed structure is in good accordance with the deprotonation pK of the $[CuL_2]$ complex, too. We found pK 7.0 for both isomers, which is close to the value of 6.8, obtained for the imidazole group in the free ligand [1–8]. This supports the concept that the change in the protonation state of the imidazole group does not affect the structures of the isomers, i.e. it does not take part in the coordination sphere of either of these species. Another possible explanation is that in the $[CuL_2]$ complex the 'LH' ligand is bound by the imidazole nitrogen, while the amino group remains protonated. The lower deprotonation pK in the complex compared to the free ligand indicates the coordination of the amino group in the $[CuL_2H_{-1}]^-$ complex. This, however, would be accompanied by altered ESR parameters and d–d energies. The accidental coincidence of all these data of the corresponding isomers is improbable (Table 2).

The ESR spectra for the various copper(II)–glycyl-L-histidine complexes are illustrated in Fig. 6, and the concentration distribution curves including also the isomers are shown in Fig. 7.

4. Conclusions

Below pH 10 the presence of the side-chain imidazole group in the glycyl-L-histidine complexes only slightly affects the mode of coordination compared to the simple dipeptides: it is bound to the metal ion only in the $[CuLH_{-1}]$ complex, and in the 'LH_{-1}' ligand of the bis complexes; in these species it displaces the carboxylate group from the third equatorial site. The 'LH' and 'L' ligands in the $[CuL_2]$ and $[CuL_2H_{-1}]^-$ complexes, respectively, are ligated through the amino nitrogen and the peptide oxygen donors, either with the first in equatorial and the second in axial position, or vice

versa. Above pH 10, the deprotonation of the pyrrolic nitrogen causes dramatic changes in the coordination. In equimolar solution, the equilibrium of three species occurs up to pH 12: the monomer $[CuLH_{-2}]^{-}$ with a deprotonated imidazole ring, the corresponding tetramer $[Cu_4L_4H_{-8}]^{4-}$ and also the mixed hydroxo complex $[CuLH_{-1}OH]^{-}$ are formed.

Acknowledgements

We thank the Hungarian Scientific Research Fund OTKA T-032929 for the financial support. We are indebted to Professor István Nagypál for helpful discussions.

References

[1] G. Brookes, L.D. Pettit, J. Chem. Soc., Dalton Trans. (1975) 2112.
[2] I. Sóvágó, E. Farkas, A. Gergely, J. Chem. Soc., Dalton Trans. (1982) 2159.
[3] G. Arena, V. Cucinotta, Ann. Chim. Rome 74 (1984) 399.
[4] A. Ensuque, A. Demaret, L. Abello, G. Lapluye, J. Chim. Phys. 84 (1987) 1013.
[5] R.P. Agarwal, D.D. Perrin, J. Chem. Soc., Dalton Trans. (1975) 268.
[6] M.J.A. Rainer, B.M. Rode, Inorg. Chim. Acta 92 (1984) 1.
[7] M.J.A. Rainer, B.M. Rode, Inorg. Chim. Acta 107 (1985) 127.
[8] P.G. Daniele, O. Zerbinati, V. Zelano, G. Ostacoli, J. Chem. Soc., Dalton Trans. (1991) 2711.
[9] T. Gajda, B. Henry, J.J. Delpuech, J. Chem. Soc., Dalton Trans. (1993) 1301.
[10] D.B. McPhail, B.A. Goodman, J. Chem. Soc, Faraday Trans. 83 (1987) 3683.
[11] (a) G. Brookes, L.D. Pettit, J. Chem. Soc., Dalton Trans. (1975) 2106. (b) A. Gergely, I. Nagypál, J. Chem. Soc., Dalton Trans. (1977) 1104.
[12] (a) B.A. Goodman, D.B. McPhail, H.K.J. Powell, J. Chem. Soc., Dalton Trans. (1981) 822. (b) B.A. Goodman, D.B. McPhail, J. Chem. Soc., Dalton Trans. (1985) 1717.
[13] M. Pasenkiewicz-Gierula, W. Froncisz, R. Basosi, W.E. Antholine, J.S. Hyde, Inorg. Chem. 26 (1987) 801.
[14] R. Pogni, G. Della Lunga, R. Basosi, J. Am. Chem. Soc. 115 (1993) 1546.
[15] A. Rockenbauer, L. Korecz, Appl. Magn. Reson. 10 (1996) 29.
[16] T. Szabó-Plánka, A. Rockenbauer, L. Korecz, Magn. Reson. Chem. 37 (1999) 484.
[17] T. Szabó-Plánka, A. Rockenbauer, L. Korecz, Polyhedron 18 (1999) 1969.
[18] T. Szabó-Plánka, A. Rockenbauer, L. Korecz, D. Nagy, Polyhedron 19 (2000) 1123.
[19] (a) A. Rockenbauer, Plenary Lecture in second Asia-Pacific EPR/ESR Symposium, 31 Oct 4 Nov, 1999, Hangzhou, China, Proceedings, p. 15. (b) A. Rockenbauer, T. Szabó-Plánka, Zs. Árkosi, L. Korecz, Section Lecture in 30th Congress AMPERE, 23–29 July, 2000, Lisbon, Portugal.
[20] L. Zékány, I. Nagypál, G. Peintler, PSEQUAD for Chemical Equilibria, Technical Software Distributors, Baltimore, MD, 1991.
[21] (a) V.G. Shtyrlin, E.L. Gogolashvili, A.V. Zakharov, J. Chem. Soc., Dalton Trans. (1989) 1293. (b) A. Gergely, E. Farkas, J. Chem. Soc., Dalton Trans. (1982) 381.
[22] J.F. Blount, K.A. Fraser, H.C. Freeman, J.T. Szimansky, C.H. Wang, Acta Crystallogr., Sect. B 22 (1967) 396.
[23] T. Szabó-Plánka, G. Peintler, A. Rockenbauer, M. Gyõr, M. Varga-Fábián, L. Institórisz, L. Balázspiri, J. Chem. Soc., Dalton Trans. (1989) 1925.
[24] H. Siegel, R.B. Martin, Chem. Rev. 82 (1982) 385.

PERGAMON

www.elsevier.nl/locate/poly

Polyhedron 19 (2000) 2059–2068

POLYHEDRON

Spectroscopic and electrochemical properties of nickel(II), iron(III) and cobalt(II) complexes with benzilbisthiosemicarbazone — importance of working conditions and the metal salt used in the final complex

Marta Cañadas [a], Elena López-Torres [a], Arturo Martínez-Arias [b], Mª. Antonia Mendiola [a,*], Mª. Teresa Sevilla [c]

[a] *Departamento de Química Inorgánica, Universidad Autónoma de Madrid, 28049 Madrid, Spain*
[b] *Instituto de Catálisis y Petroleoquímica, CSIC, Campus UAM, 28049 Madrid, Spain*
[c] *Departamento de Química Analítica y Análisis Instrumental, Universidad Autónoma de Madrid, 28049 Madrid, Spain*

Received 17 February 2000; accepted 10 July 2000

Abstract

Reactions of benzilbisthiosemicarbazone (LH_6) with nickel, cobalt and iron chloride and nitrate give different complexes depending on the salts used and the working conditions. Reactions from nickel chloride give three complexes, **1**, **2** and **3** when the solvent or the pH is modified. Complex **1** is obtained in ethanol under reflux, and in methanol, independently of temperature and also with basic medium. Complex **2** is formed by working in ethanol at room temperature. The ligand acts as a dianion in both complexes. In the presence of hydrochloric acid, the new isolated complex **3** presents the neutral form of the ligand. Reaction from nitrate yields only complex **1**. Reactions with iron chloride give two new complexes with different formulae and grade of deprotonation in the ligand. For complex **4**, obtained at room temperature, LH_6 acts as an anion with a ligand–iron ratio of 2:1 and in its neutral form with a 1:1 ratio in complex **5**, working under reflux. Reactions with iron nitrate yield complex **6**, with the ligand in an intermediate situation, as anion but a nitrate remains. Complexes **7** and **8**, with a 1:1 cobalt–ligand molar ratio are isolated from reactions with cobalt nitrate; both contain nitrate and ethanol or water to complete the co-ordination sphere. Attempts to get a macrocyclic thiosemicarbazone from reaction of benzil and LH_6 in the presence of nickel or iron salt gave the complexes obtained, in absence of the dicarbonyl molecule. Electrochemical behaviour of complexes studied by cyclic voltammetry show metal-centred reduction processes for all of them. The reduction/oxidation potential values depend on the structures of complexes. Nickel complexes exhibit waves corresponding to Ni(III)–Ni(II) process. Electrochemical response of iron complexes depends on the presence of chloride ions. © 2000 Elsevier Science Ltd. All rights reserved.

Keywords: Thiosemicarbazones; Electrochemistry; Iron complexes; EPR of iron complexes; Nickel complexes; Cobalt complexes

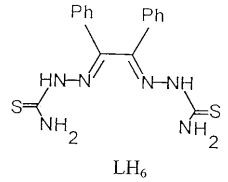
1. Introduction

The investigation of metal complexes with sulfur-containing Schiff bases is a subject of current and growing interest and it has been shown that many of them present anticancer activity [1,2]. A particular important group of such ligands includes those containing thiosemicarbazone moieties, because complexes formed with many of the first row transition metals have shown a wide range of biological properties [3–5].

It has been shown that a NNS tridentate system is present in most of the thiosemicarbazones with carcinostatic potency [6] and that copper and iron complexes usually have higher activity than the free ligands [7,8]. The chemical properties of these complexes, namely concerning their behaviour in redox reactions, relate to those observed in biological systems. For some copper complexes, a lower reduction potential seems to be related to an increased antifungal activity and with their potential abilities as SOD–mimic complexes [8–

* Corresponding author. Tel.: +34-91-397-4844; fax: +34-91-397-4833.
E-mail address: antonia.mendiola@uam.es (M. Antonia Mendiola).

0277-5387/00/$ - see front matter © 2000 Elsevier Science Ltd. All rights reserved.
PII: S0277-5387(00)00505-2



LH_6

Fig. 1. Proposed structure for benzilbisthiosemicarbazone, LH_6.

11]. Recently, iron-based SOD mimics have been reported [12–14]. The most successful mimics were obtained using macrocyclic pentadentate ligands [12]. However, these structures are quite different from the distorted trigonal bipyramidal geometry of the active site structure of Fe–SODs [15]. Some iron complexes with tripodal tetradentate ligand have activity [16]. The mimetic activity is related to the reduction potential values in the Fe(III)–Fe(II) process. The values observed in most Fe–SOD are between 0.2 and 0.4 V (versus NHE) [17]. The factors that influence the accessibility of several oxidation states for nickel are currently studied, because it is related to the bio-inorganic role of this metal ion in several redox enzymes [18,19]. Further interest in the co-ordination chemistry of nickel (I) and cobalt (I) arise from the role of these complexes in several catalytic reactions, such as electrocatalytical [20–22] and photocatalytical [23,24] reduction of CO_2. The incorporation of both soft and hard donor atoms in the co-ordination environment of the metal ion may be crucial in the stabilisation of oxidation numbers $+1$ and $+3$ for nickel [25].

Several studies on metal complexes of ligands derived from benzil and thiohydrazides with cobalt (II), zinc (II) and nickel (II) chloride and copper (II) salts have been made in our group [26,27]. Copper complexes have also been studied as SOD mimetic types [28,29]. In this paper we report the details of the synthesis, the spectroscopic characterization and the electrochemical behaviour of complexes obtained from benzilbisthiosemicarbazone (Fig. 1) and nickel (II), cobalt (II) and iron (III) salts. We have also investigated the influence of the counter-ion and the pH of the reaction medium in the behaviour of the ligand in reactions with metal chloride or nitrate.

2. Experimental

2.1. Reagents

Nickel(II) and cobalt(II) chloride and nitrate hexahydrate, iron(III) chloride hexahydrate and iron (III) nitrate nonahydrate were commercial products of highest chemical grade (Fluka). Solvents were purified according to standard procedures.

Benzilbisthiosemicarbazone LH_6 was prepared following the method previously reported [26].

2.2. Synthesis of nickel complexes

2.2.1. $NiC_{16}H_{14}N_6S_2$ (1)

A solution of nickel (II) chloride (0.20 g, 0.8 mmol) in methanol (10 cm^3) was added to a suspension of LH_6 (0.30 g, 0.8 mmol) in 20 cm^3 of the same solvent. The mixture was stirred for 3 h at room temperature. The reddish solid formed was filtered off, washed with methanol and dried in vacuo (yield 73%). ^{13}C NMR (DMSO-d_6): δ(ppm) 127.7, 128.8, 129.4, 131.6 (CPh), 153.8 (CN), 179.7 (CS). ^1H NMR (DMSO-d_6): δ(ppm) 7.6 (s, NH_2), 7.1–7.3 (m, HPh).

The same solid was obtained in ethanol under reflux [27]; in the presence of LiOH (0.028 g, 0.8 mmol) under reflux; and from nickel nitrate in ethanol at room temperature.

2.2.2. $NiC_{32}H_{30}N_{12}S_4$ (2)

This complex was prepared in the same way using ethanol and at room temperature (yield 63%) [27].

2.2.3. $NiC_{16}H_{16}N_6S_2Cl_2$ (3)

This complex was obtained following the same procedure, but in the presence of 10 cm^3 of hydrochloric acid (12 M) in methanol and under reflux (yield 58%).

2.2.4. Reactions with benzil

Working in the conditions described, but in the presence of benzil (0.17 g, 0.8 mmol) in methanol. The mixture was (a) refluxed with stirring for 3 h; (b) refluxed for 3 h in the presence of lithium hydroxide (0.034 g, 0.8 mmol); and (c) refluxed for 3 h in the presence of 10 cm^3 of hydrochloric acid (12 M). A reddish brown solid **1** was formed in procedures (a) and (b) but a brown solid **3** was formed following (c).

2.3. Synthesis of iron (III) complexes

2.3.1. $FeC_{32}H_{29}N_{12}S_4$ (4)

A solution of iron (III) chloride (0.23 g, 0.8 mmol) in 10 cm^3 of methanol was added to a suspension of LH_6 (0.30 g, 0.8 mmol) in 20 cm^3 of the same solvent. The mixture was stirred for 6 h at room temperature. The solid formed was filtered off, washed with methanol and dried in vacuo (yield 31%).

2.3.2. $FeC_{17}H_{20}N_6S_2OCl_3$ (5)

The reaction took place in the same conditions, but heating the mixture under reflux for 6 h gave a green solution, which was concentrated until a dark brown solid was formed (yield 43%). A reaction in the presence of hydrochloric acid in the reaction medium, enabled the reagents to be isolated. The reaction in the presence of LiOH (0.034 g, 0.8 mmol) in methanol under reflux for 2 h gave a yellow solid (yield 21%) [30].

Table 1
Analytical data and some physical properties for complexes [a]

	$NiLH_4$ (1)	$Ni(LH_5)_2$ (2)	$NiLH_6Cl_2$ (3)	$Fe(LH_5)(LH_4)$ (4)	$FeLH_6Cl_3$ CH_3OH (5)	$FeLH_4NO_3{\cdot}3H_2O$ (6)	$CoLH_5NO_3$ (7)	$CoLH_5NO_3{\cdot}CH_3CH_2OH$	$CoLH_5NO_3{\cdot}3H_2O$ (8)
C (%)	46.41 (46.52)	50.02 (50.00)	39.53 (39.51)	49.63 (50.12)	36.76 (37.05)	40.15 (40.07)	39.81 (41.38)		36.91 (36.23)
N (%)	18.97 (20.30)	22.02 (21.90)	17.25 (17.28)	21.82 (21.93)	14.79 (15.25)	17.45 (18.18)	18.70 (18.77)		18.26 (18.49)
H (%)	3.42 (3.39)	3.90 (3.90)	3.53 (3.29)	3.95 (3.92)	3.01 (3.63)	4.29 (4.26)	3.73 (4.02)		3.59 (3.96)
S (%)	15.49 (15.53)	16.59 (16.64)	13.19 (13.17)	17.18 (16.73)	11.88 (11.62)	12.22 (11.87)	12.23 (12.26)		12.03 (12.07)
pf (°C)	250	240	>260	242	>260	210	260		>260
Colour	reddish-brown	brown	reddish-brown	yellow	dark-brown	black	dark-brown		dark-brown
Λ_M (Ω^{-1} cm^2 mol^{-1})	3.1	2.9	25	2.5	45.5	17	31		22

[a] Found (calcd)%.

2.3.3. Reactions with benzil

Following the same procedure described for nickel (II) chloride. Using procedures (a) and (c), the reagents were recovered, but in the presence of lithium hydroxide the yellow solid obtained above was isolated.

2.3.4. $FeC_{16}H_{20}N_7S_2O_6$ (6)

A solution of iron (III) nitrate (0.52 g, 1.3 mmol) in ethanol (10 cm^3) was added to a suspension of LH_6 (0.46 g, 1.3 mmol) in 40 cm^3 of ethanol. Immediately the colour of the solution changed to dark brown, then the mixture was stirred for 8 h. The dark solid was filtered off, washed with ethanol and dried in vacuo (yield 27%).

2.4. Synthesis of cobalt(II) complexes

2.4.1. $CoC_{18}H_{21}N_7S_2O_4$ (7)

A solution of cobalt(II) nitrate (0.54 g, 1.8 mmol) in ethanol (25 cm^3) was added to a suspension of LH_6 (0.66 g, 1.8 mmol) in 40 cm^3 of ethanol. Immediately the solution changed to a dark brown colour. The mixture was stirred for 8 h. The dark solid was filtered off, washed with ethanol and dried in vacuo (yield 66%).

2.4.2. $CoC_{16}H_{21}N_7S_2O_6$ (8)

The same procedure was followed, as above, but heating the mixture under reflux with stirring for 8 h (yield 82%).

2.5. Physical measurements

Microanalyses were carried out using a Perkin–Elmer 2400 II CHNS/O elemental analyser. IR spectra in the 4000–400 cm^{-1} range were recorded as KBr pellets on a Bomen-100 spectrophotometer and in the range 550–200 cm^{-1} on a Bruker IFS 66V.

UV–Vis spectra in solution were registered on an Ati-Unicam UV2 spectrophotometer and the solid reflectance spectra on a Pye-Unicam SP-8-100. Conductivity data were measured using freshly prepared DMF solutions (ca. 10^{-3}M) at 25°C with a Metrohm Herisau model E-518 instrument.

^{1}H and ^{13}C NMR spectra were recorded on a Bruker AMX-300 spectrophotometer, using DMSO-d_6 as a solvent and Me_4Si as an internal standard.

Fast atom bombardment mass spectra were recorded on a VG Auto Spec instrument using Cs as the fast atom and *m*-nitrobenzylalcohol (*m*NBA) as the matrix.

EPR spectra were obtained with a Bruker ER 200D spectrometer operating in the X-band and calibrated with a DPPH standard ($g = 2.0036$). Portions of the samples were placed inside a quartz probe cell and subjected to brief out-gassing at room temperature (in high vacuum conditions) prior to record the spectra.

Table 2
Relevant IR spectral data and assignament of LH_6 and its complexes (cm^{-1})

	$\nu NH + \nu NH_2$	$\nu C{=}N + \delta NH_2$	Thioamide I	Thioamide IV	ν(M–N)	ν(M–X)
LH_6	3420, 3384 3342, 3328 3236, 3145	1613, 1585	1465 [a]	848		
$NiLH_4$ (1)	3450, 3273 3119	1625, 1615, 1610	1444	852	489, 432	
$Ni(LH_5)_2$ (**2**)	3456, 3419 3279, 3235 3131	1610, 1602 1588	1474, 1440	869	506, 432	
$NiLH_6Cl_2$ (**3**)	3398, 3387, 3273, 3098	1615, 1599, 1583, 1570	1460, 1444	859	487, 432	313,324
$Fe(LH_5)(LH_4)$ (**4**)	3419, 3260, 3249, 3144	1590, 1581	1479, 1470, 1440	866	503, 437, 426	
$FeLH_6Cl_3\ CH_3OH$ (**5**)	3300–3160	1617, 1507, 1575	1444	849	506, 475	382
$FeLH_4NO_3{\cdot}3H_2O$ (**6**)	3420, 3286 3219 [b]	1618 [b], 1574	1439	844	485	295 [a]
$CoLH_5NO_3\ CH_3CH_2OH$ (**7**)	3300–2700 [b]	1615	1463	848	481	340
$CoLH_5NO_3{\cdot}3H_2O$ (**8**)	3300–2700 [b]	1626 [b]	1482	835	481	342

[a] Several bands.
[b] Solvent molecules (water, methanol or ethanol).

Electrochemical measurements were performed with a BAS CV 27 voltammograph and a BAS A-4 XY register, using a carbon glassy (ϕ 5 mm) as working electrode, a platinum wire as auxiliary and a double junction, with porous ceramic wick, Ag–AgCl as reference electrode. In all cases, ferrocene was used as an external standard under the experimental conditions employed, redox couple ferricinium–ferrocene ($E_{1/2} = +0.48$ V; $\Delta E_p = 60$ mV). Cyclic voltammetry studies of ligands and complexes were carried out in 0.01 M solutions in dimethylformamide containing 0.1 M $[NBu_4]$ $[PF_6]$ and lithium chloride as supporting electrolytes. The range of potential studied was from $+1.5$ to -2.5 V. All solutions were purged with nitrogen steam for 5 min before measurements and the working electrode was polished before each experiment with diamond paste. The procedure was performed at room temperature and nitrogen atmosphere was maintained over the solution during the measurements.

3. Results and discussion

Analytical data are summarised in Table 1. From these data it can be deduced that the formulae of complexes depends on the working conditions.

For nickel reactions, three complexes were obtained: **1** ($NiLH_4$) and **2** ($Ni(LH_5)_2$), in which the ligand acts as an anion and complex **3** ($NiLH_6Cl_2$) with LH_6 in its neutral form. The last one is only obtained in the presence of hydrochloric acid, while complex **1** appears independently of the salts used, the solvent (methanol or ethanol), under reflux and in the presence of a basic medium.

Attempts to get the macrocyclic ligand from the reaction of LH_6 and benzil in the presence of nickel chloride, under the working conditions described in the experimental section, were unsuccessful. The complexes isolated from the nickel salt and benzilbisthiosemicarbazone were the same in basic or acid medium.

The nature of iron complexes is very dependent on the working conditions: temperature, salt used or the reaction medium. From the iron chloride reactions in methanol, two complexes **4** ($Fe(LH_5)(LH_4)$) and **5** ($FeLH_6Cl_3CH_3OH$) are obtained depending on the temperature. Complex **4** presents a 1:2 iron–ligand molar ratio with LH_6 acting as an anion, but complex **5** has chloride ions and the ligand is in its neutral form. In comparison with the nickel reaction, no complex is obtained by working in the presence of hydrochloric acid, while in the basic medium an iron macrocyclic complex was formed [30]. Moreover, from the nitrate reaction a new complex **6** ($FeLH_4NO_3{\cdot}3H_2O$), which has a nitrate ion, is isolated.

As in the case of nickel, attempts to get the macrocyclic ligand from the reaction of benzil and LH_6 in the presence of iron chloride, under the working conditions described in the experimental section, were unsuccessful. A macrocyclic complex was obtained working in the presence of lithium hydroxide. This complex was obtained in the absence of benzil as shown in a previous study [30].

From cobalt nitrate reactions, the obtained complexes **7** ($CoLH_5NO_3CH_3CH_2OH$) and **8** ($CoLH_5NO_3{\cdot}3H_2O$) present the ligand as partially deprotonated as in complex **6**, in contrast to the complex obtained from chloride [27]. In both cobalt complexes, solvent molecules are bonded to cobalt, ethanol in complex **7** and water in complex **8**.

The conductivity data (Table 1) indicate that all complexes are non-electrolytes, although complexes **5**, **7** and **8** show a partial solvolysis [31].

3.1. Nickel complexes

Mass spectra of all complexes show a peak at 413 amu corresponding to the $[LH_5Ni]^+$ fragment. The spectrum of complex **3** does not exhibit the molecular ion peak, but since it is a molecular complex the chloride ions must be bonded to the metal.

^{1}H NMR spectra of complexes **1** and **2** exhibit the amine and aromatic hydrogen in the same range as the free ligand. This is diagnostic of the diamagnetism for complexes, which indicates a square-planar symmetry for them in DMSO solution.

The spectrum of complex **2** confirms the presence of two non-equivalent ligand molecules. Its spectrum exhibits signals in the same position as complex **1** and the free ligand. This data indicates that one of the ligands is replaced by the DMSO. The ^{13}C NMR spectrum supports the partial substitution of one of the ligands by the solvent. The ^{13}C NMR spectrum of **1** shows a signal corresponding to the thioamide group in the same position as the free ligand, but the imine group is shifted to a lower field. These data support both azomethine groups and the primary amines being bonded to the nickel ion, as was proposed from the previous spectral data [27].

The IR spectrum of **3** shows several bands between 3398 and 3098 cm^{-1} corresponding to N–H stretching vibrations, which indicates that the ligand is present in its neutral form according to the analytical data. The shifts of the other bands in this spectrum are similar to those of complex **1**, so the behaviour of the ligand must be the same. The bands present in the far infrared spectrum of complex **3** support that the imine and thioamide nitrogen atoms are bonded to the metal ion. This spectrum shows two additional bands assignable to ν(Ni–Cl) with respect to complexes **1** and **2**, which confirm the chlorine–nickel bonds (Table 2). Electronic spectrum in DMF solution shows absorption bands at 707 nm ($\varepsilon = 333$ mol^{-1} dm^3 cm^{-1}) and 744 nm ($\varepsilon =$ 304 mol^{-1} dm^3 cm^{-1}) and three more intense bands at 430, 416 nm ($\varepsilon = 310^3$ mol^{-1} dm^3 cm^{-1}) and 312 nm ($\varepsilon = 12.244$ mol^{-1} dm^3 cm^{-1}) and in solid state at 540 and 680 nm with a shoulder at 740 nm, which are consistent with a distorted octahedral environment for the nickel [32].

3.2. Iron complexes

The reactions of iron salts with LH_6 gave three new complexes with different stoichiometry and variable grades of deprotonation in the ligand (Table 1).

From the chloride reaction, complexes **4** and **5** show both variables. The mass spectrum of **4** presents a pattern similar to that of complex **2**, which had the same stoichiometry. The IR spectrum is also close, with poorly resolved bands. Therefore, the same co-ordination behaviour of the thiosemicarbazone must be expected in both complexes, in which one ligand acts as dianion bonding through two imine nitrogen atoms and the terminal amine groups, and the other by the amine

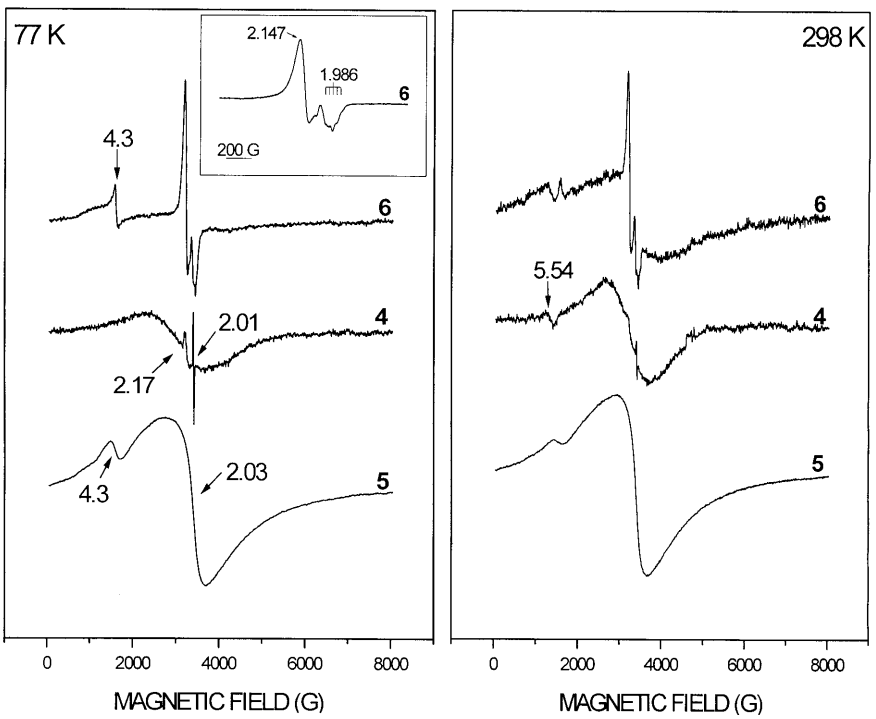


Fig. 2. EPR spectra of iron complexes in solid state, recorded at 77 and 298 K.

group [27]. Analytical data for complex **5** agree with a 1:1 molar ratio and the presence of methanol and chloride ions. Its IR spectrum confirms that the ligand acts in its neutral form and is bonded by the azomethine nitrogen atoms to the iron ion. The bands in the far IR confirm this behaviour, as do the bonds to the iron by the methanol molecule and the chloride ions.

Complex **6**, which is obtained from iron nitrate, presents an intermediate situation. The ligand acts as an anion, but a nitrate ion remains. The mass spectrum shows a peak corresponding to $[LH_4Fe]^+$. The infrared spectrum confirms the presence of the nitrate group as a ligand (mono or bidentate) and the water molecules, so it is more difficult for the assignment of the amine vibrations. By comparison with the cadmium nitrate complex in which recent X-ray data confirm a monodentate behaviour for this group [33], we propose that the nitrate is bonded by only one oxygen. The band assigned to the imine group is shifted to lower frequency, which indicates that these nitrogen atoms are involved in the bond to the iron. The iron co-ordination sphere is completed by four oxygen atoms, one from the nitrate group and the other from water molecules (Fig. 3(c)). The bands present in the far IR confirm the bond Fe–N(NC) and several Fe–O bonds (Table 2).

Electronic spectra in solution show an intense band at 400 nm ($\varepsilon = 10^3$ mol^{-1} dm^3 cm^{-1}) with a shoulder at 766 nm ($\varepsilon = 180$ mol^{-1} dm^3 cm^{-1}). The reflectance spectrum of **4** only shows a peak at 320 nm and several shoulders at lower energy. Spectra of complexes **5** and **6** show bands at 610 and 550 nm with a shoulder at lower energy in each absorption band, which support a distorted octahedral geometry for the iron ion. Electronic spectra in solution show charge transfer bands that obscure d–d bands [32].

3.2.1. EPR spectra

The EPR spectra of the iron(III) complexes in solid state, recorded at 77 and 298 K, are shown in Fig. 2. In all cases an overall intensity decrease is produced when the spectra are recorded at 298 K related to those recorded at 77 K.

The spectrum of complex **6** exhibits resonances in the low field region showing a peak at $g' = 4.3$ and a relatively broad absorption in the $g' = 9.0$–4.0 range. This is typical of high-spin iron(III) complexes in rhombically distorted low-symmetry positions [34]. For these cases the zero-field splitting terms remove the degeneracy of the spin sextet resulting in three Kramer's doublets; transitions within these states give rise to resonances in the low field region of the spectra [34]. Observation of a relatively broad resonance in this region and a narrower line at $g' = 4.3$ is consistent with the existence of a certain dispersion in the zero-field splitting terms. This could be caused by strain effects in the solid-state crystallites, giving rise to a relatively large spreading of the g resonant values [34]. In addition, complex **6** exhibits a signal at $g_\perp = 2.147$, and $g_\parallel = 1.986$ which is resolved by a hyperfine splitting of five lines in the parallel component, with $A = 29$ G, which shows intensity decreasing from the central line to the outermost components of the pattern (the inset of Fig. 2 shows details of this signal obtained in a shorter range run). This signal is typical of low-spin iron(III) complexes in a distorted octahedral environment with axial symmetry. Analysis of the g tensor values suggests that the axial ligands are weaker than the equatorial ones and that the d_{xy} orbital is lower in energy [35,36]. On the other hand, the hyperfine splitting pattern shown by this signal is consistent with a partial delocalization of the unpaired electron density into two equivalent nitrogen atoms through a superhyperfine interaction. Considering the infrared results, the nitrogen atoms responsible of this effect might be those of the imine groups. Besides, in the spectrum recorded at 298 K, the presence of a relatively broad signal with g value close to g_e is observed. This signal can be attributed to the low-spin iron(III) system, the broadening arising from the effects of magnetic exchange interactions within adjacent iron(III) species in the crystallites or a relatively fast high-low spin configurational equilibrium [36].

A similar broad signal prevails in complexes **4** and **5** indicating the presence of low-spin iron(III) configurations in them. In the former case the presence of high-spin iron(III) is apparent only in the spectrum recorded at 298 K (revealed by a peak at $g' = 5.54$), suggesting a greater relative stability of the low-spin configuration for complex **4**, while complex **5** shows the coexistence of low- and high-spin states of the iron(III) signal at low recording temperatures. In the case of complex **4** a narrower iron(III) signal in the low-spin state is evidenced by a signal at $g_1 = 2.142$, $g_2 = 2.110$ and unresolved g_3 in the spectrum recorded at 77 K. A narrow signal at $g = 2.01$, with relatively low intensity, is also observed in the spectrum of this complex. This could probably arise from location of unpaired electrons in the organic ligands of the complex or from the presence of impurity radicals.

3.3. Cobalt complexes

As it was mentioned in the experimental section and from the analytical data, two new complexes were obtained from the nitrate reaction with LH_6 (Table 1). Both complexes differ in the solvated molecules, but the ligand presents the same grade of deprotonation. The mass spectra show the peak corresponding to the $[LH_5Co]^+$ ion. IR spectra confirm the presence of the nitrate ion and the solvent molecules. The band assigned to thioamide IV remains in the same position as

in the free ligand, which indicates that this group is not involved in the bonding to the cobalt ion. The presence of solvent molecules does not permit the assignment of the NH and imine vibrations, but the bands in the far IR region indicate that the ligand is bonded by the imine nitrogen atoms (Table 2) [4].

The solid state electronic spectra of complexes **7** and **8** show bands at 580 and 500 nm with a shoulder at 690 and 680 nm, respectively, these data are consistent with a pentacoordinated or a distorted octahedral geometry for the cobalt ion [32].

An example of the different structures proposed for complexes is shown in Fig. 3, where the output of the calculation carried out using the Hyperchem program is plotted.

3.4. Electrochemical behaviour

The cyclic voltammogram of the ligand in DMF shows only two irreversible cathodic waves at -1.44 and -1.75 V, which can be attributed to the reduction of the groups present in the ligand.

3.4.1. Nickel complexes

Cyclic voltammogram of complex **1** shows the same pattern in glassy carbon electrode as in platinum [27]. The electrochemical behaviour of complex **3** differs from that complex **1**, in the same conditions, and depends on the potential range explored. On scanning from 0.0 to -2.5 V, the cyclic voltammogram (Fig. 4(a)) shows two waves in the cathodic scan at -1.10 and -1.67 V, respectively, corresponding to successive reductions of the Ni (II) ion [37–39], and in the reverse scan two anodic peaks at -1.61 and -1.05 V. Analysis of the first redox couple in the interval 25–800 mV s^{-1} shows a lineal variation of i_{pc} versus $v^{1/2}$. Small dependence of the potential peak with the scan rate is observed, and the i_{pa}–i_{pc} ratio is close to the unity. These results suggest a diffusion controlled quasirreversible Ni(II)–Ni(I) process. The more negative redox couple shows similar features, except that the potential peak values are independent of the scan rate, so this couple corresponds to a reversible process. When the positive potential limit is increased to $+1.5$ V (Fig. 4(b)), complex **3** exhibits an irreversible oxidation at $+0.87$ V, which generates a new unknown species which is turned into an irreversible reduction at -0.67 V [39–41].

Reduction potentials values of complexes **1** and **3** are similar, although slightly more negative for the latter complex due to the lower number of unsaturations for complex **3**. It is more difficult to have access to the $+1$ state for nickel in the complex with the ligand in its neutral form and two chloride ions bonded to the metal ion. The values of the oxidation process show that it is easier to oxidize complex **3** than complex **1**. This fact agrees with the presence of two chloride ligands in complex **3**. Chloride is a good π-donor, which will stabilise the higher oxidation state [41–43].

3.4.2. Iron complexes

Voltammetric studies of complexes **4**, **5** and **6** were carried out in dimethylformamide as solvent and using tetrabutylammonium hexafluorophosphate (TBAHFP)

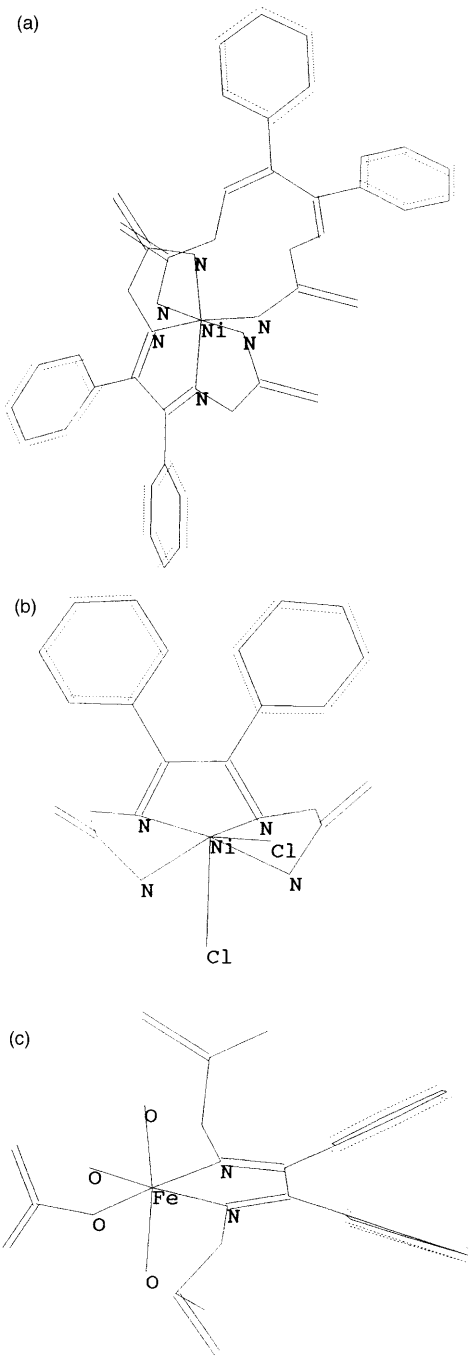


Fig. 3. Possible structures for (a) complex **2**; (b) complex **3**; (c) complex **6**.

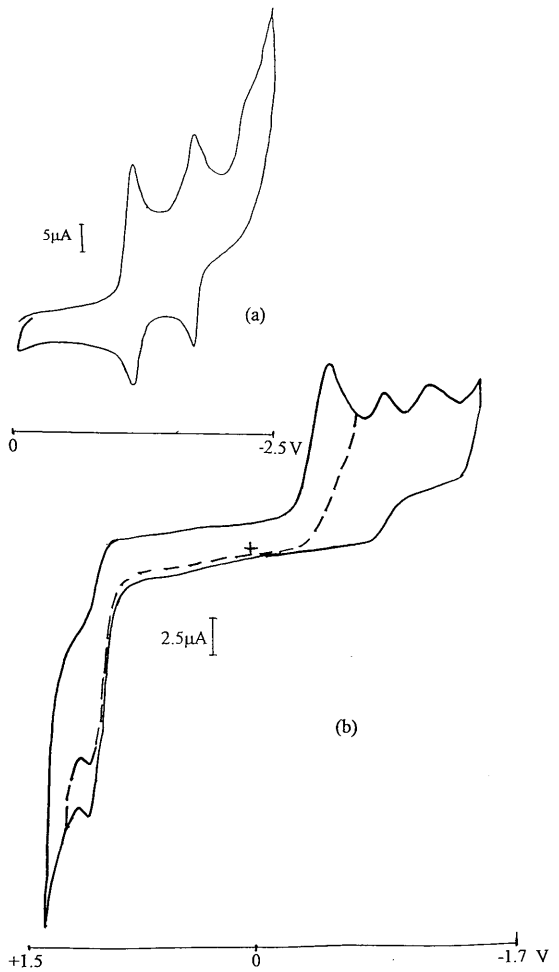


Fig. 4. Cyclic voltammogram for complex **3**; (a) potential range 0.0 to −2.5 V; (b) potential range +1.5 to −2.5 V, $v = 100$ mV s^{-1}.

and lithium chloride as electrolytes. In addition, voltammetric response in TBAHFP was recorded with successive additions of LiCl until ca. 0.1 M.

In the solutions containing TBAHFP, complexes **4**, **5** and **6** show different electrochemical behaviour. The cyclic voltammogram of complex **4** shows waves attributed to the ligand and poorly defined waves at less negative potentials. Using 2.10^{-2} M solutions the cyclic voltammogram obtained shows two waves in the range from +1 to −1.7 V. The peak at −0.75 V could be attributed to a Fe(III)–Fe(II) process. This behaviour could be explained considering the two ligands around the metal ion, without flexibility to accommodate the structural changes that accompany the reduction process. Cyclic voltammogram of complex **5** exhibits metal centred waves and other ones corresponding to the ligand reduction processes. In the range from +1 to −1 V a quasirreversible process attributed to the Fe(III)–Fe(II) couple at +0.19 V and a reduction wave at −0.72 V are observed (Fig. 5(a)). Cyclic voltammetric response of complex **6** shows poorly defined peaks due to the reduction of different species of iron(III) (Fig. 6(a)).

The three complexes show a different behaviour after the addition of LiCl. The voltammogram of complex **4** does not change, but those of complexes **5** and **6** are modified by the presence of chloride ions (LiCl). A gradual addition of chloride ions yielded a better defined cyclic voltammogram of complex **5**, which has chloride ions in its formula; a fully reversible Fe(III)–Fe(II) process is observed, although the potential values are shifted to +0.04 V. At the level of 0.1 M LiCl a well defined voltammogram is obtained (Fig. 5(b)). For complex **6**, a dramatic change in the voltammogram is produced by successive additions of LiCl, suggesting strong interaction of the complex with the anion by the replacement of the co-ordinated nitrate ion by chloride. From the first addition, a clear reversible process attributed to the Fe(III)–Fe(II) couple at +0.03 V and two peaks at more negative potential are observed (Fig. 6(b)). The features of the voltammogram depend on chloride content in the solution. A new peak at −0.62 V arises and its intensity increases when the concentration of chloride increases, so it can be related to the reduction of mixed species containing iron, ligand and chloride, $[Fe(LH_5)Cl_3)]^-$, $[Fe(LH_5)_2)]^+$, which are responsible of the electrochemical response observed in these conditions as previously described [44]. The redox process Fe(III)–Fe(II) would be accompanied by slow loss of nitrate, and therefore addition of chloride ions will improve this and hence more reversible electrochemical behaviour is observed. The voltammogram obtained at the level of 0.1 M LiCl is shown in Fig. 6(c).

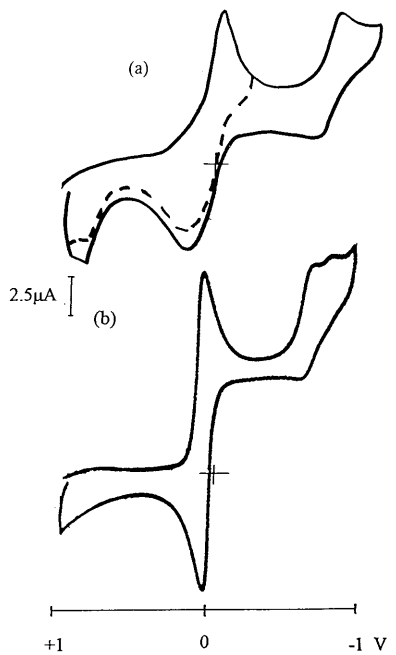


Fig. 5. Cyclic voltammogram for complex **5**; (a) in TBAHFP; (b) at the level of 0.1 M LiCl, $v = 100$ mV s^{-1}.

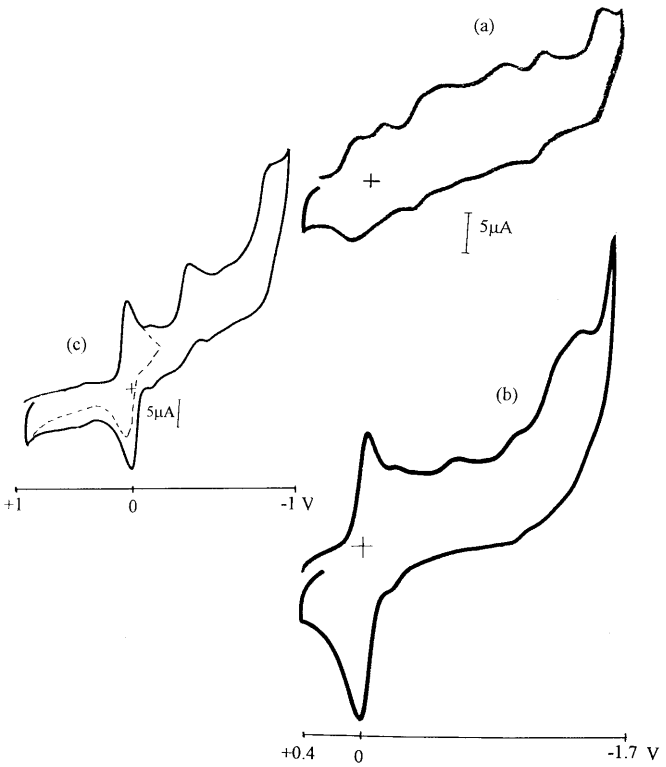


Fig. 6. Cyclic voltammogram for complex **6**; (a) in TBAHFP; (b) in TBAHFP after the addition of 0.1 ml of LiCl 0.1 M; (c) in TBAHFP at the level of 0.1 M of LiCl, $v = 100$ mV s^{-1}.

3.4.3. Chloride medium

The pattern of the cyclic voltammograms of complexes **5** and **6** are almost the same of that obtained from the addition of LiCl described above.

The reduction potential values of complexes **5** and **6** in LiCl are in the range of the Fe–SOD mimic observed [17]. Therefore, these compounds might be SOD mimetic.

3.4.4. Cobalt complexes

Voltammetric behaviour of cobalt complexes **7** and **8** was studied in the potential range from $+1$ to -2.5 V. The electrochemical behaviour of both complexes is very close according to the same geometry proposed from the spectroscopic data for these complexes. Both complexes exhibit waves only in the negative range of potential. Cyclic voltammogram of **7** (Fig. 7) shows an irreversible reduction wave at -1.85 V attributed to the insaturations of the ligand. In addition, it exhibits a cathodic wave at -0.97 with the anodic counterpart at -0.91 V corresponding to a cobalt(II) centred reduction process [45]. Study of the dependence of the voltammetric parameters with scan rate in the interval 25–800 mV s^{-1} show a lineal relationship of i_{pc} with $v^{1/2}$. The peak potential shows a small dependence with the scan rate. The ratio i_{pa}–i_{pc} is close to unity. From these data, it can be deduced that this redox couple is related to a quasirreversible process controlled by diffusion. The potential values are slightly shifted with respect to those obtained from the cobalt chloride complex in the same conditions, because in this complex chloride ions were bonded to the cobalt ion [27].

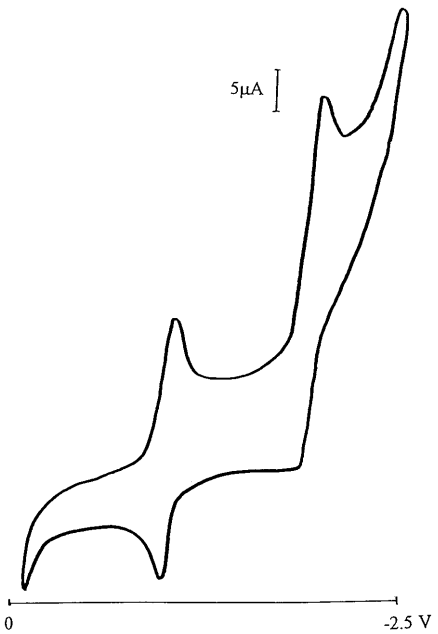


Fig. 7. Cyclic voltammogram of complex **7**, $v = 100$ mV s^{-1}.

Acknowledgements

We thank the Comunidad Autónoma de Madrid (Spain) for financial support (projects 06M/041/96 and 07M/0015/99). We also thank Professor J. Soria for the use of the EPR spectrometer.

References

[1] D.L. Klayman, J.P. Scovill, J.F. Bartosevich, J. Bruce, J. Med. Chem. 26 (1983) 35 and references therein.
[2] J.P. Scovill, D.L. Klayman, C. Lambos, G.E. Childs, J.D. Nortsch, J. Med. Chem. 27 (1984) 87.
[3] M.J.M. Campell, Coord. Chem. Rev. 15 (1975) 279.
[4] S. Padhye, G.B. Kauffman, Coord. Chem. Rev. 63 (1985) 127.
[5] D.X. West, S.B. Padhye, B.P. Sonawane, Struct. Bond. 76 (1991) 1.
[6] E.J. Blanz, F.A. French, Cancer Res. 28 (1968) 2419.
[7] S. Padhye, R. Chikate, A. Kumbhar, J.M. Shallon, M.P. Chitnis, Biometals 5 (1992) 67.
[8] D.X. West, A.E. Liberta, S.B. Padhye, R.C. Chikate, B.P. Sonawane, A.S. Kumbhar, R.G. Yerande, Coord. Chem. Rev. 123 (1993) 49.
[9] I. Haiduc, A. Silvestru, Coord. Chem. Rev. 99 (1990) 253.
[10] C.M. Liu, G. Xiong, X. You, Y. Liu, Polyhedron 15 (1996) 4565.
[11] Z. Duracková, J. Labuda, J. Inorg. Biochem. 58 (1995) 297.

[12] D. Zhang, D.H. Busch, P.L. Lennon, R.H. Weis, W.L. Neuman, D.P. Riley, Inorg. Chem. 37 (1998) 956.
[13] M. Rodriguez, I. Morgenstern-Baradau, M. Cesario, J. Guilhem, B. Keita, L. Nadjo, Inorg. Chem. 35 (1996) 7804.
[14] B. Kwak, K.W. Cho, M. Pyo, M.S. Lah, Inorg. Chim. Acta. 290 (1999) 21.
[15] M.S. Lah, M.M. Dixon, K.A. Pattridge, W.C. Stallings, J.A. Fee, M.L. Ludwing, Biochemistry 34 (1995) 1546.
[16] Y. Nishida, I. Watanabe, K. Unoura, Chem. Lett. (1991) 1517.
[17] C.K. Vance, A.-F. Miller, J. Am. Chem. Soc. 120 (1998) 461.
[18] J.R. Lancaster (Ed), The Bioinorganic Chemistry of Nickel, VCH, New York, 1988.
[19] A.F. Kolodziej, Prog. Inorg. Chem. 41 (1994) 493.
[20] M. Beley, J.P. Collin, R. Rupert, J.P. Sauvage, J. Am. Chem. Soc. 108 (1986) 7461.
[21] K. Bujno, R. Bilewicz, L. Siegfried, T. Kaden, J. Electroanal. Chem. 407 (1996) 131.
[22] H. Aga, A. Amarata, Y. Hisaeda, J. Electroanal. Chem. 437 (1997) 111.
[23] E. Kimura, S. Wada, M. Shionoya, Y. Okazaki, Inorg. Chem. 33 (1994) 770.
[24] E. Mejeritskaia, F. Luo, C.A. Kelly, B. Koch, E.M. Gundlach, E.L. Blinn, Inorg. Chim. Acta 246 (1996) 295.
[25] A. Berkessel, M. Bolte, T. Newmann, L. Seidel, Chem. Ber. 129 (1996) 1183.
[26] P. Souza, M.A. Mendiola, A. Arquero, V. Fernández, E. Gutiérrez-Puebla, C. Ruíz-Valero, Z. Naturforsch., Teil B 49 (1994) 263.
[27] A. Arquero, M.A. Mendiola, P. Souza, M.T. Sevilla, Polyhedron 15 (1996) 1657.
[28] Z. Duracková, M.A. Mendiola, M.T. Sevilla, A. Valent, Bioelectrochem. Bioenerg. 48 (1999) 109.
[29] E. Franco, E. López-Torres, M.A. Mendiola, M.T. Sevilla, Polyhedron 19 (2000) 441.
[30] A. Arquero, M. Cañadas, M. Martínez-Ripoll, M.A. Mendiola, A. Rodríguez, Tetrahedron 54 (1998) 11 271.
[31] W.J. Geary, Coord. Chem. Rev. 7 (1971) 81.
[32] A.B.P. Lever, Inorganic Electronic Spectroscopy, second ed., Elsevier, Amsterdam, 1984.
[33] E. Colacio, E. López-Torres, M.A. Mendiola, J.M. Moreno, Proc. 9a Reunion Cientifica de Química Inorgania, Bilbao (Spain) 2000.
[34] R. Aasa, J. Chem. Phys. 52 (1970) 3919.
[35] J. Costa, R. Delgado, M.G.D. Drew, V. Félix, R.T. Henriques, J.C. Waerenborgh, J. Chem. Soc., Dalton Trans. (1999) 3253.
[36] J. García-Tojal, J.L. Pizarro, L. Lezama, M.I. Arriortua, T. Rojo, Inorg. Chim. Acta 278 (1998) 150.
[37] B. Castro, C. Freire, Inorg. Chem. 29 (1990) 5113.
[38] A.J. Blake, R.O. Gould, M.A. Halcrow, M. Schröeder, J. Chem. Soc., Dalton Trans. (1993) 2909.
[39] E. Pereira, L. Gómez, B. Castro, Inorg. Chim. Acta 271 (1998) 83.
[40] M.A.A.F.C.T. Carrondo, B. Castro, A.M. Coelho, D. Domingues, C. Freire, J. Morais, Inorg. Chim. Acta 205 (1993) 157.
[41] F. Azevedo, M.A.A.F.C.T. Carrondo, B. Castro, M. Convery, D. Domingues, C. Freire, M.T. Duarte, K. Nielsen, I.C. Santos, Inorg. Chim. Acta 219 (1994) 47 and references therein.
[42] F.V. Lovecchio, E.S. Gore, D.H. Busch, J. Am. Chem. Soc. 96 (1974) 3109.
[43] A.M. Tait, F.V. Lovecchio, D.H. Busch, Inorg. Chem. 16 (1977) 2206.
[44] V.M. Leovac, L.S. Jovanovic, V.I. Cesljevic, L. Bjelica, C.B. Arion, N.V. Geberleu, Polyhedron 13 (1994) 3005.
[45] A.A. Isse, A. Gennaro, E. Vianello, J. Chem. Soc., Dalton Trans. (1993) 2091.

PERGAMON

www.elsevier.nl/locate/poly

Polyhedron 19 (2000) 2069–2075

POLYHEDRON

Tin dioxide thin films from Sn(IV) modified alkoxides — synthesis and structural characterization of $Sn(OEt)_2(\eta^2\text{-acac})_2$ and $Sn_4(\mu_3\text{-O})_2(\mu_2\text{-OEt})_4(OEt)_6(\eta^2\text{-acac})_2$

Martine Verdenelli [a], Stéphane Parola [a,*], Liliane G. Hubert-Pfalzgraf [b], Sylvain Lecocq [c]

[a] *Laboratoire des Multimatériaux et Interfaces UMR CNRS 5615, Université Claude Bernard-Lyon 1, 69622 Villeurbanne, Lyon cedex, France*
[b] *UPR 5401 IRC, 69626 Villeurbanne, Lyon cedex, France*
[c] *Laboratoire de Cristallographie UMR 5078, UCB-Lyon 1, 69622 Villeurbanne, Lyon cedex, France*

Received 29 May 2000; accepted 13 July 2000

Abstract

SnO_2 or doped SnO_2 thin films can be used as transparent conductors in various optoelectronic devices such as screens or solar cells. They usually present high optical transmittance, low resistivity and high chemical and mechanical stability. The synthesis and single crystal X-ray diffraction analysis of new tin (IV) modified alkoxides $Sn(OEt)_2(\eta^2\text{-acac})_2$ (**1**) and $Sn_4(\mu_3\text{-O})_2(\mu_2\text{-OEt})_4(OEt)_6(\eta^2\text{-acac})_2$ (**2**) (acacH = 2,4 pentanedione) are reported. **1** crystallizes in the monoclinic system (space group $P2_1/n$) while **2** crystallizes in the triclinic system (space group $P\bar{1}$). The asymmetric unit of the molecular species $Sn(OEt)_2(\eta^2\text{-acac})_2$ contains two monomers which are slightly different. $Sn_4(\mu_3\text{-O})_2(\mu_2\text{-OEt})_4(OEt)_6(\eta^2\text{-acac})_2$ is a tetranuclear species in which Sn atoms are connected together by two triply bridging oxo ligands and four bridging ethoxo groups. Six terminal ethoxo groups and two chelating β-diketonato ligands are completing the coordination of the metal atoms. Their behaviour towards hydrolysis–condensation reactions is discussed. © 2000 Elsevier Science Ltd. All rights reserved.

Keywords: Alkoxide; Tin; Tin dioxide; Sol–gel; β-Diketonate

1. Introduction

Tin dioxide thin films can be used as transparent conductors in various optoelectronic devices such as screens or solar cells. They usually present high optical transmittance, low resistivity and high chemical and mechanical stability. SnO_2 films have been previously prepared using chemical vapor deposition (CVD) [1], spray pyrolysis [2,3], or the sol–gel process [4–8]. One of the advantages of the sol–gel process is that the required temperature, which can be quite low, should allow deposition on thermosensitive substrates such as organic substrates. Tin alkoxides precipitate easily upon controlled addition of water. To avoid this precipitation one can stabilize the alkoxide precursors by substitution of alkoxo groups with less hydrolysable ones, β-diketone for instance. There is only one tin alkoxide modified with β-diketone which is structurally known, namely $[Sn(OPr^i)_3(acac)]_2$ [9], while three alkoxides have been structurally characterized, $Sn(OBu^t)_4$, $[Sn(OPr^i)_4(HOPr^i)]_2$ [10] and $[Sn(OBu^i)_4(HOBu^i)]_2$ [11]. T. Toupance have recently published F-doped SnO_2 materials by the sol–gel route using $Sn(OR^1)F(R^2COCHCOR^2)_2$ (R^1 = *tert*-amyl, isopropyl, ethyl; R^2 = methyl, *tert*-butyl) as precursors [12]. In this article we report the synthesis and structural characterization of tin (IV) modified alkoxides with β-diketone: $Sn(OEt)_2(\eta^2\text{-acac})_2$ and $Sn_4(\mu_3\text{-O})_2(\mu_2\text{-OEt})_4(OEt)_6(\eta^2\text{-acac})_2$ (acacH = 2,4 pentanedione). Their behaviour towards hydrolysis–condensation reactions is discussed and they are compared as potential precursors for film deposition.

* Corresponding author. Tel.: +33-4-724-48167; fax: +33-4-724-31568.
E-mail address: parola@univ-lyon1.fr (S. Parola).

0277-5387/00/$ - see front matter © 2000 Elsevier Science Ltd. All rights reserved.
PII: S0277-5387(00)00507-6

2. Results and discussion

β-Diketones, especially acetylacetone, are often used in order to stabilize metal alkoxides towards hydrolysis reactions during the sol–gel process [13]. The system $Sn(OBu^t)_4$–EtOH–acacH is of great interest for the elaboration of tin oxide and it has previously been used to prepare Sb^{3+} doped SnO_2 thin films for example [8].

The complexes $Sn(OEt)_2(\eta^2\text{-acac})_2$ (**1**) and $Sn_4(\mu_3\text{-}O)_2(\mu_2\text{-}OEt)_4(OEt)_6(\eta^2\text{-acac})_2$ (**2**) have been successfully prepared and isolated by reacting acetylacetone with the product of ethanolysis of $Sn(OBu^t)_4$ in a ratio acacH–Sn = 1:1. Two kinds of crystals were grown in the toluene solution, corresponding to compounds **1** and **2**. Species **1** could also be prepared by reacting acetylacetone and the product of ethanolysis of $Sn(OBu^t)_4$ in a ratio acacH–Sn = 2:1. The infrared spectrum for **1** shows two vibration bands at 1573 and 1534 cm^{-1} in the C=O region corresponding to terminal acetylacetonato ligands. The ^1H NMR spectrum at room temperature shows a singlet at 5.54 ppm attributed to the CH of the acac ligands, a quadruplet at 3.94 ppm for the CH_2, a triplet at 1.22 ppm for the CH_3 of the ethoxo groups and two singlets at 2.14 and 2.03 ppm for the methyls of the acac groups with a ratio OEt–acac = 1. The presence of two discrete and equivalent resonances associated with the CH_3 of the acetylacetone is consistent with a *cis* configuration for the alkoxide groups [7]. This was confirmed by single crystal X-ray diffraction (Fig. 1). Crystallographic data and selected bond lengths and angles are reported in Tables 1 and 2. The molecular species $Sn(OEt)_2(\eta^2\text{-acac})_2$ looks like a monomer but the asymmetric unit contains two monomers, A and B, which are different from a crystallographic point of view. The O–C–C angles of the alkoxo groups are slightly different, these angles are O11–C110–C111 = 124.7(7)° and O12–C120–C121 = 113.9(5)° for monomer A while O21–C210–C211 = 113.4(4)° and O22–C220–C221 = 114.3(5)° for monomer B. The angles around the metal atoms are also different: for example between the two ethoxo groups, O11–Sn1–O12 = 97.46(13)° for A and O22–Sn2–O21 = 101.20(12)° for B. Compound **1** presents two terminal ethoxo groups and two chelating β-diketonato ligands. The tin atom is hexacoordinated with a distorted octahedral environment. Sn–O bond lengths are varying between 1.960(3) and 2.113(2) Å with Sn–OR_t bonds shorter than Sn–η^2O bonds, which are quite similar to the Sn–O bonds in $[Sn(acac)(OPr^i)_3]_2$ [9]. The alkoxo groups are in a *cis* position surrounding the tin atom. They have the same position as the chlorine atoms in $SnCl_2(acac)_2$ [14] while the methyl groups in $Sn(CH_3)_2(acac)_2$ are in a *trans* position [15]. The *cis* configuration of compound **1** is more stable than the *trans* configuration. RO^- ligands, as well as Cl^-, act as σ- and π-donors and π-bonding is most easily accomplished if the two alkoxo groups are located in *cis* positions. Compound **2** was also prepared by reacting acetylacetone with the ethanolysis product of $Sn(OBu^t)_4$ in a ratio acacH–Sn = 1:2. The infrared spectrum shows two vibration bands in the C=O region at 1561 and 1539 cm^{-1} corresponding to terminal

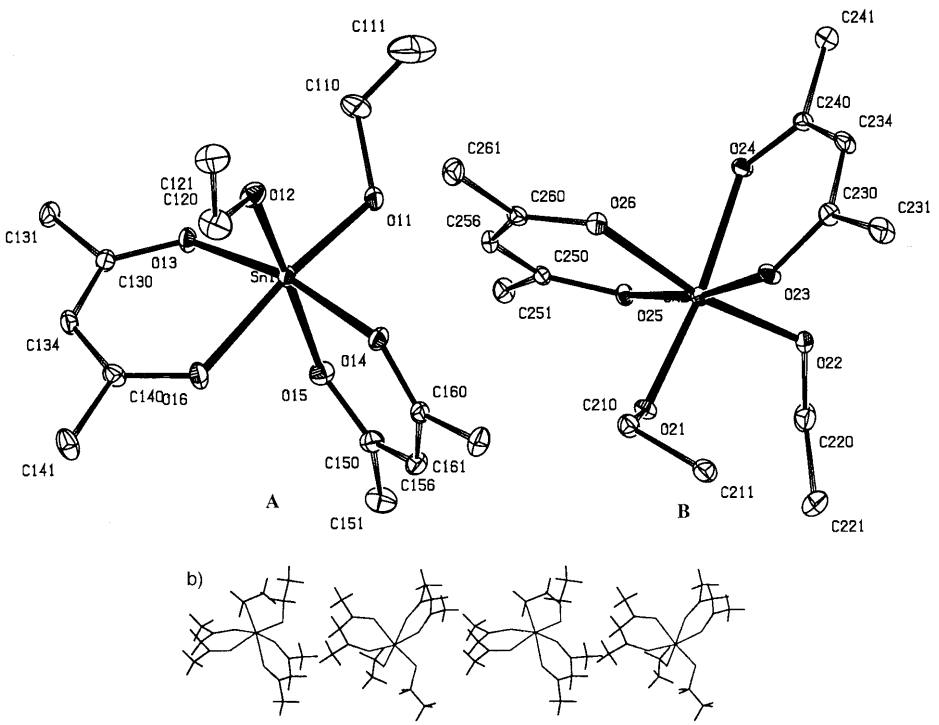


Fig. 1. ORTEP drawing and stereoview of $Sn(OEt)_2(\eta^2\text{-acac})_2$. Thermal ellipsoids are at 20% [26].

Table 1
Crystallographic data for $Sn(OEt)_2(\eta^2\text{-acac})_2$ and $Sn_4(\mu_3\text{-O})_2(\mu_2\text{-OEt})_4(OEt)_6(\eta^2\text{-acac})_2$

Compounds	$Sn(OEt)_2(acac)_2$	$Sn_4(O)_2(OEt)_{10}(acac)_2$
Empirical formula	$C_{14}H_{24}O_6Sn$	$C_{30}H_{64}O_{16}Sn_4$
Formula weight	407.03	1155.57
Temperature (K)	223(2)	293(2)
Wavelength (Å)	0.71073	0.71073
Crystal system	monoclinic	triclinic
Space group	$P2_1/n$	$P\bar{1}$
Unit cell dimensions		
a (Å)	8.485(10)	9.490(1)
b (Å)	29.378(8)	11.058(1)
c (Å)	13.878(5)	11.242(1)
α (°)	90(10)	70.46(1)
β (°)	92.89(10)	72.99(1)
γ (°)	90(10)	76.05(1)
V (Å^3)	3455(2)	1049.6(2)
Z	8	1
D_{calc} (g cm^{-3})	1.565	1.828
Absorption coefficient (mm^{-1})	1.501	2.415
Crystal size (mm)	$10.00\times0.30\times0.30$	$0.90\times0.50\times0.30$
Theta range for data collection (°)	1.39–29.59	1.98–23.53
Limiting indices	$-11\le h\le11$ $-31\le k\le40$ $-17\le l\le19$	$-10\le h\le10$ $-12\le k\le12$ $-11\le l\le12$
Reflections collected	24671	6908
Independent reflections	9522 [$R_{int}=0.0919$]	2891 [$R_{int}=0.1298$]
Absorption correction	empirical: Sortav	empirical: Sortav
Max./min. transmission	0.6617, 0.0235	0.5311, 0.2199
Refinement method	Full-matrix least-squares on F^2	Full-matrix least-squares on F^2
Data/restraints/parameters	9522/0/374	2891/7/227
Goodness-of-fit on F^2	0.963	0.995
Final R indices [$I>2\sigma(I)$]	$R_1=0.0523$, $wR_2=0.1059$	$R_1=0.0796$, $wR_2=0.1539$
R indices (all data)	$R_1=0.1081$, $wR_2=0.1194$	$R_1=0.2085$, $wR_2=0.2013$

β-diketonato groups. The ^{1}H NMR spectrum at room temperature shows a singlet at 5.60 and 5.58 ppm corresponding to the CH of the acac ligands, a quadruplet at 3.7 ppm for the CH_2, a triplet at 1.25 ppm for the CH_3 of the ethoxo groups and a singlet at 2.13 ppm for the methyles of the acac groups with a ratio OEt–acac = 5. The ^{119}Sn NMR spectrum has been measured. The compound displays several resonances with chemical shifts in the regions of δ −694, −646, −607 and −568 ppm. The tin atoms supporting the acetylacetone Sn2 and Sn2a have a more negative chemical shifts (δ = −694, −646 ppm) than Sn1 and Sn1a (δ = −607, −568 ppm). The values for Sn2 and Sn2a are in the same region as the values measured in the complexes $Sn(acac)_2(OR)_2$ (R = Me, Bu, OPr^i) ($\delta\approx-690$, −650 ppm), $Sn(acac)(OPr^i)_3$ ($\delta\approx-680$ ppm) and $Sn(bzac)(OPr^i)_3$ (bzac = benzoylacetone) ($\delta\approx-697$, −595 ppm) [9]. Correlations of ^{119}Sn chemical shift values with tin coordination numbers have been previously reported [7,16–18]. According to the data published in the literature the chemical shifts of compound **2** are consistent with six-coordinated species. This was confirmed by single-crystal X-ray diffraction analysis on **2** (Fig. 2). Crystallographic data and selected bond lengths and angles are reported in Tables 1 and 3. $Sn_4(\mu_3\text{-O})_2(\mu_2\text{-OEt})_4(OEt)_6(\eta^2\text{-acac})_2$ (**2**) is a tetrameric species. Sn atoms are connected together by two triply bridging oxo ligands and four bridging ethoxo groups. Six terminal ethoxo groups and two chelating β-diketonato ligands are completing the coordination of the metal atoms. The tin atoms are hexacoordinated with a distorted octahedral environment. The four Sn atoms are nearly co-planar. There are two kinds of tin, either connected to one chelating acetylacetonato, three alkoxo and one oxo groups for Sn2 and Sn2a or four alkoxo and two oxo groups for Sn1 and Sn1a. Sn–O bond lengths are in the range 1.926(18)–2.187(15) Å. The metal oxygen framework of **2** is similar to that adopted by $[Ti(OR)_4]_4$ species such as $[Ti(OMe)_3(OEt)]_4$ [19], $[Ti(OMe)_4]_4$ [20] or $[Ti(OEt)_4]_4$ [21]. If the solid-state structure was remaining in the solution we would expect only one ^{119}Sn resonance for Sn2 and one for Sn1. The presence of four resonances probably means that a reorganization occurs in solution with the formation of different isomers of **2**.

Compounds **1** and **2** are both soluble in ethanol and possess hydrolysable ligands. They are thus potential precursors for the preparation of tin dioxide through

Table 2
Selected bond lengths (Å) and angles (°) for $Sn(OEt)_2(\eta^2\text{-acac})_2$

Sn(1)–O(11)	1.962(3)	Sn(2)–O(21)	1.979(3)
Sn(1)–O(12)	1.965(3)	Sn(2)–O(22)	1.960(3)
Sn(1)–O(13)	2.078(3)	Sn(2)–O(23)	2.070(3)
Sn(1)–O(14)	2.082(3)	Sn(2)–O(24)	2.113(2)
Sn(1)–O(15)	2.094(3)	Sn(2)–O(25)	2.062(3)
Sn(1)–O(16)	2.093(3)	Sn(2)–O(26)	2.097(3)
O(11)–Sn(1)–O(12)	97.46(13)	O(21)–Sn(2)–O(22)	101.20(12)
O(11)–Sn(1)–O(13)	92.39(12)	O(21)–Sn(2)–O(23)	93.70(11)
O(11)–Sn(1)–O(14)	94.77(12)	O(21)–Sn(2)–O(24)	171.98(12)
O(11)–Sn(1)–O(15)	86.32(13)	O(21)–Sn(2)–O(25)	93.50(11)
O(11)–Sn(1)–O(16)	169.89(13)	O(21)–Sn(2)–O(26)	89.88(11)
O(12)–Sn(1)–O(13)	96.90(14)	O(22)–Sn(2)–O(23)	92.90(12)
O(12)–Sn(1)–O(14)	91.04(13)	O(22)–Sn(2)–O(24)	86.82(11)
O(12)–Sn(1)–O(15)	175.13(13)	O(22)–Sn(2)–O(25)	92.79(12)
O(12)–Sn(1)–O(16)	92.65(13)	O(22)–Sn(2)–O(26)	168.92(11)
O(13)–Sn(1)–O(14)	168.54(11)	O(23)–Sn(2)–O(24)	85.62(10)
O(13)–Sn(1)–O(15)	85.95(12)	O(23)–Sn(2)–O(25)	169.78(10)
O(13)–Sn(1)–O(16)	86.17(11)	O(23)–Sn(2)–O(26)	86.32(11)
O(14)–Sn(1)–O(15)	85.59(12)	O(24)–Sn(2)–O(25)	86.24(10)
O(14)–Sn(1)–O(16)	85.22(11)	O(24)–Sn(2)–O(26)	82.10(11)
O(15)–Sn(1)–O(16)	83.59(13)	O(25)–Sn(2)–O(26)	86.46(11)

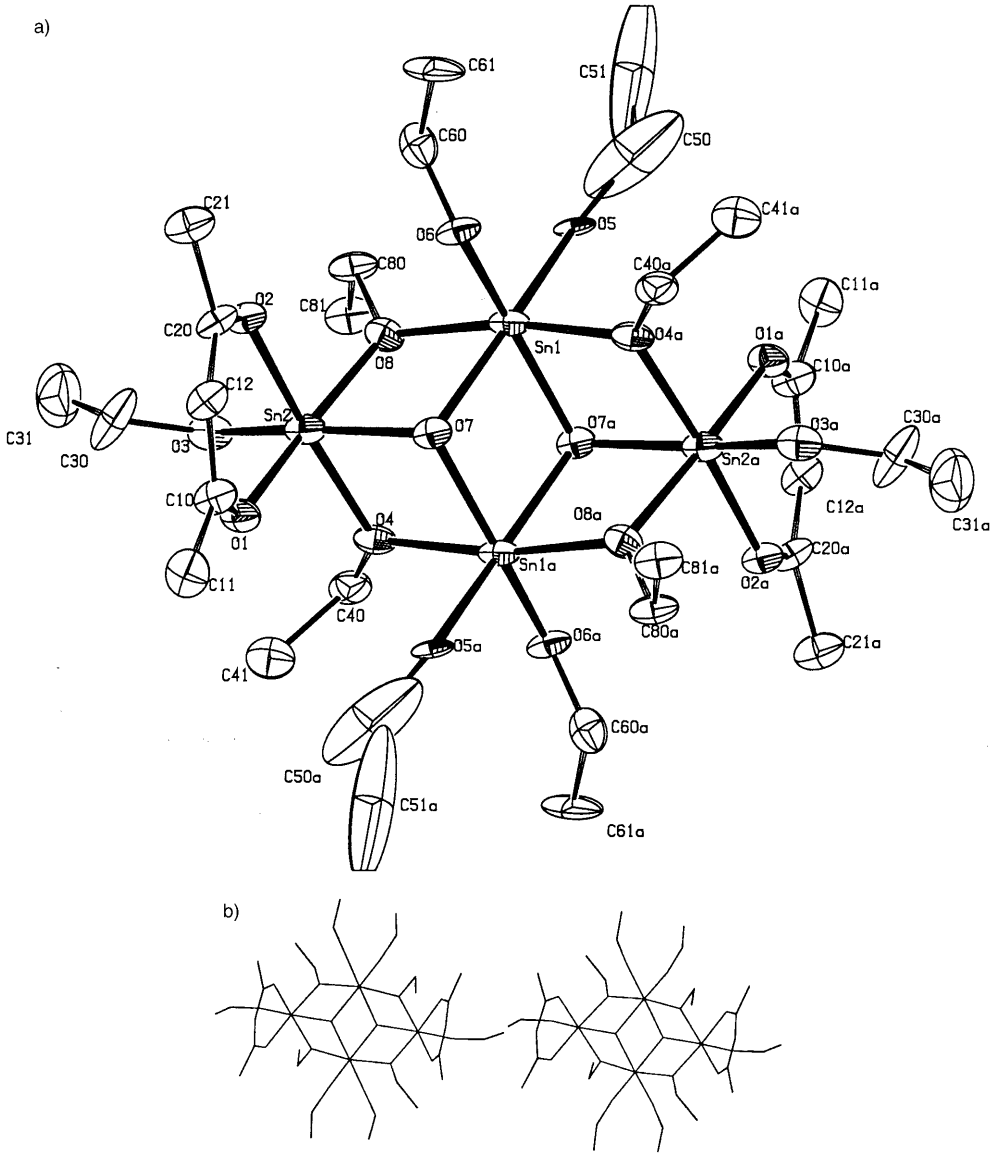


Fig. 2. ORTEP drawing and stereoview of $Sn_4(\mu_3\text{-}O)_2(\mu_2\text{-}OEt)_4(OEt)_6(\eta^2\text{-}acac)_2$. Thermal ellipsoids are at 20% [26].

the sol–gel process. Hydrolysis reactions have been conducted and various parameters have been analysed, such as the h values (degree of hydrolysis $h = [H_2O]/[M(OR)_n]$), the aging of the sols and the influence of the substitution of alkoxo groups with β-diketonato ligands. Pure tin alkoxide solutions led to clear sols for h values up to 3 and gels for h values between 3 and 8. For higher h values the precipitation starts immediately. Solutions of modified alkoxides **1** and **2** give slightly different results. Clear sols are obtained with $3 < h < 8$ and can be stable for weeks. For $h > 8$, turbid gels are obtained while precipitation occurs for high h values (50). TGA and X-ray diffraction analysis on the powder resulting from hydrolysis with $h = 50$ show that complete elimination of the remaining ligands occurs at 365°C and crystallisation of pure SnO_2 Cassiterite starts at about 350°C (Fig. 3). Films (thickness ≈ 0.6–1.3 μm) were deposited using both spin and dip-coating methods on glass substrates. They present high transmission in the visible (99%). They generally show a very smooth and homogeneous surface.

3. Conclusion

New tin oxide precursors for the sol gel process, $Sn(OEt)_2(\eta^2\text{-}acac)_2$ (**1**) and $Sn_4(\mu_3\text{-}O)_2(\mu_2\text{-}OEt)_4(OEt)_6(\eta^2\text{-}acac)_2$ (**2**), could be isolated and characterized by single crystal X-ray diffraction. These species are of great interest because ethanol is one of the most commonly used solvent for the sol–gel process. The presence of β-diketonato ligands in the coordination sphere

of the metal induces the stabilization of the precursors toward hydrolysis reaction, thus permitting the preparation of stable sols or gels with higher hydrolysis ratios.

4. Experimental

4.1. General procedures and measurements

All reactions were conducted under an inert atmosphere using Schlenk tubes and vacuum-line techniques. Solvents were purified by standard techniques. The compound $Sn(OBu^t)_4$ was prepared according to the literature [10] and purified by sublimation under vacuum. [$Sn(OEt)_4$] was obtained by alcoholysis of the pure $Sn(OBu^t)_4$ at room temperature. Infrared spectra were recorded on a Perkin Elmer Paragon 500 spectrometer as Nujol mulls. ^1H NMR spectra were recorded on a Brüker AM300 spectrometer and ^{119}Sn NMR spectra on a Brüker DRX500 spectrometer with $Sn(CH_3)_4$ as standard. Powder X-ray diffraction patterns were obtained on a Siemens D5000 diffractometer. TGA analysis were recorded with a Setaram TGDTA92 thermobalance, using Al_2O_3 crucible and heating rates of 5°C min^{-1}.

4.2. Preparation of $Sn(OEt)_2(\eta^2\text{-acac})_2$ (1) and $Sn_4(\mu_3\text{-}O)_2(\mu_2\text{-}OEt)_4(OEt)_6(\eta^2\text{-acac})_2$ (2) — method A

EtOH (1.5 ml, 25.7 mmol) was added to a solution of $Sn(OBu^t)_4$ (0.64 g, 1.56 mmol) in toluene (10 ml). The reaction medium was stirred for 30 min and evaporated to dryness. [$Sn(OEt)_4$] was dissolved in toluene (20 ml) and 2,4-pentanedione (0.16 ml, 1.56 mmoles) was added. The solution was stirred for 20 h and filtrated. Crystallization occurred at room temperature. Two kinds of crystals were simultaneously obtained, yellow prisms (**1**) and small colourless crystals (**2**).

Table 3
Selected bond lengths (Å) and angles (°) for $Sn_4(\mu_3\text{-}O)_2(\mu_2\text{-}OEt)_4(OEt)_6(\eta^2\text{-acac})_2$

Sn(1)–O(6)	1.967(13)	Sn(2)–O(1)	2.058(15)
Sn(1)–O(5)	2.185(10)	Sn(2)–O(2)	2.066(13)
Sn(1)–O(7)	2.102(13)	Sn(2)–O(3)	1.926(18)
Sn(1)–O(7a)	2.087(12)	Sn(2)–O(4)	2.045(13)
Sn(1)–O(4a)	2.128(15)	Sn(2)–O(8)	2.058(14)
Sn(1)–O(8)	2.187(15)	Sn(2)–O(7)	2.103(15)
Sn(1)···Sn(1a)	3.267(3)	Sn(1)···Sn(2)	3.287(3)
O(6)–Sn(1)–O(7)	91.4(5)	O(3)–Sn(2)–O(4)	92.0(6)
O(6)–Sn(1)–O(7a)	160.0(6)	O(3)–Sn(2)–O(1)	97.5(7)
O(7)–Sn(1)–O(7a)	77.5(6)	O(4)–Sn(2)–O(1)	92.8(6)
O(6)–Sn(1)–O(4a)	89.8(6)	O(3)–Sn(2)–O(8)	92.3(6)
O(7)–Sn(1)–O(4)	97.6(6)	O(4)–Sn(2)–O(8)	90.6(6)
O(7)–Sn(1)–O(4a)	75.5(5)	O(1)–Sn(2)–O(8)	169.6(6)
O(6)–Sn(1)–O(5)	100.1(5)	O(3)–Sn(2)–O(2)	94.1(6)
O(7)–Sn(1)–O(5)	164.0(5)	O(4)–Sn(2)–O(2)	173.9(6)
O(7a)–Sn(1)–O(5)	94.4(5)	O(1)–Sn(2)–O(2)	86.4(6)
O(4a)–Sn(1)–O(5)	93.5(5)	O(8)–Sn(2)–O(2)	89.2(5)
O(6)–Sn(1)–O(8)	97.7(6)	O(3)–Sn(2)–O(7)	165.7(5)
O(7)–Sn(1)–O(8)	76.3(6)	O(4)–Sn(2)–O(7)	76.9(5)
O(7a)–Sn(1)–O(8)	95.8(5)	O(1)–Sn(2)–O(7)	92.0(6)
O(4a)–Sn(1)–O(8)	170.4(5)	O(8)–Sn(2)–O(7)	79.1(6)
O(5)–Sn(1)–O(8)	91.1(5)	O(2)–Sn(2)–O(7)	97.1(6)

4.3. Preparation of $Sn(OEt)_2(\eta^2\text{-acac})_2$ (1) — method B

2,4-pentanedione (0.24 ml, 2.34 mmol) was added to a solution of $Sn(OBu^t)_4$ (0.48 g, 1.17 mmol) in toluene (10 ml). The reaction medium was stirred for 4 hours and ethanol (0.14 ml, 2.34 mmol) was slowly added. **1** crystallized in toluene at room temperature (0.09 g, 19%).

FT-IR (cm^{-1}): $\nu = 1573$ s, 1534 s; 1279 m, 1194 w, 1155 w, 1101 s, 1058 m, 1025 m, 938 m, 900 w (C–O + C–C); 789 m, 733 w, 680 w, 650 w; 606 w, 579 w, 445 w, 415 m (M–O); ^1H NMR ($CDCl_3$, 20°C, ppm): $\delta = 5.54$ (s, 2H, $(CH_3CO)_2CH$), 3.94 (q ($J = 7$), 4H, OCH_2CH_3), 2.14, 2.03 (s, 12H, $(CH_3CO)_2CH$), 1.22 (t ($J = 7$ Hz), 6H, OCH_2CH_3).

4.4. Preparation of $Sn_4(\mu_3\text{-}O)_2(\mu_2\text{-}OEt)_4(OEt)_6(\eta^2\text{-acac})_2$ (2) — method C

EtOH (1.5 ml, 25.7 mmol) was added to a solution of $Sn(OBu^t)_4$ (0.64 g, 1.56 mmol) in toluene (10 ml). The reaction medium was stirred for 30 min and evaporated to dryness. The white powder was dissolved in toluene (20 ml) and 2,4-pentanedione (0.08 ml, 0.78 mmol) was added. The solution was stirred for 20 h and evaporated to dryness. **2** crystallized in hexane at 4°C (0.116 g, 26%).

FT-IR (cm^{-1}): $\nu = 1561$ s, 1539 s, 1351 m; 1283 w, 1153 w, 1101 s, 1063 s, 1033 m, 940 w, 894 m, 828 w (C–O + C–C); 807 w, 723 w, 679 w, 650 w; 616 w, 591 w, 548 m, 464 w, 417 m (M–O); ^1H NMR ($CDCl_3$, 20°C, ppm): $\delta = 5.60$, 5.58 (s, 2H, $(CH_3CO)_2CH$), 3.7 (q ($J = 6.9$), 20H, OCH_2CH_3), 2.13 (s, 12H, $(CH_3CO)_2CH$), 1.25 (t ($J = 6.9$ Hz), 30H, OCH_2CH_3); ^{119}Sn NMR ($CDCl_3$, 20°C, ppm): $\delta = -694$, -647.8, -646, -645.7, -608.3, -606.8, -568.1.

4.5. Crystal-structure determination of 1 and 2

Data collections for **1** and **2** were performed on a NONIUS Kappa CCD diffractometer with Mo Kα radiation ($\lambda = 0.71069$ Å) using the program Denzo [22]. Intensities were collected by the ω–2θ scan technique. All diagrams and calculations were performed using MAXUS [23]. Hypotheses were determined using

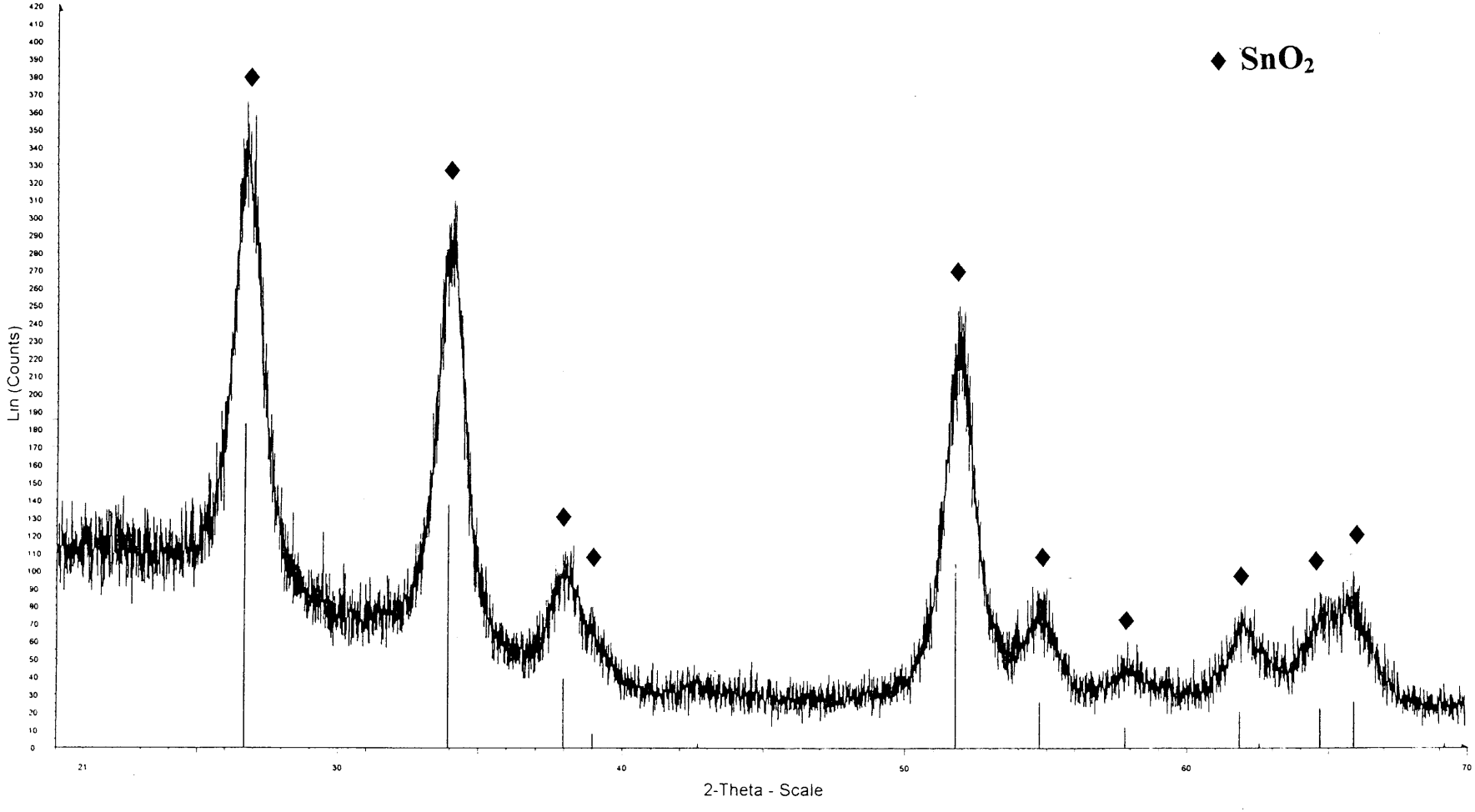


Fig. 3. Powder X-ray diffraction pattern of the xerogel prepared with complete hydrolysis of the precursor and thermal treatment at 500°C.

SIR-97 [24]. Refinement of F^2 against *all* reflections were performed using SHELXL-97 [25]. The weighted R-factor wR and goodness-of-fit S are based on F^2, conventional R-factors R are based on F, with F set to zero for negative F^2.

5. Supplementary material

Crystallographic data for the structures have been deposited with the Cambridge Crystallographic Data Centre, CCDC Nos. 141250 and 141251. Copies of this information may be obtained free of charge from The Director, CCDC, 12 Union Road, Cambridge, CB2 1EZ, UK (fax: +44-1223-336033; e-mail: deposit@ccdc.ac.uk or www: http://www.ccdc.cam.ac.uk).

References

[1] T. Maruyama, K. Tabata, J. Appl. Phys. 68 (8) (1990) 4282.
[2] E. Shanthi, A. Banerjee, V. Dutta, K.L. Chopra, J. Appl. Phys. 53 (3) (1982) 1615.
[3] A. Tiburcio-Silver, A. Maldonado, A. Escobosa, E. Saucedo, J.M. Montoya, J.A. Moreno, Appl. Surf. Sci. 70/71 (1993) 746.
[4] C.J.R. Gonzales-Olivier, I. Kato, J. Non-Cryst. Solids 82 (1986) 400.
[5] R. Puyané, I. Kato, Proc. SPIE Int. Soc. Opt. Eng. 401 (1983) 190.
[6] Y. Takahashi, Y. Wada, J. Electrochem. Soc. 137 (1) (1990) 267.
[7] L. Armelao, F.O. Ribot, C. Sanchez, Mat. Res. Soc. Symp. Proc. 435 (1996) 387.
[8] M. Guglielmi, E. Menegazzo, M. Paolizzi, G. Gasparro, D. Ganz, J. Pütz, M.A. Aegerter, L.G. Hubert-Pfalzgraf, C. Pascual, A. Duran, H.X. Willems, M. Van Bommel, L. Büttgenbach, L. Costa, J. Sol–Gel Sci. Technol. 13 (1998) 679.
[9] C.D. Chandler, G.D. Fallon, A.J. Koplick, B.O. West, Aust. J. Chem. 40 (1987) 1427.
[10] M.J. Hampden-Smith, T.A. Wark, A.L. Rheingold, J.C. Huffman, Can. J. Chem. 69 (1991) 121.
[11] C.D. Chandler, J. Caruso, M.J. Hampden-Smith, A.L. Rheingold, Polyhedron 14 (1995) 2491.
[12] A. Gamard, B. Jousseaume, T. Toupance, G. Campet, Inorg. Chem. 38 (1999) 4671.
[13] C. Sanchez, J. Livage, M. Henry, F. Babonneau, J. Non-Cryst. Solids 100 (1998) 65.
[14] G.A. Miller, E.O. Schlemper, Inorg. Chim. Acta 30 (1978) 131.
[15] G.A. Miller, E.O. Schlemper, Inorg. Chem. 12 (3) (1973) 677.
[16] R. Hani, R.A. Geanangel, Coord. Chem. Rev. 44 (1982) 229.
[17] D.J. Teff, J.C. Huffman, K.G. Caulton, Inorg. Chem. 35 (1996) 2981.
[18] M.J. Hampden-Smith, T.A. Wark, C.J. Brinker, Coord. Chem. Rev. 112 (1992) 81.
[19] R.D. Witters, C.N. Caughlan, Nature 205 (1965) 1312.
[20] D.A. Wright, D.A. Williams, Acta Crystallogr., Sect. B 24 (1968) 1107.
[21] J.A. Ibers, Nature 197 (1963) 686.
[22] Z. Otwinowski, W. Minor, Methods Enzymol. 276 (1997) 307–326.
[23] S. Mackay, C.J.Gilmore, C. Edwards, N. Stewart, K. Shankland, MAXUS — Computer Program for the Solution and Refinement of Crystal Structures, Nonius, The Netherlands; MacScience, Japan; and The University of Glasgow, 1999.
[24] A. Altomare, G. Cascarano, C. Giacovazzo, A. Guagliardi, M.C. Burla, G. Polidori, M. Camalli, J. Appl. Cryst. 27 (1994) 435.
[25] G.M. Sheldrick, SHELXL-97, Program for the Refinement of Crystal Structures, University of Göttingen, Göttingen, Germany, 1997.
[26] C.K. Johnson, ORTEP-II, A Fortran Thermal-Ellipsoid Plot Program, Report ORNL-5138, Oak Ridge National Laboratory, Oak Ridge, TN, USA, 1976.

PERGAMON

www.elsevier.nl/locate/poly

Polyhedron 19 (2000) 2077–2081

POLYHEDRON

The preparation of the first examples of sulfimide complexes of platinum; the X-ray crystal structure of $[Pt(Ph_2SNH)_4]Cl_2$

P.F. Kelly *, A.C. Macklin, A.M.Z. Slawin, K.W. Waring.

Department of Chemistry, Loughborough University, Loughborough, Leicestershire, LE11 3TU, UK

Received 25 May 2000; accepted 13 July 2000

Abstract

The reactivity of *S*,*S*-diphenylsulfimide, Ph_2SNH, (**1**) towards platinum complexes has been investigated. Solutions of **1** and $[PtCl_2(PMe_2Ph)_2]$ show an equilibrium between the starting materials and *cis*-$[PtCl(Ph_2SNH)(PMe_2Ph)_2]Cl$; addition of $[NH_4][BF_4]$ generates pure *cis*-$[PtCl(Ph_2SNH)(PMe_2Ph)_2][BF_4]$ (**2**). Four equivalents of **1** react with $[PPh_4]_2[PtCl_4]$ over a period of days to give crystalline $[Pt(Ph_2SNH)_4]Cl_2$ (**3**); the crystal structure of **3** confirms the expected square planar geometry with significant H-bonding interactions between the cation and the chlorides. © 2000 Elsevier Science Ltd. All rights reserved.

Keywords: Complexes; Platinum; Sulfimides; Hydrogen bonding

1. Introduction

We have long been interested in the ability of sulfur (and selenium)–nitrogen species to react with transition metal centres [1]. In our earlier work on such systems we tended to concentrate upon the reactivity of S–N species that were either completely devoid of substituents (eg. S_4N_4, $[S_3N_3]^-$ etc.) or had only hydrogen present in addition to the sulfur and nitrogen (e.g. $S_4N_4H_4$). In more recent studies we looked at the properties of substituent-capped long-chain species such as $Me_3SiNSNSNSNSiMe_3$, though in such cases the substantial disruption of the latter during reaction means that only unsubstituted S–N ligands are found in the products [2]. In our most recent work, however, we have prepared a range of complexes of a class of S–N ligand that bears organic groups and retains them upon coordination. Specifically we have investigated the reactivity of *S*,*S*′-diphenylsulfimide, Ph_2SNH (**1**), towards a number of metal centres.

These studies have generated a range of unexpected results, such as the unique isomerism of *trans*-$[CuCl_2(Ph_2SNH)_2]$ [3] and the concerted, directed hydrogen bonding between both sets of triple N–H units on either side of the $[Co(Ph_2SNH_2)_6]^{2+}$ cation and the chloride counterions [4]. The interesting ligand properties of **1** were further illustrated by its reactivity towards $Pt(MeCN)_2Cl_2$; now a nucleophilic attack of the sulfimide upon the coordinated nitrile is seen giving rise to the novel $Ph_2SNC(Me)NH$ ligand [5]. The key feature of this reaction is that the latter fragment cannot be formed by simple reaction of the sulfimide with MeCN in the absence of the platinum centre. Although the latter reaction was of great interest and has great potential as a source of new hybrid sulfimide/nitride fragments as free systems, the unexpected reaction of **1** with MeCN meant that simple coordination chemistry with Pt went unobserved.

One aspect of our current interests centres upon making direct contrast between the coordinating ability of **1** and of underivatised S–N species such as S_4N_4. In the previous work alluded to above, platinum complexes proved to be amongst the most versatile reagents for such reactions; thus we have an interest in observing the simple coordination chemistry of **1** with this metal. Here we report on the results of the first such studies and reveal that **1** is not only more reactive towards simple Pt species than underivatised S–N systems but that the products also exhibit interesting H-bonding structures that bode well for their use in constructing extended arrays.

* Corresponding author. Tel.: +44-1509-222-578; fax: +44-1509-223-925.

E-mail address: p.f.kelly@lboro.ac.uk (P.F. Kelly).

0277-5387/00/$ - see front matter © 2000 Elsevier Science Ltd. All rights reserved.
PII: S0277-5387(00)00508-8

2. Experimental

2.1. General

All reactions were performed under an atmosphere of dry nitrogen using dried, degassed solvents (CH_2Cl_2 and MeCN from calcium hydride, Et_2O from sodium–benzophenone). *S*,*S*′-Diphenylsulfimide was prepared by our recently reported variation of the literature method [6]; $[PPh_4]_2[PtCl_4]$ was prepared by addition of $[PPh_4]Cl$ to $K_2[PtCl_4]$ in water, $[PtCl_2(PMe_2Ph)_2]$ by addition of PMe_2Ph to $[PtCl_2(COD)]$.

2.2. Preparations

2.2.1. *[PtCl(Ph$_2$SNH)(PMe$_2$Ph)$_2$][BF$_4$] (**2**)*

A solution of $[PtCl_2(PMe_2Ph)_2]$ (50 mg, 0.09 mmol) in CH_2Cl_2 (10 ml) was treated with a solution of **1** (23 mg, 0.11 mmol) in the same volume of CH_2Cl_2. After stirring for 1 h the colourless solution was treated with solid $[NH_4][BF_4]$ (10 mg, 0.1 mmol) and the resulting mixture stirred vigorously overnight. Filtration followed by reduction of the volume in vacuo and slow diffusion of diethylether yielded a mass of well-formed colourless crystals of **2**. ^{31}P NMR of solutions before crystallisation showed an effectively quantitative yield of the product: AX spectrum, δ_A −12.7 $^1J(^{31}P-^{195}Pt)$ 3651 Hz; δ_B −20.0 ppm $^1J(^{31}P-^{195}Pt)$ 3141 Hz. Microanalysis: *Anal*. Found: C, 41.6; H, 1.4; N, 4.1. Calc. for $C_{28}H_{33}BClF_4NP_2PtS$: C, 42.3; H, 1.8; N, 4.2%. IR: in addition to peaks due to the PMe_2Ph ligands, bands also seen at 3307(m, *v*(N–H)), 1065 (s, br), 517 (m), 284(m, *v*(Pt–Cl)).

Treatment of a solution of **2** in CH_2Cl_2 with $[^nBu_4N]Cl$ resulted in the rapid establishment of an equilibrium between **2** and $[PtCl_2(PMe_2Ph)_2]$ (as shown by ^{31}P NMR).

2.2.2. *[Pt(Ph$_2$SNH)$_4$]Cl$_2$ (**3**)*

A solution of $[PPh_4]_2[PtCl_4]$ (0.1 g, 0.1 mmol) in CH_2Cl_2 (20 ml) was treated with solid **1** (0.1 g, 0.5 mmol); after stirring the solution was left to stand. Overnight a small crop of pale yellow crystals appeared; the mixture was allowed to stand for one week during which time the amount of crystalline material increased. At this point the solution was decanted from the crystals which were washed with CH_2Cl_2 and dried in vacuo. Yield: 83 mg, 79% based upon Pt. Microanalysis: *Anal*. Found C, 53.2; H, 3.9; N, 4.7. Calc. For $C_{48}H_{44}N_4S_4PtCl_2$ C, 53.8; H, 4.1; N 5.2%.

2.3. X-ray crystallography

Data were collected for **3** (using a Bruker SMART diffractometer with graphite monochromated Mo Kα radiation) using small slices: 11 178 data collected, 3293 data used ($R_{int} = 0.1197$). Data were corrected for Lorentz and polarisation effects and an empirical absorption correction was applied resulting in transmission factors ranging from 0.842 to 1.00.

Structure analysis and refinement: the structure was solved by direct methods and refined by full-matrix least-squares against F^2 leading to $R_1 = 0.0376$, $wR_2 = 0.0494$ with $I > 2\sigma(I)$. The maximum/minimum residual electron densities in the final ΔF map were 0.991 and -1.068 e Å^{-3}; calculations were performed using SHELXTL [7].

3. Results and discussion

The unexpected observation that **1** reacts with $Pt(MeCN)_2Cl_2$ to generate $[Pt(Ph_2SNH)(Ph_2SNC(Me)NH)Cl]Cl$ [5] diverted attention away from the possible simple coordination chemistry that **1** could show towards platinum. Attention to such chemistry is made worthwhile for two reasons. Firstly, we have used platinum as one of the main metal centres for reaction with binary S–N species such as S_4N_4. Contrast between the reactivity of such species and **1** is thus best achieved by looking at such complexes. Secondly, we have already noted a propensity for strong H-bonding from coordinated **1** to counterions; such interactions may well be utilised in the formation of extended array systems. As platinum has a well-defined square-planar geometry one would expect to see a significant contrast between the H-bonding arrangement in its homoleptic complexes of **1** and the aforementioned arrangement in $[Co(Ph_2SNH_2)_6]Cl_2$.

^{31}P NMR reveals that an equimolar mixture of **1** and *cis*-$PtCl_2(PMe_2Ph)_2$ in CH_2Cl_2 at room temperature contains both the platinum starting material and a complex identified by an AX spectrum. Both these features of the spectrum remain, albeit in varying ratios, even when the relative amounts of the reagents are altered; even a large excess of **1** does not remove all *cis*-$PtCl_2(PMe_2Ph)_2$ from the system. This observation suggested the presence of an equilibrium between **1**, *cis*-$PtCl_2(PMe_2Ph)_2$ and a new coordination complex and this was confirmed by removing free chloride from the system. Thus, treatment with $[NH_4][L]$, where L = $[PF_6]^-$ or $[BF_4]^-$, results in the complete conversion of the platinum starting material through to the product. Though both salts may be precipitated by addition of ether, the $[PF_6]^-$ case does not crystallise well via slow diffusion-only an oil is obtained. In the case of the $[BF_4]^-$ salt, however, slow diffusion of ether leads to colourless crystals of the product, which we have characterised as *cis*-$[PtCl(Ph_2SNH)(PMe_2Ph)_2][BF_4]$ (**2**) by a combination of NMR, IR and micro-analysis. The key evidence comes from the fact that an AX pattern is observed in the ^{31}P NMR spectrum; this rules out a

trans structure, while the $^{195}Pt-^{31}P$ coupling constants of the phosphorus atoms are consistent with P *trans* to Cl and to N. Comparison of the latter value (3141 Hz) with that for P *trans* to N(H) in the $[S_2N_2H]^-$ complex $[Pt(S_2N_2H)(PMe_2Ph)_2]^+$ (3240 Hz) serves to confirm that the ligand is *N*-bound (noting that in the aforementioned case the value for P *trans* to S is significantly different: 2595 Hz) [8]. By analogy with the latter case therefore we can be confident therefore that the sulfimide has coordinated through the nitrogen atom.

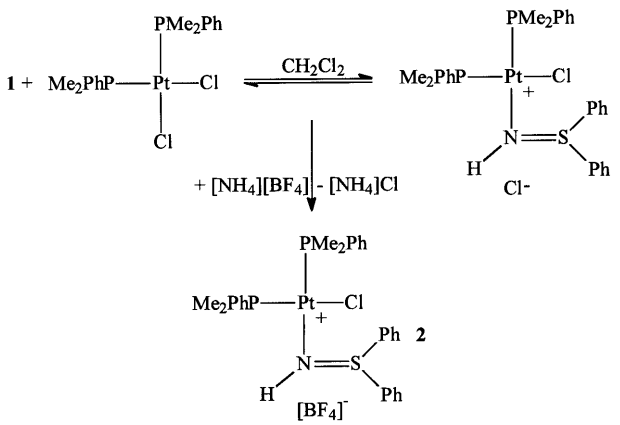
Attempts to use X-ray crystallography to confirm the structure find problems brought about by the small size and poor quality of the crystals and by disorder within the anions[1]. For this reason we do not formally present the X-ray data here though it should be noted that the solution is accurate enough to confirm the connectivity as shown in the structure in Scheme 1.

Two immediate questions come to mind as an extension to this reaction and the structure of **2**, namely (i) can more than one unit of **1** be coordinated to the platinum and (ii) is it possible to generate the *trans* isomer of **2**? On the first point, there is no evidence that, at ambient temperatures at least, a second molecule of **1** can react with **2** to generate a complex of the type $[Pt(Ph_2SNH)_2(PMe_2Ph)_2]^{2+}$. While it is possible that steric influences play a part in precluding formation of the latter, the isolation of a homoleptic sulfimide complex noted below would make this a less likely explanation. On the second point we have so far produced no evidence for the formation of the other potential isomer of **2**. Heating in toluene — a technique which can be used to generate the *trans* isomer of $[PtCl_2(PMe_2Ph)_2]$ from the *cis* — for example [9] does not appear to induce isomerisation. It may well be that again, steric considerations are paramount and mitigate against formation of the *trans*-phosphine isomer; for example, it could be argued that in the *cis* arrangement the bulky sulfimide unit has close contact with only one of the phosphines whereas it would interact with both in a *trans* structure.

If a solution of **2** in CH_2Cl_2 is treated with one equivalent of $[^nBu_4N]Cl$, ^{31}P NMR reveals the presence of both **1** and **2**. This observation confirms that the initial reaction of **1** with $[PtCl_2(PMe_2Ph)_2]$ must proceed via the kind of equilibrium shown in Scheme 1. It is only through removal of the free chloride as $[NH_4]Cl$ that the reaction can be driven to completion. That the choice of anion should have such a dramatic effect upon the ability of the product to crystallise is somewhat surprising; there would appear no obvious reason why the $[BF_4]^-$ salt should crystallise so readily while the $[PF_6]^-$ analogue generates only an oil.

The above reaction allows us to make some important comparisons between the coordinating ability of **1** and that of species such as S_4N_4. The latter is inert to $PtCl_2(PMe_2Ph)_2$ at ambient temperatures and only reacts upon either thermolysis [10] or photolysis [11]. In both cases the reaction probably proceeds via smaller anions such as $[S_3N_3]^-$; the sodium salt of the latter reacts to give $Pt(S_2N_2)(PMe_2Ph)_2$, a product which also forms when $S_4N_4H_4$ reacts in the presence of the base DBU [12]. Thus in order for underivatised S–N species to react with $PtCl_2(PMe_2Ph)_2$ a driving force such as salt elimination, photochemical disruption or simple brute force of high temperatures has to be employed. Clearly, therefore, **1** has a much stronger affinity for the platinum centre as it reacts, albeit in the equilibrium shown in Scheme 1, at ambient temperatures.

Although the above reaction appears to be limited to addition of one unit of **1** as ligand, we can in the correct circumstances generate a homoleptic platinum complex of **1**. We have previously shown that $[PPh_4]_2[PtCl_4]$ forms when $K_2[PtCl_4]$ reacts with $[PPh_4]Cl$ in water [13]. The presence of the phosphonium cation solublises the $[PtCl_4]^{2-}$ anion in CH_2Cl_2 and addition of four equivalents of **1** results in a slow reaction which eventually deposits $[Pt(Ph_2SNH)_4]Cl_2$ (**3**) as a well-formed pale yellow crystalline product after a few days standing. The product has been characterised by micro-analysis and IR spectroscopy; in the latter case the spectrum is quite distinctly similar to that of the copper analogue $[Cu(Ph_2SNH)_4]Cl_2$ [6]. Thus it shows a very strong and broad N–H stretch at 3056 cm^{-1} (3081 cm^{-1} for the Cu analogue) and a strong S–N stretch at 934 cm^{-1} (which comes at 940 cm^{-1} in the copper case). The N–H stretch is particularly pertinent — we have noted that this stretch is only strong when **1** is present on a cation and there is thus H-bonding to the anion; in neutral species it can often be hard



Scheme 1. The equilibrium present in solutions of **1** and $PtCl_2(PMe_2Ph)_2$ and the formation of **2**.

[1] Triclinic, $a = 15.724(5)$, $b = 17.407(6)$, $c = 14.64(1)$ Å; $\alpha = 112.31(3)$, $\beta = 97.537$, $\gamma = 90.86(3)°$; $V = 3466(3)$ Å^3; space group $P\bar{1}$. Due to the small size and poor quality of the crystal the refinement did not converge well. The $[BF_4]^-$ ions show signs of disorder but this could not be resolved into discrete sites.

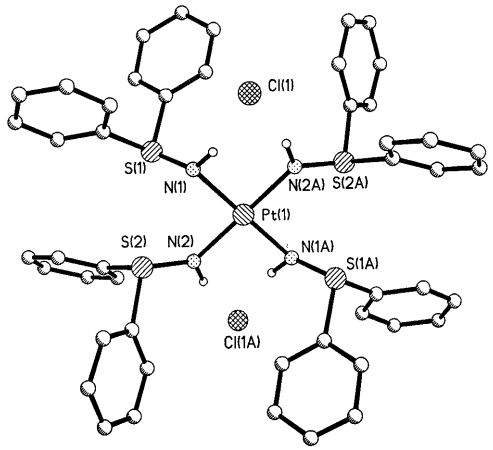


Fig. 1. The molecular structure of $[Pt(Ph_2SNH)_4]Cl_2$ (**3**).

to detect. Ultimate confirmation of the structure of **3** comes through X-ray crystallography. Fig. 1 shows its molecular structure and confirms the expected square-planar geometry; it also confirms that the ligands are all *N*-bound (an important point given the thiophilic nature platinum — note the presence of a Pt–S bound sulfimide-type unit, albeit as part of a metallocycle, in $[Pt(Ph_2SNH)(Ph_2SNC(Me)NH)Cl]Cl$ [5]). Comparison with the structure of $[Cu(Ph_2SNH)_4]Cl_2$ [6] reveals an effectively identical S–N bond distance within the ligands though the average angle at the nitrogens is less (122.6 cf. 125.3°) in **3**. Perhaps the most important observation is that, as in the Cu case, the ligands arrange themselves in such a way that the two pairs of *cis* sulfurs extend on to opposite sides of the MN_4 plane; as a result each pair of N–H groups can co-operate in H-bonding to a chloride. The overall average H–Cl bond distance is thus only 2.25 Å, with N–H–Cl angles of 168°. As mentioned earlier such cooperative H-bonding seems to be a feature of complexes of **1**; in the case of **3** Table 1 it clearly raises the possibility that insertion of the appropriate bridging H-bonding anion could result in the formation of extended structures. Thus one may envisage metathesis reactions to introduce anions such as fumarate or terepthalate into the system which could then link the cations into extended arrays. Work towards this is underway.

Table 1
Selected bond distances (Å) and angles (°) in complex **3**

Pt–N(1)	2.042(5)
Pt–N(2)	2.041(5)
N(1)–S(1)	1.589(5)
N(2)–S(2)	1.580(5)
N(1)–Pt–N(2)	92.2(2)
N(1)–Pt–N(2A)	87.8(2)
Pt–N(1)–S(1)	120.6(3)
Pt–N(2)–S(2)	124.6(3)

This reaction also provides a contrast between the reactivity of **1** and S_4N_4. In the latter case we have observed substitution of one of the chlorides of the $[PtCl_4]^{2-}$ followed by a redox reaction to give a Pt(IV) complex of $[S_4N_4]^{2-}$ [13]. Although a redox reaction is not an obvious option for **1**, the fact that no more than one chloride is substituted by the S_4N_4 (even when in excess) clearly provides further evidence of relative reactivity of the two species.

In conclusion we can say that this work clearly indicates that **1** has a powerful affinity for platinum centres; although the option to bind via sulfur is there, it prefers to coordinate through the nitrogen and is significantly more reactive than 'organo-free' sulfur nitrides such as S_4N_4. The presence of strong, concerted H-bonding interactions within **3** confirms the potential of sulfimide ligands such as **1** to act as a new class of initiator of extended array systems.

4. Supplementary material

Crystallographic data for the structural analysis has been deposited with the Cambridge Crystallographic Data Centre, CCDC No. 143910 for compound **3**. Copies of this information may be obtained free of charge from The Director, CCDC, 12 Union Road, Cambridge, CB2 1EZ, UK (fax: +44-1223-336033; e-mail: deposit@ccdc.cam.ac.uk or www: http://www.ccdc.cam.ac.uk).

Acknowledgements

We are grateful to Johnson Matthey for loans of precious metals.

References

[1] P.F. Kelly, J.D. Woollins, Chem. Soc. Rev. (1992) 245, and references therein.
[2] P.F. Kelly, A.M.Z. Slawin, A. Soriano-Rama, J. Chem. Soc., Dalton Trans. (1996) 53.
[3] P.F. Kelly, A.M.Z. Slawin, K.W. Waring, J. Chem. Soc., Dalton Trans. (1997) 2853.
[4] P.F. Kelly, A.M.Z. Slawin, K.W. Waring, Inorg. Chem. Commun 1 (1998) 249.
[5] P.F. Kelly, A.M.Z. Slawin, Chem. Commun. (1999) 1081.
[6] P.F. Kelly, S.M. Man, A.M.Z. Slawin, K.W. Waring, Polyhedron 18 (1999) 3173.
[7] Siemens SHELXTL, Revision 5.03, Siemens Analytical X-ray, Madison, WI, USA, 1995.
[8] R. Jones, C.P. Warrens, D.J. Williams, J.D. Woollins, J. Chem. Soc., Dalton Trans. (1987) 907.
[9] F.R. Hartley, Chemistry of Platinum and Palladium, Applied Science, London, 1973.

[10] J.M. Jolliffe, P.F. Kelly, J.D. Woollins, J. Chem. Soc., Dalton Trans. (1989) 2179.
[11] C.W. Allen, P.F. Kelly, J.D. Woollins, J. Chem. Soc., Dalton Trans. (1991) 1343.
[12] R. Jones, P.F. Kelly, D.J. Williams, J.D. Woollins, Polyhedron 6 (1987) 1541.
[13] P.S. Belton, V.C. Ginn, P.F. Kelly, J.D. Woollins, J. Chem. Soc., Dalton Trans. (1992) 1135.

PERGAMON

www.elsevier.nl/locate/poly

Polyhedron 19 (2000) 2083–2093

POLYHEDRON

Potentiometric and spectroscopic studies of the cobalt(II), nickel(II) and manganese(II) complexes with some aminodiphosphonic acids in aqueous solution

Barbara Kurzak [a,*], Anna Kamecka [a], Krzysztof Kurzak [a], Julia Jezierska [b], Paweł Kafarski [c]

[a] *Institute of Chemistry, University of Podlasie, 3-Maja 54, 08-110 Siedlce, Poland*
[b] *Faculty of Chemistry, University of Wrocław, 50-383 Wrocław, Poland*
[c] *Institute of Organic Chemistry, Biochemistry and Biotechnology, Technical University, 50-370 Wrocław, Poland*

Received 12 April 2000; accepted 5 July 2000

Abstract

The stoichiometries and stability constants of the manganese(II), cobalt(II) and nickel(II) complexes with seven aminodiphosphonates [$RN(CH_2PO_3H_2)_2$, L] containing iminomethylenephosphonate moieties have been determined pH-metrically at 25°C and at an ionic strength of 0.20 mol dm^{-3} (KCl). The results suggest for L = **1**–**6** only equimolar species: $[M(H_2L)]$, $[M(HL)]^-$, $[ML]^{2-}$ and hydroxo $[MH_{-1}L]^{3-}$, in the pH range of 3–11.5, the only difference is the presence of an additional $[M(H_3L)]^+$ species at low pH for *N*-3-picolyliminodi(methylenephosphonic) acid. For L = **7** the models contain protonated and non-protonated 1:2 species. From the comparative analysis of the stability and the spectroscopic (UV–VIS) data it has been established that the ligands coordinate to the metal ions only by the phosphonate group(s) in a monodentate or bidentate manner. The LMCT bands from $O^-(PO_3^{2-})$ to Ni^{2+} are at 222–211 nm. © 2000 Elsevier Science Ltd. All rights reserved.

Keywords: Potentiometry; Equilibria; Stability constants; Manganese(II); Cobalt(II); Nickel(II) complexes; Aminopolyphosphonates; UV–VIS spectra

1. Introduction

Beginning in the 1970s, the search for environmentally safer compounds focused on amino acid biosynthesis inhibitors, several of which were successfully developed as herbicides [1]. Aminoalkylphosphonic acids are broadly defined as amino acid analogues in which the carboxylic function is replaced by a phosphonic one or related function. Aminopolyphosphonic acids and their derivatives have also received considerable attention because of their interesting biological activity [2–4]. Metal aminophosphonate (aminopolyphosphonate) chemistry is attracting increasing interest because of the variety of properties that can be introduced via the phosphonate ligand [5–10]. Although metal complexes of aminophosphonic (aminopolyphosphonic) acids have been studied fairly extensively in solution, their solution chemistry is still not well understood [11–13]. Besides, glyphosate (*N*-phosphonomethylglycine, a well known herbicide) acts by inhibiting the sixth step in the initial common route of aromatic amino acid biosynthesis. The first step in aromatic metabolism is the condensation of phospho*enol*pyruvate (PEP) with erythrose-4-phosphate (E4P), a reaction catalysed by 3-deoxy-D-arabinoheptulosonate-7-phosphate (DAHP) synthase. DAHP synthase has been shown to occur in plants as two distinct isoenzymes with different roles and properties. One form, localized in the cytosol, strictly requires the presence of divalent cations (Co^{2+} in the range 0.4–0.7 mM, or Mg^{2+} at higher concentrations) [14,15]; however, the activity of the other plastidial form does not, but is stimulated three- to five-fold by 0.5 mM Mn^{2+} [16]. The activities of these two enzyme forms were

* Corresponding author. Tel.: +48-25-643-1097; fax: +48-25-644-2045.
E-mail address: bkurzak@ap.siedlce.pl (B. Kurzak).

0277-5387/00/$ - see front matter © 2000 Elsevier Science Ltd. All rights reserved.
PII: S0277-5387(00)00509-X

measured in the presence of seven different *N*-substituted aminomethylenebisphosphonic acids by Forlani et al. [17].

The manganese(II) diphosphonic acid systems is an area of Mn^{2+} chemistry in which a significant amount of structural data are not available.

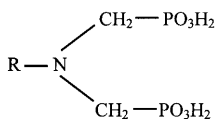
Manganese is one of the twenty-five life elements and participates in the formation of a variety of metalloenzymes: superoxide dismutase, pyruvate carboxylase [18,19], arginase and enolase [20]. Manganese catalases originating from *Thermus thermophilus* and *Lactobacillus plantarum* protect organisms from oxidative damage [21]. To explore the potential possibilities of manganese bonding to proteins, a number of investigations on manganese interactions with simple amino acids have been carried out. Many papers suggest O,O type coordination whereas the amino nitrogen remains rather uncoordinated [22–26]. In some cases the coordination through the nitrogen atom of the amino acid has been postulated [27,18]. This bonding mode is also proposed for some naturally existing enzymes [20].

For a better understanding and interpretation of the biological findings, a more detailed knowledge about complexing abilities of this type of compound with different metal ions is indispensable.

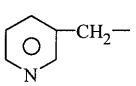
As part of our program on the coordination chemistry of divalent cations with aminopolyphosphonic acids (aminodi- and aminobisphosphonic acids), we have set out to elucidate the molecular structures and reactivities of these types of complex.

We have recently reported results on metal complexes of the same iminodi(methylenephosphonic) acids [28,29]. It has been established that the coordination in all copper(II) complexes is realized by the phosphonic group(s) and imino nitrogen [28]. The tridentate complexes with two joined five-membered chelate rings predominate in solutions at a pH of about 7–11, for the majority of the zinc systems. On the contrary, Ca^{2+} and Mg^{2+} prefer a pure phosphonate coordination [29].

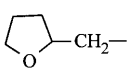
The aim of the present work was to obtain information on the protonation equilibria and the complex-forming ability of those iminodi(methylenephosphonic) acids (see Scheme 1), by establishing the compositions and stabilities of the species formed with Mn^{2+}, Co^{2+} and Ni^{2+} ions in aqueous solution.



R = (C_6H_{11}) - **1**
($(CH_3)_2CH(CH_2)_2$ - **2**
CH_3CH_2- **3**
CH_3 - **4**
(C_6H_5)CH_2 - **5**



6



7

Scheme 1. *N*-Cyclohexyliminodi(methylenephosphonic) acid (**1**); *N*-iso-pentyliminodi(methylenephosphonic) acid (**2**); *N*-ethyliminodi-(methylenephosphonic) acid (**3**); *N*-methyliminodi(methylenephosphonic) acid (**4**); *N*-benzyliminodi(methylenephosphonic) acid (**5**); *N*-3-picolyliminodi(methylenephosphonic) acid (**6**); *N*-2-methyltetrahydrofuryliminodi(methylenephosphonic) acid (**7**).

2. Experimental

2.1. Materials

Diphosphonic acids used in this paper were obtained according to previously described procedures [30,31]. The exact concentrations of the solutions of the ligands used for potentiometric studies were determined by the Gran method [32]. The concentrations of the metal(II) chloride stock solutions were standarized by complexometric ethylenediaminetetraacetate (EDTA) titration. Carbonate-free potasium hydroxide (the titrant) was prepared and standardized against a standard potassium hydrogenphthalate solution.

2.2. Potentiometry

The stability constants of the proton and metal(II) complexes were determined by pH-metric titration of 2 cm^3 samples. The ligand (L) concentration was 2×10^{-3} mol dm^{-3} and additionally 4×10^{-3} mol dm^{-3} for ligand **6** and 1×10^{-3} mol dm^{-3} for ligand **1**. The metal:ligand molar ratio was 0:1; 1:1.5; 1:2 and the ionic strength adjusted to 0.2 mol dm^{-3} with KCl in each case. The titrations were performed with a carbonate-free KOH solution under argon atmosphere over pH range 2.5–11.5 for ligand and 2.5–10.5 for metal:ligand systems. The exceptions were the Ni^{2+}–**1** and Co^{2+}–**1** systems, where precipitation was observed at pH about 9. All titration solutions were thermostatted at 25 ± 0.1°C using a constant-temperature water-bath.

The pH was measured with a MOLSPIN automatic titration system using a micro combination pH electrode (Mettler–Toledo, Type 2). Small amounts ($\Delta v = 0.001$ cm^3) of titrant were added (total volume = 0.1 cm^3). The electrode system was calibrated by periodic titrations of HCl solution (7.5×10^{-3} mol dm^{-3} in KCl) against standard KOH solution. The resulting titration data were used to calculate the standard elec-

Table 1
Protonation constants of the ligands ($\log \beta^{H}$) and stability constants of the manganese(II) complexes ($\log \beta$) at 25°C and $I = 0.2$ mol dm^{-3} (KCl) [a]

Assignments	Compound						
	1	**2**	**3**	**4**	**5**	**6**	**7**
$\log \beta_1^H$	12.5	12.3	12.2	11.75(1)	11.32(1)	10.40(1)	11.46(1)
$\log \beta_2^H$	18.59(2)	18.51(2)	18.24(3)	17.70(1)	17.51(1)	16.49(2)	17.59(2)
$\log \beta_3^H$	23.29(2)	23.38(2)	22.93(3)	22.49(1)	22.24(1)	21.42(2)	22.38(3)
$\log \beta_4^H$						24.36(4)	
pK(PO_3H^-)	6.09	6.21	6.04	5.95	6.19	6.09	6.13
pK(PO_3H^-)	4.70	4.87	4.69	4.79	4.73	4.93	4.79
pK(NH^+_{pyr})						2.94	
$\log \beta[Mn(H_3L)]^+$						22.71(7)	
$\log \beta[Mn(H_2L)]$	21.05(2)	20.74(2)	20.54(1)	19.82(3)	19.82(3)	18.78(1)	19.91(3)
$\log \beta[Mn(HL)]^-$	16.30(1)	15.99(1)	15.80(1)	15.19(1)	15.07(1)	14.07(1)	15.10(1)
$\log \beta[MnL]^{2-}$	6.58(2)	7.28(1)	7.25(1)	7.42(2)	6.96(2)	6.75(1)	7.98(3)
$\log \beta[MnLH_{-1}]^{3-}$	−4.85(4)	−3.39(2)	−3.49(3)	−4.23(15)	−4.08(5)	−4.27(5)	
$\log \beta[Mn(HL)_2]^{4-}$							29.19(5)
$\log \beta[Mn(HL)L]^{5-}$							22.00(11)
$\log \beta[MnL_2]^{6-}$							12.97(8)
$pK_{[Mn(H_2L)]}$	4.75	4.75	4.74	4.63	4.75	4.71	4.81
$pK_{[Mn(HL)]^-}$	9.72	8.71	8.55	7.77	8.11	7.32	7.12
$pK_{[MnL]^{2-}}$	11.43	10.67	10.74	11.65	11.04	11.02	
$Mn^{2+} + HL^+_{NH} \rightleftarrows Mn(HL)$ [b]	3.80	3.69	3.60	3.44	3.75	3.67	3.64
$\log K_{[MnL]^{2-}} - \Sigma pK$	−16.71	−16.10	−15.68	−15.07	−15.28	−14.67	−14.40

[a] The standard deviations are given in parentheses.
[b] $\log K = \log \beta_{[Mn(HL)]^-} - pK^+_{NH}$.

trode potentials, E^0, and the dissociation constant for water ($pK_w = 13.74$). These values were then used to calculate the hydrogen-ion concentration [H^+] from emf readings [33]. Calculations were carried out using the SUPERQUAD computer program [34].

The charges of the complexes have been omitted in the text and tables. However, for clarity, it should be mentioned, that the fully deprotonated forms have negative charges L^{4-}.

2.3. Spectroscopic measurements (UV–VIS)

The UV absorption spectra for systems with nickel(II) were recorded at room temperature on a Specord M40 spectrophotometer, digitally (20 cm^{-1}) over the range 28000–50000 cm^{-1}. The spectral data at selected ca. 1000 wavenumbers over the range 30000–50000 cm^{-1} (or 37000–50000 cm^{-1}) were employed for analysis and resolved into Gaussian components. The metal ion concentration was 5×10^{-4} mol dm^{-3}. The spectra were fitted with Gaussian bands using the CFP program [35] based on the Slavič [36] numerical algorithm, which for the last a few years has been successfully applied by us to the deconvolution of d-d (ligand field) spectra [37] (and refs. therein).

The VIS absorption spectra for systems with cobalt(II) and nickel(II) were recorded at room temperature on a Cary 5 spectrophotometer, digitally (0.5 nm) over the range 270–900 nm. The metal ion concentration was 1×10^{-2} mol dm^{-3}.

3. Results and discussion

3.1. Potentiometry

The values determined in the present work are in good agreement with those published earlier in our former works [28,29] or by others [38,39,7]. The list of these compounds is shown in Scheme 1. Although the fully protonated ligand forms contain five dissociable protons (H_5L^+) for **1**–**5** and **7** and six protons (H_6L^{2+}) for **6** (because of the additional proton on the pyridine nitrogen atom) they release only three protons in the measurable pH range: two protons from each of the phosphonic groups (PO_3H^-) and one imiono nitrogen, NRH^+. An additional proton from NH^+_{pyr} dissociates in **6** (Table 1). The characteristic pK values for dissociation of one proton from each of the PO_3H_2 groups lie in the range 1.5–2. Thus, they do not participate in the metal coordination equilibria.

3.2. Systems with manganese(II), cobalt(II) or nickel(II)

The chemical models for the ligands **1**–**6** with these metal ions contain only equimolar complexes: protonated, deprotonated and hydroxo complexes (Tables 1 and 2). The formation of the bis complexes seems to be generally hindered because of the electrostatic repulsion of the negatively charged phosphonate groups precludes coordination of the second ligand; the charge of the bis complex would be $6-$. Hence, only 1:1 complexes are formed and data collected in Tables 1 and 2 indicate lower chelating ability of the ligands towards Mn^{2+}, Co^{2+} or Ni^{2+} than Cu^{2+} [28]. However, the overall stability constants of the manganese(II) complexes are distinctly lower if compared with that obtained for the cobalt(II) and nickel(II) complexes. The chemical models for systems of ligand **7** with these metal ions are different if compared with all the other systems studied. These models contain protonated and non protonated 1:2 species (Tables 1 and 2).

The metal complex speciations derived from potentiometric calculations for compounds **2**–**6** in the range pH 3–10.5, do not differ considerably. The incipient precipitation, in the Co^{2+}–**1** and Ni^{2+}–**1** systems, caused by the formation of complex(es) and/or hydroxo complex(es) at pH near 9 makes the observation of the next step doubtful, also in the presence of higher ligand-to-metal molar ratio. The Co^{2+}–**5** and Ni^{2+}–**5** systems presented in Figs. 1 and 2 exhibit, in general, approximately the same distribution curves as those observed for the other ones, and thus is representative for all the ligands. Three complexes: $[M(H_2L)]$, $[M(HL)]^-$, $[ML]^{2-}$ and hydroxo $[MLH_{-1}]^{3-}$, are formed in the above-mentioned pH range, with the single difference found for complexes of compound **6**, namely the presence of an additional $[M(H_3L)]^+$ species at low pH. Although the concentration of this complex is very low ($\sim 5\%$), the assumption of this species improved the fit between the experimental and the calculated titration data. Since the agreement of this fit with or without the assumption of the $[MOH]^-$ species

Table 2
Stability constants of the cobalt(II) and nickel(II) complexes ($\log \beta$) at 25°C and $I = 0.2$ mol dm^{-3} (KCl) [a]

Assignments	Compound						
	1	**2**	**3**	**4**	**5**	**6**	**7**
$\log \beta[Co(H_3L)]^+$						22.86(9)	
$\log \beta[Co(H_2L)]$	21.03(2)	19.98(9)	19.86(8)	19.42(5)	19.93(3)	18.73(4)	20.06(3)
$\log \beta[Co(HL)]^-$	15.97(1)	15.42(1)	15.10(2)	15.05(1)	14.90(1)	13.78(1)	15.70(1)
$\log \beta[CoL]^{2-}$		8.08(2)	7.95(2)	8.77(1)	8.31(2)	7.75(2)	9.66(4)
$\log \beta[CoLH_{-1}]^{3-}$	−2.42(3)	−3.02(3)	−3.05(4)	−2.39(4)	−2.49(4)	−3.22(3)	
$\log \beta[Co(HL)_2]^{4-}$							30.17(5)
$\log \beta[Co(HL)L]^{5-}$							24.40(6)
$\log \beta[CoL_2]^{6-}$							13.65(4)
$pK_{[Co(H_2L)]}$	5.06	4.56	4.76	4.37	5.03	4.95	4.36
$pK_{[Co(HL)]^-}$		7.34	7.15	6.28	6.59	6.03	6.04
$pK_{[CoL]^{2-}}$		11.10	11.00	11.16	10.80	10.97	
$Co^{2+} + HL^+_{NH} \rightleftarrows Co(HL)$ [a]	3.47	3.12	2.90	3.30	3.58	3.38	4.24
$\log K_{[CoL]^{2-}} - \Sigma pK$		−15.30	−14.98	−13.72	−13.93	−13.67	−12.72
$\log \beta[Ni(H_3L)]^+$						22.70(10)	
$\log \beta[Ni(H_2L)]$	20.66(3)	19.76(11)	19.44(10)	19.13(9)	19.87(4)	18.61(3)	20.16(4)
$\log \beta[Ni(HL)]^-$	15.64(2)	15.27(1)	15.00(1)	15.01(1)	14.79(2)	13.73(1)	15.79(1)
$\log \beta[NiL]^{2-}$		8.21(1)	8.14(1)	9.00(1)	8.27(2)	7.58(1)	9.35(7)
$\log \beta[NiLH_{-1}]^{3-}$	−2.51(3)	−3.10(4)	−2.94(4)	−2.09(2)	−3.61(7)		
$\log \beta[Ni(HL)_2]^{4-}$							30.18(7)
$\log \beta[Ni(HL)L]^{5-}$							24.43(6)
$\log \beta[NiL_2]^{6-}$							12.78(11)
$pK_{[Ni(H_2L)]}$	5.02	4.49	4.44	4.12	5.08	4.88	4.37
$pK_{[Ni(HL)]^-}$		7.06	6.86	6.01	6.52	6.15	6.44
$pK_{[NiL]^{2-}}$		11.31	11.08	11.09	11.88		
$Ni^{2+} + HL^+_{NH} \rightleftarrows Ni(HL)$ [b]	3.14	2.97	2.80	3.26	3.47	3.33	4.33
$\log K_{[NiL]^{2-}} - \Sigma pK$		−15.17	−14.79	−13.49	−13.97	−13.84	−13.03

[a] The standard deviations are given in parentheses.
[b] $\log K = \log \beta_{[M(HL)]^-} - pK^+_{NH}$.

Table 3
Spectroscopic parameters for the cobalt(II) complexes[a]

Ligand	Species	pH	UV–Vis
			λ (nm), ε ($dm^3\ mol^{-1}\ cm^{-1}$)
H_2O	$[Co(H_2O)_6]^{2+}$	4.0	≈1250 (1.4), 649 (∼0.7), 511 (5.3) **A**
1	$[Co(H_2L)]$	4.1	653 (∼0.7), 518 (6.7) **A**
	$[Co(HL)]^-$	7.0	652 (∼0.85), 523 (7.3) **A**
2	$[Co(HL)]^-$	6.25	652.5 (∼0.7), 523.5 (7.4) **A**
	$[CoL]^{2-}$	9.2	652 sh, 526.5 (7.2) **A**
			808 (∼1.0) 494 (7.1) **B**
	$[CoLH_{-1}]^{3-}$	12.0	≈830 (3.0), 644.5 (45), 600 (39), 502 (20) **B**
3	$[Co(HL)]^-$	6.25	655 (∼0.7), 525 (7.7) **A**
	$[CoL]^{2-}$	8.9	652 sh, 524.5 (7.3) **A**
			803 (∼1.0), 493.5 (7.1) **B**
	$[CoLH_{-1}]^{3-}$	12.3	≈830 (4.4), 643.5 (41.4), 599 (38.4), 503 (21.9) **B**
4	$[Co(HL)]^-$	5.5	656 (∼0.8), 525 (7.6) **A**
	$[CoL]^{2-}$	9.1	650 sh, 518 (7.4) **A**
			810 (∼0.8), 497.5 (7.5) **B**
	$[CoLH_{-1}]^{3-}$	12.3	≈830 (6.1), 540–580 (13.0) **B**
5	$[Co(HL)]^-$	5.9	654(∼0.7), 523.5 (7.6) **A**
	$[CoL]^{2-}$	9.0	650 sh, 525 (7.7) **A**
			811 (∼1.2), 493 (7.7) **B**
	$[CoLH_{-1}]^{3-}$	12.4	≈820 (7.4), 642 (34.6), 596.5 (37.1), 500 (28.2) **B**
6	$[Co(H_3L)]^+$	3.1	647 (∼0.5), 511 (6.9) **A**
	$[Co(HL)]^-$	6.1	661 (∼0.4), 517 (9.6) **A**
	$[CoL]^{2-}$	8.5	660 sh, 523 (9.1) **A**
			809 (∼1.2), 493 (9.1) **B**
	$[CoLH_{-1}]^{3-}$	12.2	≈830 (6.6), 636.5 (21.7), 593.5 (27.9), 500.5 (23.4) **B**
7	$[Co(HL)L]^{5-}$	8.0–9.0	779 (6.5), 539.5 (35), 479 sh, **A**
	$[CoL]^{2-}$	9.0	784 (4.3), 540 (24.4), 480 sh, **A**

[a] Data presented in this table actually reflect the optical properties of solutions in which the given forms are the major species; sh denotes shoulder. **A**, d–d transition in an octahedral complex; **B**, d–d transition in a tetrahedral complex.

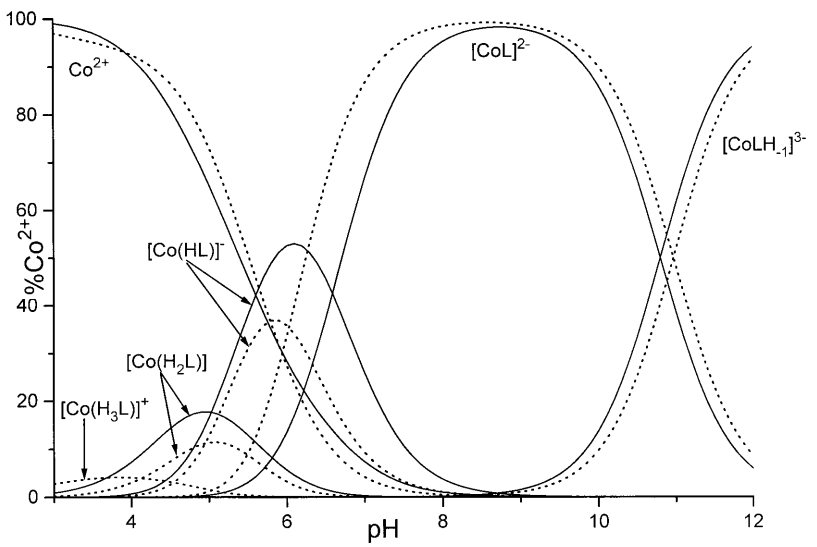


Fig. 1. Species distribution curves for the complexes formed in the Co^{2+}/ligand **5** (full line) and Co^{2+}/ligand **6** (dotted line) systems as a function of pH; $c_{Co^{2+}} = 1 \times 10^{-3}$ mol dm^{-3}; $c_L = 2 \times 10^{-3}$ mol dm^{-3}.

is within experimental error and the value of $\log K_{[M(OH)]}$ differs very much from the values in SC-Database [40], we decided to remove this species from our models.

The deprotonation constant, $pK_{[M(H_3L)]^+}$, for the reaction $[M(H_3L)]^+ \rightleftarrows [M(H_2L)] + H^+$ for the ligand **6** with Mn^{2+}, Co^{2+} or Ni^{2+}, is 3.93, 4.13 and 4.09, respectively. These values are lower than obtained for the PO_3H^{1-} groups of the free ligand (Tables 1 and 2). Thus, for the first species the pyridine nitrogen is involved in the coordination and both PO_3^{2-} and N_{imino} groups remain protonated. In this case the phosphonate O^- is unable to coordinate the metal ion due to steric reasons. This fact is supported by the absorption spectra of the Ni^{2+}–**6** system presented in Fig. 3. These spectra exhibit the changes versus pH. It has to be mentioned that at pH 3 the high-intensity charge-transfer band, being near to the d-d transitions, and is observed and distorts the visible spectra (Table 4). At a higher pH region this band disapeared. From these and the data collected in Table 4 we concluded that at this pH in the $[Ni(H_3L)]^+$ species the pyridine nitrogen is coordinated and the CT band is the consequence of the transition between N_{pyr} and Ni^{2+}.

In the systems presented, only one species, $[M(H_2L)]$, is formed as a minor species in which the protonated ligands coordinate to these metal ions by the phosphonate group(s) in a monodentate(bidentate) manner. Deprotonation of $[M(H_2L)]$ leads to the formation of $[M(HL)]^-$. The $pK_{[M(H_2L)]}$ values characteristic for the next deprotonation step for the $[M(H_2L)]$ complexes are considerably lower than the corresponding deprotona-

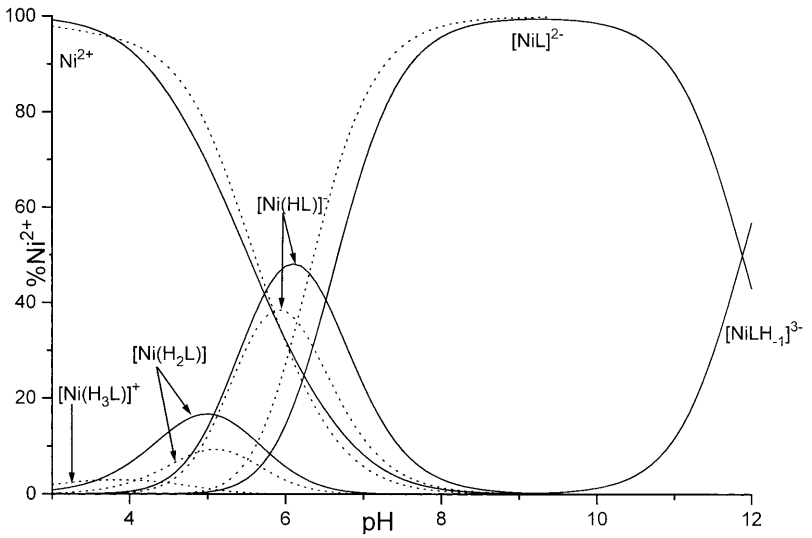


Fig. 2. Species distribution curves for the complexes formed in the Ni^{2+}/ligand **5** (full line) and Ni^{2+}/ligand **6** (dotted line) systms as a function of pH; $c_{Ni^{2+}} = 1 \times 10^{-3}$ mol dm^{-3}; $c_L = 2 \times 10^{-3}$ mol dm^{-3}.

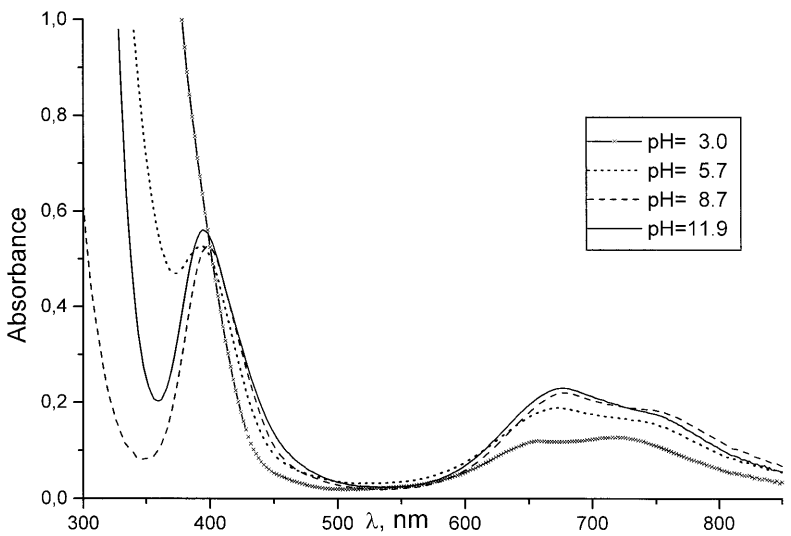


Fig. 3. pH-varied absorption spectra of the Ni^{2+}/ligand **6** system: $c_{Ni^{2+}} = 1 \times 10^{-2}$ mol dm^{-3}; $c_L = 2 \times 10^{-2}$ mol dm^{-3}; 5 cm cell.

Table 4
Spectroscopic parameters for the nickel(II) complexes

Ligand	Species	pH	UV–VIS
			λ (nm), ε ($dm^3\ mol^{-1}\ cm^{-1}$)
H_2O	$[Ni(H_2O)_6]^{2+}$	5.5	≈1159 (2.4), 720.5 (∼2.2), 657 (∼1.9), 395 (5.1)
1	$[Ni(H_2L)]$	4.4	733 (2.5), 664 (2.1), 401 (6.1)
	$[Ni(HL)]^-$	7.4	737.5 (2.4), 672 (1.9), 402.5 (6.2)
2	$[Ni(HL)]^-$	6.2	742 (2.7), 675 (2.1), 404.5 (6.5)
	$[NiL]^{2-}$	9.1	751 (3.1), 680.5 (3.8), 399 (9.5)
		9.1	217 (1429)
	$[NiLH_{-1}]^{3-}$	11.8	742 (3.74), 676 (4.86), 394 (11.0)
3	$[Ni(HL)]^-$	6.0	744.5 (2.7), 675 (2.1), 405.5 (6.3)
	$[NiL]^{2-}$	8.9	750 (3.2), 680 (3.9), 399.5 (9.5)
		9.1	215 (1375)
	$[NiLH_{-1}]^{3-}$	12.0	743 (3.5), 676.5 (4.5), 395 (10.5)
4	$[Ni(HL)]^-$	5.4	742 (2.3), 675 (1.9), 404.5 (6.0)
	$[NiL]^{2-}$	8.9	742 (3.1), 676 (3.8), 398 (8.9)
		9.1	211 (1498)
	$[NiLH_{-1}]^{3-}$	12.0	743 (3.1), 676.5 (3.9), 397.5 (9.5)
5	$[Ni(HL)]^-$	5.9	738 (2.4), 675 (2.1), 403 (6.3)
	$[NiL]^{2-}$	9.1	756 (3.4), 680.5 (4.2), 399.5 (10.4)
		9.1	218 (3145)
	$[NiLH_{-1}]^{3-}$	12.0	760 (3.2), 679 (4.4), 394 (11.7)
6	$[Ni(H_3L)]^+$	3.0	717 (4.6), 665 (5.2), CT [a]
	$[Ni(HL)]^-$	5.7	740 (3.2), 671 (3.9), 385 (11.6)
	$[NiL]^{2-}$	8.7	760 (3.5), 679.5 (4.4), 399.5 (10.6)
		9.1	222 (2012)
7	$[Ni(HL)L]^{5-}$	8.0–9.0	735 (3.3), 657 (5.0), 393 (12.5)
	$[NiL]^{2-}$	9.0	735.5 (3.2), 664.5 (4.5), 395 (10.5)
		9.2	215 (1476)
	$[NiL_2]^{6-}$	12.0	735.5 (3.6), 657 (5.3), 393 (13.5)

[a] The strong overlap between d-d band and that of the dominant high-intensity charge — transfer band.

tion constants of the free ligands (see Tables 1 and 2). It can be assigned to deprotonation of the phosphonic group promoted by the studied metal ions binding, i.e. the protonated ligand coordinates to these metal ions by the phosphonate groups in a bidentate manner. In this case the formation of an eight-membered chelate ring may be assumed [41,42]. The following deprotonation step, has the $pK_{[M(HL)]^-}$ values much lower than the pK_{NH^+} of the free ligands. On the other hand, the deprotonation of $[M(HL)]^-$ in the range pH 6–9.5, which leads to $[ML]^{2-}$, does not generate considerable changes in the spectra of cobalt(II) and nickel(II) systems, so the bonding mode in both species might be the same with O,O coordination. The only CT bands at 222–211 nm, which were observed for the systems with Ni^{2+} (Table 4) are similar to this observed for $[Ni(H_2O)_6](ClO_4)_2$ complex (198 nm) and can be reasonably assigned to the transition from PO_3^{2-} oxygen to Ni^{2+}, i.e. LMCT transition (Fig. 4). Similar studies were made on the copper(II) complexes of these ligands and in those cases two different CT bands were obtained [28].

Ligand **7** bearing the oxygen atom of the tetrahydrofuryl substituent placed in the sterically favourable position which allows it to be an additional effective metal binding site, is a more effective chelating agent than other ones. This is reflected in the higher basicity-adjusted stability constant, $\log K_{[ML]^{2-}} - \Sigma pK$ (Tables 1 and 2).

A comparison of Mn^{2+}, Co^{2+} or Ni^{2+} complexes of **5** and **7** (these ligands have the same basicity) shows significant differences. Basicity-adjusted stability constants, $\log K_{[ML]^{2-}} - \Sigma pK$ are -15.28 and -14.40 for Mn^{2+} with ligand **5** and **7**, respectively; -13.93 and -12.72 for Co^{2+} with **5** and **7**, respectively and -13.97 and -13.03 for Ni^{2+} with **5** and **7**, respectively. Taking this into account, comparison of $[M(\mathbf{5})]^{2-}$ and $[M(\mathbf{7})]^{2-}$ complexes still reveals a difference in stabilities of about 0.88 and 1.2 or 0.94 log units, respectively, suggesting interaction between Mn^{2+}, Co^{2+} or Ni^{2+} and the furyl oxygen atom.

The basicity-adjusted stability constants ($\log K_{[CoL]^{2-}} - \Sigma pK$) varies in the sequence (Table 1):

$$[Co(\mathbf{2})] < [Co(\mathbf{3})] < [Co(\mathbf{5})] < [Co(\mathbf{4})] < [Co(\mathbf{6})] < [Co(\mathbf{7})]$$

The similar sequence is observed for manganese(II) and nickel(II) complexes. This can be explained, in part, by the significant changes of the imino substituent size.

It is interesting to compare the stability of the simple complex $M^{2+} + OH^- \rightleftharpoons [M(OH)]^+$ with that of the mixed one $[ML]^{2-} + OH^- \rightleftharpoons [ML(OH)]^{3-}$. The equilibrium constant, $K_{[ML(OH)]^{3-}}$, evaluated from the computed values of the related β values according to equation: $\log K_{[ML(OH)]^{3-}} = \log \beta_{[MLH_{-1}]^{3-}} - \log \beta_{[ML]^{2-}}$, (equilibrium 3 in Tables 5 and 6 and the $[MLH_{-1}]^{3-}$ species corresponds to $[ML(OH)]^{3-}$ in terms of equilibrium) shows how tightly OH^- is bound to the simple $[ML]^{2-}$ complex. Thus, the binding strength of OH^- in mixed complexes depends on the stability of the simple complex $[ML]^{2-}$ (see Table 2).

When we consider $[ML(OH)]^{3-}$ to be a mixed-ligand complex, the difference in stability, $\Delta\log K$, between the simple and mixed-ligand species is given by:

$$\Delta\log K = \log K^{[ML]}_{[ML(OH)]} - \log K^{M}_{MOH}$$
$$= \log K^{[MOH]}_{[ML(OH)]} - \log K^{M}_{[ML]}$$

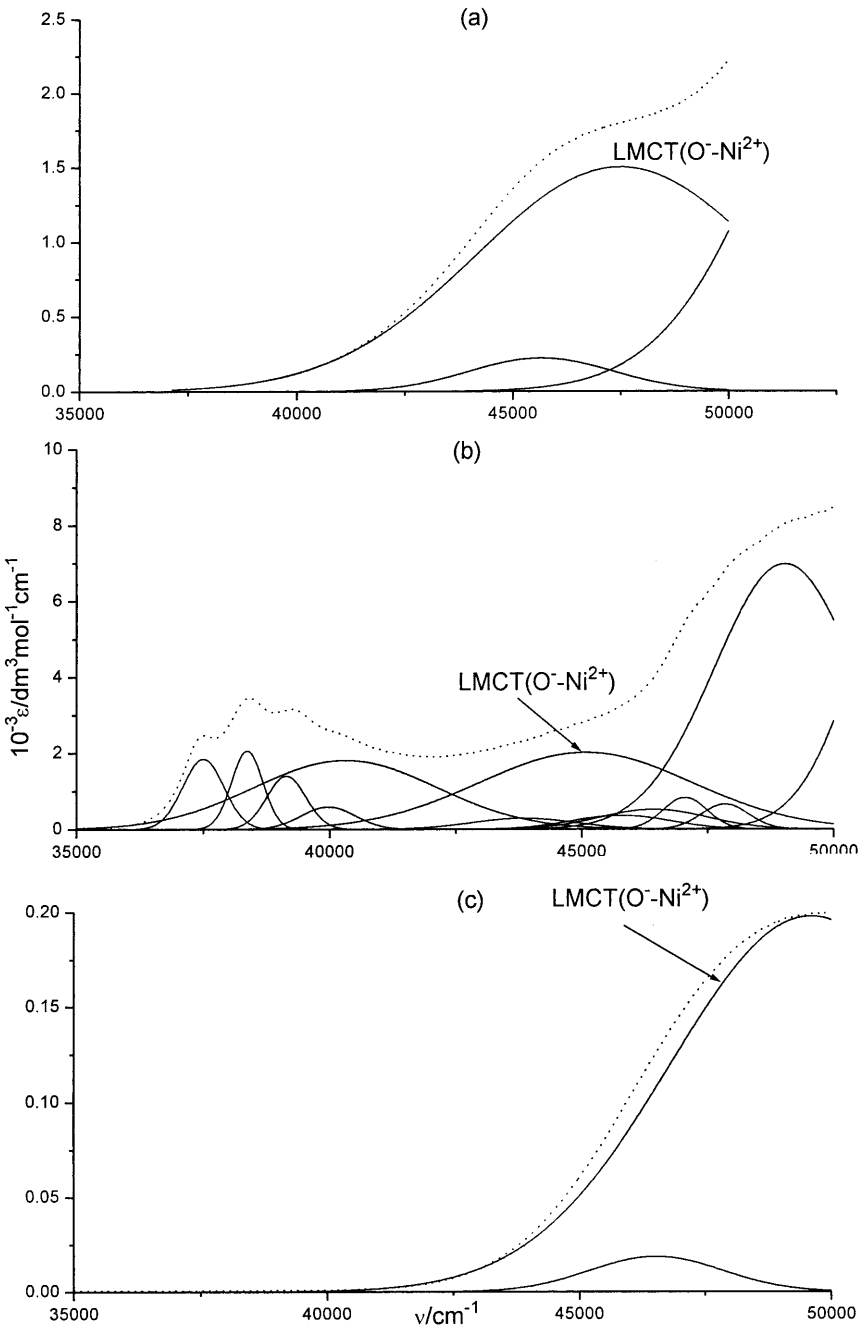


Fig. 4. Ultraviolet spectra and Gaussian line-shape analysis for: $[NiL]^{2-}$; L = **4** (a); L = **6** (b); pH 9; $[Ni(H_2O)](ClO_4)_2$ (c); experimental spectrum (grey line); component bands (black line).

Table 5
Equilibrium constants of formation cobalt(II) complexes of iminodiphosphonic acids

Equilibrium	2	3	4	5	6	7
1. $M+L \rightleftarrows ML$	8.08	7.95	8.77	8.31	7.75	9.66
2. $M+H_2O \rightleftarrows MOH+H^+$ [a]	−9.64	−9.64	−9.64	−9.64	−9.64	−9.64
3. $ML+H_2O \rightleftarrows MLOH+H^+$	−11.10	−11.00	−11.16	−10.80	−10.97	
4. $MOH+L \rightleftarrows MLOH$	6.62	6.59	7.25	7.15	6.42	
5. $MOH+ML \rightleftarrows MLOH+M$	−1.46	−1.36	−1.52	−1.16	−1.33	

[a] Ref. [43].

Table 6
Equilibrium constants of formation nickel(II) complexes of iminodiphosphonic acids

Equilibrium	2	3	4	5	6	7
1. $M+L \rightleftarrows ML$	8.21	8.14	9.00	8.27	7.58	9.35
2. $M+H_2O \rightleftarrows MOH+H^+$ [a]	−9.14	−9.14	−9.14	−9.14	−9.14	−9.14
3. $ML+H_2O \rightleftarrows MLOH+H^+$	−11.31	−11.08	−11.09	−11.88		
4. $MOH+L \rightleftarrows MLOH$	6.04	6.20	7.05	5.53		
5. $MOH+ML \rightleftarrows MLOH+M$	−2.17	−1.94	−1.95	−2.74		

[a] Ref. [44].

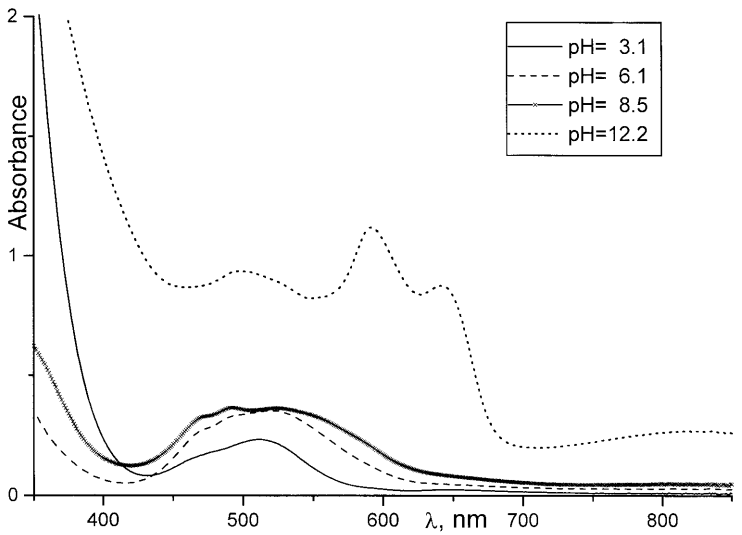


Fig. 5. pH-varied absorption spectra of the Co^{2+}/ligand **6** system: $c_{Co^{2+}} = 1 \times 10^{-2}$ mol dm^{-3}; $c_L = 2 \times 10^{-2}$ mol dm^{-3}; 4 cm cell.

The $\Delta\log K$ parameter (equilibrium 5 in Tables 5 and 6) expresses the effect of the bonded primary ligand (L) towards the incoming secondary ligand (OH^-). For comparison, also the $\log K$ values for the hydrolysis of both M^{2+} [43,44] and $[ML]^{2-}$ ions of cobalt(II)/nickel(II) are included in Tables 5 and 6. Since the OH^- group coordinates more easily with the free cobalt(II)/nickel(II) ion than with the complexed metal ion, $[ML]^{2-}$, $\Delta\log K$ should be negative. The binding strength of OH^- in mixed-ligand complexes depends on the stability of $[ML]^{2-}$ which, in our case, does not necessarily mean that it depends on the basicity of the ligand (compare values in Table 1 and equilibrium 3 in Tables 5 and 6). In a case of bulky L bonded in the Co^{2+} (Ni^{2+}) equimolar complex the coordination of OH^- is more favoured than that of the second ligand of the same kind.

3.3. Spectrophotometrical studies

Absorption spectra of the Co^{2+}-ligand **6** system presented in Fig. 5 exhibit, in general, approximately the same changes versus pH as those observed for the other above-mentioned systems with cobalt(II). Even at the pH value where the distribution of the species has a maximum, the other complexes coexist in a greater or smaller extent. Therefore, in the absorption spectra measured even at this pH value the contributions from

the other species would be included. To extract the ligand-field absorption spectrum of each species, the experimental spectrum, measured at a pH value where each species exhibits maximal contribution, was resolved into the components spectra corresponding to the individual species existing at that pH. The molecular absorptivity for the individual species was then calculated taking into account their distribution. In some cases this method has not given satisfactory results for species which the contribution was too small in the system.

The electronic spectra of cobalt(II) complexes depend on the configuration of these complexes. The difference in the ligand-field bands between various configurations, is so apparent that the electronic spectrum may be regarded as diagnostic of the stereochemistry of the cobalt(II) complexes.

The $[CoL]^{2-}$ complexes are formed from $[Co(HL)]^{-}$ at pH ca. 5.5 and they are predominant species at around pH 7–10.5 in solution. This process involves deprotonation of an imino nitrogen and is accompanied by a deviation of the complex geometry from octahedral or pseudo- octahedral and formation of the $[CoL]^{2-}$ results in distinct changes in absorption spectra. The spectrum in the visible region reveals additional d-d bands (Table 5). The deprotonation of $[CoL]^{2-}$ leads to the formation of $[CoLH_{-1}]^{3-}$ and corresponds to the subsequent dissociation of the proton from coordinated water molecule. This hydroxo species predominated above pH 11 and solutions give a deep blue color. These observations and spectroscopic results shown in Table 3 strongly suggest preorganization at Co^{2+} binding site and indicate changing geometry from octahedral towards tetrahedral. The much higher electron-donating ability of OH^{-} relative to that of H_2O is responsible for the changes in the spectra.

3.4. Ultraviolet spectroscopic studies

All the band maxima reported in this work are derived from Gaussian analysis of the experimental curves in the ultraviolet region. In general, the unique procedure (see experimental section) which starts with Gaussian analysis, through assignment of the bands, to calculation of the chemically useful parameters, is based on two assumptions: the symmetry of compound is known, and theoretical model (e.g. ligand field model for the complexes and orbital molecular model for the ligands) is adequate for the calculation of the spectral parameters. Unfortunately, the systems presented in this work are rather complex. Different structures of the particular ligands are the reason that the above mentioned interpretation makes for considerable difficulties. Thus, each system studied should be analysed separately. Therefore, the Gaussian analysis of the ultraviolet spectra in this work provides the bands which can be conclusively distinguished from the experimental (observed) spectrum. The numerical spectra $\varepsilon_i = f(\nu_i)$ and full Gaussian analysis results of all spectra are available from the authors on request. Fig. 4(a and b) present (as representative example) ultraviolet spectra $\varepsilon_i = f(\nu_i)$) along with Gaussian components for Ni^{2+}-ligand **4** and Ni^{2+}-ligand **6** systems.

Because ligands **2-4** do not have bands in the UV region, one observed band corresponds to the CT transition (for example: Ni^{2+}-ligand **4** system in Fig. 4a). Although compounds **5, 6** and **7** have their own UV absorption spectra, one new band is easily seen when their spectra are compared with those for the complexes (for example: Ni^{2+}-ligand **6** system in Fig. 4b). The CT band at 198 nm is observed for the $[Ni(H_2O)_6](ClO_4)_2$ (Fig. 4c). In this case the coordination of oxygen atoms to nickel(II) is beyond doubt. Thus, the CT band at 222–211 nm observed for the nickel(II)–**2**, –**6** and **7** systems corresponds most likely to the $O–Ni^{2+}$ LMCT transition.

From the data collected in Table 4 we conclude that the energy order of the CT transition displays a hipsochromic effect (i.e. increasing energy):

$$[\text{Ni (6)}] < [\text{Ni (5)}] \approx [\text{Ni (2)}] < [\text{Ni (3)}] \approx [\text{Ni (7)}] < [\text{Ni(4)}]$$

This effect depends predominantly on the size of the fragment R (Scheme 1) bonded to the nitrogen donor. The highest energy is observed when R = methyl group and the lowest when R involves an *N*-3-picolyl ring. A similar energy relation was observed for the systems with copper(II) [28].

4. Conclusion

The ligands **1**–**6** exhibit the model contains equimolar protonated and deprotonated complexes but neither a 1:2 species nor any polynuclear ones. Otherwise, the model for M^{2+}-ligand **7** systems includes 1:2 species. From the comparative analysis of the stability and the spectroscopic (UV–VIS) data it has been established that the coordination in $[ML]^{2-}$ is realized by both phosphonic groups $\{PO_3^{2-}, PO_3^{2-}\}$ with an eight-membered chelate ring. The N-atom is not coordinated. For all systems studied the only LMCT band from O^{-} (PO_3^{2-}) to M^{2+} exists in the UV region. Compound **7**, in which the tetrahydrofuryl oxygen atom is sterically accessible for some interaction with metal ions is a more effective chelating agent than other ones. A comparison of the basicity-adjusted stability constants, $\log K_{[ML]^{2-}} - \Sigma pK$, suggests some interaction between M^{2+} and the furyl oxygen atom. The manganese(II), cobalt(II) and nickel(II) complexes of the aromatic iminodimethylenephosphonic acids are more stable

than those of the aliphatic ones. This is reflected by the relative stability data. It can also be seen from the values of the relative stability constants (Tables 1 and 2) that the lowest affinity for the hard oxygen donor atoms is in the case of manganese(II) complexes.

References

[1] G. Kishore, D. Shah, Annu. Rev. Biochem. 57 (1988) 627.
[2] J.P. Solvin, E.M. Tobin, Biochim. Biophys. Acta 177 (1981) 637.
[3] B. Lejczak, B. Boduszek, P. Kafarski, G. Forlani, H. Wojtasek, P. Wieczorek, J. Plant Growth Regul. 15 (1996) 109.
[4] P. Kafarski, B. Lejczak, G. Forlani, R. Gancarz, C. Torreilles, J. Grembecka, A. Ryczek, P. Wieczorek, J. Plant Growth Regul. 16 (1997) 153.
[5] B. Lejczak, P. Kafarski, J. Zygmunt, Biochemistry 28 (1989) 3549.
[6] D. GrobeIny, U.B. Goli, R.E. Galardy, Biochemistry 28 (1989) 4948.
[7] K. Sawada, T. Kanda, Y. Naganuma, T. Suzuki, J. Chem. Soc., Dalton Trans. (1993) 2557.
[8] K. Sawada, T. Miyagawa, T. Sakaguchi, K. Doi, J. Chem. Soc., Dalton Trans. (1993) 3777.
[9] M. Jeżowska-Bojczuk, K. Tamas, H. Kozłowski, P. Decock, J.P. Barycki, J. Chem. Soc., Dalton Trans. (1994) 811.
[10] B. Boduszek, M. Dyba, M. Jeżowska-Bojczuk, T. Kiss, H. Kozłowski, J. Chem. Soc., Dalton Trans. (1997) 973.
[11] E. Matczak-Jon, B. Kurzak, W. Sawka-Dobrowolska, P. Kafarski, B. Lejczak, J. Chem. Soc., Dalton Trans. (1996) 3455.
[12] B. Kurzak, E. Matczak-Jon, M. Hoffmann, J. Coord. Chem. 43 (1998) 243.
[13] E. Matczak-Jon, B. Kurzak, W. Sawka-Dobrowolska, B. Lejczak, P. Kafarski, J. Chem. Soc., Dalton Trans. (1998) 161.
[14] R.J. Ganson, T.A. D'Amato, R.A. Jensen, Plant Physiol. 82 (1986) 203.
[15] R.L. Doong, J.E. Gander, R.J. Ganson, R.A Jensen, Plant Physiol. 84 (1992) 351.
[16] R.J. Ganson, T.A. D'Amato, R.A Jensen, Plant Physiol. 82 (1986) 203.
[17] G. Forlani, B. Lejczak, P. Kafarski, Pestic. Biochem. Physiol. 55 (1996) 180.
[18] H. Sigel, B.E. Fisher, B. Prijs, J. Am. Chem. Soc. 99 (1977) 4489.
[19] E. Frieden, J. Chem. Educ. 62 (1985) 916.
[20] G.C. Dismukes, Chem. Rev. 96 (1996) 2909.
[21] R.H. Holm, P. Kennepohl, E.J. Solomon, Chem. Rev. 96 (1996) 2239.
[22] Z. Ciunik, T. Głowiak, Acta Crystallogr., Sect. B 36 (1980) 1212.
[23] W. Clegg, O. Mi Lacy, B.P. Straughan, Acta Crystallogr., Sect. C 43 (1987) 794.
[24] T. Głowiak, Z. Ciunik, Acta Crystallogr., Sect. B 33 (1977) 3237.
[25] Z. Rzączyńska, R. Mrozek, T. Głowiak, J. Chem. Crystallogr. 27 (1997) 417.
[26] R. Mrozek, Z. Rzączyńska, T. Głowiak, Monatsh. Chem. 129 (1998) 129 Chemical Monthly.
[27] H. Schmidbaur, I. Bach, J. Riede, G. Muller, J. Helbig, G. Hopf, Chem. Ber. 121 (1988) 795.
[28] B. Kurzak, A. Kamecka, K. Kurzak, J. Jezierska, P. Kafarski, Polyhedron 17 (1998) 4403.
[29] E. Matczak-Jon, B., Kurzak, A. Kamecka,W. Sawka-Dobrowolska, P. Kafarski, J Chem. Soc., Dalton Trans. (1999) 3627.
[30] M. Soroka, P. Mastalerz, Pol. J. Chem. 50 (1976) 661.
[31] J. Oleksyszyn, E. Gruszecka, P. Kafarski, P. Mastalerz, Monatsh. Chem. 113 (1982) 1138.
[32] G. Gran, Acta Chem. Scand. 4 (1950) 559.
[33] M. Molina, C. Melios, J.O. Tognalli, L.C. Luchiari, M. Jafelicci, Jr., J. Electroanal. Chem. 105 (1979) 237.
[34] P. Gans, A. Sabatini, A.Vacca, J. Chem. Soc., Dalton Trans. (1985) 1195
[35] K. Kurzak, Ph.D. Thesis, Technical University of Wroclaw, Wroclaw, 1983.
[36] I.A. Slavič, Nucl. Instr. Methods 34 (1976) 285.
[37] (a) K. Kurzak, Spectrochim. Acta 47A (1991) 1041. (b) K. Kurzak, Wiad. Chem. 45 (1991), 425 in Pol. (c) K. Kurzak, A. Kolkowicz, Spectrosc. Lett. 30(5) (1997) 805.
[38] R.P. Carter, R.L. Carrol, R.R. Irani, Inorg. Chem. 6 (1967) 939.
[39] F.I. Bel'skii, I.B. Goryunova, P.V. Petrovskii, T.Ya. Medved', M.I. Kabachnik, Izv. Akad. Nauk. SSSR 31 (1982) 103.
[40] L.D. Pettit, H.K.J. Powell, SC-Database, Academic Software, Timble, Otley, Yorks, LS21 2PW, UK (1999).
[41] K. Sawada, T. Kanda, Y. Naganuma, T. Suzuki, J. Chem. Soc., Dalton Trans. (1993) 2557.
[42] K. Sawada, T. Ichikawa K. Uehara, J. Chem. Soc., Dalton Trans. (1996) 3077.
[43] P.R. Danesi, Acta Chem. Scand. 21 (1967) 143.
[44] S. Chaberek, R.C. Courtney, A.E. Martell, J Am. Chem. Soc. 74 (1952) 5057.

PERGAMON

www.elsevier.nl/locate/poly

Polyhedron 19 (2000) 2095–2100

POLYHEDRON

Syntheses, crystal structures and properties of new manganese(II) complexes with macrocyclic polyamine ligands bearing pyridyl donor pendants

Xian-He Bu [a,b,*], Wei Chen [a], Lin-Jing Mu [a], Zhi-Hui Zhang [a], Ruo-Hua Zhang [a], Thomas Clifford [c]

[a] *Department of Chemistry, Nankai University, Tianjin 300071, PR China*
[b] *State Key Laboratory on Coordination Chemistry, Nanjing University, Nanjing 210093, PR China*
[c] *Department of Chemistry, University of Kansas, 7 Mallot Hall, Lawrence, KS 66045, USA*

Received 18 May 2000; accepted 11 July 2000

Abstract

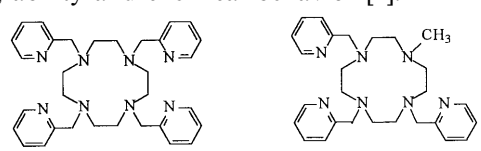
Two new Mn^{II} complexes with polydentate macrocyclic polyamine ligands functionalized with pyridyl donor pendants, 1,4,7,10-tetrakis(2-pyridylmethyl)-1,4,7,10-tetraazacyclododecane ($\mathbf{L}^1$) and 1-methly-4,7,10-tris(2-pyridylmethyl)-1,4,7,10-tetraazacyclododecane ($\mathbf{L}^2$), have been synthesized and their structures determined by X-ray diffraction analysis. In $[Mn\mathbf{L}^1](ClO_4)_2$ (**I**), the Mn^{II} central ion is eight-coordinated with all the eight donor nitrogens of $\mathbf{L}^1$ (including four pendant pyridyl nitrogens and four tertiary amines of cyclen) to form a distorted square-prism coordination geometry, and in $[Mn\mathbf{L}^2](ClO_4)_2$ (**II**), the M^{II} central ion is seven-coordinated (distorted monocapped octahedral geometry) with all the seven nitrogen donor atoms of $\mathbf{L}^2$ (including three pendant pyridyl nitrogens and four tertiary amines of cyclen) comprising the donor set. The solution chemistry of the two Mn^{II} complexes has been further studied by cyclic voltammetry (CV), UV–Vis and ESR spectral techniques. © 2000 Elsevier Science Ltd. All rights reserved.

Keywords: Crystal structures; Synthesis; Macrocyclic polyamine ligand; Manganese complexes; Octa- and hepta-coordination

1. Introduction

The coordination chemistry of macrocyclic polyamine ligands bearing functional pendant donor groups has attracted much interest in recent years, mainly as the metal complexes of such ligands might be effective models for protein-metal binding sites in metalloproteins in some biological systems, as potential therapeutic reagents or as multi-electron catalysts [1]. 1,4,7,10-Tetraazacyclododecane (cyclen) is a versatile macrocyclic polyamine ligand [2] from which many ligands have been derived by attaching functional groups on its backbone and their metal complexes show interesting properties and functions [3].

We previously reported a potential octadentate ligand, 1,4,7,10-tetrakis(2-pyridylmethyl)-1,4,7,10-tetraazacyclododecane ($\mathbf{L}^1$), by attaching four pyridyl donors to the cyclen backbone [4], which potentially provides four nitrogen donors from the flexible cyclen ring and four N donors from the pendant pyridyl donors. This ligand, in which the cyclen backbone often adopts a well-defined square and its functional arms can offer the topology suitable for effective encapsulation of large metal ions [1g,3–5], has been found to present interesting features both regarding its coordinating ability and chemical behavior [4].



$\mathbf{L}^1$ $\mathbf{L}^2$

Chart 1.

* Corresponding author. Tel.: +86-22-2350-2809; fax: +86-22-2350-0850.
E-mail address: buxh@nankai.edu.cn (X.-H. Bu).

0277-5387/00/$ - see front matter © 2000 Elsevier Science Ltd. All rights reserved.
PII: S0277-5387(00)00510-6

The discovery that Mn^{II} complexes of some macrocyclic polyamines [1h] and polydentate ligands [6,7] were effective superoxide scavengers attracted our interest, and led us to study the Mn^{II} complexes of $\mathbf{L}^1$ and a new heptadentate ligand 1-methyl-4,7,10-tris(2-pyridylmethyl)-1,4,7,10-tetraazacyclododecane) ($\mathbf{L}^2$, see Chart 1), which is potentially a heptadentate ligand. The Mn^{II} complexes of the two ligands show that both the two ligands can encapsulate Mn^{II} ion effectively using all their nitrogen donors to form octa- or hepta-coordinated complexes. Both of the complexes show superoxide scavenger activity from our preliminary cyclic voltammetry (CV) studies. We report herein the syntheses, crystal structures and solution properties of the two Mn^{II} complexes with $\mathbf{L}^1$ and $\mathbf{L}^2$.

2. Experimental

2.1. Materials and general methods

Most of the starting materials and solvents for syntheses were obtained commercially and used without further purification. 1,4,7,10-Tetrakis(2-methylpyridyl)-1,4,7,10-tetraazacyclododecane) ($\mathbf{L}^1$) [4], and 1-methyl-4,7,10-teraazacyclododecane [8] were synthesized according to published procedures. ^{1}H NMR was recorded on a Bruker AC-P200 spectrometer (200 MHz, 25°C, in $CDCl_3$, with tetramethylsilane as the internal reference). FT-IR spectra were taken on a 170SX (Nicolet) spectrometer. Elemental analysis was performed on a P-E 240C analyzer. ESR spectra were measured on a Bruker ER-200-D-SRC10 spectrometer at room temperature and 110 K, respectively. Magnetic susceptibilities were measured on a Faraday balance at room temperature and the calibration was made with Mohr's salt. Effective magnetic moment was calculated by the equation $\mu_{eff} = 2.828(\chi_M T)^{1/2}$, where χ_M is the magnetic susceptibility corrected for diamagnetism of the constituting atoms using Pascal's constants.

2.2. Synthesis

2.2.1. 1-Methyl-4,7,10-tris(2-pyridylmethyl)-1,4,7,10-tetraazacyclododecane ($\mathbf{L}^2$)

To a solution of 1-methyl-1,4,7,10-tetraazacyclododecane hydrochloride (540 mg, 1.8 mmol) in water (15 cm^3) was added NaOH (660 mg, 16.5 mmol), and this mixture was stirred for ca. 30 min. Then a solution of 2-(chloromethyl)pyridine hydrochloride (900 mg, 5.5 mmol) in CH_2Cl_2 (50 cm^3) was added dropwise over a period of ca. 2 h. The stirring was continued at 30°C for 1 week under an argon atmosphere. The organic layer was then separated and the aqueous layer was extracted with $CHCl_3$ (50×5 cm^3), and the combined organic layers were evaporated to give a residue which was purified by column chromatography on silica gel (eluent: CH_2Cl_2/CH_3OH 92:8). The product was finally recrystallized from ethanol–ether as colorless needles (Yield: 0.56 g, 60% based on 1-methyl-cyclen). ^{1}H NMR: δ1.90 (s, 3H), 2.62–2.74 (m, 16H), 3.50 (s, 6H), 7.12–7.23 (m, 8H), 7.57–7.67 (m, 4H). IR (KBr pellet, cm^{-1}): 625, 764, 1095, 1148, 1309, 1433, 1474, 1571, 1593, 1625, 2016, 2812, 2969, 3400 (br). *Anal.* Calc. for $C_{27}H_{37}N_7$: C, 70.6; H, 8.06; N, 21.4. Found: C, 70.9; H, 8.14; N, 21.0%.

2.2.2. Preparation of $Mn\mathbf{L}^1(ClO_4)_2$ (I) and $Mn\mathbf{L}^2(ClO_4)_2$ (II)

I was prepared by mixing a 1:1 molar ratio of $Mn(ClO_4)_2 \cdot 6H_2O$ (68 mg, 0.19 mmol) and $\mathbf{L}^1$ (100 mg, 0.19 mmol) in mixing solvents (CH_3CN/CH_3OH 1:1) at ca. 60°C under argon for ca. 30 min. The reaction mixture was then filtered, and crystals suitable for X-ray analysis were obtained by slow evaporation of the solvent. Yield: 88 mg, 60%. IR (KBr pellet, cm^{-1}): 630, 760, 1085, 1118, 1309, 1436, 1480, 1571, 1636, 2026, 2865, 2980, 3405, 3440 (br). *Anal.* Calc. for $C_{32}H_{40}N_8MnO_8Cl_2$: C, 48.6; H, 5.06; N, 14.2. Found: C, 48.3; H, 5.32; N, 14.4%.

II was prepared by a similar procedure to the preparation of **I**. Yield: 74 mg, 48%. IR (KBr pellet, cm^{-1}): 487, 620, 766, 1092, 1435, 1479, 1570, 1603, 2869, 2965, 3430 (br). *Anal.* Calc. for $C_{27}H_{37}MnN_7O_8Cl_2$: C, 44.6; H, 5.09; N, 15.4. Found: C, 44.4; H, 5.31; N, 15.7%.

2.3. Crystallographic studies

The data collections and determination of unit cells were performed with Mo Kα radiation ($\lambda = 0.71073$ Å) on an Enraf-Nonius CAD-4 diffractometer equipped with a graphite crystal monochromator. Unit cell parameters were obtained by least-squares refinement of one setting angle of 25 reflections in the range 9.34–12.2° (for **I**) and 9.10–10.49° (for **II**). The structures were solved by direct methods (SHELXS-86) with empirical absorption corrections. The Mn atoms were located from *E*-maps. The other non-hydrogen atoms were determined by successive difference Fourier syntheses on *F*. Final refinement was done by full matrix least-squares methods with anisotropic thermal parameters for non-hydrogen atoms. The hydrogen atoms were added theoretically, refined with riding model position parameters and fixed isotropic thermal parameters. All the calculations were performed on an IBM PC/586 computer, using the Siemens SHELTXTL-PC program package [9]. The crystallographic data and refinement details have been summarized in Table 1.

2.4. Electrochemical studies

Cyclic voltammograms were obtained by a BAS-100B electrochemical apparatus equipped with a glassy-carbon working electrode, a saturated calomel electrode (SCE) reference and a platinum auxiliary electrode. Solutions of **I** or **II** (1.0, 2.0, 3.0 mmol dm^{-3}) were prepared by dissolving appropriate amounts of the complexes in anhydrous acetonitrile with 0.1 mol dm^{-3} (n-butyl)$_4NPF_6$ ($TBAPF_6$) as supporting electrolyte. The tested system was oxygenated by bubbling pure O_2 gas at room temperature through the solution, and the concentration of O_2 was assumed to be 3 mmol dm^{-3} [6]. The cyclic voltammograms at scan rates of 50 or 100 mV s^{-1} were evaluated graphically.

Table 1
Crystal data and data collection summary for **I** and **II**

	I	**II**
Chemical formula	$C_{32}H_{40}N_8MnCl_2O_8$	$C_{27}H_{37}N_7MnCl_2O_8$
Crystal dimensions (mm)	$0.2\times0.25\times0.3$	$0.15\times0.4\times0.4$
Mr (g mol^{-1})	790.57	713.48
Crystal system	triclinic	orthorhombic
Space group	$P\bar{1}$ (no. 2)	*Pbca* (no. 61)
a (Å)	9.0730(2)	15.984(6)
b (Å)	11.354(2)	16.591(8)
c (Å)	18.614(4)	23.252(5)
α (°)	86.42(3)	90.00(0)
β (°)	81.57(3)	90.00(0)
γ (°)	69.29(3)	90.00(0)
V (Å^3)	1774(3)	6167(7)
Z	2	8
D_{calc} (g cm^{-3})	1.480	1.463
μ (mm^{-1})	0.5675	0.6124
$F(000)$	822	2968
Radiation	Mo Kα	Mo Kα
Scan modes	ω–2θ	ω–2θ
λ (Å)	0.71073	0.71073
Index range		
h	−9–9	0–17
k	−12–12	0–18
l	0–20	0–25
Temperature (K)	299 ± 1	299 ± 1
Measured reflections	5083	4730
Independent reflections	4594	4730
Observed reflections ($I\geq3\sigma(I)$)	3734	3129
Parameters refined	455	406
Absorption correction	empirical absorption correction (DIFABS) [10]	
$(\text{Absorption correction})_{min}$	0.788	0.809
$(\text{Absorption correction})_{max}$	0.966	0.986
R	0.043	0.060
R_w	0.042	0.064
$(\Delta/\alpha)_{max}$	0.004	0.18
Goodness-of-fit	0.90	3.595
Maximum residual peak (e Å^{-3})	0.43	0.73
Minimum residual hole (e Å^{-3})	−0.39	−0.47

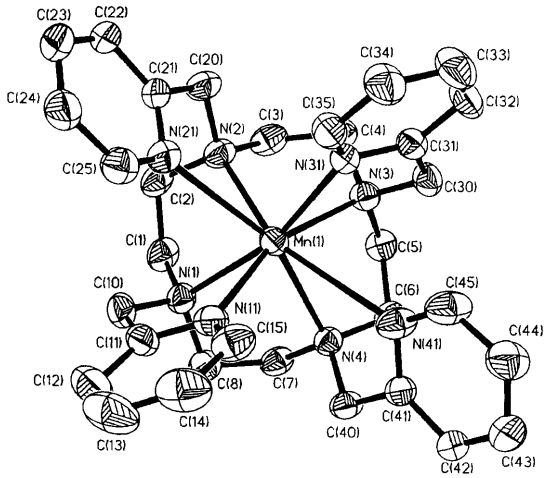


Fig. 1. ORTEP structure of **I** with 30% probability thermal ellipsoids.

3. Results and discussion

3.1. Synthesis and general characterization

$\mathbf{L}^1$ was synthesized by a method reported in our previous paper [4]. $\mathbf{L}^2$ was synthesized by a similar method. It was obtained as colorless needles in 60% yield. All the analytical and spectral data are in good agreement with the theoretical requirements of $\mathbf{L}^2$.

The syntheses of **I** and **II** were achieved by the reaction of the corresponding ligands with $Mn(ClO_4)_2\cdot6H_2O$ in nearly equimolar ratios in mixed solvent (1:1 CH_3CN–CH_3OH). The results of elemental analysis of the two complexes are consistent with the composition of $[Mn\mathbf{L}](ClO_4)_2$ ($\mathbf{L}=\mathbf{L}^1$ or $\mathbf{L}^2$). The IR spectra of the two complexes show absorption bands due to the pyridine ring skeletal vibrations and bands from the perchlorate counter anions. The electronic spectra of the colorless Mn^{II} complexes in methanol solution are essentially featureless in the range 400–800 nm, and d–d transitions are hardly observable. The effective magnetic moments of both **I** and **II** are 5.65 and 5.56 B.M. (at 293 K), corresponding to $S=5/2$ spin state (high spin) with an appreciable orbital contribution.

3.2. Description of crystal structure

3.2.1. Crystal structure of $[Mn\mathbf{L}^1]ClO_4$ (I)

The structure of **I** consists of $[Mn\mathbf{L}^1]^{2+}$ cations and ClO^{4-} counter anions. A view of the cation of **I** is given in Fig. 1 and the selected bond distances and angels are listed in Table 2.

The Mn^{II} ion in $[MnL^1]^{2+}$ cation is eight-coordinated by four N atoms of the macrocycle and the four nitrogens of the pendant pyridyl groups arranged at the corners of a square prism. Each set of N atoms [nitrogens on cyclen ring, N_{cyclen}: N(1), N(2), N(3), N(4); and nitrogens on pendant pyridine, N_{py}: N(11), N(21), N(31), N(41)] is nearly co-planar, with mean deviation of 0.006 and 0.036 Å from the corresponding least-squares planes. These two planes are essentially parallel to each other and form a 0.6° dihedral angle with each other. The nitrogen atoms thus fully encapsulate the Mn^{II} ion which lies 1.270 and 1.354 Å from the basal planes in the above-mentioned order.

Table 2
Selected bond lengths (Å) and angles (°) for **I**

Mn(1)–N(1)	2.377(3)	Mn(1)–N(2)	2.418(3)
Mn(1)–N(3)	2.386(4)	Mn(1)–N(4)	2.491(3)
Mn(1)–N(11)	2.302(4)	Mn(1)···N(21)	2.771(4)
Mn(1)–N(31)	2.306(3)	Mn(1)···N(41)	2.923(4)
N(1)–Mn(1)–N(2)	74.0(1)	N(1)–Mn(1)–N(3)	115.9(1)
N(2)–Mn(1)–N(3)	75.2(1)	N(1)–Mn(1)–N(4)	74.1(1)
N(2)–Mn(1)–N(4)	117.3(1)	N(3)–Mn(1)–N(4)	72.7(1)
N(1)–Mn(1)–N(11)	72.1(1)	N(2)–Mn(1)–N(11)	125.5(1)
N(3)–Mn(1)–N(11)	159.1(1)	N(4)–Mn(1)–N(11)	92.4(1)
N(1)–Mn(1)–N(31)	164.1(1)	N(2)–Mn(1)–N(31)	96.0(1)
N(3)–Mn(1)–N(31)	72.0(1)	N(4)–Mn(1)–N(31)	121.8(1)
N(11)–Mn(1)–N(31	105.7(1)	Mn(1)–N(1)–C(1)	110.2(3)

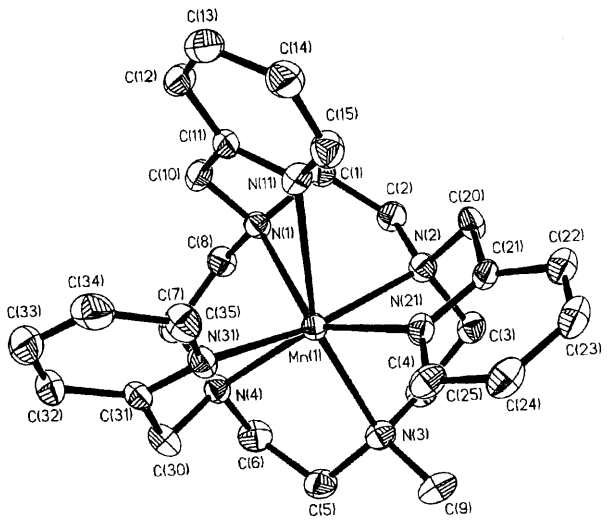


Fig. 2. ORTEP structure of **II** with 30% probability thermal ellipsoids.

Table 3
Selected bond distance (Å) and angles (°) for **II**

Mn(1)–N(1)	2.316(4)	Mn(1)–N(2)	2.327(4)
Mn(1)–N(3)	2.430(4)	Mn(1)–N(4)	2.371(4)
Mn(1)–N(21)	2.239(4)	Mn(1)–N(31)	2.334(4)
Mn(1)···N(11)	2.732(4)		
N(1)–Mn(1)–N(2)	77.6(1)	N(1)–Mn(1)–N(3)	122.4(1)
N(2)–Mn(1)–N(3)	76.5(1)	N(2)–Mn(1)–N(31)	164.1(2)
N(1)–Mn(1)–N(4)	76.7(1)	N(2)–Mn(1)–N(4)	120.7(2)
N(3)–Mn(1)–N(4)	74.2(1)	N(1)–Mn(1)–N(21)	131.6(1)
N(2)–Mn(1)–N(21)	74.1(2)	N(3)–Mn(1)–N(21)	87.8(2)
N(4)–Mn(1)–N(21)	151.6(2)	N(1)–Mn(1)–N(31)	100.2(2)
N(3)–Mn(1)–N(31)	116.9(2)	N(4)–Mn(1)–N(31)	73.3(2)
N(21)–Mn(1)–N(31	96.8(2)	Mn(1)–N(1)–C(1)	108.6(3)

The $Mn(1)–N_{cyclen}$ distances are normal Mn–N bonds. A pair of $Mn–N_{py}$ bond distances are shorter than those of $Mn(1)–N_{cyclen}$ while other two $Mn(1)–N_{py}$ are longer. The Mn(1)–N(21) and Mn(1)–N(41) bonds can be considered as semi-coordination bonds, similar to the $[Mn–(py)_3tren]^{2+}$ complex [7] which exhibits an Mn–N distance equal to 2.79 Å. The coordination geometry of **I** is similar to that found for the Mn^{II} complex with 1,4,7,10-tetrakis(pyrazol-1-ylmethyl)-1,4,7,10-tetraazacyclodecane) [1h].

The potentially octadentate ligand L^1 yields complexes with coordination numbers from six to eight, according to the stereochemical requirements of the metal ions involved. In the series of the structures, the Ni^{II} [4a], Co^{II}, Fe^{II} [11], and Mn^{II} complexes show the following fundamental features: the metal ions are always bound to the four nitrogen atoms of cyclen, whose bonding cavity is too small to accommodate those cations and completes their coordination sphere with two or four additional N donors from the pendant pyridine groups. All donor atoms of cyclen are forced to lie on the same side of the metal atom while all the donor pendant arms are forced to point to the other side of the metal ion. Analysis of the M–N bond distances and angles for these complexes reveals some regular trends: (1) on going from the complexes of Mn^{II} to Ni^{II}, the distance of the metal ion from the basal cyclen plane decrease from 1.270 to 0.901 Å; (2) the difference between N(1)–M–N(3) and N(2)–M–N(4) angles (N labels as for I) increases from Mn^{II} to Ni^{II}. Cyclen ring folds to yield six-coordinated complexes (for Ni^{II}) or remains planar in the eight-coordinated complexes (Mn^{II} and Fe^{II}); (3) in these complexes, two of the four pyridine donor pendants in non-adjacent positions interact with the central metal to form normal M–N bonds, while the other two pendants remain uncoordinated or semi-coordinated, and the distances from metal to uncoordinated or semi-coordinated donor atom (N) increased from Mn^{II} to Ni^{II}. This indicates that Mn^{II} accepts the strongest coordination from the pendant pyridines in this series of complexes.

3.2.2. Crystal structure of $[MnL^2]ClO_4$ (II)

The structure of **II** consists of a discrete monomer $[MnL^2]^{2+}$ cation and two uncoordinated perchlorate anions. The ORTEP view of **II** is shown in Fig. 2, and the selected bond distances and angles are listed in Table 3.

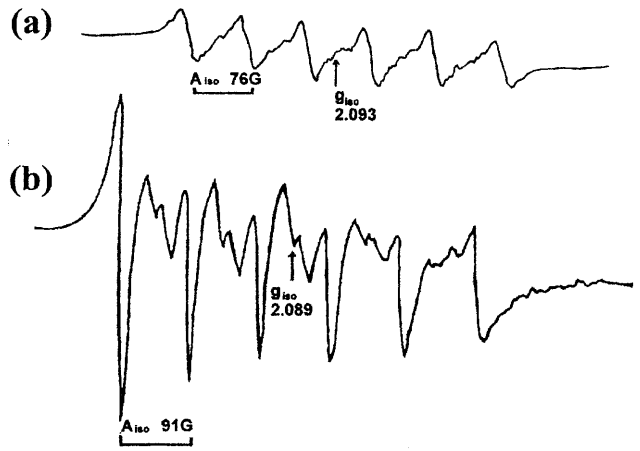


Fig. 3. The X-band ESR spectra of **II** in MeOH at room temperature and 110 K.

The structure indicates that **II** has a hepta-coordinated metal center defined by four nitrogen atoms of cyclen [N(1), N(2), N(3) and N(4)] and three nitrogen atoms of the pendant pyridine groups [N(11), N(21) and N(31)]. The coordination polyhedron may be best described as a square-prism with the basal planes defined by cyclen and the pyridine nitrogens (N_{cyclen} and N_{py}), respectively, and having a vacant donor site on the latter face. A basal least-squares plane from the four nitrogens of cyclen gave a mean deviation of only 0.009 Å while the three pyridine nitrogens form the other basal face. These two planes form a 3.6° dihedral angle and are essentially parallel to each other, and the Mn^{II} ion is displaced by 1.151 and 1.484 Å from that two planes.

In **II**, such a high coordination number is achieved at the expense of a longer Mn–N distance (Mn–N (11)) of 2.732 Å which is much longer than normal Mn–N bonds, but shorter than the sum of van der Waals radii of Mn^{II} and N. The other six normal Mn–N coordination bonds have typical Mn–N distances. The distances of Mn–N_{py} (N (21) and N (31)) are shorter than those of Mn–N_{cyclen}. The average distances from metal to N_{cyclen} or N_{py} (normal or semi-coordinated) in **II** are shorter than those distances in **I**. Thus the coordination of $\mathbf{L}^2$ to Mn^{II} in **II** is stronger than that of $\mathbf{L}^1$ in **I**, and this may be considered as the reduction of the steric hindrance due to fewer pyridyl pendants on $\mathbf{L}^2$ (see Fig. 2).

Table 4
ESR parameters of **I** and **II** in methanol solution

Complex	Room temperature		110 K	
	g	A, G (cm^{-1})	g	A, G (cm^{-1})
I	2.11	91 (8.9×10^{-3})	2.10	89 (8.7×10^{-3})
II	2.09	76 (7.4×10^{-3})	2.09	91 (8.9×10^{-3})

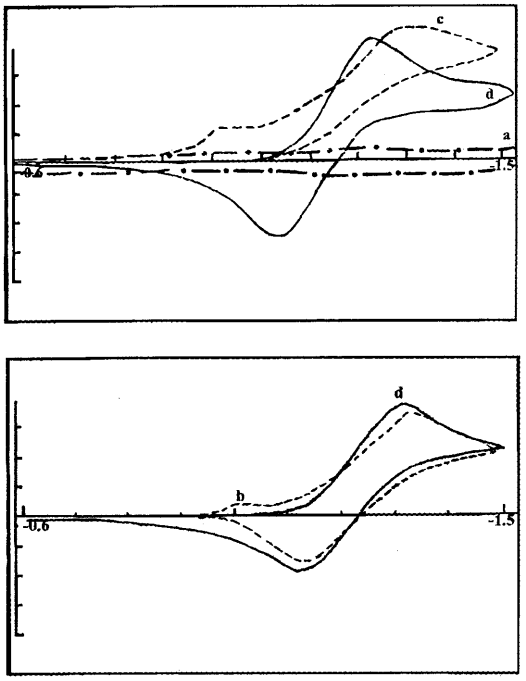


Fig. 4. Cyclic voltammograms in acetonitrile solution containing 0.1 mol dm^{-3} $TBAPF_6$ and various substrates (scan rate 50 mV s^{-1}): (a) 2.0 mmol dm^{-3} **II** only; (b) 1.0 mmol dm^{-3} **II** and 3 mmol dm^{-3} dioxygen; (c) 3.0 mmol dm^{-3} **II** and 3 mmol dm^{-3} dioxygen; (d) 3 mmol dm^{-3} dioxygen only.

3.3. ESR studies

The ESR spectra were obtained in CH_3OH solution at room temperature and 110 K, respectively, and the spectra of **II** is shown in Fig. 3. For **II**, the spectrum with a symmetry center was split into six equally spaced absorption peaks by the interaction with the $^{55}Mn^{II}$ nucleus ($I = 5/2$) at room temperature. When the solution was frozen at 110 K, these six absorption peaks split to give further hyperfine structures, perhaps due to coupling with the N atoms of the ligand. The spectrum of **I** was similar to that of **II** at room temperature, but when the sample of **I** in CH_3OH was frozen at 110 K, no change was observed in the ESR spectrum, indicating a weaker coordination to $\mathbf{L}^1$ than to $\mathbf{L}^2$, which is in agreement with the crystal structural results of the two complexes as have been discussed above and the data have been listed in Table 4.

3.4. Electrochemical studies

The mechanism of SOD (superoxide dismutase) catalyzing the dismutation of O_{2-} is commonly proposed to commence with the coordination of O_{2-} to the metal activity center of SOD and produce the intermediate metal···O_{2-} adduct [12]. Despite SOD mimics having many kinds of structures, the first step in catalyzing O_{2-} dismutation is same: formation of the intermediate

$$O_2 + [LMn^{2+}] \longrightarrow [LMn^{2+}O_2]$$
$$[LMn^{2+}O_2] + e \longrightarrow [LMn^{2+}O_2^-]$$

Scheme 1. The production of the intermediary ($\mathbf{L} = \mathbf{L}^1$ or $\mathbf{L}^2$)

$[LMn^{+}\cdots O_{2-}]$ [6]. So the propensity of the catalyst to form the superoxide adduct is a good guide to whether the model SOD can catalyze O_{2-} dismutation. The superoxide adduct can be detected under anhydrous conditions by electrochemistry.

Fig. 4 shows the cyclic voltammograms recorded with a glassy carbon working electrode and illustrates the behavior of the present system. Curve a is the cyclic voltammogram of **II** in the dehydrated system without oxygen. The cyclic voltammogram of **II** in the presence of oxygen is shown as curve b and c. Curve d shows the cyclic voltammogram of oxygen in the absence of **II**. By comparison of parts b, c and d in the dehydrated system of Fig. 4, it appears a new reduction wave at a more positive potential than that of the oxygen reduction wave. This new wave is chemically irreversible. The anodic wave corresponding to the oxidation of O_{2-} is diminished when the concentration of **II** is increased for a fixed concentration of oxygen. It should be noted that oxygen can be excluded completely from the solution by an argon stream, and the situation observed in curve a is restored. Hence the complex reacts reversibly with oxygen. For a concentration of oxygen larger than that of the metal complex, the current of the irreversible new wave increases with complex concentration. Similar phenomena can be observed in **I**; however, it shows a lower current compared to **II** under the same experimental conditions. The positive shift in the cathodic peak potential is attributable to the more positive formal potential of the $[LMn^{2+}O_2]/[LMn^{2+}O_{2-}]$ couple compared with the O_2/O_{2-} wave [13].

These observations support the interpretation of a complex-assisted O_2 reduction in the presence of **II** is one in which the O_2 and **II** forms an adduct prior to the electron transfer (Scheme 1).

In analogous systems, the precursor complex is formed prior to reduction is the accepted mechanism [14,15]. The intermediate complex product by the first step of the superoxide scavenging reaction also was detected by electrochemistry. This is good evidence of the complexes (**I** and **II**) ability to bind oxygen to produce $[LMn^{+}\cdots O_{2-}]$ which is the essential intermediate in the mechanism of SOD or its models in catalyzing O_{2-} dismutation. Thus these complexes have potential ability for scavenging superoxide.

4. Supplementary material

Supplementary data have been deposited with the Cambridge Crystallographic Data Centre, CCDC Nos. 139887 and 139888. Copies of this information may be obtained free of charge from The Director, CCDC, 12 Union Road, Cambridge, CB2 1EZ, UK (fax: +44-1223-336033; e-mail deposit@ccdc.cam.ac.uk or www: http//www.ccdc.cam.ac.uk).

Acknowledgements

This work was financially supported by the National Natural Science Foundation of China (Nos. 19771022 and 29971019) and the Natural Science Foundation of Tianjin, China and the Trans-Century Talents Training Program Foundation by the State Education Ministry of China (to X.H. Bu).

References

[1] (a) N.W. Alcock, K.P. Balakrishnan, A. Berry, P. Moore, C.J. Reader, J. Chem. Soc., Dalton Trans. (1988) 1089. (b) G. Hunter, A. McAuley, T.W. Whitcombe, Inorg. Chem. 27 (1988) 2634. (c) E. Kimura, T. Koike, K. Toriumi, Inorg. Chem. 27 (1988) 3687. (d) U. Auerbach, U. Eckert, K. Wieghardt, B. Nuber, J. Weiss, Inorg. Chem. 29 (1990) 938. (e) D. Parker, Chem. Soc. Rev. (1990) 297. (f) P.V. Bernhart, G.A. Lawrence, Coord. Chem. Rev. (1990) 297. (g) D.G. Fortier, A. McAuley, J. Chem. Soc., Dalton Trans. (1991) 101. (h) M.D. Vaira, F. Mani, P.Stoppioni, J. Chem. Soc., Dalton Trans. (1992) 1127.

[2] (a) R.M. Izatt, K. Pawlak, J.S. Bradshaw, R.L. Bruening, Chem. Rev. 91 (1991) 1721. (b) Y. Inoue, T. Kanamori, T. Yoshida, X.H. Bu, M. Shionoya, T. Koike, E. Kimura, Biol. Pharm. Bull. 17 (1994) 243. (c) T. Sawada, K. Fukumaru, H. Sakurai, Biochem. Biophys. Res. Commun. 216 (1995) 154.

[3] (a) E.T. Clarke, A.E. Martell, Inorg. Chim. Acta. 181 (1991) 27 and 37. (b) K. Kumar, M.F. Tweedle, M.F. Malley, J.Z. Gougoutas, Inorg. Chem. 34 (1995) 6472.

[4] (a) X.H. Bu, X.C. Cao, W. Chen, R.H. Zhang, T. Clifford, Polyhedron 17 (1998) 289. (b) X.H. Bu, X.C. Cao, W.Q. Zhang, R.H. Zhang, T. Clifford, Transition Met. Chem. 22 (1997) 51.

[5] G. Norante, M.D. de M. Vaira, F. Mani, S. Mazzi, P. Stoppioni, Inorg. Chem. 29 (1990) 2822.

[6] A. Deroche, I. Morgenstern-Badarau, M. Cesario, J. Guilhem, B. Keita, L. Nadjo, C. Houée-Levin, J. Am. Chem. Soc. 118 (1996) 4567.

[7] R.M. Kirchner, C. Mealli, M. Bailey, N. Howe, L.P. Torre, L.J. Wilson, L.C. Andrews, N.J. Rose, E.C. Lingafelter, Coord. Chem. Rev. 77 (1987) 89.

[8] J.E. Richman, T.J. Atkins, J. Am. Chem. Soc. 96 (1974) 2268.

[9] G.M. Sheldrick, Acta Crystallogr., Sect. A 46 (1990) 467.

[10] N. Walker, D. Stuart, Acta Crystallogr., Sect. A 39 (1983) 158.

[11] X.H. Bu, S.L. Lu, R.H. Zhang, H. Liu, H.P. Zhu, Q.T. Liu, Polyhedron 19 (2000) 431.

[12] W.S. Webley, R.R. Durand, F.C. Anson, J. Electroanal. Chem. 229 (1987) 273.

[13] W.S. Webley, R.R. Durand, Jr., F.C. Anson, J. Electroanal. Chem. 229 (1987) 273.

[14] Y. Nishida, N. Tanaka, A. Yamazaki, T. Tokii, N. Hashimoto, K. Ide, K. Iwasawa, Inorg. Chem. 34 (1995) 3616.

[15] W.S. Szulblinski, P.R. Warburton, D.H. Busch, Inorg. Chem. 32 (1993) 5368.

PERGAMON

www.elsevier.nl/locate/poly

Polyhedron 19 (2000) 2101–2110

POLYHEDRON

Reactivity, structure and electrospray mass spectrometry of pentafluoro- and pentachloro-phenoxy-substituted cyclotriphosphazenes

Craig V. Depree [a], Eric W. Ainscough [a,*1], Andrew M. Brodie [a,*2], Anthony K. Burrell [a], Cornelis Lensink [b], Brian K. Nicholson [c]

[a] *Chemistry - Institute of Fundamental Sciences, Private Bag 11222, Massey University, Palmerston North, New Zealand*
[b] *Industrial Research Limited, PO Box 31-310, Lower Hutt, New Zealand*
[c] *Department of Chemistry, University of Waikato, Hamilton, New Zealand*

Received 22 May 2000; accepted 12 July 2000

Abstract

The reaction of $N_3P_3Cl_6$ with the sodium salts of pentachloro- and pentafluorophenol, has been investigated. In contrast to the non-*geminal* substitution typified by other RO^- nucleophiles, the regiochemistry of the reaction of $C_6X_5O^-$ (X = Cl and F) with $N_3P_3Cl_6$ is dominated by *geminal* substitution. The reaction of $C_6Cl_5O^-$ with $N_3P_3Cl_6$ in refluxing tetrahydrofuran yielded *gem*-$N_3P_3Cl_2(OC_6Cl_5)_4$ (**1**) as the major product. The fully substituted derivative $N_3P_3(OC_6Cl_5)_6$ (**2**) was attained in low yield from reaction in refluxing diglyme. In contrast, the reaction of $C_6F_5O^-$ with $N_3P_3Cl_6$ in refluxing tetrahydrofuran yielded the fully substituted product $N_3P_3(OC_6F_5)_6$ (**3**) after approximately 4 h. ^{31}P NMR spectral results suggest the $C_6F_5O^-$ ion may be attacking in a 'random' fashion at low degrees of substitution, which is largely replaced by an electronic *geminal*-directing effect at tetrasubstitution. Single crystal X-ray crystallographic analyses have been carried out on compounds **1** and **3**. Electrospray mass spectrometry has been evaluated as a general technique for characterizing cyclotriphosphazenes, $N_3P_3R_6$. If R = OEt or OPh, good positive ion spectra are observed but, in contrast, if R is more strongly electron withdrawing (Cl, C_6Cl_5O or C_6F_5O) negative ion spectra are obtained. © 2000 Elsevier Science Ltd. All rights reserved.

Keywords: Pentafluoro-cyclotriphosphazene; Pentachloro-cyclotriphosphazene; X-ray structures; Electrospray mass spectrometry

1. Introduction

Phosphazenes have been extensively studied for the last forty years. Although much of the research has focussed on the synthesis of commercially useful phosphazene polymers, it is the investigation of small cyclophosphazenes which have yielded the wealth of information regarding reactivity, mechanism and structure.

While the mechanistic aspects of substitution by amine nucleophiles are well understood, less information is available for RO^- nucleophiles and consequently more uncertainty surrounds their reactivity with $N_3P_3Cl_6$. Almost invariably RO^- ions react non-*geminally*, which is proposed to be via an S_N2 backside attack [1,2]. Since an S_N2 attack favors the most electrophilic site, the observed non-*geminal* regiochemistry implies the non-*geminal* directing alkoxy and aryloxy nucleophiles are electron-releasing relative to Cl (i.e. $\equiv PCl_2$ more electrophilic than $\equiv PCl(OR)$]. This is supported by phosphazene ring-nitrogen basicity studies conducted by Shaw et al. [3], which indicate groups such as OMe, OEt, OPh and OCH_2CF_3 are all electron-donating relative to Cl. Even the latter, which is the least electron-releasing, yields only approximately 2% of *geminal* products [4]. With the possible exception of 2,6-dichlorophenoxide [5], there appears to have been no regiochemical studies conducted on electron-withdrawing RO^- nucleophiles. It is therefore not surpris-

[1] *Corresponding author.
[2] *Corresponding author. Tel.: +64-6-350-5102; fax: 64-6-350-5682; e-mail: a.brodie@massey.ac.nz

0277-5387/00/$ - see front matter © 2000 Elsevier Science Ltd. All rights reserved.
PII: S0277-5387(00)00511-8

ing that *geminal* substitution products are rare and of very low yield for the RO^- ions studied thus far.

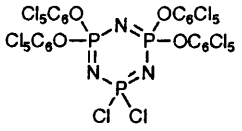
Assuming all RO^- ions react via an S_N2 mechanism, and ignoring any steric effects, one can generalize that relative to Cl, electron-releasing and electron-withdrawing RO^- ions should react non-*geminally* and *geminally*, respectively. Likewise, RO^- ions that have a net electronic effect similar to that of Cl should react via both *geminal* and non-*geminal* routes. Therefore the major intent of this study was to investigate the substitution pattern of electron-withdrawing aryloxy nucleophiles with $N_3P_3Cl_6$, and thereby determine whether the expected *geminal* substitutions occurred.

2. Results and discussion

Based on the pK_a values of the parent phenols [6–8], the sodium salts of C_6Cl_5OH and C_6F_5OH were considered to be suitable examples of strongly electron-withdrawing RO^- ions. The electron-withdrawing effect of progressively adding halogens to phenol is apparent from the following pK_a values [7]: phenol 9.92; 2-chlorophenol 8.52; 2,6-dichlorophenol 6.80; 2,4,6-trichlorophenol 5.99; 2,3,4,6-tetrachlorophenol 5.22 and pentachlorophenol 4.74.

2.1. Reaction of pentachlorophenoxide with $N_3P_3Cl_6$

The reaction of excess $NaOC_6Cl_5$ with $N_3P_3Cl_6$ in refluxing tetrahydrofuran was monitored at regular intervals by ^{31}P NMR spectroscopy. The reaction is very slow and proceeds via a predominantly *geminal* pathway (Scheme 1), with significant quantities of non-*geminal* products observed only at disubstitution. Accurate integration of the ^{31}P spectra was complicated by overlapping peaks, but approximately one-third of the disubstituted products are non-*geminal*. After 10–13 days the major product is the *gem*-tetra[3], and although there are di- and tri-substituted derivatives still present, there are no peaks in the ^{31}P spectra corresponding to higher degrees of substitution. The *gem*-tetra product, *gem*-$N_3P_3Cl_2(OC_6Cl_5)_4$ (**1**), was isolated via slow evaporation of the filtered tetrahydrofuran solution, yielding crystals suitable for single crystal X-ray crystallography.



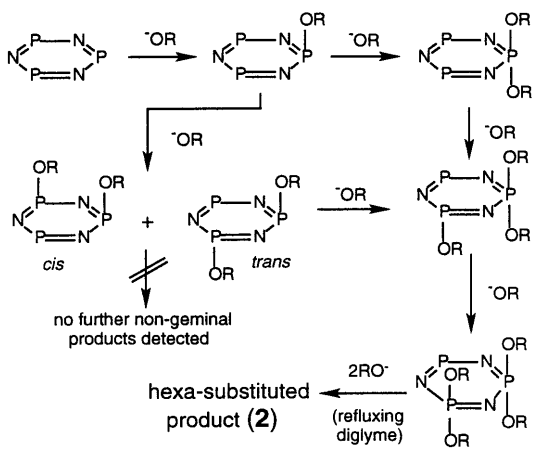
1

Reaction times in excess of approximately 13 days did not result in the formation penta- or hexasubstituted derivatives, although it is possible that low solubility may preclude their detection by ^{31}P NMR spectroscopy. Similarly, increasing the reaction temperature to 101°C (dioxane) resulted in no penta- or hexa-derivatives being observed, and presumably on account of the lower solubility of the phenoxide salt in dioxane, the reaction is significantly slower. Increasing the temperature further to 162°C (diglyme) yielded a small quantity of $N_3P_3(OC_6Cl_5)_6$ (**2**), which was recrystallized from benzene as the di-solvate. Compound **2** has been reportedly formed from $C_6Cl_5O^-$ and $N_3P_3Cl_6$ in a continuous process at room temperature (r.t.) after 0.5–1 h [9], however, characterization data was not given and our results indicate that under these conditions hexasubstitution would be unlikely.

The predominantly *geminal* substitution is consistent with an S_N2 mechanism and pentachlorophenoxide being significantly electron-withdrawing. The electron-withdrawing effect of the $C_6Cl_5O^-$ group is evident from the failure of the ring-nitrogen atoms to protonate under the conditions required for the observation of a positive ion electrospray mass spectrum of **1** (see later). Consequently, ≡PCl(OR) sites are more electrophilic than $\equiv PCl_2$ sites and are thus favored by an S_N2 attacking RO^- ion.

The non-*gem*-di-substituted isomers are most likely formed by a competing S_N2 attack at less electrophilic $\equiv PCl_2$ sites, which although electronically less favorable, are favored both sterically and statistically (i.e. two $\equiv PCl_2$ sites for every one ≡PCl(OR) site) at disubstitution. The non-*geminal* trend is not repeated at tri-substitution since *geminal* substitution is now favored both electronically and statistically with two ≡PCl(OR) sites available.

The reaction of 2,6-$Cl_2C_6H_4O^-$ with $N_3P_3Cl_6$ yields mainly *geminal* products at di- and tri-substitution [5], but in contrast to $C_6Cl_5O^-$, tetrasubstitution is pre-



Scheme 1. S_N2 substitution pathway for the reaction of $NaOC_6Cl_5$ with $N_3P_3Cl_6$.

[3] A *geminal* tetrasubstituted product has been abbreviated to *gem*-tetra, a non-*geminal* trisubstituted product to non-*gem*-tri, etc.

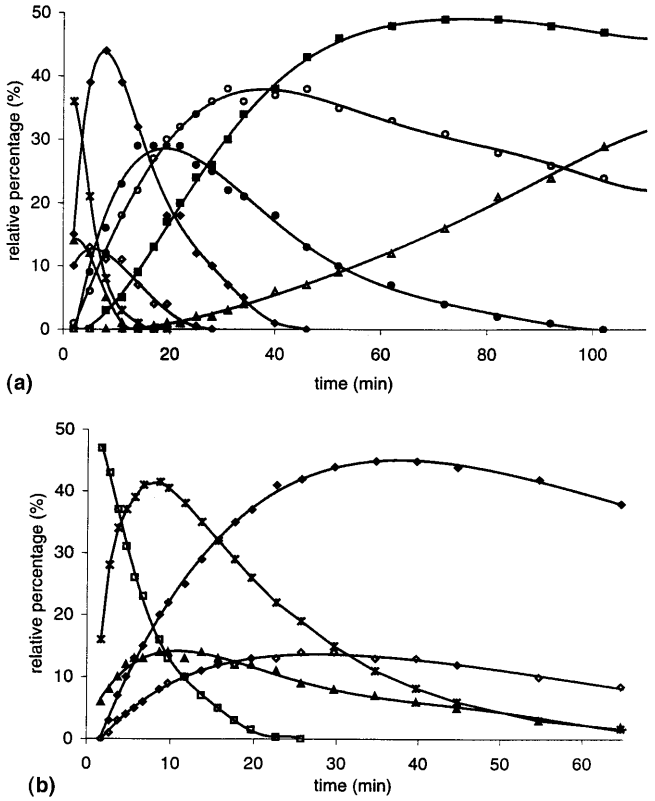
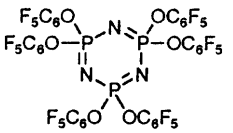


Fig. 1. Relative percentage of the substituted products (derived from ^{31}P NMR integration) from a 7:1 reaction of $C_6F_5O^-$ and $N_3P_3Cl_6$ (a) at 22°C and (b) at −10°C. Key to symbols: □ mono, ▲ *gem*-di, × non-*gem*-di, ◆ *gem*-tri, ◇ non-*gem*-tri, ○ *gem*-tetra, ● non-*gem*-tetra, ■ penta, △ hexa.

dominately non-*geminal*. The authors proposed an S_N1 mechanism with a subsequent mechanistic 'cross-over' to an S_N2 mechanism at higher degrees of substitution. As outlined for $C_6Cl_5O^-$, the reaction regiochemistry can also be accounted for by competing S_N2 reactions. The non-*geminal* preference at tetra-substitution possibly reflects the inferior electron-withdrawing nature of 2,6-$Cl_2C_6H_4O^-$, and hence a decreased electrophilicity difference between ≡PCl(OR) and ≡PCl_2 sites. Consequently for 2,6-$Cl_2C_6H_4O^-$, when steric demands are small (e.g. disubstitution), electronic effects will favor *geminal* products, whereas at higher degrees of substitution (e.g. tetra-), steric effects may transcend the slight electronic preference for *geminal* substitution-resulting in non-*geminal* products.

2.2. Reaction of pentafluorophenoxide with $N_3P_3Cl_6$

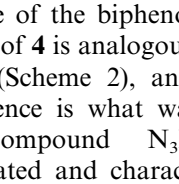
In contrast to $C_6Cl_5O^-$ the reaction of $C_6F_5O^-$ with $N_3P_3Cl_6$ in tetrahydrofuran is much faster, the reasons for which are not understood. The fully substituted derivative $N_3P_3(OC_6F_5)_6$ (**3**) was formed exclusively after approximately 4 h in refluxing tetrahydrofuran, and 30 h at r.t. Compound **3** has been reported previously [10–12], but the regiochemistry of the reaction between $C_6F_5O^-$ and $N_3P_3Cl_6$ has not been examined.



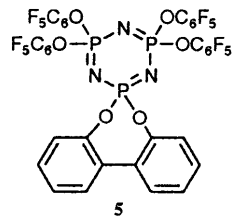
3

^{31}P NMR spectroscopy showed that non-*geminal* and *geminal* pathways appear to alternate during the progress of the reaction, as the major di- and tri-substituted products (approximately 75%) are non-*geminal* and *geminal*, respectively (Fig. 1a, b; the latter, at −10°C, shows the mono- and disubstituted products more clearly). This indicates that $C_6F_5O^-$ is attacking randomly, because at di-substitution there are twice the number of non-*geminal* ≡PCl_2 sites available on the mono-substituted compound. Therefore ignoring steric and electronic effects, two thirds of the mono-substituted product should react non-*geminally*. The observed approximately 75% of non-*gem*-di may reflect a contributing steric preference for non-*geminal* substitution. Similarly at tri-substitution, a random attack on the non-*gem*-di isomers would predict two thirds reacting *geminally* [twice as many ≡PCl(OR) sites] to give the *gem*-tri product, which accounts for the observed 75% of *gem*-tri product. The approximately 11:9 *geminal* preference at tetrasubstitution indicates that attack on the ≡PCl_2 and ≡PCl(OR) sites of the *gem*-tri is no longer random, since approximately three-quarters of the *gem*-tri has to react *geminally* to account for the observed regiochemistry. At higher degrees of substitution, the electrophilicity difference between ≡PCl(OR) and ≡PCl_2 sites must therefore become significant, resulting in the random attack being largely replaced by an electronic *geminal* preference. The proposed pathway is depicted in Scheme 2.

The change over to a *geminal* preference at higher degrees of substitution is supported by the approximately 70% *geminal* preference at disubstitution when $N_3P_3(2,2'\text{-}O_2C_{12}H_8)Cl_4$ (**4**) [13] was reacted with $C_6F_5O^-$. The presence of the biphenoxy group means that the disubstitution of **4** is analogous to the tetrasubstitution of $N_3P_3Cl_6$ (Scheme 2), and hence the observed *geminal* preference is what was expected. The fully substituted compound $N_3P_3(2,2'\text{-}O_2C_{12}H_8)(OC_6F_5)_4$ (**5**) was isolated and characterized from the corresponding 4:1 reaction. The closely related compound, $N_3P_3(2,2'\text{-}O_2C_{12}H_8)(p\text{-}FC_6H_4O)_4$ has been reported previously by Shreeve et al. [14].



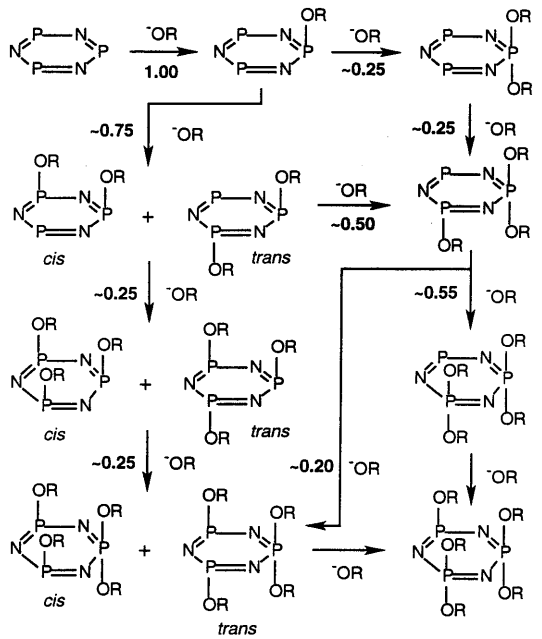
4



5

In comparison to $C_6Cl_5O^-$, the increased tendency of $C_6F_5O^-$ ions to initially react non-*geminally* with $N_3P_3Cl_6$ is presumably attributable to the much greater reactivity of the fluoro analogue. Consequently, attack by $C_6F_5O^-$ at a phosphorus center is less discriminating at di- and tri-substitution, despite the electrophilicity of $\equiv PCl(OC_6F_5)$ sites which are conducive to *geminal* substitution.

Although more examples are needed before any general conclusions can be made regarding the reactivity of electron-withdrawing RO^- nucleophiles, it appears that as for the F^- ion [15], *geminal* substitution tends to be favored for electron-withdrawing aryloxides, but is not exclusive (especially for $C_6F_5O^-$) until higher substitution is achieved.



Scheme 2. Proposed substitution pathway for the reaction of $NaOC_6F_5$ with $N_3P_3Cl_6$.

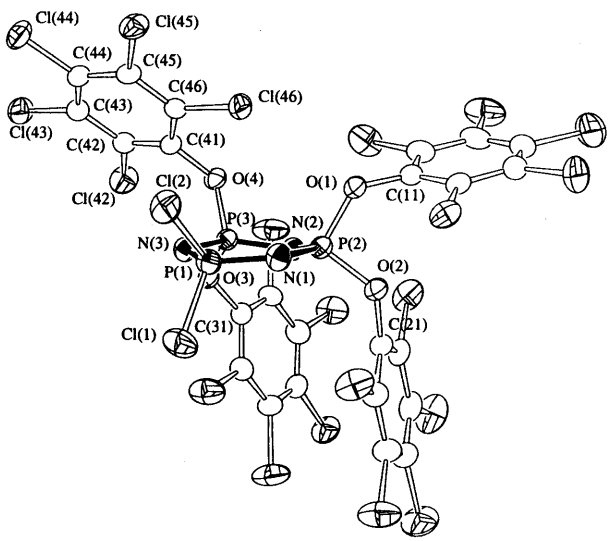


Fig. 2. ORTEP diagram of *gem*-$N_3P_3(OC_6Cl_5)_4Cl_2$ (**1**) (ellipsoids are drawn at 50% probability level); the tetrahydrofuran solvate molecule is omitted.

2.3. Structures of *gem*-$N_3P_3(OC_6Cl_5)_4Cl_2 \cdot C_4H_8O$ (**1**) and $N_3P_3(OC_6F_5)_6$ (**3**)

Compound **1**, which crystallizes with tetrahydrofuran molecules in the lattice, contains a cyclic trimeric phosphazene ring, with P(2) and P(3) each connected to two pentachloro-phenoxy groups via P–O–C linkages, and P(1) connected to two chlorine atoms (Fig. 2). The phosphazene ring is slightly puckered, with a maximum deviation from the mean ring plane of -0.136 Å for N(2). The P–N bond lengths are similar, and range from 1.576(3) to 1.582(3) Å with a mean of 1.580(1) Å. The N–P–N and P–N–P bond angles range from 117.1(2) to 118.5(2)° and 120.3(2) to 121.7(2)°, respectively. The P–O bond distances are between 1.586(2) and 1.607(2) with a mean of 1.595(4) Å. The average P–Cl bond distance is 1.999(1) Å. Selected bond lengths and bond angles of **1** are given in Table 1.

Compound **3** contains a cyclic trimeric phosphazene ring, with each phosphorus atom connected to two pentafluorophenoxy groups via P–O–C linkages (Fig. 3). The phosphazene ring is slightly puckered, with maximum deviations from the mean ring plane of 0.127 and -0.156 Å for N(3) and P(3), respectively. The P–N bond lengths range from 1.564(2) to 1.571(2) Å with a mean of 1.568(1) Å, and the N–P–N and P–N–P bond angles range from 115.90(11) to 119.11(11)° and 119.90(13) to 120.81(13)°, respectively. The P–O bond lengths range from 1.574(2) to 1.590(2), with a mean value of 1.584(3) Å. Selected bond lengths and bond angles for **3** are given in Table 2.

Because of the electron-withdrawing nature of $C_6Cl_5O^-$ and $C_6F_5O^-$, compounds **1** and **3** might be expected to exhibit long P–O bonds and short P–N bonds [15]. However, comparing these bond lengths of compounds **1** and **3** with the starting material ($N_3P_3Cl_6$) [16] and phosphazenes with electron-releasing phenoxy groups (Table 3) [17,18], does not show any significant trends in P–O and P–N bond lengths. The 1.568(1) mean P–N distance of **3** is significantly shorter than that of $P_3N_3Cl_6$ and **1**, although it is unclear whether this is indicative of the electronegativity of the $C_6F_5O^-$ group, since it is not accompanied by a correspondingly

Table 1
Selected bond lengths (Å) and angles (°) for *gem*-$N_3P_3(OC_6Cl_5)_4Cl_2$ (**1**)

P(1)–N(1)	1.583(3)
P(1)–N(3)	1.582(3)
P(1)–Cl(2)	1.9972(13)
P(1)–Cl(1)	1.9997(13)
P(2)–N(1)	1.579(3)
P(2)–N(2)	1.582(3)
P(2)–O(2)	1.586(2)
P(2)–O(1)	1.594(2)
P(3)–N(2)	1.576(3)
P(3)–N(3)	1.581(3)
P(3)–O(3)	1.593(2)
P(3)–O(4)	1.607(2)
O(1)–C(11)	1.386(4)
O(2)–C(21)	1.383(4)
O(3)–C(31)	1.385(4)
O(4)–C(41)	1.393(4)
N(3)–P(1)–N(1)	118.48(16)
N(1)–P(2)–N(2)	117.16(16)
N(2)–P(3)–N(3)	118.57(16)
P(2)–N(1)–P(1)	121.70(19)
P(3)–N(2)–P(2)	120.35(17)
P(3)–N(3)–P(1)	120.27(18)
Cl(2)–P(1)–Cl(1)	100.92(6)
O(2)–P(2)–O(1)	97.42(12)
O(3)–P(3)–O(4)	99.91(13)
C(11)–O(1)–P(2)	126.0(2)
C(21)–O(2)–P(2)	129.7(2)
C(31)–O(3)–P(3)	125.0(2)
C(41)–O(4)–P(3)	122.1(2)

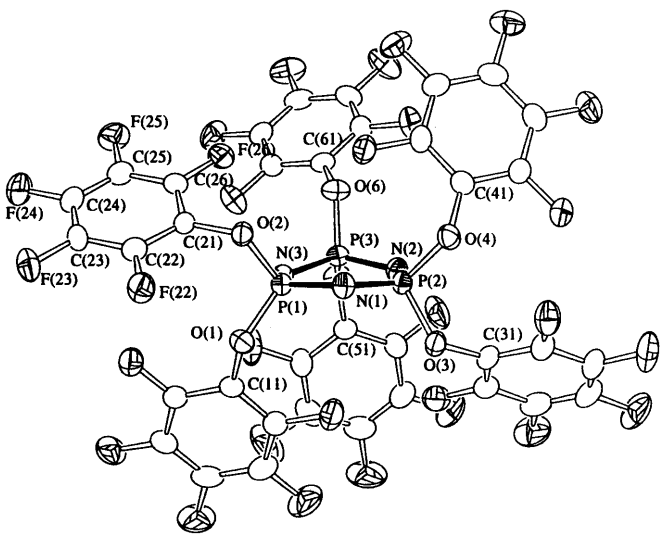


Fig. 3. ORTEP diagram of $N_3P_3(OC_6F_5)_6$ (**3**) (ellipsoids are drawn at 50% probability level).

long P–O distance. The mean P–O bond length of **1** approaches the accepted P–O single bond distance [19] of 1.61 Å; however, interpretation of this is limited since all mean P–O bond distances in Table 3 are not significantly different.

2.4. Electrospray mass spectrometry

As far as we are aware, the study of phosphazenes by electrospray mass spectrometry (ESMS) has not been reported previously. This technique has proven to be a useful alternative to EI or FAB mass spectrometry for characterizing inorganic and organometallic compounds because there is often less fragmentation and

Table 2
Selected bond lengths (Å) and angles (°) for $N_3P_3(OC_6F_5)_6$ (**3**)

P(1)–N(1)	1.564(2)
P(1)–N(3)	1.567(2)
P(2)–N(1)	1.565(2)
P(2)–N(2)	1.568(2)
P(3)–N(2)	1.570(2)
P(3)–N(3)	1.571(2)
P(1)–O(2)	1.5886(18)
P(1)–O(1)	1.5903(19)
P(2)–O(3)	1.5844(19)
P(2)–O(4)	1.5871(19)
P(3)–O(5)	1.5742(18)
P(3)–O(6)	1.5788(19)
O(1)–C(11)	1.368(3)
O(2)–C(21)	1.385(3)
O(3)–C(31)	1.378(3)
O(4)–C(41)	1.375(3)
O(5)–C(51)	1.376(3)
O(6)–C(61)	1.366(3)
N(1)–P(1)–N(3)	118.87(11)
O(2)–P(1)–O(1)	99.31(10)
N(1)–P(2)–N(2)	119.11(11)
O(3)–P(2)–O(4)	99.44(10)
N(2)–P(3)–N(3)	115.92(11)
O(5)–P(3)–O(6)	98.35(10)
P(2)–N(1)–P(1)	119.91(13)
P(2)–N(2)–P(3)	120.78(13)
P(1)–N(3)–P(3)	120.36(13)
C(11)–O(1)–P(1)	125.18(16)
C(21)–O(2)–P(1)	119.34(15)
C(31)–O(3)–P(2)	122.34(16)
C(41)–O(4)–P(2)	124.28(17)
C(51)–O(5)–P(3)	124.55(16)
C(61)–O(6)–P(3)	130.90(17)

Table 3
Comparison of selected mean bond lengths

Compound	Mean bond lengths (Å)	
	P–N	P–O
$N_3P_3Cl_6$ [a]	1.581(3)	
$N_3P_3(OC_6H_5)_6$ [b]	1.575(2)	1.582(2)
$N_3P_3(OC_6H_4–OC_6H_5)_6$ [c]	1.576(2)	1.578(3)
gem-$N_3P_3(OC_6Cl_5)_4Cl_2$ (**1**) [d]	1.580(1)	1.595(4)
$N_3P_3(OC_6F_5)_6$ (**3**) [d]	1.568(1)	1.584(3)

[a] Average P–Cl bond length = 1.993(2) Å, Ref. [16].
[b] Ref [17].
[c] Ref [18].
[d] This work.

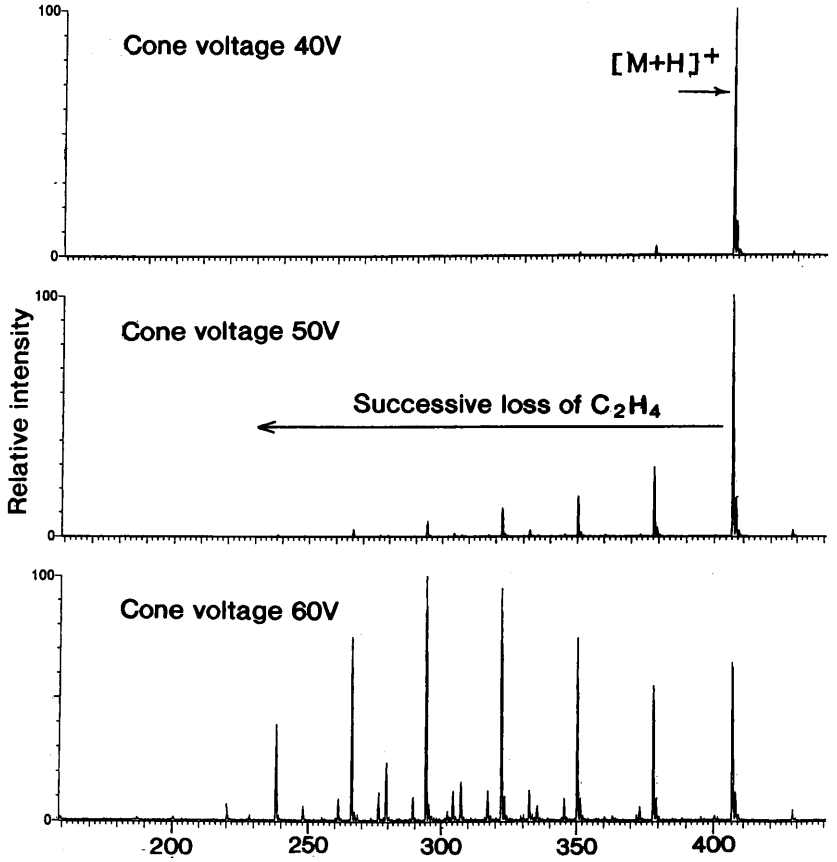


Fig. 4. The electrospray mass spectra of $N_3P_3(OEt)_6$ in $CH_3CN–H_2O$ (1:1) showing the increased net elimination of C_2H_4 (or hydrolysis) with increasing cone voltage; 40 V (a), 50 V (b) and 60 V (c).

low volatility is not a problem since the samples are introduced as solutions [20–22].

The observation of a positive-ion ESMS spectrum requires the formation of a cationic species, e.g. $[M + H]^+$ or $[M + Na]^+$. As mentioned in Section 1, basicity studies on a range of cyclotriphosphazenes have shown that the ring-nitrogen atoms are basic [3] and in fact protonated species can be isolated with metal-containing anions [23]. Hence the most likely cation binding site in the ESMS experiment is the ring-nitrogen atom. However, the basicity of this nitrogen atom is sensitive to the substituents on the phosphorus atoms, with electron-withdrawing substituents decreasing it. We were therefore interested to discover whether or not the basicity of the ring-nitrogen atoms decreased sufficiently when $C_6Cl_5O^-$ or $C_6F_5O^-$ were attached to the phosphorus atoms to preclude the observation of positive-ion ESMS spectra.

2.4.1. $N_3P_3(OEt)_6$

This gave a very clean $[M + H]^+$ peak at m/z 406 when run in $CH_3CN–H_2O$, the ion presumably forming by protonation at one of the ring nitrogen atoms. The spectrum is illustrated in Fig. 4a, which was run under relatively mild conditions (40 V cone voltage). As the cone voltage was increased to 50 and then 60 V (Fig. 4b,c) fragmentation occurred to give a series of peaks differing by 28 mass units, corresponding to successive net loss of C_2H_4 from the ethoxy groups to convert the $P–OC_2H_5$ to P–OH groups. The elimination from all six P–OR bonds presumably yields metaphosphimic acid, $[NHP(O)OH]_3$ (m/z 238), which is the phosphazene formed from tautomerization of $N_3P_3(OH)_6$ [24]. There was also a weak peak corresponding to $[2M + H]^+$ at m/z 811, where two $N_3P_3(OEt)_6$ molecules have aggregated about one proton.

To test the basicity of $N_3P_3(OEt)_6$ towards other cations, a solution in CH_3CN was treated with a drop of an aqueous solution containing all of the Group 1 cations ($Li^+–Cs^+$) at approximately 0.01 mol l^{-1}. This gave the spectrum shown in Fig. 5. One family of peaks in the 400–550 region consists of $[M + \text{cation}]^+$ signals, with H^+ cation dominating and the others in the relative order $Cs^+ > Rb^+ > K^+ > Na^+ > Li^+$. A second set around 800–950 consists of $[2M + \text{cation}]^+$, with the H^+ cation now a minor contributor. This can be understood in terms of the relative sizes. H^+ will be the most abundant cation and is a strong acid so forms $[M + H]^+$ very readily. However, it is small so aggregating two $N_3P_3(OEt)_6$ molecules to generate $[2M +$

$H]^+$ will not be favored on steric grounds. The other cations are present in equal concentrations, hence the adducts formed will depend on competition between solvation by H_2O and/or CH_3CN and coordination to the ring-nitrogen atoms. For the larger Cs^+ ion, solvation will be weaker so adducts form more readily than with the more tightly solvated Li^+ (with the other intermediate). All, however, are now large enough to form $[2M + \text{cation}]^+$ species without excessive steric hindrance.

2.4.2. $N_3P_3(OPh)_6$

This compound behaved similarly to $N_3P_3(OEt)_6$, giving strong $[M + H]^+$ ions at m/z 694 and weak $[2M + H]^+$ ions at m/z 1387 in either $CH_3CN–H_2O$ or EtOH. It too formed adducts with other cations. Particularly strong signals were found with added Ag^+, corresponding to $[M + Ag]^+$, $[M + Ag + CH_3CN]^+$ and $[2M + Ag]^+$, and, perhaps more surprisingly, a strong $PhHg^+$ adduct was seen at m/z 972 in a solution of $N_3P_3(OPh)_6$ in EtOH with added PhHgOAc. The fact that a stable, ring-nitrogen coordinated, silver(I) complex can be isolated using hexakis(2-pyridyloxy)cyclotriphosphazene [25], would support a similar interaction in the ESMS experiment, as opposed to arene ring coordination.

2.4.3. $N_3P_3(OPh)_5Cl$

This gave the expected $[M + H]^+$ and $[2M + H]^+$ ions in either $CH_3CN–H_2O$ or MeOH. Added PhHgOAc again produced a clean $PhHg^+$ adduct ion, and with Ag^+ clear $[M + Ag]^+$, $[M + Ag + CH_3CN]^+$ and

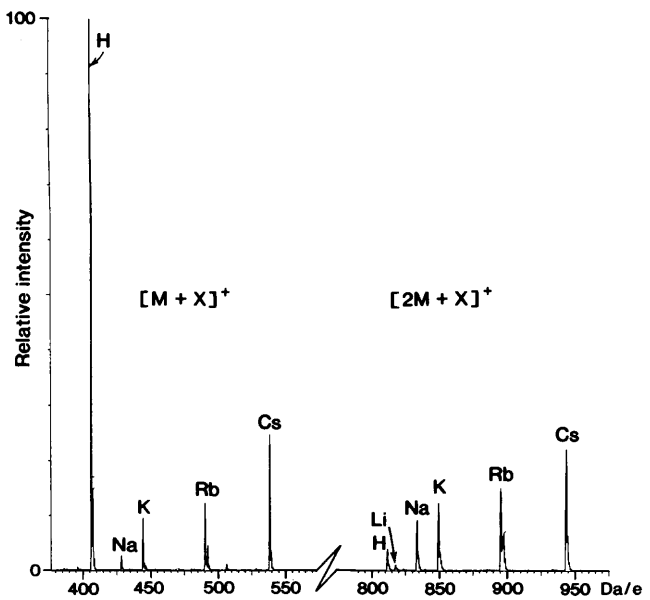


Fig. 5. The electrospray mass spectrum of $N_3P_3(OEt)_6$ in CH_3CN with an added drop of an aqueous solution containing all the Group 1 metal cations in equimolar concentration, showing the relative selectivities for both the $[M + X]^+$ and $[2M + X]^+$ aggregates.

$[2M + Ag]^+$ signals were seen. In the latter case, there was no sign of an ion $[N_3P_3(OPh)_5]^+$, which would have been formed by Cl^- abstraction. Similarly, the negative ion spectrum gave no signals, which shows that Ag^+ induced hydrolysis to give $N_3P_3(OPh)_5(OH)$ has not occurred since this would have given a $[N_3P_3(OPh)_5(O)]^-$ peak.

2.4.4. $N_3P_3(OC_6F_5)_6$ (3)

This compound behaves completely differently from those described above. In the positive ion mode no signals were detected in $CH_3CN–H_2O$ or EtOH (even with added acid), showing the basicity of the ring nitrogen atoms has been reduced through electron withdrawal by the C_6F_5O groups to the point where attachment of a proton does not take place. However, in negative ion mode a strong, clean peak at m/z 1066 corresponding to $[M - C_6F_5]^-$ is seen in $CH_3CN–H_2O$. This presumably arises from hydrolysis to give $N_3P_3(OC_6F_5)_5(OH)$ which then deprotonates to give $[N_3P_3(OC_6F_5)(O)]^-$, an anion which would be stabilized by the plethora of electron withdrawing C_6F_5O groups. This is consistent with the observation that hydrolysis rates of aryloxycyclophosphazenes are greater when the phenoxy groups contain electron-withdrawing substituents. For example, in 25 vol% aqueous diglyme, the rate constants for $R = p\text{-}NO_2$ and $R = p\text{-}Me$ are 5.16×10^{-1} and 6.93×10^{-7} mol^{-1} l s^{-1}, respectively [26]. It is therefore not surprising that similar hydrolysis is not observed for $N_3P_3(OPh)_6$ in the negative ion spectrum. Addition of $AgClO_4$ to a CH_3CN solution of $N_3P_3(OC_6F_5)_6$, gave no signals in the positive ion mode corresponding to an Ag^+ adduct, but in the negative ion showed a strong $[M + ClO_4]^-$ species at m/z 1332. For this phosphazene, aggregation with anions appears to have become more favorable than with cations.

2.4.5. $N_3P_3(OC_6F_5)_4(O_2C_{12}H_8)$ (4)

As expected by comparison with the results for **3**, this compound gave a strong signal at m/z 884 in the negative ion mode in $CH_3CN–H_2O$ or CH_3OH, corresponding to the hydrolysis product $N_3P_3(OC_6F_5)_3(O_2C_{12}H_8)O^-$. However, a weak $[M + H]^+$ peak at m/z 1052 shows that some residual basicity is still retained for **4** (in the positive-ion mode). However, there was no adduct formed with either Rb^+ or Cs^+ ions.

2.4.6. $N_3P_3Cl_6$

This compound gave no signals in positive ion mode in $CH_3CN–H_2O$. However, addition of Ag^+ ions led to a complex set of peaks from which a $[M + Ag]^+$ envelope could be found at m/z 456, but the complicated nature of the spectrum makes it unsuitable for analytical purposes. The negative ion spectrum, in contrast, gave a clean signal of $[N_3P_3Cl_5(O)]^-$, arising from a hydrolysis reaction of the parent species.

2.4.7. gem-$N_3P_3(OC_6Cl_5)_4Cl_2$ (1)

For this compound spectra were difficult to record because of poor solubility in all solvents used. However, a sufficient amount dissolved in CH_3CN to give a weak signal in negative ion mode centered about m/z 1018 corresponding to $[N_3P_3(OC_6Cl_5)_3Cl_2(O)]^-$ from hydrolysis of one of the $C_6Cl_5O^-$ groups (rather than one of the P–Cl bonds), which is consistent with the C_6Cl_5O substituent being more electron withdrawing than the Cl. More unexpectedly was a weak signal at m/z 1267 in positive ion mode under relatively harsh conditions, which corresponds to an M^+ ion (rather than a $[M+H]^+$ ion; the calibration of the instrument can distinguish these). The source of the electrospray mass spectrometer can be regarded as an unconventional cell, and redox processes giving M^+ ions are not unknown [20,27]. However there is no obvious reason why there should be an M^+ ion formed in this case, but not for any of the other samples examined. Possibly for the compounds with more basic ring-nitrogen sites, the formation of $[M+H]^+$ ions swamps a small amount of M^+ arising from oxidation, but for $N_3P_3(OC_6Cl_5)_4Cl_2$ the lack of competing protonation highlights the alternative ion-forming process.

2.4.8. $N_3P_3(OC_6Cl_5)_6$ (2)

For this sample, total insolubility precluded exploration.

In summary, ESMS is a useful technique for characterizing $N_3P_3(OR)_6$ and related species when R is an electron-releasing organic group, since strong $[M+H]^+$ ions are formed via the basic ring-nitrogen sites. Other simple cations also form strong adducts, meaning relative coordinating strengths can be assessed readily from ESMS spectra. For corresponding species with strongly electron-withdrawing R groups, protonation to give positive ions was not observed. In situ hydrolysis of these groups can occur to give –OH, which on deprotonation, allows detection of the corresponding anion. This, however, is a less satisfactory method of characterization. Hydrolysis of a P–Cl bond was also seen for $N_3P_3Cl_6$, but appears less favorable than reaction at P–OR bonds.

3. Experimental

3.1. General

All manipulations were carried out under nitrogen using standard Schlenk techniques. Analytical grade solvents were purchased from standard chemical suppliers, and with the exception of tetrahydrofuran, were used without further purification/drying. Tetrahydrofuran (THF) was distilled from Na–benzophenone and stored over activated molecular sieves. Technical grade (BDH) pentachlorophenol and hexachlorocyclotriphosphazene, $N_3P_3Cl_6$ (Aldrich), were sublimed prior to use. NaH was isolated as a pure powder from a paraffin oil mixture by washing with hexane. $N_3P_3(2,2'\text{-}O_2C_{12}H_8)Cl_4$ (**4**) [13], $N_3P_3(OEt)_6$ [28], $N_3P_3(OPh)_6$ and $N_3P_3(OPh)_5Cl$ [29] were prepared by literature methods. 2,2′-Biphenol (Aldrich) and pentafluorophenol (Aldrich) were used as received. NMR spectra were run on a JEOL GX270W MHz spectrometer and ESMS samples were run on a VG Platform II instrument. For the chlorinated samples, the m/z values quoted are for the most intense peaks in the isotopomer envelope, confirmed by simulation.

3.2. Synthesis of compounds

3.2.1. gem-$N_3P_3(OC_5Cl_5)_4Cl_2$ (1)

Pentachlorophenol (1.838 g, 6.90 mmol) was added whilst stirring to NaH (160 mg, 6.67 mmol) in dry tetrahydrofuran (30 ml). After stirring the mixture for approximately 20 min at r.t., $N_3P_3Cl_6$ (200 mg, 0.575 mmol) was added and the reaction heated to reflux. After approximately 10–13 days ^{31}P NMR showed predominantly the *gem*-tetrasubstituted product, at which time the reaction was stopped. The solvent was removed under vacuum and the solid residue washed with dilute NaOH (0.04 mol l^{-1}). The remaining residue was digested in boiling tetrahydrofuran and filtered whilst hot through kiesulghur. Slow evaporation of the filtrate yielded colorless crystals of monosolvated
gem - tetra(pentachlorophenoxy)dichloro - cyclotriphosphazene (**1**) (150 mg, 21%). m.p. 286–293°C. *Anal.* Found: C, 25.26; H, 0.42; Cl, 58.46; N, 3.12. $C_{24}N_3O_4P_3Cl_{22}\cdot C_4H_8O$ requires C, 25.11; H, 0.60; Cl, 58.24; N, 3.14%. ^{31}P NMR (THF) δ_P 0.1 (d), 26.4 (t), $J_2 = 88$ Hz. ES MS (m/z): positive ion 1267 M^+; negative ion 1018 $[P_3N_3(OC_6Cl_5)_3Cl_2(O)]^-$.

3.2.2. $N_3P_3(OC_6Cl_5)_6\cdot 2C_6H_6$ (2)

Similarly, $N_3P_3Cl_6$ (100 mg, 0.288 mmol) was added to 12 mole equivalents of sodium pentachlorophenoxide (prepared in situ as for **1**) in diglyme (20 ml), and the reaction stirred under reflux for 5 days considerable decomposition was evident from the brown color of the reaction. Once cooled, the reaction mixture was filtered and the precipitate washed ($NaHCO_3$–H_2O) and subsequently extracted with hot benzene. Slow diffusion of pentane into the benzene solution afforded, in low yield, hexa(pentachlorophenoxy)cyclotriphosphazene·$2C_6H_6$ (**2**); a colorless, micro-crystalline solid (45 mg, 8%). m.p. (dec.) >330°C. *Anal.* Found: C, 30.49; H, 0.62; Cl, 56.20; N, 2.19. Calc. for $C_{36}N_3O_6P_3Cl_{30}\cdot 2C_6H_6$: C, 30.62; H, 0.64; Cl, 56.48; N, 2.23%. ^{31}P NMR (benzene:CH_2Cl_2 2:1) δ_P 2.1 (s).

3.2.3. $N_3P_3(OC_6F_5)_6$ (3)

Similarly, $N_3P_3Cl_6$ (200 mg, 0.565 mmol) was added to seven molar equivalents of sodium pentafluorophenoxide (prepared in situ as for **1**) in tetrahydrofuran (30 ml), and the reaction stirred under reflux for 6 h. After removal of the solvent, the residue was washed (H_2O) and subsequently extracted with CH_2Cl_2 and dried with $MgSO_4$. Hexane was added and the solution cooled to 4°C, which yielded colorless crystals of hexakis(pentafluorophenoxy)cyclotriphosphazene (**3**) (490 mg, 70%). m.p. 110–111°C. *Anal.* Found: C, 35.30; N, 3.55; P, 7.51. Calc. for $C_{36}N_3O_6P_3F_{30}$: C, 35.06; N, 3.41; P, 7.53%. ^{31}P NMR (THF) δ_P 10.7 (s). ES MS (m/z): negative ion 1066 $[P_3N_3(OC_6F_5)_5(O)]^-$. Crystals suitable for single crystal X-ray studies were grown via the slow diffusion of pentane into a CH_2Cl_2 solution of **3**.

3.2.4. $N_3P_3(OC_6F_5)_4(2,2'\text{-}O_2C_{12}H_8)$ (5)

Similarly, **4** (100 mg, 0.217 mmol) was added to 4 mole equivalents of sodium pentafluorophenoxide in tetrahydrofuran (30 ml^{-1}), and the reaction stirred under reflux conditions for approximately 24 h. The reaction mixture was worked up as for **3**. Colorless crystals of (2,2′-biphenolate)tetra(pentafluorophenoxy)-cyclotriphosphazene (**5**) (91 mg, 40%) were obtained by slow evaporation from CH_2Cl_2–hexane. m.p. 148–151°C. *Anal.* Found: C, 41.24; H, 0.73; N, 4.05. $C_{36}H_8N_3O_6F_{20}P_3$ requires C, 41.13; H, 0.77; N, 4.00%. ^{31}P NMR (THF) δ_P 13.6 (d, $J_2 = 95$ Hz), 22.4 (dd, $J_2 = 90$ and 100 Hz). ES MS (m/z): positive ion 1052 $[M+H]^+$; negative ion 884 $[N_3P_3(OC_6F_5)_3\text{-}(O_2C_{12}H_8)O]^-$.

3.3. Reaction of $NaOC_6F_5$ with $N_3P_3(2,2'\text{-}O_2C_{12}H_8)Cl_4$ (4)

Similarly, **4** (100 mg, 0.217 mmol) was added to 2 mole equivalents of sodium pentafluorophenoxide in tetrahydrofuran (30 ml), and the reaction stirred under reflux conditions for approximately 18 h. ^{31}P NMR was used to determine the ratio of *geminal* and non-*geminal* disubstituted products — no further work up was performed on the reaction mixture.

3.4. Monitoring the reaction between $NaOC_6F_5$ and $N_3P_3Cl_6$

The general procedure was as follows: a solution of $N_3P_3Cl_6$ (200 mg, 0.575 mmol) in tetrahydrofuran (3 ml) was added quickly to a stirred tetrahydrofuran (7 ml) solution containing seven molar equivalents of in situ prepared $NaOC_6F_5$. After approximately 30 s stirring, 5 ml was transferred to a 10 mm NMR tube and loaded into a JEOL 270 MHz spectrometer. ^{31}P NMR spectra were acquired at routine time intervals. Similarly, the reaction was also monitored at low temperature, with the initial solutions cooled to 0°C prior to mixing and the probe temperature set to −10°C.

Similarly, using ^{31}P NMR, the reaction of pentachlorophenoxide with $N_3P_3Cl_6$ was monitored. However, because of the slow nature of the reaction, monitoring was performed once every 1–3 days.

3.5. Crystal structure determination of compound 1

Single crystals of *gem*-$N_3P_3Cl_2(OC_6Cl_5)_4\cdot C_4H_8O$ (**1**.C_4H_8O) were recrystallized from tetrahydrofuran, mounted in inert oil and transferred into the cold gas stream of a Siemens SMART CCD area-detector diffractometer. Crystal data for $C_{28}H_8N_3O_5P_3Cl_{22}$: $M = 1339.18$, monoclinic, space group; $P2_1/n$, $a = 16.8730(2)$, $b = 15.0169(2)$, $c = 19.2459(2)$ Å, $\beta = 109.60(1)°$, $V = 4593.97(9)$ Å^3, $T = 203(2)$ K, $Z = 4$, $D_{calc} = 1.936$ g cm^{-3}, $F(000) = 2624$, μ(Mo Kα) = 1.45 mm^{-1}, 27 675 reflections were collected ($2.78 < 2\theta < 55.02°$), of which 10 063 were unique ($R_{int} = 0.0376$). Data was corrected for absorption effects (SADABS); $T_{max} = 0.8803$, $T_{min} = 0.7404$. Refinement of 550 parameters converged at $R_1 = 0.0471$ [observed data: 7233 $|F_o| > 4\sigma(F_o)$], $wR_2(F^2) = 0.1025$ (all data).

3.6. Crystal structure determination of compound 3

Single crystals of $N_3P_3(OC_6F_5)_6$ (**3**) were recrystallized via slow CH_2Cl_2–pentane diffusion, mounted in inert oil and transferred into the cold gas stream of a Siemens SMART CCD area-detector diffractometer. Crystal data for $C_{36}N_3O_6P_3F_{30}$: $M = 1233.30$, monoclinic, space group; $P2_1/n$, $a = 7.9946(1)$, $b = 43.4044(2)$, $c = 12.1024(1)$ Å, $\beta = 108.863(1)°$, $V = 3974.00(6)$ Å^3, $T = 203(2)$ K, $Z = 4$, $D_{calc} = 2.061$ g cm^{-3}, $F(000) = 2400$, μ(Mo Kα) = 1.45 mm^{-1}, 14 645 reflections were collected ($5.12 < 2\theta < 50.44°$), of which 6990 were unique. Data were corrected for absorption effects (SADABS); $T_{max} = 0.9308$, $T_{min} = 0.8796$. Refinement of 703 parameters converged at $R_1 = 0.0415$ [observed data: 6097 $|F_o| > 4\sigma(F_o)$], $wR_2(F^2) = 0.0909$ (all data).

Structures of **1** and **3** solved and refined routinely using direct methods (SHELXS-97) [30] and full-matrix least-squares on F^2 (SHELXL-97) [31] respectively. All non-hydrogen atoms were refined anisotropically. The hydrogen atoms of the molecules were geometrically idealized and refined using a riding model.

4. Supplementary material

Crystallographic data for the structural analysis has been deposited with the Cambridge Crystallographic Data Centre, CCDC Nos. 144167 and 144168. Copies of this information may be obtained free of charge

from: The Director, CCDC, 12 Union Road, Cambridge, CB2 1EZ, UK (fax: +44-1223-336033; e-mail: deposit@ccdc.cam.ac.uk or www: http://www.ccdc.cam.ac.uk).

Acknowledgements

We gratefully acknowledge the financial support, including a postdoctoral fellowship for CVD, from the Massey University Research Fund. The authors also thank Mr Clem Powell for valued preliminary investigations.

References

[1] H.R. Allcock, Phosphorus–Nitrogen Compounds, Academic Press, New York, 1972, pp. 150–174 Chapter 6.
[2] M.F. Sorokin, V.K. Latov, Kinet. Catal. 7 (1966) 35.
[3] (a) D. Feakins, W.A. Last, S.N. Nabi, R.A. Shaw, P. Watson, J. Chem. Soc. A (1969) 196. (b) D. Feakins, W.A. Last, N. Neemuchwala, R.A. Shaw, J. Chem. Soc. A (1965) 2805. (c) D. Feakins, W.A. Last, N. Neemuchwala, R.A. Shaw, Chem. Ind. (1963) 164. (d) R.A. Shaw, Pure Appl. Chem. 52 (1980) 1063. (e) R.A. Shaw, Z. Naturforsch. 31B (1976) 641.
[4] J.L. Schmutz, H.R. Allcock, Inorg. Chem. 14 (1975) 2433.
[5] H.R. Allcock, D.C. Ngo, M. Parvez, K. Visscher, J. Chem. Soc., Dalton Trans. (1992) 1687.
[6] S. Li, M. Paleologou, W.C. Purdy, J. Chromatogr. Sci. 29 (1991) 66.
[7] J. Drahonovsky, Z. Vacek, Collect. Czech. Chem. Commun. 36 (1971) 3431.
[8] V.M. Vlasov, O.P. Sheremet, Izv. Sib. Otd. Akad. Nauk SSSR, Ser. Khim. Nauk. 2 (1982) 114.
[9] Romanian Patent Application: RO 84-115019 840627, CAN 108:38130.
[10] B.S. Nader, K.K. Kar, T.A. Morgan, C.E. Pawloski, W.L. Dilling, Tribol. Trans. 35 (1992) 37.
[11] A.H. Gerber, From: Gov. Rep. Announce. Index (U.S.) 77 (1977) 103.
[12] P.O. Gitel, L.F. Osipova, O.P. Solovova, Zh. Obsshch. Khim. 45 (1975) 1749.
[13] G.A. Carriedo, L. Fernández-Catuxo, F.J. García-Alonso, P. Gómez-Elipe, P.A. González, Macromolecules 29 (1996) 5320.
[14] A. Viji, S.J. Geib, R.L. Kirchmeier, J.M. Shreeve, Inorg. Chem. 35 (1996) 2915.
[15] H.R. Allcock, Phosphorus–Nitrogen Compounds, Academic Press, New York, 1972, pp. 16–35 Chapter 2.
[16] G.J. Bullen, J. Chem. Soc., Sect. A (1971) 1450.
[17] W.C. Marsh and J. Trotter, J. Chem. Soc., Sect. A (1971) 169.
[18] H.R. Allcock, S. Al-Shali, D.C. Ngo, K.B. Visscher, M. Parvez, J. Chem. Soc., Dalton Trans. (1996) 3549.
[19] D.W.J. Cruickshank, J. Chem. Soc. (1961) 5486.
[20] W. Henderson, B.K. Nicholson, L.M. McCaffrey, Polyhedron 17 (1998) 4291.
[21] R. Colton, A. D'Agostino, J.C. Traeger, Mass Spectrom. Rev. 14 (1995) 79.
[22] R.B. Cole, Electrospray Ionisation Mass Spectrometry: Fundamentals, Instrumentation and Applications, Wiley Interscience, New York, 1997.
[23] V. Chandrasekhar, K.R.J. Thomas, Appl. Organomet. Chem. 7 (1993) 1.
[24] C.W. Allen, in: I. Haiduc, D.B. Sowerby (Eds.), The Chemistry of Inorganic Homo- and Heterocycles, Academic Press, London, 1987, p. 501 Chapter 20.
[25] E.W. Ainscough, A.M. Brodie, C.V. Depree, unpublished results.
[26] (a) H.R. Allcock, E.J. Walsh, Chem. Commun. (1970) 580. (b) H.R. Allcock, E.J. Walsh, J. Am. Chem. Soc. 94 (1972) 4538.
[27] A.T. Blades, M.G. Ikonomou, P. Kebarle, Anal. Chem. 63 (1991) 2109.
[28] B.W. Fitzsimmons, R.A. Shaw, Inorg. Synth. 8 (1966) 77.
[29] E.T. McBee, K. Okuhara, C.J. Morton, Inorg. Chem. 5 (1966) 450.
[30] G.M. Sheldrick, Acta Crystallogr., Sect. A 46 (1990) 467.
[31] G.M. Sheldrick, Program for Crystal Structure Refinement, Universität Göttingen, Germany, 1997.

PERGAMON

www.elsevier.nl/locate/poly

Polyhedron 19 (2000) 2111–2118

POLYHEDRON

Tetranuclear manganese carboxylate clusters with imidazole-carboxylate chelating ligands. X-ray crystal structure of the 4-imidazoleacetate complex

Colette Boskovic, Kirsten Folting, George Christou *

Department of Chemistry and Molecular Structure Center, Indiana University, Bloomington, IN 47405-4001, USA

Received 9 May 2000; accepted 17 July 2000

Abstract

Procedures are described for the synthesis of tetranuclear manganese carboxylate complexes with ligands derived from 4-imidazoleacetic acid (imidacH) and 4-imidazolecarboxylic acid (imidcarbH). Reaction mixtures containing NBu^n_4imidac or $NHex^n_4$imidcarb generated in situ and either $[Mn_3O(O_2CMe)_6(py)_3](ClO_4)$ or $Mn(O_2CR)_2$, RCO_2H (R = Me, Ph) and NR'_4MnO_4 ($R' = Bu^n$, Hex^n) give red–brown solutions from which the products $(NBu^n_4)[Mn_4O_2(O_2CR)_7(imidac)_2]$ (R = Me (**1**); R = Ph (**2**)) and $(NHex^n_4)[Mn_4O_2(O_2CR)_7(imidcarb)_2]$ (R = Me (**3**); R = Ph (**4**)) can be obtained. The X-ray crystal structure of **2** reveals that the anion consists of an $[Mn_4(\mu_3\text{-}O)_2]^{8+}$ core with the four Mn atoms disposed in a 'butterfly' arrangement and the O atoms triply bridging each 'wing'. Peripheral ligation is provided by seven bridging O_2CPh^- ligands and two chelating $imidac^-$ groups. All available characterization data are consistent with the same core for complexes **1**, **3** and **4**, with the structures varying only in the peripheral ligation. ^1H NMR spectroscopy of all four complexes indicates that the structure is maintained in solution and the majority of the resonances have been assigned on the basis of T_1 measurements and substitution and exchange experiments. Cyclic voltammetry reveals the presence of a single quasi-reversible oxidation processes for complexes **1** and **2**. © 2000 Elsevier Science Ltd. All rights reserved.

Keywords: Polynuclear manganese-carboxylate clusters; Imidazole-carboxylate chelating ligands; Paramagnetic NMR

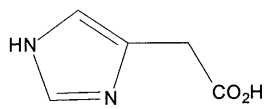
1. Introduction

The chemistry of Mn carboxylate clusters is an area of considerable interest, and numerous examples varying widely in both nuclearity and structure have been reported [1]. The interest in these species is in part due to their application to the modeling of Mn-containing proteins and enzymes, in which up to four Mn nuclearities have been identified [2,3]. We have previously described procedures that allow the synthesis of tetranuclear Mn carboxylate compounds possessing the $[Mn_4(\mu_3\text{-}O)_2]$ core and of formulation $[Mn^{III}_4O_2(O_2CR)_7(L)_2]^z$, where L is a pyridine-based N/N or N/O chelate derived from 2,2′-bipyridine (bpy), picolinic acid (picH), 8-hydroxyquinoline (hqnH) or 2-(hydroxymethyl)pyridine (hmpH) [4–6].

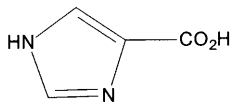
As part of a continuing exploration of tetranuclear Mn carboxylate clusters with chelating ligands, we have recently turned our attention to the use of imidazole-containing chelates in order to compare and contrast the products with those already obtained with pyridine-based chelates. We describe herein our initial results comprising the syntheses and characterization of tetranuclear clusters possessing imidazole-based N/O chelating ligands derived from 4-imidazoleacetic acid (imidacH) and 4-imidazolecarboxylic acid (imidcarbH). These species allow informative comparisons with those possessing pyridine-based chelating ligands with which they are isostructural, as well as providing access to compounds that possess either five- or six-membered chelate rings but are otherwise identical. In addition, imidazole ligation to tetranuclear Mn clusters is of interest due to the histidine ligation of the tetranuclear Mn complex responsible for water oxidation in Photosystem II [7].

* Corresponding author. Tel.: +1-812-855-2399; fax: +1-812-855-2399.

0277-5387/00/$ - see front matter © 2000 Elsevier Science Ltd. All rights reserved.
PII: S0277-5387(00)00516-7



imidacH



imidcarbH

2. Experimental

2.1. Synthesis

All manipulations were performed under aerobic conditions, using materials as received. Trinuclear $[Mn_3O]$ complexes were available from previous work [8]. $NBu^n_4MnO_4$ and $Mn(O_2CPh)_2{\cdot}2H_2O$ were prepared as described [4,9] and $NHex^n_4OH$ (Hex = hexyl) was prepared according to Giovannellio et al. [10]. WARNING: Appropriate care should be taken in the use of $NR^n_4MnO_4$, and readers are referred to the detailed warning given elsewhere [9].

2.1.1. $NHex^n_4MnO_4$

To a vigorously stirred solution of $KMnO_4$ (5.00 g, 31.6 mmol) in H_2O (100 cm^3) was added a solution of $NHex^n_4Br$ (13.50 g, 31.6 mmol) in H_2O (100 cm^3), resulting in the formation of a purple precipitate. This was filtered, washed copiously with H_2O and Et_2O and dried in vacuo at room temperature. The yield was 13.49 g, 92%.

2.1.2. $(NBu^n_4)[Mn_4O_2(O_2CMe)_7(imidac)_2]$ (**1**)

Method A: to a stirred solution of $Mn(O_2CMe)_2{\cdot}4H_2O$ (0.74 g, 3.0 mmol) and glacial acetic acid (1 cm^3) in MeCN (70 cm^3) was slowly added $NBu^n_4MnO_4$ (0.27 g, 0.75 mmol) in small portions to give a deep brown solution. To this was added a solution resulting from the combination of imidacH·HCl (0.31 g, 1.9 mmol) in MeCN (5 cm^3) and 1.0 M NBu^n_4OH in MeOH (3.8 cm^3, 3.8 mmol). The reaction mixture was stirred overnight and a brown precipitate removed by filtration. The filtrate was reduced in volume to 50 cm^3 and Et_2O (100 cm^3) was added, leading to the formation of a red–brown precipitate which could be recrystallized from MeCN–Et_2O. The yield was 0.60 g (55%). Drying in vacuo leads to the unsolvated form. Elemental analysis, *Anal.* Found: C, 41.09; H, 5.78; N, 6.08. Calc. for $C_{40}H_{67}N_5O_{20}Mn_4$: C, 41.50; H, 5.83; N, 6.05. Selected IR data (cm^{-1}): 1647(m), 1608(s), 1493(m), 1467(w), 1401(s), 1387(s), 1333(s), 1320(s), 1266(w), 1227(w), 1176(w), 1087(w), 1028(m), 943(m), 935(sh), 882(w), 802(w), 737(sh), 721(m), 678(m), 650(s), 635(sh), 613(m), 436(m).

Method B: to a stirred solution of $[Mn_3O(O_2CMe)_6(py)_3](ClO_4)$ (0.30 g, 0.34 mmol) in MeCN (20 cm^3) was added a solution resulting from the combination of imidacH·HCl (0.11 g, 0.68 mmol) in MeCN (3 cm^3) and 1.0 M NBu^n_4OH in MeOH (1.4 cm^3, 1.4 mmol). The reaction mixture was stirred overnight and a brown precipitate was removed by filtration. The filtrate was reduced in volume to 10 cm^3 and Et_2O (20 cm^3) was added, leading to the formation of a red–brown precipitate which could be recrystallized from MeCN–Et_2O. The yield was 0.14 g (47%). The product was spectroscopically identical to that obtained by method A.

2.1.3. $(NBu^n_4)[Mn_4O_2(O_2CPh)_7(imidac)_2]$ (**2**)

To a stirred solution of $Mn(O_2CPh)_2{\cdot}2H_2O$ (1.34 g, 4.0 mmol) and $PhCO_2H$ (0.86 g, 7.0 mmol) in MeCN (100 cm^3) was slowly added $NBu^n_4MnO_4$ (0.36 g, 1.0 mmol) in small portions to give a deep brown solution. To this was added a solution resulting from the combination of imidacH·HCl (0.41 g, 2.5 mmol) in MeCN (5 cm^3) and 1.0 M NBu^n_4OH in MeOH (5.0 cm^3, 5.0 mmol). The resulting solution was stirred overnight, filtered through celite, reduced in volume to 40 cm^3, and Et_2O (100 cm^3) added dropwise with vigorous stirring. This led to the formation of a red–brown precipitate, which could be recrystallized from MeCN–Et_2O. The yield was 1.45 g (73%). Crystals suitable for crystallography were grown by layering an MeCN solution of the complex with Et_2O, and they were kept in contact with the mother liquor to prevent interstitial solvent loss. Drying in vacuo leads to the unsolvated form. Elemental analysis. *Anal.* Found: C, 56.77; H, 5.66; N, 4.34. Calc. for $C_{75}H_{81}N_5O_{20}Mn_4$: C, 56.58; H, 5.13; N, 4.40. Selected IR data (cm^{-1}): 1606(s), 1571(s), 1501(w), 1490(m), 1466(w), 1448(m), 1384(s), 1331(s), 1314(m), 1303(m), 1265(m), 1231(w), 1173(m), 1143(w),1089(w), 1068(w), 1026(m), 940(m), 838(m), 720(s), 690(m), 676(m), 650(s), 630(m), 610(m), 468(m), 437(m).

2.1.4. $(NHex^n_4)[Mn_4O_2(O_2CMe)_7(imidcarb)_2]$ (**3**)

Method A: to a stirred solution of $Mn(O_2CMe)_2{\cdot}4H_2O$ (0.74 g, 3.0 mmol) and glacial acetic acid (1 cm^3) in MeCN (70 cm^3) was slowly added $NHex^n_4MnO_4$ (0.35 g, 0.75 mmol) in small portions to give a deep brown solution. To this was added a solution resulting from the combination of imidcarbH (0.21 g, 1.9 mmol) in MeCN (10 cm^3) and 0.2 M $NHex^n_4OH$ in MeOH (9.5 cm^3, 1.9 mmol). The reaction mixture was stirred overnight and a brown precipitate removed by filtration. The filtrate was reduced in volume to 50 cm^3 and Et_2O (100 cm^3) was added, leading to the formation of a red–brown precipitate which could be recrystallized from MeCN–Et_2O. The yield was 0.55 g (47%). Drying in vacuo leads to the unsolvated form. Elemental analysis. *Anal.* Found: C, 44.34; H, 6.28; N, 5.12. Calc. for $C_{46}H_{79}N_5O_{20}Mn_4$: C, 44.49; H, 6.41; N, 5.64. Selected IR data (cm^{-1}): 1681(s), 1615(s), 1579(sh), 1504(w), 1486(w), 1465(w), 1397(s), 1332(s), 1313(s), 1263(w),

1188(m), 1154(w), 1099(w), 1076(w), 1043(w), 1013(m), 933(w), 822(m), 800 (w), 776(w), 679(s), 654(s), 614(m), 569(w), 502 (m).

Method B: to a stirred solution of $[Mn_3O(O_2CMe)_6(py)_3](ClO_4)$ (0.50 g, 0.57 mmol) in MeCN (60 cm^3) was added a solution resulting from the combination of imidcarbH (0.097 g, 0.86 mmol) in MeCN (5 cm^3) and 0.2 M $NHex^n_4OH$ in MeOH (4.3 cm^3, 0.86 mmol). The reaction mixture was stirred overnight and a brown precipitate was removed by filtration. The filtrate was reduced in volume to 30 cm^3 and Et_2O (60 cm^3) was added, leading to the formation of a red–brown precipitate which could be recrystallized from MeCN–Et_2O. The yield was 0.27 g (50%). The product was spectroscopically identical to that obtained by method A.

2.1.5. $(NHex^n_4)[Mn_4O_2(O_2CPh)_7(imidcarb)_2]$ (**4**)

To a stirred solution of $Mn(O_2CPh)_2{\cdot}2H_2O$ (0.49 g, 1.5 mmol) and $PhCO_2H$ (0.32 g, 2.6 mmol) in MeCN (80 cm^3) was slowly added $NHex^n_4MnO_4$ (0.17 g, 0.36 mmol) in small portions to give a deep brown solution. To this was added a solution resulting from the combination of imidcarbH (0.10 g, 0.92 mmol) in MeCN (5 cm^3) and 0.2 M $NHex^n_4OH$ in MeOH (4.6 cm^3, 0.92 mmol). The resulting solution was stirred overnight, filtered through celite, reduced in volume to 40 cm^3, and Et_2O (100 cm^3) added dropwise with vigorous stirring. This led to the formation of a red–brown precipitate, which could be recrystallized from MeCN–Et_2O. The yield was 0.12 g (54%). Drying in vacuo leads to the unsolvated form. Elemental analysis. *Anal.* Found: C, 57.50; H, 5.57; N, 4.18. Calc. for $C_{81}H_{93}N_5O_{20}Mn_4$: C, 58.03; H, 5.59; N, 4.18. Selected IR data (cm^{-1}): 1680(s), 1610(s), 1572(s), 1508(w), 1490(w), 1464(w), 1448(m), 1375(s), 1344(sh), 1305(s), 1188(w), 1174(m), 1156(w), 1140(w), 1068(m), 1025(m), 1012(m), 936(w), 827(m), 780(w), 718(s), 688(m), 676(m), 654(s), 617(m), 563(w), 502(m), 468(m).

Table 1
Crystallographic data for complex **2**·5MeCN

Formula [a]	$C_{85}H_{96}Mn_4N_{10}O_{20}$
Formula weight	1797.50
Space group	$P\bar{1}$
Crystal system	triclinic
a (Å)	12.1886(3)
b (Å)	17.8130(5)
c (Å)	22.0268(5)
α (°)	68.1714(8)
β (°)	84.7029(8)
γ (°)	83.0696(7)
V (Å^3)	4401.2
Z	2
Temperature (°C)	−163
Crystal size (mm)	$0.60\times0.40\times0.40$
Radiation (Å) [b]	0.71073
ρ (g cm^{-3})	1.356
μ (cm^{-1})	6.344
Collected data (°)	$4.92\leq2\theta\leq54.57$
Total data	35889
Unique data	20163
R_{merge}	0.038
Observed data ($F>2\sigma(F)$)	10514
R (%) [c]	6.07
R_w (%) [d]	6.19

[a] Including solvate molecules.
[b] Graphite monochromator.
[c] $R=100\ \Sigma||F_o|-|F_c||/\Sigma|F_o|$.
[d] $R_w=100\ [\Sigma w(|F_o|-|F_c|)^2/\Sigma w|F_o|^2]^{1/2}$ where $w=1/\sigma^2(|F_o|)$.

2.2. X-ray crystallography

Data for complex **2** were collected on a Bruker platform goniometer equipped with a SMART 6000 CCD detector at −163°C; details of the diffractometry, low temperature facilities and computational procedures employed by the Molecular Structure Center are available elsewhere [11]. Data collection parameters are summarized in Table 1.

The initial survey of a limited portion of reciprocal space located a set of reflections with no symmetry or systematic absences. Solution and refinement of the structure confirmed the choice of the centrosymmetric space group $P\bar{1}$. The structure was solved using a combination of Patterson and direct methods (DIRDIF-96 [12]). Most of the atoms in the cation and anion were located from DIRDIF-96. The remaining atoms were located in successive iterations of least-squares refinement followed by generation of a difference Fourier map. In addition to the main anion of interest, the asymmetric unit contained a $NBu^n_4{}^+$ cation and five molecules of MeCN. Many of the hydrogen atoms were visible in a later difference Fourier map. On three of the solvent molecules, at least one hydrogen atom was located on the methyl carbon atom. Hydrogen atoms were then introduced in fixed calculated positions and assigned a thermal parameter of 1.0 plus the isotropic equivalent of the parent atom. In the final cycles of least-squares refinement the non-hydrogen atoms were refined using anisotropic thermal parameters, while the hydrogen atoms were fixed. The final difference map was essentially featureless, the largest peak was 1.42 e Å^{-3} located 1.05 Å from H(55) and 1.92 Å from C(93) (in the cation). The next largest peak was 0.98 e Å^{-3} also in the region of the cation, indicating a possible small disorder.

2.3. Other measurements

IR spectra (KBr pellet) were recorded on a Nicolet model 510P spectrometer. ^{1}H NMR spectra were recorded in CD_3CN at ~20°C with a 300 MHz Varian Gemini 2000 NMR spectrometer. Cyclic voltammetry employed a BAS CV-50W voltammetric analyzer and a standard three-electrode assembly (glassy-carbon work-

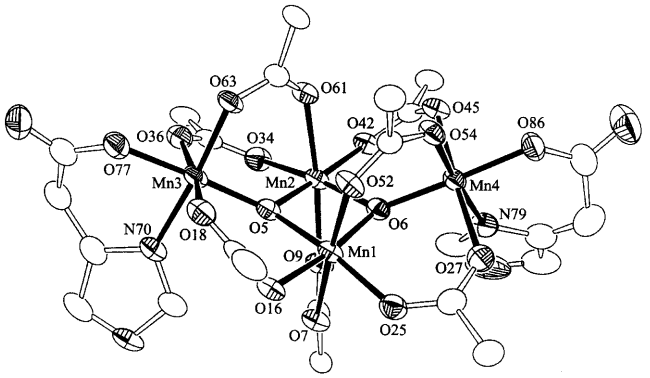


Fig. 1. ORTEP representation for the anion of complex **2** at the 50% probability level. For clarity, only the *ipso* carbon atom of each benzoate ring is included.

ing, Pt-wire auxiliary, $Ag–AgNO_3$ reference) with 0.1 M $NBu^n_4PF_6$ as supporting electrolyte. Potentials are quoted versus the ferrocene–ferrocenium couple under the same conditions. Elemental Analyses were performed by Atlantic Microlab Inc., Norcross, Georgia or in-house with a Perkin–Elmer Series II CHNS/O Analyzer 2000.

3. Results and discussion

3.1. Syntheses

In earlier reports we have described two procedures for the preparation of $[Mn^{III}_4O_2(O_2CR)_7(L)_2]^z$ complexes, where L is derived from 2,2′-bipyridine (bpy), picolinic acid (picH), 8-hydroxyquinoline (hqnH) and 2-(hydroxymethyl)pyridine (hmpH) [4–6] The first procedure involves treatment of trinuclear $[Mn_3O(O_2CR)_6(py)_3]^+$ complexes with salts of the chelating ligand L, or with the acid form of the ligand and an equivalent of base. The second procedure involves a comproportionation reaction between Mn^{II} and MnO^-_4 in the presence of RCO_2H and L. In the present study both procedures have allowed the synthesis of the analogous $imidac^-$ and $imidcarb^-$ complexes with R = Me and Ph. NBu^{n+}_4 salts of the $imidac^-$ species were isolated, while $NHex^{n+}_4$ salts of the $imidcarb^-$ species were preferred in order to obtain soluble materials. Thus, treatment of an MeCN solution of $[Mn_3O(O_2CMe)_6(py)_3]^+$ with NBu^n_4(imidac) or $NHex^n_4$(imidcarb) generated in situ afforded a brown solution from which $NBu^n_4[Mn_4O_2(O_2CMe)_7(imidac)_2]$ (**1**) or $NHex^n_4[Mn_4O_2(O_2CMe)_7(imidcarb)_2]$ (**3**) were obtained with minimal workup in good yield (47 and 50%, respectively). Employment of the second procedure, whereby a reaction mixture containing $Mn(O_2CR)_2$, NR'_4MnO_4 (R′ = Bu^n or Hex^n) and RCO_2H was similarly treated with NBu^n_4(imidac) or $NHex^n_4$(imidcarb) also resulted in brown solutions from which **1**, $NBu^n_4[Mn_4O_2(O_2CPh)_7(imidac)_2]$ (**2**), **3** and $NHex^n_4[Mn_4O_2(O_2CPh)_7(imidcarb)_2]$ (**4**) were obtained with minimal workup in good yield (55, 73, 47 and 54%, respectively). This reaction employed a 4:1 Mn^{II}:Mn^{VII} ratio, as required for preparation of a Mn^{III}_4 product (Eq. (1))

$$4Mn^{2+} + Mn^{7+} \rightarrow 5/4Mn^{3+}_4 \quad (1)$$

Compound **2** was structurally characterized, and all available characterization data for **1** are consistent with it having the same structure as **2**. Crystals of **3** and **4** suitable for X-ray crystallography could not be obtained; however, all of the characterization data are consistent with structures analogous to those of **1** and **2**.

3.2. Description of structure

An ORTEP representation of the anion of complex **2** is given in Fig. 1. Crystallographic data and selected bond distances and angles are listed in Tables 1 and 2, respectively.

Complex **2** crystallizes in the triclinic space group $P\bar{1}$. The asymmetric unit contains the complete anion, the NBu^{n+}_4 cation and five MeCN solvate molecules; the latter two will not be further discussed. The anion of **2** possesses a Mn_4O_2 core with the familiar 'butterfly' structure. Mn(1) and Mn(2) occupy the 'body' positions, while Mn(3) and Mn(4) occupy the 'wingtip' positions and O(5) and O(6) triply bridge each wing. The structure can be considered as two triangular Mn_3O units edge-shared through Mn(1) and Mn(2) with a dihedral angle of 142.2°. Unlike the planar core of the Mn_3O complexes, the μ_3-O atoms of the triangular units of the 'butterfly' structure lie slightly below the plane (Fig. 1). Two distinct Mn···Mn distances are observed, with the 'body' Mn(1)···Mn(2) separation of ca. 2.8 Å significantly shorter than the four 'body' to 'wingtip' separations of 3.3–3.4 Å. These separations are consistent with the presence of two and one bridging oxygen atoms, respectively [13]. Peripheral ligation is by seven bridging benzoate ligands and two $imidac^-$ ligands chelating the 'wingtip' Mn atoms. Each Mn atom is six-coordinate with axially elongated octahedral geometry typical of Jahn–Teller distorted high spin d^4 Mn^{III} ions. The axially elongated sites are all occupied by benzoate oxygen atoms, with both of the oxygen atoms of the unique benzoate ligand (bridging the 'body' Mn atoms) occupying JT elongated positions. The $imidac^-$ oxygen atoms are coordinated *trans* to the μ_3-O atoms at a distance of 1.9 Å, which is comparable to the other (non-JT elongated) Mn-benzoate bonds. The molecule has idealized C_2 point symmetry and, overall, the structure is extremely similar to those of the analogous bpy, pic^-, hqn^- and hmp^- complexes, with the cores of each species essentially superimposable

[4–6]. The structural differences between complex **2** and the previously reported 'butterfly' complexes arise in the vicinity of the chelating ligand. In particular, the imidac$^-$ species possesses a significantly non-planar six-membered chelate ring in contrast to the planar five-membered chelate rings of the bpy, pic$^-$, hqn$^-$ and hmp$^-$ species.

Table 2
Selected interatomic distances (Å) and angles (°) for complex **2**

Mn(1)···Mn(2)	2.816(1)	Mn(2)···Mn(3)	3.293(1)
Mn(1)···Mn(3)	3.446(1)	Mn(2)···Mn(4)	3.444(1)
Mn(1)···Mn(4)	3.319(1)		
Mn(1)–O(5)	1.915(3)	Mn(3)–O(5)	1.848(3)
Mn(1)–O(6)	1.872(3)	Mn(3)–O(18)	2.244(4)
Mn(1)–O(7)	2.156(3)	Mn(3)–O(36)	2.201(4)
Mn(1)–O(16)	1.958(3)	Mn(3)–O(63)	1.933(3)
Mn(1)–O(25)	1.981(3)	Mn(3)–O(77)	1.929(4)
Mn(1)–O(52)	2.175(3)	Mn(3)–N(70)	2.012(4)
Mn(2)–O(5)	1.869(3)	Mn(4)–O(6)	1.876(3)
Mn(2)–O(6)	1.898(3)	Mn(4)–O(27)	2.166(3)
Mn(2)–O(9)	2.240(3)	Mn(4)–O(45)	2.176(3)
Mn(2)–O(34)	1.971(4)	Mn(4)–O(54)	1.957(3)
Mn(2)–O(43)	1.942(3)	Mn(4)–O(86)	1.903(3)
Mn(2)–O(61)	2.205(3)	Mn(4)–N(79)	2.027(4)
Mn(1)–O(5)–Mn(2)	96.2(2)	Mn(1)–O(6)–Mn(4)	124.7(2)
Mn(1)–O(6)–Mn(2)	96.7(2)	Mn(2)–O(5)–Mn(3)	124.8(2)
Mn(1)–O(5)–Mn(3)	132.6(2)	Mn(2)–O(6)–Mn(4)	131.7(2)
O(5)–Mn(1)–O(6)	82.7(2)	O(5)–Mn(3)–O(18)	92.3(2)
O(5)–Mn(1)–O(7)	86.0(2)	O(5)–Mn(3)–O(36)	96.0(2)
O(5)–Mn(1)–O(16)	91.7(2)	O(5)–Mn(3)–O(63)	94.2(2)
O(5)–Mn(1)–O(25)	172.6(2)	O(5)–Mn(3)–O(77)	176.6(2)
O(5)–Mn(1)–O(52)	98.8(2)	O(5)–Mn(3)–N(70)	90.9(2)
O(6)–Mn(1)–O(7)	92.8(2)	O(18)–Mn(3)–O(36)	171.5(2)
O(6)–Mn(1)–O(16)	172.4(2)	O(18)–Mn(3)–O(63)	87.3(2)
O(6)–Mn(1)–O(25)	99.7(2)	O(18)–Mn(3)–O(77)	84.8(2)
O(6)–Mn(1)–O(52)	89.6(2)	O(18)–Mn(3)–N(70)	93.1(2)
O(7)–Mn(1)–O(16)	92.0(2)	O(36)–Mn(3)–O(63)	90.3(2)
O(7)–Mn(1)–O(25)	86.8(2)	O(36)–Mn(3)–O(77)	87.0(2)
O(7)–Mn(1)–O(52)	174.8(2)	O(36)–Mn(3)–N(70)	88.6(2)
O(16)–Mn(1)–O(25)	86.5(2)	O(63)–Mn(3)–O(77)	87.5(2)
O(16)–Mn(1)–O(52)	86.1(2)	O(63)–Mn(3)–N(70)	175.0(2)
O(25)–Mn(1)–O(52)	88.3(2)	O(77)–Mn(3)–N(70)	87.5(2)
O(5)–Mn(2)–O(6)	83.2(2)	O(6)–Mn(4)–O(27)	92.5(2)
O(5)–Mn(2)–O(9)	89.8(2)	O(6)–Mn(4)–O(45)	89.7(2)
O(5)–Mn(2)–O(34)	98.4(2)	O(6)–Mn(4)–O(54)	94.9(2)
O(5)–Mn(2)–O(43)	174.4(2)	O(6)–Mn(4)–O(86)	176.1(2)
O(5)–Mn(2)–O(61)	86.8(2)	O(6)–Mn(4)–N(79)	90.2(2)
O(6)–Mn(2)–O(9)	85.0(2)	O(27)–Mn(4)–O(45)	174.1(2)
O(6)–Mn(2)–O(34)	171.8(2)	O(27)–Mn(4)–O(54)	91.6(2)
O(6)–Mn(2)–O(43)	94.8(2)	O(27)–Mn(4)–O(86)	91.1(2)
O(6)–Mn(2)–O(61)	98.6(2)	O(27)–Mn(4)–N(79)	86.1(2)
O(9)–Mn(2)–O(34)	87.0(2)	O(45)–Mn(4)–O(54)	93.7(2)
O(9)–Mn(2)–O(43)	95.3(2)	O(45)–Mn(4)–O(86)	86.6(2)
O(9)–Mn(2)–O(61)	174.7(2)	O(45)–Mn(4)–N(79)	88.4(2)
O(34)–Mn(2)–O(43)	84.4(2)	O(54)–Mn(4)–O(86)	86.7(2)
O(34)–Mn(2)–O(61)	89.5(2)	O(54)–Mn(4)–N(79)	174.5(2)
O(43)–Mn(2)–O(61)	88.3(2)	O(86)–Mn(4)–N(79)	88.4(2)

3.3. ^1H NMR spectroscopy

The ^{1}H NMR spectra of complexes **1** and **2** in MeCN-d_3 are shown in Fig. 2 and the resonance positions are listed in Table 3 using the labeling scheme given in Fig. 2. Assignments were made on the basis of: (i) comparison with the spectrum of the O_2CMe-d_3 analog of **1** to distinguish between the resonances of the imidac$^-$ protons and those associated with the carboxylates; (ii) addition of D_2O to the NMR solution to assign the amine resonance of the imidac$^-$ ligand; (iii) T_1 measurements (inversion recovery method) correlated with the relative proton to metal centre distances to assign the remaining resonances associated with the imidac$^-$ protons; and (iv) comparison with the spectra of structurally analogous 'butterfly' complexes with other chelating ligands [5,6]. Both complexes display five resonances due to the protons of the imidac$^-$ ligand in addition to resonances due to the carboxylate protons.

For complex **1** four resonances due to the methyl protons of the four inequivalent acetate ligands are observed with an approximate intensity ratio of 2:2:2:1, indicating that the peak at 16.9 ppm (C′) can be assigned to the unique acetate bridging the 'body' Mn atoms Mn(1) and Mn(2). The resonance positions and T_1 values of these four resonances are similar to those observed for the pic$^-$ and hqn$^-$ 'butterfly' complexes and are consistent with idealized C_2 point symmetry, implying retention of the solid state structure in solution. A more complex spectrum is evident for **2** due to the presence of four inequivalent benzoate ligands. Assignment of the resonances as due to *ortho*, *meta* or *para* protons may be broadly made on the basis of the relative chemical shifts and T_1 values [14], although it is not possible to ascertain which peaks correspond to the unique benzoate ligand bridging the 'body' Mn atoms. Nevertheless, the pattern of benzoate resonances is again similar to that observed for other benzoate 'butterfly' complexes.

Five resonances of approximately equal intensity are observed for the protons of the imidac$^-$ ligands for both complexes **1** and **2**. For complex **1** the most downfield imidac$^-$ resonance at ca. 26.3 ppm is obscured by a resonance due to the protons of the unique acetate ligand and is only evident in the spectrum of the O_2CMe-d_3 analogue. Addition of a small amount of D_2O to the NMR solutions of **1** and **2** leads to the immediate disappearance of the resonances at -2.5 and -4.3 ppm, respectively. This is attributed to exchange broadening and allows assignment of these resonances to the amine proton of the imidac$^-$ ligand, H_B. Assignment of the remaining resonances relies predominantly on the correlation between the line widths, measured T_1 values and the proton to 'wingtip' metal centre [Mn(3) and Mn(4)] separations derived from the crystal

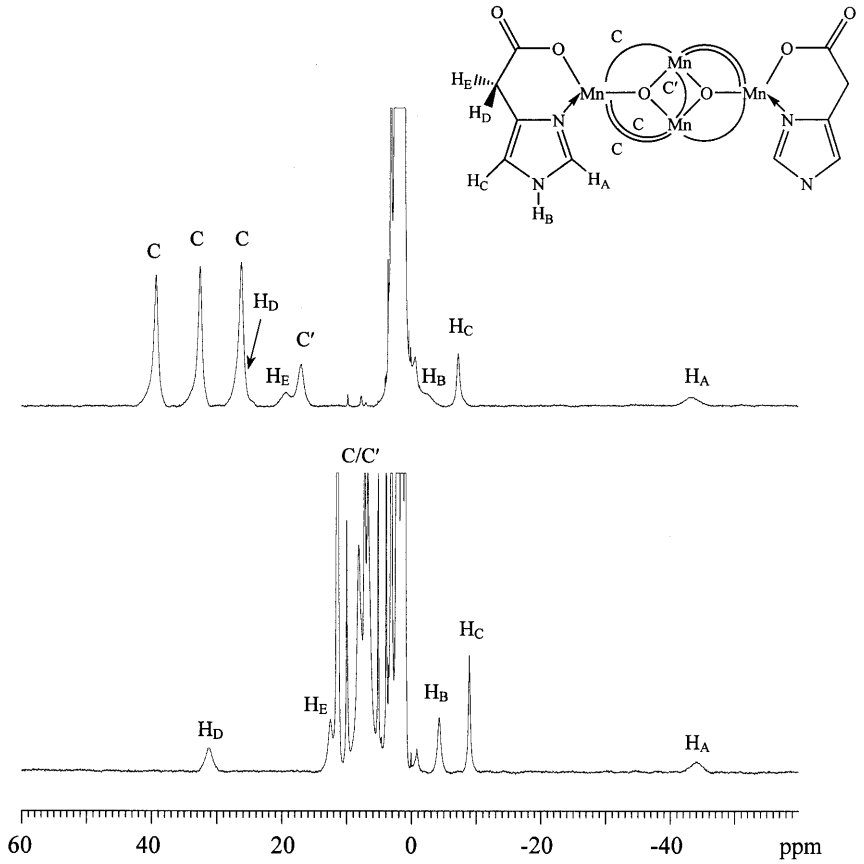


Fig. 2. Proton NMR spectra of complexes **1** (top) and **2** (bottom) in MeCN-d_3. The peaks are labeled according to the scheme shown as an inset. The band of resonances in the -1 to 5 ppm region is from the NBu_4^{n+} protons, residual protio solvent and adventitious water.

Table 3
Proton NMR data for complexes **1** and **2** in MeCN-d_3 at $T \sim 20$°C

Complex **1**		Complex **2**		Assignment [a]
δ (ppm)	T_1 (ms) [b]	δ (ppm)	T_1 (ms) [b]	
39.2	2.2			C (A)
32.4	2.4			C (A)
26.3 [c]	0.9 [c]	31.2	0.8	H_D
26.1	2.0			C (A)
19.3	1.3	12.5	2.2	H_E
16.9	2.2			C (A′) [d]
		11.5	17.3	C (*m*-B)
		11.3	16.1	C (*m*-B)
		10.0	12.2	C (*m*-B)
		8.1	2.5	C (*o*-B)
		7.2	9.2	C (*o*-B)
		6.6	5.2	C (*o*-B)
		5.1	32.1	C (*p*-B)
		3.9	31.2	C (*p*-B)
−2.5	[e]	−4.3	4.0	H_B
−7.3	3.3	−8.9	4.9	H_C
−42.9	0.5	−44.2	0.5	H_A

[a] Numbering of imidac$^-$ protons as in Fig. 2.
[b] Inversion recovery method.
[c] Determined from (O_2CMe-d_3) analog of **1**.
[d] Unique acetate bridging Mn(1) and Mn(2).
[e] Could not be determined.

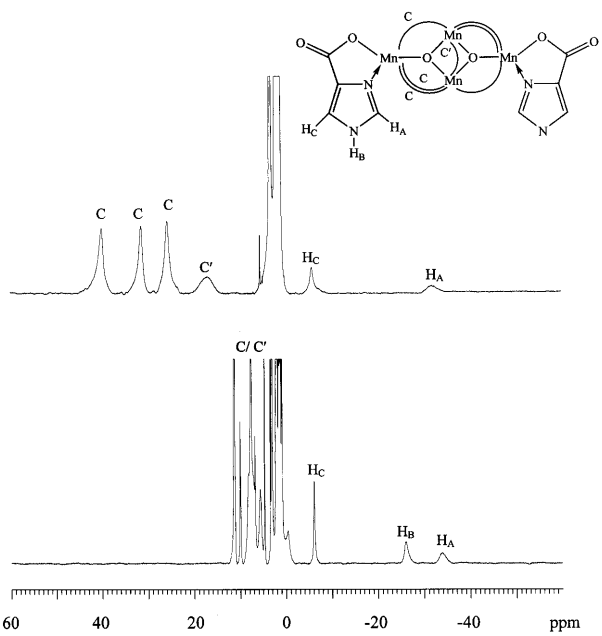


Fig. 3. Proton NMR spectra of complexes **3** (top) and **4** (bottom) in MeCN-d_3. The peaks are labeled according to the scheme shown as an inset. The band of resonances in the -1 to 5 ppm region is from the $NHex_4^{n+1}$ protons, residual protio solvent and adventitious water.

Table 4
Proton NMR data for complexes **3** and **4** in MeCN-d_3 at $T \sim 20$°C

Complex **3**		Complex **4**		Assignment [a]
δ (ppm)	T_1 (ms) [b]	δ (ppm)	T_1 (ms) [b]	
39.9	2.4			C (A)
31.3	2.4			C (A)
25.6	2.3			C (A)
16.8	2.4			C (A′) [c]
		11.3	19.0	C (*m*-B)
		11.2	18.1	C (*m*-B)
		10.0	13.8	C (*m*-B)
		8.2	[d]	C (*o*-B)
		7.6	8.9	C (*o*-B)
		6.8	12.8	C (*o*-B)
		5.7	2.4	C (*o*-B)
		4.7	36.2	C (*p*-B)
		3.4	32.5	C (*p*-B)
−5.8	2.6	−6.1	4.5	H_C
[d]	[d]	−25.8	[d]	H_B
−32.0	0.3	−33.9	0.6	H_A

[a] Numbering of imidcarb$^-$ protons as in Fig. 3.
[b] Inversion recovery method.
[c] Unique acetate bridging Mn(1) and Mn(2).
[d] Could not be determined.

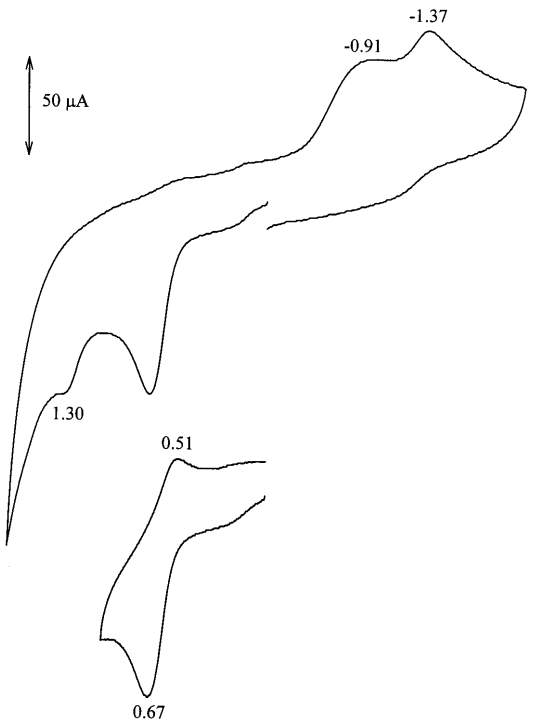


Fig. 4. Cyclic voltammogram (1 mM, 100 mV s^{-1}) for complex **2** in MeCN (0.1 M $NBu^n_4PF_6$). The potentials (V) are quoted versus ferrocene–ferrocenium.

structure of **2**. This is on the basis of previous studies that have concluded that the major contibution to the line widths in Mn^{III} complexes is dipolar broadening, which is proportional to r^{-6} [15–18]. The broadest resonance, with the smallest T_1 value, at ca. −40 ppm is assigned to the proton closest to the wingtip Mn atoms, H_A. The significant upfield chemical shift of this resonance is consistent with those observed for the proton at the position adjacent to the Mn-coordinated N atoms in the pic$^-$ and hqn$^-$ 'butterfly' compounds. The sharpest resonance with the largest T_1 value is assigned to the proton most distant from the Mn centre, H_C. Protons H_D and H_E are diastereotopic with H_D significantly closer to the Mn atom (ca. 3.5 versus 4.2 Å), and are assigned accordingly. The marked chemical shift difference between the resonances of these protons indicates the significant contribution of a dipolar mechanism to the observed isotropic shifts. The chemical shifts of resonances H_A, H_B and H_C are relatively consistent between complexes **1** and **2**, with less than 2 ppm difference observed in each case. However, slightly larger chemical shift differences of ca. 5 and 7 ppm are observed for H_D and H_E, respectively. The reason for this is unclear in the absence of a crystal structure of complex **1**.

The ^{1}H NMR spectra of complexes **3** and **4** in MeCN-d_3 are shown in Fig. 3 and the resonance positions are listed in Table 4 using the labeling scheme given in Fig. 3. Assignments were made analogously to those for **1** and **2**. The pattern of resonances due to the carboxylate protons of **3** and **4** are very similar to those observed for **1** and **2**. Three resonances due to the imidcarb$^-$ protons are observed for **4** while only two are evident for **3**. The one missing is that due to H_B, which is presumably because of exchange with adventitious water. The resonances due to H_A and H_C display very similar isotropic shifts to the equivalent resonances in **1** and **2**, while the resonance due to H_B is shifted by ca. 20 ppm, presumably due to exchange effects.

3.4. Electrochemistry

The cyclic voltammograms (CVs) of complexes **1** and **2** (1 mM) have been recorded in MeCN solution (0.1 M $NBu^n_4PF_6$) (Fig. 4). Similar results are observed for both complexes and the CV of **2** is shown in Fig. 3. Both complexes display a quasi-reversible one-electron oxidation at 0.58 and 0.59 V versus ferrocene for **1** and **2**, respectively. The peak separations at a scan rate of 100 mV s^{-1} are 187 and 154 mV, respectively, compared with that for the ferrocene–ferrocenium couple of 116 mV under the same conditions. Plots of i_p versus $v^{1/2}$ are linear in the scan rate (v) range of 10–500 mV s^{-1}, indicating a diffusion-controlled process. Both complexes also display an irreversible oxidation at peak potentials of 1.35 and 1.30 V, respectively at a scan rate of 100 mV s^{-1}. In addition two irreversible reductions are observed at peak potentials of −0.94 and −1.37 for **1** and −0.91 and −1.37 V for **2**.

The quasi-reversible oxidation at 0.59 V for **2** in MeCN is assigned to oxidation to the $Mn^{III}_3Mn^{IV}$ level

as shown in Eq. (2). The oxidation potential can be compared with the

$$[Mn_4O_2(O_2CPh)_7(imidac)_2]^- \overset{0.59\ V}{\rightleftharpoons} [Mn_4O_2(O_2CPh)_7(imidac)_2]^0 \quad (2)$$

value of 0.69 V found for the corresponding couple in $[Mn_4O_2(O_2CPh)_7(pic)_2]^-$ under the same conditions. This is consistent with the greater acidity of picH (pK_a of 5.25 [19]) versus imidacH (pK_a measured as ca. 7.0), as the more electron-donating $imidac^-$ is better able to stabilize higher oxidation states of Mn than pic^-.

Well-defined cyclic voltammograms of complexes **3** and **4** could not be obtained due to their relative insolubility in MeCN in the presence of 0.1 M $NBu^n_4PF_6$ as support electrolyte. However, poorly resolved oxidation processes with peak potentials of ca. 0.60 and 1.2 V and reduction processes at ca. −1.2 and −1.6 V were evident for **4** under these conditions.

The presence of apparently accessible oxidation processes for complexes **1** and **2** suggested the possibility of oxidation of these complexes. Indeed, oxidation of other 'butterfly' complexes has resulted in the formation of new species [20]. An investigation of similar reactivity for **1** and **2** is in progress, with preliminary studies involving electrochemical oxidation of these species resulting in insoluble red–brown solids. Further efforts are required to fully characterize these materials, although their IR spectra do not display bands associated with $NBu^n_4{}^+$, implying that they are uncharged.

4. Conclusions

Tetranuclear Mn clusters possessing imidazole-carboxylate based chelating ligands have been synthesized and found to be essentially isostructural with those possessing pyridine-based chelating ligands. ^{1}H NMR spectroscopy indicates that the species retain their structure in solution and the resonances can be assigned using the methods described in the text. An investigation of the electrochemistry of the species reveals a quasi-reversible oxidation process, similar to those observed for the analogous compounds possessing pyridine-based chelating ligands.

5. Supplementary data

Supplementary structural data for compound **2** have been deposited with the Cambridge Crystallographic Data Centre, CCDC No. 141954. Copies of this information may be obtained free of charge from The Director, CCDC, 12 Union Road, Cambridge, CB2 1EZ, UK (fax: +44-1223-336033; e-mail: deposit@ccdc.ac.uk or www: http://www.ccdc.cam.ac.uk).

Acknowledgements

This work was funded by NIH grant GM 39083.

References

[1] G. Aromi, S.M.J. Aubin, M.A. Bolcar, G. Christou, H.J. Eppley, K. Folting, D.N. Hendrickson, J.C. Huffman, R.C. Squire, H.L. Tsai, S. Wang, M.W. Wemple, Polyhedron 17 (1998) 3005 and references cited therein.
[2] V.K. Yachandra, K. Sauer, M.P. Klein, Chem. Rev. 96 (1996) 2927.
[3] J.R. Debus, Biochim. Biophys. Acta 1102 (1992) 269.
[4] J.B. Vincent, C. Christmas, H.R. Chang, Q. Li, P.D.W. Boyd, J.C. Huffman, D.N. Hendrickson, G. Christou, J. Am. Chem. Soc. 111 (1989) 2086.
[5] E. Libby, J.K. McCusker, E.A. Schmitt, K. Folting, D.N. Hendrickson, G. Christou, Inorg. Chem. 30 (1991) 3486.
[6] E. Bouwman, M.A. Bolcar, E. Libby, J.C. Huffman, K. Folting, G. Christou, Inorg. Chem. 31 (1992) 5185.
[7] X.-S. Tang, B.A. Diner, B.S. Larsen, M.L. Gilchrist, G.A. Lorigan, R.D. Britt, Proc. Nat. Acad. Sci. USA 91 (1994) 704.
[8] J.B. Vincent, H.R. Chang, K. Folting, J.C. Huffman, G. Christou, D.N. Hendrickson, J. Am. Chem. Soc. 109 (1987) 5703.
[9] J.B. Vincent, K. Folting, J.C. Huffman, G. Christou, Inorg. Chem. 25 (1986) 996.
[10] T.J. Giovanellio, J. Pecci, Clin. Chim. Acta 67 (1976) 7.
[11] M.H. Chisholm, K. Folting, J.C. Huffman, C.C. Kirkpatrick, Inorg. Chem. 23 (1984) 1021.
[12] P.T. Beurskins, G. Beurskins, W.P. Bosman, R. de Gelder, S. Garcia Granda, R.O. Gould, R. Israel, J.M.M. Smits, DIRDIF-96, A Computer Program System for Crystal Structure Determination by Patterson Methods and Direct Methods applied to Difference Structure Factors, University of Nijmegen, The Netherlands (1996).
[13] G. Christou, J.B. Vincent, in: L. Que (Ed.), ACS Symposium Series 372, American Chemical Society, Washington DC, 1988, p. 238 (Chapter 12).
[14] M.M. Glass, K. Belmore, J.B. Vincent, Polyhedron 12 (1993) 133.
[15] P. Addy, D.F. Evans, Q. De Souza, Polyhedron 6 (1987) 2003.
[16] D.R. Eaton, J. Am. Chem. Soc. 87 (1965) 3097.
[17] G.N. La Mar, F.A. Walker, J. Am. Chem. Soc. 95 (1973) 6950.
[18] G.N. La Mar, W.DeW. Horrocks, R.H. Holm (Eds.), NMR of Paramagnetic Molecules, Academic Press, New York, 1973.
[19] E.P. Sergeant, B. Dempsey, Ionisation Constants of Organic Acids in Aqueous Solution, Pergamon, Oxford, 1979.
[20] S. Wang, H.L. Tsai, K.S. Hagen, D.N. Hendrickson, G. Christou, J. Am. Chem. Soc. 116 (1994) 8376.

PERGAMON

www.elsevier.nl/locate/poly

Polyhedron 19 (2000) 2119–2125

POLYHEDRON

Complexes of heteroscorpionate trispyrazolylborate anionic ligands Part I. The crystal structure and reactivity of thiocyanato[hydrobis(3-phenylpyrazolyl)(3-*tert*-butylpyrazolyl)-borato]cobalt(II) complex

Marta Łukasiewicz [a], Zbigniew Ciunik [a], Stanisław Wołowiec [a,b,*]

[a] *Department of Chemistry, University of Wrocław, 14 Joliot-Curie Strasse, 50-383 Wrocław, Poland*
[b] *Department of Chemistry, Rzeszów Technological University, 6 Powstańców Warszawy Avenue, 35-959 Rzeszów, Poland*

Received 3 April 2000; accepted 11 July 2000

Abstract

The high-spin cobalt(II) complexes with homoscorpionate hydrotris(3-phenylpyrazolyl)borate (Tp^{Ph}) and heteroscorpionate hydrobis(3-phenylpyrazolyl)(3-*tert*-butylpyrazolyl)borate {$HB(3\text{-}Phpz)_2(3\text{-}t\text{-}Bupz)$} anionic ligands (Tp′) of the general formula Tp′Co(X) were studied. The former tripodal ligand provides intermediate steric hindrance for the central metal ion, which is able to adopt two additional donors from thiocyanate and neutral ligands like pyrazole (pzH) and methanol, or two oxygen donors from the lactate anion. Replacement of one of three 3-phenyl substituents in Tp^{Ph} by the *tert*-butyl one produces a ligand of high steric hindrance which gave tetracoordinate Tp′Co(X) complexes, where X = thiocyanate or monodentate lactate. The complexes were studied by the ^1H NMR spectroscopic method in solution and two of them, $Tp^{Ph}Co(NCS)(pzH)$ and $[HB(3\text{-}Phpz)_2(3\text{-}t\text{-}Bupz)]Co(NCS)$, were characterized structurally by X-ray crystallography. © 2000 Elsevier Science B.V. All rights reserved.

Keywords: Heteroscorpionate tris(3-*R*-pyrazolyl)borate cobalt(II) complexes; Structures; NMR

1. Introduction

Since Trofimenko's first report on the synthesis of transition metal ion complexes of tris(pyrazolyl)borate anions (Tp), they have been widely used as convenient tripodal ligands mimicking the three nitrogen donor arrangment of histidine residues in metalloenzymes [1,2]. However, in metalloenzymes the *cis*- arranged nitrogen donors are chemically different and thus form the chiral surrounding of the metal centre. Until now homoscorpionate Tp′ ligands were studied almost exclusively containing all the pyrazole residues (pz) modified by introducing variable size substituents into the 3, 4, and/or 5 position of pz [2a,3–13]. The syntheses of the first heteroscorpionate Tp′ ligand and its thallium(I) complex were briefly reported quite recently by Parkin [14]. The synthesis of chiral tris(pyrazolyl)borate anionic ligands, with three different pyrazoles remains a long-standing challenge. The promising catalytic properties of transitions metal ion complexes with homoscorpionate ligands prompted us to study mixed-pyrazole Tp′ ligands with variable steric hindrance placed at the 3- and 5-position of pyrazole to finally construct chiral Tp′ ligands with desirable steric and electronic anisotropy. Its complexes are expected to induce asymmetry in some catalytic reactions. The reported precedence is the successful attempt of enantioselective cyclopropanation of styrene by ethyldiazoacetate, catalyzed by the $Tp^{pm}Cu(I)$ complex, containing chiral substituents fused with 3,4-pz positions [15]. On our way to a chiral Tp′ ligand we have chosen 3-phenylpyrazole as a relatively chemically inert intermediate sterically hindered structural element and prepared mixed-pyrazole Tp′ ligands with 3-*tert*-butylpyrazole and 3,5-di-*tert*-butylpyrazole. Here we present the structural studies on high-spin Tp′Co(X)

* Corresponding author. Tel.: +48-17-865-1657; fax: +48-17-854-3655.

E-mail address: sw@prz.rzeszow.pl (S. Wołowiec).

0277-5387/00/$ - see front matter © 2000 Elsevier Science B.V. All rights reserved.
PII: S0277-5387(00)00512-X

complexes (where $X = [NCS]^-$ and lactate $[OOC\text{-}CH(OH)CH_3]^-$) by single-crystal X-ray crystallography and ^1H NMR spectroscopy (in solution).

2. Experimental

2.1. Methods

^1H NMR spectra were obtained with a Bruker AMX300 spectrometer operating in the quadrature mode at 300 MHz. The residual peaks of deuterated solvents were used as internal standards. The magnetic moments of complexes were measured in solution according to the modified Evan's method [16]. The FTIR spectra were recorded on a Perkin–Elmer 1725X instrument. The UV–Vis experiments were performed using a HP 8453 diode-array and a Beckman DU 640 spectrophotometer. Mass spectra were obtained using a Finnigan MAT TSQ 700 spectrometer by the ESI method at 4.5 kV ionization potential and 250°C capillary temperature in acetonitrile and tetrahydrofuran solvents. Crystal data were collected for **1** and **3·pzH** on a Kuma KM4CCD area detector single-crystal X-ray diffractometer with ω scans. Data reduction and structure solutions were carried out with KM4CCD and SHELXS-97 software packages, respectively. Least-square refinements were performed with SHELXL-97. The crystal data of both crystals are given in Table 1, together with refinement details.

Table 1
Crystal data and structure refinement

Empirical formula	$C_{26}H_{26}BN_7SCo$	$C_{31}H_{25}BN_9SCo$
Formula weight	538.34	625.40
T/K	120(1)	293(2)
λ/Å	0.71073	0.71073
Crystal system	orthorhombic	monoclinic
Space group	*Pnma*	$P2_1/n$
Unit cell dimensions		
a (Å)	18.154(4)	11.800(2)
b (Å)	15.181(3)	14.347(3)
c (Å)	9.099(2)	18.701(4)
β (°)		100.06(3)
V (Å^3)	2507.6(9)	3117.3(11)
Z	4	4
D_{calc} (Mg m^{-3})	1.426	1.333
μ (mm^{-1})	0.798	0.654
F(000)	1116	1288
Crystal size (mm)	$0.10 \times 0.10 \times 0.10$	$0.15 \times 0.10 \times 0.10$
Diffractometer	Kuma KM4CCD	Kuma KM4CCD
θ Range for data collection (°)	2.84–25.00	2.63–20.00
Range h,k,l	$-18 \le h \le 21$, $-18 \le k \le 16$, $-10 \le l \le 10$	$-11 \le h \le 10$, $-13 \le k \le 13$, $-13 \le l \le 17$
Reflections collected	13 595	10 686
Independent reflections/R_{int}	2289/0.0773	2901/0.0614
Data/parameters	2289/181	2901/389
Weighting scheme: a, b, c [a]	0.0833, 3.94, 3	0.0385, 5.93, 3
Goodness-of-fit (F^2)	1.126	1.258
Final R_1/wR_2 indices ($I > 2\sigma_I$)	0.0609/0.1556	0.0694/0.1336
Extinction coefficient		0.0005(4)
Largest difference peak/hole (e Å^{-3})	0.804/−0.429	0.310/−0.248

[a] $w = 1/[\sigma^2(F_o^2) + (a \times P)^2 + b \times P]$ where $P = [\mathrm{Max}(F_o^2, 0) + 2 \times F_c^2]/c$.

2.2. Synthesis of Tp′ ligands and Tp′Co(NCS) complexes

2.2.1. General procedure

All potassium salts of homo- and heteroscorpionate Tp′ ligands were prepared by condensation of KBH_4 with melted pyrazoles and the progress of the reaction was controlled by measurement of hydrogen gas evolved. The KTp′ salts were purified by washing out the excess pyrazoles with appropriate solvents and drying in high vacuum. In case of mixed-pyrazole salts, the stepwise condensation method was applied, the ligands were converted straightforwardly into Tp′Co(NCS) salts by dropwise addition of a tetrahydrofuran (THF) solution of KTp′ into the vigorously stirred aqueous solution of 0.1 M cobalt(II) thiocyanate and 1.0 M potassium thiocyanate. The blue solid complexes were extracted with methylene dichloride solvent, the organic layer was washed twice with water, the solvent was removed on a rotary evaporator and the solid residue was recrystallized from a THF–hexane mixture to give the crystalline material. Details on synthesis and isolation procedures are given below. Potassium hydrotris(3-phenylpyrazolyl)borate (KTp^{Ph}) was prepared by a known method [3] on a scale of 0.01 mol. The $Tp^{Ph}Co(NCS)$ complex was prepared according to the general procedure.

2.2.2. Thiocyanato[hydrobis(3-phenylpyrazolyl)-(3-tert-butylpyrazolyl)borato]cobalt(II) (1)

Potassium hydrobis(3-phenylpyrazolyl)(3-*tert*-butylpyrazolyl)borate $K[HB(3\text{-}Phpz)_2(3\text{-}t\text{-}Bupz)]$ was synthesized by the two-step condensation of 0.908 g KBH_4 (0.015 mol) with 4.32 g 3(5)-*tert*-butylpyrazole (0.03 mol) and 2.79 g 3(5)-phenylpyrazole (0.0255 mol). The excess of pyrazoles was washed out with 150 cm^3 hot hexane and 50 cm^3 pentane. 3.8 g of HTp′ salts were isolated (55% yield). The mixture of Tp′Co(NCS) complexes was obtained by addition of 0.5 g of KTp′ salts in 15 cm^3 THF into a 100 cm^3 stock solution of cobalt(II) thiocyanate. The Tp′Co(NCS) products were

isolated by a general procedure. The [HB(3-Phpz)$_2$(3-*t*-Bupz)]Co(NCS) (**1**) and [HB(3-*t*-Bupz)$_2$(3-Phpz)]Co(NCS) (**2**) complexes were separated from [HB(3-Phpz)$_3$]Co(NCS) (**3**) by repeatable crystallization from a THF–hexane mixture; the first crop gave pure crystals of violet blue **3**·(THF) [3], whereas the second crop of collected blue crystals contained **1** and **2**. The complexes **1** and **2** were separated by selectively dissolving **2** in methanol. The yields were: 51.86% **1** (1.21 g), 19.50% **3** (0.472 g), 3.25% **2**; total yield 74.6%. Using both procedures we were able to get pure blue crystals of **1**, which were grown from THF–hexane and subsequently subjected to X-ray analysis.

Elemental analysis calculated for $C_{26}H_{26}N_7BSCo$ (M.W. 538.34) C, 58.00; H, 4.87; N, 18.21. Found: C, 58.32; H, 5.01; N, 18.32%. Mass spectrum (ESI) *m*/*e*: [**1** + H$^+$] 539 (44%); [**1**–NCS]$^+$ 480 (100%). IR (KBr): $\nu_{(NCS)}$ 2065; $\nu_{(BH)}$ 2495 cm^{-1}. UV–Vis: λ [nm] (ε [mol^{-1} dm^3 cm^{-1}]): 337 (3.26×10^3), 641 (1.01×10^3). Magnetic moment (Evans's method) $\mu = 4.40$ B.M. (in $CDCl_3$ at 296 K). ^{1}H NMR ($CDCl_3$, 293 K): δ [ppm] (intensity, assignment): −6.90 (1H, B–H); 3.02 (9H, $C(CH_3)_3$); 8.98 (4H, *m*-H(3-Phpz)); 9.69 (2H, *p*-H(3-Phpz)); 19.10 (4H, *o*-H(3-Phpz)); 36.52 (2H, 5-H(3-Phpz)); 45.32 (1H, 5-H(3-*t*-Bupz)); 70.13 (2H, 4-H(3-Phpz)); 77.61 (1H, 4-H(3-*t*-Bupz)).

2.2.3. Thiocyanato[hydrobis(3-tert-butylpyrazolyl)-(3-phenylpyrazolyl)borato]cobalt(II) (2)

Potassium hydrobis(3-*tert*-butylpyrazolyl)(3-phenylpyrazolyl)borate K[HB(3-*t*-Bupz)$_2$ (3-Phpz)] was synthesized by similar procedure as above. The optimized conditions to obtain the desired Tp′ ligand required 0.6 equivalents of 3-phenylpyrazole and 2.5 equivalents of 3-*tert*-butylpyrazole. The isolated Tp′Co(NCS) complexes yielded 70% of Tp-*t*-BuCo(NCS) (**4**) and 30% of **2**.

^{1}H NMR ($CDCl_3$, 293 K) δ [ppm] (intensity, assignment): −7.00 (1H, B–H), 4.10 (18H, $C(CH_3)_3$), 9.01 (2H, *m*-H(3-Phpz)), 10.44 (1H, *p*-H(3-Phpz)), 21.60 (2H, *o*-H(3-Phpz)), 31.47 (1H, 5-H(3-Phpz)), 42.01 (2H, 5-H(3-*t*-Bupz)), 67.71 (1H, 4-H(3-Phpz)), 76.35 (2H, 4-H(3-*t*-Bupz)).

2.2.4. Thiocyanato[hydrotris(3-phenylpyrazolyl)borato]-cobalt(II) pyrazole (3·pzH)

This complex was obtained as a side-product during the synthesis of the mixed-pyrazole heteroscorpionate Tp′ ligand containing 3-phenylpyrazole and pyrazole according to general procedure. Pure crystals of **3** were grown from THF–hexane solvents, containing pyrazole. The results on cobalt(II) and thallium(I) complexes of [hydrobis(3-phenylpyrazolyl)(pyrazolyl)]$^-$ ligand will be presented separately.

Elemental analysis calculated for $C_{31}H_{26}N_9BSCo$ (M.W. 626.42): C, 59.44; H, 4.18; N, 20.12. Found: C, 59.39; H, 4.01; N, 20.20%. IR (KBr): $\nu_{(NCS)}$ 2077; $\nu_{(BH)}$ 2502 cm^{-1}. UV–Vis λ [nm] (ε [mol^{-1} dm^3 cm^{-1}]): 640 ($7.89 \cdot 10^2$) for **3**.

2.2.5. [Hydrotris(3-phenylpyrazolyl)borato]-cobalt(II)lactate (5)

The complex was obtained on a 0.005 mol scale according to the general procedure modified by the use of 0.1 M cobalt(II) lactate and 0.5 M sodium lactate instead of the thiocyanate salts as for **3**.

Elemental analysis calculated for $C_{29}H_{27}N_6O_3BCo$ (M.W. 577.32) C, 60.33; H, 4.71; N, 14.56. Found: C, 60.22; H, 4.60; N, 14.42%. ^{1}H NMR (in $CDCl_3$) δ [ppm] (intensity, assignment): −51.67 (6H, *o*-H(3-Phpz)), 2.94 (6H, *m*-H(3-Phpz)), 4.50 (3H, *p*-H(3-Phpz)), 51.07 (3H, CH_3(lactate)), 52.78 (3H, 4-H(3-Phpz)), 62.70 (3H, 5-H(3-Phpz)), 77.02 (1H, CH(lactate)), 90.76 (1H, B–H).

3. Results and discussion

3.1. Synthetic procedures

The synthesis of mixed-pyrazole Tp′ anionic ligands (heteroscorpionates) requires condensation of borohydride with an optimized equivalent number of substituted pyrazoles. The reaction can be performed in one step using appropriate amounts of pyrazole equivalents or in multistep approach used here. The reaction in melted mixtures is controlled by measurements of hydrogen gas evolved. The temperature of every step of stepwise condensation depends on: (i) number of the step; (ii) the steric and electronic properties of the R substituent at the 3, 4, and/or 5 position of the pyrazole used in the condensation; and (iii) the chemical structure of the $[(R\text{–}pz)_nBH_{(4-n)}]^-$ anion used in a given step of the reaction.

$$[BH_4]^- + (R_1\text{–}pzH) \rightarrow [(R_1\text{–}pz)BH_3]^- + H_2 \quad (1)$$

$$[(R_1\text{–}pz)BH_3]^- + (R_2\text{–}pzH) \rightarrow [(R_1\text{–}pz)(R_2\text{–}pz)BH_2]^- + H_2 \quad (2)$$

$$[(R_1\text{–}pz)(R_2\text{–}pz)BH_2]^- + (R_3\text{–}pzH) \rightarrow [(R_1\text{–}pz)(R_2\text{–}pz)(R_3\text{–}pz)BH]^- + H_2 \quad (3)$$

Thus, the optimization of synthesis of $[(R_1\text{–}pz)(R_2\text{–}pz)(R_3\text{–}pz)BH]^-$ chiral ligand requires many attempts to be done in order to drive the reaction towards the desired product with reasonable yield. We have undertaken the systematic studies on the synthesis of mixed-pyrazole Tp′ ligands. As a fixed structural element of these ligands we have chosen 3-phenylpyrazole, the substituent is of intermediate steric hindrance

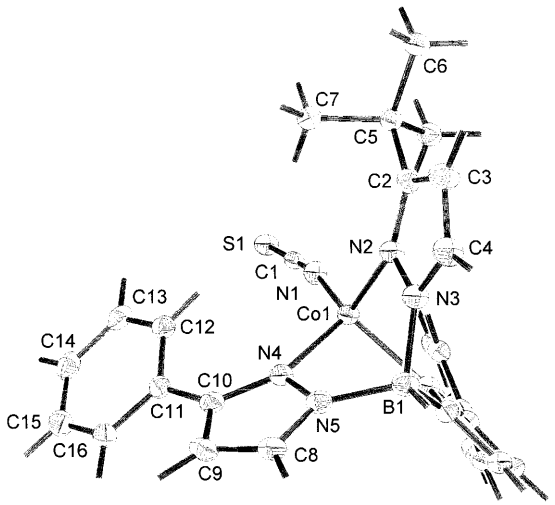


Fig. 1. ORTEP diagram for **1**. Thermal ellipsoids are drawn at the 30% probability level. Selected bond lengths (Å) and angles (°): Co(1)–N(1), 1.907(5); Co(1)–N(2), 2.023(5); Co(1)–N(4), 2.024(3); N(1)–Co(1)–N(2), 120.1(2); N(1)–Co(1)–N(4), 121.3(2); N(2)–Co(1)–N(4), 96.2(2); N(1)–Co(1)–N(4′), 121.3(2); N(2)–Co(1)–N(4′), 96.2(2); N(4)–Co(1)–N(4′), 95.4(2); where (′) denotes equivalent atoms generated by a symmetry mirror plane.

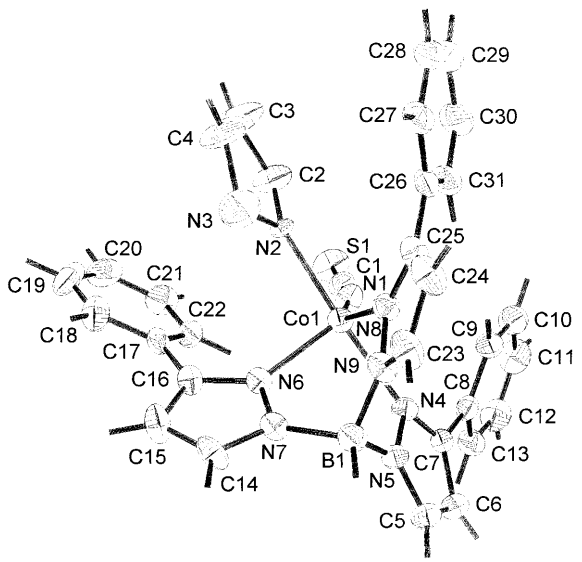


Fig. 2. ORTEP diagram for **3·pzH**. Thermal ellipsoids are drawn at the 30% probability level. Selected bond lengths (Å) and angles (°): Co(1)–N(1), 1.941(6); Co(1)–N(8), 2.064(5); Co(1)–N(6), 2.081(5); Co(1)–N(2), 2.160(4); Co(1)–N(4), 2.181(5); N(1)–Co(1)–N(8), 144.4(2); N(1)–Co(1)–N(6), 120.8(2); N(8)–Co(1)–N(6), 94.8(2); N(1)–Co(1)–N(2), 89.5(2); N(8)–Co(1)–N(2), 90.5(2); N(6)–Co(1)–N(2), 91.6(2); N(1)–Co(1)–N(4), 94.4(2); N(8)–Co(1)–N(4), 4.0(2); N(6)–Co(1)–N(4), 90.0(2); N(2)–Co(1)–N(4), 174.4(2).

and is relatively chemically inert in comparison with 3-isopropylpyrazole with similar steric hindrance [2a]. In order to construct the Tp′ ligand of rather high steric demands we have introduced the *tert*-butyl-substituents into the 3- and 5- positions of the third pyrazole instead of the 3-phenyl and synthesized the mixed-pyrazole Tp′ ligand and its high-spin Tp′Co(NCS) complexes. Obviously, the sequence (1–3) of condensations resulted in the formation of a statistic mixture of Tp′ ligands, whenever two or more R–pzH were used. These were converted into Tp′Co(NCS) complexes and separated as such. This approach allowed us first to identify the Tp′ products formed in synthetic step by ^{1}H NMR spectral measurements of paramagnetic Tp′Co(NCS) complexes, and second to isolate and characterize structurally individual Tp′Co(NCS) species. Gathering those data are necessary steps to design and synthesize a chiral Tp′ ligand. Thus, we have found that introducing two pyrazoles of intermediate steric hindrance (3-phenylpyrazole) and only one pyrazole with large steric demands (3-*tert*-butylpyrazole) produced the Tp′ ligand of high steric demands (vide infra). The synthetic route optimized for **1** required the 1:2:1.7 KBH_4:3-*tert*-butylpyrazole:3-phenylpyrazole ratio in stepwise condensation leading to 69.5:4.4:26.1% **1**:**2**:**3** distribution of products. At the second step of the synthetic route the 3-phenylpyrazole condensed with both $[H_3B(3\text{-}t\text{-Bupz})]^-$ and the substituted 3-*t*-Bupz in $[H_2B(3\text{-}t\text{-Bupz})_2]^-$ formed in the first step. The latter reaction was also observed to occur between $K[H_2B(3\text{-}t\text{-Bupz})_2]$, $K[HB(3\text{-}t\text{-Bupz})_3]$ and ten equivalents of 3-phenylpyrazole in toluene-d_9 in an NMR tube at 393 K within a 3 h time interval under ^{1}H NMR spectral examination. The synthetic procedure in dimethylacetamide did not give any superior control over the stoichiometry of the synthesis and the number of side-products was greater than in the case of the reaction between substituted pyrazoles and KBH_4 in the melt. On the other hand, the optimized synthetic route for **2** required a 1:2.5:0.6 KBH_4:3-*tert*-butylpyrazole:3-phenylpyrazole stoichiometry to avoid the formation of **1**, which otherwise could not be easily separated from **2**. Still, separation of **2** from the homoscorpionate complex **4** was not achieved. For our purposes, however, only the ^{1}H NMR spectral identification of **2** was necessary.

3.2. X-ray crystallographic studies of Tp′Co(NCS) complexes

The molecular crystals of **1** and **3·pzH** were grown from the same THF–hexane mixture of solvents. The molecular structure of complexes **1** and **3·pzH** are presented as ORTEP diagrams at Figs. 1 and 2. The geometry around the cobalt(II) ion in **1** is trigonally-elongated tetrahedral, with Co–N(pz) bond lengths of 2.023(5) Å, and a N-bonded thiocyanate inside a hydrophobic pocket formed by two 3-phenyl substituents. The phenyl substituent planes are twisted about 24.9° in relation to the pyrazole planes (Fig. 1). There is a plane of symmetry passing through the central metal ion, boron atom and 3-*tert*-butylpyrazole moiety. The crys-

tal structure of **1** showed no additional ligands present in the coordination sphere, unlike **3**·THF [3] or **3**·**pzH** (Fig. 2). For comparison the geometry around the cobalt(II) ion in **3**·**pzH** is trigonal bipyramidal with additional nitrogen-coordinated pyrazole. All the Co–N bond distances are considerably larger than those in **1**, different for all the pz(Tp^{Ph}) and very close to those found in **3**·THF. The hydrophobic pocket formed by the 3-phenyl substituents is enlarged if compare with that in **1** by an increase in the twist of the Ph/pz planes up to 33–38°.

3.3. Reactivity of complexes

The ^{1}H NMR spectroscopy for high-spin cobalt(II) complexes was proven to be very useful method for elucidation of the structure of Tp′Co(X) complexes [5,7,8,10–13]. We have applied this method to study the series of title complexes and products of their chemical conversion. The ^{1}H NMR spectrum of tetracoordinate **3** in $CDCl_3$ is presented in Fig. 3(A). For this and other tetracoordinate complexes studied till now the B–H resonance is shifted upfield to about −5.0 ppm, and the *o*-H (from the phenyl substituent of 3-phenylpyrazole) resonance is shifted downfield to 17.5 ppm. When **3** in $CDCl_3$ is titrated with CD_3OD, the B–H and *o*-H resonances shift dramatically to 80.7 and −48.2 ppm, respectively. Obviously, the new species **3**·$\mathbf{CD_3OD}$ is formed (Fig. 3(B)). For the unambiguous assignment of 5-H and 4-H resonances both in tetra- and pentacoordinate Tp′Co(XY) complexes we have compared the ^{1}H NMR spectra in a $CDCl_3$–CD_3OD mixed-solvent system for complexes **3** (i.e. Tp^{Ph}Co(NCS)) and $Tp^{Ph,Me}$Co(NCS). The 4-H resonance shifted upfield upon increase of methanol-d_4 concentration in both species, whereas the 5-H in **3** shifted downfield. Consequently, the 5-H and 4-H resonances for **3** in $CDCl_3$ were observed at 40.7 and 71.0 ppm, respectively. In the case the complex **3**·$\mathbf{CD_3OD}$ in CD_3OD they shifted into 65.1 and 53.7 ppm, respectively. A similar spectrum was produced by Tp^{Ph}Co[OOCCH(OH)CH_3] (**5**) in $CDCl_3$ (Fig. 3(C)). We were able to produce **5** in situ by addition of solid sodium lactate into **3** in $CDCl_3$. The ^{1}H NMR spectrum of the pure heteroleptic complex Tp^{Ph}CoTp has been obtained by addition of one equivalent of KTp (in CD_3OD) into the **3**·$\mathbf{CD_3OD}$ (Fig. 3(D)).

The ^{1}H NMR spectrum of the high-spin Co(II) complex **1** in $CDCl_3$, (Fig. 4(A)) consists of two 4-H resonances at 70.1 and 77.6 ppm, two 5-H resonances at 36.5 and 45.3 ppm with an integral intensity ratio of 2:1, respectively, the broad resonance of *o*-H(3-Phpz) at

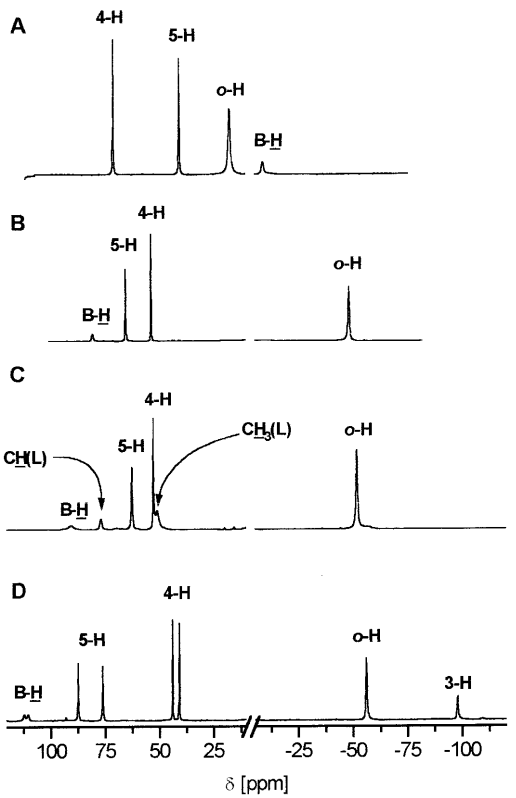


Fig. 3. The ^{1}H NMR spectra of: (A) Tp^{Ph}Co(NCS) in $CDCl_3$; (B) Tp^{Ph}Co(NCS)(CD_3OD) in CD_3OD; (C) Tp^{Ph}Co(OOCCH(OH)CH_3) in $CDCl_3$; (D) Tp^{Ph}CoTp in CD_3OD at 295 K. The 10–0 ppm region of the spectra in this and subsequent figures, containing high intensity, narrow resonances of *m*- and *p*-H (Ph) has been omitted for clarity.

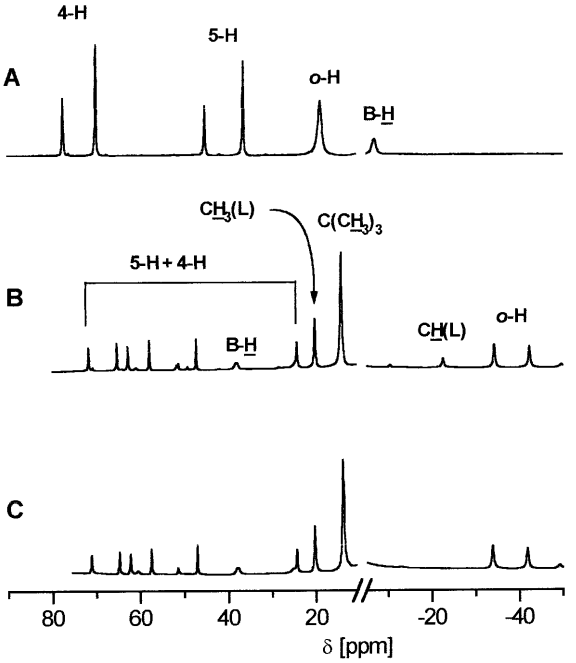


Fig. 4. The ^{1}H NMR spectra of: (A) [HB(3-Phpz)$_2$(3-*t*-Bupz)]Co(NCS) (**1**) in $CDCl_3$; (B) [HB(3-Phpz)$_2$(3-*t*-Bupz)]Co(OOCCH(OH)CH_3) in CD_3OD generated in situ by addition of ten equivalents of sodium lactate dissolved in CD_3OD into **1** dissolved in $CDCl_3$; (C) the spectrum was taken 24 h later from the same solution as B.

19.1 ppm and the broad signal of B–H at −6.9 ppm. The position of the latter is characteristic for tetracoordinate Tp′Co(II)(X) complexes (for comparison see Fig. 3(A and B)). Albeit the cobalt(II) metal centre in **1** is not able to adopt an additional ligand like THF or pzH, methanol does coordinate to the metal ion in **1**; the ^{1}H NMR spectrum of the adduct being complicated, revealing the presence of at least three species of different concentration.

The complexes **1**, **2**, and **3** could not be separated chromatographically in aerobic conditions; our attempts to isolate them on silica gel (even in the presence of [Bu_4N][SCN]) with 5% methylene dichloride in hexane as eluent), led to oxidation of Co(II) to Co(III) in **1** with putative oxidation of the Tp′ ligand, already reported for $(Tp^{iPr})_2M$ complexes (M = Mn(II), Co(II)) [17–19]. Still **3** remained intact under these conditions.

Further comparison of the reactivity of **1** and **3** was achieved at the level of metathesis reactions. The exchange of the thiocyanate anion by Tp or lactate was monitored by means of ^{1}H NMR spectroscopy. We have found that in both cases (**1** and **3**) the quantitative conversion of thiocyanate starting complexes into lactate counterparts occurred. The conversion of **1** into [HB(3-*t*-Bupz)(3-Phpz)$_2$]Co[OOCCH(OH)CH_3] (**6**) (Fig. 4(B)) was achieved by stepwise addition of ten equivalents of sodium lactate stock solution to the NMR tube containing partially dissolved **1** in methanol-d_4. The product **6** dissolves easily in methanol. It was also proven to be a high-spin cobalt(II) complex with 3.90 B.M. magnetic moment measured by Evan's method at 293 K in $CDCl_3$. A characteristic feature of the spectrum of **6** is the presence of two *o*-H(Phpz) resonances separated by 9 ppm (−42.3 and −33.3 ppm) indicating that the [HB(3-*t*-Bupz)(3-Phpz)$_2$] ligand is a very sensitive diastereotopic probe of second face chirality of the cobalt(II) complex brought up by attachment of the chiral auxiliary ligand. Variable-temperature ^{1}H NMR experiments have shown that fluxional behavior in both **5** and **6** is similar. The coalescence point was 230 K in both studied complexes, which gave a value of $\Delta G^{\neq} = 36$ kJ mol^{-1}. Below that temperature the 4-H, 5-H, and *o*-H(Phpz) resonances of **5** split into three sets, while only two sets of resonances of the 95:5 integral intensity ratio (based on *o*-H(Phpz) resonances) are produced in case of **6,** indicating the presence of two rotational isomers around Co–OOC(lactate) at 200 K in methanol-d_4. Another interesting feature of **6** was observed during ^{1}H NMR spectral studies; the lactate C–H resonance at −22.6 ppm decreased its intensity over time and eventually disappeared completely (for comparison see traces B and C in Fig. 4). The selective deuteration of lactate is not surprising in view of the known C–H bond activation properties by Tp′Co(II) and Tp′Rh(I) complexes [17–20] and will deserve further study. The coordination mode of lactate in **6** differs from that in **5**. Most probably the hydroxyl oxygen is coordinated to the metal ion in **5**, giving rise to a substantial downfield shift (76.7 ppm) of the C–H (lactate) resonance (Fig. 3C), whereas large steric hindrance introduced by the *tert*-butyl substituent in **6** hampers this kind of interaction, leading to an upfield shift of the corresponding C–H resonance to −22.6 ppm (Fig. 4(B)). The attempts to isolate **5** in crystalline form suitable for X-ray crystallographic studies failed due to decomposition of **5** into the known (κ^3-Tp^{Ph})Co(κ^2-Tp^{Ph}) [21] complex and cobalt(II) lactate. We were unable to grow crystals of **6**.

Yet another reactivity difference between **1** and **3** was observed by the ^{1}H NMR technique; **1** underwent slow reaction with chloroform-*d* to produce [HB(3-*t*-Bupz)(3-Phpz)$_2$]CoCl at room temperature within several hours, whereas **3** showed no trace of conversion into the chloride form. The replacement of thiocyanate by Tp was monitored spectrally by titration of **1** with KTp in methanol-d_4. In the case of **1** (dissolved in chloroform-*d*) titrated with a methanolic-d_4 solution of KTp no formation of the stable heteroleptic bis-tris(pyrazolyl)borate complex was found and eventually upon addition of one equivalent of KTp all the starting material disappeared. Finally, Tp_2Co and diamagnetic product from the conversion of **1** were found. This again indicates that in aerobic conditions **1** can be readily converted into its oxidized form.

4. Conclusions

The comparison of steric hindrance imposed by 3-R substituents on pyrazole in hydrotris(3-phenylpyrazolyl)borate (Tp^{Ph}) and heteroscorpionate hydrobis(3-phenylpyrazolyl)(3-*tert*-butylpyrazolyl)borate anionic ligands in their high-spin cobalt(II) complexes of the general formula Tp′Co(X,Y) have shown that in the case of the former ligand the pentacoordinate complexes with X = $[NCS]^-$, Y = pyrazole (pzH); X = $[NCS]^-$, Y = methanol; and XY = lactate (with carboxylic and hydroxyl oxygen donors) as well as heteroleptic hexacoordinate (κ^3-Tp^{Ph})Co(κ^3-Tp) (where Tp = trispyrazolylborate anion) form readily, whereas the steric hindrance from only one 3-*tert*-butyl substituent instead of the 3-phenyl one hampers the coordination of any additional ligand to form a stable complex with a cobalt(II) coordination number higher than 4.

5. Supplementary material

Crystallographic data for the structural analysis have been deposited with the Cambridge Crystallographic

Data Centre, CCDC Nos. 138237 for compound **1** and 138236 for **3·pzH**. Copies of this information may be obtained free of charge from: The Director, CCDC, 12 Union Road, Cambridge, CB2 1EZ, UK (Fax: +44-1223-336033; e-mail: deposit@ccdc.cam.ac.uk or www: http://www.ccdc.cam.ac.uk).

References

[1] S. Trofimenko, J. Am. Chem. Soc. 88 (1966) 1842.
[2] For reviews covering the data on metal ion complexes of Tp′ ligands and biomimetic studies see: (a) S. Trofimenko, Chem. Rev. 93 (1993) 943. (b) N. Kitajima, W.B. Tolman, Progr. Inorg. Chem. 43 (1995) 419.
[3] J.C. Calabrese, S. Trofimenko, J.S. Thompson, J. Chem. Soc., Chem. Commun. (1986) 1122.
[4] S. Trofimenko, J.C. Calabrese, S. Thompson, Inorg. Chem. 26 (1987) 1507.
[5] S. Trofimenko, J.C. Calabrese, P.J. Domaille, S. Thompson, Inorg. Chem. 28 (1992) 1091 and references therein.
[6] D.M. Eichhorn, W.H. Armstrong, Inorg. Chem. 29 (1990) 3607.
[7] J.C. Calabrese, P.J. Domaille, J.S. Thompson, S. Trofimenko, Inorg. Chem. 29 (1990) 4429.
[8] J.C. Calabrese, P.J. Domaille, S. Trofimenko, G.J. Long, Inorg. Chem. 30 (1991) 2975.
[9] S. Trofimenko, J.C. Calabrese, J.K. Kochi, S. Wołowiec, F.B. Hulsbergen, I. Reedijk, Inorg. Chem. 31 (1992) 3943.
[10] S. Trofimenko, J.C. Calabrese, Inorg. Chem. 31 (1992) 4810.
[11] A.L. Rheingold, R.L. Ostrander, B.S. Haggerty, S. Trofimenko, Inorg. Chem. 33 (1994) 3666.
[12] A.L. Rheingold, B.S. Haggerty, G.P.A. Yap, S. Trofimenko, Inorg. Chem. 36 (1997) 5097.
[13] A.L. Rheingold, G.P.A. Yap, L.M. Liable-Sands, I.A. Guzei, S. Trofimenko, Inorg. Chem. 36 (1997) 6261.
[14] P. Ghosh, D.G. Churchill, M. Rubinstein, G. Parkin, New J. Chem. 23 (1999) 961.
[15] M.C. Keyes, B.M. Chamberlein, S.A. Caltagirone, J.A. Halfen, W.B. Tolman, Organometallics 17 (1998) 1984.
[16] (a) D.F. Evans, J. Chem. Soc. (1959) 2003. (b) S.K. Sur, J. Magn. Reson. 82 (1989) 169.
[17] N. Kitajima, M. Osawa, M. Tanaka, Y. Moro-oka, J. Am. Chem. Soc. 113 (1991) 8952.
[18] S. Hikichi, H. Komatsuzaki, M. Akita, Y. Moro-oka, J. Am. Chem. Soc. 120 (1998) 4699.
[19] J. Egan, B.S. Haggerty, A.L. Rheingold, S.C. Sendlinger, K.H. Theopold, J. Am. Chem. Soc. 112 (1990) 2445.
[20] C.K. Ghosh, W.A.G. Graham, J. Am. Chem. Soc. 109 (1987) 4726.
[21] A. Kremer-Aach, W. Kläui, R. Bell, A. Strerath, H. Wunderlich, D. Mootz, Inorg. Chem. 36 (1997) 1552.

PERGAMON

www.elsevier.nl/locate/poly

Polyhedron 19 (2000) 2127–2133

POLYHEDRON

A new simple synthetic route to M_3Se_7 (M = Mo or W) core containing complexes: crystal structure and characterisation of $[M_3(\mu_3\text{-}Se)(\mu\text{-}Se_2)_3(dtc)_3]_2Se$

Matthew J. Almond *, Michael G.B. Drew, Helen Redman, David A. Rice

Department of Chemistry, University of Reading, P.O. Box 224, Whiteknights, Reading, Berkshire, RG6 6AD, UK

Received 29 May 2000; accepted 17 July 2000

Abstract

The reaction of $M(CO)_6$, (M = Cr, Mo or W), with elemental Se and $(Et_2NCS_2)_2$ in refluxing 1,2-dichlorobenzene has been studied. For M = Mo the previously unknown compound $[Mo_3(\mu_3\text{-}Se)(\mu\text{-}Se_2)_3(dtc)_3]_2Se$ (**1**) (dtc = Et_2NCS_2) was obtained. A single crystal X-ray crystallographic study shows that **1** contains two $[Mo_3(\mu_3\text{-}Se)(\mu\text{-}Se_2)_3(dtc)_3]$ subunits joined by a bridging selenium atom which is coordinated to the three axial Se atoms of the three Se_2 moieties in each subunit. The results of vibrational spectroscopic and mass spectrometric studies back up this crystallographic investigation. Similar reactions where $Cr(CO)_6$ or $W(CO)_6$ replace $Mo(CO)_6$ in the reaction mixture give, with $Cr(CO)_6$, the well-known complex $[Cr(dtc)_3]$ or, with $W(CO)_6$, a mixture of products including **2** which is the tungsten analogue of **1**. © 2000 Elsevier Science B.V. All rights reserved.

Keywords: Crystallographic; Selenium; Tungsten analogue; Refluxing

1. Introduction

Studies of compounds containing a core consisting of a Group 6 metal, particularly molybdenum, and sulfur have been stimulated by the search for model compounds that may be used to provide an understanding of functioning of iron- and molybdenum-containing nitrogen-fixing enzymes. A large variety of metal–sulfur cores have been identified a number of which are bonded to the dithiocarbamate ligand $[R_2NCS_2]^-$ (dtc) [1–3]. In many such studies it is found that the central metal sulfide core is in the form of the triangular $[M_3S(S_2)_3]^+$ ion. This core generally exists as a single structural unit in a monomeric species e.g. in $[Mo_3S_7(dtc)_3]Cl$ [4] or $[Mo_3S_7(dtc)_3]X$ (X = I or Br) [5].

The majority of the work in this area has been carried out on metal sulfide species. Reports of analogous selenides are rare although the monomeric species $[M_3Se_7(dtc)_4]$ (M = Mo or W) [6] has been prepared. It is also possible that two structural units may be linked together via a central chalcogen atom. Such coordination has been seen in the dimer $[Mo_3S_7(dtc)_3]_2S$ [7]. This interesting species is formed from $(NEt_4)[Mo_3S_7Br_6]$ as a starting material; this is reacted with the bidentate hydroxyquinoline ligands which are then displaced by diethyldithiocarbamate in slight excess. It is presumed that the additional S^{2-} anion is formed by hydrolysis of some of the tetraethylthiuram disulfide. A single crystal X-ray diffraction study of $[Mo_3S_7(dtc)_3]_2$ S (**4**) demonstrates that the S atom between the two clusters is coordinated to six sulfur atoms in total i.e. the three axial sulfur atoms of the three S_2 units in each Mo_3S_7 subunit. The formation of a complex $[Mo_3S(SSe)_3(dtc)_3]SeCN$ has also been reported [8]. In some aspects this complex shows a structural similarity to $[Mo_3S_7(dtc)_3]_2S$ in that the selenium atom of the $SeCN^-$ counter ion is coordinated to sulfur and selenium atoms of the SSe units in the $[Mo_3S(SSe)_3]$ core.

In the current work we report the synthesis and crystallographic and spectroscopic characterisation of the hitherto unknown selenium analogue of **4** i.e. $[Mo_3Se_7(dtc)_3]_2Se$ (**1**). One of the features of this work is the relatively high yield obtained simply by heating a

* Corresponding author. Tel.: +44-118-931-8209; fax: +44-118-931-6332.

E-mail address: m.j.almond@rdg.ac.uk (M.J. Almond).

0277-5387/00/$ - see front matter © 2000 Elsevier Science B.V. All rights reserved.
PII: S0277-5387(00)00515-5

mixture of $Mo(CO)_6$, solid elemental selenium and $(Et_2NCS_2)_2$ in refluxing 1,2-dichlorobenzene. We also report the synthesis (albeit in lower yield) and structural characterisation of the tungsten analogue of **1** i.e. $[W_3Se_7(dtc)_3]_2Se$ **2**. These preparations contrast with chemistry carried out in this laboratory where mixtures of binary carbonyls and elemental selenium are heated under reflux in the absence of any coordinating ligand. In these cases no crystalline products are seen [9,10]. Here the products are the new selenium-rich selenides $CrSe_3$ (from $Cr(CO)_6$) and $MoSe_{\sim 5}$ (from $Mo(CO)_6$) [9]. Although **1** has not previously been observed there are precedents for compounds where $[Mo_3Se_7]^{4+}$ building blocks are linked together via coordinating selenium atoms e.g. in the anions $[Mo_9Se_{40}]^{8-}$ [11] and $[Mo_{12}Se_{56}]^{12-}$ [12] which have been synthesised by hydrothermal methods.

An impetus is given to our research from the recent use of dithiocarbamate complexes as precursors to thin layers of transition metal compounds by Low Pressure Chemical Vapour Deposition processes [13]. Specific examples include the growth of layers of PbS [13,14], CdS [13] and ZnS [15]. Layers of In_2Se_3 have also been generated from the selenocarbamate [In($Se_2CN(CH_3)$*n*-hexyl)] [16]. We anticipate that complexes containing a metal–chalcogenide core surrounded by dithiocarbamate ligands might have sufficient volatility to be used as precursors in Low Pressure Chemical Vapour Deposition and that such compounds might yield layers of unusual composition [17]. The preparation of **1** and **2** by a straightforward synthetic route is thus of some interest in the context of the preparation by CVD growth of metal chalcogenides.

Table 1
Crystal data and structure refinement for (**1**) and (**2**)

	(1) [a]	(2)
Empirical formula	$C_{36}H_{80}N_6O_4S_{12}Se_{15}Mo_6$	$C_{30}H_{60}N_6S_{12}Se_{15}W_6$
Formula weight	2805.82	3177.06
Temperature (K)	293(2)	293(2)
Wavelength (Å)	0.71073	0.71073
Crystal system	orthorhombic	monoclinic
Space group	*C*2*cb* (No 41)	*C*2/*c*
Unit cell dimensions		
a(Å)	16.543(14)	54.91(5)
b(Å)	27.31(3)	12.990(15)
c(Å)	17.585(18)	23.91(3) A
β(°)		90.660(10)
V(Å^3)	7945(13)	17053(30)
Z	4	8
D_{calc} (Mg m^{-3})	2.346	2.475
Absorption coefficient (mm^{-1})	8.144	14.783
F(000)	5296	11424
2θ Range for data collection	2.73–25.95	2.56–25.98
Index ranges	$0 \le h \le 20$, $-33 \le k \le 33$, $-21 \le l \le 21$	$0 \le h \le 67$, $-15 \le k \le 15$, $-25 \le l \le 25$
Reflections collected/unique	12939/3958 [$R_{int} = 0.0698$]	20837/12222 [$R_{int} = 0.0930$]
Refinement method	Full-matrix least-squares on F^2	Full-matrix least-squares on F^2
Data/restraints/parameters	3958/3/260	12222/3/389
Goodness-of-fit on F^2	1.074	1.341
Final *R* indices [$I > 2\sigma(I)$]	$R_1 = 0.0727$, w$R_2 = 0.1769$	$R_1 = 0.1373$, w$R_2 = 0.3604$
R indices (all data)	$R_1 = 0.0946$, w$R_2 = 0.1887$	$R_1 = 0.2199$, w$R_2 = 0.4064$
Absolute structure parameter	0.09(2)	
Largest diff. peak and hole (e Å^{-3})	0.988 and −1.628	3.385 and –3.243

[a] The empirical formula for the molybdenum cluster includes one water and three ethanol molecules per molecule of $[Mo_3Se_7(S_2CN(C_2H_5)_2)_3]_2Se$.

2. Experimental

Infrared spectra were recorded on a Perkin–Elmer FTIR spectrometer (1720-X) with a resolution of ± 1 cm^{-1}. Raman spectra were recorded on a Perkin–Elmer 1700X FT spectrometer, with NIR excitation at 1032 nm and with a typical resolution of ± 1 cm^{-1}. Elemental analysis was performed by Medac Ltd. at Brunel Science Centre, University of Surrey. FAB mass spectrometry was performed by the EPSRC National Mass Spectrometry Centre, University of Swansea.

Crystal data for **1** and **2** are given in Table 1, together with refinement details. Data were collected with Mo Kα radiation using the MARresearch Image Plate System. The crystals were positioned at 70 mm from the Image Plate. 95 frames were measured at 2° intervals with a counting time of 2 min. Data analysis was carried out with the XDS program [18]. The structures were solved using direct methods with the SHELX86 program [19]. In **1**, Mo, Se and S were refined anisotropically and in **2**, W and Se were refined anisotropically with the remaining atoms isotropic. The hydrogen atoms were included in geometric positions and given thermal parameters equivalent to 1.2 times those of the atom to which they were attached. The structures were then refined using SHELXL [20]. Empirical absorption corrections were carried out using the difabs program [21]. All calculations were carried out on a Silicon Graphics R4000 Workstation.

3. Preparations

All reactions were carried out under a nitrogen atmosphere. All reagents were purchased from Aldrich and used as supplied.

3.1. $[Mo_3(\mu_3Se)(\mu Se_2)_3(dtc)_3]_2Se$ (1)

1.00 g (3.79 mmol) $Mo(CO)_6$, 1.2 g (15.20 mmol) Se, 1.1 g (3.71 mmol) $(Et_2NCS_2)_2$ were heated under reflux in 50 cm^3 1,2-dichlorobenzene for 1.5 h. The reaction mixture was allowed to cool overnight and filtered under suction to remove unreacted Se. The solution was treated with petroleum ether (100–120°C) producing a heavy orange precipitate (1.36 g) which was filtered under suction and washed with petroleum ether (40–60°C) and allowed to dry in air. The product was recrystallised from dimethylformamide. Red/orange crystals of $[Mo_3(\mu_3Se)(\mu Se_2)_3(dtc)_3]_2Se$ (**2**) were obtained. The mass of the recrystallised product was 0.71 g (52.3% yield).

Elemental analysis: *Anal.* Found: C, 15.52; H, 2.66; N, 4.03; S, 12.85; Se, 48.40. Calc.: C, 13.6; H, 2.28; N, 3.17; S, 14.31; Se, 44.70%. Infrared spectrum (wavenumber/cm^{-1}): 2980 (m), 2950 (m) (ν(C–H)); 1500 (s) (ν(C–N)); 1464 (m), 1439 (m), 1387 (w), 1361 (w), 1218 (s) ($\delta(CH_x)$); 1279 (s) (ν(C–N)); 1155 (m) ($\delta(NC_2)$), 1083 (m), 1042 (m), 856 (m), 789 (m) ($\rho(CH_x)$); 1011 (m), 923 (m) (ν(C–S)). Raman spectrum (wavenumber/cm^{-1}): 2931 (vs) (ν(C–H)); 1493 (s) (ν(C–N)); 1458 (m) ($\delta(CH_x)$); 1276 (m) (ν(C–N)); 1080 (w) ($\rho(CH_x)$); 1003 (m) (ν(C–S)); 572 (m), 413 (s) (ν(Mo–S)); 370 (s) (ν(Se–Se)); 284 (vs) (ν(Mo–Se)); 237 (vs) (ν(Mo–Mo). FAB mass spectrum (*m*/*e* values; n.b. peak positions are given for the most abundant isotopes): 1292 $[Mo_3(\mu_3Se)(\mu Se_2)_3(dtc)_3]$; 1234 $[Mo_3(\mu_3Se)(\mu Se_2)_3(dtc)_2(S_2CN)]$; 1202 $[Mo_3(\mu_3Se)(\mu Se_2)_3(dtc)_2(SCN)]$; 1176 $[Mo_3(\mu_3Se)(\mu Se_2)_3(dtc)_2(S)]$; 1144 $[Mo_3(\mu_3Se)(\mu Se_2)_3(dtc)_2]$;1060 $[Mo_3(\mu_3Se)(\mu Se_2)_3(dtc)(S_2)]$; 1028 $[Mo_3(\mu_3Se)(\mu Se_2)_3(dtc)(S)]$; 996 $[Mo_3(\mu_3Se)(\mu Se_2)_3(dtc)]$; 967 $[Mo_3(\mu_3Se)(\mu Se_2)_3(S_2CN(Et)]$; 938 $[Mo_3(\mu_3Se)(\mu Se_2)_3(S_2CN)]$.

3.2. $[W_3(\mu_3Se)(\mu Se_2)_3(dtc)_3]_2Se$ (2)

1.52g (4.32 mmol) $W(CO)_6$, 0.70g (8.87 mmol) Se, 0.65g (2.19 mmol) $(Et_2NCS_2)_2$ were heated under reflux in 75 cm^3 1,2-dichlorobenzene for 1 h and allowed to cool overnight. A brown solid was recovered on filtering under suction. Treatment of the resulting solution with diethyl ether produced dark red crystals of $[W_3(\mu_3Se)(\mu Se_2)_3(dtc)_3]_2Se$ (**2**).

Elemental analysis: *Anal.* Found: C, 13.79; H, 2.03; N, 2.60; Se, 38.00. Calc.: C, 12.37; H, 2.08; N, 2.88; Se, 40.65. Infrared spectrum (wavenumber/cm^{-1}): 2972(m) (ν(C–H)); 1499(s) (ν(C–N)); 1453(m), 1436(m), 1379(m) 1354(m), 1198(m) ($\delta(CH_x)$); 1277(s) (ν(C–N)); 1150(m) ($\delta(NC_2)$); 1096(m), 1076(w), 970(w), 844(vw), 775(w), 748(w) ($\rho(CH_x)$); 1003(w), 909(w) (ν(C–S)).

3.3. $Cr(dtc)_3$ (3)

0.84 g (3.82 mmol) $Cr(CO)_6$, 1.20 g (15.20 mmol) Se, 1.1 g (3.71 mmol) $(Et_2NCS_2)_2$ were heated under reflux in 50 cm^3 1,2-dichlorobenzene for a period of 1.5 h. The reaction mixture was allowed to cool overnight and was filtered under suction where unreacted Se was collected. Blue crystals of Cr $(dtc)_3$ (**3**) were obtained by treating the remaining solution with petroleum ether (100–120°C).

Elemental analysis: *Anal.* Found: C, 36.09; H, 5.88; N, 8.36. Calc. C, 36.12; H, 6.09; N, 8.46%. Infrared spectrum (wavenumber/cm^{-1}): 2964 (m), 2928 (m) (ν(C–H)); 1490 (s) (ν(C–N)), 1449 (m), 1430 (m), 1375 (w), 1355 (w) (δ(C–H)); 1270 (s) (ν(C–N)); 1210 (s) ($\delta(CH_x)$); 1146 (m) ($\nu(NC_2)$); 1075 (m) ($\rho(CH_x)$); 996 (m), 913 (w) (ν(C–S)); 847 (m) ($\rho(CH_x)$); 574 (w), 373 (w) (ν(Cr–S)). Raman spectrum (wavenumber/cm^{-1}): 2983 (vs), 2940 (vs) (ν(C–H)); 1497 (ν(C–N)); 1450 (s), 1372 (m) ($\delta(CH_x)$); 1273 (s) (ν(C–N)); 1209, 1075 ($\delta(CH_x)$); 1144 (m) ($\nu(NC_2)$); 998 (s); 916 (m) (ν(C–S)); 877 (w), 847 (w), 774 (w), 723 (w) ($\rho(CH_x)$); 581 (m), 426 (s), 370 (m), 323 (m) (ν(Cr–S)).

4. Results and discussion

4.1. Characterisation of 1

The structure of **1** is shown in Figs. 1 and 2; it is isostructural with **4** [7] and consists of two $[Mo_3Se(Se_2)_3(dtc)_3]$ subunits which are linked via a bridging selenium atom Se(10) over a crystallographic twofold axis. The subunit is shown in Fig. 2 with the atomic numbering scheme. The dimensions of the $[Mo_3Se(Se_2)_3(dtc)_3]$ subunit are compared to those found in **4** in Table 2. Allowing for the replacement of sulfur by the larger selenium, it is clear that the main characteristics of the subunit are maintained. The three molybdenum atoms form a triangle and pairs are bridged by three independent μ^2, Se_2 moieties. Distances of the selenium atoms from the plane are highly asymmetric (Se (41) 1.77, Se (42) –0.36, Se (51) 1.81, Se (52) –0.32, Se (61) 1.84, Se (62) –0.22 Å). Clearly the asymmetry is caused by the strongly-bound Se (11) which bridges all three molybdenum atoms with a mean Mo–Se (11) distance of 2.485 Å compared to 2.381 Å for the analogous Mo–S bonds. This capping atom Se (11), unlike Se (10) on the other side of the anion, is bound to the three molybdenum atoms and steric constraints open up the Se_3 face for its inclusion. This capping also leads to a lengthening of the three Mo–Se (n2) ($n = 4, 5, 6$) bonds closest to the bridging Se (11), defined as equatorial, and these are longer (mean 2.612 Å), than the other three Mo–Se(n1) ($n = 4, 5, 6$) defined as axial (mean 2.544 Å) which form the cavity around

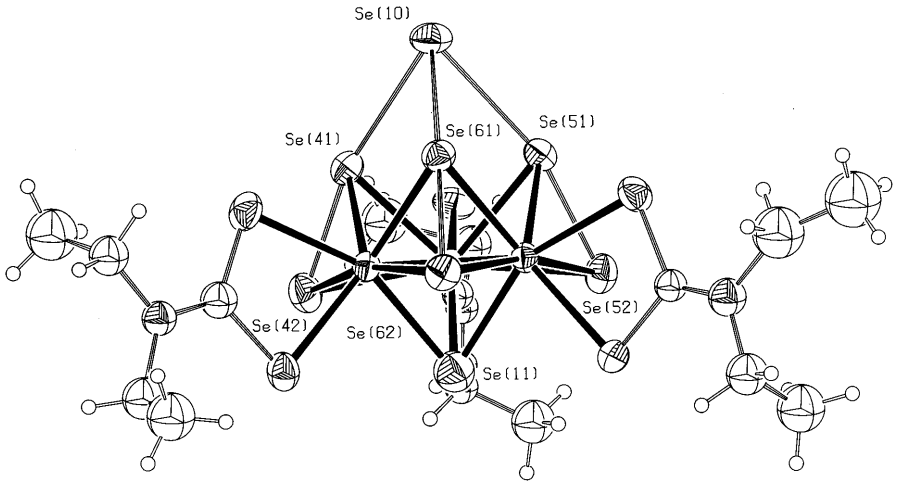


Fig. 1. The structure of the $[Mo_3Se(Se_2)_3(dtc)_3]_2Se$ dimer. Ellipsoids shown at 30% probability. Se(10) is the bridging atom and Se(11) the atom that caps the Se3 face.

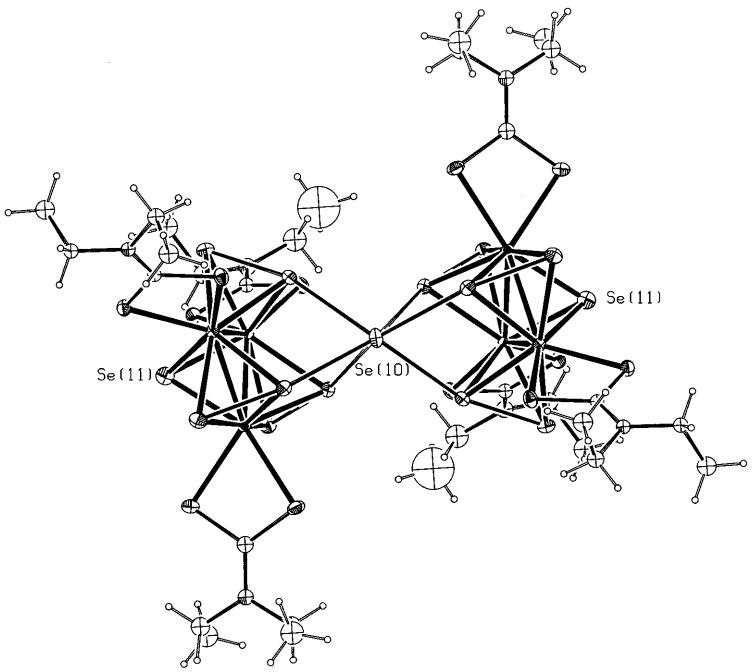


Fig. 2. The structure of the $[Mo_3Se(Se_2)_3(dtc)_3]Se$ subunit together with the atomic numbering scheme. Ellipsoids shown at 30% probability. Se(10) is the bridging atom and Se(11) the atom that caps the Se3 face.

Se(10). A very similar difference is also observed in the analogous Mo–S bonds in **4** (e.g. 2.481, versus 2.415 Å). The bonds to the dtc ligand are asymmetric with the Mo–S(n1) ($n = 1, 2, 3$)(*cis*) bonds shorter at 2.507 Å than the Mo–S(n2) ($n = 1, 2, 3$)(*trans*) bonds at 2.489 Å (comparable distances in **4** are 2.491 and 2.526 Å). Distances of sulfur atoms from the Mo_3 plane are S(11) −1.74, S(12) 1.09, S(21) −1.76, S(22) 1.07, S(31) −1.83, S(32) 0.97 Å. The Mo–Mo bond lengths are increased slightly but significantly in **1** compared to **4** by the larger size of the bridging selenium atoms with a mean Mo–Mo distance of 2.766 Å in **1** compared to 2.716 Å in **4**.

There are many examples of this $Mo_3S(S_2)_3$ core in the literature and the dimensions found in **4** are common to all the structures. However, this is the first example of the selenium analogue. It is of significant interest that in all structures containing this $[Mo_3S(S_2)_3(dtc)_3]$ core, there is found to be an additional anion approaching the three axial sulfur atoms of the complex, so clearly these three atoms form a cavity which forms an anionic binding site. In **4** the anion that is bound in the site is an additional sulfide anion, but many other examples are known, but predominantly halides. A list of 15 examples is given in Ref. [7]. These

Table 2
Comparison of dimensions (A) in **1**, **2** and **4**

	1 this work M = Mo, X = Se	**2** (this work) M = W, X = Se	**4** {ref [7]}[b] M = Mo, X = S
M–M	2.762(3) – 2.769(3)	2.737(4) – 2.763(4)	2.716
M–μ_3(X)	2.471(4) – 2.487(4)	2.478(6) – 2.502(6)	2.381
M–X(eq)	2.581(4) – 2.651(4)	2.600(5) – 2.633(6)	2.481
M–X(ax)	2.515(3) – 2.557(3)	2.558(5) – 2.570(5)	2.415
M–S(*cis*)[a]	2.503(6) – 2.535(7)	2.522(11) – 2.589(10)	2.489
M–S(*trans*)[a]	2.520(6) – 2.540(6)	2.522(10) – 2.577(8)	2.526
X(ax)–X(b)	2.816(4) – 2.905(4)	2.807(7) – 3.022(6)	2.71

[a] Defined relative to the μ(3) Se(11) atom — see text.
[b] Mean value.

additional anions are only weakly bound with distances to S (axial) of between 2.87 and 3.25 Å. However in **4** the sulfide anion forms a significantly shorter contact at 2.71 Å. In **1**, in the present structure, the selenium analogue $[Mo_3Se(Se_2)_3(dtc)_3]$, the anionic binding site remains in situ and is occupied by a selenide anion. The mean distance between this anion and the selenium atoms in the pocket is 2.86 Å. The vast majority of the examples listed in [7] show the anion forming a single unit but in **4** and in **1**, the anion bridges two such subunits. The bridge is significantly asymmetric in that the angle subtended at the anion by the axes of the two subunits (defined as being perpendicular to the Mo_3 triangles is (46, 33° in **4**)).

The spectroscopic findings back up the crystallographic determination. The IR spectrum of **1** shows bands characteristic of coordinated diethyldithiocarbamato ligands [22–26]. Of more interest perhaps is the Raman spectrum where relatively strong bands in the region 200–600 cm^{-1} are seen. These principally arise from the Mo_3Se_7 core or from Mo–S vibrations. A tentative assignment of these bands, see Section 2, has been made by comparison with the vibrational spectra of related compounds [27–30]. The FAB mass spectrum of **1** shows a fragmentation pattern entirely as expected. Although the elemental analysis for **1** does not tally precisely with the calculated values the discrepancy may be accounted for by the presence of a small amount of trapped solvent or by the presence of small quantities of other impurities. Repeated attempts further to purify **1** by recrystallisation were not successful.

4.2. Characterisation of *2*

We have extended this work by repeating the synthesis of 1 under identical conditions but using W $(CO)_6$ or $CrCO)_6$ in place of Mo $(CO)_6$. With W $(CO)_6$ a mixture of products is formed. Crystals of 2 were obtained by treatment of the brown solid obtained from the reaction mixture with diethyl ether. Unfortunately it proved to be impossible to characterise the other components of the mixture. However, a combination of single crystal X-ray diffraction, infrared and Raman spectroscopies and FAB mass spectrometry demonstrate that **2** is the tungsten analogue of **1**.

The structure of **2** is shown in Figs. 3 and 4, it is similar to both **1** and **4** and consists of two $[W_3(\mu_3-Se)(\mu-Se_2)_3(dtc)_3]$ subunits linked by a bridging selenium atom just as the corresponding Mo subunits are linked by a selenium atom in **1**. However, it is not isomorphous as no crystallographic symmetry is present. The dimensions of the Mo subunit of **1** and the W subunit of **2** are compared in Table 2. The triply bridging selenium atom (Se(11)) is strongly bound to three tungsten atoms with an average distance of 2.493 Å (cf. the corresponding Mo–Se distance of 2.485 Å in **1**). In **2** there is a smaller difference between the W–S (eq) and W–Se (ax) bonds than in **1**. As in **1**, however,

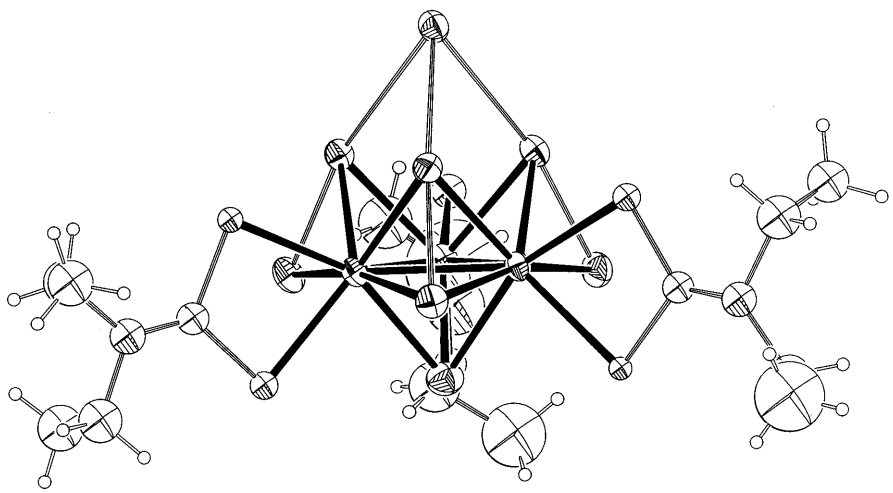


Fig. 3. The structure of the $[W_3Se(Se_2)_3(dtc)_3]Se$ subunit. Ellipsoids shown at 20% probability.

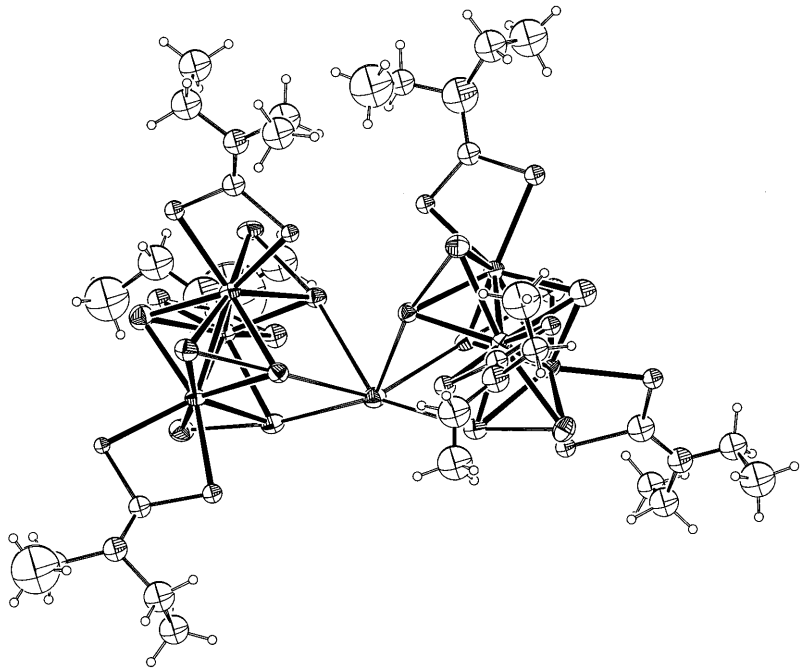


Fig. 4. The structure of the $[W_3Se(Se_2)_3(dtc)_3]_2Se$ dimer. Ellipsoids shown at 20% probability.

the bonds to the dtc ligand are asymmetric with the W–S (*cis*) bonds shorter than the W–S (*trans*) bonds (2.538 cf. 2.565 Å). Again, however, the asymmetry is not so pronounced in **2** as in **1**. The average W–W distance in **2** (2.751 Å) is shorter than the average Mo–Mo distance in 1 (2.766 Å) possibly reflecting somewhat stronger metal–metal bonding, as expected for the heavier transition metal.

The infrared spectrum of **2** is very similar to that of **1**. Most of the Raman spectrum of **2** was masked by strong fluorescence. However, strong Raman scattering was seen at 297, 237 and 202 cm^{-1} and these features were assigned to ν(W–S), ν(W–Se) and ν(W–W) stretches respectively. It may be seen that these features have all shifted to low frequency when compared to the corresponding bands of **1** reflecting the greater mass of tungsten compared to molybdenum. The FAB mass spectrum of **2** shows three distinct clusters of peaks centred around m/e values of 1636, 1588 and 1556. These are assigned to the ions $[W_3(\mu_3Se)(\mu Se_2)_3(S_2CNEt_2)_3]Se^+$, $[W_3(\mu_3Se)(\mu Se_2)_3(S_2CNEt_2)_3]S^+$ and $[W_3(\mu_3Se)(\mu Se_2)_3(S_2CNEt_2)_3]^+$ respectively. A large number of peaks were seen at lower m/e values but these could not be assigned with any degree of certainty.

4.3. Reaction of $Cr(CO)_6$

With $Cr(CO)_6$ there is no hint of any product akin to **1** or **2**. Rather the well-known compound $Cr(S_2CNEt_2)_3$ (**3**) [31] is formed in almost quantitative yield. **3** has been characterised by a combination of single crystal X-ray diffraction, IR and Raman spectroscopies and FAB mass spectrometry. The identical product, **3**, is also formed if the synthesis is repeated with no selenium in the reaction mixture. The FAB mass spectrum of **3** shows a molecular ion peak at $m/e = 496$; together with a number of other peaks including those at $m/e = 348$ and 200 corresponding to the loss of one and two dtc ligands from the parent molecule, respectively. The single crystal study confirms the nature of **3** [31]. It is not unexpected to find that chromium behaves in a different manner to molybdenum and tungsten; as expected the heavier metals readily form clusters incorporating metal-metal bonding whereas such behaviour is not seen for chromium.

5. Supplementary material

Crystallographic data for the structural analysis have been deposited with the Cambridge Crystallographic Data Centre, CCDC 144857 for compound **1** and CCDC 144858 for compound **2**. Copies of this information may be obtained free of charge from The Director, CCDC, 12 Union Road, Cambridge, CB2 1EZ, UK (fax: +44-1223-336033; e-mail: deposit@ccdc.cam.ac.uk or www: hhtp://www.ccdc.cam.ac.uk).

Acknowledgements

We thank EPSRC for the award of a studentship to H.R. We thank EPSRC and University of Reading for funds for the Image Plate System.

References

[1] T.C.W. Mak, K.S. Jasim, C. Chieh, Angew. Chem., Int. Engl. 23 (1984) 391.
[2] Y. Gea, M.A. Greaney, C.L. Coyle, E.I. Stiefel, J. Chem. Soc., Chem. Commun. 1992, 160.
[3] M.G.B. Drew, R.J. Hobson, P.E.M. Mumba, D.A. Rice, N. Turp, J. Chem. Soc., Dalton Trans. 1987, 1163
[4] V.P. Fedin, M.N. Sokolov, O.A. Geras'ko, A.V. Virovets, N.V. Podberezkaya, V.Ye. Fedorov, Inorg. Chim. Acta 192 (1992) 153.
[5] H. Zimmermann, K. Hegetscheiler, T. Keller, V. Gramlich, H.W. Schmalle, W. Petter, W. Schneider, Inorg. Chem. 30 (1991) 4336.
[6] V.P. Fedin, M.N. Sokolov, O.A. Geras'ko, A.V. Virovets, N.V. Podberezkaya, V.Ye. Fedorov, Inorg. Chim. Acta 187 (1991) 81.
[7] M.D. Meienberger, K. Hegetschweiler, H. Rüegger, V. Gramlich, Inorg. Chim. Acta 213 (1993) 157.
[8] V.P. Fedin, Y.V. Mironov, A.V. Virovets, N.V. Podberezkaya, V.Y. Fedorov, Polyhedron 11 (1992) 1959.
[9] D.A. Rice, S.J. Hibble, M.J. Almond, K.A. Hassan-Mohammad, S.J. Pearse, J. Mater. Chem. 2 (1992) 895.
[10] S.J. Hibble, D.A. Rice, M.J. Almond, K.A. Hassan-Mohammad, S.P. Pearse, J.R. Sagar, J. Mater. Chem. 2 (1992) 1237.
[11] J.H. Liao, M.G. Kanatzids, Inorg. Chem. 31 (1992) 431.
[12] J.H. Liao, M.G. Kanatzids, J. Am. Chem. Soc. 112 (1990) 7400.
[13] N.I. Fainer, M.L. Kosinova, Y.M. Rumyantsev, E.G. Salman, F.A. Kunetsov, Thin Solid Films 280 (1996) 16.
[14] T. Trindade, P. O'Brien, Chem. Vap. Dep. 3 (1997) 2.
[15] R. Nomura, T. Murai, T. Toyosaki, H. Matsuda, Thin Solid Films 271 (1995) 4.
[16] P. O'Brien, D.J. Otaway, J.R. Walsh, Chem. Vap. 3 (1997) 4.
[17] M.J. Almond, H. Redman, D.A. Rice, J. Mater. Chem., in press.
[18] W. Kabsch, J.Appl.Cryst. 21 (1988) 916.
[19] G.M. Sheldrick, SHELXL-86 Acta Crystallogr., A 46 (1990) 467.
[20] G.M. Sheldrick, SHELXL: Program for Crystal Structure Refinement, University of Göttingen, 1993.
[21] N. Walker, D. Stuart, Acta Crystallogr. 39 (1983) 158.
[22] K. Nakamoto, Infrared and Raman Spectra of Inorganic and Coordination Compounds, fourth edn, Wiley, New York, 1986.
[23] M.L. Shankranarayama, C.L. Patel, Spectrochim. Acta 21 (1965) 95.
[24] D.C. Bradley, M.H. Gitlitz, J. Chem. Soc. 1969, 1152.
[25] G.W. Watt, B.J. McCormick, Spectrochim. Acta 21 (1965) 753.
[26] K.A. Jensen, B.M. Dahl, P.H. Nielsen, G. Borch, Acta Chem. Scand. 76 (1972) 2241.
[27] V.P. Fedin, A.V. Mironov, M.N. Sokolov, B.A. Kulesov, V.Y. Fedorov, D.S. Yufit, Y.T. Structchkov, Inorg. Chim. Acta 174 (1990) 275.
[28] E. Diemann, A. Mueller, P.J. Aymonino, Z. Anorg. Allg. Chem. 479 (1981) 199.
[29] M.J. Mayor-Lopez, J. Welser, K. Hegetschweiler, M.D. Meienberger, F. Joho, S. Leoni, K. Nesper, G.J. Reiss, W. Frank, B.A. Kolesov, V.P. Fedin, V.Y. Fedorov, Inorg. Chem. 37 (1998) 2633.
[30] V.P. Fedin, B.A. Kolesov, Y.V. Mironov, V.Y. Fedorov, Polyhedron 8 (1989) 2419.
[31] C.L. Raston, A.H. White, Aust. J. Chem. 30 (1977) 2091.

PERGAMON

www.elsevier.nl/locate/poly

Polyhedron 19 (2000) 2135–2140

POLYHEDRON

Isolation and structure of a europium(III) chloride complex of 2,6-bis[(diphenylphosphino)methyl]pyridine *N*,*P*,*P*′-trioxide

E.M. Bond [a], E.N. Duesler [a], R.T. Paine [a,*], H. Nöth [b]

[a] *Department of Chemistry, University of New Mexico, Albuquerque, NM 87131, USA*
[b] *Department of Chemistry, Universität München, Butenandtstraße 5-13, 81377 Munich, Germany*

Received 7 February 2000; accepted 19 July 2000

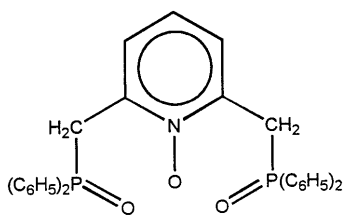
Abstract

The combination of $EuCl_3 \cdot 6H_2O$ with the trifunctional ligand 2,6-$[(C_6H_5)_2P(O)CH_2]_2C_5H_3NO$, in a 1:2 ratio, produces the coordination complex $[Eu\{[(C_6H_5)_2P(O)CH_2]_2C_5H_3NO\}_2(H_2O)_2]Cl_3 \cdot 9H_2O$. The molecular structure of the complex has been determined by single-crystal X-ray diffraction methods. The *N*,*P*,*P*′-trioxide ligands each bind to the central Eu(III) ion in a tridentate fashion along with two water molecules. The eight inner sphere oxygen atoms surrounding the Eu(III) ion form a square antiprism. These results are discussed in the context of the structures formed by lanthanide nitrates. © 2000 Elsevier Science B.V. All rights reserved.

Keywords: Lanthanide complex; Tridentate chelate; Europium(III) chloride

1. Introduction

The liquid–liquid extraction (LLE) properties of the trifunctional 2,6-bis[(diorganylphosphino)methyl]pyridine *N*,*P*,*P*′-trioxides (NOPOPO's) [1–5] have stimulated interest in the molecular structures adopted in the coordination complexes of these ligands [6–8]. For example, ligand **1** in $CHCl_3$ extracts trivalent lanthanides and americium(III) from concentrated nitric acid solutions (1–6 M HNO_3), and it reversibly releases the extracted metal ions to dilute nitric acid solutions [1,4,5].



1

The magnitudes of the distribution ratio, $K_D = [M]_{org}/[M]_{aq}$, vary from $\sim 10^{-2}$ in 0.01 M HNO_3 to $\sim 10^3$ in 10 M HNO_3 [1,4,5]. Under similar conditions, carbamoylmethyl phosphonates (CMPs) and phosphine oxides (CMPOs) show similar trends in increasing K_D values with increasing $[HNO_3]$ using $CHCl_3$ [5] or aromatic solvents [9–12] as the diluents. These types of behavior are unique since most neutral organic extractants show depressed K_D values with increasing aqueous acid concentration presumably due to increasing competition between protons and metal ions for the extractant donor sites. We have also observed that K_D varies with the concentration of ligand used in the extractions, and the slope of the dependency ($\log K_D$ versus $\log [\mathbf{1}]$) is classically interpreted to indicate the number of ligands participating in the extraction complex [9]. In the case of **1** in $CHCl_3$ solution extracting Am(III) from HNO_3 solutions, the slopes are 2.3 at 0.1 M HNO_3 and 1.8 at 1.0 M HNO_3 [1,4]. Non-integral slopes are typically interpreted to result from formation of: (a) mixtures of complexes having different L/M ratios; (b) ligand aggregates in the organic phase; (c) non-stoichiometric outer-sphere complexes and/or (d) non-ideal organic solutions. In most cases it is difficult to determine which of these features operates especially under conditions directly comparable with a LLE pro-

* Corresponding author. Tel.: +1-505-277-1661; fax: +1-505-277-2609.

E-mail address: rtpaine@unm.edu (R.T. Paine).

0277-5387/00/$ - see front matter © 2000 Elsevier Science B.V. All rights reserved.
PII: S0277-5387(00)00519-2

cess, where extractant concentration far exceeds the metal ion concentration. Furthermore, based upon extraction data, it is not possible to conclude how **1** binds to trivalent metal ions in $CHCl_3$ solution.

In support of synthetic efforts aimed at deriving new, improved extractants, it is important to obtain a more detailed molecular view of the complexes formed by **1** and its analogues. Ideally, it would be preferred to directly determine, under LLE conditions, full solution phase structures by using one or more readily available physical methods. With such data and companion molecular modeling, efficient molecular redesign of extractant structures would be possible. Limited success in identifying solution phase inner coordination sphere structures has been achieved for CMP and CMPO complexes by using IR [13], NMR [14–16] and EXAFS [17] techniques. However, additional detail is required. A 'next-best' approach involves full structure determination of isolated, crystalline coordination complexes from single-crystal X-ray diffraction data. This method is quite precise; however, there is no guarantee that the solid-state structure of the isolated complex is the same as the liquid phase solvent extraction complex. Still, crystal structure data provide useful information about how ligands organize about a metal ion. Furthermore, in the current case, it is not practical to isolate and structurally characterize Am(III) extraction complexes or to study the equilibrium speciation of the organic solvent soluble Am(III) complexes by spectroscopic techniques under the strongly ligand-loaded conditions employed in LLE. As a result, we have chosen to use stable lanthanide ions as stand-ins for the radioactive Am(III) ion. In previous studies we have reported on the structural characterization of $Ln(NO_3)_3$ complexes with **1** [6], and report here the isolation of a complex formed from $EuCl_3$ and **1**. The structure determination allows for discussion of the observed extraction behavior of **1** toward Eu(III) in HCl solutions.

Table 1
Details of the crystal data and refinement

Compound	
Empirical formula	$C_{62}H_{76}Cl_3EuN_2O_{17}P_4$
Formula weight	1503.44
Color/size (mm)	Colorless, $0.25 \times 0.18 \times 0.10$
Crystal system	Monoclinic
Space group	$P2_1/c$
a (Å)	20.245(4)
b (Å)	13.749(3)
c (Å)	26.528(5)
α (°)	90
β (°)	105.12(3)
γ (°)	90
Volume (Å^3)	7128(2)
Z	4
D_{calc} (g cm^{-3})	1.401
μ (Mo Kα) (mm^{-1})	1.146
Temperature (K)	193
$F(000)$	3088
Independent reflections	11864
Final R_1, R_w^2 ($I>2\sigma(I)$)	0.0477, 0.1062
Goodness of fit on F^2	1.051
Largest difference peak/hole (e Å^{-3})	1.391/−0.446

2. Experimental

The ligand **1** was prepared according to the published procedure [6,7]. Chloroform and ethanol were purchased from EM Science (Omnisolv) and McCormick Distilling Co., respectively, and they were used without purification. Infrared spectra were recorded from KBr pellet samples by using a Mattson 2020 FT-IR spectrometer. TGA data were obtained on a Perkin–Elmer TGA-7 analyzer using N_2 as the purge gas. NMR spectra were recorded on Bruker 250 MHz and JEOL 400 MHz spectrometers. Elemental analyses were obtained from Galbraith Laboratories.

2.1. Synthesis of the complex

The complex was prepared by addition of **1** (0.4 mmol) in $CHCl_3$ (40 ml) to a vial containing $EuCl_3(6H_2O$ (0.2 mmol) in EtOH (20 ml). The vial was shaken and then allowed to stand for 2 days. The mixture produced a colorless solid. The solid was separated from the mother liquor and washed with Et_2O to remove residual free ligand. The mother liquor was placed in the refrigerator at 10°C and crystals suitable for X-ray analysis slowly formed in the vial. The solid was hydroscopic and vacuum drying resulted in a colorless powder. The vacuum-dried powder was used for spectroscopic and compositional analyses. Infrared spectrum (KBr, cm^{-1}): 3356(m), 3054(w), 1437(m), 1227(m), 1159(s), 1127(s), 862(w), 750(m), 727(m), 696(m), 507(m). Elemental analysis. Found: C, 50.46; H, 4.47; N, 2.09. Calc. for $C_{62}H_{76}Cl_3EuN_2O_{17}P_4$: C, 49.53; H, 5.09; N, 1.86%.

2.2. Crystallographic analysis

A prism-shaped crystal was selected and mounted in a sealed glass capillary. Data collection was performed on a Siemens P4 instrument with a CCD area-detector and low-temperature device operating at 193 K. Mo Kα radiation was used with a graphite single-crystal monochromator. Pertinent data collection and refinement information are summarized in Table 1. Data were recorded in the hemisphere mode (two settings, $\Delta/\phi = 0.3°$) with a measurement rate of 10 s per frame. No extinction correction was applied and the absorption correction employed SADABS. Data reduction was accomplished by use of SAINT (Siemens Analytical In-

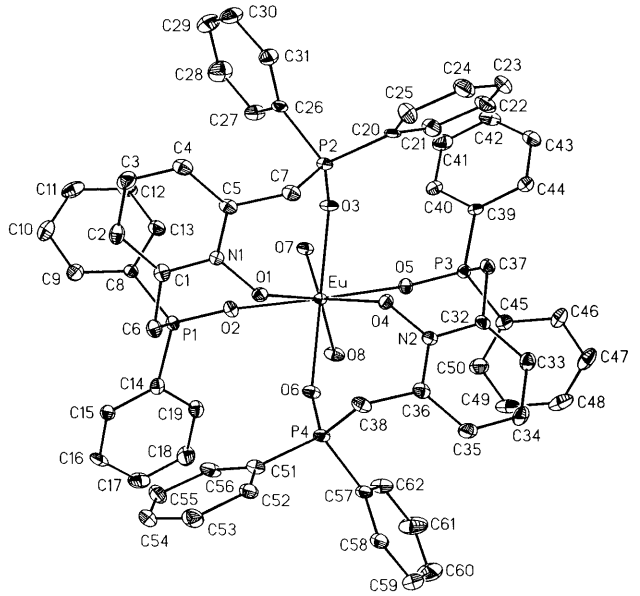


Fig. 1. ORTEP view of $[Eu\{[(C_6H_5)_2P(O)CH_2]_2C_5H_3NO\}_2(H_2O)_2]Cl_3{\cdot}9H_2O$.

struments, Version 4.1). The structure was solved by direct methods and refined by using full-matrix least-squares techniques. All non-hydrogen atoms were refined anisotropically except for one disordered outer sphere water oxygen atom: O(9) and O(10) occupancies 0.57 and 0.43, respectively. All hydrogen atoms were included (riding model) with $U_{iso} = 1.25U_{eq}$ of the parent atom.

3. Results and discussion

As noted in Section 1, previous liquid–liquid extraction studies of Am(III) from HNO_3 solutions with $CHCl_3$ solutions of **1** revealed ligand dependencies of 2.3 at 0.1 M HNO_3 and 1.8 at 1.0 M HNO_3 [1,4]. As noted above, crystallographic studies of solid-state structures do not necessarily accurately reflect all of the structural details of complexes formed in aqueous or organic solutions; however, they do provide some clues on the nature of the possible metal–extractant liquid phase interactions. For example, in prior work [6,8] $Ln(NO_3)_3{\cdot}xH_2O$ salts have been combined with **1** in EtOH or EtOH–$CHCl_3$ solutions, and 1:1 and 2:1 L/M complexes have been isolated and characterized. Single-crystal X-ray diffraction analyses show that the 1:1 complexes of these metal nitrates contain one tridentate ligand **1** and three bidentate nitrate groups bonded to the central Ln(III) ion. The resulting Ln(III) coordination number is nine. Such complexes are not likely to be present in large amounts in LLE systems where the ligand concentration in the organic phase is huge relative to the metal concentration in the acidic aqueous phase. In addition, 2:1 complexes have been isolated, and they have two tridentate coordinated molecules of **1** and one bidentate nitrate in the inner sphere giving rise to a coordination number of eight. The remaining two nitrates, and in some cases several solvent molecules, reside in the outer coordination sphere of the crystalline complexes. The structure of the 2:1 complexes is somewhat unusual since neutral acyclic ligands typically do not displace NO_3^- ions from the inner sphere in Ln(III) complexes. Of course, several macrocyclic ligands displace nitrate ions from the inner coordination sphere of Ln(III) ions [18]. Examination of space filling models of the 2:1 complexes show that the two neutral ligands nearly completely encapsulate the Ln(III) leaving only a narrow slot for one NO_3^- ion to fit in the inner sphere. The exterior of the complex is therefore, dominated by the 'greasy' organic fragments of the ligands and this is consistent with the high $CHCl_3$ solubility of the complex. No doubt this character facilitates the transfer of Ln(III) ions from aqueous acid solutions to the organic phase in extractions. Complexes with more than two ligands bonded to the central Ln(III) ion have not yet been isolated despite attempts to produce them under various conditions. This suggests that a ligand dependency of 2.3 at low nitrate concentration does not arise from a mixture of ML_3 and ML_2 complexes, but instead it may reflect the presence of aggregates or outer sphere complexes containing **1** when the ligand is present in high concentration.

Interestingly, extractions of Am(III) from 1 M HCl solutions by **1** in $CHCl_3$ produce a ligand dependency of 3.1 [2]. Due to the poor coordination ability of Cl^- relative to NO_3^-, it seemed possible that isolated coordination complexes obtained from combination of excess of **1** with $LnCl_3{\cdot}nH_2O$ salts might display a 3:1 L/Ln ratio. In this case the molecular structure might contain, for example, two tridentate ligands **1** and a monodentate ligand **1** in the inner coordination sphere although preliminary molecular modeling suggested an unfavorable 'tight-fit' for a P=O bonded monodentate ligand in the slot left by the two tridentate ligands. The tight-fit would result from steric crowding between substituents on the phosphoryl groups in the tridentate ligands and the phenyl groups on a P=O group in a monodentate ligand.

In the present study, we have examined reactions of $LnCl_3{\cdot}nH_2O$ salts with **1** in various ratios in EtOH, EtOH–$CHCl_3$ and EtOH–H_2O mixtures. Suitable single crystals were obtained in only one case where the ligand–Eu(III) ratio was 2:1 and the solvent mixture was EtOH–$CHCl_3$. The crystal structure determination reveals that the isolated complex has the composition $[Eu\{[(C_6H_5)_2P(O)CH_2]_2C_5H_3NO\}_2(H_2O)_2]Cl_3{\cdot}9H_2O$. A view of the molecular structure is shown in Fig. 1 and the eight-coordinate polyhedron is presented in Fig. 2.

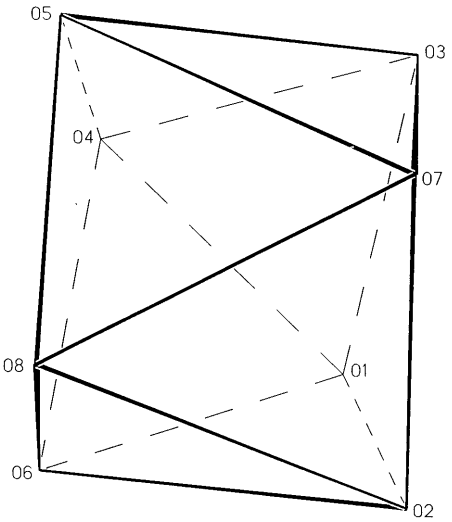


Fig. 2. Coordination polyhedron for $[Eu\{[(C_6H_5)_2P(O)CH_2]_2C_5H_3NO\}_2(H_2O)_2]Cl_3\cdot 9H_2O$.

Two tridentate molecules of **1** are present in the Eu(III) molecular structure, but a third molecule of **1** is absent both from the inner and outer spheres. The weakly binding Cl^- anions are displaced from the Eu(III) inner sphere and replaced by two water molecules. The three Cl^- anions and an additional nine molecules of water are found in the outer sphere in a complex hydrogen bonded array.

The $Eu(\mathbf{1})_2(H_2O)_2$ inner sphere complex has an approximate C2 rotation axis. The average P(O)–Eu distance, 2.355 Å (range: 2.343(3)–2.369(4) Å), is comparable with distances found in lanthanide nitrate complexes of **1** [6–8]. The average N(O)–Eu distance, 2.462 Å (range: 2.467(3)–2.458(3) Å), is longer than the P(O)–Eu distance, and a similar trend is observed in all complexes of **1** [6–8]. As in the lanthanide nitrate complexes of **1** the two tridentate ligands form a large 'mushroom cap-like' enclosure around the Eu(III) ion. Unlike the complexes containing nitrate counter ions, the remaining small coordination 'slot' is occupied by two neutral water molecules instead of one bidentate NO_3^- ion. The average H_2O–Eu distance, 2.464 Å (range: 2.479(4)–2.448(4) Å), is comparable to the N(O)–Eu distance. The fact that one of the water molecules has a significantly longer Eu–OH_2 distance suggests that it is more loosely bound, probably in response to steric crowding in the inner sphere. The average P=O distance, 1.503 Å, and N–O distance, 1.336 Å, are identical to those reported earlier for nitrate complexes [6–8]. The O(7)–Eu–O(8) bond angle is 69.9(2)° which is similar to the value for a bidentate NO_3^- ion [6].

Table 2
Selected bond lengths (Å)

$[Eu\{[(C_6H_5)_2P(O)CH_2]_2C_5H_3NO\}(H_2O)_2]Cl_3\cdot 9H_2O$			
Eu–O(1)	2.467(3)	Eu–O(4)	2.458(3)
Eu–O(2)	2.343(3)	Eu–O(5)	2.349(3)
Eu–O(3)	2.369(4)	Eu–O(6)	2.358(4)
Eu–O(7)	2.479(4)	Eu–O(8)	2.448(4)
N(1)–O(1)	1.335(5)	N(2)–O(4)	1.336(5)
P(1)–O(2)	1.498(4)	P(2)–O(3)	1.502(4)
P(3)–O(5)	1.500(4)	P(4)–O(6)	1.508(4)

The molecular structures for the corresponding 2:1 complexes $[Eu(\mathbf{1})_2(NO_3)](NO_3)_2$ [3], $[Pr(\mathbf{1})_2(NO_3)](NO_3)_2$, and $[Yb(\mathbf{1})_2(NO_3)](NO_3)_2$ [6,8] have also been obtained. As suggested above, the structures of these nitrate complexes are closely similar with two tridentate ligands **1** and a bidentate nitrate forming the eight-coordinate inner sphere geometry. In these cases the three ligand oxygen donor atoms form nearly isosceles triangular coordination footprints on the central metal with the following non-bonded O···O separations: Eu–ligand **1**: (P)O···O(N), 2.837; (P)O···O(N), 3.009; (P)O···O(P) 3.648 Å. Ligand **2**: (P)O···O(N), 2.848; (P)O···O(N), 2.965, (P)O···O(P) 3.584 Å. Pr–ligand **1**: (P)O···O(N), 2.873; (P)O···O(N), 2.986; (P)O···O(P), 3.488 Å. Pr–ligand **2**: (P)O···O(N), 2.875: (P)O···O(N), 3.029; (P)O···O(P), 3.829 Å. Yb–ligand **1**: (P)O···O(N), 2.929; (P))···O(N), 2.770; (P)O···O(P), 3.462 Å. Yb–ligand **2**: (P)O···O(N), 2.952; (P)O···O(N), 2.791; (P)O···O(P), 3.439 Å. These values can be compared with the non-bonded O···O separations in the $EuCl_3$ complex: ligand **1**: O(1)···O(2), 2.874; O(1)···O(3), 3.049; O(2)···O(3), 3.756 Å. Ligand **2**: O(4)···O(5), 2.887; O(4)···O(6), 3.057; O(5)···O(6), 3.828 Å. As we have noted before [6,7] the ligand **1** is able to accommodate a range of central metal ion radii by adjusting the size of the footprint through small conformational changes in the C(ring)–CH_2–P(O)Ph_2 arms. The largest effect appears in the non-bonded (P)O···O(P) separation which is reduced as the M(III) ionic radius decreases. The Pr(III) ionic radius (1.14 Å, CN = 8) is larger than that of Eu(III) (1.07 Å, CN = 8), hence it would be expected that the ligand footprints in the Eu(III) complexes would be significantly smaller than in the Pr(III) complex. This is the case when comparing the structures of the $[M(\mathbf{1})_2(NO_3)](NO_3)_2$ (M = Pr, Eu) complexes. However, in the present case, it appears that the sizes of the ligand footprints in $[Eu(\mathbf{1})_2(H_2O)_2]Cl_3$ more closely match those in $[Pr(\mathbf{1})_2(NO_3)](NO_3)_2$ rather than those in $[Eu(\mathbf{1})_2(NO_3)](NO_3)_2$. Therefore, the size variation between the Eu(III) nitrate and chloride complexes probably arise in response to the effective space occupied by a single inner-sphere bidentate nitrate ion compared to two inner-sphere water molecules (Table 2).

Returning to the question regarding the identity of the extraction complex, it is informative to compare the structural results with other characterization data for the complex. First, it is noted that in our relatively dry

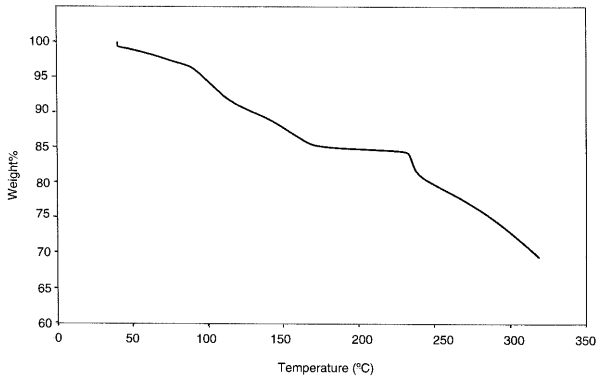


Fig. 3. Thermal gravimetric analysis (TGA) for the vacuum-dried complex.

laboratory atmosphere single crystals and bulk solid samples of the complex lose water and disintegrate into a powder. Depending upon length of exposure, analytical samples show significant variations in CHN content. In an effort to obtain consistent analytical results, samples were vacuum-dried for several hours before submission for analysis or spectroscopic studies. The observed CHN analysis (%) data are C, 50.46; H, 4.47; N, 2.09, while calculated values for $Eu(\mathbf{1})_2(Cl)_3 \cdot nH_2O$ ($n = 9$, 10 and 11) are C, 50.75, 50.14, 49.53; H, 4.95, 5.02, 5.05; N, 1.91, 1.89, 1.86, respectively. Although there is no evidence for it in the crystal structure determination, integrated peak intensities obtained from the ^1H NMR spectra of the complex suggest that one-quarter equivalent of EtOH may be present in powder samples. The calculated CHN composition for a complex $Eu(\mathbf{1})_2(Cl)_3 \cdot 1/4EtOH \cdot 9H_2O$ is C, 50.76; H, 4.97; N, 1.89. Clearly, it is difficult to arrive at a definite composition even for the isolated complex based upon these data alone. In an effort to shed further light on the composition of the vacuum-dried material, a TGA study was completed, and a typical trace is shown in Fig. 3. There appear to be several gradual weight loss events between 40 and 200°C. The total measured weight loss up to 200°C is 15.2%. At $\sim$240°C a more abrupt weight loss occurs. The complex $[Eu(\mathbf{1})_2(H_2O)_2](Cl)_3 \cdot 9H_2O$ would be expected to show a weight loss of 13.2% if all water of hydration were lost with no chemical reaction in the remaining complex. A complex with less water of hydration due to prior vacuum drying should show less weight loss. Further, the complex $Eu(\mathbf{1})_2(Cl)_3 \cdot 1/4EtOH \cdot 9H_2O$ mentioned above would produce a weight loss of 13.3% by removal of the EtOH and H_2O. Unfortunately then, the analytical and TGA data do not provide an unambiguous chemical formula for the complex prior to drying or a complete picture of the compositional changes in the isolated complex as a result of drying. Similar patterns have been found in lanthanide nitrate complexes with **1** [6,8].

Infrared analysis of the dried powdered complex shows a single band at 1227 cm^{-1} that most likely corresponds to the coordinated N–O group of **1** and a band at 1159 cm^{-1} that corresponds to the coordinated P=O groups. There is no evidence for uncoordinated functional groups that would most likely be indicated by a P=O band in the vicinity of 1190 cm^{-1} [6].

Given the data presented here, it remains to speculate over the nature of the solvent extraction complex such as formed by **1** in $CHCl_3$ when exposed to HCl solutions of $EuCl_3$. The simplest interpretation of ligand dependency of the extractions that produce a slope 3.1 is that the very high ligand–metal ratios ($\sim 10^6$) employed in the radioactive tracer analyses drives the addition of a third equivalent of **1** to the complex as it transfers to the ligand rich organic phase. It is possible that this third equivalent displaces the two inner sphere water molecules found in the isolated crystals; however, it is also likely that the extra ligand is simply included in a hydrogen bonded outer sphere structure. Indeed, this ligand may take the place of some or all of the outer sphere water found in the crystals isolated at lower ligand concentrations.

4. Supplementary material

Crystallographic data for the structural analysis have been deposited with the Cambridge Crystallographic Data Centre, CCDC No. 133406. Copies of this information may be obtained free of charge from The Director CCDC, 12 Union Road, Cambridge, CB2 1EZ, UK (Fax: +44-1223-336033 or e-mail: deposit@ccdc.com.ac.uk or www: http://www.ccdc.com.ac.uk).

Acknowledgements

R.T.P. thanks the US Department of Energy, Office of Basic Energy Sciences (grant 97ER-14446) for financial support of this research.

References

[1] E.M. Bond, U. Engelhardt, T.P. Deere, B.M. Rapko, R.T. Paine, J.R. FitzPatrick, Solvent Extr. Ion Exch. 15 (1997) 381.
[2] E.M. Bond, U. Engelhardt, T.P. Deere, B.M. Rapko, R.T. Paine, J.R. FitzPatrick, Solvent Extr. Ion Exch. 16 (1998) 967.
[3] E.M. Bond, X. Gan, J.R. FitzPatrick, R.T. Paine, J. Alloys Compd. 172 (1998) 271–273.
[4] E.M. Bond, Ph.D. Thesis, University of New Mexico, 1998.
[5] E.M. Bond, R.T. Paine, unpublished results.
[6] B.M. Rapko, E.N. Duesler, P.H. Smith, R.T. Paine, R.R. Ryan, Inorg. Chem. 32 (1993) 2164.
[7] U. Englehardt, B.M. Rapko, E.N. Duesler, D. Frutos, R.T. Paine, Polyhedron 14 (1995) 2361.

[8] X. Gan, E.N. Duesler, R.T. Paine, unpublished results.
[9] E.P. Horwitz, D.G. Kalina, L. Kaplan, G.W. Mason, H. Diamond, Sep. Sci. Technol. 17 (1982) 1261.
[10] D.G. Kalina, E.P. Horwitz, L. Kaplan, A.C. Muscatello, Sep. Sci. Technol. 16 (1981) 1127.
[11] E.P. Horwitz, A.C. Muscatello, D.G. Kalina, L. Kaplan, Sep. Sci. Technol. 16 (1981) 417.
[12] E.P. Horwitz, D.G. Kalina, A.C. Muscatello, Sep. Sci. Technol. 16 (1981) 403.
[13] K.A. Martin, E.P. Horwitz, J.R. Ferraro, Solv. Extr. Ion Exch. 4 (1986) 1149.
[14] D.G. Kalina, Solv. Extr. Ion Exch. 2 (1984) 381.
[15] N.V. Jarvis, Solv. Extr. Ion Exch. 9 (1991) 697.
[16] (a) T. Nakamura, C. Miyake, Solv. Extr. Ion Exch. 12 (1994) 931. (b) T. Nakamura, C. Miyake, Solv. Extr. Ion Exch. 12 (1994) 951.
[17] H. Diamond, H.-K. Pan, G.S. Knapp, E.P. Horwitz, Solv. Extr. Ion Exch. 1 (1983) 515.
[18] L.M. Vallarino, in: K.A. Gschneidner, Jr., L. Eyring (Eds.), Handbook of the Physics and Chemistry of Rare Earths, vol. 15, North Holland, Amsterdam, 1991, p. 443.

PERGAMON

www.elsevier.nl/locate/poly

Polyhedron 19 (2000) 2141–2147

POLYHEDRON

Synthesis, characterization and catalytic activity of addition compounds of dioxomolybdenum(VI) pyridine-2,6-dicarboxylate. Crystal structure of MoO_2(dipic)(L) (L = DMF, DMSO, $OPPh_3$)

Francisco J. Arnáiz [a,*], Rafael Aguado [a], María R. Pedrosa [a], André De Cian [b], Jean Fischer [b]

[a] *Laboratorio de Química Inorgánica, Universidad de Burgos, Pz Misael Bañuelos s/n, 09001 Burgos, Spain*
[b] *Laboratoire de Cristallochimie et Chimie Structurale (UMR 7513), Université Louis Pasteur, Institut Le Bel, 4 rue Blaise Pascal, 67000 Strasbourg, France*

Received 11 April 2000; accepted 20 July 2000

Abstract

MoO_2(dipic)(L) (dipic = pyridine 2,6-dicarboxylate (dipicolinate); L = dimethyl formamide (DMF), dimethyl sulfoxide (DMSO), hexamethyl phosphorotriamide (HMPA), triphenylphosphine oxide ($OPPh_3$), triethylamine, tripropylamine, tributylamine, pyridine, 2-methylpyridine, 3-methylpyridine, 4-methylpyridine) have been prepared by reacting equimolar amounts of $MoO_2Cl_2(L)_2$ (L = DMF, DMSO) with Na_2dipic, followed by addition of the appropriate ligand to the resulting solutions. The molecular structures of the DMF, DMSO and HMPA derivatives have been established by X-ray diffraction analysis. The ability of MoO_2(dipic)(L) (L = DMF, DMSO, HMPA, $OPPh_3$) to work as oxotransfer catalysts has been examined and compared with that of the prototypical $MoO_2(Et_2dtc)_2$ (Et_2dtc = diethyl dithiocarbamate). Dipicolinate complexes proved to be more efficient catalysts than dithiocarbamate for the deoxygenation of azoxybenzene with triphenylphosphine in boiling toluene. © 2000 Elsevier Science B.V. All rights reserved.

Keywords: Dioxomolybdenum dipicolinate; Oxygen-atom transfer; Azoxybenzene deoxygenation

1. Introduction

It has been assumed for years that the presence of sulfur atoms coordinated to molybdenum is a requisite for complexes of this metal to have oxotransfer activity, and many model compounds that mimic oxotransferases have been studied [1–7]. The first oxotransfer reaction involving a molybdenum complex without coordinated sulfur atoms was reported in 1990 [8]. This observation proved that the presence of sulfur atoms coordinated to molybdenum is not essential for oxotransfer activity in mild conditions, and since then a number of complexes of this kind have been reported [9–14]. One of the most relevant is the anionic $[MoO_2(NCS)_4]^{2-}$ species, which contains *N*-coordinated thiocyanate and has a catalytic activity greater than that of the prototypical $MoO_2(Et_2dtc)_2$ in the oxidation of PPh_3 with DMSO [9]. More recently the catalytic activity of $MoO_2(CH_3)_2(L)$ (L = bipyridine, alkyl substituted bipyridine) [15], and that of MoO_2[2,6-bis(mentyl)pyridine)] in oxotransfer processes has been mentioned [16]. In our laboratory we found that simple, air-stable complexes derived from MoO_2Cl_2 and MoO_2Br_2 are also superior to dithiocarbamates in the oxygen atom transfer from DMSO to PPh_3 at room temperature [13,14,17]. This prompted us to search for new dioxomolybdenum(VI) compounds in order to test their potentiality as oxotransfer catalysts. Here we report on the synthesis, characterization and catalytic activity of a number of dipicolinate complexes.

* Corresponding author..
E-mail address: farnaiz@ubu.es (F.J. Arnáiz).

0277-5387/00/$ - see front matter © 2000 Elsevier Science B.V. All rights reserved.
PII: S0277-5387(00)00513-1

2. Experimental

2.1. General procedures and measurements

All operations were carried out in a dry oxygen-free nitrogen atmosphere using standard Schlenck techniques, except the synthesis of the compounds with DMF, DMSO, HMPA and $OPPh_3$ which were conducted in air. Diethyl ether and toluene were distilled from sodium under nitrogen prior to use. *N*,*N*-Dimethylformamide was dried with barium oxide and distilled under reduced pressure. Acetone and amines for the preparation of amine complexes were distilled immediately before use. Triphenylphosphine was recrystallized prior to use and checked by ^{31}P NMR and melting point for purity. All other reagents were commercial products and were used without further purification. $MoO_2Cl_2(DMSO)_2$ and $MoO_2Cl_2(DMF)_2$ were prepared as reported [13]. Na_2dipic was prepared by reacting equimolar amounts of Na_2CO_3 and H_2dipic in water, crystallizing the resulting solution and heating the solid at 100°C under vacuum for 5 h. Melting points were determined with a Buchi 'Tottoli' with variable warm speed. Elemental analyses (C, H, N) were performed on a Perkin–Elmer 2400 CHN analyzer and molybdenum was determined by titration with lead(II) nitrate [18]. IR spectra were recorded on a Perkin–Elmer 843 spectrometer with Heyden and Son Spectrafile-IR version 2.2 operating software, and UV–Vis spectra on a Milton Roy Spectronic 3000 Arrays spectrometer equipped with a thermostated cell. NMR spectra were recorded on a Bruker AC-300 and a Bruker DPX 300 spectrometer (^1H, 300 MHz; ^{31}P, 121.5 MHz). Chemical shifts are relative to TMS (^1H), or external 85% H_3PO_4 (^{31}P), with downfield values reported as positive. Coupling constants J are given in Hz.

2.2. General procedure for the preparation of MoO_2(dipic)(L) (L = DMF, DMSO, HMPA, $OPPh_3$)

A mixture of Na_2dipic (2.11 g, 10.5 mmol), $MoO_2Cl_2(DMF)_2$ (3.45 g, 10 mmol) and L (12 mmol) in acetone (60 ml) was refluxed with stirring for 1 h. The white precipitate was separated by filtration and washed with acetone (10 ml). The combined filtrate and washing was concentrated to 10 ml and then diethyl ether (50 ml) was added. The resulting light yellow microcrystalline precipitate was filtered, washed with diethyl ether (2 × 10 ml) and dried under vacuum.

2.2.1. MoO_2(dipic)(DMF)

Yield 3.07 g (83.8%). — M.p. (dec.) 200–202°C. — IR (KBr) cm^{-1}: $\nu(MoO_2) = 942$ s, 905 s; $\nu(CO_2) = 1693$ s, 1489 s; ν(C=O, DMF) = 1637 s. — ^1H NMR (300 MHz, acetone-d_6, 25°C, TMS): $\delta = 8.85$ (t, $J = 7.63$, 1H, dipic), 8.46 (d, $J = 7.63$, 2H, dipic), 8.19 (s, 1H, H–CO), 3.06 (s, 3H, CH_3), 2.62 (s, 3H, CH_3). — *Anal.* Calc. for $C_{10}H_{10}MoN_2O_7$ (367.96): Mo 26.20, C 32.81, H 2.75, N 7.65. Found: Mo 26.12, C 31.67, H 2.87, N 7.56%.

2.2.2. MoO_2(dipic)(DMSO)

Yield 3.40 g (91.6%). — M.p. (dec.) 185–187°C. — IR (KBr) cm^{-1}: $\nu(MoO_2) = 942$ s, 909 s; $\nu(CO_2) = 1707$ s, 1470 s; ν(S=O) = 1081 s. — ^1H NMR (300 MHz, acetone-d_6, 25°C, TMS): $\delta = 8.81$ (t, $J = 7.73$, 1H, dipic), 8.45 (d, $J = 7.73$, 2H, dipic), 2.69 (s, 6H, CH_3). — *Anal.* Calc. for $C_9H_9MoNO_7S$ (372.92): Mo 25.85, C 29.12, H 2.44, N 3.77. Found: Mo 25.73, C 29.24, H 2.39, N 3.79%.

2.2.3. MoO_2(dipic)(HMPA)

Yield 3.62 g (76.7%). — M.p. (dec.) 234–236°C. — IR (KBr) cm^{-1}: $\nu(MoO_2) = 934$ s, 912 s; $\nu(CO_2) = 1707$ s, 1466 s; ν(P=O) = 1192 s; ν(HMPA) = 1303, 993 and 756. — ^1H NMR (300 MHz, acetone-d_6, 25°C, TMS): $\delta = 8.76$ (t, $J = 7.76$, 1H, dipic), 8.43 (d, $J = 7.76$, 2H, dipic), 2.46 (d, $J_{HP} = 9.63$, 18H, CH_3). — ^{31}P NMR (121.5 MHz, acetone-d_6, 25°C, H_3PO_4): $\delta = 29.60$. — *Anal.* Calc. for $C_{13}H_{21}MoN_4O_7P$ (474.02): Mo 20.32, C 33.06, H 4.48, N 11.86. Found: Mo 20.22, C 32.18, H 4.30, N 11.68%.

2.2.4. MoO_2(dipic)($OPPh_3$)

Yield 4.20 g (73.5%). — IR (KBr) cm^{-1}: $\nu(MoO_2) = 940$ s, 910 s; $\nu(CO_2) = 1710$ s, 1585 s; ν(P=O) = 1154 s. — ^1H NMR (300 MHz, acetone-d_6, 25°C, TMS): $\delta = 8.71$ (t, $J = 7.76$, 1H, dipic), 8.31 (d, $J = 7.93$, 2H, dipic), 7.7–7.5 (m, 15H, C_6H_5). — ^{31}P NMR (121.5 MHz, acetone-d_6, 25°C, H_3PO_4): δ = 33.07. — *Anal.* Calc. for $C_{25}H_{18}MoNO_7P$ (572.99): Mo 16.79, C 52.56, H 3.27, N 2.45. Found: Mo 16.62, C 52.42, H 3.23, N 2.50%.

2.3. General procedure for the preparation of MoO_2(dipic)(amine) (amine = pyridine (Py), 2-methylpyridine (2-MePy), 3-methylpyridine (3-MePy), 4-methylpyridine (4-MePy), triethylamine (NEt_3), tripropylamine (NPr_3), tributylamine (NBu_3))

To a solution of MoO_2(dipic)(DMF) (1.46 g, 4 mmol) in acetone (20 ml) a solution of amine (4.2 mmol) in acetone (5 ml) is added. After stirring the resulting mixture for 5 min, the white precipitate is filtered, washed with acetone (2 × 5 ml) and diethyl ether (2 × 10 ml), and dried under vacuum.

2.3.1. MoO_2(dipic)(Py)

Yield 1.41 g (95%). — IR (KBr) cm^{-1}: $\nu(MoO_2) =$ 946 s, 919 s; $\nu(CO_2) = 1730$ s, 1484 s. — *Anal.* Calc. for $C_{12}H_8MoN_2O_6$ (372.14): Mo 25.78, C 38.73, H 2.17, N 7.53. Found: Mo 25.35, C 38.52, H 2.32, N 7.25%.

2.3.2. MoO_2(dipic)(2-MePy)

Yield 1.03 g, (67%). — IR(KBr) cm^{-1}: $\nu(MoO_2)$ = 946 s and 918 s; $\nu(CO_2)$ = 1726 s, 1431 s. — *Anal.* Calc. for $C_{13}H_{10}MoN_2O_6$ (386.17): Mo 24.85, C 40.43, H 2.61, N 7.25. Found: Mo 24.85, C 40.13, H 2.38, N 7.07%.

2.3.3. MoO_2(dipic)(3-MePy)

Yield 1.24 g, (80%). — IR(KBr) cm^{-1}: $\nu(MoO_2)$ = 947 s, 914 s; $\nu(CO_2)$ = 1726 s, 1455 s. — *Anal.* Calc. for $C_{13}H_{10}MoN_2O_6$ (386.17): Mo 24.85, C 40.43, H 2.61, N 7.25. Found: Mo 23.96, C 39.62, H 2.57, N 6.95%.

2.3.4. MoO_2(dipic)(4-MePy)

Yield 1.32 g, (85%). — IR(KBr) cm^{-1}: $\nu(MoO_2)$ = 942 s, 908 s; $\nu(CO_2)$ = 1730 s, 1433 s. — *Anal.* Calc. for $C_{13}H_{10}MoN_2O_6$ (386.17): Mo 24.85, C 40.43, H 2.61, N 7.25. Found: Mo 24.98, C 39.86, H 2.77, N 6.96%.

2.3.5. MoO_2(dipic)(NEt_3)

Yield 1.17 g, (74%). — IR(KBr) cm^{-1}: $\nu(MoO_2)$ = 942 s, 912 s; $\nu(CO_2)$ = 1609 s, 1447s. — *Anal.* Calc. for $C_{13}H_{18}MoN_2O_6$ (394.24): Mo 24.34, C 39.61, H 4.60, N 7.11. Found: Mo 24.03, C 39.35, H 4.72, N 7.25%.

2.3.6. MoO_2(dipic)(NPr_3)

Yield 1.08 g, (62%). — IR(KBr) cm^{-1}: $\nu(MoO_2)$ = 937 s, 909 s; $\nu(CO_2)$ = 1690 s, 1470 s. — *Anal.* Calc. for $C_{16}H_{24}MoN_2O_6$ (436.32): Mo 21.99, C 44.04, H 5.54, N 6.42. Found: Mo 22.54, C 45.04, H 5.70, N 6.22%.

2.3.7. MoO_2(dipic)(NBu_3)

Yield 1.72 g, (90%). — IR(KBr) cm^{-1}: $\nu(MoO_2)$ = 939 s, 910 s; $\nu(CO_2)$ = 1684 s, 1467 s. — *Anal.* Calc. for $C_{19}H_{30}MoN_2O_6$ (478.40): Mo 20.26, C 47.70, H 6.32, N 5.86. Found: Mo 19.50, C 46.96, H 6.10, N 5.68%.

2.4. Preparation of Mo_2O_3(dipic)$_2$($OPPh_3$)$_2$

2.4.1. Method A

A mixture of MoO_2(dipic)($OPPh_3$) (0.71 g, 1.25 mmol) and PPh_3 (0.33 g, 1.25 mmol) in toluene (30 ml) was refluxed for 1 h under nitrogen. The dark brown powdered precipitate is filtered, washed with diethyl ether and dried under vacuum (0.61 g, 87%).

2.4.2. Method B

A mixture of MoO_2(dipic)($OPPh_3$) (0.71 g, 1.25 mmol) and PPh_3 (0.33 g, 1.25 mmol) in acetone (30 ml) was refluxed for 2 h under nitrogen. The resulting solution is concentrated to 10 ml and then treated with diethyl ether (30 ml). The dark brown precipitate is filtered, washed with diethyl ether and dried under vacuum (0.63 g, 89.5%).

IR(KBr) cm^{-1}: $\nu(MoO_2)$ = 953 s, 914 s; $\nu(CO_2)$ = 1688 s, 1438 s; $\nu(P{=}O)$ = 1160 s. — ^1H NMR (80 MHz, $CDCl_3$, 25°C, TMS): δ = 8.0–8.4 (m, J = 7.76 Hz, 3H, dipic), 7.4–7.6 (m, 15H, C_6H_5). — *Anal.* Calc. for $C_{50}H_{36}Mo_2N_2O_{13}P_2$ (1129.99): Mo 17.03, C 53.30, H 3.22, N 2.49. Found: Mo 17.23, C 53.12, H 3.06, N 2.32%.

2.5. Catalytic activity

The measurement of the catalytic activity of MoO_2(dipic)(DMSO) in the oxidation of triphenyl phosphine with dimethyl sulfoxide was followed by ^{31}P NMR spectroscopy, and compared with that of $MoO_2(Et_2dtc)_2$, as previously reported [13]. Two 5 ml DMSO (20% v/v in DMSO-d_6) solutions, at [Mo] = 0.02 mol dm^{-3} and [PPh_3] = 0.40 mol dm^{-3}, were used. At 25°C the oxidation of 50% PPh_3 required 175 min in the dipicolinate solution and 85 min in that of the dithiocarbamate. PPh_3 became undetectable with the former after 7 h. Solid PPh_3 (50 mg) was added to the dipicolinate solution that was examined after 4 h showing only the presence of $OPPh_3$. The same result was obtained when this operation was repeated after 2, 4 and 7 days.

2.6. Deoxygenation of azoxybenzene

The deoxygenation of azoxybenzene was followed in toluene at 105°C monitoring the reaction by visible spectroscopy. Samples of 2 ml were collected off by syringe from the reacting system at regular intervals, and immediately transferred to graduated rubber-capped tubes, containing 2 ml of 4 M NaOH, immersed into an ice bath. After vigorous shaking of the tubes to remove the molybdenum complexes from the toluene phase the absorbance was measured at 446 nm, wavelength at which azobenzene is the only absorbing species present in toluene.

2.7. Crystal-structure determinations

Suitable single crystals were grown at room temperature by diffusion of diethyl ether on acetone solutions of the complexes in a dry atmosphere. Crystal data MoO_2(dipic)(DMF) were collected using an Enraf–Nonius MACH3 diffractometer with graphite-monochromated Mo Kα radiation. Crystal data for the complexes MoO_2(dipic)(DMSO) and MoO_2(dipic)($OPPh_3$) were collected using a KappaCCD diffractometer with graphite-monochromated Mo Kα radiation. Hydrogen atom positions were located from difference Fourier maps. All three structures were solved using OPENMOLEN

2.2. Table 1 provides crystallographic details for these compounds.

3. Results and discussion

3.1. Synthesis and characterization of the complexes

To the best of our knowledge only a marginal reference to the synthesis and characterization by melting point and infrared spectroscopy of MoO_2(dipic)-(HMPA) has been reported [19]. More recently, in studies on the reactivity of molybdenaoxaziridine complexes, the formation of Mo_2O_3(dipic)$_2$(HMPA)$_2$ was postulated [20]. MoO_2(dipic)(HMPA) was prepared by reacting MoO_2(acac)$_2$ (acac = acetylacetonate) with dipicolinic acid and HMPA in CH_2Cl_2. In these conditions a green solution was obtained which suggests that a redox process also occurs, probably involving the acacH displaced.

To overcome this difficulty we have used the easily available $MoO_2Cl_2(L)_2$ (L = DMF, DMSO) [17] complexes instead of MoO_2(acac)$_2$. Metathetic reactions between the disodium salt of dipicolinic acid and the corresponding chlorocomplex in acetone proved to be appropriate for preparing MoO_2(dipic)(DMF) and MoO_2(dipic)(DMSO). The reaction requires about 24 h at room temperature for completion, probably because Na_2dipic is scarcely soluble in acetone, but less than 1 h when carried out to reflux. The compounds are recovered in good yield from the resulting solutions by removing most of the solvent under vacuum followed by precipitation with diethyl ether.

MoO_2(dipic)(L) (L = HMPA, $OPPh_3$, tertiary amine) were prepared by treating acetone solutions of MoO_2(dipic)(DMF) or MoO_2(dipic)(DMSO) with the corresponding ligand. MoO_2(dipic)(HMPA) and MoO_2(dipic)($OPPh_3$) are obtained by addition of diethyl ether to the resulting solutions, while the amine derivatives separated as fine white precipitates; further studies for the complete characterization of the latter are in progress. MoO_2(dipic)(HMPA) and MoO_2-(dipic)($OPPh_3$) can also be prepared by reacting $MoO_2Cl_2(L)_2$ (L = DMF, DMSO) with Na_2dipic in presence of the corresponding ligand, followed by filtration of NaCl and addition of diethyl ether to the resulting solution. In this regard the DMF complex is superior to that of DMSO since DMF is miscible with diethyl ether. The presence of minor amounts of water either in Na_2dipic or in the solvent has not significant effect on the preparation of the derivatives with DMF, DMSO, HMPA and $OPPh_3$ since these ligands are able to displace water from the coordination sphere of molybdenum. Also they have a low affinity for protons, thus precluding the formation of polymolybdates. By the contrary, the high proton basicity of tertiary amines requires the use of rigorously anhydrous conditions to obtain pure products.

No relevant features are observed in the IR spectra of the compounds. The presence of two bands in the region 900–950 cm^{-1} indicates that, as usual for dioxomolybdenum(VI) species, all the complexes contain

Table 1
Crystal data and summary of intensity data collection and structure refinement of complexes MoO_2(dipic)(DMF), MoO_2(dipic)(DMSO) and MoO_2(dipic)($OPPh_3$)

	MoO_2(dipic)(DMF)	MoO_2(dipic)(DMSO)	MoO_2(dipic)($OPPh_3$)
Empirical formula	$C_{10}H_{10}MoN_2O_7$	$C_9H_9MoNO_7S$	$C_{25}H_{18}MoNO_7P$
Molecular weight	366.14	371.18	571.34
Crystal system	triclinic	triclinic	monoclinic
Space group	$P\bar{1}$	$P\bar{1}$	$P12_1/n1$
Unit cell dimensions			
a (Å)	7.1627(9)	6.627(1)	9.5225(3)
b (Å)	7.991(1)	7.619(1)	17.9542(6)
c (Å)	13.486(4)	12.793(1)	14.5104(4)
α (°)	72.21(2)	97.164(4)	
β (°)	79.49(2)	101.912(4)	107.537(2)
γ (°)	62.19(1)	93.063(4)	
V (Å^3)	649.4(2)	625.0(2)	2365.5(2)
Z	2	2	4
D_{calc} (g cm^{-3})	1.87	1.97	1.60
μ (mm^{-1})	1.043	1.244	0.669
Number of data measured	2737	8656	18322
Number of data with $I>3\sigma(I)$	2320	2586	5009
Scan mode	$\theta/2\theta$	ϕ and ω scans	phi scans
T (K)	294	294	173
R	0.025	0.027	0.040
wR	0.041	0.043	0.056
Goodness-of-fit (GOF)	1.012	1.094	1.043

Table 2
Selected bond lengths (Å) and angles (°) for MoO_2(dipic)(DMF), MoO_2(dipic)(DMSO) and MoO_2(dipic)($OPPh_3$)

	MoO_2(dipic)(DMF)	MoO_2(dipic)(DMSO)	MoO_2(dipic)($OPPh_3$)
Mo(1)–O(5)	1.674(2)	1.696(2)	1.687(2)
Mo(1)–O(6)	1.702(2)	1.703(2)	1.700(2)
Mo(1)–O(1)	2.009(2)	2.008(2)	2.003(2)
Mo(1)–O(4)	2.010(2)	2.017(2)	2.000(2)
Mo(1)–N(1)	2.190(2)	2.198(2)	2.205(2)
Mo(1)–O(7)	2.308(2)	2.312(2)	2.247(2)
O(4)–C(7)	1.320(4)	1.335(3)	1.326(3)
O(1)–C(1)	1.325(4)	1.334(3)	1.325(3)
O(7)–X	1.233(4)	1.544(2)	1.502(2)
O(5)–Mo(1)–O(6)	105.5(1)	104.7(1)	104.6(1)
O(1)–Mo(1)–O(4)	144.68(9)	144.81(7)	145.43(8)
O(6)–Mo(1)–O(4)	106.5(1)	101.82(8)	103.86(9)
O(6)–Mo(1)–O(1)	101.8(1)	106.90(9)	104.73(8)
N(1)–Mo(1)–O(4)	72.48(8)	72.56(7)	72.95(8)
N(1)–Mo(1)–O(1)	72.79(8)	73.12(7)	73.03(7)
O(5)–Mo(1)–O(4)	95.8(1)	94.49(9)	72.95(8)
O(5)–Mo(1)–O(1)	96.6(1)	97.40(8)	95.79(9)
O(6)–Mo(1)–O(7)	82.3(1)	83.86(8)	85.04(8)
N(1)–Mo(1)–O(7)	71.76(8)	73.97(6)	71.31(7)
N(1)–Mo(1)–O(5)	100.5(1)	97.40(8)	99.06(9)
O(5)–Mo(1)–O(7)	172.0(1)	171.37(8)	170.36(9)
N(1)–Mo(1)–O(6)	153.9(1)	157.58(8)	156.35(9)

the *cis*-MoO_2 moiety [21,22]. A relationship between the basicity of the *O*-donor neutral ligand and the separation of the $\nu(MoO_2)$ bands (the higher the basicity the lower the separation) is also appreciated, but a definite explanation for this effect is not attempted since the differences in bond lengths and angles for the group *cis*-MoO_2 are not significant (see Table 2). The stretching bands for O–C, O–S and O–P of the coordinated ligands in complexes with DMF, DMSO, HMPA and $OPPh_3$ occur at 1637, 1081, 1154 and 1192 cm^{-1} respectively; they are shifted 20–25 cm^{-1} to lower wavenumbers with respect to those of the free ligands, which is indicative of coordination through the oxygen atom [23].

The ^1H NMR spectra of MoO_2(dipic)(L) (L = DMF, DMSO, HMPA and $OPPh_3$) are in agreement with those expected for octahedral complexes having a reflection plane and free rotation around the molybdenum-neutral ligand bond. The presence of two singlets for the methyl groups in MoO_2(dipic)(DMF) indicates that no free rotation exists around the C–N bond.

3.2. Molecular structures

Single-crystal X-ray diffraction studies on MoO_2(dipic)(L) (L = DMF, DMSO, $OPPh_3$) revealed that the three complexes have a closely related structure, similar to that of MoO_2(dipic)(DMF) shown in Fig. 1.

The molybdenum atom adopts the expected distorted octahedral geometry, which is determined by the usual way of coordination for the dipicolinate ligand (planar tridentate) to the angular *cis*-MoO_2 moiety.

Selected bond lengths and angles are listed in Table 2. The bond lengths for Mo–O(5) and Mo–O(6) are not identical, the former being shorter. While the Mo–O(6) distance, involving the oxygen *trans* to N(1), is nearly identical for all the complexes, the Mo–O(5) distance increases with the basicity of the *trans* ligand.

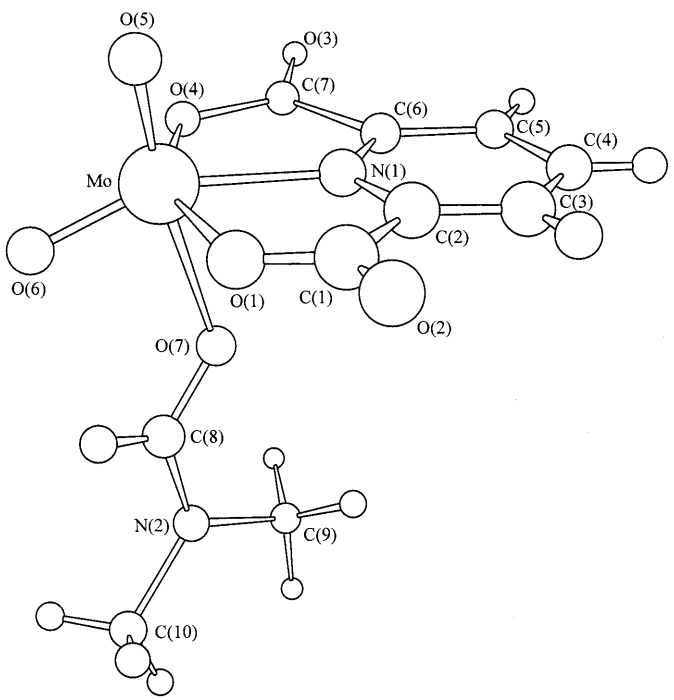


Fig. 1. Molecular structure and atom-labeling for complex MoO_2(dipic)(DMF); the hydrogen atoms are shown with small arbitrary radii.

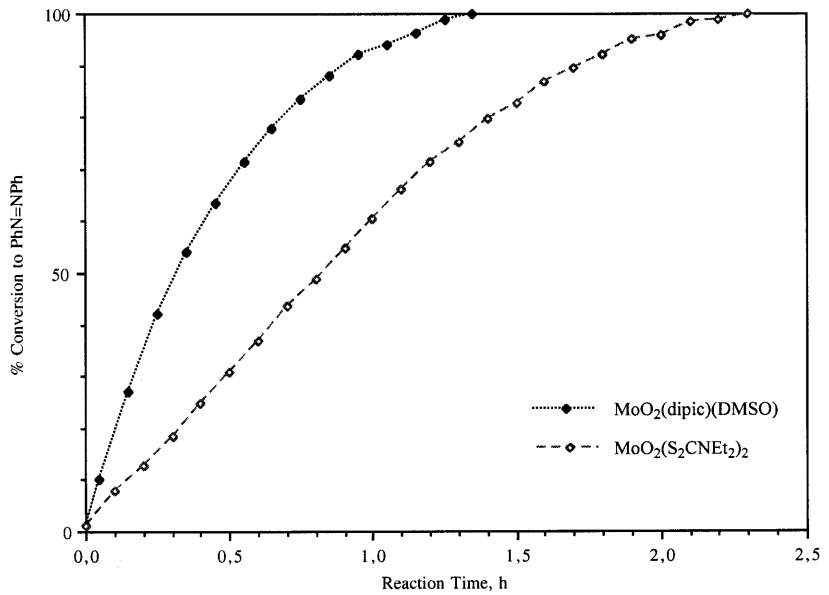


Fig. 2. Reduction of PhN(O)=NPh to PhN=NPh using PPh_3 as a funtion of time at [Mo] = 1.25 10^{-3} mol dm^{-3} and $[PPh_3]_0/[PhN(O)=NPh]_0/[Mo^{VI}]_0 = 10/1/0.05$.

The angles for the *cis*-MoO_2 group, O(5)–Mo–O(6), are very similar in the three compounds (ca. 105°), and in good agreement with those found for analogous complexes with *N*- and *O*-coordinated ligands [1,24].

3.3. Oxotransfer reactions

The oxygen atom transfer from MoO_2(dipic)(L) (L = DMF, DMSO, HMPA, $OPPh_3$) to PPh_3 has been examined. By treating acetone solutions of the complexes with PPh_3 a brown solution results at the same time that $OPPh_3$ forms. No significant difference in the behavior of the complexes MoO_2(dipic)(DMF), MoO_2(dipic)(DMSO) and MoO_2(dipic)($OPPh_3$) was observed, except for the evolution of the foul-smelling dimethyl sulfide (DMS) when the DMSO adduct was used. The only molybdenum product we could characterize, even in a large excess of PPh_3, is $Mo_2^{V}O_3$(dipic)$_2$($OPPh_3$)$_2$. Attempts to grow crystals suitable for X-ray characterization have been unsuccessful to date. Evidence — based on the ^{1}H NMR of the product — about formation of $Mo_2^{V}O_3$(dipic)$_2$(HMPA)$_2$ was found when using MoO_2(dipic)(HMPA), presumably due to the superior coordinating ability of HMPA with respect to $OPPh_3$. These results strongly suggest that: (i) $Mo^{IV}O$(dipic)(L) comproportionates as it forms with the remaining $Mo^{VI}O_2$(dipic)(L), at the same time that the coordinated DMF or DMSO are displaced by the $OPPh_3$ produced, thus leading to the dinuclear complex $Mo_2^{V}O_3$(dipic)$_2$($OPPh_3$)$_2$ which is very resistant to reduction; (ii) $Mo^{IV}O$(dipic)(DMSO) rearranges to $Mo^{VI}O_2$(dipic)(DMS) (PPh_3 is unable to deoxygenate DMSO in absence of MoO_2(dipic)(L) in the same conditions) and the resulting, soft ligand dimethyl sulfide is easily displaced from the coordination sphere of molybdenum. After this, it becomes evident that at least MoO_2(dipic)(DMSO) displays catalytic activity in oxotransfer reactions.

The catalytic activity of MoO_2(dipic)(DMSO) in the oxotransfer from DMSO to PPh_3 has been measured and compared with that of the prototypical $MoO_2(Et_2dtc)_2$ by following the formation of $OPPh_3$ by ^{31}P NMR as previously reported [13]. At 25°C the dithiocarbamate complex showed to be considerably more active than MoO_2(dipic)(DMSO). However, while $MoO_2(Et_2dtc)_2$ decomposes slowly in DMSO at room temperature, MoO_2(dipic)(DMSO) retains its catalytic activity for several days, as shown by addition of new batches of PPh_3 to the original solution.

The oxotransfer from azoxybenzene to PPh_3 has also been examined. Azoxybenzene derivatives are difficult to deoxygenate [25], and because of the low basicity of the azoxy group a weak coordinating solvent is advisable to avoid competition for the molybdenum center.

Fig. 2 shows the transformation of azoxybenzene into azobenzene with a large excess of PPh_3 in hot toluene in presence of $MoO_2(Et_2dtc)_2$ and MoO_2(dipic)(DMSO). The behavior of MoO_2(dipic)(DMF), MoO_2(dipic)(HMPA) and MoO_2(dipic)($OPPh_3$) is closely similar to that of MoO_2(dipic)(DMSO) and the results are omitted for clarity.

After completion of the deoxygenation process, $Mo_2O_3(Et_2dtc)_4$ and $Mo_2^{V}O_3$(dipic)$_2$($OPPh_3$)$_2$ could be isolated. The fact that we were unable to isolate oxomolybdenum(IV) complexes in a large excess of PPh_3 suggests that $Mo_2O_3(Et_2dtc)_4$ and $Mo_2^{V}O_3$(dipic)$_2$($OPPh_3$)$_2$ are the prevalent species in toluene solution, and that the equilibrium represented below — as well

as the analogous for $Mo_2O_3(Et_2dtc)_4$ — is strongly displaced to the left in poor coordinating solvents.

$$Mo_2O_3(dipic)_2(OPPh_3)_2 \leftrightharpoons MoO_2(dipic)(OPPh_3) + MoO(dipic)(OPPh_3)$$

4. Conclusions

(i) A number of air stable dioxomolybdenum(VI) dipicolinates can be easily prepared in good yields by reacting the readily available DMF or DMSO adducts of MoO_2Cl_2 with Na_2dipic, followed by addition of the appropriate ligand. (ii) The compounds, while showing a low catalytic activity in oxotransfer reactions at ambient temperature, display a high activity above 100°C which combined with the thermal stability of the complexes can be exploited in deoxygenation processes otherwise difficult to achieve.

5. Supplementary material

Crystallographic data for the structural analysis have been deposited with the Cambridge Crystallographic Data Centre, CCDC Nos. 137435 {for [MoO_2(dipic)(DMF)]}, 137436 {for [MoO_2(dipic)(DMSO)]} and 137437 {for [MoO_2(dipic)($OPPh_3$)]}. Copies of this information may be obtained free of charge from The Director, CCDC, 12 Union Road, Cambridge, CB2 1EZ, UK (fax: +44-1223-336033; e-mail: deposit@ccdc.cam.ac.uk or www: http://www.ccdc.cam.ac.uk).

Acknowledgements

This work was supported by the Direccion General de Enseñanza Superior (Grant PS95-0832) and Junta de Castilla y Leon (Grant BU14/98).

References

[1] R.H. Holm, Chem. Rev. 87 (1987) 1401 references therein.
[2] R.H. Holm, Coord. Chem. Rev. 100 (1990) 183 references therein.
[3] J. Kollar, Am. Chem. Soc. Div. Petr. Chem. Prepr. 23 (1978) 106.
[4] R.A. Sheldon, J.K. Kochi, Metal Catalyzed Oxidation of Organic Compounds, Academic, New York, 1981.
[5] H. Mimoun, J. Mol. Catal. 7 (1980) 1.
[6] F. Bottomley, L. Sutin, Adv. Organomet. Chem. 28 (1988) 339.
[7] H. Arzoumanian, Bull. Soc. Chim. Belg. 100 (1991) 717.
[8] S.A. Roberts, C.G. Young, C.A. Kipke, W.E. Cleland, Jr., K. Yamanouchi, M.D. Carducci, J.H. Enemark, Inorg. Chem. 29 (1990) 3650.
[9] H. Arzoumanian, R. Lopez, G. Agrifoglio, Inorg. Chem. 33 (1994) 3177.
[10] H. Arzoumanian, G. Agrifoglio, H. Krentzien, M. Capparelli, J. Chem. Soc., Chem. Commun. (1995) 655.
[11] H. Arzoumanian, G. Agrifoglio, H. Krentzien, New J. Chem. 20 (1996) 699.
[12] H. Arzoumanian, A. Bouraoui, V. Lazzeri, M. Rajzmann, H. Teruel, H. Krentzien, New J. Chem. 16 (1992) 965.
[13] F.J. Arnáiz, R. Aguado, J.M. Martínez-Ilarduya, Polyhedron 13 (1994) 3257.
[14] F.J. Arnáiz, R. Aguado, J. Chem. Educ. 72 (1995) A196.
[15] C.C. Romao, 5th FGIPS Meeting in Inorganic Chemistry, Toulouse, France, October 1999.
[16] S. Bellemin-Laponaz, K.S. Coleman, P. Dierkes, J.-P. Masson, J.A. Osborn, Eur. J. Inorg. Chem. (2000) 1645.
[17] F.J. Arnáiz, Inorg. Synth. 31 (1997) 246.
[18] R. Pürschel, E. Lassner, R.Z. Scharf, Anal. Chem. 163 (1958) 104.
[19] L.S. Liebeskind, K.B. Sharpless, R.D. Wilson, J.A. Ibers, J. Am. Chem. Soc. 100 (1978) 7061.
[20] E.R. Moller, K.A. Jörgensen, J. Am. Chem. Soc. 115 (1993) 11814.
[21] (a) P.C.H. Mitchell, Quart. Rev. 20 (1966) 103. (b) Y.L. Wong, J.F. Ma, W.F. Law, Y. Yan, W.T. Wong, Z.Y. Zhang, T.C.W. Mak, D.K.P. Ng, Eur. J. Inorg. Chem. (1999) 313.
[22] F.J. Arnáiz, R. Aguado, J. Sanz-Aparicio, M. Martinez-Ripoll, Polyhedron 13 (1994) 2745.
[23] K. Nakamoto, Infrared and Raman Spectra of Inorganic and Coordination Compounds, fifth ed., Wiley, New York, 1997.
[24] (a) J. Stiefel, in: G. Wilkinson, J.A. McCleverty (Eds.), Comprehensive Coordination Chemistry, vol. 3, Pergamon Press, Oxford, 1987, p. 1375 (Chapter 36.5). (b) Y.L. Wong, J.F. Ma, W.F. Law, Y. Yan, W.T. Wong, Z.Y. Zhang, T.C.W. Mak, D.K.P. Ng, Eur. J. Inorg. Chem. (1999) 313.
[25] (a) J.F. Vozza, J. Org. Chem. 34 (1969) 3219. (b) J.I.G. Cadogan, M. Cameron-Wood, Proc. Chem. Soc. (1962) 361. (c) G.A. Olah, B.G.B. Gupta, S.C. Narang, J. Org. Chem. 43 (1978) 4503. (d) D. Konwar, R.C. Boruah, J.S. Sandhu, Synthesis 4 (1990) 337.

PERGAMON

www.elsevier.nl/locate/poly

Polyhedron 19 (2000) 2149–2154

POLYHEDRON

Template reaction of $[Ni(ben)_3](ClO_4)_2$ with acetone. Crystal structure of 1,11-bis-benzyl-5,7,7-trimethyl-1,4,8,11-tetra-aza-undeca-4-ene nickel(II) perchlorate

Guillermo Mendoza-Díaz [a,*], Lena Ruiz-Ramírez [b], Rafael Moreno-Esparza [b]

[a] *Facultad de Química, Universidad de Guanajuato, Noria Alta s/n, Guanajuato, Gto. 36050 Mexico*
[b] *Departamento de Química Inorgánica y Nuclear, División de Estudios de Posgrado, Facultad de Química, Universidad Nacional Autónoma de México, Ciudad Universitaria, 04510 Mexico*

Received 7 February 2000; accepted 21 July 2000

Abstract

The template synthesis of a new open-chain tetra-aza ligand derived from *N*-benzylethylenediamine is reported. X-ray structural analysis of the title compound has been determined. ^{13}C CP-MAS NMR for the $[Ni(benacet)](ClO_4)_2$ complex was made and assignment of the signals was carried out by the use of the open gate decoupling technique and by comparison with the Ni(II) and Zn(II) complexes of the *trans*-[14]diene ligand as well as with the perchlorate salt of the free macrocycle. Based on the type of isolated compound, a hypothesis of the possible mechanism of reaction that explains the formation of the mesityl moiety during the template reaction is discussed. This hypothesis could also be used to explain how in the original reaction made by Curtis, a mixture of *cis*- and *trans*-isomers are formed. © 2000 Elsevier Science B.V. All rights reserved.

Keywords: Tetra-aza ligands; CP-MAS NMR; Nickel complex; Template reaction

1. Introduction

The development of multidentate ligands that form a coordination sphere surrounding a metal ion and particularly the development of synthetic procedures to obtain macrocyclic ligands is of current importance [1]. The relevance of this is due in part, to the interest in preparing simple coordination compounds that could mimic the metallo-biomolecules and their activity [2]. This type of chemistry has been defined as biomimetic chemistry and these new molecules may act as artificial enzymes, artificial oxygen carriers, etc. One of these activities is the oxidative DNA cleavage [3]. In particular, nickel macrocyclic compounds have been found to promote site- and conformation-specific oxidative cleavage of DNA [4]. Muller et al. have demonstrated that reactivity of these macrocyclic nickel complexes, depends upon the in-plane donor strength, flexibility of macrocyclic ligand and to a lesser extent on redox potential [5,6].

Template reactions have been widely studied as a synthetic route for macrocyclic ligands. In particular, the synthesis of tetra-aza macrocycle ligands developed in the 1960s, where the Ni(II) ion was employed as a templating agent, opened a field with great possibilities in preparative chemistry. In this template reaction developed by Curtis [7], the crucial step is a Schiff base condensation between the carbonyl fragment with the primary amine coordinated to the metal ion, and therefore imposing geometric restrictions to the ligand and their reactivity. It has been found that copper(II) can also act as a template agent; however nickel has usually been preferred. The formation of the ligand complexes depends significantly on the dimension of the cavity, the rigidity of the ligand, the nature of the donor atoms and the complexing properties of the anions involved in the reaction. In particular the rigidity of the tetra-aza

* Corresponding author. Tel.: +52-4-732-6885, ext. 8133; fax: +52-4-733-0177.
E-mail address: mendozag@quijote.ugto.mx (G. Mendoza-Díaz).

0277-5387/00/$ - see front matter © 2000 Elsevier Science B.V. All rights reserved.
PII: S0277-5387(00)00525-8

ligands will vary extensively depending on whether they are macrocycles, or open chains with or without bulky terminal groups. An example of the first class is the macrocyclic ligand originally prepared by Curtis, [14]diene, (see Fig. 1a); an example for the second group is the analogous ligand with an open chain structure (see Fig. 1b) [7]; however, as far as we know there is no example of direct template synthesis to obtain complexes with ligands of the third class, involving the formation of a mesytil moiety.

In the current investigation, we attempted to gain more insight about the template mechanism in the Curtis-type reaction, as well as the type of structure obtained when the amine employed is a mono-substituted ethylenediamine with a bulky group.

2. Experimental

All reactants and solvents were analytical grade and were used without further purification, with the exception of ethylenediamine which was distilled over NaOH before use.

Infrared spectra were recorded on a Perkin–Elmer 1600 series FTIR on KBr pellets. Electronic spectra were recorded on a Perkin–Elmer model lambda 4B on quartz cuvettes and methanol as solvent. ^{13}C, ^{15}N NMR CP-MAS and solution spectra were recorded on a Varian Unity-Plus spectrometer of 300 MHz equipped with a VT CP-MAS probe and a broad band 5 mm probe for solution. X-ray diffraction data were collected on a Siemens P4/PC diffractometer.

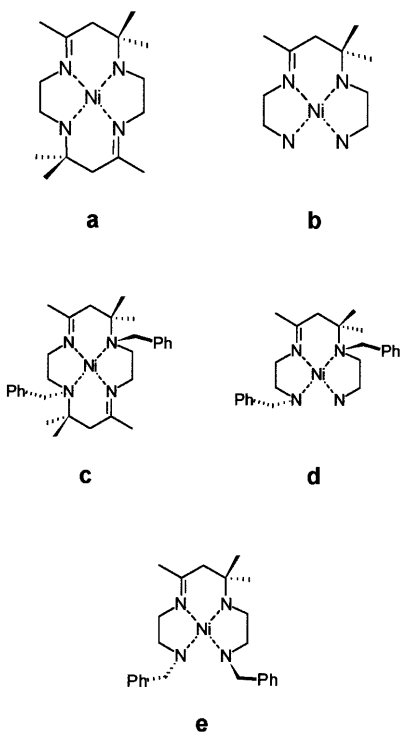


Fig. 1. Products from the Curtis template reaction: (a) the cationic macrocyclic complex: 2,4,4,9,11,11-hexamethyl-1,5,8,12-tetra-aza-tetradecacyclo-1,8-diene nickel(II) ([14]diene); (b) the cationic complex: 5,7,7-trimethyl-1,4,8,11-tetra-aza-undeca-4-ene nickel(II); (c–e) possible isomers obtained from the condensation reaction between $[Ni(ben)_3]^{2+}$ and acetone (see text for explanation).

2.1. Synthesis of products

N-Benzyl-ethylendiamine was prepared according to a previous report [8].

Tris-*N*-benzylethylendiamine nickel(II) perchlorate, $[Ni(ben)_3](ClO_4)_2$, was prepared by adapting a previously reported technique [8–10]. In the original procedure after the precipitate was filtered off, it must be washed with acetone. Instead in this preparation we used a mixture of 2:1 ethanol–ether. The precipitate was collected and dried in vacuum at 80°C. **Caution!** As with all perchlorates this compound is very sensitive and could explode on heating or shaking it. In particular, when this product was recrystallized from a methanol solution, as soon as the solution was concentrated and cooled down a massive precipitation occurred, with the consequent solvent occlusion. At this point the material becomes very sensitive and any movement could produce a violent explosion.

5,7,7,12,14,14-Hexamethyl-1,4,8,11-tetra-azacyclotetradeca-4,11-diene diperchlorate (*trans*-[14]diene perchlorate) and their complexes with Ni(II) and Zn(II) were prepared according to the literature [15].

1,11-Bis-benzyl-5,7,7-trimethyl-1,4,8,11-tetra-aza-undeca-4-ene nickel(II) perchlorate ($[Ni(benacet)](ClO_4)_2$ ($C_{24}H_{36}Cl_2N_4NiO_8$). Formula weight: 638.18, was prepared as follows: 0.830 g of $[Ni(ben)_3](ClO_4)_2$ was dissolved in 50 ml of acetone dried over molecular sieves. The mixture was stirred for 72 h. In the first 3 h the original blue color became reddish–brown and this became darker until it was not possible to appreciate any further change of color. The solution obtained was rota-evaporated until no further condensation of solvent was observed. The oily residue was then dissolved in 25 ml of methanol and stirred for 1 h. After a few minutes a yellow precipitate was formed. This precipitate was filtered off and dried under air-flow. By evaporation of the remaining solution it was possible to obtain even more of the compound. Yield: 0.558 g, 77%. Elemental analysis: Found: C, 44.97; H, 5.65; N, 8.78%. Calc. for $C_{24}H_{36}N_4O_8Cl_2Ni$: C, 45.16; H, 5.64; N, 8.78%.

2.2. Single crystal of 1,11-bis-benzyl-5,7,7-trimethyl-1,4,8,11-tetra-aza-undeca-4-ene nickel(II) perchlorate ($[Ni(benacet)](ClO_4)_2$

Orange prismatic crystals were grown by slow evaporation of a methanol solution, prepared by redissolu-

tion of the obtained product. A specimen of $0.4 \times 0.3 \times 0.3$ mm was selected and mounted on the diffractometer. Unit cell parameters were determined from 50 reflections obtained by incremental (25) and thin shell (25) methods and refined by the least-squares method. Intensities were collected with graphite monochromatized Mo Kα radiation, using the ω-scan technique, with a scan width 0.85° + separation $K\alpha_1$ and $K\alpha_2$ position and variable scan speed 4–60° min^{-1}. 4131 independent reflections were measured in the range. 3687 intensities were collected over the range $2 \leq \theta \leq 28$, 2837 of which were assumed as observed applying the condition $I \geq 2\sigma(I)$. The structure was solved by direct methods and difference Fourier map location using the program SHELXS-86 [11] and refined with SHELXS-97 [12], by full-matrix least-squares. Refinement of F^2 was made against all reflections. The weighted R-factor wR and goodness of fit S are based on F^2, conventional R-factors R are based on F, with F set to zero for negative F^2. The threshold expression of $F^2 > 2\sigma(F^2)$ is used only for calculating R-factors (gt) etc. and is not relevant to the choice of reflections for refinement. R-factors based on F^2 are statistically about twice as large as those based on F, and R-factors based on all data, will be even larger. The quantity minimized was $\Sigma w(F_o - F_c)^2$ where $w = \{\sigma^2(F_o^2) + (0.0649P)^2 + 2.1500P\}^{-1}$, where $P = (F_o^2 + 2F_c^2)/3$. Absorption correction was applied to the data. Hydrogen atoms where calculated geometrically and U-refined isotropically. All other atoms where refined anisotropically. Crystal data, bond distances and bond angles are given in Tables 1–3.

Table 1
Crystal data for the compound $[Ni(benacet)](ClO_4)_2$

Formula	$C_{24}H_{36}Cl_2N_4NiO_8$
Crystal system	Monoclinic
Space group	C_c
Unit cell dimensions	
a (Å)	20.794(2)
b (Å)	10.557(1)
c (Å)	15.875(2)
β (°)	125.73
V (Å^3)	2829.0(5)
Z	4
D_{calc} (g cm^{-3})	1.494
$F(000)$	1336
Absorption coefficient (mm^{-1})	0.928
Index ranges	$-1<h<27$, $-1<k<13$, $-20<l<17$
Reflections collected	4131
Independent reflections	3687 [$R_{int} = 0.0243$]
Observed reflections	2838 [$F>2\sigma(I)$]
Final R indices (observed data)	0.0472 ($wR = 0.1137$)
Final R indices (all data)	0.0697 ($wR = 0.1283$)
Goodness-of-fit (all)	1.041
Goodness-of-fit (observed)	1.047
Final maximum difference electron density (e Å^{-3})	0.523
Final minimum difference electron density (e Å^{-3})	−0.431
Final average difference electron density (e Å^{-3})	0.066

3. Results and discussion

As stated in the introduction, our interest was focused in gaining insight on the template mechanism involved in Curtis type reactions. The template reaction of tris-*N*-benzylethylenediamine nickel perchlorate with acetone could potentially give several products such as those illustrated in Fig. 1c–e. However we only obtained one product (Fig. 1e).

The orange–yellow product obtained was diamagnetic in the solid state and slightly paramagnetic when dissolved in DMSO or other donor solvents. The infrared spectrum shows the signals due to stretching vibrations ν(N–H) at 3255.1 cm^{-1} and ν(C=N) at 1645.7 cm^{-1}, characteristic for these imino–amino complexes. Electronic spectra in the visible region displayed a symmetric band centered at 456 nm ($\varepsilon = 116$ l mol^{-1} cm^{-1}) when dissolved in acetone, at 454 nm ($\varepsilon = 112$ l mol^{-1} cm^{-1}) in methanol and at 448 nm in water. The maximum blue shift follows almost a linear relationship with the dielectric constant of the solvent (20.7 for acetone, 32.63 for methanol and 78.54 for water). This suggest that axial interaction between the metallic center with the solvent is present and explains the paramagnetic behavior observed in solution.

The molecular structure of $[Ni(benacet)](ClO_4)_2$ is shown in Fig. 2 and bond lengths and bond angles are shown in Tables 2 and 3, respectively. In this compound, the nickel ion displays a square planar coordination surrounded by the ligand with a helical

Table 2
Bond lengths (Å) in the cationic complex $[Ni(benacet)]^{2+}$

Ni1–N1	1.934(8)	Ni1–N2	1.925(9)
Ni1–N3	1.918(8)	Ni1–N4	1.881(11)
N1–C1	1.453(14)	N4–H41N	0.9900(12)
N1–H11N	0.9901(11)	N2–H21N	0.9900(16)
N1–C11	1.485(5)	N2–C21	1.483(5)
N2–C3	1.463(13)	N3–C7	1.323(16)
N3–C2	1.489(14)	N4–C5	1.434(15)
N4–C4	1.495(14)	C1–C2	1.452(17)
C3–C4	1.544(17)	C5–C9	1.521(13)
C5–C6	1.48(2)	C5–C10	1.546(3)
C6–C7	1.49(2)	C7–C8	1.514(9)
C11–C12	1.528(8)	C12–C17	1.392(3)
C12–C13	1.392(3)	C13–C14	1.391(3)
C14–C15	1.392(3)	C15–C16	1.392(3)
C16–C17	1.392(3)	C22–C23	1.390(3)
C22–C27	1.392(3)	C23–C24	1.392(3)
C21–C22	1.495(8)	C24–C25	1.390(3)
C25–C26	1.391(3)	C26–C27	1.392(3)

Table 3
Bond angles (°) for the $[Ni(benacet)]^{2+}$ cation

N4–Ni1–N3	94.73(18)	N4–C4–C3	108.1(9)
N4–Ni1–N2	86.6(4)	N4–C5–C6	109.7(10)
N3–Ni1–N2	172.1(4)	N4–C5–C9	115.6(11)
N4–Ni1–N1	174.5(4)	C6–C5–C9	116.5(11)
N3–Ni1–N1	85.1(5)	N4–C5–C10	101.4(8)
N2–Ni1–N1	94.30(16)	C6–C5–C10	108.3(13)
C1–N1–C11	112.1(8)	C9–C5–C10	103.8(10)
C1–N1–Ni1	105.0(7)	C5–C6–C7	122.8(8)
C11–N1–Ni1	109.7(6)	N3–C7–C8	120.4(10)
C1–N1–H1N	123(4)	N3–C7–C6	122.2(10)
C11–N1–H1N	107(5)	C8–C7–C6	112.5(11)
Ni1–N1–H1N	99(4)	N1–C11–C12	111.8(8)
C21–N2–C3	109.2(7)	C17–C12–C13	121.8(10)
C21–N2–Ni1	117.8(7)	C17–C12–C11	116.3(9)
C3–N2–Ni1	108.0(7)	C13–C12–C11	121.5(9)
C21–N2–H2N	110(5)	C14–C13–C12	118.9(10)
C3–N2–H2N	90(4)	C13–C14–C15	118.2(11)
Ni1–N2–H2N	118(4)	C16–C15–C14	121.9(13)
C7–N3–C2	119.2(9)	C15–C16–C17	118.7(14)
C7–N3–Ni1	123.2(7)	C12–C17–C16	118.7(12)
C2–N3–Ni1	113.2(8)	N2–C21–C22	112.3(8)
C5–N4–C4	116.3(10)	C23–C22–C27	116.4(9)
C5–N4–Ni1	124.5(8)	C23–C22–C21	118.3(8)
C4–N4–Ni1	112.8(8)	C27–C22–C21	125.2(9)
C5–N4–H4N	96(4)	C22–C23–C24	122.2(11)
C4–N4–H4N	98(4)	C25–C24–C23	119.3(11)
Ni1–N4–H4N	102(4)	C24–C25–C26	118.9(11)
C2–C1–N1	111.5(9)	C25–C26–C27	119.3(11)
C1–C2–N3	105.3(9)	C26–C27–C22	122.0(9)
N2–C3–C4	103.1(8)		

conformation (see Fig. 2), having only one type of helix present in the crystal. Metal–nitrogen distances in the complex are very similar, however it should be noted that bonds between nickel with N1 and N4, while corresponding to the secondary amines *trans* to each other, are the shortest. The longest one is the Ni–N3 bond, corresponding to the imine group. The sum of the bond angles around nickel is 360.7°, indicative of the high level of planarity in this complex in the solid state.

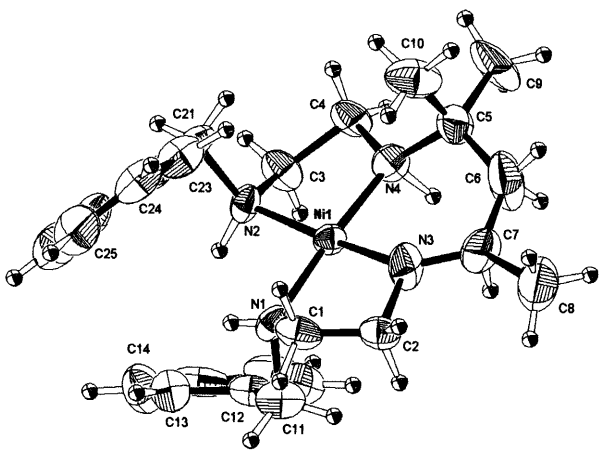


Fig. 2. ORTEP diagram [16], for the $[Ni(benacet)]^{+}$ cationic complex where the square-planar coordination for nickel and the helical structure of the ligand are shown. Observe that one of the benzyl groups is above and the other below the coordination plane.

As stated above, only one helical form of the molecule is present in the crystal. These helical molecules pack in an alternating form, where a self-complementary arrangement between the helixes is observed through a π–π interaction between the aromatic rings of the adjacent molecules. The average distance between the mean plane of one of the phenyl rings to the carbon atoms of the adjacent ring is 3.55(6) Å. The angle formed between the two mean planes is 3.45°. Therefore, the π–π interaction of the phenyl rings and the helical self-complementary arrangement should control packing. A similar type of interaction has been observed in $[Cu(ben)_2(NO_3)_2]$ [9]. This latter complex is differently packed than other *N*-alkyl-ethylenediamine complexes [13,14] supporting the assumption that the π–π interaction between phenyl rings is an important contribution in the driving force for crystal packing.

Because the complex is diamagnetic in the solid state, it was possible to obtain a CP-MAS ^{13}C-NMR spectra. Assignment of the signals was made by a comparative study using the normal spectra and the spectra collected using interrupted decoupling in order to identify the quaternary carbons. The compounds selected for this study were the free macrocycle *trans*-[14]diene (see Fig. 1a) as perchlorate and their metal complexes with Ni(II), and Zn(II). In Fig. 3 are the solid state ^{13}C NMR spectra for these compounds and the assignments made in Table 4. Three different signals for methyl carbons are observed for all compounds, similar to those ^{1}H NMR results previously reported in solution for the [14]-diene complexes. In the imino signal an interesting difference was observed. In the *trans*-[14]diene perchlorate and $[Ni(benacet)]^{2+}$ a single signal was observed, whereas for $[Ni[14]diene]^{2+}$ and $[Zn[14]diene]^{2+}$ complexes two signals were observed (splitting of 117 and 183 Hz for Ni and Zn complexes, respectively).

These observed doublets are due to the dipolar interaction between the imino carbon and ^{14}N. This effect results from the ^{14}N nuclear quadrupole moment interfering with the ability of magic angle spinning and cross polarization to average out carbon–nitrogen dipolar interactions. This splitting is given by [17] (Eq. (1))

$$S_1 = \frac{9\chi D}{20Z}(3\cos^2\beta_{CN} - 1 + \eta\sin^2\beta_{CN}\cos 2\alpha_{CN}) \qquad (1)$$

where D is the dipolar coupling between ^{13}C and ^{14}N ($D = \gamma_C\gamma_N h/4\pi^2 r^3$), Z is the Zeeman energy for ^{14}N, χ is the quadrupole coupling constant, η is the asymmetry in the quadrupole tensor and β_{CN} and α_{CN} are the polar and azimuthal angles between the C–N bond with the principal axis system of the electric field gradient tensor. This coupling is strongly dependent on the inverse

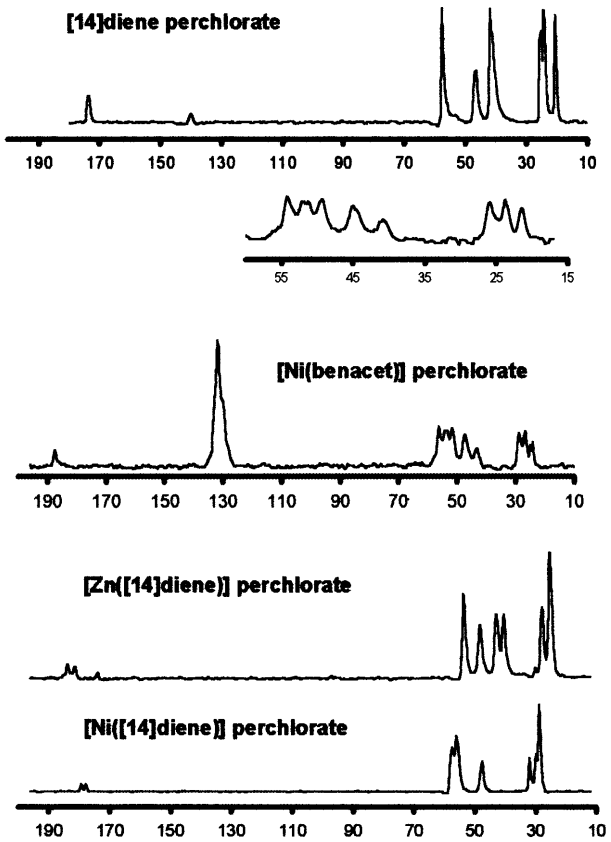


Fig. 3. CP-MAS ^{13}C NMR for the [Ni(benacet)]$(ClO_4)_2$ complex, [14]diene perchlorate and complexes with zinc and nickel.

of the cube of the carbon–nitrogen distance, the field strength, and the asymmetry of the coupling tensor. When the splitting energy is very small then the two peaks are not resolved and only a weighted average peak of the two components is observed. If it is considered that all the parameters in the above equation are similar for all the compounds studied, except in the C–N distance, then for the *trans*-[14]diene and $[Ni(benacet)]^{2+}$ a longer C–N distance than in the nickel and zinc complexes with the [14]diene ligand would be expected.

For the cationic complex $[Ni(benacet)]^{2+}$, a ^{15}N CP-MAS spectra was obtained, with signals at 232.3, −3.4 and −28.6 ppm referred to NH_4Cl (0.0 ppm). These signals were assigned to N3, the imino nitrogen; N4, the nitrogen *cis* to the imino group forming part of the mesityl moiety and N1, N2, the amine nitrogen atoms that have the benzyl groups attached, respectively. This assignment is in agreement with the crystal data described above. In particular, the chemical shift of N4 (−3.4 ppm) could be explained in terms of its geometry. From data in Table 3 it is possible to observe that this nitrogen is distorted from tetrahedral geometry, making that hybridization change from sp^3 to an intermediate between sp^3 and sp^2. This change should affect the shielding on the nitrogen nucleus protecting more than the N1 and N2 that have normal behavior.

In a previous work [9], we reported the crystal structure of $[Cu(ben)_2(NO_3)_2]$, this compound displays a *trans*-arrangement of benzyl residues. Also, similar compounds with *N*-alkyl-ethylenediamine with this arrangement have been reported [13,14]. This difference between $[Cu(ben)_2(NO_3)_2]$ and the $[Ni(benacet)]^{2+}$ where the benzyl residues are in the *cis*-position, suggests that the mechanism of this reaction involves a *cis*-condensation between two adjacent acetoimino groups, and therefore explains why it is required as a starting material to form the tris-*N*-benzylethylenediamine nickel(II) cation. The proposed mechanism is illustrated in Fig. 4.

As a key step, it is required a proton be extracted from one of the methyl groups. This extraction is carried out by free benzylethylenediamine originated from the equilibrium present in solution between the tris-complex and the bis-complex and free base. Then, the quaternary carbon of the neighboring acetoimine is in a good position for a nucleophilic attack carried out

Table 4
CP-MAS ^{13}C NMR for the [Ni(benacet)]$(ClO_4)_2$ complex and *trans*-[14]diene perchlorate ligand and their complexes with Ni(II) and Zn(II) [a]

Atom numbering following scheme I	[14]diene	[Ni(L)]	[Zn(L)]	[Ni(benacet)]	Atom numbering following Fig. 2
C2	173.5	180.8, 179.2	183.9, 181.5	187.0	C7
C3	40.7	43.1	40.3	40.3	C6
C4	57.5	53.0	53.6	53.6	C5
C6	41.6	51.7, 52.2	43.1	44.3 (51.4)	C4
C7	46.8	54.5	48.4	48.7	C2
Methyl groups	24.8	26.6	27.6	25.6	Methyl groups
	23.7	24.4	24.8	23.4	
	20.1	23.3		21.1	
				50.68	C1, C3
				51.4 (44.3)	C11
				130	C12
				128.5, 126	C13, C14, C15

[a] C4 and C11 assignment for [Ni(benacet)] is uncertain and is indicated in parenthesis.

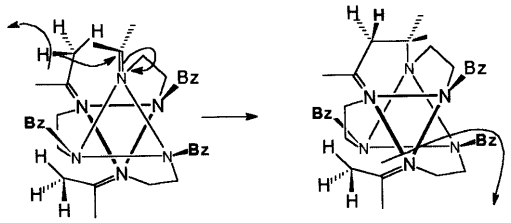


Fig. 4. Scheme illustrating the stereochemical requirements of condensation to form a mesityl residue with two acetoimino groups coordinated to nickel(II) as a possible step in the Curtis-type reaction. A proton extraction is required in the first step in order to obtain nucleophilic attack of the methylene anion to the imino-carbon. After the formation of the mesityl moiety a rearrangement of the new ligand should occur with the consequent elimination of the remaining benzylethylenediamine.

by the methylene anion to form the mesityl moiety. Finally, after this condensation takes place, the tension generated in the system due to the new bond formed is released by rearrangement of the ligand and elimination of the third *N*-benzylethylenediamine, to give the final product, where both benzyl groups are in a *cis*-positions.

This mechanism could also explain the original template reaction between $[Ni(en)_3]^{2+}$, where a mixture of *cis*- and *trans*-$[Ni([14]diene)]^{2+}$ is obtained. The process followed should be the same and once the rearrangement described above takes place, a second mesytil condensation occurs, noting the possibility that proton extraction may occur from any of the acetoimino groups and therefore allowing the formation of a *cis*- or *trans*-complex to take place. Formal kinetic studies are required to validate the proposal of this mechanism for this powerful synthetic reaction.

Finally, the helical structure of the complex reported here opens an interesting field for the development of new, potentially active compounds as oxidative nucleases that could act with more site-specificity. Preliminary studies are currently in progress.

4. Supplementary material

Crystallographic data for the structural analysis have been deposited with the Cambridge Crystallographic Data Centre, CCDC 139837. Copies of this information may be obtained free of charge from: The Director, CCDC, 12 Union Road, Cambridge, CB2 1EZ, UK (Fax: +44-1223-336-033; e-mail: deposit@ccdc.cam.ac.uk or www: http://www.ccdc.cam.ac.uk).

Acknowledgements

We thank Dr Sylvain Bernès, USAI, FQ-UNAM, México, D.F., for collecting the diffraction data of the crystal and to Dr S.P. Kasprzyk (Poland) for his valuable suggestions on the synthetic procedure. This work was partially supported by the Dirección de Intercambio Académico of Universidad Nacional Autónoma de México.

References

[1] L. Fabbrizzi, M. Licchelli, A Ma. Manotti-Lanfredi, O. Vassalli, F. Ugozzoli, Inorg. Chem. 35 (1996) 1582.
[2] R. Breslow, Acc. Chem. Res. 28 (1995) 146.
[3] D.S. Sigman, A. Mazumder, D.M. Perrin, Chem. Rev. 93 (1993) 2295.
[4] J.R. Morrow, K.A. Kolasa, Inorg. Chim. Acta 195 (1992) 245.
[5] J.G. Muller, X. Chen, A.C. Dadiz, S.E. Rokita, C.J. Burrows, Pure Appl. Chem. 65 (1993) 545.
[6] J.G. Muller, X. Chen, A.C. Dadiz, S.E. Rokita, C.J. Burrows, J. Am. Chem. Soc. 114 (1992) 6407.
[7] N.F. Curtis, Coord. Chem. Rev. 3 (1968) 3.
[8] G. Mendoza-Díaz, L. Ruiz-Ramirez, F. Cervantes-Lee, K.H. Pannell, Rev. Soc. Quim. Mex. 36 (1992) 211.
[9] K.C. Patel, D.E. Goldberg, J. Inorg. Nucl. Chem. 35 (1973) 4041.
[10] K.C. Patel, D.E. Goldberg, J. Inorg. Nucl. Chem. 36 (1974) 565.
[11] G.M. Sheldrick, Acta Crystallogr., Sect. A 46 (1997) 463.
[12] G.M. Sheldrick, SHELXL-97, Program for the refinement of crystal structures from diffraction data, Institut für Anorganische. Chemie, Göttingen, Germany, 1997.
[13] L. Grenthe, P. Paoeletti, M. Sandström, S. Glikberg, Inorg. Chem. 18 (1979) 2687.
[14] R. Härnäläinen, U. Turpeinen, M. Ahlgrén, Acta Crystallogr., Sect. B 35 (1979) 2408.
[15] A.M. Tait, D.H. Bush, Inorg. Syn. 18 (1978) 1.
[16] L. Zsolsnai, XPMA and ZORTEP molecular geometry program, Universität Heidelberg, Germany, 1997.
[17] P.J. Barrie, A. Gyani, M. Motevalli, P. O'Brien, Inorg. Chem. 32 (1993) 3862.

PERGAMON

www.elsevier.nl/locate/poly

Polyhedron 19 (2000) 2155–2161

POLYHEDRON

Magnetic properties and coordination environments of oxovanadium(IV) within $VO(IV)N_2S_2$ and $VO(IV)S_4$ chromophores

Young-Jin Kim [a,*], Young-Inn Kim [b], Sung-Nak Choi [b]

[a] *Department of Chemistry, Northwestern University, Evanston, IL 60208, USA*
[b] *Department of Chemistry, Pusan National University, Pusan 609-735, South Korea*

Received 18 January 2000; accepted 21 July 2000

Abstract

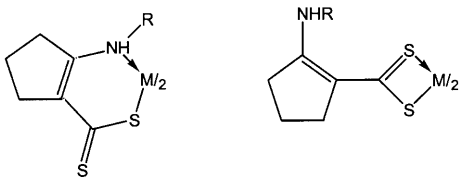
Oxovanadium(IV) complexes of the 2-amino-1-cyclopentene-1-dithiocarboxylate (acdc) and 2-methylamino-1-cyclopentene-1-dithiocarboxylate (N–CH_3acdc) anion have been synthesized and characterized by using IR, EPR, magnetic susceptibility and XPS measurements to elucidate the coordination environment of oxovanadium(IV) complexes of the acdc ligand and its derivative. The corresponding spin-Hamiltonian parameters, $\langle g \rangle$ values and hyperfine coupling constants, $\langle A \rangle$ have been examined for the prepared complexes having $VO(IV)N_2S_2$ and $VO(IV)S_4$ chromophore. The EPR data confirm its usefulness in the characterization of the coordination environments of these compounds. The XPS studies have also provided us with valuable information on the binding properties of $VO(acdc)_2$ and $VO(N–CH_3acdc)_2$. The magnetic susceptibility, coupled with the V=O stretching frequency suggest the presence of some degree of magnetic interaction in these compounds. © 2000 Elsevier Science B.V. All rights reserved.

Keywords: Dithiocarboxylate; Vanadium(IV); Magnetism; EPR; Infrared; Coordination.

1. Introduction

It is becoming increasingly apparent that the chemistry of vanadium is of great importance in many biological systems [1–4]. A more detailed understanding of the nature of vanadium and potentially biologically important ligands such as dithiocarboxylic acid necessitates a detailed knowledge of the coordination environment and oxidation states of the metal within the systems. By studying the molecular structure, electronic structure, and magnetic properties of existing compounds, it is possible to design ligand environments to introduce specific magnetic properties to oxovanadium centers. For example, most dimeric oxovanadium(IV) complexes exhibit an antiferromagnetic exchange interaction [5], and Dutta et al. have observed flexibility and diversity in the electronic and molecular structures of dinuclear vanadium complexes using the tridentate ONS donor ligand system [6]. A number of vanadium complexes having sulfur environments, covering a wide structural variety and oxidation state range, have been synthesized in recent years in order to obtain the above objectives [7–10].

Bereman et al. showed that 2-amino-1-cyclopentene-1-dithiocarboxylate and its derivatives could coordinate to metal ions in bidentate and/or tetradendate coordination modes and form either MN_2S_2 or MS_4 chromophores, depending on the type of metal ions and the geometry of the ligands. A series of M(II) complexes with *N*-alkyl-2-amino-1-cyclopentene-1-dithiocarboxylate have also been prepared and characterized using EPR, electronic absorption spectroscopy and electrochemical methods. Alkyl substituents were found to impose subtle effects on the coordination geometry and physicochemical properties of the central metal ions [11,12].



(I) (II)

(R = H, CH_3, and M = divalent metal ion)

* Corresponding author. Tel.: +1-847-491-2435; fax: +1-847-491-7713.
E-mail address: yjkim@chem.nuw.edu (Y.-J. Kim).

0277-5387/00/$ - see front matter © 2000 Elsevier Science B.V. All rights reserved.
PII: S0277-5387(00)00528-3

The 2-amino-1-cyclopentene-1-dithiocarboxylate ligand can coordinate to a metal center in two ways (type I, II). By substitution it should be able to tune the coordination of this ligand from one form to the other. Since the coordination environment around the metal is different, large effects on the electronic and magnetic properties are expected.

In this study we utilize the oxovanadium(IV) ion (d^1 electronic configuration). We show that this metal ion, being harder than copper(II), might prefer the nitrogen donor of the amine unit to the sulfur donor of the dithiocarboxylate unit. The introduction of various alkyl groups on the amino group was carried out to enhance the basicity of the nitrogen donor atom. Previously, the $VO(acdc)_2$ complex was synthesized [13], but the bonding nature of this compound has not been fully characterized. In this paper we report the coordination mode for the complexes $VO(acdc)_2$ and $VO(N–CH_3\text{-}acdc)_2$ and the magnetic interaction on monomeric oxovanadium(IV) complexes in the solid phase via IR, EPR, magnetic susceptibility and XPS.

2. Experimental

2.1. Materials

2 - Amino - 1 - cyclopentene - 1 - dithiocarboxylic acid (Hacdc) and 2-methylamino-1-cyclopentene-1-dithiocarboxylic acid ($N–CH_3$acdc) were prepared by a published method [14]. $VOSO_4·3H_2O$ was purchased from Aldrich Chemical Co. and used without further purification. All solvents were reagent grade and were distilled over 4-A molecular sieves. Spectrophotometric grade acetonitile and methylene chloride (Aldrich) were used for all spectrophotometric measurements. All manipulations were performed under an argon atmosphere using standard Schlenk techniques.

2.2. Preparation of bis(2-amino-1-cyclopentene-1-dithiocarboxylato)oxovanadium(IV), $VO(acdc)_2$

To a solution of $VOSO_4·3H_2O$ (0.217 g, 1.0 mmol) in deaerated 1:1 ethanol–water (20 ml) was added a solution of 2-amino-1-cyclopentene-1-dithiocarboxylic acid (0.319 g, 2.0 mmol) in 25 ml of aqueous sodium hydroxide (2.0 mmol) solution under vigorous stirring. After the addition was completed, the reaction mixture was stirred continuously for 2 h at room temperature under an argon atmosphere. The red–brown solid was filtered, washed successively with deaerated H_2O and EtOH, and dried in vacuo. Yield: 87%. IR (KBr): 3328(m), 3278(w), 3170(m), 3141(w), 1634(s), 1470(s), 1409(m), 1326(w), 1285(w), 946(m), 806(w), 662(w), 568(w), 552(w,br), 430(w) cm^{-1}. Elemental analysis: *Anal*. Found: C, 37.31; H, 4.23; N, 7.66; S, 33.01. Calc. for $C_{12}H_{16}N_2S_4VO$: C, 37.60; H, 4.17; N, 7.31; S, 33.46%.

2.3. Preparation of bis(2-methylamino-1-cyclopentene-1-dithiocarboxylato)oxovanadium(IV), $VO(N–CH_3acdc)_2$

To a solution of 2-methylamino-1-cyclopentene-1-dithiocarboxylic acid (2.0 mmol) in deaerated methanol (50 ml) was slowly added a solution of $VOSO_4·3H_2O$ (0.209 g, 1.0 mmol) in deaerated methanol–water (20 ml), and the mixture was stirred for 2 h at room temperature. The olive-green compound was filtered, washed with warm water, followed by cold methanol, and dried in vacuo. Yield: 63%. IR (KBr): 3412(m), 2928(m), 1610(s), 1492(s), 1381(w), 1346(s), 1281(s), 987(m), 911(w), 759(w), 610(w,br), 434(w) cm^{-1}. Elemental analysis: *Anal*. Found: C, 39.90; H, 4.96; N, 6.84; S, 32.07. Calc. for $C_{14}H_{20}N_2S_4VO$: C, 40.88; H, 4.86; N, 6.81; S, 31.18%.

2.4. Measurements

IR spectra (KBr pellets) were obtained on a Polaris FTIR spectrophotometer over the range 4000–400 cm^{-1}. EPR measurements were carried out with an ESP-300S Bruker spectrometer operating at the X-band frequency (9.45 GHz). The external magnetic field was calibrated with a microwave bridge model ER 032MR Bruker wavemeter and the temperature was controlled with a model ER4111VT Bruker device with accuracy of $\pm 1\%$. Magnetic susceptibility measurements were made on a powered sample over the temperature range 2–300 K using a Foner type100 vibrating sample magnetometer with a field calibrated at 10 000 G using the magnetic susceptibility standard $HgCo(NCS)_4$ [15]. The data were corrected for the diamagnetism of the constituent atoms using Pascal's constants. X-ray photoelectron spectra were recorded on a Perkin–Elmer Physical Electronics model 5400 X-ray photoelectron spectrometer equipped with a magnesium anode X-ray source and a hemispherical analyzer. The residual gas pressure was 5×10^{-9} torr and the binding energies were calibrated using the Au $4f_{7/2}$ peak at 84.9 eV and the Cu $2P_{3/2}$ peak at 932.4 eV. The adventitious C 1S line at 284.6 eV was used for charge referencing. Elemental analyses (C, H, N, and S) were performed at the Korea Research Institute of Standards and Science.

3. Results and discussion

IR spectra of the free ligands are characterized, in part, by prominent bands appearing at approximately 2538 and 1351 cm^{-1} due to $\nu_{N–H}$ and $\nu_{C=S}$ stretching

modes, respectively; these bands disappeared upon complexation to the metal ion (see Table 1). For the $VO(acdc)_2$ complex: (a) the C=S stretching band of the dithiocarboxylate unit is largely shifted to lower frequency at 1326 cm^{-1} upon complexation; (b) the intensity of C–S stretching band is largely reduced; and (c) a new band appears at 662 cm^{-1}. For the $VO(N–CH_3acdc)_2$ complex, the C–N stretching band appearing at 1282 cm^{-1} in the free ligand is shifted to 1288 cm^{-1}. Similar behavior has been observed in the analogous copper and nickel compounds, and is consistent with extensive π-delocalization [13]. In addition, the $VO(N–CH_3acdc)_2$ complex displays a broad band at 3412 cm^{-1}. This band is assigned to the deformation vibration of the amine group of the $NHCH_3$ unit. The intense C=S stretch appearing at 1351 cm^{-1} in the free ligand is shifted to 1385 cm^{-1} upon complexation. The results clearly indicate that the nitrogen of the amine group and the sulfur of the dithiocarboxylate unit of the ligand are coordinated to the oxovanadium(IV) ion. In these two complexes, the frequency of the vanadium–oxygen double bond stretching mode was considered to be directly proportional to the strength of the metal–ligand interaction. However, the shift of $\nu_{V=O}$ has also been found to depend on coordination numbers and the type of donor molecules [16b]. The IR spectrum of $VO(acdc)_2$ shows an intense V=O stretch at 946 cm^{-1}. The relatively low value of $\nu_{V=O}$ is consistent with the rather long V=O bond encountered for most square pyramidal oxovandium(IV) complexes [16a] [17]. The obtained value, $\nu_{V=O}$ for $VO(acdc)_2$ is almost identical to that in $VO(ddc)_2$ (945 cm^{-1}) (ddc = diethyldithiocarbamate) [18], but is substantially lower than those in VO(t-salen) (975 cm^{-1}) (t-salen = *N*,*N*′-ethylenebis(thiosalicylidene-aminato) [19], $VO(mpo)_2$ (984 cm^{-1}) (mpo = 2-mercaptopyridine *N*-oxide) [20], and slightly higher than that in $VO(Hmpp)_2$ (937 cm^{-1}) (H_2mpp = 2-mercapto-3-pyridinol) [21]. On the other hand, a strong V=O terminal stretch appearing at 982 cm^{-1} for $VO(N–CH_3acdc)_2$ is higher in energy than for the $VO(acdc)_2$ complex. In terms of Ballhausen and Gray's molecular orbit Scheme, the π-bonding between the vanadium $3d_{xz}$, $3d_{yz}$ orbitals and the oxygen $2p_x$, $2p_y$ orbitals in V=O bond is largely enhanced when ligand coordination at the sixth axial site (*trans* to the V=O bond axis) is achieved [22]. The frequency for oxovanadium(IV) complexes having $O=V(L)_2$ compositions (L = bidendate ligand) was found to be ca. 985 cm^{-1}. Variation of the frequency of the V=O vibration, due to changes in the environment of the VO^{2+} entity, has been extensively studied [23]. The V=O frequency spread for various oxovanadium (IV) complexes has been reported to be 985 ± 50 cm^{-1}, which approximately corresponds to the force constant spread, $k = 7.0 \pm 0.7$ mdynes $Å^{-1}$. Thus it is tempting to suggest that the shift to lower frequencies of the V=O stretching is due to the transfer of increasing amounts of charge onto the vanadium by ligands of increasing donor strength. Metal to ligand π-bonding is expected to play a significant role in many complexes of this sort. Therefore, the ligand series derived from vibration spectra arises primarily as a result of variations in σ-bonding by the ligands and secondarily as a result of metal-to-ligand π-bonding. However, if the complexes have an intermolecular interaction through the V=O···V=O units [22b], the V=O stretching band will appear at lower frequency. For the $VO(acdc)_2$ complex, the V=O stretching band at 946 cm^{-1} may be due to intermolecular interactions through the inter-chain interaction of V=O···V=O units or a sulfur atom of an equatorial coordinated dithiocarboxylate ligand to vanadium center may simultaneously bond to axial position of another oxovanadium center to form a bridge. These two possibilities do not rule out the intermolecular interaction of the oxovanadium complex. If the reduction of the V=O stretching frequency in the $VO(acdc)_2$ complex is due to intermolecular interactions, the molecular structure must be different in these two complexes. We postulate that the bulky alkyl groups sufficiently alter the vanadium coordination environment and significantly weaken the intermolecular interaction of V=O···V=O chains in $VO(N–CH_3acdc)_2$, leaving the V=O stretching frequency unchanged.

Zelentsov [24] suggested for the magnetic abnormality of oxovanadium(IV) complexes of substituted *N*-(2-hydroxyphenyl)-salicylidenimine which having an oxygen bridged dimeric structure, provides an appropriate symmetry for the 3d orbitals of vanadium(IV) to overlap with each other and form a strong metal–ligand bond. Symal et al. [23], for a series of Schiff base complexes of the type $VO(ONS)_3 \cdot nH_2O$, proposed a binuclear structure on the basis of their subnormal magnetic moment (1.27–1.52 B.M.). Similarly, Poddar [25] and others [26] observed subnormal magnetic moments in the case of oxovanadium(IV) complexes of

Table 1
Characteristic infrared frequencies of VO^{2+} complexes with suggested assignments

$VO(acdc)_2$		$VO(N–CH_3acdc)_2$	
Frequency (cm^{-1})	Assignment	Frequency (cm^{-1})	Assignment
1634(s)	$\nu_{C=C}$	1610(s)	$\nu_{C=C}$
1470(vs)	$\nu_{C=N}$	1492(s)	$\nu_{C=N}$
1326(w)	$\nu_{C=S}$	1385(s)	$\nu_{C=S}$
1285(w)	$\nu_{C–N}$	1282(s)	$\nu_{C–N}$
946(m)	$\nu_{V=O}$	982(m)	$\nu_{V=O}$
662(w, br)	ν_{VS4} (A_1)	610(w, br)	ν_{VS4} (A_1)
568(w)			
552(w,br)			
430(w)	ν_{VS4} (A_1 or E)	434(w) (A_1 or E)	ν_{VS4}

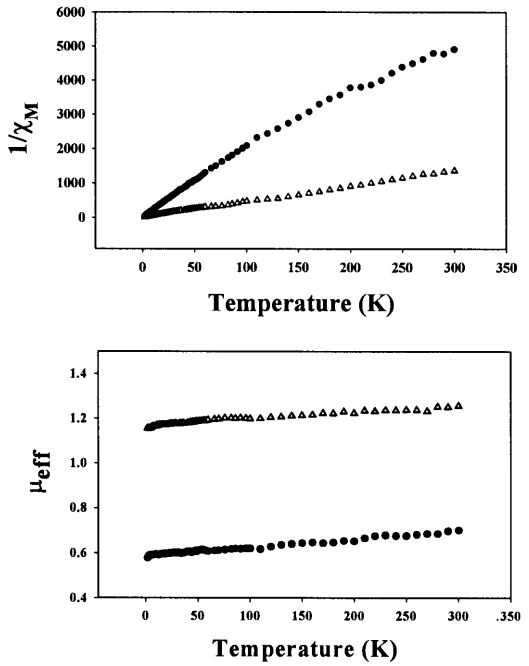


Fig. 1. Temperature variation of the magnetic susceptibility (χ_M) and magnetic moment (μ_{eff}) for the complexes: $VO(acdc)_2$ (●) and $VO(N–CH_3acdc)_2$ (▲).

bidentate Schiff base and suggested the oxygen bridged dimeric structure independently. Fig. 1 shows the temperature dependence of the magnetic behavior. The complexes exhibit near-straight lines when the inverse value of the susceptibility is plotted against temperature, satisfying the Curie–Weiss equation. At room temperature the observed values of solid-state magnetic moments for $VO(acdc)_2$ and $VO(N–CH_3acdc)_2$ complexes are 0.69 and 1.25 B.M., respectively. The moments are slightly lower than the spin-only value ($\mu_{eff} = 1.73$ B.M.) of the expected $3d^1$ configurations. This subnormal magnetic moment may be due to the presence of intra or intermolecular antiferromagnetic coupling, and/or oxidation of V(IV) to diamagnetic V(V). The magnetism of the polycrystalline sample $VO(acdc)_2$ and $VO(N–CH_3acdc)_2$ were investigated in the temperature range 2–300 K to confirm whether these complexes are of oxomonomeric- or coupled dimeric-type structure. When the orbital contribution is quenched, the magnetic moment of the complex differs from the spin-only value. This variation results from the two sources: (i) mixing in excited state having some contributions from spin–orbit coupling, and (ii) second-order Zeeman effects (temperature-independent paramagnetism). The temperature dependence of the magnetic moment predicted for a $^2T_{2g}$ ground term in octahedral symmetry is not observed, indicating that the $VO(S_4)$ and $VO(N_2S_2)$ core symmetry for these complexes is lower than octahedral. Therefore, it is expected the $^2T_{2g}(Oh)$ term is split by a near-trigonal field to give an orbital singlet $^2A_1$ as the ground state, consistent with the near-Curie-like $1/\chi_M(T)$ and $\mu_{eff}(T)$ plots, and also with EPR studies. From the variable-temperature magnetic data it should be possible to calculate the spin–orbit coupling constant, λ, for vanadium (IV) by following Figgis's estimation [27]. We obtained the spin–orbit coupling constant, λ as 180 ± 60 cm^{-1}. Thus, the value of the spin–orbit coupling constant is quite large since μ_{eff} values for $VO(acdc)_2$ and $VO(N–CH_3acdc)_2$ do not vary much with temperature. The reduction of the spin–orbit coupling constant from its free ion value is indicative of strong delocalization of the metal d-electron to ligand orbitals. The unusually low magnetic moment of the $VO(acdc)_2$ complex at 298 K was calculated from the measured magnetic susceptibility to be $\mu_{eff} = 0.69$ B.M. (vanadium), which may be due to less quenching of orbital contributions than in the mononuclear vanadium(IV) complex ($\mu_{eff} = 1.73$ B.M.), as expected for a simple $S = 1/2$ paramagnet with a d_{xy}-based ground state [28]. Therefore, from the magnetic data together with infrared data, it may be suggested that the $VO(acdc)_2$ complex exhibits a magnetic interaction through the overlap of the d_{xy} magnetic orbital on one monomeric oxovanadim(IV) with intermolecular interaction of V=O units in the solid state.

More compelling evidence could be obtained by conducting single-crystal X-ray studies. However, these complexes are quite unstable and crystal growth has been unsuccessful. Even though we could not determine the molecular crystal structure, we attempted to use EPR measurements and an XPS spectroscopic method to determine the coordination environment of $VO(acdc)_2$ and $VO(N–CH_3acdc)_2$. Fig. 2 shows the X-band EPR spectra of $VO(acdc)_2$ and $VO(N–CH_3acdc)_2$ obtained in a CH_2Cl_2 at 77 K, as well as at room temperature. These complexes gave a clear eight-line pattern indicative of ^{51}V hyperfine coupling. The g values ($g_\perp$ and $g_\parallel$) which are well within the characteristic g values for most oxovanadium(IV) compounds having a VOS_4 chromophore [29]. At room temperature, a spectrum of $VO(acdc)_2$ shows to be a typical anisotropic spectrum of a molecule with axial symmetry, and consists of an eight-line hyperfine structure indicative of electron coupling to an $I = 7/2$ ^{51}V species superimposed upon a broad background. The calculated values of $g_o = 1.970$ and $A_o = 1.887 \times 10^{-18}$ erg $= 95 \times 10^{-4}$ cm^{-1} ($a_o = 104$ G) are consistent with those observed for monomeric square-pyramidal oxovanadium(IV) complexes, in which all four coordination sites on the vanadium basal plane are occupied by sulfur atoms. The $VO(N–CH_3acdc)_2$ complex is characterized by a similar spectral pattern, and the corresponding spin-Hamiltonian parameters are $g_\parallel = 1.952$ ($A_\parallel = 182 \times 10^{-4}$ cm^{-1}) and $g_\perp = 1.984$ ($A_\perp = 59 \times$

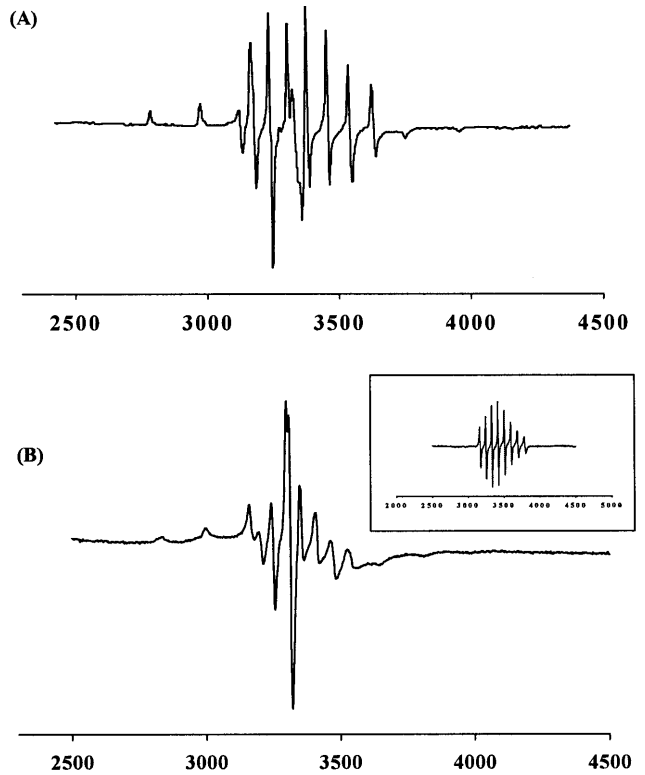


Fig. 2. X-band EPR spectrum of $VO(acdc)_2$ (A) and $VO(N–CH_3acdc)_2$ (B) in CH_2Cl_2 at 77 K; the insert shows the spectrum of $VO(N–CH_3acdc)_2$ at room temperature.

10^{-4} cm^{-1}). The parameters are summarized in Table 2, together with EPR data for complexes with related donor sets. Additional interesting features that deserving mention are the small hyperfine coupling constants and relatively large $g_\perp$ values in comparison to those observed for related complexes featuring N/O donor sets [30,31]. This indicates moderate π-interaction of sulfur in the present ligand system, leading to increased delocalization of the vanadium unpaired electron [32]. Dickson and co-workers have shown that the EPR spectra of various oxovanadium complexes yield hyperfine coupling constants (A_o) and g_o values in reasonable well-defined characteristic ranges for the type of metal–ligand bonds, i.e. g_o values increase and A_o decreases in the series of $VO(O_4)$, $VO(N_2S_2)$, $VO(N_4)$ and $VO(S_4)$ chromophores [33]. In comparison with other square pyramidal VO^{2+} complexes, the $VO(acdc)_2$ complex gives a higher g_o value and a lower A_o value than expected, whereas, the values for $VO(N–CH_3acdc)_2$ are near the average observed for the $VO(S_4)$ and $VO(N_4)$ complex systems. This is consistent with nephelauxetic series, $S > N > O$, suggesting that the sulfur atom is more covalently bound than either nitrogen or oxygen donor ligands, resulting in larger electron delocalization and ultimately a higher g_o value and a smaller A_o value. The difference in $A_\parallel$ values for the $VO(acdc)_2$ and $VO(N–CH_3acdc)_2$ complexes reflects the differences in coordination environment of VOS_4 and VON_2S_2 chromophores, respectively, and it reflects well the highly covalent nature of the metal–ligand bonding in VOS_4 chromophores.

X-ray photoelectron spectroscopy (XPS) has been particularly useful in elucidation of the structure of the complexes; it can be used for determining bonding configurations because the technique detects changes in the electronic environment of an atom, as evidenced by shifts in the binding energy of core electrons. Fig. 3 shows the XPS spectrum for the $VO(acdc)_2$ complex, the peak at 516.3 eV corresponds to vanadium $^2P_{3/2}$ in the oxidation state of IV [34]. This shows that the vanadium atoms in the $VO(acdc)_2$ and $VO(N–CH_3acdc)_2$ complex are in the same oxidation state, V(IV) and no indication for oxidation of the metal atom in the $VO(acdc)_2$ and $VO(N–CH_3acdc)_2$ complex. In general, the core binding energy of N 1s in NH_3 is 398.9 eV, while in the metal complex it shifts to

Table 2
EPR parameters of $VO(acdc)_2$, $VO(N–CH_3acdc)_2$ and related oxovanadium(IV) complexes

Compounds	Solvent	g_o	$\langle g \rangle$ [a]	$g_\parallel$	$g_\perp$	A_o (10^{-4} cm^{-1})	$\langle A \rangle$ [a] (10^{-4} cm^{-1})	$A_\parallel$ (10^{-4} cm^{-1})	$A_\perp$ (10^{-4} cm^{-1})
$VO(acdc)_2$	DMSO	1.972				95			
	CH_2Cl_2 [b]		1.996	2.000	1.993		71	120	47
$VO(N–CH_3acdc)_2$	CH_2Cl_2	1.977				102.1			
	CH_2Cl_2 [b]		1.973	1.952	1.984		100	182	59
$[VO(edt)_2]^{2-}$ [c]	DMF	1.981		1.976	1.977	71.6		133.8	39.7
$[VO(mnt)_2]^{2-}$ [d]	$CHCl_3$	1.984		1.973	1.986	71.6		135	43
$[VO(dmit)_2]^{2-}$ [e]	CH_3CN	1.990				77.1			
VO(t-salen) [f]	DMF			1.978	1.986			148	51

[a] $\langle g \rangle = 1/3(g_\parallel + 2g_\perp)$ and $\langle A \rangle = 1/3(A_\parallel + 2A_\perp)$.
[b] Frozen glasses (77 K).
[c] See Ref. [37].
[d] See Ref. [38].
[e] See Ref. [39].
[f] See Ref. [40].

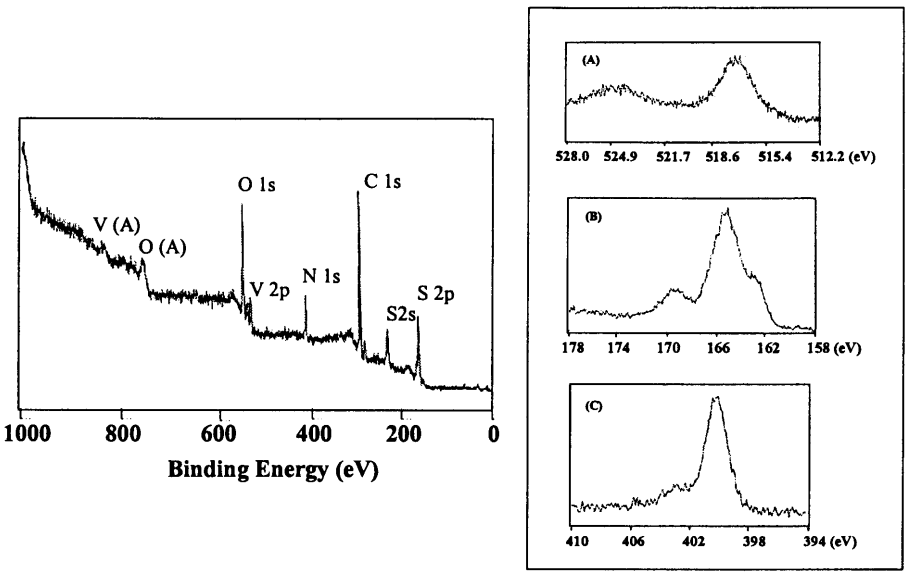


Fig. 3. XPS spectra for the $VO(acdc)_2$ complex: (A) V ($2p_{3/2}$), (B) S (2p) and (C) N (1s).

higher binding energy by ~ 1.0 eV [35]. This binding energy shifts are understandable in terms of the lower electron density on the bonded nitrogen atom as a result of the coordination to a metal ion. If the comparison of the N 1s binding energies of $VO(acdc)_2$ and $VO(N–CH_3acdc)_2$ are made, the higher values N 1s binding energies of the $VO(N–CH_3acdc)_2$ reflects the electron-donating properties of the methyl group which, in turn, likely promotes the basicity of nitrogen to participate in chelation with central metal ion. The binding energies of $VO(acdc)_2$ and $VO(N–CH_3acdc)_2$ are listed in Table 3. The sulfur ($2p_{1/2,3/2}$) binding energies for $VO(acdc)_2$ and $VO(N–CH_3acdc)_2$ are 163.9 and 163.1 eV, respectively. This indicates that the charge on vanadium(IV) within the $VO(acdc)_2$ complex is more delocalized onto the coordinated ligand and resides in large part on the sulfur atoms (equally distributed over the four equivalent sulfur atoms) than in the $VO(N–CH_3acdc)_2$ complex.

4. Conclusions

IR, EPR and XPS studies have provided us with valuable information regarding the coordination environments of the $VO(acdc)_2$ and $VO(N–CH_3acdc)_2$ complexes. Also, magnetic susceptibility data suggest that the magnetic interaction occurring within the two compounds is quite different. Simply introducing a methyl group on the nitrogen of the amine group causes a change in the coordination around the oxovanadium(IV) center. Previously, Choi et al.[36] reported on the basis of EPR studies that copper(II) reacts with 2-methylamino-1-cyclopentene-1-dithiocarboxylate to produce a CuS_4 chromophore and concluded that $Cu(acdc)_2$ and $Cu(N–CH_3acdc)_2$ have the same coordination structure. However, what we have observed in this study shows that both ligands, acdc and $N–CH_3acdc$ are coordinated quite differently to the vanadium(IV) center. Even when enhancement of the basicity of the nitrogen donor of the amine is achieved, copper(II) prefers the sulfur donor of the dithiocarboxylate unit to the nitrogen donor of the amine group. So, the reason why $VO(N–CH_3acdc)_2$ prefers one nitrogen donor of the amine and one sulfur donor of the dithiocarboxylate group is apparently due to the characteristics of the metal center. The copper(II) ion is a d^9 system while VO^{2+} is a d^1 system. The copper(II) ion is softer than vanadium(IV) on the basis of the Hard–Soft Acid–Base model and prefers the more polarizable sulfur donors. The vanadium(IV) center prefers nitrogen and sulfur donors to about the same degree. Therefore, the coordination mode of the 2-amino-1-cyclopenetene-1-dithiocarboxylate and the 2-methylamino-1-cyclopenetene-1-dithiocarboxylate ligand and toward metal ions is not simple to explain. Rather, factors affected by the intrinsic basicity of ligand donors and the hard–soft relationship seem to be intermingled.

Table 3
Binding energies (eV) of oxovanadium(IV) complexes

Compound	Vanadium		N (1s)	S (2p)	O (1s)
	$2p_{3/2}$	$2p_{1/2}$			
$VO(acdc)_2$	516.3	523.5	398.8	163.9	531.3
$VO(N–CH_3acdc)_2$	516.1	523.0	399.7	163.1	531.1

Acknowledgements

This research was financially supported by the KORSEF (921-0200-002-2). We thank Professor Joseph T. Hupp at Northwestern University, USA, for many helpful discussions.

References

[1] (a) B.G. Silbernagel, J. Catal. 56 (1979) 315. (b) N.S. Dean, S.L. Bartley, W.E. Streib, E.B. Lobkovsky, G. Chrustou, Inorg. Chem. 34 (1995) 1608.
[2] N. Pau, in: M.J. Dilworth, A.R. Glenn (Eds.), Biology and Biochemistry of Nitrogen Fixation, Elsevier, Amsterdam, 1991, p. 37.
[3] B.S. Kang, M.C. Hong, T.B. Wen, H.Q. Liu, J.X. Lu, J. Cluster Sci. 6 (1995) 379.
[4] (a) N.S. Dean, M. Mokry, M.R. Bond, C.J. O'Conor, C.J. Carrano, Inorg. Chem. 35 (1996) 2818. (b) G.R. Hanson, Y. Sun, C. Orvig, Inorg. Chem. 35 (1996) 6507. (c) Y. Sun, B.R. James, S.J. Rettig, C. Orvig, Inorg. Chem. 35 (1996) 1667. (d) R. Codd, T.W. Hambly, P.A. Lay, Inorg. Chem. 34 (1995) 877.
[5] W. Plass, Angew. Chem., Int. Ed. Engl. 35 (1996) 627.
[6] (a) S.K. Dutta, S.B. Kumar, S. Bhattacharyya, E.R.T. Tiekink, M. Chaudhury, Inorg. Chem. 36 (1997) 4954. (b) S.K. Dutta, E.R.T. Tiekink, M. Chaudhury, Polyhedron 16 (1997) 1863.
[7] J.K. Money, J.C. Huffman, G. Christou, J. Am. Chem. Soc. 109 (1987) 2210.
[8] G. Henkel, B. Krebs, W. Schmidt, Angew. Chem., Int. Ed. Engl. 31 (1992) 1367.
[9] J.G. Reynolds, S.C. Sendlinger, A.M. Murray, J.C. Huffman, G. Christou, Inorg.Chem. 34 (1995) 5745.
[10] K.K. Nanda, E. Sinn, A.W. Addision, Inorg. Chem. 35 (1996) 1.
[11] (a) R.D. Bereman, G.D. Shiedls, J. Bordner, J.R. Dorfman, Inorg. Chem. 20 (1981) 2165. (b) R.D. Bereman, M.R. Churchill, G.D. Shields, Inorg. Chem. 18 (1979) 3117.
[12] E.M. Martin, Ph.D. Thesis, North Carolina State University, 1989.
[13] S.N. Chio, J.R. Wasson, Inorg. Chem. 14 (1975) 1964.
[14] (a) T. Takeshima, M. Yokoyama, T. Imamoto, M. Akano, H. Asaba, J. Org. Chem. 34 (1969) 730. (b) B. Bordas, P. Sohar, G. Matolxsy, P. Berenxsi, J. Org. Chem. 37 (1972) 1727.
[15] H. Rade St, J. Phys. Chem. 77 (1973) 424.
[16] (a) J.K. Money, J.C. Huffman, G. Christou, Inorg. Chem. 24 (1985) 5745. (b) C.J. Ballhausen, H.B. Gray, Inorg. Chem. 1 (1962) 111.
[17] P.R. Klich, A.T. Daniher, P.R. Challen, D.B. McConvill, W.J. Youngs, Inorg.Chem. 35 (1996) 347.
[18] B.J. McCormick, Inorg. Chem. 7 (1968) 1965.
[19] J.C. Dutton, G.D. Fallon, K.S. Murray, Inorg. Chem. 27 (1988) 34.
[20] W. Tsagkalidis, D. Rodewald, D. Rehder, V. Vergopoulos, Inorg. Chim. Acta 219 (1994) 213.
[21] T.B. Wen, J.C. Shi, X. Huang, Z.N. Chen, O.T. Liu, B.S. Kang, Polyhedron 17 (1998) 331.
[22] (a) J. Selbin, Angew. Chem., Int. Ed. Engl. 5 (1965) 712. (b) A.T. Casey, J.R. Thackeray, Aust. J. Chem. 22 (1969) 2549.
[23] A. Symal, Coord. Chem. Rev. 16 (1975) 309.
[24] V.V. Zelentsov, J. Russ, Inorg. Chem. 7 (1962) 670.
[25] S.N. Poddar, K. Dey, J. Haldar, S.C. Nathsarkar, J. Indian Chem. Soc. 47 (1970) 743.
[26] Y. Kuge, S. Yamada, Bull. Chem. Soc. Japan. 45 (1972) 799.
[27] B.N. Figgis, Trans. Faraday Soc. 57 (1961) 198.
[28] D. Collison, B. Graham, C.D. Garner, F.E. Mabbs, J. Chem. Soc., Dalton Trans. (1980) 667.
[29] B.J. McCormick, Inorg. Chem. 7 (1968) 1965.
[30] C.R. Cornman, J. Kampf, M.S. Lah, V.L. Pecoraro, Inorg. Chem. 31 (1992) 2035.
[31] M. Branca, G. Micera, A. Dessi, D. Dana, K.N. Raymond, Inorg. Chem. 29 (1990) 1586.
[32] M.R. Bond, L.M. Morky, T. Otieno, J. Thompson, C.J. Carrano, Inorg. Chem. 34 (1995) 1894.
[33] F.E. Dickson, C.J. Kunsesh, E.L. McGinnis, L. Petrakis, Anal. Chem. 44 (1972) 978.
[34] E.G. Ferrer, E.J. Baran, J. Electron Spectrosc. Relat. Phenom. 57 (1991) 189.
[35] H.J.R. Vanbekkum, Carbon 33 (1995) 1021.
[36] Y.S. Kim, Y.I. Kim, S.N. Choi, Bull. Kor. Chem. Soc. 11 (1990) 85.
[37] J.K. Money, K. Folting, J.C. Huffmann, D. Collison, J. Temperley, F.E. Mabbs, G. Christou, Inorg. Chem. 25 (1986) 4583.
[38] N.M Atherton, C.J. Winscom, Inorg. Chem. 12 (1973) 383.
[39] G. Matsubayashi, K. Akiba, T. Tanaka, Inorg. Chem. 27 (1988) 4744.
[40] J.C. Dutton, G.D. Fallon, K.S Murray, Inorg. Chem. 27 (1988) 34.

PERGAMON

www.elsevier.nl/locate/poly

Polyhedron 19 (2000) 2163–2170

POLYHEDRON

Synthesis, magnetic, spectroscopic and electrochemical studies of mixed pyrimidine-2-thiolate/triphenylphosphine rhenium(V) and rhenium(III) complexes

Gianantonio Battistuzzi, Maria Cannio, Raffaele Battistuzzi *

Department of Chemistry, University of Modena and Reggio Emilia, 41100 Modena, Italy

Received 22 May 2000; accepted 24 July 2000

Abstract

Equimolar amounts of *trans*-[$ReOX_2(OEt)(PPh_3)_2$] (X = Cl, Br, I) precursors and potentially bidentate *N*,*S*-donor pyrimidine-2(1*H*)-thione (pymSH) react in refluxing acetone to give mononuclear octahedral paramagnetic *trans*-[$Re^{III}X_2(pymS)(PPh_3)_2$] (X = Cl, Br, I) species. Starting from a metal–ligand molar ratio of 1:3, in the presence of $N(C_2H_5)_3$ as deprotonating agent in refluxing ethanol, the same reaction proceeds stepwise, affording octahedral [$ReO(pymS)_3$] or [$ReO(pymS)_3$] and pentagonal-bipyramidal [$Re(pymS)_3PPh_3$] complexes as a function of the reaction time. The compounds were characterized by elemental analysis, magnetic susceptibility, UV–Vis–NIR, IR and ^1H NMR spectroscopy and by cyclovoltammetric measurements. Reaction pathways and physico-chemical properties of the complexes are discussed. © 2000 Elsevier Science B.V. All rights reserved.

Keywords: Thiopyrimidine; Rhenium(V) complexes; Rhenium(III) complexes; Cyclic voltammetry; UV–Vis–NIR, IR, ^1H NMR spectra

1. Introduction

We are particularly interested in sulfur-containing heterocyclic ligands in which the combination of soft (S) and hard (N) donors leads usually to the formation of chelate rings which stabilize rhenium centers in intermediate oxidation states. Recently [1], we have reported that the reaction of 4,6-dimethylpyrimidine-2(1*H*)-thione (Me_2pymSH) with *trans*-[$ReOX_2(OEt)(PPh_3)_2$] (X = Cl, Br, I) precursors in 1:1 molar ratio, in refluxing acetone, proceeds step-wise affording rhenium(V), [$ReOX_2(Me_2pymS)(PPh_3)$] (X = Cl, Br, I), or rhenium(V) [$ReOX_2(Me_2pymS)(PPh_3)$] (X = Cl, Br, I), and rhenium(III) *trans*-[$ReX_2(Me_2pymS)(PPh_3)_2$] (X = Cl, Br) mixed octahedral complexes, as a function of the reaction time. In this paper, we report on the reactions of the pyrimidine-2(1*H*)-thione (pymSH), with rhenium(V) *trans*-[$ReOX_2(OEt)(PPh_3)_2$] (X = Cl, Br, I) synthons in order to compare the stoichiometry, structure and the chemistry of new rhenium species with related rhenium- Me_2pymS/triphenylphosphine mixed complexes. The pymSH is the simplest and the least sterically demanding 1,3-diazine derivative containing the following group subject to the tautomeric equilibrium:

–NH–C(S)–N=↔=N–C(SH)=N–

The new *trans*-[$ReX_2(pymS)(PPh_3)_2$] (X = Cl, Br, I) complexes and the species [$ReO(pymS)_3$] and [$Re(pymS)_3PPh_3$], whose X-ray crystal molecular structures have been reported by Zubieta et al. [2], were characterized with elemental analysis, electrochemical and magnetic measurements and UV–VIS–NIR, IR and ^1H NMR spectra.

2. Experimental

2.1. Materials

trans-[$ReOX_2(OEt)(PPh_3)_2$] (X = Cl, Br, I) synthons [3–5] and pyrimidine-2(1*H*)-thione [6] were prepared by

* Corresponding author. Tel.: +39-59-205-5044; fax: +39-59-373-543.

E-mail address: battistuzzi.gianantonio@unimo.it (R. Battistuzzi).

0277-5387/00/$ - see front matter © 2000 Elsevier Science B.V. All rights reserved.
PII: S0277-5387(00)00517-9

literature methods. Acetone, ethanol (RPE, C. Erba), dichloromethane (Fluka, over molecular sieves) and deutero-chloroform (100% D, Jansen Chimica) were used as received.

2.1.1. Preparation of the trans-[$ReX_2(pymS)(PPh_3)_2$] (X = Cl, Br, I) complexes

trans-[$ReOX_2(OEt)(PPh_3)_2$] (X = Cl, Br, I) precursors (1.0 mmol) and pymSH (1.0 mmol) were suspended in acetone (20 cm^3) and refluxed with stirring for 45 min. On heating, the solutions became clear and dark-brown in color. Upon cooling to 0°C for 12 h, the red–brown crystalline products were filtered off, washed with acetone and dried in vacuo.

2.1.1.1. trans-[$ReCl_2(pymS)(PPh_3)_2$]·0.5C_3H_6O. Found: C, 54.0; H, 3.9; N, 3.0; S, 3.4. Calc. for [$ReCl_2$(pymS)-(PPh_3)$_2$]·0.5C_3H_6O: C, 54.0; H, 3.9; N, 3.0; S, 3.5%. Yield ca. 42%. $\mu_{eff} = 1.72$ BM. Selected IR bands (cm^{-1}), $pymS^-$, ring: 1553m, 1535m; ν(NCN) + ν(NCS) + ν(CS): 1259w, 1185m, 1162ms; ν(Re–Cl): 309vs, 297vs. ^1H NMR ($CDCl_3$), δ(ppm), PPh_3: 13.98(m) [12H], 8.82 (m) [18H]; $pymS^-$: 17.52 (d) [1H, –CH], 13.01(s) [1H, –CH]; 3.65(t) [1H, –C_5H]; acetone: 2.18 (s) [6H, –CH_3].

2.1.1.2. trans-[$ReBr_2(pymS)(PPh_3)_2$. Found: C, 48.8; H, 3.4; N, 2.8; S, 3.2. Calc. for [$ReBr_2$(pymS)(PPh_3)$_2$]: C, 48.9; H, 3.4; N, 2.8; S, 3.3%. Yield ca. 48%. $\mu_{eff} = 1.73$ BM. Selected IR bands (cm^{-1}), $pymS^-$, ring: 1555m, 1538m; ν(NCN) + ν(NCS) + ν(CS): 1258w, 1187s, 1160m; ν(Re − Br): 208m, 189m. ^1H NMR ($CDCl_3$), δ(ppm), PPh_3: 14.23 (m) [12H], 8.81 (m) [18 H]; $pymS^-$: 16.92(s) [1H, –CH]; 12.40(s) [1H, –CH]; 4.21(t) [1H, –C_5H].

2.1.1.3. trans-[$ReI_2(pymS)(PPh_3)_2$]. Found: C, 44.6; H, 3.0; N, 2.6; S, 2.9. Calc. for [ReI_2(pymS)(PPh_3)$_2$]: C, 44.6; H, 3.1; N, 2.6; S, 3.0%. Yield ca. 46%. $\mu_{eff} = 1.76$ BM. Selected IR bands (cm^{-1}), $pymS^-$, ring: 1553m, 1540m; ν(NCN) + ν(NCS) + ν(CS): 1259mw, 1186ms, 1163m; ν(Re–I): 164m, 156m. ^1H NMR ($CDCl_3$), δ(ppm), PPh_3: 14.36(m) [12H], 8.80(m) [18H]; $pymS^-$: 14.62(s) [1H,–CH], 9.91(s) [1H, − CH], 5.28(t) [1H, − C_5H].

2.1.2. Preparation of the [$ReO(pymS)_3$] and [$Re(pymS)_3PPh_3$] complexes

Solid *trans*-[$ReOX_2(OEt)(PPh_3)_2$] precursor (X = Cl or Br or I) (0.6 mmol) was added to a solution of pymSH (1.8 mmol) containing 1.8 mmol of $N(C_2H_5)_3$ in 30 cm^3 of absolute EtOH. The mixture was refluxed under stirring for 2 h. On heating a green microcrystalline solid precipitated immediately and the clear and green solution became red-brown in color. After standing overnight the green compound was filtered off, washed many times with ethanol and dried in vacuum.

2.1.3. [$ReO(pymS)_3$]

Found: C, 26.9; H, 1.6; N, 15.6; S, 17.9. Calc. for [$ReO(pymS)_3$]: C, 26.9; H, 1.7; N, 15.7; S, 17.9%. Yield ca. 80%. Selected IR bands (cm^{-1}), $pymS^-$, ring: 1561vs, 1544vs; ν(NCN) + ν(NCS) + ν(CS): 1260mw, 1179m, 1169ms; ν(Re≡O): 967vs. Upon rotary concentration, the residual brown mother liquor (8–10 cm^3) leads, with time, to the separation of large dark-brown crystals of [$Re(pymS)_3PPh_3$]·EtOH as a minor product of the reaction. The crystals were washed with EtOH, Et_2O and dried in vacuo. Yield ca. 13%.

2.1.4. [$Re(pymS)_3PPh_3$]·EtOH

Found: C, 46.3; H, 3.6; N, 10.0; S, 11.5. Calc. for [$Re(pymS)_3PPh_3$]·EtOH: C, 46.4; H, 3.6; N, 10.1; S, 11.6%. Diamagnetic. Selected IR bands (cm^{-1}), $\nu(OH)_{EtOH}$: 3440mbr; PPh_3,ν(C–C):1582w, 1570w, 1480ms,1432s; ν(P–C): 1090 ms; $pymS^-$, ring: 1550sh, 1544ms; ν(NCN) + ν(NCS) + ν(CS): 1260mw, 1181m, 1155m. The brown [$Re(pymS)_3PPh_3$]·EtOH compound was also obtained with a good yield (ca. 93%), starting from [$ReO(pymS)_3$] and PPh_3 1:4 molar ratio and refluxing the mixture in ethanol for about 3 h.

2.2. Analyses and physical measurements

Elemental analyses (C, H, N, S) were carried out by a C. Erba Elemental Analyzer Model 1110. IR spectra were recorded in KBr pellets (4000–400 cm^{-1}) and in powdered polyethylene pellets (400–50 cm^{-1}) on a Perkin–Elmer 1600 series FTIR and a Bruker-IFS 113 V FTIR spectrophotometers, respectively. Room temperature magnetic susceptibilities were measured by Gouy method and corrected for diamagnetism by Pascal's constants. Conductivity measurements of the complexes, were performed on fresh 10^{-3} mol dm^{-3} solutions in CH_2Cl_2 at 25°C with a Jenway 4020 Conductivity Meter. Diffuse reflectance and solution spectra (in CH_2Cl_2, *C* ca. 10^{-5} and *C* ca. 10^{-3} mol dm^{-3}) between 200–2400nm were recorded on a Perkin–Elmer UV–Vis–NIR spectrometer 19. ^1H NMR spectra of the free ligands pymSH and PPh_3 and their rhenium(III) halide-complexes, were obtained with a Bruker-AMX 400 instrument at 25 ± 0.1°C in $CDCl_3$. The residual signal of $CDCl_3$ at 7.27 ppm was used as internal standard and the chemical shifts were converted to the usual TMS scale. Cyclic voltammetric measurements were performed on 10^{-4}–10^{-5} mol dm^{-3} CH_2Cl_2 (dried over molecular sieves) solutions of the complexes with a PAR Model 273A Potentiostat/Galvanostat under argon at 25°C. Tetrabuthylammonium perchlorate (TBAP) and chloride (TBACl) were used as base electrolytes and the ionic strength of the solutions was kept constant (5×10^{-2} mol dm^{-3}). A three-electrode arrangement was employed with a glassy-carbon working electrode (GC; PAR), a plat-

inum ring (1 cm^2) as a secondary electrode and Hg/Hg_2Cl_2, Cl^-_{sat} in CH_2Cl_2 as reference electrode. Potential scan rate between 0.05 and 0.5 Vs^{-1} were used. All the potential values are referred to the SCE electrode, their accuracy was ± 0.01 V.

3. Results and discussion

3.1. General

At variance with that reported for 4,6-dimethylpyrimidine-2(1*H*)-thione (Me_2pymSH) [1], the reaction of pyrimidine-2(1*H*)-thione (pymSH) with the same synthons, *trans*-[$ReOX_2(OEt)(PPh_3)_2$] (X = Cl, Br, I), carried out with the same procedure (with a molar ratio of 1:1, in refluxing acetone for 10–15 min), does not result initially in the separation of mixed oxo-complexes of the rhenium(V) of the type [$ReOX_2$(pymS)(PPh_3)], but affords directly and exclusively *trans*-[ReX_2(pymS)-(PPh_3)$_2$] (X = Cl, Br, I) rhenium(III) species with yields close to the 50% (trans notation refers to the arrangement of phosphine ligands).

The formation of these paramagnetic, mononuclear, octahedral complexes is undoubtedly the result of a sequence of events (equilibria between isomeric rearrangements, formation of transient intermediate species etc.) that involve as fundamental steps the substitution of trans EtO^- and O^{2-} groups in the precursors and reduction of Re(V) to Re(III) centers. Reduction of Re(V) to Re(III) cannot be due to the oxidation of thiopyrimidine to the corresponding disulfide since under our experimental conditions, the yields in *trans*-[ReX_2(pymS)(PPh_3)$_2$] (X = Cl, Br, I) species are higher than 40% and not close to 33% as it would be expected in the case of oxidation of thiopyrimidine to disulfide. Therefore, it seems probable that the formation of the rhenium(III) pyrimidinethiolate/PPh_3 mixed complexes in acetone can be interpreted in terms of a *trans* → *cis* isomerization of the *trans*-[$ReOX_2(OEt)(PPh_3)_2$] precursors, followed by substitution of pymSH, in thiol form, for EtO^- and an equatorial PPh_3 ligand, with formation of the transient oxo-intermediate of the rhenium(V) species [$ReOX_2$(pymS)(PPh_3)] (X = Cl, Br; I) and the EtOH and PPh_3 compounds. Subsequently, the hypothesized oxo-intermediate reacts rapidly {as reported for the complexes [$ReOX_2(acac)(PPh_3)_2$] (X = Cl, Br, I) [7,8]} with the displaced PPh_3 (2 equiv. of PPh_3 per rhenium(V) are required), evolving to the final mixed pyrimidinethiolate/PPh_3 rhenium(III) (theoretical yield 50%) and $O=PPh_3$ species, according the overall reaction scheme previously reported [1].

In contrast with the behavior of the related *trans*-[$ReX_2(Me_2pymS)(PPh_3)_2$] (X = Cl, Br) complexes [1], the species *trans*-[ReX_2(pymS)(PPh_3)$_2$] (X = Cl, Br, I) in CH_2Cl_2 or $CHCl_3$ solution are stable also in the presence of atmospheric oxygen. In fact, they maintain their color and give electronic and ^{1}H NMR spectra, which are unchanged after 2 days at room temperature. In addition, the pymSH ligand reacts with *trans*-[$ReOX_2(OEt)(PPh_3)_2$] (X = Cl, Br, I) in refluxing ethanol in the presence of $N(C_2H_5)_3$ as deprotonating agent, in 1:3:3 molar ratio, affording mainly the green microcrystalline [$ReO(pymS)_3$] complex (yield ca. 85%), and a brown crystalline [$Re(pymS)_3PPh_3$]·EtOH species as minor product (yield ca. 13%). Despite the different starting materials and preparation methods, the close similarity of the stoichiometry and spectroscopic properties of the present complexes with those structurally characterized reported previously by Zubieta [2], provide strong evidence in favor of identical structures.

3.2. Magnetic moments, vibrational, electronic and ^{1}H NMR spectra

The chloro-, bromo- and iodo-derivatives of the rhenium(III), *trans*-[ReX_2(pymS)(PPh_3)$_2$], show room temperature magnetic moments of 1.73, 1.72 and 1.76 BM, respectively. These values are characteristic of mononuclear complexes with low-spin rhenium(III) (d^4) ions in O_h field [9], and arises because of the large spin-orbit coupling ($\xi = 2500$ cm^{-1} [10]), which gives a diamagnetic ground state.

According with the elemental analyses, the acetone- and ethanol-containing complexes *trans*-[$ReCl_2$(pymS)-(PPh_3)$_2$]·0.5 C_3H_6O and [$Re(pymS)_3PPh_3$]·EtOH, display a medium ν(C=O) and ν(O–H) absorptions centered at 1713 and 3440 cm^{-1}, respectively. The ν(NH) IR bands of pymSH ligand {ν(N–H···S) at 2620 cm^{-1}, for the free ligand in KBr [11]} are absent from the spectra of all the complexes, suggesting deprotonation of the pyrimidine ligand. Confirmation of the presence of the $pymS^-$ anion is given by the absorption bands in the 1600–1500 region, which are attributable to ν(C···C) and ν(C···N) skeletal stretching modes of "aromatic six-membered heterocyclic ring" [12,13]. Furthermore, the lowering in intensity and the shifts to smaller wavenumbers of the strong ligand bands between 1225–1182 cm^{-1} [11,14], assigned to mixed ν(NCN), ν(NCS) and ν(CS) modes, strongly suggest, in accordance with X-ray structural results reported for [$ReO(pymS)_3$], [$Re(pymS)_3PPh_3$] [2] and with related *trans*-[$ReX_2(Me_2pymS)(PPh_3)_2$] (X = Cl, Br) [15] and [$ReCl_2$(pyrS)(PPh_3)$_2$] [16] complexes, an *N*,*S*-chelation of the aromatic $pymS^-$ anion around the rhenium (V) and rhenium(III) ions. Analogously to the complexes having a $[ReO]^{3+}$ core [9], the [$ReO(pymS)_3$] compound shows a very strong IR band at 967 cm^{-1} assignable to ν(Re≡O) mode. In the far-IR region (500–50 cm^{-1}) the [ReX_2(pymS)(PPh_3)$_2$] (X = Cl, Br, I) complexes show, besides the ligand bands and absorptions

due to ν(Re–N), ν(Re–S) and ν(Re–P) modes (whose assignments have not been achieved), two strong or medium bands with a peak-to-peak separation varying from 8 to 12 cm^{-1}, readily assigned to the ν(Re–X) stretching modes of mutually *cis* halides. All the three halide-complexes show similar solid state diffuse reflectance spectra and, when dissolved in CH_2Cl_2 the non-conducting solutions give absorption spectra similar to those of the related solid species (Table 1). From this it follows that the compounds are stable and retain their identity in solution and with time. The solution spectra exhibit intense (ε, 44100–8624 $dm^3\ mol^{-1}\ cm^{-1}$) absorption bands between 230–380 nm that are the result of interligand electronic transitions of $pymS^-$[17] and PPh_3 [18] ligands. In the range 450–850 nm, the spectra show some weaker absorptions (ε, 7805–29 $dm^3\ mol^{-1}\ cm^{-1}$) which fall at higher wavelengths on going from chloro- to the bromo- and iodo-compound. These bands can be assigned to a combination of ligand-to-metal charge transfer and d–d bands. In agreement with that reported previously [1], we tentatively assign the peaks in the range 1800–1833 nm (ε, 132–440 $dm^3\ mol^{-1}\ cm^{-1}$), which are better resolved in the solution spectra, to spin-allowed $^3T_{1g}(\Gamma_3,\Gamma_5) \leftarrow {}^3T_{1g}(\Gamma_1)$ excitations between levels of the ground state $^3T_{1g}(t_{2g}^4)$ split by large spin-orbit coupling. The bands in the regions 1240–1445 nm (ε, 19–38 $dm^3\ mol^{-1}\ cm^{-1}$) and 941–1010 (ε, 4–17 $dm^3\ mol^{-1}\ cm^{-1}$) might be due to the formally spin-forbidden $^1T_{2g}(\Gamma_5) \leftarrow {}^3T_{1g}(\Gamma_1)$ and $^1E_g(\Gamma_3) \leftarrow {}^3T_{g1}(\Gamma_1)$ transitions, respectively.

The ^{1}H NMR spectrum of pymSH ligand in $CDCl_3$ contains a triplet at 7.10 ppm downfield from TMS, assigned to the –C(5)H proton and a peak at 8.60 ppm of intensity 2, assigned to the equivalent –C(4)H and –C(6)H protons. The presence of two unpaired electrons in the *trans*-$[ReX_2(pymS)(PPh_3)_2]$ (X = Cl, Br, I) complexes, affects markedly the resonance signals giving rise to large chemical shifts ($+17$ to $+3$ ppm) and narrow signals due to fast relaxation of the metal center. The sharp doublet of the pymSH free ligand at 8.60 ppm in all the halide-complexes is shifted downfield and split in two singlets, each one of intensity 1, with the –CH proton adjacent to the coordinating nitrogen shifted to higher frequency than the other. The signal of –C(5)H proton of pymSH, is also shifted from 7.10 ppm to 3.65–5.28 ppm range. The *trans*-PPh_3 ligands give rise to a single set of PPh_3 signals and exhibit a pattern which is lightly affected by the nature of the halide: the *ortho* protons appear around 14 ppm (intensity 12) downfield the meta and para protons (8.80–8.84 ppm, intensity 18). The presence of acetone of crystallization in the $[ReCl_2(pymS)(PPh_3)_2]\cdot 0.5C_3H_6O$ complex is confirmed by a singlet around $\delta = 2.18$ ppm, which on integration corresponds to six protons.

Table 1
Diffuse reflectance (DR) and CH_2Cl_2 solution (S) ($C \approx 10^{-5}$and $C \approx 10^{-3}$ mol dm^{-3}) electronic spectral data (nm) of pymSH and its Re^{III} and Re^{V} complexes at room temperature (ε, $dm^3\ mol^{-1}\ cm^{-1}$ in parentheses)

PymSH		$[ReCl_2(pymS)(PPh_3)_2$		$[ReBr_2(pymS)(PPh_3)_2]$		$[ReI_2(pymS)(PPh_3)_2]$		$[Re(pymS)_3PPh_3]$		$[ReO(pymS)_3]$	
S	DR	S	DR	S	DR	S	DR	S	DR	S	DR
237 (10 820)	233sh	225 (44 100)	230sh	225 (44 200)	230s	230 (43 390)	230sh			234 (19 755)	
		255sh	260s	260sh	260sh	260sh	265s	264 (23 340)	264s	258 (17 845)	
291 (7320)	291s							312sh		293 (12 100)	300sh
380 (740)	353sh	370 (5885)	380s	355 (8624)	376sh	381 (7441)	378sh	378 (5920)	378s	366 (6427)	
		457 (3084)	448sh	464 (4127)	453s	462 (7805)	448sh	462 (12 265)	450	414sh	398sh
		503 (2055)	510sh	510 (3192)	511s	545 (4300)	545s	540sh	535s	580sh	580sh
		602sh	560sh	620sh	792m	850 (29)	853m	710sh	727sh	653 (250)	664s
		941 (13)	945m	970 (4)	980m	1010 (17)	1008m			900sh	910sh
		1255 (33)	1270s	1340 (34)	1327s	1240 (19)	1242m	1410 (8)	1415w		
						1445 (38)	1484mbr				
	1693wbr		1703sh		1714sh		1720sh		1669m	1700 (10)	1652w
		1820 (132)	1790s	1800 (232)	1786br	1833 (440)	1813s				

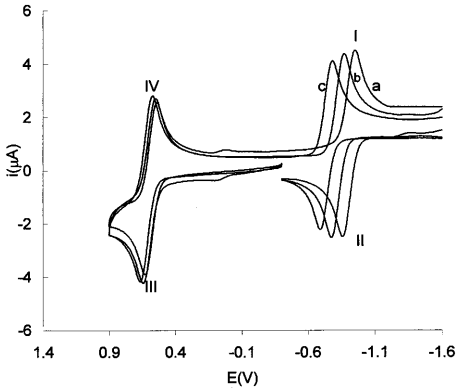


Fig. 1. Cyclic voltammograms for: (a) $[ReCl_2(pymS)(PPh_3)_2]$; (b) $[ReBr_2(pymS)(PPh_3)_2]$. $[ReI_2(pymS)(PPh_3)_2]$ complexes taken in CH_2Cl_2; $C = 4 \times 10^{-4}$ mol dm^{-3}; $v = 0.05$ V s^{-1}.

Both rhenium(V) $[ReO(pymS)_3]$ and rhenium(III) $[Re(pymS)_3PPh_3]$ are air-stable diamagnetic solids. The diamagnetism of the $[ReO(pymS)_3]$ species, according with a structural study [2] (which shows that the rhenium(V) ion adopts a distorted octahedral coordination in which the Re–O bonding of length 1.675 Å is formally a triple bond), is perfectly consistent with that expected from the simple crystal field theory for a d^2 mono-oxo complexes in a roughly C_{4v} symmetry [19]. In fact, taking the z axis as coincident with Re–O bond axis, for a C_{4v} symmetry the lowest energy non-bonding d_{xy} orbital of the rhenium(V) will accommodate the two d-electrons giving a spin-paired complex. The seven-coordinate $[Re(pymS)_3PPh_3]$ complex, contains a Re(III) metal center in a d^4 electronic configuration in an approximate pentagonal-bipyramidal environment [2]. In this geometry (pyramid base in xy plane) two of the three t_{2g} d orbitals (d_{xz}, d_{yz}) are sufficiently lowered in energy [20,21] to contain the two pairs of paired d-electrons to result in a diamagnetic species. The non-conducting CH_2Cl_2 solutions of both $[ReO(pymS)_3]$ and $[Re(pymS)_3PPh_3]$ complexes display electronic spectra (Table 1) showing a good correspondence with solid-state reflectance spectra. This strongly indicates that both species retain their identity in solution with time (after 6 days). A common feature of the absorption spectra of the $[ReO(pymS)_3]$ and $[Re(pymS)_3PPh_3]$ derivatives is the presence of the UV absorption bands (at 230–300 nm) characterizing the chromophore systems of the $pymS^-$ and/or $pymS^-$ and PPh_3 ligands. The most dominant spectral feature of the solution spectra of the green $[ReO(pymS)_3]$ species, are two band envelopes centered at 366 nm ($\varepsilon = 6427$ dm^3 mol^{-1} cm^{-1}) and at 653 nm ($\varepsilon = 250$ dm^3 mol^{-1} cm^{-1}) which contain some components. With reference to previous spectroscopic works on d^2 metal-ligand multiply bonded systems containing a $[ReO]^{3+}$ core [1,22], the relative intensity of the bands between 580–900 nm probably suggests that they are components of a $^3E_g[b_{2g}(xy)^1e_g(xz, yz)^1 \leftarrow b_{2g}(xy)^2]$ excited state that is split by strong spin–orbit coupling interactions [23]. The slightly more intense bands between 366–414nm presumably arise from mixed ligand-to-metal charge transfer and to singlet → singlet $^1E_g[(b_{2g})^1(e_g)^1] \leftarrow {}^1A_g[(b_{2g})^2]$ transitions.

Mononuclear seven-coordinate pentagonal-bipyramidal Re(III) (d^4) species, have not been deeply investigated through electronic spectroscopy. In a D_{5h} field, the five degenerate d orbitals split into three groups, a degenerate $e_1''[(xz), (yz)]$ ground state, a degenerate $e_2'[(x^2-y^2), (xy)]$ excited state and an $a_1'(z^2)$ excited state [24]. The ligand field symmetry in the $[Re(pymS)_3PPh_3]$ compound is lower than D_{5h} owing to distortions due to a $[ReN_3S_3P]$ coordination, which split the e_2' degenerate excited state. If the e_2' state is split by the distortions, then the e_1'' ground state is expected to be split too. Therefore, in accordance with that reported by Drew [25] for a diamagnetic $K_5[Mo(CN)_7]$ complex in which the Mo(II) ($4d^4$) center displays a distorted pentagonal-bipyramidal environment, and considering the energy and intensity of solution ($\varepsilon > 10^3$ dm^3 mol^{-1} cm^{-1}) and solid spectral absorptions, we suggest that the bands between 378 and 730 nm, presumably arise from a combination of d–d and metal–ligand [26] charge transfer transitions.

3.3. Cyclic voltammetry measurements

3.3.1. trans-[$ReX_2(pymS)(PPh_3)_2$] ($X = Cl, Br, I$) complexes

The cyclic voltammetric curves (CV) of these complexes, show two cathodic–anodic coupled peaks (Fig. 1). The corresponding data are reported in Table 2. The analysis of the peak current values, which depend linearly on the concentration of the complexes and on the square root of the potential scan rate, suggests that all the processes are diffusion controlled. The peak to peak separation and the ratio between the currents of the cathodic and anodic peaks also show that both the redox couples are reversible. Finally, the comparison of current values with those of p-NO_2–toluene, whose electrochemical reduction process is monoelectronic and reversible, indicates that all the processes involve one electron. Therefore, the potential peak in the cathodic range corresponds to the reduction process of Re(III) to Re(II) and its anodic counterpart to the oxidation, so the overall process is:

$$[ReX_2(pymS)(PPh_3)_2] + e \leftrightarrows [ReX_2(pymS)(PPh_3)_2]^- \quad (X = Cl, Br, I)$$

The couple in the anodic potential range corresponds to the overall process:

$$[ReX_2(pymS)(PPh_3)_2] \rightleftarrows [ReX_2(pymS)(PPh_3)_2]^+ + e$$

Table 2
The electrochemical data of $[ReX_2(pymS)(PPh_3)_2]$ complexes in CH_2Cl_2; $C = 4 \times 10^{-4}$ mol dm^{-3}, $v = 0.05$ V s^{-1}

Compounds	$-E_{pc}$(I) (V)	i_{pc}(I) (μA)	$-E_{pa}$(II) (V)	$-i_{pa}$(II) (μA)	$-E°$ (V)	E_{pa}(III) (V)	$-i_{pa}$(III) (μA)	E_{pc}(IV) (V)	i_{pc}(IV) (μA)	$E°$ (V)
$[ReCl_2(pymS)(PPh_3)_2]$	0.94	3.5	0.86	3.6	0.91	0.60	3.6	0.50	3.7	0.55
$[ReBr_2(pymS)(PPh_3)_2]$	0.86	3.8	0.77	3.7	0.82	0.63	3.7	0.53	3.8	0.58
$[ReI_2(pymS)(PPh_3)_2]$	0.77	3.6	0.69	3.5	0.73	0.64	3.7	0.54	3.9	0.59

Table 3
Dependence of the potential and current values from (a) the concentration and (b) the potential scan rate of the complex $[Re(pymS)_3(PPh_3)]$

		$-E_{pc}$(I) (V)	i_{pc}(I) (μA)	$-E_{pa}$(I) (V)	i_{pa}(I) (μA)	$-E_{pa}$(II) (V)	$-i_{pa}$(II) (μA)	E_{pa}(III) (V)	$-i_{pa}$(III) (μA)	E_{pc}(II) (V)	i_{pc}(II) (μA)	$E°$ (V)	E_{pa}(IV) (V)	$-i_{pa}$(IV) (μA)
(a) C 10^4 mol dm^{-3} [a]														
2.75		1.45	1.2	1.31	0.3	1.04	0.7	0.49	1.4	0.40	0.8	0.44	1.34	1.7
3.99		1.47	2.2	1.33	0.4	1.02	1.1	0.50	2.3	0.41	1.8	0.45	1.36	2.8
5.31		1.49	3.4	1.30	0.3	0.97	1.3	0.51	3.6	0.40	2.3	0.45	1.39	3.8
(b) v (V s^{-1}) [b]	*$v^{1/2}$* [b]													
0.05	0.224	1.46	2.3	1.33	0.5	1.02	1.2	0.50	3.0	0.41	2.5	0.45	1.36	2.8
0.1	0.316	1.51	3.3	1.32	0.7	0.99	1.5	0.50	4.3	0.39	3.1	0.44	1.37	2.54
0.2	0.447	1.54	4.5	1.30	1.1	0.95	2.4	0.52	5.8	0.38	3.8	0.45	1.23	2.73
0.4	0.632	1.56	6.1	1.29	1.2	0.93	3.8	0.52	7.6	0.36	5.9	0.44	1.20	5.0
0.5	0.707	1.56	7.4	1.29	1.2	0.92	4.2	0.54	7.9	0.37	5.9	0.45	1.18	3.92

[a] $v = 0.05$ V s^{-1}.
[b] $C = 4 \times 10^{-4}$ mol dm^{-3}.

When X = Cl, the complex is more difficult to reduce and is oxidized more easily due to the different coordinating ability of the chloride with respect to bromide or iodide ions. The CV curves of bromo- and iodo-derivatives do not change with time, therefore these complexes are stable. At variance the CV curves of the chloro-complex change with time, in fact it has been demonstrated that this compound loses the ligand molecule (Fig. 2) and completely decomposes in four hours. In the latter case the cyclic voltammetry shows the peaks of the free thiopyrimidine ligand and the solution color changes from yellow–orange to yellow–green first and finally to yellow. This color change suggests a Re(III) → Re(V) oxidative process and it is so remarkable that it can be attributed to a homogeneous reaction involving the bulk complex in solution. This is due to the TBAP used as base electrolyte. In fact this process does not occur in the presence of TBACl. The Re(III) → Re(V) oxidation was confirmed upon electrolytic oxidation of the Re(III) species at $E = 1$ V: indeed the CV curves recorded in TBAP after four hours and in TBACl after anodic electrolysis are identical.

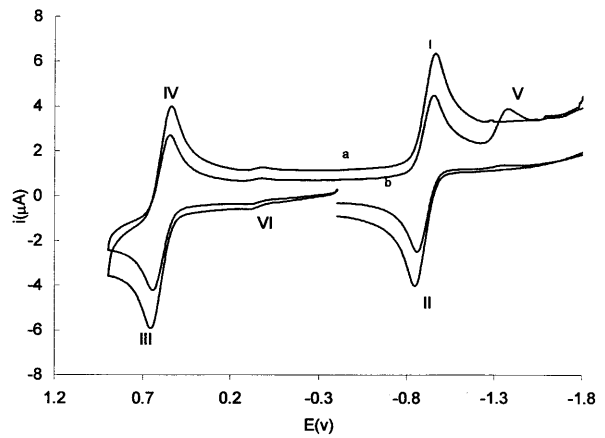


Fig. 2. CV curves of the $[ReCl_2(pymS)(PPh_3)_2]$ complex in CH_2Cl_2 ($C = 4 \times 10^{-4}$ mol dm^{-3}, $v = 0.05$ V s^{-1}): (a) recorded on fresh solution, (b) recorded after 2 h. The cathodic peak V corresponds to the oxidation to the anionic dimeric form $(pymS)_2^-$ due to the partial dimerization of the radical anion. This result agrees with the literature data [27].

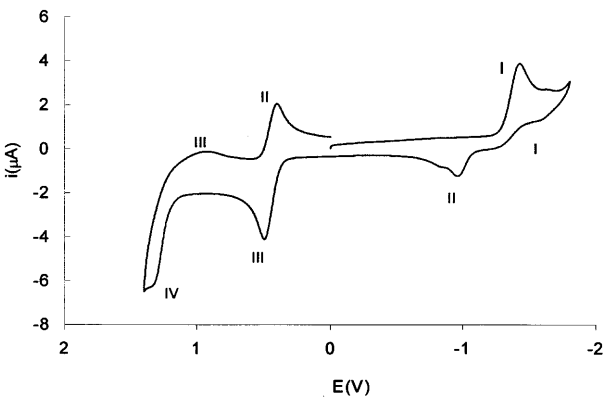


Fig. 3. Cyclic voltammogram of the $[Re(pymS)_3PPh_3]$ complex in CH_2Cl_2. $C = 4 \times 10^{-4}$ mol dm^{-3}, $v = 0.05$ V s^{-1}.

3.3.2. *[Re(pymS)$_3$PPh$_3$] complex*

A typical CV curve of the compound is reported in Fig. 3. The voltammogram shows two cathodic and four anodic peaks. The cathodic peak (I) corresponds to the reduction of Re(III) to Re(II). The process is monoelectronic and diffusion controlled: in fact the i_p values depend linearly on the complex concentration and on the square root of the potential scan rate. Its anodic counterpart shows two peaks (I) and (II): the first is controlled by a homogeneous kinetic process and it can be attributed to a structural modification after the reduction process; the second is diffusion controlled. The sum of the currents of the first and the second anodic peak corresponds to the current value of the cathodic peak and it can be attributed to the oxidation of Re(II) to the Re(III) (reaction 1). The overall process is quasi reversible. In the positive potential range, the Re(III) complex is oxidized in two different monoelectronic steps to Re(IV) (peak III) and Re(V) (peak IV), respectively. These processes are diffusion controlled. The anodic peak (III) shows a cathodic counterpart peak and the process is reversible, while the anodic peak (IV) doesn't show a definite cathodic counterpart and the redox process appears to be quasi reversible (reaction 2 and 3, respectively). The electrochemical data are reported in Table 3. CV curves were repeated several times on the same electrode surface. In all cases the CV curves are reproducible, and this suggests that the electrochemical processes do not cause decomposition of the complex. The overall scheme can be suggested:

$$[Re(pymS)_3(PPh_3)] + e \rightleftarrows [Re(pymS)_3(PPh_3)]^- \quad (1)$$

$$[Re(pymS)_3(PPh_3)] \leftrightarrows [Re(pymS)_3(PPh_3)]^+ + e \quad (2)$$

$$[Re(pymS)_3(PPh_3)]^+ \rightleftarrows [Re(pymS)_3(PPh_3)]^{2+} + e \quad (3)$$

3.3.3. *[ReO(pymS)$_3$] complex*

The CV curve is reported in Fig. 4 The voltammogram shows two cathodic peaks and four anodic peaks. The cathodic peaks I and II and the anodic peaks I and IV are diffusion controlled. The current value of the cathodic peak I is twice with respect to the II and corresponds to the IV anodic peak current. The current value of the cathodic peak II coincides with that of *p*NO_2-toluene, recorded in the same experimental conditions, therefore this peak corresponds to a monoelectronic process. Since the potential value of this peak is similar to that for the reduction of the

Table 4
Comparison of the potential values of $[ReO(pymS)_3]$ and $[Re(pymS)_3(PPh_3)]$complexes. $v = 0.05$ V s, $C = 4 \times 10^{-4}$mol dm^{-3}

Compounds	$-E_{pc}$(I) (V)	E_{pc}(II) (V)	$-E_{pa}$(I) (V)	$-E_{pa}$(II) (V)	E_{pa}(III) (V)	E_{pa}(IV) (V)
$[ReO(pymS)_3]$	0.91	−1.49	1.35	0.81	0.40	1.36
$[Re(pymS)_3(PPh_3)]$	1.47	0.40	1.33	1.03	0.50	1.36

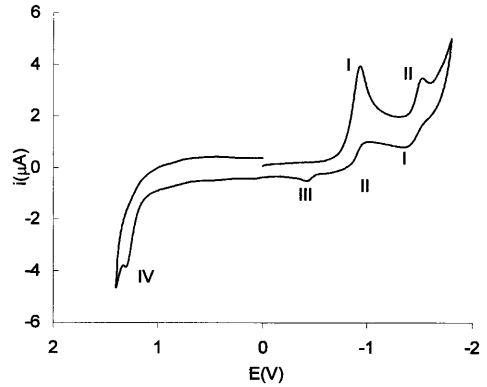


Fig. 4. CV curve of the $[ReO(pymS)_3]$ compound in CH_2Cl_2. $C = 4 \times 10^{-4}$mol dm^{-3}, $v = 0.05$ Vs^{-1}.

$[Re(pymS)_3(PPh_3)]$ complex to Re(II) species, we may attribute it to the same reduction process (Table 4). Also the corresponding oxidation process shows a behavior similar to that shown by the $[Re(pymS)_3(PPh_3)]$ complex, therefore the anodic peaks I and II indicate the oxidation of the Re(II) to Re(III) (reaction 5). The anodic peak III can be attributed to an adsorption process of the electrochemical product. The first cathodic peak corresponds to the reduction of the Re(V) complex to Re(III) species (reaction 4). The potential value of the anodic peak IV corresponds to the oxidation to Re(V) (reaction 6) and the current value indicates that it is a bielectronic process. This peak does not show a clear cathodic counterpart. The CV curves of the complex, repeated on the same electrode surface, do not change, suggesting that this compound is stable in electrochemical processes.

$$[ReO(pymS)_3] + 2e \rightarrow [ReO(pymS)3]^{2-} \quad (4)$$

$$[ReO(pymS)_3]^{2-} + e \rightleftarrows [ReO(pymS)_3]^{3-} \quad (5)$$

$$[ReO(pymS)_3]^{2-} \rightarrow [ReO(pymS)_3] + 2e \quad (6)$$

The electrochemical data are reported in Table 4. The electrochemical behavior of the $[ReO(pymS)_3]$ complex is not modified by the O_2 presence. In fact, degassing the saturated O_2 solution, the voltammogram corresponds to the initial CV curve of the compound.

Acknowledgements

Financial support by the Italian Ministero della Università e della Ricerca Scientifica e Tecnologica (P.R.I.N. 1998) is gratefully acknowledged. The NMR and Far-IR spectra were recorded in the Centro Interdipartimentale Grandi Strumenti of University of Modena and Reggio Emilia.

References

[1] G. Battistuzzi, M. Borsari, R. Battistuzzi, Polyhedron 16 (1997) 2093.
[2] D.J Rose, K.P Maresca, P.B Kettler, Y. Da Chang, V. Soghomomian, Q. Chen, M.J. Abrams, S.K. Larsen, Zubieta J. Inorg. Chem. 35 (1996) 3548.
[3] J. Chatt, G.A. Rowe, J. Chem. Soc. (1962) 4019.
[4] N.P Johnson, C.J.L. Lock, G. Wilkinson, Inorg. Synth. 8 (1967) 147.
[5] G.V. Parsal, Inorg. Synth. 17 (1977) 110.
[6] D.G. Grosby, R.V. Berthold, H.E. Johnson, Org. Synth. 43 (1963) 68.
[7] D.E. Grove, N.P. Johnson, C.J.L. Lock, G. Wilkinson, J. Chem. Soc. (1965) 490.
[8] I.D. Brown, C.J. Lock, Can. J. Chem. 52 (1974) 1704.
[9] J.E. Fergusson, Coord. Chem. Rev. 1 (1966) 459.
[10] A. Earnshaw, B.N. Figgis, J. Lewis, R.D. Peacok, J. Chem. Soc. (1961) 3132.
[11] M.J. Nowak, H. Rostkowska, L. Lapinski, J. Leszczynki, J.S. Kwiatkowski, Spectrochim. Acta, Part A 47 (1991) 339.
[12] A.R. Katrizki, Q. Rev. 13 (1959) 358.
[13] J. Spinner, Chem. Soc. (1960) 1237.
[14] D.N. Sathyanarayana, S.V.K. Raja, Spectrochim. Acta, Part A 41 (1985) 809.
[15] R. Battistuzzi, T. Manfredini, L.P. Battaglia, A. Bonamartini Corradi, A.J. Marzotto, Cryst. Spectrosc. Res. 19 (1989) 513.
[16] B. Schmidt-Brüdken, U. Abram, Z. Anorg. Allg. Chem. 626 (2000) 951.
[17] S.P. Gupta, S. Sharma, R.K. Goel, Spectrochim. Acta, Part A 42 (1986) 1171.
[18] G. Show, J. Chem. Soc., Chem. Comm. (1966) 425.
[19] J.M. Mayer, Comm. Inorg. Chem. 4 (1988) 125.
[20] J.J. Zuckerman, J. Chem. Educ. 42 (1965) 315.
[21] R. Krishnamurthy, W.B. Schaap, J. Chem. Educ. 46 (1969) 799.
[22] R. Davis, J.E. Fergusson, Inorg. Chim. Acta 4 (1970) 16.
[23] J.E. Winkles, H.B. Gray, Inorg. Chem. 24 (1985) 346.
[24] R. Hoffmann, B.F. Beier, E.L. Muetterties, A.R. Rossi, Inorg. Chem. 16 (1977) 511.
[25] M.G.B. Drew, P.C.H. Mitchell, J. Pygall, J. Chem. Soc., Dalton Trans. (1977) 1071.
[26] J. Rall, F. Weingard, D.M. Ho, M.J. Hegg, F. Tisato, E. Deutsch, Inorg. Chem. 33 (1994) 3442.
[27] R. Battistuzzi, M. Borsari, D. Dallari, G. Gavioli, C. Tavagnacco, G. Costa, J. Electroanal. Chem. 368 (1994) 227.

PERGAMON

www.elsevier.nl/locate/poly

Polyhedron 19 (2000) 2171–2175

POLYHEDRON

Alkyne complexes of tungsten(II) containing carboxylate and sulfonate substituted pyridine ligands. Water-soluble alkyne complexes of tungsten(II)

Paul K. Baker *, Alyn E. Jenkins, Margaret M. Meehan

Department of Chemistry, University of Wales, Bangor, Gwynedd, LL57 2UW, UK

Received 14 March 2000; accepted 24 July 2000

Abstract

Reaction of $[WI_2(CO)(NCMe)(\eta^2\text{-}RC_2R)_2]$ (R = Me, Ph) with one equivalent of L{L = 3-(CO_2Na)-py, 4-(CO_2Na)-py, 3,4-$(CO_2Na)_2$-py, 3,5-$(CO_2Na)_2$-py, 3-(SO_3Na)-py} in a mixture of CH_2Cl_2–CH_3OH (1:1 ratio) at room temperature gave the acetonitrile replaced products, $[WI_2(CO)L(\eta^2\text{-}RC_2R)_2]$ (**1**–**10**) in good yield. The 2-butyne complexes are slightly water-soluble, whereas the diphenylacetylene complexes are insoluble in water. Treatment of $[WI_2(CO)_3(NCMe)_2]$ with two equivalents of propiolic acid (HC_2CO_2H) in CH_2Cl_2 at 0°C yields the bis(propiolic acid) complex $[WI_2(CO)(NCMe)(\eta^2\text{-}HC_2CO_2H)_2]$ (**11**). Reaction of **11** with two equivalents of NaOH in MeOH–CH_2Cl_2 (1:1) affords the completely water-soluble complex, $[WI_2(CO)(NCMe)(\eta^2\text{-}HC_2CO_2Na)_2]$ (**12**) in 58% yield. All the new complexes **1**–**12** were characterised by elemental analysis (C, H, and N), IR and ^1H NMR spectroscopy. © 2000 Elsevier Science B.V. All rights reserved.

Keywords: Tungsten(II); Carboxylate and sulfonate substituted pyridines; Propiolic acid; Water soluble complexes

1. Introduction

The importance of water-soluble organometallic complexes in catalytic processes has become increasingly important in recent years [1,2]. Although a wide range of water-soluble organometallic complexes which have attached water-solubilising phosphine ligands have been described [3], far fewer containing water-solubilising nitrogen donor ligands have been reported. Herrmann et al. [4,5] have described several water-soluble metal-carbonyl complexes containing 2-(2′-pyridyl) pyridine-5-sulfonate as a water solubilising bidentate nitrogen donor ligand. Since our preliminary report in 1995 [6], of the first water soluble seven-coordinate complexes of tungsten(II) containing carboxylate and sulfonate substituted pyridine ligands, we have extended this work to zero-valent tetracarbonyl complexes of molybdenum and tungsten [7], and π-allyl dicarbonyl complexes of molybdenum(II) [8].

In 1986 [9], we described the reaction of the zero-valent complexes *fac*-$[M(CO)_3(NCMe)_3]$ (prepared in situ) with one equivalent of iodine at 0°C to give quantitative yields of the seven-coordinate complexes $[MI_2(CO)_3(NCMe)_2]$. In 1988, [10], we described the reactions of $[WI_2(CO)_3(NCMe)_2]$ with RC_2R (R = Me, Ph) to give the bis(alkyne) complexes $[WI_2(CO)(NCMe)(\eta^2\text{-}RC_2R)_2]$, both of which have been structurally characterised. The chemistry of the seven-coordinate complexes $[MI_2(CO)_3(NCMe)_2]$ and the alkyne complexes $[WI_2(CO)(NCMe)(\eta^2\text{-}RC_2R)_2]$(R = Me, Ph) has been extensively studied [11,12]. In this paper we describe the reactions of $[WI_2(CO)(NCMe)(\eta^2\text{-}RC_2R)_2]$-(R = Me,Ph) with one equivalent L {L = 3-(CO_2Na)-py, 4-(CO_2Na)-py, 3,4-$(CO_2Na)_2$-py, 3,5-$(CO_2Na)_2$-py, 3-(SO_3Na)-py} to give the complexes, $[WI_2(CO)L(\eta^2\text{-}RC_2R)_2]$, and the synthesis of $[WI_2(CO)(NCMe)(\eta^2\text{-}HC_2CO_2H)_2]$, and its conversion to the completely water soluble complex, $[WI_2(CO)(NCMe)(\eta^2\text{-}HC_2CO_2Na)_2]$.

* Corresponding author. Tel.: +44-1248-382-379; fax: +44-1248-370-5828.

E-mail address: p.k.baker@bangor.ac.uk (P.K. Baker).

0277-5387/00/$ - see front matter © 2000 Elsevier Science B.V. All rights reserved.
PII: S0277-5387(00)00518-0

2. Experimental

All reactions described in this paper were carried out under an inert atmosphere of dry nitrogen using standard vacuum/Schlenk line techniques. The starting materials used in this research, namely $[WI_2(CO)_3(NCMe)_2]$ [9] and $[WI_2(CO)(NCMe)(\eta^2\text{-}RC_2R)_2]$ [10] were prepared by literature methods. All chemicals used were purchased from commercial sources.

Elemental analyses (C, H and N) were determined using a Carlo Erba Elemental Analyser MOD 1108 (using helium as a carrier gas). Infrared spectra were recorded as KBr discs. ^{1}H NMR spectra were recorded on a Bruker AC 250 NMR spectrometer in DMSO-d_6 referred to $SiMe_4$.

2.1. Preparations

2.1.1. $[WI_2(CO)\{3\text{-}(CO_2Na)\text{-}py\}(\eta^2\text{-}MeC_2Me)_2]$ (1)

To $[WI_2(CO)(NCMe)(\eta^2\text{-}MeC_2Me)_2]$ (0.2 g, 0.325 mmol) dissolved in a 1:1 mixture of $EtOH/CH_2Cl_2$ (30 ml) was added 3-(CO_2Na)-py (0.047 g, 0.325 mmol). The solution was stirred for 3 h, at room temperature (r.t.), and the reaction mixture filtered through Keiselguhr. The solvent was removed in vacuo to give a yellow product. Recrystallisation of this product from $EtOH/CH_2Cl_2$ yielded the pure compound, $[WI_2(CO)\{3\text{-}(CO_2Na)\text{-}py\}(\eta^2\text{-}MeC_2Me)_2]$ (**1**) (Yield = 0.21 g, 88%).

Similar reactions of $[WI_2(CO)(NCMe)(\eta^2\text{-}MeC_2Me)_2]$ with one equivalent of L {L = 4-(CO_2Na)-py, 3,4-$(CO_2Na)_2$-py, 3,5-$(CO_2Na)_2$-py, 3-(SO_3Na)-py} gave the new complexes $[WI_2(CO)L(\eta^2\text{-}MeC_2Me)_2]$ (**2**–**5**).

2.1.2. $[WI_2(CO)\{3\text{-}(CO_2Na)\text{-}py\}(\eta^2\text{-}PhC_2Ph)_2]$ (6)

To a solution of $[WI_2(CO)(NCMe)(\eta^2\text{-}PhC_2Ph)_2]$ (0.25 g, 0.29 mmol) dissolved in a 1:1 mixture of $MeOH–CH_2Cl_2$ (30 ml) was added 3-(CO_2Na)-py (0.042 g, 0.29 mmol). The reaction mixture was stirred for 24 h, at r.t.; the solution was filtered over Keiselguhr and the solvent removed in vacuo giving a black product. The product was recrystallised from $MeOH–CH_2Cl_2$ at −17°C to give the analytically pure product, $[WI_2(CO)\{3\text{-}(CO_2Na)\text{-}py\}(\eta^2\text{-}PhC_2Ph)_2]$ (**6**). (Yield = 0.14 g, 52%).

In similar reactions, $[WI_2(CO)(NCMe)(\eta^2\text{-}PhC_2Ph)_2]$ was dissolved in a 1:1 mixture of $MeOH–CH_2Cl_2$, and reacted with one equivalent of L {L = 4-(CO_2Na)-py, 3,4-$(CO_2Na)_2$-py, 3,5-$(CO_2Na)_2$-py, 3-(SO_3Na)-py} to give the products, $[WI_2(CO)L(\eta^2\text{-}PhC_2Ph)_2]$ (**7**–**10**).

2.1.3. $[WI_2(CO)(NCMe)(\eta^2\text{-}HC_2CO_2H)_2]$ (11)

To $[WI_2(CO)_3(NCMe)_2]$ (0.5 g, 0.832 mmol) dissolved in CH_2Cl_2 (20 cm^3) was added HC_2CO_2H (0.1 g, 1.664 mmol). The solution was allowed to stir for 1 h at 0°C during which a red precipitate formed. The solvent was removed via a syringe and the product dried in vacuo to give the analytically pure product, $[WI_2(CO)(NCMe)(\eta^2\text{-}HC_2CO_2H)_2]$ (**11**) (Yield = 0.41 g, 76%).

2.1.4. $[WI_2(CO)(NCMe)(\eta^2\text{-}HC_2CO_2Na)_2]$ (12)

To a solution of $[WI_2(CO)(NCMe)(\eta^2\text{-}HC_2CO_2H)_2]$ (0.3 g, 0.464 mmol) dissolved in a 1:1 mixture of $MeOH–CH_2Cl_2$ (30 ml) was added NaOH (0.04 g, 0.928 mmol). The reaction mixture was stirred for one hour, after which the solution was filtered over Keiselguhr, and the solvent removed in vacuo giving a yellow product, which was recrystallised from H_2O–hexane at −17°C to give the analytically pure product, $[WI_2(CO)(NCMe)(\eta^2\text{-}HC_2CO_2Na)_2]$ (**12**) (Yield = 0.19 g, 58%).

3. Results and discussion

The reaction of $[WI_2(CO)(NCMe)(\eta^2\text{-}RC_2R)_2]$ with one equivalent of L in a 1:1 mixture of CH_2Cl_2 and CH_3OH at r.t. gave $[WI_2(CO)L(\eta^2\text{-}RC_2R)_2]$ {R = Me, Ph; L = 3-(CO_2Na)-py, 4-(CO_2Na)-py, 3,4-$(CO_2Na)_2$-py, 3,5-$(CO_2Na)_2$-py, 3-(SO_3Na)-py} (**1**–**10**) with the acetonitrile ligand being replaced by L. The complexes were characterised by elemental analysis (Table 1), IR spectroscopy (Table 2) and ^{1}H NMR spectroscopy (Table 3). The complexes were stable in the solid state when stored under dinitrogen at −17°C, but were very unstable in air when in solution. The complexes were soluble in dimethylsulfoxide, acetone and methanol, sparingly soluble in dichloromethane. The 2-butyne complexes **1**–**5** are slightly soluble in water, whereas the diphenylacetylene complexes **6**–**10** are insoluble in water. The total insolubility in water of the diphenylacetylene complexes **6**–**10** is probably due to the phenyl rings in the diphenylacetylene ligand.

The IR spectra of complexes **1**–**10** showed one strong carbon monoxide stretching band between 2071 and 2012 cm^{-1}. An alkyne absorption was also observed between 1668 and 1602 cm^{-1} for complexes **1**–**10**. These bands are of much lower wavenumber than for the uncoordinated alkyne due to the back donation into empty π* antibonding orbitals of the coordinated alkyne. Carbonyl stretching bands for the carboxylate units were observed for the complexes **1**–**4** and **6**–**9** between 1700 and 1733 cm^{-1}. The complexes $[WI_2(CO)\{3\text{-}(SO_3Na)\text{-}py\}(\eta^2\text{-}RC_2R)_2]$ (**5**) and (**10**) have an S=O stretching band at 1224 cm^{-1}.

The ^{1}H NMR spectra (Table 3) of complexes **1**–**5**, showed two singlets which can be assigned to the protons of the 2-butyne ligands. The proton assignments of the substituted pyridine ligands is shown in Fig. 1. The complex $[WI_2(CO)\{3\text{-}(CO_2Na)\text{-}py\}(\eta^2\text{-}MeC_2Me)_2]$ (**1**) showed resonances at 9.4 (H_a), 9.1 (H_b), 8.7 (H_c) and 7.0 ppm (H_d). The complexes **6**–**10** showed

Table 1
Physical and analytical data for the alkyne complexes of tungsten(II) [a]

Complex	Yield	Colour	C(%)	H(%)	N(%)
(**1**) $[WI_2(CO)\{3\text{-}(CO_2Na\text{-}py\}(\eta^2\text{-}MeC_2Me)_2]$	88	yellow	24.8(25.1)	2.4(2.2)	1.7(2.0)
(**2**) $[WI_2(CO)\{4\text{-}(CO_2Na)\text{-}py\}(\eta^2\text{-}MeC_2Me)_2]$	62	yellow	25.6(25.1)	2.2(2.2)	2.1(2.0)
(**3**) $[WI_2(CO)\{3,4\text{-}(CO_2Na)_2\text{-}py\}(\eta^2\text{-}MeC_2Me)_2]$	63	brown	25.2(24.5)	1.3(1.4)	1.9(1.8)
(**4**) $[WI_2(CO)\{3,5\text{-}(CO_2Na)_2\text{-}py\}(\eta^2\text{-}MeC_2Me)_2]$	83	brown	24.7(24.5)	1.5(1.4)	2.1(1.8)
(**5**) $[WI_2(CO)\{3\text{-}(SO_3Na)\text{-}py\}(\eta^2\text{-}MeC_2Me)_2]$	75	brown	22.8(22.3)	1.7(2.2)	2.0(1.9)
(**6**) $[WI_2(CO)\{3\text{-}(CO_2Na)\text{-}py\}(\eta^2\text{-}PhC_2Ph)_2]$	52	black	43.8(43.5)	2.4(2.5)	1.1(1.5)
(**7**) $[WI_2(CO)\{4\text{-}(CO_2Na)\text{-}py\}(\eta^2\text{-}PhC_2Ph)_2]$	66	yellow	42.9(43.5)	3.4(2.5)	1.7(1.5)
(**8**) $[WI_2(CO)\{3,4\text{-}(CO_2Na)_2\text{-}py\}(\eta^2\text{-}PhC_2Ph)_2]$	74	yellow	42.4(41.8)	2.5(2.2)	1.5(1.4)
(**9**) $[WI_2(CO)\{3,5\text{-}(CO_2Na)_2\text{-}py\}(\eta^2\text{-}PhC_2Ph)_2]$	78	yellow	41.8(41.8)	2.9(2.2)	1.8(1.4)
(**10**) $[WI_2(CO)\{3\text{-}(SO_3Na)\text{-}py\}(\eta^2\text{-}PhC_2Ph)_2]$	77	brown	40.1(40.7)	3.6(2.4)	2.1(1.4)
(**11**) $[WI_2(CO)(NCMe)(\eta^2\text{-}HC_2CO_2H)_2]$	76	red	16.9(16.7)	1.4(1.1)	2.5(2.2)
(**12**) $[WI_2(CO)(NCMe)(\eta^2\text{-}HC_2CO_2Na)_2]$	58	yellow	15.7(15.6)	1.2(0.7)	2.4(2.0)

[a] Calculated values in parentheses.

broad multiplets at around 7.3 ppm in their ^{1}H NMR spectra, which can be attributed to the hydrogens of the diphenylacetylene ligand. The pyridine protons in the complexes **6**–**10** have similar resonances to those observed in complexes **1**–**5** respectively. The structure of the compounds **1**–**10** is very likely to be very similar to those of $[WI_2(CO)L(\eta^2\text{-}RC_2R)_2]$ {L = NCMe, R = Me, Ph [10]; L = NCBu^t, R = Me [13]; L = $NCCH_2(3\text{-}C_4H_3S)$, R = Me [14]; L = CO, R = Me [15]}. The proposed structure for complexes **1**–**10** is shown in Fig. 2.

The reactions are likely to proceed via an associative mechanism with the formation of a seven-coordinate adduct, $[WI_2(CO)(NCMe)L(\eta^2\text{-}RC_2R)_2]$, in which each alkyne ligand donates two electrons to the metal. The loss of the acetonitrile ligand from the intermediate would allow the alkynes to donate an average of three electrons each to the metal as in the acetonitrile complexes, $[WI_2(CO)(NCMe)(\eta^2\text{-}RC_2R)_2]$. Associative mechanisms for ligand substitution reactions of molybdenum(II) and tungsten(II) have been previously proposed for this type of reaction [16,17]. Attempts to protonate **1**–**5** with $H[BF_4]$ were unsuccessful. Although reactions occurred in each case, no identifiable products could be isolated from these reactions.

The starting materials $[WI_2(CO)(NCMe)(\eta^2\text{-}RC_2R)_2]$ (R = Me, Ph) were reacted with two equivalents of L {L = 3-(CO_2Na)-py, 4-(CO_2Na)-py, 3,4-$(CO_2Na)_2$-py, 3,5-$(CO_2Na)_2$-py, 3-(SO_3Na)-py} for 24 h in a mixture of dichloromethane and methanol at r.t. did not give the expected cationic complexes $[WI(CO)L_2(\eta^2\text{-}RC_2R)_2]I$ [18]. The elemental analysis results for the products formed did not correspond to the calculated values for $[WI(CO)L_2(\eta^2\text{-}RC_2R)_2]I$, the expected products we have previously observed from the reactions of $[WI_2(CO)(NCMe)(\eta^2\text{-}RC_2R)_2]$ with simple pyridines [18]. For all of the complexes formed the analytical data were in agreement with the values expected for the reaction of $[WI_2(CO)L(\eta^2\text{-}RC_2R)_2]$ with one equivalent of L. The experiments were repeated by refluxing for 24 h to see if a second substituted pyridine ligand could be coordinated to the tungsten. However, the results were comparable with the reactions carried out at r.t.

Another approach to preparing a water-soluble alkyne complex of tungsten (II) was made by reacting the seven-coordinate complex $[WI_2(CO)_3(NCMe)_2]$ with two equivalents of propiolic acid (HC_2CO_2H) in dichloromethane at 0°C for one hour gives $[WI_2(CO)(NCMe)(\eta^2\text{-}HC_2CO_2H)_2]$(**11**). The complex was fully characterised (Tables 1–3), but was not water-soluble. In an attempt to make the alkyne complex water-soluble, the complex $[WI_2(CO)(NCMe)(\eta^2\text{-}HC_2CO_2H)_2]$(**11**) was reacted with two equivalents of NaOH in MeOH–CH_2Cl_2 (1:1) at r.t. for thirty minutes, affording the completely water-soluble complex $[WI_2(CO)(NCMe)(\eta^2\text{-}HC_2CO_2Na)_2]$(**12**). Complex **12** was characterised by elemental analysis (Table 1), IR spectroscopy (Table 2) and ^{1}H NMR spectroscopy (Table 3). Since proton resonances for the terminal alkyne protons (C≡C-*H*) for **11** and **12**, appear at $\delta = 7.1$ and 7.3 ppm, respectively, it is likely [19], the alkynes are donating a total of six-electrons to the

Table 2
IR data for the alkyne complexes of tungsten(II) [a]

Complex	ν(C≡O) (cm^{-1})	ν(C=O) (cm^{-1})	ν(C≡C) (cm^{-1})
(**1**)	2014 s	1711 s	1662 s
(**2**)	2012 s	1708 m	1668 m
(**3**)	2013 s	1700 m	1654 m
(**4**)	2016 s	1723 m	1627 s
(**5**) [b]	2017 w	1224 [b] s	1617 s
(**6**)	2065 s	1733 m	1622 s
(**7**)	2067 s	1725 s	1602 w
(**8**)	2070 s	1721 s	1622 s
(**9**)	2069 s	1722 m	1618 m
(**10**) [b]	2071 m	1224 [b] m	1626 s
(**11**)	2018 s	1730 m	1674 w
(**12**)	2013 m	1728 m	1661 m

[a] Spectra recorded as KBr discs.
[b] S=O stretching frequency; s = strong, m = medium, w = weak.

Table 3
^{1}H NMR data for the alkyne complexes of tungsten(II) [a]

Complex	^{1}H NMR (δ) ppm
1	9.4 {m, 1H$_a$, 3-(CO_2Na)-py}; 9.1 {m, 1H$_b$, 3-(CO_2Na)-*py*}; 8.7 {d, $J = 5.9$ Hz, 1H$_c$, 3-(CO_2Na)-*py*}, 8.0 {m, 1H$_d$, 3-(CO_2Na)-*py*}; 3.0, 3.2 (2s, 12H, *Me*C_2)
2	8.3 {d, $J = 7.2$ Hz, 2H$_a$, 4-(CO_2Na)-*py*}; 7.8 {d, $J = 7.3$ Hz, 2H$_b$, 4-(CO_2Na)-*py*}, 3.0, 3.2 (2s, 12H, *Me*C_2)
3	9.3 {s, 1H$_a$, 3,4-(CO_2Na)$_2$-*py*}, 8.7 {d, $J = 8.8$ Hz, 1H$_b$, 3,4-(CO_2Na)$_2$-*py*}, 7.8 {d, $J = 7.2$ Hz, 1H$_c$, 3,4-(CO_2Na)$_2$-*py*}, 2.9, 3.1 (2s, 12H, *Me*C_2)
4	9.25 {d, $J = 1.4$ Hz, 1H$_b$, 3,5-(CO_2Na)$_2$-*py*}; 8.6 {d, $J = 1.4$ Hz, 2H$_a$, 3,5-(CO_2Na)$_2$-*py*}, 3.4, 3.2 (2s, 12H, *Me*C_2)
5	8.8 {s, 1H$_a$, 3-(SO_3Na)-*py*}; 8.5 {d, 1H$_b$, $J = 6.5$ Hz, 3-(SO_3Na)-*py*}; 8.1 {d, 7.7 Hz, 1H$_c$, 3-(CO_2Na)-*py*}; 7.7 {m, 1H$_d$, 3-(SO_3Na)-*py*}; 3.2, 3.0 (2s, 12H, *Me*C_2)
6	9.5 {s, 1H$_a$, 3-(CO_2Na)-*py*}; 9.2 {d, $J = 5.9$ Hz, 1H$_b$, 3-(CO_2Na)-*py*}; 8.4 {d, $J = 7.5$ Hz, 1H$_c$, 3-(CO_2Na)-*py*}; 8.1 {m, 1H$_d$, 3-(CO_2Na)-*py*};7.35 (m, 20H, PhC_2)
7	8.7 {d, $J = 7.4$ Hz, 2H$_a$, 4-(CO_2Na)-*py*}; 7.9 {d, $J = 7.3$ Hz, 2H$_b$, 4-(CO_2Na)-*py*}; 7.3 (brm, 20H, PhC_2)
8	9.1 {s, 1H$_a$, 3,4-(CO_2Na)$_2$-*py*}; 8.9 {d, $J = 5.9$ Hz, 1H$_b$, 3,4-(CO_2Na)$_2$-*py*}; 8.6 {d, $J = 5.9$ Hz, 1H$_c$, 3,4-(CO_2Na)$_2$-*py*}; 7.35 (brm, 20H, PhC_2)
9	9.4 {s, 1H$_b$, 3,5-(CO_2Na)$_2$-*py*}; 8.8 {d, $J = 1.6$ Hz, 2H$_a$, 3,5-(CO_2Na)$_2$-*py*}; 7.15 (brm, 20H, Ph*C*$_2$)
10	9.4 {s, 1H$_a$, 3-(SO_3Na)-*py*}; 8.9 {d, $J = 7.3$ Hz, 1H$_b$, 3-(CO_2Na)-*py*}; 8.3 {d, $J = 7.8$ Hz, 1H$_c$, 3-(CO_2Na)-*py*}; 7.7 {m, 1H$_d$, 3-(SO_3Na)-*py*}; 7.4 (m, 20H, PhC_2)
11	7.1 (s, 2H, *H*C≡C), 3.6 (s, 2H, CO_2*H*); 2.2 (s, 3H, NC*Me*)
12	7.3 (s, 2H, *H*C≡C), 2.1 (s, 3H, NC*Me*)

[a] Spectra recorded in DMSO (+25°C) and referenced to $SiMe_4$.

tungsten in these complexes. This enables **11** and **12** to obey the effective atomic number rule.

Although no suitable single crystal was grown for X-ray crystallography, the structure of the complexes **11** and **12** (see Fig. 3) is likely to be similar to the structure of other [WI_2(CO)(L)(η^2-RC_2R)$_2$] complexes which have been characterised crystallographically [10,13–15]. The formal geometry of the complexes is eight-coordinate, but they can be considered to be six-coordinate with each alkyne ligand occupying a single coordination site. The two iodine atoms are mutually *cis*-, and each is *trans*- to an alkyne ligand. The acetonitrile ligand lies *trans*- to the C≡O group. The IR spectra of the complexes **11** and **12** have C≡O stretches at 2018 and 2013 cm^{-1}, respectively, C=O stretches at 1730 and 1728 cm^{-1} and C≡C stretches at 1674 and 1661 cm^{-1}, respectively.

In conclusion, we have described the preparation and characterisation of the first example of a totally water-soluble bis(alkyne) complex of tungsten(II). In view of many complexes derived from [WI_2(CO)(NCMe)(η^2-RC_2R)$_2$] being alkene metathesis catalysts [20], being able to induce water solubility in this type of complex is an important breakthrough.

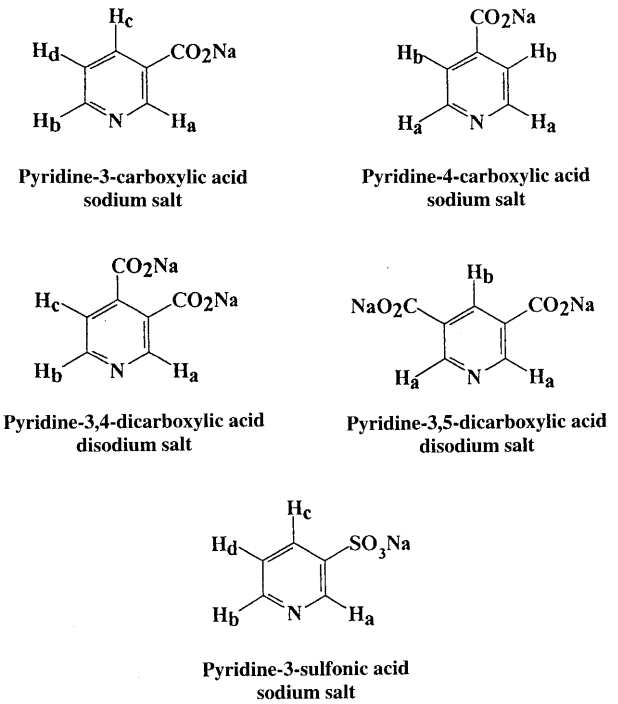


Fig. 1. ^{1}H NMR proton assignments for the carboxylate and sulfonate substituted pyridine ligands.

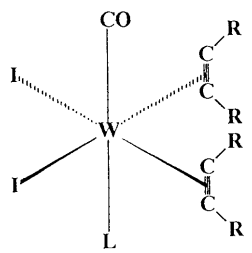


Fig. 2. Proposed structure of [WI_2(CO)L(η^2-RC_2R)$_2$] (**1**–**10**).

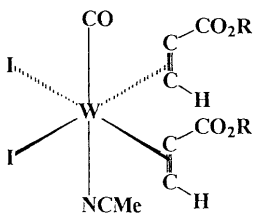


Fig. 3. Proposed structure of [WI_2(CO)(NCMe)(η^2-HC_2CO_2R)$_2$] (R = H, Na) (**11** and **12**).

Acknowledgements

A.E.J. thanks the Training for Work Scheme for support.

References

[1] A.F. Borowski, D.J. Cole-Hamilton, G. Wilkinson, New J. Chem. 2 (1978) 137.
[2] E.G. Kuntz, Chemtech. 17 (1987) 570.
[3] M. Barton, J.D. Atwood, J. Coord. Chem. 24 (1991) 43 and references cited therein.
[4] W.A. Herrmann, W.R. Thiel, J.G. Kuchler, Chem. Ber. 123 (1990) 1953.
[5] W.A. Herrmann, W.R. Thiel, J.G. Kuchler, J. Behm, E. Herdtweck, Chem. Ber. 123 (1990) 1963.
[6] P.K. Baker, A.E. Jenkins, A.J. Lavery, D.J. Muldoon, A.J. Shawcross, J. Chem. Soc., Dalton Trans. (1995) 1525.
[7] P.K. Baker, A.E. Jenkins, Polyhedron 16 (1997) 2279.
[8] P.K. Baker, A.E. Jenkins, J. Organomet. Chem. 125 (1997) 545.
[9] P.K. Baker, S.G. Fraser, E.M. Keys, J. Organomet. Chem. 309 (1986) 319.
[10] E.M. Armstrong, P.K. Baker, M.G.B. Drew, Organometallics 7 (1988) 319.
[11] P.K. Baker, Adv. Organomet. Chem. 40 (1996) 45 and references cited therein.
[12] P.K. Baker, Chem. Soc. Rev. 27 (1998) 125 and references cited therein.
[13] P.K. Baker, M.E. Harman, M.B. Hursthouse, A.J. Lavery, K.M.A. Malik, D.J. Muldoon, A.J. Shawcross, J. Organomet. Chem. 484 (1994) 169.
[14] P.K. Baker, M.G.B. Drew, S. Edge, S.D. Ridyard, J. Organomet. Chem. 409 (1991) 207.
[15] E.M. Armstrong, P.K. Baker, M.G.B. Drew, J. Organomet. Chem. 336 (1987) 377.
[16] S.R. Allen, P.K. Baker, S.G. Barnes, M. Green, L.J. Trollope, L.J. Muir, K.W. Muir, J. Chem. Soc., Dalton Trans. (1981) 873
[17] R.S. Herrick, D.M. Leazer, J.L. Templeton, Organometallics 2 (1982) 834.
[18] P.K. Baker, E.M. Armstrong, M.G.B. Drew, Inorg. Chem. 27 (1988) 2287.
[19] J.L. Templeton, Adv. Organomet. Chem. 29 (1989) 1 and references cited therein.
[20] M. Al-Jahdali, P.K. Baker, A.J. Lavery, M.M. Meehan, D.J. Muldoon, J. Mol. Catal., in press, 2000.

PERGAMON

www.elsevier.nl/locate/poly

Polyhedron 19 (2000) 2177–2181

POLYHEDRON

Charge-transfer photochemistry of the ternary complex (diselenocarbamato, dithiophosphato)copper(II)

N.D. Yordanov [a,*], B. Jeliazkova [b], D. Roussanova [a], G. Sarova [b], P. O'Brien [c], M.A. Malik [c]

[a] *Bulgarian Academy of Sciences, Institute of Catalysis, 1113 Sofia, Bulgaria*
[b] *University of Sofia, Department of Chemistry, 1, James Bourchier Blvd., 1164 Sofia, Bulgaria*
[c] *Department of Chemistry, Imperial College of Science, Technology and Medicine, South Kensington, London, SW 7 2AY, UK*

Received 19 April 2000; accepted 24 July 2000

Abstract

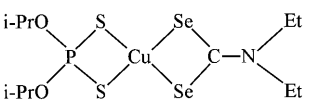
Photolysis of the ternary system consisting of diethyldiselenocarbamate (Et_2dsc), diisopropyldithiophosphate (i-Pr_2dtp) and copper(II) (1:1:1) has been studied in toluene, CH_2Cl_2, $CHCl_3$, CCl_4 and chloroalkane–EtOH solutions. The results obtained by EPR techniques and UV–Vis data indicate that a homolytic Cu–S bond cleavage involving dtp ligand appears as the primary photoprocess in Cu(dsc)(dtp) photolysis. Further conversion of the primary photoproduct $Cu^{I}(Et_2dsc)$ is discussed in terms of specific interaction with the solvent. According to quantum yield data solvent efficiencies in photolysis could be related to their oxidizing power. A reaction mechanism is proposed well fitting the experimental results. © 2000 Elsevier Science B.V. All rights reserved.

Keywords: CT photochemistry; Ternary copper(II) complexes; Diselenocarbamate and dithiophosphate ligands

1. Introduction

In recent papers [1,2] we have described the photochemical behaviour of bis(diethyldiselenocarbamato)-Cu(II), $Cu(Et_2dsc)_2$, and bis(diisopropyldithiophosphato)Cu(II), $Cu(i\text{-}Pr_2dtp)_2$, in aprotic solvents. The results obtained show that the primary photochemical act in both complexes is an intramolecular electron transfer from the equatorially bound Se (resp. S) atom of the ligand to copper(II) yielding the corresponding complex of copper(I) and the free radical from the ligand. Further reactions of the primary photoproducts are related to the redox properties of both ligands and solvents. It was also found that upon irradiation in the corresponding charge transfer band the quantum yield of $Cu(dsc)_2$ photolysis is lower than the value obtained for $Cu(dtc)_2$ in the same solvent.

In the present paper we report our data on the photochemical properties of the ternary Cu(dsc)(dtp) complex obtained with ligands of chemically different donor sets as a part of our study on the photochemistry of copper(II) chelate complexes with different chromophores.



2. Experimental

2.1. Starting materials

The complex bis(diethyldiselenocarbamato)Zn(II) was obtained and purified following a literature procedure [3,4]. Diisopropyldithiophoshoric acid and its sodium salt were prepared as previously described [5]. $CuSO_4.5H_2O$ (p.a.) was obtained from Fluka and used without further purification. The solvents were used after distillation.

* Corresponding author. Tel.: +359-2-979-2546; fax: +359-2-756-116.
E-mail address: ndyepr@bas.bg (N.D. Yordanov).

0277-5387/00/$ - see front matter © 2000 Elsevier Science B.V. All rights reserved.
PII: S0277-5387(00)00520-9

2.2. Preparation of compounds

The parent complexes $Cu(Et_2dsc)_2$ and $Cu(i\text{-}Pr_2dtp)_2$ were prepared by standard literature methods [1,2,4,5]. The ternary complex Cu(dsc)(dtp) was obtained according to the reaction:

$$Cu(Et_2dsc)_2 + Cu(i\text{-}Pr_2dtp)_2 = 2Cu(dsc)(dtp) \quad (1)$$

by mixing the corresponding equimolar solutions of $Cu(Et_2dsc)_2$ and $Cu(i\text{-}Pr_2dtp)_2$ to obtain Cu:dtc:dtp = 1:1:1. The initial solutions of the parent complexes were prepared by weighing and dissolution of the appropriate amounts.

2.3. Instrumentation

The EPR spectra were taken at room temperature on an X-band Bruker ER 200D-SRC spectrometer. The standard ER4202ST rectangular cavity (TE_{102} mode) was used. The microwave power was 3 mW and 2 G modulation amplitude of the magnetic field (at 100 kHz) during all experiments.

The electronic absorption spectra were recorded on a Specord UV–Vis (Carl Zeiss, Jena) spectrophotometer using quartz cells to record in the 250–750 nm region.

All measurements were performed at room temperature (293 K).

2.4. Irradiation and quantum yields

Photolysis experiments were performed with the full spectrum of a 250 W medium-pressure mercury lamp or through a solution filter to separate the 436 nm mercury line [5] as described previously [1,2]. For quantum yield determination the complex concentrations were such as to have essentially complete light absorption. The total amount of photolysis was limited to less than 5% to measure the quantum yield of the primary photoprocess. No correction was made for internal filter effects. The absorption values at the visible LMCT band were used to determine the concentration change of the complex during the photolysis. The incident light intensity was determined immediately after each photolysis by a ferrioxalate actinometric method [5]. At least three determinations of quantum yields were made for each complex. Photolyses of all complexes were carried out at 20 ± 1°C. The accuracy of the quantum yield measurements was found to be within 20–25%. Photolysis reactions were also monitored by measuring the UV–Vis and EPR spectra directly in the photolysis cell or by removing aliquots at various intervals to record UV–Vis absorption.

3. Results and discussion

3.1. EPR spectrum of Cu(dsc)(dtp)

The isotropic EPR spectra of the ternary complex Cu(dsc)(dtp) in $CHCl_3$, CH_2Cl_2, acetone and toluene are compared in Fig. 1 with the spectra of the parent complexes $Cu(Et_2dsc)_2$ and $Cu(i\text{-}Pr_2dtp)_2$. It is seen from Fig. 1 that the newly obtained spectrum of Cu(dsc)(dtp) exhibits four hyperfine lines due to the interaction of the copper unpaired electron with $^{63,65}Cu$ nucleus ($I = 3/2$) which are additionally split into superhyperfine (shf) lines by one ^{31}P and one ^{77}Se nuclei both with nuclear spins $I = 1/2$. However, since the natural abundance of ^{77}Se is 7.5%, only 15% of the molecules of the ternary complex contain one ^{77}Se nucleus. Thus in fact the recorded spectrum of Cu(dsc)(dtp) is a superposition of two EPR signals, one containing ^{77}Se and the other corresponding to the remaining Se isotopes ($^{74,76,78,80,82}Se$). The estimated EPR parameters of Cu(dsc)(dtp) are: $g_o = 2.034 \pm 0.002$; $A_o(^{63,65}Cu) = 78 \pm 1$ G; $A_o(^{77}Se) = 48 \pm 1$ G; $A_o(^{31}P) = 7.5 \pm 0.5$ G. The obtained g_o and $A_o(^{63,65}Cu)$ values are the average of the corresponding parameters of the parent $Cu(Et_2dsc)_2$ and $Cu(i\text{-}Pr_2dtp)_2$ complexes which are $g_o = 2.020 \pm 0.002$; $A_o(^{63,65}Cu) = 80 \pm 1$ G; $A_o(^{77}Se) = 46 \pm 1$ G about $Cu(Et_2dsc)_2$ and $g_o = 2.046 \pm 0.002$; $A_o(^{63,65}Cu) = 73 \pm 1$ G; $A_o(^{31}P) = 9.5 \pm 0{,}5$ G about $Cu(i\text{-}Pr_2dtp)_2$, respectively. Therefore, the considered EPR parameters indicate an average covalence within the chromophore CuS_2Se_2 of the ternary Cu(dsc)(dtp) complex as compared to the parent bis-chelates with CuS_4 and $CuSe_2$ chromophores according to the 'additive rule' [6,7]. This effect is due to the fact that unpaired electron occupies a 'group' orbital in which Cu and four donor atoms of the chromophore are included and the magnitudes of the EPR parameters g and A are averaged as a result. However, this is not the case with ^{31}P shf split-

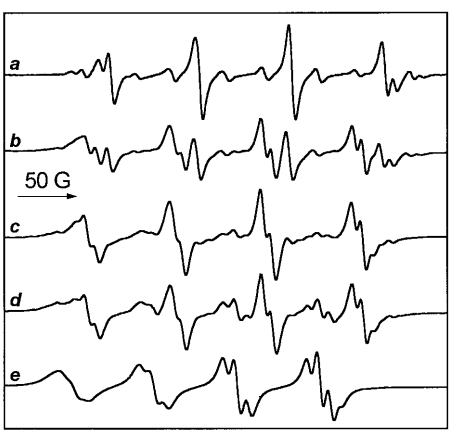


Fig. 1. EPR spectra taken after mixing of $Cu(dsc)_2$ with $Cu(dtp)_2$. The ratio $Cu(dsc)_2/Cu(dtp)_2$ is: (a) 1:0; (b) 2:1; (c) 1:1; (d) 1:2; (e) 0:1. Spectrum (c) corresponds to the Cu(dsc)(dtp) complex. Solvent: $CHCl_3$, $T = 298$ K.

Table 1
Values of λ_{max} (nm) for the complexes $Cu(Et_2dsc)(i\text{-}Pr_2dtp)$, $Cu(Et_2dsc)_2$ and $Cu(i\text{-}Pr_2dtp)_2$ in various solvents

Solvent	$Cu(Et_2dsc)(i\text{-}Pr_2dtp)$	$Cu(Et_2dsc)_2$	$Cu(i\text{-}Pr_2dtp)_2$
CH_2Cl_2	452	495	420
$CHCl_3$	455	495	420
CCl_4	455	495	420
Toluene	450	495	420
Acetone	453	495	417

ting constant which may be used [8] as the probe of precise unpaired electron distribution in mixed-ligand complexes. In the case of Cu(dsc)(dtp) ternary complex the magnitude of ^{31}P shf splitting from dtp ligand is lower than in the parent $Cu(dtp)_2$ complex, suggesting a shift of the unpaired electron density from this ligand to dsc. In the same time, ^{77}Se shf splitting in the mixed-ligand Cu(dsc)(dtp) complex is higher than in the parent $Cu(dsc)_2$. As seen from Fig. 1, equilibrium in reaction (1) is practically shifted to the right.

3.2. UV–Vis spectra of Cu(dsc)(dtp)

The visible absorption of Cu(dsc)(dtp) is due to the strongly allowed ligand to metal charge transfer (LMCT) band which appears near to 455 nm in CH_2Cl_2, $CHCl_3$, CCl_4, toluene and acetone (Table 1). Similar to the corresponding EPR parameters, the obtained λ_{max} values of Cu(dsc)(dtp) are close to the average magnitudes of λ_{max} of the parents LMCT bands which are at 495 nm about $Cu(Et_2dsc)_2$ and 420 nm about $Cu(i\text{-}Pr_2dtp)_2$.

3.3. Continuous photolysis

Solutions of Cu(dsc)(dtp) in toluene, acetone and chloroalkanes could be kept for several days in the dark without any changes in their UV–Vis and EPR spectra. The complex undergoes photolysis when irradiated with UV or visible light of $\lambda < 450$ nm. In general, the irradiation produces a colour change in solution, accompanied by changes in their UV–Vis and EPR absorption.

3.4. Photoreduction of Cu(dsc)(dtp) in toluene

EPR spectral changes obtained upon photo-irradiation of 1×10^{-3} mol dm^{-3} toluene solutions of Cu(dsc)(dtp) with visible light (because of the strong absorption of toluene in UV) are given in Fig. 2. The data show the decreasing intensity of the EPR spectrum of Cu(dsc)(dtp) because of the reduction of Cu(II) to Cu(I).

When 6×10^{-5} mol dm^{-3} toluene solutions of Cu(dsc)(dtp) are photolysed with visible light at 20°C (Fig. 3) the electronic absorption changes reveal only the bleaching of the visible LMCT absorption.

To check whether photoreduction of Cu(II) is reversible the irradiated solutions were kept for 24 h in the dark and the absorption spectra were measured again after that. The obtained spectra clearly showed that photoreduction was partly reversible due to a thermal back reaction, proceeding when photolysis was limited to less than 50%. But they were continuing to bleach when the total amount of photolysis was more than 80%.

3.5. Photoreduction of Cu(dsc)(dtp) in acetone

The LMCT absorption of Cu(dsc)(dtp) in aerated acetone and its EPR intensity gradually decrease following the reduction of Cu(II) to Cu(I) without any intermediate absorption or EPR signal upon irradiation with visible light (because of the strong absorption of acetone in UV). On keeping the irradiated solutions

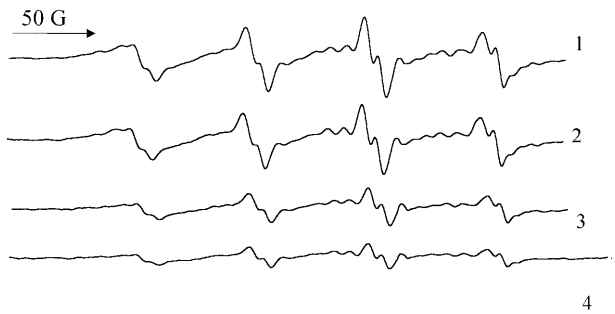


Fig. 2. Set of EPR spectra of Cu(dsc)(dtp) in toluene, 298 K, irradiated for 0 (1), 10 (2), 20 (3) and 40 s (4).

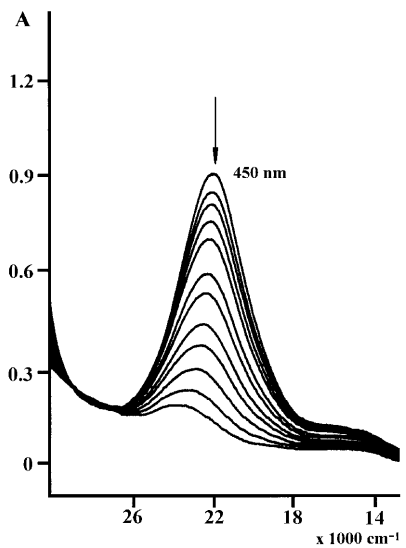


Fig. 3. Absorption spectrum of 7×10^{-5} M Cu(dsc)(dtp), irradiated for 0–285 s in toluene.

within 24 h in the dark the original spectrum is partly restored due to a thermal back reaction, proceeding when the total amount of photolysis is less than 60%.

3.6. Photoreduction of Cu(dsc)(dtp) in chloroalkanes

More complicated UV–Vis spectral changes were observed when photolysis was monitored in chloroalkanes. Fig. 4 shows the UV–Vis spectral changes obtained upon irradiation $\lambda < 450$ nm of 7×10^{-5} mol dm^{-3} Cu(dsc)(dtp) in CH_2Cl_2. It is seen that the LMCT absorption of Cu(dsc)(dtp) at about 450 nm gradually decreases in photolysis with the consecutive increases in absorption at 435 nm (22 990 cm^{-1}) and 350 nm (28 750 cm^{-1}). The new bands attain a maximum absorption and fade upon longer irradiation to give a nearly colourless solution. The observed spectral changes are rather similar to those previously reported about the photolysis of the parent $Cu(Et_2dsc)_2$ in chloroalkanes [1] proceeding with the formation of the mixed-ligand complex $Cu^{II}(Et_2dsc)Cl$ ($\lambda_{max} = 445$ nm) and its chloride-bridged dimeric form $Cu_2(Et_2dsc)_2Cl_2$ ($\lambda_{max} = 350$ nm) as intermediates. Under the same experimental conditions the other parent, $Cu(i\text{-}Pr_2dtp)_2$, exhibits a different photolysis pathway discussed before [2].

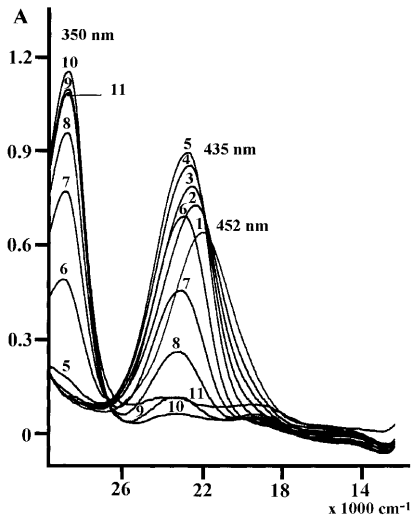


Fig. 4. Absorption spectrum of 8×10^{-5} M Cu(dsc)(dtp), irradiated for 0–94 s in CH_2Cl_2.

The intensity of the EPR spectrum of a 5×10^{-3} mol dm^{-3} Cu(dsc)(dtp) solution in CH_2Cl_2 is gradually decreasing upon photo-irradiation following the reduction of Cu(II) to Cu(I).

Partially photolyzed CH_2Cl_2 solutions of Cu(dsc)(dtp), containing both $Cu^{II}(Et_2dsc)Cl$ and $Cu_2(Et_2dsc)_2Cl_2$, left standing in the dark, undergo thermal back reaction as monitored by UV–Vis spectroscopy. When the total amount of photolysis is more than 80% and $Cu^{II}(Et_2dsc)Cl$ ($\lambda_{max} = 445$ nm, 22 470 cm^{-1}) is completely removed by a secondary photolytic process, the 350 nm band of $Cu_2(Et_2dsc)_2Cl_2$ is continuing to bleach in the dark to give a colourless solution.

Similar UV–Vis and EPR changes are observed during photo-irradiation of Cu(dsc)(dtp) solutions when CH_2Cl_2 is replaced by $CHCl_3$ as the solvent (Fig. 5) indicating that the same reaction mechanism is operative for both chloroalkane solvent systems. However, when irradiation is carried out in CCl_4 only the absorption band at 420 nm (23 800 cm^{-1}) (Fig. 6) appears in the visible part of the spectrum simultaneously with the gradual decrease in intensity of the initial charge transfer band of Cu(dsc)(dtp) at 455 nm (21 980 cm^{-1}).

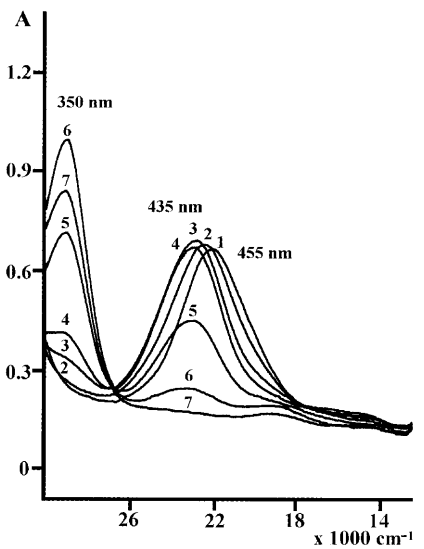


Fig. 5. Absorption spectrum of 5×10^{-5} M Cu(dsc)(dtp), irradiated for 0–55 s in $CHCl_3$.

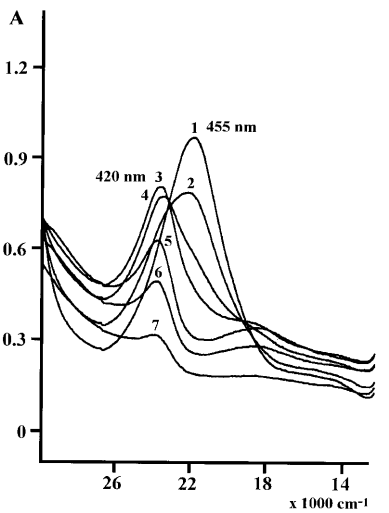


Fig. 6. Absorption spectrum of 6×10^{-5} M Cu(dsc)(dtp), irradiated for 0–50 s in CCl_4.

3.7. Quantum yield

The quantum yield proved to be sensitive to the solvent. For solutions in 20°C CCl_4 the quantum yield of 436 nm irradiation was determined to be 1.5×10^{-3} mol einstein^{-1}. In $CHCl_3$ photolysis the same light irradiation gave about 1.0×10^{-3} mol einstein^{-1}, but it was much smaller in CH_2Cl_2. A photoredox process was also seen in acetone and toluene but it gave immeasurably small quantum yield values. Therefore, the data obtained at 436 nm irradiation decreases in the following order of solvents $CCl_4 > CHCl_3 > CH_2Cl_2 >$ acetone, toluene. Because of their electron acceptor properties [9] chloromethanes act as oxidants and their Cl atom donating power increases with decreasing energy of the C–Cl bond which is 75 kcal mol^{-1} in CH_2Cl_2, 71.9 kcal mol^{-1} in $CHCl_3$ and 68 kcal mol^{-1} in CCl_4 [10,11]. In view of this the observed solvent efficiencies in photolysis could be related to their oxidizing power.

3.8. Mechanism

The evidence about $Cu^{II}(Et_2dsc)Cl$ and $Cu_2(Et_2dsc)_2Cl_2$ formation (Fig. 4) as intermediate products of Cu(dsc)(dtp) photolysis in chloroalkanes is in accordance with a scheme in which the primary photo-electron transfer to Cu(II) would occur with the participation of i-Pr_2dtp ligand to form free i-$Pr_2dtp^{\bullet}$ radical and $Cu^{I}(Et_2dsc)$. The subsequent reactions of $Cu^{I}(Et_2dsc)$ following the primary homolytic Cu-S bond cleavage are strongly solvent dependent as found before [1]. In chloroalkanes the primary photo-process is followed by a rapid $Cu^{I}(Et_2dsc)$ thermal oxidation with the chloroalkane to give $Cu^{II}(Et_2dsc)Cl$ in equilibrium with the dimeric form $Cu_2(Et_2dsc)_2Cl_2$ [1] and by a i-$Pr_2dtp^{\bullet}$ recombination to the stable disulphide (ds) of dithiophosphate. Furthermore, the products $Cu^{II}(Et_2dsc)Cl$ and $Cu_2(Et_2dsc)_2Cl_2$ undergo secondary photo-processes yielding CuCl and a free $Et_2dsc^{\bullet}$ radical as found before [1]. The details of this mechanism account for all of the observations made in this study as well as for the electron-acceptor properties of chloroalkanes and their oxidizing power.

The data of Fig. 2 compare well to those obtained in acetone, suggesting rather similar photochemical pathways of Cu(dsc)(dtp) in acetone and toluene.

4. Conclusions

The primary photo-process appearing upon UV–Vis irradiation with $\lambda < 450$ nm of Cu(dsc)(dtp) in acetone, toluene and chloroalkane (CH_2Cl_2, $CHCl_3$ and CCl_4) solutions involves the homolytic cleavage of the bond between S atom of i-Pr_2dtp and Cu(II) to give $Cu^{I}(Et_2dsc)$ and a free i-$Pr_2dtp^{\bullet}$ radical as the primary photo-products. The solvent appears to play a major role in determining further reactions of the primary photo-products.

Acknowledgements

The financial support from the Foundation 'Scientific Research' of Sofia University (Project 245/98) is gratefully acknowledged.

References

[1] G. Sarova, D. Roussanova, B. Jeliazkova, N.D. Yordanov, M.A. Malik, P. O'Brien, Spectrochim. Acta A 56 (2000) 351.
[2] B.G. Jeliazkova, N.D. Yordanov, Inorg. Chim. Acta 203 (1993) 201.
[3] M.A. Malik, P. O'Brien, Mater. Chem. 3 (1991) 999.
[4] N.D. Yordanov, M.Y. Mihaylov, P. O'Brien, Polyhedron 17 (1998) 3501.
[5] J.C. Calvert, J.N. Pitts, Photochemistry, Wiley, New York, 1967, pp. 728, 797.
[6] K. Wuetrich, Helv. Chim. Acta 48 (1965) 1012.
[7] N.D. Yordanov, V. Alexiev, Commun. Dep. Chem. Bulg. Acad. Sci. 16 (1983) 214.
[8] N.D. Yordanov, N. Savov, to be published.
[9] P.S. Engel, D.F. Keys, A. Kitamura, J. Am. Chem. Soc. 107 (1985) 4964.
[10] P. Goldfinger, G. Martens, J. Chem. Soc. (1961) 2220.
[11] J.C. Calvert, J.N. Pitts, Photochemistry, Wiley, New York, 1967, p. 824.

PERGAMON

www.elsevier.nl/locate/poly

Polyhedron 19 (2000) 2183–2188

POLYHEDRON

X-ray and spectroscopic characterisation of octahedral cobalt(II) and nickel(II) complexes with 1-allylimidazole in the solid state and electron-donor properties of the latter in aqueous solution

Krystyna Kurdziel [a,*], Tadeusz Głowiak [b]

[a] *Institute of Chemistry, Pedagogical University, Chęcińska 5, 25-020 Kielce, Poland*
[b] *Faculty of Chemistry, Wroclaw University, Joliot-Curie 14, 50-383 Wrocław, Poland*

Received 4 April 2000; accepted 24 July 2000

Abstract

Octahedral Co^{II} and Ni^{II} complexes with 1-allylimidazole (L), of general formula $[ML_6](NO_3)_2$, have been obtained in the solid state and characterised by single-crystal X-ray analysis, spectroscopic evidence (IR, far-IR, UV–Vis–NIR) and magnetochemical measurements. Effective magnetic moments of the cobalt(II) and nickel(II) complexes are 5.10 and 2.90 BM, respectively. Crystal field parameters for these high-spin, octahedral species are comparable with those of imidazole and 1-alkylimidazoles. Formation processes of successive cobalt(II), nickel(II) and copper(II) complexes with 1-allylimidazole were followed quantitatively by the potentiometric method. As was the case with imidazole and 1-alkylimidazoles, the complexation proceeded according to the Bjerrum's model with retention of the six-coordinate geometry of the central ion. The complexation pattern was also confirmed by absorption spectra taken over the visible range in aqueous solution. © 2000 Elsevier Science B.V. All rights reserved.

Keywords: Imidazole derivatives; Transition metal complexes; Crystal structure; Absorption spectra; Stability constants

1. Introduction

Histamine, histidine, pilocarpine and allantoin belong to the class of the most widely known imidazole derivatives occurring in living organisms. A crucial role in elucidation of the interaction of proteins with metal ions has been attributed to the imidazole entity in the molecule of histidine. The imidazole ring of histidine provides a link, tying a protein molecule with Fe^{II} on the histidine molecule. The mechanisms of many enzymatic reactions involve complexation processes of the Co^{2+}, Ni^{2+}, Fe^{2+}, Cu^{2+} and Zn^{2+} ions. Catalytic activity of a metal ion in the active centre of a metalloproteide has been found to depend on its tendency towards complexation and on the structure of the compounds [1]. For this reason structural and physicochemical studies of metal complexes with ligands incorporating the imidazole ring are of cognitive importance.

In the preceding paper [2], physico-chemical characterisation and X-ray structure of the nitrato complexes of copper(II) with 1-allylimidazole were presented. These were tetragonal $[CuL_2(NO_3)_2]$ and dinuclear $[Cu_2L_4(NO_3)_2]$ complexes. Again, in Ref. [3], heptacoordinate isomorphic cobalt(II) and nickel(II) complexes with 1-allylimidazole have been reported. This contribution is a continuation of our studies on coordination compounds of 1-allylimidazole and deals with octahedral Co^{II} and Ni^{II} complexes of the ligand in the solid state and with stability of the Co^{II}, Ni^{II} and Cu^{II} complexes in aqueous solution.

2. Experimental

2.1. Investigation in the solid state

2.1.1. Synthesis

A 2 mmol solution of $Co(NO_3)_2 \cdot 6H_2O$ or $Ni(NO_3)_2 \cdot 6H_2O$ in propan-2-ol containing trimethyl orthoformate was mixed with analogous 12 mmol solution of 1-

* Corresponding author. Tel.: +48-41-361-4942; fax: +48-41-361-4942.
E-mail address: krys@top.pu.kielce.pl (K. Kurdziel).

0277-5387/00/$ - see front matter © 2000 Elsevier Science B.V. All rights reserved.
PII: S0277-5387(00)00521-0

allylimidazole (Aldrich, Europe). After a few days, precipitated compounds were purified by crystallization from propan-2-ol. The crystals were washed with abs. ethyl ether and dried at room temperature under vacuum. The results of elemental analysis are as follows: cobalt(II) complex: C, 51.8; H, 5.9; N, 23.7. Calc. for $[CoL_6](NO_3)_2$ C, 51.58; H, 5.82; N, 23.57; nickel(II) complex: C, 52.1; H, 6.0; N, 23.6. Calc. for $[NiL_6](NO_3)_2$: C, 51.99; H, 5.82; N, 23.58%.

2.1.2. Physical measurements

Elemental analyses were run on a model 240 Perkin–Elmer CHN analyzer. The IR spectra were recorded on a Perkin–Elmer 180 (spectral range 50–4000 cm^{-1}) spectrophotometer in Nujol and in KBr pellets. The far-IR spectra were obtained in Nujol mulls sandwiched between polyethylene plates. The electronic spectra (5000–30 000 cm^{-1}) were recorded on a Cary 5 UV–Vis–NIR spectrophotometer in Nujol mulls. Magnetic susceptibility data were obtained at room temperature and corrected for diamagnetism by Pascal's constants.

2.1.3. Crystal data

X-ray measurements were performed on a Kuma KM4CCD diffractometer. The structures were solved by direct methods using the SHELX-97 programme [4] and refined by full-matrix least-squares methods using the SHELXL-97 programme [5]. Details of the crystal data and refinement for the cobalt(II) and nickel(II) compounds studied are shown in Table 1.

Table 1
Crystal data and structure refinement for complexes $[CoL_6](NO_3)_2$ and $[NiL_6](NO_3)_2$

	Co^{II}	Ni^{II}
Empirical formula	$C_{36}H_{48}CoN_{14}O_6$	$C_{36}H_{48}NiN_{14}O_6$
Molecular weight	831.81	831.59
Temperature (K)	100(1)	100(1)
Radiation (Å)	Mo Kα ($\lambda = 0.71073$)	Mo Kα ($\lambda = 0.71073$)
Crystal system	monoclinic	monoclinic
Space group	*Pn*	*Pn*
a (Å)	8.148(2)	8.120(2)
b (Å)	14.226(3)	14.129(3)
c (Å)	17.787(4)	17.196(3)
β (°)	99.10(3)	99.02(3)
V (Å^3)	2035.8(8)	1948.5(7)
Z	2	2
μ (mm^{-1})	0.484	0.563
2*θ* Range (°)	2.86–27.00	2.80–27.00
Data [$I > 2s(I)$]/parameters	7578/513	5330/513
Reflections collected	12727	12523
Independent reflections	7830 [$R_{int} = 0.0141$]	5409 [$R_{int} = 0.0177$]
Final *R* indices [$I > 2\sigma(I)$]	$R_1 = 0.0397$ $wR_2 = 0.1009$	$R_1 = 0.0372$ $wR_2 = 0.0940$
Absolute structure parameter	0.465(11)	0.250(11)
Largest difference peak and hole (e Å^{-3})	0.883 and −0.381	0.958 and −0.394

2.2. Solution studies

2.2.1. Potentiometric measurements

Potentiometric measurements of the metal-ion systems were carried out using a PHM-84 pH meter (radiometer) and a GK 24001 C combination electrode placed in a glass vessel (298 K thermostat) solution of constant ionic strength ($I = 0.5$ mol dm^{-3}) maintained with KNO_3. The electrode was calibrated by means of a HCl solution of known titre with a NaOH solution according to Ref. [6]. The concentration of protonated ligand (HL^+) in stock solutions used in potentiometric titrations was 0.20 mol dm^{-3}.

In the three series of measurements the metal–HL^+ molar ratios were 1:4, 1:8 and 1:10. The titration with the base was conducted in triplicate, over the pH range 2.5–7.5. The dissociation constants of the conjugate acid and stability constants, β_n, of the complexes were refined by the SUPERQUAD program. Standard deviations quoted refer to random errors only.

2.3. Spectroscopic measurements

The visible-range absorption spectra of the Co^{2+}, Ni^{2+} and Cu^{2+} complexes in aqueous solutions were recorded on a Specord M-40 (Carl Zeiss, Jena) spectrophotometer. The solutions were prepared in an analogous manner as were those for the potentiometric titrations. The initial metal concentrations were 0.04 mol dm^{-3}. The highest concentration of the protonated ligand was 0.20 mol dm^{-3}.

3. Results and discussion

3.1. Studies in the solid state

3.1.1. Description of structure

Both the labelling of atoms and molecular structures of the complexes are shown in Fig. 1. Selected bond lengths and bond angles are compiled in Table 2. A similar environment for the central ion in the $[ML_6]^{2+}$ ion is provided by 'pyridynic' nitrogen atoms of six imidazole rings. The shape of the coordination polyhedron fits onto a slightly distorted octahedron. In the nickel(II) complex, the shortest Ni–N distance is 2.046 Å and the longest is 2.133 Å, the difference being 0.087 Å. In the cobalt(II) complex the difference between these bonds is smaller (0.029 Å). The *trans*-angles in the coordination plane formed by atoms labelled N(11), N(21), N(31) and N(41) are 178.5(1) and 177.9(1)° for the cobalt(II) compound and 179.0(1) and 177.2(1)° for the nickel(II) compound.

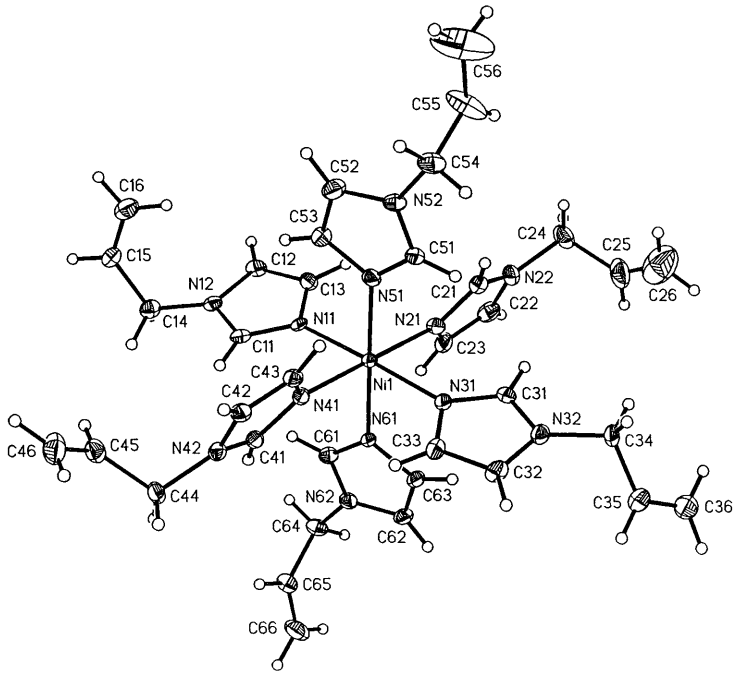


Fig. 1. The structure and numbering scheme for the complexes studied.

The angles between the aforementioned coordination plane and the planes of imidazole rings with pyridynic nitrogen atoms labelled N(11), N(21), N(31), N(41), N(51) and N(61) are respectively, 18.4(1), 67.8(1), 71.5(1), 70.1(1), 69.9(1) and 1.1(2)° in the cobalt(II) complex and 18.2(1), 67.0(1), 71.3(1), 70.0(1), 69.7(1) and 0.9(3)° in the nickel(II) complex. The bond lengths and bond angles in the 1-allylimidazole ligand are similar to those in its complexes with other metals [2,3].

3.1.2. The infrared spectra

The shapes of the IR and far-IR spectra of the complexes support the structures suggested. Coordination of the 1-allylimidazole molecules through 'pyridynic' nitrogen atoms of the imidazole rings manifests in displacement towards higher energies of the ν(C=C) vibrations coupled with those of ν(C=N) of the imidazole ring from 1508 (free 1-allylimidazole) to 1518 cm^{-1} (the cobalt(II) complex) and 1520 cm^{-1} (the nickel(II) complex). The metal–nitrogen linkage emerges in the far-IR region as a rather broad intense band at 228 and 246 cm^{-1}, respectively for cobalt(II) and nickel(II) complexes [2,3,7–9]. The lack of interaction between the nitrate group and the metal ion is indicated by the position of a band characteristic of this group. Thus, broad intense bands at 1376 and 820 cm^{-1} (the cobalt(II) complex) and at 1385 and 822 cm^{-1} (the nickel (II) complex) are assigned, respectively, to symmetric and antisymmetric vibrations of the free nitrate ion [10,11].

3.1.3. Magnetic properties and d-d electronic spectra

Magnetic moments determined for the cobalt(II) and nickel(II) complexes at room temperature are 5.10 and 2.90 BM, respectively. These values are characteristic of high-spin octahedral complexes of metals [12]. The electronic spectrum of the nickel(II) complex is typical for the six coordinate compounds of the metal. Characteristic absorption bands emerge over the visible and near-IR regions. A low-energy absorption appears as a broad band at 11 600 cm^{-1} and can be assigned to the $^3A_{2g}(F) \rightarrow {}^3T_{2g}(F)$ (ν_1) electron transition. The next two bands at 16 800 and 27 500 cm^{-1} are assignable, respectively, to the $^3A_{2g}(F) \rightarrow {}^3T_{1g}(F)$ (ν_2) and $^3A_{2g}(F) \rightarrow {}^3T_{1g}(P)$ (ν_3) transitions. The ν_2 and ν_3 frequencies were subsequently utilised to determine Dq values and the Racah parameter [12,13] (Table 3). With octahedral high-spin cobalt(II) complexes, the crystal field theory allows for three spin permissible d-d transitions, namely $^4T_{1g}(F) \rightarrow {}^4T_{2g}(F)$ (ν_1), $^4T_{1g}(F) \rightarrow {}^2A_{2g}$ (ν_2) and $^4T_{1g}(F) \rightarrow {}^4T_{1g}(P)$ (ν_3) [11]. With the cobalt(II) complex, the first of these bands appears over the near-IR range at $\nu_1 = 9560$ cm^{-1}. In the visible range of the spectrum, only one asymmetric band appears at 20 600 cm^{-1}. On the low-energy side of the band there are distinct deformations which, in the case of octahedral cobalt(II) complexes, can be explained in terms of overlapping the ν_2 and ν_3 bands as well as a spin forbidden band due to the $^4T_{1g}(F) \rightarrow {}^2T_{1g}(G)$ transition. The components of this absorption region were obtained by means of the Gaussian distribution. The maxima of the three bands

appear at 21 000, 20 000 and 18 900 cm^{-1}.The strongest 21 000 cm^{-1} band can be assigned to the $^4T_{1g}(F) \rightarrow {}^4T_{1g}(P)$ (ν_3) transition. Unfortunately, interpretation of the remaining bands is not as straightforward a priori. On the basis of the frequencies $\nu_1 = 9560$ and $\nu_3 = 21\ 000\ cm^{-1}$, parameters of the crystal field could be determined [10,12] (Table 3). By utilising the relation $\nu_2 = \nu_1 + 10$ Dq, the position of ν_2 should be around 20 200 cm^{-1}, i.e. in the immediate vicinity of the ν_1 band. The band is likely to emerge at $\nu = 18\ 900$ cm^{-1}. These asignments are supported by parameters Dq and B calculated by using frequencies ν_2 and ν_3 [13]. In this case the calculated values of Dq = 1061 and $B = 855$ are quite compatible with the parameters determined by using ν_1 and ν_3 (Table 3). With both the cobalt(II) and nickel(II) complexes, the crystal field parameters assume magnitudes matching those of imidazole and 1-alkylimidazoles and are consistent with the basicities of the ligands (Table 4). The positions of 1-allylimidazole in the spectrophotometric and nepheloauxetic rank orders closely matches those of imidazole and 1-alkylimidazoles [15].

Table 2
Bond lengths [Å] and bond angles [°] for complexes $[CoL_6](NO_3)_2$ and $[NiL_6](NO_3)_2$

	Co^{II}	Ni^{II}
M–N(11)	2.181(2)	2.112(3)
M–N(21)	2.169(2)	2.111(3)
M–N(31)	2.182(2)	2.129(3)
M–N(41)	2.175(2)	2.133(3)
M–N(51)	2.153(3)	2.078(3)
M–N(61)	2.155(3)	2.046(3)
O(1)–N(1)	1.245(4)	1.220(4)
O(2)–N(1)	1.242(3)	1.221(4)
O(3)–N(1)	1.239(3)	1.232(4)
O(4)–N(2)	1.241(4)	1.241(4)
O(5)–N(2)	1.241(4)	1.212(4)
O(6)–N(2)	1.235(4)	1.213(4)
N(21)–M–N(11)	90.1(1)	90.5(1)
N(11)–M–N(31)	178.5(1)	179.0(1)
N(11)–M–N(41)	91.0(1)	91.0(1)
N(51)–M–N(11)	89.0(1)	89.7(1)
N(61)–M–N(11)	90.4(1)	90.1(1)
N(21)–M–N(31)	90.4(1)	90.4(1)
N(21)–M–N(41)	177.9(1)	177.2(1)
N(21)–M–N(51)	90.8(1)	91.4(1)
N(61)–M–N(21)	88.5(1)	88.2(1)
N(31)–M–N(41)	88.5(1)	88.1(1)
N(51)–M–N(31)	92.4(1)	90.5(1)
N(61)–M–N(31)	88.3(1)	89.8(1)
N(31)–M–N(41)	87.4(1)	86.3(1)
N(51)–M–N(41)	93.3(1)	94.1(1)
N(61)–M–N(51)	179.0(1)	179.5(1)
O(1)–N(1)–O(2)	119.6(3)	118.1(3)
O(1)–N(1)–O(3)	121.2(3)	122.5(3)
O(2)–N(1)–O(3)	119.1(3)	119.3(3)
O(5)–N(2)–O(6)	119.7(3)	118.2(4)
O(5)–N(2)–O(4)	120.2(3)	120.4(3)
O(6)–N(2)–O(4)	120.1(3)	121.3(4)

3.2. Studies in aqueous solution

On the basis of the pH-metric measurements, the acid dissociation constant of protonated 1-allylimidazole was determined to be 9.52×10^{-8} ($pK_a = 7.02$). The dissociation constants of imidazole and selected 1-substituted imidazoles are shown in Table 4.

These data show that the basicity of 1-allylimidazole is just equal to that of imidazole and 1-alkylimidazoles. 1-Allylimidazole is, by an order of magnitude, a stronger Brönsted base than its homologue, 1-vinylimidazole ($pK_a = 5.92$). The weaker basicity of the latter is due to the negative inductive effect of the vinyl substituent. With allyl substituents, the effect is absent, because the π electrons of the double bond are isolated from the lone electron pair of the pyridynic '3' nitrogen atom of the imidazole ring. The complexation of Co^{II}, Ni^{II} and Cu^{II} with 1-allylimidazole was conducted over pH range 2.5–7.5. The equilibrium constants for these systems are summarized in Table 4. On the basis of these constants, curves of percentile molar contributions of successive complexes being formed in solution were plotted in Fig. 2.

The stability of the complexes of the three metals is compatible with the Irwing–Williams series ($Co^{II} < Ni^{II} < Cu^{II}$) as seen in the plots presented in Fig. 2. Successive Cu^{II} complexes are formed in more acidic solutions than those of the remaining metals. The regularity in variation of the successive equilibrium constants, K_n, of the cobalt(II), nickel(II) and copper(II) complexes shows that the complexation reactions in solution proceed according to the Bjerrum's model, with retention of the six coordinate geometry of the central ion, as was the case with analogous complexes of imidazole and 1-alkylimidazoles [18].

A comparison of the constants in Table 4 shows that the stability of the complexes is comparable, in terms of basicity, to that of the corresponding complexes of imidazole and 1-alkylimidazoles. Thus, 1-allylimidazole forms slightly more stable complexes than 1-vinylimidazole, in spite of the fact that the pK_a values of respective ligands suggest larger differences in their stability. As demonstrated previously [19], stability of the 1-vinylimidazole complexes is strengthened by contribution of additional $\pi_{M \rightarrow L}$ back-bonding.

The visible absorption spectra of aqueous solutions of the complexes provide further support in favour of the conclusion that the coordination reactions with 1-allylimidazole proceed without the change of the coordination number of the central ion. Upon raising concentration of free 1-allylimidazole (increasing pH), a

Table 3
The description of the electronic spectra of 1-allylimidazole, imidazole and aqua complexes of Co^{II} and Ni^{II} ($[ML_6^{2+}]$) in solid state and the 1-allylimidazole studied complexes in aqueous solution

Ligand		Reference				
Cobalt(II)	$^4T_{1g}(F) \rightarrow {}^4T_{2g}(F)$	$^4T_{1g}(F) \rightarrow {}^4A_{2g}$	$^4T_{1g}(F) \rightarrow {}^4T_{2g}(P)$	Dq	*B*	
1-Allylimidazole	9560	16 380	20 660	1077	801	this work
Imidazole	9437	18 870	20 530	1064	820	[14]
	9600	19 800	20 600	1050	800	[8]
H_2O	8100	16 000	19 400	920	830	[13,14]
1-Allylimidazole in aqueous solution			20 200; $\varepsilon = 30$ (pH 6.99)			this work
Nickel(II)	$^3A_{2g} \rightarrow {}^3T_{2g}$	$^3A_{2g} \rightarrow {}^3T_{1g}(F)$	$^3A_{2g} \rightarrow {}^3T_{1g}(P)$	Dq	*B*	
1-Allylimidazole	11 600	16 820	27 500	1045	863	this work
Imidazole	10 580	17 390	27 700	1058	895	[14]
	10 650	17 400	28 000	1065	880	[8]
H_2O	8500	15 200	25 300	885	920	[13,14]
1-Allylimidazole in aqueous solution		16 600; $\varepsilon = 7.4$ (pH 6.74)	27 500			this work
Copper(II)	$^2E_g \rightarrow {}^2T_{2g}$					
H_2O	12 600					[12]
1-Allylimidazole in aqueous solution	17 300; $\varepsilon = 68$ (pH 6.90)					this work

Table 4
Stability constants of imidazole derivatives in aqueous solution [a]

Ligand	Central ion	log β_1	log β_2	log β_3	Log β_4	log β_5	log β_6	Reference
Imidazole	Co^{2+}	2.47	4.40	5.85	6.85			[16,17]
p$K_a = 7.12$	Ni^{2+}	3.09	5.56	7.56	9.10			
	Cu^{2+}	4.31	7.84	10.76	12.90			
1-Ethylimidazole	Co^{2+}	2.32	4.17	5.42	7.02	7.42		[18]
p$K_a = 7.25$	Ni^{2+}	3.04	5.54	7.52	8.97	9.85	10.20	
	Cu^{2+}	4.40	7.99	10.98	13.22	14.20		
1-Vinylimidazole	Co^{2+}	2.25	4.00	5.25	6.17	6.37		[19]
p$K_a = 5.92$	Ni^{2+}	2.94	5.34	7.24	8.43	9.10		
	Cu^{2+}	3.60	6.70	9.30	11.35	11.90		
1-Allylimidazole	Co^{2+}	2.45(3)	4.30(3)	5.70(4)	7.20(4)			this
p$K_a = 7.02$	Ni^{2+}	3.00(2)	5.50(4)	7.50(3)	9.20(4)	10.20(3)		work
	Cu^{2+}	4.15(2)	7.70(2)	10.62(3)	13.16(4)	14.23(4)		
1-Propylimidazole	Co^{2+}	2.38	4.20	5.44	6.90	7.88	8.40	[18]
p$K_a = 7.22$	Ni^{2+}	3.06	5.56	7.60	9.18	10.33	11.00	
	Cu^{2+}	4.25	7.81	10.70	13.10	14.20		

[a] At 298 K; ionic strength $I = 0.5$ (mol dm^{-3}) (KNO_3), for imidazole $I = 0.16$ (mol dm^{-3}) (KNO_3).

hypsochromic shift in the absorption band is observed. Both the shape and position of the absorption bands as well as the magnitude of the mean molar absorptivity (Table 3) indicate the presence of six coordinate octahedral or pseudo-octahedral nickel(II) and cobalt(II) as well as tetragonal copper(II) complexes in aqueous solution.

4. Supplementary data

Crystallographic data have been deposited with the Cambridge Crystallographic Data Centre, CCD Nos. 142333 and 142334. Copies of this information may be obtained free of charge from The Director, CCDC, 12 Union Road, Cambridge, CB2 1EZ, UK

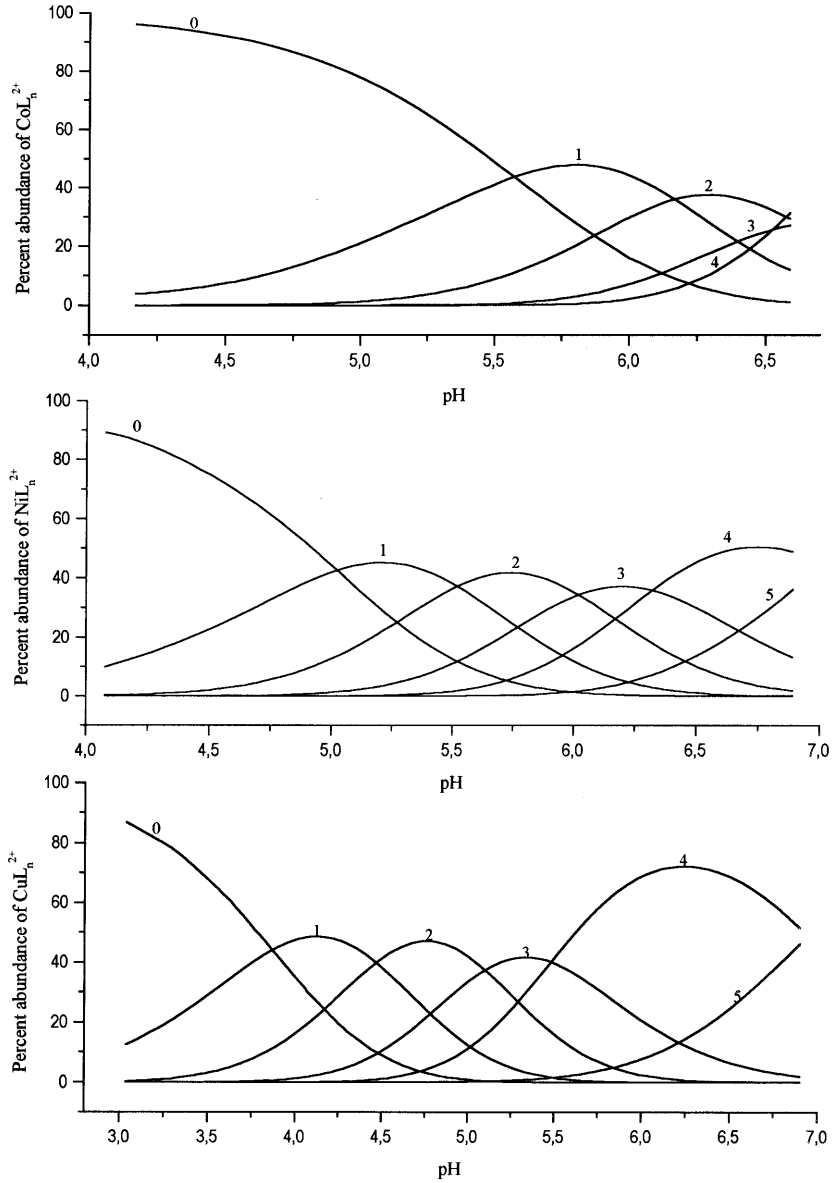


Fig. 2. Diagrams of complexes formed in M^{2+}–1-allylimidazole systems as a function of $-\log[H^+]$ at 298 K and $I = 0.5$ mol dm^{-3}. The numbers in the diagrams represent mean n in ML_n^{2+}.

(fax: +44-1233-336033; e-mail:deposit@ccdc.cam.ac.uk or www: http://www.ccdc.cam.ac.uk).

References

[1] R.D. Gillard, Inorg. Chim. Acta Rev. 6 (1967) 69.
[2] K. Kurdziel, T. Glowiak, Pol. J. Chem. 72 (1998) 2181.
[3] T. Glowiak, K. Kurdziel, J. Mol. Struct. 516 (1999) 1.
[4] G.M. Sheldrick, SHELX-97, Program for Solution of Crystal Structure, University of Göttingen, Göttingen, Germany, 1997.
[5] G.M. Sheldrick, SHELXL-97, Program for the Refinement of Crystal Structure, University of Göttingen, Göttingen, Germany, 1997.
[6] A. Braibanti, G. Ostacoli, P. Paoletti, L.D. Pettit, S. Sammartanto, Pure Appl. Chem. 59 (1987) 1721.
[7] J. Reedijk, Rec. Trav. Chim. 91 (1972) 1373.
[8] J. Reedijk, Rec. Trav. Chim. 88 (1969) 1451.
[9] K. Kurdziel, T. Glowiak, Transition Met. Chem. 24 (1999) 366.
[10] J. Davis, J. Smith, J. Chem. Soc., Sect. A (1971) 317.
[11] K. Nakamoto, Infrared and Raman Spectra of Inorganic and Coordination Compounds, fifth ed., Wiley, New York, 1986.
[12] A.B.P. Lever, Inorganic Electronic Spectroscopy, second ed., Elsevier, New York, 1984.
[13] A.E. Underhill, D.E. Billing, Nature 210 (1966) 834.
[14] W.J. Eilbeck, F. Holmes, A.E. Underhill, J. Chem. Soc., Sect. A (1967) 757.
[15] J.A. Welleman, F.B. Hulsbergen, J. Verbrest, J. Reedijk, J. Inorg. Nucl. Chem. 40 (1978) 143.
[16] E.K. Sklenskaya, M.Kh. Karapet'yants, Russ. J. Inorg. Chem. 11 (1961) 1102.
[17] G. Berthon, C. Luca, Anal. Chim. Acta 51 (1970) 239.
[18] B. Lenarcik, B. Barszcz, Pol. J. Chem. 53 (1979) 963.
[19] B. Lenarcik, K. Kurdziel, J. Chem. Res., Sect. S (1989) 240.

PERGAMON

www.elsevier.nl/locate/poly

Polyhedron 19 (2000) 2189–2193

POLYHEDRON

Syntheses and characterization of two dodecanuclear heterobimetallic Mo–Cu–S cage clusters: $[NEt_4]_2[(Mo_2Cu_2S_2O_2edt_2)_3(\mu_6\text{-}Se_2)]\cdot CH_2Cl_2$ and $[NEt_4]_2[(Mo_2Cu_2S_2O_2edt_2)_3(\mu_6\text{-}S)]\cdot 3H_2O$ (edt = $^-SC_2H_4S^-$).

Ping Lin, Xin-Tao Wu *, Ling Chen, Li-Ming Wu, Wen-Xin Du

State Key Laboratory of Structural Chemistry, Fujian Institute of Research on the Structure of Matter, the Chinese Academy of Sciences, Fuzhou, Fujian 350002, People's Republic of China

Received 8 March 2000; accepted 27 July 2000

Abstract

The reaction of Se_2 or S^{2-} with the $[MoS_2O_2(S_2C_2H_4)_2]^{2-}/2Cu^+$ yielded two novel dodecanuclear interstitial clusters having the general formula $[NEt_4]_2[(Mo_2Cu_2S_2O_2edt_2)_3(\mu_6\text{-}Se_2)]\cdot CH_2Cl_2$ (**1**) and $[NEt_4]_2[(Mo_2Cu_2S_2O_2edt_2)_3(\mu_6\text{-}S)]\cdot 3H_2O$ (**2**) (edt = $^-SC_2H_4S^-$), whose crystal structures were determined by X-ray crystallography. The anions in **1** and **2** can be viewed as a cage consisting of three $[MoS_2O_2(S_2C_2H_4)_2]^{2-}/2Cu^+$ fragments, with an Se_2^{2-} or an S^{2-} at the center, respectively. © 2000 Elsevier Science B.V. All rights reserved.

Keywords: Dodecanuclear; Mo–Cu–S cage cluster; Interstitial group

1. Introduction

Cluster compounds play an important role in bioinorganic chemistry, material science and catalysis etc. Recently, polynuclear metal cluster compounds have become even more interesting owing to their fascinating electronic, structural, chemical, magnetic and optical properties, and potential uses as heterogeneous catalysts as well as synthetic analogs of biological systems [1]. The structure of polynuclear transition metal clusters may often be described as fragments of metal aggregates stabilized by ligand shells. Many cage-like clusters containing an interstitial group have been reported, such as: $Co_6C(CO)_{12}S_2$ [2], $[Rh_9P(CO)_{21}]^{2-}$ [3a] and $[Rh_{10}P(CO)_{22}]^{3-}$ [3b] $[Cp_6Yb_6Cl_{13}]^-$ [4], $[W_6O_{19}]^{2-}$ and $[V_{10}O_{28}]^{6-}$ [5], $Ag_2C_2\cdot 8AgF$ (the interstitial group is $^-C{\equiv}C^-$) [6]. A few heterobimetallic cage-like clusters containing an interstitial group are also known, for example $[Nb_2W_4O_{19}]^{4-}$ and $[(C_5H_5)Ti(W_5O_{18})^{3-}$ [5], $[Mo_6Cu_6S_6O_6(S_2)_6(\mu_6\text{-}S)]^{2-}$ [7], $[\{M_2Cu_2S_2O_2(S_2C_2H_4)_2\}_3(\mu_6\text{-}S_2)]^{2-}$ (M=Mo, W) [8] and $[\{M_2Ag_2S_2O_2(S_2C_2H_4)_2\}_3(\mu_6\text{-}S)]^{2-}$ (M=Mo, W) [9]. In this contribution, we report the syntheses and characterization of two dodecanuclear heterometallic cage clusters $[NEt_4]_2[(Mo_2Cu_2S_2O_2edt_2)_3(\mu_6\text{-}Se_2)]\cdot CH_2Cl_2$ (**1**) and $[NEt_4]_2[(Mo_2Cu_2S_2O_2edt_2)_3(\mu_6\text{-}S)]\cdot 3H_2O$ (**2**), which contain a μ_6-Se_2 and a μ_6-S ligand, respectively. To our knowledge, **1** is the first cluster compound containing a μ_6-Se_2 group.

2. Experimental

The synthesis of compound **2** and the starting material $[Et_4N]_2[Mo_2S_2O_2edt_2]$ were carried out in air; and the synthesis of compound **1** was carried out in a nitrogen atmosphere. Infrared spectra were recorded on a Nicolet Magna 750 FT-IR spectrophotometer as KBr pellets for M-IR (4000–400 cm^{-1}) and as CsI pellets for Far-IR (600–100 cm^{-1}). Elemental analyses were performed by the Elemental Analysis Laboratories in our Institute.

* Corresponding author. Tel.: +86-591-3719238; fax: +86-591-3714946.

E-mail address: wxt@ms.fjirsm.ac.cn (X.-T. Wu).

0277-5387/00/$ - see front matter © 2000 Elsevier Science B.V. All rights reserved.
PII: S0277-5387(00)00522-2

2.1. Preparation of $[Et_4N]_2[Mo_2S_2O_2edt_2]$

H_2S gas was bubbled into a 20 ml aqueous solution of Na_2MoO_4 (4.84 g, 20 mmol). Three minutes later, the solution turned to red and was then heated to 85°C, when $Na_2S_2O_4$ (0.469 g, 3.3 mmol) and $H_6S_2C_2$ (1.6 ml, 20 mmol) were added. After stirring for 2 h, 4.2 g of $[Et_4N]Br$ (20 mmol) was added to the solution, which was cooled in air to deposit a red precipitate. The precipitate was collected and washed by C_2H_5OH and Et_2O three times, and 6.5 g of $[Et_4N]_2[Mo_2O_2S_2edt_2]$ was obtained (yield 91.3%). *Anal.* Calc. for $C_{20}H_{48}Mo_2N_2O_2S_6$: C, 32.78; H, 6.60; N, 3.82. Found: C, 32.80; H, 6.7; N, 3.81%. IR (cm^{-1}): 2972.7 (s), 2891.0 (s), 1479.4 (s), 1456.4 (s), 939.2 (vs), 472.5 (m), 443.5 (m), 339.4 (m).

2.2. Preparation of $[NEt_4]_2[(Mo_2Cu_2S_2O_2edt_2)_3(\mu_6\text{-}Se_2)]\cdot CH_2Cl_2$ (**1**)

Se powder (0.032 g, 0.4 mmol) was placed in a S tube, and 5 ml DMF solution and metallic Na (0.01 g, 0.43 mmol) was added. The solution was heated to 363 K for 1 h, and then suspension (i) was produced. To a solution of $Cu(NO_3)_2\cdot 3H_2O$ (0.242 g, 1 mmol in 30 ml of MeCN and 30 ml of CH_2Cl_2) was added $NaBH_4$ (0.038 g, 1 mmol) with stirring. After 30 min, $[Et_4N]_2[Mo_2S_2O_2edt_2]$ (0.356 g, 0.5 mmol) was added, and the mixture was stirred for 1 min, whereupon suspension (ii) was produced. Next, suspension (i) was added to suspension (ii) and stirred for 30 min and then the black precipitate was removed by filtration. The dark red filtrate was allowed to stand at room temperature under nitrogen for 15 days, after which 0.07 g of black crystals of **1** were obtained (yield: 18%). Complex **1** is slightly soluble in MeCN and CH_2Cl_2, and easily soluble in DMF. *Anal.* Calc. for $C_{29}H_{66}Cl_2Cu_6Mo_6N_2O_6S_{18}Se_2$: C, 15.13; H, 2.89; N, 1.22; Se, 6.86. Found: C, 15.15; H, 2.92; N, 1.29; Se, 6.82%. IR: (cm^{-1}): 2974.2 (s), 2890.2 (s), 1479.0 (s), 1456.4 (s), 954.6 (vs); 462.8 (m), 432.0 (m), 343.3 (m).

2.3. Synthesis of $[NEt_4]_2[(Mo_2Cu_2S_2O_2edt_2)_3(\mu_6\text{-}S)]\cdot 3H_2O$ (**2**)

To a solution of $Cu(NO_3)_2\cdot 3H_2O$ (0.242 g, 1 mmol in 60 ml of MeCN) was added $NaBH_4$ (0.038 g, 1 mmol) with stirring. After 30 min, $[Et_4N]_2[Mo_2S_2O_2edt_2]$ (0.356 g, 0.5 mmol) was added to the suspension, and the mixture was stirred for 0.5 min. Some flocculate appeared in the reaction solution. Then, two drops of $(NH_4)_2S$ aqueous solution (containing 8% S) were added to the reaction solution and stirred for 20 min, the flocculate disappeared and a black precipitate was obtained. The precipitate was filtered off, and the dark red filtrate was allowed to stand at room temperature in air for 5 days, after which 0.08 g of the black crystal of **2** was obtained (yield: 22.3%). Complex **2** is stable in air, slightly soluble in MeCN and CH_2Cl_2, and easily soluble in DMF. *Anal.* Calc. for $C_{28}H_{70}N_2Cu_6Mo_6O_9S_{19}$: C, 15.68; H, 3.29; N, 1.31. Found: C, 15.7; H, 3.32; N, 1.36. %. IR (cm^{-1}): 2973.7 (s), 2890.8 (s), 1479.2 (s), 1456.0 (s), 950.7 (vs), 470.5 (m), 439.7 (m), 352.9 (m).

2.4. Crystallographic structure determination

Crystallographic data for compounds **1** and **2** are listed in Table 1. Data were collected at room temperature on a Siemens SMART-CCD area-detector diffractometer with a graphite monochromator utilizing Mo Kα radiation ($\lambda = 0.71073$ Å). Intensity data were obtained by using an ω scan technique with scan rates of 19 s/frame and 0.3°/frame, in the range $3.26 < 2\theta < 50.32$ for **1** and $3.30 < 2\theta < 46.50°$ for **2**. Data reductions and absorption corrections were performed with SMART and SADABS softwares, respectively.

Structural analyses were performed using a Silicon Graphics in Indy workstation with the program

Table 1
Crystallographic data for compounds **1** and **2**

Complex	**1**	**2**
Empirical formula	$C_{29}H_{66}N_2Cl_2Cu_6Mo_6O_6S_{18}Se_2$	$C_{28}H_{70}N_2Cu_6Mo_6O_9S_{19}$
Molecular weight	2301.62	2144.93
Crystal colour	black	black
Crystal dimens (mm)	$0.5\times0.5\times0.4$	$0.4\times0.4\times0.3$
Space group	$P4_32_12$ (No. 96)	$P4_12_12$ (No. 92)
$a = b$ (Å)	13.188(2)	13.0936(2)
c (Å)	37.973(5)	37.7775(8)
V (Å^3)	6604.7(14)	6476.7(2)
Z	4	4
μ(Mo Kα) (mm^{-1})	4.775	3.699
D_{calc} (g cm^{-3})	2.315	2.200
$F(000)$	4472	4216
No. of independent reflections	5890	4553
R_{int}	0.0835	0.0484
No. of observed reflections [$I > 2\sigma(I)$]	5635	4114
No. of variables refined	321	234
R [a]	0.0714	0.0449
wR [b]	0.1888	0.0987
Absolute structure parameter	0.11(3)	0.04(3)
Goodness of fit on F^2	1.138	1.087
Max. shift in final cycle	0.019	0.005
Max./min. $\Delta\rho$ (e Å^{-3})	2.263/−3.350	0.898/−0.491

[a] $R = \Sigma\{||F_o|-|F_c||\}/\Sigma|F_o|\}$

[b] $wR = \{\Sigma[w(F_o^2-F_c^2)^2]/\Sigma[w(F_o^2)^2]\}^{1/2}$; $w = 1/[\sigma^2(F_o^2)+(0.1028P)^2+66.7126P]$, where $P = (F_o^2+2F_c^2)/3$ for complex **1**; $w = 1/[\sigma^2(F_o^2)+(0.0368P)^2+32.6477P]$, where $P = (F_o^2+2F_c^2)/3$ for complex **2**.

SHELXTL [10]. The structures were solved by direct methods, and the positions of heavy atoms were obtained from E maps. The remaining non-hydrogen atoms were located from successive difference Fourier maps. The refinement of structures was performed by full-matrix least-squares techniques on F^2 using SHELXL93 [11]. For **1**, all non-hydrogen atoms were treated as anisotropic. For **2**, all non-hydrogen atoms are anisotropic except the O atoms of H_2O molecules and the C, N atoms. No attempt was made to locate hydrogen atoms. The selected bond lengths and angles for **1** and **2** are listed in Tables 2 and 3, respectively.

Table 2
Selected bond distances (Å) and angles (°) in **1**[a]

Mo1–O1	1.683(10)	Mo2–S6	2.439(4)	Cu1–Se	2.301(3)	Cu3–S7*	2.357(4)
Mo1–S1	2.355(4)	Mo2–S5	2.448(4)	Cu1–S1*	2.355(4)	Cu3–S5*	2.361(4)
Mo1–S1*	2.361(4)	Mo2–Mo3	2.878(2)	Cu1–S3	2.354(4)	Se–Se*	2.257(4)
Mo1–S2	2.432(4)	Mo3–O3	1.664(9)	Cu2–S2	2.285(4)	S1–Cu1*	2.355(4)
Mo1–S3	2.457(4)	Mo3–S7	2.336(4)	Cu2–Se	2.310(3)	S1–Mo1*	2.361(4)
Mo1–Mo1*	2.882(2)	Mo3–S9	2.349(4)	Cu2–S9	2.350(4)	S6–Cu1*	2.290(4)
Mo2–O2	1.684(10)	Mo3–S8	2.446(4)	Cu2–S4	2.360(4)	S5–Cu3*	2.361(4)
Mo2–S7	2.339(4)	Mo3–S4	2.454(4)	Cu3–S8	2.305(4)	S7–Cu3*	2.357(4)
Mo2–S9	2.350(4)	Cu1–S6*	2.290(4)	Cu3–Se	2.307(3)		
S1–Mo1–S1*	102.02(12)	S6*–Cu1–S1*	113.41(15)	Se–Cu3–S7*	116.06(13)	Cu2–S2–Mo1	100.12(14)
S1–Mo1–S2	81.00(13)	Se–Cu1–S1*	116.23(12)	S8–Cu3–S5*	114.22(15)	Cu1–S3–Mo1	80.77(12)
S1*–Mo1–S3	80.05(13)	S6*–Cu1–S3	115.16(15)	Se–Cu3–S5*	110.88(13)	Cu2–S4–Mo3	80.08(12)
S2–Mo1–S3	81.54(13)	Se–Cu1–S3	110.46(13)	S7*–Cu3–S5*	81.55(14)	Cu3*–S5–Mo2	80.24(12)
S7–Mo2–S9	101.62(13)	S1*–Cu1–S3	82.32(14)	Se*–Se–Cu1	108.62(11)	Cu1*−S6–Mo2	102.48(14)
S9–Mo2–S6	81.14(13)	S2–Cu2–Se	118.80(13)	Se*–Se–Cu2	106.59(12)	Mo3–S7–Mo2	76.00(12)
S7–Mo2–S5	80.10(13)	S2–Cu2–S9	111.7(2)	Se*–Se–Cu3	106.79(7)	Mo3–S7–Cu3*	121.2(2)
S6–Mo2–S5	81.41(13)	Se–Cu2–S9	115.50(13)	Cu1–Se–Cu3	111.66(10)	Mo2–S7–Cu3*	82.60(13)
S7–Mo3–S9	101.69(13)	S2–Cu2–S4	114.0(2)	Cu1–Se–Cu2	109.20(10)	Cu3–S8–Mo3	102.83(14)
S7–Mo3–S8	80.08(14)	Se–Cu2–S4	107.69(14)	Cu3–Se–Cu2	113.71(10)	Mo3–S9–Mo2	75.55(12)
S9–Mo3–S4	81.97(13)	S9–Cu2–S4	83.99(14)	Cu1*–S1–Mo1	122.0(2)	Mo3–S9–Cu2	82.48(12)
S8–Mo3–S4	80.62(14)	S8–Cu3–Se	113.74(13)	Cu1*–S1–Mo1*	82.79(13)	Mo2–S9–Cu2	122.8(2)
S6*–Cu1–Se	115.10(13)	S8–Cu3–S7*	116.3(2)	Mo1–S1–Mo1*	75.34(11)		

[a] Symmetry transformations used to generate equivalent atoms: *, $(2-y, 2-x, 3/2-z)$.

Table 3
Selected bond distances (Å) and angles (°) in **2**[a]

Mo1–O1	1.674(7)	Mo2–S4	2.422(3)	Cu1–S	2.370(2)	Cu3–S8	2.448(3)
Mo1–S9*	2.341(3)	Mo2–S3	2.437(3)	Cu1–S6*	2.447(3)	Cu3–S3	2.486(4)
Mo1–S9	2.354(3)	Mo2–Mo3	2.8769(13)	Cu1–S7*	2.488(3)	S–Cu1*	2.370(2)
Mo1–S2	2.424(3)	Mo3–O3	1.674(7)	Cu2–S4	2.334(3)	S–Cu2*	2.375(3)
Mo1–S1	2.442(3)	Mo3–S8	2.339(3)	Cu2–S	2.375(3)	S–Cu3*	2.403(3)
Mo1–Mo1*	2.872(2)	Mo3–S7	2.357(3)	Cu2–S1	2.449(3)	S5–Cu3*	2.335(3)
Mo2–O2	1.684(7)	Mo3–S5	2.430(3)	Cu2–S9	2.481(3)	S6–Cu1*	2.447(3)
Mo2–S7	2.347(3)	Mo3–S6	2.432(3)	Cu3–S5*	2.336(3)	S7–Cu1*	2.488(3)
Mo2–S8	2.350(3)	Cu1–S2	2.337(3)	Cu3–S	2.403(3)	S9–Mo1*	2.341(3)
S9*–Mo1–S9	102.36(9)	S2–Cu1–S7*	98.14(10)	Cu1*–S–Cu2*	81.64(8)	Mo1–S1–Cu2	80.71(9)
S9*–Mo1–S2	79.88(10)	S–Cu1–S7*	109.17(9)	Cu1*–S–Cu1	147.5(2)	Cu1–S2–Mo1	92.63(10)
S9–Mo1–S1	77.62(10)	S6*–Cu1–S7*	76.08(10)	Cu1–S–Cu2*	81.10(8)	Mo2–S3–Cu3	79.93(10)
S2–Mo1−S1	81.04(10)	S4–Cu2–S	126.69(11)	Cu1*–S–Cu2	81.09(8)	Cu2–S4–Mo2	97.68(11)
S7–Mo2–S8	102.55(10)	S4–Cu2–S1	101.11(11)	Cu1–S–Cu2	81.64(8)	Cu3*–S5–Mo3	98.59(11)
S7–Mo2–S4	79.27(10)	S–Cu2–S1	128.27(10)	Cu2*–S–Cu2	115.1(2)	Mo3–S6–Cu1*	82.07(10)
S8–Mo2–S3	77.55(10)	S4–Cu2–S9	99.17(11)	Cu1*–S–Cu3	116.33(9)	Mo2–S7−Mo3	75.41(8)
S4–Mo2–S3	80.81(10)	S–Cu2–S9	110.68(11)	Cu1–S–Cu3	89.40(7)	Mo2–S7–Cu1*	111.26(11)
S8–Mo3–S7	102.58(10)	S1–Cu2–S9	75.13(10)	Cu2*–S–Cu3	155.45(11)	Mo3–S7–Cu1*	82.73(10)
S8–Mo3–S5	78.35(10)	S5*–Cu3–S	124.03(10)	Cu2–S–Cu3	85.54(6)	Mo3–S8−−o2	75.69(8)
S7–Mo3–S6	78.84(10)	S5*–Cu3–S8	105.81(11)	Cu1*–S–Cu3*	89.40(7)	Mo3–S8–Cu3	108.45(11)
S5–Mo3–S6	80.80(10)	S–Cu3–S8	111.54(9)	Cu1–S–Cu3*	116.34(9)	Mo2–S8–Cu3	82.43(9)
S2–Cu1–S	132.70(13)	S5*–Cu3–S3	102.21(11)	Cu2*–S–Cu3*	85.54(6)	Mo1*–S9–Mo1	75.41(8)
S2–Cu1–S6*	100.09(11)	S–Cu3–S3	126.57(10)	Cu2–S–Cu3*	155.44(11)	Mo1*–S9–Cu2	110.07(11)
S–Cu1–S6*	123.22(12)	S8–Cu3–S3	74.85(11)	Cu3–S–Cu3*	78.46(13)	Mo1–S9–Cu2	81.80(9)

[a] Symmetry transformations used to generate equivalent atoms: *, $(y, x, -z)$.

3. Results and discussion

3.1. Syntheses

For the synthesis of compound **1** or **2**, $[Et_4N]_2[Mo_2O_2S_2edt_2]$ and Na_2Se_2 or $(NH_4)_2S$ were used as starting materials. Cu^+ cations were introduced through the reduction of $Cu(NO_3)_2{\cdot}3H_2O$ by $NaBH_4$. Se_2^{2-} or S^{2-} was added into the reaction solution after the precursor $[Mo_2S_2O_2edt_2]^{2-}/2[Cu(MeCN)_2]^+$ fragment had been formed. Three $[Mo_2S_2O_2edt_2]^{2-}/2[Cu(MeCN)_2]^+$ fragments can be assembled together by Se_2^{2-} or S^{2-}, then compound **1** or **2** was obtained.

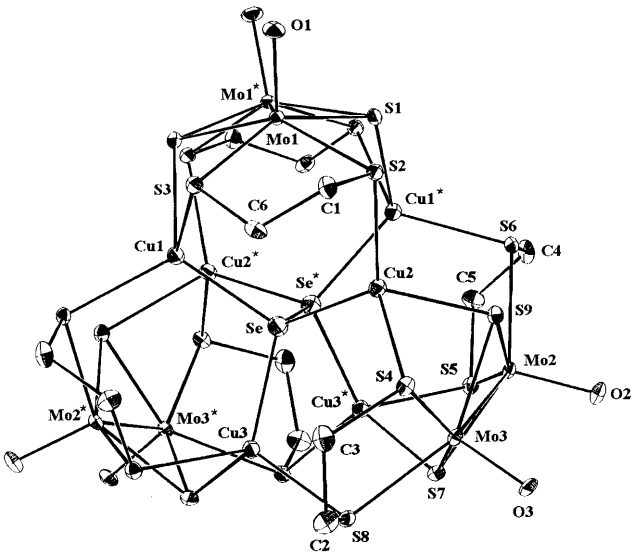


Fig. 1. ORTEP plot of the anion $[(Mo_2Cu_2S_2O_2edt_2)_3(\mu_6\text{-}Se_2)]^{2-}$ in **1** with the ellipsoids drawn at 10% probability level.

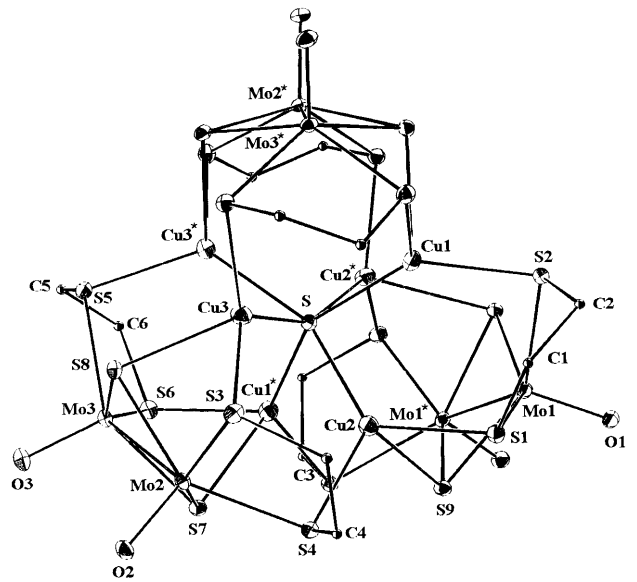


Fig. 2. ORTEP plot of the anion $[(Mo_2Cu_2S_2O_2edt_2)_3(\mu_6\text{-}S)]^{2-}$ in **2** with the ellipsoids drawn at 10% probability level.

3.2. Structure of $[NEt_4]_2[(Mo_2Cu_2S_2O_2edt_2)_3(\mu_6\text{-}Se_2)]{\cdot}CH_2Cl_2$ (1)

The structure of the anion in **1** (Fig. 1) may be viewed as a cage which is composed of three $[Mo_2S_2O_2edt_2]^{2-}/2Cu^+$ fragments assembled by an Se_2^{2-} ion at its center and bonded to six Cu atoms in μ_6 fashion. Each Se atom is bound to three Cu atoms with Se–Cu bonds having approximate sp^3 geometry. The Cu–Se–Cu angles range from 109.20 to 113.71° and the Se–Cu distances range from 2.301 to 2.310 Å, average 2.306 Å. The angles Se*–Se–Cu range from 106.59 to 108.62° and the Se–Se* bond is 2.257 Å. Each Mo atom displays tetragonal-pyramid (TPY) coordination geometry, being surrounded by two S atoms of $^-SC_2H_4S^-$ (S_{edt}), two bridging S atoms of binuclear molybdenum (S_{br}) and one terminal oxygen atom. The oxygen atom occupies the axial position of each TPY with an average M–O distance of 1.677 Å, and the four remaining sulfido atoms are equatorial. The average Mo–S_{br}–Mo angle is 75.63°. Each Mo atom is chelated by one $^-SC_2H_4S^-$ forming a five-membered ring, and the average Mo–S_{edt} distance and average S_{edt}-Mo–S_{edt} angle are 2.446 Å and 81.19°, respectively. There are three Mo–Mo metal–metal bonds and the average Mo–Mo distance is 2.886 Å. Each Cu atom is coordinated by three S atoms (two S_{edt}, one S_{br} atom) and one Se atom of the μ_6-Se_2 ligand, to give a distorted tetrahedral geometry [angles S–Cu–S and S–Cu–Se are in the wide range of 81.55(14)–118.80(13)°]. The average S_{br}–Cu and S_{edt}–Cu distances are 2.354 and 2.326 Å, respectively.

The anion of **1** has two big windows each composed of a puckered $Cu_3S_6C_6$ 15-membered ring which consists of three Cu atoms combining three $^-SC_2H_4S^-$ ligands. It has a pseudo-3-fold axis exactly along the –Se bond and approximately perpendicular to the two windows.

3.3. Structure of $[NEt_4]_2[(Mo_2Cu_2S_2O_2edt_2)_3(\mu_6\text{-}S)]{\cdot}3H_2O$ (2)

The structure of the anion in **2** (Fig. 2), which is similar to that in **1**, may be viewed as a cage with a μ_6-S^{2-} ion at the center and bonded to six Cu atoms. The average Cu–μ_6-S distance is 2.383 Å, and the Cu–μ_6-S–Cu angles range from 78.46–155.45°. There are three narrow Cu–μ_6-S–Cu angles with 81.10(8)° of Cu1–S–Cu2*, 81.09(8)° of Cu–S–Cu1*, 78.46(13)° of Cu3–S–Cu3*. Each Cu atom is coordinated by four S atoms (two S_{edt}, one S_{br} and the μ_6-S atom) to give a distorted tetrahedral geometry [angles S–Cu–S are in the wide range of 74.85(11)—132.70(13)°]. The average S_{br}–Cu distance of 2.472 Å is longer than that in anion **1** (2.354 Å), and the average S_{edt}–Cu distance of 2.398 Å is longer than that in anion **1** (2.326 Å). These may

be due to the fact that the interstitial group S^{2-} in anion **2** is small than Se_2^{2-} in anion **1**.

4. Supplementary material

Crystallographic data for the structural analysis have been deposited with the Cambridge Crystalographic Data Centre, CCDC Nos. 139119 and 139120, respectively, for compounds **1** and **2**. Copies of this information may be obtained free of charge from The Director, CCDC, 12 Union Road, Cambridge, CB2 1EZ, UK (fax: +44-1223-336033; e-mail: deposit@ccdc.cam.ac.uk or www: http://www.ccdc.cam.ac.uk).

Acknowledgements

This research was supported by grants from the State Key Laboratory of Structural Chemistry, Fujian Institute of Research on the Structure of Matter, Chinese Academy of Sciences, and the National Natural Science Foundation of China, and the Science Foundation of Fujian Province.

References

[1] (a) J. Koutecky, P. Fantucci, Chem. Rev. 86 (1986) 539. (b) J.C. Phillips, Chem. Rev. 86 (1986) 619. (c) D. Fenske, J. Oher, J. Hachgenei, K. Merzweiller, Angew. Chem., Int. Ed. Engl. 27 (1988) 1277. (d) S.C Lee, R.M. Holm, Angew. Chem., Int. Ed. Engl. 29 (1990) 840.
[2] G. Bor, G. Gervasio, R. Rossetti, P.L. Stanghellini, J. Chem. Soc., Chem. Commun. (1978) 841.
[3] (a) J.L. Vidal, W.E. Walker, R.L. Pruett, R.C. Schoening, Inorg. Chem. 18 (1979) 129. (b) J.L. Vidal, W.E. Walker, R.C. Schoening, Inorg. Chem. 20 (1981) 238.
[4] W.P. Kretschmer, J.H. Teuben, S.I. Troyanov, Angew. Chem., Int. Ed. Engl. 37 (1998) 88.
[5] V.W. Day, W.G. Klemperer, Science 228 (1985) 533.
[6] G.C. Guo, G.D. Zhou, Q.G. Wang, T.C.W. Mak, Angew. Chem., Int. Ed. Engl. 37 (1998) 630.
[7] X.T. Wu, B. Wang, Y.F. Zheng, J.X. Lu, Jiegou Huaxue (Chin. J. Struct. Chem.) 71 (1988) 47.
[8] P. Lin, X.T. Wu, Q. Huang, Q.M. Wang, T.L. Sheng, W.J. Zhang, J. Guo, J.X. Lu, Inorg. Chem. 37 (1998) 5672.
[9] P. Lin, X.T. Wu, W.J. Zhang, J. Guo, T.L. Sheng, Q.M. Wang, J.X. Lu, Chem. Commun. (1997) 1349.
[10] G.M. Sheldrick, SHELXTL-Version 5, Siemens Analytical X-ray Instruments Inc, Madison, WI, 1990.
[11] G.M. Sheldrick, SHELXTL-93: Program for the Refinement of Crystal Structure, University of Göttingen, Germany, 1993.

PERGAMON

www.elsevier.nl/locate/poly

Polyhedron 19 (2000) 2195–2201

POLYHEDRON

Preparation and structure of 2-(2-benzimidazol-2-yl)pyridine *N*-oxide and its complexes

Martina Vrbová [a], Peter Baran [a], Roman Boča [a,*], Hartmut Fuess [b], Ingrid Svoboda [b], Wolfgang Linert [c], Ulrich Schubert [c], Petra Wiede [c]

[a] *Department of Inorganic Chemistry, Slovak Technical University, SK-81237 Bratislava, Slovakia*
[b] *Materialsciences, Darmstadt University of Technology, D-64287 Darmstadt, Germany*
[c] *Institute of Inorganic Chemistry, Vienna University of Technology, Vienna, Austria*

Received 19 June 2000; accepted 27 July 2000

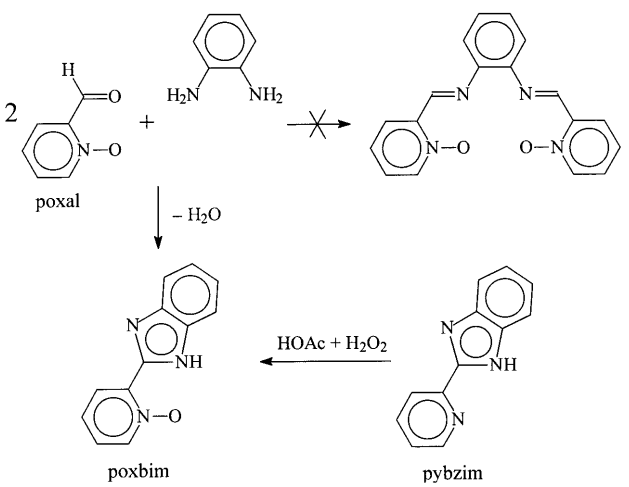
Abstract

The condensation product of pyridinecarboxaldehyde *N*-oxide with *o*-phenylenediamine yields a ligand 2-(2-benzimidazolyl)-pyridine *N*-oxide (poxbim) which has been isolated in a free form. The bidentate ligand gave a series of complexes with Mn(II), Fe(II), Co(II), Ni(II), Cu(II) and Zn(II) with 1:1, 1:2, 1:3, 1:4 and 1:5 metal-to-ligand ratios. The 1:2 cobalt(II) adduct, $[Co(poxbim)_2(H_2O)_2](ClO_4)_2$, has been structurally characterised. Its temperature-dependent magnetic susceptibility shows a behaviour that is characteristic for the octahedral $^4T_{1g}$ term under the axial distortion due to symmetry lowering to D_{4h}. The structure of a 1:4 zinc(II) adduct shows that two ligands remain uncoordinated in $[Zn(poxbim)_2(H_2O)_2](ClO_4)_2 \cdot (poxbim)_2 \cdot 2H_2O$.
© 2000 Elsevier Science B.V. All rights reserved.

Keywords: Pyridine *N*-oxide ligands; Cobat(II) complexes; Zinc(II) complexes; X-ray structures; Magnetic susceptibility

1. Introduction

In dealing with the chemistry of the pyridine *N*-oxide ligands a novel ligand Hpoxap — the product of the condensation of 2-pyridinecarboxaldehyde *N*-oxide (poxal) with *o*-aminophenol — and its Cu(II) complexes have been described recently [1]. In the present study, *o*-phenylenediamine was used instead of *o*-aminophenol. The aim was to prepare a corresponding tetradentate Schiff base, as produced by the salicylaldehyde or pyridinecarboxaldehyde upon the 2:1 condensation with *o*-phenylenediamine [2–4]. Contrary to expectations, the aldehyde used (poxal), yielded 2-(2-benzimidazolyl)pyridine *N*-oxide (poxbim) (**1**). A different route of the preparation of such a compound has already been presented: the oxidation of 2-(2-pyridyl)benzimidazol (pybzim) by the peroxoacetic acid (Scheme 1). The product has been tested as an anthelminticum [5]. To our best knowledge it was never used as a ligand in coordination compounds. This prompted us to undertake a systematic study of poxbim complexation reactions with transition metals.



Scheme 1. Possible routes of preparation of poxbim.

* Corresponding author. Tel.: +42-17-5932-5610; fax: +42-17-5249-3198.
E-mail address: boca@cvtstu.cvt.stuba.sk (R. Boča).

0277-5387/00/$ - see front matter © 2000 Elsevier Science B.V. All rights reserved.
PII: S0277-5387(00)00553-2

Table 1
Products of the L = poxbim complexation

Centra atom M	Ratio M:L	Product; $X = ClO_4^-$	Numbering
Cu	2:1	$CuLCl_2$	**3**
Fe	1:2	$FeL_2X_2{\cdot}4H_2O$	**4**
Co	1:2	$CoL_2X_2{\cdot}2H_2O$	**2**
Cu	1:1, 1:2	$CuL_2Cl_2{\cdot}H_2O$, $CuL_2X_2{\cdot}H_2O$	**5**, **6**
Zn	1:1	$ZnL_2X_2{\cdot}3H_2O$	**7**
Ni	1:2	$NiL_3X_2{\cdot}2H_2O$	**8**
Mn	1:1, 1:2	$MnL_4X_2{\cdot}5H_2O$	**9**
Co	1:4	$CoL_4X_2{\cdot}4H_2O$	**10**
Ni	1:4	$NiL_4X_2{\cdot}4H_2O$	**11**
Zn	1:2	$ZnL_4X_2{\cdot}4H_2O$	**12**
Co	1:3	$CoL_5X_2{\cdot}5H_2O$	**13**

2. Experimental

2.1. Ligand and complexes

A solution of 10.0 g (0.0708 mol) of 2-pyridinecarboxaldehyde *N*-oxide, monohydrate (prepared by the method of Jerchel [6]) in 45 cm^3 of EtOH was added to a solution of 7.65 g (0.0708 mol) of freshly recrystallised *o*-phenylenediamine in 50 cm^3 of EtOH under stirring and heating. The resulting dark-red solution was boiled for a few minutes and then cooled to room temperature (r.t.) under stirring. After 1 h an orange solid was filtered off, washed with EtOH and air-dried. Yield 3.9 g (26%). M.p. 234–235°C. *Anal*. Found: C, 68.5; H, 4.23; N, 20.0. Calc. for $C_{12}H_9N_3O$: C, 68.7; H, 4.29; N, 20.0%. Orange prisms (**1**), suitable for X-ray structure determination, were obtained upon the recrystallisation of the crude product from acetone.

2.1.1. $[Co(poxbim)_2(H_2O)_2](ClO_4)_2$ (**2**)

A solution of 0.5 mmol (0.183 g) of the metal salt $Co(ClO_4)_2{\cdot}6H_2O$ in 5 cm^3 of hot EtOH was slowly added to the solution of 1 mmol (0.211 g) of **1** in 25 cm^3 of hot EtOH under rigorous stirring. The mixture was kept boiling until the volume reduced to approximately 5 cm^3 and then cooled to r.t. under stirring. The product was filtered off, washed with EtOH and air-dried. Yield 0.294 g (82%). *Anal*. Found: C, 40.7; H, 3.01; Cl, 9.84; N, 11.7. Calc. for $C_{24}H_{22}N_6O_{12}CoCl_2$: C, 40.2; H, 3.09; Cl, 9.90; N, 11.7%.

A series of other complexes involving poxbim ligand with Mn(II), Fe(II), Co(II), Ni(II), Cu(II) and Zn(II) has been prepared; the metal to ligand stoichiometry was 1:1, 1:2, 1:3, 1:4, and 1:5 (Table 1).

2.1.2. $Cu(poxbim)Cl_2$ (**3**)

A solution of 0.106 g (0.5 mmol) of **1** in 30 cm^3 of hot EtOH was slowly added to the solution of 0.170 g (1.0 mmol) of $CuCl_2{\cdot}2H_2O$ in 13 cm^3 of hot EtOH under rigorous stirring. The dark-green solution was boiled for 5 min and a pale-green solid started to precipitate, which subsequently recrystallised to a brown product. The stirring was continued without heating for another 60 min when the product was filtered, washed with a small amount of EtOH and air-dried. Yield 0.154 g (89%). *Anal*. Found: C, 41.7; H, 2.62; Cl, 22.2; Cu, 19.9; N, 11.9**.** Calc. for $C_{12}H_9N_3OCuCl_2$: C, 41.7; H, 2.62; Cl, 20.5; Cu, 18.4; N, 12.2%.

2.1.3. $Fe(poxbim)_2(ClO_4)_2(H_2O)_4$ (**4**)

In order to eliminate traces of Fe(III) a piece of metallic Fe and three drops of concentrated perchloric acid were added to a solution of 0.181 g (0.5 mmol) of $Fe(ClO_4)_2{\cdot}6H_2O$ in 5 cm^3 of EtOH–water (2:1) mixture. After 5 min of heating the filtered mixture was added to the hot solution of 0.211 g (1.0 mmol) of **1** in 25 cm^3 of hot EtOH under rigorous stirring. The resulting dark Bordeaux solution was boiled 1 min, cooled to r.t. under stirring and let to crystallise overnight. The orange product was filtered, washed with a small amount of EtOH and air-dried. Yield 0.192 g (51%). *Anal*. Found: C, 38.7; H, 3.07; Cl, 9.94; N, 11.1. Calc. for $C_{24}H_{26}N_6O_{14}FeCl_2$: C, 38.5; H, 3.50; Cl, 9.46; N, 11.2%.

2.1.4. $Cu(poxbim)_2Cl_2(H_2O)$ (**5**), $Cu(poxbim)_2(ClO_4)_2(H_2O)$ (**6**)

A solution of 0.5 mmol of the metal salt (0.085 g of $CuCl_2{\cdot}2H_2O$ or 0.185 g of $Cu(ClO_4)_2{\cdot}6H_2O$) in 10 cm^3 of hot EtOH was slowly added to the solution of 1 mmol (0.211 g) of **1** in 50 cm^3 of hot EtOH under rigorous stirring. A green solid crystallised immediately. The mixture was cooled to r.t. under stirring, and then the products were filtered, washed with EtOH and air-dried. Yield for **5**, 0.215 g (75%). *Anal*. Found: C, 50.0; H, 3.52; Cl, 12.9; Cu, 11.6; N, 14.4. Calc. for $C_{24}H_{20}N_6O_3CuCl_2$: C, 50.2; H, 3.51; Cl, 12.3; Cu, 11.0; N, 14.6%. Yield for **6**, 0.206 g (59%). *Anal*. Found: C, 42.2; H, 2.95; Cl, 10.9; Cu, 8.51; N, 11.8. Calc. for $C_{24}H_{20}N_6O_{11}CuCl_2$: C, 41.0; H, 2.87; Cl, 10.1; Cu, 9.04; N, 12.0%.

2.1.5. $Zn(poxbim)_2(ClO_4)_2(H_2O)_3$ (**7**)

A solution of 0.211 g (1.0 mmol) of **1** in 5 cm^3 of hot EtOH was added to the hot filtered solution of 0.372 g (1.0 mmol) of $Zn(ClO_4)_2{\cdot}6H_2O$ in 10 cm^3 of EtOH under rigorous stirring. The pale-yellow solution was boiled for 1 min, cooled to r.t. under stirring and then put in a closed beaker into the refrigerator. After 1 month a product was filtered, washed with a small amount of EtOH and air-dried. Yield 0.288 g (78%). *Anal*. Found: C, 39.5; H, 3.32; Cl, 9.58; N, 11.3; Zn, 7.63. Calc. for $C_{24}H_{24}N_6O_{13}ZnCl_2$: C, 38.9; H, 3.27; Cl, 9.57; N, 11.3; Zn, 8.83%.

*2.1.6. $Ni(poxbim)_3(ClO_4)_2(H_2O)_2$ (**8**), $Mn(poxbim)_4(ClO_4)_2(H_2O)_5$ (**9**) and $Zn(poxbim)_4(ClO_4)_2(H_2O)_4$ (**12**)*

A solution of 0.5 mmol of the metal salt (0.183 g of $Ni(ClO_4)_2{\cdot}6H_2O$, 0.181 g of $Mn(ClO_4)_2{\cdot}6H_2O$) and 0.186 g of $Zn(ClO_4)_2{\cdot}6H_2O$) in 5 cm^3 of hot EtOH was slowly added to the solution of 1 mmol (0.211 g) of **1** in 25 cm^3 of hot EtOH under rigorous stirring. The mixture was kept boiling until the volume reduced to approximately 5 cm^3 and then cooled to r.t. under stirring. The products were filtered, washed with EtOH and air-dried. Yield for **8**, 0.124 g (40%). *Anal.* Found: C, 46.6; H, 3.40; Cl, 7.78; N, 13.2; Ni, 6.39. Calc. for $C_{36}H_{31}N_9O_{13}NiCl_2$: C, 46.6; H, 3.37; Cl, 7.65; N, 13.6; Ni, 6.33%. Yield for **9**, 0.237 g (81%). *Anal.* Found: C, 48.5; H, 3.68; Cl, 5.48; N, 14.0. Calc. for $C_{48}H_{46}N_{12}O_{17}MnCl_2$: C, 48.5; H, 3.90; Cl, 5.96; N, 14.1%. Yield for **12**, 0.192 g (65%). *Anal.* Found: C, 48.9; H, 3.70; Cl, 6.32; N, 14.2; Zn, 5.22. Calc. for $C_{48}H_{44}N_{12}O_{16}ZnCl_2$: C, 48.8; H, 3.75; Cl, 6.00; N, 14.2; Zn, 5.54%.

*2.1.7. $Co(poxbim)_4(ClO_4)_2(H_2O)_4$ (**10**) and $Ni(poxbim)_4(ClO_4)_2(H_2O)_4$ (**11**)*

A solution of 0.3 mmol of the metal salt (0.110 g of $Co(ClO_4)_2{\cdot}6H_2O$, 0.110 g of $Ni(ClO_4)_2{\cdot}6H_2O$) in 5 cm^3 of hot EtOH was slowly added to the solution of 1.2 mmol (0.253 g) of **1** in 10 cm^3 of hot EtOH under rigorous stirring. The mixture was boiled and then cooled to r.t. under stirring and let to crystallise. The adducts were filtered, washed with EtOH and air-dried. Yield for **11**, 0.308 g (87%). *Anal.* Found: C, 49.0; H, 3.64; Cl, 5.00; N, 14.0; Ni, 4.53. Calc. for $C_{48}H_{44}N_{12}O_{16}NiCl_2$: C, 49.1; H, 3.78; Cl, 6.04; N, 14.3; Ni, 5.00%. Yield for **10**, 0.267 g (76%). *Anal.* Found: C, 48.9; H, 3.70; Cl, 6.28; N, 14.1. Calc. for $C_{48}H_{44}N_{12}O_{16}CoCl_2$: C, 49.1; H, 3.78; Cl, 6.04; N, 14.3%.

*2.1.8. $Co(poxbim)_5(ClO_4)_2(H_2O)_5$ (**13**)*

A solution of 0.110 g (0.4 mmol) of $Co(ClO_4)_2{\cdot}6H_2O$ in 5 cm^3 of hot EtOH was slowly added to the solution of 1.2 mmol (0.253 g) of **1** in 20 cm^3 of hot EtOH under rigorous stirring. The mixture was boiled and then cooled to r.t. under stirring and let to crystallise slowly. The brown products were filtered, washed with EtOH and air-dried. Yield, 0.284 g (84%). *Anal.* Found: C, 51.4; H, 3.78; Cl, 5.19; N, 15.0. Calc. for $C_{60}H_{55}N_{15}O_{18}CoCl_2$: C, 51.3; H, 3.95; Cl, 4.20; N, 15.0%.

2.2. Instruments

IR spectra (Philips, PU 9800 FT-IR spectrometer) were recorded in the 4000–200 cm^{-1} range in Nujol suspension between CsI windows.

Magnetic susceptibility measurements (alternating current susceptometer, LakeShore, model 7221) were conducted in the temperature range 4–90 K; the field parameters were $f = 222$ Hz, $H_{AC} = 800$ A m^{-1}, $H_{DC} = 800$ A m^{-1}. The correction to the underlying diamagnetism has been calculated on the basis of Pascal constants [7]: -3.94×10^{-9} m^3 mol^{-1}.

2.3. X-ray crystal structure determination

Single-crystal data collection of **1** and **12** was performed at 299 K with an Enraf-Nonius CAD-4 diffractometer [8]. The unit cells were determined by least-squares refinements from θ values of 25 accurately measured reflections. Intensities were recorded with an ω–2θ scan. Corrections to Lorentz, polarisation and absorption (ψ empirical) effects were applied. Diffraction data of **2** were collected at 303 K on a Siemens SMART CCD area detector diffractometer using 0.3° ω-scans. The crystal-to-detector distance was 3.85 cm. Graphite-monochromated Mo Kα radiation, $\lambda =$ 0.71093 Å was used in both cases.

The structures were solved by direct methods [9] and subsequent Fourier differences techniques, and refined anisotropically by common least-squares methods [10]. The hydrogen atoms were refined with fixed distances from the parent carbon atoms. The final R indices [$I > 2\sigma(I)$] were $R_1 = 0.026$, $R_1 = 0.051$, and $R_1 = 0.075$ for **1**, **2**, and **12**, respectively. The crystal data on **1**, **2** and **12** are presented in Table 2.

3. Results and discussion

The condensation of poxal with *o*-phenylenediamine in the molar ratio 2:1 gave **1** (poxbim) in a relatively low yield (25%). The same yield (26%) was obtained upon the condensation using the molar ratio 1:1. It seems to be evident that, after the condensation of one molecule of poxal, the oxidation of the reaction intermediate (either Schiff base or imidazolidine) occurred. This is in contrast to a synthesis based on the salicylaldehyde [2] or pyridinecarboxaldehyde [4]; it illustrates a higher reactivity of pyridine *N*-oxides [11]. The observed oxidation could be a reason for the low yield. However, the yield is a bit higher than that of the direct oxidation of pybzim (19%). IR spectra were used to check the identity of the poxbim products obtained by the two routes.

The molecular structure of **1** with the atom numbering is shown in Fig. 1. The whole molecule is almost planar and bond lengths and angles are within the values typical for such a type of heterocyclic compounds. Only a negligible twist around the C(7)–C(8) bond (the pyridine ring forms the dihedral angle of 4.1° to the benzimidazole fragment) disturbs the ideal pla-

Table 2
Crystal data for **1**, **2** and **12**

	1	2	12
Empirical formula	$C_{12}H_9N_3O$	$C_{24}H_{22}Cl_2CoN_6O_{12}$	$C_{24}H_{22}ClN_6O_8Zn_{0.5}$
Formula weight	211.24	716.31	590.66
Crystal system	orthorhombic	monoclinic	triclinic
Space group	$P2_12_12_1$	$P2_1/n$	$P\bar{1}$
Unit cell dimensions			
a (Å)	5.906(1)	10.198(2)	8.528(2)
b (Å)	11.650(1)	9.315(2)	11.848(2)
c (Å)	14.360(1)	14.887(2)	12.435(1)
α (°)	90	90	87.52(1)
β (°)	90	99.418(2)	83.75(2)
γ (°)	90	90	84.02(2)
Volume (Å^3)	988.0(2)	1395.1(4)	1241.5(4)
Z	4	2	2
D_{calc} (Mg m^{-3})	1.420	1.705	1.580
Absorption coefficient (mm^{-1})	0.089	0.884	0.631
$F(000)$	440	730	608
Crystal size max., mid., min. (mm)	0.40, 0.20, 0.15	0.06, 0.04, 0.03	0.35, 0.28, 0.18
θ Range for data collection (°)	2.25–22.97	2.26–25.06	1.65–25.54
Index ranges	$-1\le h\le 6$, $-1\le k\le 12$, $-1\le l\le 15$	$-12\le h\le 12$, $-10\le k\le 11$, $-10\le l\le 17$	$-10\le h\le 10$, $-14\le k\le 14$, $-15\le l\le 15$
Reflections collected	1195	7742	9210
Independent reflections	1060 [$R_{int}=0.0138$]	1636 [$R_{int}=0.0780$]	4611 [$R_{int}=0.1125$]
Data/restraints/parameters	1060/0/181	2468/0/214	4585/10/379
Goodness-of-fit on F^2	1.064	1.084	0.996
Final R indices [$I>2\sigma(I)$]	$R_1=0.0265$, $wR_2=0.0667$	$R_1=0.0515$, $wR_2=0.0947$	$R_1=0.0747$, $wR_2=0.2102$
R indices (all data)	$R_1=0.0311$, $wR_2=0.0702$	$R_1=0.1000$, $wR_2=0.1136$	$R_1=0.1481$, $wR_2=0.3247$
Largest difference peak and hole (e Å^{-3})	0.138 and −0.109	0.268 and −0.349	1.479 and −1.824

narity. The oxygen atom of the pyridine *N*-oxide fragment lies 0.010 Å above the mean plane of the pyridine ring. The hydrogen atom on the imidazole nitrogen forms one intramolecular hydrogen bond and one intermolecular hydrogen bond with O(1′) of the neighbouring molecule. Via the net of hydrogen bonds molecules are joined into infinite chains along the crystallographic *a*-axis.

To study the coordination ability of the poxbim ligand, perchlorates as poorly coordinating anions were used for reactions of poxbim with selected first row transition metals. The complexes obtained could be divided into three groups according their metal to ligand ratio.

Only one 1:1 adduct (compound **3**) was obtained using the excess of copper(II) chloride (Table 1). Preliminary susceptibility measurements in the temperature range (80–300) K ($\mu_{eff}/\mu_B = 1.6$ at 80 K, and 2.0 at 300 K) indicate a dimeric or higher nuclearity for its molecular structure.

The second group of product with the stoichiometry of $ML_2X_2{\cdot}nH_2O$ (compounds **4**–**7**) is exemplified by the complex $[Co(poxbim)_2(H_2O)_2](ClO_4)_2$, for which the molecular and crystal structure was determined. Fig. 2 presents a view of the $[Co(poxbim)_2(H_2O)_2]^{2+}$ cation along with its atom numbering. The cobalt atom lies in the inversion centre surrounded by two bidentate chelating poxbim molecules: Co(1)–O(2) = 2.0286(2) and Co(1)–N(3) = 2.1117(4) Å. Two oxygen atoms from water molecules complete the hexacoordination: Co(1)–O(1) = 2.1422(3) Å. The ligand poxbim coordinates through the oxygen and imine nitrogen atoms of the imidazole group. This means that the poxbim ligand altered its conformation with respect to the free molecule. The intramolecular hydrogen bond was interrupted due to the rotation of the benzimidazole group around the C(7)–C(8) bond. The oxygen atom lies in the pyridine mean plane without considerable deviations (0.026 Å). The cobalt atom deviates slightly from

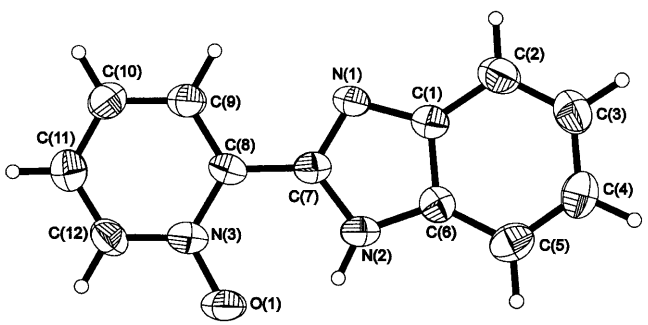


Fig. 1. View of the poxbim molecule, **1**.

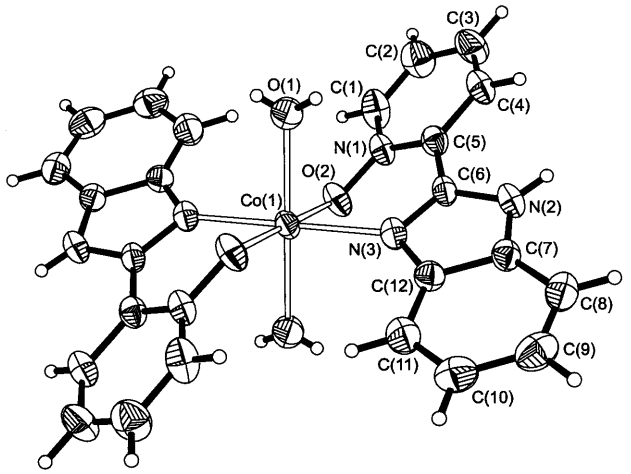


Fig. 2. View of the $[Co(poxbim)_2(H_2O)_2]^{2+}$ complex, **2**.

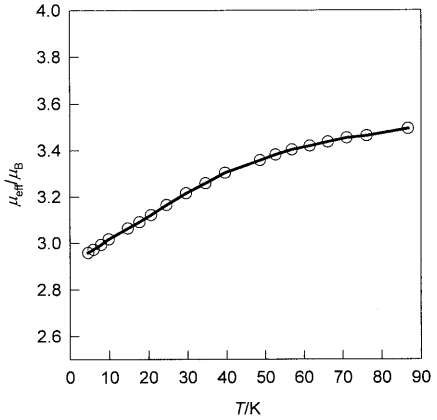


Fig. 4. Temperature dependence of the effective magnetic moment for **2**.

the mean benzimidazole plane (0.122 Å) but essentially from the pyridine plane (− 1.207 Å). A similar coordination mode of the pyridine *N*-oxide group has also been observed for other bidentate ligands: dipyridine *N*,*N*′-dioxide [12,13] or 1,10-phenanthroline *N*-oxide [14]. The Co(1)–O(2)–N(1) angle, 120.9(2)°, is close to those found in Cu(II) complexes [12,13]. It is, however, slightly lower than the angle found in [Cu(poxap)X] complexes [1] in which the central Cu(II) atoms lie in the calculated pyridine planes.

The crystal packing of **2** is determined by three hydrogen bonds involving hydrogens of coordinated water molecules and imidazole group and perchlorate oxygen atoms (Fig. 3).

The molar magnetic susceptibility for **2**, corrected to the underlying diamagnetism, has been converted to the effective magnetic moment and its temperature dependence is shown in Fig. 4.

It can be seen that the effective magnetic moment ranges from the value of $\mu_{eff}/\mu_B = 2.9$ at 4.6 K to $\mu_{eff}/\mu_B = 3.5$ at 87 K. These values are considerably lower relative to the spin-only value for three unpaired electrons ($\mu_{eff}/\mu_B = 3.87$). Such behaviour is typical for the octahedral $^4T_{1g}$ term under the axial distortion due to symmetry lowering to D_{4h} [15]. There exist a number of factors influencing the magnetic properties, namely: (i) the spin Zeeman term; (ii) the orbital Zeeman term; (iii) the spin–orbit interaction; (iv) the orbital reduction factor ($\kappa \leq 1$); (v) the Figgis T_1-term mixing parameter ($1 \leq A \leq 3/2$); and (vi) the axial crystal field splitting (Δ). These parameters enter the spin Hamiltonian of the form [16,17]:

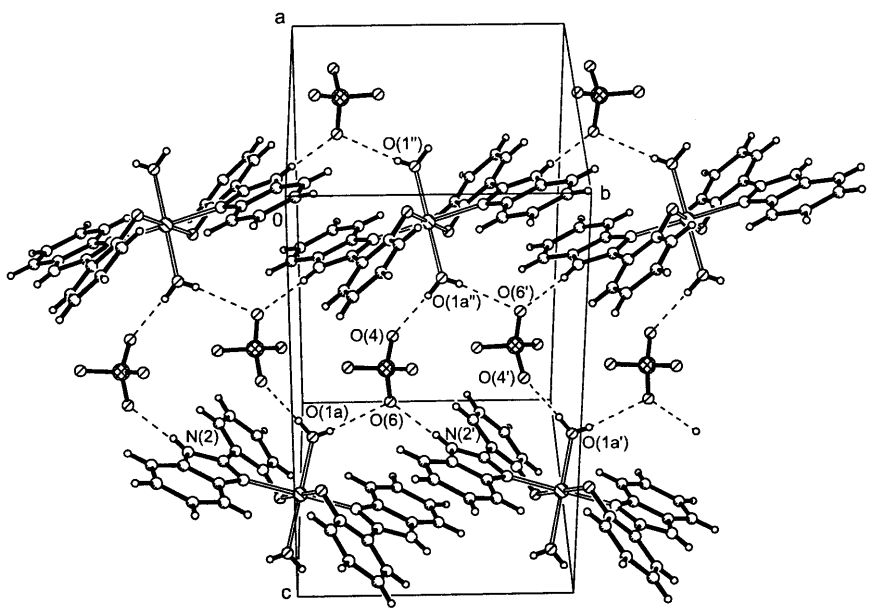


Fig. 3. Crystal packing of the $[Co(poxbim)_2(H_2O)_2](ClO_4)_2$ showing hydrogen bonding.

$$\hat{H}^{\text{spin}} = \mu_B(g_e\vec{S} + \kappa\gamma^{[\text{strong field}]}A\vec{L}) \cdot \vec{B}[\hbar^{-1}] + \kappa v_\xi^{[\text{strong field}]}A\vec{L} \cdot \vec{S}[\hbar^{-2}] + \Delta(\hat{L}_z^2 - \hat{L}^2/3)[\hbar^{-2}]$$

and they interplay in a complicated manner. Therefore it is difficult, if not impossible, to fix all of them reliably from the powder susceptibility data alone. Definitely, 12 magnetically active energy levels are partially populated in the temperature interval concerned.

However, an alternative model of the magnetism comes into consideration; this considers spin-admixed states $^4A_1$–$^2A_1$. When the excited $^2A_1$ state is close to the ground $^4A_1$ state, its thermal population results in some reduction of the magnetic productivity – the fact really observed on the basis of magnetic data for **2**. The adaptation of such a model is not a routine task since the key matrix elements of the type $\langle {}^4A_1|\hat{H}^{so}|{}^2A_1\rangle$ within the point group D_{4h} or D_{2h} have not been derived so far. An analogous model of $^6A_1$–$^4A_1$ is known for Fe(III) complexes and successful in describing the reduced magnetic productivity of iron(III) porphyrins [18,19].

The third group of products (**8**–**13**) is characterised by higher metal to ligand stoichiometry than 1:2. The IR spectra for **8**–**13** are more complex than that for ML_2X_2-type complexes in the fingerprint region. Additional peaks could be assigned to peaks of uncoordinated or differently coordinated (possibly monodentate) poxbim molecules. Parallel occurrence of two different kinds of poxbim in the crystal structure can explain higher ligand-to-metal stoichiometries as well as the IR data. The X-ray structure determination for the $Zn(poxbim)_4(ClO_4)_2{\cdot}4H_2O$ complex (**12**) gives a surprising explanation of the role of poxbim in the complexes of the third group. The structure shows that two ligands remain uncoordinated in $[Zn(poxbim)_2(H_2O)_2]$-$(ClO_4)_2{\cdot}(poxbim)_2{\cdot}2H_2O$. The geometry of the coordination polyhedron $[Zn(poxbim)_2(H_2O)_2]^{2+}$ is analogous to the $[Co(poxbim)_2(H_2O)_2]^{2+}$ in **2**. Some relevant distances are: Zn(1)–O(1) = 2.074(4), Zn(1)–N(3) = 2.094(5) and Zn(1)–O(2) = 2.130(4) Å (Fig. 5).

Two uncoordinated ligands form a pair due to the hydrogen bonds between the imidazole hydrogen and the oxygen of the *N*-oxide group. The positions of pairs $[poxbim]_2$ resemble the positions of the coordinated ligands in the $[Zn(poxbim)_2(H_2O)_2]^{2+}$ complex (Fig. 6). The separation of the best-fit planes of poxbim molecules in the $[Zn(poxbim)_2(H_2O)_2]^{2+}$ complex is 1.50 Å and it equals to 1.64 Å for two uncoordinated ligands in the $[poxbim]_2$ pair. Intermolecular O–O and O–N contacts between two $[Zn(poxbim)_2(H_2O)_2]^{2+}$ units are 2.75 and 3.14 Å. These are not too far from similar contacts between two $[poxbim]_2$ units, which are 3.39 and 3.01 Å, respectively.

Noticeable is the fact that the IR spectra of all M:L = 1:3, 1:4 and 1:5 complexes look very similar. Therefore, we assume that these compounds contain $[ML_2]^{2+}$ and $[L_2]$ units in a different ratio: repetition of $[ML_2]^{2+}$ and $[L_2]$ motifs in crystal packing in the 2:1 ratio will lead to the apparent stoichiometry $[ML_3]^{2+}$ of the nickel complex **8**, and 2:3 ratio yields the $[ML_5]^{2+}$ stoichiometry found for the cobalt complex **13**.

4. Supplementary material

Crystallographic data (X-ray data (.cif files)) for the structures reported in this paper have been deposited with the Cambridge Crystallographic Data Centre, CCDC No. 139606 for compound **1,** CCDC No. 139607 for compound **2** and CCDC No. 145870 for

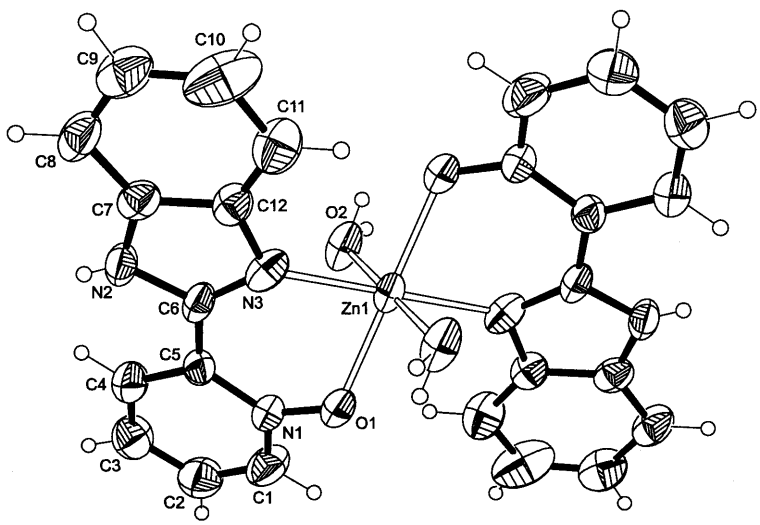


Fig. 5. View of the $[Zn(poxbim)_2(H_2O)_2]^{2+}$ cation of the compound **12**.

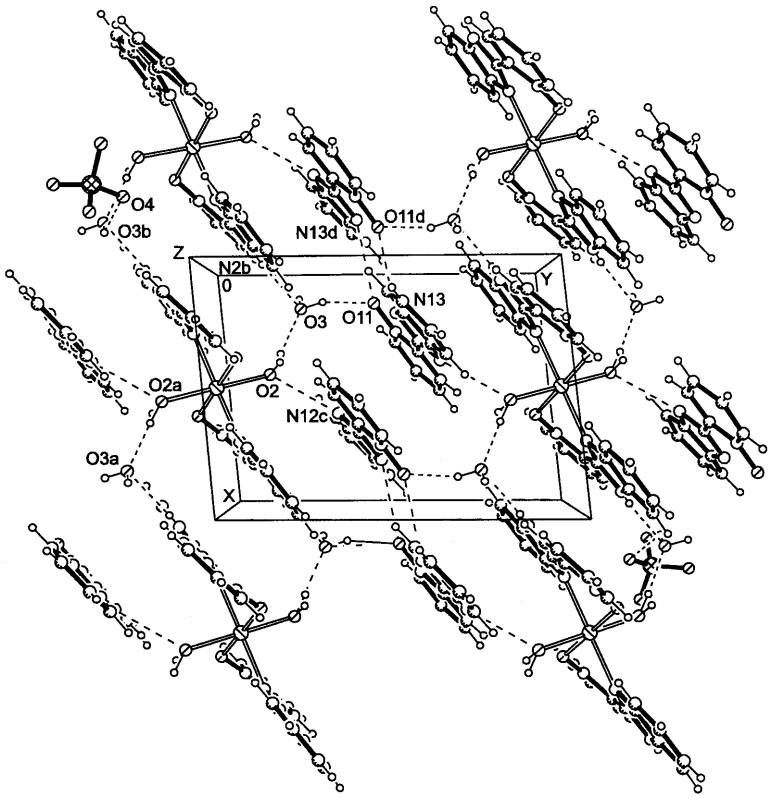


Fig. 6. Crystal packing of the $[Zn(poxbim)_2(H_2O)_2](ClO_4)_2 \cdot 2poxbim \cdot 2H_2O$ along the x-axis.

compound **12**. Copies of this information may be obtained free of charge from the Director, CCDC, 12 Union Road, Cambridge, CB2 1EZ, UK (fax: +44-1223-336033; e-mail: deposit@ccdc.cam.ac.uk or http://www.ccdc.cam.ac.uk).

Acknowledgements

Thanks are due the European Community Training and Mobility of Researchers Network (TMR) project 'Thermal and Optical Spin State Switching' (TOSS) supported by the European Community under the Contract number ERB-FMRX-CT98-0199 and to the European Science Foundation under the project 'Molecular Magnets'.

References

[1] P. Baran, C. Arnold, R. Boča, M. Breza, H. Ehrenberg, H. Elias, H. Fuess, L. Gelieňová, R. Klement, I. Svoboda, G. Wltschek, Inorg. Chim. Acta (submitted).
[2] P.C.H. Mitchel, D.A. Parker, J. Chem. Soc., Dalton Trans. (1972) 1828.
[3] X. Li, M.S. Lah, V.L. Pecoraro, Inorg. Chem. 27 (1988) 4657.
[4] Z. Zang, Z. Yin, G. Wang, Ch. Zeng, Inorg. Chem. 29 (1990) 560.
[5] R.D. Hauguito, V.L. Narayanan, U.S. Pat. 386435004, February, 1975.
[6] D. Jerchel, J. Heider, H. Wagner, Annalen 613 (1958) 153.
[7] E. König, Landolt-Börnstain, Neue Serie, Bd. II/2, Springer, Berlin, 1996, p. 1.
[8] Enraf-Nonius Diffractometer Control Software, Release 5.1, Enraf-Nonius, Delft, 1993.
[9] G.M. Sheldrick, SHELXS-86, University of Göttingen, Germany, 1986.
[10] G.M. Sheldrick, SHELXS-93, University of Göttingen, Germany, 1993.
[11] E. Oichiai, J. Org. Chem. 18 (1953) 534.
[12] P. Baran, M. Koman, D. Valigura, J. Mrozinski, J. Chem. Soc., Dalton Trans. (1991) 1385.
[13] M. Koman, P. Baran, D. Valigura, Acta Crystallogr., Sect. C 47 (1991) 2529.
[14] J. Kozíšek, P. Baran, D. Valigura, Acta Crystallogr., Sect. C 48 (1992) 31.
[15] F.E. Mabbs, D.J. Machin, Magnetism and Transition Metal Complexes, Chapman and Hall, London, 1973.
[16] R. Boča, Coord. Chem. Rev. 173 (1998) 167.
[17] R. Boča, Theoretical Foundations of Molecular Magnetism, Elsevier, Amsterdam, 1999.
[18] M. Weisbluth, Struct. Bonding 2 (1967) 1.
[19] O. Kahn, Molecular Magnetism, VCH, New York, 1993.

PERGAMON

www.elsevier.nl/locate/poly

Polyhedron 19 (2000) 2203–2209

POLYHEDRON

Spectroscopic characterization of lanthanide complexes with *N*,*N*′-tetraethyl-*N*″-benzoylphosphoryltriamide. Crystal structure of tris(*N*,*N*′-tetraethyl-*N*″-benzoylphosphoryltriamide) cerium(III) trinitrate complex

Katerina E. Gubina, Julia A. Shatrava, Vladimir A. Ovchynnikov, Vladimir M. Amirkhanov *

Faculty of Chemistry, University of Kiev, Vladimirskaya str. 64, 25201 Kiev, Ukraine

Received 28 April 2000; accepted 2 August 2000

Abstract

A new range of lanthanide compounds of the formula $Ln(HL)_3(NO_3)_3$, where Ln = La, Ce–Nd, Sm–Lu, Y; HL = $C_6H_5C(O)N(H)P(O)[N(CH_2CH_3)_2]_2$–*N*,*N*′–tetraethyl–*N*″-benzoylphosphoryltriamide have been prepared and characterized by means of IR, ^1H, ^{31}P NMR and UV–Vis spectroscopies. The compounds are isomorphous according to X-ray powder diffraction studies. The crystal and molecular structure of $Ce(HL)_3(NO_3)_3$ has been determined by X-ray diffraction studies. The complex has a molecular structure. The monodentate neutral phosphoryltriamide ligands are coordinated to the metal ion via phosphoryl oxygen atom. The coordination polyhedron of Ce is a tricapped trigonal prism, CN = 9 [6O(NO_3^-) + 3O(P=O)]. By UV–Vis spectroscopy it was shown that in acetonitrile solution the neodymium complex with molar ratio 1:3 (Nd^{3+}:HL) exists (stability constant = 2.56). © 2000 Elsevier Science B.V. All rights reserved.

Keywords: Lanthanide; Carbacylamidophosphate; NMR; X-ray data

1. Introduction

The present work is a continuation of regular studies of lanthanide complexes with carbacylamidophosphate compounds of the general formula $R_1C(O)NHP(O)R_2$, which are also potential *O*,*O*′-donor ligands for metal ions [1]. The presence of a peptide group in the compound causes its diverse biological activity and some of their *N*-ethyleneimine derivatives (at the phosphoryl group) have been proposed as anticancer drugs [2]. Carbacylamidophosphates may be regarded as powerful chelating systems, closely related to β-diketonates.

The first studies of the coordination chemistry of carbacylamidophosphates were devoted to complexes of the lanthanides because of the high affinity of the phosphoryl group for the rare-earth elements [3].

Studies of rare earth coordination compounds with bis(diethylamido)-trichloracetylamidophosphorus acid [4] and *N*,*N*′-tetramethyl-*N*″-benzoylphosphoryltriamide [5] were reported earlier.

Herein, we report the synthesis and studies of the lanthanide coordination compounds with *N*,*N*′-tetraethyl-*N*″-benzoylphosphoryltriamide in the solid state and in non-aqueous solutions and the result of X-ray studies of $Ce(NO_3)_3(HL)_3$.

2. Experimental

2.1. Preparation of $Ln(NO_3)_3(HL)_3$

N,*N*′-Tetraethyl-*N*″-benzoylphosphoryltriamide was prepared and identified according to Ref. [2].

Complex compounds were synthesized through the following reaction:

* Corresponding author. Tel.: +38-44-221-0292.

E-mail address: vamr@anorgchemie.univ.kiev.ua (V.M. Amirkhanov).

0277-5387/00/$ - see front matter © 2000 Elsevier Science B.V. All rights reserved.
PII: S0277-5387(00)00526-X

$$Ln(NO_3)_3 \cdot nH_2O + 3HL \rightarrow Ln(NO_3)_3(HL)_3 + nH_2O$$

where Ln = La–Nd, Sm–Lu and Y.

Hydrated rare earth nitrate (1 mmol) was dissolved in isopropanol (15 ml). The solution was heated to boiling point to dissolve the rare earth salt completely, and the resulting solution was added to the solution of HL (3 mmol) in methanol (15 ml). The obtained solution was allowed to stand in a vacuum desiccator over $CaCl_2$. After a while the crystals precipitated from the solution. They were filtered off, washed with cooled acetone, and dried over $CaCl_2$ (yield 80–90%). A single crystal of $Ce(HL)_3(NO_3)_3$ was prepared by slow crystallization from isopropanol.

According to X-ray diffraction, the prepared complexes are isostructural crystalline compounds. They are stable in air and slightly colored depending on the color of the Ln(III) aqua ion, soluble in methyl and ethyl alcohol, less soluble in acetone, and essentially insoluble in nonpolar aprotic solvents and water.

For all compounds the contents of metals were determined by a complexometric titration method with xylenol orange as indicator:

Ln(III)	Found/Calc.	Ln(III)	Found/Calc.
La	11.02/11.042	Dy	12.26/12.68
Ce	11.06/11.13	Ho	12.17/12.85
Pr	11.02/11.18	Er	12.84/13.0
Nd	11.33/11.42	Tm	12.95/13.12
Sm	11.72/11.85	Yb	13.39/13.27
Eu	12.02/11.96	Lu	13.32/13.52
Gd	11.96/12.32	Y	7.35/7.36
Tb	12.03/12.44		

3. Methods

IR spectra were recorded in KBr pellets on an UR-10 spectrometer (Carl Zeiss, Jena) (400–4000 cm^{-1}). X-ray diffraction patterns were recorded on a DRON-3 diffractometer using Cu Kα radiation. The ^1H (TMS) and ^{31}P (H_3PO_4 in D_2O) NMR spectra were recorded on a Bruker WP 100 SY spectrometer at room temperature in acetone-d_6 solution.

Electroconductivity measurements for $Nd(HL)_3(NO_3)_3$ were made at room temperature in acetone solutions in the concentration range 0.09–0.01 mol^{-1}.

Crystal data for the cerium compound were collected using an Enraf–Nonius CAD4 automated diffractometer. Table 1 lists the cell parameters and details of data acquisition and structure refinement. Selected geometrical parameters of $Ce(HL)_3(NO_3)_3$ are listed in Table 2. The structure was solved by direct methods and refined by the least-square method using the programs SHELXS and SHELXL-93 [6,7]. All the non-hydrogen atoms were refined anisotropically. The hydrogen atoms were calculated from the geometry of the molecule. In the final difference map, the highest peak 0.37 e $Å^{-3}$ was near the cerium ion (1.12 Å).

Table 1
Crystal data and structure refinement for $Ce(NO_3)_3(HL)_3$

Empirical formula	$C_{45}H_{70}CeN_{12}O_{15}P_3$
Temperature (K)	293(2)
Wavelength (Å)	0.71073
Crystal system	monoclinic
Space group	*Cc*
Unit cell dimensions	
a (Å)	14.666(3)
b (Å)	24.644(5)
c (Å)	17.543(4)
β (°)	103.25(2)
V ($Å^3$)	6172(2)
Z	4
Crystal size (mm)	$0.50 \times 0.45 \times 0.45$
θ Range for data collection (°)	1.65–24.9
Index ranges	$0 \le h \le 16$, $0 \le k \le 29$, $-20 \le l \le 20$
Reflections collected	5179
Independent reflections	5179
Refinement method	full-matrix least-squares on F^2
Data/restraints/parameters	4842/20/649
Goodness-of-fit on F^2	1.037
Final *R* indices [$I > 2\sigma(I)$]	$R_1 = 0.0502$, $wR_2 = 0.1058$
R indices (all data)	$R_1 = 0.0801$, $wR_2 = 0.1219$
Absolute structure parameter	0.00(2)
Largest difference peak and hole (e A^{-3})	0.368 and −0.246

UV–Vis spectra were measured at room temperature in absolute acetonitrile on a KSVU-23, LOMO adapted for an IBM PC.

Systems with a constant concentration of Nd^{3+} and various concentrations of phosphorylic ligand (HL) in acetonitrilic solutions of neodymium perchlorate were studied. The equilibrium concentration values of complexes were determined by means of measurement of integral intensities of $^4I_{9/2} \rightarrow {}^2P_{1/2}$ transitions appropriate to a solvated ion Nd^{3+} and complex. These bonds were divided by GAUSSIAN.

The number of ligands *n* in complex, was determined graphically on the equation [8]: $\log [ML]/[M] = \log \beta_n - n \log [L]$.

The stability constants of the complexes were calculated from values for the equilibrium concentrations of the components.

4. Results and discussion

4.1. IR spectroscopy

The IR spectra of the coordination compounds are very similar. The spectra reveal significantly lower frequencies of ν(PO) compared to the data for the free

Table 2
Selected bond lengths (Å) and angles (°)

Ce(1)–O(1C)	2.400(7)	P(1C)–N(2C)	1.598(13)
Ce(1)–O(1B)	2.401(10)	P(1C)–N(3C)	1.641(12)
Ce(1)–O(1A)	2.404(9)	P(1C)–N(1C)	1.664(9)
Ce(1)–O(7)	2.563(9)	P(1B)–O(1B)	1.479(10)
Ce(1)–O(3)	2.579(8)	P(1B)–N(2B)	1.57(2)
Ce(1)–O(10)	2.584(8)	P(1B)–N(3B)	1.665(14)
Ce(1)–O(9)	2.590(12)	P(1B)–N(1B)	1.700(13)
Ce(1)–O(4)	2.597(10)	O(2A)–C(7A)	1.22(2)
Ce(1)–O(6)	2.615(9)	N(1A)–C(7A)	1.36(2)
P(1A)–O(1A)	1.482(10)	O(2B)–C(7B)	1.20(2)
P(1A)–N(3A)	1.60(2)	N(1B)–C(7B)	1.38(2)
P(1A)–N(2A)	1.62(2)	O(2C)–C(7C)	1.22(2)
P(1A)–N(1A)	1.686(11)	N(1C)–C(7C)	1.35(2)
P(1C)–O(1C)	1.494(8)		
O(1C)–Ce(1)–O(1B)	91.3(3)	O(1C)–P(1C)–N(1C)	106.3(6)
O(1C)–Ce(1)–O(1A)	92.2(3)	N(3A)–P(1A)–N(2A)	107.9(9)
O(1B)–Ce(1)–O(1A)	85.6(3)	N(2B)–P(1B)–N(3B)	109.8(8)
X(1A)–Ce(1)–O(1A)	79.4(3)	N(2C)–P(1C)–N(3C)	115.9(5)
X(1B)–Ce(1)–O(1A)	97.5(3)	C(7A)–N(1A)–P(1A)	127.8(9)
X(1C)–Ce(1)–O(1A)	165.6(3)	C(7B)–N(1B)–P(1B)	124.5(12)
X(1A)–Ce(1)–O(1B)	96.4(3)	C(7C)–N(1C)–P(1C)	127.8(10)
X(1B)–Ce(1)–O(1B)	169.2(3)	O(2A)–C(7A)–N(1A)	121.2(13)
X(1C)–Ce(1)–O(1B)	82.6(3)	O(2B)–C(7B)–N(1B)	122(2)
X(1A)–Ce(1)–O(1C)	168.1(3)	O(2C)–C(7C)–N(1C)	121.6(14)
X(1B)–Ce(1)–O(1C)	78.2(3)	N(1A)–C(7A)–C(1A)	116.2(11)
X(1C)–Ce(1)–O(1C)	96.2(3)	N(1B)–C(7B)–C(1B)	115(2)
X(1C)–Ce(1)–X(1A)	93.7(3)	N(1C)–C(7C)–C(1C)	118.9(12)
X(1B)–Ce(1)–X(1A)	94.4(3)	O(8)–N(5)–Ce(1)	58.7(7)
X(1C)–Ce(1)–X(1B)	95.6(3)	O(7)–N(5)–Ce(1)	121(2)
O(1A)–P(1A)–N(1A)	104.3(6)	O(6)–N(5)–Ce(1)	121.2(13)
O(1B)–P(1B)–N(1B)	103.3(6)	O(3)–N(4)–Ce(1)	117.8(14)
O(4)–N(4)–Ce(1)	59.5(8)	N(5)–O(6)–Ce(1)	95.6(8)
O(5)–N(4)–Ce(1)	176.2(11)	N(5)–O(7)–Ce(1)	98.1(9)
O(11)–N(6)–Ce(1)	177(2)	N(6)–O(9)–Ce(1)	95.5(9)
O(10)–N(6)–Ce(1)	59.1(7)	N(6)–O(10)–Ce(1)	96.6(9)
O(9)–N(6)–Ce(1)	59.5(8)	P(1A)–O(1A)–Ce(1)	155.8(6)
N(4)–O(3)–Ce(1)	97.3(8)	P(1B)–O(1B)–Ce(1)	159.9(6)
N(4)–O(4)–Ce(1)	96.8(9)	P(1C)–O(1C)–Ce(1)	157.7(5)

ligand ($\Delta\nu$(PO) = 15–55 cm^{-1}), reflecting the coordination via the phosphoryl oxygen atom [9,10]. The ν(CO) values of the complexes (1680–1690 cm^{-1}) do not differ from the parameters for the free ligand (1675 cm^{-1}).

The broad absorption band in the IR spectrum of the free ligand at 3070 cm^{-1} can be assigned to vibrations of the NH group connected by a hydrogen bond to a phosphoryl group of a neighboring molecule [11]. By coordination to the lanthanide ion the intermolecular hydrogen bonds break up and that is why in the spectra of the complexes ν(NH) is detected near 3320–3335 cm^{-1}.

Thereby the main changes in the spectra deal with the ν(NH) and ν(PO) bands. This fact can be explained by the formation of a coordination bonding lanthanide ion with a phosphoryl ligand via a phosphoryl group.

The vibrations of the nitrate groups appear as two absorption bands in the range 1500–1300 cm^{-1}, which is evidence for the bidentate coordination of a nitrate ion [12].

4.2. UV–Vis spectroscopy

The comparison of the diffuse reflectance spectrum of the complexes of $Nd(NO_3)_3(HL)_3$, and absorption spectrum in acetonitrile solution allows one to assume the identity of the structure of the coordination spheres of this compound in the solid state and in acetonitrile.

The ratio of intensities and character of splitting of lines in the hypersensitive transition $^4I_{9/2} \rightarrow {}^4G_{5/2},{}^2G_{7/2}$ region Fig. 1 testifies to the similarity of the environment of the central atom in these compounds [13].

It was shown that the acetonitrile solutions of $Ln(HL)_3(NO_3)_3$ are weak electrolytes ($C = 3.0 \times 10^{-2}$–0.4×10^{-2} mol^{-1}, $\lambda = 23$–$43\ \Omega^{-1}$ cm^2 mol^{-1}), therefore very probably the structure of the coordination unit is preserved in acetonitrile. A decrease in complex concentration results in the values of molecular conductivity growing sharply.

A number of solutions with constant concentration of neodymium perchlorate (0.1 mol^{-1}) and different metal:ligand ratios were studied. Fig. 2 shows the absorption spectra of these solutions in the $^4I_{9/2} \rightarrow {}^2P_{1/2}$ transition region. The oscillator strength of the f–f transitions for the solutions of neodymium compounds are given in Table 3. Fade-in of f–f transitions in $^4I_{9/2} \rightarrow {}^4G_{5/2},{}^2G_{7/2}$ region up to ratio a metal:ligand ratio equal to 1:4 with an exit at a plateau observed. Data accounting for the composition of the complex and the constant of stability are given in Table 4.

The absorption spectra of neodymium perchlorate contain one band in the $^4I_{9/2} \rightarrow {}^2P_{1/2}$ transition region (428.1 nm). By addition of the ligand to the solution we can observed a new band (429.84 nm) in the spectrum. The intensity of the above-mentioned band grew with increasing concentration of HL. Apparently, this band corresponds to a complex whose concentration grows by increasing the metal: HL ratio. The ratio of the integrated intensity of these two bands was accepted for the calculation.

Plotted versus $\log[ML]/[M] = f(\log[L])$, Fig. 2, and the linear least-squares approximations for the series solutions give the equation of a straight line $y = 2.56$–$3.28x$ (with the correlation coefficient $K = 0.99$) which evidences complex formation with composition 1:3 (stability constant 2.56).

Thus, in acetonitrile solutions equilibrium takes place:

$$Nd[(Solv)_n]^{3+} + 3HL \leftrightarrows [Nd(Solv)_{n-m}(HL)_3] + mSolv$$

It is interesting to note that investigations of complex formation in solutions of a ligand, close on a structure (*N*,*N*′ - tetramethyl - *N*″ - benzoylphosphoryltriamide),

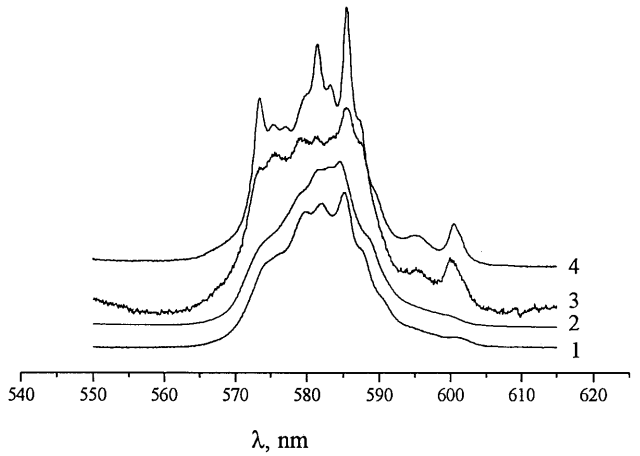


Fig. 1. $^4I_{9/2} \rightarrow {}^4G_{5/2},{}^2G_{7/2}$ in the absorption spectra of neodimium complexes: (1) $Nd(NO_3)_3(CCl_3C(O)NHP(O)[NEt_2]_2)_3$ in acetone solution; (2) $Nd(NO_3)_3(HL)_3$ in acetonitrile solution; (3) $Nd(NO_3)_3(HL)_3$ in the solid state; (4) $Nd(NO_3)_3(CCl_3C(O)NHP(O)[NEt_2]_2)_3$ in the solid state.

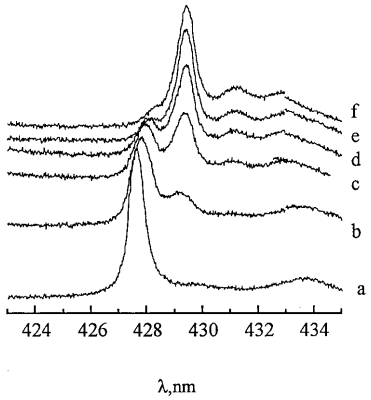


Fig. 2. $^4I_{9/2} \rightarrow {}^2P_{1/2}$ in the absorption spectra of neodimium complexes in acetonitrile solutions $C(Nd^{3+}) = 0.1$ mol l^{-1}. Ratio of metal:ligand is equal: (a) sol. $Nd(ClO_4)_3$; (b) 1:1; (c) 1:2; (d) 1:2.5; (e) 1:3; (f) 1:3.5.

concluded that in simulated conditions a complex of composition 1:2 is formed [14].

4.3. NMR spectroscopy

A rather wide range of chemical shifts in the NMR spectra of the synthesized compounds is due to the paramagnetic properties of rare-earth ions [15]. Table 5 presents the chemical shifts in the ^1H and ^{31}P NMR spectra of solutions of the $Ln(NO_3)_3(HL)_3$ complexes in acetone. The ^1H NMR spectra show the signals from the protons of the methyl and methylene groups. Broad signals of amide protons appear in the NMR spectra of the compounds of La, Ce, Sm, Yb, Lu, Y at 8.88, 12.6, 9.69, 9.55, 8.7, 8.64 ppm, respectively. The ^{31}P NMR spectra of the solutions of the complexes in acetone exhibit one singlet, indicating the magnetic equivalence of all phosphorus atoms in the molecule.

4.4. X-ray

The coordination sphere of Ce in $Ce(NO_3)_3(HL)_3$ is a tricapped trigonal prism (coordination number is nine) (Fig. 3). The O(1a), O(1b), and O(1c) oxygen atoms of the three ligands HL occupy the vertices of one triangu-

Table 3
Oscillator strength of f–f transitions for a solution of $Nd(HL)_3(ClO_4)_3$ in acetonitrile at room temperature $c = 0.125$ m l^{-1}

S′L′J′	Spectral region (Å)	$P_{exp} \times 10^8$				
	Molar ratio Nd^{3+}:HL:	1:1	1:2	1:3	1:4	1:5
$^4F_{7/2}$, $^4S_{3/2}$	7100–7750	945.79	944.66	920.86	903.59	853.89
$^4F_{9/2}$	6610–7050	64.06	63.46	64.88	66.48	63.38
$^4G_{5/2}$, $^2G_{7/2}$	5500–6100	1764.69	2205.62	2809.01	3812.35	3874.64
$^2K_{13/2}$, $^4G_{7/2}$, $^4G_{9/2}$	4900–5500	886.90	899.43	963.93	1073.97	1040.81
$^2K_{15/2}$,$^2G_{9/2}$,(^2D,$^2F)_{3/2}$,$^4G_{11/2}$	4500–4900	223.52	213.62	228.91	244.69	228.14
$^2P_{1/2}$, $^2D_{5/2}$	4130–4400	55.45	70.81	73.76	79.72	72.77
$^4D_{3/2}$,$^4D_{5/2}$, $^2I_{11/2}$, $^4D_{1/2}$,$^2L_{15/2}$	3380–3700	979.46	1045.20	1047.17	1262.29	1174.38

Table 4
Data for calculation of constant stability for the complex $[Nd(HL)_n]^{3+}$

Nd^{3+}:HL	$[Nd^{3+}]$	$[Nd(HL)_n^{3+}]$	[HL]	$\log \frac{[Nd(HL)_n^{3+}]}{[Nd^{3+}]}$	$-\log$ [HL]
1:1.5	0.078	0.048	0.139	−0.211	0.85
1:2	0.057	0.068	0.182	0.077	0.739
1:2.5	0.035	0.090	0.223	0.410	0.653
1:3	0.02	0.105	0.270	0.720	0.569

lar base of a prism, and the O(4), O(6), O(9) oxygen atoms from the three nitrate groups are located at the vertices of another triangular base. The caps adjacent to the rectangular faces of the prism are occupied by the second oxygen atoms O(3), O(7), O(10) of the coordinated nitrate groups. The symmetry of such an environment is roughly C_3. A similar structure was observed for the complex $Eu(NO_3)_3(CCl_3C(O)NHP(O)[NEt_2]_2)_3$ [4].

Table 5
^1H and ^{31}P NMR chemical shifts (ppm) for the lanthanide coordination compounds with *N*,*N*′-tetraethyl-*N*″-benzoylphosphorytrilamide

^{31}P			^1H			
Ln		Line width (Hz)	C_6H_5	CH_3	CH_2	NH
La	11.86	7	7.81	1.12	3.24	8.88
Ce	42.7	10	7.48	1.67	4.85	12.6
Pr	94.2	22	7.2	2.47	6.90	
Nd	96.0	18	7.72	1.59	4.86	
Sm	11.32	7	7.83	1.17	3.43	9.69
Eu	−134	22	8.0	0.62	1.39	
Tb	−262	52	3.4; 9.3 [a]			
Dy	−126	65	71; 20.6 [a]			
Ho	−144	49	2.1; 4.8; 5.2 [a]			
Er	−221	16	9.3	−1.95	1.5	
Tm	−167	20	8.4; 9.0; 9.9 [a]			
Yb	−42	23	8.89	1.04	3.43	9.55
Lu	13.5	7	7.84	1.12	3.26	8.7
Y	12.7	5	7.82	1.11	3.26	8.64

[a] Without assignment.

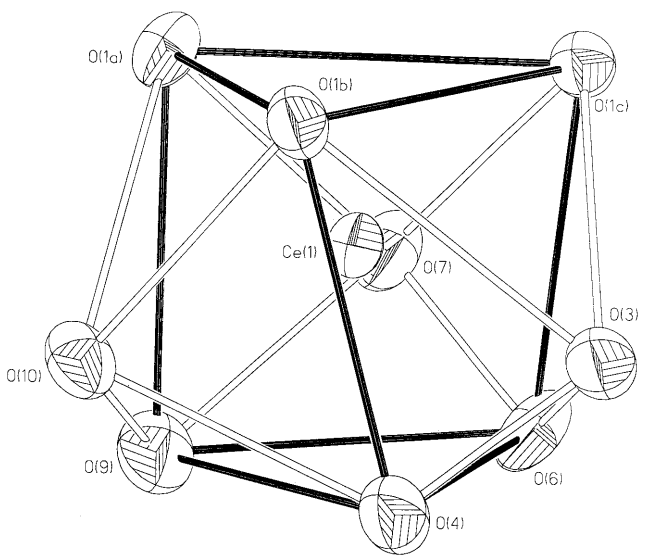


Fig. 3. Polyhedra of complex $Ce(NO_3)_3\{(C_6H_5C(O)NHP(O)[N(CH_2CH_3)_2]_2\}_3$.

The nitrate groups symmetrically coordinate the central atom, therefore the coordination polyhedron of $Ce(NO_3)_3(HL)_3$ can be conventionally considered to be a distorted pseudo-octahedron if every nitrate group is assumed to occupy one site in the coordination polyhedron ($3O(HL) + 3X$), where X is the midpoint of the line connecting the coordinated oxygen atoms of the nitrate group). All of the angles of this coordination polyhedron are close to the octahedral angle (Table 3).

In the planar four-membered CeO_2N chelate rings, the average angle CeON is 96,6°, and the average Ce–O bond length for the nitrate groups is 2.51(12) Å, which agrees well with the literature data on nitrate lanthanide complexes [6]. The coordinated nitrate groups have virtually planar triangular structures. The tightening effect of the coordination center leads to the average ONO angle of the chelate ring (118.1°) being smaller than the other angles (on average, 121.7°). The average N–O distance is 1.229(2) Å, and the bonds adjacent to the Ce–O bonds are the longest (on the average, they are 0.05 Å longer). Therefore, the coordination of the nitrate groups results in their slight distortion. Interestingly, the nitrate groups lie in three mutually perpendicular planes (the angles between these planes are in average 86°).

As in the majority of the complexes based on the phosphoryl ligand [6] the P–O and Ce–O bonds in the $Ce(NO_3)_3(HL)_3$ complex are not collinear. The CeOP angles range within 155.8(6)–159.9(6)°, which is similar for lanthanide complexes with *N*,*N*′-tetraethyl-*N*″-trichloroacetylphosphoryltriamide.

The average cerium phosphoryl oxygen distance in the complex is 2.402 Å, which falls within the bond length range typical of lanthanide complexes with phosphoryltriamide ligands.

The phosphoryl and carbonyl groups are in the *anti* position to each other (Fig. 4), The same configuration is typical of the free ligand HL [11]. However, a different conformation is observed in the structure of the complex $Ln(NO_3)_3\{C_6H_5C(O)NHP(O)[N(CH_3)_2]_2\}_2$, where the ligand is a coordinated bidentate with C=O and P=O groups in the *sin* position [16].

In as much as the structures of the three phosphoryl ligands are similar, hereafter we will consider the average geometry of the neutral ligands.

The phosphoryl group forms the OPN angles of 112.45(6)°, and 104.1(7)° with the nitrogen atoms of the diethylamino groups and benzamide group, respectively. The small value of the latter angle is probably caused by the occurrence of hydrogen bonding $NH\cdots ONO_2$.

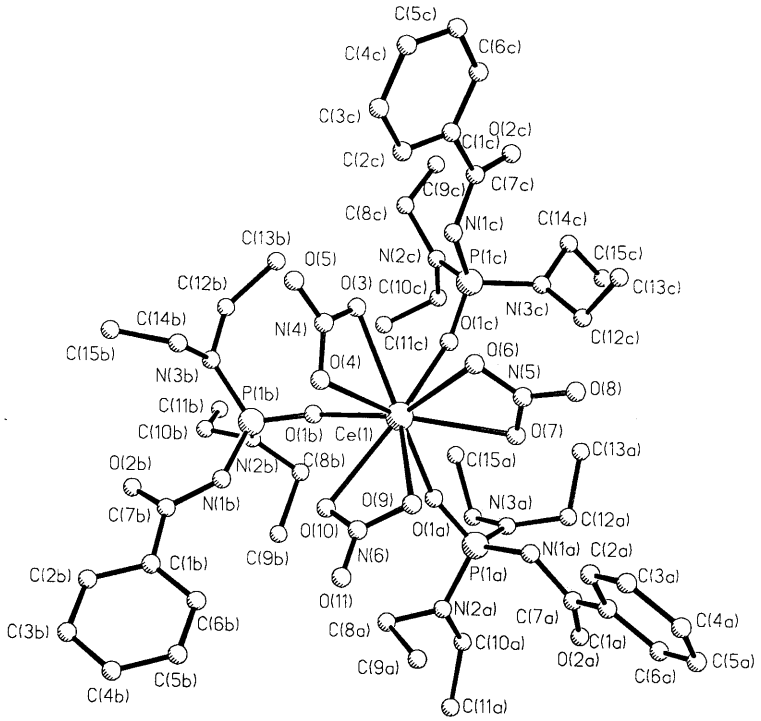


Fig. 4. Molecular structure of the complex $Ce(NO_3)_3\{(C_6H_5C(O)NHP(O)[N(CH_2CH_3)_2]_2\}_3$.

Geometry of hydrogen bond

Donor (D)	Hydrogen atom (H)	Acceptor (A)	*d* (Å)			Angle (°)
			D–H	A–H	D–A	D–H–A
N(1a)	H(1a)	O(7)	0.86	2.044	2.848	155.3
N(1b)	H(1b)	O(10)	0.86	2.09	2.881	1522.8
N(1c)	H(1c)	O(3)	0.86	2.143	2.938	153.5

The sum of the angles about the amide nitrogen atom is close to 360° (sp^2-hybridization), which is caused by delocalization of the lone pair of electrons of the nitrogen. This fact and the decrease in P–N distances in the coordinated ligand compared to the free ligand (1.616 Å in the complex, versus 1.631(2) in the free ligand) can be explain by an increase in the $d_\pi-p_\pi$ conjugation between the phosphorus atom and nitrogen atoms of diethylamide groups upon complex formation.

The carbonyl atom shows sp^2-character.

The angle between the benzene ring plane and the carbamide plane change within 6–23°, showing the presence of π-conjugation between the carbonyl group and the benzene ring. This fact can be confirmed by a decrease in the C–C bond length (1.49 Å) between these groups compared with the bond lengths of other such bonds.

5. Conclusion

The distinctions in the way of coordination by the ligand with dimethylamide substituents (bidentate coordination) from analogous with diethylamide substituents deals with steric factors: more apparent diethylamide substituents near the phosphorus atom lead to monodentate coordination.

6. Supplementary material

Crystallographic data for the structural analysis have been deposited at the Cambridge Crystallographic Data Center, CCDC No. 140547. Copies of this information may be obtained free of charge from The Director, CCDC, 12 Union Road, Cambridge, CB2 1EZ, UK (fax: +44-1223-336033; e-mail: deposit@ccdc.cam.ac.uk or www: http://www.ccdc.cam.ac.uk).

References

[1] V.M. Amirchanov, V.A. Trush, A.A. Kapshuk, V.V. Skopenko, Russ. J. Inorg. Chem. 41 (1996) 1947.
[2] O.N. Rebrova, W.N. Biyushkin, T.I. Malinovskij, Dokl. AN USSR 26 (1982) 1391.
[3] L.J. Caudle, E.N. Duesler, R.T. Paine, Inorg. Chem. 24 (1985) 4441.
[4] V.M. Amirchanov, A.A. Kapshuk, V.A. Ovchinnikov, V.V. Skopenko, Russ. J. Inorg. Chem. 41 (1996) 1405. [5]K.E. Gubina, V.A. Ovchynnikov, V.M. Amirkhanov, H. Fischer, R. Stumpf, V.V. Skopenko, Z. Naturforsch., Teil B 55 (2000) 495.
[6] G.M. Sheldrick, Acta Crystallogr., Sect. A 46 (1990) 467.
[7] G.M. Sheldrick, SHELXS-93: Program for the Refinement of Crystal Structures, University of Göttingen, Göttingen, Germany, 1993.

[8] K.B. Yacimirskiy, N.K. Davidenko, N.A. Kostromina, T.V. Ternovaya, Russ. Theor. Exp. Chem. 1 (1965) 100.
[9] V.M. Amirkhanov, V.A. Trush, Zh. Obshchei Khimii 65 (1995) 1120.
[10] V.A. Trush, K.V. Domasevitch, V.M. Amirkhanov, J. Sieler, Z. Naturforsch., Teil B 54 (1999) 451.
[11] V.M. Amirkhanov, V.A. Ovchynnikov, T. Glowiak, H.Z. Kozlowski, Z. Naturforsch., Teil. B 52 (1997) 1331.
[12] K. Nakamoto, IR and Raman Spectra of Inorganic and Coordination Compounds, 3, Wiley, New York, 1978, p. 283.
[13] V.M. Amirkhanov, V.A. Ovchinnikov, A.V. Turov, V.V. Skopenko, Russ. J. Coord. Chem. 23 (1997) 126.
[14] K.E Gubina, V.M. Amirkhanov, V.A. Ovchynnikov, Dopovidi Akademii Nauk (Ukraine) 7 (2000) 143–148.
[15] W.D. Horrocks, J.P. Sipe, III, D. Sundick, Nuclear Magnetic Resonance Shift Reagents, Academic Press, London, 1973, p. 53.
[16] V.M. Amirchanov, V.A. Ovchynnikov, T. Glowiak, H. Kozlowski, Z. Naturforsch. 52 (1997) 1331.

PERGAMON

www.elsevier.nl/locate/poly

Polyhedron 19 (2000) 2211–2213

POLYHEDRON

X-ray structural determination of a bulky phosphine complex: chloro{tris(2,4,6-trimethoxyphenyl)phosphine}gold(I), {AuCl[P($C_9H_{11}O_3$)$_3$]}

Elmer C. Alyea *, George Ferguson, Shanmugaperumal Kannan

Department of Chemistry and Biochemistry, University of Guelph, Guelph, Ont., Canada N1G 2W 1

Received 15 March 2000; accepted 11 May 2000

Abstract

The title compound, {AuCl[P($C_9H_{11}O_3$)$_3$]}, has three fold symmetry in the solid state. The Au–Cl and Au–P bond lengths are 2.294 and 2.255 Å, respectively, and the Au atom has nearly linear coordination geometry, with P–Au–Cl 176.03(9)°. The extreme bulkiness of the phosphine ligand is shown by the mean cone angle of 188° (based on O atoms defining the cone), though the cone angle is considerably smaller than 214° for trimesitylphosphine in the known analogous complex. The shorter Au–P bond distance than for Ag–P (2.379(1) Å) in the corresponding known silver chloride complex of tris(2,4,6-trimethoxyphenyl)phosphine tentatively supports an earlier conclusion that gold is smaller than silver. © 2000 Elsevier Science B.V. All rights reserved.

Keywords: Bulky phosphine; X-ray structure; Cone angle; Two-coordinate gold complex.

1. Introduction

Our long-standing interest in the steric effects of bulky phosphine ligands [1,2] led us some years ago to determine the crystal structure of chloro(trimesitylphosphine)gold(I) containing the bulkiest known phosphine [3]. Another related bulky phosphine, tris(2,4,6-trimethoxyphenyl)phosphine, has garnered recent attention [4]. Since several crystallographic studies of mono tertiarylphosphine gold(I) chloride complexes have been reported [5–28] we undertook the structural determination of the title compound to provide a relative steric profile of tris(2,4,6-trimethoxyphenyl)phosphine, particularly as compared with other bulky phosphines.

2. Results and discussion

Chloro{tris(2,4,6 - trimethoxyphenyl)phosphine}gold-(I) (**1**) has approximate threefold symmetry in the solid state (Fig. 1). The dihedral angles between the aryl ring planes and the relevant Au–P–Cln1(n = 1, 2, 3) planes are 50.4(3), 56.7(3)and 15.3(3)° for planes C11–C16, C21–C26 and C31–C36, respectively. The three aryl

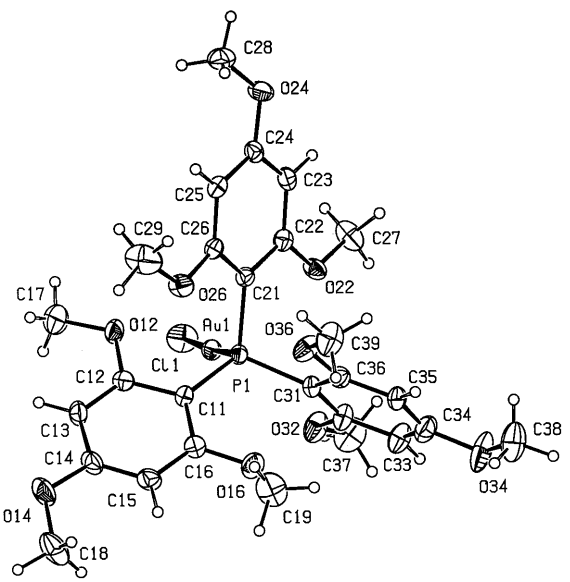


Fig. 1. A view of (**1**) with the atomic numbering scheme; displacement ellipsoids are drawn at the 30% probability level.

* Corresponding author. Tel.: +1-519-824-4120, Ext. 3031; fax: +1-519-766-1499.

E-mail address: alyea@chembio.uoguelph.ca (E.C. Alyea).

0277-5387/00/$ - see front matter © 2000 Elsevier Science B.V. All rights reserved.
PII: S0277-5387(00)00527-1

Table 1
Summary of dimensions (Å, °) for some chloro(monophosphine)gold(I) complexes

Structure	Au–Cl	Au–P	Cl–Au–P	Reference
$[(MeO)_3C_6H_2]_3PAuCl$	2.294(2)	2.255(2)	176.03(9)	this work
$(Mesityl)_3PAuCl$	2.2716(19)	2.2634(15)	178.01(8)	[3]
Ph_3PAuCl	2.279(3)	2.235(3)	179.6(1)	[5]
$(Cyclohexyl)_3PAuCl$	2.279(5)	2.242(4)	177.0(2)	[7]
$(Ethyl)_3PAuCl$	2.305(8)	2.232(9)	178.5(3)	[9]
	2.306(8)	2.231(8)	178.9(3)	
$Ph(Me_2C_4H_2)PAuCl$	2.288(2)	2.227(2)	176.1(1)	[10]
$(o\text{-}Tolyl)_3PAuCl$	2.281(3)	2.243(2)	179.4(1)	[11]
$(m\text{-}Tolyl)_3PAuCl$	2.288(2)	2.235(2)	175.1(1)	[12]
$Ph(cyclohexyl)_2PAuCl$	2.234(3)	2.234(2)	178.3(1)	[13]
$Ph(anthracenyl)_2PAuCl$	2.281	2.249	173.9	[14]
Ph_2(2-trimethylsiloxy)-PAuCl	2.285	2.229	177.3	[16]
Ph_2(trimethylsilymethyl)PAuCl	2.292	2.236	176.9	[20]
$(Me_2N)_3PAuCl$	2.289	2.222	177.9	[25]

rings of the bulky triarylphosphine ligand have very similar geometries. The P atom is displaced 0.18(1), 0.22(1) and 0.09(1) Å from the aromatic plane and the *ortho* methoxy O atoms are displaced in the opposite direction (e.g. O12 −0.04(1), O16 +0.09(1) Å). There are also weak interactions between the Au atom and the three immediately adjacent methoxy oxygens (O32, O12 and O22, Au···O separations 2.922(1), 3.112(1) and 3.122(1) Å. Comparable values for the known analogous Ag complex are: 2.818(3), 3.038(3) and 3.140(3) Å [4]. In the analogous trimesitylphosphine complex the significant Au···H interactions to the *ortho* methyl groups (mean contacts Au···C 3.229 Å and Au···H 2.40 Å) were characterized as 'remote agostic' [29]. Whether the same designation of an attractive interaction is applicable for (**1**) is not as clear from the structural data. All six *ortho* methoxy groups in (**1**) have their methyl groups oriented so that they are remote from the central P atom and are turned away from the Au atom. In the trimesitylphosphine complex the mean P–C*n*1–C*n*6 angle (117.3(6) Å) (where $n = 1$, 2, 3) is 6.7° less than the mean P–C*n*1–C*n*2 angles (124.0(6)°). Comparable angles in the present complex are 118.8(17) and 125.2(17)°, respectively. For the analogous 1:1 silver chloride and bromide complexes studied by Baker et al. [4], these angles follow the same trends. The mean Au–P–C angle and the mean C–P–C angle in (**1**) are 110.5(8) and 108.4(10)°, respectively; comparable values for the corresponding trimesitylphosphine complex are 107.6(2) and 111.2(3)°, attesting to the greater *ortho* interactions due to the larger steric bulk of the $Pmes_3$ ligand (see below). The comparable mean angles in the known silver chloride complex are identical to those found in (**1**) [4].

The Au–Cl bond length (2.294(2) Å) and P–Au–Cl bond angle (176.03(9)°) in (**1**) are comparable with those reported in other structural studies of species containing the R_3P–Au–Cl fragment (R_3P = triaryl- or trialkyl-phosphine). For comparison, relevant Au–Cl and Au–P bond lengths and P–Au–Cl angles for some selected structures of this type, revealed in a search of the Cambridge Structural Database [30], are shown in Table 1. The Au–P bond length of 2.255(2) Å (**1**) is slightly less than the Au–P bond distance in chlorotrimesitylphosphine (2.2634(15) Å), but comparable to those found in Cy_3PAuCl (2.242(4) Å) and $(o\text{-tolyl})_3PAuCl$ (2.243(2) Å). The Ag–P bond distance in previously reported chloro{tris[trimethoxyphenyl)phosphine]}silver(**I**) is 2.379(1) Å and a weak Ag···O interaction of 2.818(3) Å gives rise to a P–Ag–Cl angle of 175.0(1)° [4]. This longer distance for the Ag–P bond compared to the Au–P one in the present complex is in keeping with the recent conclusion that gold is smaller than silver based on a structural comparison of the analogous bis(trimesitylphosphine) cations [31]. However, since our much earlier structural analysis of the $[Ag(Pmes_3)_2]$ cation indicated that significant intramolecular steric distortions occur within that cation [32], the recent conclusion based on comparing the $[M(Pmes_3)_2]$ cations is clearly flawed. Our present comparison of the analogous L–M–Cl complexes provides more valid evidence for the conclusion that gold is indeed smaller than silver. However, the presence of other intramolecular interactions which are still significant in the present complex (such as the Au···O interactions) suggests that caution should still be exercised in making such a conclusion, i.e. a definitive study should involve a smaller phosphine.

In order to quantify the relative bulkiness of the tris(2,4,6-trimethoxyphenyl)phosphine and trimesitylphosphine ligands, we calculated the cone angles of these ligands from the crystallographic data for the two analogous gold complexes. By calculating semi-cone angles ($\theta/2$) using the 'ligand-profile' concept [1] with C–H at 1.08 Å, resultant average cone angles [2] of 188° and 214° were obtained for tris(2,4,6-trimethoxyphenyl)phosphine and trimesitylphosphine, respectively. The smaller estimated steric size of the former ligand is commensurate with the folding back of the methoxy groups and the observed structural data for the title complex.

3. Experimental

3.1. Compound synthesis and NMR spectral data

The compound was synthesized by stirring tris(2,4,6-trimethoxyphenyl)phosphine with (dimethylsulfide)-

gold(I) chloride in dichloromethane at room temperature for about 5 h. The yield of **1** was 90%. The colorless crystals were obtained from chloroform–toluene mixture on slow evaporation. The melting point is 503 K (dec). Spectral data: ^{31}P-NMR ($CDCl_3$): −32.9. ^{1}H-NMR ($CDCl_3$): 3.53 (s, 18H, OCH_3); 3.78 (s, 9H, OCH_3); 6.02 (d, 4 Hz, 6H, phenyl) ppm.

3.2. Crystal data and data collection parameters

$C_{27}H_{33}AuClO_9P$, $M = 764.92$, Tetragonal, $a = 15.3343(9)$, $c = 12.3291(11)$ Å, $U = 2899.1(3)$ Å^3, $T = 294$ K, space group $P4_3$, graphic monochromated Mo Kα radiation, $\lambda = 0.71073$ Å, $Z = 4$, $D_{calc} = 1.753$ Mg m^{-3}, $F(000) = 1512$, colourless crystals with dimensions $0.43 \times 0.25 \times 0.22$ mm, $\mu = 5.275$ mm^{-1}, CAD4 diffractometer, θ range for data collection 2–27°, 3331 unique reflections measured, 2562 with $I > 2\sigma(I)$.

3.3. Structure solution and refinement

The structure was solved by Patterson methods and refined full-matrix least-squares on F_o^2, using the program SHELXL-93 [33]. All data used were corrected for Lorentz-polarization factors, and for absorption (Gaussian integration, NRCVAX [34]). The hydrogen atoms were included in idealized positions as riding atoms. Final R-factors were $R = 0.0291$, $wR = 0.0556$ for observed data and $R = 0.0569$ and $wR = 0.0603$ for all data.

4. Supplementary material

Crystallographic data for the structural analysis have been deposited at the Cambridge Crystallographic Data Centre, CCDC No. 141601 for compound **1**. Copies of this information may be obtained free of charge from The Director, CCDC, 12 Union Road, Cambridge, CB2 1EZ, UK (Fax: +44-1223-336033; e-mail: deposit@ccdc.cam.ac.uk or www: http://www.ccdc.cam.ac.uk).

Acknowledgements

E.C.A. thanks NSERC (Canada) for a research grant.

References

[1] G. Ferguson, P.J. Roberts, E.C. Alyea, M.A. Khan, Inorg. Chem. 17 (1978) 2965.
[2] E.C. Alyea, G. Ferguson, J. Malito, B. Ruhl, Organometallics 8 (1989) 1188.
[3] E.C. Alyea, G. Ferguson, J.F. Gallagher, J. Malito, Acta Crystallogr., Sect. C 49 (1993) 1473.
[4] L.J. Baker, G.A. Bowmaker, D. Camp, Healy P.C. Effendy, H. Schmidbaur, O. Steigelman, A.H. White, Inorg. Chem. 31 (1992) 3656.
[5] N.C. Baenziger, W. Bennett, D.M. Soboroff, Acta Crystallogr., Sect. B 32 (1976) 962.
[6] N. Alcock, P. Mopre, P.A. Lampe, K.F. Mok, J. Chem. Soc., Dalton Trans. (1982) 207.
[7] J.A. Muir, M.M. Muir, L.B. Pulgar, P.G. Jones, G.M. Sheldrick, Acta Crystallogr., Sect. C 41 (1985) 1174.
[8] C.J.L. Lock, M.A. Turner, Acta Crystallogr., Sect. C 43 (1987) 2096.
[9] E.R.T. Tiekink, Acta Crystallogr., Sect. C 45 (1989) 1233.
[10] S. Attar, W.H. Bearden, N.W. Alcock, E.C. Alyea, J.H. Nelson, Inorg. Chem. 29 (1990) 425.
[11] C.S.W. Harker, E.R.T. Tiekink, Acta Crystallogr., Sect. C 46 (1990) 1546.
[12] C.S.W. Harker, E.R.T. Tiekink, Acta Crystallogr., Sect. C 47 (1991) 878.
[13] J.A. Muir, S.I. Cuadrado, M.M. Muir, Acta Crystallogr., Sect. C 47 (1991) 1072.
[14] T.E. Muller, J.C. Green, D.M.P. Mingoes, C.M. McPartlin, C. Wittingham, D.J. Williams, T.M. Woodroffe, J. Organomet. Chem. 551 (1998) 313.
[15] J. Thomaier, S. Boulmaaz, H. Schonberg, H. Ruegger, A. Currao, H. Grutzmacher, H. Hillebrecht, H. Pritzkow, New J. Chem. (Nouv. J. Chim.) (1998) 947.
[16] C. Hollatz, A. Schier, H. Schmidbaur, Z. Naturforsch., Teil B 54 (1999) 30.
[17] B.L. Chen, K.F. Mok, S.C. Ng, J. Chem. Soc., Dalton Trans. (1998) 4035.
[18] M.A. McWhannell, G.M. Rosair, A.J. Welsh, Acta Crystallogr. Sect. C 54 (1998) 13.
[19] J. Zanc, A. Schier, H. Schmidbaur, Z. Naturforsch., Teil B 52 (1997) 1471.
[20] P.G. Jones, A. Laguna, Eur. J. Inorg. Chem. (1998) 989.
[21] C.B. Dieleman, D. Matt, I. Neda, R. Schmutzlur, H. Thonnessen, P.G. Jones, A. Harriman, J. Chem. Soc., Dalton Trans. (1998) 2115.
[22] J.M. Lopez-Luzuriaga, A. Schier, H. Schmidbaur, Chem. Ber. 130 (1997) 221.
[23] D.F. Feng, S.S. Tang, C.W. Liu, I.J.B. Lin, Y.S. Wen, L.K. Liu, Organometallics 16 (1997) 901.
[24] W. Schnider, A. Bauer, A. Schier, H. Schmidbaur, Chem. Ber. 130 (1997) 1423.
[25] A. Bauer, M.W. Mitzel, A. Schier, D.W.H. Rankin, H. Schmidbaur, Chem. Ber. 130 (1997) 323.
[26] F. Cannales, M.C. Gimeno, P.G. Jones, A. Laguna, C. Sarroca, Inorg. Chem. 36 (1997) 5206.
[27] P.G. Jones, E. Bembeneck, Z. Kristallogr. 213 (1998) 611.
[28] P.G. Jones, C. Thone, Acta Crystallogr., Sect. C 53 (1997) 42.
[29] M. Brookhart, M.L.H. Green, L.L. Wong, in: S.J. Lippard (Ed.), Progress in: Inorgorganic Chemistry, vol. 36, Wiley, New York, pp. 1–124.
[30] Cambridge Structural Database System (CSDS), Database 5.18, Cambridge Crystallographic Data Centre, University Chemical Laboratories, Cambridge, UK, 1999.
[31] A. Bayler, A. Schier, G.A. Bowmaker, H. Schmidbaur, J. Am. Chem. Soc. 118 (1996) 7006.
[32] E.C. Alyea, G. Ferguson, A. Somogyvari, Inorg. Chem. 21 (1982) 1369.
[33] G.M. Sheldrick, SHELXS 93: Program for crystal structure refinement, University of Göttingen, Germany, 1997.
[34] E.J. Gabe, Y.L. Page, J.P. Charland, F.L. Lee, P.S. White, J. Appl. Cryst. 22 (1997) 384.

PERGAMON

www.elsevier.nl/locate/poly

Polyhedron 19 (2000) 2215–2223

POLYHEDRON

Dinuclear copper(II) complexes incorporating a novel pyrazolo-based ligand with S- and N-rich coordination spheres

Jeh-Li Chou [a,*], Jong-Pyng Chyn [a], F.L. Urbach [b], D.F. Gervasio [b]

[a] *Department of Chemistry, Chinese Military Academy, PO Box 90602-6, Fengshan 830, Taiwan, ROC*
[b] *Department of Chemistry, Case Western Reserve University, Cleveland, OH 4416-7078, USA*

Received 22 May 2000; accepted 7 August 2000

Abstract

The new binucleating ligand 3,5-bis(1′-(4′-(2″-pyridyl)-2′-thiabutyl))pyrazole (BLEPH) forms dinuclear Cu^{II} complexes which are able to bind one additional exogenous bridging molecule such as N_3^-, Cl^-, Br^- and OH^-. Three of these complexes $[Cu_2(BLEP)(\mu\text{-}N_3)(N_3)_2]$ (**1**); $[Cu_2(BLEP)(\mu\text{-}Cl)(Cl)(H_2O)]Cl$ (**2**); and $[Cu_2(BLEP)(\mu\text{-}Br)(Br)(H_2O)]Br$ (**3**) were characterized by X-ray single crystal structure analysis. The two copper centers are bridged by the central pyrazolyl group of the BLEP and one azide (in **1**), one chloro (in **2**) or bromo (in **3**) and the side arm of BLEP coordinates to each of the coppers with one pyridyl N and one thia S. Electrochemical studies of these complexes reveal that the redox waves are -247 and 15 mV for **2**; -215 and 37 mV for **3** corresponding to the $Cu^{II}Cu^{II}/Cu^{I}Cu^{II}$ and $Cu^{I}Cu^{II}/Cu^{I}Cu^{I}$ couples, and -291 mV for **1** corresponding to the $Cu^{II}Cu^{II}/Cu^{I}Cu^{I}$ process, respectively. The intramolecular magnetic exchange coupling ($J = -46.6\ cm^{-1}$) in the bromo-bridged complex shows weaker antiferromagnetic interaction than the N_3-bridged complex. The exchange coupling process through μ_2-N_3 ligand enhances the net antiferromagnetic interaction. Electronic spectra covering the 12 500–50 000 cm^{-1} region are also reported for these complexes. © 2000 Elsevier Science B.V. All rights reserved.

Keywords: Dinuclear; Antiferromagnetic interactions; Pyrazolyl groups

1. Introduction

Stimulated by the occurrence of N/S coordinated copper ions in a variety of proteins [1], numerous ligands with N and S donor atoms have been synthesized and investigated in order to model the properties of these metallobio-sites [2–4]. Biological systems like the mononuclear 'blue' type-1 copper sites and the dinuclear Cu_A center in cytochrome *c* oxidase and catalysis of catechol autoxidation are involved in electron transfer processes during enzyme turnover [1,5]. Much effort has been devoted to the study of dinuclear copper model complexes with bridging thiolates and terminal N donor atoms [6,7]. With regard to a general study of the properties of dimeric copper units in a mixed N/S environment it is of interest to also investigate inverse systems, i.e. those incorporating bridging nitrogen moieties and terminal thioether coordination. The ability of the diazole unit of pyrazolates to bridge two metal centers is well documented [8]. However, relatively few studies of pyrazolate-based ligands bearing additional side arms in the 3- and 5-positions of the heterocycle have been reported, and most of these systems possess N-donors in the substituents [9–13]. On the other hand, various mononuclear complexes of chelating ligands containing both azole and thioether moieties have been designed as model complexes for type 1 copper proteins [3,4a,14]. In the present study dinuclear copper complexes of mixed N/S donor systems based on bridging diazole heterocycles are investigated.

Binuclear copper azide systems have been of considerable interest due to the broad range of their structural and magnetic properties. In particular, azide can act as a bridging ligand in an end-on (μ-1,1) and end-to-end (*cis* μ-1,3) fashion. It is now well established that μ-1,1 bridging gives ferro- and μ-1,3 bridging antiferromagnetic coupling between the copper centers. Moreover,

* Corresponding author. Tel.: +886-7-742-9442; fax: +886-7-715-1510.
E-mail address: horng@ms31.url.com.tw (J.-L. Chou).

0277-5387/00/$ - see front matter © 2000 Elsevier Science B.V. All rights reserved.
PII: S0277-5387(00)00529-5

binuclear copper azide systems have been studied as structural models for copper-containing enzymes involved in the reversible binding and activation of dioxygen like hemocyanin (Hc) [15]. However, the vast majority of studies have focused on binuclear copper(II) azide complexes [16].

In recent work we described the synthesis of mononuclear or dinuclear complexes derived from a series of alkoxo or pyrazolate-based ligand with pendant 2-(2′-mercaptoethyl)pyridine side arms [17] and demonstrated the possibility to tune the range of accessible metal–metal separations in these systems selectively by variation of the bridging function group.

In this paper we report a new synthetic strategy to generate a new dinucleating pyrazolate-based ligand providing both S- and N-rich coordination spheres for two metal centers. Four binuclear Cu(II) complexes $[Cu_2(BLEP)(\mu\text{-}N_3)(N_3)_2]$ (**1**), $[Cu_2(BLEP)(\mu\text{-}Cl)(Cl)(H_2O)]Cl$ (**2**), $[Cu_2(BLEP)(\mu\text{-}Br)(Br)(H_2O)]Br$ (**3**) and $Cu_2(BLEP)(\mu\text{-}OH)(ClO_4)_2\cdot H_2O$ (**4**) where BLEP is deprotonated 3,5-bis(1′-(4′-(2′-pyridyl)-2′-thiabutyl)) pyrazole are prepared and structurally characterized in order to probe the coordination potential of the new ligand system. X-ray structure investigation revealed that the two copper centers are bridged by the central pyrazolyl group of the BLEP and one azide (in **1**), chloro (in **2**) or bromo ligand (in **3**), and the side arm of BLEP coordinates to each of the coppers with one pyridyl N and one thia S.

2. Experimental

2.1. Ligand synthesis

2.1.1. Methyl pyrazole-3,5-dicarboxylate

Pyrazole-3,5-dicarboxylic acid (5.04 g, 0.029 mol) and sulfuric acid (5 ml) were mixed in 250 ml methanol and refluxed for 6 h. The solution was concentrated to about 60 ml by rotary evaporation, followed by saturated sodium carbonate to bring the pH to 8. After standing at 0°C overnight, white needle crystals were obtained in about 86% yield.

2.1.2. 3,5-Bis(hydroxymethyl)pyrazole

A suspension of $LiAlH_4$ (6 g, 0.158 mol) in 400 ml dry ether under N_2 was prepared. Finely ground methyl pyrazole-3,5-dicarboxylate (3.78 g, 0.021 mol) was placed in a paper thimble of a Soxhlet apparatus that was then fitted to the flask. The ether was refluxed for 24 h with a recycle time of 10–15 min. Then, 60 ml H_2O was added dropwise to the cooled suspension over 45 min. The ether was removed under reduced pressure, and the resulting white cake was suspended in 200 ml methanol, treated with CO_2(g) for 10 min, and then refluxed for 6 h. The solid was filtered, and the filtrate was evaporated to give an oily residue (5 ml). Water in this residue was removed azeotropically with ethanol. The residue was redissolved in ethanol and filtered, and the filtrate was evaporated. The product (as the hydrochloride salt) was obtained as white needles by dissolution of this residue in 20 ml ethanolic HCl by the addition of ether; 2.36 g (70%).

2.1.3. 3,5-Bis(chloromethyl)pyrazole hydrochloride

3,5-Bis(hydroxymethyl)pyrazole (2.36 g, 0.0143 mol) in neat $SOCl_2$ (50 ml, distilled from $P(OPh)_3$) was placed in a preheated 95°C oil bath and was refluxed for 0.5 h. The excess $SOCl_2$ was removed by distillation under reduced pressure. The residue was dissolved in 75 ml ethanol and filtered, and ether was added to produce white plates, 2.67 g (92%).

2.1.4. 2-(2′-Mercaptoethyl)pyridine [21]

This compound was synthesized by a literature method.

2.1.5. 3,5-Bis(1′-(4′-(2′-pyridyl)-2′-thiabutyl))pyrazole (BLEPH)

2-(2′-Mercaptoethyl)pyridine (2.78 g, 0.02 mol) was dissolved in 50 ml absolute ethanol and deprotonated by means of one equivalent of sodium metal (0.69 g, 0.03 mol) at 0°C. 3,5-Bis(chloromethyl)pyrazole hydrochloride (2.00 g, 0.01 mol) was then added in one portion and the resulting solution was kept stirring overnight at room temperature. The solution was kept at 0°C and filtered. The filtrate was evaporated to give a white orange oily product in about 80% yield.

2.2. Metal complexes

2.2.1. $[Cu_2(BLEP)(\mu\text{-}N_3)(N_3)_2]\cdot C_3H_7OH$ (1)

Reaction of a 1:2:3 molar ratio of 3,5-bis(1′-(4′-(2″-pyridyl)-2′-thiabutyl))pyrazole, $Cu(NO_3)_2\cdot 3H_2O$ and NaN_3 in absolute ethanol for 30 min afforded dark brown microcrystals of $[Cu_2(BLEP)(\mu\text{-}N_3)(N_3)_2]$ (82%). *Anal.* Calc. for $Cu_2C_{22}S_2N_{13}H_{29}O$: C, 38.70; H, 4.28; N, 26.67. Found: C, 38.47; H, 4.02; N, 26.78%. The crystals suitable for X-ray single-crystal structure analysis were obtained by evaporation from dichrolomethane–isopropyl alcohol (4/1) mix-solvent.

2.2.2. $[Cu_2(BLEP)(\mu\text{-}Cl)(Cl)(H_2O)]Cl\cdot 2H_2O$ (2)

A solution of sodium metal (0.023 g, 1.0 mmol) and a solution of $CuCl_2\cdot 2H_2O$ (0.341 g, 2.0 mmol) in ethanol (30 ml) were added stepwise to a solution of BLEPH (0.37 g, 1.0 mmol) in CH_3CN (40 ml). Add 30 ml methanol into the deep green solution which was filtrated from the crude mixture, and it was evaporated to dryness. The resulting green powder (80%) was washed several times with small portions of ethanol. *Anal.* Calc. for $Cu_2C_{19}S_2N_4H_{27}Cl_3O_3$: C, 34.73; H, 4.14;

N, 8.53. Found: C, 34.56; H, 4.07; N, 8.47%. The crystals suitable for X-ray single-crystal structure analysis were obtained by diffusion of ether into a dichloromethane solution.

2.2.3. $[Cu_2(BLEP)(\mu\text{-}Br)(Br)(H_2O)]Br\cdot 2H_2O$ (3)

A solution of sodium metal (0.023 g, 1.0 mmol) and a solution of $CuBr_2$ (0.447 g, 2.0 mmol) in ethanol (30 ml) were added stepwise to a solution of BLEPH (0.37 g, 1.0 mmol) in absolute methanol (40 ml). The green reaction mixture was evaporated to dryness, and the resulting green powder (86%) was washed several times with small portions of ethanol. *Anal.* Calc. for $Cu_2C_{19}S_2N_4H_{27}O_3Br_3$: C, 28.87; H, 3.44; N, 7.09. Found: C, 28.62; H, 3.47; N, 6.98%. The crystals suitable for X-ray single-crystal structure analysis were obtained by diffusion of ether into a dichloromethane solution of the product.

2.2.4. $Cu_2(BLEP)(\mu\text{-}OH)(ClO_4)_2\cdot H_2O$ (4)

A solution of sodium metal (0.089 g, 3.9 mmol) and a solution of $Cu(ClO_4)_2\cdot 6H_2O$ (1.44 g, 3.9 mmol) in methanol (30 ml) were added stepwise to a solution of BLEPH (0.72 g, 1.9 mmol) in absolute methanol (40 ml). The solution filtrated from the green crude mixture was evaporated to dryness, and the resulting green powder (82%) was washed several times with small portions of methanol. *Anal.* Calc. for $Cu_2C_{19}S_2N_4H_{24}O_{10}Cl_2$: C, 31.24; H, 3.31; N, 7.67. Found: C, 31.48; H, 3.39; N, 7.70%.

2.3. Physical measurements

Elemental analyses (C, H, N) were performed at National Cheng Kung University on a Heraeus CHN-O-Rapid Analyzer. The ^1H NMR spectrum was recorded on a Varian EM390 spectrometer at National Sun Yat-sen University. Electronic absorption spectra in the visible and ultraviolet regions were recorded on Shimazu UV-210 spectrophotometer. Cyclic voltammetry was measured by using a Bioanalytical Systems instrument (model BAS-100A). The platinum-disk working electrode (1.5-mm diameter) was polished with 1-μm aluminum oxide powder prior to each series of scans. A silver wire in 0.01 M $AgNO_3$ ($Ag/AgNO_3$) served as a reference electrode and was separated from the working electrode. A platinum wire was used as an auxiliary electrode, and all scans were recorded in deoxygenated DMSO solution with N_2 blowing over the top during the scan. Tetraethylammonium perchlorate (0.1 M NEt_4ClO_4; TEAP) was used as the supporting electrolyte. The choice of solvent was based on the solubility and coordination effect of the complexes. Scan rate ranging from 50 to 200 mV s^{-1} were used. The potentials reported for the redox couples were obtained by averaging the anodic and cathodic peak potentials which were referenced to the $Ag/AgNO_3$ electrode and uncorrected for junction potential.

2.4. X-ray crystallography

The crystal data were collected on a R3M/E four-circle diffractiometer with a graphite monochromator using a Mo Kα radiation ($\lambda = 0.71073$). Intensities were measured by a θ–2θ mode. Details of crystal parameters, data collection and structure refinement are summarized in Table 1. The structure was solved by the direct method. Hydrogen atoms were not found. The final refinement (based on F) was by full-matrix least-squares. The highest peak on the final Fourier-difference map had the value of 1.15 (**1**), 0.57 (**2**) and 0.47 (**3**) e A^{-3}. All calculations were performed with the NRC-VAX package [19].

3. Results and discussion

The new binucleating ligand (BLEPH) was synthesized by the methods outlined in Scheme 1. The diol that is produced from the reduction is tenaciously bound to the aluminum and required extraction with carbonated methanol to remove it from the alumina cake. The hydrochloride salt is then readily obtained. We found that the BLEPH ligand is most efficiently produced by the reaction of equivalent amounts of $NaSCH_2CH_2Py$ and 3,5-bis(chloromethyl) pyrazole.

3.1. Synthesis and structural characterization of $[Cu_2(BLEP)(\mu\text{-}N_3)(N_3)_2]\cdot C_3H_7OH$ (1)

The dark brown complex **1** is produced when the ligand BLEPH is first deprotonated by means of sodium metal and subsequently treated with 2 equivalents of $Cu(NO_3)_2\cdot 3H_2O$ and 3 equiv. of NaN_3. Complex **1** shows good solubility in CH_2Cl_2 and proved to be stable in air over prolonged periods.

The structure of complex **1** is shown in Fig. 1. Selected bond lengths and angles are given in Table 2. Both copper ions are pentacoordinate involving a tridentate binucleating ligand, a bridging azide and a terminal azide ligand, resulting in a distorted square planar N_4S coordination sphere, better described as a distored square pyramid with the pyridyl group in the axial position, rather than as a trigonal bipyramid. The azido ligand is linked to both copper centers in an end-on (μ-1,1) fashion, with a Cu···Cu separation of 3.486(2) Å and a Cu–N5–Cu bridge angle of 116.8°, which lies almost at the longest limit of the range reported for μ-1,2-diazine(pyridazine, phthalazine, thiadiazole) [15–18] end-on (μ-1,1) azido dicopper(II) complexes. The end-on azido bridge is roughly symmetrically disposed with respect to the dinuclear

center, with a slightly different copper–nitrogen distances of 2.037(4) and 2.056(4) Å, and the same Cu–N5–N6 angles of 119°. This may be compared with the analogous complex [23] μ-1-3-azido{μ-{1,1′-[(1*H*-pyrazol-1-ido-3,5-diyl)bis[1,4,7-triazacyclo-nonane]]} dicopper(II), another pyrazolate- based ligand with two pendant 1,4,7-triazacyclononane side arms, in which the azide bound to dicopper in a μ-1,3 bridging form and the Cu···Cu distance is 4.15 Å. The Cu–S distance (2.439(2) and 2.444(2) Å) lie within the normal range usually expected for a Cu^{II} thioether bond [4,16]. The Cu···Cu distance is found to be 3.486(2) Å.

3.2. Synthesis and structural characterization of $[Cu_2(BLEP)(\mu\text{-}Cl)(Cl)(H_2O)]Cl\cdot 2H_2O$ (2)

Treatment of the deprotonated potential ligand with 2 equiv. of $CuCl_2\cdot 2H_2O$ affords the green ionic complex $[Cu_2(BLEP)(\mu\text{-}Cl)(Cl)(H_2O)]Cl\cdot 2H_2O$ (**2**), which crystallizes upon vapor diffusion of ether into a CH_2Cl_2 solution of the product. A view of the molecular structure of **2** is depicted in Fig. 2; selected distances and angles are listed in Table 3. This structure is analogous to the square pyramidal coordination found in the solid state [18] for $[Cu_2(BLEP)(\mu\text{-}Cl)(Cl)(H_2O)]Cl$ in which the two coppers are bridged in the equatorial plane by a chloride ion and apical coordination to the two coppers is provided by another chloride ion and a water molecule. The Cu–Cu distance in $[Cu_2(BLEP)(\mu\text{-}Cl)(Cl)(H_2O)]Cl$ is 3.6356(8) Å. The two square pyramidal copper ions have their apical sites located on the same side of the complex. This cofacial arrangement is ideal for apical interaction of the catechol substrate with the two copper ions in the manner suggested by Nishida and co-workers [20]. In contrast to the type of catecholate coordination found by Karlin et al. [21], a phenolate–bridged dicopper(II) complex would appear to be highly strained for **2**. In Karlin's structure the two oxygens of tetrachloro-catecholate span basal positions of the two square pyramidal copper ions [6].

3.3. Synthesis and structural characterization of $[Cu_2(BLEP)(\mu\text{-}Br)(Br)(H_2O)]Br\cdot 2H_2O$ (3)

Treatment of the deprotonated potential ligand with 2 equiv. of $CuBr_2$ affords the green ionic complex $[Cu_2(BLEP)(\mu\text{-}Br)(Br)(H_2O)]Br\cdot 2H_2O$ (**3**), which is isomorphous with **2**. Selected distances and angles are listed in Table 3. This structure is analogous to the square pyramidal coordination found in **2**, in which the two coppers are bridged in the equatorial plane by a bromide ion and apical coordination to the two coppers is provided by another bromide ion and a water molecule. The Cu–Cu distance in **3** is 3.706(2) Å that is observably longer than that in **1** (3.486(2) Å), and is slightly longer than that in **2** (3.6356(8) Å) due to the increased size of the exogenous bridging atom.

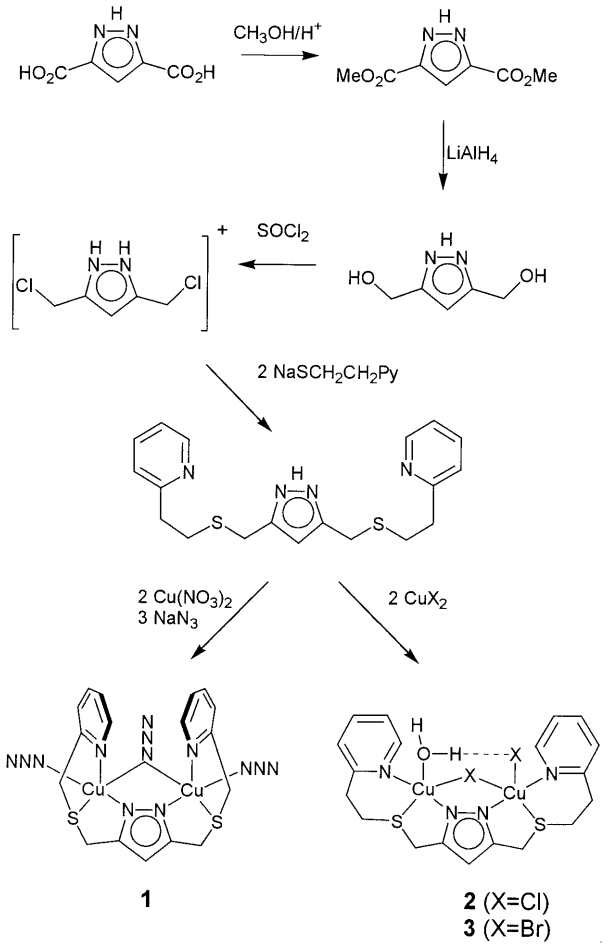
3.4. Electrochemistry

Table 4 gives the electrochemical data obtained at a platinum electrode for 5 mmol solution of complexes in

Table 1
Crystallographic data for complexes **1**, **2** and **3**

	1	**2**	**3**
Empirical formula	$Cu_2C_{22}H_{21}N_{13}S_2O_1$	$Cu_2C_{19}S_2N_4H_{27}Cl_3O_3$	$Cu_2C_{19}S_2N_4H_{27}Br_3O_3$
Formula weight	674.70	657.01	790.36
Crystal system	triclinic	triclinic	triclinic
Space group	$P\bar{1}$	$P\bar{1}$	$P\bar{1}$
Unit cell dimensions			
a(Å)	9.576(3)	8.204(1)	8.325(3)
b(Å)	13.194(3)	12.805(3)	12.972(4)
c(Å)	13.313(4)	13.649(2)	13.856(4)
α(°)	63.89(2)	100.54(2)	100.79(3)
β(°)	74.65(3)	107.07(1)	106.24(3)
γ(°)	87.85(2)	105.14(1)	105.60(3)
V (Å^3)	1450.5(7)	1269.7(4)	1326.8(7)
D_{calc} (g cm^{-3})	1.545	1.719	1.978
Z	2	2	2
F(000)	685.81	620.56	776.04
h,k,l ranges	−11–11, 0–15, −13–15	−9–9, 0–15, −16–15	−8–8, 0–13, −14–14
2θ Range	2–50	2–50	2–45
Reflections collections	5100	4803	3469
Reflections Refinement [$I>2\sigma(I)$]	4124	3871	2501
R_f [a]	0.043	0.033	0.029
R_w	0.049	0.033	0.027

[a] $R_f = \Sigma||F_o|-|F_c||/\Sigma|F_o|$.



Scheme 1. Synthesis of the ligand and complexes.

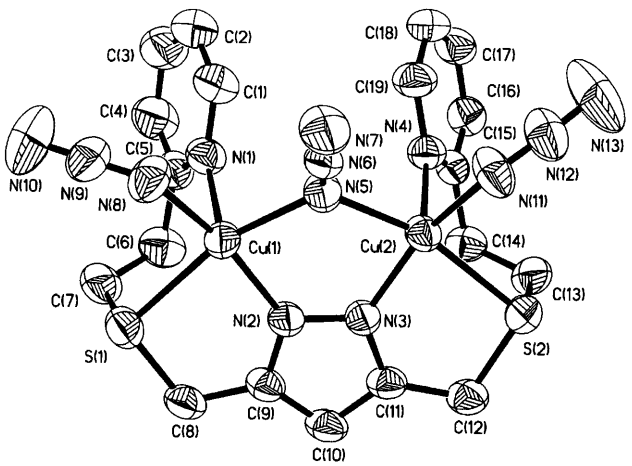


Fig. 1. The ORTEP drawing of complex **1** (50% thermal ellipsoids) with atomic numbering.

the potential range -0.8 to 0.5 V versus the Ag/$AgNO_3$ electrode in DMSO at sweep rates of 50 mV s^{-1}. Two main behaviors can be distinguished in Fig. 3. First, complex **1** exhibits a single two-electron transfer redox wave at -0.291 V with cyclic voltammetric peak separations of 206 mV. Second, complexes **2** and **3** show quasi-reversible redox processes and corresponding to successive one-electron-transfer steps observed for each complex. The redox waves are -0.247 and 0.015 V for **2** and at -0.215 and 0.037 V for **3**, correspond to the $Cu^{II}Cu^{II}/Cu^{I}Cu^{II}$ and $Cu^{I}Cu^{II}/Cu^{I}Cu^{I}$ couples, respectively. The peak potentials and half-wave potential of quasi-reversible process of complex **1** are listed in Table 4 and cyclic voltammogram is shown in Fig. 3. Reductive cyclic voltammograms of this complex show a quasi-reversible two-electron redox wave, and we attribute this to the reduction of $Cu^{II}Cu^{II}/Cu^{I}Cu^{I}$. Because the ability of σ-donation of the azide is much stronger than that of the halides, the values of reduction potentials of E_{pc}(**1**) is more negative than E_{pc}(**2**) and E_{pc}(**3**). Since the σ-donation effect will raise the energy level of the LUMO of these complexes, the half-wave potentials of reductive waves decreases with the increasing σ-donor strength of the azide complex [24,25]. These results also agree with the spectrochemical series $N_3^- > Cl^- > Br^-$ [26,27]. The difference between the two redox potentials of these complexes are about 250 mV, and the phenomenon is due to the

Table 2
Selected atom distances (Å) and angles (°) for complex **1**

Cu(1)–Cu(2)	3.486(2)	Cu(1)–S(1)	2.444(2)
Cu(1)–N(2)	1.924(4)	Cu(1)–N(5)	2.037(4)
Cu(1)–N(8)	1.951(4)	Cu(2)–S(2)	2.439(2)
Cu(2)–N(3)	1.917(4)	Cu(2)–N(5)	2.056(4)
Cu(2)–N(11)	1.944(4)		
S(1)–Cu(1)–N(2)	81.2(1)	S(1)–Cu(1)–N(5)	164.5(1)
S(1)–Cu(1)–N(8)	94.3(2)	N(2)–Cu(1)–N(5)	86.8(2)
N(2)–Cu(1)–N(8)	162.4(2)	N(5)–Cu(1)–N(8)	94.2(2)
S(2)–Cu(2)–N(3)	81.7(1)	S(2)–Cu(2)–N(5)	164.1(1)
S(2)–Cu(2)–N(11)	94.6(2)	N(3)–Cu(2)–N(5)	86.3(2)
N(3)–Cu(2)–N(11)	157.4(2)	N(5)–Cu(2)–N(11)	92.6(2)

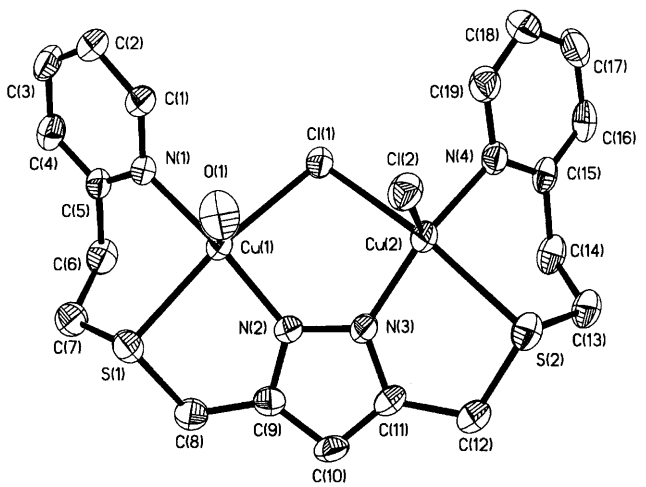


Fig. 2. The ORTEP drawing of complex **2** (50% thermal ellipsoids) with atomic numbering.

Table 3
Selected atom distances (Å) and angles (°) for isomorphous complexes **2** and **3**

	2 (X = Cl)	**3** (X = Br)		**2** (X = Cl)	**3** (X = Br)
Cu(1)–Cu(2)	3.6356(8)	3.706(2)	Cu(1)–S(1)	2.369(1)	2.361(2)
Cu(1)–N(1)	1.964(3)	1.962(4)	Cu(1)–N(2)	1.911(3)	1.923(4)
Cu(1)–O(1)	2.197(3)	2.181(4)	Cu(1)–X(1)	2.363(1)	2.484(2)
Cu(2)–S(2)	2.398(1)	2.394(2)	Cu(2)–N(3)	1.919(3)	1.914(5)
Cu(2)–N(4)	1.972(3)	1.974(5)	Cu(2)–X (1)	2.428(1)	2.541(1)
Cu(2)–X(2)	2.480(1)	2.628(1)			
X(1)–Cu(1)–S(1)	168.46(4)	167.13(6)	X (1)–Cu(1)–N(1)	93.92(9)	92.8(2)
X(1)–Cu(1)–N(2)	88.90(9)	89.3(2)	X(1)–Cu(1)–O(1)	90.93(8)	93.5(1)
S(1)–Cu(1)–N(1)	92.21(9)	92.0(2)	S(1)–Cu(1)–N(2)	82.6(1)	83.1(2)
S(1)–Cu(1)–O(1)	98.17(8)	98.0(1)	N(1)–Cu(1)–N(2)	164.1(1)	164.7(2)
N(1)–Cu(1)–O(1)	95.8(1)	94.9(2)	N(2)–Cu(1)–O(1)	99.8(1)	100.1(2)
X(1)–Cu(2)–X(2)	93.94(4)	94.96(5)	X(1)–Cu(2)–S(2)	167.69(4)	167.84(5)
X(1)–Cu(2)–N(3)	89.09(9)	89.6(1)	X(1)–Cu(2)–N(4)	90.70(9)	89.9(1)
X(2)–Cu(2)–S(2)	96.96(4)	96.38(6)	X (2)–Cu(2)–N(3)	104.9(1)	104.8(2)
X(2)–Cu(2)–N(4)	101.5(1)	100.9(1)	S(2)–Cu(2)–N(3)	82.61(9)	83.3(1)
S(2)–Cu(2)–N(4)	92.70(9)	92.3(2)	N(3)–Cu(2)–N(4)	153.6(1)	154.2(2)

Table 4
Electrochemical data for 0.005 M solutions of the complexes in DMSO (potentials in V vs. $Ag/AgNO_3$)

Compound	E_{Pc}		E_{Pa}		$E_{1/2}$		ΔE (mV)	
1	−0.394		−0.188		−0.291		206	
2	−0.291	−0.058	−0.203	0.087	−0.247	0.015	88	145
3	−0.248	−0.015	−0.182	0.088	−0.215	0.037	66	103

interaction between two copper centers through the bridging ligand and the asymmetric coordination environments of two copper centers in complexes **2** and **3**.

3.5. Electronic spectroscopy

Electronic absorption spectra in the UV–Vis region of these complexes were recorded in methanol solution and collected in Table 5. An analysis of LMCT spectra must necessarily consider the electronic structure of the free ligands and the perturbation, if any, in their absorption spectra by a spectroscopically inactive dipositive ion such as Zn(II), and Mg(II). The absorption bands below 300 nm are due to absorption of the free ligand, and the extinction coefficient corresponds to typical π to π* transition. These four complexes have similar electronic absorption and exhibit two main features (Fig. 4), one band at 320–356 nm, the other band at lower energy ca. 420 nm. In addition to these two bands, the spectrum of azide shows a medium intensity absorption ($\varepsilon = 2500$ dm^3 mol^{-1} cm^{-1}) at 495 nm, which can be assigned to be the LMCT band of N_3^- to Cu charge transfer.

3.6. Magnetic properties

Variable-temperature DC magnetic susceptibility data were collected for complex **1** and **3** at an applied field of 10.0 kG. Magnetic data μ_{eff} versus T plots of complexes **1** and **3** were displayed in Figs. 5 and 6, respectively. Fig. 5 shows plots of the effective magnetic moment (μ_{eff}) per Cu_2 versus temperature for several

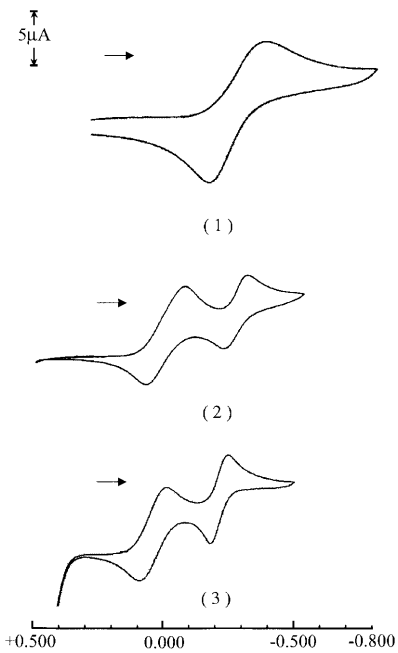


Fig. 3. Cyclic voltammograms of complexes **1**, **2**, and **3** in DMSO solvent with the TEAP as the supporting electrolyte.

Table 5
Quantitative spectral and data of complexes **1**, **2**, **3** and **4**.

Complex	λ_{max} (nm)	Extinction coefficient (M^{-1} cm^{-1})
1	204	18653
	223	13170
	255	8325
	345	4287
	420	3658
	495	18653
2	209	13852
	227	15852
	259	13573
	355	5693
	417	13852
3	208	19178
	227	21220
	253	15216
	327	6004
	356	6247
	417	19178
4	209	16325
	226	15989
	255	9750
	321	3823
	409	3138

different samples of complex **1**. As can be seen in Fig. 5, the values of μ_{eff}/Cu_2 for several different samples of complex **1** are consistent around 1.82 μ_B at 300 K. As the temperature is decreased, the values of μ_{eff}/Cu_2 decrease and reach around 0.2 μ_B at 5.0 K. If there were no exchange interaction between the metal ions in a Cu_2^{II} complex, the spin-only effective magnetic moment would be 2.45 μ_B and it would be independent of temperature. Clearly, there is appreciable antiferromagnetic exchange interaction between the two copper ions in complex **1**. However, the antiferromagnetic property is different from other ferromagnetic μ-1,1 azido dicopper complexes, we think it maybe caused by the coordinated S atoms of ligand. The curve for each sample is slightly different from each other, it indicates there is different intermolecular and/or intramolecular magnetic interactions.

In Fig. 6, the effective magnetic moment (μ_{eff}) per Cu_2 is 2.33 μ_B at 319.5 K. As the temperature is decreased, the value of μ_{eff}/Cu_2 also decreases and reaches 0.35 μ_B at 2.0 K. The value of effective moment at 319.5 K is 2.33 μ_B, slightly lower than the spin only value (2.45 μ_B), indicative of the presence weak to moderate antiferromagnetic exchange interaction between the two copper ions in complex **3**.

In order to assess the nature of exchange interaction in complexes **1** and **3**, the theoretical expression for the magnetic susceptibility per molecule is given by Eq. (1) [22],

$$\chi_m = \frac{N\mu_B^2 g^2}{3k(T-\theta)}\left[1+\left(\frac{1}{3}\right)\exp(-2J/kT)\right]^{-1}(1-\rho) + \frac{\rho N\mu_B^2 g^2}{4kT} + N\alpha \quad (1)$$

where θ is the Weiss constant which correlates to the intermolecular interaction, $N\alpha$ is temperature-independent susceptibility, ρ represents the fraction of possible magnetically impurity, and N, μ_B, and k have their usual meanings. The data for complexes **1** and **3** were fitted to Eq. (1) with g, J, ρ and θ as variables. The

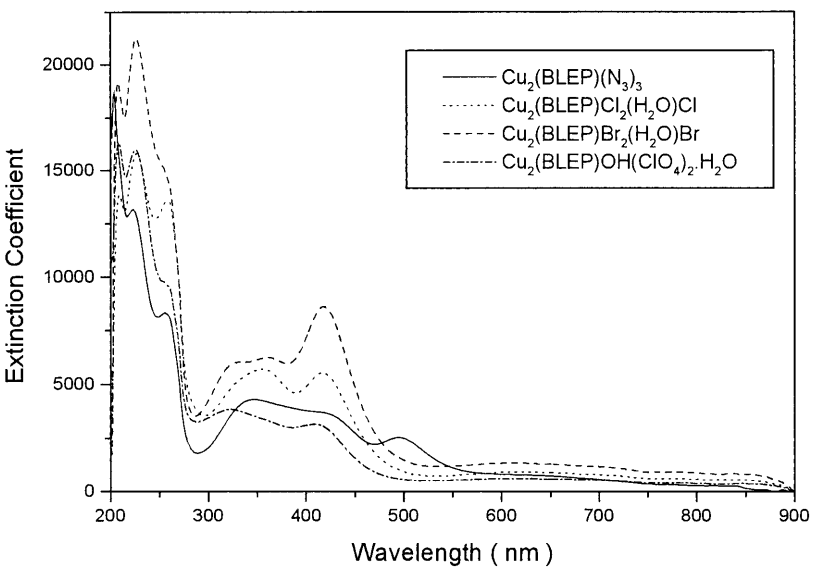


Fig. 4. Electronic absorption spectra of complexes **1**, **2**, **3** and **4** in methanol.

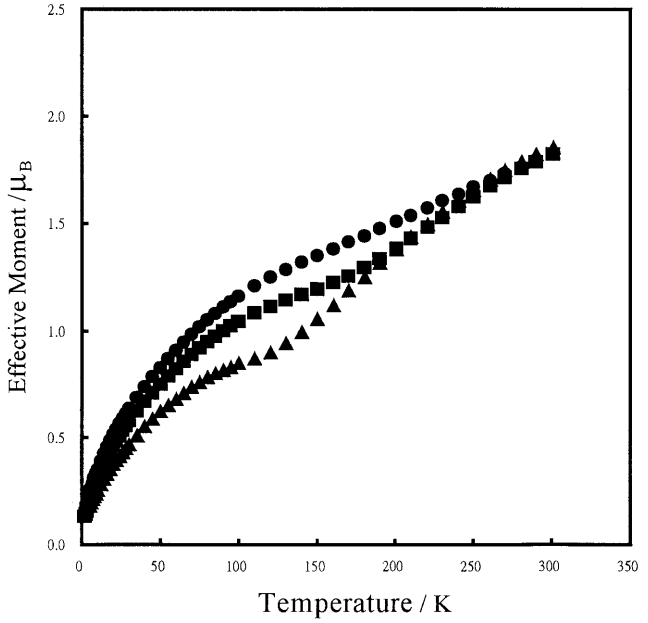


Fig. 5. The experimental data curves of magnetic moments of complex **1**.

agree factor R is defined as $(\Sigma[(\chi_m)^{obs} - (\chi_m)^{calc}]^2/\Sigma[(\chi_m)^{obs}]^2)^{1/2}$. The best fit line for complex **3** (solid line) gives $g = 1.96$, $J = -46.6$ cm^{-1}, $N\alpha = 179 \times 10^{-6}$ emu mol^{-1}, $\theta = -2.2$ K, and $\rho = 0.016$. The agreement of factor ($10^2R = 6.5$) is small, giving a good data fit. The sharp increase in susceptibility at low temperatures is associated with a small amount of paramagnetic impurity ($\rho = 0.016$). The small value of the Weiss constant ($\theta = -2.2$ K) indicates a weak antiferromagnetic intermolecular interaction, which probably results from hydrogen-bonding interaction. The intramolecular magnetic exchange coupling ($J = -46.6$ cm^{-1}) is a weaker antiferromagnetic interaction than that of $[Cu_2(PAP6Me)(\mu_2\text{-}N_3)(\mu_2\text{-}Br)Br_2]$ ($J = -162$ cm^{-1}) [16]. The exchange coupling process through μ_2-N_3 ligand enhances the net antiferromagnetic interaction.

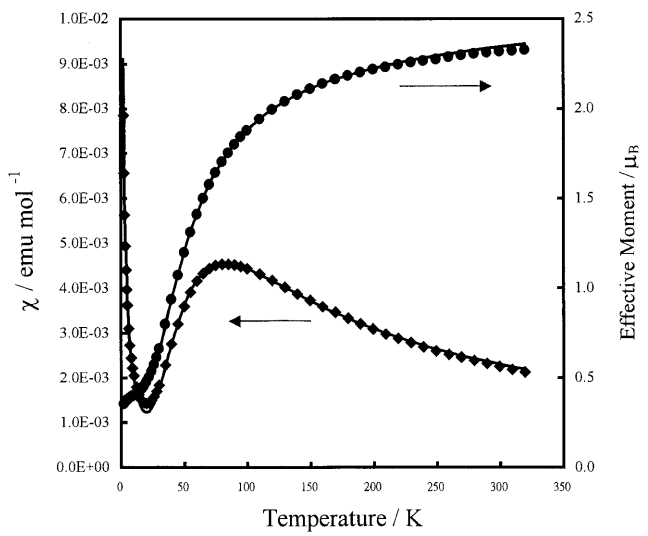


Fig. 6. The experimental data and fitted curves of magnetic susceptibility (●) and moments (◆) of complex **3**.

4. Supplementary material

Tables of atomic positional parameters, anisotropic thermal parameters, intramolecular bond distances and angles and hydrogen atom positional parameters for all complexes have been deposited with the Cambridge Crystallographic Data Centre (CCDC) No. 138833–138835. Copies may be obtained free of charge from The Director, CCDC, 12 Union Road, Cambridge, CB2 1EZ, UK (fax: +44-1223-336033; e-mail: deposit@ccdc.cam.ac.uk or www: http://www.ccdc.cam.ac.uk).

Acknowledgements

The research grants from National Science Council of Republic of China and Chinese Military Academy are highly appreciated.

References

[1] (a) W. Kaim, J. Rall, Angew. Chem. 108 (1996) 47; Angew. Chem., Int. Ed. Engl. 35 (1996) 43. (b) A.G. Sykes, Adv. Inorg. Chem. 36 (1991) 377.
[2] N. Kitajima, Adv. Inorg. Chem. 39 (1992) 2.
[3] E. Bouwman, W.L. Driessen, J. Reedijk, Coord. Chem. Rev. 104 (1990) 143.
[4] (a) K.C. Tran, J.P. Battioni, J.L. Zimmermann, C. Bois, G.J.A.A. Koolhaas, P. Leduc, E. Mulliez, H. Boumchita, J. Reedijk, J.C. Chottard, Inorg. Chem. 33 (1994) 2802. (b) R. Bentfeld, N. Ehlers, R. Mattes, Chem. Ber. 128 (1995) 1199.
[5] (a) J.A. Farrar, F. Neese, P. Lappalainen, P.M.H. Kroneck, M. Saraste, W.G. Zumft, A.J. Thomson, J. Am. Chem. Soc. 118 (1996) 11501. (b) E.I. Solomon, in: T.G. Spiro (Eds.), Copper Proteins, Wiley-Interscience, New York, 1981 (Chapter 2).
[6] (a) R.P. Houser, J.A. Halfen, B.G. Young, Jr., N.J. Blackburn, W.B. Tolman, J. Am. Chem. Soc. 117 (1995) 10745. (b) R.P Houser, B.G. Young, W.B. Tolman, J. Am. Chem. Soc. 118 (1996) 2101.
[7] (a) A.F. Stange, E. Waldhör, M. Moscherosch, W. Kaim, Z. Naturforsch. B 50 (1995) 115. (b) N.D.J. Branscombe, A.J. Blake, A. Marin-Becerra, W.-S. Li, S. Parsons, L. Ruiz-Ramirez, M. Schröder, J. Chem. Soc., Chem. Commun. (1996) 2573.
[8] (a) P.J. Steel, Coord. Chem. Rev. 106 (1990) 227. (b) A.P. Sadimenko, S.S. Basson, Coord. Chem. Rev. 147 (1996) 247.
[9] T.G. Schenck, J.M. Downes, C.R.C. Milne, P.B. Mackenzie, H. Boucher, J. Whelan, B. Bosnich, Inorg. Chem. 24 (1985) 2334.
[10] (a) T. Kamiusuki, H. Okawa, N. Matsumoto, S. Kida, J. Chem. Soc. Dalton Trans. (1990) 195. (b) T. Kamiusuki, H. Okawa, N. Matsumoto, M. Kodera, S. Kida, J. Coord. Chem. 23 (1991) 201. (c) M. Itoh, K. Motoda, K. Shindo, T. Kamiusuki, H. Sakiyama, N. Matsumoto, H. Okawa, J. Chem. Soc., Dalton Trans. (1995) 3635.

[11] B. Mernari, F. Abraham, M. Lagrenee, M. Drillon, P. Legoll, J. Chem. Soc., Dalton Trans. (1993) 1707.
[12] L. Behle, M. Neuburger, M. Zehnder, T.A. Kaden, Helv. Chim. Acta 78 (1995) 693.
[13] F. Meyer, S. Beyreuther, K. Heinze, L. Zsolnai, Chem. Ber. 130 (1997) 605.
[14] (a) S. Knapp, T.P. Keenan, J. Liu, J.A. Petanza, H.J. Schugar, Inorg. Chem. 29 (1990) 2189. (b) W.G. Haanstra, M.F. Cabral, J. de O. Cabral, W.L. Driessen, J. Reedijk, Inorg. Chem. 31 (1992) 3150. (c) R. Prins, M. Biagini-Cingi, M. Drillon, R.A.G. de Graaff, J. Hassnot, A.-M. Manotti-Lanfredi, P. Rabu, J. Reedijk, F. Ugozzoli, Inorg. Chim. Acta 248 (1996) 35.
[15] (a) E.I. Solomon, M.J. Baldwin, M.D. Lowery, Chem. Rev. 92 (1992) 521. (b) K.D. Karlin, Z. Tyeklar, Bioinorganic Chemistry of Copper, Chapman and Hall, London, 1993, pp. 143–196.
[16] (a) L.K. Thompson, S.S. Tandon, M.E. Manuel, Inorg. Chem. 34 (1995) 2356. (b) J.H. Satcher Jr., M.W. Droege, T.J.R. Weakley, R.T. Taylor, Inorg. Chem. 34 (1995) 3317. (c) G.A. van Albada, M.T. Lakin, N. Veldman, A.L. Spek, J. Reedijk, Inorg. Chem. 34 (1995) 4910. (d) M.-Y. Chow, Z.-Y. Zhou, T.C.W. Mak, Inorg. Chem. 31 (1992) 4900.
[17] (a) J.-P. Chyn, F.L. Urbach. Inorg. Chim. Acta. 189 (1991) 157. (b) J.-P. Chyn, J.-L. Chou and K.-J. Shieh, J. Chin. Chem. Soc. (1991) 38, 461. (c) J.-P. Chyn, K.-J. Shieh, J.-L. Chou, Y. Wang, G.-H. Lee, C.-P Chen, J. Chin. Chem. Soc. 38 (1991) 549.
[18] L. Bauer, L.A. Gardella, J. Org. Chem. 26 (1961) 82.
[19] A.C. Lason, F.L. Lee, P.Y. Le, M. Webster, J.P. Charland, E.J. Gabe, NRCVAX Crystal Structure System, Chemistry Division, NRC, Ottawa, Canada, 1990.
[20] N. Oishi, Y. Nishida, K. Ida, S. Kida, Bull. Chem. Soc. Jpn. 53 (1980) 2847.
[21] K.D. Karlin, Y. Gultneh, T. Nichoison, J. Zubieta, Inorg. Chem. 24 (1985) 3727.
[22] B. Bleaney, K.D. Bowers, Proc. R. Soc. London, Sect. A 214 (1952) 4519.
[23] (a) K.D. Karlin, B.I. Cohen, J.C. Hayes, A. Farooq, J. Zubieta, Inorg. Chem. 26 (1987) 147. (b) L. Casella, M. Guillotti, G. Pallanza, M. Buga, Inorg. Chem. 30 (1991) 221.
[24] R.A. Holwerda, T.F. Tekut, B.G. Gafford, J.H. Zhang, C.J. O'Connor, J. Chem. Soc. Dalton Trans. (1991) 1051.
[25] A.M. Golub, H. Kohler, V.V. Skopendo, Chemistry of the Pseudohalides, Elsevier, New York, 1986, p. 459.
[26] M. Rodriguez, A. Llobet, M. Corbella, A.E. Martell, J. Reibenspies, Inorg. Chem. 38 (1999) 2328.
[27] B. Chiari, J. Helms, O. Piovesana, T. Tarantelli, P.F. Zanazzi, Inorg. Chem. 25 (1986) 870.

PERGAMON

www.elsevier.nl/locate/poly

Polyhedron 19 (2000) 2225–2229

POLYHEDRON

Kinetic evidence of ring closure step in the substitution of *cis*-$[Cr(bpy)_2(OH_2)_2]^{3+}$ with $[M(CN)_8]^{4-}$ (M = Mo, W)

Rafał Kania, Barbara Sieklucka *

Faculty of Chemistry, Jagiellonian University, Ingardena 3, 30-060 Kraków, Poland

Received 7 July 2000; accepted 8 August 2000

Abstract

The substitution reaction of *cis*-$[Cr(bpy)_2(OH_2)_2]^{3+}$ with $[M(CN)_8]^{4-}$ (M = Mo,W) results in the formation of $\{[(bpy)_2Cr(\mu\text{-}NC)_2M(CN)_6]\}^-$. The new species exhibit intense MMCT transitions and a high degree of electronic coupling revealing a borderline localized-to-delocalized class of behavior. The complex formation reactions were studied as a function of $[M(CN)_8]^{4-}$ concentration, pH and temperature. Two consecutive reaction steps were observed: the first exhibits dependence on the $[M(CN)_8]^{4-}$ concentration and the second is concentration-independent. The mechanism has been rationalized in terms of an ion-pair formation preceding two successive anation steps: initial attachment of the N-end of the cyano ligand of the octacyanometalate moiety followed by slower intramolecular binding of the other N-site leading to ring closure. The large positive $\Delta H^{\neq}$ and large and negative $\Delta S^{\neq}$ values for the second step suggest associative character of the substitution reaction. © 2000 Elsevier Science B.V. All rights reserved.

Keywords: Kinetics; Substitution; Mechanism; *cis*-Diaquabis(2,2′-bipirydyl)chromium(III); Octacyanomolybdate(IV); Octacyanotungstate(IV)

1. Introduction

The good σ-donor ability of the N-end of terminal cyano ligands has been extensively employed to the construction of polymetallic molecular cyano-bridged systems due to their applications in electron-transfer processes, molecular electronics and as molecular magnets [1–3]. The fundamental process linking metal centers through a cyano-bridge is the substitution reaction of cyanometallate at the labile coordination site of a second complex.

Substitution of hexacyanometallates $[M(CN)_6]^{n-}$ on cationic complexes $[M'L_5(H_2O)]^{m+}$ with single available coordination sites have contributed significantly to the understanding of the mechanism of the formation of cyano-bridged species. The numerous studies revealed that substitution proceeds by a step mechanism involving the formation of an ion-pair followed by its conversion to the cyano-bridged product and have generally been interpreted in terms of the activation mode characteristic of an aqua complex [4,5].

Our interest in the possibility of binding $[M(CN)_8]^{n-}$ ions (M = Mo or W) to other metal centers [6–9] has resulted in kinetic studies of the substitution of *cis*-$[Cr(bpy)_2(OH_2)_2]^{3+}$ with $[M(CN)_8]^{4-}$ (M = Mo, W) ions. The preliminary investigations, carried out at 25°C, have shown that the reaction generally follows the accepted mechanism with substitution of two aqua ligands in a single step [10]. We have now extended this work over a wide temperature range and have been able to resolve the detailed kinetics of the two subsequent aqua ligand substitution steps. The reactivity of *cis*-$[Cr(bpy)_2(OH_2)_2]^{3+}$ with $[M(CN)_8]^{4-}$ ions involves the formation of the $\{[(bpy)_2(H_2O)Cr(\mu\text{-}NC)M(CN)_7]\}^-$ intermediate species followed by the rate-determining ring-closure step into the final $\{[(bpy)_2Cr(\mu\text{-}NC)_2M(CN)_6]\}^-$ complex.

2. Experimental

2.1. Materials

$K_4[Mo(CN)_8]$ and $K_4[W(CN)_8]$ were prepared according to the published procedure [11]. Stock solutions

* Corresponding author. Tel.: +48-126-336-377, ext. 2036; fax: +48-126-340-515.

E-mail address: siekluck@chemia.uj.edu.pl (B. Sieklucka).

0277-5387/00/$ - see front matter © 2000 Elsevier Science B.V. All rights reserved.
PII: S0277-5387(00)00531-3

Table 1
The characteristics of the MMCT transitions of $[(bpy)_2Cr(\mu\text{-}NC)_2M(CN)_6]^-$ species (M = Mo, W)

Compound	λ_{max} [a] (nm)	ν_{max} [a] (cm^{-1})	$\Delta\nu_{1/2}$ (cm^{-1})	ε_{max} [a] (M^{-1} cm^{-1})	H_{if} (cm^{-1})
$[(bpy)_2Cr(\mu\text{-}NC)_2Mo(CN)_6]^-$	515	19 417	5890	2160 ± 40	1963
$[(bpy)_2Cr(\mu\text{-}NC)_2W(CN)_6]^-$	562	17 794	6000	3040 ± 30	2248

[a] Ref. [10].

of sodium octacyano-molybdate(IV) and -tungstate(IV) were obtained by a cation-exchange technique (Dowex 50X8). A stock solution of *cis*-$[Cr(bpy)_2(OH_2)_2](ClO_4)_3$ was prepared either by hydrolysis of $[Cr(bpy)_3](ClO_4)_3$ [12,13] or substitution of *cis*-$[Cr(bpy)_2Cl_2](ClO_4)_3$ [14]. The identity and purity of *cis*-$[Cr(bpy)_2(OH_2)_2](ClO_4)_3$ and $Na_4[M(CN)_8]$ (M = Mo, W) solutions were checked by means of electronic spectra [15–17]. Other reagents of analytical grade (Aldrich) were used as received.

2.2. Measurements

Kinetic studies were performed on a Shimadzu 2101 PC spectrophotometer equipped with a thermoelectrically controlled cell holder CPS 60. Stoichiometries, the overall equilibrium constants K_T and molar absorptivity coefficients (ε_{max}) of the final products were calculated from the sets of spectrophotometric data by the application of Job's method. The stoichiometry of the substitution reaction of *cis*-$[Cr(bpy)_2(OH_2)_2]^{3+}$ by $[M(CN)_8]^{4-}$ (M = Mo, W) was found to be 1:1 directly from the Job's plots. The values of the overall equilibrium constant K_T and molar absorbance coefficient (ε_{max}) were calculated by using SPECFIT[1] software package; this is a global least-squares fitting routine for equilibrium and kinetic studies which uses a factor-analysis decomposition method [10]. Pseudo-first-order conditions for the excess of octacyanometalates [$(0.349–1.39) \times 10^{-2}$ M] over *cis*-$[Cr(bpy)_2(OH_2)_2]^{3+}$ concentration (6.96×10^{-4} M) were employed. The kinetics of the substitution reaction of the *cis*-$[Cr(bpy)_2(OH_2)_2]^{3+}$ with the $[M(CN)_8]^{4-}$ ions were followed from the build-up of the products, $[(bpy)_2Cr(\mu\text{-}NC)_2M(CN)_6]^-$ ions, monitored at 515 and 562 nm for (CrMo) and (CrW), respectively. The reaction temperature was maintained to within 0.1°C over the range 30–50°C. The $[H^+]$ ion concentration and ionic strength of the reaction solutions were maintained by means of $HClO_4$ and $NaClO_4$. Generally, the kinetic measurements were performed using an acid ($HClO_4$) concentration of 0.1 M. Some kinetic runs were performed at different $[H^+]$ concentrations in the range $0.1–5 \times 10^{-4}$ M. More details on the data-fitting procedure are given in the Section 3. All attempts to isolate pure solid products were unsuccessful.

[1] Provided by R.A. Binstead of Spectrum Software Associates, Chapel Hill, NC.

3. Results and discussion

The addition of each of the $[M(CN)_8]^{4-}$ ions to an aqueous solution of *cis*-$[Cr(bpy)_2(OH_2)_2]^{3+}$ results in slow formation of highly colored products. Job's method combined with a least-squares fitting routine was applied to determine stoichiometry, overall equilibrium constants K_T, and molar absorbance coefficients (ε_{max}) of the product [10]. The substitution of *cis*-$[Cr(bpy)_2(OH_2)_2]^{3+}$ by $[M(CN)_8]^{4-}$ proceeds according to the stoichiometry of 1:1 and results in the formation of the $[(bpy)_2Cr(\mu\text{-}NC)_2M(CN)_6]^-$ ions with K_T of $(1.0 \pm 0.1) \times 10^4$ and $(2.5 \pm 0.3) \times 10^4$ M^{-1} for Mo and W, respectively, in agreement with (Eq. (1)).

$$[Cr(bpy)_2(OH_2)_2]^{3+} + [M(CN)_8]^{4-} \overset{K_T}{\rightleftharpoons} [(bpy)_2Cr(\text{-}NC)_2M(CN)_6]^- + 2H_2O \quad (1)$$

The characteristic transitions in the visible part of the spectra of 515 nm (CrMo) and 562 nm (CrW) are not present in either the reduced or oxidized form of either complex alone and we assigned it to the optical MMCT (metal–metal charge-transfer) transition from M(IV) to Cr(III). The Hush model [18] (Eqs. (2) and (3)),

$$H_{if} = \nu_{max}\alpha = 2.05 \times 10^{-2}\left(\frac{\nu_{max}}{d}\right)\sqrt{\frac{\varepsilon_{max}\Delta\nu_{1/2}}{\nu_{max}}} \quad (2)$$

$$\alpha^2 = 4.24 \times 10^{-4}\left(\frac{\varepsilon_{max}\Delta\nu_{1/2}}{\nu_{max}d^2}\right) \quad (3)$$

where ν_{max}, $\Delta\nu_{1/2}$ and ε_{max} are the energy (cm^{-1}), bandwidth (cm^{-1}) and molar absorbance coefficient of MMCT band, has been applied to the above spectroscopic data. The intermetallic distance of 5.3 Å between metal centers has been assumed on the basis of the crystallographic data of *cis*-$[Cr(bpy)_2(OH_2)(Cl)]Cl_2$ [19] and $K_4[M(CN)_8]$ [20,21]. The electronic absorption characteristics of the MMCT bands together with the calculated Hush parameters are shown in Table 1. The high degree of electronic coupling characterized by $H_{if} = 1963$ (CrMo) and 2248 cm^{-1} (CrW) suggests that these complexes are similar to the examples of the borderline localized–delocalized class of compounds [22–26]. The H_{if} values and MMCT bandwidths, exhibiting low energy asymmetries, are significantly larger than those obtained for $[(NC)_7M^{IV}(\mu\text{-}CN)Os(NH_3)_5]^-$ (M = Mo, W) localized mixed-valence cyano-bridged complexes with H_{if} of 915 and 1030 cm^{-1} for Mo and W, respectively [27].

The kinetic studies were carried out with $[M(CN)_8^{4-}]$ (M = Mo,W) in excess. At 25°C, the observed dependencies of the pseudo-first-order rate constants k_{obs} on the concentration of the entering ligand $[M(CN)_8^{4-}]$ (M = Mo or W) were linear with small positive intercepts, consistent with an ion-pair ligand substitution mechanism depicted in Eqs. (4) and (5). The corresponding rate law is given in Eq. (6) [10].

$$[Cr(bpy)_2(OH_2)_2]^{3+} + [M(CN)_8]^{4-} \overset{K_{os}}{\rightleftharpoons} \{[Cr(bpy)_2(OH_2)_2]^{3+}, M(CN)_8]^{4-}\} \quad (4)$$

$$\{[Cr(bpy)_2(OH_2)_2]^{3+}, M(CN)_8]^{4-}\} \overset{k'_s}{\underset{k_{aq}}{\rightleftharpoons}} [(bpy)_2Cr(NC)_2M(CN)_6]^{-} \quad (5)$$

$$k_{obs} = k_{aq} + k_f[M(CN)_8^{4-}] \quad (6)$$

where $k_f = k'_sK_{os}$.

The typical kinetic plot at higher temperatures, 30–50°C, is shown in Fig. 1. The kinetic data clearly exhibited two consecutive exponential functions. The biphasic kinetic data have been analyzed in terms of Eq. (7) with the corresponding expression of A_t in Eq. (8).

$$A \overset{k^I_{obs}}{\rightarrow} B \overset{k^{II}_{obs}}{\rightarrow} C \quad (7)$$

$$A_t = A_\infty + a_1 \times \exp(-k^I_{obs} \times t) + a_2 \times \exp(-k^{II}_{obs} \times t) \quad (8)$$

where k^I_{obs} and k^{II}_{obs} are pseudo-first-order rate constants of the first and second step, respectively. The composite parameters a_1 and a_2 are the functions of the initial *cis*-$[Cr(bpy)_2(OH_2)_2]^{3+}$ ion concentration, molar absorbance coefficients and rate constants [28] (Eqs. (9) and (10)):

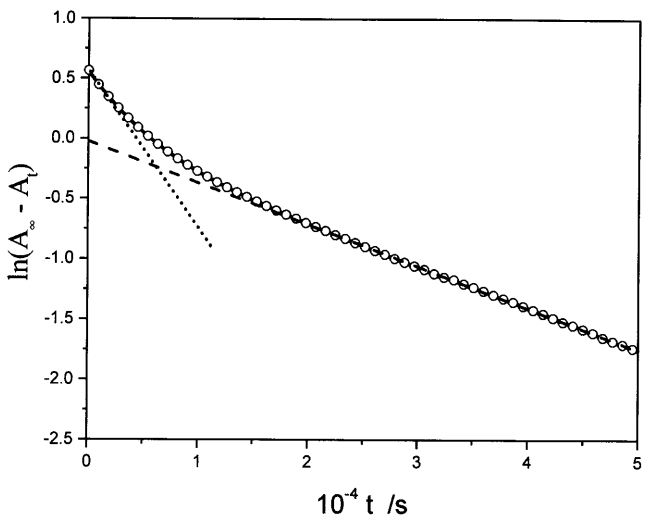


Fig. 1. Typical plot of two-step kinetics of the substitution reaction *cis*-$[Cr(bpy)_2(OH_2)_2]^{3+}$ by $[M(CN)_8]^{4-}$; M = W, $[Cr(bpy)_2(OH_2)_2^{3+}] = 6.96 \times 10^{-4}$ M, $[W(CN)_8^{4-}] = 1.18 \times 10^{-2}$ M, $[H^+] = 0.1$ M, $I =$ 1.0 M ($HClO_4 + NaClO_4$), $T = 40$°C, $\lambda = 560$ nm.

$$a_1 = \frac{[Cr(bpy)_2(OH_2)_2^{3+}]_0\{k^{II}_{obs}(\varepsilon_A - \varepsilon_C) - k^I_{obs}(\varepsilon_A - \varepsilon_B)\}}{k^{II}_{obs} - k^I_{obs}} \quad (9)$$

$$a_2 = \frac{[Cr(bpy)_2(OH_2)_2^{3+}]_0 k^I_{obs}(\varepsilon_C - \varepsilon_B)}{k^{II}_{obs} - k^I_{obs}} \quad (10)$$

The non-linear least-squares fitting procedure of the kinetic data to Eq. (8) yielded the values of A_∞, k^I_{obs}, k^{II}_{obs}, a_1 and a_2. It was not practical to obtain an experimental value of A_∞, since the reactions are characterized by very long half-lives [29]. In cases where A_∞ was experimentally determined, the difference between the calculated and the experimental value of A_∞ was less than 8%. The coupling of the exponential expressions by a_1 and a_2 variables resulted in significant errors in k^I_{obs} and k^{II}_{obs}.

The pseudo-first-order rate constants k^I_{obs} exhibited a dependence on $[M(CN)_8]^{4-}$ concentration. The application of the rate law in the form of Eq. (6) to k^I_{obs} gave inconsistent values for k_{aq}. However, the fitting of the data to the rate law in Eq. (11),

$$k^I_{obs} = k_sK_{os}[M(CN)_8^{4-}]/(1 + K_{os}[M(CN)_8^{4-}]) \quad (11)$$

gave satisfactory fitting and well-behaving values of k_s and K_{os}, the forward reaction rate constant and the ion-pair association constant, respectively. Initially, the presence of the back reaction (k'_{aq}) was expected. Eq. (11) rearranged into a linear expression including k'_{aq} and has the form of Eq. (12) [29].

$$1/(k^I_{obs} - k'_{aq}) = 1/(k_sK_{os}[M(CN)_8^{4-}]) + 1/k_s \quad (12)$$

The attempts to refine a correlation coefficient by varying the value of k_{aq}, according to the rate law in Eq. (12) were unsuccessful, indicating that the values of k_{aq} were too small to be determined. The values of k_s and K_{os} were calculated from the linear plots of $1/k^I_{obs}$ versus $1/[M(CN)_8^{4-}]$ (M = Mo or W) (Figs. 2 and 3) and the rate data along with the corresponding activation parameters are collected in Table 2. The value of the ion-pair association constant K_{os} exhibits no dependence on the temperature, which is in agreement with the temperature independence of K_{os} of $\{[Cr(NH_3)_5(H_2O)]^{3+}\ [Co(CN)_6]^{3-}\}$ and other Cr(III)-based ion-pairs [29]. The mean values of K_{os} are 23 ± 14 M^{-1} for $\{cis\text{-}[Cr(bpy)_2(OH_2)_2]^{3+}, [Mo(CN)_8]^{4-}\}$ and 27 ± 19 M^{-1} for $\{cis\text{-}[Cr(bpy)_2(OH_2)_2]^{3+}, [W(CN)_8]^{4-}\}$. The experimental value of K_{os} is in good agreement with the value of $K_{os} = 33$ M^{-1} calculated from the Eigen–Fuoss expression (assuming the hydrogen bonded ion-pair has a distance of 8.9 Å between the metal centers [19–21]) [10,30,31].

The rate constants k^{II}_{obs} show no dependence on $[M(CN)_8^{4-}]$ concentration. The mean values of k^{II}_{obs} and

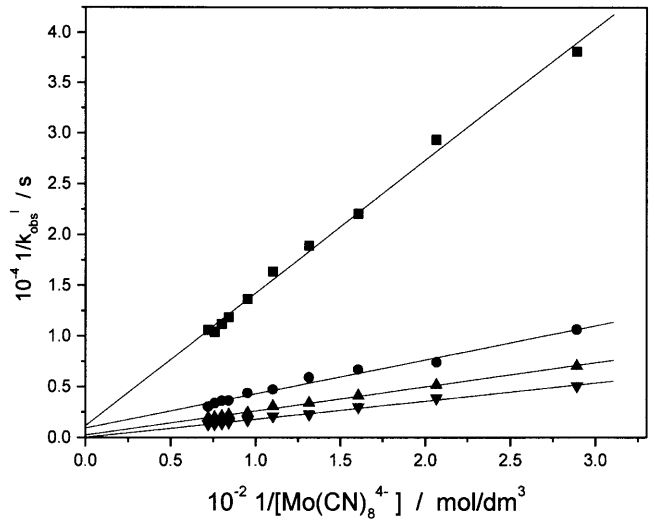


Fig. 2. The plot of $1/k^{I}_{obs}$ versus $1/[Mo(CN)_8^{4-}]$ at 30°C (■), 40°C (●), 45°C (▲) and 50°C (▼); $[Cr(bpy)_2(OH_2)_2^{3+}] = 6.96 \times 10^{-4}$ M, $[H^+] = 0.1$ M, $I = 1.0$ M ($HClO_4 + NaClO_4$).

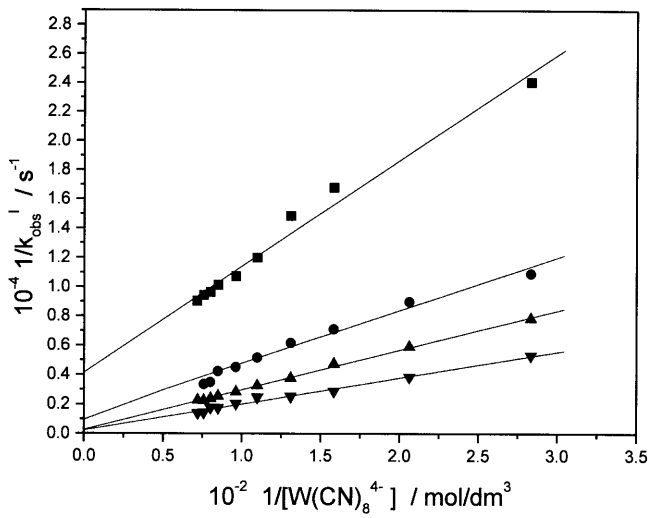
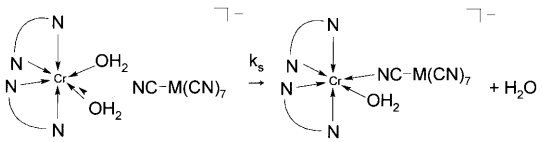
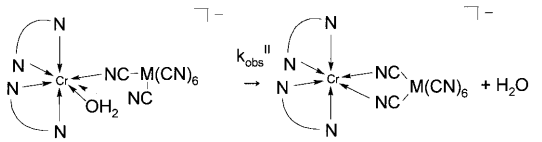


Fig. 3. The plot of $1/k^{I}_{obs}$ versus $1/[W(CN)_8^{4-}]$ at 30°C (■), 40°C (●), 45°C (▲) and 50°C (▼); $[Cr(bpy)_2(OH_2)_2^{3+}] = 6.96 \times 10^{-4}$ M, $[H^+] = 0.1$ M, $I = 1.0$ M ($HClO_4 + NaClO_4$).

corresponding activation parameters are listed in Table 2. The independence of k^{II}_{obs} on $[M(CN)_8^{4-}]$ concentration suggests a ring-closure reaction [32,33]. The substitution of $[M(CN)_8]^{4-}$ on *cis*-$[Cr(bpy)_2(OH_2)_2]^{3+}$ can be rationalized in terms of Eqs. (13) and (14), where the formation of an ion-pair (Eq. (2)) precedes two distinguishable substitution steps:



(13)



(14)

the substitution of aqua ligand within the ion-pair (k_s) followed by the rate-determining ring-closure step (k^{II}_{obs}). These results indicate that the closing of the ring by the substitution of a second aqua ligand is sterically controlled by the large, bulky octacyanide ligand.

The values of k^{I}_{obs} and k^{II}_{obs} at different $[H^+]$ are listed in Table 3. The substitution of $[M(CN)_8]^{4-}$ on *cis*-$[Cr(bpy)_2(OH_2)_2]^{3+}$ is independent of $[H^+]$ in the range 1.15×10^{-3} 0.1 M, despite the first protonation equilibrium of *cis*-$[Cr(bpy)_2(OH_2)_2]^{3+}$ ($pK_a = 3.5$ [15]) and protonation of $[M(CN)_8]^{4-}$ in acidic solution ($K_{a1} > K_{a2} > K_{a3} > 0.1$, $K_{a4} = (2.5 \pm 0.8) \cong 10^{-2}$ M) [34].

The apparent activation parameters do not give unequivocal evidence of the type of mechanism. Both reaction steps are characterized by large positive $\Delta H^{\neq}$ values. While the large positive $\Delta S^{\neq}$ value of the first substitution step is largely charge-controlled for the reaction between unlike charged species, the second ring-closure step is accompanied by large and negative activation entropy, suggesting the associative character of the substitution process [32,35,36]. The substitution

Table 2
Rate and activation parameters for the anation reaction of *cis*-$[Cr(bpy)_2(OH_2)_2]^{3+}$ by $[M(CN)_8]^{4-}$ in aqueous acidic solution (M = Mo,W) [a]

T (°C)	$[(bpy)_2Cr(NC)_2Mo(CN)_6]^-$		$[(bpy)_2Cr(NC)_2W(CN)_6]^-$	
	$10^4\ k_s$ ($M^{-1}\ s^{-1}$)	$10^5\ k^{II}_{obs}$ (s^{-1})	$10^4\ k_s$ ($M^{-1}\ s^{-1}$)	$10^5\ k^{II}_{obs}$ (s^{-1})
30	4.1 ± 0.4	1.3 ± 0.6	0.24 ± 0.03	1.7 ± 0.3
40	13 ± 3.1	4.5 ± 1.0	1.1 ± 0.3	3.1 ± 0.6
45	37 ± 8.7	6.9 ± 1.8	3.6 ± 0.8	4.7 ± 1.3
50	90 ± 51	9.7 ± 3.8	4.2 ± 1.8	6.5 ± 2.3
$\Delta H^{\neq}$ (kJ mol^{-1})	135 ± 32	80 ± 22	119 ± 12	52 ± 3
$\Delta S^{\neq}$ (J K^{-1} mol^{-1})	133 ± 14	-75 ± 14	79 ± 9	-164 ± 14

[a] $I = 1.0$ M ($NaClO_4$); $[H^+] = 0.1$ M.

Table 3
Values of k^{I}_{obs} and k^{II}_{obs} for the anation of *cis*-$[Cr(bpy)_2(OH_2)_2]^{3+}$ by $[M(CN)_8]^{4-}$ (M = Mo, W) [a]

$[H^+]$ (M)	$[(bpy)_2Cr(NC)_2Mo(CN)_6]^-$		$[(bpy)_2Cr(NC)_2W(CN)_6]^-$	
	$10^5\ k^{I}_{obs}$ (s^{-1})	$10^5\ k^{II}_{obs}$ (s^{-1})	$10^4\ k^{I}_{obs}$ (s^{-1})	$10^5\ k^{II}_{obs}$ (s^{-1})
0.1	9.45	1.67	1.11	1.43
0.01	9.91	1.97	1.04	1.77
1.15×10^{-3}	9.71	1.70	1.04	1.73
	9.69 ± 0.09	1.78 ± 0.07	1.06 ± 0.02	1.67 ± 0.07

[a] $[Cr(bpy)_2(OH_2)_2^{3+}] = 6.95\times10^{-4}$ M, $[M(CN)_8^{4-}] = 2.37\times10^{-2}$ M, $I = 1.0$ M ($NaClO_4$), $T = 30$°C.

of *cis*-$[Cr(bpy)_2(OH_2)_2]^{3+}$ by $[M(CN)_8]^{4-}$ can be compared to associative interchange substitution of $[Cr(H_2O)_6]^{3+}$ and $[Cr(H_2O)_5(OH)]^{3+}$ by $[M(CN)_8]^{4-}$, characterized by large negative values of $\Delta S^{\neq}$ [37–39] and dissociative or I_d substitution of $[Cr(NH_3)_5(H_2O)]^{3+}$ by $[Co(CN)_6]^{3-}$ ($\Delta S^{\neq} = 26$ J K^{-1} mol^{-1}) and other anionic ligands [29,40].

Acknowledgements

We thank the Polish Research Grants Committee (Grant No. 461/T09/97/13 to B.S.) for support of this research.

References

[1] H. Vahrenkamp, A. Geiss, G.N. Richardson, J. Chem. Soc., Dalton Trans. (1997) 3643.
[2] K.R. Dunbar, R.A. Heintz, Prog. Inorg. Chem. 45 (1997) 283.
[3] M. Verdaguer, A. Bleuzen, V. Marvaud, J. Vaissermann, M. Seuleiman, C. Desplanches, A. Scuiller, C. Train, R. Garde, G. Gelly, C. Lomenech, I. Rosenman, P. Veillet, C. Cartier, F. Villain, Coord. Chem. Rev. 190 (1999) 1023.
[4] B. Sieklucka, Prog. React. Kin. 15 (1989) 175.
[5] B. Sieklucka, Prog. React. Kin. Mech. 24 (1999) 165.
[6] B. Sieklucka, J. Chem. Soc., Dalton Trans. (1997) 869.
[7] B. Sieklucka, W. Lasocha, L.M. Proniewicz, R. Podgajny, H. Schenk, J. Mol. Struct. 520 (2000) 155.
[8] R. Podgajny, B. Sieklucka, W. Lasocha, J. Chem. Soc., Dalton Trans. (2000) 1799.
[9] B. Sieklucka, J. Szklarzewicz, T.J. Kemp, W. Errington, Inorg. Chem., in press.
[10] R. Podgajny, R. Kania, P. Kita, W. Lasocha, B. Sieklucka, in: G. Ondrejovic, A. Sirota (Eds.), Coordination Chemistry at the turn of the century, Slovak Technical University Press, Bratislava, 1999, p. 183.
[11] J.G. Leipold, L.D.C. Bok, P.J. Cilliers, Z. Anorg. Allg. Chem. 409 (1974) 343.
[12] B.R. Baker, B.D. Mehta, Inorg. Chem. 4 (1965) 848.
[13] K. Mesbah, P. Kita, Polish J. Chem. 67 (1993) 2047.
[14] W. Kharmawphlong, S. Choudhury, A.K. Deb, S. Goswami, Inorg. Chem. 34 (1995) 3826.
[15] M. Maestri, F. Bolletta, N. Sephone, L. Moggi, V. Balzani, Inorg. Chem. 15 (1976) 2048.
[16] R.G. Inskeep, J. Bierrum, Acta Chem. Scand. 15 (1961) 62.
[17] Z. Stasicka, A. Samotus, W. Jakób, Rocz. Chem. 40 (1966) 967.
[18] N.S. Hush, Prog. Inorg. Chem. 8 (1967) 391.
[19] W.A. Wickramasinghe, P.H. Bird, M.A. Jamieson, N. Sephone, M. Maestri, Inorg. Chim. Acta 64 (1982) L85.
[20] L.D.C. Bok, J.G. Leipold, S.S. Basson, Z. Anorg. Allg. Chem. 392 (1972) 303.
[21] L.D.C. Bok, J.G. Leipold, S.S. Basson, Acta Crystallogr., Sect. B 26 (1970) 1209.
[22] Ch.G. Atwood, W.E. Geiger, J. Am. Chem. Soc. 115 (1993) 5310.
[23] W. Bruns, W. Kaim, E. Waldhr, M. Krejcik, Inorg. Chem. 34 (1995) 663.
[24] G.A. Neyhart, C.J. Timpson, W.D. Bates, T.J. Meyer, J. Am. Chem. Soc. 118 (1996) 3730.
[25] T. Ito, T. Hamaguchi, H. Nagino, T. Yamaguchi, J. Washington, C.P. Kubiak, Science 277 (1997) 660.
[26] K.D. Demadis, G.A. Neyhart, E.M. Kober, T.J. Meyer, J. Am. Chem. Soc. 120 (1998) 7121.
[27] W.M. Laidlow, R.G. Denning, Inorg. Chim. Acta 219 (1994) 121.
[28] J.M. Espenson, T. Chao, Inorg. Chem. 16 (1977) 2553.
[29] D.C. Gaswick, S.M. Maliniak, Inorg. Chem. 32 (1993) 175.
[30] R.M. Fuoss, J. Am. Chem. Soc. 80 (1958) 5059.
[31] M. Eigen, Z. Phys. Chem. 1 (1954) 176.
[32] S. Suvachittanont, H. Hohmann, R. van Eldik, J. Reedijk, Inorg. Chem. 32 (1993) 4544.
[33] R. Romeo, G. Alibrandi, G. Arena, L.M. Scolaro, M.R. Plutino, Inorg. Chim. Acta 235 (1995) 281.
[34] A. Samotus, B. Kosowicz-Czajkowska, Rocz. Chem. 45 (1971) 1623.
[35] K.R. Ashley, R.E. Hamm, Inorg. Chem. 5 (1966) 1645.
[36] A. Roodt, S.S. Basson, J.G. Leipoldt, Polyhedron 13 (1994) 599.
[37] S.I. Ali, S. Sharma, Z. Khan, Transition. Met. Chem. 21 (1996) 222.
[38] S.I. Ali, Z. Murtaza, A.A. Khan, Z. Phys. Chem. (Leipzig) 266 (1985) 1250.
[39] S.I. Ali, Z. Murtaza, Polyhedron 4 (1986) 463.
[40] S. Castillo-Blum, A.G. Sykes, Inorg. Chem. 23 (1984) 1049.

PERGAMON

www.elsevier.nl/locate/poly

Polyhedron 19 (2000) 2231–2236

POLYHEDRON

Synthesis, characterisation and study of mercury(II) chloride complexes with triphenylphosphine and heterocyclic thiones. The crystal structures of [(benzothiazole-2-thionato)-(benzothiazole-2-thione)(bis-triphenylphosphine) chloro mercury(II)] and [(μ_2-dichloro){(bis-pyrimidine-2-thionato)-mercury(II)}{(bis-triphenylphosphine)mercury(II)}] at 100 K

S.K. Hadjikakou [a,*], M. Kubicki [b]

[a] *Department of Chemistry, Section of Inorganic and Analytical Chemistry, University of Ioannina, 45100 Ioannina, Greece*
[b] *Department of Chemistry, A. Mickiewicz, University, ul. Grunwaldzka 6, 60-78 Poznan, Poland*

Received 30 June 2000; accepted 8 August 2000

Abstract

Direct reaction of mercury(II) chloride with triphenylphosphine (PPh_3) and benzothiazole-2-thione (bzthtH) in the molar ratio of 1:1:2 results in the formation of the [Hg(PPh_3)(bzthztH)(bzthzt)Cl] (**1**) (bzthzt = the anion of benzothiazole-2-thione) while the reaction of mercury(II) chloride with triphenylphosphine (PPh_3) and pyrimidine-2-thione (pmtH) in the molar ratio of 1:1:1 gives [$Hg_2Cl_2(PPh_3)_2(pmt)_2$] (**2**) (pmt = the anion of pyrimidine-2-thione). The complexes have been characterised by their elemental analyses, melting points and their FTIR, far-IR spectroscopic data. The crystal structure of complex **1** which has been determined by single-crystal X-ray crystallography at r.t. reveals that the molecule is monomeric with tetrahedral geometry around the metal ion. A benzothiazole-2-thione molecule and a benzothiazole-2-thionato anion are coordinated, via sulfur atoms, to the mercury(II) ion [Hg–S(2A) = 2.726(2) and Hg–S(2) = 2.419(2) Å]. A triphenylphosphine molecule is also coordinated through a phosphorus atom to the metal ion [Hg–P = 2.453(2) Å] while the tetrahedral geometry around the mercury is completed by a chlorine atom [Hg–Cl = 2.633(2) Å]. The complex is covalent in the solid state. The crystal structure of complex **2** which has also been established by single-crystal X-ray crystallography at 100(1) K shows that the molecule is binuclear and consists of two different moieties with tetrahedral geometry around each mercury(II) ion. One moiety consists of a mercury(II) ion with two phosphorus atoms from phosphine ligands and two bridging chlorine atoms, while the other consists of a mercury(II) ion and two sulfur atoms of pyrimidine-2-thionato ligands. The entire complex is covalent in the solid state. The two Hg(2)–S(42) bond lengths are 2.3513(11) Å while the two Hg(1)–P(1) bond lengths are 2.4826(9) Å. The two parts of the molecule are linked to each other by two chlorine atoms with Hg(1)–Cl(1) and Hg(2)–Cl(1) bond distances of 2.5310(10) and 3.0472(10) Å, respectively. © 2000 Elsevier Science B.V. All rights reserved.

Keywords: Mercury(II) complexes; Triphenylphosphine; Benzothiazole-2-thione; pyrimidine-2-thione; Crystal structures

1. Introduction

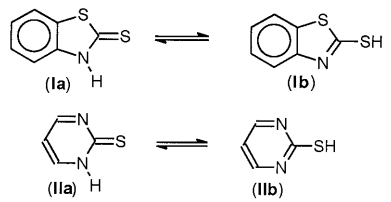
The study of the coordination and structural chemistry of mercury(II) halide complexes with ligands containing a variety of donor atoms has been a matter of interest over several decades [1–5]. The study of mercury complexes with sulfur-containing ligands has attracted considerable interest due to the relevance of this type of molecule as structural and spectroscopic models of biological systems [6–13]. Among the topics of interest in the study of the chemistry of mercury complexes with ligands containing thiolate or thione groups is the potential of these ligands for use in the detoxification of

* Corresponding author. Tel.: +30-651-98-374..
E-mail address: shadjika@cc.uoi.gr (S.K. Hadjikakou).

0277-5387/00/$ - see front matter © 2000 Elsevier Science B.V. All rights reserved.
PII: S0277-5387(00)00533-7

mercury from living systems afforded by the binding of mercury ions to the thiolato or thione groups of the ligands rather than to the cystein thiolate groups of proteins [14,15]. In the literature, there are some reports on the interaction of heterocyclic thiones and mercury ions [16–24]. On the other hand, the multiformity of the structural types which have resulted for the mercury(II) complexes with aryl-phosphine ligands provides an area of interest [25–29]. Surprisingly, there are very few reports on the structural characterisation of mixed-ligand mercury(II) complexes with heterocyclic thiones and triaryl-phosphine ligands [30].

Here we report the structural and spectroscopic characterisation of mercury(II) complexes derived from the reaction of mercury(II) chloride with triphenylphosphine and benzothiazole-2-thione (**I**, $C_7H_5NS_2$) or pyrimidine-2-thione (**II**, $C_4H_4N_2S$) in different molar ratios.



2. Experimental

2.1. Materials and instruments

All solvents used were reagent grade, mercury(II) chloride and triphenylphosphine (Merck) as well as benzothiazole-2-thione and pyrimidine-2-thione (Merck or Aldrich) were used with no other purification prior to use. Elemental analyses for C, H, N, and S were carried out with a Carlo Erba EA model 1108. Melting points were measured with a Stuart Scientific apparatus and are uncorrected. IR spectra in the region of 4000–370 cm^{-1} were obtained in KBr discs while far-IR spectra in the region of 400–50 cm^{-1} were obtained in polyethylene discs, with a Perkin–Elmer Spectrum GX FTIR spectrometer.

2.2. Synthesis of [Hg(PPh_3)(bzthztH)(bzthzt)Cl] (*1*)

A mixture of mercury(II) chloride (0.138 g, 0.5 mmol), triphenylphosphine (0.132 g, 0.5 mmol) and benzothiazole-2-thione (0.167 g, 1.0 mmol) in a 20 ml solution of 1:1 methanol–acetonitrile was stirred for 3 h. The suspension was filtered off and the clear solution was kept in darkness. Slow evaporation of the solvent at room temperature (r.t.) yielded orange crystals suitable for single-crystal analysis by crystallography. M.p. 167°C. *Anal.* Found: C: 46.87; H: 2.99; N: 3.76; S: 15.47. Calc. for $C_{32}H_{24}ClHgN_2PS_4$: C: 46.21; H: 2.91; N: 3.37; S:15.42%. IR (cm^{-1}): 1597m, 1496s, 1451s, 1433vs, 1407vs, 1332s, 1097vs, 1071vs, 1022vs, 1008vs, 985vs, 747vs, 687vs, 601vs, 519vs, 501vs, 486vs. Far-IR (cm^{-1}): 310m, 248s, 192s, 165s, 152s, 141m.

2.3. Synthesis of [$Hg_2Cl_2(PPh_3)_2$(pmt)$_2$] (*2*)

A mixture of mercury(II) chloride (0.138 g, 0.5 mmol), triphenylphosphine (0.132 g, 0.5 mmol) and pyrimidine-2-thione (0.056 g, 0.5 mmol) was suspended in a 20 ml solution of 1:1 methanol–acetonitrile and stirred for 3 h. The suspension was filtered off and the clear solution was kept in darkness. Slow evaporation of the solvent at r.t. yielded pale yellow–white crystals suitable for single-crystal analysis by crystallography. M.p. 220°C. *Anal.* Found: C: 43.29; H: 2.95; N: 4.32; S: 5.85. Calc. for $C_{44}H_{36}Cl_2Hg_2N_4P_2S_2$: C: 43.36; H: 2.97; N: 4.60; S: 5.26%. IR (cm^{-1}): 1560s, 1537s, 1481m, 1425s, 1370vs, 1201m, 1172s, 1097s, 803s;743vs, 691vs, 519s, 504vs, 489s. Far-IR (cm^{-1}): 248s, 227m, 177m, 172m, 165m, 151s, 134m.

2.4. X-ray data collection and reduction of the intensity data of the complexes

X-ray diffraction data were collected on a Kuma KM4CCD [31] diffractometer equipped with a CCD area detector. The experiment for **1** was carried out at r.t., while for **2** the temperature was set at 100(1) K, using graphite–monochromated Mo Kα ($\lambda = 0.71073$ Å) radiation. The frames were record using $\Delta\omega = 0.75°$ rotation scans. A total of 782 frames in six runs were measured for each structure. Each frame was recorded twice in order to eliminate accidental spots. Reflection indexing, Lorentz and polarisation correction, peak integration and background determinations were performed using the Kuma CRYSALIS RED software package [32]. The unit cell dimensions were initially determined from the 15 appropriately chosen frames and were then refined with all recorded images. Empirical absorption corrections were applied for both data sets; $T_{min} = 0.40$ for **1** and 0.491 for **2**, $T_{max} = 0.944$ and 0.972 for **1** and **2**, respectively. Both structures were solved by direct methods using the program SHELXS-86 [33]. For each structure, full-matrix least-squares refinement with all reflections was carried out with the program SHELXL-93 [34]. Scattering factors incorporated in SHELXL-93 were used. The function $\Sigma w(|F_o|^2 - |F_c|^2)^2$ was minimised with $w^{-1} = [\alpha^2(F_o)^2 + 0.0504P^2]$ ($P = [\max(F_o^2, 0) + 2F_c^2]/3$)). Empirical extinction corrections were also applied to compounds **1** and **2**, according to the formula $F_c' = kF_c[1 + 0.001 \times F_c^2\lambda^3/\sin 2\theta]^{1/4}$. The final values for **1** and **2** are listed in Table 1. The non-hydrogen atoms were refined with anisotropic thermal parameters. The coordinates of the other hydrogen

atoms were calculated as 1.2 times U_{eq} for the appropriate carrier carbon atom. Bond lengths and angles for both compounds are listed in Tables 2 and 3. Thermal ellipsoid representations of the molecules together with atomic numbering schemes are shown in Figs. 1 and 2.

2.5. Computational details

Extended Hückel calculations were performed using the program CACAO [35]. The calculations were carried out using crystallographic data of the molecules studied. The EHT parameters for Hg, were those established in the literature.

3. Results and discussion

3.1. General aspects

Crystals of complex **1** were prepared by slow evaporation of the solution remaining after the filtration of the initial product had deposited from the reaction of $HgCl_2$ with triphenylphosphine and benzothiazole-2-thione in a molar ratio of 1:1:2 in methanol–acetonitrile solution. Smaller yields of the same product were obtained using a 1:1:1 molar ratio of reactants. Crystals of complex **2** were similarly obtained from the reaction of $HgCl_2$ with triphenylphosphine and pyrimidine-2-thione in equimolar ratio. The formulas of the complexes were firstly deduced from their elemental analysis, m.p. and their spectroscopic data. The crystals of the complexes are air stable when they are stored in darkness at r.t.

Table 1
Crystal data and the structure refinement details for the complexes **1** and **2**

Compound	**1**	**2**
Empirical formula	$C_{32}H_{24}ClHgN_2PS_4$	$C_{44}H_{36}Cl_2Hg_2N_4P_2S_2$
Formula weight	831.78	1218.90
Crystal system	monoclinic	monoclinic
Space group	$P2_1/c$	$C2/c$
a (Å)	10.412(2)	15.7674(9)
b (Å)	29.472(6)	13.2146(7)
c (Å)	11.039(2)	20.6533(10)
β (°)	111.29(3)	99.140(4)
V (Å^3)	3156.3(11)	4248.6(2)
Z	4	2
D_{calc} (g cm^{-3})	1.75	1.91
$F(000)$	1624	2336
μ(mm^{-1})	5.30	7.55
Crystal size (mm)	$0.3\times0.3\times0.2$	$0.2\times0.2\times0.15$
θ Range (°)	2–30	2–30
hkl Range	$-11\le h\le11$, $-30\le k\le31$, $-9\le l\le11$	$-21\le h\le19$, $-18\le k\le18$, $-28\le l\le26$
Reflections measured	14771	18062
Unique reflections (R_{int})	4045 (0.069)	5511 (0.041)
Number of parameters	371	254
Weighting scheme:		
1	0.01	0.045
2	5	0.6
Extinction parameter (k)	0.00066(14)	0 0.031
R (F)	0.059	0.079
wR (F^2)	0.089	
Goodness-of-fit	1.78	1.20
Max/min $\Delta\rho$ (e Å^{-3})	0.9/−1.0	1.9/−2.6

Table 2
Selected bond lengths (Å) and angles (°) for molecule **1** with e.s.d. values in parentheses

Bond lengths			
Hg(1)–S(2)	2.419(2)	S(1A)–C(2A)	1.747(8)
Hg(1)–P(1)	2.453(2)	S(1A)–C(9A)	1.750(9)
Hg(1)–Cl(1)	2.633(2)	C(2A)–N(3A)	1.320(11)
Hg(1)–S(2A)	2.726(2)	C(2A)–S(2A)	1.690(9)
S(1)–C(9)	1.735(9)	N(3A)–C(4A)	1.392(11)
S(1)–C(2)	1.755(8)	C(4A)–C(9A)	1.386(12)
C(2)–N(3)	1.288(11)	P(1)–C(21)	1.799(8)
C(2)–S(2)	1.726(9)	P(1)–C(11)	1.802(9)
N(3)–C(4)	1.403(11)	P(1)–C(31)	1.812(8)
C(4)–C(9)	1.392(12)		
Bond angles			
S(2)–Hg(1)–P(1)	140.79(7)	N(3A)–C(2A)–S(2A)	128.2(7)
S(2)–Hg(1)–Cl(1)	101.10(8)	N(3A)–C(2A)–S(1A)	110.3(6)
P(1)–Hg(1)–Cl(1)	103.30(8)	S(2A)–C(2A)–S(1A)	121.5(5)
S(2)–Hg(1) S(2A)	108.23(8)	C(2A)–S(2A)–Hg(1)	108.4(3)
P(1)–Hg(1)–S(2A)	97.66(8)	C(2A)–N(3A)–C(4A)	116.5(7)
Cl(1)–Hg(1)–S(2A)	99.10(7)	C(5A)–C(4A)–C(9A)	121.0(9)
C(9)–S(1)–C(2)	89.2(4)	C(5A)–C(4A)–N(3A)	127.2(9)
N(3)–C(2)–S(2)	126.5(7)	C(9A)–C(4A)–N(3A)	111.8(8)
N(3)–C(2)–S(1)	115.1(6)	C(8A)–C(9A)–S(1A)	129.5(7)
S(2)–C(2)–S(1)	118.4(5)	C(4A)–C(9A)–S(1A)	110.1(6)
C(2)–S(2)–Hg(1)	97.5(3)	C(21)–P(1)–C(11)	106.7(4)
C(2)–N(3)–C(4)	111.6(7)	C(21)–P(1)–C(31)	106.6(3)
C(5)–C(4)–N(3)	125.8(8)	C(11)–P(1)–C(31)	107 7(4)
C(9)–C(4)–N(3)	114.3(8)	C(21)–P(1)–Hg(1)	109,3(3)
C(4)–C(9)–S(1)	109.8(6)	C(11)–P(1)–Hg(1)	113.0(3)
C(8)–C(9)–S(1)	129.0(8)	C(31)–P(1)–Hg(1)	113.2(3)
C(2A)–S(1A)–C(9A)	91.3(4)		

3.2. IR spectroscopy

The IR spectra of complex **1** shows distinct vibrational bands at 1496 and at 1332 cm^{-1} which have been assigned as C–N bond vibrations (thioamide bands I and II) and at 1008 and at 747 cm^{-1} which were attributed to the C–S bond vibrations (thioamide bands III and IV). The corresponding thioamide bands of the free benzothiazole-2-thione ligand are given at 1490, 1320, 1010 and 860 cm^{-1}, respectively [36,37]. The most significant change has been observed in the thioamide band IV, supporting the sulfur donation of the ligand upon its coordination to the metal ion. The

Table 3
Selected bond lengths (Å) and angles (°) for molecule **2** with e.s.d. values in parentheses [a]

Bond lengths			
Hg(1)–P(1)	2.4826(9)	N(41)–C(44)	1.333(6)
Hg(1)–Cl(1)	2.5310(10)	N(41)–C(42)	1.339(5)
Hg(2)–S(42)	2.3513(11)	C(42)–N(43)	1.328(5)
Hg(2)–Cl(1)	3.0472(10)	C(42)–S(42)	1.765(4)
P(1)–C(21)	1.805(4)	N(43)–C(46)	1.340(5)
P(1)–C(11)	1.809(4)	C(44)–C(45)	1.369(7)
P(1)–C(31)	1.814(4)	C(45)–C(46)	1.371(6)
Bond angles			
$P(1)^{i}$–Hg(1)–P(1)	116.32(4)	C(21)–P(1)–Hg(1)	114.81(12)
P(1)–Hg(1)–Cl(1)	107.10(4)	C(11)–P(1)–Hg(1)	112.85(12)
P(1)–Hg(1)–$Cl(1)^{i}$	113.72(4)	C(31)–P(1)–Hg(1)	108.11(11)
Cl(1)–Hg(1)–$Cl(1)^{i}$	97.39(4)	C(44)–N(41)–C(42)	115.4(4)
$S(42)^{i}$–Hg(2)–S(42)	168.11(5)	N(43)–C(42)–N(41)	126.6(4)
S(42)–Hg(2)–$Cl(1)^{i}$	99.20(4)	N(43)–C(42)–S(42)	119.2(3)
S(42)–Hg(2)–Cl(1)	90.11(4)	N(41)–C(42)–S(42)	114.2(3)
$Cl(1)^{i}$–Hg(2)–Cl(1)	77.21(4)	C(42) S(42)–Hg(2)	99.82(13)
Hg(1)–Cl(1)–Hg(2)	92.70(3)	C(42)–N(43)–C(46)	115.6(3)
C(21)–P(1)–C(11)	107.66(16)	N(41)–C(44)–C(45)	123.3(4)
C(21)–P(1)–C(31)	106.88(17)	C(44)–C(45)–C(46)	116.2(4)
C(11)–P(1)–C(31)	106.02(17)	N(43)–C(46)–C(45)	122.9(4)

[a] Symmetry transformations used to generate equivalent atoms: $1-x, y, -z+1/2$.

bands at 687, 519, 501 and 486 cm^{-1} have been attributed to the vibrations of the C–P bond. Further information about the complex formation was obtained from the study of far-IR spectra. The new bands at 137, 192 and 248 cm^{-1} have been assigned to the vibrations of Hg–P, Hg–S and Hg–Cl bonds, respectively [22,38,39]. The IR spectra of complex **2** shows bands at 1560 1370, 1172 and 803 cm^{-1} for the thioamide bands I, II, III and IV, respectively, while the bands observed at 690, 508, and 489 cm^{-1} are characteristic for the vibrations of the P–C bond. The corresponding thioamide bands of the free thione ligand are given at 1510, 1320, 982 and 791 cm^{-1}, respectively [40]. The far-IR spectra of complex **2** contains new bands at 141, 165 and 247 cm^{-1} which have been attributed to the Hg–P, Hg–S and Hg–Cl bonds, respectively [22,38,39].

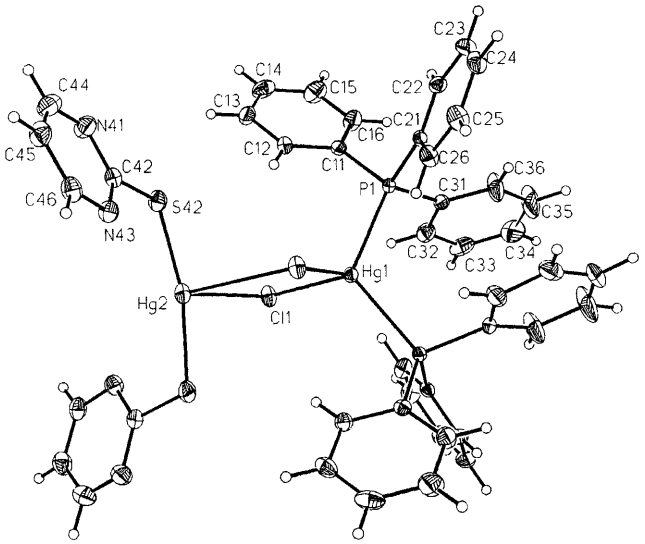


Fig. 2. Thermal ellipsoid representations of molecule **2** together with the atomic numbering scheme.

3.3. Structure of the $[Hg(PPh_3)(bzthztH)(bzthzt)Cl]$ (1)

A view of molecule **1** is shown in Fig. 1, while selected bond lengths and angles are given in Table 2. The molecule is a covalent monomer in the solid state with tetrahedral geometry around the metal ion. Two sulfur atoms, one phosphorus atom and one chlorine atom surround the mercury atom to build a distorted tetrahedron. Thus, one of the two benzothiazole-2-thione molecules has been deprotonated upon coordination. The formation of the benzothiazole-2-thionato anion during the reaction of a neutral thione molecule with the $[Cu(PPh_3)_3Cl]$ has also been observed and is described earlier [37]. The Hg(1)–S(2A) bond distance is 2.726(2) Å while the C(2A)–S(2A) and C(2A)–N(3A) bond distances are 1.690(9) and 1.320(11) Å, respectively, indicating that this ligand has been coordinated through its neutral form. The Hg(1)–S(2A) bond length is longer than those found in $[HgBr_2(meimz2SH)]_2$ (Hg–S = 2.407(2) and 2.405(2) Å)

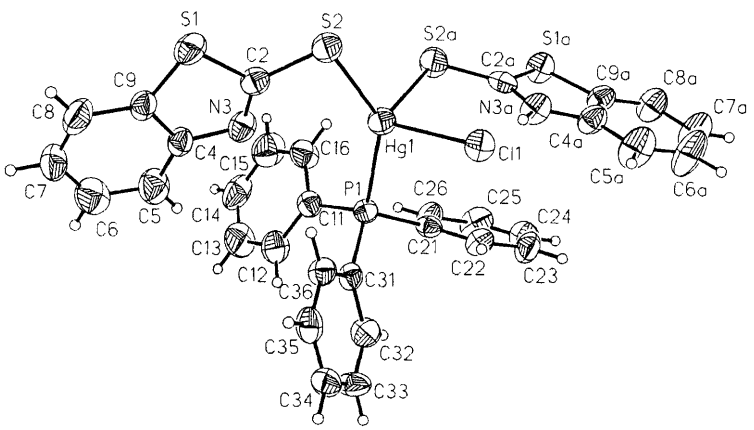


Fig. 1. Thermal ellipsoid representations of molecule **1** together with the atomic numbering scheme.

[20], $[Hg(ditet)_2Cl_2]$ (Hg–S = 2.49(1) and 2.50(1) Å) and in $[Hg(diditet)Cl_2]$ (Hg–S = 2.42(2) Å) [22], where thione ligands have been coordinated to the metal through their neutral form. The second Hg(1)–S(2) bond distance is 2.419(2) Å, while the corresponding C(2)–S(2) and C(2)–N(3) bonds are 1.726(9) and 1.288(11) Å, respectively, indicating a coordination through the anionic form of this ligand. The Hg–S bond length found earlier in $[Hg(PPh_3)_2(SCN_4Ph)_2]$ [30], where the ligand is coordinated to the mercury ion through its anionic form, is 2.566(3) Å. The Hg–P bond length is 2.453(2) Å and is similar to those found in $[Hg(PPh_3)_2(SCN_4Ph)_2]$ [30] (Hg–P = 2.500(3) Å), $[Hg(PPh_3)_2(CN)_2]$ [25] (Hg–P = 2.434(5) and 2.589(5) Å, respectively), $[Hg(PPh_3)_2(NO_3)_2]$ [25] (Hg–P = 2.451(1) Å) and in $[HgCl_2(PPh_3)_2]$ [28] (Hg–P = 2.462(2) and 2.478(2) Å). The Hg–Cl bond length is 2.633(2) Å and is longer than those measured in $[HgCl_2\{Ph_2P(S)CH_2CH_2(S)PPh_2\}]$ [3] (Hg–Cl = 2.447(3) and 2.442(3) Å, respectively), $[Hg(ditet)_2Cl_2]$ (Hg–Cl = 2.51(1) and 2.52(1) Å [22], $[\{HgCl_2(H_2L)\}_2]$ [38] (Hg–Cl = 2.532(6), 2.380(7), 2.585(6) and 2.489(7) Å) and in $[HgCl_2(PPh_3)_2]$ [28] (Hg–Cl = 2.559(2) and 2.545(3) Å). The Cl–Hg–S(2A) angle is 99.10(7)° indicating a N–H···Cl hydrogen bond while the Cl–Hg–S(2) angle is 108.23(8)° and is in accordance to those measured for the complex $[Hg(ditet)_2Cl_2]$ [22] (S(1)–Hg–Cl(1) = 108.6(3) and S(2)–Hg–Cl(1) = 104.3(3)). The P–Hg–S(2A) angle is 97.66(8)° and is in accordance to the corresponding angles found in $[Hg(PPh_3)_2(SCN_4Ph)_2]$ [30] (P–Hg–S = 100.37(6) and 95.7(1)°) while the P–Hg–S(2) angle is 140.79(7)°.

3.4. Structure of the $[Hg_2Cl_2(PPh_3)_2(pmt)_2]$ (2)

A view of molecule **2** is shown in Fig. 2, while selected bond lengths and angles are given in Table 3. The molecule is a covalent, binuclear complex which consists of two different moieties with tetrahedral geometry around each mercury(II) ion. One moiety, consists of a mercury(II) ion with two phosphorus atoms from phosphine ligands and two bridging chlorine atoms while the other, consists of a mercury(II) ion and two sulfur atoms of pyrimidine-2-thionato ligands. The whole molecule sits on a two-fold axis of symmetry passing through the two metal atoms. The two Hg–S bond lengths are 2.3513(11) Å and are in accordance with those found in $[HgBr_2(meimz2SH)]_2$ (Hg–S = 2.407(2) and 2.405(2) Å) [20], $[Hg(ditet)_2Cl_2]$ (Hg–S = 2.49(1) and 2.50(1) Å) and in $[Hg(diditet)Cl_2]$ (Hg–S = 2.42(2) Å) [22], while the two Hg–P bond lengths are 2.4826(9) Å and are similar to those found in $[Hg(PPh_3)_2(SCN_4Ph)_2]$ [30] (Hg–P = 2.500(3) Å), $[Hg(PPh_3)_2(CN)_2]$ [25] (Hg–P = 2.434(5) and 2.589(5) Å, respectively), $[Hg(PPh_3)_2(NO_3)_2]$ [25] (Hg–P = 2.451(1) Å) and in $[\{HgCl_2(PPh_3)_2\}_2]$ [29] (Hg–P = 2.406(7) Å). The two parts of the molecule are linked to each other by two chlorine atoms with Hg(1)–Cl(1) and Hg(2)–Cl(1) bond distances 2.5310(10) and 3.0472(10) Å, respectively. The corresponding bond distances between mercury(II) and bridging Cl atoms found in the $[\{HgCl_2(PPh_3)_2\}_2]$ complex [29] are Hg–Cl(2) = 2.623(8) Å and Hg–Cl(2^i) = 2.658(8) Å, respectively. The Cl(1)–Hg(1)–Cl(1^i), Hg(1)–Cl(1)–Hg(2) and the Cl(1)–Hg(2)–Cl(1^i) angles are 97.39(4), 92.70(3) and 77.21(4)°, respectively. The values of the Cl(2)–Hg–Cl(2^i) and Hg–Cl(2)–Hg^i angles measured in the $[\{HgCl_2(PPh_3)_2\}_2]$ complex [29] are 85.3(3) and 94.6(3)°, respectively. The P(1)–Hg(1)–P(1^i) angle is 116.32(4)°, slightly smaller than the value of the corresponding angle measured in $[Hg(PPh_3)_2(SCN_4Ph)_2]$ [30] (P1–Hg–P2 = 125.6(1)°). The S(42)–Hg(1)–S(42^i) angle is 168.11(5)°.

3.5. Computational study

The rather unusual formation of the complex $[Hg_2Cl_2(PPh_3)_2(pmt)_2]$ (**2**) prompted us to undertake a computational study in order to verify the factors leading the formation of this type of complex towards the formation of the $[Hg(PPh_3)(bzthztH)(bzthzt)Cl]$ (**1**) complex. As it has been evidenced, the energy of the LUMO lies 2.979 eV higher than the corresponding HOMO's energy in the case of complex **2** while the energy of the LUMO lies 3.618 eV higher than the corresponding HOMO's energy in the case of complex **1**. The differences in the HOMO–LUMO energy values computed could explain the stability of **2**. The calculated overlap population in the case of complex **1** is 0.342 and 0.657 e for the Hg(1)–Cl(1) and Hg(1)–P(1) bonds, respectively, and 0.330, 0.572 e for the two Hg(1)–S(2A) and Hg(1)–S(2) bonds. The calculated overlap population in the case of complex **2** is 0.639 e for the two Hg(1)–P bonds and 0.652 e for the two Hg(2)–S bonds, respectively, while the overlap population for the Hg(1)–Cl(1) and Hg(2)–Cl(1) bonds is.0.412 and 0.108 e, respectively. The calculated net charges for the Hg(1) and Hg(2) of complex **2** are –0.179 and 0.266, respectively.

4. Supplementary material

Crystallographic data for the structural analysis have been deposited with the Cambridge Crystallographic Data Centre, CCDC Nos. 140 847 for compound **1** and 140 848 for compound **2**. Copies of this information may be obtained free of charge from: The Director, CCDC, 12 Union Road, Cambridge, CB2 1EZ, UK (Fax: +44-1223-336033; e-mail: deposit@ccdc.cam.ac.uk or www: http://www.ccdc.cam.ac.uk).

References

[1] N.A. Bell, W. Clegg, J.R. Creighton c, E.S. Raper, Inorg. Chim. Acta 303 (2000) 12.
[2] T.S. Lobana, A. Sanchez, J.S. Casas, A. Castineiras, J. Sordo, M.S. Garcia-Tasende, E.M. Vazquez-Lopez, J. Chem. Soc., Dalton Trans. (1997) 4289.
[3] T.S. Lobana, M.K. Sandhu, M.J. Liddell, E.R.T Tiekink, J. Chem. Soc., Dalton Trans. (1990) 691.
[4] C.M.V. Stalhandske, I. Persson, M. Sandstrom, M. Aberg, Inorg. Chem. 36 (1997) 4945.
[5] K.K. Cheung, R.S. McEwen, G.A. Sim, Nature 23 (1965) 383.
[6] R.A. Santos, E.S. Gruff, S.A. Koch, G.S. Harbinson, J. Am. Chem. Soc. 113 (1991) 469.
[7] D.T. Jiang, S.M. Heald, T.K. Sham, M.J. Stillman, J. Am. Chem. Soc. 116 (1994) 11004.
[8] G. Fleissner, P.M. Kozlowski, M. Vargek, J.W. Bryson, T.V. O'Halloran, T.G. Spiro, Inorg. Chem. 38 (1999) 3523.
[9] E.S. Gruff, S.A. Koch, J. Am. Chem. Soc. 112 (1990) 1245.
[10] H. Barrera, J.C. Bayon, P. Gonzalez-Duarte, J. Sola, M.M. Vinas, J.L. Brianso, X. Solans, Polyhedron 1 (1982) 647.
[11] G. Christou, K. Folting, J.C. Huffman, Polyhedron 3 (1984) 1247.
[12] L. Carlton, D. White, Polyhedron 9 (1990) 2717.
[13] P.G. Schultz, K.G. Au, C.T. Walsh, Biochemistry 24 (1985) 6840.
[14] E. Block, M. Britto, M. Gernen, D. McGouety, H. Kang, J. Zubieta, Inorg. Chem. 29 (1990) 3172.
[15] A. Castineiras, W. Hiller, J. Strahle, J. Chem. Soc., Dalton Trans. (1986) 1945.
[16] Lobana T.S, Paul S., Castineiras A., J. Chem. Soc., Dalton Trans. (1999) 1819.
[17] E.S. Raper, Coord. Chem. Rev. 61 (1985) 115.
[18] E.S. Raper, Coord. Chem. Rev. 129 (1994) 91.
[19] E.S. Raper, Coord. Chem. Rev. 153 (1996) 199.
[20] E.S. Raper, J.R. Creighton, N.A. Bell, W. Clegg, L. Cucurull-Sanchez, Inorg. Chim. Acta 277 (1998) 14.
[21] A.R. Norris, S.E. Taylor, E. Buncel, F. Belanger-Gariery, A.L. Beauchamp, Can. J. Chem. 61 (1983) 1536.
[22] M. Cannas, F.A. Devillanova, G. Marongiu, G. Verani, J. Nucl. Chem. 43 (1981) 2383.
[23] J. Dai, M. Munakata, G. Bian, Q. Xu, T. Kuroda-Sowa, M. Maekawa, Polyhedron 17 (1998) 2267.
[24] N.A. Bell, T.N. Branston, W. Clegg, J.R. Creighton, L. Cucurull-Sanchez, M.R.J. Elsegood, E.S. Raper, Inorg. Chim. Acta 303 (2000) 220.
[25] H.B. Buergi, E. Fischer, R.W. Kunz, M. Parvez, P.S. Pregosin, Inorg. Chem. 21 (1982) 1246.
[26] T.S. Lobana, M.K. Sandhu, D.C. Povey, G.W. Smith, V. Rambas, J. Chem. Soc., Dalton Trans. (1989) 2339.
[27] P. Barbaro, F. Cecconi, C.A. Ghilardi, S. Midollini, A. Orlandini, A. Vacca, Inorg. Chem. 33 (1994) 6163.
[28] N. Bell, T.D. Dee, M. Golstein, P.J. McKenna, I.W. Nowell, Inorg. Chim. Acta 71 (1983) 135.
[29] N. Bell, M. Golstein, T. Jones, I.W. Nowell, Inorg. Chim. Acta 43 (1980) 87.
[30] H. Noth, W. Beck, K. Burger, Eur. J. Inorg. Chem. (1998) 93.
[31] Kuma KM-4CCD User Manual, Kuma Diffraction, Wrocław, Poland, 1999.
[32] CRYSALIS, Program for Reduction of the Data from Kuma CCD Diffractometer, Kuma Diffraction, Wrocław, Poland, 1999.
[33] G.M. Sheldrick, Acta Crystallogr., Sect. A 46 (1990) 467.
[34] G.M. Sheldick, SHELXL-93. Program for the Refinement of Crystal Structures, University of Göttingen, Germany, 1993.
[35] C. Mealli, D. Proserpio, J. Chem. Educ. 67 (1990) 399.
[36] J.P. Khullar, U. Agarwala, Can. J. Chem. 53 (1975) 1165.
[37] P.J. Cox, P. Aslanidis, P. Karagiannidis, S.K. Hadjikakou, Polyhedron 18 (1999) 1501.
[38] R. Baggio, M.T. Garland, M. Perec, J. Chem. Soc., Dalton Trans. (1995) 987.
[39] G.B. Deacon, J.H. Green, Chem. Commun. (1966) 629.
[40] L.J. Bellamy, The Infrared Spectra of Complex Molecules, Wiley, New York, 1966.

PERGAMON

www.elsevier.nl/locate/poly

Polyhedron 19 (2000) 2237–2242

POLYHEDRON

Polymeric and tetranuclear silver(I) chains encapsulated by a scorpion-like ligand. Synthesis and structures of $[Ag_2(tren(mim)_3)]_n(NO_3)_{2n}\cdot nH_2O$ and $[Ag_4(tren(mim)_3)_2](CF_3SO_3)_4\cdot 2H_2O$ (tren(mim)$_3$ = tris{2-[2-(1-methyl)imidazolyl]methyliminoethyl}amine)

Shi-Ping Yang, Hai-Liang Zhu, Xian-Hong Yin, Xiao-Ming Chen *, Liang-Nian Ji

School of Chemistry and Chemical Engineering, Zhongshan University, Guangzhou 510275, People's Republic of China

Received 23 May 2000; accepted 8 August 2000

Abstract

Two compounds, $[Ag_2(tren(mim)_3)]_n(NO_3)_{2n}\cdot nH_2O$ (**1**) and $[Ag_4(tren(mim)_3)_2](CF_3SO_3)_4\cdot 2H_2O$ (**2**), were obtained by self-assembly of AgX ($X = NO_3^-$, $F_3CSO_3^-$) with tren(mim)$_3$ (tren(mim)$_3$ = tris{2-[2-(1-methyl)imidazolyl]methyliminoethyl}amine). The crystal structures of **1** and **2** have been determined by X-ray diffraction analysis. In **1**, three arms of the ligand, which can be described as a scorpion-like ligand, function in both the usual bidentate chelate fashion and an unprecedented bidentate bridging mode in coordination to Ag(I) atoms; the ligands wrap the infinite Ag(I) wire with the adjacent Ag···Ag separation of approximately 3.0 Å, indicating weak metal–metal interaction, to furnish cationic helical chains. The ligand in **2** behaves in two different coordination fashions in comparison to the ligand in **1**. Two ligands encapsulate four Ag(I) atoms in an interlocking fashion. A pair of the tetranuclear cations related by an inversion center is connected to form an octanuclear cation through a ligand-unsupported metallic interaction between two Ag(I) atoms being separated at 3.117(2) Å and belonging to different tetranuclear cations. The ^{1}H NMR spectra of **1** and **2** in solution are virtually identical, indicating that **1** and **2** have similar structures in solution. © 2000 Elsevier Science B.V. All rights reserved.

Keywords: Imidazole; Schiff base; Silver complexes; Crystal structures

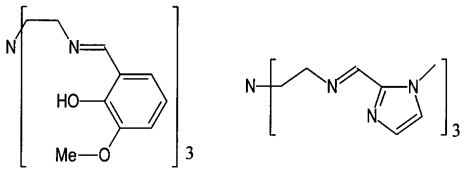
1. Introduction

Metal complexes of tripodal Schiff ligands are well explored with d- and f-block metals, which have been focused on the structural and physico-chemical properties as well as the possible application as magnetic resonance imaging agents, and the modeling of metalloenzymes such as superoxide dismutases [1,2]. Generally, these tripodal ligands are the condensation products of tris(2-aminoethyl)amine (tren) and aromatic aldehydes and contain three bidentate compartments (Scheme 1). They commonly function in the triple chelate mode, arising from the conjugation of the Schiff base group and thus complexation of these ligands with metal ions gives mononuclear complexes in six- or seven-coordination; in the later cases the amine nitrogen atom participates in coordination. A few exceptions have recently been found in some dinuclear complexes of the tripodal Schiff base tris[2-(3-methoxysalicylideneamino)ethyl]amine (tren(salmo)$_3$), in which a pair of metal atoms are bridged by the μ_2-phenolate groups [3]. In the present work, we report the synthesis and crystal structures of two novel chain-like complexes with a tripodal Schiff base as bridging agent, namely $[Ag_2(tren(mim)_3)]_n(NO_3)_{2n}\cdot nH_2O$ (**1**) and

* Corresponding author. Tel.: +86-20-8411-3986; fax: +86-20-8411-2245.

E-mail address: cescxm@zsu.edu.cn (X.-M. Chen).

0277-5387/00/$ - see front matter © 2000 Elsevier Science B.V. All rights reserved.
PII: S0277-5387(00)00534-9



tren(salmo)$_3$ tren(mim)$_3$

Scheme 1.

$[Ag_4(tren(mim)_3)_2](CF_3SO_3)_4{\cdot}2H_2O$ (**2**) (tren(mim)$_3$ = tris{2-[2-(1-methyl)imidazolyl]methyliminoethyl}amine, see Scheme 1).

2. Experimental

2.1. Materials and physical measurements

All the reagents were commercially available and used as received. The C, H, N microanalyses were carried out with a Perkin–Elmer 240 elemental analyzer. IR spectra were recorded from KBr pellets in the range 4000–400 cm^{-1} on a Nicolet Impact 420 FTIR spectrometer. ^{1}H NMR spectra were recorded with an Inova 500NB spectrometer using TMS as internal reference and DMSO-d_6 as matrix.

2.2. Synthesis of metal complexes

2.2.1. $[Ag_2(tren(mim)_3)]_n(NO_3)_{2n}{\cdot}nH_2O$ (*1*)

1-Methylimidazole-2-carbaldehyde (3 mmol, 0.33 g) was added to a solution of tren (1 mmol, 0.15 g) in dried MeOH . The mixture was refluxed for 5 h, and was then added to a solution of $AgNO_3$ (2 mmol, 0.34 g) in MeCN. A colorless crystalline solid (**1**) was obtained by vapor diffusion of diethyl ether after 3 days. *Anal*. Calc. for $C_{21}H_{32}Ag_2N_{12}O_7$: C, 32.32; H, 4.13; N, 21.54. Found: C, 32.48; H, 3.97; N, 21.43%. IR data (KBr, cm^{-1}): 3486 m, 3114 m, 2811 m, 1637 s, 1482 s, 1440 s, 1426 s, 1377 sh 1285 s 1166 m, 1089 m, 1075 m, 1046 m, 835 m, 800 m, 779 m. ^{1}H NMR (500 MHz, DMSO-d_6): $\delta = 8.63$ (3 H, s, imine), 7.47 (3 H, s, imidazole ring), 7.19 (3 H, s, imidazole ring), 3.86–3.84 (4 H, m, C=N–CH_2), 3.82 (9 H, s, CH_3), 3.15 (2 H, s, C=N–CH_2), 2.94–2.91 (6 H, m, N–CH_2).

2.2.2. $[Ag_4(tren(mim)_3)_2](CF_3SO_3)_4{\cdot}2H_2O$ (*2*)

1-Methylimidazole-2-carbaldehyde (3 mmol, 0.33 g) was added to a solution of tren (1 mmol, 0.15 g) in dried MeOH. The mixture was refluxed for 5 h, then a solution of $AgCF_3SO_3$ (2 mmol, 0.52 g) in MeCN was added. A colorless crystalline solid (**2**) was obtained by vapor diffusion of diethyl ether after 3 days. *Anal*. Calc. for $C_{46}H_{64}Ag_4N_{20}O_{14}F_{12}S_4{\cdot}2H_2O$ (**2**): C, 28.94; H, 3.38; N, 14.68. Found: C, 29.18; H, 3.17; N, 14.95%. IR data (KBr, cm^{-1}): 3121 m, 2952 sh, 2864 m, 2811 m, 1637 s, 1482 s, 1440 s, 1635 m, 1271 s, 1166 s, 1082 m, 1032 s, 765 m, 639 s, 579 m, 519 m. ^{1}H NMR (500 MHz, DMSO-d$_6$): $\delta = 8.62$ (3 H, s, imine), 7.45 (3 H, s, imidazole ring), 7.18 (3 H, s, imidazole ring), 3.86–3.84 (4 H, m, C=N–CH_2), 3.82 (9 H, s, CH_3), 3.15 (2 H, s, C=N–CH_2), 2.93–2.89 (6 H, m, N–CH_2).

Table 1
Crystallographic and experimental data for **1** and **2**

Complexes	**1**	**2**
Formula	$C_{21}H_{32}Ag_2N_{12}O_7$	$C_{46}H_{64}Ag_4N_{20}O_{14}F_{12}S_4$
Formula weight	780.33	1908.84
Crystal system	monoclinic	monoclinic
Space group	$P2_1/n$	$C2/c$
a (Å)	11.769(4)	38.838(6)
b (Å)	10.666(4)	18.150(2)
c (Å)	22.941(7)	21.390(2)
β (°)	101.21(2)	90.11(2)
V (Å^3)	2825(2)	15078(3)
Z	4	8
D_{calc} (g cm^{-3})	1.835	1.666
T (K)	293	293
λ (Mo Kα) (Å)	0.710 73	0.710 73
μ (Mo Kα)(mm^{-1})	1.451	1.229
R_1 ($I>2\sigma(I)$) [a]	0.0454	0.0747
wR_2 (all data) [a]	0.0906	0.2272

[a] $R_1 = \Sigma||F_o|-|F_c||/\Sigma|F_o|$, $wR_2 = [\Sigma w(|F_o^2|-|F_c^2|)^2/\Sigma\, w(F_o^2)^2]^{1/2}$.

2.3. X-ray crystallography

Diffraction intensities for complexes **1** and **2** were collected at 293 K on a Siemens R3m diffractometer. Lorentz-polarization and absorption corrections were applied [4]. The structure solutions and full-matrix least-square refinements based on F^2 were performed with the SHELXS-97 and SHELXL-97 program packages [5], respectively. All the nonhydrogen atoms were refined anisotropically. Hydrogen atoms of the organic were generated geometrically (C–H 0.96 Å) and those of the aqua ligands were located from the difference maps; all hydrogen atoms were assigned the same isotropic thermal parameters and included in the structure-factor calculations. Analytical expressions of neutral-atom scattering factors were employed, and anomalous dispersion corrections incorporated [6]. The crystallographic data for **1** and **2** are summarized in Table 1. Selected bond distances and angles are given in Table 2.

Table 2
Selected interatomic distances (Å) and angles (°) for **1** and **2**

1			
Ag1–N3	2.309(3)	Ag1–N4	2.477(3)
Ag1–N7	2.425(3)	Ag1–N9	2.356(3)
Ag2–N6	2.172(3)	Ag3–N1	2.137(3)
Ag1···Ag2	2.934(1)	Ag1···Ag3	3.053(1)
N7–Ag1–N4	101.7(1)	N3–Ag1–N9	118.4(1)
N3–Ag1–N7	133.7(1)	N7–Ag1–N9	71.3(1)
N3–Ag1–N4)	98.4(1)	N4–Ag1–N9	135.6(1)
Ag2···Ag1···Ag3	158.76(3)		
2			
Ag1–N5	2.589(6)	Ag1–N6	2.195(6)
Ag1–N9	2.167(5)	Ag2–N4	2.600(5)
Ag2–N8	2.230(5)	Ag2–N16	2.162(5)
Ag3–N1	2.202(5)	Ag3–N13	2.324(6)
Ag3–N14	2.486(7)	Ag4–N11	2.188(7)
Ag4–N18	2.553(7)	Ag4–N19	2.225(6)
Ag1···Ag2	2.9279(9)	Ag2···Ag3	3.1313(9)
Ag3···Ag4	2.929(1)	Ag4···Ag4a	3.117(1)[a]
N9–Ag1–N6	161.2(2)	N9–Ag1–N5	126.1(2)
N6–Ag1–N5	71.7(2)	N16–Ag2–N8	161.4(2)
N16–Ag2–N4	121.8(2)	N8–Ag2–N4	75.2(2)
N1–Ag3–N13	145.6(2)	N1–Ag3–N14	127.2(2)
N13–Ag3–N14	73.7(2)	N11–Ag4–N18	153.5(2)
N11–Ag4–N19	132.1(2)	N18–Ag4–N19	74.0(2)
Ag1···Ag2···Ag3	116.44(3)	Ag2···Ag2···Ag4	133.62(3)
Ag3···Ag4···Ag4 [a]	156.83(3)		

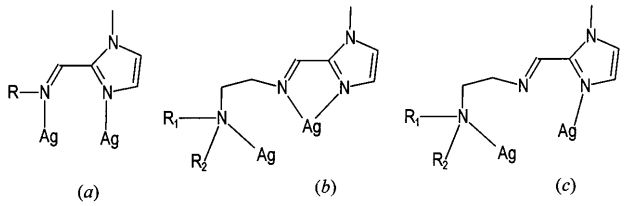
[a] Symmetry code for **2**: $1-x$, y, $1/2-z$.

3. Results and discussion

3.1. Crystal structures

3.1.1. $[Ag_2(tren(mim)_3)]_n(NO_3)_{2n}\cdot nH_2O$ (*1*)

The crystal structure of **1** features polymeric helical $[Ag_2(tren(mim)_3)]_n^{2n+}$ cations, nitrate anions and solvate water molecules. In the polymeric chain, each structural unit consists of a binuclear $[Ag_2(tren(mim)_3)]$ core, as shown in Fig. 1. The crystal structure shows that tren(mim)$_3$ acts in a very unusual fashion in coordination with the Ag(I) atoms. One of the arms functions in the usual bidentate chelate fashion to bind Ag1, whereas the other two arms act in an unusual bidentate bridging mode to ligate two Ag(I) atoms, as shown in Scheme 2(a); to our knowledge, such a bridging mode for Schiff bases has not been documented in the literature. Each of the later two arms uses its imidazole or imine nitrogen atom to bind Ag1, resulting in a highly distorted tetrahedral coordination geometry for Ag1. The remaining imine or imidazole nitrogen atom binds to Ag2 and Ag3, respectively. Both Ag2 and Ag3 are each located at a crystallographic inversion center and coordinated by a pair of imine nitrogen atoms or by a pair of imidazole nitrogen atoms in a linear arrangement, respectively. The structure is thus extended into infinite chains through the bridging coordination, in which the adjacent Ag···Ag separations are 2.9337(10) and 3.0533(11) Å for Ag1···Ag2 and Ag1···Ag3, respectively, and the metal atoms are arranged in a virtually linear fashion with the most distorted angle Ag2···Ag1···Ag3 at 158.76(2)°. The Ag···Ag distances are in accordance with the values previously reported in other Ag(I) complexes [7,8], and are well below the summed van der Waals radii of two silver atoms (3.44 Å) [9], indicating some extent of weak metal–metal interaction. Therefore, tren(mim)$_3$



Scheme 2.

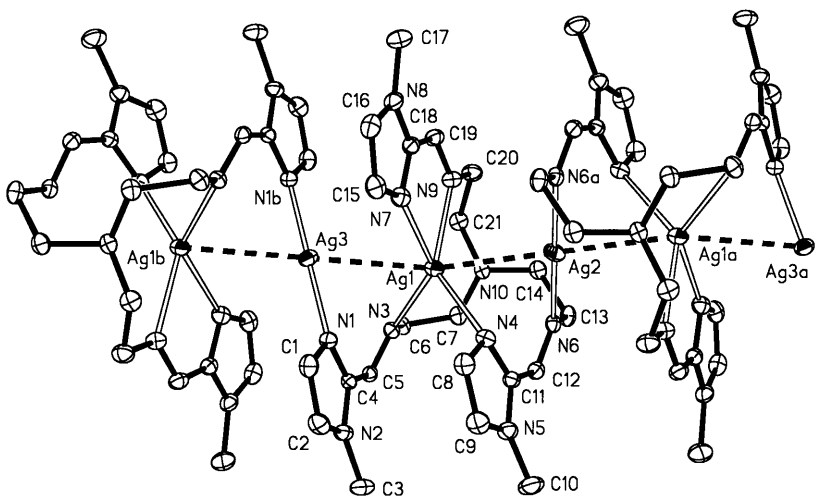


Fig. 1. ORTEP view of the coordination environment in **1**. Symmetry codes: (a) $1-x$, $1-y$, $-z$; (b) $-x$, $1-y$, $-z$.

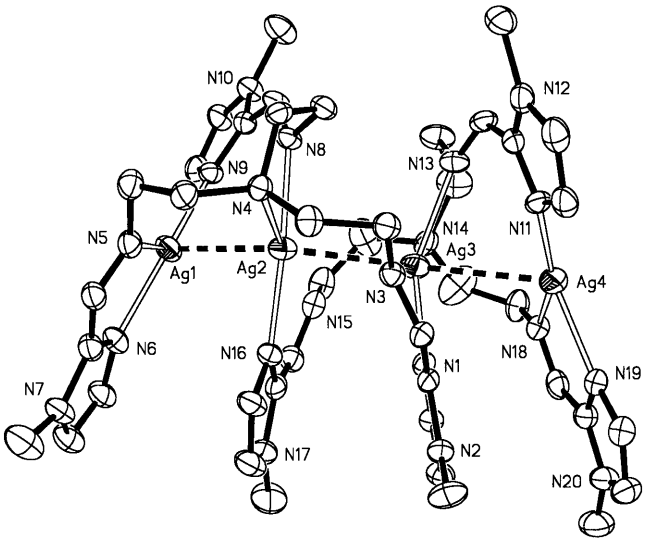


Fig. 2. ORTEP view of the $[Ag_4(tren(mim)_3)_2]^{4+}$ cation in **2**.

may be best described as a scorpion-like ligand, and it wraps the Ag(I) ions to furnish cationic helical wires. It is noteworthy that, although a number of linear oligonuclear metal complexes comprising Cr(II), Co(II), Ni(II), Rh(II), Ru(II), Pt(II,III) [10–14], as well as a linear trinuclear Ag(I) complex have been documented [8a], no analogous Ag(I) complex has been reported so far.

Detailed examination reveals that the average bond distance of Ag1–N(imine) (2.333 Å) and Ag1–N(imidazole) (2.451 Å) for the tetrahedral Ag(1) atom are significantly longer than the bond distances of Ag2–N(imine) (2.172(3) Å) and Ag3–N(imidazole) (2.137(3) Å) for the two linear coordinated Ag(I) atoms, indicating that the bond lengths are directly related to the coordination numbers. The bond angles of N–Ag1–N are from 71.260(11)–135.62(11)°, being markedly distorted from an idealized tetrahedron, such distortion is frequently observed in silver(I) chemistry. The lattice water molecule forms a hydrogen bond with the oxygen atom of the anion (O1w···O2 = 2.878(3) Å).

$[Ag_4(tren(mim)_3)_2](CF_3SO_3)_4\cdot 2H_2O$ (2). The crystal structure of **2** consists of discrete tetranuclear $[Ag_4(tren(mim)_3)_2]^{4+}$ cations, trifluoromethanesulfonate anions and water molecules. The tetranuclear $[Ag_4(tren(mim)_3)_2]^{4+}$ cation is depicted in Fig. 2, which comprises two $tren(mim)_3$ ligands and four Ag(I) atoms. The scorpion-like ligand behaves in a different coordination fashion in comparison to that found in **1**. One arm of each $tren(mim)_3$ uses its imine and imidazole nitrogen atom to bind Ag1 (or Ag4) in the bidentate chelate mode, the second arm bridges Ag1 and Ag2 (or Ag3 and Ag4) using its imidazole and imine nitrogen atoms, whereas the third arm links to Ag3 (or Ag2) using its imidazole nitrogen atom as a unique donor. The amine nitrogen atom also participates in coordination to Ag3 (or Ag2). It is worthy to note that there are three unusual bridging modes in **2**. One is similar to that found in **1** (Scheme 2(a)). The participation of the amine nitrogen atom in coordination yields two types of unusual bridging mode for the scorpion-like ligand, in which the amine nitrogen atoms bind a Ag(I) atom and a bidentate imidazole-imine entity chelates another Ag(I) atom (Scheme 2(b)), whereas another bidentate imidazole-imine entity uses only the imidazole nitrogen atom to ligate another Ag(I) atom (Scheme 2(c)). More interestingly, the ligand encapsulates the Ag(I) atoms in an interlocking fashion, being different to that found in **1**. A pair of the tetranuclear cations related by an inversion center is connected to form an octanuclear cation through a weak metallic interaction between Ag4 and Ag4a separated at 3.117(2) Å, as illustrated in Fig. 3. Since the four imidazole rings ligated to Ag4 and Ag4a are arranged in an off-set fashion, there is no significant $\pi-\pi$ interaction between imidazole groups from different tetramers, the weak metallic interaction between Ag4 and Ag4a can be described as ligand-unsupported, which is rarely observed [7b,c,15,16]. Although the Ag4···Ag4a distance is quite long, it is comparable to other ligand-supported metallic separations found in **2** (2.9279(9)–3.1313(9) Å) and **1**, and is also well below the summed van der Waals radii of two

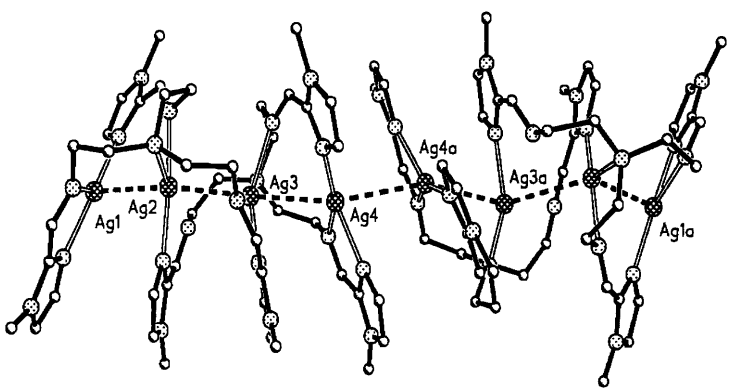


Fig. 3. Perspective view showing a dimer of the $[Ag_4(tren(mim)_3)_2]^{4+}$ cations connected by the weak Ag···Ag interaction in **2**.

silver atoms [9]. Each Ag(I) atom in the cation is coordinated in a distorted T-shape geometry, associated with a five-membered chelate ring, the metallic chain is thus in a zigzag fashion with the Ag···Ag···Ag angles in the range 116.44(3)–156.83(4)°. Among the average bond distances of Ag–N(imidazole) (2.190(6) Å), Ag–N(imine) (2.424(6) Å) and Ag–N(amine) (2.543(6) Å), Ag–N(imidazole) is the shortest while Ag–N(amine) is the longest. Finally, it should be noted that the counterions in **2** may play an important role in terminating the polymerization; the terminal Ag1 has weak interaction with one oxygen atom of the anion (Ag···O 2.967(7) Å). Similar to **1**, the lattice water molecule forms a hydrogen bond with oxygen atom of the anion (O1···F11 = 2.732(5) Å), and there are hydrogen bonds between the lattice water molecules (O1w···O2w = 2.727(6) Å).

3.2. Spectroscopy

The IR spectra of **1** and **2** show the strong bands at 1637 and 1440 cm^{-1} can be assigned to the symmetric stretching vibrations of –C=N– and –C=N–C=N–, respectively, implying direct coordination of the imine nitrogen atoms and imidazole nitrogen atoms [17]. The ^1H NMR spectra of **1** and **2**, having virtually identical patterns, indicate that they have similar structures in solution although they have different structures in the solid state. The structural differences in the solid state between **1** and **2** may apparently be attributed to the influence of the counter-ions in the crystallization process.

4. Conclusions

Self-assembly of the tripodal Schiff base containing imidazole groups with silver(I) salts yielded a tetranuclear and a polymeric helical silver(I) complex, which have been structurally characterized to exhibit three novel bridging modes for the ligands in coordination to Ag(I) atoms in the solid state, as well as ligand-unsupported weak Ag···Ag contacts. The ^1H NMR spectra implies that **1** and **2** have similar structures in solution. The different aggregations and helicities of the structures in the solid state may be attributed to the influence of the counter-ions in crystallization.

5. Supplementary material

Crystallographic data for the structural analysis have been deposited with the Cambridge Crystallographic Data Centre, CCDC Nos. 120560 and 120561. Copies of this information may be obtained free of charge from: The Director, CCDC, 12 Union Road, Cambridge, CB2 1EZ, UK (Fax: +44-1223-336033; e-mail: deposit @ccdc.cam.ac.uk or www: http://www.ccdc.cam.ac.uk).

Acknowledgements

This work was supported by the National Natural Science Foundation of China (No. 29625102, 29673057). We are indebted to the Chemistry Department of the Chinese University of Hong Kong for donation of the R3m diffractometer.

References

[1] (a) A. Deroche, I. Morgenstern-Badarau, M. Cesario, J. Guilhem, B. Keita, L. Nadjo, C.H. Levin, J. Am. Chem. Soc. 118 (1996) 4567. (b) S.H. Gou, X.Z. You, K.B. Yu, J.P. Lu, Inorg. Chem. 32 (1983) 1883. (c) P.G. Sim, E. Sinn, Inorg. Chem. 17 (1978) 1288. (e) P.G. Sim, E. Sinn, J. Am. Chem. Soc. 103 (1981) 241.

[2] (a) I. Morgenstern-Badarau, F. Lanbert, A. Deroche, M. Cesario, J. Guilherm, B. Keita, L. Nadjo, Inorg. Chim. Acta 275-276 (1998) 234. (b) C.T. Brewer, G. Brewer, M.Y. Sheng, W.R. Scheidt, I. Muller, Inorg. Chim. Acta 278 (1998) 197.

[3] (a) P. Bhattacharyya, J. Parr, A.T. Ross, A.M.Z Slawin, J. Chem. Soc., Dalton Trans. (1998) 3149. (b) J.P. Costes, F. Dahan, A. Dupuis, S. Lagrave, J.P. Laurent, Inorg. Chem. 37 (1998) 153. (c) S. Liu, L. Gelmini, S.J. Rettig, R.C. Thompson, C. Orvig, J. Am. Chem. Soc. 114 (1992) 6081. (d) S.J. Archibald, A.J. Blake, S. Parsons, M. Schröder, R.E.P. Winpenny, J. Chem. Soc., Dalton Trans. (1997) 173.

[4] AC.T. North, D.C. Phillips, F.S. Mathews, Acta Crystallogr., Sect. A 24 (1968) 351.

[5] (a) G.M. Sheldrick, SHELXS-97, Program for Crystal Structure Solution, Göttingen University, Germany, 1997. (b) G.M. Sheldrick, SHELXL-97, Program for Crystal Structure Refinement, Göttingen University, Germany, 1997.

[6] International Tables for X-ray Crystallography, A.J.C. Wilson, (Ed.) vol. C, Tables 4.2.6.8 and 6.1.1.4, Kluwer Academic, Dordrecht, 1992.

[7] (a) M.L. Tong, S.L. Zheng, X.M. Chen, Chem. Commun. (1999) 561. (b) M.L. Tong, X.M. Chen, B.H. Ye, L.N. Ji, Angew. Chem., Int. Ed. Eng. 38 (1999) 2237. (c) M.L. Tong, X.M. Chen, B.H. Ye, S.W. Ng. Inorg. Chem. 37 (1998) 5278.

[8] (a) C.M. Che, H.K. Yip, D. Li, S.M. Peng, G.H. Lee, Y.M. Wang, S.T. Liu, Chem. Commun. (1991) 1615. (b) M. Munakata, L.P. Wu, T. Kuroda-Sowa, Adv. Inorg. Chem. 46 (1997), 173. (c) P. Pyykkö, Chem. Rev. 97(1997) 597 and references therein.

[9] A Bondi, J. Phys. Chem. 68 (1964) 441.

[10] (a) J.T. Sheu, C.C. Lin, C.C. Wang, S.M. Peng, Chem. Commun. (1996) 315. (b) M.H. Yang, T.W. Lin, C.C. Chou, H.C. Lee, H.C. Chang, G.H. Lee, M.K. Leung, S.M. Peng, Chem. Commun. (1997) 2279. (c) S.J. Shie, C.C. Lee, C.C. Wang, S.M. Peng, Angew. Chem., Int. Ed. Engl. 36 (1997) 56. (d) C.C. Wang, W. C. Lo, C.C. Chou, G.H. Lee, J.M. Chen. S.M. Peng, Inorg. Chem. 37 (1998) 4059. (e) S.Y. Lai, T.W. Lin, Y.H. Chen, C.C. Wang, G.H. Lee, M.H. Yang, M.K. Leung, S.M. Peng, J. Am. Chem. Soc. 121 (1999) 250.

[11] (a) A.L. Balch, M.M. Olmstead, J. Am. Chem. Soc. 101 (1979) 3128. (b) K.P. Mann, M.J. Dipierro, T.P. Gill, J. Am. Chem. Soc. 102 (1980) 3965. (c) M.A. Ciriano, S. Sebasrian, L.A. Oro, A. Tiripicchio, M.T. Camellini, F.J. Lahoz, Angew. Chem., Int. Ed. Eng. 27 (1988) 402.

[12] (a) L. Wu, P. Field, C. Murphy, P. Nagle, B. Hathaway, C. Simmons, P. Thornton, J. Chem. Soc., Dalton. Trans. (1990) 3835. (b) S. Aduldecha, B. Hathaway. J. Chem. Soc., Dalton. Trans. (1991) 993. (c) G.J. Pyrka, M.E. Mekki, A.A. Pinkerton. Chem. Commun. (1991) 84.
[13] (a) F.A. Cotton, L.M. Daniels, G.T.I.V. Jordon, C.A. Murillo, J. Am. Chem. Soc. 119 (1997) 10377. (b) F.A. Cotton, L.M. Daniels, G.T.I.V. Jordon, Chem. Commun. (1997) 421. (c) F.A. Cotton, L.M. Daniels, C.A. Murillo, X. Wang, Chem. Commun. (1998) 39. (d) F.A. Cotton, Inorg. Chem. 37 (1998) 5710.
[14] (a) K. Matsumoto, K. Sakai, K. Nishio, Y. Tokisue, R. Ito, T. Nishide, Y. Shichi, J. Am. Chem. Soc. 114 (1992) 8110. (b) K. Sakai, Y. Tanaka, K. Hirata, T. Tsubomura, Lijima, S.A. Bhattacharjee, J. Am. Chem. Soc. 120 (1998) 8366.
[15] X-M. Chen, T.C.W. Mak, J. Chem. Soc., Dalton Trans. (1991) 3253.
[16] (a) K. Singh, J.R. Long, P. Stavropoulos, J. Am. Chem. Soc. 119 (1997) 2942. (b) M.A. Omary, H.H. Patterson, Inorg. Chem. 37 (1998) 1060.
[17] (a) G.M. Sheldrick, SHELX-97, University of Göttingen, Göttingen, Germany, 1997. (b) L.S. Long, Y.-X. Tong, X.-L. Yu, X.-M. Chen, L.-N. Ji, Transition Met. Chem. 24 (1999) 49.

PERGAMON

www.elsevier.nl/locate/poly

Polyhedron 19 (2000) 2243–2247

POLYHEDRON

Syntheses and crystal structures of four-coordinate aryloxo neodymium complexes

Li-Lu Zhang [a], Ying-Ming Yao [a], Yun-Jie Luo [a], Qi Shen [a,b,*], Jie Sun [b]

[a] *Department of Chemistry, Suzhou University, Suzhou 215006, People's Republic of China*
[b] *Laboratory of Organometallic Chemistry, Chinese Academy of Sciences, Shanghai 200032, People's Republic of China*

Received 1 March 2000; accepted 8 August 2000

Abstract

Two four-coordinate complexes of neodymium with 2,6-di-*tert*-butyl-4-methylphenolate have been synthesized and their single-crystal structures determined. Anhydrous $NdCl_3$ reacted with ArONa in a 1:3 molar ratio in THF at room temperature to yield the neutral four-coordinate complex $[(ArO)_3Nd(THF)]\cdot MePh$ (**1**), which crystallized as a solvate, in which three aryloxide ligands and one THF ligand are coordinated to neodymium to form a slightly distorted tetrahedron. The reaction of $NdCl_3$ with 4 equiv. of ArONa in THF gave $[(ArO)_4Nd][Na(THF)_6]$ (**2**). In this anion–cation pair compound, the neodymium and sodium atoms exhibit distorted tetrahedral and distorted octahedral coordination geometry, respectively. The average Nd–O(Ar) distance is 2.176 and 2.230 Å in complex **1** and **2**, respectively. © 2000 Elsevier Science B.V. All rights reserved.

Keywords: Synthesis; Crystal structure; Aryloxide; Neodymium; Anion–cation pair compound

1. Introduction

Lanthanide alkoxides and aryloxides have found a variety of applications as homogeneous catalysts for organic reactions [1] and precursors for organolanthanide syntheses [2] and high purity oxide materials [3]. The syntheses, structures and reactivities of alkoxo- and aryloxolanthanide complexes have recently attracted a great deal of attention [4–6]. Investigation into the chemistry of lanthanide complexes containing aryloxo ligands has produced complexes exhibiting a variety of structural types [7–9]. The coordination number and degree of oligomerization of the products can be controlled by varying the bulky substituents on the arene ring in the reaction of europium ingot with substituted phenols [9,10]. These facts are consistent with general expectations. From metathesis reactions, the neutral monomeric or dimeric complexes can be obtained when the bulky substituted phenoxides are used as ligands [11–13]. However, for a less bulky ligand, such as 2,6-diisopropyl phenoxide, anionic ate complexes containing alkali metals are obtained via bridging interactions to form one-dimensional chains, two-dimensional sheets or extended three-dimensional structures [14,15]. Recently, homoleptic anionic aryloxide–lanthanoid complexes have also been obtained by Clark and Deacon et al. using substituted phenoxides as ligands [16–18].

Previous studies with the 2,6-di-*tert*-butyl-4-methyl phenoxo ligand, *O*-C_6H_2-2,6-*tert*-Bu-4-Me, (OAr in this paper) have shown that it gives low-coordinate neutral monomeric complexes with scandium and samarium, $Sc(ArO)_3$ and $[Sm(ArO)_3(THF)]\cdot THF$, from the reaction of $LnCl_3$ with NaOAr [11,19]. To understand more about this reaction with the other lanthanide elements, we have studied the reaction of anhydrous $NdCl_3$ with 3 and 4 equiv. of NaOAr in THF, and the desired complex $[Nd(ArO)_3(THF)]\cdot MePh$ (**1**) and unusual compound $[Nd(ArO)_4][Na(THF)_6]$ (**2**) were synthesized. Single-crystal structure studies revealed that the latter is a disconnected anion–cation pair compound with the sodium well separated from the lanthanoid coordination sphere.

* Corresponding author. Tel.: +86-512-511-2513; fax: +86-512-511-2371.
E-mail address: qshen@suda.edu.cn (Q. Shen).

0277-5387/00/$ - see front matter © 2000 Elsevier Science B.V. All rights reserved.
PII: S0277-5387(00)00535-0

2. Experimental

All manipulations were performed under argon using the Schlenk technique. THF was distilled from sodium benzophenone ketyl before use. Anhydrous $NdCl_3$ was prepared according to the literature method [20]. NaOAr was prepared from the reaction of ArOH and Na in THF. Metal analyses were carried out using complexometric titration [21]. IR spectra were recorded on a Nicolet-550 FTIR spectrometer as KBr pellets. ^1H and ^{13}C NMR spectra were recorded on a Bruker AM-300 spectrometer in C_6D_6.

2.1. Synthesis of [Nd(ArO)$_3$(THF)]·MePh (1)

A solution of NaOAr (15.7 cm^3, 13.59 mmol) in THF was slowly added to a suspension of $NdCl_3$ (1.135 g, 4.53 mmol) in 20 cm^3 THF at room temperature. After being stirred for 72 h, the NaCl was separated from the reaction mixture by centrifugation. The solvent was removed in vacuum and toluene was added to extract the product. The dissolved portion was removed by centrifugation. The filtrate was concentrated and cooled at −20°C for crystallization. Blue single crystals suitable for X-ray determination were obtained over a few days (yield 3.15 g, 72%). Found: Nd, 14.83. Calc. for [Nd(ArO)$_3$(THF)]·(MePh): Nd, 14.92%. IR absorptions (cm^{-1}): 2957(s), 2918(w), 2873(w), 1634(s), 1434(s), 1396(m), 1362(m), 1231(m), 1151(s), 1065(m), 1027(w), 864(s), 771(s), 460(m).

2.2. Synthesis of [Nd(ArO)$_4$][Na(THF)$_6$] (2)

A solution of NaOAr (25.0 cm^3, 21.56 mmol) in THF was slowly added to a suspension of $NdCl_3$ (1.352 g, 5.39 mmol) in 25 cm^3 THF at room temperature. After stirring for 72 h, the precipitate was removed from the reaction mixture by centrifugation. The solvent was removed in vacuum and toluene was added. The precipitate was separated and the solution concentrated, and then cooled at −20°C. The yellow crystals were obtained after several weeks (4.05 g, 51%). Found: Nd, 9.62. Calc. for [Nd(ArO)$_4$][Na(THF)$_6$]: 9.75%. IR absorptions (cm^{-1}): 2962(s), 2925(m), 2876(w), 1637(s), 1437(s), 1225(s), 1159(s), 864(m), 771(m), 507(s). ^1H NMR (C_6D_6): δ 7.16(8H, Ph), 2.35(12H, Me), 1.62 (48H, THF), −1.11(72H, Bu^t). ^{13}C NMR: 123.3(PhO), 88.7(PhO), 84.2(PhO), 74.9 (PhO), −9.3(THF), −19.8(Me), −26.8(THF), −28.9(Me), −29.4(Bu^t), −29.6(Bu^t).

Table 1
Crystal data and experimental parameters

Compound	[Nd(OAr)$_3$(THF)]·MePh (**1**)	[Nd(OAr)$_4$][Na(THF)$_6$] (**2**)
Formula	$C_{56}H_{85}NdO_4$	$C_{84}H_{140}O_{10}NaNd$
Molecular weight	966.48	1477.26
Crystal size (mm)	0.20 × 0.20 × 0.30	0.20 × 0.25 × 0.30
Crystal system	monoclinic	monoclinic
Crystal color and habit	blue, prism	yellow, prism
Space group	*Cc* (No. 9)	$P2_1/c$ (No. 14)
Unit cell dimensions		
a (Å)	25.907(1)	14.414(2)
b (Å)	10.601(1)	15.119(2)
c (Å)	20.160(1)	39.686(4)
β (°)	103.38(1)	97.28(2)
V (Å^3)	5386.5(6)	8579(4)
D_{calc} (g cm^{-3})	1.192	1.144
Z	4	4
μ (mm^{-1})	1.005	0.661
F(000)	2052	3180
Temperature (K)	293(2)	293
Scan type	ω	ω
θ_{max} (°)	24.99	22.46
Number of unique reflections	3827	9139
Number of reflections with $I \geq 2.0\sigma(I)$	3819	6039
Number of parameters refined	550	637
R	0.0397	0.0640
R_w	0.1023	0.0840
Goodness-of-fit	0.965	2.93

2.3. Crystallography

Single crystals suitable for X-ray measurements were sealed in thin-walled glass capillaries under argon. Intensity data were collected in the variable ω scan mode on a Rigaku AFC 7R four-circle diffractometer using Mo Kα radiation ($\lambda = 0.71073$ Å) at 293 K. Crystallographic data are listed in Table 1.

The crystal structures of complexes **1** and **2** were determined by direct methods which yielded the positions of all non-hydrogen atoms. All the non-hydrogen atoms were refined anisotropically. Hydrogen atoms were all generated geometrically (C–H bond lengths fixed at 0.96 Å), assigned appropriate isotropic thermal parameters and allowed to ride on their parent carbon atoms. All the H atoms were held stationary and were included in the structure factor calculation in the final stage of full-matrix least-squares refinement.

3. Results and discussion

3.1. Syntheses of the complexes

The metathesis reaction between anhydrous $NdCl_3$ and NaOAr in the molar ratio 1:3 in THF at room temperature, followed by crystallization from toluene, yielded the neutral four-coordinate neodymium com-

Table 2
Selected bond lengths (Å) and angles (°) in compound **1** and **2**

[Nd(OAr)$_3$(THF)]·MePh (**1**)			
Nd(1)–O(1)	2.173(5)	Nd(1)–O(2)	2.190(5)
Nd(1)–O(3)	2.164(5)	Nd(1)–O(4)	2.444(6)
O(1)–C(1)	1.367(8)	O(2)–C(16)	1.356(8)
O(3)–C(31)	1.370(9)	O(4)–C(46)	1.450(12)
O(4)–C(49)	1.452(11)		
O(1)–Nd(1)–O(2)	115.5(2)	O(1)–Nd(1)–O(3)	119.7(2)
O(1)–Nd(1)–O(4)	100.8(2)	O(2)–Nd(1)–O(3)	116.5(2)
O(2)–Nd(1)–O(4)	107.7(2)	O(3)–Nd(1)–O(4)	90.7(2)
Nd(1)–O(1)–C(1)	162.0(5)	Nd(1)–O(2)–C(16)	147.3(4)
Nd(1)–O(3)–C(31)	155.9(5)	Nd(1)–O(4)–C(46)	120.2(5)
Nd(1)–O(4)–C(49)	130.5(5)		
[Nd(OAr)$_4$][Na(THF)$_6$] (**2**)			
Nd–O(1)	2.202(6)	Nd–O(2)	2.256(7)
Nd–O(3)	2.247(7)	Nd–O(4)	2.217(7)
Na–O(5)	2.33(2)	Na–O(6)	2.49(2)
Na–O(7)	2.36(1)	Na–O(8)	2.32(2)
Na–O(9)	2.33(2)	Na–O(10)	2.36(1)
O(1)–C(1)	1.36(1)	O(2)–C(16)	1.34(1)
O(3)–C(31)	1.35(1)	O(4)–C(46)	1.36(1)
O(1)–Nd–O(2)	108.2(2)	O(1)–Nd–O(3)	112.7(2)
O(1)–Nd–O(4)	104.3(2)	O(2)–Nd–O(3)	110.8(2)
O(2)–Nd–O(4)	111.5(3)	O(3)–Nd–O(4)	109.1(2)
O(5)–Na–O(6)	88.7(7)	O(5)–Na–O(7)	89.8(8)
O(5)–Na–O(8)	173.0(9)	O(5)–Na–O(9)	90.4(8)
O(5)–Na–O(10)	93.7(7)	O(6)–Na–O(7)	86.7(6)
O(6)–Na–O(8)	88.8(7)	O(6)–Na–O(9)	173.6(7)
O(6)–Na–O(10)	97.4(6)	O(7)–Na–O(8)	83.6(7)
O(7)–Na–O(9)	87.0(5)	O(7)–Na–O(10)	174.7(5)
O(8)–Na–O(9)	91.4(9)	O(8)–Na–O(10)	93.1(7)
O(9)–Na–O(10)	89.0(5)		

plex [Nd(ArO)$_3$(THF)]·MePh in high yield, as shown in Eq. (1).

$$NdCl_3 + 3NaOAr \xrightarrow{THF} (ArO)_3Nd(THF) + 3NaCl \quad (1)$$

This reaction is similar to the reaction of NaOAr with anhydrous $SmCl_3$ [19], but different from that of 2,6-diisopropylphenoxide which reacted with $NdCl_3$ in THF to produce K[Nd(OC$_6$H$_3$-Pr$^i_2$-2,6)$_4$] instead of Nd(OC$_6$H$_3$–Pr$^i_2$-2,6)$_3$ [14]. Subsequent studies have shown that $LnCl_3$ reacted with 4 equiv. of potassium 2,6-diisopropylphenoxide in THF, followed by crystallization from toluene, to form the 'ate' complex K[Ln(OC$_6$H$_3$–Pr$^i_2$-2,6)$_4$] in high yield as shown in Eq. (2) [15].

$$LnCl_3 + 4K\text{–}OC_6H_3\text{–}Pr^i_2\text{-}2,6 \xrightarrow[2.\ \text{Toluene}]{1.\ \text{THF}} K[Ln(OC_6H_3\text{–}Pr^i_2\text{-}2,6)_4 + 3KCL \quad (2)$$

The reaction of anhydrous $NdCl_3$ with 4 equiv. of NaOAr in THF at room temperature, did not give the 'ate' complex Na[Nd(OAr)$_4$], but rather produced the unusual compound [Nd(ArO)$_4$][Na(THF)$_6$] as illustrated in Eq. (3).

$$NdCl_3 + 4NaOAR \xrightarrow{THF} [(ArO)_4Nd][Na(THF)_6] + 3NaCl \quad (3)$$

^{1}H, ^{13}C NMR and IR studies show that there are not only phenolate ligand signals, but also THF signals. A single-crystal study reveals (see below) that compound **2** contains a discrete homoleptic aryloxoneodymium anion with the alkali metal cation well separated from the neodymium coordination sphere. To our knowledge, only three analogous complexes [Na(diglyme)$_2$][Nd(Odpp)$_4$], [Odpp = 2,6-diphenylphenolate, diglyme = bis(2-methoxyethyl) ether], [Na(diglyme)$_2$][Er(Odpp)$_4$] and [Na(DME)$_2$][Nd(Odpp)$_4$] (DME = 1,2-dimethoxyethane) have been recently reported in the literature [18]. Generally, unidentate coordinating or non-coordinating solvents were considered disadvantageous for ion pair complex formation. Watkin et al. reported that Sm(OC$_6$H$_3$–Pr$^i_2$-2,6)$_3$(THF)$_2$ reacted with one equiv. of LiC_5Me_5 in THF to form the lithium ate complex, which however reacted with an excess of TMEDA (tetramethylethylenediamine) to form a charge–separated salt [22]. In our case, the disconnected anion–cation pair compound can be crystallized from mixed THF–toluene solvent. This difference may be attributed to the large size of the substituents on the arene ring.

3.2. Structures

The molecular structures of compound **1** and **2** were determined by single-crystal studies. The selected bond lengths and angles are listed in Table 2.

3.2.1. Crystal structure of *[Nd(OAr)$_3$(THF)]·MePh* (**1**)

The molecular structure of [Nd(OAr)$_3$(THF)]·MePh is shown in Fig. 1. The compound is isostructural with [Sm(OAr)$_3$(THF)]·THF and the toluene solvent molecule replaces the THF molecule in the molecular packing [19]. The complex is a four-coordinate monomer with three aryloxo oxygen atoms and one THF oxygen atom around the neodymium forming a distorted tetrahedron. The coordination geometry around the metal is different from that in [Nd(Odpp)$_3$(THF)] which has a distorted trigonal bipyramidal array by forming an intramolecular π-bond [23]. Interestingly, in [Nd(Odpp)$_3$(DME)] [24], [Nd(Odpp)$_3$(THF)$_2$], [Nd(Odpp)$_3$(THF)] and Nd(Odpp)$_3$ [23], all of these compounds show distorted trigonal bipyramidal stereochemistry and the neodymium atoms are five- or seven-coordinate. Few examples of four-coordinate neodymium complexes are known. Evans and co-workers reported the structure of

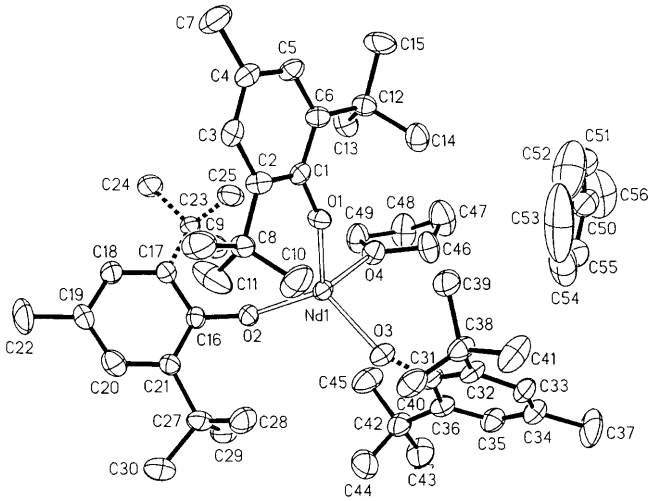


Fig. 1. Molecular structure of $[Nd(ArO)_3(THF)]\cdot(MePh)$.

a four-coordinate neodymium amide complex; however, to achieve steric saturation of the metal center, an agostic interaction between the α carbon and neodymium was observed [25]. The current difference in the coordination number can be attributed to the more bulky ArO ligand as compared to the Odpp ligand and amide.

The three aryloxo oxygen atoms around neodymium show a nearly trigonal planar array with Σ O–Nd–O = 351.7°; this value is comparable with those in $Nd(Odpp)_3(THF)$ (358.7°) and $Nd(Odpp)_3$ (353.2°) [23]. The Nd–O(Ar) distances range from 2.164(5) to 2.190(5) Å, giving the average Nd–O(Ar) distance 2.176 Å. This value is a little shorter than those in $[Nd(Odpp)_3(DME)]$ (2.191 Å) [24], $[Nd(Odpp)_3(THF)_2]$ (2.190 Å), $[Nd(Odpp)_3(THF)]$ (2.193 Å) [23], $K[Nd(OC_6H_3\text{–}Pr^i_2\text{-}2,6)$ (2.211 Å) [15] and comparable with that in $Nd(Odpp)_3$ (2.169 Å) [23]. Subtraction of the estimated radius (0.86 Å) [26] for four-coordinate Nd^{3+} from Nd–O(Ar) gives 1.31 Å, which is similar to those for $[Sm(OAr)_3(THF)]\cdot THF$ (1.31 Å) [19], and $Sc(OAr)_3$ (1.30 Å) [8], but a little longer than those for other aryloxo lanthanide complexes $[Yb(Odpp)_3(THF)_2]$ (1.27 Å) [27] $[La(Odpp)_3(THF)_2]$ (1.28 Å) [28], and $Yb(OC_6H_2Bu^t_3\text{-}2,4,6)_3(THF)$ (1.27 Å) [29]. The Nd–O(THF) distance is 2.444(6) Å, and a similar subtraction from this value gives 1.58 Å. This is much higher than the usual value 1.34 Å for organolanthanoid complexes [30], but still within the range for the complexes of bulky lanthanoid aryloxides [19,27,29].

3.2.2. Crystal structure of $[Nd(OAr)_4][Na(THF)_6]$ (2)

The molecular structure of **2** is comprised of a discrete $[Na(THF)_6]^+$ cation and a $[Nd(ArO)_4]^-$ anion (Fig. 2).

In the anion, the neodymium metal is coordinated to four oxygen atoms from aryloxide ligands in a pseudo-tetrahedral fashion. The stereochemistry around the neodymium atom is similar to that in $K[Nd(OC_6H_3\text{–}Pr^i_2\text{-}2,6)$[15], $[Na(diglyme)_2][Nd(Odpp)_4]$ and $[Na(diglyme)_2][Er(Odpp)_4]$ [18]. The Nd–O distances range from 2.202(6) to 2.256(7) Å, giving the average distance of 2.230 Å, which is somewhat longer than the average Nd–O(Ar) distance (2.176 Å) observed for complex **1**, although both of them have similar stereochemical arrangement around the central metal. This difference can be attributed to steric repulsion, as an additional ArO ligand replacing the THF ligand increases the steric repulsion among the ligands. It is also longer than that in the analogous aryloxide complex $[Na(diglyme)_2][Nd(Odpp)_4]$ [18], which is consistent with the fact that ArO is more bulky than Odpp. The Nd–O(Ar) distances in complex **2** are similar to those in $K[Nd(OC_6H_3Pr^i_2\text{-}2,6)_4]$ (average = 2.21 Å) [14] and $Na[Nd(Odpp)_4]$ (2.20 Å) [17,18], but slightly longer than those in $[Nd(Odpp)_3](THF)$ (2.193 Å) and $Nd(Odpp)_3$ (2.169 Å) [23]. The Nd–O distance is also longer than the Er–O(Ar) distance in

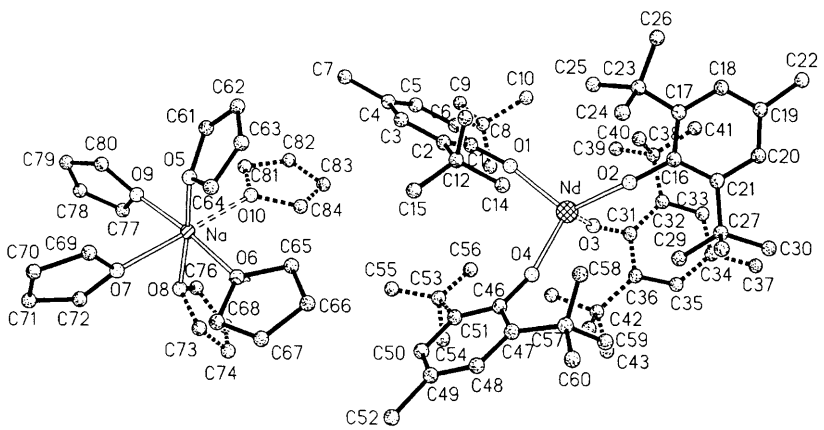


Fig. 2. Molecular structure of $[Nd(ArO)_4][Na(THF)_6]$.

$[Na(diglyme)_2][Er(Odpp)_4]$ even if the differences in ionic radii are considered [18]. This Nd–O(Ar) distance is very similar to $\langle Nd–O_{br}\rangle$ (2.211 Å) and apparently longer than $\langle Nd–O_{ter}\rangle$ (2.122 Å) of $Nd_2(O\text{-}2,3\text{-}Pr^i_2C_6H_3)_6$ [7]. The C–O distances of the phenolate ligands range from 1.34(1) to 1.36(1) Å, and are apparently shorter than the single bond length, reflecting substantial delocalization from oxygen into the aromatic rings. The average C–O bond length is 1.35 Å, and is similar to that in complex **1** (1.36 Å), $Yb(OC_6H_2Bu^t_3\text{-}2,4,6)_3(THF)$ (1.38 Å) [29], $[Yb(Odpp)_3(THF)_2]$ (1.33 Å) [27], and $[La(Odpp)_3(THF)_2]$ (1.31 Å) [28].

The six O–Nd–O angles range from 104.3(2) to 112.7(2)°, which is comparable with those angles in $[Na(diglyme)_2][Nd(Odpp)_4]$ [18]. But there are apparently differences from those in $K[(Nd(O\text{-}2,6\text{-}Pr^i_2C_6H_3)_4]$ [14], in which one of the six O–Nd–O angles (95.29°) deviates significantly from that of an ideal tetrahedron because of the interaction between the potassium atom and two aryloxide ligands. The Nd–O–C angles range from 144.6(7) to 167.9(7)°.

In the cation $[Na(THF)_6]^+$, the sodium ion is solvated and octahedrally bonded to the oxygen atoms of six THF molecules. The bond lengths of Na–O range from 2.32(2) to 2.49(2) Å and the angles for the two closest oxygen atoms to the sodium range from 83.6(7) to 97.4(6)°. These are slightly different from the values 2.380(5)–2.434(4), 2.340(10)–2.4410(10) Å and 88.2(2)–92.8(2), 88.8(4)–91.2(4)° in $[Na(THF)_6][(C_9H_7)_3Nd(\mu\text{-}Cl)Nd(C_9H_7)_3]$ [31] and $[Na(THF)_6][Cp_3Lu(\mu\text{-}H)LuCp_3]$ [32], respectively. Actually, in the last two compounds, the cations are centrosymmetrical, but in complex **2**, the O(5)–Na–O(8), O(6)–Na–O(9) and O(7)–Na–O(10) angles are 173.0(9), 173.6(7) and 174.7(5)°, respectively. These values show the cation is a distorted octahedron.

4. Supplementary data

Crystallographic data for the structural analysis have been deposited with the Cambridge Crystallographic Data Center, CCDC No. 136299 for compound **1** and CCDC No. 136300 for compound **2**. Copies of this information may be obtained free of charge from The Director, CCDC, 12 Union Road, Cambridge, CB2 1EZ, UK (fax: +44-1223-336033; e-mail:deposit@ccdc.cam.ac.uk or www:http://www.ccdc.cam.ac.uk).

Acknowledgements

This work was supported by State Project for Basic Research, Chinese National Natural Science Foundation and the Key Laboratory of Organic Synthesis of Jiangsu Province. Thanks are due to the Department of Chemistry, The Chinese University of Hong Kong, for carrying out the X-ray structure determination.

References

[1] M. Shibasaki, H. Sasai, T. Arai, Angew. Chem., Int. Ed. Engl. 36 (1997) 1236.
[2] P.B. Hitchcock, M.F. Lappert, R.G. Smith, R.A. Bartlett, P.P. Power, J. Chem. Soc., Chem. Commun. (1988) 1007.
[3] L.G. Hubert-Pfalzgraf, New J. Chem. 19 (1995) 727.
[4] R.C. Mehrotra, A. Singh, U.M. Tripathi, Chem. Rev. 91 (1991) 1287.
[5] W.J. Evans, New J. Chem. 19 (1995) 525.
[6] M.N. Bochkarev, L.N. Zakharov, G.S. Kalinina, Organoderivatives of the Rare Earths, Kluwer Academic, Dordrecht, 1996.
[7] D.M. Barnhart, D.L. Clark, J.C. Gordon, J.C. Huffman, R.L. Vincent, J.G. Watkin, B.D. Zwick, Inorg. Chem. 33 (1994) 3487.
[8] G.B. Deacon, C.M. Forsyth, P.C. Junk, B.W. Skelton, A.H. White, Chem. Eur. J. 5 (1999) 1452.
[9] W.J. Evans, M.A. Greci, J.W. Ziller, J. Chem. Soc., Dalton Trans. (1997) 3035.
[10] W.J. Evans, W.G. McClelland, M.A. Greci, J.W. Ziller, Eur. J. Solid State Inorg. Chem. 33 (1996) 145.
[11] P.B. Hitchcock, M.F. Lappert, A. Singh, J. Chem. Soc., Chem. Commun. (1983) 1499.
[12] P.B. Hitchcock, M.F. Lappert, A. Singh, Inorg. Chim. Acta 139 (1987) 183.
[13] M.F. Lappert, A. Singh, R.G. Smith, Inorg. Synth. 27 (1990) 164.
[14] D.L. Clark, J.G. Watkin, J.C. Huffman, Inorg. Chem. 31 (1992) 1554.
[15] D.L. Clark, G.C. Gordon, J.C. Huffman, R. Vincent-Hollis, J.G. Watkin, B.D. Zwick, Inorg. Chem. 33 (1994) 5903.
[16] D.L. Clark, R.V. Hollis, B.L. Scott, J.G. Watkin, Inorg. Chem. 35 (1996) 667.
[17] D.L. Clark, G.B. Deacon, T. Feng, R.V. Hollis, B.L. Scott, B.W. Skelton, J.G. Watkin, A.H. White, J. Chem. Soc., Chem. Commun. (1996) 1729.
[18] G.B. Deacon, T. Feng, P.C. Junk, B.W. Skelton, A.H. White, J. Chem. Soc., Dalton Trans. (1997) 1181.
[19] Q.Z. Qi, Y.H. Lin, J.Y. Hu, Q. Shen, Polyhedron 14 (1995) 413.
[20] Y. Li, X. Xu, L. Zhu, G. Lu, Chinese J. Appl. Chem. 5 (1987) 82.
[21] J.L. Atwood, W.E. Hunter, A.L. Wayda, W.J. Evans, Inorg. Chem. 20 (1981) 4115.
[22] R.J. Butcher, D.L. Clark, J.C. Gordon, J.G. Watkin, J. Organomet. Chem. 577 (1999) 228.
[23] G.B. Deacon, T. Feng, B.W. Skelton, A.H. White, Aust. J. Chem. 48 (1995) 741.
[24] G.B. Deacon, T. Feng, P.C. Junk, B.W. Skelton, A.H. White, Chem. Ber. 130 (1997) 851.
[25] W.J. Evans, R. Anwander, J.W. Ziller, Inorg. Chem. 34 (1995) 5927.
[26] R.D. Shannon, Acta Crystallogr., Sect. A 32 (1976) 751.
[27] G.B. Deacon, S. Nickel, P. Mackinnon, E.R.T. Tiekink, Aust. J. Chem. 43 (1990) 1245.
[28] G.B. Deacon, B.M. Gatehouse, Q. Shen, G.N. Ward, E.R.T. Tiekink, Polyhedron 12 (1993) 1289.
[29] G.B. Deacon, T. Feng, S. Nickel, M.I. Ogden, A.H. White, Aust. J. Chem. 45 (1992) 671.
[30] G.B. Deacon, P.I. Mackinnon, T.W. Hambley, J.C. Taylor, J. Organomet. Chem. 259 (1983) 91.
[31] M.Q. Chen, G. Wu, W.L. Wu, S.M. Zhuang, Z.E. Huang, Organometallics 7 (1988) 802.
[32] H. Schumann, W. Genthe, E. Hahn, M.B. Hossain, D. van der Helm, J. Organomet. Chem. 299 (1986) 67.

PERGAMON

www.elsevier.nl/locate/poly

Polyhedron 19 (2000) 2249–2254

POLYHEDRON

Cationic complexes of Re with dppm (bis(diphenylphosphinomethane)). Crystal structure of $[Re(dppm)_3]I{\cdot}CH_3OH{\cdot}CH_2Cl_2$

Mario Rivero [a], Carlos Kremer [a,*], Jorge Gancheff [a], Eduardo Kremer [a], Leopoldo Suescun [b], Alvaro Mombrú [b], Raúl Mariezcurrena [b], Sixto Domínguez [c], Alfredo Mederos [c], Stefano Midollini [d]

[a] *Cátedra de Química Inorgánica, Facultad de Química, CC 1157 Montevideo, Uruguay*
[b] *Laboratorio de Cristalografía y Química del Estado Sólido, Facultad de Química, CC 1157 Montevideo, Uruguay*
[c] *Departamento de Química Inorgánica, Universidad de la Laguna, Tenerife, Islas Canarias, Spain*
[d] *CNR-ISSECC, Florence, Italy*

Received 24 March 2000; accepted 18 April 2000

Abstract

The reaction of $[ReO_2(PPh_3)_2I]$ with bis-diphenylphosphines (dpp) only produces complexes with general formula $[ReO_2(dpp)_2]^+$. However, when the ligand used in this work (bis(diphenylphosphinomethane) (dppm)) reacts with the same precursor an interesting Re(I) complex is also afforded. By changing the reaction conditions, *trans*-$[Re^VO_2(dppm)_2]^+$ and $[Re^I(dppm)_3]I$ were obtained and characterized. The crystal structure of $[Re(dppm)_3]I{\cdot}CH_3OH{\cdot}CH_2Cl_2$ is given. In this compound, the P atoms are arranged in a strongly distorted octahedral coordination polyhedron around the rhenium center. This is the first case of a tris(dppm) complex ever reported. © 2000 Elsevier Science B.V. All rights reserved.

Keywords: Rhenium; Re complexes; Re(I); *trans*-Dioxo Re(V) complexes; Phosphines; dppm

1. Introduction

In previous works [1,2], we have reported on the preparation and crystal structure of some *trans*-Re(V) dioxo complexes with didentate diphosphines, namely, $[ReO_2(dppe)_2]I$ and $[ReO_2(dppp)_2]PF_6$ (dppe = 1,2-bis-(diphenylphosphinoethane) and dppp = 1,3-bis-(diphenylphosphinopropane)). They were obtained by reaction of $[ReO_2(PPh_3)_2I]$ with the appropriate ligand. In both cases, the sole product was the dioxo compound, unchanged in the Re oxidation state. They are useful systems to study the influence of ring size on the coordination properties.

The next step in this study was to attempt the formation of a four-membered ring with this 5d-transition metal. This can be performed using dppm (bis-(diphenylphosphinomethane)) as chelating ligand. In any case, the formation of a highly strained ring is expected. For this reason most dppm complexes show one or two phosphines connecting two metallic centers. $Re_2Cl_4(\mu\text{-dppm})_2$, $Mo_2(dppm)_2X_4$ ($X = Cl^-$, NCS^-) and $Re_2Cl_5(dppm)_2$ are good examples of this behavior [3–5]. As an alternative, dppm can participate in mixed ligand complexes, by bonding the two phosphorus atoms to the same central atom. This fact has been reported for some Re complexes in different oxidation states: *fac*-$[Re^VOCl_3(dppm)]$, *mer*-$[Re^{III}Cl_3(dppm)(PPh_3)]$, *fac*-$[Re^{III}(NCH_3)Cl_3(dppm)]$, *trans*-$[Re^VNCl_2(dppm)(PPh_3)]$ and $[Re^VNCl(dppm)_2]Cl$ [6]. It is interesting to note that the synthesis of these complexes involves the reduction of Re, presumably by the diphosphine. The identification of compounds such as $[ReCl_3(dppm)(dppom)]$ and $[ReCl_4(dppom)]$ (dppom = $Ph_2PCH_2P(=O)Ph_2$), in which dppm is partially oxidized to dppom, points in this direction [6,7]. The coordination of dppom seems to be a way to change the strained four-membered ring of dppm to a five-membered one.

* Corresponding author. Fax: +598-2-924-1906.
E-mail address: ckremer@bilbo.edu.uy (C. Kremer).

0277-5387/00/$ - see front matter © 2000 Elsevier Science B.V. All rights reserved.
PII: S0277-5387(00)00485-X

In any case, no tris(dppm)–Re complex has been reported up to now. The situation is not very different for other d-transition metals. No tris(dppm) complexes have been structurally elucidated. Only related compounds such as $\{[(Ph_2P)_2CH]_3V\}[Li(THF)_4](THF)_2$, in which dppm is deprotonated before coordination, have been reported [8].

In this work, we report on two new cationic complexes formed when $[Re^{V}O_2(PPh_3)_2I]$ reacts with dppm. During the development of procedures for the synthesis of *trans*-$[Re^{V}O_2(dppm)_2]^+$ by a substitution reaction, a novel cationic complex $[Re^{I}(dppm)_3]I$ was also obtained and characterized. This is the first time that a Re(I) complex has been prepared with dppm as the only didentate ligand. Dppm demonstrates the ability to act as didentate chelating ligand and its tendency to promote reductive reactions. The crystal structure of $[Re(dppm)_3]I{\cdot}CH_3OH{\cdot}CH_2Cl_2$ is the first case of a tris-(dppm) complex ever reported.

2. Experimental

2.1. Materials

All chemicals were of reagent grade and used as received. HPLC grade methanol and all other solvents (reagent grade) were used without further purification. Violet microcrystals of $[ReO_2(PPh_3)_2I]$ were obtained using the reported method [9] except for $NH_4[ReO_4]$, which was used in place of $H[ReO_4]$.

2.2. Physical measurements

IR spectra were recorded as KBr pellets on a Bomen MB FT-IR spectrophotometer. Proton NMR spectra were recorded at 200.133 MHz on a Bruker AC200 spectrometer. Peak positions in ppm are relative to TMS as external reference. $^{31}P\{^1H\}$ spectra were recorded on the same instruments operating at 81.015 MHz. Chemical shifts are relative to external 85% H_3PO_4 with downfield values reported as positive. Elemental analysis was accomplished on a Carlo Erba model 1108 elemental analyzer. Fast Atom Bombardment spectra were obtained from a 3-nitrobenzylalcohol matrix using a Micromass–Autospec spectrometer.

2.3. HPLC analyses

Chromatograms were obtained with an HPLC system by Merck, equipped with a variable wavelength monitor and a PRP-X200 (10 μm) cation exchange column (4 × 250 mm). A 0.02 M solution of NaCl in methanol was used as mobile phase with 1.5 ml min^{-1} flow. Detection was accomplished at 255 nm.

2.4. Potentiometry measurements

The potentiometric titrations were carried out in mixed solvent dioxane–water (70:30 v/v) solutions at 25 °C and ionic strength $I = 0.1$ mol dm^{-3} in KCl. Experimental details can be found elsewhere [1]. The autodissociation constant of the solvent pK_w was 16.0, in good agreement with reported data [10]. Measurements were taken of dppm and the complex at the concentrations $C = 1.0$, 1.5 and 2.0 mmol dm^{-3}, between pH values of 1.7 and 7.0. The experimental potentiometric data were analyzed by means of the SUPERQUAD program [11].

2.5. Preparation of the complexes

2.5.1. $[ReO_2(dppm)_2]I$ (**1**)

$[ReO_2(PPh_3)_2I]$ (0.30 g, 0.345 mmol) and dppm (1.5 g, 3.90 mmol) were stirred in dichloromethane (20 ml) for 10 min at room temperature (r.t.). A yellow solution was obtained. It was evaporated to dryness under vacuum at a temperature not higher than 30°C. From this crude material, the complex was extracted with freshly distilled methanol (5 × 10 ml). The pale yellow solution was filtered (through paper) and the solvent was evaporated again under similar conditions. The yellow solid was washed with ether (4 × 5 ml); yield 65–70%. The solid can be recrystallized from methanol; yield 70%. IR spectrum (ν, cm^{-1}): 3051 (s), 1483 (s), 1436 (vs), 1102 (s), 791 (s), 735 (vs), 725 (vs), 690 (vs), 504 (s), 477 (m), 279 (m), 247 (s). *Anal.* Calc. for $C_{50}H_{44}IO_2P_4Re$: C, 53.9; H, 4.0. Found: C, 53.8; H, 4.0%.

2.5.2. $[ReO_2(dppm)_2]PF_6$

Concentrated solutions of (**1**) showed the formation of a dark solid in CD_2Cl_2 while recording the NMR spectra. In spite of the color, IR spectrum of the solid proved to be essentially free dppm. Hexafluorophosphate salt was therefore prepared by adding a large excess of NH_4PF_6 to a methanolic solution of (**1**); yield: 40–50%. Selected NMR data (CD_2Cl_2, 293 K): ^1H NMR: 7.0–8.0 (m, 40H, C_6H_5), 5.41 ppm (t, $J_{P-H} = 5$ Hz, 4H, CH_2); $^{31}P\{^1H\}$: −45.9 ppm (s). *Anal.* Calc. for $C_{50}H_{44}F_6O_2P_5Re$: C, 53.1; H, 3.9. Found: C, 52.9; H, 4.1%.

2.5.3. $[Re(dppm)_3]I$ (**2**)

A mixture of $[ReO_2(PPh_3)_2I]$ (0.30 g, 0.345 mmol) and dppm (0.7 g, 1.90 mmol) was refluxed in freshly distilled methanol (20 ml) for 3 h. A clear yellow solution was obtained, from which a yellow crystalline solid was separated after cooling to r.t. The solid was washed with ether (4 × 5 ml); yield 25–30%. Suitable yellow crystals for X-ray diffraction were obtained by slow evaporation of a methanol–dichloromethane solution. IR spectrum (ν, cm^{-1}): 3050 (s), 1482 (s), 1433

(vs), 1310 (w), 1090 (s), 738 (vs), 726 (vs), 697 (vs), 513 (s), 485 (m), 408 (m). Selected NMR data (CD_2Cl_2, 293 K): ^1H NMR: 7.4–6.5 (m, 60H, C_6H_5), 5.51 ppm (s, broad, 6H, CH_2); $^{31}P\{^1H\}$: −50.3 ppm (s). *Anal*. Calc. for $C_{75}H_{66}IP_6Re$: C, 61.4; H, 4.5. Found: C, 61.6; H, 4.9%.

2.6. Crystallographic measurements and structure determinations

2.6.1. Crystal data

Colour: yellow. $C_{77}H_{72}Cl_2IOP_6Re$, $M = 1583.17$, orthorhombic, $a = 21.150(3)$, $b = 18.172(3)$, $c = 17.678(5)$ Å, $V = 6794(2)$ Å^3, space group $Pna2_1$, $Z = 4$, $D_{calc} = 1.548$ g cm^{-3}, μ(Mo Kα) = 2.509 mm^{-1}, $F(000) = 3176$, crystal size $0.36 \times 0.25 \times 0.22$ mm.

2.6.2. Structure determination

Data were collected at r.t. on a Rigaku AFC7S four-circle diffractometer [12] in the range $2.23 \leq \theta \leq 27.51°$, $-19 \leq h \leq 27$, $-7 \leq k \leq 23$, $-22 \leq l \leq 16$. A total of 8888 reflections were collected in the ω–2θ scan mode, of which 8825 were unique ($R_{int} = 1.64\%$) and 7381 ($I > 2\sigma(I)$) were used in the full-matrix least squares refinement with the SHELXL-97 program [13]. The structure was solved using the Patterson method with the SHELXS-97 program [14]. Non-hydrogen atoms were refined anisotropically. Hydrogen atoms were included at calculated geometrically suitable positions and refined riding on the corresponding atom, with isotropic thermal displacement parameter 1.2 times higher than the equivalent isotropic displacement parameter of the atoms bonded to them (1.5 times for the methanol solvent molecule). Final residuals were $R = 0.0312$ for a weighting scheme of $w^{-1} = (\sigma^2(F_o^2) + (0.0469P)^2 + 7.3285P)$ where $P = (F_o^2 + 2F_c^2)/3$. The goodness of fit (Goof) finished at 1.038. Mean final shift/esd was lower than 0.01. The maximum and minimum residual densities were 1.037 and −1.114 e Å^{-3}, respectively.

2.7. Calculations

Molecular mechanics calculations (MM) were performed using the MM+ force field implemented in the HyperChem package version 5.0. Geometry optimizations were carried out using the Polak–Ribière (gradient conjugated) method with a convergence criterion of 0.01 kcal mol^{-1}.

3. Results and discussion

The reaction product of $[Re^VO_2(PPh_3)_2I]$ with dppm is strongly affected by the reaction conditions. It has thus been possible to obtain Re complexes in different oxidation states. The composition of the solids, obtained by elemental analysis and confirmed by FABMS (see below), fitted with the formulae $[Re^VO_2(dppm)_2]I$ (**1**) and $[Re^I(dppm)_3]I$ (**2**). It is interesting to note that when preparation involves lower temperatures and larger dppm to Re molar ratios, the result is simply a substitution on the Re(V) core. But, if the reaction is carried out at a higher temperature and lower ligand to Re molar ratio, dppm is able to reduce the central atom and displace the two oxo groups, destroying the very stable $[ReO_2]^+$ core. The reduction of other Re precursors to yield stable dppm complexes has been previously reported [5,6], but this is the first time in which a Re(I) compound was obtained.

Positive fast atom bombardment mass spectroscopy of Pt(II) and Pd(II) dppm complexes has been previously discussed [15]. Re complexes follow a similar fragmentation pathway. The most prominent peaks of (**1**) were present at $m/z = 988$ [M$^+$ + H] and 603 [M$^+$ + H − dppm]. For (**2**), signals were found at 1335 [M$^+$ − 2H$_2$], 956 [M$^+$ + H − dppm], 877 [M$^+$ − H − dppm − Ph] and 755 [M$^+$ − H − dppm − Ph − PhP=CH$_2$].

The IR spectrum of $[Re^VO_2(dppm)_2]I$ showed a very strong absorption at 791 cm^{-1} characteristic of the linear $[O{=}Re{=}O]^+$ core. This vibration was in the expected range (775–836 cm^{-1}) for the asymmetric $[ReO_2]^+$ stretching [16]. The characteristic IR absorption of the $[O{=}Re{=}O]^+$ core is not present in (**2**), showing the complete substitution of the oxo ligands. In addition, it was also possible to observe in the IR spectra the characteristic vibrations of dppm. In particular, the scissoring of CH_2 groups (around 1483 cm^{-1}) and the P–CH_2 deformation band (around 1435 cm^{-1}) are present in the complexes (see Section 2). This is consistent with the presence of dppm in the compounds and rules out the possibility that it could be deprotonated in the complex (as, for example, in $\{[(Ph_2P)_2CH]_3V\}[Li(THF)_4](THF)_2$ [8]).

Selected bond distances and angles for $[Re(dppm)_3]I{\cdot}CH_3OH{\cdot}CH_2Cl_2$ are given in Table 1. Tables of coordinates, anisotropic temperature factors, hydrogen atom coordinates and a full listing of geometric data are available as supplementary data.

Fig. 1 illustrates the geometry and atom-numbering scheme. The structure consists of monomeric units of $[Re(dppm)_3]^+$, iodide as counterion and dichloromethane and disordered methanol as cocrystallization solvent molecules. The coordination polyhedron around Re(I) ion can be described as a distorted octahedron. The bond lengths for Re–P range from 2.400(2) to 2.467(2) Å and the P–Re–P angles for P atoms belonging to the same ligand from 68.01(6) to 69.08(6)°. No evidence for charge delocalization suggesting the presence of dppm as anion can be obtained from the structural results. On the contrary, the

Re–P*i*–C–P*j* torsion angles range from 17.1(3) to 20.3(3)°, for Re1–P3–C2–P4 and Re1–P5–C3–P6, respectively, clearly indicating non-planarity of the ligand skeleton (P*i* and P*j* belonging to the same dppm ligand). In a previously reported vanadium analogue ($\{[(Ph_2P)_2CH]_3V\}[Li(THF)_4](THF)_2$ [8]) two deprotonated dppm ligands exhibited very low torsion angles, 0.3° for V1–P4–C38–P3 and 1.7° for V1–P3–C83–P6, and only the third one corresponded to neutral dppm, with the torsion angle V1–P2–C13–P1, 14.8°.

Table 1
Selected bond lengths (Å) and angles (°) for $[Re(dppm)_3]I\cdot CH_3OH\cdot CH_2Cl_2$

Re(1)–P(1)	2.3999(19)
Re(1)–P(2)	2.4203(17)
Re(1)–P(3)	2.4232(17)
Re(1)–P(4)	2.4577(18)
Re(1)–P(5)	2.4585(17)
Re(1)–P(6)	2.4670(17)
P(1)–C(1)	1.831(7)
P(2)–C(1)	1.843(7)
P(3)–C(2)	1.847(7)
P(4)–C(2)	1.843(7)
P(5)–C(3)	1.850(7)
P(6)–C(3)	1.829(7)
P(1)–Re(1)–P(2)	68.88(6)
P(1)–Re(1)–P(3)	96.75(6)
P(2)–Re(1)–P(3)	93.95(6)
P(1)–Re(1)–P(4)	153.59(6)
P(2)–Re(1)–P(4)	89.35(6)
P(3)–Re(1)–P(4)	69.08(6)
P(1)–Re(1)–P(5)	96.04(6)
P(2)–Re(1)–P(5)	161.43(6)
P(3)–Re(1)–P(5)	98.70(6)
P(4)–Re(1)–P(5)	107.82(6)
P(1)–Re(1)–P(6)	95.25(6)
P(2)–Re(1)–P(6)	101.61(6)
P(3)–Re(1)–P(6)	162.99(6)
P(4)–Re(1)–P(6)	103.96(6)
P(5)–Re(1)–P(6)	68.01(6)
P(1)–C(1)–P(2)	95.8(3)
P(4)–C(2)–P(3)	97.2(3)
P(6)–C(3)–P(5)	97.0(3)

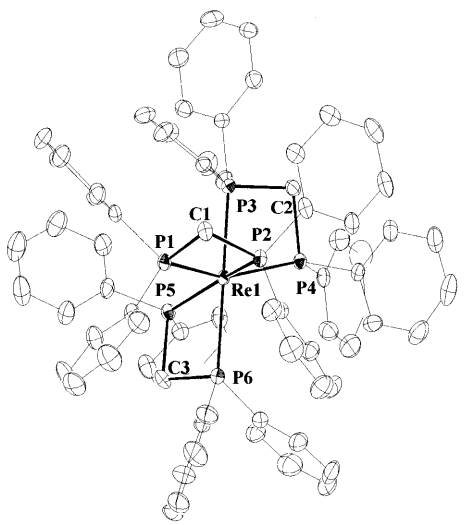


Fig. 1. ORTEP view [17] of the complex (**2**) with displacement ellipsoids drawn at 30% probability level. Hydrogens are omitted for clarity.

In spite of the distorted geometry of (**2**), the Re–P bonds present the usual lengths and fall within the range of values observed in other phosphine-containing Re complexes. Moreover, distance seems to be independent of the Re oxidation state [3].

As far as we know, this is the first structure of a tris(dppm) complex ever reported. Steric strain involved in the geometry of three four-membered rings supports the unusual appearance of these complexes. In order to know how strained the ligand in the complex is, we performed molecular mechanics calculations on the dppm. The optimized structure of dppm shows a P–C–P angle of 110.6°, not far from 106.2(3)° reported for the crystalline structure at −40°C [18]. As a second step, we optimized the structure of the ligand fixing the P–C–P angle (up to 60°) but allowing the rearrangement of the rest of the molecule. Fig. 2 shows the increase in the total energy at different P–C–P angles. As can be seen, the adjustment of the angle to 95° (the angle found in the structure of (**2**)) represents an increase of only 30% in the total energy of the molecule. This small angle does not seem to involve a large strain in the ligand, resulting in a very stable complex. The soft–soft interaction between the P atoms and the Re(I) center seems to be strong enough to compensate the strain of the three ligands.

The solid state structure found for the complexes is sustained in solution. The positive overall charge of the complexes in solution was checked by HPLC. Chromatograms in a cation exchange column show a characteristic peak at 3.9 (**1**) and 5.6 (**2**) min.

The ^1H and ^{31}P NMR spectra of the compounds agree with octahedral coordination. ^{31}P signals are very sharp, suggesting the diamagnetic character of the complexes. In particular the ^{31}P spectrum of (**1**) indicates that the two oxygens atoms are in *trans* position. Another remarkable result is the proton integration of the signals. Once more, the presence of two methylenic protons per ligand molecule is confirmed in solution.

It has been demonstrated that Re(V) dioxo complexes with didentate diphosphines, $[ReO_2(dppe)_2]^+$ and $[ReO_2(dppp)_2]^+$ can be protonated in dioxane–water (70:30 v/v) [1] according to:

$$[ReO_2(\text{phosphine})_2]^+ + 2H^+ \leftrightarrows [Re(OH)_2(\text{phosphine})_2]^{3+}$$

The titrations of $[ReO_2(dppm)_2]^+$ performed under the same conditions, show no protonation of the complex. The lower basicity of the oxo groups could be

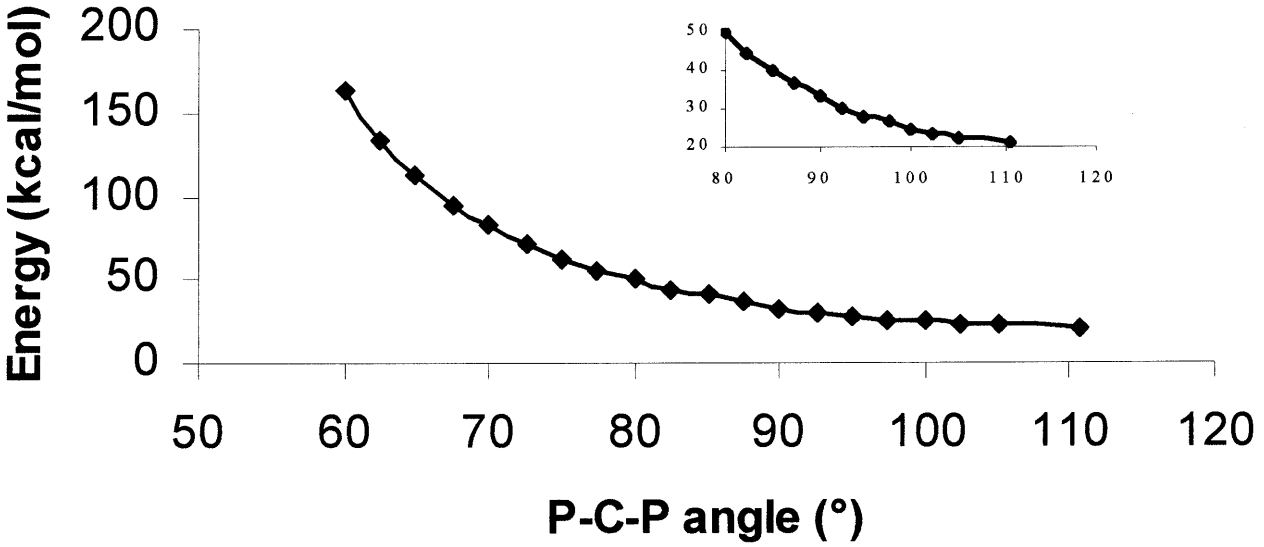


Fig. 2. Total energy of the dppm molecule as a function of the P–C–P angle, obtained by molecular mechanics calculations.

originated either in a short Re–O distance, which diminishes the availability of the lone pair of electrons of the oxygen atoms, or in the steric hindrance of the complex. IR stretching band at 791 cm^{-1} is almost at the same energy than those for $[ReO_2(dppe)_2]I$ and $[ReO_2(dppp)_2]I$ [1]. So, Re–O bond strength seems to be similar. This fact makes more probable the second argument.

For the free ligand, a simultaneous protonation of both phosphine groups is detected with $\log \beta_{12} = 3.04 \pm 0.06$ ($\chi^2 = 10.5$; $\sigma(E) = 3.50$). This value is in line with those for similar diphosphines [1].

4. Conclusions

In spite of many existing examples of complexes with dppm (including several transition metals), no reports could be found that include a tris(dppm) structure. Both the formation of a four-membered ring and the reductive character of the ligand seem to be the reason for this fact. All results reported in this work provide evidence of the formation of a tris(dppm) complex. The reasons why this unexpected compound is obtained seem to be the reductive character of the ligand, which promotes the reduction of the metallic atom, as well as the soft character of the Re(I) center. These results open up the study of a new aspect of the dppm characteristics in coordination chemistry.

5. Supplementary data

Crystallographic data for the structural analysis has been deposited with the Cambridge Crystallographic Data Centre, CCDC 133405 for compound **2**. Copies of this information may be obtained free of charge from: The Director, CCDC, 12 Union Road, Cambridge, CB2 1EZ, UK (fax: +44-1223-336033; e-mail: deposit@ccdc.cam.ac.uk or www: http://www.ccdc.cam.ac.uk).

Acknowledgements

This research received financial support from the Programa de Desarrollo de Ciencias Básicas (PEDECIBA), CONICYT (project number 305) and HCM Program (Network on Metals and Environmental Problems, EC, grant CT 94-0632).

References

[1] C. Kremer, M. Rivero, E. Kremer, L. Suescun, A. Mombrú, R. Mariezcurrena, S. Domínguez, A. Mederos, S. Midollini, A. Castiñeiras, Inorg. Chim. Acta 294 (1999) 47.
[2] L. Suescun, A. Mombrú, R. Mariezcurrena, C. Kremer, M. Rivero, E. Kremer, S. Domínguez, A. Mederos, Acta Crystallogr., Sect. C 55 (1999) 1785.
[3] W. Wu, P.E. Fanwick, R.A. Walton, Inorg. Chem. 36 (1997) 3810.
[4] E.H. Abbot, K.S. Bose, F.A. Cotton, W.T. Hall, J.C. Sekutowski, Inorg. Chem. 17 (1978) 3240.
[5] F.A. Cotton, L.W. Shive, B.R. Stults, Inorg. Chem. 15 (1976) 2239.
[6] R. Rossi, A. Marchi, L. Marvelli, L. Magon, M. Peruzzini, U. Casellato, R. Grazziani, Inorg. Chim. Acta 204 (1993) 63.
[7] X.L.R. Fontaine, E.H. Fowles, T.P. Layzell, B.L. Shaw, M. Thornton-Pett, J. Chem. Soc., Dalton Trans. (1991) 1519.
[8] J.J.H. Edema, A. Meetsma, F. Van Bolhuis, S. Gambarotta, Inorg. Chem. 30 (1991) 2056.
[9] G. Ciani, G.D. D'Alfonso, P. Romiti, A. Sironin, M. Freni, Inorg. Chim. Acta 72 (1983) 29.
[10] R. Motekaitis, A.E. Martell, J. Coord. Chem. 24 (1995) 49.

[11] P. Gans, A. Sabatini, A. Vacca, J. Chem. Soc., Dalton Trans. (1985) 1195.
[12] Molecular Structure Corporation (1993) MSC/AFC Diffractometer Control Software, Version 5.1.0. MSC, 3200 Research Forest Drive, The Woodlands, TX 77381, USA.
[13] G.M. Sheldrick, Acta Crystallogr., Sect. A 46 (1990) 467.
[14] G.M. Sheldrick, SHELXL-97: Program for the Refinement of Crystal Structures, University of Göttingen, Germany, 1997.
[15] K.A. Asker, A.W. Greenway, K.R. Seddon, A.A. Shimran, J. Organomet. Chem. 354 (1988) 257.
[16] N.P. Johnson, C.J.L. Lock, G. Wilkinson, J. Chem. Soc. (1964) 1054.
[17] L. Zsolnai, H. Pritzkow, ZORTEP: An interactive ORTEP Program, University of Heidelberg, Germany, 1995.
[18] H. Schmidbaur, G. Reber, A. Schier, F.E. Wagner, G. Muller, Inorg. Chim. Acta 147 (1988) 143.

PERGAMON

www.elsevier.nl/locate/poly

Polyhedron 19 (2000) 2255–2260

POLYHEDRON

Metal-centered redox chemistry of substituted cobalt phthalocyanines adsorbed on graphite and correlations with MO calculations and Hammett parameters. Electrocatalytic reduction of a disulfide

José H. Zagal *, Miguel A. Gulppi, Gloria Cárdenas-Jirón

Department de Quimica de Los Materiales, Facultad de Química y Biología, Universidad de Santiago de Chile, Casilla 40, Correo 33, Santiago, Chile

Received 1 October 1999; accepted 14 March 2000

Abstract

We have studied the metal-centered redox chemistry of unsubstituted cobalt–phthalocyanine (Co–Pc) and the cobalt complexes of the substituted ligands, cobalt–octaethylhexyloxyphthalocyanine (CoOEHPc), cobalt–tetramethoxyphthalocyanine (CoMeOPc), cobalt–tetraneopentoxyphthalocyanine (CoTNPPc), cobalt–tetraaminophthalocyanine (CoTAPc), cobalt–tetrasulfonatophthalocyanine (CoTSPc) and cobalt–hexadecafluorophthalocyanine ($CoPcF_{16}$) adsorbed on ordinary pyrolytic graphite (OPG). These complexes exhibit two distinct metal-centered reversible redox processes attributed to the Co(II)/Co(I) and Co(III)/Co(II) couples. The redox potentials of these couples are shifted according to the electron withdrawing or donating character of the groups located at the periphery of the phthalocyanine ligand, as seen by comparison to molecular orbital theoretical calculations. Correlations between the redox potential and the Hammett parameters of the substituents provide good linear correlations. The slopes of the linear free energy correlations give values of 0.41 and 0.49 V σ^{-1} for the Co(III)/Co(II) and Co(II)/Co(I) redox couples, respectively. We have also tested the electrocatalytic activity of these adsorbed phthalocyanines for the reduction of 2-hydroxyethyldisulfide. A plot of $\log i$ (current density at constant potential) versus the Co(II)/Co(I) redox potential gives a linear correlation where the rate of the reaction increases with the driving force of the catalyst, suggesting that that the reaction takes place via an outer-sphere mechanism. © 2000 Elsevier Science B.V. All rights reserved.

Keywords: Substituted cobalt phthalocyanines; Redox properties; Hammett parameters; Frontier orbitals; Disulfide reduction

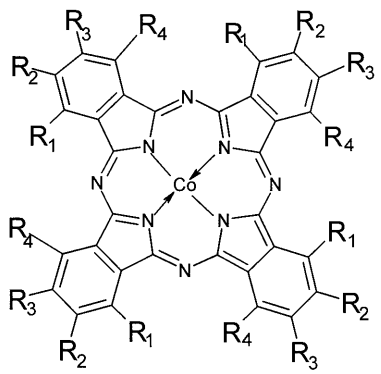
1. Introduction

Metallophthalocyanines (MPcs) are continuously attracting the attention of many research groups due to the great variety of applications of these materials in different fields such as energy conversion of visible light [1–4] sensors, [5–7] catalysis [8], electrocatalysis [9], molecular semiconductors [10–12], and electrochromic materials [10]. Redox properties of these materials are important [13,14] as they are correlated to the corresponding charge transfer spectra [13] and to catalytic and electrocatalytic properties [8,9]. Redox processes in metallophthalocyanines can be located at the ligand and at the metal center [15,16], the phthalocyanine ring can undergo successive one-electron reduction and one-electron oxidation to yield the anion and cation radicals respectively. With redox-active metals, metal oxidation or reduction occurs at potentials between those corresponding to ligand reduction or oxidation. Reduction of the ligand is associated to the position of LUMO ($M(II)\text{–}Pc(-2) + e^- \rightleftarrows [(M(II)\text{–}Pc(-3)]^{-1}$) whereas oxidation of the ligand ($(M(II)\text{–}Pc(-2)) \rightleftarrows [(M(II)\text{–}Pc(-1)]^+ + e^-$) is associated to the position of the HOMO. MPc's having a metal that possesses energy levels lying between the HOMO and the LUMO of the phthalocyanine ligand, in general will exhibit redox processes centered on the metal. This is the case for the phthalocyanines of Cr, Mn, Co and Fe [14–16], which have open d-shell structures.

* Corresponding author. Fax: +56-2-681-2108.
E-mail address: jzagal@lauca.usach.cl (J.H. Zagal).

0277-5387/00/$ - see front matter © 2000 Elsevier Science B.V. All rights reserved.
PII: S0277-5387(00)00486-1

It has been demonstrated that substituents on the periphery of the phthalocyanine ligand strongly influence the solution redox chemistry of these materials. Electron-donating groups lead to a negative shift of the redox potentials and electron-withdrawing groups to a positive shift. This has been observed with both closed d-shell metals like copper and zinc and open d-shell metals like Co–phthalocyanines [14]. On the other hand, it has been demonstrated by several authors that phthalocyanine adsorbs very strongly on graphite electrodes and that is possible to examine their electrochemical and catalytic properties in the confined state, on the electrode surface [9,14,17–22]. We are particularly interested in exploring the catalytic activity of cobalt phthalocyanines for the electrochemical oxidation of thiols [9,17–21] and reduction of molecular oxygen [21,22] and in correlating these properties with the redox potentials of the Co(II)/Co(I) and Co(III)/Co(II) reversible couples in the adsorbed phthalocyanine.



$CoF_{16}Pc$: $R_1=R_2=R_3=R_4=$-F.
CoTSPc: $R_1=R_2=R_4=$-H, $R_3=$-SO_3^-.
CoPc: $R_1=R_2=R_3=R_4=$-H.
CoTAPc: $R_1=R_2=R_4=$-H, $R_3=$-NH_2.
CoTNPPc: $R_1=R_2=R_4=$-H, $R_3=$-$O(CH_2)_2CH(CH_2)_2$.
CoMeOPc: $R_1=R_4=$-H, $R_2=R_3=$-OCH_3.
CoOEHPc: $R_1=R_4=$-H, $R_2=R_3=$-$OCH_2CH(CH_2CH_3)(CH_2)_3CH_3$

Fig. 1. General structure of cobalt phthalocyanines used in this work.

Table 1
Redox potentials of adsorbed cobalt phthalocyanine derivatives in Volts versus SCE at pH 13[a]

Compound	Co(III)/Co(II)	Co(II)/Co(I)	Refs.
$CoPcF_{16}$	0.669 [b]	−0.345	[20,21], this work
Co–TSPc	0.630	–0.518	[20–22,30]
Co–Pc	0.590	−0.605	[20–22]
Co–TAPc	0.435 [b]	−0.690	[20,30], this work
CoTNPPc	0.449	−0.685	[20–22]
CoMeOPc	0.520	−0.685	[20–22]
CoOEHPc	0.420 [b]	−0.725	[19–21], this work

[a] Obtained from cyclic voltammograms of phthalocyanines adsorbed on OPG, in NaOH 0.2 M pH 13 under nitrogen. Potential scan rate: 0.1 V s^{-1}. Potentials from average of anodic and cathodic current peaks.

[b] Estimated from Hammett parameters.

Lever [23–25], Orihashi [26,27] and Luk'yanets [28,29] have studied the variations of redox potentials of phthalocyanines with substituents, via the use of Hammett substituent constants and relatively good linear correlations have been found. All these studies have been carried out using the metallophthalocyanines dissolved in different solvents and there is only one report [30] using four phthalocyanine derivatives confined on the surface of a graphite electrode. One of the purposes of this work is to study the influence of substituents on the ligand on a great variety of cobalt phthalocyanine (adsorbed on graphite) to establish linear correlations between the Co(II)/Co(I) and Co(III)/Co(II) redox potentials with the sum of the Hammett constants. The variation of the electron density caused by the electron donating or electron withdrawing character of the substituent present on the periphery of the phthalocyanine ligand is discussed in terms of theoretical MO calculations. We also examine the effect of redox potential of the phthalocyanines on their activity for the electrochemical reduction of a 2-hydroxyethyldisulfide.

2. Results and discussion

Fig. 1 shows the structure of the phthalocyanines used in this work. We have reported in several papers the redox properties of cobalt phthalocyanine and derivatives, adsorbed on graphite electrodes and the results are summarized in Table 1. It can be seen from the data included in Table 1 that the formal potentials of both Co(III)/Co(II) and Co(II)/Co(I) redox couples are shifted to more positive values (compared with unsubstituted CoPc) by the effect of electron-withdrawing substituents in the ligand (F and $–SO_3^-$) and to more negative values by electron-donating groups ($–NH_2$, methoxy, neopentoxy and octaethylhexyloxy). Note that some values of the potentials of the Co(III)Co(II) redox couples of some phthalocyanines substituted with electron-withdrawing groups have been estimated using the Hammett parameters of the substituents, because those processes are shifted to potentials too positive, beyond the oxidation potential of the graphite substrate, and cannot be measured in aqueous solutions without damaging the electrode. The effect of the substituents on the redox potentials essentially agrees with previous reports that included other substituted cobalt phthalocyanines [14,30].

Figs. 2 and 3 compare the Co(III)/Co(II) and Co(II)/Co(I) formal potentials of the different adsorbed cobalt phthalocyanines with the energy of the highest occupied (HOMO) and the lowest unoccupied (LUMO) molecular orbital, calculated by PM3. In both cases, a linear

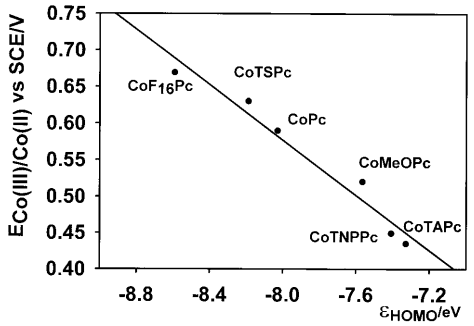


Fig. 2. Plot of Co(III)Co(II) redox potential vs. the energy of the HOMO in the phthalocyanine.

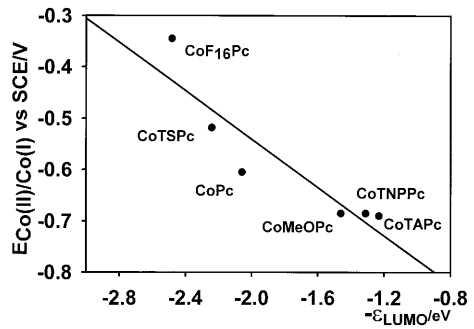


Fig. 3. Plot of Co(II)Co(I) redox potential vs. the energy (with negative sign) of the LUMO in the phthalocyanine.

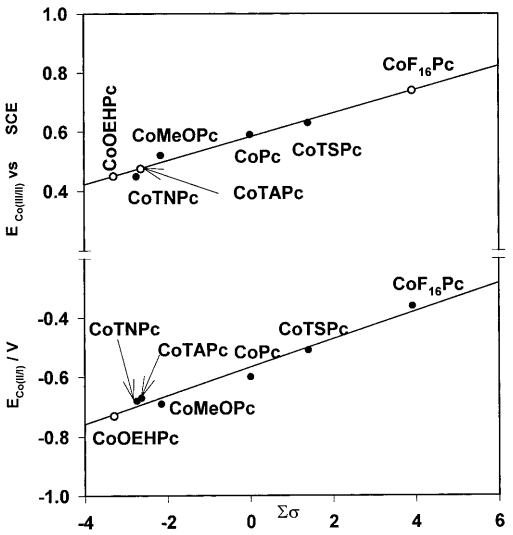


Fig. 4. Plot of Co(III)/Co(II) and Co(II)Co(I) redox potentials of the adsorbed cobalt phthalocyanines derivatives (at pH 13) vs. the Hammett $\Sigma\rho$ values. Open circles are calculated values, from Table 1.

correlation is obtained, which shows that electron-withdrawing groups F and $-SO_3^-$ stabilize the HOMO compared to Co–Pc. This is reflected in a more negative position of the energy of the HOMO. The opposite is true for electron-donating methoxy and neopenthoxy groups. Similar conclusions can be drawn from the energies of the LUMO. Note that energies of the HOMOs have negative values and energies of the LUMOs have positive values. This is why in the case of LUMO energies '$-\varepsilon_{LUMO}$' are plotted. The results in Figs. 2 and 3 essentially show the validity of the theoretical calculations, even though they have been performed only to the semi-empirical level. It is expected that those complexes with a more stable HOMO (more negative energy) will be more difficult to oxidize and will correspond to those having more positive redox potentials.

Fig. 4 illustrates plots of the Co(III)/Co(II) and Co(II)/Co(I) formal potentials of the adsorbed cobalt phthalocyanine derivatives versus the sum of the Hammett parameters of the corresponding substituent on the ligand. The Hammett parameters were obtained from the literature [31]. As pointed out by Lever [23], octasubstituted phthalocyanines such as CoOEHPc are single isomers. In contrast, the tetrasubstituted species CoTNPPc, CoTAPc, CoMeOPc, CoTSPc and CoTNPc are likely to be mixtures of isomers, randomly substituted in the two or three positions of each of the four benzene rings in the phthalocyanine ligand. There is no special reason that individual isomers will have significantly different formal redox potentials. For this reason, as suggested by Lever [23] the effect of the substituent can be correlated with the σ_p parameter (*para* substitution position) regardless of the position of the substituent, whether it is in the two or the three position in the peripheral benzene ring. In the case of the hexadeca substituted $CoF_{16}Pc$, σ parameters correspond to the arithmetical sum of the Hammett parameters in the *meta* and *para* positions. $CoF_{16}Pc$ is the only fully substituted phthalocyanine used in this study so eight fluoro groups are located at the *meta* position and eight fluoro groups in the *para* position. $\Sigma\sigma_p + \Sigma\sigma_m$ is 3.20, which fits well on the straight line. If we use only the *para* values, $\Sigma\sigma_p$ for 16 groups is 0.96, which falls well off the straight line corresponding to the Co(II)/(I) couple. The linear correlations in Fig. 4 have regression coefficients of 0.93 for the Co(III)Co(II) couple and 0.97 for the Co(II)/Co(I) couple using the data in the closed circles. The open circles for CoOEHPc correspond to data where the redox potentials are known but no data are available for the Hammett parameters, so the latter can be estimated from this figure. The opposite is true for $CoF_{16}Pc$ where the Hammett parameters are available but not the Co(III)/Co(II) redox potential. The estimated values are included in Table 1. The slopes of the lines are 0.041 V σ^{-1} for the Co(III)/Co(II) couple and 0.049 V σ^{-1} for the Co(II)/Co(I) couple, respectively. The value of 0.49 V σ^{-1} for the Co(II)/Co(I) couple compares well with 0.48 V σ^{-1} reported by Lever et al. [30] obtained from a plot using CoTNPPc, CoTAPc, CoPc and CoTSPc. It is interesting to comment at this point that the effect of substituents on the redox potentials of the phthalocyanines

is somewhat attenuated by the fact that these complexes are adsorbed on a graphite electrode. For complexes in solution, slopes are almost twice as large [23–25]. Lever et al. [30] have suggested that this could be attributed to the effect of the π-electronic system of the basal planes of the graphite substrate. This is only a speculation since redox data for a variety of substituted phthalocyanines adsorbed or immobilized on other electrode materials are not available.

Savéant et al. [32–35] have postulated in a series of papers that for outer sphere redox catalysis the redox potential of the catalyst represents the driving force of the reaction, and this was demonstrated for the reduction of vicinal alkyl dibromides. In fact it was possible to differentiate outer sphere from inner sphere redox catalysts by plotting $\log k$ (where k is the rate constant of the rate determining step) versus the redox potential of the catalyst. For outer-sphere catalysts, a straight line is obtained where $\log k$ increases with driving force. In a previous paper [20], we tested several substituted cobalt phthalocyanines adsorbed on graphite as catalysts for the electrochemical oxidation of 2-mercaptoethanol ($2R–SH \rightarrow R–SS–R + 2e^- + 2H^+$) and a plot of $\log k$ versus driving force (represented by the Co(II)/Co(I) redox potential) gives a straight line, but the rate of the reaction decreases with driving force. In other words this meant that the more the oxidative power of the phthalocyanine the less the activity for the oxidation of 2-mercaptoethanol. We attributed this observation to the fact that the oxidation of 2-mercaptoethanol activated by cobalt phthalocyanines proceeds by an inner-sphere mechanism and there other factors like the electronic coupling between donor (R–SH) and acceptor (Co–Pc), that control the rate of the reaction [20]. In this paper we have tested the catalytic activity of cobalt phthalocyanine derivatives for the reverse reaction, i.e. the reduction of 2-hydroxyethyldisulfide ($R-SS–R + 2e^- + 2H^+ \rightarrow 2R–SH$). In general the reduction of organic disulfides requires large overpotentials [36,37] and the R–SH/R–SS–R couple is very irreversible. This is associated with large activation energies as rupture of the sulfur–sulfur bond is involved [36].

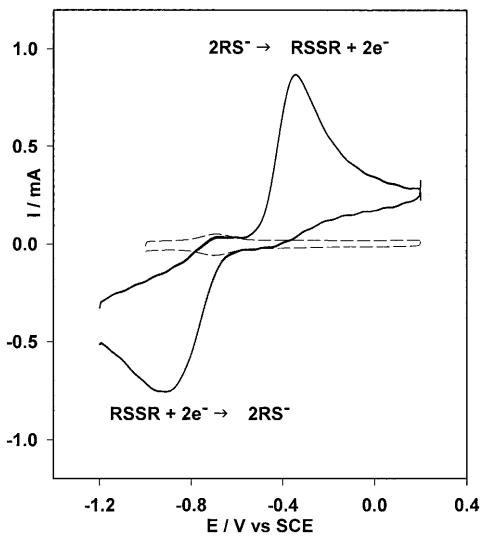


Fig. 5. Dashed lines: cyclic voltammogram of OPG modified with CoTNPPc in 0.2 M NaOH. Solid line, curve obtained after adding 0.0037 M of RSH and R–SSR to the electrolyte. Deaerated solutions. Scan rate: 0.1 V s^{-1}.

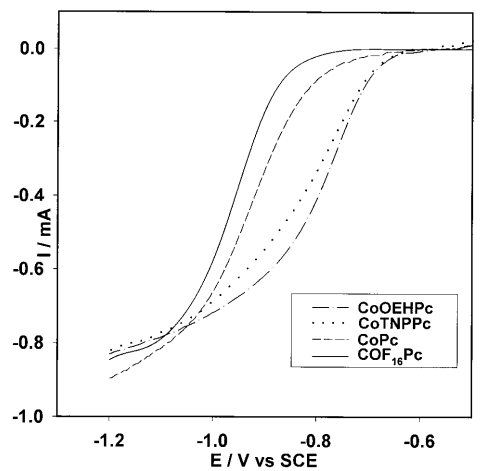


Fig. 6. Polarization curves obtained on a rotating OPG electrode modified with CoTNPPc in a solution containing 0.2 M NaOH + 0.0037 M of RSH and R–SS–R. Deaerated solution. Rotating rate 1000 rpm. Scan Rate 0.002 V s^{-1}.

In Fig. 5 the curve in dashed line illustrates the potentiodynamic response of the graphite electrode in alkaline media, modified with an adsorbed monolayer of CoTNPPc. The peak at ca. −0.685 V versus SCE corresponds to the Co(II)/Co(I) reversible couple in the adsorbed phthalocyanine. We use CoTNNPc as a typical example but similar curves are obtained with the other cobalt phthalocyanine derivatives. The curve in solid line shows a typical voltammogram obtained with the OPG/CoTNPPc modified electrode after adding 0.0037 M of both R–SS–R and R–SH to the electrolyte. The large separation between the reduction and oxidation wave (ca. 0.5 V) illustrates the irreversibility of the reaction from a kinetic point of view. A separation of 0.059 V should be observed for a one-electron transfer reversible process [38]. It also shows that the oxidation of the thiol occurs at potentials where Co(II) species predominate whereas the reduction of the disulfide occurs after the Co center is reduced to Co(I) in the adsorbed phthalocyanine.

Fig. 6 shows typical polarization curves obtained with a rotating disk OPG electrode modified with some Co–phthalocyanine derivatives taken as representative examples. A rotating disk electrode was used to minimize mass-transport limitations. The curves are shifted for the different cobalt phthalocyanine derivatives, which shows that its activity is influenced by the substituents present on the periphery of the phthalocyanine

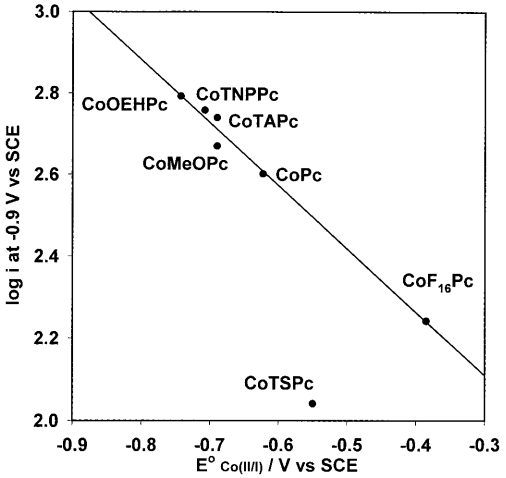


Fig. 7. Plot log log i (current density) versus the Co(II)/Co(I) redox potential for the reduction of 2-hydroxyethyldisulfide in 0.2 M NaOH.

ligand. This effect, however, is better illustrated in Fig. 7 where log i (current density at constant potential) for each phthalocyanine derivative is plotted versus the Co(II)/Co(I) redox potential. Note that we have used currents instead of the rate constants since the currents obtained experimentally are probably under mixed kinetic and mass transport control. However, the plot in Fig. 7 gives a qualitative idea of the dependence of the rates with the redox potential. The data point of Co–TSPc falls well off the straight line. This could be attributed to the negative charges on the four sulfonato groups on the periphery of the phthalocyanine ring. This could cause a change in the orientation of the adsorbed molecule on the graphite due to electrostatic repulsion at those negative potentials. Yeager et al. have suggested that CoTSPc adsorbs perpendicularly to the graphite based on in situ UV–Vis spectroscopic measurements of these molecules adsorbed on the basal plane of graphite [39]. If this is so, the graphite–Co distance would be larger compared with the other phthalocyanines and this could decrease the rate of the reaction. Apart from the data point of CoTSPc a straight line is obtained with the other phthalocyanines, which indicates that the rate of the reaction increases with driving force, i.e. the more the reductive power of the phthalocyanine the higher the activity for the reduction of the disulfide. This observation suggests that the reduction of the disulfide occurs via an outer-sphere mechanism, in contrast to what is found for the oxidation of the thiol [20]. This also indicates that the interaction of the disulfide with the cobalt center is weak. The opposite is true for the thiol. In fact, it has been demonstrated by visible spectroscopy that 2-mercaptoethanol, in alkaline media reduces the Co(II) center to Co(I) in cobalt tetrasulfonated phthalocyanine (CoTSPc) in solution [40]. In contrast, the disulfide has no effect on the spectrum of Co–TSPc. We have also demonstrated this by differential visible reflectance spectroscopy measurements [18] of Co–TSPc adsorbed on the basal plane of graphite electrodes. In alkaline medium the thiol L-cysteine reduces the adsorbed Co(II)TSPc to Co(I)TSPc. All this evidence indicates that thiols interact strongly with Co(II) but the disulfides do not. The plot in Fig. 7 indicates that the different adsorbed cobalt phthalocyanine derivatives, according to what has been suggested by Savéant [32–35], behave like outer-sphere redox catalysts, for the reduction of 2-dihydroxyethyldisulfide and probably for the reduction of other disulfides. Since the redox potential of these complexes is an important parameter in determining their catalytic and electrocatalytic activity, whether they act as outer or inner-sphere redox catalysts, it is interesting to establish linear correlations between their redox potential and the Hammett parameters of substituents in the periphery of the macrocyclic ligand. The same is valid for the semi-empirical theoretical calculations of the energies of the frontier orbitals of these molecules that correlate linearly with the redox potentials. In this fashion it is possible then to estimate redox potentials of phthalocyanines that cannot be measured directly from cyclic voltammograms as illustrated by some examples in this work and others given in the literature [23–30].

3. Experimental

3.1. Computational details

SCF molecular orbital theoretical calculations with full optimization using a PM_3 semiempirical procedure parametrized for transition metals were carried out for all substituted cobalt phthalocyanine with PC Spartan Pro package [41]. In all cases a doublet multiplicity (Co(II)) with an UHF (Unrestricted Hartree Fock) procedure was used.

Details about the origin and purification of the different substituted cobalt phthalocyanines are given in previous papers [18–20,22]. Adsorption of the complexes was achieved by placing a drop of 10^{-4} M solution of the complex on the electrode surface for 30 min. The solvent was dimethyl formamide for $CoPcF_{16}$, dimethylsulfoxide for CoPc, pyridine for CoMeOPc, CoTNPPc, CoTAPc and doubly-distilled water for CoTSPc. Adsorption of all complexes was verified by the appearance of typical peaks in the cyclic voltammograms of the modified electrodes. 2-Hydroxyethyldisulfide was spectroscopic grade from Riedel de Häen and was used as provided. Measurements were conducted on a BAS-100 potentiostat. The working electrode (Pine Instruments) was an ordinary pyrolytic graphite disk (OPG) of 0.44 cm^2. The electrode was

polished with 800 and 1200 grit emery paper and 1 μ alumina followed by ultrasonic treatment in purified water for 2 min. A saturated calomel electrode (SCE) was used as the reference, and a platinum spiral wire (14 cm^2, 99.99%, Aldrich) was used as the auxiliary electrode. The electrolyte (0.14 M NaOH + 0.5 M Na_2CO_3) was prepared from deionized, double-distilled water, and deaerated with ultra pure N_2. Electrolytes (NaOH, Na_2CO_3) were analytical grade from Merck.

Acknowledgements

This work was funded by the Presidential Chair in Science, Fondecyt Project 1970653 and Dicyt-Usach. M.A.G. ackowledges a Dicyt Doctoral fellowship.

References

[1] A.N. Snow, W.R. Barger, in: C.C. Leznoff, A.B.P. Lever (Eds.), Phthalocyanines, Properties and Applications, VCH, New York, 1989.
[2] K.Y. Law, Chem. Rev. 93 (1993) 449.
[3] D. Wöhrle, Chimia 45 (1991) 307.
[4] D. Wöhrle, L.K. Hoop, D. Schlettwein, in: C.C. Leznoff, A.B.L. Lever (Eds.), Phthalocyanines, Properties and Applications, vol. 4, VCH, New York, 1996, p. 219.
[5] X. Qi, R.P. Baldwin, Electroanalysis 6 (1994) 353.
[6] X. Qi, R.P. Baldwin, J. Electrochem. Soc. 143 (1996) 1283.
[7] A. Napier, J.P. Hart, Electroanalysis 8 (1996) 1006.
[8] B. Basu, S. Satapathy, A.K. Bhatnagar, Catal. Rev. 35 (1993) 571.
[9] J.H. Zagal, Coord. Chem. Rev. 119 (1992) 89.
[10] A. Schmidt, L.K. Chan, A. Back, N.R. Armstrong, in: C.C. Leznoff, A.B.P. Lever (Eds.), Phthalocyanines, Properties and Applications, vol. 4, VCH, New York, 1996, p. 307.
[11] H. Böttcher, J. Prakt. Chem. 334 (1992) 14.
[12] J. Simon, J.J. André, Molecular Semi-conductor, Springer, Berlin, 1985.
[13] M.M. Nichelson, in: C.C. Leznoff, A.B.P. Lever (Eds.), Phthalocyanines, Properties and Applications, vol. 3, VCH, New York, 1993, p. 71.
[14] D. Schlettwein, T. Yoshida, J. Electroanal. Chem. 441 (1998) 139.
[15] A.B.P. Lever, S.R. Pickens, P.C. Minor, S. Licoccia, B.S. Ramaswany, K. Magnell, J. Am. Chem. Soc. 103 (1981) 6800.
[16] A.B.P. Lever, S. Liccocia, K. Magnell, P.C. Minor, B.S. Ramaswamy, ACS Symp. Ser. 201 (1982) 237.
[17] J.H. Zagal, C. Páez, Electrochim. Acta 34 (1989) 243.
[18] R.O. Lezna, S. Juanto, J.H. Zagal, J. Electroanal. Chem. 452 (1998) 221.
[19] J.H. Zagal, M. Gulppi, C. Depretz, D. Lelièvre, J. Porphyr. Phthalocyanines 3 (1999) 355.
[20] J.H. Zagal, M.A. Gulppi, C.A. Caro, G. Cárdenas-Jirón, Electrochem. Commun. 1 (1999) 389.
[21] J.H. Zagal, M. Gulppi, M. Isaacs, G. Cárdenas-Jirón, M.J. Aguirre, Electrochim. Acta 44 (1998) 1349.
[22] J.H. Zagal, M. Páez, A.A. Tanaka, J.R. dos Santos, C.A. Linkous, J. Electroanal. Chem. 339 (1992) 13.
[23] A.B.P. Lever, Inorg. Chim. Acta 203 (1993) 171.
[24] A.B.P Lever, in: C.C. Leznoff, A.B.P Lever (Eds.), Phthalocyanines, Properties and Applications, vol. 3, VCH, New York, 1993, p. 1.
[25] A.B.P. Lever, J. Porphyrins Phthalocyanines 3 (1999) 488.
[26] Y. Orihashi, H. Ohno, E. Tesuchida, Mol. Cryst. Liq. Crystallogr. 160 (1988) 139.
[27] Y. Orihashi, M. Nishikawa, H. Ohno, E. Tushida, H. Matsuda, M. Kato, Bull. Chem. Soc. Jpn. 60 (1987) 3731.
[28] V.I. Gavrilov, L.G. Tomilova, V.M. Derkacheva, E.V. Chernykh, N.T. Ioffe, I.V. Shelepin, E.A. Luk'yanets, Zh. Obshch. Khim. 53 (1883) 1347.
[29] V.I. Gavrilov, E.V. Chernykh, L.G. Tomilova, V.M. Derkacheva, E.V. Chernykh, N.T. Ioffe, I.V. Shelepin, E.A. Luk'yanets, I.V. Shelepin, Zh. Obshch. Khim. 60 (1886) 1448.
[30] Y. Tse, P. Janda, H. Lam, J. Zhang, W. Pietro, A.B.P. Lever, J. Porphyr. Phthalocyanines 1 (1997) 3.
[31] C. Hansch, A. Leo, R.W. Taft, Chem. Rev. 91 (1991) 165.
[32] D. Lexa, J. Mispelter, J.M. Savéant, J. Am. Chem. Soc. 103 (1981) 6806.
[33] D. Lexa, J.M. Savéant, D.L. Wang, Organometallics 4 (1986) 1428.
[34] D. Lexa, J.M. Savéant, K.B. Su, D.L. Wang, J. Am. Chem. Soc. 109 (1987) 6464.
[35] D. Lexa, J.M. Savéant, H.J. Schäfer, K.B. Su, B. Vering, D.L. Wang, J. Am. Chem. Soc. 112 (1990) 6162.
[36] K. Daasbjerg, H. Jensen, R. Benassi, F. Taddei, S. Antonello, A. Gennaro, F. Maran, J. Am. Chem. Soc. 121 (1999) 1750.
[37] T.R. Ralph, M.L. Hitchman, J.P. Millington, F.C. Walsh, J. Electroanal. Chem. 375 (1994) 1.
[38] C.M.A. Brett, A.M. Oliveira-Brett, Electrochemistry, Principles, Methods, and Applications, Oxford University Press, New York, 1992.
[39] B.Z Nikolic, R.R. Adzic, E. Yeager, J. Electroanal. Chem. 103 (1989) 1979.
[40] K.P.S. Leung, E.A. Betterton, M.R. Hoffmann, J. Phys. Chem. 93 (1989) 430.
[41] PC Spartan Pro 1.0, Wavefunction, Inc., 18401 Von Karman Avenue, Suite 370 Irvine, CA 92612, USA.

PERGAMON

www.elsevier.nl/locate/poly

Polyhedron 19 (2000) 2261–2268

POLYHEDRON

Facile conversion of bis(alkynyl) into diyne ligand on platinum assisted by electrophilic gold phosphine

Cleber V. Ursini [a], Gilson H.M. Dias [a,*], Manfredo Hörner [b], Adailton J. Bortoluzzi [c], Milton K. Morigaki [d]

[a] *Instituto de Química, UNICAMP, Campinas, SP 13081-970, Brazil*
[b] *Departamento de Química, UFSM, Santa Maria, RS 97105-900, Brazil*
[c] *Departamento de Química, UFSC, Florianópolis, SC 88040-900, Brazil*
[d] *Departamento de Química, UFES, Vitória, ES 29060-900, Brazil*

Received 1 October 1999; accepted 15 February 2000

Abstract

^{31}P NMR spectroscopy measurements were used to establish the course for the stoichiometric-dependent reactions between $[Au(PPh_3)]^+$ and $[Pt(C{\equiv}CPh)_2(dppf)]$ (**1**), which for equimolar amounts afford as the unique product $[Pt\text{-}\{\eta^3\text{-}C(C{\equiv}CPh){=}C(Ph)Au(PPh_3)\}(dppf)]^+$ (**2**), but any excess of **1** gives also $[Pt(\eta^2\text{-}PhC{\equiv}CC{\equiv}CPh)(dppf)]$ (**3**) [dppf = 1,1′-bis(diphenylphosphine)ferrocene]. Both compounds **2** and **3** were obtained straightforwardly by the reactions of **3** with $[Au(PPh_3)]^+$ and $[Pt(C_2H_4)(dppf)]$ with 1,4-diphenylbutadiyne, respectively. The X-ray crystal structure analysis of **3** confirmed a trigonal-planar coordination geometry about the platinum atom, and a bent η^2-coordinated diyne ligand. © 2000 Elsevier Science B.V. All rights reserved.

Keywords: Platinum; Gold; Cross-coupling; Diyne; X-ray

1. Introduction

There has been a growing interest in metal-induced carbon–carbon bond-forming reactions of terminal alkynes [1]. In particular, one of the earliest experimental evidences of coupling reactions, mainly using d^8-metal complexes, has been provided by isolated *trans* and *cis*-$[Pt(C{\equiv}CPh)_2(PPh_3)_2]$, $[Pt(\eta^2\text{-}HC{\equiv}CPh)(PPh_3)_2]$, and 1,4-diphenylbuta-1,3-diyne products from the reaction between *cis*-$[PtCl_2(PPh_3)_2]$ and phenylacetylene [2]. Theoretical analysis and kinetics studies of oxidative addition and reductive elimination on d^8-metal-centered coupling of organic groups showed that a *cis* orientation or trigonal-planar geometry for the complex is necessary before occurrence of reductive elimination of the coupled product [3,4]. It is well established that the C–C elimination process at platinum(II) center is less favorable than for palladium counterparts, whereas the platinum intermediates are generally substitution-inerts in homogeneous catalysis, being therefore better candidates to carry out mechanistic studies [5,6].

One of our main objectives in the present paper was to find out whether the electrophilic metal reagent $[Au(PR_3)]^+$ behaves toward *cis*-alkynyl groups like its isolobal H^+ in formation of gold–butenynyl ligands [7,8]. This would be in contrast, therefore, to other electrophiles such $[Ag(PR_3)]^+$ and HgX_2 for which the reactions resulted in a coordinated metallic moiety at C≡C bonds of *cis*-$[Pt(C_6F_5)_2(C{\equiv}CR)_2]^{2-}$ [9]. To ascertain this premise, the reaction of complex **1** with $[Au(PPh_3)]^+$ was used as a model. The chelating dppf ligand was chosen due to its significant steric strain in square planar complexes, which ensures a *cis* configuration for the other two coordination sites. Consequently, it accelerates the formation of the coupling products [10].

* Corresponding author. Tel.: +55-19-788-3023; fax: +55-19-788-3146.
E-mail address: dias@iqm.unicamp.br (G.H.M. Dias).

0277-5387/00/$ - see front matter © 2000 Elsevier Science B.V. All rights reserved.
PII: S0277-5387(00)00487-3

2. Experimental

2.1. General

All manipulations were performed using general Schlenk and high-vacuum techniques. Solvents were appropriately dried and distilled under argon prior to use.

IR spectra were recorded as Nujol mulls on a JASCO IR 700 spectrometer, and calibrated relative to polystyrene at 1601 and 1028 cm^{-1}. The NMR spectra were recorded upon either BRÜKER AC300P (^1H 300.13, ^{13}C 75.47, ^{31}P 121.50 MHz) or VARIAN GEMINI 300 (^1H 300.08, ^{13}C 75.46, ^{31}P 121.47 MHz) Fourier-transform machines in $CDCl_3$, unless otherwise stated. ^1H and ^{13}C-{^1H} spectra were referenced to internal $SiMe_4$, and ^{31}P-{^1H} spectra referenced to external 85% H_3PO_4, and locked on the solvent deuterium signal. Reactions monitored by ^{31}P-{^1H} spectra were recorded in THF with the deuterium lock signal from D_2O, using a concentric glass capillary of this solvent in the 5 mm NMR sample-tube. Elemental analyses were performed on a Perkin–Elmer 2400 CHN microanalyzer. All percentages given are the averages of at least two independent determinations. 1,1′-Bis(diphenylphosphine)ferrocene (dppf) and phenylacetylene were purchased from Aldrich and used as received. [Ag][O_3SCF_3] (Aldrich) was recrystallized from ethyl ether–petroleum ether. 1,4-Diphenylbutadiyne [11] and the complexes [Pt(C≡CPh)$_2$(cod)] [11], [Au(PPh_3)Cl] [12] [$PtCl_2$(cod)] [13] and [Pt(cod)$_2$] [14] were prepared as described in the literature. Fresh and filtrated solutions of [Au(PPh_3)(THF)][O_3SCF_3] (0.50×10^{-2} mmol ml^{-1}) were used, prepared by an equimolar mixture of [Ag][O_3SCF_3] and [Au(PPh_3)Cl] in THF, which were stirred in the dark for 1 h, and filtered through a pad of diatomaceous earth.

2.2. Preparations

2.2.1. [Pt(C_2H_4)(dppf)] [15]

[Pt(cod)$_2$] (0.097 g, 0.23 mmol) was added in small portions to 15 ml of petroleum ether saturated with ethylene at 0°C. A solution of dppf (0.133 g, 0.24 mmol) in 15 ml of diethyl ether was then added, and the mixture stirred for 1 h at 25°C in an argon atmosphere. The resulting yellow solution was reduced to a small volume, affording a precipitate by bubbling ethylene through the solution at 0°C, which was washed with cold petroleum ether (3×5 ml) saturated with ethylene and dried under reduced pressure for 3 h. Yield of 0.167 g (93%). ^1H NMR: δ 2.14 [d, 4H, J(PtH) 60 Hz, J(PH) 2.8 Hz, C_2H_4]; 4.16 (s, 4H, η^5-C_5H_4P); 4.22 (s, 4H, η^5-C_5H_4P); 7.28–7.70 (m, 20H, C*H*, Ph); ^{31}P-{^1H} NMR: δ 29.1 [s, ^1J(PtP) 3684 Hz, Ph_2P]. *Anal.* Found: C, 55.16; H, 4.19. Calc. for $C_{36}H_{32}FeP_2Pt$: C, 55.61; H, 4.15%.

2.2.2. [Pt(C≡CPh)$_2$(dppf)] (1)

A stirred suspension of [Pt(C≡CPh)$_2$(cod)] (0.060 g, 0.12 mmol) in THF (10 ml) was treated with dppf (0.068 g, 0.12 mmol). After stirring for 1 h at 25°C, the resulting orange solution was concentrated under reduced pressure to ca. 2 ml. Addition of diethyl ether afforded a yellow solid, which was washed with diethyl ether and dried in vacuo for 2 h to give 0.089 g (78%). M.p. 225°C (dec.). IR: ν(C≡C) 2132 w, 2121 w cm^{-1}. ^1H NMR: δ 4.19 (s, 4H, η^5-C_5H_4P); 4.32 (s, 4H, η^5-C_5H_4P); 6.79 [dt, 4H, ^3J(HH) 5.4 Hz, ^4J(HH) 1.7 Hz, *o*-C*H*, C≡C*Ph*]; 6.4–7.02 (m, 6H, *m*-, *p*-C*H*, C≡C*Ph*); 7.31 [td, 8 H, ^3J(HH) 7.5 Hz, ^4J(HH) 1.3 Hz, *m*-C*H*, PPh_2]; 7.38 [td, 4H, ^3J(HH) 7.5 Hz, ^4J(HH) 1.3 Hz, *p*-C*H*, P*Ph*]; 7.85 [m, 8H, ^3J(PH) 11.2 Hz, ^3J(HH) 7.0 Hz, ^4J(HH) 1.3 Hz, *o*-C*H*, P*Ph*]. ^{13}C-{^1H} NMR: δ 72.82 (s, *C*H, η^5-C_5H_4P); 75.75 (t, *C*H, η^5-C_5H_4P); 75.82 [d, $|^1J(CP) + {}^2J(C\,P')|$ 61 Hz, *C*P, η^5-C_5H_4P]; 103.37 [dd, ^1J(PtC) 1132 Hz, $|^2J(CP) + {}^2J(CP')|$ 75 or 133 Hz, Pt*C*≡CPh]; 110.34 [m, ^2J(PtC) 308 Hz, $|^3J(CP) + {}^3J(CP')|$ 35.2 Hz, $^3J(CP) = \pm(36 \pm 2)$ Hz, $^3J(CP') = \pm(0.8 \pm 2)$ Hz, PtC≡*C*Ph]; 125.13 (s, *p*-*C*H, C≡C*Ph*); 127.21 (s, *m*-*C*H, C≡C*Ph*); 128.08 [t, $|^3J(CP) + {}^5J(CP')|$ 10.5 Hz, *m*-*C*H, P*Ph*]; 130.62 (s, *p*-*C*H, P*Ph*); 131.79 (s, *o*-*C*H, C≡C*Ph*); 133.44 [m, ^2J(PtC) 27 Hz, $|^1J(PC) + {}^3J(P'C)|$ 57.8 Hz, *ipso*-*C*, P*Ph*]; 135.19 [t, $|^2J(CP) + {}^4J(CP')|$ 11.5 Hz, *o*-*C*H, P*Ph*]. ^{31}P-{^1H} NMR: δ 15.1 [s, J(PtP) 2372 Hz]. *Anal.* Found: C, 62.70; H, 3.98. Calc. for $C_{50}H_{38}FeP_2Pt$: C, 63.10: H, 4.02%.

2.2.3. [Pt{η^3-C(C≡CPh)=C(Ph)AuPPh_3}(dppf)][O_3SCF_3] (2)

A stirred solution of **3** (0.075 g 0.078 mmol) in THF (5 ml) was treated with [Au(PPh_3)][O_3SCF_3] (0.080 mmol) in THF (16 ml) at °C. The resulting orange solution was stirred for 5 min at 5°C, and 10 min at r.t. The volume was reduced to 5 ml under vacuum, and fast addition of diethyl ether (10 ml) afforded yellow precipitate, which was washed with diethyl ether (3×5 ml) and dried under reduced pressure for 10 h. Yield of 0.106 g (87%). IR: ν(C≡C) not observed; ν(CF) 1270 vs, br; ν(SO) 1154 s, br; 1028 s, br cm^{-1}. ^1H NMR ($CDCl_3$): δ 3.79 (s, 2H, η^5-C_5H_4P); 4.28 (s, 2H, η^5-C_5H_4P); 4.50 (s, 4H, η^5-C_5H_4P); δ 6.75–6.88 (m, 9H, Ph) 6.90–6.97 [td, ^3J(HH) 7.8 Hz, ^4J(HH) 1.9 Hz, 4 H, Ph]; 7.14–7.33 (m, 12 H, Ph); 7.40 [t, ^3J(HH) 7.8 Hz, 3 H, Ph]; 7.47–7.57 (m, 9 H, Ph); 7.59 (m, 4 H, *o*-CH, Ph, dppf); 7.81 [m, ^3J(PH) 11.3 Hz, ^3J(HH) 7.8 Hz, ^4J(HH) 1.4 Hz, 4 H, *o*-CH, Ph, dppf]. ^{31}P-{^1H} NMR ($CDCl_3$): δ 20.48 [dd, ^1J(PtP) 3036 Hz, J(PP′) 16.5 Hz, J(PP″) 8.9 Hz, Pt(dppf)]; 23.58 [t, ^1J(PtP) 4364 Hz, ^2J(PP) 18.9 Hz, J(PP′) 16.5 Hz, Pt(dppf)]; 35.15 [dd, J(PtP) 209 Hz, J(P′P″) 18.9 Hz, J(PP″) 8.9 Hz, Au(PPh_3)]. *Anal.* Found: C, 53.04: H, 3.13. Calc. for $C_{69}H_{53}AuF_3O_3FeP_3PtS$: C, 53.11; H, 3.43%.

*2.2.4. [Pt(η²-PhC≡CC≡CPh)(dppf)] (**3**)*

Method A. [Pt(cod)$_2$] (0.060 g, 0.15 mmol) was added in small portions to 15 ml of petroleum ether saturated with ethylene at 0°C. A solution of dppf (0.081 g, 0.15 mmol) in 15 ml of diethyl ether was added, and the mixture stirred for 1 h at 25°C in an argon atmosphere. 1,4-Diphenylbutadiyne (0.041 g, 0.203 mmol) was then added, and the solution stirred further for 1 h. The volatiles were evaporated, and the residue extracted from benzene (3 ml). Addition of 15 ml of petroleum ether gave a yellow solid, which was washed with petroleum ether (3 × 10 ml) and dried under reduced pressure. Yield of 0.107 g (77%). IR: ν(C≡C)$_{uncoord}$ 2166 m, ν(C≡C)$_{coord}$ 1720 m cm^{-1}. ^{1}H NMR ($CDCl_3$): δ 3.95 (q, 2H, η⁵-C_5H_4P); 4.14 (t, J 1.6 Hz, 2H, η⁵-C_5H_4P); 4.32 (m, 2H, J 1.4 Hz, η⁵-C_5H_4P); 4.37 (dd, J 3.8 Hz, J 1.9 Hz, 2H, η⁵-C_5H_4P); 6.88–7.00 (m, 1H, *p*-C*H*, 2H, *m*-C*H*, PhC≡C); 7.15–7.38 (m, 19H, Ph); 7.71 [m, 4H, ^3J(PH) 11.3 Hz, ^3J(HH) 7.8 Hz, ^4J(HH) 1.9 Hz, *o*-C*H*, PPh_2]; 7.90 [m, 4H, ^3J(PH) 11.2 Hz, ^3J(HH) 8.0 Hz, ^4J(HH) 1.5 Hz, *o*-C*H*, PPh_2]. NMR ^{13}C {^{1}H} ($CDCl_3$): δ 71.02 [d, J(CP) 5.7 Hz, η⁵-C_5H_4P]; 72.08 [d, J(CP) 6.3 Hz, η⁵-C_5H_4P]; 74.29 [m, $|J(CP)+J(CP')|$ 9.5 Hz, η⁵-C_5H_4P]; 75.03 [q, $|J(CP)+J(CP')|$ 10.7 Hz, η⁵-C_5H_4P]; 80.07 [d, ^1J(CP) 51.4 Hz, CP, η⁵-C_5H_4P]; 82.77 [dd, J(CP) 12.99 Hz, J(CP′) 6.93 Hz, *C*≡CPh free]; 82.81 [dd, ^1J(CP) 50.8 Hz, ^3J(CP) 3.2 Hz, CP, η⁵-C_5H_4P]; 103.83 [d, J(PtC) 17.5 Hz, $|J(CP)+J(CP')|$ 7.4 Hz, C≡*C*Ph free]; 109.19 [dd, ^1J(PtC) 289 Hz, ^2J(CP) 78.0 Hz, ^2J(CP′) 5.5 Hz, η²-C≡C]; 125.52 [d, J(PtC) 12 Hz, $|J(CP)+J(CP')|$ 2.2 Hz, probably *ipso*-C, C≡C*Ph* free]; 126.40 (s, *p*-CH, C≡C*Ph*); 126.81 (s, *p*-CH, C≡C*Ph*); 127.77 (s, *m*-CH, C≡C*Ph*); 127.78 [d, $|J(CP)+J(CP')|$ 10.0 Hz, *m*-CH, PPh]; 127.95 (s, *m*-CH, C≡C*Ph*); 128.04 [d, $|J(CP)+J(CP')|$ 10.4 Hz, *m*-CH, PPh]; 129.34 [d, $|J(CP)+J(CP')|$ 1.4 Hz, *p*-CH, PPh); 129.90 [d, $|J(CP)+J(CP')|$ 1.0 Hz, *p*-CH, PPh]; 130.62 [d, ^4J(PtC) 37.3 Hz, $|J(CP)+J(CP')|$ 5.5 Hz, *o*-CH, η²-C≡C*Ph*]; 130.79 [d, J(PtC) 8.6 Hz, $|J(CP)+J(CP')|$ 1.9 Hz, *o*-CH, C≡C*Ph* free]; 132.36 [t, $|J(CP)+J(CP')|$ 19.0 Hz, J(PtC) 6.6 Hz, probably *ipso*-C, η²-C≡C*Ph*]; 134.00 [d, J(PtC) 20.4 Hz, $|J(CP)+J(CP')|$ 13.7 Hz, *o*-CH, P*Ph*]; 134.56 [d, J(PtC) 27.6 Hz, $|J(CP)+J(CP')|$ 14.4 Hz, *o*-CH, P*Ph*]; 135.90 [dd, ^2J(CP) 79.1 Hz, ^2J(CP′) 6.3 Hz, probably η²-C≡C]; 136.25 [d, J(PtC) 44.2 Hz, ^1J(CP) 44.6 Hz, ^3J(CP) 2.8 Hz, *ipso*-C, P*Ph*]; 136.90 [d, J(PtC) 36.7 Hz, ^1J(CP) 46.3 Hz, ^3J(CP) 2.5 Hz, *ipso*-C, P*Ph*]. ^{31}P-{^{1}H} NMR ($CDCl_3$): δ 22.1 [d, ^1J(PtP) 3630 Hz, ^2J(PP) 10.7 Hz, Ph_2*P*Pt]; 22.9 [d, ^1J(PtP) 3371 Hz, ^2J(PP) 10.7 Hz, Ph_2*P*Pt]. *Anal.* Found: C, 63.17; H, 4.00. Calc. for $C_{50}H_{38}FeP_2Pt$: C, 63.10; H, 4.02%.

Method B. A stirred solution of [Pt(C_2H_4)(dppf)] (0.160 g, 0.21 mmol) in THF (15 ml) was treated with 1,4-diphenylbutadiyne (0.050 g, 0.25 mmol) at r.t. After being stirred for 1 h, the resulting yellow solution was filtered through an alumina column and concentrated to 2 ml. Addition of diethyl ether and petroleum ether (1:1) afforded a yellow solid, which was washed with petroleum ether and dried under vacuum. Yield: 0.180 g (92%). *Anal.* Found: C, 63.17; H, 3.81. Calc. for $C_{50}H_{38}FeP_2Pt$: C, 63.10; H, 4.02%. The spectral data were identical with that of **3** prepared from the method A.

*2.2.5. Both **2** and **3** from the same reaction*

A solution of [Pt(C≡CPh)$_2$(dppf)] (0.033 g, 0.035 mmol) in THF (10 ml) was treated with [Au(PPh_3)(thf)][O_3SCF_3] (0.030 mmol) in THF (6 ml). After 3 h of stirring, the yellow solution was concentrated under reduced pressure, and diethyl ether added to the solution to give an orange precipitate, which was washed with diethyl ether (3 × 5 ml), and dried under vacuum for 2 h. This product was identified as **2**. Yield of 0.013 g (23%). *Anal.* Found: C, 53.00; H, 3.24. Calc. for $C_{69}H_{53}AuF_3O_3FeP_2PtS$: C, 53.11; H, 3.43%.

The supernatant liquid and washings were passed through an alumina column. Addition of 5 ml of petroleum ether yielded yellow crystalline solids, after leaving the solution stand overnight at −20°C. The crystals were washed with petroleum ether (3 × 5 ml), dried under reduced pressure, and identified as **3**. Yield of 0.010 g (30%). *Anal.* Found: C, 52.81; H, 2.98. Calc. for $C_{69}H_{53}AuF_3O_3FeP_3PtS$: C, 53.11; H, 3.43%. The spectral data were identical with those of **2** and **3** prepared before.

2.3. X-ray crystallography

Single crystals of **3** were grown from diethyl ether–petroleum ether 1:1 mixture. A yellow crystal (0.45 × 0.30 × 0.15 mm) of the compound was mounted on a glass fiber and used for intensity data collection. For data collection the unit cell dimensions and the orientation matrix were obtained from a least square fit of 25 reflections in the range $8.78 \le \theta \le 13.42°$. The automatic intensity search and indexing method indicated a cell belonging to the monoclinic crystal system with a P lattice. X-ray intensity data were recorded on an Enraf–Nonius CAD4 diffractometer employing the ω–2θ scan method with a scan speed of 45 sec/reflection. Every 60 min, the intensity and orientation of three standard reflections were confirmed; the observed intensity decay was less than 1.4% over the data collection. From the Bravais lattice and observed reflections, the space group was chosen to be $P2_1/n$. Lorentz and polarization corrections were made on the intensity data; due to the linear absorption coefficient of 3.96 mm^{-1} a semi-empirical absorption correction based on psi-scans was performed [16].

The structure was solved using the heavy-atom Patterson method employing SHELXS-97 [17] program and

all non-hydrogen atoms were located by subsequent Fourier difference synthesis. For structure refinement the SHELXL-97 [18] program was employed and the full-matrix least-squares method minimized on $\Sigma w(F_o^2 - F_c^2)^2$ where w is a weighting scheme indicated below. All non-hydrogen atoms were refined using anisotropic thermal parameters. Hydrogen atom sites were obtained geometrically and their displacement parameters were refined isotropically on a groupwise basis. For the final refinement of the structure, an isotropic extinction correction was included. The final refinements including 510 parameters converge to $R = 4.15$ and $R_w = 7.32\%$ with the weighting scheme, $w = 1/[s^2(F_o^2) + (0.0291P)^2 + 4.3290P]$ where $P = (F_o^2 + 2F_c^2)/3$.

*2.3.1. Crystal data: complex **3***

$C_{50}H_{38}FeP_2Pt$, $M = 951.68$, monoclinic, $a = 14.8059(2)$, $b = 17.6930(3)$, $c = 15.8196(2)$ Å, $\beta = 104.590(2)°$, space group $P2_1/n$, $Z = 4$, $V = 4010.48(10)$ Å^3.

3. Results and discussion

3.1. Synthesis and properties of complexes

Complex [Pt(C≡CPh)$_2$(dppf)] **1** is readily prepared in good yield from [Pt(C≡CPh)$_2$(cod)] [19] with the displacement of cod by dppf ligand (cod = 1,5-cyclooctadiene). Treatment of **1** with less of than 1 equiv. of [Au(thf)(PPh$_3$)][O$_3$SCF$_3$] in THF affords a mixture of [Pt{η^3-C(C≡CPh)=C(Ph)AuPPh$_3$}(dppf)]$^+$ (**2**) and [Pt(η^2-PhC≡CC≡CPh)(dppf)] (**3**). Concentration of the reactional solution, the less soluble complex **2** is selectively precipitated with diethyl ether. Crystallization of **3** is performed by adding petroleum ether into the supernatant and cooling. An increase in the relative amount of **1** towards two-fold excess in the reaction with [Au(PPh$_3$)]$^+$ favors the yield of **3**, as the main product. Complex **3** is reasonably stable in the solid state and in solution. Pure **2**, isolated as triflate salt, is stable as a solid, but is thermally unstable for prolonged periods in THF and CHCl$_3$ solutions. An authentic sample of **3** is prepared either by reaction of [Pt(cod)$_2$] with dppf and 1,4-diphenylbutadiyne in petroleum ether saturated with ethylene or by treatment of [Pt(C$_2$H$_4$)(dppf)] with diphenylbutadiyne. An alternative route for a rapid preparation of **2** in good yields is by treatment of **3** with [Au(PPh$_3$)]$^+$ in a 1:1 ratio.

3.2. Spectroscopic characterization

The IR spectrum of **1** exhibits two weak absorptions at 2132 and 2121 cm^{-1}, which correspond to the stretching frequencies of the *cis*-Pt(C≡CPh)$_2$ moiety. Compound **3** shows one band at 2166 cm^{-1} assignable to an uncoordinated alkyne, and another at 1720 cm^{-1}, owing to a carbon–carbon triple bond order is significantly reduced because of the coordination of the alkyne at the platinum atom.

A comparison between the ^{1}H NMR spectra of **1** (δ 4.19, and 4.32, 1:1) and **2** (δ 4.50, 4.28, and 3.79, 2:1:1) in the region of the cyclopentadienyl ring suggests a decrease in the symmetry of **2**. Whereas the spin system of **2** is AA′BB′CC′DD′, the single peak with double intensity is indeed two unresolved resonances [20]. The ^{1}H NMR spectrum of **3** exhibits four resonances with equal intensity for the chemically non-equivalent cyclopentadienyl protons and well-solved multiplets in the phenyl proton regions. Quaternary carbon resonances of the alkynyl ligands of **1** are observed at δ 103.4 [J(PtC) 1132 Hz] for C$_\alpha$ and at δ 110.3 [J(PtC) 308 Hz] for C$_\beta$ in the ^{13}C-{^{1}H} NMR spectrum. These carbons appear as the A part of AXX′ and AMXX′ spin system (M = ^{195}Pt, and X = ^{31}P) of a second-order spectrum, owing to the presence of chemically equivalent but magnetically non-equivalent ^{31}P nuclei.

^{31}P NMR data proved to be very useful for a better characterization of the complexes. Complex **1** displays only a singlet at high field (δ 15.1) with ^1J(PtP) of 2372 Hz, assigned to the phosphorus nuclei of the ligand dppf bound at the platinum atom. The presence of three sets of doublets in the spectrum of **2** reveals three distinct phosphorus nuclei environments. Two of these sets at δ 20.48 and 23.58, with very large platinum coupling constants ^1J(PtP) of 3036 and 4364 Hz, belong to the two P of the dppf. The smallest J(PtP) value is typical of a P atom lying *trans* to the stronger-field vinyl that is structurally well recognized, while the largest J(PtP) value shows a P atom *trans* to the weaker-field coordinated alkyne [21]. Interestingly, **2** has chemical shifts and ^1J(PtP) values near those observed for [Pt(η^3-allyl)(PR$_3$)$_2$]$^+$ [22], η^3-propargyl–allenyl [Pt(η^3-CH$_2$CCPh)(PPh$_3$)$_2$] [23], and butadienyl [Pt(η^3-CH$_2$CRCCH$_2$)(dppf)]$^+$ [24] complexes. Of particular relevance is the third set at lower field (δ 35.15) with a large J(PtP) 209 Hz, which is tentatively assigned to the P of the spacious Au(PPh$_3$) moiety bound at the vinyl group of the buta-1,3-diynyl ligand. However, we must bear in mind that we cannot rule out the possibility of an interaction between platinum and gold atoms. Additionally, a coupling constant of this magnitude is compared to those found for sp^3 carbon-bound P in complexes of the type [Pt{σ:η^2-C$_8$H$_{12}$(PR$_3$)}(dppe)]$^+$ (^3J(PtP) 223 Hz) [25], but is larger than in the bridged complex [Pt$_2$(μ-η^2,η^2-butadiyne)(PPh$_3$)$_4$] (^4J(PtP) 34 Hz) [26]. Unfortunately, no single-crystal of **2** was obtained for X-ray analysis. The basic structure of **2** appears analogous to [Ru(CO)$_2$\{C(C≡CPh)=C(Ph)HgCl\}Cl(PMe$_2$Ph)$_2$], which has the HgCl sub-

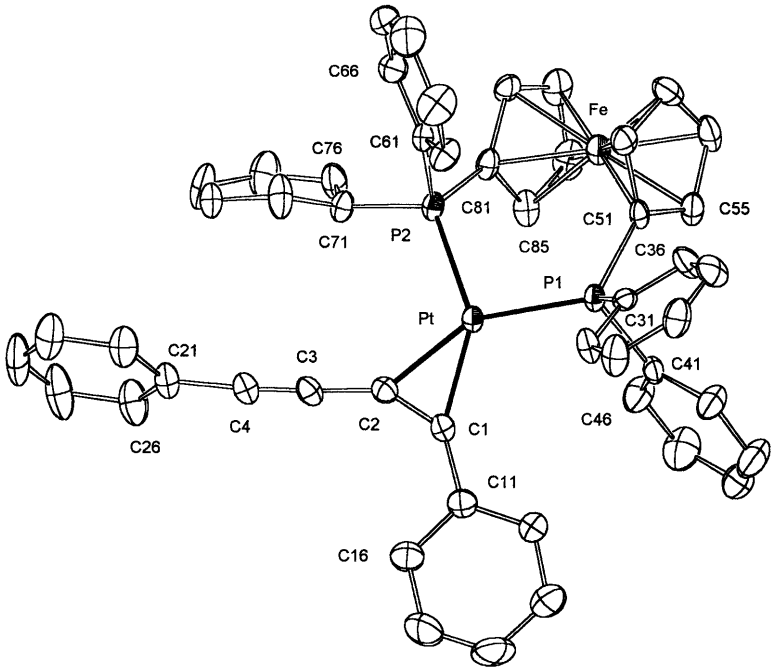


Fig. 1. ZORTEP plot with atom-labeling scheme of the structure of **3**; displacement ellipsoids at the 30% probability level.

stituent at 1-position of the η^1-but-1-en-3-yn-2-yl ligand, and also decomposes slowly in solution releasing $Me_3CC{\equiv}CC{\equiv}CCMe_3$ [27]. Taking into account a comparison between spectroscopic and reactivity data of **2** with known enynyl analogues [28], the compound **2** would be better described as an η^3-enynyl ligand rather than the alternate η^2,η^2 description. On the other hand, the assignment is unambiguous in complex **3**. The two near doublets at 22.1 and 22.9 ppm with large ^1J(PtP) of 3630 and 3371 Hz are typical of complexes [Pt(η^2-PhC≡CC≡CPh)L_2] (L = phosphine ligands) [20]. The identity of **3** is supported by X-ray study and an analogy with early data of η^2-coordinated diyne ligands, in which the complexes have been prepared and in some case structurally characterized by X-ray diffraction studies [29].

3.2.1. Crystal structure of *3*

The ZORTEP [30] drawing of the molecular structure of **3** is shown in Fig. 1. Selected bond distances and angles are given in Table 1. The list of the observed and calculated structure factors is available from the authors upon request.

The neutral complex shows a trigonal coordination of platinum by the η^2-coordinated Ph–C≡CC≡CPh ligand [Pt–C(1) = 2.050(7), Pt–C(2) = 2.040(7) Å], and the dppf ligand [Pt–P(1) = 2.2714(16), Pt–P(2) = 2.2679(18) Å]. Atoms P(1), P(2), C(2) and C(1) forms a plane (RMS deviation 0.021 Å), from which the Pt atom is moved away by 0.010(2) Å. The Pt atom is distanced 1.94 Å from the center of the C(1)–C(2) bond, and the Pt–C1 and Pt–C2 distances compare well with those reported earlier for acetylene platinum compounds [31]. The P1–Pt–P2 angle of 101.32(2)° is one the most striking feature of this bidentate ligand (95–103° range) [32].

Table 1
Selected bond lengths (Å) and angles (°) for **3** with e.s.d.s in parenthesis

Pt–C(2)	2.040(7)
Pt–C(1)	2.050(7)
Pt–P(2)	2.2679(18)
Pt–P(1)	2.2714(16)
C(1)–C(2)	1.293(9)
C(1)–C(11)	1.432(10)
C(2)–C(3)	1.394(9)
C(3)–C(4)	1.176(9)
C(2)–Pt–C(1)	36.9(2)
C(2)–Pt–P(2)	108.7(2)
C(1)–Pt–P(2)	145.50(19)
C(2)–Pt–P(1)	150.0(2)
C(1)–Pt–P(1)	113.14(19)
P(2)–Pt–P(1)	101.32(6)
C(2)–C(1)–C(1)	138.6(7)
C(2)–C(1)–Pt	71.2(5)
C(11)–C(1)–Pt	150.2(5)
C(1)–C(2)–C(3)	147.0(7)
C(1)–C(2)–Pt	72.0(4)
C(3)–C(2)–Pt	141.0(5)
C(4)–C(3)–C(2)	177.0(9)
Torsion angles	
C(1)–C(2)–P(2)–P(1)	3.0(5)
C(1)–P(1)–P(2)–C(2)	1.08(17)
C(12)–C(11)–C(1)–C(2)	175.7(9)
P(1)–C(51)–C(81)–P(2)	33.8(4)

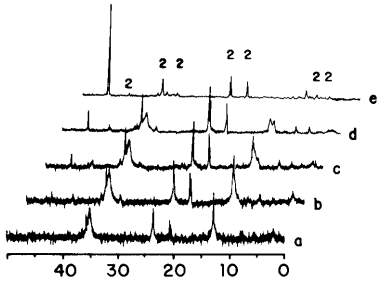


Fig. 2. Monitored ^{31}P-{^{1}H} NMR spectra (ppm) of the reaction mixture obtained by reaction between **1** and $[Au(PPh_3)]^+$ (1:1) in THF at times: (a) 15; (b) 30; (c) 45; (d) 90; (e) 300 min. The numbers **2** are the peaks due to this complex.

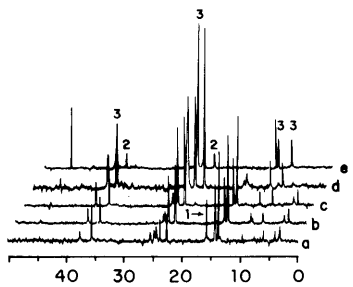


Fig. 3. Monitored ^{31}P-{^{1}H} NMR spectra (ppm) of the reaction between **1** and $[Au(PPh_3)]^+$ (2:1) in THF at times: (a) 15; (b) 30; (c) 45 min; (d) 3; (e) 12 h. The numbers **1**, **2**, and **3** are peaks due to these complexes.

Due to the η^2-coordination, the C(1)–C(2) distance is elongated to 1.293(9) compared with 1.176(9) Å for the alkynyl fragment C(3)–C(4) with C–C-triple bond character, and C(1) becomes sp^2-character [C(2)–C(1)–C(11) = 138.6(7)°].

The ferrocenyl group deviates slightly from the local D_{5d} point symmetry demonstrated by the torsion angle P(1)–C(51)–C(81)–P(2) of 33.8(4)° and the observed angle of 2.7(2)° between both cyclopentadienyl rings. These five membered rings are essentially planar: C(51)–C(52)–C(53)–C(54)–C(55) (RMS deviation 0.0035 Å) and C(81)–C(82)–C(83)–C(84)–C(85) (RMS deviation 0.0014 Å), from which the Fe(II) ion is moved away by 1.640(3) and 1.642(3) Å, respectively.

All phenyl rings are almost planar with an average RMS deviation of 0.0201 Å. One of these phenyl rings is partially disordered in that atoms C(74), C(75) and C(76) split over to the alternative positions of atoms C(74A), C(75A) and C(76A) hawing complementary occupancy factors of 43, 45 and 47%, respectively.

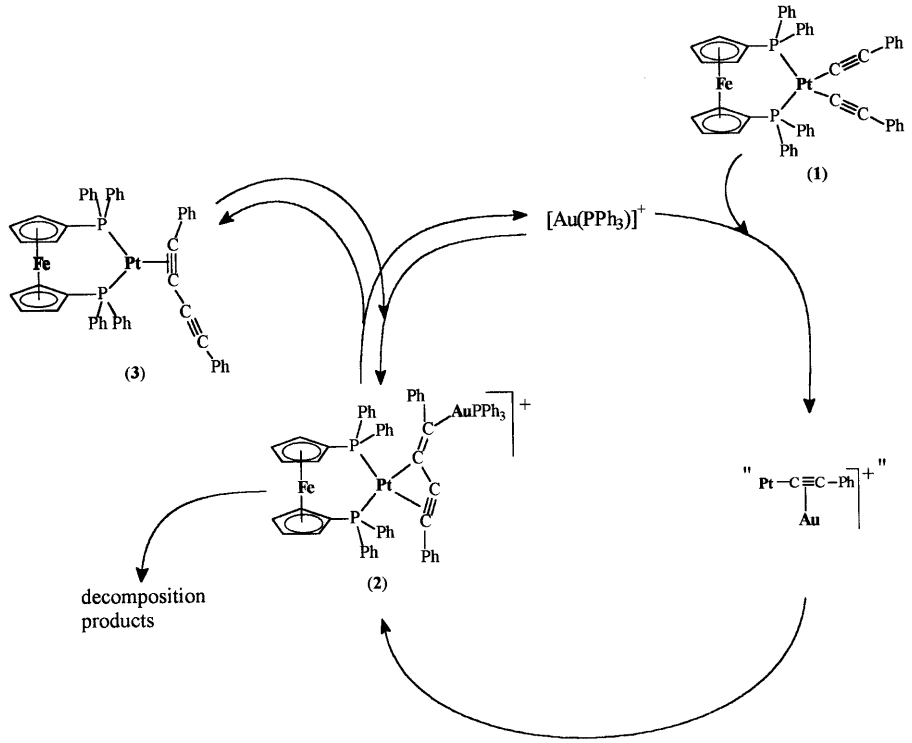
3.2.2. The course of the reactions followed by ^{31}P NMR

One characteristic of the reactional system is the formation of species that resonate in different regions of the ^{31}P NMR spectrum, allowing the stages of the reactions to be monitored. Moreover, the previous spectroscopic data of the isolated species **1**–**3** have supported the assignments (see under Section 2). Decomposition products of **2**, detected in the solution by ^{31}P NMR data in Figs. 2 and 3, were an unidentified phosphine–gold product of $[Au(PPh_3)]^+$, which resonates at 45.5 ppm in the expected high-frequency region of gold complexes [33] and $[Pt(dppf)(H_2O)_2]^{2+}$ at 9.7 ppm [34].

Reaction between $[Au(PPh_3)]^+$ and **1** in equimolar amounts in THF, shown in Fig. 2, is accompanied by immediate growth of the resonances assigned to **2** [δ 20.4, 23.6 (P_2Pt), and 35.1 (PAu)]. The set of resonances observed at δ 35 (PAu), and at δ 13 (P_2Pt, ^{1}J(PtP) 2620 Hz), which disappears completely within 3–5 h, is assigned to the intermediate with gold π-coordinated at C≡C bonds of the (dppf)Pt(C≡CPh)$_2$ moiety. The assignment is in line with data for analogous systems, whereas the addition of electrophiles to the electron-rich β-carbon of metal acetylides is the best entry into vinylidene and enynyl complexes [35]. The activation of C≡C bonds by $Au(PPh_3)^+$ would allow further rearrangements, as shown in Scheme 1. The signals associated with **1** (15.1 ppm), $[Au(PPh_3)]^+$ (30.2 ppm), and **3** (22.1, and 22.9 ppm) were not detected in all these spectra. Therefore, the product **2**, without the participation of **1**, does not rearrange into butadiyne complex **3**.

The time evolution of the ^{31}P-{^{1}H} NMR spectra recorded for the reaction between **1** and $[Au(PPh_3)]^+$ in 2:1 molar ratio in THF are shown in the Fig. 3. Transient resonances of the precursor complex **1** remain for more than 30 min, while increase the characteristic signals of **3**. The extra set of close signals that arises at 13.5 ppm (^{1}J(PtP) = 2585 Hz) and 14.0 ppm (^{1}J(PtP) = 2504 Hz), and a unique singlet at 35.5 ppm (PAu) may now be attributed to two intermediates. Probably, an intermediate has a gold atom coordinated at C≡C bonds of two *cis*-Pt(C≡C)$_2$ moieties, because there is no signal for bonded PPh_3. Signals of **2** appear only after 45 min of reaction, and remain approximately constant during the measurements, while resonances of **3** grow significantly until becoming predominant at the end of the reaction. Subsequent spectra, registered over 1 day, reveal a nearly complete conversion of the precursors into the major complex **3**. Occasionally, such spectra exhibited an extra resonance at 34.2 ppm from residual [Au(PPh$_3$)Cl], which eliminates the presence of silver derivatives of **1** in solution. Therefore, when **1** is initially employed in excess, a second reaction between **2** and **1** occurs to produce **3**.

A reaction of **1** with **2** (1:1 ratio) has been carried out in THF to better understand the contribution of **2** to the overall-reaction. ^{31}P NMR spectra show immediate formation of **3** and the usual intermediates (at 13.5, 14.0, and 35.5 ppm), which converts into **2** during reaction (Fig. 4). As the signal of $[Au(PPh_3)]^+$ (30.2



Scheme 1. Pathways to the reaction between **1** and $[Au(PPh_3)]^+$ in THF.

ppm) is not present in all spectra, such results provide a diagnostic indication that the rapid rearrangement step of **2** to **3** depends strongly on the presence of **1** for sequestering $[Au(PPh_3)]^+$ from **2**. Inversely, since $[Au(PPh_3)]^+$ also promptly reacts with **3**, any trace of unreacted $[Au(PPh_3)]^+$ in solution is consumed by available **1** or **3**, closing the formal reaction cycle. This emergent result reinforces the conclusion that the reaction of **3** by $[Au(PPh_3)]^+$ leads to the gold derivative of a but-1-en-3-yn-2-yl ligand. Therefore, the reduction/oxidation occurs reversibly in these two stages under mild condition as a very facile process (see Scheme 1). Particularly interesting for the comprehension this reaction process with electrophilic gold was the protonation at a coordinated carbon of 1,4-diphenylbutadiyne ligand of the zerovalent complex $[Ru(\eta^2\text{-}PhC{\equiv}CC{\equiv}CPh)(CO)_2(PPh_3)_2]$ [36]. Moreover, reactions of hydrides $[RuH(O_2CCF_3C)(CO)(PPh_3)_2]$ [5b] and $[(PP_3)Ru(H)(H_2)][BPh_4]$ [37] with 1,4-diphenylbutadiyne also have provided an alternate synthetic method for 1,4-diphenylbut-1-en-3-yn-2-ylruthenium(II) complexes.

Considering these facts, the proposed reaction pathways for formation of products are now outlined in Scheme 1.

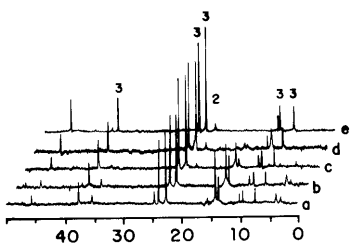


Fig. 4. Monitored $^{31}P\text{-}\{^1H\}$ NMR spectra (ppm) of the reaction between **1** and **2** (1:1) in THF at times: (a) 15; (b) 30 min; (c) 1.50; (d) 5; (e) 12 h. The numbers **2** and **3** are the peaks due to these complexes.

4. Supplementary data

Crystallographic data (excluding structure factors) for the structure reported in this paper have been deposited with the Cambridge Crystallographic Data Centre, CCDC No. 133546. Copies of this information may be obtained free of charge from The Director, CCDC, 12 Union Road, Cambridge CB2 1EZ, UK (fax: +44-1223-336033; e-mail: deposit@ccdc.cam.ac.uk or www: http://www.ccdc.cam.ac.uk).

Acknowledgements

We are very grateful to the CNPq-PADCT and CAPES-PROBRAL for financial support, Professor Dr J. Strähle (University of Tübingen) for the diffractometer facilities, and Dr B. Mann for his critical comments and his pertinent suggestions.

References

[1] See, for example: (a) B.M. Trost, C. Chan, G. Ruhter, J. Am. Chem. Soc. 109 (1987) 3486. (b) J. Ohshita, K. Furumori, A. Matsuguchi, M. Ishikawa, J. Org. Chem. 55 (1990) 3277. (c) M.I. Bruce, G.A. Koutsantonis, M.J. Liddell E.R.T. Tiekink, J. Organomet. Chem. 420 (1991) 253; (d) W.J. Evans, R.A. Keyer, J.W. Ziller, Organometallics 12 (1993) 2618. (e) M. Schäfer, N. Mahr, J. Wolf, H. Werner, Angew. Chem., Int. Ed. Engl. 32 (1993) 1315. (f) A. Santos, J. López, L. Matas, J. Ros, A. Galán, A.M. Echavarren, Organometallics 12 (1993) 4215. (g) P. Barbaro, C. Bianchini, M. Peruzzini, A. Polo, F. Zanobini, Inorg. Chim. Acta 220 (1994) 5.

[2] (a) A. Furlani, S. Licoccia, M.V. Russo, A.C. Villa, C. Guastini, J. Chem. Soc., Dalton Trans. (1984) 2197. See also (b) A. Furlani, M.V. Russo, A.C. Villa, A.G. Manfredotti, C. Guastini, J. Chem. Soc., Dalton Trans. (1977) 2154. (c) I. Collamati, A. Furlani, J. Organomet. Chem. 17 (1969) 457.

[3] (a) J.J. Low, W. Goddard, J. Am. Chem. Soc. 108 (1986) 6115. (b) K. Tatsumi, R. Hoffmann, A. Yamamoto J.K. Stille, Bull. Chem. Soc. Jpn. 54 (1981) 1857.

[4] P.J. Stang, M.H. Kowalski, J. Am. Chem. Soc. 111 (1989) 3356.

[5] (a) K. Sonogashira, Y. Tohda, N. Hagihara, Tetrahedron Lett. (1975) 4467. (b) M. Akita, H. Yasuda, A. Nakamura, Bull. Chem. Soc. Jpn. 57 (1984) 480. (c) A. Dobson, D.S. Moore, S.D. Robinson, M.B. Hursthouse, L. New, Polyhedron 4 (1985) 1119. (d) R. Rossi, A. Carpita, C. Bigelli, Tetrahedron Lett. 26 (1985) 523. (e) D. Villemin, E. Schigeko, J. Organomet. Chem. 293 (1985) C10. (f) J. Krause, K.R. Pörschke, Proceedings of the Fifth International Conference on the Chemistry of Platinum, St. Andrews (Scotland), 1993, p. A199.

[6] J.M. Brown, N.A. Cooley, Organometallics 9 (1990) 353.

[7] D.M.P. Mingos, D.J. Wales, Introduction to Cluster Chemistry, Prentice-Hall, Englewood Cliffs, 1990, p. 40.

[8] (a) M.I. Bruce, Chem. Rev. 91 (1991) 197. (b) M.I. Bruce, Pure Appl. Chem. 62 (1990) 1021. (c) L.D. Field, A.V. George, E.Y. Malouf, I.H.M. Slip, T.W. Hambley, Organometallics 10 (1991) 3842. (d) L.D. Field, A.V. George, G.R. Purches, I.H.M. Slip, Organometallics 11 (1992) 3019.

[9] (a) J. Forniés, E. Lalinde, F. Martínez, M.T. Moreno, A.J. Welch, J. Organomet. Chem. 455 (1993) 271. (b) J.R. Berenguer, J. Forniés, E. Lalinde, A. Martín, M.T. Moreno, J. Chem. Soc., Dalton Trans. (1994) 3343.

[10] (a) T. Hayashi, M. Konishi, Y. Kobori, M. Kumada, T. Higuchi, K. Hirotsu, J. Am. Chem. Soc. 106 (1984) 158. (b) D.A. Clemente, G. Pilloni, B. Longato, M.T. Camellini, Inorg. Chim. Acta 115 (1986) L9. (c) J.M. Brown, P.J. Guiry, Inorg. Chim. Acta 220 (1994) 249.

[11] I.D. Campbell, G. Eglinton, Org. Synth. 5 (1973) 517.

[12] C.A. McAuliffe, R.V. Parish, P.D. Randall, J. Chem. Soc., Dalton Trans. (1979) 1730.

[13] J.Y. McDermott, G.H. White, G.M. Whitesides, J. Am. Chem. Soc. 98 (1976) 6521.

[14] M. Green, J.A.K. Howard, J.L. Spencer, F.G.A. Stone, J. Chem. Soc., Dalton Trans. (1977) 271.

[15] This complex was previously synthesized by reducing [$PtCl_2$(dppf)] with sodium borohydride under ethylene, in the isolated yield of 78%, according to Ref. [6].

[16] Enraf–Nonius, CAD-4-Express Software. Enraf–Nonius Inc., Delft, The Netherlands, 1994.

[17] G.M. Sheldrick, SHELXS-97, Program for Crystal Structure Solution, University of Göttingen, Germany, 1990.

[18] G.M. Sheldrick, SHELXL-97, Program for Crystal Structure Refinement, University of Göttingen, Germany, 1997.

[19] R.J. Cross, M.F. Davidson, J. Chem. Soc., Dalton Trans. (1986) 1987.

[20] B.C. Ankianiec, G.B. Young, Polyhedron 10 (1991) 1411.

[21] N.W. Alcock, A.F. Hill, R.P. Melling, Organometallics 10 (1991) 3898.

[22] C. Carfagna, R. Galarini, K. Linn, J.A. López, C. Mealli, A. Musco, Organometallics 12 (1993) 3019.

[23] P.W. Blosser, D.G. Schimpff, J.C. Gallucci, A. Wojcicki, Organometallics 12 (1993) 1993.

[24] S.A. Benyunes, L. Brandt, A. Fries, M. Green, M.F. Mahon, T.M.T. Papworth, J. Chem. Soc., Dalton Trans. (1993) 3785.

[25] S. Fallis, G.K. Anderson, N.P. Rath, Organometallics 10 (1991) 3180.

[26] J.B.B. Heyns, F.G.A. Stone, J. Organomet. Chem. 160 (1978) 337.

[27] Z. Dauter, R.J. Mawby, C.D. Reynolds, D.R. Saunders, J. Chem. Soc., Dalton Trans. (1986) 433.

[28] (a) G. Jia, A.L. Rheingold, D.W. Meek, Organometallics 8 (1989) 1378. (b) A.K. McMullen, J.P. Selegue, J.G. Wang, Organometallics 10 (1991) 3421. (c) C. Bianchini, M. Peruzzini, F. Zanobini, P. Frediani, A. Albinati, J. Am. Chem. Soc. 113 (1991) 5453. (d) Y. Wakatsuki, H. Yamazaki, N. Kumegawa, T. Satoh, J.Y. Satoh, J. Am. Chem. Soc. 113 (1991) 9604.

[29] (a) H.F. Klein, H. Beck-Hemetsberger, L. Reitzel, B. Rodenhäuser, G. Cordier, Chem. Ber. 122 (1989) 43. (b) W. Bonrath, K.R. Pörschke, G. Wilke, K. Angermund, C. Krüger, Angew. Chem., Int. Ed. Engl. 27 (1988) 833. (c) P.B. Tripathy, B.W. Renoe, K. Adzamli, D.M. Roundhill, J. Am. Chem. Soc. 93 (1971) 4406. (d) M. Kersting, K. Dehnicke, D. Fenske, J. Organomet. Chem. 309 (1986) 125. (e) T. Rappert, O. Nürnberg, H. Werner, Organometallics 12 (1993) 1359. (f) N.W. Alcock, A.F. Hill, R.P. Melling, A.R. Thompsett, Organometallics 12 (1993) 641. (g) H. Werner, O. Gevert, P. Steinert, J. Wolf, Organometallics 14 (1995) 1786. (h) H. Werner, O. Gevert, P. Haquette, Organometallics 16 (1997) 803.

[30] L. Zsolnai, H. Pritzkow, ZORTEP, Program for Personal Computer, University of Heidelberg, Germany, 1996.

[31] (a) J.O. Glanville, J.M. Stewart, S.O. Grim, J. Organomet. Chem. 7 (1967) P9. (b) L.R. Favello, S. Fernández, J. Fornés, E. Lalinde, F. Martínez, M.T. Moreno, Organometallics 16 (1997) 1326.

[32] I.R. Butler, W.R. Cullen, T.J. Kim, S.J. Rettig, J. Trotter, Organometallics 4 (1985) 972.

[33] See, for example: (a) H. Schmidbaur, Gmelin Handbuch der Anorganischen Chemie. Organogold Compounds, Springer-Verlag, Berlin, 1980. (b) G. Jia, R.J. Puddephatt, J.D. Scott, J.J. Vittal, Organometallics 12 (1993) 3565.

[34] P.J. Stang, B. Olenyuk, J. Fan, A.M. Arif, Organometallics 15 (1996) 904.

[35] For general reviews see: references [8a, b] and references therein.

[36] N.W. Alcock, A.F. Hill, R.P. Melling, A.R. Thompsett, Organometallics 12 (1993) 641.

[37] C. Bianchini, C. Bohanna, M.A. Esteruelas, P. Frediani, A. Meli, L.A. Oro, M. Peruzzini, Organometallics 11 (1992) 3837.

PERGAMON

www.elsevier.nl/locate/poly

Polyhedron 19 (2000) 2269–2275

POLYHEDRON

The reaction of copper and iron species with thiuram sulfides: copper and iron dithiocarbamate derivatives

Luis I. Victoriano *

Facultad de Ciencias Químicas, Universidad de Concepción, Casilla 160-C, Concepción, Chile

Received 1 October 1999; accepted 18 April 2000

Abstract

The reaction chemistry of thiuram mono- and disulfides with copper(I), (II) and copper metal is reviewed. Cu(I) and the monosulfides afford adducts, while Cu(II) yields an oxidized form of the ligand, which is also obtained upon oxidation with ferric chloride or solutions of halogens. The disulfides and copper metal lead to Cu(I) dithiocarbamates, while oxidation of copper(I) species affords Cu(III)-containing mixed valence species. Similarly Cu(II) and the disulfides yield neutral Cu(III) complexes.
© 2000 Elsevier Science B.V. All rights reserved.

Keywords: Copper and iron species; Thiuram sulfides; Dithiocarbamate derivatives

1. Introduction

Thiuram sulfides, otherwise known as bis(*N*,*N*-dialkylthiocarbamoyl)sulfides, $R_2NC(S)S_nC(S)NR_2$ are the thiocarbamoyl esters of dialkyldithiocarbamic acids. The disulfides ($n = 2$) R_4tds are known on account of their biological activity, which leads to applications as fungicides, rubber vulcanization accelerators, agents of alcoholism therapy [1–3] and quite recently, as arrestors of human immunodeficiency virus infections such as AIDS [4]. This wide diversity of examples of biological activity has been attributed to a combination of at least two factors [5]: capability to fit into a receptor site and ability to undergo reversible redox reactions at suitable potentials. From this point of view, the equilibrium relating thiuram disulfides and dithiocarbamates is very relevant to the chemistry of the disulfides. A peculiarity of metal dithiocarbamate chemistry is the recognized ability of the ligands to stabilize unusually high oxidation states in transition metals, a property which has been attributed to the ligand ability to delocalize positive charge from the metal towards the periphery of the complex [6]. Thiuram disulfides are unique among thiolato-type ligands, in that reductive scission of the S–S bond leads to chelating systems (dithiocarbamate anions) which are particularly well suited to stabilize high oxidation states under the premise outlined above.

Coordination compounds containing ligands with sulfur atoms as donors have received much attention, due to their role as analogues of proteins containing metal–sulfur bonds [7]. Among these ligands, dithiocarbamates have been used to synthesize model compounds for enzyme activity [8,9]. Also, polynuclear metal dithiocarbamates may act as mineral analogues and thus as models of sulfide mineral degradation by microorganisms [10], a topic which has a strong relevance in connection with biolixiviation [11]. It must also be stated that one successful approach to the development of new metal sulfide catalysts involves thermolysis of discrete metal thio complexes containing coligands rich in sulfur, such as dithiocarbamates [12,13].

The monosulfides ($n = 1$) R_4tms, perhaps because they lack the wide breadth of applications known for the disulfides in agriculture and experimental medicine, have been much less extensively studied and where such studies deal with the subject of interaction of monosulfides and metal species, the field remains virtually unexplored. Exceptions have been reports dealing with the preparation and properties of the neutral complexes

* Fax: +56-41-245-974.
E-mail address: lvictori@udec.cl (L.I. Victoriano).

0277-5387/00/$ - see front matter © 2000 Elsevier Science B.V. All rights reserved.
PII: S0277-5387(00)00488-5

MR_4tmsX_2 (M = Zn [14], Hg [15], Ni and Co [16]; X = halogen) or $M'R_4tmsX$ (M′ = Ag [17]) and of the cationic $[CrR_4tmsX_2]^+$ [18]. The spectroscopic properties of the latter complexes are inconsistent with a possible oxidative addition of the ligand to the metal center and it has been suggested that their electrochemistry be examined [19]. Thiuram monosulfides may also undergo C–S bond scission to give dithiocarbamate–metal–thiocarboxamido complexes or straightforward dithiocarbamates. Examples of the former are the reaction of monosulfides with tris(triphenylphosphine)–metal halides (metal = Rh and Pt) [20] or zero valent molybdenum complexes [21], while the interaction of a series of metal halides with thiuram monosulfides has afforded metal dithiocarbamates (metal = Ni^{2+}, Pt^{2+}, Cu^{2+}, Co^{3+} and Fe^{3+}) [22].

The present article intends to review the chemistry of thiuram sulfides and copper or iron metal species. Good compilations have appeared related to the general chemical properties of thiuram disulfides [1], and these reviews have covered the information then available on the interaction of such molecules with metal species. Also, the updates of Coucouvanis [7] and McCullough [8] on the chemistry of 1,1-dithiolate complexes constitute very informative first sources. More recently, Steggerda, Cras and Willemse have touched upon the subject [6].

Typical reactions of thiurams mono and disulfides with metal species fall under three distinct categories: (a) adduct formation; (b) ligand reduction with concomitant degradation to dithiocarbamate and/or thiocarboxamide ligands; and (c) thiuram oxidation. All of the above classes are found in the case of copper. We shall address each of these in the same order. Within each section thiuram disulfides will be treated first, followed by the monosulfides.

The following abbreviations are used throughout the text: R_4tms is *N*,*N*,*N*′,*N*′-tetraalkylthiuram monosulfide. Similarly, R_4tds stands for the corresponding disulfide, while *N*,*N*-dialkyldithiocarbamates are shortened to R_2dtc.

General preparative, instrumental and analytical techniques are described in the reports where the corresponding syntheses were first published. No attempt is made here to supply full experimental details for each of the preparations. The reader is directed to the original reports. Suitable references are found in Section 2.

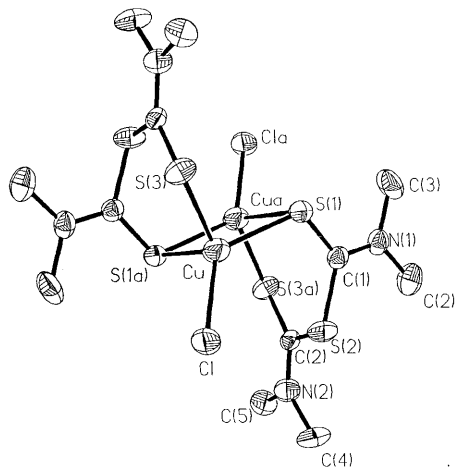


Fig. 1. The molecular structure of $[CuMe_4tmsCl]_2$.

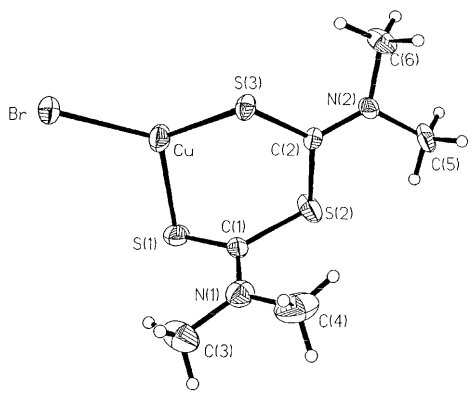


Fig. 2. The monomeric unit of the $[CuMe_4tmsBr]_n$ polymer.

2. Results and discussion

2.1. Adduct formation

Metal species which display a closed shell configuration typically react with thiuram disulfides to yield adducts, and copper(I) conforms to the rule.

Thus, R_4tms added to a cold slurry of cuprous halides in a suitable organic solvent yield solutions of the 1:1 adducts CuR_4tmsX (R = Me, Et, ^{i}Pr; X = Cl, Br, I, not all combinations) [23]. The products are typically deep orange to red diamagnetic solids soluble in organic solvents to yield non-conducting solutions. IR bands at ca. 350 cm^{-1} confirm coordination of Cu(I) to sulfur [24]. The solubility properties and low melting point of the complexes hint at a discrete non-ionic structure in the solid. This expectation is for the most part confirmed from the single crystal X-ray structure determinations [25]. Complexes $CuMe_4tmsX$ exist as chelated units formed by a molecule of the ligand and one of copper(I) halide. In all three cases, coordination about copper(I) is tetrahedral and is completed by sulfur and halogen. The chloro derivative is an S-bridged centrosymmetric dimer (see Fig. 1). All three copper–sulfur distances are slightly shorter in the chloro derivative.

The molecular structure of the bromo derivative corresponds to a polymer (Fig. 2). Association of basic chelated units generates long chains parallel to the *x* axis of the unit cell. The copper coordination is com-

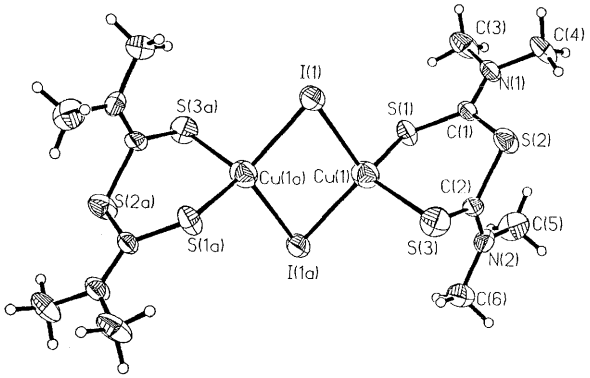


Fig. 3. The dimer $[CuMe_4tmsI]_2$.

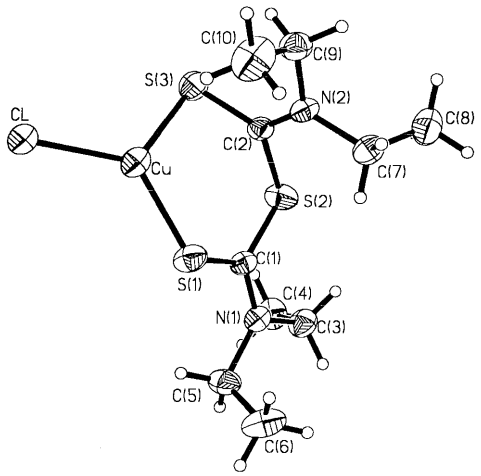


Fig. 4. The monomeric $[CuEt_4tmsCl]$.

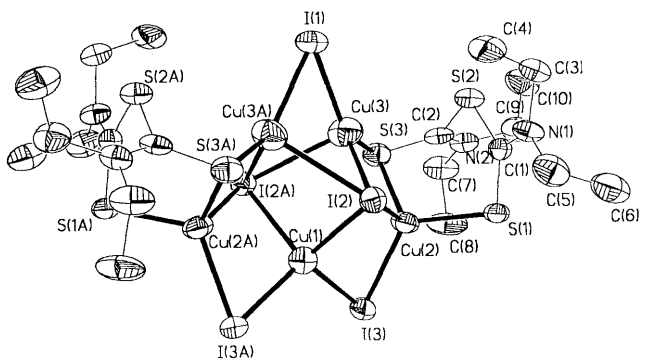


Fig. 5. The pentanuclear complex $[Cu_5(Et_4tms)_2I_5]$.

pleted by one bromine and three sulfur atoms. The iodo complex contains two μ-iodine bridged units of $CuMe_4tmsI$. As in the chloro and bromo derivatives, coordination about copper is tetrahedral and it is completed by two iodine and two sulfur atoms (Fig. 3).

Other CuR_4tmsX complexes (R = Et, X = Cl and Br [26]; R = ^{n}Pr, ^{i}Pr, X = Br [27]) feature monomers containing tricoordinate copper(I), a result which had been anticipated from the vibrational spectra [24]. The Cu–S distances are about 2.24 Å in the ethyl complexes, values which are noticeably shorter than those found in the methyl derivatives. This is attributed to the non-bridging nature of the sulfur atoms in the heavier alkyl homologues (Fig. 4).

Reaction of acetonitrile solutions of cuprous iodide and Et_4tms leads to a crystalline phase of composition $(CuI)_5(Et_4tms)_2$ [26,28]. The solid state structure of this aggregate may be described as formed by a central $(CuI)_3$ distorted octahedral element, and two additional $CuEt_4tmsI$ units fused to the central $(CuI)_3$ cage by means of sulfur and iodine bridges. The molecule displays a twofold crystallographic axis through one copper and one iodine, coincident with the long axial position of the 'octahedron' (Fig. 5).

The severely bent equatorial plane of the octahedron is defined by two additional copper and two iodine atoms. Each $CuEt_4tmsI$ unit contains one tetrahedral copper, a bidentate sulfur ligand and one iodine atom. These units are fused to two faces of the octahedron by means of two iodine bridges and by one sulfur bridge.

Discrete pentanuclear copper(I) complexes have been so far reported for $Cu_5(SPh)_7^{2-}$ [29] and $Cu_5X_7^{2-}$ (X = Br, I). The anion $Cu_5I_7^{2-}$ has been described as a pentagonal bipyramid of seven iodine atoms, where only slight deviations from C_{5h} symmetry occur [30]. In the bromo derivative, the pentagonal bipyramid of ligand atoms is more severely distorted [31]. With the hindsight afforded by the previous models we may now view the structure of the tetraethylthiuram monosulfide complex as consisting of the same basic structural unit, viz. a pentagonal bipyramid conformed by the two apical iodine atoms and by a distorted basal plane conformed by two sulfurs and three iodines. All copper atoms display tetrahedral coordination and appear as three distinct sets. The shortest metal–metal distance found (2.533(8) Å) rules out any possible metal–metal bonding. The iodine atoms are either μ_2- or μ_4-bridged and the shortest I···I contact (4.261 Å) compares well with the one found in $[Cu_2I_4^{2-}]$ [32] and other related systems [33].

The structure of the pentanuclear derivative is unique within a series of thiuram complexes known thus far. A variety of experimental conditions have failed to yield a mononuclear copper complex in combinations of copper(I) iodide and tetraethylthiuram monosulfide. Also, all efforts to isolate a species of higher nuclearity using combinations of different copper(I) halides and methyl, ^{n}Pr or ^{i}Pr substituents on the ligand have not met with any success. It is speculated that the kinetics of complexation might be slow in the case of $CuI–Et_4tms$, so that the available free CuI competes with the monomeric $CuEt_4tmsI$ for extension of the association.

Copper(II) sulfate and Me_4tms in acetonitrile lead to a solid phase $[CuL_2^+]_2SO_4^{2-}$. The crystal structure of this complex shows a CuS_4 chromophore where Cu(I) is

coordinated by two ligands in a strongly distorted tetrahedral environment (Fig. 6). The average Cu–S distance is 2.33 Å. The chelating rings display a boat conformation [34].

The tetrahedral and trigonal planar stereochemistries found in R_4tms complexes of copper(I) are not surprising. For d^{10} Cu(I), stereochemistry is dictated by charge and steric effects on the ligand, and tetrahedral and trigonal geometries are the norm [35].

The $CuMe_4$tmsX complexes show conductivities which are typical of non electrolites in acetonitrile or chloroform. Molecular weight determinations for the $CuMe_4$tmsBr derivative are consistent with a monomer. Such formulation in acetonitrile is not surprising, considering the strong coordination properties of the solvent. The halogen bridges present in the solid are broken and acetonitrile occupies the fourth coordination position on copper.

The temperature dependence of the ^{1}H NMR spectra of thiuram sulfides has been interpreted in terms of restricted rotation about the C–N bond which causes inequivalence of the alkyl groups and broadening of the signals at temperatures close to ambient [36]. This is apparent in the spectra of the complexed CuR_4tmsX and parent ligand. Two sets of CH_3 resonances are present in all the cases studied.

The spectra of $CuMe_4$tmsCl calls for additional comments. At room temperature the spectrum consists of four singlets of approximately equal height. The outer components are much broader and altogether account for three quarters of the overall integrated intensity. Below room temperature, and down to -10°C, the outer signals decrease in intensity (63% of the total) and the center of the system shifts slightly upfield (0.01 ppm). These changes are reversible and are attributed to the onset of a monomer–dimer equilibrium in solution. If the bond-making process of dimer formation from monomers were the only thermodynamically relevant event, one would expect the monomer–dimer equilibrium (exothermic) to shift to monomer at room temperature, and to dimer at lower temperatures. This allows one to assign the room temperature most intense signals as monomer, and in turn allows evaluation of the related equilibrium constant. The values thus obtained are 0.22 and 0.47 l mol^{-1} at 27 and -10°C, respectively. The limited temperature range available does not warrant further speculation as to the significance of the enthalpy value thus obtained for the dimerization process.

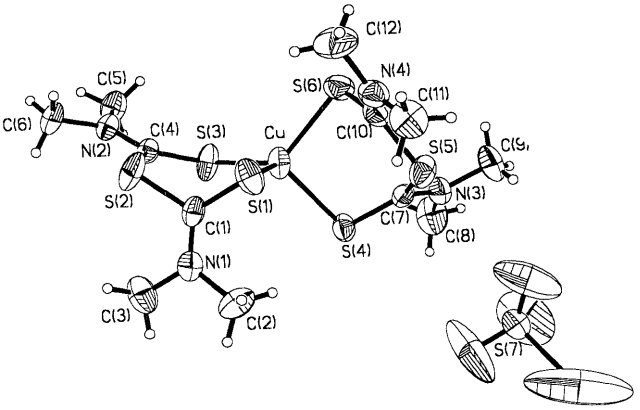


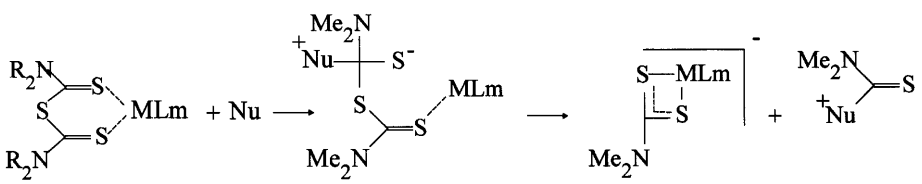
Fig. 6. The ionic complex $[Cu(Me_4tms)_2]^+$ SO_4^{2-} at room temperature.

Solutions of $CuMe_4$tmsX complexes are not stable. Upon standing or heating, decomposition is observed. One of the decomposition products is the corresponding $Cu(Me_2dtc)_2$ compound, which has been isolated and characterized by melting point, IR and elemental analyses. The ability of tetraalkylthiuram monosulfides to generate metal dithiocarbamates has been used as a synthetic alternative to the preparation of the latter compounds [22]. It is now clear, after the work of McCleverty and Morrison that rupture of the C–S bond is a consequence of the nucleophilic attack on the thiocarbamoyl carbon, by a suitable agent [37] (Scheme 1).

Possible nucleophiles in our case are the solvent or the halide ions, but efforts to determine the fate of the missing dimethylthiocarboxamido residue have been unsuccessful.

2.2. Thiuram sulfides as oxidants — degradation to dithiocarbamates

Other reactions of metal containing species with thiuram sulfides are characterized by the oxidizing properties of the thiuram. Reduction of the ligand and scission of the S–S bond results in incorporation of the dtc fragments into the metal coordination sphere. As exemplified in the modern literature, rarely are these systems fully described by redox and complexation schemes alone. Bond breaking and extensive redistribution of the ligand systems are common. In many of the early studies the redox balance in the products isolated



Scheme 1.

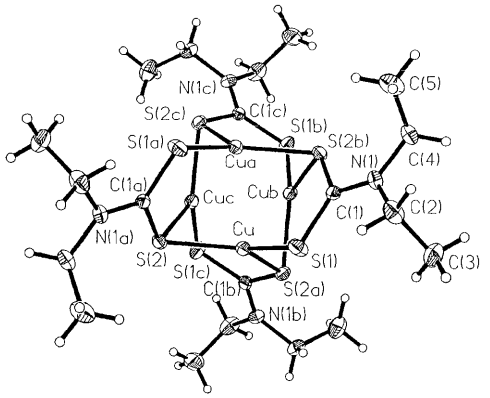


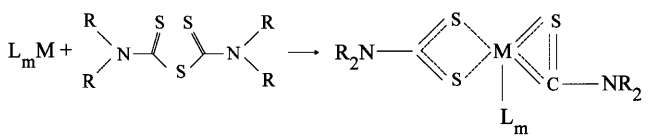
Fig. 7. The complex $[Cu(Et_2dtc)]_4$.

has not accounted for the observed reduction of the ligand [22]. In some cases, hypervalent metal states might be involved. This is now demonstrated in the case of copper(II) halides and thiuram disulfides [38]. Other systems may well behave in a similar manner. For example, tetramethylthiuram monosulfide reacts with the electron-rich species $Mo(CO)_3(MeCN)_3$ to produce a complex $[(CO)_2(Me_2NCS_2)Mo(Me_2NCS)]$ which contains bidentate dithiocarbamate and thiocarboxamide ligands [39] (Scheme 2).

Other examples illustrating the oxidizing properties of the ligand towards copper are as follows.

2.2.1. Thiuram disulfides and copper metal

Oxidation of copper powder by carbon disulfide solutions of thiuram disulfides lead to dark solutions of $Cudtc_2$, which are reduced by excess metal to the cuprous Cudtc [40–42]. The crystal structure of the ethyl derivative features a tetrameric species $(CuEt_2dtc)_4$ where the copper atoms are arranged at the corners of a tetrahedron and all ligands are bidentate with singly bridging sulfur atoms [43]. A reexamination of the structure confirms all features described (Fig. 7). While well defined bis adducts are formed with triphenylphosphine, other donors such as dimethylsulfoxide, triphenylarsine, *N*,*N*,*N*′,*N*′-tetramethylethylenediamine or tetramethylthiuram monosulfide have no effect on solutions of cuprous dithiocarbamates [42].

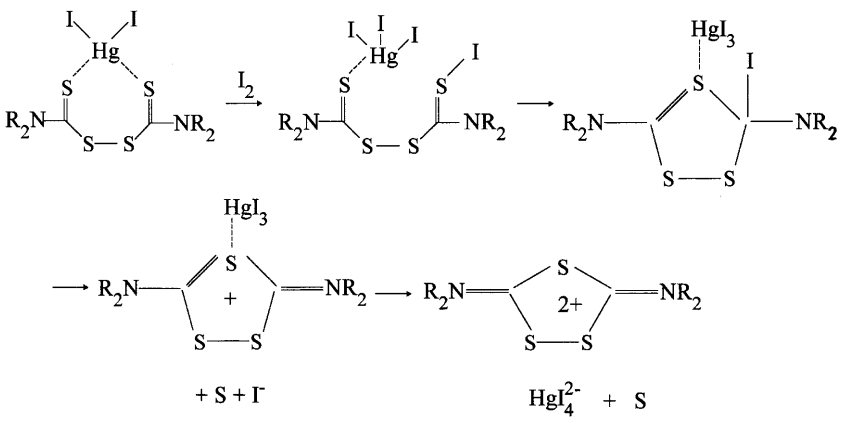


Scheme 2.

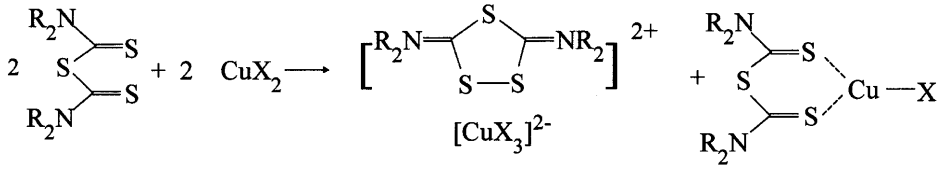
2.2.2. Thiuram disulfides and copper(I) halides

Mixed valence dithiocarbamates of general formulation $Cu_2(R_2dtc)_3X_2$ (X = Cl and Br, but not I) have been isolated by admixing solutions of Cu(I) halides and thiuram disulfides in different organic solvents [44]. IR and PE spectra are indicative of Cu(II) and Cu(III) mixtures in 1:1 mole ratios. A tentative formulation $Cu^{III}dtc_2^+$ $Cu^{II}dtcX_2^-$ is proposed [45]. Experiments performed with Me_4tds are more involved, since a variety of product compositions including CudtcCl, $Cu_4dtc_2Br_3$ and $Cu_3dtc_2Br_3$ are obtained. Based on magnetic data and spectral comparisons with known compounds, the following structures are respectively proposed. Dimeric, halogen bridged $Cu_2dtc_2Cl_2$, a polymeric network of $Cudtc_2$ and CuBr for $Cu_4dtc_2Br_3$ and ionic $Cudtc_2^+$ $Cu_2Br_3^-$ [46].

Copper(I) bromide reacts with R_4tds (R = Me, Et, ^{n}Pr and ^{n}Bu) in the appropriate soichiometric ratios to yield the compounds $Cu_n(dtc)_2Br_n$ ($n = 2$, 4 and 6). From IR, ESCA and magnetic measurements, the presence of the Cu(III)-containing cation $[Cu(dtc)_2]^+$ is inferred. The complexes are formulated as $[Cu(dtc)_2]^+$ $[Cu_{(n-1)}Br_n]^-$ [47,48]. Mixing equimolar ratios of the reactants leads to the series of complexes $Cu_2(dtc)_3X_2$ (R = Me, Et; X = Cl, Br, not all combinations) [48,49]. The crystal structure of $Cu_2(Et_2dtc)_3Br_2$ reveals chains of alternating $Cu(dtc)_2$ and $CuBr_2(dtc)$ units. The Cu–S bonds in the former are conspicuously shorter than in the latter. Therefore, the complexes seem to be better formulated as $[Cu(R_2dtc)]^+[CuX_2(R_2dtc)]^-$ [49].



Scheme 3.



Scheme 4.

2.2.3. Thiuram disulfides and copper(II) halides

Addition of copper(II) halides CuX_2 to tetrahydrofuran solutions of thiuram disulfides generate dark purple–blue $R_2dtcCuBr_2$ or brown–red $R_2dtcCuCl_2$ (R = Me, Et, ^{i}Pr). The diamagnetic products are characterized by abnormally high C–N and Cu–S stretching frequencies in the IR spectra and by high values of the observed binding energies in the photoelectron spectra. All the data are consistent with a formulation incorporating copper(III). A single crystal structure determination shows planar $C_2NCS_2CuBr_2$ monomeric units featuring a distorted square planar environment about Cu, with Cu–S and Cu–Br distances which are shorter than those found in related Cu(II) systems (Fig. 8) [50,51].

2.3. Ligand oxidation

Oxidation of metal dithiocarbamates may proceed further than the expected formation of thiuram disulfides, leading to the formation of cyclic five membered dications, usually stabilized by formation of anionic halogen complexes of the metal species. The mechanistic aspects of this oxidation are so far of a speculative nature and do not offer explanations as to the fate of the supernumerary sulfur atom (see Scheme 3). Reports dealing with this aspect of the chemistry of thiuram sulfides are as follows.

Iodine oxidation of $HgtdsI_2$ results in elimination of one sulfur atom and formation of the 3,5-bis(*N*,*N*-dialkyliminium)-1,2,4-trithiolane ($[R_4bitt\text{-}3]^{2+}$) dication referred to in the previous paragraph. This may come about through the ability of the thiocarbamoyl carbon to undergo nucleophilic attack by a suitable species.

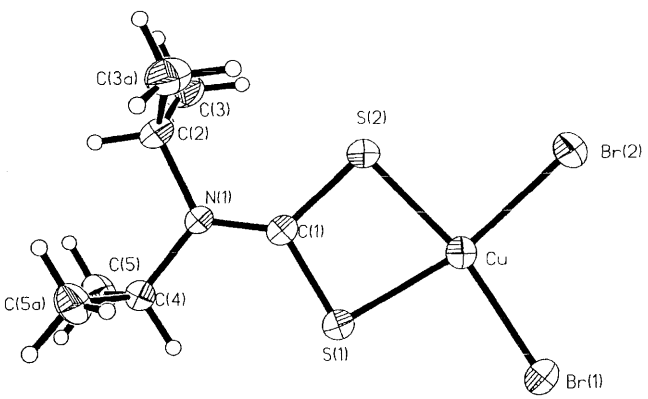


Fig. 8. The complex $[Br_2Cu\{(i\text{-}Pr)_2dtc]$.

Sulfur elimination may then follow [52]. A single crystal structure determination has confirmed the nature of the resulting $[R_4bitt\text{-}3]^{2+}HgI_4^{2-}$ species [53].

Related systems are exemplified by the reaction of Et_4tds with $FeCl_3$ [54] which results in $[Et_4bitt\text{-}3]^{2+}$ $2FeCl_4^-$, also accessible through halogen oxidation of $Fe(Et_2dtc)_3$ or $Fe(Et_2dtc)_2Cl$ [55]. A similar oxidation carried out on $Cu^I(Bu_2dtc)$ yields $[Bu_4bitt\text{-}3]^{2+}Cu_2X_6^{2-}$ (X = Cl, Br). In the absence of X-ray studies for these materials there seems to be a reasonable body of evidence based on IR spectroscopy, to support the structures proposed [55]. An interesting short lived species of formulation $[Et_4bitt\text{-}3]^{2+}2[Fe(Et_2dtc)_3]^-$ has been recently reported in a mass spectrometric study of oxidation products of $Fe(Et_2dtc)_3$ [56].

Formation of the $[R_4bitt\text{-}3]^{2+}$ cations is also apparent in reactions involving thiuram monosulfides. Thus, oxidation of the ligand accounts for reduction of two equivalents of copper(II) during the reaction of copper(II) halides with R_4tms (R = Me, Et), where one of the products isolated corresponds to the trihalocuprate(I) dianion of the $[R_4bitt\text{-}3]^{2+}$ cation [25] (see Scheme 4).

Other oxidizing agents used in the transformation of thiuram monosulfides to dialkyliminium trithiolanes have been $FeCl_3$ [57] and solutions of halogens [58].

Acknowledgements

Support was available through funding from FONDECYT 1990494 and from the University of Concepción DIUC 97210108. Nicolás Schiappacasse rendered important assistance in the scanning of figures.

References

[1] G.D Thorn, R. Ludwig, The Dithiocarbamates and Related Compounds, Elsevier, Amsterdam, 1981.
[2] E.J. Butterfield, D.C. Torgeson, Fungicides, in: H.F. Mark, D.F. Othmer, C.G. Overberger, G.T. Seaborg (Eds.), Kirk–Othmer Encyclopedia of Chemical Technology, Wiley, New York, 1991.
[3] T. Kitson, Education in Chemistry, 1985, p. 43 March.
[4] P.K. Gessner, T. Gessner, Disulfiram and its Metabolite, Diethyldithiocarbamate, Chapman and Hall, London, 1992.
[5] R.G. Compton, J.C. Eklund, A. Hallik, S. Kumbhat, L. Nei, A.M. Bond, R. Colton, Y.A. Mah, J. Chem. Soc., Dalton Trans. (1995) 1917.
[6] J.J. Steggerda, J.A. Cras, J. Willemse, Rec. Trav. Chim. 100 (1981) 41.

[7] B. Macias, M.V. Villa, M.R. Rodríguez-Gallego, Transition Met. Chem. 20 (1995) 347.
[8] B. Macias, J.J. Criado, M.V. Villa, M.R. Iglesias, M. Castillo, Polyhedron 12 (1993) 501.
[9] B. Macias, J.J Criado, M.V. Villa, J.L. Rodríguez, M. Castillo, Polyhedron 12 (1993) 2791.
[10] R.M. Golding, A.D. Rae, B.J. Ralph, L. Sulligoi, Inorg. Chem. 10 (1974) 2499.
[11] D.K. Ewart, M.N. Hughes, Adv. Inorg. Chem. 36 (1991) 103.
[12] E.R.T. Tiekink, X.F. Yan, C.G. Young, Aust. J. Chem. 45 (1992) 897.
[13] C.G. Young, T.O. Kokaba, M. Sadek, R.T. Brownlee, E.R.T. Tiekink, Aust. J. Chem. 47 (1994) 2075.
[14] (a) J.A. McCleverty, N. Morrison, J. Chem. Soc., Dalton Trans. (1976) 2169. (b) H.C. Brinkhoff, J.A. Cras, J.J. Steggerda, J. Willemse, Rec. Trav. Chim. 88 (1969) 633.
[15] (a) C.F. Barrientos, J.G. Contreras, An. Quím. 75 (1979) 245. (b) H.C. Brinkhoff, J.M. Dautzenberg, Rec. Trav. Chim. 91 (1972) 117.
[16] J.G. Contreras, H. Cortés, Inorg. Nucl. Chem. Lett. 6 (1970) 225, 639.
[17] (a) P.J.H.A.M. van de Leemput, J. Willemse, J.A. Cras, L. Groen, Rec. Trav. Chim. 98 (1979) 413. (b) J.G. Contreras, J.A. Gnecco, H.V. Carbacho, J. Coord. Chem. 19 (1989) 371.
[18] J.G. Contreras, H. Cortés, J. Inorg. Nucl. Chem. 33 (1971) 1337.
[19] D. Coucouvanis, Prog. Inorg. Chem. 26 (1979) 301.
[20] A.W. Gal, A.F.J.M. van der Ploeg, F.A. Vollenbroek, W. Bosman, J. Organomet. Chem. 96 (1975) 123.
[21] J.J. Steggerda, J.A. Cras, J. Willemse, Rec. Trav. Chim. 100 (1981) 41.
[22] I. Ojima, T. Onishi, T. Iwamoto, N. Inamoto, K. Tamaru, Inorg. Nucl. Chem. Lett. 6 (1970) 65.
[23] L.I. Victoriano, H. Cortés, J. Coord. Chem. 36 (1995) 159.
[24] L.I. Victoriano, X.A. Wolf, H. Cortés, Polyhedron 14 (1995) 2581.
[25] L. Victoriano, M.T. Garland, A. Vega, Inorg. Chem. 36 (1997) 688.
[26] L. Victoriano, M.T. Garland, A. Vega, J. Chem. Soc., Dalton Trans. (1998) 1127.
[27] L. Victoriano, M.T. Garland, A. Vega, J. Chem. Crystallogr. 29 (1999) 211.
[28] L. Victoriano, M.T. Garland, A. Vega, Inorg. Chem. 37 (1998) 2060.
[29] I.G. Dance, Aust. J. Chem. 31 (1978) 2195.
[30] H. Hartl, F. Mahdjour-Hassan-Abadi, Angew. Chem., Int. Ed. Eng. 23 (1984) 378.
[31] S. Andersson, S. Jagner, J. Crystallogr. Spectrosc. Res. 18 (1988) 591.
[32] G.A. Bowmaker, Adv. Spectrosc. 14 (1987) 1.
[33] S. Jagner, G. Helgesson, Adv. Inorg. Chem. 37 (1991) 1.
[34] L. Victoriano, M.T. Garland, A. Vega, Proceedings of the 32nd International Conference on Coordination Chemistry, Santiago, August 1997, vol. 4, pp. 23.
[35] K.N. Nanda, A.W. Addison, R.J. Butcher, M.R. McDevitt, T. Nageswara-Rao, E. Sinn, Inorg. Chem. 36 (1997) 134.
[36] H.C. Brinkhoff, A.M. Grotens, J.J. Steggerda, Rec. Trav. Chim. 89 (1970) 11.
[37] J.A. McCleverty, N.J. Morrison, J. Chem. Soc., Dalton Trans. (1976) 2169.
[38] L. Victoriano, M.T. Garland, A. Vega, Proceedings of the 32nd International Conference on Coordination Chemistry, Santiago, August 1997, vol. 8, pp. 20.
[39] H.P.M.M. Ambrosius, J. Willemse, J.A. Cras, Proceedings of the Thirrd International Conference on the Chemistry and Uses of Molybdenum, 415, Ann Arbor, Michigan, 1979.
[40] A. Fredga, Rec. Trav. Chim. 69 (1950) 416, 949.
[41] S. Akerström, Ark. Kem. 14 (1959) 387.
[42] L. Victoriano, H. Cortés, J. Coord. Chem. 39 (1996) 201.
[43] R. Hesse, Ark. Kem. 20 (1963) 481.
[44] L.I. Victoriano, H. Cortés, Proceedings of the 22nd Congreso Latinoamericano de Química, Concepción, January 7–12, 1996, p. 84.
[45] L. Victoriano, H. Cortés, Bol. Soc. Chil. Quim. 41 (1996) 5.
[46] L. Victoriano, H. Cortés, M.I. Yuseff, L. Fuentealba, J. Coord. Chem. 39 (1996) 193.
[47] P.J.H.A.M. van de Leemput, J. Willemse, J.A. Cras, Rec. Trav. Chim. Pays Bas 95 (1976) 53.
[48] L. Victoriano, H. Cortés, M.I. Yuseff, L. Fuentealba, J. Coord. Chem. 39 (1996) 193.
[49] P.J.H.A.M. van de Leemput, J.A. Cras, J. Willemse, P.T. Beurskens, E. Menger, Rec. Trav. Chim. Pays Bas 95 (1976) 191.
[50] L.I. Victoriano, M.T. Garland, A. Vega, L. Parraguez, 31st International Conference on Coordination Chemistry,Vancouver, August 18–23, 1996, pp. 12.
[51] L.I. Victoriano, J. Granifo, L. Parraguez, Polyhedron, submitted.
[52] J. Willemse, J.A. Cras, P.J.H.A.M. van de Leemput, Inorg. Nucl. Chem. Lett. 12 (1971) 255.
[53] P.T. Beurskens, W.P. Bosman, J.A. Cras, J. Cryst. Mol. Struct. 2 (1972) 183.
[54] V. Tamminen, E. Hjelt, Suom. Kem. 23B (1950) 39.
[55] J. Willemse, J.J. Steggerda, J. Chem Soc., Chem. Commun. (1969) 1123.
[56] A.M. Bond, R. Colton, A. D'Agostino, J. Harvey, J.C. Traeger, Inorg. Chem. 32 (1993) 3952.
[57] L.I. Victoriano, J.A. Gnecco, H.V. Carbacho, Polyhedron 15 (1996) 1315.
[58] H.V. Carbacho, L. Victoriano, J. Inorg. Nucl. Chem. 37 (1975) 1327.

PERGAMON

www.elsevier.nl/locate/poly

Polyhedron 19 (2000) 2277–2282

POLYHEDRON

Spectroscopic and electrochemical study of $[Ru(NH_3)_5OH_2]^{3+}$, $[Ru(NH_3)_5Cl]^{2+}$, and $[Os(NH_3)_5OH_2]^{3+}$ immobilized on thin film of Ti(IV) oxide dispersed on the silica gel surface

Devaney Ribeiro do Carmo [a], Ubirajara Pereira Rodrigues-Filho [a], Yoshitaka Gushikem [b], Douglas Wagner Franco [a,*]

[a] *Instituto de Química de São Carlos, Universidade de São Paulo Carlos, CP 780, 13560-970 São Carlos, SP, Brazil*
[b] *Instituto de Química, UNICAMP, CP 6154, 13083-970 Campinas, SP, Brazil*

Received 10 October 1999; accepted 3 April 2000

This paper is dedicated in memoriam to our master and friend Professor Waldemar Safioti

Abstract

$[Ru(NH_3)_5H_2O]^{3+}$, $[Ru(NH_3)_5Cl]^{2+}$ and $[Os(NH_3)_5H_2O]^{3+}$ were supported on the hydrated titanium alkoxide grafted on silica gel surface. The mononuclear complexes on the matrix surface have been characterized by specific surface area, elemental analysis, UV–Vis spectroscopy and electrochemical techniques (cyclic voltammetry, differential pulse polarography). These supported species exhibit one defined band on the visible region of the electronic spectrum: band $[Ru(NH_3)_5H_2O]^{3+}$ (668 nm), $[Ru(NH_3)_5Cl]^{2+}$ (676 nm) and $[Os(NH_3)_5H_2O]^{3+}$ (825 nm), attributed to $M^{III} \rightarrow Ti^{IV}$ (M = Ru(III) and Os(III)) metal to metal charge transfer process. For the mononuclear anchored species $[Ru(NH_3)_5H_2O]^{3+}$, $[Ru(NH_3)_5Cl]^{2+}$ and $[Os(NH_3)_5H_2O]^{3+}$, the ($E_{1/2}$) for the M(III)/M(II) couple at 25°C are, respectively: -0.22, -0.28, and -1.15 V versus SCE. A formation of an oxo bridge Ti–O–M$(NH_3)_5$ (M = Ru, Os) and chloro bridge Ti–Cl–Ru$(NH_3)_5$ was postulated for the grafted complexes on the SiO_2/TiO_2 surface. © 2000 Elsevier Science B.V. All rights reserved.

Keywords: Silica; Titanium(IV); Ruthenium; Osmium

1. Introduction

The versatility of the techniques for the modification of silica gel [1–5] surface provide access to quite useful new materials [6–11]. One of the aspects of this technique is the grafting of titanium alkoxide on the silica gel surface followed by further hydrolysis yielding the respective oxide on its surface [11,12]. The thin film of TiO_2 on SiO_2 surface obtained by this procedure, strongly interacts [2,11,12] with the anion complexes $[Fe(CN)_6]^{4-}$ and $[Ru(CN)_6]^{4-}$. This interaction was assumed to be electrostatic in nature.

As a natural extension of the former work [2,11,12] the interaction of the thin film oxide with cations is investigated. This paper describes the electrochemical properties of $[Ru(NH_3)_5H_2O]^{3+}$, $[Ru(NH_3)_5Cl]^{2+}$ and $[Os(NH_3)_5H_2O]^{3+}$ complex species immobilized on the titanium oxide surface.

In these complexes, whereas equatorial NH_3 ligands are well known to be kinetically inert regarding substitution reactions [13], the axial ligands Cl^- and H_2O, would exchange with other ligands in solution but at a slow rate [14–16]. The specific rate for water exchange in $[Ru(NH_3)OH_2]$ is 5×10^{-4} s^{-1} at 25°C [17] and 8.7×10^{-5} $M^{-1}s^{-1}$ at 40°C for chloride aquation [18] in $[Ru(NH_3]_5Cl]^{2+}$. Ti(IV) having a d^0 electronic configuration in solution phase is kinetically labile [19,20] and a similar behavior for the highly dispersed oxide on the silica surface should be expected. As the metal oxides are highly dispersed on the silica surface the coordination sites of titanium ions are not saturated due to the extensive Ti–O–Ti bond formation [21].

* Corresponding author. Tel.: +55-16-272-3813; fax: +55-16-273-9982.
E-mail address: douglas@iqsc.sc.usp.br (D.W. Franco).

0277-5387/00/$ - see front matter © 2000 Elsevier Science B.V. All rights reserved.
PII: S0277-5387(00)00489-7

Thus, the Lewis acid sites coordinated with water or OH^- ligands can be easily replaced. Therefore, the formation of stable complexes of the robust species of ruthenium and osmium with the grafted titanium oxide acid center (Brønsted or Lewis) is likely to occur.

2. Experimental

2.1. Chemical reagents

All reagents and solvents were of analytical grade (Merck or Aldrich) and were used as purchased. All the manipulations with air sensitive compounds were carried under argon atmosphere using standard technique [22].

2.2. Specific surface area

The specific surface area S_{BET}, was determined by BET multipoint technique. The equipment used was a Micrometrics Flow Sorb II-2300 connected to a Flow Controller 2300 FC.

2.3. Silica functionalization with titanium(IV)

Silica gel (Merck) having a specific surface area $S_{BET} = 500 \pm 76$ m^2 g^{-1} average pore diameter of 0.60 nm and particle size between 0.025 and 0.20 nm, was activated by heating at 150°C under vacuum (10^{-3} torr) before use. About 70 g of this activated material were suspended in 150 cm^3 of dry toluene and after which, 24 cm^3 of tetrabutyl orthotitanate monomer (Aldrich) was added. The solid was mechanically stirred and refluxed for 6 h under argon atmosphere and then filtered and rinsed with 350 cm^3 of dry toluene. The solvent was eliminated by heating at 110°C.

The product obtained was carefully hydrolyzed and rinsed with demineralized water. The following equations can be written to represent the functionalization steps described above:

$$n(\equiv SiOH) + Ti(OR)_4 \leftrightharpoons (\equiv SiO)_n Ti(OR)_{4-n} + n HOR \quad (1)$$

$$(\equiv SiO)_n Ti(OR)_{4-n} + (4-n)H_2O \leftrightharpoons (\equiv SiO)_n Ti(OH)_{4-n} + (4-n)HOR \quad (2)$$

where ≡SiOH is silanol and OR is butoxide groups.

The specific surface area of $(\equiv SiO)_n Ti(OH)_{4-n}$ was $S_{BET} = 456 \pm 20$ m^2 g^{-1} and the amount of Ti was determined by X-ray fluorescence analysis as equal to 0.82 mmol g^{-1}.

Complexes of $[Ru(NH_3)_5H_2O]^{3+}$, $[Ru(NH_3)_5Cl]^{2+}$ and $[Os(NH_3)_5H_2O]^{3+}$ were prepared, following procedures already described in literature [23–25].

2.4. Reaction of the complexes with ≡(SiO)$_n$Ti(OH)$_{4-n}$

These complex ions were grafted in a batch procedure, immersing about 0.5 g of $(\equiv SiO)_n Ti(OH)_{4-n}$, (for the sake of brevity, ≡TiOH), in 25 cm^3 of 1.0×10^{-3} M complex solution and the mixture shaken for 30 min. With the immobilization of these complexes on the matrix a change in the solid color from white to yellow is observed.

The solids were filtered, washed with water and dried under inert atmosphere. The resulting solids are designated as $\equiv Ti^{IV}ORu^{III}(NH_3)_5$, $\equiv Ti^{IV}ClRu^{III}(NH_3)_5$ and $\equiv Ti^{IV}OOs^{III}(NH_3)_5$ were stored in desiccators under vacuum (10^{-2} torr) and in the dark.

The amount of Ru and Os attached to the surface of silica, determined using X-ray fluorescence [11,12] and atomic absorption spectroscopy [2,5], were $(1.8 \pm 0.1) \times 10^{-2}$, $(2.2 \pm 0.1) \times 10^{-2}$ and $(1.3 \pm 0.1) \times 10^{-2}$ (mmol g^{-1}), respectively, for $\equiv Ti^{IV}ORu^{III}(NH_3)_5$, $\equiv Ti^{IV}ClRu^{III}(NH_3)_5$ and $\equiv Ti^{IV}OOs^{III}(NH_3)_5$.

Assuming that the chemical species are uniformly distributed on the matrix surface the average surface density, d, and the average intermolecular distance, l, of the attached ligands above cited, were estimated [3] by applying the equations:

$$d = (N \times N_A)/S_{BET} \quad (3)$$

$$l = (1/d)^{1/2} \quad (4)$$

where N is the number of moles of the chemical species per gram of silica and N_A is Avogadro's number. The results of these calculations are shown in Table 1.

Table 1
Chemical species, number of moles of chemical species (N), average surface density (d) and mean interatomic distance (l) of attached species on the silica gel

Silica	N (mmol g^{-1})	d (atom nm^{-2})	l (Å)
≡TiOH	8.2×10^{-1}	1.1	9.5
$\equiv Ti^{IV}ORu^{III}(NH_3)_5$	1.8×10^{-2}	2.4×10^{-2}	64
$\equiv Ti^{IV}ClRu^{III}(NH_3)_5$	2.2×10^{-2}	2.9×10^{-2}	59
$\equiv Ti^{IV}OOs^{III}(NH_3)_5$	1.3×10^{-2}	1.7×10^{-2}	77

2.5. Electrochemical measurements

Cyclic voltammetry and differential pulse polarography experiments were performed using a Princeton Applied Research (PAR) model 273 potentiostat/galvanostat. The three electrode system used in these studies consisted of a modified working electrode (modified carbon paste electrode), a reference saturated calomel electrode (SCE) and a platinum wire as the

auxiliary electrode. The voltammetric spectra of all complexes on the matrix (carbon paste mixture) were hindered by the potential range work of carbon paste (-1.1 to 1.1 V versus SCE) [26]. The measurements were carried out at 25°C. In these studies the criteria used to determine the couple M(III)/M(II) electrochemical reversibility was anodic current/cathodic current ratio approximately equal to 1.

2.6. Electronic spectra

The electronic spectra were recorded using a Hitachi U-3501 spectrophotometer. As the refraction index of carbon tetrachloride and the silica matrix are nearly the same [2], the supported complexes on the silica gel surface were immersed in spectra grade carbon tetrachloride and the electronic spectra of suspension were obtained using quartz cell of 1 mm path length.

The spectra obtained as described above were of very good agreement with those recorded using diffuse reflectance.

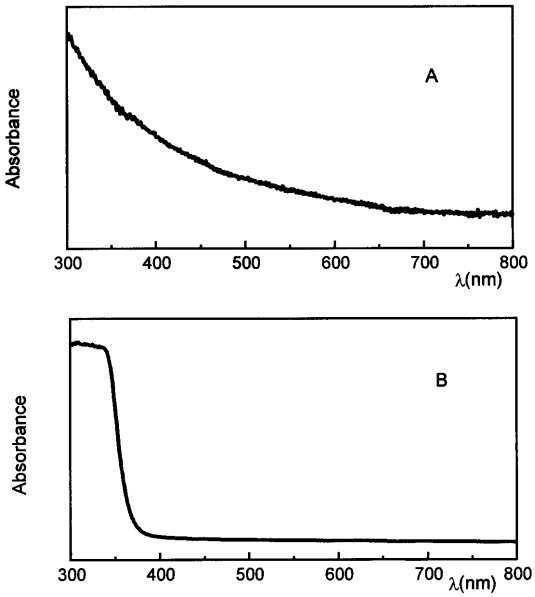


Fig. 1. Absorption spectra of (A) (SiO_2) and (B) titanium oxide dispersed on silica gel.

3. Results and discussion

The $[Ru(NH_3)_5H_2O]^{3+}$, $[Ru(NH_3)_5Cl]^{2+}$ and $[Os(NH_3)_5H_2O]^{3+}$ complexes strongly interact with ≡TiOH in acid medium at pH about 3, whereas the $[Ru(NH_3)_6]^{3+}$ complex does not. The hydroxo group in ≡TiOH, is expected to be more labile than H_2O and Cl^- ligands in the $[Ru^{III}(NH_3)_5X]^{n+}$ complexes, $n = 3$, 2. Therefore, it is reasonable to assume that $[Ru^{III}(NH_3)_5X]^{n+}$ complexes bind to Ti(IV) using X as a bridging ligand. This interaction of the complexes with these titanium acid center at pH 3, although below the pH of zero point of charge (pH_{zpc} between 5.4 ± 1) [27,28], can take place according to the following scheme:

$$\equiv TiOH + H^+ \leftrightharpoons \equiv Ti^+ + H_2O \quad (5)$$

$$\equiv Ti^+ + [M(NH_3)_5H_2O]^{3+} \leftrightharpoons \equiv Ti\text{–}O\text{–}M(NH_3)_5^{2+} + 2H^+ \quad (6)$$

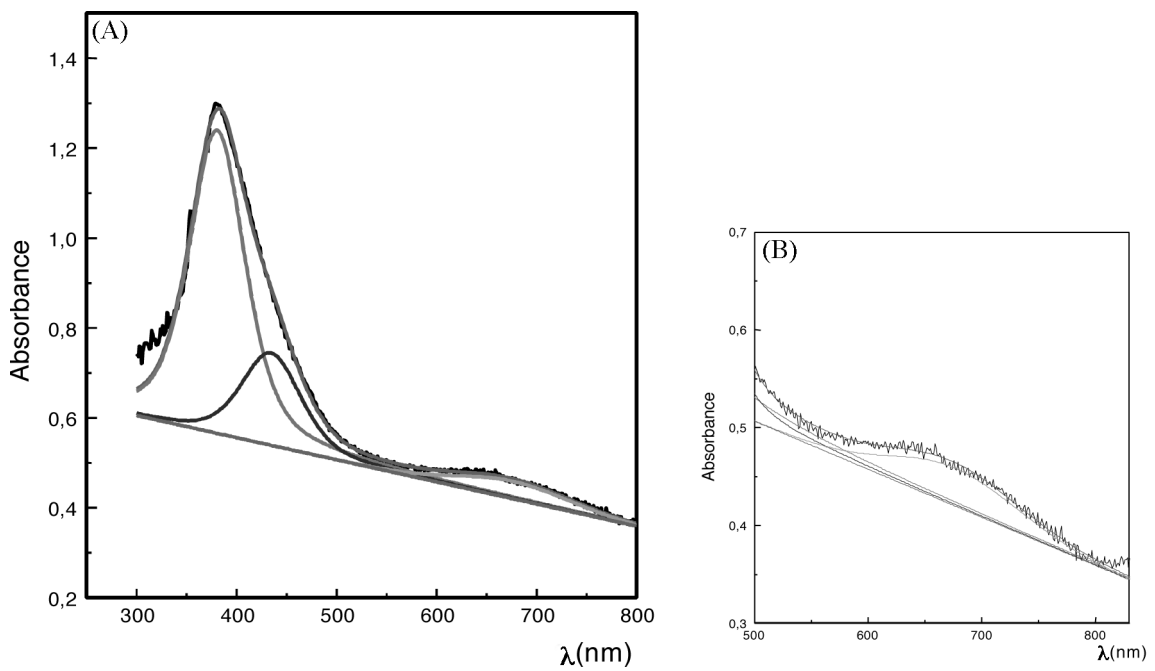


Fig. 2. Electronic absorption spectrum of grafted $[Ru(NH_3)_5Cl]^{2+}$ on the support ≡TiOH.

forming the oxo bridge between the metal and the grafted titanium oxide, or the chloro bridge:

$$\equiv Ti^{+} + [M(NH_3)_5Cl]^{2+} \leftrightharpoons \equiv Ti\text{–}Cl\text{–}M(NH_3)_5^{3+} \quad (7)$$

As the ligands in $[Ru(NH_3)_6]^{3+}$ are inert [16], the NH_3 are not able to act as bridging ligands, and since the titanium center would be as $\equiv Ti^{+}$, the hexaammine species were not able to anchor on the ≡TiOH surface.

Figs. 1(A,B) show the electronic spectra of the SiO_2 and ≡TiOH, respectively. The band gap energy for ≡TiOH was estimated as 3.34 eV that agrees fairly well with the value reported for the TiO_2/SiO_2 catalyst system [29]. This band gap is higher than for anatase (3.08 eV) which is consistent with the larger dispersion of titanium oxide on the silica gel surface (1.1 atom nm^{-2}) [29].

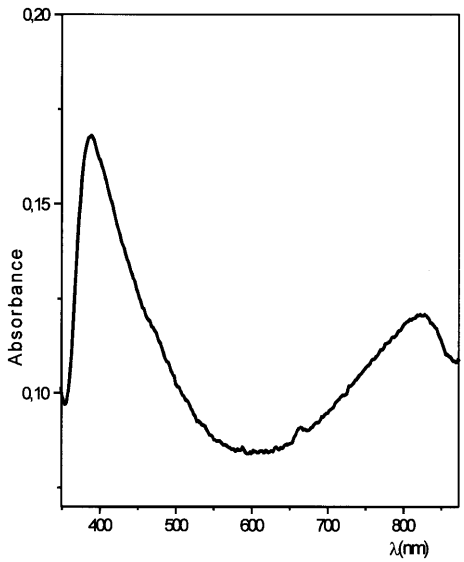


Fig. 3. Electronic absorption spectrum of grafted $[Os(NH_3)_5H_2O]^{3+}$ on the support ≡TiOH.

Table 2
Electronic and electrochemical parameters for the binuclear complexes on the matrix surface and the precursor complexes in solution

Compounds	UV–Vis λ (nm)	Assignments (nm)	$E_{1/2}$ (V)
$\equiv Ti^{IV}ORu^{III}(NH_3)_5$	362 [a], 410 [a], 668 [a]	LF, LMCT, MMCT (668)	−0.22
$\equiv Ti^{IV}ClRu^{III}(NH_3)_5$	380 [a], 431 [a], 676 [a]	LF, LMCT, MMCT (676)	−0.28
$\equiv Ti^{IV}OOs^{III}(NH_3)_5$	390, 825	LMCT, MMCT (825)	−1.15
$[Ru(NH_3)_5H_2O]^{3+}$ [b]	220 (sh) [c], 268, 320 [c]	LF, LMCT (O → Ru(III))	−0.18 [d]
$[Ru(NH_3)_5Cl]^{2+}$ [e]	260, 328	LF, LMCT (Cl → Ru(III))	−0.28 [d]
$[Os(NH_3)_5OH_2]^{3+}$ [f]	220 (sh) [c]	LF	−0.98

[a] Obtained through gaussian deconvolution.
[b] Ref. [32].
[c] Shoulder.
[d] Refs. [39,41].
[e] Refs. [30,31].
[f] Ref. [33].

Figs. 2 and 3 show the electronic spectra of the supported $[Ru(NH_3)_5Cl]^{2+}$ and $[Os(NH_3)_5H_2O]^{3+}$ species and Table 2 summarizes their more relevant spectral features.

Due to the absorption displayed by ≡TiOH at 350 nm (Fig. 1(B)) the analysis of the supported complexes spectra near 400 nm is very difficult. However, above 500 nm the electronic spectra of the grafted species are well defined. Therefore, by subtracting the support absorption and using gaussian fitting some tentative attributions have been carried out.

Both ruthenium complexes exhibit a band around 670 ± 10 nm. This band does not occur in the electronic spectra of the mononuclear pentaammine species in solution or in solid state. The energy of this transition is around 1.8 eV, therefore consistent with a Ru(III) → OTi(IV) (or Ru(III) → Ti(IV)) and a Ru(III) → ClTi(IV) metal to metal charge transfer (MMCT) process.

The grafted $[Os(NH_3)_5H_2O]^{3+}$ exhibits an absorption band at 825 nm (1.5 eV), which is not present in the electronic spectra of $[Os(NH_3)_5H_2O]^{3+}$ either in solution or in solid state. This band consistently positioned at lower energy in relation to the ones observed for the analogous Ru(III) complexes, was tentatively assigned to the charge transfer process Os(III) → OTi(IV).

In the range of potential studied (-1.0 to 1.0 V) the support ≡TiOH is not electroactive. The voltammetric spectra of the grafted $[Ru(NH_3)_5H_2O]^{3+/2+}$ complex is well defined as illustrated in Fig. 4.

Its is well known [34,35] that in solution ClO_4^- easily oxidizes $[Ru(NH_3)_5H_2O]^{2+}$ at room temperature according to:

$$8[Ru(NH_3)_5H_2O]^{2+} + ClO_4^- + 8H^+ \leftrightharpoons 8[Ru(NH_3)_5H_2O]^{3+} + Cl^- + 4H_2O \quad (8)$$

This reaction [36] is described to be first order in [Ru(II)] and in $[ClO_4^-]$ and zero order in $[H^+]$ (in the range from 10^{-3} to 10^{-2} M, $k = (2.6 \pm 0.1) \times 10^{-2}$ M^{-1}).

In our studies no evidence for the Ru(II) oxidation by perchlorate ion was observed. Indeed, the best defined cyclic voltammograms were obtained with $NaClO_4$ as a supporting electrolyte.

At first sight this behavior was not expected as a substantial oxidation of the electrochemically formed Ru(II) could occur under the conditions of the experiments ($NaClO_4$ 1.0 M). The inability of ClO_4^- to oxidize the anchored Ru(II) is probably due to matrix effects. The Ru(III) species dispersed on the matrix has a superficial density of 0.024 atom nm^{-2}, being the

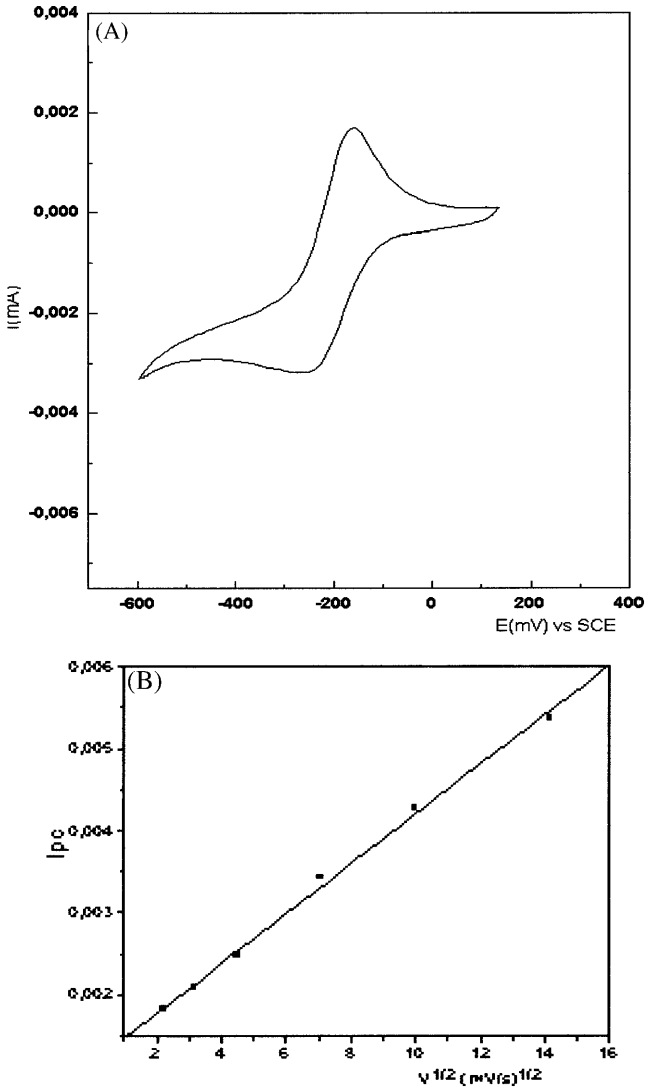


Fig. 4. Cyclic voltammograms using modified carbon paste electrode with $[Ru(NH_3)_5H_2O]$ grafted on the matrix. Conditions: $NaClO_4$ 1.0 M, 25°C; pH 3,1; $v = 20$ mV s^{-1}). The inserted graphic shows the dependence of cathodic peak with square root of the scan rates.

average distance between two ruthenium centers around 64 Å. The ClO_4^- reduction is a multi-step electron process [34], and as the ions' mobility in the carbon paste is certainly smaller than in solution, the chemical Ru(II) oxidation by ClO_4^- does not occur in the time scale of our experiments, the complete cycle was obtained in less than one minute.

For the anchored aqua ruthenium complex, the midipoint potential $E_{1/2} = (E_{pa} + E_{pc})/2$ was (-0.22 ± 0.01) V, $\Delta E_p = (E_{pa} - E_{pc}) = (0.10 \pm 0.02)$ V, and the ratio I_{pa}/I_{pc} was about (0.92 ± 0.02). The anodic and cathodic peaks intensities were directly proportional to the square root of the scan rates (see Fig. 4(B)), suggesting diffusion controlled process [37].

For the supported ruthenium ammines the peak to peak separation and $W_{1/2}$ values, (0.140 V $\pm$ 0.005) to $(W_{1/2})_a$ and $(W_{1/2})_c$ calculated from DPP data, are higher that the ones observed for the similar ions in solution. The insulator properties of SiO_2 [38] and the inability [19] of the ligands act as good electron density conductors, probably accounts on great part for these behavior.

The Os(III)/Os(II) couple in the polarogram of $\equiv Ti^{IV}OOs^{III}(NH_3)_5$ in the carbon paste electrode presents the mid-point potential with $E_{1/2} = -1.15 \pm 0.04$ V versus SCE and $I_{pa}/I_{pc} = 0.9 \pm 0.03$. The $W_{1/2}$ values calculated using DPP technique were 0.23 $(W_{1/2})_a$ and 0.25 V $(W_{1/2})_c$.

The electrochemical data of Table 2 for the supported and free complex ions in solution, suggest for the osmium and ruthenium species $\equiv Ti^{IV}OM^{III}(NH_3)_5$, a stabilization [34] of the metal center oxidation state(III) regarding to the (II) as a consequence of the association with the matrix.

Another interesting matrix effect manifestation can be observed in the $\equiv Ti^{IV}$–Cl–$Ru^{III}(NH_3)_5$ system.

The electrochemistry behavior of $[Ru(NH_3)_5Cl]^{2+}$ in aqueous has been already described [39,40]. In solution during the cathodic scan (1.0 to -0.6 V), only one wave is observed due to the reduction, Ru(III) to Ru(II), in $[Ru(NH_3)_5Cl]^{2+}$ ($E_{1/2} = -0.28$ V versus SCE) complex, which is followed by aquation of the halide ligand in the reduced complex, $k_{Cl^-} = 4.4$ s^{-1}. Thus, two waves are observed in the anodic scan: one is due to the remaining $[Ru(NH_3)_5Cl]^{2+}$ and the other originated by the oxidation of the $[Ru(NH_3)_5H_2O]^{2+}$ ($E_{1/2}$ -0.18 V versus SCE).

The cyclic voltammogram of the supported $[Ru(NH_3)_5Cl]^+$ (see Fig. 5) species exhibits only one

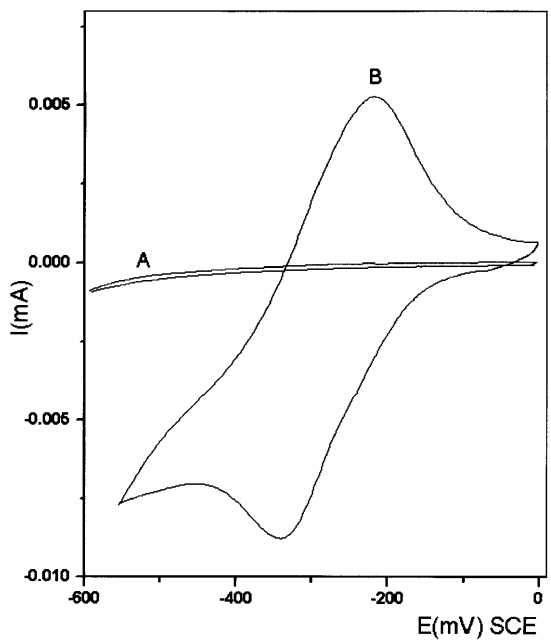


Fig. 5. Cyclic voltammograms using modified carbon paste electrodes: (A) matrix (≡TiOH) and (B) $[Ru(NH_3)_5Cl]]^{2+/+}$ grafted on the matrix ($NaClO_4$ 1.0 M, 25°C, pH 3.1; $v = 20$ mV s^{-1}).

coupled redox process: $E_{pc} = -0.34$ and $E_{pa} = -0.22$ V.

The ΔE_P for the supported $[Ru(NH_3)_5Cl]^{+2/+}$ is equal to (0.12 ± 0.01) V, is on agreement, within the limits of the experiment error with the value of $\Delta E_P = (0.10 \pm 0.01)$ V for the related $[Ru(NH_3)_5\ H_2O]^{3+/2+}$ supported system.

No distinct signal of a second electroactive species was detected, in anodic scan when the scan rate has changed from 0.005–0.5 V s^{-1} in the temperature range of 5–45°C. Therefore it seems unlikely that in the carbon paste electrode, a constrict environment, the bridge $\equiv Ti^{IV}$–Cl–Ru^{III} is disrupted, in the time scale of the experiment.

4. Conclusions

Electrochemical and spectroscopic measurements pointed out matrix effects over $[M(NH_3)_5H_2O]^{3+}$ (M = Ru(III) or Os(III)) and Ru $(NH_3)Cl]^{2+}$ grafted species. The well known fast reactions of Ru(II) with ClO_4^- and the aquation of Cl^- in the Ru $(NH_3)Cl]^{2+}$ in solution were not observed for the anchored species. The existence of a MMCT band due to the $M^{III} \rightarrow OTi^{IV}$ process and the observed shift in the $E_{1/2}$ values for the M(III)/M(II) couples in the anchored species suggest a stabilization of the M^{III} regarding the M^{II} oxidation state, as a consequence of the interaction with the matrix. Analyzing the reaction between the support and $[M(NH_3)_5H_2O]^{3+}$, $[M(NH_3)_5Cl]^{2+}$ and $[Ru(NH_3)_6]^{3+}$ a formation of a binuclear system Ti^{IV}–LM^{III}, where $L = O^{2-}$ or Cl^- has been proposed.

Acknowledgements

The authors are indebted to FAPESP, CAPES, CNPq for financial support and Angela Cristina Pregnolato Giampedro for the English manuscript revision. The loan of $RuCl_3$ from Johnson and Mathey is also acknowledged.

References

[1] L.M. Siperko, T. Kuwana, Electrochim. Acta 130 (1983) 765.
[2] Y. Gushikem, C.R.M. Peixoto, U.P. Rodrigues-Filho, L.T. Kubota, E. Stadler, J. Colloid Interface Sci. 184 (1996) 236.
[3] S. Denofre, Y. Gushikem, S.C. Castro, Y. Kawano, J. Chem. Soc., Faraday Trans. 89 (1993) 1057.
[4] M.T. Hoffmann, S.M.C. Neiva, M.R. Martins, D.W. Franco, in: H.A. Mottola, J.R. Steinmezt (Eds.), Chemically Modified Surfaces, Elsevier, New York, 1992, p. 257.
[5] S.M.C. Neiva, J.A.V. Santos, J.C. Moreira, Y. Gushikem, H. Vargas, D.W. Franco, Langmuir 9 (1995) 239.
[6] L. Lorencetti, Y. Gushikem, L.T. Kubota, G.O. Neto, J.R. Fernandes, Mikrochim. Acta 117 (1995) 239.
[7] L.T. Kubota, F. Gouvea, A.N. Andrade, B.G. Milagres, G.O. Neto, Electrochim. Acta 41 (1996) 1465.
[8] B. Rebenstorf, S.L.T. Andersson, J. Chem. Soc., Faraday Trans. 86 (1990) 2783.
[9] L.T. Kubota, B.G. Milagres, F. Gouvea, G.O. Neto, Anal. Lett. 29 (1996) 893.
[10] A. Walcarius, Electroanalysis 10 (1998) 1217.
[11] L.T. Kubota, Y. Gushikem, Electochim. Acta 37 (1992) 2477.
[12] D.R. Carmo, Y. Gushikem, D.W. Franco, in: J.P. Blitz, C.B. Little (Eds.), Fundamental and Applied Aspects of Chemically Modified Surfaces, The Royal Society of Chemistry, Cambridge, 1999, p. 325.
[13] P.C. Ford, Coord. Chem. Rev. 5 (1970) 75.
[14] H. Taube, Pure Appl. Chem. 51 (1979) 901.
[15] J.A. Stritar, H. Taube, Inorg. Chem. 8 (1969) 2281.
[16] H. Taube, Comm. Inorg. Chem. 1 (1981) 17.
[17] P. Forlano, L.M. Baraldo, J.A. Olabe, C.O. Della Védora, Inorg. Chim. Acta 223 (1994) 37.
[18] C.W.B. Bezerra, S.C. Silva, M.T.P. Gambardella, R.H.A Santos, L.M.A. Plicas, E. Tfouni, D.W. Franco, Inorg. Chem. 38 (1999) 5660.
[19] R.G. Wilkins, Kinetics and Mechanism of reactions of Transition Metal Chemistry, second ed., Wenhein, New York, 1991, p. 183.
[20] I.D. Ellis, G. Sykes, J. Chem. Soc., Dalton Trans. 573 (1973).
[21] L.T. Kubota, Ph.D. Dissertation, Unicamp, Brazil, 1993.
[22] D.F. Shriver, Manipulation of Air Sensitive Compounds, McGraw–Hill, New York, 1969.
[23] N.E. Dixon, G.A. Lawrance, P.A. Lay, A.M. Sargeson, Inorg. Chem. 23 (1984) 2940.
[24] T. Meyer, H. Taube, Inorg. Chem. 7 (1968) 2369.
[25] P.A. Lay, R.H. Mangunson, J. Sen, H. Taube, J. Am. Chem. Soc. 104 (1982) 7658.
[26] K. Kalcher, J.M. Kauffmann, J. Wang, I. Svancara, K. Vytras, Z. Neuhold, Z.C. Zang, Electroanalysis 7 (1995) 5.
[27] C. Kormann, D.W. Bahnemann, M.R. Hoffmann, Environ. Sci. Technol. 25 (1991) 494.
[28] M.M. Kondo, Ph.D. Dissertation, Delaware University, USA, 1996.
[29] S.F Cheng, S.-J. Tsai, Y.F. Lee, Catal. Today 26 (1995) 87.
[30] A. Adegite, J.F. Iyun, J.F. Ojo, J. Chem. Soc., Dalton Trans. 2 (1977) 115.
[31] A.D. Allen, J.R. Stevens, Can. J. Chem. 51 (1972) 92.
[32] H. Krentizen, Ph.D. Dissertation, Stanford University, USA, 1976.
[33] J.D. Bhur, Ph.D. Dissertation, Stanford University, USA, 1978.
[34] H. Taube, Surv. Prog. Chem. 6 (1976) 31.
[35] J.F Endicott, H. Taube, Inorg. Chem. 4 (1989) 437.
[36] J.F Endicott, H. Taube, J. Am. Chem. Soc. 84 (1962) 4984.
[37] L.T. Kubota, Y. Gushikem, J. Perez, A. Tanaka, Langmuir 11 (1995) 1009.
[38] L.T. Kubota, Y. Gushikem, J. Electroanal. Chem. 362 (1993) 219.
[39] H.S. Lim, D.J. Baclay, F. Anson, Inorg. Chem. 11 (1972) 1460.
[40] G.M. Coleman, J.W. Gesler, F.A. Shirley, J.R. Kuemptel, Inorg. Chem. 12 (1973) 1036.
[41] C. Shi, F. Anson, Inorg. Chem. 36 (1997) 2632.

PERGAMON

www.elsevier.nl/locate/poly

Polyhedron 19 (2000) 2283–2287

POLYHEDRON

The effect of hydrolysis initiator on the phase formation in sulfated sol–gel zirconia

X. Bokhimi [a,*], A. Morales [a], O. Novaro [a,1], T. López [b], R. Gómez [b]

[a] *Institute of Physics, The National University of Mexico (UNAM), A.P. 20-364, 01000 Mexico D.F., Mexico*
[b] *Department of Chemistry, Universidad Autónoma Metropolitana-Iztapalapa A.P. 55-534, 09340 Mexico D.F., Mexico*

Received 1 October 1999; accepted 18 April 2000

Abstract

Sol–gel zirconia was sulfated with sulfuric acid. Samples were analyzed with X-ray powder diffraction and thermogravimetry; crystalline phases were refined via Rietveld method. The samples annealed at 600°C crystallized into nanocrystalline tetragonal zirconia when they were prepared with acetic acid, but they crystallized into a mixture of zirconium sulfide, zirconium oxide sulfide, and zirconium sulfate when they were prepared with hydrochloric acid or ammonium hydroxide. The sulfation of the samples prepared with acetic acid also stabilized the tetragonal zirconia. © 2000 Elsevier Science B.V. All rights reserved.

Keywords: Sulfated zirconia; Tetragonal zirconia stabilization; Rietveld method; Zirconium sulfide; Zirconium oxide sulfide; Thermogravimetry of sol–gel ZrO_2

1. Introduction

Zirconia is an oxide with three polymorphs that are transformed between each other by annealing it. The room temperature polymorph has a monoclinic crystalline structure that is transformed into a tetragonal symmetry when it is annealed in air at 1170°C and eventually to a cubic symmetry when it is heated in air at 2370°C. The high-symmetry structures of zirconia can be also obtained at room temperature by dissolving in its structure atoms like Y, La, Ca and Mg, which substitute for zirconium atoms [1]. The electronic properties of these zirconia solid solutions will depend on the size and valence of the dissolved atom, providing a mechanism to produce materials with interesting properties for electronics [2–4]. When the room temperature high-symmetry zirconia solid solutions are under stress, their crystalline structure is transformed into the monoclinic symmetry of pure zirconia; this fact is used to produce high toughness materials [5].

The above observations are valid when the samples are synthesized at large temperatures to produce microcrystalline materials. But, when zirconia is produced via soft chemistry, new phenomena have been observed; for example, when it is prepared with the sol–gel technique its tetragonal phase appears at relative low temperatures [6], caused by the hydroxyls in its structure. In this case, the tetragonal phase is in reality a zirconia solid solution with the hydrogen in lattice positions that until now are unknown. Preliminary results [7] show that carboxyls can also be dissolved in zirconia to stabilize its tetragonal phase. In the two last mentioned solid solutions the hydrogen and carbon atoms should occupy interstitial sites of zirconia crystalline structure. This result is very interesting, because it gives another option on interpreting the stabilization of the tetragonal phase when pure zirconia is modified with sulfuric acid [8], which is a system of big interest in catalysis [9]. That means that in sulfated zirconia, sulfur atoms could be not only on the crystal surface but also in bulk: in the zirconia lattice interstitials. To have a better understanding of the observed behavior of sulfated zirconia, however, its crystallography must be analyzed in detail as a function of the different parameters involved in its synthesis and annealing.

* Corresponding author. Present address: Instituto Mexicano del Petróleo, Eje Central L. Cárdenas 152, A.P. 14-805, 07730 Mexico D.F., Mexico. Tel.: +52-5-333-8105; fax: +52-5-368 9203.
E-mail address: bokhimi@www.imp.mx (X. Bokhimi).
[1] Member of 'El Colegio Nacional', Mexico.

0277-5387/00/$ - see front matter © 2000 Elsevier Science B.V. All rights reserved.
PII: S0277-5387(00)00490-3

Zirconia by itself has a good catalytic activity for alkylation and dehydration reactions and fine chemistry [10,11]. Recently, it has also been found that sulfated zirconia possesses important isomerization activity [12–15]. Sulfated zirconia also shows superacidity [16–19]: acid-site number in the sample considerably increases when sulfate ions are present, which is produced by the electron deficiency in the metal cations. The acidity depends on the structure of the crystalline phase; the tetragonal phase is the most active [20].

In the present work, we analyzed the effect on the atomic distribution of sol–gel zirconia when it is sulfated with sulfuric acid. The precise knowledge of this atom distribution will provide elements to interpret from a microscopic point of view the catalytic properties of sulfated zirconia, and the origin of its superacidity that facilitates paraffin isomerization reactions at low temperatures [21]. The present crystallographic study will also provide elements to understand the nature and structure of the observed highly acidic sites. Atom distribution was measured by using X-ray powder diffraction; when it was crystalline, the structure was refined with the Rietveld method. The evolution of this distribution was analyzed as a function of temperature, and correlated with the sample weight loss detected via thermogravimetry.

2. Experimental

2.1. Sample preparation

Zirconium *n*-butoxide (10.024 mol) was dissolved at 70°C in *tert*-butyl alcohol (150 ml), under continuous refluxing and stirring. The hydrolysis initiator, HCl for pH 3, $C_2H_4O_2$ for pH 5, and NH_4OH for pH 9, was added to the solution until reaching the desired pH. The solution with the initiator was stirred and refluxed for 10 min and eventually cooled to 50°C. Thereafter, the water (25.66 ml) was dropped into it, and its temperature was again raised to 70°C, at which it was continuously stirred and refluxed until gelling. Gels were dried in air at 100°C for 24 h. Next 1 g of dried sol–gel zirconia was uniformly impregnated with 25 ml of sulfuric acid.

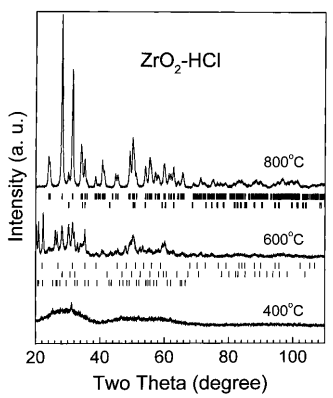


Fig. 1. X-ray diffraction pattern of the samples prepared with hydrochloric acid and annealed at different temperatures. The upper tick marks under the pattern of the sample annealed at 800°C correspond to monoclinic zirconia; the lower tick marks to tetragonal zirconia. The upper tick marks under the pattern of the sample annealed at 600°C correspond to ZrOS; the middle tick marks to ZrS_2, and the lower tick marks to $Zr(SO_4)_2$.

2.2. X-ray diffraction characterization

The crystalline structure of the samples was characterized by X-ray powder diffraction, and refined with the Rietveld technique. X-ray diffraction patterns of the specimens, prepared by packing sample powder into a glass holder, were measured at room temperature by using a Bruker D8-Advance diffractometer with Cu Kα radiation and a secondary beam monochromator. Intensity was measured by step scanning in the 2θ range between 20–110°, with a step of 0.02° and a measuring time of 2 s per point. Structure refinement was performed with DBWS-9411 code [22]; peak profiles were modeled with a pseudo-Voigt function that included average crystallite size as one of their fitting parameters [23]. Standard deviations, showing the variation of the last figures of the corresponding number, were given in parenthesis. When the number is a parameter obtained from the refinement, its standard deviation is not an estimate of the analysis as a whole, but only of the minimum possible probable error based on its normal distribution [24].

2.3. TGA characterization

This analysis was carried out in a thermoanalyzer Dupont model 950; it was performed in air from 25–1200°C at 20° min^{-1}. In order to eliminate synthesis residuals, before the thermoanalysis, sulfated samples were annealed at 400°C.

3. Results and discussion

All samples were amorphous when they were annealed below 450°C (Figs. 1–3), which reproduces previous reports for sulfated zirconia [8,25]. The amorphous character is typical for hydrated non-sulfated zirconia when it is annealed below 300°C; it is determined by the fast condensation, produced by their large number of possible nucleation sites, of the zirconyl clusters [6,26]. It is known that this zirconia is no more amorphous when it is annealed at 400°C, but a mixture of nanocrystalline tetragonal and monoclinic zirconia [6]. Therefore, the observed stabilization of the amorphous phase at 400°C in the present sulfated

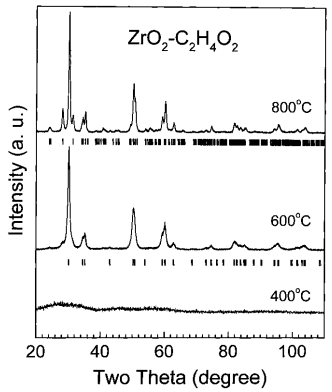


Fig. 2. X-ray diffraction pattern of the samples prepared with acetic acid and annealed at different temperatures. The tick marks under the pattern of the sample annealed at 800°C correspond to monoclinic zirconia; those under the pattern of the sample annealed at 600°C correspond to tetragonal zirconia.

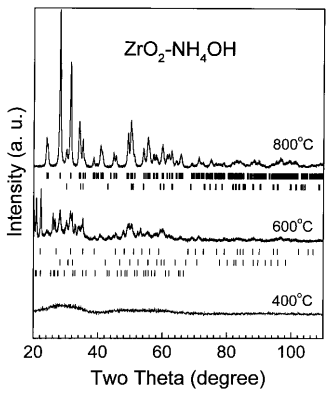


Fig. 3. X-ray diffraction pattern of the samples prepared with ammonium hydroxide and annealed at different temperatures. The upper tick marks under the pattern of the sample annealed at 800°C correspond to monoclinic zirconia; the lower tick marks to tetragonal zirconia. The upper tick marks under the pattern of the sample annealed at 600°C correspond to ZrOS; the middle tick marks to ZrS_2, and the lower tick marks to Zr $(SO_4)_2$.

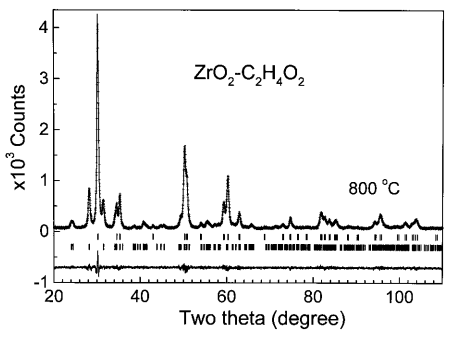


Fig. 4. Rietveld refinement plot of a sample prepared with acetic acid and annealed at 800°C. Crosses indicate the experimental data, while the calculated diffraction pattern and their difference with the experimental data are indicated with continuous lines. The upper tick marks correspond to tetragonal zirconia ($R_f = 0.008$), and the lower tick marks to monoclinic zirconia ($R_f = 0.02$).

zirconia samples should be produced by the presence of sulfate ions, which inhibit crystallization. Samples, however, crystallized when they were annealed at higher temperatures. Fig. 4 shows a typical Rietveld refinement plot, which corresponds to a sample prepared with acetic acid and annealed at 800°C.

In the samples synthesized with acetic acid as hydrolysis initiator, the tetragonal was the main phase when they were annealed at 600°C (Fig. 2 and Table 1). It is important to note, that the tetragonal phase concentration of 66(2) wt.% observed in the sulfated samples prepared with acetic acid and annealed at 800°C was larger than the concentration of 17(2) wt.% observed in the respective non-sulfated samples [6]. Because the only difference between sulfated and non-sulfated samples was the presence of the sulfate ions, the above result is an indication that sulfate ions are responsible of this additional stabilization of the tetragonal phase.

Recently, Bokhimi et al. [7] suggested that carbon atoms could be incorporated in the interstitial sites of the tetragonal zirconia lattice to stabilize it. This result could be extrapolated to the present case by assuming the presence of sulfate ions in the tetragonal phase with the sulfur atoms occupying the same interstitial sites that carbon atoms do. This would explain the stabilization of the tetragonal phase at 800°C prepared with acetic acid (Fig. 2 and Table 1). This proposition is totally new, because it has been always assumed that sulfate ions should be at the surface of the particles building the sample [8,25–29].

The stabilized tetragonal zirconia, prepared with acetic acid, was partially transformed into a monoclinic phase when samples were annealed to 800°C (Fig. 2 and Table 1). Its corresponding TGA curve showed a weight loss of 23% that occurred mainly between 500 and 700°C (Fig. 5). This weight loss was produced by evaporation from sample of those atom clusters associated with the sulfur, which can be represented with the formula SO_x. The fact that sulfate ions stabilized the amorphous structures suggests that since synthesis beginning they were in the neighborhood of zirconyl clusters, which are the zirconium oxide precursors. The neighboring contact between these atom clusters caused them to produce structures compatible with the characteristic distances between the atoms they are composed of.

In contrast to the above results, when hydrochloric acid or ammonium hydroxide were the hydrolysis initiators (Figs. 1 and 3 and Table 1), the tetragonal phase was only present in very small concentrations. Instead of this phase, monoclinic zirconia, zirconium sulfate, zirconium oxide sulfide [30], ZrOS, and zirconium sulfide [31], were formed in the traditional synthesis method, ZrOS and ZrS_2 are synthesized by heating the sample at 1300°C in flowing hydrogen sulfide [30].

Table 1
Phase composition and average crystallite size as a function of hydrolysis initiator and temperature for sulfated zirconia

Hydrolysis initiator	T (°C)	Tetragonal (wt.%)	Monoclinic (wt.%)	Tetragonal d (nm)	Monoclinic d (nm)
HCl	800	3.0(6)	97(3)	24(9)	30.3(8)
$C_2H_4O_2$	600	91(3)	8.7(2)	15.3(4)	10(1)
	800	66(2)	34(4)	28.4(1)	32(2)
NH_4OH	800	3.7(6)	96(3)	24(7)	29.5(7)

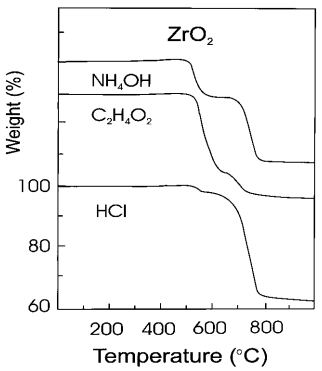


Fig. 5. TGA curves as a function of temperature of the samples prepared with different hydrolysis initiators.

For these hydrolysis initiators, the presence of Cl^- and ammonium ions avoided the contact between sulfate groups and zirconyl clusters to form the sulfur stabilized tetragonal phase. However, they catalyzed the synthesis of the above mentioned sulfur compounds, zirconium sulfate, zirconium oxide sulfide and ZrS_2, whose concentrations were not determined because the crystallography of their crystalline structures could not be refined; therefore, they were not reported in Table 1. But, since for these three compounds the main scattering centers of the X-rays were zirconium atoms, and the intensity of their main diffraction peaks was similar, then their concentrations were also similar. For these hydrolysis initiators, the above sulfur compounds were more stable than the sulfur in the tetragonal phase. However, they decomposed when the samples were annealed between 650–780°C (Fig. 4), and part of their byproducts evaporated, producing a weight loss of 31.7% for the samples prepared with HCl, and of 14.7% for those prepared with ammonium hydroxide. The samples annealed at 800°C did not contain any of these sulfur compounds and the only phase present was nanostructured monoclinic zirconia (Figs. 1 and 3 and Table 1).

According to the above results, when sulfated zirconia is used in catalysis or its properties are characterized, it is recommended to identify the phases in the sample prior to results interpretation, because these phases depend on synthesis conditions. This is especially important when synthesis is done by using sol–gel method.

4. Conclusions

Sulfating sol–gel zirconia with sulfuric acid stabilized the amorphous hydrated zirconium oxide phase. The crystalline phases that appeared in the initial crystallization step depended on the hydrolysis initiator used for the synthesis: when it was acetic acid, the formed phase was mainly tetragonal zirconia, but when it was hydrochloric acid or ammonium hydroxide the produced phases were mainly zirconium sulfate, zirconium oxide sulfide and zirconium sulfide, which disappeared when samples were annealed at 800°C. At this temperature, the tetragonal zirconia synthesized with acetic acid was very stable: its concentration was 66(2) wt.%. The present results put in alert to those who are studying or applying sulfated zirconia. Before the interpretation of their results, they must identify the crystalline phases in the samples. The present work also provides an alternative method for producing ZrOS and zirconium sulfide, at relatively low temperatures, without using hydrogen sulfide and high annealing temperatures.

Acknowledgements

We would like to thank Mr M. Aguilar for technical assistance.

References

[1] S. Somiya, N. Yamamoto, H. Yanagida, Science and Technology of Zirconia III, Advances in Ceramics, vol. 24A/B, American Ceramic Society, Westerville, OH, 1986.
[2] Y. Ohno, Y. Kaga, S. Nagata, Electr. Eng. Jpn. 107 (1987) 59.
[3] J. Fouletier, Ceramurgia 25 (1995) 209.
[4] S.P.S. Dadwal, Solid State Ionic 70/71 (1994) 83.
[5] J.F. Braza, STLE Tribol. Trans. 38 (1994) 146.
[6] X. Bokhimi, A. Morales, O. Novaro, M. Portilla, T. López, F. Tzompanzi, R. Gómez, J. Solid State Chem. 135 (1998) 28.
[7] X. Bokhimi, A. Morales, O. Novaro, T. López, R. Gómez, T.D. Xiao, P.R. Strutt, Nanostruct. Mater. 12 (1999) 593.
[8] J.R. Sohn, H.W. Kim, J. Mol. Catal. 52 (1989) 361.
[9] R.A. Keogh, B.H. Davis, Catal. Lett. 57 (1999) 33.
[10] A. Corma, V. Fornes, M.I. Juan-Rajadeli, J.M. López-Nieto, Appl. Catal. A116 (1994) 151.
[11] A. Corma, A. Martínez, C. Martínez, J. Catal. 149 (1994) 52.
[12] C. Monterra, G. Cerrato, C. Emanuel, V. Bolis, J. Catal. 142 (1993) 349.
[13] D.A. Ward, E.Y. Ko, J. Catal. 150 (1994) 18.

[14] L.M. Kustov, Y.B. Kazamsky, F. Figueras, D. Tichit, J. Catal. 150 (1994) 239.
[15] G.M. Pajonk, A. El Tamany, React. Kinet. Catal. Lett. 2 (1992) 167.
[16] Y. Yamaguchi, K. Temabe, Mater. Chem. Phys. 16 (1986) 67.
[17] P.J. Squattrito, P.R. Rudolph, A. Clearfield, Inorg. Chem. 26 (1987) 4240.
[18] T. Jin, T. Yamaguchi, K. Tanabe, Phys. Chem. 90 (1986) 4794.
[19] A. Corma, A. Martínez, Catal. Rev. Sci. Eng. 35 (1993) 483.
[20] R.A. Comelli, C.R. Vera, J.M. Parera, J. Catal. 151 (1995) 96.
[21] K. Arata, M. Hino, Mater. Chem. Phys. 26 (1990) 213.
[22] R.A. Young, A. Sakthivel, T.S. Moss, C.O. Paiva-Santos, J. Appl. Crystallogr. 28 (1995) 366.
[23] P. Thompson, D.E. Cox, J.B. Hastings, J. Appl. Crystallogr. 20 (1987) 79.
[24] E. Prince, J. Appl. Crystallogr. 14 (1981) 157.
[25] R. Srinivasan, D. Taulbee, B.H. Davis, Catal. Lett. 9 (1991) 1.
[26] D.A. Ward, E. Ko, J. Catal. 157 (1995) 321.
[27] V.I. Parvulescu, S. Coman, V. Parvulescu, G. Poncelet, Catal. Lett. 52 (1998) 231.
[28] S. Ardizzone, C.L. Bianchi, W. Cattagni, V. Ragaini, Catal. Lett. 49 (1997) 193.
[29] W. Stichert, F. Schüth, J. Catal. 174 (1998) 242.
[30] J.D. McCullough, L. Brewer, L.A. Bromley, Acta Crystallogr. 1 (1948) 287.
[31] PDF-110679, JCPDS-International Center for Diffraction Data, PA, USA, 1997

PERGAMON

www.elsevier.nl/locate/poly

Polyhedron 19 (2000) 2289–2295

POLYHEDRON

Experimental evidence of the disproportionation equilibrium in copper mixed-valence complexes

Irma G. Crivelli [a,*], Carlos Andrade [a], M. Angélica Francois [b], Daphne Boys [c], Annamaria Haberland [d], Rodrigo Segura [d], Ana María Leiva [d], Bárbara Loeb [d]

[a] *Facultad de Ciencias, Universidad de Chile, Casilla 653, Santiago, Chile*
[b] *Facultad de Ciencias, Universidad Católica de Temuco, Casilla 15-D, Temuco, Chile*
[c] *Facultad de Ciencias Físicas y Matemáticas, Universidad de Chile, Casilla 487-3, Santiago, Chile*
[d] *Facultad de Química, Pontificia Universidad Católica de Chile, Casilla 306, Santiago, Chile*

Received 1 October 1999; accepted 2 May 2000

Abstract

Experimental evidence for a dismutation equilibrium in the mixed-valence (MV) $[M^{n+}–M^{(n+1)+}]$ system type has been elusive and its existence can be established only when the oxidation–reduction processes involved are reversible. Previous research in the field of binuclear Cu(II)–Cu(II), Cu(I)–Cu(I) and the related MV Cu(II)–Cu(I) complexes allowed us to obtain electrochemical evidence for the disproportionation equilibrium in some of these systems. In this communication we report and discuss experiments with $[(RCOO)_2Cu(II)–Cu(I)(OOCR)_2]^-$ ($R = CH_3$, Ph) type MV complexes that give direct non-electrochemical experimental evidence for the presence in solution of the disproportion equilibrium:

$$2[(R–COO)_2Cu(II)–Cu(I)(OOC–R)_2]^- \Leftrightarrow (R–COO)_4Cu_2(II) + [(RCOO)_4Cu(I)_2]^{2-}$$

It was possible to isolate the different components of the disproportionation equilibrium by varying temperature and solvent conditions. To our knowledge, this is the first non-electrochemical experimental evidence of this equilibrium for copper MV complexes in solution. Furthermore, as is discussed in the text, these results may be the basis for giving an alternative point of view to that given in some studies already reported in the literature, which relate to solvent and temperature effects on the intensity and energy of the intervalence transfer bands and also to changes in the EPR spectra of MV species. © 2000 Elsevier Science B.V. All rights reserved.

Keywords: Equilibrium; Copper; Mixed valence; Disproportionation; Temperature effects

1. Introduction

Mixed-valence (MV) compounds have attracted a great deal of interest from several research groups. Different aspects of the electron transfer dynamics between the metal centers have been explored, as well as the chemical and the electrochemical behavior of such species [1]. Although the disproportionation reaction had been used in the past as a synthetic method [2], it was only in 1983 that Creutz et al. [3] postulated that a dismutation equilibrium related to the MV $[M^{n+}–M^{(n+1)+}]$ system must always be present. Nevertheless, the experimental evidence for this equilibrium has been elusive and its existence was established essentially by electrochemical methods when the oxidation–reduction processes involved are reversible [4]. For several years our research group has been working in the field of binuclear Cu(II)–Cu(II), Cu(I)–Cu(I) and the related MV Cu(II)–Cu(I) complexes as bioinorganic models [5]. For some of these systems it was possible to obtain electrochemical evidence for the disproportionation equilibrium [5c,6]. Continuing with this research, experiments were carried out in order to obtain single crystals to determine the X-ray crystal structure for copper carboxylate MV species. In this paper we report and discuss the results of such experiments which, although unsuccessful in obtaining the desired single crystals,

* Corresponding author. Tel.: +56-2-678-7367.
E-mail address: icrivelli@abello.dic.uchile.cl (I.G. Crivelli).

0277-5387/00/$ - see front matter © 2000 Elsevier Science B.V. All rights reserved.
PII: S0277-5387(00)00491-5

provide direct experimental evidence that in the solution of the MV complex the following disproportionation equilibrium (1) is present:

$$2[(R–COO)_2Cu(II)–Cu(I)(OOC–R)_2]^- \Leftrightarrow (R–COO)_4Cu_2(II) + [(R–COO)_4Cu(I)_2]^{2-} \quad (1)$$

with ($R = CH_3$, Ph). To our knowledge, this is the first direct experimental non-electrochemical evidence for the existence of the disproportionation equilibrium for copper MV complexes in solution, and the shifts of such equilibrium when the system is externally perturbed. As will be discussed in the text, these results may be the basis for giving an alternative point of view to that given in some studies already reported in the literature, which relate to solvent and temperature effects on MV compounds.

2. Experimental

2.1. Reagents

All chemicals and solvents were analytical grade and used without further purification. Argon was used to provide an inert atmosphere and also for degassing solutions. For the freezing experiments, the solutions contained in a sealed tube under argon were frozen either with liquid nitrogen or in different cold temperature mixtures.

2.2. Physical measurements

UV–Vis spectra were recorded on a Milton Roy Spectronic 3000 Diode Array and on a Varian DMS 90 spectrophotometer and the EPR spectra in the x band (9.85 GHz) on a Bruker ECS 106 spectrometer using a rectangular cavity with a 50 kHz field modulation.

2.3. Synthesis

The MV $[(R–COO)_2Cu(II)–Cu(I)(OOC–R)_2]^-$ complex with $R = CH_3$ was generated photochemically from the Cu(II)–Cu(II) parent species in a nonaqueous solution by irradiation with UV-light in a stoppered cell [5a]. The MV species with R = Ph was obtained by mixing stoichiometric quantities of $[Cu(CH_3CN)_4]ClO_4$ and $[Cu(II)(BF_4)_2]\cdot nH_2O$ (Aldrich) in a benzoic acid–sodium benzoate buffer using methanol as solvent, under an inert atmosphere [6]. The crystallization of the MV species was tried by three different methods: (1) cooling the solution at different temperatures, (2) concentrating the solution by slow vacuum evaporation of the solvent and (3) adding, after evaporation, solvents of different polarities. Only method (2) succeeded in producing single crystals.

2.4. Crystal structure determination

Data were collected with a Siemens R3m/V 4 circle diffractometer. All calculations were performed with the Siemens SHELXTL-PLUS system of programs (PC version) [7].

3. Results

As mentioned in Section 2, three methods were used in order to obtain crystals of the MV species. The results of these are the following:

3.1. Temperature effects

Fig. 1 shows the UV–Vis spectrum of the violet MV $[(CH_3–COO)_2Cu(II)–Cu(I)(OOC–CH_3)_2]^-$ complex in 95/5% (v/v) methanol–acetic acid solution, at room

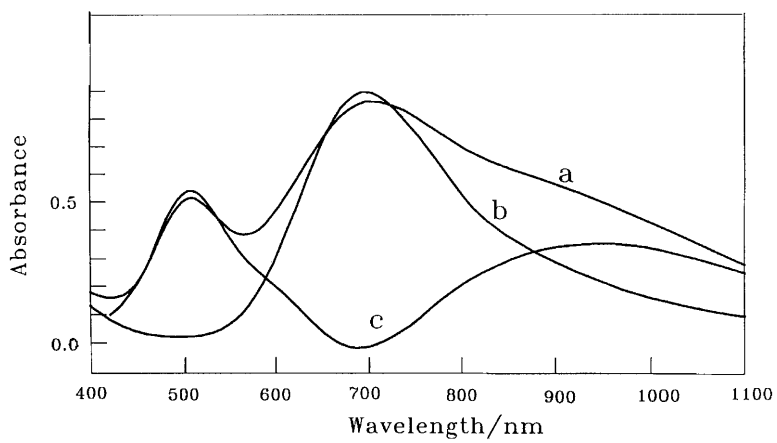


Fig. 1. UV–Vis and near IR spectra in 95/5% (v/v) methanol–acetic acid mixture as solvent for: (a) $[(CH_3–COO)_2Cu(II)–Cu(I)(OOC–CH_3)_2]^-$ MV complex generated by direct irradiation under inert atmosphere of the fully oxidized $[(CH_3–COO)_2Cu(II)–Cu(II)(OOC–CH_3)_2]$ complex whose spectrum is shown in b. (b) Non-degassed solution of $[(CH_3COO)_2Cu(II)–Cu(II)(OOC–CH_3)_2]$. (c) Differential spectrum of solution a in regard to b [5a].

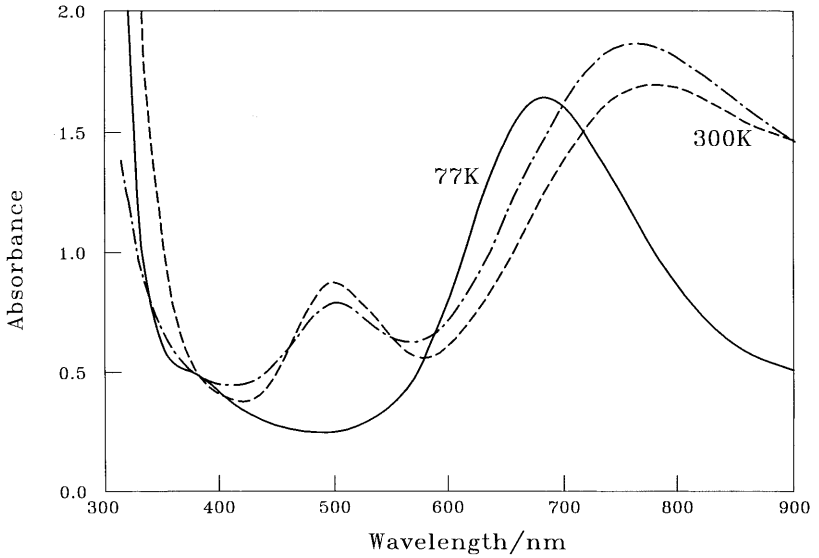


Fig. 2. Temperature effect on the UV–Vis spectra of the $[(C_6H_5–COO)_2Cu(II)–Cu(I)(OOC–C_6H_5)_2]^-$ MV complex in 4:1 ethanol–methanol solution, under inert atmosphere. (---) 300 K; (—) the same solution cooled to 77 K; (-·-·-) the same solution warmed up again to 300 K.

temperature (curve a). The spectrum for the corresponding fully oxidized $[(CH_3–COO)_2Cu(II)–Cu(II)(OOC–CH_3)_2]$ complex is also depicted (curve b). Finally, the differential spectrum (a minus b) is shown in curve c, exhibiting its two intervalence transfer (IT) bands at 508 and 960 nm [5a]. A clear temperature effect was observed for these intervalence bands: by lowering the temperature, the intensity of the IT bands decreases but, as the temperature is raised, the IT bands show up again in the spectrum. The EPR spectra also change with temperature: at room temperature, a seven-line pattern was observed, but at low temperature (77 K), the spectra mainly showed the four lines characteristic of the Cu(II) species.

The spectral pattern and behavior is maintained by other carboxylates, (e.g. R = Ph) with only slight changes in the position of the maxima. Specifically, Fig. 2 shows the changes with temperature of the UV–Vis spectrum of $[(C_6H_5–COO)_2Cu(II)–Cu(I)(OOC–C_6H_5)_2]^-$. As temperature decreases the intensity of the IT bands also decreases, disappearing completely at 77 K. No solid product is observed. At the same time, the color of the solution turns to the characteristic green color of the fully oxidized Cu(II)–Cu(II) compound. One additional experimental observation was made when the samples were taken out of the cooling media: although the solution was warmed by the surroundings, the intensity of its violet color continued to decrease. After a few minutes, the intensity started to rise and when room temperature was acquired, the IT bands at 508 and 1100 nm reappear — although with a slight intensity loss — and the solution showed the characteristic violet color. The process of losing and recovering the bands and the violet color of the solution by temperature changes is the same for both (R = CH_3 and Ph) MV species and can be repeated for several cycles.

3.2. Concentration effects

When the methanol solution of $[(C_6H_5–COO)_2Cu(II)–Cu(I)(OOC–C_6H_5)_2]^-$ was concentrated by solvent evaporation under nitrogen, calypso crystals were obtained. These crystals were isolated under strict anaerobic conditions. The X-ray crystal structure was determined (Fig. 3). It turned out to be exactly the same as that previously reported for the fully oxidized $[(C_6H_5–COO)_2Cu(II)–Cu(II)(OOC–C_6H_5)_2]$ complex [5b,8].

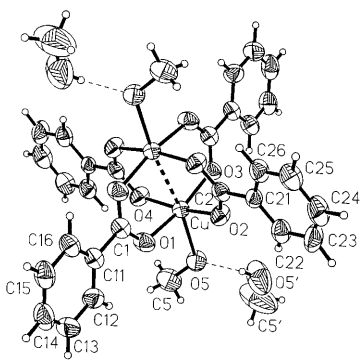


Fig. 3. Molecular structure of the crystals obtained by solvent evaporation of a solution of the $[(C_6H_5–COO)_2Cu(II)–Cu(I)(OOC–C_6H_5)_2]^-$ MV complex in equilibrium with $[(CH_3COO)_2Cu(II)–Cu(II)(OOC–CH_3)_2]$ and $[(CH_3COO)_2Cu(I)–Cu(I)(OOC–CH_3)_2]^{2-}$, as described in Eq. (1). Methanol as solvent, inert atmosphere.

3.3. Solvent polarity effects

When dichloromethane was added to the already concentrated methanolic solution of the R = Ph MV species (before any precipitation), a white solid was obtained; the white precipitate changes to a bluish-green color when exposed to air. On the other hand, when tetrahydrofurane was added, the violet color of the solution became more intense and the spectra showed an important concentration of the MV species

4. Discussion

As previously reported [5a,b] MV complexes of the type $[(R–COO)_2Cu(II)–Cu(I)(OOC–R)_2]^-$ have typical intervalence transfer bands in the 508–512 and 960–1100 nm ranges. The behavior observed in Fig. 2 may be understood in two ways: (1) as the temperature effect on the intensity of the IT band, or (2) as the dependence of the MV species concentration on temperature. Although there are many studies on the change of the energy of IT bands with either changes in temperature or in solvent [9], this is not the case for the IT band intensity dependence on temperature. Reports on this case are scarce. Nevertheless, considering that the IT band is a metal to metal charge transfer band (MMCT) results on temperature effects upon CT bands in general might be relevant. Worl and Meyer [10] reported experiments about temperature and pressure effects on the energy of the charge transfer (CT) $d_\pi \rightarrow \pi^*$ (bpy) band of the $[(bpy)Re(CO)_3Cl]$ complex in a 4:1 (v/v) ethanol–methanol mixture. Figure 1a therein reported, shows an increase in the intensity of the band when lowering the temperature from 298 to 100 K. The authors did not make a special reference to this point. However, according to this result, an inverse tendency to that observed in Fig. 2 should be expected for our system, i.e. the intensity should increase as the temperature is lowered. This seems to rule out the first interpretation given above, and therefore the results would suggest the dependence of the MV concentration on temperature. Taking into account: (a) that the concentration of the MV species is sensitive to changes in temperature, moving back and forth according to it and (b) some of the experimental details described, such as how the absorbance of the MV species in solution continues to decrease after the cooling process has ended — indicating that the system requires some time to adapt to the new conditions — shows that the possibility of an equilibrium in solution changing the concentration of the MV species should be considered. Furthermore, the solvent effect observed for the benzoate system (point 3 of Section 3) may be understood if the equilibrium is a disproportionation equilibrium as shown in Eq. (1). In this case, simple arguments as the charge differences of the three species present in solution, allows us to interpret the experimental results in the solvent polarity effects experiment as follows:

(a) In a polar solvent the uncharged Cu(II)–Cu(II) complex precipitates since the crystal X-ray structure of this solid coincides exactly with that previously reported for the $[(C_6H_5–COO)_2Cu(II)–Cu(II)-(OOC–C_6H_5)_2]$ complex [5b,8]. Thus, the equilibrium of Eq. (1) appears displaced to the right and therefore the IT band intensity decreases.

(b) The same effect (displacement of the equilibrium to the right (Eq. (1))) can be observed in nonpolar solvents, but in this case it is the higher charged complex $[(R–COO)_4Cu(I)]^{2-}$, which precipitates as a white solid.

(c) On the other hand, in a solvent of intermediate polarity such as THF, the $[(R–COO)_2Cu(II)–Cu(I)-(OOC–R)_2]^-$ species formation is favored and enhances its concentration, as shown by the increase in the intensity of the IT band. It was not possible to obtain crystals of the species under the experimental conditions used.

In a similar way, all the spectral changes observed for the MV systems described in this work, may be explained as a shifting of the disproportionation equilibrium and the dependence of the corresponding equilibrium constant, K_d, on temperature. But, taking into account that non-macrocyclic copper complexes, as the copper carboxylates, give several simultaneous equilibria in solution, the disproportionation equilibrium (Eq. (1)) may not be the only equilibrium present in solution. This situation made the evaluation of the K_d constant and its quantitative dependence with temperature and solvent more difficult.

Therefore, alternative suggestions for the experimental facts observed were tried in order to see if a different satisfactory explanation, other than the presence of the disproportionation equilibrium, could emerge.

(a) It is known that the binuclear acetate and benzoate complexes show monomer–dimer equilibrium, which has been taken into account in previous studies of these systems [5a]. On this basis, it could be possible to consider that the dimerization equilibrium — and not the disproportionation equilibrium — is governing the behavior of the system. The system could then be described by the simultaneous presence of the dimerization equilibrium (2):

$$2Cu(II) \Leftrightarrow Cu(II)–Cu(II) \quad (2)$$

(ligands omitted, for simplicity)

governed by $K_{dim}(T)$, and the Cu(II)–Cu(I) species (see Ref. [11] for the concentration values). When temperature decreases, $K_{dim}(T)$ also decreases [12], lowering the concentration of Cu(II)–Cu(II) and en-

hancing the monomeric Cu(II) concentration. However, this analysis cannot explain the disappearance of the Cu(II)–Cu(I) species at low temperature (77 K), nor can it explain its reappearance when the temperature is taken back to room temperature. The necessity of an additional equilibrium relating the Cu(II)–Cu(II) and Cu(II)–Cu(I) species makes itself evident.

(b) It is also possible to consider that the MV species is in equilibrium with the Cu(II) and Cu(I) monomer species:

$$\text{Cu(II)–Cu(I)} \Leftrightarrow \text{Cu(II)} + \text{Cu(I)} \quad (3)$$

The equilibrium would tend to the right when the temperature is lowered, therefore increasing the Cu(II) concentration, and eventually the Cu(II)–Cu(II) concentration. If this is the case, there is no reason to believe that the equilibrium

$$2\text{Cu(I)} \Leftrightarrow \text{Cu(I)–Cu(I)} \quad (4)$$

does not exist. Consequently, the following equilibria would be present in solution:

$$\text{Cu(II)–Cu(I)} \Leftrightarrow \text{Cu(II)} + \text{Cu(I)}$$

$$2\text{Cu(I)} \Leftrightarrow \text{Cu(I)–Cu(I)}$$

$$2\text{Cu(II)} \Leftrightarrow \text{Cu(II)–Cu(II)}$$

that — as a whole — are equivalent to the disproportionation equilibrium.

As an additional argument to this line of analysis, it should be taken into account that the Cu(II)–Cu(II) and Cu(I)–Cu(I) species were crushed out of the solution without lowering the temperature, and therefore these species should also be present at room temperature at some concentration.

From the preceding analysis, it can be concluded that it is not possible to explain the experimental behavior observed without considering the disproportionation equilibrium:

$$2[(\text{R–COO})_2\text{Cu(II)–Cu(I)(OOC–R)}_2]^- \Leftrightarrow (\text{R–COO})_4\text{Cu}_2\text{(II)} + [(\text{R–COO})_4\text{Cu(I)}_2]^{2-}$$

Other equilibria might also be present; however, they do not explain by themselves the main experimental evidence observed.

As an additional point, it should also be mentioned that the disproportionation equilibrium was taken into account to interpret the redox behavior of the $[(\text{CH}_3\text{–COO})_2\text{Cu(II)–Cu(I)(OOC–CH}_3)_2]^-$ and the Cu–mercaptoethylammine (Cu–MEA) systems previously reported [5c,13]. In these studies, and also in the electrochemical studies of the benzoate system [6], evidence for the following irreversible reaction for the Cu(I)–Cu(I) species was given:

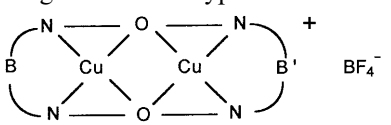
$$\text{Cu(I)–Cu(I)} \Rightarrow \text{Cu}^0 + \text{Cu(II)}$$

This reaction could be responsible for the slight degree of irreversibility in completely recovering the intensity of the IT bands.

Finally, we want to call attention to the fact that the disproportionation equilibrium could also be used to explain, from another point of view, some EPR and spectroscopic results reported previously in the literature. In the following text, this will be applied to specific cases:

(1) Sigwart et al. [14] reported the change with temperature of the EPR spectrum of a copper–carboxylate MV species: at room temperature a seven-line pattern was observed indicating that the electron is equally delocalized on both coppers. At 77 K the EPR spectra shows a large number of lines. The authors indicated 'that this spectra probably represents contributions from both the mixed-valence complex and a Cu(II) species, since the complex tends to dissociate at temperatures below -50°C'. Nevertheless, as was shown for our systems, both EPR spectra can also be adequately interpreted if we have in mind the presence of the disproportionation equilibrium and the temperature effect on K_d. In fact, at room temperature the K_d value makes the delocalized Cu(II)–Cu(I) species predominant as detected by EPR (seven line spectrum); at low temperature, the disproportionation equilibrium shifts the Cu(II)–Cu(II) and Cu(I)–Cu(I) species (K_d (RT) < K_d (77 K)) to higher concentrations so the EPR spectra shows the simultaneous presence of the Cu(II)–Cu(II) binuclear species (four line EPR pattern) and the Cu(II)–Cu(I) MV species (seven line EPR spectra), since the Cu(I)–Cu(I) species is EPR silent. This interpretation is highly possible since in a previous paper [5a] it was shown that the structure of the Sigwart compound should be very similar to the binuclear $[(\text{R–COO})_2\text{Cu(II)–Cu(I)(OOC–R)}_2]^-$ complex reported in this work. The fact that the dimeric species remain in solution at 77 K is indicated by the presence of the 370 nm band (assigned to the binuclear species [15]) at this temperature (Fig. 2).

(2) Long and Hendrickson [16] report a series of seven MV binuclear Cu(II)–Cu(I) complexes with macrocyclic ligands of the type:



with substituents indicated as B and B′. Among the results, the authors report that the EPR spectra of four of the MV species studied changes from a seven line pattern at room temperature to a four line pattern in frozen solution, manifesting in the presence of an equilibrium in solution. Although the conproportionation constants K_c ($1/K_d$) for the species were determined electrochemically, the analysis of the results was made by the authors exclusively in terms of the localized–de-

localized character of the MV species: a delocalized Cu MV complex (room temperature) has a seven line spectra, while a localized Cu MV complex (frozen solution) shows only four lines corresponding to Cu(II). Nevertheless, the same changes could be interpreted as a direct consequence of the temperature effect on the disproportionation equilibrium. From this point of view, the equilibrium should shift so that at low temperature the main species in solution are the Cu(I)–Cu(I) EPR-silent derivative and the four-line Cu(II)–Cu(II) species, while at room temperature the main species would be the delocalized MV Cu(II)–Cu(I) complex, according to the seven-line pattern observed.

Other results in Long and Hendrickson's paper can also be explained if the conproportionation equilibrium is taken into account; for example, for the quite similar complexes **I** (with $B = B' =$ propylene) and **II** (with $B = B' =$ 2,2-dimethylpropylene), the electronic spectra show the same λ_{max}, but the authors report that the ε values are different, being greater for **I** than for **II**. Nevertheless, if we take into account that K_c is 4.3×10^6 for **I** and 3.7×0^6 for **II**, at the same analytical concentration, the actual concentration of the corresponding MV species is higher for **I**, resulting in an apparently higher extinction coefficient. Therefore, this difference could just be an artifact. Finally, although in the paper additional comparisons are made, considering others of the seven species studied, it is difficult to analyze them in detail since the systems compared might have more significant structural changes.

(3) The same type of analysis can be made for the complex $[(NH_3)_5Ru^{III}–NC–Fe^{II}(CN)_5]^-$ [9b]. The authors analyzed the changes in the energy of the IT band (E_{op}) with temperature, but the system also shows changes in the absorbance intensity, (we assume that the analytical concentration of the MV species is the same). The fact that in this case the intensity I of the intervalence band also increases as the temperature increases is particularly important. In fact, $I \alpha T$, which is again not expected if the absorbance change is taken as an effect of the temperature on the intensity of a charge transfer band. It would be interesting to analyze the effect on these intensity changes in different solvents in which the system was studied, but the authors did not make a special mention of this point, because their study was focussed on the E_{op} versus T changes.

5. Conclusions

1. The results reported in this work show that the MV $[(R–COO)_2Cu(II)–Cu(I)(OOC–R)_2]^-$ species in solution are in equilibrium with the corresponding Cu(II)–Cu(II) and Cu(I)–Cu(I) parent species, giving a direct non-electrochemical experimental evidence of the presence of the disproportionation equilibrium. The experimental behavior cannot be interpreted if this type of equilibrium is not taken into account. The equilibrium can be altered by external perturbations, such as temperature changes.
2. An inverse relation between the MV species concentration and temperature exists. Since the monomer–dimer equilibrium — that may also be present — is an exothermic process, the disproportionation equilibrium could be exothermic or endothermic. This dependence on temperature, in a certain sense, is an impedance to obtaining crystals of the MV species by temperature effects.
3. The disproportionation equilibrium accounts not only for the effect of the temperature on the intensity and energy of the IT bands, but also for the changes in the EPR spectra of the MV species with temperature, as was discussed in the text.
4. The disproportionation equilibrium should also be taken into account when the effect of the temperature on the energy of the IT band is studied. Changes in the concentration of the species will change the band intensity and therefore can distort the changes in λ_{max}, particularly when the IT transfer band overlaps to some extent with the absorption bands of other complexes present in the equilibrium.

Acknowledgements

Support from Fondecyt (Grant 0643/89 and 0831/92), University of Chile (DTI-Q3066–9223), Catholic University of Temuco (DICT 92–3-06) and P. Catholic University of Chile (Grant 206/86) are gratefully acknowledged.

References

[1] K. Prassides (Ed.), Mixed Valency Systems: Applications in Chemistry, Physics and Biology, Kluwer, Dordrecht, 1991.
[2] T.J. Meyer, Ann. NY Acad. Sci. 313 (1978) 496.
[3] C. Creutz, Prog. Inorg. Chem. 30 (1983) 1.
[4] (a) C.A. Gagne, C.A. Koval, T.J. Smith, M.C. Cimolino, J. Am. Chem. Soc. 101 (1979) 4571. (b) F. Callahan, R. Keene, T.J. Meyer, D. Salmon, J. Am. Chem. Soc. 99 (1977) 1064.
[5] (a) I. Crivelli, C. Andrade, Inorg. Chim. Acta 203 (1993) 115. (b) B. Loeb, I. Crivelli, C. Andrade, Comm. Inorg. Chem. 20 (1998) 1, and references therein. (c) B. Loeb, I. Crivelli, C. Andrade, Inorg. Chim. Acta 231 (1995) 21.
[6] (a) A. Francois, MSc. in Chemistry Dissertation, Universidad de Chile, 1985. (b) A.M. Haberland, Chemistry Licentiate Thesis, P. Universidad Católica de Chile, 1992.
[7] G.M. Sheldrick, SHELXTL-PLUS, release 4.2 for Siemens Crystallographic Research System, Siemens Analytical X-ray Instruments, Inc., Madison, WI, USA, 1990.

[8] I. Brouche-Wakman, C. Bois, G.A. Popovich, L. L'Haridon, Bull. Soc. Chim. Fr. (1980) 1.
[9] (a). M.J. Powers, R.W. Callahan, D.J. Salmon, T.J. Meyer, Inorg. Chem. 15 (1976) 1457. (b) Y. Dong, J.T. Hupp, Inorg. Chem. 31 (1992) 3322. (c) T.J. Hupp, I. Dong, J. Am. Chem. Soc. 115 (1993) 6428. (d) G.A. Neyhart, C.J. Timpson, W.D. Bates, T.J. Meyer, J. Am. Chem. Soc. 118 (1996) 3730.
[10] L.A. Worl, T.J. Meyer, Chem. Phys. Lett. 143 (1988) 541.
[11] Experimentally, the MV complex was obtained in a 1.3×10^{-3} M concentration by irradiation of a 2.3×10^{-3} M solution of the Cu(II)–Cu(II) species; some Cu^0 solid was also formed [5a]. When oxygen was allowed to oxidize the solution, a concentration of 2.1×10^{-3} M for $[Cu]_{total}$ (expressed as dimer) and 1.7×10^{-3} M for the dimer, (determined from the absorbance at $\lambda = 700$ nm, where monomer and dimer absorb, and 370 nm where only dimer absorbs) was obtained [5a]. The concentration of the species in solution (if the disproportionation equilibrium is not taken into account) would then be 1.3×10^{-3} M, 4.8×10^{-4} M and 6.4×10^{-4} M for the MV, Cu(II) dimer, and Cu(II) monomer species, respectively.
[12] (a) J.K. Kochi, R.V. Subramanian, Inorg. Chem. 4 (1965) 1527. (b) I. Crivelli et al., unpublished results.
[13] I. Toledo, M. Arancibia, C. Andrade, I. Crivelli, Polyhedron 17 (1998) 174.
[14] C. Sigwart, P. Hemmerich, P. Spence, Inorg. Chem. 7 (1968) 2545.
[15] (a) P.K. Hansen, C.J. Ballhausen, Trans. Faraday Soc. 61 (1965) 631. (b) P.K. Ross, M.D. Allendorf, E.I. Solomon, J. Am. Chem. Soc. 111 (1989) 4009.
[16] R.C. Long, D.N. Hendrickson, J. Am. Chem. Soc. 105 (1983) 1513.

PERGAMON

www.elsevier.nl/locate/poly

Polyhedron 19 (2000) 2297–2302

POLYHEDRON

Influence of L-type ligands on the relative stability and interconversion of *cis–trans*-$[Ru(phen)_2L_2]^{n+}$ type complexes. A theoretical study

J. Concepción, B. Loeb *, Y. Simón-Manso, F. Zuloaga*

Facultad de Química, Pontificia Universidad Católica de Chile, Casilla 306, Santiago, Chile

Received 1 October 1999; accepted 10 January 2000

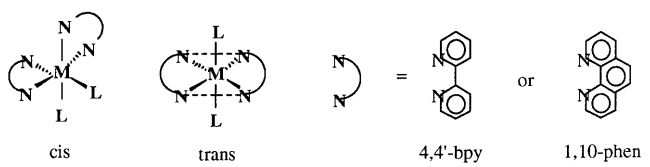
Abstract

Polipyridine complexes of type $[Ru(N\text{-}N)_2L_2]^{2+}$ are useful for the conversion of light into usable energy for which the *trans* geometry would be preferable. In this paper, the effect of distortion on *trans* structure stability was studied theoretically. A formal separation of the contributions was carried out, and it explained why the hydrogen repulsions are an important factor. A study of the main aspects related to the *cis–trans* isomers and also their mutual interconversion was analyzed. Calculations were carried out at the PM3, ZINDO and ab initio level. Energy differences between *trans* and *cis* isomers after full geometry optimizations for different L-ligands show a dependence on the L-ligand Jörgensen field strength parameter *f*. A driving coordinate was performed in order to determine the kinetic preferences for isomer formation. The analysis showed that the entrance of the second phenanthroline is favoured for the *cis* geometry in regard to the *trans* geometry. The activation barrier is also dependent on the L-ligand strength. The thermal *trans–cis* interconversion seems to be very improbable adiabatically (considering only one potential energy surface). © 2000 Elsevier Science B.V. All rights reserved.

Keywords: Ruthenium; Phenanthroline; *Cis–trans*; MO calculations; Barriers; Field strength

1. Introduction

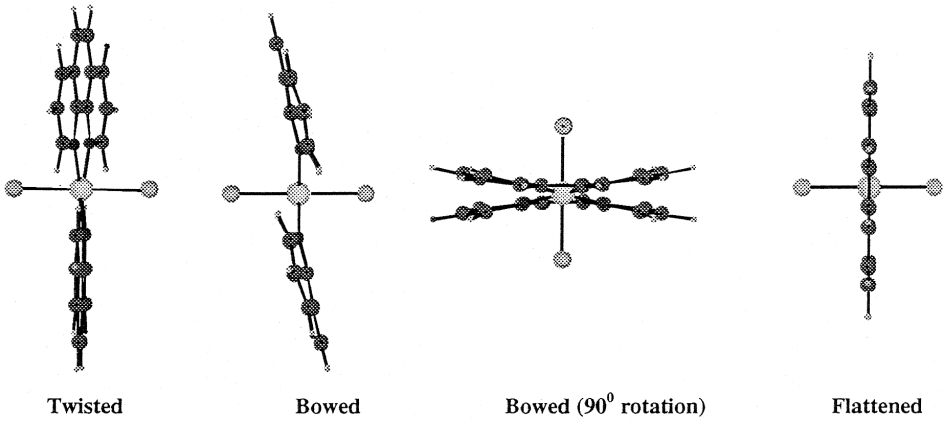
Ruthenium polypyridyl complexes of the type $[Ru(N\text{-}N)_2L_1L_2]^{n+}$ (N-N = 2,2′-bipyridine, 1,10-phenanthroline; L_1 and L_2 other ligands) have been widely studied in search of potential solar energy conversion systems [1]. Most of the work reported up until now is related to complexes having *cis* geometry, in spite of the fact that to exploit charge- and energy-transfer phenomena to their greatest effect, the *trans* geometry is more suitable [2]. Thus, the reported experimental work shows that there is a preferential formation for the *cis* isomer, and the interconversion to the *trans* isomer appears difficult to achieve.



Regarding the *trans* complexes, a significant distortion of the coordination sphere in the N_4 equatorial plane is generally observed. Two main types of distortion have been found experimentally [2c,3–6]: the twisted and the bowed configurations, as shown in Scheme 1 [3]. In the twisted configuration, each N-N ligand is planar, but twisted out of the equatorial plane of the octahedrically coordinated metal. In the bowed geometry the octahedral coordination is maintained but each N-N ligand is bent (for example non-planar bpy's) and the equatorial plane is distorted in such a way as to minimize the opposing hydrogen interactions [7]. A third geometry, called the tilt configuration, has also been reported [7] and it can be visualized as a special case of the bowed configuration where the degree of distortion of the equatorial N-N ligands changes from a minimum value (tilt configuration) to higher values of distortion (bowed configuration) depending upon the axial L_1, L_2 ligands. To our knowledge, there is no ruthenium $[Ru(N\text{-}N)_2L_1L_2]^{n+}$ type complex reported in a flattened configuration, presumably because it is not a ground state geometry.

* Corresponding authors. Tel.: +56-2-686-4404; fax: +56-2-686-4744; e-mail: bloeb@puc.cl; fzuloaga@puc.cl.

0277-5387/00/$ - see front matter © 2000 Elsevier Science B.V. All rights reserved.
PII: S0277-5387(00)00492-7



Scheme 1.

For a long time the higher stability of the *cis* isomer with respect to the *trans* isomer for $[Ru(phen)_2L_2]^{2+}$ type complexes has been explained by invoking α-hydrogen steric interactions [2]. Thus, the strong tendency of the *trans* complex to isomerize to the *cis* form is related to this kind of interaction [2b].

In this paper the *cis–trans* problem in $[Ru(N\text{-}N)_2L_2]^{2+}$ (N-N = 1,10-phen) is theoretically explored in order to deduce conditions that experimentally favour the *trans* isomer formation. Several aspects like the origin of the distortion in the equatorial N_4 plane for *trans* complexes, the relative stability of one isomer over the other, and the *cis–trans* interconversion process among them are considered.

2. Computational methods

Geometry optimization of *cis* and *trans* isomers of $[Ru(phen)_2L_2]^{2+}$ type complexes were performed by using PM3(tm) semi-empirical methods as implemented in the SPARTAN package [8a]. Moreover, equilibrium geometries were checked for some cases by means of DFT ab initio calculations [8b] and by comparison with crystallographic data, when available. Hartree Fock (HF) ab initio, DFT and Gaussian calculations were used to calculate total energies. The HYPERCHEM package [8c] was also used for spectroscopic and electronic structure calculations. Total energy differences between complexes with different L ligands were also performed, allowing the comparison of the relative stability of isomers depending upon the strength of the ligand field. Finally, the *cis–trans* interconversion barrier was studied by investigating several possible models for this process.

3. Results and discussion

3.1. Distortion in the equatorial N_4 plane in *trans*-$[Ru(phen)_2L_2]^{n+}$ complexes

The potential energy surface for *trans* complexes of type $[Ru(phen)_2L_2]^{2+}$ was explored. Starting from different initial geometries, the optimization procedures led to the two experimentally observed distorted geometries (twisted and bowed) shown in Scheme 1, as well as to the absolutely planar (flattened) configuration. The latter is not a ground state geometry but a transition state (with only one imaginary vibrational frequency) and it should correspond to a connecting path among both distorted structures mentioned above. The bowed configuration is more stable than the twisted one in most cases, although the energy difference between both ground state minima is rather small. For example, for $L = Cl^-$ the total HF/3-21G* energy is -6465.39484 a.u. for the bowed geometry, and -6465.38620 a.u. for the twisted geometry, whereas for the transition state flattened geometry the total energy achieved corresponds to -6465.38084 a.u. These figures show that the bowed conformation is

Table 1
Activation barriers (kcal mol^{-1}) for several distortion effects on the equatorial plane in *trans*-$[Ru(phen)_2L_2]^{2+}$

Complex	Activation barriers (flattened – bowed)		
	DFT	PM3	RHF/3-21G*//PM3
$[Ru(phen)_2L_2]^{2+}$			
$L = NH_3$	7.686	1.213	4.201
$L = NH_2OH$	4.890	1.470	4.708
$L = F^-$	10.635	2.964	9.600
$L = Cl^-$	10.146	2.829	8.782
$[Ru(phen)_2]^{2+}$	11.163	4.519	6.955
[(phen)$_2$]	5.779	4.092	4.526

5.4 kcal mol^{-1} more stable than the twisted geometry and that the energy barrier from bowed to twisted amounts to 8.8 kcal mol^{-1}. Thus, the interconversion process is easy to achieve, at least in the gaseous phase.

Results for the energy barrier for a series of ligands such as NH_3, NH_2OH, Cl^- and F^- are given in Table 1. Different calculation methods (DFT, PM3, etc.) were employed. Independent of the method used, the tendency is that higher energy barrier values are obtained for axial ligands as $L = F^-$ or Cl^- in reference to NH_3 or its derivatives. This shows that the energy barrier values for the interconversion process from bowed to twisted depend strongly on the nature of the ligand L. It is important to point out that although the PM3(tm) results yield lower barrier values than ab initio DFT or HF/3-21G* calculations, they follow the same trend and seem appropriate to discuss experimental effects on this matter for larger complex structures.

Several factors can be responsible for the preference of the *trans* complexes to adopt a distorted geometry. The already invoked repulsion of the neighboring hydrogens in opposite phenanthrolines is one of them. The interaction between this same type of hydrogen and the axial ligands should also be considered, as well as a possible contribution of the metal. In this sense, the interconversion barrier can be considered as a thermodynamic sum of different factors, as pictured in Fig. 1. In order to evaluate these contributions additional calculations were carried out, as described below.

The geometries of the *trans* $[Ru(phen)_2L_2]^{2+}$ complexes for all L ligands were optimized in the distorted and totally flattened configurations. Next, in the optimized structures of both geometries, the L ligands were omitted and the geometry of the $[Ru(phen)_2]^{2+}$ residue optimized. Finally, the Ru metal was omitted, obtaining the $[(phen)_2]$ moiety. A single point energy calculation was carried out for this last residue. The results obtained for $[Ru(phen)_2]^{2+}$ and $[(phen)_2]$ are also included in Table 1. The latter represents the contribution of the α hydrogens repulsion to the barrier, ΔE_{HH}, while the difference between the $[Ru(phen)_2]^{2+}$ barrier and $[(phen)_2]$ barrier represents the metal contribution to it, ΔE_M. These contributions are the same for all complexes, and, for example, in HF-3-21G* they correspond to 4.5 and 2.4 kcal mol^{-1}, respectively. Finally, the L axial ligand contributions, ΔE_L, were determined as $[Ru(phen)_2L_2]^{2+}$-$[Ru(phen)_2]^{2+}$, and the results tabulated in Table 2. From HF/3-21G* results, it can be seen that axial amino ligands play the role of lowering the energy barrier between both ground state distorted geometries, whereas halide ligands have the opposite effect in reference to the $[Ru(phen)_2]^{2+}$ intermediate. Moreover, DFT and semi-empirical PM3(tm) calculations also predict a similar effect. When analyzing the central metal atom effect one finds that the influence of ruthenium(II) is to increase the energy barrier in reference to the $[(phen)_2]$ entity, although this time PM3 results do not assign any important role to it in comparison to the other ab initio methods. Clearly PM3 underestimates this metal atom effect and DFT methods seem to overestimate it. Finally, it should be pointed out that although the ΔE_{HH} contribution to the barrier is important its order of magnitude does not greatly exceed the other contributions, therefore this factor seems to have been overestimated in the literature.

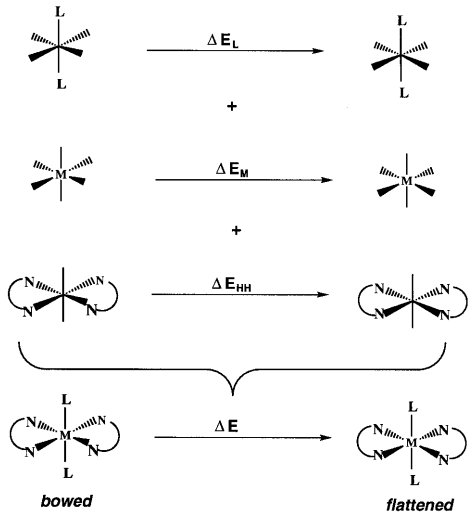


Fig. 1. Main factors that control the bowed → flattened thermodynamic interconversion barrier. ΔE_{HH}: α-hydrogen repulsion energy contribution; ΔE_L: L-ligands energy contribution; ΔE_M: metal energy contribution.

3.2. Relative stability of cis- and trans-$[Ru(phen)_2L_2]^{n+}$ complexes: energetic analysis

The total energy difference between the more stable of the *trans* configurations (bowed), and the corresponding *cis*, ΔE *trans–cis*, was calculated. ΔE *trans–cis* shows a dependence on the L ligand field strength, as can be seen in Fig. 2(a), where ΔE *trans–cis* is plotted against Jorgensen's *f* ligand field parameter [9]. In spite of the apparent data dispersion, a clear tendency is observed. A plot for a series of selected ligands (F^-, Cl^-, Br^- and I^-) is shown in Fig. 2(b). The linear curve fit gives a good correlation coefficient in this case ($R = 0.98$). The *f* value for I^- was estimated from theoretical considerations [10].[1] Noteworthy, for this ligand, the trans isomer is the more stable one.

Therefore, it can be concluded that although the *cis* isomer is generally more stable (as observed experimentally), weaker ligand fields tend to diminish the energy difference between both isomers. To get a deeper insight into the energetic and electronic reasons for this

[1] From density functional theory it is possible to obtain a relationship between the Jorgensen parameter and the Parr–Pearson indexes. Simón-Manso et al., manuscript in preparation.

Table 2
Axial ligands contribution ΔE_L (kcal mol^{-1}) to distortion, and total distortion energy HF [3-21G*] for *trans*-$[Ru(phen)_2L_2]^{2+}$ type complexes

Axial ligand	ΔE_L	ΔE [3-21G*] [a]
$L = NH_3$	−2.754	4.201
$L = NH_2OH$	−2.247	4.708
$L = F^-$	2.645	9.600
$L = Cl^-$	1.827	8.782

[a] $\Delta E = \Delta E_{HH} + \Delta E_M + \Delta E_L$; $\Delta E_{HH} = 4.526$ kcal mol^{-1}; $\Delta E_M = 2.429$ kcal mol^{-1}.

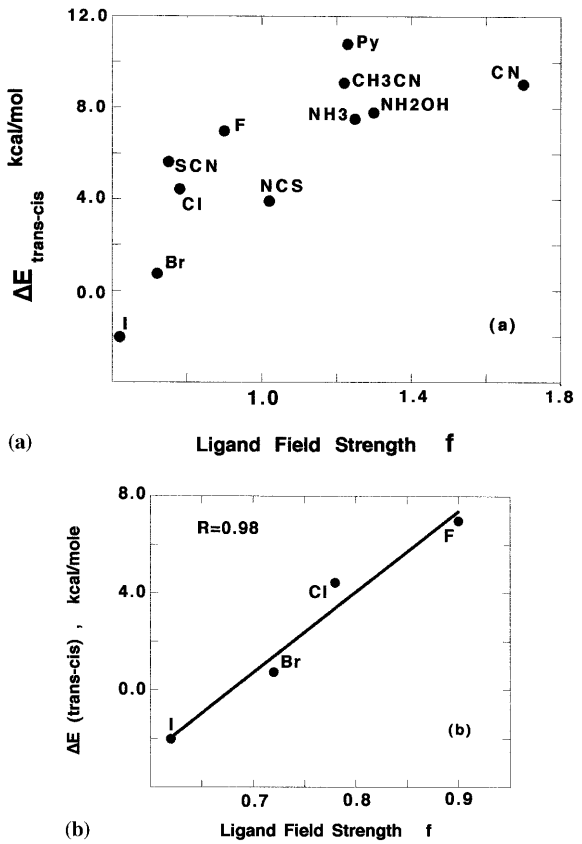


Fig. 2. Dependence of ΔE *cis–trans* on the L-ligand strength for $[Ru(phen)_2L_2]$ complexes. (a): Assorted type ligands; (b): halide series.

preference, a complex with a weak ligand such as F^- was chosen. Since experimentally the most probable situation is one in which the phen ligand coordinates to Ru in a successive way, a ZINDO/S MO diagram was built considering $Ru(phen)F_2$ and (phen) as the original fragments to build the *cis* and *trans* $[Ru(phen)_2F_2]$ complexes. The molecular orbital diagram for the frontier orbitals of Fig. 3 shows that the 'donor' phen requires a smaller energy gap for the charge transfer process when confronted with the *cis* fragment 'acceptor'. The difference in energy gap between the HOMO(phen) and LUMO$[Ru(phen)F_2]$ for the *cis* and *trans* complex formation amounts to ~ 5.1 kcal mol^{-1} in favor of the *cis* final complex molecule.

ZINDO/S calculations were also performed at CI level, using approximately 700 configurations to reproduce the experimental electronic spectra of $[Ru(phen)_3]^{2+}$, *cis*-$[Ru(phen)_2(CH_3CN)_2]^{2+}$ and *trans*-$[Ru(phen)_2(CH_3CN)_2]^{2+}$. The results are shown in Table 3. The correlation between experimental and calculated data is satisfactory, especially in the case of metal to ligand charge transfer (MLCT) bands, where solvent effects can affect the position of the band.

3.3. Preferential formation of one isomer over the other: kinetic barrier

A first approach to estimate barriers for the formation of the two isomers was by a dissociative mechanism. Starting from the optimized geometry for *trans*- and *cis*-$[Ru(phen)_2(CH_3CN)_2]^{2+}$ complexes, a coordinate driving of the distance from ruthenium to one of the N atoms of one phenanthroline was performed. The initial point was the equilibrium Ru–N distance and the last one a value of 5.3 Å, with eight steps. The geometry of each step was fully optimized. This is equivalent to the barrier that generates when a phen ligand approaches a $[Ru(phen)(CH_3CN)_2]^{2+}$ moiety. The resulting potential energy coordinate diagram is shown in Fig. 4. It can be seen that the barrier to form the *trans* isomer is considerably higher than the one to form the *cis*. Also, it is observed that the maximum appears at about 4.4 Å in both cases, indicating that barriers are mainly electrostatic in character.

In another approach, a thermal twisting mechanism was considered to estimate barrier for interconversion between isomers. Starting from the optimized geometry for the *trans* complex, successive rotations around a 'bond' between ruthenium and a centroid formed by the two N atoms of the phenanthroline and one of the L axial ligands were performed. In each rotation, the dihedral angle between the N–N vectors of both

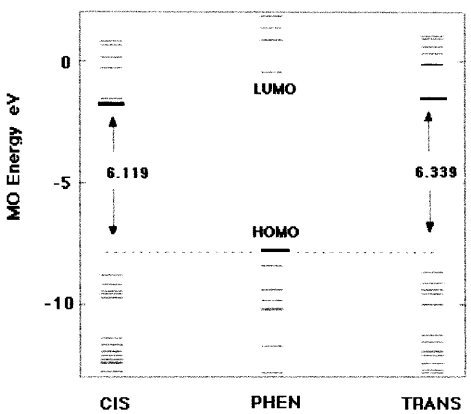


Fig. 3. MO diagram for the phen and $[Ru(phen)F_2]$ fragments responsible for the formation of the *cis*- and *trans*-$[Ru(phen)_2F_2]$ complexes.

Table 3
Calculated [a] absorption spectra of $[Ru(phen)_2L_2]^{2+}$

Calculated (gas phase) [b]			Experimental (CH_3CN)		
Energy (cm^{-1})	OS	Assignment	Energy (cm^{-1})	log ε	Assignment
$[Ru(phen)_3]^{2+}$					
23 789	0.102	MLCT	22 422	4.30	MLCT [11]
23 794	0.100				
24 358	0.073				
33 272	0.158	MLCT	not observed		
33 277	0.160				
34 200	0.305				
37 206	0.119	π–π*	38 168	5.10	
37 218	0.121				
cis-$[Ru(phen)_2(ACN)_2]^{2+}$					
23 947	0.088	MLCT	23 810	3.9	MLCT [7]
25 967	0.079	MLCT	26 110	4.0	
34 066	0.486	π–π*	38 314	4.8	
35 799	0.375				
trans-$[Ru(phen)_2(ACN)_2]^{2+}$					
24 057	0.234	MLCT	22 624	4.0	MLCT [7]
29 303	0.213	MLCT	not observed		
33 323	0.291				
35 650	0.587	π–π*	38 023	4.8	
36 838	0.177				

[a] Zindo/s method parametrized for the Ru atom (eV) as follows: $\gamma_{ss} = 7.744$, $\gamma_{sd} = 10.44$, $\gamma_{dd} = 11.60$, $\beta_s = \beta_p = -2.0$, $\beta_d = -13.0$.
[b] OS, oscillator strength.

phenanthrolines was fixed and the geometries fully optimized. After a rotation in 120° the *cis* isomer was obtained. Although some information could be extracted, this type of rotation seems difficult to observe experimentally because dissociative tendencies are present in the intermediate steps. We considered in this route a purely thermal mechanism, but photochemical routes involving triplet excited states appear to be more appropriate for this [12].

It is interesting to note that the preference of a second phenanthroline to enter in *cis* rather than in *trans* position can be analyzed by making use of the hard and soft acid and base principle [13,7]. The use of the principle that locally 'soft likes soft' and 'hard likes hard' can give an insight to determine the specific sites at which the interaction between two chemical species is going to occur. In our case, it should help to determine if the second phen will enter in a *cis* or *trans* position. Thus, we want to find hardness values at the equatorial bond sites occupied by acetonitrile molecules and also at similar sites along axial bonds.

Ab initio calculations using HF/3-21G* were carried out for $[Ru(phen)(CH_3CN)_4]^{2+}$ and phen to build the hardness map [14] encoded into the molecular electronegativity value for the above complex and for phen. The results are given in Fig. 5 for the donor (less electronegative) phen molecule and for the acceptor (more electronegative) Ru complex. The method used is described elsewhere [13]. Briefly, two possibilities exist for this reaction, one of which is a *cis* substitution and the other a *trans* substitutions of two acetonitrile solvent molecules by the bidentate phen molecule. The isosurface is the molecular electrostatic potential at the molecular electronegativity value, which is the same at any region of the molecule after electronegativity equalization. Now the change in electronegativity against a change in electron number, that is, the hardness, has

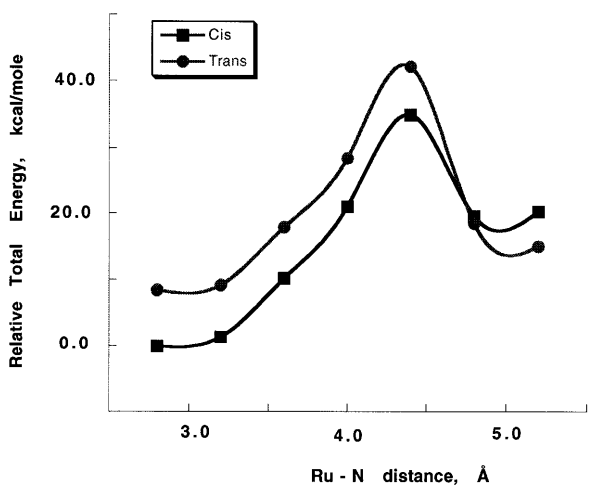


Fig. 4. Kinetic barrier for the formation of *cis*- and *trans*-$[Ru(phen)_2(CH_3CN)_2]^{2+}$ complexes from $[Ru(phen)(CH_3CN)_2]^{2+}$ and phenanthroline. Total energy values are relative to the lowest total energy value ($-120\ 826.9$ kcal mol^{-1}) used in the figure.

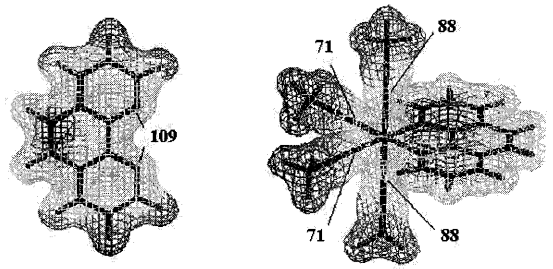


Fig. 5. Local hardness values (kcal mol^{-1}) for $[Ru(phen)(CH_3CN)_4]^{2+}$ and phenanthroline.

been encoded over that surface, yielding different values for it according to the molecule response to a given attack. Moreover, the HSAB principle states that the donor phen species (with a hardness value of 109 kcal mol^{-1} at N centers) is more willing to perform a nucleophilic attack over any of the axial sites of the acceptor Ru complex, at which the hardness value is 88 kcal mol^{-1}, forcing *cis* coordination by replacing acetonitrile molecules, one from the axial position and another from the equatorial position.

4. Conclusions

The results for the energetic analysis suggest that the thermodynamic difference between the *cis* and *trans* isomers is not sufficiently pronounced to justify the definite experimental preference to form the *cis* isomer. The kinetic factor is definitely more determinant. Thus, once a *trans* complex is formed it should be thermally stable. A good strategy to synthesize new *trans* complexes could be by derivatization of other known stable *trans* complexes.

Acknowledgements

Fondecyt support through Projects 8980007 (Líneas Complementarias) and 2970080 (Y.S.) is gratefully acknowledged. We thank Dr Alberto Vela for his comments and help on the ab initio calculations.

References

[1] (a) V. Balzani, F. Scandola, Supramolecular Photochemistry, Ellis Horwood, New York, 1990. (b) T.J. Meyer, Acc. Chem. Res. 22 (1989) 163. (c) Md.A. Masood, B.P. Sullivan, D.J. Hodgson, Inorg. Chem. 33 (1994) 4611.
[2] (a) B. Durham, S.R. Wilson, D.J. Hodgson, T.J. Meyer, J. Am. Chem. Soc. 102 (1980) 600. (b) J.L. Walsh, B. Durham, Inorg. Chem. 21 (1982) 329. (c) B.J. Coe, T.J. Meyer, P.S. White, Inorg. Chem. 32 (1993) 4012.
[3] J.L. Walsh, B. Durham, Inorg. Chem. 21 (1982) 329.
[4] B. Durham, S.R. Wilson, D.J. Hodgson, T.J. Meyer, J. Am. Chem. Soc. 102 (1980) 600.
[5] A.W. Cordes, B. Durham, P.N. Sweptson, W.T. Pennington, S.M. Condren, R. Jensen, J.L. Walsh, J. Coord. Chem. 11 (1982) 251.
[6] (a) R. Kroener, M.J. Heeg, E. Deutsch, Inorg. Chem. 27 (1988) 558. (b) H. Nagao, H. Nishimura, H. Funato, Y. Ichikawa, F.S. Howell, M. Mukaida, H. Kakihana, Inorg. Chem. 28 (1989) 3955. (c) T. Togano, H. Kuroda, N. Nagao, H. Maekawa, H. Nishimura, F.S. Howell, M. Mukaida, Inorg. Chim. Acta 196 (1992) 57.
[7] P. Bonneson, J.L. Walsh, W.T. Pennington, A.W. Cordes, B. Durham, Inorg. Chem. 22 (1983) 1761.
[8] (a) SPARTAN, version 5.1, Wavefunction Inc., 18401 Von Karman Ave. Suite 370, Irvine, CA 92612, USA, 1997. (b) Calculations were carried in the non-local approximation with the Becke's hybrid method HF exchange and LYP correlation, so-called B3LYP, using a pseudo potential for the metal. (c) HYPERCHEM, version 5.1, Hypercube Inc., 1115 N.W. 4th Street, Gainsville, FL 32601, USA, 1998.
[9] (a) C.K. Jorgensen, Absorption Spectra and Chemical Bonding, Pergamon, Oxford, 1962. (b) D. Sutton, Espectros electrónicos en los complejos de metales de transición, Editorial Reverté, Spain, 1975.
[10] R.G. Parr, R.G. Pearson, J. Am. Chem. Soc. 105 (1983) 7512.
[11] A.B.P. Lever, Inorganic Electronic Spectroscopy, Elsevier, Amsterdam, 1984.
[12] J. Concepción, B. Leob, Y. Simón-Manso, F. Zuloaga, to be submitted.
[13] R.G. Pearson, Acc. Chem. Res. 26 (1993) 250 and references therein.
[14] R. López, B. Loeb, D. Boys, F. Zuloaga, J. Chem. Soc., Perkin Trans. 2 (1998) 877.

PERGAMON

www.elsevier.nl/locate/poly

Polyhedron 19 (2000) 2303–2312

POLYHEDRON

Spectroelectrochemical and electrical characterization of poly(cobalt–tetraaminophthalocyanine)-modified electrodes: electrocatalytic oxidation of hydrazine

Ejnar Trollund [a], Pilar Ardiles [a], María J. Aguirre [a,*], Sonia R. Biaggio [b], Romeu C. Rocha-Filho [b]

[a] *Departamento de Química de los Materiales, Facultad de Química y Biología, Universidad de Santiago de Chile, Casilla 40, Correo 33, Santiago, Chile*

[b] *Departamento de Química, Universidade Federal de Sao Carlos, C.P. 676, 13560-970 Sao Carlos, SP, Brazil*

Received 1 October 1999; accepted 20 January 2000

Abstract

Polymeric complex films of cobalt–tetraaminophthalocyanine (Co–TAPc) and tetraaminophthalocyanine without the metallic center (H_2–TAPc) were grown potentiodynamically on either glassy-carbon or conducting-glass electrodes. The electrolyte used in the electropolymerization was a 0.1 M tetrabutylammonium perchlorate–DMF solution containing the monomer. The modified electrodes were characterized by UV–Vis spectroscopy, voltammetry and electrochemical impedance spectroscopy. The role of the Co(II) center and the performance of these polymeric electrodes as electrocatalysts for hydrazine oxidation in aqueous solutions of pH 13 are discussed. The results indicated that Co(II) is the species acting as the electronic receptor of hydrazine, thus enhancing the electrocatalytic effect of the poly(Co–TAPc) electrode. This was also confirmed by the charge transfer resistance values from electrochemical impedance spectroscopy obtained during hydrazine oxidation, i.e. about 6×10^3 Ω on the poly (H_2–TAPc) electrode and about 500 Ω on the poly(Co–TAPc) electrode. © 2000 Elsevier Science B.V. All rights reserved.

Keywords: Polymeric metallophthalocyanines; Modified electrodes; Electrooxidation of hydrazine; Poly(cobalt–tetraaminophthalocyanine); Impedance spectroscopy

1. Introduction

Metallophthalocyanine-modified electrodes have been extensively studied due to their application as electrocatalysts for numerous reactions such as oxygen reduction [1–18] or oxidation of hydrazine [9,12,19–25] and thiols (e.g. cysteine [26–30] and mercaptoethanol [31–34]). However, sometimes these modified electrodes may be unstable in aqueous solutions at low pH, which hinders their use in electrocatalysis. On the other hand, there are studies showing that the polymerization of metallophthalocyanines enhances their stability as well as their catalytic activity [35–39]. The nature of the ring substituents is decisive for the polymerization process to succeed [40–44] as well as to modify the macrocycle activity [45]. Besides that, the polymer structure is dependent on its synthesis procedure, since it directly affects the polymer conductivity [36,42,43,46] and therefore, its activity as electrocatalyst for different substrates [36,37,47]. All these factors make the comprehension of electrocatalysis phenomena on electrodes modified by polymeric complexes difficult. However, the adsorption of these monomeric or polymeric complexes on different metallic surfaces leads to films of nearly similar properties [47], when they are prepared by the same experimental conditions; therefore, comparisons can be made, for instance, between the electrocatalytic properties of a graphite electrode and another electrode modified with some of these complexes. Based on this assumption, information on the electrocatalysis of non-transparent electrodes modified with the polymeric complex can be obtained through the analysis of UV–Vis spectra of transparent electrodes modified with the same complex [47].

* Corresponding author. Fax: +562-681-2108.
E-mail address: maguirre@lauca.usach.cl (M.J. Aguirre).

0277-5387/00/$ - see front matter © 2000 Elsevier Science B.V. All rights reserved.
PII: S0277-5387(00)00493-9

Phthalocyanines (Pc) have two allowed electronic transitions leading to two characteristic absorption bands in the UV–Vis spectrum: the Soret band, which appears at near-UV region (200–380 nm) and the Q band at 600–750 nm [48,49]. Both absorption bands correspond to π–π^* transitions (a_2u–eg and a_1u–eg, respectively) [48]. Besides that, during the reduction of phthalocyanines containing a first-series transition metal (Me–Pc), the first electronic transfer is related to the metallic center, and the second one to the ring [50]. As a result of the increase of charge density on the metallic center, another band, related to the metal–ligand charge transfer (CT band), appears between the Soret and Q bands [51,52]. In this paper, this charge transfer band is used to analyze the role of the transition metal on the electrooxidation of hydrazine catalyzed by poly(cobalt–tetraaminophthalocyanine)-modified glassy-carbon electrodes GC/poly(Co–TAPc). To do this, a series of electrochemical and spectroelectrochemical results are compared for GC/poly(Co–TAPc) and the glassy-carbon electrode modified with the polymer without cobalt, GC/poly(H_2–TAPc). In addition, some electric parameters of the modified electrodes as well as the kinetic nature of the electrooxidation of hydrazine taking place on their surface are explored using electrochemical impedance spectroscopy (EIS).

2. Experimental

Cobalt–tetraaminophthalocyanine (Co–TAPc), from MidCentury Co., was used without further purification. The ligand, TAPc, was synthesized using a modified procedure reported by Achar et al. [53,54]. The conducting transparent electrodes were prepared by SnO_2:F deposition on a glass sheet. The glassy-carbon electrodes, from Pine, had a working geometrical area of 0.19 cm^2 and were polished with 0.25-μm alumina before each experiment.

The electrosynthesis of both polymers (with and without Co) on either conducting-glass or glassy-carbon electrodes was performed by continuously cycling the electrode potential between -0.4 and 0.9 V (versus Ag/AgCl) at 100 mV s^{-1}, for 100 potentiodynamic cycles. The electrolyte used in the electropolymerization consisted of a 0.1 M tetrabutylammonium perchlorate–DMF solution containing the monomer: either Co–TAPc ($< 10^{-3}$ M, limited by saturation) or H_2–TAPc (10^{-3} M). The electrolyte was deaerated with nitrogen and kept at room temperature (r.t.). After the polymerization, the modified electrodes were rinsed with DMF, ethanol and then with twice-distilled water.

The electrochemical experiments were performed in a three-compartment glass cell, one for each of the electrodes: the working electrode, either glassy carbon (0.19 cm^2) or conducting glass (2 cm^2); the reference electrode, saturated Ag/AgCl; the counter electrode, a Pt coil (14 cm^2). On the other hand, the UV–Vis spectroelectrochemical experiments were performed in a one-compartment quartz cubette containing similar, but smaller, counter and reference electrodes.

All the characterizations (electrochemical and spectroscopic) of the previously grown poly(Co–TAPc) and poly(H_2–TAPc) were carried out in aqueous solutions of 0.1 M Na_2CO_3, 0.1 M $NaHCO_3$ and 0.1 M NaOH mixed at different proportions in order to attain the various pHs (8.2, 10 and 13), deaerated with pure N_2. The electrocatalysis of hydrazine oxidation was investigated using a 5×10^{-3} M hydrazine (hydrazinium sulfate, p.a. from Merck) solution in these aqueous electrolytes. The EIS measurements were carried out at potentiostatic conditions, at several potentials in the range -0.4 to 0.4 V. The frequency range extended from 5 mHz to 10 kHz and the ac potential perturbation was 10 mV (rms).

An AFCBP1 Pine bipotentiostat, along with PineChem 2.5 software, was used for the electropolymerization and to obtain data on the electrooxidation of hydrazine. A Varian Cary 1E Spectrometer, along with CaryWinUV software, and coupled to a Wenking POS 73 Potentioscan, was used to obtain the UV–Vis spectra. The electrochemical-impedance-spectroscopy (EIS) measurements were carried out with a PGSTAT20 Autolab/GPES potentiostat/galvanostat system from Eco Chemie, coupled to an Eco Chemie frequency response analyzer module.

3. Results and discussion

3.1. Spectroscopic characterization of poly(Co–TAPc) and poly(H_2–TAPc)

At open-circuit potential, the UV–Vis spectra of both polymers present the two characteristic absorption bands of phthalocyanines, the Soret and Q bands, as can be seen in Fig. 1. The wavelength at the maximum of the Soret band, λ_{max}, which appears at the near-UV region, could not be determined due to the nature of the transparent electrode employed. On the other hand, the Q band is clearly shown at λ in the range ca. 700 nm. The spectra A and B in Fig. 1 were taken from transparent-glass electrodes covered by a thin film of poly(Co–TAPc) and poly(H_2–TAPc), respectively, in aqueous solution of pH 8.2. These spectra did not show significant changes with the pH, in the analyzed range (8.2–13), at open circuit potential, E_{oc}. Nevertheless, as shown in Table 1, the E_{oc} values change as the modified-electrode/solution interface is modified with the pH.

The effect of applying negative potentials, with respect to E_{oc}, on the UV–Vis absorption bands of poly(Co–TAPc) and poly(H_2–TAPc) can be seen in Fig. 2. The more negative the potential applied on the glass/poly(Co–TAPc) electrode, the more evident becomes a new band at $\lambda = 400$–500 nm and two isosbestic points at 382 and 556 nm (Fig. 2(a)). This band, which appears between the Soret and Q bands, is reproducible for all the analyzed pH and can be attributed to the metal–ligand charge transfer transition (CT band), since its intensity is comparable with that of the Q band, which is a clear indication that this band is an allowed CT band and not a d–d band. Contrary to this, Fig. 2(b) shows that the shape of the spectrum of the glass/poly(H_2–TAPc) system is not affected by this potential variation. From the results of Fig. 2 one can infer that the CT band appearing at negative potentials on the glass/poly(Co–TAPc) electrode may correspond to the reduction of Co(II) to Co(I), with the transfer of one electron to the ligand TAPc. This would give rise to two species in equilibrium, i.e. Co(I)–TAPc⇔Co(II)–TAPc$^-$, related to the isosbestic points observed in the figure. Furthermore, Fig. 3 shows that no spectra modifications occur when positive potentials are applied on either electrode, except for a decrease of the intensity of the total spectrum. This decrease is probably caused by a structural change of the polymer due to the exit of cations from the bulk of the polymer in order to reestablish electroneutrality.

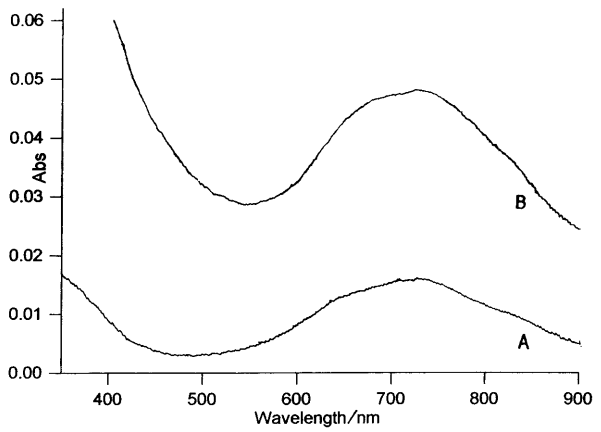


Fig. 1. UV–Vis spectra for the glass/poly(Co–TAPc) electrode (spectrum A) and for the glass/poly(H_2–TAPc) electrode (spectrum B) in aqueous solution (pH 8.2) saturated with N_2 at the open-circuit potential.

Table 1
Open-circuit potentials for poly(Co–TAPc) and poly(H_2–TAPc) on conducting glass modified electrodes, measured in aqueous solution saturated with N_2. (V vs. Ag/AgCl)

PH	E_{oc} (V)	
	poly(H_2–TAPc)	poly(Co–TAPc)
8.2	−0.092	0.014
10	−0.130	−0.012
13	−0.172	−0.071

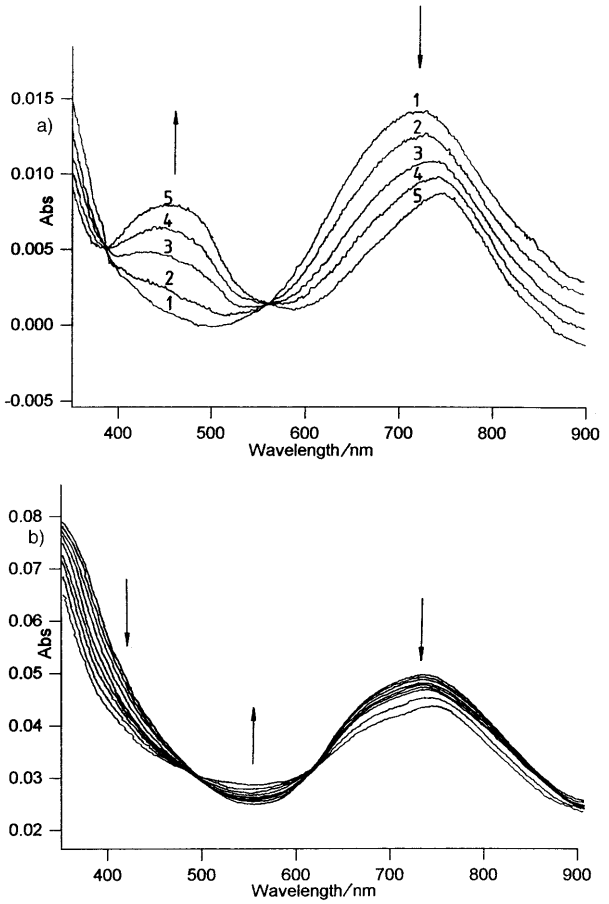


Fig. 2. (a) UV–Vis spectra for the glass/poly(Co–TAPc) electrode in aqueous solution (pH 8.2) saturated with N_2 at applied potentials increasingly more negative than the open-circuit potential: (1) 0.0 V, (2) −0.400 V, (3) −0.480 V, (4) −0.560 V and (5) −0.640 V versus Ag/AgCl. The arrows indicate the increase or the decrease of the intensity of the bands as the potential is made more negative. (b) Similar UV–Vis spectra for the glass/poly(H_2–TAPc) electrode: −0.040, −0.120, −0.200, −0.280, −0.360, −0.440, −0.520, −0.600 and −0.680 V versus Ag/AgCl.

3.2. Electrochemical characterization of poly(Co–TAPc) and poly(H_2–TAPc)

The voltammetric responses of both polymers previously electropolymerized on glassy carbon are shown in Fig. 4. Although the voltammetric profiles present the same redox peaks on either conducting glass or glassy carbon, the latter was preferred for the electrochemical analyses due to its smaller capacitive response and better peak current definition. By comparing voltammograms a and b in Fig. 4 one can attribute one of the redox peaks to the Co(II)/Co(I) couple in the complex polymer, ambiguously informed in the literature

[18,40,47,55]. Two couples, Ia/Ic and IIIa/IIIc, appearing for the modified electrodes either with or without Co, can be attributed to electron transfer processes in the ligand [18,40,47,55]. The IIa/IIc couple (at around -0.5 V) can be assigned to the metallic center Co(II)/Co(I), since it appears at a potential region where the charge-transfer band is also present (see Fig. 2(a)).

Both poly(Co–TAPc) and poly(H_2–TAPc) are stable when potentiodynamically synthesized on glassy carbon. In the pH range 8.2–13, the modified electrodes can be cycled in aqueous solutions without any change in their voltammetric profiles and the total charge involved. Fig. 4 also presents the stable i–E profile of both electrodes after several cycles (near 100) in the pH 13 electrolyte. The voltammograms obtained at pH 8.2 and 10 have the same features as the ones shown in this figure, though showing shifts of approximately 60 mV per pH unit for the peak potential values.

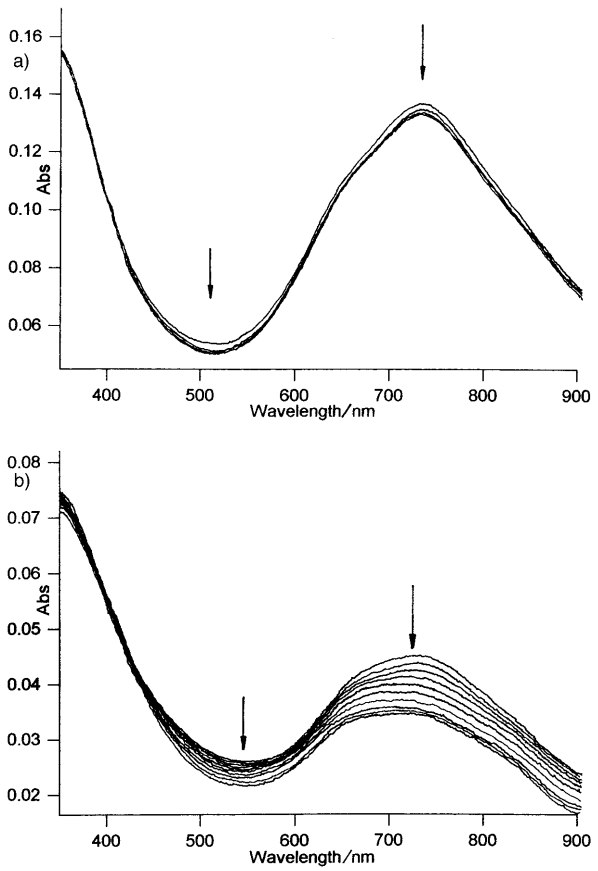


Fig. 3. (a) UV–Vis spectra for the glass/poly(Co–TAPc) electrode in aqueous solution (pH 8.2) saturated with N_2 at applied potentials increasingly more positive than the open-circuit potential (as indicated by the arrows): 0.230, 0.280, 0.360, 0.440 and 0.560 V versus Ag/AgCl. (b) Similar UV–Vis spectra for the glass/poly(H_2–TAPc) electrode: 0.114, 0.200, 0.280, 0.360, 0.440, 0.520, 0.600, 0.680, 0.760 and 0.800 V versus Ag/AgCl.

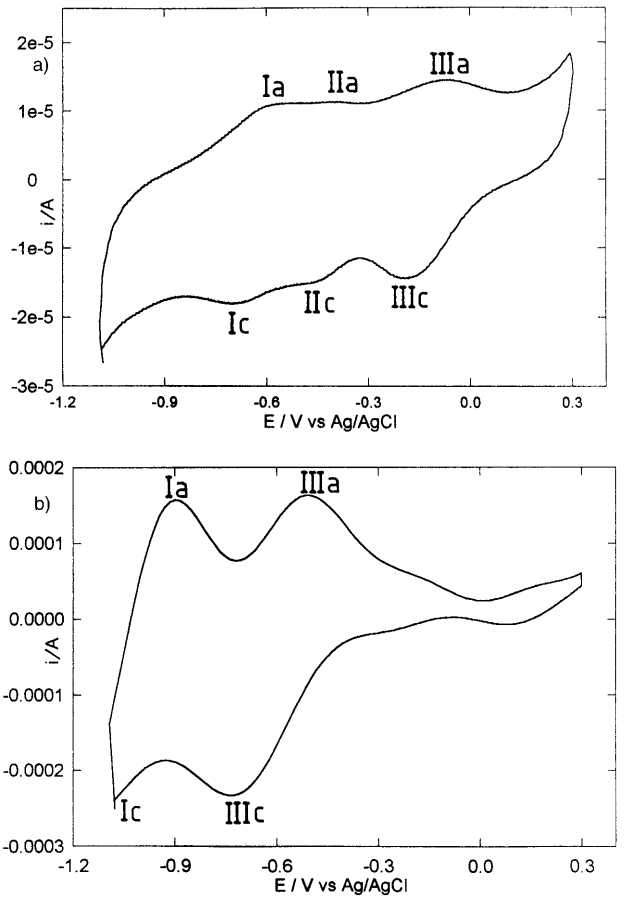


Fig. 4. (a) Cyclic voltammogram for GC/poly(Co–TAPc) electrode previously electrosynthesized by 100 continuous cycles between -0.400 and 0.90 V versus Ag/AgCl in 0.1 mol l^{-1} TBAP/DMF on a glassy-carbon electrode (GC). Sweep rate: 100 mV s^{-1}. Electrolyte: deaerated aqueous solution (pH 13). (b) Similar cyclic voltammogram for GC/poly(H_2–TAPc) electrode.

3.3. The role of the Co metallic center in the electrooxidation of hydrazine

The i–E responses for the electrooxidation of hydrazine on the GC/poly(Co–TAPc) and GC/poly(H_2–TAPc) electrodes are compared with the one on the blank electrode (bare glassy-carbon surface) in Fig. 5. The hydrazine oxidation is practically unnoted on the bare GC electrode, hardly noted on the poly(H_2–TAPc) electrode, but well noted on the poly(Co–TAPc) electrode. In the case of the poly(H_2–TAPc) electrode, the slight increase of the anodic current at potentials more positive than -0.3 V can be attributed to the catalytic oxidation of hydrazine by the ligand macrocycle. The poly(Co–TAPc) electrode clearly presents a strong electrocatalytic effect; furthermore, the onset of the oxidation process on this electrode occurs at smaller overpotentials. Though the oxidation was carried out under hydrodynamic conditions, N_2 generation on the poly(Co–TAPc) electrode at potentials more positive than -0.2 V is high enough to cause current oscilla-

tions and even the current decrease seen on the dotted curve in Fig. 5. The enhanced catalytic effect of the poly(Co–TAPc) electrode seems to be related to the metallic center, since the potential where the anodic current starts to increase coincides with the potential region of the Co(I)/Co(II) couple indicated in Fig. 4(a).

The spectroelectrochemical results for the oxidation of hydrazine on both the poly(Co–TAPc) and poly(H_2–TAPc) electrodes are shown in Figs. 6–8. Curve a in Fig. 6 shows a CT band even at open-circuit conditions (E_{oc} changes from -0.071 to -0.470 V when hydrazine is added to the electrolyte), indicating a charge transfer between hydrazine and the metallic center with the consequent reduction of Co(II) to Co(I). In the case of the poly(H_2–TAPc) electrode, the open-circuit potential also shows a significant change (from -0.172 to -0.385 V), but there is no change in its UV–Vis spectrum (see curve B of Fig. 6). In the case of poly(Co–TAPc) in the presence of hydrazine, as the potential is made more negative the CT band is increased and the Q band is decreased, while two isosbestic points become defined at 400 nm and 550 nm (Fig. 7(a)). On the other hand, these features are not present in the case of poly(H_2–TAPc), as can be seen in Fig. 7(b). In addition to this, Fig. 8 shows that for both electrodes there are no changes in the spectra as the potential is made more positive, except for an increase in the intensity of the bands in the whole spectra. However, this increase may be due to the accumulation of N_2 bubbles (product of hydrazine oxidation) at the polymer/solution interface, which leads to a change of the optical density of the system.

The results presented so far indicate that both polymers on glassy carbon catalyze the electro-oxidation of

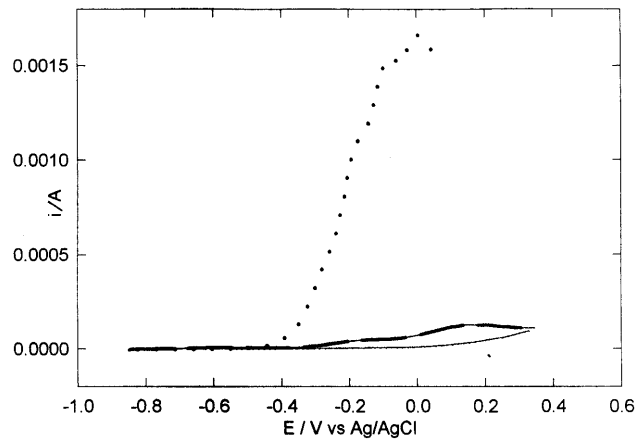


Fig. 5. Polarization curves for the electrodes of Fig. 4 and for a bare glassy-carbon (GC) electrode in the presence of 5 mmol l^{-1} hydrazine (same conditions as in Fig. 4). Potential sweep rate: 5 mV s^{-1}. Electrode rotation rate: 900 rpm. Doted line: GC/poly(Co–TAPc) electrode; hatched line: GC/poly(H_2–TAPc); continuous line: bare glassy-carbon electrode.

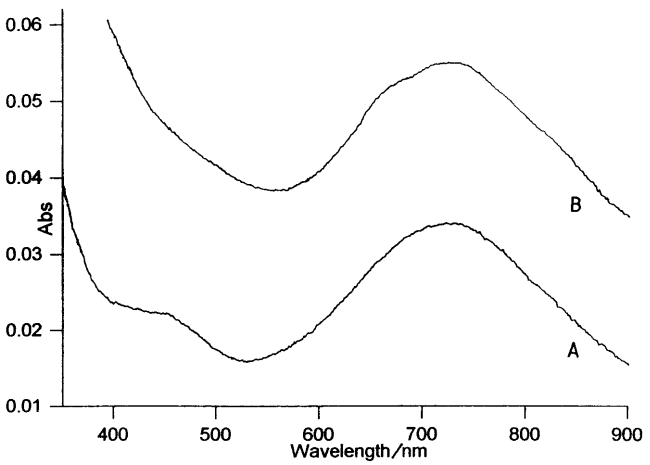


Fig. 6. UV–Vis spectra for the glass/poly(Co–TAPc) electrode (spectrum A) and for the glass/poly(H_2–TAPc) electrode (spectrum B) at the open-circuit potential in aqueous solution (pH 13) saturated with N_2 and containing 5 mmol l^{-1} hydrazine.

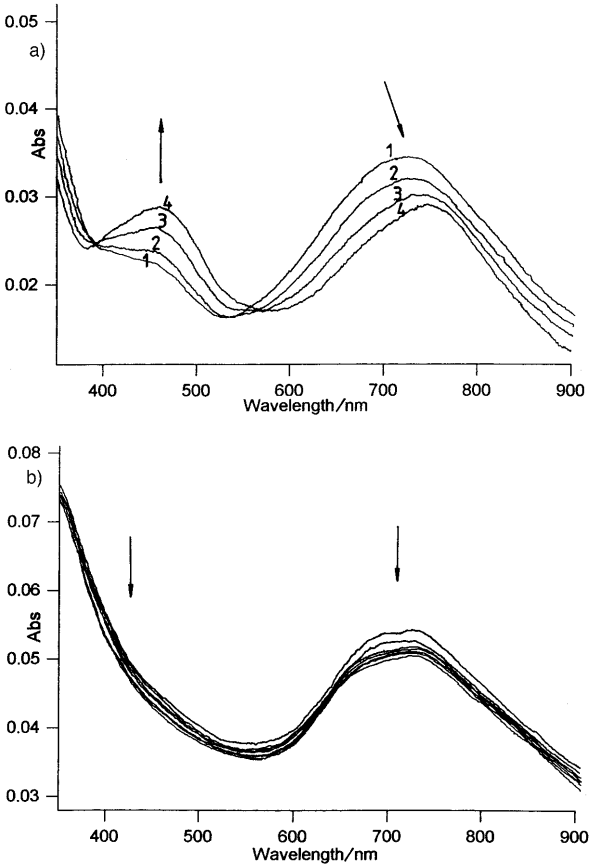


Fig. 7. (a) UV–Vis spectra for the glass/poly(Co–TAPc) electrode in aqueous solution (pH 13) containing 5 mmol l^{-1} hydrazine, saturated with N_2, at applied potentials increasingly more negative than the open-circuit potential: (1) -0.470 V, (2) -0.560 V, (3) -0.640 V and (4) -0.720 V versus Ag/AgCl. The arrows indicate the increase or the decrease of the intensity of the bands as the potential is made more negative. (b) Similar UV–Vis spectra for the glass/poly(H_2–TAPc) electrode: -0.400, -0.440, -0.480, -0.500, -0.560 and -0.600 V versus Ag/AgCl.

hydrazine in aqueous solutions. However, the polymer containing the Co center is a far more efficient electrocatalyst. One possible interpretation for this finding is that, even in the absence of applied potential (open-circuit conditions), hydrazine is able to transfer electronic charge to the polymer. If the polymer contains the metal, the charge receptor is the Co(II) center that reduces to Co(I), giving rise to the CT band. On the other hand, when the metal is absent in the polymeric matrix, hydrazine also transfers electronic charge to the ligand, but at a potential more positive than that for reducing the metal. Since the oxidation of hydrazine on poly(Co–TAPc) occurs at the potential region assigned to the Co(I)/Co(II) couple, it can be inferred that Co(II) is the species acting as the electronic receptor of hydrazine and enhancing the electrocatalytic effect of the poly(Co–TAPc) electrode. These ideas are supported by the E_{oc} changes for both polymers when hydrazine is added to the electrolyte, by the appearance of the CT band for poly(Co–TAPc) in contact with hydrazine, and by the two isosbestic points at negative potentials (related to the Co(I)–TAPc⇔Co(II)–TAPc$^-$ equilibrium).

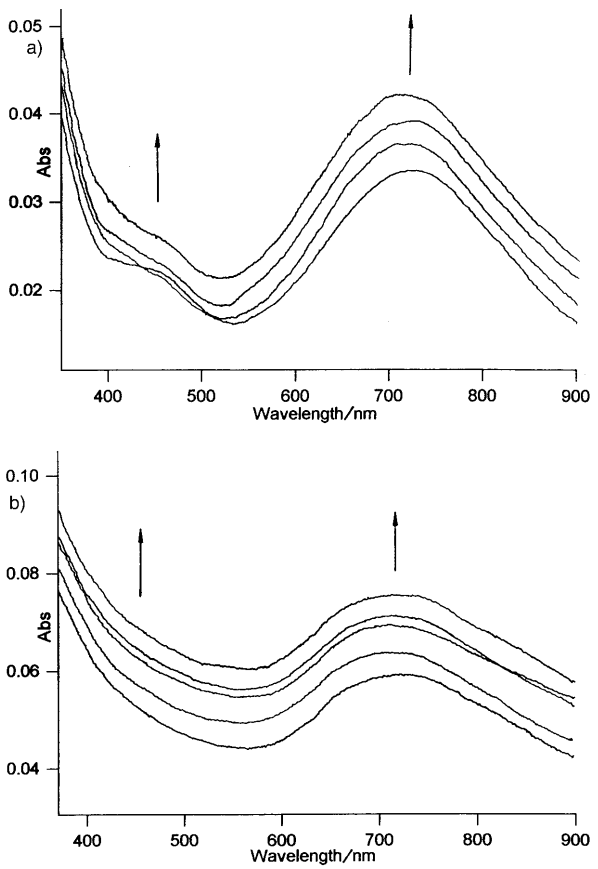


Fig. 8. (a) UV–Vis spectra for the glass/poly(Co–TAPc) electrode in aqueous solution (pH 13) containing 5 mmol l^{-1} hydrazine, saturated with N_2, at applied potentials increasingly more positive than the open-circuit potential (as indicated by the arrows): −0.120, 0.0, 0.040 and 0.160 V versus Ag/AgCl. (b) Similar UV–Vis spectra for the glass/poly(H_2–TAPc) electrode: −0.040, 0.100, 0.200, 0.300 and 0.400 V versus Ag/AgCl.

3.4. Electrical response of poly(Co–TAPc) and poly(H_2–TAPc) electrodes

Studies of the electrical properties of electrodes modified with macrocyclic molecules, using EIS, are not commonly found in the literature. Nevertheless, this technique is very useful to yield information on quantities such as the capacitance (C) or the charge transfer resistance (R_{ct}) of the electroactive interface, and to give additional information on the nature (activated charge transfer or diffusional control) of the electrocatalytic process under investigation. Data obtained from EIS measurements are usually presented in the form of complex–plane plots and Bode plots [56]. In the former, data of capacitive impedance ($Z_{imaginary}$) are plotted against the faradaic impedance (Z_{real}), while the latter is represented by plots of $\log|Z|$ versus $\log f$ or of phase angle versus $\log f$ ($|Z|$ is the impedance modulus and f the frequency).

Basically two approaches have been used to analyze impedance data of an electrode modified by a redox polymer: a kinetic model proposed by Gabrielli et al. [57], and another model proposed by Hunter et al. [58] stating that the charge transfer process occurring on an electroactive polymer phase reflects its interfacial properties and produces RC relaxation phenomena similar to those due to intercalation at an oxide/electrolyte interface. Both models lead to a physical interpretation for the impedance behavior of the modified electrode at different frequency regions:

(i) At high frequencies, one generally observes a charge transfer controlled process, defined by a semicircle in the complex–plane plot, whose characteristic time constant is related to the product of the charge transfer resistance (R_{ct}) and the double-layer capacitance of the polymer/solution interface (C_{dl}). The inverse of this quantity is the characteristic relaxation frequency for the process

$$\omega_{ct} = 1/(R_{ct}C_{dl}) \quad (1)$$

R_{ct} is determined from the semi-circle diameter [56].

(ii) At intermediate frequencies, diffusion of charge in the polymer film dominates the impedance spectrum; at this point, the complex–plane plot becomes linear with a slope of 45°. The frequency range where diffusional behavior may appear will depend on the film thickness and on the diffusion coefficient of the species.

(iii) At lower frequencies, the impedance is generally capacitive, i.e. the phase angle approaches 90°, reflecting the charge saturation set by the finite thickness of the polymer. In this case, a redox capacitance of the polymer, or low-frequency capacitance (C_{LF}) is

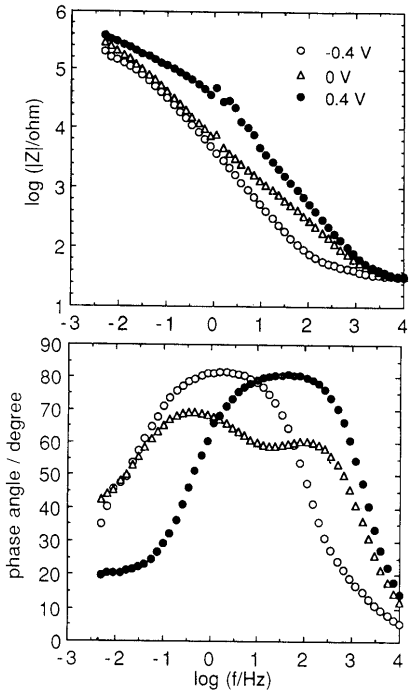


Fig. 9. Bode plots as a function of the applied potential for the GC/poly(Co–TAPc) electrode in aqueous solution (pH 13) saturated with N_2.

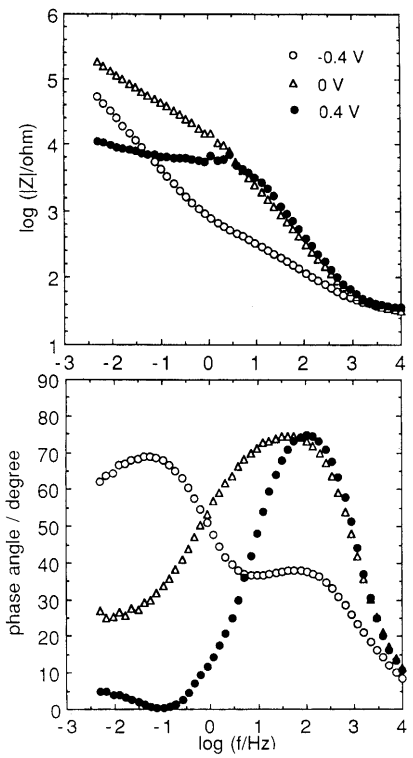


Fig. 10. Bode plots as a function of the applied potential for the GC/poly(H_2–TAPc) electrode in aqueous solution (pH 13) saturated with N_2.

defined. For very-thin films, the kinetic control region may overlap with the charge saturation and no diffusion region is defined. C_{LF} is proportional to the film thickness and to the total concentration of redox centers and can be obtained through [57,58]:

$$C_{LF} = 1/(2\pi f Z_{imag}) \quad (2)$$

A brief discussion of these models can be found elsewhere [59].

Impedance measurements were carried out for both poly(Co–TAPc) and poly(H_2–TAPc) electrodes immersed in the pH 13 electrolyte, containing hydrazine or not, at steady-state potentiostatic conditions. Figs. 9 and 10 show Bode plots for the polymeric electrodes in the electrolyte without any hydrazine, as a function of the applied potential. No charge saturation capacity can be seen in these spectra. The poly(Co–TAPc) electrode presents nearly capacitive behavior at -0.4 and 0.4 V, with a phase angle maximum of about 80° (lower part of Fig. 9). From the results of Fig. 9 (upper part), one can infer that the double-layer capacitance changes (from about 150 to about 15 μF cm^{-2}) when the oxidation state of the metallic center changes from Co(I) to Co(II); this can be attributed to a change in the polymer conformation with the potential, since Co(I) gives a less-distorted geometry for the complex macrocycle, thus leading to more redox sites at the polymer/electrolyte interface. On the other hand, the impedance results from Fig. 10 indicate that two relaxation processes with capacitive features appear for the polymeric electrode without Co center, at more negative potentials, which could be related to two different redox sites in the ring ligand.

EIS measurements for hydrazine oxidation on both electrodes were performed at -0.2 V (Figs. 11 and 12). This potential was chosen from the voltammograms of Fig. 5, where a net anodic catalytic current can be seen for both cases. The R_{ct} values for hydrazine oxidation on either electrode can be estimated from the plots

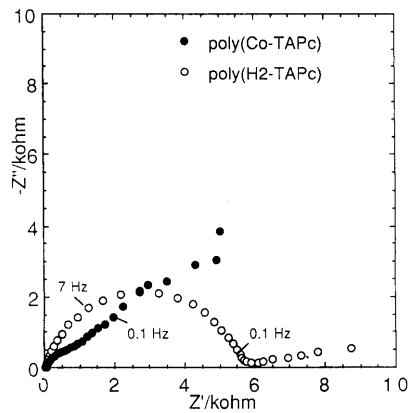


Fig. 11. Complex–plane plots at the applied potential of -0.2 V for the GC/poly(Co–TAPc) and the GC/poly(H_2–TAPc) electrodes in aqueous solution (pH 13) containing 5 mmol l^{-1} hydrazine, saturated with N_2.

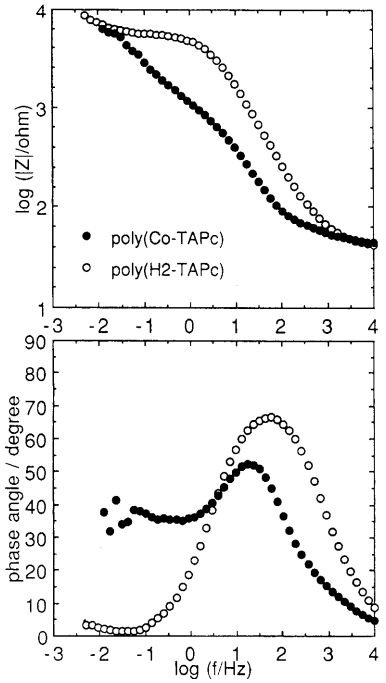


Fig. 12. Bode plots at the applied potential of −0.2 V for the GC/poly(Co–TAPc) and the GC/poly(H_2–TAPc) electrodes in aqueous solution (pH 13) containing 5 mmol l^{-1} hydrazine, saturated with N_2.

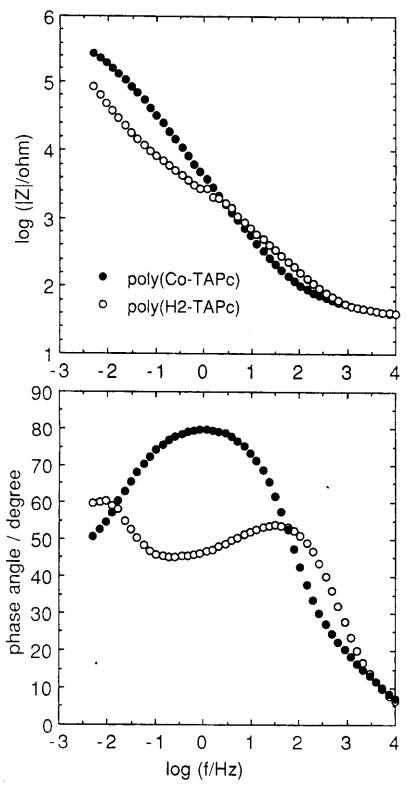


Fig. 13. Bode plots at the applied potential of −0.2 V for the GC/poly(Co–TAPc) and the GC/poly(H_2–TAPc) electrodes in aqueous solution (pH 13) saturated with N_2.

shown in Fig. 11, since both spectra present at the high-frequency region a semi-circle related to the faradaic process at the polymer/electrolyte interface. The R_{ct} value of about 500 Ω for hydrazine oxidation on poly(Co–TAPc) is much smaller than that on poly(H_2–TAPc) (about 6×10^3 Ω), confirming that the kinetic process is far more favored by the poly(Co–TAPc) material, as also indicated by the voltammetric results already presented. Furthermore, a diffusional feature can be seen in the low frequency range of Fig. 11, indicating that the thickness of these polymeric films, grown during 100 potentiodynamic cycles, is sufficient to set a diffusional regime of hydrazine species to the reaction centers. The scattering of the impedance data in the very-low-frequency limit on poly(Co–TAPc) is due to the formation of a considerable amount of the N_2 product on the electrode surface, giving rise to active area fluctuations and current instability.

Impedance studies on other redox-polymer electrodes, but in the absence of a reactant in the electrolyte, present values for R_{ct} of 100–500 Ω for glassy-carbon coated by [Ru(bpy)$_2$–poly(4′vinylpyridine)Cl]Cl [57], 300–2600 Ω for poly(vinylferrocene) on platinum [58] and 91 Ω for Ni(II)tetrakis(3-methoxy-4-hydroxyphenyl) porphyrin polymerized on glassy carbon [60].

Comparison of data obtained in the presence of hydrazine (Fig. 12) and in its absence (Fig. 13) shows that the presence of hydrazine in the electrolyte decreases the total impedance of the interface for both electrodes, but a higher effect can be noted for poly(Co–TAPc) electrode. Furthermore, the variation in the phase angle profile for the poly(H_2–TAPc) case, shown in Figs. 12 and 13 (below), from one well-defined capacitive relaxation process to two capacitive relaxation processes, is an indication that only one preferential redox site is active for hydrazine oxidation on this electrode.

4. Conclusions

The UV–Vis spectra of both poly(Co–TAPc) and poly(H_2–TAPc) retain the two characteristic absorption bands of phthalocyanines, the Soret and Q bands. When increasingly negative potentials (with respect to the open-circuit potential) are applied on the glass/poly(Co–TAPc) electrode, a new band becomes evident at $\lambda = 400$–500 nm and two isosbestic points develop at 382 nm and 556 nm. Considering that the spectrum of the glass/poly(H_2–TAPc) system is not affected by this potential variation, this band can be attributed to a metal–ligand charge transfer transition (CT band), i.e. to the reduction of Co(II) to Co(I), with the transfer of

one electron to the ligand TAPc, giving rise to two species in equilibrium, related to the isosbestic points observed: Co(I)–TAPc⇔Co(II)–TAPc$^-$. By comparing voltammograms for both systems, in the case of the glass/poly(Co–TAPc) electrode it was possible to clearly attribute one of the redox peaks (around -0.5 V) to the Co(II)/Co(I) couple in the complex polymer, since this peak appears at a potential region where the charge-transfer band is also present.

Although hydrazine oxidation was hardly noted on the poly(H_2–TAPc) electrode, it was well noted on the poly(Co–TAPc) electrode. This much enhanced catalytic effect of the poly(Co–TAPc) electrode seems to be related to the metallic center, since the potential where the anodic current starts to increase coincides with the potential region where the Co(I)/Co(II) couple was previously characterized. From the results obtained, it can be inferred that Co(II) is the species acting as the electronic receptor of hydrazine, thus enhancing the electrocatalytic effect of the poly(Co–TAPc) electrode. Furthermore, hydrazine was found to be oxidized by poly(Co–TAPc) even at open-circuit conditions, as evidenced by the appearance of a charge transfer band when hydrazine is added to the electrolyte, indicating a charge transfer between hydrazine and the metallic center, i.e. the reduction of Co(II) to Co(I). Hence, imposing anodic conditions on the poly(Co–TAPc) electrode enhances this oxidation by regenerating the Co(II) species in the polymer. Finally, the more favored electrocatalytic effect of poly(Co–TAPc) was also confirmed by the R_{ct} values obtained from EIS results during hydrazine oxidation, i.e. about 500 Ω on the poly(Co–TAPc) electrode compared with about 6×10^3 Ω on the poly(H_2–TAPc) electrode.

Acknowledgements

This work was supported by Fondecyt, Project 1980837, F. Andes/Vitae, Project B-11487/8B007, and Dicyt-Usach (Chile), and CNPq and FAPESP (Brazil). The authors acknowledge Dr Zagal's laboratory facilities.

References

[1] J.P. Randin, Electrochim. Acta 19 (1974) 83.
[2] F. Beck, J. Appl. Electrochem. 7 (1977) 191.
[3] R.K. Sen, J. Zagal, E. Yeager, Inorg. Chem. 16 (1977) 3379.
[4] J. Zagal, R.K. Sen, E. Yeager, J. Electroanal. Chem. 83 (1977) 207.
[5] J. Zagal, P. Bindra, E. Yeager, J. Electrochem. Soc. 127 (1980) 1506.
[6] A.V.D. Putten, A. Elzing, W. Visscher, E. Barendrecht, J. Electroanal. Chem. 221 (1987) 95.
[7] D.V.D. Ham, C. Hinnen, G. Magner, M. Savy, J. Phys. Chem. 91 (1987) 4743.
[8] F. Coowar, O. Contamin, M. Savy, G. Scarbeck, J. Electroanal. Chem. 226 (1988) 119.
[9] J.H. Zagal, Coord. Chem. Rev. 119 (1992) 89.
[10] J. Zagal, M. Páez, A.A. Tanaka, J.R.D. Santos, Jr., C. Linkous, J. Electroanal. Chem. 339 (1992) 13.
[11] J. Ouyang, K. Shigehara, A. Yamada, F.C. Anson, J. Electroanal. Chem. 297 (1991) 489.
[12] M. Isaacs, M.J. Aguirre, A. Toro-Labbé, J. Costamagna, M. Páez, J.H. Zagal, Electrochim. Acta 43 (1998) 1821.
[13] A.K. Shukla, C. Paliteiro, R. Manoharan, A. Hamnett, J.B. Goodenough, J. Appl. Electrochem. 19 (1989) 105.
[14] F. Coowar, O. Contamin, M. Savy, G. Scarbeck, D.V.D. Ham, J. Riga, J.J. Verbist, J. Electroanal. Chem. 282 (1990) 141.
[15] C. Hinnen, F. Coowar, M. Savy, J. Electroanal. Chem. 264 (1989) 167.
[16] G. Lalande, R. Côté, G. Tamizhmani, D. Guay, J.P. Dodelet, L. Dignard-Bailey, L.T. Weng, P. Bertrand, Electrochim. Acta 40 (1995) 2635.
[17] G. Lalande, G. Faubert, R. Côté, D. Guay, J.P. Dodelet, L.T. Weng, P. Bertrand, J. Power Sources 61 (1996) 227.
[18] Y.H. Tse, P. Janda, H. Lam, J. Zhang, W. Pietro, A.B.P. Lever, J. Porphyrins Phthalocyanines 1 (1997) 3.
[19] E.F. Perez, G. Neto, A.A. Tanaka, L.T. Kubota, Electroanalysis 10 (1998) 111.
[20] J. Zagal, S. Ureta-Zañartu, J. Electrochem. Soc. 129 (1982) 2242.
[21] J.H. Zagal, S. Lira, S. Ureta-Zañartu, J. Electroanal. Chem. 210 (1986) 95.
[22] J.H. Zagal, J. Electroanal. Chem. 109 (1980) 389.
[23] J. Zagal, E. Muñoz, S. Ureta-Zañartu, Electrochim. Acta 27 (1982) 1373.
[24] Q.Y. Peng, T.F. Guarr, Electrochim. Acta 39 (1994) 2629.
[25] F. Steinback, M. Zobel, J. Chem. Soc., Faraday Trans. I 82 (1979) 113.
[26] J.H. Zagal, P. Herrera, Electrochim. Acta 30 (1985) 449.
[27] M. Sekota, T. Nyokong, Polyhedron 16 (1997) 3279.
[28] M. Sekota, T. Nyokong, Electroanalysis 9 (1997) 1257.
[29] T.J. Mafatle, T. Nyokong, J. Electroanal. Chem. 498 (1996) 213.
[30] R.O. Lezna, S. Juanto, J.H. Zagal, J. Electroanal. Chem. 452 (1998) 221.
[31] M.J. Aguirre, M. Isaacs, F. Armijo, N. Bocchi, J.H. Zagal, Electroanalysis 10 (1998) 571.
[32] J.H. Zagal, C. Páez, Electrochim. Acta 34 (1989) 243.
[33] B.A. Retamal, M.E. Vaschetto, J.H. Zagal, J. Electroanal. Chem. 431 (1997) 1.
[34] M. Kimura, Y. Yamaguchi, T. Koyama, K. Hanabusa, H. Shirai, J. Phorphyrins Phthalocyanines 1 (1997) 309.
[35] X. Qi, P.R. Baldwin, H. Li, T.F. Guarr, Electroanalysis 3 (1991) 119.
[36] F. Xu, H. Li, Q. Peng, T.F. Guarr, Synth. Met. 55-57 (1993) 1668.
[37] F. Xu, H. Li, S.J. Cross, T.F. Guarr, J. Electroanal. Chem. 368 (1994) 221.
[38] Y.H. Tse, P. Janda, H. Lam, A.B.P. Lever, Anal. Chem. 67 (1995) 981.
[39] T.F. Kang, G.L. Shen, R.Q. Yu, Anal. Chim. Acta 354 (1997) 343.
[40] H. Li, T.F. Guarr, J. Chem. Soc., Chem. Commun. (1989) 832.
[41] C.M. Drain, F. Nifiatis, A. Vasenko, J.D. Batteas, Angew. Chem. Int. Ed. 37 (1998) 2344.
[42] M. Hannack, K. Dr, A. Lange, J. Osío-Barcina, J. Pohmer, E. Witke, Synth. Met. 71 (1995) 2275.
[43] H. Yanagi, M. Wada, Y. Ueda, M. Ashida, D. Wöhrle, Makromol. Chem. 193 (1992) 1903.

[44] T.F. Guarr, Electropolymerized phthalocyanines and their applications, Handbook of Organic Conductive Molecules and Polymers, in: H.S. Nalwa (Ed.), Conductive Polymers: Transport, Photophysics and Applications, vol. 4, Wiley, New York, 1997.
[45] G.P.G. Gassman, J. Almlöf, J. Am. Chem. Soc. 116 (1994) 1932.
[46] S. Venkatachalam, K.V.C. Rao, P.T. Manoharan, J. Polym. Sci. Part B 32 (1994) 37.
[47] B. Ortiz, S.M. Park, N. Doddapaneni, J. Electrochem. Soc. 143 (1996) 1800.
[48] N. Kobayashi, in: C.C. Leznoff, A.B.P. Lever (Eds.), Synthesis and Spectroscopic Properties of Phthalocyanine Analogues, Phthalocyanines: Properties and Applications, vol. 2, VCH, Weinheim, 1993.
[49] M.J. Stillman, Absorption and magnetic circular dichroism spectral properties of phthalocyanines. Part 2: Ring-oxidized and ring-reduced complexes, in: C.C. Leznoff, A.B.P. Lever (Eds.), Phthalocyanines, Properties and Applications, vol. 3, VCH, Weinheim, 1993.
[50] S.I. Mho, B. Ortiz, S.M. Park, D. Ingersoll, N. Doddapaneni, J. Electrochem. Soc. 142 (1995) 1436.
[51] A.B.P. Lever, S.R. Pickens, P.C. Minor, S. Licoccia, B.S. Ramaswamy, K. Magnell, J. Am. Chem. Soc. 103 (1981) 6800.
[52] P.C. Minor, M. Gouterman, A.B.P. Lever, Inorg. Chem. 24 (1985) 1892.
[53] B.N. Achar, G.M. Fohlen, J.A. Parker, J. Polym. Sci. 20 (1982) 2773.
[54] B.N. Achar, G.M. Fohlen, J.A. Parker, J. Keshavayya, J. Polym. Sci. A 25 (1987) 443.
[55] O.E. Mouahid, A. Rakotondrainibe, P. Crouigneau, J.M. Lèger, C. Lamy, J. Electroanal. Chem. 445 (1998) 209.
[56] J.R. Macdonald, Impedance Spectroscopy, Wiley, New York, 1987.
[57] G.O. Haas, H. Takenouti, J. Appl. Electrochem. 17 (1987) 82.
[58] T.B. Hunter, P.S. Tyler, W.H. Smyrl, H.S. White, J. Electrochem. Soc. 134 (1987) 2198.
[59] M.M. Musiani, Electrochim. Acta 35 (1990) 1665.
[60] T. Malinski, A. Ciszewski, J. Bennett, J.R. Fish, J. Electrochem. Soc. 138 (1991) 200.

PERGAMON

www.elsevier.nl/locate/poly

Polyhedron 19 (2000) 2313–2318

POLYHEDRON

Crystal structures, spectroscopic, TG and DSC studies of lanthanide picrate complexes with 4-methylmorpholine *N*-oxide (MMNO)

L.C. Fernandes [a], J.R. Matos [b], L.B. Zinner [a,b], G. Vicentini [a,b], J. Zukerman-Schpector [b,c,*]

[a] *Departamento de Química, Universidade Federal de Rio Grande do Norte, C.P. 1661, CEP 59072-970 Natal, RN, Brazil*
[b] *Instituto de Química, Universidade de São Paulo, C.P. 26077, CEP 05599-970 Sao Paulo, SP, Brazil*
[c] *Laboratório de Cristalografia, Estereodinâmica e Modelagem Molecular, Departamento de Química, Universidade Federal de São Carlos, C.P. 676, CEP 13565-905 Sao Carlos, SP, Brazil*

Received 1 October 1999; accepted 15 February 2000

Abstract

The crystal structures, IR absorption spectra, emission spectrum of the europium compound, TG and DSC analyses of $Ln(pic)_3 \cdot MMNO \cdot 2H_2O$ (pic = picrate, Ln = La, Nd, Eu) complexes are reported. The crystals that were grown from methanolic solutions, are isomorphous belonging to the triclinic space group $P\bar{1}$. The Ln ions are coordinated to nine oxygen atoms, six of the picrate moieties, one of the MMNO and two of water molecules, giving rise to a tricapped trigonal prism. © 2000 Elsevier Science B.V. All rights reserved.

Keywords: Crystal structures; Lanthanide complexes; Picrate; 4-Methylmorpholine; *N*-Oxide; TG; DSC

1. Introduction

The hydrated lanthanide picrates and their structures have been described already [1–4]. Lanthanide picrate complexes with several organic neutral ligands are being studied in our laboratories. These complexes with (a) sulfoxides [5–17]; (b) phosphine oxides [18,19]; (c) *N*-oxides [20–23]; (d) amides [22,24–26]; (e) phosphoramides [27,28]; and (f) lactams [29] have been described.

In this article the preparation, characterization by CHN analyses, infrared absorption spectra, emission spectrum of the europium compound, TG and DSC analyses and the single crystal X-ray structure determination of the lanthanum, neodymium and europium picrate complexes with 4-methylmorpholine *N*-oxides (MMNO) are presented. Besides our continuing interest in lanthanide picrate complexes, the use of MMNO was aimed at determining whether the presence of the methyl group attached to the N–O had any influence on the ligand properties of this substance.

2. Experimental

Compounds with composition $Ln(pic)_3 \cdot 3MMNO$ were prepared by reaction of the hydrated picrates with MMNO in absolute ethanol [30]. Recrystallization from methanol at low temperature resulted in the complexes with general formula $Ln(pic)_3 \cdot MMNO \cdot 2H_2O$ (Ln = La, Nd, Eu). These complexes were characterized by microanalytical procedures using a Perkin–Elmer model 240 instrument. Infrared absorption spectra were recorded on a Nicolet FTIR 510 using KBr pellets. Emission spectrum of the solid europium compound was determined at room temperature and at 77 K using a Hitachi Perkin–Elmer-MPF-4 spectrofluorimeter. TG data

* Corresponding author. Tel.: +55-16-260-8208; fax: 55-16-260-8350.
E-mail address: julio@power.ufscar.br (J. Zukerman-Schpector).

0277-5387/00/$ - see front matter © 2000 Elsevier Science B.V. All rights reserved.
PII: S0277-5387(00)00494-0

Table 1
Summary of analytical results (%)

Ln	Carbon		Hydrogen		Nitrogen	
	Theoretical	Experimental	Theoretical	Experimental	Theoretical	Experimental
La	28.3	28.4	2.2	2.3	14.3	14.3
Nd	28.1	28.4	2.2	2.3	14.3	14.2
Eu	27.9	28.2	2.1	2.3	14.2	14.3

were collected on a Shimadzu TGA-50, using a platinum cell, ~1.8 mg sample, dynamic air atmosphere (50 ml min^{-1}), heating rate of 2 K min^{-1}. DSC were obtained on a Shimadzu DSC-50, aluminum cell, ~1.8 mg sample, dynamic nitrogen atmosphere (50 ml min^{-1}), heating rate of 10 K min^{-1}. X-ray crystallographic data were recorded on an Enraf–Nonius CAD-4 Mach 3 diffractometer. In all cases, cell parameters were determined on the basis of 25 reflections; intensity data were obtained with graphite monochromated Mo Kα radiation ($\lambda = 0.71073$ Å) and ω–2θ scan mode at room temperature (291 K). During data collection, the intensity of three standard reflections were monitored every 30 min of X-ray exposure time showing no significant decay. Structures were solved using the standard heavy-atom Patterson procedure and difference Fourier maps and refined by full-matrix least-squares. All non-H atoms were refined anisotropically. H-atoms were located on stereochemical grounds, except that of the water molecules that were found in a difference Fourier map, and refined in the riding model with an isotropic displacement parameter amounting to 1.2 times the value of the equivalent isotropic displacement parameter of the carrier atom. Programs used: SHELXS-86 [31], SHELXL-97 [32] and ZORTEP [33]. Data were corrected for Lorentz, polarization and absorption.

3. Results and discussion

Table 1 shows a summary of CHN-analyses, showing a good accordance with the composition Ln(pic)$_3$·MMNO·2H$_2$O. Infrared absorption spectra data are presented in Table 2. Picrate bands were attributed according to Yongchi et al. [2]. The frequencies obtained for ν_s NO$_2$ are indicative of picrate coordination through the phenoxo oxygen and an oxygen of one *ortho* nitro group, behaving as a bidentate. The bands attributed to νNO, according to Maï et al. [34] at 940–988 cm^{-1}, shifted to 907–937 cm^{-1}, are indicative of coordination of MMNO through the oxygen.

The emission spectrum of the europium compound (Fig. 1), determined at 77 K, shows one band attributed to $^5D_0 \rightarrow {}^7F_0$ (578 nm), three peaks due to $^5D_0 \rightarrow {}^7F_1$ (587.5, 592, 597 nm) and five peaks due to $^5D_0 \rightarrow {}^7F_2$ (612, 612.5, 614, 616, 619.5 cm^{-1}) were attributed to a C_{3v} symmetry around the central ion [35].

TG curves (Fig. 2) show the following steps: (a) loss of humidity (300–400 K); (b) loss of two coordi-

Table 2
Absorption infrared spectra data (cm^{-1}) of the complexes with composition Ln(pic)$_3$·(MMNO)·2H$_2$O [a]

Ln	$\nu_{as}NO_2$	$\nu_s NO_2$	νC–C	νCO	νNO
La	1570s–1539s	1337s	1615s	1274s	937w
Nd	1575s–1541s	1367s–1336s	1615s	1277s	937w–907w
Eu	1575s–1542s	1368s–1334s	1614s	1277s	937w–907w

[a] s, strong; w, weak.

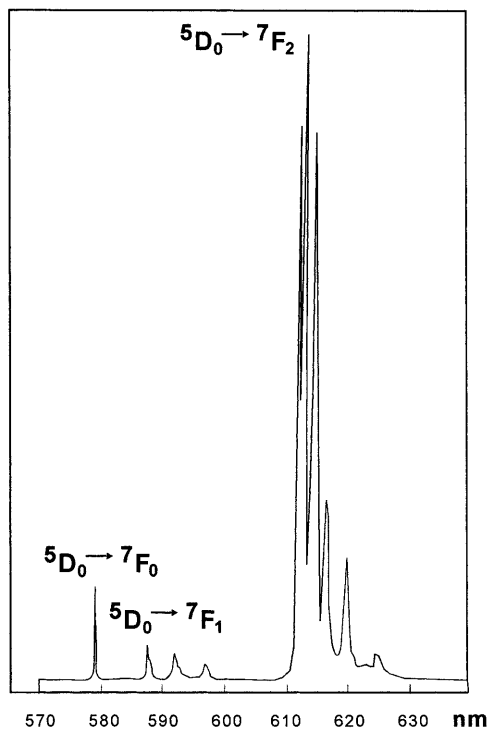


Fig. 1. Emission spectrum of the Eu complex in solid state, at 77 K.

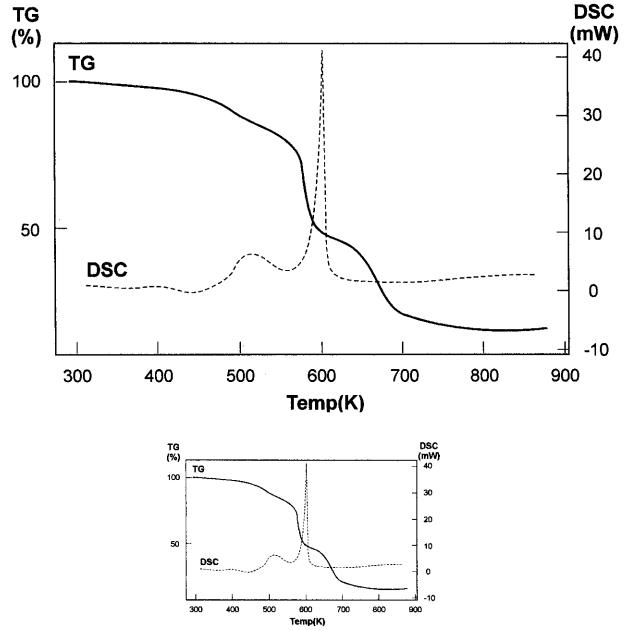


Fig. 2. TG and DSC curves of the Eu complex.

nated water molecules (400–480 K); (c) loss of MMNO and decomposition of the picrate (480–720 K); (d) the residues at 860 K are the respective oxides, Ln_2O_3 (Ln = La, Nd, Eu).

From the DSC curves (Fig. 2) the following energies were determined (in kJ mol^{-1}): for step b, 82.6 (La), 103.6 (Nd) and 124.7 (Eu); for step c, −2909 (La), −2850 (Nd) and −2790 (Eu). Experimental details and results of the crystal structure determinations are listed in Table 3. Bond lengths and angles around the Ln ion are listed in Table 4. Complete sets of atomic coordinates, anisotropic thermal parameters and distances and angles have been deposited with the Cambridge Crystallographic Data Centre. A plot of the Eu compound and of its coordination polyhedron is shown in Figs. 3 and 4, respectively.

The Ln atoms are nine-coordinated by six oxygens of three independent bidentate picrate moieties, one of the MMNO and two independent water molecules in a tricapped trigonal prism shape. The coordination of each picrate occurs via the phenoxo oxygen and one oxygen of one of the *ortho* nitro group which occupy the capping positions on the square phases of the trigonal prism. The dihedral angle between the trigonal faces being of 5.3(1), 4.6(3), 5.40(6)° in the La, Nd and Eu complexes, respectively. The average distances Eu–$O_{phenoxo}$ of 2.353 Å and Eu–O_{NO} of 2.704 Å are comparable with those found in the 2-azacyclononanone [29] compound (2.345, 2.700 Å).

Table 3
Summary of data collection and crystal parameters

	La	Nd	Eu
Empirical formula	$C_{23}H_{21}LaN_{10}O_{25}$	$C_{23}H_{21}NdN_{10}O_{25}$	$C_{23}H_{21}EuN_{10}O_{25}$
Formula weight	976.41	981.74	989.46
Temperature (K)	291(2)	291(2)	291(2)
Wavelength (Å)	0.71073	0.71073	0.71073
Crystal system, space group	triclinic, $P\bar{1}$	triclinic, $P\bar{1}$	triclinic, $P\bar{1}$
Unit cell dimensions			
a (Å)	11.9359(9)	12.032(1)	12.0311(6)
b (Å)	12.867(1)	12.711(1)	12.6639(8)
c (Å)	12.921(1)	12.881(2)	12.9876(7)
α (°)	91.997(8)	90.943(7)	90.834(5)
β (°)	106.691(8)	107.26(1)	107.457(4)
γ (°)	113.560(7)	113.99(1)	114.118(5)
V (Å^3)	1716.8(3)	1697.4(5)	1.689.58(16)
Z	2	2	2
D_{calc} (Mg m^{-3})	1.889	1.921	1.945
Absorption coefficient (mm^{-1})	1.292	1.648	1.975
F(000)	966	978	984
Crystal size (mm)	0.30 × 0.25 × 0.25	0.25 × 0.25 × 0.50	0.25 × 0.20 × 0.20
θ Range for data collection (°)	2.21–25.46	2.84–25.47	2.25–25.57
Limiting indices	$-13 \le h \le 14$, $-15 \le k \le 15$, $-15 \le l \le 0$	$-13 \le h \le 14$, $-15 \le k \le 0$, $-15 \le l \le 15$	$-14 \le h \le 13$, $-15 \le k \le 15$, $0 \le l \le 15$
Reflections collected/unique	6663/6362 (R_{int} = 0.0201)	6595/6290 (R_{int} = 0.0541)	6641/6342 (R_{int} = 0.0146)
Refinement method	Full-matrix least-squares on F^2	Full-matrix least-squares on F^2	Full-matrix least-squares on F^2
Data/restraints/parameters	6362/0/533	6290/0/533	6342/0/533
Goodness-of-fit on F^2	1.041	1.018	1.076
Final R indices [$I > 2\sigma(I)$]	R_1 = 0.0585, wR_2 = 0.1518	R_1 = 0.0739, wR_2 = 0.1849	R_1 = 0.0224, wR_2 = 0.0599
R indices (all data)	R_1 = 0.0764, wR_2 = 0.1635	R_1 = 0.1580, wR_2 = 0.2322	R_1 = 0.0244, wR_2 = 0.0609

Table 4
Distances (Å) and angles (°) around the Ln ions

Ln	La	Nd	Eu
Ln–O(1)	2.294(5)	2.244(8)	2.2201(18)
Ln–O(1C)	2.416(5)	2.364(8)	2.3100(19)
Ln–O(1A)	2.442(5)	2.389(8)	2.3448(18)
Ln–O(1B)	2.488(5)	2.443(8)	2.4052(19)
Ln–O(1W)	2.517(5)	2.447(8)	2.4072(18)
Ln–O(2W)	2.548(5)	2.482(9)	2.4435(19)
Ln–O(11A)	2.743(6)	2.686(9)	2.660(2)
Ln–O(11B)	2.760(6)	2.699(9)	2.670(2)
Ln–O(11C)	2.797(6)	2.790(10)	2.782(2)
O(1)–Ln–O(1C)	89.56 (19)	89.9(3)	89.27(7)
O(1)–Ln–O(1A)	134.5(2)	134.4(3)	135.02(7)
O(1C)–Ln–O(1A)	125.04(19)	125.4(3)	125.39(7)
O(1)–Ln–O(1B)	131.34(19)	132.8(3)	87.77(7)
O(1C)–Ln–O(1B)	78.11(18)	78.9(3)	145.98(7)
O(1A)–Ln–O(1B)	88.13(17)	86.2(3)	77.73(7)
O(1)–Ln–O(1W)	85.81(18)	86.8(3)	133.49(7)
O(1C)–Ln–O(1W)	147.07(18)	146.5(3)	78.81(7)
O(1A)–Ln–O(1W)	78.76(18)	77.7(3)	85.40(6)
O(1B)–Ln–O(1W)	80.68(17)	79.1(3)	78.86(7)
O(1)–Ln–O(2W)	80.79(19)	80.5(3)	80.51(7)
O(1C)–Ln–O(2W)	75.87(18)	76.3(3)	76.18(7)
O(1A)–Ln–O(2W)	80.69(18)	81.5(3)	81.46(7)
O(1B)–Ln–O(2W)	138.05(17)	138.1(3)	136.35(6)
O(1W)–Ln–O(2W)	134.98(17)	135.6(3)	137.08(7)
O(1)–Ln–O(11A)	73.1(2)	70.6(3)	71.05(7)
O(1C)–Ln–O(11A)	142.61(19)	142.1(3)	142.84(7)
O(1A)–Ln–O(11A)	61.5(2)	63.9(3)	64.08(6)
O(1B)–Ln–O(11A)	137.90(19)	138.0(3)	66.61(7)
O(1W)–Ln–O(11A)	66.06(17)	66.8(3)	137.40(7)
O(2W)–Ln–O(11A)	68.93(18)	68.8(3)	69.81(7)
O(1C)–Ln–O(11B)	71.12(18)	71.3(3)	71.12(7)
O(1C)–Ln–O(11B)	82.13(18)	81.7(3)	81.30(7)
O(1A)–Ln–O(11B)	134.96(18)	134.4(3)	134.70(7)
O(1B)–Ln–O(11B)	60.70(16)	61.7(3)	65.70(7)
O(1W)–Ln–O(11B)	65.52(17)	65.7(3)	62.73(6)
O(2W)–Ln–O(11B)	144.26(18)	144.0(3)	143.78(7)
O(11A)–Ln–O(11B)	120.59(18)	119.4(3)	118.86(6)
O(1)–Ln–O(11C)	141.72(19)	142.4(3)	141.54(8)
O(1C)–Ln–O(11C)	61.03(18)	61.7(3)	62.12(7)
O(1A)–Ln–O(11C)	64.26(19)	63.9(3)	63.38(7)
O(1B)–Ln–O(11C)	69.56(19)	68.9(3)	130.44(7)
O(1W)–Ln–O(11C)	132.29(19)	130.5(3)	69.01(7)
O(2W)–Ln–O(11C)	69.16(19)	69.7(3)	68.56(8)
O(11A)–Ln–O(11C)	114.76(19)	116.2(3)	115.89(7)
O(11B)–Ln–O(11C)	122.87(17)	122.4(3)	123.75

Table 5
Centroid parameters

Atom	La	Nd	Eu
Centroid radius [a] (r) (Å)	2.554	2.501	2.469
Standard deviation [b] (σ_r)	0.167	0.172	0.182
Sphericity ($1-\sigma_r/r$)	0.935	0.931	0.926
Displacement [c] (Δ) (Å)	0.083	0.090	0.093

[a] The average centroid–ligand distance.
[b] Standard deviation of r.
[c] Distance Ln–centroid.

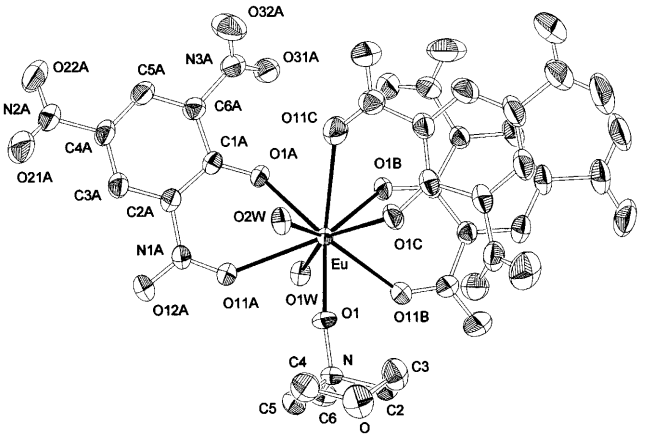


Fig. 3. Structure of the Eu(pic)$_3$·MMNO·2H$_2$O complex.

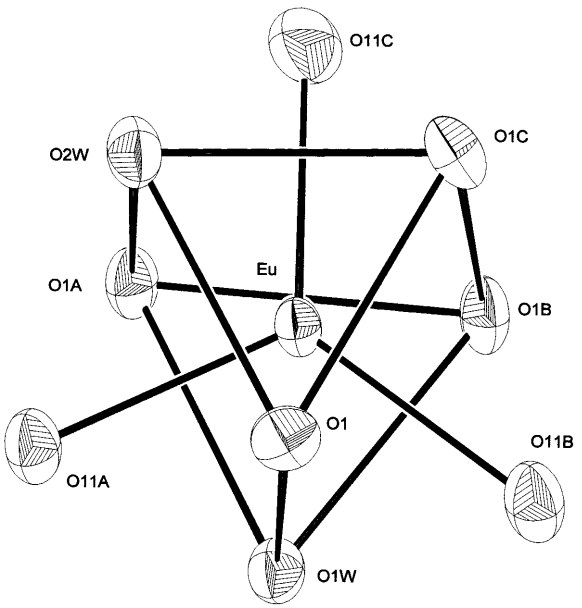


Fig. 4. Coordination polyhedron of the Eu complex.

The same trend is found for Nd, 2.399 and 2.725 Å in this work, and 2.418 and 2.676 Å in the hexamethylphosphoramide complex [25]. Several geometric parameters, introduced by Balic Zunic and Makovicky [36] and implemented in IVTON [37], in order to quantify the deformation of the coordination polyhedra as the centroid of the coordination polyhedra, i.e. the point in the coordination polyhedron with the minimum variance of distances to all ligands, the centroid–central atom distance (Δ), the average distance (r) from the centroid to the ligands, the standard deviation (σ_r) of the distances from the centroid to the ligands and the sphericity ($1-\sigma_r/r$) for the three coordination polyhedra, were calculated and are given in Table 5. It can be seen that the average centroid–ligand distances follows the lanthanidic contraction and that La complex presents the most distorted polyhedron while that of the

Table 6
Cremer and Pople's MMNO's ring puckering parameters

Atom	q_2 (Å)	q_3 (Å)	Q (Å)	θ (°)
La	0.004(9)	0.574(9)	0.574(9)	0.4(9)
Nd	0.023(9)	0.57(1)	0.57(1)	2.3(9)
Eu	0.005(4)	0.579(4)	0.579(4)	0.5(4)

Table 7
Hydrogen bond parameters [a]

D–H···A	D···A (Å)	H···A (Å)	D–H···A (°)
O1W–H1W1···O1A^{i}	2.918(3)	2.12	145.8
O1W–H2W1···O1B^{i}	2.934(3)	2.20	136.4
O1W–H2W1···O31B^{i}	2.919(4)	2.20	135.0
O2W–H1W2···O22B^{ii}	2.871(4)	1.97	170.8
O2W–H2W2···O^{iii}	2.800(3)	1.94	154.4

[a] Symmetry operations: (i) $-x$, $-y$, $-z$; (ii) x, $y-1$, z; (iii) $1-x$, $-y$, $1-z$.

Eu complex is less distorted. This is also shown by the sphericity parameter. The bond valence parameters (R_{Ln-O}) calculated for these structures being of 2.1844 (2.172), 2.0603 (2.117) and 2.0256 (20.76) for La, Nd and Eu, respectively. The values in parenthesis are those tabulated by Brese and O'Keefe [38].

In the three complexes the ring in the MMNO assumes an almost perfect chair conformation, as shown by the Cremer and Pople's [39] parameters (Table 6), the exocyclic oxygen atom O(1) being axial while the methyl group is equatorial. Unlike what occurs in the $[(MMNO)_2Mn^{III}TPP](ClO_4)$ [40] complex where the N–O bond is shortened upon complexation [1.366(10) Å], in these complexes the N–O distances of 1.380(7), 1.390(3), 1.400(15) Å for the La, Nd and Eu compounds, respectively, are closer to those found in compounds where the O atom is not involved in coordination 'bonds' nor hydrogen bonds [41,42]. On the other hand, the O–N–CH_3 angles are in good agreement, within experimental accuracy, with the values found in Refs. [40–42].

The water molecules involved in intermolecular hydrogen bonds are shown in Table 7.

4. Supplementary data

Crystallographic data for the structures reported in this paper have been deposited with the Cambridge Crystallographic Data Centre as supplementary publications No. CCDC 135296, 135297 and 135298. Copies of available material can be obtained, free of charge on application to the Director, CCDC, 12 Union Road, Cambridge, CH2 1EZ, UK (fax: +44-1223-336033 or e-mail: deposit@ccdc.cam.ac.uk or www:http://www.ccdc.cam.ac.uk).

Acknowledgements

The authors are much indebted to Fundação de Amparo à Pesquisa do Estado de São Paulo (FAPESP). This work was partially supported by CNPq and CAPES. One of us (L.C.F.) acknowledges IC-CNPq (AI) for a fellowship. The X-ray facility at the Instituto de Química, USP, was installed with a grant from FAPESP (94/2061-4).

References

[1] T. Yongchi, Y. Guangdi, L. Yingqiu, N. Jiazan, J. Mol. Sci. (China) 4 (1986) 55.
[2] T. Yongchi, L. Yingqiu, N. Jiazan, J. Mol. Sci. (China) 5 (1987) 83.
[3] J.M. Harrowfield, L. Weimin, B.W. Skelton, A.H. White, Aust. J. Chem. 47 (1994) 321.
[4] J.M. Harrowfield, B.W. Skelton, A.H. White, Aust. J. Chem. 47 (1994) 359.
[5] G. Vicentini, L.B. Zinner, K. Zinner, Koord. Khim. 17 (1991) 422.
[6] J.R. Matos, L.B. Zinner, G. Vicentini, Thermochim. Acta 214 (1993) 361.
[7] J.D. Ayala, L.B. Zinner, A. Del Pra, G. Bombieri, Inorg. Chim. Acta 211 (1993) 161.
[8] W.C. Melo, M.H. Zaim, J.R. Matos, P.C. Isolani, K. Zinner, L.B. Zinner, J. Coord. Chem. 225 (1995) 344.
[9] J.D. Ayala, G. Vicentini, A. Del Pra, G. Bombieri, Acta Crystallogr., Sect. C 50 (1994) 1458.
[10] W.C. Melo, R.E. Barrientos-Astigarraga, P.C. Isolani, L.B Zinner, M.H. Zaim, G. Vicentini, K. Zinner, An. Assoc. Bras. Quim. 44 (1995) 18.
[11] W.C. Melo, M.H. Zaim, J.R. Matos, P.C. Isolani, K. Zinner, L.B. Zinner, J. Alloys Comp. 225 (1995) 344.
[12] L.B. Zinner, J.R. Matos, M.A. Andrade da Silva, J.E.X. Matos, Thermochim. Acta 242 (1994) 253.
[13] L.B. Zinner, J.D. Ayala, M.A. Andrade da Silva, G. Bombieri, A. Del Pra, J. Cryst. Specrosc. Res. 24 (1994) 445.
[14] M.A. Andrade da Silva, M.H. Zaim, P.C. Isolani, B. Wladislaw, L.B. Zinner, K. Zinner, J. Coord. Chem. 36 (1995) 311.
[15] M.A. Andrade da Silva, J.R. Matos, M.H. Zaim, L.B. Zinner, An. Assoc. Bras. Quim. 46 (1997) 1.
[16] J.D. Ayala, G. Bombieri, A. Del Pra, A. Fantoni, G. Vicentini, Inorg. Chim. Acta 274 (1998) 122.
[17] J.D. Ayala, G. Bombieri, A. Del Pra, A. Fantoni, G. Vicentini, Inorg. Chim. Acta 274 (1998) 236.
[18] S. Braun, L.B. Zinner, G. Vicentini, An. Assoc. Bras. Quim. 41/42 (1993) 20.
[19] S.A. Jardino Filho, P.C. Isolani, G. Vicentini, J. Alloys Comp. 249 (1997) 91.
[20] G. Vicentini, F.J.S. Lima, J. Alloys Comp. 192 (1993) 277.
[21] F.J.S. Lima, P.C. Isolani, G. Vicentini, An. Assoc. Bras. Quim. 43 (1–2) (1994) 22.
[22] E. Meira da Silva, C.V.P. Melo, P.C. Isolani, K. Zinner, G. Vicentini, An. Assoc. Bras. Quim. 41/42 (1993) 17.
[23] G. Vicentini, E. Meira da Silva, J.R. Matos, K. Zinner, Thermochim. Acta 195 (1992) 39.
[24] C. Barberato, E.E. Castellano, G. Vicentini, P.C. Isolani, M.I.R. Lima, Acta Crystallogr., Sect. C 50 (1995) 351.
[25] C.V.P. Melo, G. Vicentini, E.E. Castellano, J. Zukerman-Schpector, J. Alloys Comp. 225 (1995) 354.

[26] E. Meira da Silva, G.C.L. Araujo, G. Vicentini, P.C. Isolani, C.V.P. Melo, An. Assoc. Bras. Quim. 45 (1996) 138.
[27] A.G. Silva, G. Vicentini, J. Zukerman-Schpector, E.E. Castellano, J. Alloys Comp. 225 (1995) 354.
[28] A.G. Silva, G. Vicentini, J.D. Ayala, C. Barberato, E.E. Castellano, An. Assoc. Bras. Quim. 44 (1995) 1.
[29] E.P. Marinho, D.M. Araujo Melo, L.B. Zinner, K. Zinner, E.E. Castellano, J. Zukerman-Schpector, P.C. Isolani, G. Vicentini, Polyhedron 16 (1997) 3519.
[30] L.C. Fernandes, R. Fernandes Bezerra, M.S. Costa da Camara, D.M. Araujo Melo, K. Zinner, L.B. Zinner (1999) submitted.
[31] G.M. Sheldrick, SHELXS-86, Program for the Solution of Crystal Structure, University of Göttingen, Germany, 1986.
[32] G.M. Sheldrick, SHELXL-97, Program for the Refinement of Crystal Structures, University of Göttingen, Germany, 1997.
[33] L. Zsolnai, ZORTEP, An Interactive Molecular Graphics Program, University of Heidelberg, Germany, 1995.
[34] P.T. Maï, M.-H. Herzog-Cance, A. Potier, J. Potier, Can. J. Chem. 60 (1982) 2777.
[35] J.H. Forsberg, Coord. Chem. Rev. 10 (1973) 195.
[36] T. Balic Zunic, E. Makovicky, Acta Crystallogr., Sect. B 52 (1996) 78.
[37] T. Balic Zunic, I. Vickovic, J. Appl. Crystallogr. 29 (1996) 305.
[38] N.E. Brese, M. O'Keefe, Acta Crystallogr., Sect. B 47 (1991) 192.
[39] D. Cremer, J.A. Pople, J. Am. Chem. Soc. 97 (1975) 1354.
[40] R.B. Brown, Jr., M.M. Williamson, C.L. Hill, Inorg. Chem. 26 (1987) 1602.
[41] E. Maia, A. Peguy, S. Pérez, Acta Crystallogr., Sect. B 37 (1981) 1858.
[42] E. Maia, S. Pérez, Acta Crystallogr., Sect. B 38 (1982) 849.

PERGAMON

www.elsevier.nl/locate/poly

Polyhedron 19 (2000) 2319–2325

POLYHEDRON

Toward a novel metal-based chemotherapy against tropical diseases. Part 5. Synthesis and characterization of new Ru(II) and Ru(III) clotrimazole and ketoconazole complexes and evaluation of their activity against *Trypanosoma cruzi*

Maribel Navarro [a], Teresa Lehmann [a], Efrén J. Cisneros-Fajardo [a], Alberto Fuentes [a], Roberto A. Sánchez-Delgado [a,*,1], Pedro Silva [b], Julio A. Urbina [c]

[a] *Chemistry Center, Instituto Venezolano de Investigaciones Científicas (IVIC), Apartado 21827, Caracas 1020-A, Venezuela*
[b] *Physics Center, Instituto Venezolano de Investigaciones Científicas (IVIC), Apartado 21827, Caracas 1020-A, Venezuela*
[c] *Biophysics and Biochemistry Center, Instituto Venezolano de Investigaciones Científicas (IVIC), Apartado 21827, Caracas 1020-A, Venezuela*

Received 1 October 1999; accepted 14 March 2000

Abstract

The complexes $RuCl_3(CTZ)_3{\cdot}2CH_3OH$ (**1**) and $RuCl_3(KTZ)_2(H_2O){\cdot}2H_2O$ (**2**) were prepared by reaction of $RuCl_3{\cdot}3H_2O$ with CTZ and KTZ, respectively, while $RuCl_2(KTZ)_2$ (**4**) was prepared by reaction of $RuCl_2(CH_3CN)_4$ with KTZ (CTZ = 1-[(2-chlorophenyl)diphenylmethyl-1*H*-imidazole, and KTZ = *cis*-1-acetyl-4-[4-[[2-(2,4-dichlorophenyl)-2-(1*H*-imidazol-1-ylmethyl)-1,3-dioxolan-4-yl]methoxy]phenyl]piperazine. All the complexes were characterized by NMR spectroscopy and for the paramagnetic species EPR spectroscopy was also employed. The new compounds were tested for in vitro activity against cultures of epimastigotes of *Trypanosoma cruzi*, the causative agent of Chagas disease, and compared with $RuCl_2(CTZ)_2$ (**3**) (reported previously) in order to establish some structure–activity correlations. At concentrations of 10^{-6} M (DMSO), all the complexes showed higher activity than the parental organic drug against the epimastigote form of the parasite, and Ru(II) complexes seem to be more active than their Ru(III) counterparts for a given nitrogen-donor ligand. © 2000 Elsevier Science B.V. All rights reserved.

Keywords: Ruthenium; Clotrimazole; Ketoconazole; Paramagnetic; Metal complexes; *Trypanosoma cruzi*; Chagas

1. Introduction

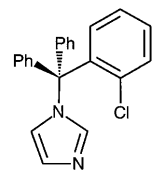
Ruthenium complexes have shown promise in the development of several types of pharmaceutical, particularly as anticancer agents [1]. As part of our research program on novel chemotherapies against tropical diseases, we have been searching for new metal-based drugs with a low level of toxicity and high biological activity against parasites responsible for ailments like malaria [2] and Chagas disease [3]. The latter is caused by *Trypanosoma cruzi*, an hemoflagelate protozoon, which is transmitted to humans by a cone-nosed bug known as Reduviid or Triatomid. This endemic and essentially incurable illness afflicts close to 20 million people in the Latin American subcontinent, ranking as the third largest parasitic disease worldwide, after malaria and schistosomiasis [4]. In view of the urgent need for an effective treatment against Chagas disease, the most varied approaches have to be considered.

Some very encouraging results have been disclosed recently by Urbina et al. [5] and by others [6] using azole-type molecules which have been found to exert their therapeutic effect through a mechanism involving the inhibition of the biosynthesis of sterols essential for

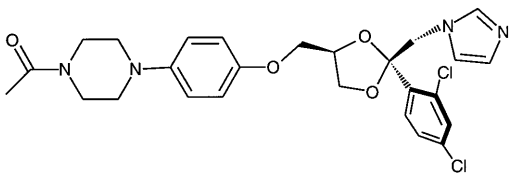
* Corresponding author. Tel.: +58-2-504-1741; fax: +58-2-504-1350.
E-mail address: rsanchez@ivic.ivic.ve (R.A. Sánchez-Delgado).
[1] John Simon Guggenheim Fellow 1998–1999.

0277-5387/00/$ - see front matter © 2000 Elsevier Science B.V. All rights reserved.
PII: S0277-5387(00)00495-2

the parasite. Another alternative which has been emerging from our laboratories as an interesting possibility makes use of such azoles (collectively known as SBIs, sterol biosynthesis inhibitors) as N-donor ligands in complexes of various metals; the general strategy we have been employing is the synthesis of metal derivatives of particular organic ligands which themselves have shown activity against *T. cruzi*, *e.g.* clotrimazole, CTZ = 1 - [(2 - chlorophenyl)diphenylmethyl-1*H* - imidazole) and ketoconazole, KTZ = *cis*-1-acetyl-4 - [4 - [[2 - (2,4 - dichlorophenyl) - 2 - (1*H* - imidazol - 1 - ylmethyl)-1,3-dioxolan-4-yl]methoxy]phenyl] piperazine [5,6].



CTZ



KTZ

Recently, we described the synthesis and characterization of a series of metal–CTZ complexes (Ru, Rh, Pt, Au and Cu) which showed promising biological activity for the case of Chagas disease. The most efficacious compound against *T. cruzi* was the Ru(II) derivative $RuCl_2(CTZ)_2$ which prompted us to study it in greater detail; this led us to a preliminary proposal for a mechanism of therapeutic action according to which the metal complex first acts as a transport agent across the parasite's membrane, and it is subsequently hydrolyzed in order to liberate CTZ which goes on to produce its known SBI action. Since a synergistic effect due to the presence of the metal fragment was observed, together with intracellular disorganization at the level of the nucleus, it was thought that Ru–DNA binding provides an additional means of damaging the parasite, and some preliminary studies indicated that some Ru–DNA interaction was in fact taking place [3]. Nevertheless, other factors such as partition coefficients at the cellular level may be influencing the selective transport and toxicity effects required for antiparasitic activity; in order to gain further insight into the mode of biological action of our complexes, we have engaged on a systematic study aimed at establishing possible structure–activity correlations.

Both CTZ and KTZ in their free forms have been evaluated against *T. cruzi*, and the latter has been found to be more active than the former [5,6]. It is also known that both Ru(II) and Ru(III) covalently bind to DNA, the binding generally being faster for the divalent state [7,8]. In order to shed some additional light on the mechanism of anti *T. cruzi* action of metal–azole derivatives, in this paper we present the synthesis, characterization and some preliminary data on the in vitro evaluation of the biological activity of a new series of Ru complexes in both the (II) and (III) oxidation states, containing either CTZ or KTZ. In this way we hope to reach a better understanding of the relative importance of the two main components of our mechanistic proposal.

2. Experimental

2.1. General procedure

Solvents of analytical grade were distilled from appropriate drying agents immediately prior to use. CTZ, KTZ, and $RuCl_3 \cdot H_2O$ were used as received. $RuCl_2(CH_3CN)_4$ and $RuCl_2(CTZ)_2$ were prepared according to the literature and characterized by comparison of their IR and NMR spectra with reported values [4]. Elemental analyses were performed at the Chemistry Center (IVIC) on a Fisons analyzer EA 1108; IR spectra were recorded on a Nicolet 5DCX FT spectrometer while UV–Vis spectra were obtained by use of a diode array Hewlett Packard 8453 instrument fitted with deuterium and mercury lamps, using chloroform solutions (10^{-4} M) of the complexes. EPR spectra were measured at room temperature (r.t.) in a Varian E-line spectrometer working in the X-band ($v = 9.3$ Hz) with a cylindrical cavity and a homemade coaxial microwave coupler for the X-band; experimental conditions (microwave power and modulation field) were adjusted to avoid saturation of signal intensity. NMR spectra were obtained in DMSO-d_6 solutions at 500 MHz with 8000 data points on a Bruker AVANCE500 spectrometer, ^{1}H NMR shifts being recorded relative to residual resonances in the deuterated solvent. For the paramagnetic complexes the NMR spectra were obtained using a 90° pulse of 10 ms. An inversion-recovery pulse sequence (180°–τ–90°–Aq) was used to obtain nonselective proton longitudinal relaxation times (T_1) with the carrier frequency set at different positions to ensure the validity of the measurements. Signal:noise ratios were improved by applying a line-broadening factor of 30 Hz to the FID prior to Fourier transformation.

2.2. $RuCl_3(CTZ)_3 \cdot 2CH_3OH$ (1)

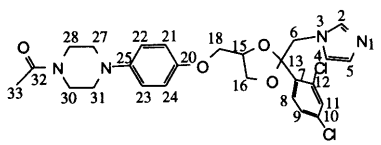
$RuCl_3 \cdot 3H_2O$ (154 mg, 0.59 mmol) was dissolved in freshly distilled methanol (15 ml), CTZ (876 mg, 2.54 mmol) in methanol (20 ml) was added to the solution which was stirred under reflux in a nitrogen atmosphere for 24 h. The volume of the solvent was reduced until precipitation began and the mixture was allowed to stand overnight at −10°C, after which the green solid obtained was filtered, washed with diethyl ether and dried under vacuum (yield, 480 mg, 62%). *Anal.* Calc. for $C_{68}H_{59}Cl_6N_6O_2Ru$: C, 62.5; H, 4.55; N, 6.4. Found: C, 62.1; H, 4.54; N, 6.9%. IR (cm^{-1}): ν(C=C) 1500, ν(C=N) 1440. λ_{max} ($CHCl_3$, 10^{-4} M) = 241, 325, 432 nm.

2.3. $RuCl_3(KTZ)_2(H_2O) \cdot 2H_2O$ (2)

$RuCl_3 \cdot H_2O$ (150 mg, 0.57 mmol) was dissolved in freshly distilled methanol (10 ml), KTZ (609 mg, 1.15 mmol) in methanol (20 ml) was added to the solution which was stirred under reflux in a nitrogen atmosphere for 24 h. The volume of the solvent was reduced until precipitation began and the mixture was allowed to stand overnight at −10°C, after which the brown solid obtained was filtered, washed with diethyl ether and dried under vacuum (yield, 70%). *Anal.* Calc. for $C_{52}H_{62}Cl_7N_8O_{11}Ru$: C, 47.1; H, 4.7; N, 8.5. Found: C, 46.8; H, 4.3; N, 8.3%. IR (cm^{-1}): ν(C=C) 1500, ν(C=N) 1440. λ_{max} ($CHCl_3$, 10^{-4} M) = 247, 296 nm.

2.4. $RuCl_2(KTZ)_2$ (4)

A 2:1 mixture of KTZ and $RuCl_2(CH_3CN)_4$ (60 mg, 0.18 mmol) was dissolved in methanol and allowed to react for 14 h at r.t., after which a white solid precipitated, which was filtered off, washed with diethyl ether and dried under vacuum (yield 60%). *Anal.* Calc. for $C_{52}H_{56}Cl_6N_8O_8Ru$): C, 50.6; H, 4.38; N, 9.09. Found: C, 51.3; H, 4.79; N, 9.28. IR (cm^{-1}): ν(C=C) 1510, ν(C=N) 1450. ^{1}H NMR ($CDCl_3$) δ, ppm: 7.92 (s, 1H) *H*(2); 7.69 (d, $J = 2.1$ Hz, 1H) *H*(11); 7.58 (d, $J = 8.7$ Hz, 1H) *H*(8); 7.46 (dd, $J^1 = 3.0$, $J^2 = 2.1$ Hz, 1H) *H*(9); 7.20 (s, 1H) *H*(4); 6.91 (s, 1H) *H*(5); 6.82 (AA′XX′, 4H) *H*(21), *H*(22), *H*(23), *H*(24); 4.62 (AB, 2H) *H*(6); 4.31 (m, 1H) *H*(15); 3.84 (m, 1H) *H*(18); 3.54 (m, 6H) *H*(27), *H*(31), *H*(16), *H*(18′); 3.43 (m, 1H) *H*(16′); 2.95 (dt, $J^1 = 3.3$, $J^2 = 4.9$ Hz, 4H) *H*(28), *H*(30); 2.02 (s, 3H) *H*(33). λ_{max} ($CHCl_3$, 10^{-4} M) = 247, 296 nm (Scheme 1).



Scheme 1. NMR numbering scheme for KTZ.

2.5. Biological tests against epimastigotes of *T. cruzi*

Tests were conducted following a method reported previously [5b]. An EP stock of the epimastigote form of *T. cruzi* was used throughout this study. The epimastigotes were cultured in liver infusion–tryptose medium supplemented with 10% calf serum at 28°C with strong stirring (120 rpm) as previously described; the cultures were initiated with a cell density of 2×10^6 epimastigotes per ml; CTZ, KTZ and compounds **1**–**4** were added as DMSO solutions (10^{-6} M) when the culture reached a cellular density of 10^7 epimastigotes per ml. Parasite proliferation was followed daily by the use of an electronic particle counter (model ZBI; counter Electronics, Inc, Hialeah, FL.) and by direct counting with an hemacytometer.

3. Results and discussion

3.1. Synthesis and characterization of the new ruthenium(III) CTZ and KTZ complexes

The Ru(III) complexes $RuCl_3(CTZ)_3$ (**1**) and $RuCl_3(KTZ)_2(H_2O) \cdot 2H_2O$ (**2**) were prepared by reaction of $RuCl_3 \cdot 3H_2O$ with CTZ (1:4) and KTZ (1:2), respectively, in methanol, yielding dark green (**1**) and brown (**2**) paramagnetic compounds which unfortunately did not provide crystals suitable for an X-ray structure determinations. The oxidation state of the ruthenium was confirmed by their characteristic rhombic EPR spectra, as shown by the data collected in Table 1. For both complexes the room temperature spectra displayed three absorption bands typical of low spin d^5 ions in an octahedral field; the theory of the EPR spectra of distorted octahedral low spin d^5 complexes (idealized t_{2g}^5, ground term $^2T_{2g}$) is well documented in the literature [9–11]. The spectra of **1** and **2** are rather compressed, g values being very close to one another in both complexes; this is attributable to a rhombic distortion with a very small anisotropy which can be ascribed to a considerable delocalization of the unpaired electron. Interestingly, an unusually high intensity of the low field line in both spectra indicates

Table 1
EPR spectroscopic data for the new Ru(III) complexes

Complex	g_1	g_2	g_3
$RuCl_3(CTZ)_3$ (**1**)	2.11	2.04	1.94
$RuCl_3(KTZ)_2(H_2O)_2 \cdot 2H_2O$ (**2**) [a]	2.22	2.21	2.07

[a] An unidentified paramagnetic impurity ($g = 2.00$) was observed in the spectrum of this compound.

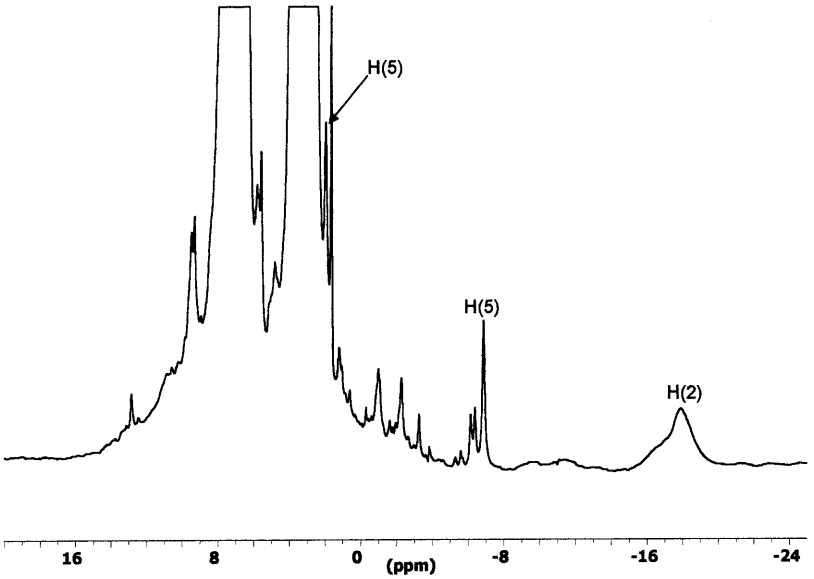


Fig. 1. ^{1}H NMR spectrum of $RuCl_3(CTZ)_3$ (**1**) in DMSO-d_6.

that the projection of the magnetic moment along the g_1 direction is large, as would be expected for systems with this type of symmetry. This spectral features are indicative also of a meridional rather than a facial structure for complex **1**; a facial Cl_3N_3 coordination would have a C_3 symmetry and therefore result in only two EPR signals [11]. A meridional arrangement of lower symmetry, which is in fact sterically more favorable for bulky ligands like CTZ, is also consistent with the NMR data presented below. In the case of **2** only two KTZ ligands can be accommodated around the ruthenium atom, presumably because of its larger size, so that the normal octahedral coordination sphere is probably attained by coordination of a water molecule; a rhombic EPR spectrum would be expected also in this case. By analogy with **1** and on the basis of NMR data reported below, a *mer* arrangement of the chlorides with two mutually *cis* KTZ ligands is the most likely stereochemistry for **2**.

3.2. NMR spectra of Ru(III) complexes

Several Ru(III) complexes containing imidazoles and related *N*-heterocycles as ligands have attracted attention, mainly because of use as radiosensitizers and of their promising antitumor properties; those compounds have been well characterized in the solid state but their solution properties are less well understood [1]; some rather extensive reports on the spectroscopic properties of imidazole complexes of Ru(III) have come out of the groups of Clarke [10] and Beauchamp [12]. We have carried out a ^{1}H NMR study of the new paramagnetic Ru(III) complexes **1** and **2**; the relaxation times (T_1) of the protons, which in the free ligand are in the range 10–0.5 s, decrease upon complexation to 3.0–0.5 s for **1** and 2.3–0.5 s for **2** (for the signals in the diamagnetic region), as a result of the contribution of the unpaired electron to the fluctuating magnetic fields that affect the relaxation of the nuclei in these systems.

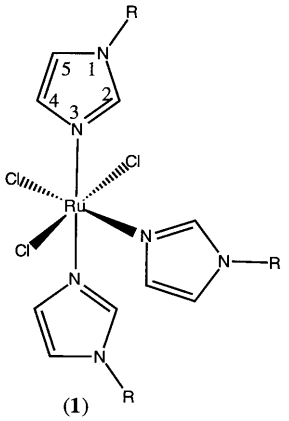
The spectrum of complex **1** in DMSO-d_6 (see Fig. 1) displays typical isotropically shifted signals for coordinated imidazoles at about -7 ppm (sharp, $T_1 = 10.1$ ms) and 2 ppm (sharp, $T_1 = 14$ ms), as well as a broad signal between -18 and -20 ppm; this high field signal is in fact composed of two peaks centered at about -17.5 and -16.5 ppm, with relative integrals of approximately 2:1 and T_1 values of 0.36 and 0.42 s, respectively (see Fig. 1). The sharp peak at 2 ppm is very close to strong signals in the diamagnetic region and therefore its integration is not reliable, but its relation to the peak at -7 ppm was established mainly on the basis of their very similar T_1 values, also close to those reported in the literature for related systems [10]. The paramagnetic region of this spectrum is further complicated by the appearance of other smaller signals between 1 and -14 ppm, possibly due to the formation of closely related solvation derivatives, as has been reported for *trans*-$[RuCl_4Im_2]^-$ in aqueous solution [12]. The spectrum of complex **2** in DMSO-d_6, shown in Fig. 2, is more straightforward as it exhibits three clearly distinct isotropically shifted signals located at -1.8 ppm (sharp), -8.7 ppm (broad) and -16.0 ppm (broad) with relative integrals 2:1:1 and T_1's of 11, 0.6, and 0.4 s. In CD_3OD two well separated signals are observed for H(5) at about -5.5 and -5.7 ppm.

On the basis of reported previously NMR spectra of other imidazoles coordinated to ruthenium(III) [10,12], the sharp signals at -5 and -2 ppm (in **1**) and at -1.8 ppm (in **2**) can be confidently assigned to the H5 protons of the CTZ and KTZ ligands, respectively. This imidazole proton is the one located furthest away from Ru and therefore it is the least affected by the paramagnetic influence of the metal center; as a result the H5 reso-

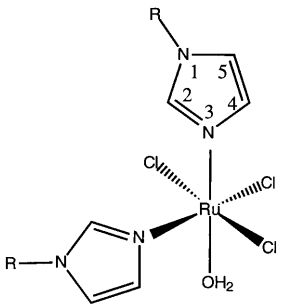
nances are the least broadened, but they experience significant upfield shifts.

As for the broad high-field signals, the situation is less clear cut, since previously reported data appear to be contradictory. Clarke's work on Ru(III)-imidazole complexes, which included extensive substitution studies in order to assign the proton resonances, concludes that the NMR signals for H(2) are broad and always appear at high fields, whereas the H(4) peak, also very broad, is generally shifted downfield although it may also be shifted upfield [10]. In contrast, Anderson and Beauchamp report spectra for Ru(III)–imidazole complexes in which two high field broad peaks are attributed to H(4) and H(2), respectively, on the basis of deuteration experiments [12]. In our case, deuteration or methylation of the ligands is not straightforward; however, the values of T_1 observed for the high field broad signals, taken together with their relative integrals and the EPR data discussed above, suggest that they correspond to two separate H(2) signals of nonequivalent CTZ (2:1) or KTZ (1:1) ligands, while the peaks corresponding to H(4) in both complexes were not observed probably because of their extreme broadness and possible location in the rather crowded diamagnetic region of the spectrum. The two separate signals observed for H(5) of **2** in CD_3OD are also in good agreement with two nonequivalent KTZ ligands.

From a perusal of the data available to us and the extensive known chemistry of Ru(III) [13], compound **1** is most likely octahedrally coordinated with the three *N*-donor atoms and the three chlorides in a *mer* stereochemistry so as to minimize the steric repulsion between the three bulky CTZ ligands; this implies that there are two (equivalent) mutually *trans* CTZ ligands while the third one is located *trans* to Cl, in accord with the 2:1 integral ratio observed for the H(2) protons in the NMR spectrum. Complex **2** is proposed to consist of an octahedral arrangement in which the three chlorines are in a meridional disposition and the two nonequivalent KTZ ligands are located mutually *cis*, thus requiring one to be *trans* to Cl, while the other is *trans* to the water molecule that completes hexacoordination.



(**1**)



(**2**)

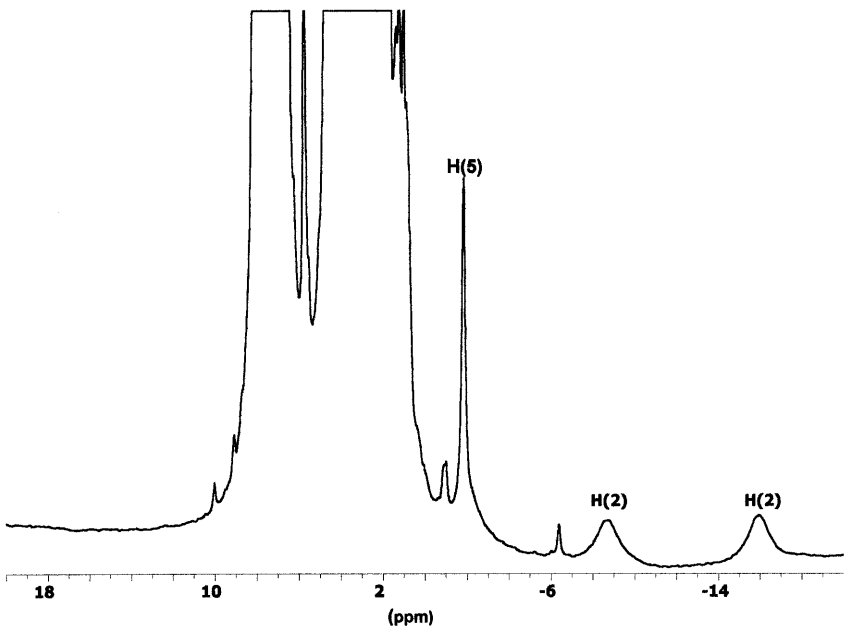


Fig. 2. ^{1}H NMR spectrum of $RuCl_3(KTZ)_2(H_2O)$ (**2**) in DMSO-d_6.

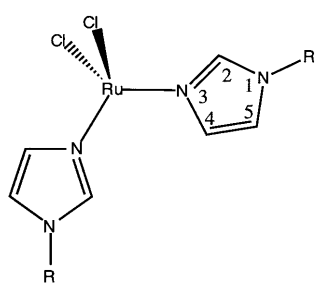
Table 2
Effect of CTZ, KTZ and their ruthenium complexes and on the proliferation of the epimastigotes of *T. cruzi* [a]

Compound	% Inhibition
CTZ	60.8
KTZ	20.3
$RuCl_2(CTZ)_2$	82.4
$RuCl_3(CTZ)_3$	65.9
$RuCl_2(KTZ)_2$	73.0
$RuCl_3(KTZ)_2$	70.3

[a] Complexes used as 10^{-6} M DMSO solutions. For details, see Section 2.

3.3. Ruthenium(II) complexes

The Ru(II) complexes **3** and **4** were prepared by displacement of the labile acetonitriles in $RuCl_2(CH_3CN)_4$ with 2 equiv. of the required ligand (CTZ or KTZ) in MeOH. We have described complex **3** in detail, as well as the X-ray structure of a closely related BTZ derivative (BTZ is the bromo analogue of the CTZ ligand) in a previous publication [3b]. These compounds are unusual diamagnetic 14-electron species with a distorted tetrahedral structure in an approximately C_{2v} arrangement of the donor atoms around the metal. Coordination through the unsubstituted N(3)-atom of the imidazole in **4** was deduced, as previously reported for **3**, from the displacement of the ^{1}H NMR signal of the proton located on the carbon atom α to that nitrogen (labeled H2 in Section 2), with respect to the free ligand ($\Delta\delta$ 0.48 ppm); this variation in chemical shift is by far larger than those observed for any other proton in the molecule. According to the analytical and NMR data and by analogy with **3**, complex **4** most likely possesses a tetracoordinated 14-electron Ru(II) configuration, which seems to be particularly adequate when the nitrogen-donor ligands are voluminous within a $RuCl_2N_2$ core. Although we have been unable to obtain crystals of **4** of X-ray quality, we presume that the structure of this complex is analogous to that of the $RuCl_2(BTZ)_2$ analogue.



(**3**, **4**)

3.4. In vitro activity of complexes **1**–**4** against epimastigotes of T. cruzi

The effect of DMSO solutions (10^{-6} M) of complexes **1**–**4** on the proliferation of in vitro cultures of the epimastigote form of *T. cruzi* (equivalent to the form present in the Reduviid vector [2]) was evaluated as described in the experimental section. Table 2 summarizes the results of such tests. The activities of the metal derivatives were all higher than the free parental compounds CTZ or KTZ, emphasizing our previous finding that binding to metal centers enhances the anti *T. cruzi* activity of azoles. Some interesting additional observations can be extracted from these preliminary biological data:

1. For CTZ, the Ru(II) complex displayed a noticeably higher activity (82.4% inhibition) than the Ru(III) derivative (73% inhibition). For KTZ the difference in activity observed was much less pronounced (73% for Ru(II) vs. 70% for Ru(III)).
2. The increase in efficacy of KTZ when attached to ruthenium is greater than that for CTZ; the trend in the activity ratio (Ru complex/free ligand) is Ru(II)–KTZ (3.60) > Ru(III)–KTZ (3.46) > Ru(II)–CTZ (1.35) > Ru(III)–CTZ (1.08).
3. At the concentrations used in this study, the most active compound was the Ru(II)–CTZ complex **3**.

In terms of our mechanistic proposal [3b], it is of interest to note that rapid metal–DNA binding is thought to be a key feature of the therapeutic action. It has been suggested that in order for DNA binding to take place, a chloro ligand must be replaced by water [14,15] but since Ru(III) is normally considered substitutionally inert in physiological conditions [16], activation by in situ reduction to a more labile Ru(II) species may actually be taking place [17]. The fact that Ru(II) appears to more active against *T. cruzi* than Ru(III) would then be in agreement with either a lower rate of hydrolysis for the Ru(III) compounds or with the need to reduce them to Ru(II) before they can exert their action. The hydrolysis of Ru(III) chloro–imidazole complexes has been studied in some detail by Anderson and Beauchamp [12] and we note that the NMR spectrum of complex **1** seems to indicate that solvolysis processes are indeed taking place in DMSO solution. Also interesting, the observed difference in activity between Ru(II) and Ru(III) was very small for KTZ, but if one takes into account that the Ru(III)–KTZ complex already contains a labile water in its coordination sphere, the need for a hydrolysis step is less pronounced. The larger increase in activity observed for KTZ with respect to CTZ as a result of coordination to Ru may be interpreted in terms of transport effects across the parasite's membrane, and/or, again, to the relative rates of hydrolysis for the different Ru complexes. Clearly more work is needed in order to further

clarify the mechanistic aspects of the observed biological activity, and a series of experiments aimed at addressing some of these issues are currently in progress.

Acknowledgements

CONICIT is gratefully acknowledged for the acquisition of the NMR spectrometer through the National NMR Laboratory at IVIC, and for funding to M.N. through Project S1-98000945. We thank Renee Lira for assistance in performing the biological tests.

References

[1] (a) M.J. Clarke, in: B.K. Keppler (Ed.), Metal Complexes in Cancer Chemotherapy, VCH, Weinheim, 1993, p. 129. (b) B.K. Keppler, K.-G. Lipponer, B. Stenzel, F. Kratz, in: B.K. Keppler (Ed.), Metal Complexes in Cancer Chemotherapy, VCH, Weinheim, 1993, p. 187. (c) N. Farrell, Transition metal complexes as drugs and chemotherapeutic agents, in: B.R. James, R. Ugo (Eds.), Catalysis by Metal Complexes, Kluwer, Dordrecht, 1989, (Chapters 1–6 and references therein). (d) I. Haiduc, C. Silvestru, Coord. Chem. Rev. 99 (1990) 253. (e) H.E. Howard-Lock, C.J.L. Lock, in: G. Wilkinson, R.D. Gillard, J.A. McCleverty (Eds.), Comprehensive Coordination Chemistry, vol. 6, Pergamon Press, New York, 1987, (Chapter 62.2). (f) Z. Guo, P.J. Sadler, Angew. Chem., Int. Ed. Engl. 38 (1999) 1512.

[2] (a) R.A. Sánchez-Delgado, M. Navarro, H. Pérez, J.A. Urbina, J. Med. Chem. 39 (1996) 1093. (b) M. Navarro, H. Pérez, R.A. Sánchez-Delgado, J. Med. Chem. 40 (1997) 1937.

[3] (a). R.A. Sánchez-Delgado, K. Lazardi, L. Rincón, J.A. Urbina, A.J. Hubert, A.F. Noels, J. Med. Chem. 36 (1993) 2041. (b) R.A. Sánchez-Delgado, M. Navarro, K. Lazardi, R. Atencio, M. Capparelli, F. Vargas, J.A. Urbina, A. Bouillez, A.J. Hubert, A.F. Noels, Inorg. Chim. Acta. 275–276 (1998) 528.

[4] World Bank, World Development Report 1993: Investing in Health, Oxford University Press, Oxford, 1993.

[5] (a) J.A. Urbina, G. Payares, J. Molina, C. Sanoja, A. Liendo, K. Lazardi, M.M. Piras, R. Piras, N. Pérez, P. Wincker, J.F. Ryley, Science 273 (1996) 969. (b) J.A. Urbina, K. Lazardi, T. Aguirre, M.M. Piras, R. Piras, Antimicrob. Agents Chemother. 32 (1988) 1237. (c) K. Lazardi, J.A. Urbina, W. De Souza, Antimicrob. Agents Chemother. 34 (1990) 2097. (d) J.A. Urbina, K. Lazardi, M. Aguirre, M.M. Piras, R. Piras, Antimicrob. Agents Chemother. 35 (1991) 730. (e) J.A. Urbina, K. Lazardi, E. Marchan, G. Visbal, M. Aguirre, M.M. Piras, R. Piras, R.A. Maldonado, G. Payares, W. De Souza, Antimicrob. Agents Chemother. 37 (1993) 580. (f) R.A. Maldonado, J. Molina, G. Payares, J.A. Urbina, Antimicrob. Agents Chemother. 37 (1993) 1353. (g) J.A. Urbina, J. Vivas, G. Visbal, L.M. Contreras, Mol. Biochem. Parasitol. 73 (1995) 199. (h) J.A. Urbina, J. Vivas, K. Lazardi, J. Molina, G. Payares, M.M. Piras, R. Piras, Chemotherapy 42 (1996) 1294.

[6] (a) R.E. McCabe, J. Infect. Dis. 158 (1988) 1408. (b) A.A.B. Moreira, H.B.W.T. De Souza, V. Amado Neto, L. Matsubara, P.L.S. Pinto, J.E. Tolezano, E.V. Nunes, M. Okumura, Rev. Inst. Med. Trop. Sao Paulo 34 (1992) 177. (c) Z. Brener, J.R. Cançado, L.M. Galvão, Z.M.P. da Luz, L. Filardi, M.E.S. Pareira, L.M.T. Santos, C.B. Cançado, Mem. Inst. Oswaldo Cruz Rio J. 88 (1993) 149. (d) R.E. Mc. Cabe, J.S. Remington, E.G. Araujo, J. Infect. Dis. 150 (1984) 594. (e) R.E. Mc. Cabe, J.S. Remington, E.G. Araujo, Trans. R. Soc. Trop. Med. Hyg. 81 (1987) 613.

[7] M. Clarke, B. Jansen, K.A. Marx, R. Kruger, Inorg. Chim. Acta 124 (1986) 13.

[8] J.R. Rubin, M. Sabat, M. Sundarlingam, Nucleic Acids Res. 11 (1983) 6571.

[9] (a) G. Feher, Electron Paramagnetic Resonance with Applications to Selected Problems in Biology, Gordon and Breach, New York, 1970. (b) K. Matsumoto, T. Matsumoto, M. Kawano, H. Ohnuki, Y. Shichi, T. Nishido, T. Sato, J. Am. Chem. Soc. 118 (1996) 3597. (c) G.K. Lahiri, S. Bhattacharya, B.K. Ghosh, A.A. Chakravorty, Inorg. Chem. 26 (1987) 4324. (d) B. Bleaney, M.C.M. O'Brien, Proc. Phys. Soc. 69 (1956) 1216. (e) H. Kamimura, J. Phys. Soc. Japan 11 (1956) 1171.

[10] (a) K.J. LaChance-Galang, P.E. Doan, M.J. Clarke, U. Rao, A. Yamano, B.M. Hoffman, J. Am. Chem. Soc. 117 (1995) 3529. (b) M.J. Clarke, V.M. Bailey, P.E. Doan, C.D. Hiller, K.J. LaChance-Galang, H. Daghlian, S. Mandal, C.M. Bastos, D. Lang, Inorg. Chem. 35 (1996) 4896. (c) V.M. Rodriguez-Bailey, K.J. LaChance-Galang, P.E. Doan, M.J. Clarke, Inorg. Chem. 36 (1997) 1873.

[11] D.A. Bardwell, D. Black, J.C. Jeffery, E. Schatz, M.D. Ward, J. Chem. Soc., Dalton Trans. (1993) 2321.

[12] (a) C. Anderson, A.L. Beauchamp, Can. J. Chem. 73 (1995) 471. (b) C. Anderson, A.L. Beauchamp, Inorg. Chem. 34 (1995) 6065.

[13] E.A. Seddon, K. Seddon, The Chemistry of Ruthenium, Elsevier, Amsterdam, 1984.

[14] E. Holler, W. Schaller, B. Keppler, Arzneim. Forsch. 41 (1991) 1065.

[15] F. Kratz, M. Hartmann, B. Keppler, L. Messori, J. Biol. Chem. 269 (1994) 2581.

[16] B.K. Keppler, M. Henn, U.M. Juhl, M.R. Berger, R. Niebl, F.E. Wagner, Prog. Clin. Biochem. Med. 10 (1989) 41.

[17] M.J. Clarke, Prog. Clin. Biochem. Med. 10 (1989) 25.

PERGAMON

www.elsevier.nl/locate/poly

Polyhedron 19 (2000) 2327–2335

POLYHEDRON

Tris(dialkyldithiocarbamato)diazenido(1-) and hydrazido(2-) molybdenum complexes: synthesis and reactivity in acid medium

Pablo C. Riveros [a], Isabel C. Perilla [a], Arnulfo Poveda [a,*], Heimo J. Keller [b], H. Pritzkow [b]

[a] *Departamento de Química, Universidad Nacional de Colombia, Santafé de Bogota, Colombia*
[b] *Anorganisch-Chemiches Institut der Universität, Im Neuenheimer Feld 270, 69120 Heidelberg, Germany*

Received 1 October 1999; accepted 24 April 2000

Abstract

A series of new molybdenum complexes, $[Mo(NNH–CO–Ph)\{S_2CN(C_2H_5)_2\}_3]$ (**1**), $[Mo(NN–CO–C_6H_4–NO_2)\{S_2CN(C_2H_5)_2\}_3]$ (**2**), $[Mo(NNH–CO–Ph)\{S_2CN(CH_3)_2\}_3]$ (**3**), $[Mo(NN–CO–C_6H_4–NO_2)\{S_2CN(CH_3)_2\}_3]$ (**4**) have been synthesized, with *p*-nitrobenzoyldiazenido(1-) and benzoylhydrazido(2-) as ligands, and dialkyldithio-carbamatos as coligands. Reactions of these compounds with aqueous and methanolic HCl were carried out but the attempted separation of the aroyl group was unsuccessful. Only the reaction of **1** and **2** with HCl in methanol gave a product, identified as $[Mo\{S_2CN(C_2H_5)_2\}_4][MoCl_4(OCH_3)_2]$. The complexes were characterized by elemental analysis, IR spectroscopy, ^1H and ^{13}C NMR, and mass spectrometry. Single crystals of **2** were obtained and the crystal structure was determined. The Mo atom is heptacoordinated; one diazenido(1-) and three diethyldithiocarbamatos act as ligands. From the latter one sulfur is in *trans*-position to the diazenido-nitrogen atom and the other five sulfur atoms lie in a plane giving a distorted pentagonal-bipyramidal coordination. © 2000 Elsevier Science B.V. All rights reserved.

Keywords: Molybdenum; Hydrazido; Diazenido; Dialkyldithiocarbamato; Hydrazines

1. Introduction

There have been several recent studies concerning the reactivity of dinitrogen coordinated to transition metal ions. Besides substitution, the reactions that give rise to N_2 derivatives such as hydrazido(2-), (1-), or diazenido(1-) are the most interesting [1–4]. Similar intermediates can be obtained by reaction of hydrazines with dioxomolybdenum complexes; however, there are not many reports in the literature of acyl or aroyl hydrazido or diazenido complexes [5]. These ligands can act as monodentate or didentate and generate derivatives that may be considered as intermediates in a cyclic process of nitrogen fixation, similarly to some rhenium complexes with phosphine ligands [6]. The aroyl and acyl derivatives could also give azido(–NNH) or hydrazido(–NNH_2) complexes by breaking the C(O)–N bond in a solvolysis reaction. All aroyl hydrazines used in this work act as monodentate. The aroyl hydrazine derivatives with dimethyldithiocarbamato coligand are stable to solvolysis whereas those with diethyldithiocarbamato react under reflux to give tetradithiocarbamato complexes.

2. Experimental

2.1. Physical measurements

Melting points were obtained with a Melt-Temp II apparatus, using glass capillaries. Elemental analyses were performed at the Microanalyses Department of the Anorganisch-Chemischen Institut of Heidelberg Universität. IR spectra were recorded for solid dispersions of 5% samples in KBr by the reflectance technique in a Nicolet 510P FT-IR spectrometer. ^1H and ^{13}C NMR spectra were obtained at room temperature (r.t.)

* Corresponding author. Tel.: +57-1-316-5000, ext. 1443; fax: +57-1-316-5220.
E-mail address: apovedap@ciencias.ciencias.unal.edu.co (A. Poveda).

0277-5387/00/$ - see front matter © 2000 Elsevier Science B.V. All rights reserved.
PII: S0277-5387(00)00496-4

in a Brucker Typ AC 300 spectrometer at 300 and 75 MHz respectively, using TMS as standard; $CDCl_3$ was used as solvent for all samples but $[MoO_2\{S_2CN(CH_3)_2\}_2]$, which was taken in $(CD_3)_2SO$. Mass spectra were recorded in a Finnigan Mat 8200 spectrometer using the FAB-Nibeol ionization technique. Small single crystals of **2** were obtained from THF solution. Crystal data were collected at −70°C with a Siemens–Stoe AED2 diffractometer using Mo Kα radiation, a graphite monochromator and omega-scan. The structure was solved by direct methods (SHELXS-86) [7]. The compound crystallizes with one half THF per molecule. The THF molecule is disordered. It was not possible to distinguish the oxygen from the carbon atoms, then the solvent molecule was refined for five carbon atoms with restrictions on the bond lengths and angles. The structure was refined by least-squares methods based on F_2 with all measured reflections (SHELXL-97 [8]) using anisotropic temperature factors for all non-hydrogen atoms except those of the THF molecule. Hydrogen atoms were inserted in calculated positions or as part of a rigid group (methyl).

2.2. Synthesis of the dioxocomplexes

2.2.1. Bis(dimethyldithiocarbamato)-dioxomolybdenum(VI), $[MoO_2\{S_2CN(CH_3)_2\}_2]$

A solution of 9.40 g (50 mmol) of $NaS_2CN(CH_3)_2\cdot 2.5H_2O$ in 100 ml H_2O was slowly added to a solution of 8.70 g (7 mmol) of $(NH_4)_6Mo_7O_{24}\cdot 4H_2O$ in 100 ml H_2O, with strong stirring. The pH was kept at about 2 by adding 1 M HNO_3. The obtained yellow precipitate was filtered off and washed with water, then dried under vacuum. Yield, 99%. The compound decomposes between 290–300°C. (Elemental analysis: *Anal*. Found: C, 28.13; H, 4.64; N, 6.40. Calc.: C, 28.30; H, 4.75; N, 6.60%).

2.2.2. Bis(diethyldithiocarbamato)dioxomolybdenum(VI), $[MoO_2\{S_2CN(C_2H_5)_2\}_2]$

The previously described procedure was employed, using 10.00 g (44 mmol) of $NaS_2CN(C_2H_5)_2\cdot 3H_2O$ in 150 ml H_2O, and 10.00 g (8 mmol) of $(NH_4)_6Mo_7O_{24}\cdot 4H_2O$ in 150 ml H_2O. The yellow compound was recrystallized in 1:1 benzene: n-hexane. Yield, 95%. m.p., 133°C. (Elemental analysis: *Anal*. Found: C, 19.27; H, 3.34; N, 7.62; S, 34.27. Calc.: C, 19.56; H, 3.28; N, 7.60; S, 34.82%).

2.3. Synthesis of the aroylhydrazine derivatives

2.3.1. Benzoylhydrazido(2-)tris(diethyldithiocarbamato)-molybdenum(V), $[Mo(NNH\text{-}CO\text{–}Ph)\{S_2CN(C_2H_5)_2\}_3]$ (1)

A suspension of 1.00 g (2.36 mmol) of $[MoO_2\{S_2CN(C_2H_5)_2\}_2]$, 0.60 g (2.66 mmol) of $NaS_2CN(C_2H_5)_2\cdot 3H_2O$, and 0.60 g (4.4 mmol) of $PhCONHNH_2$ in 20 ml methanol were boiled under reflux for 2 h with magnetic stirring. Longer times of reflux lead to lower yield, whereas shorter times cause the product to be contaminated with the reactants. The solvent was reduced to about 10 ml in a rotary evaporator and the solution was cooled to r.t. The orange solid thus obtained was filtered and washed with methanol, water, and again with a little methanol. The product was recrystallized in methanol and dried under vacuum. It can also be recrystallized in THF. Yield, 82%. The same product was obtained with 1:0:1 and 1:0:2 molar ratios of reactants respectively, but the yield decreased to 30 and 38%. Elemental analysis: *Anal*. Found: C, 38.31; H, 5.17; N, 10.14. Calc.: C, 39.21; H, 5.24; N, 10.39%.

2.3.2. Tris(diethyldithiocarbamato)-p-nitrobenzoyl-diazenido(1-)molybdenum(IV), $[Mo(NNCO\text{–}C_6H_4\text{–}NO_2)\{S_2CN(C_2H_5)_2\}_3]$ (2)

The procedure described above was employed, using 1.00 g (2.35 mmol) of $[MoO_2\{S_2CN(C_2H_5)_2\}_2]$, 0.60 g (2.66 mmol) of $NaS_2CN(C_2H_5)_2\cdot 3H_2O$, and 0.80 g (4.41 mmol) of $O_2N\text{–}C_6H_4CONHNH_2$. The red solid was recrystallized in THF and dried under vacuum for one h at 35°C. Yield, 80%. With 1:0:2 molar ratio of reactants the same product was obtained in 35% yield. (Elemental analysis: *Anal*. Found: C, 38.27; H, 5.22; N, 11.09; S, 25.15. Calc. for $[Mo(NNCO\text{–}C_6H_4\text{–}NO_2)\{S_2CN(C_2H_5)_2\}_3]\cdot 0.5THF$: C, 38.18; H, 5.07; N, 11.13; S, 25.48%). Crystals for X-ray analysis were grown by dissolving the compound in THF at 20°C and then filtering. The solution was warmed at about 60°C and after 12 h red crystals were obtained.

2.3.3. Benzoylhydrazido(2-)tris(dimethyldithiocarbamato)molybdenum(V), $[Mo(NNHCO\text{–}Ph)\{S_2CN(CH_3)_2\}_3]$ (3)

The procedure as described above was employed, using 1.00 g (2.71 mmol) of $[MoO_2\{S_2CN(CH_3)_2\}_2]$, 0.55 g (2.92 mmol) of $NaS_2CN(CH_3)_2\cdot 2.5H_2O$, and 0.60 g (4.41 mmol) of $Ph\text{–}CO\text{–}NHNH_2$. The product was recrystallized in methanol or THF and dried under vacuum. Yield, 75%. The same product was obtained in 1:0:2 molar ratio of reactants, in 33% yield. (Elemental analysis: *Anal*. Found: C, 32.56; H, 4.10; N, 11.61. Calc: C, 32.59; H, 3.93; N, 11.88%).

2.3.4. Tris(dimethyldithiocarbamato)-p-nitrobenzoyldiazenido(1-)molybdenum(IV), $[Mo(NNCO\text{–}C_6H_4\text{–}NO_2)\{S_2CN(CH_3)_2\}_3]$ (4)

The procedure described above was employed, using 1.50 g (4.07 mmol) of $[MoO_2\{S_2CN(CH_3)_2\}_2]$, 0.90 g (4.79 mmol) of $NaS_2CN(CH_3)_2\cdot 2.5H_2O$, and 1.20 g (6.63 mmol) of $O_2N\text{–}C_6H_4\text{–}CO\text{–}NHNH_2$. The product was recrystallized in THF and dried under vacuum. Yield, 81%. The same product was obtained in 30%

yield when a 1:0:2 molar ratio of reactants was used. (Elemental analysis: *Anal*. Found: C, 30.85; H, 3.75; N, 13.10; S, 29.90. Calc.: C, 30.28; H, 3.49; N, 13.24; S, 30.31%).

2.4. Solvolysis of the hydrazido(2-) and diazenido(1-) derivatives

The solvolysis of **1**, **2**, **3**, and **4** was attempted in 5% and 10% NaOH in water and in methanol at r.t. for 24 h but no reaction was observed. The reactants decomposed when refluxed at 60°C for 2 h. The same compounds did not react with 37% HCl in water at r.t. for 24 h, neither with 5% HCl below 50°C. At 60°C decomposition of the reactants was observed. IR spectroscopy was used as a probe to monitor the course of the reactions.

Only the reaction of the diethyldithiocarbamato derivatives **1** and **2** with 2.5% HCl in methanol under reflux gave an identifiable product.

2.5. Tetrakis(diethyldithiocarbamato)molybdenum(V)-tetrachlorobis(methoxy) molybdate(V), $[Mo(S_2CN(C_2H_5)_2)_4][MoCl_4(OCH_3)_2]$ (**5**)

A suspension of 0.30 g of **1** in 15 ml of a solution of concentrated HCl 2.5% *v*/*v* in methanol was placed under reflux; after 45 min a green precipitate formed, that was filtered and washed with water, diethyl ether and n-hexane. Its m.p. (143°C) and mass spectra showed it to be the unstable known compound $[Mo\{S_2CN(C_2H_5)_2\}_4]$ [9]. After refluxing for 2 h, the resultant brown solution was evaporated in a rotary evaporator until about 4 ml, then it was warmed and diethyl ether added drop to drop, until a brown solid precipitated. The solid was filtered and washed at 0°C with diethyl ether and methanol. Then it was recrystallized in methanol and dried under vacuum. Yield, 27%. The product is insoluble in acetone, diethyl ether, chloroform, and dimethyl sulfoxide (Elemental analysis: *Anal*. Found: C, 26.72; H, 4.69; Cl, 14.34; N, 5.67; S, 25.94; Calc. for $[Mo\{S_2CN(C_2H_5)_2\}_4][MoCl_4(OCH_3)_2]$: C, 26.80; H, 4.74; Cl, 13.37; N, 6.44; S, 25.63). When **2** was allowed to react by the above described procedure the same products were obtained under the same conditions but in lower yield (**5** was formed in 20% yield).

2.6. Tris(diethyldithiocarbamato)acetylhydrazido(2-)-molybdenum(V), $[Mo(NNHCO–CH_3)\{S_2CN(C_2H_5)_2\}_3]$.

A suspension of 0.50 g (1.18 mmol) of $[MoO_2\{S_2CN(C_2H_5)_2\}_2]$, 0.50 g (2.22 mmol) of $NaS_2CN(C_2H_5)_2 \cdot 3H_2O$, and 0.22 g (2.97 mmol) of $CH_3–CO–NHNH_2$ in 15 ml methanol was stirred for 12 h at r.t. The solution thus obtained was filtered and then evaporated until dryness in a rotary evaporator at 48°C. The resultant brown solid was suspended in 50 ml water and stirred for 30 min to dissolve and thus eliminate the excess of reactants. The precipitate was filtered and then washed with water, ethanol, and n-hexane. The product was recrystallized in ethanol; after three days brown microcrystals precipitated, which were filtered and washed with n-hexane, and diethyl ether. The product was dried under vacuum. Yield, 65%. ^{1}H NMR δ_H(solvent $CDCl_3$) 1.12–1.35 (18H, m, $6CH_3$), 1.95–2.20 (1H, br s, N–H), 2.17 (3H, s, CH_3–CO), 3.65–3.85 (12H, m, $6CH_2$).

2.7. Trisdiethyldithiocarbamatophenyldiazenido(1-)-molybdenum(IV), $[Mo(NNPh)\{S_2CN(C_2H_5)_2\}_3]$.

This compound was prepared following a published procedure [10].

3. Results and discussion

3.1. Synthesis of the compounds

The dioxocomplexes were synthesized by a modification of the procedure published by Moore and Larson [11]; the pH was kept below 2.0 with diluted HNO_3 in order to avoid contamination with the violet Mo(V) complex, $[\{Mo(S_2CNR_2)_2O\}_2O]$.

It has been published that the reactivity of dioxocomplexes against substituted hydrazines depends on several factors, such as the nature of the coligands and of the hydrazines, and the molar ratio of the reactants; for example, the number of substituents and the basicity of the hydrazines play an important role in the number of these that coordinate to the metal center [12–15]. In this work we found that condensation reactions between the dioxocomplexes and the hydrazides in the presence of the corresponding dialkyldithiocarbamate in methanol always give tris(dialkyldithiocarbamato) complexes of the type $[Mo(NNHCO–Ph)(S_2CNR_2)_3]$ and $[Mo(NNCO–C_6H_4–NO_2)(S_2CNR_2)_3]$ (R = $–CH_3$ or $–C_2H_5$). The same compounds are formed when no dialkyldithiocarbamate is added although in lower yield, since the additional dithiocarbamate has to be provided by decomposition of the original dithicarbamato complex.

The acyldiazenido- and acylhydrazido- ligands may be either monodentate when they are bound to the metal through the terminal nitrogen, or didentate when they are bound through the nitrogen and the oxygen. In addition, the monodentate ligand can bind the metal center in three different ways depending on the hydrazide from which it originates, as diazenido(1-), hydrazido(1-), or hydrazido(2-) [12,13]. These binding modes are shown in Fig. 1. In our case the two hydrazides act as monodentate ligands; *p*-nitrobenzohy-

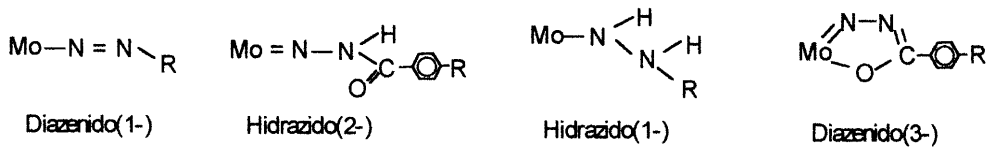


Fig. 1. Types of ligation and binding modes of the hydrazido ligands.

drazide is bound to the metal as diazenido(1-), and benzohydrazide as hydrazido(2-). A plausible explanation for this difference is that when the $-NO_2$ group is present, electron density is withdrawn from the nitrogen atom and therefore the N–H bond is unstable. Then the oxidation state of molybdenum is different with these ligands; it acts as Mo(IV) in diazenido(1-) complexes, and as Mo(V) in hydrazido(2-) complexes. The paramagnetism of the latter was proven by EPR, in which a signal at $g_{av} = 1.980$ is seen.

3.2. Reactivity of *p*-nitrobenzoyldiazenido(1-) and benzoylhydrazido(2-) complexes with acids and bases in aqueous and methanolic media

Compounds **1** and **3** are neither protonated nor deprotonated on the nitrogens of the diazenido or hydrazido ligands when boiled under reflux with base or acid in methanolic or aqueous medium. On the other hand, the same nitrogen atoms in compounds **2** and **4** are not protonated when reacting with acid in methanol, or in water. When **1** is allowed to react with HCl in methanol (2.5 ml concentrated HCl in 95 ml MeOH) under reflux, a green solid precipitates after 45 min. This precipitate is insoluble in water but soluble in chloroform, dichloromethane and acetone, indicating a non-ionic or slightly polar nature. In the solid state this compound is unstable to air, and even more in solution, and this makes difficult to take NMR spectra. The MS indicates this compound to be $[Mo(dedtc)_4]$[1], which is confirmed by its m.p., 143°C, similar to that reported in the literature [9]. The same compound was also obtained in 24% yield when **2** was allowed to react by the same procedure.

At longer reaction time (2 h) the oxidation product of $[Mo(dedtc)_4]$, $[Mo\{S_2CN(C_2H_5)_2\}_4][MoCl_4(OCH_3)_2]$ (**5**) was isolated, being the metal of the cation in the $5+$ oxidation state. Similar types of oxidation reactions have already been reported and are used for the synthesis of the cation [9,16]. Several ionic compounds that contain the $[Mo(S_2CN(C_2H_5)_2)_4]^+$ cation have been reported, which have been prepared from $[Mo_2O_2Cl_6]$ and $\{(C_2H_5)_2NH_2\}\{S_2CN(C_2H_5)_2\}$, or by oxidation of the corresponding Mo(IV) compounds [9,16,17]. The presence of the anion $[MoCl_4(OCH_3)_2]^-$ is proposed mainly on the basis of elemental analysis, since the compound is not soluble enough to allow to take NMR spectra; this anion has also been isolated from the reaction between $[Mo_2Cl_{10}]$ and CH_3OH [16].

3.3. IR spectroscopy

As expected, the dialkyldithiocarbamato coligands show IR bands due to the C=N stretching mode between 1540 and 1506 cm^{-1}, indicating a double bond character; bands due to C–S stretching are found between 1010 and 999 cm^{-1}; the C–H stretching for ethyl and methyl groups is shown in the region 2981–2858 cm^{-1}, the C–H bending modes appear as two bands around 1460 and 1380 cm^{-1} in the diethyldithiocarbamato complexes, and as only one band around 1395 cm^{-1} in the dimethyldithiocarbamato complexes [9,11,18]. The *p*-nitrobenzoyldiazenido and benzoylhydrazido ligands show bands for the =C–H stretching of the aromatic ring between 3071 and 3053 cm^{-1}, and also the out-of-plane =C–H bending modes of the aromatic rings around 700 cm^{-1}. Tables 1 and 2 show the positions of some selected bands. Two strong bands in the region 870–915 cm^{-1} assigned to *cis*-Mo=O stretchings are present in the dioxocomplexes, but disappear in the benzoylhydrazido- and *p*-nitrobenzoyldiazenidocomplexes, as expected.

The shift of the ν(C–O) and ν(N–N) IR bands according to the change in the CO bond order allows to determine whether the hydrazido and diazenido ligands act as mono- or didentate. If the IR spectrum shows bands assignable to ν(C=O) and ν(N=N), the ligand is acting as monodentate; on the other hand, if the ν(C=O) band disappears and the ν(N=N) band is

Table 1
Selected IR bands for the hidrazido and diazenido ligands

Complex	ν(=C–H)	δ(=C–H) [a]	ν(C=O)	ν(N=N)
$[Mo(NNH–CO–C_6H_5)(S_2CN(C_2H_5)_2)_3]$	3053.7	706.0	1618.5	1574.1
$[Mo(NN–CO–C_6H_4–NO_2)(S_2CN(C_2H_5)_2)_3]$	3070.1	712.8	1621.4	1591.5
$[Mo(NNH–CO–C_6H_5)(S_2CN(CH_3)_2)_3]$	3056.6	696.4	1622.3	1571.2
$[Mo(NN–CO–C_6H_4–NO_2)(S_2CN(CH_3)_2)_3]$	3070.1	709.9	1636.8	1593.4

[a] Out-of-plane bending.

[1] The MS shows a multiplet at m/z 690 which corresponds to the molecular ion, its isotopic distribution is consistent with only one molybdenum atom. Other multiplets appear at m/z 542 and 426, that correspond to $[Mo\{S_2CN(C_2H_5)_2\}_3]^+$ and $MoS\{S_2CN(C_2H_5)_2\}_2^+$, respectively.

Table 2
Selected IR bands for the dialkyldithiocarbamato ligands

Complex	ν(C=N)	ν(C–S)	ν(–C–H)	ν(–C–H)	ν(–C–H)
$[Mo(NNH–CO–C_6H_5)(S_2CN(C_2H_5)_2)_3]$	1506.6	1002.1	2980.4	2935.1	2873.3
$[Mo(NN–CO–C_6H_4–NO_2)(S_2CN(C_2H_5)_2)_3]$	1511.4	1009.9	2979.4	2935.1	2872.4
$[Mo(NNH–CO–C_6H_5)(S_2CN(CH_3)_2)_3]$	1539.4	999.2	2928.3	2858.9	
$[Mo(NN–CO–C_6H_4–NO_2)(S_2CN(CH_3)_2)_3]$	1524.9	1008.9	2931.2	2861.0	

shifted to lower frequency, the ligand is didentate. The IR spectra of **1**, **2**, **3**, and **4** show two bands in the region 1640–1570 cm^{-1} that may be assigned to either ν(C=O), ν(N=N), δ(N–H), or ν(C=C) of the aromatic ring. This fact does not allow to establish the binding mode of the above mentioned ligands. In order to make a correct assignment, $[Mo(NNHCO–CH_3)\{S_2CN(C_2H_5)_2\}_3]$ and $[Mo(NN–Ph)\{S_2CN(C_2H_5)_2\}_3]$ were synthesized, the former lacking the aromatic group and the latter, the C=O group. The IR spectrum of the former also has the above mentioned bands, therefore it can be concluded that they do not originate from the ν(C=C) of the aromatic ring of the *p*-nitrobenzoyldiazenido or benzoylhydrazido ligand. The IR spectrum of the latter does not have the band around 1620 cm^{-1} that is present in the *p*-nitrobenzoyldiazenido- and benzoylhydrazido complexes, and therefore it should correspond to ν(C=O). On the other hand, the band around 1580 cm^{-1} can still be assigned to δ(N–H) or ν(N=N). Compounds **2** and **4** do not have H bound to N, as is concluded from the ^{1}H NMR spectra but the IR spectra still show this band that can then be assigned to ν(N=N). With the assignment of these bands we can conclude that the *p*-nitrobenzoyldiazenido and benzoylhydrazido ligands are acting as monodentate in all the complexes prepared. The band corresponding to ν(N=N) is found at higher energy in the *p*-nitrobenzoyldiazenido(1-) complexes (around 1592 cm^{-1}) than in the benzoylhydrazido(2-)complexes (around 1572 cm^{-1}). This can be interpreted in terms of the decreasing N=N bond order when the ligand also has an N–H bond, since part of the electron density that is involved in the N=N bond is shifted to N–H.

3.4. NMR spectroscopy

3.4.1. ^{1}H NMR

The ^{1}H NMR spectra of **1** and **2** show the signals of the hydrogens from the diethyldithiocarbamates as complex multiplets at $\delta = 1.15–1.35$ and at $\delta = 3.62–3.93$, which are the result of overlapping of some triplets and quadruplets, respectively; this fact suggests that these coligands are not equivalent in solution. In **3** and **4** the hydrogens of the methyl groups from the dimethyldithiocarbamates give rise to four peaks in the range $\delta = 3.26–3.40$. In **1** and **3** the hydrogens of the benzyl ring of the benzoylhydrazido(2-) appear as two triplets and one doublet in the region $\delta = 7.27–8.12$, as expected [14]. In **2** and **4**, the hydrogens of the aromatic ring from the *p*-nitrobenzoyldiazenido display a multiplet at $\delta = 8.05–8.25$.

^{1}H NMR allows to determine whether the ligand is hydrazido or diazenido, since the number of hydrogens bound to the nitrogens determine the kind of ligand. The spectra of **1** and **3** show a broad signal at $\delta = 1.60–1.85$ that disappears when D_2O is used. This behavior suggests that the band corresponds to the H bound to the non-coordinated N, then in these compounds the ligand is bound as benzoyl-hydrazido(2-); a similar signal was reported for $[MoO(NNHPh)\{S_2CN(C_2H_5)_2\}_2]$ [14]. When the hydrogen is bound to the coordinated nitrogen the signal is seen at higher chemical shift due to weaker binding, as found for $[Mo(NHNPh_2)(NNPh_2)(acac)Cl_2]$ and [Mo(NHNMePh)(NNMePh)(acac)Cl_2], where the signals appear by $\delta = 12$ [13]. Compounds **2** and **4** do not show signals assignable to hydrogen bound to nitrogen, and furthermore there are not changes in the spectra with D_2O, then the ligand is bound as a *p*-nitrobenzoyldiazenido(1-).

Compound **2** shows a quintuplet at $\delta = 1.80–1.90$ that corresponds to one of the signals of THF, from the hydrogens bound to the carbons distant from oxygen. This quintuplet is not observed when the compound has not been recrystallized. The hydrogens bound to the carbons next to oxygen show a signal at $\delta = 3.70–3.80$ that overlaps with the signals from the coligands.

The integration ratios for compounds **1**, **2**, **3**, and **4** are in agreement with the presence of three dialkyldithiocarbamato coligands and one *p*-nitrobenzoyldiazenido or benzoylhydrazido ligand.

3.4.2. ^{13}C NMR

The ^{13}C NMR spectra of **1** and **3** show four signals in the region $\delta = 127–135$ that correspond to the aromatic carbons from the benzoylhydrazido. In compounds **2** and **4**, four similar signals from the *p*-nitrobenzoyldiazenido are shown at 122–150. All four compounds show a signal at $\delta = 180$ that corresponds to C from the carbonyl group. The diethyldithiocarbamato coligands

from **1** and **2** give signals around $\delta = 12$ and 42–45 from the ethyl groups, whereas the methyl groups from **3** and **4** give signals at $\delta = 37$–41. All four compounds show two signals around $\delta = 200$ and 206 that correspond to the carbons bound to sulfur in the dialkyldithiocarbamates; of these, the former signal is approximately twice as intense as the latter, suggesting that only two of the coligands are equivalent and located on the same plane, which is consistent with a nearly decaedric geometry obtained for a seven coordination number.

3.5. Mass spectrometry

Compound **2** shows a Mo-isotopic multiplet with the most intense peak at m/z 721 which can be assigned to the protonated molecular ion, $[Mo(NNHCO–C_6H_4-NO_2)\{S_2CN(C_2H_5)_2\}_3]^+$. At m/z 542 another similar multiplet is found, that corresponds to the loss of the protonated ligand –NNHCO–C_6H_4–NO_2. The additional proton is not found in the ^{1}H NMR spectrum of the complex, therefore it is gained in the ionization process; these proton additions are common when the FAB-Nibeol ionization technique is used [19].

The mass spectrum of **5** shows a multiplet with the most intense peak at m/z 690, that can be assigned to the $[Mo\{S_2CN(C_2H_5)_2\}_4]^+$ ion, its isotopic distribution corresponds to a complex with one molybdenum atom; there are also multiplets at m/z 574, assigned to $[Mo-S\{S_2CN(C_2H_5)_2\}_3]^+$; m/z 542, assigned to $[Mo\{S_2CN-(C_2H_5)_2\}]_3^+$; m/z 426, assigned to $[MoS\{S_2CN-(C_2H_5)_2\}_2]^+$; and m/z 394, that corresponds to $[Mo\{S_2CN(C_2H_5)_2\}_2]^+$.

3.6. X-ray structure of $[Mo(NNCO-C_6H_4-NO_2)\{S_2CN(C_2H_5)_2\}_3]\cdot(0.5)THF$ (2)

The X-ray structure of this compound is shown in Fig. 2. Crystal data are listed in Table 3 and the selected bond lengths and angles, in Table 4. The complete atomic coordinates, bond lengths and angles have been deposited as Supporting Information. The Mo atom is heptacoordinated, the donor atoms are arranged in a distorted pentagonal bipyramid. The atoms N5 and S1 occupy the axial positions (N5–Mo1–S1 166.1(2)°), while the atoms S2, S3, S4, S5, and S6 are located in the equatorial plane. S2 connected via C1 to the axial atom S1 deviates strongly

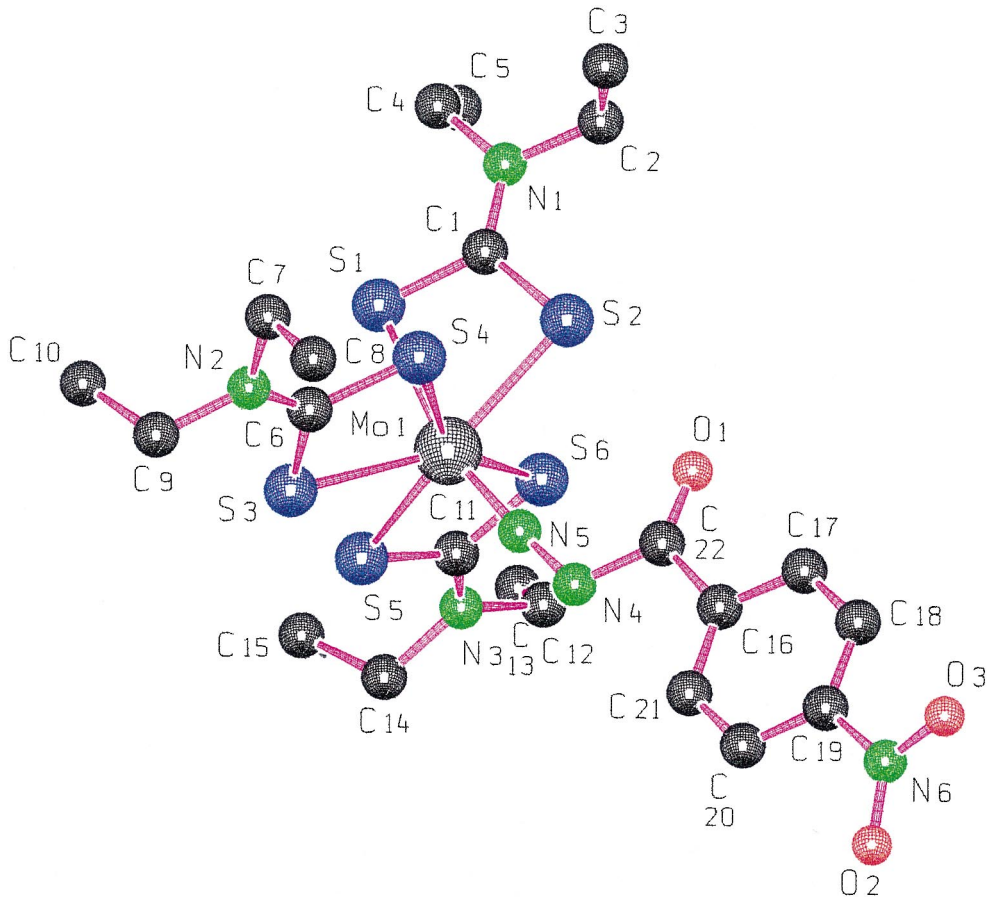


Fig. 2. Molecular structure of $[Mo(NN–CO–C_6H_4–NO_2)(S_2CN(C_2H_5)_2)_3]$ (**2**).

Table 3
Crystal data for $[Mo(NN–CO–C_6H_4–NO_2)(S_2CN(C_2H_5)_2)_3]$ (**2**)

Empirical formula	$C_{22}H_{34}MoN_6O_3S_6{\cdot}0.5C_4H_8O$
Formula weight	754.9
Crystal size (mm)	$0.05\times0.25\times0.50$
Crystal system	monoclinic
Space group	$P2_1/a$
Unit cell dimensions	
a (Å)	10.546(5)
b (Å)	27.084(14)
c (Å)	12.251(6)
α (°)	90
β (°)	110.78(4)
γ (°)	90
V (Å^3)	3437(3)
Z	4
D_{calc} (g cm^{-3})	1.46
μ (cm^{-1})	7.8
$F(000)$	1560
θ_{max}	23
hkl range	$-11\le h\le11,\ 0\le k\le29,$ $0\le l\le13$
Reflections collected	4786
Reflections unique	4786
Reflections observed	$[I>2\sigma(I)]$ 3247
Parameters	372
R_1 (for observed data only)	0.051
wR_2 (for all data)	0.124
Largest difference peak and hole (e Å^{-3})	$+0.6;\ -0.6$

Table 4
Selected bond lengths (A) and angles (°) for $[Mo(NN–CO–C_6H_4–NO_2)(S_2CN(C_2H_5)_2)_3]$ (**2**)

Mo(1)–N(5)	1.756(5)
Mo(1)–S(2)	2.490(2)
Mo(1)–S(5)	2.516(2)
Mo(1)–S(3)	2.522(2)
Mo(1)–S(6)	2.527(2)
Mo(1)–S(4)	2.531(2)
Mo(1)–S(1)	2.576(2)
C(16)–C(22)	1.513(9)
C(22)–O(1)	1.208(8)
C(22)–N(4)	1.382(9)
N(4)–N(5)	1.278(7)
N(5)–Mo(1)–S(2)	96.26(18)
N(5)–Mo(1)–S(5)	101.27(18)
N(5)–Mo(1)–S(3)	98.86(18)
N(5)–Mo(1)–S(6)	90.51(17)
N(5)–Mo(1)–S(4)	91.00(17)
N(5)–Mo(1)–S(1)	166.11(17)
S(2)–Mo(1)–S(1)	69.86(6)
S(5)–Mo(1)–S(1)	90.11(7)
S(3)–Mo(1)–S(1)	2.10(6)
S(6)–Mo(1)–S(1)	86.33(7)
S(4)–Mo(1)–S(1)	85.22(7)
O(1)–C(22)–N(4)	125.1(7)
O(1)–C(22)–C(16)	121.6(7)
N(4)–C(22)–C(16)	113.3(6)
N(5)–N(4)–C(22)	116.0(6)
N(4)–N(5)–Mo(1)	174.9(5)

from the plane through Mo1, S3, S4, S5 and S6. The MoS_2CNC_2 fragment from the diethyldithiocarbamato coligands is nearly planar as expected, and the bond distances lie in the expected ranges [9,20]. The Mo–N5–N4 group is nearly linear (175.4(9)°) indicating extensive electronic delocalization i.e., the Mo–N and N–N have double bond character or, in terms of the valence bond model, the N bound to Mo has sp hybridization. The Mo–N and N–N bond lengths (1.756(5) and 1.278(7) Å, respectively), are consistent with this character. Unfortunately, from X-ray studies it is not possible to establish whether the binding occurs as diazenido(1-) or hydrazido(2-), since comparison of bond lengths and angles (Mo–N–N–$R_{1\ or\ 2}$ fragment) for this ligands in similar compounds (Table 5) indicates that these values are within the same range. However, the double character of the Mo=N and N=N bonds is certain. There is a noticeable difference between these values and those observed for the hydrazido(1-) complexes, Mo–NH–NR_2, where the Mo–N and N–N bonds are single in character as indicated by the longer distances (1.95 and 1.38 Å, respectively), and smaller Mo–N–N angles (between 120 and 140°).

4. Conclusions

In the compounds prepared in this work, we found that bis(dialkyldithiocarbamato)-dioxocomplexes react with *p*-nitrobenzohydrazide and benzohydrazide to yield always seven-coordinate complexes, in which one oxo ligand is substituted by a hydrazide independently of the molar ratios of the hydrazide used, and the other oxoligand is substituted by an additional dialkyldithiocarbamato, even when this coligand is not added in the condensation reaction.

The aroyl hydrazines used in this work act as monodentate ligands, differently from the behavior reported for rhenium with phosphines as coligands, where the aroyl hydrazine preferentially coordinates in a didentate fashion.

Benzohydrazide and *p*-nitrobenzohydrazide have different behavior, the former gives ligands of hydrazido(2-) type while the latter, ligands of diazenido(1-) type. A plausible explanation for this difference is that when the $–NO_2$ group is present, electron density is withdrawn from the nitrogen atom and therefore the N–H bond is unstable. Molybdenum is reduced in this reactions, but the oxidation state of the metal is different in each ligand, thus Mo(V) complexes are obtained starting from Mo(VI) and benzohydrazide, while Mo(V) complexes are formed from *p*-nitrobenzohydrazide.

The study of IR spectra of the diazenido(1-) and hydrazido(2-) complexes, supported by the results of X ray diffraction and ^{1}H and ^{13}C NMR allows to make a

Table 5

Complex	Mo–N	N–N	N–C	Mo–N–N	N–N–C	Reference
Diazenido (1-)						
$[Mo(NCO_2Et)(dtc)_3]$	1.732(5)	1.274(7)	1.382(10)	178.9(5)	117.0(6)	[21]
$[Mo(NNC_6H_4\text{-}3\text{-}NO_2)(S_2CNMe_2)_3]$	1.770(6)	1.262(9)	1.410(10)	170.6(6)	117.9(7)	[22]
$[Mo(NNPh)(dmdtc)_3],CH_2Cl_2$	1.781(4)	1.233(6)	1.417(7)	171.5(4)	120.5(5)	[23]
$[Mo\{NNC_6H_4(m\text{-}NO_2)\}(dmdtc)_3]_2$, $1/2CH_2Cl_2$, $1/2H_2O$	1.765(9), 1.776(9)	1.268(13), 1.256(13)	1.421(15), 1.400(14)	170.0(9), 171.2(8)	118.0(1.0), 117.8(1.0)	[23]
$[Mo(NNC_6H_4Me\text{-}p)_2(acac)_2]$	1.80(3), 1.75(3)	1.27(3), 1.31(3)	1.37(4), 1.45(4)	176.0(28), 177.8(25)	118.0(32), 120.5(28)	[10]
$[Mo(NNC_6H4OMe)_2(acac)_2]$	1.80(2), 1.75(2)	1.24(2), 1.23(2)	1.45(2), 1.44(2)	176.8(14), 174.9(13)	120.3(14), 118.8(15)	[10]
$[Mo(PPh_3)(N\ ^{a}NCOPh)\ ^{b}(N\ ^{a}NCO\ ^{a}Ph)(C_{10}H_{11}N_2O)]$	1.785(8) [b]	1.29(1) [b]	1.40(1) [b]	171.0(6) [b]	111.9(8) [b]	[24]
Hidrazido (2-)						
$[Mo(NNMePh)(NHNMePh)(S_2CNMe_2)_2]^+$	1.752(10)	1.285(14)		169.6(7)		[25]
$[Mo(NnMe_2)O(S_2CNMe_2)_2]$	1.799(8)	1.288(10)	1.485(13), 1.529(12)	168.0(7)	121.9(8), 117.3(9)	[26]
$[Mo(NNPh_2)_2(S_2CNMe_2)_2]$	1.74(1)	1.31(1)	1.43(1), 1.45(1)	169.9(8)	118.8(5), 118.7(7)	[27]
$[Mo(NNEtPh)(S_2CN(CH_2)_5)_3]^+$	1.715(16)	1.37(2)		170(2)	118, 116	[28]
$[MoO(NNMePh)(acac)_2]$	1.789(3)	1.281(4)	1.468(4), 1.419(4)	175.6(2)	118.3(3), 119.5(5)	[29]
$[\{MoO(NNMePh)(acac)(\mu\text{-}OPr\text{-}n)\}_2]$	1.780(4)	1.292(6)	1.466(8), 1.423(6)	165.5(4)	118.7(5), 120.2(5)	[29]
$[MoI(NNHC_8H_{17})(dppe)_2]^+$	1.801(11)	1.259(14)	1.505(17)	174(1)	120(1)	[30]
Hidrazido (1-) [c]						
$[Mo(NHNPh_2)\ ^{c}(NNPh_2)\ ^{d}(acac)Cl_2]$	1.948(5) [c]	1.359(6) [c]	1.412(7), 1.432(7) [c]	140.5(4) [c]	119.4(5), 118.7(5) [c]	[11]
	1.752(4) [d]	1.313(6) [d]	1.433(7) [d]	171.9(4) [d]	118.1(4), 118.4(4) [d]	
$[Mo(NHNMePh)\ ^{e}(NNMePh)\ ^{f}(acac)Cl_2]$	1.948(2) [e]	1.339(3) [e]	1.443(4), 1.416(4) [e]	142.9(2) [e]	117.9(3), 118.7(3) [e]	[11]
	1.750(2) [f]	1.301(3) [f]	1.460(4), 1.419(4) [f]	173.8(2) [f]	116.9(2), 120.3(2) [f]	

[a] Coordinated atoms.
[b] Values correspond to this part of molecule.
[c] Values correspond to this part of molecule.
[d] Values correspond to this part of molecule.
[e] Values correspond to this part of molecule.
[f] Values correspond to this part of molecule.

conclusive assignment of ν(C=O) and ν(N=N) vibrations, which in turn allows to establish the type of binding of the hydrazines as mono o didentate.

A singular behavior is observed for the dialkyldithiocarbamato coligands, since the number of these in the complexes successively increases in each step of the syntheses.

5. Supplementary material

Crystallographic data for the structural analysis have been deposited with the Cambridge Crystallographic Data Centre, CCDC No. 137508. Copies of this information may be obtained free of charge from: The Director, CCDC, 12 Union Road, Cambridge, CB2 1EZ, UK (fax: +44-1223-336033; e-mail: deposit@ccdc.cam.ac.uk or www: http://www.ccdc.cam.ac.uk).

Acknowledgements

This work has been supported by COLCIENCIAS and the Universidad Nacional de Colombia. The authors also gratefully acknowledge the DAAD–Germany for the financial support given to Dr Poveda for a three-month visit to Heidelberg Universität, where most of the analyses were made.

References

[1] M. Hirano, M. Akita, T. Morikita, H. Kubo, A. Fukoka, S. Komiya, J. Chem. Soc., Dalton Trans. (1997) 3453.
[2] G.L. Leigh, Acc. Chem. Res. 254 (1992) 177.
[3] J. Chatt, G.A. Heath, G.J. Leigh, J. Chem. Soc., Chem. Commun. (1972) 444.
[4] M. Hidai, Y. Mizobe, Chem. Rev. 95 (1995) 1115.
[5] See Table 5.
[6] J. Chatt, J.R. Dilworth, G.J. Leigh, V.D. Gupta, J. Chem. Soc. A (1971) 2631.
[7] G.M. Sheldrick, SHELXL-86, Program for the solution of crystal structure, University of Göttingen, 1986
[8] G.M. Sheldrick, SHELXL-97, Program for the refinement of crystal structure, University of Göttingen, 1997.
[9] A.G. Sykes, in: G. Wilkinson, R.D. Gillard, J.A. McCleverty (Eds.), Comprehensive Coordination Chemistry, Pergamon Press, Oxford, 1987, p. 1229.
[10] M.W. Bishop, G. Butler, J. Chatt, J.R. Dilworth, G.J. Leigh, J. Chem. Soc., Dalton Trans. (1979) 1843.
[11] F.W. Moore, M.L. Larson, Inorg. Chem. 6 (1967) 998.
[12] J. Li-Kao, C. Bustos, D. Carrillo, F. Robert, P. Gouzerh, Transition Met. Chem. 18 (1993) 265.
[13] C. Bustos, C. Manzur, D. Carrillo, F. Robert, P. Gouzerh, Inorg. Chem. 33 (1994) 1427.
[14] J. Chatt, B.A. Crichton, J.R. Dilworth, P. Dahlstrom, R. Gutkoska, J. Zubieta, Inorg. Chem. 21 (1982) 2383.
[15] A. Nakamura, M. Nakayama, K. Sugihashi, S. Otsuka, Inorg. Chem. 18 (1979) 394.
[16] M. Decoster, F. Conan, J.E. Guerchais, Y. Le Mest, J. Sala Pala, Polyhedron 14 (1995) 1741.
[17] J. Yang, J. Cryst. Spectr. Res. 19 (1989) 929.
[18] T.C. Hsieh, J.A. Zubieta, Polyhedron 5 (1986) 305.
[19] M. Barber, R.S. Bardoli, G.J. Elliot, R.D. Sedgwick, A.N. Taylor, Anal. Chem. 54 (1982) 645A.
[20] J.M. Berg, K.O. Hodgson, Inorg. Chem. 19 (1980) 2180.
[21] G. Butler, J. Chatt, W. Hussain, G.J. Leigh, Inorg. Chim. Acta 30 (1978) L287.
[22] G. Butler, J. Chatt, G.J. Leigh, A.R.P. Smith, G.A. Williams, Inorg. Chim. Acta 28 (1978) L165.
[23] G.A. Williams, A.R.P. Smith, Aust. J. Chem. 33 (1980) 717.
[24] E. Uhlemann, E. Ludwig, W. Banße, F. Weller, Z. Anorg. Allg. Chem. 620 (1994) 955.
[25] J. Chatt, J.R. Dilworth, P.L. Dahlstrom, J. Zubieta, J. Chem. Soc., Chem. Commun. (1980) 786.
[26] M.W. Bishop, J. Chatt, J.R. Dilworth, M.B. Hursthouse, M. Motevalli, J. Chem. Soc., Dalton Trans. (1979) 1600.
[27] J. Chatt, B.A.L. Crichton, J.R. Dilworth, P. Dahlstrom, R. Gutkoska, J.A. Zubieta, Transition Met. Chem. 4 (1979) 271.
[28] F.C. March, R. Mason, K.M. Thomas, J. Organomet. Chem. 96 (1975) C43.
[29] D. Carrillo, F. Robert, P. Gouzerh, Inorg. Chim. Acta 197 (1992) 209.
[30] V.W. Day, T.A. George, S.D.A. Iske, Jr., S.D. Wagner, J. Organomet. Chem. 112 (1976) C55.

PERGAMON

www.elsevier.nl/locate/poly

Polyhedron 19 (2000) 2337–2344

POLYHEDRON

Preparation and properties of Zn–Cd films from non-aqueous colloids

Galo Cárdenas [a,*], Rodrigo Segura [a], Juan Morales [b], Hugo Soto [b], Carlos A. Lima [b]

[a] *Departamento de Polímeros, Facultad de Ciencias Químicas, Universidad de Concepcion, Casilla 160-C, Concepción, Chile*
[b] *Departamento de Física, Facultad de Ciencias Físicas y Matemáticas, Universidad de Concepción, Casilla 160-C, Concepción, Chile*

Received 1 October 1999; accepted 10 July 2000

Abstract

Bimetallic films of Zn–Cd have been prepared from colloids using several organic solvents: acetone, 2-butanone, THF, 2-propanol and 2-methoxyethanol. The colloids were prepared by simultaneous codeposition of metals and solvents at 77 K. The bimetallic films and solids were obtained by evaporation under vacuum at room temperature (r.t.) A fully chemical characterization of bimetallic films and solids was carried out by different techniques such as elemental analysis, FT-IR spectroscopy, conductivity and thermal analysis. In the IR spectra for all solvents, except for ketones, the common absorption bands appear indicating no alteration upon incorporation of metal particles. The carboxylic band disappearance in ketones may be due to some kind of interaction with metallic particle surfaces. Thermograms showed that bimetallic solids present a decomposition temperature over 400°C. The electric conductivity studies indicated that our bimetallic solids are semiconductors. © 2000 Elsevier Science B.V. All rights reserved.

Keywords: Colloids; Bimetallic films; FT-IR; Conductivity; Thermal analysis

1. Introduction

Nanoclusters with semiconductor behavior have been studied extensively [1–10]. The quantum size effect shifts the band gap of many semiconductors into the visible range and allows the possibility of nanocluster applications in light-emitting diodes. These practical applications of semiconductor nanoclusters have been hindered by surface problems due to non-radiative recombination, lowering the quantum yield of emission.

Another method of increasing the quantum yield of emission was reported more recently [11]. It involves the addition of an impurity to a quantum dot, producing a doped nanocrystalline material. Wang [12] reported a cluster of mixed semiconductors $Zn_xMn_{1-x}S$ being a magnetic semiconductor quantum dot. Manganese doped ZnS clusters have been studied by Bhargava [11,13,14] and Gallagher [15]. Sizes ranging from 35 to 75 Å were obtained and have shown photoluminescence quantum yields around 18%. Cohen [16] has synthesized semiconductor nanoclusters with controlled size and narrow size distributions using block copolymer films prepared by ring-opening methatesis polymerization. The presence of a pendant whole transport group [17] and an electron-transport group can provide, with an electrical access, to nanoclusters for device applications. Photoluminescence emission spectrum for a polymer film containing Mn-doped ZnS nanoclusters was reported [18]. The intensity of emission at 586 nm (Mn emission) was obtained as a function of the excitation wavelength. When the incident radiation decreases below 330 nm, ZnS nanoclusters begin to absorb light, and an increase in the manganese intensity is observed. The excitation of ZnS around 330 nm results in the emission at 586 nm. This proves an energy transfer from ZnS to Mn, which indicates that Mn is doped in the ZnS cluster.

Furthermore, CdS and Zn–Cd sulfide are useful as photoconductors of visible and infrared radiation [19]. These semiconductors are important to make more available photochemical and photovoltaic cells. The most promising photocell designs use their films of

* Corresponding author. Tel.: +56-41-204-256; fax: +56-41-245-974.
E-mail address: gcardena@udec.cl (G. Cárdenas).

0277-5387/00/$ - see front matter © 2000 Elsevier Science B.V. All rights reserved.
PII: S0277-5387(00)00569-6

photosensitizers interfaced with CdS in which the crystal lattice parameters of the two films are molded [20–22].

Herein, we report the results of the synthesis of zinc–cadmium films prepared from the evaporation of the solvents from colloidal dispersions prepared by chemical liquid deposition at 77 K. Films containing residual solvent of acetone, 2-butanone, THF, 2-propanol and 2-methoxyethanol are reported.

2. Experimental

2.1. Preparation of films

The films were prepared by slowly dripping the corresponding colloidal dispersions onto a substrate. To increase the speed of solvent evaporation a vacuum of 10^{-3} Torr was used over 4 h.

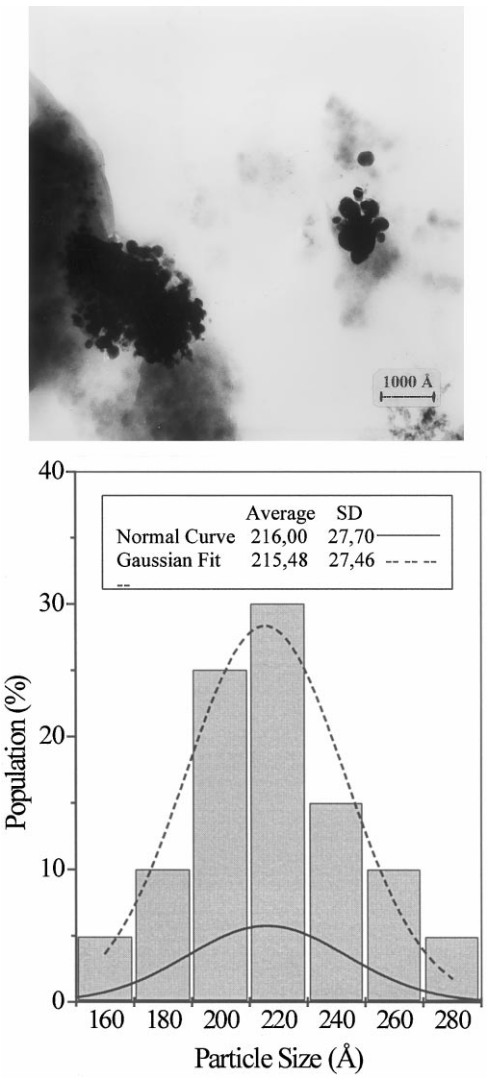


Fig. 1. The electron micrograph and histogram of Zn–acetone colloids. Magnification = 100 K. Mean size: $\mu = 216$, $\sigma = 27.70$ Å.

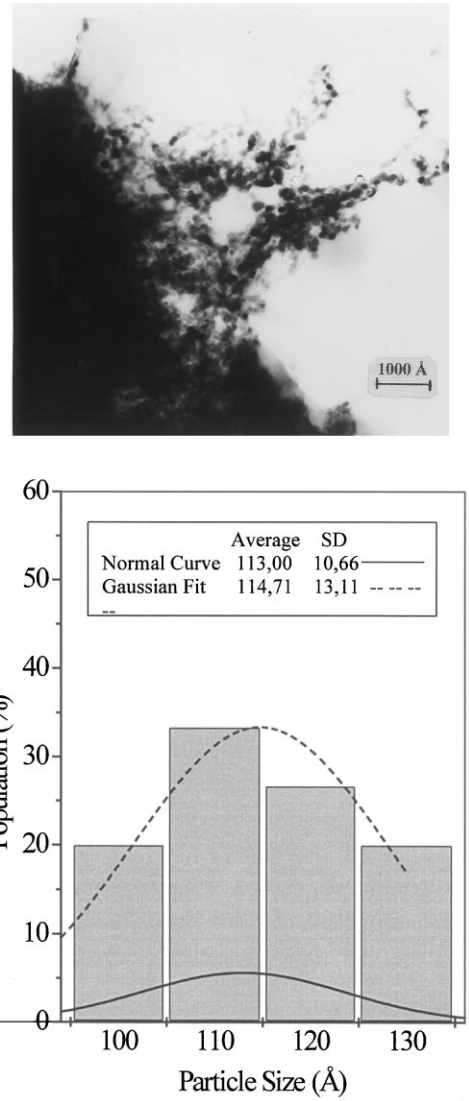


Fig. 2. The micrograph and histogram of Cd–acetone colloids. Magnification = 100 K. Mean size: $\mu = 113$, $\sigma = 10.66$ Å.

2.2. Thermogravimetric analysis

A Perkin–Elmer model TGA-7 thermogravimetric system with a microprocessor-driven temperature control unit and a TA data station, was used. The mass of the samples was generally in the range of 2–3 mg. The sample pan was placed in the balance system equipment and the temperature was raised from 25 to 550°C at a heating rate of 10°C min^{-1}. The weight of the sample pan was recorded continuously as a function of the temperature.

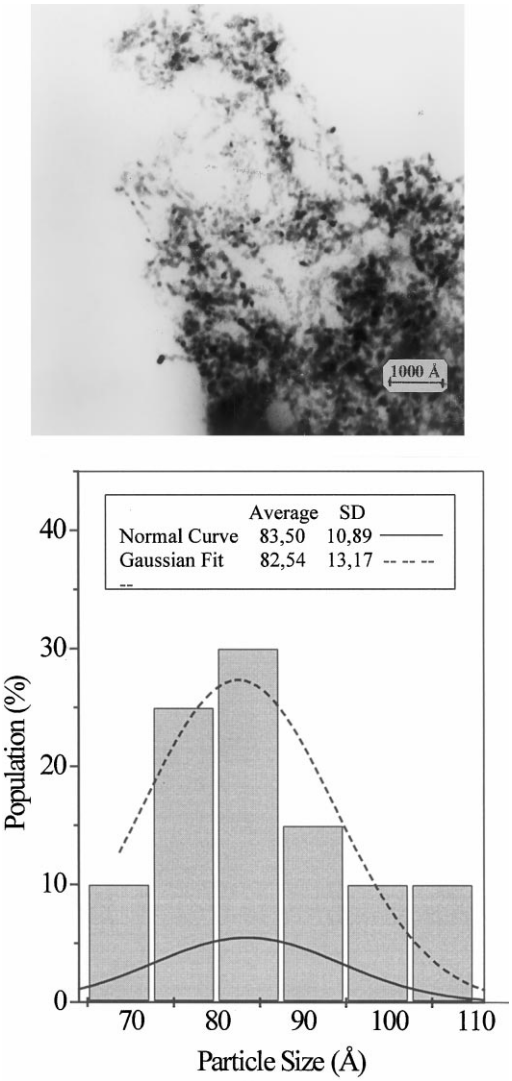


Fig. 3. The micrograph and histogram of Zn–Cd–acetone colloids. Magnification = 100 K. Mean size: $\mu = 83.50$, $\sigma = 10.89$ Å.

2.3. Infrared spectra

IR spectra were obtained using a Nicolet Magna 5PC Fourier transform infrared spectrometer. KBr pellets were prepared for all the films with 2% film concentration. A total of 128 scans were accumulated for each spectrum.

2.4. Elemental analysis

The active solids were analyzed in order to determine their elemental composition (C, H, O).

The Zn and Cd were determined by atomic absorption using a Perkin–Elmer 3100 model.

2.5. Infrared spectroscopy

The IR spectra were performed using a Nicolet Magna 5PC Fourier transform infrared spectrometer. The samples were prepared in a KBr pellet 2% w/w) at 15 000 lbs. The sample was carried out between 400 and 4000 cm^{-1} with 128 scans.

2.6. Conductivity

The electrical conductivity measurements were carried out using 120 mg sample and making a pellet at 16 600 psi.

The electrical resistance was measured using a RCL Fluke PM 6304 bridge and from the area and sample thickness the resistance was transformed to electrical resistivity, independent parameter of the sample size [23].

3. Results and discussion

The films and solids were prepared by solvent evaporation from the colloidal dispersions, using a flask connected to the vacuum line. After solvent evaporation the flask with the active solid is filled up with nitrogen gas to avoid the metal oxidation. The fine powder is later on used for complete characterization.

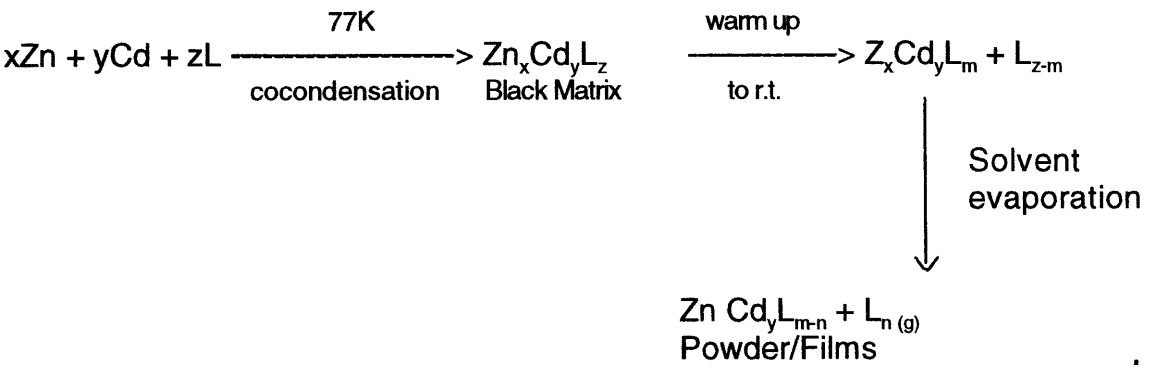


Table 1
Elemental analysis of Zn–Cd solids

Solvent	%Zn (w/w)	%Cd (w/w)	%C (w/w)	%H (w/w)	%O (w/w)
THF	28.6	47.1	4.64	1.3	18.36
THF	24.4	39.0	6.08	2.03	28.49
2-Methoxyethanol	20.1	75.7			
2-Methoxyethanol	32.0	60.9	0.62	0.22	6.26
2-Propanol	27.7	64.5	5.52	1.07	1.21
2-Propanol	30.4	50.7	2.40	0.88	15.62
2-Butanol	29.0	68.4	1.74	0.52	0.34
2-Butanol	32.0	55.4	1.92	0.85	9.83
2-Butanone	34.0	49.4	3.23	0.99	12.38
2-Butanone	27.9	47.8	2.65	0.98	20.67
Acetone	34.4	57.2	1.24	0.50	6.66
Acetone	75.8	0	0.83	0.34	23.03
Acetone	43.0	31.4	2.40	1.20	22.00
Acetone	30.0	36.6	1.45	0.66	31.29
Acetone	4.1	86.9	0.92	0.37	7.71
Acetone	0	87.6	1.35	0.46	10.59

Table 2
Elemental analysis: mole percentages

Solvent	%Zn moles	%Cd moles	%C moles	%H moles	%O moles
THF	11.89	11.39	10.50	35.05	31.18
THF	7.43	6.91	10.08	40.11	35.46
2-Methoxyethanol	12.54	27.46			
2-Methoxyethanol	28.92	32.01	3.05	12.90	23.12
2-Propanol	16.33	22.12	17.72	40.92	2.92
2-Propanol	15.68	15.21	6.74	29.44	32.93
2-Butanol	25.58	35.09	8.35	29.75	1.23
2-Butanol	18.82	18.96	6.15	32.44	23.63
2-Butanone	17.42	14.73	9.01	32.91	25.93
2-Butanone	12.79	12.74	6.61	29.14	38.72
Acetone	25.66	24.82	5.03	24.19	20.30
Acetone	38.58	0.00	2.30	11.22	47.90
Acetone	17.76	7.55	5.40	32.16	37.14
Acetone	13.05	9.26	3.43	18.63	55.63
Acetone	3.56	43.89	4.35	20.84	27.36
Acetone	0.00	38.77	5.59	22.70	32.93

In order to distinguish the differences between the colloids and the bimetallic colloids we are measuring the particle size of the colloid, Cd colloid and Zn–Cd colloid prepared with acetone. Fig. 1 shows the Zn–acetone colloid with particle size, $\mu = 216$ Å but Fig. 2 exhibits Cd–acetone with a particle size of $\mu = 113$ Å. Fig. 3 shows the particle size of the alloy ($\mu = 83.5$ Å) being smaller than the independent metal colloids.

This is good evidence for the presence of the bimetallic clusters.

3.1. Elemental analysis

Table 1 summarizes the w/w percentage of each element forming the solids, which were obtained by solvent evaporation from the colloidal dispersions.

The elemental analysis shows the incorporation between 1–10% w/w of organic materials assuming only the C, H results.

In order to observe a better ration between the elements, the weight percentages were transformed in mole percentage. Table 2 summarizes the values.

It is observed that in most of the cases the initial mole relationship of the metal is constant (50% Zn, 50% Cd) and for acetone the change in the concentration calculated initially is also shown in Table 2.

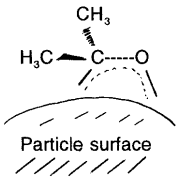
In general, we can see an excess of oxygen moles with respect to carbon, e.g. for THF (C_4H_8O) for each four carbon moles one mole oxygen should exist, and in this case we can observe that the oxygen molar is three times greater than carbon. This could be due to the presence of Zn and Cd oxides on the surface of the particles which could be due to the high oxidation potential of these metals.

These solids are very reactive to moisture and can absorb oxygen and carbon dioxide very rapidly, which also produces severe modification in the analysis.

3.2. FT-IR spectroscopy

The FT-IR spectra obtained for Zn–Cd solids show absorption bands even though the solids exhibit a low amount of solvent incorporated. The most relevant bands in each spectrum are summarized in Table 3 [24].

Most of the solvents were incorporated to the fine particles without structural changes. The acetone shows a weak C=O stretching, mainly due to planar carbonyl interaction with the particle surfaces as shown here:



Following this statement, the carbonyl band should disappear for ketones. Besides, this interaction can explain the colloid stability for ketones, due to the formation of a bond with the surface, producing a steric barrier.

Figs. 4–6 show the IR spectra of some Zn–Cd solids.

It is observed in most of the spectrum bands near 3400 cm^{-1} which corresponds to ν_{OH}. Most of the films get humidity easily during the KBr pellet preparation [24]. Similar IR results were obtained for Cd films prepared with the same solvents [25].

Also, a band at 450 cm^{-1} has been found in all the bimetallic solids. This absorption is due to the zinc and cadmium oxides [26] on the surface of the films. The C–H stretching has disappeared in the Zn–acetone solid films after the oxidation process.

3.3. Thermogravimetric analysis

The decomposition temperatures of the Zn–Cd solids are summarized in Table 4.

It was observed that most of the solids show one decomposition stage over 400°C. This fact allows us to confirm the presence of a very stable bimetallic alloy.

The solids that exhibit two decomposition stages are those in which microanalysis indicates a greater amount of organic material. As an example, THF films exhibit carbon percentages, 4.6 and 6.1, but 2-

Table 3
IR bands of Zn–Cd solids

Solvent	ν (cm^{-1})	Assignment	Observation
THF	3392.66 (m)	symmetric stretching	O–H, humidity
	2961.17 (w)	asymmetric stretching	C–H
	1577.27 (s)	scissoring	H–O–H, humidity
	1395.01 (m)	torsion	C–O
	1350.73 (m)	torsion	C–H
	1090.87 (m)	asymmetric stretching	C–O
	811.05 (w)	rocking	C–H
2-Butanol	3417.0 (m)	symmetric stretching	O–H, humidity
	2915.93 (w)	asymmetric stretching	C–H
	2852.38 (w)	symmetric stretching	C–H
	1565.80 (w)	scissoring	H–O–H, humidity
	1393.37 (m)	torsion	C–H
	1084.76 (s)	asymmetric stretching	C–O
	1022.03 (s)	symmetric stretching	C–C
	799.23 (s)	rocking	C–H
Acetone	3436.02 (w)	symmetric stretching	O–H, humidity
	2961.79 (m)	asymmetric stretching	C–H
	1750.00 (w)	symmetric stretching	C=O
	1550.00 (w)	scissoring	H–O–H, humidity
	1406.10 (m)	torsion	C–H
	1089.96 (s)	asymmetric stretching	C–O
	1023.24 (s)	symmetric stretching	C–C
	800.83 (s)	rocking	C–H

Table 4
Decomposition temperatures of Zn–Cd solids

Solvent	T_D (°C)
THF	276.43/502.60 [a]
THF	230.70/461.70 [a]
2-Methoxyethanol	441.63/523.76 [a]
2-Methoxyethanol	507.90 [a]
2-Propanol	294.86/505.33
2-Propanol	432.53
2-Butanol	486.90
2-Butanol	493.43
2-Butanone	442.56
2-Butanone	435.00
Acetone	449.10
Acetone	390.00
Acetone	517.23
Acetone	413.63
Acetone	513.03
Acetone	482.00

[a] The thermogram exhibits two decomposition temperatures.

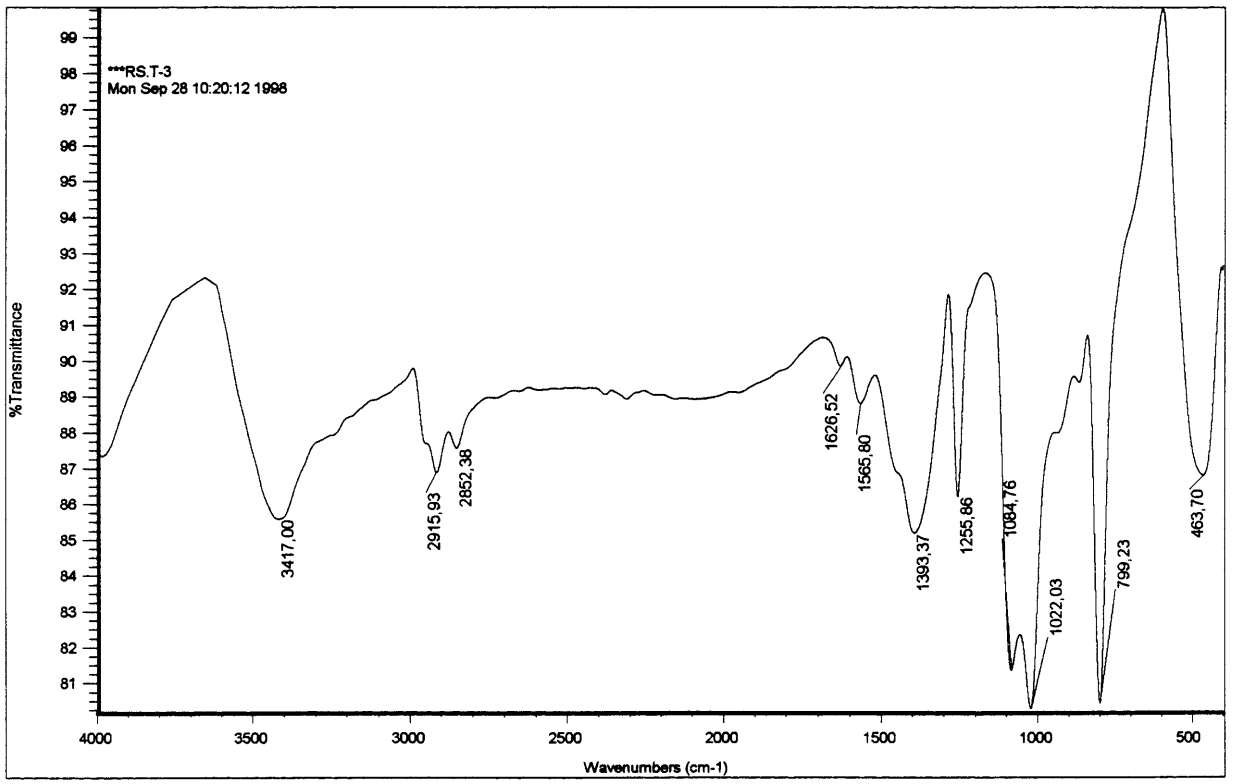


Fig. 4. FT-IR spectrum of (Zn–Cd)-2-butanol films in KBr pellet.

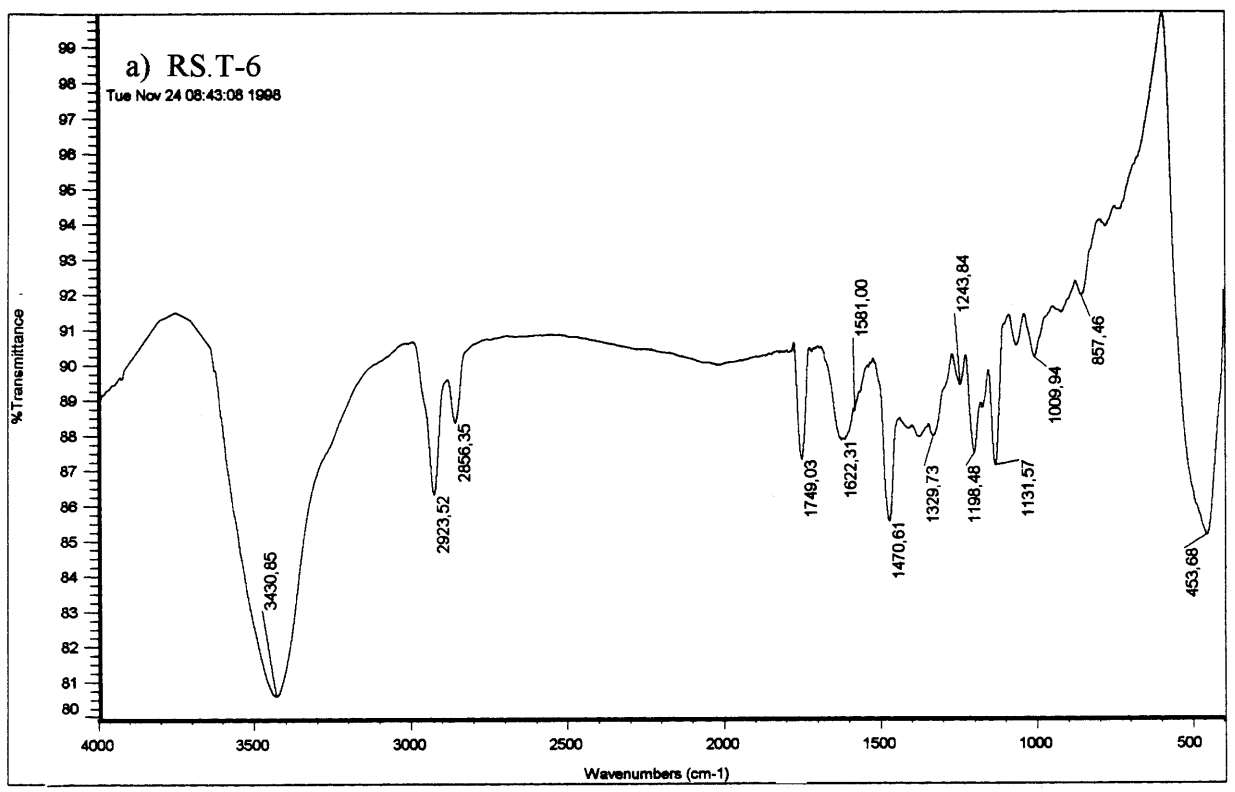


Fig. 5. FT-IR spectrum of (Zn–Cd)–acetone films in KBr pellet.

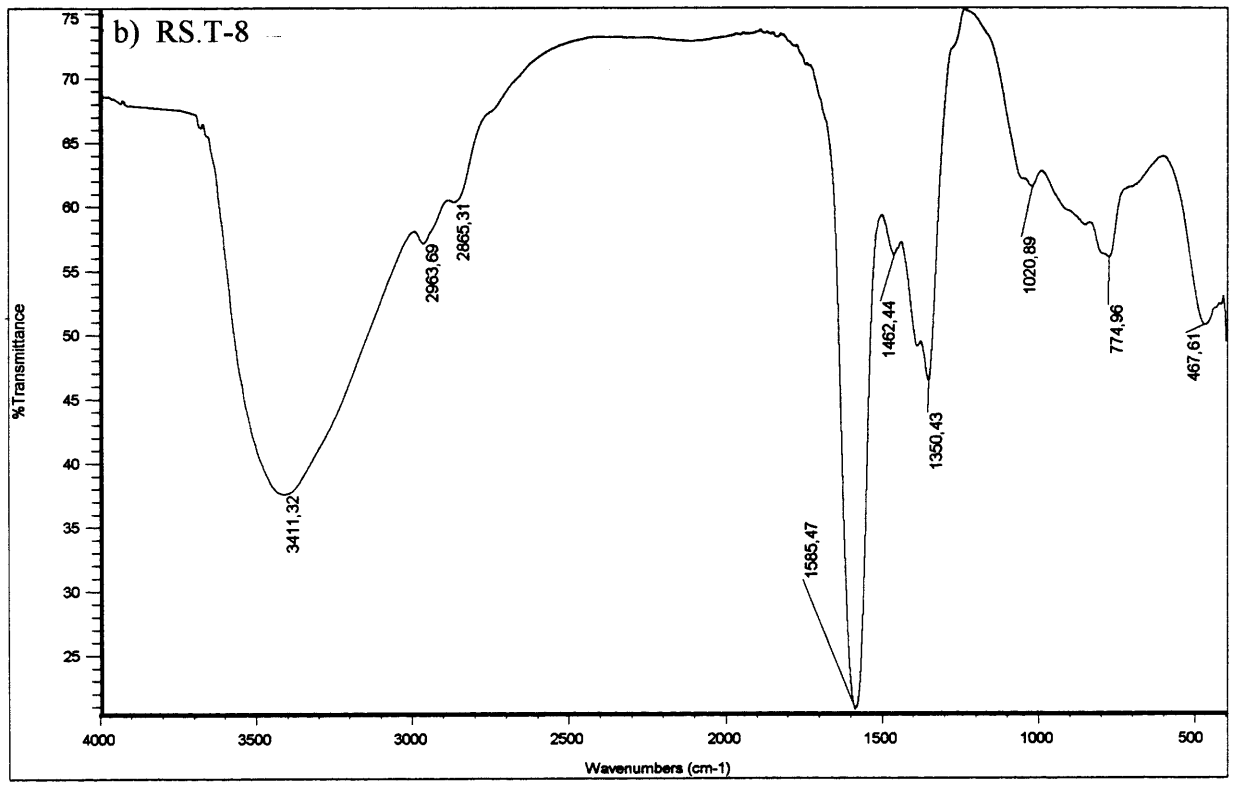


Fig. 6. FT-IR spectrum of (Zn–Cd)–THF films in KBr pellet.

propanol is 5.5% w/w. On the other hand, the other solvents only contain between 0.6 and 3.2% w/w.

This phenomenon can be explained if we consider that most of the organic solvents are physically adsorbed and not through a bond with the metal or bimetal particles. Another possibility is that solvents are occluded in the bimetal cluster particles. The electron micrograph shows spherical particles. Under these considerations we can conclude that the free solvents decompose first before the other bonded with the Zn–Cd films.

There are no tendencies in the decomposition temperatures as a function of concentration, solvent and metal percentage. For instance, the decomposition of the system is independent of the particle size or solvent structure, but is related to the amount and incorporation mechanism of the organic solvents.

It is interesting to observe that Zn–acetone [26] and Cd–acetone [25] films shown a T_D at 390 and 482°C, respectively. However, the (Zn–Cd) acetone films exhibited a T_D at 517 and 513°C, being different from the separate metals.

From the decomposition curves we can see that in most of the cases the solids are very stable without loss of weight until complete solid decomposition. This behavior is an advantage because we can have a great range of working temperatures important for future applications.

It is interesting to notice the 2-methoxyethanol films in which ($T_D = 507$°C), 2-propanol ($T_D = 505$°C), 2-butanol ($T_D = 493$°C) and acetone ($T_D = 482$°C) which are higher than the Zn melting point are showing the presence of the alloy. For THF a T_D higher than 460°C was also observed.

There is no relationship between the amount of weight loss during the decomposition and the amount of organic material obtained from the microanalysis. Most probable because the decomposition temperature near 500°C including the metal vaporization interferes with the TGA analysis.

3.4. Conductivity

The conductivity measurements were carried out for the (Zn–Cd) acetone solids. The study was performed to observe the influence of the metal percentage in the solids.

The electrical conductivities of the Zn–Cd solids are in the same range as semiconductors. These conductivities are lower than that for pure metals [27], 1.66×10^7 (s/m) for Zn and 1.38×10^7 (s/m) for Cd.

The decrease in conductivity with respect to the metals is due to the absence of a bulk structure in which the electrons can move with freedom, conducting electricity. However, we are in the presence of isolated metal particles, separated by a dielectric material [27],

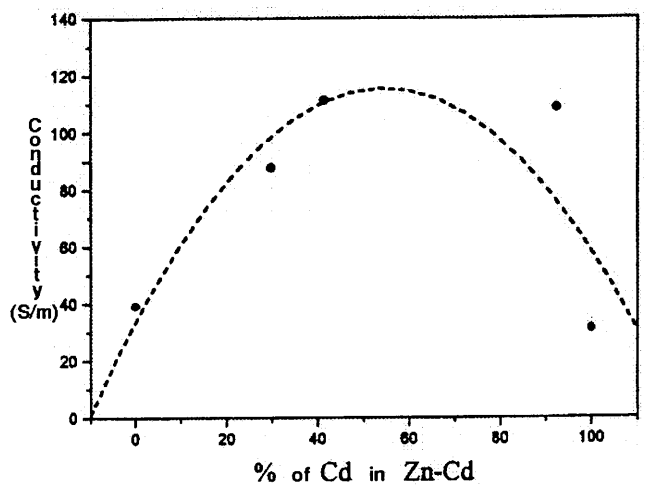


Fig. 7. Conductivity of (Zn_xCd_{1-x})–acetone films versus Cd percentage.

the organic solvent adsorbed on the surface of the metal clusters. Therefore, the conduction mechanism for these materials is different from that of the pure metals due to the availability of electrons to conduct electricity in each particle confined in potential holes separated by a greater energetic barrier (dielectric). Schmid has reported that the conduction for these metal clusters is of the tunnel effect type [28], where the electrons are excited to a higher energy level for electrical conductivity.

Another effect under study is the change in conductivity as a function of the percentage of metal incorporated in the solids. As we can observe in Fig. 7, there is an increase in the conductivity of the bimetallic solid with respect to the monometallics.

4. Conclusions

Metal films containing organometallic residues were obtained. The IR analysis showed the presence of the organic solvents in the films. These alloyed films or active powders containing solvents showed higher thermal stability than pure metals.

These active bimetallic films exhibit semiconductor properties which depend on the increase in the Cd content, keeping the measurements at r.t.

Acknowledgements

The authors would like to thank financial support from CONICYT (Grant 1960621) and technical assistance from Dirección de Investigación, Universidad de Concepción.

References

[1] A. Henglein, Chem. Rev. 89 (1861) 1989.
[2] P.E. Lippens, M. Lannoo, Phys. Rev. B39 (1989) 935.
[3] P.E. Lippens, M. Lannoo, Phys. Rev. B41 (1990) 6079.
[4] C.H. Fischer, H. Weller, L. Katsikas, A. Henglein, Langmuir 5 (1989) 429.
[5] A. Eychmuller, L. Katsikas, H. Weller, Langmuir 6 (1990) 1605.
[6] D. Schoose, A. Mews, A. Eychmuller, H. Weller, Phys. Rev. B49 (1994) 17072.
[7] Y. Wang, N. Herron, J. Caspar, Mater. Sci. Eng. B19 (1993) 61.
[8] M.G. Bawendi, A.R. Kortan, M.L. Steigerwald, L.E. Brus, J. Chem. Phys. 91 (1989) 7282.
[9] M.G. Bawendi, P.J. Carroll, W.L. Wilson, L.E. Brus, J. Chem. Phys. 96 (1992) 946.
[10] C.B. Murray, D.J. Norris, M.G. Bawendi, J. Am. Chem. Soc. 115 (1993) 8706.
[11] R.N. Bhargava, D. Gallagher, X. Hong, A. Nurmikko, Phys. Rev. Lett. 72 (1994) 416.
[12] Y. Wang, N. Herron, K. Moller, T. Bein, Solid State Commun. 77 (1991) 33.
[13] R.N. Bhargava, D. Gallagher, T. Welker, J. Lumin. 60, 61 (1994) 275.
[14] R.N. Bhargava, J. Lumin 70 (1996) 85.
[15] D. Gallagher, W.E. Heady, J.M. Racs, R.N. Bhargava, J. Cryst. Growth 138 (1994) 970.
[16] R.S. Kane, R.E. Cohen, R. Silbey, J. Phys. Chem. 100 (1996) 7928.
[17] J. Yue, R.E. Cohen, Supramol. Sci. 1 (1994) 117.
[18] J. Gratt, R.E. Cohen, Macromolecules 30 (1994) 3137.
[19] J. Torres, G. Gordillo, Thin Solid Films 207 (1992) 231.
[20] R.C. Sekhar, K.N. Raju, D.R. Reddy, B.K. Reddy, J. Phys. D. Appl. Phys. 21 (1988) 1182.
[21] J. Loeferski, J. Proceeding of the 16th IEEE Photovoltaic Specialists Conference, San Diego, CA, 1988.
[22] K.W. Boer, J. Cryst. Growth 59 (1982) 111.
[23] R.H. Hunter, Introduction to Modern Colloid Surface, Oxford Science Publications, London, 1993 (Chapter 9).
[24] R.M. Silverstein, Spectrometric Identification of Organic Compounds, third edition, Wiley, New York, 1999, p. 102.
[25] G. Cárdenas, A. Ponce, Colloid Polym. Sci. 274 (1996) 788.
[26] G. Cárdenas, R. Oliva, H. Soto, O. Pantoja, Bol. Soc. Chil. Quím. 40 (1995) 261.
[27] R.C. Weast, M.J. Astle, Handbook of Chemistry and Physics, 62nd edition, CRC Press, Boca Raton, FL, 1981, p. 1982.
[28] (a) G. Schmid, J. Chem. Soc. Dalton Trans (1998) 1077. (b) G. Schmid, Chem. Rev. 92 (1992) 1709.

PERGAMON

www.elsevier.nl/locate/poly

Polyhedron 19 (2000) 2345–2351

POLYHEDRON

Preparation and characterization of MgO powders obtained from different magnesium salts and the mineral dolomite

E. Alvarado [a], L.M. Torres-Martinez [a], A.F. Fuentes [a], P. Quintana [b,*]

[a] *Facultad de Ciencias Quimicas, DES, UANL, Monterrey, N.L., Mexico*
[b] *Cinvestav del IPN, Unidad Merida, km.6 Antigua Carretera a Progreso, C.P. 97310, Merida, Yucatan, Mexico*

Received 13 October 1999; accepted 11 May 2000

Abstract

The characterisation of the physical properties of MgO powders, obtained from three commercial magnesium compounds, $MgSO_4 \cdot 7H_2O$, $MgNO_3 \cdot 6H_2O$ and $Mg(CH_3CO_2)_2 \cdot 4H_2O$ and the mineral dolomite (natural source from Mexico), synthesised by chemical precipitation, is presented. The decomposition of the precipitated $Mg(OH)_2$ was analysed by DTA/TGA and the crystallisation process was observed by XRD. The variation of the properties with the nature of the precursors at 960°C was studied: as the crystallite size, density, specific surface area, degree of agglomeration, and the total porosity. The microstructural differences between the MgO agglomerates were examined by SEM, at different temperatures. © 2000 Elsevier Science B.V. All rights reserved.

Keywords: Magnesia; Dolomite; Crystallite size; Degree of agglomeration; X-ray diffraction; SEM

1. Introduction

Magnesia (MgO) is the most important product of the magnesium compound industry. It is usually produced for commerce by the thermal decomposition of magnesite ($MgCO_3$), from magnesium hydroxide ($Mg(OH)_2$) obtained from a seawater process or from magnesium rich-brines as the mineral dolomite [1]. Mexico is one of the major producers of MgO; the states of Nuevo Leon and Coahuila contain large deposits of high-purity dolomite; major capacity expansions took place in 1992 when Industria Peñoles started with the production of high-purity electrofused MgO in Ramos Arizpe, Coahuila [1].

The most important process for the production of MgO from seawater or brine is based on the fact that $Mg(OH)_2$ can be precipitated from solutions of magnesium salts by the addition of a strong base. The $Mg(OH)_2$ precipitate is washed, filtered and then calcined to produce MgO. Decomposition of solutions of magnesium salts is also important for the synthesis of ceramic powders. Many alternative techniques have been developed offering advantages of easy preparation of oxide powders, accurate compositional control, homogeneity and high purity [2–6].

Caustic-calcined MgO is produced at temperatures < 900°C and characterised by its moderate to high chemical reactivity. This type of magnesia has numerous applications as mineral supplement for animal feeds, in fertilisers, as a raw material for various MgO chemicals, to manufacture ceramics, cements, paper, petroleum additives, etc. Meanwhile, calcined dolomite as a source of alkali is used in agriculture, to neutralise soil acidity and adds calcium and magnesium to it; it can also can be used in the manufacture of refractories, as mineral filler, as a constituent in a glass batch, etc. [1].

The physical properties of MgO powders are affected by the type of precursor, the temperature of calcination and the impurities. Actually, one of the main problems detected in the production of caustic magnesia powders is to achieve a real density near to the ideal value, in order to obtain ceramic bodies with suitable compacting conditions. The properties of refractories in industrial processes with low densities, present undesired characteristics such as the formation of low eutectic

* Corresponding author. Tel.: +52-99-81-2960; fax: +52-99-81-2917.
E-mail address: pquint@mda.cinvestav.mx (P. Quintana).

0277-5387/00/$ - see front matter © 2000 Elsevier Science B.V. All rights reserved.
PII: S0277-5387(00)00570-2

points due to the presence of impurities, vulnerability to chemical attack and a deficient mechanical resistance [7–9].

Studies on the synthesis of materials with appropriate refractory properties had been aimed to obtain powders with certain characteristics, which may help to improve the process of sintering [10]. Among these, the following can be mentioned: high surface area, uniform particle size and chemical homogeneity. The formation of large agglomerates must be avoided, since these generate fractures in their surroundings and if present in excess, they can accelerate or delay the sinterability phenomena. The morphology of powders of MgO has been observed using scanning electron microscopy (SEM), to study the origin of the degree of agglomeration in caustic MgO and to analyse the effects during the process of sintering [7,8,11,12].

The aim of this work was to study and characterise the physical properties of MgO powders obtained by chemical precipitation from three commercial chemical compounds to be compared with dolomite (natural source from Coahuila, Mexico). Different measurements were carried out at 960°C (the surface area, the primary particle size, the crystallite size and the apparent density) to determine the degree of agglomeration between the different types of precursor. The crystallization of magnesia was studied by X-ray diffraction, and the development of the morphology was observed by SEM.

2. Experimental

Powders of MgO were synthesised by chemical precipitation from four different types of precursors, three of them commercial reagent-grade hydrated salts: $MgSO_4 \cdot 7H_2O$, $MgNO_3 \cdot 6H_2O$ and $Mg(CH_3CO_2)_2 \cdot 4H_2O$ and from the mineral dolomite ($MgCO_3 \cdot CaCO_3$) obtained from Coahuila, Mexico. The chemical analysis of dolomite used in this experiment, measured by X-ray fluorescence with Cr radiation (Diano 8000), indicates a purity of 99.8%. The principal impurities (wt%) were SiO_2 (0.01), Al_2O_3 (0.01), Fe_2O_3 (0.04), Na_2O (0.02) and P_2O_5 (0.03). The purity, for the three reagent-grade salts, taken from the catalogues of the manufacturers (Productos Quimicos Monterrey, SA), was 99.8%.

Each hydrated compound was dissolved in deionized water at room temperature to yield 0.8 M, an excess of ammonium hydroxide (13 M) was added, and vigorously stirred at 50°C, pH 10. A white precipitate of $Mg(OH)_2$ was obtained, which was thoroughly washed with distilled water and dried at 100°C for 2 h. Magnesium hydroxide powders were calcined in Pt crucibles, at different temperatures to produce MgO powders. The heating treatment was carried out in electric furnaces under air atmosphere, from 500 to 1000°C, raising the temperature 100°C every 40 min.

Natural dolomite was initially milled to 200-mesh. The decarbonation procedure was done with a progressive heating from 500 to 800°C, with a stepwise of 100°C every 0.5 h. The sample was held for 2 h and finally the temperature was increased to 900°C (0.5 h) to obtain dolima (MgO·CaO). The hydration of dolima (0.9 M) was made with a vigorously agitation and then it was mixed with a $MgCl_2$ (0.5 M) solution at 50°C, pH 11. Once $Mg(OH)_2$ appeared as a precipitate, it was washed, dried and calcined under the same conditions described above, finally a powder of MgO was obtained.

The decomposition characteristics of the salts and dolomite were determined by simultaneous differential/thermogravimetric analysis (DTA/TGA, TA-Instruments model SDT-2960). The heating rate of the sample was 10°C min^{-1}, with a flowing N_2 atmosphere, using alumina as a reference material. The powders from each calcined treatment were characterised by X-ray diffraction and the crystallite size was calculated using the Scherrer's formula, using KCl as an internal standard. A Cu Kα radiation ($\lambda = 1.5405$ Å) and Ni filter was used. The difractograms were registered in a range of 10–115 2θ (30 kV, 20 mA), in a step-scan mode of 0.01° 2θ per step and counting for 5 s/step (model Siemens D-5000).

MgO apparent density was obtained by the liquid pycnometer method according to ASTM C699, using toluene; several measurements were done until data reproducibility was obtained. The specific surface area and primary particle size of MgO powders was measured by the BET technique (Ströhlein), N_2 as an absorption gas was used. The morphology of $Mg(OH)_2$ and MgO agglomerates at different temperatures were examined by SEM (Leica S440). Powders were pelletized and coated with carbon to avoid charging during exposure to the electron beam and covered with an Au thin film by sputtering in a vacuum system.

3. Results and discussion

The decomposition path of the precipitated, $Mg(OH)_2$, was studied by DTA/TGA analysis. Results obtained from the salts were similar. A very small and a strong endothermic peak was observed; the first peak is related to the dehydration processes at temperatures < 200°C and the second to the decomposition of magnesium hydroxide, the temperature was 420, 310 and 390°C, for sulfate, acetate and nitrate, respectively. Furthermore, sulfate salt shows a continuous weight loss of 7%, between 600 and 920°C. The total weight loss was around 40% (Fig. 1). These results are in good agreement with the ones presented elsewhere [4]. In the case of dolomite, the first endothermic peak was very strong with a weight loss of 13.44 wt% and the decom-

position reaction was held at 370°C with a weight loss of 25.9%; finally at 800°C evaporation of CO_2 occurs (Fig. 1). Therefore, the complete decomposition of the acetate and nitrate can be achieved at reasonably low temperatures (< 450°C); however for the dolomite and sulfate salt this was near 800 and 950°C, respectively.

The X-ray diffraction studies on the crystallisation process for the magnesium salts showed the formation

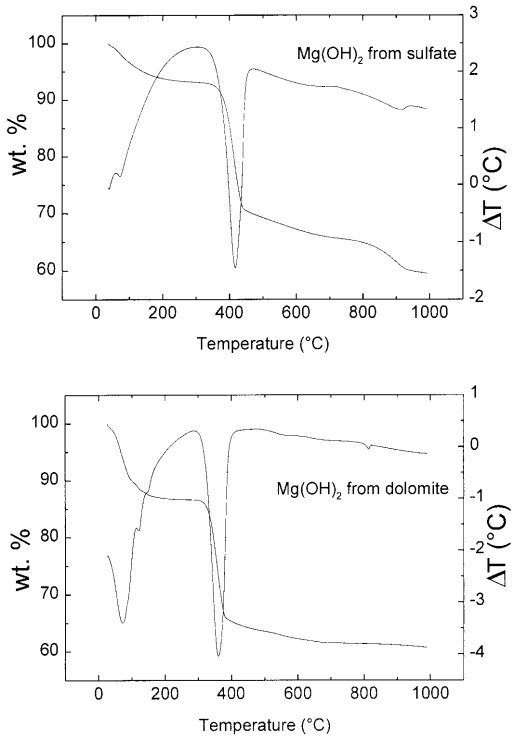


Fig. 1. DTA/TGA of $Mg(OH)_2$ obtained from two different precursors.

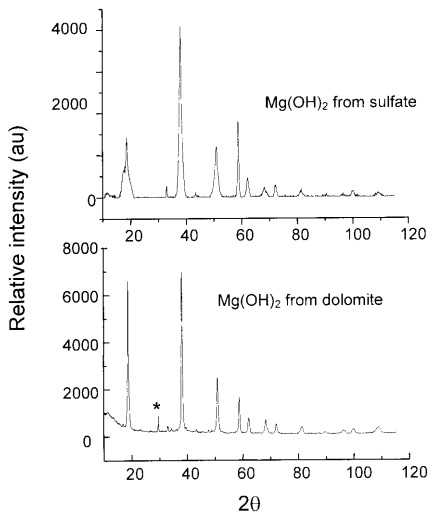


Fig. 2. Comparison of the X-ray diffraction patterns of $Mg(OH)_2$ at 100°C, between sulfate and dolomite. The latest shows the presence of $CaCO_3$ (*).

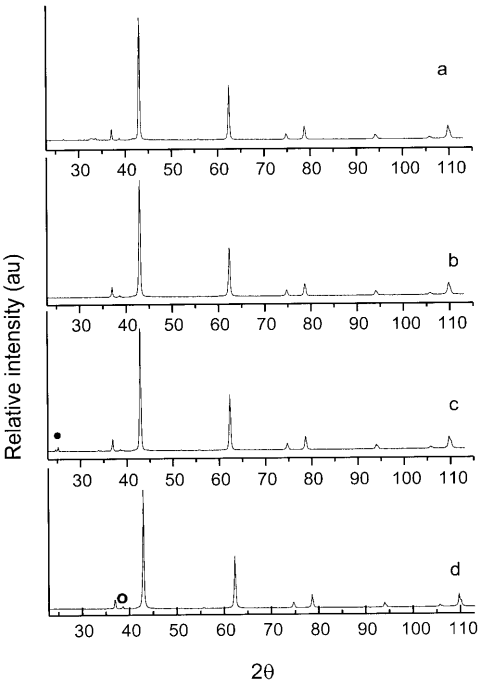


Fig. 3. Diffractograms of MgO powders obtained at 960°C from different precursors: (a) dolomite, (b) nitrate, (c) sulfate, (d) acetate. Traces of $MgSO_4$ (●) and NaF (○) are indicated.

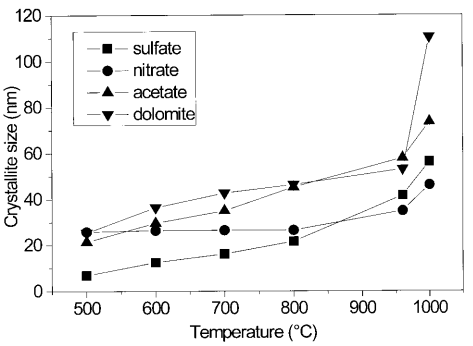


Fig. 4. Development of crystallite size with temperature on the crystallisation of MgO.

of brucite $Mg(OH)_2$ at 100°C with a very poor crystallinity, although dolomite presented stronger diffraction peaks as can be seen in Fig. 2. At higher temperature, crystals of periclase (MgO) were initially detected at 500°C after 40 min, with broad diffraction peaks, which became nice and sharp at 960°C, mainly on dolomite, since it had a higher crystallinity (Fig. 3). Additional diffraction lines were detected, as traces of NaF and magnesium sulfate phases.

Crystallite size was calculated, by means of Scherrer's equation [13] on the (200) diffraction maximum, obtained from the different powders heated 40 min at each temperature (500–1000°C). The behaviour of the crystallite growth with temperature is shown in Fig. 4. The results are very similar for the chemical com-

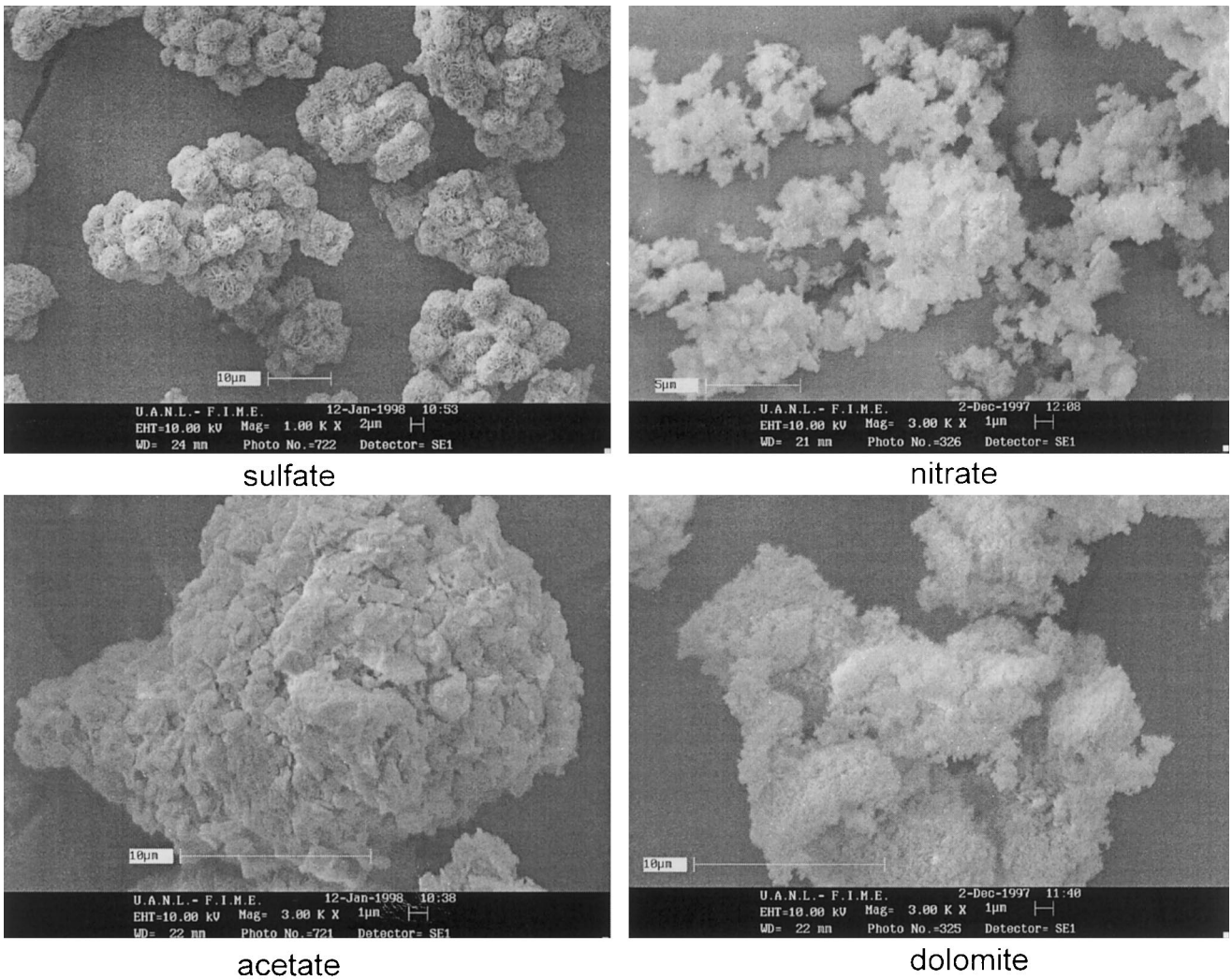


Fig. 5. Microstructure of $Mg(OH)_2$ powders obtained from the different precursors, heated at 100°C for 40 min.

pounds. Near to the decomposition temperature of brucite, the magnesium oxide formed has a very small crystallite size, showing a plateau with a slight increment, and with a crystallite growth of 10–40 nm. On raising the calcination temperature, over 850°C, a rapid increase in the crystallite size occurs; where dolomite had the highest value of 110 nm at 1000°C, which is double the value obtained for the other precursors. These data are in good agreement with the values reported in the literature for oxides prepared from different chemical precursor salts [14,15].

The apparent density measurements determined by pycnometry, ρ_{app}, at 960°C, are shown in Table 1. The density values of sulfate approach the theoretical data of periclase (3.59 g cm^{-3}), meanwhile, dolomite shows the lowest value probably due to the higher crystallite size. It has been reported that it is difficult to obtain high-density magnesia from purified raw materials [11].

Table 1
Physical properties of MgO powders obtained at 960°C (40 min) from different precursors

Precursor	ρ_{app} (g cm^{-3})	ρ_{DRX} (g cm^{-3})	Surface area [a] (m^2 g^{-1})	Surface area (m^2 g^{-1})	G_{BET} (nm)	G_{DRX} (nm)	G_{BET}/G_{DRX}	P_{tot} (%)
Sulfate	3.53	3.576	137.6	64.4	25.9	41.6	0.62	1.3
Nitrate	3.46	3.584	124.2	30.8	54.2	54.9	0.99	3.46
Acetate	3.44	3.581	105.0	28.9	57.7	57.9	0.99	3.94
Dolomite	3.42	3.585	47.3	16.5	101.1	53.1	1.90	4.60

[a] Values obtained for $Mg(OH)_2$ at 100°C, 40 min.

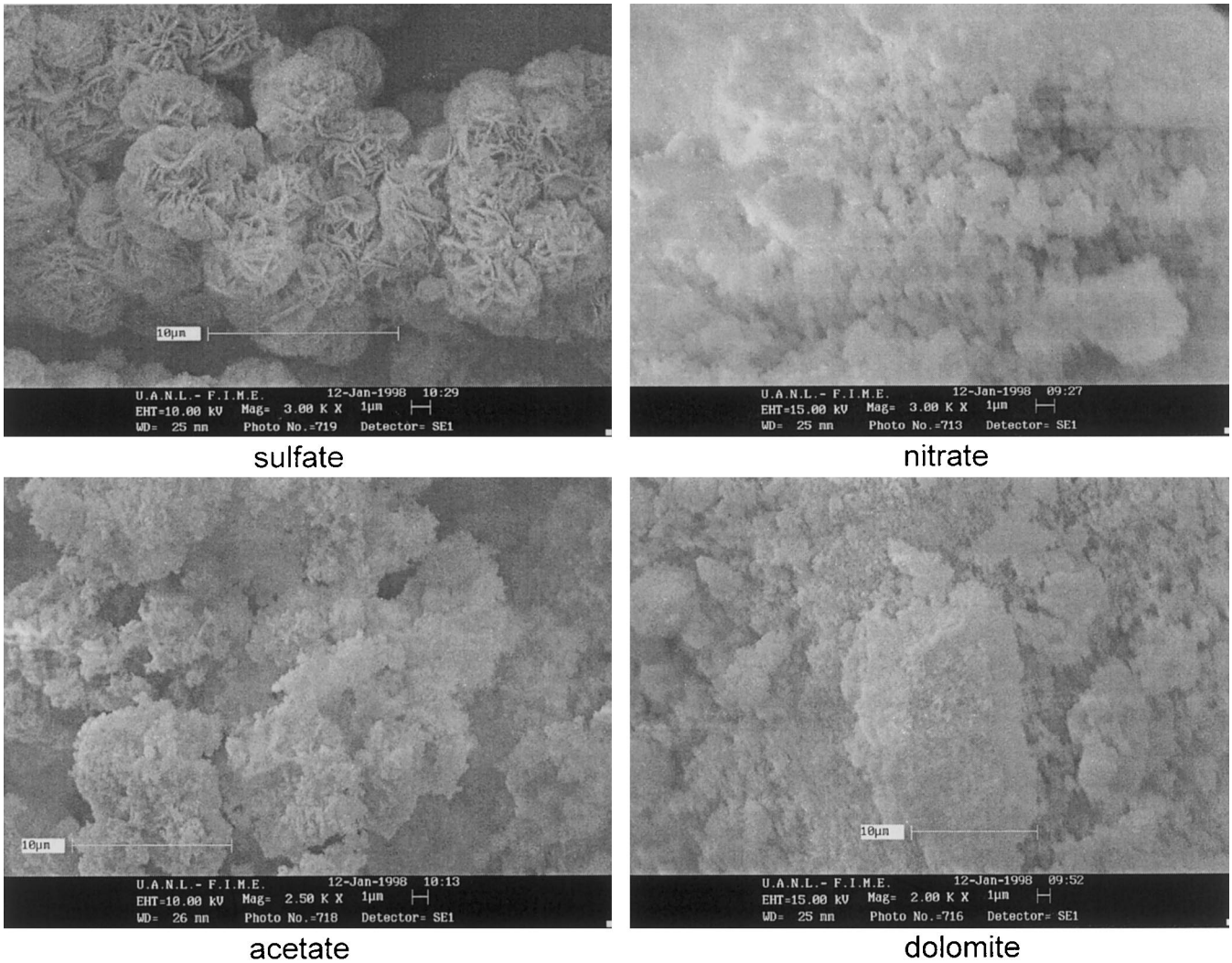


Fig. 6. SEM micrographs of MgO powders at 960°C, showing the formation of agglomerates.

Density from X-ray diffraction data was also calculated, ρ_{XRD} (same as ρ_{true}), using KCl as an internal standard and a least-square refinement program [16] to determine precisely the lattice parameter. The values obtained show good agreement with the theoretical value of periclase.

The percentage of total porosity in the different magnesia samples was calculated from

$$\%P_T = \left(1 - \frac{\rho_{app}}{\rho_{true}}\right) \times 100$$

according to [17], where the highest value was observed on powders derived from dolomite, 4.6%, and the lowest for sulfate, 1.3%. Acetate and nitrate had 3.5% and 3.9%, respectively.

The variation of the specific surface area for brucite and MgO powders can be observed in Table 1. The surface area values were higher for the powders obtained from the reagent-grade salts than those obtained from the mineral dolomite. In all cases MgO had a much lower value than the corresponding $Mg(OH)_2$. The samples obtained from sulfate show the highest values, which agrees with the smallest particle size. Meanwhile, nitrate and acetate show intermediate values. In contrast, the powders prepared from dolomite had values almost four and two orders of magnitude lower than the data obtained for sulfate and from nitrate and acetate, respectively. This effect can be related to the ρ_{app} value, which depends on the utilised precursor and the presence of impurities. The surface area obtained for periclase was in a good agreement with other reports [7,15], < 100 m^2 g^{-1}, but much higher than [14,18] due to the different route of preparation.

The degree of agglomeration G_{BET}/G_{XRD} was obtained from the primary particle size, G_{BET}, determined from the specific surface area, and from the crystallite size, G_{XRD} [8] (Table 1). The lowest agglomeration degree, 0.62, was for the sulfate sample. MgO powders obtained from the nitrate and acetate precursors were

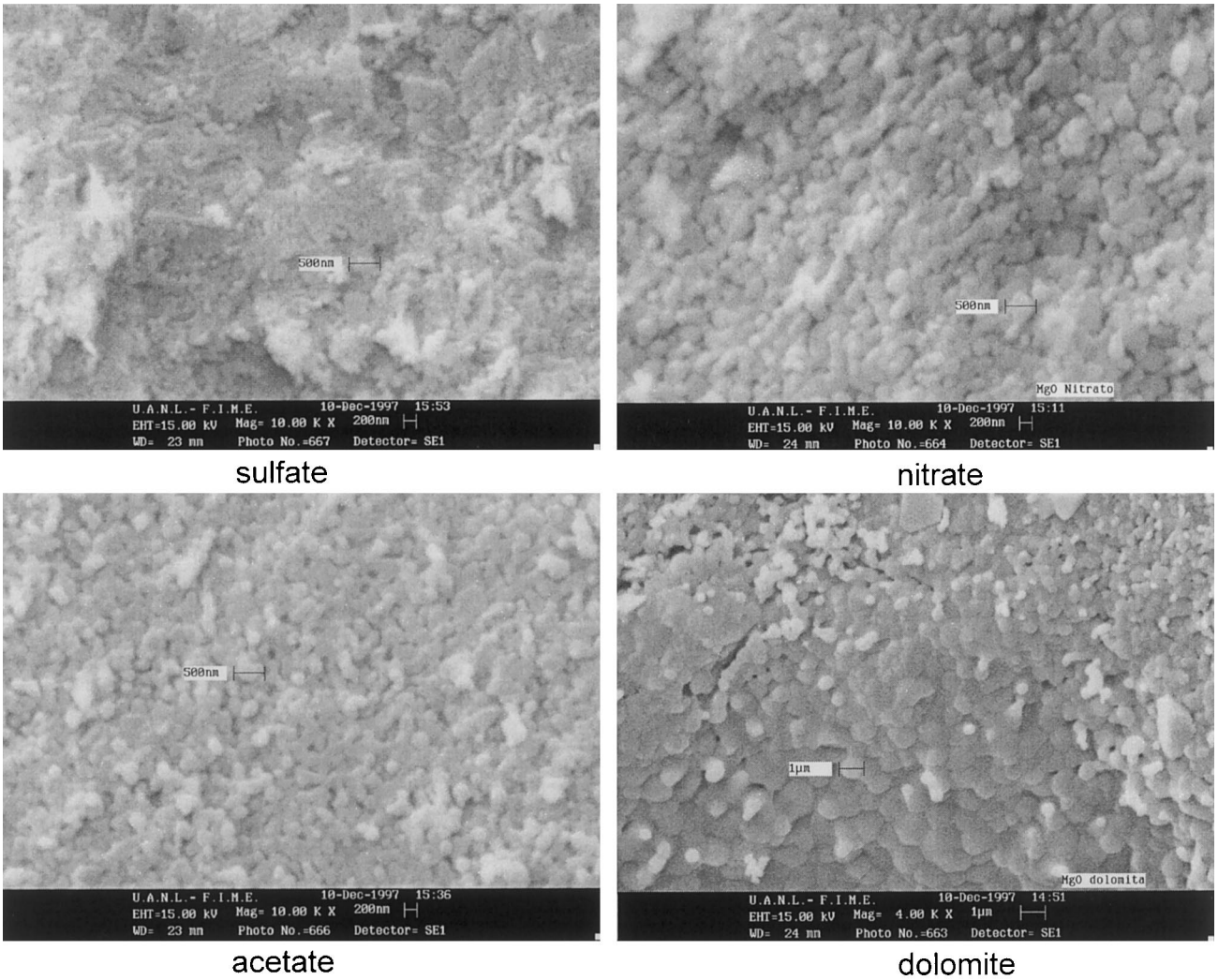


Fig. 7. Microstructure of MgO powders showing the initial stage of sintering at 1200°C (40 min).

nearly at unity, the ideal value, since the crystallite sizes were almost in accord with the primary particle sizes [8]. Meanwhile, the mineral dolomite almost doubles this value to 1.90; similar to the powder derived from the seawater magnesia process [7].

The analysis by SEM, showed the morphology of $Mg(OH)_2$ and MgO powders originating from different calcination temperatures (Figs. 5–7). At 100°C, the brucite phase is observed, which shows microstructural differences for the four precursors (Fig. 5). Samples derived from dolomite and nitrate are formed of small particles consisting of dispersed agglomerates between 5 and 10 μm, and acetate contains flakes forming large agglomerates (30 μm). At 960°C, the periclase powders for these three precursors show the presence of fine particles, less than 1 μm, forming agglomerates with a more homogeneous distribution (Fig. 6). Meanwhile, the microstructure of MgO powders calcined 1 h at 1200°C (Fig. 7), differed significantly from the precipitated hydroxide. The magnesium salt compounds showed the formation of grains with a homogeneous distribution (less than 500 nm), it was also possible to observe the initial formation of necks between particles. However, dolomite powders showed a more inhomogeneous distribution of grains, between 0.5 and 1 μm, with a higher porosity (dark zones between the grains) due to a rapid grain growth, which brings the entrapment of pores.

Magnesium hydroxide derived from sulfate show a plate-like shape, the particles were joined to each other forming spherical particles around 3 μm, which tend to form large agglomerates (30 μm). At higher temperature (960°C), a well-defined plate-like morphology was observed (with a high aspect ratio of length to thickness), which can be related to the periclase phase (Fig. 6); a similar morphology has been reported elsewhere [19]. Also, the particle size increases to 5 μm. A significant change in particle shape was observed at 1200°C, pseudomorph agglomerates were found in the calcined product (Fig. 7).

The powder activity provides the driving force for sintering, and increases with the surface area, thus with a decrease in the particle size. Moreover, a smaller value of G_{BET}/G_{XRD} indicates that the primary particle is composed of softer agglomerations of crystallites [20]. Therefore, magnesium oxide powders derived from sulfate, which showed the highest surface activity, had the softest agglomeration of crystallites among the four powders, as can be seen on the SEM image at 1200°C (Fig. 7).

It has been reported elsewhere [21], that a good densification of aggregates occurs when the growth of crystallites and pores are retarded. Therefore, from the G_{BET}/G_{DRX} data (Table 1), and from the images of SEM at 1200°C, we can conclude that powders from nitrate and acetate show the best physical properties. The mineral dolomite should be easily sintered to high-density bodies, and can be used to produce magnesia (which should be dead-burnt, i.e. chemically inactive) for the manufacture of heavy-duty basic refractories [17].

4. Conclusions

We present a comparative study on the characterisation of different physical properties of MgO powders prepared from three precursor magnesium salts and from the mineral dolomite. The samples were characterised by X-ray diffraction, thermal analysis, N_2 adsorption and SEM.

The samples at low temperatures are composed of brucite, and after 500°C pure periclase appears, where the degree of crystallinity increases with the temperature of calcination. The apparent density and the specific surface area for brucite and periclase show the following decreasing sequence: sulfate > nitrate > acetate > dolomite. Meanwhile, the particle size, the degree of agglomeration and the percentage of the total porosity, present the inverse tendency.

Magnesium powders from sulfate precursors, showed the best approach to the ideal density value, due to their high surface area, and consequently, to their smallest primary particle size. Also, the specific area value can be related to the microstructure of lamellars disposed around a central nucleus.

Microstructure studies showed that powders derived from acetate and nitrate promotes sufficient diffusion of matter into neck regions between individual particles, favouring the initial stage of sintering and a uniform grain growth. This agrees with the values obtained for the degree of agglomeration, which are near to one.

Dolomite had the biggest primary particle size due to it low surface area, therefore the degree of agglomeration is much higher in comparison with the magnesium salts. The rapid growth of crystallite size promotes the entrapment of pores between the grains, which is reflected in the higher total porosity value.

Acknowledgements

We thank CONACYT (Mexico) for supporting this project (3824P-A9607). P.Q. also acknowledges the program Catedra Patrimonial (970030-R98) and M.Sc. D.H. Aguilar for helpful comments and assistance in preparing the manuscript.

References

[1] A.N. Copp, Am. Ceram. Soc. Bull. 75 (1996) 135.
[2] L. Hench, D. Ulrich ((Eds.), Science of Ceramic Chemical Processing, Wiley, New York, 1986.
[3] J.W. Evans, L.C. De Jonghe, The Production of Inorganic Materials, Macmillan, New York, 1991.
[4] T.J. Gardner, G.L. Messing, Thermochim. Acta 78 (1984) 17.
[5] T.J. Gardner, G.L. Messing, Am. Ceram. Soc. Bull. 63 (1984) 1498.
[6] Bokhimi, A. Morales, T. Lopez, R. Gomez, J. Solid State Chem. 115 (1995) 411.
[7] K. Itatani, M. Nomura, A. Kishioka, M. Kinoshita, J. Mater. Sci. 21 (1986) 1429.
[8] K. Itatani, A. Itoh, F.S. Howell, A. Kishioka, M. Kinoshita, J. Mater. Sci. 28 (1993) 719.
[9] U. Chong, D.H. Jeong, Proceedings of UNITCR, Refractories – A, World Wide Technology, 1997, p. 1037.
[10] R.W. Rice, AIChE J. 36 (1990) 481.
[11] K. Yamamoto, K. Umeya, Am. Ceram. Soc. Bull. 60 (1981) 636.
[12] M.H. Bocanegra, J. Mater. Sci. 28 (1993) 3467.
[13] B.D. Cullity, Elements of X-Ray Diffraction, Addison-Wesley, USA, 1978.
[14] S. Ardizzone, C.L. Bianchi, B. Vercelli, J. Mater. Res. 13 (1998) 2218.
[15] S.E. Wanke, R.M.J. Fiedorow, in: K.K. Unger, et al. (Eds.), Characterization of Porous Solids, Elsevier, Amsterdam, 1998, p. 601.
[16] J. Rodriguez-Carbajal, AFFMA, Mesh Refinement Program, 1985 Filhol 1972.
[17] S.F. Estefan, M.B. Morsi, G.A. El-Shobaky, I.F. Hewaidy, Powder Tech. 49 (1987) 143.
[18] V.R. Choundhary, V.H. Rane, R.V. Gadre, J. Catal. 145 (1994) 300.
[19] J. Staron, S. Palco, Am. Ceram. Soc. Bull. 72 (1993) 83.
[20] A.M.M. Gadalla, H.W. Hennicke, Powder Met. Int. 5 (1973) 196.
[21] A.W. Hey, D.T. Livey, Trans. Brit. Ceram. Soc. 65 (1966) 627.

PERGAMON

www.elsevier.nl/locate/poly

Polyhedron 19 (2000) 2353–2360

POLYHEDRON

Fourier transform infrared and Raman spectra of uranyl bis(2-hydroxybenzaldehyde): $UO_2(sal)_2$

C.A. Téllez Soto [a,*], M. Arissawa [a], J. Gómez Lara [b], M.A. Mondragón [c]

[a] *Departamento de Físico-Química, Universidad Federal Fluminense (UFF), Instituto de Química, Morro do Valonguinho s/n, Niteroi-Centro, Cep, 24210-150 Rio de Janeiro, Brazil*

[b] *Instituto de Química UNAM, Circuito Exterior, Ciudad Universitaria, Coyoacán, 04510 Mexico D.F., Mexico*

[c] *Física Aplicada y Tecnología Avanzada, Instituto de Física, UNAM, Apdo Postal 0-1010, Querétaro, Qro 76001, Mexico*

Received 29 May 2000; accepted 14 June 2000

Abstract

The Fourier transform infrared and Raman spectra of solid uranyl bis(2-hydroxybenzaldehyde) were measured in the 4000–70 cm^{-1} region. The fundamental skeletal vibrational modes were assigned by comparison with the spectra of other uranyl complexes. The ligand bands in the complex were assigned with the aid of the infrared spectrum of the 2-hydroxybenzaldehyde calculated by the AM1 semi-empirical method, and with the aid of its experimental infrared absorption bands and Raman shifts. A normal coordinate analysis had been carried out to verify the experimental assignments of the $[UO_2L_2]$ framework. Force constants for the skeletal vibrations of this complex were calculated. The polarized Raman spectrum of 2-hydroxybenzaldehyde is also reported. © 2000 Elsevier Science B.V. All rights reserved.

Keywords: Fourier transform infrared and Raman spectra; Uranyl bis(2-hydroxybenzaldehyde); Force constants

1. Introduction

The Raman, resonance Raman and infrared spectra of potassium uranyl croconate were studied by Gonçalves et al. [1]. Recently, the Fourier transform infrared and Raman spectra of solid uranyl bis(2-hydroxy-1-naphthaldehyde) [2], abbreviated as $UO_2(2H1N)_2$, uranyl 2,4-pentanedionate: $UO_2(acac)_2$ [3], uranyl bis(1,3-diphenyl-1,3-propanedionate): $UO_2(HDBM)_2$ and uranyl bis(1,1,1,-trifluoro-2,4-pentanedionate): $UO_2(HBTF)_2$ [4] were studied. Reliable information from spectroscopic analysis on the infrared and Raman spectra of uranyl bis(2-hydroxybenzaldehyde), hereafter known as $UO_2(sal)_2$, is almost nonexistent in literature.

The aim of this paper is to report the Fourier transform infrared and Raman spectra (solid state) of $UO_2(sal)_2$, and to give the experimental assignments of the bands. The band assignments of the crystalline compound were made according the following criteria: (i) Comparison with another published uranyl complexes. (ii) Polarization studies on the Raman spectra of 2-hydroxybenzaldehyde. (iii) AM1 semiempirical calculations [5] were carry out in order to obtain the harmonic infrared spectra of the 2-hydroxy-belzaldehyde. (iv) By means of the correlation $C_{2v} \rightarrow C_s$, the fundamental ligand vibrational modes were identified and assigned. (v) A normal coordinate analysis (NCA) for the skeletal fundamentals assuming a local C_{2v} symmetry was done.

2. Experimental

$UO_2(sal)_2$ was prepared according to the synthesis proposed by Gómez Lara [6]. For the preparation of $UO_2(sal)_2$, stoichiometric quantities of an alcoholic solution of 2-hydroxybenzaldehyde were mixed with an aqueous solution of uranyl nitrate trihydrate, $UO_2(NO_3)_2 \cdot 3H_2O$. The solution was concentrated and was left to chill for crystallization.

The infrared spectrum of $UO_2(sal)_2$ was measured on a Nicolet 740 FT IR spectrometer. In the range of

* Corresponding author. Tel.: +55-21-2745-689.
E-mail address: claudio@risc1.gfq.uff.br (C.A. Téllez Soto).

0277-5387/00/$ - see front matter © 2000 Elsevier Science B.V. All rights reserved.
PII: S0277-5387(00)00571-4

4000–300 cm^{-1}, KBr pellets were used in the ratio of 1:10 ($UO_2(sal)_2$:KBr). For the 700–70 cm^{-1} range, polyethylene disks were used in the same proportion as above. The spectra were recorded with a resolution of 4 cm^{-1} for the higher region and 1 cm^{-1} for the lower region. The number of scans was 140 in both cases.

The infrared spectra of 2-hydroxybenzaldehyde in the range of 4000–600 cm^{-1} were measured using an FT IR tunnel cell (Axion Analytical). For measurements between 700 and 30 cm^{-1}, a polyethylene cell was used for liquids of 0.1 mm optical length. In this case the spectra were run on an FT IR Perkin–Elmer 2000 spectrometer.

Table 1
Infrared and Raman spectra of 2-hydroxybenzaldehyde (cm^{-1}) [a]

Infrared	Raman (ρ)	Approximate description
3292(sh)		$1658 \times 2 = 3316$
3178		ν(OH) *trans*
3129		ν(OH) *cis*
	3112 (0.03) p	ν(CH)ϕ
3098	3087 (0.09) p	ν(CH)ϕ
	3068 (0.37) p	ν(CH)ϕ
3049		
	3023 (0.27) p	ν(CH)ϕ
2845	2849	δ(CH) aldehyde group *cis*
2740	2750	δ(CH) aldehyde group *trans*
1730		$863 + 881 = 1744$
1658	1663 (0.05) p	ν(C=O) *trans* conformer
1635(sh)	1645 (1.23) dp	ν(C=O) *trans* conformer
1620	1620 (1.65) dp	ν(C=O) *trans* conformer
1598(sh)	1594 (4.91) dp	ν(C=O) *cis* conformer
1570	1580 (0.00) p	ν(C=C)+β(CCH)+γ(CCC)
	1564 (0.26) p	ν(C=C)+β(CCH)+γ(CCC)
1478		ν(C=C)+β(CCH)+γ(CCC)
1452	1458 (0.46) p	ν(C=C)+β(CCH)+γ(CCC)
1387	1387 (1.85) dp	δ(O=CH) *trans*
	1333	δ(COH) *trans*
1320	1323 (0.13) p	ν(C=C)+β(CCH)
1275	1280 (2.5) DP	δ(O=CH) *cis*
1227	1228 (0.45) p	δ(CCH) *cis*
1199	1205 (0.51) p	β(CCH)ϕ
1150	1151 (0.52) p	ν(C–OH) *trans*
1114	1116 (0.33) p	β(CCH)+ν(C=C)
	1076 (0.14)	ν(C=C)+β(CCH)
1028	1031 (0.20) p	ν(C–C=O) *cis*
979		ρ(CH)ϕ out of plane
944		ρ(CH)ϕ out of plane
881		ρ(CCH)ϕ out of plane
863		ρ(CCH)ϕ out of plane
754	768 (0.22) p	γ(CCC)ϕ
	667 (0.34) p	δ(C–C=O) *cis*
563	564 (0.61) p	χ(CCC)ϕ
451	452 (0.71) p	χ(CCC)ϕ
412	412 (0.46) p	β(CCH)
295	295 (1.0) dp	χ(CCC=O) torsion
261	260 (0.40) p	β(CCH)
	218 (1.0) dp	χ(CCCC)ϕ torsion
	150 (1.2) dp	χ(CCCC)ϕ torsion

[a] Plazeks rules applies to the depolarization of the fundamental frequencies: $0 < \rho < 6/7$ for totally symmetric modes of molecules of lower symmetry.

The Raman spectra of $UO_2(sal)_2$ and of 2-hydroxybenzaldehyde were measured on a 950 Nicolet FT Raman spectrometer equipped with an InGaAs detector, using 1064 nm radiation from a Nd-YAG laser. The resolution for the Raman spectra was of 2.0 cm^{-1} in both cases. The number of scans was 140.

In $UO_2(sal)_2$, such as in $UO_2(acac)_2$, $UO_2(HBTF)_2$, $UO_2(HDBM)_2$ and $UO_2(2H1N)_2$, the crystals did not exhibit the appropriate size and crystallinity to perform polarization measurement in the solid state. For 2-hydroxybenzaldehyde, the polarization measurements were made at 0 and 90°. The areas for the calculation of the depolarization ratio were obtained using the PEAK SOLVE software from Nicolet [7].

3. Results and discussion

3.1. Vibrational irreducible representation

Assuming a C_{2v} symmetry for the $UO_2(sal)_2$ complex, the $3n - 6 = 87$ vibrational modes can be distributed among the symmetry species:

$$\Gamma_{\text{vib.}} = 30a_1(\text{IR,R}) + 14a_2(\text{R}) + 15b_1(\text{IR,R}) + 28b_2(\text{IR,R})$$

3.2. Band assignments

3.2.1. 2-Hydroxybenzaldehyde ligands

Assuming a C_s symmetry, the vibrational modes can be described by the vibrational representation:

$$\Gamma_{\text{vib.}} = 28a' + 11a''$$

Due to the possibility of rotation of the OH group around the C–O bond, and the possibility of rotation of the –CHO group, four conformers were expected in the liquid state, one of them in *cis* position forming a H···O bond between the –OH and –CHO groups. The other three in the *trans* position.

Previous band assignment for this compound was reported by Radhi et al. [8]. The experimental vibrational assignments, which include Raman polarization measurements, are given in Table 1. The Raman spectra of 2-hydroxybenzaldehyde at 0 and 90° analyzer are shown in Fig. 1.

3.2.2. Infrared and Raman C–H stretching of the benzyl groups

For the $UO_2(sal)_2$ complex the ν(CH)ϕ for the benzyl groups can be divided into $4a_1 + 4b_2$ symmetry types. In the infrared spectrum it was possible to identified absorption bands at ~ 3040 cm^{-1} assigned as ν(CH)ϕ, and at 3010 cm^{-1} assigned as the combination band $1634 + 1379 = 3013$ cm^{-1}. The infrared spectrum for

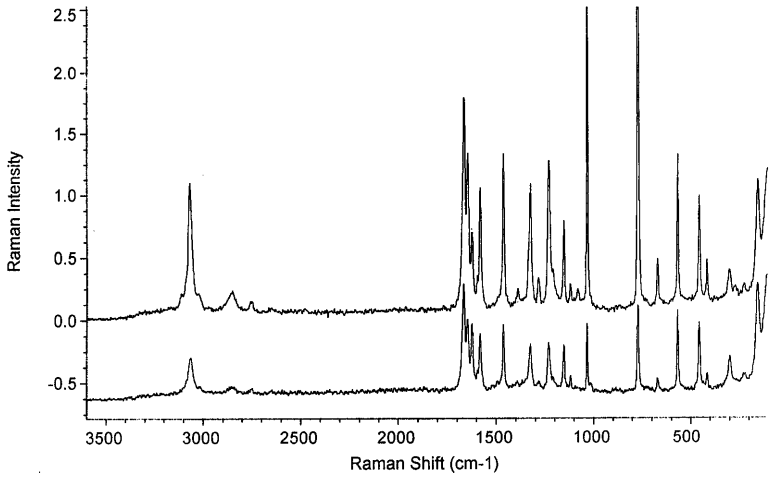


Fig. 1. Raman spectra of 2-hydroxybenzaldehyde at 0 and 90° analyzer (cm^{-1}).

the calculated conformers indicated a shift of approximately 13 cm^{-1} between the *cis* and *trans* C–H benzyl stretching, where the *cis* conformer presents the higher wavenumber. Due to the small number of allowed infrared and Raman active symmetry modes, A and B, and the poor resolution of the infrared spectrum of 2-hydroxybenzaldehyde in the benzyl stretching region, the experimental observed Raman bands were assigned to the calculated AM1 frequencies. In the Raman spectrum, bands of very weak intensity were observed at 3121, 3088, 3082sh, 3063, 3049, 3034, 3025 and 3014 cm^{-1}. In the Raman spectrum of the free ligand 2-hydroxybenzaldehyde, polarized bands at 3111, 3087, 3068 and 3023 cm^{-1} were observed. These bands can be correlated with the experimental and calculated ligand bands in the complex:

ν(CH)ϕ free ligand (C_s)	ν(CH)ϕ complex C_{2v}	AM1(*cis*)	AM1(*trans*)
3111 p (a')		3201 (3066)	3200 (3066)
3087 p (a')	3088 (a_1)	3194 (3060)	3194 (3060)
3068 p (a')	3063 (a_1)	3180 (3046)	3181 (3046)
3023 p (a')	3025 (a_1)	3174 (3041)	3163 (3030)

As can be seen, the AM1 calculated wavenumbers are overvalued. In Hollauer's work [9] on the AM1 model in the prevision of the CH vibrational frequencies, it is pointed out that the error in the AM1 calculated values is 4.2%. The values in parentheses were obtained using the correction proposed by Hollauer [9], and these values agree well with the experimental ones.

The Raman shift at 3121 cm^{-1} appears with very low intensity; for this reason it can be assigned as ν(CH)ϕ as b_2 symmetry type. The other Raman shifts that are assigned to b_2 symmetry are 3049, 3034(sh) and 3014 cm^{-1}.

3.2.3. External C–H stretching

These modes can be represented as $\Gamma_{CH} = a_1 + b_2$ and were observed in the Raman spectrum at 2897 (a_1) and at 2853 (b_2) cm^{-1}. In this case, the assignment of the symmetry type was done according to the intensity of the bands. The AM1-calculated infrared spectrum assigns these stretching at 3085 and 3089 cm^{-1}. The corrected values in 4.2% are 2955 and 2959 cm^{-1}, respectively.

3.2.4. C=O stretching

Due to the presence of four conformers in 2-hydroxybenzaldehyde, four wavenumber values for the ν(C=O) vibrational mode were expected. The infrared spectra shows absorption at 1658, 1635(sh), 1620 and 1598(sh) cm^{-1}. In the Raman spectrum, Raman shifts were found at 1663(p), 1645(dp), 1620(dp) and 1594(dp) cm^{-1}. The 1598(IR) and 1594(R) cm^{-1} wavenumbers can be assigned to the ν(C=O) vibrational mode for the *cis* conformer. The other values correspond to the ν(C=O) modes of the *trans* conformers, for which the AM1 model predict higher values than the *cis* conformer. Concerning the C=O stretching in the uranyl bis(2-hydroxybenzaldehyde) complex, the characteristic C=O wavenumber in the infrared and Raman spectra has a shift going to lower frequencies which must be considered, and by incorporating two 2-hydroxybenzaldehyde ligands to form the complex, the number of C=O stretching was increased.

Assuming a 'benzenoid resonance' structure of the 2-hydroxybenzaldehyde ligands by coordination with the UO_2^{2+} ion, equivalent internal coordinates for the C=O partial double bonds were considered. The vibrational representation for the stretching of these bonds is: $\Gamma_{C=O} = 2a_1 + 2b_2$. For the β-ketoenol complexes of Ni(II), Cu(II) and Zn(II), Thorton [10] assignments for the ν(C=O) vibrational modes were made at 1605, 1577 and 1598 cm^{-1}, respectively. For Pd(II)-acetylaceton-

ate and Cu(II) acetylacetonate the Junge and Musso's [11] assignments for the ν(C=O) stretching were for Pd(II) complex: ν_s(C=O) at 1555 cm^{-1}, ν_{as}(C=O) at 1378 cm^{-1}. For the Cu(II) complex: νs(C=O) at 1578 cm^{-1} and ν_{as}(C=O) at 1397 cm^{-1}. For $UO_2(sal)_2$, the assignments for the ν(C=O) stretching based on the above comparison and considering the intensities of the infrared and Raman bands, are:

ν_s(C=O)(a_1)	ν_{as}(C=O)(b_2)
1339(R)	1618(IR), 1616(R)
1307(IR), 1309(R)	1608(IR), 1600(R)

3.2.5. C=C stretching CCH and CCC bending of the benzene ring

In 2-hydroxybenzaldehyde, the irreducible vibrational representation for the C=C stretching is $\Gamma_{C=C} = 6$ Å. From the Hollauer study [9], in which were analyzed the CC stretching in 46 different molecules including aliphatic and cyclic compounds, the best straight line was defined by the equation $\nu(AM1) = 1.073[\nu(exp)] + 51.5$ with a correlation coefficient of 0.978. Using this equation, the prediction for the C=C stretching experimental wavenumbers is: 1619, 1603, 1507, 1468, 1338 and 1282 cm^{-1}, which gives an excellent basis to assign the experimental values found at: 1580(R), 1570(IR); 1564(IR), 1478(IR), 1458(R), 1452(IR) and 1320(IR), 1323(R) cm^{-1}.

In the uranyl bis(2-hydroxybenzaldehyde) complex, the vibration modes for the C=C stretching, CCH and CCC bending can be classified according to the representations:

$$\Gamma_{C=C} = 6a_1 + 6b_2,\ \Gamma_{CCH} = 4a_1 + 4b_2 \text{ and } \Gamma_{CCC} = 3a_1 + 3b_2$$

In benzene, wavenumbers between 1606 and 1028 cm^{-1} were assigned to the coupled modes Q(CC) + β(CCH) [12]. Higher contributions of the ΔQ(CC) internal coordinates in the coupled normal modes must be in the approximate region of 1650–1450 cm^{-1}. In the region of 1400–1000 cm^{-1} the contribution of the $\Delta\beta$(CCH) bending internal coordinates is higher [12].

For the coupling stretching and bending modes of the benzene rings, the approximate assignments were made observing the intensities of the bands in the infrared and Raman spectra. The principal contribution of the ΔQ(C=C) internal coordinates for the ν(C=C) coupled vibrational modes (wavenumbers in cm^{-1}) were found at: 1658(IR), 1665(R)(a_1); 1643(R)(a_1); 1635(IR) shoulder, 1634(R)(a_1); 1547(IR)(higher transmittance), 1540(R)(b_2); 1532(IR)(higher transmittance), 1537(R)(b_2); 1518(IR)(b_2); 1464(IR), 1461(R)(a_1); 1428(IR)(b_2); 1403(IR), 1402(R)(a_1) and 1392(IR)(b_2).

Analyzing the CCH bending in the uranyl complex, the AM1 calculated spectra for the ligand 2-hydroxybenzaldehyde was taken into account. The vibrational irreducible representation for the ligand CCH bending is $\Gamma_{CCH} = 4$ Å. The calculated AM1 wavenumbers were corrected by 8% according the suggestion given in [9]. The results in cm^{-1} units were:

AM1 (calculated)	AM1 8% corrected value	Experimental
1326	1220	1228
1285	1182	1205
1191	1096	1116
1173	1079	1076

With these results there was a basis for assigning the CCH bending in the uranyl complex, in which eight β(CCH) coupled modes were expected.

For the CCH bending or in plane β(CCH) vibrational coupled modes in the uranyl complex, the assignments are 1295(R)(a_1); 1270(IR)(b_2); 1244(IR), 1247(R)-(a_1); 1198(IR) (higher transmittance), 1200(R)(b_2); 1184(IR), 1191(R)(a_1); 1158(IR) (b_2); 1148(IR) 1147(R)-(a_1); 1033(R)(a_1).

In 2-hydroxybenzaldehyde, three γ(CCC) internal angle ring deformation of type symmetry were expected (from six internal coordinates, which represent these bending, three of them are redundant). The AM1 calculated wavenumber for these vibrational modes in the *cis* 2-hydroxybenzaldehyde were 692, 606 and 494 cm^{-1}. The experimental wavenumbers for the γ(CCC) bending were assigned at 754(IR), 768(R, p); 563(IR), 564(R, p); and 451(IR), 452(R, p).

The γ(CCC) bending modes in the complex were assigned at 760(IR), 768(R)(b_2); 584(IR), 586(R)(a_1) and 474(IR)(b_1) cm^{-1}.

3.2.6. Out of plane vibrational modes ρ(CH) and χ(CCCC) of the benzene rings

For the free ligand four ρ(CH) and three χ(CCCC) out of plane vibrational modes were expected. The AM1 calculated wavenumbers for the ρ(CH) modes in the *cis* 2-hydroxybenzaldehyde, were 1002, 969, 915 and 813 cm^{-1}. The torsion modes were ascribed at 712, 494 and 444 cm^{-1}. In the uranyl bis(2-hydroxybenzaldehyde) complex, these vibrational modes can be worked out according to the following symmetries: $\Gamma_{\rho(CH)} = 4a_2 + 4b_1$ and $\Gamma_{\chi(CCCC)} = 3a_2 + 3b_1$. The tentative assignment given in Table 2 for the out of plane bending is based on the previous $UO_2(2H1N)_2$ assignment [2] and by comparison with the assignment given through the semi-empirical AM1 calculations. The coupling vibrational modes between the ligands and the UO_2^{2+} ion are also given in Table 2.

Table 2
Infrared and Raman spectra of uranyl bis(2-hydroxy-benzaldehyde) (cm^{-1}) [a]

Infrared	Raman	Approximate description
	3112 (0.1)	ν(CH)ϕ (a_1)
	3088 (0.3)	ν(CH)ϕ (a_1)
	3082 (0.2)	ν(CH)ϕ (b_2)
	3063 (0.3)	ν(CH)ϕ (a_1)
~3040	3049 (0.4)	ν(CH)ϕ (b_2)
	3034 (0.3)	ν(CH)ϕ (b_2)
	3025 (0.2)	ν(CH)ϕ (a_1)
	3014 (0.2)	ν(CH)ϕ (b_2)
	2897 (0.2)	ν(CH) (a_1)
	2853 (0.1)	ν(CH) (b_2)
	2781 (0.1)	$1392\times2=2784$
1658 (33)	1665 (1.2)	ν(C=C)+β(CCH)+γ(CCC) (a_1)
	1643 (1.8)	ν(C=C)+β(CCH)+γ(CCC) (a_1)
1635(sh) (64)	1634 (1.6)	ν(C=C)+β(CCH)+γ(CCC) (a_1)
1618 (87)	1616 (1.5)	ν(C=O) (b_2)
1608 (88)	1600 (2.0)	ν(C=O) (b_2)
1547 (60)	1540 (2.2)	ν(C=C)+β(CCH)+γ(CCC) (b_2)
1532 (65)	1537 (2.2)	ν(C=C)+β(CCH)+γ(CCC) (b_2)
1518(sh) (38)		ν(C=C)+β(CCH)+γ(CCC) (b_2)
1464 (48)	1461 (1.5)	ν(C=C)+β(CCH)+γ(CCC) (a_1)
1458 (45)		ν(C=C)+β(CCH)+γ(CCC) (b_2)
1442 (39)	1440 (3.7)	ν(C=C)+β(CCH)+γ(CCC) (a_1)
1428 (69)		ν(C=C)+β(CCH)+γ(CCC) (b_2)
1403 (51)	1401 (1.5)	ν(C=C)+β(CCH)+γ(CCC) (a_1)
1392 (48)		ν(C=C)+β(CCH)+γ(CCC) (b_2)
	1339 (4.6)	ν(C=O) (a_1)
1307 (47)	1309 (1.2)	ν(C=O) (a_1)
	1295 (1.2)	β(CCH) (a_1)
1276(sh) (36)		$834+443=1277$
1270 (45)		β(CCH) (b_2)
1244 (24)	1247 (1.5)	β(CCH) (a_1)
1198 (53)	1200 (1.2)	β(CCH) (b_2)
1184 (38)	1191 (2.0)	β(CCH) (a_1)
1158 (49)		β(CCH) (b_2)
1148 (39)	1147 (2.5)	β(CCH) (a_1)
1139 (39)	1142 (2.5)	ν(C–OH)
1120 (27)	1127 (2.0)	$564\times2=1128$
	1033 (3.5)	β(CCH) (a_1)
1023 (13)	1028 (3.7)	ν(C–C=O)
928 (59)	930 (2.2)	ρ(CH)ϕ out of plane
924 (70)	916 (2.3)	ν_{as}(U=O) (b_1)
908 (50)	902 (2.7)	χ(CCCC)ϕ (b_2)
897 (51)		χ(CCCC)ϕ (b_1)
879 (19)		χ(CCCC)ϕ (b_1)
	845 (5.5)	ρ(CH)ρ (a_2)
	834 (10,0)	ν_s(U=O) (a_1)
774 (33)	780 (4.5)	ρ(CH)ϕ
760 (44)	768 (3.8)	γ(CCC)ϕ
752 (53)		ρ(CH)ϕ(b_1)
734 (12)	739 (2.5)	$544+198=742$
727 (12)		$544+187=731$
657 (25)	659 (2.3)	δ(COU) ring
584 (21)	586 (2.8)	γ(CCC)ϕ (a_1)
569 (24)		ρ(C=O) out of plane (b_1)
	561 (2.3)	χ(CCCO) (a_2)
532 (6)	544 (2.0)	ν_{as}(U–O) equatorial (b_2)
474 (37)		γ(CCC)ϕ (b_1)
465 (17)	463 (2.6)	ν_{as}(U–O) equatorial (b_2)
457 (17)	458 (2.8)	χ(CCCC)ϕ (b_1)
444 (11.5)	443 (4.6)	ν_s(U–O) equatorial (a_1)
430 (10.0)	433 (3.8)	ν_s(U–O) equatorial (a_1)
417 (5.1)	414 (2.8)	χ(CCCO) (b_1)
	343 (2.6)	$180+171=351$
329 (10.6)	326 (2.4)	$171+168=339$
308 (8.9)	309 (2.7)	$180+140=320$
286 (7.4)	284 (2.2)	χ(CCCO) (b_1)
	278 (2.4)	δ(OUO) equatorial (a_1)
	270 (2.3)	χ(CCCC)ϕ (a_2)
260 (16.1)	261 (2.2)	δ(OUO) axial (b_2)
241 (12)	246 (2.2)	δ(OUO) axial (a_1)
	223 (2.8)	δ(OUO)equatorial (a_2)
218 (7.4)		δ(OUO) equatorial (b_1)
	216 (2.8)	δ(OUO) equatorial (a_2)
	198 (3.8)	δ(OUO) equatorial (b_2)
185 (7.8)	187 (4.1)	δ(OUO) equatorial (a_1)
	180 (3.9)	χ(CCCO) (a_2)
	171 (3.2)	χ(CCCO) (a_2)
164 (7.5)	168 (3.3)	lattice
140 (7.5)		lattice

[a] Values for the intensity of the infrared and Raman spectra are expressed in $\%T$ and irradiance, respectively. For the Raman spectrum the intensities of the bands were scaled to the most intense band to which the value of 10 was assigned, corresponding to 16.39×10^{-3} (watts cm^2 per cm^{-1}) of irradiance.

3.2.7. U=O and U–O stretching modes

These vibrational modes can be represented as: $\Gamma_{UO}=3a_1+b_1+2b_2$, which can be subdivided as $\Gamma_{U=O}=a_1+b_1$ and $\Gamma_{U-O}=2a_1+2b_2$. In an earlier work, the band assignments for the framework vibrations of $UO_2(acac)_2$ [3], $UO_2(HBDM)_2$, $UO_2(HBTF)_2$ [4] and $UO_2(2H1N)_2$ [2] were reported. In all these cases, the axial strong bands pertaining to the ν_{as}(U=O) vibrational modes, were found at 926, 921, 908 and 920 cm^{-1}, respectively. In $UO_2(sal)_2$ the ν_{as}(U=O) was assigned to the strong infrared band at 924 cm^{-1} of b_1 symmetry type. The two b_2 equatorial U–O stretching were assigned at 544(IR,R) and 463(IR,R) cm^{-1}. The Raman shifts at 443 and at 433 cm^{-1} were assigned as ν_s(U–O) equatorial (a_1). As expected, these bands are more intense than their counterparts in the infrared spectrum. The ν_s(U=O) axial was assigned at 834(R)(very strong)–830(IR)(very weak) cm^{-1}.

3.2.8. Axial λ(OUO), and equatorial ω(OUO) and α(OUO) bending vibrations

For uranyl bis (2-hydroxy-1-naphthaldehyde),UO_2-$(2H1N)_2$, a C_{2v} symmetry was assumed [2]. In this complex, the axial and equatorial bending vibrations can be worked out according to the following representations:

$$\Gamma_{bend}=3a_1(IR,R)+2a_2(R)+2b_1(IR,R)+2b_2(IR,R)$$

Table 3
Observed and calculated wavenumbers (cm^{-1}) and valence force constants for the skeleton of $UO_2(sal)_2$

Observed	Calculated	Assignment
a_1		
834	833	ν_s(U=O) (98% S_1)
443	451	ν_s(U–O) (98% S_3)
433	433	ν_s(U–O) (100% S_2)
278	278	$\alpha\omega$(OUO) (100% S_5+S_6)
246	244	λ(OUO) (94% S_4)
187	187	$\alpha\omega$(OUO) (58% S_6+21% S_5)
a_2		
223	226	λ(OUO) (54% S_2+46% S_1)
216	214	λ(OUO) (54% S_1+46% S_2)
b_1		
924	922	ν_{as}(U=O) (91% S_1)
218	217	λ(OUO) (83% S_2)
198	202	λ(OUO) (83% S_3)
b_2		
544	544	ν_{as}(U–O) (100% S_1)
463	455	ν_{as}(U–O) (98% S_2)
261	260	λ(OUO) (87% S_3)
223	223	ω(OUO) (89% S_4)

Valence force constants [a]

$f_{(U=O)} = 6.54 \pm 0.06$	$f_{(U-O)} = 1.98 \pm 0.02$	$f_{(OUO)axial} = 0.54 \pm 0.01$
$f_{(OUO)eq.} = 1.14 \pm 0.04$	$f_{(OUO)eq.} = 1.28 \pm 0.06$	$f_{(U=O,U=O)} = -0.08 \pm 0.05$
$f_{(U-O,U-O)ad} = -0.26 \pm 0.01$	$f_{(U-O,U-O)op.} = -0.03 \pm 0.01$	$f_{(OUO,OUO)} = -0.25 \pm 0.01$
$f_{(OUO,OUO)} = 0.36 \pm 0.02$	$f_{(OUO,OUO)eq.} = 0.37 \pm 0.04$	$f_{(OUO,OUO)eq.} = 0.46 \pm 0.02$
$f_{(U=O,OUO)} = -0.38 \pm 0.04$	$f_{(U=O,OUO)} = -0.06 \pm 0.23$	$f_{(U=O,OUO)} = -0.60 \pm 0.31$
$f_{(U-O,OUO)} = -0.02 \pm 0.04$ [a]		

[a] The units are: stretching force constants in (mdyn $Å^{-1}$), bending force constants in (mdyn Å). Stretch-bending interaction in (mdyn).

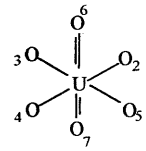
These bending can be subdivided as: $\Gamma_\lambda = a_1 + 2a_2 + 2b_1 + b_2$ (axial bending), $\Gamma_\omega = a_1$ and $\Gamma_\omega = a_1 + b_2$ (equatorial bending). For uranyl bis (2-hydroxybenzaldehyde), $UO_2(sal)_2$, the same structural framework can be considered as in $UO_2(2H1N)_2$. The wavenumbers correlation between these two complexes is:

$UO_2(2H1N)_2$ (C_{2v})	→	$UO_2(sal)_2$ (C_{2v})
260 (a_1)		278 (a_1)
251 (a_1)		246 (a_1)
198 (a_1)		187 (a_1)
273 (a_2)		223 (a_2)
246 (a_2)		216 (a_2)
216 (b_1)		218 (b_1)
140 (b_1)		198 (b_1)
243 (b_2)		261 (b_2)
		223 (b_2)

The Raman spectrum of $UO_2(sal)_2$ is illustrated in Fig. 2. Infrared and Raman spectra of $UO_2(sal)_2$ in the wavenumber region of 700–70 cm^{-1} are given in Fig. 3.

4. Normal coordinate analysis

A normal coordinate analysis for the framework structure of uranyl bis (2-hydroxybenzaldehyde) was carried out to aid the assignment of the observed wavenumbers. The skeletal structure and the internal coordinates can be described as:



	i	j		i	j	k		i	j	k
$\Delta(Q_1)$	1	6	$\Delta(\lambda_1)$	2	1	6	$\Delta(\lambda_7)$	4	1	7
$\Delta(Q_2)$	1	7	$\Delta(\lambda_2)$	3	1	6	$\Delta(\lambda_8)$	5	1	7
$\Delta(R_1)$	1	2	$\Delta(\lambda_3)$	4	1	6	$\Delta(\omega_1)$	2	1	5
$\Delta(R_2)$	1	3	$\Delta(\lambda_4)$	5	1	6	$\Delta(\omega_2)$	3	1	4
$\Delta(R_3)$	1	4	$\Delta(\lambda_5)$	2	1	7	$\Delta(\alpha)$	4	1	5
$\Delta(R_4)$	1	5	$\Delta(\lambda_6)$	3	1	7				

Geometrical parameters, which describe the framework structure of $UO_2(sal)_2$, were taken from the work of Zabokrzycka et al. [13]. The two pair of opposite planar angles OUO were chosen to be 87 and 93°. A modified general valence force field (MGVFF) potential function was used. The initial set of force constants to be refined was transferred from the force field values of $UO_2(2H1N)_2$ [2]. Force constants were adjusted to give the best wavenumber fit by a least-square procedure developed by Miyazawa [14] and Shimanouchi [15], using computer programs which have been reported previously [16]. The final valence force constants for the U=O and U–O bonds are $f_{(U=O)} = 6.54 \pm 0.06$ mdyn $Å^{-1}$ and $f_{(U-O)} = 1.98 \pm 0.02$ mdyn $Å^{-1}$. The experimental result of 6.54 mdyn $Å^{-1}$ reflects a lowering of the axial electron density through the effect of coordination with the salicylaldehyde ligands. The value of 1.98 mdyn $Å^{-1}$ is higher than the values found for $UO_2(acac)_2$, $UO_2(HBTF)_2$ and $UO_2(HDBM)_2$: 1.72, 1.71, and 1.95 mdyn $Å^{-1}$, respectively. A value of $f_{U=O} = 2.36$ mdyn $Å^{-1}$ was found for $UO_2(2H1N)_2$. The values of 1.98, 1.95 and 2.36 mdyn $Å^{-1}$ for the $UO_2(sal)_2$, $UO_2(HDBM)_2$ and $UO_2(2H1N)_2$ complex, reflect the resonance effect with the equatorial U–O bonds. The uranium–oxygen bond order can be calculated by Gordy's equation [17]: $N_{UO} = (f - 0.30)/(1.67[\chi_U \chi^2_{O/d}]^{3/4})$, where f is the U–O force constant,

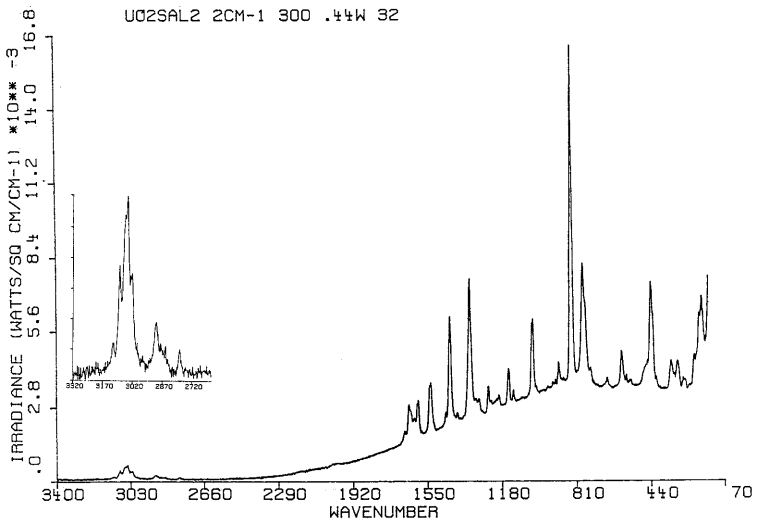


Fig. 2. Raman spectrum of uranyl bis (2-hydroxy-benzaldehyde) (cm^{-1}).

N_{UO} is the bond order, d is the U–O length and χ_U and χ_O are the U and O atom electronegativities. Using the Allred and Rochow [18] and Mulliken [19] electronegativities, the bond order for the U–O bond in $UO_2(sal)_2$ are 0.77 and 0.76, respectively.

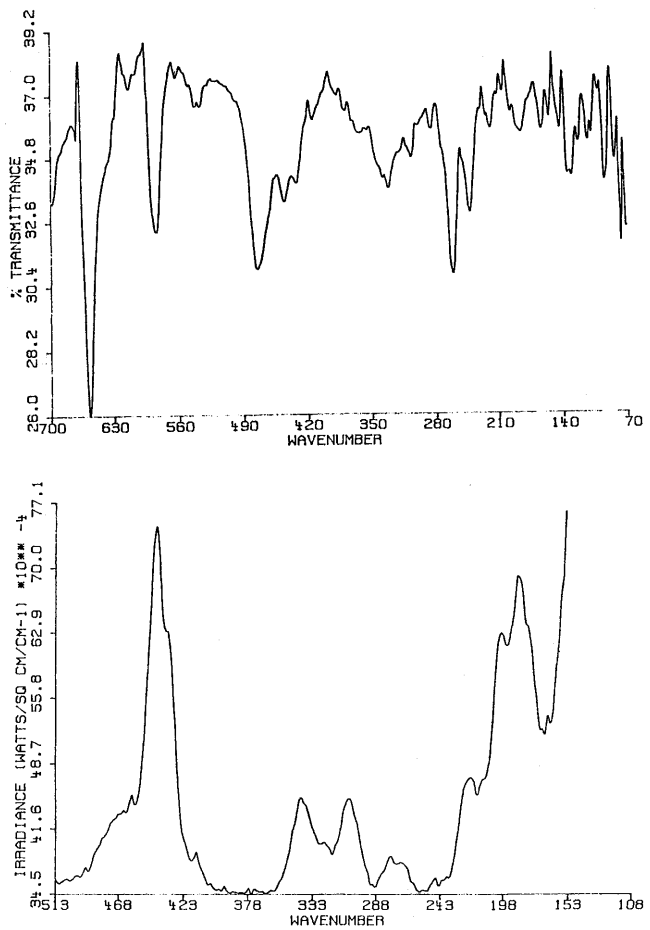


Fig. 3. Infrared and Raman spectra of uranyl bis (2-hydroxy-benzaldehyde) in the wavenumber region between 700 and 70 cm^{-1}.

According to the potential energy distribution (PED) results, there is no coupling between the ν(U=O) and ν(U–O) stretching modes in the a_1 symmetry types, and they can be considered as pure vibrational modes. In the a_1 symmetry type, coupling was found between the different equatorial angle bending and the axial bending mode appears without coupling. For the a_2 symmetry types, the two axial bending (represented as dependent internal coordinates) are coupled. For the b_1 symmetry type, PED reveals that the ν_{as}(U=O) is a pure vibrational mode. The axial bendings in this symmetry type are coupled to each other. In the b_2 symmetry type, the two ν(U–O) stretching modes, can be considered without coupling. For the bending vibrational modes the coupling is almost of 10% between them. The observed and calculated wavenumbers and the valence force constants are presented in Table 3.

Acknowledgements

One of us (C.A.T.S.) thanks the CNPq for a research grant.

References

[1] N.S. Gonçalves, L.F.C. de Oliveira, P.S. Santos, Spectrochim. Acta 50A (1994) 263.
[2] C.A. Téllez S., J. Gómez L., J. Braz. Chem. Soc. 7 (1996) 505.
[3] C.A. Téllez S., J. Gómez L., Spectrochim. Acta 51A (1995) 395.
[4] C.A. Téllez S., J. Gómez L., M.A. Mondragón, V.M. Castaño, G. Mena, Vib. Spectrosc. 9 (1995) 279.
[5] J.J.P. Stewart, Manual MOPAC 93, second review, Fujitsu Limited, 1993.

[6] J. Gómez L., Bol. Inst. Qui. UNAM. XVI (1964) 27.
[7] Peak solve (Galactic) OMNIC software, Madison, USA, 1996.
[8] M.M. Radhi, M.F. El-Bermani, Spectrochim. Acta 46A (1990) 33.
[9] J.C.S. Ramos, E. Hollauer, Quim. Nova 22 (1999) 684.
[10] D.A. Thorton, Coord. Chem. Rev. 104 (1990) 173.
[11] H. Junge, H. Musso, Spectrochim. Acta 24A (1968) 1219.
[12] L.M. Sverdlov, M.A. Kovner, E.P. Krainov, Vibrational Spectra of Polyatomic Molecules, Wiley, New York, 1974.
[13] A. Zabokrzycka, J. Brunvoll, B.N. Cyvin, S.J. Cyvin, J. Mol. Struct. (Theochem.) 87 (1982) 141.
[14] T. Miyazawa, Nippon Kagaku Zaschi 77 (1955) 1132.
[15] D.E. Mann, T. Shimanouchi, J.H. Meal, L. Fano, J. Chem. Phys. 27 (1957) 43.
[16] Y. Hase, O. Sala, Computer Programs for Normal Coordinate Analysis, Universidade de São Paulo, Brazil, 1973.
[17] W. Gordy, J. Chem. Phys. 14 (1946) 305.
[18] A.L. Allred, F.G. Rochow, J. Inorg. Nucl. Chem. 5 (1958) 264.
[19] H.O. Pritchard, H.A. Skinner, Chem. Rev. 55 (1955) 745.

PERGAMON

www.elsevier.nl/locate/poly

Polyhedron 19 (2000) 2361–2366

POLYHEDRON

Synthesis and EXAFS investigation of azomethynic copper metallochelates with an N,S,O ligand environment

A.I. Uraev [a], V.G. Vlasenko [b], B.I. Kharisov [c,*], L.M. Blanco [c], A.T. Shuvaev [b], I.S. Vasilchenko [a], A.D. Garnovskii [a], N.V. Elizondo [d]

[a] *Institute of Physical and Organic Chemistry, Rostov State University, 344090, Rostov-on-Don, Russia*
[b] *Institute of Physics, Rostov State University, 344090, Rostov-on-Don, Russia*
[c] *Facultad de Ciencias Químicas, Universidad Autónoma de Nuevo León, Apdo. Postal 18-F, Ciudad Universitaria, 66450, San Nicolás de los Garza, Nuevo León, Mexico*
[d] *Facultad de Físico-Matemáticas, Universidad Autónoma de Nuevo León, Apdo. Postal 18-F, Ciudad Universitaria, 66450, San Nicolás de los Garza, Nuevo León, Mexico*

Received 1 October 1999; accepted 10 July 2000

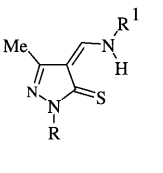
Abstract

Neutral copper complexes of different composition (CuL^1_2 and CuL^2OAc) and structure were obtained by coupling the 1-phenyl(isopropyl)-3-methyl-4-(*N*-substituted)aldimino-5-oxy(thio,seleno)pyrazoles (HL^1),and2-hydroxy(tosylamino)-*N*-(8-quinolyl)benzaldimine (HL^2) with copper(II) acetate. According to X-ray structural data, the CuL^1_2 complexes possess the pseudotetrahedral structure, and the CuL^2OAc complexes, the square-pyramidal one. The complexes were studied by EXAFS spectroscopy. EXAFS spectral data on the nearest ligand environment show a good correlation with the X-ray structural results. © 2000 Elsevier Science B.V. All rights reserved.

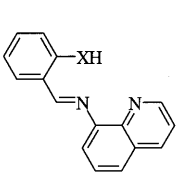
Keywords: Synthesis; EXAFS investigation; Azomethynic copper metallochelates

1. Introduction

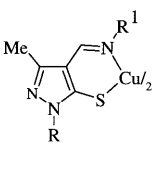
Copper chelates with an N,S,O-ligand environment are of permanent interest as models to interpret special structural, spectral, and electronic properties of the active centers of 'blue' copper proteins [1–4]. Despite the fact that such complexes have been profoundly studied [1–15], the number of adequate models, describing unusual properties of 'blue' ensymes, is limited. At present, the biomimetic copper complexes on the basis of tris-pyrazolylborate ligand systems, reported by Kitajima et al. [16–19] are the only example modeling the main peculiarities of copper center of the type I.



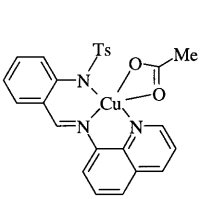
Ia: X = O, R = Ph, R1 = CH2Ph;
b: X = S, R = Ph, R1 = CH2Ph;
c : X = Se, R = Ph, R1 = CH2Ph;
d : X = S, R = i-Pr, R1 = 2-Py



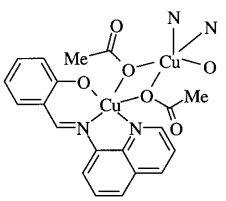
II a: X = NTs;
b: X = O



III a-d



IV



V

Using the compounds **Ia**–**d**, **IIa**,**b**, the metal chelates **IIIa**–**d**, **IV**, **V** with different combinations of N, O, S-donor atoms and geometries of a coordination polyhedra were synthesized and studied by EXAFS spectroscopy.

* Corresponding author. Tel.: +52-8-312-1228; fax: +52-8-374-0709.
E-mail address: bkhariss@ccr.dsi.uanl.mx (B.I. Kharisov).

0277-5387/00/$ - see front matter © 2000 Elsevier Science B.V. All rights reserved.
PII: S0277-5387(00)00572-6

Structures of some complexes (**IId**, **IV**, **V**) were determined by X-ray spectroscopy.

2. Experimental

2.1. Physical measurements

The Cu K-edge absorption spectra were measured at room temperature in transmission on a laboratory XAFS spectrometer [20] with a focussing quartz crystal-monochromator (1340). Fourier transform of the EXAFS spectra was carried out in the interval of wave vector of photoelectrons from $k = 2.5$ to 12.5 $Å^{-1}$, with weight function k^2. The square filter window isolated the significant Fourier transform peaks, which were then back-transformed into k-space. The best-fit distances (R), coordination numbers (N) and Debye–Waller (DW) factors were obtained from multishell fit in k-space using the back-scattering amplitude and the total phase shift calculated by the program FEFF7 [21]. In the least-squares fitting, the residual minimized and reported is $Q^2 \equiv (1/N)\Sigma k^2(\chi_I^{theor} - \chi_i^{exp})^2$ where the sum is over N data points of $k^2\chi$ between $K = 2$ and 12.5 $Å^{-1}$. The estimated uncertainty of best-fit experimental spectra to the model was less than 3%; that corresponds to an experimental error of interatomic distances and DW of 0.02 Å and 0.0005 $Å^2$, respectively.

2.2. Synthesis of ligands and complexes

The synthesis of aminomethylene derivatives **Ia**–**d** [13,15,22,23] and azomethines **IIa**,**b** [24] was carried out by interaction of ethanol or ether (0.01 M) solutions of the corresponding aldehydes with ethanol solutions (0.01 M) of amines. Solvents were purified by standard methods and distilled under argon atmosphere before use.

2.2.1. Complex *IIIa*

Hot methanol solution of copper acetate (0.1 g, 0.5 mmol) was added to hot methanol solution of the compound **Ia** (0.291 g, 1 mmol). The mixture was refluxed for 10–15 min. The brown crystalline solid formed is filtered, washed with hot ethanol and then with ether and dried in vacuo. (Yield 65%). Analytical data: Calc. for $C_{36}H_{32}N_6O_2Cu$: C, 66.70; H, 4.98; N, 12.97. Found: C, 66.43; H, 4.57; N, 12.65%.

2.2.2. Complexes *IIIb [15]*, *IIId [13]*, *IV*, *V [24]*

These were prepared according to the procedure described above.

2.2.3. Complex *IIIc*

An ethanol solution of copper acetate (0.1 g, 0.5 mmol) is added to hot ethanol solution of Ic (0.35 g, 1 mmol) by stirring under an argon atmosphere (0.35 g, 1 mmol). The mixture was refluxed for 5 min. The crystals formed were filtered, washed with ethanol and recrystallized from a toluene–heptane mixture. (Yield 78%). Analytical data: Calc. for $C_{36}H_{32}N_6Se_2Cu$: C, 56.14; H, 4.19; N, 10.91. Found: C, 55.95; H, 3.99; N, 10.72%.

3. Results and discussion

As expected, aminomethylene derivatives of 5-oxy(thio, seleno)pyrazole **Ia**–**d** in chloroform solution [25,26] have an enamine structure with a strong hydrogen bond NH···X. This is confirmed by the presence of doublet signals of NH group protons in the area $\delta =$ 13–15 ppm with $^3J_{NHCH} = 11$–14 Hz in their ^{1}H NMR spectra.

Structural data for the nearest environment of copper atoms in the chelates **IIIa**–**d**, **IV** and **V** were obtained using EXAFS spectroscopy. The Fourier transform magnitudes (FTM) of EXAFS spectra of the chelates **IIIa**–**d**, **IV**, **V** are shown in Fig. 1. Structural data obtained from fitting are presented in Table 1.

As is seen in Fig. 1, the main features of the FTM of complex **IIIa** include a large peak at $r = 1.6$ Å with a shoulder, corresponding to the first coordination sphere (CS) from light atoms N/O. This CS can be modeled well, when a copper atom in **IIIa** is surrounded by two oxygen atoms and two nitrogen atoms. The CS radii of

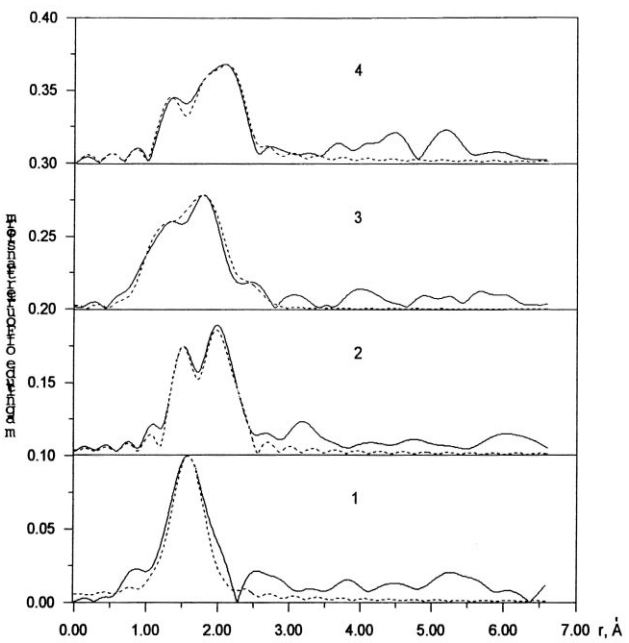


Fig. 1. FTM of the Cu K-edge EXAFS of the complexes: 1 (**IIIa**), 2 (**IIIb**), 3 (**IIId**), 4 (**IIIc**). The dashed lines show the fit using XAFS calculations from FEFF.

Table 1
Structural data obtained from the analysis of EXAFS spectra of the complexes **1**–**6**: radii of the coordination spheres (R), coordination number (N), Debye–Waller factor (σ^2) [a]

No.	Complex	R (Å)	N	σ^2 (Å)	Atom	Q (%)
1	**IIIa**	2.05	2	0.0020	N	2.5
		1.96	2	0.0038	O	
2	**IIIb**	2.00	2	0.0030		2.0
	2	2.27	2	0.0037	N	
3	**IIId** (R = Ph)	1.97	2	0.0048	N	2.0
		2.25	2	0.0055	S	
4	**IIIc**	2.04	2	0.0017	N	1.9
		2.46	2	0.0057	Se	
5	**IV**	2.01	4	0.0026	N/O	2.3
		2.58	1	0.0042	O*	
		3.02	5	0.0035	C	
6	**V**	1.99	4	0.0022	N/O	1.7
		2.54	1	0.0040	O*	
		2.96	5	0.0030	C	
		3.53	1	0.0043	Cu	

[a] The magnitude Q characterizes of quality of fit.

Cu–O and Cu–N are $R_O = 1.96$ Å and $R_N = 2.05$ Å, respectively (Table 1).

An additional peak with high r and higher amplitude in comparison with the peaks, corresponding to the CS of the light atoms N/O, is present in FTM of both **IIIb** and **IIId**. This additional peak is caused by the appearance of heavier sulfur atoms in the nearest environment of copper atoms. Very similar fits were obtained for both samples **IIIb** and **IIId** (Table 1). In the EXAFS analysis the CS can be simulated with two nitrogen atoms at $R_N = 1.97$–2.00 Å and two sulfur atoms at $R_S = 2.25$–2.27 Å. Thus, there is a good match between the distances derived from the EXAFS fit and those found in the crystal structure ($R_N = 1.982$ Å and $R_S = 2.2497$ Å) for **IIIb** and **IIId** (Table 1).

The FTM of **IIIc** is characterized by a further shift of the second main peak to a higher r, which is caused by the exchange of two sulfur atoms in the nearest environment of copper atoms by two selenium atoms. The distances of approximately 2.46 Å, obtained by the EXAFS fit, are typical for Cu–Se bonds [28].

The FTM EXAFS spectra of the complexes **IV** and **V** are shown in Fig. 2. Comparing them, two main differences are seen: slight changes in the position of the second and the third peaks and the appearance of a new peak with $r = 3.25$ Å in the FTM of **V**. The chosen model for **IV** with the coordination of the two oxygen atoms of the acetate group and three nitrogen atoms of the organic ligand to Cu atom allowed the best fit to be obtained. The structural parameters for complexes **IV** and **V** are shown in Table 1. The presence of a more distant carboxylate oxygen O* is typical for coordination of acetate groups [29]. The peaks in the area with

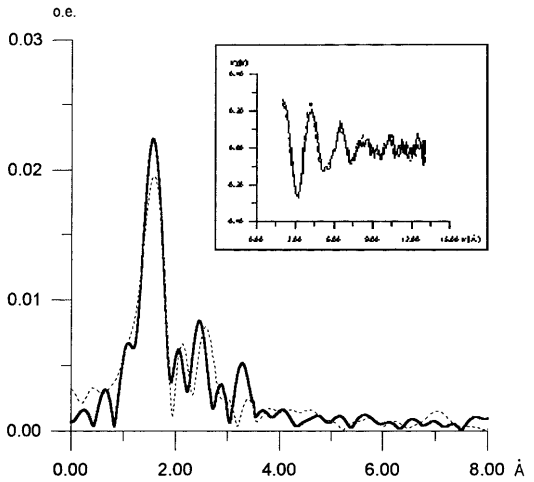


Fig. 2. FTM of the Cu K-edge EXAFS of the complexes **IV** (dash line) and **V** (solid line). The corresponding $k\chi(k)$ are shown in the insertion.

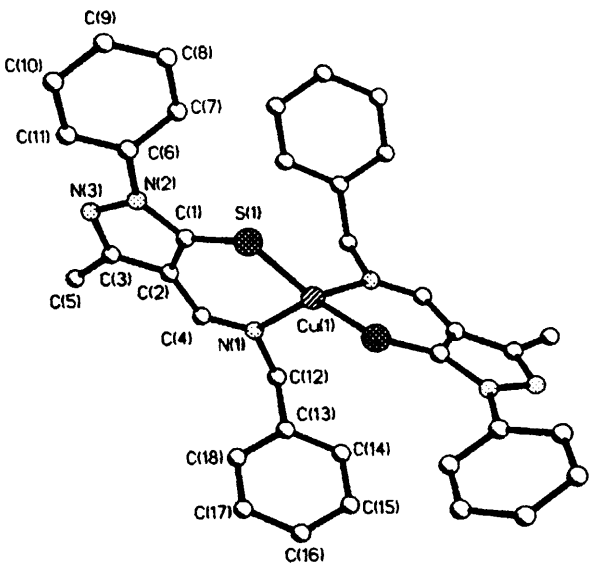


Fig. 3. Molecular structure of complex **IIIb**.

$r = 2.14$–2.16 Å which present in the FTM of both samples correspond to the distances $R_0* = 2.58$ Å for **IV** and $R_0* = 2.54$ Å for **V** (Table 1). This model was refined by the addition of a shell of five carbon atoms at $R_c = 2.96$–3.02 Å.

The most interesting feature in the FTM of complex **V** is the new peak at $r = 3.2$ Å. While it was also possible that this peak corresponds to the outer shells from carbon atoms of the azometnine ligand, the best fit was with the inclusion of the Cu–Cu interactions at $R = 3.53$ Å. The increase in the lower integration limit in the Fourier analysis (k_{min}) from 2.5 to 6.0 Å also shows that this outer shell consists of heavy atoms. This model is a good match with data found in the crystal structure for complex **V**.

Table 2
Selected bond lengths (Å) and valence angles (°) for complexes **IIIb**,**d**, **IV** and **V** according to the X-ray results

Complex	Bond	Å	Angle	°	Ref.
IIIb	Cu–S	2.2497(14)	S(1)CuN(1)	100.74(9)	[15,27]
	Cu–N	1.982(3)	S(1)CuS(1′)	98.47(6)	
			N(1)CuN(1′)	94.8(2)	
IIId	Cu–S	2.230(1)	S(1)CuN(1)	100.2(2)	[13]
	Cu–N	1.982(5)	S(1)CuS(1′)	90.92(8)	
			N(1)CuN(1′)	100.3(2)	
IV	Cu–N(1)	1.982(3)	N(1)CuN(2)	82.8(2)	[24]
	Cu–N(2)	1.990(4)	N(2)CuN(3)	162.7(2)	
	Cu–N(3)	1.952(4)	N(1)CuN(3)	90.3(2)	
	Cu–O(3)	1.949(3)	N(2)CuO(3)	91.5(2)	
	Cu–O(4)	2.646(5)	N(1)CuO(3)	162.6(2)	
			N(3)CuO(3)	99.4(2)	
			O(3)CuO(4)	54.9(2)	
V	Cu–O(1)	1.969(4)	O(1)CuO(1′)	79.2(2)	[24]
	Cu–O(3)	1.900(5)	O(1)CuO(3)	90.4(2)	
	Cu–N(1)	1.969(5)	O(1)CuN(1)	175.2(2)	
	Cu–N(2)	1.987(5)	O(1)CuN(2)	93.2(2)	
	Cu–O(1′)	2.528(4)	O(3)CuN(2)	172.6(2)	
			O(3)CuN(1)	93.2(2)	
			N(1)CuN(2)	83.5(2)	
			CuO(1)Cu	100.8(2)	

According to EXAFS fit, the Cu–Cu distance is $r = 3.53$ Å, which is typical for such bridges in natural metalloproteins [30].

Structures of some complexes were refined by X-ray structural analysis.

Among the compounds **IIIa**–**d**, **IV**, **V**, the complexes **IIIb**–**d** are of special interest, since they are the first representative compounds [1–13] of chalcogen-containing azomethinic metal chelates Cu(2+) with an open structure, which was determined by X-ray single-crystal diffraction [13,15]. In these chelates, a copper atom is in an *pseudo*-tetrahedral ligand environment N_2X_2, where X = S (complexes **IIIb**, Fig. 3, Table 2; **IIId**, Fig. 4, Table 2), X = Se (complex **IIIc**). Two planes NCuX of different metal cycles form dihedral angle **IIIb** 60.5° [15], **IIIc** 59.6°(preliminary X-ray single-crystal diffraction data), **IIId** 57.6° [13], respectively. Bond lengths of Cu–N and Cu–S (Table 2, Figs. 3 and 4) are 1.98 and 2.25 Å, respectively, similar to other tetracoordinate copper(II) chelates with an N,S-ligand environment [14]. The Cu–N distance in 'blue' copper proteins is 1.99–2.15 Å, the Cu–S distance is 2.07–2.17 Å [2,4], which is considerably shorter than those for reported biomimetic complexes [4]. The only example of model compounds, where it has been possible to register the same short bond length of Cu–S, is tris-pyrazolylborate copper complexes [16–19].

Due to the presence of the pyridyl fragment of the nitrogen atom in the complex **IIId**, it is possible to suppose the participation of the N-atom of the pyridine cycle in the formation of an additional bond. However, according to X-ray data (Table 2, Fig. 4), a nitrogen atom of a pyridine group does not form additional bonds with the copper atom and does not take part in intermolecular interactions [13]. In contrast to **IIId**, there is an additional coordination of the heterocyclic nitrogen atom in the compounds **IV** and **V**, which allows the expansion of a number of biomimetic copper complexes [3,15,27].

According to X-ray data (Table 2, Fig. 5) [23], the coordination polyhedron of **IV** is a tetragonal pyramid. The tridentate ligand is connected with the copper atom by means of three nitrogen atoms; together with the oxygen atom O(3) of the acetate group, this

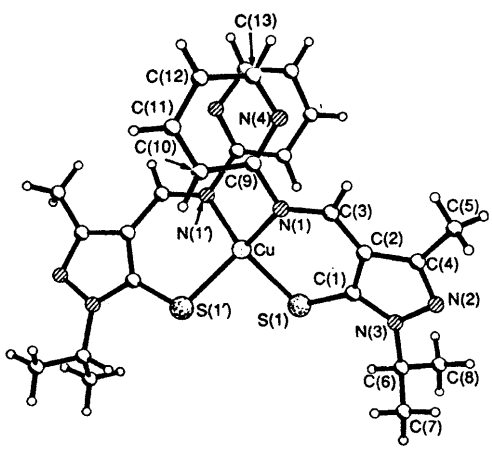


Fig. 4. Molecular structure of complex **IIId**.

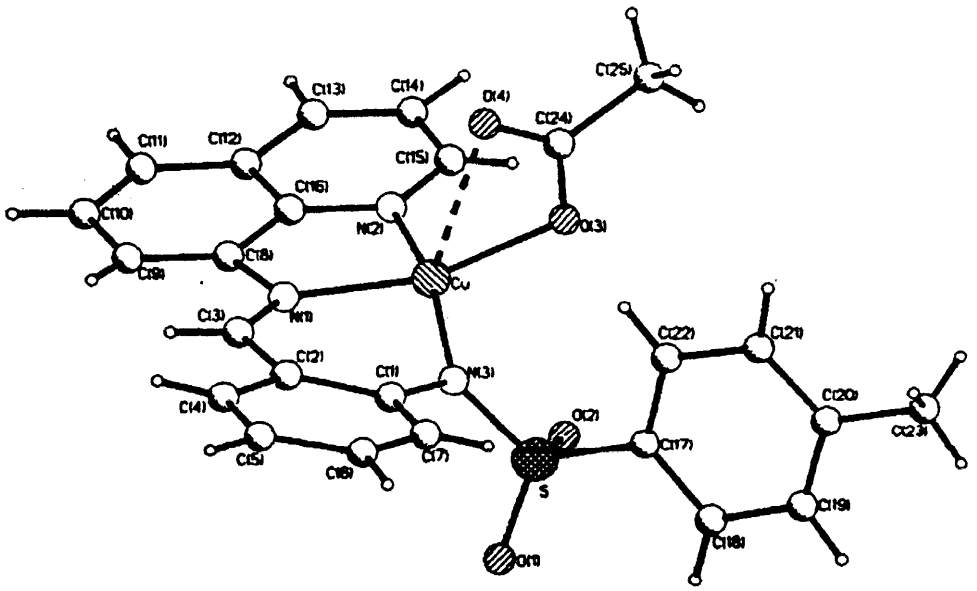


Fig. 5. Molecular structure of complex **IV**.

ligand forms an equatorial plane of a tetragonal pyramid. The apical top of this pyramid is occupied by the oxygen atom with a distance Cu–O(4) = 2.645 Å, which is slightly elongated, according to the Jahn–Teller effect. The base of the pyramid is tetrahedrally distorted: the deviation of the atoms from least-square plane is ±(0.24–0.28 Å).

As was shown by the results of X-ray structural investigation complex **V** possesses a dimeric structure which consists of two square-planar CuN_2O_2 coordination units connected one to another by the far Cu–O′ interaction. So the coordination polyhedron at the Cu atom is a square pyramid with a long apical bond (Fig. 6) [24].

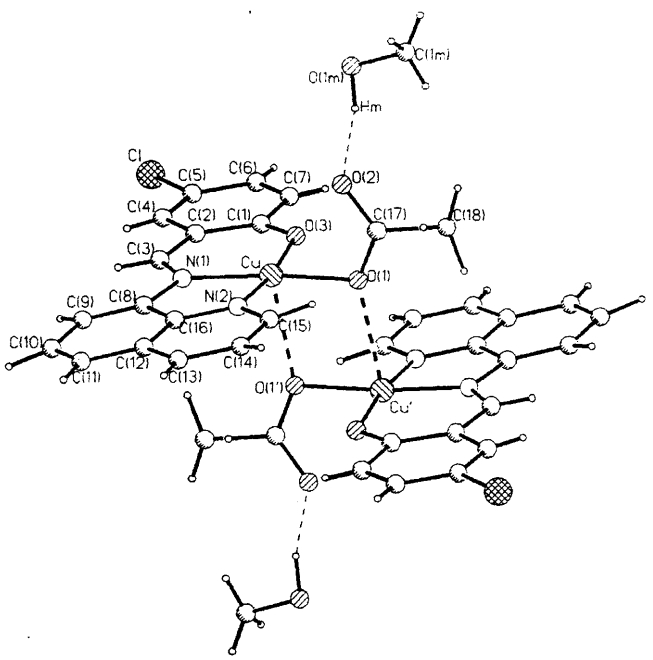


Fig. 6. Molecular structure of dimeric complex **V**.

4. Conclusions

As is shown, the structural data pertaining to the nearest-ligand environment of the central atom in the copper complexes synthesized, obtained by EXAFS spectroscopy, are in good agreement with the results obtained by X-ray single-crystal diffraction.

Acknowledgements

The authors are grateful to the Russian Foundation of Fundamental Research (grant No. 97-03-33479a).

References

[1] H. Toftlund, J. Becher, P.H. Olesen, J. Pedersen, Israel J. Chem. 25 (1985) 56.
[2] E.J. Solomon, M.J. Baldwin, M.D. Lovery, Chem. Rev. 92 (1992) 521.
[3] A.L. Nivorozhkin, A.I. Uraev, A.S. Burlov, A.D. Garnovskii, Mendeleev Chem. J. 40 (1996) 255.
[4] (a) S. Mandal, G. Das, R. Singh R. Shukla, P.K. Bharadwaj Coord. Chem. Rev.160 (1997) 191. (b) P.L. Holland, W.B. Tolman, J. Am. Chem. Soc. 121 (1999) 7020. (c) P.L. Holland, W.B. Tolman, J. Am. Chem. Soc. 122 (2000) 6331.
[5] R.D. Bereman, M.R. Churchill, G. Shields, Inorg. Chem. 18 (1979) 3117.

[6] R.D. Bereman, G.D. Shields, J. Bordner, J.R. Dorfman, Inorg. Chem. 20 (1981) 2165.
[7] R.D. Bereman, J.R. Dorfman, J. Bordner, D.P. Rillema, P. McCarthy, G.D. Shields, J. Inorg. Biochem. 16 (1982) 47.
[8] H.L. Schugar, in: K.D. Karlin, J. Zubieta (Eds.), Copper Coordination Chemistry, Biochemical and Inorganic Perspective, Chapman and Hall, New York, 1983.
[9] P. Bearwood, J.F. Gibson, J. Chem. Soc., Chem. Commun. (1983) 1099.
[10] J. Becher, H. Frydendahl, L.F. Taylor, H. Toftlund, J. Chem. Soc., Chem. Commun. (1986) 699.
[11] L. Casella, M. Gullotti, R. Vigano, Inorg. Chim. Acta 124 (1986) 121.
[12] L. Casella, M. Gullotti, A. Pintar, F. Pinciroli, R. Vigano, P. Zanello, J. Chem. Soc., Dalton Trans. (1989) 1161.
[13] A.E. Mistryukov, I.S. Vasilchenko, V.S. Sergienko, A.L. Nivorozhkin, S.G. Kochin, M.A. Porai-Koshits, L.E. Nivorozhkin, A.D. Garnovskii, Mendeleev Commun. (1992) 30.
[14] A.D. Garnovskii, A.L. Nivorozhkin, V.I. Minkin, Coord. Chem. Rev. 126 (1993) 1.
[15] A.I. Uraev, A.L. Nivorozhkin, G.I. Bondarenko, K.A. Lysenko, O. Yu. Korshunov, V.G. Vlasenko, A.T. Shuvaev, V.P. Kurbatov, M. Yu. Antipin, A.D. Garnovskii, Dokl. Akad. Nauk (Russian) 367 (1999) 67.
[16] N. Kitajima, K. Fujisawa, Y. Moro-oka, J. Am. Chem. Soc. 112 (1990) 3210.
[17] N. Kitajima, K. Fujisawa, M. Tanaka, Y. Moro-oka, J. Am. Chem. Soc. 114 (1992) 9232.
[18] D. Qiu, L.T. Kilpatrick, N. Kitajima, T.G. Spiro, J. Am. Chem. Soc. 116 (1994) 2585.
[19] N. Kitajima, W.R. Tolman, Progr. Inorg. Chem. 42 (1995) 291.
[20] A.T. Shuvaev, B. Ya. Helmer, T.A. Lubeznova, V.A. Shuvaeva, J. Synchrotron Rad. 6 (1999) 158.
[21] S.I. Zabinsky, J.J. Rehr, A. Ancudinov, R.C. Albes, M.J. Eller, Phys. Rev. 52 (1995) 2995.
[22] A.L. Nivorozhkin, M.S. Korobov, L.E. Konstantinovskii, L.E. Nivorozhkin, V.I. Minkin, Zh. Obshch. Khim. (Russian) 55 (1985) 849.
[23] A.D. Garnovskii, A.S. Antsyshkina, I.S. Vasilchenko, V.S. Sergienko, S.G. Kochin, A.L. Nivorozhkin, A.E. Mistryukov, A.I. Uraev, D.A. Garnovskii, Zh. Neorg. Khim. (Russian) 40 (1995) 67.
[24] I.S. Vasilchenko, A.S. Antsyshkina, G.G. Sadikov, et al., Zh. Neorg. khim. 44 (1999) 1278.
[25] L.N. Kurkovskaya, N.N. Shapet'ko, I.Ya. Kvitko, Yu.N. Koshelev, E.D. Samartseva, Russ. J. Org. Chem. 10 (1974) 2210.
[26] V.I. Minkin, A.D. Garnovskii, J. Elguero, A.R. Katritzky, O. Denisko, Adv. Heter. Chem. 76 (2000) 157.
[27] A.I. Uraev, A.L. Nivorozhkin, G.I. Bondarenko, K.A. Lysenko, O.Yu. Korshunov, V.G. Vlasenko, A.T. Shuvaev, V.P. Kurbatov, M. Yu. Antipin, A.D. Garnovskii, Izv. Akad. Nauk. Ser. Khim. (Russian) (2000) N11, 1892.
[28] D.Lippkow, P.Borthen, D.Hecht, H.-H.Strehblow; HASYLAB Annual Report, 1996, Band 1, 817.
[29] N. Kitajima, N. Tamura, H. Amagai, H. Fukui, Y. Moro-oka, Y. Mizutani, T. Kitagawa, R. Mathur, K. Heerwegh, C.A. Reed, C.R. Randall, L. Que, Jr., K. Tatsumi, J. Am. Chem. Soc. 116 (1994) 9071.
[30] K.A. Magnus, H. Ton-That, J.E. Carpente, Chem. Rev. 94 (1994) 727.

PERGAMON

www.elsevier.nl/locate/poly

Polyhedron 19 (2000) 2367–2372

POLYHEDRON

Catalytic properties of dinuclear copper complexes with an N_6 pyridazine-derived ligand

J. Manzur [a,*], A.M. García [a], B. Gómez [b], E. Spodine [b]

[a] *Facultad de Ciencias Físicas y Matemáticas, Universidad de Chile, Casilla 2777, Santiago, Chile*
[b] *Facultad de Ciencias Químicas y Farmacéuticas, Universidad de Chile, Casilla 233, Santiago, Chile*

Received 27 May 2000; accepted 1 September 2000

Abstract

Binuclear copper(II) complexes of the ligands 3,6-bis(di-2-pyridylmethyl)pyridazine (bdpdz) and 3,6-bis[(6-methyl-2-pyridyl)(2-pyridyl)methyl]pyridazine (mbdpdz), Cu_2LX_4 (X = Cl, Br) were prepared and characterized by UV-visible spectra, conductivity and voltammetry. These complexes were used as a catalyst for the oxidation of 3,5-di-*tert*-butylcatechol to 3,5-di-*tert*-butyl-*o*-benzoquinone. The reaction rate was determined in the presence and absence of a base (KOH) in methanol. The kinetic data are interpreted postulating one reactive species towards molecular oxygen: a copper (I) complex, which is generated by a redox equilibrium between the binuclear copper(II) complex and the substrate. © 2000 Elsevier Science B.V. All rights reserved.

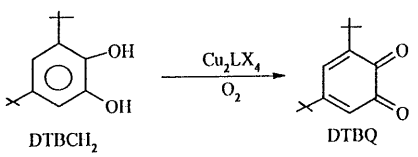
Keywords: Oxidation; Catalysis; 3,5-Di-*tert*-butylcatechol; Kinetics; Copper binuclear complexes

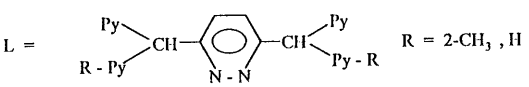
1. Introduction

Quadridentate (N_4) ligands, based on pyridazine and phthalazine as the binucleating fragments involving nitrogen donor centers, have been shown to generate principally binuclear copper(II) complexes [1–3]. These symmetrically arranged complexes present antiferromagnetic coupling and positive reduction potentials, which makes them good model systems for the active sites of copper metalloproteins. These are characteristic features of certain binuclear copper protein sites, such us tree lactase ($E_{1/2} = 0.434$ V) [4] and tyrosinase ($E_{1/2} = 0.360$ V) [5].

We have broadened the scope of these biomimetic systems by preparing binuclear complexes with hexadentate (N_6) ligands, [Cu_2LX_4], which present the pyridazine spacer. (L = bdpdz: 3,6-bis(di-2-pyridylmethyl)-pyridazine and mbdpdz: 3,6-bis[(6-methyl-2-pyridyl)(2-pyridyl)methyl]pyridazine; X = Cl, Br). The syntheses and magneto-structural characterization of these compounds have been described previously [6,7].

Recently a large number of binuclear copper(II) complexes have been reported in the literature as model compounds of tyrosinase. [8–15]. In the present paper we report the UV–Vis spectroscopic and electrochemical studies of these binuclear species in methanol, together with their catechol oxidase activity.





2. Experimental

2.1. Reagents

All reagents and solvents were of high purity grade and were purchased from commercial sources and used as received unless noted otherwise. 3,6-bis(di-2-pyridylmethyl)pyridazine (bdpdz) and 3,6-bis[(6-methyl-2-

* Corresponding author. Fax: +56-2-699-4119.
E-mail address: jmanzur@quimba.dqb.uchile.cl (J. Manzur).

0277-5387/00/$ - see front matter © 2000 Elsevier Science B.V. All rights reserved.
PII: S0277-5387(00)00573-8

pyridyl)(2-pyridyl)methyl] pyridazine (mbdpdz), and the corresponding $Cu_2(bdpdz)X_4$ and $Cu_2(mbdpdz)X_4$ complexes (X = Cl, Br) were prepared as reported elsewhere [6,7].

2.2. Measurements

The C, H, N elemental analyses were performed at CEPEDEQ (University of Chile) on a Fison-Carlo Erba EA 1108 model analyzer. Electronic spectra were recorded on a Perkin–Elmer Lambda 11 spectrophotometer using methanol (Chrom AR HPLC, Mallinckrodt) as a solvent.

Electrochemistry was performed in the methanol solution using 0.05 tetra-*n*-methyl ammonium perchlorate as an electrolyte. The cyclic voltammograms were recorded at a glassy carbon electrode, with a saturated calomel reference electrode and a Pt wire as an auxiliary electrode, on an EG&G Parr model 362 scanning potentiostat. All potential values are reported versus SCE.

Kinetic measurements were spectrophotometrically on a Unicam spectrophotometer, model UV-3, following the appearance of the reaction product, 3,5-di-*tert*-butylquinone (DTBQ), over time at 28°C (400 nm absorbance maximum, $\varepsilon = 1600\ M^{-1}\ cm^{-1}$ in methanol).

Conductance data, in methanol as a solvent, were obtained at 28°C on a Wayne Kerr Universal bridge.

3. Results and discussion

3.1. Spectral and conductivity studies

Conductance data indicate that all four complexes $[Cu_2(bdpdz)(H_2O)Cl_3]Cl$ (**1**), $[Cu_2(bdpdz)Br_4]CH_3CN$ (**2**), $[Cu_2(mbdpdz)Cl_4]\cdot 2H_2O$ (**3**), and $[Cu_2(mbdpdz)Cl_4]\cdot H_2O$ (**4**), correspond to 1:2 electrolytes in a methanol solution. The conductivity of the solutions does not change with time; thus indicating the dissociation of the halide ligands is instantaneous. All complexes have approximately the same conductance in a methanol solution (Table 1). The reported crystal structures show that in the solid state **1** is an ionic complex with one terminal chloro ligand, while **2** is a neutral species with two symmetrically disposed terminal bromo ligands [2]. The structures of **3** and **4** are unknown, since good quality crystals for X-ray diffraction were not obtained. The fact that the ionic complex **1** and the neutral complex **2** have similar conductivities suggests that the solvent replaces all terminal ligands. The binuclear structure of the complexes with the chloro or bromo bridges then remain intact in the solution.

The UV–Vis spectra show the typical absorption bands corresponding to d–d transitions of copper(II) in octahedral geometry (Table 1). The reflectance spectra of the chloro and bromo complexes with bdpdz, **1** and **2**, show bands centered at 775 and 780 nm, respectively. The bands of the copper(II) complexes in methanol solution are shifted towards higher energies with respect to the solid state spectra. This shift can be explained by the replacement of the terminal halogen ligands by solvent molecules. The effect is more pronounced for the bromo complex **2** where the two terminal bromides are replaced by the solvent, as compared with the chloro analogue that has only one terminal chloride.

Addition of 3,5-di-*tert*-butylcatechol ($DTBCH_2$), under anaerobic conditions, to a solution of the chloro complexes **1** and **3** did not produce a measurable change in the absorption spectra. For the bromo complexes **2** and **4** a decrease in absorbance as a function of the catechol concentration was clearly detected for the d–d bands. This decrease is rationalized by the following equilibrium:

$$\mathrm{Cu(II)–Cu(II)} + \mathrm{DTBCH_2} \overset{K}{\leftrightarrow} \mathrm{Cu(I)–Cu(I)} + \mathrm{DTBQ} + 2\mathrm{H^+} \quad (1)$$

The variation of the absorbance was used to estimate the value of $K = 1 \times 10^{-11}$ for the bromo complexes **2** and **4**. The fact that no measurables change in absorbance is observed for **1** and **3**, permits to predict lower values for K for these complexes.

Table 1
Spectral and conductivity data for complexes **1** to **4**

Compound	d–d (λ nm)		Λ_M (Ω^{-1} cm^2 mol^{-1}) (10^{-3} M methanol solution)
	Reflectance	Methanol solution	
1	775	770	150
2	780	745	170
3	[a]	748	130
4	[a]	770	130

[a] Ill defined band precludes the identification of the absorption maxima.

Table 2
Electrochemical data for complexes **1** to **4**

Compound	E_c (V)	E_a (V)
1	0.12 (0.30, 0.12) [a]	0.22, 0.40
2	0.13 (0.33, 0.14) [a]	0.22, 0.44
3	0.13	0.28; (0.36) [b]
4	0.14	0.44

[a] Second cycle.
[b] It appears as a shoulder on the signal at 0.28 V.

3.2. Electrochemistry

The redox behavior of the antiferromagnetically coupled binuclear copper(II) complex **1**, involving the chloro bridges, consists of a one-step two electron transfer at a positive potential of 0.12 V. The electrochemical data show that the reduction potentials of all four complexes do not depend significantly on the presence of the methyl groups substituted at the pyridine ring of the ligands (Table 2). The copper (I) complex is oxidized in a two step process at 0.22 and 0.40 V. The oxidized species formed in the first sweep towards reduction is different from the initially dissolved complex, since it reduces at 0.3 V during the second redox cycle. A typical voltammogram for complex **1** is shown in Fig. 1(A). The gross electrochemical behavior of the bromo complex **2** is similar.

The addition of $DTBCH_2$ to a solution of the copper complex **1** does not alter the peaks due to the Cu(II)/Cu(I) couple, observed in the voltammogram Fig. 1(B). However, if the voltammogram is recorded in the presence of base (Cu(II)–Cu(II):$DTBCH_2$:OH^- = 1:1:2) the followings peaks are observed Fig. 1(C):

1. During the first sweep towards oxidation a signal at 0.22 V and a second signal at 0.40 V are observed, corresponding to the one-electron re-oxidation of the copper (I) complex formed by the reaction with the catechol:

$$\text{Cu(II)–Cu(II)} + \text{DTBCH}_2 + 2\text{OH}^- \rightarrow \text{Cu(I)–Cu(I)} + \text{DTBQ} + 2\text{H}_2\text{O} \quad (2)$$

2. During the first sweep towards reduction a signal at -0.08 V is recorded corresponding to the reduction of the quinone in the presence of the copper (I) complex. An identical reduction peak is obtained for an in situ complex formation by a mixture of a solution of $Cu(AN)_4ClO_4$ with the corresponding ligand and quinone.

$$\text{Cu(I)–Cu(I)} + \text{DTBQ} + \text{e}^- \rightarrow [\text{Cu(I)–Cu(II)(DTBC}^{2-})] \quad (3)$$

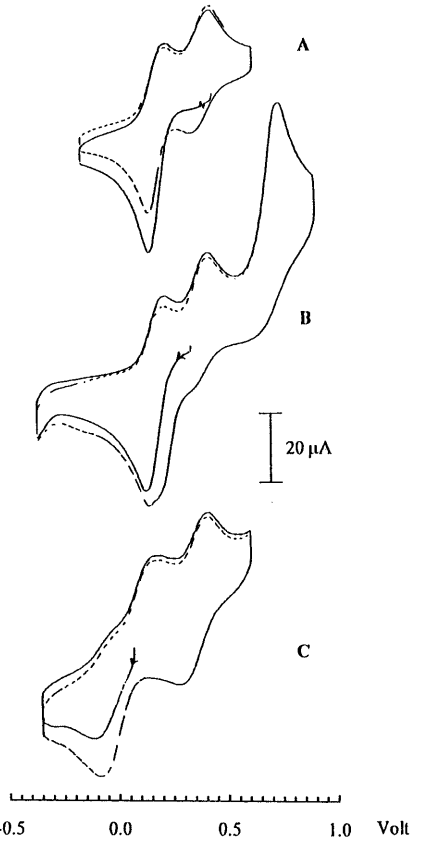


Fig. 1. Cyclic voltammograms for: (A) $[Cu_2(bdpdz)(H_2O)Cl_3]Cl$ (**1**) 5×10^{-4} M. (B) $[Cu_2(bdpdz)(H_2O)Cl_3]Cl$ and $DTBCH_2$ 5×10^{-4} M. (C) $[Cu_2(bdpdz)(H_2O)Cl_3]Cl$ and $DTBCH_2$ 5×10^{-4} M and KOH 1×10^{-3} M, scanning towards reduction. Electrolyte: 0.05 M tetra-*n*-butylammonium perchlorate in methanol.

A methanolic solution of pure quinone is reduced at -0.30 Volt.

3. Continuing the sweep towards oxidation, the [Cu(I)–Cu(II)($DTBC^{2-}$)] species produces quinone at 0.08 V.

$$[\text{Cu(I)–Cu(II)(DTBC}^{2-})] \rightarrow \text{Cu(I)–Cu(I)} + \text{DTBQ} + \text{e}^- \quad (4)$$

All four complexes exhibit the same general behavior just described, in the presence of added $DTBCH_2$ and a base.

3.3. Kinetic studies

Since DTBQ shows a characteristic band at 400 nm, the absorbance at this wavelength was used to measure the progress of the oxidation of the substrate $DTBCH_2$. The concentration of copper(II) complex, or the concentration of copper(I) complex generated by the redox reaction in presence of catechol, is too small to interfere with the measured absorbance value.

3.3.1. Kinetic data for the system without an added base (KOH)

The method of initial rates was used to determine the experimental kinetic law. The behavior of the system is similar for all four binuclear copper(II) complexes. Therefore the figures in the text refer mostly to [Cu(bdpdz)$Cl_3(H_2O)$]Cl, (**1**). Fig. 2 shows the data obtained for a concentration range of complex **1** of 2.0 to 60×10^{-6} M and at a constant concentration of $DTBCH_2$ (1×10^{-3} M). The non-linear dependence of the experimental rate on the analytical concentration of the complex can be rationalized in terms of the above mentioned equilibrium (1).

$$\text{Cu(II)–Cu(II)} + \text{DTBCH}_2 \overset{K}{\leftrightarrow} \text{Cu(I)} \text{–Cu(I)} + \text{DTBQ} + 2\text{H}^+ \quad (1)$$

The Cu(I)–Cu(I) species is assumed to be the actual reactive species towards oxygen and its concentration was calculated with the following equilibrium constant values: 1×10^{-12} (complex **1**), 1×10^{-11} (complex **2** and **4**) and 1×10^{-13} (complex **3**).

$$\text{Cu(I)–Cu(I)} + \text{O}_2 \rightarrow \text{Cu(II)–}(\text{O}^{2-})\text{–Cu(II)} \text{ (rate determining)} \quad (5)$$

The peroxo species generated in reaction (5) would rapidly decompose to give the Cu(II)–Cu(II) complex. Even though Casella et al. [8] report a combined mechanism in which, the possibility of direct oxidation of catechol by the peroxo binuclear copper(II) species is also considered together with the decomposition reaction, the former step has not been considered in the postulated mechanism. This due to the fact that in the catechol concentration range used in this study the reaction rate results independent of the substrate.

Since the kinetic runs were done at constant concentration of oxygen the experimental rate law becomes:

$$\text{Rate} = k[\text{Cu(I)–Cu(I)}]$$

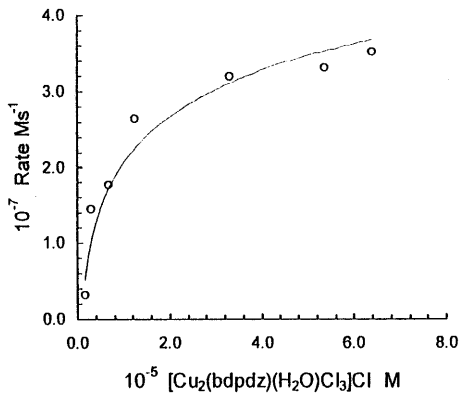


Fig. 2. Rate of oxidation of $DTBCH_2$ versus concentration of [Cu_2(bdpdz)(H_2O)Cl_3]Cl (**1**) at constant concentration of $DTBCH_2$ (1×10^{-3} M). ○: experimental data; --- simulated curve using $K = 1 \times 10^{-12}$ and $k = 0.04$ M s^{-1}.

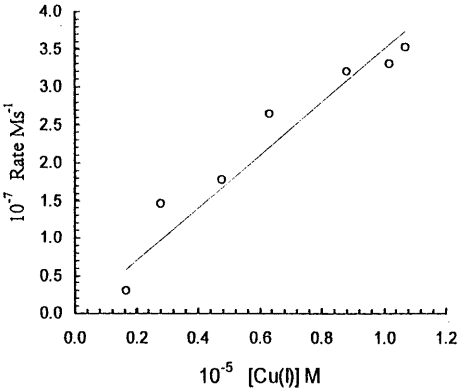


Fig. 3. Rate of oxidation of $DTBCH_2$ versus the calculated concentration of copper(I) complex derived from [Cu_2(bdpdz)(H_2O)Cl_3]Cl (**1**), using $K = 1 \times 10^{-12}$.

Fig. 3 shows the dependence of the rate on the calculated concentration of copper (I) complex for the oxidation of $DTBCH_2$ with dioxygen catalyzed by complex **1**. A linear relationship resulted for all four complexes. Calculated value for the experimental pseudo first order rate constants for complexes **1** to **4** are quoted in Table 3.

Complex **3** shows the greatest value for the rate constant while the complexes with the ligand without the methyl substituent show the lowest values. Complex **3** also shows the lowest value for the equilibrium constant equilibrium (1). These results indicate that the copper(I) complex formed is more easily oxidized, by molecular oxygen to the copper(II) state and that at least for the studied complexes the steric effect imposed by the substituent does not prevent the interaction of the substrate with the catalyst. Inspection of the potential values for the re-oxidation of the copper(I) complexes formed during the first sweep towards reduction shows that complex **3** is oxidized to copper(II)–copper(II) at a lower potential, in accordance with the kinetic results.

3.3.2. Kinetic data for the system with an added base (KOH)

Kinetic runs, carried out with concentration of complex **1** at constant values of 5.3×10^{-6} and 6.4×10^{-6} M and of $DTBCH_2$ at 1×10^{-3} M, showed a behavior which is depicted in Fig. 4. As the concentration of base increases the rate increases until a molar ratio of com-

Table 3
Kinetic and equilibrium constant data for complexes **1** to **4**

Compound	k (s^{-1})	K (equilibrium (1))
1	0.04	1×10^{-12}
2	0.03	1×10^{-11}
3	0.16	1×10^{-13}
4	0.05	1×10^{-11}

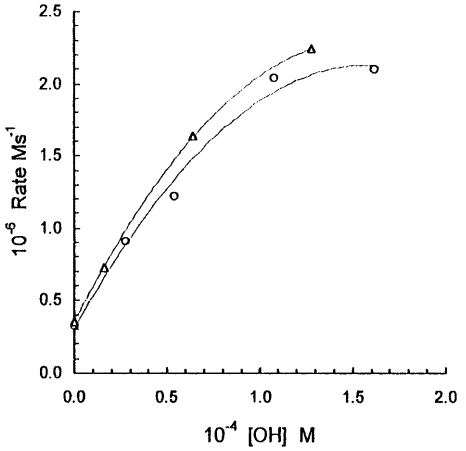


Fig. 4. Dependence of the rate of oxidation of $DTBCH_2$ on the concentration of base, at constant concentration of the catalyst; ○, $[Cu_2(bdpdz)(H_2O)Cl_3]Cl$ 5.3×10^{-5} M; △, $[Cu_2(bdpdz)(H_2O)Cl_3]Cl$ 6.4×10^{-5} M.

plex: OH of 1:2 is reached, the dependence of the rate on [OH] becomes independent above this ratio. The fact that an asymptotic value of the rate of production of DTBQ is observed as the concentration of the base is increased can be explained by the existence of equilibrium (1), which was detected by cyclic voltammetry.

Experimental data obtained for a series of kinetic runs at constant complex to base ratio of 1:2, where the copper(II) complex has been reduced completely to the copper(I) complex, show a linear dependence on this concentration. The reaction rates obtained from these experimental data permit to calculate a rate constant equal to that obtained from experiments without added base. This fact confirms that the used values of K are the correct ones.

The kinetic behavior of the studied binuclear copper(II)-complexes in the presence of base is different from the one observed earlier for mononuclear copper(II)-complexes $CuLCl_2$ (L = 6-methyl-2,2′-dipyridylmethane and 6,6′-dimethyl-2,2′-dipyridylmethane) [16]. In The case of these last compounds two active species towards molecular oxygen were detected, Cu(I)L and $Cu(II)L(DTBC^{2-})$, while in the present study a binuclear copper(I) is postulated. However, in both systems a similar equilibrium was observed in the absence of base, giving account of the reduction of the initial copper(II) species in the presence of catechol.

If the catecholase activity of the mononuclear Cu(I)L [16] and the Cu(I)–Cu(I) complex with the monomethylated ligands is compared, the binuclear species is found to be one order of magnitude more active.

Binuclear copper(II) complexes with square-pyramidal geometry and pyrazolate bridges reported by Urbach et al. [17] are found to be more efficient catalyst for the oxidation of 3,5-di-*tert*-butylcatechol. Even though the copper-copper distance reported for these complexes is of the same order of magnitude as for **1** and **2**, the geometry around the metal centers is quite different, since the latter are octahedral. This factor may explain in part the difference in the observed catecholase activity, as the interaction between the copper centers and the substrate is more favorable for the former complexes than for those reported in this paper. It has been shown that the electron transfer from catechol to copper(II) takes place only after the copper(II)-catecholate intermediate is formed. A suitable coordination site on the metal must exist for the formation of the intermediate [18]. Therefore the reported results reaffirm that the geometry around the copper ions is a dominant feature in determining the catalytic activity of synthetic model systems [19,20].

Acknowledgements

The support of this research by the Consejo Nacional de Ciencia y Tecnología (project FONDECYT 1990185) is gratefully acknowledged. B.G. acknowledges a leave of absence from Universidad Tecnológica Metropolitana (UTEM).

References

[1] F. Abraham, M. Lagrene, S. Sueur, B. Mernari, C. Bremard, J. Chem. Soc. Dalton Trans. (1991) 1443.
[2] L. Chen, L.K. Thompson, J.N. Bridson, Inorg. Chim. Acta 244 (1996) 87.
[3] L.K. Thompson, F.L. Lee, E.J. Gabe, Inorg. Chem. 27 (1988) 39.
[4] B.R.M. Reinhammer, Biochim. Biophys. Acta 275 (1972) 245.
[5] N. Makino, P. McMahill, H.S. Mason, J. Biol. Chem. 29 (1974) 6062.
[6] J. Manzur, A.M. García, R. Letelier, E. Spodine, O. Peña, D. Grandjean, M.M. Olmstead, B.C. Noll, J. Chem. Dalton Trans. (1993) 905.
[7] E. Spodine, A.M. Atria, J. Manzur, A.M. García, M.T. Garland, A. Hocquet, E. Sanhueza, R. Baggio, O. Peña, J.Y. Saillard, J. Chem. Soc. Dalton Trans. (1997) 3683.
[8] E. Monzani, L. Quinti, A. Perotti, L. Casella, M. Gullotti, L. Randaccio, S. Geremia, G. Nardin, P. Faleschini, G. Tabbi, Inorg. Chem. 37 (1998) 553.
[9] J.H. Satcher, M.W. Droege, T.J.R. Weakleay, R.T. Taylor, Inorg. Chem. 34 (1995) 3317.
[10] M. Lubben, R. Hage, A. Meetsma, K. Byma, B.L. Feringa, Inorg. Chem. 34 (1995) 2217.
[11] L. Casella, E. Monzani, M. Gullotti, D. Cavagnino, G. Cerina, L. Santagostini, R. Ugo, Inorg. Chem. 35 (1996) 7516.
[12] L. Casella, O. Carugo, M. Gullotti, S. Garofani, P. Zanello, Inorg. Chem. 32 (1993) 2056.
[13] M.N. Nasir, K.D. Karlin, D. McGowty, J. Zubieta, J. Am. Chem. Soc. 113 (1991) 698.
[14] M. Mahroof-Tahir, N.N. Murthy, K.D. Karlin, N.J. Blackburn, S.N. Shaikh, J. Zubieta, Inorg. Chem. 31 (1992) 3001.
[15] J.D. Crame, D.E. Fenton, J.M. Latour, A.J. Smith, J. Chem. Soc. Dalton Trans. (1991) 2979.

[16] J. Manzur, A.M. García, V. Rivas, A.M. Atria, J. Valenzuela, E. Spodine, Polyhedron 16 (1997) 2299.
[17] J.P. Chyn, F.L. Urbach, Inorg. Chim. Acta 189 (1991) 157.
[18] M.R. Malachowski, B. Dorsey, J.G. Sackett, R.S. Kelly, A.L. Ferk, R.N. Hardin, Inorg. Chim. Acta 249 (1996) 85.
[19] M.R. Malachowski, H.B. Huynh, L.J. Tomlinson, R.S. Kelly, J.W. Furbeejun, J. Chem. Soc. Dalton Trans. (1995) 31.
[20] K.D. Karlin, J. Zubieta (Eds.), Coordination Chemistry: Biochemical and Inorganic Perspectives, Adenine, Guilderland, NY, 1983.

PERGAMON

www.elsevier.nl/locate/poly

Polyhedron 19 (2000) 2373–2381

POLYHEDRON

Bis-bipyridine hexa-aza-macrocycle complexes of zinc(II) and nickel(II) and the catalytic reduction of carbon dioxide

J. Canales [a], J. Ramirez [a], G. Estiu [b], J. Costamagna [a,*]

[a] *Faculty of Chemistry and Biology, Universidad de Santiago de Chile, Santiago-33, Chile*
[b] *CEQUINOR, Faculty of Exact Sciences, Universidad Nacional de La Plata, CC 962, CP 1900, La Plata, Argentina*

Received 1 October 1999; accepted 11 May 2000

Abstract

Aza-macrocyclic complexes have gained importance in catalysis for the activation of small molecules, like carbon dioxide. Bis-bipyridine hexa-aza-macrocycles efficiently co-ordinate as a tetradentate ligand, to give complexes of Zn(II), Ni(II) and other transition metal ions that are essentially planar. Spectroscopic, electrochemical and chemical characterizations of these systems are presented in this article. Electrochemical studies performed in a carbon dioxide atmosphere render preliminary information about its electrocatalytical reduction. Quantum chemical calculations are used to understand the origin of the manifested properties of both the ligands and the metal complexes. They show, in this case, the importance of delocalized π interactions, which are responsible for their different structural and electronic characteristics in protic and non-protic media. © 2000 Elsevier Science B.V. All rights reserved.

Keywords: Aza-macrocycles; Electroreduction; Carbon dioxide; Delocalized π interactions

1. Introduction

The synthesis and characterization of coordination compounds with aza-macrocyclic ligands has evolved during the last years as one of the main research areas in coordination chemistry [1–4]. Aza-type ligands appear as very promising for catalysis and are, thence, one of the most frequently discussed chelating systems in the related literature [5–11]. Not much interest has been focused, however, on azamacrocycles derived from the condensation of bipyridines, i.e. bis-bipyridine hexa-azamacrocycle (3,10-dihydrotetrapyrido [2,1,6-de:2′,1′,6′-gh:2″,1″,6″-kl:2‴,1‴,6‴-na] [1,3,5,8,12] hexa-aza-cyclotetradecine), bis-azabipy hereafter. The lack of information on this subject seems to be related to the low yield observed in the synthesis of these ligands [12–15]. However, recent publications have shown that the rigorous elimination of humidity, and the use of chromatographic separations lead to a significant increase in the yields. Additional information related to the spectroscopic and electrochemical properties of these ligands and of some of their transition metal complexes is now available [16,17]. It shows that the complexation capabilities of polyaza macrocycles are mainly governed by the macrocyclic ring size. Their N-functionalization, on the other hand, enhances the metal-ion selectivity and the stability of metal complexes through the co-ordination properties of pendant substituents [18].

Aza-macrocyclic ligands, as well as their coordination and organometallic compounds play important roles in catalysis in the activation of small molecules, showing catalytic activity in electrochemically assisted reactions with several substrates [19,20]. Carbon dioxide has been tested in some of these systems, in the search for a way of lowering its high reduction potential [21–23]. Ligands that favor low oxidation states and are effective for electron transfer processes are expected to behave more efficiently for this purpose [20].

Carbon dioxide is a small molecule of utmost importance for the production and/or energy storage in non-conventional resources. Its reduction is a process of applicability in ambient chemistry related issues, such as the synthesis of ecological naphtas or the control of

* Corresponding author.
E-mail address: jcostama@lauca.usach.cl (J. Costamagna).

0277-5387/00/$ - see front matter © 2000 Elsevier Science B.V. All rights reserved.
PII: S0277-5387(00)00574-X

the greenhouse effect, responsible for disruption in the natural environment [24]. Coordination compounds have shown catalytic activity toward these reactions, and have become very promising because they allow their rational optimization by means of properly designed modifications of either the ligand or the central metal atom. The first step towards this rational design relies on a detailed study of the structural, electronic and spectroscopic characteristics of these complexes, which will help to understand the main steps of the mechanisms involved in the catalytic mediation.

This article deals with the study of the aza-macrocycle, shown in Fig. 1, that results from the condensation of bipyridine precursors [13,14]. We focus on the spectroscopic, electrochemical and theoretical characteristics of this ligand and its Ni and Zn complexes. This knowledge will allow us to properly analyze their effect on the electro-activation of carbon dioxide.

2. Experimental

2.1. Instruments

Solid IR-TF spectra were registered using a Bruker IFS-66V spectrophotometer as KBr pellets in the 4000–400 cm^{-1} and polyethylene pellets in the 400–150 cm^{-1} ranges. ^1H NMR spectra in CD_3Cl, CD_3COOD, and CF_3COOH were registered using a Bruker AC-200P spectrophotometer; TMS has been used as an internal standard. UV–Vis spectra in chloroform and acetic acid solutions were registered using a Varian Cary 1E spectrophotometer. Zinc and nickel elemental analysis were performed using a Perkin–Elmer 2380 atomic absorption spectrophotomether. Carbon, nitrogen and hydrogen elemental analysis were performed using a Fisons EA 1108 apparatus. Melting points were registered using an Electrothermal IA9000 apparatus.

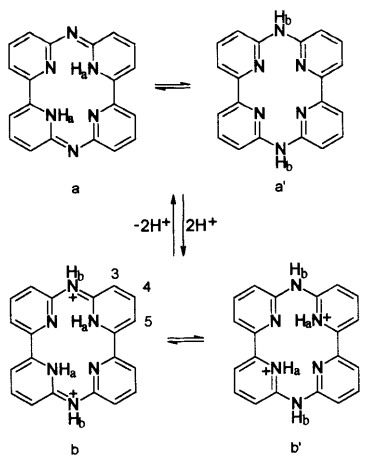


Fig. 1. Amine (**1a**, **1b**) and imine (**1a′**, **1b′**) tautomers of the bis-azabipy ligand.

2.2. Electrochemical procedures

The experiments were carried out on a PAR 173 potentiostat/galvanostat instrument with a PAR 175 model universal programmer coupled to a PAR 179 digital coulometer. The voltammograms and the simultaneous current intensity–time plots for electrolysis were registered in a X-Y Houston-Ommigraphic 2000 recorder. Cyclic voltammetry, and controlled potential electrolysis coulometry at room temperature (r.t.) (approximately 25°C) under either inert (N_2) or saturated CO_2 atmosphere were performed in a specially designed air-tight electrochemical cell with a double three-electrode system, to obtain cyclic voltammograms 'in situ' for the electrolytically generated products. All electrodes were introduced into the cell body by means of a ST glass joint, and caps with Teflon-faced-silicone septa were used for the needles that bubble and exit gases. Coulometric measurements were performed using a reticulated vitreous carbon (ERG) and a saturated calomel as working and reference electrodes, respectively. The last one was supplied by a vycor tip glass end. Platinum spiral wire counter electrode was separated by means of a salting bridge through sinterized glass ends. For cyclic voltammetry experiments a vitreous carbon-polished teflon-coated button was used as a working electrode. The reference and counter electrode were the same as above.

2.3. Synthesis

The reagents and solvents employed in the synthesis were analytical grade and were used without further purification. The synthetic procedures are mainly based on the literature [14,25], with some modifications that are indicated in the text. Fig. 2 shows a general scheme of the synthesis.

2.3.1. 6,6′-Dichloro-2,2′-bipyridine

2,2′-Bipyridine (20 g, 0.128 mol) were dissolved in 70 ml of dimethyl sulfate under nitrogen; the solution was refluxed until the appearance of a white hygroscopic solid, 1,1′-dimetil-2,2′-bipiridine sulfate, which was washed with ether under nitrogen and dissolved without further purification in 500 ml of water below 5°C for the following step. Potassium ferricianide (120 g,

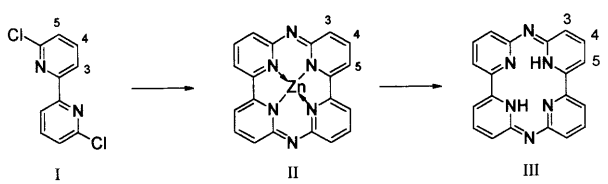


Fig. 2. General scheme of synthesis.

0.365 mol, dissolved in 400 ml of water) and sodium hydroxide (150 g, 3.75 mol, dissolved in 500 ml of water) were simultaneously added dropwise to the former solution for 3 h. The pH was adjusted to 8–9 with some drops of 37% hydrochloric acid at the end of the addition. The product, 1,1′-dimethyl-2,2′-bipyridine-6,6′(1H,1′H)-dione, was extracted with chloroform and precipitated by evaporation. It was recrystallized from chloroform, yielding 12 g. Then, 7 g, 0.0324 mol, were mixed under nitrogen with 15 g, 0.0719 mol, of phosphorus(V) chloride and 140 ml of phosphoryl chloride; the solution refluxed for 20 h and the excess of phosphoryl chloride removed by vacuum destilation. The remaining solid, 6,6′-dichloro-2,2′-bipyridine, was neutralized with ammonia and recrystallized from chloroform. Yield: 3.6 g, 50%; FTIR, ν (cm^{-1}): ν_{C-H}, 3035(s); ν_{C-C} and ν_{C-N}, 1575(m), 1545(m), 1418(m), ρ_{C-H}, 788(s); ν_{C-Cl}, 730(m). ^1H NMR in $CDCl_3$, δ (ppm): (see in Fig. 2(**I**)) H_3, 8.3(d); H_4, 7.7(t); H_5, 7.3(d).

2.3.2. Zn-bis-azabipy

6,6′-Dichloro-2,2′-bipyridine (2 g, 0.0089 mol) and ammonium tetrachloro zincate (15 g, 0.0712 mol), previously prepared from zinc chloride and ammonium chloride [25], were mixed in a mortar and then heated at 320–330°C under nitrogen over 6 h. The product was washed with water and 10% sodium hydroxide, and dried at 100°C and then sublimated at 200°C under vacuum for 3 h to separate a secondary product, 6,6′-diamino-2,2′-bipiridine. The remaining product, zinc azabipyridyl macrocycle, was dissolved in 5% acetic acid, reprecipitated with 10% sodium hydroxide and dried at 100°C. It melts above 400°C. Yield: 759 mg, 42%. *Anal.* Calc. for $ZnC_{20}N_6H_{12}\cdot 6H_2O$: C, 47.1; H, 4.7; N, 16.3; Zn, 12.9; Found: C, 47.7; H, 4.1; N, 16.5; Zn, 12.1%. FTIR, ν (cm^{-1}): ν_{C-N}, 1615(s), ν_{C-C} and ν_{C-N}, 1636(s), 1585(vs), 1544(s), 1470(vs), ρ_{C-H}, 795(m); ν_{Zn-N}, 428(m), 326(br), 275(w) (s, strong; vs, very strong; m, medium, br, broad, w, weak). ^1H NMR in CF_3COOH, δ (ppm) (see Fig. 2(**II**)): H_4, 8.4(t); H_5, 8.3(d); H_3, 7.6(d); H–N, 9.3(s) (d, doublet; t, triplet; s, singlet).

2.3.3. Bis-azabipi ligand [25]

Zinc bis-azabipy (760 mg, 1.90 mmol) was dissolved with stirring sulfuric acid (in 30 ml of 98%). Gaseous hydrogen chloride was bubbled in the solution during 6 h. Zinc chloride was separated by filtration and 25% ammonia was added to obtain a basic solution from which the azabipi ligand precipitates. It melts above 400°C. Yield: 316 mg, 35%. Color: orange. *Anal.* $C_{20}N_6H_{14}\cdot 6H_2O$: C, 53.8; H, 5.8; N, 19.1. Found: C, 52.5; H, 5.1; N, 18.8%. FTIR, ν (cm^{-1}): ν_{N-H}, 3400(s), 2800(w); ν_{C-N}, 1630(m); ν_{C-C}, 1587(m), 1534(vs), 1456(m); ρ_{C-H}, 784(m). ^1H NMR in CF_3COOH, δ (ppm) (see Fig. 1(**b**); Fig. 2(**III**)), H_3, 8.5(d); H_4, 8.6(t); H_5, 7.9(d); H_b, 10.4(s); H_a, 17.2(s).

2.3.4. Ni-bis-azabipy

This has been synthesized following a procedure described for analogous macrocyclic complexes derived from phenanthroline [17]: the azabipiridyl macrocycle (80 mg; 237.0 mmol) and nickel(II) acetate tetrahydrate (61.9 mg; 248.6 mmol), dissolved in nitrobenzene and benzyl alcohol, respectively, were mixed and refluxed under N_2 atmosphere with stirring during 3 h. The solution changed from orange to red. The red product was precipitated by addition of acetone, centrifuged and washed with nitrobenzene and water. A total of 40 mg of the complex (44% yield) were obtained after drying at 100°C. It melts above 400°C. Color: red. *Anal.* for $NiC_{20}N_6H_{12}$: C, 60.8; H, 3.1; N, 21.3; Ni, 14.9. Found: C, 60.5; H, 3.3; N, 20.5; Ni, 14.2%. IR-TF, ν (cm^{-1}), ν_{C-H}, 3075(w); ν_{C-N}, 1606(m); ν_{C-C}, 1554(m), 1480(vs), 1462(s); ρ_{C-H}, 785(m); ν_{N-M}, 470(m), 426(m), 327(w). ^1H NMR in CF_3COOH, δ (ppm), H_3, 8.3(s); H_4, 8.5(s); H_5, 7.7 (s); H-N, 10.6 (s).

2.4. Details of the computational procedure

X-ray diffraction data are not available for either the ligand or the coordination complexes. Thus, the first step of the study implies a full geometry optimization of the structures to be analyzed. Optimization is based on a minimization of the energy gradient, calculated analytically, using the BFGS algorithm to update the Hessian matrix in successive geometry cycles. PM3 and AM1 Hamiltonians [26] have been compared for the ligand and the Zn complex. Tautomer species that can coexist in equilibria have been considered for the ligand, in both their neutral and protonated forms (Fig. 1), as a way of modeling effect of protic and aprotic environments. Only PM3 calculations have been used to optimize the geometry of the Ni complex, as no parameters for Ni are available at the AM1 level. All self-consistent field (SCF) calculations were of the restricted Hartree Fock (RHF) type.

For the optimized structures, the electronic characteristics and the UV–Vis spectra have been examined by means of the INDO/S methodology [27,28], parametrized for spectroscopy [29–31], at the configuration interaction single (CIS) level of theory (ZINDO/S [32]). Several different CI calculations have been performed. As for the geometry optimization step, tautomeric and protonated structures were analyzed. The feasibility of the different structures has been decided on the basis of the best reproduction of the experimental spectra. With this objective in mind, not only monomers, but also more extended systems have been considered in order to model the different experimental situations.

A number of configurations larger than 1200 have been included in the CI calculations, which were generated by single electronic excitations from the upper 60

occupied to the lower 15 virtual orbitals, in both monomer and dimer compounds. This pattern was kept constant regardless of the size of the system. The orbital space has been selected to include all the n, and all the n and the d orbitals, for the ligand and the complexes, respectively. Oscillator strengths were evaluated with the dipole-length operator [33], retaining all one center terms. C_{2v} symmetry has been defined for the calculations whenever it applies.

3. Results and discussion

Results on electron transfer processes measured by cyclic voltammetry and coulometry; electronic spectra in solution for the bis-aza-bipy ligand and its Zn(II) and Ni(II) complexes; and geometry optimization and spectra interpretation through quantum chemical calculations will be shown and discussed next.

3.1. Electron transfer process: cyclic voltammetry and coulometry

In terms of potential applications to catalysis it is of particular interest to establish the nature of the redox processes and characterize them. In some cases, i.e. phthalocyanines, it is important to learn whether this process involves either one or both metal center together with the ligand [34]. We have reported cyclic voltammetry results in the cathodic region for Ni(II) and Cu(II) hexa-aza-macrocyclic complexes derived from phenantholine and suggested the stabilization of both Ni(I) and Cu(I) at -0.85 and -0.80 V versus SCE, respectively. Coulometric measurements indicate that these reactions involve one-electron reduction [35].

Fig. 3 shows electrochemical results of the bis-azabipy ligand and its nickel(II) complex in nitrogen and carbon dioxide in the cathodic region. The presence of a low-intensity redox process in the free ligand (in carbon dioxide) suggest that the CO_2 reduction process in the nickel(II) complex is probably occurring on the metal center [17]. The Zn azabipi complex shows a redox behavior similar to the free ligand, i.e. a significant catalytic process was not observed. Also depicted, in Fig. 3, is the clear modification of the cyclic voltammogram for the nickel complex, measured in carbon dioxide media. The intensity of the cathodic peak (approximately 1.5 V versus SCE) increases approximately three times when nitrogen is changed to carbon dioxide. Similar results have been obtained for fluorinated Ni(cyclam)$^{2+}$ complexes [34,36]. In addition, it has been found that coulometry by controlled potential electrolysis at -1.6 V in CO_2 medium has a constant intensity for a long period of time, while the behavior in nitrogen atmosphere is normal and shows one electron reduction process. The observed results confirm the electrocatalytic activity of the complexes for the reduction of carbon dioxide. Similar results have been previously observed in analogous systems such as Ni(cyclam)$^{2+}$ complexes [20,37]. The reduction of carbon dioxide might produce formic acid, -0.61 V; carbon monoxide, -0.52 V; formaldehyde, -0.48 V; methanol, -0.38 V or methane, -0.24 V (versus NHE), in multielectron transfer reactions [38]. A comparison of these electron transfers with the one-electron reduction of carbon dioxide to CO_2^-, -1.2 V; or to CO_2H, -0.60 V (versus NHE), shows that the thermochemical advantage is balanced by the kinetic constrains that are imposed by the requirement of multi-electron transfers. Adducts of CO_2 are probably involved in the reduction mechanism, as it has been found in radiolytic studies previously performed [39].

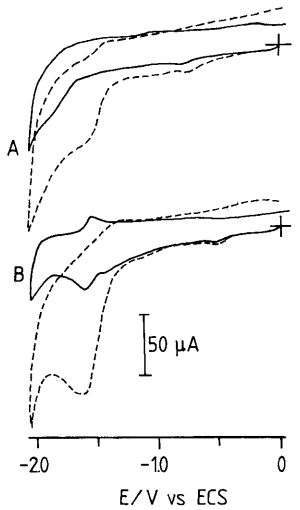


Fig. 3. Cyclic voltammograms, in *N*,*N*′-dimethylformamide, under N_2 (—) and CO_2 (----) for: (A) bis-azabipi; (B) Ni-bis-azabipi; approximately 0.1 mM; scan rate 0.2 V s^{-1}.

A quantitative evaluation of electrocatalytic properties such as turnover cycles, percentage of average current efficiency, selectivity by gas chromatographic identifications is currently being developed and will be published later.

3.2. Electronic spectra in solution

Bis-azabipy complexes are sparingly soluble in methanol and water. However, the solubility in these solvents increases by the addition of acids. Electronic spectra for the free ligand and the Zn(II) and Ni(II) complexes are shown in Fig. 4.

When the spectra obtained in protic and aprotic solvents are analyzed comparatively, the most important difference that becomes evident is related to the presence of a band structure in the visible region that only develops in the latter. As will be further discussed, the band in the visible region is assigned, on a theoret-

ical basis, to the influence of stabilizing intermolecular interactions originated in the delocalization of the pi system. On the other hand, the main influence of the protic solvent would be a protonation of the external nitrogen atoms of the macrocyclic ligand and complexes [15,16].

A previous quantum chemical INDO study of the geometry (INDO/1), electronic structure and spectroscopy (INDO/S) for phenanthroline and similar hexaazamacrocycle complexes have shown that the complexes, which are planar and neutral, bear a negative electronic density on the external nitrogen atoms [40]. The results are shown in Fig. 5 for the ligands under study and confirm the proposed protonation process [41].

3.3. Quantum chemical calculations

3.3.1. Bis-azabipy ligands

3.3.1.1. Geometry optimization. The tautomeric structures that can coexist in equilibrium in aprotic and protic media are shown in Fig. 1. Following previous publications [12–14,25] we will name them amine (**1a**, **1b**) and imine (**1a′**, **1b′**) tautomers.

Different optimized geometries result from PM3 and AM1 calculations for the deprotonated amine structure. Whereas PM3 stabilizes a completely planar structure, AM1 favors a bent one that minimizes the repulsion between the H atoms bonded to the inner nitrogens (Fig. 6(**A**)). This result is a consequence of the different parametrization used for the treatment of the hydrogen

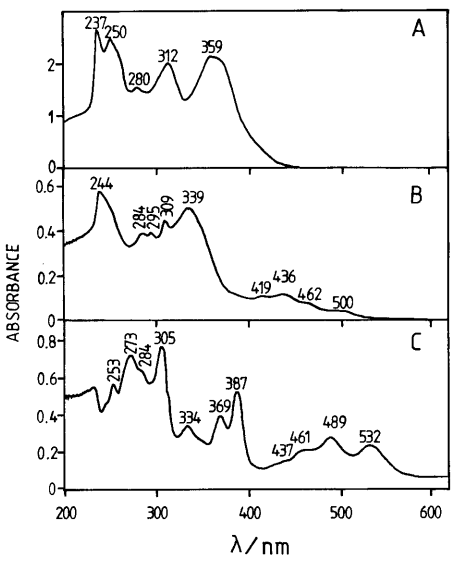


Fig. 4. UV–Vis spectra for: (A) bis-azabipy ligand 1.32×10^{-4} M in acetic acid; (B) bis-azabipy ligand 3.28×10^{-5} M in $CHCl_3$; and (C) Ni-bis-azabipy complex 1.27×10^{-4} M in $CHCl_3$.

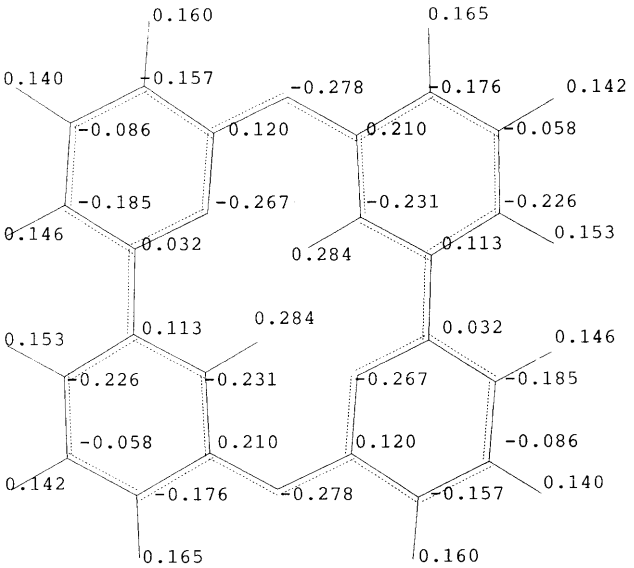


Fig. 5. Local density charges on the atomic centers of bis-azabipy ligand derived from AM1 calculations.

bond at both levels of calculation. The stabilization of H bonds between adjacent N-atoms define a more extended delocalized π system which is responsible for planarity. Due to the small energy difference between planar and bent structures, both of them have been considered for the calculation of the UV–Vis spectrum.

On the other hand, Fig. 7 shows that no planarity is associated to either the imine tautomer or the protonated structures. The stabilized geometry is the result of the influence of the aza bridge on the torsional angle defined by the pyridine rings, which is distorted from the value characteristic of biphenyl structures. Both effects converge to a NCCN angle close to 20°.

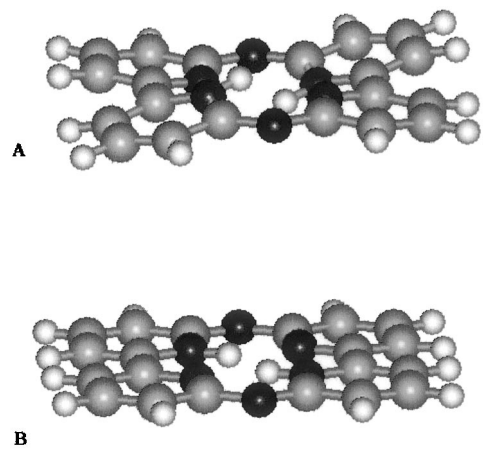


Fig. 6. Structural characteristics of the bis-azabipy ligand as result from AM1 (**A**) and PM3 (**B**) geometry optimizations. More details in the text.

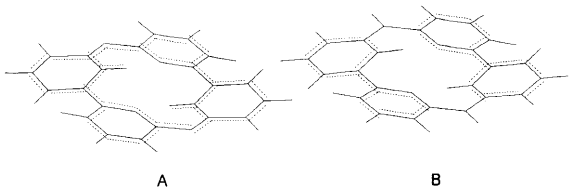


Fig. 7. Calculated structural characteristics of the bis-azabipy ligand in aprotic (**A**); and protic media (**B**).

In all the neutral structures, regardless of the semiempirical model used (AM1, PM3, ZINDO/S), a Mulliken population analysis shows the largest electron density located on the aza nitrogens.

3.3.1.2. UV–Vis spectroscopy. The UV–Vis spectrum of the macrocyclic ligand is largely dependent on the characteristics of the solvent, showing a band structure in the low energy region that only develops in non-protic environments (Fig. 4). This behavior has been previously explained on the basis of an amine–imine tautomeric equilibrium [12–14,25]. The fully conjugated amine form, stable in non-protic solvents, was supposed to be responsible of the low energy features, which disappear in protic media where the imine form becomes stabilized. However, no bands in the low energy region are predicted by the ZINDO/S CI calculations regardless of the planarity of the system or the tautomeric form considered.

Table 1 shows the observed electronic transition bands in UV–Vis region for 1.32×10^{-4} M bis-azabipy ligand in acetic acid. They are compared with the calculated bands for the system defined by a single molecule (Fig. 1(**b**)). Absorption bands start to develop in the 400 nm region. They are associated to electronic excitations from π orbitals, mainly centered on the aza N but delocalized in the π system, to fully delocalized π orbitals. The agreement between experimental and calculated spectra is remarkable. This evaluation is based on the consideration that some bands, as the lowest energy one, calculated as Laporte forbidden, can gain intensity through vibronic coupling.

When a single molecule is used to model the system in a non-protic media the spectrum of Table 2 (column 3) is calculated. No bands result for energy values lower than 420 nm. As the assignments are the same in this case and for protic media, it becomes evident that a more extended delocalized π system should be capable of decreasing the calculated energy of the transitions. We have modeled, thence, our system, by means of two ligand molecules, in a parallel arrangement (see Fig. 8(**A**)) that allows their mutual stabilization by π-interactions. Table 2 (column 1) shows the calculated electronic transition bands in UV–Vis region for our model system. They are compared (column 5) with the experimental bands for the bis-azabipy ligand in chloroform. The comparative analysis of the spectra demonstrate the feasibility of the model. The assignment of the transitions does not

Table 1
Bis-azabipy ligand 1.32×10^{-4} M in 5% (v/v) acetic acid: observed and calculated electronic transition bands [a]

E_{calc} [b]	Osc. str.	E_{exp} [c]
409.9	0.0000	412
355.0	0.9900	359(16 200)
312.5	0.6300	312(15 200)
288.0	0.0060	
283.9	0.0130	280(11 500)
280.3	0.0000	
273.2	0.0130	
267.1	0.1450	250(18 800)
266.2	0.0010	250
260.2	0.2000	250
260.1	0.1200	250
241.3	0.2000	237(20 100)
241.5	0.1100	237

[a] Values in nm.
[b] See text for assignments.
[c] ε, molar extintion coefficient, L cm^{-1} mol^{-1}.

Table 2
Bis-azabipy ligand 3.28×10^{-5} M in chloroform: observed and calculated electronic transition bands [a]

E_{calc} [b,d]	Osc. str. [b]	E_{calc} [b,d]	Osc. Str [c]	E_{exp} [e]
504.1	0.0000			500(1200)
463.6	0.0275			462(2300)
439.1	0.0055			436(3400)
417.6	0.0940	423.6	0.0000	419(3100)
368.5	0.0126			419
354.5	0.3603	364.5	0.9200	339(15 200)
351.6	0.6863	333.7	0.6403	339
338.8	0.0001	318.6	0.0000	
337.7	0.8671	314.7	0.0000	339
333.3	0.0146			
308.1	0.2522	304.3	0.5561	309(13 400)
306.3	0.0124			
305.7	0.0231			
299.1	0.0150			
297.7	0.3956	275.1	0.1448	295(11 600)
293.5	0.0267			295
292.8	0.4627			295
277.1	0.2000			284(11 600)
275.1	0.1488			284
270.8	0.4199			284
262.8	0.7026	259.4	0.2510	241(17 400)

[a] Values in nm.
[b] Dimeric structure.
[c] Monomeric structure.
[d] See text for assignments.
[e] ε, molar extintion coefficient, L cm^{-1} mol^{-1}.

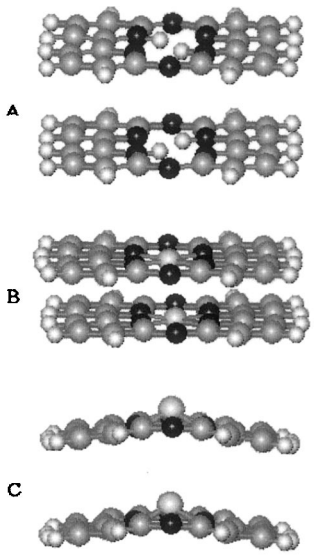


Fig. 8. Dimeric structures for: (**A**) bis-azabipy ligand; (**B**) Ni-bis-azabipy complex; (**C**) Zn-bis-azabipy complex; used to calculate the spectra reported in Tables 2–4.

change, relative to the monomers, but the orbitals involved are delocalized over the entire dimeric system.

The role of non-covalent interactions between aromatic moieties has been largely studied, as they influence the stability of nucleic acids [42], proteins [43], porphyrins and phtalocyanines, among others [44]. Because of the weak nature of the interactions, correlated ab initio calculations with split basis including polarization, define the minimum requirement for their proper computational modeling [45]. Semiempirical calculations are not parametrized for weak interactions and a geometry optimization at this level leads to the separation of the system in two monomeric units. Molecular mechanic force fields include non-bonded interactions in the van der Waals and electrostatic energy terms. They are capable of simulating the 'staking' stabilization between aromatic rings with a precision that compares the ab initio one [45].

We have preferred to use, for our calculations, the experimental information provided by the low energy features of the UV–Vis spectrum, and adjust the distance between the moieties until best fitting of the ZINDO/S-CI calculated spectrum to the experimental data. This procedure has been extensively tested [46,47], and its credibility is, nowadays, out of discussion. A dimer built up on the PM3 stabilized planar structure, with an interplanar separation of 3.3 Å between the monomers, defines the best model of the azamacrocycle ligand in non-protic media. This distance is in agreement with the one derived from molecular mechanics calculations, and is close to the one calculated in Ref. [45] for toluene dimers.

As has been previously mentioned, no dimerization is necessary to reproduce the spectrum in protic media (Table 1). Perfect agreement with experiment is attained when the ligand is modeled by the structure shown in Fig. 1(**b**). Protonation of the macrocycles destroy the stability of the dimers, a fact that is reflected, in the spectrum, in the lack of bands in the low-energy region (Fig. 4(A)).

3.3.2. Zn(II) and Ni(II) complexes

3.3.2.1. Geometry optimization. The structure of the zinc complex is slightly distorted from planarity in the orientation of the cycles, an effect originated in the position of the metal ion, which defines, with the co-ordinating nitrogen atoms, a square-based pyramidal structure (Fig. 8(**C**)). The same result is attained when either PM3 or AM1 calculations are performed.

Table 3
Zinc-bis-azabipy complex in chloroform [a]: observed and calculated electronic transition bands [b]

E_{calc} [c,e]	Osc. str. [c]	E_{calc} [d,e]	Osc. str. [d]	E_{exp}
556.6	0.0000			
540.8	0.0045			520
464.7	0.0046			467
445.4	0.0000			
430.5	0.0011	440.2	0.0000	424
417.1	0.0000			
381.8	0.0006			
367.8	1.1265	370.7	0.7341	375
349.6	0.9409	352.8	1.0409	340
349.5	0.1138	324.5	0.0000	340
342.8	0.0011	318.7	0.0082	
338.8	0.0001			
337.5	0.0000			
326.5	0.0381			
324.5	0.0000			
320.5	0.0214			
316.7	0.0008			
310.9	0.0007			
310.5	0.5154	305.1	0.3284	310
308.2	0.0000	301.5	0.0000	
303.3	0.3013	286.2	0.0000	290
301.5	0.0000	273.9	0.0010	
297.5	0.0000	269.9	0.3740	
293.5	0.0000			
292.5	0.0000			
290.7	0.0001			
290.3	0.0034			
286.7	0.0084			
286.0	0.0000			
283.0	0.0053			
281.9	0.1493			
275.3	0.3900			

[a] Saturated solutions, approximately 10^{-5} MS.
[b] Values in nm.
[c] Dimeric structure.
[d] Monomeric structure.
[e] See text for assignments.

A planar structure is calculated, on the other hand, for the nickel complex (Fig. 8(**B**)), as the smaller size of the Ni(II) ion is compatible with the size of the cavity defined by the co-ordinating nitrogen atoms.

A Mulliken population analysis describe the electronic distribution on the Zn(II) complex by a positive charge on the metal atom, counterbalanced by negative charges on the nitrogens. The positive charge is larger (0.68) after AM1 than after ZINDO/S (0.25) calculations, with the negative densities uniformly distributed on the N centers in the first case, but concentrated in the aza nitrogens in the second. A similar description holds for the Ni complex, which, at the ZINDO/S level of calculation, shows zero charge on the metal atom. AM1 and PM3 has not been considered for the electronic description of this complex. Whereas AM1 is not parametrized for Ni, PM3 is known to fail in the electronic description of systems containing amine groups [48,49]

Table 4
Nickel-bis-azabipy complex 1.27×10^{-4} M in chloroform: observed and calculated electronic transition bands [a]

E_{calc} [b,d]	Osc. str. [b]	E_{calc} [c,d]	Osc. str. [c]	E_{exp} [e]
525.3	0.0000	510.7	0.0000	532(1800)
506.8	0.0000			
501.1	0.0000			
496.0	0.0000			
495.9	0.0000			
480.5	0.0000	496.0	0.0000	489(2200)
461.2	0.0000	463.4	0.0000	461(1700)
456.9	0.0000	459.5	0.0000	
456.8	0.0000	403.4	0.0000	
435.9	0.0000			437(1300)
397.9	0.0000			
397.9	0.0000	390.9	0.6494	
382.6	0.0000			
380.6	1.0144			387(4100)
376.3	0.0002	376.2	0.7331	
359.6	1.0573			369(3100)
352.5	0.0000			
348.8	0.0144	332.1	0.0000	334(2600)
312.1	0.2315	322.7	0.0000	305(6000)
311.7	0.0007	311.1	0.1315	
308.1	0.0034			284(5000)
287.3	0.0034			
283.9	0.0005			
280.1	0.0101	279.3	0.2794	
277.6	0.0000	272.8	0.0401	
276.9	0.0000	271.7	0.3947	
276.7	0.0107			273(5500)
274.5	0.5395			273
273.2	0.1868			273
270.1	0.0000			
269.2	0.2842	267.1	0.0513	273
268.8	0.0000	263.8	0.2720	
268.6	0.0755	245.7	0.2575	273

[a] Values in nm.
[b] Dimeric structure.
[c] Monomeric structure.
[d] For assignment see text.
[e] ε, molar extintion coefficient, L cm^{-1} mol^{-1}.

3.3.2.2. UV–Vis spectroscopy. The influence of the solvent, previously described for the ligand, also becomes evident for the Zn(II) and Ni(II) complexes. A band structure develops in both cases, in the low energy region, in aprotic, but not in protic solvents (Fig. 4).

When the Zn(II) complex is considered, the low-energy region can only be reproduced when a dimeric model, with the monomers separated 3.8 Å, is used for the calculations. Results are shown in Table 3. The d orbitals of the metal lie very low in energy and are, thence, not involved in transitions. The transitions are originated, as in the case of the ligand, in electron promotions from π orbitals, mainly centered on the aza nitrogens (N) to π^* delocalized over the aromatic system.

The Ni complex is the unique case for which low energy bands are calculated even when a monomeric structure is considered (Table 4). They are associated, in the monomer, to $d \rightarrow d$ transitions. The best agreement with the experiment is attained, however, when calculations are based on a dimeric model, modeled on an interplanar separation of 3.4 Å (Table 4). For this model, $d \rightarrow d$ and $N \rightarrow \pi^*$ transitions share the low energy region. The best fitting to the experiment is attained, however, against the calculated $N \rightarrow \pi^*$ transitions, where N stands for the same orbital type previously described for the Zn complexes. We associate to the latter, which gain intensity through vibronic coupling, the origin of the bands around 500 nm.

Acknowledgements

This work has been financed by the Consejo Nacional de Investigaciones Científicas y Técnicas (CONICET), the Universidad Nacional de La Plata (Argentina), and FONDECYT (Chile), project No. 01970354 and Universidad de Santiago de Chile, project DICYT No. 9942CM. G.E. is a member of the research staff of CONICET (Argentina).

References

[1] F.H. Fry, B.Graham, L. Spiccia, D.C.R.Hockles, E.R.T. Tiekink, J. Chem. Soc., Dalton Trans. (1997) 827.
[2] M. Rosignoli, P.V. Bernhardt, G.A. Lawrence, M. Maeder, J. Chem. Soc., Dalton Trans. (1997) 323.
[3] X. Xu, Q. Luo, M. Shen, X. Huang, Q. Wu, Polyhedron 915 (1997) 16.
[4] A.J. Blake, I.A. Fallis, R.O. Gould, S. Parsons, S.A. Ross and M. Schröder, J. Chem. Soc., Dalton Trans. (1996) 4379.
[5] N.F. Curtis, Coord. Chem. Rev. 3 (1968) 3.
[6] L.F. Lindoy, D. Busch, Prep. Inorg. React. 1 (1971) 6.

[7] L.F. Lindoy, Chem. Soc. Rev. 29 (1975) 4212.
[8] M. Kasuga, T. Tsutsui, Coord. Chem. Rev. 67 (1980) 32.
[9] A.B.P. Lever, Pure Appl. Chem. 58 (1986) 1467 and references therein.
[10] R.H. Holm, Chem. Rev. 67 (1987) 1401.
[11] F.C.J.M van Vegge, W. Verboom, D.N. Reinhoudt, Chem. Rev. 94 (1994) 279.
[12] S. Ogawa, J. Chem. Soc., Perkin Trans. I (1977) 214.
[13] S. Ogawa, T. Yamaguchi, N. Gotoh, J. Chem. Soc., Perkin Trans. I (1974) 976.
[14] S. Ogawa, T. Yamaguchi, N. Gotoh, J. Chem. Soc., Chem. Commun. (1972) 577.
[15] M. Seno, S. Tsuchida, S. Ogawa, J. Am. Chem. Soc. 99 (1977) 3014.
[16] J. Costamagna, J. Canales, J. Vargas, M. Camalli, F. Caruso, E. Rivarola, Pure Appl. Chem. 65 (1993) 1251.
[17] J. Costamagna, J. Canales, J. Vargas, A. Alvarado, G. Ferraudi, J. Indian Chem. Soc. 70 (1993) 987.
[18] S.W.A. Blight, N. Choi, C.F.G.C.Geraldes, S.Knoke, M. McPartlin, M.J. Sanganee, T.M. Woodroffe, J. Chem. Soc., Dalton Trans. (1997) 4119.
[19] J. Zagal, M. Paez, C. Fierro, in: S. Srinivasan, S. Wagner, H. Wrobloba (Eds.), Electrode Materials and Processes for Energy Conversion and Storage, vols. 87–12, The Electrochem. Soc, Princeton, New Jersey, 1987, p. 198.
[20] F. Abba, G. De Santis, L. Fabbrizzi, M. Licchelli, A.M. Manotti, P. Pallavicini, A. Poggi, F. Ugozzolli, Inorg. Chem. 33 (1994) 1366.
[21] B.R. Eggins, J. McNeil, J. Electroanal. Chem. 148 (1983) 17.
[22] I. Taniguchi, in: J.O.M. Bockris, E. White, B.E. Conway (Eds.), Modern Aspects of Electrochemistry, Plenum Press, New York, 1989, p. 327.
[23] J.P. Sauvage, J. Am. Chem. Soc. 108 (1986) 7461.
[24] C. Baird, Environmental Chemistry, W.H. Freeman & Co, New York, 1995.
[25] S. Ogawa, S. Shiraishi, J. Chem. Soc., Perkin Trans. I (1980) 2527.
[26] J.J.P. Stewart, MOPAC, Version 7.0, F.J. Seiler, Research Laboratory, United States Air Force Academy, CO 80840, USA, 1994.
[27] J.A. Pople, D.P. Santry, G.A. Segal, J. Chem. Phys. 43 (1965) S129.
[28] J.A. Pople, D.L. Beveridge, P.A. Dobosh, J. Chem. Phys 47 (1967) 47.
[29] J. Ridley, M.C. Zerner, Theor. Chim. Acta 32 (1973) 111.
[30] J. Ridley, M.C. Zerner, Theor. Chim. Acta 42 (1976) 223.
[31] M.C. Zerner, G. Loew, R. Kirchner, U. Mueller-Westerhoff, J.Am. Chem. Soc. 102 (1980) 589.
[32] M.C. Zerner, ZINDO Package, Quantum Theory Project, University of Florida, Gainesville, USA, 1999.
[33] M.G. Cory, M.C. Zerner, Chem. Rev. 91 (1991) 813.
[34] J. Costamagna, G. Ferraudi, J. Canales, J. Vargas, Coord. Chem. Rev. 148 (1996) 221.
[35] J.A. Costamagna, J. Canales, J. Vargas, G. Ferraudi, Pure Appl. Chem. 67 (1995) 1045.
[36] M. Shionoya, E. Kimura, Y. Iitaka, J. Am. Chem. Soc. 112 (1990) 9237.
[37] M. Fujihira, Y. Hirata, K. Suga, J. Electroanal. Chem. 292 (1990) 199.
[38] A.J. Bard ((Ed.), Encyclopedia of Electrochemistry of the Elements, M. Dekker, New York, 1988.
[39] J. Vargas, G. Ferraudi, J. Canales, J.A. Costamagna, Inorg. Chim. Acta 226 (1994) 151.
[40] G. Estiú, A. Jubert, J. Molina, J. Costamagna, J. Canales, J. Vargas, Inorg. Chem. 34 (1995) 1212.
[41] G. Estiú, A. Jubert, J. Molina, J. Costamagna, J. Canales, J. Vargas, J. Mol. Str. 330 (1995) 201.
[42] W. Saenger, Principles in Nucleic Acid Structure, New York, Springer-Verlag, 1984.
[43] (a) T. Blundel, J. Singh, J. Thornton, S.K. Burley, G.A. Petsko, Science 234 (1986) 1005. (b) S.K. Burley, G.A. Petsko, Adv. Protein Chem. 39 (1988) 125. (c) C.A. Hunter, J. Singh, J.M. Thornton, J. Mol. Biol. 218 (1991) 837
[44] M.J. Stillman, Chapter 5, in: C.C. Leznof, A.B.P. Lever (Eds.), Phthalocyanines, Properties and Applications, VCH, New York, 1993.
[45] C. Chipot, R. Jaffe, B. Maigret, D.A. Pearlman, P.A. Kollman, J. Am. Chem. Soc. 118 (1996) 11217.
[46] G.L. Estiu, M.C. Zerner, J. Am. Chem. Soc. 121 (1999) 1893.
[47] G.L. Estiu, M.C. Zerner, J. Phys. Chem. 99 (1995) 13819.
[48] G.L. Estiu, J. Mol. Struct., Theochem. 401 (1997) 157.
[49] S.M. Bachrach, Population analysis and electron densities from quantum mechanics, in: K.B. Lipkowitz, D.B. Boyd (Eds.), Reviews in Computational Chemistry, vol. 5, VCH, New York, 1994.

PERGAMON

www.elsevier.nl/locate/poly

Polyhedron 19 (2000) 2383–2386

POLYHEDRON

Aggregation properties of metallic tetrasulfophthalocyanines embedded in sol–gel silica

M.A. Garcia-Sanchez *, A. Campero

Department of Chemistry, Universidad Autonoma Metropolitana-Iztapalapa, PO Box 55-534, Mexico, D.F., 09340, Mexico

Received 27 May 2000; accepted 1 September 2000

Abstract

The aggregation properties of metallic 2,9,6,23-tetrasulfophthalocyanines MTSPc (M = Fe, Co, Ni, Cu and Al) embedded in transparent monolithic gels of silica prepared by the sol–gel method have been followed by UV–Vis spectroscopy. These studies are necessary to follow the various complex stages of the hydrolysis–condensation reactions forming the monolithic gels. In view of the fact that under the experimental conditions used in this work (OH)AlTSPc does not show any agglomeration tendencies, it has been used as a label to determine the optimum conditions for the inclusion of the MTSPc molecules. Dimethyl formamide (DMF) and pyridine (py) have been selected as agglomeration control agents. The utilization of DMF gives materials less prone to fracture and of better optical properties than those obtained by the use of pyridine. In the case of CuTSPc and CoTSPc species with DMF (4% v/v) some color fading in the gels was observed. © 2000 Elsevier Science B.V. All rights reserved.

Keywords: Sol–gel; Aggregation; Tetrasulfophthalocyanines; Monolith; Macrocycle; Silica

1. Introduction

There is at present a good deal of interest concerning the use of new materials as active laser devices and as optical converters of ultraviolet or infrared light into visible light. The last two decades have witnessed substantial efforts, thanks to which progress in our knowledge of the synthesis and the properties of metallic oxide glasses prepared by the sol–gel method has increased. Since 1984 [1], this procedure has allowed the trapping of many types of pigments in metallic oxide gels [2–7]. The optical and lasing properties of these systems have been studied [1,6,8]. However, the important group of macrocycles known as the metallic phthalocyanines (MPc) has been less well studied in this respect [9–12].

Semiconductivity, photoconductivity, as well as the catalytic and optical properties are quite important in metallic phtalocyanines. In recent years, these compounds received considerable attention because of their non-linear optical properties [13,14], the possibility of their use as optical limiters [15,16], and in optical information storage systems [17].

Phthalocyanine is a well known macrocyclic molecule featuring an 18-π conjugated electron system which imparts extremely high chemical and thermal stability to the macrocycle [17–21]. Many metallic phthalocyanines are known to have melting points, higher than 550°C [18], while demetallation, which occurs only in 16 M H_2SO_4 solution, depends on the central cation.

Non-substituted phthalocyanines are insoluble in common solvents such as water or ethanol, whereas those with substituent groups such as sulfo (–SO_3H) and carboxyl (–COOH) in the periphery of the macrocycle (Fig. 1), become soluble. In this work we synthesize the metallic 2, 9, 16, 23-tetrasulfophthalocyanines MTSPc (M = Fe, Co, Ni, Cu and Al) and study their inclusion in gels of silica obtained by the sol–gel method using tetraethoxysilane (TEOS) as a precursor.

It is a well known fact that free and metallic phthalocyanines dimerize and may even form larger and more complex aggregates. These aggregation phenomena are deleterious to the desired electrical, optical, and catalytic properties of these compounds. Thus, it is important to improve our understanding of the dimerization phenomenon and seek the means to avoid it. Exper

* Corresponding author. Tel.: +52-5-804-4677; fax: +52-5-804-4666.

E-mail address: mags@xanum.uam.mx (M.A. Garcia-Sanchez).

0277-5387/00/$ - see front matter © 2000 Elsevier Science B.V. All rights reserved.
PII: S0277-5387(00)00575-1

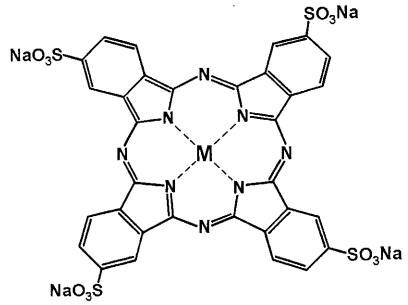


Fig. 1. Structure of tetra sodium salt of metallic 2,9,16,23-tetrasulfophthalocyanine, MTSPc (M = Fe, Co, Ni, Cu and Al).

imentally, it is found that dimer stability decreases in the series CuTSPc > H_2TSPc > FeTSPc > (VO)TSPc > CoTSPc [22].

Absorption spectra in the UV–Vis region were interpreted in terms of π–π^* transitions in the energy level diagram of the delocalized system of the macrocyclic ligand [23]. A typical spectrum of a monomeric metallic phthalocyanine is composed of two prominent bands, as well as of some other less important satellite bands (Fig. 2). The most intense band, known as the 'Q' band at around 670 nm is assigned to an $a_{1u}(\pi) \rightarrow e_g(\pi^*)$ transition while a less intense 'B', or 'Soret' band at around 350 nm is assigned to an $a_{2u}(\pi) \rightarrow e_g(\pi^*)$ transition [17]. A weak satellite band observed near 610 nm, known as the 'Q_{III}' band, is of vibrionic nature [24]. When the phthalocyanine macrocycle is allowed to dimerize, the UV–Vis spectrum is modified and only two bands are seen, namely: the Soret band at 340 nm and the type Q band at 630 nm. It has been found that the dimerization can be inhibited by using some solvents such as dimethyl formamide (DMF), pyridine (py), dimethylsulfoxide (DMSO), ethanol, etc. [25,26].

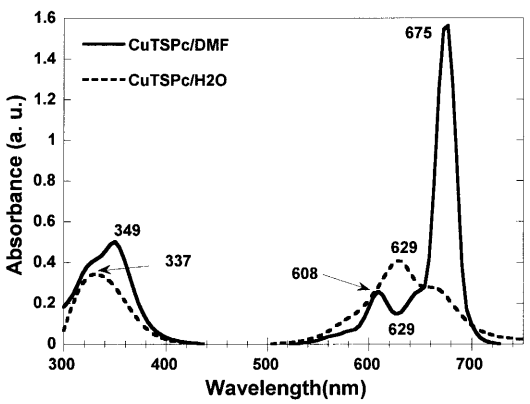


Fig. 2. UV–Vis absorption spectra of monomeric CuTSPc in (—) DMF and dimeric CuTSPc form in (---) water.

2. Experimental

Metallic tetrasulfophthalocyanines MTSPc were synthesized following the method of Weber and Buch [27].

The various components necessary to prepare the reacting sols were mixed using the following molar concentration ratios: [TEOS:H_2O:HCl:MTSPc] = [1:19:0.05:5×10^{-6}]. This mixture was prepared by the addition of 5.0 ml of the macrocyclic molecule solution (with or without aggregation control agent) to 19.8 ml of a homogeneous mixture of 9.8 ml of TEOS and 10 ml of a 0.234 M solution of HCl to give a final volume of 24.8 ml (V_f). To simplify, we state the quantity of aggregation control agent added in the 5 ml of the macrocyclic complex solution, as percent with respect to the final mixture volume.

These sols were divided in three subsets: to the first, 1% of pyridine is added, to the second, 2 or 4% of DMF is added, while no dimerization inhibiting agent is used in the last subset. The gelling sol mixtures were put into plastic cells and covered with parafilm paper. The gellation process is monitored by UV–Vis spectroscopy using a Cary 5E instrument. After monoliths separated from the cell walls (approx. 1400 h) small holes are made in the parafilm. Samples are dried at room temperature (r.t.) for 3 weeks. The final monoliths are then dried for 3 days at 70°C and 1 day at 120°C.

A second series of monoliths was prepared using CoTSPc sols, to which either 6 or 8% of DMF was added, while a last series of samples was prepared by adding either 2 or 4% of pyridine to the NiTSPc-containing sol.

3. Results and discussion

Preliminary exploratory experiments showed that the phenomenon of aggregation is totally inhibited in solutions containing 20% of DMF, 10% of pyridine, 40% of ethanol, or 60% of DMSO. Such high concentrations of the last two inhibiting agents give rise to extremely small, non-transparent and brittle monolithic gels. Thus, our efforts concentrated in the study of the dimerization inhibiting effects of DMF and pyridine.

The final volume of the monoliths is about one-tenth of that of the solution containing the polymerizing sol (V_f). (OH)AlTSPc does not show any chemical modification or dimerization while in aqueous solution or in gels; so we used it as a label which allowed us to find the proper conditions under which the gels obtained are strong and non brittle.

However, we have recently reported that if a gelling mixture containing (OH)AlTSPc plus 1% pyridine is used, formation of dimers via oxo-bridges is induce [28]. This fact is firmly based on the special features of

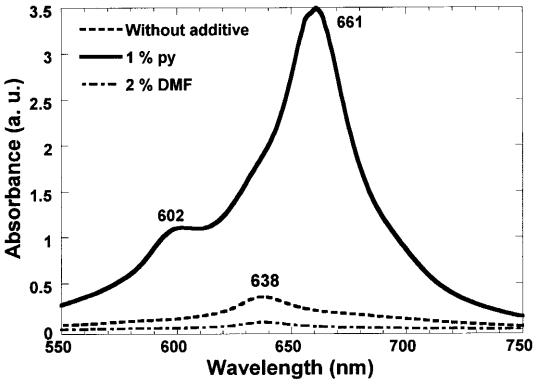


Fig. 3. UV–Vis absorption spectra of (OH)FeTSPc monolithic gels, obtained with and without addition of aggregation control additive, 1809 h after preparation.

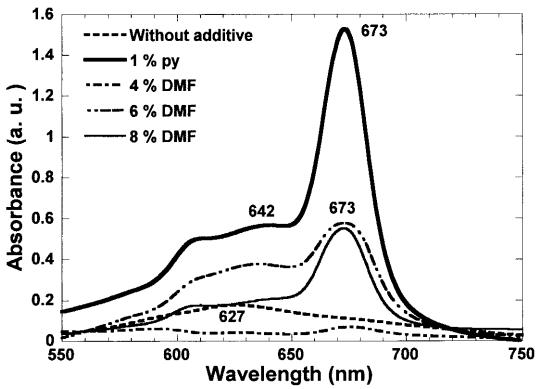


Fig. 4. UV–Vis absorption spectra of CoTSPc monolithic gels, obtained with and without addition of aggregation control additive, 2370 h after preparation.

the UV–Vis spectrum of the gel. We observe a Q band blue shifted 28 nm (674–646 nm), assigned to a μ-oxo dimer [29]. In other words, pyridine behaves as a base, with respect to Al(III) species, allowing the generation of the (O^-)AlTSPc anion which, bonding to a similar species forms the complex TSPcAl–O–AlTSPc [17,30–32]. We have also shown that the formation of this oxo-bridge complex is favored by the encapsulation conditions prevailing in the large cavities of the amorphous gel. This oxo-bridge complex does not form, for example, in a solution under reflux conditions. With the only exception of this important peculiarity, the Al(III) species stays unmodified if the pyridine concentration is lower than 0.2%.

Previous work shows that CuTSPc mixtures to which 1% of pyridine has been added, gel within 5 min after their preparation; however, these materials are non transparent and brittle. Similar mixtures to which DMF is added in concentrations between 2 and 8% give very strong and non-brittle materials which have lost their original blue color [28].

This phenomenon can be assigned to an interaction between DMF and the macrocycle of the CuTSPc molecule, leading to the formation of a species not far in nature to a lactam, involving the central Cu (II) ion and the nitrogen aza atoms of the macrocycle. The set of conjugated double bonds of the macrocycle is thus broken and the $\pi-\pi^*$ transitions necessary for the color to exist can no longer take place. One fact favoring the latter assumption is that the pH of the gelling solution is high enough to discard any possibility of macrocycle demetallation [18,19]. Even if this demetallation might take place, it is well known that the free macrocycle still features these strong $\pi-\pi^*$ transitions. Besides, we have observed that this phenomenon is seen only in the complexes of cations with an oxidation state of $+2$ which, by comparison with the M(III) complexes (OH)FeTSPc and (OH)AlTSPc, do not feature axial ligands. This fact leads us to think that DMF coordinates its nitrogen atom to these divalent cations at the same time that the oxygen of the carboxyl group interacts with the aza nitrogen atoms. A final consequence of this interaction is that the metallic complex loses its planarity.

When gels are prepared containing the species (OH)FeTSPc, using either DMF, or no dimerization inhibiting agent (Fig. 3), monoliths are obtained having the metallic species in the μ-oxo dimer form. However, if similar monoliths are prepared, containing this time 1% pyridine, one finds the species in the monomeric form predominantly, even after 1810 h.

A similar result is obtained with CoTSPc, which dimerizes easily if no additive is used (Fig. 4). Using 1% pyridine inhibits efficiently the formation of aggregates, but the gels obtained are not transparent and are very brittle. Furthermore, when 4% of DMF is added to sols containing CoTSPc, dimerization is inhibited weakly and the gels do not show any color, an observation similar to the one made in the case of the CuTSPc species.

In order to determine if higher concentrations of additives successfully inhibit dimerization, mixtures containing CoTSPc and 6 and 8% DMF were prepared (Fig. 4). It is found that though with 6% DMF dimerization is avoided at the start, the gels so obtained contain at the end, a mixture of the monomer and the dimer forms. Nevertheless, with 8% of DMF added, virtually all aggregation phenomena are inhibited, and the gels obtained are very strong, non-brittle, and the color does not fade with time.

For the case of gels containing the NiTSPc species, even though 1% pyridine is not enough to avoid dimerization, DMF concentrations higher than 4% are quite efficient for the same purpose (Fig. 5).

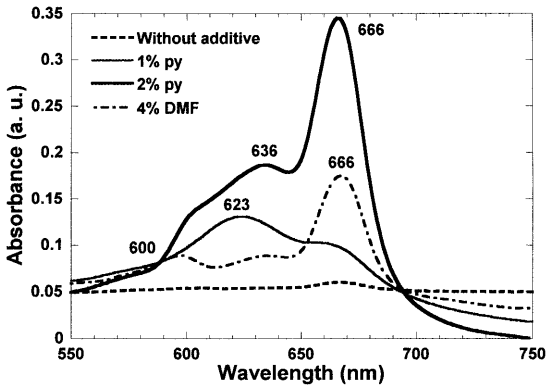


Fig. 5. UV–Vis absorption spectra of NiTSPc monolithic gels, obtained with and without addition of aggregation control additive, 1809 h after preparation.

4. Conclusions

It is possible to successfully avoid dimerization phenomena of metallic tetrasulfophthalocyanines trapped in monolithic silica gels if use is made of some inhibiting agents in appropriate minimum concentrations: 4% DMF, 2% pyridine, 8% ethanol or 12% DMSO. In practice, monoliths prepared with the last two agents, because of the high concentrations needed, are small, brittle and non-transparent which renders their utilization less interesting.

With DMF as the additive, the gels are normally stronger and of higher optical quality. However, CuTSPc and CoTSPc materials tend to fade with time because of interactions between DMF and the complex, which disrupt the conjugated double bond system of the organic macrocycle.

The use of DMF as a dimerization-inhibiting agent is efficient in the control of aggregation of MTSPc (M = Fe, Co, Ni) species embedded in gels of silica. The use of pyridine is equally effective, and though a lower concentration of the latter is necessary, the final monoliths are brittle and non-transparent; however, the use of these systems in catalysis is commendable.

The comparative study of gels prepared with the M(II)TSPc (M = Cu, Ni and Co) species and (OH)M(III)TSPc (M = Fe and Al) species has shown that loss of color in the monoliths and μ-oxo dimer formation take place easily.

Acknowledgements

The authors wish to thank CONACYT (México) for its financial support (project 30728).

References

[1] D. Avnir, D. Levy, R. Reisfeld, J. Phys. Chem. 88 (1984) 5957.
[2] D. Avnir, D. Levy, R. Reisfield, J. Non-Cryst. Solids 74 (1985) 395.
[3] V.R. Kaufman, D. Levy, D. Avnir, J. Non-Cryst. Solids 82 (1986) 103.
[4] A. Makishima, T. Tani, J. Am. Ceram. Soc. 69 (1986) 4.
[5] V.R. Kaufmann, D. Avnir, R. Reisfield, J. Non-Cryst. Solids 99 (1988) 379.
[6] J.C. Pouxviel, B. Dunn, J.I. Zink, J. Phys. Chem. 93 (1989) 2134.
[7] J. Fitremann, S. Doeuff, C. Sanchez, Ann. Chim. Fr. 15 (1990) 421.
[8] D. Levy, F. del Monte, J.M. Oton, G. Fiksman, I. Mat'as, P. Datta, M. López-Amo, J. Sol–Gel Sci. Technol. 8 (1997) 931.
[9] Y. Kobayashi, Y. Imai, Y. Kurokawa, J. Matt, Sci. Lett. 7 (1988) 1148.
[10] P.D. Fuqua, K. Mansour, D. Alvarez, S.R. Marder, J.W. Perry, B. Dunn, in: J.D. Mackenzie (Ed.), Proceedings of the SPIE Conference on Sol–gel Optics II, vol. 1758, SPIE, Bellingham, WA, 1992.
[11] F. Bentivegna, et al., Appl. Phys. Lett. 62 (1993) 1721.
[12] P.D. Fuqua, B. Dunn, J. Sol–Gel Sci. Technol. 11 (1998) 241.
[13] T.H. Wei, D.J. Hagan, M.J. Sence, E.W. Stryland, J.W. Perry, D.R. Coutler, Appl. Phys. B54 (1992) 46.
[14] M. Hanack, M. Lang, Adv. Mater. 6 (1994) 819.
[15] J.S. Shirk, et al., Appl. Phys. Lett. 55 (1989) 1287.
[16] R.A. Norwood, J.R. sounik, Appl. Phys. Lett. 60 (1992) 295.
[17] C.C. Leznoff, A.B.P. Lever, in: C.C. Leznoff, A.B.P. Lever (Eds.), Phtalocyanines Properties and Applications, VCH, New York, 1989.
[18] E.A. Lawton, J. Phys. Chem. 62 (1958) 384.
[19] B.D. Berezin, Russ. J. Inorg. Chem. 7 (1962) 11.
[20] B.D. Berezin, Russ. J. Inorg. Chem. 258 (1962) 36.
[21] A.B.P. Lever, in: H.J. Emeléus, A.G. Sharp (Eds.), Advances in Organic Chemistry and Radiochemistry, Academic Press, New York, 1965.
[22] H. Sigel, P. Walmaier, B. Prijs, Inorg. Nucl. Chem. Lett. 7 (1971) 161.
[23] N.H. Sabell, C.A. Melendres, J. Am. Chem. Soc. 86 (1982) 4342.
[24] M. Gouterman, J. Chem. Phys. 30 (1959) 30.
[25] E.W. Abel, J.M. Pratt, R. Whelan, J. Chem. Soc., Dalton Trans. (1976) 509.
[26] Y.C. Yang, J.R. Ward, R.P. Seiders, Inorg. Chem. 24 (1985) 1765.
[27] J.H. Weber, D.H. Buch, Inorg. Chem. 4 (1965) 469.
[28] M.A. García-Sánchez, A. Campero, J. Sol–Gel Sci. Techol. 13 (1998) 651.
[29] H. Homborg, K.S. Murray, Z. Anorg. Allg. Chem. 517 (1984) 149.
[30] R.D. Joyner, M.E. Kenney, J. Am. Chem. Soc. 82 (1960) 5790.
[31] J.E. Owen, M.E. Kenney, Inorg. Chem. 1 (1962) 334.
[32] P.M. Kuznesof, R.S. Nohr, K.J. Wynne, M.E. Kenney, J. Macromol. Sci.-Chem. A16 (I) (1981) 299.

PERGAMON

www.elsevier.nl/locate/poly

Polyhedron 19 (2000) 2387–2388

POLYHEDRON

Foreword

This is the second issue of Polyhedron devoted to the Italian–Spanish Conference on Thermodynamics of Metal Complexes. The first one was published in 1999 and is referred to the meeting held in Girona (Spain) organised by Professors Victoria Salvadó and Antoni Llobet.

The first meeting on this field held in collaboration among the different Spanish and Italian researchers was organised in Peñíscola (Spain) by Professor Juan Faus of the University of Valencia in 1990, then each year alternatively in Italy and in Spain congresses on this field have been organised.

In 1999 the Xth Italian–Spanish Congress was organised in S. Martino al Cimino a little town near Viterbo (Italy) by Professor Aldo Napoli of the University of Tuscia (ISMEC'99).

Nearly one hundred researchers from different countries attended the congress, presenting several communications on different topics. Indeed, the congress has focused on most of the fundamental and applied aspects of interest on thermodynamics and equilibria of metal complexes and closely related topics: solution equilibria; thermodynamic properties and chemical structure correlations; computer methods for equilibrium studies; thermodynamics of ionic exchange; complexes in non aqueous solvents; complexes with macrocyclic ligands; complexes with biological, medicine or environmental interest; complexes with analytical and technical applications; host–guest binding studies; thermodynamic aspects of macromolecular or supramolecular interactions.

The meeting was organised into 1 h plenary lectures, 40 min keynotes, 20 min oral contributions and posters. The opening plenary lecture entitled 'Transition metal and anion complexes with dinucleating hexaaza macrocyclic ligands' was addressed by Professor Antoni Llobet of the University of Girona (Spain). Other plenary lectures were 'Solution speciation of bioactive Al(III) and VO(IV) complexes' by Thamás Kiss from Jòzsef Attila University of Szeged (Hungary), 'From Stability Constants to Speciation. A database which is both easy to access and easy to apply' by Gwyneth and Leslie Pettit, Academic Software (U.K.) and finally 'Simple polyazacyclophane receptors in anion recognition and catalysis' by Enrique Garcia España and co-workers.

Two keynotes were presented by Silvia Canepari from the University of Rome (Ligand properties of β-amino-alcohols) and by Vincenzo Romano from University of Palermo, Italy (The extension of equilibrium analysis).

For the present special issue of Polyhedron devoted to the ISMEC'99 symposium, we have selected 16 contributions which have been divided into five sections:

1. Reviews
2. Solution equilibria
3. Oxygen binding ligands
4. Structure
5. Others

The paper in Section (A) is the review of Professor Thamás Kiss and co-workers which deals with the importance of biospeciation of aluminum(III) and VO(IV) and the application of speciation results in understanding the biological effects of these elements.

Five papers in Section (B) are dedicated to solution equilibria of metal complexes by the teams of Professors Ciavatta, Pulidori, Portanova, Crisponi and Magrì.

In Section (C) two papers deal with oxygen binding (Professors Bianchi, Paoletti, Tinè and co-workers), one on the solubility of oxygen in water (Professor Braibanti).

Three papers in Section (D) refer to structural contributions by Professors Niclós and Llobet and finally in Section (E) works by Professors Malatesta, Micheloni, Secco and Bucci are reported.

Following the success of the previous meetings, in 2000 Professor E. Garcia España organised the XIth edition of the Spanish–Italian Congress on Thermodynamics of Metal Complexes in Valencia (Spain) from the 4th to 7th of June. The next meeting will be organised in Parma, Italy, in June 2001.

Aldo Napoli
Guest co-editor
and Chairperson ISMEC'99
Silvia Canepari
Guest co-editor

0277-5387/00/$ - see front matter © 2000 Elsevier Science B.V. All rights reserved.
PII: S0277-5387(00)00536-2

PERGAMON

www.elsevier.nl/locate/poly

Polyhedron 19 (2000) 2389–2401

POLYHEDRON

Review

Solution speciation of bioactive Al(III) and VO(IV) complexes

Tamás Kiss [a,*], Tamás Jakusch [a], Melinda Kilyén [a], Erzsébet Kiss [b], Andrea Lakatos [c]

[a] *Department of Inorganic and Analytical Chemistry, József Attila University, PO Box 440, H-6701 Szeged, Hungary*
[b] *Department of Inorganic and Analytical Chemistry, Kossuth Lajos University, PO Box 21, H-4010 Debrecen, Hungary*
[c] *Biocoordination Chemistry Research Group, József Attila University, PO Box 440, H-6701 Szeged, Hungary*

This paper is dedicated to the memory of Professor Kálmán Burger.

Abstract

The speciation of the toxic Al(III) and the beneficial VO(IV) in various biofluids and tissues is discussed in order to describe the solution state of these metal ions in the organism. The importance of ternary complex formation with relevant biomolecules is emphasized. The interactions of Al(III) and VO(IV) with oligopeptides are also dealt with. The importance of the biospeciation of Al(III) ion in its transport and involvement in neurological disorders, and of insulin mimetic VO(IV) complexes is discussed.
© 2000 Elsevier Science B.V. All rights reserved.

Keywords: Biospeciation; Al(III) complexes; VO(IV) complexes; Insulin-mimetics

1. Introduction

The chemical speciation of an element, either essential or toxic, may be of basic relevance as concerns its biology, as the chemical form in which an element enters the body mostly determines its absorption and transport properties, and hence in part its biological and physiological activities. It is also true that to some extent independently of how this essential or toxic element was absorbed (or the form, e.g. a metal ion-containing drug, in which it was administered), it undergoes transformation because of the possible ligand-exchange reactions with the many potential metal ion-binding biomolecules in the biofluids or tissues.

In biological fluids, a majority of the metal ions are bound to proteins. In fact, only a small proportion of them are bound to low-molecular-mass (l.m.m.) compounds, mainly amino acids, biophosphates, carboxylates or hydroxycarboxylates. Free metal aquaions exist in biological fluids only in extremely low concentrations, and at these concentrations cannot play a significant role in physiological processes. In contrast, metals bound to l.m.m. compounds play major roles in many biological processes, such as intestinal absorption, cell absorption, transport and renal excretion. An understanding of these processes requires an accurate knowledge of the proportions of the l.m.m. and protein-bound fractions of the metal ions and of the delicate equilibria which determine these proportions.

Specific experimental techniques such as gel filtration, ion chromatography, ultrafiltration, ultracentrifugation, atomic absorption spectrophotometry, etc., are available to separate and determine l.m.m. and high molecular mass (h.m.m.) bound metals. On the other hand, computer programs developed to deal with multiple chemical equilibria can be actively applied not only for speciation calculations of laboratory solutions, but also for the simulation of naturally occurring mixtures of metal ions and ligands [1].

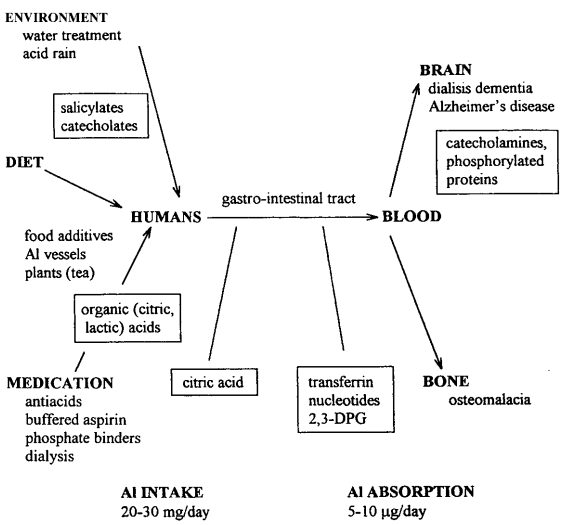
The present paper gives a brief literature survey and an insight into our recent research connected with some biospeciation problems relating to the toxic aluminum and the beneficial vanadium. Several examples are provided to emphasize the importance of a knowledge of the solution state of these metals, and it is demonstrated how this speciation information may be used for a better understanding of the effects of these metal ions in biological systems.

* Corresponding author. Tel.: +36-62-54-4337; fax: +36-62-42-0505.
E-mail address: tkiss@chem.u-szeged.hu (T. Kiss).

0277-5387/00/$ - see front matter © 2000 Elsevier Science B.V. All rights reserved.
PII: S0277-5387(00)00537-4

2. Characterization of Al(III) binding to small biomolecules

Aluminium is a well-established neurotoxic element [2]. Scheme 1 gives the various routes through which Al can enter the human organism from the environment, the diet or medication. A total of 10–30 mg of Al is estimated to be ingested each day, but only a very small proportion of this Al (5–10 μg) is absorbed. In many countries, aluminum sulfate is used as a coagulant in water treatment. Acid rain considerably increases the Al load from the environment. Al compounds, e.g. alums, are used as additives in different food-producing processes, for instance as baking powder in some countries. Some plants, e.g. tea, can accumulate an enormous amount of Al: the Al content of old tea leaves can reach even 3%. A significant amount of Al(III) may be liberated from Al vessels used in the kitchen when acidic meals are cooked in them. Some antacids and buffered medicines also contain Al. Al can accumulate dangerously in children with an impaired renal function who are treated with orally taken Al(III)-containing phosphate binders. Some forms of medical treatment, e.g. long-term haemodialysis, can also elevate the Al level in humans if the water used has a high Al content. Under normal conditions, i.e. with a normal daily load and a healthy organism, this amount is well tolerated (although the physiological effects of long-term low aluminum load, e.g. from the drinking water are still not clear [3]), as a consequence of the efficient defence mechanism, involving the formation of poorly-soluble phosphates and hydroxides in the gastro-intestinal tract, which are easily excreted. However, an abnormally high Al load and/or with an impaired renal function, an excess of Al(III) can be absorbed and transported to various target organs, where it may accumulate and exert harmful effects, e.g. osteomalacia in the bones, microcytic anemia in the red blood cells, or neurodegenerative diseases in the brain.



Scheme 1.

Al(III) is a typical hard metal ion, and the most likely binding sites of $Al(H_2O)^{3+}$ in biosystems are therefore O donors, and especially negatively-charged O donors. Carboxylate, phenolate, catecholate and phosphate are the strongest Al(III) binders. Biomolecules containing such functions may be involved in the uptake and transport processes, and also in the biological and physiological actions of Al(III) in living systems. These small biomolecules (given in the frames in Scheme 1) are either of biological importance or can mimic larger biomolecules. For example, salicylate and catecholate derivatives can serve as good model compounds to study the metal ion- binding properties of the larger soil organic material humic and fulvic acids. Small organic acids, such as citric acid for example, are important small molecule Al binders in biological fluids. Transferrin plays an essential role in the Al(III) transport in the plasma. 2,3-Diphosphoglycerate is important in the binding and accumulation of Al(III) in the red blood cells, resulting in a special kind of anemia. Other phosphates, such as nucleosidephosphates, e.g. ATP, are widely distributed in living systems, and a large variety of the reactions which take place in living organisms involve ATP. Catecholamines occur in fairly high concentration in the brain, where other potent Al(III) binders, e.g. transferrin or citrate, occur at relatively low concentrations, so that catecholamines can be of importance in the binding of Al(III) in the brain. Phosphorylated proteins, which are rich in abnormal neurone degradation products occurring in various neurological disorders, may play roles in the accumulation of Al(III).

In recent years, we have studied the interactions of such small biomolecules with Al(III) and described the speciation and solution structures of the complexes formed [4–18], in order to obtain the necessary stability constants and knowledge promoting characterization the solution state of Al(III) in biological fluids and tissues. Because of the possibility of the rather slow formation of complicated oligonuclear mixed hydroxo complexes in many of these Al(III)–ligand systems, pH-potentiometric solution speciation measurements were carried out at different metal ion concentrations (usually at $c_{Al} = 1–4$ mmol dm^{-3}) and at various metal ion to ligand ratios (usually at 1:1–1:10), and thermodynamic equilibrium was rigorously checked [14,17,18]. Those titration points, when 10 min was not enough to reach thermodynamic equilibrium state were omitted from speciation calculations.

Table 1
Total concentrations of components in computer model [a] of serum

Components	Concentration l^{-1}
High molecular mass (h.m.m)	
Albumin	630 μmol
Transferrin	37.0 μmol
Histidine	77.0 μmol
Lactate	1.51 mmol
Oxalate	9.20 μmol
Low molecular mass (l.m.m.)	
Phosphate	1.10 mmol
Citrate	99.0 μmol
Carbonate	24.9 mmol
Cistine	10.9 μmol
Cysteine	33.0 μmol
Glycine	2.30 mmol
Glutamate	60.0 μmol
Sulfate	330 μmol
H^+ (free)	39.8 nmol
OH^- (free)	417 nmol
Al^{3+}	3.00 μmol
Ca^{2+} (free)	1.37 mmol
Mg^{2+} (free)	580 μmol
Zn^{2+}	10.0 μmol

[a] Data are taken from Ref. [19].

Table 2
Simulated species distribution of low molecular mass Al(III) in blood serum [a]

Protein-bound Al(III)	Al(III) l.m.m. fraction [b]	Refs.
80%	$[Al(CitH_{-1})(OH)]^{2-}$: 94%; $[Al(CitH_{-1})]^-$: 3%; $Al(PO_4)$: 1.5%; $[Al(Oxalate)(OH)_2]^-$: 1.4%	[23]
50%	$Al(PO_4)$: 62%; $[Al(CitH_{-1})]^-$: 23%; $[Al(PO_4)(CitH)]^{2-}$: 10%	[21]
57%	$Al(OH)_3$: 51%; $Al(PO_4)$: 41.5%; $[Al_2(PO_4)(OH)_2]^+$: 7.2%	[20]
83%	Al-citrate: 98%; Al-hydroxide: 2% (phosphate not considered)	[22]
81%	$[Al(PO_4)(OH)]^-$: 80%; $Al(PO_4)$: 2%; $[Al(CitH_{-1})]^-$: 10%; $Al(OH)_3$: 4%; $[Al(OH)_4]^-$: 3%	[19]
77%	Al-citrate: 80%; Al-phosphate: 20%	[16]

[a] Based on models reported in Ref. [25].
[b] Total is 100%.

3. Biospeciation of Al(III) in blood serum

Absorbed Al(III) is transported through the blood stream, but its speciation in the blood serum is still not known. The chemical composition of the serum given in Table 1 is taken from Ref. [19]. As listed in Table 2, different speciation models [16,19–24] have been reported in the literature.

As concerns the h.m.m. components, all models agree that most of the Al(III) is bound to transferrin; albumin, the other potential h.m.m. carrier protein, is a much weaker metal ion binder and is not assumed to be able to compete for a significant amount of Al(III) [25]. Among the l.m.m. binders, citrate and phosphate are the most important. Amino acids [17], lactic acid, oxalic acid [13] and inorganic anions are not competitive binders in the presence of citrate and phosphate [13,24]. The picture is much more controversial as concerns these l.m.m. Al(III) binders. Daydé et al. [20], Jackson [21] and Harris [19] propose inorganic phosphate as the main Al(III) binder, while Clevette and Orvig [22], Duffield et al. [23] and Öhman and Martin [24] suggest that citrate (Cit) is the only important l.m.m. binder. Our earlier results [16] led us to conclude that both the phosphato and citrato complexes of Al(III) contribute to the l.m.m. fractions in the blood plasma, although about 80% of the Al(III) binds to transferrin.

The reason of such contradictory results is the lack of reliable speciation data [13,26]. In the Al(III)–phosphate (A^{3-}) system, under model conditions in the mmol dm^{-3} concentration range precipitation occurs at $pH > 3.5$, and we need to extrapolate from these data to physiological conditions, which are entirely different from the model conditions. We used LFER relationships to obtain more reliable speciation data for the Al(III)–phosphate system: $\log \beta\ ([AlAH]^+) = 17.6$, $\log \beta\ (AlA) = 13.5$, $\log \beta\ ([AlAH_{-1}]^-) = 7.2$ at 25°C and $I = 0.2$ mol dm^{-3} (KCl) [14].

Further, there are rather slow oligomerization reactions in the Al(III)–citrate (A^{3-}) system, which are strongly concentration dependent. As first reported by Öhman [27,28], at mmol dm^{-3} model concentrations a trinuclear species $[Al_3(CitH_{-1})_3(OH)]^{4-}$ predominates in a wide pH range including the physiological pH, when the thermodynamic equilibrium state is monitored by potentiometric titration (equilibration may take hours, especially in equimolar metal ion to ligand solutions). This trinuclear species is formed, but in a rather slow process, via the interactions of mononuclear 1:1 and 1:2 complexes, which exist at the beginning of complex formation and also predominates at high excesses of ligand [29]. The slow formation of the trinuclear complex through one or two intermediate species is nicely demonstrated by the changes in the ^1H NMR spectra at pH ~ 5 (see Fig. 1); after mixing, the signals are poorly resolved, broad and merged, indicating dynamic changes in the system. The complexation processes and/or ligand exchange between the initially formed mononuclear complexes and the intermediate species seem to be fairly fast. In the equilibrium state the characteristic, but rather complicated pattern of the trinuclear complex $[Al_3(AH_{-1})_3(OH)]^{4-}$ predominates in the spectrum. It is a reasonable question whether this approach provides a realistic description of the Al(III) speciation under physiological conditions: when the Al(III) concentration really exceeds a few μmol dm^{-3}, the ligand excess for potential binders is at least 1000–

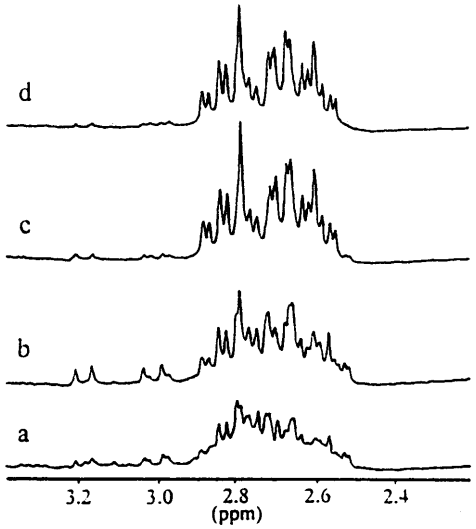


Fig. 1. ^{1}H NMR spectra of the Al(III)–citrate (A^{3-}) system, 1:1, at pH 5.0 as a function of time: (a) 15 min, (b) 40 min, (c) 10 h and (d) 30 h after mixing of the components, with $c_{Al(III)} = 0.04$ mol dm^{-3} (taken from Ref. [30]).

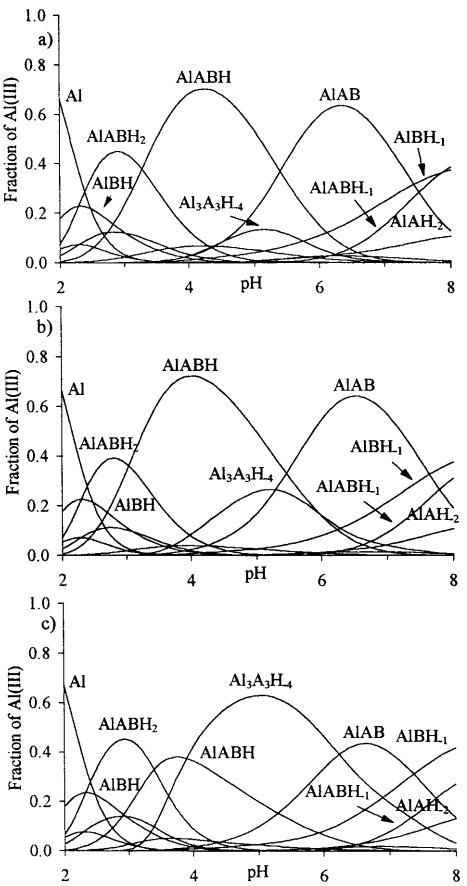


Fig. 2. Time-dependent speciation curves of Al(III)–citrate (A^{3-})–phosphate (B^{3-}) system at a 1:1:4 metal ion to ligand ratio: (a) 5 min, (b) 40 min and (c) 30 h after mixing of the components, with $c_{Al(III)} = 0.04$ mol dm^{-3}.

10 000-fold, and in consequence of the continuous metabolism, the biological fluids are open systems, which never reach real thermodynamic equilibrium. The problem of time-dependent speciation is a real challenge in Al(III) bioinorganic chemistry. Speciation model and stability constants for complexes formed in the Al(III)–citrate system at 25°C and $I = 0.2$ mol dm^{-3} (KCl) are as follows: $\log\beta$ ($[AlCitH]^{+}$) = 10.15, $\log\beta$ (AlCit) = 7.86, $\log\beta$ ($[AlCitH_{-1}]^{-}$) = 4.15, $\log\beta$ ($[AlCitH_{-2}]^{2-}$) = −1.71, $\log\beta$ ($[AlCit_2]^{3-}$) = 12.75, $\log\beta$ ($[AlCit_2H_{-1}]^{4-}$) = 7.94 and $\log\beta$ ($[Al_3(CitH_{-1})_3(OH)]^{4-}$) = 16.35 [30,31].

With a single exception, the results listed in Table 2 were obtained by ignoring the formation of ternary complexes between citrate and phosphate.

We recently have studied the Al(III)–citrate (A^{3-})–phosphate (B^{3-}) ternary system and monitored the time-dependent speciation by pH-potentiometry and multinuclear ^{1}H, ^{13}C and ^{31}P NMR spectroscopy. A detailed description of the role of time in the speciation of this system is given elsewhere [32]. Here, we focus only on the application of these results in order to obtain a reliable description of the speciation of Al(III) under serum conditions. The speciation curves obtained by pH-metry at different times after mixing of the necessary amounts of the stock solutions of Al(III) and citric acid adjusted to the required pH are shown in Fig. 2.

It can be seen that the ternary species $[AlABH]^{2-}$, $[AlAB]^{3-}$ and $[AlABH_{-1}]^{4-}$ predominate throughout the whole pH range from mixing until real thermodynamic equilibrium is reached. Time affects only the concentration of the trinuclear species, which is formed in a rather slow process from the mononuclear species $[AlAH_{-1}]^{-}$ and OH^{-}:

$$3[AlAH_{-1}]^{-} + H_2O = [Al_3(AH_{-1})_3(OH)]^{4-} + H^{+}$$

In the physiological pH range, Al(III) is bound in the ternary species $[AlAB]^{3-}$ and $[AlABH_{-1}]^{4-}$, and the binary species with phosphate, $[AlBH_{-1}]^{-}$, and citrate, $[AlAH_{-2}]^{2-}$. The results were rather surprising as the monodentate phosphate proved to be at least as efficient an Al(III) binder as the tridentate citrate. Multinuclear NMR measurements confirmed this result. It can be seen in Fig. 3, that when phosphate was added in twofold excess to a solution of the trinuclear species, the phosphate slowly displaced citrate from the oligomeric complex and in a few days the characteristic quartet of citrate was observed in the ^{1}H NMR spectrum.

Similarly, the ^{31}P NMR spectrum (Fig. 4) of the Al(III)–citrate–phosphate system at pH $\sim$7 exhibits three signals, a sharp resonance at $\sim$2 ppm, ascribed to free phosphate and two broad resonances at -3.3 and -13 ppm, ascribed to Al(III)-bound phosphates [14]. A comparison of the NMR spectrum with the speciation curves calculated for the experimental condi-

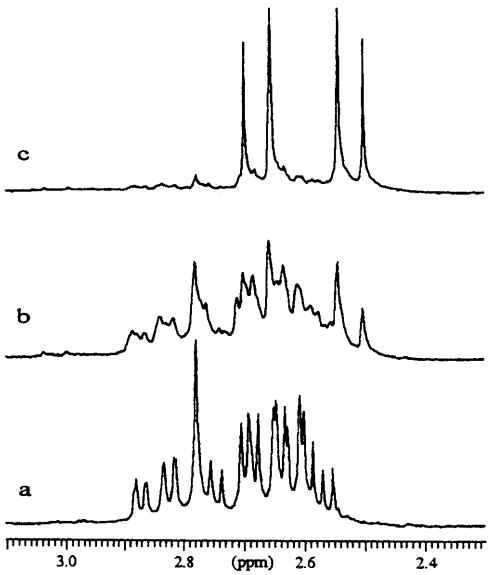


Fig. 3. ^{1}H NMR spectra at pH 7.4 of: (a) $[Al_3(CitH_{-1})_3(OH)]^{4-}$, 10 mmol dm^{-3}; (b) 10 h after the addition of phosphate to the sample in 20 mmol dm^{-3} concentration; and (c) 5 days after the addition of the phosphate to the solution (equilibrium state) (taken from Ref. [32]).

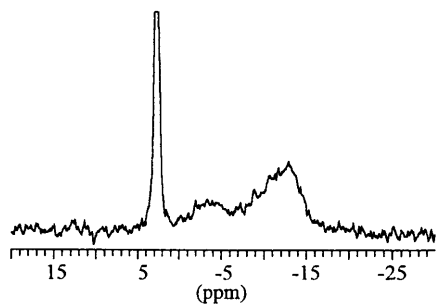


Fig. 4. ^{31}P NMR spectrum of the Al(III)–citrate (A^{3-})–phosphate (B^{3-}) system, 1:1:2, at pH 7.4 in the thermodynamic equilibrium state, with $c_{Al(III)} = 0.04$ mol dm^{-3}.

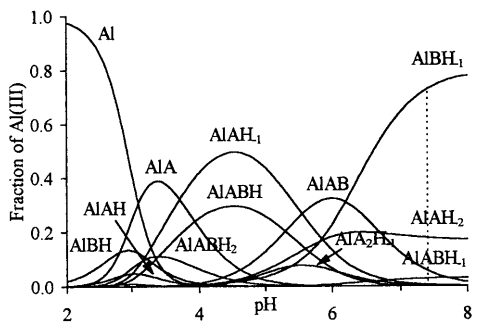


Fig. 5. Speciation curves for the complexes formed in the Al(III)–citrate (A^{3-})–phosphate (B^{3-}) system mimicking serum conditions: $c_{Al(III)} = 0.6$ μmol dm^{-3} (20% of the total $c_{Al(III)}$ in the serum, which is bound to l.m.m. ligands), $c_{citrate} = 99.0$ μmol dm^{-3}, and $c_{phosphate} = 1.1$ mmol dm^{-3}.

tions of the NMR measurements indicates practically complete agreement between the speciation results obtained by the two independent methods. Fig. 5 depicts the species distribution of Al(III) under plasma conditions. At physiological pH, phosphate seems to be the more efficient Al(III) binder, although citrate-bound Al(III) also occurs in significant concentration, in accordance with the results of Sadler et al. [33], who detected Al(III)-bound citrate in native serum by means of ^{1}H NMR.

4. Interactions of Al(III) with oligopeptides

Another Al(III) speciation problem relates to the interactions of Al(III) with proteins or peptides and their phosphorylated derivatives. This is connected with the involvement of Al(III) in Alzheimer's disease (AD), which is again a rather controversial issue [34]. There are probably a majority who deny any connection between Al(III) and AD. The crucial question is whether Al(III) is present at elevated concentrations in neurofibrillary (NF) tangles and/or senile plaques, which are common intracellular and extracellular markers of AD. According to our rather modest view, Al(III) is certainly not a causative factor in AD but it can be a risk factor as it can enhance plaque and tangle formation [35,36]. It has been clearly demonstrated by CD and FT-IR methods that Al(III) can interact with O-donors, such as Asp–COO^{-}, Glu–COO^{-} or Ser–OH, Thr–OH or Tyr–O^{-} rich fragments of β-amyloids or NF-proteins either via intramolecular complexation, causing conformational changes, or via intermolecular complex formation, linking peptide chains together through the carboxylates or phosphorylated Ser or Tyr sites. And this leads to the aggregation of neuronal degradation products.

The above mentioned results led us to attempt to obtain quantitative equilibrium-speciation and solution structural information concerning these interactions. Accordingly, we first studied the interactions of Al(III) with the building blocks of these compounds, i.e. amino acids, such as Asp, Glu, Ser, etc. [17], and also with phosphorylated Ser and Tyr [18]. Then we continued with small peptide model systems, first the Al(III)–Asp-Asp (H_3A) system. As demonstrated in Fig. 6, in the weakly acidic pH range the formation of mono complexes in different protonation states, $[AlAH_2]^{2+}$, $[AlAH]^{+}$, AlA and $[AlAH_{-1}]^{-}$ was detected, but, depending on the metal to ligand ratio, precipitation occurred at pH $\sim$5–6. This indicates that the terminal COO^{-} groups of Asp (or Glu) are not sufficient in such a small peptide to keep Al(III) in solution and to prevent precipitation of $Al(OH)_3$. To achieve this, a more specific arrangement of suitable side-chain donors is necessary.

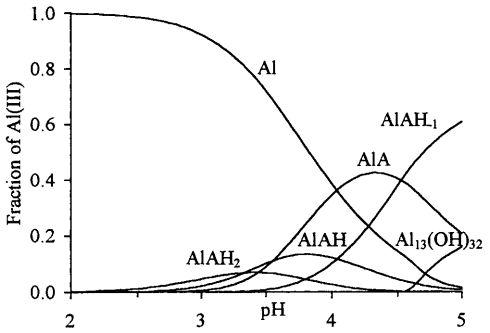
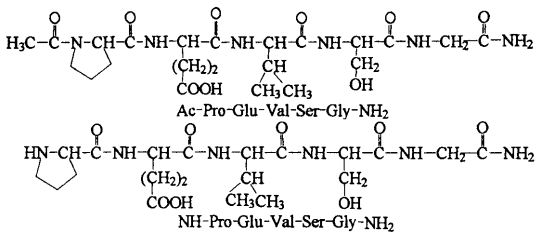


Fig. 6. Speciation curves for the complexes formed in the Al(III)–AspAsp (A^{2-}) system at a 1:4 metal ion to ligand ratio, with $c_{Al(III)} = 1.0$ mmol dm^{-3}.



Scheme 2.

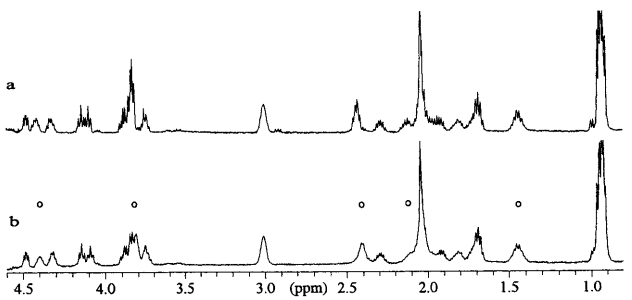


Fig. 7. ^{1}H NMR spectra of Ac–LysSerProValValGluGly (H_2A) at 4.0 mmol dm^{-3} at pH 4.0 (a) in the absence and (b) in the presence of 4.0 mmol dm^{-3} Al(III).

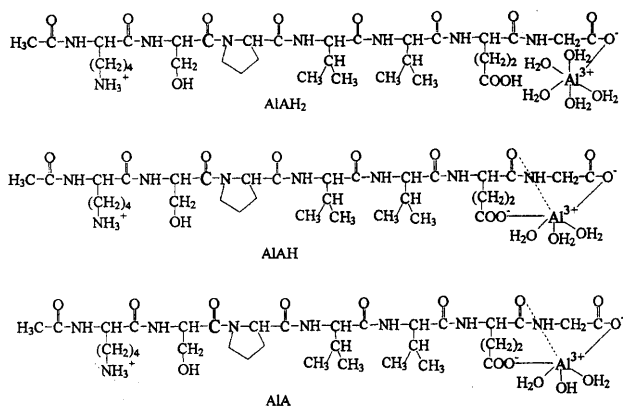
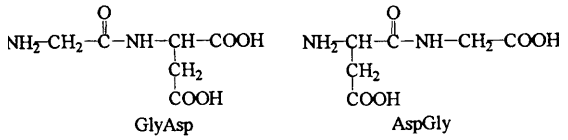


Fig. 8. Suggested binding modes in the Al(III) complexes of Ac–LysSerProValValGluGly (H_2A).

We have studied several penta- and heptapeptides. Only preliminary data are available on these systems at present and a full speciation and structural description of the Al(III) complexes formed with oligopeptides will be reported later. In the first group, pentapeptides were studied, which were rich in Glu and Ser, and had a protected C-terminus and a free or protected N-terminus, e.g. Ac–ProGluValSerGly–NH_2 (HA) and its analogue HN–ProGluValSerGly–NH_2 (HA)(see Scheme 2). We found that the Al(III)-binding capabilities of the peptides were stronger when they had a free Pro–NH function at the N-terminus. This is rather surprising as Al(III), is known [17,37] to have a low affinity for amines, and the N-terminal Pro–NH group is therefore not expected to be a strong binding site. As the C-terminal COO^- was blocked in both peptides, we would expect coordination via the side-chain Glu–carboxylate and Ser–alcoholate groups. Instead, coordination seems to be much more likely through the N-terminal donor groups. In a second group the peptides had a free C-terminus, but a blocked N-terminus. With these heptapeptides, 1:1 complexes could again be detected by pH-metry; for one of these peptides, Ac–LysSerProValValGluGly (H_2A, the formula is given in Fig. 8), the stability constants obtained were as follows: $\log \beta$ ($[AlAH_2]^{3+}$) = 17.11, $\log \beta$ ($[AlAH]^{2+}$) = 13.30, $\log \beta$ ($[AlA]^{+}$) = 9.36 $\log \beta$ ($AlAH_{-1}$) = 4.72, $\log \beta$ ($[AlAH_{-2}]^{-}$) = -0.42. ^{1}H NMR indicated a weak interaction of the peptide with Al(III) in the slightly acidic pH range. Fig. 7 depicts the ^{1}H NMR spectra of the peptide at pH ~ 4 in the absence and the presence of equimolar Al(III).

The significant selective line broadening indicates interactions between the peptide and the metal ion. The rate of the ligand-exchange reaction is roughly comparable with the NMR time scale; hence, there is no shift in the position of the resonances, and there is no increase in the number of signals. The preliminary assignments of the signals indicate mostly that the signals of the protons near the C-terminus undergo broadening mostly, which suggests that coordination starts at the terminal-COO^-, (complex $[AlAH_2]^{3+}$) and Al(III) then chelates through the terminal-COO^- of the peptide and the side chain-COO^- of Glu with participation of the central peptide-carbonyl, through the formation of a joint chelate system (complex $[AlAH]^{2+}$), and then parallel overlapping deprotonation of the non-coordinating protonated amino donor and a coordinated water molecule subsequently takes place ($[AlA]^{+}$, $AlAH_{-1}$ and $[AlAH_{-2}]^{-}$) (see Fig. 8). Two-dimensional carbon–proton correlation NMR measurements are in progress in order to achieve a complete assignment of the protons. Molecular dynamic calculations indicate favored arrangements of the terminal carboxylate and the side-chain-COO^- of Glu for the chelation of Al(III). It is interesting, however, that at



Scheme 3.

pH ~ 7 the two spectra (in the presence and absence of Al(III)) are barely different and direct coordination of Al(III) is therefore not confirmed. However, since no precipitation was observed in the solution, it is very likely that Al(III)-hydroxo species in some metastable state (which occurs fairly commonly in aqueous Al(III) solutions), form outer-sphere complexes through hydrogen-bonding with the hydrated oligopeptides. We are now going further with similar oligopeptides, and also with their phosphorylated derivatives, as interchain links involving Al(III) between oligopeptides can play an even more important role in the aggregation of neuropeptides, than intramolecular Al(III) binding.

To summarize, although the results are not always straightforward, these studies confirm that neurofilament non-phosphorylated peptides can bind Al(III), and this can trigger conformational changes resulting in aggregation processes of β-amyloids and NF tangles.

5. Characterization of VO(IV)–peptide interactions

Vanadium is an important trace metal with a great variety of physiological effects. It can act, for instance, as an enzyme regulator in various phosphate-metabolizing reactions, suggesting binding between vanadium and the protein side-chains [38]. In oxidation states III, IV and V, vanadium binds to transferrin, the essential metal ion transport protein in the serum [39]. Its interactions with oligopeptides in the physiological pH range, via coordination of the deprotonated peptide-N^- group, have been proved to involve vanadium in oxidation state V [40–42].

Vanadium in its high oxidation states $+4$ and $+5$ is a rather hard metal ion, like Al(III), and forms complexes of fairly high stability with ligands containing O-donor atoms, but it binds more weakly to N- or S-donor containing biogenic ligands [43] in solution. It was seen above that Al(III) is able to bind to peptides at either the N-terminal or the C-terminal end, involving mostly O-donor groups, but is not able to induce deprotonation and subsequent coordination of the peptide amide. And what about VO(IV)? The amide coordination of a few synthetic ligands to VO(IV) has been observed in the solid state [44]. Tasiopoulos et al. [45] recently isolated the first VO(IV) complexes of dipeptides containing a deprotonated peptide-N^- group. In aqueous solution, however, no unambiguous proof has been obtained for VO(IV)-promoted amide deprotonation and coordination, although this was strongly suggested in some glycine/alanine dipeptide complexes by CD and EPR measurements [46]. Among various binding isomers, a species with the usual (NH_2, N^-, COO^-) coordination involving deprotonated amide-N^- was also assumed at pH ~ 8. Interestingly, no amide deprotonation was observed with the tripeptide GlyGlyGly [47]. It has been found for many metal ions that the presence of a suitable anchoring donor which can bind metal ions strongly enough and promote deprotonation of the amide plays a crucial role in amide deprotonation [48]. In aqueous solution, the terminal-NH_2 is not a particularly good anchoring donor for the hard VO(IV) ion.

In order to make the arrangement of the donor groups more favorable for VO(IV) binding, we studied how the presence of an extra negatively charged O-donor side-chain COO^- group at the C- or N-terminus of simple dipeptides affects the VO(IV) binding of GlyAsp and AspGly (H_2A, Scheme 3) [49]. The results were very similar to those for simple dipeptides: no amide deprotonation could be detected with GlyAsp, but was suggested with AspGly at pH ~ 8 after dissolution of the precipitate $VO(OH)_2$. The side-chain O-donors near the terminal -NH_2 or COO^- groups did not favor amide deprotonation and coordination, as new competitive binding sites in chelating positions were developed in the molecules, and these bound the metal ions.

In the next step, the terminal $-NH_2$ group was replaced by a hard phenolate as anchoring donor group: the dipeptide analogue salicylglycine (SalGly) ($HOC_6H_4C(O)NHCH_2COOH$, 2-hydroxyhippuric acid, H_2A) proved to be an efficient VO(IV) binder: no precipitate occurred in the pH range 1–12, and EPR unambiguously indicated the presence of a N donor around the metal ion [50]. As may be seen in Table 3, the fairly high g values and low A values strongly suggest the presence of a coordinated amide-N^- in the equatorial plane of the species $[VOAH_{-1}]^-$ and $[VOAH_{-2}]^{2-}$ (Scheme 4).

We recently started investigations of the tripeptide analogue SalGly–L–Ala (H_2A) too, where the terminal amino acid is an L enantiomer, and thus we can also use CD to obtain information regarding the binding modes of the ligand. Our preliminary results indicate that both CD and EPR suggest coordination of the peptide-amides in the pH range 4–9. For example, a further decrease in the coupling constants A and an increase in the g factor of the complex $[VOAH_{-2}]^{2-}$ ($g_o = 1.983$, $A_o = 85$, $g_{\|} = 1.963$, $A_{\|} = 157$ and $g_{\perp} = 1.985$, $A_{\perp} = 51$) is a fairly unambiguous indications of the presence of N donors in the equatorial coordination sphere of VO(IV) (Scheme 5). Interestingly, with SalGlyAla the formation of various dimeric species pre-

Table 3
Speciation and EPR data on VO(IV)–SalGly system [a]

Species	log β	g_o	A_o (10^{-4} cm^{-1})	$g_{\|}$	$A_{\|}$ (10^{-4} cm^{-1})	$g_{\perp}$	$A_{\perp}$ (10^{-4} cm^{-1})
$[VOAH]^+$	10.24(3)						
VOA	7.05(2)	1.964	101	1.938	175		
$[VOAH_{-1}]^-$	2.29(2)	1.971	92	1.949	165	1.980	57
$[VOAH_{-2}]^{2-}$	−5.28(3)	1.971	89	1.951	163	1.980	55
$[VOA_2H_{-1}]^-$	5.55(6)						

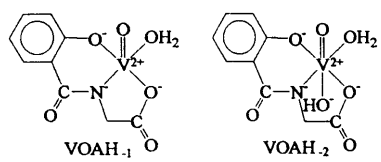
[a] Data are taken from Ref. [50].

dominates in the pH range 4–10 and through stepwise deprotonation of the species $[(VO)_2A_2]^{2-}$ to $[(VO)_2A_2H_{-4}]^{6-}$ the coordination mode changes from $2 \times (COO^-,=O,=O,O^-)$ to $2 \times (COO^-,N^-,N^-,O^-)$. The driving force of dimer formation is presumably the stacking interaction between the aromatic rings. The CD results suggest that the stepwise deprotonation and coordination of the amide start at the C-terminal end of the ligand. Accordingly, the terminal COO^- and not the phenolate seems to be the primary anchor. Further studies with various peptides, pseudopeptides and derivatives in a search for efficient anchors which can promote amide deprotonation are currently in progress in our laboratories. For example, in connection with the phenolate and carboxylate anchors, we have been studying the VO(IV) complexation with *N*,*N*′-bis(5-sulphosalicyl)ethylenediamine and *N*,*N*′-bis(malonyl)-ethylenediamine, when phenolate or carboxylate anchors, respectively, are available at both ends of the molecules. With various *N*-D-gluconylamino acids, EPR and CD measurements indicated the formation of species containing a deprotonated peptide-N^- donor. Alcoholic-OH groups of the sugar moiety in appropriate steric arrangements proved to be efficient anchors [51]. Similarly, thiolate-S^- in mercaptopropyonylglycine [52,53] and gluthathione [52,54,55] seem to be suitable anchoring donors towards VO(IV) to induce amide deprotonation not only in the solid state [52], but also in solution [53–55]. Phosphonic ($-PO_3^{2-}$) groups of diphosphono-dipeptides has been shown to act as efficient anchoring donors towards Cu(II) [56], and we are now studying their interactions with VO(IV).

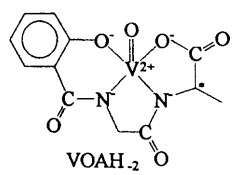
6. Vanadium complexes as insulin mimetics

Vanadium is a nutritional element present in mammalian tissues. It is available in anionic and cationic forms, the most common ones under physiological conditions being vanadate(V) ($H_2VO_4^-$) and oxovanadium-(IV) (VO^{2+}). Many studies have been performed on the biological significance of vanadium compounds during the past two decades. The insulin-like effect of vanadium is one of the most noteworthy findings and the relationship between vanadium and diabetes mellitus has been extensively studied [57–60]. Since the first report of the insulin-mimetic activities of vanadium compounds in vitro in 1979 [57], and in vivo in 1985 [60], great efforts have been made to prepare vanadium-(IV) and vanadium(V) complexes of high biological activity and low toxicity which are readily absorbed. Among others Orvig et al. and Sakurai et al. prepared many oxovanadium(IV) complexes with various coordination modes, such as $VO(O_4)$ [61–63], $VO(S_2N_2)$ [64], $VO(S_4)$ [65,66], $VO(N_3O)$ [67], and $VO(N_2O_2)$ [68–70], and examined the relationship between their structures and insulin-mimetic activities by evaluating both the in vitro and the in vivo experimental results.

With regard to the coordination chemistry of VO(IV), fairly stable complexes can be expected with O-donor ligands, but not with N,S donors. These complexes will presumably decompose and liberate most of the carrier ligands when they dissolve after oral administration. Even if they form strong complexes at neutral pH, at the pH ~ 2 of the gastric juice in the stomach they will almost completely dissociate, being labile complexes. Accordingly, other biomolecules that are potential metal ion binders present in biological fluids may partially or completely displace the original VO(IV)-carrier molecules from the coordination sphere of the metal. Ternary complex formation should therefore be taken into account in a speciation description of these complexes in biological fluids. Such ternary complexes



Scheme 4.



Scheme 5.

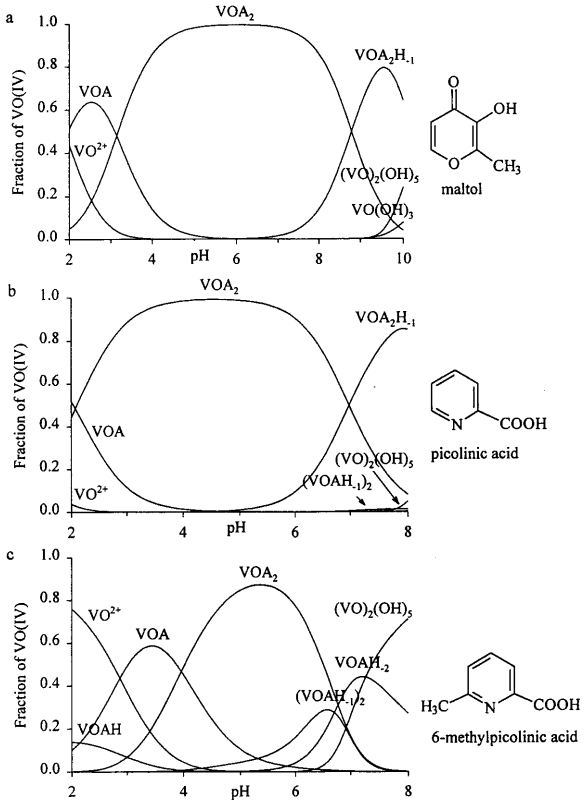


Fig. 9. Speciation curves for complexes formed in the systems: (a) Al(III)–maltolate (A^-), (b) VO(IV)–picolinate (A^-) and (c) VO(IV)–6-Me-picolinate (A^-) systems at a 1:4 metal ion to ligand ratio, with $c_{VO(IV)} = 0.002$ mol dm^{-3}. Calculated with stability constants reported in Refs. [71,72].

might be of great importance in the absorption and transport processes of the various potential insulin-mimetic drugs, such as VO(maltolate)$_2$, VO(picolinate)$_2$ and VO(6-Me-picolinate)$_2$ and even in their physiological activity. In order to describe the speciation of these insulin mimetics in various biological systems, we are currently studying their interactions with l.m.m. biomolecules in the organism, such as phosphate (gastro-intestinal tract), adenosinenucleotides (intracellular fluids), hydroxycarboxylic acids, lactic acid and citric acid (blood serum) and catecholamines, e.g. dopamine (brain). Here, mostly results on the ternary complex formation of VO(maltolate)$_2$ are presented [71].

7. Biospeciation of insulin-mimetic VO(IV) complexes in biofluids

We shall consider first the solution speciation of the insulin-mimetic compounds: VO(maltolate)$_2$, VO(picolinate)$_2$ and VO(6-Me-picolinate)$_2$ [71–73]. As may be seen in Fig. 9, mono and bis complexes are formed in these systems, but there are great differences between the stability constants of the complexes formed. Maltol forms the most stable complexes with the VO(IV) ion via the formation of five-membered chelates through the oxo and alcoholate groups. The neutral bis complex, which may have good membrane transport properties, exists in the pH range 5–7.5. Picolinic acid and 6-methylpicolinic acid also form mono and bis complexes via the pyridine N and carboxylate groups. However, the methyl group in 6-methylpicolinic acid has a very marked effect on the VO(IV)-binding capabilities of the ligands: presumably because of the steric effect of the methyl group, the stabilities of these complexes are significantly lower. This is more pronounced for the 1:2 complexes. In the VO(IV)–picolinic acid system, the bis complex is predominant in the pH range 2–7, while for 6-methylpicolinic acid VOA_2 exists in the pH range 4–6. The VO(IV)-binding abilities of the ligands studied exhibit the sequence maltol > picolinic acid > 6-methylpicolinic acid. The EPR parameters of the bis complexes listed in Fig. 10 also support this sequence. The value of the hyperfine constant, $A_{\|}$ increases, while the $g_{\|}$ value decreases in this direction, which reveals the formation of bonds with different strengths in these systems. The EPR results show that the bis complexes

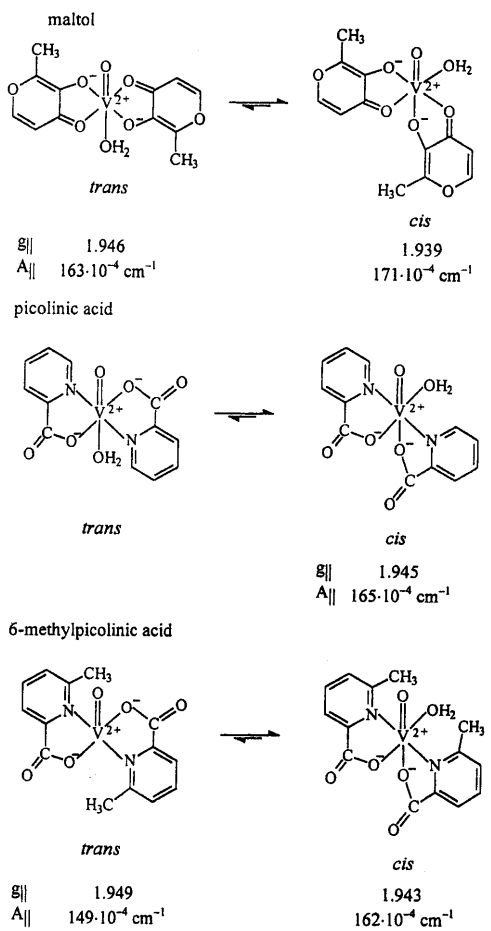


Fig. 10. Geometric isomers and EPR parameters of VO(maltolate)$_2$, VO(picolinate)$_2$ and VO(6-Me-picolinate)$_2$.

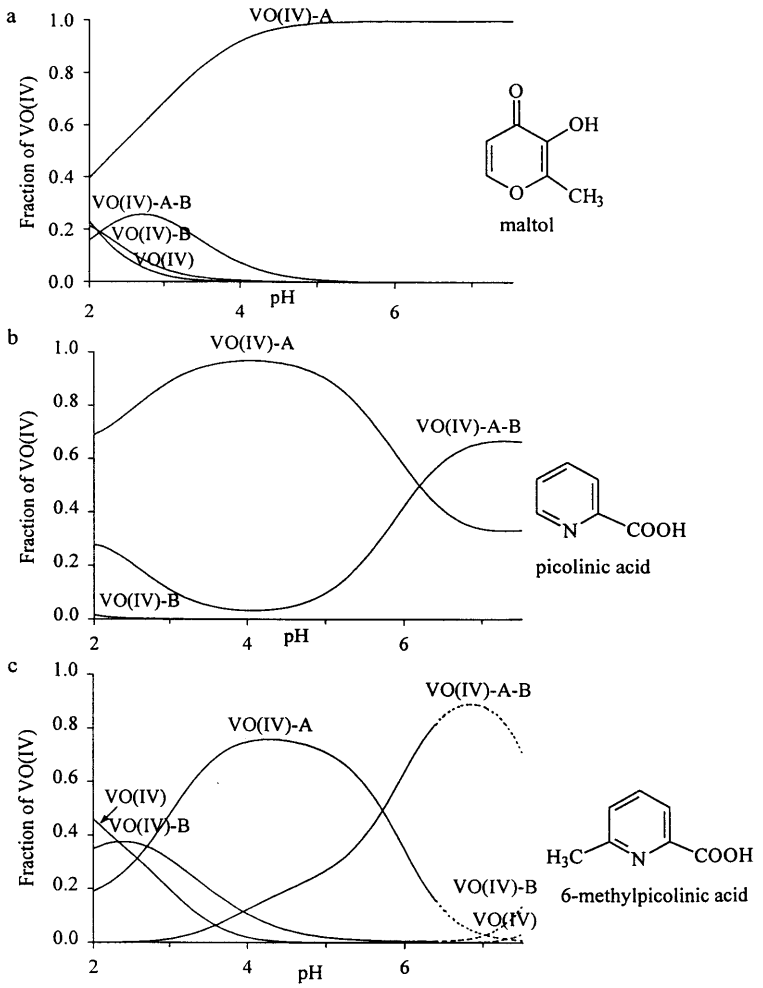


Fig. 11. Predominance diagram of the systems (a) VO(IV)–maltolate (A^-)–phosphate (B^{3-}), (b) VO(IV)–picolinate (A^-)–phosphate (B^{3-}), and (c) VO(IV)–6-Me-picolinate (A^-)–phosphate (B^{3-}) systems at a 1:5:5 metal ion to ligand ratio, with $c_{VO(IV)} = 0.001$ mol dm^{-3}.

form two geometric isomers, depending on the position of the solvent molecule in the coordination sphere of the VO(IV): the water molecule can be either *cis* or *trans* to the oxo group of the vanadium ion (see Fig. 10). In aqueous solution at room temperature and at neutral pH, the *cis* form of the bis complexes has been found to predominate with these three ligands. 6-Methylpicolinic acid proved to be the weakest VO(IV) binder, but it has the most hydrophobic character and hence its complex may provide a more efficient absorption via passive transport across the hydrophobic membranes [69].

Phosphate, as the most important l.m.m. component in the gastro-intestinal tract, may play a role in the absorption of these insulin-mimetic compounds. Predominance curves (the sum of the VO(IV) fractions bound in the binary complexes with ligand A or B and those bound in the ternary complexes with ligand A and B) for the systems VO(IV)–insulin mimetic (A^-)–phosphate (B^{3-}) are depicted in Fig. 11. It is seen that the parent complexes $[VOA]^+$ and $[VOA_2]°$ of maltol are the predominant species at pH >4, a range including the physiological pH, and the presence of phosphate affects the speciation of the VO(IV)–maltol system only slightly. Ternary complexes occur only in the pH range 2–4, but they never become predominant species. They are favored, however, with picolinic acid and 6-methylpicolinic acid. In the weakly acidic pH range and at neutral pH, mixed ligand complexes are the predominant species [72]. Accordingly, phosphate will certainly not affect the absorption of VO(maltolate)$_2$, but might have some (though not necessarily beneficial) influence on the absorption of the two picolinates. The ternary complexes are certainly charged species (the coordinating hydrogenphosphate HPO_4^{2-} a charge 2–, while the picolinate displaced by the phosphate molecule is mononegatively charged), in contrast with the neutral binary complex, and this may hinder at least the passive transport of VO(IV) through the membrane.

Adenosinenucleotides occurs in mmol dm^{-3} concentration in cellular fluids, and their interactions with

'exogenous' compounds in the organism are very likely. The predominance diagram for the VO(IV)–maltol (A^-)–ATP (B^{3-}) system (see Fig. 12) clearly indicates that maltol forms ternary complexes in the weakly acidic pH range (4.5–5.5), as detected by both pH-metry and EPR spectroscopy. The EPR spectra depicted in Fig. 13 show that a new species is present in practically the same pH range, and is presumably the mixed-ligand complex $[VOAB]^{2-}$. However, at physiological

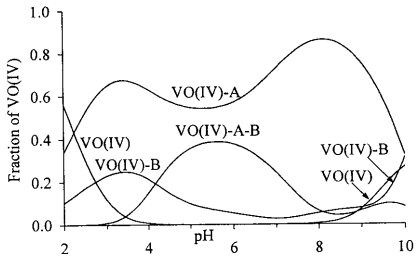


Fig. 12. Predominance diagram of the VO(IV)–maltolate (A^-)–ATP (B^{3-}) system at a 1:2:2 metal ion to ligand ratio, with $c_{VO(IV)} = 0.002$ mol dm^{-3}.

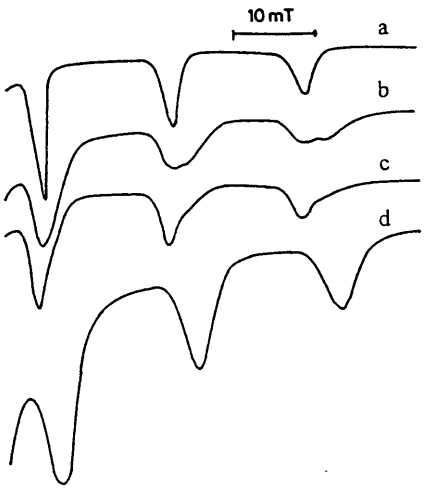


Fig. 13. High field parallel region of frozen solution EPR spectra (X band) recorded at 140 K: (a) VO(IV)–maltolate, 1:2, pH 5.5; (b) VO(IV)–maltol–ATP, 1:1:1, pH 4.5; (c) VO(IV)–maltol–ATP, 1:1:1, pH 5.5; (d) VO(IV)–ATP, 1:2, pH 5.5; $c_{VO(IV)} = 0.004$ mol dm^{-3} (taken from Ref. [71]).

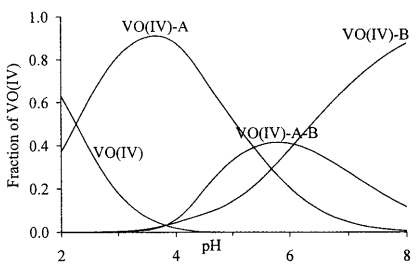


Fig. 14. Predominance diagram of the VO(IV)–maltolate (A^-)–dopamine (B^{2-}) system at a 1:2:2 metal ion to ligand ratio, with $c_{VO(IV)} = 0.002$ mol dm^{-3}.

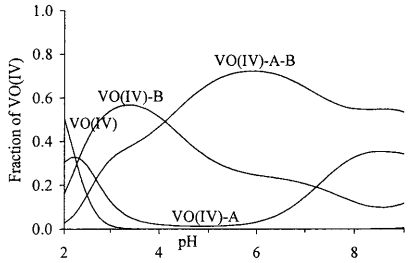


Fig. 15. Predominance diagram of the VO(IV)–maltolate (A^-)–citrate (B^{3-}) system at a 1:2:2 metal ion to ligand ratio, with $c_{VO(IV)} = 0.002$ mol dm^{-3}.

pH, maltol seems to be more competitive and VO(IV) is bound mostly to maltol. At pH >10, maltol is displaced and the ribose part of the nucleotides binds the metal [71].

The concentrations of catecholamines in the brain are fairly high. Catechol derivatives are extremely strong VO(IV) binders; they can even displace the oxo group of VO(IV) and form non-oxo $3 \times (O^-,O^-)$-coordinated tris complexes [74–76]. The high affinity of catecholates for VO(IV) is hindered in the acidic pH range because of the high proton competition on the phenolate functions. At the same time, maltol, which is also a strong VO(IV) binder, has a high affinity for VO(IV) in the acidic pH range, owing to the weaker proton competition on the maltolate chelating function. Accordingly, in the VO(IV)–maltol (A^-)–dopamine (B^{2-}) system, maltol is the predominant metal ion binder at pH <4.5; the ternary complexes of VOABH and $[VOAB]^-$ then become predominant up to pH ~ 6, while at around the physiological pH range the catechols are more efficient VO(IV) binders and displace maltol completely (see Fig. 14).

As discussed above, citrate is an important constituent of the blood serum: its concentration is ~ 0.1 mmol dm^{-3} (see Table 1). It generally behaves as a tridentate ligand in its complexes and is regarded as the strongest l.m.m. hard metal ion binder in the serum. As shown in Fig. 15, pH-metric speciation measurements and spectral studies unambiguously suggest enhanced ternary complex formation in the pH range 4–8. A considerable intensity decrease in the EPR spectrum of VO(IV)–citrate (B^{3-}) in neutral solution, due to the formation of oxo-bridged dinuclear species [77], is not observed, but the spectrum indicate the formation of new mononuclear complexes, presumably the ternary $[VOABH]^-$, $[VOAB]^{2-}$ and $[VOABH_{-1}]^{3-}$, in a wide pH range. These data strongly suggest that, if they meet, citrate will certainly react with $VO(maltolate)_2$, and this potential drug may be transported in the blood serum, presumably in the form of its ternary species with citrate. A more detailed study of the biospeciation of various insulin-mimetics in the serum is at present in progress in our laboratory.

Acknowledgements

This research was carried out in the frame of a COST D8 project. The authors wish to express their thanks to Professors G. Micera (University of Sassari, Italy), J. Costa Pessoa (University of Lisbon, Portugal), R. Bertani (C.N.R., Padova, Italy), M. Hollosi (Eotvos University, Budapest, Hungary), Zs. Majer (Eotvos University, Budapest, Hungary), Gy. Dombi (Medical University Szeged, Hungary), G. Toth (Medical University Szeged, Hungary) and P. Buglyo (Kossuth University, Debrecen, Hungary) for their valuable contributions to this work. Financial support was provided by the Hungarian Research Fund (OTKA T23776/97) and the Hungarian Ministry of Education (FKFP 0013/97).

References

[1] Chemical Speciation and its Potential Application to Medicine, in: G. Berthon (Ed.), Handbook of Metal–Ligand Interactions in Biological Fluids, Bioinorganic Chemistry, Vol. 2, Part V, Marcell Dekker, New York, 1995, 1119–1299.
[2] Research Issues in Aluminum Toxicity, J. Toxicol. Environ. Health (Special Issue) 48 (1996) 527–686.
[3] J.A. Varner, K.F. Jensen, W. Horvath, R.L. Isaacson, Brain Res. 784 (1998) 284.
[4] T. Kiss, I. Sóvágó, R.B. Martin, J. Am. Chem. Soc. 111 (1989) 3611.
[5] I. Sóvágó, T. Kiss, R.B. Martin, Polyhedron 9 (1990) 189.
[6] T. Kiss, I. Sóvágó, R.B. Martin, Inorg. Chem. 30 (1991) 2130.
[7] T. Kiss, K. Atkári, M-J. Bojczuk, P. Decock, J. Coord. Chem. 29 (1993) 81.
[8] E. Pereira, M.M.L. Fiallo, A. Garnier, T. Kiss, H. Kozlowski, J. Chem. Soc., Dalton Trans. (1993) 455.
[9] T. Kiss, I. Sóvágó, R.B. Martin, J. Pursiainen, J. Inorg. Biochem. 55 (1994) 53.
[10] E. Farkas, E. Kozma, T. Kiss, I. Tóth, B. Kurzak, J. Chem. Soc., Dalton Trans. (1995) 477.
[11] T. Kiss, Arch. Geront. Geriatrics 21 (1995) 99.
[12] B. Corain, T. Kiss, P. Zatta, Coord. Chem. Rev. 149 (1996) 329.
[13] T. Kiss, E Farkas, Chapter 4, in: R.W. Hay, J.R. Dilworth, K.B. Nolan (Eds.), Perspectives on Bioinorganic Chemistry, vol. 3, Jai Press, London, 1996.
[14] K. Atkári, T. Kiss, R. Bertani, R.B. Martin, Inorg. Chem. 35 (1996) 7089.
[15] W.R. Harris, G. Berthon, J.P. Day, C. Exley, T.P. Flaten, W.F. Forbes, T. Kiss, C. Orvig, P.F. Zatta, J. Toxicol. Environ. Health 48 (1996) 543.
[16] T. Kiss, A. Lakatos, E. Kiss, R.B. Martin, in: N.D. Hadjiliadis (Ed.), Cytotoxic, Mutagenic and Carcinogenic Potential of Heavy Metals Related to Human Environment, NATO ASI Series, vol. 26, Kluwer, Dordrecht, 1997, p. 241.
[17] T. Kiss, I. Sóvagó, I. Tóth, A. Lakatos, R. Bertani, A. Tapparo, G. Bombi, R.B. Martin, J. Chem. Soc., Dalton Trans. (1997) 1967.
[18] E. Kiss, A. Lakatos, I. Bányai, T. Kiss, J. Inorg. Biochem. 69 (1998) 145.
[19] W.R. Harris, J. Clin. Chem. 38 (1992) 1809.
[20] S. Dayde, M. Filella, G. Berthon, J. Inorg. Biochem. 38 (1990) 241.
[21] G.E. Jackson, Polyhedron 9 (1990) 163.
[22] D.J. Clevette, C. Orvig, Polyhedron 9 (1990) 151.
[23] J.R. Duffield, K. Edwards, D.A. Evans, D.M. Morrish, R.A. Vobe, D.R. Williams, J. Coord. Chem. 23 (1991) 277.
[24] L-O. Ohman, R.B. Martin, Clin. Chem. 40 (1994) 598.
[25] G. Berthon, Coord. Chem. Rev. 149 (1996) 241.
[26] L.D. Pettit, H.K.J. Powell, The IUPAC Stability Constant Database, Academic Software and IUPAC, Royal Society of Chemistry, London, 1992–1997.
[27] L-O. Ohman, S. Sjoberg, J. Chem. Soc., Dalton Trans. (1983) 2513.
[28] L-O. Ohman, Inorg. Chem. 27 (1988) 2565.
[29] J.E. Gregor, H.K.J. Powell, Aust. J. Chem. 39 (1986) 1851.
[30] A. Lakatos, I. Banyai, T. Kiss, P. Decock, Eur. J. Inorg. Chem. (submitted).
[31] M. Matzapetalis, C.P. Raptopoulou, A. Terzis, A. Lakatos, T. Kiss, A. Salifoglou, Inorg. Chem. 38 (1999) 618.
[32] A. Lakatos, T. Kiss, F. Evanics, Gy. Dombi, J. Biol. Inorg. Chem. (in preparation).
[33] J.D. Bell, G. Kubal, S. Radulovic, P. Sadler, A. Tucker, Analyst 118 (1993) 241.
[34] J. Savory, C. Exley, W.B. Forbes, Y. Huang, J.G. Joshi, T. Kruck, D.R.C. McLachlan, I. Wakayama, J. Toxicol. Environ. Health 48 (1996) 615.
[35] M. Hollosi, L. Urge, A. Perczel, J. Kajtar, I. Teplan, L. Otvos, G.D. Fasman, J. Mol. Biol. 223 (1992) 673.
[36] C. Exley, N.C. Price, S.M. Kelly, J.D. Birchall, FEBS Lett. 324 (1993) 293.
[37] R.B. Martin, in: M. Nicolini, P.F. Zatta, B. Corain (Eds.), Aluminum in Chemistry, Biology and Medicine, Cortina International, Verona, 1991.
[38] D.C. Crans, R.L. Bunch, L.A. Theisen, J. Am. Chem. Soc. 111 (1989) 7597.
[39] D. Rehder, Chapter 1, in: H. Sigel, A. Sigel (Eds.), Metal Ions in Biological Systems, Marcel Dekker, New York, 1995.
[40] D. Rehder, Inorg. Chem. 27 (1988) 4312.
[41] M. Fritzsche, V. Vergopoulos, D. Rehder, Inorg. Chim. Acta 211 (1993) 11.
[42] K. Elvingson, M. Fritzsche, D. Rehder, L. Pettersson, Acta Chim. Scand. 48 (1994) 878.
[43] L.F. Vilas Boas, J. Costa Pessoa, in: G. Wilkinson, R.D. Gillard, J.A. McCleverty (Eds.), Comprehensive Coordination Chemistry, vol. 3, Pergamon Press, Oxford, 1987, p. 453.
[44] (a) G.R. Hanson, T.A. Kabanos, A.D. Keramidas, D. Mentzafos, A. Terzis, Inorg. Chem. 31 (1992) 2587. (b) A.S. Borovik, T.M. Dewey, K.N. Raymond, Inorg. Chem. 32 (1993) 413. (c) C.R. Cornman, K.M. Geiser-Bush, P. Singh, Inorg. Chem. 33 (1994) 4621.
[45] (a) A.J. Tasiopoulos, A.T. Vlahos, A.D. Keramidas, T.A. Kabanos, Y.G. Deligiannakis, C.P. Raptopoulou, A. Terzis, Angew. Chem., Int. Ed. Engl. 35 (1996) 2531. (b) A.J. Tasiopoulos, Y.G. Deligiannakis, J.D. Woolins, A.M.Z. Slawin, T.A. Kabanos, J. Chem. Soc., Chem. Commun (1998) 569.
[46] J. Costa Pessoa, S.M. Luz, R. Duarte, J.J.G. Moura, R.D. Gillard, Polyhedron 23 (1993) 2857.
[47] J. Costa Pessoa, S.M. Luz, R.D. Gillard, J. Chem. Soc., Dalton Trans. (1997) 569.
[48] I. Sóvágó, in: K. Burger (Ed.), Biocoordination Chemistry, Ellis Horwood, New York, 1990, p. 139.
[49] J. Costa Pessoa, T. Gajda, R.D. Gillard, T. Kiss, S.M. Luz, J.J.G. Moura, I. Tomaz, J.P. Telo, I. Torok, J. Chem. Soc., Dalton Trans. (1998) 3587.
[50] T. Kiss, K. Petrohan, P. Buglyo, D. Sanna, G. Micera, J. Costa Pessoa, C. Madeira, Inorg. Chem. 37 (1998) 6389.
[51] B. Gyurcsik, T. Jakusch, Book of Abstracts of XXXIII. ICCC, Florence, 1998, p. 257.
[52] A.T. Tasiopoulos, A.N. Troganis, A. Evangelou, C.P. Raptopolou, A. Terzis, Y. Deligiannakis, T.A. Kabanos, Eur. J. Chem. 5 (1999) 910.

[53] P. Buglyo, I. Tomaz, T. Jakusch, J. Costa Pessoa, T. Kiss (in preparation).
[54] A. Dessi, G. Micera, D. Sanna, J. Inorg. Biochem. 52 (1993) 275.
[55] I. Tomaz, J. Costa Pessoa, T. Kiss, P. Buglyo, E. Kiss, J. Inorg. Biochem. 74 (1999) 315.
[56] T. Kiss, E. Farkas, H. Kozlowski, Z. Siatecki, P. Kafarski, J. Chem. Soc., Dalton Trans. (1989) 1053.
[57] E.L. Tolman, E. Barris, M. Burns, A. Pansini, R. Partridge, Life Sci. 25 (1979) 1159.
[58] Y. Schechter, S.J.D. Karlish, Nature 284 (1980) 556.
[59] S. Tamura, T.A. Brown, R.E. Dubler, J. Larner, Biochem. Biophys. Res. Commun. 113 (1984) 80.
[60] C.E. Heylinger, A.G. Tahiliani, J.H. McNeill, Science 227 (1985) 1474.
[61] J.H. McNeill, V.G. Yuen, H.R. Hoveyda, C. Orvig, J. Med. Chem. 35 (1992) 1489.
[62] P. Caravan, L. Gelmini, N. Glover, F.G. Herring, H. Li, J.H. McNeill, S.J. Rettig, I.A. Setyawati, E. Shuter, Y. Sun, A.S. Tracey, V.G. Yuen, C. Orvig, J. Am. Chem. Soc. 117 (1995) 12759.
[63] V.G. Yuen, P. Caravan, L. Gelmini, N. Glover, J.H. McNeill, I.A. Setyawati, Y. Zhou, C. Orvig, J. Inorg. Biochem. 68 (1997) 109.
[64] H. Sakurai, K. Tsuchiya, M. Nukatsuka, J. Kawada, S. Ishikawa, H. Yoshida, M. Komatsu, J. Clin. Biochem. Nutr. 8 (1990) 193.
[65] H. Watanabe, M. Nakai, K. Komazawa, H. Sakurai, J. Med. Chem. 37 (1994) 876.
[66] H. Sakurai, H. Watanabe, H. Tamura, H. Yasui, R. Matsushita, J. Takada, Inorg. Chim. Acta 283 (1998) 175.
[67] K. Kawabe, T. Suekuni, T. Inada, K. Yamato, M. Tadokoro, Y. Kojima, Y. Fujisawa, H. Sakurai, Chem. Lett. (1998) 1155.
[68] H. Sakurai, K. Fujii, H. Watanabe, H. Tamura, Biochem. Biophys. Res. Commun. 214 (1995) 1095.
[69] S. Fujimoto, K. Fujii, H. Yasui, R. Matsushita, J. Takada, H. Sakurai, J. Clin. Biochem. Nutr. 23 (1997) 113.
[70] K. Kawabe, M. Tadokoro, Y. Kojima, Y. Fujisawa, H. Sakurai, Chem. Lett. (1998) 9.
[71] T. Kiss, E. Kiss, G. Micera, D. Sanna, Inorg. Chim. Acta 283 (1998) 202.
[72] P. Buglyó, E. Kiss, I. Fábián, T. Kiss, D. Sanna, E. Garriba, G. Micera, Inorg. Chim. Acta 306 (2000) 174.
[73] E. Kiss, K. Petrohán, D. Sanna, G. Garribba, G. Micera, T. Kiss, Polyhedron 19 (2000) 55.
[74] S.R. Cooper, Y.B. Koh, K.N. Raymond, J. Am. Chem. Soc. 104 (1982) 5092.
[75] P. Buglyo, T. Kiss, J. Coord. Chem. 22 (1991) 259.
[76] P. Buglyo, A. Dessi, T. Kiss, G. Micera, D. Sanna, J. Chem. Soc., Dalton Trans. (1993) 2057.
[77] T. Kiss, P. Buglyo, D. Sanna, G. Micera, P. Decock, D. Dewaele, Inorg. Chim. Acta 239 (1993) 145.

PERGAMON

www.elsevier.nl/locate/poly

Polyhedron 19 (2000) 2403–2407

POLYHEDRON

Formation equilibria of tin(II) orthophosphate complexes

Liberato Ciavatta [a,*], Mauro Iuliano [b]

[a] *Dipartimento di Chimica dell'Università 'Federico II', Via Cinthia, 80126 Naples, Italy*
[b] *Dipartimento di Scienze Ambientali della II Università di Napoli, Via Vivaldi, 43-81100 Caserta, Italy*

Abstract

The complexation equilibria of Sn^{2+} ion with orthophosphate ions have been studied, at 25°C in 3 M $NaClO_4$ ionic medium, by potentiometric titrations with Sn^{2+}/Sn–Hg and glass electrodes. The concentrations of the metal and of the ligand ranged from 2.5×10^{-4} to 2.5×10^{-3} M and from 0.01 to 0.3 M, respectively. The hydrogen ion concentration varied between 0.1 and $10^{-5.8}$ M. The potentiometric data are consistent with the formation of the complexes: $SnH_2PO_4^+$, $Sn(H_2PO_4)_2$(aq), $SnH_2PO_4HPO_4^-$, $SnHPO_4$(aq), $Sn(HPO_4)_2^{2-}$, $Sn(HPO_4)_3^{4-}$ and $SnPO_4^-$. Stability constants for their formation in 3 M $NaClO_4$ and in dilute solution are reported. © 2000 Elsevier Science B.V. All rights reserved.

Keywords: Tin(II); Phosphato complexes; Solution equilibria; Speciation

1. Introduction

Cilley [1] has studied the reaction between Sn^{2+} and PO_4^{3-} ions at 25°C in 0.2 M $NaClO_4$ by measuring the solubility of the sparingly soluble $SnHPO_4 \cdot 0.5H_2O$ as a function of the orthophosphate concentration in the range 3×10^{-4}–0.09 M. The pH was kept constant at 2.48. Cilley explained the data by assuming the equilibria: $SnHPO_4(s) \rightleftarrows Sn^{2+} + HPO_4^{2-}$ (solubility product $= 1.5 \times 10^{-13}$), $Sn^{2+} + HPO_4^{2-} \rightleftarrows SnHPO_4(aq)$ and $Sn^{2+} + 3HPO_4^{2-} \rightleftarrows Sn(HPO_4)_3^{4-}$ with constants 6.7×10^7 and 1.1×10^{10}, respectively.

Measurements at a constant pH gives no information on the number of protons bound in the complex species. Furthermore, the solubility method does not allow any decision on whether the complexes are mono- or polynuclear in the central ion. It was, therefore, worth a reinvestigation of the system by potentiometric methods in an as wide as possible concentration range of the reagents.

In the present work the complex formation equilibria were investigated at 25°C in 3 M $NaClO_4$ ionic medium by potentiometric titrations based on Sn^{2+}/Sn–Hg as well as glass half-cells.

2. Experimental

2.1. Cells and equations

Titrations were carried out with cells (M) and (H)

$(-)$Sn(0.2%)–Hg/test solution/RE$(+)$ (M)

$(-)$RE/test solution/glass electrode$(+)$ (H)

where RE is the reference electrode: Ag/AgCl/0.01 M NaCl, 2.99 M $NaClO_4$/3 M $NaClO_4$. The test solutions had the general composition (molarities): $Sn(ClO_4)_2$ (C_M), $HClO_4$ (C_A), H_3PO_4 (C_0), NaH_2PO_4 (C_1), Na_2HPO_4 (C_2), $NaClO_4$ ($3\text{-}C_1\text{-}2C_2\text{-}C_A\text{-}2C_M$). Total phosphate concentration, $C_P = C_0 + C_1 + C_2$, was chosen to vary from 0.01 to 0.3 M. The hydrogen ion concentration ranged from 0.1 to $10^{-5.8}$ M. The C_M values were between 2.5×10^{-4} and 2.5×10^{-3} M. At $C_M < 2.5.10^{-4}$ M, the EMF of cell (M) reached constancy too slowly. The higher limit of C_M was imposed by the precipitation of solid Sn(II) phosphates.

The EMFs of cells (M) and (H) can be written at 25°C as Eqs. (1) and (2)

$$E_M = E_{0M} - 0.02958 \log([Sn^{2+}]y_M) - E_j \quad (1)$$

$$E_H = E_{0H} + 0.05916 \log([H^+]y_H) + E_j \quad (2)$$

in which E_{0M} and E_{0H} are constants in each run, y_M and y_H symbolize activity coefficients of Sn^{2+} and H^+ ions, respectively. E_j is the liquid junction potential

* Corresponding author.
E-mail address: ciavatta@chemistry.unina.it (L. Ciavatta).

0277-5387/00/$ - see front matter © 2000 Elsevier Science B.V. All rights reserved.
PII: S0277-5387(00)00538-6

arising at the boundary: test solution/3 M $NaClO_4$. The standard states are chosen so that activity coefficients tend to unity as the composition of test solution approaches 3 M $NaClO_4$.

In each experiment, the E_0 values were determined from measurements with solutions of $C_A < 0.01$ and $C_M < 0.0025$ M where phosphate was absent. Under these conditions activity coefficients are with good approximation equal to unity and the liquid junction potential can be evaluated, in accordance with Biedermann and Sillén [2], from $E_j = -0.017[H^+]$. The $[Sn^{2+}]$ and $[H^+]$ values, obtained from C_M and C_A after a small correction for the hydrolysis of the Sn^{2+} ion [3], were inserted in Eqs. (1) and (2) to yield E_{0M} and E_{0H} constant to within $\pm 5 \times 10^{-5}$ V or better.

In the presence of phosphate, medium changes, caused by the replacement of inert ions with reagent species (mainly as $H_2PO_4^-$ ion), affect to some extent E_j and activity coefficients. E_j can be considered a function of $[H^+]$ and $[H_2PO_4^-]$, whilst the activity coefficients are essentially a function of $[H_2PO_4^-]$ only. As described elsewhere [4,5],

$$E_j = -0.017[H^+] - 0.003[H_2PO_4^-] \quad (3)$$

and

$$0.05916 \log y_H = 0.018[H_2PO_4^-] \quad (4)$$

On the other hand, the dependence of y_M on $[H_2PO_4^-]$ cannot be estimated exactly. As shown later, the substitution of $[Sn^{2+}]$ with $[Sn^{2+}]y_M$ has no serious consequences on the deduction of the composition of the reaction products. However, it affects the value of some equilibrium constants.

Values of $[H^+]$ and $[Sn^{2+}]y_M$ were calculated from Eqs. (1)–(4) and mass balances of C_P and $C_H = C_A + C_0 - C_2$. According to previous results [6], in our solutions H^+ and PO_4^{3-} ions associate to form, in addition to H_3PO_4, $H_2PO_4^-$ and HPO_4^{2-}, also $H_6(PO_4)_2$, $H_5(PO_4)_2^-$, $H_4(PO_4)_2^{2-}$ and $H_3(PO_4)_2^{3-}$. Then, in presence of $SnH_{-n}(H_2PO_4)_m^{2-n-m}$ complexes of molarity $c_{n,m}$, one has

$$C_P = [H_3PO_4] + [H_2PO_4^-] + [HPO_4^{2-}] + 2([H_6(PO_4)_2] + [H_5(PO_4)_2^-] + [H_4(PO_4)_2^{2-}] + [H_3(PO_4)_2^{3-}]) + \sum m c_{n,m} \quad (5)$$

$$C_H = [H^+] + [H_3PO_4] - [HPO_4^{2-}] + 2[H_6(PO_4)_2] + [H_5(PO_4)_2^-] - [H_3(PO_4)_2^{3-}] - \sum n c_{n,m} \quad (6)$$

Sufficiently accurate $[H_2PO_4^-]$ values could be deduced from Eq. (7) neglecting the last term, since $C_P \gg C_M$, and using constants of the H^+-PO_4^{3-} system determined previously [6]

$$C_P + C_H = [H^+] + [H_2PO_4^-] + 2[H_3PO_4] + 4[H_6(PO_4)_2] + 3[H_5(PO_4)_2^-] + 2[H_4(PO_4)_2^{2-}] + [H_3(PO_4)_2^{3-}] + \sum (m-n) c_{n,m} \quad (7)$$

First, preliminary $[H^+]$ and $[Sn^{2+}]y_M$ concentrations were calculated setting $[H_2PO_4^-] = C_P$. Then, a better value of $[H_2PO_4^-]$ was found from Eq. (7) and the cycle repeated to convergence.

The potentiometric titrations were performed according to two procedures: (1) at variable C_P while $[H^+]$ was maintained essentially constant; and (2) at constant C_P and variable $[H^+]$.

2.2. Reagents and analysis

Tin(II) perchlorate solutions of exactly known composition were prepared in situ by constant-potential coulometry employing electrolysis cell (C)

$$(-)\text{AE/test solution/Hg(Sn 0.2\%)}(+) \quad \text{(C)}$$

where AE = Hg/Hg_2Cl_2/0.1 M NaCl, 2.9 M $NaClO_4$/3 M $NaClO_4$. The test solution formed the anodic compartment and the anode was polarized at -0.4 V against RE, the reference electrode of cell (M). At this potential, current intensities higher than 2×10^{-3} A were recorded and the metal was oxidized as tin(II). Since no significant quantities of metal ions are transferred from test solution to the salt bridge, the [Sn(II)] equals half the number of Faradays passed per cubic decimeter of solution.

Tin amalgam was prepared by bringing into contact bidistilled mercury and tin metal, shot 99.999%, supplied by Aldrich, under dilute $HClO_4$ in an inert atmosphere of argon gas.

Argon gas, from commercial cylinders, was freed from traces of oxygen by passing it through 0.1 M chromium(II) chloride and then washed with water and ionic medium.

Sodium perchlorate, sodium mono- and dihydrogen phosphates and other chemicals were prepared as described elsewhere [6].

2.3. Apparatus

EMF measurements were carried out at 25.00 ± 0.02°C, by immersing the cell assembly in a silicone oil thermostat. The cell arrangement was similar to that described by Forsling et al. [7]. Silver/silver chloride electrodes were prepared according to Brown [8]. The glass electrode, type 60102-100, supplied by Metrohm, acquired stable potentials within 15 min after the addition of reagents. They remained constant within 5×10^{-5} V for several hours. An Amel Instruments potentiostat–galvanostat, model 2051, was employed as

constant potential source of the coulometric circuit. The current intensity–time integral was obtained with a computer controlled data acquisition unit. The potentiometric titrations were carried out with a programmable computer controlled data acquisition unit 3421A, supplied by Hewlett–Packard. The EMF of cell (H) was measured using a Keithley 642 Type Digital Electrometer.

3. Data and calculations

The primary data (C_P, C_M, $[Sn^{2+}]y_M$, $[H^+]$) were analyzed by graphical and numerical procedures to determine the composition of the reaction products $SnH_{-n}(H_2PO_4)_m^{2-n-m}$ and equilibrium constants $*\beta_{n,m}$ for their formation according to Eq. (8)

$$Sn^{2+} + nH_2O + mH_2PO_4^- \rightleftarrows SnH_{-n}(H_2PO_4)_m^{2-n-m} + nH^+, *\beta_{n,m} \quad (18)$$

The calculations were based on the mass balance Eqs. (5) and (9)

$$*C_M = C_M - \sum p[Sn_p(OH)_q^{2p-q}] = [Sn^{2+}](1 + \sum *\beta_{n,m}[H_2PO_4^-]^m[H^+]^{-n}y_M y_L^m y_H^{-n} y_{n,m}^{-1}) \quad (9)$$

where hydrolytic species $Sn_p(OH)_q^{2p-q}$ were accounted for according to Tobias [3] and y_M, y_L, y_H and $y_{n,m}$ are activity coefficients of Sn^{2+}, $H_2PO_4^-$, H^+ and $SnH_{-n}(H_2PO_4)_m^{2-n-m}$, respectively. The activity coefficient of a species 'i' in the medium scale is a function of $[H_2PO_4^-]$ and can be expressed, according to the specific interaction theory [9,10], as Eq. (10)

$$\log y_i = \{b(i, H_2PO_4^-) - b(i, ClO_4^-)\}[H_2PO_4^-] \quad (10)$$

in which b stands for the specific interaction coefficient. As $\log y_i$ is expected to deviate from zero by no more than ± 0.1, we may write Eq. (11)

$$y_i \approx 1 + 2.303\{b(i, H_2PO_4^-) - b(i, ClO_4^-)\}[H_2PO_4^-] = 1 + \xi_i[H_2PO_4^-] \quad (11)$$

Introducing Eq. (11) into Eq. (9) yields Eq. (12)

$$F = \log\{*C_M/([Sn^{2+}]y_M)\} = \log(1 + \sum \Phi_{n,m}[H_2PO_4^-]^m[H^+]^{-n}) \quad (12)$$

where for brevity

$$\Phi_{01} = *\beta_{01} - \xi_M \quad (13)$$

whereas for all other (n, m) values is valid Eq. (14)

$$\Phi_{n,m} = *\beta_{n,m} + *\beta_{n,(m-1)}\{(m-1)\xi_L - n\xi_H - \xi_{n,(m-1)}\} \quad (14)$$

Subscripts M, L, H and n, m refer respectively to Sn^{2+}, $H_2PO_4^-$, H^+ and $SnH_{-n}(H_2PO_4)_m^{2-n-m}$.

3.1. Graphical treatment

The data are represented in Figs. 1 and 2. To construct Fig. 1, $[H_2PO_4^-]$ values were found from Eq. (7) as described above. Since points of different C_M fall on the same curve, mononuclear complexes in tin predominate. Furthermore, data of forward titrations coincide within experimental uncertainty with those of reverse titrations. Therefore, true equilibrium was attained.

Points of different acidity form different curves (Fig. 1). Thus, complexes with $n \geq 0$ are present.

At a given $[H^+]$, the shape of the curve is consistent with the formation of complexes with $m = 1$ and 2. To ascertain the most probable n values the experimental plot was compared with model curves calculated with various n and $\Phi_{n,m}$. An acceptable fit, shown in Fig. 1, was found assuming the presence of $SnH_2PO_4^+$, $Sn(H_2PO_4)_2(aq)$, $SnH_{-1}(H_2PO_4)_2^-$, $SnH_{-1}(H_2PO_4)(aq)$ and $SnH_{-2}(H_2PO_4)_2^{2-}$ with $\Phi_{n,m}$ values given in Table 1.

To explain the data represented in Fig. 2 we simply assumed the species and $\Phi_{n,m}$ values deduced above. This model fits the measurements of $\log[H^+] \geq -3$ satisfactorily, but as shown by the dashed curves in Fig.

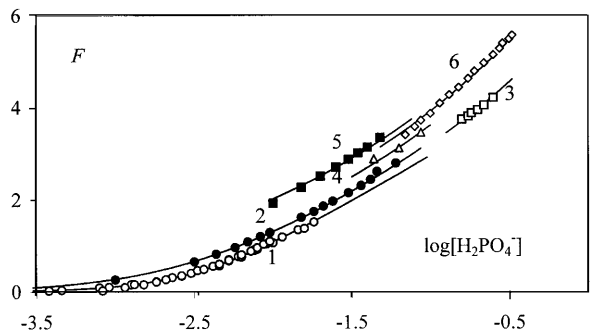


Fig. 1. F (Eq. (12)) as a function of $\log[H_2PO_4^-]$ for data of different acidity levels; $-\log[H^+](curve) = 1.0$ (1), 1.8 (2), 2.5 (3), 2.7 (4), 3.0 (6), 3.5 (5). The curves were calculated with the constants in Table 1.

Table 1
Survey of the calculated $\Phi_{n,m}$ and $*\beta_{n,m}$ values

(n, m)	$\log \Phi_{n,m}$ graphical	$\log \Phi_{n,m}$ least-squares (3σ)	$\log *\beta_{n,m}$
(0, 1)	$2.3_8 \pm 0.2$	2.17 ± 0.02	2.17 ± 0.03
(0, 2)	$4.9_5 \pm 0.2$	4.816 ± 0.006	4.816 ± 0.007
(1, 1)	1.31 ± 0.05	1.287 ± 0.006	1.287 ± 0.006
(1, 2)	$2.3_3 \pm 0.2$	2.148 ± 0.014	2.17 ± 0.04
(2, 2)	$-1.5_7 \pm 0.2$	-1.36 ± 0.01	-1.32 ± 0.03
(2, 1)	$-2.4_3 \pm 0.1$	-2.41 ± 0.01	-2.41 ± 0.01
(3, 3)	-6.1 ± 0.1	-6.10 ± 0.01	-6.10 ± 0.01

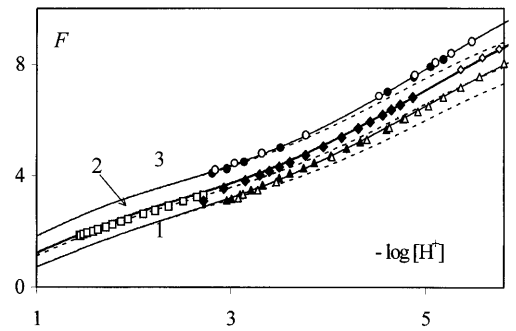


Fig. 2. F (Eq. (12)) as a function of $\log[H^+]$ at different phosphate concentrations: 0.05 (curve 1), 0.1 (curve 2) and 0.3 M (curve (3). Curves calculated with constants in Table 1. Dashed lines represent a model which neglects $SnH_{-2}(H_2PO_4)^-$ and $SnH_{-3}(H_2PO_4)_3^{4-}$ complexes.

Table 2
Equilibrium constants in the infinite dilution reference state

	log (equilibrium constant)
$Sn^{2+} + H_2PO_4^- \rightleftarrows SnH_2PO_4^+$	2.8 ± 0.2
$Sn^{2+} + 2H_2PO_4^- \rightleftarrows Sn(H_2PO_4)_2(aq)$	5.9 ± 0.2
$Sn^{2+} + HPO_4^{-2} \rightleftarrows SnHPO_4(aq)$	9.5 ± 0.2
$Sn^{2+} + H_2PO_4^- + HPO_4^{-2} \rightleftarrows SnHPO_4H_2PO_4^-$	10.3 ± 0.2
$Sn^{2+} + 2HPO_4^{-2} \rightleftarrows Sn(HPO_4)_2^{2-}$	13.4 ± 0.2
$Sn^{2+} + PO_4^{-3} \rightleftarrows SnPO_4^-$	18.0 ± 0.2
$Sn^{2+} + 3HPO_4^{-2} \rightleftarrows Sn(HPO_4)_3^{4-}$	12.9 ± 0.2

2, systematic deviations occur at lower acidities. A good explanation was obtained adding the complexes $SnH_{-2}(H_2PO_4)^-$ and $SnH_{-3}(H_2PO_4)_3^{4-}$. The most probable Φ_{21} and Φ_{33} values are given in Table 1.

3.2. Treatment by numerical methods

As a check of the results from the graphical approach the whole set of data was processed by the program SUPERQUAD [11]. The computer sought the minimum of the sum

$$U = \sum (Y - Y^{calc})^2 \quad (15)$$

where $Y = 0.02958 \log([Sn^{2+}]y_M)$ and Y^{calc} is a value calculated with a given set of parameters. The calculations were founded on the stoichiometric conditions (5), (6) and (12). It is important to observe that the last term in Eq. (5) was replaced by $\Sigma m\Phi_{n,m}[Sn^{2+}]y_M[H_2PO_4^-]^m[H^+]^{-n}$. This is not completely correct, however the difference between rigorous and approximate expressions is at most 0.2% therefore without appreciable effect on the final results. In the computations equilibrium constants of the phosphoric acid system and of the hydrolysis of the Sn^{2+} ion, taken from Ref. [3,6], were not allowed to vary. The best fit, $\sigma(Y) = 4 \times 10^{-4}$ V, was found by assuming the set of complexes evidenced graphically. The introduction of additional complexes, such as $Sn(H_2PO_4)_3^-$ or $Sn(PO_4)_2^{4-}$ or $Sn_2(OH)_2(H_2PO_4)_2(aq)$ or $Sn_3(OH)_4(H_2PO_4)_3^-$, did not produce lower agreement factors. The results, given in Table 1, are seen to match the graphical results satisfactorily.

4. Discussion

The Sn^{2+} and PO_4^{3-} ions form a series of ternary complexes $SnH_{-n}(H_2PO_4)_m^{2-n-m}$ with $(n, m) = (0, 1)$, $(0, 2)$, $(1, 1)$, $(2, 2)$, $(3, 3)$, $(1, 2)$ and $(2, 1)$. The complexes, except $SnH_{-1}(H_2PO_4)_2^-$, can formally be considered as binary of $H_2PO_4^-$ in $(0, 1)$ and $(0, 2)$, of HPO_4^{2-} for $n = m$ and of PO_4^{3-} in $(2, 1)$. The $(1, 2)$ species, on the other hand, is a mixed $H_2PO_4^- - HPO_4^{2-}$ complex. From equilibrium studies alone it is impossible to assess whether $SnHPO_4(aq)$ and $SnPO_4^-$ are effectively binary or ternary hydroxo complexes as $Sn(OH)H_2PO4(aq)$ and $Sn(OH)_2H_2PO_4^-$.

In agreement with (14) $^*\beta_{11} = \Phi_{11}$, $^*\beta_{21} = \Phi_{21}$, $^*\beta_{33} = \Phi_{33}$. To evaluate other $^*\beta_{n,m}$ from Eq. (14), we employed $\xi_L = 0$, since interaction coefficients of ions bearing the same charge sign are with good approximation equal to zero [9], $\xi_H = 0.70 \pm 0.05$, deduced by inserting Eq. (4) in Eq. (11), $\xi_M = -0.6 \pm 0.6$ and $\xi_{01} = \xi_{11} = \xi_{21} = -0.3 \pm 0.3$. The ξ parameter pertaining to the metal ion was estimated supposing that $b(Sn^{2+}, H_2PO_4^-)$ falls within -0.2 and 0.3 and setting $b(Sn^{2+}, ClO_4^-) = 0.30$, as calculated from the linear dependence of $b(i, ClO_4^-)$ with the reciprocal of the ionic radius of cations [9]. The ξ values of the complex species were estimated with the empirical rule suggested elsewhere [10]. The results of calculations of $^*\beta_{n,m}$ are given in Table 1. Only for $^*\beta_{22}$ and $^*\beta_{12}$ the effect of medium changes exceeds the experimental uncertainty.

The magnitude of the association constants in the infinite dilution reference state (Table 2) was found by assuming the validity of the specific interaction theory [9,10]. The equilibrium constants in Table 1 were transformed from molar to molal units using densities of $NaClO_4$ solutions compiled by Söhnel and Novotný [12]. Interaction coefficients were taken or estimated with rules given elsewhere [9,10]. The interaction coefficient of $Sn(HPO_4)_3^{4-}$ was set equal to $(3/2)b(Na^+, HPO_4^{2-})$. The extrapolated $^*\beta_{n,m}$ values were finally combined with the infinite dilution protolysis constants [13] $10^{-7.198}$, for $H_2PO_4^- \rightleftarrows HPO_4^{2-} + H^+$, and $10^{-12.35}$, for $HPO_4^{2-} \rightleftarrows PO_4^{3-} + H^+$, to yield the results in Table 2.

The stabilities of $SnHPO_4(aq)$ and of $SnPO_4^-$ are noticeable. This can be due to the particular structures of the complexes in which the phosphate group acts as a bidentate or a tridentate ligand. It also seems plausible that the complexes are mixed hydroxo species such as $Sn(OH)H_2PO_4(aq)$ and $Sn(OH)_2H_2PO_4^-$.

Acknowledgements

This work was financially supported by MURST, Rome.

References

[1] W.A. Cilley, Inorg. Chem. 7 (1968) 612.
[2] G. Biedermann, L.G. Sillén, Arkiv Kemi. 5 (1953) 425.
[3] R.S. Tobias, Acta Chem. Scand. 12 (1958) 198.
[4] L. Ciavatta, M. Iuliano, R. Porto, Ann. Chim. (Rome) 83 (1993) 19.
[5] L. Ciavatta, M. Iuliano, R. Porto, Ann. Chim. (Rome) 86 (1996) 411.
[6] L. Ciavatta, M. Iuliano, R. Porto, E. Vasca, Polyhedron 10 (1991) 2587.
[7] W. Forsling, S. Hietanen, L.G. Sillén, Acta Chem. Scand. 6 (1952) 901.
[8] A.S. Brown, J. Am. Chem. Soc. 56 (1934) 646.
[9] L. Ciavatta, Ann. Chim. (Rome) 70 (1980) 551.
[10] L. Ciavatta, Ann. Chim. (Rome) 80 (1990) 255.
[11] P. Gans, A. Sabatini, A. Vacca, J. Chem. Soc. (1985) 1195.
[12] O. Söhnel, P. Novotný, Densities of Aqueous Solutions of Inorganic Substances, Elsevier, Amsterdam, 1985.
[13] J.P. Hershey, M. Fernandez, F.J. Millero, J. Sol. Chem. 18 (1989) 875.

PERGAMON

www.elsevier.nl/locate/poly

Polyhedron 19 (2000) 2409–2419

POLYHEDRON

Copper complexes of dipeptides with L-Lys as C-terminal residue: a thermodynamic and spectroscopic study

Maurizio Remelli [a,*], Chiara Conato [a], Alessandra Agarossi [a], Fernando Pulidori [a], Piotr Młynarz [b], Henryk Kozłowski [b]

[a] *Department of Chemistry, University of Ferrara, via L. Borsari 46, I-44100 Ferrara, Italy*
[b] *Faculty of Chemistry, University of Wrocław, F. Joliot-Curie 14, 50-383 Wrocław, Poland*

Abstract

Complex-formation equilibria of some dipeptides (glycyl-lysine, alanyl-lysine, histidyl-lysine and β-alanyl-lysine) with the Cu(II) ion have been studied in aqueous solution, at $I = 0.1$ mol dm^{-3} (KNO_3) and $T = 25$°C. Protonation and complex-formation constants have been determined potentiometrically; complex-formation model and species stoichiometry have been checked carefully by means of different spectroscopic techniques (visible absorption, CD, EPR). The structure of the main complex species is discussed, on the basis of thermodynamic data obtained by direct calorimetry. The formation of binuclear species is demonstrated and it is suggested that the side amino group of lysine participates in complex formation at alkaline pH values.
© 2000 Elsevier Science B.V. All rights reserved.

Keywords: Copper-dipeptide complexes; Glycyl-lysine; Alanyl-lysine; Histidyl-lysine; β-alanyl-lysine

1. Introduction

The side ε-NH_2 group of the lysine (Lys) residue in peptides and proteins is one of the potential donor sites for metal (especially copper) ion complexation. However, its coordination to the metal centre generally involves the formation of unusually large chelate rings. This fact, together with its high pK value, makes ε-NH_2–Cu(II) bond formation unfavourable at neutral or acidic pH [1]. The same is true for Lys itself [2]. On the other hand, in the alkaline pH range, metal ions become more competitive with respect to protons: ε-NH_2 coordination in binuclear complexes of Cu(II) and oligopeptides has been reported, both in solution [3–5] and in the solid state [6].

A case of special interest is represented by the human liver-cell growth-factor glycyl-histidyl-lysine (GHK), found in human plasma at a concentration of about 200 ng ml^{-1} [7]. GHK was found in the albumin and α-globulin fractions and it co-isolated with an approximately equimolar amount of copper and about one-fifth molar amount of iron [8]. GHK proved to stimulate the growth and differentiation of a number of cell lines [9] and, in general, to be a good serum substitute in cellular culture media. In further studies it was recognised that GHK is endowed with a wide range of biological activities, mainly in the acceleration of wound healing and bone repair [10]. GHK was found to act synergistically with copper and iron ions, and it has been suggested that it plays a role in cellular copper ion uptake [11]. A GHK structure–activity study revealed that the His-Lys sequence and Lys side chain are essential for its biological activity, and an action mechanism has been suggested in which the first two residues of the tripeptide bind a copper ion to form a 1:1 complex while the side chain of Lys is involved in the recognition with a hypothetical receptor on the cell surface [11].

In view of its importance, not only in metal ion complexation but also in metal–peptide biological activity, the behaviour of ε-amino-N of the Lys residue in Cu(II) complex formation has been investigated in depth by means of a number of experimental techniques. Four dipeptides were employed as ligands, i.e. glycyl-lysine (Gly-Lys, GK), alanyl-lysine (Ala-Lys, AK), histidyl-lysine (His-Lys, HK) and β-alanyl-lysine (β-Ala-Lys, β-AK).

* Corresponding author.
E-mail address: rmm@unife.it (M. Remelli).

0277-5387/00/$ - see front matter © 2000 Elsevier Science B.V. All rights reserved.
PII: S0277-5387(00)00539-8

2. Experimental

2.1. Materials

Dipeptides were high purity products (Sigma) and were used without further purification. Cu(II) nitrate was an extra pure Merck product. The concentration of a stock solution of this salt was determined by ethylenediaminetetraacetate titration. The carbonate-free stock solutions of KOH were prepared by diluting a saturated KOH (Aldrich, semiconductor grade) solution and then standardised potentiometrically by titrating with potassium hydrogen phthalate. The HNO_3 stock solution was prepared by diluting concentrated HNO_3 (Merck, Suprapur) and then standardised with KOH. All sample solutions were prepared with freshly tetradistilled CO_2-free water. The ionic strength was adjusted to 0.1 mol dm^{-3} by adding KNO_3 (Merck, Suprapur). Grade A glassware was employed throughout.

2.2. Potentiometric measurements

Potentiometric titrations were performed with the following equipment: an Orion EA 940 pH meter (resolution 0.1 mV, accuracy 0.2 mV) equipped with a combined glass electrode (Metrohm EA125); a Hamilton MicroLab M motor burette (resolution 0.1 μl, accuracy 0.2 μl) equipped with a Hamilton syringe (delivery volume 0.5 cm^3). The potentiometer and burette were interfaced with an IBM PS/2 model 30 computer with which the titrations were performed automatically by means of a suitable program written in IBM-BASIC. Constant-speed magnetic stirring was applied throughout. The temperature of the titration cell was kept at 25 ± 0.02°C by means of a Haake F3C circulation thermostat. UPP grade nitrogen, previously saturated with H_2O (0.1 mol dm^{-3} KNO_3, 25°C) was blown onto the test solution in order to maintain an inert atmosphere. The electrode couple was standardised on the $pH = -\log c_{H+}$ scale by titrating HNO_3 (0.01 mol dm^{-3}) with standard KOH at 25°C and $I = 0.1$ mol dm^{-3} (KNO_3), before each titration. Aliquots (2 cm^3) of sample solution, containing suitable amounts of Cu(II), HNO_3 and the ligands, were titrated with standard KOH in the 3–11 pH range; precipitate or opalescence were never observed. Copper concentration ranged from 2 to 5 mmol dm^{-3}, and metal-to-ligand ratios were 1:1, 1:2, 1:3. A minimum of four pairs of titrations for each copper–ligand system were performed.

2.3. Spectroscopic measurements

The absorption spectra were recorded with a Uvicon 931 (Kontron) spectrophotometer, with a glass cell (W110/S4, 1 cm path length); the temperature was controlled at 25.0 ± 0.1°C by means of a Kontron GTD-900 circulation thermostat.

EPR spectra were recorded on a Bruker ESP 300E spectrometer at X-band frequency (9.3 GHz) at 120 K. Circular dichroism (CD) spectra were recorded on a Jasco J 720 spectropolarimeter in the 800–200 nm range. Metal concentration in EPR, CD and visible measurements was adjusted from 2 to 3 mmol dm^{-3} and metal to ligand ratios were 1:1 and 1:2.

2.4. Calorimetric measurements

The $\Delta H°$ values were determined by titration calorimetry with a Tronac model 450 isoperibol calorimeter equipped with a 4 cm^3 reaction vessel. The calorimetric measurements were carried out titrating in double aliquots of 3 ml of solutions containing the metal and the ligand in the various ratios with a standard solution of HNO_3. The ionic strength was kept constant at $I = 0.1$ mol dm^{-3} by adding KNO_3. The ligand concentrations ranged from 5 to 9 mmol dm^{-3}. For each system at least 250 experimental points were utilised to calculate the thermodynamic quantities. The reaction heats, which were corrected for non-chemical contributions, which are particularly important when using small volume dewars [12], and for the dilution heats computed from literature data [13], were calculated by considering the calorie as equivalent to 4.184 J.

2.5. Calculations

Calculations concerning the $E°$ of the electrode system were performed by the least-square computer programs ESAB [14], which refines acid–base titration parameters, and BEATRIX [15] based on the Gran method. The Cu(II) complex formation constants were calculated by means of the least-square computer program SUPERQUAD [16]. To obtain the species distribution within the pH ranges explored, the computer programs DISDI [17] or HYSS [18] were used. Computer simulations of potentiometric titrations, useful in setting up the experimental conditions and comparing results with predictions, were obtained using the program SCALPO [19].

Protonation and complex-formation enthalpy and entropy were computed from experimental calorimetric titration by means of the computer program DOEC [20].

A pK_w value of 13.74 and a $\Delta H°_w = 13.35$ kcal mol^{-1}, determined by separate experiments, were employed in the calculations; the Cu(II) hydrolytic constants and corresponding formation enthalpies have been taken from Arena et al. [21].

Throughout, the accuracy of thermodynamic parameter values has been estimated as approximately

three times the precision value given by SUPERQUAD or DOEC, in the cumulative calculations, and it is expressed as deviation over the last significant figure.

3. Results and discussion

3.1. Ligand protonation

Thermodynamic parameters of ligand protonation are reported in Table 1.

The most basic group is the ε-amino group of the Lys residue: its protonation constant and related enthalpy value are practically identical for all the ligands considered and they are very close to those of free Lys and of a number of alkyl amines [22]. Most likely this group is too far from the rest of the molecule to be affected by the structural changes in the ligand. This result is in agreement with previous literature data referring to other oligopeptides having Lys as C-terminal residue [23]. Entropy change values are rather low: the protonation process does not involve any charge separation and reorganisation of the hydration spheres is minimal. The latter consideration appears to hold true for all protonation processes involving nitrogen atoms.

The terminal amino group is less basic than the ε-amino group of the Lys residue, due to the proximity of the electron-withdrawing carbonyl group of the peptide bond. In the case of β-AK the two groups are separated by an additional carbon atom and the terminal amino group pK value is 1.5 units higher than the other ligands. All these pK values are 1–1.5 units lower than those of the corresponding free amino acids [22] where the peptidic group is replaced by a carboxylate; only in the case of β-AK is the difference rather small (0.3 units) for the same reasons as indicated above.

Imidazole pK value of the His residue in HK is practically identical to that of free His (6.1 [22]), since it is not affected by the peptide linkage.

The pK value of the terminal Lys residue carboxylic group is much higher than that of free Lys (2.1 [22]), except in the case of HK, where the difference is smaller. In dipeptides, an amido group replaces the Lys α-amino group and its electron-withdrawing effect is reduced. When the first amino acid is His, the effect of the aromatic group is added to that of the peptide group. It is worth noting that, in the case of carboxylic group deprotonation, the process is almost entirely entropic: in fact, it consists of a charge separation and of a resulting large-scale reorganisation of the solvent around the reacting partners.

3.2. Cu(II)–Gly-Lys and Ala-Lys complexes

Thermodynamic parameters of Cu(II) complexes with the considered ligands are reported in Table 2. The corresponding distribution diagrams are shown in Fig. 1.

The results obtained for the Cu(II)–GK system are in good agreement with what was previously reported by Rainer and Rode [23], at 37°C, although they found some minor species (120 and $12-1$) in the alkaline pH range, instead of the binuclear complexes. It is also possible to compare the thermodynamic data reported in Table 2 with other literature data referring to dipeptides having Gly or Ala as C-terminal residue, in the place of Lys. However, to make such a comparison, it is necessary to 'clean' the data in Table 2, clearing away the contribution due to protonation of the side amino group of Lys. The results are also reported in Table 2 along with some reference data.

The species formed in the Cu(II)–GK system at the most acidic pH value is the 111 complex, which reaches only moderate concentrations before deprotonating. This is the analogue of the 110 species of the Cu(II)–GG system where one ligand is bound to the metal ion by means of its terminal amino group and the adjacent carbonyl oxygen [24] (NO species), as happens for most

Table 1
Thermodynamic parameters of dipeptide protonation, at 25°C and $I = 0.1$ mol·dm^{-3} (KNO_3)

Ligand	Donor group	log K_{step}	$-\Delta H^{\circ}_{step}$ (kcal mol^{-1})	ΔS°_{step} (cal mol^{-1} K^{-1})
GK	NH_2 (Lys)	10.50(1)	12.9(3)	5(1)
	NH_2 (terminal)	8.01(1)	10.2(3)	2(1)
	COO^-	2.96(1)	−0.7(6)	16(2)
AK	NH_2 (Lys)	10.51(1)	13.3(3)	3(1)
	NH_2 (terminal)	7.93(1)	10.9(3)	0(1)
	COO^-	3.04(1)	−0.2(5)	15(1)
HK	NH_2 (Lys)	10.49(1)	12.5(3)	6(1)
	NH_2 (terminal)	7.41(1)	9.6(3)	2(1)
	N (Im)	5.91(1)	7.9(3)	0(1)
	COO^-	2.50(1)	−0.5(3)	14(1)
β-AK	NH_2 (Lys)	10.52(1)	13.9(3)	2(1)
	NH_2 (terminal)	9.29(1)	11.4(3)	4(1)
	COO^-	3.02(1)	−0.3(6)	15(1)

Table 2
Thermodynamic parameters of binary complex formation with Cu(II), at 25°C and $I = 0.1$ mol·dm^{-3} (KNO_3).

	Species	log β	log K_{step} (kcal mol^{-1})	log β − log K_{011}	$-\Delta H°$ (kcal mol^{-1})	$-(\Delta H° - \Delta H°_{011})$ (kcal mol^{-1})	$\Delta S°$ (cal mol^{-1} K^{-1})	$-(\Delta S° - \Delta S°_{011})$ (cal mol^{-1} K^{-1})
GK	**111**	15.72 (3)		5.22	20 (1)	7.1	4 (3)	−1
	110	11.88 (1)	3.86	1.38	11.8 (2)	−1.1	15 (1)	10
	11-1	2.9 (1)	9.0	−7.6	5 (8)	−5.5	−4 (20)	−9
	11-2	−7.30 (3)	10.2		n.d.		n.d.	
	121	25.97 (2)		4.97 [a]	30.9 (3)	5.1 [b]	15 (1)	5 [c]
	22-1	17.9 (1)		−3.1 [a]	n.d.		n.d.	
	22-2	9.34 (8)	8.6	−1.16	14 (3)	1.1	−4 (10)	−9
AK	**110**	12.13 (1)		1.62	13.0 (2)	−0.3	12 (1)	9
	11-2	−6.83 (6)			−6 (3)		−11 (13)	
	121	25.69 (4)		4.67 [a]	33.5 (6)	6.9 [b]	5 (2)	−1 [c]
	12-1	5.6 (1)			n.d.		n.d.	
	22-1	18.7 (1)		−2.3 [a]	20 (2)	−7 [b]	20 (7)	14 [c]
	22-2	9.94 (9)	8.8	−0.57	14 (1)	0.7	−2 (3)	−5
HK	**112**	22.13 (5)		5.73 [d]	n.d.		n.d.	
	111	19.03 (2)	3.10	8.54	26 (1)	13	1(3)	−5
	11-1	3.96 (6)			8 (2)		−8 (6)	
	11-2	−6.93 (9)	10.89		4 (6)		−44 (18)	
	123	40.56 (4)		19.58 [a]	50 (1)	24 [b]	18 (3)	6 [c]
	122	36.00 (4)	3.44	15.02 [a]	49 (1)	23 [b]	−1 (3)	−13 [c]
	121	26.93 (6)	9.07	5.95 [a]	41 (2)	15 [b]	−14 (7)	−26 [c]
	220	28.88 (9)		7.88 [a]	43 (3)	18 [b]	−12 (9)	−24 [c]
	22-1	19.6 (1)	9.3	−1.4 [a]	39 (9)	14 [b]	−43 (31)	−55 [c]
β-AK	**110**	11.40(2)		0.88	12.2 (3)	−1.7	11.2 (9)	9.2
	11-2	−8.40 (6)			n.d.		n.d.	
	121	24.86 (9)		3.82 [a]	30.6 (6)	2.8 [b]	11 (2)	7 [c]
	120	15.1 (1)	9.8	4.58	n.d.		n.d.	
	22-1	15.6 (3)		−5.44 [a]	20 (1)	−7.8 [b]	5 (3)	1 [c]
	22-2	6.92 (9)	8.68	−3.6	n.d.		n.d.	
GG [e]	**110**	5.56			6.9		2	
	11-1	1.33	4.23		−0.7		8.4	
	11-2	−8.04	9.37		−11		0.2	
	12-1	4.46			6.7		−2.4	
	22-3	−4.51			−9.1		9.8	

[a] log $\beta - 2$ log K_{011}.
[b] $\Delta H - 2\Delta H_{011}$.
[c] $\Delta S - 2\Delta S_{011}$.
[d] log β − log K_{011} − log K_{013}.
[e] Ref. [24]; n.d. = not determined.

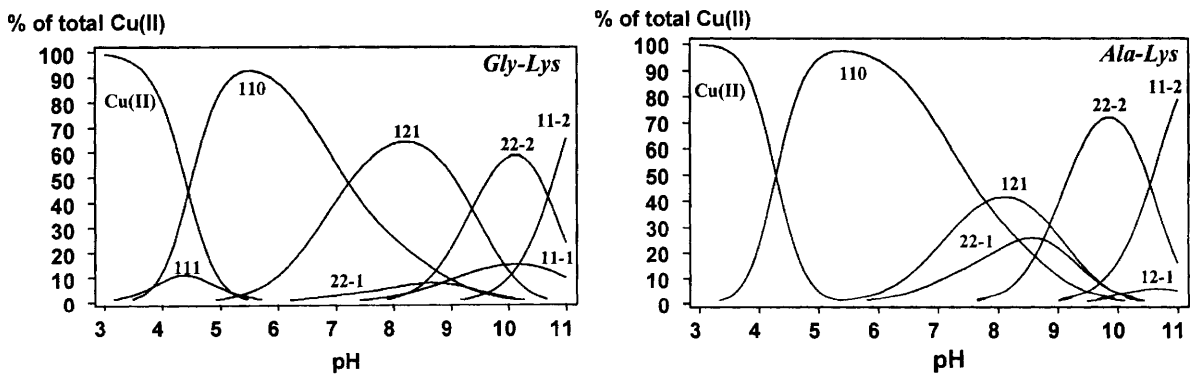


Fig. 1. Distribution diagrams of Cu(II)–dipeptide complexes at 25 °C and $I = 0.1$ mol dm^{-3} (KNO_3). [Cu(II)] = 4 mmol dm^{-3}; [Ligand] = 8 mmol dm^{-3}.

oligopeptides [1]. The thermodynamic parameters reported in Table 2 (corrected for protonation) are in excellent agreement with those of the 110 complex of GG; in particular, the value of $\Delta H^{\circ}_{111} - \Delta H^{\circ}_{011}$ (7.1 kcal mol^{-1}) corresponds to the formation of a coordination bond between a neutral nitrogen and the Cu(II) ion [25]. Moreover, the wavelength of maximum absorption in the visible range (see Tables 3 and 4) is shifted to a value of about 745 nm at the pH of maximum formation of the 111 complex, as expected from the empirical calculation of Sigel and Martin [26] for the coordination of an amino and a carbonyl group to the Cu(II) ion.

It was not possible to determine the thermodynamic parameters of the 111 complex for the Cu(II)–AK system, most likely due to its low amount. However, spectral parameters in the pH range of interest are very similar to those of the Cu(II)–GK system, suggesting the presence of the same complex species.

Starting at pH 4.5 and working down to neutral pH, the 110 complex becomes the predominant species, involving practically all the Cu(II) ions present in solution. Following the literature [1,26] and comparing the thermodynamic data with those of the system Cu(II)–GG (Table 2), it can be suggested that in the 110 complex GK (or AK) is bound to the metal ion with its terminal amino and deprotonated peptido nitrogen atoms, thus forming a five-membered chelate ring; the terminal carboxylic group is most likely coordinated, in the equatorial plane of the complex, as well. The deprotonation pK value of the 111 complex, 3.86, confirms that the Cu(II) ion is able to promote amido group deprotonation at a pH value lower than 4 [26]. CD spectra show, in both these cases, the typical CT band, at about 313 nm, due to the coordination of a deprotonated amido nitrogen to the Cu(II) ion [27]. 'Cleaned' logβ, ΔH° and ΔS° values are similar to those found for the $11-1$ complex in the Cu(II)–GG system; these values take into account both the endothermic amido nitrogen deprotonation and its exothermic coordination to the metal ion. The slightly higher values of thermodynamic parameters found for the 110 complex in the Cu(II)–AK system could be ascribed to a possible minor contribution of the, undetected, 111 complex.

As the pH is raised, the 110 complex loses first one and then two protons, giving rise to the $11-1$ and

Table 3
Spectral data for Cu(II)/Gly-Lys system, at a metal-to-ligand ratio of 1:2

		UV-Vis		CD		EPR	
pH	Main species	λ (nm)	ε	λ (nm)	$\Delta\varepsilon$	$A_{\parallel}$	$g_{\parallel}$
3.0						120	2.414
4.0	**111**	744	13	660	−0.20	121	2.412
				313	0.11		
				269	−0.18		
4.4	**110**	641	36	658	−0.40	147	2.331
				314	0.23		
				269	−0.33		
5.4	**110**	634	91	657	−0.64	172	2.250
				313	0.38		
				269	−1.20		
6.6	**110, 121**	629	89	653	−0.64		
				313	0.39		
				268	−1.78		
7.4	**110, 121**	625	92	653	−0.63	178	2.243
				313	0.40		
				268	−1.87		
8.2–8.4	**121**	620	91	649	−0.63		
				312	0.40		
				268	−1.89		
9.0	**121, 22-2**	615	97	646	−0.62	153	2.233
				311	0.42		
				266	−1.91		
10.0	**22-2**	611	96	644	−0.61	162	2.229
				513sh	−0.15		
				311	0.44		
				265	−1.93		
11.0	**11-2**	622	91	648	−0.60	164	2.229
				507sh	−0.16		
				309	0.43		
				260	−2.04		

Table 4
Spectral data for Cu(II)/Ala-Lys system, at a metal-to-ligand ratio of 1:2

pH	Main species	UV-Vis		CD		EPR	
		λ (nm)	ε	λ (nm)	$\Delta\varepsilon$	$A_{\parallel}$	$g_{\parallel}$
3.1						118	2.416
4.0	**110**	642	25	646	−0.41	177	2.248
				313	0.27		
				266	−0.96		
5.1-6.0	**110**	629	96	645	−0.72	178	2.246
				313	0.48		
				267	−1.54		
7.1	**110, 121**	627	101	654	−0.68		
				312	0.48		
				267	−1.63		
7.4	**110, 121**	623	101	641	−0.68		
				312	0.48		
8.2	**121, 22-1**	622	101	639	−0.64	161	2.227
				312	0.48		
				271	−1.62		
9.1	**121, 22-1, 22-2**	619	100	634	−0.63		
				311	0.50		
				266	−1.78		
9.4	**22-2**	613	99			164	2.226
10.0	**22, 2**	610	99	635	−0.65	161	2.229
				309	0.54		
				260	−2.04		
10.5	**22-2, 11-2**	611	96			156	2.247
11.1	**11-2**	618	94			151	2.241

$11-2$ species. The ligand coordination in the complex's equatorial plane remains unchanged, the two protons being lost from a water molecule bound to copper and by the ε-NH_2 group of the Lys residue. The $11-2$ complex can be directly compared with the same $11-2$ species in the Cu(II)–GG system: both $\log\beta_{11-2}$ and ΔH°_{11-2} are higher in the case of GK and AK, suggesting the involvement of ε nitrogen in complex formation. In particular, the difference between the corresponding ΔH°_{11-2} values for AK and GG (5 kcal mol^{-1}) is close to the Cu–N bond formation enthalpy. Moreover, the CD spectra agree with this suggestion: at pH 10 a new band appears at 510 nm and it grows when the pH is raised, while the $11-2$ complex becomes the most abundant species. The corresponding EPR spectra show a significant decrease in the $g_{\parallel}$ value. The ε-amino-nitrogen coordination should be axial, since, in the pH range of interest, the visible spectra show a decrease in the transition energy and also the $A_{\parallel}$ value of EPR spectra is shifted to lower values.

In both the Cu(II)–GK and Cu(II)–AK systems binuclear species are formed, in the alkaline pH range, even at ligand-to-metal ratios equal to or higher than two. In particular, in both systems, the $22-2$ complex reaches high concentration levels (see Fig. 1). Binuclear complex formation was previously reported by Gergely and Nagypál [24] and by Brookes and Pettit [28] for the Cu(II)–GG system (see Table 2) while it was not found by Rainer and Rode [23] in the Cu(II)–GK system. The presence of binuclear species is supported by the low intensity of EPR spectra recorded at $pH > 10$, even if the signal does not completely disappear. Brookes and Pettit suggested, for the $22-3$ complex, an equatorial coupling of two $2N/COO^{-}$ mono-complexes, via one OH^{-} bridge; this hypothesis has been accepted by Gergely and Nagypál, on the basis of the entropy and enthalpy data. A similar structure can be suggested here for both the $22-1$ and $22-2$ complexes: both the ε-nitrogens should be protonated in the former while only one is protonated in the latter species. It is worth noting that the $\log K$ value of this deprotonation step ($=\log\beta_{22-1}-\log\beta_{22-2}=8.6$–$8.8$) is noticeably lower than the corresponding pK_{011}, suggesting that this deprotonation is assisted and promoted by copper ions. It is also worth observing that, once the protonation contribution of one ε-NH_2 group has been 'cleaned' away, both $\log\beta_{22-2}$ and ΔH°_{22-2} are significantly higher than the corresponding values for the Cu(II)–GG $22-3$ complex. Moreover, at pH 10, the CD band at 510 nm is already clearly visible in the Cu(II)–GK system, while the $11-2$ complex (see above) is only a minor species. All these results tip the scales in favour of the involvement of one deprotonated ε-NH_2 group in the $22-2$ complex formation.

Finally, in the presence of an excess of ligand, some bis-complexes also form in solution, the most important

of which is the 121 species. This complex becomes the main species at a pH value of about 8 and, assuming that both the ε-NH_2 groups are protonated, it is the analogue of the $12-1$ complex found in the Cu(II)–GG system. This hypothesis is confirmed by the 'cleaned' thermodynamic parameters of 121 complexes, reported in Table 2: they are very close to the corresponding reported values for the Cu(II)–GG system, especially in the case of AK. Both $\log\beta_{121}$ and ΔH°_{121} values are close to the sum of the values found for the corresponding 111 and 110 complexes, thus suggesting that one ligand should be coordinated in the $2N/COO^-$ way, while the other should be bidentate and coordinate to copper in the NO fashion. Obviously, is it not possible for both ligands to be bound to the metal in the equatorial plane of the complex: as a consequence, the bidentate ligand should be coordinated in an equatorial–axial manner, as first suggested by Kaneda and Martell [29]. This hypothesis is supported here by the spectroscopic results, which show only minor changes when the pH is raised from 6 (where the 110 complex dominates) to 8 (where the 121 complex is the most abundant species). Similar results were also reported by Shtyrlin et al. [30] in their spectrophotometric investigation of the Cu(II)–GG system.

3.3. Cu(II)–His-Lys complexes

The presence of four nitrogens which can act as donor atoms makes possible the formation of a rather large number of complexes of different stoichiometries, between HK and the Cu(II) ion, as already found with many His derivatives [31]. HK starts to bind copper at a pH value as low as 3 (see Fig. 2). It is interesting to note how different the distribution diagrams of the Cu(II)–HK look when the ligand-to-metal ratio is close to unity (Fig. 2a) or higher (Fig. 2b). The most relevant difference concerns the pH range around neutrality, where, in the first case, the binuclear 220 complex contains all the copper present in solution; conversely, in the second case, the 122 bis-complex largely dominates. This macroscopic and uncommon difference is reflected by spectroscopic results (see Tables 5 and 6).

The coordination of HK to copper starts in the usual NO manner, with the 112 complex, but the presence of the imidazole nitrogen allows the coordination mode to change, with the formation of the 2N (α-amino and π-imidazole) 111 complex, from pH approximately equal to 4. This is always the main species in the acidic pH range. Its $\log\beta_{111}$ value, 'cleaned' of the ε-NH_2 protonation of the Lys residue, is considerably higher than $\log\beta_{110}$ for the Cu(II)–GG system, as would be expected; the corresponding 'cleaned' ΔH°_{111} value (13 kcal mol^{-1}) reflects the coordination of two nitrogen atoms in the equatorial plane of the complex, as in the case of the Cu(II)–histamine binary 110 complex [25]. CD spectra for the 1:2 Cu(II)–HK ratio (Table 6) show an intense absorption band at about 330 nm; this can be attributed to a ligand-to-metal CT transition due to the $N_{imidazole}$–Cu bond. Visible spectra show an absorption maximum at about 650 nm which is slightly lower than expected [26] for a NH_2–$N_{imidazole}$ coordination and is instead compatible with the further interaction, in the equatorial plane, of the terminal carboxylic group, although this implies the formation of a nine-membered ring.

When the pH is raised over neutrality, if Cu(II) and HK are nearly equimolar, over 90% of the metal forms the binuclear 220 species. EPR spectra recorded in this pH range do not show any detectable signal. Corresponding CD spectra show some interesting features: at about 340 nm the CT band is overcome by a new band at about 320 nm, with the opposite sign of its $\Delta\varepsilon$ value, attributed to the formation of N_{amido}–Cu bond(s). Moreover, a distinct shoulder appears at about 502 nm, most likely due to the coordination of three nitrogen atoms to the same Cu(II) ion. The whole of these data can be rationalised suggesting that, as a first step, when the pH is increased, HK changes its coordination mode from bidentate $N_{amino}/N_{imidazole}$ to tridentate $N_{amino}/$

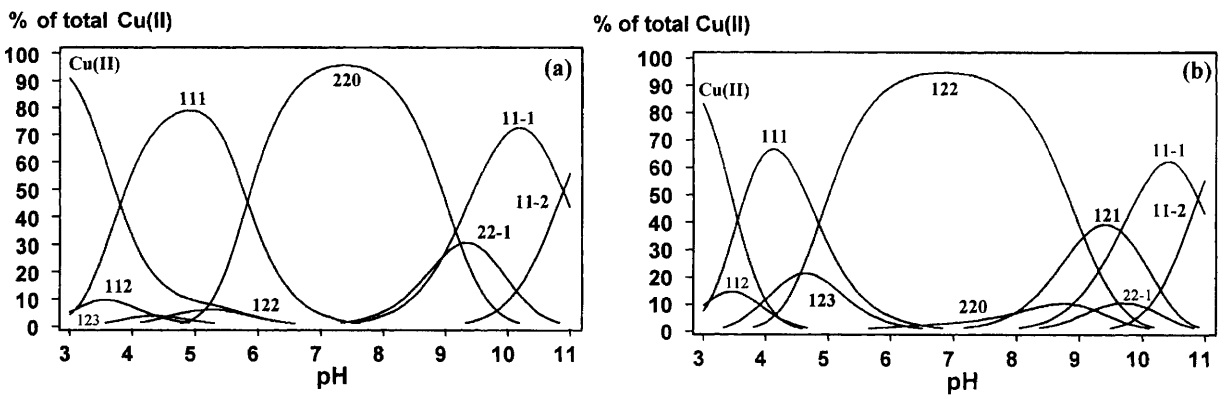


Fig. 2. Distribution diagrams of Cu(II)–HK complexes at 25 °C and $I = 0.1$ mol dm^{-3} (KNO_3). (a) [Cu(II)] = 4 mmol dm^{-3}; [HK] = 4 mmol dm^{-3}; (b) [Cu(II)] = 4 mmol dm^{-3}; [HK] = 8 mmol dm^{-3}.

Table 5
Spectral data for Cu(II)/His-Lys system, at a metal-to-ligand ratio of 1:1

pH	Main species	UV-Vis		CD		EPR	
		λ (nm)	ε	λ (nm)	$\Delta\varepsilon$	$A_{\parallel}$	$g_{\parallel}$
2.9		786	15			124	2.306
3.6	**112,111**	695	23			157	2.182
5.0	**111**	649	66	752	0.12	160	2.173
6.0	**111,220**	622	87	757	0.07		
				624	−0.11		
				360	−0.03		
				319	0.08		
7.0–8.0	**220**	617	102	629	−0.27		
				502sh	−0.04		
				320	0.37		
9.0	**220, 22-1, 11-1**	606	110	630	−0.33	158	2.201
				501sh	−0.09		
				319	0.40		
10.1	**11-1**	607	109	640	−0.41	180	2.220
				504	−0.12		
				318	0.55		
				250	−2.98		
11.0	**11-1, 11-2**	610	105	649	−0.43	172	2.243
				503	−0.15		
				317	0.56		
				252	−3.08		

Table 6
Spectral data for Cu(II)/His-Lys system, at a metal to ligand ratio of 1:2

pH	Main species	UV-Vis		CD		EPR	
		λ (nm)	ε	λ (nm)	$\Delta\varepsilon$	$A_{\parallel}$	$g_{\parallel}$
3.5	**112, 111**	685	24	611	−0.03	163	2.301
				331	−0.04		
4.0	**111**	660	38	767	0.07	167	2.295
4.8	**111, 123, 122**	646	77	714	0.20	177	2.161
				329	−0.16		
5.4	**111, 122**	645	88	699	0.43	177	2.243
				329	−0.24		
6.6	**122**	638	101	699	0.60	178	2.238
				583	−0.02		
				336	−0.24		
8.4	**122, 121**	631	103	698	0.50	180	2.237
				592	−0.07		
				350	−0.15		
9.0	**122, 121, 11-1**	622	104	707	0.24		
				599	−0.17		
				360	−0.07		
				317	0.07		
10.0	**121, 11-1**	613	104	624	−0.32	181	2.235
				516	−0.11		
				320	0.32		
11.0	**11-1, 11-2**	615	103			163	2.238

N_{amido}/COO^{-}, as reported for the Cu(II)–HG system [32]. However, in the present case, this complex (110) does not reach significant concentration levels: the presence of a free imidazole residue facilitates the formation of dimer species. The structure of the 220 binuclear complex should be similar to that found for L-carnosine in the solid state [33] and in the Cu(II)–glycyl-spinacine system [34]: the two metal centres of two 110 complexes

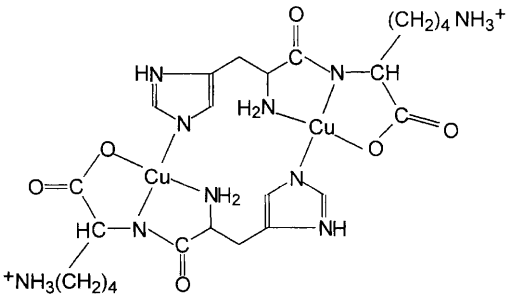


Fig. 3. Structural hypothesis for the Cu(II)–HK 220 complex. Charges around the metal centres are omitted for the sake of simplicity.

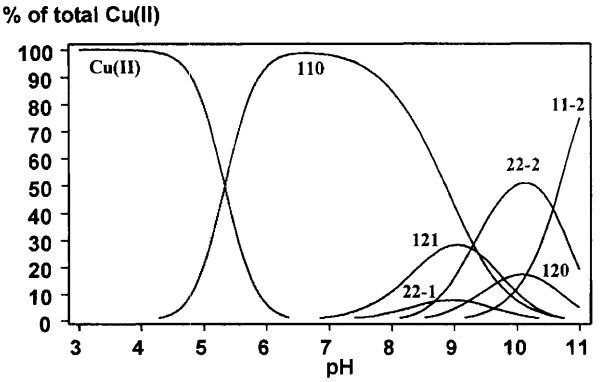


Fig. 4. Distribution diagrams of Cu(II)–β-AK complexes at 25°C and $I = 0.1$ mol dm^{-3} (KNO_3). [Cu(II)] = 4 mmol dm^{-3}; [β-AK] = 8 mmol dm^{-3}.

could be bridged by one or both the ligands, the τ-$N_{imidazole}$ atom of which is bound to the free equatorial plane position of the adjacent complex (see Fig. 3). Molecular models show that this arrangement does not give rise to molecular strain. The ΔH°_{220} value, 'cleaned' of two ε-NH_2 protonation contributions, is rather high but compatible with the coordination of two further nitrogens to copper ions, besides the tridentate coordination of the two ligands, described above. Deprotonation of the 220 complex gives rise to the $22-1$ binuclear species, most likely a hydroxo-complex, which never reaches high concentration levels.

If the ligand-to-metal ratio is 2 or higher, in the pH range from 5 to about 9, the bis-complex 122 largely prevails. In this complex the two ligands should both be bound to copper through their terminal amino and imidazole nitrogens, as suggested by Brookes and Pettit [31] for the 120 complex in the Cu(II)–HG system; the Lys ε-amino groups should be protonated. Once the two protonation contributions (12.5 kcal mol^{-1}) have been subtracted, the corresponding enthalpy of complex formation (49 kcal mol^{-1}, see Table 2) becomes 24 kcal mol^{-1}, a value compatible with the coordination of four nitrogens. The corresponding wavelength of maximum absorption (~ 630 nm) is noticeably higher than expected, and this can be explained by observing that the four nitrogen atom arrangement around the copper is most likely not strictly planar; CD spectra around pH 7 show two bands (at about 700 and 590 nm) compatible with a twisted $2 \times \{NH_2, N_{imidazole}\}$ binding.

At high pH values the 121 complex forms: the corresponding $\log K_{step}$ and ΔH°_{step} values (Table 2) are compatible with the hypothesis of Lys residue deprotonation, promoted by an apical interaction with the metal centre of the complex; the d–d absorption band shows a moderate shift towards lower wavelengths, while the $A\|$ value increases slightly. More important changes in spectroscopic data can be observed when the pH value is raised above 9, where, independently of the metal-to-ligand ratio, the new $11-1$ and $11-2$ complexes form. At a 1:2 metal-to-ligand ratio, the visible spectra show a decrease of about 20 nm in the wavelength of maximum absorption, while in CD spectra, signals appear at about 320 (pH 9) and 510 (pH 10); at a metal-to-ligand ratio of 1:1 a new intense band can be observed at about 250 nm as well. These results clearly mean a change in the coordination mode from bidentate $N_{amino}/N_{imidazole}$ to tridentate $N_{amino}/N_{amido}/COO^-$. When the pH is raised over 10, the ε-NH_2 group most likely interacts with the metal ion in axial position, as previously observed for the systems above, giving rise to the new CD bands (510 nm for 1:2 solutions and 250 for 1:1 solutions) observed.

3.4. Cu(II)–β-Ala-Lys complexes

Species distribution diagram for the Cu(II)–β-AK system is reported in Fig. 4, while thermodynamic parameters for complex formation equilibria are shown in Table 2. First of all it can be observed that, except for some minor complexes (120 instead of 121), the model is very close to the one previously discussed for AK. The system is dominated, from acidic pH to pH about 9, by the 110 complex, where the ligand is bound to copper in the normal tridentate $N_{amino}/N_{amido}/COO^-$ manner, with the formation of two adjacent rings which, in this case, are of different sizes, since there is one more carbon atom, separating the two nitrogens, than in the other ligands. The wavelength of maximum absorption in the visible region and the presence of the characteristic Cu(II)–N_{amido} band in the CD spectrum (at about 315 nm) confirm this structural hypothesis (see Table 7). The fact that the first chelate ring is larger is reflected by the fact that the values of the 'cleaned' thermodynamic parameters are lower than the corresponding data for the Cu(II)–GG, Cu(II)–GK and Cu(II)–AK complexes. Increasingly greater differences have been reported between the 110 complexes of Cu(II)–Ala and Cu(II)–β-Ala [22]. Moreover, it is worth noting that the molar absorption coefficients of

Table 7
Spectral data for Cu(II)–β-Ala-Lys system, at different metal-to-ligand ratio of 1:2

		UV-Vis		CD		EPR	
pH	Main species	λ (nm)	ε	λ (nm)	$\Delta\varepsilon$	$A_{\parallel}$	$g_{\parallel}$
5.0	**110**	652	15				
5.5		627	44	645	−0.64	178	2.255
				315	0.42		
7.5		620	63	644	−0.83	185	2.249
				314	0.56		
8.6	**110, 121**	611	62	639	−0.79	180	2.252
				313	0.53		
9.1	**110, 121, 22-2**	605	62	634	−0.76	188	2.226
				314	0.48		
9.9	**22-2**	591	65	624	−0.74	192	2.227
				311	0.43		
10.6	**22-2, 11-2**	592	64	621	−0.75	194	2.227
				312	0.40		
10.9	**11-2**	594	62			189	2.223

visible spectra recorded at different pH values are considerably lower than those found with the ligand discussed above, even though the complex formation is complete.

In the alkaline pH range some bis-complexes are formed, the most important of which is the 121 species. It most likely has a structure similar to that already discussed for the Cu(II)–AK system, but a lower formation constant, once 'cleaned' of the ε-NH_2 protonation contributions. The consequence is a low formation percentage. The loss of one proton from the 121 complex leads to the 120 species: the corresponding pK value (see Table 2) suggests the deprotonation of one ε-amino group, assisted by the Cu(II) ion. The hypothesis of an interaction between this side group and copper is also supported by the rather high 'cleaned' $\log\beta_{120}$ value, by the decrease in the visible wavelength of maximum absorption and by the increase in the $A_{\parallel}$ and corresponding decrease in $g_{\parallel}$ values of EPR spectra, when the pH exceeds 9. The same behaviour should be followed by the $22-2$ and $11-2$ complexes, as well. They are the main species in the most alkaline pH range: in fact the spectral data do not show significant variations when the pH is changed from 10 to 11. The structure of these complexes is most likely the same as discussed above for the other ligands.

4. Conclusions

The ε-NH_2 of the Lys residue proved to act as a good donor group for the Cu(II) ion at alkaline pH, where deprotonated mononuclear or binuclear complexes are formed. For the present systems no direct evidence could be put forward that this group can bridge two metal ions or two mononuclear complexes. The likely hypothesis is that ε-NH_2 may coordinate to the metal centre to which the ligand is bound, although its involvement in dimer formation cannot be excluded. No deprotonation of ε-NH_2 (and subsequent interaction with copper) was found at neutral pH: this result confirms that, under physiological conditions, the protonated Lys residue of metal-peptides can act as an 'anchor' for biological receptors [5,11].

Acknowledgements

Financial support by Italian MURST (COFIN 98) is gratefully acknowledged.

References

[1] (a) I. Sóvágó, in: K. Burger (Ed.), Biocoordination Chemistry: Coordination Equilibria in Biologically Active Systems, Ellis Horwood, Chichester, 1990, pp. 135–184. (b) L.D. Pettit, J.E. Gregor, H. Kozlowski, in: R.W. Hay, J.R. Dilworth, K.B. Nolan (Eds.), Perspectives in Bioinorganic Chemistry, vol. 1, JAI Press, London, 1991, pp. 1–41.
[2] (a) E.W. Wilson, Jr., M.H. Kasperian, R.B. Martin, J. Am. Chem. Soc. 92 (1970) 5365. (b) G. Brookes, L.D. Pettit, J. Chem. Soc., Dalton Trans. (1976) 42.
[3] B. Radomska, I. Sóvágó, T. Kiss, J. Chem. Soc., Dalton Trans. (1990) 289.
[4] B. Radomska, T. Glowiak, M. Kubiak, J. Mol. Struct. 323 (1994) 169.
[5] W.L. Puspita, A. Odani, O. Yamauchi, J. Inorg. Biochem. 73 (1999) 203.
[6] B. Radomska, M. Kubiak, T. Glowiak, H. Kozlowski, T. Kiss, Inorg. Chim. Acta 159 (1989) 111.
[7] L. Pickart, L. Thayer, M.M. Thaler, Biochem. Biophys. Res. Commun. 54 (1973) 562.
[8] L. Pickart, M.M. Thaler, M. Millard, J. Chromatogr. 175 (1979) 65.
[9] L. Pickart, In Vitro 17 (1981) 459.

[10] H. Pohunkova, J. Stehlik, J. Vachal, O. Cech, M. Adam, Biomaterials 17 (1996) 1567.
[11] L. Pickart, J.H. Freedman, W.J. Loker, J. Peisach, C.M. Perkins, R.E. Stenkamp, B. Weinstein, Nature 288 (1980) 715.
[12] L.D. Hansen, T.E. Jensen, S. Mayne, D.J. Eatough, R.M. Izatt, J.J. Christensen, J. Chem. Thermodyn. 7 (1975) 919.
[13] V.B. Parker, Thermal Properties of Aqueous Uni-Univalent Electrolytes, Natl. Stand. Ref. Data Ser. N.B.S. (U.S.) 2, U.S. Government Printing Office, 1965.
[14] C. Rigano, M. Grasso, S. Sammartano, Ann. Chim. (Rome) 74 (1984) 537.
[15] A. Braibanti, C. Bruschi, E. Fisicaro, M. Pasquali, Talanta 33 (1986) 471.
[16] P. Gans, A. Sabatini, A. Vacca, J. Chem. Soc., Dalton Trans. (1985) 1195.
[17] R. Maggiore, S. Musumeci, S. Sammartano, Talanta 23 (1976) 43.
[18] L. Alderighi, P. Gans, A. Ienco, D. Peters, A. Sabatini, A. Vacca, Coord. Chem. Rev. 184 (1999) 311.
[19] A. De Robertis, C. De Stefano, S. Sammartano, Anal. Chim. Acta 222 (1989) 385.
[20] C. Rigano, E. Rizzarelli, S. Sammartano, Thermochim. Acta 33 (1979) 211.
[21] G. Arena, R. Calì, E. Rizzarelli, S. Sammartano, Thermochim. Acta 16 (1976) 315.
[22] R.M. Smith, A.E. Martell, Critical Stability Constants, vol. 6, Plenum, London, 1989.
[23] M.J.A. Rainer, B.M. Rode, Inorg. Chim. Acta 107 (1985) 127.
[24] A. Gergely, I. Nagypál, J. Chem. Soc., Dalton Trans. (1977) 1104.
[25] G. Borghesani, F. Pulidori, M. Remelli, R. Purrello, E. Rizzarelli, J. Chem. Soc., Dalton Trans. (1990) 2095.
[26] H. Sigel, R.B. Martin, Chem. Rev. 82 (1982) 385.
[27] P.G. Daniele, E. Prenesti, G. Ostacoli, J. Chem. Soc., Dalton Trans. (1996) 3269.
[28] G. Brookes, L.D. Pettit, J. Chem. Soc., Dalton Trans. (1975) 2106.
[29] A. Kaneda, A.E. Martell, J. Coord. Chem. 4 (1975) 37.
[30] V.G. Shtyrlin, E.L. Gogolashvili, A.V. Zakharov, J. Chem. Soc., Dalton Trans. (1989) 1293.
[31] M. Remelli, C. Munerato, F. Pulidori, J. Chem. Soc., Dalton Trans. (1994) 2049.
[32] G. Brookes, L.D. Pettit, J. Chem. Soc., Dalton Trans. (1975) 2112.
[33] H.C. Freeman, J.T. Szymanski, Acta Crystallogr., Sect. B 22 (1967) 406.
[34] C. Conato, M. Remelli, R. Guerrini, F. Pulidori, Ann. Chim. (Rome) 88 (1998) 91.

PERGAMON

www.elsevier.nl/locate/poly

Polyhedron 19 (2000) 2421–2425

POLYHEDRON

On the reaction of iron(III) with chromium(III)–DTPA chelating agent

R. Bucci [a], A.D. Magrì [a], A.L. Magrì [a,*], A. Napoli [b]

[a] *Dipartimento di Chimica, Università di Roma 'La Sapienza', 00185 Rome, Italy*
[b] *Dipartimento di Scienze Ambientali, Università della Tuscia, 01100 Viterbo, Italy*

Abstract

The reaction of iron(III) with chromium(III)–DTPA 'chelating agent' has been investigated, in aqueous solution, by measuring both hydrogen ion concentration and emf of the iron(III)/iron(II) couple. In acidic medium (pH < 2.3) and with ligand excess, a 1:1 (metal–ligand molar ratio) fully deprotonated complex has been evidenced. In the same experimental conditions the iron(III) reacts with iminodiacetic acid forming a similar 1:1 deprotonated species. The stability constants of the above equilibria have been calculated at 20°C in $NaClO_4$ 1.0 mol dm^{-3}. The comparison of these constants, considering the basicity of the ligands, proved the coordination of iron(III) occurs by one iminodiacetic group. The iron(III)–chromium(III)–DTPA complex has been precipitated and the solid compound characterized by IR and thermoanalytical techniques. © 2000 Elsevier Science B.V. All rights reserved.

Keywords: Iron(III); Chromium(III); DTPA; Complexes; Thermal properties; Thermodynamics

1. Introduction

The research on the complexation reactions has always been of great interest because of the numerous applications, not only in the analytical field. It could flow from the transformation of two chemical species (the metal ion and the ligand) in a new compound (the complex) which has certain properties different from those of its components, assumed separately.

The above is confirmed by the recent application of the magnetic resonance imaging (MRI) in the study of the human body. In fact, the employment of this technique as diagnostic medium requires the use of paramagnetic contrast agents, i.e. species that have unpaired electrons. There are many transition and lanthanide metals with unpaired spins, but the main problem with these species in the native form is their toxicity. Investigation has been focused to create thermodynamically and kinetically stable complexes which, without altering paramagnetic properties of the metal ion, are much less toxic than both the metal ion and the ligand in the unbound state. Among the tested compounds, some complexes of strongly paramagnetic metal ions, such as chromium(III), iron(III) and gadolinium(III), with diethylenetriaminepentaacetic acid (DTPA, H_5L) seem to have both the required characteristics.

The chromium(III) - diethylenetriaminepentaacetate (CrL^{2-}) is a stable and very inert complex that can act as a chelating agent by the uncoordinated iminodiacetic group [1]. The reaction of this chelating agent with some metal ions has already been studied in aqueous solution as well as in the solid state [2–6].

In the present paper we report the main results found in the study of the reactions of iron(III) with chromium(III)–DTPA and with iminodiacetic acid (H_2Im) alone, in $NaClO_4$ 1.0 mol dm^{-3} aqueous solution, at 20°C. Moreover, some spectroscopic (IR), magnetic and thermal (TG and DSC) behavior of the complexes obtained in the solid state are described.

2. Experimental

2.1. Apparatus

The free hydrogen ion concentration ($[H^+]$) and that of iron(III) ($[Fe^{3+}]$) were measured with an Amel 337

* Corresponding author. Tel.: +39-06-499-13371.
E-mail address: almagri@uniroma1.it (A.L. Magrì).

0277-5387/00/$ - see front matter © 2000 Elsevier Science B.V. All rights reserved.
PII: S0277-5387(00)00540-4

potentiometer (precision 0.1 mV) by an Ingold glass electrode, calibrated in concentration units, and by a platinum wire, in the presence of iron(II) ions, respectively. The reference was an Ag/AgCl electrode, prepared according to Brown [7]. The calculated stability constants are referred to $t = 20°C$ and $I = 1$ mol dm^{-3} (sodium perchlorate).

The following electrochemical cells were employed

A(−)Glass El.	$Fe(ClO_4)_3 C_{M1}$ $Fe(ClO_4)_2 C_{M2}$ $HClO_4 C_H$ $NaClO_4(1.00 - C_H)$ M	$NaClO_4$ 1.00 M	$NaClO_4$ 0.99 M NaCl 0.01 M	Ag,AgCl(+)
B(−)Ag/AgCl	$NaClO_4$ 0.99 M NaCl 0.01 M	$NaClO_4$ 1.00 M	$Fe(ClO_4)_3 C_{M1}$ $Fe(ClO_4)_2 C_{M2}$ $HClO_4 C_H$ $NaClO_4(1.00 - C_H)$ M	Pt(+)

As the activity coefficients are unchanged in a constant ionic medium [8], the activities can be substituted by concentrations and the emf of cells A and B can be expressed, in mV units, by the following equations

$$E_A = E_A^\circ - 58.17 \log [H^+] = E_A^\circ - 58.17 \log C_H$$

$$E_B = E_B^\circ + 58.17 \log \frac{[Fe^{3+}]}{[Fe^{2+}]}$$

Perchloric acid (or sodium hydrogen carbonate) was added to maintain constant $[H^+]$ after each addition of the ligand solution (0.025 mol dm^{-3} of Na_2CrL or Na_2Im in $NaClO_4$ 1.0 mol dm^{-3}), so that the junction potential, which remain unchanged, was included in the $E°$ values. In each set of measurements, the value of E_A was constant and that of E_B° was calculated, in the absence of the ligand, by the iron concentrations (C_{M1} and C_{M2}). After each addition of the ligand the $[Fe^{3+}]$ was determined by the emf values, knowing the hydrolysis constants of iron(III) [9] and the equilibrium constants of the complexes iron(II)–chromium(III)–DTPA [4] and iron(II)–Im.

The thermal measurements were carried out using a Perkin–Elmer TGS-2 thermal analyzer, connected to a model 3600 Data Station, and a 1020 series DSC-7 thermal analysis system equipped with a multitasking software for instrument control and data analysis. Unless otherwise specified, thermogravimetry and differential scanning calorimetry runs were made on samples of about 1–2 mg (TG) and 0.3–0.5 mg (DSC) in a stream of nitrogen or oxygen (flow rate, 50 ml min^{-1}), heating rate 10°C min^{-1}.

IR spectra were recorded on a Perkin–Elmer FTIR 1600 grating spectrophotometer.

The measurements of the magnetic susceptibility were performed by the Gouy method at 8000 gauss in the temperature range 78–300 K. The instrument was calibrated with $Hg[Co(NCS)_4]$ [10].

2.2. Reagents

Iminodiacetic acid (BDH), diethylenetriaminepentaacetic acid, chromium(III) disodium salt hexahydrate (Aldrich), diethylenetriaminepentaacetic acid, and iron(III) disodium salt dihydrate (Aldrich) were used. The purity of these compounds was checked by potentiometric titration with sodium hydroxide and by thermal analysis.

Iron(III) perchlorate stock solution was prepared and standardized as already indicated [11].

Iron(II) perchlorate was prepared by catalytic reduction of iron(III) perchlorate over platinum black with purified hydrogen. Metal ion concentration was determined by permanganate titration.

Other chemicals were of analytical grade. Distilled–deionised water was used.

2.3. Preparation of the solid compound

The iron(III)–chromium(III)–DTPA complex was prepared by adding 25 cm^3 of ethanol to 50 cm^3 of an equimolar (40 mmol dm^{-3}) aqueous solution of iron(III) ions and CrL^{2-} 'metal–ligand chelating agent'. The violet precipitate was filtered off, washed with 1:1 water:ethanol ratio, then with ethanol and finally dried in vacuum, over silica gel. The chemical analysis of this compound suggested the formula $FeCrL(OH)(H_2O)_6$.

The chromium(III)–DTPA complex in the acid form $[H_2CrL(H_2O)_2]$ was prepared as reported in Ref. [2].

3. Results and discussion

3.1. Study in aqueous solution

The measurements were performed at several constant values of free hydrogen ions concentration in the

range $-\log[H^+]$ from 1.5 to 2.3 (at lower values the complexation reaction is almost negligible but at higher values hydrolysis of iron(III) ions becomes important). The iron(III) concentration was varied in the range from 0.5 to 2 mmol dm^{-3}, while the ligand concentration was progressively increased ($C_L/C_M = 1 \rightarrow 10$). In these experimental conditions it has been evidenced that iron(III) forms a 1:1 (metal:ligand molar ratio) fully deprotonated complex species with chromium(III)–DTPA. In fact, the same value of the stability constant (β_{101}) was obtained at different pH, iron(III) and ligand concentrations.

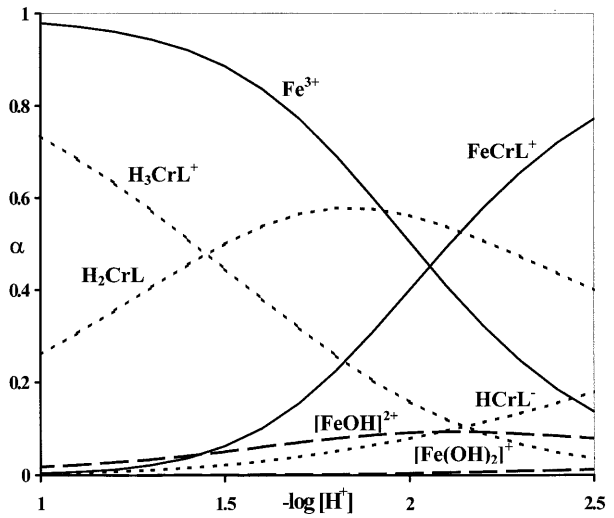


Fig. 1. Distribution diagram for the system iron(III)–chromium(III)–DTPA calculated at $t = 20°C$, $I = 1.0$ mol dm^{-3} [$NaClO_4$], $C_L/C_M = 2$ [where C_L and C_M are the analytical concentrations of the ligand ⟨chromium(III)–DTPA⟩ and metal ion ⟨iron(III)⟩].

Table 1
Equilibrium constants, used and found, in the study of iron(III) reactions with iminodiacetic acid (H_2Im) and chromium(III)–DTPA (H_2CrL) [a,b]

Equilibrium	Log K	Reference
$CrL^{2-} + H^+ \rightleftharpoons HCrL^-$	6.15	1
$HCrL^- + H^+ \rightleftharpoons H_2CrL$	2.85	1
$H_2CrL + H^+ \rightleftharpoons H_3CrL^+$	1.45	1
$Fe^{3+} + H_2O \rightleftharpoons Fe(OH)^{2+} + H^+$	−2.74	9
$Fe^{3+} + 2H_2O \rightleftharpoons Fe(OH)_2^+ + 2H^+$	−6.05	9
$2Fe^{3+} + 2H_2O \rightleftharpoons Fe_2(OH)_2^{2+} + 2H^+$	−2.85	9
$Fe^{2+} + CrL^{2-} \rightleftharpoons FeCrL$	4.95	4
$Fe^{3+} + CrL^{2-} \rightleftharpoons FeCrL^+$	8.15 ± 0.05	this work
$Im^{2-} + H^+ \rightleftharpoons HIm^-$	9.35 ± 0.01	this work
$HIm^- + H^+ \rightleftharpoons H_2Im$	2.55 ± 0.02	this work
$H_2Im + H^+ \rightleftharpoons H_3Im^+$	1.75 ± 0.02	this work
$Fe^{2+} + Im^{2-} \rightleftharpoons FeIm$	6.10 ± 0.05	this work
$FeIm + Im^{2-} \rightleftharpoons FeIm_2^{2-}$	4.45 ± 0.05	this work
$Fe^{3+} + Im^{2-} \rightleftharpoons FeIm^+$	10.95 ± 0.05	this work

[a] $t = 20°C$, $I = 1.0$ mol dm^{-3} $NaClO_4$.
[b] Estimated uncertainties represent standard deviations ($N \geq 5$).

The conditional stability constants (K') were calculated, at different values of acidity, according to the following equation:

$$K' = \frac{[FeCrL^+]}{[Fe^{3+}][CrL']}$$

where:

$$[FeCrL^+] = C_M - [Fe^{3+}]$$

$$[CrL'] = C_L - [FeCrL^+]$$

$[Fe^{3+}]$ = free iron(III) concentration determined by the emf values.

By each value of K', the stability constant (β_{101}) of the above complex has been calculated, using the equation:

$$\beta_{101} = K'\alpha_{CrL}$$

where:

$$\alpha_{CrL} = 1 + \Sigma\, \beta_{0i1}[H^+]^i$$

β_{0i1} is the protonation constant of the chromium–DTPA complex [1].

Fig. 1 shows how the mole fraction of each species, in the iron(III)–chromium(III)–DTPA system, changes with the acidity of the aqueous solution.

Also the reactions of iron(III) with iminodiacetic acid were investigated and only a similar 1:1 deprotonated species was evidenced. In order to calculate its stability constant, the values of the equilibrium constants of the iminodiacetic acid alone and those of the iron(II) complexes are needed. Therefore, they have been re-determined in our experimental conditions.

The overall results are collected in the Table 1.

By comparison of the obtained values of the stability constants, the iron(III) complex with iminodiacetic acid appears more stable than that with chromium(III)–DTPA, according to the greater basicity of the ligand. Furthermore, by calculating the ratio $\log \beta_{101}/\log \beta_{031}$ [12] nearly equal values for both ligands were obtained (0.80 for iminodiacetic acid and 0.78 for chromium (III)–DTPA) proving that in all cases the coordination of iron(III) occurs by one iminodiacetic group.

3.2. Study of the solid compounds

To improve the analysis of $FeCrL(OH)(H_2O)_6$ the IR spectrum of this complex was compared with those of the $H_2CrL(H_2O)_2$ and $Na_2FeL(H_2O)_2$ compounds.

In the heterobinuclear complex, the intense bands at 1652 and 1374 cm^{-1} (assigned to antisymmetric (ν_a) and symmetric (ν_s) stretching frequencies of coordinated carboxylate anion) with a difference $\Delta_\nu = 278$ cm^{-1} and the absence of the band at 1600 cm^{-1} [ionic or free carboxylate groups in $Na_2FeL(H_2O)_2$], as well as

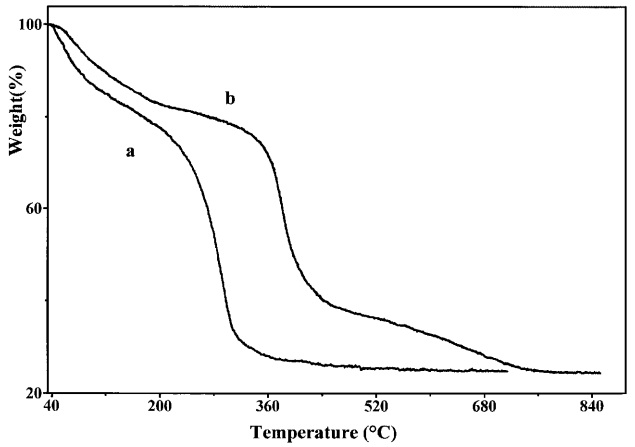


Fig. 2. TG curves in oxygen (a), and nitrogen (b), for FeCrL(OH)$(H_2O)_6$.

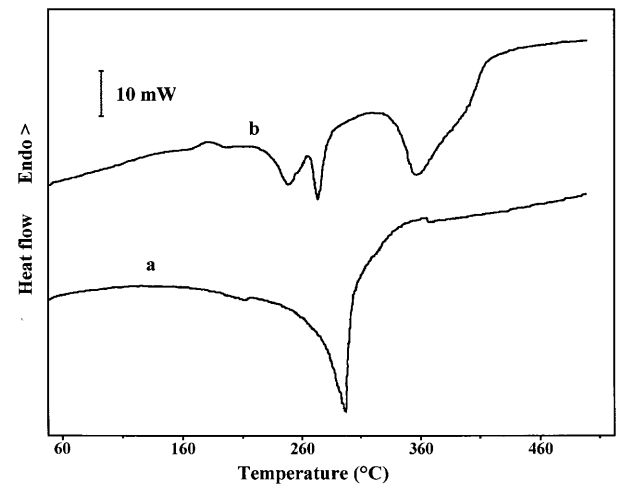


Fig. 3. DSC curves in oxygen for FeCrL(OH)$(H_2O)_6$ (a), and $Na_2FeL(H_2O)_2$ (b).

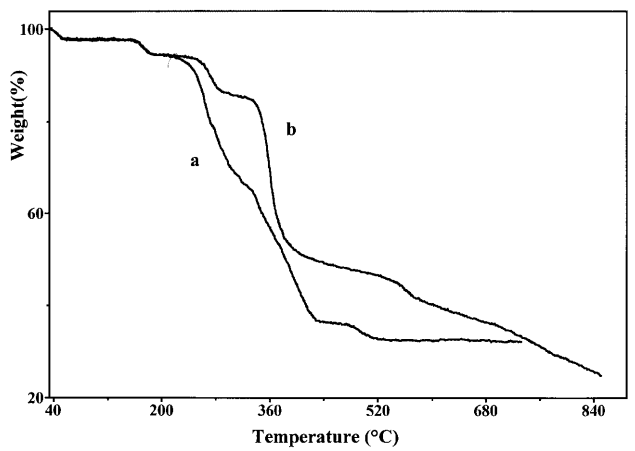


Fig. 4. TG curves in oxygen (a), and nitrogen (b), for $Na_2FeL(H_2O)_2$.

those at 1740–1705 cm^{-1} [COOH groups in $H_2CrL(H_2O)$], prove that all the carboxylate groups are involved in the metal ions chelation with high degree of covalence in the metal–oxygen bond [13].

The magnetic properties of the heterobinuclear complex were measured over a temperature range 78–300 K and the plot $1/\chi'_m$ versus T was a straight-line ($y = 12.978 + 0.426x$). The magnetic moment ($\mu = 4.35$ B.M.) and the Weiss constant ($\theta = -30.5$ K) were calculated from the slope and the intercept, respectively, on the T axis of the above line. These results prove the paramagnetic character of the complex and the formation of some degree of metal–metal interaction.

The thermal decomposition trend of the FeCrL(OH)$(H_2O)_6$ complex is greatly conditioned by the furnace atmosphere. According to termogravimetry in O_2 (Fig. 2, curve a), the dehydration reaction occurs up to approximately 120°C (for $6H_2O$, *Anal.* Calc. 17.38. Found 17.3%), beyond which the decomposition process of the anhydrous starts, first slowly (mass loss about 5% up to 185°C) then rapidly (maximum rate at 290°C). This is an oxidative process (Fig. 3, curve a) and occurs with a strong exothermic reaction ($t_p = 298$°C; $\Delta H = -4.5$ 10^3 kJ mol^{-1}). The decomposition is completed at 360°C and the residue, which remains constant up to 700°C, consists of Fe_2O_3 and Cr_2O_3 (*Anal.* Calc. 25.09. Found 25.0%). In the nitrogen atmosphere (Fig. 2, curve b), dehydration occurs in the same temperature range, but the decomposition of the anhydrous is delayed and occurs in two separate steps. The first, in the range 280–510°C (maximum rate at 380°C), forms a $Cr_2O_3 + Fe_2(CO_3)_3$ mixture (*Anal.* Calc. 35.71, Found 36.5%); the second (maximum rate at 655°C) gives at 760°C the same residue found in oxygen (found 25.0%). DSC curve shows only one, small, endothermic peak in this decomposition range ($t_p = 380$°C).

As the thermal behavior of the complex $Na_2FeL(H_2O)_2$ is unknown, we have extended this investigation to the above compound. According to the thermogram, the two water molecules of this complex depart in separate processes, the former up to 55°C and the latter in the range 140–180°C (*Anal.* Calc. 6.84. Found 6.9%). In the DSC curve (Fig. 3, curve b) an endothermic process is evident only in correspondence of the evolution of the second water molecule ($t_p = 185$°C; $\Delta H = 49$ kJ mol^{-1}). The anhydrous compound, in an oxygen atmosphere (Fig. 4, curve a), is stable up to about 210°C, then it decomposes through several steps partly overlapping one another. The thermal decomposition is completed at 520°C and the residue, stable up to 760°C at least, consists mainly of Fe_2O_3 and Na_2CO_3 (*Anal.* Calc. 35.32. Found 34.8%). This oxidative decomposition of the complex is evident in the DSC curve, which shows three strongly exothermic peaks of which two, partly overlapped, in the temperature range from 210–295°C ($t_p = 250$ and 275°C; $\Delta H = -1.2$ 10^3 kJ mol^{-1}) and one at $t_p = 359$°C ($\Delta H = -2.4$ 10^3 kJ mol^{-1}). In a dynamic N_2 atmosphere (Fig. 4, curve b), the anhydrous

compound is more stable (up to 240°C) and the decomposition is a two-step process with maximum rate at 265 and 352°C, respectively. The residue at 455°C likely consists of a $Fe_2(CO_3)_3$ and Na_2CO_3 mixture (*Anal.* Calc. 47.86. Found 47.8%) but it suffers a continuous mass loss and it does not reach a constant weight up to 840°C. The whole decomposition process, as expected, is connected with only weakly endothermic peaks.

Comparison of these data with those reported for analogous heterobinuclear chelates and chromium(III)–DTPA disodium salt chelating agent proves that iron(III) chelation causes a strong destabilising effect on the thermal stability of the compounds. Particularly, FeCrL(OH) complex is the least stable of all the studied compounds, with the exception of CuCrL.

Acknowledgements

Thanks are due to Mr G. Minelli for the technical help in the magnetic measurements. The Italian Research Council (CNR) and Italian Ministry of the University and Scientific Technological Research (MURST) are gratefully acknowledged for financial support.

References

[1] R. Bucci, A.L. Magrì, A. Napoli, J. Coord. Chem. 24 (1991) 169.
[2] A. Napoli, R. Bucci, A.D. Magrì, A.L. Magrì, Ann. Chim. (Rome) 81 (1991) 693.
[3] M. Belcastro, A. Napoli, Ann. Chim. (Rome) 83 (1993) 451.
[4] R. Bucci, A.D. Magrì, A.L. Magrì, A. Napoli, Thermochim. Acta 217 (1993) 213.
[5] A. Napoli, R. Bucci, A.D. Magrì, A.L. Magrì, J. Therm. Anal. 46 (1996) 1865.
[6] R. Bucci, A.D. Magrì, A.L. Magrì, A. Napoli, Ann. Chim. (Rome) 88 (1998) 25.
[7] A.S. Brown, J. Am. Chem. Soc. 56 (1934) 646.
[8] G. Biederman, L.G. Sillèn, Ark. Kemi. 5 (1953) 425.
[9] D.D. Perrin, J. Chem. Soc. (1959) 1710.
[10] B.N. Figgs, R.S. Nyholm, J. Chem. Soc. (1958) 4190.
[11] A. Napoli, J. Inorg. Nucl. Chem. 34 (1972) 987.
[12] T.J. Lane, J.W. Thompson, J. Am. Chem. Soc. 82 (1960) 4179.
[13] K. Nakamoto, Infrared and Raman Spectra of Inorganic and Coordination Compounds, Wiley, New York, 1977.

PERGAMON

www.elsevier.nl/locate/poly

Polyhedron 19 (2000) 2427–2434

POLYHEDRON

Lanthanide(III) complex formation with diethylenetriamine in anhydrous *N*,*N*-dimethylformamide

Clara Comuzzi [a], Plinio Di Bernardo [b,*1], Pierluigi Polese [a], Roberto Portanova [a], Marilena Tolazzi [a,*2], Pier Luigi Zanonato [b]

[a] *Dipartimento di Scienze e Tecnologie Chimiche, Università di Udine, Via Cotonificio 108, I-33100 Udine, Italy*
[b] *Dipartimento di Chimica Inorganica, Metallorganica ed Analitica, Università di Padova, via Loredan 4, I-35131 Padua, Italy*

Abstract

The formation of diethylenetriamine (dien) complexes of the lanthanide(III) ions has been studied in *N*,*N*-dimethylformamide (dmf) containing 0.1 mol dm^{-3} tetraethylammoniumtrifluoromethanesulfonate as constant ionic medium at 298 K. The stability constants have been obtained by potentiometry using the method of competitive reactions, silver(I) being the auxiliary central ion. The thermodynamic investigations have therefore been extended also to this metal ion. The data concerning lanthanide(III) complexation are well explained in terms of formation of two successive mononuclear complexes which are enthalpy stabilized, entropy changes being unfavourable. Dien coordinates with all N atoms both in ML and ML_2 lanthanide(III) complexes; with silver(I), tridentation is achieved only when the first mononuclear complex is formed. The trends in enthalpy and entropy values of the lanthanide(III) complexes are discussed taking into account the presence of multiple solvation equilibria which involve the bare ions and the complexes in solution. Comparison with similar data previously obtained in dimethylsulfoxide (dmso) both for the lanthanide(III)- and silver(I)-dien systems, shows the remarkable influence of the solvent on the thermodynamics of complex formation. © 2000 Elsevier Science B.V. All rights reserved.

Keywords: Lanthanides(III); Silver(I); Diethylenetriamine; *N*,*N*-dimethylformamide; Complexes; Thermodynamics

1. Introduction

Owing to their ability to give ionic bonding, combined with high charge density, high coordination number and rapid ligand exchange, the lanthanide(III) ions are rapidly gaining importance in homogeneous and heterogeneous catalysis and in coordination chemistry [1–5]. Moreover, they are extensively used as luminescent probes in biochemistry [6,7], as shift reagents in NMR [8] and, more recently, as contrast agents in magnetic resonance imaging (MRI) [9].

Due to their scientific, industrial and technological importance, any additional information concerning also particular aspects of the coordination chemistry of lanthanides would be of interest and utility.

So far much attention has been paid to the solution chemistry of lanthanide(III) ions in aqueous solution [1–3,10,11], where, as a consequence of the great tendency of lanthanide(III) ions to form hydroxo complexes, only slightly basic ligands have been studied. Progress in non-aqueous media, where strongly basic donors can also be investigated, has been rather slow [4,5,12–14] mainly because of the difficulty of working under anhydrous conditions with the 'water-hungry' Ln(III) ions.

With the goal of enhancing the understanding of Ln(III) coordination chemistry and with the prospective of an improvement of the methods used for rare earth separation, we have recently studied the thermodynamics of the complexation of lanthanide(III) ions in non-aqueous solutions. In particular, data have been reported on the complexation of rare earth ions by linear amines and polyamines in dimethylsulfoxide (dmso) [15–17] and acetonitrile (an) [18,19].

The investigations in dmso have shown that the formation constants of LnL_j complexes (L = ethylenediamine (en), $j = 1–3$; L = diethylenetriamine (dien) and

[1] Corresponding author. Tel. +39-049-275-213; fax: +39-049-827-5161.
[2] Corresponding author. Tel. +39-0432-558-882; fax: +39-0432-558-803.

0277-5387/00/$ - see front matter © 2000 Elsevier Science B.V. All rights reserved.
PII: S0277-5387(00)00541-6

triethylenetetramine (trien), $j = 1, 2$) increase almost linearly with increasing atomic number of the metal ions and that, for the same lanthanide(III) ion, $\log \beta_1$ values increase on going from en to dien to trien. These data, together with luminescence results, proved that polyamines are able to give a strong chelate effect in dmso while *n*-butylamine (*n*-but) is not able to coordinate Ln(III) in the same solvent [19], despite this ligand possessing a larger donor number than dmso (DN*n*-but = 42.0; $DN_{dmso} = 29.8$ [20]). On the other hand, it has been shown [19] that *n*-but is able to form strong complexes with partially undissociated lanthanide(III) trifluoromethanesulfonates (triflates) in a poorly coordinating solvent such as an ($DN_{an} = 14.1$ [20]). This emphasizes the great influence of the solvent on the composition and stability of the complexes.

As an extension of our previous work, we report here the results of a thermodynamic investigation on the complexation of Ln(III) ions with diethylenetriamine in anhydrous *N*,*N*-dimethylformamide (dmf), a solvent whose chemical and physical properties are intermediate between those of dmso and an, as shown by the values of the relative permittivities, ε, donor numbers, DN, and acceptor numbers, AN, reported for the various solvents: dmf, $\varepsilon = 36.7$, DN = 26.6, AN = 16.0; dmso, $\varepsilon = 46.4$, DN = 29.8, AN = 19.3; an, $\varepsilon = 36.0$, DN = 14.1, AN = 19.3 [21–23].

The stoichiometry and the stability constants of the complexes formed in solution have been obtained by means of potentiometric measurements using silver(I) as auxiliary competitive metal ion. Consequently, as required by this experimental procedure [24], preliminary determination of the silver(I) stability constants with the same ligand in dmf has been performed. The enthalpy changes have been determined by direct calorimetric titrations for all the lanthanide(III)-dien systems as well as for the silver(I)-dien system.

The present investigation was performed at 298 K using tetraethylammoniumtrifluoromethansulfonate (triflate) 0.1 mol dm^{-3} as supporting electrolyte.

2. Experimental

N,*N*-Dimethylformamide (Aldrich 99.9%) was distilled under reduced pressure and stored over 4 Å molecular sieves in a dark bottle. Ln(III) triflates were prepared from reaction of slight excess of the oxides (Aldrich 99.9%) with concentrated trifluoromethanesulfonic acid (triflic acid, Aldrich > 98%) in water. The excess of oxide was removed by filtration and the hydrated products ($Ln(trif)_3 \cdot nH_2O$, $trif = CF_3SO_3^-$, $n = 2,3$) were obtained in 2 weeks by slow evaporation of water under reduced pressure (at $t < 80$°C). The anhydrous salts were then obtained by heating the hydrated products in a Buchi TO-51 drying tube under high vacuum ($P < 10^{-4}$ Torr) at about 80°C. Stock anhydrous solutions of the salts were prepared by dissolving weighed amounts of these compounds in anhydrous dmf and were standardized by complexometry with EDTA [25].

The molar conductivities of solutions of some 1.00 and 10.0 mmol dm^{-3} Ln(III) triflates (respectively about 205 and 148 Ω^{-1} mol^{-1} cm^2) were measured with a Metrohm 712 conductometer and were found in good agreement with the accepted value for 1:3 electrolytes in dmf [26].

The Ag(I) triflate salt (Aldrich > 99%) and NEt_4trif (Fluka > 98%) were purified as described before [18,19]. The dien ligand was purified as described earlier [27] and the solutions of the ligand were prepared by dissolving weighed amounts of the anhydrous amine in anhydrous dmf. All solutions were prepared and stored in a glove box, under controlled atmosphere of N_2, with less than 2 ppm of water. The water content in the stock solutions (typically 10–30 ppm) was determined with a Metrohm 684 KF Coulometer.

2.1. Potentiometric measurements

The potentiometric apparatus and the titration procedure used were similar to those previously described [15,19]. The e.m.f. values were collected with a data acquisition system using an Amel model 338 pH-meter equipped with a Metrohm 6.0331.010 silver electrode as a working electrode and a Metrohm 6.0726.100 silver electrode as a reference. The e.m.f. values of cells containing Ln^{3+} and Ag^+ ions in the range $10^{-5} < [Ag^+] < 10^{-2}$ mol dm^{-3} proved that the silver(I) electrode behaved according to Nernst's law in our systems.

Each experimental series was carried out adding to a silver(I)–Ln(III) solution known amounts of the ligand solution with concentration C_L° ($100 < C_L^\circ < 300$ mmol dm^{-3}). In order to get reliable values for the formation constants and to check the absence of mixed Ag–L–Ln complexes in solution, at least three different initial concentrations of Ln(III) ($5.00 < C_{Ln}^\circ < 33.0$ mmol dm^{-3}) and at least two different silver(I) initial concentrations ($1.00 < C_{Ag}^\circ < 10.0$ mmol dm^{-3}) were used.

The same apparatus [19], in the absence of Ln(III) triflates, was used to obtain the e.m.f. data necessary to calculate the stability constants for the silver(I)-dien system in dmf ($1.00 < C_{Ag}^\circ < 20.0$ mmol dm^{-3}). To exclude moisture, all titrations were performed in a dry box. The computer program Superquad [28] was used for the calculation of the stability constants.

Table 1
Overall stability constants and thermodynamic functions of the lanthanide(III)- and silver(I)-dien complexes in dmf at 298 K and $I = 0.1$ mol dm^{-3}; estimated three standard deviations in parentheses

Metal ion	ML_j	$\log \beta_j$	$-\Delta G^\circ_{\beta_j}$ (kJ mol^{-1})	$-\Delta H^\circ_{\beta_j}$ (kJ mol^{-1})	$-T\Delta S^\circ_{\beta_j}$ (kJ mol^{-1})
Ag(I)	$j=1$	10.21 ± 0.04	58.3 ± 0.2	90.4 ± 0.6	32.1
	$j=2$	13.18 ± 0.07	75.2 ± 0.4	108.8 ± 0.5	33.6
La (1.061) [a]	$j=1$	5.29 ± 0.06	30.2 ± 0.3	44.9 ± 1.8	14.7
	$j=2$	8.36 ± 0.06	47.7 ± 0.3	89.7 ± 0.9	42
Ce (1.034)	$j=1$	5.58 ± 0.03	31.8 ± 0.1	54.0 ± 0.9	22.2
	$j=2$	9.12 ± 0.03	52.0 ± 0.2	102.3 ± 0.5	50.3
Pr (1.013)	$j=1$	5.76 ± 0.03	32.9 ± 0.2	59.7 ± 1.8	26.8
	$j=2$	9.48 ± 0.03	54.1 ± 0.2	107.1 ± 2.1	53
Nd (0.995)	$j=1$	5.90 ± 0.03	33.7 ± 0.2	61.6 ± 0.9	27.9
	$j=2$	10.11 ± 0.03	57.7 ± 0.3	109.9 ± 0.5	52.2
Sm (0.964)	$j=1$	5.74 ± 0.03	32.8 ± 0.2	54.8 ± 1.2	22
	$j=2$	10.31 ± 0.03	58.8 ± 0.2	113.6 ± 0.5	54.8
Eu (0.950)	$j=1$	5.66 ± 0.02	32.3 ± 0.1	52.3 ± 0.9	20
	$j=2$	10.11 ± 0.02	57.7 ± 0.2	111.8 ± 0.6	54.1
Gd (0.938)	$j=1$	5.69 ± 0.03	32.5 ± 0.2	46.8 ± 1.2	14.3
	$j=2$	10.25 ± 0.03	58.5 ± 0.2	111.4 ± 1.1	52.9
Tb (0.923)	$j=1$	5.73 ± 0.03	32.7 ± 0.2	47.6 ± 1.2	14.9
	$j=2$	9.70 ± 0.04	55.3 ± 0.2	104.8 ± 1.0	49.5
Dy (0.908)	$j=1$	6.03 ± 0.03	34.4 ± 0.2	47.0 ± 0.6	12.6
	$j=2$	10.08 ± 0.04	57.5 ± 0.2	102.2 ± 0.3	44.7
Ho (0.894)	$j=1$	6.19 ± 0.05	35.3 ± 0.3	47.7 ± 0.6	12.4
	$j=2$	10.19 ± 0.06	58.2 ± 0.3	100.9 ± 1.2	42.7
Er (0.881)	$j=1$	6.39 ± 0.02	36.5 ± 0.1	46.3 ± 0.9	9.8
	$j=2$	10.43 ± 0.03	59.5 ± 0.2	94.5 ± 1.5	35
Tm (0.869)	$j=1$	6.57 ± 0.05	37.5 ± 0.3	49.1 ± 0.9	11.6
	$j=2$	10.68 ± 0.06	61.0 ± 0.3	96.9 ± 0.6	35.9
Yb (0.858)	$j=1$	6.74 ± 0.03	38.5 ± 0.2	50.3 ± 0.5	11.8
	$j=2$	10.82 ± 0.05	61.7 ± 0.3	98.2 ± 0.5	36.5
Lu (0.848)	$j=1$	6.87 ± 0.06	39.2 ± 0.3	51.6 ± 0.6	12.4
	$j=2$	11.20 ± 0.09	63.9 ± 0.5	101.6 ± 0.7	37.7

[a] Lanthanide(III) ionic radii in Å [31].

2.2. Calorimetric measurements

A Tronac model 87-558 precision calorimeter was employed to measure the heats of reaction. Thecalorimeter was checked by titration of tris(hydroxymethyl)aminomethane (tham) with a HCl standard solution in water. The experimental value of tham neutralization heat was found to be $\Delta H^\circ = -47.58$ kJ mol^{-1}, in good agreement with the accepted value of -47.53 ± 0.13 kJ mol^{-1} [29].

The calorimetric titrations were performed at 298.15 ± 0.02 K by adding known volumes of ligand solutions ($100 < C^\circ_L < 300$ mmol dm^{-3}) to 20 ml of lanthanide(III) ($5.00 < C^\circ_{Ln} < 33.0$ mmol dm^{-3}) or silver(I) ($2.00 < C^\circ_{Ag} < 20.0$ mmol dm^{-3}) solutions. In order to reach higher ligand-to-metal ratios, some 'reverse' calorimetric titrations were carried out. In these titrations Ln(III) ion solutions ≈ 100 mmol dm^{-3} were added to solutions of ligand ≈ 30 mmol dm^{-3}. The heats of dilution of the reactants, determined in separate runs, were found to be negligible. The computer program Letagrop Kalle [30] was used for the calculation of the enthalpy changes.

3. Results

The computer treatment of the potentiometric experimental data shows that the best fit is achieved when formation of two mononuclear successive complexes is taken into account for all the systems. The overall stability constants obtained from the potentiometric data minimization procedures, with the corresponding limits of error, are listed in Table 1 for the reactions $M + jL \rightarrow ML_j$ ($M = Ln^{3+}$ or Ag^+; L = dien and $j =$ 1,2). The enthalpy and entropy changes for the complex formation are also reported.

Fig. 1 shows plots of n, the average number of ligands per metal ion, versus $-\log[L]$ for the formation of dien complexes of La^{3+} and Lu^{3+}, where [L] is the free ligand concentration. The relationship $n = (C_L - n'C_{Ag} - [L]/C_M$ was used to calculate n, where n' is the average number of ligands bound to silver(I) ion and C_L is the analytical ligand concentration. The values of n' and [L] were obtained from the measured free silver(I) concentration calculated from the e.m.f. data and the stability constants of the silver(I) complexes. The overlapping of the complex-formation curves at differ-

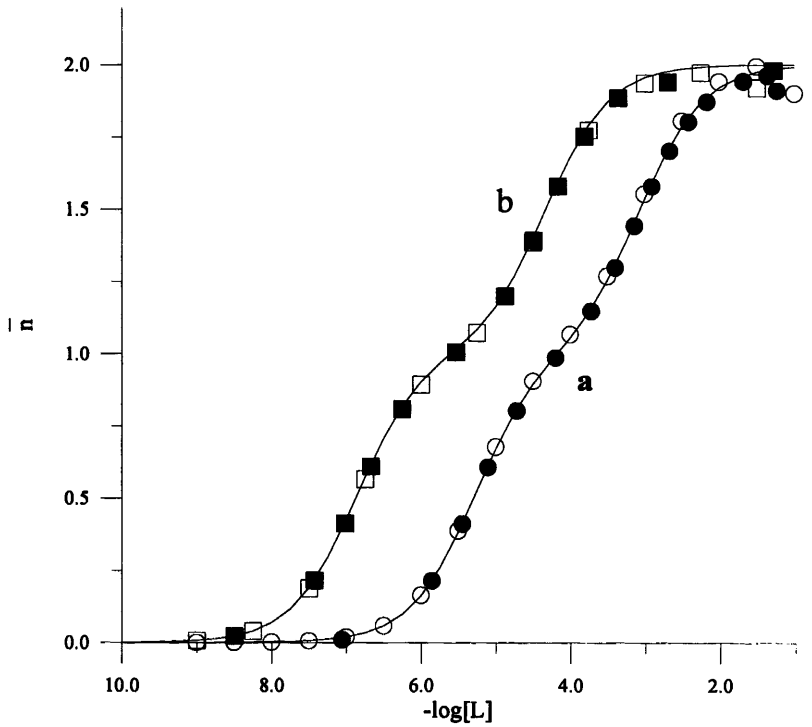


Fig. 1. Average ligand number $\bar{n}$ versus $-\log[L]$ for (a) lanthanum- and (b) lutetium-dien systems in dmf. (a) (○) C°_{La} 10.03, C°_{Ag} 1.98; (●) C°_{La} 27.78, C°_{Ag} 9.87; (b) (□) C°_{Lu} 9.57, C°_{Ag} 1.98; (■) C°_{Lu} 28.34, C°_{Ag} 9.87 mmol dm^{-3}. Only some of the experimental points, chosen at random, have been plotted. The full curves were calculated from the stability constants in Table 1.

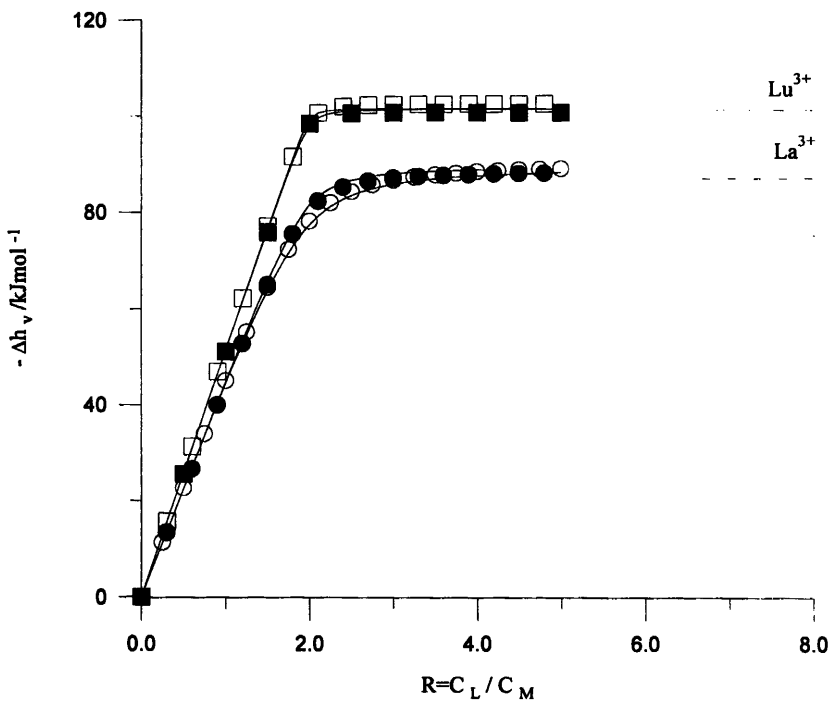


Fig. 2. The total molar enthalpy changes, Δh_v, as a function of $R = C_L/C_M$ for lanthanide(III)-dien systems in dmf. (a) (○) 8.02, (●) 20.52 mmol dm^{-3} in La^{3+}; (b) (□) 7.93, (■) 19.80 mmol dm^{-3} in Lu^{3+}. Only some of the experimental points, chosen at random, have been plotted. The solid lines have been calculated from the values of β_j and $\Delta H^{\circ}_{\beta_j}$ in Table 1. The dashed lines represent the values of enthalpy per mole of added metal obtained by the 'reverse' titrations (see text for details).

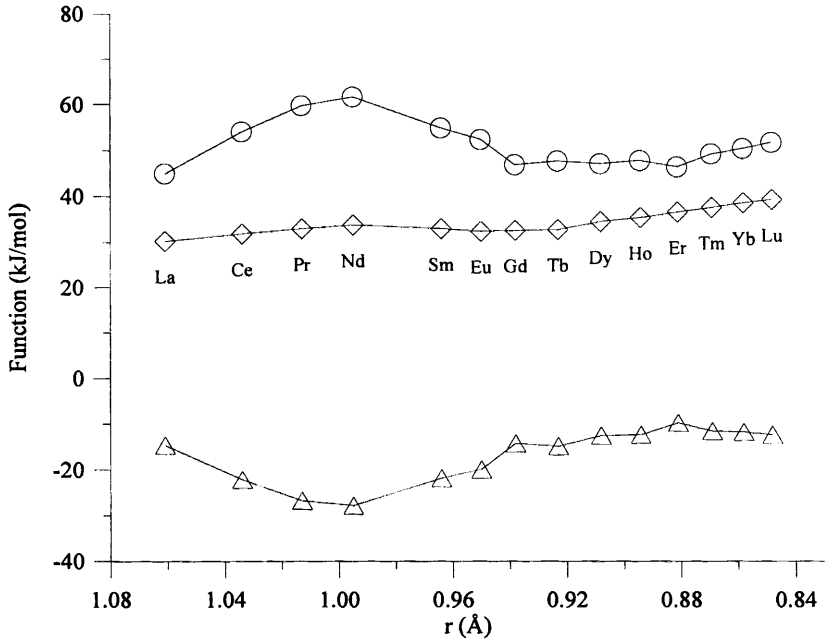


Fig. 3. Lanthanide(III)-dien thermodynamic functions for the 1:1 complex formation versus the ionic radius in dmf at 298 K and $I = 0.1$ mol dm^{-3}: (◇) $-\Delta G^{\circ}_{\beta_1}$; (○) $-\Delta H^{\circ}_{\beta_1}$; (△) $T\Delta S^{\circ}_{\beta_1}$.

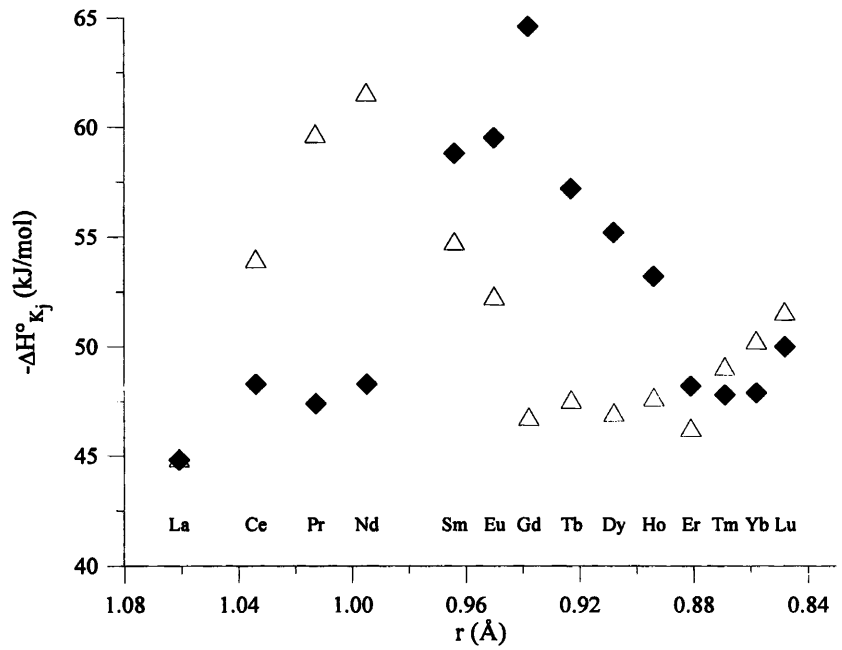


Fig. 4. Lanthanide(III)-dien stepwise $\Delta H^{\circ}_{K_j}$ functions versus the ionic radius in dmf at 298 K and $I = 0.1$ mol dm^{-3}: (△) ΔH°_{Kj}; (◆) ΔH°_{Kj}.

ent Ln^{3+}/Ag^{+} ratios and their shapes, indicate that neither polynuclear nor mixed complexes are formed in appreciable amounts and that two successive complexes are formed in stepwise equilibria.

The total heats of reaction per mole of metal ion, Δh_v, are reported as a function of $R = C_L/C_M$ in Fig. 2 for La and Lu respectively. The dotted lines in Fig. 2 refer to the values of enthalpy per mole of metal added, $\Delta h'_v$, obtained by the 'reverse' titrations. $\Delta h'_v$ is equal to Δh_v at $R \geq 2$ for the Lu(III)-system excluding the formation of higher complexes beyond the second one. For the La(III)-dien system the direct and reverse curves superimpose at slightly higher R values, as expected given the lower stabilities for the two complexes formed.

The experimental heats of reaction and the overall stability constants in Table 1 were used to calculate the full lines in Fig. 2. The experimental data fit is quite

good, indicating that the systems are described satisfactorily. Similar results are obtained for the other lanthanides.

The trend in the thermodynamic functions for the 1:1 lanthanide(III) complex formation in dmf are reported in Fig. 3 versus the lanthanide ionic radius [31]. In Fig. 4 the same plot has been drawn for the stepwise enthalpy functions, $\Delta H^{\circ}_{K_1}$ and $\Delta H^{\circ}_{K_2}$.

Some potentiometric and calorimetric titrations were also performed in dmf using the uncoordinating perchlorate as background anion [4]. No differences were observed between the data obtained with perchlorate and triflate for lanthanum and lutetium systems, so the safer triflate [19] was used in this study.

4. Discussion

4.1. Lanthanide(III)-dien systems

The data in Fig. 3 show that the stability constants of the 1:1 lanthanide(III) complexes increase almost regularly from La to Nd and from Tb to Lu, whereas almost constant values are observed from Nd to Tb. This trend, likely due to different factors acting in opposite directions, is unexpected as the increasing charge density along the series should give a monotonous increase of the stability constants [1,5].

The analysis of the enthalpy and entropy values accompanying the complex formation gives an explanation for the observed trend.

The negative enthalpy values here found (Table 1) are typical of reactions involving complexation of metal ions by neutral ligands in aprotic solvents [5,12,13,17,19,32,33]. The entropy terms, also negative, oppose the complex formation. Likely, the release of solvent molecules from the coordination sphere of the metal cations, which always accompanies complexation, does not compensate the decrease in internal entropy of the ligand and the negative entropy change due to the loss of translational entropy of the reagents when the complexes are formed.

The stability constants and the enthalpy changes of the 1:1 Ln(III)-dien complexes in dmf are much higher amd more exothermic, respectively, than those in dmso where dien was shown to act as tridentate [17]. Moreover, the thermodynamic data here reported are quite different from our unpublished results which indicate much lower stabilities and exothermicities for the complexation of lanthanides(III) by the unidentate *n*-butylamine (*n*-but) in dmf [34]. Thus, both the stability constants and the enthalpies of formation indicate that dien forms inner sphere complexes acting as tridentate in dmf too.

The trends of the $\Delta H^{\circ}_{\beta_1}$ and $\Delta S^{\circ}_{\beta_1}$ values along the lanthanide series show several discontinuities. Fig. 3 shows that the $-\Delta H^{\circ}_{\beta_1}$ values increase remarkably in the order La < Ce < Pr < Nd, then steadily decrease from Nd to Gd and thereafter slightly increasing values are observed until Lu(III). The variation of $-\Delta S^{\circ}_{\beta_1}$ along the series is similar to $-\Delta H^{\circ}_{\beta_1}$. A series of successive solvation equilibria can explain these trends. The increasing exothermicity from La to Nd can be interpreted by taking into account that La–Nd ions are present in dmf solutions in two differently solvated species. Cossy and Merbach and Pisaniello [35,36] have evidenced that the equilibrium (Eq. (1)) occurs for La, Ce, Pr and Nd ions:

$$[Ln(dmf)_9]^{3+} \rightleftharpoons [Ln(dmf)_8]^{3+} + dmf \quad (1)$$

and that this equilibrium is shifted to the right in the order La < Ce < Pr < Nd. As ΔH° for Eq. (1) is positive ($\Delta H^{\circ} = +14.8$ kJ mol^{-1} and $\Delta S^{\circ} = +69$ J K^{-1} mol^{-1} for Nd [37]), the complexation of $[Ln(dmf)_9]^{3+}$ would be less exothermic than that of $[Ln(dmf)_8]^{3+}$ to give the same $[LnL(dmf)_x]^{3+}$ species. Thus, the systematic increase in $-\Delta H^{\circ}_{\beta_1}$ from La to Nd might reflect the decrease of the desolvation enthalpy on going toward higher *Z*. The entropy changes, which decrease from La to Nd, agree with this hypothesis.

The eight-coordinated $[Ln(dmf)_8]^{3+}$ species predominates from Nd to Lu [4]. The decrease of $-\Delta H^{\circ}_{\beta_1}$ and $-\Delta S^{\circ}_{\beta_1}$ from Nd to Gd could be reasonably explained by admitting a second solvation equilibrium (Eq. (2)) that involves in this case the complexes formed instead of the bare ions and that is progressively shifted to the right from Nd to Gd.

$$[LnL(dmf)_x]^{3+} \rightleftharpoons [LnL(dmf)_{x-1}]^{3+} + dmf \quad (2)$$

In this scheme, the slight increase of $-\Delta H^{\circ}_{\beta_1}$ from Gd^{3+} to Lu^{3+} may be related to a situation where both the equilibria (1) and (2) are almost completely shifted to the right and so the enthalpy change mainly depend on the charge density of the metal ion.

The similarity of the thermodynamic functions for the formation of La^{3+} and Gd^{3+}-dien complexes as well as the difference between the $\Delta H^{\circ}_{\beta_1}$ and the $\Delta S^{\circ}_{\beta_1}$ for the formation of La/Gd-dien and Nd-dien complexes (~ 16 kJ mol^{-1} and ~ 45 J K^{-1} mol^{-1}, respectively), which are close to the binding parameters of a dmf molecule (Eq. (1)), nicely fit this interaction scheme.

The values of K_1/K_2 (in the range $10–10^2$) are not so helpful in describing the behaviour of the second ligand in $[Ln(dien)_2]^{3+}$; on the other hand the high exothermicity associated with the stepwise formation of the bis-dien complex (Fig. 4) suggests that also in this case dien behaves as tridentate.

The above mentioned interaction scheme, based on desolvation equilibria, can be successfully employed to explain also the thermodynamics of formation of the second complex. As previously suggested, 1:1 dien complexes of the lighter lanthanides (La–Nd) have the same

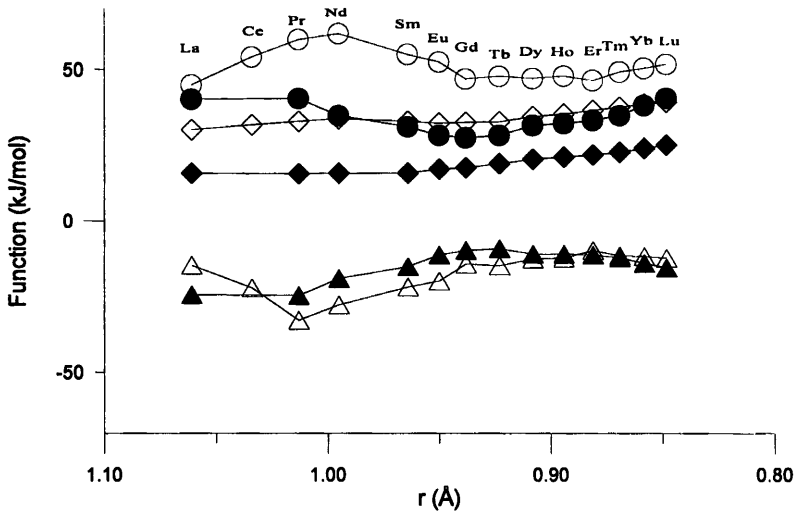


Fig. 5. Lanthanide(III)-dien thermodynamic functions for the 1:1 complex formation versus the ionic radius in dmf ((◇) $-\Delta G^{\circ}_{\beta_1}$; (○) $-\Delta H^{\circ}_{\beta_1}$; (▲) $T\Delta S^{\circ}_{\beta_1}$) and dmso ((◆) $-\Delta G^{\circ}_{\beta_1}$; (●) $-\Delta H^{\circ}_{\beta_1}$; (△) $T\Delta S^{\circ}_{\beta_1}$) at 298 K and $I = 0.1$ mol dm^{-3}.

coordination number. Thus, the slight increase of the stepwise $-\Delta H^{\circ}_{K_2}$ observed from La(III) to Nd(III) is due to the increase of the metal-ligand interaction in the hypothesis that Eq. (3) is the only equilibrium in solution.

$$[\mathrm{LnL(dmf)}_x]^{3+} + \mathrm{L} \rightleftharpoons [\mathrm{LnL_2(dmf)}_{x-n}]^{3+} + n\,\mathrm{dmf} \quad (3)$$

From Nd to Gd, equilibrium (2) is more and more shifted to the right. After gadolinium, all the 1:1 complexes have the same coordination number. So, the increase of $-\Delta H^{\circ}_{K_2}$ for the 1:2 Nd–Gd complexes is due to the lower energy required to desolvate $[\mathrm{LnL(dmf)}_x]^{3+}$ complexes to obtain species with the same stoichiometry. The decrease of the heat of reaction from Gd to Er, is likely due to the equilibrium (4) involving the solvation sphere of the ML_2 complex and shifted to the right in the order Gd < Tb < Dy < Ho < Er.

$$[\mathrm{LnL_2(dmf)}_y]^{3+} \rightleftharpoons [\mathrm{LnL_2(dmf)}_{y-1}]^{3+} + \mathrm{dmf} \quad (4)$$

From Er to Lu both the 1:1 and 1:2 complexes of the lanthanides have the same stoichiometry, so no large difference in the $-\Delta H^{\circ}_{K_2}$ values is expected, and observed, along this series.

The trend in the stepwise entropy values agree, also in this case, with the proposed interaction scheme.

For comparison, in Fig. 5 the thermodynamic data for the Ln(III)-dien complexes in dmf and in dmso [17] are plotted. It can be observed that the lanthanide(III)-dien complexes are always more stable and more enthalpy stabilized in dmf than in dmso: this feature is an example of the remarkable influence of the solvent in complex formation. In fact, although the difference in DN between dmf and dmso is low [20], nevertheless it is sufficient to highly favor complexation reactions in dmf. In this context it is noteworthy to underline that in dmso monoamines do not coordinate lanthanide(III) ions, while in dmf they do [34].

The order of magnitude of the entropy changes and the general trends of entropy and enthalpy values versus the ionic radii are similar in the two solvents. From this, it follows: (i) solvation equilibria similar to those proposed here might be taken into account also to explain the data obtained in dmso;(ii) the solvent bulk does not seem to be significantly influenced by the coordination of a neutral ligand to a lanthanide ion. So, the specific interactions of the solvent and of the ligand with the metal ion should be considered mainly responsible for the stability trends along the lanthanide series.

4.2. Silver(I)-dien system

Negative values of enthalpy and entropy are obtained also for this system as a consequence of the formation of strong covalent Ag–N bonds and the relatively weak solvation of the species [23].

The 1:1 complex formed in dmf is much more stable than the analogous tridentate complex in dmso for which $\log \beta_1 = 7.46$ [38]. The silver ion is tetrahedrally coordinated both in dmso and in dmf [39] and the similarity of thermodynamic data (in dmso $\Delta H^{\circ}_{\beta_1} = -78.2$ and $T\Delta S^{\circ}_{\beta_1} = -32.5$ kJ mol^{-1}) suggests retention of this structure when complexation occurs in both solvents. Therefore, it is likely that dien behaves as tridentate also in dmf, forming two fused five-membered chelate rings with the fourth tetrahedral position occupied by a solvent molecule[3].

[3] Tridentation is moreover confirmed by a comparison with preliminary values of $\log \beta_1$ and $\Delta H^{\circ}_{\beta_1}$, respectively about 4.80 (0.06) and −36 (2) kJ mol^{-1}, obtained in our laboratory for silver(I) complexation with the unidentate *n*-butylamine in dmf.

The very high value of the ratio $K_1/K_2 \approx 10^7$, together with the stepwise enthalpy and entropy values associated with the formation of AgL_2^+ complex ($\Delta H^\circ_{k_2} = -18.4$ and $T\Delta S^\circ_{k_2} = -1.5$ kJ mol^{-1}) are in agreement with the formation of one five-membered chelate ring by each of the two ligands.

The higher stability of the silver(I) complexes in dmf with respect to dmso can be mainly attributed to the weaker solvation of metal ion in the former solvent. Transfer functions from dmf to dmso of silver(I) are in fact $\Delta G^\circ_{tr,dmf\rightarrow dmso} = -14.0$ and $\Delta H^\circ_{tr,dmf\rightarrow dmso} = -18.3$ kJ mol^{-1} [40].

Comparison of the thermodynamic stabilities of the complexes in dmf and in water gives a good example of the ligand solvation influence in these complexation reactions. In fact, despite the larger solvation of metal ion in dmf than in water [40], the thermodynamic stability of the 1:1 complex in water is lower than in dmf ($\log \beta_{1(water)} = 6.10$ [10]). This can be connected with the larger solvation of the amine in water, through strong hydrogen bonds, which evidently compensates for the stronger solvation of Ag^+ in dmf ($\Delta G^\circ_{tr,H_2O\rightarrow dmf} = -21$ and $\Delta H^\circ_{tr,H_2O\rightarrow dmf} = -35$ kJ mol^{-1} [40]).

References

[1] G.R. Choppin, J. Less-Common Met. 112 (1985) 193. In: Lanthanide Probes in Life, Chemical and Earth Sciences, Elsevier, Amsterdam, 1989, chapter 1.
[2] G. Xian Xu, Pure Appl. Chem. (1988) 8.
[3] E.N. Rizkalla, G.R. Choppin, in: K.A. Gschneidener, L. Eyring (Eds.), Handbook on the Physics and Chemistry of Rare Earths, vol. 15, North-Holland, Amsterdam, 1991, pp.393–441.
[4] S.I. Ishiguro, K. Kato, R. Takahashi, S. Nakasone, Rare Earths 27 (1995) 61 and refs cited therein.
[5] J.-C.G. Bünzli, A. Milicic-Tang, Handbook of the Physics and Chemistry of Rare Earths, Elsevier, Amsterdam, 1995, pp. 21, 305.
[6] A.K. Saha, K. Kross, E.D. Kloszewski, D.A. Upson, J.L. Toner, R.A. Snow, C.D.V. Black, V.C. Desai, J. Am. Chem. Soc. 115 (1993) 11032.
[7] J.-C.G. Bunzli, in: G.R.Choppin, J.-C.G. Bunzli (Eds.), Lanthanide Probes in Life, Chemical and Earth Sciences, Elsevier, Amsterdam, 1989, chapter 7.
[8] J.A. Peters, J. Huskens, D.J. Raber, Prog. NMR Spectrosc. 28 (1996) 283.
[9] S. Aime, M. Botta, M. Fasano, E. Terreno, Chem. Soc. Rev. 27 (1998) 19 and refs. cited therein.
[10] D.D. Perrin, Stability Constants of Metal Ion Complexes, IUPAC Chemical Data Series no. 22, Pergamon, Oxford, 1979, part B.
[11] R.M. Smith, A.E. Martell, Sci. Total Environ. 64 (1987) 125.
[12] J.H. Forsberg, Coord. Chem. Rev. 10 (1973) 195.
[13] F. Arnaud-Neu, Chem. Soc. Rev. (1994) 235.
[14] M.A. McKervey, M.J. Schwing-Weill, F. Arnaud-Neu, in: G.W. Gokel (Ed.), Comprehensive Supramolecular Chemistry, vol. 1, Elsevier, Oxford, 1996, p. 537 and refs. cited therein.
[15] A. Cassol, P. Di Bernardo, R. Portanova, M. Tolazzi, G. Tomat, P. Zanonato, J. Chem. Soc., Dalton Trans. (1992) 469.
[16] Z. Wang, G.R. Choppin, P. Di Bernardo, P.L. Zanonato, R. Portanova, M. Tolazzi, J. Chem. Soc., Dalton Trans. (1993) 2791.
[17] A. Cassol, G.R. Choppin, P. Di Bernardo, R. Portanova, M. Tolazzi, G. Tomat, P. Zanonato, J. Chem. Soc., Dalton Trans. (1993) 1695 and refs. cited therein.
[18] P. Di Bernardo, G.R. Choppin, R. Portanova, P.L. Zanonato, Inorg. Chim. Acta 207 (1993) 85.
[19] A. Cassol, P. Di Bernardo, R. Portanova, M. Tolazzi, P. Zanonato, Inorg. Chim. Acta 262 (1997) 1.
[20] V. Guttmann, Coordination Chemistry in Non-Aqueous Solution, Springer-Verlag, Vienna, 1968.
[21] V. Guttmann, The Donor Acceptor Approach to Molecular Interactions, Plenum, New York, 1978.
[22] J.A. Riddick, W.B. Burger, T.K. Sakano, Organic Solvents, Wiley-Interscience, New York, 4th edn. 1986.
[23] S. Ahrland, in: J.J. Lagowski (Ed.), The Chemistry of Non-aqueous Solvents, vol. 5a, Academic Press, New York, 1978, chapter 1.
[24] F.J.C. Rossotti, H. Rossotti, The Determination of Stability Constants, McGraw-Hill, New York, 1961, p. 58.
[25] S.L. Lyle, Md.M. Rahmer, Talanta (1963) 1177.
[26] W.J. Geary, Coord. Chem. Rev. 7 (1971) 81.
[27] A. Cassol, P. Di Bernardo, P. Zanonato, R. Portanova, M. Tolazzi, J. Chem. Soc., Dalton Trans. (1987) 657.
[28] P. Gans, A. Sabatini, A. Vacca, J. Chem. Soc., Dalton Trans. (1985) 1995.
[29] R.M. Smith, A.E. Martell, Critical Stability Constants, vol. 6, Plenum, New York, 2nd suppl., 1989.
[30] R. Arnek, Ark. Kemi 32 (1970) 81.
[31] F.A. Cotton, G. Wilkinson, Advanced Inorganic Chemistry, Wiley, New York, 4th edn., 1980, p. 1011.
[32] Y. Liu, T.-B. Lu, M.-Y. Tau, T. Hakushi, Y. Iaoue, J. Phys. Chem. 97 (1993) 4548.
[33] A. Del Zotto, P. Di Bernardo, M. Tolazzi, P.L. Zanonatao, J. Chem. Soc., Dalton Trans. (1999) 979.
[34] For the Tm–*n*-but system, for example, $\log \beta_1 = 2.0(2)$ and $\Delta H^\circ_{\beta 1} = -17(3)$ kJ mol^{-1} have been found.
[35] D.L. Pisaniello, L. Helm, P. Meier, A.E. Merbach, J. Am. Chem. Soc. 105 (1983) 4528.
[36] C. Cossy, A.E. Merbach, Pure Appl. Chem. 60 (1988) 1785.
[37] D.L. Pisaniello, P.J. Nichols, Y. Ducommun, A.E. Merbach, Helv. Chim. Acta 65 (1982) 1025.
[38] A. Cassol, P. Di Bernardo, P. Zanonato, R. Portanova, M. Tolazzi, G. Tomat, V. Cucinotta, D. Sciotto, J. Chem. Soc., Faraday Trans. 1 85 (1989) 2445.
[39] Y. Tsutsui, K. Sugimoto, H. Wasada, Y. Inada, S. Funahashi, J. Phys. Chem. A 101 (1997) 2900.
[40] Y. Marcus, Ion Solvation, Wiley, New York, 1985.

PERGAMON

www.elsevier.nl/locate/poly

Polyhedron 19 (2000) 2435–2440

POLYHEDRON

Spectrophotometric and potentiometric study on platinum(II) chelates of mercapto carboxylic acids

Guido Crisponi [a,*], Franco Cristiani [a], Valeria Marina Nurchi [a], Rosalba Pinna [a], Tiziana Pivetta [a], María José Tapia Estévez [b]

[a] *Dipartimento di Chimica Inorganica e Analitica, Università degli Studi di Cagliari, Complesso Universitario di Monserrato, 09042 Monserrato Cagliari, Italy*

[b] *Área de Química Física, Departamento de Química, Universidad de Burgos, Plaza Misael Bañuelos, 09001 Burgos, Spain*

Abstract

The coordination of Pt(II) with different mercapto and dimercapto compounds has been studied using both potentiometric titration at 25°C in KCl 0.1 M and UV–Vis spectroscopy. The slow complex formation kinetics has been followed spectrophotometrically for several days on samples with different ligand molar fractions ranging from 0.1 to 1, keeping the ligand and metal concentration below 8×10^{-4} M. For the potentiometric titration, the ligand concentrations were kept constant at 10^{-3} M, and the 0.25, 0.5, 0.75 and 1.00 metal/ligand ratios were titrated in the pH range 2.5–11 for each ligand. The solutions were kept in a thermostatted bath at 25°C for 2 days before titration. The stabilization of the absorbance values under these conditions after 2 days, and the back titration with hydrochloric acid 0.1 M, led us to conclude that the proper equilibrium complex formation is reached under these conditions. Using KCl 0.1 M as an ionic strength medium, the reported formation constants are referred to the complexation reaction starting from $[PtCl_4]^{2-}$. Some models are proposed on the basis of the estimated stoichiometries.
© 2000 Elsevier Science B.V. All rights reserved.

Keywords: *meso*-2,3-Dimercaptosuccinic acid; Potentiometry; UV–Vis spectroscopy; Formation constants; Ionization constants; Kinetic measurements

1. Introduction

The use of chelating agents in the treatment of human metal intoxication is a field of great interest to health sciences [1–4]. Particularly, platinum intoxication is an important side effect suffered by patients treated with the antitumour drug *cis*-dichlorodiammine platinum(II) (cisplatin). Nephrotoxicity is the most serious complication due to cisplatin treatment: this has been ascribed to Pt^{2+} binding by sulphide groups of proteins in kidney tubules [5]; as a consequence, several studies have shown that compounds containing thiolic groups can reduce the toxicity of this drug without affecting its antitumour activity [6–8].

The principal aspect of platinum(II) behaviour that is to be taken into account when planning a chelating therapy, is that platinum is strongly bounded intracellularly [9]. A chelating agent such as DMSA (*meso*-2,3-dimercapto succinic acid), however, is not capable of permeating cell membranes at a physiological pH, because of its high charge due to deprotonations of the carboxylic groups. Nevertheless, thanks to the properties of DMSA in the treatment of heavy metal poisoning, in other words its low toxicity and good adsorption in the intestinal tract, it could be used as an oral chelator. This has added considerable interest to the study of its lipophilic analogues, monomethyl and dimethyl dimercapto succinates, that could be used conveniently in platinum chelation.

In this paper we present the equilibrium studies of both monomethyl and dimethyl dimercapto succinates and their parent compound, *meso*-2,3-dimercapto succinic acid (DMSA), as well as those of mercaptosuccinic acid, which is similar to DMSA except for the fact that it has only one –SH binding group. The formulas of the studied molecules are shown in Table 1.

* Corresponding author. Tel. +39-070-675-4476; fax: +39-070-675-4478.

E-mail address: crisponi@vaxca1.unica.it (G. Crisponi).

0277-5387/00/$ - see front matter © 2000 Elsevier Science B.V. All rights reserved.
PII: S0277-5387(00)00542-8

Table 1
Names, formulae and acronyms of the used compounds

mercapto succinic acid	*meso*-2,3-dimercapto succinic acid	*meso*-monomethyl dimercapto succinate	*meso*-dimethyl dimercapto succinate
COOH CHSH CH_2 COOH	COOH CHSH CHSH COOH	COOH CHSH CHSH $COOCH_3$	$COOCH_3$ CHSH CHSH $COOCH_3$
MSA	**DMSA**	**MMS**	**DMS**

The ionization constants of the above molecules, determined in a previous work [10] are reported in Table 2.

2. Experimental

2.1. Reagents

The KOH standard solutions, potassium tetrachloroplatinate(II) 99.99%, KCl, mercapto succinic acid, and *meso*-2,3-dimercapto succinic acid were Aldrich products; monomethyl and dimethyl dimercapto succinates were synthesized according to Gerecke [11]. The commercial compounds were used without further purification, the others were checked by elemental analysis with a CHN-S Fisons instrument and by ^{13}C NMR and IR spectra.

The daily procedure for use of the solutions of DMSA and its derivatives is as described in a previous work on Pd(II) complexes [12]. The Pt(II) solution was prepared by dissolving the weighted amount of potassium tetrachloroplatinate(II) in a KCl 0.1 M aqueous solution.

Table 2
Ionization constants for the four molecules in Table 1 [a]

	pK_{C1}	pK_{C2}	pK_{S1}	pK_{S2}
Mercapto succinic acid	3.12(1)	4.52(1)	10.24(3)	
meso-2,3-Dimercapto succinic acid	2.71(1)	3.43(2)	9.65(3)	12.05(3)
meso-Monomethyl dimercapto succinate	2.80(1)		7.15(2)	9.98(2)
meso-Dimethyl dimercapto succinate			5.23(1)	7.32(3)

[a] pK_{C1} and pK_{C2} refer to the ionization of the first and second COOH, pK_{S1} and pK_{S2} to the ionization of the first and second SH. Values in parentheses are standard deviations of the last significant figure.

2.2. Potentiometric measurements

Titrations were performed on a Dosimat 665 Metrohm automatic titrator connected to a Metrohm 691 pH meter. We used a thermostatted glass cell equipped with a magnetic stirring system, a Metrohm glass electrode for highly alkaline solutions, a thermometric probe, a microburet delivery tube, an inlet–outlet tube for argon, and a salt bridge connected with the reference cell, filled with a KCl 0.1 M solution, in which a saturated calomel electrode was dipped. The solutions were titrated at 25°C with carbonate-free KOH 0.1 M. The electrode was calibrated for hydrogen ion concentration by titrating HCl with KOH in KCl 0.1 M; the resulting data were analysed with the Gran [13] procedure using our GRANPLOT program. The ionization and formation constants were calculated with the PSEQUAD program [14]. All the solutions at variable ligand/metal ratios were stored at 25°C for 2 days before potentiometric analysis because of their very slow complexation. For each ligand we titrated 20 ml of the ligand–Pt(II) mixtures at an ionic strength of 0.1 M KCl with KOH 0.1 M. The ligand was always 10^{-3} M, while Pt(II) was varied according to the following ligand/metal molar ratios: 4:1, 4:2, 4:3 and 4:4. The number of experimental points for each titration was 100 in the 2.5–11 pH range. The reversibility of the equilibria was proved by carrying out an acidic titration after each basic titration.

2.3. Kinetic measurements

The formation reaction was monitored with a Hewlett–Packard 8452 diode array spectrophotometer. The absorption spectra of the samples with 8×10^{-4} M ligand and metal concentrations at an ionic strength 0.1 M of KCl were recordered every 5 min for 2 days in a 1 cm cell at 25°C.

In all the experiments the reaction proceeded under pseudo-first-order conditions and the absorbance increase due to the complex formation is given by the equation

$$A = p_1 \exp(-t/\tau) + p_2 \quad (1)$$

where τ is the relaxation time, p_1 and p_2 are constants

connected to absorbance values of reagents and products.

The kinetic measurements were evaluated fitting Eq. (1) to the absorbance value at several wavelengths, using the Marquardt algorithm. No systematic deviations between the experimental points and the fitted curves were observed.

3. Results and discussion

Platinum(II) equilibria are infrequently studied because of the inherent difficulties that are basically of two kinds: the presence of multiple equilibria with Cl^- and OH^-, and the kinetic slowness in reaching equilibrium. The equilibria among Pt(II) and chloride are quantitatively shifted to $[PtCl_4]^{2-}$ when KCl 0.1 M is used as an ionic strength medium. The reported formation constants are thus referred to the complexation reaction which starts from $[PtCl_4]^{2-}$. These conditions are quite similar to the actual plasma (103 mM in chloride) [15] in the treatment of Pt(II) poisoning in humans. As regards the slowness in reaching equilibrium, we proved that the limiting step was the complex formation when ligand and metal ions were mixed together.

The complex requires hours to form, while the equilibrium is reached rapidly after each base addition. Therefore each titration started 2 days after prepearing the ligand–Pt mixture, and delay times of 1 min between base additions were applied. The experimental titration curves were fitted with the models and the formation constants reported in Table 3, using the PSEQUAD program. Table 3 also shows the pK values for the deprotonation steps, that are reported for a better reading.

The experimental titration data for mercapto succinic acid (MSA) were fitted using a model $Pt_2L_4H_x$ with x ranging from 6 to zero; a possible structure of $Pt_2L_4H_6$ could be that presented in Fig. 1 in which the two platinum(II) ions are held together by two sulphur bridges, and the square planar coordination is completed by two ligand molecules bonded to the platinum(II) ions via the sulphide and carboxylic groups.

Table 3
Models, ligand/metal ratios of each model, logarithm of formation constants, and pK of complex deprotonations estimated for the systems with the four studied ligands [a]

Model	L/M	log(β)	pK	Model	L/M	log(β)	pK
MSA				MMS			
$Pt_2L_4H_6$	2	92.9		$Pt_2L_3H_4$	1.5	73.3	
$Pt_2L_4H_5$		88.6	4.3	$Pt_2L_3H_3$		70.0	3.3
$Pt_2L_4H_4$		84.0	4.6	Pt_2L_3H		58.3	5.8
$Pt_2L_4H_3$		78.5	5.5	PtL_2H_3	2	46.9	
$Pt_2L_4H_2$		72.3	6.2	PtL_2H_2		41.1	5.8
Pt_2L_4H		64.6	7.7				
Pt_2L_4		55.0	9.6				
DMSA				DMS			
$Pt_2L_3H_3$	1.5	66.4		$Pt_2L_3H_2$	1.5	53.5	
$Pt_2L_3H_2$		59.1	7.3	Pt_2L_3H		50.1	3.4
Pt_2L_3H		49.6	9.5	Pt_2L_3		41.4	8.7
$Pt_2L_4H_7$	2	102.2		PtL_4H_4	4	67.4	
$Pt_2L_4H_6$		97.6	4.6	PtL_4H_3		60.8	6.6
$Pt_2L_4H_5$		92.2	5.4	PtL_4H_2		51.9	8.9
$Pt_2L_4H_4$		85.6	6.6				
$Pt_2L_4H_3$		77.0	8.6				
Pt_2L_4H		56.1	10.5				

[a] The individual standard deviations of log(β) are not reported in the table, but they all range between 0.1 and 0.3.

This complex, which was completely formed at pH 3, loses the first two protons at pK 4.3 and 4.6. These values are comparable to pK 4.52 relating to the second ionization of the free ligand. The remaining four protons are lost at progressively higher pK values 5.5, 6.2, 7.7 and 9.6, because of an increasing negative charge on the complex.

On considering the *meso*-2,3-dimercapto succinic acid (DMSA), two different complexes appear, one with a similar stoichiometry to mercaptosuccinic acid, the other characterized by three ligands binding two Pt(II) ions. The structures tentatively proposed for these complexes in the most protonated form are shown in Fig. 2.

The difference between these two complexes consists in the substitution of one of the bridge ligands by a μ-water molecule. The structures in Fig. 2B, where

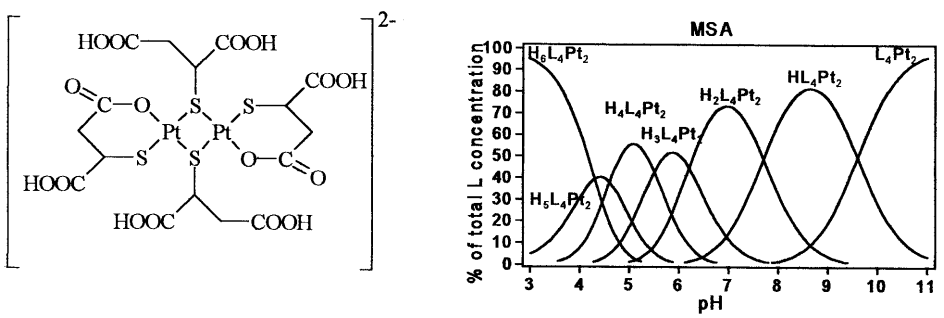


Fig. 1. The distribution curves for the MSA–Pt(II) system are reported on the right as a function of pH, [Pt(II)] being 1 mM and [MSA] 2 mM. A possible structure for the $H_6L_4Pt_2$ complex is proposed on the left.

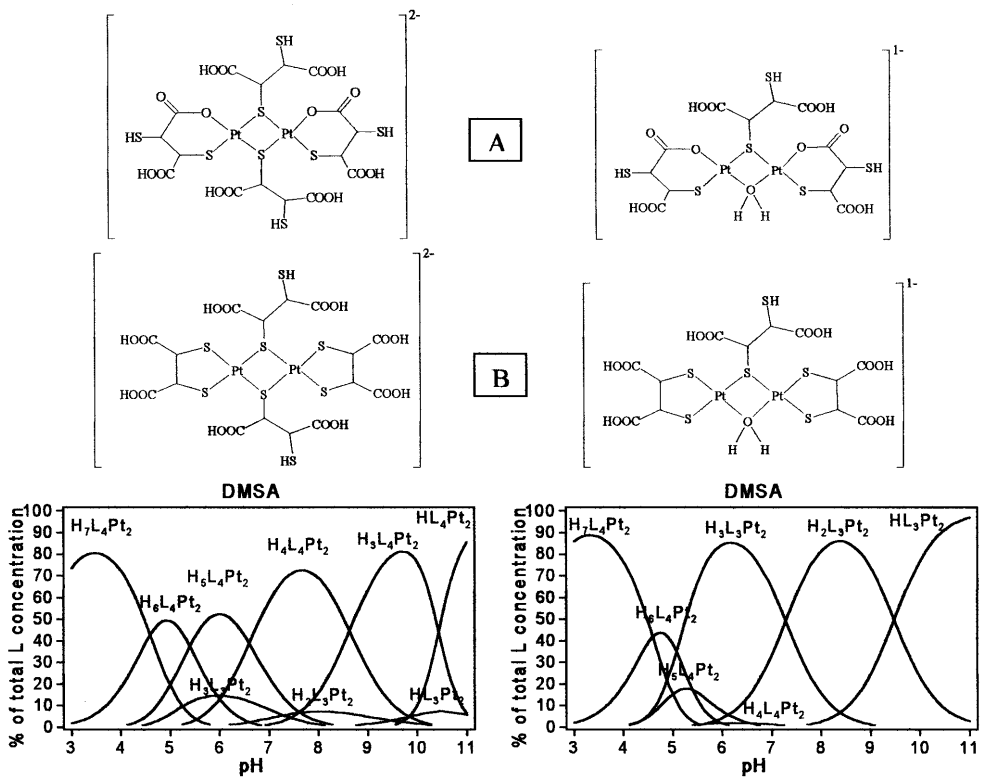


Fig. 2. The distribution curves for the DMSA–Pt(II) system are presented in the lower part, [DMSA] being always 2 mM and [Pt(II)] 2 mM in the right plot and 1 mM in the left. Possible structures of $Pt_2L_4H_{10}$ (left) and $Pt_2L_3H_7$ (right) are shown in the upper part. The structures A and B differ in the coordination of the external ligands.

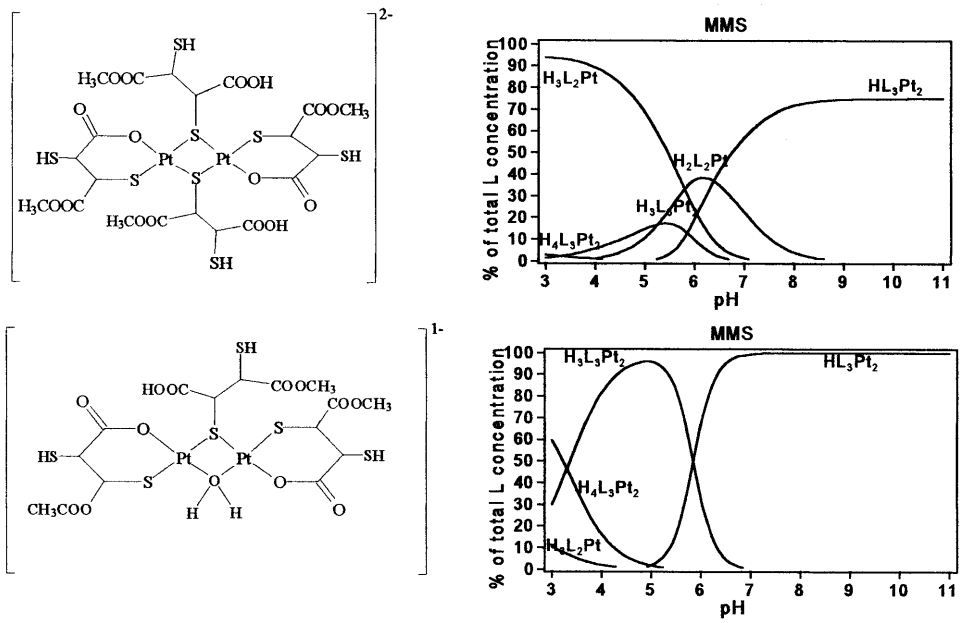


Fig. 3. The distribution curves for the MMS–Pt(II) system are presented on the right, [MMS] being always 2 mM and [Pt(II)] 2 mM in the upper plot and 1 mM in the lower. Possible structures of $Pt_2L_4H_6$ and $Pt_2L_3H_4$ are shown respectively in the upper and lower parts.

coordination of external ligands takes place using both mercapto groups, are as acceptable as those in Fig. 2A. The existing species at pH 3 loses three protons from carboxylic groups, unlike the complex with mercapto succinic acid. This is also consistent with the fact that the two carboxylic groups in DMSA are more acidic respectively by 0.4 and 1.1 pK units (see Table 2).

The model derived for *meso*-monomethyl dimercapto succinate (MMS), can be represented by the structures proposed in Fig. 3. The two stoichiometries, which

seem different at first sight, can actually be represented by very similar structures. In fact, as in the case of MSA and DMSA, PtL_2H_3 can be assumed to have the structure in the upper left part of Fig. 3. In such a model it is supposed that only one mercapto group per ligand will take part in coordination. Ionization at pK 5.8 therefore, which is slightly higher than in the free ligand both for the negative -2 charge on the entire molecule and for the inductive effect of Pt(II) coordination at the mercapto group, relates to the carboxylic group. For the same reasons, the deprotonation of –SH groups not implied in complexation takes place at pK values greater than 11 and is not experimentally observed in potentiometric measurements.

$Pt_2L_3H_4$, which appears at a 1:1 L/M ratio, can be represented with the structure in the lower left part of Fig. 3, which is very similar to the upper part, and differs only by the substitution of a bridge ligand between two Pt(II) ions with a μ-water. The latter ionizes at pK 3.3, while the only carboxylic group loses its proton at the same pK 5.8 as with $Pt_2L_3H_4$. With MMS, as with DMSA, two structures are possible when the ligand binds through the two –SH groups.

On the other hand the behaviour of *meso*-dimethyl dimercapto succinate (DMS) is quite different. At high L/M ratios, the PtL_4H_4 species is formed, where each ligand behaves as monodentate. The first two of the second –SH protons of each ligand is lost at 6.6 and 8.9, respectively at a lower and higher value than that of the free ligand 7.32. The loss of the last two protons is not experimentally observed. At lower L/M ratios a $Pt_2L_3H_2$ species is formed as in the previously observed complexes for DMSA and its monomethyl derivative. In this case the $Pt_2L_3H_2 \rightarrow Pt_2L_3H$ transition, i.e. the formation of the second pentatomic ring, occurs at pK 3.4. Here this is the only possible structure, since a coordinating carboxylic group is not available (Fig. 4).

For all four ligands, a strong increase in absorbance was observed in the 250–450 nm range during the formation reaction (Fig. 5), but no significant spectrophotometric changes were observed during the basic titration of the samples. For this reason, potentiometric measurements were used to determine formation constants and the kinetics of the complex formation was monitored through changes in the absorption spectra. These changes are very similar in all systems.

Spectra were decomposed using the SPECPEAK program [16] in four Gaussian peaks with maxima at about 250, 275, 315 and 365 nm. Absorbance data at these wavelengths for samples with a 1:1 Ligand/metal ratio fit Eq. (1) well and a first-order observed kinetic constant ($k = 1/\tau$) can be determined.

The observed kinetic constants measured at the peak at 275 nm are 6.8×10^{-5} s^{-1} for mercaptosuccinic acid (MSA), 7.3×10^{-6} s^{-1} for *meso*-2,3-dimercapto succinic acid (DMSA), 1.4×10^{-5} s^{-1} for *meso*-monomethyl dimercapto succinate (MMS), and 2.6×10^{-5} s^{-1} for *meso*-dimethyl dimercapto succinate (DMS). Therefore, the formation of complexes between these ligands and Pt(II) follows a very slow kinetics.

Generally speaking, the lower the number of close binding groups (–SH and/or –COOH), the faster the complex formation reaction (MSA and DMS). The slowest reaction is for DMSA, which has two –SH and two –COOH groups.

The tendency of platinum to form polynuclear planar complexes is well known. With MSA, which is the

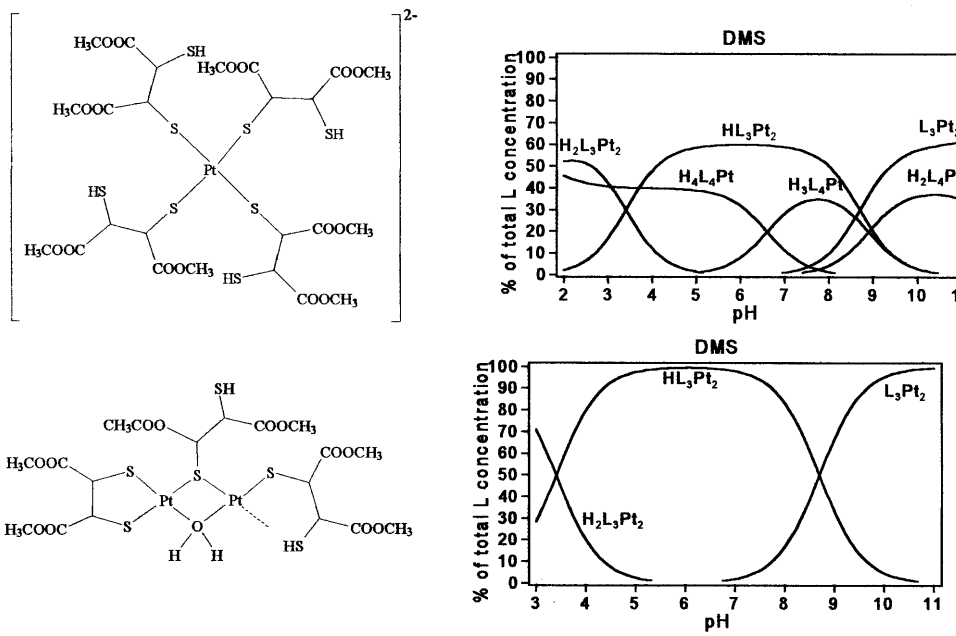


Fig. 4. The distribution curves for the DMS–Pt(II) system are presented on the right, [DMS] being always 2 mM and [Pt(II)] 2 mM in the upper plot and 1 mM in the lower. The possible structures of $Pt_4L_4H_4$ (upper) and $Pt_2L_3H_2$ (lower) are shown on the left.

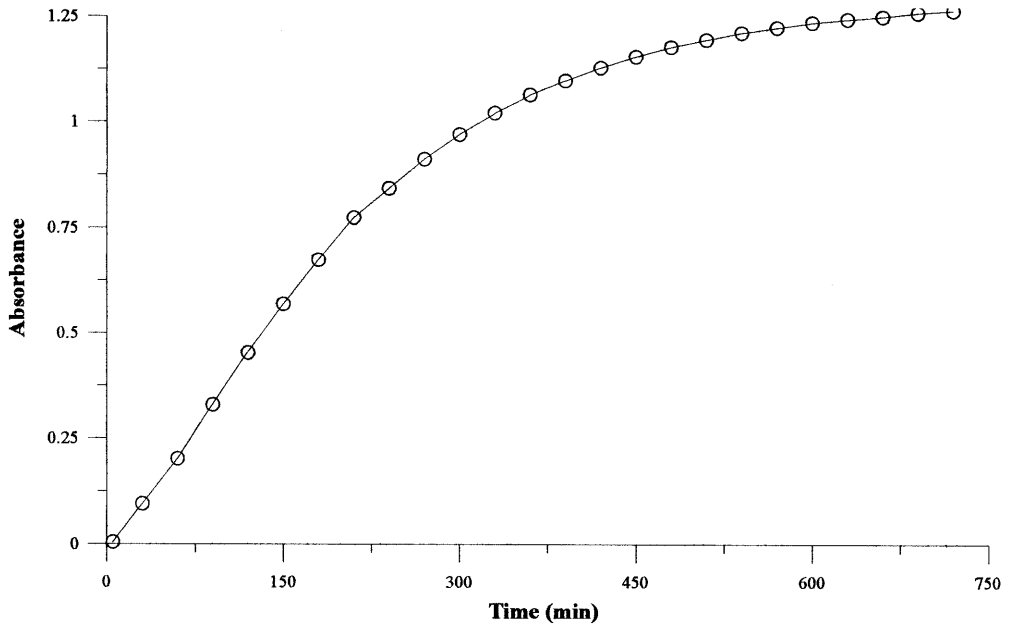


Fig. 5. Height of the peak at 275 nm versus time for the reaction of complex formation between Pt(II) and meercapto succinic acid.

ligand with the fastest complexation with Pt(II), in the case of only one –SH group, the structure proposed in Fig. 1 cannot be extended to form polynuclear complexes, because no free –SH groups are available to form bridges with other Pt(II) atoms. This could explain the faster reaction. In the other cases, the free –SH groups allow the proposed structures to spread in two dimensions. The formation of a more complex structure would justify both the slower kinetics and the powdery aspect of the isolated solids, which never crystallize. In the particular case of DMSA, which is the ligand with the slowest kinetics, the fact that it has a higher tendency to form a precipitate compared to the other ligands also after 2 days, confirms that due to its four binding groups a more complex structure is formed.

Acknowledgements

We would like to thank the University of Burgos for a grant to M.J.T.E.

References

[1] J. Aaseth, Human Toxicol. 2 (1983) 257.
[2] H.V. Aposhian, M.M. Aposhian, Rev. Pharmacol. Toxicol. 30 (1990) 279.
[3] H.V. Aposhian, R.M. Maiorino, D. Gonzales-Ramirez, M. Zuniga-Charles, Z. Xu, K.M. Hurlbut, P. Junco-Muñoz, R.C. Dart, M.M. Aposhian, Toxicology 97 (1995) 23.
[4] C.A. Bowden, E.P. Krenzelok, Drug Safety 16 (1997) 9.
[5] R.F. Borch, M.E. Pleasants, Proc. Natl. Acad. Sci. USA 76 (1979) 6611.
[6] S.B. Howell, C.E. Pfeifle, W.E. Wung, R.A. Olshen, Cancer Res. 43 (1983) 1426.
[7] M.A. Basinger, M.M. Jones, M.A. Holscher, Toxicol. Appl. Pharmacol. 103 (1990) 1.
[8] M.M. Jones, M.A. Basinger, J. Appl. Toxicol. 9 (1989) 229.
[9] D.D. Choie, A.A. Del Campo, A.M. Guarino, Toxicol. Appl. Pharmacol. 55 (1980) 245.
[10] M.C. Aragoni, M. Arca, G. Crisponi, F. Cristiani, F. Isaia, V.M. Nurchi, Talanta 43 (1996) 1357.
[11] M. Gerecke, E.A.H. Friedheim, A. Brossi, Helv. Chim. Acta 44 (1961) 955.
[12] G. Crisponi, F. Cristiani, V.M. Nurchi, R. Pinna, M.J. Tapia Estévez, Polyhedron 18 (1999) 3257.
[13] G. Gran, Analyst 77 (1952) 661.
[14] L. Zekany, I. Nagypal, in: D.J. Leggett (Ed.), Computational Methods for the Determination of Formation Constants, Plenum, New York, 1985, Chapter 8.
[15] H.G. Seiler, H. Sigel, A. Sigel (Ed.), Handbook on Toxicity of Inorganic Compounds, Marcel Dekker, New York, 1988, p.12.
[16] M.C. Aragoni, M. Arca, G. Crisponi, V.M. Nurchi, Anal. Chim. Acta 316 (1995) 195.

PERGAMON

www.elsevier.nl/locate/poly

Polyhedron 19 (2000) 2441–2445

POLYHEDRON

Cobalt(II) dioxygen carriers based on dinucleating ligands.☆ Part 1. Thermodynamics of dioxygen binding in aqueous solution

Andrea Bencini [a], Antonio Bianchi* [a,1], Claudia Giorgi [a], Piero Paoletti* [a,2], Barbara Valtancoli [a], Norberto Ceccanti [b], Rodolfo Pardini [b]

[a] *Department of Chemistry, University of Florence, Via Maragliano 75/77, 50144 Florence, Italy*
[b] *Department of Chemistry and Industrial Chemistry, University of Pisa, Via Risorgimento, 35, 56126 Pisa, Italy*

Dedicated to the late Professor Sergio Cabani.

Abstract

The equilibria involving the uptake of dioxygen (O_2) to the dicobalt(II) complexes of the macrocyclic ligands [27]aneN_9 (1,4,7,10,13,16,19,22,25-nonaazacycloheptacosane) and [30]aneN_{10} (1,4,7,10,13,16,19,22,25,28-decaazacyclotriacontane), and of the acyclic polyamine Me_2octaen (1,25-dimethyl-1,4,7,10,13,16,19,22,25-nonaazapentacosane) have been studied by potentiometric measurements in 0.15 mol dm^{-3} $NaClO_4$ aqueous solution at 298.1 ± 0.1 K, and the relevant equilibrium constants have been reported. All three ligands form stable oxygenated complexes of the type $[Co_2L(O_2)]^{4+}$ and $[Co_2L(O_2)OH]^{3+}$, in which the O_2 molecule is bound in the end-on mode to a single metal ion. In the case of the macrocyclic complexes the coordination of O_2 and OH^- reveals a cooperativity effect, i.e. a significant stability increase is observed when one of these species coordinates to a dinuclear complex containing the other one, with respect to the same reactions involving $(Co_2L)^{4+}$. This behaviour suggests the interaction via hydrogen bonding between the two species (O_2 and OH^-) coordinated to different cobalt(II) ions. © 2000 Elsevier Science B.V. All rights reserved.

Keywords: Dioxygen carriers; Dioxygen binding; Cobalt; Polynuclear complexes; Polyamines; Thermodynamics of complexation

1. Introduction

The binding, transport, and activation of molecular oxygen by metal complexes is a topic of wide current interest due to the many implications that such metal containing systems have in both biomimetic and abiotic processes involving dioxygen (O_2) [1–6]. In this respect, Co(II) complexes with polyamine ligands containing binding units suited either for the coordination of a single metal ion or for the assembling of dimetallic centres have proved particularly useful [1].

Among the authors who have supported the investigation in this field, the late Professor Sergio Cabani, to whom this paper is dedicated, gave an important contribution to the understanding of the thermodynamic and kinetic aspects governing dioxygen uptake [6–17].

Polynuclear metal complexes able to bind dioxygen can be used as biomimetic models for natural non-heme respiratory proteins, such as hemocyanin and hemerythrin. Hemocyanin is a dinuclear copper(I) protein typical of molluscs and arthropods, while hemerythrin is a protein, containing two iron(II) ions at its active site, occurring among several marine invertebrates. These proteins bind O_2 according to different coordination modes: (i) coordination to both metal centres to form a peroxide-bridging complex in oxyhemocyanin; (ii) end-on coordination to a single metal centre in oxyhemerythrin [18]. Among dioxygen complexes containing dimetallic centres, the bridging oxyhemocyanin-like coordination is the most common O_2 binding mode.

In hemocyanin the two Cu(I) ions display equal coordination environments, while in hemerythrin the two Fe(II) are differently coordinated [18]. It has been recently noted that dinuclear complexes of ligands containing different coordination sites are able to bind

☆ For Part 2 see Ref. [30].

[1] *Corresponding author. Tel.: +39-055-321-6334; fax: +39-055-354-845; e-mail: bianchi@chim1.unifi.it

[2] *Corresponding author.

0277-5387/00/$ - see front matter © 2000 Elsevier Science B.V. All rights reserved.
PII: S0277-5387(00)00543-X

dioxygen, providing important new reactivity patterns, and may be useful as model systems for hemerythrin, reproducing the situation in which dioxygen is bound to one of the metal ions but is reduced by two electrons, one from each of the metals, to form a peroxide ligand bound to one metal [19].

In order to get insight into the relation between the coordination environment of dicobalt(II) complexes and their oxygenation properties, we have undertaken a thermodynamic study on the dioxygen uptake to the dicobalt(II) complexes of the polyamines [27]aneN_9, [30]aneN_{10} and Me_2octaen. The first two ligands have a macrocyclic structure while the third one is an acyclic ligand. [27]aneN_9 and Me_2octaen contain an odd number of donor atoms and form dinuclear complexes in which the metal ion has a different coordination environment (see Scheme 1).

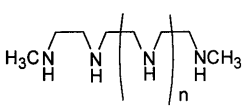
2. Experimental

2.1. Reagents

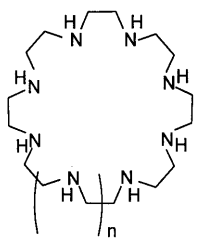
The ligands Me_2octaen, [27]aneN_9 and [30]aneN_{10} were synthesised as described previously [20–22] and used as their hydrochloric salts.

2.2. E.m.f. measurements

All pH-metric measurements ($pH = -\log[H^+]$) were carried out in 0.15 mol dm^{-3} $NaClO_4$, CO_2-free solutions at 298.1 ± 0.1 K, by using equipment and the methodology that has previously been described [23]. The combined Ingold 405 S7/120 electrode was calibrated as a hydrogen concentration probe by titrating known amounts of HCl with CO_2-free NaOH solutions, and determining the equivalent point by Gran's method [24]. This allows one to determine the standard potential $E°$ and the ionic product of water ($pK_w = 13.73(1)$ at 298.1 ± 0.1 K in 0.1 mol dm^{-3} $NaClO_4$). Measurements performed to determine the equilibrium constants for the formation of the dioxygen complexes were carried out by maintaining a constant pressure (1 atm) of O_2 in the potentiometric cell. The concentration of O_2 in solution (1.21×10^{-3} mol dm^{-3}), at the operating pressure, temperature and ionic strength, was obtained from published data [25]. The complexation reactions are rather slow; for this reason 30 min were allowed to elapse after each titration (NaOH solution) addition in order to get stable e.m.f. readings. At least three potentiometric titrations (about 100 data points for each one) were performed for each system in the pH range 2.5–10.5. In order to ensure the achievement of equilibrium conditions, a reduced number of experimental points (10–15) was obtained for each system, in separated experiments performed by adopting longer equilibration times (2 h). In all experiments the ligand concentration [L] was varied in the range 0.5×10^{-3}–1×10^{-3} mol dm^{-3}, while the metal ion concentration [M] was [M] = 2[L], in order to vary the ratio between O_2 and complex concentrations. A modification of the computer program HYPERQUAD [26] was used to calculate the equilibrium constants of the oxygenated complexes from e.m.f. data. Such modification was made in order to consider the presence of a chemical species (O_2) involved in the complexation equilibria, whose free concentration is kept constant during the measurement. Ligand protonation [20–22] and metal ion complexation [27,28] constants employed in the calculations were determined in previous works under anaerobic conditions. All titration curves, including those obtained with longer equilibration times, were treated either as a single set or as separated entities without significant variation in the value of the stability constants.



n = 6, Me_2octaen



n = 2, [27]aneN_9

n = 3, [30]aneN_{10}

Scheme 1.

3. Result and discussion

3.1. Cobalt(II) complexes

As indicated by previous studies [27,28], Me_2octaen, [27]aneN_9 and [30]aneN_{10} are able to form both mono and dinuclear Co(II) complexes under anaerobic conditions. Due to the large number of amine groups constituting their molecular structure, these ligands display a particular propensity to form dinuclear complexes. As a matter of fact, in solutions containing ligand and Co(II) in 1:2 molar ratios, the mononuclear complexes formed by Me_2octaen and [27]aneN_9 are minor species, while [30]aneN_{10} forms only dinuclear complexes (Fig. 1).

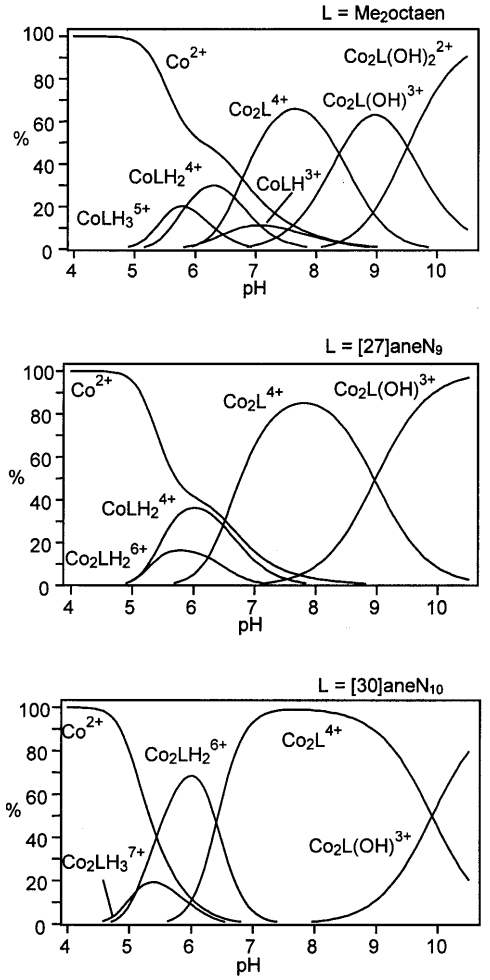


Fig. 1. Speciation diagrams for the anaerobic systems Co(II)/L (L = Me_2octaen, [27]aneN$_9$, [30]aneN$_{10}$). [L] = 1×10^{-3} mol dm^{-3}, [Co(II)] = 2×10^{-3} mol dm^{-3}; 0.15 mol dm^{-3} $NaClO_4$, 298.1 K.

As shown by the species distribution diagrams reported in Fig. 1, such dinuclear complexes form very stable hydroxylated species, indicating that the complexes present a good tendency to coordinate additional species from the medium. This is, of course, a promising starting point for the use of such compounds as O_2 binders.

3.2. Dioxygen binding

As expected, the binuclear complexes of the three ligands considered in this work are able to bind molecular oxygen giving rise to the formation of stable oxygenated complexes. The equilibrium constants determined for the O_2 complexes are reported in Table 1, while Fig. 2 displays the distribution diagrams of the complexed species formed as a function of pH in the systems Co(II)/O_2/L (L = ligands).

In contrast with the complexation equilibria taking place under anaerobic conditions [27,28], in the presence of dissolved O_2 only dicobalt(II) complexes are formed in solution containing the ligand and metal ion in a 1:2 molar ratio. This applies for all three ligands, in spite of the fact that in the absence of O_2 Me_2octaen and [27]aneN$_9$ would also form mononuclear species. Evidently the dinuclear complexes of the three ligands are more efficient, from a thermodynamic point of view, than the mononuclear one in the binding of molecular dioxygen.

It is quite interesting to note that the binding of O_2 prevents the formation of protonated complexes. A comparison of the species distribution diagrams reported in Figs. 1 and 2 for the anaerobic and aerobic systems, respectively, clearly visualises this aspect. Such behaviour indicates that the binding of O_2 to the metal centres gives rise to a strengthening of the metal to ligand bonds, overcoming the competitive effect of ligand protonation, and promoting the coordination of all donor atoms even in acidic solutions. On the other hand, the oxygenated complexes display a good ability to form hydroxylated species from neutral (Me_2octaen, [27]aneN$_9$) or slightly alkaline ([30]aneN$_{10}$) pH values (Fig. 2).

As shown by the equilibrium constants for the addition of O_2 to $(Co_2L)^{4+}$, the complex of the acyclic Me_2octaen ligand displays a greater ability to bind molecular dioxygen (Table 1) than the complexes of the macrocyclic ones ([27]aneN$_9$, [30]aneN$_{10}$), while among the macrocyclic complexes, the $(Co_2L)^{4+}$ species formed by [27]aneN$_9$ bind O_2 more strongly than the

Table 1
Logarithms of the equilibrium constants for the formation of oxygenated dicobalt(II) complexes and not-oxygenated analogues, determined in 0.15 mol dm^{-3} $NaClO_4$ solution at 298.1 ± 0.1 K

	Reaction	Me_2octaen	[27]aneN$_9$	[30]aneN$_{10}$
		Log K		
	$2Co^{2+} + L + O_2 = [Co_2L(O_2)]^{4+}$	29.23(5) [a]	24.63(5)	26.51(5)
	$2Co^{2+} + L + O_2 + H_2O = [Co_2L(O_2)OH]^{3+} + H^+$	20.71(5)	16.64(5)	18.48(5)
1	$(Co_2L)^{4+} + O_2 = [Co_2L(O_2)]^{4+}$	7.5(1)	5.8(1)	4.7(1)
2	$[Co_2L(O_2)]^{4+} + OH^- = [Co_2L(O_2)OH]^{3+}$	5.2(1)	5.7(1)	5.7(1)
3	$[Co_2L(OH)]^{3+} + O_2 = [Co_2L(O_2)OH]^{3+}$	7.4(1)	6.8(1)	6.5(1)
	$2Co^{2+} + L = (Co_2L)^{4+}$	21.69 [b]	18.85 [c]	21.85 [c]
	$2Co^{2+} + L + H_2O = [Co_2L(OH)]^{3+} + H^+$	13.31 [b]	9.88 [c]	11.94 [c]
4	$(Co_2LO_2)^{4+} = [Co_2L(O_2)OH]^{3+}$	5.35 [b]	4.76 [c]	3.82 [c]

[a] Values in parentheses are standard deviation on the last significant figures.
[b] Taken from Ref. [28].
[c] Taken from Ref. [27].

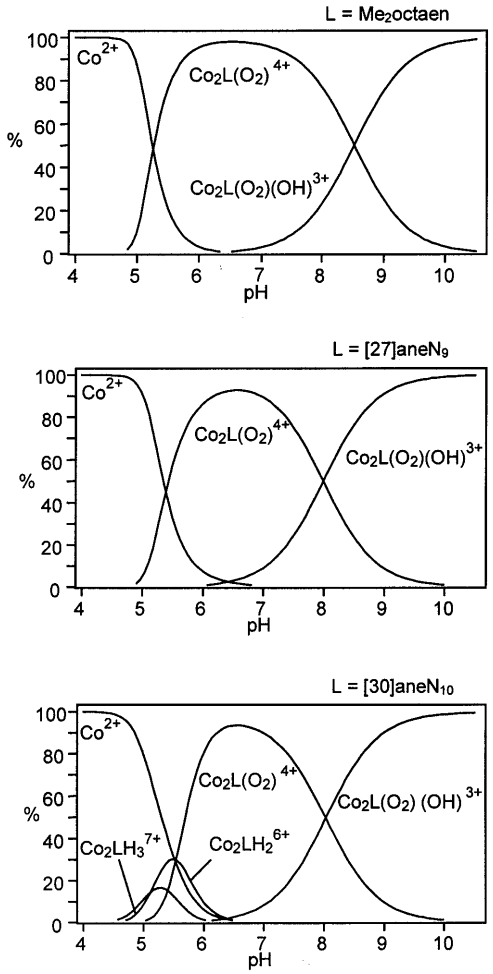


Fig. 2. Speciation diagrams for the aerobic systems Co(II)/L/O_2 (L = Me_2octaen, [27]aneN_9, [30]aneN_{10}). [L] = 1×10^{-3} mol dm^{-3}, [Co(II)] = 2×10^{-3} mol dm^{-3}, constant concentration of free O_2 [O_2] = 1.21×10^{-3} mol dm^{-3}; 0.15 mol dm^{-3} $NaClO_4$, 298.1 K.

dicobalt(II) complex of [30]aneN_{10}. A similar stability trend was also observed for the addition of OH^- to the dinuclear not-oxygenated complexes. While the different binding abilities of the macrocyclic complexes can be interpreted in terms of different numbers of coordination sites available on the metal centres for the exogen ligands, a justification for the greater binding ability of the acyclic complex with respect to the macrocyclic one is not simple, especially in the absence of structural information. A previous study dealing with the kinetics of O_2 binding by the Co(II)/[30]aneN_{10} system suggested that the dioxygen molecule acts as monodentate ligand coordinating to the binuclear complex in a end-on fashion [14]. Such kinetic information is consistent with the present thermodynamic data, since a bridging coordination of the O_2 molecule to the complex would fulfil the coordination sphere of both metal ions, opposing the binding of further species, such as OH^-. On the contrary, $[Co_2[30]aneN_{10}(O_2)]^{4+}$ displays a very good tendency to bind OH^-.

By considering the close similarity between the binding features of $[Co_2[30]aneN_{10}]^{4+}$ and $[Co_2[27]aneN_9]^{4+}$ towards both O_2 and OH^- (Table 1), an end-on coordination of O_2 is also expected to occur with the latter complex.

It is noteworthy that O_2 and OH^- manifest a clear cooperativity in the binding to the dicobalt(II) complexes of the macrocyclic ligands. As a matter of fact, a significant stability increase is observed (Table 1) when one of this species coordinates to a dinuclear complex containing the other one, with respect to the same reactions involving $(Co_2L)^{4+}$ (compare the equilibrium constants for reactions 2 and 3 with those for 4 and 1, respectively, reported in Table 1). A similar cooperativity can be explained by assuming a direct interaction via hydrogen bonding between O_2 and OH^- in the complexes, as observed in oxyhemerythrin [18]. In a previous paper [29] dealing with Ni(II) complexes it was shown that in the crystal structure of $\{Ni_2[30]aneN_{10}(H_2O)_2\}^{4+}$ the two coordination sites occupied by the water molecules are located on opposite sides of the centrosymmetric dinuclear complex, and spectral data obtained for the same compound suggested that the same structure is maintained in solution. If a similar structure also occurs for the analogous dicobalt(II) complexes in solution, and considering that the binding of O_2 and OH^- should occur at the positions occupied by the water molecules, the dicobalt(II) complex would require an important reorganisation to allow the formation of an hydrogen bond between the coordinated oxygen molecule and the hydroxide ion.

The uptake of molecular oxygen to the dicobalt(II) complex of the acyclic ligand Me_2octaen displays different thermodynamic characteristics with respect to the analogous complexes with [27]aneN_9 and [30]aneN_{10}. As already observed, the dicobalt(II) complex with the acyclic ligand Me_2octaen is a strong O_2 binder but, in contrast to the behaviour of the macrocyclic complexes, the equilibrium constants for the binding of O_2 and OH^- (Table 1) do not suggest any cooperative effect.

In the absence of structural information regarding both the oxygenated complex and the non-oxygenated one, it is rather difficult to give an interpretation of such thermodynamic properties displayed by the dicobalt(II) complex of Me_2octaen. Nevertheless, both the spectral features of the oxygenated complexes and the kinetic data for O_2 uptake are quite similar for all three ligands considered here [30], suggesting that the coordination mode adopted by O_2 in the oxygenated complexes should also be the same for all three ligands. Hence, we expect that in $[Co_2Me_2octaen(O_2)]^{4+}$ and $[Co_2Me_2octaen(O_2)OH]^{3+}$ the dioxygen molecule is end-on bound to a single metal centre, although it seems unable to give rise to hydrogen bonding interaction with OH^- in the hydroxylated complex. Assuming

that in this complex O_2 and OH^- are bound to different Co(II) ions, the absence of hydrogen bonding between the two species could be ascribed to a greater ability of dinuclear complexes with the acyclic, more flexible ligand in locating the metal centres at a longer distance to reduce the electrostatic repulsion between positive charges.

Alternatively, both O_2 and OH^- might be coordinated to the same metal centre in $[Co_2Me_2octaen(O_2)OH]^{3+}$. The experimental information we have presently collected does not allow us to exclude such possibility.

4. Conclusions

Dicobalt(II) complexes with ligands Me_2octaen, [27]aneN_9, and [30]aneN_{10} of the type $(Co_2L)^{4+}$ and $[Co_2L(OH)]^{3+}$ are efficient receptors of molecular dioxygen in aqueous solution, giving rise to the formation of $[Co_2L(O_2)]^{4+}$ and $[Co_2L(O_2)(OH)]^{3+}$ oxygenated species. In the case of the macrocyclic complexes, cooperativity is observed in the binding of O_2 in the presence of coordinated OH^- and vice versa, the presence of one of these species in the complex assisting the coordination of the other one via direct hydrogen bonding as observed in hemerythrin. This evidence suggests that the uptake of O_2 and OH^- takes place on different metal centres, the dioxygen molecule being in end-on coordination mode. On the other hand, the dicobalt(II) complex with the acyclic ligand Me_2octaen does not display any cooperativity in the binding of O_2 and OH^-, in spite of the fact that $[Co_2Me_2octaen]^{4+}$ presents a higher tendency than macrocyclic complexes to bind O_2. Nevertheless, both the spectral features of the oxygenated complexes and the kinetic data for O_2 uptake are quite similar for all three ligands, suggesting that, in the case of Me_2octaen, O_2 is also end-on coordinated to cobalt.

The kinetics of O_2 binding, of which a few aspects have been anticipated in this paper, is the subject of a concurrent publication [30].

Acknowledgements

This work has been supported by the Ministero dell'Università e della Ricerca Scientifica e Tecnologica (MURST, Rome) within the program COFIN 98.

References

[1] A.E. Martell, D.T. Sawyer (Eds.), Oxygen Complexes and Oxygen Activation by Transition Metals, Plenum, New York, 1988.
[2] L.I. Simandi (Ed.), Dioxygen Activation and Homogeneous Catalytic Oxidation, Elsevier, Amsterdam, 1991.
[3] T.D. Smith, J.P. Pilbrow, Coord. Chem. Rev. 39 (1981) 295.
[4] A.E. Martell, Acc. Chem. Rev. 15 (1982) 155.
[5] E.C. Niederhoffer, J.H. Timmons, A.E. Martell, Chem. Rev. 84 (1984) 137.
[6] S. Cabani, N. Ceccanti, M.R. Tinè, Pure Appl. Chem. 63 (1991) 1455.
[7] S. Cabani, N. Ceccanti, M.R. Tinè, Pure Appl. Chem. 63 (1991) 1455.
[8] S. Cabani, N. Ceccanti, G. Conti, P. Gianni, Gazz. Chim. Ital. 112 (1982) 159.
[9] S. Cabani, N. Ceccanti, G. Conti, J. Chem. Soc., Dalton Trans. (1983) 1247.
[10] S. Cabani, N. Ceccanti, G. Conti, Inorg. Chim. Acta L21 (1984) 89.
[11] S. Cabani, N. Ceccanti, P. Gianni, J. Chem. Soc., Dalton Trans. (1984) 307.
[12] S. Cabani, N. Ceccanti, M.R. Tinè, J. Soln. Chem. 15 (1986) 177.
[13] S. Cabani, N. Ceccanti, M.R. Tinè, J. Chem. Soc., Dalton Trans. (1988) 373.
[14] A. Bencini, A. Bianchi, S. Cabani, N. Ceccanti, P. Paoletti, M.R. Tiné, J. Chem. Soc., Dalton Trans. (1993) 695.
[15] S. Cabani, N. Ceccanti, R. Pardini, M.R. Tiné, Gazz. Chim. Ital. 124 (1994) 327.
[16] S. Cabani, React. Funct. Polym. 28 (1996) 167.
[17] S. Cabani, N. Ceccanti, R. Pardini, M.R. Tiné, A. Bencini, A. Bianchi, P. Paoletti, Ann. Chim. 89 (1999) 99.
[18] T.M. Loehr, in: A.E. Martell, D.T. Sawyer (Eds.), Oxygen Complexes and Oxygen Activation by Transition Metals, Plenum, New York, 1988, pp. 17–32.
[19] B. Bosnich, Inorg. Chem. 38 (1999) 2554.
[20] J. Aragó, A. Bencini, A. Bianchi, E. Garçia España, M. Micheloni, P. Paoletti, J.A. Ramirez, P. Paoli, Inorg. Chem. 30 (1991) 1843.
[21] A. Bencini, A. Bianchi, E. Garçia España, M. Giusti, M. Micheloni, P. Paoletti, Inorg. Chem. 26 (1987) 681.
[22] A. Bencini, A. Bianchi, E. Garçia España, M. Giusti, S. Mangani, M. Micheloni, P. Orioli, P. Paoletti, Inorg. Chem. 26 (1987) 1243.
[23] A. Bianchi, L. Bologni, P. Dapporto, M. Micheloni, P. Paoletti, Inorg. Chem. 23 (1984) 1201.
[24] G. Gran, Analyst (London) 77 (1952) 661.
[25] R. Battino (Ed.), Oxygen and Ozone, Solubility Data Series, Elsevier Science, New York, 1981.
[26] P. Gans, A. Sabatini, A. Vacca, Talanta 43 (1996) 1739.
[27] (a) A. Bencini, A. Bianchi, E. Garçia España, M. Micheloni, P. Paoletti, Inorg. Chem. 28 (1989) 2480. (b) A. Bencini, A. Bianchi, P. Paoletti, S. Cabani, N. Ceccanti, M.R. Tinè, E. Garçia España, Inorg. Chim. Acta 204 (1993) 227.
[28] A. Bencini, A. Bianchi, V. Fusi, P. Paoletti, B. Valtancoli, A. Andres, J. Arago, E. Garçia España, Inorg. Chim. Acta 204 (1993) 221.
[29] A. Bencini, A. Bianchi, M. Castellò, P. Dapporto, J. Faus, E. Garçia-España, M. Micheloni, P. Paoletti, P. Paoli, Inorg. Chem. 28 (1989) 3175.
[30] N. Ceccanti, R. Pardini, F. Secco, M.R. Tinè, M. Venturini, A. Bianchi, P. Paoletti, Polyhedron 19 (2000) 2447.

PERGAMON

www.elsevier.nl/locate/poly

Polyhedron 19 (2000) 2447–2455

POLYHEDRON

Cobalt(II) dioxygen carriers based on dinucleating ligands Part 2. Kinetics of dioxygen binding

Norberto Ceccanti [a], Rodolfo Pardini [a], Fernando Secco [a], Maria Rosaria Tinè [a,*], Marcella Venturini [a], Antonio Bianchi [b], Piero Paoletti [b]

[a] *Dipartimento di Chimica e Chimica Industriale, Università di Pisa, Via Risorgimento 35, I-56126 Pisa, Italy*
[b] *Dipartimento di Chimica, Università di Firenze, Via Maragliano, 75, I-50144 Florence, Italy*

Abstract

We consider here the kinetics of the reaction of formation of dioxygenated Co(II) complexes with the binucleating ligands 1,23-bis(methylamino)-3,6,9,12,15,18,21-heptaazatricosane (Me_2Octaen), 1,4,7,10,13,16,19,22,25-nonaazacycloheptacosane ([27]aneN_9), 1,4,7,10,13,16,19,22,25,28-decaazacyclotriacontane ([30]aneN_{10}), and 1,4,7,10,13,16,19,22,25,28,31-undecaazacyclotritriacontane ([33]aneN_{11}). The most important result is that the Co(II) complexes with these polyamines in aqueous solution and at room temperature are very flexible in binding dioxygen: by changing the value of the ligand to cobalt concentration ratio ($R = C^0_L/C^0_{Co}$) and the pH of the solution, it is possible to modulate the dioxygen uptake obtaining two-to-one or one-to-one, Co/O_2 superoxo complexes. As to the kinetics of the formation of these complexes, we find that the rate-determining step is the transformation of a cobalt-ligand precursor complex, inert towards dioxygen, to yield an active form, whereas the reaction of dioxygen uptake is fast in all the investigated systems. © 2000 Elsevier Science B.V. All rights reserved.

Keywords: Dioxygen carriers; Cobalt; Dinuclear complexes; Dinucleating ligands; Polyamines; Kinetics; Dioxygen binding

1. Introduction

The ability of Co(II) complexes to bind molecular dioxygen has been the subject of intensive studies both for modeling biological dioxygen carriers and for possible applications in transport, storage or activation of molecular dioxygen [1–7]. The structure of these synthetic dioxygen carriers, as well as the kinetics and thermodynamics of their formation, is strongly affected by the nature of the ligand. Simple tetraazotate or pentaazotate ligands form oxygenated Co(II) complexes in which dioxygen bridges two complexed subunits. The thermodynamics and the kinetics of the formation of these complexes have been extensively studied by some of the authors (N.C., R.P. and M.R.T.) under the guidance of the late Prof. Sergio Cabani to whom this work is dedicated [8–15]. In this work we consider the kinetic features of the reaction of formation in aqueous solution of the dioxygen adducts of Co(II) complexes with some dinucleating ligands.

The use of polynucleating ligands represents an evolution in synthetic Co(II) dioxygen carriers. These ligands contain a sufficient number of oxygen and/or nitrogen donor centers to coordinate more than one Co(II) ion and can act as biomimetic models of natural non-heme type (hemerythrin, hemocyanin) carriers. Martell et al. [16] examined the Co(II) complexes with the dinucleating ligands BISTREN, BISDIEN and BISBAMP in aqueous solution and obtained several interesting results. The Co_2(II)BISTREN complex shows an unexpected low affinity with dioxygen and a very slow metal-centered degradation to Co_2(III)BISTREN complexes. As a consequence, the Co_2(II)BISTREN-(μO_2)(μOH)[1] complex is a very good dioxygen carrier and many cycles of uptake-release of O_2 are possible by simply heating and cooling its aqueous solutions. More recently, Bosnich has pointed out the interest, as oxygenation catalysts, of suitable designed bimetallic peroxo-complexes where dioxygen is bound to one metal [17].

* Corresponding author. Tel.: +39-050-918311; fax: +39-050-918260.

E-mail address: mrt@dcci.unipi.it (M.R. Tinè).

[1] Throughout this paper charges are omitted for the sake of simplicity.

0277-5387/00/$ - see front matter © 2000 Elsevier Science B.V. All rights reserved.
PII: S0277-5387(00)00544-1

As a part of general research within our laboratories involving the synthetic systems for dioxygen transport and activation, we have begun the study of the thermodynamics and the kinetics of the reaction of formation of dioxygenated Co(II) complexes with large polyazaalkanes. Owing to their ability to form dinuclear complexes, large polyazaalkanes are good candidates for studying O_2 binding; actually they produce two binding sites in which the two Co(II) ions possess variable surroundings in geometry and number of coordinated donors atoms. The ligands considered in this work are the acyclic polyamine 1,23-bis(methylamino)-3,6,9,12,15,18,21-heptaazatricosane (Me_2Octaen) and the macrocyclic polyamines 1,4,7,10,13,16,19,22,25-nonaazacycloheptacosane ([27]aneN_9), 1,4,7,10,13,16,19,22,25,28-decaazacyclotriacontane ([30]aneN_{10}), and 1,4,7,10,13,16,19,22,25,28,31-undecaazacyclotritriacontane ([33]aneN_{11}). They react with cobalt under anaerobic conditions forming mononuclear or dinuclear complexes, depending on the ligand/cobalt concentration ratio and on the pH of the solution. The acidity constants of the protonated ligands [18–21] and the equilibrium formation constants of their Co(II) complexes in anaerobic conditions have been previously determined [22–24]. Some preliminary results, concerning dioxygenated Co(II) complexes with these ligands, have been already reported [25,26].

2. Experimental

2.1. Materials

The ligands were prepared according to the procedure previously described: Me_2Octaen [18], [27]aneN_9 [19], [30]aneN_{10} [20], [33]aneN_{11} [21]. They have been used as hydrochloride salts. Their purity was checked by elemental and NMR analysis. All other chemicals were reagent-grade products and were used without further purification.

2.2. Apparatus

Dioxygen concentration was measured by means of a Beckman Oxygen Analyser (model 0260) equipped with an oxygen electrode capable of measuring oxygen concentrations up to a maximum of 199.0 ppm. The electrode was calibrated in air-saturated 0.15 mol dm^{-3} $NaClO_4$ aqueous solutions [9,12]. The cell was designed to contain the oxygen sensor, a glass electrode for pH measurements, and two openings for introducing the reagents by means of microsyringes or titration microburettes. It was filled, leaving no vapour space, with aqueous solutions of the ligand in 0.15 mol dm^{-3} $NaClO_4$ saturated with dioxygen or with air and adjusted to the selected pH values. The solution was thermostated at 298.1 ± 0.1 K and magnetically stirred. Known amounts of $Co(NO_3)_2$ were added and the pH of the solution was kept constant to the selected value by adding known amounts of NaOH stock solutions as long as the reaction of formation of the dioxygen adducts proceeded. A Crison Micro TT 2050 automatic titrating system equipped with a combined glass electrode was used for the pH measurements and NaOH additions. The glass electrode was calibrated as a hydrogen concentration probe by titration of known amounts of HCl with CO_2-free NaOH solutions. In this investigation pH is defined as the logarithm of a concentration, $-\log [H^+]$. The free dioxygen concentration in solution, C_{O_2}, has been monitored, during the dioxygen binding reaction, as a function of time in experiments carried out at different pH values and at different values of the cobalt/ligand concentration ratio $R = C^0_L/C^0_{Co}$, where C^0_L and C^0_{Co} are, respectively, the initial concentration of the ligand and of cobalt. The dioxygen bound/cobalt concentration ratio as a function of time, $R_{O_2}(t)$, was calculated as $R_{O_2}(t) = (C^0_{O_2} - C_{O_2}(t))/C^0_{Co}$, where $C^0_{O_2}$, is the initial dioxygen concentration. Spectrophotometric measurements were performed at 298.1 K by using a Perkin–Elmer Lambda 6 UV–Vis spectrophotometer and a Hewlett–Packard 8452 Diode Array spectrophotometer equipped with a rapid mixing apparatus (Applied Photophysics model RX1000) with an empirical dead-time lower than 1.5×10^{-2} s. Both the measuring cell and the mixing device were thermostated at 298.1 ± 0.1 K.

3. Results and discussion

3.1. Characterization of the oxygenated complexes

The characterization of the oxygenated Co(II) complexes with Me_2Octaen, [27]aneN_9, [30]aneN_{10}, and [33]aneN_{11}, and the study of the kinetics of their formation and of their further evolution has been carried out by means of the analysis of the binding dioxygen curves, proton balances, and UV–Vis spectra, carried out in a large field of the cobalt/ligand concentration ratio (R ranging from 0.5 to 2) and of the pH of the solution (from 7 to 12). In each experiment the values of R and pH were selected in order to ensure that only mononuclear or only dinuclear Co(II)/L precursor complexes were present in anaerobic conditions.

Fig. 1 shows some dioxygen binding curves, $R_{O_2}(t)$, for the system Co/[27]aneN_9/O_2. This phenomenology is common to all the systems considered in this work with only minor differences.

The combined analysis of the whole set of the dioxygen binding curves and of potentiometric measurements allows us to obtain a significant picture of the nature and of the formation conditions of the various dioxy-

gen adducts. The main features of the formation processes can be summarised as follows: (i) at $R = 0.5$ and pH ranging from 7 to 10, a dinuclear complex of stoichiometry $Co_2LO_2(OH)_j$ ($j = 0, 1$) rapidly forms, the number of bound hydroxo groups depending on the pH of the solution; (ii) at $R = 0.5$ and pH > 11.3, the step of formation of this complex is slowed down and is followed by the slow consumption of a further equivalent of dioxygen; (iii) at $R > 1.5$ and pH > 8, the investigated polyazaalkanes form oxygenated mononuclear cobalt complex $CoLH_j(O_2)$ ($j = 0, 1$ depending on the pH of the solution). We will describe the main features and the behavior of these complexes by distinguishing between dinuclear and mononuclear species. In any case it is important to put in evidence two interesting results which emerge from our analysis. The first is that the Co(II) complexes with these polyamines are very flexible in bonding dioxygen: by changing the value of the ligand/cobalt concentration ratio and the pH of the solution, it is possible to obtain one-to-one or two-to-one Co/O_2 dioxygen adducts. The second result is that one-to-one Co(II) dioxygen complexes form in aqueous solution and at room temperature. This is a rather unusual behavior for synthetic dioxygen carriers and, to the best of our knowledge, only a few cases are reported in the literature [27–29].

3.2. Dinuclear complexes

At $R = 0.5$ and pH ranging from 7 to 10, $Co_2LO_2(OH)_j$ ($j = 0, 1$) is the prevailing oxygenated species for all the ligands considered in this work, the number of bound hydroxo groups depending on the pH of the solution. The formation constants of these complexes are reported in the first paper of this series [30]. The stability trends observed for the formation of such oxygenated complexes are in agreement with a complex structure of superoxo type, in which dioxygen is end-on bonded to a single cobalt atom. A similar not-bridging arrangement of the coordinated dioxygen molecule seems to be also in agreement with the rather long metal to metal distance, ranging from 5.75 to 7.26 Å, observed in several crystal structures of dinuclear complexes with [30]aneN$_{10}$ [31,20].

Fig. 2 shows the UV–Vis spectrum of the $Co_2LO_2(OH)_j$ complex and its evolution in time, when the ligand is Me_2Octaen. Two absorption bands with maxima at $\lambda = 320$ nm and at $\lambda = 395$ nm are initially present, but they tend to slowly disappear while a new band arises with a maximum at $\lambda = 370$ nm. The UV–Vis spectrum is the same between pH 7 and 10, but the rate of the transformation increases as the pH increases. The decay at $\lambda = 320$ nm obeys a first-order kinetic law, the molar extinction coefficient at $t = 0$ and the half-life time being $\varepsilon_{320} = 6165 \pm 60$ mol^{-1} dm^3 cm^{-1} and $t_{1/2} = 60 \pm 5$ min at pH 7 and $\varepsilon_{320} = 6110 \pm 80$ mol^{-1} dm^3 cm^{-1} and $t_{1/2} = 11.5 \pm 0.5$ min at pH 10. Such spectral evolution is essentially due to a conformational rearrangement of the oxygenated acyclic complex. An analogous behavior is displayed by the Co(II) complexes with the macrocyclic polyazaalkanes, but the spectral evolution is slower than for the acyclic Me_2Octaen and becomes slower and slower as the dimension of the macrocyclic ring increases; for [30]aneN$_{10}$ and [33]aneN$_{11}$ it overlaps with the reaction of irreversible oxidation which leads to the decrease of the absorbance in the spectral range 300–500 nm.

In order to study the kinetics of the formation of the $Co_2LO_2(OH)_j$ complex, the absorbance has been monitored at $\lambda = 320$ nm, by means of a diode array spec-

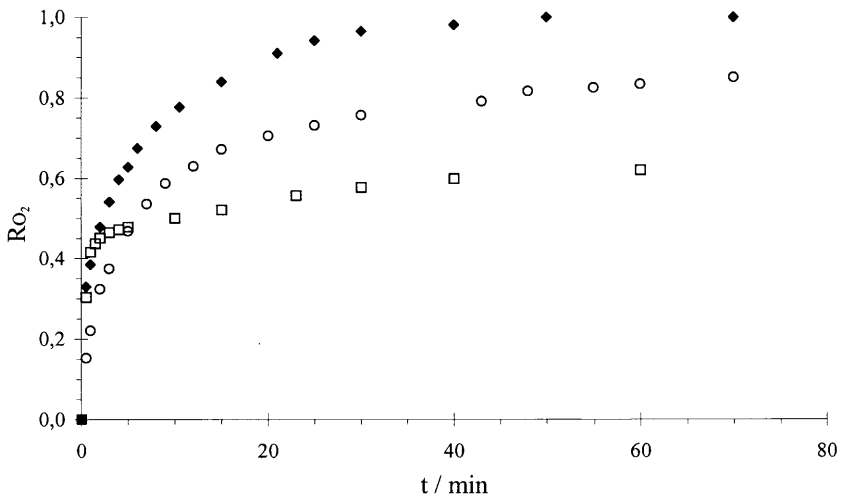


Fig. 1. Dioxygen binding curves, $R_{O_2}(t)$, for Co(II)–[27]aneN$_9$ complexes in aqueous solution at various R and pH: $C^0_{Co} = 4.43 \times 10^{-4}$ mol dm^{-3}, $R = 0.5$, pH 9.8 (□); $C^0_{Co} = 3.67 \times 10^{-4}$ mol dm^{-3}, $R = 0.5$, pH 11.4 (○); $C^0_{Co} = 3.98 \times 10^{-4}$ mol dm^{-3}, $R = 2$, pH 8.5 (◆). $R_{O_2}(t) = (C^0_{O_2} - C_{O_2}(t)/C^0_{Co}$; $R = C^0_L/C^0_{Co}$.

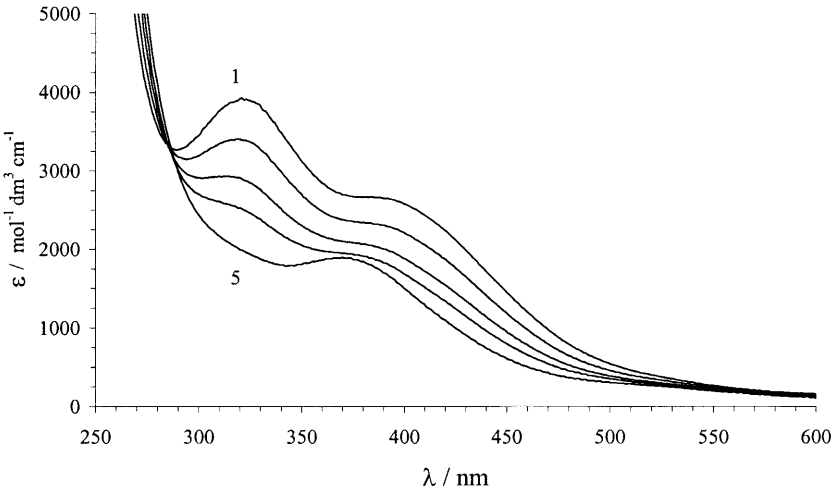


Fig. 2. Spectral evolution with time of the complex $Co_2Me_2OctaenO_2(OH)_j$ ($\varepsilon = A/C^0_{Co}$). Spectra recorded after 1.5, 12, 40, 120, and 600 min (pH 9.4, $C^0_{Co} = 5.80 \times 10^{-4}$ mol dm^{-3}; $C^0_L = 2.70 \times 10^{-4}$ mol dm^{-3}, $p_{O_2} = 101$ kPa).

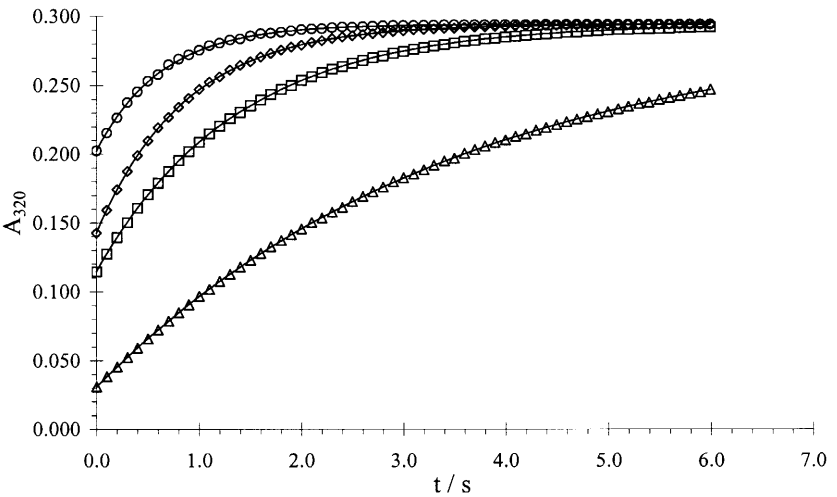


Fig. 3. Absorbance at $\lambda = 320$ nm as a function of time for the system $Co/Me_2Octaen/O_2$ (continuous lines are the fitting curves): $C^0_{Co} = 9.64 \times 10^{-5}$ mol dm^{-3}; $C^0_L = 4.82 \times 10^{-5}$ mol dm^{-3}; $C^0_{O_2} = 2.04 \times 10^{-4}$ mol dm^{-3}; pH 8.40 (△), pH 8.94 (□), pH 9.40 (◇), pH 9.94 (○).

trophotometer equipped with a rapid mixing apparatus. For each system, oxygenated solutions of the ligand were mixed with oxygenated solutions containing $Co(NO_3)_2$. The solutions were saturated with dioxygen or with air at 1 atm. Spectrophotometric measurements were carried out at different cobalt concentrations in the pH range from 8.4 to 10 by using solutions of the ligand suitably buffered with sodium tetraborate and NaOH. Each experiment was repeated at least five times.

The kinetic behavior is independent of the initial dioxygen concentration, indicating that O_2 is involved only in a fast step following the rate-determining one. In Fig. 3, we report, as an example, the experimental results of single runs at four pH values for the system $Co/Me_2Octaen/O_2$. The increase of the absorbance at 320 nm strongly depends on pH and exhibits a positive intercept at $t = 0$. By considering that only the oxygenated complexes absorb at 320 nm, this intercept indicate that a first rapid reaction leading to formation of an oxygenated complex immediately occurs. This reaction, too fast to be studied with our apparatus, is followed by a second slower process which falls in the range-time of our instrumentation and can so be monitored. The kinetics of this second process follows a first-order law:

$$A = A^0 + (A^\infty - A^0)(1 - e^{-\eta t}) \quad (1)$$

where η is the apparent kinetic constant whereas A^0 and A^∞ represent the absorbance values at $t = 0$ and $t = \infty$, respectively. The parameters A^0, A^∞ and η were determined by means of a least-square procedure and

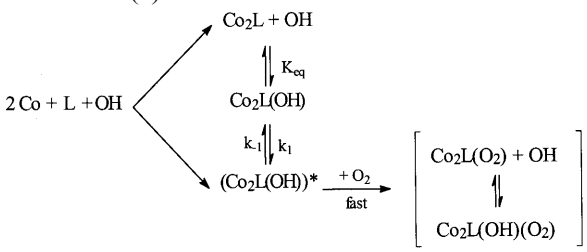
Table 1
Kinetic constants for the reaction $Co_2LOH \rightarrow Co_2LOH^*$ and log K_{eq} values for the equilibrium $Co_2L + OH \rightleftharpoons Co_2LOH$

Ligand	k_1 (s^{-1})	Log K_{eq}	Log K_{eq} [a]
Me_2Octaen	1.81 ± 0.05	4.8 ± 0.3	5.62 ± 0.04
[27]aneN_9	0.33 ± 0.03	5.1 ± 0.7	5.03 ± 0.04
[30]aneN_{10}	0.81 ± 0.05	4.5 ± 0.5	3.52 ± 0.04
[33]aneN_{11}	1.5 ± 0.2	4 ± 1	2.09 ± 0.04

[a] Determined by independent potentiometric measurements [22–24].

their reproducibility was of 5% on A^0, 1% on A^∞ and 3% on η. In the same figure the calculated functions are compared with the experimental data. A^0 and η depend on the pH.

By considering that preliminary results on the kinetics of formation of the dinuclear Co_2L complexes in anaerobic conditions indicate that the formation of these complexes seems to be faster than the slower reaction of formation of their dioxygen adducts, the experimental behavior is consistent with the following mechanism (2):



(2)

where the kinetic controlling step is the transformation of the cobalt-ligand precursor complex to yield an active form. The precursors, Co_2L, Co_2LOH, and Co_2LOH^*, exhibit different reactivities toward dioxygen, Co_2LOH^* being the most active form. Co_2LOH^* directly formed by the reaction of the cobalt with the ligand, immediately binds dioxygen and this reaction is responsible of the absorption at $t = 0$. Because the Co_2LOH^* concentration is higher at higher pH, A^0 increases with pH. The slow step involve the formation of the intermediate species Co_2L, and Co_2LOH the latter being converted in the active form Co_2LOH^* in the rate-determining step. Thereafter the rate of the formation of the oxygenated complex is controlled by the rate of formation of Co_2LOH^*.

According to this mechanism the apparent kinetic constant of the slow step, η, depends on the pH as:

$$\eta = \frac{k_1 K_{eq}[OH]}{1 + K_{eq}[OH]} + k_{-1} \quad (3)$$

where $K_{eq} = [Co_2LOH]/([Co_2L][OH])$. The values of K_{eq} and k_1 reported in Table 1 for all the systems with the different ligands, have been obtained by means of a non-linear best-fitting procedure on Eq. (3). The value of k_{-1} is in any case too small to be determined with sufficient precision, indicating that the equilibrium between the two hydroxo species is largely displaced towards the active one. The agreement between the experimental and calculated η values is very good for all the investigated systems (see as an example Fig. 4). The values of log K_{eq} obtained by this procedure are in fair agreement with the log K_{eq} values already determined by independent potentiometric measurements [22–24].

The different reactivity of the two equilibrium species, Co_2LOH and Co_2LOH^*, can be justified if one considers that the coordination positions of the cobalt atom not occupied by the nitrogen atoms of the ligand in Co_2LOH are directed towards the inner part of the

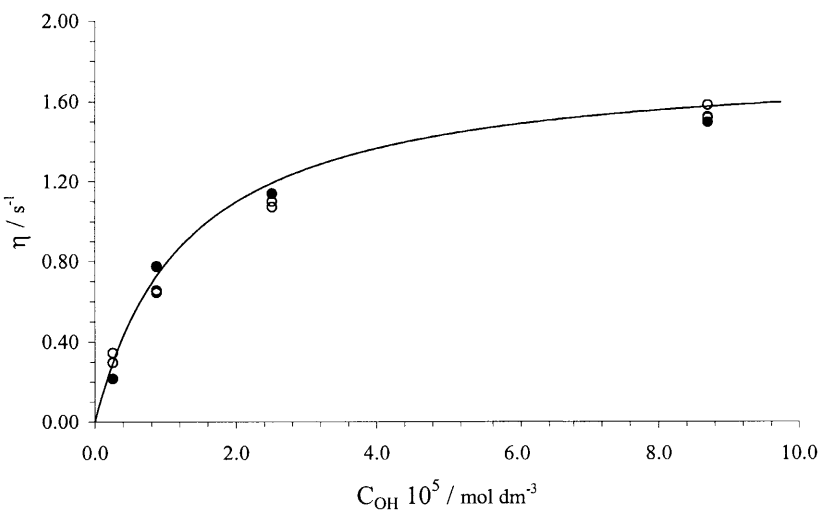


Fig. 4. Dependence of the apparent kinetic constant of formation of the $Co_2Me_2OctaenO_2(OH)_j$ complex, η, from the OH^- concentration, C_{OH}. Continuous line represents the fitting curve; (○) are the experimental η values obtained in measurements carried out at $C^0_{O_2} = 2.0 \times 10^{-4}$ mol dm^{-3}; (●) are the experimental η values in measurements carried out at $C^0_{O_2} = 1.0 \times 10^{-3}$ mol dm^{-3}.

Table 2
Values of the kinetic constants k_1 and k_2 for the formation of the $Co_2L(O_2)(OH)_2^*$ and $Co_2L(O_2)_2(OH)_2^*$ complexes, respectively ($R = 0.5$ and pH >11.5)

Ligand	$k_1 \times 10^3$ (s^{-1})	$k_2 \times 10^3$ (s^{-1})
Me_2Octaen	5.2 ± 0.7	0.68 ± 0.09
[27]aneN_9	4.3 ± 0.5	0.12 ± 0.06
[30]aneN_{10}	2.2 ± 0.6	0.05 ± 0.02
[33]aneN_{11}	3.3 ± 0.7	0.22 ± 0.09

complex molecule requiring a molecular rearrangement in order to expose the cobalt ion to the dioxygen attack or, as suggested by the thermodynamic study [30], the Co_2LOH species needs a rearrangement in order to give rise to a $Co_2L(OH)(O_2)$ complex stabilized by direct interactions via hydrogen bonding between the bound O_2 and OH^- species.

The inspection of the k_1 values in Table 1 shows that the reaction $Co_2LOH \rightarrow Co_2LOH^*$ is faster the more flexible the ligand is. The largest value of k_1 corresponds to the reaction with the acyclic Me_2Octaen whereas, concerning the series of the cyclic ligands, k_1 increases with the cycle size.

At $R = 0.5$ and pH >11, $Co_2L(OH)_2$ is the prevailing species in anaerobic conditions for Me_2Octaen [6,23]. Although the formation of dihydroxo dicobalt(II) complexes with the macrocyclic ligands was not observed in the speciation study performed at pH <10.5 [22], these species are formed in more alkaline solutions (pH >11) as demonstrated by proton balance measures we have performed in the pH range 11.0–11.5. The reaction of dioxygen uptake at these R and pH values is much slower than at lower pH and its course has been followed by monitoring the dioxygen consumption as a function of time through measurements of the free dioxygen concentration in solution, C_{O_2}. We observe a first dioxygen uptake-which occurs in about 10 min and consumes about 0.5 mols of dioxygen per mole of cobalt — followed by a further slower dioxygen consumption. The kinetics of these reactions does not depend on the initial dioxygen concentration and C_{O_2} changes according to the kinetic law of a two-step first-order mechanism. Additional UV–Vis spectrophotometric measurements at 320 nm show an initial increase and a subsequent decrease of absorbance. These results indicate the formation of non-negligible amounts of an intermediate species and support the following reaction scheme:

$$Co_2L(OH)_2 \underset{k_1}{\rightarrow} (Co_2L(OH)_2)^* \overset{+O_2}{\underset{\text{fast}}{\rightarrow}} Co_2L(OH)_2(O_2) \underset{k_2}{\rightarrow} (Co_2L(OH)_2(O_2))^* \overset{+O_2}{\underset{\text{fast}}{\rightarrow}} \text{products} \quad (4)$$

where the kinetic controlling steps are the transformation of the precursor $Co_2L(OH)_2$ and the intermediate $Co_2L(O_2)(OH)_2$ species in order to give the active forms $Co_2L(OH)_2^*$ and $Co_2L(O_2)(OH)_2^*$. According to this scheme the function $C_{O_2} = f(t)$ is given by:

$$C_{O_2} = C^0_{O_2} - C^0_{Co} + \frac{C^0_{Co}}{(k_1 - k_2)}\left(\frac{k_1}{2} - k_2\right) e^{-k_1 t} + \frac{C^0_{Co}}{(k_1 - k_2)} \frac{k_1}{2} e^{-k_2 t} \quad (5)$$

By means of a non-linear best-fitting procedure we obtained the k_1 and k_2 values reported in Table 2.

As an example in Fig. 5 the experimental C_{O_2} values are compared with the calculated curve for the Co(II)-[33]aneN_{11} system. In Fig. 6 the concentration as a function of time of the Co_2[33]ane$N_{11}(O_2)(OH)_2$ intermediate, as calculated by using the kinetic constants determined from dioxygen consumption, is compared with that obtained by spectrophotometric data at 320

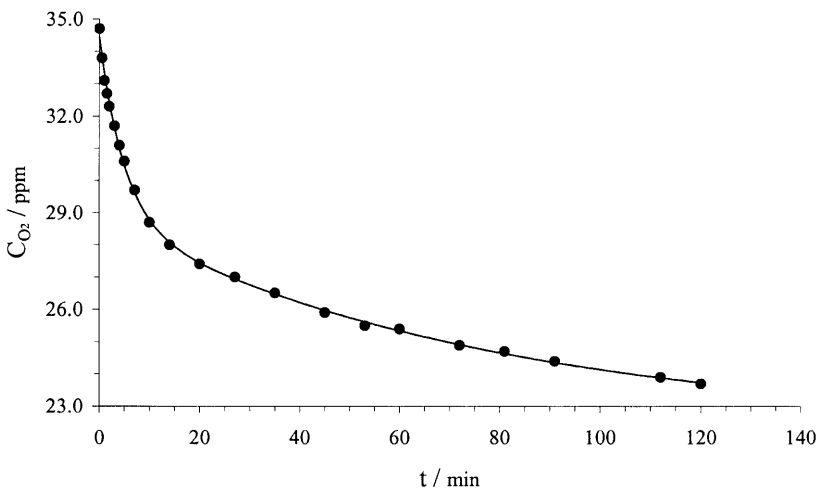


Fig. 5. Evolution of the free dioxygen concentration, C_{O_2}, in solution for the system Co(II)/[33]aneN_{11}/O_2 at $R = 0.5$ and pH >11.5. Continuous line represents the fitting curve; (●) are the experimental values ($C^0_{Co} = 4.06 \times 10^{-4}$ mol dm^{-3}; $C^0_L = 2.03 \times 10^{-4}$ mol dm^{-3}; $C^0_{O_2} = 1.08 \times 10^{-3}$ mol dm^{-3}; pH 11.50).

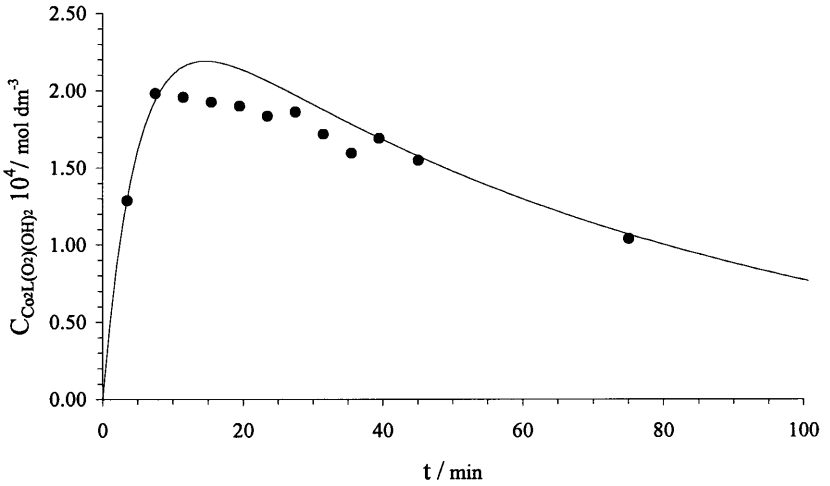


Fig. 6. Evolution with time of the concentration of the species $Co_2[33]aneN_{11}(O_2)(OH)_2$ calculated by the kinetic constants determined from oxygen consumption (continuous line), and by independent spectrophotometric measurements at 320 nm (●).

nm. The agreement between the data obtained with the two methods is good for all the ligands here considered.

The analysis of the k_1 values in Table 2 shows that the presence of the second hydroxo group in the cobalt-ligand precursor complex slows down the rate of formation of a species reactive towards dioxygen.

As shown by the spectral modifications occurring along with the dioxygen uptake process, the final complex species obtained at pH >11.5 after consumption of one equivalent of O_2 per metal ion has undergone a significant transformation with respect to the precursor complex. Nevertheless, the nature of such final di-cobalt(II) complex as well as the actual fate of the oxygen consumed in the last stage of the process remain an intriguing issue. While in the case of the 9-dentate ligands Me_2Ocaten and [27]aneN_9 the formation of a $Co_2L(O_2)_2(OH)_2$ species, in which at most one nitrogen donor atom of the ligand would not be involved in the coordination, could be invoked to rationalize the overall process the formation of a similar complex seems less probable with [30]aneN_{10} and [33]aneN_{11} considering the marked tendency these ligands have in involving all their donor atoms in metal ion coordination.

Further studies are being undertaken to identify the nature of these final complex species.

3.3. Mononuclear complexes

At $R>1.5$ and pH >8, the investigated polyazaalkanes form with the cobalt mononuclear complexes [6] able to bind one dioxygen molecule. The kinetics of formation of these oxygenated complexes has been studied by monitoring the decay of the dioxygen concentration in solution as a function of time. Several measurements were carried out at different values of R, pH (ranging from 8 to 11), and initial dioxygen concentration.

The kinetic behavior is similar to that of the dinuclear complex at the lower pH values. The binding curves show an initial rapid step ($1 \div 2$ min) up to a R_{O_2} ratio ranging from 0.05 to 0.2 and a second slow process (about 2 h) up to $R_{O_2}=1$. R_{O_2} is the bound dioxygen/cobalt concentration ratio. In this latter process C_{O_2} decays according to a first order kinetic law:

$$C_{O_2} = C^0_{O_2} - C^0_{Co}(1 - e^{-k_1 t}) \quad (6)$$

The experimental behavior is consistent with the mechanism (7):

$$\mathrm{Co + LH_j} \rightleftharpoons \mathrm{CoLH_j} \xrightarrow{k_1} \mathrm{(CoLH_j)^*} \xrightarrow[\text{fast}]{+O_2} \mathrm{CoLH_j(O_2)} \quad (7)$$

$CoLH_j^*$ is responsible for the first rapid dioxygen uptake, the slow process, independent of pH, being kinetically controlled by the transformation of $CoLH_j$ to yield the active form $CoLH_j^*$. This mechanism suggests that in the two equilibrium species $CoLH_j$ and $CoLH_j^*$ ($j=0$, 1 depending on the pH value) the metal ions are characterized by different coordination environments containing, presumably, six and five nitrogen atoms of the ligand in $CoLH_j$ and $CoLH_j^*$, respectively.

In Table 3 are reported the values of the kinetic constants, k_1, obtained by means of a non-linear best

Table 3
Values of the kinetic constant, k_1, for the formation of the $CoLH_j(O_2)$ complex

Ligand	$k_1 \times 10^3$ (s^{-1})
Me_2Octaen	0.5 ± 0.2
[27]aneN_9	1.7 ± 0.2
[30]aneN_{10}	0.7 ± 0.1
[33]aneN_{11}	1.0 ± 0.2

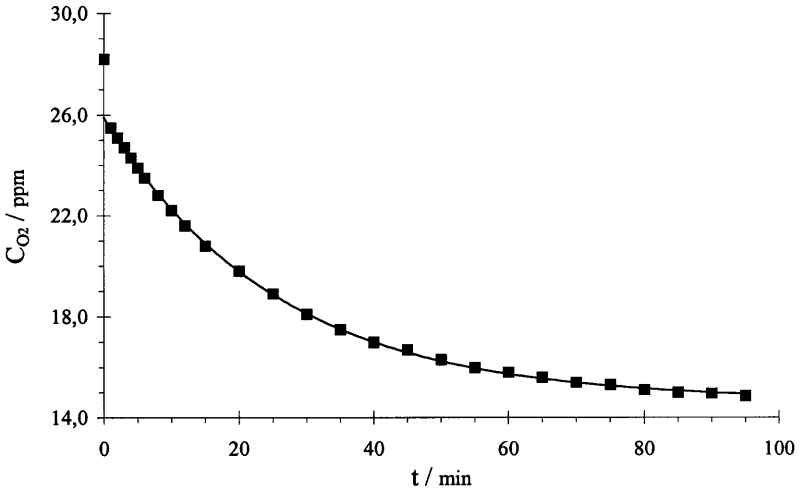


Fig. 7. Evolution of the free dioxygen concentration, C_{O_2}, in solution for the system CoII)/[30]aneN$_{10}$/O$_2$ at $R > 1.5$. Continuous line represents the fitting curve; (■) are the experimental values ($C^0_{Co} = 4.25 \times 10^{-4}$ mol dm^{-3}; $C^0_L = 7.61 \times 10^{-4}$ mol dm^{-3}; $C_{O_2} = 8.81 \times 10^{-4}$ mol dm^{-3}; pH 8.14).

fitting procedure to Eq. (6). Fig. 7 compares the experimental and calculated dioxygen concentration decay for the system Co/[30]aneN$_{10}$/O$_2$. The agreement is very good for all the ligands considered in this work.

The k_1 values given in Table 3 show that the formation of the active species is slower for the Me$_2$Octaen complex than for the more strained macrocyclic complexes.

4. Conclusions

The reaction of dioxygen addition on Co(II) complexes with the polyazaalkanes considered in this work shows some relevant differences if compared with the same reaction on Co(II) complexes with the ligands previously studied [8–15] both for the type of dioxygen adducts formed and for the kinetics of their formation. In fact, Co(II) bound to simple ligands form, in aqueous solution and at room temperature, μ-peroxo complexes in which the dioxygen bridges two cobalt ions of different subunits. The formation of end-on oxygenated complexes in water requires superstructured ligands able to form a protective cavity around the metal atom to prevent the reaction with another Co(II) complex forming a bridged μ-peroxocomplex. Examples of this kind of supramolecular structures are provided by the cobalt-cyclidenes superoxo complexes [27,28] and by oxygenated coboglobins [32–34]. Although polyazaalkanes are ligands with a relatively simple structure, nevertheless they form with cobalt mononuclear or dinuclear Co(II) complexes able to bind dioxygen giving end-on superoxo structures.

The complex behavior of these ligands arises from the manifold complexed structures they give with cobalt in solution: this is well highlighted by the kinetics of formation of their dioxygen adducts. The rate of formation of these adducts is slower than for Co(II) complexes with simple ligands and the determining rate step is in all cases the formation of an equilibrium species active towards dioxygen.

Acknowledgements

This work has been supported by the Ministero dell'Università e della Ricerca Scientifica e Tecnologica (MURST, Roma) within the program COFIN 98.

References

[1] A.E. Martell, D.T. Sawyer ((Eds.), Oxygen Complexes and Oxygen Activation by Transition Metals, Plenum Press, New York, 1988.
[2] L.I. Simandi ((Ed.), Dioxygen Activation and Homogeneous Catalytic Oxidation, Elsevier, Amsterdam, 1991.
[3] A.E. Martell, Acc. Chem. Rev. 15 (1982) 155.
[4] T.D. Smith, J.P. Pilbrow, Coord. Chem. Rev 39 (1981) 295.
[5] E.C. Niederhoffer, J.H. Timmons, A.E. Martell, Chem. Rev. 84 (1984) 137.
[6] S. Cabani, N. Ceccanti, M.R. Tiné, Pure Appl. Chem. 63 (1991) 1455.
[7] S. Cabani, React. Func. Polym. 28 (1996) 167.
[8] S. Cabani, N. Ceccanti, G. Conti, P. Gianni, Gazz. Chim. Ital. 112 (1982) 159.
[9] S. Cabani, N. Ceccanti, G. Conti, J. Chem. Soc., Dalton Trans. (1983) 1247.
[10] S. Cabani, N. Ceccanti, G. Conti, Inorg. Chim. Acta 21 (1984) 89.
[11] S. Cabani, N. Ceccanti, P. Gianni, J. Chem. Soc., Dalton Trans. (1984) 307.
[12] S. Cabani, N. Ceccanti, M.R. Tinè, J. Sol. Chem. 15 (1986) 177.

[13] S. Cabani, N. Ceccanti, M.R. Tinè, J. Chem. Soc., Dalton Trans. (1988) 373.
[14] S. Cabani, N. Ceccanti, R. Pardini, M.R. Tinè, Gazz. Chim. Ital. 124 (1994) 327.
[15] S. Cabani, N. Ceccanti, R. Pardini, M.R. Tinè, Polyhedron 18 (1999) 3295.
[16] A.E. Martell, R.J. Motekaitis, D. Chen, I. Murase, Pure Appl. Chem. 65 (1993) 959.
[17] B. Bosnich, Inorg. Chem. 38 (1999) 2554.
[18] J. Aragó, A. Bencini, A. Bianchi, E. Garçia España, M. Micheloni, P. Paoletti, J.A. Ramirez, P. Paoli, Inorg. Chem. 30 (1991) 1843.
[19] A. Bencini, A. Bianchi, E. Garçia España, M. Giusti, M. Micheloni, P. Paoletti, Inorg. Chem. 26 (1987) 681.
[20] A. Bencini, A. Bianchi, E. Garçia España, M. Giusti, S. Mangani, M. Micheloni, P. Orioli, P. Paoletti, Inorg. Chem. 26 (1987) 1243.
[21] A. Bencini, A. Bianchi, E. Garçia España, M. Micheloni, P. Paoletti, Inorg. Chem. 27 (1988) 176.
[22] A. Bencini, A. Bianchi, E. Garçia España, M. Micheloni, P. Paoletti, Inorg. Chem. 28 (1989) 2480.
[23] A. Bencini, A. Bianchi, V. Fusi, P. Paoletti, B. Valtancoli, A. Andres, J. Arago, E. Garçia España, Inorg. Chim. Acta 204 (1993) 221.
[24] A. Bencini, A. Bianchi, P. Paoletti, S. Cabani, N. Ceccanti, M.R. Tinè, E. Garçia España, Inorg. Chim. Acta 204 (1993) 227.
[25] A. Bencini, A. Bianchi, S. Cabani, N. Ceccanti, P. Paoletti, M.R. Tiné, J. Chem. Soc., Dalton Trans. (1993) 695.
[26] S. Cabani, N. Ceccanti, R. Pardini, M.R. Tinè, A. Bencini, A. Bianchi, P. Paoletti, Ann. Chim. 89 (1999) 99.
[27] J.C. Stevens, D.H. Busch, J. Am. Chem. Soc. 102 (1980) 3285.
[28] H.E. Tweedy, N.W. Alcock, N. Matsumoto, P.A. Padolik, N.A. Stephenson, D.H. Busch, Inorg. Chem. 29 (1990) 616.
[29] A. Marchaj, A. Bakac, J.H. Espenson, Inorg. Chem. 37 (1992) 4164.
[30] A. Bencini, A. Bianchi, C. Giorgi, P. Paoletti, B. Valtancoli, N. Ceccanti, R. Pardini, Polyhedron 19 (2000) 2441.
[31] A. Bencini, A. Bianchi, M. Castellò, M.D. Vaira, J. Faus, E. Garçia España, M. Micheloni, P. Paoletti, Inorg. Chem. 28 (1989) 347.
[32] T. Yonetani, H. Yamamoto, G.V. Woodrow, J. Biol. Chem. 249 (1974) 682.
[33] B.H. Hoffman, D.H. Petering, Proc. Natl. Acad. Sci. USA 67 (1970) 637.
[34] T. Yonetani, H. Yamamoto, F. Kayne, G.V. Woodrow, Biochem. Soc. Trans. 109 (1973) 83.

PERGAMON

www.elsevier.nl/locate/poly

Polyhedron 19 (2000) 2457–2461

POLYHEDRON

Solubility of oxygen and inert substances in water

A. Braibanti *, E. Fisicaro, C. Compari

Pharmaceutical Department, Applied Physical Chemistry Section, University of Parma, I-43100 Parma, Italy

Abstract

The solubility of oxygen in water at different temperatures has been analysed in the light of a statistical thermodynamic model. According to the model, the oxygen–water system is considered as a convoluted ensemble consisting of a *reacting* system, formed by oxygen molecules and structured solvent with enthalpy difference ΔH^{ϕ} between discrete enthalpy levels, and of a *non-reacting* system with continuous distribution of enthalpy levels. The enthalpy change of the reaction between oxygen and water, as determined either by measuring the solubility of substances in water at different temperatures either by measuring heat calorimetrically, is partially absorbed by some n_w water molecules. The relaxed water molecules occupy part of the cavity formed around solute. The part of heat absorbed, ΔH_w depends linearly upon the temperature and causes the observed changes with temperature of apparent enthalpy ΔH_{app} for the dissolution of oxygen and many other inert substances in water. The number n_w is proportional to the size of solute as shown by comparison with noble gases and other inert substances slightly soluble in water. The solubilization process of all these substances is clearly analogous. © 2000 Elsevier Science B.V. All rights reserved.

Keywords: Solubility; Oxygen; Solubilization enthalpy; Solubilization entropy; Cavity

1. Introduction

With the aim of studying the properties of perfluorocarbon emulsions used as injectable oxygen carriers which show enhanced capability of dissolving oxygen in aqueous solution, we have undertaken an analysis of the solubilization process of gaseous oxygen in water. The analysis of the thermodynamic parameters of the dissolution process in water of oxygen and other non-polar substances, either gaseous or liquid, has been connected [1–20] to the study of the so-called 'hydrophobic bond'. We have now examined the dissolution of oxygen and other inert substances in water in the light of a statistical thermodynamic molecular model [21–24]. The model is based on the distinction between *non-reacting* systems, with continuous distribution of enthalpy levels and *reacting* systems, with discrete quantized distribution of enthalpy levels. A *non-reacting* system is represented by a canonical partition function:

$$\zeta_A = \exp(s/R) = \exp(h/RT) \quad (1)$$

where s and h are partial molar entropy and enthalpy, respectively, whereas a *reacting* system is represented by a grand canonical partition function:

$$Z_M = \exp(-\Delta G^{\phi}/RT) \quad (2)$$

where ΔG^{ϕ} is the free energy change of the reaction. An ensemble composed of *reacting* species and *non-reacting* solvent W is represented by a convoluted partition function obtained as the product of partition functions:

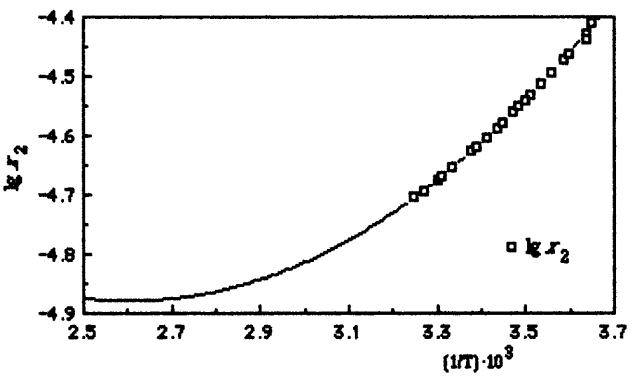


Fig. 1. Solubility of gaseous oxygen in water: affinity function lg x_2 as the function of $1/T$. Data from Benson and Krause [25] with interpolation polynomial, Eq. (16).

* Corresponding author. Tel.: +39-052-190-5024; fax: +39-052-190-5006.

E-mail address: braiban@ipruniv.cce.unipr.it (A. Braibanti).

0277-5387/00/$ - see front matter © 2000 Elsevier Science B.V. All rights reserved.
PII: S0277-5387(00)00545-3

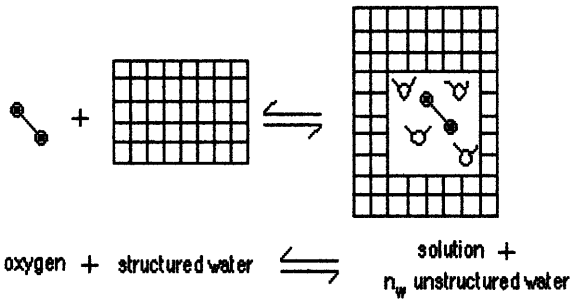


Fig. 2. The solubilization process of oxygen in water is determined by formation of a zone with n_w destructured water molecules in the cavity around solute.

$$\Xi_{MW} = Z_M \zeta_W \tag{3}$$

The model is suited to explain the changes of thermodynamic functions with the temperature in aqueous systems.

The affinity function in thermodynamic space [21–24]

$$(-\Delta G^{\phi}/RT) = \ln Z_M \tag{4}$$

in particular for oxygen or any inert gas solubility, takes the form

$$(-\Delta G^{\phi}_{app}/RT) = 2.302 \lg x_2 \tag{5}$$

where the solubility is identified, as usually with the molar fraction x_2 at unit pressure, with index 2 indicating the solute. At unit pressure, the molar fraction, x_2 is the reciprocal of the Henry constant, K_H. When the affinity function $\lg x_2$ for oxygen measured at different temperatures [25] is plotted against the reciprocal temperature $(1/T)$, it appears as a curve with a minimum at temperature $T = 400$ K (Fig. 1).

Analogous behaviour is shown by many other inert substances dissolved in water at different temperatures [26–28]. The analogy suggests that the molecular mechanisms underlying the dissolution processes of inert substances in water are similar to one another. The proposed mechanism consists in the formation of a cavity around the solute which is partially occupied, together with the solute, by some destructured water molecules (Fig. 2).

The solubility of a gas such as oxygen in water can be treated as a heterogeneous equilibrium between oxygen O_2 and x water molecules W followed by a homogeneous equilibrium:

$$O_2 + xW = (O_2W_x) = (O_2W_{(x-n_w)}) + n_wW \tag{6}$$

where xW is the portion of the bulk solvent involved in the solubilization process, and $O_2W_{(x-n_w)}$ is the oxygen molecule trapped in a cavity. The n_w water molecules are no more structured as in the bulk solvent. The constant of this equilibrium is:

$$K_s = [O_2W_{(x-n_w)}][W]^{n_w}/[O_2] \tag{7}$$

At constant gas pressure, the concentration $[O_2W_{(x-n_w)}]$ measures the solubility. With these assumption, Eq. (7) can be rewritten as a function of solubility product:

$$P_s = [W]^{n_w}/K_H = x_2[W]^{n_w} \tag{8}$$

where P_s includes the conversion factor deriving from the inhomogeneity of the concentration scales of gas and water and $K_H = 1/x_2$ is the Henry constant. By taking the logarithm of Eq. (8), we move from probability space to thermodynamic space [23]:

$$\ln x_2 = \ln P_s - n_w \ln[W] \tag{9}$$

The solubility can be expressed in thermodynamic space ($\ln x_2 = -\Delta G^{\phi}_{app}/RT$) as the function of the reciprocal temperature by a polynomial.

By calculating the first derivative of the polynomial with respect to the reciprocal temperature, we get at any temperature T:

$$\{\partial \ln x_2/\partial (1/T)\}_T = \{\partial \ln P_s/\partial(1/T)\}_T - n_w\{\partial \ln[W]/\partial(1/T)\}_T \tag{10}$$

which can be identified for a combinations of enthalpies

$$-\{\Delta H_{app}\}_T = -\{\Delta H^{\phi}\}_T + \{\Delta H_w\}_T \tag{11}$$

The left hand member, $\{\Delta H_{app}\}_T$ can be obtained from Eq. (10) from the first derivative at $T \to \infty$ of $\ln x_2 = f(1/T)$. The enthalpy $\{\Delta H^{\phi}\}_T$ can be assumed that at a first approximation it is constant, $\{\Delta H^{\phi}\}_T = \Delta H^{\phi}$. On the other hand, the enthalpy $\{\Delta H_w\}_T$ of the second term of r.h.s. of Eq. (12) can be obtained from the dependence of ln[W] upon T which can be expressed [27] as:

$$-n_w \partial \ln[W]/\partial \ln T = n_w C_{p,w}/R \tag{12}$$

where $C_{p,w}$ is the molar heat capacity of water. Eq. (12) is the mathematical expression of the concept of *thermal equivalent dilution* [29].

By transformation into the derivative with respect to $1/T$, Eq. (12) yields:

$$n_w T \partial \ln[W]/\partial(1/T) = \{-\Delta H_w/R\}_T = n_w C_{p,w} T/R \tag{13}$$

By combining Eq. (12) with Eq. (13) we get:

$$\Delta H_{app} = \Delta H_0 + n_w C_{p,w} T \tag{14}$$

where n_w is the number of water molecules involved in the reaction and $C_{p,w}$ is the molar isobaric heat capacity of water ($C_{p,w} = 75.38$ J mol^{-1} K^{-1}).

We recall that the slope of the affinity function of Fig. 1 at each point is given by the van't Hoff equation:

$$\partial(-\Delta G^{\phi}_{app}/RT)/\partial(1/T) = -\Delta H_{app}/R \tag{15}$$

Therefore, the slope of the curve at each point depends on the enthalpy of the dissolution process in water for any inert substance. The slope of the solubility curve, however, is changing with the temperature and reaches

zero at the minimum of the solubility curve. In particular, for the dissolution of oxygen or any other similar substance such as noble gases, nitrogen, hydrogen, etc., the solubility data are interpolated by a polynomial:

$$\lg x_2 = a + by + cy^2 + \cdots \quad (16)$$

with $y = 1/T$. For oxygen, the data reported in Fig. 1 give $a = -2.001$, $b = 2.209$, and $c = 0.424$ whereby values of ΔH_{app} at each temperature can be calculated from the derivative of Eq. (16) at $T \to \infty$. When the calculated values ΔH_{app} are plotted against T, the enthalpy values come out to be a linear function of T according to the Eq. (14), which is the result of an extrapolation of the solubility curve to $T \to 0$. Even if the enthalpy is measured calorimetrically at different temperatures [27], the values conform to Eq. (14).

Eq. (14) shows how the apparent enthalpy, ΔH_{app} is a linear function of the variable temperature, T with slope $\Delta C_{p,app} = n_w C_{p,w}$. This means that the contribution to heat by solvent molecules participating in the solubilization process should depend linearly upon the absolute temperature and hence should produce a change of the tangent, $\{-\Delta H_{app}/R\}_T$ of the solubility curve, what is actually observed (cf. Fig. 1). The linear dependence of ΔH_{app} upon T is shown in general by the substance examined either if the enthalpy is calculated from the tangent of the solubility curve or if it is experimentally determined by calorimetry. The slope of the line, which is different for each solute and increases with the complexity of the solute molecule gives the number of water molecules, n_w involved in the reaction.

The model has been successfully applied to other problems, to treat changes with the temperature of the solubility in water of inert gases and liquids, of denaturation enthalpy, and of micelle formation enthalpy. In all these processes, the enthalpy can be expressed as a linear function of the temperature.

The specific contribution of the number n_w of solvent molecules depends on the size of solute molecule. This can be shown by the series of gases of Table 1. Values of n_w, when plotted against parameters which are proportional to the size of solute such as the polarizability volume (Fig. 3), appear to be continuous functions of these parameters. When treating denaturation enthalpy of macromolecules, values of n_w grow up to values of a 100 or more.

By interpreting these series of processes in terms of a homogeneous molecular mechanism, a possible formation of a cavity to lodge the solute, can be put forward. The number n_w is then related to destructuring ($n_w > 0$) of water molecules around the solute as shown in Fig. 2. Roughly speaking n_w depends on the surface of the

Table 1
Solution of gases in water extrapolated enthalpy $\Delta H°$, apparent heat capacity $\Delta C_{p,app}$, and number of water molecules, n_w

Compound	Method	ΔH^{ϕ} (kJ mol^{-1})	$\Delta C_{p,app}$ (J mol^{-1} K^{-1})	n_w	Ref.	α-plz [b] (10^{-30} m^3)
He	sol. [a]	−35.7	118.0	1.57	[30]	0.205
	cal.	−40.9	135	1.79	[31]	
Ne	sol. [a]	−45.3	141.0	1.87	[30]	0.395
	cal.	−47.0	145	1.94	[31]	
Ar	sol. [a]	−68.6	187.0	2.48	[30]	1.64
	cal.	−71.5	200	2.64	[31]	
Kr	sol. [a]	−78.9	214.1	2.84	[30]	2.48
	cal.	−80.9	220	2.92	[31]	
Xe	sol. [a]	−92.6	244.2	3.24	[30]	4.04
	cal.	−93.3	250	3.30	[31]	
Rn	sol.	−108.4	291.7	3.87	[30]	5.86
H_2	sol. [a]	−45.9	140	1.86	[30]	0.819
N_2	sol. [a]	−76.9	223	2.96	[30]	1.77
O_2	sol. [a]	−72.7	204	2.70	[30]	1.60
	sol. [a]	−66.3	181	2.40	[25]	1.60
	cal.	−73.9	205	2.72	[31]	
CO	sol. [a]	−68.9	194	2.57	[30]	1.98
CH_4	sol. [a]	−75.8	208	2.76	[30]	2.60
	sol.	−83.5	244	3.24	[32]	
	cal.	−75.7	209	2.77	[33]	
	cal.	−85.1	242	3.20	[31]	

[a] Values obtained by calculating ΔH_{app} from the first derivative of the interpolation polynomial and then by plot against T.
[b] α-plz is the polarizability volume.

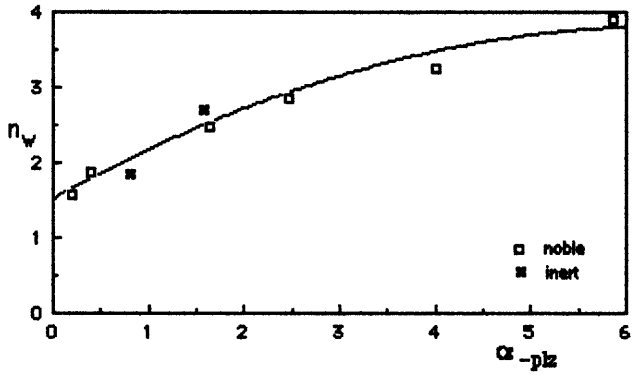


Fig. 3. Comparison of solubilization behaviour of oxygen and other inert gases. The number n_w of water molecules is a function of polarizability volume (α-plz, Table 1) thus suggesting that even n_w is a function of size of dissolved solute.

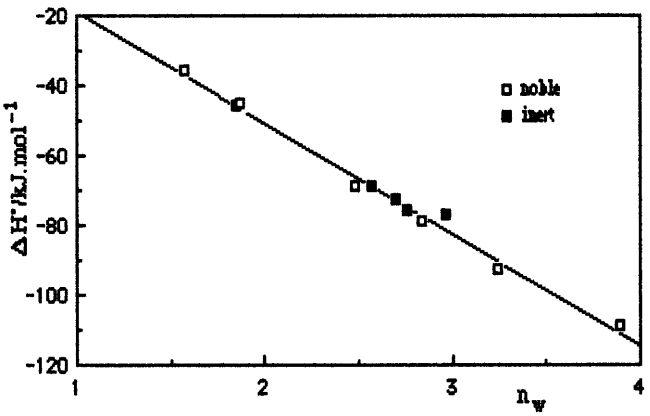


Fig. 4. Extrapolated enthalpy (Table 1) as a function of n_w.

Table 2
Solubilization entropy [30]

Compound	T_{min} (K)	$\lg x_{2,\,min}$	$\Delta S_{min}{}^{\phi}$ (J mol^{-1} K^{-1})	n_w
H_2	327.5	−0.607	−11.621	1.86
N_2	344.7	−0.760	−14.550	2.96
O_2	357.9	−0.867	−16.598	2.70
Air	360.3	−0.886	−16.962	2.39
He	305.4	−0.387	−7.409	1.57
Ne	323.1	−0.566	−10.836	1.87
Ar	369.2	−0.952	−18.226	2.48
Kr	374.1	−0.988	−18.915	2.84
Xe	396.1	−1.136	−21.749	3.24
Rn	371.5	−0.969	−18.552	3.89

solute although it is less than the number of water molecules needed to occupy the whole surface. These water molecules, according to the model of Hinz [12] and that of Costa and Silveston [10,11], should be relaxed water molecules occupying a cavity around the solute. The extrapolated enthalpy corresponds to the reaction between oxygen (or gas) and structured water before some heat is absorbed by relaxed water molecules. Actually, values of $\Delta H°$ are well correlated with n_w (Fig. 4). The correlation equation:

$$\Delta H° = 13.239 - 31.239 n_w \quad (17)$$

allows the calculation of enthalpy change per water molecule which is $\Delta h_w = -31.2$ kJ mol^{-1} per water. The order of magnitude of enthalpy change is about that for hydrogen bonds.

The entropy of the solubilization process can be calculated from the minimum of solubility. The free energy change at the minimum ΔG^{ϕ}_{min} is equal to $-T\Delta S^{\phi}_{min}$ and this property can also be employed to obtain thermodynamic functions of the solubilization process of oxygen and other substances in water (Table 2). The point of minimum solubility T_{min} is the point at which the solubilization process is adiabatic ($\Delta H^{\phi}/R = 0$). Below this temperature, the solubility of nonpolar substances has the unusual property of increasing in magnitude as the temperature is lowered. This fact is paralleled by the hydrophobic interaction effect which is decreasing in magnitude as the temperature is lowered. The parallelism is a further good argument for searching connections between the two processes. At T_{min} the affinity function $-\Delta G^{\phi}/T_m$ is equal to the entropy change:

$$-\Delta G^{\phi}/T_{min} = \Delta S^{\phi} \quad (18)$$

The values of entropy change for different compounds can be plotted against $(1/T_{min})$. A nice correlation (Fig. 5) is obtained:

$$\Delta S^{\phi} = -69.96 + 19\ 107\ (1/T_{min}) \quad (19)$$

indicating that the entropy change is composed of two parts, $\Delta S^{\phi}_a = -70.0$ J K^{-1} mol^{-1} independent of temperature and $\Delta S^{\phi}_b = 19\ 107\ (1/T_{min})$ J K^{-1} mol^{-1}. The latter portion is dependent upon the temperature and can be considered as an enthalpy change divided by temperature:

$$\Delta S^{\phi}_b = \Delta H^{\phi}_b\ (1/T_{min}) \quad (20)$$

with $\Delta H^{\phi}_b = 19.11$ kJ mol^{-1} indicating an endothermic process of cavity formation.

2. Conclusions

The logarithm of solubility $\lg x_2$ of oxygen in water at different temperatures is a measure of the affinity between gas and water. The enthalpy change of the solubilization process is a linear function of temperature. The dependence of enthalpy from the temperature is a consequence of the involvement of some water molecules. This behaviour is common to any inert gas and indicates that the molecular mechanism underlying the solubilization process is general. The experimental enthalpy data either obtained from solubility equilibria

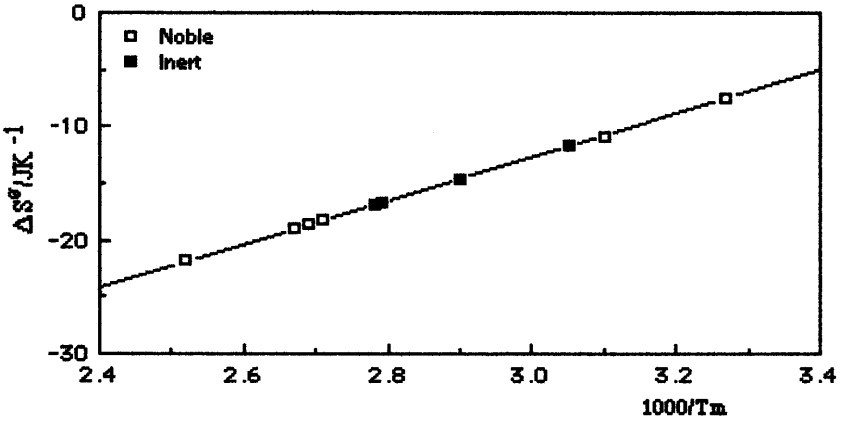


Fig. 5. Entropy change for solubilization of oxygen and inert gases in water as a function of $(1/T_{min})$.

or from calorimetric experiments are consistent with the formation of a cavity in structured water to allocate the solute. Some water molecules, the number dependent on the size of solute, become relaxed and absorb part of the enthalpy released by the reaction between water and gas. The reaction between gas and water is exothermic with enthalpy change $\Delta h_w = -31.2$ kJ mol^{-1}per water molecule. This energy is a little greater than free energy for hydrogen bonds $\Delta G_{HB} \approx -28$ kJ mol^{-1} and it is explained by considering that solubilization in water takes place by overcoming water–water hydrogen bonds. On the other hand, the solubilization process is entropically disfavoured by the entropy change $\Delta S_a^{\phi} = -70.0$ J K^{-1} mol^{-1} for transfer of a gas molecule into the cavity and entropically favoured by the endothermic reaction ($\Delta H_b^{\phi} = 19.11$ kJ mol^{-1}) for cavity formation. In conclusion, the analysis of the solubilization process of oxygen in water in comparison with the solubilization process of other inert gases has led to values of enthalpy and entropy changes of the process which are in reasonable balance with the free energy change of hydrogen bond formation.

Acknowledgements

This work is part of a Project 'Molecular Systems for Transport and Activation of Oxygen' supported (COFIN 98) by MURST (Ministry of University and Scientific and Technological Research), Rome and by University of Parma, Parma.

References

[1] H.S. Frank, M.W. Evans, J. Phys. Chem. 13 (1945) 507.
[2] W. Kauzmann, Adv. Protein Chem. 14 (1959) 507.
[3] C. Tanford, The Hydrophobic Effect: Formation of Micelles and Biological Membranes, Wiley-Interscience, New York, 1980.
[4] K. Shinoda, M. Fujiara, Bull. Chem. Soc. Jpn 41 (1968) 1.
[5] K. Shinoda, J. Phys. Chem. 81 (1977) 1300.
[6] A. Hvidt, Acta Chem. Scand., Ser A 37 (1983) 99.
[7] D. Patterson, M. Barbe, J. Phys. Chem. 80 (1976) 2435.
[8] P.L. Privalov, S.J. Gill, Adv. Protein Chem. 39 (1988) 191.
[9] P.L. Privalov, S.J. Gill, Pure Appl. Chem. 61 (1989) 1097.
[10] R. Silveston, B Kronberg, J. Phys. Chem. 93 (1989) 6241.
[11] M. Costas, B. Kronberg, R. Silveston, J. Chem. Soc., Faraday Trans. 90 (1994) 1513.
[12] T. Abou-Aiad, U. Becker, R. Biedenkamp, R. Brengelmann, R. Elsebrock, H.-J. Hinz, M. Sockhausen, Ber. Bunsenges. Phys. Chem. 101 (1997) 1921.
[13] M. Costa, B. Kronberg, R. Silveston, J. Chem. Soc., Faraday Trans. 90 (1994) 1513.
[14] R.L. Mancera, B. Kronberg, M. Costa, R. Silveston, Biophys. Chem. 70 (1998) 57.
[15] B. Lee, Biophys. Chem. 51 (1994) 271.
[16] B. Lee, Biophys. Chem. 51 (1994) 279.
[17] B. Lee, Biophys. Chem. 51 (1994) 263.
[18] B. Lee, Biopolymers 51 (1991) 993.
[19] B. Lee, Methods Enzymol. 259 (1995) 555.
[20] G. Graziano, Can. J. Chem. 76 (1998) 437.
[21] A. Braibanti, E. Fisicaro, C. Compari, Thermochem. Acta 320 (1998) 253.
[22] A. Braibanti, E. Fisicaro, C. Compari, Thermochem. Acta 320 (1998) 264.
[23] A. Braibanti, E. Fisicaro, C. Compari, Thermochem. Acta 320 (1998) 101.
[24] A. Braibanti, E. Fisicaro, C. Compari, Thermochem. Acta 320 (1998) 277.
[25] B.B. Benson, D. Krause, Jr., J. Chem. Phys. 64 (1976) 689.
[26] A. Braibanti, E. Fisicaro, F. Dallavalle, J.D. Lamb, J.L. Oscarson, R. Sambasiva Rao, J. Phys. Chem. 98 (1994) 626.
[27] A. Braibanti, E. Fisicaro, A. Ghiozzi, C. Compari, M. Panelli, J. Solut. Chem. 24 (1995) 703.
[28] A. Braibanti, E. Fisicaro, F. Dallavalle, J.D. Lamb, J.L. Oscarson, F.X. Ughi, J. Phys. Chem. 97 (1993) 8071.
[29] A. Braibanti, E. Fisicaro, C. Compari, J. Phys. Chem. B 102 (1998) 8537.
[30] E. Wilhelm, R. Battino, R.J. Wilcock, Chem. Rev. 77 (1977) 219.
[31] G. Olofsson, A.A. Oshodi, E. Qvarnström, I. Wadsö, J. Chem. Thermodyn. 16 (1984) 1041.
[32] A. Ben-Naim, J. Wilf, H. Yaacobi, J. Phys. Chem. 77 (1973) 95.
[33] H. Naghibi, S.F. Dec, S.J. Gill, J. Phys. Chem. 90 (1986) 4621.

PERGAMON

www.elsevier.nl/locate/poly

Polyhedron 19 (2000) 2463–2471

POLYHEDRON

Metal chelates of *N*-carbamoylmethyl-iminodiacetate(2 −) ion. Part III. Synthesis, XRD structures and properties of *N*-carbamoylmethyl-iminodiacetic acid (H_2ADA) and *cis*-diaqua(*N*-carbamoylmethyl-iminodiacetato)nickel(II), [Ni(ADA)$(H_2O)_2$]

E. Bugella-Altamirano [a], J.M. González-Pérez [a], A.G. Sicilia-Zafra [a], J. Niclós-Gutiérrez [a,*], A. Castiñeiras-Campos [b]

[a] *Department of Inorganic Chemistry, Faculty of Pharmacy, University of Granada, E-18071 Granada, Spain*
[b] *Department of Inorganic Chemistry, Faculty of Pharmacy, University of Santiago de Compostela, E-15706 Santiago de Compostela, Spain*

Abstract

N-(Carbamoylmethyl)iminodiacetic [$H_2ADA = H_2NCOCH_2N(CH_2CO_2H)_2$)] has been crystallised from water and characterised by X-ray crystallography (final value $R_1 = 0.051$). This compound exhibits a zwitterionic structure ($H_2ADA^{\pm}$) whose conformation is stabilised by an intra-molecular hydrogen bond interaction between the 'ammonium' hydrogen atom and the *O*-amide atom as acceptor one. All the other polar bonds give hydrogen bonds, which link adjacent zwitterions, one of them is a rather symmetrical and linear link (170(2)°). The appropriate stoichiometric reaction of nickel(II) hydroxycarbonate, $NiCO_3{\cdot}2Ni(OH)_2{\cdot}4H_2O$, and H_2ADA in water yields crystalline, green samples of *cis*-diaqua(*N*-carbamoylmethyl-iminodiacetato)nickel(II), [Ni(ADA)$(H_2O)_2$] (**I**). Its single crystal X-ray diffraction study was also carried out (final $R_1 = 0.031$). The crystal of complex **I** consists of slightly asymmetrical, octahedral coordination units linked in a three-dimensional network stabilised by hydrogen bonds where the water molecules play the most relevant role. Coordination bond distances in **I** (Å): Ni(1)–N(1) = 2.072(2), Ni(1)–O(11) = 2.051(2), Ni(1)–O(21) = 2.045(2) and Ni(1)–O(31, amide) = 2.065(2) with ADA, and Ni(1)–O(1) = 2.000(2) and Ni(1)–O(2) = 2.106(2) with aqua ligands. ADA acts as tetradentate chelating ligand, which is in contrast with chelating and bridging functions for such ligand in the polymeric Cu(II) derivative, where the metal exhibits a square base pyramidal coordination (type 4 + 1). © 2000 Elsevier Science B.V. All rights reserved.

Keywords: *N*-(Carbamoylmethyl)iminodiacetic acid; *N*-(2-Amidomethyl)-iminodiacetic acid; *N*-(2-Acetamide)-iminodiacetic acid; *cis*-Diaqua(*N*-carbamoylmethyl-iminodiacetato)nickel(II); Molecular and crystal structure; Magnetic and spectral properties; Thermal stability

N-Carbamoylmethyl-iminodiacetic acid or *N*-(2-amidomethyl)iminodiacetic acid (also named *N*-(2-acetamide)iminodiacetic acid) [$H_2ADA = H_2NCOCH_2N(CH_2CO_2H)_2$)] is widely used in biological buffers of pH 6.0–7.4. Since many years, metal ion-ADA chelation in solution has been studied for a variety of divalent ions (M = Mg, Ca, Sr, Ba, Mn, Co, Ni, Cu, Zn, Cd, Hg, Pb) [1]. These initial results of Schwarzenbach et al. have been partially supported by more recent studies [2–5] about the stoichiometry and stability of ADA complexes in solution. These works also showed cases where the de-protonation reaction of the primary amide takes place for $M(ADA)_2$ chelates (M = Co or Zn) [2]. Cu(II) de-chelation has also been claimed upon ADA amide de-protonation [6,7]. In contrast, studies concerning ADA complexes in solid state are scarce ones. In fact, crystal structure determinations were limited to only two different *oxo*-ADA–vanadium compounds [8–10] both having ADA as a tripodal-tetradentate ligand. It is worth noting that the structure of the free acid H_2ADA has not been reported, in spite of being a commercially available and widely used

* Corresponding author. Tel.: +34-958-243-855; fax: +34-958-246-219.
E-mail addresses: jniclos@ugr.es (J. Niclós-Gutiérrez), qiac01@usc.es (A. Castiñeiras-Campos).

0277-5387/00/$ - see front matter © 2000 Elsevier Science B.V. All rights reserved.
PII: S0277-5387(00)00546-5

chelating agent. In addition, studies on ADA–metal chelates in solid state seem a suggestive matter as a source of structural information of the chelating role of the ADA bivalent anion [$H_2NCOCH_2N(CH_2CO_2^-)_2$] as well as of the way in which its 'primary amide' group could be involved in the chelation of different metal ions. In this sense and as a part of our program on mixed-ligand Cu(II) complexes [11] we have synthesised and reported very recently for the first time the structure of compounds poly-[(*N*-carbamoylmethyl-iminodiacetato)copper(II) monohydrate], $\{[Cu(ADA)]\cdot H_2O\}_n$ [13], (imidazole)(*N*-carbamoylmethyl-iminodiacetato)-copper(II), [Cu(ADA)(ImH)] [12] and (2,2′-bipyridine)-(*N*-carbamoylmethyl-iminodiacetato)copper(II) three-hydrate, $[Cu(ADA)(bipy)]\cdot 3H_2O$ [13]. Such XRD studies [12,13] are our precedent reports in this series and they revealed again that ADA acts as tripodal-tetradentate but with remarkable differences in its ligand roles as well as in the coordination polyhedron of Cu(II) atom. The aim of this work is to report the structure of H_2ADA itself and to extend our contribution on ADA chelates to other metal ions with the synthesis and study of the structure and properties of its nickel(II) derivative.

1. Experimental

1.1. *N*-carbamoylmethyl-iminodiacetic acid (H_2ADA)

This compound was purchased from Aldrich. Crystals suitable for X-ray structure determination were obtained by re-crystallisation of the commercial available product in water. To this purpose, 500 mg of H_2ADA were dissolved in approximately 80 ml of doubly-distilled water, with stirring and heating (approximately 60°C) for 2 h. The resulting solution was left to cool and then filtered over a crystallisation dish. Evaporation at room temperature (r.t.) produces abundant and well-shaped crystals of this free acid, which were collected by filtration and air-dried.

1.2. Synthesis of cis-diaqua(*N*-carbamoylmethyl-iminodiacetato)nickel(II), $[Ni(ADA)(H_2O)_2]$, complex **I**

It was obtained by stoichiometric reaction of $NiCO_3\cdot 2Ni(OH)_2\cdot 4H_2O$ (250.9 mg, 0.66 mmol, Merck) and H_2ADA (380.3 mg, 2 mmol) in doubly-distilled water (100 ml) in a Kitasato flask, heating ($t < 50$°C) and stirring under reduced pressure (to remove the CO_2, by-product) for 1 h. Then the reacting mixture was heated and stirred 20 h at 60°C. The resulting clear and green solution was left to cool and then slowly filtered to remove an almost inappreciable amount of non-reacted NiO (insoluble by-product). After 3 weeks of slow evaporation at r.t. (remaining volume of 10–15 ml) the solution was filtered over a little crystallisation dish which was partially covered with a watch glass. That reduces the evaporation rate. After several days, well-shaped green crystals of complex **I** appeared, many of them were suitable for X-ray diffraction studies. For a few days, additional amounts of product were collected by the same way. If super-saturation of mother liquor arises, the addition of little volumes of water and ethanol and further slow evaporation of the solution induce again the crystallisation process. The product was collected by filtration, washed with a little of cool water and air-dried. It can be re-crystallised several times from water. Yield: variable but usually $< 55\%$. Calc. for complex **I** ($C_6H_{12}N_2NiO_7$): C, 25.48; H, 4.28; N, 9.90; Ni, 20.75. Found: C, 25.19; H, 4.36; N, 9.72; Ni, 20.7% (complexometry [14]).

1.3. X-ray data collection and reduction, structure solution and refinement

A colourless prismatic crystal of H_2ADA or a green plate crystal of $[Ni(ADA)(H_2O)_2]$ was mounted on a glass fibre and used for data collection. Cell constants and an orientation matrix for data collection were obtained by least-squares refinement of the diffraction data from 25 reflections in the range of $8.834 < \theta < 18.278$ or of $9.551 < \theta < 20.927$, respectively, in an Enraf Nonius MACH3 automatic diffractometer [15]. Data were collected at 293 K using Mo Kα radiation ($\lambda = 0.71073$ Å) and the ω-scan technique, and corrected for Lorentz and polarisation effects [16]. A semi-empirical absorption correction (ψ-scan) was made [17]. The structure was solved [18] by direct methods or by Paterson and Fourier methods, respectively, which revealed the position of all non-hydrogen atoms, and refined on F^2 by a full-matrix least-squares procedure using anisotropic displacement parameters [19]. All hydrogen atoms were located from difference Fourier maps and were refined isotropically. Atomic scattering factors were from the 'International Tables for X-ray Crystallography' [20]. Molecular graphics were prepared with the programs PLATON-97 or PLATON-98 [21] or ZORTEP [22]. A summary of the crystal data, experimental details and refinement results are listed in Table 1.

1.4. Physical measurements

Nickel(II) titration was carried out by standard EDTA complexometry [14]. For this purpose, a sample (534.9 mg) of compound **I** was placed in a precipitation device (250 ml) and mineralised with 2 N sulphuric acid (10 ml) and 10 N hydrogen peroxide (5 ml) solutions. The mineralisation process of the complex would be carried out covering the reaction device of the resulting

green solution with a watch glass and then smoothly heating it a few minutes. Such reaction and the decomposition of H_2O_2 (in excess) lead to an acid solution of nickel(II) sulfate which was quantitatively diluted with doubly-distilled water into a volumetric flask (250 ml). Aliquots (25 ml) of this solution were diluted with approximately 100 ml of doubly-distilled water in the corresponding Erlenmeyer flasks. Each aliquot was added of buffer solution pH 10 (ammonia/ammonium chloride, 10 ml) and murexide (Merck, mixed at a 1:2000 ratio with potassium nitrate) as metal-indicator. Such mixtures were heated to approximately 60°C prior to initiate each titration with 10^{-2} M Na_2H_2EDTA (Merck) solution (standardised with a reference $ZnCl_2$ solution and eriochrome black T (Merck) as indicator [14]). Elemental analysis (C, H and N) were performed in the Scientific Instrumental Centre of the University of Granada as described earlier [11]. FTIR spectra were obtained by the KBr disc technique (with KBr Aldrich FTIR grade) on a Nicolet FTIR 20SXB or a Jasco FTIR 410 instrument. Thermogravimetric studies of both compounds (22–550°C) in air flow (100 ml min^{-1}) and the corresponding spectra of evolved gases were recorded using a Shimazu Thermobalance TGA-DTG-50H coupled with a FTIR Nicolet Magma 550 (and a mass spectrometer Fisons Thermolab). The electronic (reflectance) spectrum of **I** (175–3300 nm) was obtained in a Cary 5E spectrophotometer. The magnetic susceptibility of **I** was measured in the temperature range 80–300 K using a Manics DM magnetometer. The susceptometer was calibrated with mercury tetrakis(thiocyanato)cobaltate(II). Corrections for the diamagnetism (122×10^{-6} cm^3 mol^{-1}) were estimated from Pascal constants [23].

Table 1
Crystal data and structure refinement for H_2ADA and complex $[Ni(ADA)(H_2O)_2]$ (**I**)

	H_2ADA	Complex **I**
Empirical formula	$C_6H_{10}N_2O_5$	$C_6H_{12}N_2NiO_7$
Formula weight	190.16	282.89
Temperature (K)	293(2)	293(2)
Wave length (Å)	0.71073	0.71073
Crystal system, space group	monoclinic, $P2(1)/n$	monoclinic, $C2/c$
Unit cell dimensions		
a (Å)	8.426(1)	11.133(1)
b (Å)	11.334(1)	8.914(2)
c (Å)	8.991(2)	20.255(2)
β (°)	107.61(1)	104.66(1)
Volume (Å^3)	818.4(2)	1944.6(4)
Z, calculated density (Mg m^{-3})	4, 1.543	8, 1.932
Absorption coefficient (mm^{-1})	0.135	2.021
$F(000)$	400	1168
Crystal size (mm)	$0.35 \times 0.15 \times 0.15$	$0.35 \times 0.35 \times 0.15$
Theta range for data collection (°)	2.90–30.41	2.97–27.97
Index ranges	$0h12$, $-16k0$, $-12l12$	$-14h0$, $-11k0$, $-25l26$
Reflections collected/unique	2618/2471 [$R_{int} = 0.0393$]	2462/2349 [$R_{int} = 0.0222$]
Completeness	95.5% (to $2\theta = 30.41$)	47.1% (to $2\theta = 27.97$)
Absorption correction	Psi-scan	Psi-scan
Max. and min. transmission	0.961 and 0.906	0.976 and 0.770
Refinement method	Full-matrix least-squares on F^2	Full-matrix least-squares on F^2
Data/restraints/parameters	2471/0/158	2349/0/193
Goodness-of-fit on F^2	0.963	1.106
Final R indices [$I>2\sigma(I)$]	$R_1 = 0.051$, $wR_2 = 0.098$	$R_1 = 0.031$, $wR_2 = 0.068$
R indices (all data)	$R_1 = 0.222$, $wR_2 = 0.132$	$R_1 = 0.061$, $wR_2 = 0.080$
Largest difference peak and hole (e Å^{-3})	0.242 and −0.272	0.359 and −0.500

2. Results and discussion

2.1. Structure and properties of *N*-(carbamoylmethyl)iminodiacetic acid (H_2ADA)

Bond lengths and angles between non-hydrogen atoms and hydrogen bond distances and angles of this compound are given in Table 2. The crystal consists of a hydrogen bonded network of molecules where all polar N–H and O–H bonds are involved as 'H-donor' in this interactions. The acid dissociation constants of H_2ADA=H_2L have pK_a values ($I = 0.1$ (KNO_3) and 25°C) of $pK_0 = 1.59 < pK_1 = 2.31 \ll pK_2 = 8.98$ for the dissociation of the species H_3L^+ (cationic), H_2L (neutral), and HL^- (anionic), respectively [2]. Consequently it should be assumed that its protonated species and, in particular, its neutral molecule will exist as a zwitterion in solution (such as $H_2ADA^{\pm}$ for the molecular species). Our structural results indicate that the molecule also exists as a dipolar ion in solid state, and it represents the asymmetric unit of the crystal.

Two structural features of this amino-polycarboxylic acid seem of major interest. Firstly, its conformation seems intra-stabilised by only one hydrogen bond which is made up by the ammoniun proton with the O(31) amide atom as 'acceptor'. In spite of that, the C(32)–O(31) bond distance (1.231(3) Å) is not lengthened compared to the averaged distance of the C=O(amide) bond in primary amides (1.24(1) Å) [24]. The distance (2.590(3) Å) and angle (113(2)°, close to the tetrahedral angle) of this intra-molecular hydrogen bond agree reasonably well with those reported for a variety of amino-polycarboxylic acids such as iminodiacetic acid and many others [25]. It is worth noting that the *O*-amide atom should be preferred to a negatively

Table 2
Selected bond lengths (Å) and angles (°) for H_2ADA with e.s.d. values in parentheses [a]

Non-hydrogen atoms

O(11)–C(12)	1.222(3)	C(31)–N(1)–C(21)	13.0(2)
O(12)–C(12)	1.272(3)	C(31)–N(1)–C(11)	11.7(2)
O(21)–C(22)	1.212(3)	C(21)–N(1)–C(11)	12.2(2)
O(22)–C(22)	1.297(3)	N(1)–C(11)–C(12)	12.1(2)
O(31)–C(32)	1.231(3)	O(11)–C(12)–O(12)	27.0(2)
N(1)–C(31)	1.491(3)	O(11)–C(12)–C(11)	16.9(2)
N(1)–C(21)	1.493(3)	O(12)–C(12)–C(11)	16.0(2)
N(1)–C(11)	1.497(3)	N(1)–C(21)–C(22)	13.2(2)
N(32)–C(32)	1.319(3)	O(21)–C(22)–O(22)	26.6(2)
C(11)–C(12)	1.516(3)	O(21)–C(22)–C(21)	19.3(2)
C(21)–C(22)	1.513(3)	O(22)–C(22)–C(21)	14.1(2)
C(31)–C(32)	1.511(3)	N(1)–C(31)–C(32)	07.3(2)
O(31)–C(32)–N(32)	124.4(2)		
O(31)–C(32)–C(31)	118.8(2)		
N(32)–C(32)–C(31)	116.7(2)		

Hydrogen bonds

D–H···A	*d*(D–H)	*d*(H···A)	*d*(D···A)	<(DHA)
N(1)–H(1)···O(31)	0.93(3)	2.09(3)	2.590(3)	113(2)
O(12)–H(12) ···O(22) # 1	1.25(4)	1.23(4)	2.477(2)	170(2)
N(32)–H(32A) ···O(11) # 2	0.89(3)	2.12(3)	2.970(3)	161(3)
N(32)–H(32B) ···O(21) # 3	0.89(4)	2.18(4)	3.062(3)	170(3)

[a] Symmetry transformations used to generate equivalent atoms: i: # 1 = $-x+1/2$, $y+1/2$, $-z+3/2$; ii: # 2 = $-x+1/2$, $y-1/2$, $-z+5/2$; iii: # 3 = $x-1$, y, z.

charged *O*-carboxylate atom. This is not the case for other *N*-substituted-iminodiacetic acids having a suitable 'acceptor' atom in the *N*-side chain. In such compounds the ammonium hydrogen atom forms a hydrogen bond with the 'acceptor' atom of the *N*-side chain as well as with one ('bifurcated' cases [25–27]) or with two ('trifurcated cases' [25,28]) *O*-carboxylate atoms of the acetate arms. Secondly, carboxylic and carboxylate groups from pairs of adjacent dipolar ions $H_2ADA^{\pm}$ (related by the symmetry code # 1 = i: $-x+1/2$, $y+1/2$, $-z+3/2$) are linked by a rather short, symmetrical and nearly linear hydrogen bond O(12)–H(12)···O(22^{i}) with an overall distance of 2.477(2) Å and angle of 170(2)° (see Fig. 1 and Table 2). This unique hydrogen bond is consistent with the rather similar ratio of carbon–oxygen bond distances (Å) in the two linked 'carboxyl' groups, C(12)–O(12)/C(12)–O(11) (1.272(3)/1.222(3)) = 1.041 and C(22)–O(22)/C(22)–O(21) (1.297(3)/1.212(3)) = 1.070. Indeed it is on the basis of the small difference in such ratios that the acid hydrogen atom could be formally assigned to the O(12) atom. In other words, the consideration of a carboxylic –C(12)O(11)O(12)H(12) group and a carboxylate –C(22)O(21)O(22)$^{-}$ one to the zwitterion H_2ADA in the crystal (as depicted in Fig. 1) is in some ways a practical approach or a simplification.

With necessary caution, we can attempt to correlate our crystal structure results with the high pK_a value of the studied amino-amide acid derivative. With this aim, it is instructive to consider that H_2ADA acid is the result of replacing the secondary amino hydrogen atom from the iminodiacetic acid (H_2IDA=HN(CH_2CO_2H)$_2$) by the *N*-(2-amidomethyl) or *N*-(carbamoylmethyl) arm. It is generally assumed that this latter neutral group (–CH_2CONH_2) displays a moderate electron withdrawing effect ($-I$) [24] but in fact it should be operative in the hydrogen bonding intra-stabilisation, as our structural results have stated. These two effects will act in an opposite sense and the final state should depend on the balance within them. Several sets of acidity (pK_a) or protonation constants are available for H_2IDA acid or IDA(2$-$) ion, respectively, for a ionic strength of $I = 0.1$ M (KNO_3) and 25°C [29]. For example, a complete set of pK_a dissociation constant values, p$K_0 = 1.80$, p$K_1 = 2.58$ and p$K_2 = 9.27$, for the three dissociation steps of the cationic species (H_3IDA^{+}) of iminodiacetic acid is available [30]. Consequently, it can be seen that the three pK_a values of H_2ADA are approximately 0.2–0.3 pK_a units lower than the corresponding values of H_2IDA.

Concerning the vibrational properties, the relative simplicity of groups in H_2ADA molecule allow us the following tentative assignations of bands (wave-numbers in cm^{-1}) in its IR spectrum [31]: ν(OH) of carboxylic group at 3400–3384, $\nu_{as}(NH_2)$ and $\nu_s(NH_2)$ of primary amide group at 3320 and 3250, ν_{as} and ν_s of CH_2 at 3014 and 2990, and 3295, ν(C=O) of carboxylic group at approximately 1730 (shoulder), $\nu_{as}(COO^{-})$ overlapped with ν(C=O) of primary amide group (also called 'amide I' band) at 1700, and $\delta(NH_2)$ of this latter group (so-called 'amide II' band) at 1681, $\delta(CH_2)$ at 1442, and $\nu_s(COO^{-})$ at 1366. In this connection it is interesting to keep in mind that certain assignations concerning the amide primary group are only the best approximations. These are the cases of 'amide I and II' bands. The former is not due to a pure C=O stretching mode but is appreciably coupled with a C–N stretch and to some extent with the –NH_2 band [31a]. There is more controversy over the amide II band, but it is generally accepted that it is mainly due to the scissoring mode of the –NH_2 amide group. A band at 3050 cm^{-1} is assigned to a combination mode $\delta(NH_2$, amide) + $\nu_s(COO^{-}$, carboxylate group) (1681 + 1366 = 3047). Concerning the zwitterionic form of this compound, an interesting finding is a series of weak bands observed in the region of 2880–2000 cm^{-1} (in our case at 2860, 2825 and 2730 cm^{-1}, among others). They are frequently observed in the IR spectrum of amino-polycar-

boxylic acids hydrochlorides. The band at 2730 can be related with the stretching mode of the ammonium group $-N^{+}-H$ [31b,32]. In this connection, it should be noted that the asymmetric stretching mode of the carboxylate group (expected in the range 1600–1560 cm^{-1}) is moved to higher frequencies and overlapped in a broad band near 1700 cm^{-1}. Both effects are consistent with the unique symmetrical and nearly linear hydrogen bond linking the carboxylic and carboxylate group. The TG analysis with FTIR spectra of evolved gases of an anhydrous sample (7.053 mg) in air flow shows two overall pyrolytic steps (207–335 and 335–500°C) with production of H_2O, CO_2, CO, NH_3, NO and NO_2. The decomposition starts with the production of H_2O, CO_2 and traces of CO suggesting that it corresponds to the decarboxylation of two hydrogen bonded *N*-carboxymethyl arms (207–215°C).

2.2. Structure and properties of *cis*-diaqua(*N*-carbamoylmethyl-iminodiacetato)nickel(II)

Selected bond lengths and angles between non-hydrogen atoms and hydrogen bond distances and angles of this compound are given in Table 3. Complex **I** consist of molecular units $[Ni(ADA)(H_2O)_2]$ (see Fig. 2). Each molecule represents the asymmetric unit of the crystal, and eight molecules compose the unit cell. The crystal is built up by means of a three-dimensional hydrogen bonding network involving all polar bonds, from the $-NH_2$ amide group of the ADA ligand and O–H bonds of aqua ones (Table 3). The atoms N(1), O(11), O(21) and O(31, amide) of the tetradentate ADA^{2-} ion and the atoms O(1) and O(2) of coordinated water molecules define an octahedral surrounding to the nickel(II) atom. That is recognised as the most common geometry for nickel(II) coordination compounds [33] as it is observed in a host of nickel(II) complexes with an extremely wide range of mono- and polydentate ligands. The four donor atoms of the tripodal ligand ADA are similar in length (average 2.058(2) Å) whereas the two *cis*-Ni–O(water) bonds (2.000(2) and 2.102(2) Å) are the shortest and the longest ones. Additionally the *trans*-angles involving such Ni–O(water) bonds (175.6 and 179.3(1)°) are close to 180°, but the *trans*-angle O–Ni–O with donors of chelating ADA is significantly the closest (163.8(1)°). As a consequence, both ADA and aqua ligands are responsible in some way for the moderate but irregular distortion of the Ni(II) coordination polyhedron. Otherwise the internal geometry of the Ni(II) coordination and ADA ligand have usual values compared to related compounds. This includes the ADA ligand in known metal–ADA complexes [8–10,12,13], several Ni–IDA chelates [34] and a variety of compounds involving Ni(II)–O(amide) bonds [35]. These latter compounds include diaqua-tetrakis(acetamide)nickel(II) [35a], bis-(iminodiacetamide)nickel(II) diperchlorate [35d] and bis-(imidazole) (nitrilopropionamidediacetato) nickel(II) monohydrate [35g].

The tripodal chelating role of ADA represents the formation of two nearly coplanar Ni–glycinate-like rings and a third Ni–glycinamide-like one, all three sharing the Ni–N(1, amino) bond. The mean planes of both Ni–glycinate-like rings (P(2) and P(3) involving

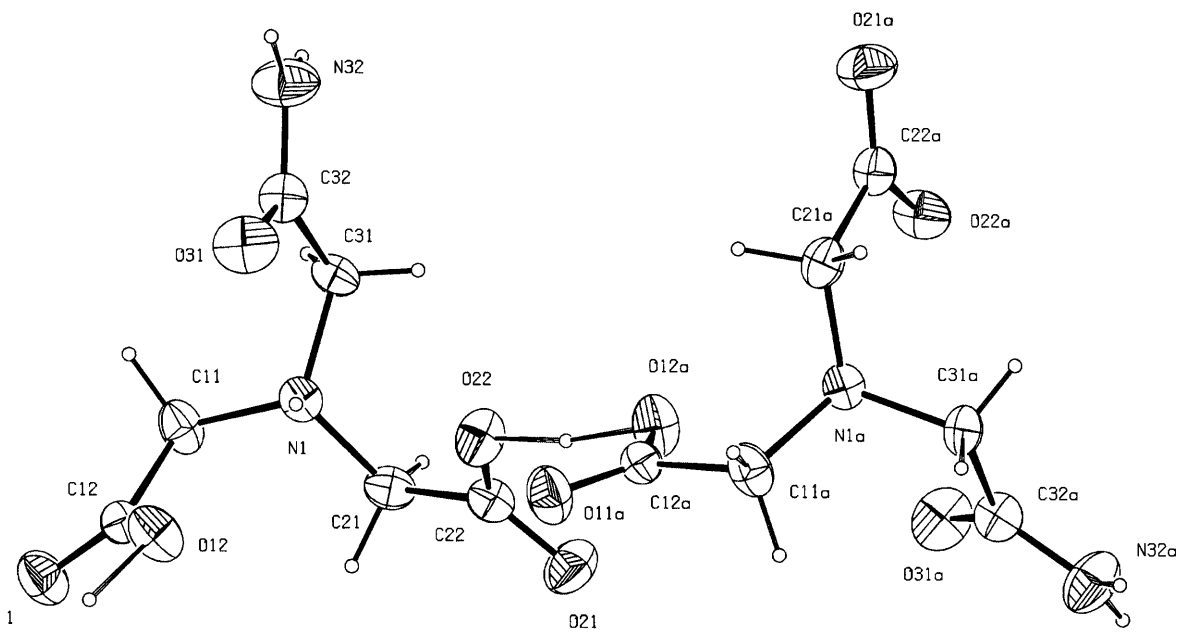


Fig. 1. Structure of the acid *N*-(carbamoylmethyl)iminodiacetic acid (H_2ADA) showing the symmetrical and nearly linear inter-molecular hydrogen bond between two adjacent zwitterions. Symmetry code $a = \#1 = i$: $-x+1/2,\ y+1/2,\ -z+5/2$.

Table 3
Selected bond lengths (Å) and angles (°) for $[Ni(ADA)(H_2O)_2]$ (**I**) with e.s.d. values in parentheses [a]

Nickel(II) environment			
Ni(1)–O(1)	2.000(2)	O(1)–Ni(1)–O(21)	95.8(1)
Ni(1)–O(21)	2.045(2)	O(1)–Ni(1)–O(11)	92.1(1)
Ni(1)–O(11)	2.051(2)	O(21)–Ni(1)–O(11)	92.2(1)
Ni(1)–O(31)	2.065(2)	O(1)–Ni(1)–O(31)	99.9(1)
Ni(1)–N(1)	2.072(2)	O(21)–Ni(1)–O(31)	163.8(1)
Ni(1)–O(2)	2.106(2)	O(11)–Ni(1)–O(31)	90.7(1)
Ni–Ni^{vi}	5.192(1)	O(1)–Ni(1)–N(1)	175.5(1)
Ni–Ni^{iv}=Ni–Ni^{vii}	6.869(1)	O(21)–Ni(1)–N(1)	82.3(1)
		O(11)–Ni(1)–N(1)	84.0(1)
		O(31)–Ni(1)–N(1)	82.1(1)
		O(1)–Ni(1)–O(2)	88.4(1)
		O(21)–Ni(1)–O(2)	87.1(1)
		O(11)–Ni(1)–O(2)	179.3(1)
		O(31)–Ni(1)–O(2)	89.8(1)
		N(1)–Ni(1)–O(2)	95.5(1)
ADA aqua ligands			
O(11)–C(11)	1.247(3)	C(12)–N(1)–C(22)	111.8(2)
O(21)–C(21)	1.276(3)	C(12)–N(1)–C(32)	111.7(2)
O(22)–C(21)	1.237(3)	C(22)–N(1)–C(32)	113.9(2)
O(31)–C(31)	1.279(4)	O(11)–C(11)–N(11)	122.9(3)
O(32)–C(31)	1.245(3)	O(11)–C(11)–C(12)	121.9(2)
N(1)–C(12)	1.477(4)	N(11)–C(11)–C(12)	115.2(3)
N(1)–C(22)	1.482(4)	N(1)–C(12)–C(11)	112.9(2)
N(1)–C(32)	1.483(4)	O(22)–C(21)–O(21)	125.1(2)
N(11)–C(11)	1.320(4)	O(22)–C(21)–C(22)	117.5(2)
C(11)–C(12)	1.510(4)	O(21)–C(21)–C(22)	117.3(2)
C(21)–C(22)	1.533(4)	N(1)–C(22)–C(21)	112.1(2)
C(31)–C(32)	1.528(4)	O(32)–C(31)–O(31)	124.8(3)
		O(32)–C(31)–C(32)	117.2(3)
		O(31)–C(31)–C(32)	117.9(2)
		N(1)–C(32)–C(31)	112.0(2)
O(1)–H(1A)	0.76(3)	H(1A)–O(1)–H(1B)	116(3)
O(1)–H(1B)	0.74(4)		
O(2)–H(2A)	0.87(4)	H(2A)–O(2)–H(2B)	105(3)
O(2)–H(2B)	0.82(4)		

Hydrogen bonds

D–H···A	*d*(D–H)	*d*(H···A)	*d*(D···A)	<(DHA)
O(1)–H(1A) ···O(22) # 1	0.76(3)	1.88(3)	2.637(3)	169(3)
O(1)–H(1B) ···O(32) # 2	0.74(4)	2.04(4)	2.757(3)	163(4)
O(2)–H(2A) ···O(31) # 2	0.87(4)	1.89(4)	2.756(3)	170(4)
O(2)–H(2B) ···O(32) # 3	0.82(4)	2.02(4)	2.832(3)	174(3)
N(11)–H(11A) ···O(21) # 4	0.84(4)	2.09(4)	2.910(4)	163(4)
N(11)–H(11B) ···O(11) # 5	0.80(4)	2.55(4)	3.060(3)	123(3)

[a] Symmetry transformations used to generate equivalent atoms: i: # 1 = $x-1/2$, $y+1/2$, z; ii: # 2 = $-x$, $-y$, $-z$; iii: # 3 = $x+1/2$, $y+1/2$, z; iv: # 4 = $-x+1/2$, $y-1/2$, $-z+1/2$; v: # 5 = $-x$, y, $-z+1/2$; vi: # 6 = $1-x$, $1-y$, $1-z$; vii: # 4 = $1/2-x$, $1/2+y-$, $1/2-z$.

O(11) and O(21) atoms, respectively) define a dihedral angle of 81.1°. The mean plane P(4) of Ni–glycinamide-like ring defines dihedral angles of 80.5° and 18.5° with P(2) and P(3) planes, respectively. The most distorted chelate ring is that involving the O(11) atom, with maximum deviations of −0.034 and 0.029 Å for O(11) and C(11) atoms, respectively, from the mean plane P(2) of the five atoms forming such a ring. These three chelate rings exhibit slightly distorted asymmetric-envelope conformation, rather common for α-amino-acidato and α-aminopolycarboxylato ligands in its metal ion chelates (with both carbon atoms lying on the same side of the plane defined by its corresponding atoms Ni, N and O of each ring) [36]. In this respect, the greatest unequal deviations correspond to C(21) (0.44 Å) and C(22) (0.69 Å) from the plane of Ni(1)N(1)(21) atoms.

The IR spectrum of complex **I** permits the identification of bands from main characteristic absorption modes expected for aqua and ADA ligands. The following tentative assignations can be made (wave-numbers in cm^{-1}) in its IR spectrum: ν(OH) of the aqua ligand at 3436 and 3364, $\nu_{as}(NH_2)$ and $\nu_s(NH_2)$ of the primary amide group at approximately 3300 (as a shoulder of the second ν(OH) band) and 3160, $\nu_{as}(CH_2)$ at 2992 and 2973, $\nu_s(CH_2)$ at 2931 and 3910, ν(C=O) of the primary amide group (also called 'amide I' band) at 1667, $\delta(H_2O)$ at 1627, $\delta(NH_2)$ of this latter group (also called 'amide II' band) overlapped with $\nu_{as}(COO^-)$ at 1603 and 1587, $\delta(CH_2)$ at 1471 and 1433, and $\nu_s(COO^-)$ at 1391. The difference $\Delta(COO) = \nu_{as}(COO) - \nu_s(COO) = 196\ cm^{-1}$ is in accordance with the expected mainly ionic nature of the Ni(II)–O(carboxylato) bonds. Obviously, in this spectrum the ν_{as}(C=O) of carboxylic group (as a shoulder at approximately 1730 cm^{-1} in the ligand spectrum) is now missing. The two bands of the primary amide group have lower frequencies in the complex spectrum than in that of the H_2ADA. Such displacements should be regarded with care because, as mentioned above, the bands 'amide I and II' are not pure C=O stretching and scissoring $-NH_2$ amides, respectively [28a]. The TG analysis (with FTIR spectra of evolved gases) of an anhydrous sample of complex **I** (7.221 mg) in air flow shows two rather separate steps (165–275 and 275–400°C). The first step corresponds to the water loss (exp. 13.329%, calc. for $2H_2O$ 12.737%). The second one is that of the ADA pyrolysis with production of H_2O, CO_2, CO (traces), N_2O and NH_3, and NO_2. The ADA decomposition starts slowly with production of H_2O, CO_2 and traces of N_2O suggesting that it corresponds to the *N*-carbamoylmethyl arm of the ligand. But such process shows a very sharp weight loss near to 378°C with overlapped production of the referred gasses. The dehydration and ADA pyrolysis leaves a residue of crude NiO (exp. 27.023%, calc. for pure NiO 26.410%). The electronic spectrum shows bands $\nu_1 = 9560$ (shoulder at approximately 14250), $\nu_2 = 16077$ and $\nu_3 = 25445\ cm^{-1}$

due to the electronic transitions $^3A_{2g}(F) \rightarrow {}^3T_{2g}$ (with a shoulder for $^3A_{2g}(F) \rightarrow {}^1E_g$), $^3A_{2g}(F) \rightarrow {}^3T_{1g}(F)$ and $^3A_{2g}(F) \rightarrow {}^3T_{1g}(P)$. This spectrum is typical of an octahedral Ni(II) surrounding [33]. Since it can be assumed that $\nu_1 = 10\ Dq = \Delta_o$, a value of 856 cm^{-1} is obtained for the Racah parameter B', that is 83% of the B parameter in the free ion. These data are in accordance with the predominant ionic nature of the Ni(II) atom in the complex **I**. The values of Δ_o and B' in this compound are higher than those of hexaaquanickel(II) (8500 and 945 cm^{-1}, respectively) as expected for the substitution of four aqua ligands with the ADA one. Indeed the Δ_o values yield the following series of complexes: $[Ni(H_2O)_6]^{2+} < [Ni(ADA)(H_2O)_2] < [Ni(NH_3)_6]^{2+}$ ($\Delta_o = 10750\ cm^{-1}$) $< [Ni(en)_3]^{2+}$ ($\Delta_o = 11200\ cm^{-1}$) [33]. These spectral data support the placement of ADA ligand between aqua and ammonia or ethylendiamine in the nephelauxetic series. A plot of $1/\chi$ data versus T (K) ($T = 80$–298 K) is linear (with a statistical r^2 factor of 0.9993) according to a Curie–Weiss behavior, $\chi_{mol} = C/(T - \theta)$ (Fig. 3). The Curie constant is $C = 1.10$ K·emu·mol^{-1} and a Weiss constant of $\theta = 5.58$. The experimental value of μ_{eff} for Ni(II) atom in the studied complex **I** is 2.97 BM, in accordance with the molecular and crystal structure here reported where the shortest inter-metallic Ni–Ni[vi] distances is 5.193(1) Å (symmetry code vi: $\#6 = 1 - x, 1 - y, 1 - z$). This value lies within the range of typical experimental ones (2.8–3.5 BM) in mononuclear octahedral Ni(II) complexes with a $^3A_{2g}$ ground state [37]. It is slightly higher than the spin-only one ($\mu_{eff} = g[S(S+1)]^{1/2} = 2.83$) suggesting that there is a small orbital angular moment contribution to the effective magnetic moment of the nickel(II) atom.

3. Concluding remarks

The nickel(II) atom exhibits an octahedral coordination in the molecule of complex **I**, which represents a common feature for this metal(II) ion. However, that differs from the square base pyramidal coordination reported for the corresponding copper(II) derivative which has a polymeric structure [12]. In addition, it is worth noting that two *cis*-aqua ligands in the nickel(II) complex gives the possibility for further studies of mixed-ligand complexes of such a metal ion, ADA, and a variety of mono- and bi-dentate ligands. At present, we continue working to evaluate these possibilities [38] on the basis of our present results and keeping in mind the structure of bis(imidazole)(nitrilopropionamidediacetato)nickel(II) monohydrate [35g] reported some years ago.

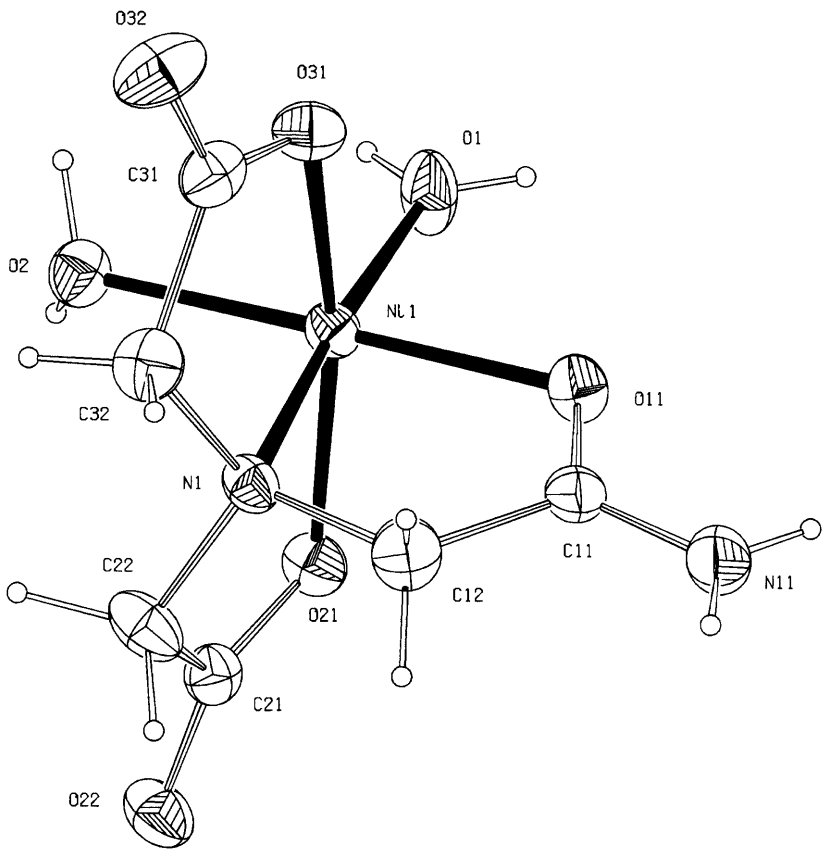


Fig. 2. Asymmetric unit in the crystal of compound $[Ni(ADA)(H_2O)_2]$ (**I**).

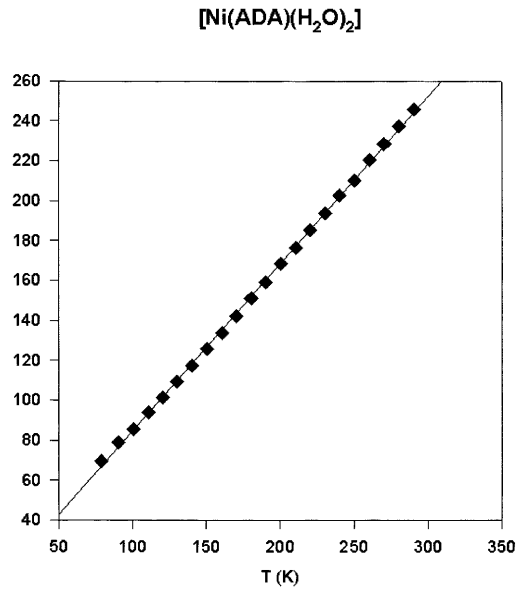


Fig. 3. Thermal variation of $\chi_M T$ for complex **I** (◆). The solid line corresponds to the best theoretical fit (see text).

4. Supplementary material

Crystallographic data for the structures reported in this paper have been deposited with the Cambridge Crystallographic Data Centre, CCDC no. 134789 for H_2ADA and CCDC No. 134790 for $[Ni(ADA)(H_2O)_2]$ (**I**). Copies of this information may be obtained free of charge from the Director, CCDC, 12 Union Road, Cambridge, CB2 1EZ, UK (fax: +44-1223-336033; e-mail: deposit@ccdc.cam.ac.uk or http://www.ccdc.cam.ac.uk).

Acknowledgements

This paper is devoted in memoriam of Prof. Sergio Cabani (University of Pisa, Italy) recently deceased. He encouraged many contributions on thermodynamics and kinetics of metal complexes. We are grateful to the Dirección General de Enseñanza Superior e Investigación Científica, MEC, Spain, for financial support (Project PB-98-0605-C03-03). A.C. thanks the Xunta de Galicia for the financial support (Project XUGA20309B97). A research grant to E.B.A. from Ministerio de Educación y Cultura is gratefully acknowledged.

References

[1] G. Schwarzenbach, G. Anderegg, W. Schneider, H. Senn, Helv. Chim. Acta 38 (1955) 4147.
[2] E. Lance, R. Nakon, Inorg. Chim. Acta 55 (1981) L1.
[3] J. Nepal, S. Dubey, Indian J. Chem. 26A (1987) 269.
[4] H.A. Azaab, A. Hassan, Bull. Soc. Chim. Fr. I (1989) 599.
[5] H.A. Azaab, Monatsh. Chem. 123 (1992) 1107.
[6] E.A. Lance, Ch.W. Rhodes, R. Nakon, Anal. Biochem. 133 (1979) 492.
[7] P.D. Parr, Ch. Rhodes, R. Nakon, Inorg. Chim. Acta 80 (1983) L11.
[8] M. Sivák, J. Tyršelová, S. Pavelík, J. Marek, Polyhedron 15 (1996) 1062.
[9] G.J. Colpas, B.H. Hamstra, J.W. Kampf, V.L. Pecoraro, J. Am. Chem. Soc. 18 (1996) 3469.
[10] B.J. Hamstra, A.L.P. Houseman, G.J. Coplas, J.W. Kampf, R. LoBrutto, W.D. Frasch, V.L. Pecoraro, Inorg. Chem. 36 (1997) 4866.
[11] M.J. Román-Alpiste, J.D. Martín-Ramos, A. Castiñeiras-Campos, E. Bugella-Altamirano, A.G. Sicilia-Zafra, J.M. González-Pérez, J. Niclós-Gutiérrez, Polyhedron 18 (1999) 3341 and several references therein.
[12] E. Bugella-Altamirano, J.M. González-Pérez, A.G. Sicilia-Zafra, J. Niclós-Gutiérrez, A. Castiñeiras-Campos, Polyhedron 18 (1999) 3333.
[13] (a) E. Bugella-Altamirano, A. Castiñeiras-Campos, J.M. González-Pérez, A.G. Sicilia-Zafra, J. Niclós-Gutiérrez, X Italian–Spanish Congress on Thermodynamics of Metal Complexes, S. Martino al Cimino, Italy, 1999, Report C-17. (b) A. Castiñeiras-Campos, E. Bugella-Altamirano, J.M. González-Pérez, A.G. Sicilia-Zafra, J. Niclós-Gutiérrez, Metal chelates of *N*-carbamoylmethyl-iminodiacetate(II) ion. Part II. Synthesis, XRD structures and properties of poly-[(*N*-carbamoylmethyl-iminodiacetato)-copper(II) monohydrate], $\{[Cu(ADA)]\cdot H_2O\}_n$, and (2,2′-bipyridine)(*N*-carbamoylmethyl-iminodiacetato)copper(II) three-hydrate, $[Cu(ADA)(bipy)]\cdot 3H_2O$ (submitted).
[14] W.B. Guenther, Quantitative Chemistry: Measurements and Equilibrium, Addison-Wesley, MA, 1968, pp. 341–343.
[15] B.V. Nonius, CAD4-Express Software, Release 5.1/1.2, Enraf Nonius, Delft, The Netherlands, 1994.
[16] M. Kretschmar, GENHKL, Program for the Reduction of CAD4 Diffractometer Data, University of Tuebingen, Germany, 1997.
[17] A.C.T. North, D.C. Phillips, F.S. Mathews, Acta Crystallogr., Sect. A 24 (1968) 351.
[18] G.M. Sheldrick, Acta Crystallogr., Sect. A 46 (1990) 467.
[19] G.M. Sheldrick, SHELXL-97. Program for the Refinement of Crystal Structures, University of Göttingen, Germany, 1997.
[20] International Tables for X-ray Crystallography, Vol. C, Kluwer Academic Publishers, Dordrecht, The Netherlands, 1995.
[21] A.L. Spek, Acta Crystallogr., Sect. A 46 (1990) C34.
[22] L. Zsolnai, ZORTEP. A Program for the Presentation of Thermal Ellipsoids, University of Heidelberg, Germany, 1997.
[23] F.E. Mabbs, D.J. Machin, Magnetism and Transition-metal Complexes, Chapman and Hall, London, 1973.
[24] B.C. Challis, J.A. Challis, Chapter 9.9: Amides and related compounds, in: D. Barton, W.D. Ollis (Eds.), Comprehensive Organic Chemistry, Pergamon Press, Oxford, 1979.
[25] L.M. Shkol'nikova, N.M. Dyatlova, M.A. Porai-Koshits, Zh. Strukt. Khim. 27 (1986) 138.
[26] L.M. Shkol'nikova, A.E. Obodnoskaya, Zh. Strukt. Khim. 27 (1986) 125.
[27] L.M. Shkol'nikova, V.Y. Temkina, N.M. Dyatlova, Y. Podlaga, Zh. Strukt. Khim. 23 (1982) 135.
[28] E. Bugella-Altamirano, D. Choquesillo-Lazarte, J.M. González-Pérez, J. Niclós-Gutiérrez, A. Castiñeiras-Campos, J.D. Martín-Ramos, Stacking interactions between pyridyne rings in *N*-(2-pyridylmethyl)iminodiacetic acid monohydrate, poly-[(*N*-(2-pyridylmethyl)imino-diacetato) copper(II) dihydrate] and aqua(imidazole)(*N* - (2 - pyridylmethyl)iminodiacetato)copper(II) trihydrate. Synthesis, XRD structures and properties of these compounds (in preparation).

[29] L.D. Pettit, K.J. Powell, The IUPAC Stability Constant Data Base, Academic Software, Sourby Old Farm, Timble, Otley, Yorks LS21 2PW, UK, 1997 Web: http://www.acadsoft.co.uk.
[30] M. Maeda, M. Ohnishi, G. Nakagawa, J. Inorg. Nucl. Chem. 43 (1981) 407.
[31] L.J. Bellamy, The Infrared Spectra of Complex Molecules, vol. 1, 3rd ed., Chapman and Hall, London, 1975 (a) Chapter 12. (b) Chapter 14.
[32] J. Niclós Gutiérrez, Ph.D Thesis, Faculty of Pharmacy, University of Granada, Granada, Spain, 1980.
[33] M. Schröeder, in: R.B. King (Ed.), Encyclopedia of Inorganic Chemistry: Nickel: Inorganic and coordination compounds, vol. 5, Wiley, New York, 1994, pp. 2392–2412 and references cited therein.
[34] (a) V.M. Agre, T.F. Sisoeva, V.K. Trunov, N.M. Dyatlova, A.Ya. Fridman, Zh. Strukt. Khim. 25 (1984) 141. (b) N.J. Mammano, D.H. Templeton, A. Zalkin, Acta Crystallogr., Sect. B 33 (1977) 1251. (c) F.G. Kramarenko, T.N. Polynova, M.A. Porai-Koshits, V.P. Chalyi, N.D. Mitrofanova, Zh. Strukt. Khim. 15 (1974) 161. (d) N.J. Mammano, D.H. Templeton, A. Zalkin, Acta Crystallogr., Sect. B 33 (1977) 1251.
[35] (a) M.E. Stone, B.E. Robertson, E. Stanley, J. Chem. Soc. A (1971) 3632. (b) Tsong-Jen Lee, Arlohun Wang, Ta-Yung Chi, Chung-Sun Chung, Acta Crystallogr., Sect. C 49 (1993) 1485. (c) V. Kh. Sabirov, R.M. Kurbanbaev, M.A. Porai-Koshits, Yu.T. Struchkov, Koord. Khim. 19 (1993) 637. (d) M. Sekizaki, Acta Crystallogr., Sect. B 32 (1976) 1568. (e) Chung Chieh, Fang-Jy Wu, Sue-Lein Wang, Chin-Hohn Len, Chung-Sun Chung, Acta Crystallogr., Sect. C 45 (1989) 1076. (f) A. Masuko, T. Nomura, Y.Saito, Bull. Chem. Soc. Jpn. 40 (1967) 511. (g) L.M. Shkol'-nikova, K.D. Suyarov, A.A. Masyuk, A.L. Poznyak, N.M. Dyatlova, Koord. Khim. 16 (1990) 1096. (h) R.W. Hay, A. Perotti, R. Oberti, L. Ungaretti, Transition Met. Chem. 18 (1993) 570.
[36] C.J. Hawkins, Absolute Configuration of Metal Complexes, Wiley-Interscience, New York, 1971 Chapter 3.
[37] W.E. Hatfield, Magnetism of transition metal ions, in: R.B. King (Ed.), Encyclopedia of Inorganic Chemistry, vol. 4, John Wiley and Sons, Chichester and New York, 1994, pp. 2066–2075 And references therein.
[38] E. Bugella-Altamirano, J.M. González-Pérez, A. Castiñeiras-Campos, A.G. Sicilia-Zafra, J. Niclós-Gutiérrez, X Italian-Spanish Congress on Thermodynamics of Metal Complexes, S. Martino al Cimino, Italy, 1999. Report P-8.

PERGAMON

www.elsevier.nl/locate/poly

Polyhedron 19 (2000) 2473–2481

POLYHEDRON

Metal chelates of *N*-carbamoylmethyl-iminodiacetate(2 −) ion Part IV. Isostructural ternary mixed-ligand cobalt(II) and nickel(II) chelates with *N*-carbamoylmethyl-iminodiacetate(2 −) ion, imidazole and aqua ligands. Synthesis, molecular and crystal structures and properties of $[M(ADA)(Him)(H_2O)]\cdot 1.5H_2O$ (M = Co, Ni)

E. Bugella-Altamirano [a], J.M. González-Pérez [a], A.G. Sicilia Zafra [a], J. Niclós-Gutiérrez [a,*], A. Castiñeiras-Campos [b]

[a] *Department of Inorganic Chemistry, Faculty of Pharmacy, University of Granada, E-18071 Granada, Spain*
[b] *Department of Inorganic Chemistry, Faculty of Pharmacy, University of Santiago de Compostela, E-15706 Santiago de Compostela, Spain*

Abstract

Stoichiometric reaction of $CoCO_3\cdot Co(OH)_2\cdot 2H_2O$, or $NiCO_3\cdot 2Ni(OH)_2\cdot 4H_2O$ with H_2ADA and imidazole (Him) in water yields crystalline samples of compounds aqua(imidazole)(*N*-carbamoylmethyl-iminodiacetato)metal(II), $[M(ADA)(Him)(H_2O)]\cdot 1.5H_2O$ (M = Co, compound **I**, dark pink; M = Ni, compound **II**, bluish). Single-crystal X-ray diffraction studies were carried out. Both complexes are isostructural (orthorhombic system, space group *Pna*2(1), $Z = 8$). These crystals consist of slightly asymmetrical octahedral coordination units linked in a tridimensional network stabilised by hydrogen bonds where all N–H bonds of ADA and Him and probably O–H bonds of water molecules are involved. The asymmetric unit has two independent but very similar complex molecules and three water ones. Coordination bond distances for **I** (average in Å): Co–N(amino) = 2.14(1), Co–O(carboxyl) = 2.06(1), Co–O(carboxyl) = 2.08(1) and Co–O(amide) = 2.15(1) with ADA, Co–N(Him) = 2.04(1), and Co–O(aqua) = 2.13(1). Coordination bond lengths for **II** (average in Å): Ni–N(amino) = 2.08(1), Ni–O(carboxyl) = 2.04(1), Ni–O(carboxyl) = 2.06(1) and Ni–O(amide) = 2.012(1) with ADA, Ni–N(Him) = 2.01(1), and Ni–O(aqua) = 2.12(1). The ADA ligand acts as a tripodal tetradentate chelating one. On the basis of the octahedral structures of $[Ni(ADA)(H_2O)_2]$, reported in the literature, and of the new compounds, it is concluded that there is a preference for the N(Him)donor atom to occupy the *trans*-position to the M–N(ADA) bond. © 2000 Elsevier Science B.V. All rights reserved.

Keywords: *N*-carbamoylmethyl-iminodiacetic acid; *N*-(2-amidomethyl)-iminodiacetic acid; *N*-(2-acetamido)-iminodiacetic acid; Imidazole; Mixed-ligand complexes; Aqua(imidazole)(*N*-carbamoylmethyl-iminodiacetato)nickel(II) sesquihydrate; Aqua(imidazole)(*N*-carbamoylmethyl-iminodiacetato)cobalt(II) sesquihydrate; Molecular and crystal structures; Magnetic, spectral and thermal properties

N-carbamoylmethyl-iminodiacetic acid also named *N*-(2-acetamido)-iminodiacetic acid or *N*-(2-amidomethyl)-iminodiacetic acid [$H_2ADA{=}H_2NCOCH_2N(CH_2CO_2H)_2$)] is a well known chelating agent, also used in 'biological buffers' of pH 6.0–7.4 [1]. Metal(II) ion–ADA chelation in solution has been known for a long time (metal = Mg, Ca, Sr, Ba, Mn, Co, Ni, Cu, Zn, Cd, Hg, Pb) [2]. The results of this study agree with more recent ones [3–6] about the stoichiometry and stability of ADA complexes in solution [2] which show that 'primary amide' deprotonation reactions for ML_2 chelates of Co(II) or Zn(II) [3] can arise in alkaline solutions. In alkaline solutions, Cu(II) dechelation processes have also been claimed upon ADA amide deprotonation [7,8].

Several papers have appeared in recent years concerning the mixed-ligand complexes of a variety of

* Corresponding author. Tel.: + 34-958-243-855; fax: + 34-958-246-219.
E-mail addresses: jniclos@.ugr.es (J. Niclós-Gutiérrez), qiac01@usc.es (A. Castiñeiras-Campos).

0277-5387/00/$ - see front matter © 2000 Elsevier Science B.V. All rights reserved.
PII: S0277-5387(00)00547-7

metal ions and ADA as primary ligand. Such compounds have salicylhydroxamate [9a], thiosemicarbazide [9b], dithiocarbazate [9b], aromatic acids [9c], amino acids [9d,e] or salicylic acid derivatives [9f] as secondary ligands. A certain number of such mixed-ligand metal complexes having ADA have been obtained in solid state and characterised by spectral and other physico-chemical methods. However structural studies in this context were noticeably limited to one aqua–*oxo*-ADA complex with vanadium(IV) [10] and the potassium salt of an *oxo*-peroxo-ADA-vanadium(V) complex [11,12]. In such compounds, ADA acts as a tripodal-tetradentate ligand.

The structural research of ADA–metal chelates in solid state seems a useful tool because it can provide information about the chelating role of the divalent anion $H_2NCOCH_2N(CH_2CO_2^-)_2$. Particular interest focuses on the way in which its 'primary amide group' takes part in metal ion chelation. In this sense and as a part of our studies on mixed-ligand Cu(II) complexes having IDA or IDA-derivatives and *N*-heterocyclic ligands, we have synthesised for the first time the compound (imidazole)(*N*-carbamoylmethyl-iminodiacetato)-copper(II), [Cu(ADA)(ImH)] [13a]. In recent reports we reported the structures of compounds $\{[Cu(ADA)]\cdot H_2O\}_n$ and $[Cu(ADA)(bipy)]\cdot 3H_2O$ (bipy = 2,2′-bipyridine) [13b] and of the H_2ADA acid itself and the nickel derivative *cis*-$[Ni(ADA)(H_2O)_2]$ [13c]. Again, the XRS study of these complexes has revealed that ADA acts as a tripodal-tetradentate ligand. In the case of the octahedral Ni(II)–ADA chelate, the *cis*-coordination of both aqua ligands suggests several possibilities for substitution by other ligands which we consider in our research projects. For example, replacing only one water molecule by an imidazole (Him) in this latter complex, two different possibilities of linking Him ligand to the nickel(II) atom arise. These are in *cis*- or *trans*-position versus the metal–N(ADA) bond. The aim of the present work is to find an answer to this question. In this connection, we report the synthesis, crystal structure and properties of two new mixed-ligand complexes of nickel(II) or cobalt(II) having aqua, ADA and Him as choice ligand set.

1. Experimental

1.1. Synthesis of aqua(imidazole)(*N*-carbamoylmethyl-iminodiacetato)-metal(II) sesquihydrate for cobalt(II) and nickel(II)

$[M(ADA)(Him)(H_2O)]\cdot 1.5H_2O$, compounds **I** (Co) or **II** (Ni), were obtained by stoichiometric reaction between $CoCO_3\cdot Co(OH)_2\cdot 2H_2O$ (252.2 mg, 1 mmol, Merck, Co ≥ 47%) or $NiCO_3\cdot 2Ni(OH)_2\cdot 4H_2O$ (250.0 mg, 0.67 mmol, Merck, Ni ≥ 47%) and H_2ADA (380.3 mg, 2 mmol, Aldrich, 98%) in water (100 ml) in a Kitasato flask, heating ($t < 50$°C) and stirring under reduced pressure (to remove the CO_2 by-product) for 3 h. These mixtures were still stirred 24 h at ~60°C and then slowly filtered to remove an almost inappreciable amount of non-reacted CoO or NiO (insoluble by-products). The pH of the reacting mixtures was not controlled during the synthesis processes. The resulting pink or green solutions were left to cool and imidazole (136.2 mg, 2 mmol, Merck, >99%) was added with stirring, which produces colour intensification (Co) or a change to a bluish colour (Ni). After 3 weeks of slow evaporation at room temperature (the remaining volume being 10–15 ml) the solutions were filtered over a small crystallisation dish and covered with a watch glass to reduce the rate of evaporation. After several days, well-shaped dark pink or bluish crystals of complexes **I** or **II**, respectively, appeared, which were suitable for X-ray diffraction studies. Additional amounts of products were formed again and collected in the same way. If mother liquor super-saturation arises, the addition of small volumes of water and ethanol and slow evaporation as before can induce the crystallisation. These products were collected by filtration, washed with a little of cool water and carefully air-dried. They can be re-crystallised several times from water. Yield: variable but usually <60%. *Anal.* Calc. for compound $C_9H_{17}CoN_4O_{7.5}$ (**I**): C, 30.01; H, 4.76; N, 15.56; Co, 16.36. Found: C, 30.20; H, 4.95; N, 15.65; Co, 16.27%. *Anal.* Calc. for complex $C_9H_{17}N_4NiO_{7.5}$ (**II**): C, 30.03; H, 4.76; N, 15.57; Ni, 16.31. Found: C, 30.27; H, 4.64; N, 15.36; Ni, 16.24%.

1.2. X-ray data collection and reduction, structure solution and refinement

A prismatic crystal of compound **I** (dark pink) or **II** (bluish) was mounted on a glass fibre and used for data collection. Cell constants and an orientation matrix for data collection were obtained by least-squares refinement of the diffraction data from 25 reflections in the range of $7.794 < \theta < 11.448$ or of $9.966 < \theta < 10.501$, respectively, in an Enraf Nonius MACH3 automatic diffractometer [14]. Data were collected at 293 K using Mo Kα radiation ($\lambda = 0.71073$ Å) and the ω-scan technique, and corrected for Lorentz and polarisation effects [15]. A semi-empirical absorption correction (ψ scan) was made [16]. The structure was solved by direct methods [17] and subsequent difference Fourier maps and refined on F^2 by a full-matrix least-squares procedure using anisotropic displacement parameters [18]. All hydrogen atoms were located in their calculated positions (C–H 0.93–0.97 Å) and were refined using a rigid model. Hydrogen atoms of water were not located. The absolute configuration was established [19].

Atomic scattering factors were taken from the 'International Tables for X-ray Crystallography' [20]. Molecular graphics were prepared with the program PLATON-98 [21]. A summary of the crystal data, experimental details and refinement results are listed in Table 1.

1.3. Physical measurements

Cobalt(II) or Nickel(II) titration was carried out by standard EDTA complexometry using xilenol orange as metallochromic indicator [22a]. Alternative procedures using murexide indicator in weak alkaline solution (for Co and Ni) or alizarin complexone in weak acid solution (for Co) are available [22b]. For this purpose an accurately weighted sample (≥ 0.5 g) of each of the studied compounds was mineralised with 2 N sulphuric acid and hydrogen peroxide solutions in a precipitation vessel covered with a watch glass. The reaction and decomposition of H_2O_2 in excess were favoured by heating carefully and the resulting green solution of nickel(II) sulfate or pink solution of cobalt(II) sulfate was quantitatively diluted with doubly-distilled water into a 250 ml volumetric flask. Aliquots (25 ml) of these solutions were titrated as described elsewhere [13c,22]. Elemental analysis (C, H, N) were performed in the Scientific Instrumental Centre of the University of Granada as described earlier [13]. Infrared (IR) spectra were obtained by the KBr disc technique on a Nicolet FTIR 20SXB or a JASCO FTIR 410 instrument. TG (pyrolysis) of studied compounds and analysis of evolved gases were recorded (295–775 K) in air flow (100 ml min^{-1}) using a Shimazu Thermobalance TGA-DTG-50H coupled with an IR-FT Nicolet Magma 550 (and mass spectrometer Fisons Thermolab). Electronic (reflectance) spectra (175–3300 nm) were obtained in a Cary 5E spectrophotometer. The magnetic susceptibilities of **I** and **II** were measured in the temperature range 80–300 K using a Manics DM magnetometer. The susceptometer was calibrated with mercury tetrakis(thiocyanato)-cobaltate(II). Corrections for the diamagnetism of ligands and metal atom (150×10^{-6} cm^3 mol^{-1} for both compounds) were estimated from Pascal constants [23,24].

Table 1
Crystal data and structure refinement for complex [Co(ADA)(Him(H_2O))·1.5H_2O (**I**) and complex [Ni(ADA)(Him)(H_2O)]·1.5H_2O (**II**)

	Compound **I**	Compound **II**
Empirical formula	$C_9H_{17}CoN_4O_{7.5}$	$C_9H_{17}N_4NiO_{7.5}$
Formula weight	360.19	359.95
Temperature (K)	293(2)	293(2)
Wave length (Å)	0.71073	0.71073
Crystal system, space group	orthorhombic, *Pna*2(1) (no. 33)	orthorhombic, *Pna*2(1) (no. 33)
Unit cell dimensions		
a (Å)	15.364(2)	15.191(4)
b (Å)	7.120(2)	7.093(2)
c (Å)	27.699(10)	26.517(5)
α, β, γ (°)	90	90
Volume (Å^3)	2818.4(2)	2857.6(11)
Z, D_{calc} (Mg m^{-3})	8, 1.629	8, 1.664
Absorption coefficient (mm^{-1})	1.217	1.401
F(000)	1472	1480
Crystal size (mm)	$0.25 \times 0.20 \times 0.15$	$0.25 \times 0.15 \times 0.10$
Theta range for data collection (°)	2.65–26.20	2.68–28.45
Index ranges	$0h19$, $-8k0$, $-33l0$	$-20h0$, $-9k0$, $-35l0$
Reflections collected/unique	2991/2991 [$R_{int} = 0.0393$]	3681/3681 [$R_{int} = 0.0000$]
Completeness	99.7% (to $2\theta = 26.20$)	99.9% (to $2\theta = 28.45$)
Absorption correction	Psi-scan	Psi-scan
Max. and min. transmission	0.961 and 0.902	0.918 and 0.934
Refinement method	Full-matrix least-squares on F^2	Full-matrix least-squares on F^2
Data/restraints/parameters	2991/1/358	3681/0/358
Goodness-of-fit on F^2	0.978	0.918
Final *R* indices [$I > 2\sigma(I)$]	$R_1 = 0.063$, $wR_2 = 0.124$	$R_1 = 0.054$, $wR_2 = 0.092$
R indices (all data)	$R_1 = 0.290$, $wR_2 = 0.174$	$R_1 = 0.313$, $wR_2 = 0.133$
Absolute structure parameter	0.00	0.00
Largest difference peak and hole (e Å^{-3})	0.905 and −1.028	0.664 and −1.2100

2. Results and discussion

2.1. Molecular and crystal structure of aqua(N-carbamoylmethyl-iminodiacetato)metal(II) sesquihydrate with cobalt(II) or nickel(II) ions

Selected bond lengths and angles between non-hydrogen atoms and hydrogen bonding data of compounds **I** and **II** are given in Tables 2 and 3, respectively. From the data shown in Tables 1–3, it follows that both compounds are isostructural. Consequently, they could be discussed at the same time. The crystal of these compounds consist of complex units [M(ADA)(Him)(H_2O)] (hereafter M = Co or Ni) and non-bonded to the metal water molecules linked in a tridimensional hydrogen bonding network involving all polar N–H bonds of the ADA amide group and Him ligand, and probably O–H bonds of water molecules (see Tables 2 and 3). The asymmetric unit of the crystal of such compounds contains twice the formula (see Fig. 1 for nickel(II) derivative). Thus, each asymmetric unit contains two non-equivalent complex molecules from a crystallographic point of view and three non-coordinated water molecules. However, these complex

Table 2
Selected bond lengths (Å) and angles (°) for complex $[Co(ADA)(Him(H_2O)]\cdot 1.5H_2O$ (**I**) (e.s.d. values in parenthesis)

Cobalt(II) coordination			
Co(1)–N(12)	2.047(14)	Co(2)–N(22)	2.0311
Co(1)–O(11)	2.074(12)	Co(2)–O(21)	2.0446
Co(1)–O(13)	2.084(11)	Co(2)–O(23)	2.0659
Co(1)–O(1)	2.121(12)	Co(2)–N(21)	2.1016
Co(1)–O(15)	2.165(12)	Co(2)–O(2)	2.1349
Co(1)–N(11)	2.178(12)	Co(2)–O(25)	2.1438
Co(1)–Co(1)^{ii}	7.012(1)	Co(2)–Co(2)^{ii}	7.012(1)
Co(1)–Co(1)^{iv}	7.012(1)	Co(2)–Co(2)^{iv}	7.012(1)
N(12)–Co(1)–O(11)	105.1(5)	N(22)–Co(2)–O(21)	100.4
N(12)–Co(1)–O(13)	95.4(5)	N(22)–Co(2)–O(23)	93.2
O(11)–Co(1)–O(13)	91.1(5)	O(21)–Co(2)–O(23)	92.6
N(12)–Co(1)–O(1)	92.0(5)	N(22)–Co(2)–N(21)	175.7
O(11)–Co(1)–O(1)	87.0(5)	O(21)–Co(2)–N(21)	83.0
O(13)–Co(1)–O(1)	172.6(4)	O(23)–Co(2)–N(21)	84.0
N(12)–Co(1)–O(15)	98.6(5)	N(22)–Co(2)–O(2)	90.9
O(11)–Co(1)–O(15)	156.1(4)	O(21)–Co(2)–O(2)	89.8
O(13)–Co(1)–O(15)	89.4(5)	O(23)–Co(2)–O(2)	174.8
O(1)–Co(1)–O(15)	89.5(5)	N(21)–Co(2)–O(2)	91.8
N(12)–Co(1)–N(11)	174.8(6)	N(22)–Co(2)–O(25)	98.1
O(11)–Co(1)–N(11)	79.2(5)	O(21)–Co(2)–O(25)	161.3
O(13)–Co(1)–N(11)	81.6(5)	O(23)–Co(2)–O(25)	88.8
O(1)–Co(1)–N(11)	91.1(5)	N(21)–Co(2)–O(25)	78.7
O(15)–Co(1)–N(11)	77.2(5)	O(2)–Co(2)–O(25)	87.4

Hydrogen bonds [a]

D–H···A	*d*(D–H)	*d*(H···A)	*d*(D···A)	<(DHA)
N(13)–H(13)···O(14) # 1	0.86	1.91	2.74(2)	160.1
N(16)–H(16A)···O(25)	0.86	2.20	3.01(2)	157.4
N(16)–H(16B)···O(13) # 2	0.86	2.10	2.94(2)	166.7
N(23)–H(23)···O(24) # 3	0.86	1.83	2.66(4)	160.7
N(26)–H(26A)···O(15)	0.86	2.27	3.07(2)	155.1
N(26)–H(26B)···O(23) # 4	0.86	2.06	2.90(2)	165.7

[a] Symmetry transformations used to generate equivalent atoms: i: $\#1 = x-1/2,\ -y+3/2,\ z$; ii: $\#2 = x,\ y-1,\ z$; iii: $\#3 = x+1/2,\ -y-3/2,\ z$; iv: $\#4 = x,\ y+1,\ z$.

molecules are very similar from a chemical point of view. In both compounds the octahedral coordination polyhedron of the metal(II) atom is built up by means of the atom N(amino), two O(carboxyl) ones and the O(amide) donor of the tetradentate ADA^{2-} ion as well as the N(pyridine-like) atom of the Him ligand plus the O(aqua) donor of the coordinated water molecule. As regards the cobalt(II) derivative, it is widely recognised that such a $3d^7$ transition divalent metal ion adopts two major stereochemistries, distorted octahedral and tetrahedral [25]. In this connection, the ligand polarisability plays a discriminating role. Less polarisable or hard donors (as most O donor and N(amine) ones) favour octahedral structures in pink to violet cobalt(II) coordination compounds [25]. The reported case falls in this group and consequently its stereochemistry will be considered normal. On the other hand, the octahedral coordination of nickel(II) atom in compound **II** should be expected because it has been recently reported for $[Ni(ADA)(H_2O)_2]$ [13c] and it is the most frequent stereochemistry for this $3d^8$ divalent transition metal ion [25]. In contrast, it is worth noting that the structure of an analogous mixed-ligand Co(II)–ADA–H_2O complex remains unknown and all attempts to obtain X-ray quality crystals of this compound in our laboratories have been unsuccessful. Because the effective ionic radii of octahedral Ni(II) (0.72 Å [26]) and Co(II) (0.745 Å, high spin [25]) are very similar, there is no comment to add about the isostructural feature in the studied compounds. Otherwise the M(II) coordination polyhedron and the internal geometry of the ADA ligand have usual bonds and angles compared with related compounds. That includes known metal–ADA complexes [8–10,12,13], cobalt(II)–IDA chelates [27] or nickel(II)–IDA ones [28] as well as a variety of mixed-ligand complexes of cobalt(II) [29] or nickel(II) [30] having from one to four Him ligands.

The metal chelation of the tripodal ADA ligand in **I** and **II** represents the formation of two nearly coplanar M–glycinate-like rings and one M–glycinamide-like one sharing the M–N(amino) bond. One of the M–glycinate-like rings falls nearly coplanar to the plane [M, N(Him), O(aqua)] (hereafter so-called G ring). This chelate ring is less distorted (deviations from its mean ring plane ranging 0.00–0.08 Å) than the other two ones. Moreover such a G ring exhibits a slightly puckered configuration (both carbon atoms displaced at opposite side of its plane N–M–O) in complex units of Co(1) and Ni(1) atoms, and a slightly asymmetrical envelope configuration (both carbon atoms at the same side of its N–M–O plane) in complex units of Co(2) and Ni(2) atoms [30]. The remaining M–glycinate-like ring and the M–glycinamide-like one are nearly coplanar to each other (angle between mean planes of $14.4 \pm 1.7°$). These rings fall not coplanar/ nearly perpendicular to the plane [M, N(Him), O(aqua)] (and then, hereafter will be so-called R and R′ rings, respectively). All R and R′ chelate rings in the studied compounds (max. deviations of the atoms from its mean ring plane ≤ 0.28 Å) are significantly more distorted than the corresponding G one (max. deviations of the atoms from its mean ring plane ≤ 0.08 Å). In addition, these rings adopt invariably an asymmetrical envelope configuration (with both carbon atoms at the same side of its N–M–O plane) rather common in metal-amino acid chelates and closely related compounds [31].

On the other hand, the Him ligand is, as expected, planar within 0.03(1) Å. The metal ion is out of the Him plane at a distance ranging from only 0.008(1) Å for Ni(1) up to 0.130(1) Å for Ni(2) (being of 0.050(1) and 0.076(1) Å for Co(1) and Co(2) cases, respectively). The Him plane is slightly twisted ($< 10°$) versus the mean plane defined by its N(pyridine-like) donor atom and the three ADA donors involved in the R and R′ chelate rings. This fact means that the heterocyclic

Table 3
Selected bond lengths (Å) and angles (°) for complex [Ni(ADA)(Him)(H_2O)]·1.5H_2O (**II**) (e.s.d. values in parenthesis)

Nickel(II) coordination			
Ni(1)–N(12)	2.013(9)	Ni(2)–O(21)	2.0317
Ni(1)–O(11)	2.054(8)	Ni(2)–O(23)	2.0481
Ni(1)–O(13)	2.065(8)	Ni(2)–N(21)	2.0849
Ni(1)–N(11)	2.076(10)	Ni(2)–O(2)	2.1177
Ni(1)–O(15)	2.101(8)	Ni(2)–O(25)	2.1317
Ni(1)–O(1)	2.112(9)	Ni(2)–N(22)	2.0155
Ni(1)–Ni(1)[ii]	7.093(1)	Ni(2)–Ni(2)[ii]	7.093(1)
Ni–1)–Ni(1)[iv]	7.093(1)	Ni(2)–Ni(2)[iv]	7.093(1)
N(12)–Ni(1)–O(11)	99.6(4)	N(22)–Ni(2)–O(21)	100.3
N(12)–Ni(1)–O(13)	94.4(4)	N(22)–Ni(2)–O(23)	92.8
O(11)–Ni(1)–O(13)	88.8(4)	O(21)–Ni(2)–O(23)	92.6
N(12)–Ni(1)–N(11)	177.3(4)	N(22)–Ni(2)–N(21)	175.7
O(11)–Ni(1)–N(11)	82.4(4)	O(21)–Ni(2)–N(21)	83.1
O(13)–Ni(1)–N(11)	83.8(4)	O(23)–Ni(2)–N(21)	84.4
N(12)–Ni(1)–O(15)	99.0(4)	N(22)–Ni(2)–O(2)	91.2
O(11)–Ni(1)–O(15)	161.3(3)	O(21)–Ni(2)–O(2)	89.9
O(13)–Ni(1)–O(15)	91.2(4)	O(23)–Ni(2)–O(2)	174.8
N(11)–Ni(1)–O(15)	79.0(4)	N(21)–Ni(2)–O(2)	91.4
N(12)–Ni(1)–O(1)	91.2(4)	N(22)–Ni(2)–O(25)	98.2
O(11)–Ni(1)–O(1)	87.7(4)	O(21)–Ni(2)–O(25)	161.4
O(13)–Ni(1)–O(1)	173.9(3)	O(23)–Ni(2)–O(25)	88.9
N(11)–Ni(1)–O(1)	90.7(4)	N(21)–Ni(2)–O(25)	78.6
O(15)–Ni(1)–O(1)	90.5(4)	O(2)–Ni(2)–O(25)	87.3

Hydrogen bonds [a]

D–H···A	*d*(D–H)	*d*(H···A)	*d*(D···A)	<(DHA)
N(13)–H(13)···O(14) # 1	0.86	1.89	2.73(2)	164.0
N(16)–H(16A)···O(25)	0.86	2.24	3.04(2)	155.4
N(16)–H(16B)···O(13) # 2	0.86	2.09	2.93(2)	167.9
N(23)–H(23)···O(24) # 3	0.86	1.88	2.71(2)	160.9
N(26)–H(26A)···O(15)	0.86	2.25	3.04(2)	151.9
N(26)–H(26B)···O(23) # 4	0.86	2.05	2.90(2)	166.3

[a] Symmetry transformations used to generate equivalent atoms: i: # 1 = $x-1/2$, $-y+3/2$, z; ii: # 2 = x, $y-1$, z; iii: # 3 = $x+1/2$, $-y-3/2$, z; iv: # 4 = x, $y+1$, z.

ligand falls nearly perpendicular to the other two sets of roughly coplanar four donor atoms. An interesting structural correlation follows the structures of compounds **I** and **II**. That is, the preference of Him ligand for the *trans*-position to the N(ADA) donor one. Such correlation can not be inferred either from the structure of the complex [Cu(ADA)(Him)] [13a] because of its five-coordinated stereochemistry or from the structure of the closely related octahedral complex in the compound bis(imidazole)(nitrilopropionamide-diacetato)-nickel(II) monohydrate [30k] because of the presence of two Him ligands together with a tetradentate nitrilopropionamide-diacetate(2 −) ion.

It seems instructive to carry out a comparison of averaged coordination bond distances and *trans*-angles in [Ni(ADA)(H_2O)$_2$] [13c] and compounds **I** and **II** (Table 4). The following insights arise: (1) It should be noted the remarkable similarity of the average value for all six metal–ligand bond lengths. Such similarity is obviously higher for the two closely related nickel(II) compounds (with and without the Him ligand instead of an aqua one). (2) In these three compounds, the coordination bonds to four donor atoms of the tripodal ligand ADA are noticeably similar in length to each other (being more significant for [Ni(ADA)(H_2O)$_2$]). (3) In both new compounds the longest bond is that of M–O(amide). That is not observed for the diaqua–ADA–nickel(II) complex. (4) *Trans*-angles involving a M–O(aqua) bond or the M–N(Him) bond are nearly close to 180° (ranging from 173.7° to 179.3°) but the remaining *trans*-angle O(carboxyl)–M–O(amide) with both donors from ADA chelating ligand is significantly below this angle (in the range of 156–164°). These data reveal that the main source of the moderate but irregular distortion at the M(II) coordination polyhedron in the studied compounds arises from the chelate ring

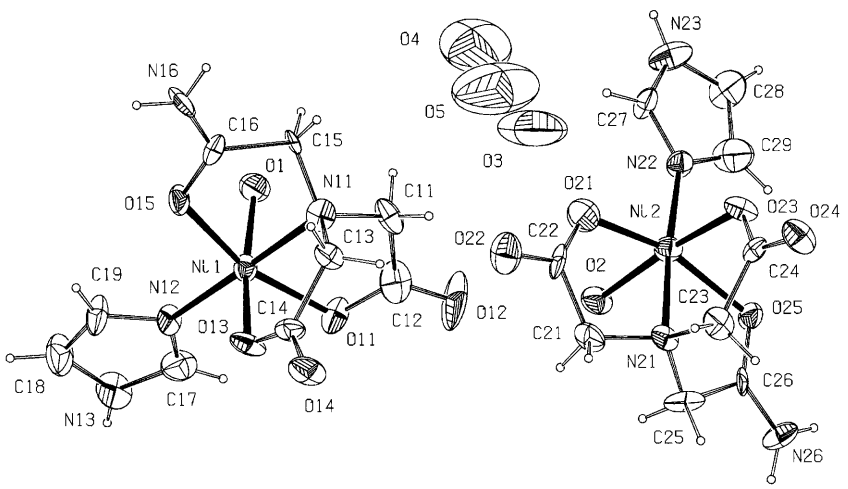


Fig. 1. Asymmetric unit in the crystal of compound [Ni(ADA)(Him)(H_2O)]·1.5H_2O (**II**).

Table 4
Structural relationships in mixed-ligand complexes $[Ni(ADA)(H_2O)_2]$ [13c] and $[M(ADA)(Him)(H_2O)]\cdot 1.5H_2O$ (M = Ni in **II**, Co in **I**): bond lengths (Å) and *trans*-angles (°)

Bond	$[Ni(ADA)(H_2O)_2]$	Compound **II** [a]	Compound **I** [a]
Bond lengths			
M–O(carboxyl, ADA)	2.051(2)	2.043	2.042
M–O(carboxyl, ADA)	2.045(2)	2.056	2.075
M–O(amide, ADA)	2.065(2)	2.116	2.154
M–N(amide, ADA)	2.072(2)	2.081	2.133
M–O(aqua) or N(Him)	2.000(2)	2.014	2.078
M–O(aqua)	2.106(2)	2.115	2.128
Average M–L bond	2.057	2.071	2.102
Bond angles			
N(amino)–M–O(aqua) or N(Him)	175.6	176.5	175.3
O(carboxyl)–M–O(aqua)	179.3	174.4	173.7
O(carboxyl)–M–O(amide)	163.8	161.4	158.7

[a] Average values for the two crystallographic independent complex units.

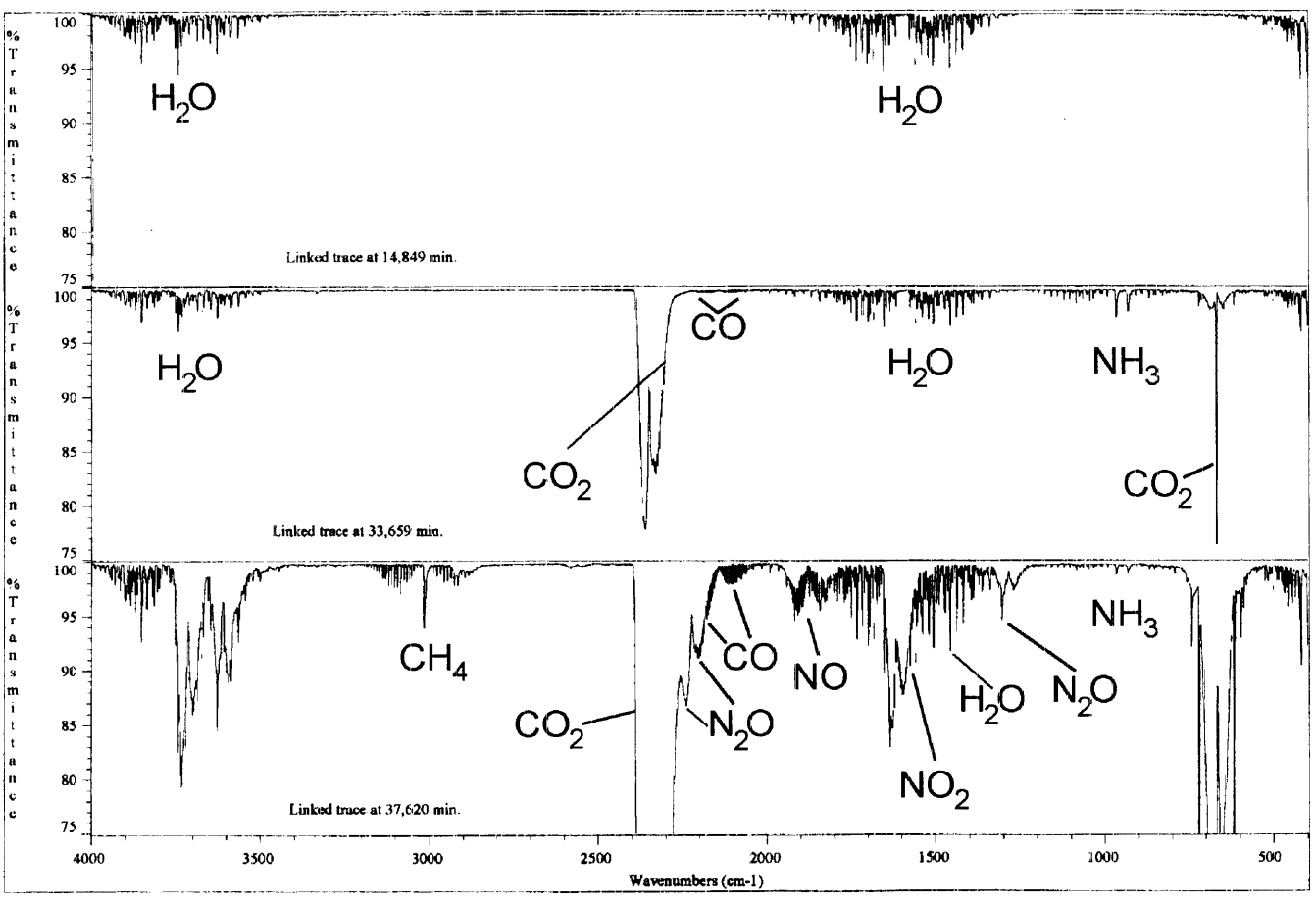


Fig. 2. Selected FTIR spectra from three steeps of the thermo-gravimetric analysis for compound **I**. (a) Spectrum at $t = 14.849$ min from first step showing only bands of water in first steep. (b) Spectrum at $t = 33.659$ min from second step with bands of water, CO_2, CO (traces) and ammonia. (c) Spectrum at $t = 37.620$ min from the beginning of third step showing bands of water, CO_2, CH_4, N_2O, NO and NO_2.

constraints in the tripodal ADA ligand. In this connection, it is worth noting that just the most distorted set of four nearly coplanar donor atoms in compounds **I** and **II** is that of the four oxygen ones (three from ADA, one from aqua). Indeed these four oxygen atoms define a folded square with a mean plane P[4(O)] from which both *trans*-pairs of oxygen donor atoms are displaced similarly but in opposite sense ($\pm 0.13(2)$ Å),

whereas the atoms of the other two sets of roughly coplanar four-donor ones deviates $< 0.06(2)$ Å from its corresponding mean plane. The metal atom is also largely moved (0.20–0.29(2) Å) out of such P[4(O)] plane towards the Him ligand (whereas the deviation of the metal atom from the other two referred mean planes is $< 0.04(2)$ Å).

2.2. Properties of aqua(*N*-carbamoylmethyl-iminodiacetato)metal(II) sesquihydrate for cobalt(II) and nickel(II)

The TG analysis in air-flow (with FTIR spectra of evolved gases) of compounds **I** and **II** are similar and show three steps. The first step (85–187°C for **I** and 135–235°C for **II**) corresponds to the loss of non-coordinated water, as it is supported by FTIR spectra (Fig. 2(a)). The other two steps corresponds to the overlapped pyrolysis of organic ligands (Fig. 2(b,c)) to give probably Co_2O_3 or $NiO{\cdot}Ni(NO_3)_2$ at 425°C. The weight loss and evolved gases in the second step (187–335°C, Fig. 2(b) for compound **I**) correspond to the loss of coordinated water plus the 2-amidomethyl arm of ADA, the organic ligand which begins the oxidative pyrolysis.

Since the isostructural relationship of compounds **I** and **II**, their IR spectra are extremely similar. They allow the identification of the main characteristic absorption bands (wave-numbers in cm^{-1}) expected for aqua and ADA ligands [32]: A very broad band (3800–2500) including ν(OH) of water, $\nu_{as}(NH_2)$ and $\nu_s(NH_2)$ of primary amide group at 3330 and 3141(3128), ν(C=O) of primary amide group ('amide I' band) at 1675, $\delta(H_2O)$, $\delta(NH_2)$ ('amide II' band) and $\nu_{as}(COO^-)$ overlapped at 1610 (1611), δ(N–H) of Him at 1542, and $\nu_s(COO^-)$ at 1403. Difference $\Delta(COO) = 207 \pm 1$ cm^{-1} in accordance with the expected ionic nature of the M(II)–O(carboxylato) bonds.

Electronic spectra of compounds **I** and **II** are typical of Co(II) (ground state $^4T_{1g}(F)$) and Ni(II) (ground state $^3A_{2g}(F)$) octahedral complexes, respectively. The spectrum of **I** shows bands at $\nu_1 = 8420$, $\nu_2 = 16\,100$ (shoulder) and $\nu_3 = 19\,350$ cm^{-1}, which fall between those of the hexaaqua-ion and the $[Co(NH_3)_6]^{2+}$ ion [25]). The spectrum of **II** shows bands $\nu_1 = 9930$ (shoulder at $\sim 14\,500$), $\nu_2 = 16\,420$ and $\nu_3 = 25\,975$ cm^{-1}. It can be assumed that $\nu_1 = 10\,Dq = \Delta_o$, and a value of 856 cm^{-1} is obtained for the Racah parameter B', 83% of the B parameter in the free ion. Δ_o and B' in **II** are higher than those of *cis*-diaqua(*N*-carbamoylmethyl-iminodiacetato)nickel(II) [13c] as expected for the substitution of one aqua ligand by Him.

For both compounds studied, a plot of $1/\chi$ data versus T (K) ($T = 80$–290 K) is linear (with a statistical factor r^2 of 0.9997) according to a Curie–Weiss behaviour, $\chi_{mol} = C/(T - \theta)$, (see Fig. 3(a) for cobalt(II) case). The experimental value of the effective magnetic moment (μ_{eff}) for the metal(II) atom is 5.10 or 3.22 BM for **I** or **II**, respectively, within the corresponding ranges for mononuclear high-spin octahedral cobalt(II) [25] or in octahedral nickel(II) [26], in agreement with the structures reported, where the shortest inter-metallic distances are > 7 Å.). The μ_{eff} value for the cobalt(II) complex largely exceeds the spin-only value [24] suggesting that there is an appreciable contribution of orbital angular momentum [25]. That can be attributed to its T ground term resulting in temperature-dependent orbital contributions to the magnetic moment. Accordingly, experimental values of μ_{eff} fall of with decreasing temperature (Fig. 3(b)).

3. Concluding remarks

Compounds **I** and **II** have octahedral stereochemistry for cobalt(II) and nickel(II) atoms, respectively, a rather common coordination for these metal(II) ions in moderate ligand fields. Such stereochemistry has been also observed in *cis*-diaqua(*N*-carbamoylmethyl-iminodiacetato)-nickel(II) [13c], the 'parent' complex of

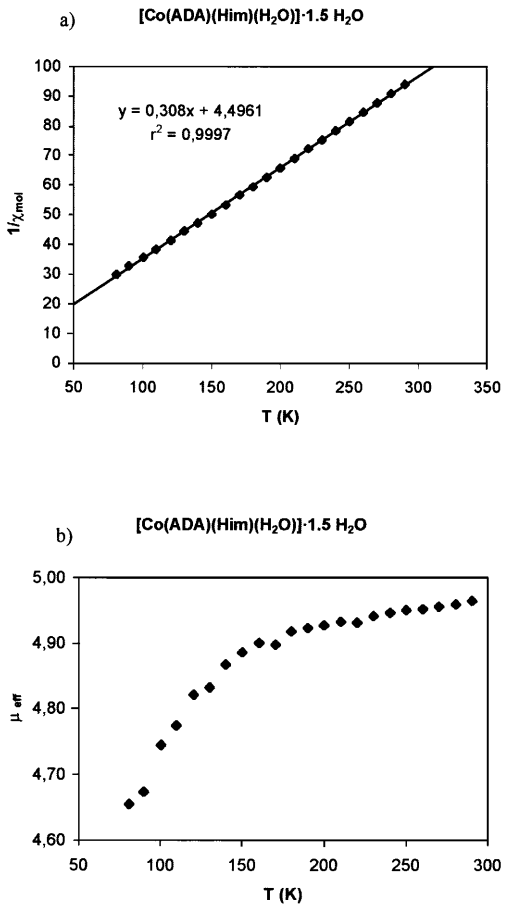


Fig. 3. Magnetic properties of compound **I**. (a) A plot of $1/\chi_{mol} = f(T)$: (◆, experimental; solid straight line represents the best theoretical fit to the linear form of the Curie–Weiss law). (b) Dependence of the effective magnetic moment versus the temperature.

compound **II**. This is in contrast to the distorted square-base pyramidal coordination found in the corresponding copper(II) derivatives, $\{[Cu(ADA)]\cdot H_2O\}_n$ (which has a polymeric structure [13b]) and [Cu(ADA)(Him)] [13a].

On the basis of the octahedral Ni(II) coordination in the above referred chelates, new structural relationships can be inferred [13c]. This study reveals that imidazole comes in the complex $[Ni(ADA)(H_2O)_2]$ replacing the aqua ligand just in *trans* to the bond Ni(II)–N(amino) with ADA. This ligand substitution reaction does not seem to cause significant changes in bond lengths and angles around the Ni(II) atom. In compounds **I** and **II**, one aqua ligand remains linked to the metal atom. That could permit further ligand substitution reactions. This possibility promotes new studies on mixed-ligand metal complexes with ADA and a variety of mono- and bi-dentate ligands.

The structure of the aqua–ADA–cobalt(II) complex remains unknown. Efforts will be made to cover this lack of information. On the other hand, at this moment, all known structures show ADA as an effective tripodal tetradentate ligand [11–13]. This feature suggests a remarkable ligand flexibility, but additional studies for metal ions with different crystallo-chemical properties will be required.

4. Supplementary material

Crystallographic data for the structures reported in this paper have been deposited with the Cambridge Crystallographic Data Centre, CCDC no. 134849 for compound $[Co(ADA)(Him(H_2O)]\cdot 1.5H_2O$ (**I**) and CCDC no. 134848 for compound $[Ni(ADA)(Him)(H_2O)]\cdot 1.5H_2O$ (**II**). Copies of this information may be obtained free of charge from the Director, CCDC, 12 Union Road, Cambridge, CB2 1EZ, UK (fax: +44-1223-336-033; e-mail: deposit@ccdc.cam.ac.uk or http://www.ccdc.cam.ac.uk).

Acknowledgements

This paper is devoted to the memory of Prof. Sergio Cabani (University of Pisa, Italy) recently deceased. He encouraged many contributions on thermodynamics and kinetics of metal complexes. We are grateful to the Dirección General de Enseñanza Superior e Investigación Científica, MEC, Spain, for financial support (Project PB-98-0605-C03-03). A.C. thanks the Xunta de Galicia for the financial support (Project XUGA20309B97). A research grant to E.B.A. from Ministerio de Educación y Cultura is gratefully acknowledged.

References

[1] T. Minami, H. Matsubara, M.O. Higashi, M. Kimura, K. Kubo, N. Okabe, Y. Okazaki, J. Chromatogr. B: Biomed. Appl. 685 (1996) 353.
[2] G. Schwarzenbach, G. Anderegg, W. Schneider, H. Senn, Helv. Chim. Acta 38 (1955) 4147.
[3] E. Lance, R. Nakon, Inorg. Chim. Acta 55 (1981) L1.
[4] J. Nepal, S Dubey, Indian J. Chem. 26A (1987) 269.
[5] H.A. Azaab, A. Hassan, Bull. Soc. Chim. Fr. I (1989) 599.
[6] H.A. Azaab, Monatsh. Chem. 123 (1992) 1107.
[7] E.A. Lance, Ch.W. Rhodes, III, R. Nakon, Anal. Biochem. 133 (1979) 492.
[8] P.D. Parr, Ch. Rhodes, R. Nakon, Inorg. Chim. Acta 80 (1983) L11.
[9] (a) E.M. Khairy, M.M. Mohamed, M.M. Khalil, M.M.A. Mohamed, Trans. Metal Chem. 21 (1996) 176. (b) I.T. Ahmed, O.M. El-Roudi, A.A. Boraei, A.A. Ahmed, S.A. Ibrahim, J. Chem. Eng. Data 41 (1996) 386. (c) I.T. Ahmed, Synth. React. Inorg. Met.-org. Chem. 26 (1996) 1455. (d) M.M. Shoukry, E.M. Khairy, M. Ezzat, M.M.A. Mohamed, Ann. Chim. (Rome) 86 (1996) 167. (e) M.R. Mahmoud, M.I. Abdel-Hamid, N.M. Ismail, I.T. Ahmed, Pol. J. Chem. 70 (1996) 544. (f) I.T. Ahmed, A.A. Boraei, S.A. Ibrahim, Synth. React. Inorg. Met.-org. Chem. 27 (1997) 169.
[10] B.J. Hamstra, A.L.P. Houseman, G.J. Colpas, J.W. Kampf, R. LoBruto, W.D. Frasch, V.L. Pecoraro, Inorg. Chem. 36 (1997) 4866.
[11] M. Sivák, J. Tyršelová, S. Pavelík, J. Marek, Polyhedron 15 (1996) 1062.
[12] G.J. Colpas, B.H. Hamstra, J.W. Kampf, V.L. Pecoraro, J. Am. Chem. Soc. 118 (1996) 3469.
[13] (a) E. Bugella Altamirano, J.M. González Pérez, A.G. Sicilia Zafra, J. Niclós Gutiérrez, A. Castiñeiras Campos, Polyhedron 18 (1999) 3333. (b) A. Castiñeiras Campos, E. Bugella Altamirano, J.M. González Pérez, A.G. Sicilia Zafra, J. Niclós Gutiérrez, Metal chelates of *N*-carbamoylmethyl-iminodiacetate(2-) ion. Part II. Synthesis, XRD structures and properties of poly-[(*N*-carbamoylmethyl-iminodiacetato)copper(II) monohydrate], $\{[Cu(ADA)]\cdot H_2O\}_n$, and (2,2′-bipyridine)(*N*-carbamoylmethyl-iminodiacetato)copper(II) three-hydrate, $[Cu(ADA)(bipy)]\cdot 3H_2O$ (submitted, 2000). (c) A. Castiñeiras Campos, E. Bugella Altamirano, J.M. González Pérez, A.G. Sicilia Zafra, J. Niclós Gutiérrez, Polyhedron 19 (2000) 2463.
[14] B.V. Nonius, CAD4-Express Software, Release 5.1/1.2, Enraf Nonius, Delft, The Netherlands, 1994.
[15] M. Kretschmar, GENHKL, Program for the Reduction of CAD4 Diffractometer Data, University of Tuebingen, Germany, 1997.
[16] A.C.T. North, D.C. Phillips, F.S. Mathews, Acta Crystallogr., Sect. A 24 (1968) 351.
[17] G.M. Sheldrick, Acta Crystallogr., Sect. A 46 (1990) 467.
[18] G.M. Sheldrick, SHELXL-97. Program for the Refinement of Crystal Structures, University of Göttingen, Germany, 1997.
[19] H.D. Flack, Acta Crystallogr., Sect. A 39 (1983) 876.
[20] International Tables for X-ray Crystallography, Vol. C, Kluwer Academic Publishers, Dordrecht, The Netherlands, 1995.
[21] A.L. Spek, PLATON. A Multipurpose Crystallographic Tool, Utrecht University, Utrecht, The Netherlands, 1998.
[22] (a) W.B. Guenther, Quantitative Chemistry: Measurements and Equilibrium, Addison-Wesley, Massachusetts 1968, pp. 341–343. (b) T.S. West, Complexometry with EDTA and Related Reagents, BDH Chemicals Ltd., Broglia Press, Bournemouth, 1969, pp. 180–181, 197–199.
[23] F.E. Mabbs, D.J. Machin, Magnetism and Transition-Metal Complexes, Chapman and Hall, London, 1973.

[24] W.E. Hatfield, Magnetism of transition metal ions, in: R.B. King (Ed.), Encyclopedia of Inorganic Chemistry, vol. 4, John Wiley and Sons, Chichester and New York, 1994, pp. 2066–2075 and references therein.
[25] D.A. Buckingham, Cobalt: inorganic and coordination compounds, in: R.B. King (Ed.), Encyclopedia of Inorganic Chemistry, vol. 2, John Wiley and Sons, Chichester and New York, 1994, pp. 712–733 and references therein.
[26] M. Schröeder, Nickel: inorganic and coordination compounds, in: R.B. King (Ed.), Encyclopedia of Inorganic Chemistry, vol. 5, John Wiley and Sons, Chichester and New York, 1994, pp. 2392–2412 and references therein.
[27] (a) Ya.M. Nesterova, T.N. Polynova, M.A. Porai-Koshits, F.G. Kramarenko, N.M. Muratova, Zh. Strukt. Khim. 20 (1979) 960. (b) Xu Duanjun, Cheng Caorong, Xu Yuanzhi, Hu Shengzhi, Jiegou Huaxue 8 (1989) 81. (c) I.V. Kuz'menko, T.N. Polynova, M.A. Porai-Koshits, A.L. Poznyak, Koord. Khim. 18 (1992) 620.
[28] (a) V.M. Agre, T.F. Sisoeva, V.K. Trunov, N.M. Dyatlova, A.Ya. Fridman, Zh. Strukt. Khim. 25 (1984) 141. (b) N.J. Mammano, D.H. Templeton, A. Zalkin, Acta Crystallogr., Sect. B 33 (1977) 1251. (c) F.G. Kramarenko, T.N. Polynova, M.A. Porai-Koshits, V.P. Chalyi, N.D. Mitrofanova, Zh. Strukt. Khim. 15 (1974) 161. (d) N.J. Mammano, D.H. Templeton, A. Zalkin, Acta Crystallogr., Sect. B 33 (1977) 1251.
[29] (a) Xiao-Ming Chen, Bao-Hui Ye, Xiao-Chun Huang, Zhi-Tao Xu, J. Chem. Soc., Dalton Trans. (1996) 3465. (b) W.D. Horrocks Jr., J.N. Ishley, R.R. Whittle, Inorg. Chem. 21 (1982) 3265. (c) Long-Gen Zhu, You-Xiang Wang, Chun-Ying Duan, Xing-Shui Yang, Xiao-Zeng You, Jin-Shun Huang, Huaxue Xuebao 50 (1992) 583. (d) Li Jianmin, Zhang Yugeng, Lin Wenbin, Liu Shixiong, Huang Jinling, Polyhedron 11 (1992) 419. (e) L.H. Abdel-Rahman, L.P. Battaglia, D. Cauzzi, P. Sgarabotto, M.R. Mahmoud, Polyhedron 15 (1996) 1783. (f) M. Doring, W. Ludwig, E. Uhlig, S. Wocadlo, U. Muller, Z. Anorg. Allg. Chem. 611 (1992) 61.
[30] (a) L.P. Battaglia, A.B. Corradi, L. Antolini, G. Marcotrigiano, L. Menabue, G.C. Pellacani, J. Am. Chem. Soc. 104 (1982) 2407. (b) H.C. Freeman, J.M. Guss, Acta Crystallogr., Sect. B 28 (1972) 2090. (c) J.A.C. van Ooijen, J. Reedijk, A.L. Spek, Inorg. Chem. 18 (1979) 1184. (d) Shaohua Gou, Xiaozeng You, Zheng Xu, Zhongyuan Zhou, Kaibe Yu, Polyhedron 10 (1991) 2659. (e) K.K. Nanda, L.K. Thompson, J.N. Bridson, K. Nag, J. Chem. Soc., Chem. Commun. (1994) 1337. (f) A. Marzotto, D.A. Clemente, A. Ciccarese, G. Valle, J. Crystallogr. Spectrosc. Res. 23 (1993) 119. (g) Zongwan Mao, Degang Fu, Qinwei Hang, Wenxia Tang, Kaibei Yu, J. Chem. Soc., Dalton Trans. (1993) 3169. (h) L.H. Abdel-Rahman, L.P. Battaglia, D. Cauzzi, P. Sgarabotto, M.R. Mahmoud, Polyhedron 15 (1996) 1783. (i) M. Koman, E. Jona, A. Maslejova, Acta Crystallogr., Sect. C 47 (1991) 1206. (j) D. Deguenon, P. Castan, F. Dahan, Acta Crystallogr., Sect. C 47 (1991) 433. (k) L.M. Shkol'nikova, K.D. Suyarov, A.A. Masyuk, A.L. Poznyak, N.M. Dyatlova, Koord. Khim. 16 (1990) 1096.
[31] C.J. Hawkins, Absolute Configuration of Metal Complexes, Wiley-Interscience, New York, 1971 Chapter 3.
[32] L.J. Bellamy, The Infrared Spectra of Complex Molecules, vol. 1, 3rd ed., Chapman and Hall, London, 1975.

PERGAMON

www.elsevier.nl/locate/poly

Polyhedron 19 (2000) 2483–2491

POLYHEDRON

A theoretical analysis of how geometrical distortions on $Cu(\mu\text{-}Cl)_2Cu$ dimers influence their electronic and magnetic properties

Montserrat Rodríguez [a], Antoni Llobet [a,*], Montserrat Corbella [b]

[a] *Departament de Química, Universitat de Girona, Campus de Montilivi, E-17071 Girona, Spain*
[b] *Departament de Química Inorgànica, Universitat de Barcelona, Martí i Franquès, 1-11, 08028 Barcelona, Spain*

Abstract

A structural classification of dimers, containing the $Cu(\mu\text{-}Cl)_2Cu$ core, based on data obtained from X-ray diffraction analysis reported in the literature has been performed. In these complexes, the local geometry around the copper metal center is generally a square pyramid, with a different degree of distortion towards a trigonal bipyramid. The global geometry of the dinuclear complex can be described in terms of the relative arrangement of the two square pyramids, giving rise to three types of geometries, termed: coplanar bases, parallel bases and perpendicular bases. Ideal models representing these geometries were defined and EH calculations were performed in each case, showing the different molecular orbitals involved in their corresponding frontier orbitals, together with their energy. EH calculations were also carried out for dimers embodying different type of structural distortions from the ideal models. The results obtained from those EH calculations have proven to be extremely useful for the proper interpretation and correlation of the magnetic data and dimer structure for those $Cu(\mu\text{-}Cl)_2Cu$ complexes reported in the literature. © 2000 Elsevier Science B.V. All rights reserved.

Keywords: Magnetic properties; Dimers; Geometrical distortions; Magnetostructural correlations

1. Introduction

The magnetic properties of transition metal complexes are of tremendous importance both from a basic research point of view and also because of their multiple technological applications [1–3]. As a consequence, there has been substantial interest, over the years, in correlating magnetic properties and molecular structure. On the other hand, the propagation of magnetic information over large distances is a topic that has attracted considerable interest in recent years [4–10].

For dihydroxo bridged dinuclear copper complexes [11–24], a good degree of success has been accomplished in correlating structure and magnetic properties. In sharp contrast, no unique magneto-structural correlation has been found for dichloro bridged dinuclear copper complexes. Furthermore, a recent report has presented a new compound that constitutes the first example of a ferromagnetic dinuclear copper with a spin-ladder disposition and moderate interactions [25].

Given the current interest in dinuclear dichloro bridged copper complexes, we have undertaken a theoretical analysis on the different geometrical factors that influence their electronic and magnetic properties, in order to offer a framework for future reference.

2. Experimental

Molecular orbital calculations have been carried out using CACAO 4.0 (computer-aided composition of atomic orbitals) [26], which is a program based on extended Hückel (EH) type of analysis.

Ideal models were used as the starting point of our analysis. In the models, the N atoms of the ligands were substituted for simple amino groups. EH calculations for complex $[Cu_2(dpt)_2Cl_2]Cl_2$ (**34**) (see Table 1) [25], showed that there is no significant difference for both energies and frontier orbital topologies between the real complex and the model.

* Corresponding author. Tel.: +34-972-418262; fax: +34-972-418150.
E-mail address: llobet@fc.udg.es (A. Llobet).

0277-5387/00/$ - see front matter © 2000 Elsevier Science B.V. All rights reserved.
PII: S0277-5387(00)00548-9

For each model, all bonding angles between Cu and the bonded ligand atoms, arranged in a *cis* fashion, were taken as 90°. All Cu–N bond distances were taken as 2.0 Å, while we distinguished between basal and apical Cu–Cl bond distances. The former was taken as 2.51 Å, whereas we used 2.70 Å for the latter. In the perpendicular bases case, we took both Cu–Cl bond distances as 2.51 Å.

The three models used, together with the drawing of their corresponding HOMO and LUMO frontier orbitals, are depicted in Fig. 1.

Throughout the present paper, the description of atomic orbital participation is only considered if it has a contribution of more than 1% to the corresponding molecular orbital.

3. Results and discussion

A number of dichloro bridged dicopper complexes have been reported in the literature so far [25,27–53]. At first glance their molecular structure shows that there is a whole variety of bond distances and angles, in sharp contrast with dihydroxo bridged dicopper complexes, that display a more homogeneous behavior from this perspective. Moreover, a closer examination of their structural parameters shows that, in dihydroxo bridged copper complexes, the geometry around the copper metal center is basically a square pyramid. The two pyramids are spatially arranged so that they share a basal edge, which contains the two OH^- bridging ligands, and the corresponding apical positions are

Table 1
$\Delta E_{S\text{-}T}$ and Magnetostructural correlation parameters for selected binuclear copper complexes containing the $Cu(\mu\text{-}Cl)_2Cu$ core

Compound [a]	Geometry type [b]	α	α/R	$\Delta E_{S\text{-}T}$ (cm^{-1})	Reference
(**1**) $[Cu(Cl)_2(TMSO)]_2$	PAR	88.5	29.3	−17.0	[27]
(**2**) $[Cu_2(baamo)_2Cl_2]$	PAR	82.9	29.52	12	[28]
(**3**) $[Cu(2\text{-}pic)_2Cl_2]_2$	PAR	100.63	29.9	−7.4	[29]
(**4**) $[Cu(tmen)Cl_2]_2$	PAR	96.8	30.7	−5.6	[30]
(**5**) $[Cu(Me_3en)Cl_2]_2$	PAR	84.84	31.4	−2.1	[31]
(**6**) $[Cu(Pypep)Cl]_2{\cdot}2H_2O$	PAR	91.1	32.18	−4.6	[32]
(**7**) $[CuCl_2(TTPP1)]_2$	PAR	86.87	32.15	−7.4	[33]
(**8**) $[Cu(dmg)Cl_2]_2$	PAR	88	32.6	6.3	[34]
(**9**) $[Cu_2(terpy)_2Cl_2][PF_6]_2$	PAR	89.9	33.02	−5.9	[35]
(**10**) $[Cu(dien)Cl]_2(ClO_4)_2$	PAR	92.05	33.5	0.4	[36]
(**11**) $[Cu(bpdio)Cl_2]_2$	PAR	96.68	33.99	4.87	[37]
(**12**) $[Cu_2Cl_3(C_7H_6N_2)_5]Cl{\cdot}4H_2O$	PAR	89.1	34.01	5.6	[38]
(**13**) $[CuCl_2(TTPP2)]_2$	PAR	90.94	34.18	−20.8	[33]
(**14**) $[Cu(4\text{-}Meox)_2Cl_2]_2$	PAR		34.4	−2.6	[36]
(**15**) $[Cu(Et_3en)Cl_2]_2$	PAR	94.84	34.8	0.1	[51]
(**16**) $[Rh(en)_3]_2[Cu_2Cl_8]Cl_2{\cdot}2H_2O$	PAR	94.58	34.96	−13.8	[39]
(**17**) $[Cu(4\text{-}Metz)(DMF)Cl_2]_2$	PAR	95.3	35.0	−3.4	[51]
(**18**) $[Ir(en)_3]_2[Cu_2Cl_8]Cl_2{\cdot}2H_2O$	PAR	94.83	35.06	−13.0	[39]
(**19**) $[Co(en)_3]_2[Cu_2Cl_8]Cl_2{\cdot}2H_2O$	PAR	95.2	35.2	−14.6	[38]
(**20**) $[Cu_2Cl_4(2pyq)_2]$	COP	95.7	38.7	−10	[40]
(**21**) $[Cu(Guan)Cl_3]_2{\cdot}2H_2O$	COP	97.9	40.0	−82.6	[53]
(**22**) $[(C_5H_5N)NH_2]_2Cu_2Cl_6$	COP	94.9	40.73	42	[41]
(**23**) $(4\text{-}BzpipdH)_2[Cu_2Cl_6]$	COP	95.3	41.62	41.7	[42]
(**24**) $[Cu_2Cl_2(HB(1\text{-}pz)_3)_2]$	COP	94.4	40.76	33.7	[52]
(**25**) $(Me_2NH_2)_2[Cu_2Cl_6]$	COP	95.6	41.57	≈20	[43]
(**26**) $(i\text{-}PrNH_3)_2[Cu_2Cl_6]$	COP	95.5	41.34	−19.46	[44]
(**27**) $(paraquat)[Cu_2Cl_6]$	COP	97.5	42.61	−26.41	[42]
(**28**) $(melH_2)[Cu_2Cl_6]$	COP	95.8	40.82	−37.53	[45]
(**29**) $K_2[Cu_2Cl_6]$	COP	95.9	41.30	−38.23	[46]
(**30**) $(morphH)_2[Cu_2Cl_6]$	COP	95.8	41.82	−61.16	[47]
(**31**) $(DBTTF)[Cu_2Cl_6]$	COP	96.2	41.88	−93.12	[48]
(**32**) $(Ph_4As)_2[Cu_2Cl_6]$	COP	93.8		45.1	[49]
(**33**) $(Ph_4P)_2[Cu_2Cl_6]$	COP	93.2		53.4	[50]
(**34**) $[Cu_2(dpt)_2Cl_2]Cl_2$	PER	91.4	35.91	42.94	[25]

[a] Ligand abbreviations: baamo: 8-amino-5-aza-4-methyl-3-octene-2-onate; bpdio: 2,2-bis-(2-pyridyl)-1,3-dioxolane; 4-BzpipdH: 4-benzilpyperidinic cation; DBTTF: dibenzotetratiafulvalenic cation; dien: diethylenetriamine; dmg: dimethylglioxime; en: ethylendiamine; Et_3en: *N*,*N*,*N*′-triethylethylendiamine; Guan: guaninic cation (2-aminohypoxantinic, $C_5H_5N_5O$); HB(1-pz)$_3$: hydrotris(1-pirazolyl)borate; i-Pr: isopropyl; Me_3en: *N*,*N*,*N*′-trimethylethylendiamine; $melH_2$: melaminic cation, $C_3H_2N_3(NH_2)_3^{2+}$; 4-Meox: 4-methyloxazole; 4-Metz: 4-methyltriazole; morphH: morpholinic cation (tetrahydro-1,4-oxazinic); paraquat: 1,1′-dimethil-4,4′-bipyridinic cation; 2-pic: 2-methylpyridine; Pypep: pyperidinic cation, *N*-(2-(4-imidazolyl)ethyl)-2-pyridine-2-carboxamidic; 2pyq: 2-(2′-pyridyl)quinoxaline; tmen: *N*,*N*,*N*′,*N*′-tetramethylethylendiamine; TMSO: tetramethylsulfoxide; trpy: 2,2′:6′,2″-terpyridine; TTPP1: 2,5,8-trithia [9](2,5)thiophenophane; TTPP2: 2,5,9,12-tetrathia [13](2,5)thiophenophane.

[b] COP stands for coplanar bases, PAR for parallel bases and PER for perpendicular bases.

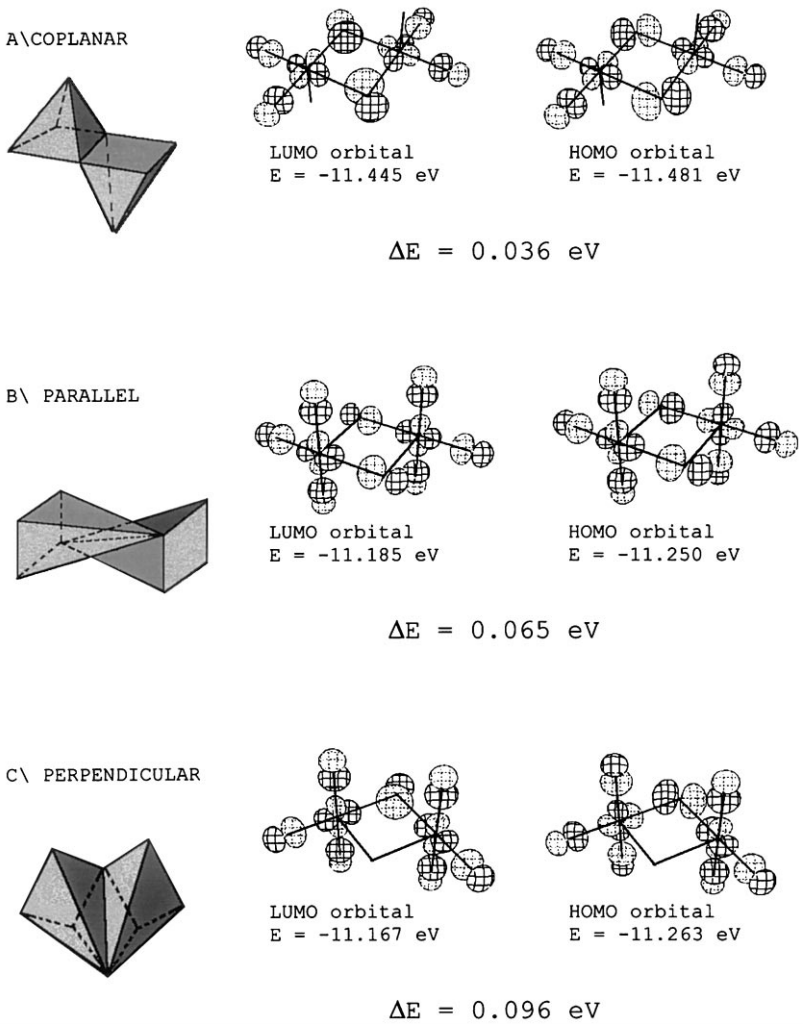


Fig. 1. Polygon arrangements found for $N_3Cu(\mu\text{-}Cl)_2CuN_3$ type of dimers together with their EH calculated HOMO and LUMO frontier orbitals for ideal models (see Section 2 for details): (A) coplanar bases; (B) parallel bases; (C) perpendicular bases.

situated in opposite directions. This geometry, termed coplanar bases, is shown in Fig. 1(A) for the homologous Cu_2Cl_2 complexes, and it is invariably the type of structural arrangement observed for most of dihydroxo bridged complexes reported to date.

For dinuclear dichlorobridged pentacoordinated copper complexes, the local geometry around the copper metal center is also generally a square pyramid, although the degree of distortion is somewhat greater than in the hydroxo case. In sharp contrast, and due to the relatively larger bond distances and angles presented, dichloro bridged complexes exhibit two more different geometries with regard to the relative arrangement of squared pyramids, besides to the coplanar bases case. Those two new geometries are termed parallel bases and perpendicular bases, and are represented in Fig. 1(B and C), respectively.

3.1. Ideal models

In the parallel bases case, the two square pyramids share a base-to-apex edge so that the Cl atom situated at the vertex of one base becomes the apical vertex of the other square pyramid, and just the opposite happens for the other Cl bridging ligand. In the perpendicular bases case, the two square pyramids share a base to apex edge, but now the apical chloro ligand of one pyramid is also the apical of the other one, and the same happens for the other chloro ligand: in both pyramids it lies on the base.

Fig. 1 presents, for the three possible geometries adopted by dinuclear dichloro bridging copper com-

plexes, the schematic structural drawings, idealized polygon arrangements and the drawings and energies of EH calculated frontier orbitals based on ideal models. EH analysis for the ideal coplanar bases case gives an energy gap of 0.036 eV between HOMO and LUMO orbitals (see Fig. 1(A)) which, in turn, are about 0.8 eV above occupied orbitals. The calculations indicate, for the HOMO orbital, the following orbital participation: Cu d orbitals, 42%; N p orbitals, 32%; basal Cl p orbitals, 24%. For LUMO orbital: Cu d orbitals, 44%; N p orbitals, 32%; basal Cl p orbitals 24%. The contribution from the apical N ligand to both frontier orbitals is less than 1%. A summary of the results obtained from EH analysis performed for the three different arrangements is shown in Table 2.

As it can be observed in Fig. 1, the Cu metal centers use $d_{x^2-y^2}$ type orbitals for a σ^* interaction with p_N and p_{Cl} orbitals, for any of the structural arrangements. For the coplanar bases case, the LUMO orbital is an antisymmetric $d_{Cu}-d_{Cu}$ orbital combination, whereas the HOMO orbital is a $d_{Cu}-d_{Cu}$ symmetric combination. For both parallel and perpendicular bases cases, the LUMO orbital is the symmetric combination of these $d_{Cu}-d_{Cu}$ orbitals, and the HOMO corresponds to the antisymmetric one.

In the frontier orbitals, for the parallel bases case, each bridging Cl ligand interacts, in a sigma fashion, only with one of the Cu metals. It is interesting to note that, for perpendicular bases case, the contribution to frontier orbitals of the apical Cl ligand is less than 1% in both HOMO and LUMO orbitals.

3.2. Distortions from ideal models

In this section we described how frontier orbitals topology and energy were affected by structural distortions. The distortions chosen are those that lead to the type of distorted structures found for real complexes, or those that help to understand the magnetic behavior of copper dimers reported in the literature.

3.2.1. Coplanar bases

The first distortion considered in this case consists on an elongation of the Cu–Cl bond distances, maintaining bond angles intact, therefore producing a symmetric enlargement of the squared core. As the Cu–Cl distance is progressively enlarged from 2.2 to 2.8 Å, the energy gap between frontier orbitals is gradually decreased. At this point the two orbitals are nearly degenerate. This is due to the fact that, as the Cu–Cl bond distance is increased, the effective bonding decreases and therefore the two Cu centers become basically independent.

The second distortion considered was a symmetric increase and decrease of the Cu–Cl–Cu bond angles that produces, as a consequence, a decrease and increase of the Cu–Cl bond distances, respectively. In this case, the frontier orbitals energy gap reaches a minimum at CuClCu bond angle equal to 90°; for this angle, the overlap between the p_{Cl} orbitals and the d_{Cu} orbitals is practically identical in both HOMO and LUMO orbitals, due to the orthogonality of p_{Cl} orbitals involved (see Fig. 1(A)). As the angle is increased, both orbitals increase in energy, but the LUMO increases at a faster pace. On the other hand, when the angle decreases, both frontier orbitals do stabilize, but now the HOMO does it faster.

The third distortion considered was the Cu geometrical transformation from a square pyramid (sqp) to a trigonal bipyramid (tbp)(see Fig. 2). In this case, the frontier orbitals energy and the gap remain practically constant over the exerted distortion. However, orbital composition and shape are substantially different. The frontier orbitals involved in the tbp geometry resemble now a orbital (Fig. 2(C)), and some degree of participation from the apical ligand orbitals was found.

3.2.2. Parallel bases

For this geometry we have considered two different distortions. The first distortion, represented in Fig. 3, consisted on the transformation of a sqp to tbp geome-

Table 2
Energies and participation of atomic orbitals to HOMO and LUMO orbitals calculated for ideal models

Geometry type	Coplanar bases	Parallel bases	Perpendicular bases
Energy GAP between HOMO and LUMO orbitals (eV)	0.036	0.065	0.096
Energy above occupied orbitals (eV)	0.8	1.5	1.3
HOMO Cu d orbitals participation (%)	42	44	42
HOMO N p orbitals participation (%)	32	44	42
HOMO basal Cl p orbitals participation (%)	24	12	12
LUMO Cu d orbitals participation (%)	44	42	44
LUMO N p orbitals participation (%)	32	44	44
LUMO basal Cl p orbitals participation (%)	24	10	10

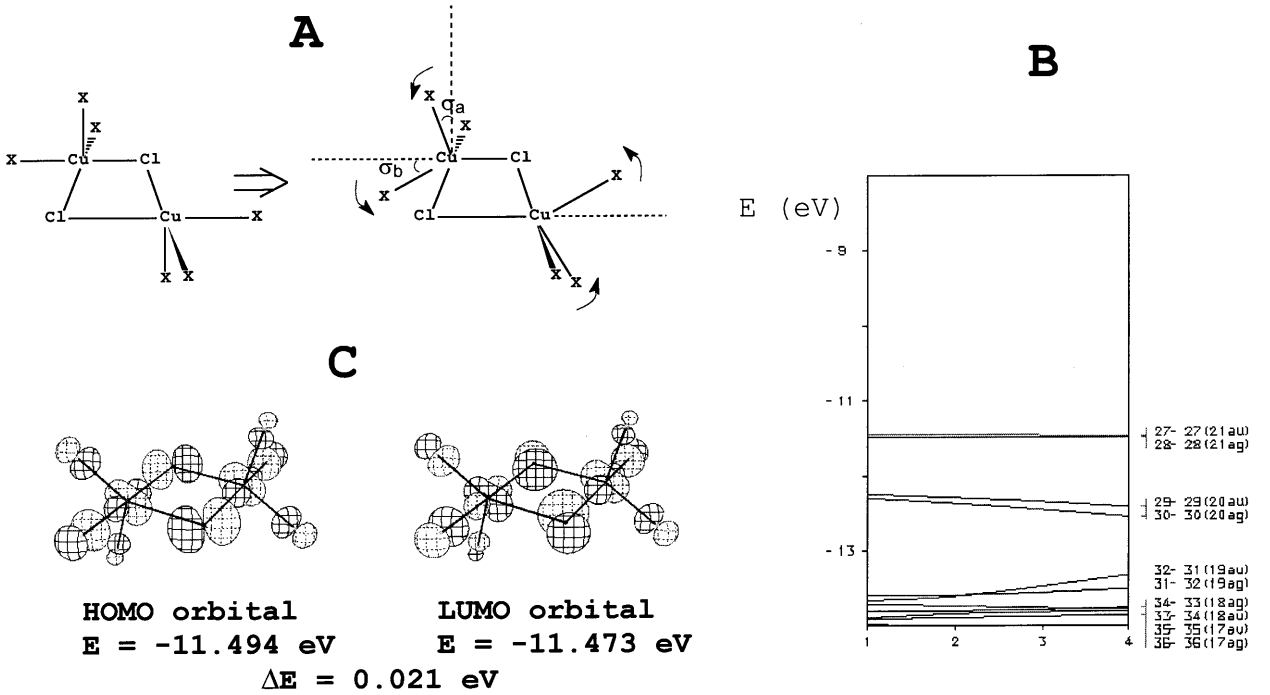


Fig. 2. Distortion from the coplanar bases ideal model. (A) Schematic diagram showing the applied distortion from sqp to tbp through a modification of the indicated angles σ_a (apical) and σ_b (basal). (B) Walsh diagram showing the energy as function of synchronized variations of σ_a and σ_b (step 1: initial idealized coplanar bases; step 2: $\sigma_a = 5°$, $\sigma_b = 10°$; step 3: $\sigma_a = 10°$, $\sigma_b = 20°$; step 4: $\sigma_a = 15°$, $\sigma_b = 30°$). (C) Drawing of HOMO and LUMO frontier orbitals obtained in step 4.

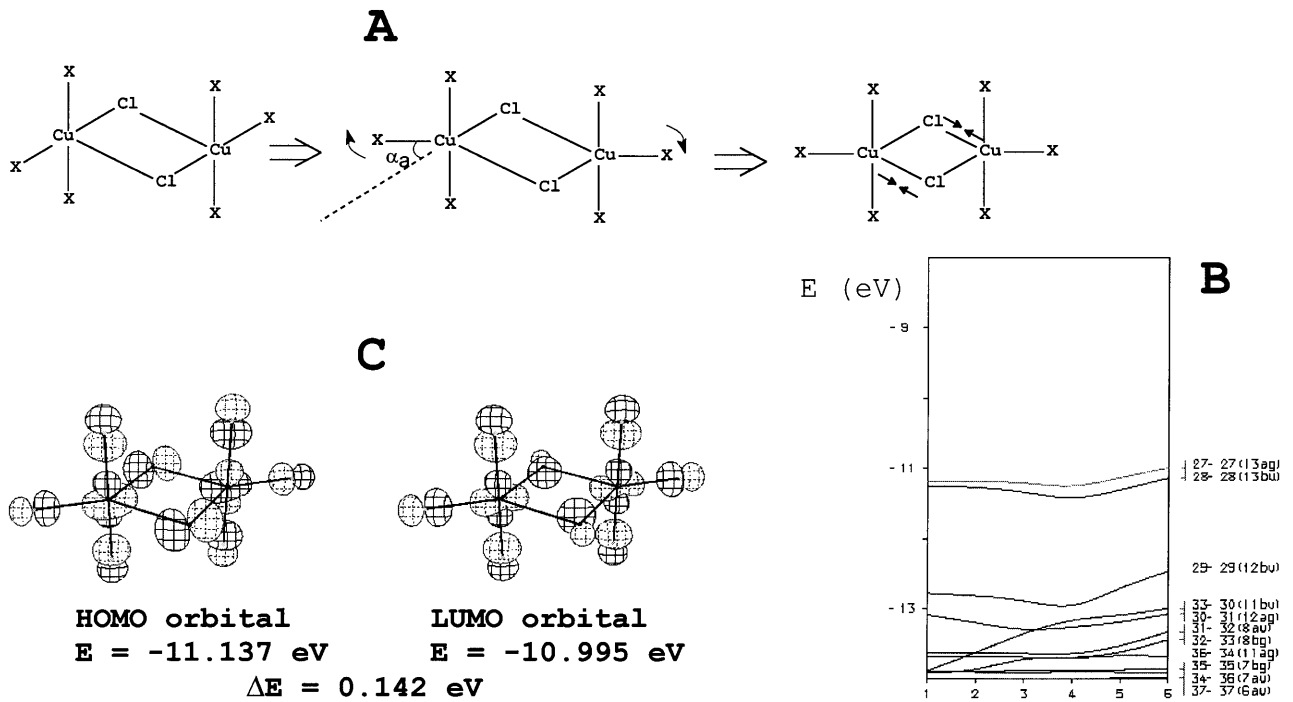


Fig. 3. Distortion from the parallel bases ideal model I. (A) Schematic diagram showing the applied distortion from sqp to tbp through a modification of the indicated bond angles and distances. (B) Walsh diagram showing the energy as function of angle (step 2–4) and bond (step 5–6) variations (step 1: initial idealized parallel bases; step 2, 3 and 4, $\alpha_a = 15$, 30 and 45°, respectively; step 4, 5 and 6 Cu–Cl bond distance 2.7, 2.5 and 2.3 respectively). (C) Drawing of HOMO and LUMO frontier orbitals obtained in step 6.

try for the Cu metal center. As in the previous case, the d_{Cu} metal orbitals involved change from type to, and some overlap between each bridging Cl and both Cu metal centers is observed. In sharp contrast with the previous case, an important increase of the gap takes place here. As shown in Fig. 3(B), this is mainly due to the angular variation (step 2–4) since upon decreasing bond distances (step 5 and 6) both

frontier orbitals increase in energy, but in similar magnitudes.

The second distortion described consisted, first, on the modification of bond angles for terminal ligands, reaching 120° (see Fig. 4, steps 2–3), and then increasing Cu–Cl bond distances (steps 5–6). The final step of this distorsion was a tbp type of geometry, frequently observed in real cases. The angular alteration produced a strong increase on the gap, which was then progressively decreased as the distances were elongated. Nevertheless, the final geometry still possesses a much higher gap than the initial. Again, the d_{Cu} metal orbitals involved change from $d_{x^2-y^2}$ type to d_{z^2}, and an effective overlap is observed between the two Cu metal centers through both the bridging chlorines.

It is worth mentioning that in the present case, the two distortions described produce a substantial increase in the energy gap with regard to the ideal model.

3.2.3. Perpendicular bases

The first distortion studied in this case involved the variation of the Cu–Cl–Cu bond angle for the apical bridging chloro ligand, maintaining the rest of the structural parameters constant except, obviously, the Cu–Cl(apical) bond distance. Upon applying this variation the gap remains constant, in agreement with the fact that the orbitals belonging to this ligand do not participate in the frontier orbitals (see Fig. 1(C)).

A second variation consisted on the same type of distortion, but now applied to the Cu–Cl(basal) bond angle (see Fig. 5). In this case, a direct relationship between the bond angle and the energy gap was found. That is, as the angle decreases (from 94.18 to 86.10), the energy gap increases, nearly linearly, from 0.045 to 0.140 eV (see Walsh diagram in Fig. 5(B)).

A third distortion consisting on synchronized variation of both apical and basal Cu–Cl–Cu bond angles gave the same results as in the previous case, as expected.

3.3. Magneto-structural correlations

Structural and magnetic data for a series of dinuclear dichlorobridged copper complexes are presented in Table 1. As can be observed, either ferromagnetic or antiferromagnetic coupling can be found for real compounds. Those of PAR type of geometry present, in general, smaller values of $\Delta E_{S\text{-}T}$ than the coplanar bases geometry dimers.

Two different type of correlations between structure and magnetic properties for dichlorobridged copper dimers can be found in the literature. One of them relates the magnetic interaction to α/R (Fig. 6(A)) [51], where α represents the Cu–Cl–Cu angle, and the second one finds a dependence of $\Delta E_{S\text{-}T}$ on the angle α (Fig. 6(B)) [52]. In both cases, it can be noticed that the majority of complexes are situated along two different lines. Therefore, there are no simple structural parameters that can correlate structure and magnetic properties. A closer examination of the graphs reveals that complexes with the same type of geometry are gathered

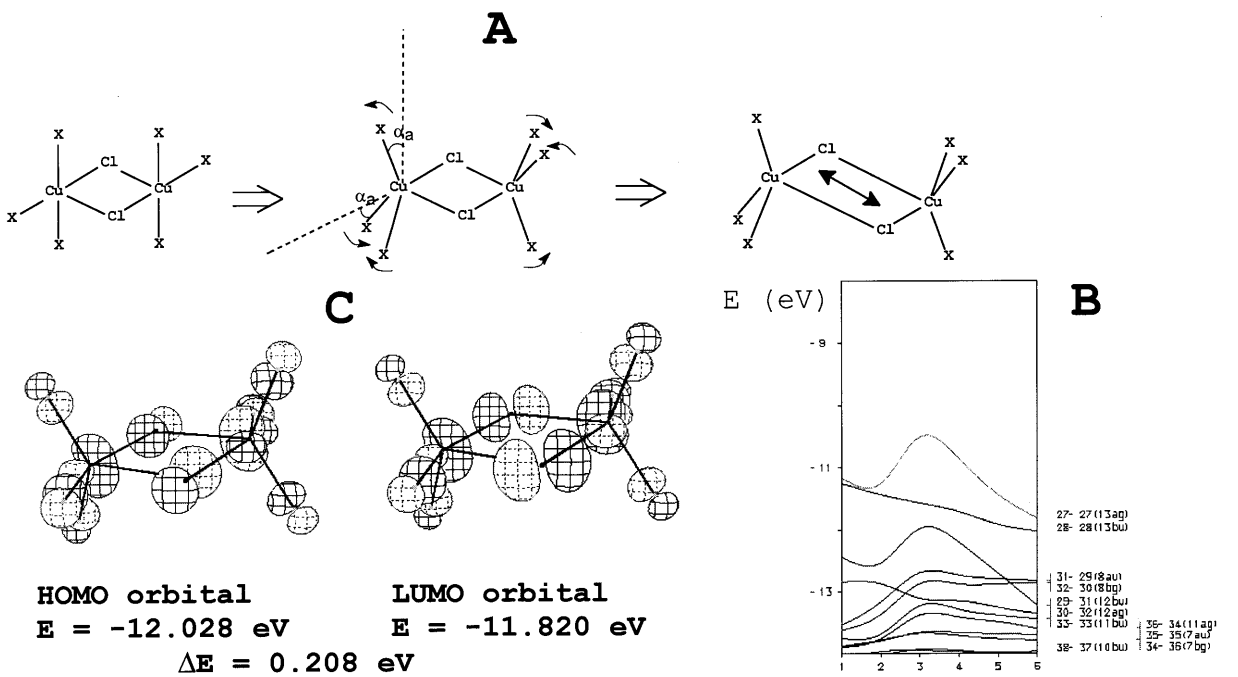


Fig. 4. Distortion from the parallel bases ideal model II. (A) Schematic diagram showing the applied distortion from sqp through a modification of the indicated bond angles and distances. (B) Walsh diagram showing the energy as function of angle (step 2–3) and bond (step 4–6) variations (step 1: initial idealized parallel bases; step 2 and 3, $\alpha_a = 15$ and 30°, respectively; step 3, 4, 5 and 6 Cu–Cl bond distance 2.51, 2.60, 2,8 and 3.04, respectively). (C) Drawing of HOMO and LUMO frontier orbitals obtained in step 6.

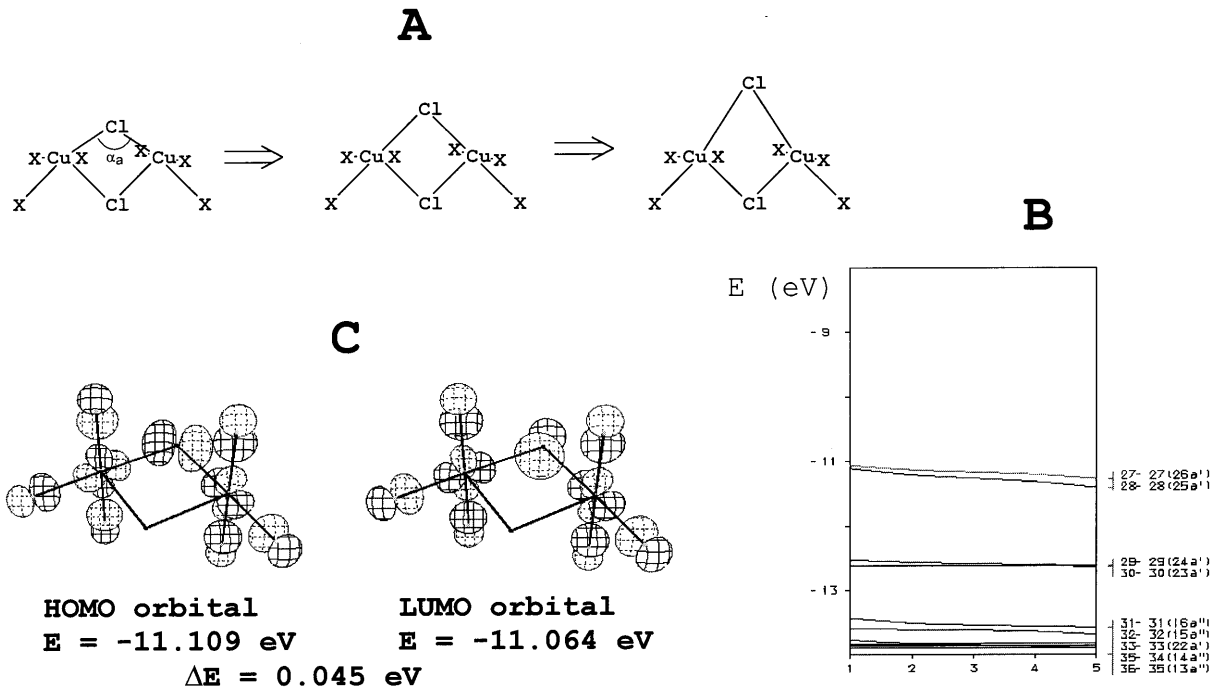


Fig. 5. Distortion from the perpendicular bases ideal model. (A) Schematic diagram showing the applied distortion through a modification of the indicated bond angle. (B) Walsh diagram showing the energy as function of the α_a angle (step 3: initial idealized perpendicular bases; step 1, 2, 4 and 5, $\alpha_a = 94.18$, 91.47, 88.56, and 86.10°, respectively). (C) Drawing of HOMO and LUMO frontier orbitals obtained in step 1.

close to straight lines, and that complex $[Cu_2(dpt)_2Cl_2]Cl_2$ (**34**) [25], which is the only one with perpendicular bases arrangement, is not placed close to any of the previous lines. The line that fits the magnetic behavior of complexes with a coplanar bases type of geometry (graph in Fig. 6(A)) has a slope of -95.54 $cm^{-1}/(°/Å)$ and an intercept at 41.56°/Å. In the graph in Fig. 6(B), the corresponding straight line has a slope of -48.65 $cm^{-1}/°$ and the intercept at 95.1°.

For this geometry, the modification of the Cu–Cl–Cu bond angle, either above or below 90°, produces a significant increment of the gap (see Section 3.2.1). Since all complexes reported to date, and belonging to this type of symmetry, have Cu–Cl–Cu bond angles higher than 90°, it follows that the higher the Cu–Cl–Cu bond angle the more antiferromagnetic character, which is actually what is found experimentally (see Fig. 6(B)) [52].

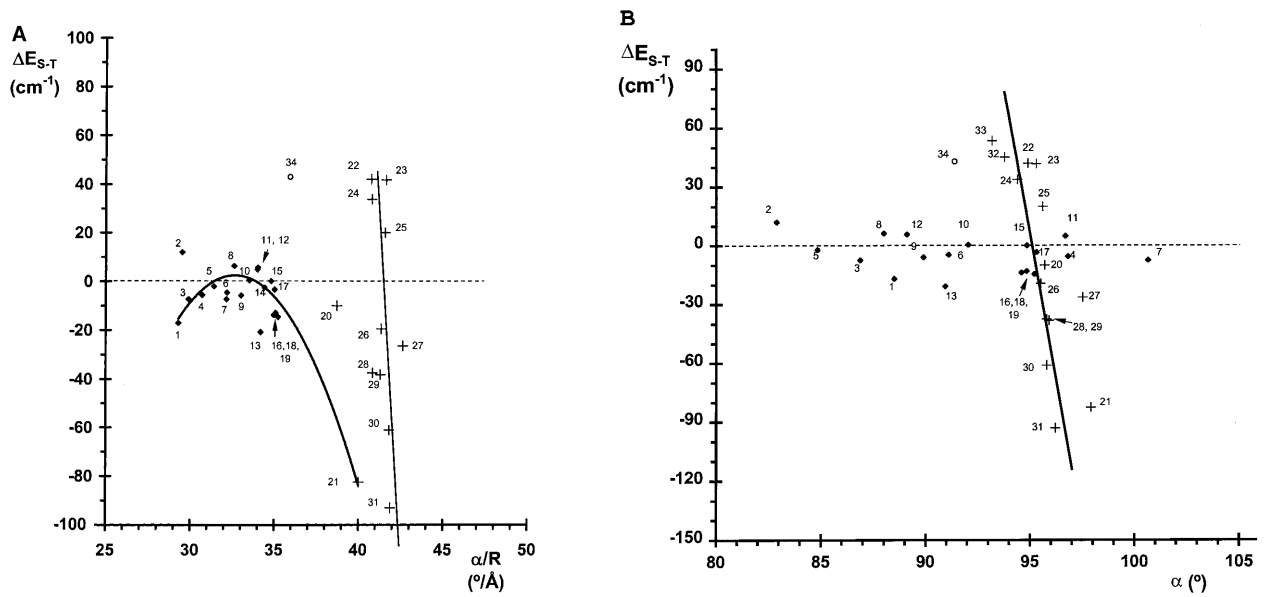


Fig. 6. Magneto-structural correlations: (A) $\Delta E_{S\text{-}T}$ (cm^{-1}) versus α/R (°/Å) and (B) $\Delta E_{S\text{-}T}$ (cm^{-1}) versus α (°) for $Cu(\mu\text{-}Cl)_2Cu$ dimers.

In sharp contrast, for this arrangement, a change of the local copper geometry from sqp by tbp practically does not change the gap. As a consequence of this, complexes **21**, **22**, **23**, **25** and **27**, bearing coplanar bases type of geometry, deviate from the established linearity (see Fig. 6(B)) basically due to the type of distortion depicted in Fig. 2(A), which involves a deviation, from their original position, of the apical ligand (with a σ_a angle) and of one of the terminal basal ligands (with a σ_b angle), leading to a tbp type of geometry around each copper atom. The complexes undergoing this type of distortion show an enhancement of the forecasted ferromagnetic character, then being placed on the right side of the straight line in Fig. 6(B). This is in agreement with the overlap theory proposed by Khan [54,55] in which this type of distortion is responsible for the increase of the effective Cu–Cl–Cu orbital overlap (the apical ligands also contribute to the HOMO and LUMO orbitals, see Fig. 2(B)) and, as a consequence, of the ferromagnetic contribution to the coupling constant *J*.

EH calculations for the ideal parallel bases type of geometry (Fig. 1(B)) show that the magnetic interaction between the copper metal centers will take place mainly through a π* type of interaction between the Cu $d_{x^2-y^2}$ and the apical p_{Cl} orbitals. Therefore in this geometry very small magnetic coupling constants (*J*) are expected which again is consistent with the experimental values listed in Table 1. What is interesting in this case, is that small geometric deviations produce large gaps as shown in Fig. 3 and Fig. 4. As a consequence of those two effects, the complexes adopting this type of symmetry are randomly scattered close to the *x* axis. Complex **21** [53], was originally assigned as forming part of the correlation followed by the compounds marked with rhombus in Fig. 6(A) [51].The fact that this complex in both graphs (Fig. 6(A and B)) is aligned close to the complexes with the coplanar type of geometry demands a reexamination of its geometrical classification. Indeed, a careful inspection of its structural parameters combined with its magnetic properties clearly shows that it is much better defined as having a coplanar bases type of geometry with a slight distortion of the local Cu geometry towards tpb. This result invalidates the empirical magnetostructural correlation proposed early by Hatfield and coworkers [51]. It is also worth mentioning that complexes **1**, **13**, **16**, **18** and **19,** which also belong to the parallel bases type of geometry, are the ones situated farther from the *x*-axis. This is due to the presence of other coordinating atoms than N, whose overall effect is an increase of the antiferromagnetic character.

Up to now there is only one fully characterized complex that presents the perpendicular bases type of geometrical arrangement [25]. For this complex, as mentioned in a previous section, only orbitals of the basal Cl bridging ligand participate in frontier orbitals. Thus from a magnetic point of view the system can be described as having only one bridging ligand. However the apical Cl has a key role in overcoming the steric hindrance leading to a $Cu–Cl_{(basal)}–Cu$ bond angle of only 91.4°. For a monobridged core the Cu–Cl–Cu bond angle would be much higher due to steric repulsions and therefore this would substantially change magnetic properties. As a result of this low angle, the overlap between $d_{Cu} - p_{Cl(basal)} - d_{Cu}$ is very similar for both frontier orbitals thus yielding relatively close energies. This similarity of energies for the HOMO and LUMO orbitals is in turn consistent with the experimental ferromagnetic behavior displayed by the complex.

In contrast with the coplanar bases type of symmetry, here the decrease of the $Cu–Cl_{(basal)}–Cu$ angle from 94.18 to 86.10° produces a nearly linear increase of the gap. Therefore if more complexes existed with this type of symmetry, this theoretical analysis would predict a very good magneto-structural correlation with the $Cu–Cl_{(basal)}–Cu$ angle.

As a summary, complexes bearing the $Cu(\mu\text{-}Cl)_2Cu$ core need to be classified in terms of their relative arrangement of square pyramids into coplanar, parallel and perpendicular bases. EH calculations indicate that in each case a completely different type of orbitals is involved in their respective frontier orbitals. Distortions from ideal models provides understanding of the different structural parameters that influence the energy gap between frontier orbitals and therefore allows to forecast the behavior of their magnetic properties.

Acknowledgements

This research has been supported by DGICYT of Spain through grants PB96-0467 and PB96-0163. CIRIT of Catalunya is also gratefully acknowledged for an aid SGR-3102-UG-01 and for the allocation of a FI doctoral grant to M.R.

References

[1] R.L. Carlin, Magnetochemistry, Springer–Verlag, Berlin, 1986.
[2] J. Reedijk, Bioinorganic Catalysis, Marcel Dekker, New York, 1993.
[3] E.I. Salomon, D.E. Wilcox, in: D. Gatteschi, O. Kahn, R.D. Willett (Eds.), Magneto-structural correlations in exchange coupled systems. In: NATO Advanced Study Institute Series, vol. C140, Reidel, Dordrecht, The Netherlands, 1984.
[4] E. Dagotto, T.M. Rice, Science 271 (1996) 618.
[5] D.N. Hendrickson, in: R.D. Willett, D. Gatteschi, O. Kahn (Eds.), Magneto-Structural Correlations in Exchange Coupled Systems, Reidel, Dordrecht, The Netherlands, 1985, p. 523.
[6] C.J. O'Connor, Prog. Inorg. Chem. 29 (1982) 203.
[7] R.E. Coffman, G.R. Buettner, J. Phys. Chem. 83 (1979) 2387.

[8] L.C. Francesconi, D.R. Corbin, A.W. Clauss, D.N. Hendrickson, G.D. Stucky, Inorg. Chem. 20 (1981) 2059.
[9] B. Chiari, W.E. Hatfield, O. Piovesana, T. Tarantelli, L.W. ter Haar, P.F. Zanazzi, Inorg. Chem. 22 (1983) 1468.
[10] B. Chiari, O. Piovesana, T. Tarantelli, P.F. Zanazzi, Inorg. Chem. 23 (1984) 2542.
[11] P.J. Hay, J.C. Thibeault, R. Hoffmann, J. Am. Chem. Soc. 97 (1975) 4884.
[12] V.H. Crawford, H.W. Richardson, J.R. Wasson, D.J. Hodgson, W.E. Hatfield, Inorg. Chem. 15 (1976) 2107.
[13] T.P. Mitchell, W.H. Bernard, J.R. Wasson, Acta Crystallogr., Sect. B 26 (1970) 2096.
[14] D.Y. Jeter, D.L. Lewis, J.C. Hempel, D.J. Hodgson, W.E. Hatfield, Inorg. Chem. 11 (1972) 1958.
[15] D.L. Lewis, W.E. Hatfield, D.J. Hodgson, Inorg. Chem. 11 (1972) 2216.
[16] D.L. Lewis, K.T. McGregor, W.E. Hatfield, D.J. Hodgson, Inorg. Chem. 13 (1974) 1013.
[17] E.D. Estes, W.E. Hatfield, D.J. Hodgson, Inorg. Chem. 13 (1974) 1654.
[18] D.J. Hodgson, Prog. Inorg. Chem. 19 (1975) 173.
[19] K.T. McGregor, N.T. Watkins, D.L. Lewis, D.J. Hodgson, W.E. Hatfield, Inorg. Nucl. Chem. Lett. 9 (1973) 423.
[20] J.A. Barnes, W.E. Hatfield, D.J. Hodgson, Chem. Commun. (1970) 1593.
[21] A.T. Casey, B.F. Hoskins, F.D. Whillans, Chem. Commun. (1970) 904.
[22] A. Bencini, D. Gatteschi, Inorg. Chim. Acta 31 (1978) 11.
[23] R.M. Countryman, W.T. Robinson, E. Sinn, Inorg. Chem. 13 (1974) 2013.
[24] M.F. Charlot, O. Kahn, S. Jeannin, Y. Jeannin, Inorg. Chem. 19 (1980) 1410.
[25] M. Rodríguez, A. Llobet, M. Corbella, J. Reibenspies, A.E. Martell, Inorg. Chem. 38 (1999) 2328.
[26] C. Mealli, D.M. Proserpio, J. Chem. Edu. 67 (1990) 399.
[27] D.D. Swank, G.F. Needham, R.D. Willett, Inorg. Chem. 18 (1979) 761.
[28] E. Kwiatkowski, M. Kwiatkowski, A. Olechnowicz, J. Mrozinski, D.M. Ho, E. Deutsch, Inorg. Chim. Acta 158 (1989) 37.
[29] W.E. Marsh, W.E. Hatfield, D.J. Hodgson, Inorg. Chem. 21 (1982) 2679.
[30] E.D. Estes, W.E. Estes, W.E. Hatfield, D.J. Hodgson, Inorg. Chem. 14 (1975) 106.
[31] D.W. Phelps, W.H. Goodman, D.J. Hodgson, Inorg. Chem. 15 (1976) 2266.
[32] S.J. Brown, X. Tao, T.A. Wark, D.W. Stephan, P.K. Mascharak, Inorg. Chem. 27 (1988) 1581.
[33] C.R. Lucas, S. Liu, L.K. Thompson, Inorg. Chem. 29 (1990) 85.
[34] M. Megnamisi-Bélombé, M.A. Novotny, Inorg. Chem. 19 (1980) 2470.
[35] T. Rojo, M.I. Arriortua, J. Ruiz, J. Darriet, G. Villeneuve, D. Beltran-Porter, J. Chem. Soc. Dalton Trans. (1987) 285.
[36] S.K. Hoffmann, D.K. Towle, W.E. Hatfield, K. Wieghardt, P. Chaudhuri, J. Weiss, Mol. Cryst. Liq. Cryst. 107 (1984) 161.
[37] C.J. O'Connor, Inorg. Chim. Acta 127 (1987) L29.
[38] A. Tosik, W. Maniukievicz, M. Bukowska-Strzyzewska, J. Mrozinski, M.P. Sigalas, C.A. Tsipis, Inorg. Chim. Acta 190 (1991) 193.
[39] S.K. Hoffmann, D.J. Hodgson, W.E. Hatfield, Inorg. Chem. 24 (1985) 1194.
[40] E.G. Bakalbassis, J. Mrozinski, S.P. Perlepes, N. Hadjiliadis, F. Lianza, A. Albinati, Polyhedron 13 (1994) 3209.
[41] J.T. Blanchette, R.D. Willett, Inorg. Chem. 27 (1988) 843.
[42] S. O'Brien, R.M. Gaura, C.P. Landee, B.L. Ramakhrishna, R.D. Willett, Inorg. Chim. Acta 141 (1988) 83.
[43] C. Chow, R.D. Willett, B.C. Gerstein, Inorg. Chem. 14 (1975) 205.
[44] S.A. Roberts, D.R. Bloomquist, R.D. Willett, H.W. Dodgen, J. Am. Chem. Soc. 103 (1981) 2103.
[45] A. Colombo, L. Menabue, A. Motori, G.C. Pellacani, W. Porzio, F. Sandrolini, R.D. Willett, Inorg. Chem. 24 (1985) 2900.
[46] M. Inoue, M. Kishita, M. Kubo, Inorg. Chem. 6 (1967) 900.
[47] B. Scott, U. Geiser, R.D. Willett, B. Patyal, C.P. Landee, R.E. Greeney, T. Manfredini, G.C. Pellacani, A.B. Corradi, L.P. Battaglia, Inorg. Chem. 27 (1988) 2454.
[48] M. Honda, C. Katayama, J. Tanaka, M. Tanaka, Acta Crystallogr., Sect. C 41 (1985) 197.
[49] R.D. Willett, C. Chow, Acta Crystallogr., Sect. B 30 (1974) 207.
[50] M. Textor, E. Dubler, R. Oswald, Inorg. Chem. 13 (1974) 1361.
[51] W.E. Marsh, K.C. Patel, W.E. Hatfield, D.J. Hodgson, Inorg. Chem. 22 (1983) 511.
[52] S.G.N. Roundhill, D.M. Roundhill, D.R. Bloomquist, C. Landee, R.D. Willett, D.M. Dooley, H.B. Gray, Inorg. Chem. 18 (1979) 831.
[53] J.A. Carrabine, M. Sundaralingam, J. Am. Chem. Soc. 92 (1970) 369.
[54] O. Kahn, Angew. Chem., Int. Ed. Engl. 24 (1985) 834.
[55] O. Kahn, Comm. Inorg. Chem. 3 (1984) 105.

PERGAMON

www.elsevier.nl/locate/poly

Polyhedron 19 (2000) 2493–2500

POLYHEDRON

Activity coefficients of 3:3 electrolytes in aqueous solutions

Francesco Malatesta *, Sara Trombella, Ambrogio Giacomelli, Massimo Onor

Dipartimento di Chimica e Chimica Industriale, Università di Pisa, Via Risorgimento 35, 56126 Pisa, Italy

Dedicated to the memory of Professor Sergio Cabani.

Abstract

Activity coefficients of 3:3 electrolytes have not been liable to determination until 1994, when one of the authors devised a new type potentiometric cell able to trace $La[Fe(CN)_6]$ down to about 5×10^{-6} mol kg^{-1}. $La[Co(CN)_6]$, $[Co(en)_3][Co(CN)_6]$, and $[Co(en)_3][Fe(CN)_6]$, are now studied by the same method. Like $La[Fe(CN)_6]$, these electrolytes display in the dilute regions large negative deviations from the limiting slope instead of the moderate positive deviations predicted by the Debye–Hückel theory. Although the negative deviations can be easily interpreted in terms of only a partial dissociation, one should not conclude that the 3:3 salts are only sparingly dissociated. Theoretical calculations are presented, showing how long-range interactions, in a population of non associated $+3$ and -3 charged spheres, are able to produce effects that simulate the behaviour of a weak electrolyte. Preliminary information is provided of an unexplored method, here devised, to determine the mean activity coefficients in mixed electrolyte solutions. © 2000 Elsevier Science B.V. All rights reserved.

Keywords: 3:3 Electrolytes; Activity coefficients; Electrolytic solutions; High-charge salts; High valency electrolytes; Mixed electrolytes

1. Introduction

About 1 century since Lewis' concept of the activity coefficient [1] and 76 years since the Debye–Hückel theory [2], experimental and theoretical information regarding 3:3 electrolytes is still lacking. Only in the last few years have potentiometric cells suitable for such salts and for the high dilution levels required become available [3–11], and only $La[Fe(CN)_6]$ has been studied appropriately [6]. Owing to the paucity of experimental data, essentially all restricted to $La[Fe(CN)_6]$, theoretical treatments have not been able to reach ultimate conclusions either. For instance, the conductivity data for $La[Fe(CN)_6]$ have long been interpreted as evidence of a significant association of the electrolyte, comparable to formic acid [12]; conversely, the activity coefficients recently determined with the method of the liquid membrane cells [6] have proved identical to those expected for a theoretical model of charged spheres free from any association, the so-called 'primitive' model [6,7]. (The only partial dissociation of $La[Fe(CN)_6]$ evidenced from the conductivity data relies on a theoretical framework that is incorrect for high-charge electrolytes).

As no general value can be obtained from $La[Fe(CN)_6]$ alone, three more salts of the same 3:3 type, lanthanum hexacyanocobaltate(III), tris(ethylenediamine)cobalt(III) hexacyanocobaltate(III), and tris(ethylenediamine)cobalt(III) hexacyanoferrate(III) are now examined. These salts are sparingly soluble, e.g. $[Co(en)_3][Fe(CN)_6]$ does not reach 5×10^{-4} mol kg^{-1}, but this does not represent a problem, as the liquid membrane cells in many electrolytes are able to provide stable and reproducible emf values down to 1×10^{-5} mol kg^{-1} and less. Moreover, a later reported thermodynamic relationship (Eq. (3)), allows us to derive the values of the activity coefficients of a 3:3 electrolyte from the corresponding relative activity coefficients, regardless of the ability of directly performing extrapolation to zero for the 3:3 electrolyte.

* Corresponding author. Fax: +39-050-918-260.
E-mail address: franco@dcci.unipi.it (F. Malatesta).

0277-5387/00/$ - see front matter © 2000 Elsevier Science B.V. All rights reserved.
PII: S0277-5387(00)00549-0

2. Experimental

2.1. Apparatus

The fundamentals of the method, cell design, and instrumentation, are the same as in the previous papers [3–9]. The cells used in the present study, are

$$Ag,\ AgCl\ |\ KCl(m_0)\ |\ K^+\ |\ K_3X(m_1)\ |\ X^{3-}\ |\ AX(test;\ m)\ |\ A^{3+}\ |\ ACl_3(m_2)\ |\ AgCl,\ Ag \quad \text{(cell 1)}$$

for the 3:3 salts (AX), and

$$Ag,\ AgCl\ |\ KCl(m_3)\ |\ Cl^-\ |\ ACl_3(test;\ m)\ |\ A^{3+}\ |\ ACl_3(m_2)\ |\ AgCl,\ Ag \quad \text{(cell 2)}$$

$$Ag,\ AgCl\ |\ KCl(m_0)\ |\ K^+\ |\ K_3X(m_1)\ |\ X^{3-}\ |\ K_3X\ (test;\ m)\ |\ K^+\ |\ KCl(m_2)\ |\ AgCl,\ Ag \quad \text{(cell 3)}$$

$$Ag,\ AgCl\ |\ KCl(m_3)\ |\ Cl^-\ |\ KCl(test;\ m)\ |\ K^+\ |\ KCl(m_2)\ |\ AgCl,\ Ag \quad \text{(cell 4)}$$

for the auxiliary salts ACl_3, K_3X, and KCl. Cells of very similar structure have been described elsewhere, including the recent assemblage details [6,9]. Briefly, sections $|K^+|$, $|X^{3-}|$, etc. indicate the organic phases (the 'membranes') able to interchange the corresponding ions (but no ions of opposite sign) with the neighbouring aqueous solutions. $|K^+|$ and $|A^{3+}|$ are composed of the salts KTFPB and $A(TFPB)_3$ dissolved in 2-nitrophenyl octyl ether, $|X^{3-}|$ of the liquid salts $(TDA)_3Fe(CN)_6$ or $(TDA)_3[Co(CN)_6]$, without solvent, and $|Cl^-|$ of TDACl dissolved in 3,4-dichlorotoluene. $TFPB^-$ stands for *tetrakis*[3,5-bis(trifluoromethyl)-phenyl] borate anion, $(C_8H_3F_6)_4B^-$, and TDA^+ for tetradodecylammonium cation, $(C_{12}H_{23})_4N^+$. The two chains of phases (Ag, AgCl, the aqueous solutions, and the membranes) lying on the left and on the right of the test solution (test; m) are assembled in two PTFE hallow cylinders, to form two composite electrodes, for the anion (shown in Fig. 1) and the cation. These electrodes are dipped in a larger vessel, also made of PTFE, containing the test solution (approximately 15 cm^3). A small magnetic bar (approximately 5×2 mm, usually at a rotation rate of approximately 1–3 rps), ensures moderate stirring conditions. The entire assembly is contained in an air bath thermostat at 25.00 ± 0.02°C. In order to monitor the temperature a platinum resistance thermometer (± 0.001 K) is used.

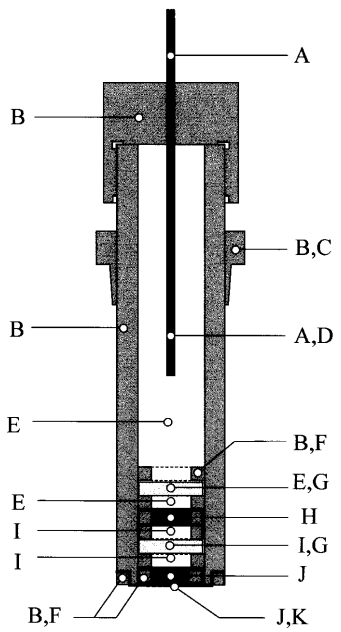


Fig. 1. Diagram of the anion responsive electrode: A = silver; B = PTFE; C = sliding ring; D = silver chloride; E = KCl solution (m_0); F = pressing ring; G = fritted glass; H = $|K^+|$, the potassium-exchange liquid membrane (17% KTFPB in NPOE); I = K_3X solution (m_1); J = $|X^{3-}|$, the anion-exchange liquid membrane, $(TDA)_3[Co(CN)_6]$ or $(TDA)_3[Fe(CN)_6]$ as appropriate; K = one of the four sheets of porous PTFE which bracket the two liquid membranes.

Emf measurements were performed using a Digital Adret Electronique 103A DC-current and voltage standard as supplier for potentials (± 0.001 mV) and a Keithley 614 electrometer (input impedance $> 10^{14}$ Ω) as null point (± 0.01 mV) detector. The measurements take ca. 90 min per solution, 60 of which as waiting time, and 30 for the emf readings — one every five min, whose average values and standard deviations are reported in the tables of the experimental results.

2.2. Reagents

Preparation and purification of the membrane salts KTFPB, $[Co(en)_3](TFPB)_3$, $La(TFPB)_3$, TDACl, $(TDA)_3[Fe(CN)_6]$, and $(TDA)_3[Co(CN)_6]$, are described elsewhere [3–5,11]. The salts KCl, $LaCl_3 \cdot nH_2O$ ($n \cong 7$), $[Co(en)_3]Cl_3$, $K_3[Fe(CN)_6]$, and $K_3[Co(CN)_6]$, were all derived from stocks of purified salts used in previous works [3–6,11,13]. $La[Co(CN)_6]$, $[Co(en)_3][Co(CN)_6]$, and $[Co(en)_3][Fe(CN)_6]$ were obtained by metathesis from $LaCl_3$ or $[Co(en)_3]Cl_3$, and $K_3[Co(CN)_6]$ or $K_3[Fe(CN)_6]$, as appropriate. While $La[Co(CN)_6]$ and $[Co(en)_3][Co(CN)_6]$ were of good quality, crude $[Co(en)_3][Fe(CN)_6]$ contained considerable amounts of potassium ions, and required leaching, and prolonged digestion in hot water, and later in cold water, under stirring conditions (some soluble unidentified red compounds were formed during digestion in hot water). The resulting salt was free of potassium, and the UV–Vis spectra of its solutions (λ range, 200–550 nm) coincided with the sum of $K_3[Fe(CN)_6]$ and $[Co(en)_3]Cl_3$.

$La[Co(CN)_6]$, $[Co(en)_3][Co(CN)_6]$, and $[Co(en)_3][Fe(CN)_6]$ were analyzed for water content by acidimetric titration, via cation exchange (Dowex $50w \times 8$ resin in the hydrogen form) dropping the resulting acid on a weighed excess of Na_2CO_3, then back-titrating (to the potentiometric end-point in the

case of $H_3[Fe(CN)_6]$) with standard HCl. The same method was also applied to lanthanum chloride. The resulting molecular weights were, respectively, 425.9 ± 1.9 (theoretical, 426.00 for $La[Co(CN)_6]\cdot 4H_2O$), 473.2 ± 1.5 (theoretical, 472.29 for $[Co(en)_3][Co(CN)_6]\cdot H_2O$), and 481.3 ± 3.5 (intermediary between 469.20, theoretical for $[Co(en)_3][Fe(CN)_6]\cdot H_2O$, and 487.21, theoretical for $[Co(en)_3][Fe(CN)_6]\cdot 2H_2O$; 1.67 ± 0.02 mol of water per mol of salt on average). For verification, $[Co(en)_3][Co(CN)_6]$ and $[Co(en)_3][Fe(CN)_6]$ were oven heated at reduced pressure (10–20 mbar). Significant weight losses were observed between 50 and 80°C, and were consistent with 1 mol of water (1.08 ± 0.12) per mol of salt for $[Co(en)_3][Co(CN)_6]$, and 1.6–1.7 (1.63 ± 0.09) for $[Co(en)_3][Fe(CN)_6]$. For $La[Co(CN)_6]$, the check analyses were performed by precipitation as oxalate and determination as La_2O_3; once again, the results were consistent with 4 (3.8 ± 0.3) mol of water per mol of salt.

All solutions were prepared by weight, from the salts or the corresponding standardized solutions as appropriate.

2.3. Principles and procedures

In the absence of interfering amounts of foreign ions able to enter the membranes, the emf values of cells such as cells 1–4 obey the relationship (Eq. (1)) [3,10]:

$$E = E^* + [(v_+ + v_-)/(z_+ v_+ F)]RT \ln m\gamma_{\pm\,\mathrm{dir}} \quad (1)$$

where z_+ is the charge of the cation, v_+ and v_- the number of cations and anions in the electrolyte, and (Eq. (2)) [10]:

$$\ln \gamma_{\pm\,\mathrm{dir}} = \ln \gamma_\pm + [w/(v_+ + v_-)] \ln a_1 \quad (2)$$

where a_1 is the activity of water in the test solutions and w the number of water molecules that follow one 'molecule' of the electrolyte when its ions leave the test solution and enter the neighboring membranes. In this respect, La^{3+} carries 12 molecules of water when entering the membrane [5]. $[Co(en)_3]^{3+}$, $[Co(CN)_6]^{3-}$ and $[Fe(CN)_6]^{3-}$ are, expectedly, nonhydrated. The difference between $\ln \gamma_\pm$ and $\ln \gamma_{\pm\,\mathrm{dir}}$ can generally be neglected if $m < 0.01$ mol kg^{-1}. E^* depends on the choice for m_0, m_1, etc. inside the invariant sections of the cell (the 'electrodes'), and also includes the numeric constant allowing for the fact that we use m instead of $m_\pm$ in Eq. (1).

Like $E°$ for classic cells without transport, E^* is generally identified by an extrapolation to ionic strength zero, with the aid of a 'guideline' like the Debye–Hückel theory (DHT), Bjerrum's ion-pair theory, etc. No problems are generally encountered for 1:1, 1:2 and 1:3 electrolytes, as the different guidelines lead to the same extrapolation values, when applied to the very diluted solutions permitted by the liquid membrane cells. Unfortunately, the diluted solutions of the 2:2, 2:3, and 3:3 electrolytes deviate from the limiting slope in the 'wrong' (in terms of DHT) direction. Bjerrum's ion-pair theory, Mayer's theory, and the numerical accurate integration of the Poisson–Boltzmann equation (IPBE), which imply (like DHT) a single adjustable parameter a, predict these reverted deviations, and prove reliable for the 2:2 and 2:3 electrolytes [8,9,11,13]. However, for a 3:3 electrolyte, even starting from a dilution level beyond 10^{-5} mol kg^{-1}, the extrapolation process may be critical. Thus, a different method able to by-pass the extrapolation problem is used [5]. Cells 1–4 correspond to alternate ways of assembling the same set of four electrodes and four solutions, and a useful thermodynamic relationship (Eq. (3)) links their E^* values [5]:

$$E^*(AX) = E^*(ACl_3) + E^*(K_3X) - E^*(KCl) - RTF^{-1} \ln 9 \quad (3)$$

Eq. (3) makes it possible to calculate the unknown value E^* of the 3:3 salt as a combination of those of much easier determination, of two 1:3 and one 1:1 auxiliary salts. There is no need for any new extrapolation for ACl_3, K_3X, and KCl, as their activity coefficients are already known [3–6,11,14–17]. Thus, four emf measurements at a known concentration, for AX, ACl_3, K_3X and KCl, can suffice to obtain $E^*(AX)$. As the value of E^* is liable to change, the relevant information is more conveniently stored in the form of the value of the activity coefficient, $\gamma_{\pm\,\mathrm{ref}}$, of a reference solution.

3. Results and discussion

The activity coefficient values that Eq. (3) yields, are $\ln \gamma_{\pm\,\mathrm{ref}} = -1.241 \pm 0.015$ for 1.000×10^{-3} m $La[Co(CN)_6]$, -1.515 ± 0.014 for 4.048×10^{-4} m $[Co(en)_3][Co(CN)_6]$, and -1.301 ± 0.015 for 2.242×10^{-4} m $[Co(en)_3][Fe(CN)_6]$. In turn, these values rely on $\ln \gamma_{\pm\,\mathrm{ref}} = -0.242$ (± 0.004 estimated) for 1.000×10^{-3} m $LaCl_3$ [5,14], -0.345 ± 0.003 for 2.000×10^{-3} m $K_3[Co(CN)_6]$ [11,15], -0.257 (± 0.004 estimated) for 1.000×10^{-3} m $[Co(en)_3]Cl_3$ [4,16], -0.265 (± 0.004 estimated) for 1.000×10^{-3} m $K_3[Fe(CN)_6]$ [6], and -0.0357 ± 0.0003 for 1.000×10^{-3} m KCl [3,17]. The ranges of uncertainty of the 3:3 salts are those of the auxiliary salts, combined with the variance of $E^*(AX)$ (three to four sequential runs for cell 1 and cell 4 alternate to cell 2 and cell 3). Should some correction be needed by any of the component salts, let us consider that a shift $\Delta \ln \gamma_\pm$ for the 1:3 (1:1) salt shifts the 3:3 salt by two (three) times this quantity, in the same direction.

Table 1
$La[Co(CN)_6]$

Series	m	E	E_{ref}	$\ln \gamma_{\pm dir}$ [a]	$\ln \gamma_{\pm}$ [b]
1	1.000×10^{-3}	-19.50 ± 0.01		(-1.241)	-1.241 ± 0.015
1	7.204×10^{-4}	-23.10 ± 0.01	-19.58 ± 0.08	-1.118 ± 0.005	-1.118 ± 0.016
1	4.836×10^{-4}	-27.62 ± 0.03	-19.66 ± 0.08	-0.979 ± 0.005	-0.979 ± 0.016
1	3.285×10^{-4}	-32.03 ± 0.03	-19.75 ± 0.08	-0.844 ± 0.005	-0.844 ± 0.016
1	2.144×10^{-4}	-37.13 ± 0.01	-19.83 ± 0.08	-0.711 ± 0.005	-0.711 ± 0.016
1	1.000×10^{-3}	-19.91 ± 0.01			
2	1.000×10^{-3}	-19.88 ± 0.01			
2	1.448×10^{-4}	-42.01 ± 0.02	-19.94 ± 0.06	-0.597 ± 0.004	-0.597 ± 0.016
2	9.656×10^{-5}	-47.33 ± 0.02	-20.00 ± 0.06	-0.499 ± 0.004	-0.499 ± 0.015
2	6.493×10^{-5}	-52.67 ± 0.01	-20.06 ± 0.06	-0.410 ± 0.004	-0.410 ± 0.015
2	4.331×10^{-5}	-58.39 ± 0.05	-20.13 ± 0.06	-0.335 ± 0.005	-0.335 ± 0.016
2	2.933×10^{-5}	-63.90 ± 0.02	-20.19 ± 0.06	-0.263 ± 0.004	-0.263 ± 0.015
2	1.000×10^{-3}	-20.25 ± 0.02			
3	1.000×10^{-3}	-20.00 ± 0.01			
3	1.924×10^{-5}	-69.77 ± 0.02	-20.05 ± 0.05	-0.193 ± 0.003	-0.193 ± 0.015
3	1.295×10^{-5}	-75.81 ± 0.03	-20.09 ± 0.05	-0.147 ± 0.003	-0.147 ± 0.015
3	8.641×10^{-6}	-82.08 ± 0.02	-20.14 ± 0.05	-0.106 ± 0.003	-0.106 ± 0.015
3	5.835×10^{-6}	-88.07 ± 0.02	-20.18 ± 0.05	-0.060 ± 0.003	-0.060 ± 0.015
3	3.835×10^{-6}	-94.63 ± 0.02	-20.23 ± 0.05	-0.021 ± 0.003	-0.021 ± 0.015
3	1.000×10^{-3}	-20.27 ± 0.03			
4	1.000×10^{-3}	-19.71 ± 0.01			
4	2.216×10^{-2}	7.54 ± 0.03	-19.79 ± 0.08	-2.743 ± 0.005	-2.741 ± 0.016
4	1.503×10^{-2}	4.54 ± 0.02	-19.87 ± 0.08	-2.526 ± 0.005	-2.524 ± 0.016
4	1.019×10^{-2}	1.43 ± 0.02	-19.95 ± 0.08	-2.314 ± 0.005	-2.313 ± 0.016
4	6.843×10^{-3}	-1.98 ± 0.03	-20.04 ± 0.08	-2.109 ± 0.005	-2.109 ± 0.016
4	4.702×10^{-3}	-5.30 ± 0.02	-20.12 ± 0.08	-1.923 ± 0.005	-1.923 ± 0.016
4	1.000×10^{-3}	-20.20 ± 0.02			
5	1.000×10^{-3}	-20.00 ± 0.01			
5	3.209×10^{-3}	-8.74 ± 0.02	-20.07 ± 0.07	-1.745 ± 0.004	-1.745 ± 0.016
5	2.166×10^{-3}	-12.52 ± 0.03	-20.14 ± 0.07	-1.568 ± 0.004	-1.568 ± 0.016
5	1.479×10^{-3}	-16.32 ± 0.03	-20.22 ± 0.07	-1.404 ± 0.004	-1.404 ± 0.016
5	1.000×10^{-3}	-20.29 ± 0.01			
6	1.000×10^{-3}	-66.08 ± 0.03			
6	2.933×10^{-5}	-109.34 ± 0.04	-66.10 ± 0.02	-0.236 ± 0.003	-0.236 ± 0.015
6	1.448×10^{-4}	-88.13 ± 0.02	-66.10 ± 0.02	-0.593 ± 0.002	-0.593 ± 0.015
6	7.204×10^{-4}	-69.59 ± 0.01	-66.15 ± 0.02	-1.113 ± 0.001	-1.113 ± 0.015
6	3.209×10^{-3}	-54.72 ± 0.01	-66.17 ± 0.02	-1.738 ± 0.001	-1.738 ± 0.015
6	1.000×10^{-3}	-66.19 ± 0.01			

[a] The errors do not include the contribution of the reference point.
[b] The errors are inclusive of the uncertainty of the reference point.

Tables 1–3 report the experimental values for the different solutions of the 3:3 salts. The measurements are divided into different series, any of which starts, and terminates, in the reference solution. When reloading the cell, leaching effects occur at membrane surfaces, and may cause shifts, that summate along the series (relaxation is slow). To counterbalance the effect, the calculation of the relative activity coefficients, via Eq. (1), rely on E_{ref} values that are estimated by interpolation, between the extreme values of the series.

The trend of the activity coefficients (including $La[Fe(CN)_6]$ [6] for comparison) is shown in Fig. 2. There are no appreciable differences between $[Co(CN)_6]^{3-}$ and $[Fe(CN)_6]^{3-}$, but $[Co(en)_3]^{3+}$ differs very much from La^{3+}. The activity coefficients display the characteristic negative deviations from the limiting law (i.e. opposite in direction to predicted by DHT), typical of the high charge electrolytes, whose interpretation is often given in terms of ion association. The ion–ion cloud electrostatic interactions are also capable of causing the same effects. For 2:2, 2:3, and 3:3 electrolytes, DHT fails to reproduce the primitive model even in the sign of the second derivative of $\ln \gamma_{\pm}$ in the origin. Under these conditions, the behaviour of the primitive model can only be guessed from the predictions of other approximations of a higher level. The Mayer theory [18], and IPBE [19,20], are possible examples. Even Bjerrum's theory of ion pairs is to be considered as an approximate treatment of the primitive model, as the fictitious 'ion pair' is a short-cut to avoid the untraceable problem of the radial distribution functions in the closer neighbourhood of an ion, not an

Table 2
$[Co(en)_3][Co(CN)_6]$

Series	m	E	E_{ref}	$\ln \gamma_{\pm}$ [a]
1	4.209×10^{-4}	-33.30 ± 0.02		(-1.552 ± 0.014)
1	3.000×10^{-4}	-36.71 ± 0.01	-33.32 ± 0.02	-1.410 ± 0.015
1	2.230×10^{-4}	-39.78 ± 0.01	-33.34 ± 0.02	-1.293 ± 0.015
1	1.622×10^{-4}	-43.08 ± 0.01	-33.36 ± 0.02	-1.166 ± 0.015
1	1.114×10^{-4}	-47.09 ± 0.01	-33.38 ± 0.02	-1.024 ± 0.015
1	8.086×10^{-5}	-50.65 ± 0.02	-33.40 ± 0.02	-0.910 ± 0.016
1	4.209×10^{-4}	-33.41 ± 0.02		
2	4.209×10^{-4}	-33.07 ± 0.01		
2	5.519×10^{-5}	-54.81 ± 0.01	-33.08 ± 0.01	-0.789 ± 0.015
2	3.998×10^{-5}	-58.67 ± 0.01	-33.10 ± 0.01	-0.691 ± 0.015
2	2.599×10^{-5}	-64.06 ± 0.01	-33.11 ± 0.01	-0.574 ± 0.015
2	1.839×10^{-5}	-68.55 ± 0.01	-33.12 ± 0.01	-0.487 ± 0.015
2	1.273×10^{-5}	-73.24 ± 0.03	-33.13 ± 0.01	-0.395 ± 0.016
2	8.662×10^{-6}	-78.57 ± 0.03	-33.15 ± 0.01	-0.320 ± 0.016
2	6.013×10^{-6}	-83.29 ± 0.04	-33.16 ± 0.01	-0.231 ± 0.016
2	4.209×10^{-4}	-33.17 ± 0.01		
3	4.209×10^{-4}	-32.68 ± 0.01		
3	1.833×10^{-5}	-67.57 ± 0.05	-32.71 ± 0.03	-0.453 ± 0.017
3	3.998×10^{-5}	-58.30 ± 0.03	-32.73 ± 0.03	-0.691 ± 0.016
3	8.086×10^{-5}	-50.20 ± 0.01	-32.76 ± 0.03	-0.921 ± 0.016
3	1.632×10^{-4}	-42.43 ± 0.01	-32.79 ± 0.03	-1.168 ± 0.016
3	2.995×10^{-4}	-36.35 ± 0.01	-32.81 ± 0.03	-1.419 ± 0.016
3	4.209×10^{-4}	-32.84 ± 0.01		

[a] The range of uncertainty is inclusive of the uncertainty of the reference point.

Table 3
$[Co(en)_3][Fe(CN)_6]$

Series	m	E	E_{ref}	$\ln \gamma_{\pm}$ [a]
1	2.242×10^{-4}	-41.35 ± 0.06		(-1.301 ± 0.015)
1	2.989×10^{-4}	-38.39 ± 0.04	-41.39 ± 0.04	-1.413 ± 0.018
1	2.030×10^{-4}	-42.46 ± 0.03	-41.43 ± 0.04	-1.261 ± 0.018
1	1.681×10^{-4}	-44.53 ± 0.04	-41.48 ± 0.04	-1.191 ± 0.018
1	1.261×10^{-4}	-47.71 ± 0.03	-41.52 ± 0.04	-1.086 ± 0.018
1	9.453×10^{-5}	-50.98 ± 0.02	-41.56 ± 0.04	-0.987 ± 0.018
1	2.242×10^{-4}	-41.60 ± 0.04		
2	2.242×10^{-4}	-41.11 ± 0.05		
2	7.093×10^{-5}	-53.61 ± 0.09	-41.20 ± 0.09	-0.874 ± 0.022
2	5.318×10^{-5}	-57.11 ± 0.06	-41.29 ± 0.09	-0.785 ± 0.021
2	3.989×10^{-5}	-60.86 ± 0.05	-41.39 ± 0.09	-0.711 ± 0.021
2	2.992×10^{-5}	-64.62 ± 0.03	-41.48 ± 0.09	-0.638 ± 0.021
2	2.242×10^{-4}	-41.58 ± 0.01		
3	2.242×10^{-4}	-40.87 ± 0.06		
3	2.243×10^{-5}	-67.37 ± 0.08	-41.03 ± 0.08	-0.536 ± 0.022
3	1.682×10^{-5}	-71.34 ± 0.05	-41.11 ± 0.08	-0.475 ± 0.021
3	1.262×10^{-5}	-75.18 ± 0.05	-41.19 ± 0.08	-0.407 ± 0.021
3	1.262×10^{-5}	-75.68 ± 0.03	-41.19 ± 0.08	-0.436 ± 0.020
3	1.262×10^{-5}	-75.75 ± 0.02	-41.19 ± 0.08	-0.441 ± 0.020
3	2.242×10^{-4}	-41.28 ± 0.05		

[a] The range of uncertainty is inclusive of the uncertainty of the reference point.

additional chemical species [21]. All these treatments agree, qualitatively, on the occurrence of negative deviations in the dilute solutions of the high charge electrolytes.

From a quantitative point of view, the Mayer theory found unsatisfactory for $La[Fe(CN)_6]$ [3,7] for $m > 10^{-3}$ mol kg^{-1} (a consideration that extends to the practically identical $La[Co(CN)_6]$), is totally unfit for

$[Co(en)_3][Co(CN)_6]$ and $[Co(en)_3][Fe(CN)_6]$. Clearly, with these extreme salts the truncation of the cluster series [22] causes a much earlier failure than usual. Conversely, IPBE and the Bjerrum theory of the ion pair maintain an astounding ability to trace the experimental curves (Fig. 3). Except for the extreme dilution levels (where H^+, OH^-, and the ions released by the membranes cause increasing interference) the IPBE approximation, for a around 0.46 nm for $[Co(en)_3][Fe(CN)_6]$ and $[Co(en)_3][Co(CN)_6]$, and 0.66 nm for $La[Fe(CN)_6]$ and $La[Co(CN)_6]$, agrees with the activity coefficients of the actual salts, approximately within the experimental error. The same observations apply to Bjerrum's theory, excluding the slightly different values requested for a. Once allowance has been made for the ion-cloud electrostatic interactions, even the impressive negative deviations displayed by $[Co(en)_3][Fe(CN)_6]$ and $[Co(en)_3][Co(CN)_6]$ do not require any additional hypothesis such as ion association.

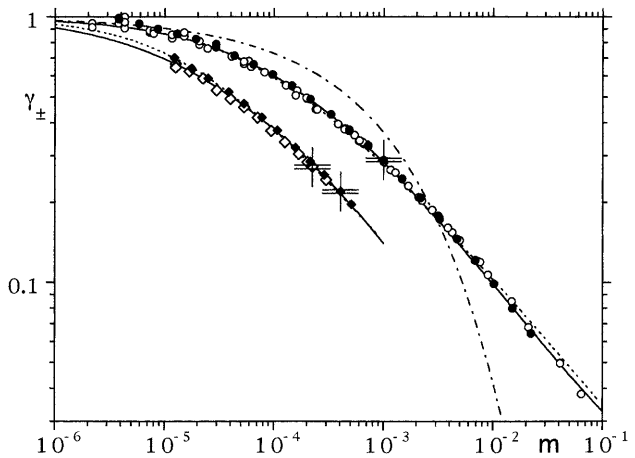


Fig. 2. Activity coefficients of $[Co(en)_3][Co(CN)_6]$ (◆), $[Co(en)_3][Fe(CN)_6]$ (◇), $La[Co(CN)_6]$ (●), and $La[Fe(CN)_6]$ (from Ref. [6]; ○), as a function of molality, compared with the Debye–Hückel limiting law (– · – · –), IPBE (full lines, $a = 0.66$ nm the upper, $a = 0.46$ nm the lower) and Bjerrum theory (dotted lines, $a = 0.67$ nm the upper, $a = 0.51$ nm the lower).

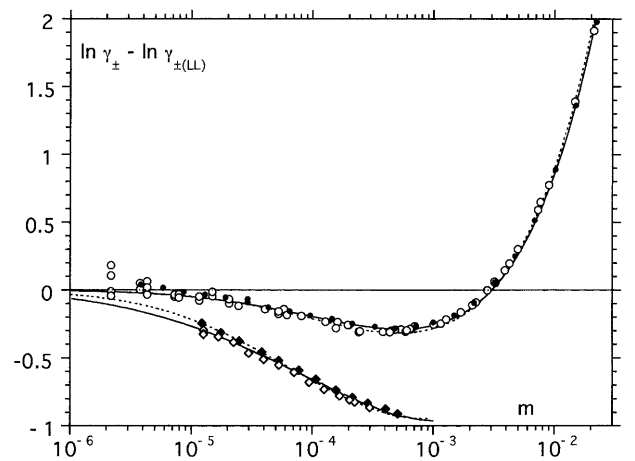


Fig. 3. An expanded view of the deviation of the activity coefficients of the 3:3 salts from the limiting law, in the dilute regions. For comparisons, the trend predicted for the primitive model, according to IPBE and the Bjerrum theory. Symbols as in Fig. 1.

The moderate, residual differences visible in Figs. 2 and 3, at the highest dilutions, between IPBE and the Bjerrum curves for $[Co(en)_3][Fe(CN)_6]$ and $[Co(en)_3][Co(CN)_6]$, are derived in part by the calculation (at very high dilution, our IPBE chains [20] lose precision), and in part correspond to a different prediction of the behaviour of the primitive model using the two treatments. We are unable to decide which trend is more correct. As an application of Murphy's laws, around 10^{-5} mol kg^{-1} (where even the experimental results are no longer very accurate) $[Co(en)_3][Fe(CN)_6]$ and $[Co(en)_3][Co(CN)_6]$ seem to suggest an IPBE-like and a Bjerrum-like trend respectively, as if the real salts, too, were not aware of the correct trend to be obeyed. Application of improved calculation methods (e.g. those from Outhwaite [23]) will be advisable in the future.

It is worth mentioning that the original Bjerrum treatment assumes $q = z^2e_0/(2\varepsilon kT)$ as the cut-off distance d that discerns between 'free ions' and 'ion pairs'. For a 3:3 electrolyte in water, $q = 3.22$ nm at 298 K; correspondingly, the fictitious association constant of the ion pairs takes the considerable value of 3.9×10^4 for $[Co(en)_3][Fe(CN)_6]$ and $[Co(en)_3][Co(CN)_6]$ ($a \approx 0.51$ nm), and of 8.3×10^3 for $La[Co(CN)_6]$ and $La[Fe(CN)_6]$ ($a \approx 0.67$ nm). As Guggenheim noted [24], there are no particularly sound reasons for imposing $d = q$. By choosing a different value for d, the value of the 'association constant', the 'associated' and 'free' ion fractions, and the activity coefficient of the 'free ions' change; however, after the recombination of the contributions of the free ions and ion pairs, the activity coefficients one obtains are found to be substantially unchanged. These considerations also apply to the 'extreme' conditions of the solutions of $[Co(en)_3][Fe(CN)_6]$ and $[Co(en)_3][Co(CN)_6]$; e.g. imposing $d = 5$ nm (instead of 3.22 nm) does not cause appreciable deviation out of the thickness of the relevant curve of Fig. 2, even in the concentration regions where the discrepancies between IPBE and the Bjerrum theory are appreciable. Under these conditions, however, the value of K_{ass} does not vary appreciably either, only from 3.93×10^4 to 4.04×10^4. This narrow range of variation for K_{ass} may suggest the occurrence of ion pairs as real chemical species, but this is an extrapolation of a mathematical concept that takes its origin from a particular way of facing the primitive model, is probably incorrect. As a matter of fact, the UV–Vis spectra of the solutions, measured at approximately 4×10^{-4} mol kg^{-1} (i.e. in a situation where the electrolyte would be about 80% associated) do not evidence any discrepancy from the mathematical sum of the corresponding 1:3 and 3:1 salts.

The a values are appreciably smaller than those expected from the ionic radii of the corresponding ions [25]; i.e. ion–ion interactions are stronger than they should be for a population of spheres of correct size and charge, in a continuum having the same dielectric properties as bulk water. This fact can suggest the actual presence of some association effects. However, it is worth considering that, when the primitive model is used to simulate a real system, the only available parameter, a, is forced to carry all the model deficiencies. In particular, the model counterbalances the effect of the decreased value of the average dielectric constant, in the closer neighbourhoods of an ion, by simulating a lower value for the ion–ion distances. The higher values for a, of the lanthanum salts compared with tris(ethylenediamine) cobalt(III) salts, should be related to the different character of the hydration shells of the corresponding ions (lanthanum, for instance, carries 12 molecules of water [5], while $[Co(en)_3]^{3+}$ does not carry any water [4], when entering the oil phase of the respective membrane).

4. Conclusions

The present study of 3:3 electrolytes provides sound experimental information on a class of salts, whose behaviour has been a mystery for a long time. Together with the 2:3 electrolytes (also unknown before our investigations [2,5,11]), 2:2 electrolytes (whose activity coefficients in literature, now revised, have in some cases been found biased by 10–16% [6,7]), 1:4 electrolytes (still untreated), and also 1:3 and 1:2 electrolytes, whose systematic revision is in progress (systematic errors by 2–6% are possible, for salts explored only in the concentration range covered by the isopiestic measurements), these results intend to provide a solid basis of reliable and precise data, aimed at supporting theoretical treatments. The final goal, however, is to reach a definite insight also in the much more important field of mixed electrolyte solutions, viz. to be able to obtain reliable predictions for chemical equilibrium and kinetics in real situations of practical interest.

Mixed electrolytes are a much harder subject than single electrolytes, not only because of the difficulties involved by theoretical treatments, but, even more, because of the lack of general experimental methods able to validate the theory, determining the real values of the activity coefficients in mixed solutions. The data available are so far limited to: (i) electrolytes liable to be studied with cells without transport (e.g. HCl in the presence of other ionic species); and (ii) saturated solutions of sparingly soluble salts in the presence of other salts. The methods so far available have been reviewed by Harned and Robinson [26]. By connecting a membrane to classic electrodes, only a limited number of further situations have become accessible, e.g. a membrane electrode for M^{n+}, matched to a silver | silver chloride electrode, makes it possible to study MCl_n in the presence of other salts of the same cation. However, the liquid membrane cells, owing to their very nature, are unable to provide a real answer to the problem of mixed solutions [3].

With regard to this problem, we shall now suggest a very simple idea which, like the liquid membrane cells that solve the problem of the single electrolytes, can solve the problem of the mixed electrolyte solutions with a single anion. Let us consider two phases, Mix (composed of an aqueous solution of the electrolytes A_aX_x, B_bX_y, C_cX_z, etc.; X^{t-}, the anion), and Org, a hydrophobic solution (in a hydrocarbon, or some more polar solvent if needed) of a neutral carrier, L for short, insoluble in water. Let L be able to keep selectively A^{s+} rather than the other cations. If the two phases are allowed to reach equilibrium, A^{s+} (but no other cations in appreciable amounts), together with the equivalent quantity of X^{w-}, will exist both in Mix and Org. The chemical potentials will be the same, $\mu(A_aX_x, \text{Mix}) = \mu(A_aX_x, \text{Org})$. In turn, $\mu(A_aX_x, \text{Org})$ can be calibrated by separate experiments, equilibrating Org with a series of solutions of pure A_aX_x in water, where the activities are known or can be determined. All we need is to be able to identify the equilibrium concentration in the various phases with sufficient precision.

Method settlement will require the selection, or synthesis, of suitable neutral carriers. The latter should be: (i) sufficiently insoluble in the aqueous phase (even in the coordinated, ionic, form $[AL]^{s+}$), as it is necessary to leave the number of significant Mix components unchanged; (ii) sufficiently selective, as it is needed to leave $\mu(A_aX_x, \text{Org})$ the same, as it would be in the complete lack of other salts dissolved in Org; (iii) not so strong, as to yield $[AL]^{s+}$ quantitatively, independently of the activity of A_aX_x in the aqueous phase. Unfortunately, there seems to be no realistic possibilities of also finding the required features in a ligand for anions; otherwise, the limitation of the presence of a single anion would cease.

As far as we know, nobody has so far utilized or even devised this route. There is no doubt that solving the practical difficulties implied by the method is no simple matter; nevertheless, a difficult track is better than no track at all, and the obvious importance of the activity coefficients in mixed electrolyte solutions could justify the efforts.

Acknowledgements

Financial support from CNR and MURST (COFIN'98) is gratefully acknowledged.

References

[1] G.N. Lewis, Proc. Am. Acad. Sci. 37 (1901) 45.
[2] P. Debye, E. Hückel, Phys. Z. 24 (1923) 185.
[3] F. Malatesta, G. Carrara, J. Solut. Chem. 21 (1992) 1251.
[4] F. Malatesta, G. Carrara, M.P. Colombini, A. Giacomelli, J. Solut. Chem. 22 (1993) 733.
[5] F. Malatesta, A. Giacomelli, R. Zamboni, J. Solut. Chem. 23 (1994) 11.
[6] F. Malatesta, J. Solut. Chem. 24 (1995) 241.
[7] F. Malatesta, Química Analítica, 15 (Suppl. 1) (1966) S9
[8] F. Malatesta, A. Giacomelli, R. Zamboni, J. Solut. Chem. 25 (1996) 61.
[9] F. Malatesta, R. Zamboni, J. Solut. Chem. 26 (1997) 791.
[10] F. Malatesta, L. Carbonaro, N. Fanelli, S. Ferrini, A. Giacomelli, J. Solut. Chem. 28 (1999) 597.
[11] F. Malatesta, F. Bruni, S. Trombella, R. Zamboni, J. Solut. Chem. 29 (2000) 449.
[12] R.A. Robinson, R.H. Stokes, Electrolyte Solutions, Butterworths, London, 1970, p. 398.
[13] F. Malatesta, R. Zamboni, J. Chem. Soc. Faraday I 76 (1980) 2510.
[14] H.S. Harned, Proc. Natl. Acad. Sci. USA 40 (1954) 551.
[15] R.A. Wynveen, J.L. Dye, Jr., C.H. Brubaker, J. Am. Chem. Soc. 82 (1960) 4441.
[16] D.J. Karl, J.L. Dye, J. Phys. Chem. 66 (1952) 550.
[17] W.J. Hamer, Y.-C. Wu, J. Phys. Chem. Ref. Data 1 (1972) 1047.
[18] E.J. Mayer, Chem. Phys. 18 (1950) 1426.
[19] E.A. Guggenheim, Trans. Faraday. Soc. 56 (1960) 1152.
[20] F. Malatesta, T. Rotunno, Gazz. Chim. Ital. 113 (1983) 783.
[21] J.F. Côté, G. Perron, J.E. Desnoyers, G.C. Benson, B.C.Y. Lu, J. Solut. Chem. 27 (1998) 685.
[22] H.L. Friedman, Ionic Solution Theory, Interscience, New York, 1962.
[23] C.W. Outhwaite, M. Molero, L.B. Bhuiyan, J. Chem. Soc. Faraday I 89 (1993) 1315.
[24] E.A. Guggenheim, Disc. Faraday Soc. 24 (1957) 53.
[25] Y. Marcus, Ion Properties, Marcel Dekker, New York, 1997.
[26] H.S. Harned, R.A. Robinson, Equilibrium properties of electrolyte solutions, in: Multicomponent Electrolyte Solutions, vol. 2, in: The International Encyclopedia of Physical Chemistry and Chemical Physics, Pergamon, Oxford, 1968.

PERGAMON

www.elsevier.nl/locate/poly

Polyhedron 19 (2000) 2501–2505

POLYHEDRON

Synthesis and ligational properties of a new tetra-azamacrocycle containing an anisolic function

Mauro Formica, Vieri Fusi* [1], Mauro Micheloni* [2], Roberto Pontellini, Paolo Romani

Institute of Chemical Sciences, University of Urbino, P.za Rinascimento 6, I-61029 Urbino, Italy

Abstract

The synthesis and characterization of the new tetra-azamacrocycle 1,4,7,10-tetraaza[12]-(2,6)anisolephane (**L**) are reported. The stepwise basicity constants were determined using potentiometric (0.15 mol dm^{-3} NMe_4Cl, 298 ± 0.1 K) and NMR (^1H and ^{13}C) techniques. **L** behaves as a tetraprotic base: $\log K_1 = 9.62$; $\log K_2 = 9.03$; $\log K_3 = 5.44$; $\log K_4 = 1.9$. NMR experiments allowed the determination of the protonation sequence. The influence of the anisolic group inside the macrocyclic cavity upon the basicity behaviour is discussed. The equilibrium constants of the species formed by **L** with Co(II), Cu(II), Zn(II), Cd(II) and Pb(II) are reported and discussed. The formation constants for the oxygenated species $[CoLO_2]^{2+}$, $[CoLHO_2]^{3+}$ and $[CoL(OH)O_2]^{+}$ are: $\log K = 7.6(1)$, 15.8(1) and −1.3(1), respectively. © 2000 Elsevier Science B.V. All rights reserved.

Keywords: Macrocycles; Synthesis; Complexes; Equilibria

1. Introduction

Synthetic macrocycles are a growing class of compounds with varying chemistry, a wide range of different molecular topologies and sets of donor atoms [1–10]. The chemical properties of macrocyclic complexes can be tuned to force metal ions to adopt unusual coordination geometry.

In the present study, a new aza-macrocycle containing the anisolic function, which can be seen as precursor of the phenolic fragment, was synthesized. The crowding of its macrocyclic cavity together with the low number of coordination sites available allows this ligand to form metal complexes without saturating the coordination request of the metal centre. The acid–base behaviour of the ligand and its coordination properties toward some transition metal ions are reported. In the case of the cobalt(II) complexes the reversible addition of molecular oxygen has been investigated.

2. Results and discussion

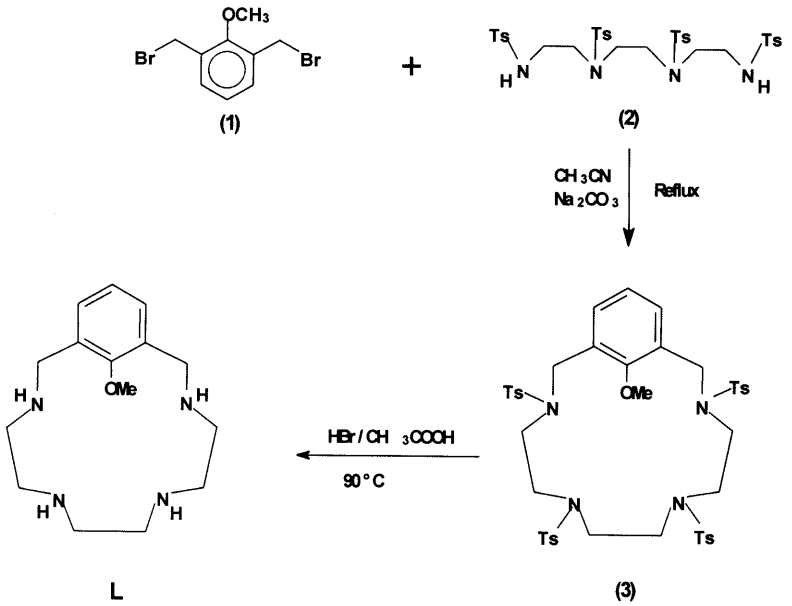
2.1. Synthesis

The synthetic pathway used to obtain ligand **L** is depicted in Scheme 1. The reaction employed to obtain the tosylated macrocycle (**3**), a modification of the Richman–Atkins method,[11] involves the cyclization of the tosylated polyamine (**2**) with 1 equiv. of the 2,6-bis(bromomethyl)anisole (**1**), in the presence of an alkaline carbonate base. The pure product, derived using a 1 + 1 cyclization scheme, is easily reached by recrystallization from CH_3CN. Finally, by treating (**3**) with a mixture of $HBr–CH_3COOH$ and phenol it is possible to selectively remove the tosyl groups, obtaining the macrocycle **L** in good yield as tetrahydrobromide salt. It should be noted that this synthetic procedure is a promising route by which to produce other azamacrocycles containing the anisole function by substitution of (**2**) with tosylated open-chain polyamine compounds. Moreover, after removal of the ethereal methyl group of the anisole, compound **L** can give a new aza-macrocycle having the phenol group as coordinating and optical sensor group.

[1] *Corresponding author.

[2] *Corresponding author. Fax: +39-0722-350-032; e-mail: mauro@chim.uniurb.it(M.Micheloni).

0277-5387/00/$ - see front matter © 2000 Elsevier Science B.V. All rights reserved.
PII: S0277-5387(00)00550-7



Scheme 1.

2.2. Solution studies

2.2.1. Protonation of *L*

The protonation equilibria of **L** were studied in a 0.15 mol dm^{-3} NMe_4Cl aqueous solution at 298 ± 0.1 K by means of potentiometric pH ($-\log[H^+]$) measurements; the results are reported in Table 1. Compound **L** binds up to four protons in aqueous solution in the pH range 2–11 investigated. The equilibrium constants of the first two protonation steps are very similar, with $\log K_2$ only slightly smaller than $\log K_1$ (see Table 1). This is a clear indication that the two protonation sites do not influence each other significantly. Another characteristic of the basicity behaviour of **L** is that the values themselves of $\log K_1 = 9.62$ and $\log K_2 = 9.03$, are very low compared with those of tetra-azamacrocycles not having any group inside the macrocyclic cavity [12]. These results indicate that the presence of the bulky anisolic group strongly influences the first two protonation sites of **L**, isolating them and preventing the formation of the hydrogen bond network which usually stabilizes the protonated species in tetra-azamacrocycles [12]. As expected, in the third protonation step the basicity of **L** is significantly reduced: $\log K_3 = 5.44$ (see Table 1); this reduction in basicity can be explained by the electrostatic repulsion between positively charged nitrogen atoms, which is even more marked in the last protonation step where four positive charges are forced to stay close each other.

Further information on the protonation mechanism of **L** was obtained by recording ^1H and ^{13}C NMR spectra in aqueous solution at various pH values. All the peak assignments were made on the basis of ^1H–^1H homonuclear and ^1H–^{13}C heteronuclear correlation experiments at the different pH values studied. The ^{13}C NMR spectrum of **L** at pH 12, where the unprotonated amine predominates in solution, exhibits nine peaks at δ 46.3 ppm attributed to the carbon atoms C3, 47.7 (C1), 48.0 (C2), 48.2 (C4), 62.7 (C9), 125.8 (C8), 132.3 (C7), 134.2 (C5) and 159.8 (C6). The ^1H spectrum at the same pH shows a singlet at 2.41 ppm attributed to the hydrogen atoms of the ethylenic chain H1 integrating four protons, a multiplet at 2.58 (eight protons, the hydrogens of the ethylenic chains H2 and H3 a doublet at 3.53 (two protons, the hydrogens $H4_A$ of the methylenic chain), a singlet at 3.84 (three protons, the hydrogens of the methyl group), a doublet at 4.17 (two protons, the hydrogens $H4_B$ of the methylenic chain), a triplet at 7.21 (one proton, the hydrogen of the aromatic group H8) and a doublet at 7.34 (two protons, the aromatic protons H7). The methylenic chains (H4) in the ^1H spectrum give rise to an AB coupling system ($\nu_A = 4.17$, $\nu_B = 3.53$ ppm, $J_{AB} = 14.1$ Hz). Moreover, the ^{13}C NMR spectrum presents only one resonance for the same group (C4). This aspect is probably due to the bulk of the ethereal methyl group which precludes the

Table 1
Protonation constants of L ($\log K$) in aqueous solution (298 ± 1 K, $I = 0.15$ mol dm^{-3} NMe_4Cl)

Reaction	
$\mathbf{L} + H^+ = H\mathbf{L}^+$	9.62(1) [a]
$H\mathbf{L}^+ + H^+ = H_2\mathbf{L}^{2+}$	9.03(1)
$H_2\mathbf{L}^{2+} + H^+ = H_3\mathbf{L}^{3+}$	5.44(1)
$H_3\mathbf{L}^{3+} + H^+ = H_4\mathbf{L}^{4+}$	1.9(3)

[a] Values in parenthesis are S.D. on the last significant figure.

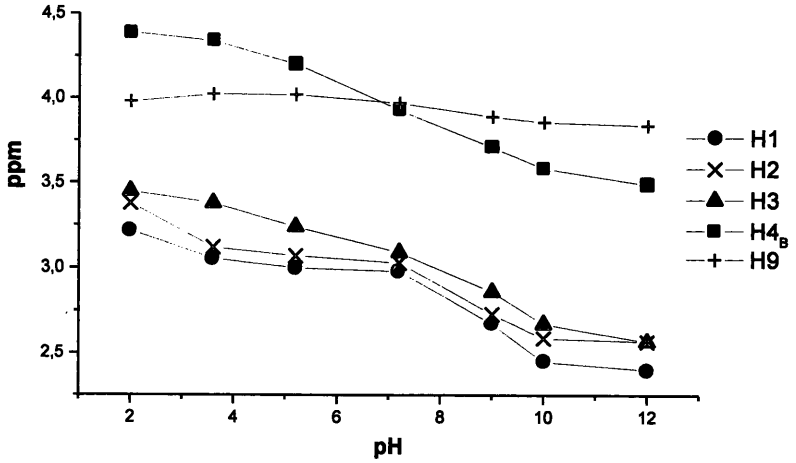


Fig. 1. Experimental ^{1}H NMR chemical shifts of **L** as a function of pH.

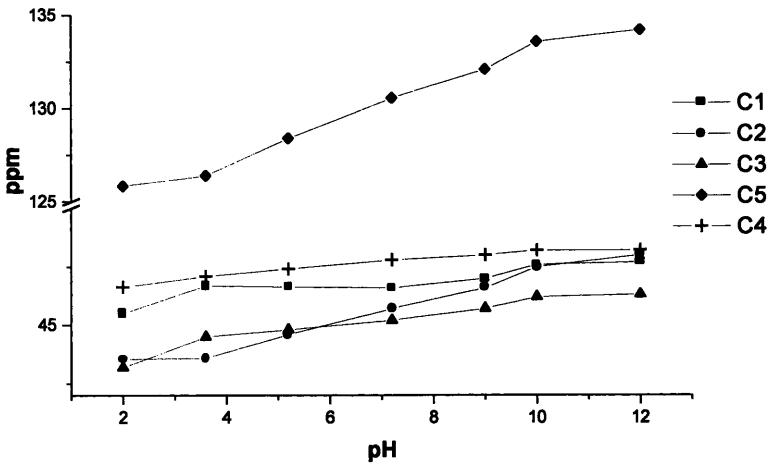


Fig. 2. Experimental ^{1}H NMR chemical shifts of **L** as a function of pH.

free rotation of the aromatic group inside the macrocyclic cavity, giving rise to a C_s time-averaged symmetry which is preserved throughout all the pH range investigated.

Figs. 1 and 2 show, respectively, the most significant ^{1}H and ^{13}C chemical shifts of **L** as a function of pH. In the pH range 7–11, in which two protons bind to the ligand, all the signals of the hydrogen atoms in α position to the nitrogen atoms exhibit a marked downfield shift (Fig. 1). This suggests that all the four nitrogen atoms are involved in the stabilization of the two acidic protons, with the two protons located on alternate nitrogen atoms as expected on the basis of a simple electrostatic model. This hypothesis was confirmed by ^{13}C NMR spectra recorded in the same pH range (Fig. 2), which show the upfield shift of all the resonance of the carbon atoms in β position with respect to the four nitrogen atoms, in good agreement with the β shift reported for protonation of polyamines [13].

In the pH range 3–5, where the triprotonated species are formed, only the hydrogen atoms H3 and H4, in α with respect to the nitrogen atoms in benzylic position, experience a considerable downfield shift, while the other resonances remain unchanged. Moreover, only the carbon signals C2 and C7, in β position with respect to the same nitrogen atoms, show an upfield shift. This suggests that the third protonation step involves only the benzylic nitrogen atom showing a proton disposition such as that depicted in Fig. 3. The fourth protonation step, which occurs only at low pH values, is instead located on the remaining free nitrogen atom.

2.2.2. Metal complexes

Table 2 reports the stability constants of complexed species of **L** with different metal ions. Under the exper-

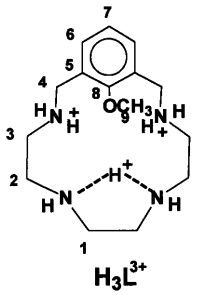


Fig. 3. Atom labelling of **L** and protonation sites for the triprotonted species.

imental conditions investigated, only mononuclear species are formed, which are much less stable than complexes formed with related tetra-azamacrocycles without any group within the macrocyclic cavity [12]. The presence of the hindering anisolic group reduces the ability of the ligand to adapt itself to the stereochemical requirements of the bound metal ion. Even the Cu(II) ion forms a 1:1 complex much less stable ($\log K_{ML} = 14.4$) than those formed with other tetra-azamacrocycles [12]. All of the other metal ions investigated form protonated species $[ML H]^{3+}$; in any case, if we consider the addition of one proton to the mononuclear species $[ML]^{2+}$ to form $[ML H]^{3+}$, the equilibrium constant is always very high (see Table 2) and comparable to that of the protonation of the free ligand (see Table 1). This is a clear indication that the nitrogen atom, which accepts the proton in the metal complex, is at most weakly interacting with the central metal ion. In the case of Co(II) and Zn(II), even the stepwise addition of the second proton to form the diprotonated species $[ML H_2]^{4+}$ (see Table 2) is characterised by a high constant, indicating that very likely a second nitrogen atom is either weakly or not at all involved in binding the metal ion. This situation with the metal ion binding sites not engaged, make the Co(II) complexes able to reversibly bind molecular oxygen. The following equilibria were found: (a) $Co^{2+} + L + O_2 = [CoLO_2]^{2+}$, $\log K = 7.6(1)$; (b) $Co^{2+} + L + H^+ + O_2 = [CoLHO_2]^{3+}$, $\log K = 15.8(1)$; (c) $Co^{2+} + L + O_2 + H_2O = [CoL(OH)O_2]^+ + H^+$, $\log K = -1.3(1)$.

3. Experimental

3.1. Synthesis

Compounds 2,6-bis(bromomethyl)anisole **1** [14] and *N*,*N*′,*N*″,*N*‴-tetrakis(*p*-tolysulphonyl)-3,6-dioctane-1,8-diamine **2** [15] were prepared as reported in the literature. All reactions were carried out in inert atmosphere.

3.1.1. 1,4,7,10-Tetrakis(p-tolylsulphonil)-1,4,7,10-tetraaza[12]-(2,6)anisolephane (3)

Over a period of 4 h, a solution of **1** (2.9 g, 0.01 mol) in 100 cm^3 of acetonitrile was added to a refluxing suspension of **2** (7.6 g, 0.01 mol) and of Na_2CO_3 (5.3 g, 0.05 mol) in 250 cm^3 of acetonitrile. The reaction mixture was maintained under reflux for a further 5 days, after which the mixture was cooled to room temperature (r.t.) and the resulting suspension was evaporated under reduced pressure. The crude product was suspended in chloroform (150 cm^3) and the suspension was filtered. The organic layer was evaporated under reduced pressure, giving a white solid which was recrystallized in a minimum amount of hot acetonitrile. Yield: 7.1 g (79%). *Anal.* Calc. for $C_{43}H_{50}N_4O_9S_4$: C, 57.70; H, 5.63; N, 6.26. Found: C, 57.9; H, 5.7; N, 6.4%. MS (FAB): 896 ($M + H^+$). ^1H NMR ($CDCl_3$, 25°C): 2.23 (s, 12H), 2.38 (s, 4H), 2.51 (m, 8H), 4.26 (d, 2H), 4.39 (s, 4H), 4.58 (d, 2H), 7.21 (t, 1H), 7.36 (d, 8H), 7.79 (d, 4H), 7.83 (d, 4H), 7.96 (d, 2H) ppm. ^{13}C NMR ($CDCl_3$, 25°C): 21.8, 46.2, 47.2, 49.2, 63.8, 125.9, 127.5, 127.6, 129.4, 130.0, 130.2, 131.9, 135.6, 135.9, 143.8, 144.0, 156.9 ppm.

3.1.2. 1,4,7,10-tetraaza[12]-(2,6)anisolephane (L4HBr)

Tetratosylated macrocycle **3** (4.5 g, 5.0 mmol) and phenol (47 g, 0.5 mol) were dissolved in HBr–CH_3COOH (33%, 450 cm^3). The solution was stirred at 90°C for 22 h. The resulting suspension was filtered and the solid washed with CH_2Cl_2 for several times. The yellowish solid was recrystallized from a water–ethanol mixture to give **L** as its tetrahydrobromide salt. Yield: 2.3 g (76%). *Anal.* Calc. for $C_{15}H_{30}N_4Obr_4$: C, 29.93; H, 5.02; N, 9.31. Found: C, 29.7; H, 5.1; N, 9.2%. MS (FAB): 279 ($M + H^+$). ^1H NMR D_2O, (pH 3, 25°C): 3.17 (s, 4H), 3.33 (m, 4H), 3.43 (m, 4H), 4.01 (s, 3H),

Table 2
Stability constants of **L** with Co(II), Cu(II), Zn(II), Cd(II) and Pb(II) in aqueous solution (298.1 ± 0.1 K, Me_4NCl 0.15 mol^{-1})

Reaction	Co^{2+}	Cu^{2+}	Zn^{2+}	Cd^{2+}	Pb^{2+}
$M^{2+} + L = ML^{2+}$	6.34 (1) [a]	14.40(1)	7.51(1)	7.36(1)	8.44(1)
$ML^{2+} + H^+ = MLH^{3+}$	7.86 (3)	6.80(1)	7.38(1)	7.29(1)	6.80(1)
$MLH^{3+} + H^+ = MLH_2^{4+}$	7.37 (4)	2.89(2)	6.78(2)		
$ML^{2+} + OH^- = MLOH^+$	3.66 (3)	4.50(3)	5.54(2)	3.03(1)	
$MLOH^+ + OH^- = ML(OH)_2$			2.12(9)		

[a] Values in parentheses are S.D. on the last significant figure.

4.36 (D, 2H), 4.61(d, 2H), 7.47 (t, 1H), 7.67 (d, 2H) ppm. ^{13}C NMR 42.8, 43.0, 44.5, 45.8, 64.9, 125.6, 128.4, 136.0, 159.2 ppm.

3.2. General

3.2.1. NMR spectroscopy

^{1}H, ^{13}C spectra were recorded on a Bruker AC-200 instrument, operating at 200.13 and 50.33 MHz, respectively. In ^{1}H NMR experiments peak positions are reported in relation to HOD (4.75 ppm), dioxane was used as a reference standard in ^{13}C NMR spectra ($\delta = 67.4$ ppm). For the spectra recorded in $CDCl_3$, the peak positions are reported with respect to TMS. Small amounts of NaOD or DCl solutions were added to a solution of the ligand to adjust the pD. The pH was calculated from the measured pD values using the following relationship: $pH = pD - 0.40$ [16].

3.2.2. Spectrophotometric titrations

Absorption spectra were recorded on a Varian Cary-100 spectrophotometer.

3.2.3. Potentiometric measurements

All potentiometric measurements were carried out in 0.15 mol dm^{-3} Me_4NCl at 298.1 ± 0.1 K, in the pH range 2.5–10, using the fully automatic equipment that has been already described [17]. The EMF data were acquired with the PASAT computer program [18]. The electrode was calibrated as a hydrogen concentration probe by titrating known amounts of HCl with CO_2-free Me_4NOH solutions and determining the equivalent point by Gran's method [19], which gives the standard potential $E°$ and the ionic product of water K_w. At least three measurements were performed. The HYPERQUAD computer programs were used to process the potentiometric data and calculate the protonation constants [20].

Acknowledgements

Support for this research by MURST (Ministero per l'Università e la Ricerca Scientifica e Tecnologica) COFIN98 is gratefully acknowledged.

References

[1] (a) C.J. Pedersen, J. Am. Chem. Soc. 89 (1967) 7017. (b) J.M. Lehn, Pure Appl. Chem. 49 (1977) 857. (c) D.J. Cram, J.M. Cram, Science 183 (1984) 4127.
[2] R.M. Izatt, J.J. Christensen, Synthetic Multidentate Macrocyclic Ligands, Academic Press, New York, 1978.
[3] F. Vögtle, E. Weber, Host Guest Complex Chemistry Macrocycles, Springer-Verlag, Berlin, 1985.
[4] L.F. Lindoy, The Chemistry of Macrocyclic Ligands Complexes, Cambridge University Press, Cambridge, 1989.
[5] G.W. Gokel, in: J.F. Stoddart (Ed.), Crown Ethers and Cryptands (Monographs in Supramolecular Chemistry), The Royal Society of Chemistry, Cambridge, 1992.
[6] B. Dietrich, P. Viout, J.M. Lehn, Macrocyclic Chemistry, VCH, Weinheim, 1993.
[7] D. Parker, Macrocycle Synthesis: A Practical Approach, Oxford University Press, Oxford, 1996.
[8] D.J. Cram, J.M. Cram, Container Molecules and Their Guests, Monographs in Supramolecular Chemistry, The Royal Chemistry Society, Cambridge, 1997.
[9] Y.A. Zolotov, Macrocyclic Compounds in Analytical Chemistry, Wiley, New York, 1997.
[10] A. Bianchi, K. Bowman-James, E. Garcia-España, Supramolecular Chemistry of Anions, Wiley-VCH, New York, 1997.
[11] J.E. Richman, T.J. Atkins, J. Am. Chem. Soc. 96 (1974) 2268.
[12] A. Bianchi, M. Micheloni, P. Paoletti, Coord. Chem Rev. 101 (1991) 17.
[13] (a)J.C. Batchelor, J.H. Prestegard, R.J. Cushley, S.R. Lipsy, J. Am. Chem. Soc. 95 (1973) 6558. (b) A.R. Quirt, J.R. Lyerla, I.R. Peat, J.S. Cohen, W.R. Reynold, M.F. Freedman, J. Am. Chem. Soc. 96 (1974) 570. (c) J.C. Batchelor, J. Am. Chem. Soc. 96 (1975) 3410. (d) A. Bencini, A. Bianchi, E. Garcia-España, M. Micheloni, J.A. Ramirez, Coord. Chem. Rev.188 (1999) 97.
[14] E. Chapoteau, M.-S. Chowdhary, B.-P. Czech, A. Kumar, W. Zazulak, J. Org. Chem. 57 (1992) 2804.
[15] A. Bencini, A. Bianchi, E. Garcia-España, M. Giusti, M. Micheloni, P. Paoletti, Inorg. Chem. 26 (1987) 681.
[16] A.K. Covington, M. Paabo, R.A. Robinson, R.G. Bates, Anal. Chem. 40 (1968) 700.
[17] A. Bianchi, L. Bologni, P. Dapporto, M. Micheloni, P. Paoletti, Inorg. Chem. 23 (1984) 1201.
[18] M. Fontanelli, M. Micheloni, I Spanish–Italian Congr. Thermodynamics of Metal Complexes, Peñiscola, June 3–6, 1990, University of Valencia, Spain, 1990, p. 41.
[19] (a) G. Gran, Analyst 77 (1952) 661. (b) F.J. Rossotti, H. Rossotti, J. Chem. Educ. 42 (1965) 375.
[20] P. Gans, A. Sabatini, A. Vacca, Talanta 43 (1996) 1739.

PERGAMON

www.elsevier.nl/locate/poly

Polyhedron 19 (2000) 2507–2513

POLYHEDRON

Equilibria and kinetics of complex formation between nickel(II) and the polyamine Me_2octaen

F. Secco [a,*], M.R. Tinè [a], M. Venturini [a], A. Bencini [b], C. Giorgi [b], B. Valtancoli [b]

[a] *Dipartimento di Chimica e Chimica Industriale della Università di Pisa, Via Risorgimento 35, I-56126 Pisa, Italy*
[b] *Dipartimento di Chimica, Università di Firenze, Via Maragliano 75, I-50144 Florence, Italy*

Abstract

The kinetics and the equilibria of complex formation between Ni(II) and 1,25-dimethyl-1,4,7,10,13,16,19,22,25-nonaazapentacosane (Me_2Octaen) have been investigated in aqueous solution between pH 3 and 4.5 by the stopped-flow method and UV spectrometry. Me_2Octaen is a linear polyamine made by the union of eight *en* units bearing two methyl residues at the ends of the chain. Spectrophotometric titrations and kinetic experiments indicated that below pH 4.5 the binding of Ni(II) to the ligand gives rise to several 1:1 complexes differing in their degree of protonation, whereas above pH 4.5 binuclear complexes are formed as well. Concerning the mononuclear species, the ratios of the formation to the dissociation rate constants are in agreement with the equilibrium constants measured by static spectrometry. The analysis of the kinetic data reveals that the mostly reactive form of the ligand (denoted in its fully protonated form as H_9L^{9+}) is H_5L^{5+}, whereas the much more abundant species H_6L^{6+} yields only a minor contribution to the overall process of complex formation. Measurements at different ionic strengths have shown positive salt effects, as expected for reactive processes involving particles with charges of the same sign. Addition of sodium acetate resulted in a large enhancement of the rate of the complex formation reaction, whereas the complex dissociation rate was found to be almost insensitive to the presence of the buffer. Analogous, although more modest, effects have been found with sodium chloroacetate. This behaviour is explained by assuming that the anion of the buffer could bind to Ni^{2+} and/or to the ligand, thus reducing the repulsion between the positively charged reaction partners. © 2000 Elsevier Science B.V. All rights reserved.

Keywords: Me_2Octaen; Polyamines; Nickel(II); Equilibria; Kinetics; Stopped-flow

1. Introduction

The kinetics of the binding of divalent metal ions to linear polyamines have been subjected to thorough investigations in past decades [1–7] since these ligands appeared to behave anomalously with respect to most ligands (including ammonia). Rorabacher et al. [1,2] measured the rates of complex formation between Ni^{2+} and a variety of oligoamines (ranging from *en* to *tetren*) and observed that the reactivity of these ligands toward Ni^{2+} was higher than that predicted by the Eigen–Wilkins argument [8]. This observation led Rorabacher [2] to postulate a special mechanism, defined as internal conjugate base (or ICB) mechanism, the key feature of which is the formation of a hydrogen bridge between a water molecule in the inner coordination shell of the metal ion and a nitrogen atom of the polyamine. The hydrogen bridge can exert two effects: the first results in the stabilisation of the outer-sphere complex, whose formation is a prerequisite for replacement of coordinated water by the ligand [8]. The second (more modest) effect consists in the labilisation of the remaining five coordinated water molecules. Both effects contribute to the enhancement of the rate of the binding process. The more recent availability of longer polyamines makes this kind of study even more interesting, owing to the ability of the ligand not only to form polynuclear species [9], but also to interact with anions of different nature [10].

In this paper we present the results of an investigation of the binding of Ni(II) to Me_2Octaen [1,25-dimethyl-1,4,7,10,13,16,19,22,25-nonaazapentacosane], a linear polyamine represented in Fig. 1 in its fully unprotonated form. This investigation, besides being of

* Corresponding author. Tel.: +39-050-918259; fax: +39-050-918260.
E-mail address: ferdi@dcci.unipi.it (F. Secco).

0277-5387/00/$ - see front matter © 2000 Elsevier Science B.V. All rights reserved.
PII: S0277-5387(00)00551-9

interest in itself, can provide useful information about the mode of binding of Co(II) to polynucleating ligands. Since Co(II) and Ni(II) are known to form complexes with the same mechanism [8], mechanistic details gained from this study could be profitably used to throw light on the mechanism of formation of oxygenated complexes of Co(II).

2. Experimental

2.1. Materials

Me_2Octaen was synthesised and purified as described elsewhere [9]. Nickel perchlorate (Fluka) was dissolved in 0.01 mol dm^{-3} perchloric acid in order to prevent precipitation of the hydroxide. The obtained stock solution was standardised by EDTA titrations at pH 10 using murexide as an indicator [11]. All other chemicals were analytical grade and were used without further purification. Doubly distilled water was used to prepare the solutions and as a reaction medium. All measurements were performed at ionic strength 0.1 mol dm^{-3} obtained by suitable additions of sodium perchlorate.

2.2. Physical measurements

2.2.1. Equilibria

Spectrophotometric titrations were performed with a Perkin–Elmer lambda 17 spectrophotometer equipped with thermostated cell holders able to maintain the temperature constant with fluctuations within ± 0.1°C. Increasing amounts of nickel perchlorate were added by a microsyringe directly into the measuring cell containing a known volume (usually 2 ml) of the ligand solution. The data were subsequently analysed by a non-linear least-square fitting procedure provided by the Jandel (AISN software) program.

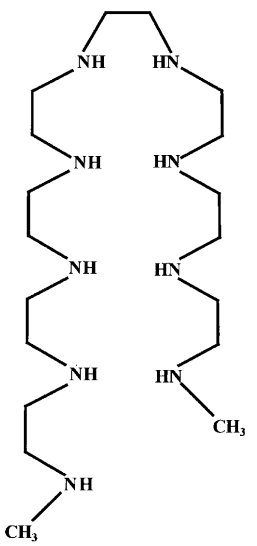


Fig. 1. Me_2Octaen represented in its neutral, fully unprotonated form.

The acid dissociation constants of the ligand were measured by pH titrations. These were performed by a Crison Micro TT 2050 automatic titrator equipped with a combined glass electrode. The instrument was calibrated by titrating an exactly known amount of HCl with NaOH. Current pH measurements were performed with a PHM 84 research pH meter (Radiometer, Copenhagen). A suitable calibration procedure [12] enabled us to convert the pH meter output into hydrogen ion concentration.

2.2.2. Kinetics

The course of the complex formation reaction was monitored at 230 nm using a stopped-flow apparatus constructed in our laboratory. A Hi-Tech SF-61 mixing unit was coupled to a spectrophotometric line through two optical guides. The UV radiation produced by a Hamamatsu L248102 'quiet' lamp was passed through a Bausch and Lomb 338875 high intensity monochromator and then split into two beams. The reference beam was sent directly to a 1P28 photomultiplier. The measuring beam was sent through an optical quartz guide to the observation chamber and then through a second optical guide, to the measuring photomultiplier, also 1P28. The outputs of the two photomultipliers were balanced before each shot and the signal revealing the course of the reaction was sent to a Tektronix 2212 digital oscilloscope with a maximum sampling rate of 4000 data points in 200 μs and a minimum sampling rate of 4000 data points in 500 s. Finally, the acquired signal was transferred to a personal computer via a GPIB interface and analysed by a non-linear least-square procedure expressly devised to fit multiexponential functions [13]. Chemical relaxation experiments were performed on a temperature-jump instrument manifactured by Messanlagen studien geselleshaft (Göttingen, Germany).

3. Results and discussion

3.1. Equilibria

The acid dissociation constants of Me_2Octaen were determined by gradual neutralisation with NaOH of the ligand initially present in the fully protonated form, H_9L^{9+}. Since both the equilibria and the kinetics are strongly dependent on the ionic strength, it was found important to use acid dissociation constants of Me_2Octaen determined under conditions identical to those of the kinetic study ($I = 0.1$ mol dm^{-3} ($NaClO_4$), $T = 25$°C). The values are reported in Table 1 where, for comparison, the literature data at $I = 0.15$ mol

Table 1
Acid dissociation and stability constants of the Ni(II)–Me_2Octaen system at 25°C; $K_i = [MH_iL]/[M][H_iL]$, $K_{Ai} = [H][H_{i-1}L]/[H_iL]$ and $K_{Ci} = [H][MH_{i-1}L]/[MH_iL]$

	$I = 0.1$ mol dm^{-3}	$I = 0.15$ mol dm^{-3} [a]
pK_{A1}	10.14	10.58
pK_{A2}	9.51	9.72
pK_{A3}	9.20	9.35
pK_{A4}	8.39	8.70
pK_{A5}	7.81	7.93
pK_{A6}	5.24	5.10
pK_{A7}	3.80	3.88
pK_{A8}	3.00	2.98
pK_{A9}	2.08	2.74
pK_{C5}	3.04	
$\log K_4$	7.38	7.43 [b]
$\log K_5$	2.60	

[a] Ref. [9].
[b] Ref. [14].

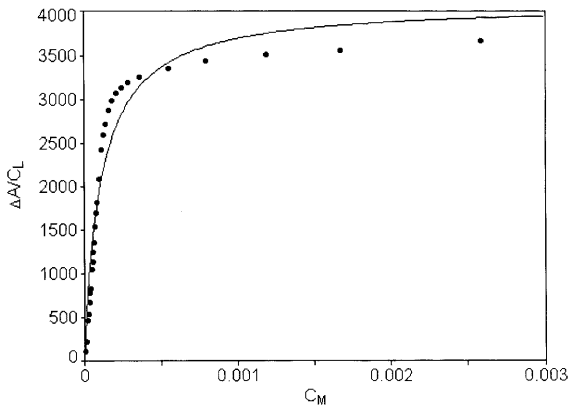


Fig. 2. Spectrophotometric titration of the nickel(II)–Me_2Octaen system. pH 4.8, $I = 0.1$ mol dm^{-3}, $T = 25$°C, $\lambda = 230$ nm. The continuous line deviating from experiment is calculated neglecting the binuclear species.

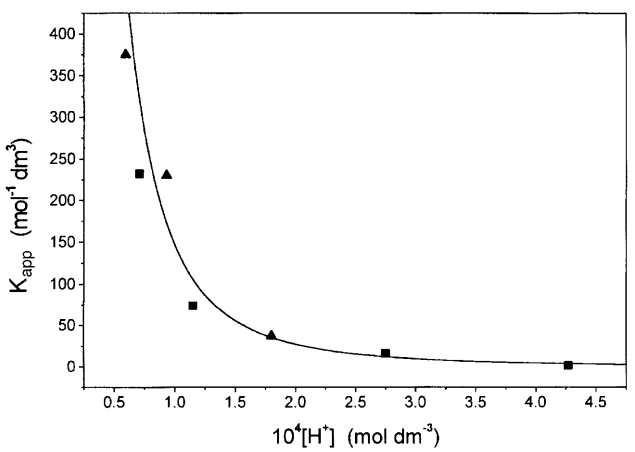


Fig. 3. Dependence of the apparent stability constant for the Ni(II)–Me_2Octaen complex, K_{1app}, on $[H^+]$. ▲, Thermodynamics, ■, kinetics. $I = 0.1$ mol dm^{-3}, $T = 25$°C.

dm^{-3} are also given [9]. The spectrophotometric titrations were carried out at 230 nm by using solutions of the ligand as much diluted as possible. Under these circumstances very small amounts of buffer are sufficient to prevent noticeable acidity variations during titration. At constant pH the equilibria of the system could be conveniently described by the apparent reactions

$$M_f + L_f \rightleftharpoons ML_T \quad (1)$$

$$2M_f + L_f \rightleftharpoons M_2L_T \quad (2)$$

where M_f and L_f indicate the free reactants, whereas ML_T and M_2L_T indicate the total mononuclear and binuclear species respectively. The equilibrium constants of reactions (1) and (2), denoted as K_{1app} and K_{2app} respectively, have been evaluated by a non-linear least-square procedure applied to the equation

$$\Delta A/C_L = \frac{\Delta\varepsilon_1 K_{1app}[M] + \Delta\varepsilon_2 K_{2app}[M]^2}{1 + K_{1app}[M] + K_{2app}[M]^2} \quad (3)$$

where $\Delta A = (A - \varepsilon_L C_L - \varepsilon_M C_M)$, C_L and C_M are the total ligand and metal concentrations, [M] is the metal equilibrium concentration, $\Delta\varepsilon_1 = \varepsilon_{ML} - \varepsilon_L$, $\Delta\varepsilon_2 = \varepsilon_{M2L} - \varepsilon_L$ and ε_i is the molar extinction coefficient of the ith species participating in reactions (1) and (2). The optical path length is 1 cm. The method of analysis is shown in Fig. 2 where the continuous line deviating from experiment represents the trend calculated disregarding the formation of the binuclear complex. However, the deviations between calculated and experimental trends become less and less evident as the pH is decreased, until they disappear for pH values less than 4.5. This finding indicates that below that pH value only mononuclear complexes are formed, in agreement with previous potentiometric results [9].

Owing to the complexity of the system, we have concentrated our attention on the results obtained at pH values between 3.3 and 4.5. The best representation of the dependence of K_{1app} on the hydrogen ion concentration is provided by the equation

$$K_{1app} = \left(A + \frac{B}{[H^+]}\right)\alpha_{H_5L} \quad (4)$$

A plot of K_{1app} versus $[H^+]$ is shown in Fig. 3. The equilibrium parameters A and B were obtained by a non-linear least-square fitting to Eq. (4) and the continuous line represents the calculated trend. Models requiring replacements of α_{H_5L} by α_{H4L} or by α_{H6L} gave definite deviations from the experimental trend and models leading to three term equations did not improve the results. These findings enable us to state that the prevailing species between pH 3.3 and 4.5 are MH_5L^{7+} and MH_4L^{6+} and that $A = K_5$, $B = K_4K_{A5}$ and that the values of K_4, K_5 and $K_{C5} = K_{A5}K_4/K_5$ are reported in Table 1 in logarithm form. Our value of log K_4 is in fair

agreement with the literature datum [14] of 7.43, obtained at $I = 0.15$ mol dm^{-3}. Note that the equilibrium constants of the individual steps are defined as $K_i = [MH_iL]/[M][H_iL]$, $K_{Ai} = [H][H_{i-1}L]/[H_iL]$, $K_{Ci} = [H][MH_{i-1}L]/[MH_iL]$ and $\alpha_{H_5L} = [H_5L]/C_L$.

3.2. Kinetics

The kinetic experiments were carried out under pseudo first-order conditions. Below pH 4.5 the kinetic curves are fitted by single exponential functions. For pH values between 4.5 and 5.0 the curves become biexponential only for $C_M > 5 \times 10^{-3}$ mol dm^{-3}, whereas above pH 5.0 two exponentials are observed even at the lowest of the employed metal ion concentrations ($C_M = 1 \times 10^{-3}$ mol dm^{-3}). Fig. 4 shows a stopped-flow signal recorded at pH 5.5. The experimental points are perfectly fitted by a biexponential curve whereas the monoexponential fit displays remarkable deviations from experiment, as indicated by the smooth continuous line. Fig. 5 shows the metal ion concentration dependence of the observed time constant, $1/\tau$, measured below pH 4.5 where only reaction (1) contributes to the kinetic behaviour of the system. For $C_M \gg C_L$ the observed time constant is expressed by the relationship

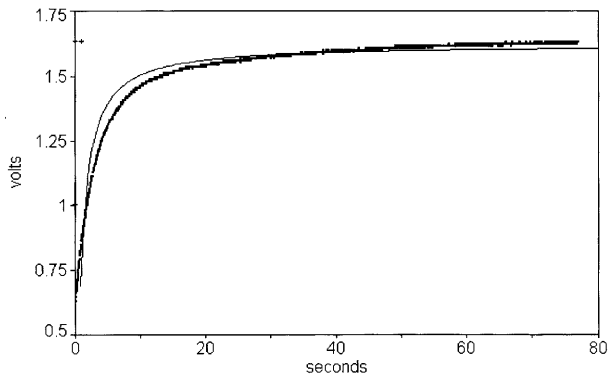


Fig. 4. Stopped-flow experiments for the Ni(II)–Me$_2$Octaen system, $C_L = 1 \times 10^{-4}$ mol dm^{-3}, $C_M = 0.025$ mol dm^{-3}, pH 5.5, $I = 0.1$ mol dm^{-3}, $T = 25$°C, $\lambda = 230$ nm. The curve is biexponential and indicates that mononuclear and binuclear complexes are being formed. The continuous line deviating from experiment is calculated according to a single exponential.

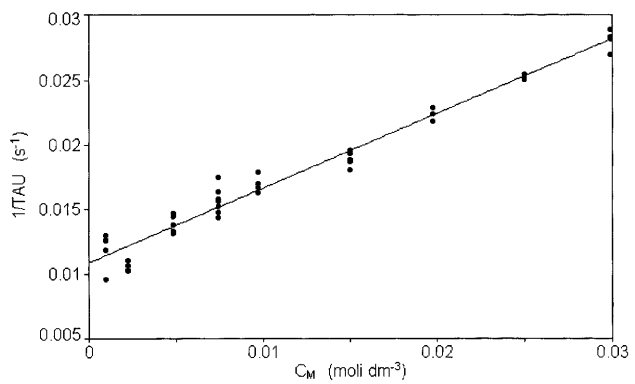
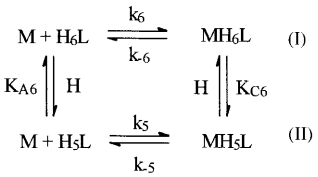


Fig. 5. Dependence of $1/\tau$ on the metal concentration for the Ni(II)–Me$_2$Octaen system, pH 3.94, $I = 0.1$ mol dm^{-3}, $T = 25$°C.

$$\frac{1}{\tau} = k_f C_M + k_d \quad (5)$$

where k_f and k_d are respectively the formation and dissociation rate constants of reaction (1) and could be evaluated from slope and intercept of the straight line of Fig. 5. Both the apparent rate constants change with $[H^+]$. This observation not only confirms the existence of several acid–base equilibria between the differently protonated forms of the ligand and between the differently protonated forms of the mononuclear complex, but could also indicate which forms are able to bind the metal ion. In the investigated range of pH ($3.3 \leq pH \leq 4.5$) the species H_3L^{3+}, H_2L^{2+} HL^+ and L could not make any contribution to the reaction rate, owing to their extremely low concentrations. All the remaining species, in principle, should be considered as possible candidates to participate in the binding process. The model which, among the tested ones, provides the best representation of the kinetic behaviour is that depicted below (charges have been omitted for the sake of simplicity):



According to the above reaction scheme the dependence of k_f and k_d on the hydrogen ion concentration is provided by the relationships

$$k_f = \left(k_5 + \frac{k_6[H^+]}{K_{A6}}\right)\alpha_{H_5L} \quad (6)$$

$$k_d = \left(k_{-5} + \frac{k_{-6}[H^+]}{K_{C6}}\right)\alpha_{MH_5L} \quad (7)$$

where $\alpha_{H_5L} = [H_5L]/C_L$ and $\alpha_{MH_5L} = [MH_5L]/C_L$. The values of the rate parameters are $k_5 = 20.6$ mol^{-1} dm^3 s^{-1}, $k_6 = 0.154$ mol^{-1} dm^3 s^{-1}, $k_{-5} = 0.059$ s^{-1} and $k_{-6}/K_{C6} = 67$ mol^{-1} dm^3 s^{-1}.

Fig. 6 shows the dependence of k_f on $[H^+]$ whereas the dependence of k_d on $[H^+]$ is shown in Fig. 7. The continuous lines represent the calculated values according to Eqs. (6) and (7) respectively. It should be noted that a good representation of the experiments is also obtained by considering only H_5L^{5+} as the reactive species. In such a case the analysis of the data yields $k_5 = 22.2$ mol^{-1} dm^3 s^{-1} and $k_{-5} = 0.061$ s^{-1}. These results, being very similar to those obtained including

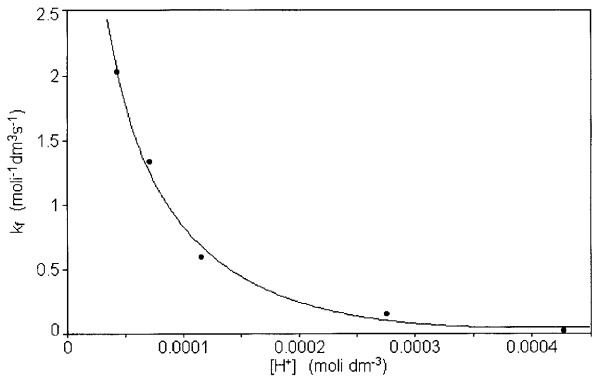


Fig. 6. Dependence of k_f on the hydrogen ion concentration for the Ni(II)–Me_2Octaen system, $I = 0.1$ mol dm^{-3}, $T = 25$°C. The continuous line is calculated according to Eq. (5).

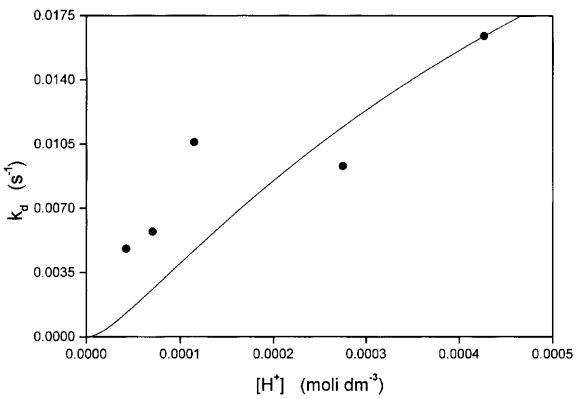


Fig. 7. Dependence of k_d on the hydrogen ion concentration for the Ni(II)–Me_2Octaen system, $I = 0.1$ mol dm^{-3}, $T = 25$°C. The continuous line is calculated according to Eq. (6).

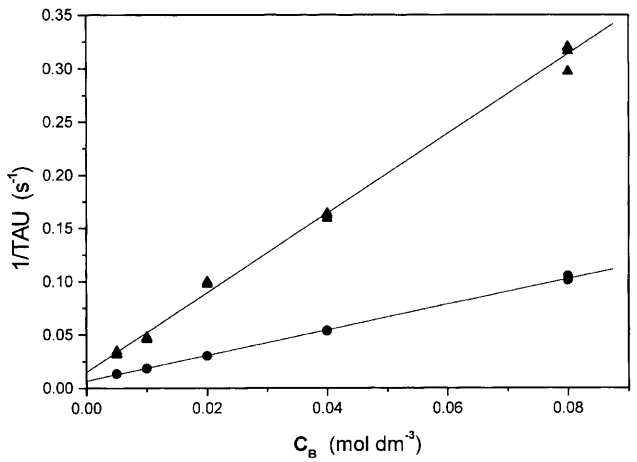


Fig. 8. Dependence of $1/\tau$ on the sodium acetate concentration (C_B) for the Ni(II)–Me_2Octaen system. ▲ $C_M = 3.0 \times 10^{-2}$ mol dm^{-3}, ● $C_M = 9.8 \times 10^{-3}$ mol dm^{-3}, pH 4.37, $I = 0.1$ mol dm^{-3}, $T = 25$°C.

step I as well, indicate that the contribution of this step to the overall reaction is of minor importance and that H_5L^{5+} is the main reactive species in the investigated range of pH.

3.3. The ionic strength effect

Changes of ionic strength from 0.1 mol dm^{-3} to 0.25 mol dm^{-3} by addition of sodium perchlorate lead to an increase by a factor 2 in k_f and to an even larger decrease in k_d. The effect on k_d should be fully ascribed to the influence of the ionic strength on α_{MH_5L}, because the specific rates of dissociation of the complexes, k_{-5} and k_{-6}, corresponding to monomolecular processes, are scarcely sensitive to salt effects. By contrast, the change observed in k_f should be ascribed to a combination of a secondary salt effect (influence on α_{H_5L}) and a primary salt effect (influence on k_5 and k_6). However the system of equilibria involved in the reaction mechanism is too complex to enable us to provide a quantitative evaluation of the experiments.

3.4. The buffer effect

Fig. 8 shows that $1/\tau$ changes linearly with the concentration of sodium acetate for two series of experiments both performed at pH 4.2, but differing in the metal concentration. The slope and the intercept values of the straight line associated with the set of experiments performed at $C_M = 3 \times 10^{-2}$ mol dm^{-3} are higher than the corresponding values derived from experiments performed at $C_M = 9.8 \times 10^{-3}$ mol dm^{-3}. Additionally, two series of experiments were carried out by changing C_M at constant C_B (total buffer concentration) and pH. The reaction parameters in the presence of buffer were derived from plots like that of Fig. 5 and are collected in Table 2. One can observe that buffer addition influences mainly the apparent complex formation constant k_f^b whereas the complex dissociation constant k_d^b remains almost unaffected (the superscript b indicates that the reaction parameters have been derived in the presence of buffer). In the light of these results, the expression for the time constant could be written in the form of eq. (8) where $(k_f + k'_f C_B)$ and $(k_d + k'_d C_B)$ correspond respectively to k_f^b and k_d^b of Table 2.

$$\frac{1}{\tau} = (k_d + k'_d C_B) + (k_f + k'_f C_B) C_M \quad (8)$$

Table 2
The buffer effect. Values of the apparent rate constants, k_f^b (mol^{-1} dm^3 s^{-1}) and k_d^b (s^{-1}) for the Ni(II)–Me_2Octaen system in the presence of different concentrations of sodium acetate (C_B); pH 4.37, $I = 0.1$ mol dm^{-3}, $T = 25$°C

C_B (mol dm^{-3})	k_f^b (mol^{-1} dm^3 s^{-1})	k_d^b (s^{-1})
0.02	2.1	4.5×10^{-3}
0.08	12.5	6.1×10^{-3}

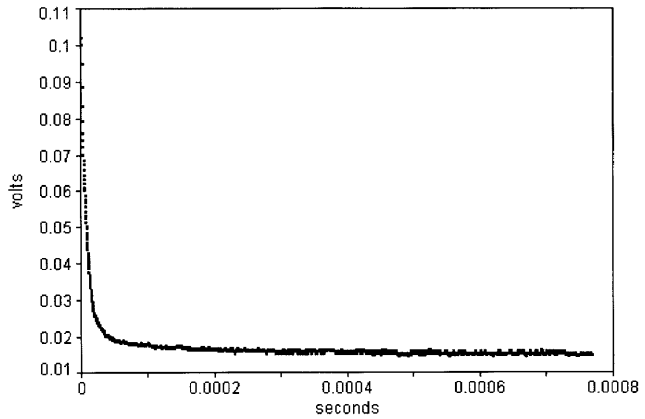
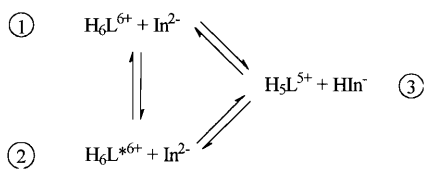


Fig. 9. Temperature jump experiment on the Me_2Octaen–chlorophenol red system. Two relaxation effects are clearly observable. $C_L = 5 \times 10^{-5}$ mol dm^{-3}, $C_{ind} = 1 \times 10^{-4}$mol dm^{-3}, pH 5.5, $I = 0.1$ mol dm^{-3}, $T = 25$°C, $\lambda = 570$ nm.

Qualitatively similar, but less pronounced, effects were obtained in the presence of sodium chloroacetate.

The most common interpretation forwarded to explain the buffer effect on reactions in which hydrogen ions have to be removed from the reaction site is based on the idea that the process of proton removal would be rate determining [15]. In order to assess whether such an explanation could hold for our system as well, the rate of the proton transfer reaction between Me_2Octaen and chlorophenol red, an acid–base indicator with p$K_A = 6.0$, was measured by the temperature-jump method. Fig. 9 shows a kinetic curve recorded at pH 5.5. Two relaxation effects, differing in the time scale by a factor of about 20, are visible. The pH of the solution is sufficiently low to ensure the exclusion of any contribution to the rate of proton transfer coming from the hydrolysis path. A possible contribution from the protolysis path could not be detected since its relaxation time, calculated with the help of the Debye equation [16], turns out to be 0.3 μs, which is much faster than the instrumental heating time (4 μs). Under these circumstances only a single relaxation effect, ascribed to the direct proton exchange between ligand and indicator, should be observed. The presence of two effects reveals that proton exchange is not a simple step. However, the observed behaviour could be rationalised by assuming that the protonated ligand is distributed between two forms, one of which, indicated as H_6L^{*6+}, is characterised by an internal hydrogen bridge of the type $>N\cdots H-N<$. The proton transfer process in such a case is reasonably represented by the cycle



(9)

which displays two relaxation effects. The first of these effects should be associated with the unhindered proton exchange step 1⇔3. This step is fast in both directions, actually displaying its maximum (diffusion controlled) velocity in the thermodynamically favoured direction $1 \rightarrow 3$ and a velocity only slightly lower in the reverse direction $3 \rightarrow 1$ because the ΔpK value is small ($pK_{Hin} - pK_{H6L} = 0.26$). The experimental relaxation time of this effect is $\tau_{fast} = 8$ μs, which agrees with the value of 7 μs calculated by the Debye equation [16]. In contrast, the second relaxation effect, which is associated mainly with the hindered proton exchange step 2⇔3, displays a longer relaxation time ($\tau_{slow} = 140$ μs). This result could be rationalised by considering that the transfer of the proton from H_6L^{*6+} to In^{2-} requires an additional amount of energy to break the intramolecular hydrogen bond present in H_6L^{*6+}. From the value of $1/\tau_{slow}$ the approximate value of 10^8 mol^{-1} dm^3 s^{-1} has been derived for the rate constant of the process $2 \rightarrow 3$. Such a value is more than one order of magnitude lower than that expected for a non-hindered proton transfer reaction but, still, is very high. This fact enables us to exclude that the process of ligand deprotonation in the Ni(II)–Me_2Octaen system could be rate determining. The rate enhancement observed by buffer addition should be thus rationalised otherwise.

A reasonable explanation of the buffer effect can be given if one takes into account the ability of the buffer anion to interact with the metal ion giving species of reduced charge like $NiOAc^+$. In addition, OAc^- could interact with Me_2Octaen giving ligand–anion complexes, thus reducing the positive charge of the ligand as well. Such a kind of complex between organic anions and polyamines has been already observed [10]. Charge reduction on both the reaction partners means reduction of electrostatic repulsion and, consequently, rate enhancement.

We could try now to evaluate the ICB effect displayed by the Ni(II)–Me_2Octaen system by comparing $k^*_{H_5L}$, the first-order rate constant for the conversion of the outer-sphere to the inner-sphere complex in the Ni(II)–H_5L system, with the rate constant of the analogous conversion in the Ni(II)–NH_3 system. According to the Eigen and Tamm argument [17], the second-order rate constant for the binding of Ni^{2+} ion to H_5L^{5+} should be given by the relationship $k_5 = K_{os}k^*_{H_5L}$, where K_{os} is the stability constant of the outher sphere complex. By using the Eigen–Fuoss equation [18,19] one could estimate $K_{os} = 2.6 \times 10^{-5}$ mol^{-1} dm^3 for a distance between the charge centres of 5×10^{-8} cm. This leads to $k^*_{H_5L} = 8.5 \times 10^5$ s^{-1}, whereas the value of k^*_{NH3} for the Ni(II)–NH_3 system [2,4] is 4.6×10^3 s^{-1}. Thus the observed ICB effect is

$$k^*_{H_5L}/k^*_{NH_3} = 185 \quad (10)$$

Note that this value does constitute a lower limit since, to be more precise, the above ratio should be multiplied by a factor larger than unity which accounts for steric and statistical effects [6]. The ICB effect for the Ni(II)–*en* system is 200 [6]. The closeness of this to our result suggests that both ligands bind to Ni(II) with the same mechanism, irrespective of the chain length, a mechanism where the formation of the first Ni–N< bond is rate determining [2].

Acknowledgements

We thank Dr H. Diebler of the Max Planck Institut für Biophysikalische Chemie, Göttingen (Germany), for valuable discussions. This work has been supported by Ministero dell'Università per la Ricerca Scientifica e Tecnologica (MURST, Rome) within the program COFIN 98.

References

[1] D.W. Margerum, D.B. Rorabacher, F.G. Clarke, Inorg. Chem. 2 (1963) 667.
[2] D.B. Rorabacher, Inorg. Chem. 5 (1966) 1981.
[3] D.B. Rorabacher, T.S. Turan, J.A. Defever, W.G. Nickels, Inorg. Chem. 8 (1969) 1498.
[4] D.B. Rorabacher, C.A. Menendz-Chepeda, J. Am. Chem. Soc. 93 (1971) 6071.
[5] T.S. Turan, R.B. Rorabacher, Inorg. Chem. 11 (1972) 288.
[6] R.W. Taylor, H.K. Stepien, D.B. Rorabacher, Inorg. Chem. 13 (1974) 1282.
[7] T.S. Turan, Inorg. Chem. 13 (1974) 1584.
[8] M. Eigen, R.G. Wilkins, Adv. Chem. Ser. 49 (1965) 55.
[9] J. Aragò, A. Bencini, A. Bianchi, E. Garcia-Espana, M. Micheloni, P. Paoletti, J.A. Ramirez, P. Paoli, Inorg. Chem. 30 (1991) 1843.
[10] A. Bencini, A. Bianchi, P. Paoletti, S. Cabani, N. Ceccanti, M.R. Tinè, E. Garcia-Espana, Inorg. Chim. Acta 204 (1993) 227.
[11] S.W. Schwarzenbach, H. Flaschka, Complexometric Titrations, Methuen, London, 2nd edn., 1969, p. 48.
[12] H. Diebler, F. Secco, M. Venturini, J. Phys. Chem. 88 (1984) 4229.
[13] S.W. Provencher, J. Chem. Phys. 64 (1976) 2772.
[14] A. Bencini, A. Bianchi, V. Fusi, P. Paoletti, B. Valtancoli, J. Agarò, E. Garcia Espana, Inorg. Chim. Acta 20 (1993) 221.
[15] A.A. Frost, R.G. Pearson, Kinetics and Mechanism, Wiley, New York, 2nd edn., 1961, chapter 9, p. 213.
[16] P. Debye, Trans. Electrochem. Soc. 42 (1942) 265.
[17] M. Eigen, K. Tamm, Z. Elektrochem. 66 (1962) 107.
[18] R.M. Fuoss, J. Am. Chem. Soc. 80 (1958) 5059.
[19] M. Eigen, Z. Elektrochem. 64 (1960) 115.

PERGAMON

www.elsevier.nl/locate/poly

Polyhedron 19 (2000) 2515–2520

POLYHEDRON

Spectroscopic characteristics and thermal properties of divalent metal complexes of diclofenac

R. Bucci [a], A.D. Magrì [a], A.L. Magrì [a,*], A. Napoli [b]

[a] *Dipartimento di Chimica, Università di Roma 'La Sapienza', 00185 Rome, Italy*
[b] *Dipartimento di Scienze Ambientali, Università della Tuscia, 01100 Viterbo, Italy*

Abstract

The spectroscopic characteristics (IR and diffuse reflectance) and the thermal properties (TG, DTG and DSC) of the solid compounds obtained by the reaction of diclofenac (DH) with manganese(II), iron(II), cobalt(II), nickel(II), copper(II) and zinc(II) are reported and discussed. The complexes agreed with the empirical formula $MeD_2 \cdot (H_2O)_x$ and the metal ions are co-ordinated through the carboxylate group of the ligand. The furnace atmosphere (N_2 or O_2) greatly influences the thermal decomposition trend of the complexes, less their thermal stability. On the contrary, the initial decomposition temperature depends on the co-ordinated metal ion, especially in the case of iron(II) and copper(II) compounds, which are much less stable than other complexes. © 2000 Elsevier Science B.V. All rights reserved.

Keywords: Diclofenac; Metal(II) compounds; Spectroscopic properties; Thermal properties

1. Introduction

Diclofenac (DS), sodium salt of [2-[(2,6-dichlorophenyl)amino]phenyl] acetic acid, is a potent non-steroidal anti-inflammatory agent for the treatment of rheumatoid arthritis. The pharmacological effects of this drug are thought to be related to the inhibition of the conversion of arachidonic acid to prostaglandins, which are the mediators of the inflammatory process [1–3].

The literature reports several methods for determination of diclofenac [4–19] but only few data on the complexing ability of this drug with metal ions [20–26].

In a previous paper [27] we reported the main results of an extensive investigation on chemical, spectroscopic and thermoanalytical behaviour of DS and proposed new methods for its determination in pharmaceutical formulations. Since it is well-known that the interaction of the metal ions may influence the biological activity of drugs administered for therapeutic reasons, because many drugs act via chelation or by inhibiting the activity of metal-enzymes, in the present paper we extend the above study on the reaction of diclofenac with the Irving and Williams series of divalent metal ions: manganese(II), iron(II), cobalt(II), nickel(II), copper(II) and zinc(II).

2. Experimental

2.1. Apparatus

UV–Vis spectra were acquired with 1 cm quartz cells on a Perkin–Elmer 320 UV–Vis spectrophotometer connected to a model 3600 Data Station equipped with software packages 'IF-320', for instrument control. The scan speed was adjusted at 30 nm min^{-1}, slit width = 1 nm, response time = 0.5 s. The spectrophotometer was connected with a 'Colora' ultra-thermostat (25.0 ± 0.1°C).

IR and diffuse reflectance spectra were recorded using a Perkin–Elmer 1600 FT-IR and a Beckman DGB spectroreflectometer.

The thermal measurements were carried out using a Perkin–Elmer TGS-2 thermal analyser, connected to a model 3600 Data Station, and a 1020 series DSC-7 thermal analysis system equipped with a multitasking software for instrument control and data analysis. Unless specified otherwise, thermogravimetry and differen-

* Corresponding author. Tel: +39-06-499-13371.
E-mail address: antonio.magri@uniromal.it (A.L. Magrì).

0277-5387/00/$ - see front matter © 2000 Elsevier Science B.V. All rights reserved.
PII: S0277-5387(00)00552-0

tial scanning calorimetry runs were made on sample of about 1–2 mg (TG) and 0.3–0.5 mg (DSC) in a stream of nitrogen or oxygen (flow rate, 50 ml min^{-1}, heating rate 10°C min^{-1}).

The acidity of the aqueous solutions was checked with an Orion EA 940 pH-meter with an Orion 81-02 Ross combination pH electrode.

Millipore filtering apparatus fitted with 0.45 μm membrane discs.

2.2. Reagents

Diclofenac sodium salt 'Sigma' was used without further purification. Purity of dry material, checked by potentiometric titration, was 99.8% ($S_r = 0.05\%$, $N = 5$). The metal ions were in the form of perchlorate 'Aldrich'.

Distilled, deionised and, if necessary, O_2 and/or CO_2-free water was used. All other chemicals were of analytical-reagent grade.

2.3. Preparation of the solid compounds

The following general procedure was applied: 20 cm^3 of 0.01 mol dm^{-3} aqueous solution of the metal ion were added to 40 cm^3 of 0.01 mol dm^{-3} aqueous solution of the ligand ($C_L/C_M = 2$), maintaining the pH of the mixture in the range from 5.5 to 6, by the addition of small quantities of NaOH solution. The mixture was stirred for about 2 h, at room temperature, and then the precipitate was filtered off, washed with water and dried in vacuo, over silica gel, for at least 48 h.

The analysis of all the solid compounds agreed with the empirical formula $MD_2 \cdot (H_2O)_x$ [where M and D are, respectively the metal and the diclofenate ions and $x = 0$ for M = Fe(II), $x = 1$ for M = Mn(II), Co(II), Ni(II), $x = 3$ for Cu(II) and $x = 4$ for Zn(II)].

The compounds were prepared also in hot aqueous solution [23] achieving the same results.

3. Results and discussion

The main data of the spectroscopic and thermoanalytical investigation are summarised in Tables 1 and 2.

Because all the complexes showed similar spectroscopic characteristics and thermal behaviour, for the sake of brevity, we give below, as an example, a more detailed discussion of the first compound of the series and only a short presentation of the related studies of other complexes underlining its peculiar features.

3.1. Bis(dichlorophenylaminophenylacetato)manganese(II)

This compound, a pale pink powder, has the empirical formula $Mn(C_{14}H_{10}Cl_2NO_2)_2 \ (H_2O)$.

It is slightly soluble in water, but soluble in ethanol and this solution exhibits a spectrum with two maxima at $\lambda = 445$ nm and $\lambda = 370$ nm.

The diffuse-reflectance spectrum, which shows only a weak band at about 21 300 cm^{-1}, does not give a sure proof of the stereochemistry of the complex, because of the interference of the ligand absorption which mask the d–d bands.

The IR spectrum (Fig. 1) shows a strong band at 3570 cm^{-1} attributed to the presence of co-ordinated water. In fact, this band is absent in the anhydrous compound obtained by heating the sample at 150°C (see TG curves). The single band at 3320 cm^{-1} (ν_{NH}), similar to that found for diclofenac in the protonated form [27], instead of the two strong bands at 3388 cm^{-1} (ν_{NH}) and 3260 cm^{-1} ($\nu_{NH\cdots O}$ due to intramolecular hydrogen bonding), which appears in DS [22], proves the co-ordination of the metal ion through the carboxylate groups, but it can't exclude that there is an interaction between NH group and the metal ion. This hypothesis is confirmed by the $\nu_{as\,COO^-}$ and $\nu_{s\,COO^-}$ bands. The difference $\Delta_\nu = (1554-1420 =)134$ cm^{-1} is less than that of the DS free ion [$\Delta_\nu = (1572-1402 =)$ 170 cm^{-1}] as expected for bidentate co-ordination.

Table 1
Spectroscopic data from visible, diffuse reflectance and infrared spectra of bis(dichlorophenylaminophenylacetato)metal(II) compounds

Compound	Colour	Absorption maximum		Diagnostic IR [b] bands (cm^{-1})	
		Visible [a] (nm)	Diffuse reflectance (cm^{-1})	$\nu_{as\,COO^-}$	$\nu_{s\,COO^-}$
DH ($C_{14}H_{11}Cl_2NO_2$)	white			1694	1304
DS ($C_{14}H_{10}Cl_2NO_2Na$)	white			1572	1402
$Mn(C_{14}H_{10}Cl_2NO_2)_2 \cdot (H_2O)$	pale pink	370–445	21 300	1554	1420
$Fe(C_{14}H_{10}Cl_2NO_2)_2$	bronze		11 100–21 300	1578	1400
$Co(C_{14}H_{10}Cl_2NO_2)_2 \cdot (H_2O)$	blue	350–528	7700–17 400–18 900	1578	1400
$Ni(C_{14}H_{10}Cl_2NO_2)_2 \cdot (H_2O)$	pale green	403–675–750	8500–13 500–15 100–25 000	1578	1400
$Cu(C_{14}H_{10}Cl_2NO_2)_2 \cdot (H_2O)_4$	green	725	14 500–25 600	1616–1558	1415–1394
$Zn(C_{14}H_{10}Cl_2NO_2)_2 \cdot (H_2O)_3$	white			1560	1432

[a] In ethanol solution.
[b] KBr disc.

Table 2
Thermogravimetric data for the analysed compounds in the temperature range 30–850°C

Compound	Gas	t range [a] (°C)	(t_{max}) [b] (°C)	Weight loss (%)		Residue	
				Calculated [c]	Found	Calculated [c]	Found
$Mn(C_{14}H_{10}Cl_2NO_2)_2\cdot(H_2O)$	N_2	105–125	(115)	2.74 [H_2O]	2.7		97.3
		223–280	(250)		78.3	17.50 [$MnCO_3$]	19.0
		280–440			1.6		17.4
		440–700	(630)	5.89 [$CO_{1.66}$]	5.6		11.8
	O_2	223–280	(236, 247)		20.0		77.3
		280–390			3.0		74.3
		390–585	(485, 520)		62.5	11.61 [Mn_3O_4]	11.8
$Fe(C_{14}H_{10}Cl_2NO_2)_2$	N_2	165–260	(230)		73.6		26.4
		260–680			9.0	17.92 [$FeCO_3$]	17.4
		680–800	(738)	5.57 [$CO_{1.5}$]	5.5		11.9
	O_2	140–165	(148)		8.3		91.7
		165–305	(240)		41.7		50.0
		305–390			4.2		45.8
		390–520	(490)		33.6	12.36 [Fe_2O_3]	12.2
$Co(C_{14}H_{10}Cl_2NO_2)_2\cdot(H_2O)$	N_2	30–100	(60)	2.70 [H_2O]	2.8		97.2
		227–280	(253)		78.5		18.7
		280–400			1.0	17.82 [$CoCO_3$]	17.7
		400–680	(600)	5.78 [$CO_{1.66}$]	5.9		11.8
	O_2	227–287	(259)		64.6		32.6
		287–405			1.3		31.3
		405–490	(470)		7.0		24.3
		490–615	(572)		11.1	12.03 [Co_3O_4]	13.2
$Ni(C_{14}H_{10}Cl_2NO_2)_2\cdot(H_2O)$	N_2	30–120	(72)	2.70 [H_2O]	2.8		97.2
		228–310	(265)		66.0		31.2
		310–700			20.1		11.1
	O_2	228–340	(268)		36.1		61.1
		340–410			4.9		56.2
		410–565	(525)		44.4	11.20 [NiO]	11.8
$Cu(C_{14}H_{10}Cl_2NO_2)_2\cdot(H_2O)_4$	N_2	55–100	(75)	9.92 [$4H_2O$]	9.4		90.6
		154–185	(175)		2.4		88.2
		185–280	(234)		38.9		49.3
		280–850			29.2		20.1
	O_2	154–185	(175)		2.4		88.2
		185–356	(234)		28.5		59.7
		356–665	(493,604)		48.9	10.96 [CuO]	10.8
$Zn(C_{14}H_{10}Cl_2NO_2)_2\cdot(H_2O)_3$	N_2	70–100	(78)	7.61 [$3H_2O$]	7.7		92.3
		245–286	(272)		75.3	17.67 [$ZnCO_3$]	17.0
		286–600	(520)	6.20 [CO_2]	5.9		11.1
	O_2	245–286	(272)		72.2		20.1
		286–372			2.9		17.2
		372–520	(470)		6.0	11.6 [ZnO]	11.2

[a] Decomposition temperature range (water loss in O_2 occurs as in N_2 and it is not reported).
[b] t_{max} is the temperature of the maximum decomposition rate (by DTG analysis of TG curves).
[c] Volatile products and supposed residues are reported in brackets.

The thermal decomposition trend of this complex is greatly conditioned by the furnace atmosphere. According to thermogravimetry in O_2 (Fig. 2, curve a) this compound loss its water molecule in the temperature range from 105 to 125°C (*Anal*. Calc.: 2.74, Found: 2.7%) and the anhydrous is stable up to about 223°C. The first decomposition process takes place between 223 and 280°C, with about 20% weight loss, and it is a two-step overlapped process ($t_{max} = 236$ and 247°C). Upon further heating the sample slowly loses mass up to about 390°C, then the decomposition speeds up suddenly with a new two-step partly overlapped process ($t_{max} = 485$ and 520°C). At 585°C the residue consists mainly of Mn_3O_4 (*Anal*. Calc.: 11.61, Found: 11.8%) or a mixture of different oxides. In N_2 atmosphere (Fig. 2, curve b) the thermal behaviour is similar to that in O_2 only up to 223°C, then the decomposition rate increases ($t_{max} = 250$°C) and, with an apparent one-step process, at 280°C the residue is about 19% (*Anal*. Calc. for $MnCO_3$: 17.50%). This residue slowly loses mass (about 1.6% up to 440°C) then, between 440 and 700°C, it changes into the final metal oxide. DSC curves (Fig. 3,

curves a and b) confirm the influence of the furnace atmosphere on the decomposition mechanism of the complex showing exo- and/or endothermic peaks connected with the weight losses in TG. An endothermic process accompanies the water evolution ($t_p = 120$°C; $\Delta H = 46$ kJ mol^{-1}) both in O_2 and N_2 atmosphere. Then, several exothermic reactions characterise the oxidative thermal decomposition of the complex, whereas, in N_2, the initial decomposition stage occurs with an exothermic reaction partly neutralised by the overlapped endothermic one. Another wick endothermic peak appears up to 500°C.

3.2. Other complexes

All the complexes are fairly soluble in water and soluble in ethanol.

The diffuse reflectance spectra suggest an octahedral geometry around the metal ion for cobalt(II), nickel(II) and copper(II) complexes [23,28] whereas in the case of iron(II) and zinc(II) as reported for manganese(II) compound, the ligand interference is enough to mask the d–d bands.

A comparison of the IR spectra, in the range from 1700 to 1300 cm^{-1}, with those of the ligand in sodium (DS) and protonated (DH) form suggests the carboxylic group is involved in the metal ions complexation and the formed oxygen-metal bond has a different degree of covalent character: in the Fe(II), Co(II) and Ni(II) complexes the bonding is primarily ionic whereas in Cu(II) complex it is primarily covalent [29]. The Cu(II), Ni(II) and Zn(II) complexes show a strong absorption at 3550 cm^{-1} attributed to OH stretching of co-ordinated water molecules.

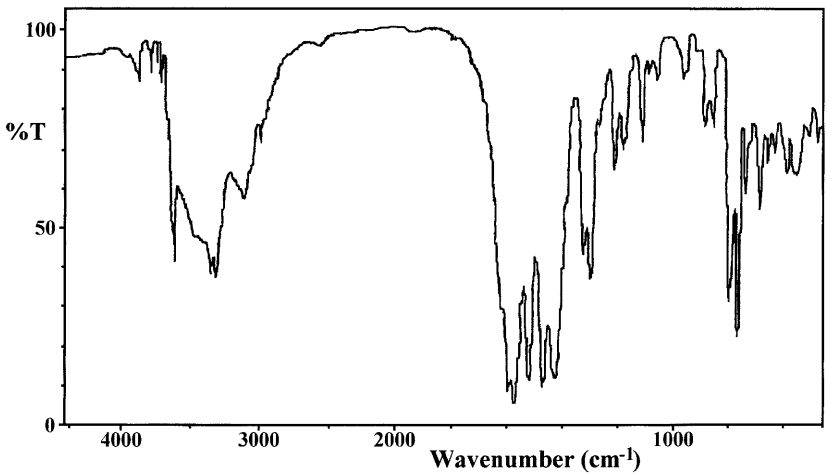


Fig. 1. IR spectra (KBr disc) of bis(dichlorophenylaminophenylacetato)manganese(II).

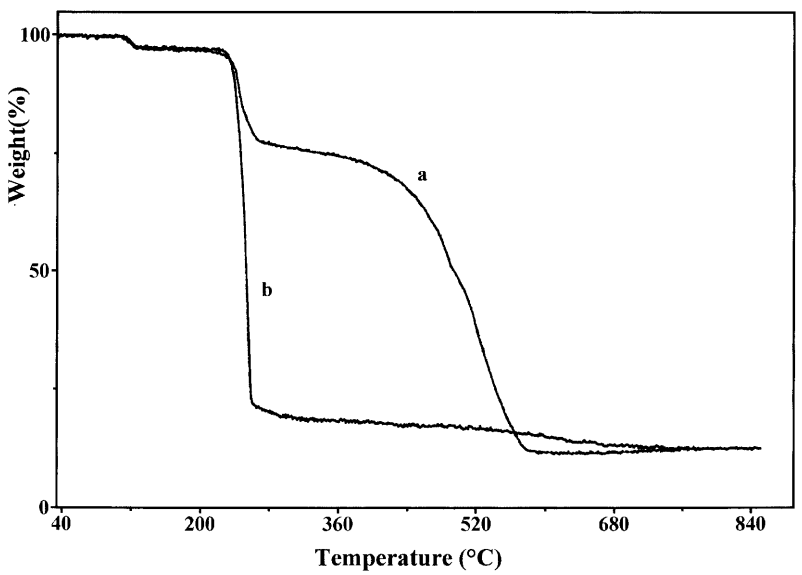


Fig. 2. TG of bis(dichlorophenylaminophenylacetato)manganese(II) in O_2 (curve a) and in N_2 (curve b) atmosphere.

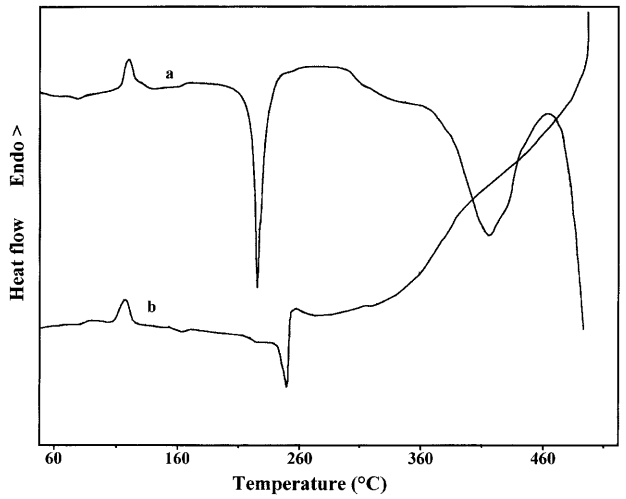


Fig. 3. DSC of bis(dichlorophenylaminophenylacetato)manganese(II) in O_2 (curve a) and in N_2 (curve b) atmosphere.

According to the thermograms (TG) in a dynamic O_2 atmosphere, the water content of the complexes departs at temperature up to about 125°C. The anhydrous compounds are more stable than DH ($t_d = 140$°C) but less than DS ($t_d = 265$°C) [27]. The thermal decomposition occurs through a multi-step process, so conclusion is drawn that the partial reactions take place consecutively, partly overlapping one another. At about 650°C the residues consist mainly of the metal oxides. In a dynamic N_2 atmosphere the first decomposition step occurs at the same temperature than in O_2 but with a more quick and a higher mass loss. An exception is the thermal behaviour of the iron(II) complex. The decomposition delay observed in N_2 can be explained by the inhibition of the oxidative decomposition of the complex, which probably occurs through iron(II) to iron(III) transition. In fact, in O_2, the decomposition begins with an exothermic peak at 145°C whereas DSC in N_2 shows an endothermic peak at about 175°C.

4. Conclusions

This study enriches the knowledge of diclofenac with some aspects of its complexing ability and, although the reaction medium is very different from the biological environment, however the obtained results enable to suppose that the administration of this drug for long time could decrease the bioavailability of some important metal ions. In fact diclofenac reacts with divalent metal ions forming 1:2 (metal to ligand ratio) very slightly water-soluble complexes, so much so that the stability constants were not determined.

The spectroscopic analysis of the solid compounds proved the carboxylate group of the ligand is involved in the complexation reaction with different degree of covalency in the formed metal(II)–oxygen bonds and, with regard to cobalt(II), nickel(II) and copper(II) complexes, an octahedral geometry around the metal ion.

The thermal analysis evidenced a great dependence of the thermal decomposition trend of these complexes by the furnace atmosphere. It was found that, in nitrogen, the decomposition occurs through the $MeCO_3$ intermediate (this mechanism was particularly evident in TG curves of manganese(II), iron(II), cobalt(II) and zinc(II) compounds). The kind of the bonded metal ion influenced the thermal stability order that, calculated by the initial decomposition temperature (t_d) of the anhydrous compounds (in N_2), resulted $Zn > Ni \geq Co \geq Mn \gg Fe > Cu$. It does not agree fully with that expected for analogous series of metal(II) complexes [30] leading to suppose different structures and/or inter–intramolecular interactions. In particular we emphasise the thermal behaviour of iron(II) complex, the only one precipitated in anhydrous form. This compound, as found in a precedent case [31], is more stable than copper(II) complex only and, in O_2 atmosphere, it becomes the least stable of all the analysed complexes. This behaviour could be justified by the initial oxidation reaction of iron(II) to iron(III) that favours the thermal decomposition of the compound.

Acknowledgements

The authors acknowledge the National Research Council of Italy (CNR) for the financial support.

References

[1] Martindale, The Extrapharmacopeia, 29th ed., The Pharmac. Press, London, 1980.
[2] P.A. Todd, E.M. Sorkin, Drugs 35 (1988) 244.
[3] P. Moser, A. Sallmann, I. Wiesemberg, J. Med. Chem. 33 (1990) 2358.
[4] A. Shumaker, H.E. Geissler, E. Mutschler, J. Chromatogr. 181 (1980) 512.
[5] W. Schneider, P.H. Degen, J. Chromatogr. 217 (1981) 263.
[6] K.K.H. Chan, K.H. Vyas, K. Wnuck, Anal. Lett. 15 (1982) 1649.
[7] J. Godbilon, S. Gauron, J.P. Metayer, J. Chromatogr. 338 (1985) 151.
[8] C. Sarbu, J. Chromatogr. 367 (1986) 286.
[9] B. Henning, A. Steup, R. Benecke, Pharmazie 42 (1987) 861.
[10] D. Grandjean, J.C. Beolor, M.T. Quincon, E. Savel, J. Pharm. Sci. 78 (1989) 247.
[11] M.R. Borenstein, Y. Xue, S. Cooper, T. Tzeng, J. Chromatogr. B 685 (1996) 59.
[12] C.S. Sastry, A.R.M. Rao, T.N.V. Prasad, Anal. Lett. 20 (1987) 349.
[13] C.S.P. Sastry, A.S.R.P. Tipirneni, M.V. Suryanarayana, Analyst 114 (1989) 513.
[14] B.V. Kamath, K. Shivram, Indian J. Pharm. Sci 54 (1992) 81.
[15] B.V. Kamath, K. Shivram, G.P. Oza, S. Vangani, Anal. Lett 26 (1993) 665.

[16] B.V. Kamath, K. Shivram, Anal. Lett 26 (1993) 903.
[17] H. Fabre, S.W. Sun, B. Mandrou, H. Maillols, Analyst 118 (1993) 1061.
[18] J.C. Botello, G. Perez-Caballero, Talanta 42 (1995) 105.
[19] I. Kramancheva, I. Dobrev, L. Brakalov, A. Andreeva, Anal. Lett. 30 (1997) 2235.
[20] S.A. Abdel Fattah, S.Z. El-Khateeb, S.A. Abdel Razeg, M. Tawakkol, Spect. Lett. 21 (1988) 533.
[21] S.A. Kustrin, L. Zivanovic, D. Radulovic, M. Vasiljevic, Analyst 116 (1991) 753.
[22] D. Kovala-Demertzi, D. Mentzafos, A. Terzis, Polyhedron 12 (1993) 1361.
[23] R. Kesharwani, P. Singh, J. Indian Chem. Soc. 72 (1995) 803.
[24] A. Fini, G. Feroci, G. Fazio, M.J. Fernandez-Hervas, M.A. Olgado, A.M. Rabasco, Int. J. Pharm. Adv. 1 (1996) 269.
[25] S. Agatonovic-Kustrin, L. Zivanovic, M. Zecevic, D. Radulovic, J. Pharm. Biomed. Anal. 16 (1997) 147.
[26] C. Castellari, G. Feroci, S. Ottani, Acta Crystallogr., Sect. C 55 (1999) 907.
[27] R. Bucci, A.D. Magrì, A.L. Magrì, Fresenius J. Anal. Chem. 362 (1998) 577.
[28] A.B.P. Lever, Inorganic Electronic Spectroscopy, Elsevier, Amsterdam, 1968.
[29] R.E. Sievers, J.C. Bailer, Jr, Inorg. Chem. 1 (1962) 174.
[30] A.L. Magrì, A.D. Magrì, F. Balestrieri, E. Cardarelli, G. D'Ascenzo, Thermochim. Acta 38 (1980) 225.
[31] R. Bucci, A.D. Magrì, A.L. Magrì, A. Napoli, Thermochim. Acta 217 (1993) 213.

PERGAMON

www.elsevier.nl/locate/poly

Polyhedron 19 (2000) 2521–2527

POLYHEDRON

Hydrothermal syntheses, structures and magnetic properties of coordination cation metavanadates, $Cu(tn)_2(VO_3)_2$ and $Ni(NH_3)_2(VO_3)_2$

Bi-Zhou Lin [a,b,*], Shi-Xiong Liu [a]

[a] *Department of Chemistry, Fuzhou University, Fuzhou, Fujian 350002, People's Republic of China*
[b] *Institute of Material Physical Chemistry, Huaqiao University, Quanzhou, Fujian 362011, People's Republic of China*

Received 14 June 2000; accepted 27 July 2000

Abstract

Two new metavanadates, $Cu(tn)_2(VO_3)_2$ (tn = 1,3-diaminopropane) and $Ni(NH_3)_2(VO_3)_2$, have been prepared under hydrothermal conditions and their single-crystal structures determined by X-ray diffraction. Both structures consist of corner-sharing VO_4 tetrahedral chains with complex cations occupying the interchain positions. While there dominantly exist electrostatic interactions between the $Cu(tn)_2^{2+}$ fragments and the vanadium oxide chains in $Cu(tn)_2(VO_3)_2$, the $Ni(NH_3)_2^{2+}$ moieties in the $Ni(NH_3)_2(VO_3)_2$ bridge the vanadium oxide chains into a three-dimensional framework structure by Ni–O covalent interactions. The magnetic properties were measured in the temperature ranging from 4 to 275 K. It is shown that $Cu(tn)_2(VO_3)_2$ possesses well-separated Cu^{2+} centers and that the magnetic behavior of $Ni(NH_3)_2(VO_3)_2$ can be explained based on a one-dimensional Ising model. © 2000 Elsevier Science B.V. All rights reserved.

Keywords: Crystal structures; Metavanadate complexes; Nickel complexes; Copper complexes; Hydrothermal synthesis; Magnetic properties

1. Introduction

Self-assembly of inorganic molecular precursors or subunits in a quest for supramolecular chemistry is one of the highly recognized areas of chemical research [1]. The significant contemporary interest in organic/inorganic hybrid materials reflects their diverse applications or potential applications in the areas such as catalysis, molecular electronics, magnetism and photochemistry [2]. The chemistry of the transition metal-phosphates, prepared by hydrothermal synthetic techniques, has been extensively studied due to their inherent potential for the development of supramolecular chemistry [3]. The recent success in the hydrothermal assembly of the low-dimensional and microporous oxometalate hybrid materials using metal coordination complexes suggests a novel approach towards rational synthesis of metal oxide/organic solids [4–8].

As a continuation of our effort in the hydrothermal assembly of metal oxide-based solid materials, we seek to explore the assembly of the vanadate anions and the coordination complexes [9]. We report herein the syntheses, structures, IR spectra and magnetic properties of two new hybrid solids, $Cu(tn)_2(VO_3)_2$ (**1**) and $Ni(NH_3)_2(VO_3)_2$ (**2**), where tn = 1,3-diaminopropane. Both structures consist of one-dimensional chains, formed by corner-sharing VO_4 tetrahedra. The chains are similar to those found in anhydrous metavanadates, such as $LiVO_3$ [10], $NaVO_3$ [11], KVO_3, NH_4VO_3 and $TlVO_3$ [12]. While there mainly are electrostatic interactions between the $Cu(tn)_2^{2+}$ fragments and the vanadium oxide chains in the structure of **1**, the adjacent chains in the structure of **2** are held together through $\{Ni(\mu\text{-}O)_4N_2\}$ octahedral moieties, and forming a three-dimensional framework.

* Corresponding author. Tel.: +86-595-269-1567; fax: +86-595-268-6969.
E-mail address: bzlin@hqu.edu.cn (B.-Z. Lin).

0277-5387/00/$ - see front matter © 2000 Elsevier Science B.V. All rights reserved.
PII: S0277-5387(00)00581-7

2. Experimental

2.1. General procedures

Reagents were purchased commercially and used without further purification. The hydrothermal reaction was carried out in 17 ml of Teflon-lined stainless steel autoclaves under autogenous pressure with a fill factor of approximately 40%. The reactants were stirred briefly before heating. The infrared spectra were obtained on a Perkin-Elmer FTIR 2000 Spectrometer with pressed KBr pellets in the 4000–400 cm^{-1} region. The magnetic susceptibility data were measured using Quantum Design PPMS 6000 magnetometer in the temperature range from 4 to 275 K at an applied magnetic field of 5 kG. The diamagnetic corrections were estimated form Pascal's constants.

2.2. Synthesis of $Cu(tn)_2(VO_3)_2$

A mixture of V_2O_5 (0.135 g), CuO (0.058 g), 1,3-diaminopropane (0.38 ml), H_3BO_3 (0.653 g) and H_2O (7.0 ml) in a mole ratio of 1:1:5.8:14.4:533 was heated at 165°C for 48 h. This gave deep brown prismatic crystals of **1** as major product (in the yield of approximately 80% based on vanadium), and a small amount of H_3BO_3 was found. The acidity of the medium kept pH $\sim$9.5 before and after the synthesis. Attempts to synthesize **2** without H_3BO_3 proved unsuccessful. *Anal.* Calc. for $C_6H_{20}CuN_4O_6V_2$: C, 17.59; H, 4.92; N, 13.68; V, 24.87. Found: C, 17.52; H, 4.89; N, 13.74; V, 24.80%.

2.3. Synthesis of $Ni(NH_3)_2(VO_3)_2$

A mixture of NH_4VO_3 (0.117 g), $Ni(NO_3)_2{\cdot}6H_2O$ (0.174 g), and H_2O (5.5 ml) in a mole ratio of 1:0.6:389 was heated at 130°C for 48 h.The acidity of the medium kept the value of pH at approximately 5.5 before and after the synthesis. Green thin plates of **2** were purely obtained from the above hydrothermal reaction, and the yield was approximately 85% based on vanadium. *Anal.* Calc. for $H_6N_2NiO_6V_2$: H, 2.08; N, 9.64; V, 35.05. Found: H, 2.10; N, 9.59; V, 35.11%.

2.4. X-ray crystallography

X-ray diffraction data on crystals of **1** with $0.26 \times 0.18 \times 0.10$ mm and of **2** with $0.25 \times 0.15 \times 0.10$ mm were collected on a Rigaku AFC5R four-circle diffractometer at 23°C with graphite-monochromated Mo Kα ($\lambda = 0.71069$ Å), the scan mode being ω–2θ at a scan speed of 8° min^{-1} in ω. Cell dimensions were refined using 25 reflections in the rang $20 < 2\theta < 30°$. The diffraction data were corrected for Lorentz and polarization effects.

The structures were solved by direct methods using SHELXS-86 software package [13]. All non-hydrogen atoms in both structures were refined anisotropically by the full-matrix least-squares methods. All hydrogen atoms were localized in the difference electron density maps and included in the refinements with fixed positional and isotropically thermal parameters. The refinements of the structures were performed using SHELXL-93 crystallographic software package [14]. The crystallographic data are given in Table 1.

Table 1
Crystallographic data for $Cu(tn)_2(VO_3)_2$ and $Ni(NH_3)_2(VO_3)_2$

Empirical formula	$C_6H_{20}CuN_4O_6V_2$	$H_6N_2NiO_6V_2$
Formula weight	409.68	290.66
Crystal system	orthorhombic	orthorhombic
Space group	$Pna2_1$	*Pnma*
Unit cell dimensions		
a (Å)	11.455(2)	5.535(1)
b (Å)	8.402(2)	10.661(2)
c (Å)	14.322(3)	11.772(2)
V (Å^3)	1378.4(5)	694.6(2)
Z	4	4
D_{calc} (g cm^{-3})	1.974	2.779
μ(Mo Kα) (mm^{-1})	2.883	5.302
Crystal size (mm)	$0.26 \times 0.18 \times 0.10$	$0.25 \times 0.15 \times 0.10$
Color	brown	green
Shape	prism	plate
θ_{max} (°)	26	26
No. of data collected	1592	835
No. of unique data	1410	717
No. of observed data ($I > 2\sigma(I)$)	1143	614
No. of variables	172	55
Goodness-of-fit	1.09	1.10
R_1/wR_2	0.0408/0.1018	0.0271/0.0786

3. Results and discussion

3.1. Syntheses and infrared spectra

In principle, the hydrothermal technique has many variables, which can affect the result significantly. The H_3BO_3 in the preparation of **1** takes a role as the acid buffering agent. This species appears to be needed in the syntheses, although it is not incorporated in the final structure. Without H_3BO_3 or H_3BO_3 replaced by CH_3COOH, attempts to synthesize **1** proved fruitless and black $(H_3N(CH_2)_3NH_3)V_4O_{10}$, which was reported previously[15], was obtained. On the other hand, $NH_4V_3O_8$ [16] is formed under very similar synthetic conditions to those employed for compound **2** except for the initial pH value of **6** rather than 5.5. It is shown that the kinetic parameters (nucleation, crystal, etc.) are important and strongly influenced by small changes of the synthetic parameters.

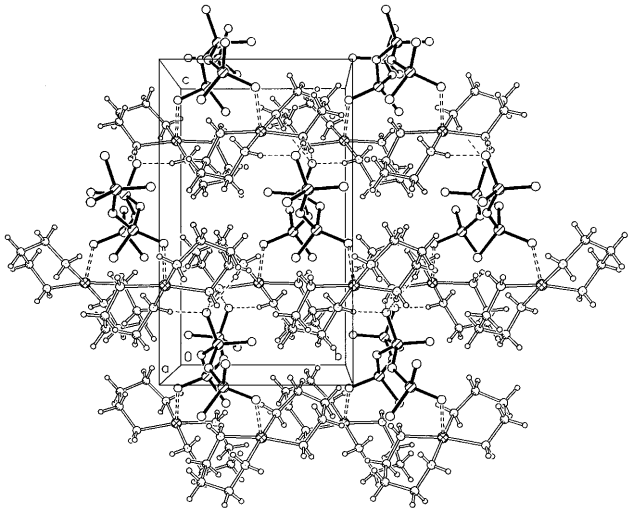


Fig. 1. The packing of $Cu(tn)_2(VO_3)_2$ showing the hydrogen bonds, where cross-hatched circles for Cu, stripped ones for V, big open ones for O, dotted ones for N, shaded ones for C, and small open ones for H.

The bands at 952 and 905 cm^{-1} in the IR spectrum of 1977 and 933 cm^{-1} in **2** are related to the VO_2 symmetric stretching involving the exterior oxygen atoms and to that involving the backbone oxygen atoms, respectively [17]. The bands at 832 in **1** and 835 cm^{-1} in **2** are assigned to the VO_2 antisymmetric stretching, while the feature at 635 in **1** and 639 cm^{-1} in **2** are attributed to the symmetric and antisymmetric stretching of V–O–V.

3.2. Structure of $Cu(tn)_2(VO_3)_2$

The metavanadate anion in the structure of compound **1** consists of infinite one-dimensional chains of corner-sharing VO_4 tetrahedra, which extend parallel to the *a* axis, as shown in Fig. 1. The complex cations $Cu(tn)^{2+}$ provide charge balance and are located between the chains.

The vanadium oxide chains are similar to those found in other anhydrous metavanadates, such as $LiVO_3$ [10], $NaVO_3$ [11], KVO_3, NH_4VO_3 and $TlVO_3$ [12]. As listed in Table 2, two crystallographically-independent vanadium sites V(1) and V(2) both exhibit distorted geometry. The oxygen atoms shared by two adjacent VO_4 tetrahedra have longer V–O bond lengths ranging from 1.782(8) to 1.811(8)Å, while the terminal vanadly oxygen atoms have shorter V–O bond lengths between 1.614(9) and 1.660(7) Å. The values are in good agreement with those found in metavanadates MVO_3 ($M = Li^+$, Na^+, K^+, NH_4^+ and Tl^+) [10–12]. Valence sum calculations [18] resulted in 4.96 for V(1) and 5.08 for V(2), both very close to the ideal value of 5 for V(V).

The $Cu(tn)_2^{2+}$ complexes are arranged alternately on each side of the vanadium oxide chain. The copper atom adopts a CuN_4 square planar geometry, where the four nitrogen atoms come from two bidentate ligands 1,3-diaminopropane with Cu–N distances between 2.005(8) and 2.039(8) Å. The least-square plane is defined by the four nitrogen atoms with the mean deviation of 0.057 Å. The copper atom protrudes from the plane by 0.119(5) Å. The closest distance between

Table 2
Selected bond lengths (Å) and angles (°) for $Cu(tn)_2(VO_3)_2$ [a]

Cu(1)–N(2)	2.005(8)	Cu(1)–N(4)	2.008(8)	Cu(1)–N(1)	2.039(8)
Cu(1)–N(3)	2.039(7)	V(1)–O(1)	1.628(7)	V(1)–O(4)	1.660(7)
V(1)–O(2)	1.782(8)	V(1)–O(3)	1.797(8)	V(2)–O(5)	1.614(9)
V(2)–O(6)	1.635(8)	V(2)–O(2a)	1.796(8)	V(2)–O(3)	1.811(8)
Cu(1)···O(1)	2.406(8)	N(1)···O(6c)	3.17(1)	N(1)···O(6d)	2.99(1)
N(2)···O(4a)	3.07(1)	N(2)···O(6c)	2.97(1)	N(3)···O(4a)	3.01(1)
N(4)···O(4)	3.09(1)	N(4)···O(6d)	2.91(1)		
N(2)–Cu(1)–N(4)	176.5(4)	N(2)–Cu(1)–N(1)	88.1(3)		
N(4)–Cu(1)–N(1)	91.9(3)	N(2)–Cu(1)–N(3)	93.0(3)		
N(4)–Cu(1)–N(3)	86.3(3)	N(1)–Cu(1)–N(3)	170.0(4)		
O(1)–V(1)–O(4)	106.3(4)	O(1)–V(1)–O(2)	110.5(4)		
O(4)–V(1)–O(2)	110.1(4)	O(1)–V(1)–O(3)	108.7(4)		
O(4)–V(1)–O(3)	107.7(4)	O(2)–V(1)–O(3)	113.1(4)		
O(5)–V(2)–O(6)	107.0(5)	O(5)–V(2)–O(2a)	108.4(5)		
O(6)–V(2)–O(2a)	107.9(4)	O(5)–V(2)–O(3)	113.4(5)		
O(6)–V(2)–O(3)	107.8(4)	O(2a)–V(2)–O(3)	112.0(4)		
V(1)–O(3)–V(2)	144.4(5)	V(1)–O(2)–V(2b)	141.4(5)		
N(1)–H(11A)–O(6c)	139.2(3)	N(1)–H(11B)–O(6d)	168.9(3)		
N(2)–H(12A)–O(4a)	154.1(3)	N(2)–H(12B)–O(6c)	146.5(3)		
N(3)–H(13A)–O(4a)	175.1(3)	N(4)–H(14A)–O(4)	152.6(3)		
N(4)–H(14B)–O(6d)	169.0(3)				

[a] Symmetry codes: (a) $x+1/2, -y+3/2, z$; (b) $x-1/2, -y+3/2, z$; (c) $-x+1, -y+1, z-1/2$; (d) $-x+1/2, y-1/2, z-1/2$.

Cu and O is 2.406(8) Å for Cu(1)···O(1). If this interaction is considered significant, the environment around the copper atom can be also viewed as distorted square-pyramidal geometry connected to every other vanadium site in the vanadium oxide chains. As depicted in Fig. 2, the two chelate rings each composed of Cu and C, N atoms of 1,3-diaminopropane illustrate a distinctly chainlike configuration.

There exists extensive hydrogen bonding between the N–H groups from the complex fragments $Cu(tn)_2^{2+}$ and the oxygen atoms from the inorganic anion chains, with N···O interatomic distances ranging from 2.91(1) to 3.17(1) Å (see Fig. 1).

3.3. Structure of $Ni(NH_3)_2(VO_3)_2$

The substitute of $Cu(tn)_2^{2+}$ by $Ni(NH_3)_2^{2+}$ conduced to compound **2**. Figs. 3 and 4 are two projections of the structure of **2** along the *a* and *b* directions, respectively.

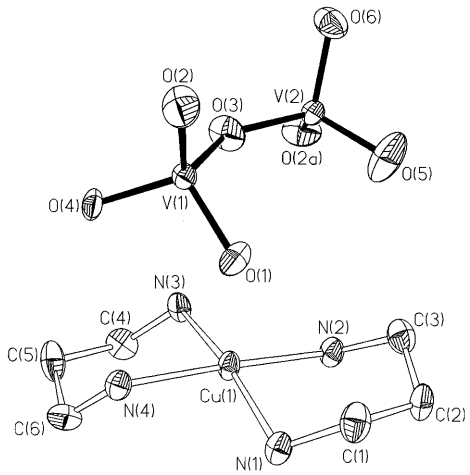


Fig. 2. The asymmetric unit in $Cu(tn)_2(VO_3)_2$, showing the metal-atom coordination environments with 50% probability displacement ellipsoids.

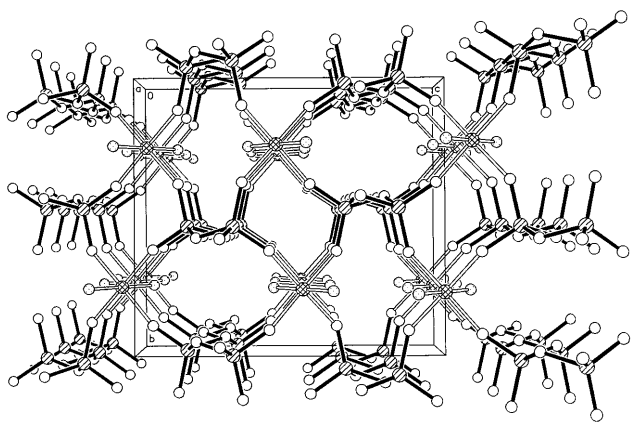


Fig. 3. The structure of $Ni(NH_3)_2(VO_3)_2$ projected along the *a* axis,where cross-hatched circles for Ni, stripped ones for V, open ones for O, and dotted ones for N.

The three-dimensional framework structure of **2** is built up from the corner-sharing VO_4 tetrahedral chains hold together by the complex fragments $Ni(NH_3)_2^{2+}$ through the Ni–O covalent interactions.

The coordination spheres centered V and Ni atoms are shown in Fig. 5. Four oxygen atoms are coordinated to V(1) with a distorted tetrahedral geometry. As listed in Table 3, the two oxygen atoms bridging two adjacent VO_4 tetrahedra have longer V–O bond distances of 1.800(3) and 1.802(3) Å, and the others linking one VO_4 tetrahedron and one NiO_4N_2 octahedron have shorter V–O bond distances of 1.632(3) and 1.652(3) Å. Although these values are in accord with those observed in metavanadates MVO_3 ($M = Li^+$, Na^+, K^+, NH_4^+ and Tl^+) [10–12], the shorter V–O

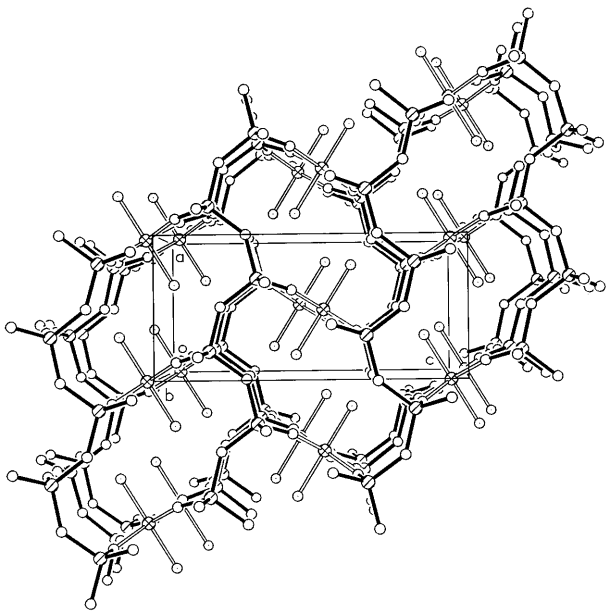


Fig. 4. The structure of $Ni(NH_3)_2(VO_3)_2$ projected along the *b* axis.

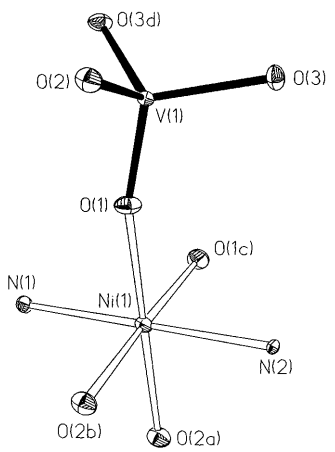


Fig. 5. The asymmetric unit in $Ni(NH_3)_2(VO_3)_2$, showing the metal-atom coordination environments with 50% probability displacement ellipsoids.

Table 3
Bond lengths (Å) and angles (°) for $Ni(NH_3)_2(VO_3)_2$ [a]

Ni(1)–O(1)	2.035(3)	Ni(1)–O(2a)	2.029(3)	Ni(1)–N(1)	2.037(4)
Ni(1)–N(2)	2.060(4)	V(1)–O(1)	1.632(3)	V(1)–O(2)	1.652(3)
V(1)–O(3d)	1.800(3)	V(1)–O(3)	1.802(3)	N(2)···O(3f)	2.806(4)
O(2b)–Ni(1)–O(1)	91.6(1)	O(1c)–Ni(1)–O(1)	90.1(2)		
O(2a)–Ni(1)–O(2b)	86.7(2)	O(2a)–Ni(1)–O(1c)	91.6(1)		
O(2a)–Ni(1)–O(1)	178.1(1)	O(2b)–Ni(1)–O(1c)	178.1(1)		
O(2a)–Ni(1)–N(1)	91.7(1)	O(2b)–Ni(1)–N(1)	91.7(1)		
O(1c)–Ni(1)–N(1)	89.3(2)	O(1)–Ni(1)–N(1)	89.3(2)		
O(2a)–Ni(1)–N(2)	88.3(1)	O(2b)–Ni(1)–N(2)	88.2(1)		
O(1c)–Ni(1)–N(2)	90.7(1)	O(1)–Ni(1)–N(2)	90.7(1)		
N(1)–Ni(1)–N(2)	179.9(2)	O(1)–V(1)–O(2)	109.9(2)		
O (1)–V(1)–O(3d)	107.8(2)	O(2)–V(1)–O(3d)	111.5(2)		
O(1)–V(1)–O(3)	109.5(2)	O(2)–V(1)–O(3)	109.0(1)		
O(3d)–V(1)–O(3)	109.2(1)	V(1)–O(1)–Ni(1)	163.8(2)		
V(1)–O(2)–Ni(1b)	146.3(2)	V(1e)–O(3)–V(1)	133.0(2)		
N(2)–H(4)–O(3f)	142.7(1)				

[a] Symmetry codes: (a) $-x+1$, $y+1/2$, $-z+1$; (b) $-x+1$, $-y$, $-z+1$; (c) x, $-y+1/2$, z; (d) $x-1/2$, y, $-z+3/2$; (e) $x+1/2$, y, $-z+3/2$; (f) $x+1/2$, $-y+1/2$, $-z+3/2$.

bond lengths are slightly shorter than those found in recently reported metavanadates with the coordination cations covalently attached to the anion chains, such as $Cu(en)(VO_3)_2$ (1.670 and 1.687Å), $Cu(bpy)(VO_3)_2$ (1.667Å), $Cu(bpy)_2(VO_3)_2$ (1.678Å) [5] and $Cu(dien)(VO_3)_2{\cdot}H_2O$ (1.687 Å) [19]. Valence sum calculations [18] were 5.10 for V. It is close to the ideal value for V(V). The octahedral geometry about each nickel atom is nearly ideal, with no derivations of more than 4° from the ideal octahedral geometry. In the six coordination atoms of each Ni atom, apart from the two nitrogen atoms from two NH_3 ligands with Ni–N distances of 2.037(4) and 2.060(4) Å, the four oxygen atoms come from the four adjacent vanadium oxide chains surround each $Ni(NH_3)_2^{2+}$ fragment with Ni–O distances of 2.035(3) and 2.029(3) Å.

The structure of **2** along the *a* axis, as illustrated in Fig. 3, shows a screw-like spiral arrangement of seemingly six-membered rings composed of O–O edges of four VO_4 tetrahedra and two NiO_4N_2 octahedra or 12-membered rings counting metal and oxygen atoms individually. A cell unit is passed through four such channels with two in a left-handed fashion and the others in a right-handed fashion. Along the *b* axis, the structure also illustrates left- and right-handed six-membered spiral channel arrangements (Fig. 4). There are the angles of 90° and 84.4° between the two types of six-membered cross-sectional rings in the left- and right-handed spiral channels along the *a* and *b* axes, respectively. Fig. 3 also shows that the four-membered windows formed by two VO_4 and two NiO_4N_2 polyhedra packed in the *a* direction.

It is notable that the connections between complex fragments and metavanadate chains in **2** are different from those in **1** and in other known coordination cation metavanadates. The electrostatic interactions are dominant between the fragments and the metavanadate chains in **1** and $Ni(en)_3(VO_3)_2$ [9]. In $Cu(bpy)_2(VO_3)_2$ [5] and $Cu(dien)(VO_3)_2{\cdot}H_2O$ [19], each complex fragment is covalently bound through a single oxygen atom to very other tetrahedral unit in the vanadium oxide chain. In $Cu(en)(VO_3)_2$, $Cu(bpy)(VO_3)_2$ [5] and $Cu(NH_3)_2(VO_3)_2$ [20], each copper atom adopts a square planar configuration with two oxygen atoms from adjacent VO_4 units in the chain. However, each complex fragment in **2** is joined to its four adjacent vanadium oxide chains into a three-dimensional framework. These differences may originate from the nature of the transition metal ions employed. While the copper(II) ion favors four-coordinated square-planar or five-coordinated square-pyramidal geometry because of its strong Jahn–Teller effects, the nickel(II) ions tends to six-coordinated octahedral geometry.

In the structure of **2**, significant hydrogen bonding between H(4) on N(2) and O(3) with nitrogen–oxygen distance of 2.806(4) Å is observed, as listed in Table 3.

3.4. Magnetic properties

The temperature dependencies of the magnetic susceptibilities and inverse susceptibilities of **1** are illustrated in Fig. 6. The effective magnetic moment (μ_{eff}) of **1** at 275 K ($1.79\mu_B$), determined from the equation $\mu_{eff} = 2.828(\chi_m T)^{1/2}$, is consistent with that expected for an isolate paramagnetic system with $S = 1/2$ ($\mu_{eff} = 1.73\mu_B$). The χ_m^{-1} versus T curve is almost linear in the whole temperature range, suggesting principally paramagnetism in **1**. The magnetic susceptibility data was analyzed with the Curie–Weiss law:

$$\chi_m = Ng^2\mu_B^2 S(S+1)/3k(T-\theta) \quad (1)$$

A least-squares fit obtains the parameters, $g = 2.06(5)$, $\theta = 0.04(2)$ K and the agreement factor $F = [\Sigma(\chi_{obs} - \chi_{cal})^2/\Sigma\chi^2_{obs}]^{1/2} = 0.124\%$. The very small θ demonstrates that no distinct magnetic interactions exist. The nearest Cu···Cu distance in the structure of **1** is greater than 7.22 Å, and the exchange couplings thus can have to be excluded.

The magnetic behavior of compound **2** is shown in Fig. 7. The μ_{eff} value of **2** per nickel(II) at 275 K is $2.95\mu_B$. It is greater than the spin-only value for $S = 1$ ($\mu_{eff} = 2.83\mu_B$), indicating the presence of a ferromagnetic coupling between Ni(II) ions. This is further suggested by a positive Weiss constant $\theta = +5.27(4)$ K, derived from the Curie–Weiss law fit in the temperature ranging from 25 to 275 K (Fig. 7). In the structural parameters of **2**, the magnetic super-exchange would most likely occur through the –Ni–O–V–O–Ni– bonding pathway with nearest Ni···Ni distance of 5.419(1) Å. It is shown that a one-dimensional $S = 1$ Ising model with ion anisotropy can explain well the origin of the magnetic super-exchange interactions in **2**.

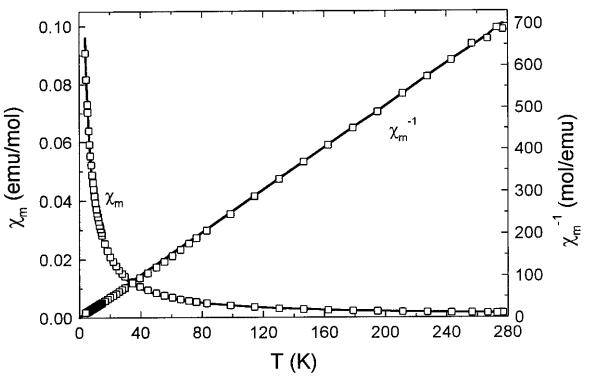


Fig. 6. Thermal variations of the magnetic susceptibility (χ_m) and inverse susceptibility data (χ_m^{-1}) of $Cu(tn)_2(VO_3)_2$, where □ plots for observed results and solid lines for fitting calculations based on the Curie–Weiss law.

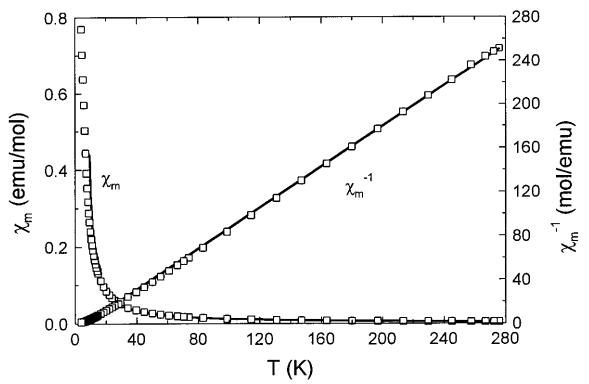


Fig. 7. Thermal variations of the magnetic susceptibility (χ_m) and inverse susceptibility data (χ_m^{-1}) of $Ni(NH_3)_2(VO_3)_2$, where □ plots for observed results, and solid lines attached χ_m and χ_m^{-1} for fitting calculations based on the one-dimensional Ising model and the Curie–Weiss law, respectively.

The behavior of a one-dimensional Ising linear chain has been described by O'Brien [21]. The equation to describe the effect of a molecular exchange field is:

$$\chi_m = \frac{Ng^2\mu_B^2 S(S+1)}{kT} \frac{e^{2d}(e^j\lambda_+ - 1 + e^j)}{F_\lambda} \quad (2)$$

where J is the exchange parameter, D is the zero-field splitting parameter, $d = D/2kT$, $j = 2J/kT$, and λ_+ and F_λ are complicated expressions in terms of D and J, as defined in [21].

The magnetic susceptibility data of **2** was analyzed with Eq. (2). A least-square fit using $T > 15$ K data shows the parameters, $J/k = 2.58(5)$ K, $D/k = -1.26(4)$ K, $g = 2.36(5)$ and $F = 0.424\%$. The positive J value demonstrate a ferromagnetic exchange propagated between paramagnetic centers, and the negative D denotes that the $M_s = 0$ states lies below the $M_s = \pm 1$ states in the nickel octahedral field.

In conclusion, this paper demonstrates two new examples of hydrothermally assembling vanadium oxides through the templating effects of transition metal complexes for preparation of composite organic/inorganic solids. The title compounds show two interaction types between coordination complexes and vanadium oxides. While compound **1** dominantly possesses the electrostatic interactions between the fragments and the vanadium oxide chains, the coordination groups in **2** are covalently bound to the vanadium oxide, and form a three-dimensional framework structure. This suggests that templates, along with the hydrothmal parameters, may influence the resulted structural complexity. Varying the reactive conditions and combining different transition element complexes with oxides, materials with potentially interesting and useful properties may be synthesized.

4. Supplementary material

Crystallographic data for the structures reported in this paper have been deposited with the Cambridge Crystallographic Data Centre, CCDC No. 145084 for compound **1** and CCDC No. 145085 for compound **2**. Copies of this information may be obtained free of charge from the Director, CCDC, 12 Union Road, Cambridge, CB2 1EZ, UK (fax: +44-1223-336033; e-mail: deposit@ccdc.cam.ac.uk or http://www.ccdc.cam.ac.uk).

Acknowledgements

The authors thank the financial support of the Natural Science Foundation of Fujian Province of China.

References

[1] A. Müll, H. Reuter, Angew. Chem., Int. Ed. Engl. 34 (1995) 2328.
[2] (a) P. Cox, Transition Metal Oxides, Clarendon Press, UK, 1995. (b) S.L. Suib, Chem. Rev. 88 (1988) 125. (c) A.K. Cheethan, P. Day, Solid State Chemistry, vols. 1–2, Clarendon Press, UK, 1992. (d) V. Day, W. Klemperer, Science 228 (1985) 533.
[3] (a) R.C. Haushalter, L.A. Mundi, Chem. Mater. 3 (1992) 31. (b) J. Zubieta, Comments Inorg. Chem. 16 (1994) 153. (c) G.D. Stucky, Nature 388 (1997) 735. (d) D. Riou, G. Férey, Inorg. Chem. 34 (1995) 6520.
[4] Y. Zhang, P.J. Zapf, L.M. Meyer, R.C. Haushalter, A. Clearfield, J. Zubieta, Angew. Chem., Int. Ed. Engl. 35 (1996) 989.
[5] J.R. DeBord, Y. Zhgang, R.C. Haushalter, J. Zubieta, C.J. O'Connor, J. Solid State Chem. 122 (1996) 251.
[6] M.I. Khan, E. Yohannes, D. Powell, Inorg. Chem. 38 (1999) 212.
[7] P.J. Hagrman, C. Bridges, J.E. Greedan, J. Zubieta, J. Chem. Soc., Dalton Trans. (1999) 2901.
[8] R.L. LaDuca Jr., R. Finn, J. Zubieta, Chem. Commun. (1999) 1669.
[9] S.X. Liu, B.Z. Lin, S. Lin, Inorg. Chim. Acta 304 (2000) 33.
[10] R.D. Shannon, C. Calvo, Can. J. Chem. 51 (1973) 265.
[11] F. Marumo, M. Isobe, S. Iwai, Y. Kondo, Acta Crystallogr., Sect. B 30 (1974) 1628.
[12] F.C. Hawthorne, C. Calvo, J. Solid State Chem. 22 (1977) 157.
[13] G.M. Sheldrick, SHELXS-86 Program for Solution of Crystal Structure, University of Göttingen, Germany, 1986.
[14] G.M. Sheldrick, SHELXL-93 Program for Refinement of Crystal Structure, University of Göttingen, Germany, 1993.
[15] (a) D. Riou, G. Férey, Inorg. Chem. 34 (1995) 6520. (b) Y. Zhang, R.C. Haushalter, A. Clearfield, Inorg. Chem. 35 (1996) 4950.
[16] B.Z. Lin, S.X. Liu, Acta Crystallogr., Sect. C 55 (1999) 1961.
[17] S.H. Tang, Z.X. Shen, C.W. Ong, M.H. Huok, J. Mol. Struct. 354 (1995) 29.
[18] I.D. Brown, D. Altermatt, Acta Crystallogr., Sect. B 41 (1985) 244.
[19] L.-M. Zheng, J.-Z. Zhou, K.-H. Lii, L.-Y. Zhang, Y. Liu, X.-Q. Xin, J. Chem. Soc., Dalton Trans. (1999) 939.
[20] S. Aschwanden, H.W. Schmalle, A. Reller, H.R. Oswald, Mater. Res. Bull. 28 (1993) 45.
[21] S. O'Brien, R.M. Gaura, C.P. Landee, R.D. Willett, Solid State Commun. 39 (1981) 1333.

PERGAMON

www.elsevier.nl/locate/poly

Polyhedron 19 (2000) 2529–2532

POLYHEDRON

Synthesis, structure and magnetic properties of di-carboxylato-bridged complex $[Cu_2(phen)_2(Hpht)_2(NO_3)(H_2O)]NO_3{\cdot}2H_2O$

Licun Li *[1], Daizheng Liao, Zonghui Jiang *[2], Shiping Yan

Department of Chemistry, Nankai University, Tianjin 300071, People's Republic of China

Received 4 July 2000; accepted 2 August 2000

This paper is dedicated to Professor Olivier Kahn

Abstract

The binuclear complex $[Cu_2(phen)_2(Hpht)_2(NO_3)(H_2O)]NO_3{\cdot}2H_2O$ (Hpht = hydrogen phthalate and phen = 1,10-phenanthroline) has been synthesized and structurally characterized. The structure consists of unsymmetrical di-μ-carboxylato-bridged $[Cu_2(phen)_2(Hpht)_2(NO_3)(H_2O)]^+$ cation, one NO_3^- anion and two H_2O solvate molecules. The temperature dependence of the magnetic susceptibilities of the complex have been studied in the range 5–300 K, giving the exchange coupling parameter $J = -79.2\ cm^{-1}$, indicating a moderately strong antiferromagnetic interaction between the copper(II) ions within the binuclear unit. © 2000 Elsevier Science B.V. All rights reserved.

Keywords: Carboxylato-bridged copper(II) complex; Crystal structure; Magnetic properties

1. Introduction

The magneto-structural characterization of binuclear copper(II) complexes has played a key role in the development of magnetochemistry [1,2]. One of the more appealing examples concerns the carboxylato-bridged binuclear copper(II) complexes. Among several types, the antiferro-magnetically coupled tetra- and di-μ-carboxylato-bridged binuclear copper(II) complexes have been extensively studied [3–7]. For tetra-μ-carboxylato-bridged dicopper(II) complexes, the strong intramolecular antiferromagnetic interaction has been observed in the range -160 to $-350\ cm^{-1}$ depending on the nature of carboxylic acid and the apical ligand [9]. The mechanism of this interaction has been demonstrated to be a superexchange of magnetic $d_{x^2-y^2}$ orbitals through the bridging acetates. In di-μ-carboxylato-bridged binuclear copper(II) complexes, the magnetic exchange coupling is still antiferromagnetic, but the strength of this exchange coupling becomes weaker than in the above tetra-μ-carboxylato-bridged binuclear copper(II) series. Tokii et al. [8] have ascribed this diminished coupling predominantly to the fact that the latter complexes contain only two bridging carboxylates in contrast to four in the above series.

The magneto-structural relationship for symmetrically carboxylato-bridged copper(II) complexes shows the magnitude of the exchange coupling dependence on the number of bridges and Cu–O–Cu(α) angle [9]. The present work stems from our interest in exploring this correlation for unsymmetrical carboxylato-bridged copper(II) complexes. Herein we present the synthesis, crystal structure and magnetic properties of $[Cu_2(phen)_2(Hpht)_2(NO_3)(H_2O)]NO_3{\cdot}2H_2O$.

2. Experimental

2.1. Materials

1,10-Phenanthroline, copper(II) nitrate trihydrate and sodium azide were purchased from commercial sources and used as received.

[1] *Corresponding author. Tel.: +86-022-235-09657; e-mail: coord@sun.nankai.edu.cn

[2] *Corresponding author.

0277-5387/00/$ - see front matter © 2000 Elsevier Science B.V. All rights reserved.
PII: S0277-5387(00)00524-6

2.2. Synthesis of $[Cu_2(phen)_2(Hpht)_2(NO_3)(H_2O)]NO_3\cdot 2H_2O$

An enthanolic solution (10 ml) of 1,10-phenanthroline hydrate (1 mmol, 198 mg) was added to a solution of $Cu(NO_3)_2\cdot 3H_2O$ (1 mmol, 241 mg) in ethanol (10 ml), then mixed with an ethanolic solution (10 ml) of phthalic acid (1 mmol, 166 mg) followed by the addition of an aqueous solution (5 ml) of sodium azide (1 mmol, 65 mg). The reaction mixture was stirred at room temperature (r.t.) for 1 h, then filtered and the filtrate, on slow evaporation at r.t., gave blue crystals after 1 week. *Anal*. Calc. for $C_{40}H_{32}N_6O_{17}Cu_2$: C, 48.24; H, 3.21; N, 8.43. Found: C, 47.29; H, 3.15; N, 8.33%.

2.3. Measurements

Elemental analysis for C, H and N were carried out on a Perkin–Elmer model 240 elemental analyzer. Variable temperature magnetic susceptibilities were measured on an MPMS-7 SQUID magnetometer. Diamagnetic corrections were made with Pascal's constants for all constituent atoms, and the magnetic moments were calculated using the equation $\mu_{eff} = 2.828(\chi_M T)^{1/2}$. Experimental susceptibilities were also corrected for the temperature-independent paramagnetism (60×10^{-6} cm^3 mol^{-1} per Cu(II)).

3. Crystal structure determination and refinement

A blue crystal ($0.30 \times 0.25 \times 0.20$) was selected and mounted in Bruker Smart 1000 diffractometer equipped with graphite-monochromated Mo Kα radiation ($\lambda = 0.71073$ Å). The data were collected at r.t. and a total of 19 213 reflections were collected in the range $0.96 < \theta < 26.41°$ including 8323 independent reflections ($R_{int} = 0.0588$). Selected crystallographic data are given in Table 1. The structure was solved with direct methods using the SHELXS-97. The H atoms were assigned with common isotropic displacement factors and included in the final refinement by use of geometrical restraints. Full matrix least-squares refinement on F^2 was carried out using SHEHXL-97 and the goodness-of-fit on F^2 was 0.978. The final agreement factor values are $R_1 = 0.0470$, $wR = 0.1047(I > 2\sigma)$, $R_1 = \Sigma(||F_o| - |F_c||)/\Sigma|F_o|$, $wR_2 = (\Sigma\, w(|F_o|^2 - |F_c|^2)^2/\Sigma\, w|F_o|^2)^2$. Selected bond distances and angles are given in Table 2.

Table 1
Crystallographic data and processing parameters for $[Cu_2(phen)_2(Hpht)_2(NO_3)(H_2O)]NO_3\cdot 2H_2O$

Empirical formula	$C_{40}H_{32}N_6O_{17}Cu_2$
Formula weight	995.80
Crystal system	monoclinic
Space group	$P2_1/n$
a (Å)	10.1396(7)
b (Å)	42.454(3)
c (Å)	10.5856(7)
α (°)	90
β (°)	116.9630(10)
γ (°)	90
V (Å^3)	4061
wR_2	0.10475(5)
Z	4
D_{calc} (g cm^{-3})	1.629
μ (Mo Kα mm^{-1})	1.134
F(000)	2032
R_1	0.0470

Table 2
Selected bond distances (Å) and bond angles (°) for $[Cu_2(phen)_2(Hpht)_2(NO_3)(H_2O)]NO_3\cdot 2H_2O$

Cu(1)–O(3)	1.945(3)	Cu(1)–O(1)	1.966(3)
Cu(1)–N(1)	1.990(3)	Cu(1)–N(2)	2.005(4)
Cu(1)–O(6)	2.251(3)	Cu(2)–O(2)	1.940(3)
Cu(2)–O(4)	1.960(3)	Cu(2)–N(4)	1.983(4)
Cu(2)–N(3)	2.014(3)	Cu(2)–O(5)	2.219(4)
O(1)–C(25)	1.248(5)	O(2)–C(25)	1.249(5)
O(3)–C(27)	1.250(5)	O(4)–C(27)	1.254(5)
O(9)–C(26)	1.204(5)	O(10)–C(26)	1.301(5)
O(11)–C(28)	1.294(5)	O(12)–C(28)	1.213(5)
O(3)–Cu(1)–O(1)	90.30(12)	O(3)–Cu(1)–N(1)	175.80(14)
O(1)–Cu(1)–N(1)	90.68(13)	O(3)–Cu(1)–N(2)	95.50(14)
O(1)–Cu(1)–N(2)	159.46(13)	N(1)–Cu(1)–N(2)	82.22(15)
O(3)–Cu(1)–O(6)	87.75(13)	O(1)–Cu(1)–O(6)	92.73(14)
N(1)–Cu(1)–O(6)	96.28(13)	N(2)–Cu(1)–O(6)	107.14(14)
O(2)–Cu(2)–O(4)	92.68(13)	O(2)–Cu(2)–N(4)	175.56(14)
O(4)–Cu(2)–N(4)	91.38(13)	O(2)–Cu(2)–N(3)	93.30(14)
O(4)–Cu(2)–N(3)	162.17(13)	N(4)–Cu(2)–N(3)	82.29(14)
O(2)–Cu(2)–O(5)	88.11(15)	O(4)–Cu(2)–O(5)	96.92(13)
N(4)–Cu(2)–O(5)	93.19(15)	N(3)–Cu(2)–O(5)	100.05(13)
C(25)–O(1)–Cu(1)	123.6(3)	C(25)–O(2)–Cu(2)	136.8(3)
C(27)–O(3)–Cu(1)	127.5(3)	C(27)–O(4)–Cu(2)	131.7(3)
O(1)–C(25)–O(2)	126.2(4)	O(9)–C(26)–O(10)	124.4(5)
O(3)–C(27)–O(4)	126.8(4)	O(12)–C(28)–O(11)	123.5(5)

4. Result and discussion

4.1. Description of the structure of $[Cu_2(phen)_2(Hpht)_2(NO_3)(H_2O)]NO_3\cdot 2H_2O$

The structure of the title complex is made up of the di-μ-carboxylato-bridged $[Cu_2(phen)_2(Hpht)_2(NO_3)(H_2O)]^+$ cation, one NO_3^- anion and two H_2O solvate molecules. The labeled diagram of $[Cu_2(phen)_2(Hpht)_2(NO_3)(H_2O)]NO_3\cdot 2H_2O$ is shown in Fig. 1. The coordination around each copper(II) atom is distorted square–pyramidal with two nitrogen atoms of a phenanthroline, two oxygen atoms of the carboxylate groups of hydrogen phthalate and one

water O(5) and one nitrate O(6) occupy the apical positions for Cu(1) and Cu(2), respectively. In two basal planes, the average Cu–N distance is 1.99 Å and the Cu–O distance is 1.95 Å, in good agreement with those structurally analogous complexes [8,10,11]. The deviations of Cu(1) from the N(1), N(2), O(1), O(3) plane and Cu(2) from the N(3), N(4), O(2), O(4) plane are 0.2008 and 0.1544 Å, respectively. The values of the two axial Cu–O bonds are 2.251(3) and 2.219(4) Å for NO_3^- and H_2O, respectively, which are longer than those of the basal planes. The deprotonated carboxylate groups act as *syn–syn* carboxylato bridges which connect the two basal planes of the copper(II) ions, whereas protonated carboxylate remains uncoordination. The Cu(1)···Cu(2) distance is 3.154 Å. Unlike symmetrically carboxylato-bridged copper(II) complexes, the Cu–O–C angles of the title complex are over the greater range 123.6(3)–136.8(3)°. One uncoordinated water and one uncoordinated carboxylate oxygen form an intramolecular hydrogen bond (2.598 Å and 174.43° for O(10)···O(17) and O(10)···H(17w)–O(17), respectively). The intermolecular hydrogen bond occurs between the uncoordinated carboxylate of one unit and one coordinated water of another (2.561 Å and 160.30° for O(12)···O(16) and O(12)···H(16w)–O(16), respectively). The dihedral angle between the two basal planes around the copper(II) ions is 24.4° and the angle between two phen planes is 2.0°.

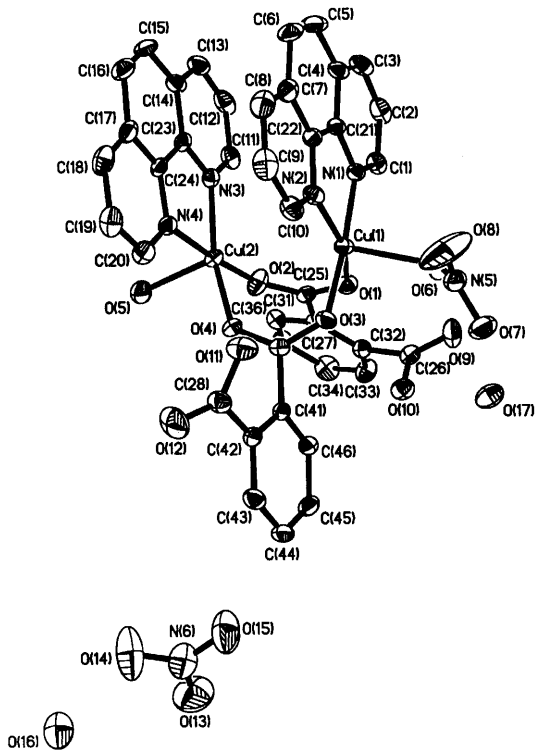


Fig. 1. The labeled diagram of the complex $[Cu_2(phen)_2(Hpht)_2(NO_3)(H_2O)]NO_3{\cdot}2H_2O$. Thermal ellipsoids are at the 30% probability level.

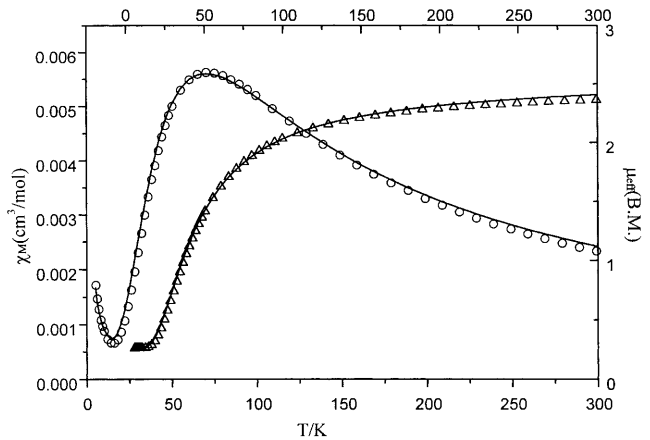


Fig. 2. Plots of χ_M (○) and μ_{eff} (△) of $[Cu_2(phen)_2(Hpht)_2(NO_3)(H_2O)]NO_3{\cdot}2H_2O$ versus T. Solid lines represent the best theoretical fits.

4.2. Magnetic properties

The Variable-temperature magnetic susceptibility of the title complex was measured in the temperature range 5–300 K and the results are shown in Fig. 2. For the complex, the χ_M values increase as the temperature decreases, reaching a maximum at about 100 K, then decreases on cooling and increases again below 10 K, which indicates that antiferromagnetic interaction occurs between Cu(1) and Cu(2). The μ_{eff} value at r.t. is 2.30 B.M., which is smaller than the expected value for two uncoupled copper(II) ions. According to the structure of the present complex, we use Bleaney–Bowers equation [12] to fit the magnetic susceptibility data. In addition, to obtain satisfactory results at low temperature, the paramagnetic monomeric impurity ρ was introduced [2]. Following the equation, we obtained a very satisfactory fit for the data in the range 5–300 K. $J = -79.2\ cm^{-1}$, $g = 2.02$, $\rho = 0.010$, $R = 3.0 \times 10^{-6}$ (R is an agreement factor defined as $R = \Sigma[(\chi_M)_{obs} - (\chi_M)_{calc}]^2/\Sigma[(\chi_M)_{obs}]^2$). From this data, a moderately strong antiferromagnetic interaction exists in the title complex and it is smaller than the corresponding values reported for the tetra-μ-carboxylate-bridges species [4,13,14]. This may be explained by the reduced overlap between the atomic orbitals of the copper atoms and the appropriate Mos of the carboxylato bridge as the number of carboxylate bridges decreases [15]. Wieghardt [9] has proposed a parametric approach to the J value by means of the relationship between J/n and the Cu–O–C bond angle (α) in which n is the number of carboxylate bridges. For the title complex, the Cu–O–C bond angles change over the greater range 123–136° because of the unsymmetrical carboxylate bridges, however, if the average Cu–O–C bond angle (129.5°) was considered, the experimental results obey Wieghardt's proposition.

We can compare the structure and magnetic properties with those reported for the $[Cu_2(CH_3CO_2)_2(phen)_2(H_2O)_2](NO_3)_2{\cdot}4H_2O$ complex [8] which is structurally analogous. For this complex, the Cu–O–C bond angle is 128° and the magnetic exchange coupling is $-86\ cm^{-1}$ between copper(II) ions. In the title complex, the average Cu–O–C bond angle is 129.5°, which is greater than that of the previous complex, therefore a smaller magnetic exchange interaction would be expected and it is agreement with experimental results ($J = -79.2\ cm^{-1}$).

In conclusion, the number of bridges and the Cu–O–C bond angle for unsymmetrical carboxylato-bridged binuclear copper(II) complexes determined the magnitude of magnetic exchange between the copper(II) ions.

5. Supplementary data

Crystallographic data for the structural analysis have been deposited with the Cambridge Crystallographic Data Center, CCDC No. 146141 for the title compound. Copies of this information may be obtained free of charge from The Director, CCDC, 12 Union Road, Cambridge, CB2 1EZ, UK (fax: +44-1223-336033; e-mail: deposit@ccdc.cam.ac.uk or www: http://www.ccdc.cam.ac.uk).

Acknowledgements

This project was supported by the Tianjin Natural Science Foundation-Tianjin the 21st Century Science Foundation for Youth (No. 983700511).

References

[1] R.D. Willet, D. Gatteschi, O. Kahn (Eds.), Magneto–Structural Correlation in Exchange Coupled Systems, Reidel, Dordrecht, 1985.
[2] O. Kahn, Molecular Magnetism, VCH, Weinheim, 1993.
[3] R.J. Doedens, Prog. Inorg. Chem. 21 (1976) 209.
[4] M. Kato, Y. Muto, Coord. Chem. Rev. 92 (1988) 45.
[5] T. Kanata, H. Uekasa, S. Ohba, Y. Saito, S. Iwata, M. Kato, T. Tokii, Y. Muto, O.W. Steward, Acta Crystallogr., Sect. B 47 (1991) 344.
[6] R.W. Jotham, S.F.A. Kettle, J.A. Marks, J. Chem. Soc., Dalton Trans. (1972) 428
[7] Y. Muto, T. Tokii, K. Chijiwa, M. Kato, Bull. Chem. Soc. Jpn. 57 (1984) 1008.
[8] T. Tokii, N. Watanabe, M. Nakashima, Y. Muto, M. Murooka, S. Ohba, S. Ohba, Y. Saito, Bull. Chem. Soc. Jpn. 63 (1990) 364.
[9] K.S. Bürger, P. Chaudhuri, K. Eieghardt, Inorg. Chem. 35 (1996) 2704.
[10] S.P. Perlepes, J.C. Huffman, G. Christou, Polyhedron (1992) 1471
[11] E. Dubler, U.K. Häring, K.H. Scheller, P. Baltzer, H. Sigel, Inorg. Chem. 23 (1984) 3785.
[12] B. Bleaney, K.D. Bowers, Proc. R. Soc. Lond., Ser. A 214 (1952) 451.
[13] T. Kanata, H. Uekasa, S. Ohba, T. Furukawa, T. Tokii, Y. Muto, M. Kato, Acta Crystallogr., Sect. B 48 (1992) 253.
[14] G.A. Clay, C.H.L. Kennard, J. Chem. Soc. (1961) 5244
[15] A. Escuer, R. Vicente, F.A. Mautner, M.A.S. Goher, Inorg. Chem. 36 (1997) 1233.

PERGAMON

www.elsevier.nl/locate/poly

Polyhedron 19 (2000) 2533–2538

POLYHEDRON

Spectral characteristics of the copper(III) and nickel(III) coordination compounds with open-chain and macrocyclic dioxotetraamines

Yaroslaw D. Lampeka *, Sergey P. Gavrish

L.V. Pisarzhevskii Institute of Physical Chemistry of the National Academy of Sciences of Ukraine, Prospekt Nauki 31, Kiev 03039, Ukraine

Received 13 June 2000; accepted 2 August 2000

Abstract

Electronic absorption spectra of copper(III) and nickel(III) complexes with open-chain and macrocyclic ligands containing two amide and two amine groups have been described. The absorption bands assigned to the σ- (high-energy) and π- (low energy) LMCT transitions show definite dependence on the structure of the ligands. Thus, the spectra of the complexes with a five-membered chelate ring bearing an isolated carbonyl group are most closely related to the spectra of metal(III) peptides. In some cases the splitting of the σ-LMCT band is observed. Two absorption bands are also characteristic for the spectra of oxamide derived complexes, though several nickel(III) compounds display only a low-energy π-LMCT transition. The most typical spectral feature of the coordination compounds of malonamide derived ligands is the lack of well-resolved low energy bands which could be assigned to π-LMCT transitions and only one band is observed in the UV region which apparently includes both possible transitions. © 2000 Elsevier Science B.V. All rights reserved.

Keywords: Asorption spectra; Copper(III); Nickel(III); Dioxotetraamines; Macrocyclic ligands

1. Introduction

Because of their biological relevance the stability, structure and spectral characteristics of metal complexes with oligopeptides have been the subjects of numerous investigations for many years [1,2]. The ability of such amide-containing ligands to stabilise the high oxidation states of transition metal ions, in particular, copper(III) and nickel(III), and the presence of these metal(III) ions in active sites of native enzymes lent a further impetus to the study of these compounds [3,4].

However, in spite of a wide variability of oligopeptides studied as the ligands, almost all works done were restricted to the compounds built up from α-amino-acid residues. When co-ordinated to the metal ions such ligands form only five-membered chelate rings with each ring bearing one carbonyl oxygen (Chart 1), thus the complexes are very similar from a structural point of view. It is evident that only two variables both exerting mainly electronic effects, i.e. the substituents R^n (typically aliphatic group) and the number of deprotonated amide groups, can be taken into consideration when the influence of ligand structure on the properties of this type complexes is considered. Therefore, it seems quite expectable that irrespective of the ligand structure the electronic absorption spectra of metal(III) oligopeptide complexes are very similar with negligible influence of the substituent R^n, though a moderate bathochromic shift of absorption bands is observed when the number of deprotonated amide groups in the complexes is reduced [5,6].

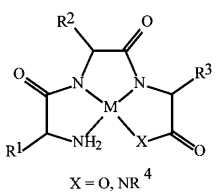


Chart 1.

* Corresponding author. Tel.: +38-44-265-2570; fax: +38-44-265-6216.

E-mail address: ditop@iphch.kiev.ua (Y.D. Lampeka).

0277-5387/00/$ - see front matter © 2000 Elsevier Science B.V. All rights reserved.
PII: S0277-5387(00)00557-X

Metal complexes of non-peptidic tetradentate ligands containing two amide and two amine donor groups represent the class of compounds which can be successfully used as appropriate structural models to mimic the properties of oligopeptide complexes. At the same time, much higher structural variability is inherent of these compounds – both structural parameters (open-chained or macrocyclic nature of the ligand, the size and the set of chelate rings) and electronic characteristics (the number and relative position of carbonyl oxygen atom(s) in chelate rings, the nature of the substituent in the macrocycle) can be varied. Therefore, the study of physicochemical properties of the complexes formed by this class of ligands allows one to gain deeper insight into the question how the metal ion and the ligand are interacting in oligopeptide complexes.

In the ranges of our investigation of the thermodynamic and kinetic aspects of redox behaviour of the complexes with non-peptidic amides, the series of nickel and copper compounds with ligands shown in Fig. 1 was studied by different physicochemical methods [7–14]. The goal of the present work is to discuss the main peculiarities of electronic absorption spectra of metal(III) compounds of this type and to establish the influence of the ligand structural parameters on spectral characteristics. In addition, the comparison of these data with spectral properties of copper(III) and nickel(III) ions in some naturally occurring enzymes could serve as useful tool in elucidation of the structure of their active sites.

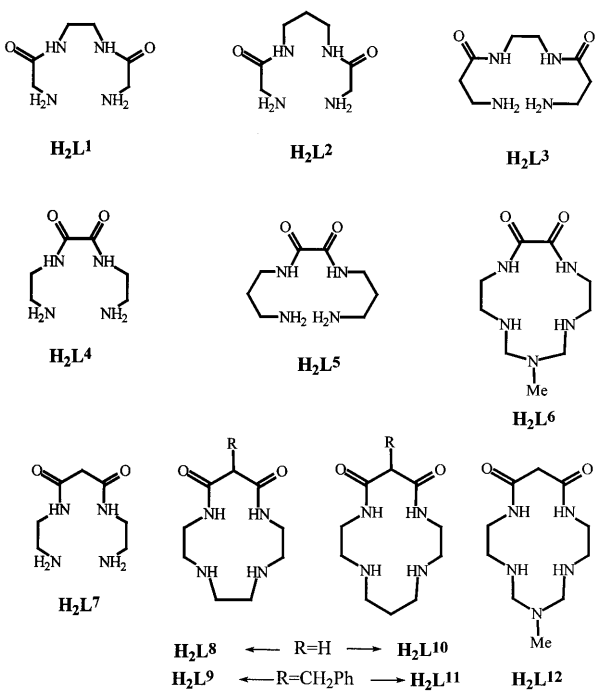


Fig. 1. Ligands containing two amide and two amine groups.

2. Experimental

Amide ligands H_2L^n and their copper(II) and nickel(II) complexes $M^{II}L$ were obtained as described [11]. Corresponding metal(III) compounds $M^{III}L$ were generated in aqueous solution in situ by oxidation of starting $M^{II}L$ complexes with potassium peroxodisulfate. Electronic absorption spectra were recorded on Specord M-40 and Specord UV–Vis (Karl Ceiss, Jena) spectrophotometers.

The values of molar extinction coefficient ε for the metal(III) complexes were determined as follows. 0.5 cm^3 of 5.0×10^{-3} mol dm^{-3} $K_2S_2O_8$ solution was added to 1.0 cm^3 of 2.5×10^{-3} mol dm^{-3} $M^{II}L$ solution and after some time (1.5–10 min, depending on the rate of the oxidation reaction for a given complex) 0.5 cm^3 of 4.0×10^{-1} mol dm^{-3} $HClO_4$ was added. After recording the absorption, 0.5 cm^3 of 1.2×10^{-4} mol dm^{-3} $K_4[Fe(CN)_6]$ solution was added and the absorption was measured again. This procedure was repeated several times. Extinction coefficients were calculated from the drop of absorption after addition of hexacyanoferrate(II) solution with an accuracy of about 5%.

3. Results and discussion

3.1. Solution properties of the complexes

The interaction of copper(II) and nickel(II) ions with diamidodiamines H_2L^n proceeds with the abstraction of two protons from the ligands and leads to the formation of neutral species $M^{II}L$, thus this equilibrium is pH-dependent. It is completely shifted to the formation of the complexes in neutral or mildly alkaline solutions. The metal(III) compounds $M^{III}L^+$ were obtained via oxidation of corresponding metal(II) complexes with peroxodisulfate and their authenticity was confirmed by the redox titration (vide supra) and, for nickel(III) species, by EPR measurements [11]. The choice of this oxidant was determined by its high redox potential and by the fact that neither it itself nor the products of its reduction absorb in the visible and near UV spectral region. The disadvantage of using of such an oxidant consists in insufficiently high rates of its redox reaction. In the cases when the rates of the formation of $M^{III}L^+$ and its redox decomposition were comparable we were unable to reach full conversion of $M^{II}L$ into $M^{III}L^+$, and for some complexes (CuL^3, CuL^5, NiL^3, NiL^8, NiL^9) no accumulation of essential amounts of $M^{III}L^+$ was observed at all.

The method of generation of $M^{III}L^+$ species presumes that in neutral aqueous solutions some amounts of starting $M^{II}L$ complexes persist which prevent accurate determination of the positions and intensities of absorption bands of oxidised forms. To overcome this

Table 1
Spectral characteristics [a] of the copper(III) complexes with diamidodiamine ligands in aqueous solution containing 0.1 mol dm^{-3} $HClO_4$

Complex	σ-LMCT transition	π-LMCT transition	LF transition
$Cu^{III}L^1$	38 500 (10050)	24 600 (6200 ± 90)	
$Cu^{III}L^2$	37 100 (11700), 32 500 (11550 ± 300)	23 200 (5050)	
$Cu^{III}L^4$	37 000 (6950)	30 900 (6980 ± 100)	22 200 (800)
$Cu^{III}L^7$	35 700 (13500 ± 600)	31 000 (8300) sh	
$Cu^{III}L^8$	33 500 (12900 ± 300)	28 000 (7300) sh	22 000 (1250) sh
$Cu^{III}L^9$	33 000 (12100 ± 300)	27 000 (4900) sh	22 000 (1450) sh
$Cu^{III}L^{10}$	33 500 (14600 ± 300)	30 000 (12600) sh	21 000 (1400) sh
$Cu^{III}L^{11}$	34 000 (13700) sh	31 000 (14900 ± 300)	21 000 (1470) sh
$Cu^{III}L^{12}$	33 600 (14900 ± 330)	31 000 (12800) sh	20 500 (1800) sh

[a] Absorption maxima in cm^{-1} and molar extinction coefficient ε in dm^3 mol^{-1} cm^{-1}; the accuracy in determination of ε was indicated for the bands used for redox titration; sh, shoulder.

complication and to register the spectra of 'pure' metal(III) compounds, the well known property of metal(II) complexes to dissociate rapidly in acidic solutions was used [15]. $M^{III}L^+$ are much more stable under these conditions [7]. Thus, extinction coefficients of UV absorption bands were determined as described in Section 2 by redox titration with $K_4[Fe(CN)_6]$. Reaction of ferrocyanide with peroxodisulfate can be neglected since the interaction of copper(III) and nickel(III) species with $[Fe(CN)_6]^{4-}$ is very fast [16]. This is also supported by the fact that the ε values obtained in such a way were independent on the concentration of $S_2O_8^{2-}$ used to generate metal(III) complexes.

3.2. Spectra of the metal(III) peptide complexes

As follows from the literature data [17,18] UV–Vis spectra of copper(III) oligopeptide complexes are typically characterised by the presence of two intensive absorption bands in the region 40 000–25 000 cm^{-1}. Based on their intensities and keeping in mind the high oxidation state of the metal ion, one can conclude that these bands have a ligand-to-metal charge-transfer (LMCT) nature. Sometimes ligand field (LF) transitions are also observed in such systems as band with moderate intensity located at approximately 22 000 cm^{-1} but in the majority of complexes it is masked with low-energy LMCT absorption. In principle, LMCT transition could originate from the orbitals of different donor atoms of the ligand – deprotonated amide nitrogen, amine nitrogen or carboxylate oxygen. Since the same spectral patterns are characteristic of the complexes with the donor set consisting of only amidic nitrogen atoms, it is assumed that the main contribution to the spectra observed is made by LMCT transitions from N_{amide} while CT bands from the donor atoms of other chemical nature, if present, are overlapped with those. The presence of two LMCT bands in the spectra of copper(III) peptide complexes is explained by the fact that the $N_{amide} \rightarrow Cu^{III}$ component of the metal chromophore has both σ- and π-symmetry molecular orbitals relative to copper(III)-N_{amide} bond. Among the two bands observed, the assignment of the low-energy one to π- and high-energy band to σ-LMCT is based on the analysis of the charge transfer spectra of other transition metal complexes [19].

In general, the spectra of nickel(III) oligopeptide complexes are similar to those of the copper(III) species. They are also characterised by two absorption bands in the UV (approximately 40 000 cm^{-1}) and near UV (approximately 30 000 cm^{-1}) regions with relatively high intensities ($\log \varepsilon$ approximately 3–4). Analogously, the high energy band is assigned to the σ- and the low-energy band to the π-LMCT transition [6].

3.3. Spectra of the metal(III) complexes with diamidodiamine ligands

Analogously to the spectra of oligopeptide compounds, the solution spectra of the metal(III) complexes with the ligands under consideration are characterised by the presence of several intensive absorption bands in

Table 2
Spectral characteristics [a] of the nickel(III) complexes with diamidodiamine ligands in aqueous solution containing 0.1 mol dm^{-3} $HClO_4$

Complex	σ-LMCT transition	π-LMCT transition
$Ni^{III}L^1$	40 300 (11250), 35 000(6100) sh	26 400 (3700 ± 50)
$Ni^{III}L^2$	38 500 (12700), 33 000(7550) sh	27 500 (4000 ± 60)
$Ni^{III}L^4$		32 200 (6050 ± 50)
$Ni^{III}L^5$	39 000 (13200) sh	30 000 (8770 ± 100)
$Ni^{III}L^6$		32 800 (7550 ± 70)
$Ni^{III}L^7$	35 100 (14900 ± 600)	30 000 (7300) sh
$Ni^{III}L^{10}$	34 900 (15000 ± 140)	30 000 (10350) sh
$Ni^{III}L^{11}$	35 000 (12300 ± 300)	30 000 (8500) sh
$Ni^{III}L^{12}$	34 900 (14800 ± 100)	30 000 (9300) sh

[a] Absorption maxima in cm^{-1} and molar extinction coefficient ε in dm^3 mol^{-1} cm^{-1}; the accuracy in determination of ε was indicated for the bands used for redox titration; sh, shoulder.

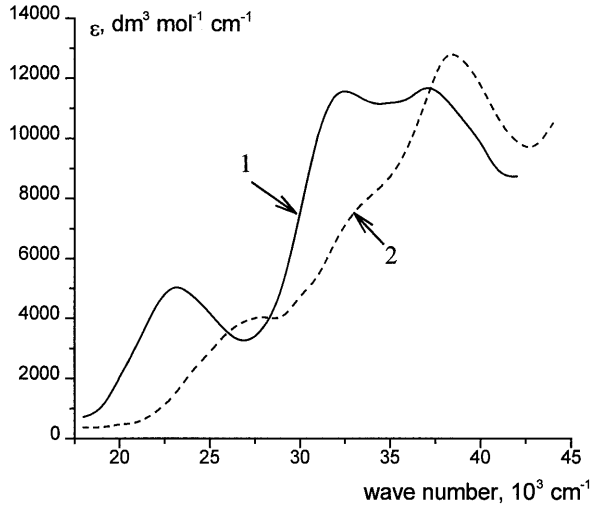


Fig. 2. Absorption spectra of $Cu^{III}L^2$ (1) and $Ni^{III}L^2$ (2) in 0.1 mol dm^{-3} $HClO_4$.

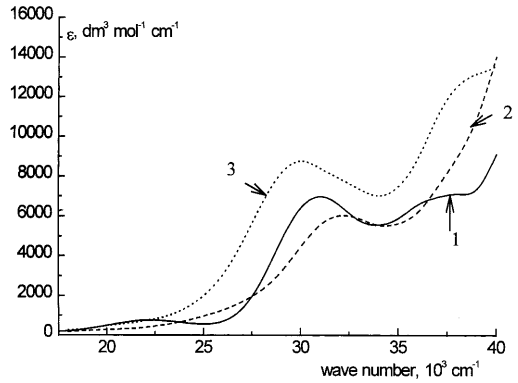


Fig. 3. Absorption spectra of $Cu^{III}L^4$ (1), $Ni^{III}L^4$ (2) and $Ni^{III}L^5$ (3) in 0.1 mol dm^{-3} $HClO_4$.

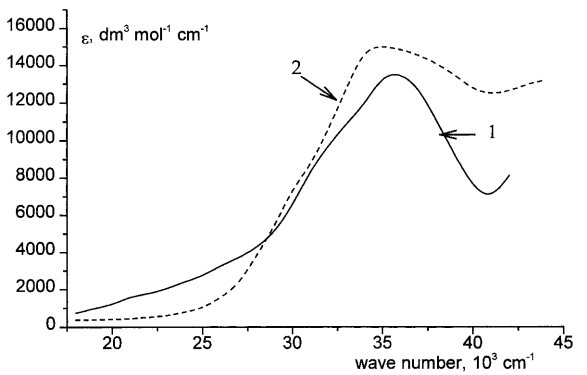


Fig. 4. Absorption spectra of $Cu^{III}L^7$ (1) and $Ni^{III}L^7$ (2) in 0.1 mol dm^{-3} $HClO_4$.

the UV and near UV region (Tables 1 and 2). However, the number of bands observed and general shapes of the spectra in these cases differ from the those of the former and show definite dependence on the structure of the ligands.

Generally, from the point of view of structural peculiarities, the complexes studied can be classified into three groups.

The first group comprises the metal(III) compounds with the ligands H_2L^1 and H_2L^2. The main structural motif present in $M^{III}L^1$ and $M^{III}L^2$ is the five-membered chelate ring bearing isolated carbonyl group. It is just the fragment which is inherent of peptide complexes (see Chart 1). Therefore, it comes as no surprise that their CT spectra most closely resemble those of oligopeptide complexes – as for the former, two well-resolved absorption bands are characteristic of these compounds (Tables 1 and 2, as an example the spectra of $M^{III}L^2$ are shown in Fig. 2).

It seems quite reasonable, similar to the literature data (vide supra), to assign the high- and low-energy bands to σ- and π-LMCT transition, respectively (see Tables 1 and 2). At the same time, distinct splitting of one of these bands is observed for these compounds that is especially evident for $M^{III}L^2$ (Fig. 2). The question, what band having either σ- or π-LMCT nature is split, is ambiguous, since low real symmetry of the chromophore permits both σ- and π-transition to be split into two allowed transitions [17]. Based on the relative intensities of the bands and the distances between the maxima of components we are inclined to believe that the lowering of symmetry removes the degeneracy of the band corresponding to the σ-LMCT transition. This is further confirmed by analogous assignment of the split bands in the copper(III) complex of cyclic tetrapeptide *cyclo*-(β-alanylglycine-β-alanylglycine) [20].

The second structural group consists of complexes formed by both the open-chain and macrocyclic ligands having oxamide fragment, H_2L^4, H_2L^5 and H_2L^6. As for the former group, the only characterised copper(III) complex with this type of ligand, $[Cu^{III}L^4]^+$, possesses two absorption bands which can be assigned to σ- (high-energy) and π- (low-energy) LMCT transitions (Fig. 3). Similar spectral patterns are characteristic also for the nickel(III) complex with H_2L^5. At the same time, in the spectra of the nickel complexes with a 5,5,5-set of chelate rings ($Ni^{III}L^4$ and $Ni^{III}L^6$) only one absorption band is present (Fig. 3). Accepting that this band corresponds to π-type of LMCT, as is quite reasonable, one can conclude that σ-LMCT transition in these compounds must be located at $\nu > 40\,000$ cm^{-1} and thus be higher than for all other types of complexes studied.

The third group includes the coordination compounds of the ligands derived from malonamide, i.e. forming a six-membered chelate ring bearing two carbonyl groups (H_2L^7–H_2L^{12}). The most typical feature of the spectra of these compounds is the lack of well-resolved low energy bands that could be assigned to π-LMCT transitions. Instead, only one broad non-symmetric band is observed which apparently includes both σ- and π-transitions (Fig. 4). A redistribution of the

relative intensities of the constituents of a single band observed when an benzyl substituent is introduced in the malonamide fragment can serve as indirect evidence confirming this suggestion (Fig. 5). In our opinion, such an effect can be assigned to the interaction of the π-system of the aromatic ring with π-electrons of the chromophore influencing the MO diagram of the molecule as a whole.

Thus, the results obtained show that the CT spectra of copper(III) and nickel(III) complexes with diamidodiamines, despite being characterised by the absorption bands of a similar nature, show a distinct dependence on the structure of the ligands. As far as the energy of the σ-LMCT transition is considered, it is the highest for the first two groups of copper(III) complexes and essentially lower for malonamide derivatives, while quite the opposite picture is observed for the energy of the π-LMCT band. An analogous tendency is also observed for the energy of the σ-LMCT transition in the case of nickel(III) complexes, but the dependence of the π-LMCT energies on the structure of the ligands in this case differs. Though again this band has the lowest energy in the complexes of the first group, it is nearly the same for the remaining compounds. It was shown formerly for the copper(III) peptide complexes that the energy separation ΔE between the two CT bands varies in the ranges $(10.4 \div 12.6) \times 10^3$ cm^{-1} and is dependent on the number of α-methyl groups in the ligand [5,21]. In the present case the range of ΔE is much higher (from approximately 5×10^3 cm^{-1} for malonamide ligands to 13.9×10^3 cm^{-1} for CuL^1 or CuL^2, see Table 1) and is not connected with the inductive effect of the substituents.

It was shown also that the increase of the number of deprotonated amide groups in the coordination sphere of the copper(III) and nickel(III) oligopeptide complexes results in the blue shift of the π-LMCT bands and is accompanied by the lowering of the formal $M^{III/II}L$ couple potentials E_f [5,6]. In the present case the spectral changes are determined by the variation of the structural characteristics of the ligands, not by the nature of the donor atoms. Therefore, it was of interest to estimate whether an analogous relationship between spectral and redox characteristics can be valid for the non-peptide type of complexes. The analysis of available data allows one to conclude that, for the copper complexes for which a distinct π-LMCT band can be identified, its energy decreases in the series CuL^4–CuL^1–CuL^2, thus correlating with the increase of the E_f values (cf. with 0.49, 0.59 and 0.75 V versus SCE [11], respectively). In general, a similar tendency is inherent also for the nickel(III) species – the redox potentials of the complexes derived from oxamide ligands are much less positive (by approximately 70–100 mV) than for the compounds with H_2L^1 and H_2L^2 [11] which are characterised by a lower energy of π-LMCT transition as compared to the former. At the same time, this correlation can not be considered as general. For example, copper(III) complexes with isomeric ligands H_2L^2 and H_2L^7 possess very similar redox potentials [11] but are characterised by different absorption spectra. The same is also true for the nickel complexes with these ligands.

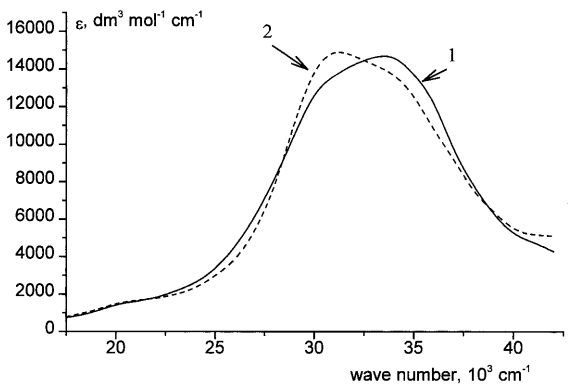


Fig. 5. Absorption spectra of $Cu^{III}L^{10}$ (1) and $Cu^{III}L^{11}$ (2) in 0.1 mol dm^{-3} $HClO_4$.

In addition to the electronic transitions discussed above, one more band in the visible region is present in the spectra of several copper(III) complexes (Table 1). Based on its relative low intensity and as well on the dependence of its energy on the set of chelate rings in complexes one can assign it to the ligand field transition in the low-spin d^8 electron configuration of the copper(III) ion. An analogous band, though at lower energy, was observed formerly in the copper(III) complex of tetraglycine [21].

To summarise, the results of our study of the spectra of copper(III) and nickel(III) complexes revealed that open-chain and macrocyclic ligands containing two amide and two amino groups can be considered as appropriate structural models of oligopeptides. In general, spectral characteristics of metal(III) complexes with these ligands have much in common with the spectra of oligopeptide compounds. For both types of species the absorption bands observed in the UV and visible spectral region have a ligand-to-metal charge transfer nature (LMCT) and depending on their energy were assigned to σ- (high-energy) and π- (low energy) LMCT transitions. At the same time, in contrast to oligopeptide coordination compounds, the spectral characteristics of the complexes under consideration show a definite dependence on the structure of the ligands despite a similar chromophore of the metal ions. Thus, the spectra of the complexes possessing a five-membered chelate ring with isolated carbonyl group are most closely related to the spectra of metal(III) peptides displaying two well-resolved absorption bands. In some cases the splitting of the σ-LMCT band is observed. Two absorption bands are also

present in the spectra of complexes with oxamide derived ligands which form a five-membered chelate ring bearing vicinal carbonyl groups, though in several nickel(III) compounds of this type only low-energy π-LMCT transition is observed. The most typical spectral feature of the coordination compounds of malonamide derived ligands is the lack of well-resolved low energy bands which could be assigned to π-LMCT transitions and only one broad non-symmetric band is observed in the UV region which apparently includes both possible transitions.

Acknowledgements

The authors wish to thank the Department of Basic Research of the Ministry of Science and Technologies of Ukraine for financial support (Grant 4F/375-97).

References

[1] R.W. Hay, J.R. Dilworth, K.B. Nolan ((Eds.), Perspectives on Bioinorganic Chemistry, vol. 1, JAI Press, London, 1991 and Vol. 2, 1993; and references cited therein.
[2] J.K. Moran, C.F. Meares, in: R.B. King (Ed.), Encyclopedia of Inorganic Chemistry, Vol. 6, Wiley, Chichester, 1994, pp. 3067-3079.
[3] J.R. Lancaster, The Bioinorganic Chemistry of Nickel, VCH Publishers, New York, 1988.
[4] P.F. Knowles, N. Ito, in: R.W. Hay, J.R. Dilworth, K.B. Nolan (Eds.), Perspectives on Bioinorganic Chemistry, vol. 2, JAI Press, London, 1993, pp. 207–244.
[5] F.P. Bossu, K.L. Chellappa, D.W. Margerum, J. Am. Chem. Soc. 99 (1977) 2195.
[6] F.P. Bossu, D.W. Margerum, Inorg. Chem. 16 (1977) 1210.
[7] Ya.D. Lampeka, S.P. Gavrish, J. Coord. Chem. 21 (1990) 351.
[8] S.P. Gavrish, Ya.D. Lampeka, J. Coord. Chem. 24 (1990) 351.
[9] S.P. Gavrish, Ya.D. Lampeka, Russ. J. Inorg. Chem. 38 (1993) 1211.
[10] S.P. Gavrish, Ya.D. Lampeka, Theor. Exp. Chem. 29 (1993) 229.
[11] S.P. Gavrish, PhD Dissertation Thesis, Kiev, 1993.
[12] S.P. Gavrish, Ya.D. Lampeka, Theor. Exp. Chem. 31 (1995) 95.
[13] S.P. Gavrish, Ya.D. Lampeka, J. Coord. Chem. 38 (1996) 295.
[14] S.P. Gavrish, Ya.D. Lampeka, Russ. J. Inorg. Chem. 42 (1997) 742.
[15] R.W. Hay, M.P. Pujari, F. McLaren, Inorg. Chem. 23 (1984) 3033.
[16] J.M. Anast, D.W. Margerum, Inorg. Chem. 21 (1982) 3494.
[17] A.W. Hamburg, D.W. Margerum, Inorg. Chem. 22 (1983) 3884.
[18] J.P. Hinton, D.W. Margerum, Inorg. Chem. 25 (1986) 3248.
[19] W.R. Mason, H.B. Gray, Inorg. Chem. 7 (1968) 55.
[20] J.S. Rybka, D.W. Margerum, Inorg. Chem. 20 (1981) 1453.
[21] J.S. Rybka, J.L. Kurtz, T.A. Neubecker, D.W. Margerum, Inorg. Chem. 19 (1980) 2791.

PERGAMON

www.elsevier.nl/locate/poly

Polyhedron 19 (2000) 2539–2546

POLYHEDRON

Reactions of trichlorovinylmercurials with potential non-chelating bidentate ligands. Crystal structures of [$(C_2Cl_3)_2Hg$ (4,4′-bipyridyl)] (**1**), [C_2Cl_3Hg(2-pyridyl thiolate)] (**12**) and polymeric $HgBr_2$(2,2′-dipyridyl disulfide) (**10**)

Norman A. Bell [a,*], Thomas Gelbrich [b], Michael B. Hursthouse [b], Mark E. Light [b], Annette Wilson [a]

[a] *Division of Chemistry, Sheffield Hallam University, Pond Street, Sheffield, S1 1WB, UK*
[b] *Department of Chemistry, University of Southampton, Highfield, Southampton, SO17 1BJ, UK*

Received 27 June 2000; accepted 14 August 2000

Abstract

Reactions of C_2Cl_3HgX (X = C_2Cl_3, Cl, Br) with the potential bidentate ligands, bis(diphenylphosphino)methane, 2,4′-bipyridyl, 4,4′-bipyridyl and 2,2′-dipyridyl disulfide(PySSPy), in a 2:1 molar ratio have been studied and the thermal and infrared spectral characteristics of the products have been examined. Complexes were isolated for $(C_2Cl_3)_2Hg$ and C_2Cl_3HgCl in all cases apart from between $(C_2Cl_3)_2Hg$ and the diphosphine. The diphosphine and 2,2′-dipyridyl disulfide formed 1:1 complexes (**7**, **6**) with C_2Cl_3HgCl, whereas with $(C_2Cl_3)_2Hg$ the latter ligand formed [$\{(C_2Cl_3)_2Hg\}_2$(PySSPy)] (**3**) which on standing formed C_2Cl_3HgSPy (**12**). 4,4′-Bipyridyl and 2,4′-bipyridyl differed in the stoichiometry of the isolated complexes. $(C_2Cl_3)_2Hg$ formed 1:1 complexes (**1**, **2**) with both ligands whereas C_2Cl_3HgCl formed a 1:1 complex (**4**) with the former ligand but a 1:2 complex (**5**) with the latter. All four ligands caused disproportionation of C_2Cl_3HgBr with resulting isolation of the mercury(II) bromide complexes (**8**–**11**). The structure of [$(C_2Cl_3)_2Hg$ (4,4′-bipyridyl)] (**1**) shows that only one nitrogen is weakly coordinated to mercury so that C–Hg–C is approximately linear in the monomeric structure but there are four intramolecular chlorines closer to mercury than the sum of the van der Waals radii. The C–Hg–S angle in [C_2Cl_3Hg(2-pyridyl thiolate)] (**12**) is only slightly distorted from linearity due to secondary bonding to nitrogen. There are two weak intramolecular contacts between mercury and chlorine and two intermolecular mercury–sulfur contacts to form pairs of molecules which form double chains along the *b* axis. [$HgBr_2$(2,2′-dipyridyl disulfide)] (**10**) is polymeric and contains four-coordinate mercury with the ligand bridging between mercury atoms via coordination to nitrogen. © 2000 Elsevier Science B.V. All rights reserved.

Keywords: Trichlorovinyl; Mercury(II); Crystal structures; Complexes; Bidentate ligands

1. Introduction

Unlike the mercury(II) halides which form a wide range of complexes [1], mercury dialkyls form few complexes. The presence of electronegative substituents in the organic group attached to mercury or replacement of one of the organic groups by a halogen enhances the Lewis acidity of mercury, so that bis(trinitromethyl) mercury [2] and bis(pentafluorophenyl) mercury [3] are stronger acceptors than the unsubstituted compounds. Likewise trichlorovinylmercury chloride and bromide [4] are slightly stronger acceptors than bis(trichlorovinyl)mercury [5] with bidentate chelating ligands.

Coordination between mercury and a hetero atom in the same molecule has been increasingly used to explain the several anomalies in physical properties of organomercury compounds as well as interpret many of their reactions [6]. In particular, special features of infrared (IR), NQR spectra, dipole moments as well as anomalous effects of ortho substituents are explained

* Corresponding author. Tel.: +44-114-225-3002; fax: +44-114-225-3066.
E-mail address: n.a.bell@shu.ac.uk (N.A. Bell).

0277-5387/00/$ - see front matter © 2000 Elsevier Science B.V. All rights reserved.
PII: S0277-5387(00)00554-4

by such coordinative interactions [7–9]. X-ray structure determination and electron diffraction are often used to ascertain the possible presence of these interactions and unusual features in the ^{35}Cl NQR spectra of a range of chlorinated organomercurials have been ascribed to intramolecular interaction of chlorine and mercury. [10–24]. While NQR data indicate the possibility of secondary Hg–Cl bonding in complexes of bis(trichlorovinyl)mercury [5], the X-ray structure of the 3,4,7,8-tetramethyl-1,10-phenanthroline complex did not provide any conclusive evidence [25]. In furtherance of our studies on the coordination behaviour of chlorovinylmercurials and Hg···Cl secondary interactions, we have studied the reactions and determined the crystal structures of some of the complexes formed by such organomercurials with potential bidentate ligands in which the positions of the donor atoms renders chelation improbable.

2. Experimental

The ligands were commercially available and were used without further purification. Microanalyses were carried out by Elemental Micro-Analysis Ltd at Beaworthy. Thermal measurements were recorded using a Mettler TA 3000 thermal analyser. Samples were heated at a rate of 10°C min^{-1} under a flow of nitrogen of 50 cm^3 min^{-1}. IR spectra (2000–600 cm^{-1}), were recorded as KBr discs using an ATI Mattson Genesis Series FTIR spectrometer using WINFRIST software. Melting points were obtained using an electrothermal melting point apparatus and are uncorrected.

2.1. Reagents

Bis(trichlorovinyl) mercury (m.p. 72–73°C, lit. [26] 72–73°C), trichlorovinylmercury chloride (m.p. 105–107°C, lit. [26] 109°C) and trichlorovinylmercury bromide (m.p. 98–100°C, lit. [26] 99–100°C) were prepared as previously described.

2.2. Preparation of complexes

The complexes were prepared by adding an ethanolic solution of the ligand to the organomercurial also in ethanol in 1:2 mole ratio, the solutions being warmed where necessary to dissolve the materials. After mixing the solutions, solvent was evaporated to crystallisation and the deposit then recrystallised and dried in vacuo. A representative synthesis is shown below. Solvents for recrystallisation, analytical data, melting points and appearance are reported in Table 1.

2.2.1. Preparation of [{$(C_2Cl_3)_2Hg$}$_2$(2,2′-dipyridyl disulfide)] (3)

A warm solution of 2,2′-dipyridyl disulfide (0.23 g, 1.04 mmol), dissolved in ethanol (25 cm^3), was added to bis(trichlorovinyl)mercury (0.92 g, 1.99mmol) also dissolved in ethanol. The clear solution was evaporated to low volume (10 cm^3) and the deposit filtered off and recrystallised from ethanol/water as colourless needles. Yield: 0.46g, 40%.

2.3. X-ray crystallography

Crystals of **1**, **10** and **12**, suitable for X-ray analysis, were grown by slow evaporation of ethanolic solutions of the complexes.

Table 1
Solvents for recrystallisation, analytical data, melting points and appearance for complexes **1–11**

Complex	Appearance	Found (%)			Calculated (%)			M.p. (°C)
		C	H	N	C	H	N	
$[(C_2Cl_3)_2Hg(4,4'\text{-bipy})]$ (**1**)	needles [a]	27.31	1.30	4.46	27.23	1.31	4.54	80
$[(C_2Cl_3)_2Hg(2,4'\text{-bipy})]$ (**2**)	needles [b]	27.24	1.12	4.40	27.23	1.31	4.54	78
[{$(C_2Cl_3)_2Hg$}$_2$(2,2′-dipyridyl disulfide)] (**3**)	needles [c]	18.61	0.66	2.59	18.92	0.71	2.45	115
$[C_2Cl_3HgCl\ (4,4'\text{-bipy})]$ (**4**)	cubes [a]	27.19	1.46	5.28	27.58	1.54	5.36	200
$[C_2Cl_3HgCl\ (2,4'\text{-bipy})_2]$ (**5**)	needles [a]	38.70	2.25	8.81	38.93	2.37	8.25	175
$[C_2Cl_3HgCl(2,2'\text{-dipyridyl disulfide})]$ (**6**)	needles [a]	24.19	1.41	4.74	24.56	1.37	4.77	170
$[C_2Cl_3HgCl(Ph_2PCH_2PPh_2)]$ (**7**)	needles [a]	43.23	3.18	-	43.19	2.95	-	245
$[HgBr_2(4,4'\text{-bipy})]$ (**8**)	powder [a]	23.51	1.41	5.24	23.25	1.56	5.42	345
$[HgBr_2(2,4'\text{-bipy})_2]$ (**9**)	needles [a]	35.06	2.25	8.07	35.71	2.39	8.32	150
$[HgBr_2(2,2'\text{-dipyridyl disulfide})]$ [d] (**10**)	needles [a]	21.86	1.35	4.78	20.65	1.37	4.81	170
$[HgBr_2(Ph_2PCH_2PPh_2)]$ (**11**)	powder [a]	40.31	3.37		40.30	2.98		155

[a] Solvent for recrystallisation: ethanol.
[b] Solvent for recrystallisation: hexane.
[c] Solvent for recrystallisation: ethanol/water.
[d] Calculated for $[C_2Cl_3HgBr(2,2'\text{-dipyridyl disulfide})]$: C, 22.83; H,1.1.28; N, 4.44%.

Table 2
Crystallographic data for complexes **1**, **12** and **10**

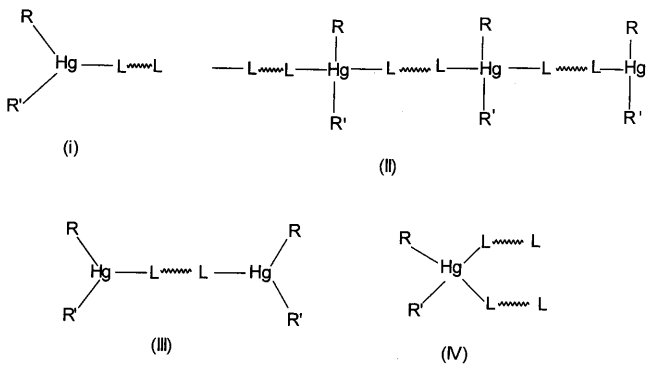
	1	**12**	**10**
Crystal	colourless block	colourless plate	colourless prism
Size	$0.15\times0.15\times0.1$	$0.2\times0.15\times0.05$	$0.15\times0.15\times0.1$
Chemical formula	$C_{14}H_8Cl_6HgN_2$	$C_7H_4Cl_3HgNS$	$(C_{10}H_8Br_2Hg\text{-}N_2S_2)_n$
Unit cell dimensions			
a (Å)	12.6531(3)	12.328(2)	9.1068(4)
b (Å)	15.0642(4)	4.0434(6)	13.5042(7)
c (Å)	9.5394(2)	22.219(5)	11.7830(5)
β (°)	94.633(1)	102.45(8)	104.566(3)
Crystal system	monoclinic	monoclinic	monoclinic
Space group	$C2/c$	$P2_1/n$	$P2_1/n$
Z	4	4	4
Total reflections	5143	1620	7353
Unique (R_{int})	1751, 0.0452	1180, 0.0409	2392, 0.0499
Completeness to $\theta=25°$	98.3%	61.7%	96.8
R_1 [$F^2>2\sigma(F^2)$]	0.0287	0.0697	0.035
wR_2 (all data)	0.0711	0.1983	0.0891
Parameters	124	119	155

Cell dimensions and intensity data were recorded at 298 K, using a Nonius Kappa CCD area detector diffractometer mounted at the window of a rotating anode operating at 50 kV, 90 mA, with a molybdenum anode (λ(Mo Kα) = 0.71073 Å). The crystal-to-detector distance was 30 mm and ϕ and Ω scans (2° increments, 10 s exposure time) were carried out to fill the Ewald sphere. Data collection and processing were carried out using the programs COLLECT [27], DENZO [28] and MAXUS [29] and an empirical absorption correction was applied using SORTAV [30,31].

The structures were solved via direct methods [32] and refined by full-matrix least-squares [32] on F^2. Non-hydrogen atoms were refined anisotropically. Hydrogen atoms for **1** were located from the difference map and fully refined, whilst hydrogen atoms for **10** and **12** were placed in idealised positions and refined using a riding model. Summary details are presented in Table 2.

3. Results and discussion

Reactions between $(C_2Cl_3)_2Hg$, C_2Cl_3HgCl and C_2Cl_3HgBr and a range of bidentate ligands, bis-(diphenylphosphino)methane, 2,4′-bipyridyl, 4,4′-bipyridyl, 2,2′-dipyridyl disulfide and 4,4′-dipyridyl disulfide were studied by reaction of the mercurial and ligand in 2:1 mole ratio in ethanolic solution. The ligands chosen differed from the chelating ligands studied earlier [4,5] such that in the case of 2,4′-bipyridyl, 4,4′-bipyridyl and 4,4′-dipyridyl disulfide, the positions of the donor atoms precluded chelation, whereas for bis(diphenylphosphino)methane and 2,2′-dipyridyl disulfide the size of ring which would be formed in chelation is improbable. A surprising variety of stoichiometries for the isolated complexes was found and the structural possibilities for these complexes are shown in I–IV (R = C_2Cl_3, R′ = C_2Cl_3, Cl or Br and L ∼ L is the bidentate ligand). Bis(phenylethynyl)-mercury forms only 2:1 complexes with 4,4′-bipyridyl and 4,4′-dipyridyl disulfide which are expected to be of type III [33].



We initially attempted to obtain the crystal structure of the parent organomercurial, bis(trichlorovinyl)-mercury, to ascertain if there was crystallographic evidence for secondary Hg–Cl interactions to support the NQR evidence found earlier [5]. The molecule was triclinic but, despite repeated attempts, the structure was not amenable to solution. However, we were able to determine the structure of two other trichlorovinylmercury complexes and these can be compared with the structures of the wide range of organomercurials which have recently been reviewed [34].

Bis(diphenylphosphino)methane does not complex with the weak acceptor $(C_2Cl_3)_2Hg$ but with the stronger Lewis acid C_2Cl_3HgCl a 1:1 complex (**7**) was isolated. Chelation is improbable in this complex due to the bite of the ligand and it is most likely to be of type II in which the ligand acts as a bridge between mercury atoms, thereby resulting in four-coordinate mercury, although a type I structure, in which the ligand is monodentate with a pendant phosphine group and the mercury only three coordinate, is possible.

2,4′-Bipyridyl forms complexes of different stoichiometry with $(C_2Cl_3)_2Hg$ and C_2Cl_3HgCl. The weaker acceptor $(C_2Cl_3)_2Hg$ forms a 1:1 complex (**2**), steric effects preventing the entry of a second ligand into the coordination site around mercury and the similarity in the IR spectrum of this complex and the 4,4′-bipyridyl complex of $(C_2Cl_3)_2Hg$, whose crystal structure has

been determined, is indicative of a type I complex. The stronger acceptor C_2Cl_3HgCl is less sterically encumbered than $(C_2Cl_3)_2Hg$ and forms the usual four-coordinate mercury(II) (**5**) by attachment of two 2,4′-bipyridyl ligands. Both of these trichlorovinylmercurials form 1:1 complexes with 4,4′-bipyridyl for which the $(C_2Cl_3)_2Hg$ complex (**1**) has been confirmed crystallographically to be monomeric and of type I, whereas C_2Cl_3HgCl (4,4′-bipyridyl) may be associated (type II) due to less steric crowding around mercury, though the similarity in the IR spectra of the two complexes suggests similar structures. The structure of the 1:1 complex (**1**) of $(C_2Cl_3)_2Hg$ with 4,4′-bipyridyl is shown in Fig. 1, with selected bond lengths and angles in Table 3. The molecule is centrosymmetric and the most notable features of the structure are (i) the slight distortion of the C–Hg–C angle (169.9(3)°) from linearity, reflecting the tendency of organomercury compounds towards linearity in contrast to mercury(II) halides which tend to become pseudotetrahedral, (ii) the long Hg–N bond (2.690(6) Å, cf. 2.00–2.20 Å in a wide range of Hg–N compounds [34]) indicating only weak interaction, (iii) only one of the nitrogen atoms in the bipyridyl is coordinated to mercury, also indicative of weak coordination and (iv) the two intramolecular contacts between Hg and Cl(1) and Cl(3) (3.318(5) and 3.346(6) Å, respectively) and in the symmetry related other half of the molecule. Though these Hg···Cl contacts are less than the sum of the van der Waals radii, they appear to be an inherent feature of the structure and do not reflect significant intramolecular shortening of the Hg···Cl distances due to secondary interactions as these would tend to narrow the angles around C(1) and C(2), adjacent to mercury, to less than 120°. The Cl(1)–C(1)–Hg angle is in fact normal (120.3(3)°) for an sp^2 hybridised carbon and the C(1)–C(2)–Cl angles are slightly greater than 120° with the Cl(2)–C(2)–Cl(3) angle being significantly less (112.3(3)°), The planes of the two pyridine rings are twisted by 37.6(3)° to reduce interactions between hydrogens on neighbouring rings. Thus the complex is of type I, rather than the expected polymeric arrangement of type II in which both nitrogens would be coordinated to different mercury atoms, reflecting the poor acceptor character of $(C_2Cl_3)_2Hg$ compared to $HgBr_2$ for which the 2,2′-dipyridyl disulfide complex has both nitrogens coordinated to different mercury atoms (type II). This weak interaction between a variety of ligands and organomercurials in which mercury only undergoes slight distortion from linearity on complexation with nitrogen containing Lewis bases has previously been demonstrated [25].

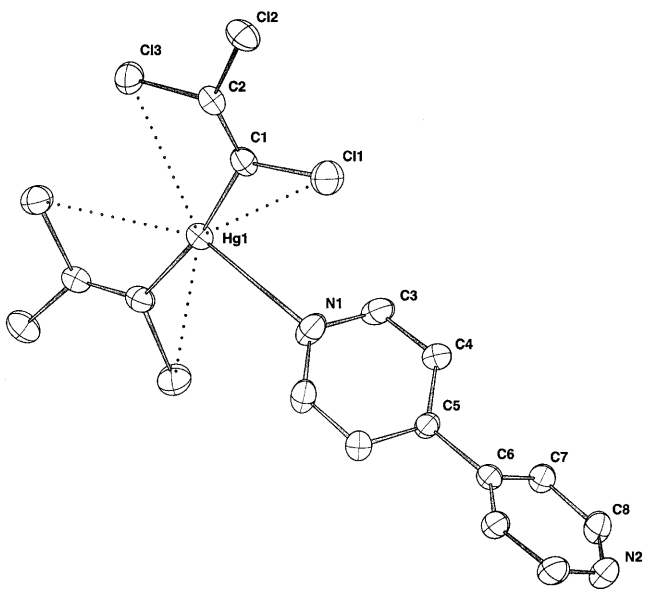


Fig. 1. Molecular structure of $[(C_2Cl_3)_2Hg(4,4'bipyridyl)]$ (**1**) with ellipsoids at 30% probability.

Although 4,4′-dipyridyl disulfide formed brown solutions with the trichlorovinylmercurials, from which complexes could not be isolated, 2,2′-dipyridyl disulfide does form isolable complexes with C_2Cl_3HgX (X = C_2Cl_3, Cl). Bis(trichlorovinyl)-mercury being a relatively weak acceptor [5] requires only one nitrogen atom per mercury to satisfy its coordination deficiency and thus forms $[(C_2Cl_3)_2Hg]_2$-(2,2′-dipyridyl disulfide) (**3**) (type III) although a weak interaction with sulfur may occur. An attempt to obtain the crystal structure of this complex which is analogous to the 2:1 adduct of bis-(pentafluorophenyl)mercury(II) and bis(diphenylarsino)-methane, whose structure was determined with a high *R* value almost 30 years ago [35] showed that, on standing, cleavage of the disulfide bond had occurred and the structure obtained was that for C_2Cl_3HgSPy (**12**). Heterocyclic thionates have been prepared in situ by splitting the disulfide bond of a heterocyclic disulfide either thermally or photochemically and organometallic chelate complexes of heterocyclic thionates have been prepared by these means [36]. The stronger, less sterically crowded, acceptor C_2Cl_3HgCl [4] require two nitrogen atoms for coordinative saturation and so forms a 1:1 complex (**6**) which is likely to be polymeric (type II) as found for the corresponding mercury(II) bromide complex described herein.

The structure of $C_2Cl_3Hg(PyS)$ (**12**) is shown in Fig. 2 with bond lengths and angles in Table 3. The crystal structure of MeHg(PyS) has been described previously [37] and also $Me_2Tl(PyS)$ and $Me_2Sn(PyS)_2$ [38]. In the former complex the ligand is η^1-sulfur donating with secondary bonding to nitrogen and to two neighbouring thionate sulfur atoms so that the overall geometry around mercury is distorted trigonal bipyramidal [37]. In the thallium compound the ligand is η^1-nitrogen donating with secondary Tl···S bonding to the ligand and also to a neighbouring ligand so that the metal becomes five-coordinate, whereas in the tin compound the metal becomes octahedrally coordinated as the lig-

Table 3
Bond lengths (Å) and bond angles (°) for compounds **1**, **10** and **12**

(a)

Compound ***1***

Hg1–C1	2.083(5)	Hg1–C1 [a]	2.083(5)	Hg1–N1	2.690(6)
Cl1–C1	1.737(5)	Cl2–C2	1.732(6)	Cl3–C2	1.730(5)
N1–C3 [a]	1.344(7)	N1–C3	1.344(7)	N2–C8	1.329(7)
N2–C8 [a]	1.329(7)	C1–C2	1.314(7)	C3–C4	1.383(7)
C4–C5	1.389(6)	C5–C4 [a]	1.389(6)	C5–C6	1.500(9)
C6–C7 [a]	1.393(6)				
C6–C7	1.393(6)	C7–C8	1.381(7)		
Hg1–Cl1	3.318(5)	Hg1–Cl3	3.346(6)		

Compound ***12***

Hg1–C6	2.06(2)	N1–C1	1.33(3)	C3–C4	1.37(4)
Hg1–S1	2.350(6)	N1–C5 [c]	1.44(3)	C4–C5	1.49(4)
Cl1–C7 [b]	1.76(2)	C1–C2	1.42(3)	C5–N1 [c]	1.44(3)
Cl2–C7	1.73(2)	C2–C3 [c]	1.27(3)	C6–C7	1.30(3)
Cl3–C6	1.75(3)	C3–C2 [c]	1.27(3)	C7–Cl1 [d]	1.76(2)
S1–C1	1.82(3)	Hg(1)–Cl(3)	3.271(5)	Hg(1)–Cl(2)	3.374(4)
Hg1–S1 [I]	3.329(3)	Hg1–S1 [II]	3.359(5)		

Compound ***10***

C1–N1	1.326(8)	C1–C2	1.370(9)	C1–S1	1.786(6)
C2–C3	1.369(10)	C3–C4	1.380(11)	C4–C5	1.358(10)
C5–N1	1.347(8)	C6–N2	1.335(9)	C6–C7	1.373(10)
C7–C8	1.373(10)	C8–C9	1.373(10)	C9–C10	1.376(9)
C10–N2	1.338(8)	C10–S2	1.785(6)	N1–Hg1	2.529(5)
N2–Hg1	2.633(5)	S1–S2 [e]	2.029(3)	S2–S1 [f]	2.029(3)
Br1–Hg1	2.4468(7)	Br2–Hg1	2.4671(7)		

(b)

Compound ***1***

C1–Hg1–C1 [a]	169.9(3)	C1–Hg1–N1	95.03(13)	C1 [a]–Hg1–N1	95.03(13)
C3 [a]–N1–C3	115.4(6)	C3 [a]–N1–Hg1	122.3(3)	C3–N1–Hg1	122.3(3)
C8–N2–C8 [a]	116.6(7)	C2–C1–Cl1	117.4(4)	C2–C1–Hg1	122.2(4)
Cl1–C1–Hg1	120.3(3)	C1–C2–Cl3	121.7(5)	C1–C2–Cl2	126.0(4)
Cl3–C2–Cl2	112.3(3)	N1–C3–C4	124.7(5)	N1–C3–H3	114(4)
C4–C3–H3	121(4)	C3–C4–C5	118.5(5)	C3–C4–H4	119(3)
C5–C4–H4	123(3)	C4–C5–C4 [a]	118.4(6)	C4–C5–C6	120.8(3)
C4 [a]–C5–C6	120.8(3)	C7 [a]–C6–C7	118.3(6)	C7 [a]–C6–C5	120.9(3)
C7–C6–C5	120.9(3)	C8–C7–C6	118.1(6)	C8–C7–H7	123(3)
C6–C7–H7	119(3)	N2–C8–C7	124.5(6)	N2–C8–H8	117(4)
C7–C8–H8	118(4)				

Compound ***12***

C6–Hg1–S1	170.7(7)	C1–S1–Hg1	94.9(8)	C1–N1–C5 [c]	119(2)
N1–C1–C2	124(2)	N1–C1–S1	113.9(18)	C2–C1–S1	122.2(19)
C3 [c]–C2–C1	118(2)	C2 [c]–C3–C4	125(3)	C3–C4–C5	118(3)
N1 [c]–C5–C4	116(2)	C7–C6–Cl3	118.0(18)	C7–C6–Hg1	124(2)
Cl3–C6–Hg	117.9(13)	C6–C7–Cl2	121.7(18)	C6–C7–Cl1 [d]	125.1(19)
Cl2–C7–Cl1 [d]	113.2(13)				

Compound ***10***

N1–C1–C2	123.0(6)	N1–C1–S1	112.1(4)	C2–C1–S1	124.9(5)
C3−C2−C1	118.0(7)	C2−C3−C4	120.6(7)	C5–C4–C3	117.2(7)
N1–C5–C4	123.6(7)	N2–C6–C7	123.0(7)	C6–C7–C8	119.0(7)
C8–C9–C10	118.3(7)	N2–C10–C9	123.5(6)	C7–C8–C9	119.1(7)
N2–C10–S2	111.4(4)	C9–C10–S2	125.1(5)	N1–Hg1–N2	83.75(19)
C1–N1–C5	117.6(6)	C1–N1–Hg1	127.4(4)	Br2–Hg1–N2	102.29(11)
C5–N1–Hg1	113.5(4)	C6–N2–C10	117.2(6)	Br1–Hg1–N2	92.69(11)
C6–N2–Hg1	111.3(4)	C10–N2–Hg1	129.6(4)	Br2–Hg1–N1	92.20(12)
C1–S1–S2 [e]	104.6(2)	C10–S2–S1 [f]	105.1(2)	Br1–Hg1–N1	111.85(12)
Br1–Hg1–Br2	153.01(3)				

[a] $-x,\ y,\ -z+0.5$.
[b] $x,\ y+0.5,\ z$.
[c] $-x+1,\ -y,\ -z+1$.
[d] $x,\ y-1,\ z$
[e] $x-1,\ y,\ z$.
[f] $x+1,\ y,\ z$.
[I] $x,\ 1+y,\ z$
[II] $1-x,\ 1-y,\ -z$.

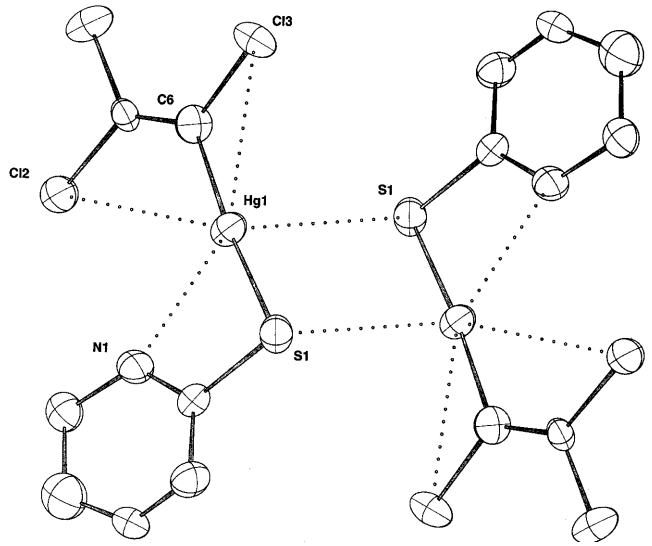


Fig. 2. Molecular structure of $[C_2Cl_3Hg(2\text{-pyridyl thiolate})]$ (**12**) with ellipsoids at 30% probability.

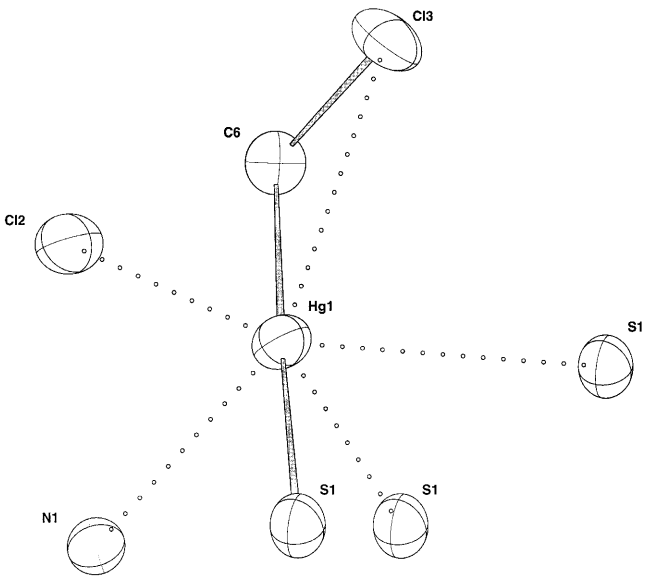


Fig. 3. Coordination around mercury in $[C_2Cl_3Hg(2\text{-pyridyl thiolate})]$ (**12**) with ellipsoids at 30% probability.

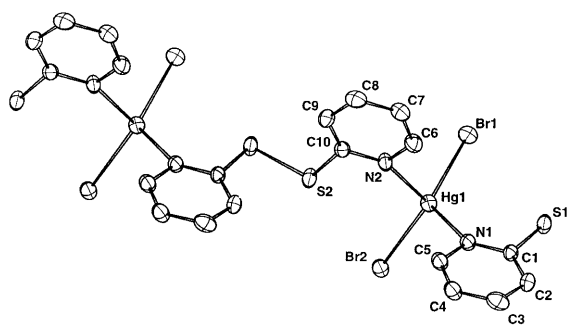


Fig. 4. Molecular structure of $[HgBr_2(2,2'\text{-dipyridyl disulfide})]_n$ (**10**) with ellipsoids at 30% probability.

and is S,N-chelating [38]. In $C_2Cl_3Hg(PyS)$ (**12**) the complex contains essentially two-coordinate mercury(II) with a shorter η^1-sulfur donating ligand than in the methyl analogue (2.350(6) cf. 2.374(2) Å). The C–S bond length (1.82(3) Å) (cf. 1.776(1) Å in the methyl analogue) lies in the range for a single bond, showing that the ligand is in the thiol form. There is a secondary interaction with nitrogen (Hg–N = 2.809(7) Å) which results in slight distortion from linearity at mercury (170.7(7)°). This distortion is larger than the 176.4(2) found in the methyl analogue [37] but there is a shorter Hg–C bond length (2.06(2) Å) than in the methyl compound (2.089(7) Å) and in $(C_2Cl_3)_2Hg(4,4'\text{-bipy})$ (2.083(5) Å) due to less steric crowding around mercury. In addition to the Hg(1)···N(1) interaction there are two further intramolecular contacts, less than the sum of the van der Waals radii (Hg(1)···Cl(3), 3.271(5) Å and Hg(1)···Cl(2), 3.374(4) Å), as well as two intermolecular contacts ($Hg(1)\cdots S(1)^{I}$, 3.329(3) Å and $Hg(1)\cdots S(1)^{II}$, 3.359(5) Å). The intermolecular contacts link adjacent molecules into pairs (Fig. 2) and these are linked by contacts above and below (Fig. 3) to form double chains along the *b* axis. Mercury, C6, C7 and all of the chlorine atoms are coplanar as also found in the structure of **1**.

Reaction of C_2Cl_3HgBr with 2,2′-dipyridyl disulfide gave a crystalline complex that was initially thought to be a 1:1 complex on the basis of the analytical data, like the corresponding chloride. However the peaks due to C=C and C–Cl appeared to be absent in its IR spectrum. The X-ray structure of the compound showed it to be the 1:1 complex (**10**) of mercury(II) bromide which had similar theoretical C, H and N analytical data to that for the C_2Cl_3HgBr complex. Data for both are shown in Table 1 for comparison. Bis(diphenylphosphino)methane, 4,4′-bipyridyl and 2,4′-bipyridyl also caused disproportionation of C_2Cl_3HgBr resulting in the formation of the 1:1 complexes (**11**, **8**) of $HgBr_2$ with the former two ligands and $HgBr_2(2,4\text{-bipy})_2$ (**9**) with the latter.

The structure of $[HgBr_2(PySSPy)]_n$ (**10**) is shown in Fig. 4 and selected bond lengths and angles in Table 3. The structure consists of a pseudotetrahedral distribution around mercury of two bromines and two nitrogens from different 2,2′-dipyridyl disulfide molecules, thus creating a polymeric chain with the ligand bridging two mercury atoms, as found for the chloro analogue [39]. There are no mercury–sulfur interactions as the Hg–S distances (3.586(7), 3.732(7) Å) are very long. The Hg–Br distances (2.4468(7), 2.4671(7) Å) are similar to those found in $HgBr_2(pyridine)_2$ (2.478(3), 2.483(3) Å [40]), whereas the Hg–N distances (2.529(5), 2.633(5) Å) are significantly longer (2.38(2). 2.39(2) Å) but are similar to those found in the chloro analogue (2.527(5), 2.632(3) Å) [39]. The Br–Hg–Br angle is remarkably large (153.01(3)°) and is similar to that found in the corresponding chloride (154.8(1)°), result-

Table 4
Thermal characteristics of complexes of trichlorovinylmercurials

Compound	Temperature (°C)	Thermal behaviour [a]
$[(C_2Cl_3)_2Hg(4,4'\text{-bipy})]$ (**1**)	98–308	95.4% mass loss in single step
$[(C_2Cl_3)_2Hg(2,4'\text{-bipy})]$ (**2**)	114–297	major mass loss (85.2%) in single step
	297–410	slow mass loss leaving ~3% residue
$[\{(C_2Cl_3)_2Hg\}_2(2,2'\text{-dipyridyl disulfide})]$ (**3**)	155–227	38.8% mass loss
	227–387	39.0% mass loss
	387–800	slow mass loss leaving ~3% residue
$[C_2Cl_3HgCl\ (4,4'\text{-bipy})]$ (**4**)	111–260	mass loss 42.9%
	260–376	mass loss 41.4%
$[C_2Cl_3HgCl(2,4'\text{bipy})_2]$ (**5**)	138–228	mass loss 87.8%
	228–261	mass loss 10.3% leaving ~2% residue
$[C_2Cl_3HgCl(2,2'\text{-dipyridyl disulfide})]$ (**6**)	197–308	mass loss 59.6%
	308–367	mass loss 23.2%
	367–600	slow mass loss leaving ~3% residue
$[C_2Cl_3HgCl\text{-}(Ph_2PCH_2PPh_2)]$ (**7**)	182–249	mass loss 16.9%
	249–323	mass loss 36.2%
	323–480	mass loss 26.0% leaving 20.9% residue
$[HgBr_2(4,4'\text{-bipy})]$ (**8**)	118–367	single step mass loss 98.1%
$[HgBr_2(2,4'\text{-bipy})_2]$ (**9**)	95–363	single step mass loss 97.2%
$[HgBr_2(2,2'\text{-dipyridyl disulfide})]$ (10)	123–499	mass loss 83.0%
	500–582	mass loss 2.7%
$[HgBr_2(Ph_2PCH_2PPh_2)]$ (**11**)	224–412	mass loss 66.7%
	412–480	mass loss 15.5% leaving 17.8% residue

[a] Mass loss and residue are expressed as % of the mass of the original compound.

ing from bridging by the nitrogen ligand whereas in a chelate complex such as (*N*,*N*,*N*′,*N*′-tetramethyl-*o*-phenylenediamine)$HgBr_2$ [41] the Br–Hg–Br angle is 123.04(8)° and N-Hg-N is 73.2(4)° compared to 83.75(19)° in the bromide described herein and 81.1(2)° in the chloride analogue [39]. The other angles and distances are similar to those found in the free ligand [42].

Comparison of the IR spectra of the complexes with those of the parent mercurials show that the strong absorptions at 1530 and 845 cm^{-1} due to C=C and C–Cl vibrations respectively are not significantly moved on complexation. The most notable feature of the spectra is the increase in intensity of the 845 cm^{-1} peak in $[\{(C_2Cl_3)_2Hg\}_2(2,2'\text{-dipyridyl disulfide})]$ (**3**) compared to the free ligand and the $(C_2Cl_3)HgCl(2,2'\text{-dipyridyl disulfide})$ complex (**6**). The spectra of all the complexes show bands which are characteristic of the parent organomercurials and the ligands. However, it is to be noted that the bands of the ligands are only slightly modified in the complexes. The similarity in the IR spectra of the 2,2′-dipyridyl disulfide complexes with those of 2,2'-bipyridyl complexes [4,5] leads us to the conclusion that coordination takes place through nitrogen in all cases rather than sulfur, since the weak nature of the Hg–N interaction in organomercury–nitrogen complexes as illustrated by the crystal structure of $(C_2Cl_3)_2Hg$(3,4,7,8-tetramethyl-1,10-phenanthroline in which C–Hg–C is little distorted from linearity and the Hg–N bonds are long [25] and the low coordination number of the metal is unlikely to modify the spectra significantly.

The thermal characteristics of the complexes are shown in Table 4. For some of the complexes, e.g. $(C_2Cl_3)_2Hg(4,4'\text{-bipy})$ (**1**) mass loss occurred in a single step, though often over a wide temperature range, usually leaving a slight residue, doubtless from thermal degradation of the complexes. In two cases mass losses corresponded closely with values expected for the formation of intermediates in the decomposition schemes as shown below:

$$[\{(C_2Cl_3)_2Hg\}_2(2,2'\text{-dipyridyl disulfide})] \xrightarrow{155-227^\circ C} (C_2Cl_3)_2Hg\uparrow + (C_2Cl_3)_2Hg(2,2'\text{-dipyridyl disulfide})$$

(mass loss found 38.8%; calc. 40.4%)

$$\xrightarrow{227-387^\circ C} 2,2'\text{-dipyridyldisulfide} + (C_2Cl_3)_2Hg\uparrow$$

(mass loss found 39.0%; calc. 40.4%)

$$(C_2Cl_3)HgCl(Ph_2PCH_2PPh_2) \xrightarrow{182-323^\circ C} (C_2Cl_3)HgCl\uparrow + Ph_2PCH_2PPh_2$$

(mass loss found 53.1%; calc. 51.7%)

For the remaining complexes decomposition was complex and, though in some cases the TG traces showed evidence for the formation of intermediates, it was not possible to predict the nature of these simply from the mass losses.

4. Supplementary material

Crystallographic data for the structures reported in this paper have been deposited with the Cambridge

Crystallographic Data Centre, CCDC No. 146176 for compound **1**, CCDC No. 146177 for compound **12** and CCDC No. 146178 for compound **10**. Copies of this information may be obtained free of charge from the Director, CCDC, 12 Union Road, Cambridge, CB2 1EZ, UK (fax: +44-1223-336033; e-mail: deposit@ccdc.cam.ac.uk or http://www.ccdc.cam.ac.uk).

Acknowledgements

The authors gratefully acknowledge a grant from the Royal Society of Chemistry Research Fund in support of this work.

References

[1] (a) C.A. McAuliffe, The Chemistry of Mercury, McMillan, London, 1977. (b) P.A.W. Dean, Prog. Inorg. Chem. 24 (1978) 109.
[2] A.L. Fridman, T.N. Ivshina, V.A. Tartakovskii and S.K. Novikov, Izv. Akad. Nauk SSSR, Ser. Khim. (1968) 2839.
[3] A.J. Canty, G.B. Deacon, Aust. J. Chem. 24 (1971) 489.
[4] N.A. Bell, I.W. Nowell, D.J. Starkey, Inorg. Chim. Acta 48 (1981) 139.
[5] N.A. Bell, I.W. Nowell, P.A. Reynolds, R.J. Lynch, J. Organomet. Chem 193 (1980) 147.
[6] L.V. Vilkov, M.G. Anashkin, Zhur. Strukt. Khim 9 (1968) 690.
[7] A.K. Prokof'ev, V. Bregadze, O.Yu. Okhlobystin, Uspekhi Khim 39 (1970) 412.
[8] E.F. Kiefer, W.L. Waters, D.A. Carlson, J. Am. Chem. Soc. 90 (1968) 5127.
[9] E.F. Kiefer, W. Gericke, S.J. Amimoto, J. Am. Chem. Soc. 90 (1968) 5131.
[10] G. Wulfsberg, R. West, J. Am. Chem. Soc. 93 (1971) 4085.
[11] G. Wulfsberg, R. West, V.N.M Rao, J. Am. Chem. Soc. 95 (1973) 8658.
[12] T.A. Babushkina, E.V. Bryukhova, F.K. Velichko, V.I. Pakhomov, G.K. Semin, J. Struct. Chem. 9 (1968) 153.
[13] E.V. Bryukhova, F.K. Velichko, G.K. Semin, Bull. Acad. Sci. USSR, Chim. Ser. (1969) 880.
[14] F.K. Velichko, L.A. Nikonova, G.K. Semin, Bull. Acad. Sci. USSR, Chem. Ser. (1967) 78.
[15] V.I. Bregadze, T.A. Babushkina, O.Yu. Okhlobystin, G.K. Semin, Theor. Exp. Chim. 3 (1968) 325.
[16] E.V. Bryukhova, T.A. Babushkina, M.V. Kashutina, O.Yu. Okhlobystin, G.K. Semin, Proc. Acad. Sci. USSR 183 (1968) 1035.
[17] G.K. Semin, V.I. Robas, in: I.P. Biryukov, M.G. Voronkov, I.A. Safin (Eds.), Tables of NQR Frequencies, Israel Programme for Scientific Translations, Jerusalem, 1969, p. 24.
[18] D.N. Kravtson, A.P. Zhukov, B.A. Faingor, E.M. Rokhlina, G.K. Semin, A.N. Nesmayanov, Bull. Acad. Sci. USSR, Chem. Ser. (1968) 1161.
[19] A.N. Nesmayanov, O.Yu. Oklobystin, E.V. Bryukhova, V.I. Bregadge, D.N. Kravtsov, B.A. Faingor, L.S. Golovchenko, G.K. Semin, Bull. Acad. Sci. USSR, Chem. Ser. (1969) 1785.
[20] G. Wulfsberg, R. West, V.N.M. Rao, J. Organomet. Chem. 86 (1975) 303.
[21] G. Wulfsberg, J. Organomet. Chem. 86 (1975) 321.
[22] V.I. Pakhomov, A.I. Kitaigorodskii, J. Struct. Chem. 7 (1966) 798.
[23] I.A. Ronova, O.Yu. Okhlobystin, Yu.T. Struchkov, A.K. Prokof'ev, Russ. J. Struct. Chem. 13 (1972) 183.
[24] A.G. Davies, J.P. Goddard, M.B. Hursthouse, N.P.C. Walker, J. Chem. Soc., Dalton Trans. (1985) 471.
[25] N.A. Bell, I.W. Nowell, Acta Crystallogr., Sect. B 37 (1980) 447.
[26] D. Seyferth, R.H. Towe, Inorg. Chem. 1 (1962) 185.
[27] 'Collect' Data Collection Software, B.V. Nonius, 1998.
[28] Z. Otwinowski, W. Minor, Processing of X-ray diffraction data collected in oscillation mode, in: C.W. Carter, R.M. Sweet (Eds.), Methods in Enzymology: Macromolecular Crystallography, Part A, vol. 276, Academic Press, New York, 1997, p. 307.
[29] S. Mackay, C.J. Gilmore, C. Edwards, M. Tremayne, N. Stuart, K. Shankland, maXus: A Computer Program for the Solution and Refinement of Crystal Structures from Diffraction Data.
[30] R.H. Blessing, Acta Crystallogr., Sect. A 51 (1995) 33.
[31] R.H. Blessing, J. Appl. Crystallogr. 30 (1997) 421.
[32] G.M. Sheldrick, SHELX-97: Programs for Crystal Structure Analysis (Release 97-2), Institüt für Anorganische Chemie der Universität, Göttingen, Germany, 1998.
[33] N.A. Bell, P. Culshaw, Unpublished observations.
[34] C.E. Holloway, M. Melnik, J. Organomet. Chem. 495, 1. (b) J.S. Casas, M.S. Garcia-Tasende, J. Sordo, Coord. Chem. Rev. 193–195 (1999) (1995) 283.
[35] A.J. Canty, B.M. Gatehouse, J. Chem. Soc., Dalton Trans. (1972) 511.
[36] E.S. Raper, Coord. Chem. Rev. 153 (1996) 199 and references therein.
[37] A. Castineiras, W. Hiller, J. Strahle, J. Bravo, J. Casas, M. Gayoso, J. Sordo, J.Chem. Soc., Dalton Trans. (1986) 1945.
[38] M.V. Casteno, A. Macias, A. Castineiras, A.S. Gonzales, E.G. Martinez, J.S. Casas, J. Sordo, W. Hiller, E.E. Castellano, J. Chem. Soc., Dalton Trans. (1990) 1001.
[39] M.M. Kadooka, E. Hilti, L.G. Warner, K. Seff, Inorg. Chem. 15 (1976) 1186.
[40] A.J.Canty, C.L. Raston, B.W. Skelton, A.H. White, J. Chem. Soc., Dalton Trans. (1982) 15.
[41] C.M. Hughes, M.C. Favos, B.W. Skelton, A.H. White, Aust. J. Chem. 38 (1985) 1521.
[42] N.V. Raghavan, K. Seff, Acta Crystallogr., Sect. B 37 (1977) 386.

PERGAMON

www.elsevier.nl/locate/poly

Polyhedron 19 (2000) 2547–2555

POLYHEDRON

Strontium β-diketonate complexes with polyamine donor ligands: the synthesis and structural characterization of $[Sr(thd)_2(L)]_n$ ($n = 2$; L = diethylenetriamine, $n = 1$; L = triethylenetetramine, tetraethylenepentamine and tris(2-aminoethyl)amine) complex

Jung Woo Park [a], Jun Tae Kim [a], Sang Man Koo [a,*], Chang Gyun Kim [b], Yun Su Kim [b]

[a] *Department of Industrial Chemistry and Ceramic Processing Research Center, College of Engineering, Hanyang University, Seoul 133-791, South Korea*

[b] *Thin Film Materials Laboratory, Advanced Material Division, Korea Research Institute of Chemical Technology, Taejon 305-600, South Korea*

Received 15 June 2000; accepted 14 August 2000

Abstract

Four novel $[Sr(thd)_2(L)]_n$ ($n = 2$; L = diethylenetriamine (**I**), $n = 1$; L = triethylenetetramine (**II**), tetraethylenepentamine (**III**), and tris(2-aminoethyl)amine (**IV**)) complexes were synthesized by the reaction of $Sr(thd)_2$ with corresponding polyamines in THF and characterized by FTIR, ^1H NMR and single-crystal X-ray crystallography. Complex **I** exists as a dimmer in the solid state in which two strontium atoms are bridged by two thd ligands. Complexes **II** and **III** exist as monomers in the solid state and in both complexes, the polyamine ligands are coordinated to the central strontium atom in a meridional fashion, with the two thd ligands on opposite sides of the neutral ligand plane. Complex **IV** also exist as a monomer in the solid state. In this molecule, strontium atom is eight-coordinate with all of the nitrogens of the amine ligand and all oxygens of the thd ligand binding to the metal atom. The amine ligand is coordinated to one side of the metal atom and resulting in a *cis*-relationship. Thermogravimetric analysis shows that complexes **I**, **II**, **III** and **IV** are sufficiently volatile and sublimed without residue. © 2000 Elsevier Science B.V. All rights reserved.

Keywords: Strontium; Polyamine ligand; Thd ligand; Precursor

1. Introduction

There has been a continuing interest in the synthesis of alkaline earth metal β-diketonate complexes (particularly Ca, Sr and Ba), because they have been used as promising metal organic chemical vapor deposition (MOCVD) precursors for perovskite metal oxides and ceramic superconductors [1,2]. A useful MOCVD precursor must not only have appropriate reactivity for the desired film growth process but also low volatility and stable vapor pressure characteristics [3]. Monomeric complexes are expected to exhibit an enhanced volatility in comparison to oligomeric complexes because of minimizing intermolecular solid-state interactions and connectivities. Heavier alkaline earth metal bis(β-diketonate) complexes usually exist as oligomeric species ($Ca_3(thd)_6$ [4], $Sr_3(thd)_6$(H–thd) [5], and $Ba_4(thd)_8$ [6]) (thd = 2,2,6,6-tetramethyl-3,5-heptanedionate) in the solid state. They have relatively low volatility and undergo severe deterioration during storage. They have also unstable vapor pressure as a result of tendency to oligomerize. The main reason for these problems is, among other factors, the large size of the heavier Group II metal ions. To circumvent this problem, recent research interests have been focused on the synthesis of coordinatively saturated Group II metal precursors by introducing ancillary Lewis base ligands. For example, polyether adducts of strontium and bar-

* Corresponding author. Tel.: +82-2-2290-0527; fax: +82-2-2281-4800.

E-mail address: sangman@email.hanyang.ac.kr (S. Man Koo).

0277-5387/00/$ - see front matter © 2000 Elsevier Science B.V. All rights reserved.
PII: S0277-5387(00)00555-6

ium complexes, $Sr(Ph_2acac)_2$(tetraglyme) [7], $Sr(thd)_2$-(tetraglyme) [7], $Ba(thd)_2$(triglyme) [8], $Ba(thd)_2$-(tetraglyme) [7] are reported. Although these adduct complexes exist as monomeric, exhibiting higher vapor pressure than those of $[M(thd)_2]_n$ complexes, the low Lewis acidity of barium and strontium ions weaken the bonding of the adducted polyether chain resulting in dissociation of polyether ligands upon attempted sublimation of the solid and thus have unstable vapor pressure [7,9]. Another approach to improve the volatility and vapor pressure stability of precursors is the introduction of fluorinated β-diketonate ligands [10–13]. However, in many cases, the use of fluorinated β-diketonates necessitates the addition of water vapor as a reactant gas to prevent the formation of undesirable metal fluorides [14,15]. Polyamine adducts of strontium and barium complexes, $Sr(hfac)_2(bpy)_2$ [16](hfac = 1,1,1,5,5,5 - hexafluoro - 2,4 - pentanedionate, bpy = 2,2′-dipyridyl), $Ba(hfac)_2(Phen)_2$ [17](Phen = *o*-phenanthroline), $Ba(thd)_2$(pmdt) (pmdt = 1,1,4,7,7-pentamethyldiethylenetriamine) [18], $Ba(thd)_2$(hmtt) (hmtt = 1,1,4,7,10,10 - hexamethyltriethylenetetramine) [18], $[Ba(thd)_2(diethylenetriamine)]_2$ [19], $[Ba(thd)_2$-(triethylenetetramine)$]_2$ [19] and $[Ba(tfa)_2(hmtt)]$(tfa = 1,1,1,-trifluoro-2,4,-pentanedionate) [20], $[Ba(thd)_2$-(pmdt)](pmdt = pentamethyldiethylenetriamine) [20] $[Ba(thd)_2(hmtt)]$(hmtt = hexamethyltriethyleneteramine) [21] have also been reported recently and proven to be effective in reducing molecular aggregation through the coordinative saturation. Because of the increased basicity of amines compared to ethers, it is expected that nitrogen-donor ligands make stronger bonds with metal than analogous oxygen-donor ligands. In this respect, when the polyamines were introduced as neutral ligands to the metal diketonates, it was expected that precursors would exhibit more stable thermal behavior than polyether adducts and simple monodentate Lewis base adducts.

In this article, we report the synthesis and characterization of $[Sr(thd)_2(L)]_n$ ($n = 2$; L = diethylenetriamine, $n = 1$; L = triethylenetetramine, tetraethylenepentamine, and tris(2-aminoethyl)amine) complexes which can be used as potential MOCVD precursors for ferroelectric BST($(Ba,Sr)TiO_3$) thin films.

2. Experimental

All manipulations were performed using standard Schlenk line techniques and under dinitrogen atmosphere. Tetrahydrofuran (THF) was distilled after being refluxed with sodium/benzophenone. Acetonitrile, *n*-pentane, *n*-hexane were distilled after being refluxed over CaH_2 before use. Diethylenetriamine, triethylenetetramine, and tetraethylenepentamine (Aldrich) were used as received. $[Sr(thd)_2]_n$ was synthesized from strontium metal and Hthd in anhydrous THF.

2.1. $[Sr(thd)_2(diethylenetriamine)]_2$ (I)

A 250-ml Schlenk flask was charged with $Sr(thd)_2$ (6.61 mmol, 3 g) and a stirring bar. To this flask 100 ml of THF was added via cannula and then diethylenetriamine (6.66 mmol, 0.72 ml) was injected slowly by syringe while stirring at an ambient temperature. The reaction mixture was stirred for a further 4 h and then filtered through a fine porosity funnel. The solvent was removed by vacuum, 30 ml of acetonitrile was then added to the resulting oily crude product, and the solution was stirred for 10 min. Finally white powders were isolated by filtration and dried under vacuum. Yield: 85%. Colorless crystals for single-crystal X-ray structural determination were grown from hot *n*-hexane solutions. M.p. 128–135°C. Calc. for $C_{52}H_{102}N_6O_8Sr_2$: C, 56.03; H, 9.22; N, 7.54. Found: C, 56.20; H, 9.27; N, 7.58%. FTIR: $\nu(NH_2,NH)$; 3386, 3340, 3293 cm^{-1}, ν(C=O); 1596 cm^{-1}. ^1H NMR (benzene-d_6): δ (CH in thd ligand); 5.81 (*s*,1H), δ (CH_3 in thd ligand); 1.31 (*s*,18H), δ (CH_2 in amine ligand); 2.37 (br,2H), 2.22 (br,2H).

2.2. $[Sr(thd)_2(triethylenetetramine)]$ (II)

A 250-ml Schlenk flask was charged with Sr(thd)2 (6.61 mmol, 3 g) and a stirring bar. To this flask 100 ml of THF was added via cannula and then triethylenetetramine (6.71 mmol, 1.00 ml) was injected slowly by syringe while stirring at an ambient temperature. The reaction mixture was stirred for a further 12 h and filtered through a fine porosity funnel. The solvent was removed by vacuum, 30 ml of acetonitrile was then added to the resulting oily crude products and stirred for 10 min. Finally white powders were isolated by filtration and dried under vacuum. Yield: 90%. Colorless crystals for single-crystal X-ray structural determination were grown from hot *n*-hexane solutions. M.p. 100–106°C. Calc. for $C_{28}H_{56}N_4O_4Sr$: C, 56.01; H, 9.40; N, 9.33. Found: C, 56.25; H, 9.78; N, 9.70%. FTIR: $\nu(NH_2,NH)$; 3382, 3359, 3281, 3316 cm^{-1}, δ (C=O); 1596 cm^{-1}. ^1H NMR (benzene-d_6): δ (CH in thd ligand); 5.82 (*s*,1H), δ (CH_3 in thd ligand); 1.34 (*s*,18H), δ (CH_2 in amine ligand); 2.45 (*d*,2H), 2.22 (br,4H).

2.3. $[Sr(thd)_2(tetraethylenepentamine)]$ (III)

A 250-ml Schlenk flask was charged with $Sr(thd)_2$ (6.61 mmol, 3 g) and a stirring bar. To this flask 100 ml of THF was added via cannula and then tetraethylenepentamine (6.64 mmol, 1.26 ml) was injected slowly by syringe stirring at ambient temperature. The reaction mixture was stirred for a further 12 h and filtered

through a fine porosity funnel. The solvent was removed by vacuum, 30 ml of acetonitrile was then added to the resulting oily crude products and then stirred for 10 min. Finally white powders were isolated by filtration and dried under vacuum. Yield: 85%. Colorless crystals for single-crystal X-ray structural determination were grown from hot *n*-hexane solutions. M.p. 84–90°C. Calc. for $C_{30}H_{61}N_5O_4Sr$: C, 56.00; H, 9.56; N, 10.88. Found: C, 56.12; H, 9.86; N, 10.73%. FTIR: ν(NH_2,NH); 3394, 3332, 3281 cm^{-1}, ν(C=O); 1596 cm^{-1}. ^1H NMR (benzene-d_6): δ (CH in thd ligand); 5.74 (*s*,1H), δ (CH_3 in thd ligand); 1.31 (*s*,18H), δ (CH_2 in amine ligand); 2.66 (*d*,2H), 2.46 (*d*,4H), 2.22 (br,2H).

2.4. [Sr(thd)$_2$(tris(2-aminoethyl)amine)] (IV)

A 250-ml Schlenk flask was charged with Sr(thd)$_2$ (6.61 mmol, 3 g) and a stirring bar. To this flask 100 ml of THF was added via cannula and then tris(2-aminoethyl)amine (6.68 mmol, 1.00 ml) was injected slowly by syringe stirring at an ambient temperature. The reaction mixture was stirred for a further 12 h and filtered through fine porosity funnel. The solvent was removed by vacuum, 30 ml of acetonitrile was then added to the resulting oily crude products and stirred for 10 min. Finally white powders were isolated by filtration and dried under vacuum. Yield: 85%. Colorless crystals for single-crystal X-ray structural determination were grown from hot *n*-hexane solutions. M.p. 76–84°C. Calc. for $C_{24}H_{56}N_4O_4Sr$: C, 56.01; H, 9.40; N, 9.33. Found: C, 56.12; H, 9.34; N, 9.27%. FTIR: ν(NH_2,NH); 3370, 3332 cm^{-1}, ν(C=O); 1596 cm^{-1}. ^1H NMR (benzene-d_6): δ (CH in thd ligand); 5.80 (*s*,1H), δ (CH_3 in thd ligand); 1.35 (*s*,18H), δ (CH_2 in amine ligand); 2.29 (*d*,3H), 1.93 (*d*,3H).

2.5. X-ray crystallography

Single crystals of complexes **I**, **II**, **III** and **IV** were obtained directly from saturated *n*-hexane solutions. All of the crystals were subsequently mounted into glass capillary under N_2 atmosphere and then sealed. A summary of the X-ray diffraction data is presented in Table 1. The diffraction data was collected at an ambient temperature on Bruker P4 four circle diffractometer using Mo–K_α radiation. The intensity data was collected using a θ–2θ step scan technique and for all data sets the condition of the crystal was monitored by measuring two standard reflections. The solutions of structures **I**, **II**, **III** and **IV** were carried out by a combination of heavy atom Patterson techniques, direct methods, and Fourier techniques. The refinements of the structures by full-matrix-least-squares methods were based on 9051 unique reflections ($2\theta = 45$, $I > 2\sigma$) for **I**, 8485 unique reflections ($2\theta = 45$, $I > 2\sigma$) for **II**, 2455 unique reflections ($2\theta = 45$, $I > 2\sigma$) for **III**, and 2283 unique reflections ($2\theta = 45$, $I > 2\sigma$) for **IV**. Anisotropic temperature factors were used for all non-hydrogen atoms in **I**, **II**, **III**, and **IV**. At the current stage of refinement on 779 parameters for **I**, 715 parameters for **II**, 212 for **III**, and 206 for **IV** with all atoms present in the asymmetric units, $R = 0.0693$, $R_w = 0.1612$ for **I**, $R = 0.0700$, $R_w = 0.1755$ for **II**, $R = 0.0559$, $R_w = 0.1448$ for **III**, and $R = 0.0813$, $R_w = 0.2088$ for **IV**.

Table 1
Crystallographic data for [Sr(thd)$_2$(diethylenetriamine)]$_2$ (**I**), [Sr(thd)$_2$(triethylenetetramine)] (**II**), [Sr(thd)$_2$(tetraethylenepentamine)] (**III**) and [Sr(thd)$_2$(tris(2-aminoethyl)amine)](**IV**)

	I	II	III	IV
Formula	$Sr_2N_6O_8C_{52}H_{102}O_2$	$SrN_4O_4C_{28}H_{56}$	$SrN_5O_4C_{30}H_{61}$	$SrN_4O_4C_{24}H_{56}$
Formula weight	1114.64	600.39	643.36	552.3
Crystal system	monoclinic	monoclinic	orthorhombic	orthorhombic
Space group	$P2_1/c$ (No.14)	$P2_1/c$ (No.14)	*Pccn* (No.56)	*Pnma* (No.62)
a (Å)	20.528(3)	11.411(4)	11.437(2)	12.178(2)
b (Å)	12.106(2)	16.164(2)	15.868(3)	25.712(5)
c (Å)	26.638(5)	38.508(6)	20.917(6)	11.060(2)
α (°)	90	90	90	90
β (°)	95.06(1)	94.66(2)	90	90
γ (°)	90	90	90	90
Z	4	8	4	4
V (Å)^3	6594(2)	7079(3)	3796(2)	3463.1(11)
T (°C)	20	20	20	20
λ (Å)	0.71073	0.71073	0.71073	0.71073
ρ_{calc} (g cm^{-3})	1.123	1.127	1.124	1.163
μ (cm^{-1})	1.664	1.556	1.455	1.590
R [a] ($I>2\sigma(I)$)	0.0693	0.0700	0.0559	0.0813
R_w [b] ($I>2\sigma(I)$)	0.1612	0.1755	0.1448	0.2088

[a] $R = \Sigma||F_o|-|F_c||/|F_o|$.
[b] $R_w = [\Sigma\, w(|F_o|-|F_c|)^2/\Sigma\, w(|F_o|^2)]^{1/2}$, where $w = 1/\sigma^2|F_o|)$.

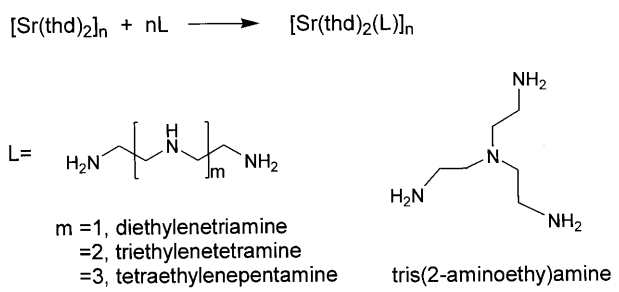
2.6. Other physical measurements

^{1}H NMR spectra (300 MHz) were obtained with Varian Gemini 300 spectrometer. Infrared spectra were measured with a Nicolet Magna-IR 760 spectrometer. CHN analyses were obtained with Thermoquest EA-1110 CHNS analyzer. A controlled thermal analysis of the complexes was investigated using a Perkin–Elmer TGA7 thermogravimetric analyzer, connected to a DECpc personal computer via a TAC 7/DX thermal analysis instrument controller. The weight of the samples investigated was between 6 and 8 mg. The measurements were performed in alumina crucibles under an atmosphere of flowing dry nitrogen gas (25 cm^3 min^{-1}), using heating rates of 5°C min^{-1}.

3. Results and discussion

3.1. Synthesis

The large ionic radius of barium and strontium metal ions (1.18 Å (Ba^{2+}) and 1.35 Å (Sr^{2+}) for C.N. = 6) render coordinatively unsaturation to their complex with average size ligands [22]. Therefore these metal ions will display typically high coordination numbers and their compounds often spontaneously oligomerize. The barium and strontium β-diketonate complexes $M(thd)_2$ exist as tetramer and trimer, respectively, and are highly sensitive to moisture. We have investigated the reaction of the homoleptic $M(thd)_2$ (M = Ba and Sr) complexes with chelating N-donor lewis base ligands. Our previous studies [19] reveal that polyamine ligands can efficiently saturate the coordination sphere of the barium cation and reduce the molecular aggregation. We have investigated the reaction of the homoleptic $Sr(thd)_2$ complexes with the chelating N-donor lewis base ligands. The strontium bis(diketonate) with polyamine adduct complexes $[Sr(thd)_2(L)]_n$ ($n = 2$; L = diethylenetriamine (**I**), $n = 1$; L = triethylenetetramine (**II**), tetraethylenepentamine (**III**), and tris(2-aminoethyl)amine (**IV**)) can be obtained from the reaction shown in Scheme 1. The reaction of $Sr(thd)_2$ with one equivalent of polyamines in THF solution proceeds readily at an ambient temperature, under N_2 atmosphere, to give a pale yellow solution. The crude white products were purified by recrystalization in *n*-hexane solution and the slightly excess polyamine can be removed easily by washing with acetonitrile. All of the complexes were obtained as colorless crystals in an excellent yield on the crystallization from saturated hot *n*-hexane solution.



Scheme 1.

The complexes **I**, **II**, **III** and **IV** are highly soluble in non-polar hydrocarbon solvents such as *n*-pentane, *n*-hexane and in polar solvents like diethylether, THF and toluene but insoluble in CH_3CN. If 2 equivalents of polyamines are used in the preparation of **I**, **II**, **III**, and **IV** then generally oily products result. Also, all of the complexes **I**, **II**, **III** and **IV** are readily dissolved in small amounts of polyamines. This indicates that the complexes are highly soluble in an excess of the Lewis base, presumably forming more highly ligated complexes. When the commercially available hydrated complex $Sr(thd)_2{\cdot}H_2O$ was used as starting materials, the yield was very low and unidentified insoluble powders in hydrocarbon solvents were precipitated. All complexes are relatively stable in air and moisture. The melting points of **I**, **II** and **III** are 128–135, 100–106, 84–90, and 76–84°C respectively, which are significantly lower than that of $Sr(thd)_2$ (200–203°C).

3.2. Spectroscopic data

All of the complexes were characterized by IR, NMR, and elemental analysis. The infrared spectrum of **I**, **II**, **III**, and **IV** exhibit the characteristic N–H stretching vibrational peaks from the amine ligand in the region 3200–3400 cm^{-1}. Also all of the complexes show strong absorption bands at 1596 cm^{-1} due to the C=O stretching vibrational peaks from thd ligands. ^{1}H NMR spectra of all four complexes in C_6D_6 show only a characteristic signal for one type of thd and polyamine ligand environment at room temperature. The ethylene proton resonances of coordinated polyamines are broad and unresolved sharply in all four spectra. The integration ratio of thd to polyamine ligand was observed to be 2:1 which indicate all four complexes have $Sr(thd)_2(L)$ formula in solution state which are in agreement with elemental analyses. Analytical and spectroscopic data for all four complexes are in accordance with the structures determined by X-ray crystallography, discussed in detail in the following section.

3.3. Single-crystal X-ray structures

To investigate the structure in the solid state, X-ray single–crystal structural studies were undertaken for all four complexes, which reveal that **I** exists as a dinuclear complex, $[Sr(thd)_2(diethylenetriamine)]_2$. On the other

hand, **II**, **III**, and **IV** exist as mononuclear complexes, [Sr(thd)$_2$(triethylenetetramine)], [Sr(thd)$_2$(tetraethylenepentamine)], [Sr(thd)$_2$(tris(2-aminoethyl)amine)], respectively. The selected bond distances and angles of complex **I**, **II**, **III**, and **IV** are presented in Tables 2 and 3.

3.4. [Sr(thd)$_2$(diethylenetriamine)]$_2$ (I)

The single-crystal X-ray structure of complex **I** is shown in Fig. 1. In complex **I**, each strontium metal is a eight coordinate, with a distorted propellane fashion, where a terminal amine ligand and three thd ligands are coordinated to strontium metal. The two strontium atoms are bridged by two thd ligands, in which two amine ligands and two terminal thd ligands are coordinated as *trans* fashion. Each strontium atom in complex **I** is coordinated with three nitrogen atoms (Sr–N average 2.77 Å) from diethylenetriamine and five oxygen atoms, two from the terminal thd ligand and three from the bridging thd ligand. The distances in bridging Sr–O_{thd} (average 2.634 Å) are significantly longer than those in terminal chelating ones (average 2.521 Å) as expected. The O–Sr–O chelate angles for the terminal thd ligands are 67.6(3)° (O(1)–Sr(1)–O(2)) and 69.6(3)°(O(5)–Sr(1)–O(6)). These values are larger than those observed in bridging thd ligands (66.7(2)° for O(3)–Sr(1)–O(4) and 66.2° for O(7)–Sr(1)–O(8)). The N–Sr–N angles for amine ligands are nearly identical and are in the range from 62.4(5)°–63.6(5)°.

3.5. [Sr(thd)$_2$(triethylenetetramine)] (II)

For complex **II**, there are two molecules in the asymmetric unit that are nearly identical within the precision of experiment. In Fig. 2, their structures and relative positioning were illustrated. In each molecule, strontium atom is eight coordinate with all of the nitrogens of the triethylenetetramine ligand and all oxygens of the thd ligand binding to the metal atom. Both Sr(1) and Sr(2) are coordinated in an meridional fashion by triethylenetetramine ligands, with two bidentate thd ligands on opposite sides of the amine ligand mean plane. This coordination environment is similar to the coordination pattern found in eight coordinated Ba and Ca triglyme adducts, Ca(thd)$_2$(triglyme) and Ba(thd)$_2$-(triglyme) complexes [8], but is different from those in Sr(hfac)$_2$(bpy)$_2$ [16], where the central Sr atom is eight coordinated with two hfac moieties on one side and the two bpy ligands on the other side. The Sr–O thd distances are in the range from 2.480(7)–2.555(6) Å (average 2.513 Å) for Sr(1) and from 2.458(6)–2.511(6) Å (average 2.491 Å) for Sr(2) which are slightly shorter than those in complex **I**. The Sr–N distances (average 2.75 Å in each molecule) are slightly shorter than those of complex **I**. The O–Sr–O chelate angles for the terminal thd ligands in both molecules are little different (average 67.95 (O–Sr(1)–O) and 68.8°(O–Sr(2)–O) and are comparable for those in complex **I**. The N–Sr–N angles for amine ligands are nearly identical and are in the range from 63.1(4)–64.6(3)°.

3.6. [Sr(thd)$_2$(tetraethylenepentamine)] (III)

The single-crystal X-ray structure of complex **III** is shown in Fig. 3. Strontium atom and N(1) atom are located on crystallographic 2-fold axis, and thus half of the molecule had to be determined. Strontium atom is nine coordinate with all of the nitrogens of the tetra-

Table 2
Selected bond lengths (Å) for complexes **I**, **II**, **III** and **IV**

*Complex **I***							
Sr(1)–O(1)	2.505(9)	Sr(2)–O(3)	2.718(8)	Sr(1)–N(1)	2.760(11)	Sr(2)–N(4)	2.751(12)
Sr(1)–O(2)	2.548(9)	Sr(2)–O(5)	2.470(9)	Sr(1)–N(2)	2.74(2)	Sr(2)–N(5)	2.83(2)
Sr(1)–O(3)	2.618(8)	Sr(2)–O(6)	2.515(9)	Sr(1)–N(3)	2.819(11	Sr(2)–N(6)	2.724(12)
Sr(1)–O(4)	2.536(8)	Sr(2)–O(7)	2.616(8)				
Sr(1)–O(7)	2.584(8)	Sr(2)–O(8)	2.554(10)				
*Complex **II***							
Sr(1)–O(1)	2.511(6)	Sr(1)–N(1)	2.774(10)	Sr(2)–O(5)	2.502(6)	Sr(2)–N(5)	2.763(12)
Sr(1)–O(2)	2.505(6)	Sr(1)–N(2)	2.742(10)	Sr(2)–O(6)	2.494(7)	Sr(2)–N(6)	2.749(11)
Sr(1)–O(3)	2.555(6)	Sr(1)–N(3)	2.775(10)	Sr(2)–O(7)	2.511(6)	Sr(2)–N(7)	2.779(12)
Sr(1)–O(4)	2.480(7)	Sr(1)–N(4)	2.723(8)	Sr(2)–O(8)	2.458(6)	Sr(2)–N(8)	2.720(11)
*Complex **III***							
Sr–O(1A)	2.515(4)	Sr–N(1)	2.743(10)	Sr–N(3A)	2.786(7)		
Sr–O(1)	2.515(4)	Sr–N(2)	2.768(11)				
Sr–O(2A)	2.576(4)	Sr–N(2A)	2.768(11)				
Sr–O(2)	2.576(4)	Sr–N(3)	2.786(7)				
*Complex **IV***							
Sr–O(1)	2.656(7)	Sr–N(1)	2.702(13)	Sr–N(3)	2.768(8)		
Sr–O(2)	2.466(7)	Sr–N(2)	2.773(10)				

Table 3
Selected bond angles (°) for complexes **I**, **II**, **III** and **IV**

Complex ***I***					
O(1)–Sr(1)–O(4)	87.6(3)	N(2)–Sr(1)–N(1)	62.9(5)	O(6)–Sr(2)–N(6)	73.7(5)
O(1)–Sr(1)–O(2)	67.6(3)	O(1)–Sr(1)–N(3)	135.9(4)	O(8)–Sr(2)–N(6)	143.1(5)
O(4)–Sr(1)–O(2)	144.4(3)	O(4)–Sr(1)–N(3)	136.4(4)	O(7)–Sr(2)–N(6)	84.2(5)
O(1)–Sr(1)–O(7)	114.7(3)	O(2)–Sr(1)–N(3)	72.1(4)	O(3)–Sr(2)–N(6)	74.1(4)
O(4)–Sr(1)–O(7)	79.0(3)	O(7)–Sr(1)–N(3)	80.6(4)	O(5)–Sr(2)–N(4)	79.5(4)
O(2)–Sr(1)–O(7)	88.3(3)	O(3)–Sr(1)–N(3)	72.4(4)	O(6)–Sr(2)–N(4)	72.2(4)
O(1)–Sr(1)–O(3)	147.2(3)	N(2)–Sr(1)–N(3)	62.9(5)	O(8)–Sr(2)–N(4)	67.3(5)
O(4)–Sr(1)–O(3)	66.7(2)	N(1)–Sr(1)–N(3)	118.5(5)	O(7)–Sr(2)–N(4)	117.6(4)
O(2)–Sr(1)–O(3)	144.2(3)	O(5)–Sr(2)–O(6)	69.6(3)	O(3)–Sr(2)–N(4)	162.1(4)
O(7)–Sr(1)–O(3)	81.4(3)	O(5)–Sr(2)–O(8)	81.5(3)	N(6)–Sr(2)–N(4)	112.5(6)
O(1)–Sr(1)–N(2)	88.4(4)	O(6)–Sr(2)–O(8)	133.6(3)	O(5)–Sr(2)–N(5)	141.6(4)
O(4)–Sr(1)–N(2)	133.8(4)	O(5)–Sr(2)–O(7)	129.9(3)	O(6)–Sr(2)–N(5)	93.2(4)
O(2)–Sr(1)–N(2)	73.0(4)	O(6)–Sr(2)–O(7)	157.9(3)	O(8)–Sr(2)–N(5)	87.4(4)
O(7)–Sr(1)–N(2)	142.5(4)	O(8)–Sr(2)–O(7)	66.2(3)	O(7)–Sr(2)–N(5)	76.3(4)
O(3)–Sr(1)–N(2)	94.9(4)	O(5)–Sr(2)–O(3)	84.5(3)	O(3)–Sr(2)–N(5)	132.4(4)
O(1)–Sr(1)–N(1)	67.1(4)	O(6)–Sr(2)–O(3)	94.9(3)	N(6)–Sr(2)–N(5)	63.6(5)
O(4)–Sr(1)–N(1)	73.3(4)	O(8)–Sr(2)–O(3)	118.2(3)	N(4)–Sr(2)–N(5)	62.4(5)
O(2)–Sr(1)–N(1)	115.9(4)	O(7)–Sr(2)–O(3)	79.0(2)	Sr(1)–O(3)–Sr(2)	94.9(3)
O(7)–Sr(1)–N(1)	152.2(3)	O(5)–Sr(2)–N(6)	135.3(5)	Sr(1)–O(7)–Sr(2)	98.2(3)
O(3)–Sr(1)–N(1)	85.5(4)				
Complex ***II***					
O(4)–Sr(1)–O(1)	137.3(2)	N(4)–Sr(1)–N(3)	63.3(3)	O(8)–Sr(2)–N(8)	80.3(4)
O(4)–Sr(1)–O(2)	92.7(2)	N(2)–Sr(1)–N(3)	64.6(3)	O(6)–Sr(2)–N(8)	72.4(4)
O(1)–Sr(1)–O(2)	68.2(2)	O(4)–Sr(1)–N(1)	81.0(3)	O(5)–Sr(2)–N(8)	119.2(4)
O(4)–Sr(1)–O(3)	67.7(2)	O(1)–Sr(1)–N(1)	121.4(3)	O(7)–Sr(2)–N(8)	77.2(4)
O(1)–Sr(1)–O(3)	147.3(2)	O(2)–Sr(1)–N(1)	67.9(3)	N(6)–Sr(2)–N(8)	121.8(5)
O(2)–Sr(1)–O(3)	141.8(2)	O(3)–Sr(1)–N(1)	76.5(3)	O(8)–Sr(2)–N(7)	139.0(3)
O(4)–Sr(1)–N(4)	90.3(3)	N(4)–Sr(1)–N(1)	164.5(4)	O(6)–Sr(2)–N(7)	102.8(4)
O(1)–Sr(1)–N(4)	73.5(3)	N(2)–Sr(1)–N(1)	64.1(4)	O(5)–Sr(2)–N(7)	82.6(3)
O(2)–Sr(1)–N(4)	125.7(3)	N(3)–Sr(1)–N(1)	112.6(4)	O(7)–Sr(2)–N(7)	82.6(3)
O(3)–Sr(1)–N(4)	88.3(3)	O(8)–Sr(2)–O(6)	83.4(2)	N(6)–Sr(2)–N(7)	63.2(4)
O(4)–Sr(1)–N(2)	144.2(3)	O(8)–Sr(2)–O(5)	135.0(2)	N(8)–Sr(2)–N(7)	63.9(4)
O(1)–Sr(1)–N(2)	72.9(3)	O(6)–Sr(2)–O(5)	67.6(2)	O(8)–Sr(2)–N(5)	80.0(4)
O(2)–Sr(1)–N(2)	81.7(3)	O(8)–Sr(2)–O(7)	70.0(2)	O(6)–Sr(2)–N(5)	120.5(3)
O(3)–Sr(1)–N(2)	95.3(3)	O(6)–Sr(2)–O(7)	142.4(2)	O(5)–Sr(2)–N(5)	86.0(4)
N(4)–Sr(1)–N(2)	121.6(4)	O(7)–Sr(2)–N(5)	149.2(2)	O(5)–Sr(2)–O(7)	81.3(4)
O(4)–Sr(1)–N(3)	128.4(2)	O(8)–Sr(2)–N(6)	131.3(3)	N(6)–Sr(2)–N(5)	63.1(4)
O(1)–Sr(1)–N(3)	79.5(2)	O(6)–Sr(2)–N(6)	142.0(3)	N(8)–Sr(2)–N(5)	154.8(5)
O(2)–Sr(1)–N(3)	138.9(2)	O(5)–Sr(2)–N(6)	75.4(3)	N(7)–Sr(2)–N(5)	126.3(4)
O(3)–Sr(1)–N(3)	68.0(2)	O(7)–Sr(2)–N(6)	73.9(3)		
Complex ***III***					
O(1A)–Sr–O(1)	92.6(2)	N(2A)–Sr–N(3)	153.3(3)	N(1)–Sr–(2A)	64.0(3)
O(2A)–Sr–N(2)	75.6(2)	O(1)–Sr–O(2)	67.26(12)	O(2)–Sr–(3A)	118.9(2)
O(2)–Sr–N(3)	80.4(2)	O(1)–Sr–N(2A)	87.5(3)	O(2A)–Sr–N(1)	70.52(8)
O(1A)–Sr–O(2A)	67.26(12)	O(1A)–Sr–N(3A)	72.3(2)	N(2)–Sr–N(2A)	128.0(5)
O(2)–Sr–N(2)	87.5(2)	O(2A)–Sr–O(2)	141.0(2)	N(1)–Sr–N(3A)	118.3(2)
N(1)–Sr–N(3)	118.3(2)	O(2A)–Sr–(2A)	87.5(2)	O(2)–Sr–N(1)	70.52(8)
O(1)–Sr–O(2A)	147.91(14)	O(1)–Sr–N(3A)	69.4(2)	O(1A)–Sr–N(3)	69.4(2)
N(1)–Sr–N(2)	64.0(3)	O(1A)–Sr–N(1)	133.6(1)	N(2)–Sr–N(3A)	153.3(3)
N(2)–Sr–N(3)	61.5(3)	O(2)–Sr–N(2A)	75.6(2)	O(1A)–Sr–N(2)	87.5(3)
O(1A)–Sr–O(2)	147.91(14)	O(2A)–Sr–(3A)	80.4(2)	O(1)–Sr–N(3)	72.3(2)
O(1A)–Sr–N(2A)	130.5(3)	O(1)–Sr–N(1)	133.6(1)	N(2A)–Sr–(3A)	61.5(3)
Complex ***IV***					
O(2)–Sr–O(1)	66.1(2)	O(1)–Sr–O(1A)	130.5(3)	O(2)–Sr–O(2A)	73.5(3)
N(1)–Sr–N(2)	66.8(3)	N(2)–Sr–N(3)	64.6(2)	N(1)–Sr–N(3)	113.9(4)
N(3)–Sr–N(3A)	81.5(4)				

ethylenepentamine ligand and all oxygens of the thd ligand binding to the metal atom. The amine ligand is observed to be located on a meridional plane, with two bidentate thd ligands lying respectively above and below the plane. Similar coordination fashion was found in those of $Ba(thd)_2$(tetraglyme) [7], $Ba(hfa)_2$(tetraglyme) [25], $Ca(hfa)_2$(tetraglyme) [8] and $Ca(thd)_2$(tetraethylenepentamine) [26] complexes. But in the case of Ca complexes, only four out of five donor atoms in the ancillary ligand are coordinated to the central Ca atom and coordination number is eight in those complexes.

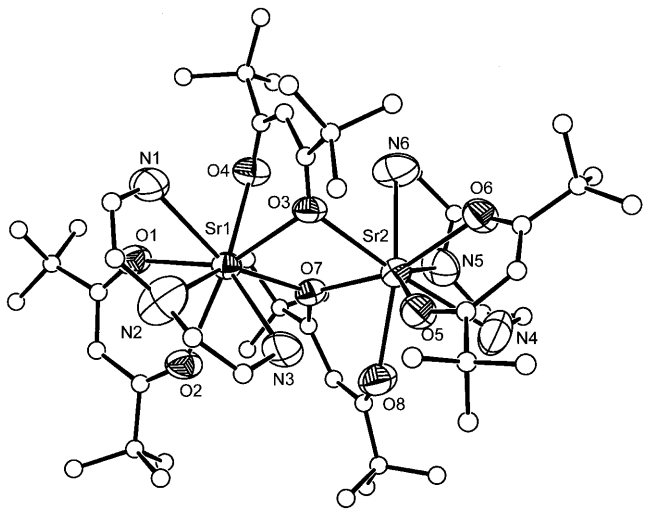


Fig. 1. Molecular structure and labeling of $[Sr(thd)_2$(diethylenetriamine)$]_2$ (**I**). Thermal ellipsoids as drawn by ORTEP represent the 40% probability surfaces. Hydrogen atoms have been omitted for clarity.

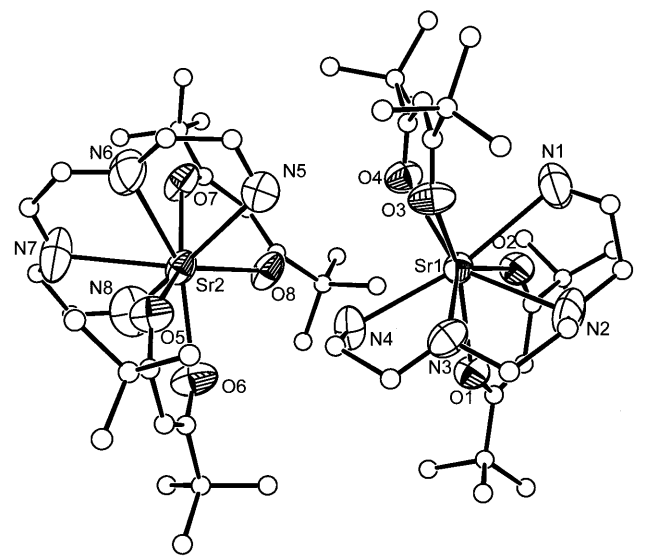


Fig. 2. Molecular structure, labeling and relative positions of the two molecules of $[Sr(thd)_2$(triethylenetetramine)] (**II**). Thermal ellipsoids as drawn by ORTEP represent the 40% probability surfaces. Hydrogen atoms have been omitted for clarity.

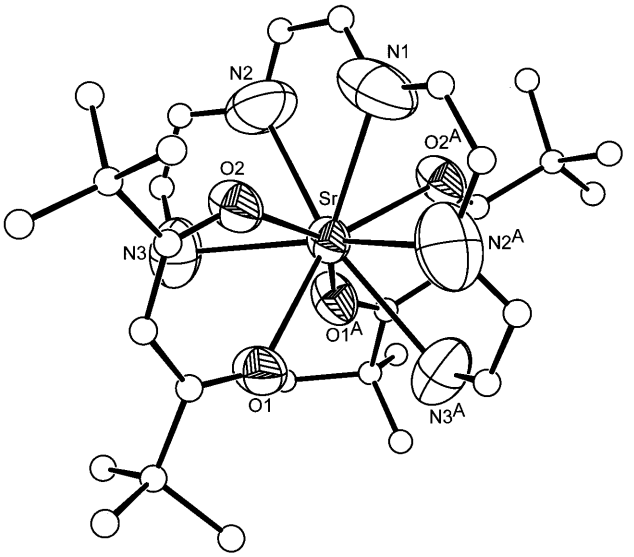


Fig. 3. Molecular structure and labeling of $[Sr(thd)_2$(tetraethylenepentamine)] (**III**). Thermal ellipsoids as drawn by ORTEP represent the 40% probability surfaces. Hydrogen atoms have been omitted for clarity. Symmetry-generated atoms have the suffix A.

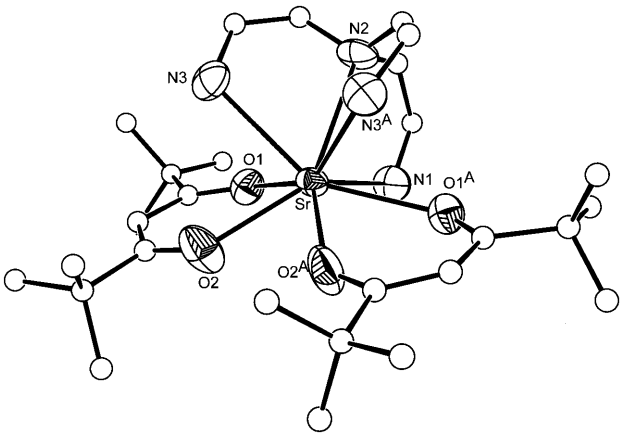


Fig. 4. Molecular structure and labeling of $[Sr(thd)_2$(tris(2-aminoethyl)amine)] (**IV**). Thermal ellipsoids as drawn by ORTEP represent the 40% probability surfaces. Hydrogen atoms have been omitted for clarity. Symmetry-generated atoms have the suffix A.

This difference between our strontium analogues and other barium analogues may be due to the smaller ionic radius of the Ca cation than those of barium and strontium. The Sr–O thd distances are in the range from 2.515(4)–2.576(4)Å (average 2.546 Å) which are apparently longer than those in complex **I** and **II**. These longer Sr–O distances in complex **III** reflect the strong chelating effect and higher denticity of tetraethylenepentamine ligand. The Sr–N(1) distance (2.720 Å) is significantly shorter than that of Sr–N(2) (2.768 Å) and Sr–N(3)(2.786 Å). The O–Sr–O chelate angles for the thd ligands are 67.26(12)° and the N–Sr–N angles for amine ligands are in the range from 61.5(4)–64.0(3)°.

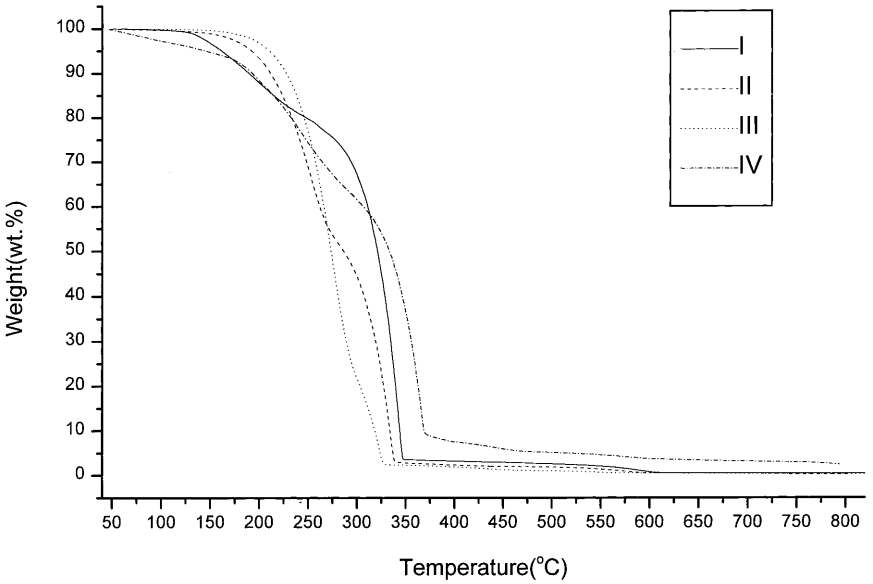


Fig. 5. Thermogravimetric analyses of complexes **I**, **II**, **III** and **IV** under N_2 with a temperature ramp of 5°C min^{-1}.

3.7. [Sr(thd)$_2$(tris(2–aminoethylene)amine)] ((IV)

The single-crystal X-ray structure of complex **IV** are shown in Fig. 4. The molecule in **IV** occupies a crystallographic mirror plane in which strontium, N(2) and N(3) atoms are located on a mirror plane. In this molecule, strontium atom is eight coordinate with all of the nitrogens of the amine ligand and all oxygens of the thd ligand binding to the metal atom. The amine ligand is coordinated to one side of the metal atom and resulting in a *cis*–relationship of the thd ligands with an O–M–O angle of 66.1(2). This coordination environment is similar to the coordination pattern found in $Sr(hfac)_2(bpy)_2$ [16], $[Ba(hfac)_2(CH_3OCH_2CH_2)_3N]$ [23], but is different from those in complex **II**, **III** and polyglyme adducts of barium and strontium β-diketonates, where polyamine or polyglyme ligands are coordinated to metal atom in meridional fashion with two β-diketonate moieties being positioned on either side of this plane. The Sr–N distances show different patterns in two molecules.

3.8. Thermal analyses

Thermogravimetric data for complexes **I**, **II**, **III** and **IV** which were collected under an N_2 atmosphere with a 5°C min^{-1} temperature ramp rate are shown in Fig. 4. It is immediately apparent that all complexes are sufficiently volatile and sublime or evaporate without residue. Upon heating under nitrogen, complex **I** and **II** undergo two major steps of weight loss. The first weight loss occurs at ca 100–250°C (ca. 20%) for **I** and ca 150–275°C (ca. 45%) for **II** and this represents the loss of amine ligand in the complexes. A similar result was reported earlier for [Sr(thd)(tetraglyme)] complex [7] in which the loss of tetraglyme ligand occurs at 150–260°C. The DSC plot for complex **I** and **II** reveals only two endotherms. The first sharp isotherms are attributed to the melting, centered at 134.21°C for **I** and 105.52°C for **II** which are in agreement with a visual observation. The second broad isotherms are centered at 342.39°C for **I** and 359.69°C for **II**, which are presumably due to separation and evaporation of amine ligand. However in complexes **III** and **IV**, there is no evidence for loss of amine ligand. Fig. 4 shows that complex **III** and **IV** sublime and vaporize without decomposition over the temperature range ca. 150–330°C and ca. 100–370°C, respectively. The DSC plot for complex **III** and **IV** reveals only one endotherm centered at 88.29°C for **III** and 70.96°C for **IV** which is attributed to the melting. All four complexes show enhanced thermal stability than those of $Sr(thd)_2$(H–thd) [24] and $Sr(thd)_2$(tetraglyme) [7]. In $Sr(thd)_2$(H–thd) complex, the loss of H–thd occurs below 200°C and followed by sublimation of the remaining $[Sr(thd)_2]_n$ between ca. 270–390°C to give a residue of 3.4% Fig. 5.

4. Conclusion

A new class of volatile strontium bis(diketonate) with polyamine adducts has been successfully synthesized and characterized. From the molecular structures determined by single-crystal X-ray analyses, it is possible to explain that the minimum coordination number for saturating strontium cation coordination sphere is 8. In fact, coordinatively unsaturated $Sr(thd)_2$(diethylenetriamine) (coordination number 7) exist as a dimmer by bridging one of oxygen atom from thd ligand in adja-

cent molecule and thus satisfy coordinative saturation number 8. On the other hand, coordinatively saturated complexes **II**, **III** and **IV** exist as monomer. These complexes, when compared to $Sr(thd)_2$, offer the advantages of air/moisture stability and enhanced thermal stability. Therefore it is expected that these complexes are promising MOCVD precursors for BST thin films.

5. Supplementary data

Crystallographic data for the structural analysis have been deposited with the Cambridge Crystallographic Data Center, CCDC No. 145280 for complex **I**, CCDC No. 145281 for complex **II**, CCDC No. 145282 for complex **III** and CCDC No. 145283 for complex **IV**. Copies of this information may be obtained free of charge from The Director, 12 Union road, Cambridge, CB2 1EZ, UK (fax: +44-1223-336033; e-mail: deposit @ccdc.cam.ac.uk or www: http://www.ccdc.cam.ac.uk).

Acknowledgements

This work has been generously supported by grants from the Korean Ministry of Science & Technology (System IC 2010, TS-9824).

References

[1] L.G. Hubert-Pfalzgraf, H. Guillon, Appl. Organomet. Chem. 12 (1998) 221.
[2] W.S. Rees, Jr., CVD of Nonmetas, VCH, Weinheim, 1996.
[3] A.C. Jones, Chem. Vap. Depos. 4 (1983) 169.
[4] V.C. Arunasalam, S.R. Drake, M.B. Hursthouse, K.M. A. Malik, S.A.S. Miller, D.M.P. Mingos, J. Chem. Soc., Dalton Trans. (1996) 2435.
[5] S.R. Drake, M.B. Hursthouse, K.M.A. Malik, D.J. Otway, J. Chem. Soc., Dalton Trans. (1993) 2883.
[6] A.A. Drozdov, S.I. Troynov, Polyhedron 11 (1992) 2877.
[7] S.R. Drake, S.A.S. Miller, M.B. Hursthouse, K.M.A. Malik, Polyhedron 12 (1993) 1621.
[8] S.R. Drake, S.A.S. Miller, D.J. Williams, Inorg. Chem. 32 (1993) 3227.
[9] R. Gardiner, D.W. Brown, P.S. Kirlin, A.L. Rheingold, Chem. Mater. 3 (1991) 1053.
[10] J.A.P. Nash, J.C. Barnes, D.J. Cole-Hamilton, B.C. Richards, S.L. Cook, M.L. Hitchman, Adv. Mater. Opt. Eelectron. 5 (1995) 1.
[11] M. Motevalli, P. O'Brien, I.M. Watson, Polyhedron 15 (1996) 1865.
[12] M. Motevalli, P. O'Brien, I.M. Watson, Acta. Crystallogr., Sect. C 52 (1996) 3028.
[13] J.A. Belot, D.A. Neumayer, C.J. Reedy, D.B. Studebaker, B.J. Hinds, C.L. Stern, T.J. Marks, Chem. Mater. 9 (1997) 1638.
[14] S. Matsuno, F. Uchikawa, S. Utsunomiya, S. Nakabayashi, Appl. Phys. Lett. 60 (1992) 2427.
[15] B.N. Hanses, B.M. Hyberston, R.M. Barkley, R.E. Sievers, Chem. Mater. 4 (1992) 749.
[16] Y. Shen, Y. Pan, G. Dong, X. Sun, X. Huang, Polyhedron 17 (1997) 69.
[17] N. Kuzmina, M. Ryazanov, S. Troyanov, Polyhedron 18 (1999) 2177.
[18] R.A. Gardiner, D.C. Gordon, G.T. Stauf, B.A. Vaartstra, Chem. Mater. 6 (1994) 1967.
[19] J.W. Park, S.M. Koo, Bull. Kor. Chem. Soc. 20 (1999) 1257.
[20] S.R. Drake, M.B. Hursthouse, K.M.A. Malik, S.A.S. Miller, D.J. Otway, Inorg. Chem. 32 (1993) 4464.
[21] R.A. Gardiner, D.C. Gordon, G.T. Stauf, B.A. Vaartstra, R.L. Ostrander, A.L. Rheingold, Chem. Mater. 6 (1994) 1967.
[22] T.P. Hanusa, Chem. Rev. 93 (1993) 1023.
[23] Y. Yokota, R.A. Jacobson, B.C. Logsdon, S. Ringrose, A.T. Setterdahl, J.G. Verkade, Polyhedron 18 (1999) 2519.
[24] J.A. Darr, S.R. Drake, D.J. Otway, S.A.S. Miller, D.M.P. Mingos, I. Baxter, M.B. Hursthouse, K.M.A. Malik, Polyhedron 16 (1997) 2581.
[25] P. van der Sluis, A.L. Spek, K. Timmer, D.A. Meinema, Acta Crystallogr., Sect. C 46 (1990) 1741.
[26] T. Hänninen, I. Mutikainen, V. Saanila, M. Ritala, M. Leskelä, Chem. Mater. 9 (1997) 1234.

PERGAMON

www.elsevier.nl/locate/poly

Polyhedron 19 (2000) 2557–2564

POLYHEDRON

Solvent influences on the molecular aggregation of magnesium aryloxides: synthesis, crystal structure, and solution characterization of $Mg(OAr)_2(L)_3$ (OAr = DMP, DIP, TCP) and $[Mg(DIP)_2]_3$

Cecilia A. Zechmann [a], Timothy J. Boyle [a,*], Mark A. Rodriguez [a], Richard A. Kemp [b]

[a] *Sandia National Laboratories, Advanced Materials Laboratory, 1001 University Boulevard S.E., Albuquerque, NM 87106, USA*
[b] *Union Carbide Corporation, Westhollow Research Center, 3333 Highway 6 South, Houston, TX 77082, USA*

Received 8 May 2000; accepted 16 August 2000

Abstract

Magnesium aryloxides were prepared in a variety of solvents through the reaction of dibutyl magnesium with sterically varied aryl alcohols: 2,6-dimethylphenol (H-DMP), 2,6-diisopropylphenol (H-DIP), and 2,4,6-trichlorophenol (H-TCP). Upon using a sufficiently strong Lewis-basic solvent, the solvated monomeric species $Mg(DMP)_2(py)_3$ (**1**, py = pyridine), $Mg(DIP)_2(THF)_3$, (**2a**, THF = tetrahydrofuran) $Mg(TCP)_2(THF)_3$ (**3**) were isolated. Each of these complexes possesses a five-coordinate magnesium that adopts a trigonal bipyramidal geometry. In the absence of a Lewis base, the reaction with H-DIP yields a soluble trinuclear complex, $[Mg(DIP)_2]_3$ (**2b**). The Mg metal centers in **2b** adopt a linear arrangement with a four-coordinate central metal while the outer metal centers are reduced to just three-coordinate. Solution spectroscopic methods suggest that while **2b** remains intact, the monomeric species (**1**, **2a**, and **3**) are involved in equilibria which facilitate intermolecular ligand transfer. © 2000 Elsevier Science B.V. All rights reserved.

Keywords: Magnesium; Aryloxide; Structure; Adduct

1. Introduction

Magnesium alkoxides ($Mg(OR)_2$) were first prepared and reported in the early 1900s [1–3]. Since that time they have found applications in such areas as Ziegler–Natta catalyst support precursors [4] and reagents for organic synthesis [5,6]. Although they are widely used, only a handful of structurally characterized $Mg(OR)_2$ complexes have been reported, including, the complex structure for the methoxide methanolate, $Mg(OMe)_2 \cdot 3.5MeOH$ [7], two tetrameric alkoxyether magnesium aggregates, $[Mg_4(OCH_2CH(CH_2)_3O)_6Cl_2]$ [8] and $[Mg(OCH(CH_3)CH_2OCH_3)_2]_4$ [9], and a siloxide, $[(RSiO_3)_2(R(OH)SiO_2]_2Mg(THF)_5$ where R = (2,6-*i*-$Pr_2C_6H_3$)(Me$_3$Si)N [10]. A number of magnesium aryloxides have also been reported including a series of dimeric complexes prepared by Ittel et al. ($[Mg(OAr)_2]_2$ where OAr = $OC_6H_2(CMe_3)_2Me$ (BHT), $OC_6H_2(CMe_3)_2$ (BHB)) [11] and a similar fluorinated derivative, $Mg(OC_6H_2(CF_3)_3)_2(THF)_3$, reported by Roesky et al. [12].

We have utilized a series of sterically and electronically varied aryloxide ligands (where OAr = $OC_6H_3(Me)_2$-2,6 (DMP), $OC_6H_3(CHMe_2)_2$-2,6 (DIP), and $OC_6H_2(Cl)_3$-1,3,5 (TCP) to further probe the structural aspects of $Mg(OAr)_2$. Aryloxides were chosen as they can be easily derivatized and often result in complexes with increased solubility and decreased oligomerization. Products isolated were identified by single crystal X-ray diffraction as $Mg(DMP)_2(py)_3$ (**1**), $Mg(DIP)_2(THF)_3$ (**2a**), $[Mg(DIP)_2]_3$ (**2b**), and $Mg(TCP)_2(THF)_3$ (**3**).

* Corresponding author. Tel.: +1-505-272-7625; fax: +1-505-272-7336.
E-mail address: tjboyle@sandia.gov (T.J. Boyle).

0277-5387/00/$ - see front matter © 2000 Elsevier Science B.V. All rights reserved.
PII: S0277-5387(00)00566-0

2. Experimental

All compounds were handled under an inert atmosphere using standard glovebox or Schlenk techniques. Toluene, tetrahydrofuran (THF), and hexanes were dried over and distilled from Na/benzophenone immediately prior to use. Pyridine was dried over and distilled from CaO. The following chemicals were obtained from Aldrich and used as received: 1.0 M di-*n*-butylmagnesium in heptane ($Mg(Bu)_2$), 2,6-dimethylphenol (H-DMP), 2,6-diisopropylphenol (H-DIP), and 2,4,6-trichlorophenol (H-TCP). ^1H and ^{13}C NMR solution spectral data were collected on a Brucker 400 MHz spectrometer. All spectra were referenced against the residual proton impurity in the appropriate dried, deuterated solvent. FTIR data were obtained on a Bruker Vector 22 using KBr pressed pellets under a N_2 purge. Elemental analyses were performed on a Perkin–Elmer 2400 CHN-S/O Elemental Analyzer.

2.1. $Mg(DMP)_2(py)_3$ (**1**)

$Mg(Bu)_2$ (71.4 ml, 25 mmol) was placed in a 500 ml three-neck round bottom, diluted with THF (37 ml) and pyridine (18.5 ml), and cooled to 0°C in an ice bath. A solution containing H-DMP (17.51 g, 68.5 mmol) dissolved in THF (50 ml) was transferred slowly via cannula to the cooled $Mg(Bu)_2$ solution. The reaction mixture was allowed to warm slowly to room temperature (r.t.) and stirred overnight. The resulting clear, colorless solution was then heated to reflux temperature for 2 h. The solution was then allowed to cool and the solvent removed in vacuo yielding an off-white powder. Yield: 30.3 g (84.2%). ^1H NMR (400.1 MHz, pyridine-d_5) δ 7.23 (d, 2H, $OC_6H_3(CH_3)_2$-2,6, $^3J_{H-H}=$ 7.2 MHz), 6.67 (t, 1H, $OC_6H_3(CH_3)_2$-2,6, $^3J_{H-H}=7.2$ MHz), 2.47 (s, 6H, $OC_6H_3(CH_3)_2$-2,6). FTIR (KBr pellet, cm^{-1}) 3066(m), 3007(w), 2958(w), 2920(m), 2899(w), 2851(w), 1589(m), 1472(s), 1437(s), 1324(m), 1268(w), 1211(m), 1090(m), 1068(w), 1036(w), 1009(w), 878(w), 752(s), 699(s), 623(w), 548(w), 425(m). *Anal.* Calc. for $C_{31}H_{33}MgN_3O_2$: C, 73.89; H, 6.60; N, 8.33. Found: C, 72.58; H, 6.43; N, 7.96%.

2.2. $Mg(DIP)_2(THF)_3$ (**2a**)

$Mg(Bu)_2$ (34 ml, 34 mmol) was diluted with THF (35 ml) and cooled in an ice bath. A solution containing H-DIP (12.22 g, 68.5 mmol) dissolved in THF (15 ml) was slowly cannula transferred to the $Mg(Bu)_2$ solution. The reaction mixture was warmed to room temperature and allowed to stir for 4 h yielding a clear colorless solution. The solvent was removed in vacuo yielding an off-white powder. Yield: 18.8 g (93%). ^1H NMR (400.1 MHz, THF-d_8) δ 6.77 (4H, d, OC_6H_3-2,6-$CH(CH_3)_2$, $^3J_{H-H}=7.6$ Hz), 6.27 (2H, t, OC_6H_3-2,6-$CH(CH_3)_2$, $^3J_{H-H}=7.6$ Hz), 3.50 (4H, sept, OC_6H_3-2,6-$CH(CH_3)_2$, $^3J_{H-H}=6.8$ Hz), 1.13 (12H, d, OC_6H_3-2,6-$CH(CH_3)_2$, $^3J_{H-H}=6.8$ Hz). FTIR (KBr pellet, cm^{-1}) 2961(s), 2868(m), 1588(w), 1438(s), 1361(m), 1346(w), 1285(w), 1261(m), 1192(w), 1151(w), 1108(w), 1040(m), 888(m), 860(w), 743(m), 695(w), 589(w), 557(w), 405(w). *Anal.* Calc. for $C_{36}H_{58}MgO_5$: C, 72.65; H, 9.82. Found: C, 73.04; H, 9.43%.

2.3. $[Mg(DIP)_2]_3$ (**2b**)

$Mg(Bu)_2$ (25 ml, 25 mmol) was diluted with toluene (25 ml) and cooled to 0°C in an ice bath. A solution containing H-DIP (8.95 g, 68.5 mmol) dissolved in toluene (10 ml) was cannula transferred to the $MgBu_2$ solution. The reaction mixture was warmed to r.t. and allowed to stir overnight yielding a colorless clear solution. The solvent was removed in vacuo resulting in an off-white gummy solid. The solid was washed with hexanes (50 ml) and dried to yield an off-white free-flowing powder. Yield: 8.4 g (89%). ^1H NMR (400.1 MHz, C_6D_6) δ 7.04 (4H, dd, $OC_6H_3\{CH(CH_3)_2\}_2$-2,6, $^3J_{H-H}=7.8$ Hz, $^4J_{H-H}=1.5$ Hz), 7.03 (4H, d, $OC_6H_3\{CH(CH_3)_2\}_2$-2,6, $^3J_{H-H}=7.6$ Hz), 6.831 (2H, t, $OC_6H_3\{CH(CH_3)_2\}_2$-2,6, $^3J_{H-H}=7.6$ Hz), 6.825 (4H, dd, $OC_6H_3\{CH(CH_3)_2\}_2$-2,6, $^3J_{H-H}=7.8$ Hz, $^3J_{H-H}=$ 7.7 Hz) 6.73 (dd, $OC_6H_3\{CH(CH_3)_2\}_2$-2,6, $^3J_{H-H}=$ 7.7 Hz, $^4J_{H-H}=1.5$ Hz), 3.62 (4H, sept, $OC_6H_3\{CH(CH_3)_2\}_2$-2,6, $^3J_{H-H}=6.8$ Hz), 2.71 (4H, sept, $OC_6H_3\{CH(CH_3)_2\}_2$-2,6, $^3J_{H-H}=6.8$ Hz), 2.38 (4H, sept, $OC_6H_3\{CH(CH_3)_2\}_2$-2,6, $^3J_{H-H}=6.7$ MHz), 1.42 (12H, d, $OC_6H_3\{CH(CH_3)_2\}$-2,6, $^3J_{H-H}=6.8$ Hz), 1.37 (12H, d, $OC_6H_3\{CH(CH_3)_2\}$-2,6, $^3J_{H-H}=6.8$ Hz), 1.10 (12H, d, $OC_6H_3\{CH(CH_3)_2\}$-2,6, $^3J_{H-H}=6.8$ Hz), 0.96 (12H, d, $OC_6H_3\{CH(CH_3)_2\}$-2,6, $^3J_{H-H}=6.7$ Hz), 0.79 (12H, d, $OC_6H_3\{CH(CH_3)_2\}$-2,6, $^3J_{H-H}=6.7$ Hz), 0.34 (12H, d, $OC_6H_3\{CH(CH_3)_2\}$-2,6, $^3J_{H-H}=6.8$ Hz). FTIR (KBr pellet, cm^{-1}) 3066(w), 3027(w), 2961(s), 2870(m), 1590(w), 1452(m), 1438(s), 1346(w), 1321(w), 1284(w), 1260(m), 1193(m), 1110(w), 1042(w), (907(w), 843(m), 754(s), 686(w), 574(w), 508(w), 417(w). *Anal.* Calc. for $C_{24}H_{34}MgO_2$: C, 76.09; H, 9.05. Found: C, 75.18; H, 8.91%.

2.4. $Mg(TCP)_2(THF)_3$ (**3**)

A THF (5 ml) solution containing H-TCP (2.33 g, 11.8 mmol) was added (via cannula transfer) to a 0°C solution containing $Mg(Bu)_2$ (5.9 ml, 5.9 mmol) diluted with THF (6 ml). The resulting clear colorless solution was stirred at r.t. overnight followed by removal of the solvent in vacuo to yield a white solid. Yield: 3.45 g (92%). ^1H NMR (400.1 MHz, THF-d_8) δ 7.12 ($OC_6H_2Cl_3$). FTIR (KBr pellet, cm^{-1}) 2988(m), 2890(m), 1566(w), 1480(s), 1388(w), 1325(w), 1245(m), 1174(w), 1038(s), 911(w), 896(w), 876(w), 861(w),

852(w), 803(w), 788(m), 759(s), 735(w), 596(w), 494(m), 433(w). *Anal.* Calc. for $C_{24}H_{28}Cl_6MgO_5$: C, 45.50; H, 4.46. Found: C, 43.63; H, 4.08%.

2.5. X-ray structure determinations

Data collection parameters for all compounds are given in Table 1. Additional information is supplied in the Supporting Information. A suitable crystal of each sample was mounted on a glass fiber from a pool of Fluorolube™ HO-125 then immediately placed under a liquid N_2 stream on a Bruker AXS diffractometer. The radiation used was graphite monochromatized Mo Kα radiation ($\lambda = 0.71073$ Å). Lattice determination and data collection were carried out using SMART software [13]. Data reduction was performed using SAINT+ software [14]. Structure solution and refinement was performed using SHELXTL-5.1 software [15]. Absorption correction using SADABS [16] in SHELXTL-5.1 was carried out only for **3**. The structures were solved using direct methods and yielded positions for the heavy atoms. Subsequent Fourier synthesis gave the remaining non-hydrogen atom positions. Hydrogen atoms were fixed in positions of ideal geometry and refined within the XSHELL software [17]. These idealized hydrogen atoms had their isotropic temperature factors fixed at 1.2 or 1.5 times the equivalent isotropic U of the C atoms to which they were bonded. The final refinements include anisotropic thermal parameters on all non-hydrogen atoms. Disorder in the isopropyl methyl groups on the phenyl rings of **2b** was noted (C71 and C72). Acceptable thermal parameters were obtained by refining over two partially occupied positions. Due to the disorder, hydrogen atoms were not assigned to C71 or C72.

3. Results and discussion

3.1. Syntheses

The $Mg(OAr)_2$ isolated in this study were prepared by the reaction of $Mg(Bu)_2$ with 2 equiv. of the appropriate HOAr (Eq. (1)). Typically, the $Mg(OAr)_2$ products were insoluble in standard non-polar solvents, however, when the reaction was carried out in the presence of a *sufficiently* strong Lewis-basic solvent (L), a soluble adduct was formed (Eq. (2)). For example, in the reaction with H-TCP, use of THF as a solvent resulted in the formation of a soluble product while the reaction with H-DMP yielded a soluble species *only* when a stronger Lewis base (i.e. pyridine) was available.

$$Mg(Bu)_2 + 2HOAr \rightarrow [Mg(OAr)_2]_n + 2H\text{-}Bu \quad (1)$$

$$Mg(Bu)_2 + 2HOAr + xsL \rightarrow [Mg(OAr)_2](L)_3 + 2H\text{-}Bu \quad (2)$$

In contrast, $Mg(DIP)_2$ was found to yield a soluble product independent of the solvent employed. However, the aggregate size was found to vary depending on the presence or absence of a donor solvent.

The generation of a heteroleptic product was attempted (in the presence of a Lewis base) through the reaction of $Mg(Bu)_2$ with 1 equiv. of H-DIP to form

Table 1
Data collection parameters for **1**–**3**

Compound	**1**	**2a**	**2b**	**3**
Chemical formula	$C_{31}H_{33}MgN_3O_2$	$C_{36}H_{58}MgO_5$	$C_{72}H_{102}Mg_3O_6$	$C_{24}H_{28}Cl_6MgO_5$
Formula weight	503.91	595.13	1136.47	633.47
Temperature (K)	168(2)	168(2)	168(2)	168(2)
Space group	$C2/c$	$Pna2_1$	$P2_1/c$	$C2/c$
Unit cell dimensions				
a (Å)	13.647(1)	17.233(1)	22.242(2)	12.553(2)
b (Å)	11.719(1)	15.308(1)	12.715(1)	11.107(2)
c (Å)	19.076(1)	13.631(1)	25.536(2)	20.666(3)
β (°)	104.585(2)		107.388(2)	99.864(3)
V (Å^3)	2952.6(4)	3596.0(4)	6891.5(11)	2793.5(7)
Z	4	4	4	4
D_{calc} (Mg m^{-3})	1.134	1.099	1.095	1.506
μ (mm^{-1}) (Mo Kα radiation)	0.090	0.087	0.092	0.671
[a]R_1 (%)	3.74	6.37	5.35	4.78
[b]wR_2 (%) [$I > 2\sigma(I)$]	10.89	15.63	11.15	11.81
[a]R_1 (%, all data)	4.89	10.18	15.96	9.00
[b]wR_2 (%, all data)	11.49	17.59	14.12	13.53

[a] $R_1 = \sigma \| F_o | - | F_c \| / \sigma | F_o |$.

[b] $wR_2 = \left[\Sigma[w(F_o^2 - F_c^2)^2] / \Sigma[w(F_o^2)^2] \right]^{1/2}$.

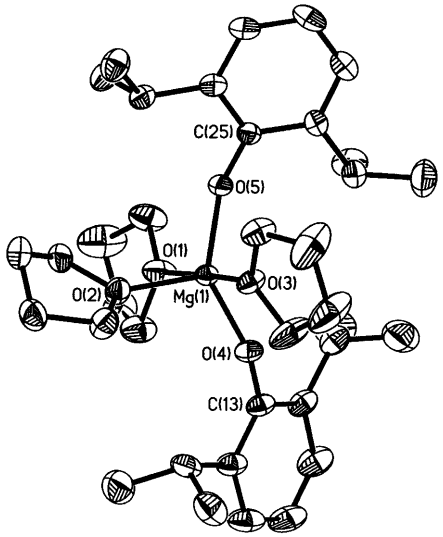


Fig. 1. Thermal ellipsoid plot of $Mg(DMP)_2(py)_3$ (**1**). Ellipsoids are drawn at 30% probability and protons are omitted for clarity.

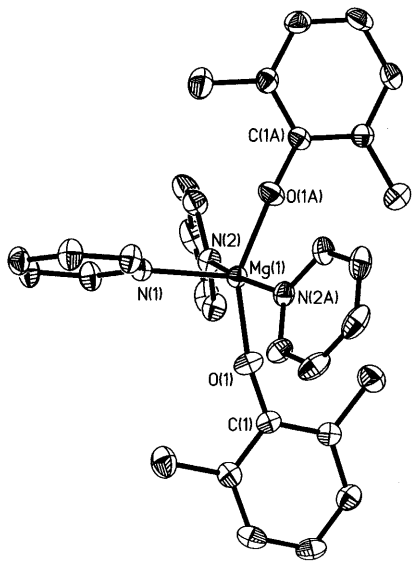


Fig. 2. Thermal ellipsoid plot of $Mg(DIP)_2(THF)_3$ (**2a**). Ellipsoids are drawn at 30% probability and protons are omitted for clarity.

the 'BuMg(DIP)' intermediate, **4**, followed by the addition of 1 equiv. of H-TCP to give the mixed ligand product, 'Mg(DIP)(TCP)$(L)_x$', **5**. Eqs. (3) and (4) summarize the reaction path for the general mixed-ligand case. The stability of the alkyl/aryloxy intermediate, **4**, toward disproportionation was not rigorously established.

$$Mg(Bu)_2 + 2HOAr + xsL \rightarrow [(Bu)Mg(OAr)]_n + H\text{-}Bu \quad (3)$$

$$[(Bu)Mg(OAr)]_n + 2HOAr' + xsL \rightarrow [Mg(OAr)(OAr')]_n + H\text{-}Bu \quad (4)$$

Work by Ashby et al. on similar alkyl/alkoxy species (i.e. MeMg(OR)) revealed that, while the mixed species did not disporportionate and could be isolated as crystalline solids, they were often involved in complex solution equilibria [18]. Unfortunately, a single crystalline product could not be isolated for the mixed alkoxide, **5**. This likely results from subsequent disproportionation of the heteroleptic product to give a complex mixture which includes both homoleptic $Mg(OAr)_2$ species.

3.2. Solid-state structures

Compounds **1**, **2a**, and **3** were isolated as monomeric complexes with five-coordinate, trigonal bipryamidal (tbp) Mg cations. Figs. 1–3 show the thermal ellipsoid plots of complexes **1**, **2a**, and **3**, respectively, and a summary of their metrical data is listed in Table 2. For each complex, the two OAr and a coordinated solvent occupy the equatorial positions with the remaining two solvent molecules located in the axial sites. The stronger ligand (i.e. OAr) avoids geometrical arrangements that force a *trans* configuration. This arrangement for $Mg(OAr)_2(L)_3$ has been previously observed by Roesky et al. in $(Mg(OC_6H_2(CF_3)_3)_2(THF)_3)$ using a fluorinated aryloxide [12]. In **2a** and **3** the donor solvent is THF while pyridine fills in the coordination sphere of **1**. The average Mg–O bond lengths for the aryloxides in **1**, **2a** and **3** do not deviate significantly from each other (1.90, 1.90, and 1.91 Å, respectively). The O–M–O angles involving the alkoxide oxygens are 15–20° larger than ideal likely due to their steric bulk. However, the largest deviation occurs for the DMP analog, **1**, which possesses the least hindering aryloxide. The same complex also displays the largest deviation in linearity for the axial solvent sites. Both of these observations can be accounted for by the stronger *trans* influence of pyridine in **1** over THF in **2a** and **3**.

Due to the absence of a Lewis base, the structure of **2b** differs significantly from the monomeric complexes previously discussed. Oligomerization is the only means by which the low-oxidation state magnesium cation can satisfy its coordination sphere. The number of bridging OAr was minimized by the bulky isopropyl substituents on the phenyl ring resulting in a trimeric product as can be seen in Fig. 4. Table 3 contains a partial list of the interatomic distances observed in **2b**. The three Mg atoms are nearly linear at 176° with Mg···Mg distances of 2.91 Å. The central Mg cation adopts a four-coordinate distorted tetrahedral environment employing four bridging OAr ligands. While the outer metal centers and each of their three ligated oxygens are coplanar, one of the O–M–O angles surrounding each outer Mg is significantly smaller than the idealized 120°. This angle is constrained by one of two four-membered rings. The average Mg–O distance in **2b** is 1.91 Å and

is almost identical to the averages for the five-coordinate monomeric complexes.

Control over the nuclearity of $Mg(OAr)_2$ based upon solvent choice has been previously observed by Ittel et al. [11]. They reported a series of dimeric magnesium aryloxide complexes, $[Mg(OAr)_2]_2$ where OAr = $OC_6H_2(CMe_3)_2Me$ (BHT), $OC_6H_2(CMe_3)_2$ (BHB), which maintained their solid-state structures in non-donor solvents. The dinuclear BHT and BHB derivatives were also found to be very soluble in donor solvents. However, based upon NMR studies, the dimers appeared to be disrupted by Lewis-basic solvents forming tetrahedral monomeric complexes, '$M(OAr)_2(solv)_2$'. The bulkiest ligand, DIP, in this study gave a three- and four-coordinate solvent-free trinuclear complex and five-coordinate monomeric solvent adduct. In contrast, the BHT and BHB ligands are more sterically hindering and allow only three-coordinate dimeric solvent-free magnesium centers and four-coordinate monomers even in the presence of small Lewis bases. Nuclearity dependence on solvent has also been documented for the '$Y(DMP)_3$' system in which both monomeric and dimeric products could be isolated [19]. However, instead of isolating an adduct and a solvent-free species as observed for the Mg examples, both yttrium complexes possess coordinated solvent.

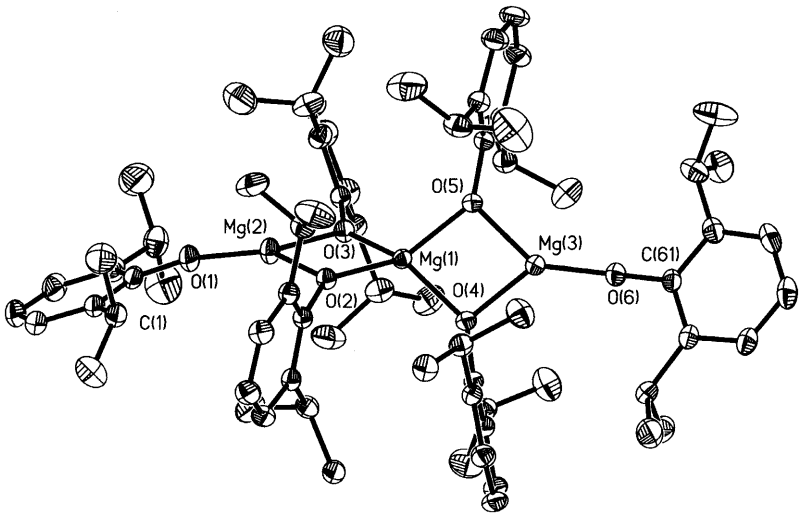


Fig. 3. Thermal ellipsoid plot of $Mg(TCP)_2(THF)_3$ (**3**). Ellipsoids are drawn at 30% probability and protons are omitted for clarity.

Table 2
Comparison of the interatomic distances (Å) and angles (°) for the monomeric complexes, **1**, **2a**, and **3**

	1		**2a**		**3**	
Bond distances						
Mg–(OAr)	Mg(1)–O(1)	1.887(1)	Mg(1)–O(4)	1.879(2)	Mg(1)–O(1)	1.914(2)
			Mg(1)–O(5)	1.896(2)		
Mg–(Solv)	Mg(1)–N(1)	2.172(1)	Mg(1)–O(1)	2.120(2)	Mg(1)–O(2)	2.079(2)
	Mg(1)–N(2)	2.258(1)	Mg(1)–O(2)	2.065(2)	Mg(1)–O(3)	2.059(3)
			Mg(1)–O(3)	2.145(2)		
Bond angles						
(ArO)–Mg–(OAr)	O(1)–Mg(1)–O(1′)	148.20(7)	O(4)–Mg(1)–O(5)	138.95(10)	O(1)–Mg(1)–O(1′)	134.52(14)
(ArO)–Mg–(Solv)	O(1)–Mg(1)–N(1)	105.90(3)	O(4)–Mg(1)–O(1)	91.61(10)	O(1)–Mg(1)–O(2)	88.89(7)
	O(1)–Mg(1)–N(2)	87.81(4)	O(4)–Mg(1)–O(2)	113.10(10)	O(1)–Mg(1)–O(3)	112.74(7)
	O(1)–Mg(1)–N(2′)	89.14(4)	O(4)–Mg(1)–O(3)	87.80(10)	O(1)–Mg(1)–O(2')	93.77(8)
			O(5)–Mg(1)–O(1)	89.52(10)		
			O(5)–Mg(1)–O(2)	107.94(10)		
			O(5)–Mg(1)–O(3)	92.67(9)		
(Solv)–Mg–(Solv)	N(1)–Mg(1)–N(2)	95.59(3)	O(1)–Mg(1)–O(2)	87.56(11)	O(2)–Mg(1)–O(3)	86.56(6)
	N(2)–Mg(1)–N(2′)	168.83(5)	O(1)–Mg(1)–O(3)	177.27(10)	O(2)–Mg(1)–O(2′)	173.11(12)
			O(2)–Mg(1)–O(3)	90.22(10)		
Mg–O–C(OAr)	Mg(1)–O(1)–C(1)	167.38(9)	Mg(1)–O(4)–C(13)	157.4(2)	Mg(1)–O(1)–C(1)	144.27(17)
			Mg(1)–O(5)–C(25)	149.8(2)		

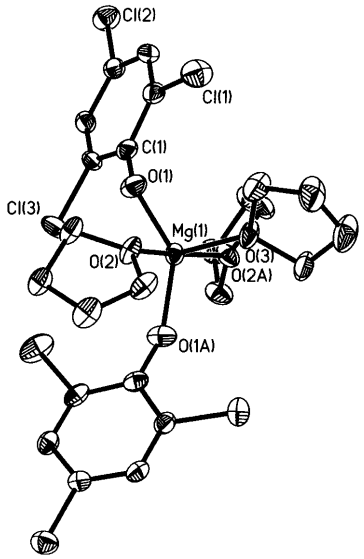


Fig. 4. Thermal ellipsoid plot of $[Mg(DIP)_2]_3$ (**2b**). Ellipsoids are drawn at 30% probability and protons are omitted for clarity.

Ongoing work in our laboratory has revealed a similar solvent dependence on the nuclearity of lithium aryloxides [20].

3.3. Solution structures

Metal alkoxides often display dynamic behavior in solution thereby accessing structural configurations not observed in the solid state. This possibility was investigated for **1**–**3** and **5** using solution spectroscopic methods. The ^{1}H NMR of the solvated monomers (**1**, **2a**, and **3**) revealed a single ligand environment. This observation can be explained in two possible ways: (i) the complexes remain monomeric in solution, or (ii) the complexes are involved in a dynamic process that is fast on the NMR time scale. In an effort to distinguish between these two possibilities, the solution behavior of the heteroleptic complex, **5** $[Mg(TCP)(DIP)(THF)_x]$, was investigated.

While the ^{1}H NMR of **5**, was expected to contain a single environment for each TCP and DIP ligand (analogous to the homoleptic compounds, **2a** and **3**), two environments for each ligand were observed. The presence of a single sterically hindered product could be ruled out by the observation of two triplets arising from the *para* proton on the phenyl ring of the DIP. A single product, possessing no symmetry, would give rise to a doublet of doublets from coupling to two inequivalent *meta* protons. Therefore, an equilibrium in which the heteroleptic and homoleptic products interconvert (Eq. (5)) must be considered.

$$2\underset{\mathbf{5}}{Mg(DIP)(TCP)(THF)_x} \rightleftharpoons \underset{\mathbf{3}}{Mg(TCP)_2(THF)_x} + \underset{\mathbf{2a}}{Mg(DIP)_2(THF)_x} \quad (5)$$

An equilibrium was observed in this system through the addition of a large amount of **3** to a solution of **5**. The phenyl region of the NMR spectrum for the mixture revealed just one doublet and one triplet for the DIP ligand, a large peak corresponding to the excess **3** as well as a much smaller TCP resonance. The observable phenyl resonances must arise from the remaining heteroleptic species, **5**. The large excess of **3** has caused the equilibrium in Eq. (5) to shift toward **5** and has diminished **2a** to the extent that it is only detectable as a very small doublet in the methyl region of the spectrum. Ligand transfer is likely an associative process

Table 3
Selected bond distances (Å) and bond angles (°) for $[Mg(DIP)_2]_3$ (**2b**)

Bond distances				
Mg···Mg	Mg(1)···Mg(2)	2.917(1)	Mg(2)···Mg(3)	2.913(1)
Mg–(Oar)	Mg(2)–O(1)	1.785(2)	Mg(3)–O(6)	1.790(2)
Mg–(μ-OAr)	Mg(1)–O(2)	1.959(2)	Mg(2)–O(2)	1.932(2)
	Mg(1)–O(3)	1.956(2)	Mg(2)–O(3)	1.926(2)
	Mg(1)–O(4)	1.953(2)	Mg(3)–O(4)	1.931(2)
	Mg(1)–O(5)	1.956(2)	Mg(3)–O(5)	1.935(2)
Bond angles				
Mg···Mg···Mg	Mg(2)···Mg(1)···Mg(3)	175.94(4)		
(ArO)–Mg–(μ-OAr)	O(1)–Mg(2)–O(2)	135.34(8)	O(6)–Mg(3)–O(4)	134.15(8)
	O(1)–Mg(2)–O(3)	139.84(8)	O(6)–Mg(3)–O(5)	141.70(8)
(μ-OAr)–Mg–(μ-OAr)	O(2)–Mg(2)–O(3)	83.44(6)	O(3)–Mg(1)–O(4)	135.82(7)
	O(2)–Mg(1)–O(3)	81.97(6)	O(3)–Mg(1)–O(5)	112.05(7)
	O(2)–Mg(1)–O(4)	115.53(7)	O(4)–Mg(1)–O(5)	82.34(6)
	O(2)–Mg(1)–O(5)	138.34(7)	O(4)–Mg(3)–O(5)	83.47(7)
Mg–(μ-OAr)–Mg	Mg(1)–O(2)–Mg(2)	97.14(7)	Mg(1)–O(4)–Mg(3)	97.15(7)
	Mg(1)–O(3)–Mg(2)	97.45(7)	Mg(1)–O(5)–Mg(3)	96.94(7)

accomplished through the formation of a dimeric or oligomeric intermediate. This dynamic process should be considered general for $Mg(OAr)_2(L)_3$ (**1**, **2a**, and **3**) complexes and, although not detectable by NMR, must occur in solutions of the homoleptic monomeric species as well.

Solution ^1H NMR of **2b** confirms that the solid-state structure remains intact upon dissolution in non-coordinating solvents. The solid-state structure reveals two OAr environments (bridging and terminal). If the molecule is fluxional or monomeric in solution, a single OAr environment would be expected. If the molecule remains intact with rapid and free rotation about all O–C bonds, only two methyl doublets should be present in a 2:1 ratio (two bridging:one terminal). In the ^1H NMR spectrum of **2b**, six equal intensity methyl doublets are observed indicating that the molecule remains trimeric in solution. The additional resonances further suggest that rotation about the C–O bonds is greatly hindered thereby reducing the time-averaged symmetry. This rotation is likely impeded by the bulky isopropyl substituents on the phenyl rings. Their steric bulk may be sufficient such that isopropyl groups on ligands bridging the same Mg centers cannot adopt an eclipsed configuration. If this is the case, then the molecular symmetry is reduced to D_3 (no mirror planes) and the molecule should exhibit two methyl signals from the terminal ligands and four from the bridging ligands. Such steric congestion may render the bridging oxygens sufficiently labile as to be replaced by coordinating solvent (Eq. (6)). Indeed, when **2b** is dissolved in THF-d_8, the resulting spectrum is identical to that observed for crystalline **2a**.

$$[\underset{\mathbf{2b}}{Mg(DIP)_2}]_3 \overset{THF}{\rightarrow} 3\underset{\mathbf{2a}}{Mg(DIP)_2}(THF)_3 \quad (6)$$

4. Conclusions

A series of magnesium aryloxides was prepared by the reaction of $Mg(Bu)_2$ with a variety of HOAr and identified in the solid state as $Mg(DMP)_2(py)_3$ (**1**), $Mg(DIP)_2(THF)_3$ (**2a**), $[Mg(DIP)_2)]_3$ (**2b**), and $Mg(TCP)_2(THF)_3$ (**3**). Oligomeric species were generally obtained in the absence of a donor solvent. Through exposure to THF, five-coordinate monomers were readily obtained for the TCP, **3**, and DIP, **2a**, analogs. Although the TCP and DMP products are both oligomeric in the absence of a Lewis base, a stronger donor (i.e. pyridine) was required to disrupt the insoluble DMP species. The necessity of a stronger donor can be attributed to the differing acidity of their parent HOAr. Presence of chlorine substituents on the TCP ring results in a lower pK_a for H-TCP and thus removes electron density from the aryloxide oxygen. Bridging OAr oxygens in $[Mg(TCP)_2]_n$ should then be more labile in comparison to those in the oligomeric $[Mg(DMP)_2]_n$. Conversely, a steric argument can be made for the ease of the trinuclear (**2b**) to monomer (**2a**) conversion observed for the DIP products. Solution NMR studies revealed that the trinuclear species, **2b**, remained intact (in non-coordinating solvents), while the monomeric complexes are components of an equilibrium that facilitates intermolecular ligand transfer. The variation in nuclearity observed in this work and for analogous complexes (BHT and BHB) [11] suggests that through judicious choice of ligand and solvent it is possible to isolate soluble $Mg(OAr)_2$ species with tailored aggregate sizes.

5. Supplementary material

Crystallographic data for the structures reported in this paper have been deposited with the Cambridge Crystallographic Data Centre, CCDC Nos. 143924, 143925, 143926, and 143927. Copies of this information may be obtained free of charge from the Director, CCDC, 12 Union Road, Cambridge, CB2 1EZ, UK (fax: +44-1223-336033; e-mail: deposit@ccdc.cam.ac.uk or http://www.ccdc.cam.ac.uk).

Acknowledgements

For support of this research, the authors would like to thank the United States Department of Energy under contract DE-AC04-94AL85000 and Union Carbide Corporation. Sandia is a multiprogram laboratory operated by Sandia Corporation, a Lockheed Martin Company, for the United States Department of Energy.

References

[1] V. Cerchez, Bull. Soc. Chim. 43 (1928) 762.
[2] H. Lund, J. Bjerrum, Chem. Ber. B64 (1931) 210.
[3] D.C. Bradley, R.C. Mehrotra, D.P. Gaur, Metal Alkoxides, Academic Press, New York, 1978.
[4] E.P.J. Moore, Polypropylene Handbook, Hanser/Gardner Publications, Cincinnati, 1996.
[5] S.G. Hegde, D.C. Myles, Synth. Commun. 27 (1997) 2111.
[6] S. Kanemasa, M. Nishiuchi, E. Wada, Tetrahedron Lett. 33 (1992) 1357.
[7] Z.A. Starikova, A.I. Yanovsky, E.P. Turevskaya, N.Y. Turova, Polyhedron 16 (1997) 967.
[8] P. Sobota, J. Utko, Z. Janas, S. Szafert, Chem. Commun. (1996) 1923.
[9] L. Albaric, N. Hovnanian, A. Julbe, C. Guizard, A. Alvarezlarena, J.F. Piniella, Polyhedron 16 (1997) 587.
[10] A. Klemp, H.W. Roesky, H.G. Schmidt, H.S. Park, M. Noltemeyer, Organometallics 17 (1998) 5225.
[11] J. Calabrese, M.A. Cushing, S.D. Ittel, Inorg. Chem. 27 (1988) 867.

[12] H.W. Roesky, M. Scholz, M. Noltemeyer, Chem. Ber. 123 (1990) 2303.
[13] SMART Version 5.054, Bruker Analytical X-ray Systems, Inc., 6300 Enterprise Lane, Madison, WI 53719, 1998.
[14] SAINT Version 6.01, Bruker Analytical X-ray Systems, Inc., Madison, WI 53719, 1998.
[15] SHELXTL/NT Version 5.10, Bruker Analytical X-ray Instruments, Inc., Madison, WI 53719, 1997.
[16] G. Sheldrick, SADABS, First Release, University of Göttingen, Germany, 1996.
[17] XSHELL Version 3.0, Bruker Analytical X-ray Systems, Inc., 6300 Enterprise Lane,Madison, WI 53719, 1998.
[18] E.C. Ashby, J. Nackashi, G.E. Parris, J. Am. Chem. Soc. 97 (1975) 3162.
[19] W.J. Evans, J.M. Olofson, J.W. Ziller, Inorg. Chem. 28 (1989) 4308.
[20] T.J. Boyle, D.M. Pedrotty, T.M. Alam, S.C. Vick, M.A. Rodriguez, Inorg. Chem. 39 (2000) 5133.

PERGAMON

www.elsevier.nl/locate/poly

Polyhedron 19 (2000) 2565–2572

POLYHEDRON

Structure and chemical bonding in *cis*- and *trans*-$M(NO)_2(O_2CR)_2$ (M = Cr and Mo) complexes

Ludmiła Szterenberg [a], Szczepan Roszak [b], Renata Matusiak [a], Antoni Keller [a,*]

[a] *Faculty of Chemistry, University of Wrocław, Joliot-Curie 14, 50-383 Wrocław, Poland*
[b] *Institute of Physical and Theoretical Chemistry, Wrocław University of Technology, Wyb. Wyspiańskiego 27, 50-370 Wrocław, Poland*

Received 28 February 2000; accepted 18 August 2000

Abstract

New *cis*- and *trans*-nitrosyl complexes of the formula $M(NO)_2(O_2CR)_2$ (M = Cr and Mo) were synthesized and characterized spectroscopically. The supporting theoretical studies indicate the deviation of molecules from their ideal geometries. The most striking consequence is the deformation of the ON–M–NO fragment from its linear form, in *trans* complexes. This deformation leads to the additional weak ν_s(NO) vibration. © 2000 Elsevier Science B.V. All rights reserved.

Keywords: Nitrosyl complex; Chromium; Molybdenum; Carboxylate; DFT

1. Introduction

The unique physical and chemical properties of metal nitrosyl complexes [1–9], their importance related to biological and medical aspects [10–15], and their potential application in organic synthesis [16] have led to the constant interest in these compounds observed for more then 100 years [17]. The molecular unit $\{M(NO)_x\}^n$ (n is the number of d electrons of the metal [2]) is formed, inside which the electron density can move within a wide range. The relation between electronic density distribution in $\{M(NO)_x\}^n$ and the nature of the central atom and other coordinated ligands is still an important issue in structural physicochemistry, biochemistry (because of the biological importance of some complexes ([10–15]) and in catalysis. Complexes of this group are known as catalysts of oxidation [18–23], hydrogenation [24–26], oligomerization and polymerization [27–33], isomerization [34–38], and metathesis [23–34,39,40] reactions. The most active catalysts of the reaction of olefin metathesis are nitrosyl complexes of molybdenum [34,41–43] and tungsten [43,39,44]. These compounds also catalyze oligomerization and polymerization reactions of alkenes and alkynes [30–33,45,46].

The nitrosyl complexes with ligands coordinated via oxygen atoms are especially important. Carbene complexes of the type $[M(NO)_2(=CHR)L_2(AlCl_2)_2]$ (M = Cr, Mo; L = alkoxy or carboxylate ligands), were obtained in reactions of dinitrosyl complexes of the $\{M(NO)_2(OR)_2\}_n$ and $M(NO)_2(O_2CR)_2$ type with $RAlCl_2$ [32,47,48]. In the case of molybdenum, stable alkylidene complexes are formed. Here, coordinated alkylidene ligands have nucleophilic character in spite of the low oxidation state of the metals. Thus, these compounds are different carbene complexes than the Fischer (low oxidation states, electrophilic carbene ligands) or Schrock (high oxidation state, nucleophilic carbene ligands) compounds. In the synthesis of these compounds, $RAlCl_2$ plays two roles — as an alkylating agent, but first of all it is a Lewis acid, emptying the coordination sites at the metal due to breaking the bridging (in polymeric complexes) or chelate bonds [32,47,48]. A similar effect is also caused by other Lewis acids, like $M'Cl_4$ (M′ = Ti, Sn) [31–33]. Terminal acetylenes, present in such systems, could generate the formation of dinitrosylcarbene (vinylidene) catalysts. These complexes should contain low oxidation state metals. Their stoichiometries, $M(NO)_2(=CRR')L_2(LA)_2$, are similar to those of the dinitrosylcarbene complexes obtained earlier in our laboratory [32,47,48], but the carbene groups are electrophilic in character.

* Corresponding author. Tel.: +48-71-320-4334; fax: +48-71-328-2348.
E-mail address: akeller@wchuwr.chem.uni.wroc.pl (A. Keller).

0277-5387/00/$ - see front matter © 2000 Elsevier Science B.V. All rights reserved.
PII: S0277-5387(00)00556-8

Synthesis of new *trans*- and *cis*-dinitrosylchromium complexes, their spectroscopic characterization and the theoretical study of the structure and chemical bonding of these types of chromium and molybdenum complexes are the subject of this paper.

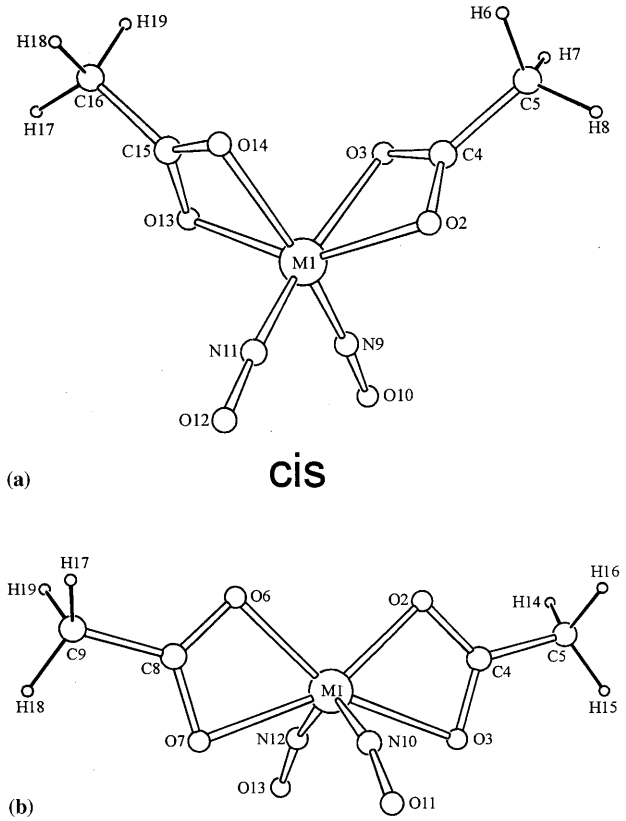


Fig. 1. The *cis* (a) and *trans* (b) structures of $M(NO)_2(O_2CR)_2$ (M = Cr or Mo) complexes. The corresponding geometrical parameters are given in Tables 1 and 2.

Table 1
The relative energies (ΔE) and structural parameters of *cis*- and *trans*-$Cr(NO)_2(O_2CCH_3)_2$ complexes from DFT calculations performed in LanL2DZ (L) and LanL2DZ supplemented by the polarization function (L+p) basis sets [a]

Parameters	*cis* L	*cis* L+p	*trans* L	*trans* L+p
ΔE	0	0	25.3	26.6
$Cr–O_2$	2.03	2.016	2.02	2.16
$Cr–O_3$	2.09	2.08	2.17	2.01
$Cr–N_1$	1.70	1.70	1.73	1.73
$N_1–O_1$	1.20	1.16	1.20	1.16
$N_1–Cr–N_{11}$	93.9	92.0	132.2	130.1
$Cr–N_1–O_1$	176.2	174.8	163.0	161.4
$O_2–Cr–O_3$	64.6	64.2	63.0	62.6
$O_2–Cr–O_{12}$	148.0	147.8	139.2	140.6
$O_2–Cr–O_{13}$	91.0	84.5	94.7	94.1

[a] Energy is measured in (kcal mol^{-1}), distance in (Å), angles in (°).

Table 2
The relative energies (ΔE) and structural parameters for the *cis*- and *trans*-$Mo(NO)_2(O_2CCH_3)_2$ complexes from calculations performed in LanL2DZ (L) and LanL2DZ supplemented by the single polarization function (L+p) basis sets [a]

Parameters	*cis* L	*cis* L+p	*trans* L	*trans* L+p
ΔE	0	0	28.6	29.5
$Mo–O_2$	2.16	2.15	2.14	2.27
$Mo–O_3$	2.23	2.22	2.29	2.14
$Mo–N_1$	1.83	1.83	1.86	1.86
$N_1–O_1$	1.21	1.17	1.21	1.18
$N_1–Mo–N_{11}$	92.1	91.4	132.4	131.4
$Mo–N_1–O_1$	179.9	174.3	164.2	163.6
$O_2–Mo–O_3$	60.5	60.2	59.3	59.0
$O_2–Mo–O_{12}$	145.9	145.8	141.5	142.3
$O_2–Mo–O_{13}$	82.9	83.4	99.8	99.6

[a] Energy is measured in (kcal mol^{-1}), distance in (Å), angles in (°).

2. Experimental

All experiments presented here were performed under an argon atmosphere using standard Schlenk techniques and vacuum-line procedures. Solvents were purified and distilled under argon from appropriate agents. The *trans* complexes $[Cr(NO)_2(CO)_2(MeNO_2)_2](BF_4)_2$, $[Cr(NO)_2(MeNO_2)_4](BF_4)_2$ and $\{Cr(NO)_2(OR)_2\}_n$ (R = Et, ^{i}Pr) were prepared according to the published procedure [32]. The IR spectra were measured on an Impact 400 (Nicolet) spectrophotometer. The ^{1}H NMR spectra were recorded using a Bruker 300 spectrometer and referenced to Me_4Si. Molecular weights were determined using a Perkin–Elmer 115 instrument.

2.1. Synthesis of trans-$Cr(NO)_2(O_2CMe)_2$ (1) and trans-$Cr(NO)_2(O_2CCPh_3)_2$ (2)

NaO_2CR (8.6 mmol, R = CH_3, CPh_3) in MeOH was added to $[Cr(NO)_2(CO)_2(MeNO_2)_2](BF_4)_2$ or $[Cr(NO)_2(MeNO_2)_4](BF_4)_2$ (4.3 mmol) in $MeNO_2$ (20 ml) at room temperature. The reaction mixtures were stirred for 15 min after which the solutions were filtered and removed under vacuum. The complexes were extracted from the remainder with a small amount of CH_2Cl_2 and precipitated with hexane.

2.2. $Cr(NO)_2(O_2CMe)_2$

IR (Nujol mulls): ν(NO) 1778 sh, 1698 vs; $\nu_{as}(CO_2)$ 1580 vs, $\nu_s(CO_2)$ 1421 s. ^{1}H NMR (in CD_3CN at 20°C): δ 2.10 (s, 6H, CH_3) ppm. *Anal.* Calc. for $C_4H_6CrN_2O_6$: C, 20.88; H, 2.63; N, 12.17. Found: C, 20.96; H 2.70; 12.01%.

2.3. $Cr(NO)_2(O_2CCPh_3)_2$

IR (Nujol mulls): ν(NO) 1777 sh, w, 1696 vs; $\nu_{as}(CO_2)$ 1559 vs, $\nu_s(CO_2)$ 1447 m. ^{1}H NMR (in acetone-d_6 at 20°C): δ 7.26 (m, 30H, Ph) ppm. *Anal*. Calc. for $C_{40}H_{30}CrN_2O_6$: C, 69.97; H, 4.40; N, 4.08. Found: C, 70.08; H, 4.51; N, 4.00%.

2.4. Synthesis of cis-$\{Cr(NO)_2(OR)_2\}_n$ (R = Et (**3a**), ^{i}Pr (**4a**))

A solution of *trans*-$\{Cr(NO)_2(OEt)_2\}_n$ in toluene was stirred for 30 min at 60°C. The green precipitate of the *cis*-isomer was filtered off, washed with CH_2Cl_2 and dried in vacuo.

Table 3
Calculated and experimental frequencies ν(NO) (cm^{-1}) and intensities I (km mol^{-1}) for *cis*- and *trans*-$M(NO)_2(O_2CCH_3)_2$ (M = Cr, Mo) [a]

		Calculated						Experimental			
		ν		I		Iv_s/Iv_{as}		ν	Iv_s/Iv_{as}	ν_{calc}/ν_{exp}	
		L	L+p	L	L+p	L	L+p			L	L+p
M = Cr											
cis	ν_{as}	1727	1857	1117	1348	0.44	0.50	1699 [b]	0.43		
	ν_s	1829	1977	498	676			1849 [b]			
	$\Delta\nu$ [c]	102	102					150 [b]			
trans	ν_{as}	1697	1840	1431	1708	0.14	0.18	1698	0.14	1.00	1.08
	ν_s	1778	1926	203	314			1778		1.00	1.08
	$\Delta\nu$ [c]	81	86					80			
M = Mo											
cis	ν_{as}	1670	1811	1098	1294	0.43	0.44	1650 [d]	0.42	1.01	1.09
	ν_s	1759	1903	472	570			1770 [d]		0.99	1.07
	$\Delta\nu$ [c]	89	92					120 [d]			
trans	ν_{as}	1625	1772	1675	1733	0.12	0.17	1665 [e]			
	ν_s	1710	1857	201	293						
	$\Delta\nu$ [c]	85	85								

[a] Calculations were done in LanL2DZ (L) and LanL2DZ supplemented by the polarization function (L+p) basis sets.
[b] For *cis*-$\{Cr(NO)_2(OEt)_2\}_n$.
[c] $\Delta\nu = \nu_s - \nu_{as}$.
[d] Ref. [62].
[e] For *trans*-$[Mo(NO)_2(Hsal\text{-}INH)_2]$ [59].

Table 4
Frequencies of ν(NO) and relative intensities Iv_s/Iv_{as} of other known *cis*- and *trans*-dinitrosyl complexes of chromium and molybdenum

Complex	ν_s(NO) (cm^{-1})	ν_{as}(NO) (cm^{-1})	$\Delta\nu$(NO) [a] (cm^{-1})	Iv_s/Iv_{as}	Ref.
trans-$Cr(NO)_2(O_2CCPh_3)_2$	1777	1696	81	0.12	[b]
trans-$\{Cr(NO)_2(OEt)_2\}_{2n}$		1720			[32]
trans-$\{Cr(NO)_2(O^iPr)_2\}_n$		1718			[32]
trans-$[Cr(NO)_2(MeCN)_4]^{2+}$		1793			[32,50]
trans-$[Cr(NO)_2(MeNO_2)_4]^{2+}$		1798			[32]
trans-$[Cr(NO)_2(CO)_2(MeNO_2)_2]^{2+}$		1791			[32]
trans-$[Cr(NO)_2(bipy)_2]^{2+}$		1702			[32]
cis-$\{Cr(NO)_2(O^iPr)_2\}_n$	1854	1698	156	0.41	[b]
cis-$[Cr(NO)_2(OEt)_2(SnCl_4)]$	1887	1766	121	0.45	[b]
cis-$[Cr(NO)_2(O_2CCPh_3)_2(SnCl_4)_2]$	1885	1763	122	0.48	[b]
trans-$[Mo(NO)_2(Hsal\text{-}BZH)_2]$		1678			[49]
trans-$[Mo(NO)_2(Hvan\text{-}BZH)_2]$		1671			[49]
trans-$[Mo(NO)_2(Hvan\text{-}INH)_2]$		1678			[49]
cis-$\{Mo(NO)_2(OEt)_2EtOH\}_n$	1740	1616	124	0.45	[66]
cis-$\{Mo(NO)_2(O^iPr)_2\}_n$	1772	1630	142	0.44	[66]
cis-$Mo(NO)_2(O_2CPh)_2$	1790	1682	118	0.43	[62]

[a] $\Delta\nu(NO) = \nu_s(NO) - \nu_{as}(NO)$.
[b] This work.

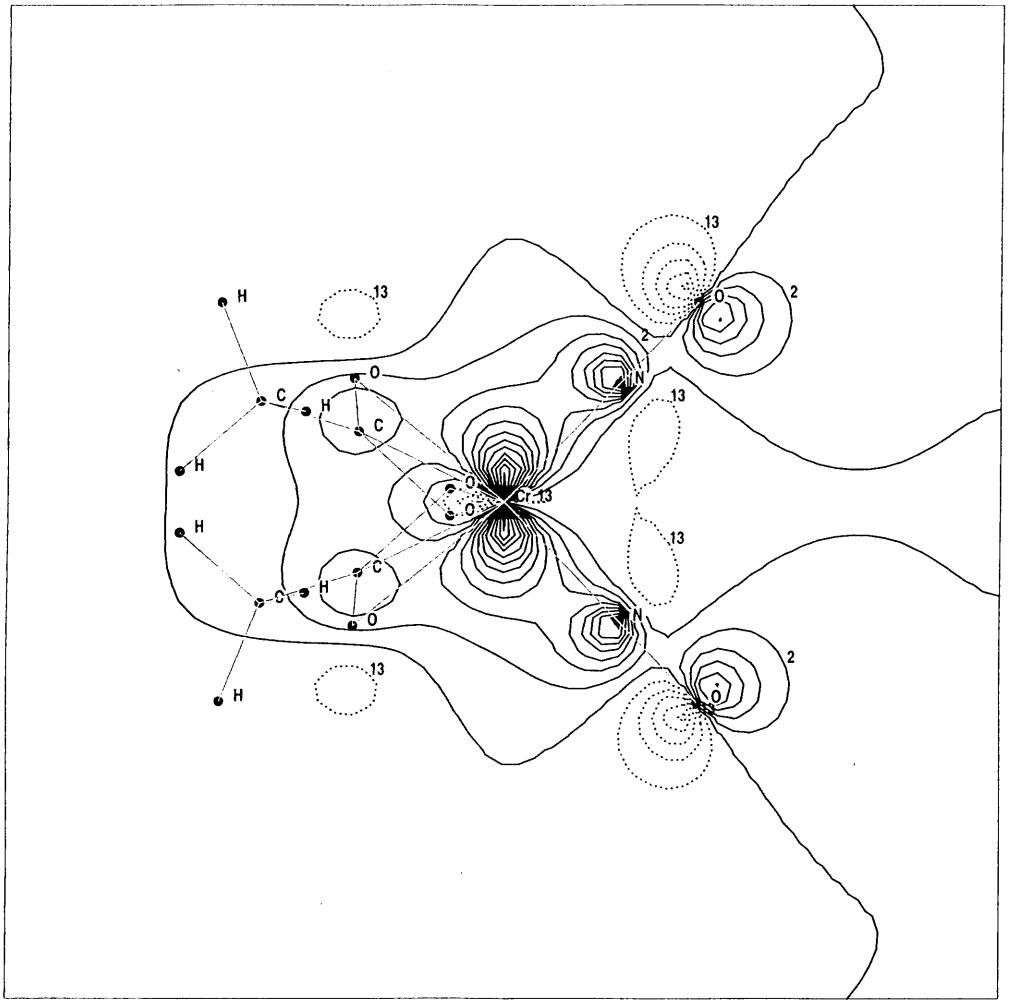


Fig. 2. The HOMO for the *cis*-$Cr(NO)_2(O_2CR)_2$ molecule plotted in the N–Cr–N plane. The contour lines from 1–12 are positive (increasing order), from 13–17 are negative (decreasing order). The contour 1 denotes zero. The spacing between lines is 0.0125 units. Note the π character of the Cr–N bond in the orbital.

2.5. $\{Cr(NO)_2(OEt)_2\}_n$

IR (Nujol mulls): ν_s(NO) 1849 s, ν_{as}(NO) 1699 vs, ν(OR) 1093 m, 1050 m, 1025 sh. ^{1}H NMR (acetone-d_6): δ 3.62, 3.35 (s, br, 6H, CH_3CH_2), 1.35, 1.06 (s, 9H, CH_3CH_2) ppm. *Anal.* Calc. for $C_4H_{10}CrN_2O_4$: C, 23.77; H, 4.99; N, 13.86. Found: C, 23.89; H, 5.04; N, 13.73%.

2.6. $\{Cr(NO)_2(O^1Pr)_2\}_n$

IR (Nujol mulls): ν_s(NO) 1854 s, ν_{as}(NO) 1698 vs.

2.7. Synthesis of cis-$\{Cr(NO)_2(OEt)_2(SnCl_4)\}_n$ (**5**) and cis-$\{Cr(NO)_2(O_2CCPh_3)_2(SnCl_4)_2\}_n$ (**6**)

$SnCl_2$ in CH_2Cl_2 was added to a stirred solution of the appropriate $\{Cr(NO)_2L_2\}_n$ complex (L = OEt, O_2CCPh_3) in CH_2Cl_2 in a 1:2 molar ratio. The yellow–brown adduct precipitates were filtered off, washed with CH_2Cl_2 and dried in vacuo.

2.8. $[Cr(NO)_2(OEt)_2(SnCl_4)]$

IR (Nujol mulls): ν_s(NO) 1887 s, ν_{as}(NO) 1766 vs, ν(OR) 1088 m, 1008 m, 993 sh. ^{1}H NMR (in CD_3CN at 20°C): δ 4.54, 3.64 (s, br, 4H, CH_2CH_3), 1.26, 0.91 (s, br, 6H, CH_2CH_3) ppm. *Anal.* Calc. for $C_4H_{10}Cl_4CrN_2O_4$ Sn: C, 10.38; H, 2.18; Cl, 30.65; N, 6.05. Found: C, 10.44; H, 2.27; Cl, 35.71; N, 5.97%.

2.9. $[Cr(NO)_2(O_2CCPh_3)_2(SnCl_4)_2]$

IR (Nujol mulls): ν_s (NO) 1885 s, ν_{as} (NO) 1763 vs, ν_{as}(CO) 1550 vs, ν_s(CO) 1421 s. ^{1}H NMR (in CD_3CN at 20°C): δ 7.26 (m, 30H, Ph) ppm. *Anal.* Calc. for

$C_{40}H_{30}Cl_8CrN_2O_6Sn_2$: C, 39.78; H, 2.50; Cl, 23.48; N, 2.32. Found: C, 39.87; H, 2.54; Cl, 23.55; N, 2.27%.

3. Details of theoretical studies

The studies presented here were performed applying density functional theory (DFT) [49]. The DFT approach utilized Becke's three parameters hybrid functional (B3LYP) [50], based on earlier works [51,52]. Calculations were performed within the LanL2DZ [53,54] basis set. Additional calculations were performed with the LanL2DZ basis supplemented by the single five-component d function on heavy atoms. The exponents of polarization functions for chromium and molybdenum are 0.058317 and 0.1270, respectively. Exponents for other atoms were adopted from Huzinaga et al. [55]. The computations presented were made using the program GAUSSIAN-94 [56].

4. Results and discussion

The structure and the nature of bonding in nitrosyl complexes were discussed in 1974 by Enemark and Feltham [2]. In the case of dinitrosyl complexes possessing the $\{M(NO)_2\}^n$ fragment the important problem concerns the N–M–N angle. The number of d electrons, n, determines the linearity ($D_{\infty h}$) or nonlinearity (C_{2v}) of the N–M–N angle. The six-coordinated dinitrosyl complexes of Group 6 metals should contain the nonlinear $M(NO)_2$ fragment. All the structurally characterized compounds, including $Mo(NO)_2TTP$, possess nitrosyl ligands in the *cis* position [6,57]. However, the dinitrosylchromium complex $[Cr(NO)_2(MeCN)_4](PF_6)_2$, synthesized 30 years ago by Connolly et al. [58], is *trans* with regard of the nitrosyl groups. Only a single band in the region of the ν(NO) frequency was observed in the IR spectrum of this compound. The replacement of acetonitrile ligands by sulfur chelating ones ($S_2CNEt_2^-$

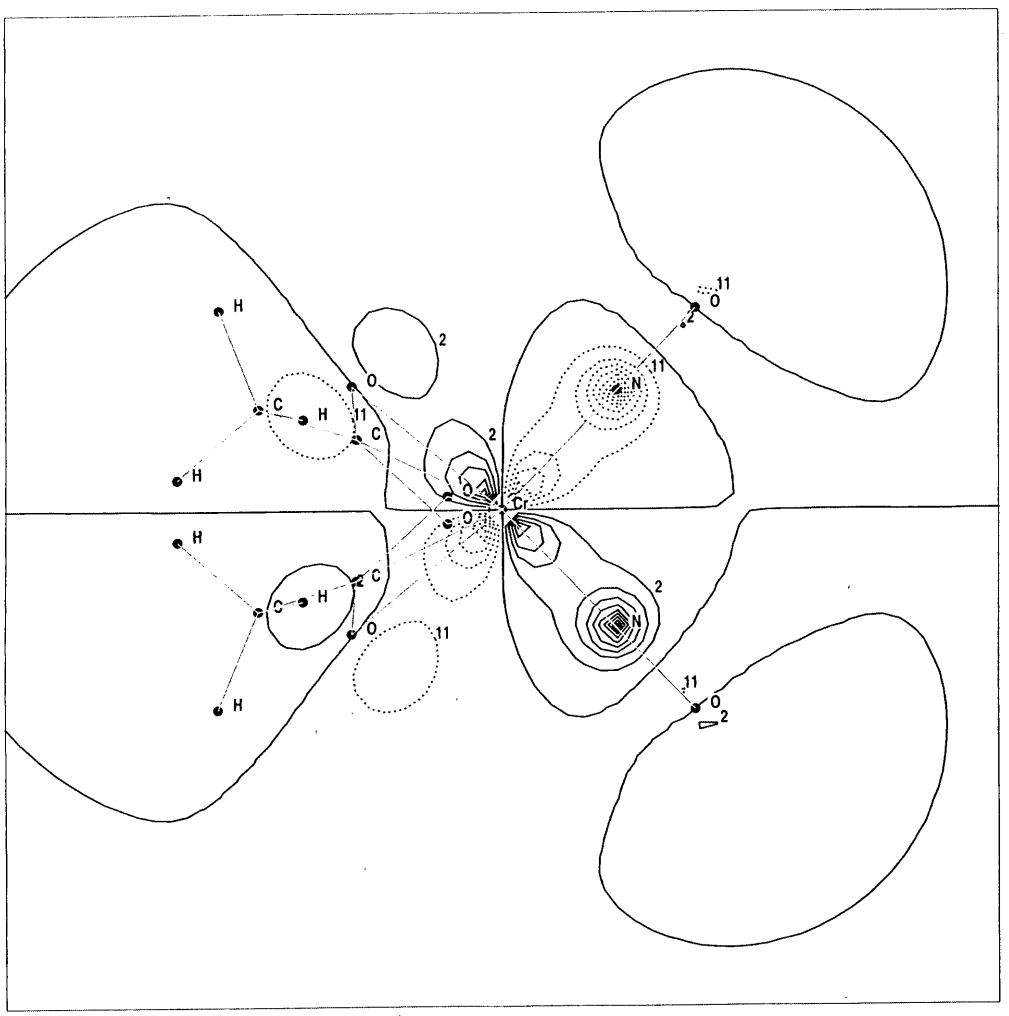


Fig. 3. The HOMO-1 for the *cis*-$Cr(NO)_2(O_2CR)_2$ molecule plotted in the N–Cr–N plane. The contour lines from 1–12 are positive (increasing order), from 13–17 are negative (decreasing order). The contour 1 denotes zero. The spacing between lines is 0.0125 units. Note the σ character of the Cr–N bond in the orbital.

and/or $S_2C_2(CN)_2^{2-}$) leads to the formation of respective *cis*-dinitrosylchromium complexes. Recently, the *trans*-dinitrosylmolybdenum complexes with Schiff bases were also synthesized [59]. A number of diatomic *trans*-dinitrosylchromium complexes were obtained in our laboratory [32]. The reaction of complexes containing the *trans*-$[Cr(NO)]^{2+}$ core with M^IOR ($M^I = Na$, Li) leads to the formation of respective *trans* complexes. A similar reaction Eq. (1) yields dicarboxylatochromium complexes, i.e. $Cr(NO)_2(O_2CR)_2$ (where $R = CH_3$ or CPh_3).

$$[Cr(NO)_2(CO)_2(MeNO_2)_2](BF_4)_2 \quad \text{or} \quad \underset{(L = MeCN \text{ or } MeNO_2)}{[Cr(NO)_2L_4](BF_4)_2} + 2NaO_2CR \underset{(R = Me\ (\mathbf{1})\ \text{or}\ CPh_3\ (\mathbf{2}))}{\rightarrow} Cr(NO)_2(O_2CR)_2 + 2NaBF_4 \quad (1)$$

The brown complex **1**, soluble in donor solvents (MeCN, $MeNO_2$, MeOH) is polymeric ($\{Cr(NO)_2(O_2CMe)_2\}_n$). The $\Delta\nu(CO_2) = \nu_{as} - \nu_s$ splitting equals 151 cm^{-1} confirms the above [60,61]. Very low $\Delta\nu(CO_2)$ values (< 105) generally indicate chelation [61]. For example, in $[Mo(NO)_2(O_2CMe)_2]\cdot MeOH$, $\Delta\nu(CO_2)$ is 97 cm^{-1} [62]. The ^1H NMR spectrum of **1** in CD_3NO_2 contains one methyl proton signal at 2.10 ppm.

Complex **2** (soluble in CH_2Cl_2, benzene, toluene, CCl_4) exists in the monomeric form as indicated by its molecular weight (Found: 683.91. Calc. for $Cr(NO)_2(O_2CCPh_3)_2$: 686.68). The $\Delta\nu(CO_2)$ value for chelate triphenylacetate ligands is 112 cm^{-1}. The ^1H NMR spectrum (in CD_2Cl_2 at 20°C) exhibits a multiplet at 7.26 ppm due to phenyl protons. The IR spectra of **1** and **2** are similar to all the *trans*-dinitrosylchromium complexes [32,58] and are characterized by a single strong band at 1700 cm^{-1} related to the ν(NO) vibration. However weak shoulders at 1778 and 1777 cm^{-1} may also be observed.

Dinitrosylchromium complexes with alkoxy ligands (i.e. *trans*-$\{Cr(NO)_2(OR)_2\}_n$, R = Et (**3**), ^{i}Pr (**4**)), when heated (60°C) in noncoordinating solvents, undergo isomerization to *cis* complexes (**3a**, **4a**). However, only the *cis*-$\{Cr(NO)_2(OEt)_2\}_n$ (**3a**) complex was obtained in pure form, as a brown powder soluble only in polar solvents. Complex **4** partially disintegrates during such treatment, while complex **2** does not isomerize at all and at higher temperatures decomposes. Complex **1** is not soluble in noncoordinating solvents.

The IR spectra of complexes **3a** and **4a** (see Section 2) contain two ν(NO) frequencies characteristic for the *cis*-$\{Cr(NO)_2\}^6$ unit (C_{2v} symmetry), corresponding to symmetric and asymmetric stretching motions of the N–O bond. The ν(CO) frequencies of RO^- ligands (e.g. for R = Et 1093, 1050 and 1025 cm^{-1}) may indicate the presence of bridging as well as terminal alkoxy ligands in these complexes [32,63]. The ^1H NMR spectrum of the complex **3a** (see Section 2) also confirms the above. It contains two resonance signals for the CH_2 and CH_3 protons corresponding to the terminal and bridging ethoxy ligands.

Reactions of complexes **2** and **3** with Lewis acids (e.g. $SnCl_4$) induce similar *trans*-$[Cr(NO)_2] \rightarrow$ *cis*-$[Cr(NO)_2]$ transformations, in 1:1 as well as in 1:2 molar ratios of reagents. The adducts *cis*-$[Cr(NO)_2(OEt)_2(SnCl_4)]$ (**5**) and *cis*-$[Cr(NO)_2(O_2CCPh_3)_2(SnCl_4)_2]$ (**6**) are produced in such reactions. Their IR spectra contain two characteristic ν(NO) frequencies. The character of the spectrum of complex **5**, in the range of ν(OEt) frequencies, indicates the bridging and terminal coordination of ethoxy ligands [32,63]. Examination of the ^1H NMR spectrum (see Section 2) also leads to the same conclusion.

4.1. Theoretical results

Theoretical studies were performed for the $M(NO)_2(O_2CMe)_2$ (M = Cr and Mo) complexes. The valence orbitals of chromium and molybdenum undergo the d^5s^1 hybridization which leads to a trigonal bipyramid structure. In the molecules studied, however, the metal–acetate rings destroy the perfect D_{4h} symmetry. Two equilibrium structures were located (Fig. 1) with the *cis* isomers (C_2 symmetry) being more stable then its *trans* partners (C_{2v} symmetry) (Tables 1 and 2). The X-ray structures for the *trans*-dinitrosyl complexes of Group 6 metals are unknown. The main structural difference between the ideal structures of the *cis* and *trans* isomers concerns the N–M–N angle. In the ideal *trans* structure the ON–M–NO fragment is linear. The studies performed, however, indicated a significant deviation from linearity with the N–M–N angle being 130.1 and 163.6° for Cr and Mo compounds, respectively. In the case of the *cis* isomers N–M–N angles of 92.0° (Cr) and 91.0° (Mo) are close to the values found for the perfect geometry (90.0°). The M–N–O branch was also found to be nonlinear. It was noted several years ago [64] that slightly bent M–N–O fragments are a common feature of polynitrosyl complexes. The electronic rationalization of this phenomenon was given by Kettle [65]. In an every molecule studied, the O–M–O angles of metal–acetate rings amount to about 60°, again far from the 90° expected for the ideal D_{2h} symmetry. This distortion leads to two different M–O bonds within the same ring.

The vibrational spectra of studied compounds reflects the geometry of the molecules. Two different frequencies for NO vibrations (asymmetrical and symmetrical) were expected and both are observed. The calculated and experimental frequencies are presented in Table 3. The most striking effect comparing this structure to the ideal is that there are two, instead of just one, vibra-

tional motions for NO in the *trans* case. The frequencies calculated applying the LanL2DZ basis set closely reproduces the available experimental spectra. The extension of the basis set by the polarization functions, however, leads to the systematically higher values of frequencies which have to scaled by 0.9 to reproduce experimental data. This scaling factor reflects the quality of the method and the basis set applied. The excellent agreement of the smaller basis results with experimental values has to be treated with caution. The differences between asymmetric and symmetric modes of N–O vibrations are reproduced satisfactorily. The calculated ratio of Iv_s/Iv_{as} is also close to that observed experimentally. This agreement gives us confidence in the calculations performed for *trans* isomers where experimental results are scarce. The inflection observed in the wide band of the *trans* isomer in the Cr based molecule fits the theoretically found symmetric vibration. The much lower ratio of Iv_s/Iv_{as} (0.14) for the *trans* isomer compared to that of the *cis* form (0.43) is consistent with molecular structures. The weak symmetric band would vanish in the case of the perfect D_{4h} structure. Table 4 collects the ν(NO) frequencies and relative intensities Iv_s/Iv_{as} of other known *cis*- and *trans*-dinitrosyl complexes of chromium and molybdenum.

The nature of bonds formed by the metal are similar in Cr and Mo compounds. The analysis of bonding performed here is based on the Mulliken population analysis. The two highest molecular orbitals (Figs. 2 and 3) describe the Me–NO bonds. These bonds are covalent, and may be described as two three-centered N–Me–N σ and π bonds. The central metal atom donates 0.5 of an electron to the acetate rings, although the total loss of electrons in d orbitals amounts to 1.2 electrons. Due to the rearrangement of the electronic density of metal, its s orbitals gain 0.4 of an electron, while 0.3 of an electron is shifted to the metal p orbitals. The involvement of p orbitals in the formation of bonds indicates the deviation from the d^5s hybridization and in effect the distortion of the perfect D_{2h} symmetry. The electronic structure of the center of coordination is similar in both the *cis* and *trans* isomers, and is visible as an almost equal occupation of the orbitals on the central atom.

5. Conclusions

The number of d electrons in the $\{M(NO)_2\}^n$ fragment determines its structural properties. The six-coordinated dinitrosyl complexes of Group 6 metals should have the *cis* form. However, *trans* isomers containing Cr or Mo are also known (Tables 3 and 4) and some of them were synthesized in this work. X-ray structures are not known for *trans*-dinitrosyl complexes of Group 6. Based on the previous IR studies [32,50,51], D_{2h} symmetry was expected for *trans* structures with a linear ON–M–NO fragment.

Theoretical studies determined two isomers (Fig. 1): *cis* (C_2 symmetry) and *trans* (C_{2v} symmetry), with the *cis* forms being energetically more stable (Tables 1 and 2). The *trans* NO groups are divided by a plane defined by the acetate rings. The latter structures are significantly distorted from ideal geometries. The expected D_{2h} symmetry of *trans* complexes, due to the nonlinearity of the ON–M–NO fragment, is lowered to C_{2v}. This distortion is observed as an additional symmetric NO vibration. The weak band corresponding to ν_s(NO) may be easily hidden in the strong one associated with the ν_{as}(NO) vibrational motion. In the case of compounds **1** and **2**, the single bands at about 1700 cm^{-1} is related to ν_{as}(NO), but weak shoulders at 1778 and 1777 cm^{-1} may correspond to the symmetrical NO vibrations. The reasonable reproduction of the properties of the *cis* isomers gives confidence for the overall theoretical studies presented. The calculated intensities of observed bands are comparable in the *cis* case, while the second (symmetrical) vibration in the *trans* molecule is barely seen. The calculations led to the distortion of ON–M–NO structures in every isomer studied. The study of structures of other complexes would help to answer if this is a property of Cr and Mo complexes only or if this is a more general feature of nitrosyl complexes. The M–N–O branches were also distorted from linearity in every structure studied. The geometry optimization also indicated a significant deformation of the acetate rings. Different lengths of M–O bonds within the same rings were observed.

The electronic density rearrangement on the central atom is almost the same in both *cis* and *trans* isomers. The change in the electronic density is due to the transfer of electrons from d orbitals to the acetate rings (0.5 electron) and s and p orbitals (0.7 electron).

The reported results, including the charge distribution picture on the central and ligand atoms confirm the suggested mechanism of the formation of carbene and vinylidene catalysts in *cis*-$M(NO)_2(O_2CR)_2$–Lewis acid and $\{M(NO)_2(OR)_2\}_n$–Lewis acid systems [31–33,47,48,54,66]. The favorable conditions for the electrophilic attack of Lewis acid molecules on the carboxylate ligand oxygen atoms are in the equatorial plane (M1O3O14N9N11 plane in Fig. 1). In the same plane, on the side opposite to the NO groups, carbene and vinylidene ligands will coordinate.

Acknowledgements

We thank the State Committee for Scientific Research (grant no 3T09A 059 17) and Wrocław University of Technology (grant no 341-831) for supporting

this work. We would like to thank Poznań and Wrocław Supercomputing and Networking Centers and Interdisciplinary Center for Mathematical and Computational Modeling of Warsaw University for the generous allotment of computer time.

References

[1] W.P. Griffith, Adv. Organomet. Chem. 7 (1968) 211.
[2] J.H. Enemark, R.D. Feldham, Coord. Chem. Rev. 13 (1974) 339.
[3] K.G. Caulton, Coord. Chem. Rev. 14 (1975) 327.
[4] F. Bottomley, Coord. Chem. Rev. 26 (1978) 7.
[5] J.A. McCleverty, Chem. Rev. 79 (1979) 53.
[6] R.D. Feltham, J.H. Enemark, in: G.L. Geoffroy (Ed.), Topics in Inorganic and Organometallic Stereochemistry, Wiley, New York, 1981 (Chapter 4).
[7] L.W. Gladfelter, Adv. Organomet. Chem. 24 (1985) 41.
[8] G.B. Richter-Addo, P. Legzdins, Chem. Rev. 88 (1988) 991.
[9] B.L. Wescott, J.H. Enemark, Inorg. Elect. Struct. 2 (1999) 403.
[10] S. Moncada, S.A. Marletta, J.B. Hibbis, M. Feelisch, in: R. Busse (Ed.), The Biology of Nitric Oxide, vols. 1–4, Portland Press, Colchester, 1992, p. 1994.
[11] S.S. Stamler, D.J. Singel, J. Loscaizo, Science 258 (1992) 1898.
[12] G.B. Richter-Addo, P. Legzdins, Metal Nitrosyls, Oxford University Press, Oxford, 1992.
[13] A.R. Butler, D. Lyn, H. Williams, Chem. Soc. Rev. 22 (1993) 233.
[14] R.J.P. Williams, Chem. Soc. Rev. 25 (1996) 77.
[15] G. Stochel, E. Ilkowska, M. Pawelec, A. Wanat, M. Wolak, ACH-Models Chem. 135 (1998) 847.
[16] K.K. Pandey, Coord. Chem. Rev. 51 (1983) 69.
[17] K.A. Hofmann, Z. Anorg. All. Chem. 12 (1896) 146.
[18] J. Smidt, R. Jira, Chem. Ber. 3 (1960) 162.
[19] B.S. Tovorg, S.E. Diamond, F. Mares, A. Szalkiewicz, J. Am. Chem. Soc. 103 (1981) 3522.
[20] R.D. Tiwari, K.K. Pandey, U.C. Agarwala, Inorg. Chem. 21 (1982) 845.
[21] B.W. Graham, K.R. Laing, C.J. O'Connor, W.R. Roper, J. Chem. Soc., Dalton Trans. (1972) 1237.
[22] J. Fleischer, D. Schnurpfeil, K. Seyfert, R. Taube, J. Prakt. Chem. 319 (1977) 995.
[23] A. Keller, J.M. Sobczak, R. Matusiak, J. Mol. Catal. 136 (1998) 115.
[24] C.W. Bird, Transition Metal Intermediates in Organic Synthesis, Academic Press, New York, 1967, p. 248.
[25] R.A. Sanchez-Deigado, A. Andriollo, O.L. Deochoa, T. Suarez, N. Valencia, J. Organomet. Chem. 209 (1981) 77.
[26] W. Strohmeier, K. Holke, J. Organomet. Chem. 193 (1980) C63.
[27] J.P. Candlin, W.H. Janes, J. Chem. Soc. C (1968) 1856.
[28] D. Ballivet-Tkatchenko, C. Billard, A. Revillon, J. Polym. Sci. 19 (1981) 1697.
[29] I. Tkatchenko, J. Organomet. Chem. 124 (1977) C39.
[30] A. Sen, R.R. Thomas, Organometallics 1 (1982) 1251.
[31] A. Keller, R. Matusiak, J. Mol. Catal. 142 (1999) 317.
[32] A. Keller, R. Matusiak, J. Mol. Catal. 145 (1999) 127.
[33] R. Matusiak, A. Keller, Polym. Bull. 43 (1999) 199.
[34] E.A. Zuech, W.B. Hughes, D.H. Kubicek, E.T. Kittleman, J. Am. Chem. Soc. 93 (1970) 528.
[35] S.T. Wilson, J.A. Osborn, J. Am. Chem. Soc. 93 (1971) 3068.
[36] C.G. Pierpont, R. Eisenberg, Inorg. Chem. 11 (1972) 1094.
[37] G. Dolcetti, Inorg. Nucl. Chem. Lett. 9 (1973) 705.
[38] A. Keller, J. Mol. Catal. 70 (1991) 143.
[39] R.J. Haines, Chem Soc. Rev. 4 (1975) 155.
[40] K.J. Ivin, Olefin Metathesis, Academic Press, London, 1983.
[41] R. Taube, K. Seyferth, Rev. Inorg. Chem. 8 (1986) 31.
[42] A. Keller, L. Szterenberg, J. Mol. Catal. 57 (1989) 207.
[43] A. Keller, J.M. Sobczak, J.J. Ziólkowski, in: E.R. Braithwaite, J. Haber (Eds.), Studies in Inorganic Chemistry, vol. 19, Elsevier Science, Amsterdam, 1994, p. 618 (Chapter 11).
[44] M. Leconte, Y. Ben Taarit, J.L. Bilhon, J.M. Basset, J. Mol. Catal. 8 (1980) 263.
[45] A. Keller, J. Mol. Catal. 78 (1993) L15.
[46] A. Keller, R. Matusiak, J. Mol. Catal. 104 (1996) 213.
[47] A. Keller, J. Organomet. Chem. 407 (1991) 237.
[48] A. Keller, J. Organomet. Chem. 436 (1992) 199.
[49] R.G. Parr, W. Wang, Density Functional Theory of Atoms and Molecules, Oxford University Press, Oxford, 1989.
[50] A.D. Becke, J. Chem. Phys. 104 (1996) 1040.
[51] C. Lee, W. Yang, R.G. Parr, Phys. Rev. 37 (1988) 785.
[52] S.H. Vosko, L. Wilk, M. Nusair, Can. J. Phys. 58 (1980) 1200.
[53] P.J. Hay, W.R. Wadt, J. Chem. Phys. 82 (1985) 270.
[54] T.H. Dunning, Jr., P.J. Hay, in: H.F. Schaefer III (Ed.), Modern Theoretical Chemistry, vol. 3, Plenum, New York, 1976, p. 1.
[55] S. Huzinaga (Ed.), GAUSSIAN Basis Sets for Molecular Calculations, Elsevier, Amsterdam, 1984.
[56] M.J. Frisch, G.W. Trucks, H.B. Schlegel, P.M.W. Gill, B.G. Johnson, M.A. Robb, J. Cheeseman, T. Keith, G.A. Petersson, J.A. Montgomery, K. Raghavachari, M.A. Al.-Laham, V.G. Zakrzewski, J.V. Oritz, J.B. Foresman, J. Cioslowski, B.B. Stefanov, A. Nanayakkara, M. Challacombe, C.Y. Peng, P.Y. Ayala, W. Chen, M.W. Wong, J.L. Andres, E.S. Replogle, R. Gomperts, R.L. Martin, D.J. Fox, J.S. Binkley, D.J. Defrees, J.J. Baker, J.P. Srewart, M. Head-Gordon, C. Gonzales, J.A. Pople, GAUSSIAN-94, Gaussian, Pittsburgh, PA, 1995.
[57] T. Diebold, M. Schappacher, B. Chevrier, R. Weiss, J. Chem. Soc., Chem. Commun. (1979) 693.
[58] N.G. Connolly, L.F. Dahl, Chem. Commun. (1970) 880.
[59] M.R. Mauyra, S. Gopinathan, C. Gopinathan, Polyhedron 12 (1993) 159.
[60] (a) N.N Greenwood (Senior Reporter), Spectroscopic Properties of Inorganic and Organometallic Compounds, A Special Periodical Report, vol. 1, The Chemical Society, London, 1968, p. 199. (b) N.N Greenwood (Senior Reporter), Spectroscopic Properties of Inorganic and Organometallic Compounds, A Special Periodical Report, vol. 2, The Chemical Society, London, 1969, p. 333.
[61] G.B. Deacon, R.J. Phillips, Coord. Chem. Rev. 33 (1980) 227.
[62] A. Keller, L. Szterenberg, Z. Naturforsch., Teil. B 47 (1992) 1469.
[63] D.C. Bradley, Proc. Symp. Coord. Chem. (1965) 1964.
[64] G. Johansson, W.N. Lipscomb, Acta Crystallogr. 11 (1958) 594.
[65] S.F.A. Kettle, Inorg. Chem. 4 (1965) 1661.
[66] A. Keller, Inorg. Chim. Acta 149 (1988) 165.

PERGAMON

www.elsevier.nl/locate/poly

Polyhedron 19 (2000) 2573–2577

POLYHEDRON

Study of copper(II) chloro- and dichloropropionates, crystal and molecular structure of *trans*-bis(methyl-3-pyridylcarbamate)bis(α,α-dichloropropionato)copper(II)

Ján Moncoĺ [a,*], Marian Koman [a], Milan Melník [a], Marta Černáková [b], Tadeusz Glowiak [c]

[a] *Department of Inorganic Chemistry, Slovak Technical University, SK-81237 Bratislava, Slovak Republic*
[b] *Department of Environmental Sciences, Slovak Technical University, SK-81237 Bratislava, Slovak Republic*
[c] *Institute of Chemistry, University of Wroclaw, PL-50383 Wroclaw, Poland*

Received 4 February 2000; accepted 18 August 2000

Abstract

The synthesis and characterization of the complexes CuX_2L_2 {where $X = CH_3CHClCOO^-$, $CH_3CCl_2COO^-$ or $ClCH_2CHClCOO^-$, and L = nicotinamide (na), isonicotinamide (ina) or methyl-3-pyridylcarbamate (mpc)} are reported. Characterization of the compounds was based on elemental analysis, IR, electronic and EPR spectra. All the CuX_2L_2 compounds seem to possess octahedral copper(II) stereochemistry with differing tetragonal distortion. Complex $[Cu(CH_3CCl_2COO)_2(mpc)_2]$ was also studied by X-ray analysis. The structure of $[Cu(CH_3CCl_2COO)_2(mpc)_2]$ is centrosymmetric. The Cu(II) atom is *pseudo*-octahedrally *trans*-coordinated by four carboxylic oxygen atoms of α,α-dichloropropionate anions [Cu(1)–O(1) = 1.959(2) Å (2 ×) and Cu(1)–O(2) = 2.677(2) Å (2 ×)], and by two nitrogen atoms two methyl-3-pyridylcarbamate ligands [Cu(1)–N(1) = 1.981(2) Å (2 ×)]. The antibacterial effects have been tested on various strains of bacteria, yeasts and micromycetes. © 2000 Elsevier Science B.V. All rights reserved.

Keywords: Copper(II); Chloropropionate; Crystal structure; EPR; Bio-activity

1. Introduction

Some derivatives of propionic acid, as for example, 2-(2-fluorophenyl)propionic acid and 2-(4-isobutylphenyl)propionic acid are used as an antirheumatic drugs. These acids, like other antirheumatic drugs, inhibit the biosynthesis of prostaglandins, but they differ from most of them having an additional inhibitory effect on prostaglandin receptors [1].

The interaction of copper(II) atom, which plays a vital role in a number of quite different biological processes, with therapeutically administered drugs is a subject of considerable interest [2].

On the basis of spectral and magnetic properties of some copper(II) chloropropionate with nicotinamide, a *pseudo*-octahedral environment around the copper(II) atom was proposed [3]. The aim of this study is to investigate the complexation of copper(II) chloro- and dichloropropionate complexes with nicotinamide (na), isonicotinamide (ina) and methyl-3-pyridylcarbamate (mpc). The compounds of the composition CuX_2L_2 ($X = CH_3CHClCOO^-$, $CH_3CCl_2COO^-$ or $ClCH_2CHClCOO^-$ and L = na, ina or mpc) were prepared and studied by spectral methods, as well as their bio-activities.

The complex $[Cu(CH_3CCl_2COO)_2(mpc)_2]$ was also studied by X-ray analysis. These structure data are discussed and compared with other copper(II) compounds.

* Corresponding author. Tel.: +42-7-5249-3198; fax: 42-7-5249-5180.
E-mail address: moncol@chtf.stuba.sk (J. Moncoĺ).

0277-5387/00/$ - see front matter © 2000 Elsevier Science B.V. All rights reserved.
PII: S0277-5387(00)00559-3

Bio-activity of the complexes was tested on *Micrococcus luteus*, *Bacillus subtilis*, *Escherichia coli*, *Pseudomonas aeruginosa*, *Saccharomyces cerevisiae*, *Candida albicans* and *Aspergillus niger*.

2. Experimental

2.1. Preparation of compounds

A solution of the sodium salt of α-chloropropionic, α,α-dichloropropionic or α,β-dichloropropionic acid was prepared and pH adjusted to 4.5–5 and an aqueous solution of copper(II) sulfate in the molar ratio 1:2 was added. These were left to stand at room temperature (r.t.), and the green products of the composition $CuX_2 \cdot nH_2O$ ($n = 1$, 0, 1, respectively) were isolated.

The copper(II) compounds of composition CuX_2L_2 ($X = CH_3CHClCOO^-$, $CH_3CCl_2COO^-$ or $ClCH_2$-$CHClCOO^-$ and L = nicotinamide (na); isonicotinamide (ina) or methyl-3-pyridylcarbamate (mpc)) were prepared by reaction between CuX_2 and L in hot methanol solution (1.75×10^{-2} mol of CuX_2 and a small amount of the corresponding free acid were dissolved in 50 ml of methanol). To this blue–green solution was added 3.5×10^{-2} mol of L in 50 ml of methanol. The resultant blue solution was concentrated to approximately 50 ml and cooled to r.t. The blue or violet microcrystalline precipitate was filtered, washed with cold methanol and dried at r.t. Crude products were recrystallized from methanol ($CuX_2(na)_2$ and $CuX_2(ina)_2$) or acetone ($CuX_2(mpc)_2$) solution. Fine crystals were isolated and washed with cold methanol. Elemental analyses of isolated copper(II) compounds are given in Table 1.

2.2. Spectroscopic studies

Electronic spectra in the region from 10 000 to 28 000 cm^{-1} were measured with a Perkin–Elmer 450 spectrophotometer using a Nujol suspension. EPR spectra of microcrystalline samples were run on a Varian model E4 spectrometer at r.t. Infrared spectra of the compounds were recorded in the range 400–3600 cm^{-1} using the Magma-750 FTIR.

2.3. Structure determination

Data collection and cell refinement were carried out using SYNTEX $P2_1$ diffractometer software [4]. Intensity data were corrected for Lorenz and polarization factors. The structure was solved by the heavy atom method with SHELXS-86 [5], and subsequent Fourier synthesis using SHELXL-93 [6], anisotropic thermal parameters were refined for all non-hydrogen atoms. Geometrical analysis was performed using SHELXL-93 [6]. The structure was drawn using ORTEP-III [7]. The final parameters after refinement are summarized in Table 3. Selected inter-atomic distances and bond angles are given in Table 4.

2.4. Bio-test

The antimicrobial activity of the newly prepared copper(II) complexes was evaluated by a dilution method in test tubes [8] using G^+ bacterial strains *Micrococcus luteus* CCM 1569, *Bacillus subtilis* CCM 2216 and G^- bacterial strains *Escherichia coli* CCM 5172, *Pseudomonas aeruginosa* CCM 1960. The effect of these compounds on the yeasts *Saccharomyces cerevisiae* CCY 22-3-1 and *Candida albicans* CCY 29-3-15. Cultivation of bacteria was on nutrient broth medium and yeasts on malt extract. The cultures of bacteria and

Table 1
Elemental analyses for the compounds [a]

Compound	Cu%		C%		H%		N%	
	Calc.	Found	Calc.	Found	Calc.	Found	Calc.	Found
1	12.15	11.98	41.35	40.96	3.80	3.95	10.72	10.80
2	10.74	11.0	36.54	36.65	3.07	3.12	9.47	9.55
3	10.74	10.53	36.54	37.03	3.07	2.83	9.47	9.52
4	12.17	12.20	41.78	41.87	3.12	3.65	10.83	10.81
5	12.17	12.36	41.78	41.29	3.12	3.77	10.83	10.78
6	10.74	10.42	36.54	36.06	3.07	3.33	9.47	9.20
7	10.74	10.83	36.54	36.54	3.07	3.17	9.47	9.77
8	10.57	10.28	39.97	40.06	4.36	4.24	9.32	9.63
9	9.75	9.80	36.85	37.50	3.29	3.40	8.59	8.85
10	9.75	9.66	36.85	36.38	3.29	3.44	8.59	8.56

[a] Compounds are: (**1**) $Cu(CH_3CHClCOO)_2(na)_2 \cdot 2H_2O$; (**2**) $Cu(CH_3CCl_2COO)_2(na)_2$; (**3**) $Cu(ClCH_2CHClCOO)_2(na)_2$; (**4**) α-$Cu(CH_3CHClCOO)_2(ina)_2$; (**5**) β-$Cu(CH_3CHClCOO)_2(ina)_2$; (**6**) $Cu(CH_3CCl_2COO)_2(ina)_2$; (**7**) $Cu(ClCH_2CHClCOO)_2(ina)_2$; (**8**) $Cu(CH_3CHClCOO)_2(mpc)_2 \cdot H_2O$; (**9**) $Cu(CH_3CCl_2COO)_2(mpc)_2$; (**10**) $Cu(ClCH_2CHClCOO)_2(mpc)_2$.

Table 2
IR, ES and EPR data for CuX_2L_2

	IR (cm^{-1})			Electronic spectra (cm^{-1})	EPR					Ref.
	ν_{as}(COO)	ν_s(COO)	ν(C=N)		g_1	$g_\perp$	g_2	g_3 $g_\parallel$	g_{av}	
1				15 015		2.06		2.27	2.13	[3]
2				16 129					2.07	[3]
3	1580	1428	1615	15 500		2.0533		2.222	2.11	[this work]
4	1600	1426	1616	14 900	2.025		2.063	2.248	2.112	[this work]
5	1617	1423	1629	14 166	2.037		2.083	2.302	2.141	[this work]
6	1605	1424	1620	14 800		2.049		2.206	2.101	[this work]
7	1605	1422	1613	15 700		2.0132		~2.207	2.078	[this work]
8	1586	1410	1605	14 400		2.056		2.279	2.130	[this work]
9	1575	1418	1607	14 900, sh 18 100					2.054	[this work]
10	1588	1420	1611	14 900		2.056		2.256	2.123	[this work]

yeasts were incubated on medium during static culturing for 2 days at 28°C. The time course of absorbance (A_{600}) was determined in three experiments. The filamentous fungi *Aspergillus niger* F-384 was tested by a macrodilution technique on solidified broth medium during static culturing for 4 days at 28°C [9].

Chromatographically pure compounds were dissolved in dimethylsulfoxide. The concentration of complexes under study ranged from 10^{-5} to 4 mmol l^{-1}.

The antimicrobial activity was characterized by the IC_{50} values (concentration of a derivative which inhibits microbial growth by 100%). The IC_{50} and MIC values were read from toxicity curves.

3. Results and discussion

The IR spectra of the studying compounds show the carboxylate stretching frequencies $\nu_{as}(COO^-)$ at ~ 1600 cm^{-1} and $\nu_s(COO^-)$ at 1420 cm^{-1} (Table 2). The stretching vibration of the C=N bond in the pyridine ring (nicotinamide, isonicotinamide or methyl-3-pyridylcarbamate) appears at 1590 cm^{-1}, and on complexation a shift to higher frequencies is observed [10]. In the compounds this shift to about 1615 cm^{-1} (Table 2) may suggest bond formation by the copper(II) atom to the pyridine ring nitrogen, thereby increasing the dipolar contribution of C=N in the heterocyclic ring.

The electronic spectra of the compounds show intraligand transition bands (Table 2). These types of d–d spectrum are typical for a tetragonal arrangement around Cu(II) atom. The electronic spectrum of α-$[Cu(CH_3CHClCOO)_2(ina)_2]$ exhibits the band at about 14 900 cm^{-1}, while β-$[Cu(CH_3CHClCOO)_2(ina)_2]$ at 14 166 cm^{-1}. The higher value of the band of the α-isomer indicates a somewhat greater tetragonal distortion about the Cu(II) atom for the α- than the β-isomer.

As can be seen in Table 2, the intraligand transition bands range from 14 166 cm^{-1} for β-$[Cu(CH_3CHClCOO)_2(ina)_2]$ to 16 129 cm^{-1} for $[Cu(CH_3CCl_2COO)_2(mpc)_2]$. The 'blue-shift' of d–d band indicates that tetragonal distortion increases in the given order.

EPR spectra of the powdered isomers (α- and β-$[Cu(CH_3CHClCOO)_2(ina)_2]$) are *pseudo*-rhombic. While the EPR spectra of $[Cu(CH_3CCl_2COO)_2(na)_2]$ [1] and $[Cu(CH_3CCl_2COO)_2(mpc)_2]$ are isotropic. In all remain-

Table 3
Crystal data and structure refinement for $Cu(CH_3CCl_2COO)_2(mpc)_2$

Empirical formula	$C_{20}H_{22}Cl_4CuN_4O_8$
Formula weight	651.76
Temperature (K)	293(2)
Wavelength (Å)	0.71073
Crystal system	monoclinic
Space group	$P2_1/c$
Unit cell dimensions	
a (Å)	12.853(3)
b (Å)	6.246(1)
c (Å)	17.237(3)
β (°)	109.73(3)
Volume (Å^3)	1302.5(4)
Z	2
D_{calc} (Mg m^{-3})	1.662
Absorption coefficient (mm^{-1})	1.301
F(000)	662
Crystal size (mm)	$0.5 \times 0.2 \times 0.05$
θ Range for data collection (°)	1.68–27.58
Index ranges	$0 \le h \le 15$, $-8 \le k \le 8$, $-22 \le l \le 21$
Reflections collected/unique	5905
Refinement method	Full-matrix least-squares on F^2
Data/restraints/parameters	2889/0/172
Goodness-of-fit on F^2	0.807
Final R indices [$I > 2\sigma(I)$]	$R = 0.0447$, $wR_2 = 0.0759$
R indices (all data)	$R = 0.1191$, $wR_2 = 0.1070$
Largest difference peak and hole (e Å^{-3})	0.425 and −0.226

Table 4
Selective bond lengths (Å) and angles (°) for $[Cu(CH_3CCl_2COO)_2(mpc)_2]$ (**I**) and $[Cu(CH_3CH_2COO)_2(mpc)_2]\cdot 0.25H_2O$ (**II**)

	I	II
Cu(1)–O(1)	1.959(2)	1.955(2)
Cu(1)–N(1)	1.981(3)	1.955(2)
Cu(1)–O(2)	2.677(2)	2.653(2)
O(1)–C(1)	1.251(4)	1.268(4)
O(2)–C(1)	1.223(4)	1.227(4)
C(1)–C(2)	1.540(4)	1.503(5)
N(1)–C(4)	1.331(4)	1.330(3)
N(1)–C(8)	1.354(4)	1.342(3)
O(1)–Cu(1)–N(1)	89.1(2)	89.39(8)
O(1)–Cu(1)–O(2)	54.0(8)	54.23(8)
C(1)–O(1)–Cu(1)	106.4(2)	107.2(2)
C(4)–N(1)–Cu(1)	120.9(2)	121.0(2)
C(8)–N(1)–Cu(1)	120.6(2)	119.4(2)
O(1)–C(1)–C(2)	115.3(3)	116.1(3)
O(2)–C(1)–C(2)	119.2(3)	121.2(3)
C(4)–N(1)–C(8)	118.5(3)	119.3(2)
Ref.	[this work]	[11]

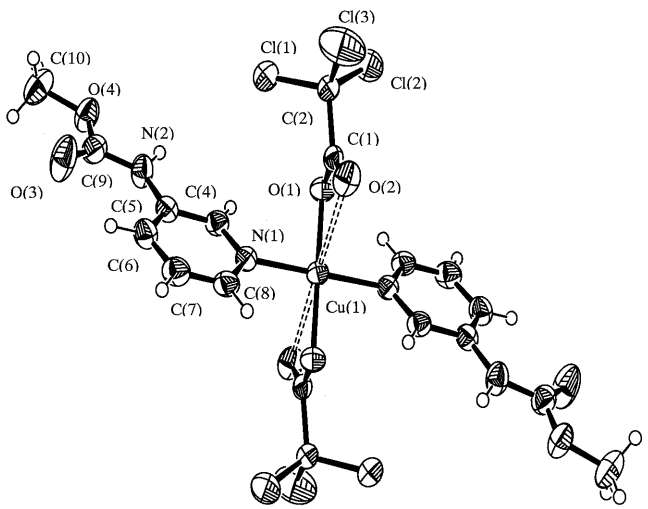


Fig. 1. Perspective of complex $[Cu(CH_3CCl_2COO)_2(mpc)_2]$ (**9**), with the atom numbering scheme. Thermal ellipsoids are drawn at the 50% probability level.

ing samples, the spectra are of axial type. The g-values are given in Table 2.

The structure of $[Cu(CH_3CCl_2COO)_2(mpc)_2]$ is shown in Fig. 1. As one can see, the stereochemistry around the Cu(II) centre may be described as an axially elongated octahedral. Molecules of the complex lie on a crystallographic inversion centre, with the Cu(II) atom coordinated by the pyridyl N atoms of two different methyl-3-pyridylcarbamate molecules and by an O atom from each of the two α,α-dichloropropionate anions to give a *trans*-square-planar arrangement, with Cu–N(1) and Cu–O(1) bond distances of 1.981(2) and 1.959(2) Å, respectively. The remaining carboxylate O atoms in each α,α-dichloropropionates participates in much longer axial bonding, Cu–O(2) 2.677(2) Å, to complete an axially elongated octahedral environment about Cu(II). The C(1)–O(1) and C(1)–O(2) distances [1.251(4) and 1.223(4) Å, respectively] are significantly different.

The α,α-dichloropropionate chelate angle O(1)–Cu–O(2) is very acute at 54.0(1)°. The two chlorine atoms and the methyl carbon atom of the group $-CCl_2CH_3$ are disordered occupying three statistical positions, presented by Cl(1), Cl(2) and Cl(3) with the site occupancy factors of 0.741(5), 0.618(5) and 0.641(6), respectively.

In Table 4 are given selective bond distances (Å) and bond angles (°) for the familiar structures of $[Cu(CH_3CCl_2COO)_2(mpc)_2]$ and $[Cu(CH_3CH_2COO)_2(mpc)_2]\cdot 0.25H_2O$ [11]. As can be seen, the Cu–N as well as Cu–O bond distances are somewhat longer in the former than in the latter. There are at least two reasons, the first α,α-dichloropropionate is much bulky than propionate and the second there is somewhat 'lower' electronic densities on O atoms in the former than in the latter.

On the basis of spectral data, for all remaining copper compounds, can be proposed a tetragonal bipyramidal coordination about copper(II) atoms with a different degree of distortion.

The results of preliminary screening are presented in Table 5; this shows the tested compounds differ in their bio-activities againts bacteria, yeasts and micromycetes:

1. Bio-activities of the compounds increase in the sequence > micromycetes < yeasts < bacteria.
2. The compounds are more active against G^- that G^+ bacteria. From the G^- bacteria, *P. aeruginosa* is more resistance than the other one. The reason for the resistance is that *P. aeruginosa* contains the most effective enzymes. These enzymes are available to destroy PCP, PCB, pesticides and some other pollutants.
3. The complex $[Cu(CH_3CCl_2COO)_2(na)_2]$, which is most active against *A. niger* at 1 mmol l^{-1}, was growing instead of a black colony a white one. *A niger* lost the spores and therefore lost its reproductive ability. When the white colony was added on cultivation medium without the compound, the colony became black again.
4. Nicotinamid as a neutral ligand is a part of the pyridine nucleotides as NAD^+ and $NADP^+$, which takes a part in redox reactions. These are most important for transfer of hydrogen in the cell breath (biological oxidation).

4. Supplementary material

Crystallographic data (atomic coordinates, anisotropic displacement parameters for non-hydrogen atoms and all bond lengths and angles) for the structure

Table 5
Bio-activities against bacteria, yeasts and micromycetes of copper(II) chloro and dichloropropionates (IC_{50} and MIC (mmol l^{-1}))

Compounds	Bacteria								Yeasts				Filamentous fungi	
	E. coli		*P. aeruginosa*		*M. luteus*		*B. subtilis*		*S. cerevisiae*		*C. albicans*		*A. niger*	
	IC_{50}	MIC	IC_{50}	MIC	IC_{50}	MIC	IC_{50}	MIC	IC_{50}	MIC	IC_{50}	MIC	IC_{50}	MIC
1	0.09	2.4	0.67	2.4	0.43	3.0	0.52	3.07	0.34	2	0.31	3.8	0.05	2
2	0.17	2.4	0.41	2.4	0.41	2.7	0.09	2.72	0.43	2	0.31	2	0.25	2
3	0.13	2.4	0.25	2.4	0.35	2.6	0.29	2.72	0.45	2	0.31	2	0.15	2
4	0.08	2.2	0.05	2.75	0.02	3.0	0.34	2.9	0.32	2	0.39	2	[a]	[a]
6	0.10	2.4	0.09	3.2	0.34	2.32	0.32	2.4	1.2	3.9	1.0	3.9	0.19	2
7	0.37	3.25	0.83	3.25	0.18	3.15	0.08	2.77	0.34	2	0.21	2	0.42	3.9
8	0.07	2.3	0.37	2.3	0.09	2.4	0.09	2.4	0.46	2.7	0.61	3.9	0.19	3.9
9	0.09	2.6	0.26	2.75	0.09	3.95	0.41	2.15	1.1	3.2	0.25	2	0.19	2
10	0.07	2.6	0.15	2.95	0.04	2.7	0.39	2.4	0.35	2.2	0.27	3.7	0.32	2

[a] Not tested.

reported in this paper have been deposited with the Cambridge Crystallographic Data Centre, CCDC No. 139867 for $[Cu(CH_3CCl_2COO)_2(mpc)_2]$. Copies of this information may be obtained free of charge from the Director, CCDC, 12 Union Road, Cambridge, CB2 1EZ, UK (fax: +44-1223-336033; e-mail: deposit@ccdc.cam.ac.uk or http://www.ccdc.cam.ac.uk).

References

[1] R.J. Flower, Pharm. Rev. 22 (1974) 33.
[2] M. Melník, I. Potočňák, Ł. Macášková, D. Mikloš, C.E. Holloway, Polyhedron 13 (1996) 2159.
[3] (a) M. Melník, J. Mroziński, C.E. Holloway, J. Coord. Chem. 29 (1993) 209. (b) M. Melník, C.E. Holloway, D. Mrozińska, J. Mroziński, Bull. Pol. Acad. Sci. Chem. 40 (1992) 169.
[4] F. Pavelčík, Program $XP2_1$, Comenius University Pharmaceutical Faculty, Bratislava, Slovakia, 1993.
[5] G.M. Sheldrick, SHELXS-86, in: G.M. Sheldrick, C. Krueger, R. Goddard (Eds.), Crystallographic Computing 3, Oxford University Press, Oxford, 1985, p. 175.
[6] G.M. Sheldrick, SHELXL-93, Program for Refinement of Crystal Structure, University of Göttingen, Germany, 1994.
[7] (a) M.N. Burnett, C.K. Johnson, ORTEP-III (Oak Ridge Thermal Ellipsoids Plot Program for Crystal Structure Illustrations), Report ORNL-6895, Oak Ridge National Laboratory, Tennessee, 1996. (b) L.J. Farrugia, J. Appl. Crystallogr. 30 (1997) 565.
[8] S. Jantová, D. Hudecová, S. Stankovský, K. Špirková, Ł. Ruzetová, Folia Microbiologica (1995) 611.
[9] D. Hudecová, S. Jantová, M. Melník, M. Uher, Folia Microbiologica (1996) 473.
[10] Y. Morimoto, A.E. Martell, J. Am. Chem. Soc. 83 (1961) 4528.
[11] M. Koman, M. Melník, T. Glowiak, Acta Crystallogr., Sect C. 54 (1998) 1604.

PERGAMON

www.elsevier.nl/locate/poly

Polyhedron 19 (2000) 2579–2584

POLYHEDRON

Binaphtholato complexes of tungsten(VI) from tris(1,2-ethanediolato)tungsten(VI). Synthesis and X-ray structures of [W(bino)(diolato)$_2$] complexes

Ari Lehtonen *, Reijo Sillanpää

Department of Chemistry, University of Turku, FIN-20014 Turku, Finland

Received 23 June 2000; accepted 18 August 2000

Abstract

Racemic 6,6′-disubstituted-1,1′-bi-2-naphthols H_2X_2bino (X = H, Br) and corresponding binaphthyl acetates react with trisdiolatetungsten(VI) complexes [W(eg)$_3$] and [W(eg)(pin)$_2$] (eg = ethanediolate dianion, pin = pinacolate dianion) forming heteroleptic complexes [W(X_2bino)(diolato)$_2$]. The X-ray crystal structure determinations confirmed that the isolated compounds are made of monomeric tris(diolate)tungsten(VI) molecules in which the central tungsten atom is bonded to six oxygen atoms forming a distorted octahedral coordination sphere around the metal ion. © 2000 Elsevier Science B.V. All rights reserved.

Keywords: Binaphtholato complexes; Tungsten(VI); X-ray structures

1. Introduction

Chelating oxygen donor ligands, e.g. 1,1′-bi-2-naphthols have confirmed to be useful chiral accessories in enantiospecific organic syntheses with early transition metals [1,2]. The hard Lewis-base character of the phenoxide group makes these compounds ideal for attaching to the metal ions having high oxidation states. Therefore, binaphtholates of Ti(IV), Zr(IV), W(VI) and Mo(VI), often with other ligands, have been used successfully to catalyse organic reactions [3]. For example, tungsten(VI) chlorocomplexes with substituted binaphtholato ligands are known to be suitable catalyst precursors for ring-opening metathesis polymerisation of norbornene [4]. They can be prepared by a direct alcoholysis reaction between WCl_6 and corresponding binaphthol, when the composition of these compounds is depending on the substituents in 3 and 3′ positions of used binaphthol molecules. 3,3′-Ph_2-1,1′-bi-2-naphthol ($H_2$33′Phbino) reacts with WCl_6 forming a monosubstituted [W(33'Phbino)Cl_4], while sterically less hindered 3,3′-Me_2-1,1′-bi-2-naphthol ($H_2$33′Mebino) forms a complex *cis*-[W(33'Mebino)$_2Cl_2$]. Racemic H_2bino with no substituents in *ortho* positions reacts with WCl_6 producing a mixture of different isomers of trisdiolato complex [W(bino)$_3$].

The reactions of metal alkoxides with phenols or phenyl acetates are easy approaches to the metal phenoxides, as presented by the following equations:

$$M(OR)_n + xArOH \leftrightarrow M(OR)_{n-x}(OAr)_x + xROH \quad (1)$$

$$M(OR)_n + xR'C(O)OAr \leftrightarrow M(OR)_{n-x}(OAr)_x + xR'C(O)OR \quad (2)$$

These reactions, alcohol-exchange and transesterification, has confirmed to be useful in the preparation of metal phenoxides [5]. They are very efficient methods, especially if suitable metal alkoxides can be easily prepared from metal oxides, because they make it possible to avoid the use of air and moisture sensitive metal chlorides.

As a part of our ongoing project related to the tungsten catalysed olefin metathesis reactions, we are interested in the use of diolate complexes of W(VI) as air-stable starting materials for catalytically active systems [6]. We have earlier studied preparation of W(VI) phenoxides by the reaction of [W(eg)$_3$] (**1**) (eg = ethyleneglycolate, 1,2-ethanediolate dianion) with

* Corresponding author. Tel.: +358-2-333-6733; fax: +358-2-333-6700.

E-mail address: ari.lehtonen@utu.fi (A. Lehtonen).

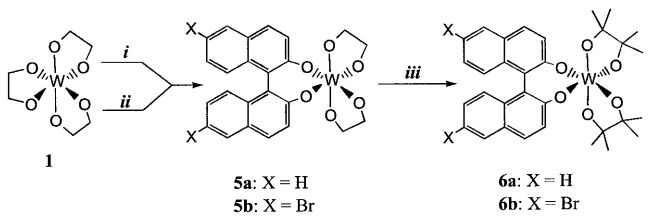
0277-5387/00/$ - see front matter © 2000 Elsevier Science B.V. All rights reserved.
PII: S0277-5387(00)00560-X

phenyl acetates [7]. In the present study, we have employed the above-mentioned ligand-exchange reactions to prepare new binaphtholate complexes of W(VI). Syntheses and structural studies of $[W(X_2bino)(eg)_2]$ (X = H, Br) and $[W(X_2bino)(pin)_2]$ (pin = pinacolate, 2,3-dimethyl-2,3-butanediolate dianion) are reported.

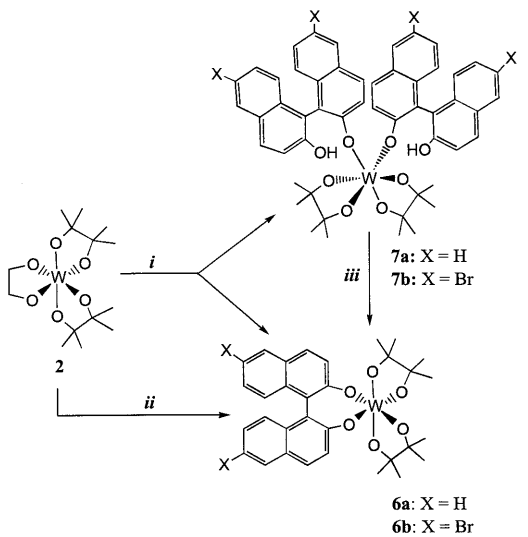
2. Results and discussion

2.1. Synthesis of the $[W(X_2bino)(eg)_2]$ (5) complexes

Mixed-ligand complexes of the type $[W(X_2bino)(eg)_2]$ (**5**) were prepared by the reaction of **1** with a stoichiometric amount of racemic 6,6′-X_2-1,1′-bi-2-naphthols (H_2X_2bino) (**3**) in a toluene solution at reflux temperature (see path *i* in Scheme 1 The identical compounds were also prepared by using corresponding binaphthyl acetates ($Ac)_2X_2bino$ (**4**) as ligand precursors (see path *ii* in Scheme 1). Binaphthyl acetates reacted slowly in toluene, but more readily if chlorobenzene was used as a reaction medium. As the reaction employing free binaphthol can be promoted by fractionating out the liberated ethanediol as a toluene azeotrope, it seems to lead to the better yields (according to TLC analyses).



Scheme 1. (i)H_2X_2bino/PhMe, reflux; (ii)$X_2bino(Ac)_2$/PhCl, reflux; (ii)$2H_2pin$/PhMe.



Scheme 2. (i)H_2X_2bino/PhMe, reflux; (ii)$X_2bino(Ac)_2$/PhCl, reflux; (iii)xylene, reflux.

However, the use of binaphthyl acetates as starting materials is preferred due to the good solubility of ligand precursor in common solvents, which avails purification by recrystallisation from CH_2Cl_2 or toluene. Compounds **5** are orange crystalline materials, stable as solids when stored under an atmosphere of dry air or nitrogen. They are moderately soluble in chlorinated hydrocarbons, ethers and aromatic solvents but practically insoluble in hexane. The crystals of **5** obtained from CH_2Cl_2 contain about 1/4 molecule of CH_2Cl_2 per one molecule of $[W(X_2bino)(eg)_2]$.

Our attempts to further substitute eg ligands by chlorides and prepare compounds of type $[W(bino)Cl_4]$ failed. Treatment of complexes **5** with a variety of chloride sources (HCl, $AlCl_3$, AcOCl, and $SOCl_2$) always led to the formation of dark solids. Extraction of these solids by toluene resulted in the isolation of small amounts of $[W(bino)_3]$, which seems to be a thermodynamically more stable product than heteroleptic binaphtholate chlorides [4]. Our efforts to prepare complexes of type $[W(bino)_2(eg)]$ or $[W(bino)_3]$ were unsuccessful as reaction of **1** with 2 or 3 equiv. of H_2bino (or its diacetate) yields complex **5** and unreacted ligand precursor.

2.2. Synthesis of the $[W(X_2bino)(pin)_2]$ (6) complexes

Complexes of the type **6** formed when ethanediolato ligands of compounds **5** were substituted by 2 equiv. of pinacol (see path *iii* in Scheme 1.). The substitution reactions were carried out in refluxing toluene and the product was purified by column chromatography. Yellow, air-stable crystalline compounds **6** are soluble in common organic solvents and can be crystallised from hot hexane. In the case **6a** the unit cell contains 1/2 molecule of hexane per one molecule of $[W(bino)(pin)_2]$. These compounds were also prepared from pinacolate complex $[W(eg)(pin)_2]$ (**2**), which reacts readily with binaphthols in refluxing toluene (path *i* in Scheme 2.). This reaction leads also to the formation of minor quantities of $[W(pin)_2(X_2Hbino)_2]$ (**7**) (see below). Compounds **6** are as well formed if complex **2** is allowed to react with binaphthol acetates in chlorobentsene at reflux temperature, but reactions are remarkably slower and long reaction times (few days) are required to reach practical yields (path *ii* in Scheme 2).

2.3. Formation of $[W(pin)_2(X_2Hbino)_2]$ (7) complexes

Synthesis of complexes **6** from pinacolato complex **2** and binaphthols leads also to the development of bis(hydrogenbinaphtholato) complexes $[W(pin)_2(HX_2bino)_2]$ (**7**) in small quantities (see path *i* in Scheme 2). These by-products can be turned to compounds **6** by heating in xylene at reflux temperature. Compounds **7** are soluble in chlorinated solvents and toluene. They

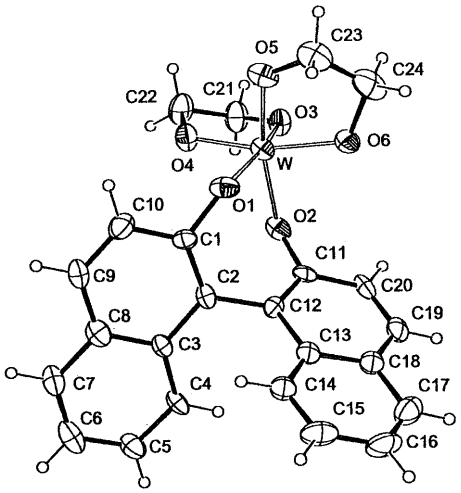


Fig. 1. An ORTEP [13] drawing of complex [W(bino)(eg)$_2$] (**5a**) with 30% probability ellipsoids.

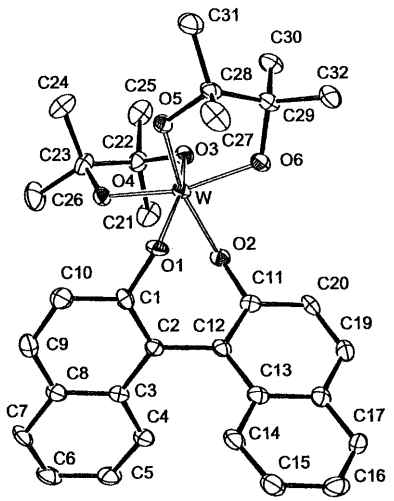


Fig. 2. An ORTEP [13] drawing of complex [W(bino)(pin)$_2$] (**6a**) with 30% probability ellipsoids. Hydrogen atoms are omitted for clarity.

can be crystallised from a hexane–toluene mixture as orange prisms. X-ray analysis of **7a** showed that in these compounds the hydrogendiolate groups act as monodentate phenoxides. Our earlier studies have shown that simple non-*ortho*-substituted phenols can not displace the any of the diolate ligands from the first coordination sphere of trisdiolato complexes. It was interesting to notice that two bulky difunctional phenols can replace ethanediolato ligand from **2** and then both coordinate in a monofunctional manner to a W(VI) centre.

2.4. Structures of complexes

Compounds **5a**, **6a** and **6b** form monomeric molecules in which six oxygen donors surround the central tungsten atoms (Figs. 1–3). The distorted octahedral WO_6 units are generally similar in all these compounds, as seen from the bonding parameters presented in Table 1. Bonding parameters of diolato groups are also closely similar to the parameters reported for the tungsten(VI) diolato complexes with simple phenoxides, e.g. [W(eg)$_2$(OPhR$_2$-2,6)$_2$] and [W(pin)$_2$(OPh)$_2$] [7,8]. In the solid state, compounds **5a** and **6a** adopt a $\Delta(\lambda\lambda\lambda)$ (or its optical isomer $\Lambda(\delta\delta\delta)$) configuration, whereas in **6b** bino ligand and one pin ligand has a λ conformation and another pin ligand is settled to δ conformation, the whole structure showing $\Delta(\lambda\lambda\delta)$ configuration. The ^{1}H NMR spectra of compounds **5** and **6** show typical resonances for bino ligands [4]. In the aliphatic region of the spectra of complexes **5** are seen multiplets for diolate groups, which implies that there are two different environments for these methylene protons. The aliphatic resonances in the spectra of compounds **6** indicate that all pinaco-

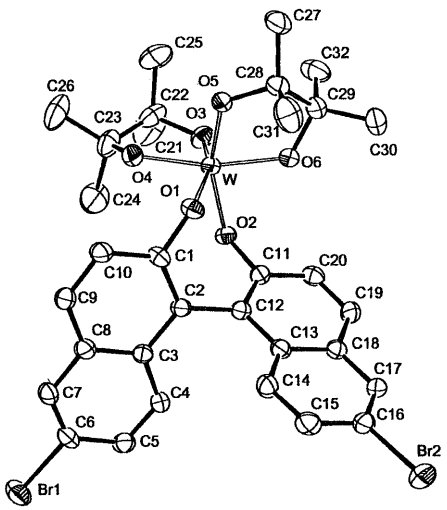


Fig. 3. An ORTEP [13] drawing of complex [W(Br$_2$bino)(pin)$_2$] (**6b**) with 30% probability ellipsoids. Hydrogen atoms are omitted for clarity.

Table 1
Selected bonding distances (Å) and angles (°) for complexes **5a**, **6a** and **6b**

	5a	6a	6b
W–O(1)	1.930(8)	1.934(4)	1.940(4)
W–O(2)	1.908(8)	1.946(4)	1.932(4)
W–O(3)	1.894(7)	1.888(4)	1.882(4)
W–O(4)	1.891(8)	1.904(4)	1.909(4)
W–O(5)	1.879(8)	1.897(4)	1.888(4)
W–O(6)	1.925(8)	1.910(4)	1.910(4)
W–O(1)–C(1)	130.1(7)	122.6(3)	124.4(3)
W–O(2)–C(11)	127.1(7)	131.8(3)	124.6(3)
W–O(3)–C	121.0(8)	120.8(4)	122.6(4)
W–O(4)–C	120.7(8)	120.5(3)	121.4(4)
W–O(5)–C	121.3(8)	121.4(3)	121.5(4)
W–O(6)–C	118.1(8)	119.6(3)	120.9(4)

late methyl groups have different environments. The different signals for the axial and equatorial methyl groups are indications of a rigid chelate ring, which prevents fast transformations of the ligand configuration. Similar signals for ethanediolate and pinacolate hydrogens are seen in the spectra of comparable W(VI) phenoxides, e.g. $[W(eg)_2(OPhR_2\text{-}2,6)_2]$ and $[W(pin)_2(OPh)_2]$ [7,8].

The structure of compound **7a** is depicted in Fig. 4 and its main structural parameters are shown in Table 2. It is a six-coordinated W(VI) complex with two bidentate pin ligands (one in a λ and the other in a δ conformation) and two monodentate hydrogennaphtholato ligands in *cis*-positions. Only one proton of the phenolic OH groups takes part in H-bonding. This is a quite weak intramolecular H-bond, which is indicated by the O6···O1 distance of 2.947(9) Å.

In order to get information of the influence of more bulky ligand X to a $W(pin)_2X_2$-coordination unit (X is a monodentate phenolate type ligand) we can compare the W–O bond parameters of $[W(pin)_2(Hbino)_2]$ to those of $[W(pin)_2(OPh)_2]$ [8]. In former W–O(alif.) bond lengths are from 1.876(5) to 1.940(5) Å while in the latter they are from 1.889(5) to 1.920(5) Å. The W–O(arom.) bond lengths in **7a** are 1.908(6) and 1.932(5) Å while in $[W(pin)_2(OPh)_2]$ they are 1.884(5) and 1.916 Å. The *trans*-O(alif.)–W–O(alif.) angles are 169.3(2) and 163.2(2)° for **3a** and $[W(pin)_2(OPh)_2]$, respectively. All *trans*-O(alif.)–W–O(arom.) angles are 169.3(2) in both compounds are about 160° (159.7 and 158.8° in **7a** compared to 160.2 and 163.6° in $[W(pin)_2(OPh)_2]$). The above suggests that two bulky X^- ligands can distort the coordination sphere of $W(pin)_2X_2$-unit making it probably more labile. The ^1H NMR spectra of compounds **7** show complicated pattern of signals for monodentate binaphtholato ligands. The resonances of the aliphatic protons indicate that all pinacolate methyl groups have different environments. The different signals for the axial and equatorial methyl groups are indications of a rigid chelate ring, which prevents fast transformations of the ligand configuration

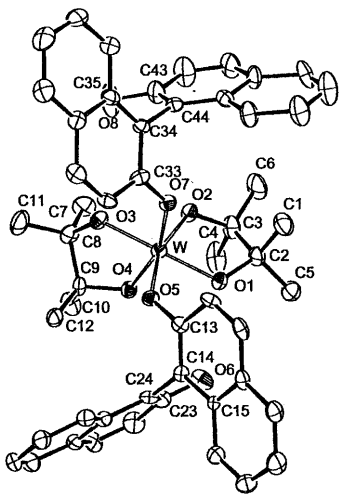


Fig. 4. An ORTEP [13] drawing of complex $[W(pin)_2(Hbino)_2]$ (**7a**) with 30% probability ellipsoids. Hydrogen atoms are omitted for clarity.

Table 2
Selected bonding distances (Å) and angles (°) for complex **7a**

W–O(1)	1.940(5)	W–O(1)–C(2)	118.8(5)
W–O(2)	1.876(5)	W–O(2)–C(3)	121.6(6)
W–O(3)	1.925(6)	W–O(3)–C(8)	120.3(5)
W–O(4)	1.884(6)	W–O(4)–C(9)	120.7(5)
W–O(5)	1.932(5)	W–O(5)–C(13)	136.0(5)
W–O(7)	1.908(6)	W–O(7)–C(33)	137.3(6)

3. Conclusion

Our studies on the synthesis of mixed W(VI) diolate-phenoxides continue as an extension of our search for novel catalyst precursors for olefin metathesis. We have shown that trisdiolatotungsten(VI) complexes $[W(eg)_3]$ and $[W(eg)(pin)_2]$ (eg = ethanediolate dianion, pin = pinacolate dianion) reacts with 6,6′-disubstituted-1,1′-bi-2-naphthols *rac*-H_2X_2bino (X = H, Br) and corresponding binaphthyl acetates forming heteroleptic complexes $[W(X_2bino)(diolate)_2]$. $[W(X_2bino)(eg)_2]$ reacts further with pinacol to form $[W(X_2bino)(pin)_2]$. The X-ray crystal structure determinations confirm that compounds are monomeric molecules presenting distorted octahedral coordination around the W(VI) cation.

4. Experimental

Chemicals were from commercial origins and were used without subsequent purification. Trisdiolatotungsten(VI) complexes **1** and **2** were prepared as described earlier [9]. Racemic binaphthols and binaphthyl acetates were prepared using published procedures [10–12]. Preparative TLC was carried out using 20 × 20 cm plates made from aqueous slurries (Aldrich, silica gel G) followed by drying in air at 80°C. CH_2Cl_2 was used as an eluent in analytical TLC (Merck, Silica Gel 60). NMR spectra were recorded on Bruker AM-200 spectrometer. IR spectra were measured on a Mattson Galaxy FTIR spectrometer as Nujol mulls. Elemental analyses were obtained using a Perkin–Elmer CHNS-Analyzer 2400. Samples were dried in vacuo at 40°C for 2 h before elemental and spectral analyses.

*4.1. Preparation of the $[W(X_2bino)(eg)_2]$ (**5**) complexes (where X = H (**5a**) or Br (**5b**)*

4.1.1. Method A. From binaphthols

Complex **1** (1.0 mmol, 365 mg) was heated with 1 equiv. of binaphthol **3** in 50 ml of toluene at reflux to

form a red solution. The H_2eg that formed was removed by azeotropic distillation with toluene. After 6 h the solvent was removed in vacuo, the red oily residue was dissolved in CH_2Cl_2 and filtered. Drastic reduction of the solution volume and refrigeration at −20°C yielded orange–red crystalline products. Compounds **5a** ($R_f = 0.35$) and **5b** ($R_f = 0.40$) were isolated in yields 48% (285 mg) and 43% (320 mg), respectively. Analytical samples were purified by preparative TLC in 50-mg scale (CH_2Cl_2 as an eluent) followed by extraction with CH_2Cl_2 and drying in vacuo. Crystals of **5a** for X-ray measurements were obtained after slow evaporation of CH_2Cl_2. For **5a**: δ_H ($CDCl_3$, standard $SiMe_4$): 7.90 (m, 4H, aromatics), 7.40 (d, 2H, aromatics), 7.25 (m, 6H, aromatics), 5.60 (m, 4H, CH_2), 5.20 (m, 4H, CH_2). IR: 1327(s), 1271(w), 1242(s), 1219(s), 1155(w), 1061(vs), 1030(vs), 955(s), 918(s), 860(w), 828(m), 818(s), 779(m), 758(s), 733(m), 660(s), 629(vs), 606(vs), 594(s), 552(s), 540(s), 529(m). Found: C, 48.6; H, 3.4. $C_{24}H_{20}O_6W$ requires C, 49.0; H, 3.5%. For **5b**: δ_H ($CDCl_3$, standard $SiMe_4$): 8.03 (2H, aromatics), 7.79 (d, 2H, aromatics), 7.44 (d, 2H, aromatics), 7.25 (d, 2H, aromatics), 7.10 (d, 2H, aromatics), 5.55 (m, 4H, CH_2), 5.20 (m, 4H, CH_2). IR: 1327(s), 1271(w), 1242(s), 1219(s), 1155(w), 1061(vs), 1030(vs), 955(s), 918(s), 860(w), 828(m), 818(s), 779(m), 758(s), 733(m), 660(s), 629(vs), 606(vs), 594(s), 552(s), 540(s), 529(m). Found: C, 38.4; H, 2.2. $C_{24}H_{18}Br_2O_6W$ requires C, 38.7; H, 2.5%.

4.1.2. Method B. From binaphthyl acetates

Complex **1** (reaction scale 1.0 mmol) was heated with 1 equiv. of binaphthyl acetate **4** in 30 ml of chlorobenzene at reflux for 16 h to form a red solution. The bulk of the solvent was removed by distillation and finally at reduced pressure. The red oily residue were dissolved in CH_2Cl_2 and filtered. Drastic reduction of the solution volume and refrigeration at −20°C yielded orange–red microcrystals in yields of 54% (320 mg) for **5a** and 53% (395 mg) for **5b**, respectively. Compounds were identical to those prepared by method A.

4.2. Preparation of the [W(X$_2$bino)(pin)$_2$] (6) complexes (where X = H (6a) or Br (6b)

4.2.1. Method A. From binaphthols

To the solution of **2** (0.5 mmol, 240 mg) in toluene (50 ml) was added 1 equiv. of binaphthol **3**. The solution was allowed to reflux for five hours, and the H_2eg that formed was removed by azeotropic distillation. After the solvent had been removed in vacuo, the orange residue was purified by flash chromatography (30% of toluene in hexane as an eluent). Compounds were crystallised from hot hexane to give orange prisms in yields of 73% (255 mg) for **6a** ($R_f = 0.83$) and 68% (290 mg) for **6b** ($R_f = 0.90$), respectively. For **6a**: δ_H ($CDCl_3$, standard $SiMe_4$): 7.89 (m, 4H, aromatics), 7.42 (d, 2H, aromatics), 7.23 (m, 6H, aromatics), 1.55 (6H, CH_3), 1.31 (6H, CH_3) 1.27 (6H, CH_3), 1.09 (6H, CH_3). IR: 1460(s), 1377(s), 1329(s), 1270(w), 1242(s), 1217(m), 1140(vs), 1072(m), 1010(w), 955(vs), 900(s), 885(vs), 818(s), 770(m), 756(s), 733(s), 716(s), 669(m), 631(vs), 604(s), 567(w), 515(m). Found: C, 54.2; H, 5.0. $C_{32}H_{36}O_6W$ requires C, 54.9; H, 5.2%. For **6b**: δ_H ($CDCl_3$, standard $SiMe_4$): 8.02 (2H, aromatics), 7.81 (d, 2H, aromatics), 7.46 (d, 2H, aromatics), 7.24 (d, 2H, aromatics), 7.08 (d, 2H. aromatics), 1.53 (6H, CH_3), 1.31 (6H, CH_3), 1.27 (6H, CH_3) 1.09 (6H, CH_3). IR: 1462(s), 1375(s), 1329(s), 1267(w), 1240(s), 1217(m), 1142 (vs), 1067(m), 1003(w), 951(vs), 906(m), 889(vs), 876(s), 814(m), 735(w), 716(s), 629(vs), 590(w), 525(w). Found: C, 45.2; H, 4.1. $C_{32}H_{34}Br_2O_6W$ requires C, 44.8; H, 4.0%. The synthesis of complex **6a** was accompanied also by the formation of 12 mg of complex **7a** ($R_f = 0.45$), which was crystallised from a hot hexane–toluene mixture (5 + 5 ml). Formation of **7b** was also detected by TLC ($R_f =$ 0.55), but only negligible amounts of that was isolated. Compounds **7** were turned quantitatively to compounds **6** by heating in xylene at reflux temperature (b.p. = 135°C). For **7a**: δ_H ($CDCl_3$, standard $SiMe_4$): 8.00–7.68 (several peaks, 6H, aromatics), 7.50 (m, 6H. aromatics), 7.35 (m, 6H, aromatics), 7.27 (m, aromatics), 1.35 (6H, CH_3), 1.26 (6H, CH_3), 1.15 (6H, CH_3) 1.09 (6H, CH_3).IR: 3418(br), 1460(s), 1375(s), 1335(s), 1270(w), 1256(s), 1233(vs), 1217(m), 1175(m), 1142(vs), 1072(m), 1010(w), 990(vs), 955(vs), 900(s), 887(vs), 812(vs), 770(m), 746(s), 733(s), 716(s), 669(w), 631(vs), 617(s), 592(m), 515(m). Found: C, 64.0; H, 5.2. $C_{52}H_{50}O_8W$ requires C, 63.3; H, 5.1%.

4.2.2. Method B. From binaphthyl acetates

Complex **2** (0.5 mmol, 24 mg) was heated with 1 equiv. of binaphthyl acetate (**4**) in 30 ml of chlorobenzene at reflux temperature for 3 days to form a red solution. The solvents were removed at reduced pressure, and red oily residues were purified as described above to obtain compounds in yields of 31% (110 mg) **6a** and 32% (145 mg) for **6b**, respectively. Compounds were identical to those prepared by method A.

4.2.3. Method C. From complexes 5

To the red solution of complex **5** (reaction scale 0.5 mmol) in 50 ml of toluene was added pinacol (140 mg, 1.2 mmol) and the mixture was heated at reflux. The colour of the solution turned yellow during reaction. The H_2eg that formed was removed by azeotropic distillation with toluene during 6 h. Compounds were separated and purified as described above to obtain

Table 3
Crystal data and experimental details of studied complexes

	5a	**6a**	**6b**	**7a**
Formula	$C_{24}H_{20}O_6W\cdot 1/4CH_2Cl_2$	$C_{32}H_{36}O_6W$	$C_{32}H_{34}Br_2O_6W\cdot 1/2C_6H_{14}$	$C_{52}H_{50}O_8W$
M_r	609.48	700.46	901.35	986.77
Crystal system	monoclinic	monoclinic	triclinic	triclinic
Space group	$C2/c$ (15)	$P2_1/n$ (14)	$P\bar{1}$ (2)	$P\bar{1}$ (2)
Unit cell dimensions				
a (Å)	26.018(5)	9.496(2)	12.853(5)	14.468(5)
b (Å)	15.535(4)	12.855(4)	13.754(7)	16.533(4)
c (Å)	11.674(8)	24.417(2)	11.753(7)	10.681(2)
α (°)	90	90	106.28(5)	100.72(2)
β (°)	103.36(3)	100.13(1)	107.34(4)	110.13(2)
γ (°)	90	90	101.38(4)	71.81(2)
U (Å^3)	4591(3)	2934.1(2)	1812(2)	2270(2)
Z	8	4	2	2
Observed reflections	4015	5165	6386	7993
Parameters	285	352	397	560
[a]R_1	0.134 (0.053)	0.067 (0.033)	0.062 (0.036)	0.104 (0.055)
[a]wR_2	0.132 (0.111)	0.062 (0.074)	0.081 (0.089)	0.120 (0.107)

[a] Values in parentheses for reflections with $I>2.0\sigma(I)$. $R_1=\Sigma||F_o|-|F_c||/\Sigma|F_o|$. $wR_2=\{\Sigma[w(F_o^2-F_c^2)^2]/\Sigma[w(F_o^2)^2]\}^{1/2}$ and $w=1/[\sigma^2(F_o^2)+(aP)^2+bP)]$, where $P=(2F_c^2+F_o^2)/3$.

yellow crystals in yields of 76% (265 mg) for **6a** and 69% (310 mg) for **6b**, respectively.

4.3. X-ray crystal determinations

Crystal data for compounds **5a**, **6a** and **6b**, along with other experimental details, are summarised in Table 3. Single-crystal data collections, reduction and subsequent calculations were essentially as described in other related papers from our laboratory [7].

5. Supplementary data

Crystallographic data for the structures reported in this paper have been deposited with the Cambridge Crystallographic Data Centre, CCDC No. 146181 for **5a**, CCDC No. 146182 for **6a**, CCDC No. 146183 for **6b** and CCDC No. 146184 for **7a**. Copies of this information may be obtained free of charge from the Director, CCDC, 12 Union Road, Cambridge, CB2 1EZ, UK (fax: +44-1223-336033; e-mail: deposit@ccdc.cam.ac.uk or http://www.ccdc.cam.ac.uk).

Acknowledgements

We thank the Academy of Finland for financial support of this research.

References

[1] For example: (a) A. Van der Linden, C.J. Schaverien, N. Meijboom, C. Ganter, A.G. Orpen, J. Am. Chem. Soc. 177 (1995) 3008. (b) K.M. Totland, T.J. Boyd, G.G. Lavoie, W.M. Davis, R.R. Schrock, Macromolecules 29 (1996) 6114. (c) M. Chavarot, J. Byrne, P.Y. Chavant, J. Pardillos-Guindet, Y. Vallée, Tetrahedron Asymm. 9 (1998) 3889.
[2] L. Pu, Chem. Rev. 98 (1998) 2405.
[3] (a) M. Bandin, S. Casolari , P.G. Cozzi, G. Proni, E. Schmohel, G.P. Spada, E. Tagliavini, A. Umani-Ronchi, Eur. J. Org. Chem. (2000) 491. (b) K. Mikami, M. Terada, T. Nakai, J. Am. Chem. Soc. 111 (1989) 1940. (c) X.-W. Yang, J.-H. Sheng, C.-S. Da, H.-S. Wang, W. Su, R. Wang, A.S.C. Chan, J. Org. Chem. 65 (2000) 295. (d) N.W. Eilerts, J.A. Heppert, Polyhedron 14 (1995) 3255. (e) D.S. La, J.G. Ford, E.S. Sattely, P.J. Bonitatebus, R.R. Schrock, A.H. Hoveyda, J. Am. Chem. Soc. 121 (1999) 11604.
[4] S.D. Dietz, N.W. Eilerts, J.A. Heppert, M.D. Morton, Inorg. Chem. 32 (1993) 1698.
[5] M.H. Chisholm, I.P. Rothwell, in: G. Wilkinson (Ed.), Comprehensive Coordination Chemistry, vol. 2, Pergamon, New York, 1987, pp. 335–364.
[6] A. Lehtonen, R. Sillanpää, J. Catal. 161 (1996) 867.
[7] A. Lehtonen, R. Sillanpää, Polyhedron 18 (1999) 175.
[8] A. Lehtonen, R. Sillanpää, J. Chem. Soc., Dalton Trans. (1995) 2701.
[9] A. Lehtonen, R. Sillanpää, Polyhedron 13 (1994) 2519.
[10] M. Noji, M. Nakajima, K. Koga, Tetrahedron Lett. 35 (1994) 7983.
[11] Q.-S. Hu, D. Vitharana, X.-F. Zheng, C. Wu, C.M.S. Kwan, L. Pu, J. Org. Chem. 61 (1996) 8370.
[12] G.D.Y. Sogah, D.J. Cram, J. Am. Chem. Soc. 101 (1979) 3035.
[13] L.J. Farrugia, J. Appl. Crystallogr. 30 (1997) 565.

PERGAMON

www.elsevier.nl/locate/poly

Polyhedron 19 (2000) 2585–2592

POLYHEDRON

The reactivity of the 'P_2N' ligand 2-(diphenylphosphino)-*N*-[2-(diphenylphosphino)benzylidene]--benzeneamine towards sulfur and acid

Eric W. Ainscough [1]*, Andrew M. Brodie [2]*, Anthony K. Burrell, Xiaohong Fan, Michael J.R. Halstead, Steven M.F. Kennedy, Joyce M. Waters

Chemistry-Institute of Fundamental Sciences, Massey University, Private Bag 11-222, Palmerston North, New Zealand

Received 26 June 2000; accepted 20 August 2000

Abstract

The reaction of 2-(diphenylphosphino)-*N*-[2-(diphenylphosphino)benzylidene]benzeneamine (PNCHP) with sulfur in a 1:1 molar ratio shows the phosphorus atom nearest the imine nitrogen to be preferentially oxidised. The overall product distribution, determined by synthesising each component independently, is: 50% 2-(diphenylphosphinothioyl)-*N*-[2-(diphenylphosphino)-benzylidene]benzeneamine (SPNCHP), 7% 2-(diphenylphosphino)-*N*-[2-(diphenylphosphinothioyl)benzylidene]benzeneamine (PNCHPS) and 27% 2-(diphenylphosphinothioyl)-*N*-[2-(diphenylphosphinothioyl)benzylidene]benzeneamine SPNCHPS (27%) with 16% of the reactant, PNCHP, remaining. The structures of PNCHP and SPNCHP have been determined by single-crystal X-ray diffraction. The PNCHP molecule has an approximate centre of symmetry with the two phosphorus atoms adopting a *trans* orientation with respect to each other. The two phosphorus atoms in SPNCHP also adopt a *trans* arrangement to minimise non-bonded steric interactions. The –CH=N– 'bridge' linking the two phenyl rings is not coplanar with its associated phenyl ring. The single crystal X-ray structure of the solvate, $SPNCHP{\cdot}CH_2Cl_2$, shows that the extent of this non-planarity is influenced by the presence of a CH_2Cl_2 solvent of crystallisation. Reaction of PNCHP with the strong acids, $HClO_4$ and HBF_4 results in protonation of the imine nitrogen followed by nucleophilic attack on the imine carbon by the phosphorus nearest the imine nitrogen to form the phosphonium salt [$\overline{PNHCH}$P]X (X = ClO_4 and BF_4), the structures of which have been determined by X-ray crystallography. A new P–C bond is formed thus producing a five-membered heterocyclic ring. © 2000 Elsevier Science B.V. All rights reserved.

Keywords: Crystal structures; Phosphine sulfides; Phosphonium salt

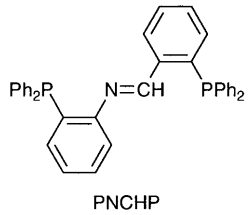
1. Introduction

The chemistry of mixed donor multidentate ligands containing organophosphorus and nitrogen donors is appearing more frequently in the literature in such diverse areas as chiral complexes in catalysis [1], stabilized oxygen carriers [2], cyclometallation [3], building blocks in radiopharmacology [4] and resolving agents [5]. The non-dissociative character of chelating polyphosphines may be a disadvantage in some catalytic processes whereas hybrid polydentate ligands offer the possibility of supplying vacant coordination sites at the metal by dissociation of an N or O or P donor [6–8]. In this paper we report the single crystal X-ray structure and some fundamental reactivity studies towards sulfur and acid on the new hybrid ligand, 2 - (diphenylphosphino) - *N* - [2 - (diphenylphosphino)-benzylidene]benzeneamine (PNCHP), which binds to a range of metals [9–12] (Scheme 1).

[1] *Corresponding author. Tel.: +64-6-350-4780; fax: +64-6-350-5682; e-mail: e.ainscough@massey.ac.nz

[2] *Corresponding author. Tel.: +64-6-350-5102; fax: +64-6-350-5682; e-mail: a.brodie@massey.ac.nz

0277-5387/00/$ - see front matter © 2000 Elsevier Science B.V. All rights reserved.
PII: S0277-5387(00)00558-1



PNCHP

Scheme 1. Structure of PNCHP.

2. Results and discussion

2.1. Oxidation of PNCHP and its synthetic components with sulfur

In an effort to understand the reactivity of PNCHP we have examined its oxidation with sulfur since its inequivalent phosphorus atoms provide an opportunity to investigate if there is any preference for one site or the other when the molecule is oxidised by one mole equivalent of sulfur. The ^{31}P-{^{1}H} NMR spectrum of such a reaction mixture showed resonances at 42.2, 41.9, 41.1, 35.8, 33.6, −13.9 and −15.3 ppm plus the signals at −14.2 and −14.8 ppm for unreacted PNCHP.

To identify the possible products independent syntheses of the three sulfur oxidised species, viz. SPNCHP, PNCHPS and SPNCHPS, were undertaken (Scheme 2). The amino phosphine, 2-PNH$_2$, was oxidised with S to produce 2-aminophenyldiphenylphosphine sulfide (2-SPNH$_2$) which was reacted with 2-PCHO to give SPNHCP. Similarly, PNCHPS was prepared by oxidising the aldehyde substituted phosphine, 2-PCHO, with sulfur to produce phenyl-2-carbaldehydediphenylphosphine sulfide (2-SPCHO) which was then reacted with 2-PNH$_2$. Finally, oxidation of PNCHP with sulfur in a 1:2 mole ratio resulted in SPNCHPS. The mass spectra (LSIMS) of all three sulfur derivatives of PNCHP exhibited peaks corresponding to [MH]$^+$ protonated parent ions. However, in addition for SPNCHPS, a peak at m/z 746, assignable to the [M + Cs]$^+$ ion, was observed which must arise from the interaction of the disulfide with the caesium ion beam in the mass spectrometer. Indeed, it is possible to isolate stable metal ion complexes with this ligand, e.g. the three coordinate copper(I) complex, [Cu(SPNCHPS)]ClO$_4$ [13].

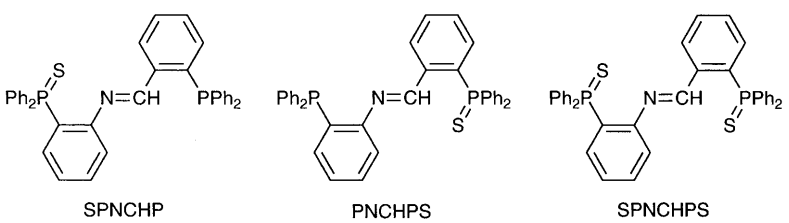
Table 1
Selected ^{1}H and ^{31}P-{^{1}H} NMR data for the compounds [a]

Compound	^{1}H (δ (ppm))	^{31}P-{^{1}H} (δ (ppm)) [b]
2-PNH$_2$	4.14 [s, broad, 2H(NH$_2$)	−20.2
2-PCHO	10.50 [d, J = 5.5 Hz [c], 1H(CHO)]	−11.6
2-SPNH$_2$	5.16 [s, broad, 2H(NH$_2$)]	39.8
2-SPCHO	10.71 [s, 1H(CHO)]	40.3
PNCHP	8.92 [d, J = 5.5 Hz [c], 1H(CH=N)]	−14.2, −14.8
SPNCHP	8.87 [d, J = 6.2 Hz [c], 1H(CH=N)]	42.2, −15.3
PNCHPS	9.02 [s, 1H(CH=N)]	40.9, −13.9
SPNCHPS	8.91 [s, 1H(CH=N)]	41.9, 41.1
[PNHCHP]ClO$_4$		38.1, −17.0
[PNHCHP]BF$_4$		39.0, −16.2

[a] In CDCl$_3$.
[b] With reference to 85% H$_3$PO$_4$.
[c] ^{4}J(PH)/Hz.

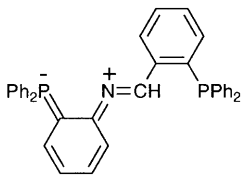
Selected ^{1}H and ^{31}P-{^{1}H} NMR data for 2-SPCHO, 2-SPNH$_2$, SPNCHP, PNCHPS, SPNCHPS as well as their un-oxidised precursors are given in Table 1. The ^{31}P-{^{1}H} NMR data show the chemical shifts for the phosphorus(III) atoms occur in the range −11 to −20 ppm whereas the signals for the phosphorus(V) atoms lie in the range 40–42 ppm. The isomers PNCHPS and SPNCHP may be clearly distinguished from one another since the chemical shift for each type of phosphorus atom is different in both compounds. Similarly SPNCHPS may be distinguished from PNCHPS and SPNCHP. Comparing the values observed for the mono-phosphine sulfides with those seen for the precursor molecule (Table 1) would suggest that the PNCHP signal at −14.2 ppm can be assigned to the P atom nearest to the imine nitrogen and one at −14.8 ppm to the other P.

In the ^{1}H NMR spectrum for 2-PCHO a doublet signal is observed at 10.50 ppm for the aldehyde proton and for PNCHP the imine proton resonance near 8.92 ppm is also a doublet as a result of ^{4}J(P–H) coupling. A decoupling experiment for PNCHP shows that the imine proton is not coupled to the phenyl protons. When the phosphorus atom nearest to the imine or aldehyde protons is oxidised with sulfur to form PNCHPS and 2-SPCHO the imine and aldehyde protons appear as singlets, the ^{4}J(P–H) coupling now being reduced.



SPNCHP PNCHPS SPNCHPS

Scheme 2. Structures of SPNCHP, PNCHPS and SPNCHPS.



Scheme 3. Possible resonance structure of PNCHP.

In contrast, when the phosphorus atom nearest the imine N of PNCHP is oxidised to give SPNCHP, the imine proton resonance remains as a doublet [^4J(P–H) 6.2Hz], thus allowing the two isomers PNCHPS and SPNCHP to be distinguished. In the fully oxidised compound SPNCPS the imine proton is observed as a singlet resonance.

Returning to the reaction of PNCHP with one mole equivalent of sulfur, the ^{31}P-{^{1}H} NMR spectrum is now easily assigned. The major product is SPNCHP (50%) with a minor amount of its isomer PNCHPS (7%), as well as SPNCHPS (27%) and unreacted PNCHP (16%). The fact that the PNCHPS:SPNCHP ratio is not 1:1 suggests that the phosphorus atom nearest the imine nitrogen is more reactive than the other. This is supported by the possible resonance structure which shows an enhanced basicity for this phosphorus atom (Scheme 3).

This would account for the observed results since the first step in the reaction of tertiary phosphines with elemental sulfur is the nucleophilic attack of the P atom on an S atom of the S_8 ring to produce a chain species, e.g. $Ph_3P^+–S–(S)_6–S^-$. The rate of reaction has been observed to increase with electron releasing substituents on the aromatic ring of the phosphine [14].

The synthesis of an isomeric pair of tertiary phosphine sulfides is rare and is successful in this case because of the synthetic methods utilised above. Seyferth et al. [15] first prepared the unsymmetrical ligand $Ph_2P(S)CH_2PR^1R^2$ (R^1, R^2 are alkyl groups) and others have been synthesised by Grim et al. [16] The preparations involve the production of $Ph_2P(S)CH_2Li$ from Ph_3PS and CH_3Li, followed by reaction of the appropriate R_2PCl. Careful control of reaction conditions are required and yields range from 10 to 50%. When $Ph_2P(S)CH_2PMe_2$ is heated to approximately 160°C in diglyme, the transfer of sulfur from the less basic diphenyl phosphine site to the more basic dimethyl phosphine site occurs [17]. A similar experiment with PNCHPS in boiling toluene does not yield SPNCHP.

2.2. Single-crystal structures of PNCHP, SPNCHP and SPNCHP·CH_2Cl_2

The phosphine sulfide precursor, PNCHP, crystallises with two crystallographically distinct, but chemically identical, molecules in the asymmetric unit. One of these molecules is depicted in Fig. 1 with selected bond distances and angles for both. Each molecule has an approximate centre of symmetry at the mid-point of the –C=N– imine bond, giving each an overall *trans* configuration. It is unlikely that the difference in the imine bond length between N(1)–C(3) and N(4)–C(2) is a real effect but both clearly establish the multiple bond character. The range of P–C bond lengths and C–P–C angles are in agreement with those found in other tertiary phosphines [18]. Calculation of planes of 'best fit' through the phenyl rings and the –N=CH– bridge shows that some rotation has occurred about the C(phenyl)–N and C(phenyl)–C bonds but there are differences in these rotations for the two molecules. In molecule A the plane through atoms N(1), C(3), C(112), C(312) makes angles of 36.8(3) and 35.0(4)° with phenyl rings C(111)–C(116) and C(311)–C(316), respectively. This is in contrast with the comparable angles in molecule B of 7.4(8) and 7.7(8)° between the planes containing atoms N(2), C(4), C(212), C(412) and

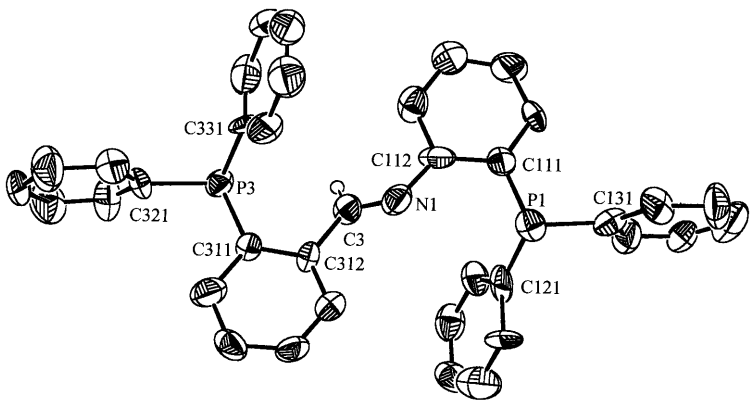


Fig. 1. ZORTEP [26] diagram of PNCHP (molecule A). The thermal ellipsoids are drawn at the 50% probability level. Selected bond lengths (Å) and angles (°) for molecule A: N(1)–C(3) 1.298(6), N(1)–C(112) 1.394(13), C(3)–C(312) 1.481(13), C(3)–N(1)–C(112) 123.3(7), N(1)–C(3)–C(312) 118.9(6); for molecule B: N(4)–C(2) 1.229(6), N(4)–C(412) 1.358(14), C(2)–C(212) 1.491(13), C(2)–N(4)–C(412) 126.9(7), N(4)–C(2)–C(212) 124.8(6).

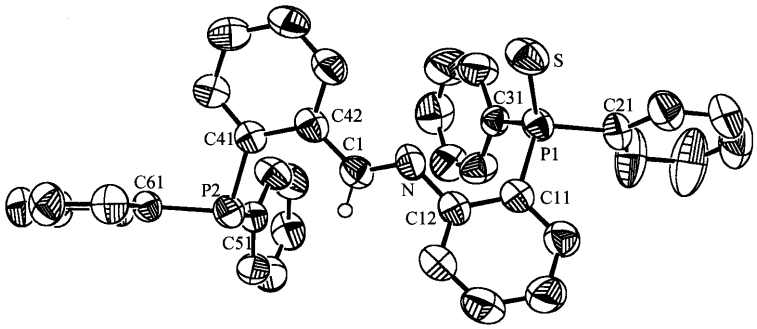


Fig. 2. ORTEP3 [27] diagram of SPNCHP. The thermal ellipsoids are drawn at the 50% probability level. Selected bond lengths (Å) and angles (°) for SPNCP: P(1)–S 1.945(2), C(1)–N 1.257(6), C(1)–C(42) 1.476(7), N–C(12) 1.423(6), N–C(1)–C(42) 122.2(5), C(1)–N–C(12) 122.7(4); for SPNCHP·CH_2Cl_2: P(1)–S 1.939(2), C(1)–N 1.261(5), C(1)–C(42) 1.455(5), N–C(12) 1.404(4), N–C(1)–C(42) 124.0(4), C(1)–N–C(12) 122.0(4).

the rings C(211)–C(216) and C(411)–C(416), respectively. As well, the two phenyl rings in both molecule A and molecule B are approximately parallel to one another and this results in a 'step' occurring in each. In molecule A ring atoms C(111)–C(116) are displaced by approximately 0.51 Å from the plane of atoms C(311)–C(316) whereas a smaller 'step' of approximately 0.18 Å is observed in molecule B.

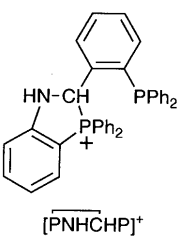
A diagram of the SPNCHP molecule is shown in Fig. 2 with selected bond lengths and angles for it, and the CH_2Cl_2 solvate. The data show a close correspondence between the two sets of distances and angles. For example, the P–S bond lengths at 1.945(2) and 1.939(2) Å are not significantly different and are in good agreement with the range of distances (1.92–1.97 Å [19]) found for other tertiary phosphine sulfides and indicate some multiple bond character. The S–P–C angles (mean 113.6 and 113.5° for the two structures) are all greater than the C–P–C angles in line with the presence of the larger S atom. However, the C–P–C angles show some differences at the two P atoms, with those associated with P(1) being a little larger than their counterparts at P(2) (mean C–P(1)–C 105.1 and 105.1°; mean C-P(2)–C 102.2 and 102.5° for the two structures respectively). The most notable difference observed between the two structure determinations is associated with the planes of 'best fit' data. For SPNCHP·CH_2Cl_2 the plane containing the 'bridge' atoms [N, C(1), C(12), C(42)] lies at an angle of 31° to the plane containing the aromatic ring atoms C(11)–C(16) and 23° to the plane of atoms C(41)–C(46). However, in the non-solvated structure the comparable angles are 39° and 5°. In neither structure are the aromatic rings on either side of the imine bridge parallel to one another. In the solvated structure the two aromatic rings make an angle of approximately 11° with one another whereas in the non-solvated counterpart the angle is 35°. Thus it appears that there is considerable flexibility in the molecule and the precise overall geometry is influenced not only by electron delocalisation but also by crystal packing forces.

2.3. Reaction of PNCHP with acid

When aqueous acids, such as $HClO_4$ and HBF_4, are added to PNCHP in ethanol/dichloromethane solution the yellow solution goes colourless immediately. On standing, in the presence of the acid, the white salt, [$\overline{\text{PNHCH}}$P]X (X = ClO_4 and BF_4), is isolated. The appearance of two singlet phosphorus signals at approximately 38 and −17 ppm (Table 1) in the NMR is indicative of the presence of a phosphonium salt as well as free phosphine. The single crystal X-ray structures (see below) showed the compounds contain a five-membered ring phosphonium salt (Scheme 4).

For the perchlorate salt, the ^{13}C-{^1H} NMR spectrum showed a quartet (due to coupling to the two P nuclei) at 59.6 ppm [^1J(P–C) 56.8 and ^3J(P–C) 27.4 Hz] assignable to the ring carbon (the former imine C). Consistent with this is the disappearance of the ν(C=N) stretching frequency in the IR spectrum of the products and the appearance of a ν(N–H) stretching frequency at approximately 3300 cm^{-1}. As well in the IR, strong bands are seen near 1100 cm^{-1} assignable to the ν(Cl–O) or ν(B–F) frequency of ionic perchlorate or tetrafluoroborate [20]. For the perchlorate, the conductivity in nitromethane was 78 S cm^2 mol^{-1} consistent with a 1:1 electrolyte [21].

It can be envisaged that the cation, [$\overline{\text{PNHCH}}$P]$^+$, is formed by the initial protonation of the imine nitrogen followed by nucleophilic attack by the most basic phosphine atom on the imine carbon with subsequent elec-



[$\overline{\text{PNHCH}}$P]$^+$

Scheme 4. Structure of [$\overline{\text{PNHCH}}$P]$^+$.

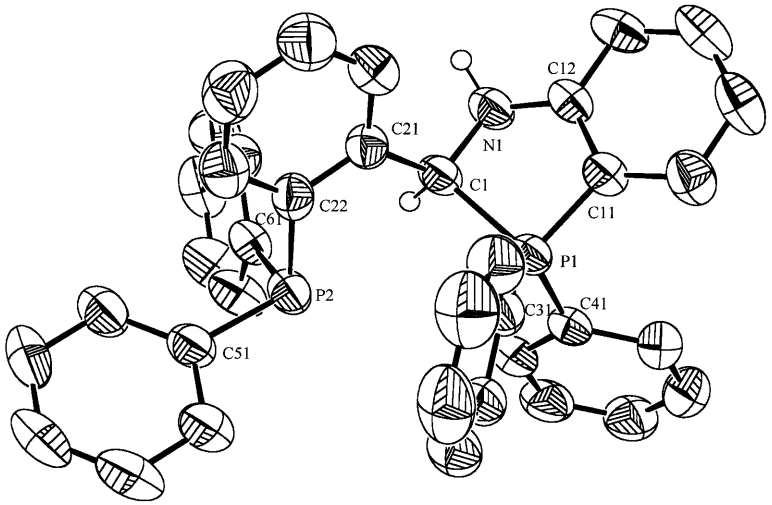


Fig. 3. ZORTEP [26] diagram of the cation in $[\overline{PNHC}HP]ClO_4$. The thermal ellipsoids are drawn at the 40% probability level. Selected bond lengths (Å) and angles (°) for $[\overline{PNHC}HP]ClO_4$: P(1)–C(11) 1.671(4), P(1)–C(1) 1.935(4), N(1)–C(12) 1.346(5), N(1)–C(1) 1.399(5), C(11)–C(12) 1.438(6), C(11)–P(1)–C(1).91.4(2), C(12)–N(1)–C(1) 111.5(4), N(1)–C(1)–P(1) 103.0(3); for $[\overline{PNHC}HP]BF_4$: P(1)–C(11) 1.755(5), P(1)–C(1) 1.856(5), N(1)–C(12) 1.367(6), N(1)–C(1) 1.444(6), C(11)–C(12) 1.389(7), C(11)–P(1)–C(1) 93.0(2), C(12)–N(1)–C(1) 116.5(4), N(1)–C(1)–P(1) 100.6(3).

tron re-arrangement to produce a five-membered ring phosphonium salt. Addition of base, such as triethylamine, reverses the reaction to re-form PNCHP.

2.4. Single-crystal X-ray structures of $[\overline{PNHC}HP]X$ ($X = ClO_4$ and BF_4)

The structure of the salt of the $[\overline{PNHC}HP]^+$ cation is given in Fig. 3 with selected bond lengths and angles for both salts ($X = ClO_4$ and BF_4). The structures show that there is a five-membered heterocyclic ring with P(2) being assigned as the tertiary phosphorus atom and P(1) as the quaternary phosphonium one. The ring carbon, C(1), is chiral and the salts crystallize as racemic mixtures. The bond lengths and angles found in the two structures are similar; hence the discussion will focus on mean bond parameters. The N(1)–C(1) bond length at 1.422 Å is considerably longer than expected for a C=N imine bond [as found in PNCHP (mean 1.258 Å) for example]. However, it is shorter than expected for a C–N single bond (1.47 Å [22]) as is N(1)–C(12) at 1.357 Å which suggests some electron delocalisation around this region of the ring. The average P–C bond distance in the two cations is 1.804 Å. Both the longest and shortest P–C distances are associated with the heterocyclic ring, viz. P(1)–C(1) 1.896 Å and P(1)–C(11) 1.713 Å. The ring C(11)–P(1)–C(1) angle at 92.2° is considerably smaller than the other angles about this atom [100.2(2)–115.5(2)°] presumably due to the steric constraints imposed by the rest of the ring. In fact it is comparable to the C–P–C angle [88.2(4)°] in the similar five-membered ring of 1*H*-1,3,-benzazaphosphole [23]. The atoms in the heterocyclic ring deviate considerably from coplanarity. A calculation of the plane of 'best fit' through the three ring atoms, P(1), C(1) and C(11), shows that C(12) and N(1) lie above this plane by 0.362(7) and 0.585(7) Å for the perchlorate and by 0.398(8) and 0.552(8) Å for the tetrafluoroborate.

3. Conclusions

The two phosphorus atoms in the PNCHP molecule are inequivalent, the one nearer the imine nitrogen being more readily oxidised by elemental sulfur than the other. This same phosphorus atom is involved in forming a P–C bond when PNCHP is treated with strong acid. The product is the cyclic phosphonium salt, $[\overline{PNHC}HP]^+$, which contains a five-membered PCNCC heterocyclic ring.

4. Experimental

Solvents were purified and dried in the usual manner and all reactions were performed under dinitrogen or argon. 2 - (Diphenylphosphino) - *N* - [2 - (diphenylphosphino)-benzylidene]benzeneamine (PNCHP) [12], phenyl-2-carbaldehydediphenylphosphine (2-PCHO) [24] and 2-aminophenyldiphenylphosphine (2-PNH_2) [25] were prepared according to literature methods. Microanalyses were performed by the Campbell Microanalytical Laboratory, University of Otago. Nuclear magnetic resonance (NMR) spectra were recorded on a JEOL GX270W spectrometer and infrared (IR) spectra on a BIORAD FTS-40 instrument as Nujol mulls between KBr discs. Mass spectra were obtained using a

Varian BG70-250S double focussing magnetic sector mass spectrometer by the method of liquid secondary ion mass spectrometry (LSIMS) at the Horticulture and Food Research Institute of New Zealand Limited, Palmerston North. Samples were dissolved in CH_2Cl_2 with *m*-nitrobenzylalcohol as a matrix.

4.1. Syntheses

4.1.1. Phenyl-2-carbaldehydediphenylphosphine sulfide (2-SPCHO)

2-PCHO (0.290 g, 1.0 mmol) and sulfur (0.032 g, 1.0 mmol) were dissolved in 15 cm^3 of toluene and the solution was heated under reflux for 30 min. After standing at 4°C for 1 day the cream coloured product that formed was filtered and washed with toluene. Yield: 0.32 g, 65%. Found: C, 70.52; H, 4.92; S, 9.70. Calc. for $C_{19}H_{15}OPS$: C, 70.81; H, 4.66; S, 9.94%. M.p. 117–119°C. MS: *m*/*z* (relative intensity) 323 (100%) $[MH]^+$. IR: 639 cm^{-1} [*ν*(PS)].

4.1.2. 2-Aminophenyldiphenylphosphine sulfide (2-SPNH$_2$)

2-PNH_2 (0.416 g, 1.5 mmol) and sulfur (0.048 g, 1.5 mmol) were dissolved in 15 cm^3 of CH_2Cl_2 and 8 cm^3 of ethanol and the solution refluxed for 80 min. After standing at room temperature (r.t.) for 1 day, white needles of the product which formed were filtered and washed with ethanol. Yield: 0.40 g, 85%. Found: C, 69.90; H, 5.65; N, 4.64; S, 10.03. Calc. for $C_{18}H_{16}NPS$: C, 69.90; H, 5.18; N, 4.53; S, 10.36%. M.p. 184–185°C. MS: *m*/*z* (relative intensity) 310 (100%) $[MH]^+$. IR: 628 cm^{-1} [*ν*(PS)].

4.1.3. 2-(Diphenylphosphinothioyl)-N-[2-(diphenylphosphino)benzylidene]benzeneamine methanol hemisolvate (SPNCHP·0.5MeOH)

2-PCHO (0.464 g, 1.6 mmol), 2-$SPNH_2$ (0.469 g, 1.6 mmol) and toluene-*p*-sulfonic acid (8 mg) were added to benzene (200 cm^3). The solution was refluxed under argon for 7 h using a Dean–Stark trap. Upon removal of the solvent with a rotary evaporator the resulting yellow oil was dissolved in a small amount of CH_2Cl_2 and methanol added until crystallisation began. After standing overnight at 4°C, pale yellow crystals of the product were filtered off and washed with methanol and dried in vacuo. Yield: 0.76 g, 83%. Found: C, 75.79; H, 5.53; N, 2.66; S, 5.81. Calc. for $C_{37.5}H_{31}NO_{0.5}P_2S$: C, 75.38; H, 5.19; N, 2.35; S, 5.36%. M.p. 189–191°C. MS: *m*/*z* (relative intensity) 582 (100%) $[MH]^+$. IR: 1613 [*ν*(C=N)], 632 cm^{-1} [*ν*(PS)].

4.1.4. 2-(Diphenylphosphino)-N-(2-diphenylphosphinothioyl)benzylidene]benzeneamine methanol hemisolvate (PNCHPS·0.5MeOH)

This was prepared by a method similar to that for SPNCHP·0.5MeOH above, with the new reagents 2-SPCHO (0.208 g, 0.64 mmol), 2-PNH_2 (0.178 g, 0.64 mmol) and toluene-*p*-sulfonic acid (8 mg). Yield: 0.20 g, 52%. Found: C, 75.28; H, 5.36; N, 2.55. Calc. for $C_{37.5}H_{31}NO_{0.5}P_2S$: C, 75.38; H, 5.19; N, 2.35%. M.p. 224–225°C. MS: *m*/*z* (relative intensity) 582 (100%) $[MH]^+$. IR: 1620 [*ν*(C=N)], 634 cm^{-1} [*ν*(PS)].

4.1.5. 2-(Diphenylphosphinothioyl)-N-[2-diphenylphosphinothioyl)benzylidene]benzeneamine (SPNCHPS)

To a solution of PNCHP (110 mg, 0.20 mmol) dissolved in 15 cm^3 CH_2Cl_2 and 4 cm^3 ethanol was added sulfur (14 mg, 0.40 mmol) After 30 min heating under reflux, the solution changed colour from orange to yellow and on standing overnight at r.t. a light yellow precipitate of the product formed. This was recrystallised from a $CHCl_3$–toluene mixture. Yield: 0.11 g, 88%. Found: C, 72.14; H, 4.81; N, 2.34; S, 10.57. Calc. for $C_{37}H_{29}NP_2S_2$: C, 72.43; H, 4.73; N, 2.28; S, 10.44%. M.p. 301–303°C. MS: *m*/*z* (relative intensity) 746 (18%) $[M + Cs]^+$, 614 (55%) $[MH]^+$. IR: 1614 [*ν*(C=N)], 635 cm^{-1} [*ν*(PS)].

4.1.6. Reaction of PNCHP with sulfur in a 1:1 molar ratio

PNCHP (0.138 g, 0.25 mmol) and sulfur (0.008 mg, 0.25 mmol) were dissolved in 10 cm^3 CH_2Cl_2 and 2.5 cm^3 ethanol and the solution refluxed for 10 min. The reaction solution was taken to dryness by rotary evaporation and the solid which formed redissolved in $CDCl_3$ for a ^{31}P-{^1H} NMR spectrum. The following compounds were identified (see Section 2): PNCHP, SPNCHP, PNCHPS and SPNCHPS.

4.1.7. [PNHCHP]ClO_4

To PNCHP (0.22 g, 0.4 mmol) dissolved in cold ethanol–dichloromethane was added aqueous $HClO_4$ (0.5 mmol). A clear solution resulted and on standing for 2 days [PNHCHP]ClO_4 crystallised. The product was filtered off, washed with ethanol and dried in vacuo. Yield 0.20 g 76%. Found: C, 67.91; H, 4.67; N, 2.43. Calc. for $C_{37}H_{30}ClN\ O_4P_2$: C, 68.37; H, 4.65; N, 2.15%. MS: *m*/*z* (relative intensity) 550 (100%) $[M–ClO_4]^+$. IR: 3280 [*ν*(NH)], 1103 cm^{-1} [*ν*(ClO)].

4.1.8. [PNHCHP]BF_4

This was prepared using the above method for [PNHCHP]ClO_4 but using tetrafluoroboric acid. Found: C, 69.54; H, 4.78; N, 2.09; P, 9.72. Calc. for $C_{37}H_{30}BF_4NP_2$: C, 69.72; H, 4.74; N, 2.20; P, 9.72%. IR: 3303 [*ν*(NH)], 1064 cm^{-1} [*ν*(BF)].

4.2. Determination of crystal structures

Single crystals of PNCHP, SPNCHP and SPNCHP·CH_2Cl_2 were grown from dichloromethane–

methanol and of the salts, [PNHCHP]ClO_4 and [PNHCHP]BF_4, from dichloromethane–ethanol. All crystals were secured to the end of a glass fibre with cyanoacrylate glue and mounted on a CAD4 diffractometer with a graphite monochromator. Intensity data were collected at room temperature with Mo Kα radiation ($\lambda = 0.71073$ Å). No absorption corrections were applied. Crystallographic data are summarised below. Initially for PNCHP the distinction between the C and N atoms of the C=N imine bond was not clearcut and this raised the possibility of there being disorder, giving rise to centrosymmetric data and the space group $P2_1/c$. This hypothesis was tested but rejected on the basis of systematic absence violations and on the statistical evidence which strongly favoured a non-centrosymmetric space group. As well, refinement in $P2_1/c$ was much less satisfactory. The labels were eventually assigned mainly on the basis of the lengths of the (C,N)–C(phenyl) bonds and with reference to the relative thermal parameters of the imine bridge atoms. For all structures, anisotropic thermal parameters were assumed for all non-hydrogen atoms. Hydrogen atoms were included at calculated sites riding on the atoms to which they were attached and with fixed thermal parameters except for HN(1) attached to N(1) in both [PNHCHP]ClO_4 and [PNHCHP]BF_4. These latter H were located from difference maps but once located were not refined.

4.2.1. Crystal data for PNCHP

$C_{37}H_{29}NP_2$, $M = 549.55$, monoclinic, $a = 15.026(3)$, $b = 11.600(2)$, $c = 17.261(3)$ Å, $\beta = 98.51(3)°$, $U = 2975.5(9)$ Å^3, $T = 293$ K, space group $P2_1$ (no. 4), $Z = 2$, μ(Mo Kα) 0.173 mm^{-1}, 5736 reflections measured, 5515 unique ($R_{int} = 0.0131$). The final $wR_2[I > 2\sigma(I)] = 0.0996$, $R_1[I > 2\sigma(I)] = 0.0469$.

4.2.2. Crystal data for SPNCHP

$C_{37}H_{29}NP_2S$, $M = 581.61$, monoclinic, $a = 19.200(4)$, $b = 10.122(4)$, $c = 17.040(3)$ Å, $\beta = 111.30(5)°$, $U = 3085(1)$ Å^3, $T = 293$ K, space group $P2_1/c$ (no. 14), $Z = 4$, μ(Mo Kα) 0.235 mm^{-1}, 5618 reflections measured, 5413 unique ($R_{int} = 0.0821$). The final $wR_2[I > 2\sigma(I)] = 0.1432$, $R_1[I > 2\sigma(I)] = 0.0612$.

4.2.3. Crystal data for SPNCHP·CH_2Cl_2

$C_{38}H_{31}Cl_2NP_2S$, $M = 666.54$, triclinic, $a = 8.766(2)$, $b = 9.637(3)$, $c = 21.160(4)$ Å, $\alpha = 101.71(2)$, $\beta = 94.69(2)$, $\gamma = 102.34(2)°$, $U = 1695.2(7)$ Å^3, $T = 293$ K, space group $P\bar{1}$ (no. 2), $Z = 2$, μ(Mo Kα) 0.326 mm^{-1}, 6370 reflections measured, 4558 unique ($R_{int} = 0.0239$). The final $R_1[I > 2\sigma(I)] = 0.0772$.

4.2.4. Crystal data for [PNHCHP]ClO_4

$C_{37}H_{30}ClNO_4P_2$, $M = 650.01$, monoclinic, $a = 10.161(2)$, $b = 9.286(2)$, $c = 35.447(7)$ Å, $\beta = 90.97(3)°$, $U = 3344$ (1) Å^3, $T = 293$ K, space group $P2_1/c$ (no. 14), $Z = 4$, μ(Mo Kα) 0.250 mm^{-1}, 6578 reflections measured, 5800 unique ($R_{int} = 0.013$). The final $wR_2[I > 2\sigma(I)] = 0.1403$, $R_1[I > 2\sigma(I)] = 0.0524$.

4.2.5. Crystal data for [PNHCHP]BF_4

$C_{37}H_{30}BF_4NP_2$, $M = 637.37$, monoclinic, $a = 8.950(2)$, $b = 19.188(4)$, $c = 18.656(4)$ Å, $\beta = 99.39(3)°$, $U = 3160.9(12)$ Å^3, $T = 298$ K, space group $P2_1/n$ (no. 14), $Z = 4$, μ(Mo Kα) 0.189 mm^{-1}, 5925 reflections measured, 5546 unique ($R_{int} = 0.0382$). The final $wR_2[I > 2\sigma(I)] = 0.1368$, $R_1[I > 2\sigma(I)] = 0.0548$.

5. Supplementary material

Crystallographic data for the structures reported in this paper have been deposited with the Cambridge Crystallographic Data Centre, CCDC No. 146136 for PNCHP, CCDC No. 146137 for SPNCHP, CCDC No. 146138 for SPNCHP·CH_2Cl_2, CCDC No. 146139 for [PNHCHP]BF_4 and CCDC No. 146140 for [PNHCHP]ClO_4. Copies of this information may be obtained free of charge from the Director, CCDC, 12 Union Road, Cambridge, CB2 1EZ, UK (fax: +44-1223-336033; e-mail: deposit@ccdc.cam.ac.uk or http://www.ccdc.cam.ac.uk).

Acknowledgements

We thank Massey University for financial support and Mr J. Allen, Horticulture and Food Research Institute of New Zealand Limited, for mass spectra.

References

[1] C. Bianchini, E. Farnetti, L. Glendenning, M. Graziani, G. Nardin, M. Peruzzini, F. Zanobini, Organometallics 14 (1995) 1489.
[2] P. Barbaro, C. Bianchini, F. Laschi, S. Midollini, S. Moneti, G. Scapacci, P. Zanello, Inorg. Chem. 33 (1994) 1622.
[3] S.D. Perera, B.L. Shaw, J. Chem. Soc., Dalton Trans. (1995) 641.
[4] F. Tisato, F. Refosco, A. Moresco, G. Bandoli, A.D. Domella, C. Bolzati, Inorg. Chem. 34 (1995) 1779.
[5] N.W. Alcock, D.I. Hulmes and J.M. Brown, J. Chem. Soc., Commun. (1995) 395.
[6] (a) A. Bader and E. Lindner, Coord. Chem. Rev. 108 (1991) 27. (b) G.R. Newkome, Chem. Rev. 93 (1993) 2067.
[7] C. Bianchini, E. Farnetti, M. Graziani, G. Nardin, A. Vacca, F. Zanobini, J. Am. Chem. Soc. 112 (1990) 9190.
[8] H. Yan, M. Alvarez, N. Lugan and R. Mathieu, J. Chem. Soc., Chem. Commun. (1995) 1721.
[9] E.W. Ainscough, A.M. Brodie, M.J. Halstead, J.M. Waters, Abstracts of the 9th National Convention of the Royal Australian Chemical Institute, Melbourne, 1992, T1–37.
[10] E.W. Ainscough, A.M. Brodie, X. Fan and J.M. Waters,

Abstracts of the 1995 International Chemical Congress of Pacific Basin Societies, Honolulu, 1995, INOR 062.
[11] E.W. Ainscough, A.M. Brodie, A.K. Burrell, S.M.F. Kennedy, J. Organomet. Chem. 609 (2000) 2.
[12] E.W. Ainscough, A.M. Brodie, P.D. Buckley, A.K. Burrell, S.M.F. Kennedy, J.M. Waters, J. Chem. Soc., Dalton Trans. (2000) 2663.
[13] E.W. Ainscough, A.M. Brodie, X. Fan, J.M. Waters, unpublished results.
[14] H.R. Hudson, in: F.R. Hartley (Ed.), The Chemistry of Organophosphorus Compounds, vol. 1, John Wiley and Sons, Chichester, 1990, p. 445.
[15] D. Seyferth, D.W. Welch, J. Organomet. Chem. 2 (1964) 1.
[16] S.O. Grim, R.C. Barth, J.D. Mitchell, J.D. Gaudio, Inorg. Chem. 16 (1977) 1776.
[17] S.O. Grim, G.T. Andrews, I.J. Colqu-Houn, W. McFarlane, J. Chem. Soc., Dalton Trans. (1982) 2353.
[18] D.G. Gilheany, in: F.R. Hartley (Ed.), The Chemistry of Organophosphorus Compounds, vol. 1, John Wiley and Sons, Chichester, 1990, p. 14.
[19] D.G. Gilheany, in: F.R. Hartley (Ed.), The Chemistry of Organophosphorus Compounds, vol. 2, John Wiley and Sons, Chichester, 1992, p. 11.
[20] K. Nakamoto, Infrared and Raman Spectra of Inorganic and Coordination Compounds Part B, 5th ed., John Wiley and Sons, New York, 1997.
[21] W.J. Geary, Co-ord. Chem. Rev. 7 (1971) 81.
[22] International Tables for X-ray Crystallography, Vol. 3, Kynoch Press, Birmingham, 1962.
[23] G. Becker, W. Massa, O. Mundt, R.E. Schmidt, C. Witthauer, Z. Anorg. Allg. Chem. 540-541 (1986) 336.
[24] M.K. Cooper, J.M. Downes, P.A. Duckworth, Inorg. Synth. 25 (1989) 129.
[25] J.E. Hoots, T.B. Rauchfuss, D.A. Wrobleski, Inorg. Synth. 21 (1982) 175.
[26] L. Zsolnai, Program ZORTEP, University of Heidelberg, 1994.
[27] L.J. Farrugia, ORTEP3 for Windows, University of Glasgow, 1996.

PERGAMON

www.elsevier.nl/locate/poly

Polyhedron 19 (2000) 2593–2598

POLYHEDRON

Electron-rich and electron-poor heterobimetallic butterfly clusters: synthesis and structure of $[Ru_3Ir(CO)_8(\mu_3\text{-}H)(\mu\text{-}Cl)_2(\mu\text{-}P^tBu_2)_2(^tBu_2PH)]$ and $[Ru_3Au(CO)_{10}(\mu\text{-}Cl)(^tBu_2PH)]$

Hans-Christian Böttcher *, Marion Graf, Kurt Merzweiler, Christoph Wagner

Department of Chemistry, Martin Luther University, Halle-Wittenberg, Kurt-Mothes-Str. 2, D-06120 Halle/Saale, Germany

Received 6 June 2000; accepted 21 August 2000

Dedicated to Prof. Helmut Hartung on the occasion of his 65th birthday.

Abstract

The cluster $[Ru_3Ir(CO)_8(\mu_3\text{-}H)(\mu\text{-}Cl)_2(\mu\text{-}P^tBu_2)_2(^tBu_2PH)]$ (**3**) has been isolated from the reaction of $[Ru_3(CO)_{12}]$ with $[Ir(^tBu_2PH)_3Cl]$ in refluxing toluene. The analogous reaction of $[Ru_3(CO)_{12}]$ with $[Au(^tBu_2PH)Cl]$ in refluxing THF gave $[Ru_3Au(CO)_{10}(\mu\text{-}Cl)(^tBu_2PH)]$ (**4**) in good yield. The single-crystal X-ray structure analyses reveal both clusters to contain a Ru_3M butterfly skeleton. With respect to the EAN electron count of 62e, **3** can be considered as electron-rich (64e), while **4** is electron-poor (60e). © 2000 Elsevier Science B.V. All rights reserved.

Keywords: Ruthenium; Iridium; Gold; Electron-rich; Cluster; Phosphido-bridged; Crystal structures

Heterometallic metal clusters are of current interest in view of their site-selective reactivity and synergetic effects in catalytic reactions [1]. Recently, we reported the synthesis and X-ray crystal structures of the phosphido-bridged heterometallic clusters $[Ru_3Ir(CO)_7(\mu\text{-}H)_2(\mu_3\text{-}Cl)(\mu\text{-}P^tBu_2)_2(^tBu_2PH)]$ (**1**) and $[Ru_3Rh(CO)_7(\mu_3\text{-}H)(\mu\text{-}Cl)_2(\mu\text{-}P^tBu_2)_2(^tBu_2PH)]$ (**2**) [2,3]. These compounds were obtained by condensation of $[Ru_3(CO)_{12}]$ with mononuclear complexes $[M(^tBu_2PH)_3Cl]$ (M = Rh, Ir). An important feature in these reactions is, that the latter complexes bear secondary phosphine ligands, which are able to form phosphido bridges upon thermolysis. It seems that such reactions preferably work for 4d and 5d metal complexes. On the contrary, the thermal reaction of tri-ruthenium-dodecacarbonyl with $[\{Cu(^tBu_2PH)Cl\}_4]$ affords only homotrinuclear ruthenium clusters, i.e. the copper complex acts merely as ligand transfer reagent [4]. In this paper, we describe new results on the reactions of $[Ru_3(CO)_{12}]$ with $[Ir(^tBu_2PH)_3Cl]$ and $[Au(^tBu_2PH)Cl]$, respectively, yielding two novel tetrametallic butterfly clusters with Ru_3M core.

1. Results and discussion

1.1. Reaction of $[Ru_3(CO)_{12}]$ with $[Ir(^tBu_2PH)_3Cl]$

A more intense study of the ^{31}P NMR spectra of crude product mixtures, obtained from reactions of $[Ru_3(CO)_{12}]$ with $[Ir(^tBu_2PH)_3Cl]$ in refluxing toluene, showed beside the cluster **1** and the compound $[Ru_3(CO)_8(\mu\text{-}H)_2(\mu_3\text{-}PBu^t)(^tBu_2PH)]$, respectively, another unidentified product containing phosphido bridging ligands. Now we could show that using a molar ratio of 1:2 (Ru_3/Ir) results in decreased yields of **1** but leads instead to enhanced yields in the novel product (**3**). After column chromatography on alumina with hexane–diethylether mixtures the novel cluster

* Corresponding author. Tel.: +49-345-552-5634; fax: +49-345-552-7028.

E-mail address: boettcher@chemie.uni-halle.de (H.-C. Böttcher).

0277-5387/00/$ - see front matter © 2000 Elsevier Science B.V. All rights reserved.
PII: S0277-5387(00)00561-1

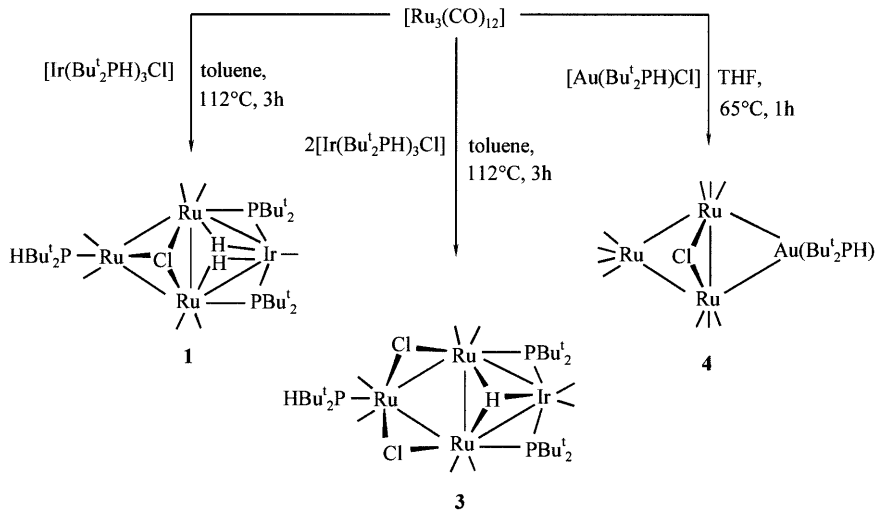
$[Ru_3Ir(CO)_8(\mu_3\text{-}H)(\mu\text{-}Cl)_2(\mu\text{-}P^tBu_2)_2(^tBu_2PH)]$ (**3**) could be isolated in approximately 55% yield (Scheme 1). The molecular structure of **3** in the solid has been unambiguously established by X-ray crystallography (vide infra). Thus it could be shown that a closely related iridium analogue to the complex $[Ru_3Rh(CO)_7(\mu_3\text{-}H)(\mu\text{-}Cl)_2(\mu\text{-}P^tBu_2)_2(^tBu_2PH)]$ (**2**) exists. However in contrast to **2**, electron counting reveals the cluster **3** to be a species containing 64 cluster valence electrons (c.v.e.). By the effective atomic number rule (EAN) for a butterfly configured tetrametal core with five metal-metal bonds 62 c.v.e. are predicted. Therefore, **3** has be to considered as electron-rich cluster [5].

The IR spectrum of **3** in the solid exhibits ν(CO) absorption bands only in the region characteristic of carbonyls in a terminal coordination mode. The $^{31}P\{^1H\}$ NMR spectrum of this compound consists of a signal at δ 267.2 (d, $^3J_{PP} = 15.4$ Hz, μ-P^tBu_2) and a corresponding resonance at δ 45.6 (t, $^3J_{PP} = 15.4$ Hz, $^tBu_2PH$). These data indicate two chemically equivalent phosphorus nuclei of two phosphido bridges across metal-metal bonds which couple with a phosphorus nucleus of a phosphine ligand. A comparison of the ^{31}P chemical shifts for the phosphido bridges in **1** and **3** shows that these ligands resonate for **3** at higher field (**1**: δ 318.2). That is a further indication exhibiting **3** as an electron-rich cluster. (These upfield shifts correlate with increased Ru–P–Ru angles and therefore with an elongation of the Ru–Ru bonds bridged by the phosphido groups.) In accordance with the ^{31}P NMR results, the ^1H NMR spectrum of **3** exhibits the corresponding signals for both phosphine and phosphido ligands. Furthermore a resonance in the metal hydride region at δ −13.77 (t, $^2J_{PP} = 15.5$ Hz, 1H, μ-H) is observed. According to the splitting pattern of the three phosphorus nuclei in the $^{31}P\{^1H\}$ NMR spectrum and the lack of a second coupling in the hydride signal in the proton NMR spectrum a capping position (μ_3) of the hydride on the Ru_2Ir triangle is assumed. Furthermore, the mass spectrum of **3** also confirms the composition; the molecular ion peak and fragment peaks resulting from successive loss of carbonyl ligands were observed.

In the context with the electron-precise compound **2** the evidence of a hypothetical electron-rich cluster $[Ru_3Rh(CO)_8(\mu_3\text{-}H)(\mu\text{-}Cl)_2(\mu\text{-}P^tBu_2)_2(^tBu_2PH)]$ is of interest. In the course of some investigations on **2** we have to note that no reaction of **2** with carbon monoxide under normal conditions (1 bar CO, r.t.) for several hours could be realized. The unchanged starting material was recovered as indicated by NMR measurements. At elevated pressure (60 bar CO, 24 h) a reaction occurs and investigations in this field are under way.

1.2. Reaction of $[Ru_3(CO)_{12}]$ with $[Au(^tBu_2PH)Cl]$

As mentioned above the synthesis of heteronuclear Ru_3Cu frameworks failed by reaction of $[Ru_3(CO)_{12}]$ with the copper(I) complex containing both the chloro and the secondary phosphine ligand. In this context we were interested in the reaction of the ruthenium carbonyl with $[Au(^tBu_2PH)Cl]$ (**5**), which was described by Schmidbaur and Aly [6]. Thus, treatment of **5** with equimolar amounts of $[Ru_3(CO)_{12}]$ in refluxing THF for 30 min results in a colour change of the solution from orange to deep red. Removal of the solvent and recrystallization from hexane yields deep red crystals which were identified by elemental analysis, spectroscopic means, and crystal structure analysis as $[Ru_3Au(CO)_{10}(\mu\text{-}Cl)(^tBu_2PH)]$ (**4**) (Scheme 1). The IR spectrum of **4** in the solid shows ν(CO) absorption bands only in the region characteristic of terminal carbonyl groups. The $^{31}P\{^1H\}$ NMR spectrum of **4** shows merely a singlet at δ 90.55 ($^tBu_2PH$). Therefore,



Scheme 1.

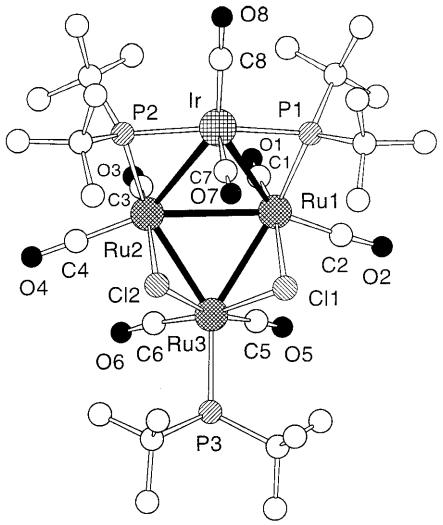


Fig. 1. The molecular structure of $[Ru_3Ir(CO)_8(\mu_3\text{-}H)(\mu\text{-}Cl)_2(\mu\text{-}P^tBu_2)_2(^tBu_2PH)]$ (**3**).

Table 1
Selected bond lengths (Å) and angles (°) for **3**

Ru(1)–Ru(2)	3.1176(7)	Ru(1)–C(2)	1.865(4)
Ru(2)–Ru(3)	2.9246(5)	Ru(2)–C(3)	1.849(4)
Ru(1)–Ru(3)	2.9305(5)	Ru(2)–C(4)	1.860(4)
Ru(1)–Ir	2.9882(4)	Ru(3)–C(5)	1.853(4)
Ru(2)–Ir	3.0309(4)	Ru(3)–C(6)	1.850(4)
Ru(1)–Cl(1)	2.4498(10)	Ir–C(7)	1.979(5)
Ru(3)–Cl(1)	2.4181(10)	Ir–C(8)	1.855(4)
Ru(2)–Cl(2)	2.4247(10)	Ru(1)–P(1)	2.3180(9)
Ru(3)–Cl(2)	2.4347(10)	Ru(2)–P(2)	2.3151(10)
Ru(3)–P(3)	2.4095(9)	Ir–P(1)	2.3361(10)
Ru(1)–C(1)	1.846(4)	Ir–P(2)	2.3343(10)
Ru(1)–Ru(2)–Ru(3)	57.920(13)	C(1)–Ru(1)–Cl(1)	157.86(11)
Ru(1)–Ru(3)–Ru(2)	64.344(14)	C(2)–Ru(1)–Cl(1)	86.85(13)
Ru(3)–Ru(1)–Ru(2)	57.737(13)	P(1)–Ru(1)–Cl(1)	107.21(3)
Ru(1)–Ir–Ru(2)	62.386(13)	Ru(1)–Cl(1)–Ru(3)	74.02(3)
Ru(2)–Ru(1)–Ir	59.479(8)	C(3)–Ru(2)–Cl(2)	154.87(12)
Ru(1)–P(1)–Ir	79.89(3)	C(4)–Ru(2)–Cl(2)	86.00(13)
Ru(2)–P(2)–Ir	81.37(3)	P(2)–Ru(2)–Cl(2)	106.81(3)
Ru(1)–Ir–C(7)	93.52(16)	C(3)–Ru(2)–C(4)	86.01(18)
C(7)–Ir–C(8)	96.17(19)	C(5)–Ru(3)–Cl(1)	94.66(13)
Ru(1)–Ir–C(8)	147.88(13)	C(6)–Ru(3)–Cl(1)	170.95(13)
Ru(2)–Ir–C(8)	146.65(13)	C(5)–Ru(3)–Cl(2)	167.46(11)
P(1)–Ir–C(8)	98.62(13)	C(6)–Ru(3)–Cl(2)	97.33(14)
P(2)–Ir–C(8)	97.90(13)	P(3)–Ru(3)–Cl(1)	98.17(3)
C(1)–Ru(1)–Ir	94.29(11)	P(3)–Ru(3)–Cl(2)	97.72(3)
C(2)–Ru(1)–Ir	147.02(13)	P(1)–Ir–P(2)	156.19(3)
C(3)–Ru(2)–Ir	103.01(12)	Ru(1)–Ru(2)–P(2)	107.09(3)
C(4)–Ru(2)–Ir	145.76(14)	Ru(2)–Ru(1)–P(1)	109.44(3)

the cluster contains only one terminal phosphine ligand, i.e. not any phosphido bridge was formed in the course of the reaction. In accordance with the $^{31}P\{^1H\}$ NMR spectrum, the proton NMR spectrum of **4** exhibits the corresponding signals for the phosphine ligand at δ 4.37 (d, $J_{PH} = 334.5$ Hz, $^tBu_2PH$) and 1.40 (d, $^3J_{PH} = 15.8$ Hz, $^tBu_2PH$). The mass spectrum of **4** confirms the composition, i.e. the molecular ion peak and fragments resulting from successive loss of carbonyl groups were observed.

*1.3. Molecular structures of $[Ru_3Ir(CO)_8(\mu_3\text{-}H)(\mu\text{-}Cl)_2(\mu\text{-}P^tBu_2)_2(^tBu_2PH)]$ (**3**) and $[Ru_3Au(CO)_{10}(\mu\text{-}Cl)(^tBu_2PH)]$ (**4**)*

Compound **3** crystallizes from hexane in the monoclinic space group $P2_1/a$ with four molecules in the unit cell. A representation of the molecule is shown in Fig. 1, selected bond lengths and angles are listed in Table 1. The molecule possesses a butterfly configured tetrametal framework with the iridium occupying one of the wing tips. The metal core is folded with a dihedral angle of 144.96(1)° between the planes [Ru(1)–Ru(2)–Ru(3)] and [Ru(1)–Ru(2)–Ir]. For the compounds **1** and **2** corresponding dihedral angles of 166° and 149°, respectively, were found. The Ru_3Ir core of **3** can be discussed as closed tetrametal framework, although the hinge bond Ru(1)–Ru(2) is with 3.1176(7) Å considerably elongated and the two Ru–Ir bonds can also be considered as long. Therefore, **3** can be discussed as an electron-rich M_4 cluster [5]. The other two Ru–Ru bonds in the Ru_3 triangle are shorter and in good accordance with the closely related situation in **2** [for **2**: Ru(1)–Ru(3), 2.953(1); Ru(2)–Ru(3), 2.956(1) Å]. However, compound **2** is not directly comparable with **3**, because cluster **2** is a 62 c.v.e. species. Nevertheless, an elongated hinge bond was also detected in **2**, and up to now an explanation for this circumstance is lacking.

The presence of two or more phosphido bridges is often a recurring feature of formally electron-rich clusters as outlined by Carty and coworkers [5]. These bridging ligands practise a stabilizing influence towards fragmentation even in the case if an excess of electrons in the cluster core is present. From our laboratory we can confirm this by the closed 52e-cluster $[Ru_3(CO)_9(\mu\text{-}H)(\mu\text{-}PCy_2)_3]$ [7], whereas the closed 50e-cluster $[Ru_3(CO)_6(\mu\text{-}Cl)_3(\mu\text{-}P^tBu_2)(^tBu_2PH)]$ contains only one phosphido bridge [4]. An inspection of the metal-metal distances in the Ru_3Ir clusters **1** and **3** yields a generally expanded metal framework for **3** [**1**: Ru(1)–Ru(2), 2.651(1); Ru(1)–Ru(3), 2.798(1); Ru(2)–Ru(3), 2.724(1); Ru(1)–Ir, 2.748(1), Ru(2)–Ir, 2.720(1) Å; for **3** see Table 1]. As reviewed by Carty and coworkers the cluster expansion of **3** shows the form of three long and two normal bonds, and in the first instance one would expect a similar situation as described for the 64e clusters $[Ru_4(CO)_{13}(\mu\text{-}PR_2)_2]$ (R = Ph, ^{i}Pr, OEt, N^{i}Pr$_2$; **5a–d**) [5,8]. However a remarkable difference between the structures of **5a–d** and **3** exists: the Ru_4 butterfly frameworks of **5a–d** are almost planar with dihedral angles between the two Ru_3 triangles of 173°–180°, whereas **3** is more folded (145°). Therefore, it seems not meaningful to use the EHMO calculations for **5a–d**,

which include a distribution of the additional two electrons in an antibonding molecular orbital localized on the $M_3(\mu\text{-}PR_2)_2$ triangle [8]. The hydrido ligand in **3** could not be located directly during the X-ray analysis, however by means of the observed NMR data (vide supra) a capping position of the latter on the Ru_2Ir triangle is reasonable to assume. In contrast to the molecule of **2**, in which the rhodium bears only one carbonyl group, the coordination sphere of the iridium in **3** is completed by a further carbonyl ligand. The same effect was observed in the two complexes $[CoRh(CO)_4(\mu\text{-}H)(\mu\text{-}P^tBu_2)(^tBu_2PH)]$ [9] and $[CoIr(CO)_5(\mu\text{-}H)(\mu\text{-}P^tBu_2)(^tBu_2PH)]$ [10]. Thus, that confirms the tendency of the iridium to pursuit of higher coordination numbers.

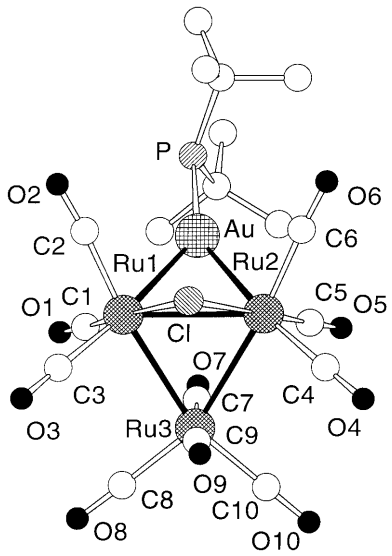


Fig. 2. The molecular structure of $[Ru_3Au(CO)_{10}(\mu\text{-}Cl)(^tBu_2PH)]$ (**4**).

Table 2
Selected bond lengths (Å) and angles (°) for **4**

Ru(1)–Ru(2)	2.8581(13)	Ru(2)–C(4)	1.918(13)
Ru(1)–Ru(3)	2.8148(12)	Ru(2)–C(5)	1.851(10)
Ru(3)–Ru(2)	2.8196(12)	Ru(2)–C(6)	1.949(9)
Ru(1)–Au	2.7548(11)	Ru(2)–Cl	2.428(2)
Ru(2)–Au	2.7679(15)	Ru(3)–C(7)	1.944(11)
Ru(1)–C(1)	1.859(10)	Ru(3)–C(8)	1.915(10)
Ru(1)–C(2)	1.934(11)	Ru(3)–C(9)	1.950(11)
Ru(1)–C(3)	1.925(11)	Ru(3)–C(10)	1.915(11)
Ru(1)–Cl	2.437(2)	Au–P	2.313(3)
Ru(1)–Ru(2)–Ru(3)	59.44(3)	C(5)–Ru(2)–Cl	171.5(3)
Ru(3)–Ru(1)–Ru(2)	59.60(3)	C(6)–Ru(2)–Cl	89.7(3)
Ru(1)–Au–Ru(2)	62.33(3)	C(5)–Ru(2)–Ru(1)	117.4(3)
Ru(1)–Ru(2)–Au	58.61(3)	C(6)–Ru(2)–Ru(1)	114.0(3)
Ru(2)–Ru(1)–Au	59.06(4)	C(4)–Ru(2)–C(5)	91.3(4)
Ru(1)–Cl–Ru(2)	71.95(7)	C(4)–Ru(2)–C(6)	99.7(5)
Ru(2)–Ru(1)–Cl	53.87(6)	C(5)–Ru(2)–C(6)	93.5(4)
Ru(3)–Ru(2)–Cl	87.90(6)	C(4)–Ru(2)–Cl	95.9(3)
Ru(1)–Ru(2)–Cl	54.18(6)	C(7)–Ru(3)–Ru(1)	85.6(3)
Ru(3)–Ru(1)–Cl	87.82(7)	C(8)–Ru(3)–Ru(1)	97.8(3)
P–Au–Ru(1)	144.58(13)	C(9)–Ru(3)–Ru(1)	86.8(4)
P–Au–Ru(2)	153.02(12)	C(10)–Ru(3)–Ru(1)	162.2(3)
C(1)–Ru(1)–Ru(2)	117.5(3)	C(7)–Ru(3)–Ru(2)	87.5(3)
C(2)–Ru(1)–Ru(2)	113.5(3)	C(8)–Ru(3)–Ru(2)	158.6(3)
C(3)–Ru(1)–Ru(2)	131.6(4)	C(9)–Ru(3)–Ru(2)	82.8(3)
C(1)–Ru(1)–Cl	171.4(3)	C(10)–Ru(3)–Ru(2)	101.3(3)
C(2)–Ru(1)–Cl	90.5(3)	C(7)–Ru(3)–C(8)	93.5(4)
C(3)–Ru(1)–Cl	93.5(3)	C(9)–Ru(3)–C(8)	94.3(4)
C(1)–Ru(1)–C(2)	93.9(5)	C(10)–Ru(3)–C(8)	100.0(5)
C(1)–Ru(1)–C(3)	93.0(4)	C(9)–Ru(3)–C(10)	92.5(5)
C(2)–Ru(1)–C(3)	99.7(5)	C(7)–Ru(3)–C(10)	92.5(4)

Compound **4** crystallizes from hexane in the triclinic space group $P\bar{1}$ with two molecules in the unit cell. The molecular structure of **4** is shown in Fig. 2, selected bond lengths and angles are summarized in Table 2. The molecule exhibits a 'butterfly' tetrametal framework with the gold atom in one of the wing tip positions. A localized bonding description in butterfly clusters suggests a total valence electron count of 62. Because **4** exhibits only 60 c.v.e the compound can be considered in the sense of the EAN rule as electron-poor species. The metal core of **4** is strongly folded with a dihedral angle of 120.11(1)° between the planes [Ru(1)–Ru(2)–Ru(3)] and [Ru(1)–Ru(2)–Au]. A closely related molecular structure was described for the cluster $[Ru_3Au(CO)_{10}(\mu\text{-}Cl)(PPh_3)]$ (**6**) [11]. The geometric features and bondlength characteristics between **4** and **6** are in very good agreement. As described for the latter, also we found that **4** is only stable under mild conditions, i.e. heating in solvents with higher boiling points like THF leads to rapid decomposition. Attempts to synthesize phosphido-bridged heteronuclear clusters containing gold failed by this way.

2. Experimental

2.1. General considerations

All reactions were performed under argon atmosphere, using conventional Schlenk techniques. Solvents were dried over sodium/benzophenone ketyl or molecular sieves and were distilled under argon prior to use. Starting materials were either commercially available or were prepared as described before: $[Ir(^tBu_2PH)_3Cl]$ [12]; $[Au(^tBu_2PH)Cl]$ was prepared in analogy to the synthesis of $[Au(Ph_2PH)Cl]$ [13]. IR spectra were obtained using a Mattson 5000 instrument. The NMR spectra were recorded on a Bruker WP 200 spectrometer (^1H at 199.975 MHz, reference TMS; $^{31}P\{^1H\}$ NMR at 80.950 MHz, reference 85% H_3PO_4 as external standard). The mass spectra were obtained on a Hitachi Perkin–Elmer RMU 6, Nermag R 30-10 instrument. The elemental analyses were performed by the Analytisches Laboratorium des Institutes für Organische Chemie, Martin-Luther-Universität Halle.

Table 3
Crystal data and details of the X-ray analysis for **3** and **4**

Complex	**3**	**4**
Empirical formula	$C_{32}H_{55}Cl_2IrO_8P_3Ru_3$	$C_{18}H_{18}AuClO_{10}PRu_3$
Formula weight	1226.98	960.92
Temperature (K)	220(2)	293(2)
Wavelength (Å)	0.71073	0.71073
Crystal system	monoclinic	triclinic
Space group	$P2_1/a$	$P\bar{1}$
Unit cell dimensions		
a (Å)	17.766(3)	9.418(2)
b (Å)	12.0943(15)	11.584(3)
c (Å)	21.401(4)	13.363(3)
α (°)	90	91.73(3)
β (°)	109.88(2)	103.25(3)
γ (°)	90	103.69(3)
V (Å^3)	4324.3(12)	1373.1(6)
Z	4	2
D_{calc} (g cm^{-3})	1.885	2.324
Absorption coefficient (mm^{-1})	4.372	7.144
$F(000)$	2396	898
θ Range for data collection (°)	2.08–26.12	2.55–25.00
Index ranges	$-21 \le h \le 21$, $-14 \le k \le 14$, $-26 \le l \le 24$	$-11 \le h \le 11$, $-13 \le k \le 13$, $-15 \le l \le 15$
Reflections collected	26878	9861
Independent reflections	8426	4547
Refinement method	Full-matrix least-squares on F^2	
Data/restraints/parameters	8426/0/629	4547/0/307
Goodness-of-fit on F^2	1.021	1.054
Final R indices $[I>2\sigma(I)]$	$R_1 = 0.0246$	$R_1 = 0.0508$
	$wR2 = 0.0591$	$wR2 = 0.1303$
R indices (all data)	$R1 = 0.0311$	$R1 = 0.0608$
	$wR2 = 0.0612$	$wR2 = 0.1377$
Largest difference peak and hole (e Å^{-3})	1.801/−1.348	3.466/−2.377

2.2. Preparation of *[Ru$_3$Ir(CO)$_8$(μ_3-H)(μ-Cl)$_2$(μ-P^{t}Bu$_2$)$_2$(^{t}Bu$_2$PH)]* (**3**)

A mixture of [Ir(^{t}Bu$_2$PH)$_3$Cl] (1.33 g, 2 mmol) and [Ru$_3$(CO)$_{12}$] (0.64 g, 1 mmol) was heated in refluxing toluene (40 cm^3) for 3 h. After cooling to room temperature (r.t.) and removing the solvent, the remaining residue was extracted three times with 20 ml portions of heptane. The volume of the combined extracts was reduced to 10 cm^3 and separated by column chromatography on alumina with hexane as eluent. The orange–red fraction contains complex **3** which was crystallized from hexane at −30°C. Yield: 0.68 g (55%) based on [Ru$_3$(CO)$_{12}$].

2.2.1. Analytical data for **3**

Found: C, 31.47, H, 4.52, Cl, 5.83, P, 7.89; Calc. for $C_{32}H_{56}Cl_2IrO_8P_3Ru_3$: C, 31.30, H, 4.60, Cl, 5.77, P, 7.57%. IR (KBr pellet, cm^{-1}): ν(CO): 2020(s), 1991(s), 1962(m), 1940(s), 1915(sh). ^{1}H NMR ($CDCl_3$): δ 5.14 (d, $J_{PH} = 326.4$ Hz, 1H, ^{t}Bu$_2$P*H*), 1.54 (d, $^3J_{PH} = 14.8$ Hz, 18H, ^{t}Bu$_2$PH), 1.52 (d, $^3J_{PH} = 15.2$ Hz, 36H, μ-P^{t}Bu$_2$), −13.77 (t, $^2J_{PH} = 15.5$ Hz, 1H, μ-H). ^{31}P{^{1}H} NMR ($CDCl_3$): δ 267.2 (d, $^3J_{PP} = 15.5$ Hz, μ-*P*^{t}Bu$_2$); 45.7 (t, $^3J_{PP} = 15.5$ Hz, ^{t}Bu$_2$*PH*). Mass spectrum: $m/z = 1228$ $[M]^+$, 1200 $[M-CO]^+$, 1172 $[M-2CO]^+$, 1144 $[M-3CO]^+$, 1116 $[M-4CO]^+$, 1088 $[M-5CO]^+$, 1060 $[M-6CO]^+$, 1032 $[M-7CO]^+$, 1004 $[M-8CO]^+$.

2.3. Preparation of *[Ru$_3$Au(CO)$_{10}$(μ-Cl)(^{t}Bu$_2$PH)]* (**4**)

A sample of [Au(^{t}Bu$_2$PH)Cl] (0.38 g, 1 mmol) was dissolved in 30 cm^3 of THF in a Schlenk tube and [Ru$_3$(CO)$_{12}$] (0.64 g, 1 mmol) was added. The mixture was stirred under reflux for 30 min. After cooling to r.t. and removal of the solvent, the residue was dissolved with hexane (30 cm^3). The complex **4** was crystallized from the hexane solution at −30°C as red crystals. Yield: 0.69 g (72%) based on [Ru$_3$(CO)$_{12}$].

2.3.1. Analytical data for **4**

Found: C, 22.34, H, 2.11, Cl, 4.02, P, 3.05; Calc. for $C_{18}H_{19}AuCl_{10}O_{10}PRu_3$: C, 22.48, H, 1.99, Cl, 3.69, P, 3.22%. IR (KBr pellet, cm^{-1}): ν(CO): 2088(m), 2050(s), 2024(vs), 1987(vs), 1976(sh), 1966(m), 1955(s). ^{1}H NMR ($CDCl_3$): δ 4.37 (d, $J_{PH} = 334.5$ Hz, 1H, ^{t}Bu$_2$P*H*), 1.40 (d, $^3J_{PH} = 15.8$ Hz, ^{t}Bu$_2$PH). ^{31}P{^{1}H} NMR (C_6D_6): δ 90.55 (s, ^{t}Bu$_2$PH). Mass spectrum: $m/z = 962$ $[M]^+$, 934 $[M-CO]^+$, 906 $[M-2CO]^+$, 878 $[M-3CO]^+$, 850 $[M-4CO]^+$, 822 $[M-5CO]^+$, 794 $[M-6CO]^+$, 766 $[M-7CO]^+$.

2.4. X-ray crystal structure determinations of **3** and **4**

Crystal data, data collection and refinement parameters are summarized in Table 3. Crystals of **3** and **4** suitable for X-ray diffraction studies were grown by crystallization from hexane. For data collection the diffractometer Stoe-IPDS was used. The structure was solved by direct methods and refined on F^2 [14]. The refinement of the crystal structure of **4** showed, that there is some positional disorder in the P^{t}Bu$_2$ groups. There seem to be two alternative orientations of the phosphido groups which are only 0.88 Å apart from each other. Therefore, the disorder could not be resolved completely and only a splitting of the phosphorus positions (ratio 77:23) could be taken into account.

3. Supplementary material

Crystallographic data for the structures reported in this paper have been deposited with the Cambridge

Crystallographic Data Centre, CCDC No. 142329 for **3** and CCDC No. 142328 for **4**. Copies of this information may be obtained free of charge from the Director, CCDC, 12 Union Road, Cambridge, CB2 1EZ, UK (fax: +44-1223-336033; e-mail: deposit@ccdc.cam.ac.uk or http://www.ccdc.cam.ac.uk).

Acknowledgements

We thank the Kulturministerium des Landes Sachsen-Anhalt and the Fonds der Chemischen Industrie for financial support as well as Degussa AG for a generous loan of $RuCl_3 \cdot 3H_2O$ and $HAuCl_4 \cdot 3H_2O$.

References

[1] P. Braunstein, L.A. Oro, P.R. Raithby ((Eds.), Metal Clusters in Chemistry, Wiley-VCH, Weinheim, 1999.
[2] H.-C. Böttcher, M. Graf, K. Merzweiler, J. Organomet. Chem. 531 (1997) 107.
[3] H.-C. Böttcher, M. Graf, K. Merzweiler, J. Organomet. Chem. 534 (1997) 43.
[4] H.-C. Böttcher, M. Graf, K. Merzweiler, C. Bruhn, Polyhedron 16 (1997) 3253.
[5] J.F. Corrigan, Y. Sun, A.J. Carty, New J. Chem. 18 (1994) 77.
[6] H. Schmidbaur, A.A.M. Aly, Z. Naturforsch. 34b (1979) 23.
[7] H.-C. Böttcher, M. Graf, K. Merzweiler, C. Bruhn, Polyhedron 17 (1998) 3433.
[8] J.F. Corrigan, M. Dinardo, S. Doherty, G. Hogarth, Y. Sun, N.J. Taylor, A.J. Carty, Organometallics 13 (1994) 3572.
[9] B. Walther, H.-C. Böttcher, M. Scheer, G. Fischer, D. Fenske, G. Süss-Fink, J. Organomet. Chem. 437 (1992) 307.
[10] H.-C. Böttcher, M. Graf, K. Merzweiler, J. Organomet. Chem. 525 (1996) 191.
[11] G. Lavigne, F. Papageorgiou, J.-J. Bonnet, Inorg. Chem. 23 (1984) 609.
[12] H.-C. Böttcher, M. Graf, K. Merzweiler, Polyhedron 16 (1997) 341.
[13] J. Vicente, M.T. Chicote, P.G. Jones, Inorg. Chem. 32 (1993) 4960.
[14] G.M. Sheldrick, Acta Crystallogr., Sect. A 46 (1990) 467.

PERGAMON

www.elsevier.nl/locate/poly

Polyhedron 19 (2000) 2599–2604

POLYHEDRON

Crystal structure and antitumor activity of some rare earth metal complexes with Schiff base

Zheng-Yin Yang [a,*], Ru-Dong Yang [a], Fa-Shen Li [b], Kai-Bei Yu [c]

[a] *Department of Chemistry, Lanzhou University, Lanzhou 730000, People's Republic of China*
[b] *Department of Physics, Lanzhou University, Lanzhou 730000, People's Republic of China*
[c] *Chengdu Center of Analysis and Determination, Chengdu Branch, Chinese Academy of Sciences, Chengdu, People's Republic of China*

Received 14 June 2000; accepted 23 August 2000

Abstract

The ligand 1-phenyl-3-methyl-5-hydroxy-4-pyrazolyl phenyl ketone (PMBP) isonicotinoyl hydrazone (H_2L) was prepared by condensation of PMBP with isoniazid. Seven complexes of rare earth metals with H_2L were synthesized and characterized on the basis of elemental analyses, IR, UV, ^1H NMR spectra and thermal analyses. The general formula of the complexes is $Ln(HL)_3{\cdot}3.5H_2O$ (where Ln(III) = La, Eu, Gd, Tb, Dy, Ho and Er). X-ray diffraction analysis showed that the coordination polyhedron of the Eu complex is a tricapped trigonal prism. The La and Eu complexes possess antitumor activity, and the inhibitory rates for leukemia cells (L_{1210}) are 87.1% and 78.5%, respectively. © 2000 Elsevier Science B.V. All rights reserved.

Keywords: Rare earth complex; Crystal structure; Antitumour activity; Hydrazone

1. Introduction

Complexes of Schiff bases with paramagnetic metal ions have received the most attention as a new class of potential magnetic resonance imaging (MRI) contrast agent [1–3], and manganese Schiff base complexes have been demonstrated to be effective as imaging agents for liver and kidneys [3]. In addition, a great many Schiff base complexes with metals have also provoked wide interest because they possess a diverse spectrum of biological and pharmaceutical activities, such as antitumor and antioxidative activities, as well as the inhibition of lipid peroxidation and so on [4–9]. Our previous works showed that the light rare earth complexes with PMBP-isonicotinoyl hydrazone (H_2L) have certain scavenger effects on $OH^{\bullet}$ and $O_2^{-\bullet}$ radicals, and inhibitory action on lipid peroxidation [10]. In order to investigate further their pharmaceutical activity, several additional rare earth complexes have been synthesized on the basis of our previous work, and the crystal structure of the Eu complex was determined by X-ray diffraction analysis (Fig. 1).

2. Experimental

2.1. Material

1-Phenyl-3-methyl-4-benzoyl-5-pyrazolone (PMBP) and isoniazid were produced in China. The hydrated rare earth (III) chlorides were prepared by dissolving Ln_2O_3 in concentrated HCl, then crystallizing the products. All chemicals used were of analytical grade.

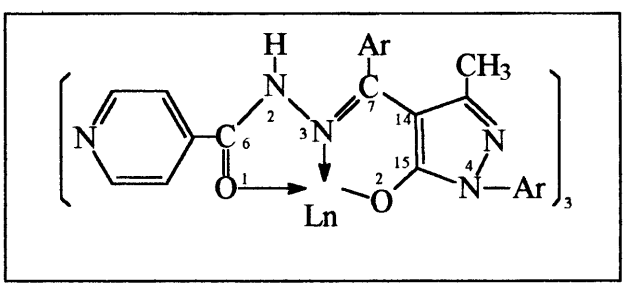


Fig. 1. Diagram of the complexes.

* Corresponding author. Tel.: 86-931-891-3515; fax: +86-931-891-2582.
E-mail address: yangzy@lzu.edu.cn (Z.-Y. Yang).

0277-5387/00/$ - see front matter © 2000 Elsevier Science B.V. All rights reserved.
PII: S0277-5387(00)00562-3

Table 1
Elemental analysis and molar conductivity

Formula	Color	Yield (%)	C (%)		H (%)		N (%)		Ln(%)		Λ (U) [a]
			Calc.	Found	Calc.	Found	Calc.	Found	Calc.	Found	
$C_{23}H_{19}N_5O_2$	yellow	82	69.50	69.43	4.82	4.89	17.26	17.08			
$LaC_{69}H_{61}N_{15}O_{9.5}$	yellow	64	59.57	59.36	4.42	4.39	15.10	15.08	9.98	10.02	3.24
$EuC_{69}H_{61}N_{15}O_{9.5}$	yellow	65	59.02	59.24	4.38	4.24	14.96	14.91	10.82	11.01	3.75
$GdC_{69}H_{61}N_{15}O_{9.5}$	yellow	68	58.79	58.86	4.36	4.32	14.90	14.93	11.11	11.21	8.51
$TbC_{69}H_{61}N_{15}O_{9.5}$	yellow	72	58.72	59.01	4.36	4.39	14.89	14.71	11.26	11.28	4.69
$DyC_{69}H_{61}N_{15}O_{9.5}$	yellow	74	58.58	58.46	4.35	4.36	14.85	14.75	11.40	11.51	6.72
$HoC_{69}H_{61}N_{15}O_{9.5}$	yellow	73	58.48	58.67	4.34	4.31	14.85	14.67	11.60	11.68	7.65
$ErC_{69}H_{61}N_{15}O_{9.5}$	yellow	69	58.38	58.59	4.33	4.21	14.80	14.63	11.78	11.80	5.23

[a] $U = \Omega^{-1}\ cm^2\ mol^{-1}$.

2.2. Physical measurements

Carbon, hydrogen and nitrogen were analyzed on a Carlo Erba 1106 elemental analyzer. The metal contents of the complexes were determined by titration with EDTA volumetric method using xylenol orange tetrasodium salt (1% alcoholic solution) as an indicator [11]. Infrared spectra (4000–400 cm^{-1}) were determined with KBr optics on a Nicolet 5DX IR spectrophotometer. Ultraviolet spectra were recorded on a Shimadzu UV-240 spectrophotometer. The thermal behavior was monitored on a PCT-2 differential thermal analyzer. The molar conductance values were determined in ethanol on a DSS-11A conductivity meter. An orange yellow crystal of the Eu complex ($0.50 \times 0.44 \times 0.36$ mm) was mounted on a Siemens P_4 diffractometer, and determined with Mo Kα radiation. Intensities were measured using $\theta/2\theta$ scan technique, 2θ range $3.44 \leq 2\theta \leq 54.98°$ ($h = -1$–24, $k = -24$–1, $l = -1$–44); 6295 independent reflections were collected with Siemens XSCANS program at 295(2) K, 5452 observed [$I > 3\sigma(I)$] which were used to solve the structure and least-squares refinement. The diffraction data were corrected by the LP factor; absorption correction was made semi-empirically from ψ-scans. The europium atom was located from a Patterson function and the other non-hydrogen atoms from Fourier synthesis. The structure was refined by full-matrix least-squares on F^2. All hydrogen atoms, except ones on C_{11} and C_{12}, were located from a difference-Fourier synthesis. The final R index [$I > 2\sigma(I)$] was equal to 0.0457 ($R_w = 0.1394$), $\Delta/\sigma_{max} = 1.304$, $F(000) = 4368$, μ(Mo Kα) = 0.0940 cm^{-1}. All calculation was completed on a PC486 computer with the SHELXTL 5.03 program.

2.3. Preparation of the ligand

1.08 g of isoniazid (8 mmol) and 2.23g of PMBP (8 mmol) were dissolved in ethanol (300 ml), and refluxed on a water bath for 1 h [10]. The color of the solution changed from light yellow to deep red. After cooling to room temperature, a large amount of red precipitate separated out. The product was purified by crystallization with anhydrous ethanol, yield 82%. m.p. 244–245°C. *Anal.* Found: C, 69.43; H, 4.89; N, 17.08. Calc. for $C_{23}H_{19}N_5O_2$: C, 69.50; H, 4.82; N, 17.26%. ^{1}H NMR (DMSO-d_6), δ (ppm): 1.50 (3H, singlet, CH_3); 7.10–7.90 (11H, multiplet, 2 phenyl, –NH–); 8.20 (2H, doublet, $J = 6$ Hz, H^3, H^5 of pyridine ring); 8.76 (2H, broadband, H^2, H^6 of pyridine ring).

2.4. Preparation of the complexes

1.58 g of ligand H_2L (8 mmol) was added to water (80 ml), the pH of which was adjusted to 7 by the addition of an aqueous solution of NaOH (10%); the solution turned light yellow. Then a solution of $EuCl_3 \cdot 6H_2O$ (3 mmol) in water (20 ml) was added dropwise to the system. After stirring at 50°C for 0.5 h, a yellow precipitate was separated by filtration, washed several times with water, and hot ethanol, respectively, and dried in a vacuum, yield]: 65% (Table 1). The other complexes were also synthesized by this method.

20 mg of Eu complex was dissolved in 20 ml of methanol, then the solution was filtrated and diluted with 40 ml of ethanol. After a week at room temperature, the crystalline complex separated out. *Anal.* Found: C, 58.46; H, 4.38; N, 14.54; Eu, 10.31. Calc. for $EuC_{69.5}H_{63}N_{15}O_{10}$: C, 58.77; H, 4.47; N, 14.79; Eu, 10.70%.

3. Results and discussion

All complexes are yellow, soluble in DMSO, ethanol and methanol, a little soluble in water, insoluble in benzene and diethyl ether. The molar conductivity of the complexes is around 3.24–8.51 $\Omega^{-1}\ cm^2\ mol^{-1}$ in ethanol (Table 1). This shows that all the complexes are non-electrolytes in ethanol [12]. The elemental analyses

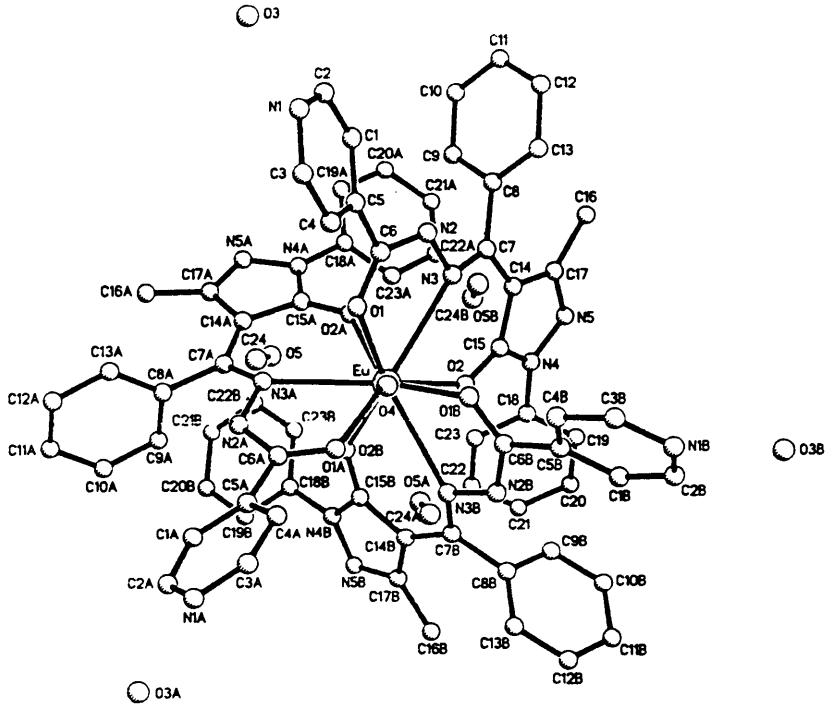


Fig. 2. Structure of the Eu complex.

(Table 1) show the formula of the complexes is $Ln(HL)_3{\cdot}3.5H_2O$ (Ln = La, Eu, Gd–Er), with three and a half H_2O for each complex confirmed by thermal analyses.

3.1. Description of the crystal structure

The crystal of the Eu complex is rhombohedral, space group R_3 with $Z = 6$, unit-cell dimensions $a =$ 19.1354(11), $b = 19.1354(11)$, $c = 33.918(4)$ Å, $\alpha = \beta =$ 90°, and $\gamma = 120°$, $V = 10756(2)$ Å^3, $D_c = 1.316$ g cm^{-3}. The complex in water is a yellow powder, but it is an orange yellow crystal after crystallizing in a mixed solvent of methanol and ethanol (1:2). The formula of the complex in the crystalloid form is $C_{69.5}H_{63}$-$EuN_{15}O_{10}$. It is different from the complex in powder form, which has been confirmed by elemental analyses. X-ray diffraction analyses show that there are not only three and a half lattice waters but also a half methanol molecule in each complex unit, $Eu(HL)_3{\cdot}3.5H_2O{\cdot}$ $0.5HOCH_3$ (Fig. 2), and six complex units in the unit cell. The coordination polyhedron is a tricapped trigonal prism configuration with the nine-coordinate atoms composed of three nitrogens and six oxygens from three ligand (HL–) (Fig. 3). The crystal is a highly symmetric rhomb with a principal axis, 3, of symmetry. Some important bond lengths and angles are given in Tables 2 and 3, respectively. The data for C6–O1 (1.231 Å) and C15–O2 (1.268 Å) bond lengths show that the carbonyl 6 is still a double bond, but carbonyl 15 inclines to a monobond in the complexes (Fig. 1). The C6–N2 is similar to a double bond, confirmed by C15–N4 (1.365 Å) > C6–N2 (1.325 Å) > C7–N3 (1.304 Å). All of these demonstrate that the oxygen (O2) of carbonyl 15 takes part in coordination by the enolic form, and its active hydrogen is replaced by Eu,

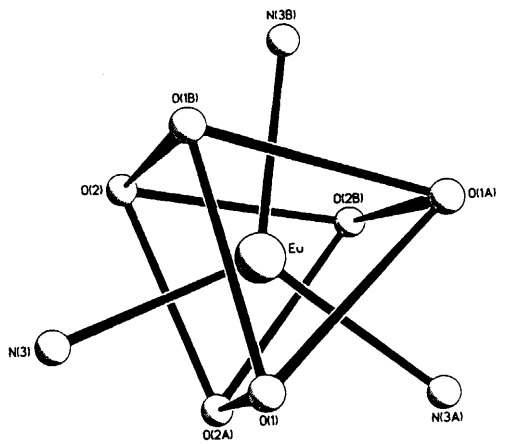


Fig. 3. The coordination polyhedron.

Table 2
Important bond lengths (Å)

Eu–O2	2.301(3)	Eu–O2A	2.301(3)	Eu–N3	2.725(4)
Eu–O2B	2.301(3)	Eu–O1B	2.462(3)	Eu–N3A	2.725(4)
Eu–O1	2.462(3)	Eu–O1A	2.462(3)	Eu–N3B	2.725(4)

Table 3
Important bond angles (°)

O2–Eu–O2A	82.92(12)	O2–Eu–O2B	82.92(12)
O2A–Eu–O2B	82.92(12)	O2–Eu–O1B	85.49(12)
O2A–Eu–O1B	141.68(11)	O2B–Eu–O1B	131.58(11)
O2–Eu–O1	131.58(10)	O2A–Eu–O1	85.49(12)
O2B–Eu–O1	141.68(11)	O1B–Eu–O1	75.38(12)
O2–Eu–O1A	141.68(11)	O2A–Eu–O1A	131.58(10)
O2B–Eu–O1A	85.49(12)	O1B–Eu–O1A	75.38(12)
O1–Eu–O1A	75.38(13)	O2–Eu–N3	69.62(10)
O2A–Eu–N3	69.33(11)	O2B–Eu–N3	142.64(11)
O1B–Eu–N3	72.39(11)	O1–Eu–N3	62.30(10)
O1A–Eu–N3	131.65(11)	O2–Eu–N3B	69.33(11)
O2A–Eu–N3B	142.64(11)	O2B–Eu–N3B	69.62(10)
O1B–Eu–N3B	62.30(10)	O1–Eu–N3B	131.65(11)
O1A–Eu–N2B	72.39(11)	N3–Eu–N3B	119.768(13)
O2–Eu–N3A	142.64(11)	O2A–Eu–N3A	69.62(10)
O2B–Eu–N3A	69.33(11)	O1B–Eu–N3A	131.65(11)
O1–Eu–N3A	72.39(11)	O1A–Eu–N3A	62.30(10)
N3–Eu–N3A	119.768(12)	N3B–Eu–N3A	119.768(13)
C6–O1–Eu	124.3(3)	C15–O2–Eu	138.2(3)
N2–N3–Eu	110.3(2)	C7–N3–Eu	131.6(3)

but those (O1) of the carbonyl 6 do not have the enolic form. The data of plane 1 (Table 4) indicate that the five-membered ring composed of Eu, O1, C6, N2 and N3 with the six-membered ring Eu, N3, O2, C7, C14 and C15 is coplanar, forming a large conjugation chelate ring.

3.2. Thermal analysis

Some data of thermal analyses are listed in Table 5. The DTA curves of the complexes have an endothermic peak between 86 and 90°C, the corresponding TG curves show that the weight loss in each complex is equal to three and a half water molecules. These results are in accordance with the compositions of the complexes determined by elemental analyses. Three exothermic peaks appear around 346–363, 458–478 and 628–701°C, respectively. Initial temperature of decomposition is greater than 346°C; this indicates that the thermal stability of the complexes is higher than that of the free ligand which decomposes at 278°C.

3.3. Ultraviolet spectra

UV spectral data of complexes are listed in Table 6. The free ligand exhibits a strong absorption band at 298 nm, and a shoulder peak at 286 nm. The complexes yield two new peaks at approximately 366 and 383 nm, respectively. The two absorption bands approach the region observed. This shows that there is a large conjugate system formed by enolization of the ligand in the complexes. Therefore, the complexes should be a chelate containing both a five-membered and a six-membered ring. This is a reason why the complexes exhibit high thermal stability.

3.4. Infrared spectra

The main stretching frequencies of the IR spectra of the ligand (H_2L) and its complexes are tabulated in Table 7. The aqueous ν(OH) for the complexes appears at 3350 cm^{-1}. $\nu(C_{(6)}{=}O)$ and $\nu(C_{(15)}{=}O)$ vibrations of the free ligand are at 1616 and 1560 cm^{-1}, respectively; these peaks for the complexes shift to 1602, 1434–1441 cm^{-1}. $\Delta\nu$ ($\nu_{ligand} - \nu_{complex}$) of carbonyls 6 and 15 is equal to 14, and 119–126 cm^{-1}. δ_{NNH} vibrations of the free ligand at 1532 cm^{-1} and its complexes at 1539–

Table 4
Planar fragments of the complex; plane 1: $-1.860x + 13.61y + 21.585z = 16.261$

Atom	Eu	O_1	O_2	N_2	N_3	C_6	C_7	C_{14}	C_{15}	N_4	N_5	C_{17}
Δ [a]	−0.2812	−0.1009	0.0390	0.0639	0.1126	−0.0132	−0.0550	−0.0024	0.0180	−0.0166	−0.0110	−0.0207

[a] Δ = deviation.

Table 5
Thermal analysis data of the complexes

Complex	D [a] (°C)	M.p. (°C)	Process	%H_2O loss		Decomposed (°C)			Process	Residue
				Calc.	Found	t_1	t_2	t_3		
H_2L		243	endothermic			278	395	543	exothermic	
$La(HL)_3{\cdot}3.5H_2O$	87		endothermic	4.52	5.1	352	458	628	exothermic	La_2O_3
$Eu(HL)_3{\cdot}3.5H_2O$	90		endothermic	4.49	4.5	361	473	642	exothermic	Eu_2O_3
$Gd(HL)_3{\cdot}3.5H_2O$	89		endothermic	4.47	4.5	359	469	647	exothermic	Gd_2O_3
$Tb(HL)_3{\cdot}3.5H_2O$	91		endothermic	4.46	4.6	346	458	701	exothermic	Tb_4O_7
$Er(HL)_3 \times 3.5H_2O$	86		endothermic	4.44	4.5	363	478	638	exothermic	Er_2O_3

[a] D = Dehydration.

Table 6
Ultraviolet spectral data

Complex	λ_{max} (nm), $\varepsilon \times 10^{-3}$ (L mol^{-1} cm^{-1})									
	λ_1	ε_1	λ_2	ε_2	λ_3	ε_3	λ_4	ε_4	λ_5	ε_5
H_2L	198	1.23	286	5.81	298	6.34				
$La(HL)_3{\cdot}3.5H_2O$	200	4.49	290	6.10	297	30.17	365	12.57	391	7.82
$Eu(HL)_3{\cdot}3.5H_2O$	198	6.81	296	31.36	297	32.55	366	13.61	383	10.95
$Gd(HL)_3{\cdot}3.5H_2O$	198	7.14	285	29.36	297	30.55	368	14.24	393	11.50
$Tb(HL)_3{\cdot}3.5H_2O$	198	7.15	286	29.14	297	40.24	367	18.78	384	15.80
$Dy(HL)_3{\cdot}3.5H_2O$	199	6.91	285	29.94	297	39.89	365	19.20	384	14.80
$Ho(HL)_3{\cdot}3.5H_2O$	199	6.93	285	38.93	298	29.24	365	9.02	383	16.53
$Er(HL)_3{\cdot}3.5H_2O$	197	3.74	285	29.54	298	29.54	364	10.15	383	15.03

Table 7
Some IR data of the ligand and its complexes

Complex	ν_{OH}	ν_{NH}	$\nu_{C(6)=O}$	$\nu_{C=N}$	$\nu_{C(15)=O}$	δ_{HOH}	δ_{NNH}	ν_{M-O}	ν_{M-N}
H_2L		3058m	1616m	1588w	1560s		1532m		
$La(HL)_3{\cdot}3.5H_2O$	3353m	3051m	1602m	1571w	1434s	1638s	1539s	456w	405w
$Eu(HL)_3{\cdot}3.5H_2O$	3360m	3058m	1602m	1574w	1434m	1638s	1546m	456w	410w
$Gd(HL)_3{\cdot}3.5H_2O$	3353m	3051m	1602m	1574w	1434m	1638s	1546s	456w	408w
$Tb(HL)_3{\cdot}3.5H_2O$	3360m	3058m	1602m	1574w	1441m	1638s	1546m	456w	405w
$Dy(HL)_3{\cdot}3.5H_2O$	3360m	3058m	1602m	1574w	1434m	1638s	1546m	456w	406w
$Ho(HL)_3{\cdot}3.5H_2O$	3360m	3058m	1602m	1574w	1441m	1638s	1546m	456w	405w
$Er(HL)_3{\cdot}3.5H_2O$	3360m	3058m	1602m	1574w	1434m	1638s	1546m	456w	405w

Table 8
Test results of inhibitory tumor cells [a]

Complex	Tested cells	Dose (μg ml^{-1})	Effect	Result	Inhibitory rate (%)
$La(HL)_3{\cdot}3.5H_2O$	HCT-8	10, 1	>10	−	
	L1210	10, 1	<10	+	87.1, 32.4
$Eu(HL)_3{\cdot}3.5H_2O$	HCT-8	10, 1	<10	+	53.5, 0
	L1210	10, 1	<10	+	78.5, 12.5
$H_2L{\cdot}LaCl_3$	HCT-8	10, 1	>10	−	
	L1210	10, 1	>10	−	

[a] 'Effect' means that the tested complex, of dose less than 10 μg ml^{-1}, has an inhibitory effect for the tested cells; 'Result' is the result of 'Effects', + having an inhibitory effect, − no inhibitory effect; 'Inhibitory rate' is 100%(control group − test group)/control group.

1546 cm^{-1} show that the active hydrogen of the –NHN= group still exists in the complexes. The band at 456 cm^{-1} is assigned to ν(M–O). All of these demonstrate that the oxygens of carbonyl have formed a coordinate bond with the rare earth metal ions, one of which ($C_{(15)}$=O) is in the enolic form as confirmed above by the crystal structure analyses. The band at 1588 cm^{-1} for the free ligand is assigned to the ν(C=N) stretch; it shifts to 1571–1574 cm^{-1} for its complexes. The weak bands at 405–410 cm^{-1} are assigned to ν(M–N). This further confirms that the nitrogen of the imino-group bonds to rare earth metal ions. All of these data confirm the fact that there is a conjugate chelate ring formed by ligand enolization in the complexes. This is consistent with the results of the crystal structure of the Eu complex.

3.5. Antitumor activity

Test results of the complexes, $La(HL)_3{\cdot}3.5H_2O$ and $Eu(HL)_3{\cdot}3.5H_2O$, for hepatic carcinoma (HCT-8), and leukemia cells (L_{1210}) are summarized in Table 8. It is clear that both complexes can affect L_{1210} cells. The inhibitory rates of $La(HL)_3{\cdot}3.5H_2O$ and $Eu(HL)_3{\cdot}3.5H_2O$ for L_{1210} cells are 87.1% and 78.5% respectively, and that of the Eu complex for HCT-8 cells is 53.5%, but free ligand H_2L and $LaCl_3$ cannot affect L_{1210} and HCT-8 cells. This shows that the coordination improves the antitumor activity of the two complexes. The acute toxicity data of tested complexes are summarized in Table 9. LD_{50} values of $La(HL)_3{\cdot}3.5H_2O$ and $Eu(HL)_3{\cdot}3.5H_2O$ are 348.9 ± 32 mg kg^{-1} and 279.1 ± 31 mg kg^{-1}, respectively. The toxic

Table 9
Acute toxicity data of La and Eu complexes for mice

Number	Dose (mg kg^{-1})	Number of mice tested	Number of dead mice	
			La complex	Eu complex
1	960.0	10	10	
2	768.0	10	9	10
3	614.4	10	8	8
4	491.5	10	6	7
5	393.2	10	5	6
6	314.6	10	4	5
7	251.7	10	3	4
8	201.3	10	2	3
9	161.1	10	1	2
10	128.9	10	0	1
11	103.1	10		0
LD_{50} (mg kg^{-1})			348.9 ± 32	279.1 ± 31

ity of the Eu complex is greater than that of the La complex.

4. Supplementary material

Supplementary data have been deposited with the Cambridge Crystallographic Data Centre, CCDC No. 137232. Copies of this information may be obtained free of charge from The Director, CCDC, 12 Union Road, Cambridge, CB2 1EZ, UK (fax: +44-1223-336033; e-mail: deposit@ccdc.cam.ac.uk or www: http://www.ccdc.cam.ac.uk).

Acknowledgements

This research was supported by The Chinese Academy of Medical Sciences and Lanzhou Medical College. The project was supported by the National Natural Science Foundation in China (29975012).

References

[1] J.L. Sesser, T.D. Mody, G.W. Hemmi, V. Lynch, Inorg. Chem. 32 (1993) 3175.
[2] P.S. Smith, J.R. Brainard, D.E. Morris, G.D. Jarvinen, R.R. Ryan, J. Am. Chem. Soc. 111 (1989) 7437.
[3] S.C. Jackels, B.R. Kroos, W.H. Hinson, N. Karstaodt, P.R. Moran, Radiology 159 (1986) 525.
[4] L.F. Wang, Y. Zhu, Z.Y. Yang, J.G. Wu, Q. Wang, Polyhedron 10 (1991) 2477.
[5] S.Y. Yu, S.X. Wang, Q.H. Luo, L.F. Wang, Polyhedron 12 (1993) 1093.
[6] S. Padhy, G.B. Kauffman, Coord. Chem. Rev. 63 (1985) 127.
[7] Z.Y. Yang, L.F. Wang, J.Q. Wu, X.Y. Li, Chinese J. Appl. Chem. 9 (1992) 31.
[8] J.G. Wu, R.W. Deng, Z.N. Chen, Transition Met. Chem. 18 (1993) 23.
[9] S. Chandra, K.K. Sharma, Transition Met. Chem. 9 (1984) 1.
[10] Z.Y. Yang, R.D. Yang, Q. Li, F.S. Li, Syn. Reac. Inorg. Metal-Org. Chem. 29 (1999) 205.
[11] Z.Y. Yang, R.D. Yang, L.F. Wang, X.P. Yang, Bull. Soc. Chim. Belg. 104 (1995) 129.
[12] W.J. Geary, Coord. Chem. Rev. 7 (1971) 81.

PERGAMON

www.elsevier.nl/locate/poly

Polyhedron 19 (2000) 2605–2611

POLYHEDRON

Redox responsive binuclear complexes using 5,6-dihydroxy-1,10-phenanthroline as a bridging ligand: synthesis, characterization and physicochemical studies

Atindra D. Shukla, Amitava Das *

Central Salt and Marine Chemicals Research Institute, Bhavnagar 364002, Gujarat, India

Received 21 June 2000; accepted 23 August 2000

Abstract

A set of new binuclear complexes has been synthesized and characterized using redox active bridging ligands (BL), 5,6-dihydroxy-9,10-phenanthroline ($dpcatH_2$) and $M(bipy)_2Cl_2$ (M is Ru(II) or Os(II))/$Ru(tpzea)Cl_2$ (tpzea is tris(*N*-pyrazolyl ethyl) amine) as the building blocks. For all binuclear complexes a large degree of stabilization of the semiquinone (sq) state for the $Ru(bpy)_2(dpsq)^+$ fragment has been observed. UV–Vis, electrochemical and spectroelectrochemical studies clearly show that the first two redox processes involve only the bridging ligand. Further experimental results show that auxiliary ligands coordinated to the metal center do not have any appreciable effect on the redox behavior of the bridging ligand. © 2000 Elsevier Science B.V. All rights reserved.

Keywords: Synthesis; Semiquinone; Ruthenium; Spectroelectrochemical studies; Redox

1. Introduction

The study of electronic interaction between two redox active metal centers with well defined structure, linked by a conjugated bridging ligand, has attracted much recent attention [1]. For multicomponent systems in which each component is a complex metal moiety, the bridging ligand (BL) plays a crucial role in successful design as it determines the separation, relative spatial arrangement of the metal core and the electronic interaction between the ends [2]. However, until now much attention has focused on the use of redox-innocent bridging ligands or linkers in which metal-based redox processes precede bridge-based. The use of non-innocent redox active bridging ligands offers the possibility to modulate the energy of the bridging ligand with a change in potential and thus to affect or manipulate the electronic coupling of the redox active metal cores that it links [3]. Metal complexes containing 'non-innocent' dioxolene ligands (member of catechol-semiquinone-quinone redox series) as one of the binding sites in a binucleating bridging ligand are important as its redox activity is retained even when coordinated to a metal core. Thus 5,6-dihydroxy-1,10-phenanthroline ($dpcatH_2$) is one of the most versatile bridging ligands in this regard [3–9] as it has pendant 1,10-phenanthroline and catechol as two chelating centers with well explored coordination chemistry of their respective mononuclear components. Also, the effect of an auxiliary ligand on redox processes involving the bridging ligand is relevant in the context of the tuning of the redox and magnetic properties of these binuclear complexes. Recently we have reported binuclear complexes derived from a bischelating ligand having 2,2′-bipyridyl (bpy) and catechol as the coordinating sites [8]. Having a much shorter and more planar structure, $dpcatH_2$ is expected to transmit better electronic interaction between the metal centers. In this paper we report the synthesis, characterization, physicochemical and spectroelectrochemical studies of homo and hetero binuclear complexes using $dpcatH_2$ as the bridging ligand. Also, both N–N bound and O–O bound monometallic complexes have been synthesized for comparison of the physicochemical properties with those of bimetallic species.

* Corresponding author. Fax: +91-278-426970.
E-mail address: salt@csir.res.in (A. Das).

0277-5387/00/$ - see front matter © 2000 Elsevier Science B.V. All rights reserved.
PII: S0277-5387(00)00563-5

2. Experimental

Microanalyses (C, H, N) were performed using a Perkin–Elmer 4100 elemental analyzer. IR spectra were recorded as KBr pellets using a Perkin–Elmer spectrum GX 2000 spectrometer. Electronic spectra were recorded on a Shimadzu UV-3101 PC spectrophotometer. ^{1}H NMR spectra were recorded on a Bruker 200 MHz FT NMR (model Avance-DPX 200). Fast-atom bombardment measurement was carried out on a VG-ZAB instruments using 3-nitrobenzyl alcohol as matrix. EPR spectra were recorded at room temperature and at 77 K on a Bruker ESP-300 spectrometer. Electrochemical experiments were performed using a CH 660A (USA) electrochemical instrument; a conventional three-electrode cell assembly was used. Saturated Ag/AgCl as reference and platinum as working electrodes were used for this purpose. Ferrocene was added at the end of each experiment as internal standard; all potentials are quoted versus the ferrocene/ferrocenium (Fc/Fc^+) couple. Spectra of the electro-reduced/oxidized species were recorded either by a Shimadzu UV-3101 PC model under dinitrogen atmosphere or in situ with a fiber optic deep probe attached to an Ocean Optics 2000 CCD spectrophotometer.

$Ru(bpy)_2Cl_2\cdot 2H_2O$ [10], $Os(bpy)_2Cl_2$ [11], $[\{Ru(bpy)_2\}_2(bpesq)]$ [8], $Ru(DMSO)_4Cl_2$ [12], tris(*N*-pyrazolyl ethyl) amine (tpzea) [13], 5,6-dihydroxy-1,10-phenanthroline ($dpcatH_2$) [14] and ferrocenium hexafluorophosphate ($FcPF_6$) [15] were prepared following known methods. $[Bu_4N]PF_6$ was used as background electrolyte for electrochemical studies. Acetonitrile, used as solvent in electrochemical analysis, was dried and distilled before use. All reactions were performed under argon atmosphere.

2.1. Synthesis

2.1.1. *[Ru(2,2′-bipy)$_2$dpcatH$_2$](PF$_6$)$_2$ (I)*

$Ru(bpy)_2Cl_2\cdot 2H_2O$ (200 mg, 0.385 mmol) and 97.5 mg (0.46 mmol) of $dpcatH_2$ were refluxed in 50 cm^3 ethanol–water mixture (1:1; v/v) for 7 h and then concentrated under vacuo to $\sim$10 cm^3. To this, a saturated aqueous solution of KPF_6 was added and kept refrigerated overnight. A dark red precipitate was filtered off, air dried and the crude product was purified by column chromatography using silica column and CH_3CN-saturated aqueous solution of NH_4PF_6 (98:2%, v/v) as eluant. The first major fraction was collected and concentrated in vacuo ($\sim$5 cm^3). Excess NH_4PF_6 was removed by solvent extraction in the aqueous layer. The desired compound was collected in the CH_2Cl_2 layer and dried in vacuo. Yield: 155 mg, 44%. *Anal.* Found: C, 42.0; H, 2.6; N, 9.1. Calc. for $RuC_{32}H_{24}N_6O_2P_2F_{12}$: C, 41.97; H, 2.62; N, 9.18%. FAB MS: m/z 913 (M^+, $\sim$2%), 768 ($M^+ - PF_6$, $>$5%), 623 ($M^+ - 2PF^6$, 30%). IR (KBr, cm^{-1}): 3445 (br, –OH), 1610, 1580 (C=C and C=N), 835 (PF_6^-). ^{1}H NMR (200 MHz, CD_3CN): δ 8.62–8.59 (6H, m), 8.13 (4H, t, 5.9Hz), 8.08 (2H, d, 5.6Hz), 7.98 (4H, d, 5.6Hz), 7.58 (2H, t, 5.6Hz), 7.51 (4H, t, 5.9Hz).

2.1.2. *[Os(bpy)$_2$dpcatH$_2$](PF$_6$)$_2$ (II)*

$Os(2,2'\text{-bipy})_2Cl_2\cdot 2H_2O$ (100 mg, 0.164 mmol), and $dpcatH_2$ (47 mg, 0.164 mmol) were refluxed in 50 cm^3 ethanol–water (1:1, v/v) for 24 h and then concentrated under vacuo to $\sim$10 cm^3. The desired complex was precipitated by adding saturated aqueous solution of KPF_6 and filtered off. This was purified following a method similar to that for complex **I**. The first orange–brown fraction was collected and dried. Excess of NH_4PF_6 was removed in the aqueous layer while the desired complex was partitioned in the CH_2Cl_2 layer and dried in vacuo. Yield: 62 mg, 38%. *Anal.* Found: C, 39.0; H, 2.4; N, 8.3. Calc. for $OsC_{32}H_{24}N_6O_2P_2F_{12}$: C, 38.25; H, 2.39; N, 8.4%. FAB MS: m/z 1004 (M^+, $\sim$3%), 859 ($M^+ - PF_6$, $\sim$5%), 714 ($M^+ - 2PF_6$, 25%). IR (KBr, cm^{-1}): 3449 (br. –OH), 1604, 1585 (C=C and C=N), 840 (PF_6^-). ^{1}H NMR (200 MHz, CD_3CN): δ 8.45–8.37 (6H, m), 8.1 (4H, m), 8.02 (2H, d, 5.4Hz), 7.89 (4H, d, 5.4Hz), 7.53–7.49 (6H, m).

2.1.3. *[Ru(bpy)$_2$(dpsq)](PF$_6$) (III)*

$Ru(bpy)_2Cl_2\cdot 2H_2O$(200 mg, 0.385 mmol), $dpcatH_2$ (110 mg, 0.385 mmol) and KOH (44 mg, 0.78 mmol) were refluxed in ethanol (50 cm^3) for 6 h. To this resulting mixture $FcPF_6$ (0.127 mg, 0.385 mmol) was added and stirred at room temperature for 30 min. Then the desired compound was precipitated after reducing the volume to $\sim$5 cm^3 and adding aqueous KPF_6 solution. The purification procedure is similar to that for complex **I**. Yield: 145 mg, 49%. *Anal.* Found: C, 49.4; H, 3.0; N, 10.6%. Calc. for $RuC_{32}H_{22}N_6O_2PF_6$: C, 50.0; H, 2.86; N, 10.94%. FAB MS: m/z 768 (M^+, $\sim$2%), 623 ($M^+ - PF_6$, $<$10%). IR (KBr, cm^{-1}): 1612, 1590 (C=C, C=N), 1446 (semiquinone stretching), 835 (PF_6^-).

2.1.4. *[{Ru(bpy)$_2$}$_2$dpsq](PF$_6$)$_2$ (IV)*

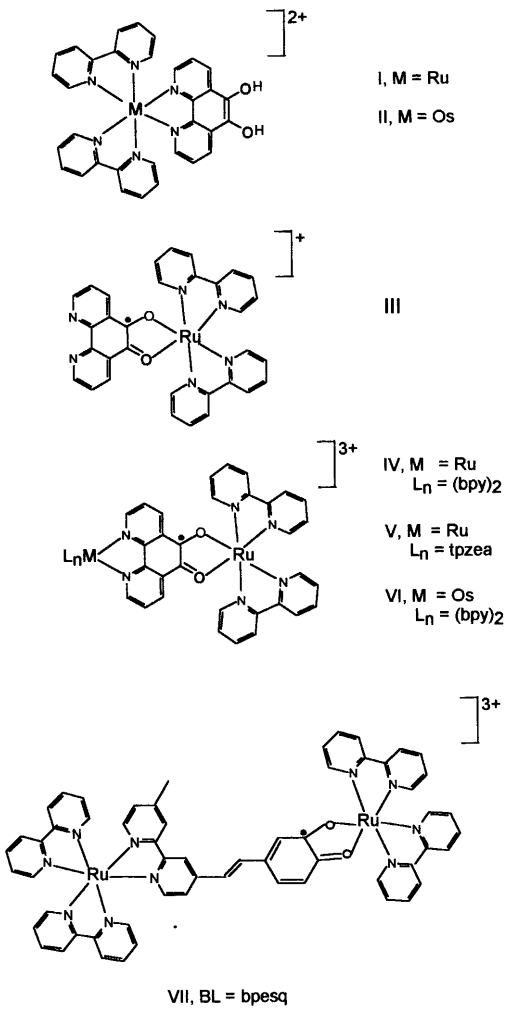
Method 1: $Ru(bpy)_2Cl_2\cdot 2H_2O$ (200 mg, 0.385 mmol) and $dpcatH_2$ (40.8 mg, 0.192 mmol) were refluxed under argon in 50 cm^3 water–ethanol mixture (1:1, v/v) for 7 h. To this, $FcPF_6$ (127 mg, 0.385 mmol) was added and stirred at room temperature for 30 min. Ethanol was removed under vacuo, aqueous KPF_6 solution was added and kept refrigerated overnight. A dark red color precipitate appeared which was filtered and the desired complex was purified following a procedure similar to that for complex **I**. Yield: 250 mg, 44%.

Method 2: Complex **I** (100 mg, 0.11 mmol), $Ru(bpy)_2Cl_2\cdot 2H_2O$ (52 mg, 0.1 mmol) and KOH (11.2 mg, 0.2 mmol) were refluxed in C_2H_5OH–CH_3CN mix-

ture (10:1, v/v) under argon for 3 h. Following workup the procedure is similar to that of method 1. Yield: 180 mg, 74%. *Anal.* Found: C, 42.2; H, 2.6; N, 9.6%. Calc. for $Ru_2C_{52}H_{38}N_{10}O_2P_3F_{18}$: C, 42.42; H, 2.58; N, 9.52%. FAB MS: m/z 1326 ($M^+ - PF_6$, $<2\%$), 1181 ($M^+ - 2PF_6$, $\sim 5\%$), 1036 ($M^+ - 3PF_6$, $\sim 15\%$). IR (KBr, cm^{-1}): 1608, 1585 (C=C and C=N), 1444 (semiquinone streaching), 840 (PF_6^-).

2.1.5. *[Ru(2,2′-bipy)$_2$dpsqRu(tpzea)](PF$_6$)$_3$ (V)*

$Ru(DMSO)_4Cl_2$ (168 mg, 0.35 mmol) was added to a methanolic solution (~ 30 cm^3) of tpzea (100 mg, 0.33 mmol) and was allowed to stir at 50°C for 30 min. The color of the solution changes from pale yellow to bright orange. To this resulting reaction mixture, KOH (48 mg, 0.68 mmol) and complex **I** (315 mg, 0.34 mmol) were added and refluxed for 3 h. The color of the solution changes to reddish brown. The volume of the solution was reduced to ~ 15 cm^3, aqueous KPF_6 was added and kept refrigerated overnight. The precipitate was filtered off, dried and purified by column chromatography following the method adopted for complex **IV**. Yield: 175 mg, 32%. *Anal.* Found: C, 39.3; H, 3.0; N, 12.3%. Calc. for $Ru_2C_{47}H_{43}N_{13}P_2O_3F_{18}$: C, 38.68; H, 2.95; N, 12.48%. FAB mass: m/z 1168 ($M^+ - 2PF_6$, $\sim 5\%$), 1023 ($M^+ - 3PF_6$, 15%). IR (KBr, cm^{-1}): 1607, 1600 (C=C, C=N), 1442 (semiquinone stretching), 840 (PF_6).



Scheme 1.

2.1.6. *[Os(2,2′-bipy)$_2$dpsqRu(2,2′-bipy)$_2$](PF$_6$)$_3$ (VI)*

$Os(bpy)_2Cl_2$ (60 mg, 0.104 mmol) and complex **III** (85 mg, 0.11 mmol) were refluxed in ethanol–water 1:1 (50 cm^3) for 24 h. The volume of reaction mixture was reduced to about 10 cm^3 and the desired complex was precipitated by adding excess aqueous KPF_6 solution. Crude product was filtered, air dried and purified by column chromatography in a similar fashion adopted for complex **I**, and the second major brown fraction was collected and dried. Excess NH_4PF_6 was removed by solvent extraction in the aqueous layer, while pure compound was collected in the CH_2Cl_2 layer and dried in vacuo. Yield: 30 mg, 20%. *Anal.* Found: C, 39.4; H, 2.4; N, 9.0%. Calc. for $OsRuC_{52}H_{38}N_{10}O_2P_3F_{18}$: C, 40.0; H, 2.43; N, 8.97%. FAB mass: m/z 1415 ($M^+ - PF_6$, $\sim 1\%$), 1270 ($M^+ - 2PF_6$, 3%), 1125 ($M^+ - 3PF_6$, $\sim 8\%$). IR (KBr, cm^{-1}): 1610, 1597 (–C=C, –C=N), 1440 (semiquinone stretching), 843 (PF_6).

3. Results and discussion

3.1. Synthesis and characterization

Proposed formulations for all the complexes (Scheme 1) were confirmed by elemental analysis, FAB mass analysis, UV–Vis, IR and ^1H NMR or ESR spectroscopy. Complexes **I** and **II** were prepared by reaction of $dpcatH_2$ with $M(bpy)_2Cl_2$ (M is Ru(II) for **I** or Os(II) for **II**) and were purified by column chromatography. In the absence of externally added base, $dpcatH_2$ preferentially coordinates to Ru(II) and Os(II) centers via N–N binding site of the phen functionality. However, in the presence of KOH, $dpcatH_2$ exists in solution as $dpcat^{2-}$ and reacts with $Ru(bpy)_2Cl_2$ via dioxolene binding site. Isolated complex **III** is found to be paramagnetic and is in the semiquinone (dpsq) oxidation state (vide infra). $Ru(bpy)_2(dpcat)$ complex forms initially, and partially converts to the $Ru(bpy)_2(dpsq)^+$ fragment during aerobic work-up. To ensure the complete conversion to the semiquinone form, crude reaction mixture was treated with 1 equiv. of $FcPF_6$ at room temperature for 30 min and single product was isolated. Complex **III**, having a pendant N–N donor phen group available for further coordination, was used as a precursor for synthesis of the complexes **IV**, **V** and **VI**. For synthesis of complex **V**, $Ru(tpzea)Cl_2$ was generated in situ as characterization of this complex was difficult for its extreme hygroscopic nature.

Table 1
UV–vis spectroscopic data for the complexes

Complex	λ_{max} (nm) ($10^3\varepsilon$ (M^{-1} cm^{-1}))
I [a]	244 (62), 285 (94), 438 (23)
II [a]	244 (64), 288 (95), 403 (17), 690 (sh)
III [a]	242 (48), 285 (40), 429 (7), 929 (0.7)
IV [a]	244 (48), 285 (81), 438 (18.3), 938 (9.3)
V [a]	243 (53), 280 (89), 433 (12), 948 (1.0)
VI [a]	238 (65), 292 (134), 338 (sh), 420 (22), 463 (21), 487 (sh), 554 (sh), 686 (4.5), 840 (sh)
VII [b]	244 (52), 288 (113), 455 (25), 576 (576), 989 (9)
$[(bpy)_2Rudpcat]^{+}$ [c]	447 (7.4), 960 (0.38)
$[(bpy)_2Rudpq]^{3+}$ [c]	435 (6.9)
$[(bpy)_2RudpcatRu(bpy)_2]^{+}$ [c]	429 (19.4), 550 (sh), 660 (sh), 952 (0.93)
$[(bpy)_2RudpqRu(bpy)_2]^{3+}$ [c]	432 (18)
$[(bpy)_2RudpcatRu(tpzea)]^{+}$ [c]	430 (10), 1005 (0.35)
$[(bpy)_2RudpqRu(tpzea)]^{3+}$ [c]	429 (9.5)
$[(bpy)_2RubpecatRu(bpy)_2]^{+}$ [c]	450 (26.2), 595 (sh), 662 (sh), 1004 (0.88)
$[(bpy)_2RubpeqRu(bpy)_2]^{3+}$ [c]	442 (24)

[a] Spectra recorded in CH_3CN.
[b] Ref. [8].
[c] Spectra of the electroreduced and oxidized species were recorded with in the range 360–1100 nm in the presence of 0.1 M $[Bt^n_4N]BF_4$ in CH_3CN; sh shoulder.

Table 2
Effect of solvent on λ_{max} (nm) for $Ru(\pi) \rightarrow sq(\pi^*)$ MLCT transition

Complex	CH_2Cl_2	C_2H_5OH	$HCON(CH_3)_2$
III	915	926	933
IV	929	943	949
V	934	982	989

3.2. UV–Vis spectral studies

Details of the electronic spectra of these complexes are presented in Table 1. Complexes **I** and **II** have spectra similar to those reported for $Ru(bpy)_2(phen)^{2+}$ and $Os(bpy)_2(phen)^{2+}$ respectively [16]. Complex **III** shows a more intense and red shifted MLCT band than that reported for $Ru(bpy)_2(sq)^{+}$ species ($\lambda_{max} = 890$ nm and $\varepsilon = 6.4 \times 10^3$ dm^3 mol^{-1}, sq is the semiquinone form of 1,2-dihydroxybenzene [17,18]. The observed red shift is due to the lower energy of the orbital based on the semiquinone fragment in complex **III** as compared to $Ru(bpy)_2(sq)^{+}$ species; this can be explained on the basis of extended conjugation in the bridging ligand, dpsq. This is further supported by the higher red shift observed for $Ru(d\pi) \rightarrow dpsq(\pi^*)$ charge transfer in complex **VII** for more extended delocalization in $bpecatH_2$ [8]. Higher ε value and transitional dipole moment for the $Ru(d\pi) \rightarrow dpsq(\pi^*)$ transition is understandable, as the semiquinone fragment in complex **III** is more electronegative than that in $Ru(bpy)_2(sq)^{+}$ [17–20]. The spectrum for complex **IV** is very similar to the combined spectra for complexes **I** and **III**. Higher values for λ_{max} and ε for the $Ru(d\pi) \rightarrow dpsq(\pi^*)$ transition (Table 1) are due to the coordination of the pendant N–N donor phen functionality to the Ru(II) center of the cationic $Ru(bpy)_2^{2+}$ fragment. The spectrum for complex **VI** shows bands ascribable to each of the two chromophores, $Ru(bpy)_2(dpsq)$ and $Os(bpy)_2(phen)$, with appreciable blue shift (840 nm) for the $Ru(d\pi) \rightarrow dpsq(\pi^*)$ transition (Table 1). This can only be explained if one considers that greater extension of the metal d-orbitals for osmium can enhance the metal–ligand back bonding and better energy match with the dpsq fragment compared to the Ru counterpart in complex **IV**. However, the spectrum in this region is complicated by an absorption band (~ 690 nm) attributed to $Os(d\pi)bpy(^3\pi^*)$ singlet to triplet transition [21]. Higher full width at half maximum (fwhm) values for complexes **IV** and **V** compared to **III** are due to the large Franck–Condon barrier to the MLCT transition. For the valence trapped model the $Ru(d\pi) \rightarrow sq(\pi^*)$ transition results in a charge separated state consisting of partially Ru(III) and dpcat, which is expected to be associated with appreciable nuclear reorganization and accounts for the higher fwhm value. Moreover, the dependence of λ_{max} of the $Ru(d\pi) \rightarrow sq(\pi^*)$ transition for complexes **III**, **IV** and **V** on solvent polarity (Table 2) is also indicative of the solvent stabilization of a charge separated species. As predicted by earlier work for a similar feature in related complexes to a transition from an $Ru(d\pi)$ to semiquinone based singly occupied molecular orbital (SOMO), we attribute this transition as $Ru(d\pi) \rightarrow sq(SOMO\ \pi^*)$ transition [3a,8,22].

3.3. Electrochemical studies

All complexes were studied by cyclic and square wave voltammetry in MeCN and results are summarized in Table 3 (all potentials are quoted versus the Fc/Fc^{+} couple). Both complexes **I** and **II** show anticipated redox processes in addition to an irreversible oxidation process. Peak potential for this irreversible process ($\sim +0.45$ V) is determined by square wave voltammogram. 1,2-dihydroxy benzene is known to undergo oxidation to form quinone, which involves loss of protons and is expected to be irreversible in aprotic solvents, e.g. MeCN [23]. For complex **III**, there is a quasireversible Ru(II)/(III) couple (1.10 V) along with two ligand centered reductions at extreme negative potential (-1.90 and -2.08 V) for two coordinated bpy groups. In addition to these, two reversible redox processes are present. These can be assigned to two dioxolene-based processes, dpcat/dpsq couple at -0.40 V and dpsq/dpq couple at 0.27 V. For complex **IV**, in

Table 3
Electrochemical data for complexes [a]

Complex	Dioxolene-based redox process	Ru(II/III) couple	Os(II/III) couple	bpy-Based reduction
I	0.7 [b]	1.02 (90)		−1.90, −2.08
II	0.68 [b]		0.95 (100)	−1.88, −2.05
III	0.27, −0.40 (80)	1.10 (90)		−1.87, −2.07
IV	0.26 (75), −0.48 (80)	1.15 (130)		−1.8, −1.92, −2.1
V	0.27 (90), −0.42 (100)	0.73 (qr), 1.12 (85)		−1.76, −2.07
VI	0.13 (95), −0.55 (85)	1.14 (95)	1.00 (110)	−1.83, −1.9, −1.98, −2.15

[a] Recorded in CH_3CN at a scan rate of 100 mV s^{-1}; potentials are in volts versus the Fc/Fc^+ couple. For nearly reversible waves, peak–peak separation (mV) values are given in parentheses.
[b] Not reversible, qr quasireversible.

addition to the phen/bpy-based reductions at extreme negative potentials, three reversible one-electron processes are observed; two are dioxolene based (dpcat/dpsq redox couple at −0.48 V and dpsq/dpq redox couple at 0.26 V) and the third is in fact two overlapping seemingly reversible Ru(II)/(III) couples of $Ru(bpy)_2(dpphen)^{2+}$ and $Ru(bpy)_2(dpsq)^+$ fragments (Fig. 1). Neither cyclic nor square wave voltammetry could clearly distinguish these two processes. The presence of a cationic $Ru(bpy)_2(phen)^{2+}$ core makes dpsq → dpcat reduction easier (−0.69 V for $Ru(bpy)_2(sq)^+$ [9,17,18]) whereas dpsq → dpq oxidation (+0.16 V for $Ru(bpy)_2(sq)^+$ [9,17,18]) is difficult. Behavior of complex **VI** is very similar to that of complex **IV**; a reversible Os(II)/(III) couple appears at 1.0 V and Ru(II)/(III) couples of $Ru(bpy)_2(sq)$ and Ru(tpzea)phen fragments appear at 1.12 and 0.73 V respectively. The redox process dpsq → dpcat has become difficult by 70 mV, while the dpsq → dpq process has become easier by 130 mV. This agrees well with the UV–Vis spectral observation (vide supra) and is concomitant with the fact that closer energy matching of the π^*_{BL} and Os(dπ) orbitals results a stronger π-interaction and leads to a more efficient electronic drain on the bridging ligand and thereby facilitates the oxidation processes, dpsq → dpq. Further it is also possible to quantify the extent of stabilization of the dpsq state by evaluating the conproportionation constant, K_c ($\log K_c = \Delta E°/0.059$), where $\Delta E°$ is the difference between the two well resolved, reversible one-electron steps associated with BL for the ligand based process. Thus, K_c(sq) values (2sq ⇄ q + Hq) calculated for complexes **III**–**VI** are in the order of $\sim 10^{10}$, emphasizing the large degree of stabilization of the semiquinone state.

3.4. Spectroelectrochemical studies

To obtain further information about the spectral changes associated with the change in the redox states of the binding ligand, spectroelectrochemical studies were carried out. UV–Vis data of complexes **III**–**VII** for various redox states of the BL are summarized in Table 3 and reveal that these complexes show rich spectral responses to the variation in applied potential. Fig. 2A shows the changes in spectral features of complex **III** when the bridging ligand is selectively reduced from dpsq to the dpcat oxidation state by bulk electrolysis at −0.4 V (versus Ag/AgCl); the MLCT band for Ru(dπ) → sq(π*) transition at 929 nm decreases while increases in absorbance at 650, 545 and 440 nm were observed. Shoulders at ∼560 and 650 nm are assigned to intraligand dpcat(π) → dpphen(π*) and interligand dpcat(π) → bpy(π*) charge transfer transitions. Fig. 2B shows successive changes in spectral features on selective oxidation of the binding mode from semiquinone to quinone species by bulk electrolysis at 0.8 V (versus Ag/AgCl); absorbance at 938 nm is replaced by a much weaker and broader band λ_{max} at ∼1000 nm, attributed to the Ru(dπ) → q(π*) MLCT process. The observed red shift is presumably due to better π-acidic nature of the quinone ligand. Fig. 2C

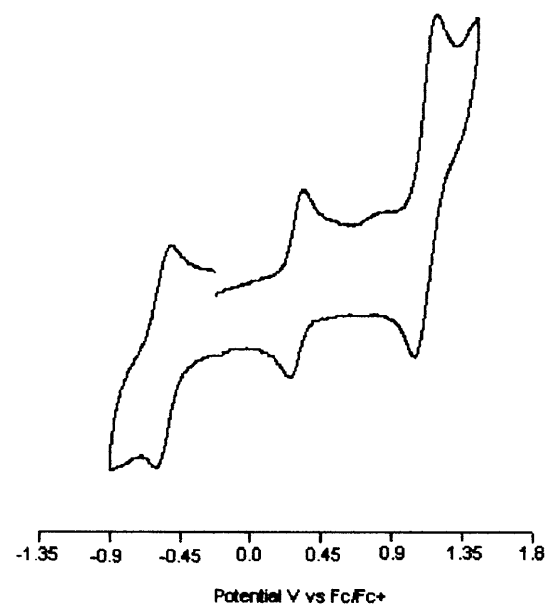


Fig. 1. Cyclic voltammogram of complex **IV** recorded at 500 mV s^{-1} in CH_3CN.

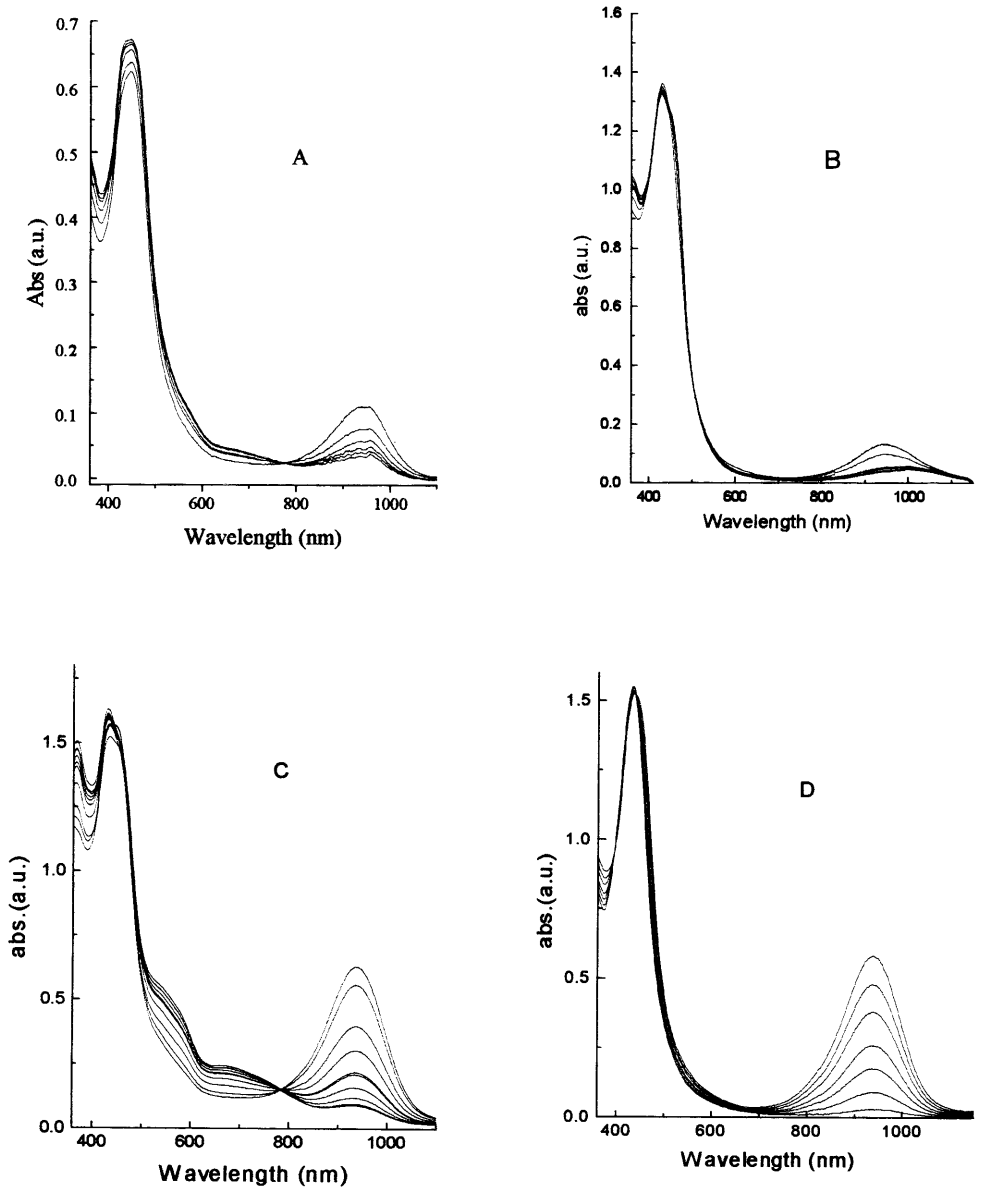


Fig. 2. UV–Vis spectra recorded during bulk electrolysis: (a) complex **III** selectively reduced at −0.40 V (versus Ag/AgCl standard electrode), (b) complex **III** selectively oxidized at 0.8 V (versus Ag/AgCl standard electrode), (c) complex **IV** selectively reduced at −0.40 V (versus Ag/AgCl standard electrode), (d) complex **IV** selectively oxidized at 0.8 V (versus Ag/AgCl standard electrode).

shows the changes in spectral features for complex **IV**, similar to that for **III**, except better resolved shoulders appear at 550 and 660 nm for cat(π) → bpy/phen(π^*) transitions respectively. The observed red shift of ~10 nm is due to coordination of a cationic Ru(II) species at the remote side of BL. This is further supported by the fact that on selective reduction of the dpsq → dpcat state in complex **VII**, the same intraligand charge transfer band appears at much lower energy (595 nm) as extended conjugation in BL is responsible for lowering the energy of the substituted bpy ligand which is coordinated to the remote $Ru(bpy)_2$ core, whereas the shoulder at 662 nm for interligand charge transfer (bpecat(π) → bpy(π^*)) remains unaffected with the change in BL. This further reveals that a change either in conjugation or coordination at the remote side of BL does not affect the energy for the dpcat(π) → dpbpy(π^*) transition. For selective oxidation of the dpsq to dpq binding mode, the spectral change recorded is almost identical to that observed for complex **III** (Fig. 2D). Spectroelectrochemical behavior of complex **V** is almost identical to that of complex **III**. This can be explained if one considers that tpzea, being a much weaker π-acceptor ligand compared to bpy in complex **IV**, does not have any appreciable MLCT (Ru($d\pi$) → tpzea(π^*)) transition and thereby cannot influence the electron density of the BL and the spectral behavior of the complex. However, unambiguous assignment of the spectroelec-

trochemical response of complex **VI** is difficult due to the number of overlapping absorption bands at the region of the $Ru(d\pi) \rightarrow BL(\pi^*)$ transition.

3.5. ESR spectroscopy

Complexes **III**–**VI** are paramagnetic due to the semiquinone coordinating mode and were studied by ESR spectroscopy. All these complexes show a room temperature spectrum consisting of a broadened free radical signal centered at $g \approx 2.003$ in acetonitrile. At 77 K (in a frozen CH_3CN–toluene glass), spectra recorded do not show any hyperfine structure and are apparently an axial spectrum with $g_\perp \approx 1.98$ and $g_\parallel \approx 2.050$. The difference between $g_\perp$ and $g_\parallel$ is smaller than that observed for other Ru(II)–sq complexes [17,18]; but the apparent axial symmetry suggests that the MO containing the unpaired electron for both complexes is partially localized on the metal and is consistent with the electronic spectral studies.

4. Supplementary material

Supplementary information (1 page) concerning the spectroscopic data is available from the authors (A.D.) on request.

Acknowledgements

This work is supported by Department of Science and Technology (India). The authors are thankful to Dr P.K. Ghosh and Dr R.V. Jasra of CSMCRI, Bhavnagar for their keen interest in the work. A.D.S. is also thankful to CSIR (India) for a Sr. Research Fellowship.

References

[1] (a) J.A. McCleverty, M.D. Ward, Acc. Chem. Res. 31 (1998) 842. (b) D. Astruc, Acc. Chem. Res. 30 (1997) 383. (c) A. Das, A.D. Shukla, H.C. Bajaj, Indian J. Chem. 77 (2000) 51. (d) E. Ishow, A. Gourdon, J.-P. Launay, C. Chiorboli, F. Scandola, Inorg. Chem. 38 (1999) 1504. (e) T.J. Rutherford, F.R. Keene, J. Chem. Soc., Dalton Trans. (1999) 1155. (f) E. Psillakis, P.K.A. Shonfield, A.-A. Jouaiti, J.P. Maher, J.A. McCleverty, M.D. Ward, J. Chem. Soc., Dalton Trans. (2000) 241.

[2] (a) M.D. Ward, Chem. Soc. Rev. (1995) 121. (b) V. Balzani, A. Juris, M. Venturi, S. Campagna, S. Serroni, Chem. Rev. 96 (1996) 759. (c) K. Prassides (Ed.), Mixed Valency Systems: Application in Chemistry, Physics and Biology, Kluwer, Dordrecht, 1991.

[3] (a) T.E. Keyes, R.J. Forster, P.M. Jayaweera, C.G. Coates, J.J. McGarvey, J.G. Vos, Inorg. Chem. 37 (1998) 5925. (b) F. Hartl, T.L. Snoeck, D.J. Stufkens, A.B.P. Lever, Inorg. Chem. 34 (1995) 3887. (c) D.F. Joulie, E. Schatz, M.D. Ward, F. Weber, L.J. Yellowless, J. Chem. Soc., Dalton Trans. (1994) 799.

[4] G.A. Fox, S. Bhattacharya, C.G. Pierpont, Inorg. Chem. 30 (1991) 2895.

[5] B. Whittle, N.S. Everest, C. Howard, M.D. Ward, Inorg. Chem. 34 (1995) 2025.

[6] P.L. Hill, L.Y. Lee, T.R. Younkin, S.D. Orth, L.M. White, Inorg. Chem. 36 (1997) 5655.

[7] F. Calderazzo, F. Marchetti, G. Pampaloni, V. Passarelli, J. Chem. Soc., Dalton Trans. (1999) 4389.

[8] A.D. Shukla, B. Whittle, H.C. Bajaj, A. Das, M.D. Ward, Inorg. Chim. Acta 285 (1999) 89.

[9] A.B.P. Lever, H. Masui, R.A. Metcalfe, D.J. Stufkens, E.S. Dodsworth, P.R. Auburn, Coord. Chem. Rev. 125 (1993) 317.

[10] B.P. Sullivan, D.J. Salmon, T.J. Meyer, Inorg. Chem. 17 (1978) 3334.

[11] E.M. Kober, J.V. Caspar, B.P. Sullivan, T.J. Meyer, Inorg. Chem. 27 (1988) 4587.

[12] I.P. Evans, A. Spencer, G. Wilkinson, J. Chem. Soc., Dalton Trans. (1973) 204.

[13] T.N. Sorrell, D.L. Jameson, Inorg. Chem. 21 (1982) 1014.

[14] W. Paw, R. Eisenberg, Inorg. Chem. 36 (1997) 2287.

[15] (a) S. Decurtins, F. Felix, J. Ferguson, H.U. Güdel, A. Ludi, J. Am. Chem. Soc. 102 (1980) 4102. (b) K. Kalyansundaram, Photochemistry of Polypyridine and Porphyrin Complexes, Academic Press, San Diego, CA, 1992.

[16] N.G. Connelly, W.E. Geiger, Chem. Rev. 96 (1996) 877.

[17] (a) J. Rebek Jr., Acc. Chem. Res. 17 (1984) 258. (b) S.R. Boone, C.G. Pierpont, Inorg. Chem. 26 (1987) 1769. (c) A.B.P. Lever, P.R. Auburn, E.S. Dodsworth, M. Haga, W. Liu, M. Melnik, W.A. Nevin, J. Am. Chem. Soc. 110 (1988) 8076.

[18] H. Masui, A.B.P. Lever, P.R. Auburn, Inorg. Chem. 30 (1991) 2402.

[19] M. Haga, E.S. Dodsworth, A.B.P. Lever, Inorg. Chem. 25 (1986) 447.

[20] Transitional dipole strength (D) is related to the oscillator strength (f) (K.A. Gscheidner Jr., L. Eyring, Handbook of Physics and Chemistry of Rare Earths, Elsevier, 1998) by $D = (2.127 \times 10^{-30} f)/\nu_o$ [ν_o is the wavenumber for $Ru(d\pi) \rightarrow$ dpsq(π^*), MLCT transition] and f is related to the fwhm $\nu_{1/2}$ by $f = 4.60 \times 10^{-9}\ \varepsilon_{max}\ \nu_{1/2}$ (P. Chen, T.J. Meyer, Chem. Rev. 98 (1998) 1439). Thus, D values for complexes **III**, **IV**, and **V** are found to be 9.68×10^{-37}, 1.42×10^{-35} and 1.69×10^{-36} respectively. Evaluation of f and D for the same transition of complex **VI** was difficult due to a number of overlapping absorption bands in that region.

[21] (a) K.S. Schanze, G.A. Neyhart, T.J. Meyer, J. Phys. Chem. 90 (1986) 2182. (b) J.T. Hupp, G.A. Neyhart, T.J. Meyer, J. Am. Chem. Soc. 108 (1986) 5349.

[22] (a) A.B.P. Lever, Inorganic Electronic Spectroscopy, Elsevier, Amsterdam, 1984. (b) S. Ernst, V. Kasack, W. Kaim, Inorg. Chem. 27 (1988) 1146. (c) V.L. Berre, L. Angely, N.S. Guegnen, J. Simonet, Nouv. J. Chim. 9 (1985) 419.

[23] (a) G.D. Storrier, K. Takada, H.D. Abruna, Inorg. Chem. 38 (1999) 559. (b) G. Hilt, T. Jarbawi, W.R. Heineman, E. Steckhan, Chemistry Eur. J. 3 (1997) 79.

PERGAMON

www.elsevier.nl/locate/poly

Polyhedron 19 (2000) 2613–2619

POLYHEDRON

Oxovanadium(IV) complexes of quinic acid. Synthesis, characterization and potentiometric study

Y. Allegretti, E.G. Ferrer, A.C. González Baró, P.A.M. Williams *

Centro de Química Inorgánica (CEQUINOR), Facultad de Ciencias Exactas, Universidad Nacional de La Plata, C. Correo 962, 1900 La Plata, Argentina

Received 27 May 2000; accepted 21 August 2000

Abstract

The synthesis, characterization and speciation of the VO^{2+}–quinic acid system is described. Three new solid complexes were obtained: $[VO(quin)(H_2O)_3]$ (**I**), $Na_4[VO(quin)_2SO_4]\cdot 4H_2O$ (**II**) and $Na_6[VO(quin)_2SO_4]\cdot 4H_2O$ (**III**), at pH 3.5, 6 and 12, respectively. They were characterized by elemental analysis, diffuse reflectance, FTIR and Raman spectroscopies, and thermal behavior. Their stability constants were determined at 298 K and at a constant ionic strength of 0.150 M using potentiometric methods. In aqueous solution three different complexes appeared as the main species at the pH values indicated above as shown in the species distribution curves. Up to pH 8 the system behaves as a 2-hydroxyacid/metal-like compound, while at higher pH further deprotonations were observed, which resulted in the formation of sugar–VO^{2+}-like complexes. UV–Vis spectra were also reported. © 2000 Elsevier Science B.V. All rights reserved.

Keywords: Vanadium complexes; Quinic acid complexes; IR spectra; Raman spectra; Thermal behavior; Potentiometric titrations

1. Introduction

Vanadium is thought to be a trace metal in most higher animals and it is known to be essential to some organisms, including tunicates and mushrooms. The best evidence for a biological role of this element comes from bacteria and plants (vanadium containing nitrogenase and haloperoxidases) [1]. Vanadium has the exceptional ability to interact with biomolecules in both cationic and anionic forms and in its several oxidation states. Among its biological functions, many important therapeutic effects have been described, including hormonal, cardiovascular, anticarcinogenic and insulin mimetic activities [2]. The coordination chemistry and reactivity of vanadium plays a predominant role. Because of the physiological relevance of this metal, its complexation behavior with organic ligands is of great interest for a better understanding of the interactions with biomolecules.

Quinic acid (quin), Fig. 1 is a precursor of shikimic acid and it can be used as a carbon source when incorporated in the synthesis pathway. Shikimic acid is involved in the biosynthesis of many natural products which contain an aromatic ring, including essential amino acids and folic acid, in microorganisms and plants [3]. It is also used as raw material, or building block, in the synthesis of new pharmaceutical preparations that are still under clinical trials phase. Quin is a naturally occurring hydroxy compound, with antimicrobial effects [4]. It is involved in plant metabolism as a metal carrier because of its polyglycolic nature. It also participates in the photosynthetic process, where the presence of metal ions, in the form of coordination compounds, modifies the effect of the ligand itself [5]. The ester of quinic acid with caffeic acid (chlorogenic

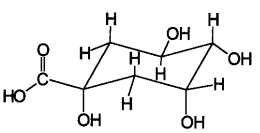


Fig. 1. Schematic structure of quinic acid (quin).

* Corresponding author. Fax: +54-221-425-9485.
E-mail address: williams@quimica.unlp.edu.ar (P.A.M. Williams).

0277-5387/00/$ - see front matter © 2000 Elsevier Science B.V. All rights reserved.
PII: S0277-5387(00)00567-2

acid) is the fruit's first line of defense against fungal invasion. It occurs widely in fruits other than grapes.

The oxovanadium(IV)–vanadyl cation interacts with sugar molecules in the presence of extra substituents (e.g. carboxylate) that anchor the VO^{2+} at low pH values in solution [6–9]. Once bonded to the metal, the ligand can deprotonate the OH groups and coordinate through these positions. Only sugars containing *cis* OH groups can adopt the mentioned chelating behavior. The polyhydroxy-substituted ring of quin has also typical characteristics of a sugar molecule. The interest in the study of its interaction with vanadyl(IV) arises from the several functionals available for binding: both 2-hydroxy acid and deprotonated *cis* diol groups can coordinate the metal center. There is a little information about the crystal structure of metal complexes with quin [10] and only few reports related to vanadium [11]. In the present work, three VO^{2+} quin complexes were precipitated from solutions at different pH values. The solids were characterized by IR and Raman spectroscopies and thermal analysis. The electronic spectra of solutions were analyzed and the species distribution diagram was obtained by potentiometric titrations.

2. Experimental

2.1. Reagents and instrumentation

All chemicals were of analytical grade and were used without further purification. Quinic acid, $VOSO_4 \cdot 5H_2O$ and $VOCl_2$ (50% aqueous solution) were purchased from Sigma, Merck and Carlo Erba, respectively.

IR spectra of powdered samples were measured with a Bruker IFS 66 FTIR-spectrophotometer from 4000 to 400 cm^{-1} in the form of pressed KBr pellets.

Raman spectra were obtained with a Spex-Ramalog double monochromator spectrometer, using the 514.5 nm line of an argon ion laser for excitation. The rotating disk technique was used, in order to avoid burning of the compound by the laser light.

Electronic absorption spectra were recorded on a Hewlett–Packard 8453 diode-array spectrophotometer, using 1 cm quartz cells. Diffuse reflectance spectra were performed with a Shimadzu UV-300 instrument, using MgO as an internal standard. Thermogravimetric (TG) and differential thermal analysis (DTA) were performed on a Shimadzu system (models TG-50 and DTA-50, respectively), working in an oxygen flow (60 ml min^{-1}) and at a heating rate of 10°C min^{-1}. Sample quantities ranged between 10 and 20 mg. Al_2O_3 was used as a DTA standard. Vanadium contents were determined by the tungsto-phosphovanadic method [12] and sodium by flame photometry. C, H and S were determined using Carlo Erba EA 1108 equipment.

2.2. Potentiometric titrations

The EMF measurements were determined with a Schott Gerate TS165 pH meter and the added volumes were measured using a Techware (Sigma) Digitrate (25 ml).

$VOSO_4 \cdot 5H_2O$ was used without further purification and dried at 60°C until constant weight. The 'formula weight' was re-calculated ($VOSO_4 \cdot 4.84H_2O$; 250.12) on the basis of a thermogravimetric analysis, before preparing the solutions. NaCl was dried until constant weight and stored in a desiccator. All solutions were made in freshly boiled tridistilled water cooled under a constant flow of nitrogen. The solutions were freshly prepared prior to their use. Diluted solutions of HCl (Merck) were standardized against TRISMA-base (hydroxymethyl aminomethane). Diluted NaOH solutions were prepared from a saturated NaOH solution and standardized against the HCl. In order to assess the degree of carbonate contamination, the method of Gran [13] was used. Cell compartments were kept at 25 ± 0.1°C with circulating water from a thermostated bath. The ionic strength was fitted at 0.150 M with NaCl in the solutions. The glass electrode was calibrated separately in a solution with known $[H^+]$ before and after each titration.

In a first step, ligand solutions were titrated with standard NaOH, in the absence of metal, to determine the pK_a value. Further, titrations of the vanadium/ligand solution were performed in order to establish the equilibria in the H^+/quin/VO^{2+} system.

The formation constants denoted β_{pqr} correspond to the general notation:

$$pM^{2+} + qL^{2-} + rH^+ \leftrightarrow (M^{2+})_p(L^{2-})_q(H^+)_r$$

A value of $pK_w = 13.76$ (corresponding to $\log \beta_{00\text{-}1} = -13.76$) was assumed for the experimental conditions ($T = 298$ K, $I = 150$ mM).

2.3. Preparative

The solid complexes were prepared mixing 1 mmol of $VOSO_4 \cdot 5H_2O$ with 2 mmol of quinic acid, under nitrogen atmosphere.

2.3.1. Compound $[VO(quin)(H_2O)_3]$ (I)

A mixture of 15 ml of methanol in 5 ml of water was used as the solvent. The solution was cooled with an ice bath and the pH was adjusted with $NaOCH_3$ to 3.5. After 15 min of stirring a light blue precipitated was formed. The solid was filtered under vacuum, washed with cooled methanol and dried over $CaCl_2$. Yield: 81%. *Anal.* Calc.. for $C_7H_{16}O_{10}V$: C, 27.00; H, 5.14; V, 16.40. Found: C, 27.24; H, 4.90; V, 16.75%.

2.3.2. Compound $Na_4[VO(quin)_2SO_4]\cdot 4H_2O$ (II)

The reactants were added to 5 ml of water. The pH of the solution was fitted to a final value of 6 with solid $NaHCO_3$. The excess of bicarbonate was eliminated by filtration. The addition of absolute ethanol to the resulting solution produced a violet precipitate, which was filtered, washed with absolute ethanol and dried in an oven at 60°C. Yield: 75%. *Anal.* Calc. for $C_{14}H_{28}Na_4O_{21}VS$: C, 23.76; H, 3.96; Na, 13.01; S, 4.53; V, 7.21. Found: C, 24.00; H, 3.85; Na, 13.5; S, 4.30; V, 7.55%.

2.3.3. Compound $Na_6[VO(quin)_2SO_4]\cdot 4H_2O$ (III)

Quinic acid and vanadyl sulfate were dissolved in 5 ml of water. Solid NaOH was added until a final pH value of 12 was reached. Addition of excess absolute ethanol produced the precipitation of a green solid complex. The microcrystalline powder was filtered, washed with absolute ethanol and dried at 60°C. Yield: 53%. *Anal.* Calc. for $C_{14}H_{26}Na_6O_{21}VS$: C, 22.37; H, 3.46; Na, 18.38; S, 4.26; V, 6.79. Found: C, 22.45; H, 3.44; Na, 18.82; S, 4.53; V, 7.03%.

3. Results and discussion

3.1. UV–Vis spectra

At pH 3.5 three different components in solution exist simultaneously. The majority species is VO(quin) (63.8%), as detected by potentiometric titrations (see below). Free VO^{2+} is present at 17.8% and $VO(quin)_2$ at 15.5%. The subtraction of the bands corresponding to the two latter species in their respective percentages gave the electronic spectrum of VO(quin) with bands at: 568 nm (9.05 M^{-1} cm^{-1}) and 790 nm (30.06 M^{-1} cm^{-1}). The typical electronic spectrum of $[VO(H_2O)_5]^{2+}$ consists of three bands: $b_2 \rightarrow e$, $b_2 \rightarrow b_1$ and $b_2 \rightarrow a_1$ (generally obscured by overlapping with a charge transfer band), corresponding to a C_{4v} geometry [14]. When carboxylate coordinates to vanadyl(IV) the $b_2 \rightarrow e$ and the $b_2 \rightarrow b_1$ bands shifts to the red and to the blue, respectively, due to the stronger ligand crystal field [15–22].

The spectrum of the violet single species present at pH 6 show bands at 415 nm (21.6 M^{-1} cm^{-1}), 530 nm (22.60 M^{-1} cm^{-1}), 615 nm (18.00 M^{-1} cm^{-1}) and 780 nm (14.40 M^{-1} cm^{-1}). These four bands are typical of 2-hydroxyacids coordinated to vanadyl(IV) cation, forming chelate complexes with two ligand molecules coordinating the metal ion through the carboxylate and deprotonated hydroxyl groups and are indicative of the predominance of the *trans* isomer in solution [6,10].

At pH 12 the typical three-band pattern corresponding to the interaction of VO^{2+} with sugars is observed [7,8,23]. The new bands are located at 422 nm (18.60 M^{-1} cm^{-1}), 542 nm (19.20 M^{-1} cm^{-1}) and 664 nm (16.00 M^{-1} cm^{-1}). The considerable variation in the UV–Vis spectrum is in accordance with the variation on the donor set involved in the VO^{2+} coordination When increasing the pH of the solution consecutive proton dissociation of the hydroxyl groups of the coordinated ligands takes place. This dissociation is followed by coordination of the second hydroxyl function (replacing carboxylate), i.e. the formation of two chelate rings involving four deprotonated hydroxyl groups [7,8,23–33]. In these complexes the carboxylate group acted as the anchoring site for oxovanadium(IV) ion. In the absence of a binding site readily available at low pH, the hydrolysis of oxovanadium(IV) is favored over complex formation with the ligand.

3.2. Diffuse reflectance spectra

The diffuse reflectance data agree with the UV–Vis spectrum. In complex **I** obtained at pH 3.5 two bands located at 550 and 780 nm were observed denoting coordination of the vanadyl(IV) cation through the carboxylate group of quinic acid, as has already been stated in the difference UV–Vis spectrum. Complex **II**, obtained at pH 6, shows four bands at 415, 530, 615 and 780 nm. The three bands of complex **III** appeared at 425, 525 and 660 nm.

3.3. Infrared spectra

From the data in Table 1 the following can be stated:

1. The ν(COOH) band of the free ligand splits into two components when the coordination occurs, Table 1. The Δ value $[\nu_a(COO^-) - \nu_s(COO^-)]$ of complexes **I** and **II** (approximately 270 cm^{-1}) is in

Table 1
Assignments of some characteristic IR bands (cm^{-1}) of quinic acid and $[VO(quin)(H_2O)_3]$ (**I**), $Na_4[VO(quin)_2SO_4]\cdot 4H_2O$ (**II**) and $Na_6[VO(quin)_2SO_4]\cdot 4H_2O$ (**III**) [a]

Quinic acid	I	II	III	Assignments
1681 (vs)				ν(COOH)
	1635 (s)	1634 (s)	1631 (s)	$\nu_a(COO^-)$
	1363 (m)	1363 (m)	1457 (m)	$\nu_s(COO^-)$
1228 (s)	1186 (sh)			δ(C–OH)
		1131 (vs)	1131 (vs)	$\nu(SO_4^{2-})$
		996 (s)	996 (s)	$\nu(SO_4^{2-})$
	1151 (s)	1157 (m)	1152 (m)	see text
1137 (vs)	1116 (s)	1118 (s)	1125 (s)	see text
1079 (s)	1089 (sh)	1086 (s)	1086 (sh)	see text
1062 (s)	1067 (s)	1066 (s)	1062 (s)	see text
	986 (s)	968 (s)	929 (s)	ν(V=O)
		631 (s)	638 (s)	$\nu(SO_4^{2-})$
		619 (s)	621 (s)	$\nu(SO_4^{2-})$
613 (m)	613 (m)			

[a] vs, very strong; s, strong; m, medium; w, weak; sh, shoulder.

agreement with a unidentate coordination of the carboxylate group. Complex **III** exhibits a significantly lower Δ value (ca. 174 cm^{-1}) suggesting that the carboxylate group is present in an ionic form without coordination to the metal center [34].

2. The free sulfate anion have a T_d point group. Of the four fundamentals, only ν_3 and ν_4 are IR active (1104 (vs) and 613 (s) cm^{-1}, respectively). When sulfate coordinates to a metal, its symmetry is lowered and the spectrum is affected due to the changes in the selection rules and different modes can be activated depending on its coordination mode [34]. The bands located at 1131 (vs), 996 (s), 631 (s) and 619 (s) cm^{-1} in the spectra of **II** and **III** indicate the presence of the sulfate anion in those complexes. The absence of the $\nu_3(SO_4^{2-})$ strong band at 1170 cm^{-1} allows us to discard the bridging bidentate coordination of this group. The strong band at 996 cm^{-1} ($\nu_1(SO_4^{2-})$) together with the strong $\nu_4(SO_4^{2-})$ band in the 600–650 cm^{-1} range are indicative of a unidentate coordination of the sulfate group. The absence of the very strong band in the 1150–1000 cm^{-1} range allowed a conclusion that the solid **I**, obtained at pH 3.5, is a unique species. Neither $VOSO_4$ nor complex **II**, present in the solution, coprecipitated with it. When the complexes were precipitated at pH ≥ 6 the sulfate is involved in the coordination sphere, as mentioned above.
3. In order to record the bands that are masked by the sulfate anion, the complexes at pH 6 and 12 were prepared in a similar manner, using $VOCl_2$ instead of $VOSO_4$. For carbohydrates, the bands in the 1200–1060 cm^{-1} region are assigned as a coupling of C–O and C–C vibrations with some C–O–H and C–C–H bending components [35,36]. The band of the free ligand at 1137 cm^{-1} splits into two components in the three complexes. This fact can be indicative of either coordination or deprotonation of the C–OH groups.
4. When vanadyl(IV) interacts with carboxylate anion (complex **I**) the position of the ν(V=O) band is located at approximately 990 cm^{-1} [19,22,37]. The intermediate value of ν(V=O) observed in complex **II** is characteristic of complexes of hydroxycarboxylates with oxovanadium(IV) [6,38]. The decrease in the V=O IR stretch from compound **I** to **II** can be explained on the basis of the sulfate coordination. The position of ν(V=O) in the spectrum of **III**, is the same of that for the vanadyl complexes with sugars, denoting that the coordination occurs through the deprotonated hydroxy groups [7,9,31]. The weakening of the V=O bond in compound **III** [7,29–33,38] can be due to an increase of the σ-donor character of the ligands in the coordination sphere of the vanadium center.

3.4. Raman spectra

In order to determine sulfate anion and carboxylate group stretching modes, Raman spectra were recorded. Fluorescence is observed in the case of complex **II** so the Raman spectrum was measured with the complex prepared using $VOCl_2$ instead of $VOSO_4$. The most important features have been observed (Table 2):

1. The intensity of the antisymmetric stretching COO^- band lowered and the symmetric mode is increased with respect to the FTIR, as expected.
2. Raman active modes of sulfate anion shown in complex **III** are in agreement with the lowering of symmetry caused by coordination.
3. Typical bands of the sugar moiety are observed.
4. The ν(V=O) remains in the same position as the IR spectra with higher intensity.

3.5. Thermogravimetric behavior

The thermal behavior of the free ligand and the three complexes was investigated by means of TG and DTA measurements under O_2 atmosphere up to 1000°C (Fig. 2).

3.5.1. Quinic acid

The degradation starts at 150°C with a loss of 10.12% accompanied by a medium endothermic peak located at 172.5°C (s, *endo*) (DTA signal). Finally, two consecutive events are observed with losses of 84.54% (322.5°C, s, *exo*) and 4.62% (472°C, m, *exo*), respectively.

3.5.2. Complex *I*

As can be seen from the thermogram shown in Fig. 2 the three water molecules are removed in two steps,

Table 2
Assignments of some characteristic Raman bands (cm^{-1}) of quinic acid and $[VO(quin)(H_2O)_3]$ (**I**), $[VO(quin)_2]^{2-}$, prepared using $VOCl_2$ instead of $VOSO_4$ (**II**, $VOCl_2$) and $Na_6[VO(quin)_2SO_4]\cdot 4H_2O$ (**III**) [a]

Quinic acid	**I**	**II** ($VOCl_2$)	**III**	Assignments
1680 (s)				ν(COOH)
	1630 (w)	1641 (m)	1633 (w)	$\nu_a(COO^-)$
	1358 (s)	1358 (s)	1451 (s)	$\nu_s(COO^-)$
1228 (m)	1200 (m)			δ(C–OH)
			1131 (sh)	$\nu(SO_4^{2-})$
			994 (vs)	$\nu(SO_4^{2-})$
	1141 (m)	1157 (m)	1151 (w)	see text
1137 (s)	1116 (m)	1118 (m)	1127 (m)	see text
1073 (sh)	1095 (w)	1090 (w)	1074 (m)	see text
	1047 (m)	1048 (m)	1058 (w)	see text
	987 (vs)	960 (vs)	927 (vs)	ν(V=O)
			627 (s)	$\nu(SO_4^{2-})$
613 (w)	607 (m)			

[a] vs, very strong; s, strong; m, medium; w, weak; sh, shoulder.

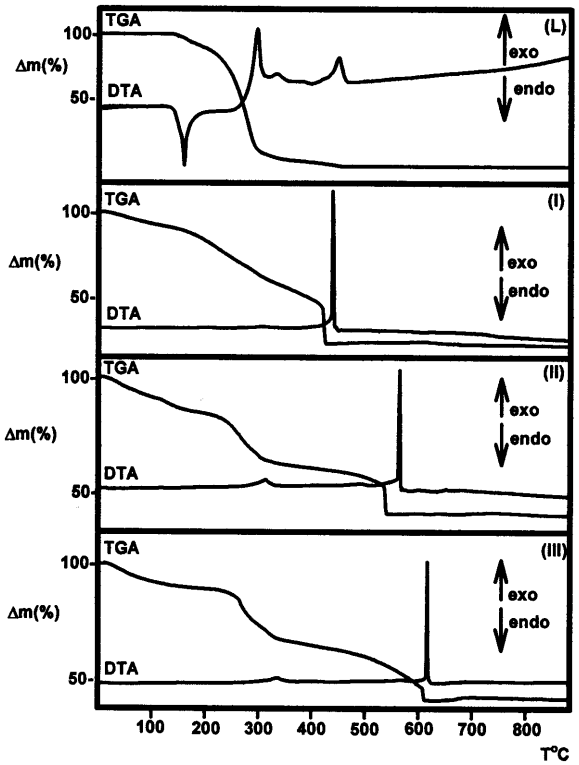


Fig. 2. TG and DTA curves of the thermal decompositions of quinic acid (L), $[VO(quin)(H_2O)_3]$ (**I**), $Na_4[VO(quin)_2SO_4]\cdot 4H_2O$ (**II**) and $Na_6[VO(quin)_2SO_4]\cdot 4H_2O$ (**III**). Oxygen flow: 50 ml min^{-1}, rate: 10°C min^{-1}.

with losses of 5.57% and 11.57% in the ranges of 50–100°C and 100–230°C, respectively. The theoretical mass loss is 5.78% for the first water molecule and 11.74% for the two remaining molecules, in excellent agreement with the observed values. After dehydration a complex series of consecutive events is observed: 9.94%, 13.58% (328°C, w, *exo*), 28.27% (445°C, vs, *exo*), 2.04%. The weight of the residue at 1000°C is 29.03% in good agreement with the theoretical value (29.26%). The total stoichiometry of this process is proposed as follows:

$$2[VO(quin)(H_2O)_3] \xrightarrow{O_2} V_2O_5 + \text{volatile products}$$

3.5.3. Complex *II*

The loss of two water molecules of hydration occurs in the 25–85°C range ($\Delta\omega_{exp} = 5.39\%$ and $\Delta\omega_{calc} = 5.09\%$). This step is followed by the loss of the two remaining water molecules in the 85–145°C range ($\Delta\omega_{exp} = 5.04\%$ and $\Delta\omega_{calc} = 5.09\%$). Two successive degradation steps 27.07% (337°C, vw, *exo*) and 20.13% (568°C, vs, *exo*) leads to the final residue at 1000°C. The overall reaction pattern can be formulated as:

$$2Na_4[VO(quin)_2SO_4]\cdot 4H_2O \xrightarrow{O_2} 2Na_2SO_4 + V_2O_5 + 2Na_2O + \text{volatile products}$$

for which a mass loss of 58.28% is calculated, in good agreement with the experimental value of 57.63%.

3.5.4. Complex *III*

The dehydration occurs in a single stage and covers the 25–160°C range with the elimination of four water molecules ($\Delta\omega_{exp} = 9.79\%$ and $\Delta\omega_{calc} = 9.59\%$). Immediately after, the decomposition is accompanied by three successive steps with losses of 16.58%, 9.02% (358°C, vw, *exo*) and 17.27% (587°C, vw, *exo*; 633°C, vs, *exo*). The total degradation is postulated as:

$$2Na_6[VO(quin)_2SO_4]\cdot 4H_2O \xrightarrow{O_2} 2Na_2SO_4 + V_2O_5 + 4\ Na_2O + \text{volatile products}$$

with a theoretical total residue of 47.54% at 1000°C (exp. residue = 47.34%).

The final residues of the three complexes have been characterized on the basis of IR spectroscopy. In all cases V_2O_5 is detected. The presence of this oxide is also demonstrated by a very weak endothermic DTA signal in the 660–670°C range corresponding to the melting point (658°C) [39].

The thermal studies performed suggest that complex **I** is more stable than the other complexes because of the higher degradation temperature (approximately 230°C). The presence of the sulfate anion in the coordination sphere of complexes **II** and **III** may enhance their reactivity.

3.6. Potentiometric titrations

The acidity constants for quinic acid were determined from three titrations using pK_a values and Best calculation programs [40]. Solutions of 20 mM quinic acid were titrated with NaOH over a 2.3–12 pH range. In these conditions only the first two deprotonation constants ($\log\beta_{012} = 15.32$ and $\log\beta_{011} = 12.0$) could be estimated. These data compare well with literature values [41]. On these basis L^{2-} has been considered as the proper component of the system, even when the ligand has three more potential acidic protons.

To estimate the formation constants of the ternary system $VO^{2+}/L^{2-}/H^+$ the data collected from four titrations were analyzed with BEST and SUPERQUAD [42] calculation programs.

The experiments were performed on a 2.3–12 pH range. Total vanadyl(IV) concentration in the titration vessel was 10 mM while the ligand concentration was 20 mM. The usual criteria used to select equilibrium models of speciation using these sorts of programs (CHI^2 and *R* values, S.D. values, etc.) was the comparison with the spectroscopic results.

In Table 3 the proposed species and the corresponding β values for this system are shown. Due to the very low total vanadium concentration in the experimental

conditions the $(VO)_2(OH)_2^{2+}$ species was neglected. The species distribution as a function of pH was obtained with the SPECIES program (see Fig. 3).

It can be seen that complexation occurs in the whole pH range, according to the spectroscopic results and physicochemical characterization discussed above. No precipitation nor hydrolysis of VO^{2+} species was observed during the experiments. At the initial pH value of 2.3, potentiometric titration curves of quinic acid with and without vanadyl(IV) are not superimposable indicating that complex formation occurs at low pH. This observation is consistent with the fact that monodentate carboxylate binding takes place. Carboxylic protons are strongly acidic in the vanadyl complexes than in the free ligand as can be seen in Fig. 3 ($pK_{a1} = 3.32$).

In the 2.3–6.0 pH range more than one species contributes to the electronic spectrum of the solution in a significant percentage. At pH between 6 and 8, the titration curve corresponds to that of only one main species. This was confirmed by UV–Vis spectroscopy. The position of the bands is similar to that of α-hydroxy-acid complexes with vanadyl(IV) [6,11]. From Fig. 3 it can be seen that at least four different species coexist in solution with a reaccomodation of the ligand around the metal center. Finally, at pH 12 a new deprotonation of the ligand takes place and the majority of species correspond to an alkoxide-linked complex. Since $VO(OH)_3^-$ is present in such small amounts its UV spectrum could not be observed and the spectrum shows mainly the three-band pattern of VO^{2+}/carbohydrate complexes [7,8,23–33].

Table 3
Composition, notation and formation constants (β) for the $VO^{2+}/L^{2-}/H^+$ system (0.150 M NaCl, 25°C) [a]

Species	Formula	log β
012	LH_2	15.32
011	LH	12.00
110	ML	11.56
11-1	MLH_{-1}	6.28
120	ML_2	22.01
12-1	ML_2H_{-1}	11.34
12-2	ML_2H_{-2}	0.54

[a] In the final calculation log β for vanadium hydrolysis products were: −5.50, −17.90 and −21.85 for MH_{-1}, MH_{-3} and M_2H_{-5}, respectively.

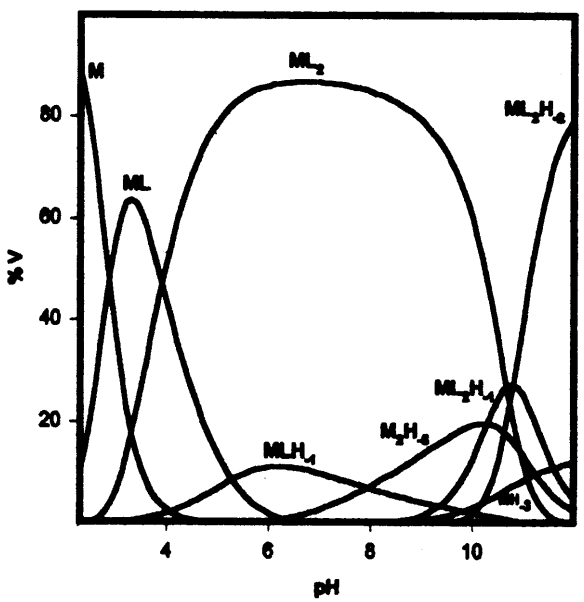


Fig. 3. Concentration distribution of the complexes present in the vanadyl(IV)–quinic acid system as a function of pH at 25°C, I = 0.150 M NaCl.

Acknowledgements

E.G.F. is member of the Research Career from CONICET. P.A.M.W. is member of the Research Career from CICPBA. This study has been partially supported by CONICET, CICPBA and Agencia Nacional de Promoción Científica y Tecnológica (PICT 119). E.G.F. acknowledges support from Fundación 'Antorchas'.

References

[1] D. Redher, Coord. Chem. Rev. 182 (1999) 297.
[2] K.H. Thompson, J.H. Mc. Neill, C. Orvig, Chem. Rev. 99 (1999) 2561.
[3] Y. Inomata, T. Haneda, F.S. Howell, J.Inorg.Biochem. 76 (1999) 13.
[4] D. Stead, Lett. Appl. Microbiol. 18 (1994) 112.
[5] S.E. Castillo-Blum, N. Barbra-Behrens, Coord. Chem. Rev. 196 (2000) 3.
[6] G. Barr-David, T.W. Hambley, J.A. Irwin, R.J. Judd, P.A. Lay, B.D. Martin, R. Bramley, N.E. Dixon, P. Hendry, J.Y. Ji, R.S.U. Baker, A.M. Bonin, Inorg. Chem. 31 (1992) 4906.
[7] S.B. Etcheverry, P.A.M. Williams, E.J. Baran, Carbohydr. Res. 302 (1997) 131.
[8] P.A.M. Williams, S.B. Etcheverry, E.J. Baran, Carbohydr. Res. 329 (2000) 41.
[9] S.B. Etcheverry, P.A.M. Williams, E.J Baran, J. Inorg. Biochem. 63 (1996) 285.
[10] T. Haneda, Y. Inomata, F.S. Howell, J. Inorg. Biochem. 67 (1997) 303 and references therein.
[11] R. Codd, T.W. Hambley, P.A. Lay, Inorg. Chem. 34 (1995) 877.
[12] M. Onishi, Photometric Determination of Traces of Metals, Part II, 4th ed., Wiley, New York, 1988.
[13] G. Gran, Analyst 77 (1952) 661.
[14] C.J. Ballhausen, H.B. Gray, Inorg. Chem. 1 (1972) 111.
[15] C.R. Johnson, R.E. Shepherd, Bioinorg. Chem. 8 (1978) 115.
[16] K. Wüthrich, Helv. Chim. Acta 48 (1965) 779.
[17] E.J. Baran, A.H. Jubert, A.L. Rocha, J. Raman Spectr. 20 (1989) 801.
[18] E.G. Ferrer, P.A.M. Williams, E.J. Baran, Biol. Trace Elem. Res. 30 (1991) 175.
[19] E.G. Ferrer, P.A.M. Williams, E.J. Baran, J. Inorg. Biochem. 50 (1993) 253.

[20] P. Kögerler, E.G. Ferrer, E.J. Baran, Monatsh. Chem. 127 (1996) 801.
[21] P.A.M. Williams, P. Kögerler, E.J. Baran, Acta Farm. Bonaerense 17 (1998) 31.
[22] S.B. Etcheverry, P.A.M. Williams, D.A. Barrio, V.C. Sálice, E.G. Ferrer, A.M. Cortizo, J. Inorg. Biochem. 80 (2000) 169.
[23] P.A.M. Williams, E.J. Baran, J. Inorg. Biochem. 50 (1993) 101.
[24] G. Micera, A. Dessí, H. Kozlowski, B. Radomska, J. Urbanska, P. Decock, B. Dubois, I. Olivier, Carbohydr. Res. 188 (1989) 25.
[25] M. Branca, G. Micera, A. Dessí, H. Kozlowski, J. Chem. Soc., Dalton Trans. (1989) 1283.
[26] M. Branca, G. Micera, D. Sanna, A. Dessí, H. Kozlowski, J. Chem. Soc., Dalton Trans. (1990) 1997.
[27] M. Branca, A. Dessí, D. Sanna, J. Inorg. Biochem. 45 (1992) 169.
[28] P.A.M. Williams, S.B. Etcheverry, E.J. Baran, J. Inorg. Biochem. 65 (1997) 133.
[29] C.P. Rao, S.P. Kaiwar, Inorg. Chim. Acta 186 (1991) L11.
[30] A. Sreedhara, M.S.S. Raghavan, C.P. Rao, Carbohydr. Res. 264 (1994) 227.
[31] A. Sreedhara, C.P. Rao, B.J. Rao, Carbohydr. Res. 289 (1996) 39.
[32] R.P. Bandar, C.P. Rao, J. Inorg. Biochem. 68 (1997) 1.
[33] S.B. Etcheverry, P.A.M. Williams, E.J. Baran, Biol. Trace Elem. Res. 51 (1996) 169.
[34] K. Nakamoto, Infrared and Raman Spectra of Inorganic and Coordination Compounds, 4th ed., Wiley, New York, 1986.
[35] J.J. Cael, J.L. Koenig, J. Blackwell, Carbohydr. Res. 32 (1974) 79.
[36] M. Mathlouthi, J.L. Koenig, Adv. Carbohydr. Chem. Biochem. 44 (1986) 7.
[37] P.A.M. Williams, E.G. Ferrer, E.J. Baran, J. Coord. Chem. 42 (1997) 261.
[38] S.L. Castro, M.E. Cass, F.J. Hollander, S.L. Bartley, Inorg. Chem. 34 (1995) 466.
[39] R.J.H. Clark, Vanadium, Comprehensive Inorganic Chemistry, vol. 3, Pergamon Press, Oxford, 1973, p. 511.
[40] A.E. Martell, R.J. Motekaitis, Determination and Use of Stability Constants, 2nd ed., VCH, New York, 1992.
[41] C.F. Timberlake, J. Chem. Soc. (1959) 2795.
[42] P. Gans, A. Sabatini, A. Vacca, J. Chem. Soc., Dalton Trans. (1985) 1195.

PERGAMON

www.elsevier.nl/locate/poly

Polyhedron 19 (2000) 2621–2627

POLYHEDRON

Anhydrous copper(II) hexanoate from cuprous and cupric oxides. The crystal and molecular structure of $Cu_2(O_2CC_5H_{11})_4$

Adriana Doyle [a], Judith Felcman [a,*], Maria Teresa do Prado Gambardella [b], Cláudio Nazari Verani [c], Maria Luiza Bragança Tristão [d]

[a] *Department of Chemistry, Pontifícia Universidade Católica do Rio de Janeiro (PUC-RJ), Rua Marquês de São Vicente, 225, Gávea, 22453-900 Rio de Janeiro, RJ, Brazil*

[b] *Department of Chemistry and Molecular Physics, Instituto de Química de São Carlos, Universidade de São Paulo (USP) – São Carlos, Caixa Postal 780, 13560-250 São Carlos, SP, Brazil*

[c] *Max-Planck-Institut für Strahlenchemie, Stiftstrasse, 34–36, D-45470 Mülheim, Germany*

[d] *Cenpes/Petrobrás, Cidade Universitária, Avenida 1, Quadra 7, Ilha do Fundão, 21910-900 Rio de Janeiro, RJ, Brazil*

Received 14 January 2000; accepted 24 August 2000

Abstract

The synthesis and spectroscopic, magnetic and structural characterization of a complex of copper(II) with hexanoic acid, $Cu_2(O_2CC_5H_{11})_4$ are described. The same complex is formed by synthesis using either CuO or Cu_2O. The compound exhibits a typical dinuclear paddle-wheel type structure, consisting of two copper(II) ions in square-pyramidal geometry bridged by four carboxylate anions in the *xy* plane. The IR spectrum shows that the $\Delta\nu_{COO}$ for this complex appears at 171 cm^{-1} which corresponds to a bridging bidentade mode of coordination of carboxylate-to-metal. Elemental analysis, EPR spectra and TG analysis were also performed. The magnetic susceptibility measurement confirms the antiferromagnetic nature of the copper–carboxylate coupling which is in agreement with the X-ray crystallography results. © 2000 Elsevier Science B.V. All rights reserved.

Keywords: Copper complexes; Carboxylate complexes; Dinuclear complexes; Crystal structures; Cuprous oxide; Cupric oxide.

1. Introduction

Due to their varied geometric structures and physicochemical properties, copper(II) complexes have received considerable attention in the last years. They have several applications in many areas which include biochemical and industrial ones.

The complexes with carboxylic acids are very interesting [1] because they can contain two or more antiferromagnetically coupled metal centers [2–9]. Since each carboxylate oxygen atom has two lone pairs they can either have only one lone pair involved in the coordination resulting in a dinuclear paddle-wheel structure or have the second lone pair donated to a metal ion of another paddle-wheel structure resulting in a polymeric structure. Although polymeric structures can also occur when the ligand bridges two units, it seems that all anhydrous copper(II) carboxylates adopt the structure in which the bridge is between the metal of one paddle-wheel like structure and the carboxylate of a second one [10]. Several copper(II) alcanoates have been studied [4,5,9–12]. All these compounds have a molar susceptibility anomalously low compared to those of other copper(II) compounds and show a paramagnetic susceptibility with a maximum at about 270 K, falling steeply with the decreasing of temperature[12].

Usually copper(II) carboxylates are prepared from copper(II) acetate and the corresponding carboxylic acid [13], or $CuSO_4 \cdot 5H_2O$ and the sodium salt of the carboxylic acid [3,14,15] or any other compound of copper(II), such as carbonate [11,12] and the corresponding carboxylic acid.

In this paper, copper(II) hexanoate was prepared by reaction of both cupric and cuprous oxides with hexanoic acid. In both cases the resulting compound was

* Corresponding author. Tel.: +55-21-529-9571; fax: +55-21-529-9569.

E-mail addresses: adoyle@connection.com.br (A. Doyle), felcman@rdc.puc-rio.br (J. Felcman), teca@iqsc.sc.usp.br (M.T.P. Gambardella), mlu@cenpes.petrobras.br (M.L.B. Tristão).

0277-5387/00/$ - see front matter © 2000 Elsevier Science B.V. All rights reserved.
PII: S0277-5387(00)00568-4

anhydrous copper(II) hexanoate. The synthesis of the complex starting from cuprous oxide represents the inverse reaction of thermal decomposition of copper(II) carboxylates in the presence of reducing agents as described in the literature [16]. The resulting copper(I) complex is easily oxidized on exposure to the atmosphere. We also describe its structure, spectroscopic and magnetic properties. Up to now this compound had been synthesized only from copper(II) acetate [13] and also did not have its crystal structure and other properties studied. We found references [11,13,16,17] that describe the IR spectra of some anhydrous copper(II) carboxylates, but only in the region between 4000 and 400 cm^{-1}. Here, we performed IR spectra in this region and in the range from 600 to 50 cm^{-1}.

2. Experimental

2.1. Synthesis and chemical characterization of the complex

Syntheses were carried out through the reaction of both cuprous and cupric oxides with hexanoic acid. All chemicals and solvents used were commercially available reagent grade ones, with no further treatment.

The green crystals, which were formed in both cases after several days reaction, were vacuum filtered, thoroughly washed with acetone and left to dry at room temperature (r.t.). In the case of the reaction with cuprous oxide it appeared at the same time a deposit of metallic copper.

The crystal obtained from cuprous oxide will be called crystal A and the one obtained from cupric oxide will be called crystal B. Both complexes were practically insoluble in water, ethanol and acetone.

The copper content was determined by atomic absorption spectrometry in a Varian AA5 Instrument. A total of 5.0 mg of the compound was digested with a small amount of nitric acid and diluted to 50 ml. The measurements were taken using the wavelength of 324.7 nm and a slit of 0.1 nm.

Carbon, hydrogen and oxygen determinations were performed in an elemental analyzer EA 1110 from CE Instruments. The composition, in %, found for crystal A and crystal B can be seen in Table 1.

2.2. Magnetic measurements

Temperature dependent (2–298 K) magnetization data were recorded on a SQUID magnetometer (MPMS Quantum Design) in an external magnetic field of 1 T. The experimental susceptibility data were corrected for underlying diamagnetism by use of tabulated Pascal's constants.

Electron paramagnetic resonance measurements were carried out both in the crystals and the green solution from which the crystals were formed, on a Bruker 300 E ESR spectrometer operating at X-band frequency (9.45 GHz at 77 K) using a rectangular standard cavity TE 102, with signal modulation at 100 kHz, modulation amplitude 7.052 Gauss and microwave potency of 4.01×10^{-1} mW.

2.3. Physical measurements

IR spectra of the studied crystals were obtained in a Nicolet 760 Magna IR spectrometer with 128 scans and a spectral resolution of 4 cm^{-1}, at r.t. For the spectrum over the wave-number range from 4000 to 400 cm^{-1}, the crystals were pressed into pellets with KBr and the instrument was equipped with a KBr beam splitter and a DTGS detector with CsI windows. Over the wave-number range from 600 to 50 cm^{-1}, the crystals were pressed with polyethylene and the instrument was equipped with a solid substance and a DTGS detector.

Thermogravimetric analysis was performed with a Perkin–Elmer TGA 7. The temperature range used was from 20 to 900°C, with a scanning rate of 10.0°C min^{-1}.

2.4. X-ray structure analysis

A crystal of copper(II) hexanoate (crystal A) was mounted in the Enraf-Nonius CAD4 diffractometer, and using 25 reflections automatically centered, the cell parameters were obtained and refined [18]. Crystal data and numerical details on collection and refinement are presented in Table 2. The intensity data were reduced to F_o and corrected by absorption factor according to an empirical method, ψ-scan [19,20].

The structure was solved by SIR-92 [21], difference Fourier synthesis, and refined on F^2 by full-matrix least-squares using the SHELXL-97 [22]. The hydrogen atoms were positioned geometrically and a riding model was used during the refinement, with U_{iso} amounting to 1.5 (methyl H atoms; C–H = 0.97 Å)

Table 1
Elemental analysis of the crystals of copper(II) hexanoate

Crystal	Values of elements (%) (calculated values in brackets)			
	C	H	O	Cu
Crystal A	48.67 (49.06)	7.12 (7.49)	21.77 (21.80)	19.81 (21.63)
Crystal B	49.22 (49.06)	8.51 (7.49)	20.73 (21.80)	20.70 (21.63)

Table 2
Crystallographic data for $Cu_2(O_2CC_5H_{11})_4$

Molecular formula	$Cu_2(O_2CC_5H_{11})_4$
Molecular weight	587.67
Colour	Green
Crystal size (mm)	$0.05 \times 0.20 \times 0.62$
Crystal system	triclinic
Space group	$P\bar{1}$
Z	1
Unit cell dimensions	
a (Å)	5.1538(7)
b (Å)	8.498(1)
c (Å)	17.050(3)
α (°)	84.18(1)
β (°)	85.88(1)
γ (°)	76.21(1)
V (Å^3)	720.6(2)
D_{calc} (g cm^{-3})	1.354
$F(000)$	310
μ_{calc} (cm^{-1})	1.52
Data collection	
T (K)	243
Total data	4851
Total unique data	4174
Total $F^2 \geq 2\sigma(F^2)$ data	3512
Absorption correction	ψ scan
T_{min}, T_{max}	0.657, 0.774
Refinement	
No. refinement parameters	156
Final R [$F^2 \geq 2\sigma(F^2)$], $wR(F^2)$	0.031, 0.075
S	1.036
w^{-1}	$\sigma^2(F_o^2)+(0.03896P)+0.19P$ $P=(F_o^2+2F_c^2)/3$
$\Delta\rho_{max}$, $\Delta\rho_{min}$ in final cycle	0.43, −0.30

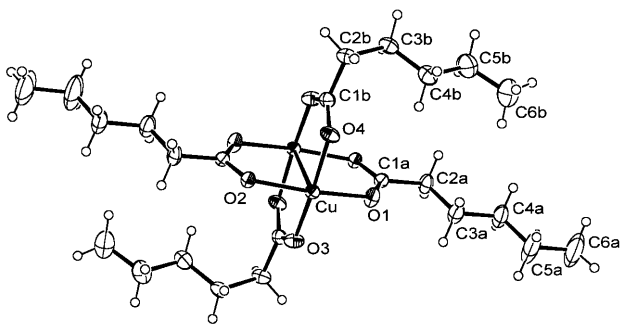


Fig. 1. Molecular structure of anhydrous copper(II) hexanoate. H atoms have been omitted for clarity.

or 1.2 (for the remaining; C–H = 0.98 Å) times the value of U_{eq} of the atom to which they are attached. All non-hydrogen atoms were refined anisotropically. The maximum and minimum electron density observed at the end of refinement were 0.43 (0.88 Å from Cu) and −0.30 (1.36 Å from O_2).

Crystal B showed the same X-ray results.

3. Results and discussion

23.1. General

Starting from cuprous oxide, the synthesis of the anhydrous copper(II) hexanoate led to the formation of a green solution and a deposit of metallic copper almost immediately after the addition of the cuprous oxide to the hexanoic acid. Several days after, small green needle-shaped crystals of X-ray quality were formed. The deposition of metallic copper shows that the copper(I) disproportionates into copper(II) and metallic copper: $2Cu^{1+} \leftrightarrow Cu^0 + Cu^{2+}$. Then, the Cu(II) ions react with the hexanoic acid to give the desired complex. This synthesis led to a yield of 68%. When cupric oxide was used, the formation of the green solution was observed a month after the addition of the reagent and it took several months for the deposition of the same green needle-shaped crystals. This synthesis gave a yield of 57%.

Elemental analysis of the crystals corresponds in both cases to the copper(II) hexanoate. The structures were determined and were shown to consist of dinuclear paddle-wheel like units.

All other experimental data obtained for both complexes and which are described below were similar and permitted the conclusion that they were the same compound.

3.2. X-ray crystallography

The molecular structure of copper(II) hexanoate representation is given in Fig. 1. The copper–copper distance is 2.5791(5) Å, and metal centers are bridged by four hexanoate ligands. The extended polymeric structure (Fig. 2) consists of chains of dimeric units with adjacent non-bonded coppers separated by 3.2357(5) Å. Selected bond lengths and angles are given in Table 3.

Both copper atoms have a distorted square-pyramidal geometry, with equatorial Cu–O distance of the O involved in the chain extension being slight longer than

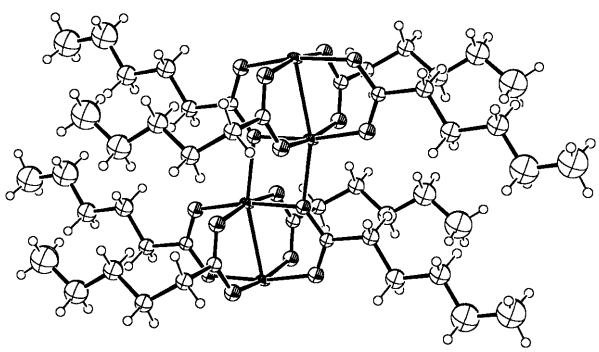


Fig. 2. Polymeric structure of $[Cu_2(O_2CC_5H_{11})_4]_n$.

Table 3
Selected bond distances (Å) and angles (°) of copper(II) hexanoate [a]

Cu–Cu^{i}	2.5791(5)	Cu–O4	1.947(1)
Cu–O1	1.964(1)	Cu–O2^{ii}	2.206(1)
Cu–O2	2.011(1)	Cu–Cu^{ii}	3.2357(5)
Cu–O3	1.940(1)		
O1–Cu–O2	169.88(5)	O2–Cu–Cu^{i}	82.34(4)
O1–Cu–O3	89.89(6)	O3–Cu–O4	169.75(5)
O1–Cu–O4	88.64(6)	O3–Cu–O2^{ii}	93.94(5)
O1–Cu–O2^{ii}	110.23(5)	O3–Cu–Cu^{i}	83.07(4)
O1–Cu–Cu^{i}	87.55(4)	O4–Cu–O2^{ii}	96.09(5)
O2–Cu–O3	88.99(6)	O4–Cu–Cu^{i}	86.73(4)
O2–Cu–O4	90.67(6)	Cu–O2–Cu^{i}	100.11(5)
O2–Cu–O2^{ii}	79.89(5)		

[a] Symmetry code: i: $-x+1$, $-y+2$, $-z+1$ and ii: $-x+2$, $-y+2$, $-z+1$.

Table 4
Selected IR absorption bands (cm^{-1}) of anhydrous copper(II) hexanoate

$Cu_2(O_2CC_5H_{11})_4$	Assignment
2955 (m)	$\nu_{CH_3,\ as}$
2932 (m)	$\nu_{CH_2,\ as}$
2873 (w)	$\nu_{CH_3,\ s}$
2861 (w)	$\nu_{CH_2,\ s}$
1588 (s)	$\nu_{COO,\ as}$
1417 (m)	$\nu_{COO,\ s}$
387 (s)	ν_{Cu-O}
341 (m)	ν_{Cu-O}
301 (m)	
245 (s)	
235 (s)	δO–Cu–O
188 (m)	δO–Cu–O
146 (m)	δCu–Cu–O
100 (m)	δCu–Cu–O
171	Δ_{COO}



Fig. 3. Schematic representation of the carboxylate–metal bridging (I) and chelating (II) types of coordination.

the others three Cu–O_{eq} distances. The copper distance to the basal plane is 0.1743(6) Å, and the apical Cu–O bond length is 2.206(1) Å.

The results presented agree well with those determined for plenty of polymeric copper(II) carboxilates [4,5,9,12,23–30].

3.3. Infrared spectrum

The IR spectra of the compounds produced in both preparations were similar and showed the asymmetric and symmetric stretching vibrations of methyl and methylene groups, ν_{as} and ν_s (CH_3 and CH_2) at wavenumbers that correspond to hydrocarbons with oxygen atoms (see Table 4) [31].

The asymmetric and symmetric stretching vibrations of the coordinate carboxylate groups, $\nu_{COO,\ as}$ and $\nu_{COO,\ s}$ appear at 1588 (crystal A), 1589 (crystal B) and 1417 cm^{-1} (crystal A and B), respectively, and are characteristic of dicopper tetracarboxylates [32]. Several authors [2,3,13,16,32–35] have proposed that the position of these two bands ($\Delta\nu_{COO} = \nu_{COO,\ as} - \nu_{COO,\ s}$) helps to elucidate the type of carboxylate-to-metal complexation structure present in a given metal carboxylate. It was also found in the literature that a $\Delta\nu_{COO}$ band at approximately 150–170 cm^{-1} corresponds to a bridging bidentade mode of coordination, while chelating bidentade structures usually appears at approximately 100 cm^{-1}. These modes of coordination are shown in Fig. 3(I) and (II). Note that the complexes studied have a $\Delta\nu_{COO} = 171$ cm^{-1} for crystal A and 172 cm^{-1} for crystal B, corresponding to a bridging bidentade mode of coordination which is in agreement with the results of X-ray crystallography.

The comparison of the bands found in the spectra of our complexes at 387 (or 386) and 341 cm^{-1} with those of similar systems [36] leads to the conclusion that they could be Cu–O vibrations. The main bands and their assignments are shown in Table 4.

3.4. TG analysis

The decomposition of $Cu_2(O_2CC_5H_{11})_4$ was observed by TG analysis. A TG curve of crystal A is presented in Fig. 4. Our experiment showed that the anhydrous copper(II) hexanoate was stable up to 120°C. At this temperature it began to decompose releasing water, carbon monoxide and a mixture of metallic copper and cuprous oxide. After 287°C the copper and the cuprous

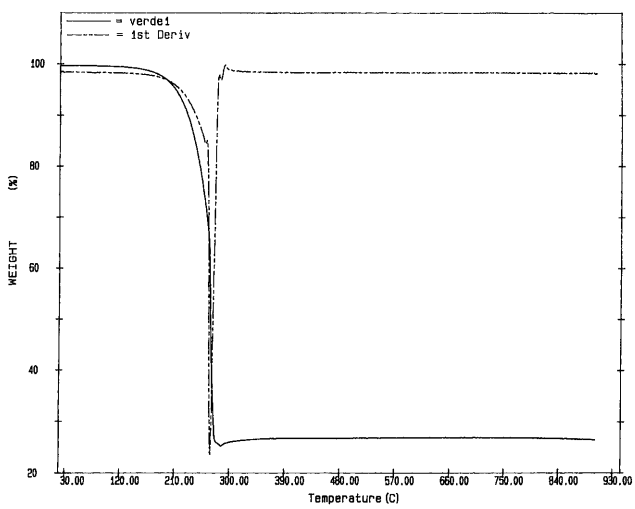


Fig. 4. TG curve for $Cu_2(O_2CC_5H_{11})_4$.

Table 5
Mass of residuals (%) after TG analysis of $Cu_2(O_2CC_5H_{11})_4$

	$Cu_2(O_2CC_5H_{11})_4$
Experimental	25.33
Calculated for Cu_2O	24.36
Calculated for 2CuO	27.09
Calculated for CuO	13.54
Calculated for CuO+Cu	24.36
Calculated for 2Cu	21.63

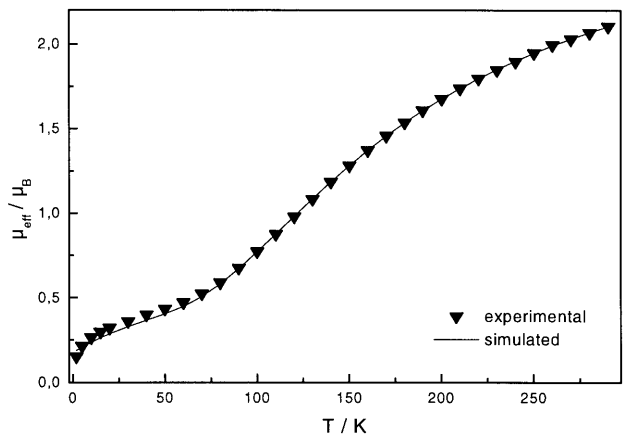


Fig. 5. Plots of the effective moment/Bohr moment versus absolute temperature of the complex.

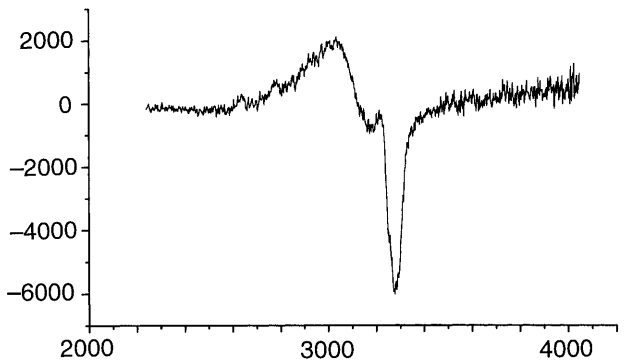


Fig. 6. ESR spectrum of the green solution of cuprous oxide in hexanoic acid.

oxide were gradually oxidized to cupric oxide, which maintained a constant weight up to 900°C [37]. The same behavior was found for crystal B. The final product of the thermal decomposition of crystal A approximately corresponds to cupric oxide and for crystal B to a mixture of CuO, Cu_2O and Cu. Similarly, CuO is the thermal decomposition product of copper(II) formate, acetate and propionate complexes [14,16,38]. The residual mass data are given in Table 5.

3.5. Magnetic susceptibility

Mononuclear copper(II) complexes have essentially temperature-dependent magnetic moments, in the range of 1.75–2.20 BM [39–43] indicating interactions between unpaired electrons. On the other hand, there is a class of copper(II) complexes that have moments smaller than these values, which are attributed to the magnetic exchange of an antiferromagnetic nature. This can be due to either the formation of a weak bond between two copper atoms or a superexchange process via the intervening oxygen [44]. These compounds have pairs of Cu(II) ions which are held close together and are so strongly coupled that the compound is diamagnetic [39,43,45,46]. In this second class we may include anhydrous copper(II) hexanoate. The values formed for copper(II) hexanoate suggest that the structure might be a distorted square-pyramidal as it is confirmed in the polymeric structure (Fig. 2).

At 290 K the anhydrous copper(II) hexanoate exhibits a μ_{eff} value of 2.10 BM, which is lower than the theoretical value of $\mu_{eff} = 2.44$ BM expected for compounds with two non-coupled spins of $S_1 = S_2 = 1/2$. It indicates that the system is weakly coupled at r.t.

By lowering the temperature from 290 to 2 K, the μ_{eff} decreases monotonically, approaching a broad minimum of 0.15 BM at 2 K. This value is very near to that of $S = 0$, expected for the ground state of an antiferromagnetically coupled dinuclear copper(II) complex.

The magnetic analysis was carried out using the Heisenberg–Dirac–van Vleck model [47] based on the spin Hamiltonian for an isotropic magnetic exchange, $H = -2JS_1 \cdot S_2$, where $S_1 = S_2 = 1/2$ for the cupric ion.

A full-matrix diagonalization approach performed by the JULE software [48] was employed to fit the experimental data. The approach includes exchange ($-2JS_1 \cdot S_2$) and Zeeman interactions, together with axial single-ion zero-field interactions (DS_Z^2) when necessary. The best fit shown as the solid line in Fig. 5 yields $J = -156\ cm^{-1}$, and $g_1 = g_2 = 2.174$ and $\rho = 1\%$ (paramagnetic impurity) confirms the antiferromagnetic nature of the couplings. The solution is not unique and small variation of the J value (-162 to $-154\ cm^{-1}$) with further changes in the g values ($2.14 \leq g \leq 2.18$) also gave an acceptable fitting.

These data are in excellent agreement with the expected values for two antiferromagnetic copper(II) ions bounded to carboxylate bridges. Such compounds were extensively investigated in the past years [49] and the coupling can be attributed to a super-exchange mechanism acting via the carboxylate π-bonds.

3.6. Electronic paramagnetic resonance

Both crystals gave no EPR signals in spite of being a Cu(II) complex; this also confirms its antiferromag-

netism [2]. The green solution of both preparations gave an EPR signal that indicates the presence of copper(II) (Fig. 6). In the case of the solution prepared with hexanoic acid and cuprous oxide this observation leads to the conclusion that the Cu(I) was oxidized to Cu(II).

4. Conclusions

All the experimental data obtained for both compounds synthesized from hexanoic acid with either cuprous oxide or cupric oxide are quite similar. For this reason it can be concluded that they are the same compound. The oxidation and reduction of copper(I) to metallic copper and copper(II) in the presence of hexanoic acid leads to a more efficient reaction than the one that occurs when cupric oxide is used.

The results obtained here are in concordance with those of several polymeric copper(II) carboxylates.

5. Supplementary material

Crystallographic data (excluding structure factors) for the structure reported in this paper have been deposited with the Cambridge Crystallographic Data Centre, CCDC No. 136713. Copies of this information may be obtained free of charge from the Director, CCDC, 12 Union Road, Cambridge, CB2 1EZ, UK (fax: +44-1223-336033; e-mail: deposit@ccdc.cam.ac.uk or http://www.ccdc.cam.ac.uk).

Acknowledgements

The authors are grateful to Dr. Douglas Wagner Franco and Mario Sergio Schultz of the Chemistry Department, Universidade de São Paulo (USP) – São Carlos, Brazil, for measuring the X-band EPR spectra (FAPESP process no. 92/3515-3); Dr. P. Chaudhuri of the Max-Planck-Institut für Strahlenchemie, Mülheim, Germany, for making possible the magnetochemical measurements and for critical suggestions. We also thank CNPq, Brazil for their financial support.

References

[1] R.C. Mehrotra, R. Bohra, Metal Carboxylates, Academic Press, London, 1983.
[2] B.P. Baranwal, S.S. Das, P. Singh, Synth. React. Inorg. Met.-Org. Chem. 28 (1998) 1689.
[3] E.J. Baran, S.B. Etcheverry, M.H. Torre, E. Kremer, Polyhedron 13 (12) (1994) 1859.
[4] G.C. Campbell, J.F. Haw, Inorg. Chem. 27 (1988) 3706–3709.
[5] G.C. Campbell, J.H. Reibenspies, J.F. Haw, Inorg. Chem. 30 (1991) 171.
[6] R.D. Harcourt, F.L. Skrezenek, R.G.A.R. Maclagan, J. Am. Chem. Soc. 108 (1986) 5403.
[7] R.D. Harcout, G.E. Martin, J. Chem. Soc., Faraday Trans. II 73 (1977) 114.
[8] M. Kato, Y. Muto, Coord. Chem. Rev. 92 (1988) 45.
[9] F.P.W. Agterberg, H.A.J. Provó Kluit, W.L. Driessen, H. Oevering, W. Buijs, M.T. Lakin, A.L. Spek, J. Reedijk, Inorg. Chem. 36 (1997) 4321.
[10] M. Yamanaka, H. Uekusa, S. Ohba, Y. Saito, S. Iwata, M. Kato, T. Tokii, Y. Muto, O.W. Steward, Acta Crystallogr., Sect. B 47 (1991) 344.
[11] M.F. Ramos Moita, M.L.T.S. Duarte, R. Fausto, Spectrosc. Lett. 27 (1994) 1421.
[12] M.J. Bird, T.R. Lomer, Acta Crystallogr., Sect. B 28 (1972) 242.
[13] M.F. Ramos Moita, M.L.T.S. Duarte, R. Fausto, J. Chem. Soc., Faraday Trans. 90 (1994) 2953.
[14] M. Petric, I. Leban, P. Segedin, Polyhedron 14 (1995) 983.
[15] G.B. Deacon, R.J. Phillips, Coord. Chem. Rev. 33 (1980) 227.
[16] S.J. Kirchner, S.A. Schubert, et al., Inorg. Chim. Acta 27 (1978) L80.
[17] N.E. Ghermani, C. Lecomte, Acta Crystallogr., Sect. B 50 (1994) 157.
[18] CAD4 Express Software, Enraf-Nonius, Delft, The Netherlands, 1992.
[19] L.J.J Farrugia, Appl. Crystallogr. 32 (1999) 837.
[20] A.C.T. North, D.C. Phillips, F.S. Matheus, Acta Crystallogr., Sect. A 24 (1968) 351.
[21] A. Altomare, G. Cascarano, C. Giacovazzo, A. Guagliardi, J. Appl. Crystallogr. 26 (1993) 343.
[22] G.M. Sheldrick, SHELXL-97. Program for Crystal Structure Analysis, University of Göttingen, Germany, 1997.
[23] T.R. Lomer, K. Perera, Acta Crystallogr., Sect. B 30 (1974) 2912.
[24] T.R. Lomer, K. Perera, Acta Crystallogr., Sect. B 30 (1974) 2913.
[25] J.D. Zubkowski, D. Washington, N. Njoroge, E.J. Valente, T. Cannon, C.D. Parks, P. Berdahl, D.L. Perry, Polyhedron 16 (1997) 2341.
[26] Y.H. Chung, H.H. Wei, Y.H. Liu, G.H. Lee, Y. Wang, Polyhedron 17 (1998) 449.
[27] W.H. Chan, T.C.W. Mak, W.H. Yip, G. Smith, E.J. O'Reilly, C.H.L. Kennard, Polyhedron 6 (1987) 881.
[28] S.I. Troyanov, E.G. Ilina, K.M. Dunaeva, Koord. Khim. 17 (1991) 1692.
[29] S.I. Ilina, S.I. Troyanov, K.M. Dunaeva, Koord. Khim. 18 (1992) 882.
[30] M.R. Baumgartner, H. Schmalle, E. Dubler, Inorg. Chim. Acta. 252 (1996) 319.
[31] C.N.R. Rao, Chemical Applications of Infrared Spectroscopy, Academic Press, New York, 1963, p. 130.
[32] D.P. Strommen, A.M. Giroud-Godquin, P. Maldivi, J.C. Marchon, B. Marchon, Liq. Cryst. 2 (1987) 689.
[33] R. Fausto, M.F. Ramos Moita, M.L.T.S. Duarte, J. Mol. Struct. 349 (1995) 439.
[34] F.P.W. Agterberg, H.A.J. Provó Kluit, W.L. Driessen, J. Reedijik, H. Oevering, W. Buijs, N. Veldman, M.T. Lakin, A.L. Spek, Inorg. Chim. Acta 267 (1998) 183.
[35] K. Nakamoto, Infrared Spectra of Inorganic and Coordination Compounds, 4th ed., John Wiley, New York, 1986, pp. 231–233.
[36] Y. Mathey, D.R. Greig, D.F. Shriver, Inorg. Chem. 21 (1982) 3409.
[37] C. Duval, Inorganic Thermogravimetric Analysis, 2nd ed., Elsevier, New York, 1963, pp. 374–386.
[38] M.A. Bernard, A. Busnot, F. Busnot, A. Leclaire, Thermochim. Acta 31 (1985) 189.
[39] F.A. Cotton, G. Wilkinson, Advanced Inorganic Chemistry, 2nd ed., Interscience Publishers, New York, 1967, p. 902.

[40] M.S. Hingorani, B.V. Agarwala, Synth. React. Inorg. Met.-Org. Chem. 20 (1990) 123.
[41] H. Zechang, Z. Rouhua, L. Tong, Synth. React. Inorg. Met.-Org. Chem. 22 (1992) 363.
[42] M.A.H. Hafez, A.A. El-Asmy, F.I.M. Taha, E.M. Saad, Synth. React. Inorg. Met.-Org. Chem. 25 (1995) 551.
[43] G.A. Kolawole, Synth. React. Inorg. Met.-Org. Chem. 26 (1996) 1307.
[44] B.N. Figgis, D.J. Martin, Inorg. Chem. 5 (1966) 100.
[45] N.T. Akinchan, R. Akinchan, P.M. Drozdzewski, Y.H. Yang, Synth. React. Inorg. Met.-Org. Chem. 26 (1996) 1735.
[46] J.R. Wasson, C. Shyr, C. Trapp, Inorg. Chem. 7 (1968) 469.
[47] A.P. Ginsberg, Inorg. Chim. Acta Rev. 5 (1971) 45.
[48] C. Krebs, Ph.D. Thesis, Ruhr-Universität, Bochum, 1997.
[49] M. Melnik, Coord. Chem. Rev. 36 (1981) 1.

PERGAMON

www.elsevier.nl/locate/poly

Polyhedron 19 (2000) 2629–2637

POLYHEDRON

Synthesis, characterization and spectra of lanthanide(III) hydrazone complexes The X-ray molecular structures of the erbium(III) complex and the ligand

Damianos G. Paschalidis [a,*], Ioannis A. Tossidis [a], Maria Gdaniec [b]

[a] *Department of Chemistry, Aristotle University, 54006 Thessaloniki, Greece*
[b] *Faculty of Chemistry, A. Mickiewicz University, 60-780 Poznan, Poland*

Received 4 April 2000; accepted 28 August 2000

Abstract

A series of nine new lanthanide(III) complexes of the type $[Ln(PBH)_2(NO_3)_2]NO_3{\cdot}xH_2O$ (PBH = 2-pyridinecarboxaldehyde benzoylhydrazone) have been prepared and studied by IR, UV–Vis and mass spectra. In addition the crystal structures of $PBH{\cdot}H_2O$ and $[Er(PBH)_2(NO_3)_2]NO_3{\cdot}1.5H_2O$ have been solved. Erbium atom is ten-coordinate and the coordination polyhedron is best described as a distorted bicapped square antiprism. © 2000 Elsevier Science B.V. All rights reserved.

Keywords: Lanthanide; Erbium complex; Hydrazone

1. Introduction

The chemistry of the trivalent lanthanide ions has expanded rapidly in the last 40 years. The interest in the lanthanide complexes is chiefly ruled by their promising utilization due to their low toxicity and their powerful paramagnetic and luminescent properties [1–3]. Even though the lanthanide complexes are associated with important biological uses as diagnostic tools [4–7]. It is known that a considerable amount of work has been done on complexes with hydrazones because of their ability to chelate with metal ions [8–19], but little work has been reported on crystal structures of such derivatives of lanthanide elements [20–22]. In the course of our studies of the chemistry of lanthanide chelate compounds we have prepared and characterized a considerable number of chelates containing hydrazones as ligands, thus we report here a series of nine new lanthanide(III) complexes of the type $[Ln(PBH)_2(NO_3)_2]NO_3{\cdot}xH_2O$, the crystal structure of the erbium complex and the structure of the free ligand.

* Corresponding author. Tel.: +30-31-90-8171; fax: +30-31-90-8171.

E-mail address: dpasch@chem.auth.gr (D.G. Paschalidis).

2. Experimental

2.1. Starting materials and procedures

Lanthanide nitrates (99.9%) $Ln(NO_3)_3{\cdot}xH_2O$ ($x = 5$ for Eu, Tb, Dy, Ho, Er, Yb and $x = 6$ for Y, Nd, Gd) were purchased from Aldrich Chemicals and were used without further purification. Lanthanide salts were stored in a dessicator to prevent hydration. The PBH ligand was prepared as previously described [23]. All solvents were reagent grade and anhydrous. Microanalyses (C, H, N) were taken with a Perkin–Elmer analyzer model 2400. Melting points were determined with a Büchi silicon oil bath apparatus and are uncorrected. Molar conductivities were measured on a WTW model LF 530 conductivity bridge employing a calibrated immersion type cell, which had a cell constant of 0.996. This represents a mean value calibrated at 25°C with potassium chloride solutions. Temperatures were controlled with an accuracy of ± 0.1°C using a Haake thermoelectric circulating system of water. Experimental and theoretical details for the conductivity measurements were reported elsewhere [24]. Room temperature magnetic susceptibility measurements in solid state were

0277-5387/00/$ - see front matter © 2000 Elsevier Science B.V. All rights reserved.
PII: S0277-5387(00)00580-5

done with a Johnson Matthey magnetic susceptibility balance MSB-MKI type. IR spectra were recorded in the 4000-250 cm^{-1} region on a Perkin–Elmer 1650 FT-IR spectrophotometer using KBr pellets. Calibration of frequency reading was made with polystyrene film. Electronic spectra in the region 200–1100 nm were measured on a Shimadzu-160A dual beam spectrophotometer using 1 cm, teflon stoppered, quartz absorption cells. The absorption spectra of solid compounds were measured on mulls that were prepared by grinding the dry solid and then regrinding it into a paste with paraffin oil (Nujol). This paste was spread on a disk of filter paper; the proper thickness of the sample was determined by trial and error. A disk of filter paper, dampened with paraffin oil, was placed in the reference position. All spectroscopic measurements were made at room temperature ($\sim$20°C). Mass spectra were measured on a RMU-6L Hitachi Perkin–Elmer mass spectrometer with ionization source of T-2p type operating at 70 eV.

2.2. Ligand

The ligand 2-pyridinecarboxaldehyde benzoylhydrazone (PBH), was prepared according to a procedure reported elsewhere [23] and recrystallized a minimum of three times from a hot methanol–water mixture. The ligand was crystallized from an acetonitrile solution by slow evaporation at 20–22°C. After a few days prismatic crystals were isolated from the solution. Analytical data for PBH are summarized in Table 1.

2.3. Preparation of Y, Nd, Eu, Gd, Tb, Dy, Ho, Er, and Yb complexes of PBH. General procedure

A methanol solution (5 ml) of PBH (973 mg, 4 mmol) was added slowly to a methanol solution (5 ml) of the appropriate lanthanide nitrate hydrated (2 mmol). The solution was allowed to stand at 20–22°C. After a few days crystals were isolated from the solution. Crystals suitable for the X-ray structure determination were obtained only in the case of Er-complex. The crystals were of poor quality, fragile and usually twinned. After inspection of a big number of crystals by microscopy a transparent crystal was isolated and used for data collection. Table 1 reports analytical data of the compounds.

2.4. Crystal structure determinations

The X-ray data for PBH were collected on a Kuma KM-4 diffractometer using graphite monochromatized Cu Kα radiation. The structure was solved by direct methods using the SHELXS-97 program [25]. Full-matrix least squares refinement was carried on F^2 with SHELXS-97 program [26]. All non hydrogen atoms have been refined anisotropically. The hydrogen atoms have been placed in calculated positions and refined using a riding model.

The data for the Er-complex were collected on a KumaCCD diffractometer using graphite monochromatized Mo Kα radiation with detector-to-crystal distance of 6 cm. More than a hemisphere of reciprocal space was covered by combination of four sets of exposures; each set had a different φ-angle (0, 90, 180, 270) and each exposure of 30s covered 0.75° in ω. Coverage of the unique set is over 98% complete. The collected data were reduced using the program KM4RED [27]. The structure was solved by direct methods with the program SHELXS-97 [25] and refined by full-matrix least-squares on F^2 with SHELXL-97 program [26]. Non-coordinated nitrate anion has been found disordered over two positions with occupancy factor equal to 1/2. A relatively high electron density maximum at hydrogen bond distance from its symmetry equivalent at position $1-x$, y, $1.5-z$ and at hydrogen bond dis-

Table 1
Colours, partial elemental analyses, molar conductivities and magnetic susceptibilities of the PBH ligand and for lanthanide(III) chelates

Compound	Colour	Melting point (°C)	Found (calc.%)			ΛM [a]	μ (B.M.)
			C	H	N		
$PBH{\cdot}H_2O$	white	103	64.02 (64.18)	5.38 (5.38)	17.34 (17.27)		
$[Y(NO_3)_2(PBH)_2]NO_3{\cdot}2H_2O$	white	225	41.09 (41.01)	3.46 (3.44)	16.61 (16.55)	101	dia.
$[Nd(NO_3)_2(PBH)_2]NO_3{\cdot}0.5H_2O$	light pink	237	39.60 (39.54)	2.95 (2.93)	15.92 (15.96)	110	3.58
$[Eu(NO_3)_2(PBH)_2]NO_3{\cdot}1.5H_2O$	cream	238	38.22 (38.29)	3.05 (3.09)	15.40 (15.45)	88	3.60
$[Gd(NO_3)_2(PBH)_2]NO_3{\cdot}H_2O$	white	231	38.53 (38.46)	2.97 (2.98)	15.57 (15.53)	102	7.34
$[Tb(NO_3)_2(PBH)_2]NO_3{\cdot}H_2O$	yellow	247	38.28 (38.39)	2.95 (2.97)	15.46 (15.49)	94	9.53
$[Dy(NO_3)_2(PBH)_2]NO_3{\cdot}1.5H_2O$	light yellow	225	37.92 (37.80)	3.02 (3.05)	15.20 (15.26)	87	10.41
$[Ho(NO_3)_2(PBH)_2]NO_3{\cdot}1.5H_2O$	yellow	221	37.61 (37.69)	3.05 (3.04)	15.17 (15.21)	108	10.21
$[Er(NO_3)_2(PBH)_2]NO_3{\cdot}1.5H_2O$	pale yellow	207	37.62 (37.58)	3.00 (3.03)	15.19 (15.17)	89	9.42
$[Yb(NO_3)_2(PBH)_2]NO_3{\cdot}2H_2O$	yellow	212	37.07 (36.93)	3.12 (3.10)	14.95 (14.90)	90	4.63

[a] Units: mol^{-1} cm^2 Ω^{-1} in CH_3OH.

Table 2
Crystal data and structure refinement parameters

Empirical formula	$C_{13}H_{13}N_3O_2$	$C_{26}H_{25}ErN_9O_{12.5}$
Formula weight	243.26	830.81
Crystal size (mm)	$0.45\times0.45\times0.30$	$0.25\times0.25\times0.15$
Crystal colour	pale yellow	pale yellow
Temperature (K)	293(2)	293(2)
Crystal system	orthorhombic	monoclinic
Space group	*Pbca*	*C2/c*
Unit cell dimensions		
a (Å)	7.1431(9)	26.902(1)
b (Å)	11.990(1)	18.390(1)
c (Å)	29.475(2)	15.259(1)
α (°)	90	90
β (°)	90	123.06(1)
γ (°)	90	90
V (Å^3)	2524.4(4)	6326.9(6)
Z	8	8
D_{calc} (Mg m^{-3})	1.280	1.744
D_{obs} (Mg m^{-3})		1.73
Wavelength (Å)	1.54178	0.71073
Monochromator	graphite	graphite
Absorption coefficient (mm^{-1})	0.730	2.731
Diffractometer used	Kuma KM-4	KumaCCD
F(000)	1024	3296
θ Range (°)	3.00–67.61	4.16–28.28
Index ranges	$0\le h\le8$	$-35\le h\le35$
	$0\le k\le14$	$-24\le k\le24$
	$0\le l\le35$	$-17\le l\le0$
Reflections collected	2273	18947
Independent reflections	2273	7722 [$R_{int}=0.0283$]
Completeness to θ (%)	99.2	98.4
Absorption correction	none	ψ scan
Refinement method	full-matrix least-squares on F^2	full-matrix least-squares on F^2
Data/restraints/parameters	2273/0/216	7722/14/433
Goodness-of-fit on F^2	1.055	0.928
Final R indices [$I>2\sigma(I)$]	$R_1=0.0397$, $wR_2=0.1128$	$R_1=0.0366$, $wR_2=0.0885$
R indices (all data)	$R_1=0.0515$, $wR_2=0.1226$	$R_1=0.0665$, $wR_2=0.0943$
Largest diff. peak and hole (e Å^{-3})	0.217 and −0.142	1.990 and −0.810

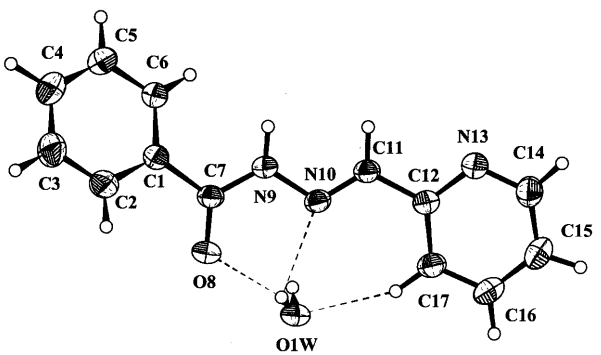


Fig. 1. Crystal structure of $C_{13}H_{11}N_3O\cdot H_2O$ showing the atom numbering scheme. The thermal ellipsoids are drawn at 30% probability.

tance to N(9A) and O(2D) has been attributed to a water molecule. Because this water molecule was situated only 1 Å from O(1C) of the disordered nitrate ion its occupancy has to be fractional and equal to that of the nitrate anion D. The disordered nitrate anions and disordered water molecule have been refined with isotropic displacement parameters. All other non-hydrogen atoms have been refined anisotropically. The hydrogen atoms have been placed in calculated positions and refined using a riding model. Restraints have been imposed on bond distances, angles and planarity of disordered nitrate groups. Crystallographic and structure determination data, for both structures, are listed in Table 2.

3. Results and discussion

3.1. General characteristics

The PBH is a white crystalline solid. The analytical results agree with the molecular formula $C_{13}H_{13}N_3O_2$ ($PBH\cdot H_2O$). The $[Ln(PBH)_2(NO_3)_2]NO_3\cdot xH_2O$ complexes synthesized and investigated in this work were crystalline solids. The analytical results agree with the molecular formula $LnC_{26}H_{22}N_9O_{11}\cdot nH_2O$ where $n=0.5$ for Ln=Nd complex, $n=1$ for Gd and Tb complexes, $n=1.5$ for Eu, Dy, Ho and Er complexes and $n=2$ for Y and Yb complexes. The complexes can be easily dissolved in alcohol, methanol, acetonitrile, dimethylformamide and dimethylsulfoxide but they are not soluble in nonpolar organic solvents. The room temperature magnetic moments of the complexes, corrected for diamagnetism, show very little deviation from van Vleck values [28], indicating minor participation of 4f-electrons in the bond formation. The molar conductivity measurements show that the complexes are 1:1 electrolytes.

3.2. Description of the structure of the ligand

The crystals of PBH are made up of orthorhombic unit cells, each containing eight monomeric $C_{13}H_{11}N_3O$ molecules and eight water molecules. A displacement ellipsoid plot of the PBH molecule with the atomic numbering is shown in Fig. 1, selected bonds lengths and angles are given in Table 3. The bonds and angles observed in this structure are normal and the molecule

Table 3
Selected bond lengths (Å) and angles (°) for $PBH\cdot H_2O$

O(8)–C(7)	1.224(2)	C(12)–N(13)–C(14)	117.65(13)
N(9)–N(10)	1.373(2)	C(7)–N(9)–N(10)	118.86(12)
C(7)–N(9)	1.352(2)	N(9)–N(10)–C(11)	116.04(12)
N(10)–C(11)	1.268(2)	O(8)–C(7)–N(9)	122.49(13)
C(11)–C(12)	1.465(2)	O(8)–C(7)–C(1)	121.56(12)
C(7)–C(1)	1.493(2)	N(9)–C(7)–C(1)	115.92(13)
N(13)–C(12)	1.335(2)	N(10)–C(11)–C(12)	121.01(13)
N(13)–C(14)	1.336(2)		

Table 4
Hydrogen bonds (Å) and angles (°) for PBH·H_2O

D–H···A	d(D–H)	d(H···A)	d(D···A)	<(DHA)
O(1W)–H(1W)···O(8) [a]	0.85(3)	2.24(3)	3.010(2)	152(2)
O(1W)–H(1W)···N(10) [a]	0.85(3)	2.50(3)	3.097(2)	129(2)
O(1W)–H(2W)···N(13) [b]	0.87(3)	2.02(3)	2.873(2)	166(3)
N(9)–H(9A)···O(1W)	0.88(2)	1.99(2)	2.852(2)	165(1)
C(11)–H(11A)···O(1W)	0.96(2)	2.49(2)	3.266(2)	138(1)
C(6)–H(6A)···O(1W)	0.96(2)	2.45(2)	3.310(2)	149(1)

[a] Symmetry transformations used to generate equivalent atoms: $-x+1/2,\ y-1/2,\ z$.
[b] Symmetry transformations used to generate equivalent atoms: $x+1/2,\ -y+1/2,\ -z+1$.

is in the keto tautomeric form. The C(7)–O(8) [1.224(2)] and N(9)–N(10) [1.373(2) Å] bond lengths indicate bond orders of two and one, respectively, confirming that the crystal contains the keto tautomer [29]. The structural conformation of the molecule is the *E* isomer (at the N(10)=C(11) double bond), the most common conformation for analogous derivatives [30]. The dihedral angles between the mean planes of the phenyl and pyridine rings is 28.23(9)°; these two rings make angles of 22.64(10) and 5.65(9)° with the central hydrazone mean plane [O(8)–C(7)–N(9)–N(10)–C(11)]. The hydrazone molecules are approximately aligned perpendicular to the *a*-axis. The crystal structure is stabilized by extensive hydrogen bonding involving the water and the hydrazone molecules. The water molecule present is involved in a variety of N–H···O, O–H···O, C–H···O and H–O···N hydrogen bonds. Selected hydrogen-bond parameters are given in Table 4.

3.3. Description of the structure of $[Er(C_{13}H_{11}N_3O)_2(NO_3)_2]NO_3\cdot 1.5H_2O$

The X-ray study revealed that the crystals of $[Er(PBH)_2(NO_3)_2]NO_3\cdot 1.5H_2O$ are made up of monoclinic unit cells, each containing eight monomeric complex cations $[Er(PBH)_2(NO_3)_2]^+$, 16 ionic nitrates with occupancy of 1/2 and 16 water molecules eight of which have occupancy of 1/2. A diagram of the molecular structure and the atom numbering system used is shown in Fig. 2. The two ligand molecules coordinated with the same metal atom are labeled A and B. Selected bond lengths and angles are given in Table 5. The Er^{III} atom is ten-coordinate by linking to two tridentate PBH ligands and two bidentate nitrate ligands. Non-coordinated nitrate anion has been found to be disordered over two positions with occupancy factor equal to 1/2. The linking of the PBH ligand to the metal atom is accomplished through the pyridine nitrogen, the azomethine nitrogen and the carbonyl oxygen. Thus two five-membered chelate rings are formed.

As expected, the situation with respect to the coordination polyhedra for ten-coordination is complex. Three polyhedra are generally considered [31]: the bicapped square antiprism, the bicapped dodecahedron, and a polyhedron of C_{2v} symmetry derived from the triangular faced dodecahedron. Calculation of the ligand–ligand repulsion energies, reported elsewhere [32], shows that the bicapped square antiprism is the favored arrangement. In our case the coordination polyhedron around the Er atom is a distorted bicapped square antiprism and is shown in Fig. 3. O(2B), O(8B), O(2A), N(13B) define the one square face of the polyhedron

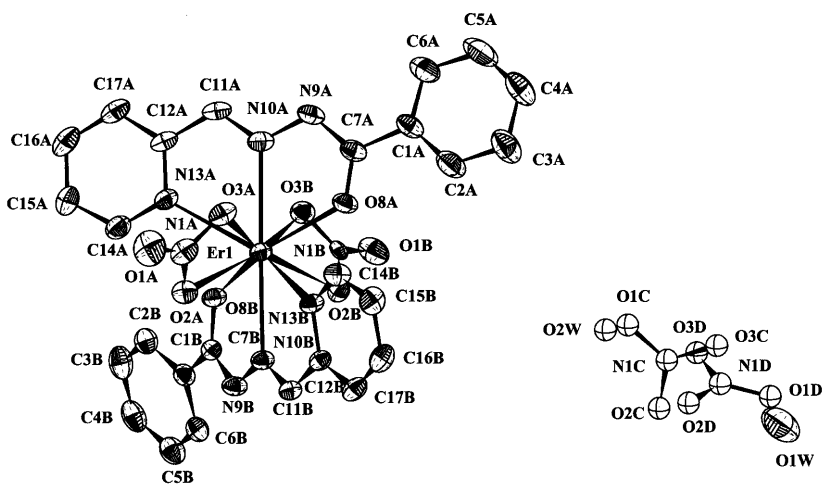


Fig. 2. Crystal structure of $[Er(C_{13}H_{11}N_3O)_2(NO_3)_2]NO_3\cdot 1.5H_2O$ showing the atom numbering scheme. The thermal ellipsoids are drawn at 30% probability; hydrogen atoms are omitted for clarity.

Table 5
Selected bond lengths (Å) and angles (°) for $[Er(C_{13}H_{11}N_3O)_2(NO_3)_2]NO_3{\cdot}1.5H_2O$

Er(1)–O(8A)	2.366(3)	Er(1)–O(8B)	2.361(3)
Er(1)–O(3A)	2.420(3)	Er(1)–O(2B)	2.450(3)
Er(1)–O(2A)	2.447(3)	Er(1)–O(3B)	2.465(3)
Er(1)–N(13A)	2.603(3)	Er(1)–N(10B)	2.535(3)
Er(1)–N(10A)	2.574(3)	Er(1)–N(13B)	2.556(3)
O(8B)–Er(1)–O(2B)	76.20(10)	O(8A)–Er(1)–O(3A)	85.08(12)
O(8A)–Er(1)–O(3B)	72.81(10)	O(8A)–Er(1)–O(2B)	71.90(10)
O(8B)–Er(1)–N(10B)	62.68(10)	O(8A)–Er(1)–N(10A)	61.66(11)
O(2A)–Er(1)–N(10B)	68.74(10)	O(3A)–Er(1)–N(10A)	69.17(11)
O(2B)–Er(1)–N(10B)	66.63(10)	O(3B)–Er(1)–N(10A)	67.53(11)
O(8A)–Er(1)–N(13B)	68.99(10)	O(8B)–Er(1)–N(13A)	69.71(10)
O(3A)–Er(1)–N(13B)	73.26(10)	O(3A)–Er(1)–N(13A)	72.46(10)
O(2A)–Er(1)–N(13B)	74.70(10)	O(2A)–Er(1)–N(13A)	71.58(10)
O(2B)–Er(1)–N(13B)	82.81(11)	O(3B)–Er(1)–N(13A)	88.94(11)
N(10B)–Er(1)–N(13B)	61.92(10)	N(10A)–Er(1)–N(13A)	61.67(11)
O(8B)–Er(1)–O(2A)	85.53(10)		

and O(3B), O(8A), O(3A), N(13A) define the other. The two capping atoms are N(10A) and N(10B). The polygon formed by N(13A), . . . , O(3B) is very close to a square. The internal angles range from 85.18(12)–95.90(13)° averaging to 89.55°; the sides of this face have lengths in the interval [2.868, 3.552] Å with a mean value of 3.157 Å. The figure formed by O(2A), . . . , O(8B) is less distorted than the other with internal angles in the range 93.07–87.31° and sides from 2.969–3.266 Å. The two square faces are essentially parallel and the angle between them is 0.92(12)°. The angle N(10A)–Er(1)–N(10B) is 178.04(11)° slightly distorted from the ideal value of 180°. Similar coordination geometry was found in other ten-coordinate lanthanides, e.g. in tetraaquatri(nitrato)yttrium(III) dihydrate [33] and $HLa(EDTA){\cdot}7H_2O$ [34].

The Er–O distances range between 2.361(3) and 2.465(3) Å. Similarly the Er–N distances range between 2.535(3) and 2.603(3) Å. These distances are considerably shorter than the corresponding distances observed in the analogous Ce-complex: $[Ce(NO_3)_3(PBH)_2]{\cdot}CH_3COCH_3{\cdot}2H_2O$ [22]. The Ce–O distances range between 2.528(3) and 2.759(4) Å and the Ce–N distances range between 2.725(4) and 2.848(4) Å. In both PBH ligands coordinated with erbium the benzene and pyridine rings have normal dimensions. The dihedral angles between the mean planes of the pyridine and phenyl rings is 9.2(3)° in the coordinated PBH molecule A and 13.4(3)° in B, respectively.

In each nitrate group the non coordinated O-atom is closer to N [1.203(10) and 1.212(7) Å] than the other two [1.237(5)–1.293(5) Å] and the metal bound O–N–O angles [115.34(46) and 116.57(30)°] are significantly smaller than the other O–N–O angles [118.75(40)–124.68(36)°], which is a common property of all bidentate nitrate groups [35].

All the water molecules are involved in hydrogen bond formation with PBH ligands. The crystal structure is stabilized by a complicated hydrogen-bond network in which imine hydrogen forms a hydrogen bond with a water oxygen atom. One oxygen of each non-coordinated nitrate ion is hydrogen bonded to a water molecule. Additional hydrogen bonding occurs between water–water molecules. A diagram showing this network is given in Fig. 4. Selected hydrogen bond lengths and angles are given in Table 6.

3.4. IR spectroscopic studies

The IR spectra of the complexes in the region 4000–250 cm^{-1} are analyzed in comparison with that of the free ligand. This data gives evidence for the coordination of the PBH to the metal ion via two nitrogen atoms and one oxygen. The complexes and the free PBH show an IR band at 3420–3490 cm^{-1}. This band is reasonably attributable to the water molecule. The vibration attributable to the ν(N–H) mode is observed at 3186 cm^{-1} for the free ligand and at 3191–3220 cm^{-1} for the complexes. This fact suggests that PBH function as a neutral ligand to the lanthanide(III) ions [36]. For the complexes, the bands assignable to the ν(C=O) and ν(C=N) vibrations are observed at 1608–1610 cm^{-1} and 1567–1572 cm^{-1}, respectively, whereas the corresponding bands for the free ligand are ob-

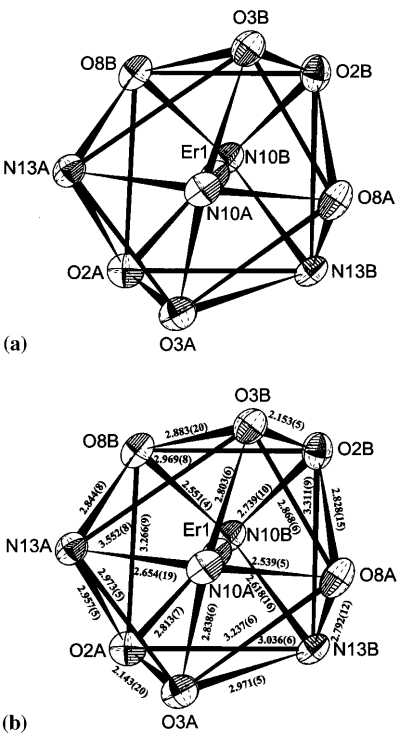


Fig. 3. (a) The coordination polyhedron around each Er^{3+} ion. (b) The coordination polyhedron around each Er^{3+} ion. Dimensions of the edges are in Å.

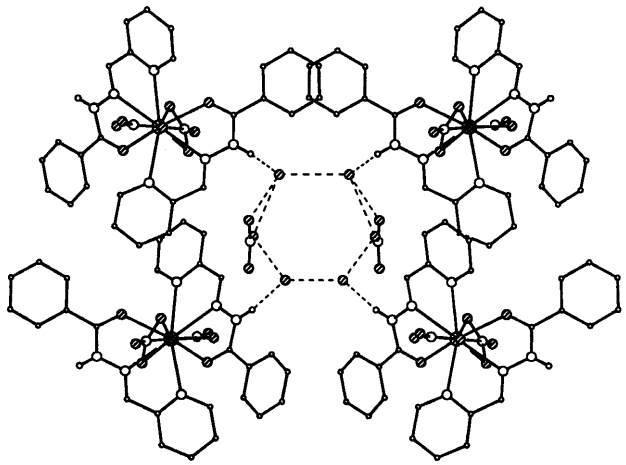


Fig. 4. View of the hydrogen bond network of Er-complex.

served at 1657 and 1600 cm^{-1}, respectively. The shifts of the ν(C=O) and ν(C=N) vibrations of the bonds toward lower wave numbers on complexation indicate that carbonyl oxygen and azomethine nitrogen coordinate to the metal [36]. The low energy pyridine ring in-plane and out-of-plane vibrations observed in the spectrum of the ligand at 625 and 406 cm^{-1}, respectively, whereas the corresponding bands for the complexes are shifted to higher frequencies at 633–634 and 415–422 cm^{-1}, respectively, which is a good indication of the coordination of the heterocyclic nitrogen [37] (Table 7).

The infrared spectra of the complexes demonstrate the presence of coordinated and ionic nitrates. The two strong bands associated with the asymmetric stretch (C_{2v} symmetry, coordinated NO_3^- group) appear at 1473–1478 and 1284–1311 cm^{-1}. The separation of the nitrate stretching fundamentals at $\sim$1400 and $\sim$ 1300 cm^{-1} ($\Delta\nu$) has been used as a criterion to distinguish between the degree of covalency of the nitrate coordination [37]. $\Delta\nu$ increases as the coordination of the nitrate group increases for monodentate to bidentate and/or bridging. The magnitude is used to establish the type of nitrate coordination. In our complexes $\Delta\nu \sim 170$ cm^{-1} and is typical of bidentate bonding of nitrates [37]. The band at 1384 cm^{-1} is characteristic for ionic nitrates (D_{3h} symmetry, free NO_3^- ion). The data indicate that the chelates contain both coordinated bidentate and ionic nitrate groups.

3.5. Electronic spectral studies

The electronic spectral data of the lanthanide(III) complexes both in the solid state (Nujol) and in solutions of DMF are similar (Table 8). The assignments are made by comparison with Carnall's data on aqueous solutions [38]. This suggests that the complexes seem to maintain the same stereochemistry in solid and solution phases. The electronic spectral data of the complexes and the PBH recorded in methanol (Table 9) and Nujol (Table 10) and they are almost identical. The ligand shows an intense absorption band at 44 444 (methanol solution), 40 322 cm^{-1} (Nujol) which shifts to a higher wavelength with increasing solvent polarity and is assigned to $\pi \rightarrow \pi^*$ transition of the rings [17]. A red shift is observed for this transition when the nitrogen of the pyridine ring is metal coordinated [17]. The position of the maximum varies between the chelates of different lanthanides (38 000–45 000 cm^{-1}). Another intense absorption band in the region $\sim$33 000 cm^{-1} in the spectrum of the free ligand is attributed to intraligand transition of $\pi \rightarrow \pi^*$ type located mainly on the C=N group [17]. This band also occurs in the spectra of the complexes, but is shifted toward higher frequencies, a fact which further supports the coordination of the hydrazones via azomethine nitrogen atom. A third intense band appears in the 24 000–29 000 cm^{-1} region which is assigned to an $n \rightarrow \pi^*$ transition located on the carbonyl group. Complex formation through the carbonyl group should cause a blue shift of

Table 6
Hydrogen bonds (Å) and angles (°) for $[Er(C_{13}H_{11}N_3O)_2(NO_3)_2]NO_3 \cdot 1.5H_2O$

D–H···A	d(D–H)	d(H···A)	d(D···A)	<(DHA)
N(9A)–H(9A)···O(2W)	0.90	1.94	2.798(9)	157.9
N(9A)–H(9A)···O(1C)	0.90	1.94	2.818(10)	164.4
N(9B)–H(9B)···O(1W) [a]	0.90	2.04	2.894(6)	157.6
C(14B)–H(14B)···O(1B) [b]	0.96	2.47	3.234(6)	136.0
C(16B)–H(16B)···O(3B) [a]	0.96	2.47	3.296(5)	144.4
O(1W)…O(1A) [c]	3.157(7)		O(2W)···O(2D)	2.684 (17)
O(1W)···O(3C)	3.036 (14)		O(1W)···O(1W) [d]	3.267 (12)
O(1W)···O(1D)	2.927 (11)		O(2W)···O(2W) [d]	2.986 (18)
O(1W)···O(2D)	2.900 (12)			

[a] Symmetry transformations used to generate equivalent atoms: $-x+1/2, y+1/2, -z+1/2$.
[b] Symmetry transformations used to generate equivalent atoms: $x, -y+1, z+1/2$.
[c] Symmetry transformations used to generate equivalent atoms: $-x+1/2, -y+1/2, -z+1$.
[d] Symmetry transformations used to generate equivalent atoms: $-x+1, y, -z+3/2$.

Table 7
Infrared spectral data (cm^{-1}) for the PBH ligand and its lanthanide(III) chelates

Compound	ν(O–H) water	ν(N–H)	ν(C=O)	ν(C=N)	$\nu_4(NO_3^-)$	$\nu_3(NO_3^-)$	$\nu_1(NO_3^-)$	Pyridine [a]	
								In plane	Out-of-plane
$PBH{\cdot}H_2O$	3459	3186	1657	1600				625	406
$[Y(NO_3)_2(PBH)_2]NO_3{\cdot}2H_2O$	3450	3200	1611	1570	1478	1384	1284	633	420
$[Nd(NO_3)_2(PBH)_2]NO_3{\cdot}0.5H_2O$	3445	3192	1608	1567	1476	1384	1308	633	415
$[Eu(NO_3)_2(PBH)_2]NO_3{\cdot}1.5H_2O$	3420	3196	1610	1568	1477	1384	1311	633	418
$[Gd(NO_3)_2(PBH)_2]NO_3{\cdot}H_2O$	3447	3220	1610	1568	1478	1384	1306	633	418
$[Tb(NO_3)_2(PBH)_2]NO_3{\cdot}H_2O$	3490	3191	1610	1568	1478	1384	1307	633	419
$[Dy(NO_3)_2(PBH)_2]NO_3{\cdot}1.5H_2O$	3441	3191	1610	1569	1477	1384	1305	633	420
$[Ho(NO_3)_2(PBH)_2]NO_3{\cdot}1.5H_2O$	3440	3193	1610	1569	1478	1384	1309	634	420
$[Er(NO_3)_2(PBH)_2]NO_3{\cdot}1.5H_2O$	3452	3200	1611	1570	1473	1384	1305	634	422
$[Yb(NO_3)_2(PBH)_2]NO_3{\cdot}2H_2O$	3420	3192	1612	1572	1477	1384	1302	634	420

[a] Low energy pyridine ring vibrations.

Table 8
Electronic spectral data of the lanthanide(III) chelates for DMF solutions and Nujol mull spectra ($t = 20°C$) in the visible region

Compound	DMF solution		Nujol	Assignments
	Frequency (cm^{-1})	log ε	Frequency (cm^{-1})	
$[Nd(NO_3)_2(PBH)_2]NO_3{\cdot}0.5H_2O$	11 507	0.46	11 481	$^4I_{9/2} \rightarrow {}^4F_{3/2}$
	12 531	0.94	12 531	$^4I_{9/2} \rightarrow {}^4F_{5/2}$
	13531	0.84	13 568	$^4I_{9/2} \rightarrow {}^4F_{7/2}$, $^3S_{3/2}$
			14 727	$^4I_{9/2} \rightarrow {}^4F_{9/2}$
	17 182	0.98	17 271	$^4I_{9/2} \rightarrow {}^4G_{5/2}$, $^2G_{7/2}$
	19 047	0.63	18 975	$^4I_{9/2} \rightarrow {}^4G_{7/2}$
	19 531	0.42	19 493	$^4I_{9/2} \rightarrow {}^4G_{9/2}$
			20 964	$^4I_{9/2} \rightarrow {}^4G_{11/2}$
$[Dy(NO_3)_2(PBH)_2]NO_3{\cdot}1.5H_2O$			10 267	$^6H_{15/2} \rightarrow {}^6H_{5/2}$
	11 001	0.37	10 881	$^6H_{15/2} \rightarrow {}^6F_{7/2}$
	12 391	0.25	12 515	$^6H_{15/2} \rightarrow {}^6F_{5/2}$
			13 315	$^6H_{15/2} \rightarrow {}^6F_{3/2}$
$[Ho(NO_3)_2(PBH)_2]NO_3{\cdot}1.5H_2O$	15 528	0.64	15 600	$^5H_8 \rightarrow {}^5F_5$
	18 587	0.72	18 691	$^5H_8 \rightarrow {}^5F_4$
	20 618	0.29	20 661	$^5H_8 \rightarrow {}^5F_3$
$[Er(NO_3)_2(PBH)_2]NO_3{\cdot}1.5H_2O$	10 298	0.05	10 288	$^4I_{15/2} \rightarrow {}^4I_{11/2}$
	15 337	0.35	15 408	$^4I_{15/2} \rightarrow {}^4F_{9/2}$
	19 194	0.98	19 305	$^4I_{15/2} \rightarrow {}^2H_{11/2}$, $^4G_{11/2}$
	20 534	0.39	20 576	$^4I_{15/2} \rightarrow {}^4F_{7/2}$
$[Yb(NO_3)_2(PBH)_2]NO_3{\cdot}2H_2O$	10 235	0.66	10 256	$^2F_{7/2} \rightarrow {}^2F_{5/2}$

the $n \rightarrow \pi^*$ transition. In our complexes this band is shifted by 1000–2000 cm^{-1}. The electronic spectral data of the complexes further support the coordination of the ligand to the lanthanide through the carbonyl oxygen, azomethine nitrogen and pyridine nitrogen.

3.6. Mass spectral studies

The electron impact mass spectra of all the complexes and the PBH are summarized in the Table 11. The mass spectrum of the Eu complex shows fragments due to $[Eu(NO_3)_2(PBH)_2]^{+\bullet}$ radical cation and $[Eu(NO_3)_2(PBH)]^+$ cation, which are formed from the expulsion of the $-NO_3^{\bullet}$ and after the $[PBH]^{\bullet}$ radical from the molecular ion of the complex. The fragment due to $\{[Y(NO_3)_2(PBH)]NO_3\}^{+\bullet}$ radical cation is formed from the expulsion of the $[PBH]^{\bullet}$ radical from the molecular ion of the complex (Fig. 5). The spectra of Y and Dy complexes show fragments due to $[Y(PBH_{an})]^{2+}$ and $[Dy(PBH_{an})]^{2+}$, respectively (PBH_{an} represents the anionic form of the PBH). The major peaks of the spectra of all complexes can be explained following the fragmentation path of the PBH (Fig. 6).

Table 9
Electronic spectral data of the PBH ligand and its lanthanide(III) chelates for methanol solutions (t = 20°C)

Compound	Assignments					
	$\pi \rightarrow \pi^*$		$\pi \rightarrow \pi^*$		$n \rightarrow \pi^*$	
	Frequency (cm^{-1})	log ε (max)	Frequency (cm^{-1})	log ε (max)	Frequency (cm^{-1})	log ε (max)
PBH·H_2O	44 444	3.92	32 787	4.23	27 397	3.73
$[Y(NO_3)_2(PBH)_2]NO_3 \cdot 2H_2O$	39 370	4.33	34 602	4.34	27 397	4.48
$[Nd(NO_3)_2(PBH)_2]NO_3 \cdot 0.5H_2O$	45 662	4.40	33 112	4.51	27 397	4.32
$[Eu(NO_3)_2(PBH)_2]NO_3 \cdot 1.5H_2O$	45 454	4.22	33 112	4.49	27 397	4.05
$[Gd(NO_3)_2(PBH)_2]NO_3 \cdot H_2O$	45 871	4.39	33 112	4.49	27 397	4.35
$[Tb(NO_3)_2(PBH)_2]NO_3 \cdot H_2O$	45 454	4.46	33 783	4.57	27 397	4.38
$[Dy(NO_3)_2(PBH)_2]NO_3 \cdot 1.5H_2O$	45 662	4.42	33 112	4.58	27 472	4.37
$[Ho(NO_3)_2(PBH)_2]NO_3 \cdot 1.5H_2O$	44 444	4.23	34 722	4.30	27 397	4.52
$[Er(NO_3)_2(PBH)_2]NO_3 \cdot 1.5H_2O$	44 444	4.30	34 602	4.32	27 174	4.55
$[Yb(NO_3)_2(PBH)_2]NO_3 \cdot 2H_2O$	45 662	4.19	33 112	4.44	27 322	4.06

Table 10
Electronic spectral data of the ligand PBH and its lanthanide(III) chelates from Nujol mull spectra (solid state, $t = 20°C$)

Compound	Assignments		
	$\pi \rightarrow \pi^*$	$\pi \rightarrow \pi^*$	$n \rightarrow \pi^*$
	Frequency (cm^{-1})	Frequency (cm^{-1})	Frequency (cm^{-1})
PBH·H_2O	40 322	33 445	29 239
$[Y(NO_3)_2(PBH)_2]NO_3 \cdot 2H_2O$	40 816	33 222	27 777
$[Nd(NO_3)_2(PBH)_2]NO_3 \cdot 0.5H_2O$	40 650	33 333	24 691
$[Eu(NO_3)_2(PBH)_2]NO_3 \cdot 1.5H_2O$	40 816	33 557	24 691
$[Gd(NO_3)_2(PBH)_2]NO_3 \cdot H_2O$	39 062	33 222	26 809
$[Tb(NO_3)_2(PBH)_2]NO_3 \cdot H_2O$	38 168	33 112	24 272
$[Dy(NO_3)_2(PBH)_2]NO_3 \cdot 1.5H_2O$	38 610	33 112	27 777
$[Ho(NO_3)_2(PBH)_2]NO_3 \cdot 1.5H_2O$	38 910	33 222	26 455
$[Er(NO_3)_2(PBH)_2]NO_3 \cdot 1.5H_2O$	40 650	33 333	24 691
$[Yb(NO_3)_2(PBH)_2]NO_3 \cdot 2H_2O$	40 486	33 333	24 875

Table 11
Relative abundances (%) of the ions in the EI mass spectra of the PBH ligand and its complexes

m/z	Assignments	Relative abundances (%)									
		PBH	Y	Nd	Eu	Gd	Tb	Dy	Ho	Er	Yb
51	VIII	50	65			47	89	66	36	37	
77	IV	50	32	7		47	87	69	37	32	
78	VII	51	100	5		47	89	68	39	31	
93	V	72	69	3		25		33		67	
105	III	50	72	4	16	44	100	69	33		13
119	VI	65	37	2	15	24	11	29			8
121	II	48	62		7	55		71			
147	I	9	23				15				65
223	$[PBH]^{+\bullet} - H_2$		4		100	23	45	72			
224	$[PBH]^{+\bullet} - H^{\bullet}$		2		12		60	47		21	
225	$[PBH]^{+\bullet}$	28	5		13	55	17	60		20	
314	$[Y(PBH)]^{2+}$		19								
388	$[Dy(PBH)]^{2+}$							11			
500	$\{[Y(NO_3)_2(PBH)]NO_3\}^{+\bullet}$		5								
501	$[Eu(NO_3)_2(PBH)]^{+}$				5						
726	$[Eu(NO_3)_2(PBH)_2]^{+\bullet}$				3						

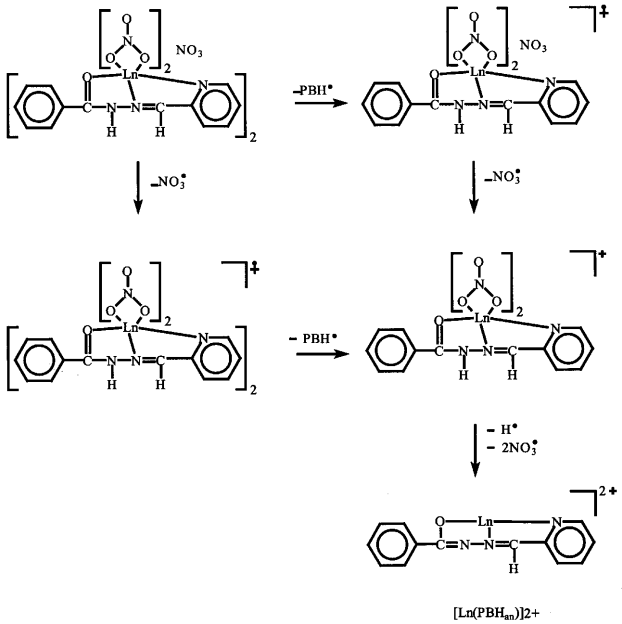


Fig. 5. The fragmentation pattern of the lanthanide(III) complexes (Ln represents the lanthanide(III) ions).

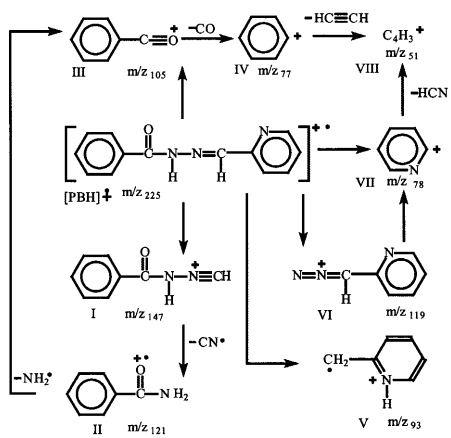


Fig. 6. The fragmentation path of the ligand PBH.

4. Supplementary material

Crystallographic data for the structural analysis have been deposited with the Cambridge Crystallographic Data Centre, CCDC deposition numbers: 142156 for PBH and 141461 for $[Er(PBH)_2(NO_3)_2]NO_3 \cdot 1.5H_2O$. Copies of this information may be obtained free of charge from: The Director, CCDC, 12 Union Road, Cambridge, CB2 1EZ, UK (Fax: +44-1223-336033; e-mail: deposit@ccdc.cam.ac.uk or www: http://www.ccdc.cam.ac.uk).

References

[1] N. Sabbatini, M. Guardigli, J. Lehn, Coord. Chem. Rev. 123 (1993) 201.

[2] Z. Pikramenou, J. Yu, R.B. Lessard, A. Ponce, P.A. Wong, D.G. Nocera, Coord. Chem. Rev. 132 (1994) 181.

[3] R. Reisfeld, C.K. Jørgensen, Lasers and Excited States of Rare Earths, Springer, Berlin, 1977.

[4] C.H. Evans, Biochemistry of the Lanthanides, Plenum, New York, 1990.

[5] T.J. Meade, Coord. Chem. Rev. 184 (1999) 1.

[6] L. Thunus, R. Leyeune, Coord. Chem. Rev. 184 (1999) 125.

[7] K. Wang, R. Li, Y. Cheng, B. Zhu, Coord. Chem. Rev. 190–192 (1999) 297.

[8] M.F. Iskander, S.R. Zaynan, M.A. Khalifa, L. El-Sayed, J. Inorg. Nucl. Chem 36 (1974) 551.

[9] L. El-Sayed, M.F. Iskander, Inorg. Chim. Acta 33 (1971) 435.

[10] N.S. Biradar, B.R. Hanivale, Inorg. Chim. Acta 17 (1976) 157.

[11] K.K. Narang, A. Aggarwal, Inorg. Chim. Acta 9 (1974) 137.

[12] M. Katyal, Y. Dutt, Talanta 22 (1975) 151.

[13] T.A. Manuel, Adv. Organomet. Chem. 3 (1965) 181.

[14] J.D. Curry, M.A. Robinson, D.H. Busch, Inorg. Chem. 8 (1967) 1570.

[15] D. Nicholls, C.N. Elgy, M.R. Harrison, Inorg. Chim. Acta 57 (1982) 21.

[16] I.A. Tossidis, C.A. Bolos, Inorg. Chim. Acta 112 (1986) 93.

[17] I.A. Tossidis, C.A. Bolos, P.N. Aslanidis, G.A. Katsoulos, Inorg. Chim. Acta 133 (1987) 275.

[18] R.L. Dutta, M.M. Hossain, J. Sci. Ind. Res. 44 (1985) 635.

[19] V.S. Sergienko, V.L. Abramenko, L.L. Minacheva, M.A. Porai-Koshits, V.G. Sakharova, Koord. Khim. 19 (1993) 28.

[20] J.E. Thomas, R.C. Palenik, G.J. Palenik, Inorg. Chim. Acta 37 (1979) L459.

[21] J. Dan, S. Seth, S. Chakraborty, Acta Crystallogr., Sect. C 45 (1998) 1018.

[22] P.C. Christidis, I.A. Tossidis, D.G. Paschalidis, Acta Crystallogr., Sect. C 55 (1999) 707.

[23] T.E. Khalil, L. Labib, M.F. Iskander, Polyhedron 13 (1994) 2569.

[24] W.J. Geary, Coord. Chem. Rev. 7 (1971) 81.

[25] G.M. Sheldrick, SHELXS-97 Program for the solution of crystal structures, University of Göttingen, Germany, 1997.

[26] G.M. Sheldrick, SHELXL-97 Program for the refinement of crystal structures, University of Göttingen, Germany, 1997.

[27] KUMA Diffraction, KM4RED, Version 1.157a, Wrocław, Poland 1999.

[28] J.H. van Vleck, A. Frank, Phys. Rev. 34 (1929) 1494.

[29] H.K. Fun, K. Sivakumar, Z.L. Lu, C.Y. Duan, Y.P. Tian, X.Z. You, Acta Crystallogr., Sect. C 52 (1996) 986.

[30] R. Velevan, K. Sivakumar, Acta Crystallogr., Sect. C 51 (1995) 1227.

[31] A.R. Al-Karaghouli, J.S. Wood, Inorg. Chem. 11 (1972) 2293.

[32] R.B. King, J. Am. Chem. Soc. 92 (1970) 6460.

[33] B. Ribar, N. Milinski, Z. Budovalcev, I. Krstanovic, Cryst. Struct. Comm. 9 (1980) 203.

[34] M.D. Lind, B. Lee, J.L. Hoard, J. Am. Chem. Soc. 87 (1965) 1611.

[35] B. Ribar, P. Radivojevic, G. Argay, A. Kalman, Acta Crystallogr., Sect. C 44 (1988) 595.

[36] M. Sakamoto, Inorg. Chim. Acta 131 (1987) 139.

[37] W. Radecka-Paryzek, E. Jankowska, Inorg. Chim. Acta 134 (1987) 179.

[38] W.T. Carnall, in: K.A. Gschneidner, Jr., L.R. Eyring (Eds.), Handbook on the Physics and Chemistry of Rare Earths, vol. 3, North Holland, Amsterdam, 1979, p. 171 (Chapter 24).

PERGAMON

www.elsevier.nl/locate/poly

Polyhedron 19 (2000) 2639–2648

POLYHEDRON

Release of free nucleobases from oligomers by copper(II)–peroxide adduct

Teruyuki Kobayashi [b], Mami Kunita [a], Satoshi Nishino [a], Hideaki Matsushima [c], Tadashi Tokii [c], Hideki Masuda [b], Hisahiko Einaga [b], Yuzo Nishida [a,*]

[a] *Department of Chemistry, Faculty of Science, Yamagata University, Yamagata 990-8560, Japan*
[b] *Department of Applied Chemistry, Nagoya Institute for Technology, Shouwa-ku, Nagoya 466-8585, Japan*
[c] *Department of Chemistry, Faculty of Science and Engineering, Saga University, Saga 840-8502, Japan*

Received 2 May 2000; accepted 1 September 2000

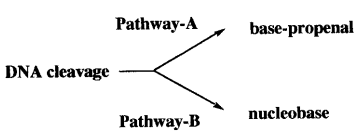
Abstract

The release of nucleobases from oligonucleotides (12-mer, d(5′-CGCTTTAAAGCG)$_2$, 8-mer, d(5′-AAACGTTT)$_2$, 7-mer, d(TCGCGCG)$_2$, and 6-mer, d(CGCGCG)$_2$) by copper(II) complex and hydrogen peroxide systems was investigated in terms of HPLC. The [Cu(bdpg)Cl]Cl complex gave a large quantity of free nucleobases in the reaction mixture, but the activities of other compounds, such as [Cu(tpa)Cl]ClO_4, were much lower than that of the (bdpg)-complex; where (bdpg) and (tpa) represent a *N*,*N*-bis(2-pyridylmethyl) derivative of β-alanineamide and 2-aminomethylpyridine, respectively. The above results and the electrospray mass spectral data on the solutions strongly suggest that the remarkable activity of the (bdpg)-compound is due to the high electrophilic nature of the copper(II)–hydroperoxide adduct, whose formation is greatly promoted through hydrogen bonding with the amide-oxygen atom coordinated to the copper(II) atom, and this electrophilic copper(II)–peroxide adduct attacks the sugar ring of nucleoside, to give the corresponding hydroxylated species, and from which free nucleobases are released.
© 2000 Elsevier Science B.V. All rights reserved.

Keywords: Release of free nucleobases from oligomers; Copper(II)–peroxide adduct; DNA cleavage; Electrospray mass spectrometry

1. Introduction

Two types of monomeric products have been isolated and identified during Fe-BLM mediated degradation of DNA: free nucleobase and base propenal (see Scheme 1) [1]. The base-propenal formation requires O_2 in addition to that required to form activated-BLM and is accompanied by DNA strand scission and phosphoglycolate termini production. The free base release requires no additional O_2 and is accompanied by production of an oxidatively damaged sugar in the intact DNA strand [2,3]. At present there is no clear elucidation as to why two ways are present in the strand scission of DNA.



Scheme 1.

In order to clarify the origin of the presence of two pathways in DNA cleavage reaction, we have investigated the DNA degradation by several metal compounds including Fe(III) and Cu(II) compounds in the presence of hydrogen peroxide (for the chemical structures of the ligands, see Fig. 1) [4–6]. As the results indicate, we have found that the copper(II) complexes used in our previous studies are divided into two types based on the activity of DNA degradation, e.g. [Cu(bdpg)Cl]$^+$ complex effects the complete degradation of DNA (pBR322, supercoiled Form I), however [Cu(tpa)Cl]$^+$ complex gives only Form II DNA under the same experimental conditions (for the chemical structures of the ligands, see Fig. 1). This difference observed for DNA cleavage reaction in [Cu(bdpg)Cl]$^+$ and [Cu(tpa)Cl]$^+$ was also observed in the different

* Corresponding author. Tel.: +81-023-6284603; fax: +81-023-6284510.
E-mail address: yuzo@sci.kj.yamagata-u.ac.jp (Y. Nishida).

0277-5387/00/$ - see front matter © 2000 Elsevier Science B.V. All rights reserved.
PII: S0277-5387(00)00576-3

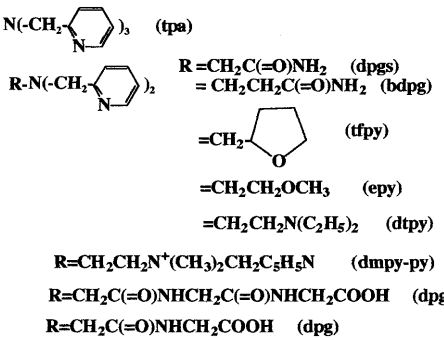


Fig. 1. Chemical structures of ligands cited in this paper.

Table 1
Crystal data of $[Cu(dmpy\text{-}py)Cl](ClO_4)_2$

Formula weight	660.40
Crystal system	triclinic
Lattice parameters	
a (Å)	12.572(5)
b (Å)	12.745(6)
c (Å)	11.052(3)
α (°)	109.13(3)
β (°)	99.22(4)
γ (°)	118.42(3)
Space group	$P\bar{1}$
Z	2
D_{calc} (g cm^{-3})	1.612
μ (Mo Kα) (cm^{-1})	11.54
Number of observations ($I>3\sigma(I)$)	3785
Number of variables	352
Residuals; R, R_w	0.052, 0.062

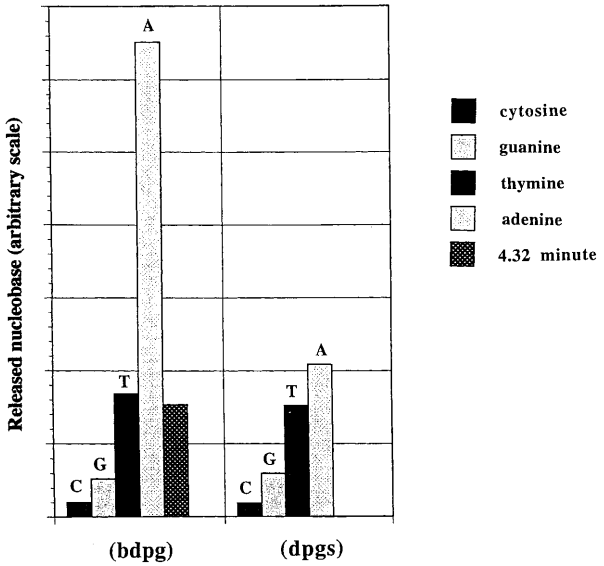


Fig. 3. Illustration of relative quantity of released nucleobases from 8-mer based on the result in Fig. 2.

Table 2
Percentage (%) of released nucleobases to the original oligomers by [Cu(bdpg)Cl]Cl and hydrogen peroxide system [a]

	Cytosine	Guanine	Adenine	Thymine
12-mer	15.3	15.9	7.1	7.1
8-mer	0.6	2.8	3.6	4.1
6-mer	6.2	4.5	nd	nd
7-mer	4.2	8.2	nd	4.1

[a] (nd): not detected.

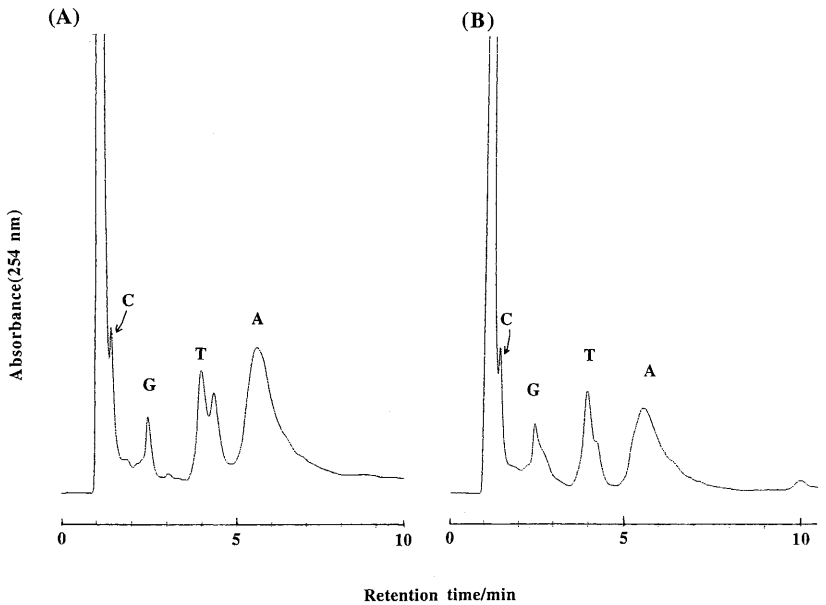
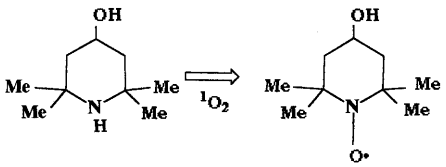


Fig. 2. HPLC of the solution containing a copper(II) complex, H_2O_2, and 8-mer measured at 60 min after H_2O_2 was added. Peaks at 1.44, 2.46, 4.05 and 5.51 min were attributed to C (cytosine), G (guanine), T (thymine), and A (adenine), respectively, confirmed by the use of authentic samples. The peak at 4.32 min observed for the (bdpg)-complex is not known. (A): [Cu(bdpg)Cl]Cl; (B): $[Cu(dpgs)Cl]ClO_4$.

behavior towards the spin-trapping reagent for singlet oxygen ($^1\Delta_g$), 2,2,6,6-tetramethyl-4-piperidinol (TMPN); i.e. the former complex gives no nitrone radical in the reaction with TMPN, however much formation of the nitrone radical was observed when TMPN was reacted with $[Cu(tpa)Cl]^+$ complex in the presence of hydrogen peroxide (see the scheme below) [5]. This is suggesting that the structure and reactivity of a copper(II)–hydroperoxide adduct are highly affected by the peripheral organic group and also TMPN, and demonstrating that the different DNA cleavage patterns observed for the copper(II) compounds should be due to the different reactivity of the copper(II)–peroxide adduct formed during the course of the reaction [5].



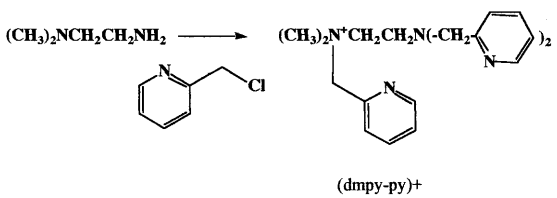
TMPN nitrone radical

In order to confirm the validity of our conclusion on the intrinsic active-species for the DNA cleavage reaction, in this study we have investigated the degradation of several oligomers by the copper(II)–H_2O_2 systems in terms of HPLC, and we have also measured the electrospray mass spectra (ESI-MS) of the solutions.

2. Experimental

2.1. Materials

Chemical structures of the ligands used in this study are illustrated in Fig. 1. The ligands except for (dmpy-py), were obtained according to the published method [4,5,7]. From the reaction mixture of *N*,*N*-dimethylaminoethylamine (1 mol) and picolyl chloride (2 mol), we have obtained the $[Cu(dmpy\text{-}py)Cl](ClO_4)_2$, where three molecules of picolyl chloride reacted with one molecule of *N*,*N*-dimethylaminoethylamine (see below), which is quite different from the case of *N*,*N*-diethylaminoethylamine.



(dmpy-py)+

2.2. Crystal structure determination of $[Cu(dmpy\text{-}py)Cl](ClO_4)_2$

A blue–green prism having approximate dimensions of $0.3 \times 0.3 \times 0.5$ mm was mounted on a glass fiber. All measurements were made on a Rigaku AFC5S diffractometer with graphite monochromated Mo Kα radiation and a 12 kW rotating anode generator at Saga University. Cell constants and an orientation matrix for data collection, obtained from a least-squares refinement using the setting angles of 25 carefully centered reflections, and the crystal data of the compounds are summarized in Table 1. The structure was solved by direct methods. The non-hydrogen atoms were refined anisotropically. The final cycle of full-matrix least-squares refinement was based on the observed reflections ($I > 3.00\sigma(I)$), and $R = \Sigma||F_o| - |F_c||/\Sigma|F_o|$ and $R_w = [(\Sigma\ \omega(|F_o| - |F_c|)^2/\Sigma\ \omega|F_o|^2)]^{1/2}$ were listed in Table 1. Neutral atom scattering factors were taken from Cromer and Weber [8]. Anomalous dispersion effects were included in $F_{calc.}$ The values for $\Delta F'$ and $\Delta F''$ were those of Cromer [9]. All calculations were performed using TEXSAN the crystallographic software package of Molecular Structure Corporation [10].

2.3. HPLC containing the oligomer, copper(II) complex, and hydrogen peroxide

A copper(II) complex was dissolved in the solution (20 ml) containing an oligomer (12-mer, d(5′-CGCTTTAAAGCG)$_2$, 8-mer, d(5′-AAACGTTT)$_2$, 7-mer, d(TCGCGCG)$_2$, and 6-mer, d(CGCGCG)$_2$, purchased from Rikaken Co., Nagoya, Japan; the latter two oligomers are left-handed Z-DNA [11]), and the mixture was treated with hydrogen peroxide; final concentrations are $[Cu^{2+}] = 1.67$ mM, $[H_2O_2] = 16.7$ mM, and oligomer, 0.2 mM in Tris–HCl buffer (pH 7.8). The reaction mixture was stirred under air at 298 K, and analyzed by HPLC ($5C_{18}$-AR column, eluted with 10% methanol solution containing 0.1 mol of ammonium acetate [12] at a flow rate of 1.6 ml min^{-1}; detected by absorbance at 254 nm; see Fig. 2). The quantity of detected nucleobases was evaluated by measuring the area of HPLC peak by the use of the authentic sample (see Fig. 3 and Table 2).

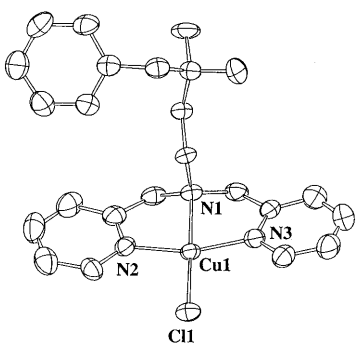


Fig. 4. ORTEP drawing of $[Cu(dmpy\text{-}py)Cl]^{2+}$. Cu1–Cl1, 2.244(2); Cu1–N1, 2.052(4); Cu1–N2, 1.977(4); Cu1–N3, 1.975(3) Å; Cl1–Cu1–N1, 172.4(1); Cl1–Cu1–N2, 97.78(1); Cl1–Cu1–N3, 97.2(1); N1–Cu1–N2, 82.2(2); N1–Cu1–N3, 82.0(2); N2–Cu1–N3, 163.2(2)°.

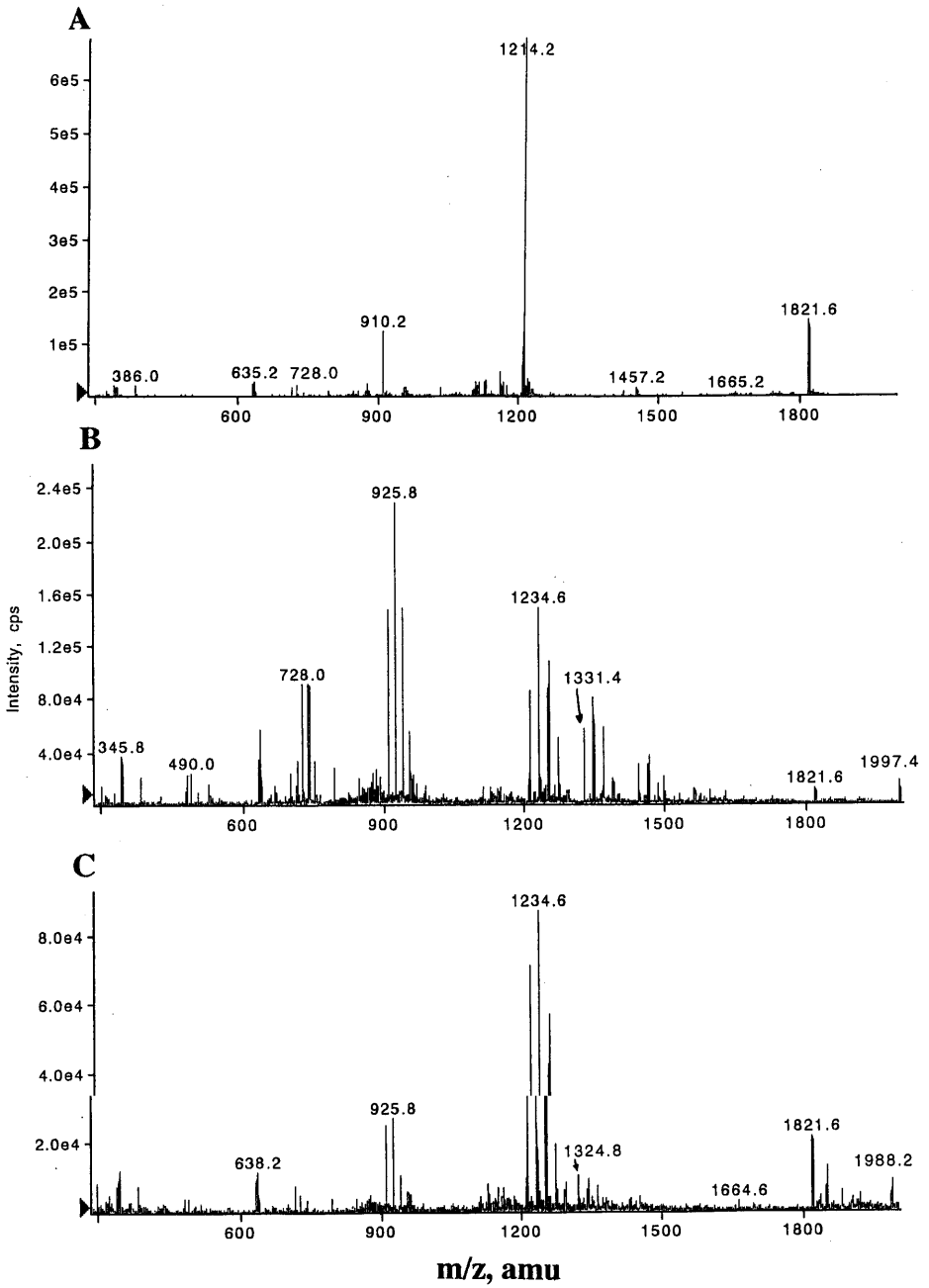


Fig. 5. ESI-mass spectra (negative pattern) of solutions containing 12-mer and copper(II) complex. (A): 12-mer; (B): 12-mer + [Cu(tpa)Cl]ClO_4; (C): 12-mer + [Cu(bdpg)Cl]Cl.

2.4. ESI-mass spectrometry

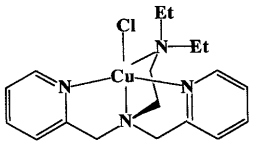
ESI-mass spectra were obtained with an API 3000 triple quadrapole mass spectrometer at the Institute for Molecular Science, Okazaki, Japan. At first, the solutions of a metal chelate (5 mM aqueous solution) and oligomer (300 μM aqueous solution) were prepared. The metal complex (6 μl) and oligomer (20 μl) solutions were then mixed, and the ESI-mass spectra of the solution was measured after the addition of ammonium acetate (2μl, 150 mM) and acetonitrile (30 μl).

3. Results and discussion

3.1. Structural features of copper(II) compounds

The crystal structure of [Cu(dmpy-py)Cl]$(ClO_4)_2$ is illustrated in Fig. 4; the copper(II) compound contains a tridentate *N*,*N*-bis(2-pyridylmethyl)amine moiety and chloride ion in the basal plane; in this compound the ligand contains a positive nitrogen atom as shown before and this positive nitrogen atom cannot coordinate to a copper(II) ion, leading to the square planar

four-coordinated species. In the case of *N*,*N*-diethylaminoethylamine, a tetradentate ligand (dtpy) is obtained, and from this a square pyramidal five-coordinated complex was prepared (see the figure below) [13].



(1)

[Cu(dtpy)Cl]$^+$

The structure of [Cu(bdpg)Cl]$^+$ is a square pyramide [7] and is similar to those of complexes with (dpgs), (dtpy), and others [5,7]. The [Cu(tpa)Cl]$^+$ is a trigonal bipyramide.

3.2. ESI-MS

The interaction between a metal compound and oligomer was extensively studied by Stubbe et al. by the use of NMR spectroscopy, especially for cobalt-bleomycins (Co-BLM) [14–16]. We have recently confirmed the binding of Fe-BLM towards several oligomers in terms of ESI-mass spectroscopy [17]. In this study, we have investigated the interaction between copper(II) chelate and oligomer (12- and 8-mers) in terms of the ESI-MS.

As shown in Fig. 5, we can observe several peaks in the ESI-mass spectra (negative pattern) of the 12-mer. Based on the calculated isotope patterns, the signals at $m/z = 1821.6$, 1214.2, 910.2, and 728.0 are attributed to (-2), (-3), (-4), and (-5) species of the single strand 12-mer. The signal at $m/z = 1457.2$ is due to (-5) species of the double-strand. When a copper(II) complex was added to the solution containing NH_4CH_3COO and 12-mer, new signals have appeared as shown in Fig. 5 traces B and C and also Table 3. Strong signals in the range $m/z = 1234.6$–1275 and 925.8–957 are due to species of acetic acid adducts of 1214.2 and 910.2 species, respectively (see also Table 3). The signals at $m/z = 1331.4$ and 1997.4 are due to [1:1] adduct of the Cu(II)–(tpa) complex and single-strand 12-mer, as determined by the calculated isotope patterns. Corresponding signals are observed at $m/z =$ 1324.8 and 1988.2 in the case of the (bdpg)-complex (see Fig. 5, trace C and Table 3). Analogous signals due to the 1:1 adduct have been observed for all the solutions containing a copper(II) complex (see Table 3). Although the peak intensity is very small, the signals due to species where 2 or 3 copper(II) complexes are bound to a single-strand chain are detected in the spectra (see Table 3). The results obtained for 8-mer (in the positive pattern) were illustrated in Fig. 6. The peaks at $m/z = 1205.6$, 1606.8 and 2409.4 may be attributed to $(+2)$, $(+3)$, and $(+4)$ species of the double-strand of 8-mer. The peaks at $m/z = 1381.2$ (trace B in Fig. 6) and 1371.0 (trace C in Fig. 6) can be assigned to the copper-bound species ([1:1] in single-strand, or [2:1] in the double-strand where two copper compounds are bound to the double-strand) for the Cu(II)–(tpa) and Cu(II)–(bdpg) complexes, respectively. In this case, the binding of multiple copper(II)

Table 3
Assignment of signals in ESI-mass spectra of 12-mer and copper(II) compounds (calculated for the single-strand) (m/z (deprotonated number form 12-mer), total charge of complex; HAcO represents acetic acid)

Formula	bdpg	dpgs	dpg	dpgt	tpa
[(12mer)+Cu(L)$^{2+}$]	1988.2 ($-4H^+$, -2)	1980.2 ($-4H^+$, -2)	2009.6 ($-3H^+$, -2)	2038.4 ($-4H^+$, -2)	1997.4 ($-4H^+$, -2)
	1324.8 ($-5H^+$, -3)	1320.2 ($-5H^+$, -3)	1339.8 ($-4H^+$, -3)	1358.4 ($-5H^+$, -3)	1331.4 ($-5H^+$, -3)
+HAcO	1345.2 ($-5H^+$, -3)	1340.8 ($-5H^+$, -3)	1359.6 ($-4H^+$, -3)	1379.2 ($-5H^+$, -3)	1351.8 ($-5H^+$, -3)
+2HAcO	1365.2 ($-5H^+$, -3)	1360.8 ($-5H^+$, -3)	1380.4 ($-4H^+$, -3)	1400.0 ($-5H^+$, -3)	1372.4 ($-5H^+$, -3)
+3HAcO	1385.8 ($-5H^+$, -3)	1381.6 ($-5H^+$, -3)	1401.0 ($-4H^+$, -3)		1393.0 ($-5H^+$, -3)
[(12mer)+2Cu(L)$^{2+}$]	1435.0 ($-7H^+$, -3)	2139.2 ($-6H^+$, -2)	2198.2 ($-3H^+$, -2)	1502.8 ($-7H^+$, -3)	2173.2 ($-4H^+$, -2)
		1426.0 ($-7H^+$, -3)	1464.6 ($-5H^+$, -3)		1448.4 ($-5H^+$, -3)
+HAcO	1456.8 ($-7H^+$, -3)	1446.4 ($-7H^+$, -3)	1485.6 ($-5H^+$, -3)	1523.2 ($-7H^+$, -3)	2203.7 ($-4H^+$, -2)
					1469.2 ($-5H^+$, -3)
+2HAcO	1476.4 ($-7H^+$, -3)	1467.0 ($-7H^+$, -3)	1506.2 ($-5H^+$, -3)	1543.6 ($-7H^+$, -3)	1489.4 ($-5H^+$, -3)
+3HAcO			1527.0 ($-5H^+$, -3)	1564.0 ($-7H^+$, -3)	1510.6 ($-5H^+$, -3)
[(12mer)+3Cu(L)$^{2+}$]		2299.2 ($-8H^+$, -2)	1590.0 ($-6H^+$, -3)	1647.2 ($-9H^+$, -3)	2349.3 ($-8H^+$, -2)
		1532.4 ($-9H^+$, -3)			1565.8 ($-9H^+$, -3)
+HAcO		1552.4 ($-9H^+$, -3)	1610.0 ($-6H^+$, -3)		1587.2 ($-9H^+$, -3)
[2(12mer)+Cu(L)$^{2+}$]		1901.4 ($-6H^+$, -4)			1343.8 ($-4H^+$, -3)
[(12mer)+Cu(L)Cl$^+$]		1332.0 ($-4H^+$, -3)			

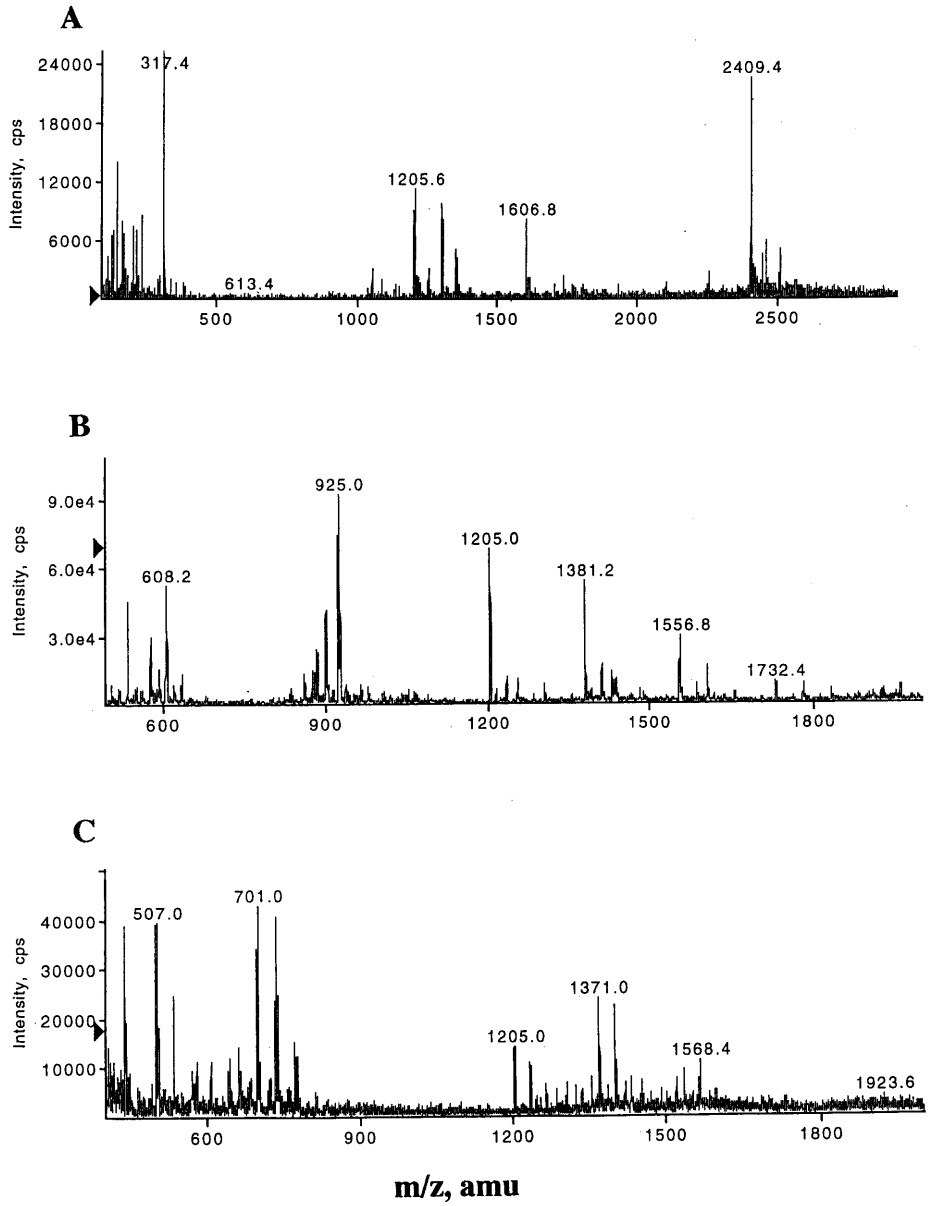


Fig. 6. ESI-mass spectra (positive pattern) of solutions containing 8-mer and copper(II) complex. (A): 8-mer; (B): 12-mer + [Cu(tpa)Cl]ClO_4; (C): 12-mer + [Cu(bdpg)Cl]Cl.

complexes towards a single-strand was also found (2 or 3 copper(II) complexes to single-strand; see Table 4). These clearly demonstrate that the copper(II) complexes used in this study show high affinity towards DNA strand at the oxygen atom of the phosphoric bridge (see Fig. 7), although its position is not specified by the compound as exemplified in the HPLC results described below.

When hydrogen peroxide was added to the solution containing a copper(II) complex and oligomer ($[H_2O_2]/[Cu^{2+}] = 10$), the ESI-mass spectrum remains unchanged in the case of [Cu(tpa)Cl]ClO_4 (see Fig. 8), but the main signals observed for the solution containing [Cu(bdpg)Cl]Cl and the oligomer have disappeared. In the latter case, the disappearance of the signals should be due to degradation of the oligomer by the addition of hydrogen peroxide; which is consistent with the results obtained in HPLC developed in the later section.

3.3. Release of nucleobases from oligomers and DNA cleavage reaction

As stated in the previous section [4,5] we have reported that the copper(II) complexes used in our

previous studies are divided into two types based on the activity for DNA (supercoiled) degradation, e.g. $[Cu(bdpg)Cl]^+$ and $[Cu(dpgs)Cl]^+$ effect the complete degradation of DNA (pBR322, supercoiled Form I), however $[Cu(tpa)Cl]^+$ and other compounds used in this study give only Form II DNA under the same experimental conditions. In order to get more detailed information on this problem, we have investigated the reaction between the copper(II) complex and oligomer in the presence of hydrogen peroxide, and the part of the results is represented in Fig. 2. According to the work by Hecht et al. [18] the Fe(III)–BLM–H_2O_2 system gives much cytosine and cytosine–propenal in the reaction with the 12-mer under aerobic conditions, and their result was reconfirmed in this study.

Table 4
Assignment of main peaks in ESI-mass spectra (m/z, positive pattern) of 8-mer (copper complex binds with DNA stand as+2 charged species with dissociation of chloride or perchlorate ions)

8-mer	2409.4	[double-strand+$2H^+$]$^{2+}$
	1606.8	[double-strand+$3H^+$]$^{3+}$
	1205.6	[double-strand+$4H^+$]$^{4+}$
8-mer+[Cu(tpa)Cl]ClO_4	1381.2	[(double-strand)+2Cu(II)-complex)]$^{4+}$
	1556.8	[(double-strand-$4H^+$) +4Cu(II)-complex)]$^{4+}$
	1732.4	[(double-strand-$8H^+$) +6Cu(II)-complex]$^{4+}$
8-mer+[Cu(bdpg)Cl]Cl	1371.0	[(double-strand) +2Cu(II)-complex)]$^{4+}$
	1537.4	[(double-strand-$4H^+$) +4Cu(II)-complex)]$^{4+}$
8-mer+[Cu(dpgs)Cl]ClO_4	1363.6	[(double-strand) +2Cu(II)-complex)]$^{4+}$
	1523.0	[(double-strand-$4H^+$) +4Cu(II)-complex)]$^{4+}$
	1682.0	[(double-strand-$8H^+$) +6 Cu(II)-complex]$^{4+}$

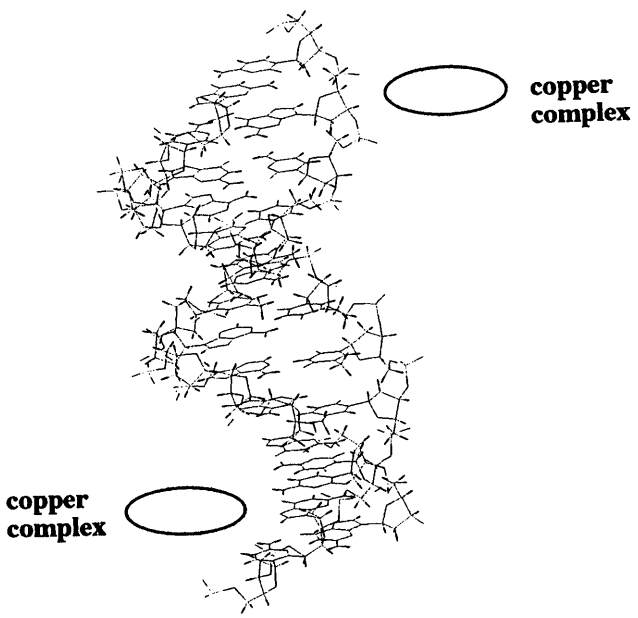


Fig. 7. Schematic illustration of binding of copper(II) complex to double-strand 12-mer.

We have found that the $[Cu(bdpg)Cl]^+$ complex gave large quantities of four nucleobases in the reaction with the 12-mer (see Fig. 9 and Table 2), however release of the free nucleic acids is much smaller in the cases of (tpa) and (dpgt), and other compounds (see Fig. 9). The formation of cytosine–propenal was not detected for all the copper(II)–H_2O_2 systems examined. The order of the activity to release the nucleic acids from 12-mer is as follows: (bdpg) > (dpgs) ≫ (dtpy) ∼ (dpgt) ∼ (dmpy-py) ∼ (tpa). The positive charge on the ligand of the (dmpy-py)-complex has little effect on the reaction. Similar results were found when other oligomers were used instead of 12-mer (see Figs. 10–12). The release of four nucleobases from 12-mer by the Cu(II)–(bdpg) complex indicates that this complex binds to 12-mer randomly; the binding position of the copper(II) complex is not specified by the chelate structure; this is quite different from that of Fe-BLM towards DNA. Since multiple binding of copper(II) complexes towards DNA single strand has no effect on the cleavage behavior of the copper(II) compounds (see the case of 8-mer in Table 2), it seems quite likely that the intrinsic active species for DNA cleavage is a monomeric copper species.

Based on the previous [5,19,20] and present results, and generally accepted proposal that the release of free nucleobases occurs through the formation of the 4′-hydroxylated form of the sugar moiety [1,21–24] it seems quite reasonable to consider that the remarkable activity of the (bdpg)-compound is due to its high electrophilic nature of a copper(II)–hydroperoxide adduct (see Scheme 2), whose formation is greatly promoted through hydrogen bonding with the amide–oxygen atom coordinated to the copper(II) atom, and this electrophilic copper(II)–peroxide adduct attacked to the sugar ring of nucleoside, to give the corresponding hydroxylated species, and from which free nucleobases have been released. The poor activities of other compounds to degrade the oligomers should be due to their negligible ability to form a peroxide adduct, as exemplified in many reactions [7,25]. These discussions clearly support our previous proposal that in the case of Cu-(tpa) complex, formation and activation of a copper(II)–peroxide adduct is assisted by the organic groups of supercoiled DNA chains (see Scheme 3), and that the reactivity of the peroxide adduct thus formed

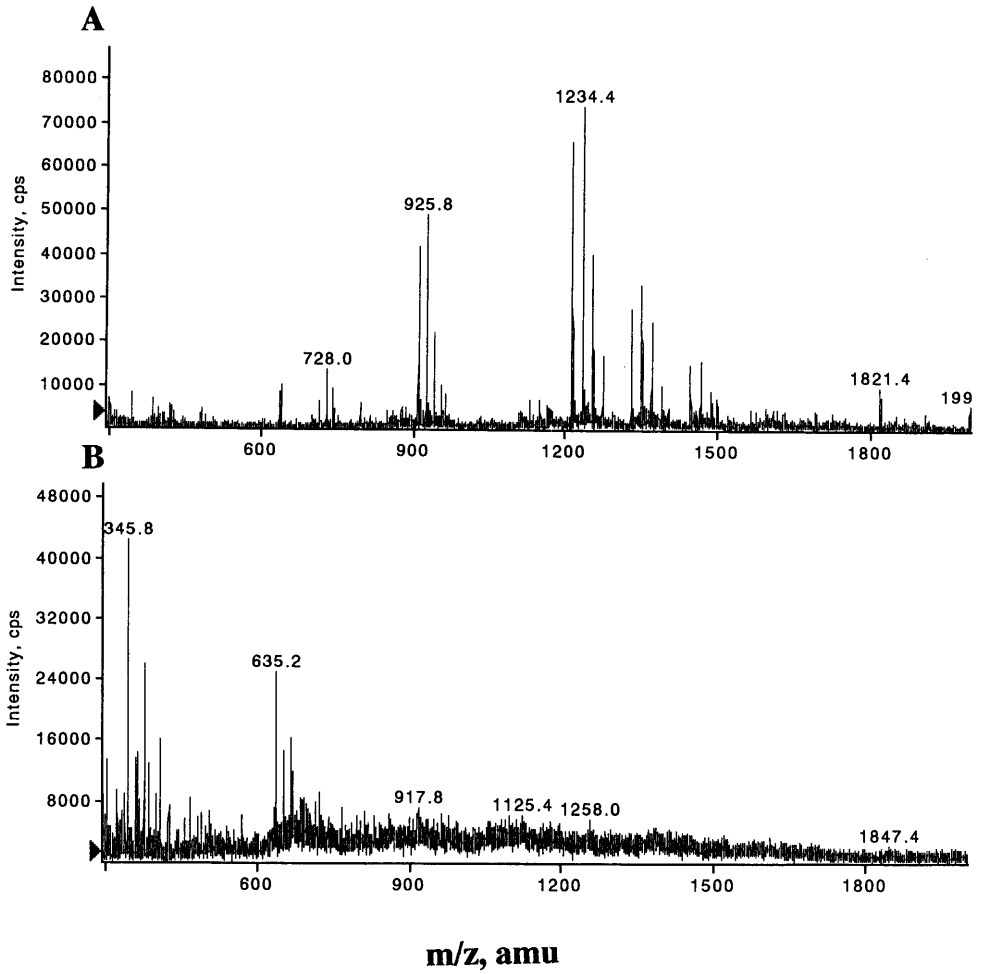


Fig. 8. ESI-mass spectra (negative pattern) of solutions containing 12-mer, copper(II) complex, and hydrogen peroxide. (A): $[Cu(tpa)Cl]ClO_4$; (B): [Cu(bdpg)Cl]Cl.

is quite different from that of the Cu–(bdpg) compound; the latter may explain the fact [4,5] that the $[Cu(bdpg)Cl]^+$ complex effects the complete degradation of DNA (pBR322, supercoiled Form I); however, $[Cu(tpa)Cl]^+$ complex gives only Form II DNA under the same experimental conditions.

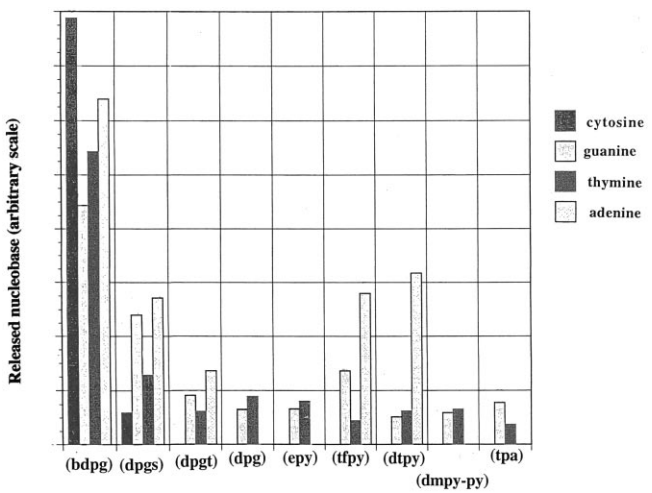


Fig. 9. Schematic illustration of quantity of released nucleobases from 12-mer by the copper(II)–H_2O_2 systems (after 60 min).

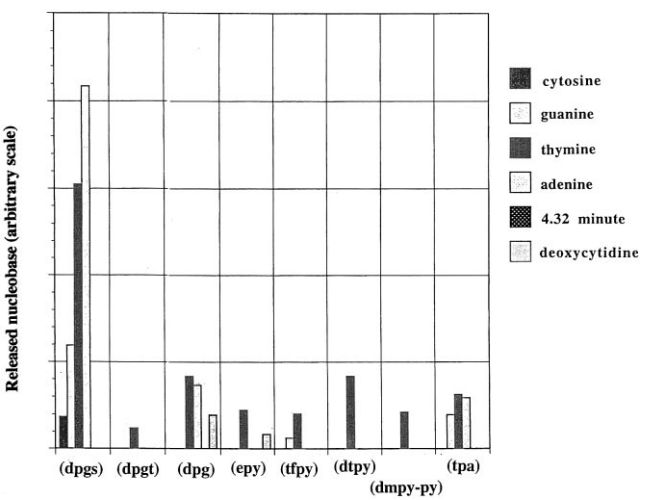


Fig. 10. Schematic illustration of quantity of released nucleobases from 8-mer by the copper(II)–H_2O_2 systems (after 60 min).

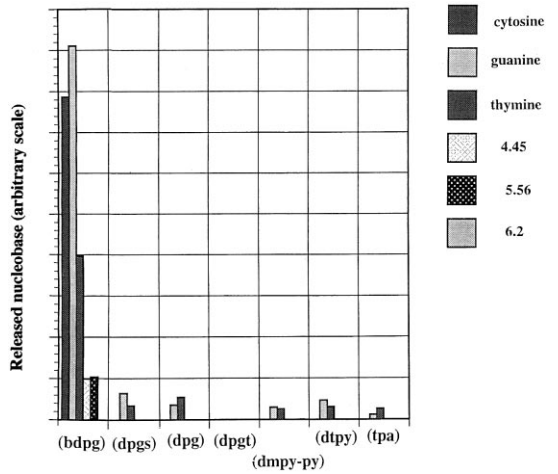


Fig. 11. Schematic illustration of quantity of released nucleobases from 7-mer by the copper(II)–H_2O_2 systems (after 60 min).

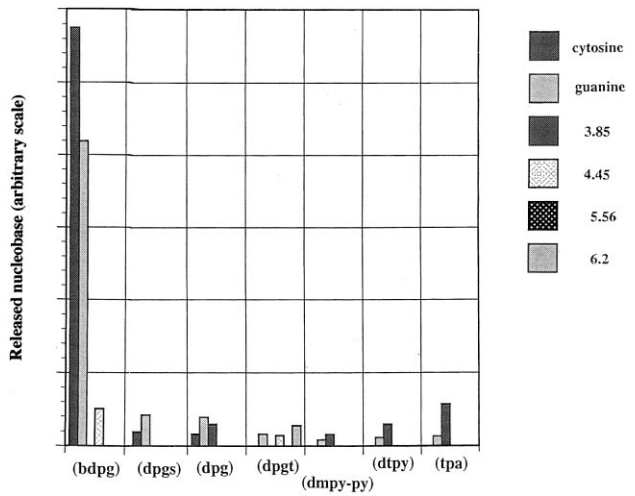
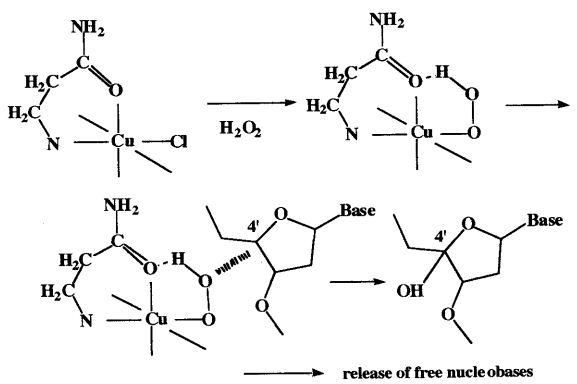
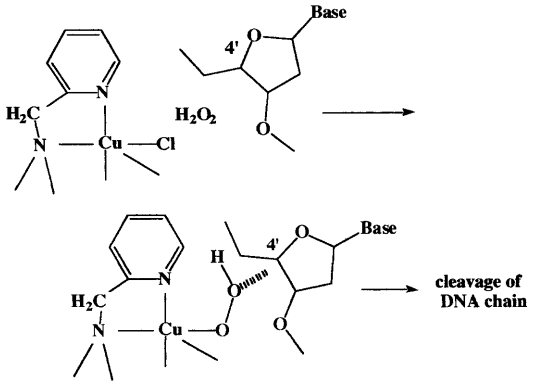


Fig. 12. Schematic illustration of quantity of released nucleobases from 6-mer by the copper(II)–H_2O_2 systems (after 60 min).



Scheme 2.



Scheme 3.

4. Supplementary material

Crystallographic data for the structural analysis have been deposited with the Cambridge Crystallographic Data Centre, CCDC No. 146878. Copies of this information may be obtained free of charge from: The Director, CCDC, 12 Union Road, Cambridge, CB2 1EZ, UK (Fax: +44-1223-336033; e-mail: deposit@ccdc.cam.ac.uk or www: http://www.ccdc.cam.ac.uk).

References

[1] (a) J. Stubbe, J.W. Kozarich, Chem. Rev. 87 (1987) 1107. (b) R.M. Burger, Chem. Rev. 98 (1998) 1153. (c) W.K. Pogpzelski, T.D. Tullius, Chem. Rev. 98 (1998) 1089.
[2] M.J. Absalon, W. Wu, J.W. Kozarich, J. Stubbe, Biochemistry 34 (1995) 2076.
[3] B.M. Burger, K. Deloca, B. Birdsall, J. Biol. Chem. 269 (1994) 25978.
[4] T. Kobayashi, T. Okuno, T. Suzuki, M. Kunita, S. Ohba, Y. Nishida, Polyhedron 17 (1998) 1553.
[5] (a) S. Nishino, T. Kobayashi, M. Kunita, S. Ito, Y. Nishida, Z. Naturforsch. C 54 (1999) 94. (b) Y. Nishida, Recent Res. Dev. Pure Appl. Chem. 3 (1999) 123.
[6] T. Kobayashi, L.L. Guo, Y. Nishida, Z. Naturforsch. C 53 (1998) 867.
[7] T. Okuno, S. Ohba, Y. Nishida, Polyhedron 16 (1997) 3765.
[8] D.T. Cromer, J.T. Waber, International Tables for X-ray Crystallography, vol. IV, Kynoch, Birmingham, 1974.
[9] J.A. Ibers, W.C. Hamilton, Acta Crystallogr. 17 (1964) 781.
[10] TEXSAN–TEXRAY Structure Analysis Package, Molecular Structure Corporation, 1985.
[11] T. Schwartz, M.A. Rould, K. Lowenhaupt, A. Hebert, A. Rich, Science 284 (1999) 1841.
[12] H. Kasai, S. Nishimura, Nucl. Acids Res. 12 (1984) 2137.
[13] Y. Kani, S. Ohba, M. Kunita, Y. Nishida, Acta Crystallogr., Sect. C 56 (2000) e198.
[14] (a) W. Wu, D.E. Vanderwall, S.M. Lui, X.-J. Tang, C.J. Turner, J.W. Kozarich, J. Stubbe, J. Am. Chem. Soc. 118 (1996) 1268. (b) W. Wu, D.E. Vanderwall, S.M. Lui, X.-J. Tang, C.J. Turner, J.W. Kozarich, J. Stubbe, J. Am. Chem. Soc. 118 1996 1281.
[15] (a) J.C. Cortes, H. Sugiyama, K. Ikudome, I. Saito, A.H.-J. Wang, Biochemistry 36 (1997) 9995. (b) J.C. Cortes, H. Sugiyama, K. Ikudome, I. Saito, A.H.-J. Wang, Eur. J. Biochem. 244 (1997) 818.

[16] P. Fulmer, C. Zhao, W. Li, E. DeRose, W.E. Antholine, D.H. Petering, Biochemistry 36 (1997) 4367.
[17] T. Kobayashi, S. Nishino, H. Masuda, H. Einaga, Y. Nishida, Inorg. Chem. Commun., in press.
[18] A. Natrajan, S.M. Hecht, G.A. van der Marel, J.H. van Boom, J. Am. Chem. Soc. 112 (1990) 3997.
[19] Y. Nishida, M. Kunita, S. Nishino, Inorg. Chem. Commun. 2 (1999) 156.
[20] S. Nishino, M. Kunita, T. Kobayashi, H. Matsushima, T. Tokii, Y. Nishida, Z. Naturforsch. B 54 (1999) 1272.
[21] I. Saito, T. Morii, H. Sugiyama, T. Matsuura, C.F. Meares, S.M. Hecht, J. Am. Chem. Soc. 111 (1989) 2307.
[22] L.E. Rabow, J. Stubbe, J.W. Kozarich, J. Am. Chem. Soc. 112 (1990) 3196.
[23] G.H. McGall, L.E. Rabow, G.W. Ashley, S.H. Wu, J.W. Kozarich, J. Stubbe, J. Am. Chem. Soc. 114 (1992) 4958.
[24] P. Fulmer, D.H. Petering, Biochemistry 33 (1994) 5319.
[25] Y. Nishida, S. Nishino, Z. Naturforsch. C 54 (1999) 1107.

PERGAMON

www.elsevier.nl/locate/poly

Polyhedron 19 (2000) 2651–2655

POLYHEDRON

Synthesis and characterization of two tris-chelate complexes of cobalt(III) with 3,5-dimethyl-1-(*N*-methyl/ethyl)thiocarbamyl-pyrazole (HL_1, HL_2) — biologically important bidentate ligands with one ambidentate donor site

Anil Kumar Barik [a], Sachindranath Paul [a], Ray J. Butcher [b], Susanta Kumar Kar [a,*]

[a] *Department of Chemistry, University College of Science, 92 A.P.C. Road, Calcutta 700 009, India*
[b] *Department of Chemistry, Howard University, 2400 Sixth Street N.W., Washington, DC 20059, USA*

Received 26 April 2000; accepted 2 August 2000

Abstract

Cobalt(III) complexes, of two potentially pyrazole-derived bidentate ligands (with one ambidentate donor site), 3,5-dimethyl-1-(*N*-methyl/ethyl)thiocarbamylpyrazole (HL_1 for *N*-methyl, HL_2 for *N*-ethyl) have been synthesized and characterized by elemental analyses, IR, UV–Vis and ^{1}H NMR spectral studies. The structure of $Co(L_2)_3$ has been determined by single-crystal X-ray diffraction studies. The complex (triclinic, space group $P\bar{1}$) has a distorted octahedral structure with the ambidentate ligands coordinated to the Co(III) ion as uninegative bidentate chelating agents via the pyrazole ring nitrogen (tertiary) and the thiocarbamyl iminyl nitrogen atoms. The distortion from the regular octahedral geometry is ascribed to the stereochemical limitations imposed by the planar bidentate ligands. © 2000 Elsevier Science B.V. All rights reserved.

Keywords: Cobalt(III) complex; Thiocarbamylpyrazole; Spectroscopic study; X-ray crystal structure

1. Introduction

The well-documented bio-activity of pyrazole-derivatives often ascribed to the chelation phenomena [1,2] with trace metal ions has generated a significant growth of literature in the coordination chemistry of pyrazole-derived ligands, amply reflected through review articles of Trofimenko [3–5]. In continuation of our recent report [6] on the synthesis and structural characterization of Cu(II) and Ni(II) complexes with 3,5-dimethyl-1-(*N*-methyl/ethyl) thiocarbamylpyrazole, (HL_1, HL_2, respectively, Fig. 1), the present communication aims at reporting the synthesis and spectroscopic characterization of two cobalt(III) complexes with the same ligands (HL_1, HL_2) together with X-ray crystal structure studies of $Co(L_2)_3$. However, while in the $Ni(L_2)_2$ complex [6] the two ligand molecules in their deprotonated forms bind individually, the Ni(II) ion through the pyrazole ring nitrogen (tertiary) and thiolato sulfur (of thiocarbamyl group), the present Co(III) species have their individual three deprotonated ligands bonded through the expected ring nitrogen (Pz ring) and iminyl nitrogen (of thiocarbamyl group) to the central metal ion. Thus the ambidentate nature of the ligands at their thiocarbamyl end is finally established through the supportive evidence of the crystal structure analysis of the present $Co(L_2)_3$ complex (Fig. 2).

2. Experimental

2.1. Chemicals

Solvents and reagents were obtained from commercial sources and used without further purification. Spectrograde solvents were used for spectral and conductance measurements. $CDCl_3$ (Aldrich) was used for recording ^{1}H NMR spectral data.

* Corresponding author. Tel.: +91-033-350-8386; fax: +91-033-351-9755.
E-mail address: skkar@cucc.ernet.in (S.K. Kar).

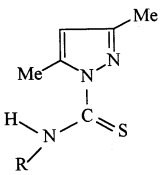
0277-5387/00/$ - see front matter © 2000 Elsevier Science B.V. All rights reserved.
PII: S0277-5387(00)00523-4

Table 1
Analytical data and other pertinent physico-chemical properties of the complexes

Complex	Elemental analyses found (Calc.)			Conductivity at 30°C in MeOH (Ω^{-1} cm^2 mol^{-1})
	%C	%H	%N	
$[Co(L_1)_3]$	44.85 (44.76)	5.29 (5.33)	22.59 (22.38)	9
$[Co(L_2)_3]$	47.79 (47.61)	5.99 (5.95)	20.48 (20.83)	9

Table 2
^{1}H NMR spectral data for the ligands and the Co(III) complexes in $CDCl_3$

Compound	NH	C_4–H	C_3–CH_3	C_5–CH_3	N–CH_3	N–CH_2–CH_3	N–CH_2–CH_3
HL_1	9.18	5.86	2.07	2.63	3.06		
HL_2	9.07	5.82	2.04	2.60		3.56	1.16
$[Co(L_1)_3]$		5.96	2.17	2.81	3.19		
$[Co(L_2)_3]$		6.00	2.96	3.02		4.00	1.47



HL_1, R = Me

HL_2, R = Et

Fig. 1.

2.2. Preparation

The ligands 3,5-dimethyl-1-(*N*-methyl)thiocarbamylpyrazole [HL_1] and 3,5-dimethyl-1-(*N*-ethyl)-thiocarbamylpyrazole [HL_2] were synthesized and characterized according to the method as described in our recent report [6].

The metal complexes were prepared by reacting an ethanolic solution (15 cm^3) of $CoCl_2 \cdot H_2O$ (1.19 g, 0.005 mol), with an ethanolic solution (15 cm^3, 0.015 mol) of the appropriate ligand. The pH of the solution was adjusted to approximately 8 by dropwise addition of dilute ammonia (1:1) solution. The result was a dark red (for HL_1) and an orange–red (for HL_2) solution, and after concentration at water-bath temperature, this afforded a dark red compound (for HL_1) and an orange–red compound (for HL_2) approximately 70% in each case. The compounds were collected by filtration, washed with cold ethanol and dried over fused calcium chloride. The X-ray quality crystals for $Co(L_2)_3$ were grown by slow evaporation of an acetonitrile solution of the complex at room temperature.

The different instrumental techniques used for characterization of the compounds have been described in our earlier reports [6,7]. Analytical data are presented in Table 1.

2.3. Crystallography

A single crystal of dimensions ($0.4 \times 0.6 \times 0.4$ mm) of the complex, $Co(L_2)_3$ was selected and mounted on an automatic Enraf–Nonius CAD-4 diffractometer equipped with a graphite monochromator and Mo Kα radiator ($\lambda = 0.71013$ Å). Unit-cell dimensions and intensity data were measured at 293 K.

The structure was solved by direct methods refined by full-matrix least-squares based on F^2 with anisotropic thermal parameters for non-hydrogen atoms using XCAD-49 (data reduction) and SHELXTL (absorption correction, structure solution/refinement and molecular graphics). The H-atoms were included in structure factor calculations in their idealized positions. The crystallographic data are summarized in Table 3 and the final positional parameters are available as supplementary material (see Section 5).

3. Results and discussion

When $CoCl_2 \cdot 6H_2O$ in ethanol was stirred with the title ligands HL_1 and HL_2 in air, (the pH was approximately 8, made by dilute ammonia solution), an immediate color change took place demonstrating a facile complex formation reaction. The most probable oxidizing agent in these syntheses is dioxygen. However, no attempt was made to monitor the metallation reaction under strictly anaerobic conditions.

These cobalt(III) complexes were isolated as dark red and orange–red microcrystalline solids which were highly soluble in polar organic solvents. The molar conductance values for the complexes in methanol indicate their nonelectrolytic nature. The complexes are diamagnetic as expected for a spin-paired d^6-ion.

3.1. Spectral studies

The breathing motion of the pyrazole ring is shifted to a higher frequency upon complexation and is consistent with pyrazole ring nitrogen (tertiary) coordination. Coordination of the pyrazole ring nitrogen to cobalt(III) is further suggested by the shift of the ν(C=N) band (at 1585 cm^{-1} for HL_1 and at 1560 cm^{-1} for HL_2) to higher frequency by 5–15 cm^{-1} upon complexation along with the occurrence of the ν(Co–N) band at 265 cm^{-1} in the complexes. This also conforms with our earlier report [6]. The disappearance of the broad ν(N–H) band at 3390–3210 cm^{-1} in the free ligand spectra after complexation suggests that deprotonation of the ligand takes place prior to the metallation reaction. The thioamide I band (at 1255 cm^{-1} for HL_1 and at 1260 cm^{-1} for HL_2), which contains considerable ν(C=S) character, is of the same intensity in the complexes and is found almost at the same frequency, suggesting noncoordination of the metal through sulfur after deprotonation. Participation of the thiocarbamyl iminyl nitrogen in coordination is indicated by a red-shift of 10–15 cm^{-1} of the ligand ν(C–N) mode (1570 cm^{-1} for HL_1 and at 1545 cm^{-1} for HL_2) of the thioacetamide II band [8,9] after complexation. The band at approximately 260 cm^{-1} in both complexes in their far IR spectra indicated the presence of ν_{Co-N} (thiocarbamyl).

Table 3
Crystal data and structure refinement for $[Co(L_2)_3]$

Empirical formula	$C_{24}H_{36}CoN_9S_3$
Formula weight	605.73
Temperature (K)	293(2)
Wavelength (Å)	0.71073
Crystal system	triclinic
Space group	$P\bar{1}$
Unit cell dimensions	
a (Å)	11.5328(11)
b (Å)	11.5617(10)
c (Å)	11.7971(10)
α (°)	100.715(5)
β (°)	104.417(5)
γ (°)	93.293(6)
Z (Å^3)	1488.0(2)
D_{calc} (Mg m^{-3})	1.352
Absorption coefficient (mm^{-1})	0.817
F(000)	636
Crystal size (mm)	$0.4 \times 0.6 \times 0.4$
θ Range for data collection (°)	2.20–28.50
Limiting indices	$0 \le h \le 15$, $-15 \le k \le 15$, $-15 \le l \le 15$
Reflections collected	7875
Independent reflections	7510 ($R_{int} = 0.0144$)
Absorption correction	Semi-empirical from ψ-scans
Max. and min. transmission	0.5411 and 0.4651
Refinement method	Full-matrix least-squares on F^2
Data/restraints/parameters	7502/0/379
Goodness-of-fit on F^2	1.081
Final R indices [$I > 2\sigma(I)$]	$R_1 = 0.0437$, $wR_2 = 0.1004$
R indices (all data)	$R_1 = 0.0669$, $wR_2 = 0.1193$
Largest difference peak and hole (e Å^{-3})	0.389 and −0.413

The visible absorption spectra of the Co(III) complexes may be expected theoretically to consist of transitions from the $^1A_{1g}$ ground state to other singlet states [9,10]. Although the entire energy-level pattern is not known in greater detail, usually the complex species of Co(III) give rise to two spin-allowed and two spin-forbidden ligand field bands in the solid-state spectrum of an authentic Co(III) octahedral species [11,12]. However, the diffuse reflectance spectra of the complexes, under discussion, consist of only one broad band at approximately 24 000 cm^{-1} corresponding to one spin-allowed transition ($^1A_{1g} \rightarrow {}^1T_{2g}$) for the low-spin Co(III) octahedral species. Methanolic solutions of the complexes, in addition to showing the intra-ligand charge transfer band at approximately 33 000 cm^{-1} ($\varepsilon \sim 21\,000$ l cm^{-1} mol^{-1}), display an $N \rightarrow Co^{III}$ charge-transfer transition (LMCT) at approximately 25 300 cm^{-1} ($\varepsilon \sim 3\,500$ l cm^{-1} mol^{-1}). In the electronic spectra of the present complexes, however, no d–d band is observed, probably due to the intrusion of tails of intense charge-transfer bands into the visible portion of the spectra which masks the expected d–d bands.

Table 2 represents a listing of the ^1H NMR assignments for both the ligands (HL_1 and HL_2) and their Co(III) complexes in order to have supportive evidence regarding the bonding sites of the ligands towards the Co(III) ion which has also been inferred from IR spectral studies as previously discussed. The disappearance of the broad singlet at δ 9.18 (for HL_1) and 9.07 (for HL_2) in the free ligand upon complexation strongly suggests that deprotonation of the iminothioketo form of the free ligands takes place during the complexation process. The C_4–H (ring) signal in the complex is shifted downfield from its original position in the uncomplexed ligand upon coordination of the tertiary nitrogen of the pyrazole ring, which reduces electron density at C_4 (ring Pz). The coordination of the pyrazole ring nitrogen is further substantiated by the shifting of both C_3– and C_5–CH_3 protons towards the lower fields as shown in Table 2. Coordination of the uninegative nitrogen atom of the –C(S)–$\overset{\ominus}{N}$–R group (R = CH_3 for HL_1 and CH_3–CH_2– for HL_2) to the central Co(III) ion is substantiated by the deshielding of the primary –CH_3 protons for HL_1 and both secondary and primary (–CH_3) protons of HL_2 bonded to the coordinating

Table 4
Selected bond lengths (Å) and angles (°) for the $[Co(L_2)_3]$ complex with e.s.d. values in parentheses

Co–N(13)	1.922(2)	Co–N(21)	1.933(2)
Co–N(11)	1.933(2)	Co–N(23)	1.933(2)
Co–N(31)	1.937(2)	Co–N(33)	1.937(2)
N(13)–Co–N(21)	88.19(8)	N(13)–Co–N(11)	81.47(8)
N(21)–Co–N(11)	95.73(8)	N(13)–Co–N(23)	95.44(9)
N(21)–Co–N(23)	81.40(8)	N(11)–Co–N(23)	175.88(8)
N(13)–Co–N(31)	174.69(8)	N(21)–Co–N(31)	96.28(8)
N(11)–Co–N(31)	95.20(8)	N(23)–Co–N(31)	88.08(8)
N(13)–Co–N(33)	94.48(8)	N(21)–Co–N(33)	175.47(8)
N(11)–Co–N(33)	88.29(8)	N(23)–Co–N(33)	94.68(9)
N(31)–Co–N(33)	81.25(8)		

iminyl nitrogen. In the case of the $Co(L_2)_3$ complex, the $–CH_2–$ protons being relatively close to the above donor site in the complex suffer a relatively higher amount of downfield shift ($\delta = 0.44$ ppm) than the $–CH_3$ protons ($\delta = 0.31$ ppm) which is as a result of being positioned one carbon away from the donor N atom. ^{1}H NMR spectra thus provide tacit support for the bonding characteristics of the primary ligand (HL_1/HL_2) in forming complexes with cobalt(III) through pyrazolyl ring nitrogen (^{2}N) and the iminyl nitrogen of the substituted thiocarbamyl group.

3.2. Description of the crystal and molecular structure of the $Co(L_2)_3$ complex

A perspective view of the complex together with the atom numbering scheme is shown in Fig. 2. Selected bond lengths and bond angles are listed in Table 4. The compound consists of a discrete mononuclear $[Co(C_8H_{12}N_3S)_3]$ neutral unit. The cobalt(III) ion in the complex, $Co(L_2)_3$ is in a six-coordinate environment of six nitrogen atoms from the three ligand molecules to form a CoN_6 chromophore. Each ligand molecule behaves as a bidentate *N*,*N*-chelating agent via the pyrazolyl ring nitrogen atom and the thiocarbamyl nitrogen atom. The ligands are present as singly deprotonated bidentate ones. The deprotonation, which actually takes place from the imino nitrogen of the thiocarbamyl group, is not accompanied by tautomerisation to the 'thiol' form. For the sake of convenience, these three molecules of the ligand are designated as ligand **1**, ligand **2** and ligand **3**, and the individual atoms in the ligand are identified with suffix **1**, **2** and **3** where necessary.

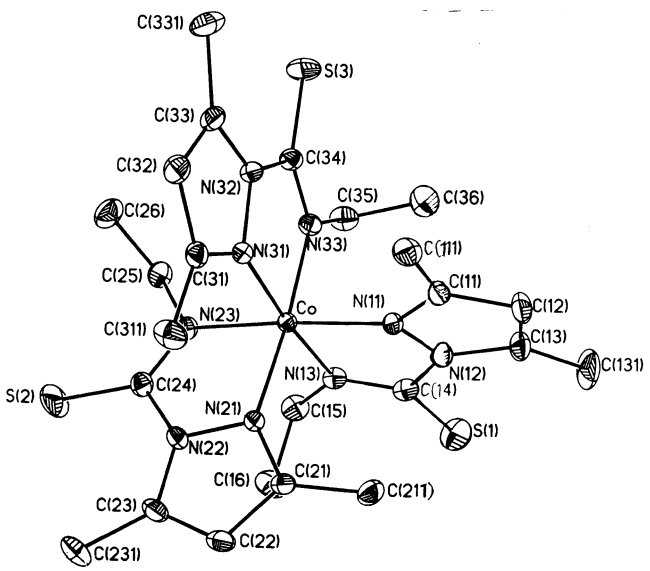


Fig. 2. A perspective view of the complex $Co(L_2)_3$ showing atom numbering scheme.

The cobalt atom is in an octahedral environment, with similar types of donor atom (either pyrazolyl N or thiocarbamyl N) from three ligand molecules occupying a facial plane. The best description of the geometry around cobalt is obtained when N(13), N(21), N(31) and N(33) are considered to form a square plane and N(11) and N(23) act as axial donor sites. Angles generated at the Co(III) center by the chelating donor points (pyrazolyl N and thiocarbamyl N) differ slightly in the three coordinating ligands (Table 4). It appears that the angles at the Co(III) center in the chelate rings are controlled to some extent by the ligand geometry. The coordination sphere of the cobalt atom in the present complex may be considered as a distorted octahedron. The twelve angles subtended at the Co(III) ion by the adjacent donor atoms range from 81.25(8) to 96.28(8)° compared to 90° required for a perfect octahedron. This distortion from the idealized geometry may be attributed to the restricted bite angles imposed by the planar bidentate ligands. From the study of all the bond angles around the central cobalt atom, it is evident that except for the three angles (viz., N(11)–Co–N(33), N(13)–Co–N(21) and N(23)–Co–N(31) angles, 88.29(8), 88.19(8) and 88.08(8)°, respectively) no other angles in this six-coordinated cobalt(III) complex are close to idealized values expected for a regular octahedral geometry, indicating that distortion is a common phenomenon in tris-ligand cobalt(III) complexes of planar *N*,*N* bidentate chelating agents. The average Co^{III}–N(pyrazole) distance in the complex is the same within experimental error, the average value being 1.934(2) Å. The average Co^{III}–N(thiocarbamyl) length is 1.931(2) Å which is close to the Co^{III}–N(pyrazole) length. The observed average Co–N bond distance is, however, shorter than that (1.947 Å) found in the complex $[Co(L4M)_2]BF_4$ [13] (L4M = anion (loss of ^{3}N proton) of 2-acetylpyridine-^{4}N-methylthiosemicarbazone) and longer than that (1.918 Å) in the complex $[Co(MPzSB)_2]Cl$ [14]

(MPzSB = anion (loss of ^{3}N proton) of *S*-benzyldithiocarbazate of 5-methyl-3-formyl pyrazole). For the ligand moiety, the interatomic distances and angles are within normal ranges.

4. Conclusion

In continuation of our earlier report [6], this study reports the characterization of cobalt(III) complexes with two potentially bidentate pyrazole-derived ligands with one ambidentate donor site at the thiocarbamyl part. Since the substituted thiocarbamyl sites function as ambidentate donor, the mode of binding to different metal ions depends upon the relative softness or hardness of the metal ions. The difference in the ligational behavior at the thiocarbamyl part towards Ni(II) and Co(III) ions is reasonably ascribed to a strong coordination of harder base N (of thiocarbamyl part) with harder Co(III) ion and that of softer base S with softer Ni(II) ion.

5. Supplementary material

Crystallographic data for the structural analysis have been deposited with the Cambridge Crystallographic, CCDC No. 141946 for compound $Co(L_2)_3$. Copies of this information may be obtained free of charge from The Director, CCDC, Data Center, 12 Union Road, Cambridge, CB2 1EZ, UK (fax: +44-1223-336033; e-mail: deposit@ccdc.cam.ac.uk or www:http://www.ccdc.cam.ac.uk).

Acknowledgements

The financial support from the University Grants Commission, New Delhi, India to two authors (A.B. and S.P.) is gratefully acknowledged.

References

[1] R.C. Elderfield (Ed.), Heterocyclic Compounds, Wiley, New York, 1959, p. 565.
[2] H.E. Skipper, R.K. Robins, J.R. Thomson, C.C. Cheng, R.W. Brockman, Jr., F.M. Schabel, Cancer Res. 17 (1957) 579.
[3] S. Trofimenko, Chem. Rev. 72 (1972) 479.
[4] S. Trofimenko, Progr. Inorg. Chem. 34 (1986) 117.
[5] S. Trofimenko, Chem. Rev. 93 (1993) 943.
[6] A.K. Barik, P. Bandyopadhyay, S.K. Kar, Polyhedron 18 (1999) 001.
[7] A.K. Barik, S. Paul, S.K. Kar, R.J. Butcher, J.C. Bryan, Polyhedron 18 (1999) 571.
[8] S. Burman, D.N. Satyanarayan, J. Inorg. Nucl. Chem. 43 (1981) 3403.
[9] G.J. Sutton, Aust. J. Chem. Soc. 22 (1969) 2474.
[10] F.A. Cotton, G. Wilkinson, Advanced Inorganic Chemistry, 5th Edn., Wiley, New York, 1988, p. 734.
[11] A. Monaci, F. Tarli, A.M.M. Lanfredi, M.T. Tiripicchio, M.T. Camellini, J. Chem. Soc., Dalton Trans. (1979) 1435.
[12] A.B.P. Lever, Inorganic Electronic Spectroscopy, Elsevier, New York, 1984, pp. 463–478.
[13] D.X. West, H. Gebremedhin, T.J. Romack, Inorg. Chim. Acta 216 (1994) 229.
[14] A. Mitra, T. Banerjee, P. Roychowdhury, S. Chaudhuri, P. Bera, N. Saha, Polyhedron 16 (1997) 3735.

PERGAMON

www.elsevier.nl/locate/poly

Polyhedron 19 (2000) 2657–2659

POLYHEDRON

Synthesis and structure of a novel molybdenum imido calix[6]arene

Carl Redshaw [a,*], Mark R.J. Elsegood [b]

[a] *School of Chemical Sciences, University of East Anglia, Norwich NR4 7TJ, UK*
[b] *Department of Chemistry, Loughborough University, Loughborough, Leicestershire LE11 3TU, UK*

Received 28 June 2000; accepted 28 August 2000

Abstract

Treatment of *p-tert*-butylcalix[6]areneH_6 (H_6L) with $[Mo(OBu^t)_2\{[2,2'\text{-}(N)\text{-}C_6H_4]_2(CH_2CH_2)\}]$ in refluxing toluene affords, after work-up, the complex $[Mo(2\text{-}NC_6H_4CH_2CH_2C_6H_4NHC(Me)NH\text{-}2')LH_2]\cdot 4MeCN$ (**1**), which contains an 11-membered metallocyclic ring as characterised by Synchrotron X-radiation. © 2000 Elsevier Science B.V. All rights reserved.

Keywords: 11-Membered metallocyclic ring; Synchrotron radiation; Metallocalix[6]arene

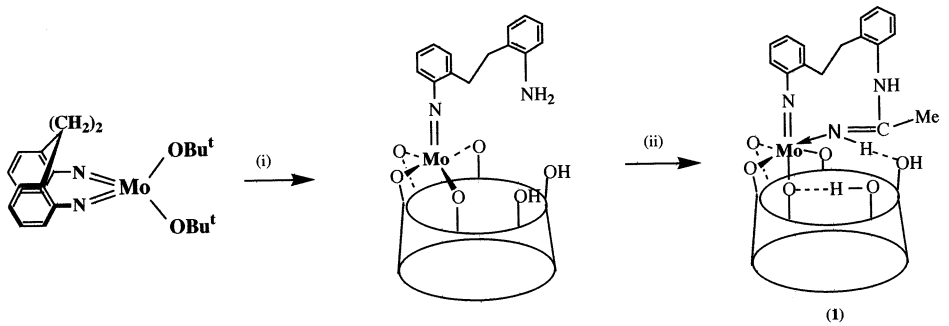
The chemistry of transition metal complexes of the simplest of the calixarenes, the calix[4]arene system, is relatively well developed [1]. In general, these complexes retain the cone-like conformation of the parent ligand [2]. By contrast, transition-metal compounds containing the larger ring systems are still quite rare [3], presently being restricted to W (calix[5]), and Ti (calix[6]), Pt, Pd, Re (diphosphinite of calix[6]) and Zr, Ti, V, Mo (calix [6] and [8]). In recent work we have been investigating routes to imidometal calixarenes, for example, treatment of $[Mo(NAr)_2(OBu^t)_2]$ ($Ar = C_6H_3Pr^i_2\text{-}2,6$) with calix[4]arene$H_4$ (H_4L^1) and calix[8]areneH_8 (H_8L^2) affords, via alkoxide and imido displacement reactions, the novel mono and dimetallocalixarene complexes $[Mo(NAr)L^1(NCMe)]$ and $[\{Mo(NAr)(NCMe)\}_2L^2]$, respectively [4]. Since we had already characterised the first chelating or *ansa* bis(imido) metal derivatives [5], we chose to prepare a range of metallocalix[n]arene species with pendant amino functionalities utilising the bis(imido) complex $\{Mo(OBu^t)_2[(2\text{-}NC_6H_4)_2CH_2CH_2]\}$ and the alkoxide/imido displacement methodology. Here we describe a novel metallocalix[6]arene complex $[Mo(2\text{-}NC_6H_4CH_2CH_2C_6H_4NHC(Me)NH\text{-}2')LH_2]$ (**1**), containing an 11-membered metallocyclic ring formed on intramolecular insertion of the pendant amino group into a molybdenum–acetonitrile bond.

Treatment of the chelating bis(imine) complex $[Mo(OBu^t)_2\{[2,2'\text{-}(N)\text{-}C_6H_4]_2(CH_2CH_2)\}]$[5] with H_6L in toluene affords, after work-up, the complex $[Mo(2\text{-}NC_6H_4CH_2CH_2C_6H_4NHC(Me)NH\text{-}2')LH_2]$ (**1**)[1]. Stoichiometrically, **1** is formed via loss of two molecules of *tert*-butanol followed by proton transfer to N(2) to release a pendant amino group – see Scheme 1. The intermediate formed prior to the addition of acetonitrile must therefore contain two phenolic groups. The IR spectrum of this intermediate contains a broad feature (weak) in the ν(N–H) region (3364 cm^{-1}) together with a strong ν(C–N) stretch at approximately 1270 cm^{-1}. A second broad feature at 3124 cm^{-1} is assigned to ν(OH), which appears as a broad singlet (integrating to 2 H) at δ 10.38 ppm in the ^{1}H NMR (C_6D_6). Following addition of acetonitrile, an intramolecular insertion of the pendant NH_2 group into a molybdenum–acetonitrile bond, in an analogous fashion to the reaction of $[ReCl_4(NCMe)_2]$ with aniline [6], results in

* Corresponding author. Tel.: +44-1603-593-137; fax: +44-1603-259-396.
E-mail address: carl.redshaw@uea.ac.uk (C. Redshaw).

[1] Satisfactory elemental analyses have been obtained. $[Mo(OBu^t)_2\{[2,2'\text{-}(N)\text{-}C_6H_4]_2(CH_2CH_2)\}]$[4] (1.0 g, 2.22 mmol) and *p-tert*-butylcalix[6]areneH_6 (2.1 g, 2.16 mmol) were refluxed in toluene (40 cm^3) for 12 h. After allowing to cool to room temperature, the volatiles were removed under reduced pressure and the residue extracted with MeCN (30 cm^3). Prolonged standing at ambient temperature afforded small red–brown prisms (0.89 g, 28%). Selected spectroscopic data for **1**: ^{1}H NMR ($CDCl_3$, 298 K): δ 4.94 [d, $^2J_{HH}$ 12 Hz, $ArCH_2Ar$], 4.73 [d, $^2J_{HH}$ 14 Hz, $ArCH_2Ar$], 4.45 [d, $^2J_{HH}$ 13 Hz, $ArCH_2Ar$], 3.48 [d, $^2J_{HH}$ 12 Hz, $ArCH_2Ar$], 3.38 [d, $^2J_{HH}$ 14 Hz, $ArCH_2Ar$], 3.13 [d, $^2J_{HH}$ 14 Hz, $ArCH_2Ar$]. IR: ν(NH) 3350w(sh), ν(OH) 3132, 3124bs, ν(C=N) 1628s, ν(Mo–O) 825, 800m.

0277-5387/00/$ - see front matter © 2000 Elsevier Science B.V. All rights reserved.
PII: S0277-5387(00)00579-9



Scheme 1. Reagents and conditions: (i) H_6L, toluene, reflux, 12 h; (ii) MeCN, ~72 h.

an amidine ligand bound to the metal centre through the imine nitrogen. Small crystals of **1**, only suitable for an X-ray diffraction analysis using synchrotron radiation[2] [6], were grown from acetonitrile at room temperature in approximately 30% yield. The molecular structure is shown in Fig. 1, with selected bond lengths and angles given in the caption. The core geometry is best described as distorted octahedral with angles ranging from 83.7(3) to 96.2(3)°. The bite angle [N(1)–Mo(1)–N(3)] of the metallocyclic ring is 94.4(3)°, the conformation of which is somewhat folded with the aromatic rings approximately coplanar and separated by a CH_2CH_2 step. The distance of 1.742(8) Å for the Mo(1)–N(1) bond and 1.388(11) Å for the N–C(*ipso*) bond, combined with Mo(1)–N(1)–C(1) angle of 173.1(7)°, are consistent with a linear arylimido ligand, which is reflected in the long *trans* Mo(1)–O(4) bond length [2.051(6) Å versus 1.905(6) for O(2), 1.953(6) for O(1) and 1.989(6) Å for O(3)]. The amidine(imine) to Mo bond length [2.162(8) Å] is indicative of a dative bond, hence indicating a formal +VI oxidation state for the molybdenum centre. The macrocycle (L^1) adopts a severly twisted 'hump-like' or partial cone

[2] X-ray crystallography. Crystal data for **1**·4MeCN ($C_{82}H_{97}MoN_3O_6{\cdot}4C_2H_3N$), $M = 1480.78$, monoclinic, space group $P2_1/c$, $a = 28.412(3)$, $b = 11.3105(14)$, $c = 25.466(3)$ Å, $\beta = 94.651(3)°$, $V = 8156.7(16)$ Å^3, $T = 160$ K, $Z = 4$, μ (Mo Kα) $= 0.218$ mm^{-1}, crystal size $0.02 \times 0.06 \times 0.12$ mm, 43 324 data measured of which 15 738 were unique, $R_{int} = 0.125$, all unique data used in refinement against F^2 values to give final $wR = 0.3523$ (on F^2 for all data), $R = 0.1339$ {for 9320 data with $F^2 > 4\sigma(F^2)$}. Silicon 111 monochromated Synchrotron radiation ($\lambda = 0.6878$ Å) at Daresbury SRS Station 9.8 was used as described previously [6]. Twofold positional disorder was modelled with restraints for some calixarene *p*-^{t}Bu groups.

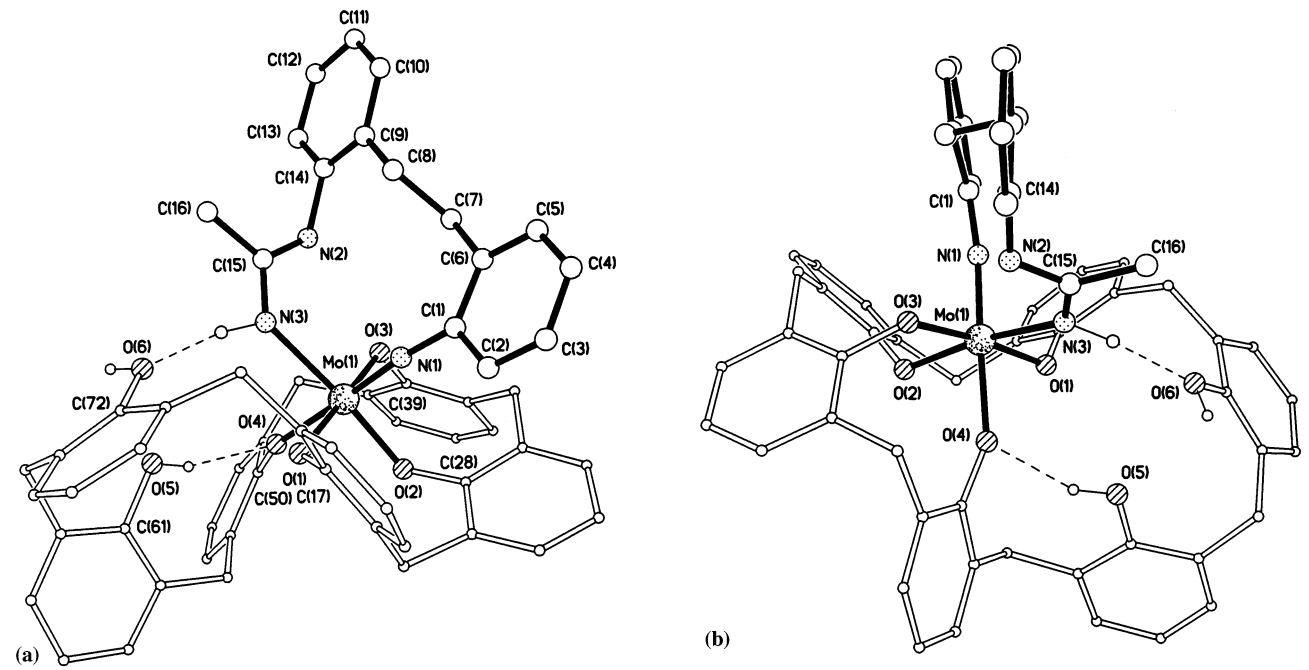


Fig. 1. (a) Molecular structure of **1**. Selected dimensions (Å and °): Mo(1)–N(1) 1.742(8), Mo(1)–N(3) 2.162(8) 2.162(8), Mo(1)–O(1) 1.953(6), Mo(1)–O(2) 1.905(6), Mo(1)–O(3) 1.989(6), Mo(1)–O(4) 2.051(6); Mo(1)–N(1)–C(1) 173.1(7), M0(1)–N(3)–C(15) 133.2(6). (b) Molecular structure of **1** showing the stepped geometry of the *N*,*N*-chelate ligand. Selected H-bond dimensions (Å and °): O(4)···H 1.90, O(6)···H 1.91; O(5)–H···O(4) 157, N(3)–H···O(6) 169.

(up-up-out) conformation, only previously seen for the palladium(II) chloride complex $[PdCl_2L^1P]$ (where L^1P is a calix[6]arene derived diphosphite) [3b]. The phenolic protons of O(5) and O(6) are involved in intramolecular H-bonding with O(4) and N(3), respectively, which results in the lowered stretching constants for ν(PhO–H) (see caption to Fig. 1(b) for H-bond geometry).

1. Supplementary material

Crystallographic data for the structures reported in this paper have been deposited with the Cambridge Crystallographic Data Centre, CCDC no. 146026. Copies of this information may be obtained free of charge from the Director, CCDC, 12 Union Road, Cambridge, CB2 1EZ, UK (fax: +44-1223-336033; e-mail: deposit@ccdc.cam.ac.uk or http://www.ccdc.cam.ac.uk).

Acknowledgements

The Leverhulme Trust (Special Research Fellowship to C.R.), Professor V.C. Gibson (Imperial College) and The University of East Anglia are thanked for financial support. The EPSRC are thanked for provision of the Bruker AXS SMART diffractometers at Daresbury Laboratory, and for the award of beam time at Daresbury. We would like to thank Professor W. Clegg for use of the crystallographic computing facilities in Newcastle.

References

[1] (a) D.M. Roundhill, Prog. Inorg. Chem 43 (1995) 533. (b) C. Wiser, C.B. Dielman, D. Matt, Coord. Chem Rev. 165 (1997) 93.
[2] (a) A. Zanotti-Gerosa, E. Solari, L. Giannini, C. Floriani, A. Chiesi-Villa, C. Rizzoli, J. Am. Chem. Soc. 120 (1998) 437. (b) L. Giannini, E. Solari, C. Floriani, N. Re, A. Chiesi-Villa, C. Rizzoli, Inorg. Chem. 38 (1999) 1438. (c) L. Giannini, E. Solari, A. Zanotti-Gerosa, C. Floriani, A. Chiesi-Villa, C. Rizzoli, Angew. Chem., Int. Ed. Engl. 36 (1997) 753. (d) B. Castellano, E. Solari, C. Floriani, R. Scopelliti, N. Re, Inorg. Chem. 38 (1999) 3406. (e) A. Zanotti-Gerosa, E. Solari, L. Giannini, C. Floriani, A. Chiesi-Villa, C. Rizzoli, Chem. Commun. (1997) 183. (f) L. Giannini, E. Solari, A. Zanotti-Gerosa, C. Floriani, A. Chiesi-Villa, C. Rizzoli, Angew. Chem., Int. Ed. Engl. 35 (1996) 85. (g) B. Castelleno, A. Zanotti-Gerosa, E. Solari, C. Floriani, A. Chiesi-Villa, C. Rizzoli, Organometallics 15 (1996) 4894. (h) L. Giannini, A. Casella, E. Solari, C. Floriani, A. Chiesi-Villa, C. Rizzoli, N. Re, A. Sgamellotti., J. Am. Chem. Soc. 119 (1997) 1998.
[3] (a) M. Fan, H. Zhang, M. Lattman, Chem. Commun. (1998) 99. (b) F.J. Parlevliet, A. Olivier, W.G.J. de Lange, P.C.J. Kamer, H. Kooijman, A.L. Spek, P.W.N.M. van Leevwan, Chem. Commun. (1996) 583. (c) S.G. Bott, A.W. Coleman, J.L. Atwood, Chem. Commun. (1986) 610. (d) G.E. Hofmeister, F.E. Halm, S.F. Pedersen, J.Am.Chem.Soc. 111 (1989) 2318. (e) G.E. Hofmeister, E. Alvarado, J.A. Leary, D.I. Yoon, S.F. Pedersen, J.Am.Chem.Soc. 112 (1990) 8843. (f) V.C. Gibson, C. Redshaw, W. Clegg, M.R,J. Elsegood, Chem. Commun. (1995) 2371. (g) F.J. Parlevliet, M.A. Zuideveld, C. Kiener, H. Kooijman, A.L. Spek, P.C.J. Kamer, P.W.N.M. van Leevwan, Organometallics 18 (1999) 3394. (h) C. Redshaw, M.R.J. Elsegood, Inorg. Chem. 39 (2000) 5164.
[4] V.C. Gibson, C. Redshaw, W. Clegg, M.R.J. Elsegood, U. Siemeling, T. Türk, J. Chem. Soc. Dalton Trans. (1996) 4513.
[5] G. Rouschias, G. Wilkinson, J. Chem. Soc. (A) (1968) 489.
[6] W. Clegg, M.R.J. Elsegood, S.J. Teat, C. Redshaw, V.C. Gibson, J. Chem. Soc. Dalton Trans. (1998) 3037.

PERGAMON

www.elsevier.nl/locate/poly

Polyhedron 19 (2000) 2661–2666

POLYHEDRON

Synthesis and characterisation of nickel(II) complexes with tripodal ligand tris[4-(3-(5-methylpyrazolyl)-3-aza-3-butenyl] amine (MPz_3tren): X-ray crystal structure of $[Ni(MPz_3tren)](BF_4)_2\cdot 0.5H_2O$

Sachindranath Paul [a], Anil Kumar Barik [b], Ray J. Butcher [c], Susanta Kumar Kar [a,*]

[a] *Department of Chemistry, University College of Science, 92 A.P.C. Road, Calcutta 700 009, India*
[b] *Department of Chemistry, St. Paul's C.M. College, 33/1 Raja Rammohan Roy Sarani, Calcutta 700 009, India*
[c] *Department of Chemistry, Howard University, 2400 Sixth Street, NW, Washington, DC 20059, USA*

Received 28 June 2000; accepted 30 August 2000

Abstract

Nickel(II) complexes of the tripodal ligand (MPz_3tren) of the general formula $[Ni(MPz_3tren)]X_2\cdot nH_2O$ (X = Cl, Br, NO_3, ClO_4 and BF_4; $n = 0$ for Cl and Br; $n = 0.5$ for NO_3, ClO_4 and BF_4) have been prepared by template methodology and characterised by elemental analyses, magnetic susceptibility and conductivity measurements at RT, IR and electronic spectra. The molar conductivities measured in MeOH for all the complexes show them to be 1:2 electrolytes. The hexadentate character of the ligand in all the complexes is inferred from IR spectral studies. The electronic spectra in solid state and in MeOH solution suggest octahedral geometry for all the complexes. The structure of $[Ni(MPz_3tren)](BF_4)_2\cdot 0.5H_2O$ has been determined by single-crystal X-ray diffraction studies (monoclinic, $c2/c$). Nickel(II) is in a trigonal antiprismatic N_6 donor environment and the crystal structure is stabilised by a network of strong H-bonding. © 2000 Elsevier Science B.V. All rights reserved.

Keywords: Ni(II) complexes; Tripodal ligand; Crystal structures; Spectroscopic studies

1. Introduction

Currently, there is a growing interest in defining the coordination chemistry of tripodal ligands [1–4]. Transition metal complexes with these ligands display special physical, chemical or structural properties, such as unusual conformation, high thermodynamic stability and virtual kinetic inertness. Furthermore, these ligands can serve as precursors to the synthesis of interesting macrobicyclic [5,6] compounds which usually require high-dilution techniques [7] or the use of metal ions as templates [8,9] for their formation. We have synthesised the present hexadentate tripodal ligand with six nitrogen donor sites in situ following a method that does not employ high-dilution conditions. The title tripodal ligand upon formation of the octahedral complexes by wrapping around the metal ion leaves an open face with three groups positioned in such a way that it may be capped by suitable reagents. One of the advantages in this procedure is that the donor atoms as well as the substituents in the tripodal arms may be varied which may result in tuning the shape of the metal-ion containing cavity described by the resulting macrobicyclic ligands. The conformations of the complexes formed by these ligands must be influenced by the balance between a number of factors including (a) the electronic configuration and size of the metal ion, (b) the geometric and electronic properties of the ligand and (c) the repulsions between atoms in different ligand arms.

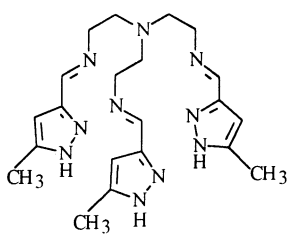


Fig. 1. MPz_3tren.

* Corresponding author. Tel.: +91-33-350-8386; fax: +91-33-351-9755.
E-mail address: skkar@cucc.ernet.in (S. Kumar Kar).

0277-5387/00/$ - see front matter © 2000 Elsevier Science B.V. All rights reserved.
PII: S0277-5387(00)00577-5

Complexes of metal ions with pyrazole-derived ligands are of great importance in part because of their pharmacological interest [10]. The publication of several reviews and books covering various aspects of pyrazole-derived ligands is witness to the great importance attached to them [11–14]. Most of the metal chelates of tripodal ligands have been derived from Tren [tris(2-aminoethyl) amine] and pyridine containing carbonyl compounds. However, no work has been initiated on the metal chelates of similar ligands derived from Tren and 5-methyl-pyrazole-3-carbaldehyde. In the present paper, we report the synthesis and characterisation of a few nickel(II) complexes of tris[4-(3-(5-methylpyrazole)-3-aza-3-butenyl]amine (henceforth abbreviated as MPz_3tren, Fig. 1). The structural aspects of these complexes are confirmed by the X-ray crystallographic studies on a representative complex, $[Ni(MPz_3tren)](BF_4)_2{\cdot}0.5H_2O$.

2. Experimental

All physical measurements and analytical procedures were similar to those described previously [15,16].

2.1. Preparation of the complexes

A template methodology by interaction of the reactants viz., 5-methylpyrazole-3-carbaldehyde and Tren in the presence of nickel(II) salts has yielded the reported metal chelates. A 20 cm^3 methanolic solution of 5-methylpyrazole-3-carbaldehyde (0.003 mol, 0.33 g) was refluxed with a 10 cm^3 methanolic solution of Tren (0.001 mol, 0.146 g) for 2 h. Divalent nickel salt (0.001 mol) dissolved in a minimum quantity of methanol (10 cm^3) was added to the refluxing mixture, discontinuing the reflux further. A few drops of methanolic solution of ammonia were also added to the mixture to adjust the pH to approximately 8. The solution was stirred continuously for 2–3 h at room temperature (r.t.). The mixture was filtered and concentrated to half of its original volume and kept at r.t. for slow evaporation for 3 days. The complexes were filtered, washed with cold methanol and dried over fused $CaCl_2$.

The blue–violet crystals, so isolated for $[Ni(MPz_3tren)](BF_4)_2{\cdot}0.5H_2O$ were found to be suitable for X-ray diffraction studies.

2.2. X-ray crystallography

The crystal, a blue–violet prism of approximate dimensions $0.42 \times 0.60 \times 0.58$ mm was measured on an Enraf-Nonius CAD-4 diffractometer using Mo Kα radiation ($\lambda = 0.71073$ Å) and a graphite monochromator at -80°C. The unit cell dimensions were obtained from a least-squares fit to the setting angles of 25 accurately determined reflections. The data were collected using the ω–2θ scan technique with a 2θ range of 4–55° and were corrected by an empirical method for absorption and Lorentz and polarisation effects. Calculations were carried out using XCAD-49 (data reduction), SHELXTL (absorption corrections, structure solution refinement and molecular graphics). Crystal data and details of data collection are listed in Table 1.

The structure was solved using direct methods and refined on F^2 by full-matrix least-squares techniques with anisotropic displacement factors for all non-hydrogen atoms. The positions of the hydrogen atoms were calculated from the geometry of the molecular skeleton and their thermal displacement parameters were refined isotropically on a groupwise basis. Selected bond lengths and angles for the complex are reported in Table 2.

Table 1
Crystal data and structure refinement for $[Ni(MPz_3tren)](BF_4)_2{\cdot}0.5H_2O$

Empirical formula	$C_{21}H_{31}B_2F_8N_{10}NiO_{0.50}$
Formula weight	663.89
Temperature (K)	293(2)
Wavelength (Å)	0.71073
Crystal system	monoclinic
Space group	$c2/c$
Unit cell dimensions	
a (Å)	13.9604(14)
b (Å)	19.7105(14)
c (Å)	22.564(2)
α (°)	90
β (°)	107.075(7)
γ (°)	90
Volume, z (Å^3)	5935.1(9)
D_{calc} (Mg m^{-3})	1.486
Absorption coefficient (mm^{-1})	0.737
$F(000)$	2728
Crystal size (mm)	$0.42 \times 0.60 \times 0.58$
θ Range for data collection (°)	2.07–27.50
Limiting indices	$0 \le h \le 18$, $0 \le k \le 25$, $-29 \le l \le 28$
Reflections collected	7092
Independent reflections	6820 ($R_{int} = 0.0232$)
Completeness to $\theta = 27.50$°	100.0%
Absorption correction	empirical
Max. and min. transmission	0.4262 and 0.3241
Refinement method	Full-matrix least-squares on F^2
Data/restraints/parameters	6820/19/459
Goodness-of-fit on F^2	1.020
Final R indices [$I > 2\sigma(I)$]	$R_1 = 0.0583$, $wR_2 = 0.1461$
R indices (all data)	$R_1 = 0.0935$, $wR_2 = 0.1655$
Extinction coefficient	0.00043(11)
Largest difference peak and hole (e Å^{-3})	0.523 and -0.444

Table 2
Selected bond distances (Å) and bond angles (°) for $[Ni(MPz_3tren)](BF_4)_2\cdot 0.5H_2O$ [a]

Ni–N(1A)	2.088(3)	Ni–N(3A)	2.122(3)
Ni–N(1B)	2.094(3)	Ni–N(3B)	2.113(3)
Ni–N(1C)	2.081(3)	Ni–N(3C)	2.122(3)
N(1C)–Ni–N(1A)	94.79(11)	N(1C)–Ni–N(1B)	93.02(11)
N(1A)–Ni–N(1B)	94.13(11)	N(1C)–Ni–N(3B)	91.50(11)
N(1A)–Ni–N(3B)	169.81(11)	N(1B)–Ni–N(3B)	77.51(11)
N(1C)–Ni–N(3A)	170.36(12)	N(1A)–Ni–N(3A)	77.62(12)
N(1B)–Ni–N(3A)	93.44(11)	N(3B)–Ni–N(3A)	96.87(12)
N(1C)–Ni–N(3C)	77.54(12)	N(1A)–Ni–N(3C)	91.84(11)
N(1B)–Ni–N(3C)	169.23(11)	N(3B)–Ni–N(3C)	97.35(11)
N(3A)–Ni–N(3C)	96.59(11)	C(7A)–N–C(7B)	118.7(4)
C(7A)–N–C(7C)	117.4(3)	C(7B)–N–C(7C)	117.5(3)

[a] Numbers in parentheses are estimated standard deviations.

3. Results and discussion

3.1. Crystal structure of $[Ni(MPz_3tren)](BF_4)_2\cdot 0.5H_2O$

A perspective view of the complex $[Ni(MPz_3tren)](BF_4)_2\cdot 0.5H_2O$ is shown in Fig. 2. The structure consists of a $[Ni(MPz_3tren)]^{2+}$ cation and a BF_4^- anion. In the crystal structure the potentially heptadentate MPz_3tren ligand coordinates to the metal through the three imine and the three pyrazole nitrogen atoms. Three imine nitrogen atoms are at the vertices of one equilateral triangle and three pyrazole nitrogen atoms are at the vertices of another. Another similar type tripodal ligand tris[4-(2-pyridyl)-3-aza-3-butenyl]amine(Py_3tren) which has also six potential N-donor sites (except the bridgehead one) has been found [17] to bind nickel(II) in a similar fashion. Among the distances from the metal to the seven potentially ligating atoms, the tertiary amine N(7) is longer. Thus, the direct interaction between N(7) (bridgehead) and the metal ion is small compared to the interactions with the other six nitrogen atoms [18].

The coordination polyhedron of the said complex is best described as trigonal antiprism (TAP). Even that is not a perfect description because there is some trigonal distortion (rotation of opposing triangular faces tending towards a trigonal prism) of the complex. The σ-only ligand field splitting pattern for a trigonal antiprism (D_3) consists of three levels a_1 (d_z^2), 1e ($d_{x^2-y^2}$, d_{xy}) and 2e (d_{xz},d_{yz}). The lone pair of the tertiary nitrogen atom (bridgehead, i.e. N7) capping the trigonal antiprismatic face interacts directly with the a_1 orbital. The Ni–N(7) distance (3.275 Å) in the complex is 0.125 Å longer than the sum of the van der Waal's radii ($r_{Ni-VDW} + r_{N-VDW} = 3.15$ Å) and the

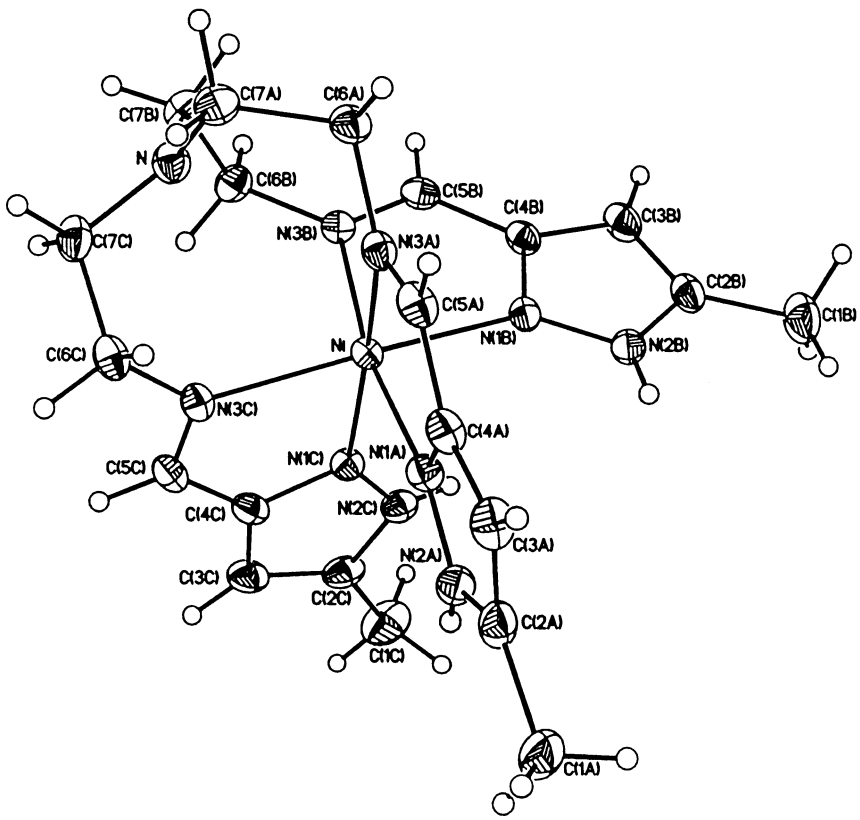


Fig. 2. A perspective view of the $[Ni(MPz_3tren)]^{2+}$ cation.

Table 3
Non-bonding atomic distances (from Fig. 3) in Å

N(2AB)···F(24A)	2.799
N(2BB)···F(21B)	2.729
N(2CB)···F(11A)	2.803
O(1WA)···F(12A)	2.743
Ni–N(bridgehead, OB)	3.27

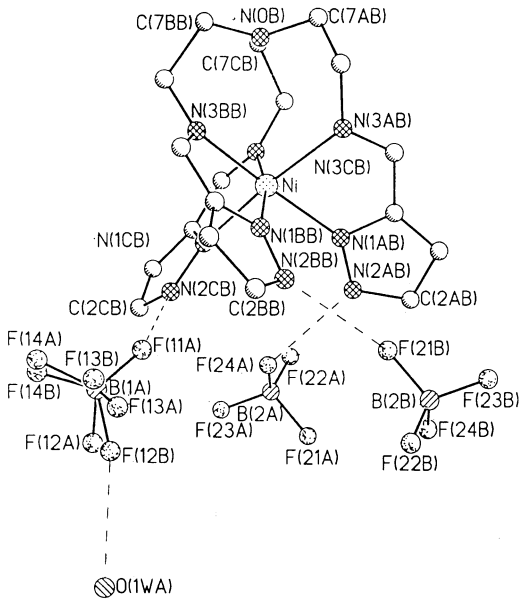


Fig. 3. A portion of the packing diagram of the $[Ni(MPz_3tren)](BF_4)_2 \cdot 0.5H_2O$ showing hydrogen bonding as dotted lines.

bridgehead nitrogen is thus uncoordinated [19]. The above observed distance is almost same as the value obtained for $[Ni(Py_3tren)](BF_4)_2$ and $[Ni(Py_3tren)](PF_6)_2$ [2] which are 3.227(4) and 3.235(4) Å, respectively, where Py_3tren = tris[4-(2-pyridyl)-3-aza-3-butenyl]amine. The remaining six Ni–N bond distances (excluding the bridgehead) are considerably shorter than the sum of the van der Waal's radii. The average value being 2.103(3) Å is, however, comparable to the reported value for the crystal structure of bis[3-hydroxyiminobutanone(4-phenyl thiosemicarbazone] nickel(II) nitrate monohydrate [2.047(6) Å] [20] and that of bis-{*S*-methyl-β-*N*-(6-methylpyrid-2-yl)methylinedithiocarbazato}nickel(II) complex [2.103(6) Å] [21].

It is also noteworthy that the bond angle C–N–C at the N(7) is ~118° which also agrees well with that in $[Ni(Py_3tren)](BF_4)_2/(PF_6)_2$ [2]. The tertiary amine nitrogen atom N(7) corresponds to a three-ribbed umbrella that has been inverted by the winds. As the a_1 and 1e levels are filled, the repulsion increases which is reflected through the increment of Ni–N(7) distance resulting in the flattening of the umbrella.

From the survey of non-bonding distances (Table 3) it is evident that all the pyrazolyl nitrogen atoms N(2AB), N(2BB) and N(2CB) are strongly hydrogen bonded with the fluorine atoms F(24A), F(21B) and F(11A), respectively, of three BF_4^- ions (Fig. 3). Each of two BF_4^- ions bridges two asymmetric units through severe H-bonding interactions involving F(24) and F(21) with pyrazolyl N atom (uncoordinated). Again the third pyrazolyl N-atom (also uncoordinated) of the third arm of the ligand molecule in the complex is also H-bonded with the third BF_4^- ion which is further H-bonded with a water molecule in the crystal lattice. However, the third BF_4^- ion is disordered.

Thus in crystal lattice, the molecules are interconnected to give a three dimensional network through significantly strong H-bonding interactions.

3.2. Vibrational and electronic spectra

The analytical data of the metal complexes are given in Table 4, which show that chelates may be represented by the general formula $[Ni(MPz_3tren)]X_2 \cdot nH_2O$ where X = Cl, Br, NO_3, ClO_4 and BF_4; $n = 0$ for Cl, Br; $n = 0.5$ for NO_3, ClO_4, BF_4. The molar conductance values in methanol show that these complex species are 1:2 electrolytes [22]. The magnetic moments of the complexes lie in the 3.09–3.25 BM range at r.t. and are close to the predicted values for octahedral geometry around the metal atom [23].

The IR spectra of all the complexes, except the chloro and the bromo, exhibit a hump around 3530 cm^{-1} which infer the presence of lattice water in these

Table 4
Analytical data and pertinent physico-chemical properties of the complexes

Complex	Colour	Elemental analyses found(calc.)			μ_{eff} at 298 K (BM)	Conductivity ($\wedge_M$) ($cm^2\ \Omega^{-1}\ mol^{-1}$)
		%C	%H	%N		
$[Ni(MPz_3tren)]Cl_2$	red	45.52(45.67)	5.39(5.43)	25.43(25.37)	3.16	173
$[Ni(MPz_3tren)]Br_2$	red	39.21(39.33)	4.69(4.68)	21.73(21.85)	3.09	167
$[Ni(MPz_3tren)](NO_3)_2 \cdot 0.5H_2O$	blue–violet	41.52(41.06)	4.98(5.05)	22.92(22.81)	3.23	179
$[Ni(MPz_3tren)](ClO_4)_2 \cdot 0.5H_2O$	blue–violet	36.99(36.64)	4.43(4.50)	20.15(20.35)	3.18	189
$[Ni(MPz_3tren)](BF_4)_2 \cdot 0.5H_2O$	blue–violet	38.04(37.74)	4.56(4.64)	21.08(20.96)	3.21	195

complexes [24]. There is no absorption band at approximately 1670 cm^{-1} due to the free aldehyde group [25]. The absence of stretching and bending vibrations of the (C–O) group at approximately 1530 and 1275 cm^{-1} substantiates the absence of this group [25]. The strong bands appearing at approximately 1590 ± 10 cm^{-1} may be assigned to ν(C=N) vibrations and point towards the coordinated azomethine groups [26,27]. The appearance of a strong band at approximately 1050 cm^{-1} in the spectra of the metal chelates indicates the tertiary nitrogens of the Pz rings as the possible binding sites [28]. This is also in conformity with our previous work [15,16] and X-ray crystallographic studies of several pyrazole-metal complexes [29–31]. Therefore, it is clear from the IR spectra that the three NH_2 groups of Tren have condensed with the three aldehyde groups of three 5-methylpyrazole-3-carbaldehyde molecules to give rise to an N_6 arrangement of three azomethine and three pyrazole ring (tertiary) nitrogen atoms equally suitable for coordination.

The diffuse reflectance spectra of the complexes exhibit three main bands in the region at approximately 10 822–11 299 cm^{-1}(ν_1); 17 035–18 083 cm^{-1}(ν_2) and 27 322–27 932 cm^{-1}(ν_3). Octahedral nickel(II) complexes are characterised by three spin-allowed ligand field bands [32] corresponding to transition from the $^3A_{2g}$ ground state to the $^3T_{2g}$, $^3T_{1g}$ and $^3T_{1g}$(P) excited states. Calculation of ligand field parameters [32] for the complexes gives $D_q = 1082–1130$ cm^{-1}, $B = 778–796$ cm^{-1} and $\beta = 0.5$ (in all cases). These data are quite consistent with those of authentic octahedral Ni(II) species as reported by earlier authors [33,34].

The solution electronic spectra of the complexes recorded in methanol are characterised by two bands in the region at approximately 10977–11299 cm^{-1} ($\varepsilon \sim 9.88–25.71$ l mol^{-1} cm^{-1}) and approximately 17 482–19 084 cm^{-1} ($\varepsilon \sim 13.62–29.38$ l mol^{-1} cm^{-1}) assignable to ν_1 and ν_2 bands, respectively. These bands are not significantly different from those in the solid state thereby suggesting no electronic or geometric change upon dissolution of the complexes in the said solvent. The ν_3 band is masked by the high intensity charge transfer band at approximately 40 000 cm^{-1} which is probably a result of an intraligand transition. In addition, the extent of distortion from ideal octahedral geometry is reflected in the intensities and sometimes splitting of these bands. For complexes which are octahedral or slightly distorted from the octahedral, molar absorption coefficients lie below 30 l mol^{-1} cm^{-1}. The intensities of the two ligand-field bands obtained for the complexes are consistent with their near-octahedral structure. Various bands in the spectra do not follow any regular pattern and they seem to be anion independent.

4. Supplementary material

Crystallographic data for the structure reported in this paper have been deposited with the Cambridge Crystallographic Data Centre, CCDC no. 145858. Copies of this information may be obtained free of charge from the Director, CCDC, 12 Union Road, Cambridge, CB2 1EZ, UK (fax: +44-1223-336-033; e-mail: deposit@ccdc.cam.ac.uk or http://www.ccdc.cam.ac.uk).

Acknowledgements

Acknowledgement is made to the University Grants Commission, New Delhi, India for awarding a Research Fellowship to S.P. and also for the financial assistance to S.K.K. The authors also like to thank Dr. K. Pramanik of IACS, Calcutta for his helpful suggestion about the crystal structure description. Finally, the authors wish to thank Professor N. Saha, Vice-Chancellor of Kalyani University, India for his valuable suggestion and help during the entire period of work.

References

[1] C. Orvig, D.J. Berg, S.J. Rettig, J. Am. Chem. Soc. 113 (1991) 2528.
[2] R.M. Kirchner, C. Mealli, M. Bailey, M. Howe, L.P. Torre, L.J. Wilson, L.C. Andrews, N.J. Rose, E.C. Lingafelter, Coord. Chem. Rev. 77 (1987) 89.
[3] K.G. Ragunathan, P.K. Bharadwaj, J. Chem. Soc., Dalton Trans. (1992) 2417.
[4] P. Ghosh, R. Shukla, D.K. Chand, P.K. Bharadwaj, Tetrahedron 51 (1995) 3265.
[5] L.R. Gahan, T.M. Donlevy, T.W. Hambley, Inorg. Chem. 19 (1990) 1451.
[6] A.M. Sargeson, Pure Appl. Chem. 56 (1984) 1603.
[7] K. Ziegler, Methodes der Organischen Chemie, Part 2, vol. 4, Houben-weyl, Georg-Thieme-verlag, Stuttgart, 1955, p. 729.
[8] J. Hunter, J. Nelson, C. Harding, M. McCann, V. McKee, J. Chem. Soc., Chem. Commun. (1990) 1148.
[9] T.M. Garrett, T.J. McMurry, M.W. Hosseini, Z.E. Reyes, F.E. Hahn, K.N. Raymond, J. Am. Chem. Soc. 113 (1991) 2965 and references therein.
[10] H.E. Skipper, R.K. Robins, J.R. Thomson, C.C. Cheng, R.W. Brockman, F.M. Schabel, Jr., Cancer Res. 17 (1957) 579.
[11] S. Trofimenko, Chem. Rev. 72 (1972) 497.
[12] S. Trofimenko, Prog. Inorg. Chem. 34 (1986) 117.
[13] S. Trofimenko, Chem. Rev. 93 (1993) 943.
[14] R.C. Elderfield, Heterocyclic Compounds, John Wiley, New York, 1959, p. 565.
[15] A.K. Barik, P. Bandyopadhyay, S.K. Kar, Polyhedron 18 (1999) 01.
[16] A.K. Barik, S. Paul, S.K. Kar, R.J. Butcher, J.C. Bryan, Polyhedron 18 (1999) 571.
[17] L.J. Wilson, N.J. Rose, J. Am. Chem. Soc. 90 (1968) 6041.
[18] J.E. Huheey, E.A. Keiter, R.L. Keiter, Inorganic Chemistry, Principles of Structure and Reactivity, 4th ed., Harper Collins, New York, 1993.

[19] W. Radeeka-Paryzek, E. Jankowska, E. Luks, Polyhedron 7 (1988) 439 and references therein.
[20] S.K. Chattopadhyay, D. Chattopadhyay, T. Banerjee, R. Kuroda, S. Ghosh, Polyhedron 16 (1997) 1925.
[21] M.A. Ali, S.M.M. Majumder, R.J. Butcher, J.P. Jasinski, J.M. Jasinski, Polyhedron 16 (1997) 2749.
[22] W.J. Gearey, Coord. Chem. Rev. 7 (1971) 81.
[23] F.A. Cotton, G. Wilkinson, C.A. Murillo, M. Bochmann, Advanced Inorganic Chemistry, 6th ed., Wiley, New York, 1999.
[24] X. Shen, D. Wu, X. Huang, Q. Liu, Z. Huang, B. Kang, Polyhedron 16 (1997) 1477.
[25] K. Nakamoto, Infrared and Raman Spectra of Inorganic and Coordination Compounds, 4th ed., Wiley, New York, 1987.
[26] D.P. Singh, N. Shishodia, B.P. Yadav, N.B. Rana, Polyhedron 16 (1997) 2229.
[27] D.X. West, H. Gebremedhin, T.J. Romack, Inorg. Chim. Acta 216 (1994) 229.
[28] A. Mitra, T. Banerjee, P. Roychoudhury, S. Chandhuri, P. Bera, N. Saha, Polyhedron 16 (1997) 3735.
[29] F.A. Chavez, M.M. Olmsted, P.K. Mascharak, Inorg. Chim. Acta. 269 (1998) 269.
[30] C.H. Cheng, J.S. Lain, Y.J. Klu, S.L. Wang, Acta Cryst C46 (1990) 208.
[31] N. Adhikari, S. Chaudhuri, R.J. Butcher, N. Saha, Polyhedron 18 (1999) 1323.
[32] A.B.P. Lever, Inorganic Electronic Spectroscopy, Elsevier, New York, 1984.
[33] M.A. Ali, S.E. Livingstone, D.J. Philips, Inorg. Chim. Acta. 6 (1972) 39.
[34] M. Mohan, A. Agarwal, N.K. Jha, J. Inorg. Biochem. 34 (1988) 41.

PERGAMON

www.elsevier.nl/locate/poly

Polyhedron 19 (2000) 2667–2672

POLYHEDRON

Synthesis and structural characterisation of the oxo-rhenium(V) complexes with spirophosphorane derived bidentate ligand ($P \sim O^-$). Crystal structure of *trans*-$ReOCl_2[OCMe_2CMe_2OP(OCMe_2CMe_2O)](PPh_3)$

Tadeusz Głowiak, Witold K. Rybak *, Anna Skarżyńska

Faculty of Chemistry University of Wrocław, 14 F. Joliot-Curie, 50-383 Wrocław, Poland

Received 4 July 2000; accepted 4 September 2000

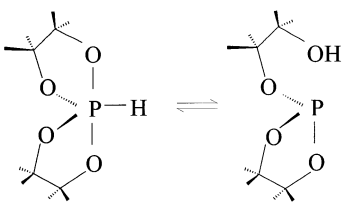
Abstract

The reactions of $ReO(OEt)Cl_2L_2$, L = py, PPh_3 or $ReOCl_3(Me_2S)(OPPh_3)$, with spirohydrophosphorane $HP(OCMe_2CMe_2O)_2$ – abbreviated here as HP ~ O – in toluene yield $ReOCl_2(P \sim O)L$ complexes, L = py (**1**), PPh_3 (**2**) and $OPPh_3$ (**3**), respectively. The encountered bidentate phosphite pinacolato $(OCMe_2CMe_2O)POCMe_2CMe_2O^-$ ligand ($P \sim O^-$) is afforded by means of a spirophosphorane ring-opening reaction. All the pink–violet compounds **1**–**3** were characterised by NMR, IR and UV–Vis spectroscopies. The structure of *trans*-$ReOCl_2(P \sim O)PPh_3$ (**2**) was determined crystallographically. The rhenium atom adopts distorted octahedral geometry with a *trans* multiply bonded terminal oxo ligand ($Re–O_t = 1.698(2)$ Å) *trans* to pinacolate oxygen (Re–O = 1.880(2) Å). Two phosphorus atoms as well as two chlorides are mutually in a *trans* arrangement. © 2000 Elsevier Science B.V. All rights reserved.

Keywords: Spirophosphorane ring-opening; Phosphite diolato(1 −) ligand; Crystal structures

1. Introduction

The chemistry of pentacoordinate phosphorus and, in particular, spirophosphorane compounds has been an area of extensive investigation for some time [1]. However, to our knowledge, there are few reports on their metal coordination ability. Basically there are two known routes to obtain transition metal derivatives of spirophosphorane: replacement of the chloride ion in chlorophosphorane with a metal carbonyl anion [2] and deprotonation of spirohydrophosphorane, both resulting in corresponding metal phosphoranide complexes [3,4]. In most of these cases, spirophosphorane ligands coordinate only via phosphorus atoms forming monodentate metallophosphorane arrangements. On the other hand, cyclic hydrophosphoranes are known to be in equilibrium with ring-opened hydroxyl tautomers tricoordinate towards phosphorus (Eq. (1)) [5].



(1)

Several factors, e.g. temperature, solvent basicity, ring size and the bulkiness of substituents on the ring may affect the distribution of tautomers [6]. This points to another possible way of coordination by hydrophosphorane as a ligand, i.e. through a bidentate ring-opened hydroxyl tautomer.

This paper reports on the synthesis and structural characterisation of oxo-rhenium(V) complexes containing a phosphite pinacolato(1 −) $(OCMe_2CMe_2O)POCMe_2CMe_2O^-$ anionic ligand ($P \sim O^-$) which derives from a corresponding tautomeric form of spirophosphorane HP ~ O (Eq. 1).

* Corresponding author. Tel.: +48-71-3204-335; fax: +48-71-3282-348.

E-mail address: rybak@wchuwr.chem.uni.wroc.pl (W.K. Rybak).

0277-5387/00/$ - see front matter © 2000 Elsevier Science B.V. All rights reserved.
PII: S0277-5387(00)00582-9

2. Experimental

2.1. General procedures

All preparations were performed in an atmosphere of dry, oxygen-free nitrogen using conventional Schlenk techniques. Solvents were carefully dried and deoxygenated by standard methods [7]. $ReOCl_2(OEt)py_2$ [8] was prepared by modified procedure described below. $ReOCl_3(Me_2S)(OPPh_3)$ [9], $ReOCl_2(OEt)(PPh_3)_2$ [10] were obtained according to the literature procedures. Pinacol $HOCMe_2CMe_2OH$, triethylamine NEt_3 and phosphorus trichloride PCl_3 were purified according to the standard procedures [7].

2.2. Instrumentation

The IR and FIR measurements were made in KBr pellets either with Nicolet FTIR Impact 400 or in Nujol with Brucker IFS 113V. ^1H, ^{13}C, ^{31}P NMR spectra were obtained on a Bruker AMX (300 MHz for H NMR). The chemical shifts δ are given in ppm towards the TMS (^1H, ^{13}C) and H_3PO_4 (^{31}P) using deuterated solvents as lock and reference (^1H, ^{13}C), respectively. UV–Vis spectra in CH_2Cl_2 solution were obtained on a HP 8452A. Elemental analyses were performed on a Perkin–Elmer 2400 CHN by the Laboratory of Elemental Analyses in our Department.

2.3. Synthesis of the ligand

The ligand $HP(OCMe_2CMe_2O)_2$, 2,2,3,3,7,7,8,8-octamethyl-1,4,6,9-tetraoxa-5-phospha(5-P^v) spiro[4.4]-nonane (HP ~ O) was readily obtained in a route adopting general procedures described in the literature [11]. To a stirred solution of pinacol $(Me_2COH)_2$ (11.8 g, 0.1 mol) and NEt_3 (20.9 cm^3, 0.15 mol) in diethyl ether (250 cm^3) at 0°C, the solution of PCl_3 (4.4 cm^3, 0.05 mol) in ethyl ether (40 cm^3) was slowly added in a dropwise manner. After that, the mixture was stirred for 10 h at room temperature (r.t.). The solution was filtered and evaporated to dryness. The crude product was extracted with pentane and crystallised twice from pentane in a freezer to give the pure spirophosphorane ligand (5.28 g, 40% yield).

^1H NMR ($C^2H_2Cl_2$, 25°C): δ 1.0 (s, 12, CH_3), 1.1 (s, 12, CH_3), 7.5 (d, 1, $J_{PH} = 810$Hz); $^{31}P\{^1H\}$ NMR ($C_6^2H_6$, 25°C): δ −40.15 (s), ^{31}P NMR −40.15 (d, $J_{PH} = 796$Hz); ^{13}C NMR ($C_6^2H_6$, 25°C) δ 23.65, 23.95, 24.18, 24.33 (CH_3), 78.48s, 78.5s (CCH_3); IR (KBr, cm^{-1}) 1150s, 1218s ν(C–O–P), 2385m ν(P–H).

2.4. Synthesis of the complexes

2.4.1. *cis*-$ReOCl_2(P \sim O)py$ (1)

(a) A suspension of the blue complex $ReOCl_2$-$(EtO)py_2$ (0.87 g, 1.82 mmol) and spirophosphorane ligand HP ~ O (0.96 g, 3.64 mmol) in toluene (30 cm^3) was refluxed for 4 h until the starting rhenium compound reacted and a light-violet crystalline solid was afforded. The product was filtered, washed with Et_2O and dried in vacuo (0.98 g, 88%). Pure **1** was recrystallised from dichloromethane/ethyl ether solution as pink–violet crystals. (b) A suspension of the pink–violet complex $ReOCl_2(P \sim O)OPPh_3$ (**3**) (0.1053 g, 0.129 mmol) and pyridine (0.02 cm^3, 0.258 mmol) in toluene (25 cm^3) was refluxed for 4 h until the started rhenium compound reacted and a light-violet solid was afforded. The product was filtered, washed with toluene and diethyl ether, dried under vacuum (0.061 g, 75.9%). *Anal.* Calc. for $C_{17}H_{29}O_5Cl_2NPRe$ (mol. wt. calc. 615.5): C, 33.17; H, 4.75; Cl, 11.51; N, 2.27; P, 5.03; Found: C, 31.83; H, 4.58; Cl, 12.46; N, 2.29; P, 3.71%; IR (KBr, cm^{-1}) 958vs ν(Re=O), 931s, 1020s ν(C–O–P), 1604 ν(C=N); FIR (nujol, cm^{-1}) 249s, 291s, 303s ν(Re–Cl), ν(Re–N), ν(Re–P).

2.4.2. *trans*-$ReOCl_2(P \sim O)(PPh_3)$ (2)

(a) A mixture of $ReOCl_2(OEt)(PPh_3)_2$ (0.8 g, 0.95 mmol), toluene (40 cm^3) and spirophosphorane ligand HP ~ O (0.50 g, 1.90 mmol) was stirred and boiled for 6 h until the starting compound reacted and deep-orange solution appeared. The solution was concentrated by half to obtain a pink–violet precipitate of **2**.The product was filtered, washed with Et_2O and dried under vacuum (0.6 g, 80% yield). (b) A suspension of the pink–violet complex $ReOCl_2(P \sim O)OPPh_3$ (**3**) (0.10 g, 0.12 mmol) and PPh_3 (0.06 g, 0.24 mmol) in toluene (25 cm^3) was refluxed for 4 h until the starting rhenium compound reacted and an orange solution appeared. The solution was concentrated in vacuo to obtain pink precipitate. The product was filtered, washed with toluene and diethyl ether, dried under vacuum (0.078 g, 80%). *Anal.* Calc. for $C_{30}H_{39}O_5Cl_2P_2Re$ (mol. wt. calc. 798.7): C, 45.11;H, 4.92; Cl, 8.87; P, 7.75; Found: C, 45.40; H, 4.73; Cl, 8.76; P, 7.64%; IR (KBr, cm^{-1}) 955vs ν(Re=O) 940s, 1020s ν(C–O–P); FIR (nujol, cm^{-1}) 228m, 252s, 303s ν(Re–Cl), ν(Re–P).

2.4.3. *trans*-$ReOCl_2(P \sim O)(OPPh_3)$ (3)

A suspension of $ReOCl_3(Me_2S)(OPPh_3)$ (0.5 g, 0.77 mmol) and HP ~ O (0.61 g, 2.31 mmol) in toluene was stirred and boiled until the starting rhenium compound reacted (4 h) and a pink–orange solution appeared. The solution was concentrated by half to obtain a pink–violet precipitate of **3**. The product was filtered, washed with absolute ethyl alcohol, ethyl ether and dried under vaccum (0.29 g, 61% yield). The crude **3** was recrystallised from toluene/dichloromethane solution. *Anal.* Calc. for $C_{30}H_{39}O_6Cl_2P_2Re$ (mol. wt. calc.

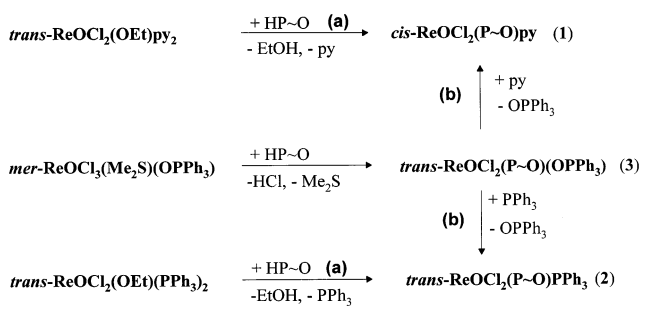
814.7): C, 44.23; H, 4.83; Cl, 8.70; P, 7.60; Found: C, 44.7; H, 4.71; Cl, 8.41; P, 8.05%; IR (KBr, cm^{-1}) 956vs ν(Re=O), 993s, 1025s ν(C–O–P); FIR (nujol, cm^{-1}) 249s, 254s, 303s ν(Re–Cl), ν(Re–P).

2.4.4. *trans-ReOCl$_2$(OEt)py$_2$ [8]*

A suspension of $ReOCl_3(Me_2S)(OPPh_3)$ (2 g, 3.08 mmol) and pyridine (0.75 cm^3, 9 mmol) in freshly distilled dry ethanol (100 cm^3) was stirred and boiled until the starting rhenium compound reacted and the dark-blue colour of solution appeared (2 h). The solution was cooled in an ice bath to obtain blue crystals. The product was filtered and washed with ethyl alcohol and diethyl ether. Yield 1.18 g (81%).

Table 1
Crystallographic experimental data of complex $ReOCl_2(P\sim O)PPh_3$ (**2**)

Empirical formula	$C_{30}H_{39}Cl_2O_5P_2Re$
Formula weight	798.65
Temperature (K)	100(1)
Wavelength (Å)	0.71073
Crystal system	monoclinic
Space group	$C2/c$
Unit cell dimensions	
a (Å)	18.066(4)
b (Å)	13.615(3)
c (Å)	26.210(5)
β (°)	102.20(3)
Volume (Å^3)	6301(2)
Z	8
D_{calc} (Mg m^{-3})	1.684
Crystal size (mm)	$0.10\times0.15\times0.15$
Absorption coefficient (mm^{-1})	4.165
$F(000)$	3184
θ Range for data collection (°)	$3.48\leq27.00$
Index ranges h, k, l	$-23\rightarrow23$, $-17\rightarrow15$, $-33\rightarrow32$
Reflections collected / unique	20334/6851
GOF	1.054
Final R and wR_2 indices	$R_1=0.0239$, $wR_2=0.0507$
Largest difference peak and hole (e Å^{-3})	1.304 and −1.028



Scheme 1.

2.5. Crystallography

Pink-violet prisms of the *trans*-$ReOCl_2(P\sim O)PPh_3$ complex (**2**) suitable for X-ray structural analysis were obtained by slow diffusion of Et_2O vapour into CH_2Cl_2 solution. Table 1 summarises the data relevant to structure analyses. All measurements of the crystal were performed on a Kuma KM4CCD κ-axis diffractometer, with graphite-monochromated Mo Kα radiation. The crystal was positioned at 65 mm from the KM4CCD camera. A total of 612 frames were measured at 0.75° intervals with a counting time of 30 s. The data were corrected for Lorentz and polarisation effects. No absorption correction was applied. Data reduction and analysis were carried out using the Kuma Diffraction (Wrocław) programs. The structure was solved by means of heavy atom methods using SHELXS-97 and refined by the full-matrix least-squares method on all F^2 using SHELXL-97 procedures [12]. Non-hydrogen atoms were refined with anisotropic thermal parameters. Hydrogen atoms were included from the $\Delta\rho$ maps and refined with isotropic thermal parameters. Atomic positional and thermal parameters, as well as lists of bond lengths and angles were deposited as supplementary material.

3. Results and discussion

3.1. Synthesis and characterisation of the $ReOCl_2(P\sim O)L$ complexes

Neutral oxo-rhenium(V) complexes containing a bidentate phosphite pinacolato ligand $P\sim O^-$, which derives from a tautomer of the corresponding hydrophosphorane $HP\sim O$ (Eq. 1), can be obtained via routes outlined in Scheme 1. All three direct syntheses of the $ReOCl_2(P\sim O)L$ complexes (L = py (**1**), PPh_3 (**2**), $OPPh_3$ (**3**)) were carried out in boiling toluene solutions, both to move the tautomeric equilibrium into a phosphite form and to facilitate the separation of sparingly soluble **1**–**3** from reaction mixtures. Apart from the reaction employing $ReOCl_3(Me_2S)(OPPh_3)$ as the substrate, rhenium alkoxide compounds seem to be the precursors of choice in preparation of these complexes. A twofold molar excess of a moisture sensitive $HP\sim O$ ligand in reactions with $ReOCl_2(OEt)py_2$ or $ReOCl_2(OEt)(PPh_3)_2$ is sufficient to afford complexes **1** and **2** in yields of approximately 85% (route (a)). In the case of parent $ReOCl_3(Me_2S)(OPPh_3)$, a larger excess of $HP\sim O$ is required, possibly to trap liberating HCl. Complexes **1** and **2** can also be obtained in a simple ligand substitution reaction (route (b)) starting with the most labile complex **3**. Complexes **1**, **2** and **3** are obtained as pink–violet solids stable in air and moderately soluble in CH_2Cl_2, except for the more soluble **3**,

Table 2
^{1}H NMR, ^{31}P NMR, UV–Vis spectroscopic data of **1**–**3** in dichloromethane solution at room temperature

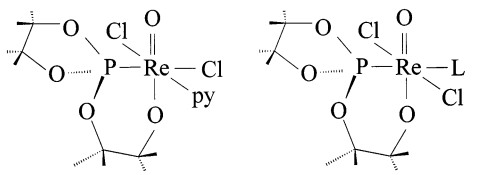
Complex	^{1}H NMR δ (ppm) (int., mult., J/Hz)		^{31}P{^{1}H} NMR δ (ppm) (mult., J (Hz))	UV–vis (λ_{max} (nm)) (ε (M^{-1} cm^{-1}))
	methyl	aryl		
cis-$ReOCl_2(P\sim O)py$ (**1**)	0.87, 1.01, 1.15, 1.31, 1.40, 1.46, 1.52, 1.54 (24H, s′s)	7.67 (2H, t, 7), 7.97 (1H, t, 8), 8.84 (2H, d, 5)	91.03(s)	314 (3570), 500 (120), 620 (14)
trans-$ReOCl_2(P\sim O)(PPh_3)$ (**2**)	0.73, 1.39, 1.42, 1.56, (8H, s′s)	7.45, 7.73 (5H, m′s)	2.44 (d, 585), 85.6 (d, 585)	318 (1320), 458 (153), 652 (24)
trans-$ReOCl_2(P\sim O)(OPPh_3)$ (**3**)	0.95, 1.35, 1.44, 1.55, (8H, s′s)	7.53, 7.91 (5H, m′s)	44.25 (d, 44), 93.30 (d, 44)	266 sh, 532 (66), 668 (23)

which is also soluble in CH_3CN and slightly soluble in $C_6H_5CH_3$.

The hybrid phosphite pinacolato ligand $P\sim O^-$ containing both 'soft' phosphorus and 'hard' alkoxide oxygen donor atoms stabilise the rhenium centre in the intermediate oxidation state (5+) [13]. While the reduction of $ReOCl_3L_2$ (L = py, PR_3, $P(OR)_3$) complexes using phosphines PR_3 is quite feasible [14], compounds **1**–**3** do not undergo reduction to the corresponding rhenium(III) complexes. Attempted oxidation reaction with H_2O_2 resulted in $P\sim O^-$ ligand decay.

The IR spectra of **1**–**3** show intensive bands characteristic for coordinated ligands. The ν(Re=O) bands at about 950 cm^{-1} were discerned by means of subtraction of the free $HP\sim O$ spectrum, due to partial overlapping $P\sim O^-$ ligand vibrations in the same (1000–900 cm^{-1}) spectral region. These bands are in the usual range of ν(Re=O) stretching vibrations [15] (e.g. *trans*-$ReOCl_2(OEt)L_2$: L = py 962 cm^{-1} [8a], PPh_3 946 cm^{-1} [16], *trans*-$ReOCl_2(OMe)py_2$, 960 cm^{-1} [17]) and suggest *trans* coordination mode O=Re–O– of oxygen donor atoms in complexes **1**–**3**. The ν(Re–Cl) bands for complexes **1**–**3** in FIR spectra were not confidently identified because in the same spectral region (350–250 cm^{-1}) ν(Re–N) and ν(Re=P) vibrations also occur [18].

NMR spectra, which are more informative, are summarised in Table 2. The ^{1}H NMR spectrum of **1** at r.t. shows eight singlets of equal intensity in the aliphatic range (0.8–1.6 ppm) indicating the non-equivalence of all the eight methyl groups in $P\sim O^-$ ligand. The spectrum in the aromatic region, consisting of two triplets and one doublet, is typical of coordinated pyridine. Apart from the broadening and a small upfield shift of signals at low temperature (220 K), the pattern of resonances is preserved. NMR data indicate C_1 symmetry of metal-ligand arrangements and suggest *cis* geometry of chloride ions for complex **1** (Chart 1). Unlike complex **1**, complexes **2** and **3** have disparate patterns of NMR spectra. Their ^{1}H NMR spectra at r.t. exhibit only four singlets (Table 2) due to the eight methyl groups of the $P\sim O^-$ ligand. It might suggest C_S symmetry around the metal centre for complexes **2** and **3** and *trans* geometry of chloride ions (Chart 1). However, complexes **2** and **3** exhibit variable temperature ^{1}H NMR spectra. At low temperature (203 K), the spectrum of **3** consists of eight singlets related to the eight methyl groups. As the temperature is raised, these signals broaden and coalesce ultimately to give four single sharp resonances noticed at r.t. Thus, these results demonstrate the fluxional behaviour of the ligand $P\sim O^-$, presumably consisting of two concomitant conformation changes, that of the chelating metallacycle –ReOCCOP– and that of the phosphorus cycle –POCCO–. Furthermore, while the ^{31}P{^{1}H} NMR spectrum of **1** shows a singlet, the spectra of **2** and **3** are connected with the AX system and comprised of two doublets with $^2J_{PP}$ 585 Hz and $^3J_{PP}$ 44 Hz, respectively. These data indicate a vertical coupling of the two phosphorus atoms [13a,19] and ultimately corroborate the anticipated C_S symmetry of **2** and **3**.



cis -**1** [OC-6-52] *trans* - **2,3** (L=PPh_3, $OPPh_3$) [OC-6-13]

Chart 1.

Other characteristic features of the complexes **1**–**3** are their pink–violet colour and their UV–Vis spectra. Electronic absorption spectra are summarised in Table 2. The large extinction values ε at about 300 nm imply CT bands. On the other hand, low values of ε for two visible absorption bands (at about 500 and 650 nm) are consistent with ligand field electronic transitions nd-σ*d and nd-π*d usually observed for metal complexes with the $4-5d^2$ electronic configuration [15,20]. Similar absorption bands are also shown by other complexes with a meridional arrangement of O_{oxo}, $P\sim O$ donor atoms, e.g. 662 nm (ε 23), 526 (56) for *trans*-

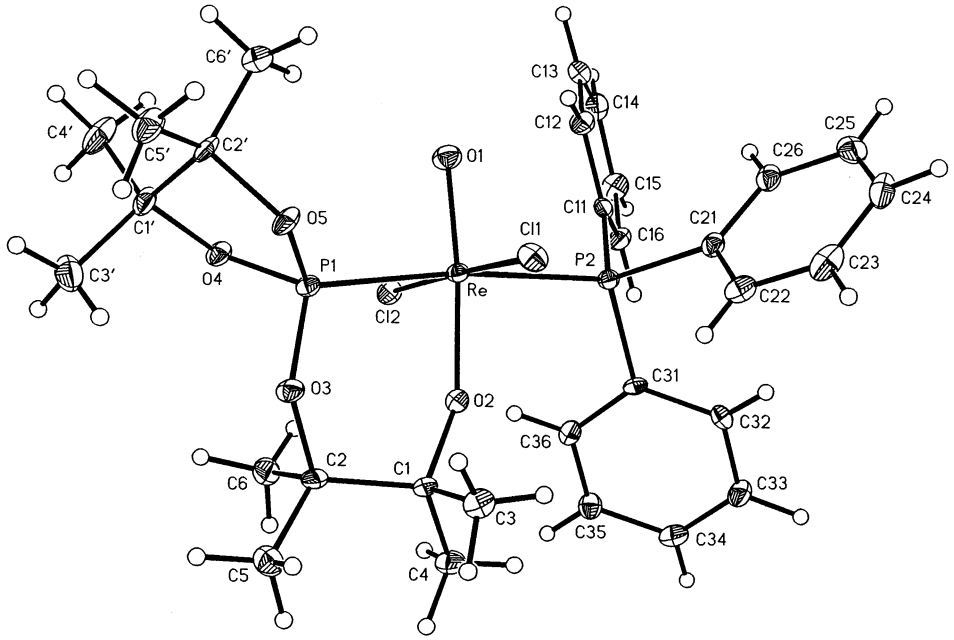


Fig. 1. Crystallographic structure of *trans*-$ReOCl_2(P \sim O)(PPh_3)$ (**2**).

$ReOCl_2(OEt)(PPh_3)_2$, and 830 (15), 610 (80) for *cis*-$ReOCl(OC_6H_4PPh_2)_2$, as reported elsewhere [21]. In order to determine the molecular structure of **2**, we undertook single crystal X-ray analysis.

3.2. Crystal structure of *trans*-$ReOCl_2(P \sim O)(PPh_3)$ (**2**)

The molecular structure of **2** is shown in Fig. 1 and salient bond lengths and angles are summarised in Table 3. Complex **2** has a six-coordinate distorted octahedral geometry with three sets of donor atoms: chlorides, both phosphorus and two oxygens in *trans* arrangements, respectively. Thus, the local coordination symmetry at rhenium is near C_S. The rhenium atom lies out of P(1)Cl(1)P(2)Cl(2) equatorial mean plane by 0.1 Å toward the terminal oxo ligand. The rhenium oxo ligand distance Re–O(1) of 1.698(2) Å is short and fits well into the usual range of multiply bonded mono-oxo groups (1.69 Å mean value) [15]. Also the Re–O(2) (pinacolate) bond length of 1.880(2) Å is shortened in a way characteristic of the *trans* O=Re–O(alcoholate) arrangement, in which total bond order in O=Re–O is close to four [22]. Similarly, both *trans* Re–Cl(1) and Re–Cl(2) distances 2.403(1) and 2.405(1) Å, respectively are in the normal range (2.35–2.45 Å) for complexes of this type [22b,23]. However, the Re–P bond lengths show some disparities. Whereas the Re–P(2) (phosphine) bond length at 2.532(1) Å appears to be within the wide range (2.42–2.57Å) reported for analogous PR_3 derivatives [19,22–24], the Re–P(1) (phosphite) distance of 2.388(1) Å in **2** is rather short. This shortening can be explained by the strong π-acceptor character of the phosphite moiety [25] and is consistent with the Re–P distances reported for other phosphite derivatives [26]. The distortions from an ideal rhenium-centred octahedron are also manifested in related angle distributions. The bite angle P(1)–Re–O(2) is acute (81.80(6)°), while the *trans*-related angle P(2)–Re–O(1) is obtuse (95.57(7)°). The angles O(1)–Re–O(2) 173.17(9)°, P(1)–Re–P(2) 172.98(3)° and Cl(1)–Re–Cl(2) 177.40(2)° accomplish non-linear axes in an approximate octahedron. Both phosphorus-pertinent cycles are puckered. The six-membered metal-containing cycle is fixed to the δ-skew half chair conformation with the torsion angle O(2)–Re–P(1)–O(3) = 10.4°, whilst the five-membered phosphorus cy-

Table 3
Selected bond lengths (Å), bond angles (°) and torsion angles (°) for $ReOCl_2(P \sim O)PPh_3$ (**2**)

Re–O(1)	1.698(5)	Re–P(2)	2.5318(9)
Re–O(2)	1.880(2)	Re–Cl(1)	2.4035(8)
Re–P(1)	2.3881(9)	Re–Cl(2)	2.4057(8)
O(1)–Re–O(2)	173.17(9)	Cl(1)–Re–Cl(2)	177.40(2)
O1–Re–P(1)	91.41(7)	O(1)–Re–P(2)	95.57(7)
O(2)–Re–P(1)	81.80(6)	O(2)–Re–P(2)	91.22(6)
O1–Re–Cl(1)	90.51(8)	P(1)–Re–P(2)	172.98(3)
O(2)–Re–Cl(1)	88.30(7)	Cl(1)–Re–P(2)	93.13(3)
P(1)–Re–Cl(1)	85.98(3)	Cl(2)–Re–P(2)	87.76(3)
O(1)–Re–Cl(2)	91.83(8)	O(3)–P(1)–O(4)	110.26(11)
O(2)–Re–Cl(2)	89.25(7)	O(3)–P(1)–Re	111.67(8)
P(1)–Re–Cl(2)	92.84(3)	O(4)–P(1)–Re	117.22(8)
O(2)–Re–P(1)–O(3)	10.44(10)	Re–O(2)–C(1)–C(2)	43.7(4)
P(1)–Re–O(2)–C(1)	−20.0(4)	P(1)–O(3)–C(2)–C(1)	68.8(3)
Re–P(1)–O(3)–C(2)	−43.7(2)	O(2)–C(1)–C(2)–O(3)	−53.9(3)

cle adopts λ-skew envelope conformation with the torsion angle O(4)–P(1)–O(5)–C(2′) = −10.7. To summarise, except for the large disparity between the Re–P bond lengths, the molecular structure of **2** does not show extraordinary features.

4. Supplementary material

Crystallographic data for the structure reported in this paper have been deposited with the Cambridge Crystallographic Data Centre, CCDC no. 146153. Copies of this information may be obtained free of charge from the Director, CCDC, 12 Union Road, Cambridge, CB2 1EZ, UK (fax: +44-1223-336-033; e-mail: deposit@ccdc.cam.ac.uk or http://www.ccdc.cam.ac.uk).

References

[1] (a) D.E.C. Corbridge, Phosphorus an Outline of its Chemistry, Biochemistry and Technology, Studies in Inorganic Chemistry 10, 4th ed., Elsevier, 1990. (b) R.R. Holmes, Pentacoordinated Phosphorus-Structure and Spectroscopy, ACS Monographs 175–176, vols. 1–2, American Chemical Society, Washington DC, 1980. (c) J.G. Verkade, L.D. Quin, Phosphorus – ^{31}P NMR Spectroscopy in Stereochemical Analysis, VCH, Deerfield Beach, 1987. (d) D. Hellwinkel, G.M. Kosolapoff, L. Maier, Organo Phosphorus Compounds, vol. 3, Wiley-Interscience, New York, 1972.

[2] (a) M. Lattman, B.N. Anand, S.S. Chu, R.D. Rosenstein, Organometallics 3 (1984) 670. (b) M. Lattman, S.A. Morse, A.H. Cowely, J.G. Lasch, N.C. Norman, Inorg. Chem. 24 (1985) 1364. (c) B.N. Anand, R. Bains, K. Aggarwald, K. Usha, Ind. J. Chem. 34A (1995) 27.

[3] R. Faw, C.D. Montgomery, S.J. Rettig, B. Shurmer, Inorg. Chem. 37 (1998) 4136.

[4] (a) D.V. Khasnis, M. Lattman, U. Siriwardane, Inorg. Chem. 28 (1989) 681. (b) M. Lattman, E.G. Burns, S.K. Chopra, A.H. Cowley, A.M. Arif, Inorg. Chem. 26 (1987) 1926.

[5] (a) R.R. Holmes, J. Am. Chem. Soc. 26 (1974) 4143. (b) R. Burgada, Bull. Soc. Chim. (1975) 407. (c) A. Munoz, Bull.Soc.Chim. (1977) 728. (d) R. Burgada, R. Setton, in: F.R. Hartley (Ed.), The Chemistry of Organophosphorus Compounds, vol. 3, Wiley-Interscience, New York, 1993, p. 185. (e) S. Kojima, M. Nakamoto, K. Kajiyama, K. Akiba, Tetrahedron Lett. 36 (1995) 2261.

[6] D. Bernard, C. Laurenco, R. Burgada, J. Organomet. Chem. 47 (1973) 113.

[7] D.D. Perrin, W.L.F. Armarego, Purification of Laboratory Chemicals, 3rd ed., Pergamon Press, Oxford, 1988.

[8] (a) N.P. Johnson, F.J.M. Taha, G.W. Wilkinson, J. Chem. Soc. (1964) 2614. (b) M. Freni, D. Giusto, P. Romiti, G. Minghetti, Gazz. Chim. Ital. 99 (1969) 286. (c) A. Guest, C.J.L. Lock, Can. J. Chem. 49 (1971) 603.

[9] (a) J.C. Bryan, R.E. Stenkamp, T.H. Tulip, J.M. Mayer, Inorg. Chem. 26 (1987) 2283. (b) D.E. Grove, G. Wilkinson, J. Chem. Soc. (A) (1966) 1224.

[10] N.P. Johnson, C.J.L. Lock, Inorg. Synth. 9 (1967) 145.

[11] L.W. Nesterov, R.A. Sabirova, N.E. Krepisheva, R.I. Mutalapova, Dokl. Akad. Nauk S.S.S.R. 148 (1963) 1085.

[12] (a) G.M. Sheldrick, SHELXS-97 Programme for the Solution of Crystal Structures, University of Göttingen, Germany, 1997. (b) G.M. Sheldrick, SHELXL-97 Programme for the Refinement of Crystal Structures, University of Göttingen, Germany, 1997.

[13] (a) H. Luo, I. Setyawati, S.J. Rettig, C. Orvig, Inorg. Chem. 34 (1995) 2287. (b) C. Bolzati, F. Tisato, F. Refosco, G. Bandoli, A. Dolmella, Inorg. Chem. 35 (1996) 6221.

[14] (a) J. Chatt, G.A. Rowe, J. Chem. Soc. (1962) 4019. (b) G. Rouschias, Chem. Rev. 74 (1974) 531, (c) K.A. Conner, R.A. Walton, in: G. Wilkinson, R.D. Gillard, J.A. McCleverty (Eds.), Comprehensive Coordination Chemistry, vol. 4, Pergamon Press, Oxford, 1987, p. 125.

[15] W.A Nugent, J.M. Mayer, Metal-Ligand Multiple Bonds, Wiley, New York, 1988.

[16] N.P. Johnson, C.J.L. Lock, G. Wilkinson, J. Chem.Soc. (1964) 1054.

[17] S. Fortin, A.L. Beauchamp, Inorg. Chim. Acta 279 (1998) 159.

[18] (a) K. Nakamoto, Infrared Spectra of Inorganic and Coordination Compounds, 4th ed., Wiley Interscience, New York, 1986. (b) J.E. Fergusson, P.F. Heveldt, J. Inorg. Nucl. Chem. 38 (1976) 2231.

[19] F. Connac, Y. Lucchese, M. Gressier, M. Dartiquenave, A.L. Beauchamp, Inorg.Chim.Acta 304 (2000) 52.

[20] M. Baluka, J. Hanuza, B. Jezowska-Trzebiatowska, Bull. Acad. Pol. Sci., Ser. Chim. 20 (1972) 20.

[21] U. Oetliker, S. Savoie, C. Reber, F. Connac, A.L. Beauchamp, F. Loiseau, M. Dartiguenave, Chem. Commun. (1998) 657.

[22] (a) G.F. Ciani, G. D'Alfonso, P.F. Romiti, A. Sironi, M. Freni, Inorg. Chim. Acta 72 (1983) 29. (b) R. Graziani, U. Castellato, R. Rossi, A. Marchi, J. Crystallogr., Spectrosc. Res., 15 (1985) 573. (c) A.-M. Lebuis, C. Roux, A.L. Beauchamp, Acta Crystallogr., Sect. C 49 (1993) 33.

[23] (a) V.S. Sergienko, M.A. Porai-Koshits, V.E. Mistriukov, K.B. Kotegov, Koord. Khim. 8 (1982) 230. (b) V.S. Siergienko, M.A. Porai-Koshits, Koord. Khim. 8 (1982) 251. (c) A.-M. Lebuis, A.L. Beauchamp, Can. J. Chem. 71 (1993) 441. (d) H. Luo, C. Orvig, S.J. Rettig, Acta Crystallogr., Sect. C, 52 (1996) 1377. (e) A.L. Ondracek, P.E. Fanwick, R.A. Walton, Inorg. Chim. Acta 267 (1998) 123.

[24] (a) K.V. Katti, C.L. Barnes, Inorg. Chem. 31 (1992) 4231. (b) H. Luo, I. Setyawati, S.J. Rettig, Ch. Orvig, Inorg. Chem. 34 (1995) 2287. (c) C. Bolzati, F. Tisato, F. Refosco, G. Bandoli, A. Dolmella, Inorg. Chem. 35 (1996) 6221.

[25] (a) C.A. Tolman, Chem. Rev. 77 (1977) 313. (b) T.B. Brill, S.J. London, Chem. Rev. 84 (1984) 577. (c) M.M. Rachman, H.Y. Lin, A. Prock, W.P. Giering, Organometallics 6 (1987) 650.

[26] (a) M.F.N.N. Carvalho, A.J.L. Pombeiro, U. Schubert, O. Orama, C.J. Pickett, R.L. Richards, J. Chem. Soc., Dalton Trans. (1985) 2079. (b) A.T. Patton, C.E. Strouse, C.B. Knobler, J.A. Gladysz, J. Am. Chem. Soc. 105n (1983) 5804. (c) T. Głowiak, W.K. Rybak, A. Skarżyńska, Polyhedron 17 (1998) 3153.

PERGAMON

www.elsevier.nl/locate/poly

Polyhedron 19 (2000) 2673–2678

POLYHEDRON

Complexes of ytterbium(III) nitrate and triflate with homoazacalix[*n*]arenes ($n = 3, 4$)

Pierre Thuéry [a,*], Martine Nierlich [a], Jacques Vicens [b], Hiroyuki Takemura [c]

[a] *CEA/Saclay, SCM (CNRS URA 331), Bât. 125, 91191 Gif-sur-Yvette, France*
[b] *ECPM, Laboratoire de Chimie des Interactions Moléculaires Spécifiques (CNRS UMR 7512), 25 rue Becquerel, 67087 Strasbourg, France*
[c] *Department of Chemistry, Faculty of Science, Kyushu University, Ropponmatsu 4-2-1, Chuo-ku, Fukuoka 810-8560, Japan*

Received 17 July 2000; accepted 4 September 2000

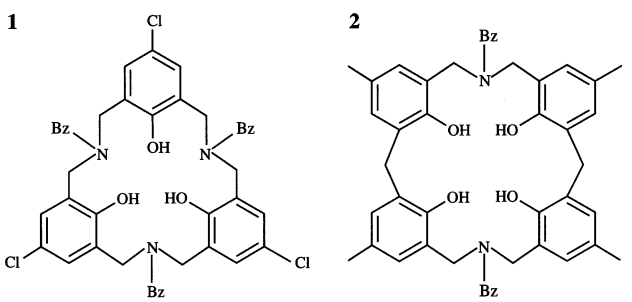
Abstract

The synthesis and crystal structures of three ytterbium(III) complexes of homoazacalixarenes are reported. In all cases, the complexes are obtained without addition of a base, the protons of the complexing phenolic moieties being transferred to the amine groups upon complexation. The 1:1 complex between *p*-chloro-*N*-benzylhexahomotriazacalix[3]arene (**1**) and $Yb(NO_3)_3$ is analogous to the neodymium(III) complex reported previously, with the metal ion bound to three phenoxide groups and three nitrate ions. A second 1:1 complex is obtained with $Yb(NO_3)_3$ and *p*-methyl-*N*-benzyltetrahomodiazacalix[4]arene (**2**), in which the metal ion is bound to two phenoxide groups only. The replacement of nitrate by triflate counter-ions results in the formation of a 1:2 'sandwich' complex with **1**, in which two divergent calixarene molecules are bridged by the metal ion, the counter-ions being non-bonding. © 2000 Elsevier Science B.V. All rights reserved.

Keywords: Ytterbium(III); Lanthanides; Calixarenes; Homoazacalixarenes; Crystal structure

1. Introduction

When dissolved in a basic medium, calixarenes unmodified on the lower rim are poly-aryloxide ligands well suited for complexation of lanthanide and actinide (mainly uranyl) ions [1]. We have recently started an investigation of homoazacalixarenes [2], in which at least one methylene bridge is replaced by a CH_2–N(R)–CH_2 group, as ligands for those ions [3,4]. The first results obtained showed that a specificity of azacalixarenes, by comparison with classical calixarenes and homooxacalixarenes, was to give complexes without addition of a basic agent, the protons of the complexing phenolic groups being transferred to the amine groups, which results in a poly-zwitterionic form of the ligand being the complexing species. Crystal structure determinations evidenced similar features in the complex of neodymium(III) nitrate with *p*-chloro-*N*-benzylhexahomotriazacalix[3]arene (**1**) (Scheme 1) [3] and in those of uranyl nitrate with **1** or *p*-methyl-*N*-benzyltetrahomodiazacalix[4]arene (**2**) [4]. In all cases, the mononuclear complexes formed are neutral and the metal ion, bound to two (UO_2^{2+}) or three (Nd^{3+}) phenoxide groups, remains bound to its nitrate counter-ions. Notwithstanding the usual bonding to phenoxide groups, the location of the metal ion is different from that in comparable phenolic calixarene and homooxacalixarene complexes. The oxacalixarene analogous to **1**, *p-tert*-butylhexahomotrioxacalix[3]arene gives μ-aryl-



Scheme 1. The homoazacalixarenes under study. Bz = benzyl, CH_2–C_6H_5.

* Corresponding author. Tel.: +33-1-6908-6329; fax: +33-1-6908-6640.

E-mail address: thuery@drecam.cea.fr (P. Thuéry).

0277-5387/00/$ - see front matter © 2000 Elsevier Science B.V. All rights reserved.
PII: S0277-5387(00)00583-0

oxo-bridged dimeric complexes with lanthanide(III) ions, in which the metal ions are displaced out of the plane defined by the three oxygen atoms towards the calixarene cavity [5]. In the case of uranyl ion complexes of homooxacalixarenes, the metal ion is located close to the mean plane defined by the bonding oxygen atoms of the calixarene [1b,c,6]. On the other hand, in the case of the homoazacalixarenes **1** and **2**, the positive charges located on the nitrogen atoms, in the calixarene framework, push the cation out of the plane of the bonding atoms, towards the exterior of the macrocycle. It ensues that, in the resulting complexes, the metal ion has a dissymmetrical environment, with about one half of the space occupied by the calixarene donor atoms and the other half by the counter-ions. In order to investigate the possibility of obtaining other coordination modes, we investigated the complexes formed with a lanthanide ion smaller than Nd^{3+} and with different counter-ions. We report herein the synthesis and the crystal structures of three ytterbium(III) complexes with the two azacalixarenes **1** and **2**, with, in the case of **1**, two different counter-ions, i.e. the nitrate ion used in the previous studies and the less-coordinating triflate (trifluoromethanesulfonate, $CF_3SO_3^-$) ion.

2. Experimental

2.1. Synthesis

The ligands *p*-chloro-*N*-benzylhexahomotriazacalix[3]arene (**1**) and *p*-methyl-*N*-benzyltetrahomodiazacalix[4]arene (**2**) were synthesized as reported previously [3,4].

2.1.1. *[Yb(NO$_3$)$_3$(**1**)]·2CH$_3$CN (**3**)*

Compound **1** (0.070 g, 0.08 mmol) was dissolved in 10 ml of CH_3CN–$CHCl_3$ (1:1) and a solution of $Yb(NO_3)_3{\cdot}5H_2O$ (0.070 g, 0.15 mmol) in 10 ml of CH_3CN was added dropwise, giving a pale yellow solution immediately. Single crystals suitable for X-ray crystallography were obtained upon slow evaporation of the solution. FAB-MS: m/z 1075.2 corresponding to $[Yb(NO_3)_2\ (\mathbf{1}) - 2H^+]$; 1012.2 corresponding to the loss of a nitrate ion; 949.2 corresponding to the loss of another nitrate ion; such successive departures of nitrate ions have already been observed in the case of the related neodymium complex [3]. The microanalysis results were unsatisfactory, having been performed on a mixture of crystals and heterogeneous powder.

2.1.2. *[Yb(NO$_3$)$_3$(**2**)][Yb(NO$_3$)$_3$(**2**)(CH$_3$CN)]·CH$_3$CN·CHCl$_3$·3H$_2$O (**4**)*

Compound **2** (0.160 g, 0.22 mmol) was dissolved in 10 ml of CH_3CN–$CHCl_3$ (1:1) and a solution of $Yb(NO_3)_3{\cdot}5H_2O$ (0.100 g, 0.22 mmol) in 10 ml of CH_3CN was added dropwise, giving a pale yellow solution immediately. Single crystals suitable for X-ray crystallography were obtained by slow evaporation of the solution. Three mass peaks were detected by FAB-MS: m/z 952.1 corresponding to $[Yb(NO_3)\ (\mathbf{2}) - 2H^+]$; 890.1 corresponding to the loss of a nitrate ion and $2H^+$; 719.2 corresponding to the loss of the metal ion and H^+. Anal. Calc. for $[UO_2(NO_3)_2\ (\mathbf{3})]{\cdot}CHCl_3{\cdot}H_2O$, $UC_{46}H_{45}Cl_6N_5O_{12}$: C, 50.31; H, 4.52. Found: C, 50.27; H, 4.55%.

2.1.3. *[Yb(**1**)$_2$](CF$_3$SO$_3$)$_3$·3CH$_3$CN (**5**)*

Compound **1** (0.050 g, 0.06 mmol) was dissolved in 15 ml of CH_3CN–$CHCl_3$ (1:1) and a solution of $Yb(CF_3SO_3)_3$ (0.020 g, 0.03 mmol) in 10 ml of CH_3CN was added dropwise, giving a pale yellow solution immediately. Single crystals suitable for X-ray crystallography were obtained by slow evaporation of the solution. ^{1}H NMR (200 MHz, 1:1 mixture of $CDCl_3$–CD_3CN) in ppm referenced to TMS: δ 7.50 (s, 6H, Ar–H); 7.32 (s, 9H, Ar–H); 6.98 (bs, 6H, Ar–H_{calix}); 4.76 (bs, 12H, Ar_{calix}–CH_2–N); 3.75 (bs, 6H, Ar–CH_2–N). FAB-MS: five mass peaks were detected: m/z 2029.1 corresponding to $[Yb(CF_3SO_3)_2\mathbf{1}]$; 1879.1 corresponding to the loss of another triflate ion and the related peak at 940.1 for the doubly charged ion; 1729.1 corresponding to the loss of the last triflate ion and the related peak at 865.1 for the doubly charged ion.

2.2. Crystallography

The data were collected on a Nonius Kappa-CCD area detector diffractometer [7] using graphite-monochromated Mo Kα radiation (0.71073 Å). The crystals were introduced in Lindemann glass capillaries with a protecting 'Paratone' oil (Exxon Chemical Ltd.) coating. The data were processed with DENZO-SMN [8]. The structures were solved by direct methods with SHELXS-97 [9] and subsequent Fourier-difference synthesis and refined by full-matrix least-squares on F^2 with SHELXL-97 [10]. Absorption effects were corrected empirically with the program MULABS from PLATON [11]. Hydroxyl and ammonium protons were introduced as found on the Fourier difference maps whereas all other hydrogen atoms were introduced at calculated positions (except in the disordered parts in **3** and on the chloroform and water molecules in **4**). All hydrogen atoms were treated as riding atoms with a displacement parameter equal to 1.2 (OH, NH, CH, CH_2) or 1.5 (CH_3) times that of the parent atom. All non-hydrogen atoms were refined anisotropically, except the disordered ones in **3** and the oxygen atoms of the water molecules in **4**. Special features are indicated in the following.

2.2.1. Compound 3

One benzyl group and one acetonitrile molecule were found disordered over two sites each. Each of those benzyl positions overlaps one of the positions of the acetonitrile molecule. The occupation factors have been refined so as to take into account the impossibility for two overlapping positions to be simultaneously occupied. The two other acetonitrile molecules have been affected with a 0.5 occupation factor in order to keep reasonable displacement parameters. The disordered benzyl groups have been refined as idealized hexagons and some soft restraints have been applied to the badly resolved acetonitrile molecules.

2.2.2. Compound 5

In order to respect electroneutrality as well as to obtain physically significant displacement parameters, one of the triflate counter-ions was affected with a 0.5 occupation factor. One of the solvent acetonitrile molecules, located close to this triflate anion, was equally affected with a 0.5 occupation factor in order to take into account the impossibility of a simultaneous occupation of both sites.

Crystal data and structure refinement parameters are given in Table 1 and selected bond lengths and angles in Table 2. The molecular plots were drawn with SHELXTL [12]. All calculations were performed on a Silicon Graphics R5000 workstation.

3. Results and discussion

The asymmetric unit in $[Yb(NO_3)_3(\mathbf{1})]\cdot 2CH_3CN$ (**3**) comprises one molecule, without any crystallographic symmetry (Fig. 1), which is similar to the neodymium(III) complex molecule already reported [3]. The three nitrogen atoms are protonated and involved in bifurcated $(N–H)^+\cdots O^-$ hydrogen bonds with the two

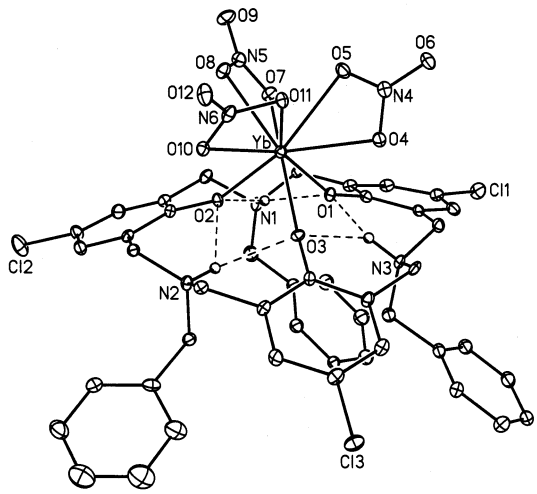


Fig. 1. View of complex **3**. Hydrogen bonds in dashed lines. Ammonium protons represented as small spheres of arbitrary radii. Other hydrogen atoms and solvent molecules omitted for clarity. Only one component of the disordered parts is represented.

Table 1
Crystal data and structure refinement details for **3**–**5**

	3	**4**	**5**
Empirical formula	$C_{49}H_{48}Cl_3N_8O_{12}Yb$	$C_{101}H_{113}Cl_3N_{12}O_{29}Yb_2$	$C_{99}H_{93}Cl_6F_9N_9O_{15}S_3Yb$
Formula weight	1220.34	2411.46	2301.74
Temperature (K)	110(2)	110(2)	110(2)
Crystal system	monoclinic	monoclinic	triclinic
Space group	$P2_1/n$	$C2/c$	$P\bar{1}$
a (Å)	15.806(1)	25.1287(11)	13.0501(10)
b (Å)	14.160(1)	17.7998(8)	14.9337(6)
c (Å)	24.719(2)	47.1010(11)	15.0187(12)
α (°)	90	90	75.412(5)
β (°)	98.923(5)	103.351(2)	71.785(3)
γ (°)	90	90	75.896(4)
V (Å^3)	5465(1)	20498(2)	2647(1)
Z	4	8	1
μ (mm^{-1})	1.923	1.977	1.174
Reflections collected	37 625	56 420	18 167
Independent reflections	8986	14 934	9200
Observed reflections [$I>2\sigma(I)$]	5269	9239	7530
R_{int}	0.103	0.118	0.071
R_1	0.060	0.058	0.056
wR_2	0.134	0.142	0.137

neighboring phenoxide oxygen atoms. The Yb^{3+} cation is displaced by 1.489(4) Å from the mean plane defined by O(1), O(2) and O(3), i.e. somewhat less than Nd^{3+} (1.591(2) Å), in agreement with coordination bond lengths shorter by 0.115 Å. The coordination number is nine (whereas it is six in the Lu^{3+} complex of *p-tert*-butylhexahomotrioxacalix[3]arene), and the geometry of the coordination polyhedron is that of a very distorted tricapped trigonal prism. The values of the dihedral angles between the three phenolic rings and the mean plane defined by the phenolic oxygen atoms are 12.6(5), 21.2(4) and 26.4(4)°, different from those in the neodymium complex and indicating a more symmetrical, pseudo-trigonal, conformation. The cavity is far more shallow than in the uranyl or lanthanide ion complexes of *p-tert*-butylhexahomotrioxacalix[3]arene [5,6b], in which the closer approach of the cation pushes the three bonding oxygen atoms away from each other. The mean plane defined by the three amine nitrogen atoms is close to being parallel to that defined by the three phenoxide oxygen atoms (dihedral angle 2.2(4)°), the distance between the two planes being about 1.04 Å. Apart from the slight modifications reported above, the replacement of Nd^{3+} (ionic radius 0.995 Å) by Yb^{3+} (0.858 Å) has no effect on the overall structure of the complex. In the case of complexes with *p-tert*-butylhexahomotrioxacalix[3]arene, the more notable effect when replacing Lu^{3+} (0.85 Å) by La^{3+} (1.061 Å), apart from slight geometrical modifications of the calixarene conformation, is the involvement of the three ether oxygen atoms in coordination in the second case, whereas only one is coordinated in the first one.

The asymmetric unit in $[Yb(NO_3)_3(\mathbf{2})][Yb(NO_3)_3(\mathbf{2})(CH_3CN)]\cdot CH_3CN\cdot CHCl_3\cdot 3H_2O$ (**4**) comprises two different molecules, noted A and B (Fig. 2), which does not possess any symmetry element. In both of them, the cation is located outside the lower rim array and is bound to two phenoxide oxygen atoms only, in a manner similar to that observed in the uranyl ion complex of **2** [4]. The protons of the two bonding oxygen atoms from the calixarene have been transferred to the two nitrogen atoms, which results in the formation of a cyclic hydrogen bonding array. The conformation of the calixarene, with a pseudo-symmetry plane containing the nitrogen atoms and perpendicular to the mean plane of the molecule, is different from that of its uncomplexed form, which contains bifurcated hydrogen bonds, and close to that in the uranyl ion complex. The main difference between molecules A and B lies with the environment of the Yb^{3+} cation, which is eight-coordinated in A and nine-coordinated in B, the three nitrate ions in the latter molecule being arranged differently to permit the bonding of an acetonitrile molecule. In both cases, the four oxygen atoms are located in a plane (rms deviation 0.04 and 0.02 Å in A and B,

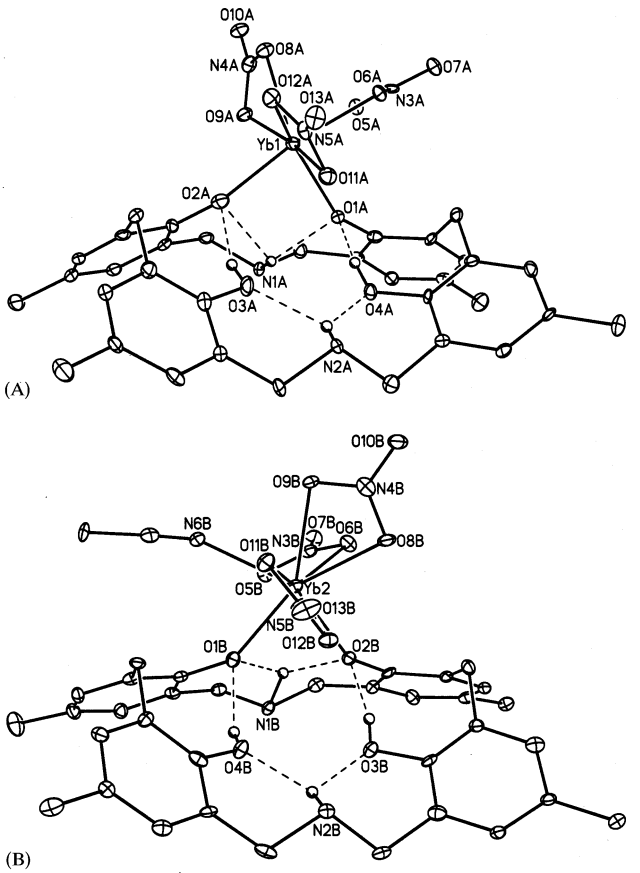


Fig. 2. View of molecules A and B in complex **4**. Hydrogen bonds in dashed lines. Hydroxyl protons represented as small spheres of arbitrary radii. Other hydrogen atoms, benzyl groups and solvent molecules omitted for clarity.

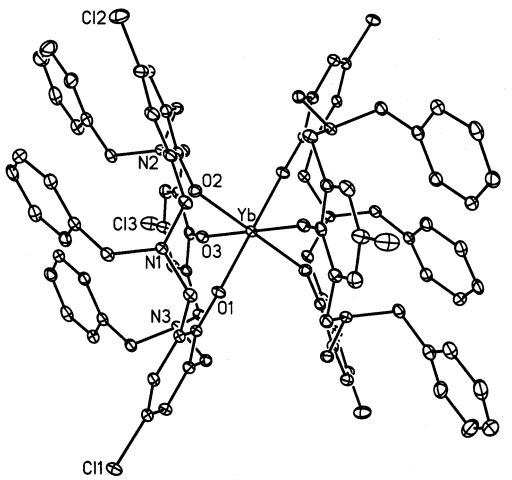


Fig. 3. View of complex **5**. Hydrogen atoms and hydrogen bonds, counter-ions and solvent molecules omitted for clarity.

respectively) with the Yb^{3+} cation located at 1.397(7) and 1.450(6) Å from this plane. The two amine nitrogen atoms are inequivalent with respect to this plane, N(1) being far more distant from it (2.43(1) in A, 2.30(1) Å in B) than N(2) (0.46(1) in A, 0.68(1) Å in B). This is

related to the more 'vertical' position of the phenolic rings adjacent to N(1) (mean dihedral angle with the O_4 mean plane 64(1)°, including both molecules) with respect to those adjacent to N(2) (20(6)°). The same conformation has been observed in the uranyl ion complex.

The complex $[Yb(\mathbf{1})_2](CF_3SO_3)_3\cdot 3CH_3CN$ (**5**) shows the effect of changing the counter-ion on the stoichiometry and geometry of the complex. Whereas the nitrate ions in **3**, **4** and the cases reported previously [3,4] remained coordinated to the metal cation, the less-coordinating triflate ion is not bound to it, which permits the formation of a centrosymmetric 'sandwich' complex by coordination of a second calixarene moiety (Fig. 3). As in complex **3**, the three amine groups are protonated and involved in bifurcated hydrogen bonds with the three phenoxide groups. The Yb^{3+} cation is located at 1.355(2) Å from the mean plane defined by the three oxygen atoms, i.e. nearer to it than in **3**, which is related to lower Yb–O bond lengths in **5** (mean value 2.18(3) Å) than in **3** (2.23(2) Å) as a consequence of a lower coordination number. The six-coordinate metal cation in **5** is in a quite regular octahedral environment (mean angle between adjacent Yb–O bonds 90(5)°). One of the phenolic rings is more tilted than the two other ones and also than those in **3**, the dihedral angles being 42.0(2), 11.89(8) and 15.9(1)°. Such an arrangement comprising two divergent calixarene molecules centered on one metal ion (or an assemblage of metal ions) has already been often encountered with various metal ions and has also been intentionally devised recently [13] in order to obtain koiland-type molecules [14]. The three flexible benzyl arms in **5**, if properly oriented by a guest, could in

Table 2
Selected bond lengths (Å) and angles (°) in compounds **3**–**5**

Ytterbium environment							
3							
Yb–O(1)	2.243(6)	Yb–O(4)	2.459(6)	Yb–O(7)	2.549(7)	Yb–O(10)	2.475(7)
Yb–O(2)	2.211(6)	Yb–O(5)	2.437(7)	Yb–O(8)	2.426(6)	Yb–O(11)	2.431(6)
Yb–O(3)	2.232(6)						
4							
Yb(1)–O(1A)	2.152(6)	Yb(1)–O(5A)	2.436(6)	Yb(1)–O(8A)	2.373(6)	Yb(1)–O(11A)	2.430(7)
Yb(1)–O(2A)	2.173(6)	Yb(1)–O(6A)	2.381(6)	Yb(1)–O(9A)	2.398(7)	Yb(1)–O(12A)	2.340(7)
Yb(2)–O(1B)	2.210(6)	Yb(2)–O(5B)	2.412(6)	Yb(2)–O(8B)	2.428(7)	Yb(2)–O(11B)	2.424(7)
Yb(2)–O(2B)	2.211(6)	Yb(2)–O(6B)	2.486(6)	Yb(2)–O(9B)	2.414(6)	Yb(2)–O(12B)	2.454(6)
Yb(2)–N(6B)	2.492(9)						
5							
Yb–O(1)	2.141(3)	Yb–O(2)	2.187(4)	Yb–O(3)	2.202(3)		
Hydrogen bonds							
3							
N(1)···O(1)	2.808(9)	N(1)–H	0.836	H···O(1)	2.093	N(1)–H···O(1)	143.4
N(1)···O(2)	2.846(10)			H···O(2)	2.206	N(1)–H···O(2)	133.4
N(2)···O(2)	2.792(9)	N(2)–H	0.820	H···O(2)	2.216	N(2)–H···O(2)	127.5
N(2)···O(3)	2.838(10)			H···O(3)	2.155	N(2)–H···O(3)	140.8
N(3)···O(1)	2.718(9)	N(3)–H	0.986	H···O(1)	2.179	N(3)–H···O(1)	112.8
N(3)···O(3)	2.795(9)			H···O(3)	1.924	N(3)–H···O(3)	145.8
4							
N(1A)···O(1A)	2.775(10)	N(1A)–H	0.979	H···O(1A)	2.035	N(1A)–H···O(1A)	130.4
N(1A)···O(2A)	2.984(11)			H···O(2A)	2.321	N(1A)–H···O(2A)	124.6
N(2A)···O(3A)	2.765(10)	N(2A)–H	0.726	H···O(3A)	2.150	N(2A)–H···O(3A)	141.6
N(2A)···O(4A)	2.703(10)			H···O(4A)	2.157	N(2A)–H···O(4A)	132.7
O(3A)···O(2A)	2.735(9)	O(3A)–H	0.906	H···O(2A)	1.869	O(3A)–H···O(2A)	157.8
O(4A)···O(1A)	2.677(9)	O(4A)–H	0.931	H···O(1A)	1.755	O(4A)–H···O(1A)	166.2
N(1B)···O(1B)	2.739(10)	N(1B)–H	1.174	H···O(1B)	1.896	N(1B)–H···O(1B)	124.5
N(1B)···O(2B)	2.706(10)			H···O(2B)	1.804	N(1B)–H···O(2B)	129.5
N(2B)···O(3B)	2.693(10)	N(2B)–H	1.146	H···O(3B)	1.938	N(2B)–H···O(3B)	119.5
N(2B)···O(4B)	2.669(10)			H···O(4B)	1.850	N(2B)–H···O(4B)	125.1
O(3B)···O(2B)	2.662(8)	O(3B)–H	0.727	H···O(2B)	2.006	O(3B)–H···O(2B)	150.2
O(4B)···O(1B)	2.634(9)	O(4B)–H	0.734	H···O(1B)	1.966	O(4B)–H···O(1B)	149.8
5							
N(1)···O(1)	3.015(6)	N(1)–H	1.054	H···O(1)	2.494	N(1)–H···O(1)	109.6
N(1)···O(2)	2.837(6)			H···O(2)	2.075	N(1)–H···O(2)	127.0
N(2)···O(2)	2.778(6)	N(2)–H	0.770	H···O(2)	2.232	N(2)–H···O(2)	128.6
N(2)···O(3)	2.866(6)			H···O(3)	2.180	N(2)–H···O(3)	148.6
N(3)···O(1)	3.156(6)	N(3)–H	0.936	H···O(1)	2.586	N(3)–H···O(1)	119.7
N(3)···O(3)	2.794(6)			H···O(3)	1.980	N(3)–H···O(3)	144.3

principle constitute a second and deeper pseudo-trigonal cavity able to hold the terminal part of a symmetrical guest as a 'connector', leading to a koilate structure.

4. Supplementary data

Crystallographic data for the structural analysis has been deposited with the Cambridge Crystallographic Data Centre, CCDC no. 146346 for compound **3**, CCDC no. 146347 for compound **4** and CCDC no. 146348 for compound **5**. Copies of this information may be obtained free of charge from the Director, CCDC, 12 Union Road, Cambridge, CB2 1EZ, UK (fax: +44-1223-336033; e-mail: deposit@ccdc.cam.ac.uk or www:http://www.ccdc.cam.ac.uk).

References

[1] For reviews, see: (a) J.C. Bünzli, J.M. Harrowfield, in: J. Vicens, V. Böhmer (Eds.), Calixarenes: A Versatile Class of Macrocyclic Compounds Kluwer, Dordrecht 1991, pp. 211–231. (b) J. Harrowfield, Gazz. Chim. Ital. 127 (1997) 663. (c) P. Thuéry, M. Nierlich, J. Harrowfield, M. Ogden, in: Z. Asfari, V. Böhmer, J. Harrowfield, J. Vicens (Eds.), Calix 2001: Recent Developments in Calixarene Chemistry, Kluwer, Dordrecht, in press.

[2] (a) H. Takemura, K. Yoshimura, I.U. Khan, T. Shinmyozu, T. Inazu, Tetrahedron Lett. 33 (1992) 5775. (b) I.U. Khan, H. Takemura, M. Suenaga, T. Shinmyozu, T. Inazu, J. Org. Chem. 58 (1993) 3158. (c) H. Takemura, T. Shinmyozu, H. Miura, I.U. Khan, T. Inazu, J. Inclusion Phenom. 19 (1994) 193. (d) H. Takemura, T. Shinmyozu, T. Inazu, Coord. Chem. Rev. 156 (1996) 183.

[3] P. Thuéry, M. Nierlich, J. Vicens, H. Takemura, J. Chem. Soc. Dalton Trans. (2000) 279.

[4] P. Thuéry, M. Nierlich, J. Vicens, B. Masci, H. Takemura, Eur. J. Inorg. Chem., in press.

[5] C.E. Daitch, P.D. Hampton, E.N. Duesler, T.M. Alam, J. Am. Chem. Soc. 118 (1996) 7769.

[6] (a) J.M. Harrowfield, M.I. Ogden, A.H. White, J. Chem. Soc. Dalton Trans. (1991) 979. (b) P. Thuéry, M. Nierlich, B. Masci, Z. Asfari, J. Vicens, J. Chem. Soc. Dalton Trans. (1999) 3151.

[7] Nonius B.V., Kappa-CCD Software, Delft, The Netherlands, 1998

[8] C.W. Carter, Jr., R.M. Sweet (Eds.), Methods in Enzymology, Macromolecular Crystallography, Part A, vol. 276, Academic Press, New York, 1997, pp. 307–326.

[9] G.M. Sheldrick, Acta Crystallogr. Sect. A 46 (1990) 467.

[10] G.M. Sheldrick, SHELXL-97, Program for the Refinement of Crystal Structures, University of Göttingen, Germany, 1997.

[11] A.L. Spek, PLATON, University of Utrecht, The Netherlands, 1998.

[12] G.M. Sheldrick, SHELXTL, Version 5.1, University of Göttingen, Germany, 1999.

[13] G. Mislin, E. Graf, M.W. Hosseini, A. Bilyk, A.K. Hall, J.M. Harrowfield, B.W. Skelton, A.H. White, Chem. Commun. (1999) 373.

[14] M.W. Hosseini, A. De Cian, Chem. Commun. (1998) 727.

PERGAMON

www.elsevier.nl/locate/poly

Polyhedron 19 (2000) 2679–2687

POLYHEDRON

Intervalence electron transfer through a thiolate bridge ligand: a $Fe^{III}-S-R-Fe^{II}$ mixed valence complex

Carlos Díaz [a,*], Alejandra Arancibia [b]

[a] *Departamento de Química, Facultad de Ciencias, Universidad de Chile, Casilla 653, Santiago, Chile*
[b] *Facultad de Quimica, P. Universidad Catolica de Chile, Casilla 306, Santiago, Chile*

Received 15 May 2000; accepted 5 September 2000

Abstract

The reaction of Cp(dppe)FeI with the ligands 2,2′- and 4,4′-dithiobispyridine ($S_2(Py)_2$) give the mononuclear or binuclear complexes of the type [Cp(dppe)Fe-$S_2(Py)_2$]PF_6, [Cp(dppe)Fe–SPy]PF_6 or [{Cp(dppe)Fe}$_2$-μ-SPy]$(PF_6)_2$ depending on the reaction condition. Reaction of Cp(dppe)FeI with dithiobispyridines in presence of $TlPF_6$ as halide abstractor and using CH_2Cl_2 as a solvent gives the complexes [Cp(dppe)Fe-4,4′-$S_2(Py)_2)_2$]PF_6 (**1**) and [CpFe(dppe)-2,2′-$S_2(Py)_2$]PF_6 (**2**) whereas the same reaction using CH_3OH as a solvent and NH_4PF_6 as the halide abstractor leads to the formation of the Fe^{III}–thiolate complex [Cp(dppe)Fe-2,2′-SPy]PF_6 (**3**) and the mixed-valence complex [Cp(dppe)Fe^{III}-μSPy-Fe^{II}(dppe)Cp]$(PF_6)_2$ (**4**). Magnetic and ESR measurements are in agreement with one unpaired electron delocalized between them. Mössbauer data indicate clearly the presence of two different iron sites, each one of the N-bonded and S-bonded iron atoms, with intermediate oxidation state Fe^{II}–Fe^{III}. An electron transfer intervalence absorption was observed for this complex at 780 nm (in CH_2Cl_2). By applying the Hush theory the intervalence parameters were obtained; $\alpha = 0.028$, $H_{ab} = 361\ cm^{-1}$ which indicate Class II Robin–Day. Estimation of the rate electron transfer affords a value $k_{th} = 6.5 \times 10^6\ s^{-1}$. Solvent effect on the intervalence transition follow the Hush prediction for high dielectric constants solvents which permit the evaluation of the outer and inner-sphere reorganizational parameters, which were analyzed and discussed. The electronic interaction parameters compare well with those found for electron transfer in metalloproteins. © 2000 Elsevier Science B.V. All rights reserved.

Keywords: Thiolate-bridged complexes; Mixed-valence; Electron-transfer; Iron

1. Introduction

A variety of metalloproteins are known to contain sulfur as part of the coordination environments of metal ions [1–9]. Iron, copper and the molybdenum ion are especially common in metalloenzymes containing sulfur ligands. In several of such metalloproteins the metal–thiolate bond is involved in the active site [5–9], specifically iron–thiolate clusters are involved in the electron transfer behavior of ferredoxin and cytochrome P_{450}, [5–8]. Thus, the enzyme sulfite reductase from *Escherichia coli* (EcSiR) which catalyzes the reduction of sulfite to sulfide contains a covalently bridged cluster-siroheme assembly [9]. The bridging ligand is probably a cysteinyl sulfur atom but this can not be proven from the X-ray data. The assimilatory sulfide reductase from *Desulfovibrio vulgaris* (DvSiR) has been proposed to contain a moiety Fe_4S_4–S–Siroheme, however no X-ray structure data is available for such enzymes [9]. Mixed-valence complexes in which two metals enter are connected by a bridging group provide a simple and useful model for comparison with most complex biological systems [10,11]. In the case of iron–thiolate containing metalloproteins, no available iron–thiolate–iron mixed valence models have been reported [12–15].

In previous work [16,17] we have shown that the products of the reaction of organic disulfide with Cp(dppe)FeI depend on the reaction conditions i.e. solvent and halide abstractor used (see Scheme 1).

Now we have investigated the reaction of Cp(dppe)-FeI with 2,2′-dithiobispyridine and with 4,4′thiolate–irondithiobispyridine ligands. Potentially, dithio-

* Corresponding author. Tel.: +56-2-6787-396; fax: +56-2-2713-888.
E-mail address: cdiaz@abello.dic.uchile.cl (C. Díaz).

0277-5387/00/$ - see front matter © 2000 Elsevier Science B.V. All rights reserved.
PII: S0277-5387(00)00587-8

bispyridines can act as a N and S monodentate ligand and as a N and S bridging ligand between two metal centers. Examples of some of these coordination types have appeared recently [18,19].

2. Results and discussion

The reaction of Cp(dppe)FeI with 2,2′-dithiobispyridine and with 4,4′-dithiobispyridine afford different products (see Scheme 2) depending on the solvent and halide abstractor used. Thus, the reaction of CpFe(dppe)I with dithiobispyridines in the presence of $TlPF_6$ and using CH_2Cl_2 as a solvent gives the complexes [Cp(dppe)Fe-2,2′-S_2(py)]PF_6 (**1**) and [Cp(dppe)-Fe-4,4′-S_2(py)]PF_6 (**2**). On the other hand the same reaction with 2,2-dithiopyridine and using methanol as the solvent and NH_4PF_6 as the halide abstractor gives the blue thiolate iron(III) complex [CpFe(dppe)-Spy]PF_6 (**3**).

Thus the reaction of Cp(dppe)FeI with 4,4′-dithiobispyridine, in CH_3OH as the solvent and in presence of NH_4PF_6 affords the unexpected thiolate bridged valence mixed complex [Cp(dppe)Fe^{III}-4-SPy-Fe^{II}(dppe)Cp]$(PF_6)_2$ (**3**).

The formation of the bridging pyridinethiolate ligand arises from the oxidative addition of the organometallic fragment Cp(dppe)Fe^+ by the 4,4′-dithiobispyridine ligand followed by coordination of the pyridine pendant nitrogen by other CpFe(dppe)$^+$ fragment. In this reaction the ligand has the dual role: affording the S–N moiety as well as oxidizing the fragment from [Cp(dppe)Fe^{II}]$^+$ to [Cp(dppe)Fe^{III}]$^{+2}$

$$Py–SS–Py + 2e^- \rightarrow 2S–Py^- \quad (1)$$

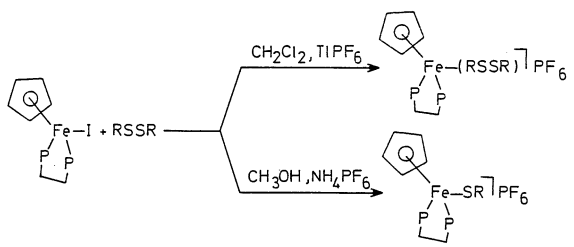
A limited number of complexes of pyridine-4-thiol are known; however, coordination occurs usually at the sulfur atom in the thione form [18–23]. The most usual pyridine-2-thiol can act as an unidentate, bidentate or bridging ligand, the latter being the most common coordination mode.

In complexes **1** and **2,** dithiopyridine acts as a disulfide ligand [24,25]. Their IR spectra exhibit the expected bands of the CpFe(dppe) moiety [26] as well as those of the PySSPy ligand and PF_6 anion [27]. ^{1}H NMR signals of the disulfide ligands are observed normally [28]. Values are given in Section 4. The ^{13}P NMR spectra of the complexes **1** and **2** show the typical singlet signal of dppe in [Cp(dppe)FeL]PF_6 complexes [29,30], and the septet corresponding to the PF_6^- anion. UV–Vis spectra of the complexes exhibit one d–d absorption band around 450 nm typical of [Cp(dppe)FeL]PF_6 complexes where L is neutral donor ligand [29,30]. The formation of the Fe^{II}-dithioeter complex instead of the Fe^{III}-thiolate complex can be explained by the low dielectric medium of the reaction (CH_2Cl_2), as well as by the low acidic environment provided by the iodide abstractor, $TlPF_6$ salt [16,17].

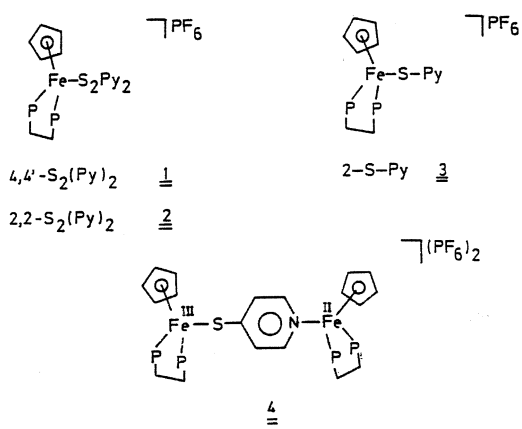
In complex **3**, the formation of a thiolate ligand instead of the disulfide complex can be due to the high dielectric (CH_3OH) and acidic medium (NH_4PF_6). On the other hand the possible formation of the binuclear complex by coordination of the pendant nitrogen pyridine side of the 2,2′-dithiopyridine to an Cp(dppe)Fe^+ fragment (as occurs with the 4,4′-dithiopyridine reaction, see below) is precluded probably due to steric effect of the bulky Cp(dppe)Fe moiety [16,17].

The violet mixed-valence complex [Cp(dppe)Fe^{III}-4-S(Py)-Fe^{II}(dppe)Cp]$(PF_6)_2$ (**4**) was characterized by elemental analysis, IR, ESR, Mössbauer and UV–Vis spectroscopy as well as electrochemical and magnetic methods. An NMR characterization of this complex was precluded due to their paramagnetism. On the other hand, despite many attempts, it was not possible to grow single crystals of this complex, therefore structural determination could not be made. The IR spectrum showed the typical bands for the Cp(dppe)Fe moiety [26] and the expected band at 838 cm^{-1} corresponding to $\nu(PF_6)$. Bands of the thiobispyridine group appear around 1570 cm^{-1}.

At room temperature a value of $\mu_{eff} = 1.4$ BM in solid state (considering the two iron atoms) is in good agreement with the expectation of one unpaired electron by two iron atoms $\mu_{eff} = 1.22$ BM, spin-only value.



Scheme 1.



Scheme 2.

Table 1
EPR, Mössbauer and electrochemical data for complex **4**

Temperature (K)	EPR		Mössbauer [b]			VC [c]		
	Solid	Solution [a]	δ_1	ΔE_a	δ_2	ΔE_b	$E_{1/2}$ [d]	$E_{1/2}$ [e]
300	2.0738	2.0685	0.31	0.92	0.49	0.99	0.26	0.11
77	2.0841	2.1481(g_1) 2.0691(g_2) 1.9316(g_3)						

[a] In dichloromethane.
[b] Iron as reference.
[c] Dichloromethane solution, $[NBu_4]PF_6$ as supporting electrolyte.
[d] Half-wave potential assigned to the iron link to the nitrogen atom.
[e] Half-wave potential assigned to the iron link to the sulfur atom.

The same reduced value with respect to that calculated ($\mu_{teo} = 1.7$ BM) can be due to some antiferromagnetic interaction in solid state. Detailed magnetic temperature studies are in progress.

The ESR spectrum of complex **4** in solid state showed a single broad band with no observable coupling. The g values extracted from spectra are collected in Table 1. The broadening can be attributed to the exchange interaction between two magnetically nonequivalent sites (Fe–S; Fe–N) [31]. A similar single signal was observed in the ESR of the mixed valence complex Cp*Fe(dppe)–CH=CH–CH=CH–Fe(dppe)Cp* [32]. On the other hand, the ESR spectrum in CH_2Cl_2 solution at room temperature also exhibits a single sharp signal at $g = 2.0685$ G (see Fig. 1(a)). At low temperature (77 K) in solid state a single, but broader signal than expected, is observed ($g = 2.0841$ G). In a dichloromethane solution (see Fig. 1(b)) at 77 K, the spectrum shows three separated features corresponding to the three components of the g tensor as expected for d^5 low spin iron(III) complexes in pseudooctahedral geometry [33,34]. Hyperfine coupling with the 2 equiv. ^{31}P nuclei with partial resolution was observed AP(43G) [31]. As recently documented [33], the observation of this behavior may constitute definitive evidence for delocalization of mixed valence complexes in the EPR time scale. Thus this suggests a decrease in electron-delocalization at low temperature.

The ^{57}Fe Mössbauer spectrum of **4** is shown in Fig. 2. The observed parameters are listed in Table 1. It is well known that Mössbauer spectroscopy is very useful to identify the oxidation states of iron in mixed-valence compounds [35–42]. Mononuclear iron(II) complexes of the type (η^5-C_5R_5)Fe(dppe)R exhibits Mössbauer parameters in the range $\delta = 0.13$–0.28; $\Delta E_Q = 1.95$–2.08 while that for similar iron(III) derivatives, parameters are in the range $\delta = 0.25$–0.35 mm s^{-1} and $\Delta E_Q = 0.76$–0.8 mm s^{-1}. Then ΔE_Q is characteristic, of the oxidation state of the iron metal. For binuclear mixed valence iron complexes, the presence of two distinct doublets in the spectrum is diagnostic of a localized valence whereas observation of a single average doublet is diagnostic of detrapped valence. The spectrum of complex **4** showed a two-doublet signal with quadrupole splitting and isomer shift values corresponding to intermediate states Fe^{II}–Fe^{III}. The parameters found for complex **4** are in agreement with some intermediate situation, showing some average valence II–III, which suggests a certain degree of delocalization of the electron. The presence of two similar signals indicate two slight different iron sites which can arise from the asymmetry of the bridging ligand, which induce different iron environments (the asymmetry of

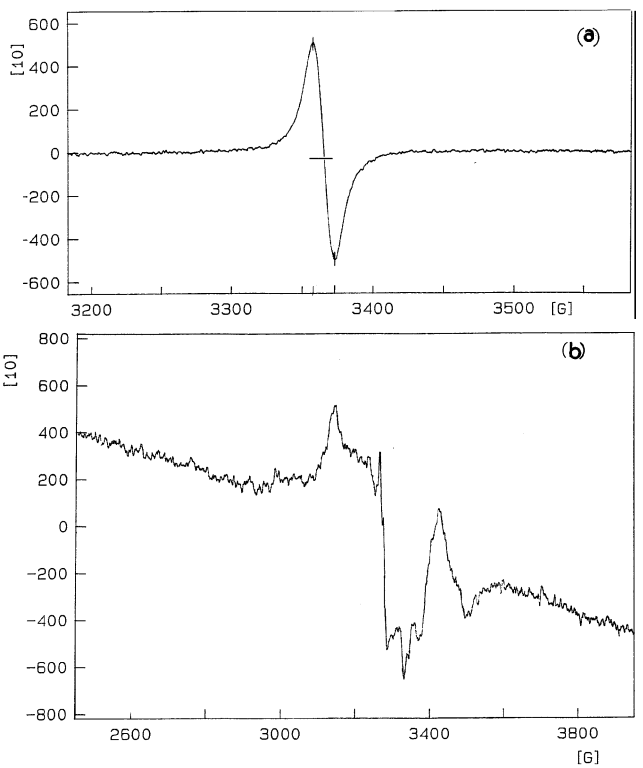


Fig. 1. EPR spectra of complex **4** in dichloromethane solution (a) at room temperature and (b) at 77 K.

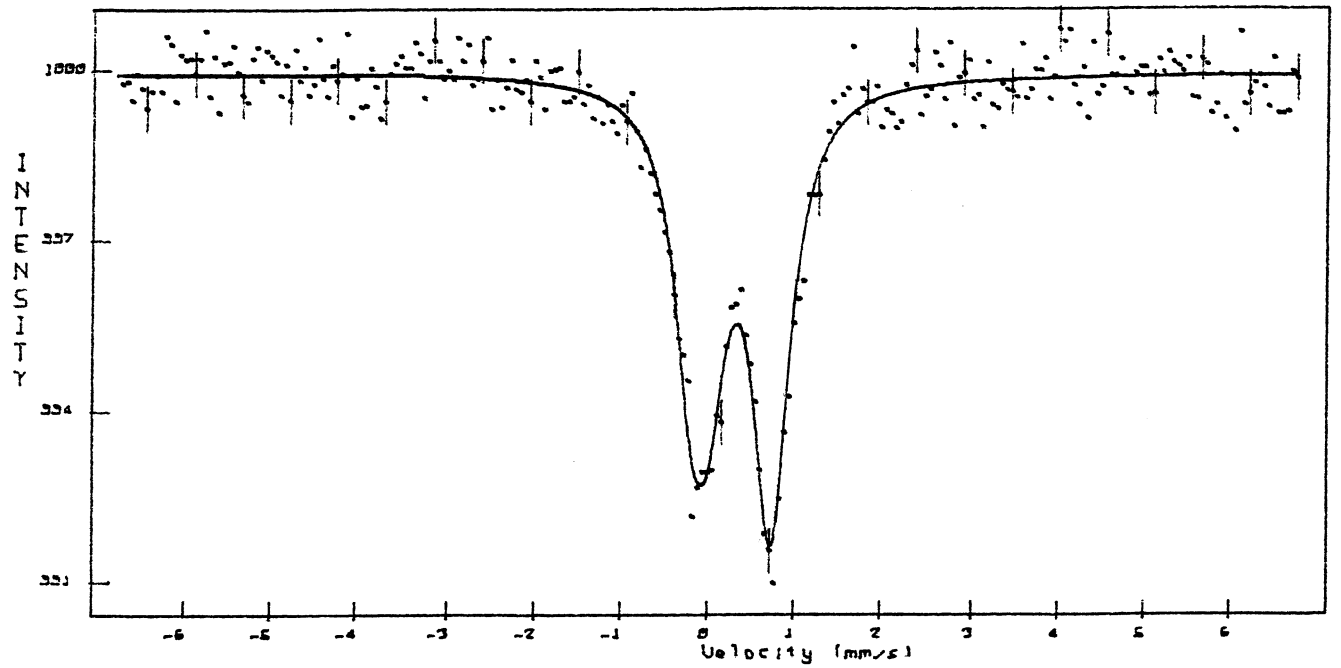


Fig. 2. Mössbauer spectrum of complex **4** at room temperature.

the ligand, see structure in Scheme 2, is also shown by the results of the UV–Vis, which shows the presence of Fe^{III}–S as well as Fe^{III}–N chromophores, see below) Consistent with this, the presence of two Fe^{III} centers having different auxiliary ligands and linked with a symmetrical bridge exhibit two slightly different signals ($\delta = 0.192, \ -0.033$ mm s^{-1}) but almost the same quadrupole values (1.978, 1.958 mm s^{-1}). A localized valence situation may induce the presence of a signal with high quadrupole values (>1.9 mm s^{-1}) corresponding to Fe^{II} as well as a signal at low quadrupole values (<0.9 mm s^{-1}) corresponding to Fe^{III}. For instance the Fe^{II}–Fe^{III} localized mixed valence complex $[Cp^*Fe(CO)_2C{\equiv}CC{\equiv}CCp^*Fe(dppe)]PF_6$ exhibit two doublets slightly separated with ΔE_Q 1,990; 0,865, corresponding to the Fe^{II} and Fe^{III} centers, respectively [39]. If complex **4** holds a localized Fe^{II}–Fe^{III} situation, a signal with a ΔE_Q value near 1.9, as is observed in $[CpFe(dppe)(NCCH_3]PF_6$ (having a Fe–N bond exhibits a quadrupole value of 1.96 mm s^{-1}[42]), might be observed. Hence the highest quadrupole value for complex **4** suggests clearly the presence of a detrapped valence situation. Thus data for complex **4** compares well with data for another delocalized Fe^{II}–Fe^{III} valence mixed complexes: $Cp^*Fe(dppe)$–C≡C–C_6H_4–C≡C–$Fe(dppe)Cp^*)PF_6$ $\Delta E_Q = 1.1$ mm s^{-1} [37], Cp^*-$Fe(dppe)$=C=CH–CH=C=$Fe(dppe)Cp^*)PF_6$ $\Delta E_Q = 1.3$ mm s^{-1} [35], and $(Cp^*Fe(dppe)$–C≡C–C≡C–Fe-$(dppe)Cp^*)PF_6$ $\Delta E_Q = 1.0$ mm s^{-1} [32]. The ΔE_Q value for the complex **4** is also in agreement with the Fe^{II}–Fe^{III} average-mixed-valence complexes, biferricenium$^+$TCA$^-$·2TCAA, $\Delta E_Q = 0.903$, and 1′,6′-diiodobiferrocene, $\Delta E_Q = 1.20$ mm s^{-1} [40]. Most recently [41] the detrapped Fe^{II}–Fe^{III} mixed-valence complexes $[Fe^{II}Fe^{III}(bpmp)(L)][BF_4]_2$ exhibit ΔE_Q values in the range 0.88–1.02 mm s^{-1}, similar to the values found for complex **4**. Mössbauer spectroscopy can also be used to monitor the intramolecular electron transfer rate in mixed valence compounds in solid state. When the intermetallic electron transfer rate is slower than 10^6 s^{-1}, localized valence is observed, whereas observation of a single average-valence quadrupole doublet is diagnostic of an electron transfer faster than 10^9 s^{-1}. Then the electron transfer rate for the complex **4** in solid state could be near 10^9 s^{-1}.

The UV–Vis spectrum of the complex **4** (see Fig. 3) exhibits, in addition (without maxima) to the characteristic absorptions of $[Cp(dppe)Fe^{II}L]^+$ L = neutral donor ligand around 450 nm [29,30], the typical absorption band of the iron(III)–thiolate chromophores around 560 nm [16,17]. This corroborates the presence of Fe^{III}–S as well as the Fe^{II}–N bond in the proposed structure of the mixed-valence complex. For comparison purposes, λ_{max} is 439 nm for the complex $[Cp(dppe)Fe$–$NC_5H_5]PF_6$ [29,30], while λ_{max} for the complex $[Cp(dppe)Fe$–$S_2(Py)_2]PF_6$ is 450 nm. The broad band around 790 nm is not present in the mononuclear precursors $[Cp(dppe)Fe$–$NC_5H_5]PF_6]$, [29] nor $[Cp(dppe)Fe$–$SR]PF_6$ [16,17], then it was assigned to an intervalence transition (IT) $Fe^{II} \rightarrow Fe^{III}$ [43,44]. Consistently with this, upon reduction with Red Al (sodium bis (2-methoxy ethoxy) aluminum) this intervalence band disappears as is shown in Fig. 3.

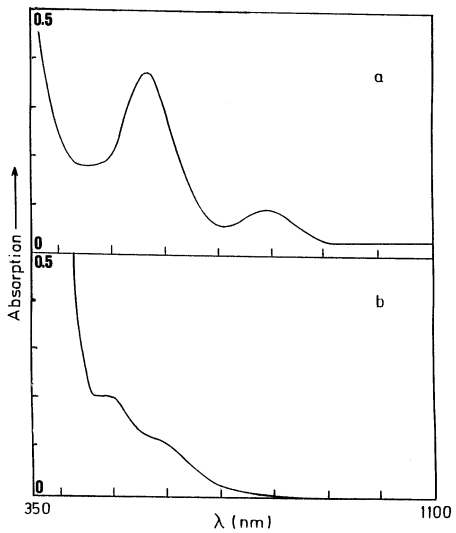


Fig. 3. UV–Vis spectra of (a) the complex [{Cp(dppe)Fe}$_2$-μ-S(Py)](PF$_6$)$_2$ before the reduction; (b) after reduction with Red Al.

Information about the electron transfer interaction between the metallic centers can be obtained by applying the Hush theory [45–47]. According to this model, the degree of electronic delocalization (α) can be calculated from Eq. (2) (Table 2).

$$\alpha^2 = \frac{(4.2 \times 10^{-4})\varepsilon_{max} v_{1/2}}{v_{max} d^2} \quad (2)$$

where v_{max} and $v_{1/2}$ are given in cm^{-1} and the intermetallic distance in Å. Since the d value for complex **4** is unknown, we have used an average value (7.6 Å), obtained from Fe–S in CpFe(CO)$_2$SC$_2$H$_5$ [48] and from mean values [49] for S–C, C=C and Fe–N (pyridine) bonds. This is an approximation usually used and accepted in the absence of the most reliable crystallographic data [43,44]. The estimated value in CH_2Cl_2 $\alpha = 0.028$ indicate an interaction Class II Robin–Day [50,51]. Values calculated in other solvents are similar as is shown in Table 3. The degree of interaction between the metal center can be estimated through the electronic coupling element H_{ab} [10,43,44,52].

$$H_{ab}\ (cm^{-1}) = \frac{2.06 \times 10^{-2}(\varepsilon_{max} v_{max} \Delta v_{1/2})^{1/2}}{d} \quad (3)$$

The value 361 cm^{-1} suggests a moderate electronic interaction between the metal centers similar to that found in mixed-valence complexes with large bridge ligands containing pyridine groups linked to the metals [53]. Comparisons of H_{ab} values are displayed in Table 3. This value is close to that observed for some metalloproteins [5–8]. The thermal first-order electron transfer rate constant can be expressed as [43,44,50,51,50–53]:

$$K_{th} = [H_{ab}^2/h][\pi/kT\lambda]^{1/2} e[-E_a/RT] \quad (4)$$

where λ is the reorganization energy of the electron transfer, which can be calculated from the maximum of the IT absorption band of the electron transfer by $E_{op} = \lambda$ and the activation energy E_a can be estimated from:

$$E_a = [\lambda^2/4\lambda] \quad (5)$$

The value calculated $K_{th} = 6.5 \times 10^6$ is in general of the order for rate constants for other mixed-valence complexes (containing pyridine bridging ligands) as can be viewed from Table 3. Thus this value compares well with electron transfer rate estimated recently for some metalloproteins [5–8].

Solvent dependence of intervalence transition of a mixed valence complex gives information about reorganizational energy arising from rearrangements of the inner and outer coordination spheres [10,45–47,50,51]. From a dielectric continuum model, Hush derived the expression:

$$E_{op} = \lambda = \lambda_i + \lambda_0 = \lambda + e^2(1/2a_1 + 1/2a_2 - 1/a) \times (1/D_{op} - 1/D_s) \quad (6)$$

where λ and λ_0 are the inner and outer-sphere reorganizational parameters respectively, e is the unit electron charge, a_1 and a_2 are the molecular radius of the redox sites, d is the internuclear separation and D_{op} and D_s are the optical and static dielectric constants of the

Table 2
Intervalence transition parameter for [{Cp(dppe)Fe}$_2$-μ-S(Py)](PF$_6$)$_2$ in several solvents

Solvent	E_{op}(cm^{-1})	α [a]	$\Delta v_{1/2}$ (cm^{-1}) [b]	H_{ab} (cm^{-1}) [c]	E_a (cm^{-1}) [d]	$k_{th} \times 10^6$ (s^{-1}) [e]
Acetonitrile	12 682.3	0.028	1615	362	3170.6	6.3
Ethylmethylcetone	12 674.3	0.030	1689	388	3168.5	9.1
Acetone	12 674.3	0.030	1592	385	3168.6	7.2
Dichloromethane	12 698.4	0.028	1616	361	3174.6	6.5
Methanol	12 690.4	0.026	2233	331	3172.6	2.4

[a] Calculated using Eq. (2).
[b] Calculated using $\Delta v_{1/2} = (2310 E_{op})^{1/2}$.
[c] Calculated using Eq. (3).
[d] Calculated using Eq. (5).
[e] Calculated using Eq. (4).

Table 3
Electronic coupling element H_{ab} [a], rate constant [b] and comproportionation constant [c] for mixed-valence complexes containing pyridine bridged ligands

Complex	H_{ab} (cm^{-1})	k_{th} (cm^{-1})	K_c
$[Cp(dppe)Fe–S–C_5H_4N–Fe(dppe)Cp]^+$	361	6.5×10^6	3.5×10^2
$[(NH_3)_5Ru–NCC_5H_4N–Ru(NH_3)_5]^{5+}$	535	7.0×10^6	4.4×10^4
$[(NH_3)_5Ru–NC_5H_4(CH=CH)C_5H_4N–Ru(NH_3)_5]^{5+}$	240	4.7×10^7	10
$[(NH_3)_5Ru–NC_5H_4(CH=CH)_2C_5H_4N–Ru(NH_3)_5]^{5+}$	220	1.1×10^8	10
$[(NH_3)_5Ru–NC_5H_4-(CH=CH)_3C_5H_4N–Ru(NH_3)_5]^{5+}$	180	6.1×10^8	9
$[(NH_3)_5Ru–NC_5H_4SSC_5H_4N–Ru(NH_3)_5]^{5+}$	310	8.7×10^9	8.0×10^4
$[(NH_3)_5Ru–NC_5H_4SC_5H_4N–Ru(NH_3)_5]^{5+}$	150	3.7×10^6	158
$[(NH_3)_5Ru–NC_5H_4–C(O)O–Ru(NH_3)_5]^{4+}$	300	2.9×10^3	2.6×10^7
$[(NH_3)_5Ru–NC_5H_4–C(O)NH–Ru(NH_3)_5]^{4+}$	510	8.8×10^7	1.3×10^9
$[(NH_3)_5Ru–NC_5H_4–C_5H_4N–Ru(NH_3)_5]^{5+}$	390	6.5×10^8	20
$[(NH_3)_5Ru–NC_5H_4–CH_2–C_5H_4N–Ru(NH_3)_5]^{5+}$	100	7.3×10^5	73
$[(NH_3)_5Ru–NC_5H_4–NH–C_5H_4N–Ru(NH_3)_5]^{5+}$	500	9.6×10^8	26
$[(NH_3)_5Ru–NC_5H_4–C\equiv C–C_5H_4N–Ru(NH_3)_5]^{5+}$	285	3.8×10^7	14

[a] Estimated from Eq. (3), and using data Refs. [9,15,16,20–22].
[b] Estimated from Eq. (4).
[c] Estimated from Eq. (7).

medium. The intercept of the near linear plot E_{op} versus $(1/D_{op}-1/D_s)$ for the several solvents (see Fig. 4) affords the approximate λ_i value, $\lambda_i = 12\,470\ cm^{-1}$ (the solvent CH_2Cl_2 fall out from correlation is due probably to the ion pairing effects [43,44]). From Eq. (6), the value for λ_0 can be calculated ($\lambda_0 = 227\ cm^{-1}$).

The low value of the outer-sphere reorganization contribution respect to the inner-sphere reorganization appears to be associated to the spherical symmetry of the groups $(\eta^5\text{-}C_5R_5)Fe(dppe)^+$ [11,43,44,54]. The high variations of the metal–ligand bond distances during the electron-transfer indicated by the high values of λ_i, appears to be characteristic of mixed-valence complexes containing the moiety $(\eta^5\text{-}C_5R_5)Fe(dppe)^+$ (compare for instance with $[\{Cp^*Fe(dppe)\}_2\text{-}\mu\text{-}(C\equiv C–(C_6H_4)_n–C\equiv C)](PF_6)_2$, $n=0,\ 1$ $\lambda_i = 7100\ cm^{-1}$, $\lambda_0 = 500 cm^{-1}$ [35]) however an inverse tendency $\lambda_0 > \lambda_i$ has been reported recently for $[\{CpFe(dppe)\}_2\text{-}\mu\text{-}CN]PF_6$ [43,44]. The high delocalized behaviour for **4** in spite of the high inner reorganizational energies can be due to a considerable contribution from the vibrational modes of the bridging ligand to the reorganization energy [55,56]. The total reorganization energy $\lambda = 12\,697\ cm^{-1}$ is slightly higher than those reported for electron transfer in metalloproteins, which is reasonable because of the most bulky environment of the active site of metal proteins.

The cyclic voltammogram for the $[\{CpFe(dppe)\}_2\text{-}\mu\text{-}SPy](PF_6)_2$ complex exhibits two close, one electron electrochemical quasi-reversible waves. Values are shown in Table 1. The first at 0.26 V is chemically quasi-reversible ($i_{p_c}/i_{p_a} = 1.25$) and can be assigned to the oxidation of the Fe–Py moiety by comparison with data for $[CpFe(dppe)L]PF_6$ complexes [29,30]. On the other hand the lowest oxidation at 0.11 V (although not well defined) is electrochemically quasi-irreversible ($\Delta E_p = 0.08$ V), but chemically irreversible and is assigned to the Fe^{III}–S/Fe^{II}–S couple [57,58]. Thus an irreversible oxidation peak at 1.3 V corresponding to the oxidation of R–SS–R, as well as a quasi-irreversible oxidation peak at -0.55 V assigned to the oxidation of RS^- were observed, behavior typical of the redox properties of $[CpFe(dppe)SR]PF_6$ [57] and other metal–thiolate complexes [58]. Although the second oxidation wave described above is chemically irreversible, a rough estimation can be made of the comproportionation constant $K_c = 3.5\times10^2$ for the reaction:

$$[Fe^{II}-S-py-Fe^{II}]^+ + [Fe^{III}-Spy-Fe^{III}]^{3+} \overset{K_c}{\rightleftarrows} 2[Fe^{II}-Spy-Fe^{III}]^{2+} \quad (7)$$

The relatively high value of K_c agrees with the relatively high electron coupling between the iron centers and also provides a more efficient electron delocalization than X = methylene, ethylene and acetylene groups (considering the NC_5H_4–X–C_5H_4N moiety) [53]. Data shown in Table 3 also suggests that the thiolate bridging ligand is more efficient in electron delocalization than organic sulfide ligands (R_2S), but somewhat less efficient than the disulfide ligands. These conclusions are in agreement with the rate of redox chromium exchange reactions,

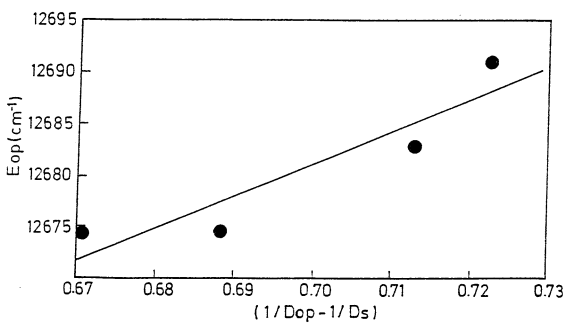


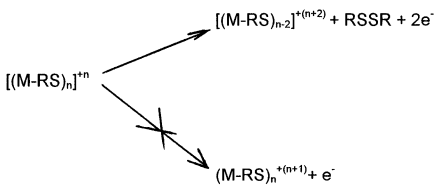
Fig. 4. Plot of E_{op} versus $(1/D_{op}-1/D_s)$ for the mixed valence complex $[Cp(dppe)Fe\text{-}S(Py)Fe(dppe)Cp]\ (PF_6)_2$.

$$*Cr^{2+} + [(H_2O)_5CrSR]^{2+} \Leftrightarrow Cr^{2+} + [(H_2O)_5^{*}CrSR]^{2+} \quad (8)$$

where the rates of reduction were found to be fast mediated by the thiolate sulfur ligand which functions as an extremely efficient electron-transfer bridge between chromium(II) and chromium(III) [1]. It is interesting to note that the only sulfur ligand bridging in mixed-valence complexes are sulfides and disulfides, then the complex $[\{Cp(dppe)Fe\}_2\text{-}\mu S(Py)](PF_6)_2$ is to our knowledge the first thiolate acting as a bridge of the form M–SR–M between metal centers in mixed valence compounds $[LnM\text{–}X\text{–}MLn]^{z+}$ X = bridging ligand [59,60].

The unexpected formation of the Fe^{III}–Fe^{II} thiolate complex can be explained assuming the formation of the iron(III)–thiolate mononuclear complex — the expected product using CH_3OH as a solvent and NH_4PF_6 as a halide abstractor — and subsequently the coordination of the nitrogen coordination pendant site by an $Cp(dppe)Fe^{+}$ fragment. To our knowledge this is the first Fe^{II}–Fe^{III} mixed valence complex, containing an thiolate ligand bridge [12–15,59,60] where the Fe^{III} is bonded to the sulfur–thiolate and the Fe^{II} is linked to some donor atom contained in R.

The scarcity of mixed-valence compounds containing this type of bridging ligand can be due to the difficulty in obtaining the mixed-valence complex by oxidation of the corresponding Fe^{II}-(μ-thiolate)–Fe^{II} complex owing to the known oxidation of the thiolate ligand instead the oxidation of the metallic center:



The efficient electron transfer between the iron centers through the pyridinethiolate ligand can be explained by the effective π-system formed by overlapping of the SOMO($Cp(dppe)Fe^{III}$)–HOMO($S\text{-}C_6H_5$) orbitals as well as HOMO($Cp(dppe)Fe^{II}$)–LUMO(NC_5H_5) overlap. The electron transfer from Fe^{II} to the pyridine ring can involve the HOMO of the fragment Cp(dppe)Fe which is π in character [16,17] and the LUMO of pyridine which also has π character [61] (see Fig. 5).

On the other hand electron transfer from the pyridine–thiolate ligand to $Cp(dppe)Fe^{III}$ fragment [16,17] through the thiolate side can involve the HOMO of the thiolate [62,63] which has a π character and the π-SOMO orbital of the Fe^{III} fragment. The possible π system involved in the Fe^{II}–Fe^{III} electron transfer is depicted in Fig. 5. In this orbital interaction diagram the structure of the iron–pyridine moiety was established according to data from iron–pyridine complexes

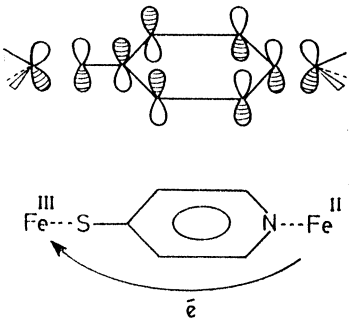


Fig. 5. Molecular orbitals probably involved in the electron transfer process. Interaction of the pyridine and thiolate side of the pyridinethiolate ligand with the iron fragments was deduced from HOMO of thiolate and LUMO of pyridine (see text).

[64] and those for the iron–thiolate side of the bridging ligand was made according to iron–thiolate structural data [16,17,48]. HOMO-thiolate [62,63] and LUMO-pyridine [61] was according literature data. SOMO of $Cp(dppe)Fe^{2+}$ and HOMO of $Cp(dppe)Fe^{+}$ has been reported previously [16,17].

3. Conclusions

From the study of the reaction of Cp(dppe)FeI with dithiopyridines, a new mixed valence binuclear complex containing a thiolate bridge was isolated and identified. The nature of the Fe^{III}–Fe^{II} interaction through the thiolate bridge, determined from ESR, Mössbauer and the Hush parameters, appears to be similar to the electron transfer in some metalloproteins, although the reorganizational energy is greater in the binuclear model than the biological systems. Recent studies on electron transfer between sulfur surface modified gold electrodes and cytochrome *c* reveal that the 4-pyridinethiolate ligand can act as an efficient bridge conductor between the cytochrome and the electrode [65].

4. Experimental

All reactions were carried out under purified N_2 or Ar using standard Schlenk techniques and the solvents used (methanol, dichloromethane, diethyl ether and *n*-hexane) were appropriately distilled and dried before use. The precursor complex Cp(dppe)FeI was prepared according to literature methods [42,66]. 4,4′- and 2,2′-dithiobispyridine, $[NBu_4]PF_6$, NH_4PF_6, (Aldrich) were used as received. $TlPF_6$ (**caution**! Thallous salts are very poisonous and should be handled with caution) was prepared from Tl_2CO_3 and HPF_6. IR spectra were recorded as KBr pellets on a FT-Bruker 66V spectrometer.

NMR spectra were run in CD_2Cl_2 or $(CD_2)_2CO$ solution at room temperature (r.t.) on a Bruker AMX 300 spectrometer with TMS(H) $\delta = 0.0$ ppm as internal standard or 85% H_3PO_4 and downfield positive to the reference as external standard for the ^{31}P measurements. UV–Vis spectra were run on a Varian DMS-9 spectrophotometer with 1 cm optical path cuvettes. Cyclic voltammetry was carried out at r.t. in CH_2Cl_2 using a Parc model 370 electrochemistry system equipped with a three electrode device, employing a glassy carbon working electrode, platinum wire, counter electrode and saturated calomel reference electrode. Solution was 10^{-3} M in the complex and 0.1 M in Bu_4PF_6 as supporting electrolyte. Under the same experimental conditions $E_{1/2}$ for the ferrocene/ferrocenium couple was 0.45 V with separations of about 0.060 V. Magnetic measurements were carried out by a Gouys method at r.t. (25°C) on a Johnson Matthey balance using mercury terathiocyanate cobaltate(II) as the calibrate. ESR spectra were carried out using an ESR Bruker ECS 106 spectrometer using a rectangular mode cavity with a 50 Hz field modulation. The measurements were made with the microwave band X (9.79 G Hz). For the solid sample the crushed powder was used. The Mössbauer spectrum, as a fine powder sample was obtained in a conventional spectrometer with constant acceleration. The source was 10mCi^{57} Co in a Pd matrix. The gamma ray detection was carried out with a Reuter–Stoke detector connected to an Ortec amplifying and selecting system. A 1024 channel Camberra multichannel analyzer was used for the acquisition of information. The reported shift values are relative to iron.

4.1. Reaction of Cp(dppe)FeI with 2,2′-dithiobispyridine in CH_2Cl_2

A mixture of 0.15 g (0.23 mmol) of Cp(dppe)FeI [31] and 0.08 g (0.36 mmol) of 2,2′-dithiobispyridine in 30 ml dichloromethane and in the presence of 0.16 g $TIPF_6$ (0.46 mmol) was stirred at r.t. for 24 h. The solution was filtered through Celite and the filtrate was concentrated under reduced pressure to a volume of $\approx$10 ml. Then 5 ml of an *n*-hexane–diethyl ether 1:1 mixture was added. The brown–orange precipitate was washed twice with diethyl ether and dried under vacuo. Yield 0.16 g; 78%. *Anal.* Found: C, 56.68; H, 4.09; N, 2.7. Calc. for $C_{41}H_{37}N_2F_6S_2P_3Fe$: C, 55.69; H, 4.18; N 3.16%.

Ir (KBr, cm^{-1}): 1088 $\nu(C_5H_5)$; 698 ν(dppe); 1576 $\nu(S_2(Py_2))$; 840 $\nu(PF_6)$.

^1H NMR (acetone-d_6 solution, ppm) 8.46m,7.68m,7.65m,7.23m $S_2(Py)_2$; 7.33m dppe; 4.76s Cp; 3.4m CH_2. ^{31}P NMR (acetone-d_6 ppm) 92.4 dppe; -138.8 PF_6.

4.2. Reaction of Cp(dppe)FeI with 4,4′-dithiobispyridine in CH_2Cl_2

A solution of Cp(dppe)FeI 0.15 g (0.23 mmol) and 4,4′-dithiobispyridine 0.08 g (0.36 mol) in the presence of $TIPF_6$ 0.16 g (0.46 mmol) in 30 ml dichloromethane was stirred at r.t. for 24 h. The separation procedure, similar to that above for 2,2′-dithiobispyridine, affords red–brown solid. Yield 0.14 g; 68%. *Anal.* Found: C, 55.7; H, 4.2; N, 3.2. Calc. for $C_{41}H_{37}F_6N_2S_2P_3Fe$: C, 55.65; H, 4.18; N, 3.16%.

Ir (Kbr, cm^{-1}) 1082 $\nu(C_5H_5)$; 694 ν(dppe); 1565 $\nu(S_2(Py)_2)$; 847 $\nu(PF_6)$.

^1H NMR (acetone-d_6 cm^{-1}) 7.62m, 7.54m, 7.41m, 7.19m S_2 $(Py)_2$; 7.33m (dppe) 4.76s C_5H_5; 3.4m CH_2. ^{31}P NMR (acetone-d_6 ppm) 92.3 dppe; -138.8 PF_6.

4.3. Reaction of Cp(dppe)FeI with 4,4′-dithiobispyridine in CH_3OH

Cp(dppe)FeI 0.15 g (0.23 mmol) was stirred with 4,4′-dithiobispyridine 0.08 g (0.36 mmol) in the presence of NH_4PF_6 0.06 g (0.37 mmol) in CH_3OH (30 ml) for 24 h at r.t. The solvent was evaporated under vacuo and the black solid residue was extracted with dichloromethane (15 ml). Upon addition of a 1:1 mixture of *n*-hexane–diethyl ether, a blue–black microcrystals precipitated which were washed several times with diethyl ether and dried under reduced pressure. Yield approximately 70%. *Anal.* Found: C, 55.98; H, 4.17; N, 1.1. Calc. for $C_{67}H_{62}NF_{12}SP_6Fe_2$: C, 55.93; H, 4.31; N, 0.97%.

Ir (KBr, cm^{-1}) 1094 $\nu(C_5H_5)$; 695 ν(dppe); 1565 $\nu(S_2(Py)_2)$; 839 $\nu(PF_6)$.

4.4. Reaction of Cp(dppe)FeI with 2,2′-dithiobispyridine in methanol

Cp(dppe)FeI 0.15 g (0.23 mmol) and 2,2′-dithiobispyridine 0.08 g (0.36 mmol) in the presence of NH_4PF_6 0.06 g (0.37 mmol) in CH_3OH (30 ml) were stirred for 24 h at r.t. Separation and purification procedures similar to the above reaction with 4,4′-dithiobispyridine afford a blue solid. Yield 0.13 g; 65%. *Anal.* Found: C, 55.9; H, 4.3; N, 1.7. Calc. for $C_{36}H_{33}F_6NSP_3Fe$: C, 55.82; H, 4.26; N, 1.8%.

Ir (KBr, cm^{-1}) 1094 $\nu(C_5H_5)$; 695 ν(dppe); 1565 $\nu(S_2Py)$; 838 $\nu(PF_6)$

Acknowledgements

This work was partially supported by Fondecyt (Project 1000672).

References

[1] J.J. Lippard (Eds.), Progress in Inorganic Chemistry, vol. 27, Wiley, New York, 1980, p. 153.
[2] A.I. Thompson, F. Armstrong, J. Am. Chem. Soc. 119 (1997) 9729.
[3] J.G. Dance, Polyhedron 5 (1986) 1037.
[4] J.R. Winkley, H.B. Gray, Chem. Rev. 92 (1982) 369.
[5] J.G. Dance, Polyhedron 5 (1986) 1037.
[6] H. Beinert, R.H. Holm, E. Múnck, Science 277 (1977) 653 and reference therein.
[7] J.H. Dawson, M. Sono, Chem. Rev. 87 (1987) 1255.
[8] J.R. Long, R.H. Holm, Inorg. Chim. Acta 229 (1995) 229.
[9] H.Y. Lin, B. Scharbert, R.H. Holm, J. Am. Chem. Soc. 113 (1991) 9529 and reference therein.
[10] R.A. Marcus, N. Sutin, Biochim. Biophys. Acta 811 (1985) 265.
[11] T. Guarr, G. McLendon, Coord. Chem. Rev. 68 (1985) 1.
[12] For extensive recent review on mixed valence $LnM–X–MLn^{z+}$ systems see: G.A. Carriedo, in: Recent Research Development in Organometallic Chemistry, vol. 1, 1996.
[13] K. Kalyanasundaram, K. Nazeeruddin, Inorg. Chim. Acta 224 (1994) 213.
[14] V. Balzani, A. Juris, M. Venturi, S. Campagna, S. Serroni, Chem. Rev. 96 (1996) 759.
[15] For a Fe_4S_4–Fe models, see Ref. [8].
[16] C. Díaz, C. Leal, N. Yutronic, J. Organomet. Chem. 516 (1996) 59.
[17] C. Díaz, C. Leal, N. Yutronic, Bol. Soc. Chil. Quim. 41 (1996) 99.
[18] I. de Sousa Moreira, D.W. Franco, Inorg. Chem. 33 (1994) 1607.
[19] I. de Sousa Moreira, D.W. Franco, J. Chem. Soc. Chem. Commun. 5 (1992) 450.
[20] For the related ligand thiopyridine see: E.S. Raper, Coord. Chem. Rev. 61 (1985) 115.
[21] F. Canales, M. Concepción Gimeno, P.C. Jones, A. Laguna, C. Sarroca, Inorg. Chem. 36 (1997) 5206 and reference therein.
[22] M. Berardini, J. Lee, D. Freedman, T. Lee Jae, J.C. Brennan, Inorg. Chem. 36 (1997) 5772 and reference therein.
[23] S.E. Kabir, M.M. Karim, K. Kundu, S.M.B. Ullah, K.I. Hardcastle, J. Organomet. Chem. 517 (1996) 155.
[24] D. Carrillo, Coord. Chem. Rev. 119 (1992) 137.
[25] C. Diaz, Polyhedron 10 (1991) 1319.
[26] M.M. Campos, C. Díaz, K. Figueroa, L. Padilla, N. Lara, Vib. Spectrosc. 7 (1994) 61.
[27] K. Nakanishi, Infrared Absorption Spectroscopy, Holden-Day, San Francisco, 1962.
[28] A. Forchioni, C.C. Pappalardo, Spectrochim. Acta 31A (1975) 1367.
[29] C. Díaz, A. Arancibia, Polyhedron 13 (1994) 117.
[30] C. Díaz, C. Leal, Polyhedron 15 (1996) 2825.
[31] W. Kaim, Coord. Chem. Rev. 76 (1987) 187.
[32] M. Guillermot, L. Toupet, C. Lapinte, Organometallics 17 (1991) 1928.
[33] S. Le Stang, F. Paul, C. Lapinte, Organometallic 19 (2000) 1035.
[34] C. Diaz, Bol. Soc. Chil. Quim. 44 (1999) 315.
[35] N. LeNarvor, L Toupet, C. Lapinte, J. Am. Chem. Soc. 117 (1995) 7129.
[36] C. Roger, P. Hamon, L. Toupet, H. Rabaa, J.I. Seillard, J.R. Hamon, C. Lapinte, Organometallics 10 (1991) 1045.
[37] N. LeNarvor, C. Lapinte, Organometallics 14 (1995) 634.
[38] N. Connelly, M.P. Gamasa, J. Gimeno, C. Lapinte, E. Lastra, J.P. Maher, N. Le Narvor, P.M. Rieger, J. Chem. Soc., Dalton Trans. (1993) 2575.
[39] F. Coats, M.A. Guillevic, L. Toupet, F. Paul, C. Lapinte, Organometallics 16 (1997) 5988.
[40] W.H. Morrison, D.N. Hendrickson, Inorg. Chem. 14 (1975) 2331.
[41] T. Manago, S. Hayami, H. Oshio, S. Osaki, H. Hasuyama, R.H. Herber, Y. Maeda, J. Chem. Soc., Dalton. Trans. (1999) 1001.
[42] C. Diaz, R. Latorre, Bol. Soc. Chil. Quim. 37 (1992) 211.
[43] For valence-mixed complexes containing the fragment $Cp(dppe)Fe^{+}$ see C. Díazand A. Arancibia, Inorg. Chim. Acta 269 (1998) 246.
[44] C. Diaz, A. Arancibia, Polyhedron 19 (2000) 137.
[45] N.S. Hush, Prog. Inorg. Chem. 8 (1967) 391.
[46] N.S. Hush, Electrochim. Acta 13 (1968) 1005.
[47] N.S. Hush, Coord. Chem. Rev. 64 (1985) 135.
[48] R.E. English, L.R. Nassimbeni, R.J. Haines, J. Chem. Soc., Dalton Trans. (1978) 1379.
[49] C. Orpen, L. Brammer, F.H. Alíen, O. Kermmand, D.C. Watson, R. Taylor, J. Chem. Soc., Dalton Trans. (1987) sup. 1 and 2.
[50] C. Creutz, Prog. Inorg. Chem. 30 (1983) 1.
[51] N. Sutin, B.S. Brunschwig, C. Creutz, J.R. Winkler, Pure Appl. Chem. 60 (1988) 1817.
[52] M.H. Chou, C. Creutz, N. Sutin, Inorg. Chem. 31 (1992) 2318.
[53] A.C. Rebou, J.P. Launay, K. Takahashi, T. Nikira, 5. Tarutani, Ch. W. Spangler; Inorg. Chem. 33 (1994) 1325.
[54] V. Balzani, A. Juris, M. Venturi, S. Campagna, S. Serroni, Chem. Rev. 96 (1996) 759.
[55] P. Forlano, F.D. Cukiernik, O. Poizat, J.A. Olabe, J. Chem. Soc., Dalton Trans. (1997) 1595.
[56] K.S. Doorn, P.O. Stoutland, R.B. Dyer, H.W. Wodruff, J. Am. Chem. Soc. 114 (1992) 3133.
[57] C. Díaz, E. Araya, M.A. Santa Ana, Polyhedron 17 (1998) 222.
[58] J.C Kotz, W. Coco Vinning, R. Rosen, A. Romao Dias, M.H. García, Organometallics 2 (1983) 68.
[59] The complex $(Me_2S)Cl_2W$ $(SEt)_3WC1_2(SMe_2)$ possessing three symmetrical bridging thiolate ligands has been postulated as a tungsten (III, IV) mixed valence complex, however non intervalence absorption studies were done; P.M. Boorman, V.D. Patel, K.A. Kerr, P.W. Codding, P. Van Roey, Inorg. Chem. 19 (1980) 3508.
[60] Similarly the complex $[NEt_4][V_2(edt)_4]$ (edt = ethane-1,2-dithiolate) containing four thiolate bridging ligand has been recently reported but no intervalence absorption studies have been make on the $V^{III}–V^{IV}$ centres; J.R. Rambo, S.L. Castro, K. Folting, S.L. Bartley, R.A. Heintz, C. Christou, Inorg. Chem. 35 (1996) 6844.
[61] For electronic structure of pyridine and their complexes see: H. Daamen, A. Oskam, Inorg. Chim. Acta 26 (1978) 81.
[62] For electronic structure of thiolate complexes see: M.T. Ashby, J.H. Enemark, D.L. Lichtenberg, Inorg. Chem. 27 (1988) 191.
[63] M.T. Ashby, J.H. Enemark, J. Am. Chem. Soc. 108 (1986) 730.
[64] F.A. Cotton, J.M. Troup, J. Am. Chem. Soc. 96 (1974) 3438.
[65] B.D. Lansp, D. Hobara, M.D. Porter, K. Wiki, Th.M. Cotton, Langmuir 13 (1997) 736.
[66] C.A. Barrado, G. Carriedo, C. Díaz, V. Riera, Inorg. Chem. 30 (1991) 4416.

PERGAMON

www.elsevier.nl/locate/poly

Polyhedron 19 (2000) 2689–2695

POLYHEDRON

Synthesis, spectral properties, crystal structures and antimicrobial effects of copper(II) pyridinecarboxylate adducts with chelating ligands

Martina Palicová [a,*], Peter Segl'a [a], Dušan Mikloš [a], Miroslava Kopcová [a], Milan Melník [a], Barbora Dudová [b], Daniela Hudecová [b], Tadeusz Glowiak [c]

[a] *Department of Inorganic Chemistry, Slovak Technical University, 812 37 Bratislava, Slovak Republic*
[b] *Department of Biochemistry and Microbiology, Slovak Technical University, 812 37 Bratislava, Slovak Republic*
[c] *Institute of Chemistry, University of Wroclaw, F. Joliot-Curie 14, 50 383 Wroclaw, Poland*

Received 27 July 2000; accepted 8 September 2000

Abstract

The reaction of an ethanolic solution of copper(II) pyridinecarboxylates $CuX_2 \cdot nH_2O$ (where X is nicotinate (nic) ($n = 0$) or isonicotinate (isonic) ($n = 4$)) with ethylenediamine (en) in a molar ratio of 1:2 lead to the isolation of solid tetragonally distorted octahedral complexes of the type $[Cu(en)_2(H_2O)_2]X_2 \cdot nH_2O$ ($n = 1$ for nic; $n = 0$ for isonic). The analogous reaction of $CuX_2 \cdot nH_2O$ with diethylenetriamine (dien) in a molar ratio of 1:1 leads to the formation of square-pyramidal pentacoordinated complexes of the type $[CuX(dien)(H_2O)]X$. On the other hand, the reaction of equimolar quantities of copper(II) nitrate and dien with nicotinate anions (equimolar quantities of pyridinecarboxylic acid and NaOH) in ethanolic solutions gives a solid monomeric complex $[Cu(nic)(NO_3)dien)(H_2O)] \cdot H_2O$ in which the coordination polyhedron around the Cu(II) atom is a $(4 + 1 + 1)$ distorted tetragonal bipyramid. Based on the molecular structure the electronic and IR spectra are discussed. Moreover, the results of the quantitative determination of antimicrobial activity of the isonic complexes $[Cu(isonic)_2(H_2O)_4]$, $[Cu(en)_2(H_2O)_2](isonic)_2$, $[Cu(isonic)(dien)(H_2O)](isonic)$, as well as isonicotinic acid, ethylenediamine and diethylenetriamine alone are discussed. © 2000 Elsevier Science B.V. All rights reserved.

Keywords: Chelating ligands; Crystal structures; Copper(II) complexes; Pyridinecarboxylate complexes; Antimicrobial activity

1. Introduction

Carboxylatocopper(II) complexes are interesting from both a chemical and biological point of view. Different possible coordinations of the carboxyl group to the central atom lead to the existence of compounds with distinct crystal structures. Pyridinecarboxylic acid and its derivatives possessing very interesting pharmaceutical properties constitute an important group of anthelmintics and vitamins. It is known that some drugs act via chelation [1] or via inhibition of metalloenzymes [2], but little is known about the modification of activity of most drugs when their ligating potential is utilized.

Synthesis, spectral and thermal properties of various complexes $CuX_2 \cdot nH_2O$ (where X is pyridine-3-carboxylate or nicotinate (nic) and pyridine-4-carboxylate or isonicotinate (isonic); $n = 0$–4) have been reported [3,4]. Only a few structures of $[CuX_2(H_2O)_4]$ [5] and their adducts with chelating ligands 1,10-phenanthroline and 2,2′-bipyridine have been reported [6,7]. Different coordination modes of the pyridinecarboxylate (coordinated not only through the carboxylate group, but also through the nitrogen atom of the pyridine ring) lead to formation of mononuclear [5] or polynuclear [6,7] structures. Recently, we have studied [8] the adducts of Cu(II) isonicotinate with ethylenediamine (en) and diethylenetriamine (dien), prepared $[Cu(en)_2(H_2O)_2](isonic)_2$ and $[Cu(isonic)(dien)(H_2O)_{1.5}] \cdot 0.5SO_4 \cdot 2.5H_2O$ and solved their structures by X-ray analysis.

* Corresponding author. Tel.: +421-7-593-25611; fax: +421-7-524-93198.
E-mail address: palicova@chtf.stuba.sk (M. Palicová).

0277-5387/00/$ - see front matter © 2000 Elsevier Science B.V. All rights reserved.
PII: S0277-5387(00)00585-4

Table 1
Analytical data [a] for the complexes

Complex	Calculated (%) (Found) (%)			
	Cu	C	H	N
$[Cu(nic)_2$	20.7 (20.5)	46.8 (46.5)	2.6 (2.6)	9.1 (8.9)
$[Cu(en)_2(H_2O)_2](nic)_2 \cdot H_2O$	13.2 (13.4)	39.9 (40.2)	6.7 (6.3)	17.4 (17.5)
$[Cu(nic)(dien)(H_2O)]nic$	14.2 (13.9)	43.0 (42.7)	5.6 (5.8)	15.7 (16.0)
$[Cu(nic)(NO_3)(dien)(H_2O]\cdot H_2O$	16.4 (16.1)	31.1 (31.4)	5.7 (5.6)	18.1 (18.1)
$[Cu(dien)(isonic)(H_2O)]isonic$	14.8 (14.6)	44.8 (45.2)	4.9 (5.0)	16.3 (16.5)

[a] Microanalysis results obtained with maximum deviations: Cu, ± 0.3; C, ± 0.5; H, ± 0.4; N, ± 0.3%.

Table 2
Crystal data and structure refinement for $[Cu(nic)(NO_3]dien)(H_2O]\cdot H_2O$

Empirical formula	$C_{10}H_{21}CuN_5O_7$
Formula weight	386.86
Crystal size (mm)	$0.15 \times 0.15 \times 0.15$
Crystal system	Triclinic
Space group	$P\bar{1}$
Z	2
Unit cell dimensions	
a (Å)	7.303(2)
b (Å)	8.147(2)
c (Å)	13.164(3)
α (°)	96.00(3)
β (°)	91.53(3)
γ (°)	94.18(3)
V (Å^3)	776.4(3)
D_{calc} (Mg m^{-3})	1.655
$F(000)$	402
Linear absorption coefficient (μ) (mm^{-1})	1.451
Radiation type (Å)	Mo Kα, $\lambda = 0.71073$
Temperature (K)	100(1)
θ Range for data collection	3.79–28.71
Index ranges	$-7 \le h \le 9$, $-10 \le k \le 10$, $-17 \le l \le 17$
No. reflections collected	5531
No. independent reflections	3505 [$R_{int} = 0.0304$]
Refinement method	Full-matrix least-squares on F^2
Data/restraints/parameters	3082/0/293
Goodness-of-fit on F^2	1.093
Final R indices ($I > 2\sigma(I)$)	$R = 0.0261$, $R_w = 0.0701$
R indices (all data)	$R = 0.0313$, $R_w = 0.0717$
Largest difference peak and hole (e Å^{-3})	0.458/−0.487

In the present paper, we report as a part of our investigation of metal ion–drug interactions the complexation of isonic and nic in the presence of en and dien. The stereochemistry and the mode of ligand coordination in solid copper(II) complexes have been determined by IR and electronic measurements. The crystal and molecular structure of one of the products, $[Cu(nic)(NO_3)(dien)(H_2O)]\cdot H_2O$, has also been solved. Moreover, for some of the isonicotinate complexes antimicrobial activity has been determined.

2. Experimental

2.1. Chemical reagents

All the chemicals used were of reagent grade and without further purification. All organic reagents were purchased from Aldrich; their purity was checked by IR spectra.

2.2. Analysis and physical measurements

Copper was determined by electrolysis after mineralization of the complexes; carbon, hydrogen, nitrogen and sulfur were determined by microanalytical methods (Carlo Erba Instruments EA 1180). Besides the elemental analysis, the water content in the hydrates was determined from thermogravimetrical curves. The yields of products were related to the metal contents in the reacting mixtures. Analytical data for solid complexes are given in Table 1.

Electronic spectra (9000–50 000 cm^{-1}) of the powdered samples in nujol mulls were recorded at room temperature (r.t.) on a Specord 200. IR spectra in the region of 100–4000 cm^{-1} were recorded on a Philips Analytical PU 9800 FTIR spectrometer and on a Magna 750 spectrometer at r.t. Spectra of solid samples were obtained in nujol mulls and KBr pellets (1 wt%).

2.3. X-ray structure determination

Data collection and cell refinement (see Table 2) for the complex $[Cu(nic)(NO_3)(dien)(H_2O)]\cdot H_2O$ were carried out using a KUMA KM4 diffractometer and software [9]. The diffraction intensities were corrected for Lorentz-polarization effects. The structure was solved by Patterson methods using XFPS [10] and subsequent Fourier difference maps. Anisotropic thermal parameters were refined for all non-hydrogen atoms. All hydrogen atoms were found from the difference Fourier maps and their positional parameters refined. Geometrical analysis was performed using SHELXL-93 [11]. The structure of the complex was drawn by ORTEP [12] (Fig. 1). Basic crystallographic data are summarized in Table 2.

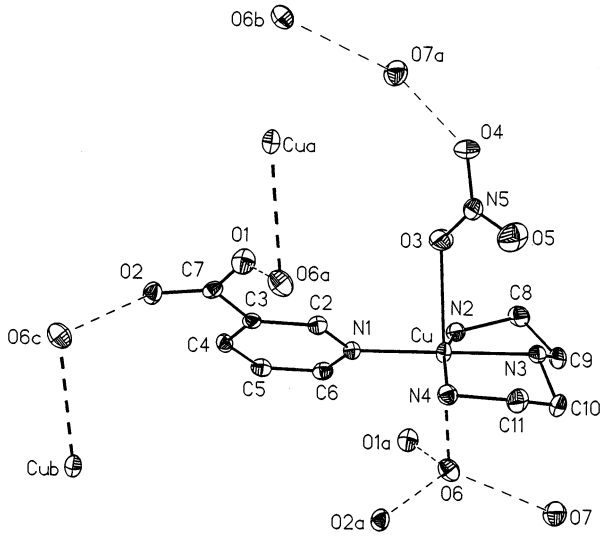


Fig. 1. ORTEP plot of $[Cu(nic)(NO_3)(dien)(H_2O)]\cdot H_2O$ also indicating the hydrogen bonds interconnecting neighbouring molecules (thermal ellipsoids are shown at the 50% probability level).

2.4. Preparation of the complexes

$[Cu(nic)_2]$ was prepared similarly as described by Kleinstein [4]. Aqueous solution (10 cm^3) of the nicotinic acid and an equimolar quantity of sodium hydroxide (10 mmol) were added to 30 cm^3 of an aqueous solution of copper(II) sulfate (5 mmol), and the reaction mixture was refluxed for 15 min. The blue precipitate was filtered off in a nearly quantitative yield (95%).

The violet complex $[Cu(en)_2(H_2O)_2](nic)_2\cdot H_2O$ was formed in an ethanolic solution (30 cm^3) of $[Cu(nic)_2]$ (1.25 mmol) by adding ethylenediamine (in the molar ratio of 1:2). Similarly, the blue complexes $[Cu(nic)(dien)(H_2O)](nic)$ and $[Cu(isonic)(dien)(H_2O)](isonic)$ were formed in an ethanolic solution (30 cm^3) of 1.25 mmol $[Cu(nic)_2]$ or $[Cu(isonic)_2(H_2O)_4]$ [8] by adding diethylenetriamine (in the molar ratio of 1:1), respectively. All resulting solutions were left to slowly evaporate at r.t. In isolating the above complexes, it was necessary to add acetone to the concentrated solution. Precipitates of the complexes were filtered off, washed with ethanol and finally dried in vacuo (yields of the complexes $[Cu(en)_2(H_2O)_2](nic)_2\cdot H_2O$, $[Cu(nic)(dien)(H_2O)](nic)$ and $[Cu(isonic)(dien)(H_2O)](isonic)$ were 66, 72 and 75%, respectively).

The blue crystals of $[Cu(nic)(NO_3)(dien)(H_2O)]\cdot H_2O$ were obtained dissolving copper(II) nitrate (1.25 mmol) and dien (1.25 mmol) in 20 cm^3 of ethanol. The solution was heated for 1 h at 70°C, then 20 cm^3 of an aqueous solution of the nicotinic acid and an equimolar quantity of sodium hydroxide (1.25 mmol) were slowly added. The resulting solution was left to slowly evaporate at r.t. In isolating the crystals, it was necessary to add a few cm^3 of acetone to the concentrated reaction solution. Well-shaped crystals, suitable for X-ray structure analysis, were collected after a few hours by filtration, washed with acetone and finally dried in vacuo (yield 83%).

2.5. Antimicrobial assays

The antimicrobial activity of the isonic complexes $[Cu(isonic)_2(H_2O)_4]$, $[Cu(en)_2(H_2O)_2](isonic)_2$, $[Cu(isonic)(dien)(H_2O)](isonic)$, as well as isonicotinic acid, ethylenediamine and diethylenetriamine alone was evaluated by a macrodilution method using G^+ *Staphylococcus aureus* CCM 3953, G^- *Escherichia coli* CCM 3988 and the yeasts *Candida parapsilosis* (purchased from the Laboratory of Medical Mycology, Postgraduate Medical Institute, Bratislava) in L-shaped tubes. The cultures of bacteria and yeasts were incubated under vigorous shaking [13]. The efficiency of prepared compounds on filamentous fungi *Rhizopus oryzae*, *Alternaria alternata*, *Fusarium moniliforme* (obtained from the Collection of Microorganisms of Department of Biochemistry and Microbiology, Slovak University of Technology), *Botrytis cinerea* CCM F-16 and *Microsporum gypseum* (received from the Laboratory of Medical Mycology, Postgraduate Medical Institute, Bratislava) was tested by macrodilution technique on solidified broth medium during static culturing [14].

Chromatographically pure compounds were dissolved in dimethylsulfoxide, its final concentration never exceeded 1.0 vol.% in either control or treated samples. The concentration of tested compounds used in all experiments ranged from 1.0 to 10.0 mmol l^{-1} for filamentous fungi and from 0.125 to 5.0 mmol l^{-1} for yeasts and bacteria.

The antimicrobial activity was characterized by the IC_{50} values (concentration of a compound which in comparison to the control inhibits the growth of microorganisms to 50%) and MIC values (minimal inhibitory concentration of a compound which inhibits microbial growth by 100%). The IC_{50} and MIC values were read from toxicity curves.

MIC experiments on subculture dishes were used to assess the minimal microbicidal concentration (MMC). Subcultures were prepared separately in Petri dishes containing competent agar medium and incubated at 30°C for 48 h (bacteria, yeasts) and at 25°C for 96 h (filamentous fungi). The MMC value was taken as the lowest concentration which showed no visible growth of microbial colonies in the subculture dishes.

3. Results and discussion

3.1. Crystal structure description of complex $[Cu(nic)(NO_3)(dien)(H_2O)]\cdot H_2O$

In the structure of $[Cu(nic)(NO_3)(dien)(H_2O)]\cdot H_2O$ (Fig. 1) the coordination polyhedron around the Cu(II) atom is a $(4+1+1)$ distorted tetragonal bipyramid, where three of the equatorial positions are occupied by three nitrogen atoms of the diethylenetriamine ligand, the Cu–N distances ranging from 2.017(2) to 2.035(2) Å (Table 3) and the N–Cu–N angles for dien being nearly the same [N2–Cu–N3 84.95(6)° and N3–Cu–N4 85.14(6)°, respectively], while in the fourth equatorial position the nic anion is coordinated through the nitrogen atom of the pyridine ring with the Cu–N1 distance of 2.025(2) Å. One axial position is occupied by the oxygen atom O3 of the NO_3^- anion at a distance of 2.457(2) Å, the other axial position being occupied by the oxygen atom O6 of a water molecule at a considerably longer distance of 2.716(2) Å.

A system of hydrogen bonds is interconnecting each of the molecules with other molecules (a) via the coordinated water molecule (O6) which creates two hydrogen bonds [2.708(2) and 2.731(2) Å, respectively] with two carboxyl oxygen atoms O1a, O2a of two different neighbouring molecules and a hydrogen bond [2.851(2) Å] with the uncoordinated water molecule (O7), (b) via the two carboxyl oxygen atoms O1, O2 with the water molecules (O6a, O6c), and (c) via the nitrate oxygen atom O4 creating a hydrogen bond [2.817(2) Å] with the uncoordinated water molecule (O7a).

Table 3
Bond lengths (Å) and angles (°) for $[Cu(nic)(NO_3)(dien)(H_2O)]\cdot H_2O$

Cu–N3	2.0169(14)	N1–C6	1.358(2)
Cu–N4	2.0179(15)	N2–C8	1.495(2)
Cu–N1	2.0249(14)	N3–C9	1.478(2)
Cu–N2	2.0346(16)	N3–C10	1.481(2)
Cu–O3	2.4572(16)	N4–C11	1.493(2)
Cu–O6	2.7161(16)	C2–C3	1.399(2)
O1–C7	1.259(2)	C3–C4	1.394(2)
O2–C7	1.2646(19)	C3–C7	1.519(2)
O3–N5	1.2664(19)	C4–C5	1.399(2)
O4–N5	1.2641(19)	C5–C6	1.387(2)
O5–N5	1.2441(19)	C8–C9	1.523(2)
N1–C2	1.350(2)	C10–C11	1.523(2)
N3–Cu–N4	85.14(6)	N1–C2–C3	122.74(15)
N3–Cu–N1	178.60(5)	C4–C3–C2	118.52(15)
N4–Cu–NI	93.69(6)	C4–C3–C7	121.89(14)
N3–Cu–N2	84.95(6)	C2–C3–C7	119.58(14)
N4–Cu–N2	164.27(6)	C3–C4–C5	118.91(14)
N1–Cu–N2	96.35(6)	C6–C5–C4	119.26(15)
C2–N1–C6	118.31(14)	N1–C6–C5	122.26(15)
C2–NI–Cu	119.70(11)	O1–C7–O2	126.20(15)
C6–NI–Cu	121.95(11)	O1–C7–C3	117.02(14)
C8–N2–Cu	107.59(11)	O2–C7–C3	116.78(14)
O5–N5–O4	119.81(14)	N2–C8–C9	107.82(13)
O5–N5–O3	120.72(14)	N3–C9–C8	106.97(13)
O4–N5–O3	119.47(14)	N3–C10–C11	107.16(13)
C9–N3–C10	117.29(13)	N4–C11–C10	109.64(14)
C9–N3–Cu	108.50(10)	H61–O6–H62	106(2)
C10–N3–Cu	107.51(10)	H71–O7–H72	107(3)
C11–N4–Cu	109.25(11)		

3.2. Spectroscopic data

All the typical features of IR spectra are clearly compatible with the structural characteristics of the complexes under study.

The most characteristic bands in the IR spectra correspond to carboxyl group stretching vibrations in the expected regions [15]. The carboxylate stretching frequencies $\nu_{as}(COO^-)$ and $\nu_s(COO^-)$ for each of the complexes under study are given in Table 4. The difference between the antisymmetric stretch and symmetric stretch, which gives information on the carboxylate bonding mode for the complexes, could not be determined accurately due to an overlap of $\nu_{as}(COO^-)$ with the stretching vibration of C=N of the pyridine ring. Moreover, the positions of the absorption bands are strongly affected by hydrogen bonding interactions of the carboxyl group of nic or isonic with other ligands as confirmed by the crystal structures of some of the complexes. However, considerable splitting of bands assigned to $\nu_{as}(COO^-)$ and $\nu_s(COO)$ for anhydrous $[Cu(nic)_2]$ confirms that the nicotinic acid anion as a ligand is most probably coordinated via a bridging carboxyl group.

The *N*-coordination of the nicotinate or isonicotinate in complexes $[Cu(nic)_2]$, $[Cu(isonic)_2(H_2O)_4]$, $[Cu(nic)(NO_3)(dien)(H_2O)]\cdot H_2O$ and $[Cu(isonic)(dien)(H_2O)_{1.5}]\cdot 0.5SO_4\cdot 2.5H_2O$ is in agreement with the positions of absorption bands in the region from 650 to 667 cm^{-1} and in the region from 423 to 447 cm^{-1}, respectively, which are due to in-plane ring deformation and out-of-plane deformation of the coordinated pyridine ring [15]. However, the positions of bands above 450 cm^{-1} can not be assigned accurately, because they are obscured with the Cu–O stretching frequencies [16] (Table 4). On the other hand, in the IR spectra of both complexes $[Cu(en)_2(H_2O)_2](nic)_2\cdot H_2O$ and $[Cu(en)_2(H_2O)_2](isonic)_2$, which contain en, medium bands are observed at 620 and 615 cm^{-1} as well as at 398 and 395 cm^{-1}, respectively, which are assigned to in-plane ring deformation and out-of-plane deformation of a non-coordinated pyridine ring [15].

In the spectra of complexes $[Cu(nic)(dien)(H_2O)](nic)$ and $[Cu(isonic)(dien)(H_2O)](nic)$ the positions of bands assigned to in-plane ring deformation and out-of-plane deformation are characteristic for a coordinated as well as for a non-coordinated pyridine ring [15].

In the IR spectrum of complex $[Cu(nic)(NO_3)(dien)(H_2O)]\cdot H_2O$, strong bands were observed at 1313 and 1007 cm^{-1} which were assigned to $\nu_s(NO_2)$ and

Table 4
Spectral data [a] for the copper(II) complexes

Complex	IR spectra (cm^{-1})							Electronic spectra (kK)	
	Carboxylic group			Pyridine ring				Band I	Band II
	$\nu_{as}(COO^-)$		$\nu_s(COO^-)$	δ(py)		γ(py)			
$[Cu(nic)_2$	1653s 1630s	1426m	1371s 1386s	650m		447m [c] 432sh		13.5br 11.8sh	
$[Cu(en)_2(H_2O)_2](nic)_2\cdot H_2O$	1590s [c] 1620sb		1387s,br		620m		398m	18.4br	31.2sb
$[Cu(nic)(dien)(H_2O)]nic$	1618sbr		1388s,br	654m	625m	458m [c] 440sh	391m	16.9br 12.7sh	
$[Cu(nic)(NO_3)(dien)(H_2O)]\cdot H_2O$	1622s 1611s		1377sbr	653m		449m		17.6br	
$[Cu$ (isonic)$(dien)H_2O)]$isonic	1613sbr		1375s,br	673m	624w	456m [c] 445sh	392m	16.6br 12.5sh	27.5sh
$[Cu(isonic)_2(H_2O)_4]$ [b]	1649s 1597s,br [c]	1418s	1381s,br	667s		436s		15.3br	28.4sh
$[Cu(en)_2(H_2O)_2](isonic)_2$ [b]	1590s [c]		1375s,br		615m		395m	18.5br	
$[Cu(isonic)(dien)(H_2O)_{1.5}]\cdot 0.5SO_4\cdot 2.5H_2O$ [b]	1603s,br [c]		1375s	667m		423m		17.3br	27.5sh

[a] s, strong; m, medium; w, weak; sh, shoulder; br, broad.
[b] The values are taken from a paper by Seg'la et al. [8].
[c] Mixed bands or some of the observed bands also belong to another vibrational mode.

ν(NO), typical for the unidentate coordination mode of nitrato groups [15] (see the crystal structure).

The electronic spectra (Table 4) of both complexes $[Cu(nic)(dien)(H_2O)](nic)$ and $[Cu(isonic)(dien)(H_2O)]$-(nic) exhibit a broad asymmetrical band with a maximum at 16 900 and 16 600 cm^{-1} (band I) and shoulders on its low energy side which are typical for five-coordinated copper(II) complexes with almost a square-pyramidal structure [17]. The solid-state electronic spectra of all other copper(II) complexes under study (Table 4) exhibit a symmetrical broad ligand field band with a maximum in the range of 18 500 to 13 500 cm^{-1}. For some of the complexes, there is also a charge transfer band at about 30 000 cm^{-1} (band II). This type of d–d spectrum is typical for tetragonally distorted octahedral copper(II) complexes [17].

3.3. Structure of solid complexes

The reaction of ethanolic solution of copper(II) pyridinecarboxylates $CuX_2\cdot nH_2O$ (where X is nic or isonic, $n = 0$ and 4, respectively) with en in a molar ratio of 1:2 lead to isolation of solid complexes of the type $[Cu(en)_2(H_2O)_2]X_2\cdot nH_2O$ ($n = 1$ and 0) which contain uncoordinated pyridinecarboxylate anions. Moreover, the crystal structure of $[Cu(en)_2(H_2O)_2](isonic)_2$, which comprises $[Cu(en)_2(H_2O)_2]_2$, cations and isonicotinate anions, has been determined [8]. The four N atoms of en form the coordination plane around the copper(II) atom, and oxygen atoms of the water molecules, lying in the axial positions, complete an elongated octahedral coordination sphere. The analogous reaction of $CuX_2\cdot nH_2O$ with dien in a molar ratio of 1:1 leads to formation of pentacoordinated complexes of the type $[CuX(dien)(H_2O)]X$ (X = nic or isonic), which contain coordinated and non-coordinated pyridinecarboxylate anions. In these complexes the copper(II) atom is coordinated in a square-pyramidal arrangement by three N atoms of dien and one N atom of the pyridine ring of nic or isonic in equatorial positions, and by one water molecule in an axial position. The analogous structure of the pentacoordinated complex cation has been found by X-ray structure analysis [18] for $[Cu(isonic)(dien)(H_2O)]PF_6$. On the other hand, the reaction of equimolar quantities of copper(II) sulfate or nitrate and dien with pyridinecarboxylate anions (equimolar quantities of pyridinecarboxylic acid and NaOH) in ethanolic solutions gives solid monomeric complexes $[Cu(isonic)(dien)(H_2O)_{1.5}]\cdot 0.5SO_4\cdot 2.5H_2O$ [8] and $[Cu(nic)(NO_3)(dien)(H_2O)]\cdot H_2O$, respectively. The crystal structure of the sulfate complex contains two cations — a pentacoordinated $[Cu(isonic)(dien)(H_2O)]^+$, and a hexacoordinated $[Cu(isonic)(dien)(H_2O)_2]^+$ sulfate anions and water molecules. In the crystal structure of the nitrate complex the coordination polyhedron around the Cu(II) atom is a (4 + 1 + 1) distorted tetragonal bipyramid (see Section 3.1).

All the above complexes with chelating ligands (en and dien) are monomeric, and the complexes with en contain only non-coordinated pyridinecarboxylate anions, while the complexes with dien contain both non-coordinated and *N*-coordinated anions. In the case of the sulfate or nitrate complexes only *N*-coordinated anions in the equatorial plane are present. On the other hand, another type of nic coordination has been revealed by a previous structure determination of the polymeric complex [Cu(nic)(1,10-phenanthroline)(aqua)$_2$]$NO_3 \cdot 2H_2O$ [6] in which the nicotinate anions bridge the adjacent Cu(II) atoms through both the pyridine N atom and the carboxyl O atom to form zigzag polymeric chains along the *b* axis. Similarly, in the complex [Cu(nic)(2,2′-bipyridine)(aqua)]$NO_3 \cdot 2H_2O$ [7], the nicotinate anions bridge the adjacent Cu(II) atoms through both the pyridine N atom and the carboxyl group to form infinite chains. The carboxyl group of the nicotinate anion coordinates to the Cu(II) atom as a chelate.

3.4. Antimicrobial activities

Results of the quantitative determination of anti microbial activity, characterized by the IC_{50} and MIC values of the isonic complexes [Cu(isonic)$_2$(H_2O)$_4$], [Cu(en)$_2$(H_2O)$_2$](isonic)$_2$,[Cu(isonic)(dien)(H_2O)](isonic), as well as isonicotinic acid, ethylenediamine and diethylenetriamine alone are presented in Table 5. From among the tested compounds, the compound [Cu(isonic)$_2$(H_2O)$_4$] has shown the highest antibacterial activity against G^+ *S. aureus* ($IC_{50} = 1.9$ mmol.l^{-1}). Isonicotinic acid (isonicH) at a concentration of 5 mmol l^{-1} has not influenced the *S. aureus* growth, inhibition of the bacteria growth by compound [Cu(isonic)$_2$(H_2O)$_4$] at the same concentration was approximately 90%. Although ethylenediamine (en) alone has partially inhibited the *S. aureus* growth, ($IC_{50} = 2.6$ mmol l^{-1}), this influence has not manifested itself with [Cu(en)$_2$(H_2O)$_2$](isonic)$_2$. The effect of the compounds on G^- *E. coli* was considerably lower. IsonicH at a concentration of 5 mmol.l^{-1} did not influence the *E. coli* growth, inhibition of the growth by complexes [Cu(isonic)$_2$(H_2O)$_4$], [Cu(en)$_2$(H_2O)$_2$](isonic)$_2$, and [Cu(isonic)(dien)(H_2O)](isonic) at the same concentration was approximately 50% ($lC_{50} = 5$ mmol l^{-1}).

The highest effect against the yeasts *C. parapsilosis* was observed for the compounds [Cu(isonic)$_2$(H_2O)$_4$] and [Cu(isonic)(dien)(H_2O)](isonic) ($IC_{50} = 2.1$ and 3.3 mmol l^{-1}). While isonicotinic acid alone at a concentration of 5 mmol l^{-1} has not inhibited the yeasts growth, growth inhibition by the compounds [Cu(isonic)$_2$(H_2O)$_4$] and [Cu(en)$_2$(H_2O)$_2$](isonic)$_2$ at the same concentration was 70–80%. Similarly as in the case of *S. aureus* the partial inhibitory activity of en against *C. parapsilosis* ($IC_{50} = 3.7$ mmol l^{-1}) was not observed in the activity of its Cu-adduct ([Cu(en)$_2$(H_2O)$_2$](isonic)$_2$, $IC_{50} > 5$ mmol l^{-1}).

The growth of filamentous fungi, phytopathogenic fungi *B. cinerea*, *F. moniliforme* and a dermatophytic fungus *M. gypseum* was practically not influenced by

Table 5
Antimicrobial activity of copper(II) isonicotinates, isonicotinic acid (isonicH), ethylenediamine (en) and diethylenetriamine (dien) characterized by IC_{50} and MIC (mmol l^{-1}) [a]

Microrganism	Compound											
	[Cu(isonic)$_2$(H_2O)$_4$]		[Cu(en)$_2$(H_2O)$_2$]-(isonic)$_2$		[Cu (isonic)(dien)H_2O)]isonic		isonicH		en		dien	
	IC_{50}	MIC	IC_{50}	MIC	IC_{50}	MIC	IC_{50}	MIC	IC_{50}	MIC	IC_{50}	MIC
Staphylococcus aureus	>5	>5	1.9	>5	>5	>5	>5	>5	2.6	5[s]	>5	>5
Escherichia coli	>5	>5	5	>5	5	>5	5	>5	3.2	5[s]	>5	>5
Candida paropsilosis	>5	>5	2.1	>5	>5	>5	3.3	>5	3.7	>5	>5	>5
Rhizopus oryzae	>10	>10	3.7	>10	6.8	>10	2.2	5[c]	>10	>10	7.2	>10
Alternaria alternata	>10	>10	>10	>10	5	>10	5	>10	>10	>10	>10	>10
Botrytis cinerea	>10	>10	>10	>10	>10	>10	>10	>10	>10	>10	4.1	>10
Fusarium moniliforme	>10	>10	>10	>10	>10	>10	>10	>10	>10	>10	>10	>10
Microsporum gypseum	8	>10	>10	>10	>10	>10	>10	>10	>10	>10	3.1	>10

[a] c, microbicidal effect; s, microbistatical effect.

the tested copper compounds at a concentration of 10 mmol l^{-1} ($IC_{50} > 10$ mmol l^{-1}). The growth of *R. oryzae* was most significantly inhibited by the compounds [Cu(isonic)(dien)H_2O](isonic) and [Cu(isonic)$_2$-(H_2O)$_4$], $IC_{50} = 2.2$ and 3.7 mmol l^{-1}, respectively. The inhibition activity decreases in the order [Cu(isonic)-(dien)H_2O](isonic) > [Cu(isonic)$_2$(H_2O)$_4$] > [Cu(en)$_2$-(H_2O)$_2$](isonic)$_2$ > dien > isonic = en. The copper(II) adducts — compounds [Cu(en)$_2$(H_2O)$_2$](isonic)$_2$ and [Cu(isonic)(dien)H_2O](isonic) — have partially inhibited the growth of *A. alternata* (approximately at the same level, $IC_{50} = 5$ mmol l^{-1}) and also strongly inhibited sporulation.

4. Supplementary material

Supplementary materials including all atomic coordinates (Table S1), anisotropic displacement parameters for non-hydrogen atoms (Table S2) and all interatomic distances and bond angles (Table S3) for the compound [Cu(nic)(NO_3)(dien)(H_2O)]·H_2O have been deposited with the Cambridge Crystallographic Data Centre, CCDC no. 147398. Copies of this information may be obtained free of charge from The Director, CCDC, 12 Union Road, Cambridge, CB2 1EZ, UK (fax: +44-1223-336033; e-mail: deposit@ccdc.cam.ac.uk or www.http://www.ccdc.cam.ac.uk). Observed and calculated structure factors are available on request from the authors.

Supplementary material (available from the authors) concerning the antimicrobial activities include figures S1–S6 containing graphs on: growth inhibition of *S. aureus* by [Cu(isonic)$_2$(H_2O)$_4$] (Fig. S1); growth inhibition of *C. parapsilosis* by [Cu(isonic)$_2$(H_2O)$_4$] (Fig. S2); colony growth inhibition of *R. oryzae* by [Cu(isonic)$_2$-(H_2O)$_4$] (Fig. S3); colony growth inhibition of *R. oryzae* by [Cu(isonic)(dien)(H_2O)]isonic (Fig. S4); colony growth inhibition of *A. alternata* by [Cu(en)$_2$(H_2O)$_2$]-(isonic)$_2$ (Fig. S5); effect of [Cu(en)$_2$(H_2O)$_2$](isonic)$_2$ on the sporulation of *A. alternata* (Fig. S6).

Acknowledgements

This work was financially supported by grants 1/6106/20 and 1/7342/20 from the Slovak Grant Agency for Science.

References

[1] A. Albert, Selective Toxicity, The Physico-Chemical Basis of Therapy, 6th ed., Chapman and Hall, London, 1979.
[2] M.N. Hughes, The Inorganic Chemistry of Biological Processes, 2nd ed., Wiley, New York, 1981.
[3] G. D'Ascenzo, W.W. Wendlandt, Anal. Chim. Acta 50 (1970) 79.
[4] A. Kleinstein, G.A. Webb, J. Inorg. Nucl. Chem. 33 (1971) 405.
[5] K. Waizumi, M. Takuno, N. Fukushima, H. Masuda, J. Coord. Chem. 44 (1998) 269.
[6] D. Xu, A. Xie, Y. Xu, K. Nishikawa, N. Yasuoka, J. Coord. Chem. 43 (1998) 115.
[7] D. Xu, A. Xie, Y. Xu, C. Zhang, W. Chen, J. Coord. Chem. 39 (1996) 273.
[8] P. Segl'a, M. Palicová, M. Koman, D. Mikloš, M. Melník, Inorg. Chem. Comm. 3 (2000) 120.
[9] Kuma. Kuma KM4 User's Guide, Version 3.1. Kuma Diffraction, Wroclaw, 1991.
[10] F. Pavelčík, C. Rizzoli, G.D. Andreetti, Program for Automatic Structure Determination by Fourier, Patterson and Superposition Methods, Comenius University, Bratislava, Slovakia, and University of Parma, Italy, 1990.
[11] G.M. Sheldrick, SHELXL-93. Program for the Refinement of Crystal Structures, University of Göttingen, Germany, 1993.
[12] C.K. Johnson, ORTEP IL Report ORNL-5138, Oak Ridge National Laboratory, Tennessee, USA, 1976.
[13] V. Betina, D. Mičeková, P. Nemec, J. Gen. Microbiol. 71 (1972) 343.
[14] D. Hudecová, S. Jantová, M. Melnik, M. Uher, Folia Microbiol. 41 (1996) 473.
[15] K. Nakamoto, Infrared and Raman Spectra of Inorganic and Coordination Compounds, Part B, 5th ed., Wiley, New York, 1997 pp. 23, 56, 79.
[16] D. Xu, A. Xie, Y. Xu, K. Nishikawa, N. Yasuoka, J. Coord. Chem. 43 (1998) 115.
[17] A.B.P. Lever, Inorganic Electronic Spectroscopy, 2nd ed., Elsevier, Amsterdam, 1984, p. 480 and 554.
[18] F.M. Nie, Z.M. Wang, Y.M. Li, X.H. Zhao, Ch.H. Yan, Acta Crystallogr., Sect. C 54 (1998) 1853.

PERGAMON

www.elsevier.nl/locate/poly

Polyhedron 19 (2000) 2697–2705

POLYHEDRON

Tetrakis(triphenylphosphine oxide) complexes of the lanthanide nitrates; synthesis, characterisation and crystal structures of $[La(Ph_3PO)_4(NO_3)_3]\cdot Me_2CO$ and $[Lu(Ph_3PO)_4(NO_3)_2]NO_3$

William Levason *, Elizabeth H. Newman, Michael Webster

Department of Chemistry, University of Southampton, Southampton, SO17 1BJ, UK

Received 2 August 2000; accepted 8 September 2000

Abstract

The reaction of $Ln(NO_3)_3\cdot 6H_2O$ (Ln = La, Ce, Pr or Nd) with a sixfold excess of Ph_3PO in acetone formed $[Ln(Ph_3PO)_4(NO_3)_3]\cdot Me_2CO$. The crystal structure of the La complex shows a nine-coordinate metal centre with four phosphine oxides, two bidentate and one monodentate nitrate groups, and PXRD studies show the same structure is present in the other three complexes. In CH_2Cl_2 or Me_2CO solutions, ^{31}P NMR studies show that the complexes are essentially completely decomposed into $[Ln(Ph_3PO)_3(NO_3)_3]$ and Ph_3PO. Similar reactions in ethanol gave $[Ln(Ph_3PO)_3(NO_3)_3]$ only. In contrast for Ln = Sm, Eu or Gd, only the $[Ln(Ph_3PO)_3(NO_3)_3]$ are formed from either acetone or ethanol solutions. For the later lanthanides Ln = Tb–Lu, acetone solutions of $Ln(NO_3)_3\cdot 6H_2O$ and Ph_3PO gave $[Ln(Ph_3PO)_3(NO_3)_3]$ only, even with a large excess of Ph_3PO, but from cold ethanol $[Ln(Ph_3PO)_4(NO_3)_2]NO_3$ (Ln = Tb, Ho–Lu) were obtained. The structure of $[Lu(Ph_3PO)_4(NO_3)_2]NO_3$ shows an eight-coordinate metal centre with four phosphine oxides and two bidentate nitrate groups. In solution in CH_2Cl_2 or Me_2CO the tetrakis-complexes show varying amounts of decomposition into mixtures of $[Ln(Ph_3PO)_3(NO_3)_3]$, $[Ln(Ph_3PO)_4(NO_3)_2]NO_3$ and Ph_3PO as judged by $^{31}P\{^1H\}$ NMR spectroscopy. The $[Ln(Ph_3PO)_3(NO_3)_3]$ also partially decompose in solution for Ln = Dy–Lu, forming some tetrakis(phosphine oxide) species. © 2000 Elsevier Science B.V. All rights reserved.

Keywords: Lanthanides; Phosphine oxides; X-ray structures

1. Introduction

Phosphine oxides have proved popular ligands for complexing to lanthanide metal ions and are used widely in solvent extraction and separation processes for the lanthanides [1]. The reaction of Ph_3PO with lanthanide nitrates in ethanol or acetone in an Ln:Ph_3PO ratio $1:\leq 4$ produces the $[Ln(Ph_3PO)_3(NO_3)_3]$ which contain nine-coordinate metal centres based upon three phosphine oxides and three bidentate nitrates [2–5]. A lower Ln:Ph_3PO ratio in ethanol gives $[Ln(Ph_3PO)_2(EtOH)(NO_3)_3]$ which also contain nine-coordinate metal ions. There are also reports of $Ln(Ph_3PO)_4(NO_3)_3$ complexes [2] formed only by certain lanthanide ions, whose structures are unclear. None of the tetrakis(Ph_3PO) complexes have been characterised structurally and the spectroscopic data are limited and inconclusive. Here we report some systematic attempts to prepare $Ln(Ph_3PO)_4(NO_3)_3$ complexes for all the lanthanides (except Pm); a number of the known $[M(Ph_3PO)_3(NO_3)_3]$ were also synthesised to provide comparative spectroscopic data. We have reported elsewhere [6] the synthesis and characterisation of $[Y(R_3PO)_4(NO_3)_2]NO_3$ ($R_3 = Ph_3$, Ph_2Me, Me_3), and $[Sc(Ph_2MePO)_4(NO_3)_2]NO_3$.

2. Results and discussion

2.1. $[M(Ph_3PO)_4(NO_3)_3]\cdot Me_2CO$ (M = La, Ce, Pr or Nd)

The reaction of $M(NO_3)_3\cdot 6H_2O$ (M = La, Ce, Pr or Nd) with ≥ 6 equiv. of Ph_3PO in ice-cold acetone

* Corresponding author. Tel.: +44-2380-593-792; fax: +44-2380-593-781.

E-mail address: wxl@soton.ac.uk (W. Levason).

0277-5387/00/$ - see front matter © 2000 Elsevier Science B.V. All rights reserved.
PII: S0277-5387(00)00588-X

Table 1
$^{31}P\{^{1}H\}$ NMR data [a]

Complex	300 K [b]	220 K
$[La(Ph_3PO)_4(NO_3)_3]$	33.3 (300)	34.3, 27.0
$[La(Ph_3PO)_4(NO_3)_3]$ [c]	35.3 (500)	37.0, 27.0
$[La(Ph_3PO)_3(NO_3)_3]$	33.6 (10)	
$[Ce(Ph_3PO)_4(NO_3)_3]$	71 (1100)	93, 27.0
$[Ce(Ph_3PO)_4(NO_3)_3]$ [c]	78 (1600)	95, 27.0
$[Ce(Ph_3PO)_3(NO_3)_3]$	71 (400)	93
$[Pr(Ph_3PO)_4(NO_3)_3]$	125 (6500)	169, 27.0
$[Pr(Ph_3PO)_3(NO_3)_3]$	125 (500)	
$[Nd(Ph_3PO)_4(NO_3)_3]$	140.5 (4900)	173, 27.0
$[Nd(Ph_3PO)_3(NO_3)_3]$	141 (600)	
$[Sm(Ph_3PO)_3(NO_3)_3]$	32.5 (60)	
$[Eu(Ph_3PO)_3(NO_3)_3]$	−121 (260)	
'$[Dy(Ph_3PO)_4(NO_3)_2]NO_3$'	see text −199 (500) [d]	
$[Dy(Ph_3PO)_3(NO_3)_3]$	−139 (2000), −199 (480) [d]	
$[Ho(Ph_3PO)_4(NO_3)_2]NO_3$	27.0, −136 (1050), −152 (380) [d]	
$[Ho(Ph_3PO)_3(NO_3)_3]$	−136 (1100), −152 (360) [d]	
$[Er(Ph_3PO)_4(NO_3)_2]NO_3$	−119 (200) [d], −168 (600)	
$[Er(Ph_3PO)_3(NO_3)_3]$	−119 (180) [d], −168 (600)	
$[Tm(Ph_3PO)_4(NO_3)_2]NO_3$	27.0, −55.5 (250) [d], −120 (1350)	
$[Tm(Ph_3PO)_3(NO_3)_3]$	−55 (220) [d], −120 (1300)	
$[Yb(Ph_3PO)_4(NO_3)_2]NO_3$	27.0, 22 (50) [d], −6(vw)	
$[Yb(Ph_3PO)_3(NO_3)_3]$	22 (50) [d], −6 (150)	
$[Lu(Ph_3PO)_4(NO_3)_2]NO_3$	39.0 (5) [d], 35.5(w), 27.0	38.0(10) [d], 36.3, 27.0
$[Lu(Ph_3PO)_3(NO_3)_3]$	39.2 (10)	

[a] In CH_2Cl_2–$CDCl_3$ (10%) unless indicated otherwise. Shifts relative to external 85% H_3PO_4.
[b] $W_{1/2}$ (Hz) in parentheses.
[c] In Me_2CO-d^6–Me_2CO (5%).
[d] Resonance attributed to tetrakis(Ph_3PO) complex.

resulted in precipitation of complexes of formula $[M(Ph_3PO)_4(NO_3)_3]\cdot Me_2CO$. The La and Ce complexes have been described briefly before [2], but contrary to that report, we find that Pr and Nd also form analogous complexes. The fifth lanthanide, Pm, is radioactive and unavailable, but the next, samarium formed only the known [2] $[Sm(Ph_3PO)_3(NO_3)_3]\cdot 2Me_2CO$ under similar conditions (see Section 2.2). The CsI disc IR spectra each show single intense and broad ν(PO) vibrations at approximately 1155–1160 cm^{-1} with ill-defined shoulders at higher frequency, for M = La, Ce, Pr and Nd, and no band corresponding to free Ph_3PO at 1195 cm^{-1}, which demonstrates that all four phosphine oxides are coordinated, and suggests a relatively symmetric geometry. The C=O vibration of the acetone is approximately 1705 cm^{-1} lowered from the vapour phase value of 1740 cm^{-1}, but the X-ray structure of the lanthanum complex shows the acetone is not coordinated, and similar lowering is found in $[Eu(Ph_3PO)_3(NO_3)_3]\cdot Me_2CO$ [4]. The nitrate vibrations are difficult to identify but bands at approximately 1475, 1310, 1030, and 815 cm^{-1} are tentatively associated with the bidentate nitrate groups. Careful comparisons of the CsI disc spectra of $[M(Ph_3PO)_4(NO_3)_3]\cdot Me_2CO$ and $[M(Ph_3PO)_3(NO_3)_3]$ (M = La or Ce) were made in an attempt to identify the monodentate nitrate group vibrations; weak bands at 1227 and 825 cm^{-1} are tentatively attributed to this group, but in such complex spectra any assignment is not definitive. In 10^{-3} mol dm^{-3} solution in either Me_2CO or CH_2Cl_2[1] the complexes are non-electrolytes, and the conductivities do not increase with added Ph_3PO.

The $[M(Ph_3PO)_4(NO_3)_3]\cdot Me_2CO$ are usually obtained as powders, and attempts to grow crystals from pre-isolated complexes from acetone or chlorocarbons gave crystals of the corresponding $[M(Ph_3PO)_3(NO_3)_3]$. Small thin plates of $[La(Ph_3PO)_4(NO_3)_3]\cdot Me_2CO$ were obtained directly from one synthesis, and the X-ray crystal structure (below) showed the lanthanum to be nine-coordinate, bonded to four phosphine oxides, two bidentate and one monodentate nitrate groups. X-ray powder diffraction showed that the Ce, Nd and Pr samples had very similar patterns and all four showed strong similarities with the chief difference being the relative intensities of the two strongest lines at 2θ 8° (I_1) and 10° (I_2). For the La compound, comparison between the observed ($I_1 < I_2$) and calculated [7] ($I_1 > I_2$) patterns showed differences which we believe are due to

[1] Although neither acetone nor CH_2Cl_2 is regarded as an ideal solvent for conductance measurements, they were used in the present case for consistency with the NMR measurements.

the platy nature of the La crystallites. (The powder XRD was recorded on the same sample that yielded the single crystal.) The calculated relative intensity of these lines matches the Nd and Pr sample very well and we conclude that all four samples are likely to be isomorphous with the same or very similar structures.

The $^{31}P\{^{1}H\}$ NMR spectrum (Table 1) of $[La(Ph_3PO)_4(NO_3)_3]$ shows a very broad resonance at 300 K of δ 33.3 (CH_2Cl_2) or 35.3 (Me_2CO), which on cooling the solution resolve into two resonances in the ratio 3:1 identified as $[La(Ph_3PO)_3(NO_3)_3]$ and Ph_3PO by comparison of the chemical shifts. Addition of Ph_3PO to either solution showed fast exchange on the phosphorus NMR timescale at 300 K, but on cooling separate resonances are resolved. Addition of a fivefold molar excess of Ph_3PO and cooling to 190 K failed to generate any new resonance showing that even in the presence of excess ligand, the tetrakis complex is essentially completely dissociated into Ph_3PO and the corresponding tris complex. The Ce, Pr and Nd complexes behave similarly (Table 1), with the added complication that contact shifted $^{31}P\{^{1}H\}$ NMR resonances of these paramagnetic complexes show a large temperature variation, and some line broadening [8]. In these three complexes, exchange with added Ph_3PO is slow at 273 K in CH_2Cl_2 solution. Of the first four lanthanide(III) ions, only La is diamagnetic and ^{139}La has far from ideal nuclear properties for NMR studies (^{139}La, 99.9%, $I = 7/2$, $Q = 0.21 \times 10^{-28}$ m^2, $\Xi = 14.13$ MHz, $D_c = 336$) although spectra from some complexes have been recorded successfully [9]. However attempts to observe ^{139}La spectra from solutions of $[La(Ph_3PO)_4(NO_3)_3]\cdot Me_2CO$ in either acetone or CH_2Cl_2 solution failed. Nor were we any more successful with $[La(Ph_3PO)_3(NO_3)_3]$ or $[La(Ph_3PO)_2(EtOH)(NO_3)_3]$, and it seems that the combination of ligand lability and the moderate quadrupole moment result in unobservable broad lines, consequent from fast relaxation.

2.2. $[M'(Ph_3PO)_3(NO_3)_3]$ ($M' = Sm$, Eu or Gd)

The reaction of $M'(NO_3)_3\cdot 6H_2O$ ($M' = Sm$, Eu or Gd) with Ph_3PO ($1: \geq 3$) in either acetone or ethanol[2] gave only the known [2] $[M'(Ph_3PO)_3(NO_3)_3]$ (from acetone as solvates $[M'(Ph_3PO)_3(NO_3)_3]\cdot 2Me_2CO$). Moreover the $[M'(Ph_3PO)_3(NO_3)_3]$ are non-electrolytes in CH_2Cl_2 solutions, and the conductances do not increase significantly on addition of Ph_3PO (twofold molar excess). The $^{31}P\{^{1}H\}$ NMR spectrum of $[Sm(Ph_3PO)_3(NO_3)_3]$ in CH_2Cl_2 is a single relatively sharp line at δ 32.5. Addition of a tenfold molar excess of Ph_3PO to this solution showed only resonances for the tris complex and free ligand. For $[Eu(Ph_3PO)_3(NO_3)_3]$ the $^{31}P\{^{1}H\}$ NMR spectrum was a singlet at δ -121, but on addition of a tenfold molar excess of Ph_3PO a weak resonance at δ -101 was seen (integral $\sim 5\%$ of that of the tris-complex), possibly due to the formation of some tetrakis(phosphine oxide) complex. We have not observed a $^{31}P\{^{1}H\}$ NMR spectrum from solutions of $[Gd(Ph_3PO)_3(NO_3)_3]$, presumably due to unfavourable relaxation, but since solutions of $[Gd(Ph_3PO)_3(NO_3)_3]$ plus excess Ph_3PO are non-electrolytes, it seems that formation of a tetrakis(phosphine oxide) complex in solution does not occur to any great extent.

2.3. $[M''(Ph_3PO)_4(NO_3)_2]NO_3$ ($M'' = Tb$, Ho, Er, Tm, Yb or Lu)

The reaction of $Lu(NO_3)_3\cdot 6H_2O$ with a four–sixfold excess of Ph_3PO in acetone gave only the $[Lu(Ph_3PO)_3(NO_3)_3]\cdot 2Me_2CO$ consistent with literature reports [2]. However, using a Lu:Ph_3PO ratio of $1: \geq 6$ in ice-cold ethanol resulted in a $Lu(Ph_3PO)_4(NO_3)_3$ complex. Cousins and Hart [2] reported that this reaction yielded the ethanol solvate $[Lu(Ph_3PO)_4(NO_3)_3]\cdot EtOH$, from which the ethanol was removed on heating in vacuo. However, in our hands the unsolvated complex was obtained, shown most clearly by the X-ray crystal structure of the complex described below, the crystals used being obtained directly from the synthesis. The crystal structure of the lutetium complex shows an eight-coordinate metal centre with two chelating nitrates and four phosphine oxides and one ionic nitrate group (below). In the IR spectrum we identified weak peaks at approximately 1360, 1350 and 833 cm^{-1} which are absent in the corresponding spectrum of $[Lu(Ph_3PO)_3(NO_3)_3]$, and which may be tentatively associated with the ionic nitrate group [10]. The $^{31}P\{^{1}H\}$ NMR spectrum of $[Lu(Ph_3PO)_4(NO_3)_2]NO_3$ in CH_2Cl_2 solution at 300 K revealed a sharp resonance at δ 39.0 and a very weak broader feature at approximately δ 35.5. On cooling this solution to 200 K the spectrum consisted of a relatively sharp resonance at 38.0, a weaker feature at 36.3 and some Ph_3PO at 27.0. Integration of the 200 K spectrum shows that the δ 38.0:36.3:27.0 features have approximate intensity ratios 20:3:2. Addition of excess Ph_3PO to this solution at 200 K resulted in the disappearance of the feature at δ 36.3. The conductivity of a 10^{-3} mol dm^{-3} solution of $[Lu(Ph_3PO)_4(NO_3)_2]NO_3$ in CH_2Cl_2 was $\Lambda_M = 19$ Ω^{-1} cm^2 mol^{-1}, which increased slightly in the presence of excess Ph_3PO. These values may be compared with that of 22 Ω^{-1} cm^2 mol^{-1} for a similar concentration of $[N^nBu_4][BF_4]$, and shows that the lutetium complex approximates to a 1:1 electrolyte. Although CH_2Cl_2 has been criticised as a solvent for conductance measurements [11], it was used here to maintain the same

[2] We confirm the report of Cousins and Hart [2] that traces of solid $[Ln(Ph_3PO)_2(EtOH)(NO_3)_3]$ cause preferential crystallisation of this ethanol complex even from solution with high Ph_3PO:Ln ratios.

solvent system used for the NMR studies. Taken together, the $^{31}P\{^1H\}$ NMR results and conductance data suggest that $[Lu(Ph_3PO)_4(NO_3)_2]NO_3$ is present mostly as the tetrakis(Ph_3PO) cation in chlorocarbon solution, with only a small amount of decomposition into Ph_3PO, possibly $[Lu(Ph_3PO)_3(NO_3)_3]$ (which due to its very similar phosphorus shift may not show a resonance resolved from that of the tetrakis complex). A further unidentified minor species with $\delta = 36.3$ at 200 K and which undergoes fast exchange with Ph_3PO at ambient temperatures (which $[Lu(Ph_3PO)_3(NO_3)_3]$ does not) is present also, and this is lost in the presence of a large excess of Ph_3PO.

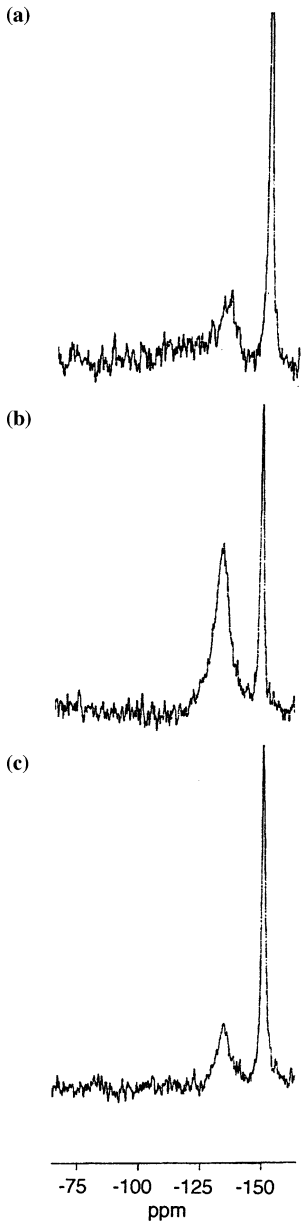


Fig. 1. $^{31}P\{^1H\}$ NMR spectra of (a) $[Ho(Ph_3PO)_4(NO_3)_2]NO_3$; (b) $[Ho(Ph_3PO)_3(NO_3)_3]$; and (c) $[Ho(Ph_3PO)_3(NO_3)_3]$ + excess Ph_3PO: all in CH_2Cl_2–$CDCl_3$ solutions at 300 K.

For the elements Tb, Ho, Er, Tm and Yb, $[M''(Ph_3PO)_4(NO_3)_2]NO_3$ complexes separated slowly from the appropriate nitrate salts and Ph_3PO in a 1: ≥ 6 ratio in ethanol solution below 0°C. If concentrated solutions were used (resulting in immediate precipitation of solid) or crystallisation occurred at room temperature, impure materials or even $[M''(Ph_3PO)_2(EtOH)(NO_3)_3]$ were sometimes formed. The crude complexes sometimes appear to incorporate some ethanol of solvation, which is removed on gentle warming in vacuum. Curiously several attempts to isolate $[Dy(Ph_3PO)_4(NO_3)_2]NO_3$ resulted in samples which based upon analysis, IR and ^{31}P NMR spectra appeared to contain both $[Dy(Ph_3PO)_4(NO_3)_2]NO_3$ and $[Dy(Ph_3PO)_2(EtOH)(NO_3)_3]$, and the pure tetrakis(phosphine oxide) complex has so far eluded us. The IR spectra (CsI disc) of the $[M''(Ph_3PO)_4(NO_3)_2]NO_3$ are very similar to that of the Lu complex, and they are assigned similar structures in the solid state. However, in CH_2Cl_2 solutions the behaviour is more complex: for example most have molar conductances (see Section 3) approximately half those expected for 1:1 electrolytes, which increase significantly on addition of Ph_3PO but are still less than that of the Lu analogue. In CH_2Cl_2 solution the $^{31}P\{^1H\}$ NMR spectra show in each case (except M″ = Tb for which no resonances were observed probably due to extreme line-broadening) two resonances, one relatively sharp and one much broader (Table 1), and upon addition of excess Ph_3PO to such solutions, the sharper resonance increases in relative intensity and the broader one decreases, and a third resonance due to Ph_3PO is also present (Fig. 1 shows a typical example). However even with a large (~ tenfold molar) excess of Ph_3PO it does not appear to be possible to suppress the broader resonance completely. $^{31}P\{^1H\}$ NMR spectra were also obtained from solutions of the corresponding $[M''(Ph_3PO)_3(NO_3)_3]$ in CH_2Cl_2 and these showed for each M″ the two resonances due to coordinated phosphine oxide with identical chemical shifts to those obtained from solutions of the tetrakis complexes. Similar behaviour was observed for $[Y(Ph_3PO)_4(NO_3)_2]NO_3$ and $[Y(Ph_3PO)_3(NO_3)_3]$ [6], although the yttrium system was also studied by ^{89}Y NMR spectroscopy, which allowed direct deduction of the number of bound phosphine oxides via the resolved phosphorus couplings. Thus we conclude that dissolution of $[M''(Ph_3PO)_4(NO_3)_2]NO_3$ or $[M''(Ph_3PO)_3(NO_3)_3]$ in CH_2Cl_2 results in a mixture of both complexes[3], which are not exchanging rapidly on the NMR timescale with Ph_3PO, but for which the proportion of the tetrakis(phosphine

[3] For the $[M''(Ph_3PO)_3(NO_3)_3]$ solutions mass balance requires another M″ species is formed, since none are seen in the $^{31}P\{^1H\}$ NMR spectra, these are probably phosphine oxide free, although the identity remains unclear (see also Ref. [6]).

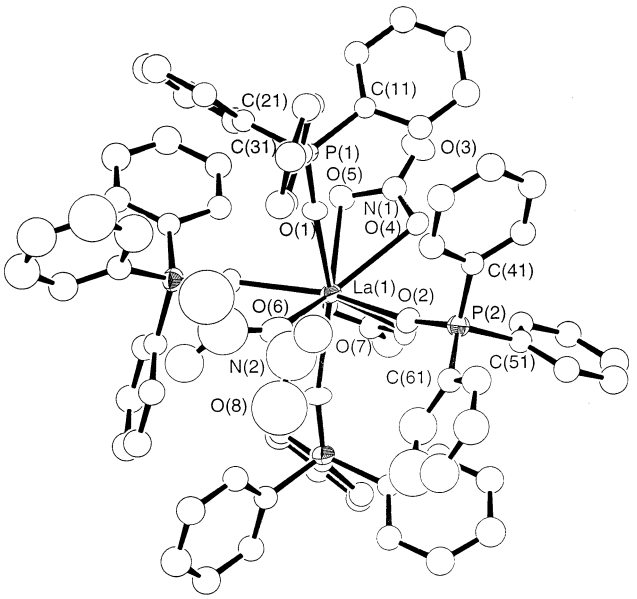


Fig. 2. Structure of $[La(Ph_3PO)_4(NO_3)_3]\cdot Me_2CO$ showing the atom numbering scheme. The ellipsoids are drawn at the 30% probability level.

oxide) complex is increased easily by addition of excess Ph_3PO. We noted above that $[M''(Ph_3PO)_3(NO_3)_3]\cdot 2Me_2CO$ were easily obtained pure from acetone solution, and hence we also recorded $^{31}P\{^1H\}$ NMR spectra for two examples $[M''(Ph_3PO)_3(NO_3)_3]$ and $[M''(Ph_3PO)_4(NO_3)_2]NO_3$ (M′ = Ho or Er) from acetone solutions. These spectra also showed that both tris- and tetrakis(phosphine oxide) complexes were present in acetone solution, but whilst the solid $[M''(Ph_3PO)_4(NO_3)_2]NO_3$ dissolve easily in acetone, $[M''(Ph_3PO)_3(NO_3)_3]$ dissolve with difficulty, and hence the ready isolation of the tris-complex from acetone reflects its low solubility, rather than different solution speciation. The mixture of complexes in solution also accounts for the conductance data reported above. For dysprosium, $[Dy(Ph_3PO)_3(NO_3)_3]\cdot 2Me_2CO$ was isolated easily from acetone solutions, and on dissolution in CH_2Cl_2, the $^{31}P\{^1H\}$ NMR spectrum showed a broad resonance at δ −139 ($W_{1/2}$ = 2000 Hz) and a sharper feature at −199 ($W_{1/2}$ = 480 Hz), the relatively intensities of the resonances shifting in favour of the latter on addition of excess Ph_3PO. The resonance at δ −199 is thus assigned to $[Dy(Ph_3PO)_4(NO_3)_2]NO_3$, suggesting the behaviour is similar to the other later metals, and our failure to isolate this complex presumably reflects unfavourable solubilities (similar behaviour was observed in $Y(NO_3)_3$–Ph_2MePO or Me_3PO systems [6]).

2.4. Crystal structure of $[La(Ph_3PO)_4(NO_3)_3]\cdot Me_2CO$

Crystals for this and the following structure were only obtained from the bulk preparation. It has not proved possible to grow crystals by usual routes and the crystals used, cleaved from a clump of plates, were both small and of modest quality. The structure consists of discrete molecules with the La and O(6) atoms located on a twofold axis (Fig. 2, Table 2(a)). The La atom is coordinated by four O atoms from Ph_3PO in an approximately square planar arrangement. Two bidentate nitrate ligands are on one side of the square plane and a disordered monodentate NO_3 on the other side. The O(6)–La(1)–O(P) angles are all $<90°$ and the phosphine oxide groups bend away from the two bidentate nitrate groups. The geometry of the Ph_3PO is unexceptional and the monodentate coordination of one nitrate is seen clearly in the La(1)–O–N angles which are 98°(av) for the two bidentate NO_3 groups and 134° for the single monodentate group and the La(1)···O(7) distance (4.3 Å). The solvate Me_2CO is also on a twofold axis. The bond distances to La may be compared with $[La(Ph_3PO)_3(NO_3)_3]\cdot EtOH\cdot CHCl_3$

Table 2
Selected bond lengths (Å) and angles (°) for $[La(Ph_3PO)_4(NO_3)_3]\cdot Me_2CO$ and $[Lu(Ph_3PO)_4(NO_3)_2]NO_3$

(a) $[La(Ph_3PO)_4(NO_3)_3]\cdot Me_2CO$ [a]			
La(1)–O(1)	2.488(7)	P(1)–O(1)	1.482(8)
La(1)–O(2)	2.449(8)	P(2)–O(2)	1.486(8)
La(1)–O(4)	2.656(8)		
La(1)–O(5)	2.695(8)		
La(1)–O(6)	2.585(17)		
N(1)–O(3)	1.22(1)	N(2)–O(6)	1.29(2)
N(1)–O(4)	1.24(1)	N(2)–O(7)	1.26(2)
N(1)–O(5)	1.28(1)	N(2)–O(8)	1.28(2)
P–C	1.755(9)–1.798(7)		
La(1)–O(1)–P(1)	164.5(6)	La(1)–O(2)–P(2)	169.4(5)
O(1)–La(1)–O(1i)	147.8(4)	O(2)–La(1)–O(2i)	155.1(4)
O(1)–La(1)–O(6)	73.9(2)	O(2)–La(1)–O(6)	77.6(2)
O(4)–La(1)–O(5)	47.2(3)		
La(1)–O(4)–N(1)	99.7(7)	La(1)–O(5)–N(1)	96.7(7)
La(1)–O(6)–N(2)	134(3)		
O(3)–N(1)–O(4)	123(1)	O(3)–N(1)–O(5)	120(1)
O(4)–N(1)–O(5)	116(1)	O(6)–N(2)–O(7)	127(2)
O(6)–N(2)–O(8)	120(2)	O(7)–N(2)–O(8)	113(2)
O–P–C	110.7(5)–112.5(5)	C–P–C	106.3(4)–108.0(4)
(b) $[Lu(Ph_3PO)_4(NO_3)_2]NO_3$ [b]			
Lu(1)–O(1)	2.220(9)	P(1)–O(1)	1.504(9)
Lu(1)–O(2)	2.181(9)	P(2)–O(2)	1.532(9)
Lu(1)–O(4)	2.429(10)	N(1)–O(3)	1.230(15)
Lu(1)–O(5)	2.406(9)	N(1)–O(4)	1.230(15)
		N(1)–O(5)	1.261(14)
O(1)–Lu(1)–O(2)	154.8(4)	O(3)–N(1)–O(4)	121.6(13)
O(1)–Lu(1)–O(1i)	91.3(5)	O(3)–N(1)–O(5)	119.6(14)
O(2)–Lu(1)–O(2i)	90.0(5)	O(4)–N(1)–O(5)	118.8(12)
O(1)–Lu(1)–O(2i)	94.8(4)	Lu(1)–O(1)–P(1)	166.6(6)
O(4)–Lu(1)–O(5)	52.6(3)	Lu(1)–O(2)–P(2)	166.9(6)
O–P–C	109.0(7)–113.3(6)		

[a] Symmetry operation: $i = -x, y, 1/2-z$.
[b] Symmetry operation: $i = 1/2-x, 1/2-y, z$.

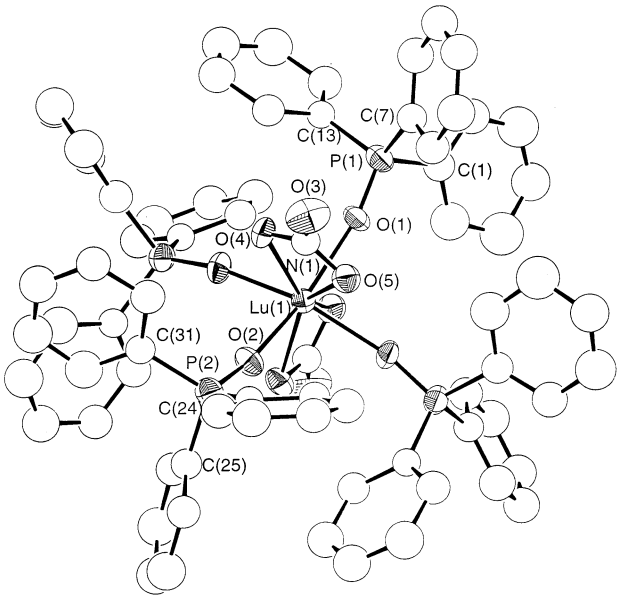


Fig. 3. Structure of the cation in $[Lu(Ph_3PO)_4(NO_3)_2]NO_3$ showing the atom numbering scheme. The ellipsoids are drawn at the 40% probability level.

[14] which is the *mer* pseudo-octahedral isomer (with the bidentate NO_3 being regarded conceptually as a monatomic group). Here the La–O(P) seem a little shorter (2.373, 2.427, 2.415 Å) than in the present compound and the La–O(N) (2.583–2.681 Å) are very similar (Table 2(a)). (Note that the bond lengths were calculated from the coordinates in the Cambridge structural database [12], refcode Kakruj and no e.s.d.s are available). All our attempts to grow crystals of $[La(Ph_3PO)_3(NO_3)_3]$ from petroleum ether (40–60°C)–CH_2Cl_2 or Et_2O–CH_2Cl_2 gave small poor quality crystals of a CH_2Cl_2 solvate which again was the *mer* isomer [13]. As our results parallel those of Huang et al. [14] but were marginally poorer, the data are not reported.

2.5. Crystal structure of $[Lu(Ph_3PO)_4(NO_3)_2]NO_3$

The crystal structure of the lutetium complex shows an eight-coordinate metal centre with two chelating nitrates and four phosphine oxides, and one ionic nitrate group (see Fig. 3 and Table 2(b)). The Lu atom is located on a twofold axis and following our earlier formalism can be regarded as *trans* pseudo-octahedral. The nitrate ion (N(1)) is symmetrically coordinated to Lu but does not show the distortions in bond lengths and angles noted in the La complexes but this is probably a reflection of the data quality. The ionic nitrate is also on a twofold axis but shows disorder, which was partially modelled. The closest structural analogue appears to be the $[La(Ph_3PO)_4(NO_3)_2]^+$ cation in $[La(Ph_3PO)_4(NO_3)_2]_2[Ni(C_4N_2S_2)_2]\cdot 2CH_3OH$ [15]. The mean La–O(P) (2.404) and La–O(N) (2.602 Å) are longer than the corresponding Lu values (2.200, 2.418 Å) reflecting the smaller ionic radius of Lu^{3+}.

3. Experimental

Physical measurements were made as described previously [6]. $^{31}P\{^1H\}$ NMR spectra were obtained at 145.5 MHz on a Bruker AM360 from solutions in CH_2Cl_2–5% $CDCl_3$, and with chemical shifts reported relative to external 85% H_3PO_4. The lanthanide (La, Ce, Sm, Lu, Tm, Tb) nitrate hexahydrates and Ph_3PO were obtained from Aldrich and used as received. Other lanthanide nitrates (Yb, Pr, Nd, Gd, Er, Ho, Dy, Eu) were made by reacting an excess of the appropriate M_2O_3 with hot aqueous HNO_3, filtering off unreacted oxide and pumping the solution to dryness in vacuum. The synthesis of $[Ln(Ph_3PO)_3(NO_3)_3]\cdot 2Me_2CO$ for all of the lanthanide nitrates was carried out as described [2], and several $[Ln(Ph_3PO)_3(NO_3)_3]$ were made in solvate free form from ethanol. Our IR data are in agreement with literature values to ± 2 cm^{-1} and hence are not given. The $^{31}P\{^1H\}$ NMR data have not been reported previously and are given in Table 1 for comparison.

The syntheses used for other complexes were generally similar and representative examples are described.

3.1. $[Ce(Ph_3PO)_4(NO_3)_3]\cdot Me_2CO$

An ice-cold solution of Ph_3PO (2.68 g, 10 mmol) in acetone (10 cm^3) was added to one of cerium(III) nitrate hexahydrate (0.43 g, 1.0 mmol) in acetone (15 cm^3). The solution was left at ambient temperature for 24 h when white crystals separated. Yield 0.73 g (50%). *Anal.* Found: C, 60.1; H, 4.5; N, 2.7. Calc. for $C_{75}H_{66}CeN_3O_{14}P_4$: C, 60.2; H, 4.4; N, 2.8%. IR (cm^{-1}) (CsI disc) 2950w, 1707m, 1591w, 1477m, 1439m, 1371m, 1313m, 1227w, 1191sh, 1160s (PO), 1122s, 1092m, 1073m, 1034s, 998m, 825w, 816m, 760s, 726s, 696s, 541s, 495m, 445m, 408m, 313w, 296m. ^1H NMR (300 K, $CDCl_3$) 2.2(s), 7.4–7.7(m), 8.4(s).

The following were made by very similar routes.

3.1.1. $[La(Ph_3PO)_4(NO_3)_3]\cdot Me_2CO$

Anal. Found: C, 59.9; H, 4.2; N, 2.6. Calc. for $C_{75}H_{66}LaN_3O_{14}P_4$: C, 60.2; H, 4.6; N, 2.8%. IR (cm^{-1}) (CsI disc) 2950w, 1708m, 1592w, 1473m, 1439s, 1365s, 1314m, 1227w, 1188sh, 1158s (PO), 1122s, 1092m, 1073m, 1034m, 998m, 825w, 817m, 758s, 725s, 697s, 543s, 464w, 445m, 408m, 312w, 296m. ^1H NMR (300 K, $CDCl_3$) 2.2(s), 7.3–7.7(m).

3.1.2. $[Pr(Ph_3PO)_4(NO_3)_3]\cdot Me_2CO$

Anal. Found: C, 59.7; H, 4.7; N, 2.7. Calc. for $C_{75}H_{66}N_3O_{14}P_4Pr$: C, 60.1; H, 4.4; N, 2.8%. IR (cm^{-1}) (CsI disc) 3000w, 1704m, 1589w, 1480m, 1437s, 1365s, 1311m, 1297(sh), 1226m, 1188(sh), 1155s(PO), 1121s, 1090m, 1070m, 1034m, 995m, 823w, 815m, 756s, 720s, 693s, 618m, 543s. ^1H NMR (300 K, $CDCl_3$) 2.2(s), 7.2–7.7(m), 10.1(br, s).

3.1.3. $[Nd(Ph_3PO)_4(NO_3)_3]\cdot Me_2CO$

Anal. Found: C, 59.6; H, 4.4; N, 2.6. Calc. for $C_{75}H_{66}N_3NdO_{14}P_4$: C, 60.0; H, 4.4; N, 2.8%. IR (cm^{-1}) (CsI disc) 3060w, 1702m, 1479s, 1439s, 1362s, 1310m, 1297(sh), 1226m, 1189sh, 1157s (PO), 1121s, 1091m, 1072m, 1036m, 1026w, 997m, 862w, 834w, 814m, 756s, 724s, 698s, 617m, 542s. ^1H NMR (300 K, $CDCl_3$) 2.2(s), 7.5–7.7(m), 8.9(br,s).

3.2. $[Lu(Ph_3PO)_4(NO_3)_2]NO_3$

An ice-cold solution of Ph_3PO (1.67 g, 6.2 mmol) in ethanol (15 cm^3) was added to one of lutetium(III) nitrate hexahydrate (0.36 g, 0.76 mmol) in ethanol (5 cm^3). The solution was left at $<0°C$ for 24 h when white crystals separated. The product was dried at 50°C in vacuo. Yield 0.67 g (60%). *Anal.* Found: C, 58.2; H, 4.1; N, 2.8. Calc. for $C_{72}H_{60}LuN_3O_{13}P_4$: C, 58.6; H, 4.1; N, 2.8%. IR (cm^{-1}) (CsI disc) 2950w, 1592w, 1509s, 1485s, 1439s, 1361s, 1350sh, 1303s, 1188sh, 1158s (PO), 1122s, 1093m, 1074m, 1034s, 999s, 930w, 833w, 817m, 750s, 724s, 694s, 541s, 463m, 445m, 416w, 305m. ^1H NMR ($CDCl_3$, 300 K) 7.1–7.6(m). Λ_M (CH_2Cl_2, 10^{-3} mol dm^{-3}) = 19 Ω^{-1} cm^2 mol^{-1}.

The following were made by very similar routes.

3.2.1. $[Yb(Ph_3PO)_4(NO_3)_2]NO_3$

Anal. Found: C, 58.7; H, 3.7; N, 2.7. Calc. for $C_{72}H_{60}N_3O_{13}P_4Yb$: C, 58.8; H, 4.1; N, 2.9%. IR (cm^{-1}) (CsI disc) 2950w, 1592w, 1505s, 1485s, 1439m, 1358s, 1300s, 1189sh, 1157s (PO), 1122s, 1093m, 1074w, 1033m, 999m, 930w, 834w, 817m, 750s, 724s, 695s, 541s, 463w, 445w, 406w. ^1H NMR ($CDCl_3$, 300 K) 7.6–5.7(m). Λ_M (CH_2Cl_2, 10^{-3} mol dm^{-3}) = 17 Ω^{-1} cm^2 mol^{-1}.

3.2.2. $[Tm(Ph_3PO)_4(NO_3)_2]NO_3$

Anal. Found: C, 58.7; H, 4.1; N, 2.8. Calc. for $C_{72}H_{60}N_3O_{13}P_4Tm$: C, 58.9; H, 4.1; N, 2.9%. IR (cm^{-1}) (CsI disc) 2950w, 1592w, 1500s, 1485s, 1439s, 1351s, 1300m, 1189sh, 1154s (PO), 1122m, 1093m, 1033m, 999m, 855w, 833w, 817m, 750s, 724s, 696s, 541s, 462m, 445w, 415w. ^1H NMR ($CDCl_3$, 300 K) 6.5–4.5(m). Λ_M (CH_2Cl_2, 10^{-3} mol dm^{-3}) = 14 Ω^{-1} cm^2 mol^{-1}.

3.2.3. $[Er(Ph_3PO)_4(NO_3)_2]NO_3$

Anal. Found: C, 59.1; H, 4.2; N, 2.8. Calc. for $C_{72}H_{60}ErN_3O_{13}P_4$: C, 59.0; H, 4.1; N, 2.9%. IR (cm^{-1}) (CsI disc) 2950w, 1593w, 1482s, 1435s, 1365s, 1298s, 1190sh, 1153s (PO), 1122m, 1092m, 1073w, 1032m, 999m, 932w, 858w, 833w, 817m, 750s, 729s, 694s, 541s, 463m, 445m, 416w, 311m. Λ_M (CH_2Cl_2, 10^{-3} mol dm^{-3}) = 13 Ω^{-1} cm^2 mol^{-1}.

3.2.4. $[Ho(Ph_3PO)_4(NO_3)_2]NO_3$

Anal. Found: C, 58.5; H, 4.0; N, 2.7. Calc. for $C_{72}H_{60}HoN_3O_{13}P_4$: C, 59.1; H, 4.1; N, 2.9%. IR (cm^{-1}) (CsI disc) 2950w, 1593w, 1510w, 1477s, 1439s, 1359s, 1316s, 1190sh, 1155s (PO), 1122s, 1093m, 1073m, 1032m, 999w, 875w, 835w, 817m, 750s, 725s, 693s, 542s, 463m, 445m, 415w. Λ_M (CH_2Cl_2, 10^{-3} mol dm^{-3}) = 12 Ω^{-1} cm^2 mol^{-1}.

3.2.5. $[Tb(Ph_3PO)_4(NO_3)_2]NO_3$

Anal. Found: C, 59.0; H, 4.1; N, 3.0. Calc. for $C_{72}H_{60}N_3O_{13}P_4Tb$: C, 59.3; H, 4.2; N, 2.9%. IR (cm^{-1}) (CsI disc) 2950w, 1593w, 1503s, 1472br,s, 1358s, 1310s, 1186sh, 1161s(PO), 1123s, 1094m, 1074w, 1031m, 999w, 930w, 833w, 818m, 749s, 726s, 694s, 541s, 463m, 447m, 417w. Λ_M (CH_2Cl_2, 10^{-3} mol dm^{-3}) = 10 Ω^{-1} cm^2 mol^{-1}.

3.3. Crystal structure determinations

Small modest-quality crystals of both materials were obtained from the preparation and diffraction data were measured on either a Rigaku AFC7S (Lu) or Nonius ccd (La) diffractometer using Mo Kα radiation ($\lambda = 0.71073$ Å).

3.3.1. $[La(Ph_3PO)_4(NO_3)_3.]\cdot Me_2CO$

The data were collected as triclinic even though data collection software suggested a monoclinic cell and solved in space group $P\bar{1}$ (no. 2) ($Z = 2$) using PATT in SHELXS-86 [16]. From La, P and some of the phenyl rings, the model was developed by standard methods. The third NO_3 group was difficult to locate; the O bonded to La was clear but the remaining NO_2 was very weak in the difference Fourier maps. The resulting structure showed excellent two-fold symmetry about the La atom except for the weak NO_2 residue.

The data were transformed to the monoclinic C lattice and the structure solution repeated with La(1) and O(6) now located on a twofold axis in the space group $C2/c$. The symmetry now requires that either the monodentate NO_3 lies on the twofold axis or is off-axis and disordered and the latter is found. N(2), O(7) and O(8) appeared as the three largest peaks on a

later Fourier map and restraints (DFIX) were used on N–O and O···O distances around N(2). The phenyl rings were constrained to be regular hexagons. The R factor was lower for the $C2/c$ space group and this is regarded as the preferred model. Full-matrix least-squares refinement on F^2 was carried out using SHELXL-97 [17] (Table 3).

Table 3
Crystallographic data for $[La(Ph_3PO)_4(NO_3)_3]\cdot Me_2CO$ and $[Lu(Ph_3PO)_4(NO_3)_2]NO_3$

Compound	$[La(Ph_3PO)_4(NO_3)_3]\cdot Me_2CO$	$[Lu(Ph_3PO)_4(NO_3)_2]NO_3$
Molecular formula	$C_{72}H_{60}LaN_3O_{13}P_4 + C_3H_6O$	$C_{72}H_{60}LuN_3O_{13}P_4$
Molecular weight	1496.10	1474.08
Crystal system	monoclinic	orthorhombic
Space group	$C2/c$ (no. 15)	$Pccn$ (no. 56)
Unit cell dimensions		
a (Å)	20.8697(9)	17.070(6)
b (Å)	17.5901(9)	15.412(7)
c (Å)	20.2428(12)	26.700(8)
α (°)	90.0	90.0
β (°)	90.523(4)	90.0
γ (°)	90.0	90.0
U (Å^3)	7430.8(7)	7024(5)
2θ Range for cell (°)		14.2–16.0
Temperature (K)	298	298
D_{calc} (g cm^{-3})	1.337	1.394
Z	4	4
$F(000)$ (e)	3064	2992
Crystal size (mm)	$0.20\times0.10\times0.05$	$0.55\times0.30\times0.25$
Scan mode (diffractometer)	$\omega\&\phi$ (ccd area detector)	ω (Rigaku AFC7S)
Observations	32 434	6172
Unique observations	6459 ($R_{int}=0.31$)	6172
hkl range	−24 to 24, −20 to 20, −23 to 24	0–20, 0–18, 0–31
Absorption correction	sortav	Ψ-scan
Max/min transmission	0.973, 0.701	1.000, 0.752
Data in refinement	6459	6172
Parameters/restraints	169/6	225/4
Weighing scheme (w^{-1}) [a]	$\sigma^2(F_o^2)+(0.16P)^2$	$\sigma^2(F_o^2)+(0.18P)^2$
λ (Å) (Mo Kα)	0.71073	0.71073
μ (cm^{-1})	7.24	15.6
Max 2θ (°)	49.9	50.0
S	0.965	0.97
Maximum shift/e.s.d.	0.02	0.09
Residual electron density (e Å^{-3})	−0.80 to +1.01	−1.91 to +1.88
R [b] ($F_o>n\sigma(F_o)$)	0.096 ($n=4$, 2888 refs)	0.078 ($n=4$, 2645 refs)
R [b] (all data)	0.216	0.193
wR_2 (all data)	0.306	0.292

[a] $P=[\mathrm{Max}(F_o^2,0)+2F_c^2]/3$.
[b] $R=\Sigma||F_o|-|F_c||/\Sigma|F_o|$; $wR_2=[\Sigma\, w(F_o^2-F_c^2)^2/\Sigma\, wF_o^4]^{1/2}$.

3.3.2. $[Lu(Ph_3PO)_4(NO_3)_2]NO_3$

Althought the data were weak, SHELXS-86 [16] gave a plausible solution for the Lu, P and some lighter atoms which was developed into a model for the cation with Lu positioned on a twofold axis (4c site). The NO_3 anion was identified with both N(2) and O(6) again on a twofold (4d) site, but too many peaks were found in the difference Fourier map to account for the remaining eightfold O(7) atom and a disordered model (O(7A), O(7B) with restraints added) was adopted. Full-matrix least-squares refinement on F^2 was carried out using SHELXL-97 [17] with anisotropic Lu, P and O(1) to O(5) atomic displacement parameters only. Apart from two peaks close to Lu and one near the disordered NO_3 group all peaks in the residual electron density are <1.0 e Å^{-3}.

4. Conclusions

Although all the lanthanides form $[Ln(Ph_3PO)_2(EtOH)(NO_3)_3]$ and $[Ln(Ph_3PO)_3(NO_3)_3]$ complexes, the tetrakis(phosphine oxide) complexes exhibit a varying pattern along the series. For the largest four ions La–Nd (Ln^{3+} radii: 104.5–98 pm) [18] nine-coordinate $[Ln(Ph_3PO)_4(\eta^2\text{-}NO_3)_2(\eta^1\text{-}NO_3)]$ are formed. For the smaller later metals Tb–Lu (Ln^{3+} radii: 92–86 pm) the complexes contain the eight-coordinate cations $[Ln(Ph_3PO)_4(\eta^2\text{-}NO_3)_2]NO_3$, whilst tetrakis complexes do not seem to form under similar conditions for the middle elements Sm–Gd. Whilst this might seem simply a consequence of the differing steric demands of Ph_3PO and nitrate groups operating against a background of decreasing metal cation radius, the solution behaviour (especially the ^{31}P NMR data) show other factors are involved. For the earlier metals La–Gd only $[Ln(Ph_3PO)_3(NO_3)_3]$ are present in solution even with excess Ph_3PO, for Tb–Tm $[Ln(Ph_3PO)_4(NO_3)_2]^+$ and $[Ln(Ph_3PO)_3(NO_3)_3]$ are both present, and for the later elements Yb and Lu, $[Ln(Ph_3PO)_4(NO_3)_2]^+$ show little decomposition in solution. This suggests that the affinity for Ph_3PO over nitrate increase down the series. We note that Y^{3+} (90 pm) conforms to this pattern. These studies are currently being extended to Ph_2MePO and Me_3PO complexes to explore these factors further, and preliminary data show, for example, that solid $[La(Ph_2MePO)_4(NO_3)_3]$ contains ten-coordinate La with three bidentate nitrate ions [19].

5. Supplementary data

Crystallographic data for the structures have been deposited with the Cambridge Crystallographic Data Centre (CCDC) and given numbers 139145 (Lu) and 147405 (La). Copies of the data can be obtained upon

request from CCDC, 12 Union Road, Cambridge, CB2 1EZ, UK, quoting the deposition numbers (fax: +44-1223-336033; e-mail: deposit@ccdc.cam.ac.uk or www: http://www.ccdc.cam.ac.uk).

Acknowledgements

We thank Professor M.B. Hursthouse for the data collection on the Nonius ccd diffractometer, Dr P.F. Henry for the powder X-ray diffraction measurements, and M. Bosson for preliminary studies of the Pr and Nd complexes.

References

[1] For a review see; T.S. Lobana, in: F.R. Hartley (Ed.), The Chemistry of Organophosphorus Compounds, vol. 2, Wiley, New York, 1992, p. 409.
[2] D.R. Cousins, F.A. Hart, J. Inorg. Nucl. Chem. 29 (1967) 1745.
[3] A.M.G. Massabni, M.L.R. Gibran, O.A. Serra, Inorg. Nucl. Chem. Lett. 14 (1978) 419.
[4] G. Valle, G. Casotto, P.L. Zanonato, B. Zarli, Polyhedron 5 (1986) 2093.
[5] J. Sakamoto, C. Miyake, Kidorui 22 (1993) 154. (Chem. Abs. 1995, 122, 278608y).
[6] L. Deakin, W. Levason, M.C. Popham, G. Reid, M. Webster, J. Chem. Soc., Dalton Trans. (2000) 2439.
[7] K. Yvon, W. Jeitscho, E. Parthe, J. Appl. Cryst. 10 (1977) 73.
[8] G.N. La Mar, W. DeW. Horrocks Jr., R.H. Holm (Eds.), NMR of Paramagnetic Molecules, Academic Press, New York, 1973, Chapters 12 and 13.
[9] D. Rehder, in: P.S. Pregosin (Ed.), Transition Metal Nuclear Magnetic Resonance, Elsevier, New York, 1991.
[10] S.D. Ross, Inorganic Infrared and Raman Spectra, McGraw Hill, London, 1972 Chapter 4.
[11] W.J. Geary, Coord. Chem. Rev. 7 (1971) 81.
[12] F.H. Allen, O. Kennard, Chem. Des. Autom. News, 8 (1993) 1 and 31-37.
[13] $[La(Ph_3PO)_3(NO_3)_3]\cdot xCH_2Cl_2$ ($x = 0.6$). Triclinic, space group $P\bar{1}$ (no. 2), $a = 11.3713(2)$, $b = 22.2680(5)$, $c = 24.3798(5)$ Å, $\alpha = 84.928(1)$, $\beta = 89.523(1)$, $\gamma = 77.764(1)°$, $V = 6009.1(2)$ Å^3, $T = 298$ K, $Z = 4$, $R = 0.097$ (15 091 reflections, $I > 2\sigma(I)$).
[14] Huang Chunhui, Xu Rongfang, Zhou Yongfeng, Xu Guangxian, Guo Fang, Zhu Naijue, Acta Phys.-Chim. Sin. 3 (1987) 491. (Chem. Abs. 108 (1988) 123246r).
[15] D.-L. Long, H.-M. Hu, J.-T. Chen, J.-S. Huang, Acta Crystallogr, Sect. C 55 (1999) 1664.
[16] G.M. Sheldrick, SHELXS 86, Program for the Solution of Crystal Structures, University of Göttingen, 1985.
[17] G.M. Sheldrick, SHELXL 97, Program for the Refinement of Crystal Structures, University of Göttingen, 1997.
[18] R.D. Shannon, C.T. Prewitt, Acta Crystallogr., Sect. B 26 (1970) 1046. The radii quoted are ionic radii for six-coordination rather than eight- or nine-coordination as present in the complexes, but for the purposes of comparison the trend across the series is important not the absolute values.
[19] M. Bosson, W. Levason, M. Webster, unpublished work.

PERGAMON

www.elsevier.nl/locate/poly

Polyhedron 19 (2000) 2707–2711

POLYHEDRON

Synthesis and structural characterization of mixed ligand η^1-2-hydroxyacetophenone complexes of cobalt(III)

Nijhuma Mondal [a], Dilip K. Dey [a], Samiran Mitra [a,*1], K.M. Abdul Malik [b,*2]

[a] *Department of Chemistry, Jadavpur University, Calcutta 700 032, India*
[b] *Department of Chemistry, Cardiff University, PO Box 912, Park Place, Cardiff, CF10 3TB, UK*

Received 29 June 2000; accepted 12 September 2000

Abstract

A tridentate Schiff base ligand $[(CH_3)_2NCH_2CH_2N{=}C(CH_3)C_6H_4OH)]$ (LH) has been synthesized from 2-hydroxyacetophenone and 2-dimethylaminoethylamine. This ligand forms the neutral complexes $[Co(L)(N_3)\{o\text{-}(CH_3C{=}O)C_6H_4O\}]$ (**1**) and $[Co(L)(SCN)\{o\text{-}(CH_3C{=}O)C_6H_4O\}]\cdot 1/2H_2O$ (**2**) in presence of equivalent amount of Co(II) acetate, and sodium azide for **1** and sodium thiocyanate for **2**. The complexes have been characterized by spectroscopic and crystallographic methods. The coordination geometry around Co(III) in both the complexes is distorted octahedral with one tridentate ligand L, one bidentate 2-hydroxyacetophenone and one monodentate azide for **1** and thiocyanate for **2**. The azide and thiocyanate ligands in the two complexes occupy different positions relative to the coordination sites of L. © 2000 Elsevier Science B.V. All rights reserved.

Keywords: Cobalt; 2-Hydroxyacetophenone; Azide; Thiocyanate; Crystal structure

1. Introduction

Cobalt(III) complexes derived from symmetrical and nonsymmetrical Schiff bases have drawn considerable attention in the past for their important biological applications [1–3]. Many model complexes of cobalt in both +2 and +3 oxidation states have been prepared and investigated, with particular emphasis on the reactivity of the metal ions in the transmethylation reaction and the reversible absorption of molecular oxygen [4–6]. In contrast, Co(III) complexes with uninegative tridentate Schiff base ligands have received less attention. We therefore carried out a study on the synthesis, structural characterization and reactivity of monomeric Co(III) mixed-ligand complexes derived from uninegative Schiff base ligands and η^1-bonded 2-hydroxyacetophenone. Aldehyde and ketone complexes of transition metals have been known from many years, but related studies on the formation and reaction of such complexes have been reported only relatively recently [7–12]. It has been found that both aldehydes and ketones can coordinate with metal centres in either η^1 or η^2 bonding mode and rarely in the η^3 fashion [7], and the bonded aldehydes and ketone groups can undergo various types of chemical transformation. These types of complexes are also used as catalysts in organic synthesis. Hersh and co-workers [13,14] have characterized an η^1-aldehyde complex of tungsten, which was used as a catalyst for Diels–Alder reaction [13,14]. The optically active η^2-aldehyde complex of rhenium was found to produce an optically active alcohol [15]. The structural studies on aldehyde complexes reveal that cationic-aldehyde complexes exhibit an η^1-bonding mode, while the neutral complexes show an η^2-bonding mode [16].

Recently Bharadwaj and co-workers [17] reported several η^1-aldehyde complexes of Mn(III), Fe(III) and Cu(II) metal ions. In the Mn(III) complexes, the bonded aldehyde group was reported to react readily with reagents such as 2-aminophenol, 2-aminothiophenol and 2-aminoethanol, producing mononuclear neutral Mn(III) complexes. The Cu(II) complex showed catalytic activity in the oxidation of olefins to epoxides in the presence of 2-methylpropanol and molecular oxygen. In a previous paper, we [18] described the synthesis and characterization of a neutral complex of

[1] *Corresponding author. E-mail: pkbose@cal.vsnl.net.in
[2] *Corresponding author. Tel.: +44-29-2087-4950; fax: +44-29-2087-4030; e-mail: malikka@cardiff.ac.uk

0277-5387/00/$ - see front matter © 2000 Elsevier Science B.V. All rights reserved.
PII: S0277-5387(00)00584-2

M(III), where the aldehyde group of salicylaldehyde is bonded to the metal in an η^1-mode. In this complex, the salicylaldehyde ligand showed enhanced reactivity towards primary monoamine and formed mixed-ligand complexes of Mn(III). To our knowledge, the structurally characterized 2-hydroxyacetophenone complex of Co(III) has not been reported so far. In the present article we report on the synthesis and characterization of two mixed-ligand complexes of Co(III) where the carbonyl group of 2-hydroxyacetophenone is bonded to the metal ion in an η^1-fashion.

2. Experimental

Reagent grade 2-hydroxyacetophenone (Merck), $Co(OAc)_2{\cdot}4H_2O$, sodium azide and sodium thiocyanate (Loba Chemie), and 2-dimethylaminoethylamine (Fluka) were used as received. Elemental analyses were carried out using a Perkin–Elmer 2400 II elemental analyser. Infrared spectra were recorded on a Perkin–Elmer 883-IR instrument as KBr pellets and electronic spectra were recorded on a Hitachi U-3400 (UV–Vis-NIR) spectrophotometer from a solution in methanol. ^1H and ^{13}C NMR spectra were recorded on a Bruker DPX-300 in $CDCl_3$ with TMS as internal standard. Magnetic susceptibilities were measured at room temperature using a vibrating sample magnetometer.

2.1. Synthesis of the ligand

The Schiff base ligand $(CH_3)_2NCH_2CH_2N{=}C(CH_3)C_6H_4OH$ (LH) was obtained by boiling a methanolic solution (25 ml) of 2-hydroxyacetophenone (1 mmol) and 2-dimethylamino-ethylamine (1 mmol) for 30 min under reflux. The orange solution containing the ligand was purified by column chromatography [silica gel (SRL) 60–120 mesh size, light petroleum–ethyl acetate mixture], and the purity confirmed by elemental analyses and ^1H NMR spectrum [^1H NMR (300 MHz): $\delta = 2.1$(s), 2.4(s), 2.8(t), 3.4(t), 6.9(m), 13.0(s)].

2.2. Synthesis of [Co(L)(N_3){o-($CH_3C{=}O$)C_6H_4O}] (1)

$Co(OAc)_2{\cdot}4H_2O$ (1 mmol, 0.249 g) in 5 ml methanol and an equivalent amount of 2-hydroxyacetophenone (0.12 ml) were added to a methanolic solution of the Schiff base ligand (1 mmol, 0.021 g). The resulting mixture was stirred for 5 min with addition of sodium azide (1 mmol, 0.065 g) in a minimum amount of water. On standing overnight, dark brown crystals of **1** were formed, which were collected by filtration and dried in vacuo over P_2O_5. *Anal.* Found: C, 54.22; H, 5.50; N, 15.71. Calc. for $C_{20}H_{24}CoN_5O_3$: C, 54.43; H, 5.48; N, 15.86%. ^1H NMR (300 MHz): δ (ppm) = 1.94(s), 2.22–2.78(m), 4.01(s), 6.48–6.66(m), 6.90–7.00(m), 7.43–7.61(m), 7.76(d). ^{13}C NMR (75 MHz): δ (ppm) = 18.54 (–N=C–CH_3), 28.41 (–C(CH_3)=O), 47.94 (N–CH_3), 52.12 (N–CH_3), 55.45 (N–CH_2–), 63.02 (N–CH_2–), 201.56 (C=O), 172.24 (C–O), 166.23 (C=N).

2.3. Synthesis of [Co(L)(NCS){o-($CH_3C{=}O$)C_6H_4O}]·1/2H_2O (2)

$Co(OAc)_2{\cdot}4H_2O$ (1 mmol, 0.249 g) in 5 ml methanol and an equivalent amount of 2-hydroxyacetophenone were added to a methanolic solution of the Schiff base ligand (1 mmol, 0.21 g). The mixture was stirred for 5 min with the addition of sodium thiocyanate (1 mmol, 0.081 g) in a minimum amount of water. Dark brown crystals appeared within 3 h, which were collected by filtration and dried in vacuo over P_2O_5. *Anal.* Found: C, 55.52; H, 5.32; N, 9.07. Calc. for $C_{21}H_{25}CoN_3O_{3.5}S$: C, 54.08; H, 5.40; N, 9.00%. ^1H NMR (300 MHz): δ (ppm) = 1.99(s), 2.46–2.87(m), 3.49(s), 4.09(s), 6.42–6.50(m), 6.79(d), 6.95–7.07(m), 7.45(d). ^{13}C NMR (75 MHz): δ (ppm) = 18.96 (–N=C–CH_3), 27.02 (–C(CH_3)=O), 48.75 (N–CH_3), 51.04 (N–CH_3), 54.32 (N–CH_2–), 62.0 (N–CH_2–), 202.21 (C=O), 171.73 (C–O), 167.80 (C=N).

2.4. X-ray crystallography

Crystallographic measurements were made at 150 K on an Enraf–Nonius Kappa CCD area detector diffractometer mounted at the window of a FR591 rotating anode generator for **1** [19] and on an Enraf–Nonius Turbo CAD4 diffractometer (non-profiled ω scan) for **2** [20] using Mo Kα radiation ($\lambda = 0.71073$ Å). Accurate cell parameters were obtained by least-squares refinement of the diffractometer angles for the entire data set in a 10° ϕ range for **1** and for 25 reflections in the range $17.0 < \theta < 18.0°$ for **2**. Absorption corrections were carried out by using multiple and symmetry related data measurements via the program SORTAV [21] for **1** and DIFABS [22] for **2**. The structures were solved by a direct method (SHELXS-86) [23] and refined by full-matrix least-squares on F^2 using all unique data (SHELXL-96) [24]. In both structures, the phenyl rings were treated as idealized hexagons (C–C = 1.390 Å, C–C–C = 120.0°). Crystals of **2** contained a disordered water solvate, for which two oxygen positions (occupancies 0.12 and 0.38) were refined with an ISOR = 0.01 restraint. Two partially occupied hydrogen atoms were obtained from difference map, which were included in the model but not refined. Other hydrogen atoms in both the structures were included in calculated positions (riding model) with U_{iso} tied with the U_{eq} of the parent atom. A summary of the crystallographic data and refinement details, and important bond lengths and angles for both complexes are given in Tables 1 and 2, respectively.

3. Results and discussion

The analytical data for the complexes **1** and **2** are in good agreement with the calculated values. The diamagnetic character of the complexes indicated that the cobalt atom in both cases has a low spin d^6 configuration and $+3$ oxidation state.

3.1. Infrared and NMR spectroscopy

The IR stretching frequencies for the metal bonded imine group and the η^1-bonded carbonyl group are very similar [25,26]. Strong peaks at ca. 1610 cm^{-1} for both complexes are attributable to the imine and η^1-bonded carbonyl stretching vibrations. The $\nu(N_3)$ appeared at 2035 cm^{-1} for **1** and ν(CN) for (SCN) was found at 2120 cm^{-1} for **2**. The ^1H and ^{13}C NMR spectra of the complexes are consistent with the X-ray determined structures (discussed below). In the spectrum of the free ligand, the OH proton appears at 13 ppm; this signal is absent in the spectra of the complexes, which suggests that the cobalt atom is bonded to the ligand through the replacement of the phenolic hydrogens. The ^1H NMR signals for both the complexes are basically similar, with those for **1** being slightly broader than in **2**. In ^{13}C NMR, the signals for the C=O and C=N groups are comparable. These features suggest structural similarity between the two complexes. The signals for all other aromatic and aliphatic carbon atoms appear at the usual positions.

Table 1
Crystal data and details of data collection and structure refinement for **1** and **2** [a]

	Compound **1**	Compound **2**
Chemical formula	$C_{20}H_{24}CoN_5O_3$	$C_{21}H_{24}CoN_3O_3S\cdot 1/2H_2O$
Formula weight	441.37	466.43
a (Å)	14.7508(3)	7.016(2)
b (Å)	6.6224(2)	23.218(3)
c (Å)	20.5799(5)	13.315(2)
β (°)	97.7477(13)	94.72(2)
V (Å^3)	1992.01(9)	2161.6(6)
Space group	$P2_1/c$ (no. 14)	$P2_1/n$ (no. 14)
Crystal size (mm)	$0.20\times0.075\times0.075$	$0.35\times0.25\times0.20$
Shape	needle-like	prism
Color	red	brown
θ Range for data collection (°)	3.20–25.10	3.04–25.17
Reflections collected	18 331	3849
Unique reflections	3539	3487
R_{int}	0.0611	0.0221
Data/parameters in the refinement	3539/242	3487/257
Goodness-of-fit on F^2	0.976	1.028
Final R [b] indices	$R_1 = 0.1198$, (0.0754) [c] $wR_2 = 0.2021$, (0.1904) [c]	$R_1 = 0.1082$, (0.0441) [c] $wR_2 = 0.1187$, (0.0774) [c]

[a] Details in common: monoclinic, $Z=4$, Mo Kα radiation, $\lambda=0.71073$ Å, $T=150(2)$ K.

[b] $R_1=\Sigma(F_o-F_c)/\Sigma(F_o)$; $wR_2=[\Sigma\{w(F_o^2-F_c^2)^2\}/\Sigma\{w(F_o^2)\}^2]^{1/2}$.

[c] R_1 and wR_2 values for all unique data; those calculated for data with $I>2\sigma(I)$ are given in parentheses.

Table 2
Important bond lengths (Å) and bond angles (°) for **1** and **2**

	(**1**)	(**2**)
Co(1)–O(1)	1.860(5)	1.850(3)
Co(1)–O(2)	1.905(5)	1.911(2)
Co(1)–O(3)	1.902(4)	1.860(3)
Co(1)–N(1)	2.007(5)	2.007(3)
Co(1)–N(2)	1.895(5)	1.893(3)
Co(1)–N(3)	1.937(6)	1.906(3)
O(1)–C(1)	1.314(6)	1.334(3)
O(2)–C(13)	1.286(8)	1.258(4)
O(3)–C(19)	1.350(6)	1.331(3)
N(2)–C(7)	1.293(8)	1.294(5)
N(2)–C(8)	1.479(8)	1.482(5)
N(3)–N(4)	1.199(7)	
N(4)–N(5)	1.163(7)	
N(3)–C(21)		1.160(5)
C(21)–S(1)		1.628(4)
O(1)–Co(1)–O(2)	89.5(2)	86.02(11)
O(1)–Co(1)–O(3)	87.4(2)	89.15(12)
O(1)–Co(1)–N(1)	177.7(2)	176.39(12)
O(1)–Co(1)–N(2)	94.8(2)	96.06(12)
O(1)–Co(1)–N(3)	89.7(2)	88.90(13)
O(2)–Co(1)–O(3)	92.5(2)	93.47(11)
O(2)–Co(1)–N(1)	92.2(2)	91.56(11)
O(2)–Co(1)–N(2)	86.6(2)	177.64(12)
O(2)–Co(1)–N(3)	178.4(2)	88.37(12)
O(3)–Co(1)–N(1)	91.0(2)	88.33(12)
O(3)–Co(1)–N(2)	177.6(2)	87.70(12)
O(3)–Co(1)–N(3)	88.9(2)	177.21(13)
N(1)–Co(1)–N(2)	86.8(2)	86.42(13)
N(1)–Co(1)–N(3)	88.6(2)	93.71(13)
N(2)–Co(1)–N(3)	92.0(2)	90.53(13)
Co(1)–N(3)–N(4)	116.6(5)	
Co(1)–N(3)–C(21)		175.0(3)
N(3)–N(4)–N(5)	177.1(7)	
N(3)–C(21)–S(1)		179.5(4)
Co(1)–O(1)–C(1)	125.5(4)	124.9(2)
Co(1)–O(2)–C(13)	127.0(5)	125.9(2)
Co(1)–O(3)–C(19)	122.6(4)	123.5(2)
Co(1)–N(1)–C(9)	104.2(4)	103.8(2)
Co(1)–N(2)–C(7)	127.0(5)	127.2(3)
Co(1)–N(2)–C(8)	112.4(4)	112.4(2)

3.2. Electronic spectroscopy

Two main bands, $^1A_{1g}\rightarrow{}^1T_{1g}$ and the $^1A_{1g}\rightarrow{}^1T_{2g}$, are normally observed in the d–d spectra of Co(III) complexes. In the present case, however, we observed only the lower energy band at 552 nm ($\varepsilon=540$ dm^3 mol^{-1} cm^{-1}) for **1** and at 555 nm ($\varepsilon=290$ dm^3 mol^{-1} cm^{-1}) for **2**. The higher energy band was probably obscured by the ligand to metal charge transfer band.

3.3. Crystal structures

The molecular structures of $[Co(L)(N_3)\{o\text{-}(CH_3C{=}O)C_6H_4O\}]$ (**1**) and $[Co(L)(NCS)\{o\text{-}(CH_3C{=}O)C_6H_4O\}]$ (**2**) are shown in Figs. 1 and 2, respectively, and important bond lengths and bond angles both compounds are listed in Table 2. The atom numbering scheme adopted is the same for both compounds except the azide and thiocyanate anions. Crystals of **2** also contain 0.5 molecule of H_2O per mole of complex, which is partially occupied and disordered, and is not shown in the figure.

In both compounds, the Co(III) ion is hexacoordinated with a N_3O_3 donor set arising from one tridentate Schiff base ligand (L), one bidentate 2-hydroxyacetophenone, and one monodentate azide (**1**) or thiocyanate (**2**). The coordination geometry is distorted octahedral in both cases, with the *trans* and *cis* angles lying in the ranges 176.39(12)–178.4(2) and 86.02(11)–96.06(12)°, respectively. The basic geometry is very similar in the two compounds but there are significant differences in the arrangements of the ligands around the metal atoms. This is evident from Figs. 1 and 2, in which the molecules are viewed approximately along the normal to the plane of the N(1), N(2) and O(1) donor atoms of the ligand L. If we consider these three atoms of L to occupy three corners of the equatorial plane, then the fourth corner is occupied by the phenolate oxygen [O(3)] in **1** but by the keto oxygen [O(2)] in **2**. This also means that the keto oxygen on **1** and the phenolate oxygen in **2** occupy one of the axial sites in the respective octahedron. The other axial position is occupied by the azide group in **1** and by the thiocyanate group in **2**. It is important to note that, in the former, the azide group lies *trans* to the O(2) atom of the acetophenolate ligand, whereas in the latter the thiocyanate group lies *trans* to the O(3) atom of the same ligand. The $[Co(L)(L')\{o\text{-}(CH_3C{=}O)C_6H_4O\}]$ (L′=NNN or NCS) molecules in the present work clearly represent two structural isomers of an octahedral complex containing one tridentate, one bidentate and one unidentate ligands.

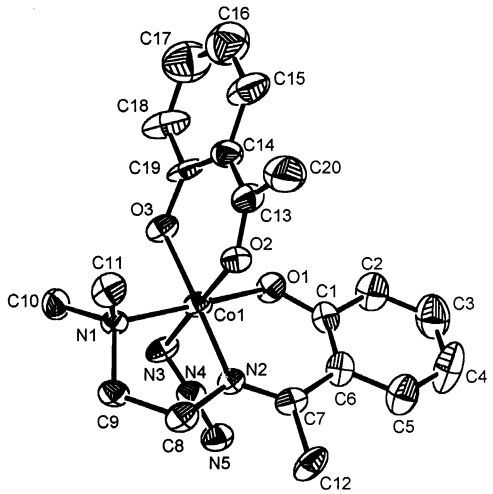


Fig. 1. X-ray structure of **1** with atom numbering scheme. The thermal ellipsoids are drawn at 40% probability level. For clarity, the hydrogen atoms are not shown.

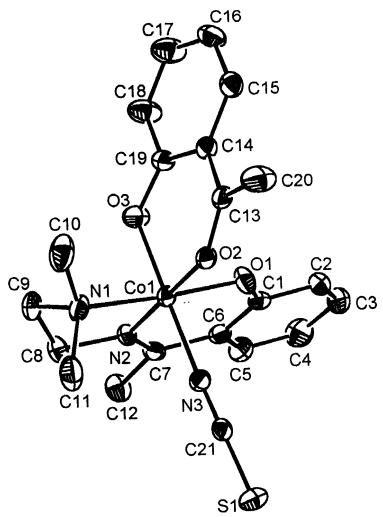


Fig. 2. X-ray structure of **2** with atom numbering scheme. The thermal ellipsoids are drawn at 40% probability level. For clarity, the hydrogen atoms are not shown.

The corresponding Co–O and Co–N distances in the two molecules are quite close. In fact, the Co(1)–N(1), Co(1)–N(2), Co(1)–O(1) and Co(1)–O(3)/O(2) distances in the equatorial plane in the two molecules are virtually identical [2.007(5), 1.895(5), 1.860(5) and 1.902(4) Å respectively in **1**, and 2.007(3), 1.893(3), 1.850(3) and 1.911(2) Å in **2**]. The Co–N(1) distance is ca. 0.12 Å longer than the Co–N(2) distance and reflects the different state of hybridization of the two nitrogen atoms. In both **1** and **2**, the Co–O distances fall in the range reported for other Schiff base complexes of Co(III) [5,6]. It may be noted here that the Co–O distances in the equatorial plane in the present complexes do not depend on the nature of the oxygen atom, i.e. whether it belongs to the phenolate (**1**) or the keto group (**2**). In contrast, the Co–O distances in the axial positions seem to be affected by the nature of the ligand *trans* to it. Thus the Co(1)–O(2) distance [1.905(5) Å] in **1** is somewhat longer than the Co–O(3) distance [1.860(3) Å] in **2**, which may be the result of greater *trans* influence of the azide compared with the thiocyanate group. In **1**, the bond lengths involving the azide group, Co(1)–N(3), N(3)–N(4) and N(4)–N(5) distances are 1.937(6), 1.199(7) and 1.163(7) Å, respectively, and are comparable to the corresponding values in other Co(III) azido complexes [27,28]. The azide group is almost linear [N(5)–N(4)–N(3) = 177.1(7)°] and coordinates to the cobalt atom in a bent fashion [N(4)–N(3)–Co(1) = 116.6(5)°]. In **2**, the NCS group is

also linear [N(3)–C(21)–S(1) = 179.5(4)°] and nearly coaxial with the Co(1)–N(3) bond [C(21)–N(3)–Co(1) = 175.0(3)°]. The N–C and C–S distances [1.160(5) and 1.628(4) Å, respectively] are comparable with the corresponding distances in other molecules, e.g. 1.146(4) and 1.638(3) Å in $[Ni(pn)(py)_2(NCS)_2]$ [19]. The corresponding geometry parameters in the tridentate and bidentate ligands in **1** and **2** are comparable. The N(2)–(C7) distance [1.293(8) Å (**1**), 1.294(5) Å (**2**)] clearly indicates its double bond character. The NCH_2CH_2N chelate adopts a *gauche* conformation in both the molecules. Of the C–O distances, those in the keto group are somewhat shorter than those in the phenolate groups.

4. Supplementary data

Full details of data collections and structure determinations have been deposited with the Cambridge Crystallographic Data Centre, CCDC nos. 146 366 (**1**) and 146 367 (**2**). Copies of this information may be obtained free of charge from: The Director, CCDC, 12 Union Road, Cambridge CB2 1EZ, UK (fax: +44-1223-336033; e-mail: deposit@ccdc.cam.ac.uk or www: http://www.ccdc.cam.ac.uk).

Acknowledgements

We thank CSIR, DST and UGC (New Delhi, India) for financial assistance, and Professor M.B. Hursthouse (Southampton University) for access to the EPSRC supported X-ray Crystallography Service (data for **2**).

References

[1] R.K. Parashar, R.C. Sharma, A. Kumar, G. Mohan, Inorg. Chim. Acta 151 (1988) 201.
[2] S. Brückner, M. Calligaris, G. Nardin, L. Randaccio, Inorg. Chim. Acta 4 (1968) 386.
[3] H. Chen, D. Han, H. Yan, W. Tang, Y. Yang, H. Wang, Polyhedron 12 (1993) 1097.
[4] J.P. Costes, G. Cros, M.H. Darbieu, J.P. Laurent, Inorg. Chim. Acta 60 (1982) 111.
[5] A. Böttcher, T. Takeuchi, K.I. Hardcastle, T.J. Meade, H.B. Gray, D.C. Wikel, M. Kapon, Z. Dori, Inorg. Chem. 36 (1997) 2498.
[6] A. Clearfield, R. Gopal, R.J. Kline, M. Sipski, L.O. Urban, J. Coord. Chem. 7 (1978) 163.
[7] Y. Huang, J.A. Gladysz, J. Chem. Educ. 65 (1988) 298.
[8] (a) D.B. Dombek, J. Chem. Educ. 63 (1986) 210. (b) D.B. Dombek, Adv. Catal. 32 (1983) 325.
[9] R. Noyori, T. Ohkuma, M. Kitamura, H. Takaya, N. Sayo, H. Kumobayashi, S. Akutagawa, J. Am. Chem. Soc. 109 (1987) 7560.
[10] J.W. Faller, J.A. John, M.R. Mazzieri, Tetrahedron Lett. 30 (1989) 1769.
[11] E.R. Burkhardt, R.G. Bergman, C.H. Heathcock, Organometallics 9 (1990) 30.
[12] J.H. Freudenberger, A.W. Konradi, S.F. Pederson, J. Am. Chem. Soc. 111 (1989) 8014.
[13] P.V. Bonesen, C.L. Puckett, R.V. Honeychuck, W.H. Hersh, J. Am. Chem. Soc. 111 (1989) 6070.
[14] P.V. Bonesen, C.L. Puckett, R.V. Honeychuck, J. Farahi, W.H. Hersh, J. Org. Chem. 52 (1987) 5293.
[15] J.M. Fernandez, K. Emerson, R.H. Larsen, J.A. Gladysz, J. Am. Chem. Soc. 108 (1986) 8268.
[16] R.M. Bullock, B.J. Rappoli, J. Am. Chem. Soc. 113 (1991) 1659.
[17] G. Das, R. Shukla, S. Mondal, R. Singh, P.K. Bharadwaj, J.V. Hall, K.H. Whitemire, Inorg. Chem. 36 (1997) 323.
[18] T. Gupta, M.K. Saha, S. Sen, S. Mitra, A.J. Edwards, W. Clegg, Polyhedron 18 (1998) 197.
[19] K.M.A. Malik, S. Mitra, R.K.B. Singh, J. Chem. Crystallogr. 29 (1999) 877.
[20] CAD4 Express Software, Enraf–Nonius, 1994.
[21] (a) R.H. Blessing, Acta Crystallogr., Sect. A 51 (1995) 33. (b) J. Appl. Crystallogr. 30 (1997) 421.
[22] A.C.T. North, D.C. Phillips, F.S. Mathews, Acta Crystallogr., Sect. A 24 (1968) 351.
[23] G.M. Sheldrick, Acta Crystallogr., Sect. A 46 (1990) 467.
[24] G.M. Sheldrick, SHELXL-96, Program for Crystal Structure Refinement, University of Göttingen, Germany, 1996.
[25] K. Nakamoto, Infrared and Raman Spectra of Inorganic and Co-ordination Compounds, 3rd Edn., Wiley, New York, 1978, p. 231.
[26] R.H. Holm, W.G. Everett, A. Chakraborty, Prog. Inorg. Chem. 7 (1986) 83.
[27] M.A.S. Goher, R.J. Wang, T.C.W. Mak, Polyhedron 11 (1992) 829.
[28] M.S. Massoud, F.A. Mautner, M. Abu-Youssef, N.M. Shuaib, Polyhedron 18 (1999) 2287.

PERGAMON

www.elsevier.nl/locate/poly

Polyhedron 19 (2000) 2713–2717

POLYHEDRON

Copper(II)-activated transformation of azomethine to imidate: synthetic and structural studies

Nimma Rajaiah Sangeetha, Satyanarayan Pal, Samudranil Pal *

School of Chemistry, University of Hyderabad, Hyderabad 500 046, India

Received 29 June 2000; accepted 20 September 2000

Abstract

The Schiff base 2-pyridine–carboxaldehyde 4-dimethylaminobenzoylhydrazone (HL, **1**) was prepared by reacting 2-pyridine–carboxaldehyde and 4-dimethylaminobenzoylhydrazine in a 1:1 molar ratio in methanol. Reaction of HL (**1**) with $Cu(O_2CCH_3)_2{\cdot}H_2O$ (in a 1:1 molar ratio) in methanol afforded a dinuclear copper(II) complex, $[Cu_2(\mu\text{-}O_2CCH_3)_2L'_2]{\cdot}2H_2O$ (**2**). The azomethine functionality (–CH=N–) of **1** is converted to imidate (–C(OMe)=N–) in the complexed ligand L'^-. Molecular structures of both **1** and **2** were determined by X-ray crystallographic studies. The dinuclear molecule of **2** is centrosymmetric and contains two monoatomic bridging acetate groups. Each copper(II) centre is in a square-pyramidal N_2O_3 coordination sphere. The ligand, L'^- coordinates the metal ion via the pyridine-N, the imidate-N, and the deprotonated amide-O atoms. One of the acetate oxygen atoms completes the N_2O_2 square-plane. The oxygen of the symmetry-related acetate fills the apical coordination site. Structural parameters are consistent with both copper ions being in a +2 oxidation state. The room temperature magnetic moment is 1.89 μ_B (per Cu). In powder phase the complex displays an axial EPR spectrum at 298 K. The complex is nonconducting in methanol solution. The electronic spectrum shows a ligand field absorption at 680 nm and charge transfer bands in the range 426–215 nm. © 2000 Elsevier Science B.V. All rights reserved.

Keywords: Copper(II); Azomethine; Imidate; Crystal structures

1. Introduction

Continuing interest in the metal-assisted transformations of organic functionalities is primarily due to the quest for convenient synthetic methods and regio- and stereoselective processes [1–5]. We have been working on the transition-metal complexes of amide containing aroylhydrazones to obtain high-valent metal complexes and amide oxygen bridged dinuclear species. Our interest is to study the effect of amide protonation and deprotonation on the coordination geometry, metal redox and interaction between metal centres in dinuclear species [6–11]. In our attempt to prepare a bivalent copper complex by treating pyridine-N, imine-N and amide-O donor 2-pyridine–carboxaldehyde 4-dimethylaminobenzoylhydrazone (HL, **1**) with $Cu(O_2CCH_3)_2{\cdot}H_2O$ in methanol, we have observed an interesting reaction in which the azomethine group present in HL is transformed to imidate in the complex, $[Cu_2(\mu\text{-}O_2CCH_3)_2L'_2]{\cdot}2H_2O$ (**2**). The syntheses and X-ray structures of the free hydrazone and the copper(II) complex of the transformed ligand are described in this report.

2. Experimental

The chemicals and solvents used in this work were of analytical grade available commercially and were used without further purification.

2.1. Preparation of HL (*1*)

To a methanol solution (30 cm^3) of 4-dimethylaminobenzoylhydrazine (380 mg, 2.12 mmol), 0.2 cm^3 (225 mg, 2.10 mmol) of 2-pyridine–carboxaldehyde was added and the mixture was refluxed for 6 h. The solution was then evaporated on a steam bath to 5 cm^3

* Corresponding author. Tel.: +91-40-301-0500; fax: +91-40-301-2460.

E-mail address: spsc@uohyd.ernet.in (S. Pal).

0277-5387/00/$ - see front matter © 2000 Elsevier Science B.V. All rights reserved.
PII: S0277-5387(00)00595-7

and cooled to room temperature. A light yellow crystalline solid separated was collected by filtration, washed with *n*-hexane and dried in air. Yield: 462 mg (82%). Found: C, 67.0; H, 5.9; N, 20.8. Calc. for $C_{15}H_{16}N_4O$: C, 67.15; H, 6.01; N, 20.88%. ^{1}H NMR data [δ (J) (ppm (Hz)) (multiplicity)]: $N(CH_3)_2$, 3.03 (s); azomethine-H, 9.53 (s); amide-H, 8.21 (s); aroyl H-atoms, 6.68 (9) (d), 7.85 (9) (d); pyridine H-atoms, 7.25 (m), 7.7 (m), 8.12 (8) (d), 8.56 (5) (d). Electronic spectral data in CH_3OH solution [λ_{max} (ε) (nm (mol^{-1} dm^3 cm^{-1}))]: 417sh (2100), 345 (33 500), 302 (15 000), 290sh (14 000), 232sh (10 100). Selected IR bands (cm^{-1}): 3216m, 1636s, 1608s, 1557s, 1526s, 1470m, 1435m, 1375m, 1339m, 1283s, 1194s, 1134s, 1069m, 1028m, 947m, 918m, 824s, 781m, 756m, 667m, 598w, 523w.

2.2. Preparation of $[Cu_2(\mu\text{-}O_2CCH_3)_2L'_2]\cdot 2H_2O$ (2)

A methanol solution (15 cm^3) of $Cu(O_2CCH_3)_2\cdot H_2O$ (25 mg, 0.125 mmol) was added to another methanol solution (25 cm^3) of 2-pyridine–carboxaldehyde 4-dimethylaminobenzoylhydrazone (HL) (34 mg, 0.127 mmol). The brown mixture was refluxed for 1 h. The clear brown solution was cooled to room temperature and 40 cm^3 of xylene was added followed by slow evaporation in air at room temperature. A dark crystalline solid separated in about 2 weeks and was collected by filtration and dried in air. The single crystal for structure determination was chosen from this material. Yield obtained by this procedure was 17 mg (31%). Found: C, 49.2; H, 4.9; N, 12.5. Calc. for $Cu_2C_{36}H_{44}N_8O_{10}$: C, 49.37; H, 5.06; N, 12.79%. Electronic spectral data in CH_3OH solution [λ_{max} (ε) (nm (mol^{-1} dm^3 cm^{-1}))]: 680sh (120), 426 (32 500), 304sh (13 100), 281 (15 300), 238sh (15 500), 215sh (18 000). Selected IR bands (cm^{-1}): 3468w, 1636s, 1601s, 1528w, 1462m, 1379s, 1329s, 1263m, 1188s, 1057w, 964w, 936m, 824m, 793m, 752m, 683m, 650m, 611m, 494w.

2.3. Physical measurements

Microanalytical data (C,H,N) were obtained with a Perkin–Elmer model 240C elemental analyser. Infrared spectra were collected by using KBr pellets of the compounds on a JASCO-5300 FT-IR spectrophotometer. A Shimadzu 3101-PC UV–Vis/NIR spectrophotometer was used to obtain the electronic spectrum. A ^{1}H NMR spectrum of HL in $CDCl_3$ solution was recorded on a Bruker 200 MHz spectrometer using $Si(CH_3)_4$ as internal standard. A JEOL FE-3X spectrometer was used to collect the X-band EPR spectrum. The spectrum was calibrated with respect to DPPH ($g = 2.0037$). Magnetic susceptibilities were measured by using a Cahn magnetic susceptibility system consisting of a model 4600 adjustable gap electromagnet and a model 1000 electrobalance. Diamagnetic corrections calculated from Pascal's constants [12] were used to obtain the molar paramagnetic susceptibilities. Electrical conductivity measurements were performed by using a Digisun conductivity meter model DI-909.

2.4. X-ray crystallography

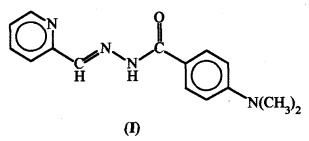
Single crystals of HL (**1**) were obtained by slow evaporation of a methanol solution. One of these solvent loss sensitive crystals was taken in a glass capillary with mother liquor and sealed. The crystal of complex **2** was mounted at the end of a glass fibre. The data were collected on an Enraf–Nonius Mach3 diffractometer using graphite-monochromated Mo Kα radiation ($\lambda = 0.71073$ Å) by ω-scan method at 293 K. Unit cell parameters of **1** and **2** were determined by the least-squares fit of 25 reflections having 2θ values in the range 18–23 and 19–22°, respectively. Intensities of three check reflections were measured after every 1.5 h during the data collection. No decay was observed in the 22 h (**1**) and 49 h (**2**) of exposure to X-radiation. The ψ-scans [13] of four reflections with θ and χ values in the ranges 3–13 and 85–87°, respectively, were used for the empirical absorption correction of the dataset of **2**.

The structures were solved by direct methods and refined by full-matrix least-squares on F^2 and difference-Fourier techniques. The structure of **1** was solved in the space group $P2_1/c$. The asymmetric unit consists of a molecule of **1** with one methanol molecule. The copper(II) complex crystallises as dihydrate (**2**) in the space group *Pccn* and the asymmetric unit contains half of the dinuclear species and one water molecule. For both structures, all the non hydrogen atoms were refined anisotropically. Hydrogen atoms were added at idealised positions for structure factor calculations, but not refined. Calculations were done using the programs of XTAL software [14] for data reduction, DATCOR program [15] for absorption correction and SHELX-97 programs [16] for structure solution and refinement. The ORTEX6a package [17] was used for molecular graphics. Crystal parameters and refinement residuals are listed in Table 1.

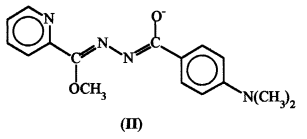
3. Results and discussion

3.1. Synthesis

The hydrazone (HL, **1**) was prepared by condensing 1 equiv. of 2-pyridine–carboxaldehyde with 1 equiv. of 4-dimethylaminobenzoylhydrazine in boiling methanol. The procedure is similar to that reported earlier [18,19]. The elemental analysis, infrared and ^{1}H NMR spectral data are as expected for structure **I**.



(I)



(II)

The complex (**2**) was obtained as a crystalline solid in ~30% yield by reacting $Cu(O_2CCH_3)_2{\cdot}H_2O$ with HL in a 1:1 molar ratio in hot methanol, followed by addition of xylene to the deep brown reaction mixture and slow evaporation in air. The remaining mother liquor was of light yellow colour. The elemental analysis of the complex is satisfactory with the empirical formula $Cu(O_2CCH_3)(L')(H_2O)$, where L'^- is the deprotonated form (**II**) of the transformed HL.

The hydrazone (HL) was synthesised in methanol and can be recrystallized from the same solvent. Thus, the azomethine to imidate conversion happens after it coordinates the metal ion. There are at least two possible pathways for the transformation of the azomethine group of the copper(II)-coordinated hydrazone: (i) a nucleophilic attack at the polarised azomethine carbon by a methoxide followed by one electron reduction of the coordinated metal ion, homolytic cleavage of (OMe)C–H and formation of (OMe)C=N, and finally aerial oxidation of copper(I) to copper(II) and (ii) addition of methanol to the polarised azomethine group followed by oxidation to the final product, $[Cu_2(\mu\text{-}O_2CCH_3)_2L'_2]$ by a portion of the copper(II) complex initially formed. The low yield of $[Cu_2(\mu\text{-}O_2CCH_3)_2L'_2]$ with respect to total copper supports this second hypothesis. Addition of water or alcohol to a metal ion coordinated azomethine group has been reported [20,21]. In the presence of water, coordinated azomethine to amide conversion has been observed before and a mechanism similar to (ii) has been suggested [22].

Table 1
Crystallographic data for $HL{\cdot}CH_3OH$ (**1**·CH_3OH) and $[Cu_2(\mu\text{-}O_2CCH_3)_2L'_2]{\cdot}2H_2O$ (**2**)

Compound	**1**·CH_3OH	**2**
Chemical formula	$C_{16}H_{20}N_4O_2$	$Cu_2C_{36}H_{44}N_8O_{10}$
Crystal system	monoclinic	orthorhombic
Space group	$P2_1/c$	$Pccn$
a (Å)	6.6704(13)	21.625(4)
b (Å)	29.778(3)	14.6815(17)
c (Å)	8.010(2)	12.279(3)
α (°)	90	90
β (°)	97.913(14)	90
γ (°)	90	90
V (Å^3)	1575.9(6)	3898.6(12)
Z	4	4
Reflections measured	2269	5016
Reflections unique	2194	4496
Reflections $I>2\sigma_I$	1267	1770
Parameters	203	257
R_1 [a], wR_2 [b] ($I>2\sigma_I$)	0.0488, 0.1241	0.0600, 0.1401

[a] $R_1 = \Sigma||F_o|-|F_c||/\Sigma|F_o|$.

[b] $wR_2 = \{\Sigma[(F_o^2-F_c^2)^2]/\Sigma[w(F_o^2)^2]\}^{1/2}$; $w = 1/[\sigma^2(F_o^2)+(aP)^2+bP]$, where $a = 0.0875$ and 0.0888 for **1**·CH_3OH and **2**, respectively, and $b = 0.0$ for both.

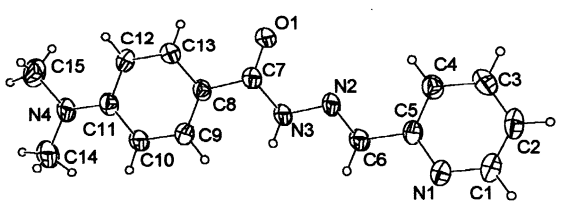


Fig. 1. Molecular structure of HL with the atom-labelling scheme. All atoms are represented by their 40% probability thermal ellipsoids.

3.2. Physical properties of $[Cu_2(\mu\text{-}O_2CCH_3)_2L'_2]{\cdot}2H_2O$ (2)

The complex (**2**) is electrically nonconducting in methanol solution. In solid state the room temperature (298 K) magnetic moment (1.89 μ_B) per metal ion is very close to the spin-only moment for a d^9 system indicating no significant spin–spin interaction.

At room temperature the complex in powder phase displays an axial EPR spectrum ($g_\parallel = 2.28$ and $g_\perp = 2.09$). No hyperfine splitting is observed. Such spectra are typical for square-planar or square-pyramidal copper(II) species [23,24]. Similar powder EPR spectra have been observed for dicopper(II) complexes containing two monoatomic bridging acetate ions [11,24].

A weak band observed at 3468 cm^{-1} in the infrared spectrum of the complex is likely to be due to the lattice H_2O molecules [25]. The peak observed at 1636 cm^{-1} is possibly due to the ν_{as} stretch of the unidentate acetate group [25]. The origin of the strong peak at 1601 cm^{-1} is probably the =N–N=C(O^-)– moiety of the ligand [26,27].

The electronic spectrum of the complex in methanol shows a weak absorption at 680 nm followed by several intense absorptions in the range 426–215 nm. Weak bands observed in the range 620–675 nm for copper(II) complexes of Schiff bases and related ligands are assigned to d–d transitions [9,11,28,29]. The intense absorptions are most probably due to the ligand-to-metal charge transfer and intraligand transitions.

3.3. Description of structures

The molecular structure of the hydrazone (HL) is shown in Fig. 1. Selected bond distances and angles are listed in Table 2. The molecule is essentially planar. The largest and smallest deviations from the least-squares plane observed are 0.108(3) and −0.001(3) Å for N4 and C11, respectively. The mean deviation from the least-squares plane is 0.051 Å. The C7–O1 (1.224(3) Å)

Table 2
Selected bond distances (Å) and angles (°) for $HL{\cdot}CH_3OH$ ($\mathbf{1}{\cdot}CH_3OH$)

O(1)–C(7)	1.224(3)	N(3)–C(7)	1.362(3)
N(2)–N(3)	1.377(3)	N(2)–C(6)	1.271(3)
O(1)–C(7)–N(3)	121.4(2)	O(1)–C(7)–C(8)	122.2(3)
C(8)–C(7)–N(3)	116.4(2)	C(7)–N(3)–N(2)	117.6(2)
N(3)–N(2)–C(6)	116.5(2)	N(2)–C(6)–C(5)	120.1(3)

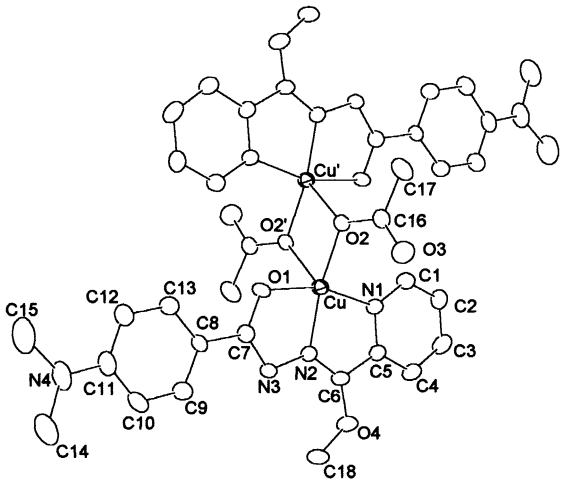


Fig. 2. Molecular structure of $[Cu_2(\mu\text{-}O_2CCH_3)_2L'_2]$ showing the 25% probability thermal ellipsoids and the atom-labelling scheme. Hydrogen atoms are omitted for clarity.

Table 3
Selected bond distances (Å) and angles (°) for $[Cu_2(\mu\text{-}O_2CCH_3)_2L'_2]{\cdot}2H_2O$ (**2**) [a]

Cu–O(1)	1.944(4)	Cu–O(2)	1.948(4)
Cu–O(2′)	2.309(4)	Cu–N(1)	2.006(5)
Cu–N(2)	1.931(5)	O(1)–C(7)	1.286(7)
N(3)–C(7)	1.330(7)	N(2)–N(3)	1.376(6)
N(2)–C(6)	1.280(7)	C(6)–O(4)	1.326(7)
O(1)–Cu–O(2)	99.22(17)	O(1)–Cu–O(2′)	94.59(17)
O(1)–Cu–N(1)	160.73(19)	O(1)–Cu–N(2)	79.80(19)
O(2)–Cu–O(2′)	75.52(17)	O(2)–Cu–N(1)	99.4(2)
O(2)–Cu–N(2)	164.82(19)	N(1)–Cu–N(2)	80.9(2)
N(1)–Cu–O(2′)	95.00(18)	N(2)–Cu–O(2′)	119.65(18)
Cu–O(2)–Cu′	104.48(17)	N(2)–C(6)–C(5)	114.7(5)

[a] Symmetry transformation used to generate equivalent atoms: $-x+1, -y, -z$.

and C7–N3 (1.362(3) Å) distances are consistent with the keto form of the amide functionality. The C6–N2 (1.271(3) Å) is typical for a C=N distance. The bond distances and angles in the pyridine and the benzene rings are unexceptional. The methanol molecule is hydrogen bonded with the amide-O of the hydrazone. The distance between the methanol oxygen and the amide-O is 2.753(3) Å.

The structure of the dinuclear complex, $[Cu_2(\mu\text{-}O_2CCH_3)_2L'_2]$ is illustrated in Fig. 2. Selected bond distances and angles are given in Table 3. The unit cell contains eight $Cu(O_2CCH_3)(L')(H_2O)$ fragments as asymmetric units. Each two $Cu(O_2CCH_3)(L')$ moieties form four centrosymmetric dinuclear molecules. The acetate ions are monoatomic bridging. The water molecules are hydrogen bonded with the nonbridging oxygen atoms of the acetate ions. The O3···O(water) distance is 2.809(9) Å. Each copper(II) centre is in distorted square-pyramidal N_2O_3 coordination geometry. The tridentate planar ligand binds the metal centre via the deprotonated amide-O, the imidate-N and the pyridine-N atoms. The oxygen of one of the acetates completes the N_2O_2 square-plane. The oxygen of the symmetry related acetate fills the apical site. There is a noticeable distortion of the basal plane towards tetrahedral geometry. The deviations of O1 and N1 from the mean plane are 0.11 and 0.10 Å, respectively, whereas those of O2 and N2 are -0.08 and -0.12 Å, respectively. The metal centre is 0.15 Å above the mean plane towards the apical O2′. The chelate bite angles in the five-membered rings formed by the amide-O and the imidate-N, and the pyridine-N and the imidate-N are very similar. The average value is 80.3°. Comparison of the N–N (1.376(6) Å), N–C (1.330(7) Å) and C–O (1.286(7) Å) distances in the $=N-N=C(O^-)-$ fragment of the coordinated ligand (L′) with the corresponding distances (Fig. 1, Table 2) in HL clearly suggests the deprotonation of the amide functionality in the complex. The C=N distance (1.280(7) Å) of the imidate moiety is identical with that (1.271(3) Å) of the azomethine group in HL. The Cu–N(pyridine) distance is comparable with the distances observed for other structurally characterised copper(II) complexes containing coordinated pyridine-N [30,31]. The distance corresponding to the Cu–N(imidate) bond is similar to the Cu–N(imine) distances reported earlier [8,9,11,32–36]. As expected the metal to deprotonated amide-O distance is shorter than that in complexes where copper(II) is coordinated to protonated amide-O [8,34–36]. The Cu–O–Cu′ bridge angle is 104.48(17)° and the metal–metal distance is 3.373(1) Å. The planar Cu_2O_2 fragment is unsymmetrical with respect to the Cu–O distances (Cu–O2, 1.948(4) Å and Cu–O2′, 2.309(4) Å). Such Cu–O distances (one short and one long) have been observed before in some dinuclear copper(II) complexes containing similar monoatomic bridging acetate [11,24,37–40].

4. Concluding remarks

In an attempt to prepare a copper(II) complex from a methanolic medium using 2-pyridine–carboxaldehyde 4-dimethylaminobenzoylhydrazone (HL), a transformation of the azomethine group of HL to imidate in the complex has been realised. The common method for the

preparation of imidates is the Pinner synthesis. In this method nitriles are treated with hydrogen halide in the presence of alcohol [41,42]. There is a report of imidate formation by reacting Schiff base with *t*-butylhypochloride in alcohol [43]. However, to the best of our knowledge no example of a metal ion activated azomethine to imidate transformation was previously known.

5. Supplementary material

Crystallographic data are available from the Cambridge Crystallographic Data Centre, 12 Union Road, Cambridge, CB2 1EZ, UK on request, quoting the deposition numbers CCDC-145601 and 145602 for **1**·CH_3OH and **2**, respectively. Copies of this information may be obtained free of charge from The Director, CCDC, 12 Union Road, Cambridge, CB2 1EZ, UK (fax: +44-1223-336033; e-mail: depsit@ccdc.cam.uk or www: http://www.ccdc.cam.ac.uk).

Acknowledgements

Funding for this work was provided by the Council of Scientific and Industrial Research, New Delhi (Grant No. 01(1422)/96/EMR-II). Ms N.R. Sangeetha acknowledges the University Grants Commission, New Delhi, for a research fellowship. X-ray crystallographic studies were performed at the National Single Crystal Diffractometer Facility, School of Chemistry, University of Hyderabad established by the Department of Science and Technology, New Delhi.

References

[1] T. Katsuki, Coord. Chem. Rev. 140 (1995) 189.
[2] M. Schuster, S. Blechert, Angew. Chem., Int. Ed. Engl. 36 (1997) 2036.
[3] R.A. Gossage, L.A. van de Kuil, G. van Koten, Acc. Chem. Res. 31 (1998) 423.
[4] A. Yamamoto, J. Chem. Soc., Dalton Trans. (1999) 1027.
[5] S. Kobayashi, H. Ishitani, Chem Rev. 99 (1999) 1069.
[6] N.R. Sangeetha, C.K. Pal, P. Ghosh, S. Pal, J. Chem. Soc., Dalton Trans. (1996) 3293.
[7] A.V. Lakshmi, N.R. Sangeetha, S. Pal, Ind. J. Chem. 36A (1997) 844.
[8] N.R. Sangeetha, S. Pal, J. Chem. Crystallogr. 29 (1999) 287.
[9] N.R. Sangeetha, K. Baradi, R. Gupta, C.K. Pal, V. Manivannan, S. Pal, Polyhedron 18 (1999) 1425.
[10] N.R. Sangeetha, S. Pal, Bull. Chem. Soc. Jpn. 73 (2000) 357.
[11] N.R. Sangeetha, S. Pal, Polyhedron 19 (2000) 1593.
[12] W.E. Hatfield, in: E.A. Boudreaux, L.N. Mulay (Eds.), Theory and Applications of Molecular Paramagnetism, Wiley, New York, 1976, p. 491.
[13] A.C.T. North, D.C. Philips, F.S. Mathews, Acta Crystallogr., Sect. A 24 (1968) 351.
[14] S.R. Hall, G.S.D. King, J.M. Stewart (Eds.), XTAL3.4 User's Manual, University of Western Australia, Perth, 1995.
[15] J. Reibenspies, Q & D Crystallographic Program Package, Texas A & M University, College Station, TX, 1989.
[16] G.M. Sheldrick, SHELX-97, Structure Determination Software, University of Göttingen, Göttingen, Germany, 1997.
[17] P. McArdle, J. Appl. Crystallogr. 28 (1995) 65.
[18] G. Struv, J. Prakt. Chem. 50 (1894) 295.
[19] L. Sacconi, Z. Anorg. Allg. Chem. 275 (1954) 249.
[20] D.H. Busch, J.C. Bailar, Jr., J. Am. Chem. Soc. 78 (1956) 1137.
[21] C.M. Harris, E.D. McKenzie, Nature 196 (1962) 670.
[22] M. Menon, S. Choudhury, A. Pramanik, A.K. Deb, S.K. Chandra, N. Bag, S. Goswami, A. Chakravorty, J. Chem. Soc., Chem. Commun. (1994) 57.
[23] P. O'Brien, J.R. Thornback, Inorg. Chim. Acta 64 (1981) 135.
[24] S.J. Brown, X. Tao, D.W. Stephan, P.K. Mascharak, Inorg. Chem. 25 (1986) 3377.
[25] K. Nakamoto, Infrared and Raman Spectra of Inorganic and Coordination Compounds, Wiley, New York, 1986, pp. 228–233.
[26] L. El-Sayed, M.F. Iskander, J. Inorg. Nucl. Chem. 33 (1971) 435.
[27] S. Choudhury, M. Kakoti, A.K. Deb, S. Goswami, Polyhedron 11 (1992) 3183.
[28] H.S. Maslen, T.N. Waters, Coord. Chem. Rev. 17 (1975) 137.
[29] S. Karunakaran, M. Kandaswamy, J. Chem. Soc., Dalton Trans. (1995) 1851.
[30] H. Oshio, U. Nagashima, Inorg. Chem. 31 (1992) 3295.
[31] K.J. Catalan, S. Jackson, J.D. Zubkowski, D.L. Perry, E.J. Valente, L.A. Feliu, A. Polanco, Polyhedron 14 (1995) 2165.
[32] S.K. Mandal, L.K. Thompson, M.J. Newlands, E.J. Gabe, K. Nag, Inorg. Chem. 29 (1990) 1324.
[33] P. Cheng, D. Liao, S. Yan, Y.Z. Jiang, G. Wang, X. Yao, H. Wang, Inorg. Chim. Acta 248 (1996) 135.
[34] Y. Shiping, C. Peng, L. Diazeng, J. Zonghui, W. Honggen, Y. Xinkan, Polyhedron 11 (1992) 879.
[35] E.W. Ainscough, A.M. Brodie, A.J. Dobbs, J.D. Ranford, J.M. Waters, Inorg. Chim. Acta 267 (1998) 27.
[36] V.V. Lukov, V.A. Kogan, S.I. Levchenkov, L.V. Zavada, K.A. Lyssanko, O.V. Shisbkin, Zh. Neorg. Khim. 43 (1998) 421.
[37] R. Hamalainen, M. Ahlgren, U. Tuspeinen, Acta Crystallogr., Sect. B 38 (1982) 1577.
[38] Y. Boukari, A. Busnot, F. Busnot, A. Leclaire, M.A. Bernard, Acta Crystallogr., Sect. B 38 (1982) 2458.
[39] J.P. Costes, F. Dahan, J.P. Laurent, Inorg. Chem. 24 (1985) 1018.
[40] B. Chiari, J.H. Helms, O. Piovesana, T. Tarantelli, P.F. Zanazzi, Inorg. Chem. 25 (1986) 870.
[41] R. Roger, D.G. Neilson, Chem. Rev. 61 (1961) 179.
[42] G. Neilson, in: S. Patai (Ed.), The Chemistry of Functional Groups; The Chemistry of Amidines and Imidates, Wiley, New York, 1975, p. 385.
[43] H. Paul, A. Weise, R. Dettmer, Chem. Ber. 98 (1965) 1450.

PERGAMON

www.elsevier.nl/locate/poly

Polyhedron 19 (2000) 2719–2738

POLYHEDRON

Author Index to Volume 19

Abe, I., see Hiroi, K., 525
Abram, U., Voigt, A. and Kirmse, R., The reaction of rhenium nitrido complexes with $^{+}CPh_3$. Synthesis, structures and EPR spectra of rhenium imido compounds, 1741
Abu-Reziq, R., see Blum, J., 509
Abu-Surrah, A.S., Lappalainen, K., Repo, T., Klinga, M., Leskelä, M. and Hodali, H.A., Palladium(II) complexes bearing ethylene-bridged S∩As and S∩P donor ligands: synthesis, crystal structure and reactivity towards the polymerization of norbornene, 1601
Adams, R.D. and Perrin, J.L., The catalytic transformation of thiiranes to cyclic disulfides by tungsten carbonyl complexes, 521
Agarossi, A., see Remelli, M., 2409
Ágoston, C.G., Várnagy, K., Bényei, A., Sanna, D., Micera, G. and Sóvágó, I., Solution equilibria and structural characterisation of the transition metal complexes of glycyl-L-cysteine disulfide, 1849
Aguado, R., see Arnáiz, F.J., 2141
Aguirre, M.J., see Trollund, E., 2303
Ahmed, S.I., Burgess, J., Fawcett, J., Parsons, S.A., Russell, D.R. and Laurie, S.H., The structures of bis-maltolato-zinc(II) and of bix-3-hydroxy-1,2-dimethyl-4-pyridinonato–zinc(II) and –lead(II), 129
Ainscough, E.W., Brodie, A.M., Burrell, A.K., Fan, X., Halstead, M.J.R., Kennedy, S.M.F. and Waters, J.M., The reactivity of the 'P_2N' ligand 2-(diphenylphosphino)-*N*-[2-(diphenylphosphino)-benzylidene]-benzeneamine towards sulfur and acid, 2585
Ainscough, E.W., see Depree, C.V., 2101
Airoldi, C., see Arakaki, L.N.H., 367
Akilan, P., see Amudha, P., 1769
Allegretti, Y., Ferrer, E.G., González Baró, A.C. and Williams, P.A.M., Oxovanadium(IV) complexes of quinic acid. Synthesis, characterization and potentiometric study, 2613
Almond, M.J., Drew, M.G.B., Redman, H. and Rice, D.A., A new simple synthetic route to M_3Se_7 (M = Mo or W) core containing complexes: crystal structure and characterisation of $[M_3(\mu_3\text{-}Se)(\mu\text{-}Se_2)_3(dtc)_3]_2Se$, 2127
Al-Salem, N.A., see Goher, M.A.S., 1465
Alshehri, S., Burgess, J., Fawcett, J., Parsons, S.A. and Russell, D.R., Structures of bis-ethylmaltolatodichloro-tin(IV) and -titanium(IV) and of trichloro(1-methyl-2-ethyl-3-hydroxy-4*H*-pyridin-4-onato)-aquatin(IV), 399
Al Shihadeh, Y., Benito, A., Lloris, J.M., Martínez-Máñez, R., Pardo, T., Soto, J. and Marcos Martínez, M., Aza–oxa macrocyclic ligands functionalised with naphthylmethyl fluorescent groups, 1867
Alvarado, E., Torres-Martinez, L.M., Fuentes, A.F. and Quintana, P., Preparation and characterization of MgO powders obtained from different magnesium salts and the mineral dolomite, 2345
Alvarez, J., see Longo, C., 487
Alvarez-Larena, A., see Chadghan, A., 855
Alyea, E.C., Ferguson, G. and Kannan, S., X-ray structural determination of a bulky phosphine complex: chloro{tris(2,4,6-trimethoxyphenyl)phosphine}gold(I), $\{AuCl[P(C_9H_{11}O_3)_3]\}$, 2211
Alzuet, G., Ferrer-Llusar, S., Borrás, J. and Martínez-Mánez, R., New Cu(II) and Zn(II) complexes of benzolamide with dithylenetriamine: synthesis, spectroscopy and X-ray structures, 725
Alzuet, G., see Borrás, E., 1859
Alzuet, G., see García-Raso, Á., 991
Amirkhanov, V.M., see Gubina, K.E., 2203
Amudha, P., Akilan, P. and Kandaswamy, M., Synthesis, spectral, electrochemical and magnetic properties of new phenoxo-bridged dicopper(II) complexes derived from unsymmetrical binucleating ligands with imino and amino side arms, 1769
Anderson, G.K., see Moser, J.A., 1329
Anderson, K.M., see Rice, C.R., 495
Andrade, C., see Crivelli, I.G., 2289
Andruh, M., see Tanase, S., 1967
Anson, C.E., Hartmann, S., Kelsey, R.D. and Stephenson, G.R., X-ray crystallographic proof of regioselectivity in a nitrosobenzene cycloaddition, and development of a novel in situ heterocycloaddition trap for use during decomplexation of tricarbonyliron diene complexes in hippeastrine synthesis, 569
Antonia Mendiola, M., see Cañadas, M., 2059
Arai, K., see Yanagihara, N., 1311
Arakaki, L.N.H. and Airoldi, C., Ethylenimine in the synthetic routes of a new silylating agent: chelating ability of nitrogen and sulfur donor atoms after anchoring onto the surface of silica gel, 367
Arancibia, A., see Díaz, C., 2679
Arancibia, A., see Diaz, C., 137
Ardiles, P., see Trollund, E., 2303
Arissawa, M., see Téllez-Sara, C.A., 2353
Arnáiz, F.J., Aguado, R., Pedrosa, M.R., De Cian, A. and Fischer, J., Synthesis, characterization and catalytic activity of addition compounds of dioxomolybdenum(VI) pyridine-2,6-dicarboxylate. Crystal structure of MoO_2(dipic)(L) (L = DMF, DMSO, $OPPh_3$), 2141
Arnold, D.P., see Jiang, J., 1381
Asada, H., Fujiwara, M. and Matsushita, T., Structures of dichloromanganese(IV) complexes with bidentate and tetradentate Schiff base ligands, 2039
A. Savel'eva, Z., V. Romanenko, G., A. Sheludyakova, L. and V. Larionov, S., Synthesis and structure of a complex with the coordinated triaminoguanidinium(2+) ion, $[Cu(TAGH_2)Cl_3]Cl{\cdot}H_2O$, 1737
Asfari, Z., see Thuéry, P., 1749
A. Sheludyakova, L., see A. Savel'eva, Z., 1737
Aslanidis, P., see Cox, P.J., 1615
Atwood, J.L. and Junk, P.C., Formation and crystal structures of novel seven-coordinate 15-crown-5 complexes of manganese(II), iron(II) and cobalt(II), 85
Aubol, S.L., see Parker, O.J., 623
Aucott, S.A., Slawin, A.M.Z. and Woollins, J.D., The preparation and characterisation of platinum and palladium phosphine thiocarbonate complexes $M(PR_3)_2(CS_3)$ and $Pt(PR_3)_2(CseS_2)$, 499
Aury, S., see Giroux, S., 1567

PII: S0277-5387(00)00652-5

Averbuj, C., see Kaftanov, J., 563
Avnir, D., see Blum, J., 509
Azam, K.A., Dilshad, R., Kabir, S.E., Mottalib, M.A., Hursthouse, M.B. and Malik, K.M.A., Metallation of 2-methyl-2-thiazoline at a triosmium cluster: X-ray structure of $[(\mu\text{-H})Os_3(CO)_{10}(\mu\text{-}\eta^2\text{-}CH_2\overline{C{=}NCH_2CH_2S})]$, 1081

Babonneau, F. and Maquet, J., Nuclear magnetic resonance techniques for the structural characterization of siloxane–oxide hybrid materials, 315
Bachmann, C., see Oberhauser, W., 913
Baidina, I.A., see Isakova, V.G., 1097
Baker, P.K. and Meehan, M.M., Synthesis and spectral properties of some new cobalt/tungsten chain triphos $\{PhP(CH_2CH_2PPh_2)_2\}$ bridged multimetallic complexes, 1585
Baker, P.K., Jenkins, A.E. and Meehan, M.M., Alkyne complexes of tungsten(II) containing carboxylate and sulfonate substituted pyridine ligands. Water-soluble alkyne complexes of tungsten(II), 2171
Baker, P.K., Samson, E., Veale, P.L. and Drew, M.G.B., Monodentately coordinated *o*-phenylenediacetonitrile seven-coordinate complexes of molybdenum(II) and tungsten(II): X-ray crystal structure of $[WI_2(CO)_3\{1,2\text{-}C_6H_4(CH_2CN)_2\text{-}N\}_2]$, 147
Bandini, M., Cozzi, P.G. and Umani-Ronchi, A., The first catalytic enantioselective Nozaki–Hirama–Kishi reaction, 537
Banerjee, R., see Mondal, B., 1213
Baran, P., see Boča, R., 835
Baran, P., see Vrbová, M., 2195
Barba-Behrens, N., see Ceniceros-Gómez, A.E., 1821
Barba-Behrens, N., see Quiroz-Castro, E., 1479
Barbier, J.-P., see Jubert, C., 1447
Bardají, M., see Romeo, I., 1837
Baricelli, P., see Longo, C., 487
Barik, A.K., Paul, S., Butcher, R.J. and Kar, S.K., Synthesis and characterization of two tris-chelate complexes of cobalt(III) with 3,5-dimethyl-1-(*N*-methyl/ethyl)thiocarbamylpyrazole (HL_1, HL_2) — biologically important bidentate ligands with one ambidentate donor site, 2651
Barton, A.J., Connolly, J., Levason, W., Mendia-Jalon, A., Orchard, S.D. and Reid, G., Synthesis and spectroscopic characterisation of tritelluroether, triselenoether, and trithioether complexes of Cr(0), Mo(0) and W(0), 1373
Barton, A.J., Levason, W., Reid, G. and Tolhurst, V.-A., Synthesis and properties of ditelluroether complexes of osmium, *trans*-$[OsCl_2(L\text{-}L)_2]$ and *trans*-$[OsCl(PPh_3)(L\text{-}L)_2]PF_6$ (L-L = *o*-$C_6H_4(TeMe)_2$, $RTe(CH_2)_3TeR$ (R = Ph or Me)), 235
Basuli, F., Kumar Das, A., Mostafa, G., Peng, S.-M. and Bhattacharya, S., Chemistry of ruthenium with some phenolic ligands: synthesis, structure and redox properties, 1663
Battistuzzi, G., Cannio, M. and Battistuzzi, R., Synthesis, magnetic, spectroscopic and electrochemical studies of mixed pyrimidine-2-thiolate/triphenylphosphine rhenium(V) and rhenium(III) complexes, 2163
Battistuzzi, R., see Battistuzzi, G., 2163
Becher, J., Hazell, A., McKenzie, C.J. and Vestergaard, C., Divalent transition metal complexes of alkylpyridyl derivatized dmit ligands, 665
Bednarek, E., see Szłyk, E., 965
Bekaroğlu, Ö., see Kandaz, M., 115
Beletskaya, I.P. and Kazankova, M.A., Catalyzed and non-catalyzed addition reactions to the triple bond, 597
Belicchi Ferrari, M., Gasparri Fava, G., Pelosi, G. and Tarasconi, P., Versatile chelating behavior of aliphatic thiosemicarbazones in zinc and cobalt complexes, 1895
Bell, N.A., Coles, S.J., Hursthouse, M.B., Light, M.E., Malik, K.A. and Mansor, R., Mercury halide complexes of tertiary phosphines. Part XVI. Dimer–monomer trend in the 1:1 complexes of mercury(II) halides with bulky tris(2,6-dimethoxyphenyl)phosphine (DMPP), 1719
Bell, N.A., Gelbrich, T., Hursthouse, M.B., Light, M.E. and Wilson, A., Reactions of trichlorovinylmercurials with potential non-chelating bidentate ligands. Crystal structures of $[(C_2Cl_3)_2Hg$ (4,4′-bipyridyl)] (**1**), $[C_2Cl_3Hg$(2-pyridyl thiolate)] (**12**) and polymeric $HgBr_2$(2,2′-dipyridyl disulfide) (**10**), 2539
Bell, V., see Veinot, J.G.C., 331
Belokon', A.I., see Turevskaya, E.P., 705
Bencini, A., Bianchi, A., Giorgi, C., Paoletti, P., Valtancoli, B., Ceccanti, N. and Pardini, R., Cobalt(II) dioxygen carriers based on dinucleating ligands. Part 1. Thermodynamics of dioxygen binding in aqueous solution, 2441
Bencini, A., see Secco, F., 2507
Benito, A., see Al Shihadeh, Y., 1867
Bényei, A., see Ágoston, C.G., 1849
Benzo, F., Beyer, L., Bozoglián, F., Hallmeier, K.-H. and Sienra, B., Inductive effect of methyl groups on acidopentaaminecobalt(III) complexes, 971
Bermejo, E., see Castiñeiras, A., 1873
Bermejo, M.R., see Maneiro, M., 47
Bermejo, M.R., see Sanmartín, J., 185
Bernardinelli, G., see Fromm, K.M., 1783
Bernasek, S.L., see Schwartz, J., 505
Bernès, S., see Ceniceros-Gómez, A.E., 1821
Bernès, S., see Gasque, L., 649
Bernès, S., see Quiroz-Castro, E., 1479
Beyer, L., see Benzo, F., 971
Bhattacharya, A.K., see Mondal, B., 1213
Bhattacharya, S., see Basuli, F., 1663
Bhattacharya, S., see Das, A., 1227
Bhattacharya, S., see Sinha, P.K., 1673
Bhattacharyya, P., Slawin, A.M.Z. and Woollins, J.D., Synthesis and characterisation of platinum(II) complexes containing heterobidentate *S*,*N*-chelating ligands: X-ray crystal structure of *cis*-$[Pt\{SPPh_2N{=}C(Me)NH\text{-}S,N\})PMe_2Ph)_2]Cl$, 809
Bhrahma, G.S., see Mondal, B., 1213
Biaggio, S.R., see Trollund, E., 2303
Bianchi, A., see Bencini, A., 2441
Bianchi, A., see Ceccanti, N., 2447
Bilakhiya, A.K., Tyagi, B. and Paul, P., Dinuclear ruthenium(II) and/or osmium(II) complexes of bipyridyl ligands bridged by rigid spacers: synthesis, characterization, electrochemical behavior and luminescence properties, 1233
Blanco, L.M., see Uraev, A.I., 2361
Blum, J., Gelman, F., Abu-Reziq, R., Miloslavski, I., Schumann, H. and Avnir, D., Sol–gel entrapped heteronuclear transition metal catalysts, 509
Boča, R., Nemečková, M., Vrbová, M., Baran, P., Svoboda, I. and Fuess, H., Tetrahydropoxen: 2,2′-(1,2-ethanediylbis(iminomethylene))bis(pyridine N-oxide) and its complexes. X-ray structure of $[Cu(H_4\text{-poxen})H_2O](ClO_4)_2{\cdot}H_2O$ and $[Co(poxen)H_2O(ClO_4)_2$, 835
Boča, R., see Vrbová, M., 2195
Bocarsly, A.B., see Schwartz, J., 505
Bocelli, G., see Thirumaran, S., 1279
Bogdanović, G., see Rogan, J., 1415
Boggess, R.K., see Mink, L.M., 1057
Boillot, M.-L., see Tuna, F., 1643
Bokhimi, X., Morales, A., Novaro, O., López, T. and Gómez, R., The effect of hydrolysis initiator on the phase formation in sulfated sol–gel zirconia, 2283
Bombicz, P., see Madarász, J., 457
Bond, E.M., Duesler, E.N., Paine, R.T. and Nöth, H., Isolation and structure of a europium(III) chloride complex of 2,6-bis[-(diphenylphosphino)methyl]pyridine *N*,*P*,*P*′-trioxide, 2135
Bonini, B.F., Comes-Franchini, M., Fochi, M., Mazzanti, G., Ricci, A. and Varchi, G., Silylcupration of acylimidazolides: a new synthesis of α-aminoacylsilanes and their synthetic applications, 529

Bontchev, P.R., Ivanova, B.B., Bontchev, R.P., Mehandjiev, D.R. and Ivanov, D.S., Complexes of Cu(II) with α-[(ethylamino)methyl]-3-hydroxy, benzenemethanol (Effortil). Crystal structure of the mononuclear Cu(II) complex with Effortil, 1843
Bontchev, R.P., see Bontchev, P.R., 1843
Borrás, E., Alzuet, G., Borrás, J., Server-Carrió, J., Castiñeiras, A., Liu-González, M. and Sanz-Ruiz, F., Coordination chemistry of sulfamethizole: crystal structures of $[Cu(sulfamethizolate)_2(py)_2(OH_2)]\cdot H_2O$, $[M(sulfamethizolate)_2(py)_2(OH_2)_2]$ [M = Co and Ni] and $\{Cu(sulfamethizolate)_2(dmf)_2\}_\infty$, 1859
Borrás, E., see García-Raso, Á., 991
Borrás, J., see Alzuet, G., 725
Borrás, J., see Borrás, E., 1859
Borrás, J., see García-Raso, Á., 991
Bortoluzzi, A.J., see de Sousa, G.F., 841
Bortoluzzi, A.J., see Ursini, C.V., 2261
Borzov, M.V., see Qian, C.-T., 1955
Boskovic, C., Folting, K. and Christou, G., Tetranuclear manganese carboxylate clusters with imidazole-carboxylate chelating ligands. X-ray crystal structure of the 4-imidazoleacetate complex, 2111
Böttcher, H.-C., Graf, M., Merzweiler, K. and Wagner, C., Electron-rich and electron-poor heterobimetallic butterfly clusters: synthesis and structure of $[Ru_3Ir(CO)_8(\mu_3\text{-}H)(\mu\text{-}Cl)_2(\mu\text{-}P'Bu_2)_2('Bu_2PH)]$ and $[Ru_3Au(CO)_{10}(\mu\text{-}Cl)('Bu_2PH)]$, 2593
Boyle, T.J., see Zechmann, C.A., 2557
Boys, D., see Crivelli, I.G., 2289
Bozoglián, F., see Benzo, F., 971
Braibanti, A., Fisicaro, E. and Compari, C., Solubility of oxygen and inert substances in water, 2457
Brasuń, J., see Kowalik-Jankowska, T., 241
Bravo-Vasquez, J.P. and Hill, R.H., Photolithographic deposition of conducting gold films from thin amorphous films of $AuPR_3X$ ($X = NO_3$, RCO_2) on silicon surfaces, 343
Brechbiel, M.W., see Park, G., 1155
Bregadze, V.I., see Sivaev, I.B., 627
Breit, B. and Zahn, S.K., Stereoselective hydroformylation, cuprate addition and domino reactions with the aid of a catalyst directing group, 513
Breitzer, J.G. and Rauchfuss, T.B., Studies on α-$C_3S_5^{2-}$ ($dmit^{2-}$) and its dinuclear Ni(II) complex: spectroscopic and structural characterization, 1283
Brellochs, B., see Sivaev, I.B., 627
Brenčič, J.V., see Modec, B., 1407
Brenčič, J.V., see Modec, B., 1219
Breneman, G.L., see Parker, O.J., 623
Breza, M., The electronic structure of planar phosphazene rings, 389
Bricklebank, N., Hargreaves, S. and Spey, S.E., Modification of the solid state structures of dithiadiazolyl radicals: crystal structure of *p*-iodophenyl-1,2,3,5-dithiadiazolyl, 1163
Bridgewater, B.M., see Hascall, T., 1063
Brodie, A.M., see Ainscough, E.W., 2585
Brodie, A.M., see Depree, C.V., 2101
Brooker, S., Croucher, P.D., Davidson, T.C. and Smith, P.D., Dimetallic thiolate-bridged complexes: synthesis and rich electrochemistry of dinickel(II) and dizinc(II) monothiolate complexes, 1887
Brown, C.A., see de Sousa, G.F., 841
Bruce, D.W., see Guillevic, M.-A., 249
Brüggeller, P., see Oberhauser, W., 913
Brunner, H., Köllnberger, A., Burgemeister, T. and Zabel, M., Optically active transition metal complexes: Part 125. Preparation and epimerization of chiral-at-metal pentamethylcyclopentadienylrhodium(III) and iridium(III) half-sandwich complexes, 1519
Bucci, R., Magrì, A.D., Magrì, A.L. and Napoli, A., On the reaction of iron(III) with chromium(III)–DTPA chelating agent, 2421
Bucci, R., Magrì, A.D., Magrì, A.L. and Napoli, A., Spectroscopic characteristics and thermal properties of divalent metal complexes of diclofenac, 2515
Bugella-Altamirano, E., González-Pérez, J.M., Sicilia-Zafra, A.G., Niclós-Gutiérrez, J. and Castiñeiras-Campos, A., Metal chelates of *N*-carbamoylmethyl-iminodiacetate(2 −) ion. Part III. Synthesis, XRD structures and properties of *N*-carbamoylmethyl-iminodiacetic acid (H_2ADA) and *cis*-diaqua(*N*-carbamoylmethyl-iminodiacetato)nickel(II), $[Ni(ADA)(H_2O)_2]$, 2463
Bugella-Altamirano, E., González-Pérez, J.M., Sicilia Zafra, A.G., Niclós-Gutiérrez, J. and Castiñeiras-Campos, A., Metal chelates of *N*-carbamoylmethyl-iminodiacetate(2 −) ion: Part IV. Isostructural ternary mixed-ligand cobalt(II) and nickel(II) chelates with *N*-carbamoylmethyl-iminodiacetate(2 −) ion, imidazole and aqua ligands. Synthesis, molecular and crystal structures and properties of $[M(ADA)(Him)(H_2O)]\cdot 1.5H_2O$ (M = Co, Ni), 2473
Burgemeister, T., see Brunner, H., 1519
Burgess, J., see Ahmed, S.I., 129
Burgess, J., see Alshehri, S., 399
Burgess, J., see Matoga, D., 1503
Burrell, A.K., see Ainscough, E.W., 2585
Burrell, A.K., see Depree, C.V., 2101
Butcher, R.J., see Barik, A.K., 2651
Butcher, R.J., see Paul, S., 2661
Bu, W.-M., see Zhang, L., 1105
Bu, W.-M., see Zhang, Z.-H., 1559
Bu, W., see Zhang, F., 1941
Bu, X.-H., Chen, W., Mu, L.-J., Zhang, Z.-H., Zhang, R.-H. and Clifford, T., Syntheses, crystal structures and properties of new manganese(II) complexes with macrocyclic polyamine ligands bearing pyridyl donor pendants, 2095
Bu, X.-H., Lu, S.-L., Zhang, R.-H., Liu, H., Zhu, H.-P. and Liu, Q.-T., Synthesis, characterization and crystal structure of the cobalt(II) and iron(II) complexes with an octadentate ligand, 1,4,7,10-tetrakis(2-pyridylmethyl)-1,4,7,10-tetraazacyclododecane (**L**), $[ML]^{2+}$, 431
Bu, X.-H., see Zhang, Z.-H., 1559
Byrne, R.H., see Klungness, G.D., 99
Byrom, C., Malik, M.A., O'Brien, P., White, A.J.P. and Williams, D.J., Synthesis and X-ray single crystal structures of bis(diisobutyldithiophosphinato)cadmium(II) or zinc(II): potential single-source precursors for II/VI materials, 211

Cabaleiro, S., Castro, J., García-Vázquez, J.A., Romero, J. and Sousa, A., Direct electrochemical synthesis of cobalt(II) complexes of tosylamides: crystal structures of $[CoL_2py_2]$, $[CoL_2DMF_2]$, $[CoL_2bipy]$ and $[CoL_2phen]$, L = [(4-methylphenyl)sulfonyl]-2-pyridylamide, 1607
Caldeira, M.M., Ramos, M.L., Pereira, G.G. and Gil, V.M.S., A multinuclear NMR study of the complexation of W(VI) with meso-2,3-dimercaptosuccinic acid (DMSA), 193
Campero, A., see Garcia-Sanchez, M.A., 2383
Cañadas, M., López-Torres, E., Martínez-Arias, A., Mendiola, M.A. and Sevilla, M.T., Spectroscopic and electrochemical properties of nickel(II), iron(III) and cobalt(II) complexes with benzilbisthiosemicarbazone — importance of working conditions and the metal salt used in the final complex, 2059
Canales, J., Ramirez, J., Estiu, G. and Costamagna, J., Bis-bipyridine hexa-aza-macrocycle complexes of zinc(II) and nickel(II) and the catalytic reduction of carbon dioxide, 2373
Cannio, M., see Battistuzzi, G., 2163
Cantoni, A., see Thirumaran, S., 1279
Cárdenas, G., Segura, R., Morales, J., Soto, H. and Lima, C.A., Preparation and properties of Zn–Cd films from non-aqueous colloids, 2337
Cárdenas-Jirón, G., see Zagal, J.H., 2255
Carmalt, C.J. and Steed, J.W., Homoleptic silyl complexes of arsenic and antimony, 1639
Carmalt, C.J., Morrison, D.E. and Parkin, I.P., Liquid-mediated metathetical synthesis of binary and ternary transition-metal pnictides, 829

Carvalho, A., Domingos, Â., Isolani, P.C., Marques, N., Pires de Matos, A. and Vicentini, G., Synthesis, luminescence studies and crystal structures of two europium(II) hydrotris(pyrazol-1-yl)borate complexes: $Eu(HBpz_3)_2 \cdot 2DPSO$ and $Eu(HBpz_3)_2 \cdot 2BPMU$, 1707
Carvalho, A., García-Montalvo, V., Domingos, Â., Cea-Olivares, R., Marques, N. and Pires de Matos, A., Synthesis and characterization of thorium and uranium tetraphenylimidophosphinate complexes. Crystal and molecular structures of $Th(tpip)_4$, $U(tpip)_4$ and $UCl(tpip)_3$, 1699
Casabó, J., see Chadghan, A., 855
Casabó, J., see Ruiz, J., 1627
Casas, J.S., Castiñeiras, A., Condori, F., Couce, M.D., Russo, U., Sánchez, A., Sordo, J. and Varela, J.M., Reaction of the diethyltin(IV) cation with pyridoxine (PN, vitamin B_6) in the presence of various anionic species: the crystal structure of $\{SnEt_2(PN-H)\}Cl$, 813
Casey, M., Lawless, J. and Shirran, C., The Heck reaction: mechanistic insights and novel ligands, 517
Castillo-Blum, S.E., see Ceniceros-Gómez, A.E., 1821
Castiñeiras, A., Garcia, I., Bermejo, E. and West, D.X., Structures of 2-pyridineformamide thiosemicarbazone and its complexes with cadmium halides, 1873
Castiñeiras, A., see Borrás, E., 1859
Castiñeiras, A., see Casas, J.S., 813
Castiñeiras, A., see García-Raso, Á., 991
Castiñeiras, A., see Labisbal, E., 1255
Castineiras, A., see Lobana, T.S., 899
Castiñeiras-Campos, A., see Bugella-Altamirano, E., 2473
Castiñeiras-Campos, A., see Bugella-Altamirano, E., 2463
Castro, J., see Cabaleiro, S., 1607
Catalano, V.J. and Craig, T.J., Synthesis and X-ray crystal structures of several dinuclear ruthenium cymene complexes based on the tetradentate ligand, 2,2′-(1*H*-pyrazole-3,5-diyl)bis(6-methylpyridine) (Me_2DppzH), 475
Catalano, V.J., Heck, R.A., Öhman, A. and Hill, M.G., Synthesis, characterization, and electrocatalytic oxidation of benzyl alcohol by a pair of geometric isomers of $[Ru(trpy)(4,4'\text{-}Me_2dppi)(OH_2)]^{2+}$ where 4,4′-dppi is 3,6-di-(4-methylpyrid-2-yl)pyridazine, 1049
Cataldo, F., ^{13}C NMR and FT-IR spectra of thiocyanogen, $S_2(CN)_2$, selenocyanogen, $Se_2(CN)_2$, and related compounds, 681
Caubet, A., see Chadghan, A., 855
Cea-Olivares, R., see Carvalho, A., 1699
Cea-Olivares, R., see López-Cardoso, M., 1539
Ceccanti, N., Pardini, R., Secco, F., Tinè, M.R., Venturini, M., Bianchi, A. and Paoletti, P., Cobalt(II) dioxygen carriers based on dinucleating ligands: Part 2. Kinetics of dioxygen binding, 2447
Ceccanti, N., see Bencini, A., 2441
Ceniceros-Gómez, A.E., Barba-Behrens, N., Quiroz-Castro, M.E., Bernès, S., Nöth, H. and Castillo-Blum, S.E., Synthesis, X-ray and spectroscopic characterisation of chromium(III) coordination compounds with benzimidazolic ligands, 1821
Černáková, M., see Moncol', J., 2573
Cervantes-Lee, F., see Pannell, K.H., 291
Cerveau, G., Corriu, R.J.P. and Framery, E., Influence of the nature of the catalyst on the textural properties of organosilsequioxane materials, 307
Chadghan, A., Pons, J., Caubet, A., Casabó, J., Ros, J., Alvarez-Larena, A. and Piniella, J.F., Cobalt(II) complexes with pyrazole-derived ligands: crystal structure of {bis[3-phenyl-5-(2-pyridyl) pyrazole]aquachlorocobalt(II)}chloride monohydrate, 855
Chai, J.-F., see Tang, L.-F., 1949
Chan, A.S.-C., see Liu, Q., 453
Chang, C.-S., see Li, Y.-I., 413
Chao, H., Ye, B.-H., Li, H., Li, R.-H., Zhou, J.-Y. and Ji, L.-N., Synthesis, electrochemical and spectroscopic properties of ruthenium(II) complexes containing 1,3-bis([1,10]phenanthroline-[5,6-*d*]imidazol-2-yl)benzene, 1975
Chapman, J., see Nel, A., 1621
Charistos, D., see Tsiamis, C., 2003
Chatterjee, D., see Ward, M.S., 1339
Chattopadhyay, P., see Pal, S., 1263
Chaudhuri, S., see Rahaman Laskar, I., 1803
Chen, A.-J., see Yeh, A.-C., 545
Chen, C.-B., see Tsai, C.-H., 633
Cheng, T.-H., Wang, Y.-M., Lee, W.-T. and Liu, G.-C., Synthesis of two *N*′-2-pyridylmethyl and *N*′-2-hydroxypropyl derivatives of diethylenetriaminepentaacetic acid and the stabilities of their complexes with Ln^{3+}, Ca^{2+}, Cu^{2+} and Zn^{2+}, 2027
Chen, H.-Y., see Lin, X., 925
Chen, J.-H., see Li, J.-M., 1117
Chen, J.-H., see Li, Y.-I., 413
Chen, J.-H., see Tsai, C.-H., 633
Chen, J.-T., see Yeh, A.-C., 545
Chen, L., see Lin, P., 2189
Chen, S.-I., see Yeh, A.-C., 545
Chen, W., see Bu, X.-H., 2095
Chen, X.-M., see Tong, M.-L., 1809
Chen, X.-M., see Yang, S.-P., 2237
Chia, L.M.L., Wheatley, A.E.H., Feeder, N., Davies, J.E. and Halcrow, M.A., Syntheses, structures and electrochemistry of $[Zn(L^1)_2](BF_4)_2 \cdot 2H_2O$ and $[Zn(L^1)(Tp^R)]BF_4$ (L^1 = 1-{pyrid-2-yl}-3-{2′,5′-dimethoxyphenyl}pyrazole; $[Tp^R]-$ = tris-{3-arylpyrazolyl}borate), 109
Chi, L.-S., see Lin, X., 925
Chinea, E., see Hernández-Padilla, M., 1175
Chisholm, M.H., Folting, K., Huffman, J.C., Li, H., Macintosh, A.M. and Wu, D.-D., d^3–d^3 Diolates of dimolybdenum and ditungsten. Part 4. Molybdenum derivatives of *S*(−)-1,1-diphenyl-1,2-propanediol, *S*(−)-1,1,2-triphenyl-1,2-ethanediol and (1*R*,2*R*)-(−)-1,2-dicyclohexyl-1,2-ethanediol, 375
Choi, J.-C., see Sakakura, T., 573
Choi, S.K., see Kim, C., 1031
Choi, S.-N., see Kim, Y.-J., 2155
Chou, J.-L., Chyn, J.-P., Urbach, F.L. and Gervasio, D.F., Dinuclear copper(II) complexes incorporating a novel pyrazolo-based ligand with S- and N-rich coordination spheres, 2215
Christou, G., see Boskovic, C., 2111
Chyn, J.-P., see Chou, J.-L., 2215
Ciavatta, L. and Iuliano, M., Formation equilibria of tin(II) orthophosphate complexes, 2403
Ciavatta, L., Iuliano, M., Porto, R., Innocenti, P. and Vacca, A., Phosphato complexes of beryllium(II): a ^{31}P and ^{9}Be nuclear magnetic resonance study, 1043
Cindrić, M., Pavlović, G., Vrdoljak, V. and Kamenar, B., Hexanuclear complexes of molybdenum(V) containing $[Mo_6O_{12}(OCH_3)_4(acac)_3]^-$ anion, 1471
Cini, R., see Pifferi, C., 69
Cisneros-Fajardo, E.J., see Navarro, M., 2319
Ciunik, Z., see Łukasiewicz, M., 2119
Clegg, W., see Sen, S., 1881
Clifford, T., see Bu, X.-H., 2095
Clifford, T., see Hay, R.W., 1485
Coe, B.J., McDonald, C.I., Couchman, S.M., Jeffery, J.C., Rees, L.H., Coles, S.J., Gelbrich, T. and Hursthouse, M.B., Axial ligand substitution and photoisomerization reactions in ruthenium(II) *trans* mixed-chelate complexes containing the ligands 1,2-phenylenebis(dimethylarsine) and 2,2′-bipyridine or 1,10-phenanthroline, 1193
Coles, S.J., Faulds, P., Hursthouse, M.B., Kelly, D.G. and Toner, A.J., Synthesis and reactivity of copper(I) phosphine–alkene complexes: X-ray crystal structure of $CuCl(Ph_2PCPh{=}CH_2)_2$, 1271
Coles, S.J., Hursthouse, M.B., Kelly, D.G. and Toner, A.J., Titanium(IV) complexes of the crystallographically characterised fluorene-Schiff base *N*-2-fluorenyl(salicylideneimine) and related bi- and tetradentate ligands, 177

Coles, S.J., see Bell, N.A., 1719
Coles, S.J., see Coe, B.J., 1193
Collinson, S.R., see Guillevic, M.-A., 249
Collison, D., see Zhang, Y.-J., 1757
Collman, J.P., see Rose, E., 581
Comerlato, N.M., see Harrison, W.T.A., 821
Comes-Franchini, M., see Bonini, B.F., 529
Compari, C., see Braibanti, A., 2457
Comuzzi, C., Di Bernardo, P., Polese, P., Portanova, R., Tolazzi, M. and Zanonato, P.L., Lanthanide(III) complex formation with diethylenetriamine in anhydrous *N*,*N*-dimethylformamide, 2427
Conato, C., see Remelli, M., 2409
Concepción Gimeno, M., see Romeo, I., 1837
Concepción, J., Loeb, B., Simón-Manso, Y. and Zuloaga, F., Influence of L-type ligands on the relative stability and interconversion of *cis*–*trans*-$[Ru(phen)_2L_2]^{n+}$ type complexes. A theoretical study, 2297
Condori, F., see Casas, J.S., 813
Connolly, J., see Barton, A.J., 1373
Constable, E.C., Hannon, M.J., Harverson, P., Neuburger, M., Smith, D.R., Wanner, V.F., Whall, L.A. and Zehnder, M., Synthesis and coordination chemistry of 4′,4″-disubstituted 2,2′:6′,2″:6″,2‴-quaterpyridines and crystal and molecular structures of nickel(II) and cobalt(II) complexes, 23
Contreras, R., see Quiroz-Castro, E., 1479
Corbella, M., see Rodríguez, M., 2483
Corriu, R.J.P., see Cerveau, G., 307
Costa-Filho, A.J., see Sanmartín, J., 185
Costamagna, J., see Canales, J., 2373
Cotton, F.A., Dikarev, E.V., Petrukhina, M.A. and Stiriba, S.-E., Studies of dirhodium(II) tetrakis(trifluoroacetate). Part 8. One-dimensional polymers of $Rh_2(O_2CCF_3)_4$ with aromatic ligands: benzene, *p*-xylene and naphthalene, 1829
Couce, M.D., see Casas, J.S., 813
Couchman, S.M., see Coe, B.J., 1193
Coulais, Y., see Loiseau, F., 1111
Cox, P.J., Aslanidis, P. and Karagiannidis, P., Binuclear copper(I) complexes containing bis(diphenylphosphino)ethane bridges: the crystal structure of bis[{μ-bis(diphenylphosphino)ethane}(pyridine-2-thione)copper(I)bromide], 1615
Cozar, O., see David, L., 1917
Cozzi, P.G., see Bandini, M., 537
Crăciun, C., see David, L., 1917
Craig, T.J., see Catalano, V.J., 475
Crisponi, G., Cristiani, F., Nurchi, V.M., Pinna, R., Pivetta, T. and José Tapia Estévez, M., Spectrophotometric and potentiometric study on platinum(II) chelates of mercapto carboxylic acids, 2435
Cristiani, F., see Crisponi, G., 2435
Crivelli, I.G., Andrade, C., Francois, M.A., Boys, D., Haberland, A., Segura, R., María Leiva, A. and Loeb, B., Experimental evidence of the disproportionation equilibrium in copper mixed-valence complexes, 2289
Crosbie, M.J., see Jones, A.C., 351
Croucher, P.D., see Brooker, S., 1887
Cruywagen, J.J. and Heyns, J.B.B., Molybdenum(VI) equilibria at high perchloric acid concentration, 907
Cui, C., Hao, H., Noltemeyer, M., Schmidt, H.-G. and Roesky, H.W., Synthesis and characterization of 1-aza-allyl complexes of aluminum, gallium and bismuth, 471
Ćurić, M., see Tušek-Božić, L., 937
Czugler, M., see Madarász, J., 457

Daier, V., see Rizzotto, M., 417
Dalgaard, P., Hazell, A., McKenzie, C.J., Moubaraki, B. and Murray, K.S., Dicopper(II) complexes of a phenolate-hinged ditopic ligand with solvent-derived ancillary ligands bound at the potentially dimetallic exogenous site, 1909
D'Alpaos, M., see Tušek-Božić, L., 937
Daniels, L.M., see Modec, B., 1407
Danis, J.A., Hawkins, H.T., Scott, B.L., Runde, W.H., Scheetz, B.E. and Eichhorn, B.W., X-ray structure determination of two related uranyl phosphate crown ether compounds, 1551
Danks, M.J., see Guillevic, M.-A., 249
Dartiguenave, M., see Loiseau, F., 1111
Das, A., Peng, S.-M. and Bhattacharya, S., Chemistry of 2-(phenylazo)pyridine complexes of osmium: synthesis, characterization and reactivities, 1227
Das, A., see Shukla, A.D., 2605
Das, B.K. and Kanatzidis, M.G., Solvothermal synthesis and structure of iron tellurido carbonyl clusters, 1995
Das, D., see Laskar, I.R., 1015
Das, D., see Pal, S., 1263
Dash, A.C., see Mondal, B., 1213
Dastych, D., see Pastorek, R., 1713
Datt, M.S., see Sacht, C., 1347
David, L., Crăciun, C., Rusu, M., Cozar, O., Ilea, P. and Rusu, D., Spectroscopic and electrochemical investigations of the $K_8[P_2VMoW_{16}O_{62}]\cdot 31H_2O$ heteropolyoxometalate, 1917
Davidson, T.C., see Brooker, S., 1887
Davies, H.O., see Jones, A.C., 351
Davies, J.E., see Chia, L.M.L., 109
Díaz, C. and Arancibia, A., Intervalence electron transfer through a thiolate bridge ligand: a Fe^{III}–S–R–Fe^{II} mixed valence complex, 2679
Díaz, J.G., see Hvastijová, M., 1021
de Barbarín, C.R., see Gasque, L., 649
de Castro, B., see Santos, I.C., 655
De Cian, A., see Arnáiz, F.J., 2141
De Jesús Gutiérrez, M., see Gasque, L., 649
DeKock, C.W., see Kim, G.-S., 1363
Demšar, A., see Petriček, S., 199
de Oliveira, A.I., see Harrison, W.T.A., 821
Depree, C.V., Ainscough, E.W., Brodie, A.M., Burrell, A.K., Lensink, C. and Nicholson, B.K., Reactivity, structure and electrospray mass spectrometry of pentafluoro- and pentachloro-phenoxy-substituted cyclotriphosphazenes, 2101
de Sousa, G.F., West, D.X., Brown, C.A., Swearingen, J.K., Valdés-Martínez, J., Toscano, R.A., Hernández-Ortega, S., Hörner, M. and Bortoluzzi, A.J., Structural and spectral studies of aheterocyclic N(4)-substituted bis(thiosemicarbazone), $H_2$2,6Achexim·H_2O, its heptacoordinated tin(IV) complex [Bu_2Sn(2,6Achexim)], and its binuclear zinc(II) complex [Zn(2,6Achexim)]$_2$, 841
de Souza, A.R., see Nothenberg, M.S., 1305
Devereux, M., McCann, M., Leon, V., Geraghty, M., McKee, V. and Wikaira, J., Synthesis and fungitoxic activity of manganese(II) complexes of fumaric acid: X-ray crystal structures of [Mn(fum)(bipy)(H_2O)] and [Mn(Phen)$_2$(H_2O)$_2$](fum)·4H_2O (fumH_2 = fumaric acid; bipy = 2,2′-bipyridine; phen = 1,10-phenanthroline), 1205
Dey, D.K., see Mondal, N., 2707
Dias, G.H.M., see Ursini, C.V., 2261
Diaz, C. and Arancibia, A., TCNE and TCNQ ligands as efficient bridges in mixed-valence complexes containing iron–cyclopentadienyl and other organometallic systems, 137
Di Bernardo, P., see Comuzzi, C., 2427
Dikarev, E.V., see Cotton, F.A., 1829
Dilshad, R., see Azam, K.A., 1081
Ding, J., see Kong, D.-Y., 217
Di Vaira, M., see Lewtas, M.R., 751
Djuran, M.I. and Milinković, S.U., Selective hydrolysis of the unactivated peptide bond in *N*-acetylated L-histidylglycine catalyzed by various palladium(II) complexes: dependence of the hydrolysis rate on the steric bulk of the catalyst, 959

Djurdjević, P., Stankov, M.J. and Odović, J., Study of solution equilibria between iron(III) ion and ciprofloxacin in pure nitrate ionic medium and micellar medium, 1085
do Carmo, D.R., Rodrigues-Filho, U.P., Gushikem, Y. and Franco, D.W., Spectroscopic and electrochemical study of $[Ru(NH_3)_5OH_2]^{3+}$, $[Ru(NH_3)_5Cl]^{2+}$, and $[Os(NH_3)_5OH_2]^{3+}$ immobilized on thin film of Ti(IV) oxide dispersed on the silica gel surface, 2277
Domingos, Â., see Carvalho, A., 1707
Domingos, Â., see Carvalho, A., 1699
Domínguez, S., see Hernández-Padilla, M., 1175
Domínguez, S., see Rivero, M., 2249
Dopke, N.C., see McGaff, R.W., 1245
Douthwaite, R.E., Synthesis, crystal structure and reactivity of the dihydroborate $[Li(Et_2O)][B(C_6F_5)_2(H)_2]$, 1579
Doxsee, K.M. and Juliette, J.J.J., Regioselectivity of metallacycle formation via intramolecular CH activation, 879
Doyle, A., Felcman, J., Gambardella, M.T.P., Verani, C.N. and Tristão, M.L.B., Anhydrous copper(II) hexanoate from cuprous and cupric oxides. The crystal and molecular structure of $Cu_2(O_2CC_5H_{11})_4$, 2621
Do, Y., see Rhee, S.W., 1961
Dozol, J.-F., see Thuéry, P., 1749
Drake, J.E., Khasrou, L.N., Mislankar, A.G. and Ratnani, R., The X-ray crystal structures of (*O*,*O*-2,3-dimethylbutylene and *O*,*O*-2-dimethylpropylene dithiophosphato)diphenyltellurium(IV) derivatives, $Ph_2Te[S_2\overline{POCMe_2CMe_2O}]_2$ and $2Ph_2Te[S_2\overline{POCH_2CMe_2CH_2O}]_2{\cdot}2Ph_2TeCl_2{\cdot}CS_2$ and those of (*O*,*O*-2,3-dimethylbutylene and *O*,*O*-2-dimethylpropylene dithiophosphoric acids, $HS_2\overline{POCMe_2CMe_2O}$ and $HS_2\overline{POCH_2CMe_2CH_2O}$, 407
Drew, M.G.B., see Almond, M.J., 2127
Drew, M.G.B., see Baker, P.K., 147
Drillon, M., see Hornick, C., 259
Duan, C.-Y., see Song, Y., 1461
Duarte, M.T., see Santos, I.C., 655
Dudová, B., see Palicová, M., 2689
Duesler, E.N., see Bond, E.M., 2135
Dürichen, P., see Ruwisch, L.M., 323
Du, W.-X., see Lin, P., 2189

Eccles, H., see Zhang, Y.-J., 1757
Edwards, A.J., see Sen, S., 1881
Edwards, D.A., Mahon, M.F. and Paget, T.J., Diphenylphosphinoacetate, nicotinate and thiophenoxyacetate as bridging ligands in heterometallic complexes involving bis(η-cyclopentadienyl)titanium(IV) and group 10 or 11 metal chlorides. Crystal structures of $[(\eta\text{-}C_5H_5)_2Ti\{OC(O)CH_2PPh_2\}_2]$ and $[(\eta\text{-}C_5H_5)_2Ti\{\mu\text{-}OC(O)CH_2PPh_2\}_2PdCl_2]$, 757
Eichhorn, B.W., see Danis, J.A., 1551
Einaga, H., see Kobayashi, T., 2639
El Fallah, M.S., see Mondal, N., 1935
Elizondo, N.V., see Uraev, A.I., 2361
El-Safty, S.A., see Zaki, A.B., 1317
Elsegood, M.R.J., see Redshaw, C., 2657
El-Sheikh, M.Y., see Zaki, A.B., 1317
Enyedy, É.A., see Farkas, E., 1727
Errington, W., see Willey, G.R., 1799
Espinosa, E., see García-Raso, A., 673
Espinosa, E., see García-Raso, Á., 991
Estiu, G., see Canales, J., 2373
Evans, J., see Zaki, A.B., 1317
Evans, J.S.O., see O'Hare, D., 297
Exarchos, G. and Robinson, S.D., Observations concerning the constitution of some 'rhodium(II) dithiocarbamato complexes', 123
Exarchos, G., Robinson, S.D. and Steed, J.W., The synthesis and characterisation of $[Pd(S_2CNEt_2)\{Ph_2P(CH_2)_nPPh_2\}]^+$ salts of some chlorometallate anions ($n = 1$, 3, 4): X-ray crystal structures of the salts $[Pd(S_2CNEt_2)\{Ph_2P(CH_2)_nPPh_2\}]_2[MCl_4]$ ($n = 1$, 4; M = Cd; $n = 3$; M = Hg), 1511

Fallis, A.G., Forgione, P., Woo, S., Legoupy, S., Py, S., Harwig, C. and Rietveld, T., Organometallic reagents and protocols for synthesis, 533
Falvello, L.R., see Sinha, P.K., 1673
Fan, H.-J., see Peng, Y., 733
Fan, L., Liu, W., Gan, X., Tang, N., Tan, M., Jiang, W. and Yu, K., Synthesis, crystal structure and fluorescence emission of complexes of lanthanide picrates with 2,2′ = [1,2-phenylenebis(oxy)]bix(*N*,*N*-diphenylacetamide)(PBD), 779
Fanwick, P.E., see Mulford, D.R., 35
Fan, X., see Ainscough, E.W., 2585
Farah, A.A., see Veinot, J.G.C., 331
Farkas, E., Enyedy, É.A., Micera, G. and Garribba, E., Coordination modes of hydroxamic acids in copper(II), nickel(II) and zinc(II) mixed-ligand complexes in aqueous solution, 1727
Farouq, J.A., see Richburg, L.M., 1815
Faulds, P., see Coles, S.J., 1271
Faure, R., see Hueso-Ureña, F., 689
Fawcett, J., see Ahmed, S.I., 129
Fawcett, J., see Alshehri, S., 399
Fawcett, J., see Matoga, D., 1503
Feeder, N., see Chia, L.M.L., 109
Felcman, J., see Doyle, A., 2621
Feng, S., see Zhang, F., 1941
Ferbinteanu, M., see Tanase, S., 1967
Ferguson, G., see Alyea, E.C., 2211
Fernandes, L.C., Matos, J.R., Zinner, L.B., Vicentini, G. and Zukerman-Schpector, J., Crystal structures, spectroscopic, TG and DSC studies of lanthanide picrate complexes with 4-methylmorpholine *N*-oxide (MMNO), 2313
Fernández, M., see Longo, C., 487
Ferrari, R., see Gasque, L., 649
Ferrer, E.G., see Allegretti, Y., 2613
Ferrer-Llusar, S., see Alzuet, G., 725
Filgueiras, C.A.L., see Teles, W.M., 739
Fiol, J.J., see García-Raso, A., 673
Fiol, J.J., see García-Raso, Á., 991
Fischer, J., see Arnáiz, F.J., 2141
Fisicaro, E., see Braibanti, A., 2457
Fleeting, K.A., see Jones, A.C., 351
Fochi, M., see Bonini, B.F., 529
Fogg, A., see O'Hare, D., 297
Folting, K., see Boskovic, C., 2111
Folting, K., see Chisholm, M.H., 375
Fondo, M., see Maneiro, M., 47
Font-Bardia, M., see Resino, I., 225
Forgione, P., see Fallis, A.G., 533
Formica, M., Fusi, V., Micheloni, M., Pontellini, R. and Romani, P., Synthesis and ligational properties of a new tetra-azamacrocycle containing an anisolic function, 2501
Framery, E., see Cerveau, G., 307
Franco, D.W., see do Carmo, D.R., 2277
Franco, E., López-Torres, E., Mendiola, M.A. and Sevilla, M.T., Synthesis, spectroscopic and cyclic voltammetry studies of copper(II) complexes with open chain, cyclic and a new macrocyclic thiosemicarbazones, 441
Francois, M.A., see Crivelli, I.G., 2289
Freire, C., see Santos, I.C., 655
Fromm, K.M., Goesmann, H. and Bernardinelli, G., H-bonded polymer structures of different dimensionality: syntheses and crystal structures of $[Ca(DME)_n(H_2O)_m]I_2{\cdot}(DME)_x$ (**1**: $n = 3$, $m = 3$, $x = 1$; **2**: $n = 2$, $m = 4$, $x = 0$) and $[Ca\{CH_3(OCH_2)_3OCH_3\}(H_2O)_4]I_2$, 1783
Fronczek, F.R., see Isovitsch, R.A., 1437

Fuentes, A.F., see Alvarado, E., 2345
Fuentes, A., see Navarro, M., 2319
Fuess, H., see Boča, R., 835
Fuess, H., see Iskander, M.F., 949
Fuess, H., see Iskander, M.F., 1181
Fuess, H., see Vrbová, M., 2195
Fujiwara, M., see Asada, H., 2039
Fujiwara, T., see Takeda, T., 593
Fun, H.K., see Manonmani, J., 2011
Fun, H.-K., see Zhu, D.-R., 2019
Furlani, A., see Tušek-Božić, L., 937
Fusi, V., see Formica, M., 2501

Galloro, J., see Veinot, J.G.C., 331
Gambardella, M.T.P., see Doyle, A., 2621
Gancheff, J., see Rivero, M., 2249
Gan, X., see Fan, L., 779
Gao, Y.-C., see Wang, Y.-Y., 891
Garía-Deibe, A.M., see Sanmartín, J., 185
García, A.M., see Manzur, J., 2367
García-Montalvo, V., see Carvalho, A., 1699
García-Raso, A., Fiol, J.J., López-Zafra, A., Mata, I., Espinosa, E. and Molins, E., Synthesis of Zn*N*-salicylidene-L-aminoacidatos: X-ray structure of [(*N*-salicylidene-L-alaninato)(aqua)zinc-(II)]·0.25H_2O and [(*N*-salicylidene-L-valinato)(aqua)zinc(II)], 673
García-Raso, Á., Fiol, J.J., Rigo, S., López-López, A., Molins, E., Espinosa, E., Borrás, E., Alzuet, G., Borrás, J. and Castiñeiras, A., Coordination behaviour of sulfanilamide derivatives. Crystal structures of [Hg(sulfamethoxypyridazinato)$_2$], [Cd(sulfadimidinato)$_2$-(H_2O)]·2H_2O and [Zn(sulfamethoxazolato)$_2$-(pyridine)$_2$(H_2O)$_2$], 991
García-Vázquez, J.A., see Cabaleiro, S., 1607
García-Vázquez, J.A., see Labisbal, E., 1255
García y García, P., see López-Cardoso, M., 1539
Garcia, I., see Castiñeiras, A., 1873
Garcia-Sanchez, M.A. and Campero, A., Aggregation properties of metallic tetrasulfophthalocyanines embedded in sol–gel silica, 2383
Garnovskii, A.D., see Uraev, A.I., 2361
Garribba, E., see Farkas, E., 1727
Garribba, E., see Kiss, E., 55
Gasowska, A., see Lomozik, L., 1145
Gasparri Fava, G., see Belicchi Ferrari, M., 1895
Gasque, L., Bernès, S., Ferrari, R., de Barbarín, C.R., De Jesús Gutiérrez, M. and Mendoza-Díaz, G., Complexation of lead(II) by L-aspartate: crystal structure of polymeric Pb(aspH(NO_3), 649
Gavrish, S.P., see Lampeka, Y.D., 2533
Gawalt, E.S., see Schwartz, J., 505
Gdaniec, M., see Paschalidis, D.G., 2629
Geiger, W.E., see MacLachlan, M.J., 275
Gelbrich, T., see Bell, N.A., 2539
Gelbrich, T., see Coe, B.J., 1193
Gelman, F., see Blum, J., 509
Georgiev, I.O., see Karasik, A.A., 1455
Geraghty, M., see Devereux, M., 1205
Gervasio, D.F., see Chou, J.-L., 2215
Ghosh, A., see Laskar, I.R., 1015
Ghosh, A., see Rahaman Laskar, I., 1803
Giacomelli, A., see Malatesta, F., 2493
Gil, V.M.S., see Caldeira, M.M., 193
Giner, J., see Ruiz, J., 1627
Giorgi, C., see Bencini, A., 2441
Giorgi, C., see Secco, F., 2507
Giroux, S., Rubini, P., Henry, B. and Aury, S., Complexes of praseodymium(III) with D-gluconic acid, 1567
Głowiak, T., Rybak, W.K. and Skarżyńska, A., Synthesis and structural characterisation of the oxo-rhenium(V) complexes with spirophosphorane derived bidentate ligand (P ~ O^-). Crystal structure of *trans*-$ReOCl_2$[$OCMe_2CMe_2OP(OCMe_2CMe_2O)$]-($PPh_3$), 2667
Głowiak, T., see Kurdziel, K., 2183
Glowiak, T., see Moncol, J., 2573
Glowiak, T., see Palicová, M., 2689
Goesmann, H., see Fromm, K.M., 1783
Goher, M.A.S., Al-Salem, N.A. and Mak, T.C.W., Synthesis, spectral and crystal structures of two new copper(I) complexes of di-2-pyridyl ketone (DPK) containing uncoordinated N-protonated ligand; [(DPK)H][CuX_2] (X = I and NCS), 1465
Goher, M.A.S. and Mautner, F.A., Spectral and structural characterization of copper(I) halide, nitrate and perchlorate complexes of pyrazine carboxamide (pyza) and X-ray crystal structure of polymeric [Cu(pyza)$_2$I]$_n$ complex, 601
Goher, M.A.S., Yang, Q.-C. and Mak, T.C.W., Synthesis, structural and spectroscopic study of polymeric copper(I) thiocyanato complexes [Cu(NCS)L]$_n$ (L = methyl nicotinate and ethyl nicotinate) and [HL][Cu(NCS)$_2$] (HL = H-ethyl isonicotinate), 615
Golič, L., see Modec, B., 1407
Golič, L., see Modec, B., 1219
Golič, L., see Petriček, S., 199
Gómez, B., see Manzur, J., 2367
Gómez-Lara, J., see Téllez-Sara, C.A., 2353
Gómez, R., see Bokhimi, X., 2283
González, A.M., see Maneiro, M., 47
González Baró, A.C., see Allegretti, Y., 2613
González Garmendia, M.J., see Seco, J.M., 1005
González-Pérez, J.M., see Bugella-Altamirano, E., 2473
González-Pérez, J.M., see Bugella-Altamirano, E., 2463
Graf, M., see Böttcher, H.-C., 2593
Gramlich, V., see Mondal, N., 1935
Grodzicki, A., see Szłyk, E., 965
Grove, D.I., see Mink, L.M., 1057
Gubina, K.E., Shatrava, J.A., Ovchynnikov, V.A. and Amirkhanov, V.M., Spectroscopic characterization of lanthanide complexes with *N*,*N*′-tetraethyl-*N*″-benzoylphosphoryltriamide. Crystal structure of tris(*N*,*N*′-tetraethyl-*N*″-benzoylphosphoryltriamide) cerium(III) trinitrate complex, 2203
Guillevic, M.-A., Danks, M.J., Harries, S.K., Collinson, S.R., Pidwell, A.D. and Bruce, D.W., Structure–property relationships in ortho-metallated imine complexes of Re(I), 249
Guillon, E., see Jubert, C., 1447
Guiry, P.J., see McCarthy, M., 541
Gulppi, M.A., see Zagal, J.H., 2255
Gupta, R. and Mukherjee, R., Synthesis and properties of [$CuLCl_2$] and [$CuL(N_3)(OClO_3)$]·H_2O (L = α,α′-bis(pyrazolyl)-*m*-xylene): X-ray structure of [$CuLCl_2$]$_2$, 719
Gupta, R., Hotchandani, R. and Mukherjee, R., Magnetic interactions in dicopper(II) complexes of a new endogenous alkoxo bridging ligand with exogenous pyrazolate, azide and acetate bridges. X-ray structure of [$Cu_2L(\mu\text{-}C_3H_3N_2)(OClO_3)(H_2O)$][$ClO_4$]·$H_2O$ (HL = 1,3-bis[*N*-methyl-*N*-(2-pyridylethyl)amino]propan-2-ol), 1429
Gushikem, Y., see do Carmo, D.R., 2277
Guzman-Jimenez, I., see Khan, S.R.A., 975
Guzman-Jimenez, I., see Khan, S.R.A., 983

Haase, W., see Iskander, M.F., 949
Haase, W., see Iskander, M.F., 1181
Haberland, A., see Crivelli, I.G., 2289
Hadjikakou, S.K. and Kubicki, M., Synthesis, characterisation and study of mercury(II) chloride complexes with triphenylphosphine and heterocyclic thiones. The crystal structures of [(benzothiazole-2-thionato)(benzothiazole-2-thione)(bis-triphenylphosphine) chloro mercury(II)] and [(μ_2-dichloro){(bis-pyrimidine-2-thionato)mercury(II)}{(bis-triphenylphosphine)mercury(II)}] at 100 K, 2231

Haid, R., see Oberhauser, W., 913
Halcrow, M.A., see Chia, L.M.L., 109
Hallmeier, K.-H., see Benzo, F., 971
Halstead, M.J.R., see Ainscough, E.W., 2585
Hanif, K.M., Kabir, S.E., Mottalib, M.A., Hursthouse, M.B., Malik, K.M.A. and Rosenberg, E., Dithiolate complexes of ruthenium and osmium: X-ray structures of $[Ru_2(CO)_6(\mu\text{-}SCH_2CH_2S)]$ and $[\{(\mu\text{-}H)M_3(CO)_{10})\}_2(\mu\text{-}SCH_2CH_2CH_2S)]$ (M = Ru, Os), 1073
Hannon, M.J., see Constable, E.C., 23
Hao, H., see Cui, C., 471
Harding, M.M., see Long, G.V., 1067
Hargreaves, S., see Bricklebank, N., 1163
Harries, S.K., see Guillevic, M.-A., 249
Harris, K.D.M., see Hix, G.B., 765
Harrison, W.T.A., Howie, R.A., Wardell, J.L., Wardell, S.M.S.V., Comerlato, N.M., Sodre Costa, L.A., Silvino, A.C., de Oliveira, A.I. and Mendonca Silva, R., Crystal structures of three [bis(1,3-dithiole-2-thione-4,5-dithiolato)zincate^{2-} salts: $[Q]_2[Zn(dmit)_2]$ (Q = 1,4-Me_2-pyridinium or NEt_4) and $[PPh_4]^{2-}$ $[Zn(dmit)_2]\cdot$DMSO. Comparison of the dianion packing arrangements in $[Q]_2[Zn(dmit)_2]$, 821
Hartman, J.S. and Shoemaker, J.A.W., Chelated fluoroboron cations. II. Synthesis and NMR studies involving aromatic chelating ligands, 165
Hartmann, S., see Anson, C.E., 569
Harverson, P., see Constable, E.C., 23
Harwig, C., see Fallis, A.G., 533
Hascall, T., Bridgewater, B.M. and Parkin, G., Reactivity of $Mo(PMe_3)_5H_2$ towards catecholborane: synthesis and structure of $Mo(PMe_3)_4(\eta^2\text{-}H_2BCat)H$, 1063
Hasebe, H., see Ohta, K., 267
Hawkins, H.T., see Danis, J.A., 1551
Hayashi, R.K., see McGaff, R.W., 1245
Hay, R.W., Clifford, T., Richens, D.T. and Lightfoot, P., Binuclear copper(II), nickel(II), cobalt(II) and zinc(II) complexes of the macrocycle 1,4,7,16,19,22-hexaaza[9.9]metacyclophane (L). Crystal structure of $[Cu_2LCl_4]_{0.5}\cdot[Cu_2LCl_3]ClO_4\cdot$dmf and the copper complex catalysed hydrolysis of the phosphotriester 2,4-dinitrophenyldiethylphosphate, 1485
Hazell, A., McKenzie, C.J. and Nielsen, L.P., Synthesis, structural characterisation and electronic behaviour of iron(II) and nickel(II) complexes of *N*,*N*-bis(2-pyridylmethyl)aniline, 1333
Hazell, A., see Becher, J., 665
Hazell, A., see Dalgaard, P., 1909
Heck, R.A., see Catalano, V.J., 1049
Henry, B., see Giroux, S., 1567
Herbst-Irmer, R., see Muthiah, C., 63
Hernández-Ortega, S., see de Sousa, G.F., 841
Hernández-Padilla, M., Chinea, E., Domínguez, S., Mederos, A., Muñoz, M.C. and Lloret, F., Synthesis, crystal structure, thermal and magnetic properties of $[Mn(H_2O)_6][Cu(pdta)]\cdot2H_2O$ (pdta = 1,3-propylenediamine-*N*,*N*,*N*′*N*′-tetraacetate), 1175
Heuer, B., Pope, S.J.A. and Reid, G., Synthesis, spectroscopic and structural characterisation of copper, silver and gold complexes of the mixed P/O-donor ligand $Ph_2P(CH_2)_2O(CH_2)_2O(CH_2)_2PPh_2$, 743
Hey-Hawkins, E., see Karasik, A.A., 1455
Heyns, J.B.B., see Cruywagen, J.J., 907
Hill, M.G., see Catalano, V.J., 1049
Hill, R.H., see Bravo-Vasquez, J.P., 343
Hiroi, K., Suzuki, Y., Kaneko, Y., Kato, F., Abe, I. and Kawagishi, R., Palladium-catalyzed asymmetric reactions enantiocontrolled by chiral organosulfur functionality, 525
Hix, G.B., Maddocks, V.C. and Harris, K.D.M., Polymerization of aniline on copper phosphonate materials, 765
Hiyama, T., see Mori, A., 567
Hodali, H.A., see Abu-Surrah, A.S., 1601
Hodson, A.G.W. and Thind, R.K., Stereochemistry of chiral, substituted η^3-butadienyl molybdenum(II) complexes, 791
Hörner, M., see de Sousa, G.F., 841
Hörner, M., see Ursini, C.V., 2261
Hornick, C., Rabu, P. and Drillon, M., Hybrid organic–inorganic multilayer materials: influence of π electrons as magnetic media in a series of bridged-layer compounds $M_2(OH)_{4-x}A_{x/2}$ (M = Cu(II) or Co(II), A = dicarboxylate anion), 259
Hor, T.S.A., see Yan, Y.-K., 641
Hotchandani, R., see Gupta, R., 1429
Hou, X., see Wang, Y.-Y., 891
Howie, R.A., see Harrison, W.T.A., 821
Huang, J.-Q., see Peng, Y., 733
Huang, J., see Liu, Q., 453
Huang, X.-Y., see Kong, D.-Y., 217
Hubert-Pfalzgraf, L.G., see Verdenelli, M., 2069
Hudecová, D., see Palicová, M., 2689
Hueso-Ureña, F., Illán-Cabeza, N.A., Moreno-Carretero, M.N., Peñas-Chamorro, A.L. and Faure, R., Ni(II) and Cu(II) complexes with the dianionic N,N,O-tridentate Schiff base 6-amino-5-formyl-1,3-dimethyluracil-benzoylhydrazone. Crystal structure of the monodimensionally hydrogen-bonded aqua-(6-amino-1,3-dimethyluracilato-benzoyl-hydrazone(2-)-N_6,N_{51},O_{52}]copper(II) hydrate, 689
Huffman, J.C., see Chisholm, M.H., 375
Huffman, J.C., see Santos, E.C., 1777
Hundal, G., see Lobana, T.S., 899
Huo, S., see Negishi, E.-i., 591
Hurlburt, P.K., see Santos, E.C., 1777
Hursthouse, M.B., see Azam, K.A., 1081
Hursthouse, M.B., see Bell, N.A., 2539
Hursthouse, M.B., see Bell, N.A., 1719
Hursthouse, M.B., see Coe, B.J., 1193
Hursthouse, M.B., see Coles, S.J., 177
Hursthouse, M.B., see Coles, S.J., 1271
Hursthouse, M.B., see Hanif, K.M., 1073
Hussain Reddy, K., see Sambasiva Reddy, P., 1687
Hu, S., see Zhang, F., 1941
Hvastijová, M., Kohout, J., Kožíšek, J., Jäger, L. and Díaz, J.G., Cyanamidonitrate–nickel(II) and –cobalt(II) complexes of imidazole ligands: X-ray crystallography and spectroscopic investigation, 1021
Hwang, L.-P., see Tsai, C.-H., 633

Ichikawa, N., see Nakashima, S., 205
Igumenov, I.K., see Isakova, V.G., 1097
Ilea, P., see David, L., 1917
Illán-Cabeza, N.A., see Hueso-Ureña, F., 689
Inagaki-Oka, Y., see Ohta, K., 267
Incarvito, C.D., see Richburg, L.M., 1815
Ingersoll, J.E., see Mink, L.M., 1057
Innocenti, P., see Ciavatta, L., 1043
Isakova, V.G., Baidina, I.A., Morozova, N.B. and Igumenov, I.K., γ-Halogenated iridium(III) acetylacetonates, 1097
Iskander, M.F., Khalil, T.E., Werner, R., Haase, W., Svoboda, I. and Fuess, H., Synthesis, characterization and magnetochemical studies of some imidazole and imidazolate copper(II) ternary complexes derived from *N*-salicylidenearoylhydrazines. X-ray crystal and molecular structures of [(*N*-salicylidene-*p*-chlorobenzoylhydrazine)*ONO*(−2)imidazole]copper(II) monohydrate and dimeric [(*N*-salicylidene-*p*-methylbenzoylhydrazine)*ONO*(−2)imidazole]-copper(II) hemihydrate, 1181
Iskander, M.F., Khalil, T.E., Werner, R., Haase, W., Svoboda, I. and Fuess, H., Synthesis, reactivity and magnetochemical studies on copper(II) complexes derived from *N*-salicylidenearoylhydrazines. X-ray structure of [mononitrato*OO*(−1)(*N*-salicylidenatobenzoylhydrazine)*ONO*(−1)]copper(II) monohydrate, 949

Isolani, P.C., see Carvalho, A., 1707
Isovitsch, R.A., May, J.G., Fronczek, F.R. and Maverick, A.W., Photoredox reactions of oxomolybdenum(V) with phosphines, 1437
Iuliano, M., see Ciavatta, L., 2403
Iuliano, M., see Ciavatta, L., 1043
Ivanova, B.B., see Bontchev, P.R., 1843
Ivanov, D.S., see Bontchev, P.R., 1843

Jäger, L., see Hvastijová, M., 1021
Jain, P.U., Munshi, P., Walawalkar, M.G., Rath, S.P., Rajak, K.K. and Lahiri, G.K., Ruthenium dithiophosphates: synthesis, X-ray crystal structure, spectroscopic and electrochemical properties, 801
Jakusch, T., see Kiss, T., 2389
James, A.J., see Kannan, S., 155
Jasper, S.A., see Santos, E.C., 1777
Jastrzab, R., see Lomozik, L., 1145
Jastrzebski, J.T.B.H., see Kronenburg, C.M.P., 553
Jeffery, J.C., see Coe, B.J., 1193
Jeliazkova, B., see Yordanov, N.D., 2177
Jenkins, A.E., see Baker, P.K., 2171
Jevtović, V.S., see Rychlewska, U., 1
Jezierska, J., see Kurzak, B., 2083
Jiang, C., see Yan, Y.-K., 641
Jiang, J., Rintoul, L. and Arnold, D.P., Raman spectroscopic characteristics of phthalocyanine and naphthalocyanine in sandwich-type (na)phthalocyaninato and porphyrinato rare earth complexes, 1381
Jiang, W., see Fan, L., 779
Jiang, Z.-H., see Zhang, L., 1105
Jiang, Z., see Li, L., 2529
Jiang, Z., see Li, L., 1575
Jia, W.-L., see Tang, L.-F., 1949
Jia, W.-L., see Tang, L.-F., 381
Ji, L.-N., see Chao, H., 1975
Ji, L.-N., see Yang, S.-P., 2237
Jin, G., see Tan, W., 1545
Jin, Q., see Tan, W., 1545
Jin, W., see Yang, L., 93
Ji, W., see Tan, W., 1545
Johansson, A. and Kessler, V.G., Synthesis and X-ray single crystal study of the bi- and trimetallic alkoxides of molybdenum(VI) and tantalum, $Mo_2Ta_4O_8(OMe)_{16}$, $Mo_4Ta_4O_{16}(O^iPr)_{12}$ and $LiMo_4Ta_3O_{14}(O^iPr)_9(OC_2H_4OMe)_3$, 1791
Jones, A.C., Leedham, T.J., Davies, H.O., Fleeting, K.A., O'Brien, P., Crosbie, M.J., Wright, P.J., Williams, D.J. and Lane, P.A., Metal–organic chemical vapour deposition of lead candium tantalate: chemical issues and precursor selection, 351
José Tapia Estévez, M., see Crisponi, G., 2435
Jubert, C., Mohamadou, A., Guillon, E. and Barbier, J.-P., Molecular structure and spectroscopic characterization of cobalt and copper complexes with a hexadentate nitrogen ligand, 1,10-bis(2-pyridylmethyl)-1,4,7,10-tetraazadecane, 1447
Juliette, J.J.J., see Doxsee, K.M., 879
Junk, P.C., see Atwood, J.L., 85

Kabir, S.E., see Azam, K.A., 1081
Kabir, S.E., see Hanif, K.M., 1073
Kafarski, P., see Kurzak, B., 2083
Kaftanov, J., Averbuj, C., Vais-Morlender, N., Liard, A. and Marek, I., Synthesis and reactivity of polymetallated olefins and functionalized metalloalkynes, 563
Kajiro, H., see Mori, A., 567
Kamecka, A., see Kurzak, B., 2083
Kamenar, B., see Cindrić, M., 1471
Kamieński, B., see Szłyk, E., 965
Kanatzidis, M.G., see Das, B.K., 1995
Kandaswamy, M., see Amudha, P., 1769
Kandaswamy, M., see Manonmani, J., 2011
Kandaz, M., Yılmaz, İ. and Bekaroğlu, Ö., Synthesis and characterization of novel symmetrical phthalocyanines substituted with mono- or bimacrocycles, 115
Kaneko, Y., see Hiroi, K., 525
Kang, B.-S., see Xiao, W., 1295
Kang, S.B., see Yoo, J., 549
Kania, R. and Sieklucka, B., Kinetic evidence of ring closure step in the substitution of *cis*-$[Cr(bpy)_2(OH_2)_2]^{3+}$ with $[M(CN)_8]^{4-}$ (M = Mo, W), 2225
Kannan, S., James, A.J. and Sharp, P.R., Dinuclear diimine palladium(II) and platinum(II) hydroxo and amido complexes: synthesis and X-ray crystal structures, 155
Kannan, S., see Alyea, E.C., 2211
Karagiannidis, P., see Cox, P.J., 1615
Karanović, L., see Rogan, J., 1415
Karasik, A.A., Georgiev, I.O., Sinyashin, O.G. and Hey-Hawkins, E., Synthesis of novel water-soluble heterocyclic phosphino amino acids with bulky aromatic substituents on phosphorus, 1455
Kar, S.K., see Barik, A.K., 2651
Kato, F., see Hiroi, K., 525
Kavounis, C.A., see Tsiamis, C., 2003
Kawabe, K., see Yanagihara, N., 1311
Kawagishi, R., see Hiroi, K., 525
Kazankova, M.A., see Beletskaya, I.P., 597
Keller, A., see Szterenberg, L., 2565
Keller, H.J., see Riveros, P.C., 2327
Kelly, D.G., see Coles, S.J., 177
Kelly, D.G., see Coles, S.J., 1271
Kelly, P.F., Macklin, A.C., Slawin, A.M.Z. and Waring., K.W., The preparation of the first examples of sulfimide complexes of platinum; the X-ray crystal structure of $[Pt(Ph_2SNH)_4]Cl_2$, 2077
Kelsey, R.D., see Anson, C.E., 569
Kemp, R.A., see Zechmann, C.A., 2557
Kennedy, S.M.F., see Ainscough, E.W., 2585
Kessler, V.G., see Johansson, A., 1791
Keum, G., see Yoo, J., 549
Keypour, H., Salehzadeh, S., Pritchard, R.G. and Parish, R.V., Cadmium(II) complexes of fully condensed Schiff-base ligands derived from two different symmetrical and asymmetrical tripodal tetraamines and 2-acetylpyridine; the novel observations for heptadentate mono-capped trigonal antiprismatic Schiff-base complexes, 1633
Khalil, T.E., see Iskander, M.F., 949
Khalil, T.E., see Iskander, M.F., 1181
Khandar, A.A. and Nejati, K., Synthesis and characterization of a series of copper(II) complexes with azo-linked salicylaldimine Schiff base ligands. Crystal structure of Cu_5PHAZOSALTN·$CHCl_3$, 607
Khan, S.R.A., Guzman-Jimenez, I., Whitmire, K.H. and Khokhar, A.R., Synthesis and characterization of piperidine platinum(II) complexes with dicarboxylates: crystal and molecular structure of *cis*-$[Pt(piperidine)_2Cl_2]·H_2O$, 975
Khan, S.R.A., Guzman-Jimenez, I., Whitmire, K.H. and Khokhar, A.R., Synthesis and characterization of platinum(II) complexes with 3-methylpiperidine: crystal and molecular structure of [Pt(3-methylpiperidine)$_2$(malonato)]·H_2O, 983
Kharisov, B.I., see Uraev, A.I., 2361
Khasrou, L.N., see Drake, J.E., 407
Khokhar, A.R., see Khan, S.R.A., 975
Khokhar, A.R., see Khan, S.R.A., 983
Kilyén, M., see Kiss, T., 2389
Kim, B., see Kim, C., 1031
Kim, C., Choi, S.K. and Kim, B., Synthesis of layered dendritic carbosilanes, 1031
Kim, C.G., see Woo Park, J., 2547
Kim, G.-S. and DeKock, C.W., Syntheses, molecular structures, and dynamic solution behavior of nitrido (oxo) molybdenum(VI) siloxides, 1363

Kim, J., see Rhee, S.W., 1961
Kim, J.T., Park, J.W. and Koo, S.M., The synthesis and structural characterization of $[Et_4N]_2[Ti(SPh)_6]$ and trimeric $[Ti_3O(SPh)_3Cl_4(CH_3CN)_5]\cdot CH_3CN\cdot(C_2H_5)_2O$ complexes, 1139
Kim, Y.-I., see Kim, Y.-J., 2155
Kim, Y.-J., Kim, Y.-I. and Choi, S.-N., Magnetic properties and coordination environments of oxovanadium(IV) within $VO(IV)N_2S_2$ and $VO(IV)S_4$ chromophores, 2155
Kim, Y., see Yoo, J., 549
Kim, Y.S., see Woo Park, J., 2547
Kinkead, S.A., see Santos, E.C., 1777
Kirmse, R., see Abram, U., 1741
Kiruschenkov, E.N., see Turevskaya, E.P., 705
Kiss, E., Petrohán, K., Sanna, D., Garribba, E., Micera, G. and Kiss, T., Solution speciation and spectral studies on oxovanadium(IV) complexes of pyridinecarboxylic acids, 55
Kiss, E., see Kiss, T., 2389
Kiss, T., Jakusch, T., Kilyén, M., Kiss, E. and Lakatos, A., Solution speciation of bioactive Al(III) and VO(IV) complexes, 2389
Kiss, T., see Kiss, E., 55
Klinga, M., see Abu-Surrah, A.S., 1601
Klungness, G.D. and Byrne, R.H., Comparative hydrolysis behavior of the rare earths and yttrium: the influence of temperature and ionic strength, 99
Kobayashi, T., Kunita, M., Nishino, S., Matsushima, H., Tokii, T., Masuda, H., Einaga, H. and Nishida, Y., Release of free nucleobases from oligomers by copper(II)–peroxide adduct, 2639
Kohout, J., see Hvastijová, M., 1021
Koh, W., see Yan, Y.-K., 641
Kojima, T., see Ma, T., 1167
Kojima, Y., see Yanagihara, N., 1311
Kolawole, G., see Nel, A., 1621
Köllnberger, A., see Brunner, H., 1519
Komac, M., see Tušek-Božić, L., 937
Koman, M., see Moncoľ, J., 2573
Komatsu, H., see Nakashima, S., 205
Kong, D.-Y. and Xie, Y.-Y., Synthesis, structural characterization and potentiometric studies of divalent metal complexes with an octadentate tetraazamacrocyclic ligand and their DNA cleavage ability, 1527
Kong, D.-Y., Meng, L.-H., Ding, J., Xie, Y.-Y. and Huang, X.-Y., New tetraazamacrocyclic ligand with neutral pendent groups 1,4,7,10-tetrakis(2-cyanoethyl)1,4,7,10-tetraazacyclododecane (L) and its cobalt(II), nickel(II) and copper(II) complexes: synthesis, structural characterization and antitumor activity, 217
Koo, S.M., see Kim, J.T., 1139
Koo, S.M., see Park, S.K., 1037
Kopacka, H., see Oberhauser, W., 913
Kopacka, H., see Scheffter, B., 871
Kopcová, M., see Palicová, M., 2689
Korecz, L., see Szabó-Plánka, T., 2049
Korecz, L., see Szabó-Plánka, T., 1123
Košmrlj, J., see Petriček, S., 199
Kowalik-Jankowska, T., Leśniak, W., Brasuń, J., Stasiak, M. and Leplawy, M.T., Copper(II) complexes of deltakephalin and its analogues containing α-hydroxymethylserine, 241
Kozłowski, H., see Remelli, M., 2409
Kožíšek, J., see Hvastijová, M., 1021
Kremer, C., see Rivero, M., 2249
Kremer, E., see Rivero, M., 2249
Kress, J., see Lorber, C.Y., 1693
Kronenburg, C.M.P., Jastrzebski, J.T.B.H. and van Koten, G., Structure and reactivity of cyanocuprates containing the monoanionic C,N-chelating aminoaryl ligands $[C_6H_4CH_2NMe_{2-}2]^-$, 553
Kubicki, M., see Hadjikakou, S.K., 2231
Kumara Swamy, K.C., see Muthiah, C., 63
Kumar Barik, A., see Paul, S., 2661
Kumar Das, A., see Basuli, F., 1663
Kumar Kar, S., see Paul, S., 2661
Kumar Maji, T., see Rahaman Laskar, I., 1803
Kumar Saha, M., see Sen, S., 1881
Kunita, M., see Kobayashi, T., 2639
Kuppayee, M., see Manonmani, J., 2011
Kurdziel, K. and Głowiak, T., X-ray and spectroscopic characterisation of octahedral cobalt(II) and nickel(II) complexes with 1-allylimidazole in the solid state and electron-donor properties of the latter in aqueous solution, 2183
Kurzak, B., Kamecka, A., Kurzak, K., Jezierska, J. and Kafarski, P., Potentiometric and spectroscopic studies of the cobalt(II), nickel(II) and manganese(II) complexes with some aminodiphosphonic acids in aqueous solution, 2083
Kurzak, K., see Kurzak, B., 2083
Kwak, B., Rhee, H. and Lah, M.S., Hexanuclear manganese metallamacrocycles with tripled hydrophobic tails, 1985

Labisbal, E., Sousa, A., Castiñeiras, A., García-Vázquez, J.A., Romero, J. and West, D.X., Spectral and structural studies of metal complexes of isatin 3-hexamethyleneiminylthiosemicarbazone prepared electrochemically, 1255
Lage, C., see Sanmartín, J., 185
Laguna, M., see Romeo, I., 1837
Lahiri, G.K., see Jain, P.U., 801
Lah, M.S., see Kwak, B., 1985
Lakatos, A., see Kiss, T., 2389
Lam, K.-C., see Yim, H.W., 849
Lampeka, Y.D. and Gavrish, S.P., Spectral characteristics of the copper(III) and nickel(III) coordination compounds with open-chain and macrocyclic dioxotetraamines, 2533
Lane, P.A., see Jones, A.C., 351
Langes, C., see Oberhauser, W., 913
Lappalainen, K., see Abu-Surrah, A.S., 1601
Laskar, I.R., Ghosh, A., Mostafa, G., Das, D., Mondal, A. and Ray Chaudhuri, N., *Cis–trans* isomerism in nickel(II)–diamine nitrite: synthesis and single crystal structure of an unusual *cis*-dinitronickel(II) complex, $[NiL_2(NO_2)_2]$ (L = 1,2-diamino-2-methylpropane), 1015
Laurie, S.H., see Ahmed, S.I., 129
Lawless, J., see Casey, M., 517
Lecas-Nawrocka, A., see Rose, E., 581
Lecocq, S., see Verdenelli, M., 2069
Leedham, T.J., see Jones, A.C., 351
Lee, G.-H., see Yeh, A.-C., 545
Lee, H.-J. and Noh, D.-Y., Electrochemistry and strong near-IR absorption of the $[Ni(dphdt)_2]^n$ complexes ($n = -1, 0$; dphdt = 5,6-diphenyl-1,4-dithin-2,3-dithiolate); X-ray crystal structure of $(Ph_4P)[Ni(dphdt)_2](CH_2Cl_2)$, 425
Lee, W.-T., see Cheng, T.-H., 2027
Lee, Y.E., see Park, S.K., 1037
Legoupy, S., see Fallis, A.G., 533
Lehmann, T., see Navarro, M., 2319
Lehtonen, A. and Sillanpää, R., Binaphtholato complexes of tungsten(VI) from tris(1,2-ethanediolato)tungsten(VI). Synthesis and X-ray structures of $[W(bino)(diolato)_2]$ complexes, 2579
Lehtonen, A., see Liimatainen, J., 1133
Lemenovskii, D.A., see Qian, C.-T., 1955
Lensink, C., see Depree, C.V., 2101
Leong, W.K., see Yan, Y.-K., 641
Leon, V., see Devereux, M., 1205
Leplawy, M.T., see Kowalik-Jankowska, T., 241
Leskelä, M., see Abu-Surrah, A.S., 1601
Leśniak, W., see Kowalik-Jankowska, T., 241
LeSuer, R., see MacLachlan, M.J., 275
Levason, W., Newman, E.H. and Webster, M., Tetrakis(triphenylphosphine oxide) complexes of the lanthanide nitrates; synthesis, characterisation and crystal structures of $[La(Ph_3PO)_4(NO_3)_3]\cdot Me_2CO$ and $[Lu(Ph_3PO)_4(NO_3)_2]NO_3$, 2697

Levason, W., see Barton, A.J., 1373
Levason, W., see Barton, A.J., 235
Lewtas, M.R., Morley, C.P. and Di Vaira, M., The reactions of $[M(dppe)_2]$ (M = Pd, Pt) with elemental selenium or tellurium: preparation and structure of the platinum polyselenide $[PtSe_4(dppe)]$, 751
Liable-Sands, L.M., see MacLachlan, M.J., 275
Liao, D., see Li, L., 2529
Liao, D., see Li, L., 1575
Liao, D.-Z., see Zhang, L., 1105
Liao, F.-L., see Li, Y.-I., 413
Liao, F.-L., see Tsai, C.-H., 633
Liard, A., see Kaftanov, J., 563
Li, F.-S., see Yang, Z.-Y., 2599
Lightfoot, P., see Hay, R.W., 1485
Light, M.E., see Bell, N.A., 2539
Light, M.E., see Bell, N.A., 1719
Li, H., see Chao, H., 1975
Li, H., see Chisholm, M.H., 375
Liimatainen, J., Lehtonen, A. and Sillanpää, R., *cis*-Dioxomolybdenum(VI) complexes with tridentate and tetradentate Schiff base ligands. Preparation, structures and inhibition of aerial oxidation of aldehydes, 1133
Li, J.-M., Zhang, Y.-G., Chen, J.-H., Rui, L., Wang, Q.-M. and Wu, X.-T., Microporous networks co-assembled by both rigid and flexible building blocks, 1117
Li, L., Liao, D., Jiang, Z. and Yan, S., A new one-dimensional $[Ni(phen)(N_3)_2]_n$ compound with alternating end-on and end-to-end bridging azido ligands, 1575
Li, L., Liao, D., Jiang, Z. and Yan, S., Synthesis, structure and magnetic properties of di-carboxylato-bridged complex $[Cu_2(phen)_2(Hpht)_2(NO_3)(H_2O)]NO_3{\cdot}2H_2O$, 2529
Lima, C.A., see Cárdenas, G., 2337
Lin, B.-Z. and Liu, S.-X., Hydrothermal syntheses, structures and magnetic properties of coordination cation metavanadates, $Cu(tn)_2(VO_3)_2$ and $Ni(NH_3)_2(VO_3)_2$, 2521
Linert, W., see Vrbová, M., 2195
Lin, J., see Yang, L., 93
Lin, P., Wu, X.-T., Chen, L., Wu, L.-M. and Du, W.-X., Syntheses and characterization of two dodecanuclear heterobimetallic Mo–Cu–S cage clusters: $[NEt_4]_2[(Mo_2Cu_2S_2O_2edt_2)_3(\mu_6\text{-}Se_2)]{\cdot}CH_2Cl_2$ and $[NEt_4]_2[(Mo_2Cu_2S_2O_2edt_2)_3(\mu_6\text{-}S)]{\cdot}3H_2O$ (edt = $^-SC_2H_4S^-$)., 2189
Lin, X., Chen, H.-Y., Chi, L.-S., Lu, C.-Z. and Zhuang, H.-H., Syntheses and structures of two complexes with incomplete cuboidal $Mo_3Te_4^{4+}$ and $Mo_3(\mu_3\text{-}S)Te_3^{4+}$ cluster cores, 925
Liou, S.-Y., see Negishi, E.-i., 591
Li, R.-H., see Chao, H., 1975
Lisowski, J. and Starynowicz, P., Chiral macrocyclic Nd(III) and Tm(III) complexes, 465
Liu, G.-C., see Cheng, T.-H., 2027
Liu-González, M., see Borrás, E., 1859
Liu, H.-Q., see Xiao, W., 1295
Liu, H., see Bu, X.-H., 431
Liu, J.-F., see Sun, Z.-G., 125
Liu, Q., see Sun, Z.-G., 125
Liu, Q., Shen, X., Huang, J., Qian, Y., Chan, A.S.-C. and Wong, W.-T., Synthesis and crystal structure of lanthanide sandwich complexes with mixed cyclooctatetraenyl and chelating ether side chain-cyclopentadienyl ligands: crystal structures of $(\eta^5\text{-}MeOCH_2CH_2Cp)Nd(\eta^8\text{-}C_8H_8)(THF)$ and $(\eta^5\text{-}C_4H_7OCH_2\text{-}C_5H_4)La(\eta^8\text{-}C_8H_8(THF)$, 453
Liu, Q.-T., see Bu, X.-H., 431
Liu, S.-X., see Lin, B.-Z., 2521
Liu, W., see Fan, L., 779
Liu, X.-X. and Wong, W.-T., Synthesis, characterization and crystal structure of a series of ruthenium nitrosonaphthol complexes, 7
Livens, F.R., see Zhang, Y.-J., 1757
Li, Y.-I., Chang, C.-S., Tung, J.-Y., Tsai, C.-H., Chen, J.-H., Liao, F.-L. and Wang, S.-L., Molecular structure of *N*-tosylimido-*meso*-tetraphenylprophyrinatozinc(II), Zn(N-NTs-tpp), 413
Llobet, A., see Rodríguez, M., 2483
Lloret, F., see Hernández-Padilla, M., 1175
Lloris, J.M., see Al Shihadeh, Y., 1867
Lobana, T.S., Verma, R., Hundal, G. and Castineiras, A., Metal–heterocyclic thione interactions. 12. Heterocyclic 2-thiolates of platinum(II) and palladium(II): the crystal structures of first examples of *cis*-$[M(\eta^1\text{-}S\text{-}pyridine\text{-}2\text{-}thiolato)_2(L\text{-}L)]$ {M = Pt, Pd, L-L = 1,2-bis(diphenylphosphino)ethane; M = Pt, L-L = 1,2-bis(diphenylphosphino)ethene} complexes, 899
Loeb, B., see Concepción, J., 2297
Loeb, B., see Crivelli, I.G., 2289
Loiseau, F., Lucchese, Y., Dartiguenave, M. and Coulais, Y., Bidentate phosphinophenol ligand: synthesis and characterization of oxo and phenylimido rhenium(V) complexes of 2-diisopropylphosphinophenol, 1111
Lomozik, L., Jastrzab, R. and Gasowska, A., Interactions in binary and ternary systems including Cu(II), uridine, uridine 5′-monophosphate or diamine, 1145
Long, D., see Tan, W., 1545
Long, G.V., Harding, M.M. and Turner, P., X-ray structure of the zinc complex of the central metal chelation site of the antitumour drug streptonigrin, 1067
Long, N., see Nel, A., 1621
Longo, C., Alvarez, J., Fernández, M., Pardey, A.J., Moya, S.A., Baricelli, P. and Mdleleni, M.M., Water as hydride source in the reduction of nitrobenzene to aniline catalyzed by cis-$[Rh(CO)_2(2\text{-}picoline)_2](PF_6)$ in aqueous 2-picoline under CO atmosphere: kinetics study, 487
López-Cardoso, M., García y García, P., Rogers-Sakuma, A. and Cea-Olivares, R., Organometallic tin(IV) derivatives of the ambidentate *O*-cholesteryl-*O*-phenyl phosphorothioate ligand, 1539
López, G., see Ruiz, J., 1627
López, G., see Sánchez, G., 1395
López-López, A., see García-Raso, Á., 991
López-Torres, E., see Cañadas, M., 2059
López-Torres, E., see Franco, E., 441
López, T., see Bokhimi, X., 2283
López-Zafra, A., see García-Raso, A., 673
Lorber, C.Y., Youinou, M.-T., Kress, J. and Osborn, J.A., Isomerization of 2-methyl-3-butyn-2-ol into prenal: mechanistic observations on tricomponent catalyst systems of the type $Ti(OR)_4$–CuCl–$R'CO_2H$. Crystal structure of $[CuCl(Me_2C(OH)C{\equiv}CH)]_4$, 1693
Lough, A.J., see MacLachlan, M.J., 275
Lucchese, Y., see Loiseau, F., 1111
Lu, C.-Z., see Lin, X., 925
Lu, G., see Schwartz, J., 505
Lu, J., see Matteson, D.S., 587
Łukasiewicz, M., Ciunik, Z. and Wołowiec, S., Complexes of heteroscorpionate trispyrazolylborate anionic ligands: Part I. The crystal structure and reactivity of thiocyanato[hydrobis(3-phenylpyrazolyl)(3-*tert*-butylpyrazolyl)borato]cobalt(II) complex, 2119
Luo, Y.-J., see Zhang, L.-L., 2243
Lu, S.-L., see Bu, X.-H., 431
Lu, T.-H., see Pal, S., 1263
Lu, X. and Wang, Z., Role of halide ions in palladium(II) catalyzed nucleophile alkyne-α,β-unsaturated carbonyl coupling reactions, 577
Lu, X.-F., see Peng, Y., 733
Lu, Z.-L., see Xiao, W., 1295
Lyčka, A., see Tušek-Božić, L., 937

Macintosh, A.M., see Chisholm, M.H., 375
Macklin, A.C., see Kelly, P.F., 2077

MacLachlan, M.J., Zheng, J., Thieme, K., Lough, A.J., Manners, I., Mordas, C., LeSuer, R., Geiger, W.E., Liable-Sands, L.M. and Rheingold, A.L., Synthesis, characterization, and ring-opening polymerization of a novel [1]silaferrocenophane with two ferrocenyl substituents at silicon, 275
Madarász, J., Bombicz, P., Czugler, M. and Pokol, G., Comparison of theophyllinato Cu(II) complexes of ethanolamine and diethanolamine. Part 2: Structure and thermal study of the dimeric complex with diethanolamine, 457
Maddocks, V.C., see Hix, G.B., 765
Madrakian, T., see Shamsipur, M., 1681
Magrì, A.D., see Bucci, R., 2421
Magrì, A.D., see Bucci, R., 2515
Magrì, A.L., see Bucci, R., 2421
Magrì, A.L., see Bucci, R., 2515
Mahon, M.F., see Edwards, D.A., 757
Maji, T.K., Mostafa, G., Mukherjee, P.S., Mondal, A., Welch, A.J., Okamoto, K.-i. and Ray Chaudhuri, N., Synthesis, characterization of triamine complexes of nickel(II)selenocyanate and their thermally induced dimerization: X-ray single crystal structures of $[Ni(dpt)(SeCN)_2(H_2O)]$ and $[Ni(aepn)(SeCN)_2(H_2O)]$ (dpt = bis(3-aminopropyl)amine and aepn = (2-aminoethyl)(3-aminopropyl)amine), 1903
Mak, C.S.K., see Tanner, P.A., 863
Mak, T.C.W., see Goher, M.A.S., 1465
Mak, T.C.W., see Goher, M.A.S., 615
Mak, T.C.W., see Tanner, P.A., 863
Malatesta, F., Trombella, S., Giacomelli, A. and Onor, M., Activity coefficients of 3:3 electrolytes in aqueous solutions, 2493
Malik, K.A., see Bell, N.A., 1719
Malik, K.M.A., see Azam, K.A., 1081
Malik, K.M.A., see Hanif, K.M., 1073
Malik, K.M.A., see Mondal, N., 2707
Malik, K.Z., Robinson, S.D. and Steed, J.W., Ruthenium carboxylate complexes $[Ru(O_2CR)_2(H_2O)(Me_2SO)_3]$ (R = Me, CF_3)-synthesis and X-ray crystal structures., 1589
Malik, M.A., see Byrom, C., 211
Malik, M.A., see Yordanov, N.D., 2177
Malleier, R., see Scheffter, B., 871
Maneiro, M., Bermejo, M.R., Sousa, A., Fondo, M., González, A.M., Sousa-Pedrares, A. and McAuliffe, C.A., Synthesis and structural characterisation of new manganese(II) and (III) complexes. Study of their photolytic and catalase activity and X-ray crystal structure of $[Mn(3\text{-Ome, 5-Br-}salpn)(EtOH)H_2O)]ClO_4$, 47
Maneiro, M., see Sanmartín, J., 185
Man Koo, S., see Woo Park, J., 2547
Manners, I., see MacLachlan, M.J., 275
Manonmani, J., Thirumurugan, R., Kandaswamy, M., Kuppayee, M., Sundara Raj, S.S., Ponnuswamy, M.N., Shanmugam, G. and Fun, H.K., Synthesis of mononuclear nickel(II) and copper(II) complexes using compartmental ligands: X-ray and electrochemical studies, 2011
Mansor, R., see Bell, N.A., 1719
Manzur, J., García, A.M., Gómez, B. and Spodine, E., Catalytic properties of dinuclear copper complexes with an N_6 pyridazine-derived ligand, 2367
Maquet, J., see Babonneau, F., 315
María Leiva, A., see Crivelli, I.G., 2289
Marcos Martínez, M., see Al Shihadeh, Y., 1867
Marek, I., see Kaftanov, J., 563
Marek, J., see Pastorek, R., 1713
Mariezcurrena, R., see Rivero, M., 2249
Marques, N., see Carvalho, A., 1707
Marques, N., see Carvalho, A., 1699
Martínez-Arias, A., see Cañadas, M., 2059
Martínez-Máñez, R., see Al Shihadeh, Y., 1867
Martínez-Mánez, R., see Alzuet, G., 725
Masuda, H., see Kobayashi, T., 2639
Mata, I., see García-Raso, A., 673
Mathonière, C., see Tanase, S., 1967
Ma, T., Kojima, T. and Matsuda, Y., Synthesis and characterization of a novel macrocyclic ligand containing catechol donor groups and its oxovanadium(IV) complex, 1167
Matoga, D., Szklarzewicz, J., Samotus, A., Burgess, J., Fawcett, J. and Russell, D.R., Preparation and characterisation of $[M(CN)_4O(pz)]^{2-}$ complexes (M = Mo or W) and their reactivity towards molecular oxygen, 1503
Matos, J.R., see Fernandes, L.C., 2313
Matos, J.R., see Nothenberg, M.S., 1305
Matsuda, Y., see Ma, T., 1167
Matsushima, H., see Kobayashi, T., 2639
Matsushita, T., see Asada, H., 2039
Matteson, D.S., Singh, R.P., Lu, J., Yang, J. and Pharazyn, P.S., Asymmetric synthesis of trisubstituted pyrrolidines via boronic esters, 587
Matusiak, R., see Szterenberg, L., 2565
Mautner, F.A., see Goher, M.A.S., 601
Maverick, A.W., see Isovitsch, R.A., 1437
May, J.G., see Isovitsch, R.A., 1437
Ma, Z.-H., see Zhang, Z.-H., 1559
Mazzanti, G., see Bonini, B.F., 529
McAuliffe, C.A., see Maneiro, M., 47
McCann, M., see Devereux, M., 1205
McCarthy, M. and Guiry, P.J., A new quinazoline-containing axially chiral ligand for asymmetric catalysis, 541
McDonald, C.I., see Coe, B.J., 1193
McGaff, R.W., Dopke, N.C., Hayashi, R.K., Powell, D.R. and Treichel, P.M., Synthesis and crystal structures of five new rhenium acetamidate complexes, 1245
McKee, V., see Devereux, M., 1205
McKenzie, C.J., see Becher, J., 665
McKenzie, C.J., see Dalgaard, P., 1909
McKenzie, C.J., see Hazell, A., 1333
Mdleleni, M.M., see Longo, C., 487
Mederos, A., see Hernández-Padilla, M., 1175
Mederos, A., see Rivero, M., 2249
Meehan, M.M., see Baker, P.K., 2171
Meehan, M.M., see Baker, P.K., 1585
Mehandjiev, D.R., see Bontchev, P.R., 1843
Mehrotra, R.C., see Sharma, M., 77
Melník, M., see Moncoĺ, J., 2573
Melník, M., see Palicová, M., 2689
Mendia-Jalon, A., see Barton, A.J., 1373
Mendiola, M.A., see Franco, E., 441
Mendonca Silva, R., see Harrison, W.T.A., 821
Mendoza-Díaz, G., Ruiz-Ramírez, L. and Moreno-Esparza, R., Template reaction of $[Ni(ben)_3](ClO_4)_2$ with acetone. Crystal structure of 1,11-bis-benzyl-5,7,7-trimethyl-1,4,8,11-tetra-aza-undeca-4-ene nickel(II) perchlorate, 2149
Mendoza-Díaz, G., see Gasque, L., 649
Meng, L.-H., see Kong, D.-Y., 217
Merzweiler, K., see Böttcher, H.-C., 2593
Messersmith, P.B., see Murphy, W.L., 357
Miao, S.-B., see Zheng, H.-B., 713
Micera, G., see Ágoston, C.G., 1849
Micera, G., see Farkas, E., 1727
Micera, G., see Kiss, E., 55
Micheloni, M., see Formica, M., 2501
Midollini, S., see Rivero, M., 2249
Mikloš, D., see Palicová, M., 2689
Milinković, S.U., see Djuran, M.I., 959
Milliron, D.J., see Schwartz, J., 505
Miloslavski, I., see Blum, J., 509

Mink, L.M., Voce, J.W., Ingersoll, J.E., Nguyen, V.T., Boggess, R.K., Washburn, H. and Grove, D.I., Platinum(IV) tetraphenylporphyrin dibromide complexes: synthesis, characterization, and electrochemistry, 1057
Miravitlles, C., see Ruiz, J., 1627
Mironov, Y.V., Tetrahedral chalcogeno thiocyanate cluster complexes $[Re_4Q_4(SCN)_{12}]^{4-}$ (Q = S, Se, Te): synthesis and crystal structures, 437
Mislankar, A.G., see Drake, J.E., 407
Misra, T.K., see Pal, S., 1925
Mitra, S., see Mondal, N., 2707
Mitra, S., see Mondal, N., 1935
Mitra, S., see Sen, S., 1881
Młynarz, P., see Remelli, M., 2409
Modec, B., Brenčič, J.V. and Golič, L., Octanuclear oxomolybdenum(V) clusters with pyridine or alkyl-substituted pyridines: crystal structures of $[Mo_8O_{16}(OCH_3)_8L_4]$ (L = 3-methylpyridine, 3,5-lutidine), 1219
Modec, B., Brenčič, J.V., Golič, L. and Daniels, L.M., Oxomolybdenum coordination compounds with alkyl-substituted pyridines. Solvothermal syntheses and structural characterization of $[Mo_{10}O_{26}(3,5\text{-Lut})_8]\cdot 2(3,5\text{-Lut})$, $[Mo_{10}O_{26}(3\text{-MePy})_8]\cdot(3\text{-MePy})$, $[Mo_{10}O_{26}(3\text{-MePy})_8]$ and $[Mo_{12}O_{28}(OCH_3)_2Cl_2(3\text{-MePy})_8]$, 1407
Mohamadou, A., see Jubert, C., 1447
Molins, E., see García-Raso, A., 673
Molins, E., see García-Raso, Á., 991
Molins, E., see Ruiz, J., 1627
Mombrú, A., see Rivero, M., 2249
Moncol, J., Koman, M., Melník, M., Černáková, M. and Glowiak, T., Study of copper(II) chloro- and dichloropropionates, crystal and molecular structure of *trans*-bis(methyl-3-pyridylcarbamate)bis(α,α-dichloropropionato)copper(II), 2573
Mondal, A., see Laskar, I.R., 1015
Mondal, A., see Maji, T.K., 1903
Mondal, B., Bhattacharya, A.K., Banerjee, R., Bhrahma, G.S. and Dash, A.C., Kinetics of oxidation of ascorbic acid by the $[Mn_3^{IV}(\mu\text{-}O)_4(bipy)_4(H_2O)_2]^{4+}$ ion (bipy = 2,2′-bipyridine), 1213
Mondal, N., Dey, D.K., Mitra, S. and Malik, K.M.A., Synthesis and structural characterization of mixed ligand η^1-2-hydroxyacetophenone complexes of cobalt(III), 2707
Mondal, N., Saha, M.K., Mitra, S., Gramlich, V. and El Fallah, M.S., Synthesis, characterization and crystal structure of cyano-bridged dinuclear copper–iron complexes, 1935
Mondal, S., see Rajak, K.K., 931
Mondragón, M.A., see Téllez-Sara, C.A., 2353
Mondry, A. and Starynowicz, P., Optical spectroscopy of neodymium(III) complexes with diethylenetriaminepentaacetic acid in solution and in $[C(NH_2)_3]_2[Nd(dtpa)(H_2O)]\cdot 7H_2O$ single crystal, 771
Monfort, M., see Resino, I., 225
Morales, A., see Bokhimi, X., 2283
Morales, J., see Cárdenas, G., 2337
Mordas, C., see MacLachlan, M.J., 275
Moreno-Carretero, M.N., see Hueso-Ureña, F., 689
Moreno-Esparza, R., see Mendoza-Díaz, G., 2149
Moreno, V., see Rizzotto, M., 417
Mori, A., Takahisa, E., Kajiro, H., Nishihara, Y. and Hiyama, T., Stereodivergent hydrosilylation of 1-alkynes catalyzed by $RhI(PPh_3)_3$ leading to (*E*)- and (*Z*)-alkenylsilanes and the application to polymer synthesis, 567
Morigaki, M.K., see Ursini, C.V., 2261
Moriguchi, T., Uchiyama, K., Yasutake, M., Shinmyozu, T., Sakata, K. and Tsuge, A., Syntheses, spectroscopic properties and X-ray crystal structures of tris(tfacacmetacyclophane)(bpy)-europium(III) and piperidinium tetrakis(*p*-tolutfacac)europate(III) complexes, 785
Morley, C.P., see Lewtas, M.R., 751
Morozova, N.B., see Isakova, V.G., 1097
Morrison, D.E., see Carmalt, C.J., 829
Moser, J.A., Stockland, R.A., Jr. and Anderson, G.K., Preparation and solution behavior of diphosphinepalladium nitrite complexes, 1329
Mostafa, G., see Basuli, F., 1663
Mostafa, G., see Laskar, I.R., 1015
Mostafa, G., see Maji, T.K., 1903
Motevalli, M., see Nel, A., 1621
Mottalib, M.A., see Azam, K.A., 1081
Mottalib, M.A., see Hanif, K.M., 1073
Moubaraki, B., see Dalgaard, P., 1909
Moya, S.A., see Longo, C., 487
Mukherjee, P.S., see Maji, T.K., 1903
Mukherjee, R., see Gupta, R., 1429
Mukherjee, R., see Gupta, R., 719
Mukherjee, R., see Patra, A.K., 1423
Mulford, D.R., Fanwick, P.E. and Rothwell, I.P., Group 4 and 5 metal derivatives of 2,2′-methylene-bis(6-phenylphenoxide), 35
Mu, L.-J., see Bu, X.-H., 2095
Muñoz, M.C., see Hernández-Padilla, M., 1175
Munshi, P., see Jain, P.U., 801
Murphy, W.L. and Messersmith, P.B., Compartmental control of mineral formation: adaptation of a biomineralization strategy for biomedical use, 357
Murray, K.S., see Dalgaard, P., 1909
Muthiah, C., Said, M.A., Pülm, M., Herbst-Irmer, R. and Kumara Swamy, K.C., New phospharanes with five- and seven-membered rings: influence of the nature of the substituents on hydrogen bonding, 63
Mu, Y., see Zhang, F., 1941

Nagy, D., see Szabó-Plánka, T., 1123
Nagy, N., see Szabó-Plánka, T., 2049
Nakashima, S., Ichikawa, N., Komatsu, H., Yamada, K. and Okuda, T., Host–guest interaction and dynamics of haloferrocenes enclathrated in deoxycholic acid as inferred from ^{57}Fe Mössbauer measurements, 205
Napoli, A., see Bucci, R., 2421
Napoli, A., see Bucci, R., 2515
Navarro, M., Lehmann, T., Cisneros-Fajardo, E.J., Fuentes, A., Sánchez-Delgado, R.A., Silva, P. and Urbina, J.A., Toward a novel metal-based chemotherapy against tropical diseases. Part 5. Synthesis and characterization of new Ru(II) and Ru(III) clotrimazole and ketoconazole complexes and evaluation of their activity against *Trypanosoma cruzi*, 2319
Negishi, E.-i., Liou, S.-Y., Xu, C. and Huo, S., A general method for the synthesis of *E* and/or *Z* oligoisoprenoids based on Pd-catalyzed homoallylalkenyl and homopropargyl-alkenyl cross coupling and Zr-catalyzed carboalumination, 591
Nejati, K., see Khandar, A.A., 607
Nel, A., Chapman, J., Long, N., Kolawole, G., Motevalli, M. and O'Brien, P., The synthesis and characterisation of two mononuclear tungsten pentacarbonyl complexes of 4,4′-bipyridine and 1,2-bis(4-pyridyl)ethane, 1621
Nemečková, M., see Boča, R., 835
Neuburger, M., see Constable, E.C., 23
Newman, E.H., see Levason, W., 2697
Nguyen, V.T., see Mink, L.M., 1057
Nicholson, B.K., see Depree, C.V., 2101
Niclós-Gutiérrez, J., see Bugella-Altamirano, E., 2473
Niclós-Gutiérrez, J., see Bugella-Altamirano, E., 2463
Nielsen, L.P., see Hazell, A., 1333
Nierlich, M., see Thuéry, P., 2673
Nierlich, M., see Thuéry, P., 1749
Nie, W.-L., see Qian, C.-T., 1955
Nishida, Y., see Kobayashi, T., 2639
Nishihara, Y., see Mori, A., 567
Nishino, S., see Kobayashi, T., 2639

Noh, D.-Y., see Lee, H.-J., 425
Noltemeyer, M., see Cui, C., 471
Nothenberg, M.S., de Souza, A.R. and Matos, J.R., Synthesis and physicochemical characterization of rhodium sulfosalicylate, 1305
Nöth, H., see Bond, E.M., 2135
Nöth, H., see Ceniceros-Gómez, A.E., 1821
Nöth, H., see Quiroz-Castro, E., 1479
Novaro, O., see Bokhimi, X., 2283
Nurchi, V.M., see Crisponi, G., 2435
Nyokong, T., see Oni, J., 1355
Nyokong, T., see Vilakazi, S., 229

Oberhauser, W., Stampfl, T., Bachmann, C., Haid, R., Langes, C., Kopacka, H., Ongania, K.-H. and Brüggeller, P., Palladium(II), platinum(II), and platinum(IV) complexes containing *trans*-1,2-bis(diphenylphosphino)ethene or *cis*,*trans*,*cis*-1,2,3,4-tetrakis(-diphenylphosphino)cyclobutane: complete X-ray structural characterization of binuclear compounds, 913
O'Brien, P., see Byrom, C., 211
O'Brien, P., see Jones, A.C., 351
O'Brien, P., see Nel, A., 1621
O'Brien, P., see Yordanov, N.D., 2177
O'Brien, S., see O'Hare, D., 297
Odović, J., see Djurdjević, P., 1085
O'Hare, D., Evans, J.S.O., Fogg, A. and O'Brien, S., Time-resolved, in situ X-ray diffraction studies of intercalation in lamellar hosts, 297
Oh, K.E., see Yoo, J., 549
Öhman, A., see Catalano, V.J., 1049
Ohta, K., Inagaki-Oka, Y., Hasebe, H. and Yamamoto, I., Discotic liquid crystals of transition metal complexes. 25: influence of the central metal on columnar mesomorphism and π-acceptor properties of the octa-alkoxy-substituted bis(diphenyldithiolene) metal complexes, 267
Okamoto, K.-i., see Maji, T.K., 1903
Okuda, T., see Nakashima, S., 205
Ongania, K.-H., see Oberhauser, W., 913
Ongania, K.-H., see Scheffter, B., 871
Oni, J. and Nyokong, T., Interaction between iron(II) tetrasulfophthalocyanine and the neurotransmitters, serotonin and dopamine, 1355
Onor, M., see Malatesta, F., 2493
Orchard, S.D., see Barton, A.J., 1373
Osborn, J.A., see Lorber, C.Y., 1693
Ovchynnikov, V.A., see Gubina, K.E., 2203
Ozeki, T., Sakaguchi, M. and Yagasaki, A., Synthesis and structure of a novel dimeric molybdenum oxyhalide anion, 43

Paget, T.J., see Edwards, D.A., 757
Paine, R.T., see Bond, E.M., 2135
Palicová, M., Segl'a, P., Mikloš, D., Kopcová, M., Melník, M., Dudová, B., Hudecová, D. and Glowiak, T., Synthesis, spectral properties, crystal structures and antimicrobial effects of copper(II) pyridinecarboxylate adducts with chelating ligands, 2689
Pal, S., Das, D., Chattopadhyay, P., Sinha, C., Panneerselvam, K. and Lu, T.-H., Synthesis, spectral and electrochemical properties of 1-alkyl-2-(naphthyl-β-azo)imidazole complexes of platinum(II) and the reaction with pyridine bases. Single-crystal X-ray structure of dichloro-[1-ethyl-2-(naphthyl-β-azo)imidazole]platinum(II), 1263
Pal, S., Misra, T.K., Sinha, C., Slawin, A.M.Z. and Woollins, J.D., Ruthenium(II) complexes of α-diimines: synthesis, spectral characterisation, electrochemical properties and single-crystal X-ray structure of bis(2,2′-bipyridine){1-benzyl-2-(*p*-tollylazo)imidazole}-ruthenium(II) perchlorate, 1925
Pal, S., see Sangeetha, N.R., 2713
Pal, S., see Sangeetha, N.R., 2713
Pal, S., see Sangeetha, N.R., 1593
Pandian, R.P., see Rose, E., 581
Panneerselvam, K., see Pal, S., 1263
Pannell, K.H., Wang, F., Sharma, H.K. and Cervantes-Lee, F., Bis(ferrocenylsilyl)thiophenes and ferrocenylene(silylene)thiophene oligomers, 291
Paoletti, P., see Bencini, A., 2441
Paoletti, P., see Ceccanti, N., 2447
Pardey, A.J., see Longo, C., 487
Pardini, R., see Bencini, A., 2441
Pardini, R., see Ceccanti, N., 2447
Pardo, T., see Al Shihadeh, Y., 1867
Parish, R.V., see Keypour, H., 1633
Park, B.B., see Rhee, S.W., 1961
Parker, O.J., Aubol, S.L. and Breneman, G.L., Crystal structure of a copper stabilized hydrate of di-2-pyridyl ketone, 623
Park, G., Ye, N., Rogers, R.D., Brechbiel, M.W. and Planalp, R.P., Effect of metal size on coordination geometry of *N*,*N*′,*N*″-tris(2-pyridylmethyl)-*cis*,*cis*-1,3,5-triaminocyclohexane: synthesis and structure of $[M^{II}L](ClO_4)_2$ (M = Zn, Cd and Hg), 1155
Parkin, G., see Hascall, T., 1063
Parkin, I.P., see Carmalt, C.J., 829
Park, J.W., see Kim, J.T., 1139
Park, S.K., Koo, S.M. and Lee, Y.E., Heterometallic lithium niobium complexes: synthesis and molecular structures of LiNbO(O-2,6-$PhMe_2)_4$·3THF and $[LiNbCl_3(O\text{-}2,6\text{-}PhMe_2)_2\cdot 2THF]_2$, 1037
Parola, S., see Verdenelli, M., 2069
Parsons, S.A., see Ahmed, S.I., 129
Parsons, S.A., see Alshehri, S., 399
Paschalidis, D.G., Tossidis, I.A. and Gdaniec, M., Synthesis, characterization and spectra of lanthanide(III) hydrazone complexes: The X-ray molecular structures of the erbium(III) complex and the ligand, 2629
Pastorek, R., Trávníček, Z., Marek, J., Dastych, D. and Šindelář, Z., Ni(II)-piperidinedithiocarbamate complexes with bidentate phosphorus-donor ligands, 1713
Patra, A.K., Ray, M. and Mukherjee, R., Magneto–structural studies of monohydroxo-bridged dicopper(II) complexes $M[Cu_2L_2(OH)]\cdot 2H_2O$ (M = Na^+ (**1**) and K^+ (**2**); H_2L = 2,6-bis[*N*-(phenyl)-carbamoyl]pyridine). Effect of Cu–OH–Cu bridge angle on antiferromagnetic coupling, 1423
Patron, L., see Tuna, F., 1643
Paul, P., see Bilakhiya, A.K., 1233
Paul, S., Kumar Barik, A., Butcher, R.J. and Kumar Kar, S., Synthesis and characterisation of nickel(II) complexes with tripodal ligand tris[4-(3-(5-methylpyrazolyl)-3-aza-3-butenyl] amine (MPz_3tren): X-ray crystal structure of $[Ni(MPz_3tren)](BF_4)_2\cdot 0.5H_2O$, 2661
Paul, S., see Barik, A.K., 2651
Pavlović, G., see Cindrić, M., 1471
Pazderski, L., see Szłyk, E., 965
Pedrosa, M.R., see Arnáiz, F.J., 2141
Pelosi, G., see Belicchi Ferrari, M., 1895
Peñas-Chamorro, A.L., see Hueso-Ureña, F., 689
Peng, S.-M., see Basuli, F., 1663
Peng, S.-M., see Das, A., 1227
Peng, S.-M., see Sinha, P.K., 1673
Peng, Y., Lu, X.-F., Fan, H.-J., Wu, Q.-J., Yu, R.-M. and Huang, J.-Q., Synthesis, crystal structure and bonding features of a trinuclear cluster $[Mo_3X(S_2)_3(dtp)_3I_3]$ (X = O,S) with layer-like packing, 733
Pereira, G.G., see Caldeira, M.M., 193
Pérez, J., see Sánchez, G., 1395
Perilla, I.C., see Riveros, P.C., 2327
Peringer, P., see Scheffter, B., 871
Perrin, J.L., see Adams, R.D., 521

Petriček, S., Demšar, A., Golič, L. and Košmrlj, J., New complexes of lanthanide chlorides. Reversible isomerization in octahedral $[LaCl_3(HMPA)_3]$ and the crystal structure of *fac*-$[SmCl_3(HMPA)_3]$, 199
Petrohán, K., see Kiss, E., 55
Petrović, D.M., see Rogan, J., 1415
Petrukhina, M.A., see Cotton, F.A., 1829
Pharazyn, P.S., see Matteson, D.S., 587
Picchi, M.P., see Pifferi, C., 69
Pidwell, A.D., see Guillevic, M.-A., 249
Piedade, M.F.M., see Santos, I.C., 655
Pietro, W.J., see Veinot, J.G.C., 331
Pifferi, C., Picchi, M.P. and Cini, R., Vanadium complexes as models for vanadium species of marine organisms. Synthesis, X-ray structure of oxo(*O*,*O*-sulfate)(2,2′:6′,2″-terpyridine)vanadium(IV) hydrate, and density functional geometry optimization analysis of vanadyl complexes, 69
Piniella, J.F., see Chadghan, A., 855
Pinkerton, A.B., see Santos, E.C., 1777
Pinna, R., see Crisponi, G., 2435
Pires de Matos, A., see Carvalho, A., 1707
Pires de Matos, A., see Carvalho, A., 1699
Pivetta, T., see Crisponi, G., 2435
Planalp, R.P., see Park, G., 1155
Pokol, G., see Madarász, J., 457
Polese, P., see Comuzzi, C., 2427
Poleti, D., see Rogan, J., 1415
Ponnuswamy, M.N., see Manonmani, J., 2011
Pons, J., see Chadghan, A., 855
Pontellini, R., see Formica, M., 2501
Pope, S.J.A., see Heuer, B., 743
Portanova, R., see Comuzzi, C., 2427
Porto, R., see Ciavatta, L., 1043
Poveda, A., see Riveros, P.C., 2327
Powell, A.K., see Zhang, Y.-J., 1757
Powell, D.R., see McGaff, R.W., 1245
Power, P.P., see Wehmschulte, R.J., 1649
Pritchard, R.G., see Keypour, H., 1633
Pritzkow, H., see Riveros, P.C., 2327
Pulidori, F., see Remelli, M., 2409
Pülm, M., see Muthiah, C., 63
Purvis, K.L., see Schwartz, J., 505
Py, S., see Fallis, A.G., 533

Qian, C.-T., Zou, G., Nie, W.-L., Sun, J., Lemenovskii, D.A. and Borzov, M.V., Stereoselective synthesis and structural characterization of *rac*-planar chiral bis(2-methoxyethylindenyl)lanthanum and yttrium tetrahydroborates, 1955
Qian, Y., see Liu, Q., 453
Quelquejeu, M., see Rose, E., 581
Quintana, P., see Alvarado, E., 2345
Quirós, M., see Seco, J.M., 1005
Quiroz-Castro, E., Bernès, S., Barba-Behrens, N., Tapia-Benavides, R., Contreras, R. and Nöth, H., Structural and spectroscopic characterisation of tris(2-benzimidazolylmethyl)amine coordination compounds of Zn(II), Cd(II) and Hg(II), 1479
Quiroz-Castro, M.E., see Ceniceros-Gómez, A.E., 1821

Rabinovich, D., see Richburg, L.M., 1815
Rabinovich, D., see Yim, H.W., 849
Rabu, P., see Hornick, C., 259
Radanović, D.D., see Rychlewska, U., 1
Radanović, D.J., see Rychlewska, U., 1
Rahaman Laskar, I., Kumar Maji, T., Chaudhuri, S., Ghosh, A. and Ray Chaudhuri, N., Synthesis and characterization of *cis* and *trans* isomers of $[NiL_2(NCS)_2]$ [L = 1-(2-aminoethyl)pyrrolidine]: X-ray single-crystal structures, 1803
Rahim, M.A., see Takeda, T., 593
Rajak, K.K., Mondal, S. and Rath, S.P., Synthesis, structure and properties of mononuclear oxovanadium(V) alkoxides incorporating chelated ethane-1,2-diol and propane-1,3-diol, 931
Rajak, K.K., see Jain, P.U., 801
Ramalingam, K., see Thirumaran, S., 1279
Ramirez, J., see Canales, J., 2373
Ramos, M.L., see Caldeira, M.M., 193
Ramírez de Arellano, M.C., see Sánchez, G., 1395
Rath, S.P., see Jain, P.U., 801
Rath, S.P., see Rajak, K.K., 931
Ratnani, R., see Drake, J.E., 407
Rauchfuss, T.B., see Breitzer, J.G., 1283
Ray Chaudhuri, N., see Laskar, I.R., 1015
Ray Chaudhuri, N., see Maji, T.K., 1903
Ray Chaudhuri, N., see Rahaman Laskar, I., 1803
Ray, M., see Patra, A.K., 1423
Redman, H., see Almond, M.J., 2127
Redshaw, C. and Elsegood, M.R.J., Synthesis and structure of a novel molybdenum imido calix[6]arene, 2657
Rees, L.H., see Coe, B.J., 1193
Reid, G., see Barton, A.J., 1373
Reid, G., see Barton, A.J., 235
Reid, G., see Heuer, B., 743
Remelli, M., Conato, C., Agarossi, A., Pulidori, F., Młynarz, P. and Kozłowski, H., Copper complexes of dipeptides with L-Lys as C-terminal residue: a thermodynamic and spectroscopic study, 2409
Repo, T., see Abu-Surrah, A.S., 1601
Resino, I., Monfort, M., Ribas, J., Font-Bardia, M. and Solans, X., Synthesis and crystal structure of a new mononuclear compound containing alternate nickel(II) and sodium ions in the sheet $[Ni(en)_2(NO_2)_2]NaClO_4 \cdot H_2O$, 225
Rhee, H., see Kwak, B., 1985
Rhee, S.W., Park, B.B., Do, Y. and Kim, J., Electronic and NMR properties of *meso*-monosubstituted ferrocenylporphyrin: evidence of π-conjugation between porphyrin and ferrocene, 1961
Rheingold, A.L., see MacLachlan, M.J., 275
Rheingold, A.L., see Richburg, L.M., 1815
Rheingold, A.L., see Yim, H.W., 849
Ribas, J., see Resino, I., 225
Ricart, G., see Rose, E., 581
Ricci, A., see Bonini, B.F., 529
Rice, C.R. and Anderson, K.M., A new synthesis of a potentially versatile ligand 2,2′-bi-(1,10-phenanthroline): crystal structure and complexation chemistry, 495
Rice, D.A., see Almond, M.J., 2127
Richburg, L.M., Farouq, J.A., Incarvito, C.D., Rheingold, A.L. and Rabinovich, D., Zinc bis(pyrazolyl)silane complexes, 1815
Richens, D.T., see Hay, R.W., 1485
Riedel, R., see Ruwisch, L.M., 323
Rietveld, T., see Fallis, A.G., 533
Rigo, S., see García-Raso, Á., 991
Rintoul, L., see Jiang, J., 1381
Rivero, M., Kremer, C., Gancheff, J., Kremer, E., Suescun, L., Mombrú, A., Mariezcurrena, R., Domínguez, S., Mederos, A. and Midollini, S., Cationic complexes of Re with dppm (bis(diphenylphosphinomethane)). Crystal structure of $[Re(dppm)_3]I \cdot CH_3OH \cdot CH_2Cl_2$, 2249
Riveros, P.C., Perilla, I.C., Poveda, A., Keller, H.J. and Pritzkow, H., Tris(dialkyldithiocarbamato)diazenido(1-) and hydrazido(2-) molybdenum complexes: synthesis and reactivity in acid medium, 2327
Rivière, E., see Tuna, F., 1643
Rizzotto, M., Moreno, V., Signorella, S., Daier, V. and Sala, L.F., Electron paramagnetic resonance and potentiometric studies of the interactions of Cr(VI) and Cr(V) with D-ribose-5-phosphate and nucleotides, 417

Robertson, E.W., Wilkin, O.M. and Young, N.A., The spectroscopic characterisation of *cis*-$Fe(CO)_4IBr$ and *cis*-$Fe(CO)_4ICl$ and an investigation of their halogen exchange reactions in solution and the vapour, 1493
Robinson, S.D., see Exarchos, G., 1511
Robinson, S.D., see Exarchos, G., 123
Robinson, S.D., see Malik, K.Z., 1589
Rocha-Filho, R.C., see Trollund, E., 2303
Rockenbauer, A., see Szabó-Plánka, T., 2049
Rockenbauer, A., see Szabó-Plánka, T., 1123
Rodríguez, M., Llobet, A. and Corbella, M., A theoretical analysis of how geometrical distortions on $Cu(\mu\text{-}Cl)_2Cu$ dimers influence their electronic and magnetic properties, 2483
Rodríguez, V., see Ruiz, J., 1627
Rodrigues-Filho, U.P., see do Carmo, D.R., 2277
Rodriguez, M.A., see Zechmann, C.A., 2557
Roesky, H.W., see Cui, C., 471
Rogan, J., Poleti, D., Karanović, L., Bogdanović, G., Spasojević-de Biré, A. and Petrović, D.M., Mixed ligand Co(II), Ni(II) and Cu(II) complexes containing terephthalato ligands. Crystal structures of diaqua(2,2′-dipyridylamine)(terephthalato)metal(II) trihydrates (metal = cobalt or nickel), 1415
Rogers, R.D., see Park, G., 1155
Rogers-Sakuma, A., see López-Cardoso, M., 1539
Romani, P., see Formica, M., 2501
Rombaut, G., see Tanase, S., 1967
Romeo, I., Bardají, M., Concepción Gimeno, M. and Laguna, M., Gold(I) complexes containing the cationic ylide ligand bis(-methyldiphenylphosphonio)methylide, 1837
Romero, J., see Cabaleiro, S., 1607
Romero, J., see Labisbal, E., 1255
Rose, E., Quelquejeu, M., Pandian, R.P., Lecas-Nawrocka, A., Vilar, A., Ricart, G., Collman, J.P., Wang, Z. and Straumanis, A., Synthesis of porphyrins: models of natural hemoproteins and impressive catalysts for asymmetric epoxidation of olefins, 581
Rosenberg, E., see Hanif, K.M., 1073
Ros, J., see Chadghan, A., 855
Roszak, S., see Szterenberg, L., 2565
Rothwell, I.P., see Mulford, D.R., 35
Roussanova, D., see Yordanov, N.D., 2177
Rubini, P., see Giroux, S., 1567
Rui, L., see Li, J.-M., 1117
Ruiz, J., Giner, J., Rodríguez, V., López, G., Casabó, J., Molins, E. and Miravitlles, C., Synthesis and characterization of heterodinuclear thiolate complexes containing the $Pd(\eta^3\text{-allyl})^+$ moiety. Crystal structure of $[(dppe)Pd(\mu\text{-}SC_6H_4Me\text{-}p)_2Pd(\eta^3\text{-}C_3H_5)][ClO_4]$, 1627
Ruiz-Ramírez, L., see Mendoza-Díaz, G., 2149
Runde, W.H., see Danis, J.A., 1551
Russell, D.R., see Ahmed, S.I., 129
Russell, D.R., see Alshehri, S., 399
Russell, D.R., see Matoga, D., 1503
Russo, U., see Casas, J.S., 813
Rusu, D., see David, L., 1917
Rusu, M., see David, L., 1917
Ruwisch, L.M., Dürichen, P. and Riedel, R., Synthesis of silyl substituted organoboranes by hydroboration of vinylsilanes, 323
Rybak, W.K., see Głowiak, T., 2667
Rychlewska, U., Radanović, D.D., Jevtović, V.S. and Radanović, D.J., Synthesis and X-ray structural study of magnesium (1,3-propanediaminetetraacetato)cuprato(II) octahydrate, $Mg[Cu(1,3\text{-}pdta)]\cdot 8H_2O$. Stereochemistry of hexadentate copper(II)–edta-type complexes in relation to the structure of the ligand, 1

Sacht, C. and Datt, M.S., Synthesis and characterisation of mixed-ligand platinum(II)–sulfoxide complexes, [PtCl(DMSO)(L)], for potential use as chemotherapeutic agents (HL = *N*,*N*-dialkyl-*N*′-(3-*R*-benzoyl)thiourea), 1347
Saha, M.K., see Mondal, N., 1935
Said, M.A., see Muthiah, C., 63
Saito, Y., see Sakakura, T., 573
Sakaguchi, M., see Ozeki, T., 43
Sakakura, T., Choi, J.-C., Saito, Y. and Sako, T., Synthesis of dimethyl carbonate from carbon dioxide: catalysis and mechanism, 573
Sakata, K., see Moriguchi, T., 785
Sako, T., see Sakakura, T., 573
Sala, L.F., see Rizzotto, M., 417
Salehzadeh, S., see Keypour, H., 1633
Sambasiva Reddy, P. and Hussain Reddy, K., Transition metal complexes of benzil-α-monoxime (BMO); X-ray structure determination of $Co(BMO)_3$, 1687
Samotus, A., see Matoga, D., 1503
Samson, E., see Baker, P.K., 147
Sánchez, A., see Casas, J.S., 813
Sánchez-Delgado, R.A., see Navarro, M., 2319
Sánchez, G., Serrano, J.L., Ramírez de Arellano, M.C., Pérez, J. and López, G., Reactivity of the di-μ-hydroxo-complexes $[\{Pd(N\text{–}N)\}_2(\mu\text{-}OH)_2][ClO_4]_2$ (N–N = bis(pyrazol-1-yl)alkanes) towards protic electrophiles. Hydration of coordinated nitriles at a palladium(II) site, 1395
Sangeetha, N.R. and Pal, S., Dimeric and polymeric square-pyramidal copper(II) complexes containing equatorial–apical chloride or acetate bridges, 1593
Sangeetha, N.R., Pal, S. and Pal, S., Copper(II)-activated transformation of azomethine to imidate: synthetic and structural studies, 2713
Sanmartín, J., Bermejo, M.R., Garía-Deibe, A.M., Maneiro, M., Lage, C. and Costa-Filho, A.J., Mono- and polynuclear complexes of Fe(II), Co(II), Ni(II), Cu(II), Zn(II) and Cd(II) with *N*,*N*′-bis(3-hydroxysalicylidene)-1,3-diamino-2-propanol, 185
Sanna, D., see Ágoston, C.G., 1849
Sanna, D., see Kiss, E., 55
Santos, E.C., Pinkerton, A.B., Kinkead, S.A., Hurlburt, P.K., Jasper, S.A., Sellers, C.W., Huffman, J.C. and Todd, L.J., Syntheses of *nido*-9,11-X_2-7,8-$C_2B_9H_{10}^-$ anions (X = Cl, Br or I) and the synthesis and structural characterization of $N(C_2H_5)_4[commo\text{-}3,3'\text{-}Co(4,7\text{-}Br_2\text{-}3,1,2\text{-}CoC_2B_9H_9)_2]$, 1777
Santos, I.C., Vilas-Boas, M., Piedade, M.F.M., Freire, C., Duarte, M.T. and de Castro, B., Electrochemical and X-ray studies of nickel(II) Schiff base complexes derived from salicylaldehyde. Structural effects of bridge substituents on the stabilisation of the +3 oxidation state, 655
Sanz-Ruiz, F., see Borrás, E., 1859
Sarova, G., see Yordanov, N.D., 2177
Scarcia, V., see Tušek-Božić, L., 937
Scheetz, B.E., see Danis, J.A., 1551
Scheffter, B., Schuh, W., Ongania, K.-H., Kopacka, H., Malleier, R., Wurst, K. and Peringer, P., Host–guest interactions of the cluster $[triangulo\text{-}Hg_3(\mu\text{-}dppm)_3]^{4+}$ (dppm = bis(diphenylphosphino)methane) with halides and pseudohalides, 871
Schmidt, H.-G., see Cui, C., 471
Schubert, U., see Vrbová, M., 2195
Schuh, W., see Scheffter, B., 871
Schumann, H., see Blum, J., 509
Schwartz, J., Gawalt, E.S., Lu, G., Milliron, D.J., Purvis, K.L., Woodson, S.J., Bernasek, S.L., Bocarsly, A.B. and VanderKam, S.K., Organometallic chemistry at the interface with materials science, 505
Scott, B.L., see Danis, J.A., 1551
Secco, F., see Ceccanti, N., 2447
Secco, F., Tinè, M.R., Venturini, M., Bencini, A., Giorgi, C. and Valtancoli, B., Equilibria and kinetics of complex formation between nickel(II) and the polyamine Me_2octaen, 2507

Seco, J.M., Quirós, M. and González Garmendia, M.J., Synthesis, X-ray crystal structure and spectroscopic, magnetic and EPR studies of copper(II) dimers with methoxy-di-(2-pyridyl)methoxide as bridging ligand, 1005
Segl'a, P., see Palicová, M., 2689
Segura, R., see Cárdenas, G., 2337
Segura, R., see Crivelli, I.G., 2289
Sellers, C.W., see Santos, E.C., 1777
Semioshkin, A.A., see Sivaev, I.B., 627
Sen, S., Kumar Saha, M., Mitra, S., Edwards, A.J. and Clegg, W., Synthesis, characterisation and crystal structure of a 1,4-diazacycloheptane complex of copper(II), 1881
Serrano, J.L., see Sánchez, G., 1395
Server-Carrió, J., see Borrás, E., 1859
Sevilla, M.T., see Franco, E., 441
Shamsipur, M. and Madrakian, T., Competitive lithium-7 NMR study of the complexation of some alkaline earth and transition metal ions with 18-crown-6 in acetonitrile and its 50:50 mixtures with nitrobenzene and nitroethane, 1681
Shanmugam, G., see Manonmani, J., 2011
Sharma, H.K., see Pannell, K.H., 291
Sharma, M., Singh, A. and Mehrotra, R.C., Synthesis and characterization of homo- and hetero-bimetallic diethanolaminates of alkaline earth metals, 77
Sharp, P.R., see Kannan, S., 155
Shatrava, J.A., see Gubina, K.E., 2203
Shen, Q., see Zhang, L.-L., 2243
Shen, X., see Liu, Q., 453
Shepherd, R.E., see Ward, M.S., 1339
Shinmyozu, T., see Moriguchi, T., 785
Shi, Q., see Wang, Y.-Y., 891
Shi, Q.-Z., see Wang, Y.-Y., 891
Shirran, C., see Casey, M., 517
Shi, Z., see Zhang, F., 1941
Shoemaker, J.A.W., see Hartman, J.S., 165
Shukla, A.D. and Das, A., Redox responsive binuclear complexes using 5,6-dihydroxy-1,10-phenanthroline as a bridging ligand: synthesis, characterization and physicochemical studies, 2605
Shuvaev, A.T., see Uraev, A.I., 2361
Sicilia Zafra, A.G., see Bugella-Altamirano, E., 2473
Sicilia-Zafra, A.G., see Bugella-Altamirano, E., 2463
Sieklucka, B., see Kania, R., 2225
Sienra, B., see Benzo, F., 971
Signorella, S., see Rizzotto, M., 417
Sillanpää, R., see Lehtonen, A., 2579
Sillanpää, R., see Liimatainen, J., 1133
Silva, P., see Navarro, M., 2319
Silvino, A.C., see Harrison, W.T.A., 821
Simón-Manso, Y., see Concepción, J., 2297
Šindelář, Z., see Pastorek, R., 1713
Singh, A., see Sharma, M., 77
Singh, R.P., see Matteson, D.S., 587
Sinha, C., see Pal, S., 1925
Sinha, C., see Pal, S., 1263
Sinha, P.K., Falvello, L.R., Peng, S.-M. and Bhattacharya, S., Chemistry of some ruthenium phenolates: synthesis, structure and redox properties, 1673
Sinyashin, O.G., see Karasik, A.A., 1455
Sivaev, I.B., Semioshkin, A.A., Brellochs, B., Sjöberg, S. and Bregadze, V.I., Synthesis of oxonium derivatives of the dodecahydro-closo-dodecaborate anion $[B_{12}H_{12}]^{2-}$. Tetramethylene oxonium derivative of $[B_{12}H_{12}]^{2-}$ as a convenient precursor for the synthesis of functional compounds for boron neutron capture therapy, 627
Sjöberg, S., see Sivaev, I.B., 627
Skarżyńska, A., see Głowiak, T., 2667
Slawin, A.M.Z., see Aucott, S.A., 499
Slawin, A.M.Z., see Bhattacharyya, P., 809
Slawin, A.M.Z., see Kelly, P.F., 2077
Slawin, A.M.Z., see Pal, S., 1925
Slawin, A.M.Z., see Smith, M.B., 695
Smith, D.R., see Constable, E.C., 23
Smith, M.B. and Slawin, A.M.Z., New *E*-unidentate $[Ph_2P(O)NP(E)Ph_2]^-$ (E = S or Se) complexes of palladium(II) and platinum(II), 695
Smith, P.D., see Brooker, S., 1887
Sodre Costa, L.A., see Harrison, W.T.A., 821
Solans, X., see Resino, I., 225
Song, Y., see Zhu, D.-R., 2019
Song, Y., Zhu, D.-R., Zhang, K.-L., Xu, Y., Duan, C.-Y. and You, X.-Z., Magnetic properties of two 1D complexes with mixed bridging ligands, 1461
Sordo, J., see Casas, J.S., 813
Soto, H., see Cárdenas, G., 2337
Soto, J., see Al Shihadeh, Y., 1867
Sousa, A., see Cabaleiro, S., 1607
Sousa, A., see Labisbal, E., 1255
Sousa, A., see Maneiro, M., 47
Sousa-Pedrares, A., see Maneiro, M., 47
Sóvágó, I., see Ágoston, C.G., 1849
Spasojević-de Biré, A., see Rogan, J., 1415
Spey, S.E., see Bricklebank, N., 1163
Speziali, N.L., see Teles, W.M., 739
Spodine, E., see Manzur, J., 2367
Spry, M.P., see Willey, G.R., 1799
Stampfl, T., see Oberhauser, W., 913
Stankov, M.J., see Djurdjević, P., 1085
Starikova, Z.A., see Turevskaya, E.P., 705
Starynowicz, P., see Lisowski, J., 465
Starynowicz, P., see Mondry, A., 771
Stasiak, M., see Kowalik-Jankowska, T., 241
Steed, J.W., see Carmalt, C.J., 1639
Steed, J.W., see Exarchos, G., 1511
Steed, J.W., see Malik, K.Z., 1589
Stephenson, G.R., see Anson, C.E., 569
Stiriba, S.-E., see Cotton, F.A., 1829
Stockland, R.A., Jr., see Moser, J.A., 1329
Straumanis, A., see Rose, E., 581
Strenger, I., see Tanase, S., 1967
Su, C.-Y., see Xiao, W., 1295
Suescun, L., see Rivero, M., 2249
Sundara Raj, S.S., see Manonmani, J., 2011
Sundara Raj, S.S., see Zhu, D.-R., 2019
Sun, J., see Qian, C.-T., 1955
Sun, J., see Zhang, L.-L., 2243
Sun, Z.-G., Liu, Q. and Liu, J.-F., Synthesis and spectroscopic characterization of organophosphoryl polyoxotungstates $[C_6H_{11}P(O)]_2X^{n+}$-$W_{11}O_{39}^{(8-n)-}$ $X^{n+} = P^{5+}$, Si^{4+}, B^{3+}, Ga^{3+}), 125
Suzuki, Y., see Hiroi, K., 525
Svoboda, I., see Boča, R., 835
Svoboda, I., see Iskander, M.F., 949
Svoboda, I., see Iskander, M.F., 1181
Svoboda, I., see Vrbová, M., 2195
Swearingen, J.K., see de Sousa, G.F., 841
Szabó-Plánka, T., Nagy, N., Rockenbauer, A. and Korecz, L., An ESR study of the copper(II)-glycyl-L-histidine system in aqueous solution by the simultaneous analysis of multi-component spectra. Formation constants and coordination modes, 2049
Szabó-Plánka, T., Rockenbauer, A., Korecz, L. and Nagy, D., An electron spin resonance study of coordination modes in the copper(II)–histamine and copper(II)–L-histidine systems in fluid aqueous solution, 1123
Szklarzewicz, J., see Matoga, D., 1503

Szłyk, E., Grodzicki, A., Pazderski, L., Bednarek, E. and Kamieński, B., Heteronuclear multiple-quantum correlation $^{15}N-^{1}H$, cross-polarized magic angle spinning ^{13}C, ^{15}N nuclear magnetic resonance and infrared spectroscopic studies of 1,2,4-triazolo-[1,5α]-pyrimidine and its Zn(II) halide and thiocyanate complexes, 965
Szterenberg, L., Roszak, S., Matusiak, R. and Keller, A., Structure and chemical bonding in *cis*- and *trans*-$M(NO)_2(O_2CR)_2$ (M = Cr and Mo) complexes, 2565

Tae Kim, J., see Woo Park, J., 2547
Takahisa, E., see Mori, A., 567
Takamori, M., see Takeda, T., 593
Takeda, T., Rahim, M.A., Takamori, M., Yanai, K. and Fujiwara, T., Synthesis of carbocycles and heterocycles by the titanocene(II)-promoted reactions of thioacetals, 593
Takemura, H., see Thuéry, P., 2673
Takeuchi, R., Iridium complex-catalyzed allylic alkylation, 557
Tanase, S., Ferbinteanu, M., Andruh, M., Mathonière, C., Strenger, I. and Rombaut, G., Synthesis and characterization of a new molecular magnet, $[Ni(ampy)_2]_3[Fe(CN)_6]_2\cdot 6H_2O$, and synthesis, crystal structure and magnetic properties of its mononuclear precursor, *trans*-$[Ni(ampy)_2(NO_3)_2]$ (ampy = 2-aminomethylpyridine), 1967
Tang, L.-F., Wang, Z.-H., Chai, J.-F., Jia, W.-L., Xu, Y.-M. and Wang, J.-T., Novel five- and six-coordinate diorganotin(IV) complexes with bis(triazol-1-yl)alkanes: linkage coordination polymers, 1949
Tang, L.-F., Wang, Z.-H., Jia, W.-L., Xu, Y.-M. and Wang, J.-T., Synthesis of diorganotin derivatives containing asymmetric disubstituted bis(pyrazol-1-yl)methanes: X-ray crystal structures of (3-isopropylpyrazol-1-yl-5′-isopropylpyrazol-1-yl)methane diphenyltin(IV) dibromide and bis(5-isopropylpyrazol-1-yl)methane diphenyltin(IV) dibromide, 381
Tang, N., see Fan, L., 779
Tang, Y., see Zhang, Z.-H., 1559
Tan, M., see Fan, L., 779
Tanner, P.A., Mak, C.S.K. and Mak, T.C.W., Synthesis, structure and spectroscopy of rare earth hypophosphites: 3. Ytterbium hypophosphite, 863
Tan, W., Zheng, H., Jin, Q., Jin, G., Ji, W., Long, D. and Xin, X., Synthesis, crystal structure and third-order optical nonlinearity of a 'flywheel'-shaped cluster, $[MoS_4Cu_3(dppm)_3][BF_4]\cdot 2H_2O$, 1545
Tapia-Benavides, R., see Quiroz-Castro, E., 1479
Tarasconi, P., see Belicchi Ferrari, M., 1895
Teles, W.M., Speziali, N.L. and Filgueiras, C.A.L., Synthesis of a polymetallic Pt, Sn complex containing square planar and trigonal bipyramidal platinum centres. Crystal and molecular structure of bis{chlorotriethylphosphinoplatinum(II)}μ-2,3,5,6-tetrakis(α-pyridyl)pyrazinetetrakis(trichlorostannyl)triethylphosphinoplatinate(II), 739
Téllez-Sara, C.A., Arissawa, M., Gómez-Lara, J. and Mondragón, M.A., Fourier transform infrared and Raman spectra of uranyl bis(2-hydroxybenzaldehyde): $UO_2(sal)_2$, 2353
Teresa Sevilla, M., see Cañadas, M., 2059
Thieme, K., see MacLachlan, M.J., 275
Thind, R.K., see Hodson, A.G.W., 791
Thirumaran, S., Ramalingam, K., Bocelli, G. and Cantoni, A., Spectral and single crystal X-ray structural studies on disulfide complexes: reaction of bis(dialkyldithiocarbamato)M(II) with iodine and crystal structure determination of diiodo(bipiperidinethiuramdisulfide)M(II) (M = zinc, cadmium), 1279
Thirumurugan, R., see Manonmani, J., 2011
Thuéry, P., Nierlich, M., Asfari, Z., Vicens, J. and Dozol, J.-F., Complexes of sodium and caesium perrhenates with calix[4]arene bis(crown-6): a model for pertechnetate ion extraction, 1749
Thuéry, P., Nierlich, M., Vicens, J. and Takemura, H., Complexes of ytterbium(III) nitrate and triflate with homoazacalix[*n*]arenes (*n* = 3, 4), 2673
Tinè, M.R., see Ceccanti, N., 2447
Tinè, M.R., see Secco, F., 2507
Todd, L.J., see Santos, E.C., 1777
Tokii, T., see Kobayashi, T., 2639
Tolazzi, M., see Comuzzi, C., 2427
Tolhurst, V.-A., see Barton, A.J., 235
Toner, A.J., see Coles, S.J., 177
Toner, A.J., see Coles, S.J., 1271
Tong, M.-L., Zheng, S.-L. and Chen, X.-M., Synthesis and structures of two-dimensional coordination polymers constructed by metal salts and 4,4′-bipyridine, 1809
Torres-Martinez, L.M., see Alvarado, E., 2345
Toscano, R.A., see de Sousa, G.F., 841
Tossidis, I.A., see Paschalidis, D.G., 2629
Trávníček, Z., see Pastorek, R., 1713
Treichel, P.M., see McGaff, R.W., 1245
Tristão, M.L.B., see Doyle, A., 2621
Trollund, E., Ardiles, P., Aguirre, M.J., Biaggio, S.R. and Rocha-Filho, R.C., Spectroelectrochemical and electrical characterization of poly(cobalt–tetraaminophthalocyanine)-modified electrodes: electrocatalytic oxidation of hydrazine, 2303
Trombella, S., see Malatesta, F., 2493
Tsai, C.-H., see Li, Y.-I., 413
Tsai, C.-H., Tung, J.-Y., Chen, J.-H., Liao, F.-L., Wang, S.-L., Wang, S.-S., Hwang, L.-P. and Chen, C.-B., Crystal of *meso*-*p*-tolyl-porphyrinato copper(II) Cu(tptp) and di-cation ion-pair complex $[H_4tptp]^{2+}[CF_3SO_3]^{2-}$ formation during the reaction of $Cu(CF_3SO_3)_2$ with *meso*-*p*-tolyl-porphyrin in $CDCl_3$, 633
Tsiamis, C., Voulgaropoulos, B., Charistos, D., Voutsas, G.P. and Kavounis, C.A., Ligand reactivity, substituent effects and solvent interactions in the spectra and structure of some oxovanadium(V) chelates with Schiff bases. Proof for dimeric species, 2003
Tsuge, A., see Moriguchi, T., 785
Tuna, F., Patron, L., Rivière, E. and Boillot, M.-L., Magnetic and spectral properties of two five-coordinate Lewis-base adducts of cobalt(II) Schiff-base complexes with a N_3O_2 ligand environment, 1643
Tung, J.-Y., see Li, Y.-I., 413
Tung, J.-Y., see Tsai, C.-H., 633
Turevskaya, E.P., Belokon', A.I., Starikova, Z.A., Yanovsky, A.I., Kiruschenkov, E.N. and Turova, N.Y., Scandium alkoxides: the first mixed-ligand alkoxides containing the $[M_5O(OR)_8]$ core, scandium alkoxoaluminates, 705
Turner, P., see Long, G.V., 1067
Turova, N.Ya., see Turevskaya, E.P., 705
Tušek-Božić, L., Komac, M., Ćurić, M., Lyčka, A., D'Alpaos, M., Scarcia, V. and Furlani, A., Five-membered [C,N] and [N,O] metallocyclic complexes of palladium(II) with monoalkyl [α-(4-benzeneazoanilino)-*N*-benzyl]phosphonates: synthesis, characterization and antitumour activity, 937
Tyagi, B., see Bilakhiya, A.K., 1233

Uchiyama, K., see Moriguchi, T., 785
Umani-Ronchi, A., see Bandini, M., 537
Uraev, A.I., Vlasenko, V.G., Kharisov, B.I., Blanco, L.M., Shuvaev, A.T., Vasilchenko, I.S., Garnovskii, A.D. and Elizondo, N.V., Synthesis and EXAFS investigation of azomethynic copper metallochelates with an N,S,O ligand environment, 2361
Urbach, F.L., see Chou, J.-L., 2215
Urbina, J.A., see Navarro, M., 2319
Ursini, C.V., Dias, G.H.M., Hörner, M., Bortoluzzi, A.J. and Morigaki, M.K., Facile conversion of bis(alkynyl) into diyne ligand on platinum assisted by electrophilic gold phosphine, 2261

Vacca, A., see Ciavatta, L., 1043
Vais-Morlender, N., see Kaftanov, J., 563
Valdés-Martínez, J., see de Sousa, G.F., 841
Valtancoli, B., see Bencini, A., 2441

Valtancoli, B., see Secco, F., 2507
VanderKam, S.K., see Schwartz, J., 505
van Koten, G., see Kronenburg, C.M.P., 553
Varchi, G., see Bonini, B.F., 529
Varela, J.M., see Casas, J.S., 813
Várnagy, K., see Ágoston, C.G., 1849
Vasilchenko, I.S., see Uraev, A.I., 2361
Veale, P.L., see Baker, P.K., 147
Veinot, J.G.C., Farah, A.A., Galloro, J., Zobi, F., Bell, V. and Pietro, W.J., Surface functionalization of cadmium sulfide quantum confined nanoclusters. 6: evidence of facile electronic communications between remote surface sites, 331
Venturini, M., see Ceccanti, N., 2447
Venturini, M., see Secco, F., 2507
Verani, C.N., see Doyle, A., 2621
Verdenelli, M., Parola, S., Hubert-Pfalzgraf, L.G. and Lecocq, S., Tin dioxide thin films from Sn(IV) modified alkoxides — synthesis and structural characterization of $Sn(OEt)_2(\eta^2\text{-acac})_2$ and $Sn_4(\mu_3\text{-}O)_2(\mu_2\text{-}OEt)_4(OEt)_6(\eta^2\text{-acac})_2$, 2069
Verma, R., see Lobana, T.S., 899
Vestergaard, C., see Becher, J., 665
Vicens, J., see Thuéry, P., 2673
Vicens, J., see Thuéry, P., 1749
Vicentini, G., see Carvalho, A., 1707
Vicentini, G., see Fernandes, L.C., 2313
Victoriano, L.I., The reaction of copper and iron species with thiuram sulfides: copper and iron dithiocarbamate derivatives, 2269
Vilakazi, S. and Nyokong, T., Interaction of nitric oxide with cobalt(II) tetrasulfophthalocyanine, 229
Vilar, A., see Rose, E., 581
Vilas-Boas, M., see Santos, I.C., 655
V. Larionov, S., see A. Savel'eva, Z., 1737
Vlasenko, V.G., see Uraev, A.I., 2361
Voce, J.W., see Mink, L.M., 1057
Voigt, A., see Abram, U., 1741
Voulgaropoulos, B., see Tsiamis, C., 2003
Voutsas, G.P., see Tsiamis, C., 2003
Vrbová, M., Baran, P., Boča, R., Fuess, H., Svoboda, I., Linert, W., Schubert, U. and Wiede, P., Preparation and structure of 2-(2-benzimidazol-2-yl)pyridine *N*-oxide and its complexes, 2195
Vrbová, M., see Boča, R., 835
Vrdoljak, V., see Cindrić, M., 1471
V. Romanenko, G., see A. Savel'eva, Z., 1737

Wagner, C., see Böttcher, H.-C., 2593
Walawalkar, M.G., see Jain, P.U., 801
Wang, F., see Pannell, K.H., 291
Wang, G.-L., see Zhang, L., 1105
Wang, J., see Zhang, F., 1941
Wang, J.-T., see Tang, L.-F., 1949
Wang, J.-T., see Tang, L.-F., 381
Wang, Q.-M., see Li, J.-M., 1117
Wang, S.-L., see Li, Y.-I., 413
Wang, S.-L., see Tsai, C.-H., 633
Wang, S.-S., see Tsai, C.-H., 633
Wang, X.-J., see Xiao, W., 1295
Wang, Y.-M., see Cheng, T.-H., 2027
Wang, Y., see Yeh, A.-C., 545
Wang, Y.-Y., Shi, Q., Shi, Q.-Z., Gao, Y.-C. and Hou, X., Molecular structure, characterization and magnetic properties of novel mixed-valence copper(I,II) α,β-unsaturated carboxylate complexes with triphenylphosphine and methanol ligands, 891
Wang, Z.-H., see Tang, L.-F., 1949
Wang, Z.-H., see Tang, L.-F., 381
Wang, Z., see Lu, X., 577
Wang, Z., see Rose, E., 581
Wang, Z.-X., see Zheng, H.-B., 713
Wanner, V.F., see Constable, E.C., 23
Wardell, J.L., see Harrison, W.T.A., 821
Wardell, S.M.S.V., see Harrison, W.T.A., 821
Ward, M.S., Chatterjee, D. and Shepherd, R.E., Formation of a mixed-valence Ru(IV)–Fe(II) binuclear complex via the reaction of $[Ru^{III}(edta)(H_2O)]^-$ and $[Fe^{III}(CN)_6]^{3-}$ in aqueous solution, 1339
Waring., K.W., see Kelly, P.F., 2077
Washburn, H., see Mink, L.M., 1057
Waters, J.M., see Ainscough, E.W., 2585
Webster, M., see Levason, W., 2697
Wehmschulte, R.J. and Power, P.P., Primary alanes and alanates: useful synthetic reagents in aluminum chemistry, 1649
Welch, A.J., see Maji, T.K., 1903
Werner, R., see Iskander, M.F., 949
Werner, R., see Iskander, M.F., 1181
West, D.X., see Castiñeiras, A., 1873
West, D.X., see de Sousa, G.F., 841
West, D.X., see Labisbal, E., 1255
Whall, L.A., see Constable, E.C., 23
Wheatley, A.E.H., see Chia, L.M.L., 109
White, A.J.P., see Byrom, C., 211
Whitmire, K.H., see Khan, S.R.A., 975
Whitmire, K.H., see Khan, S.R.A., 983
Wiede, P., see Vrbová, M., 2195
Wikaira, J., see Devereux, M., 1205
Wilkin, O.M., see Robertson, E.W., 1493
Willey, G.R., Spry, M.P. and Errington, W., Crown ether complexation of Te(IV): formation and crystal structure of $[(18\text{-crown-}6)Te(Cl)(\mu\text{-}O)_2Te(Cl)(18\text{-crown-}6)][SbCl_6]_2$, 1799
Williams, D.J., see Byrom, C., 211
Williams, D.J., see Jones, A.C., 351
Williams, P.A.M., see Allegretti, Y., 2613
Wilson, A., see Bell, N.A., 2539
Wocadlo, S., see Zhang, Y.-J., 1757
Wołowiec, S., see Łukasiewicz, M., 2119
Wong, W.-T., see Liu, Q., 453
Wong, W.-T., see Liu, X.-X., 7
Woodson, S.J., see Schwartz, J., 505
Woollins, J.D., see Aucott, S.A., 499
Woollins, J.D., see Bhattacharyya, P., 809
Woollins, J.D., see Pal, S., 1925
Woo Park, J., Tae Kim, J., Man Koo, S., Kim, C.G. and Kim, Y.S., Strontium β-diketonate complexes with polyamine donor ligands: the synthesis and structural characterization of $[Sr(thd)_2(L)]_n$ ($n = 2$; L = diethylenetriamine, $n = 1$; L = triethylenetetramine, tetraethylenepentamine and tris(2-aminoethyl)amine) complex, 2547
Woo, S., see Fallis, A.G., 533
Wright, P.J., see Jones, A.C., 351
Wu, D.-D., see Chisholm, M.H., 375
Wu, L.-M., see Lin, P., 2189
Wu, Q.-J., see Peng, Y., 733
Wurst, K., see Scheffter, B., 871
Wu, X.-T., see Li, J.-M., 1117
Wu, X.-T., see Lin, P., 2189

Xiao, W., Lu, Z.-L., Wang, X.-J., Su, C.-Y., Yu, K.-B., Liu, H.-Q. and Kang, B.-S., Chemistry of aroylhydrazones II. Enol-form coordination of 4,5-diazafluorene-9-one salicyloylhydrazone (H_2L) to transition metals and crystal structures of H_2L, $Mn(HL)_2(H_2O)_2$ and $Co(HL)_2(DMF)_2$, 1295
Xie, Y.-Y., see Kong, D.-Y., 1527
Xie, Y.-Y., see Kong, D.-Y., 217
Xin, X., see Tan, W., 1545
Xu, C., see Negishi, E.-i., 591
Xu, Y.-M., see Tang, L.-F., 1949
Xu, Y.-M., see Tang, L.-F., 381
Xu, Y., see Song, Y., 1461
Xu, Y., see Zhu, D.-R., 2019

Yagasaki, A., see Ozeki, T., 43
Yamada, K., see Nakashima, S., 205
Yamamoto, I., see Ohta, K., 267
Yanagihara, N., Yumoto, Y., Arai, K., Kawabe, K. and Kojima, Y., Thermal decomposition of oxovanadium(IV) complexes with *N*,*N*′-ethylenebis(amino acids), 1311
Yanai, K., see Takeda, T., 593
Yang, J., see Matteson, D.S., 587
Yang, L., Jin, W. and Lin, J., Synthesis, crystal structure and magnetic properties of novel dinuclear complexes of manganese, cobalt and nickel with 4-acetylbispyrazolone, 93
Yang, Q.-C., see Goher, M.A.S., 615
Yang, R.-D., see Yang, Z.-Y., 2599
Yang, S.-P., Zhu, H.-L., Yin, X.-H., Chen, X.-M. and Ji, L.-N., Polymeric and tetranuclear silver(I) chains encapsulated by a scorpion-like ligand. Synthesis and structures of $[Ag_2(tren(mim)_3)]_n(NO_3)_{2n}\cdot nH_2O$ and $[Ag_4(tren(mim)_3)_2](CF_3SO_3)_4\cdot 2H_2O$ (tren(mim)$_3$ = tris{2 - [2 - (1 - methyl)imidazolyl]methyliminoethyl}-amine), 2237
Yang, Z.-Y., Yang, R.-D., Li, F.-S. and Yu, K.-B., Crystal structure and antitumor activity of some rare earth metal complexes with Schiff base, 2599
Yanovsky, A.I., see Turevskaya, E.P., 705
Yan, S.-P., see Zhang, L., 1105
Yan, S., see Li, L., 2529
Yan, S., see Li, L., 1575
Yan, Y.-K., Koh, W., Jiang, C., Leong, W.K. and Hor, T.S.A., Amine-oxide-mediated oxidative methanolysis of metal–metal bonds in $[MM'(CO)_{10}]$ (M = Mn, Re; M′ = Re) and $[Os_3(CO)_{12}]$: crystal structure of *fac*-[Re{OC(O)OMe}]$CO)_3(\eta^2$-dppf)], 641
Yao, Y.-M., see Zhang, L.-L., 2243
Yasutake, M., see Moriguchi, T., 785
Ye, B.-H., see Chao, H., 1975
Yeh, A.-C., Chen, S.-I., Chen, A.-J., Lee, G.-H., Wang, Y. and Chen, J.-T., Addition of the alkenyl C–H bond of enamines to η^3-allenyl/propargyl complexes leading to the formation of pyrrole derivatives, 545
Ye, N., see Park, G., 1155
Yim, H.W., Lam, K.-C., Rheingold, A.L. and Rabinovich, D., Bismuth(III) thioether chemistry: synthesis and structure of a coordination polymer derived from $BiCl_3$ and $MeSi(CH_2SMe)_3$, 849
Yin, X.-H., see Yang, S.-P., 2237
Yılmaz, İ., see Kandaz, M., 115
Yoo, J., Oh, K.E., Keum, G., Kang, S.B. and Kim, Y., Indium-mediated monoallylation of carbonyl compounds with allylic chlorides and bisallylation of 2-pyridyl carboxylates with allylic halides in aqueous media, 549
Yordanov, N.D., Jeliazkova, B., Roussanova, D., Sarova, G., O'Brien, P. and Malik, M.A., Charge-transfer photochemistry of the ternary complex (diselenocarbamato, dithiophosphato)copper-(II), 2177
Youinou, M.-T., see Lorber, C.Y., 1693
Young, N.A., see Robertson, E.W., 1493
You, X.-Z., see Song, Y., 1461
You, X.-Z., see Zhu, D.-R., 2019
Yu, K.-B., see Xiao, W., 1295
Yu, K.-B., see Yang, Z.-Y., 2599
Yu, K., see Fan, L., 779
Yumoto, Y., see Yanagihara, N., 1311
Yu, R.-M., see Peng, Y., 733

Zabel, M., see Brunner, H., 1519
Zagal, J.H., Gulppi, M.A. and Cárdenas-Jirón, G., Metal-centered redox chemistry of substituted cobalt phthalocyanines adsorbed on graphite and correlations with MO calculations and Hammett parameters. Electrocatalytic reduction of a disulfide, 2255
Zahn, S.K., see Breit, B., 513
Zaki, A.B., El-Sheikh, M.Y., Evans, J. and El-Safty, S.A., Characteristic mechanisms of the homogeneous and heterogeneous oxidation of aromatic amines with transition metal–oxalate complexes, 1317
Zanonato, P.L., see Comuzzi, C., 2427
Zechmann, C.A., Boyle, T.J., Rodriguez, M.A. and Kemp, R.A., Solvent influences on the molecular aggregation of magnesium aryloxides: synthesis, crystal structure, and solution characterization of $Mg(OAr)_2(L)_3$ (OAr = DMP, DIP, TCP) and $[Mg(DIP)_2]_3$, 2557
Zehnder, M., see Constable, E.C., 23
Zhang, F., Mu, Y., Wang, J., Shi, Z., Bu, W., Hu, S., Zhang, Y. and Feng, S., Synthesis and crystal structures of unbridged bis(4-R-1,2-diphenylcyclopentadienyl)zirconium dichlorides (R = phenyl, cyclohexyl), and catalysis for olefin polymerization, 1941
Zhang, K.-L., see Song, Y., 1461
Zhang, L., Bu, W.-M., Yan, S.-P., Jiang, Z.-H., Liao, D.-Z. and Wang, G.-L., Weaker magnetic interactions of oxalato-copper(II) binuclear compounds: synthesis, spectroscopy, crystal structure and magnetism, 1105
Zhang, L.-L., Yao, Y.-M., Luo, Y.-J., Shen, Q. and Sun, J., Syntheses and crystal structures of four-coordinate aryloxo neodymium complexes, 2243
Zhang, R.-H., see Bu, X.-H., 2095
Zhang, R.-H., see Bu, X.-H., 431
Zhang, Y.-G., see Li, J.-M., 1117
Zhang, Y.-J., Collison, D., Livens, F.R., Powell, A.K., Wocadlo, S. and Eccles, H., Synthesis, spectroscopic, and X-ray crystallographic characterisation of thorium(IV) and uranium(IV) malonato and substituted malonato compounds, 1757
Zhang, Y., see Zhang, F., 1941
Zhang, Y., see Zhu, D.-R., 2019
Zhang, Z.-H., Bu, X.-H., Ma, Z.-H., Bu, W.-M., Tang, Y. and Zhao, Q.-H., Synthesis, crystal structure and properties of two new binuclear complexes bridged by end-to-end azido: $[Ni_2(TLA)_2(N_3)_3]^+$ and $[Mn_2(TLA)_2(N_3)_3]^+$, [TLA = tris(6-methyl-2-pyridylmethyl)amine], 1559
Zhang, Z.-H., see Bu, X.-H., 2095
Zhao, Q.-H., see Zhang, Z.-H., 1559
Zheng, H.-B., Miao, S.-B., Wang, Z.-X., Zhou, Z.-Y. and Zhou, X.-G., Chemical reactivity of $[(\mu\text{-Rse})(\mu\text{-S})\{Fe_2(CO)_6\}_2(\mu_4\text{-S})]^-$: synthesis and characterization of $(\mu\text{-Rse})(\mu\text{-R'S})\{Fe_2(CO)_6\}_2(\mu_4\text{-S})$ and $(\mu_3\text{-S})_2Fe_3(CO)_8[Se(Ph)Fe(CO)_2Cp]$, 713
Zheng, H., see Tan, W., 1545
Zheng, J., see MacLachlan, M.J., 275
Zheng, S.-L., see Tong, M.-L., 1809
Zhou, J.-Y., see Chao, H., 1975
Zhou, X.-G., see Zheng, H.-B., 713
Zhou, Z.-Y., see Zheng, H.-B., 713
Zhuang, H.-H., see Lin, X., 925
Zhu, D.-R., see Song, Y., 1461
Zhu, D.-R., Song, Y., Xu, Y., Zhang, Y., Sundara Raj, S.S., Fun, H.-K. and You, X.-Z., Syntheses, crystal structures and properties of the novel Co(II) and Ni(II) complexes with 4-(*p*-methylphenyl)-3,5-bis(pyridin-2-yl)-1,2,4-triazole, 2019
Zhu, H.-L., see Yang, S.-P., 2237
Zhu, H.-P., see Bu, X.-H., 431
Zinner, L.B., see Fernandes, L.C., 2313
Zobi, F., see Veinot, J.G.C., 331
Zou, G., see Qian, C.-T., 1955
Zukerman-Schpector, J., see Fernandes, L.C., 2313
Zuloaga, F., see Concepción, J., 2297

PERGAMON

www.elsevier.nl/locate/poly

Polyhedron 19 (2000) 2739–2770

POLYHEDRON

Subject Index to Volume 19

Ab initio methods
Cyclic phosphazenes, Electronic structures, Group theory, 389
Absorption spectra
Imidazole derivatives, Transition metal complexes, Crystal structure, Stability constants, 2183
Absorption spectroscopy
α,α′-Bis(pyrazolyl)-*m*-xylene, Copper(II) complexes, X-ray structure, Network structures, Electron spin resonance, 719
π-acceptors
Discotic complexes, Columnar complexes, Liquid crystals, Dithiolene, 267
Acetamidate
Trirhenium(III) clusters, Rhenium clusters, Dimolybdenum(II), MALDI, Mass spectroscopy, 1245
Acetonitrile
Macrocyclic polyether 18-crown-6, Alkaline earth metal ions, Transition metal ions, 1681
Acetylacetonates
Iridium, Halogenation, 1097
α-Acetylenic alcohols
Isomerization, Rearrangement, Heterobimetallic titanium–copper systems, 1693
Acid–base congeners
Dicopper complexes, Solvent-derived ancillary ligands, 1909
Acid–base
Dithiolene, Nickel, Dinuclear complexes, Solvatochromism, Carbon disulfide, 1283
Acid dissociation constants
Acidopentaaminecobalt(III) complexes, ESCA studies, ESI + mass spectra, 971
Acidopentaaminecobalt(III) complexes
ESCA studies, ESI + mass spectra, Acid dissociation constants, 971
Activity coefficients
3:3 Electrolytes, Electrolytic solutions, High-charge salts, High valency electrolytes, Mixed electrolytes, 2493
Acylthiourea
Platinum(II), Sulfoxide, *N*,*N*-Dialkyl-*N*′-(3-*R*-benzoyl)thiourea, NMR, Chemotherapeutic agents, 1347
Addition reactions
Alkoxyalkynes, Aminoalkynes, Organophosphorus halides, Organosilane halides, Organogermane halides, Pd-catalyzed cross-coupling reactions, 597
Additions
Alkylation, Insertions, Nucleophilic, Schiff bases, Titanium, 177
Adduct
Magnesium, Aryloxide, Structure, 2557
Aerial oxidation of aldehydes
Molybdenum complexes, 1133
Aggregation
Sol–gel, Tetrasulfophthalocyanines, Monolith, Macrocycle, Silica, 2383
Alanate
Alane, Aluminum hydride, Alumoxane, Reduction, 1649
Alane
Aluminum hydride, Alanate, Alumoxane, Reduction, 1649
β-alanyl-lysine
Copper-dipeptide complexes, Glycyl-lysine, Alanyl-lysine, Histidyl-lysine, 2409
Alanyl-lysine
Copper-dipeptide complexes, Glycyl-lysine, Histidyl-lysine, β-alanyl-lysine, 2409
Alcohol oxidation
Ruthenium, Polypyridine, Terpyridine, Electrocatalytic oxidation, Isomerization, 1049
Al(III) complexes
Biospeciation, VO(IV) complexes, Insulin-mimetics, 2389
Alkaline Earth
Calcium, H-bonding, Inorganic Polymers, X-ray structure, 1783
Alkaline earth metal ions
Macrocyclic polyether 18-crown-6, Acetonitrile, Transition metal ions, 1681
Alkaline earth metals
Heterobimetallic diethanolaminates, Homobimetallic diethanolaminates, 77
Alkaline metal extraction
Phthalocyanine complexes, Phthalonitrile derivatives, Crown-ether, Copper, Nickel, Cobalt, 115
Alkaloid synthesis
Nitrosobenzene cycloaddition, Regioselectivity, Organoiron compounds, Decomplexation, Heterocycloaddition trap, 569
Alkene
Phosphine, Polymerization, Hydroboration, Copper(I) complexes, 1271
Alkenylation
Enamine, Pyrrole, 545
Alkenylsilanes
Hydrosilylation, $RhI(PPh_3)_3$, Polyaddition, Stereodivergent, 567
Alkoxides
Indium tin oxide, Surface modification, Interfaces, 505
Alkoxides
Molybdenum, Nitrides, Synthesis, X-ray structures, NMR fluxionality, Pseudorotation, 1363
Alkoxides
Scandium, Crystal structures, Volatility, 705
Alkoxide
Tin, Tin dioxide, Sol–gel, β-Diketonate, 2069
Alkoxo compounds of oxovanadium(V)
Crystal structure of compounds of oxovanadium(V), Hydrazonato compounds of oxovanadium(V), Oxovanadium(V) dimers, Reactivity of bis(β-dionato)-oxovanadium(IV) chelates, Hydrazonato tridentate Schiff base ligands, 2003
Alkoxyalkynes
Aminoalkynes, Addition reactions, Organophosphorus halides, Organosilane halides, Organogermane halides, Pd-catalyzed cross-coupling reactions, 597
Alkylation
Additions, Insertions, Nucleophilic, Schiff bases, Titanium, 177
Alkyl-substituted pyridines
Oxomolybdenum(V) compounds, Clusters, $Mo_2O_4^{2+}$ unit, Pyridine, 1219
Alkyl-substituted pyridines
Solvothermal synthesis, Crystal structures, Oxomolybdenum(V) coordination compounds, Mo(V, VI) compounds, 1407
Alkyne complexes
Multimetallic, Cobalt carbonyl complexes, Tungsten(II), Chain triphos-bridged, 1585
Alkynes
Functionalized metalloalkynes, Olefins, Polymetallated olefins, Titanium, 563
Allenes
C–H activation, Intramolecular bonds, Titanium, Metallacycles, Carbometalation, 879

PII: S0277-5387(00)00653-7

Allylation
Aqueous reactions, Esters, Indium, Indium compounds, Pyridines, 549
π-Allyl complexes
Allylic substitutions, Iridium, Regioselectivity, Stereoselectivity, Phosphites, 557
Allyl complexes
Palladium, Platinum, Thiolate complexes, 1627
Allylic alkylation
Axially chiral phosphinamine, Hydroboration, Quinazolines, 541
Allylic substitutions
π-Allyl complexes, Iridium, Regioselectivity, Stereoselectivity, Phosphites, 557
Alternating chain
Dimer complex, Crystal structure, Magnetic properties, 1461
Aluminum complexes
1-Aza-allyl, Bismuth complexes, Crystal structures, Gallium complexes, 471
Aluminum hydride
Alane, Alanate, Alumoxane, Reduction, 1649
Alumoxane
Alane, Aluminum hydride, Alanate, Reduction, 1649
Amberlite anion-exchange resin
Aromatic amines, Oxalate anions, Metal–oxalate complexes, Oxidation, Homogeneous and heterogeneous, 1317
Amido
Diimine, Dimer, Hydroxo, Palladium, Platinum, 155
Amine oxide
Methanolysis, Rhenium, Osmium, Carbonyl, Methylcarbonate, 641
Amino acids
closo-Dodecaborate, Oxonium derivatives, Functional derivatives, Boron neutron capture therapy, 627
α-Aminoacylsilanes
β-Amino alcohols, Lewis acid, Silylcupration, Statine analogues, 529
β-Amino alcohols
α-Aminoacylsilanes, Lewis acid, Silylcupration, Statine analogues, 529
Aminoalkynes
Alkoxyalkynes, Addition reactions, Organophosphorus halides, Organosilane halides, Organogermane halides, Pd-catalyzed cross-coupling reactions, 597
(2-Aminoethyl)(3-aminopropyl)amine
Nickel(II)selenocyanate, Bis(3-aminopropyl)amine, Bis(2-aminoethyl)-methylamine, Thermochromism, 1903
1-(2-Aminoethyl)pyrrolidine
Nickel(II)thiocyanate, Crystal structures, *cis*/*trans* Isomers, 1803
Aminophosphate complexes
Palladium(II) complexes, Metallocycles, Spectroscopy, Antitumour activity, 937
Aminopolyphosphonates
Potentiometry, Equilibria, Stability constants, Manganese(II), Cobalt(II), Nickel(II) complexes, UV–VIS spectra, 2083
Aniline polymerization
Copper phosphonates, Intercalation compounds, 765
Anion–cation pair compound
Synthesis, Crystal structure, Aryloxide, Neodymium, 2243
Anticancer drugs
Rhodium(II) complexes, Rhodium(II) carboxylates, Rhodium sulfosalicylate, Thermogravimetric analysis, Spectroscopic analysis, 1305
Antiferromagnetic interactions
Dinuclear, Pryrazolyl groups, 2215
Antimicrobial activity
Chelating ligands, Crystal structures, Copper(II) complexes, Pyridinecarboxylate complexes, 2689
Antimonides
Arsenides, Metathesis, Phosphides, 829
Antimony
Homoleptic silyl complexes, Arsenic, 1639
Antitumor activity
Transition metals, Synthesis, Structural characterization, 217
Antitumour activity
Palladium(II) complexes, Metallocycles, Aminophosphate complexes, Spectroscopy, 937
Antitumour activity
Rare earth complex, Crystal structure, Hydrazone, 2599
Antitumour
Streptonigrin, 2,2′-Bipyridyl, 6,6′-Dicarboxy-2,2′-bipyridyl, Zinc, 1067
Aqua(imidazole)(*N*-carbamoylmethyl-iminodiacetato)cobalt(II) sesquihydrate
N-carbamoylmethyl-iminodiacetic acid, *N*-(2-amidomethyl)-iminodiacetic acid, *N*-(2-acetamido)-iminodiacetic acid, Imidazole, Mixed-ligand complexes, Aqua(imidazole)(*N*-carbamoylmethyl-iminodiacetato)nickel(II) sesquihydrate, Molecular and crystal structures, Magnetic, spectral and thermal properties, 2473
Aqua(imidazole)(*N*-carbamoylmethyl-iminodiacetato)nickel(II) sesquihydrate
N-carbamoylmethyl-iminodiacetic acid, *N*-(2-amidomethyl)-iminodiacetic acid, *N*-(2-acetamido)-iminodiacetic acid, Imidazole, Mixed-ligand complexes, Aqua(imidazole)(*N*-carbamoylmethyl-iminodiacetato)cobalt(II) sesquihydrate, Molecular and crystal structures, Magnetic, spectral and thermal properties, 2473
Aqueous reactions
Allylation, Esters, Indium, Indium compounds, Pyridines, 549
Arene coordination
Dirhodium(II) compounds, Trifluoroacetate, One-dimensional polymers, π-Complexes, Crystal structures, 1829
Aromatic amines
Amberlite anion-exchange resin, Oxalate anions, Metal–oxalate complexes, Oxidation, Homogeneous and heterogeneous, 1317
Aromatic diamines
Transition metal complexes, Terephthalate ions, Crystal structures, Spectral data, 1415
Arsenic
Homoleptic silyl complexes, Antimony, 1639
Arsenides
Antimonides, Metathesis, Phosphides, 829
Aryloxide
Magnesium, Structure, Adduct, 2557
Aryloxide
Synthesis, Crystal structure, Neodymium, Anion–cation pair compound, 2243
Aryloxide
Titanium, Tantalum, Nobium, Bisphenol, Hydrogenation, 35
Ascorbic acid
Kinetics, Manganese(IV), Electroprotic reactions, 1213
Asorption spectra
Copper(III), Nickel(III), Dioxotetraamines, Macrocyclic ligands, 2533
Aspartate
Lead(II), Structures, 649
Asymmetrical complexes
Cadmium(II) complexes, Schiff-base ligands, Symmetrical complexes, Heptadentate ligands, 1633
Asymmetric alkylation
Asymmetric rearrangements, Chiral ligands, Chiral sulfoxides, Palladium catalysts, 525
Asymmetric rearrangements
Asymmetric alkylation, Chiral ligands, Chiral sulfoxides, Palladium catalysts, 525
Asymmetric synthesis
Hydroformylation, Organocopper reagents, Catalysis, Domino reactions, 513
Asymmetric synthesis
Kainoids, Boronic esters, Pyrrolidine, 587
Axially chiral phosphinamine
Allylic alkylation, Hydroboration, Quinazolines, 541
1-Aza-allyl
Aluminum complexes, Bismuth complexes, Crystal structures, Gallium complexes, 471
Aza-macrocycles
Electroreduction, Carbon dioxide, Delocalized π interactions, 2373
Aza–oxa crowns
Macrocyclic ligands, Naphthylmethyl fluorescent groups, 1867
Azide
Cobalt, 2-Hydroxyacetophenone, Thiocyanate, Crystal structure, 2707
Azido-bridged nickel(II) compounds
Crystal structures, Magnetic properties, 1575
Azoimine
Ru–bipyridine, Tris-chelates, X-ray structures, Electrochemistry, Emission spectra, 1925

Azomethine
Copper(II), Imidate, Crystal structures, 2713
Azomethynic copper metallochelates
Synthesis, EXAFS investigation, 2361
Azoxybenzene deoxygenation
Dioxomolybdenum dipicolinate, Oxygen-atom transfer, 2141

Barriers
Ruthenium, Phenanthroline, *Cis–trans*, MO calculations, Field strength, 2297
^{9}Be NMR spectroscopy
Beryllium, Phosphato complexes, Solution equilibria, ^{31}P NMR spectroscopy, Speciation, 1043
Benzil-α-monoxime
Transition metal complexes, Electronic spectral data, Oximes, 1687
Benzolamide
Divalent metals, Zinc, Copper, Diethylenetriamine, Ternary complexes, 725
Benzothiazole-2-thione
Mercury(II) complexes, Triphenylphosphine, pyrimidine-2-thione, Crystal structures, 2231
Beryllium
Phosphato complexes, Solution equilibria, ^{31}P NMR spectroscopy, ^{9}Be NMR spectroscopy, Speciation, 1043
Bidentate ligands
Trichlorovinyl, Mercury(II), Crystal structures, Complexes, 2539
Bidentate Schiff base ligands
Dichloromanganese(IV) complexes, Tetradentate Schiff base ligands, Crystal structures, Photosystem II, 2039
Bimetallic complexes
Crystal structures, Palladium complexes, Platinum complexes, Diphosphine complexes, Tetraphosphine complexes, 913
Bimetallic complexesw
Molybdenum(II), Tungsten(II), Crystal structures, *o*-Phenylenediacetonitrile, Trimetallic complexes, Nitrile-bridged complexes, Seven-coordinate complexes, Halocarbonyls, 147
Bimetallic films
Colloids, FT-IR, Conductivity, Thermal analysis, 2337
Binaphtholato complexes
Tungsten(VI), X-ray structures, 2579
Binuclear copper compounds
Crystal structures, Magnetism, Oxalato-bridged compounds, 1105
Binuclear Cu(II) complexes
Magnetic properties, Electrochemistry, ESR, 1769
Binuclear manganese(II) complex
Binuclear nickel(II) complex, Crystal structures, Magnetic properties, Tris(6-methyl-2-pyridylmethyl)amine, 1559
Binuclear nickel(II) complex
Binuclear manganese(II) complex, Crystal structures, Magnetic properties, Tris(6-methyl-2-pyridylmethyl)amine, 1559
Binuclear zinc complexes
Heterocyclic bis(thiosemicarbazone), Heptacoordinate complexes, Organotin(IV) complexes, 841
Binucleating hexa-aza macrocycle
Copper(II), Nickel(II), Cobalt(II), Zinc(II), Crystal structures, Phosphotriester, Hydrolysis, 1485
Binucleating ligand
Nickel complexes, Copper complexes, Crystal structures, Redox chemistry, 2011
Bioactive groups
Phosphorothiates, Organotin(IV), Cholesteryl, 1539
Bio-activity
Copper(II), Chloropropionate, Crystal structure, EPR, 2573
Biomimetics
Calcium phosphates, Biomineralization, Liposomes, 357
Biomineralization
Calcium phosphates, Biomimetics, Liposomes, 357
Biospeciation
Al(III) complexes, VO(IV) complexes, Insulin-mimetics, 2389
2,2′-Bipyridine
1,8-Bis(dimethylamino)naphthalene, Boron-11 NMR, Chelated fluoroboron cations, Fast atom bombardment mass spectrometry, Fluorine-19 NMR, 1,10-Phenanthroline, 2,2′,6′,2″-Terpyridine, 165
4,4′-Bipyridine
Coordination polymers, Copper(II) complexes, Cadmium(II) complexes, 1809
1,4-Bipyridine
Mononuclear, Tungsten pentacarbonyl complexes, 1,2-Bis(4-pyridyl)ethane, 1621
2,2′-Bipyridyl
Streptonigrin, 6,6′-Dicarboxy-2,2′-bipyridyl, Antitumour, Zinc, 1067
Bis(2-aminoethyl)methylamine
Nickel(II)selenocyanate, Bis(3-aminopropyl)amine, (2-Aminoethyl)(3-aminopropyl)amine, Thermochromism, 1903
Bis(3-aminopropyl)amine
Nickel(II)selenocyanate, (2-Aminoethyl)-(3-aminopropyl)amine, Bis(2-aminoethyl)methylamine, Thermochromism, 1903
2,6-Bis(2-benzimidazolyl)pyridine
Chromium(III) complexes, Tris(2-benzimidazolylmethyl)amine, 2-Guanidinobenzimidazole, 2-(2-Pyridyl)benzimidazole, Crystal structures, 1821
Bis(η-cyclopentadienyl)titanium(IV)
Crystal structures, Diphenylphosphinoacetate, Heterometallics, Nicotinate, Thiophenoxyacetate, 757
1,8-Bis(dimethylamino)naphthalene
2,2′-Bipyridine, Boron-11 NMR, Chelated fluoroboron cations, Fast atom bombardment mass spectrometry, Fluorine-19 NMR, 1,10-Phenanthroline, 2,2′,6′,2″-Terpyridine, 165
Bis(methyldiphenylphosphonio)methylide salts
Gold(I) complexes, Cationic ylide ligand, P-alkylation, 1837
Bismuth complexes
Aluminum complexes, 1-Aza-allyl, Crystal structures, Gallium complexes, 471
Bismuth
Thioether, Coordination polymers, Crystal structures, Electrospray, 849
Bisphenol
Titanium, Tantalum, Nobium, Aryloxide, Hydrogenation, 35
Bisphosphines
Heterocyclic thiones, Palladium(II) complexes, Platinum(II) complexes, Pyridyl, 899
α,α′-Bis(pyrazolyl)-*m*-xylene
Copper(II) complexes, X-ray structure, Network structures, Absorption spectroscopy, Electron spin resonance, 719
Bis(pyrazolyl)silanes
Zinc, Crystal structures, Nitrogen-donor ligands, 1815
1,2-Bis(4-pyridyl)ethane
Mononuclear, Tungsten pentacarbonyl complexes, 1,4-Bipyridine, 1621
4,5-bis(2-pyridylethylsulfanyl)-1,3-dithiole-2-thione
Copper, Cobalt, Nickel, Palladium, dmit, 4,5 - bis(2 - pyridylmethylsulfanyl) - 1,3-dithiole-2-thione, 665
4,5-bis(2-pyridylmethylsulfanyl)-1,3-dithiole-2-thione
Copper, Cobalt, Nickel, Palladium, dmit, 4,5 - bis(2 - pyridylethylsulfanyl) - 1,3-dithiole-2-thione, 665
Bonding
Hydroborates, Lithium, Titanium(IV), Crystal structures, 1579
Boron
Halogenated carborane anions, Cobalt bis(dicarbollide), Carborane, Halogenation, 1777
Boronic esters
Kainoids, Asymmetric synthesis, Pyrrolidine, 587
Boron neutron capture therapy
closo-Dodecaborate, Oxonium derivatives, Functional derivatives, Amino acids, 627
Boron-11 NMR
2,2′-Bipyridine, 1,8-Bis(dimethylamino)-naphthalene, Chelated fluoroboron cations, Fast atom bombardment mass spectrometry, Fluorine-19 NMR, 1,10-Phenanthroline, 2,2′,6′,2″-Terpyridine, 165
Bpy ligands
Polypyridine ligands, Ruthenium(II) complexes, 1975
Bridged structures
Crystal structures, Heteronuclear multiple bond coherence, *N*-Tosyl ligands, Zinc porphyrin complexes, 413
Bridging ligands
Butadienyl, Chiral substituents, Molybdenum, 791

Bridging oxygen atoms
μ-oxo-Bridged cations, Crown ether complexation, Crystal structures, 1799
Bromide
Platinum(II), Platinum(IV), Porphyrins, Electrochemistry, Voltammetry, 1057
Bulky phosphine
X-ray structure, Cone angle, Two-coordinate gold complex., 2211
Butadienyl
Bridging ligands, Chiral substituents, Molybdenum, 791

Cadmium complexes
Mercury complexes, Sulfamides, X-ray structure, Zinc complexes, 991
Cadmium halides
2-Pyridineformamide, Thiosemicarbazone, Crystal structures, 1873
Cadmium(II) complexes
4,4′-Bipyridine, Coordination polymers, Copper(II) complexes, 1809
Cadmium(II) complexes
Schiff-base ligands, Symmetrical complexes, Asymmetrical complexes, Heptadentate ligands, 1633
Cadmium(II)
Zinc(II), Mercury(II), Tris(2-benzimidazolylmethyl)amine, X-ray diffraction structures, NMR data, 1479
Caesium ion
Calixcrowns, Sodium ion, Perrhenate ion, Pertechnetate ion, Nuclear reprocessing, 1749
Calcium
H-bonding, Inorganic Polymers, Alkaline Earth, X-ray structure, 1783
Calcium phosphates
Biomimetics, Biomineralization, Liposomes, 357
Calixarenes
Ytterbium(III), Lanthanides, Homoazacalixarenes, Crystal structure, 2673
Calixcrowns
Caesium ion, Sodium ion, Perrhenate ion, Pertechnetate ion, Nuclear reprocessing, 1749
Carbacylamidophosphate
Lanthanide, NMR, X-ray data, 2203
Carboalumination
1,5-diene, Cross coupling, Terpenoids, Palladium, 591
Carbometalation
C–H activation, Intramolecular bonds, Titanium, Metallacycles, Allenes, 879
Carbon dioxide
Aza-macrocycles, Electroreduction, Delocalized π interactions, 2373
Carbon dioxide
Dimethyl carbonate, Homogeneous catalysis, Mechanism, Supercritical conditions, 573
Carbon disulfide
Dithiolene, Nickel, Dinuclear complexes, Acid–base, Solvatochromism, 1283
Carbonyl
Amine oxide, Methanolysis, Rhenium, Osmium, Methylcarbonate, 641
Carbonyl clusters
Solvothermal synthesis, Polytelluride, Iron telluride, Iron cluster, Iron carbonyl, 1995
Carborane
Halogenated carborane anions, Cobalt bis(dicarbollide), Boron, Halogenation, 1777
Carbosilanes
Dendrimers, Platinum catalysts, Hydrosilation, 1031
Carboxylate and sulfonate substituted pyridines
Tungsten(II), Propiolic acid, Water soluble complexes, 2171
Carboxylate complexes
Copper complexes, Dinuclear complexes, Crystal structures, Cuprous oxide, Cupric oxide., 2621
Carboxylate
Nitrosyl complex, Chromium, Molybdenum, DFT, 2565
Carboxylates
Crystal structures, Ruthenium, Dimethyl sulfoxide, Complexes, Catalysis, 1589
Carboxylato-bridged copper(II) complex
Crystal structure, Magnetic properties, 2529
Carcinogenic
Chromium, Nucleotides, 417
Catalase
Manganese complexes, Schiff bases, Manganoenzymes, Photolysis, Dioxygen, 47
Catalysis
Chromium, Salen, Manganese, Enantioselection, Nozaki–Hiyama–Kishi reaction, 537
Catalysis
Crystal structures, Ruthenium, Dimethyl sulfoxide, Carboxylates, Complexes, 1589
Catalysis
Hydroformylation, Organocopper reagents, Asymmetric synthesis, Domino reactions, 513
Catalysis
Oxidation, 3,5-Di-*tert*-butylcatechol, Kinetics, Copper binuclear complexes, 2367
Catalysis
Zirconocene, Crystal structures, Olefin polymerizations, 1941
Catalysts
Palladium(II) complexes, Peptides, Hydrolysis, 959
Catecholborane
Reactivity, 1063
Catechols
Macrocyclic ligands, Oxovanadium complexes, ESR parameters, Distorted square-pyramid, Hydrophobic cavities, 1167
Cationic ylide ligand
Gold(I) complexes, Bis(methyldiphenylphosphonio)methylide salts, P-alkylation, 1837
Cavity
Solubility, Oxygen, Solubilization enthalpy, Solubilization entropy, 2457
Cd(II)
Hg(II), tachpyr, Torsion angles, Twist angles, Zn(II), 1155
CdS nanoclusters
Ruthenium(II) polypyridyls, Functionalized nanoclusters, Mesophase materials, Molecular devices, 331
C–H activation
Intramolecular bonds, Titanium, Metallacycles, Allenes, Carbometalation, 879
Chagas
Ruthenium, Clotrimazole, Ketoconazole, Paramagnetic, Metal complexes, *Trypanosoma cruzi*, 2319
Chain triphos-bridged
Multimetallic, Cobalt carbonyl complexes, Tungsten(II), Alkyne complexes, 1585
Chelated fluoroboron cations
2,2′-Bipyridine, 1,8-Bis(dimethylamino)-naphthalene, Boron-11 NMR, Fast atom bombardment mass spectrometry, Fluorine-19 NMR, 1,10-Phenanthroline, 2,2′,6′,2″-Terpyridine, 165
Chelating ligands
Crystal structures, Copper(II) complexes, Pyridinecarboxylate complexes, Antimicrobial activity, 2689
Chemotherapeutic agents
Platinum(II), Sulfoxide, *N*,*N*-Dialkyl-*N*′-(3-*R*-benzoyl)thiourea, Acylthiourea, NMR, 1347
Chiral-at-metal complexes
Configurational stability, Epimerisation, Equilibria, X-ray structure analyses, 1519
Chiral catalysts
Porphyrins, Hemoprotein models, Epoxidation, Olefins, 581
Chiral complexes
Macrocycles, Lanthanide complexes, NMR of paramagnetic compounds, 465
Chiral ligands
Asymmetric alkylation, Asymmetric rearrangements, Chiral sulfoxides, Palladium catalysts, 525
Chiral nematic phases
Metallomesogens, Rhenium, Nematic phases, 249
Chiral substituents
Bridging ligands, Butadienyl, Molybdenum, 791
Chiral sulfoxides
Asymmetric alkylation, Asymmetric rearrangements, Chiral ligands, Palladium catalysts, 525
Chloride metathesis
Palladium(II) complexes, Platinum(II) complexes, X-ray crystallography, Heterodifunctional ligands, 695
Chloroboranes
Hydroboration, Polysilazanes, Precursors, Vinylsilanes, 323
Chloropropionate
Copper(II), Crystal structure, EPR, Bioactivity, 2573

Cholesteryl
Phosphorothiates, Organotin(IV), Bioactive groups, 1539
Chromium
Carcinogenic, Nucleotides, 417
Chromium(III) complexes
Tris(2-benzimidazolylmethyl)amine, 2-Guanidinobenzimidazole, 2,6-Bis(2-benzimidazolyl)pyridine, 2-(2-Pyridyl)benzimidazole, Crystal structures, 1821
Chromium(III)
Iron(III), DTPA, Complexes, Thermal properties, Thermodynamics, 2421
Chromium
Nitrosyl complex, Molybdenum, Carboxylate, DFT, 2565
Chromium
Salen, Manganese, Catalysis, Enantioselection, Nozaki–Hiyama–Kishi reaction, 537
Chromium
Selenoether, Telluroether, Sulfur macrocycles, Molybdenum, Tungsten, 1373
Ciprofloxacin
Iron(III), Solution equilibria, Surfactants, 1085
cis - Diaquabis(2,2′ - bipirydyl)chromium(III)
Kinetics, Substitution, Mechanism, Octacyanomolybdate(IV), Octacyanotungstate(IV), 2225
cis - Diaqua(*N* - carbamoylmethyl - iminodiacetato)nickel(II)
N-(Carbamoylmethyl)iminodiacetic acid, *N*-(2-Amidomethyl)-iminodiacetic acid, *N*-(2-Acetamide)-iminodiacetic acid, Molecular and crystal structure, Magnetic and spectral properties, Thermal stability, 2463
Cis–trans isomerism
Crystal structures, 1,2-Diamino-2-methylpropane, Nickel(II)nitrite, 1015
cis/*trans* Isomers
Nickel(II)thiocyanate, 1-(2-Aminoethyl)pyrrolidine, Crystal structures, 1803
Cis–trans
Ruthenium, Phenanthroline, MO calculations, Barriers, Field strength, 2297
closo-Dodecaborate
Oxonium derivatives, Functional derivatives, Amino acids, Boron neutron capture therapy, 627
Clotrimazole
Ruthenium, Ketoconazole, Paramagnetic, Metal complexes, *Trypanosoma cruzi*, Chagas, 2319
Cluster compounds
Molybdenum complexes, Tellurium-rich compounds, De-tellurium reaction, Crystal structures, 925
Cluster
Ruthenium, Iridium, Gold, Electron-rich, Phosphido-bridged, Crystal structures, 2593
Clusters
Mercury, Thiocyanante, Host–guest chemistry, 871
Clusters
Oxomolybdenum(V) compounds, $Mo_2O_4^{2+}$ unit, Pyridine, Alkyl-substituted pyridines, 1219
Cobalt bis(dicarbollide)
Halogenated carborane anions, Boron, Carborane, Halogenation, 1777
Cobalt carbonyl complexes
Multimetallic, Tungsten(II), Alkyne complexes, Chain triphos-bridged, 1585
Cobalt complexes
Crystal structures, 855
Cobalt complexes
Schiff bases, Spin crossover, Photosensitive ligands, LD-LISC effect, 1643
Cobalt complexes
Thiosemicarbazones, Electrochemistry, Iron complexes, EPR of iron complexes, Nickel complexes, 2059
Cobalt complex
Zinc complexes, α-Ketoglutaric acid, Thiosemicarbazones, Crystal structures, Spectroscopic properties, 1895
Cobalt
Copper, Nickel, Palladium, dmit, 4,5-bis(2-pyridylmethylsulfanyl)-1,3-dithiole-2-thione, 4,5-bis(2-pyridylethylsulfanyl)-1,3-dithiole-2-thione, 665
Cobalt
Crystal structures, Magnetic properties, Dinuclear complexes, Manganese, Nickel, 93
Cobalt
Dioxygen carriers, Dinuclear complexes, Dinucleating ligands, Polyamines, Kinetics, Dioxygen binding, 2447
Cobalt
Dioxygen carriers, Dioxygen binding, Polynuclear complexes, Polyamines, Thermodynamics of complexation, 2441
Cobalt
Electrocatalysis, Nitric oxide, Oxidation, Phthalocyanine, Reduction, 229
Cobalt
2-Hydroxyacetophenone, Azide, Thiocyanate, Crystal structure, 2707
Cobalt(II)
Binucleating hexa-aza macrocycle, Copper(II), Nickel(II), Zinc(II), Crystal structures, Phosphotriester, Hydrolysis, 1485
Cobalt(II) complexes
Crystal structures, Iron(II) complexes, Octadentate ligands, 431
Cobalt(II) complexes
Electrochemical synthesis, Crystal structures, Tosylamide complexes, 1607
Cobalt(II) complexes
Pyridine *N*-oxide ligands, Zinc(II) complexes, X-ray structures, Magnetic susceptibility, 2195
Cobalt(II) complex
Syntheses, Crystal structures, Nickel(II) complex, 4-(*p*-Methylphenyl)-3,5-bis-(pyridin-2-yl)-1,2,4-triazole, ESIMS, 2019
Cobalt(II)
Cyanamidonitrate, Electronic spectra, Imidazole ligands, IR spectra, Nickel(II), X-ray crystallography, 1021
Cobalt(III) complex
Thiocarbamylpyrazole, Spectroscopic study, X-ray crystal structure, 2651
Cobalt(III)
Copper(II), NMR spectroscopy, Pyridylmethyl-tetraazadecane, 1447
Cobalt(II)
Potentiometry, Equilibria, Stability constants, Manganese(II), Nickel(II) complexes, Aminopolyphosphonates, UV–VIS spectra, 2083
Cobalt
Phthalocyanine complexes, Phthalonitrile derivatives, Crown-ether, Copper, Nickel, Alkaline metal extraction, 115
Colloids
Bimetallic films, FT-IR, Conductivity, Thermal analysis, 2337
Columnar complexes
Discotic complexes, Liquid crystals, π-acceptors, Dithiolene, 267
Complexation chemistry
Crystal structures, 1,10-Phenanthroline, 495
Complexation
D-Gluconic acid, D-Galactonic acid, D-Gulonic acid, Praseodymium(III), 1567
Complexes
Crystal structures, Ruthenium, Dimethyl sulfoxide, Carboxylates, Catalysis, 1589
π-Complexes
Dirhodium(II) compounds, Trifluoroacetate, One-dimensional polymers, Arene coordination, Crystal structures, 1829
Complexes
Iron(III), Chromium(III), DTPA, Thermal properties, Thermodynamics, 2421
Complexes
Lanthanides(III), Silver(I), Diethylenetriamine, *N*,*N*-dimethylformamide, Thermodynamics, 2427
Complexes
Macrocycles, Synthesis, Equilibria, 2501
Complexes
Platinum, Sulfimides, Hydrogen bonding, 2077
Complexes
Trichlorovinyl, Mercury(II), Crystal structures, Bidentate ligands, 2539
Conductivity
Colloids, Bimetallic films, FT-IR, Thermal analysis, 2337
Cone angle
Bulky phosphine, X-ray structure, Two-coordinate gold complex., 2211
Configurational stability
Chiral-at-metal complexes, Epimerisation, Equilibria, X-ray structure analyses, 1519
π-Conjugation
Ferrocenylporphyrin, Electrochemical communication, Intramolecular hydrogen bonding, NH tautomerism, 1961

Contrast agents
Crystal structures, Diethylenetriaminepentaacetate, Lanthanides, Neodymium, 771
Cooperative vibronic transitions
Infrared spectroscopy, Raman spectroscopy, Electronic absorption spectroscopy, Crystal structures, Hypophospite complexes, Two-centre transitions, 863
Coordination compounds
Uranium, Thorium, Tetraphenylimidophosphinate ligand, X-ray crystal structures, 1699
Coordination.
Dithiocarboxylate, Vanadium(IV), Magnetism, EPR, Infrared, 2155
Coordination
Iron, Phthalocyanine, Dopamine, Serotonin, 1355
Coordination modes
Electron spin resonance, Copper(II) complexes, Histamine, L-Histidine, Isomerism, 1123
Coordination modes
ESR, Copper(II) complexes, Glycyl-L-histidine, Formation constants, Isomerism, 2049
Coordination polymers
4,4′-Bipyridine, Copper(II) complexes, Cadmium(II) complexes, 1809
Coordination polymers
Bismuth, Thioether, Crystal structures, Electrospray, 849
Copper and iron species
Thiuram sulfides, Dithiocarbamate derivatives, 2269
Copper binuclear complexes
Oxidation, Catalysis, 3,5-Di-*tert*-butylcatechol, Kinetics, 2367
Copper
Cobalt, Nickel, Palladium, dmit, 4,5-bis-(2 - pyridylmethylsulfanyl) - 1,3 - dithiole-2-thione, 4,5-bis(2-pyridylethylsulfanyl)-1,3-dithiole-2-thione, 665
Copper complexes
Binucleating ligand, Nickel complexes, Crystal structures, Redox chemistry, 2011
Copper complexes
Carboxylate complexes, Dinuclear complexes, Crystal structures, Cuprous oxide, Cupric oxide., 2621
Copper complexes
Crystal structures, Metavanadate complexes, Nickel complexes, Hydrothermal synthesis, Magnetic properties, 2521
Copper complexes
Crystal structures, Nickel complexes, Schiff bases, Uracil, 689
Copper complexes
Schiff bases, X-ray structure, 5-Phenylazosalicylaldehyde, Cyclic voltammetry, 607
Copper complexes
Silver complexes, Gold complexes, 743
Copper complexes
Thiosemicarbazones, Macrocyclic ligands, Electrochemistry, Dithio-Schiff base complexes, 441
Copper compounds
Tetrathiometalate, Nonlinear optical properties, Synthesis, Crystal structures, Dppm, 1545
Copper-dipeptide complexes
Glycyl-lysine, Alanyl-lysine, Histidyl-lysine, β-alanyl-lysine, 2409
Copper
Divalent metals, Zinc, Benzolamide, Diethylenetriamine, Ternary complexes, 725
Copper
Equilibrium, Mixed valence, Disproportionation, Temperature effects, 2289
Copper
gem-Diol,di-2-pyridyl ketone, Di(2-pyridyl)methanediol, Crystal structures, 623
Copper(I) bromide complexes
Heterocyclic thione complexes, Diphosphine complexes, Dinuclear complexes, Crystal structures, 1615
Copper(I) complexes
Crystal structures, Electronic spectra, Emission spectra, Pyrazine carboxamide complexes, Vibrational spectra, 601
Copper(I) complexes
Di-2-pyridyl ketone, Crystal structures, Electronic and IR spectra, 1465
Copper(I) complexes
Phosphine, Alkene, Polymerization, Hydroboration, 1271
Copper(II)
Azomethine, Imidate, Crystal structures, 2713
Copper(II)
Binucleating hexa-aza macrocycle, Nickel(II), Cobalt(II), Zinc(II), Crystal structures, Phosphotriester, Hydrolysis, 1485
Copper(II)
Chloropropionate, Crystal structure, EPR, Bio-activity, 2573
Copper(II)
Cobalt(III), NMR spectroscopy, Pyridylmethyl-tetraazadecane, 1447
Copper(II) complexes
4,4′-Bipyridine, Coordination polymers, Cadmium(II) complexes, 1809
Copper(II) complexes
α,α′-Bis(pyrazolyl)-*m*-xylene, X-ray structure, Network structures, Absorption spectroscopy, Electron spin resonance, 719
Copper(II) complexes
Chelating ligands, Crystal structures, Pyridinecarboxylate complexes, Antimicrobial activity, 2689
Copper(II) complexes
Deltakephalins, Stability constants, 241
Copper(II) complexes
Deprotonated pyridine-2,6-dicarboxamide ligands, Singly hydroxo-bridged, Crystal structures, Magnetism, 1423
Copper(II) complexes
Dinuclear and polynuclear, Crystal structures, Equatorial–apical bridge, Paramagnetic, 1593
Copper(II) complexes
Dinucleating alkoxide ligands, X-ray structures, Hetero-bridged complexes, Magnetism, Magneto-structural trends, 1429
Copper(II) complexes
Electron spin resonance, Coordination modes, Histamine, L-Histidine, Isomerism, 1123
Copper(II) complexes
ESR, Glycyl-L-histidine, Formation constants, Coordination modes, Isomerism, 2049
Copper(II) complexes
N-salicylidenearoylhydrazines, X-ray crystal structures, Molecular structures, Magnetic properties, Infrared spectra, 949
Copper(II)
Diamines, Uridine, Uridine 5′-monophosphate, 1145
Copper(II)
1,4-Diazacycloheptane, Trichloroacetate, Crystal structures, 1881
Copper(II)–edta-type complexes
Crystal structures, Stereochemistry, 1
Copper(III)
Asorption spectra, Nickel(III), Dioxotetraamines, Macrocyclic ligands, 2533
Copper(I,II) complexes
α,β-Unsaturated carboxylates, Triphenylphosphine, Magnetic properties, Crystal structures, 891
Copper(II) imidazolate ternary complexes
N-salicylidenearoylhydrazine copper(II) complexes, Copper(II) imidazole ternary complexes, X-ray crystal structures, Molecular structures, Magnetic properties, Infrared spectra, 1181
Copper(II) imidazole ternary complexes
N-salicylidenearoylhydrazine copper(II) complexes, Copper(II) imidazolate ternary complexes, X-ray crystal structures, Molecular structures, Magnetic properties, Infrared spectra, 1181
Copper(II), nickel(II) and zinc(II) complexes
Mixed-ligand complexes, Solution equilibrium, Hydroxamic acid, 1727
Copper(II)–peroxide adduct
Release of free nucleobases from oligomers, DNA cleavage, Electrospray mass spectrometry, 2639
Copper–iron complexes
Cyano-bridge, Crystal structures, IR spectra, 1935
Copper(I) thiocyanate complexes
Methyl nicotinates, Ethyl nicotinates, Ethyl isonicotinate complexes, Crystal structures, Trigonal planar anions, 615
Copper phosphonates
Aniline polymerization, Intercalation compounds, 765
Copper
Phthalocyanine complexes, Phthalonitrile derivatives, Crown-ether, Nickel, Cobalt, Alkaline metal extraction, 115

Coupling reactions
Palladium catalyzed reactions, Halide ions, Protonolysis, 577
CPMAS ^{13}C NMR spectroscopy
Thorium(IV), Uranium(IV), Dicarboxylate complexes, X-ray crystallography, 1757
CP-MAS NMR
Tetra-aza ligands, Nickel complex, Template reaction, 2149
CPMAS
Zn(II) complexes, 1,2,4-Triazolo-[1,5α]-pyrimidine, ^{15}N NMR, HETCOR, 965
Cross coupling
1,5-diene, Terpenoids, Carboalumination, Palladium, 591
Cross-coupling
Platinum, Gold, Diyne, X-ray, 2261
15-Crown-5 complexes
Liquid clathrates, X-ray crystallography, Oxonium ion, 85
Crown ether complexation
μ-oxo-Bridged cations, Crystal structures, Bridging oxygen atoms, 1799
Crown-ether
Phthalocyanine complexes, Phthalonitrile derivatives, Copper, Nickel, Cobalt, Alkaline metal extraction, 115
Crown
Uranium, Uranyl, Phosphate, Crystal structures, 1551
Cryoscopy
Cyanocuprates, Ionic, Reactivity, Structures, 553
Crystal engineering
Dimolybdenum, Dimolybdenum diolates, 375
Crystallite size
Magnesia, Dolomite, Degree of agglomeration, X-ray diffraction, SEM, 2345
Crystallographic
Selenium, Tungsten analogue, Refluxing, 2127
Crystal structure
Alternating chain, Dimer complex, Magnetic properties, 1461
Crystal structure
Carboxylato-bridged copper(II) complex, Magnetic properties, 2529
Crystal structure
Cobalt, 2-Hydroxyacetophenone, Azide, Thiocyanate, 2707
Crystal structure
Copper(II), Chloropropionate, EPR, Bioactivity, 2573
Crystal structure
Imidazole derivatives, Transition metal complexes, Absorption spectra, Stability constants, 2183
Crystal structure of compounds of oxovanadium(V)
Alkoxo compounds of oxovanadium(V), Hydrazonato compounds of oxovanadium(V), Oxovanadium(V) dimers, Reactivity of bis(β-dionato)oxovanadium(IV) chelates, Hydrazonato tridentate Schiff base ligands, 2003
Crystal structure
Rare earth complex, Antitumour activity, Hydrazone, 2599
Crystal structures
Aluminum complexes, 1-Aza-allyl, Bismuth complexes, Gallium complexes, 471
Crystal structures
Azido-bridged nickel(II) compounds, Magnetic properties, 1575
Crystal structures
Binuclear copper compounds, Magnetism, Oxalato-bridged compounds, 1105
Crystal structures
Binuclear nickel(II) complex, Binuclear manganese(II) complex, Magnetic properties, Tris(6-methyl-2-pyridylmethyl)-amine, 1559
Crystal structures
Binucleating hexa-aza macrocycle, Copper(II), Nickel(II), Cobalt(II), Zinc(II), Phosphotriester, Hydrolysis, 1485
Crystal structures
Binucleating ligand, Nickel complexes, Copper complexes, Redox chemistry, 2011
Crystal structures
Bis(η-cyclopentadienyl)titanium(IV), Diphenylphosphinoacetate, Heterometallics, Nicotinate, Thiophenoxyacetate, 757
Crystal structures
Bismuth, Thioether, Coordination polymers, Electrospray, 849
Crystal structures
Bridged structures, Heteronuclear multiple bond coherence, *N*-Tosyl ligands, Zinc porphyrin complexes, 413
Crystal structures
Chelating ligands, Copper(II) complexes, Pyridinecarboxylate complexes, Antimicrobial activity, 2689
Crystal structures
Chromium(III) complexes, Tris(2-benzimidazolylmethyl)amine, 2-Guanidinobenzimidazole, 2,6-Bis(2-benzimidazolyl)-pyridine, 2-(2-Pyridyl)benzimidazole, 1821
Crystal structures
Cis–trans isomerism, 1,2-Diamino-2-methylpropane, Nickel(II)nitrite, 1015
Crystal structures
Cluster compounds, Molybdenum complexes, Tellurium-rich compounds, Detellurium reaction, 925
Crystal structures
Cobalt complexes, 855
Crystal structures
Cobalt(II) complexes, Iron(II) complexes, Octadentate ligands, 431
Crystal structures
Complexation chemistry, 1,10-Phenanthroline, 495
Crystal structures
Contrast agents, Diethylenetriaminepentaacetate, Lanthanides, Neodymium, 771
Crystal structures
Copper complexes, Carboxylate complexes, Dinuclear complexes, Cuprous oxide, Cupric oxide., 2621
Crystal structures
Copper, *gem*-Diol,di-2-pyridyl ketone, Di(2-pyridyl)methanediol, 623
Crystal structures
Copper(I) bromide complexes, Heterocyclic thione complexes, Diphosphine complexes, Dinuclear complexes, 1615
Crystal structures
Copper(I) complexes, Di-2-pyridyl ketone, Electronic and IR spectra, 1465
Crystal structures
Copper(I) complexes, Electronic spectra, Emission spectra, Pyrazine carboxamide complexes, Vibrational spectra, 601
Crystal structures
Copper(II), Azomethine, Imidate, 2713
Crystal structures
Copper(II) complexes, Deprotonated pyridine-2,6-dicarboxamide ligands, Singly hydroxo-bridged, Magnetism, 1423
Crystal structures
Copper(II) complexes, Dinuclear and polynuclear, Equatorial–apical bridge, Paramagnetic, 1593
Crystal structures
Copper(II), 1,4-Diazacycloheptane, Trichloroacetate, 1881
Crystal structures
Copper(II)–edta-type complexes, Stereochemistry, 1
Crystal structures
Copper(I,II) complexes, α,β-Unsaturated carboxylates, Triphenylphosphine, Magnetic properties, 891
Crystal structures
Copper–iron complexes, Cyano-bridge, IR spectra, 1935
Crystal structures
Copper(I) thiocyanate complexes, Methyl nicotinates, Ethyl nicotinates, Ethyl isonicotinate complexes, Trigonal planar anions, 615
Crystal structures
Cu dimers, Di-(2-pyridyl)ketone, Ferromagnetic dimers, Magnetic properties, Spin triplet, 1005
Crystal structures
Cu^{2+} porphyrin complexes, Protonated porphyrins, SAT complexes, Electron spin resonance, Nuclear magnetic resonance, 633
Crystal structures
Cyclic voltammetry, Nickel bisdithiolenes, Strong near-IR absorption, 425
Crystal structures
Diazafluorenone aroylhydrazone, Transition metal aroylhydrazone complexes, Enolization, ^1H NMR spectroscopy, IR, 1295
Crystal structures
Dichloromanganese(IV) complexes, Bidentate Schiff base ligands, Tetradentate Schiff base ligands, Photosystem II, 2039

Crystal structures
Diethyltin, Pyridoxine, 813
Crystal structures
Dirhodium(II) compounds, Trifluoroacetate, One-dimensional polymers, Arene coordination, π-Complexes, 1829
Crystal structures
Electrochemical synthesis, Cobalt(II) complexes, Tosylamide complexes, 1607
Crystal structures
Electrochemistry, EPR, Nickel(II)/(III) complexes, Schiff base complexes, 655
Crystal structures
2-Ethyl-3-hydroxy-4-pyranonate, Ethylmaltol, 1-Methyl-2-ethyl-3-hydroxy-4-pyridinonate, Tin(IV), Titanium(IV), 399
Crystal structures
Europium(III) complexes, Non-planar conjugated ligands, Fluorescence spectra, 785
Crystal structures
Fac isomers, Isomerization, Lanthanide chloride complexes, Octahedral complexes, 199
Crystal structures
Hydroborates, Lithium, Titanium(IV), Bonding, 1579
Crystal structures
Imidazole, Schiff base, Silver complexes, 2237
Crystal structures
Infrared spectroscopy, Raman spectroscopy, Electronic absorption spectroscopy, Hypophospite complexes, Cooperative vibronic transitions, Two-centre transitions, 863
Crystal structures
Lanthanide complexes, Picrate, 4-Methylmorpholine, *N*-Oxide, TG, DSC, 2313
Crystal structures
Lanthanide picrate, PBD, Fluorescence, 779
Crystal structures
Magnetic properties, Dinuclear complexes, Manganese, Cobalt, Nickel, 93
Crystal structures
Manganese(II) complexes, Fumaric acid, Fungitoxic activity, 1205
Crystal structures
Mercury(II) complexes, Triphenylphosphine, Benzothiazole-2-thione, pyrimidine-2-thione, 2231
Crystal structures
Mercury(II) halides, Phosphine complexes, 1719
Crystal structures
Metavanadate complexes, Nickel complexes, Copper complexes, Hydrothermal synthesis, Magnetic properties, 2521
Crystal structures
Molybdenum complexes, Tungsten complexes, Pyrazine complexes, Peroxo ligands, 1503
Crystal structures
Molybdenum(II), Tungsten(II), *o*-Phenylenediacetonitrile, Bimetallic complexesw, Trimetallic complexes, Nitrile-bridged complexes, Seven-coordinate complexes, Halocarbonyls, 147
Crystal structures
Molybdenum, Oxocluster complexes, Hantzsch synthesis, Hexanuclear molybdenum(V) complexes, 1471
Crystal structures
Molybdenum–oxo complexes, Photochemistry, Photooxidation, Phosphines, Phosphine oxides, 1437
Crystal structures
Molybdenum, Tantalum, Trimetallic alkoxides, 1791
Crystal structures
Mo–S clusters, Electronic structures, Layer-like packing, 733
Crystal structures
Nickel complexes, Copper complexes, Schiff bases, Uracil, 689
Crystal structures
Nickel(II), Iron(II), Electronic spectra, 1333
Crystal structures
Nickel(II), Mononuclear compounds, Nitrito ligands, Magnetic measurements, 225
Crystal structures
Nickel(II)thiocyanate, 1-(2-Aminoethyl)-pyrrolidine, *cis*/*trans* Isomers, 1803
Crystal structures
Ni(II) complexes, Tripodal ligand, Spectroscopic studies, 2661
Crystal structures
Nitrosonaphthol, Ruthenium nitrosonaphthol complexes, 7
Crystal structures
Organolanthanide complexes, Ether-side chain cyclopentadienyl, Cyclooctatetraenyl, 453
Crystal structures
μ-oxo-Bridged cations, Crown ether complexation, Bridging oxygen atoms, 1799
Crystal structures
Oxovanadium(V) alkoxides, Mononuclear chelation, Hydrogen bonded helical structures, 931
Crystal structures
Palladium complexes, Platinum complexes, Diphosphine complexes, Tetraphosphine complexes, Bimetallic complexes, 913
Crystal structures
Palladium, Hydroxo complexes, Pyrazolylalkane complexes, 1395
Crystal structures
Phosphine sulfides, Phosphonium salt, 2585
Crystal structures
Platinum complexes, 3-methylpiperidine, Dicarboxylates, Synthesis, 983
Crystal structures
Platinum(II) complexes, Piperidine, Synthesis, 975
Crystal structures
1,3-propylenediaminetetraacetate, Cu(II) complexes, Mn(II) complexes, Thermal properties, Magnetic properties, 1175
Crystal structures
2-Pyridineformamide, Thiosemicarbazone, Cadmium halides, 1873
Crystal structures
Rhenium, Metal clusters, Sulfur, Selenium, Tellurium, 437
Crystal structures
Ruthenium, Dimethyl sulfoxide, Carboxylates, Complexes, Catalysis, 1589
Crystal structures
Ruthenium, Iridium, Gold, Electron-rich, Cluster, Phosphido-bridged, 2593
Crystal structures
Scandium, Alkoxides, Volatility, 705
Crystal structures
Solvothermal synthesis, Oxomolybdenum(V) coordination compounds, Mo(V, VI) compounds, Alkyl-substituted pyridines, 1407
Crystal structures
Spirophosphorane ring-opening, Phosphite diolato(1 −) ligand, 2667
Crystal structures
Sulfamethizole, Metal complexes, Spectroscopic properties, 1859
Crystal structures
Syntheses, Cobalt(II) complex, Nickel(II) complex, 4-(*p*-Methylphenyl)-3,5-bis-(pyridin-2-yl)-1,2,4-triazole, ESIMS, 2019
Crystal structures
Synthesis, Macrocyclic polyamine ligand, Manganese complexes, Octa- and hepta-coordination, 2095
Crystal structures
Tetrathiometalate, Nonlinear optical properties, Synthesis, Copper compounds, Dppm, 1545
Crystal structures
Thiolate, Electrochemistry, Macrocycle, 1887
Crystal structures
Thiophosphoryl guanidines, Platinum complexes, 809
Crystal structures
Thiosemicarbazone, Isatin, Zinc, Lead, Hexamethyleneimine, Metal(II) complexes, 1255
Crystal structures
Transition metal complexes, Terephthalate ions, Aromatic diamines, Spectral data, 1415
Crystal structures
Trichlorovinyl, Mercury(II), Complexes, Bidentate ligands, 2539
Crystal structures
Uranium, Uranyl, Phosphate, Crown, 1551
Crystal structure
Synthesis, Aryloxide, Neodymium, Anion–cation pair compound, 2243
Crystal structures
Zinc, Bis(pyrazolyl)silanes, Nitrogen-donor ligands, 1815
Crystal structures
Zinc complexes, Cobalt complex, α-Ketoglutaric acid, Thiosemicarbazones, Spectroscopic properties, 1895

Crystal structures
Zinc complexes, Lead(II) complexes, Maltol, 3-Hydroxy-4-pyranone, 3-Hydroxy-4-pyridinone, 1,2-Dimethyl, 129
Crystal structures
Zinc, Tris-pyrazolylborate, Electrochemistry, 109
Crystal structures
Zirconocene, Catalysis, Olefin polymerizations, 1941
Crystal structure
Ytterbium(III), Lanthanides, Calixarenes, Homoazacalixarenes, 2673
CT photochemistry
Ternary copper(II) complexes, Diselenocarbamate and dithiophosphate ligands, 2177
Cu dimers
Crystal structures, Di-(2-pyridyl)ketone, Ferromagnetic dimers, Magnetic properties, Spin triplet, 1005
Cu(II) complexes
Effortil, Structures, Stability constants, EPR, Magnetochemical data, 1843
Cu(II) complexes
1,3-propylenediaminetetraacetate, Mn(II) complexes, Crystal structures, Thermal properties, Magnetic properties, 1175
Cu(II) complex
Structure, Triaminoguanidinium(2 +) ion, 1737
Cu^{2+} porphyrin complexes
Crystal structures, Protonated porphyrins, SAT complexes, Electron spin resonance, Nuclear magnetic resonance, 633
Cupric oxide.
Copper complexes, Carboxylate complexes, Dinuclear complexes, Crystal structures, Cuprous oxide, 2621
Cuprous oxide
Copper complexes, Carboxylate complexes, Dinuclear complexes, Crystal structures, Cupric oxide, 2621
Cyanamidonitrate
Cobalt(II), Electronic spectra, Imidazole ligands, IR spectra, Nickel(II), X-ray crystallography, 1021
Cyano-bridge
Copper–iron complexes, Crystal structures, IR spectra, 1935
Cyanobridged complexes
Mixed-valence complexes, Ruthenium–edta complexes, Ferricyanide, Intramolecular electron transfer, 1339
Cyano-bridged heteropolynuclear complexes
Molecular magnets, Iron complexes, Nickel complexes, Ferromagnetic coupling, 1967
Cyanocuprates
Cryoscopy, Ionic, Reactivity, Structures, 553
Cyclic oligomers
Thiophenes, Ferrocenes, 291
Cyclic phosphazenes
Ab initio methods, Electronic structures, Group theory, 389
Cyclic voltammetry
Crystal structures, Nickel bisdithiolenes, Strong near-IR absorption, 425
Cyclic voltammetry
Schiff bases, Copper complexes, X-ray structure, 5-Phenylazosalicylaldehyde, 607
Cyclic voltammetry
Thiopyrimidine, Rhenium(V) complexes, Rhenium(III) complexes, UV–Vis–NIR, IR, ^{1}H NMR spectra, 2163
Cycloadditions
Dienes, Indium, Magnesium, Trienes, 533
Cycloalkenes
Thioacetal, Titanocene(II), Ring-closing metathesis, Intramolecular carbonyl olefination, Heterocyclic compounds, 593
Cyclooctatetraenyl
Organolanthanide complexes, Ether-side chain cyclopentadienyl, Crystal structures, 453
Cymene
Nitration, Pyrazolyl, Ruthenium, Structure, Synthesis, 475

Decomplexation
Nitrosobenzene cycloaddition, Regioselectivity, Organoiron compounds, Heterocycloaddition trap, Alkaloid synthesis, 569
Degree of agglomeration
Magnesia, Dolomite, Crystallite size, X-ray diffraction, SEM, 2345
Delocalized π interactions
Aza-macrocycles, Electroreduction, Carbon dioxide, 2373
Deltakephalins
Copper(II) complexes, Stability constants, 241
Dendrimers
Carbosilanes, Platinum catalysts, Hydrosilation, 1031
Density functional theory
Vanadium, Vanadyl, Terpyridine, 69
Deoxycholic acid
Ferrocene derivatives, Inclusion compounds, Molecular motion, ^{57}Fe Mössbauer spectroscopy, Powder X-ray diffraction patterns, 205
Deprotonated pyridine-2,6-dicarboxamide ligands
Copper(II) complexes, Singly hydroxo-bridged, Crystal structures, Magnetism, 1423
De-tellurium reaction
Cluster compounds, Molybdenum complexes, Tellurium-rich compounds, Crystal structures, 925
DFT
Nitrosyl complex, Chromium, Molybdenum, Carboxylate, 2565
D-Galactonic acid
D-Gluconic acid, D-Gulonic acid, Praseodymium(III), Complexation, 1567
D-Gluconic acid
D-Galactonic acid, D-Gulonic acid, Praseodymium(III), Complexation, 1567
D-Gulonic acid
D-Gluconic acid, D-Galactonic acid, Praseodymium(III), Complexation, 1567
Dialkoxo-bridged binuclear Cu(II) complexes
Model of metal–guanine interaction, Single crystal structures, Thermal decompostion, Theophylline, Diethanolamine-(2,2′-iminodiethanol), 457
Dialkyldithiocarbamato
Molybdenum, Hydrazido, Diazenido, Hydrazines, 2327
Diamines
Copper(II), Uridine, Uridine 5′-monophosphate, 1145
1,2-Diamino-2-methylpropane
Cis–trans isomerism, Crystal structures, Nickel(II)nitrite, 1015
1,4-Diazacycloheptane
Copper(II), Trichloroacetate, Crystal structures, 1881
Diazafluorenone aroylhydrazone
Transition metal aroylhydrazone complexes, Crystal structures, Enolization, ^{1}H NMR spectroscopy, IR, 1295
Diazenido
Molybdenum, Hydrazido, Dialkyldithiocarbamato, Hydrazines, 2327
6,6′-Dicarboxy-2,2′-bipyridyl
Streptonigrin, 2,2′-Bipyridyl, Antitumour, Zinc, 1067
Dicarboxylate-based compounds
Hybrid copper(II) compounds, Magnetic properties, Layered magnets, Long-range ferromagnetism, 259
Dicarboxylate complexes
Thorium(IV), Uranium(IV), CPMAS ^{13}C NMR spectroscopy, X-ray crystallography, 1757
Dicarboxylates
Platinum complexes, 3-methylpiperidine, Synthesis, Crystal structures, 983
Dichloromanganese(IV) complexes
Bidentate Schiff base ligands, Tetradentate Schiff base ligands, Crystal structures, Photosystem II, 2039
Diclofenac
Metal(II) compounds, Spectroscopic properties, Thermal properties, 2515
Dicopper complexes
Solvent-derived ancillary ligands, Acid–base congeners, 1909
1,5-diene
Cross coupling, Terpenoids, Carboalumination, Palladium, 591
Dienes
Cycloadditions, Indium, Magnesium, Trienes, 533
Diethanolamine(2,2′-iminodiethanol)
Dialkoxo-bridged binuclear Cu(II) complexes, Model of metal–guanine interaction, Single crystal structures, Thermal decompostion, Theophylline, 457
Diethyldithiocarbamate
Palladium, Diphosphines, Tetrachlorometallate anions, X-ray crystal structures, 1511

Diethylenetriamine
Divalent metals, Zinc, Copper, Benzolamide, Ternary complexes, 725
Diethylenetriamine
Lanthanides(III), Silver(I), *N*,*N*-dimethylformamide, Complexes, Thermodynamics, 2427
Diethylenetriaminepentaacetate
Contrast agents, Crystal structures, Lanthanides, Neodymium, 771
Diethyltin
Crystal structures, Pyridoxine, 813
Dihydrodithiins
Thiiranes, Tungsten carbonyls, 521
Diimine
Amido, Dimer, Hydroxo, Palladium, Platinum, 155
β-Diketonate
Alkoxide, Tin, Tin dioxide, Sol–gel, 2069
Dimer
Amido, Diimine, Hydroxo, Palladium, Platinum, 155
Dimer complex
Alternating chain, Crystal structure, Magnetic properties, 1461
Dimers
Magnetic properties, Geometrical distortions, Magnetostructural correlations, 2483
Dimethyl carbonate
Carbon dioxide, Homogeneous catalysis, Mechanism, Supercritical conditions, 573
Dimethyl sulfoxide
Crystal structures, Ruthenium, Carboxylates, Complexes, Catalysis, 1589
1,2-Dimethyl
Zinc complexes, Lead(II) complexes, Maltol, 3-Hydroxy-4-pyranone, 3-Hydroxy-4-pyridinone, Crystal structures, 129
Dimolybdenum
Crystal engineering, Dimolybdenum diolates, 375
Dimolybdenum diolates
Crystal engineering, Dimolybdenum, 375
Dimolybdenum(II)
Trirhenium(III) clusters, Rhenium clusters, Acetamidate, MALDI, Mass spectroscopy, 1245
Dinuclear and polynuclear
Copper(II) complexes, Crystal structures, Equatorial–apical bridge, Paramagnetic, 1593
Dinuclear
Antiferromagnetic interactions, Pryrazolyl groups, 2215
Dinuclear complexes
Copper complexes, Carboxylate complexes, Crystal structures, Cuprous oxide, Cupric oxide., 2621
Dinuclear complexes
Copper(I) bromide complexes, Heterocyclic thione complexes, Diphosphine complexes, Crystal structures, 1615
Dinuclear complexes
Crystal structures, Magnetic properties, Manganese, Cobalt, Nickel, 93
Dinuclear complexes
Dioxygen carriers, Cobalt, Dinucleating ligands, Polyamines, Kinetics, Dioxygen binding, 2447
Dinuclear complexes
Dithiolene, Nickel, Acid–base, Solvatochromism, Carbon disulfide, 1283
Dinucleating alkoxide ligands
Copper(II) complexes, X-ray structures, Hetero-bridged complexes, Magnetism, Magneto-structural trends, 1429
Dinucleating ligands
Dioxygen carriers, Cobalt, Dinuclear complexes, Polyamines, Kinetics, Dioxygen binding, 2447
Dioxomolybdenum dipicolinate
Oxygen-atom transfer, Azoxybenzene deoxygenation, 2141
Dioxotetraamines
Asorption spectra, Copper(III), Nickel(III), Macrocyclic ligands, 2533
Dioxygen binding
Dioxygen carriers, Cobalt, Dinuclear complexes, Dinucleating ligands, Polyamines, Kinetics, 2447
Dioxygen binding
Dioxygen carriers, Cobalt, Polynuclear complexes, Polyamines, Thermodynamics of complexation, 2441
Dioxygen carriers
Cobalt, Dinuclear complexes, Dinucleating ligands, Polyamines, Kinetics, Dioxygen binding, 2447
Dioxygen carriers
Dioxygen binding, Cobalt, Polynuclear complexes, Polyamines, Thermodynamics of complexation, 2441
Dioxygen
Manganese complexes, Schiff bases, Manganoenzymes, Photolysis, Catalase, 47
Diphenylphosphinoacetate
Bis(η-cyclopentadienyl)titanium(IV), Crystal structures, Heterometallics, Nicotinate, Thiophenoxyacetate, 757
Diphosphine complexes
Copper(I) bromide complexes, Heterocyclic thione complexes, Dinuclear complexes, Crystal structures, 1615
Diphosphine complexes
Crystal structures, Palladium complexes, Platinum complexes, Tetraphosphine complexes, Bimetallic complexes, 913
Diphosphines
Palladium, Diethyldithiocarbamate, Tetrachlorometallate anions, X-ray crystal structures, 1511
Diphosphines
Palladium, Platinum, Nitrite, Isomerism, Fluxionality, 1329
Di-2-pyridyl ketone
Copper(I) complexes, Crystal structures, Electronic and IR spectra, 1465
Di-(2-pyridyl)ketone
Crystal structures, Cu dimers, Ferromagnetic dimers, Magnetic properties, Spin triplet, 1005
Di(2-pyridyl)methanediol
Copper, *gem*-Diol,di-2-pyridyl ketone, Crystal structures, 623
Dirhodium(II) compounds
Trifluoroacetate, One-dimensional polymers, Arene coordination, π-Complexes, Crystal structures, 1829
Discotic complexes
Columnar complexes, Liquid crystals, π-acceptors, Dithiolene, 267
Diselenocarbamate and dithiophosphate ligands
CT photochemistry, Ternary copper(II) complexes, 2177
Disodium or dipotassium 1,3-di(carboxylatomethyl)-5-aryl-1,3,5-diazaphosphorinanes
Water-soluble phosphines, Phosphino amino acid salts, 1455
Disproportionation
Equilibrium, Copper, Mixed valence, Temperature effects, 2289
Distorted square-pyramid
Catechols, Macrocyclic ligands, Oxovanadium complexes, ESR parameters, Hydrophobic cavities, 1167
Disulfide
Peptides, Transition metal ions, 1849
Disulfide reduction
Substituted cobalt phthalocyanines, Redox properties, Hammett parameters, Frontier orbitals, 2255
Disulfides
Thioureides, Dithiocarbamates, Tetrahedral coordination, 1279
Ditelluroether
Osmium, X-ray structures, 235
3,5-Di-*tert*-butylcatechol
Oxidation, Catalysis, Kinetics, Copper binuclear complexes, 2367
Dithiadiazolyl radicals, 1163
Dithiocarbamate derivatives
Copper and iron species, Thiuram sulfides, 2269
Dithiocarbamates
Disulfides, Thioureides, Tetrahedral coordination, 1279
Dithiocarbamates
Rhodium(II), 123
Dithiocarboxylate
Vanadium(IV), Magnetism, EPR, Infrared, Coordination., 2155
Dithiolate complexes
Ruthenium, Osmium, X-ray structures, 1073
Dithiolene
Discotic complexes, Columnar complexes, Liquid crystals, π-acceptors, 267
Dithiolene
Nickel, Dinuclear complexes, Acid–base, Solvatochromism, Carbon disulfide, 1283
1,3-dithiole-2-thione-4,5-dithiolates
dmit complexes, Zinc dmit compounds, Zincates, 821
Dithiophosphinates
Low-pressure metal organic chemical vapour deposition, II/VI Semiconductors, 211

Dithio-Schiff base complexes
Thiosemicarbazones, Macrocyclic ligands, Electrochemistry, Copper complexes, 441
Divalent metals
Zinc, Copper, Benzolamide, Diethylenetriamine, Ternary complexes, 725
Diyne
Platinum, Gold, Cross-coupling, X-ray, 2261
dmit complexes
1,3-dithiole-2-thione-4,5-dithiolates, Zinc dmit compounds, Zincates, 821
dmit
Copper, Cobalt, Nickel, Palladium, 4,5-bis(2-pyridylmethylsulfanyl)-1,3-dithiole-2-thione, 4,5-bis(2-pyridylethylsulfanyl)-1,3-dithiole-2-thione, 665
DNA cleavage activities
Tetraazamacrocyclic ligand, Transition metal, Synthesis, Structural characterization, Stability constants, 1527
DNA cleavage
Release of free nucleobases from oligomers, Copper(II)–peroxide adduct, Electrospray mass spectrometry, 2639
Dodecanuclear
Mo–Cu–S cage cluster, Interstitial group, 2189
Dolomite
Magnesia, Crystallite size, Degree of agglomeration, X-ray diffraction, SEM, 2345
Domino reactions
Hydroformylation, Organocopper reagents, Catalysis, Asymmetric synthesis, 513
Dopamine
Iron, Phthalocyanine, Serotonin, Coordination, 1355
dppm
Rhenium, Re complexes, Re(I), *trans*-Dioxo Re(V) complexes, Phosphines, 2249
Dppm
Tetrathiometalate, Nonlinear optical properties, Synthesis, Copper compounds, Crystal structures, 1545
DSC
Crystal structures, Lanthanide complexes, Picrate, 4-Methylmorpholine, *N*-Oxide, TG, 2313
DTPA
Iron(III), Chromium(III), Complexes, Thermal properties, Thermodynamics, 2421

Effortil
Cu(II) complexes, Structures, Stability constants, EPR, Magnetochemical data, 1843
Electrocatalysis
Cobalt, Nitric oxide, Oxidation, Phthalocyanine, Reduction, 229
Electrocatalytic oxidation
Ruthenium, Polypyridine, Terpyridine, Alcohol oxidation, Isomerization, 1049
Electrochemical communication
Ferrocenylporphyrin, π-Conjugation, Intramolecular hydrogen bonding, NH tautomerism, 1961
Electrochemical studies
Heterodinuclear complexes, Homodinuclear complexes, Luminescence properties, Osmium(II) complexes, Ruthenium(II) complexes, Syntheses, 1233
Electrochemical synthesis
Cobalt(II) complexes, Crystal structures, Tosylamide complexes, 1607
Electrochemical synthesis
Mononuclear complexes, Phenoxo bridges, Polyhydroxyl ligands, Polynuclear complexes, Schiff base ligands, 185
Electrochemistry
Azoimine, Ru–bipyridine, Tris-chelates, X-ray structures, Emission spectra, 1925
Electrochemistry
Binuclear Cu(II) complexes, Magnetic properties, ESR, 1769
Electrochemistry
Crystal structures, EPR, Nickel(II)/(III) complexes, Schiff base complexes, 655
Electrochemistry
Naphthylazoimidazoles, Platinum(II), PtN_4 coordination, X-ray structures, 1263
Electrochemistry
Platinum(II), Platinum(IV), Bromide, Porphyrins, Voltammetry, 1057
Electrochemistry
Thiolate, Macrocycle, Crystal structures, 1887
Electrochemistry
Thiosemicarbazones, Iron complexes, EPR of iron complexes, Nickel complexes, Cobalt complexes, 2059
Electrochemistry
Thiosemicarbazones, Macrocyclic ligands, Copper complexes, Dithio-Schiff base complexes, 441
Electrochemistry
Zinc, Tris-pyrazolylborate, Crystal structures, 109
3:3 Electrolytes
Activity coefficients, Electrolytic solutions, High-charge salts, High valency electrolytes, Mixed electrolytes, 2493
Electrolytic solutions
3:3 Electrolytes, Activity coefficients, High-charge salts, High valency electrolytes, Mixed electrolytes, 2493
Electronic absorption spectroscopy
Infrared spectroscopy, Raman spectroscopy, Crystal structures, Hypophospite complexes, Cooperative vibronic transitions, Two-centre transitions, 863
Electronic and IR spectra
Copper(I) complexes, Di-2-pyridyl ketone, Crystal structures, 1465
Electronic spectra
Cobalt(II), Cyanamidonitrate, Imidazole ligands, IR spectra, Nickel(II), X-ray crystallography, 1021
Electronic spectra
Copper(I) complexes, Crystal structures, Emission spectra, Pyrazine carboxamide complexes, Vibrational spectra, 601
Electronic spectral data
Transition metal complexes, Oximes, Benzil-α-monoxime, 1687
Electronic spectra
Nickel(II), Iron(II), Crystal structures, 1333
Electronic structures
Ab initio methods, Cyclic phosphazenes, Group theory, 389
Electronic structures
Mo–S clusters, Crystal structures, Layer-like packing, 733
Electron-rich
Ruthenium, Iridium, Gold, Cluster, Phosphido-bridged, Crystal structures, 2593
Electron spin resonance
α,α′-Bis(pyrazolyl)-*m*-xylene, Copper(II) complexes, X-ray structure, Network structures, Absorption spectroscopy, 719
Electron spin resonance
Copper(II) complexes, Coordination modes, Histamine, L-Histidine, Isomerism, 1123
Electron spin resonance
Crystal structures, Cu^{2+} porphyrin complexes, Protonated porphyrins, SAT complexes, Nuclear magnetic resonance, 633
Electron-transfer
Thiolate-bridged complexes, Mixed-valence, Iron, 2679
Electrooxidation of hydrazine
Polymeric metallophthalocyanines, Modified electrodes, Poly(cobalt–tetraaminophthalocyanine), Impedance spectroscopy, 2303
Electroprotic reactions
Kinetics, Manganese(IV), Ascorbic acid, 1213
Electroreduction
Aza-macrocycles, Carbon dioxide, Delocalized π interactions, 2373
Electrospray
Bismuth, Thioether, Coordination polymers, Crystal structures, 849
Electrospray mass spectrometry
Pentafluoro-cyclotriphosphazene, Pentachloro-cyclotriphosphazene, X-ray structures, 2101
Electrospray mass spectrometry
Release of free nucleobases from oligomers, Copper(II)–peroxide adduct, DNA cleavage, 2639
Emission spectra
Azoimine, Ru–bipyridine, Tris-chelates, X-ray structures, Electrochemistry, 1925
Emission spectra
Copper(I) complexes, Crystal structures, Electronic spectra, Pyrazine carboxamide complexes, Vibrational spectra, 601
Enamine
Alkenylation, Pyrrole, 545

Enantioselection
Chromium, Salen, Manganese, Catalysis, Nozaki–Hiyama–Kishi reaction, 537
Enolization
Diazafluorenone aroylhydrazone, Transition metal aroylhydrazone complexes, Crystal structures, ^{1}H NMR spectroscopy, IR, 1295
Enthalpy
Yttrium, Rare earth elements, Hydrolysis, Ionic strength, Spectrophotometry, 99
Epimerisation
Chiral-at-metal complexes, Configurational stability, Equilibria, X-ray structure analyses, 1519
Epoxidation
Porphyrins, Hemoprotein models, Chiral catalysts, Olefins, 581
EPR
Copper(II), Chloropropionate, Crystal structure, Bio-activity, 2573
EPR
Crystal structures, Electrochemistry, Nickel(II)/(III) complexes, Schiff base complexes, 655
EPR
Dithiocarboxylate, Vanadium(IV), Magnetism, Infrared, Coordination, 2155
EPR
Effortil, Cu(II) complexes, Structures, Stability constants, Magnetochemical data, 1843
EPR of iron complexes
Thiosemicarbazones, Electrochemistry, Iron complexes, Nickel complexes, Cobalt complexes, 2059
EPR spectroscopy
Rhenium, Nitrido complexes, Imido complexes, X-ray structures, 1741
EPR spectroscopy
Vanadium, Molybdenum, Heteropolyoxometalate, IR spectroscopy, UV–Vis spectroscopy, 1917
Equatorial–apical bridge
Copper(II) complexes, Dinuclear and polynuclear, Crystal structures, Paramagnetic, 1593
Equilibria
Chiral-at-metal complexes, Configurational stability, Epimerisation, X-ray structure analyses, 1519
Equilibria
Macrocycles, Synthesis, Complexes, 2501
Equilibria
Me_2Octaen, Polyamines, Nickel(II), Kinetics, Stopped-flow, 2507
Equilibria
Potentiometry, Stability constants, Manganese(II), Cobalt(II), Nickel(II) complexes, Aminopolyphosphonates, UV–VIS spectra, 2083
Equilibrium constants
Molybenum(VI) cations, Thermodynamic quantities, 907
Equilibrium
Copper, Mixed valence, Disproportionation, Temperature effects, 2289
Erbium complex
Lanthanide, Hydrazone, 2629
ESCA studies
Acidopentaaminecobalt(III) complexes, ESI + mass spectra, Acid dissociation constants, 971
ESI + mass spectra
Acidopentaaminecobalt(III) complexes, ESCA studies, Acid dissociation constants, 971
ESIMS
Syntheses, Crystal structures, Cobalt(II) complex, Nickel(II) complex, 4-(*p*-Methylphenyl)-3,5-bis(pyridin-2-yl)-1,2,4-triazole, 2019
ESR
Binuclear Cu(II) complexes, Magnetic properties, Electrochemistry, 1769
ESR
Copper(II) complexes, Glycyl-L-histidine, Formation constants, Coordination modes, Isomerism, 2049
ESR parameters
Catechols, Macrocyclic ligands, Oxovanadium complexes, Distorted square-pyramid, Hydrophobic cavities, 1167
Esters
Allylation, Aqueous reactions, Indium, Indium compounds, Pyridines, 549
Ether-side chain cyclopentadienyl
Organolanthanide complexes, Cyclooctatetraenyl, Crystal structures, 453
Ethylenimine
Immobilization, 3-Mercaptopropyltrimethoxysilane, Silica gels, 367
2-Ethyl-3-hydroxy-4-pyranonate
Crystal structures, Ethylmaltol, 1-Methyl-2-ethyl-3-hydroxy-4-pyridinonate, Tin(IV), Titanium(IV), 399
Ethyl isonicotinate complexes
Copper(I) thiocyanate complexes, Methyl nicotinates, Ethyl nicotinates, Crystal structures, Trigonal planar anions, 615
Ethylmaltol
Crystal structures, 2-Ethyl-3-hydroxy-4-pyranonate, 1-Methyl-2-ethyl-3-hydroxy-4-pyridinonate, Tin(IV), Titanium(IV), 399
Ethyl nicotinates
Copper(I) thiocyanate complexes, Methyl nicotinates, Ethyl isonicotinate complexes, Crystal structures, Trigonal planar anions, 615
Europium compounds
Hydrotris(pyrazolyl)borate ligands, Luminescence studies, X-ray crystal structures, 1707
Europium(III) chloride
Lanthanide complex, Tridentate chelate, 2135
Europium(III) complexes
Crystal structures, Non-planar conjugated ligands, Fluorescence spectra, 785
EXAFS investigation
Synthesis, Azomethynic copper metallochelates, 2361
Fac isomers
Crystal structures, Isomerization, Lanthanide chloride complexes, Octahedral complexes, 199
Fast atom bombardment mass spectrometry
2,2′-Bipyridine, 1,8-Bis(dimethylamino)-naphthalene, Boron-11 NMR, Chelated fluoroboron cations, Fluorine-19 NMR, 1,10-Phenanthroline, 2,2′,6′,2″-Terpyridine, 165
^{57}Fe Mössbauer spectroscopy
Deoxycholic acid, Ferrocene derivatives, Inclusion compounds, Molecular motion, Powder X-ray diffraction patterns, 205
Ferricyanide
Mixed-valence complexes, Ruthenium–edta complexes, Cyanobridged complexes, Intramolecular electron transfer, 1339
Ferrocene derivatives
Deoxycholic acid, Inclusion compounds, Molecular motion, ^{57}Fe Mössbauer spectroscopy, Powder X-ray diffraction patterns, 205
Ferrocenes
Cyclic oligomers, Thiophenes, 291
Ferrocenophane
Inorganic polymers, Silanol, Mössbauer spectroscopy, Ring-opening polymerization, 275
Ferrocenylporphyrin
π-Conjugation, Electrochemical communication, Intramolecular hydrogen bonding, NH tautomerism, 1961
Ferroelectric oxides
Metal–organic chemical vapour deposition, Precursors, Lead scandium tantalate, 351
Ferromagnetic coupling
Molecular magnets, Cyano-bridged heteropolynuclear complexes, Iron complexes, Nickel complexes, 1967
Ferromagnetic dimers
Crystal structures, Cu dimers, Di-(2-pyridyl)ketone, Magnetic properties, Spin triplet, 1005
Field strength
Ruthenium, Phenanthroline, *Cis–trans*, MO calculations, Barriers, 2297
Fluorescence
Lanthanide picrate, PBD, Crystal structures, 779
Fluorescence spectra
Crystal structures, Europium(III) complexes, Non-planar conjugated ligands, 785
Fluorine-19 NMR
2,2′-Bipyridine, 1,8-Bis(dimethylamino)-naphthalene, Boron-11 NMR, Chelated fluoroboron cations, Fast atom bombardment mass spectrometry, 1,10-Phenanthroline, 2,2′,6′,2″-Terpyridine, 165
Fluxionality
Palladium, Platinum, Nitrite, Diphosphines, Isomerism, 1329
Force constants
Fourier transform infrared and Raman spectra, Uranyl bis(2-hydroxybenzaldehyde), 2353

Formation constants
ESR, Copper(II) complexes, Glycyl-L-histidine, Coordination modes, Isomerism, 2049
Formation constants
meso-2,3-Dimercaptosuccinic acid, Potentiometry, UV–Vis spectroscopy, Ionization constants, Kinetic measurements, 2435
Fourier transform infrared and Raman spectra
Uranyl bis(2-hydroxybenzaldehyde), Force constants, 2353
Frontier orbitals
Substituted cobalt phthalocyanines, Redox properties, Hammett parameters, Disulfide reduction, 2255
FT-IR
Colloids, Bimetallic films, Conductivity, Thermal analysis, 2337
Fumaric acid
Manganese(II) complexes, Crystal structures, Fungitoxic activity, 1205
Functional derivatives
closo-Dodecaborate, Oxonium derivatives, Amino acids, Boron neutron capture therapy, 627
Functionalized metalloalkynes
Alkynes, Olefins, Polymetallated olefins, Titanium, 563
Functionalized nanoclusters
CdS nanoclusters, Ruthenium(II) polypyridyls, Mesophase materials, Molecular devices, 331
Fungitoxic activity
Manganese(II) complexes, Fumaric acid, Crystal structures, 1205

Gallium complexes
Aluminum complexes, 1-Aza-allyl, Bismuth complexes, Crystal structures, 471
gem-Diol,di-2-pyridyl ketone
Copper, Di(2-pyridyl)methanediol, Crystal structures, 623
Geometrical distortions
Magnetic properties, Dimers, Magnetostructural correlations, 2483
Glycyl-L-histidine
ESR, Copper(II) complexes, Formation constants, Coordination modes, Isomerism, 2049
Glycyl-lysine
Copper-dipeptide complexes, Alanyl-lysine, Histidyl-lysine, β-alanyl-lysine, 2409
Gold complexes
Copper complexes, Silver complexes, 743
Gold(I) complexes
Cationic ylide ligand, Bis(methyldiphenylphosphonio)methylide salts, P-alkylation, 1837
Gold
Photochemistry, Surface chemistry, Photochemical metal organic deposition, Lithography, 343
Gold
Platinum, Cross-coupling, Diyne, X-ray, 2261
Gold
Ruthenium, Iridium, Electron-rich, Cluster, Phosphido-bridged, Crystal structures, 2593
Group theory
Ab initio methods, Cyclic phosphazenes, Electronic structures, 389
2-Guanidinobenzimidazole
Chromium(III) complexes, Tris(2-benzimidazolylmethyl)amine, 2,6-Bis(2-benzimidazolyl)pyridine, 2-(2-Pyridyl)benzimidazole, Crystal structures, 1821

Halide ions
Palladium catalyzed reactions, Coupling reactions, Protonolysis, 577
Halocarbonyls
Molybdenum(II), Tungsten(II), Crystal structures, *o*-Phenylenediacetonitrile, Bimetallic complexesw, Trimetallic complexes, Nitrile-bridged complexes, Seven-coordinate complexes, 147
Halogenated carborane anions
Cobalt bis(dicarbollide), Boron, Carborane, Halogenation, 1777
Halogenation
Halogenated carborane anions, Cobalt bis(dicarbollide), Boron, Carborane, 1777
Halogenation
Iridium, Acetylacetonates, 1097
Halogen exchange reactions
Iron carbonyl halides, NMR, XAFS spectroscopy, Matrix isolation, 1493
Hammett parameters
Substituted cobalt phthalocyanines, Redox properties, Frontier orbitals, Disulfide reduction, 2255
Hantzsch synthesis
Molybdenum, Oxocluster complexes, Crystal structures, Hexanuclear molybdenum(V) complexes, 1471
H-bonding
Calcium, Inorganic Polymers, Alkaline Earth, X-ray structure, 1783
Heck reactions
Palladium, Phosphane, Sulfane, Ligands, Mechanism, 517
Helical structures
Supramolecular chemistry, Transition metals, X-ray crystal structures, 23
Hemoprotein models
Porphyrins, Chiral catalysts, Epoxidation, Olefins, 581
Heptacoordinate complexes
Heterocyclic bis(thiosemicarbazone), Organotin(IV) complexes, Binuclear zinc complexes, 841
Heptadentate ligands
Cadmium(II) complexes, Schiff-base ligands, Symmetrical complexes, Asymmetrical complexes, 1633
HETCOR
Zn(II) complexes, 1,2,4-Triazolo-[1,5α]-pyrimidine, ^{15}N NMR, CPMAS, 965
Heterobimetallic diethanolaminates
Alkaline earth metals, Homobimetallic diethanolaminates, 77
Heterobimetallic titanium–copper systems
α-Acetylenic alcohols, Isomerization, Rearrangement, 1693
Hetero-bridged complexes
Dinucleating alkoxide ligands, Copper(II) complexes, X-ray structures, Magnetism, Magneto-structural trends, 1429
Heterocyclic bis(thiosemicarbazone)
Heptacoordinate complexes, Organotin(IV) complexes, Binuclear zinc complexes, 841
Heterocyclic compounds
Thioacetal, Titanocene(II), Ring-closing metathesis, Intramolecular carbonyl olefination, Cycloalkenes, 593
Heterocyclic thione complexes
Copper(I) bromide complexes, Diphosphine complexes, Dinuclear complexes, Crystal structures, 1615
Heterocyclic thiones
Bisphosphines, Palladium(II) complexes, Platinum(II) complexes, Pyridyl, 899
Heterocycloaddition trap
Nitrosobenzene cycloaddition, Regioselectivity, Organoiron compounds, Decomplexation, Alkaloid synthesis, 569
Heterodifunctional ligands
Palladium(II) complexes, Platinum(II) complexes, Chloride metathesis, X-ray crystallography, 695
Heterodinuclear complexes
Electrochemical studies, Homodinuclear complexes, Luminescence properties, Osmium(II) complexes, Ruthenium(II) complexes, Syntheses, 1233
Heterometallic aryloxides
Lithium niobate, Monomeric compounds, Niobium, Percursors, 1037
Heterometallics
Bis(η-cyclopentadienyl)titanium(IV), Crystal structures, Diphenylphosphinoacetate, Nicotinate, Thiophenoxyacetate, 757
Heteronuclear catalysts
Immobilization, Nanoparticles, Sol–gel matrices, 509
Heteronuclear multiple bond coherence
Bridged structures, Crystal structures, *N*-Tosyl ligands, Zinc porphyrin complexes, 413
Heteropolyoxometalate
Vanadium, Molybdenum, IR spectroscopy, UV–Vis spectroscopy, EPR spectroscopy, 1917
Heteroscorpionate tris(3-*R*-pyrazolyl)borate cobalt(II) complexes
Structures, NMR, 2119
Hexamethyleneimine
Thiosemicarbazone, Isatin, Crystal structures, Zinc, Lead, Metal(II) complexes, 1255
Hexanuclear clusters
Metallamacrocycles, Manganese complexes, Pentadentate ligands, Hydrophobic aliphatic tripled tails, 1985

Hexanuclear molybdenum(V) complexes
Molybdenum, Oxocluster complexes, Hantzsch synthesis, Crystal structures, 1471
Hg(II)
Cd(II), tachpyr, Torsion angles, Twist angles, Zn(II), 1155
High acidity
Polyoxometalate, Oxyhalide, Molybdenum, X-ray structure, 43
High-charge salts
3:3 Electrolytes, Activity coefficients, Electrolytic solutions, High valency electrolytes, Mixed electrolytes, 2493
High valency electrolytes
3:3 Electrolytes, Activity coefficients, Electrolytic solutions, High-charge salts, Mixed electrolytes, 2493
Histamine
Electron spin resonance, Copper(II) complexes, Coordination modes, L-Histidine, Isomerism, 1123
Histidyl-lysine
Copper-dipeptide complexes, Glycyl-lysine, Alanyl-lysine, β-alanyl-lysine, 2409
^{1}H NMR spectroscopy
Diazafluorenone aroylhydrazone, Transition metal aroylhydrazone complexes, Crystal structures, Enolization, IR, 1295
Homoazacalixarenes
Ytterbium(III), Lanthanides, Calixarenes, Crystal structure, 2673
Homobimetallic diethanolaminates
Alkaline earth metals, Heterobimetallic diethanolaminates, 77
Homodinuclear complexes
Electrochemical studies, Heterodinuclear complexes, Luminescence properties, Osmium(II) complexes, Ruthenium(II) complexes, Syntheses, 1233
Homogeneous and heterogeneous
Aromatic amines, Amberlite anion-exchange resin, Oxalate anions, Metal–oxalate complexes, Oxidation, 1317
Homogeneous catalysis
Carbon dioxide, Dimethyl carbonate, Mechanism, Supercritical conditions, 573
Homoleptic silyl complexes
Arsenic, Antimony, 1639
Host–guest chemistry
Mercury, Clusters, Thiocyanante, 871
Hush theory
Iron complexes, Mixed valence, TCNE complexes, TCNQ complexes, 137
Hybrid copper(II) compounds
Dicarboxylate-based compounds, Magnetic properties, Layered magnets, Long-range ferromagnetism, 259
Hybrid materials
Sol-gel, NMR, Siloxane, Silicon-29, Oxygen-17, 315
Hydrazido
Molybdenum, Diazenido, Dialkyldithiocarbamato, Hydrazines, 2327
Hydrazines
Molybdenum, Hydrazido, Diazenido, Dialkyldithiocarbamato, 2327
Hydrazonato compounds of oxovanadium(V)
Alkoxo compounds of oxovanadium(V), Crystal structure of compounds of oxovanadium(V), Oxovanadium(V) dimers, Reactivity of bis(β-dionato)oxovanadium(IV) chelates, Hydrazonato tridentate Schiff base ligands, 2003
Hydrazonato tridentate Schiff base ligands
Alkoxo compounds of oxovanadium(V), Crystal structure of compounds of oxovanadium(V), Hydrazonato compounds of oxovanadium(V), Oxovanadium(V) dimers, Reactivity of bis(β-dionato)-oxovanadium(IV) chelates, 2003
Hydrazone
Lanthanide, Erbium complex, 2629
Hydrazone
Rare earth complex, Crystal structure, Antitumour activity, 2599
Hydroborates
Lithium, Titanium(IV), Bonding, Crystal structures, 1579
Hydroboration
Allylic alkylation, Axially chiral phosphinamine, Quinazolines, 541
Hydroboration
Phosphine, Alkene, Polymerization, Copper(I) complexes, 1271
Hydroboration
Polysilazanes, Precursors, Vinylsilanes, Chloroboranes, 323
Hydroformylation
Organocopper reagents, Catalysis, Asymmetric synthesis, Domino reactions, 513
Hydrogenation
Pyriding N-oxides, Metal complexes, Structures, 835
Hydrogenation
Titanium, Tantalum, Nobium, Aryloxide, Bisphenol, 35
Hydrogen bonded helical structures
Oxovanadium(V) alkoxides, Mononuclear chelation, Crystal structures, 931
Hydrogen bonding
Complexes, Platinum, Sulfimides, 2077
Hydrogen bonding
Phosphoranes, Pentacoordination, X-ray structure, 63
Hydrolysis
Binucleating hexa-aza macrocycle, Copper(II), Nickel(II), Cobalt(II), Zinc(II), Crystal structures, Phosphotriester, 1485
Hydrolysis
Palladium(II) complexes, Catalysts, Peptides, 959
Hydrolysis
Yttrium, Rare earth elements, Enthalpy, Ionic strength, Spectrophotometry, 99
Hydrophobic aliphatic tripled tails
Metallamacrocycles, Hexanuclear clusters, Manganese complexes, Pentadentate ligands, 1985
Hydrophobic cavities
Catechols, Macrocyclic ligands, Oxovanadium complexes, ESR parameters, Distorted square-pyramid, 1167
Hydrosilation
Dendrimers, Carbosilanes, Platinum catalysts, 1031
Hydrosilylation
Alkenylsilanes, $RhI(PPh_3)_3$, Polyaddition, Stereodivergent, 567
Hydrothermal synthesis
Crystal structures, Metavanadate complexes, Nickel complexes, Copper complexes, Magnetic properties, 2521
Hydrotris(pyrazolyl)borate ligands
Europium compounds, Luminescence studies, X-ray crystal structures, 1707
Hydroxamic acid
Mixed-ligand complexes, Solution equilibrium, Copper(II), nickel(II) and zinc(II) complexes, 1727
Hydroxo
Amido, Diimine, Dimer, Palladium, Platinum, 155
Hydroxo complexes
Palladium, Pyrazolylalkane complexes, Crystal structures, 1395
2-Hydroxyacetophenone
Cobalt, Azide, Thiocyanate, Crystal structure, 2707
3-Hydroxy-4-pyranone
Zinc complexes, Lead(II) complexes, Maltol, 3-Hydroxy-4-pyridinone, 1,2-Dimethyl, Crystal structures, 129
3-Hydroxy-4-pyridinone
Zinc complexes, Lead(II) complexes, Maltol, 3-Hydroxy-4-pyranone, 1,2-Dimethyl, Crystal structures, 129
Hypophospite complexes
Infrared spectroscopy, Raman spectroscopy, Electronic absorption spectroscopy, Crystal structures, Cooperative vibronic transitions, Two-centre transitions, 863

II/VI Semiconductors
Dithiophosphinates, Low-pressure metal organic chemical vapour deposition, 211
Imidate
Copper(II), Azomethine, Crystal structures, 2713
Imidazole-carboxylate chelating ligands
Polynuclear manganese-carboxylate clusters, Paramagnetic NMR, 2111
Imidazole derivatives
Transition metal complexes, Crystal structure, Absorption spectra, Stability constants, 2183
Imidazole ligands
Cobalt(II), Cyanamidonitrate, Electronic spectra, IR spectra, Nickel(II), X-ray crystallography, 1021
Imidazole
N-carbamoylmethyl-iminodiacetic acid, *N*-(2-amidomethyl)-iminodiacetic acid, *N*-(2-acetamido)-iminodiacetic acid, Mixed-ligand complexes, Aqua(imidazole)(*N* - carbamoylmethyl - iminodiacetato)nickel(II) sesquihydrate, Aqua(imidazole)(*N* - carbamoylmethyl - iminodiacetato)cobalt(II) sesquihydrate, Molecular and crystal structures, Magnetic, spectral and thermal properties, 2473

Imidazole
Schiff base, Silver complexes, Crystal structures, 2237
Imido complexes
Rhenium, Nitrido complexes, EPR spectroscopy, X-ray structures, 1741
Immobilization
Ethylenimine, 3-Mercaptopropyltrimethoxysilane, Silica gels, 367
Immobilization
Heteronuclear catalysts, Nanoparticles, Sol–gel matrices, 509
Impedance spectroscopy
Polymeric metallophthalocyanines, Modified electrodes, Electrooxidation of hydrazine, Poly(cobalt–tetraaminophthalocyanine), 2303
Inclusion compounds
Deoxycholic acid, Ferrocene derivatives, Molecular motion, ^{57}Fe Mössbauer spectroscopy, Powder X-ray diffraction patterns, 205
Indenyl
Planar chiral, Structure, Yttrium, Lanthanum, Tetrahydroborate, 1955
Indium
Allylation, Aqueous reactions, Esters, Indium compounds, Pyridines, 549
Indium compounds
Allylation, Aqueous reactions, Esters, Indium, Pyridines, 549
Indium
Cycloadditions, Dienes, Magnesium, Trienes, 533
Indium tin oxide
Surface modification, Alkoxides, Interfaces, 505
Infrared
Dithiocarboxylate, Vanadium(IV), Magnetism, EPR, Coordination., 2155
Infrared spectra
N-salicylidenearoylhydrazine copper(II) complexes, Copper(II) imidazole ternary complexes, Copper(II) imidazolate ternary complexes, X-ray crystal structures, Molecular structures, Magnetic properties, 1181
Infrared spectra
N-salicylidenearoylhydrazines, Copper(II) complexes, X-ray crystal structures, Molecular structures, Magnetic properties, 949
Infrared spectroscopy
Raman spectroscopy, Electronic absorption spectroscopy, Crystal structures, Hypophospite complexes, Cooperative vibronic transitions, Two-centre transitions, 863
Inorganic Polymers
Calcium, H-bonding, Alkaline Earth, X-ray structure, 1783
Inorganic polymers
Ferrocenophane, Silanol, Mössbauer spectroscopy, Ring-opening polymerization, 275
Insertion reactions
Platinum(II) complexes, Platinum–tin bimetallics, 2,3,5,6-Tetrakis(α-pyridyl)-pyrazine, 739
Insertions
Additions, Alkylation, Nucleophilic, Schiff bases, Titanium, 177
In situ X-ray diffraction
Intercalation, Layered compounds, Solid state, Synchrotron radiation, 297
Insulin-mimetics
Biospeciation, Al(III) complexes, VO(IV) complexes, 2389
Intercalation compounds
Aniline polymerization, Copper phosphonates, 765
Intercalation
In situ X-ray diffraction, Layered compounds, Solid state, Synchrotron radiation, 297
Interfaces
Indium tin oxide, Surface modification, Alkoxides, 505
Interstitial group
Dodecanuclear, Mo–Cu–S cage cluster, 2189
Intramolecular bonds
C–H activation, Titanium, Metallacycles, Allenes, Carbometalation, 879
Intramolecular carbonyl olefination
Thioacetal, Titanocene(II), Ring-closing metathesis, Cycloalkenes, Heterocyclic compounds, 593
Intramolecular electron transfer
Mixed-valence complexes, Ruthenium–edta complexes, Ferricyanide, Cyano-bridged complexes, 1339
Intramolecular hydrogen bonding
Ferrocenylporphyrin, π-Conjugation, Electrochemical communication, NH tautomerism, 1961
Ionic
Cryoscopy, Cyanocuprates, Reactivity, Structures, 553
Ionic strength
Yttrium, Rare earth elements, Hydrolysis, Enthalpy, Spectrophotometry, 99
Ionization constants
meso-2,3-Dimercaptosuccinic acid, Potentiometry, UV–Vis spectroscopy, Formation constants, Kinetic measurements, 2435
IR
Diazafluorenone aroylhydrazone, Transition metal aroylhydrazone complexes, Crystal structures, Enolization, ^{1}H NMR spectroscopy, 1295
Iridium
Acetylacetonates, Halogenation, 1097
Iridium
π-Allyl complexes, Allylic substitutions, Regioselectivity, Stereoselectivity, Phosphites, 557
Iridium
Ruthenium, Gold, Electron-rich, Cluster, Phosphido-bridged, Crystal structures, 2593
Iron carbonyl halides
NMR, XAFS spectroscopy, Halogen exchange reactions, Matrix isolation, 1493
Iron carbonyl
Solvothermal synthesis, Polytelluride, Iron telluride, Iron cluster, Carbonyl clusters, 1995
Iron cluster
Solvothermal synthesis, Polytelluride, Iron telluride, Iron carbonyl, Carbonyl clusters, 1995
Iron complexes
Hush theory, Mixed valence, TCNE complexes, TCNQ complexes, 137
Iron complexes
Molecular magnets, Cyano-bridged heteropolynuclear complexes, Nickel complexes, Ferromagnetic coupling, 1967
Iron complexes
Thiosemicarbazones, Electrochemistry, EPR of iron complexes, Nickel complexes, Cobalt complexes, 2059
Iron(II) complexes
Crystal structures, Cobalt(II) complexes, Octadentate ligands, 431
Iron(III)
Chromium(III), DTPA, Complexes, Thermal properties, Thermodynamics, 2421
Iron(III)
Ciprofloxacin, Solution equilibria, Surfactants, 1085
Iron(II)
Nickel(II), Crystal structures, Electronic spectra, 1333
Iron
Phthalocyanine, Dopamine, Serotonin, Coordination, 1355
Iron
Selenium, Sulfur, Synthesis, Reaction, 713
Iron telluride
Solvothermal synthesis, Polytelluride, Iron cluster, Iron carbonyl, Carbonyl clusters, 1995
Iron
Thiolate-bridged complexes, Mixed-valence, Electron-transfer, 2679
IR spectra
Cobalt(II), Cyanamidonitrate, Electronic spectra, Imidazole ligands, Nickel(II), X-ray crystallography, 1021
IR spectra
Copper–iron complexes, Cyano-bridge, Crystal structures, 1935
IR spectra
Vanadium complexes, Quinic acid complexes, Raman spectra, Thermal behavior, Potentiometric titrations, 2613
IR spectroscopy
Vanadium, Molybdenum, Heteropolyoxometalate, UV–Vis spectroscopy, EPR spectroscopy, 1917
Isatin
Thiosemicarbazone, Crystal structures, Zinc, Lead, Hexamethyleneimine, Metal(II) complexes, 1255
Isomerism
Electron spin resonance, Copper(II) complexes, Coordination modes, Histamine, L-Histidine, 1123

Isomerism
ESR, Copper(II) complexes, Glycyl-L-histidine, Formation constants, Coordination modes, 2049
Isomerism
Palladium, Platinum, Nitrite, Diphosphines, Fluxionality, 1329
Isomerization
α-Acetylenic alcohols, Rearrangement, Heterobimetallic titanium–copper systems, 1693
Isomerization
Crystal structures, *Fac* isomers, Lanthanide chloride complexes, Octahedral complexes, 199
Isomerization
Ruthenium, Polypyridine, Terpyridine, Electrocatalytic oxidation, Alcohol oxidation, 1049

Kainoids
Boronic esters, Asymmetric synthesis, Pyrrolidine, 587
Ketoconazole
Ruthenium, Clotrimazole, Paramagnetic, Metal complexes, *Trypanosoma cruzi*, Chagas, 2319
α-Ketoglutaric acid
Zinc complexes, Cobalt complex, Thiosemicarbazones, Crystal structures, Spectroscopic properties, 1895
Kinetic control
Monophasic hybrid materials, Silsesquioxane gels, Sol–gel polymerization, 307
Kinetic measurements
meso-2,3-Dimercaptosuccinic acid, Potentiometry, UV–Vis spectroscopy, Formation constants, Ionization constants, 2435
Kinetics
Dioxygen carriers, Cobalt, Dinuclear complexes, Dinucleating ligands, Polyamines, Dioxygen binding, 2447
Kinetics
Manganese(IV), Ascorbic acid, Electroprotic reactions, 1213
Kinetics
Me_2Octaen, Polyamines, Nickel(II), Equilibria, Stopped-flow, 2507
Kinetics
Oxidation, Catalysis, 3,5-Di-*tert*-butylcatechol, Copper binuclear complexes, 2367
Kinetics
Substitution, Mechanism, *cis*-Diaquabis(2,2′-bipirydyl)chromium(III), Octacyanomolybdate(IV), Octacyanotungstate(IV), 2225

Lanthanide
Carbacylamidophosphate, NMR, X-ray data, 2203
Lanthanide chloride complexes
Crystal structures, *Fac* isomers, Isomerization, Octahedral complexes, 199
Lanthanide complexes
Crystal structures, Picrate, 4-Methylmorpholine, *N*-Oxide, TG, DSC, 2313
Lanthanide complexes
Macrocycles, Chiral complexes, NMR of paramagnetic compounds, 465
Lanthanide complex
Tridentate chelate, Europium(III) chloride, 2135
Lanthanide
Erbium complex, Hydrazone, 2629
Lanthanide picrate
PBD, Fluorescence, Crystal structures, 779
Lanthanides
Contrast agents, Crystal structures, Diethylenetriaminepentaacetate, Neodymium, 771
Lanthanides(III)
Silver(I), Diethylenetriamine, *N*,*N*-dimethylformamide, Complexes, Thermodynamics, 2427
Lanthanides
Phosphine oxides, X-ray structures, 2697
Lanthanides
Phthalocyanines, Naphthalocyanines, Porphyrins, Raman, Sandwich complexes, 1381
Lanthanides
Ytterbium(III), Calixarenes, Homoazacalixarenes, Crystal structure, 2673
Lanthanum
Planar chiral, Structure, Indenyl, Yttrium, Tetrahydroborate, 1955
Layered compounds
In situ X-ray diffraction, Intercalation, Solid state, Synchrotron radiation, 297
Layered magnets
Hybrid copper(II) compounds, Dicarboxylate-based compounds, Magnetic properties, Long-range ferromagnetism, 259
Layer-like packing
Mo–S clusters, Crystal structures, Electronic structures, 733
LD-LISC effect
Schiff bases, Cobalt complexes, Spin crossover, Photosensitive ligands, 1643
Lead(II)
Aspartate, Structures, 649
Lead(II) complexes
Zinc complexes, Maltol, 3-Hydroxy-4-pyranone, 3-Hydroxy-4-pyridinone, 1,2-Dimethyl, Crystal structures, 129
Lead scandium tantalate
Metal–organic chemical vapour deposition, Precursors, Ferroelectric oxides, 351
Lead
Thiosemicarbazone, Isatin, Crystal structures, Zinc, Hexamethyleneimine, Metal(II) complexes, 1255
Lewis acid
α-Aminoacylsilanes, β-Amino alcohols, Silylcupration, Statine analogues, 529
L-Histidine
Electron spin resonance, Copper(II) complexes, Coordination modes, Histamine, Isomerism, 1123
Ligands
Heck reactions, Palladium, Phosphane, Sulfane, Mechanism, 517
Liposomes
Calcium phosphates, Biomimetics, Biomineralization, 357
Liquid clathrates
15-Crown-5 complexes, X-ray crystallography, Oxonium ion, 85
Liquid crystals
Discotic complexes, Columnar complexes, π-acceptors, Dithiolene, 267
Lithium
Hydroborates, Titanium(IV), Bonding, Crystal structures, 1579
Lithium niobate
Heterometallic aryloxides, Monomeric compounds, Niobium, Percursors, 1037
Lithography
Photochemistry, Surface chemistry, Photochemical metal organic deposition, Gold, 343
Long-range ferromagnetism
Hybrid copper(II) compounds, Dicarboxylate-based compounds, Magnetic properties, Layered magnets, 259
Low-pressure metal organic chemical vapour deposition
Dithiophosphinates, II/VI Semiconductors, 211
Luminescence properties
Electrochemical studies, Heterodinuclear complexes, Homodinuclear complexes, Osmium(II) complexes, Ruthenium(II) complexes, Syntheses, 1233
Luminescence studies
Europium compounds, Hydrotris(pyrazolyl)borate ligands, X-ray crystal structures, 1707

Macrocycles
Lanthanide complexes, Chiral complexes, NMR of paramagnetic compounds, 465
Macrocycle
Sol–gel, Aggregation, Tetrasulfophthalocyanines, Monolith, Silica, 2383
Macrocycles
Synthesis, Complexes, Equilibria, 2501
Macrocycle
Thiolate, Electrochemistry, Crystal structures, 1887
Macrocyclic ligands
Asorption spectra, Copper(III), Nickel(III), Dioxotetraamines, 2533
Macrocyclic ligands
Catechols, Oxovanadium complexes, ESR parameters, Distorted square-pyramid, Hydrophobic cavities, 1167
Macrocyclic ligands
Naphthylmethyl fluorescent groups, Aza–oxa crowns, 1867
Macrocyclic ligands
Thiosemicarbazones, Electrochemistry, Copper complexes, Dithio-Schiff base complexes, 441
Macrocyclic polyamine ligand
Crystal structures, Synthesis, Manganese complexes, Octa- and hepta-coordination, 2095

Macrocyclic polyether 18-crown-6
Acetonitrile, Alkaline earth metal ions, Transition metal ions, 1681
Magnesia
Dolomite, Crystallite size, Degree of agglomeration, X-ray diffraction, SEM, 2345
Magnesium
Aryloxide, Structure, Adduct, 2557
Magnesium
Cycloadditions, Dienes, Indium, Trienes, 533
Magnetic and spectral properties
N-(Carbamoylmethyl)iminodiacetic acid, *N*-(2-Amidomethyl)-iminodiacetic acid, *N*-(2-Acetamide)-iminodiacetic acid, *cis*-Diaqua(*N* - carbamoylmethyl - iminodiacetato)nickel(II), Molecular and crystal structure, Thermal stability, 2463
Magnetic measurements
Nickel(II), Mononuclear compounds, Crystal structures, Nitrito ligands, 225
Magnetic properties
Alternating chain, Dimer complex, Crystal structure, 1461
Magnetic properties
Azido-bridged nickel(II) compounds, Crystal structures, 1575
Magnetic properties
Binuclear Cu(II) complexes, Electrochemistry, ESR, 1769
Magnetic properties
Binuclear nickel(II) complex, Binuclear manganese(II) complex, Crystal structures, Tris(6-methyl-2-pyridylmethyl)amine, 1559
Magnetic properties
Carboxylato-bridged copper(II) complex, Crystal structure, 2529
Magnetic properties
Copper(I,II) complexes, α,β-Unsaturated carboxylates, Triphenylphosphine, Crystal structures, 891
Magnetic properties
Crystal structures, Cu dimers, Di-(2-pyridyl)ketone, Ferromagnetic dimers, Spin triplet, 1005
Magnetic properties
Crystal structures, Dinuclear complexes, Manganese, Cobalt, Nickel, 93
Magnetic properties
Crystal structures, Metavanadate complexes, Nickel complexes, Copper complexes, Hydrothermal synthesis, 2521
Magnetic properties
Dimers, Geometrical distortions, Magnetostructural correlations, 2483
Magnetic properties
Hybrid copper(II) compounds, Dicarboxylate-based compounds, Layered magnets, Long-range ferromagnetism, 259
Magnetic properties
N-salicylidenearoylhydrazine copper(II) complexes, Copper(II) imidazole ternary complexes, Copper(II) imidazolate ternary complexes, X-ray crystal structures, Molecular structures, Infrared spectra, 1181
Magnetic properties
N-salicylidenearoylhydrazines, Copper(II) complexes, X-ray crystal structures, Molecular structures, Infrared spectra, 949
Magnetic properties
1,3-propylenediaminetetraacetate, Cu(II) complexes, Mn(II) complexes, Crystal structures, Thermal properties, 1175
Magnetic, spectral and thermal properties
N-carbamoylmethyl-iminodiacetic acid, *N*-(2-amidomethyl)-iminodiacetic acid, *N*-(2-acetamido)-iminodiacetic acid, Imidazole, Mixed-ligand complexes, Aqua(imidazole)(*N* - carbamoylmethyl-iminodiacetato)nickel(II) sesquihydrate, Aqua(imidazole)(*N* - carbamoylmethyl-iminodiacetato)cobalt(II) sesquihydrate, Molecular and crystal structures, 2473
Magnetic susceptibility
Pyridine *N*-oxide ligands, Cobalt(II) complexes, Zinc(II) complexes, X-ray structures, 2195
Magnetism
Copper(II) complexes, Deprotonated pyridine-2,6-dicarboxamide ligands, Singly hydroxo-bridged, Crystal structures, 1423
Magnetism
Crystal structures, Binuclear copper compounds, Oxalato-bridged compounds, 1105
Magnetism
Dinucleating alkoxide ligands, Copper(II) complexes, X-ray structures, Hetero-bridged complexes, Magneto-structural trends, 1429
Magnetism
Dithiocarboxylate, Vanadium(IV), EPR, Infrared, Coordination, 2155
Magnetochemical data
Effortil, Cu(II) complexes, Structures, Stability constants, EPR, 1843
Magnetostructural correlations
Magnetic properties, Dimers, Geometrical distortions, 2483
Magneto-structural trends
Dinucleating alkoxide ligands, Copper(II) complexes, X-ray structures, Hetero-bridged complexes, Magnetism, 1429
MALDI
Trirhenium(III) clusters, Rhenium clusters, Acetamidate, Dimolybdenum(II), Mass spectroscopy, 1245
Maltol
Zinc complexes, Lead(II) complexes, 3-Hydroxy-4-pyranone, 3-Hydroxy-4-pyridinone, 1,2-Dimethyl, Crystal structures, 129
Manganese
Chromium, Salen, Catalysis, Enantioselection, Nozaki–Hiyama–Kishi reaction, 537
Manganese complexes
Crystal structures, Synthesis, Macrocyclic polyamine ligand, Octa- and hepta-coordination, 2095
Manganese complexes
Metallamacrocycles, Hexanuclear clusters, Pentadentate ligands, Hydrophobic aliphatic tripled tails, 1985
Manganese complexes
Schiff bases, Manganoenzymes, Photolysis, Catalase, Dioxygen, 47
Manganese
Crystal structures, Magnetic properties, Dinuclear complexes, Cobalt, Nickel, 93
Manganese(II) complexes
Fumaric acid, Crystal structures, Fungitoxic activity, 1205
Manganese(II)
Potentiometry, Equilibria, Stability constants, Cobalt(II), Nickel(II) complexes, Aminopolyphosphonates, UV–VIS spectra, 2083
Manganese(IV)
Kinetics, Ascorbic acid, Electroprotic reactions, 1213
Manganoenzymes
Manganese complexes, Schiff bases, Photolysis, Catalase, Dioxygen, 47
Mass spectroscopy
Trirhenium(III) clusters, Rhenium clusters, Acetamidate, Dimolybdenum(II), MALDI, 1245
Matrix isolation
Iron carbonyl halides, NMR, XAFS spectroscopy, Halogen exchange reactions, 1493
Mechanism
Carbon dioxide, Dimethyl carbonate, Homogeneous catalysis, Supercritical conditions, 573
Mechanism
Heck reactions, Palladium, Phosphane, Sulfane, Ligands, 517
Mechanism
Kinetics, Substitution, *cis*-Diaquabis(2,2′-bipirydyl)chromium(III), Octacyanomolybdate(IV), Octacyanotungstate(IV), 2225
11-Membered metallocyclic ring
Synchrotron radiation, Metallocalix[6]arene, 2657
Me_2Octaen
Polyamines, Nickel(II), Equilibria, Kinetics, Stopped-flow, 2507
3-Mercaptopropyltrimethoxysilane
Ethylenimine, Immobilization, Silica gels, 367
Mercury
Clusters, Thiocyanante, Host–guest chemistry, 871
Mercury complexes
Cadmium complexes, Sulfamides, X-ray structure, Zinc complexes, 991
Mercury(II) complexes
Triphenylphosphine, Benzothiazole-2-thione, pyrimidine-2-thione, Crystal structures, 2231
Mercury(II) halides
Phosphine complexes, Crystal structures, 1719

Mercury(II)
Trichlorovinyl, Crystal structures, Complexes, Bidentate ligands, 2539
Mercury(II)
Zinc(II), Cadmium(II), Tris(2-benzimidazolylmethyl)amine, X-ray diffraction structures, NMR data, 1479
meso-2,3-dimercaptosuccinic acid
Multinuclear NMR, Tungsten, 193
meso-2,3-Dimercaptosuccinic acid
Potentiometry, UV–Vis spectroscopy, Formation constants, Ionization constants, Kinetic measurements, 2435
Mesophase materials
CdS nanoclusters, Ruthenium(II) polypyridyls, Functionalized nanoclusters, Molecular devices, 331
Metal clusters
Rhenium, Sulfur, Selenium, Tellurium, Crystal structures, 437
Metal complexes
Pyriding N-oxides, Hydrogenation, Structures, 835
Metal complexes
Ruthenium, Clotrimazole, Ketoconazole, Paramagnetic, *Trypanosoma cruzi*, Chagas, 2319
Metal complexes
Sulfamethizole, Crystal structures, Spectroscopic properties, 1859
Metal(II) complexes
Thiosemicarbazone, Isatin, Crystal structures, Zinc, Lead, Hexamethyleneimine, 1255
Metal(II) compounds
Diclofenac, Spectroscopic properties, Thermal properties, 2515
Metallacycles
C–H activation, Intramolecular bonds, Titanium, Allenes, Carbometalation, 879
Metallamacrocycles
Hexanuclear clusters, Manganese complexes, Pentadentate ligands, Hydrophobic aliphatic tripled tails, 1985
Metallation
Osmium, X-ray structures, 1081
Metallocalix[6]arene
11-Membered metallocyclic ring, Synchrotron radiation, 2657
Metallocycles
Palladium(II) complexes, Aminophosphate complexes, Spectroscopy, Antitumour activity, 937
Metallomesogens
Rhenium, Nematic phases, Chiral nematic phases, 249
Metal–organic chemical vapour deposition
Precursors, Lead scandium tantalate, Ferroelectric oxides, 351
Metal–oxalate complexes
Aromatic amines, Amberlite anion-exchange resin, Oxalate anions, Oxidation, Homogeneous and heterogeneous, 1317
Metathesis
Antimonides, Arsenides, Phosphides, 829
Metavanadate complexes
Crystal structures, Nickel complexes, Copper complexes, Hydrothermal synthesis, Magnetic properties, 2521
Methanolysis
Amine oxide, Rhenium, Osmium, Carbonyl, Methylcarbonate, 641
Methylaluminoxane (MAO)
Palladium(II) complexes, Mixed donor ligands, *Trans*-influence, X-ray crystallography, Norbornene, Polymerization, 1601
Methylcarbonate
Amine oxide, Methanolysis, Rhenium, Osmium, Carbonyl, 641
1-Methyl-2-ethyl-3-hydroxy-4-pyridinonate
Crystal structures, 2-Ethyl-3-hydroxy-4-pyranonate, Ethylmaltol, Tin(IV), Titanium(IV), 399
4-Methylmorpholine
Crystal structures, Lanthanide complexes, Picrate, *N*-Oxide, TG, DSC, 2313
Methyl nicotinates
Copper(I) thiocyanate complexes, Ethyl nicotinates, Ethyl isonicotinate complexes, Crystal structures, Trigonal planar anions, 615
3-methylpiperidine
Platinum complexes, Dicarboxylates, Synthesis, Crystal structures, 983
Mixed donor ligands
Palladium(II) complexes, *Trans*-influence, X-ray crystallography, Methylaluminoxane (MAO), Norbornene, Polymerization, 1601
Mixed electrolytes
3:3 Electrolytes, Activity coefficients, Electrolytic solutions, High-charge salts, High valency electrolytes, 2493
Mixed-ligand complexes
N-carbamoylmethyl-iminodiacetic acid, *N*-(2-amidomethyl)-iminodiacetic acid, *N*-(2-acetamido)-iminodiacetic acid, Imidazole, Aqua(imidazole)(*N*-carbamoylmethyl-iminodiacetato)nickel(II) sesquihydrate, Aqua(imidazole)(*N*-carbamoylmethyl - iminodiacetato)cobalt(II) sesquihydrate, Molecular and crystal structures, Magnetic, spectral and thermal properties, 2473
Mixed-ligand complexes
Solution equilibrium, Hydroxamic acid, Copper(II), nickel(II) and zinc(II) complexes, 1727
Mixed-valence complexes
Ruthenium–edta complexes, Ferricyanide, Cyanobridged complexes, Intramolecular electron transfer, 1339
Mixed valence
Equilibrium, Copper, Disproportionation, Temperature effects, 2289
Mixed valence
Hush theory, Iron complexes, TCNE complexes, TCNQ complexes, 137
Mixed-valence
Thiolate-bridged complexes, Electron-transfer, Iron, 2679
Mn(II) complexes
1,3-propylenediaminetetraacetate, Cu(II) complexes, Crystal structures, Thermal properties, Magnetic properties, 1175
MO calculations
Ruthenium, Phenanthroline, *Cis–trans*, Barriers, Field strength, 2297
Mo–Cu–S cage cluster
Dodecanuclear, Interstitial group, 2189
Model of metal–guanine interaction
Dialkoxo-bridged binuclear Cu(II) complexes, Single crystal structures, Thermal decompostion, Theophylline, Diethanolamine(2,2′-iminodiethanol), 457
Modified electrodes
Polymeric metallophthalocyanines, Electrooxidation of hydrazine, Poly(cobalt–tetraaminophthalocyanine), Impedance spectroscopy, 2303
Molecular and crystal structure
N-(Carbamoylmethyl)iminodiacetic acid, *N*-(2-Amidomethyl)-iminodiacetic acid, *N*-(2-Acetamide)-iminodiacetic acid, *cis*-Diaqua(*N* - carbamoylmethyl - iminodiacetato)nickel(II), Magnetic and spectral properties, Thermal stability, 2463
Molecular and crystal structures
N-carbamoylmethyl-iminodiacetic acid, *N*-(2-amidomethyl)-iminodiacetic acid, *N*-(2-acetamido)-iminodiacetic acid, Imidazole, Mixed-ligand complexes, Aqua(imidazole)(*N* - carbamoylmethyl - iminodiacetato)nickel(II) sesquihydrate, Aqua(imidazole)(*N* - carbamoylmethyl - iminodiacetato)cobalt(II) sesquihydrate, Magnetic, spectral and thermal properties, 2473
Molecular devices
CdS nanoclusters, Ruthenium(II) polypyridyls, Functionalized nanoclusters, Mesophase materials, 331
Molecular magnets
Cyano-bridged heteropolynuclear complexes, Iron complexes, Nickel complexes, Ferromagnetic coupling, 1967
Molecular motion
Deoxycholic acid, Ferrocene derivatives, Inclusion compounds, ^{57}Fe Mössbauer spectroscopy, Powder X-ray diffraction patterns, 205
Molecular structures
N-salicylidenearoylhydrazine copper(II) complexes, Copper(II) imidazole ternary complexes, Copper(II) imidazolate ternary complexes, X-ray crystal structures, Magnetic properties, Infrared spectra, 1181
Molecular structures
N-salicylidenearoylhydrazines, Copper(II) complexes, X-ray crystal structures, Magnetic properties, Infrared spectra, 949
Molybdenum
Bridging ligands, Butadienyl, Chiral substituents, 791
Molybdenum complexes
Aerial oxidation of aldehydes, 1133
Molybdenum complexes
Cluster compounds, Tellurium-rich compounds, De-tellurium reaction, Crystal structures, 925

Molybdenum complexes
Tungsten complexes, Pyrazine complexes, Peroxo ligands, Crystal structures, 1503
Molybdenum
Hydrazido, Diazenido, Dialkyldithiocarbamato, Hydrazines, 2327
Molybdenum(II)
Tungsten(II), Crystal structures, *o*-Phenylenediacetonitrile, Bimetallic complexesw, Trimetallic complexes, Nitrile-bridged complexes, Seven-coordinate complexes, Halocarbonyls, 147
Molybdenum
Nitrides, Alkoxides, Synthesis, X-ray structures, NMR fluxionality, Pseudorotation, 1363
Molybdenum
Nitrosyl complex, Chromium, Carboxylate, DFT, 2565
Molybdenum
Oxocluster complexes, Hantzsch synthesis, Crystal structures, Hexanuclear molybdenum(V) complexes, 1471
Molybdenum–oxo complexes
Photochemistry, Photooxidation, Phosphines, Phosphine oxides, Crystal structures, 1437
Molybdenum
Polyoxometalate, Oxyhalide, X-ray structure, High acidity, 43
Molybdenum
Selenoether, Telluroether, Sulfur macrocycles, Chromium, Tungsten, 1373
Molybdenum
Tantalum, Trimetallic alkoxides, Crystal structures, 1791
Molybdenum
Vanadium, Heteropolyoxometalate, IR spectroscopy, UV–Vis spectroscopy, EPR spectroscopy, 1917
Molybenum(VI) cations
Equilibrium constants, Thermodynamic quantities, 907
Monolith
Sol–gel, Aggregation, Tetrasulfophthalocyanines, Macrocycle, Silica, 2383
Monomeric compounds
Heterometallic aryloxides, Lithium niobate, Niobium, Percursors, 1037
Mononuclear chelation
Oxovanadium(V) alkoxides, Crystal structures, Hydrogen bonded helical structures, 931
Mononuclear complexes
Electrochemical synthesis, Phenoxo bridges, Polyhydroxyl ligands, Polynuclear complexes, Schiff base ligands, 185
Mononuclear compounds
Nickel(II), Crystal structures, Nitrito ligands, Magnetic measurements, 225
Mononuclear
Tungsten pentacarbonyl complexes, 1,4-Bipyridine, 1,2-Bis(4-pyridyl)ethane, 1621
Monophasic hybrid materials
Silsesquioxane gels, Kinetic control, Sol–gel polymerization, 307
$Mo_2O_4^{2+}$ unit
Oxomolybdenum(V) compounds, Clusters, Pyridine, Alkyl-substituted pyridines, 1219
Mo–S clusters
Crystal structures, Electronic structures, Layer-like packing, 733
Mössbauer spectroscopy
Ferrocenophane, Inorganic polymers, Silanol, Ring-opening polymerization, 275
Mo(V, VI) compounds
Solvothermal synthesis, Crystal structures, Oxomolybdenum(V) coordination compounds, Alkyl-substituted pyridines, 1407
Multimetallic
Cobalt carbonyl complexes, Tungsten(II), Alkyne complexes, Chain triphos-bridged, 1585
Multinuclear NMR
meso-2,3-dimercaptosuccinic acid, Tungsten, 193

N-(2-Acetamide)-iminodiacetic acid
N-(Carbamoylmethyl)iminodiacetic acid, *N*-(2-Amidomethyl)-iminodiacetic acid, *cis*-Diaqua(*N*-carbamoylmethyl-iminodiacetato)nickel(II), Molecular and crystal structure, Magnetic and spectral properties, Thermal stability, 2463
N-(2-acetamido)-iminodiacetic acid
N-carbamoylmethyl-iminodiacetic acid, *N*-(2-amidomethyl)-iminodiacetic acid, Imidazole, Mixed-ligand complexes, Aqua(imidazole)(*N* - carbamoylmethyl-iminodiacetato)nickel(II) sesquihydrate, Aqua(imidazole)(*N* - carbamoylmethyl-iminodiacetato)cobalt(II) sesquihydrate, Molecular and crystal structures, Magnetic, spectral and thermal properties, 2473
N-(2-Amidomethyl)-iminodiacetic acid
N-(Carbamoylmethyl)iminodiacetic acid, *N*-(2-Acetamide)-iminodiacetic acid, *cis*-Diaqua(*N* - carbamoylmethyl-iminodiacetato)nickel(II), Molecular and crystal structure, Magnetic and spectral properties, Thermal stability, 2463
N-(2-amidomethyl)-iminodiacetic acid
N-carbamoylmethyl-iminodiacetic acid, *N*-(2-acetamido)-iminodiacetic acid, Imidazole, Mixed-ligand complexes, Aqua(imidazole)(*N* - carbamoylmethyl - iminodiacetato)nickel(II) sesquihydrate, Aqua(imidazole)(*N* - carbamoylmethyl - iminodiacetato)cobalt(II) sesquihydrate, Molecular and crystal structures, Magnetic, spectral and thermal properties, 2473
Nanoparticles
Heteronuclear catalysts, Immobilization, Sol–gel matrices, 509
Naphthalocyanines
Phthalocyanines, Porphyrins, Raman, Sandwich complexes, Lanthanides, 1381
Naphthylazoimidazoles
Platinum(II), PtN_4 coordination, Electrochemistry, X-ray structures, 1263
Naphthylmethyl fluorescent groups
Macrocyclic ligands, Aza–oxa crowns, 1867
N-(Carbamoylmethyl)iminodiacetic acid
N-(2-Amidomethyl)-iminodiacetic acid, *N*-(2-Acetamide)-iminodiacetic acid, *cis*-Diaqua(*N*-carbamoylmethyl-iminodiacetato)nickel(II), Molecular and crystal structure, Magnetic and spectral properties, Thermal stability, 2463
N-carbamoylmethyl-iminodiacetic acid
N-(2-amidomethyl)-iminodiacetic acid, *N*-(2-acetamido)-iminodiacetic acid, Imidazole, Mixed-ligand complexes, Aqua(imidazole)(*N* - carbamoylmethyl-iminodiacetato)nickel(II) sesquihydrate, Aqua(imidazole)(*N* - carbamoylmethyl-iminodiacetato)cobalt(II) sesquihydrate, Molecular and crystal structures, Magnetic, spectral and thermal properties, 2473
Nematic phases
Metallomesogens, Rhenium, Chiral nematic phases, 249
Neodymium
Contrast agents, Crystal structures, Diethylenetriaminepentaacetate, Lanthanides, 771
Neodymium
Synthesis, Crystal structure, Aryloxide, Anion–cation pair compound, 2243
Network structures
α,α′-Bis(pyrazolyl)-*m*-xylene, Copper(II) complexes, X-ray structure, Absorption spectroscopy, Electron spin resonance, 719
NH tautomerism
Ferrocenylporphyrin, π-Conjugation, Electrochemical communication, Intramolecular hydrogen bonding, 1961
N′-2-Hydroxypropyl derivatives
N′-2-Pyridylmethyl derivatives, Stability constant, 2027
Nickel bisdithiolenes
Crystal structures, Cyclic voltammetry, Strong near-IR absorption, 425
Nickel complexes
Binucleating ligand, Copper complexes, Crystal structures, Redox chemistry, 2011
Nickel complexes
Crystal structures, Copper complexes, Schiff bases, Uracil, 689
Nickel complexes
Crystal structures, Metavanadate complexes, Copper complexes, Hydrothermal synthesis, Magnetic properties, 2521
Nickel complexes
Molecular magnets, Cyano-bridged heteropolynuclear complexes, Iron complexes, Ferromagnetic coupling, 1967
Nickel complexes
Thiosemicarbazones, Electrochemistry, Iron complexes, EPR of iron complexes, Cobalt complexes, 2059

Nickel complex
Tetra-aza ligands, CP-MAS NMR, Template reaction, 2149
Nickel
Copper, Cobalt, Palladium, dmit, 4,5-bis(2-pyridylmethylsulfanyl)-1,3-dithiole-2-thione, 4,5-bis(2-pyridylethylsulfanyl)-1,3-dithiole-2-thione, 665
Nickel
Crystal structures, Magnetic properties, Dinuclear complexes, Manganese, Cobalt, 93
Nickel
Dithiolene, Dinuclear complexes, Acid–base, Solvatochromism, Carbon disulfide, 1283
Nickel(II)
Binucleating hexa-aza macrocycle, Copper(II), Cobalt(II), Zinc(II), Crystal structures, Phosphotriester, Hydrolysis, 1485
Nickel(II)
Cobalt(II), Cyanamidonitrate, Electronic spectra, Imidazole ligands, IR spectra, X-ray crystallography, 1021
Nickel(II) complexes
Potentiometry, Equilibria, Stability constants, Manganese(II), Cobalt(II), Aminopolyphosphonates, UV–VIS spectra, 2083
Nickel(II) complex
Syntheses, Crystal structures, Cobalt(II) complex, 4-(*p*-Methylphenyl)-3,5-bis-(pyridin-2-yl)-1,2,4-triazole, ESIMS, 2019
Nickel(III)
Asorption spectra, Copper(III), Dioxotetraamines, Macrocyclic ligands, 2533
Nickel(II)/(III) complexes
Crystal structures, Electrochemistry, EPR, Schiff base complexes, 655
Nickel(II)
Iron(II), Crystal structures, Electronic spectra, 1333
Nickel(II)
Me_2Octaen, Polyamines, Equilibria, Kinetics, Stopped-flow, 2507
Nickel(II)
Mononuclear compounds, Crystal structures, Nitrito ligands, Magnetic measurements, 225
Nickel(II)nitrite
Cis–trans isomerism, Crystal structures, 1,2-Diamino-2-methylpropane, 1015
Nickel(II) piperidinedithiocarbamate complexes
Synthesis, X-ray structure, 1713
Nickel(II)selenocyanate
Bis(3-aminopropyl)amine, (2-Aminoethyl)(3-aminopropyl)amine, Bis(2-aminoethyl)methylamine, Thermochromism, 1903
Nickel(II)thiocyanate
1-(2-Aminoethyl)pyrrolidine, Crystal structures, *cis*/*trans* Isomers, 1803
Nickel
Phthalocyanine complexes, Phthalonitrile derivatives, Crown-ether, Copper, Cobalt, Alkaline metal extraction, 115
Nicotinate
Bis(η-cyclopentadienyl)titanium(IV), Crystal structures, Diphenylphosphinoacetate, Heterometallics, Thiophenoxyacetate, 757
Ni(II) complexes
Tripodal ligand, Crystal structures, Spectroscopic studies, 2661
Niobium
Heterometallic aryloxides, Lithium niobate, Monomeric compounds, Percursors, 1037
Nitration
Cymene, Pyrazolyl, Ruthenium, Structure, Synthesis, 475
Nitric oxide
Cobalt, Electrocatalysis, Oxidation, Phthalocyanine, Reduction, 229
Nitrides
Molybdenum, Alkoxides, Synthesis, X-ray structures, NMR fluxionality, Pseudorotation, 1363
Nitrido complexes
Rhenium, Imido complexes, EPR spectroscopy, X-ray structures, 1741
Nitrile-bridged complexes
Molybdenum(II), Tungsten(II), Crystal structures, *o*-Phenylenediacetonitrile, Bimetallic complexesw, Trimetallic complexes, Seven-coordinate complexes, Halocarbonyls, 147
Nitrite
Palladium, Platinum, Diphosphines, Isomerism, Fluxionality, 1329
Nitrito ligands
Nickel(II), Mononuclear compounds, Crystal structures, Magnetic measurements, 225
Nitrobenzene catalytic reduction
Rhodium complexes, 2-picoline, Water gas shift reaction, 487
Nitrogen-donor ligands
Zinc, Bis(pyrazolyl)silanes, Crystal structures, 1815
Nitrosobenzene cycloaddition
Regioselectivity, Organoiron compounds, Decomplexation, Heterocycloaddition trap, Alkaloid synthesis, 569
Nitrosonaphthol
Crystal structures, Ruthenium nitrosonaphthol complexes, 7
Nitrosyl complex
Chromium, Molybdenum, Carboxylate, DFT, 2565
NMR data
Zinc(II), Cadmium(II), Mercury(II), Tris(2-benzimidazolylmethyl)amine, X-ray diffraction structures, 1479
NMR fluxionality
Molybdenum, Nitrides, Alkoxides, Synthesis, X-ray structures, Pseudorotation, 1363
NMR
Heteroscorpionate tris(3-*R*-pyrazolyl)-borate cobalt(II) complexes, Structures, 2119
NMR
Iron carbonyl halides, XAFS spectroscopy, Halogen exchange reactions, Matrix isolation, 1493
NMR
Lanthanide, Carbacylamidophosphate, X-ray data, 2203
NMR of paramagnetic compounds
Macrocycles, Lanthanide complexes, Chiral complexes, 465
NMR
Platinum(II), Sulfoxide, *N*,*N*-Dialkyl-*N*′-(3-*R*-benzoyl)thiourea, Acylthiourea, Chemotherapeutic agents, 1347
NMR
Sol-gel, Hybrid materials, Siloxane, Silicon-29, Oxygen-17, 315
NMR spectroscopy
Copper(II), Cobalt(III), Pyridylmethyl-tetraazadecane, 1447
N,*N*-Dialkyl-*N*′-(3-*R*-benzoyl)thiourea
Platinum(II), Sulfoxide, Acylthiourea, NMR, Chemotherapeutic agents, 1347
N,*N*-dimethylformamide
Lanthanides(III), Silver(I), Diethylenetriamine, Complexes, Thermodynamics, 2427
N,*N*′-Ethylenebis(amino acid)
Oxovanadium(IV) complexes, TG-DTA, 1311
^{15}N NMR
Zn(II) complexes, 1,2,4-Triazolo-[1,5α]-pyrimidine, HETCOR, CPMAS, 965
Nobium
Titanium, Tantalum, Aryloxide, Bisphenol, Hydrogenation, 35
Nonlinear optical properties
Tetrathiometalate, Synthesis, Copper compounds, Crystal structures, Dppm, 1545
Non-planar conjugated ligands
Crystal structures, Europium(III) complexes, Fluorescence spectra, 785
Norbornene
Palladium(II) complexes, Mixed donor ligands, *Trans*-influence, X-ray crystallography, Methylaluminoxane (MAO), Polymerization, 1601
N-Oxide
Crystal structures, Lanthanide complexes, Picrate, 4-Methylmorpholine, TG, DSC, 2313
Nozaki–Hiyama–Kishi reaction
Chromium, Salen, Manganese, Catalysis, Enantioselection, 537
N′-2-Pyridylmethyl derivatives
N′-2-Hydroxypropyl derivatives, Stability constant, 2027
N-salicylidenearoylhydrazine copper(II) complexes
Copper(II) imidazole ternary complexes, Copper(II) imidazolate ternary complexes, X-ray crystal structures, Molecular structures, Magnetic properties, Infrared spectra, 1181
N-salicylidenearoylhydrazines
Copper(II) complexes, X-ray crystal structures, Molecular structures, Magnetic properties, Infrared spectra, 949

N-Salicylidene derivatives
Schiff base complexes, X-ray structures, Zn(II) complexes, 673
N-Tosyl ligands
Bridged structures, Crystal structures, Heteronuclear multiple bond coherence, Zinc porphyrin complexes, 413
Nuclear magnetic resonance
Crystal structures, Cu^{2+} porphyrin complexes, Protonated porphyrins, SAT complexes, Electron spin resonance, 633
Nuclear reprocessing
Calixcrowns, Caesium ion, Sodium ion, Perrhenate ion, Pertechnetate ion, 1749
Nucleophilic
Additions, Alkylation, Insertions, Schiff bases, Titanium, 177
Nucleotides
Carcinogenic, Chromium, 417

Octa- and hepta-coordination
Crystal structures, Synthesis, Macrocyclic polyamine ligand, Manganese complexes, 2095
Octacyanomolybdate(IV)
Kinetics, Substitution, Mechanism, *cis*-Diaquabis(2,2′-bipirydyl)chromium(III), Octacyanotungstate(IV), 2225
Octacyanotungstate(IV)
Kinetics, Substitution, Mechanism, *cis*-Diaquabis(2,2′-bipirydyl)chromium(III), Octacyanomolybdate(IV), 2225
Octadentate ligands
Crystal structures, Cobalt(II) complexes, Iron(II) complexes, 431
Octahedral complexes
Crystal structures, *Fac* isomers, Isomerization, Lanthanide chloride complexes, 199
Olefin polymerizations
Zirconocene, Crystal structures, Catalysis, 1941
Olefins
Alkynes, Functionalized metalloalkynes, Polymetallated olefins, Titanium, 563
Olefins
Porphyrins, Hemoprotein models, Chiral catalysts, Epoxidation, 581
One-dimensional polymers
Dirhodium(II) compounds, Trifluoroacetate, Arene coordination, π-Complexes, Crystal structures, 1829
O,O-Alkylene dithiophosphate acids and ligands
Organotellurium(IV), 407
o-Phenylenediacetonitrile
Molybdenum(II), Tungsten(II), Crystal structures, Bimetallic complexesw, Trimetallic complexes, Nitrile-bridged complexes, Seven-coordinate complexes, Halocarbonyls, 147
Organocopper reagents
Hydroformylation, Catalysis, Asymmetric synthesis, Domino reactions, 513
Organogermane halides
Alkoxyalkynes, Aminoalkynes, Addition reactions, Organophosphorus halides, Organosilane halides, Pd-catalyzed cross-coupling reactions, 597
Organoiron compounds
Nitrosobenzene cycloaddition, Regioselectivity, Decomplexation, Heterocycloaddition trap, Alkaloid synthesis, 569
Organolanthanide complexes
Ether-side chain cyclopentadienyl, Cyclooctatetraenyl, Crystal structures, 453
Organophosphorus halides
Alkoxyalkynes, Aminoalkynes, Addition reactions, Organosilane halides, Organogermane halides, Pd-catalyzed cross-coupling reactions, 597
Organophosphoryl polyoxotungstate
Polyoxometalate, Synthesis, ^{183}W NMR, 125
Organosilane halides
Alkoxyalkynes, Aminoalkynes, Addition reactions, Organophosphorus halides, Organogermane halides, Pd-catalyzed cross-coupling reactions, 597
Organotellurium(IV)
O,O-Alkylene dithiophosphate acids and ligands, 407
Organotin(IV) complexes
Heterocyclic bis(thiosemicarbazone), Heptacoordinate complexes, Binuclear zinc complexes, 841
Organotin(IV)
Phosphorothiates, Bioactive groups, Cholesteryl, 1539
Organotin(IV)
Poly(pyrazol-1-yl)alkanes, X-ray structure, 381
Organotin(IV)
Poly(triazol-1-yl)alkanes, X-ray structure, 1949
Osmium
Amine oxide, Methanolysis, Rhenium, Carbonyl, Methylcarbonate, 641
Osmium
Ditelluroether, X-ray structures, 235
Osmium
Dithiolate complexes, Ruthenium, X-ray structures, 1073
Osmium(II) complexes
Electrochemical studies, Heterodinuclear complexes, Homodinuclear complexes, Luminescence properties, Ruthenium(II) complexes, Syntheses, 1233
Osmium
Silica, Titanium(IV), Ruthenium, 2277
Osmium
Triphenylphosphine, 2-(Phenylazo)-pyridine, Synthesis, Structures, Reactivities, 1227
Osmium
X-ray structures, Metallation, 1081
Oxalate anions
Aromatic amines, Amberlite anion-exchange resin, Metal–oxalate complexes, Oxidation, Homogeneous and heterogeneous, 1317
Oxalato-bridged compounds
Crystal structures, Binuclear copper compounds, Magnetism, 1105
Oxidation
Aromatic amines, Amberlite anion-exchange resin, Oxalate anions, Metal–oxalate complexes, Homogeneous and heterogeneous, 1317
Oxidation
Catalysis, 3,5-Di-*tert*-butylcatechol, Kinetics, Copper binuclear complexes, 2367
Oxidation
Cobalt, Electrocatalysis, Nitric oxide, Phthalocyanine, Reduction, 229
Oximes
Transition metal complexes, Electronic spectral data, Benzil-α-monoxime, 1687
μ-oxo-Bridged cations
Crown ether complexation, Crystal structures, Bridging oxygen atoms, 1799
Oxocluster complexes
Molybdenum, Hantzsch synthesis, Crystal structures, Hexanuclear molybdenum(V) complexes, 1471
Oxo ligands
Thiolates, Titanium, Trimers, 1139
Oxomolybdenum(V) compounds
Clusters, $Mo_2O_4^{2+}$ unit, Pyridine, Alkyl-substituted pyridines, 1219
Oxomolybdenum(V) coordination compounds
Solvothermal synthesis, Crystal structures, Mo(V, VI) compounds, Alkyl-substituted pyridines, 1407
Oxonium derivatives
closo-Dodecaborate, Functional derivatives, Amino acids, Boron neutron capture therapy, 627
Oxonium ion
15-Crown-5 complexes, Liquid clathrates, X-ray crystallography, 85
Oxovanadium complexes
Catechols, Macrocyclic ligands, ESR parameters, Distorted square-pyramid, Hydrophobic cavities, 1167
Oxovanadium(IV) complexes
N,*N*′-Ethylenebis(amino acid), TG-DTA, 1311
Oxovanadium(IV) complexes
Pyridinecarboxylic acids, pH-metry, Spectral studies, Speciation, 55
Oxovanadium(V) alkoxides
Mononuclear chelation, Crystal structures, Hydrogen bonded helical structures, 931
Oxovanadium(V) dimers
Alkoxo compounds of oxovanadium(V), Crystal structure of compounds of oxovanadium(V), Hydrazonato compounds of oxovanadium(V), Reactivity of bis(β-dionato)oxovanadium(IV) chelates, Hydrazonato tridentate Schiff base ligands, 2003
Oxygen-atom transfer
Dioxomolybdenum dipicolinate, Azoxybenzene deoxygenation, 2141
Oxygen-17
Sol-gel, NMR, Hybrid materials, Siloxane, Silicon-29, 315
Oxygen
Solubility, Solubilization enthalpy, Solubilization entropy, Cavity, 2457

Oxyhalide
Polyoxometalate, Molybdenum, X-ray structure, High acidity, 43

P-alkylation
Gold(I) complexes, Cationic ylide ligand, Bis(methyldiphenylphosphonio)methylide salts, 1837
Palladium
Amido, Diimine, Dimer, Hydroxo, Platinum, 155
Palladium catalysts
Asymmetric alkylation, Asymmetric rearrangements, Chiral ligands, Chiral sulfoxides, 525
Palladium catalyzed reactions
Halide ions, Coupling reactions, Protonolysis, 577
Palladium complexes
Crystal structures, Platinum complexes, Diphosphine complexes, Tetraphosphine complexes, Bimetallic complexes, 913
Palladium
Copper, Cobalt, Nickel, dmit, 4,5-bis(2-pyridylmethylsulfanyl) - 1,3 - dithiole - 2-thione, 4,5-bis(2-pyridylethylsulfanyl)-1,3-dithiole-2-thione, 665
Palladium
1,5-diene, Cross coupling, Terpenoids, Carboalumination, 591
Palladium
Diethyldithiocarbamate, Diphosphines, Tetrachlorometallate anions, X-ray crystal structures, 1511
Palladium
Heck reactions, Phosphane, Sulfane, Ligands, Mechanism, 517
Palladium
Hydroxo complexes, Pyrazolylalkane complexes, Crystal structures, 1395
Palladium(II) complexes
Bisphosphines, Heterocyclic thiones, Platinum(II) complexes, Pyridyl, 899
Palladium(II) complexes
Catalysts, Peptides, Hydrolysis, 959
Palladium(II) complexes
Metallocycles, Aminophosphate complexes, Spectroscopy, Antitumour activity, 937
Palladium(II) complexes
Mixed donor ligands, *Trans*-influence, X-ray crystallography, Methylaluminoxane (MAO), Norbornene, Polymerization, 1601
Palladium(II) complexes
Platinum(II) complexes, Chloride metathesis, X-ray crystallography, Heterodifunctional ligands, 695
Palladium
Platinum, Nitrite, Diphosphines, Isomerism, Fluxionality, 1329
Palladium
Platinum, Phosphine thiocarbonates, 499
Palladium
Platinum, Selenium, Tellurium, 751
Palladium
Platinum, Thiolate complexes, Allyl complexes, 1627
Paramagnetic
Copper(II) complexes, Dinuclear and polynuclear, Crystal structures, Equatorial–apical bridge, 1593
Paramagnetic NMR
Polynuclear manganese-carboxylate clusters, Imidazole-carboxylate chelating ligands, 2111
Paramagnetic
Ruthenium, Clotrimazole, Ketoconazole, Metal complexes, *Trypanosoma cruzi*, Chagas, 2319
PBD
Lanthanide picrate, Fluorescence, Crystal structures, 779
Pd-catalyzed cross-coupling reactions
Alkoxyalkynes, Aminoalkynes, Addition reactions, Organophosphorus halides, Organosilane halides, Organogermane halides, 597
Pentachloro-cyclotriphosphazene
Pentafluoro-cyclotriphosphazene, X-ray structures, Electrospray mass spectrometry, 2101
Pentacoordination
Phosphoranes, X-ray structure, Hydrogen bonding, 63
Pentadentate ligands
Metallamacrocycles, Hexanuclear clusters, Manganese complexes, Hydrophobic aliphatic tripled tails, 1985
Pentafluoro-cyclotriphosphazene
Pentachloro-cyclotriphosphazene, X-ray structures, Electrospray mass spectrometry, 2101
Peptides
Disulfide, Transition metal ions, 1849
Peptides
Palladium(II) complexes, Catalysts, Hydrolysis, 959
Percursors
Heterometallic aryloxides, Lithium niobate, Monomeric compounds, Niobium, 1037
Peroxo ligands
Molybdenum complexes, Tungsten complexes, Pyrazine complexes, Crystal structures, 1503
Perrhenate ion
Calixcrowns, Caesium ion, Sodium ion, Pertechnetate ion, Nuclear reprocessing, 1749
Pertechnetate ion
Calixcrowns, Caesium ion, Sodium ion, Perrhenate ion, Nuclear reprocessing, 1749
1,10-Phenanthroline
2,2′-Bipyridine, 1,8-Bis(dimethylamino)-naphthalene, Boron-11 NMR, Chelated fluoroboron cations, Fast atom bombardment mass spectrometry, Fluorine-19 NMR, 2,2′,6′,2″-Terpyridine, 165
1,10-Phenanthroline
Crystal structures, Complexation chemistry, 495
Phenanthroline
Ruthenium, *Cis–trans*, MO calculations, Barriers, Field strength, 2297
Phenolic ligands
Ruthenium, Synthesis, Structure, Redox properties, 1663
Phenolic ligands
Ruthenium, Synthesis, Structure, Redox properties, 1673
Phenoxo bridges
Electrochemical synthesis, Mononuclear complexes, Polyhydroxyl ligands, Polynuclear complexes, Schiff base ligands, 185
2-(Phenylazo)pyridine
Osmium, Triphenylphosphine, Synthesis, Structures, Reactivities, 1227
5-Phenylazosalicylaldehyde
Schiff bases, Copper complexes, X-ray structure, Cyclic voltammetry, 607
pH-metry
Oxovanadium(IV) complexes, Pyridinecarboxylic acids, Spectral studies, Speciation, 55
Phosphane
Heck reactions, Palladium, Sulfane, Ligands, Mechanism, 517
Phosphates
Ruthenium, X-ray crystal structures, 801
Phosphate
Uranium, Uranyl, Crown, Crystal structures, 1551
Phosphato complexes
Beryllium, Solution equilibria, ^{31}P NMR spectroscopy, ^{9}Be NMR spectroscopy, Speciation, 1043
Phosphato complexes
Tin(II), Solution equilibria, Speciation, 2403
Phosphides
Antimonides, Arsenides, Metathesis, 829
Phosphido-bridged
Ruthenium, Iridium, Gold, Electron-rich, Cluster, Crystal structures, 2593
Phosphine
Alkene, Polymerization, Hydroboration, Copper(I) complexes, 1271
Phosphine complexes
Mercury(II) halides, Crystal structures, 1719
Phosphine oxides
Lanthanides, X-ray structures, 2697
Phosphine oxides
Molybdenum–oxo complexes, Photochemistry, Photooxidation, Phosphines, Crystal structures, 1437
Phosphines
Molybdenum–oxo complexes, Photochemistry, Photooxidation, Phosphine oxides, Crystal structures, 1437
Phosphines
Rhenium, Re complexes, Re(I), *trans*-Dioxo Re(V) complexes, dppm, 2249
Phosphine sulfides
Crystal structures, Phosphonium salt, 2585
Phosphine thiocarbonates
Platinum, Palladium, 499

Phosphino amino acid salts
Water-soluble phosphines, Disodium or dipotassium 1,3-di(carboxylatomethyl)-5-aryl-1,3,5-diazaphosphorinanes, 1455
Phosphinophenols
Rhenium, 1111
Phosphite diolato(1 −) ligand
Spirophosphorane ring-opening, Crystal structures, 2667
Phosphites
π-Allyl complexes, Allylic substitutions, Iridium, Regioselectivity, Stereoselectivity, 557
Phosphonium salt
Crystal structures, Phosphine sulfides, 2585
Phosphoranes
Pentacoordination, X-ray structure, Hydrogen bonding, 63
Phosphorothiates
Organotin(IV), Bioactive groups, Cholesteryl, 1539
Phosphotriester
Binucleating hexa-aza macrocycle, Copper(II), Nickel(II), Cobalt(II), Zinc(II), Crystal structures, Hydrolysis, 1485
Photochemical metal organic deposition
Photochemistry, Surface chemistry, Lithography, Gold, 343
Photochemistry
Molybdenum–oxo complexes, Photooxidation, Phosphines, Phosphine oxides, Crystal structures, 1437
Photochemistry
Surface chemistry, Photochemical metal organic deposition, Lithography, Gold, 343
Photoisomerization
Ruthenium, 1193
Photolysis
Manganese complexes, Schiff bases, Manganoenzymes, Catalase, Dioxygen, 47
Photooxidation
Molybdenum–oxo complexes, Photochemistry, Phosphines, Phosphine oxides, Crystal structures, 1437
Photosensitive ligands
Schiff bases, Cobalt complexes, Spin crossover, LD-LISC effect, 1643
Photosystem II
Dichloromanganese(IV) complexes, Bidentate Schiff base ligands, Tetradentate Schiff base ligands, Crystal structures, 2039
Phthalocyanine
Cobalt, Electrocatalysis, Nitric oxide, Oxidation, Reduction, 229
Phthalocyanine complexes
Phthalonitrile derivatives, Crown-ether, Copper, Nickel, Cobalt, Alkaline metal extraction, 115
Phthalocyanine
Iron, Dopamine, Serotonin, Coordination, 1355
Phthalocyanines
Naphthalocyanines, Porphyrins, Raman, Sandwich complexes, Lanthanides, 1381
Phthalonitrile derivatives
Phthalocyanine complexes, Crown-ether, Copper, Nickel, Cobalt, Alkaline metal extraction, 115
2-picoline
Nitrobenzene catalytic reduction, Rhodium complexes, Water gas shift reaction, 487
Picrate
Crystal structures, Lanthanide complexes, 4-Methylmorpholine, *N*-Oxide, TG, DSC, 2313
Piperidine
Platinum(II) complexes, Synthesis, Crystal structures, 975
Planar chiral
Structure, Indenyl, Yttrium, Lanthanum, Tetrahydroborate, 1955
Platinum
Amido, Diimine, Dimer, Hydroxo, Palladium, 155
Platinum catalysts
Dendrimers, Carbosilanes, Hydrosilation, 1031
Platinum complexes
Crystal structures, Palladium complexes, Diphosphine complexes, Tetraphosphine complexes, Bimetallic complexes, 913
Platinum complexes
3-methylpiperidine, Dicarboxylates, Synthesis, Crystal structures, 983
Platinum
Complexes, Sulfimides, Hydrogen bonding, 2077
Platinum complexes
Thiophosphoryl guanidines, Crystal structures, 809
Platinum
Gold, Cross-coupling, Diyne, X-ray, 2261
Platinum(II) complexes
Bisphosphines, Heterocyclic thiones, Palladium(II) complexes, Pyridyl, 899
Platinum(II) complexes
Insertion reactions, Platinum–tin bimetallics, 2,3,5,6-Tetrakis(α-pyridyl)-pyrazine, 739
Platinum(II) complexes
Palladium(II) complexes, Chloride metathesis, X-ray crystallography, Heterodifunctional ligands, 695
Platinum(II) complexes
Piperidine, Synthesis, Crystal structures, 975
Platinum(II)
Naphthylazoimidazoles, PtN_4 coordination, Electrochemistry, X-ray structures, 1263
Platinum(II)
Platinum(IV), Bromide, Porphyrins, Electrochemistry, Voltammetry, 1057
Platinum(II)
Sulfoxide, *N*,*N*-Dialkyl-*N*′-(3-*R*-benzoyl)-thiourea, Acylthiourea, NMR, Chemotherapeutic agents, 1347
Platinum(IV)
Platinum(II), Bromide, Porphyrins, Electrochemistry, Voltammetry, 1057
Platinum
Palladium, Nitrite, Diphosphines, Isomerism, Fluxionality, 1329
Platinum
Palladium, Phosphine thiocarbonates, 499
Platinum
Palladium, Selenium, Tellurium, 751
Platinum
Palladium, Thiolate complexes, Allyl complexes, 1627
Platinum–tin bimetallics
Insertion reactions, Platinum(II) complexes, 2,3,5,6-Tetrakis(α-pyridyl)-pyrazine, 739
4-(*p*-Methylphenyl)-3,5-bis(pyridin-2-yl)-1,2,4-triazole
Syntheses, Crystal structures, Cobalt(II) complex, Nickel(II) complex, ESIMS, 2019
^{31}P NMR spectroscopy
Beryllium, Phosphato complexes, Solution equilibria, ^{9}Be NMR spectroscopy, Speciation, 1043
Polyaddition
Alkenylsilanes, Hydrosilylation, $RhI(PPh_3)_3$, Stereodivergent, 567
Polyamine ligand
Strontium, Thd ligand, Precursor, 2547
Polyamines
Dioxygen carriers, Cobalt, Dinuclear complexes, Dinucleating ligands, Kinetics, Dioxygen binding, 2447
Polyamines
Dioxygen carriers, Dioxygen binding, Cobalt, Polynuclear complexes, Thermodynamics of complexation, 2441
Polyamines
Me_2Octaen, Nickel(II), Equilibria, Kinetics, Stopped-flow, 2507
Poly(cobalt–tetraaminophthalocyanine)
Polymeric metallophthalocyanines, Modified electrodes, Electrooxidation of hydrazine, Impedance spectroscopy, 2303
Polyhydroxyl ligands
Electrochemical synthesis, Mononuclear complexes, Phenoxo bridges, Polynuclear complexes, Schiff base ligands, 185
Polymeric metallophthalocyanines
Modified electrodes, Electrooxidation of hydrazine, Poly(cobalt–tetraaminophthalocyanine), Impedance spectroscopy, 2303
Polymerization
Palladium(II) complexes, Mixed donor ligands, *Trans*-influence, X-ray crystallography, Methylaluminoxane (MAO), Norbornene, 1601
Polymerization
Phosphine, Alkene, Hydroboration, Copper(I) complexes, 1271
Polymetallated olefins
Alkynes, Functionalized metalloalkynes, Olefins, Titanium, 563
Polynuclear complexes
Dioxygen carriers, Dioxygen binding, Cobalt, Polyamines, Thermodynamics of complexation, 2441

Polynuclear complexes
Electrochemical synthesis, Mononuclear complexes, Phenoxo bridges, Polyhydroxyl ligands, Schiff base ligands, 185
Polynuclear manganese-carboxylate clusters
Imidazole-carboxylate chelating ligands, Paramagnetic NMR, 2111
Polyoxometalate
Organophosphoryl polyoxotungstate, Synthesis, ^{183}W NMR, 125
Polyoxometalate
Oxyhalide, Molybdenum, X-ray structure, High acidity, 43
Poly(pyrazol-1-yl)alkanes
Organotin(IV), X-ray structure, 381
Polypyridine ligands
Bpy ligands, Ruthenium(II) complexes, 1975
Polypyridine
Ruthenium, Terpyridine, Electrocatalytic oxidation, Alcohol oxidation, Isomerization, 1049
Polysilazanes
Hydroboration, Precursors, Vinylsilanes, Chloroboranes, 323
Polytelluride
Solvothermal synthesis, Iron telluride, Iron cluster, Iron carbonyl, Carbonyl clusters, 1995
Poly(triazol-1-yl)alkanes
Organotin(IV), X-ray structure, 1949
Porphyrins
Hemoprotein models, Chiral catalysts, Epoxidation, Olefins, 581
Porphyrins
Phthalocyanines, Naphthalocyanines, Raman, Sandwich complexes, Lanthanides, 1381
Porphyrins
Platinum(II), Platinum(IV), Bromide, Electrochemistry, Voltammetry, 1057
Potentiometric titrations
Vanadium complexes, Quinic acid complexes, IR spectra, Raman spectra, Thermal behavior, 2613
Potentiometry
Equilibria, Stability constants, Manganese(II), Cobalt(II), Nickel(II) complexes, Aminopolyphosphonates, UV–VIS spectra, 2083
Potentiometry
meso-2,3-Dimercaptosuccinic acid, UV–Vis spectroscopy, Formation constants, Ionization constants, Kinetic measurements, 2435
Powder X-ray diffraction patterns
Deoxycholic acid, Ferrocene derivatives, Inclusion compounds, Molecular motion, ^{57}Fe Mössbauer spectroscopy, 205
Praseodymium(III)
D-Gluconic acid, D-Galactonic acid, D-Gulonic acid, Complexation, 1567
Precursors
Hydroboration, Polysilazanes, Vinylsilanes, Chloroboranes, 323
Precursors
Metal–organic chemical vapour deposition, Lead scandium tantalate, Ferroelectric oxides, 351
Precursor
Strontium, Polyamine ligand, Thd ligand, 2547
Propiolic acid
Tungsten(II), Carboxylate and sulfonate substituted pyridines, Water soluble complexes, 2171
1,3-propylenediaminetetraacetate
Cu(II) complexes, Mn(II) complexes, Crystal structures, Thermal properties, Magnetic properties, 1175
Protonated porphyrins
Crystal structures, Cu^{2+} porphyrin complexes, SAT complexes, Electron spin resonance, Nuclear magnetic resonance, 633
Protonolysis
Palladium catalyzed reactions, Halide ions, Coupling reactions, 577
Pryrazolyl groups
Dinuclear, Antiferromagnetic interactions, 2215
Pseudohalogens
Selenocyanogen, Thiocyanogen, 681
Pseudorotation
Molybdenum, Nitrides, Alkoxides, Synthesis, X-ray structures, NMR fluxionality, 1363
PtN_4 coordination
Naphthylazoimidazoles, Platinum(II), Electrochemistry, X-ray structures, 1263
Pyrazine carboxamide complexes
Copper(I) complexes, Crystal structures, Electronic spectra, Emission spectra, Vibrational spectra, 601
Pyrazine complexes
Molybdenum complexes, Tungsten complexes, Peroxo ligands, Crystal structures, 1503
Pyrazolylalkane complexes
Palladium, Hydroxo complexes, Crystal structures, 1395
Pyrazolyl
Cymene, Nitration, Ruthenium, Structure, Synthesis, 475
Pyridinecarboxylate complexes
Chelating ligands, Crystal structures, Copper(II) complexes, Antimicrobial activity, 2689
Pyridinecarboxylic acids
Oxovanadium(IV) complexes, pH-metry, Spectral studies, Speciation, 55
2-Pyridineformamide
Thiosemicarbazone, Crystal structures, Cadmium halides, 1873
Pyridine *N*-oxide ligands
Cobalt(II) complexes, Zinc(II) complexes, X-ray structures, Magnetic susceptibility, 2195
Pyridine
Oxomolybdenum(V) compounds, Clusters, $Mo_2O_4^{2+}$ unit, Alkyl-substituted pyridines, 1219
Pyridines
Allylation, Aqueous reactions, Esters, Indium, Indium compounds, 549
Pyriding N-oxides
Metal complexes, Hydrogenation, Structures, 835
Pyridoxine
Crystal structures, Diethyltin, 813
2-(2-Pyridyl)benzimidazole
Chromium(III) complexes, Tris(2-benzimidazolylmethyl)amine, 2-Guanidinobenzimidazole, 2,6-Bis(2-benzimidazolyl)pyridine, Crystal structures, 1821
Pyridyl
Bisphosphines, Heterocyclic thiones, Palladium(II) complexes, Platinum(II) complexes, 899
Pyridylmethyl-tetraazadecane
Copper(II), Cobalt(III), NMR spectroscopy, 1447
pyrimidine-2-thione
Mercury(II) complexes, Triphenylphosphine, Benzothiazole-2-thione, Crystal structures, 2231
Pyrrole
Enamine, Alkenylation, 545
Pyrrolidine
Kainoids, Boronic esters, Asymmetric synthesis, 587

Quinazolines
Allylic alkylation, Axially chiral phosphinamine, Hydroboration, 541
Quinic acid complexes
Vanadium complexes, IR spectra, Raman spectra, Thermal behavior, Potentiometric titrations, 2613

Raman
Phthalocyanines, Naphthalocyanines, Porphyrins, Sandwich complexes, Lanthanides, 1381
Raman spectra
Vanadium complexes, Quinic acid complexes, IR spectra, Thermal behavior, Potentiometric titrations, 2613
Raman spectroscopy
Infrared spectroscopy, Electronic absorption spectroscopy, Crystal structures, Hypophospite complexes, Cooperative vibronic transitions, Two-centre transitions, 863
Rare earth complex
Crystal structure, Antitumour activity, Hydrazone, 2599
Rare earth elements
Yttrium, Hydrolysis, Enthalpy, Ionic strength, Spectrophotometry, 99
Reaction
Iron, Selenium, Sulfur, Synthesis, 713
Reactivities
Osmium, Triphenylphosphine, 2-(Phenylazo)pyridine, Synthesis, Structures, 1227
Reactivity
Catecholborane, 1063
Reactivity
Cryoscopy, Cyanocuprates, Ionic, Structures, 553

Reactivity of bis(β-dionato)oxovanadium(IV) chelates
Alkoxo compounds of oxovanadium(V), Crystal structure of compounds of oxovanadium(V), Hydrazonato compounds of oxovanadium(V), Oxovanadium(V) dimers, Hydrazonato tridentate Schiff base ligands, 2003
Rearrangement
α-Acetylenic alcohols, Isomerization, Heterobimetallic titanium–copper systems, 1693
Re complexes
Rhenium, Re(I), *trans*-Dioxo Re(V) complexes, Phosphines, dppm, 2249
Redox chemistry
Binucleating ligand, Nickel complexes, Copper complexes, Crystal structures, 2011
Redox properties
Ruthenium, Phenolic ligands, Synthesis, Structure, 1663
Redox properties
Ruthenium, Phenolic ligands, Synthesis, Structure, 1673
Redox properties
Substituted cobalt phthalocyanines, Hammett parameters, Frontier orbitals, Disulfide reduction, 2255
Redox
Synthesis, Semiquinone, Ruthenium, Spectroelectrochemical studies, 2605
Reduction
Alane, Aluminum hydride, Alanate, Alumoxane, 1649
Reduction
Cobalt, Electrocatalysis, Nitric oxide, Oxidation, Phthalocyanine, 229
Refluxing
Crystallographic, Selenium, Tungsten analogue, 2127
Regioselectivity
π-Allyl complexes, Allylic substitutions, Iridium, Stereoselectivity, Phosphites, 557
Regioselectivity
Nitrosobenzene cycloaddition, Organoiron compounds, Decomplexation, Heterocycloaddition trap, Alkaloid synthesis, 569
Re(I)
Rhenium, Re complexes, *trans*-Dioxo Re(V) complexes, Phosphines, dppm, 2249
Release of free nucleobases from oligomers
Copper(II)–peroxide adduct, DNA cleavage, Electrospray mass spectrometry, 2639
Rhenium
Amine oxide, Methanolysis, Osmium, Carbonyl, Methylcarbonate, 641
Rhenium clusters
Trirhenium(III) clusters, Acetamidate, Dimolybdenum(II), MALDI, Mass spectroscopy, 1245
Rhenium(III) complexes
Thiopyrimidine, Rhenium(V) complexes, Cyclic voltammetry, UV–Vis–NIR, IR, ^{1}H NMR spectra, 2163
Rhenium
Metal clusters, Sulfur, Selenium, Tellurium, Crystal structures, 437
Rhenium
Metallomesogens, Nematic phases, Chiral nematic phases, 249
Rhenium
Nitrido complexes, Imido complexes, EPR spectroscopy, X-ray structures, 1741
Rhenium
Phosphinophenols, 1111
Rhenium
Re complexes, Re(I), *trans*-Dioxo Re(V) complexes, Phosphines, dppm, 2249
Rhenium(V) complexes
Thiopyrimidine, Rhenium(III) complexes, Cyclic voltammetry, UV–Vis–NIR, IR, ^{1}H NMR spectra, 2163
$RhI(PPh_3)_3$
Alkenylsilanes, Hydrosilylation, Polyaddition, Stereodivergent, 567
Rhodium complexes
Nitrobenzene catalytic reduction, 2-picoline, Water gas shift reaction, 487
Rhodium(II) carboxylates
Rhodium(II) complexes, Rhodium sulfosalicylate, Thermogravimetric analysis, Spectroscopic analysis, Anticancer drugs, 1305
Rhodium(II) complexes
Rhodium(II) carboxylates, Rhodium sulfosalicylate, Thermogravimetric analysis, Spectroscopic analysis, Anticancer drugs, 1305
Rhodium(II)
Dithiocarbamates, 123
Rhodium sulfosalicylate
Rhodium(II) complexes, Rhodium(II) carboxylates, Thermogravimetric analysis, Spectroscopic analysis, Anticancer drugs, 1305
Rietveld method
Sulfated zirconia, Tetragonal zirconia stabilization, Zirconium sulfide, Zirconium oxide sulfide, Thermogravimetry of sol–gel ZrO_2, 2283
Rigid and flexible ligands
Self-assembly, Supramolecules, X-ray structure, 1117
Ring-closing metathesis
Thioacetal, Titanocene(II), Intramolecular carbonyl olefination, Cycloalkenes, Heterocyclic compounds, 593
Ring-opening polymerization
Ferrocenophane, Inorganic polymers, Silanol, Mössbauer spectroscopy, 275
Ru–bipyridine
Azoimine, Tris-chelates, X-ray structures, Electrochemistry, Emission spectra, 1925
Ruthenium
Clotrimazole, Ketoconazole, Paramagnetic, Metal complexes, *Trypanosoma cruzi*, Chagas, 2319
Ruthenium
Crystal structures, Dimethyl sulfoxide, Carboxylates, Complexes, Catalysis, 1589
Ruthenium
Cymene, Nitration, Pyrazolyl, Structure, Synthesis, 475
Ruthenium
Dithiolate complexes, Osmium, X-ray structures, 1073
Ruthenium–edta complexes
Mixed-valence complexes, Ferricyanide, Cyanobridged complexes, Intramolecular electron transfer, 1339
Ruthenium(II) complexes
Bpy ligands, Polypyridine ligands, 1975
Ruthenium(II) complexes
Electrochemical studies, Heterodinuclear complexes, Homodinuclear complexes, Luminescence properties, Osmium(II) complexes, Syntheses, 1233
Ruthenium(II) polypyridyls
CdS nanoclusters, Functionalized nanoclusters, Mesophase materials, Molecular devices, 331
Ruthenium
Iridium, Gold, Electron-rich, Cluster, Phosphido-bridged, Crystal structures, 2593
Ruthenium nitrosonaphthol complexes
Crystal structures, Nitrosonaphthol, 7
Ruthenium
Phenanthroline, *Cis–trans*, MO calculations, Barriers, Field strength, 2297
Ruthenium
Phenolic ligands, Synthesis, Structure, Redox properties, 1663
Ruthenium
Phenolic ligands, Synthesis, Structure, Redox properties, 1673
Ruthenium
Phosphates, X-ray crystal structures, 801
Ruthenium
Photoisomerization, 1193
Ruthenium
Polypyridine, Terpyridine, Electrocatalytic oxidation, Alcohol oxidation, Isomerization, 1049
Ruthenium
Silica, Titanium(IV), Osmium, 2277
Ruthenium
Synthesis, Semiquinone, Spectroelectrochemical studies, Redox, 2605

Salen
Chromium, Manganese, Catalysis, Enantioselection, Nozaki–Hiyama–Kishi reaction, 537
Sandwich complexes
Phthalocyanines, Naphthalocyanines, Porphyrins, Raman, Lanthanides, 1381
SAT complexes
Crystal structures, Cu^{2+} porphyrin complexes, Protonated porphyrins, Electron spin resonance, Nuclear magnetic resonance, 633
Scandium
Alkoxides, Crystal structures, Volatility, 705
Schiff base complexes
Crystal structures, Electrochemistry, EPR, Nickel(II)/(III) complexes, 655

Schiff base complexes
N-Salicylidene derivatives, X-ray structures, Zn(II) complexes, 673
Schiff base
Imidazole, Silver complexes, Crystal structures, 2237
Schiff-base ligands
Cadmium(II) complexes, Symmetrical complexes, Asymmetrical complexes, Heptadentate ligands, 1633
Schiff base ligands
Electrochemical synthesis, Mononuclear complexes, Phenoxo bridges, Polyhydroxyl ligands, Polynuclear complexes, 185
Schiff bases
Additions, Alkylation, Insertions, Nucleophilic, Titanium, 177
Schiff bases
Cobalt complexes, Spin crossover, Photosensitive ligands, LD-LISC effect, 1643
Schiff bases
Copper complexes, X-ray structure, 5-Phenylazosalicylaldehyde, Cyclic voltammetry, 607
Schiff bases
Crystal structures, Nickel complexes, Copper complexes, Uracil, 689
Schiff bases
Manganese complexes, Manganoenzymes, Photolysis, Catalase, Dioxygen, 47
Selenium
Crystallographic, Tungsten analogue, Refluxing, 2127
Selenium
Iron, Sulfur, Synthesis, Reaction, 713
Selenium
Palladium, Platinum, Tellurium, 751
Selenium
Rhenium, Metal clusters, Sulfur, Tellurium, Crystal structures, 437
Selenocyanogen
Pseudohalogens, Thiocyanogen, 681
Selenoether
Telluroether, Sulfur macrocycles, Chromium, Molybdenum, Tungsten, 1373
Self-assembly
Rigid and flexible ligands, Supramolecules, X-ray structure, 1117
Semiquinone
Synthesis, Ruthenium, Spectroelectrochemical studies, Redox, 2605
SEM
Magnesia, Dolomite, Crystallite size, Degree of agglomeration, X-ray diffraction, 2345
Serotonin
Iron, Phthalocyanine, Dopamine, Coordination, 1355
Seven-coordinate complexes
Molybdenum(II), Tungsten(II), Crystal structures, *o*-Phenylenediacetonitrile, Bimetallic complexesw, Trimetallic complexes, Nitrile-bridged complexes, Halocarbonyls, 147
Silanol
Ferrocenophane, Inorganic polymers, Mössbauer spectroscopy, Ring-opening polymerization, 275
Silica gels
Ethylenimine, Immobilization, 3-Mercaptopropyltrimethoxysilane, 367
Silica
Sol–gel, Aggregation, Tetrasulfophthalocyanines, Monolith, Macrocycle, 2383
Silica
Titanium(IV), Ruthenium, Osmium, 2277
Silicon-29
Sol-gel, NMR, Hybrid materials, Siloxane, Oxygen-17, 315
Siloxane
Sol-gel, NMR, Hybrid materials, Silicon-29, Oxygen-17, 315
Silsesquioxane gels
Monophasic hybrid materials, Kinetic control, Sol–gel polymerization, 307
Silver complexes
Copper complexes, Gold complexes, 743
Silver complexes
Imidazole, Schiff base, Crystal structures, 2237
Silver(I)
Lanthanides(III), Diethylenetriamine, *N*,*N*-dimethylformamide, Complexes, Thermodynamics, 2427
Silylcupration
α-Aminoacylsilanes, β-Amino alcohols, Lewis acid, Statine analogues, 529
Single crystal structures
Dialkoxo-bridged binuclear Cu(II) complexes, Model of metal–guanine interaction, Thermal decompostion, Theophylline, Diethanolamine(2,2′-iminodiethanol), 457
Singly hydroxo-bridged
Copper(II) complexes, Deprotonated pyridine-2,6-dicarboxamide ligands, Crystal structures, Magnetism, 1423
Sodium ion
Calixcrowns, Caesium ion, Perrhenate ion, Pertechnetate ion, Nuclear reprocessing, 1749
Sol–gel
Aggregation, Tetrasulfophthalocyanines, Monolith, Macrocycle, Silica, 2383
Sol–gel
Alkoxide, Tin, Tin dioxide, β-Diketonate, 2069
Sol–gel matrices
Heteronuclear catalysts, Immobilization, Nanoparticles, 509
Sol-gel
NMR, Hybrid materials, Siloxane, Silicon-29, Oxygen-17, 315
Sol–gel polymerization
Monophasic hybrid materials, Silsesquioxane gels, Kinetic control, 307
Solid state
In situ X-ray diffraction, Intercalation, Layered compounds, Synchrotron radiation, 297
Solubility
Oxygen, Solubilization enthalpy, Solubilization entropy, Cavity, 2457
Solubilization enthalpy
Solubility, Oxygen, Solubilization entropy, Cavity, 2457
Solubilization entropy
Solubility, Oxygen, Solubilization enthalpy, Cavity, 2457
Solution equilibria
Beryllium, Phosphato complexes, ^{31}P NMR spectroscopy, ^{9}Be NMR spectroscopy, Speciation, 1043
Solution equilibria
Ciprofloxacin, Iron(III), Surfactants, 1085
Solution equilibria
Tin(II), Phosphato complexes, Speciation, 2403
Solution equilibrium
Mixed-ligand complexes, Hydroxamic acid, Copper(II), nickel(II) and zinc(II) complexes, 1727
Solvatochromism
Dithiolene, Nickel, Dinuclear complexes, Acid–base, Carbon disulfide, 1283
Solvent-derived ancillary ligands
Dicopper complexes, Acid–base congeners, 1909
Solvothermal synthesis
Crystal structures, Oxomolybdenum(V) coordination compounds, Mo(V, VI) compounds, Alkyl-substituted pyridines, 1407
Solvothermal synthesis
Polytelluride, Iron telluride, Iron cluster, Iron carbonyl, Carbonyl clusters, 1995
Speciation
Beryllium, Phosphato complexes, Solution equilibria, ^{31}P NMR spectroscopy, ^{9}Be NMR spectroscopy, 1043
Speciation
Oxovanadium(IV) complexes, Pyridinecarboxylic acids, pH-metry, Spectral studies, 55
Speciation
Tin(II), Phosphato complexes, Solution equilibria, 2403
Spectral data
Transition metal complexes, Terephthalate ions, Aromatic diamines, Crystal structures, 1415
Spectral studies
Oxovanadium(IV) complexes, Pyridinecarboxylic acids, pH-metry, Speciation, 55
Spectroelectrochemical studies
Synthesis, Semiquinone, Ruthenium, Redox, 2605
Spectrophotometry
Yttrium, Rare earth elements, Hydrolysis, Enthalpy, Ionic strength, 99
Spectroscopic analysis
Rhodium(II) complexes, Rhodium(II) carboxylates, Rhodium sulfosalicylate, Thermogravimetric analysis, Anticancer drugs, 1305
Spectroscopic properties
Diclofenac, Metal(II) compounds, Thermal properties, 2515

Spectroscopic properties
Sulfamethizole, Metal complexes, Crystal structures, 1859
Spectroscopic properties
Zinc complexes, Cobalt complex, α-Ketoglutaric acid, Thiosemicarbazones, Crystal structures, 1895
Spectroscopic studies
Ni(II) complexes, Tripodal ligand, Crystal structures, 2661
Spectroscopic study
Cobalt(III) complex, Thiocarbamylpyrazole, X-ray crystal structure, 2651
Spectroscopy
Palladium(II) complexes, Metallocycles, Aminophosphate complexes, Antitumour activity, 937
Spin crossover
Schiff bases, Cobalt complexes, Photosensitive ligands, LD-LISC effect, 1643
Spin triplet
Crystal structures, Cu dimers, Di-(2-pyridyl)ketone, Ferromagnetic dimers, Magnetic properties, 1005
Spirophosphorane ring-opening
Phosphite diolato(1 −) ligand, Crystal structures, 2667
Stability constant
N′-2-Pyridylmethyl derivatives, *N*′-2-Hydroxypropyl derivatives, 2027
Stability constants
Copper(II) complexes, Deltakephalins, 241
Stability constants
Effortil, Cu(II) complexes, Structures, EPR, Magnetochemical data, 1843
Stability constants
Imidazole derivatives, Transition metal complexes, Crystal structure, Absorption spectra, 2183
Stability constants
Potentiometry, Equilibria, Manganese(II), Cobalt(II), Nickel(II) complexes, Aminopolyphosphonates, UV–VIS spectra, 2083
Stability constants
Tetraazamacrocyclic ligand, Transition metal, Synthesis, Structural characterization, DNA cleavage activities, 1527
Statine analogues
α-Aminoacylsilanes, β-Amino alcohols, Lewis acid, Silylcupration, 529
Stereochemistry
Copper(II)–edta-type complexes, Crystal structures, 1
Stereodivergent
Alkenylsilanes, Hydrosilylation, $RhI(PPh_3)_3$, Polyaddition, 567
Stereoselectivity
π-Allyl complexes, Allylic substitutions, Iridium, Regioselectivity, Phosphites, 557
Stopped-flow
Me_2Octaen, Polyamines, Nickel(II), Equilibria, Kinetics, 2507
Streptonigrin
2,2′-Bipyridyl, 6,6′-Dicarboxy-2,2′-bipyridyl, Antitumour, Zinc, 1067
Strong near-IR absorption
Crystal structures, Cyclic voltammetry, Nickel bisdithiolenes, 425
Strontium
Polyamine ligand, Thd ligand, Precursor, 2547
Structural characterization
Tetraazamacrocyclic ligand, Transition metal, Synthesis, Stability constants, DNA cleavage activities, 1527
Structural characterization
Transition metals, Synthesis, Antitumor activity, 217
Structure
Cu(II) complex, Triaminoguanidinium-(2 +) ion, 1737
Structure
Cymene, Nitration, Pyrazolyl, Ruthenium, Synthesis, 475
Structure
Magnesium, Aryloxide, Adduct, 2557
Structure
Planar chiral, Indenyl, Yttrium, Lanthanum, Tetrahydroborate, 1955
Structure
Ruthenium, Phenolic ligands, Synthesis, Redox properties, 1663
Structure
Ruthenium, Phenolic ligands, Synthesis, Redox properties, 1673
Structures
Cryoscopy, Cyanocuprates, Ionic, Reactivity, 553
Structures
Effortil, Cu(II) complexes, Stability constants, EPR, Magnetochemical data, 1843
Structures
Heteroscorpionate tris(3-*R*-pyrazolyl)borate cobalt(II) complexes, NMR, 2119
Structures
Lead(II), Aspartate, 649
Structures
Osmium, Triphenylphosphine, 2-(Phenylazo)pyridine, Synthesis, Reactivities, 1227
Structures
Pyriding N-oxides, Metal complexes, Hydrogenation, 835
Substituted cobalt phthalocyanines
Redox properties, Hammett parameters, Frontier orbitals, Disulfide reduction, 2255
Substitution
Kinetics, Mechanism, *cis*-Diaquabis(2,2′-bipirydyl)chromium(III), Octacyanomolybdate(IV), Octacyanotungstate(IV), 2225
Sulfamethizole
Metal complexes, Crystal structures, Spectroscopic properties, 1859
Sulfamides
Cadmium complexes, Mercury complexes, X-ray structure, Zinc complexes, 991
Sulfane
Heck reactions, Palladium, Phosphane, Ligands, Mechanism, 517
Sulfated zirconia
Tetragonal zirconia stabilization, Rietveld method, Zirconium sulfide, Zirconium oxide sulfide, Thermogravimetry of sol–gel ZrO_2, 2283
Sulfimides
Complexes, Platinum, Hydrogen bonding, 2077
Sulfoxide
Platinum(II), *N*,*N*-Dialkyl-*N*′-(3-*R*-benzoyl)thiourea, Acylthiourea, NMR, Chemotherapeutic agents, 1347
Sulfur
Iron, Selenium, Synthesis, Reaction, 713
Sulfur macrocycles
Selenoether, Telluroether, Chromium, Molybdenum, Tungsten, 1373
Sulfur
Rhenium, Metal clusters, Selenium, Tellurium, Crystal structures, 437
Supercritical conditions
Carbon dioxide, Dimethyl carbonate, Homogeneous catalysis, Mechanism, 573
Supramolecular chemistry
Helical structures, Transition metals, X-ray crystal structures, 23
Supramolecules
Rigid and flexible ligands, Self-assembly, X-ray structure, 1117
Surface chemistry
Photochemistry, Photochemical metal organic deposition, Lithography, Gold, 343
Surface modification
Indium tin oxide, Alkoxides, Interfaces, 505
Surfactants
Ciprofloxacin, Iron(III), Solution equilibria, 1085
Symmetrical complexes
Cadmium(II) complexes, Schiff-base ligands, Asymmetrical complexes, Heptadentate ligands, 1633
Synchrotron radiation
In situ X-ray diffraction, Intercalation, Layered compounds, Solid state, 297
Synchrotron radiation
11-Membered metallocyclic ring, Metallocalix[6]arene, 2657
Syntheses
Crystal structures, Cobalt(II) complex, Nickel(II) complex, 4-(*p*-Methylphenyl)-3,5-bis(pyridin-2-yl)-1,2,4-triazole, ES-IMS, 2019
Syntheses
Electrochemical studies, Heterodinuclear complexes, Homodinuclear complexes, Luminescence properties, Osmium(II) complexes, Ruthenium(II) complexes, 1233
Synthesis
Crystal structure, Aryloxide, Neodymium, Anion–cation pair compound, 2243
Synthesis
Crystal structures, Macrocyclic polyamine ligand, Manganese complexes, Octa- and hepta-coordination, 2095

Synthesis
Cymene, Nitration, Pyrazolyl, Ruthenium, Structure, 475
Synthesis
EXAFS investigation, Azomethynic copper metallochelates, 2361
Synthesis
Iron, Selenium, Sulfur, Reaction, 713
Synthesis
Macrocycles, Complexes, Equilibria, 2501
Synthesis
Molybdenum, Nitrides, Alkoxides, X-ray structures, NMR fluxionality, Pseudorotation, 1363
Synthesis
Nickel(II) piperidinedithiocarbamate complexes, X-ray structure, 1713
Synthesis
Organophosphoryl polyoxotungstate, Polyoxometalate, ^{183}W NMR, 125
Synthesis
Osmium, Triphenylphosphine, 2-(Phenylazo)pyridine, Structures, Reactivities, 1227
Synthesis
Platinum complexes, 3-methylpiperidine, Dicarboxylates, Crystal structures, 983
Synthesis
Platinum(II) complexes, Piperidine, Crystal structures, 975
Synthesis
Ruthenium, Phenolic ligands, Structure, Redox properties, 1663
Synthesis
Ruthenium, Phenolic ligands, Structure, Redox properties, 1673
Synthesis
Semiquinone, Ruthenium, Spectroelectrochemical studies, Redox, 2605
Synthesis
Tetraazamacrocyclic ligand, Transition metal, Structural characterization, Stability constants, DNA cleavage activities, 1527
Synthesis
Tetrathiometalate, Nonlinear optical properties, Copper compounds, Crystal structures, Dppm, 1545
Synthesis
Transition metals, Structural characterization, Antitumor activity, 217

tachpyr
Cd(II), Hg(II), Torsion angles, Twist angles, Zn(II), 1155
Tantalum
Molybdenum, Trimetallic alkoxides, Crystal structures, 1791
Tantalum
Titanium, Nobium, Aryloxide, Bisphenol, Hydrogenation, 35
TCNE complexes
Hush theory, Iron complexes, Mixed valence, TCNQ complexes, 137
TCNQ complexes
Hush theory, Iron complexes, Mixed valence, TCNE complexes, 137
Tellurium
Palladium, Platinum, Selenium, 751
Tellurium
Rhenium, Metal clusters, Sulfur, Selenium, Crystal structures, 437
Tellurium-rich compounds
Cluster compounds, Molybdenum complexes, De-tellurium reaction, Crystal structures, 925
Telluroether
Selenoether, Sulfur macrocycles, Chromium, Molybdenum, Tungsten, 1373
Temperature effects
Equilibrium, Copper, Mixed valence, Disproportionation, 2289
Template reaction
Tetra-aza ligands, CP-MAS NMR, Nickel complex, 2149
Terephthalate ions
Transition metal complexes, Aromatic diamines, Crystal structures, Spectral data, 1415
Ternary complexes
Divalent metals, Zinc, Copper, Benzolamide, Diethylenetriamine, 725
Ternary copper(II) complexes
CT photochemistry, Diselenocarbamate and dithiophosphate ligands, 2177
Terpenoids
1,5-diene, Cross coupling, Carboalumination, Palladium, 591
2,2′,6′,2″-Terpyridine
2,2′-Bipyridine, 1,8-Bis(dimethylamino)-naphthalene, Boron-11 NMR, Chelated fluoroboron cations, Fast atom bombardment mass spectrometry, Fluorine-19 NMR, 1,10-Phenanthroline, 165
Terpyridine
Ruthenium, Polypyridine, Electrocatalytic oxidation, Alcohol oxidation, Isomerization, 1049
Terpyridine
Vanadium, Vanadyl, Density functional theory, 69
Tetra-aza ligands
CP-MAS NMR, Nickel complex, Template reaction, 2149
Tetraazamacrocyclic ligand
Transition metal, Synthesis, Structural characterization, Stability constants, DNA cleavage activities, 1527
Tetrachlorometallate anions
Palladium, Diethyldithiocarbamate, Diphosphines, X-ray crystal structures, 1511
Tetradentate Schiff base ligands
Dichloromanganese(IV) complexes, Bidentate Schiff base ligands, Crystal structures, Photosystem II, 2039
Tetragonal zirconia stabilization
Sulfated zirconia, Rietveld method, Zirconium sulfide, Zirconium oxide sulfide, Thermogravimetry of sol–gel ZrO_2, 2283
Tetrahedral coordination
Disulfides, Thioureides, Dithiocarbamates, 1279
Tetrahydroborate
Planar chiral, Structure, Indenyl, Yttrium, Lanthanum, 1955
2,3,5,6-Tetrakis(α-pyridyl)pyrazine
Insertion reactions, Platinum(II) complexes, Platinum–tin bimetallics, 739
Tetraphenylimidophosphinate ligand
Uranium, Thorium, Coordination compounds, X-ray crystal structures, 1699
Tetraphosphine complexes
Crystal structures, Palladium complexes, Platinum complexes, Diphosphine complexes, Bimetallic complexes, 913
Tetrasulfophthalocyanines
Sol–gel, Aggregation, Monolith, Macrocycle, Silica, 2383
Tetrathiometalate
Nonlinear optical properties, Synthesis, Copper compounds, Crystal structures, Dppm, 1545
TG
Crystal structures, Lanthanide complexes, Picrate, 4-Methylmorpholine, *N*-Oxide, DSC, 2313
TG-DTA
Oxovanadium(IV) complexes, *N*,*N*′-Ethylenebis(amino acid), 1311
Thd ligand
Strontium, Polyamine ligand, Precursor, 2547
Theophylline
Dialkoxo-bridged binuclear Cu(II) complexes, Model of metal–guanine interaction, Single crystal structures, Thermal decompostion, Diethanolamine(2,2′-iminodiethanol), 457
Thermal analysis
Colloids, Bimetallic films, FT-IR, Conductivity, 2337
Thermal behavior
Vanadium complexes, Quinic acid complexes, IR spectra, Raman spectra, Potentiometric titrations, 2613
Thermal decompostion
Dialkoxo-bridged binuclear Cu(II) complexes, Model of metal–guanine interaction, Single crystal structures, Theophylline, Diethanolamine(2,2′-iminodiethanol), 457
Thermal properties
Diclofenac, Metal(II) compounds, Spectroscopic properties, 2515
Thermal properties
Iron(III), Chromium(III), DTPA, Complexes, Thermodynamics, 2421
Thermal properties
1,3-propylenediaminetetraacetate, Cu(II) complexes, Mn(II) complexes, Crystal structures, Magnetic properties, 1175
Thermal stability
N-(Carbamoylmethyl)iminodiacetic acid, *N*-(2-Amidomethyl)-iminodiacetic acid, *N*-(2-Acetamide)-iminodiacetic acid, *cis*-Diaqua(*N*-carbamoylmethyl-iminodiacetato)nickel(II), Molecular and crystal structure, Magnetic and spectral properties, 2463

Thermochromism
Nickel(II)selenocyanate, Bis(3-aminopropyl)amine, (2-Aminoethyl)(3-aminopropyl)amine, Bis(2-aminoethyl)methylamine, 1903
Thermodynamic quantities
Equilibrium constants, Molybenum(VI) cations, 907
Thermodynamics
Iron(III), Chromium(III), DTPA, Complexes, Thermal properties, 2421
Thermodynamics
Lanthanides(III), Silver(I), Diethylenetriamine, *N*,*N*-dimethylformamide, Complexes, 2427
Thermodynamics of complexation
Dioxygen carriers, Dioxygen binding, Cobalt, Polynuclear complexes, Polyamines, 2441
Thermogravimetric analysis
Rhodium(II) complexes, Rhodium(II) carboxylates, Rhodium sulfosalicylate, Spectroscopic analysis, Anticancer drugs, 1305
Thermogravimetry of sol–gel ZrO_2
Sulfated zirconia, Tetragonal zirconia stabilization, Rietveld method, Zirconium sulfide, Zirconium oxide sulfide, 2283
Thiiranes
Dihydrodithiins, Tungsten carbonyls, 521
Thioacetal
Titanocene(II), Ring-closing metathesis, Intramolecular carbonyl olefination, Cycloalkenes, Heterocyclic compounds, 593
Thiocarbamylpyrazole
Cobalt(III) complex, Spectroscopic study, X-ray crystal structure, 2651
Thiocyanante
Mercury, Clusters, Host–guest chemistry, 871
Thiocyanate
Cobalt, 2-Hydroxyacetophenone, Azide, Crystal structure, 2707
Thiocyanogen
Pseudohalogens, Selenocyanogen, 681
Thioether
Bismuth, Coordination polymers, Crystal structures, Electrospray, 849
Thiolate-bridged complexes
Mixed-valence, Electron-transfer, Iron, 2679
Thiolate complexes
Palladium, Platinum, Allyl complexes, 1627
Thiolate
Electrochemistry, Macrocycle, Crystal structures, 1887
Thiolates
Oxo ligands, Titanium, Trimers, 1139
Thiophenes
Cyclic oligomers, Ferrocenes, 291
Thiophenoxyacetate
Bis(η-cyclopentadienyl)titanium(IV), Crystal structures, Diphenylphosphinoacetate, Heterometallics, Nicotinate, 757
Thiophosphoryl guanidines
Platinum complexes, Crystal structures, 809
Thiopyrimidine
Rhenium(V) complexes, Rhenium(III) complexes, Cyclic voltammetry, UV–Vis–NIR, IR, ^{1}H NMR spectra, 2163
Thiosemicarbazone
Isatin, Crystal structures, Zinc, Lead, Hexamethyleneimine, Metal(II) complexes, 1255
Thiosemicarbazone
2-Pyridineformamide, Crystal structures, Cadmium halides, 1873
Thiosemicarbazones
Electrochemistry, Iron complexes, EPR of iron complexes, Nickel complexes, Cobalt complexes, 2059
Thiosemicarbazones
Macrocyclic ligands, Electrochemistry, Copper complexes, Dithio-Schiff base complexes, 441
Thiosemicarbazones
Zinc complexes, Cobalt complex, α-Ketoglutaric acid, Crystal structures, Spectroscopic properties, 1895
Thioureides
Disulfides, Dithiocarbamates, Tetrahedral coordination, 1279
Thiuram sulfides
Copper and iron species, Dithiocarbamate derivatives, 2269
Thorium(IV)
Uranium(IV), Dicarboxylate complexes, CPMAS ^{13}C NMR spectroscopy, X-ray crystallography, 1757
Thorium
Uranium, Coordination compounds, Tetraphenylimidophosphinate ligand, X-ray crystal structures, 1699
Tin
Alkoxide, Tin dioxide, Sol–gel, β-Diketonate, 2069
Tin dioxide
Alkoxide, Tin, Sol–gel, β-Diketonate, 2069
Tin(II)
Phosphato complexes, Solution equilibria, Speciation, 2403
Tin(IV)
Crystal structures, 2-Ethyl-3-hydroxy-4-pyranonate, Ethylmaltol, 1-Methyl-2-ethyl-3-hydroxy-4-pyridinonate, Titanium(IV), 399
Titanium
Additions, Alkylation, Insertions, Nucleophilic, Schiff bases, 177
Titanium
Alkynes, Functionalized metalloalkynes, Olefins, Polymetallated olefins, 563
Titanium
C–H activation, Intramolecular bonds, Metallacycles, Allenes, Carbometalation, 879
Titanium(IV)
Crystal structures, 2-Ethyl-3-hydroxy-4-pyranonate, Ethylmaltol, 1-Methyl-2-ethyl-3-hydroxy-4-pyridinonate, Tin(IV), 399
Titanium(IV)
Hydroborates, Lithium, Bonding, Crystal structures, 1579
Titanium(IV)
Silica, Ruthenium, Osmium, 2277
Titanium
Oxo ligands, Thiolates, Trimers, 1139
Titanium
Tantalum, Nobium, Aryloxide, Bisphenol, Hydrogenation, 35
Titanocene(II)
Thioacetal, Ring-closing metathesis, Intramolecular carbonyl olefination, Cycloalkenes, Heterocyclic compounds, 593
Torsion angles
Cd(II), Hg(II), tachpyr, Twist angles, Zn(II), 1155
Tosylamide complexes
Electrochemical synthesis, Cobalt(II) complexes, Crystal structures, 1607
trans-Dioxo Re(V) complexes
Rhenium, Re complexes, Re(I), Phosphines, dppm, 2249
Trans-influence
Palladium(II) complexes, Mixed donor ligands, X-ray crystallography, Methylaluminoxane (MAO), Norbornene, Polymerization, 1601
Transition metal aroylhydrazone complexes
Diazafluorenone aroylhydrazone, Crystal structures, Enolization, ^{1}H NMR spectroscopy, IR, 1295
Transition metal complexes
Electronic spectral data, Oximes, Benzil-α-monoxime, 1687
Transition metal complexes
Imidazole derivatives, Crystal structure, Absorption spectra, Stability constants, 2183
Transition metal complexes
Terephthalate ions, Aromatic diamines, Crystal structures, Spectral data, 1415
Transition metal ions
Disulfide, Peptides, 1849
Transition metal ions
Macrocyclic polyether 18-crown-6, Acetonitrile, Alkaline earth metal ions, 1681
Transition metals
Helical structures, Supramolecular chemistry, X-ray crystal structures, 23
Transition metals
Synthesis, Structural characterization, Antitumor activity, 217
Transition metal
Tetraazamacrocyclic ligand, Synthesis, Structural characterization, Stability constants, DNA cleavage activities, 1527
Triaminoguanidinium(2 +) ion
Cu(II) complex, Structure, 1737
1,2,4-Triazolo-[1,5α]-pyrimidine
Zn(II) complexes, ^{15}N NMR, HETCOR, CPMAS, 965
Trichloroacetate
Copper(II), 1,4-Diazacycloheptane, Crystal structures, 1881
Trichlorovinyl
Mercury(II), Crystal structures, Complexes, Bidentate ligands, 2539

Tridentate chelate
Lanthanide complex, Europium(III) chloride, 2135
Trienes
Cycloadditions, Dienes, Indium, Magnesium, 533
Trifluoroacetate
Dirhodium(II) compounds, One-dimensional polymers, Arene coordination, π-Complexes, Crystal structures, 1829
Trigonal planar anions
Copper(I) thiocyanate complexes, Methyl nicotinates, Ethyl nicotinates, Ethyl isonicotinate complexes, Crystal structures, 615
Trimers
Oxo ligands, Thiolates, Titanium, 1139
Trimetallic alkoxides
Molybdenum, Tantalum, Crystal structures, 1791
Trimetallic complexes
Molybdenum(II), Tungsten(II), Crystal structures, *o*-Phenylenediacetonitrile, Bimetallic complexes, Nitrile-bridged complexes, Seven-coordinate complexes, Halocarbonyls, 147
Triphenylphosphine
Copper(I,II) complexes, α,β-Unsaturated carboxylates, Magnetic properties, Crystal structures, 891
Triphenylphosphine
Mercury(II) complexes, Benzothiazole-2-thione, pyrimidine-2-thione, Crystal structures, 2231
Triphenylphosphine
Osmium, 2-(Phenylazo)pyridine, Synthesis, Structures, Reactivities, 1227
Tripodal ligand
Ni(II) complexes, Crystal structures, Spectroscopic studies, 2661
Trirhenium(III) clusters
Rhenium clusters, Acetamidate, Dimolybdenum(II), MALDI, Mass spectroscopy, 1245
Tris(2-benzimidazolylmethyl)amine
Chromium(III) complexes, 2-Guanidinobenzimidazole, 2,6-Bis(2-benzimidazolyl)pyridine, 2-(2-Pyridyl)benzimidazole, Crystal structures, 1821
Tris(2-benzimidazolylmethyl)amine
Zinc(II), Cadmium(II), Mercury(II), X-ray diffraction structures, NMR data, 1479
Tris-chelates
Azoimine, Ru–bipyridine, X-ray structures, Electrochemistry, Emission spectra, 1925
Tris(6-methyl-2-pyridylmethyl)amine
Binuclear nickel(II) complex, Binuclear manganese(II) complex, Crystal structures, Magnetic properties, 1559
Tris-pyrazolylborate
Zinc, Crystal structures, Electrochemistry, 109
Trypanosoma cruzi
Ruthenium, Clotrimazole, Ketoconazole, Paramagnetic, Metal complexes, Chagas, 2319
Tungsten analogue
Crystallographic, Selenium, Refluxing, 2127
Tungsten carbonyls
Thiiranes, Dihydrodithiins, 521
Tungsten complexes
Molybdenum complexes, Pyrazine complexes, Peroxo ligands, Crystal structures, 1503
Tungsten(II)
Carboxylate and sulfonate substituted pyridines, Propiolic acid, Water soluble complexes, 2171
Tungsten(II)
Molybdenum(II), Crystal structures, *o*-Phenylenediacetonitrile, Bimetallic complexesw, Trimetallic complexes, Nitrile-bridged complexes, Seven-coordinate complexes, Halocarbonyls, 147
Tungsten(II)
Multimetallic, Cobalt carbonyl complexes, Alkyne complexes, Chain triphos-bridged, 1585
Tungsten
meso-2,3-dimercaptosuccinic acid, Multinuclear NMR, 193
Tungsten pentacarbonyl complexes
Mononuclear, 1,4-Bipyridine, 1,2-Bis(4-pyridyl)ethane, 1621
Tungsten
Selenoether, Telluroether, Sulfur macrocycles, Chromium, Molybdenum, 1373
Tungsten(VI)
Binaphtholato complexes, X-ray structures, 2579
Twist angles
Cd(II), Hg(II), tachpyr, Torsion angles, Zn(II), 1155
Two-centre transitions
Infrared spectroscopy, Raman spectroscopy, Electronic absorption spectroscopy, Crystal structures, Hypophosphite complexes, Cooperative vibronic transitions, 863
Two-coordinate gold complex.
Bulky phosphine, X-ray structure, Cone angle, 2211

α,β-Unsaturated carboxylates
Copper(I,II) complexes, Triphenylphosphine, Magnetic properties, Crystal structures, 891
Uracil
Crystal structures, Nickel complexes, Copper complexes, Schiff bases, 689
Uranium(IV)
Thorium(IV), Dicarboxylate complexes, CPMAS ^{13}C NMR spectroscopy, X-ray crystallography, 1757
Uranium
Thorium, Coordination compounds, Tetraphenylimidophosphinate ligand, X-ray crystal structures, 1699
Uranium
Uranyl, Phosphate, Crown, Crystal structures, 1551
Uranyl bis(2-hydroxybenzaldehyde)
Fourier transform infrared and Raman spectra, Force constants, 2353
Uranyl
Uranium, Phosphate, Crown, Crystal structures, 1551
Uridine
Copper(II), Diamines, Uridine 5′-monophosphate, 1145
Uridine 5′-monophosphate
Copper(II), Diamines, Uridine, 1145
UV–Vis–NIR, IR, ^1H NMR spectra
Thiopyrimidine, Rhenium(V) complexes, Rhenium(III) complexes, Cyclic voltammetry, 2163
UV–VIS spectra
Potentiometry, Equilibria, Stability constants, Manganese(II), Cobalt(II), Nickel(II) complexes, Aminopolyphosphonates, 2083
UV–Vis spectroscopy
meso-2,3-Dimercaptosuccinic acid, Potentiometry, Formation constants, Ionization constants, Kinetic measurements, 2435
UV–Vis spectroscopy
Vanadium, Molybdenum, Heteropolyoxometalate, IR spectroscopy, EPR spectroscopy, 1917

Vanadium complexes
Quinic acid complexes, IR spectra, Raman spectra, Thermal behavior, Potentiometric titrations, 2613
Vanadium(IV)
Dithiocarboxylate, Magnetism, EPR, Infrared, Coordination, 2155
Vanadium
Molybdenum, Heteropolyoxometalate, IR spectroscopy, UV–Vis spectroscopy, EPR spectroscopy, 1917
Vanadium
Vanadyl, Terpyridine, Density functional theory, 69
Vanadyl
Vanadium, Terpyridine, Density functional theory, 69
Vibrational spectra
Copper(I) complexes, Crystal structures, Electronic spectra, Emission spectra, Pyrazine carboxamide complexes, 601
Vinylsilanes
Hydroboration, Polysilazanes, Precursors, Chloroboranes, 323
VO(IV) complexes
Biospeciation, Al(III) complexes, Insulin-mimetics, 2389
Volatility
Scandium, Alkoxides, Crystal structures, 705
Voltammetry
Platinum(II), Platinum(IV), Bromide, Porphyrins, Electrochemistry, 1057

Water gas shift reaction
Nitrobenzene catalytic reduction, Rhodium complexes, 2-picoline, 487

Water soluble complexes
Tungsten(II), Carboxylate and sulfonate substituted pyridines, Propiolic acid, 2171
Water-soluble phosphines
Phosphino amino acid salts, Disodium or dipotassium 1,3-di(carboxylatomethyl)-5-aryl-1,3,5-diazaphosphorinanes, 1455
^{183}W NMR
Organophosphoryl polyoxotungstate, Polyoxometalate, Synthesis, 125

XAFS spectroscopy
Iron carbonyl halides, NMR, Halogen exchange reactions, Matrix isolation, 1493
X-ray crystallography
Cobalt(II), Cyanamidonitrate, Electronic spectra, Imidazole ligands, IR spectra, Nickel(II), 1021
X-ray crystallography
15-Crown-5 complexes, Liquid clathrates, Oxonium ion, 85
X-ray crystallography
Palladium(II) complexes, Mixed donor ligands, *Trans*-influence, Methylaluminoxane (MAO), Norbornene, Polymerization, 1601
X-ray crystallography
Palladium(II) complexes, Platinum(II) complexes, Chloride metathesis, Heterodifunctional ligands, 695
X-ray crystallography
Thorium(IV), Uranium(IV), Dicarboxylate complexes, CPMAS ^{13}C NMR spectroscopy, 1757
X-ray crystal structure
Cobalt(III) complex, Thiocarbamylpyrazole, Spectroscopic study, 2651
X-ray crystal structures
Europium compounds, Hydrotris(pyrazolyl)borate ligands, Luminescence studies, 1707
X-ray crystal structures
Helical structures, Supramolecular chemistry, Transition metals, 23
X-ray crystal structures
N-salicylidenearoylhydrazine copper(II) complexes, Copper(II) imidazole ternary complexes, Copper(II) imidazolate ternary complexes, Molecular structures, Magnetic properties, Infrared spectra, 1181
X-ray crystal structures
N-salicylidenearoylhydrazines, Copper(II) complexes, Molecular structures, Magnetic properties, Infrared spectra, 949
X-ray crystal structures
Palladium, Diethyldithiocarbamate, Diphosphines, Tetrachlorometallate anions, 1511
X-ray crystal structures
Ruthenium, Phosphates, 801
X-ray crystal structures
Uranium, Thorium, Coordination compounds, Tetraphenylimidophosphinate ligand, 1699
X-ray data
Lanthanide, Carbacylamidophosphate, NMR, 2203
X-ray diffraction
Magnesia, Dolomite, Crystallite size, Degree of agglomeration, SEM, 2345
X-ray diffraction structures
Zinc(II), Cadmium(II), Mercury(II), Tris-(2-benzimidazolylmethyl)amine, NMR data, 1479
X-ray
Platinum, Gold, Cross-coupling, Diyne, 2261
X-ray structure analyses
Chiral-at-metal complexes, Configurational stability, Epimerisation, Equilibria, 1519
X-ray structure
α,α′-Bis(pyrazolyl)-*m*-xylene, Copper(II) complexes, Network structures, Absorption spectroscopy, Electron spin resonance, 719
X-ray structure
Bulky phosphine, Cone angle, Two-coordinate gold complex, 2211
X-ray structure
Cadmium complexes, Mercury complexes, Sulfamides, Zinc complexes, 991
X-ray structure
Calcium, H-bonding, Inorganic Polymers, Alkaline Earth, 1783
X-ray structure
Nickel(II) piperidinedithiocarbamate complexes, Synthesis, 1713
X-ray structure
Organotin(IV), Poly(pyrazol-1-yl)alkanes, 381
X-ray structure
Organotin(IV), Poly(triazol-1-yl)alkanes, 1949
X-ray structure
Phosphoranes, Pentacoordination, Hydrogen bonding, 63
X-ray structure
Polyoxometalate, Oxyhalide, Molybdenum, High acidity, 43
X-ray structure
Rigid and flexible ligands, Self-assembly, Supramolecules, 1117
X-ray structures
Azoimine, Ru–bipyridine, Tris-chelates, Electrochemistry, Emission spectra, 1925
X-ray structures
Binaphtholato complexes, Tungsten(VI), 2579
X-ray structure
Schiff bases, Copper complexes, 5-Phenylazosalicylaldehyde, Cyclic voltammetry, 607
X-ray structures
Dinucleating alkoxide ligands, Copper(II) complexes, Hetero-bridged complexes, Magnetism, Magneto-structural trends, 1429
X-ray structures
Dithiolate complexes, Ruthenium, Osmium, 1073
X-ray structures
Lanthanides, Phosphine oxides, 2697
X-ray structures
Molybdenum, Nitrides, Alkoxides, Synthesis, NMR fluxionality, Pseudorotation, 1363
X-ray structures
Naphthylazoimidazoles, Platinum(II), PtN_4 coordination, Electrochemistry, 1263
X-ray structures
Osmium, Ditelluroether, 235
X-ray structures
Osmium, Metallation, 1081
X-ray structures
Pentafluoro-cyclotriphosphazene, Pentachloro-cyclotriphosphazene, Electrospray mass spectrometry, 2101
X-ray structures
Pyridine *N*-oxide ligands, Cobalt(II) complexes, Zinc(II) complexes, Magnetic susceptibility, 2195
X-ray structures
Rhenium, Nitrido complexes, Imido complexes, EPR spectroscopy, 1741
X-ray structures
Schiff base complexes, *N*-Salicylidene derivatives, Zn(II) complexes, 673

Ytterbium(III)
Lanthanides, Calixarenes, Homoazacalixarenes, Crystal structure, 2673
Yttrium
Planar chiral, Structure, Indenyl, Lanthanum, Tetrahydroborate, 1955
Yttrium
Rare earth elements, Hydrolysis, Enthalpy, Ionic strength, Spectrophotometry, 99

Zincates
1,3-dithiole-2-thione-4,5-dithiolates, dmit complexes, Zinc dmit compounds, 821
Zinc
Bis(pyrazolyl)silanes, Crystal structures, Nitrogen-donor ligands, 1815
Zinc complexes
Cadmium complexes, Mercury complexes, Sulfamides, X-ray structure, 991
Zinc complexes
Cobalt complex, α-Ketoglutaric acid, Thiosemicarbazones, Crystal structures, Spectroscopic properties, 1895
Zinc complexes
Lead(II) complexes, Maltol, 3-Hydroxy-4-pyranone, 3-Hydroxy-4-pyridinone, 1,2-Dimethyl, Crystal structures, 129
Zinc
Divalent metals, Copper, Benzolamide, Diethylenetriamine, Ternary complexes, 725
Zinc dmit compounds
1,3-dithiole-2-thione-4,5-dithiolates, dmit complexes, Zincates, 821
Zinc(II)
Binucleating hexa-aza macrocycle, Copper(II), Nickel(II), Cobalt(II), Crystal structures, Phosphotriester, Hydrolysis, 1485

Zinc(II)
Cadmium(II), Mercury(II), Tris(2-benzimidazolylmethyl)amine, X-ray diffraction structures, NMR data, 1479
Zinc(II) complexes
Pyridine *N*-oxide ligands, Cobalt(II) complexes, X-ray structures, Magnetic susceptibility, 2195
Zinc porphyrin complexes
Bridged structures, Crystal structures, Heteronuclear multiple bond coherence, *N*-Tosyl ligands, 413
Zinc
Streptonigrin, 2,2′-Bipyridyl, 6,6′-Dicarboxy-2,2′-bipyridyl, Antitumour, 1067
Zinc
Thiosemicarbazone, Isatin, Crystal structures, Lead, Hexamethyleneimine, Metal(II) complexes, 1255
Zinc
Tris-pyrazolylborate, Crystal structures, Electrochemistry, 109
Zirconium oxide sulfide
Sulfated zirconia, Tetragonal zirconia stabilization, Rietveld method, Zirconium sulfide, Thermogravimetry of sol–gel ZrO_2, 2283
Zirconium sulfide
Sulfated zirconia, Tetragonal zirconia stabilization, Rietveld method, Zirconium oxide sulfide, Thermogravimetry of sol–gel ZrO_2, 2283
Zirconocene
Crystal structures, Catalysis, Olefin polymerizations, 1941
Zn(II)
Cd(II), Hg(II), tachpyr, Torsion angles, Twist angles, 1155
Zn(II) complexes
Schiff base complexes, *N*-Salicylidene derivatives, X-ray structures, 673
Zn(II) complexes
1,2,4-Triazolo-[1,5α]-pyrimidine, ^{15}N NMR, HETCOR, CPMAS, 965